Cover Picture

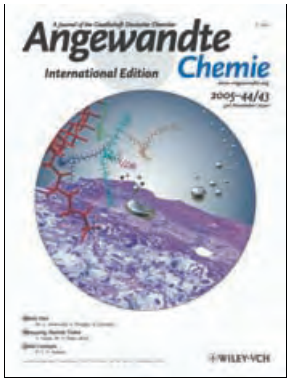

Justin M. Wiseman, Satu M. Puolitaival, Zoltán Takáts, R. Graham Cooks,* and Richard M. Caprioli*

Desorption electrospray ionization is applied to the mass spectrometric profiling of phospholipids. In their Communication on page 7094 ff., R. G. Cooks, R. M. Caprioli, and co-workers report the rapid analysis of untreated biological tissues, including the tumor region of liver tissue. The impact of charged liquid microdroplets on liver tissue in air and the release of lipids and other molecules as ions for analysis is illustrated in the cover picture (prepared by Z. Ouyang, J. Wiseman, and R. Shreve).

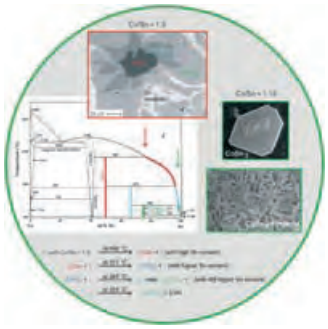

Solid-State Synthesis
A large number of new phases have been synthesized in recent years by using a metal flux. The advantages of employing liquid metals as solvents in the preparation of intermetallic compounds are presented by M. G. Kanatzidis et al. in their Review on page 6996 ff.

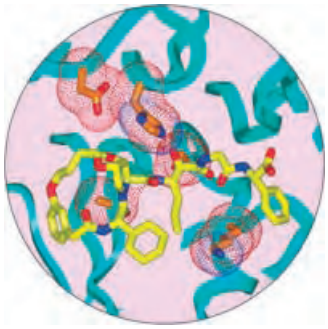

Hepatitis Virus Inhibitor
A proline-based macrocycle binds tightly with the Ala156 methyl group of hepatitis C virus (HCV) NS3 protease. In their Communication on page 7024 ff., K. X. Chen and co-workers show why the macrocycle is a potent HCV inhibitor.

Noncovalent Interactions
M. J. Krische and H. Gong show in their Communication on page 7069 ff. how aminopyrazolones, through interactions between their amide and amidine groups, can self-assemble into 1D architectures or aggregates to give macrocyclic quartets.

Contents

The following Communications have been judged by at least two referees to be "very important papers" and will be published online at www.angewandte.org soon:

*C. Drago, L. Caggiano, R. F. W. Jackson**
Vanadium-Catalyzed Sulfur Oxidation/Kinetic-Resolution Process for the Synthesis of Enantiomerically Pure Alkyl Aryl Sulfoxides

*Q. Qing, F. Chen, P. Li, W. Tang, Z. Wu, Z. Liu**
Finely Tuning the Metallic Nanogap Size with Electrodeposition Utilizing High-Frequency Impedance in Feedback

X. Rocquefelte, S. E. Boulfelfel, M. B. Yahia, J. Bauer, J.-Y. Saillard,* J.-F. Halet**
The Structural Preferences of Boron and Carbon within MB_2C_2 (M = Mg,Sc,Ca,Y,Ln) Phases: The "Coloring Problem" Revisited by DFT Calculations

G. C. Lloyd-Jones, R. G. Margue, J. G. de Vries*
Rate Enhancement by Ethylene in the Ru-Catalyzed Ring-Closing Metathesis of Enynes: Evidence for an "Ene-then-Yne" Pathway That Diverts through a Second Catalytic Cycle

S. Klaus, H. Neumann, A. Zapf, D. Strübing, S. Hübner, J. Almena, T. Riermeier, P. Groß, M. Sarich, W.-R. Krahnert, K. Rossen, M. Beller**
A General and Efficient Method for the Formylation of Aryl and Heteroaryl Bromides

N. Martín, Á. Martín-Domenech, S. Filippone, M. Altable, L. Echegoyen,* C. M. Cardona*
Retrocycloaddition Reactions of Pyrrolidinofullerenes

News

Nobel Prizes 2005: Chemistry, Physiology or Medicine, Physics ____ **6982**

Books

Electronic and Photoelectron Spectroscopy — Andrew Ellis, Miklos Feher, Timothy Wright — *reviewed by G. Hohlneicher* ____ **6983**

Highlights

Peptide–Polymer Hybrids

M. A. Balbo Block, S. Hecht* ____ **6986 – 6989**

Wrapping Peptide Tubes: Merging Biological Self-Assembly and Polymer Synthesis

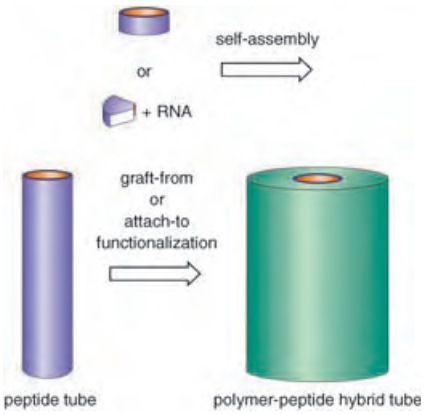

It's a wrap: Self-assembling peptide tubes are wrapped in polymer sheaths by using efficient graft-from or attach-to routes (see scheme). The properties of the peptide tubes are tuned by the polymer sheath, and the resulting peptide–polymer hybrids could prove useful for various future applications.

InterScience
© 2005 Wiley-VCH Verlag GmbH & Co. KGaA, Weinheim

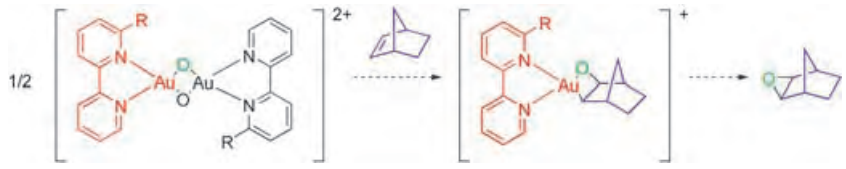

Staking claims: New aspects of gold catalysis—nucleophilic additions to unactivated olefins, auraoxetanes as the first observed organometallic intermediates, and the exciting experiments addressing the oxidation state of the catalyst—are discussed, and future challenges in this dynamic field are pointed out.

Gold Catalysis

A. S. K. Hashmi* ——— **6990 – 6993**

The Catalysis Gold Rush: New Claims

Reviews

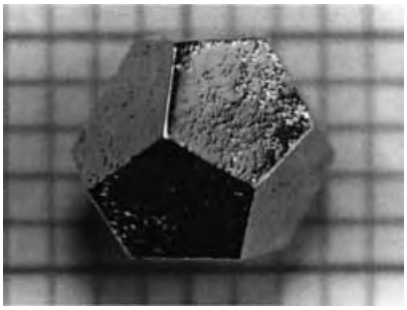

In flux: Syntheses in metal fluxes have a huge potential for generating new intermetallic species, and in recent years many new phases, sometimes with very unusual compositions, have been prepared by this method. The advantages of this approach lie in the enhanced diffusion of the elements that are dissolved in the metal solvent and the lower reaction temperatures that can be employed.

Synthesis in Metal Flux

M. G. Kanatzidis,* R. Pöttgen,* W. Jeitschko* ——— **6996 – 7023**

The Metal Flux: A Preparative Tool for the Exploration of Intermetallic Compounds

Communications

Life-saving donut: Macrocyclization through a Mitsunobu reaction was used to synthesize a 17-membered macrocycle. The bicyclic acetal core was prepared completely diastereoselectively. The macrocyclic peptidomimetic surrogate of the P2–P3 dipeptide moiety was designed to function as a hepatitis C virus (HCV) NS3 serine protease inhibitor, and the pentapeptide α-ketoamides derived from the macrocycle were shown to be potent HCV inhibitors.

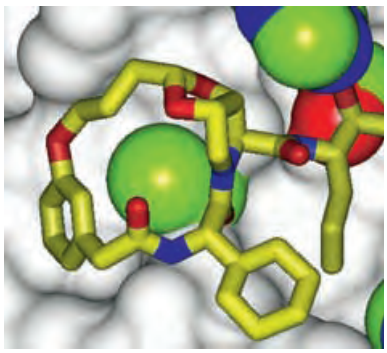

Protease Inhibitors

K. X. Chen,* F. G. Njoroge, B. Vibulbhan, A. Prongay, J. Pichardo, V. Madison, A. Buevich, T.-M. Chan ——— **7024 – 7028**

Proline-Based Macrocyclic Inhibitors of the Hepatitis C Virus: Stereoselective Synthesis and Biological Activity

For the USA and Canada:
ANGEWANDTE CHEMIE International Edition (ISSN 1433-7851) is published weekly by Wiley-VCH PO Box 191161, D 69451 Weinheim, Germany. Air freight and mailing in the USA by Publications Expediting Inc. 200 Meacham Ave., Elmont, NY 11003. Periodicals postage paid at Jamaica NY 11431. US POSTMASTER: send address changes to *Angewandte Chemie*, Wiley-VCH, 111 River Street, Hoboken, NJ 07030. Annual subscription price for institutions: US$ 5685/5168 (valid for print and electronic / print or electronic delivery); for individuals who are personal members of a national chemical society prices are available on request. Postage and handling charges included. All prices are subject to local VAT/sales tax.

© 2005 Wiley-VCH Verlag GmbH & Co. KGaA, Weinheim

The best in chemistry –

for more than a hundred years

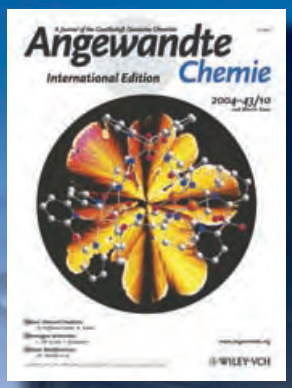

A Journal of the Gesellschaft Deutscher Chemiker

Angewandte International Edition **Chemie**

www.angewandte.org

1888: ***The beginning of a success story***

Constant Innovations

1962: First issue of the International Edition
1976: Graphical abstracts
1979: Cover pictures
1988: Centenary of Angewandte
1989: Routine use of color
1991: New section: Highlights
1992: Computerized editorial tracking system
1995: Internet service for readers
1998: Regular press service; full-text online
2000: New section: Essays; EarlyView: Communications available online ahead of the printed version
2001: New section: Minireviews
2002: Online submission of manuscripts
2003: Weekly publication; new section: News; new layout
2004: Backfiles (1962-1997); ManuscriptXpress: Online system for authors and referees

Angewandte's advisors...

Rolf Thauer
MPI für terrestrische Mikrobiologie, Marburg

» *In 1970 Karl Decker, Kurt Jungermann, and I published a review on "Energy Production in Anaerobic Organisms" in* ***Angewandte Chemie****. We were soon surprised how many scientists from all over the world had read the article. Ever since then I have admired the broad scope, the high impact, and internationality of this Journal and I am therefore very proud, as a "chemical microbiologist", to be a member of its Editorial Board.* «

Angewandte Chemie International Edition *is a journal of the German Chemical Society (GDCh)*

GDCh

WILEY InterScience® DISCOVER SOMETHING GREAT

WILEY-VCH

11991404_gu

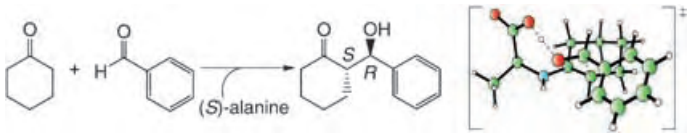

Combined forces: Theory and experiment are used together to determine the mechanism of primary amino acid catalyzed intermolecular aldol reactions. A six-membered chairlike structure is determined to be the transition state for the reaction between benzaldehyde and cyclohexanone catalyzed by (*S*)-alanine (see scheme), and a carboxylic acid catalyzed enamine mechanism is shown to be the most favorable reaction pathway.

Homochirality

A. Bassan, W. Zou, E. Reyes, F. Himo,*
A. Córdova* ——— **7028 – 7032**

The Origin of Stereoselectivity in Primary Amino Acid Catalyzed Intermolecular Aldol Reactions

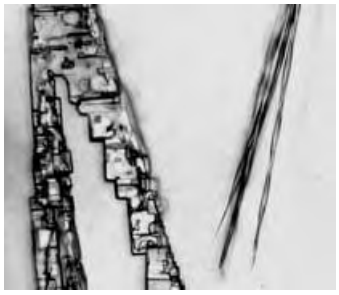

At long last, the crystal structure of the metastable form of benzamide, whose existence has been known of for over 170 years, has finally been solved by using a combination of in situ crystallization, high-speed synchrotron X-ray powder diffraction, and global-optimization methods of structure determination (see picture).

Crystallography

W. I. F. David, K. Shankland, C. R. Pulham, N. Blagden, R. J. Davey,*
M. Song ——— **7032 – 7035**

Polymorphism in Benzamide

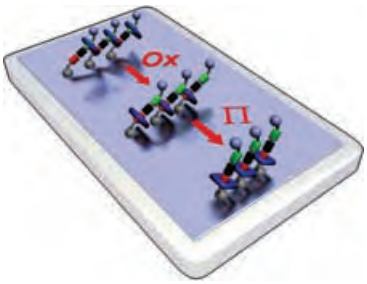

On the move! Upon oxidation in situ, a positively charged ring travels a few nanometers along the dumbbell-shaped component of a monolayer of soaplike, bistable [2]rotaxanes on water (see picture). This motion was probed by surface-sensitive X-ray scattering and establishes that bistable rotaxanes retain their switching capabilities even in condensed monolayer phases.

Molecular Devices

K. Nørgaard, B. W. Laursen, S. Nygaard, K. Kjaer, H.-R. Tseng, A. H. Flood, J. F. Stoddart,
T. Bjørnholm* ——— **7035 – 7039**

Structural Evidence of Mechanical Shuttling in Condensed Monolayers of Bistable Rotaxane Molecules

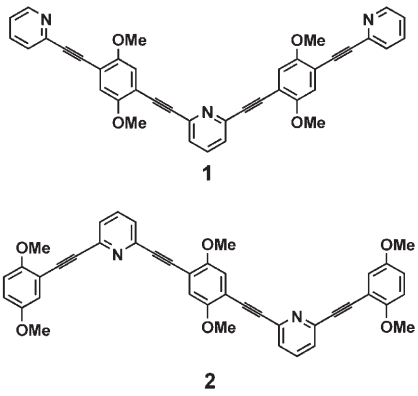

Pick of the bunch: Banana-shaped molecules **1** and **2** containing dimethoxybenzene and pyridine units are highly efficient emitters of violet light despite the interruption of the π conjugation because of *meta* substitution. The contrasting solvent dependencies of the fluorescence quantum yield values of **1** and **2** are explained by the disparity between the difference density distributions in the excited states of the molecules.

Luminescence

Y. Yamaguchi,* S. Kobayashi, T. Wakamiya, Y. Matsubara, Z.-i. Yoshida* **7040 – 7044**

Banana-Shaped Oligo(arylene-ethynylene)s: Synthesis and Light-Emitting Characteristics

© 2005 Wiley-VCH Verlag GmbH & Co. KGaA, Weinheim

Contents

Biosynthesis

S. F. Brady,* J. Clardy ——— **7045 – 7048**

Systematic Investigation of the *Escherichia coli* Metabolome for the Biosynthetic Origin of an Isocyanide Carbon Atom

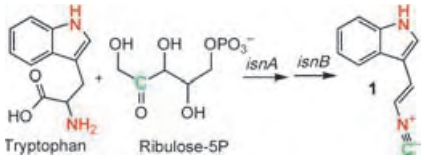

Feeding studies were conducted in which *E. coli* metabolism was controlled through the systematic use of strains that carry mutations in primary metabolic pathways, thus allowing the origin of the isocyanide carbon atom in antibiotic **1** to be determined. This carbon atom was shown to be derived from the C2 atom of ribulose-5P, or a tautomerically equivalent sugar (see scheme; *isnA* and *isnB* are the genes responsible for the biosynthetic pathway of **1**).

Hybrid Materials

W. Schmitt,* J. P. Hill, S. Malik, C. A. Volkert, I. Ichinose, C. E. Anson, A. K. Powell* ——— **7048 – 7053**

Thermolysis of a Hybrid Organic–Inorganic Supramolecular Coordination Assembly: Templating the Formation of Nanostructured Fibrous Materials and Carbon-Based Microcapsules

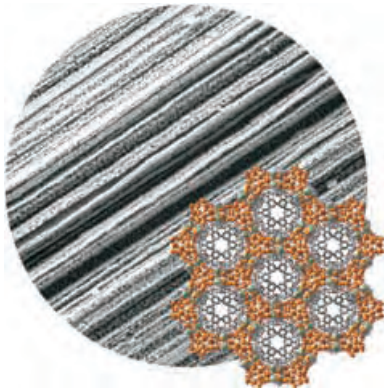

Burning a honeycomb: An exceptional hybrid organic–inorganic coordination assembly with an extended 3D structure that contains vast separated organic and inorganic regions has been prepared (see picture of its supramolecular structure and a scanning electron micrograph image). This hybrid is used as a template in thermolysis reactions to yield nano- and microsized products whose properties are determined by those of the precursor compounds.

Mesoporous Polymers

Y. Meng, D. Gu, F. Q. Zhang, Y. F. Shi, H. F. Yang, Z. Li, C. Z. Yu, B. Tu, D. Y. Zhao* ——— **7053 – 7059**

Ordered Mesoporous Polymers and Homologous Carbon Frameworks: Amphiphilic Surfactant Templating and Direct Transformation

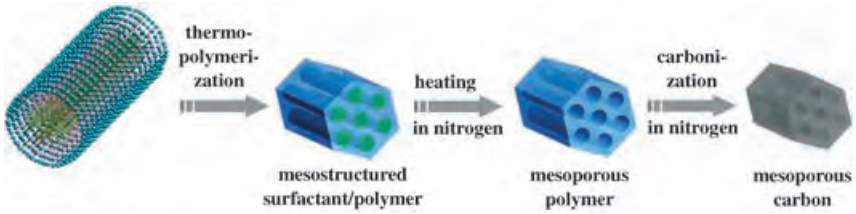

Ultrahigh stability (> 1400 °C) is found for the highly ordered mesoporous polymers and carbon frameworks synthesized from polymerization of phenol and formaldehyde around triblock copolymer templates. Calcination and carbonization lead to removal of the templates and formation of hexagonal and cubic carbon mesostructures with large uniform pores and surface areas (see schematic diagram).

Crystal Engineering

K. Sada,* K. Inoue, T. Tanaka, A. Epergyes, A. Tanaka, N. Tohnai, A. Matsumoto, M. Miyata* ——— **7059 – 7062**

Multicomponent Organic Alloys Based on Organic Layered Crystals

Random layer: Multicomponent organic solid solutions were obtained by treating equimolar mixtures of two or more aliphatic carboxylic acids with 1-naphthylmethylamine (NMA; see scheme). The single sharp XRD peaks of the crystalline products indicate specific pairing of alkyl groups between the NMA layers to form mixed crystals rather than eutectic mixtures of the components.

© 2005 Wiley-VCH Verlag GmbH & Co. KGaA, Weinheim

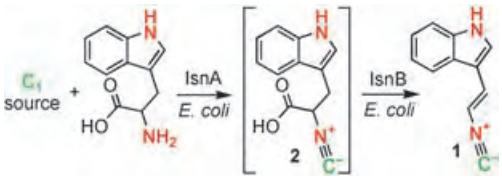

One gene, *isnA*, encodes the enzyme that converts the precursor amine functionality of tryptophan into the isocyanide moiety. The isolation and characterization of the isocyanide-containing environmental-DNA-derived antibiotic **1**, its biosynthetic genes (*isnA* and *isnB*), and the general outline of the biosynthesis of **1** via intermediate **2** are presented (see scheme).

Biosynthesis

S. F. Brady,* J. Clardy ——— **7063 – 7065**

Cloning and Heterologous Expression of Isocyanide Biosynthetic Genes from Environmental DNA

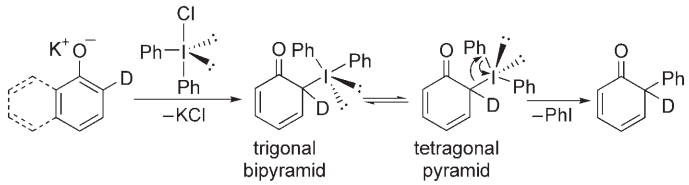

Dearomatization: Treatment of phenols and naphthols substituted at the *ortho* position by a small electron-donating group D with chlorodiphenyl-λ^3-iodane leads to their regioselective *ortho* phenylation to give cyclohexa-2,4-dienone derivatives (see scheme). The mechanism of this reaction involves a nonradical direct coupling of the ligands.

Regioselective Reactions

A. Ozanne-Beaudenon, S. Quideau* ——— **7065 – 7069**

Regioselective Hypervalent-Iodine(III)-Mediated Dearomatizing Phenylation of Phenols through Direct Ligand Coupling

The fab four: Aminopyrazolones which incorporate two ditopic hydrogen-bond donor–acceptor pairs of amide and amidine functional groups can self-assemble through formation of four hydrogen bonds. Single-crystal X-ray diffraction analysis reveals that homomeric aggregation (amide–amide, amidine–amidine) affords 1D architectures while heteromeric aggregation (amide–amidine) generates macrocyclic quartets (see picture).

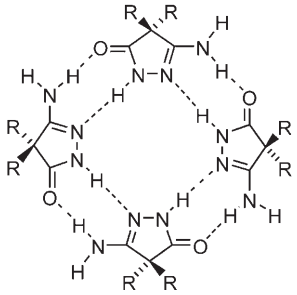

Self-Assembly

H. Gong, M. J. Krische* ——— **7069 – 7071**

Hydrogen-Bond-Mediated Self-Assembly of Aminopyrazolones: Macrocyclic Quartets—Single and Stacked One-Dimensional Motifs

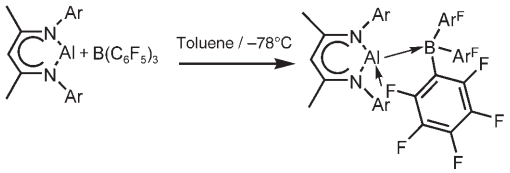

Some elements go both ways: The reaction of [LAl] (L = HC(CMeNAr)$_2$, Ar = 2,6-*i*Pr$_2$C$_6$H$_3$) with BAr$^F_3$ (Ar^F = C$_6$F$_5$) yields [LAlBAr$^F_3$] (see scheme). Crystallographic studies and ab initio calculations show the formation of an Al–F bond, which shows the aluminum center having both Lewis base and Lewis acid character.

Aluminum Complexes

Z. Yang, X. Ma, R. B. Oswald, H. W. Roesky,* H. Zhu, C. Schulzke, K. Starke, M. Baldus, H.-G. Schmidt, M. Noltemeyer ——— **7072 – 7074**

Janus-Faced Aluminum: A Demonstration of Unique Lewis Acid and Lewis Base Behavior of the Aluminum Atom in [LAlB(C$_6$F$_5$)$_3$]

© 2005 Wiley-VCH Verlag GmbH & Co. KGaA, Weinheim

Contents

Biosynthesis

A. Bhatt, C. B. W. Stark, B. M. Harvey, A. R. Gallimore, Y. A. Demydchuk, J. B. Spencer, J. Staunton, P. F. Leadlay* ——— **7075 – 7078**

Accumulation of an *E*,*E*,*E*-Triene by the Monensin-Producing Polyketide Synthase when Oxidative Cyclization is Blocked

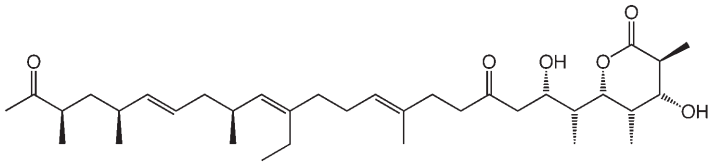

Evidence for the intermediate in the polyether biosynthesis of the ionophore antibiotic monensin A has been obtained. A tridecaketide *E*,*E*,*E*-triene (see formula) has been isolated by using mutant strains of *Streptomyces cinnamonensis*. Characterization of this intermediate allows the likely biosynthetic route to monensin to be discriminated.

Enzyme Reaction Mechanisms

D. Spiteller, C. L. Waterman, J. B. Spencer* ——— **7079 – 7082**

A Method for Trapping Intermediates of Polyketide Biosynthesis with a Nonhydrolyzable Malonyl-Coenzyme A Analogue

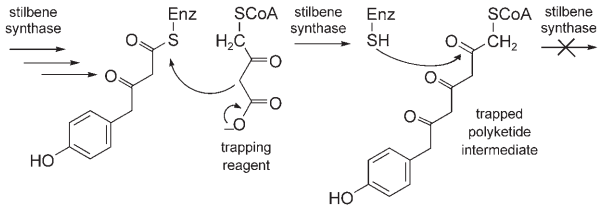

Trapped in the middle: To investigate the mechanistic details of polyketide biosynthesis, intermediates are trapped by a nonhydrolyzable malonyl-coenzyme A analogue that reacts with a growing polyketide chain formed by a stilbene synthase. As the reverse transesterification reaction is not possible, the polyketide intermediates accumulate attached to the analogue (see scheme; Enz = enzyme, CoA = coenzyme A).

Diels–Alder Reactions

Y. Yamamoto, H. Yamamoto* ——— **7082 – 7085**

Catalytic Asymmetric Nitroso-Diels–Alder Reaction with Acyclic Dienes

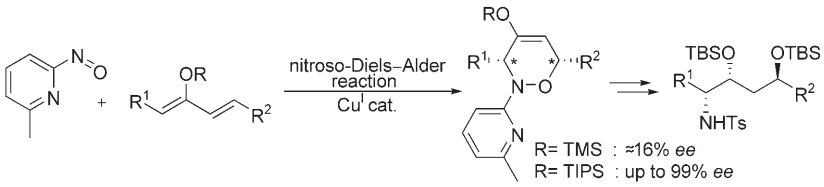

Bigger, bulkier, better: Catalytic asymmetric nitroso-Diels–Alder reactions of nitrosopyridines with silyloxydienes lead to adducts with excellent enantioselectivities (see scheme). The bulk of the silyl group (TMS = trimethylsilyl, TIPS = triisopropylsilyl) forces the diene to adopt an *s-cis* configuration in favor of the typical concerted [4+2] cycloaddition. The Diels–Alder adducts can then be converted into protected amino alcohols.

Composite Films

Y. Yu, C.-H. Chen,* J.-L. Shui, S. Xie ——— **7085 – 7089**

Nickel-Foam-Supported Reticular CoO–Li_2O Composite Anode Materials for Lithium Ion Batteries

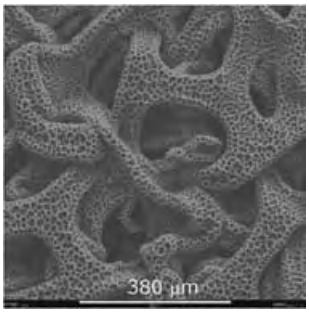

Although considered to be the inactive component, Li_2O plays three important roles in the carbon-free CoO–Li_2O composite films (see SEM image) that have now been prepared: It prohibits CoO particle growth during synthesis, it oxidizes Co^{2+} to Co^{3+}, and it acts as a structural buffer. The composite films, supported on a conducting nickel-foam substrate, were prepared by the electrostatic spray deposition technique. They display large initial discharge capacities and low first-cycle capacity losses.

© 2005 Wiley-VCH Verlag GmbH & Co. KGaA, Weinheim

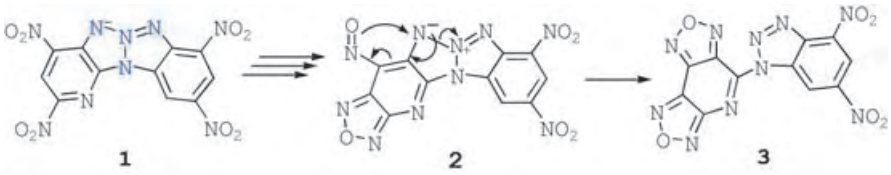

Off with a bang: The thermally stable high-energy **1** was prepared in a more efficient synthetic route. An unexpected ring scission of the tetraazapentalene T-shaped isomer **1** (distinctive nitrogen atom arrangement indicated in blue) occurs through an intramolecular electron rearrangement activated by highly-reactive ψ-dinitroso substituents of intermediate **2** to give **3**.

Explosives

M. H. V. Huynh,* M. A. Hiskey,* D. E. Chavez, R. D. Gilardi _ **7089 – 7094**

Tetraazapentalene Chemistry: Unexpected Intramolecular Electron Rearrangement Induced by Highly Reactive ψ-Dinitroso Substituents

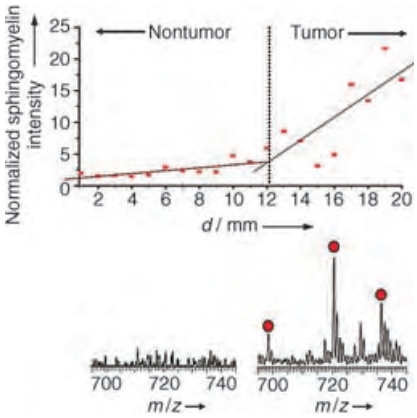

Direct chemical profiling of biological tissues, including metastatic human-liver adenocarcinoma, was carried out by using mass spectrometry under ambient conditions. Desorption electrospray ionization revealed enhanced signals from sphingolipids and increased unsaturation levels of the phospholipids in the tumor region of the tissue (see picture).

Phospholipids

J. M. Wiseman, S. M. Puolitaival, Z. Takáts, R. G. Cooks,* R. M. Caprioli* _____ **7094 – 7097**

Mass Spectrometric Profiling of Intact Biological Tissue by Using Desorption Electrospray Ionization

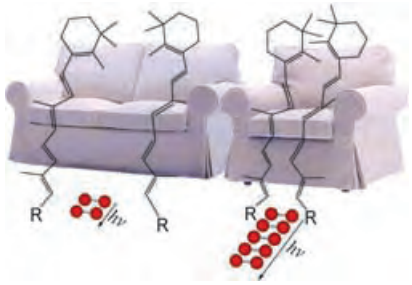

Up close and personal: Intimate retinoid polyenes, shown on the right chair, were found to react readily with oxygen (shown in red) to give the polyoxygenated species. On the other hand, when the polyenes are separated, shown on the left sofa, the oxidation is limited.

Superoxidation

I. Washington, S. Jockusch, Y. Itagaki, N. J. Turro,* K. Nakanishi* _ **7097 – 7100**

Superoxidation of Bisretinoids

Five are too many: It is known experimentally that $[(Cp')_2Zr(N_2)Zr(Cp')_2]$ ($Cp' = C_5H_{5-n}Me_n$) with $n = 4$ activates N_2 for hydrogenation, but the complex with $n = 5$ does not. This difference in reactivity arises from the N_2 coordination mode (see scheme): For $n = 0$–4, N_2 is side-on coordinated—the most suitable mode for hydrogenation—whereas for $n = 5$, N_2 is end-on coordinated owing to steric repulsion between five Me groups.

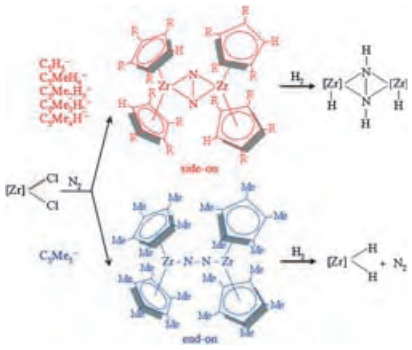

Nitrogen Fixation

P. Bobadova-Parvanova, Q. Wang, K. Morokuma,* D. G. Musaev* _____ **7101 – 7103**

How Many Methyl Groups in $[\{(\eta^5\text{-}C_5Me_nH_{5-n})_2Zr\}_2(\mu_2,\eta^2,\eta^2\text{-}N_2)]$ Are Needed for Dinitrogen Hydrogenation? A Theoretical Study

© 2005 Wiley-VCH Verlag GmbH & Co. KGaA, Weinheim

Contents

Epoxidation Catalysts

M. Kodera,* M. Itoh, K. Kano, T. Funabiki, M. Reglier ——— **7104 – 7106**

A Diiron Center Stabilized by a Bis-TPA Ligand as a Model of Soluble Methane Monooxygenase: Predominant Alkene Epoxidation with H_2O_2

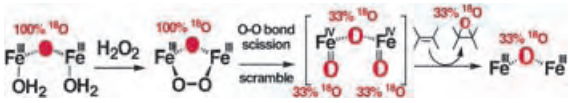

Double act: The diiron(II) complex $[Fe_2(6\text{-HPA})(O)(OH_2)_2](ClO_4)_4$ (**1**) catalyzes alkene epoxidation with H_2O_2 via a peroxodiiron complex. Detailed isotope-labeling experiments with μ-^{18}O-**1** reveal incorporation of both oxo- and peroxo-derived oxygen atoms into the epoxide reaction product (see scheme; 6-HPA = 1,2-bis[2-{bis(2-pyridylmethyl)-aminomethyl}-6-pyridyl]ethane).

Host–Guest Systems

Y. Liu, R. Warmuth* ——— **7107 – 7110**

A "Through-Shell" Binding Isotope Effect

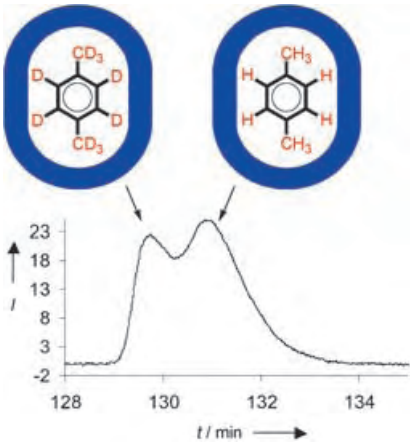

Small, but very significant: Partial separation of two hemicarceplexes which differed only in the degree of guest deuteration could be achieved by normal-phase chromatography (see picture). The difference in retention time arises from a variation in the interaction between the hemicarceplex and the silica surface as a consequence of a 0.005-Å difference in the C–H and C–D bond lengths of the guest molecules.

Magnetic Compounds

G. Leibeling, S. Demeshko, S. Dechert, F. Meyer* ——— **7111 – 7114**

Hysteretic Magnetic Bistability Based on a Molecular Azide Switch

Like a molecular toggle switch, the bridging azide ion in a highly preorganized dinickel(II) complex turns strong antiferromagnetic coupling on or off (see picture). Single crystals of the compound stay intact over the entire temperature range studied and feature hysteretic bistability not far from ambient temperature.

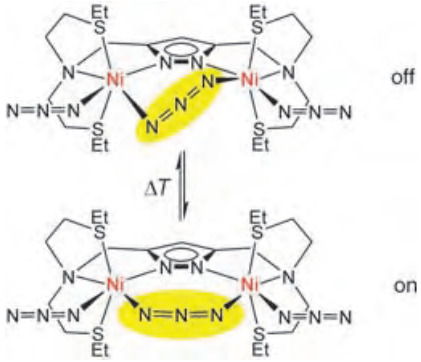

Synthetic Methods

V. Gandon, D. Leboeuf, S. Amslinger, K. P. C. Vollhardt, M. Malacria, C. Aubert* ——— **7114 – 7118**

Chemo-, Regio-, and Stereoselective Cobalt-Mediated [2+2+2] Cycloaddition of Alkynyl Boronates to Alkenes: 1,3- and 1,4-Diboryl-1,3-cyclohexadienes

Diborylated compounds are obtained by means of CpCo-mediated cocyclization of alkynyl(pinacol)boronic esters to alkenes followed by oxidative demetalation (see scheme). This strategy for the rapid and efficient construction of highly functionalized 1,3-cyclohexadienes and arenes is compatible with various substrates.

© 2005 Wiley-VCH Verlag GmbH & Co. KGaA, Weinheim

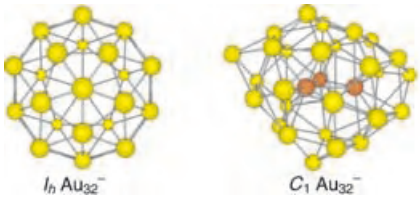

A heart of gold: The structure of the Au_{32}^- cluster has been elucidated by comparison of the results from photoelectron spectroscopy with those from theoretical calculations. Although DFT calculations suggest a high-symmetry hollow-cage structure (I_h, left) to be the lowest in energy at 0 K, the spectrum calculated for a low-symmetry (C_1, right) distorted cage containing three Au atoms inside agrees best with the experimental results.

Gold Clusters

M. Ji, X. Gu, X. Li, X. G. Gong,* J. Li,* L.-S. Wang* ——— **7119 – 7123**

Experimental and Theoretical Investigation of the Electronic and Geometrical Structures of the Au_{32} Cluster

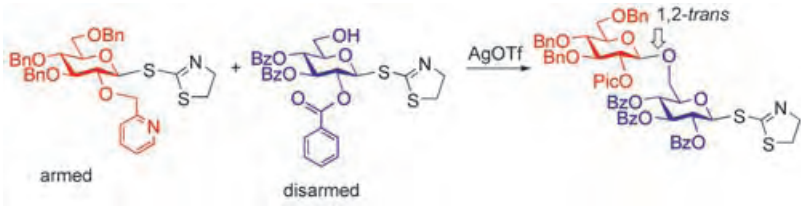

Armed and dangerous: A new armed–disarmed glycosylation strategy (see picture) allows chemoselective introduction of a 1,2-*trans* glycosidic linkage prior to other linkages through the use of a 2-*O*-picolyl moiety. This neighbouring group is capable of efficient participation through a six-membered intermediate while retaining the glycosyl donor in the armed state. Bn = benzyl, Bz = benzoyl, Tf = trifluoromethanesulfonyl, Pic = picolyl.

Selective Glycosylations

J. T. Smoot, P. Pornsuriyasak, A. V. Demchenko* ——— **7123 – 7126**

Development of an Arming Participating Group for Stereoselective Glycosylation and Chemoselective Oligosaccharide Synthesis

A pseudo-benziodoxazine structure with intramolecular secondary I···O bonding, as shown by X-ray analysis, is seen in a series of *N*-(2-iodylphenyl)acylamides prepared from 2-iodoaniline (see scheme). These compounds contain a six-membered pseudocyclic scaffold about an iodine(v) center and are able to oxidize either alcohols or sulfides, with the reactivity depending largely on the substitution pattern on the amide group adjacent to the iodyl moiety.

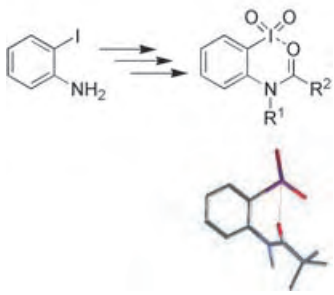

Synthetic Methods

U. Ladziata, A. Y. Koposov, K. Y. Lo, J. Willging, V. N. Nemykin,* V. V. Zhdankin* ——— **7127 – 7131**

Synthesis, Structure, and Chemoselective Reactivity of *N*-(2-Iodylphenyl)acylamides: Hypervalent Iodine Reagents Bearing a Pseudo-Six-Membered Ring Scaffold

A small number of isolated Au^{3+} ions (0.02 Au^{3+}/nm^2) heterogenized on a zirconia surface from a cheap inorganic source ($HAuCl_4$) is able to grant high catalytic activity for the selective hydrogenation of 1,3-butadiene (see picture). The catalytic turnover and mass activity rates of the Au^{3+} ions are respectively one and two orders of magnitude higher than those of metallic gold nanoparticles.

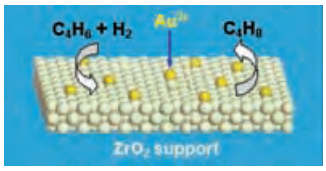

Supported Au Catalysts

X. Zhang, H. Shi, B.-Q. Xu* **7132 – 7135**

Catalysis by Gold: Isolated Surface Au^{3+} Ions are Active Sites for Selective Hydrogenation of 1,3-Butadiene over Au/ZrO_2 Catalysts

© 2005 Wiley-VCH Verlag GmbH & Co. KGaA, Weinheim

Contents

Helical Structures

K. Nakano, Y. Hidehira, K. Takahashi, T. Hiyama, K. Nozaki* ——— **7136 – 7138**

Stereospecific Synthesis of Hetero[7]helicenes by Pd-Catalyzed Double *N*-Arylation and Intramolecular *O*-Arylation

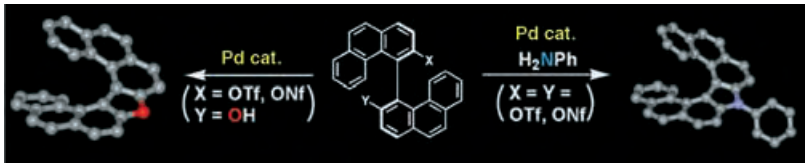

Enantioenriched aza- and oxa[7]helicenes are synthesized from an enantiopure biphenanthryldiol in a highly stereoselective manner. An *N*-phenylaza[7]helicene is prepared by a palladium-catalyzed double *N*-arylation of aniline with disulfonate derivatives (see scheme, right), whereas an oxa[7]helicene is obtained by a palladium-catalyzed intramolecular *O*-arylation of monosulfonate derivatives (see scheme, left).

Sources

Product and Company Directory

You can start the entry for your company in "Sources" in any issue of *Angewandte Chemie*.

If you would like more information, please do not hesitate to contact us.

Wiley-VCH Verlag – Advertising Department
Tel.: 0 62 01 - 60 65 65
Fax: 0 62 01 - 60 65 50
E-Mail: MSchulz@wiley-vch.de

Service

Keywords ——— *7140*

Authors ——— *7141*

Vacancies ——— *7139*

Preview ——— *7143*

© 2005 Wiley-VCH Verlag GmbH & Co. KGaA, Weinheim

Nobel Prizes 2005

Chemistry

The Nobel Prize in Chemistry is shared equally by Yves Chauvin (Institut Français du Pétrole, near Paris, France), Robert H. Grubbs (California Insitute of Technology, Pasadena, USA), and Richard R. Schrock (Massachusetts Institute of Technology, Cambridge, USA) for the development of the metathesis method in organic synthesis. While metathesis is now a well understood, many-flavored reaction with numerous industry-strength applications,[1] this was not the case when Chauvin started his investigations of its mechanism—many years after it had first been observed. In fact, he was put on the right track by publications in 1964 by Nobel laureates G. Natta (1963) and E. O. Fischer[2] (1973) as well as Banks and Bailey. Chauvin's groundbreaking paper on the mechanism appeared in 1971 and paved the way for the research of Grubbs and Schrock.[3]

Y. Chauvin

R. H. Grubbs

R. R. Schrock

Both Grubbs and Schrock have made outstanding contributions to the field of organometallic chemistry directed towards organic and polymer synthesis. Grubbs is famous for the development of a range of ruthenium-containing catalysts for olefin metathesis;[4] Schrock's name is associated with tungsten alkylidene complexes and ring-opening-metathesis polymerization.[5] Grubbs received his PhD in 1968 at Columbia University in New York under the direction of R. Breslow. In 1968 and 1969 he worked as a postdoc in the research group of J. P. Collman (Stanford University), and then as assistant and associate professor at Michigan State University in East Lansing. Since 1978 he has held a position as professor at the California Institute of Technology in Pasadena. He is the editor of the 2003 *Handbook of Metathesis* published by Wiley-VCH. Schrock earned his PhD in 1971 at Harvard University with J. A. Osborn. He subsequently worked for a year at Cambridge University (UK), and for three years at DuPont de Nemours. He has been active at the Massachusetts Institute of Technology since 1975, and as professor since 1980. Both Grubbs and Schrock serve on the boards of *Advanced Synthesis & Catalysis* and the *Journal of Polymer Science Part A: Polymer Chemistry*. Individually, they have received numerous awards, but only one jointly: In September this year, they received the German Chemical Society's prestigious August Wilhelm von Hofmann Medal. Chauvin worked at the Institut Français du Pétrole, an independent research, industrial development, and training institute, until his retirement about 10 years ago; he is still an honorary director there. His research encompassed organometallic chemistry and catalysis, as well as ionic liquids and polymers. He is a corresponding member of the French Academy of Sciences and recently contributed an introductory chapter to the handbook *Multiphase Homogeneous Catalysis* (Cornils et al. (Eds.), Wiley-VCH, 2005). Chauvin was surprized to have received the prize: "I am a bit embarrassed. I have enjoyed a quiet life until now. My American colleagues have demonstrated that my 35-year-old research was actually important. I owe the prize to them."

Physiology or Medicine

This year's laureates have indeed contributed to solving a common problem: Barry J. Marshall (QEII Medical Centre, University of Western Australia) and J. Robin Warren (formerly at the Royal Perth Hospital, Australia) were recognized for their research on the bacterium *Helicobacter pylori* and identifying its role in gastritis and peptic ulcer disease.

Physics

The Nobel Prize in Physics was awarded with one half to Roy J. Glauber (Harvard University, USA) for his contribution to the quantum theory of optical coherence and jointly to John L. Hall (National Institute of Standards and University of Colorado, Boulder, USA), and Theodor W. Hänsch (Universität München and Max Planck Institute of Quantum Optics, Germany) for their contributions to the development of laser-based precision spectroscopy, including the optical frequency comb technique. Their work made it possible to measure frequencies with an accuracy of fifteen digits, which is useful for high-precision clocks, satellite navigation, and telecommunications.

This year, the prizes are worth 1.3 million US Dollars each. They are presented traditionally by the King of Sweden on December 10, the anniversary of Alfred Nobel's death.

[1] a) *Handbook of Metathesis* (Ed. R. H. Grubbs), Wiley-VCH, Weinheim, **2003**; b) Thematic Olefin Metathesis Issue: A. Fürstner, R. H. Grubbs, R. R. Schrock, *Adv. Synth. Catal.* **2002**, *344*, 567.

[2] a) M. Rouhi, *Chem. Eng. News* **2002**, *80*, December 23, p. 34; b) G. Natta, G. Dall'Asta, G. Mazzanti, *Angew. Chem.* **1964**, *76*, 765; *Angew. Chem. Int. Ed. Engl.* **1964**, *3*, 723; c) E. O. Fischer, A. Maasböl, *Angew. Chem.* **1964**, *76*, 645; *Angew. Chem. Int. Ed. Engl.* **1964**, *3*, 580.

[3] J.-L. Hérisson, Y. Chauvin, *Makromol. Chem.* **1971**, *141*, 161.

[4] R. H. Grubbs, T. M. Trnka in *Ruthenium in Organic Synthesis* (Ed.: S.-I. Murahashi), Wiley-VCH, Weinheim, **2005**, pp. 153–177.

[5] R. R. Schrock, A. H. Hoveyda, *Angew. Chem.* **2003**, *115*, 4740; *Angew. Chem. Int. Ed.* **2003**, *42*, 4592.

DOI: 10.1002/anie.200503509

InterScience
© 2005 Wiley-VCH Verlag GmbH & Co. KGaA, Weinheim

Peptide–Polymer Hybrids

DOI: 10.1002/anie.200502436

Wrapping Peptide Tubes: Merging Biological Self-Assembly and Polymer Synthesis**

*Marco A. Balbo Block and Stefan Hecht**

Keywords:
bionanotechnology · hybrid materials · peptides · polymers · self-assembly

Transmembrane channels and pores are among Nature's most admirable devices, especially with regard to their almost perfect selectivity, speed, and gating of transport processes. Their modular architectural design is often based on bundles of α-helices, best exemplified by the potassium channel,[1] but alternative structures such as barrel proteins and β-helices have also evolved as illustrated by the gramicidin A channel.[2] In addition to modifying existing biological pores,[3] a wide variety of tubular structures based on synthetic backbones has been prepared.[4] In particular, peptide-based tubular systems have received significant attention, and herein we highlight both general design concepts and major recent advances in this rapidly developing field.

The β-sheet motif present in various forms in α-peptides[5] has proven to be a tremendously fruitful design element to mimic Nature's channel-forming structures. The parallel or antiparallel multiple-hydrogen-bonding array between building blocks with a varying degree of curvature leads to the formation of stable assemblies ranging from β-barrels, through hollow β-helices, to stacked macrocycles (Figure 1).

Natural β-barrel proteins such as α-hemolysin[6] have inspired the construction of β-barrels from staves consisting of β-sheets. On the one hand, the design of rigid-rod β-barrels by Matile and co-workers is based on the finite assembly of rigid octa(*p*-phenylene)s that carry short α-peptide side chains interdigitated with side chains of adjacent staves to form antiparallel β-sheets.[7] On the other hand, Percec and co-workers created pores from amphiphilic dendritic α-dipeptides that self-assemble into a helical arrangement of short staves.[8,9] Whereas in the first approach the internal diameter is tuned by the incorporation of a varying number of staves and α-peptide side chains of differing lengths, the latter pore-forming construct produces various diameters by changing the configuration of the dipeptide fragment. In both approaches, the length is controlled indirectly by assembly of the tube within the constraint of a lipid bilayer.

An alternative design used in channel construction is illustrated by the gramicidin family.[2] A α-peptide strand with an alternating sequence of D- and L-α-amino acids is twisted to form a single-stranded β-helix in which the intramolecular hydrogen bonding resembles that in parallel β-sheets. Further interactions between different strands allow either stacked or intertwined β-helices. The number of amino acid residues per turn (4.8–8.2 units) is greater than in α-helices which leads to a wider inner cavity with diameters between 2.3 and 4.7 Å. Whereas diameter control is largely dependent on the cationic guest species, length control is intimately connected to the length of the amino acid sequence.

In an elegant extension of the β-helix design, Ghadiri et al. pioneered peptide tubes based on stacked macrocycles consisting of an even number of alternating D- and L-α-amino acids.[10] The high aspect ratio and the chemical stability of the tubular assembly originates from strong hydrogen-bonding

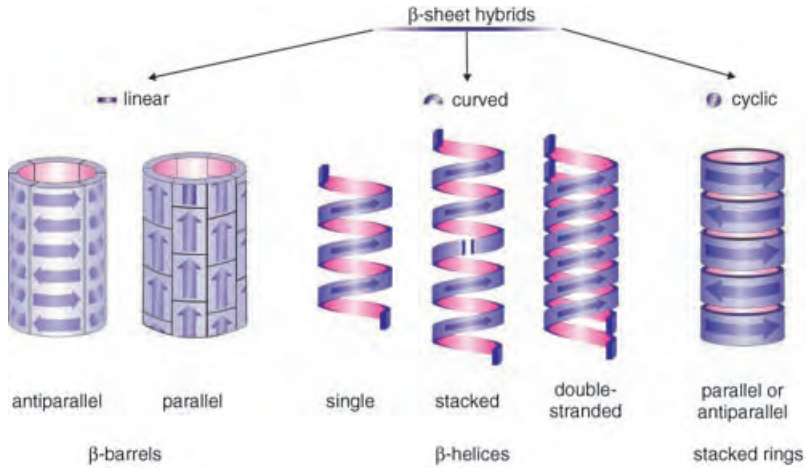

Figure 1. Tubular structures derived from the β-sheet hydrogen-bonding motif present in linear, curved, or cyclic form.

[*] M. A. Balbo Block, Dr. S. Hecht
Max-Planck-Institut für Kohlenforschung
Kaiser-Wilhelm-Platz 1
45470 Mülheim an der Ruhr (Germany)
Fax: (+49) 30-306-2979
E-mail: hecht@mpi-muelheim.mpg.de

[**] Generous support by the Max Planck Society is gratefully acknowledged. MABB is indebted to the Studienstiftung des deutschen Volkes for providing a doctoral fellowship.

InterScience
© 2005 Wiley-VCH Verlag GmbH & Co. KGaA, Weinheim

interactions between the individual rings to yield an extended, circular two-dimensional β-sheet. An increase in the number of repeat units per cycle from cyclooctamer to cyclododecamer leads to an increase in the inner diameter from 7 to 13 Å with a constant periodicity of 4.7 Å between stacked rings.[11] Control of the length of the tubes is again only possible by assembly within a lipid bilayer.[12]

From this brief overview it is apparent that a multitude of approaches to peptide tubes exists. But some unsolved problems and future challenges still face this field:

- The control of the length of a self-assembled tubular object without the external constraint of a bilayer is still unconquered territory.[13] One possible solution involves the addition of terminating agents to the supramolecular polymerization mixtures,[14] for example, Janus macrocycles that engage in hydrogen bonding on only one face of the ring.[15] Nevertheless, a broad distribution of lengths cannot be avoided. Perhaps the most promising approach to date towards finite self-assembly is that of Stupp et al. by means of crowded side chains, as exemplified by his nanomushrooms.[16]
- Controlled functionalization of the interior and exterior surfaces is absolutely crucial to render the tubular structures functional. Whereas inner functionalization affects both the efficiency and selectivity of transport processes, functional groups present at the periphery of the tubes mediate integration into bilayers or other hierarchically organized materials. In particular, peripheral modification with polymers represents an attractive route to tune materials properties and control pattern formation on the nanometer scale.[17] Peptide–polymer hybrids[18] can be prepared conveniently through controlled radical-polymerization techniques[19] that involve either post-functionalization by graft-from or attach-to routes or assembly from suitable macromonomers.[20]
- It is essential that the tubular building blocks be isolated and integrated into hierarchically organized structures to harness their beneficial properties by constructing hybrid materials.

Very recently, the group of Biesalski reported an interesting approach to address some of these issues.[21] They demonstrated the utility of a graft-from polymerization route initiated at the outer surface of self-assembled peptide nanotubes to tune their properties (Figure 2). Octameric D,L-alternating cyclo-α-peptides that bear bromoisobutyramide initiators on the lysine side chains were assembled into peptide nanotubes. After subsequent addition of *N*-isopropylacrylamide monomer and polymerization catalyst mixture, Biesalski and co-workers took advantage of the controlled nature of atom-transfer radical polymerization (ATRP) to grow a poly(*N*-isopropylacrylamide) (PNIPAM) shell of homogeneous thickness around the intact cylindrical peptide core. With the aid of atomic force microscopy (AFM) imaging before and after post-polymerization, it was shown that bundles of peptide nanotubes ranging from 100–500 nm in length were broken up to distinct rod-shaped structures with dimensions of 80 ± 20 nm length and 12 ± 3 nm height. The observed shorter length suggests the possibility of using synthetic control over molecular weight of the polymer arms to tune local steric crowding and therefore influence the length of the tubular hybrid assembly.

In a related, however very different, approach, Francis and co-workers demonstrated polymer functionalization of the tobacco mosaic virus (TMV), a well-defined tubular self-assembled entity. They utilized various novel bioconju-

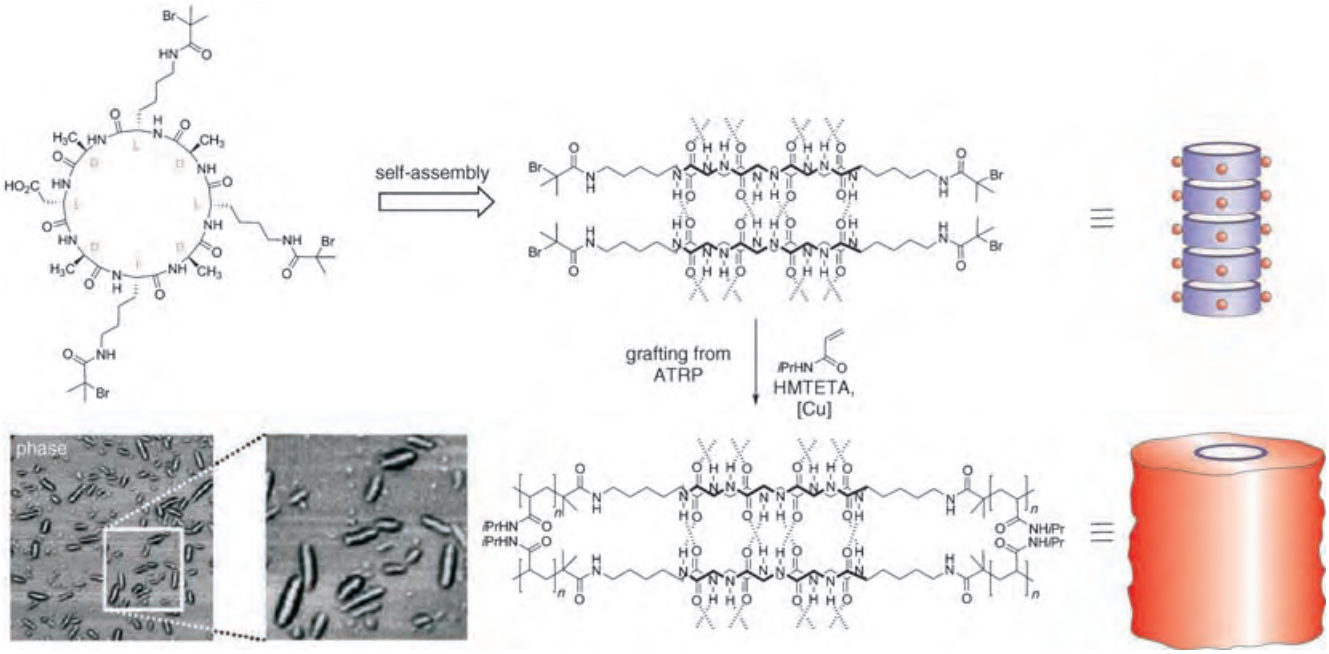

Figure 2. Grafting a polymer shell from preassembled peptide tubes:[21] D,L-Cyclo-α-peptides carrying initiator groups stack to form tubular structures from which PNIPAM is grown by ATRP; HMTETA = 1,1,4,7,10,10-hexamethyltriethylene. Bottom left depicts AFM images of peptide-PNIPAM hybrids (scales: 2 μm and 800 nm). Reproduced in part with permission from reference [21].

© 2005 Wiley-VCH Verlag GmbH & Co. KGaA, Weinheim

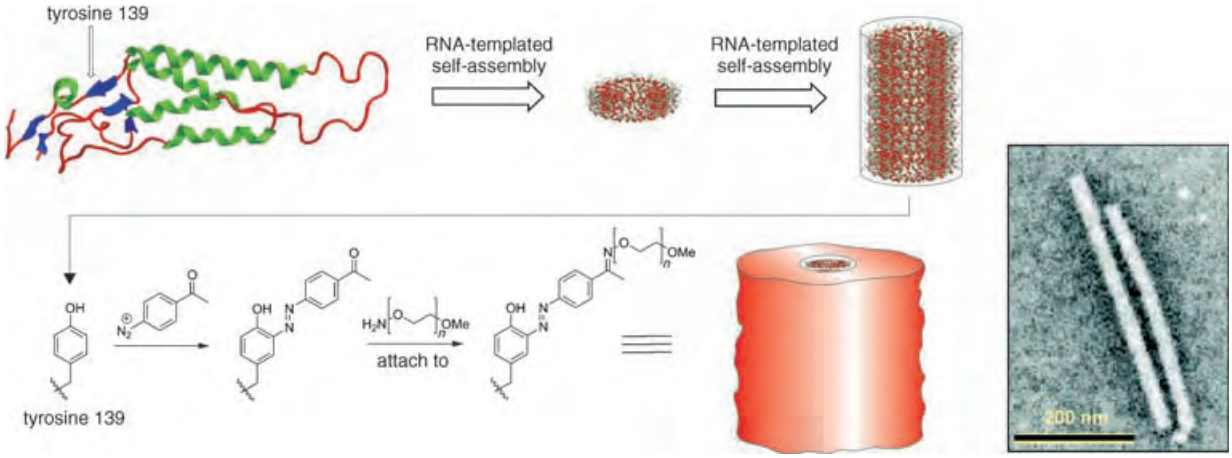

Figure 3. Attaching a polymer shell to preassembled TMV tubes:[23] Tyr 139 at the periphery of the TMV coat protein (protein data bank code: 1ei7) is functionalized by means of diazonium coupling chemistry to yield a ketone platform to which PEG-based hydroxylamines are attached. Bottom right shows a TEM image of the PEG-TMV hybrid after transfer to an organic solvent, that is, $CHCl_3$. Reproduced in part from reference [23].

gation approaches[22] to decorate the outer and inner surfaces of the TMV coat protein.[23] For instance, chemo- and regioselective modification of Tyr 139 located at the outer periphery of the TMV by means of electrophilic aromatic substitution was used to install ketone functionalities,[24] which reacted efficiently with various hydroxylamines, including poly(ethylene glycol) (PEG) derivatives (Figure 3). This attach-to route affords intact tubes that are readily soluble in a variety of organic solvents and therefore allow the use of conventional processing steps for materials applications of the PEG–TMV hybrids. Notably, this system enables the unique possibility of length control owing to the discrete nature of the interior RNA strand, which templates and directs self-assembly of the TMV-coat protein.

The work described herein truly represents the continuing trend of merging classical disciplines namely biology, organic synthesis, and polymer chemistry. Meshing the characteristics of these often-complementary fields helps to surpass limitations and greatly expands the freedom of designing custom-tailored de novo hybrid materials. The controlled modification of peptides and peptide-based objects by modern polymerization techniques will continue to thrive, and the ability to tune properties promises interesting new applications in the emerging bionanotechnology area.

[1] R. MacKinnon, *Angew. Chem.* **2004**, *116*, 4363 – 4376; *Angew. Chem. Int. Ed.* **2004**, *43*, 4265 – 4277.

[2] *Gramicidin and Related Ion Channel-Forming Peptides*, (Eds.: D. J. Chadwick, E. D. Cardew), Wiley, Chichester, **1999**.

[3] a) U. Koert, *Phys. Chem. Chem. Phys.* **2005**, *7*, 1501 – 1506; b) H. Bayley, P. S. Cremer, *Nature* **2001**, *413*, 226 – 230.

[4] a) D. T. Bong, T. D. Clark, J. R. Granja, M. R. Ghadiri, *Angew. Chem.* **2001**, *113*, 1016 – 1041; *Angew. Chem. Int. Ed.* **2001**, *40*, 988 – 1011; b) M. A. Balbo Block, C. Kaiser, A. Khan, S. Hecht, *Top. Curr. Chem.* **2005**, *245*, 89 – 150.

[5] a) N. Sewald, H.-D. Jakubke, *Peptides: Chemistry and Biology*, Wiley-VCH, Weinheim, **2002**; for alternative peptide structures based on homologous amino acids, see: b) *Pseudo-Peptides in Drug Discovery* (Ed.: P. Nielsen), Wiley-VCH, Weinheim, **2004**; and c) D. Seebach, A. K. Beck, D. J. Bierbaum, *Chem. Biodiversity* **2004**, *1*, 1111 – 1239.

[6] L. Song, M. R. Hobaugh, C. Shustak, S. Cheley, H. Bayley, J. E. Gouaux, *Science* **1996**, *274*, 1859 – 1866.

[7] N. Sakai, J. Mareda, S. Matile, *Acc. Chem. Res.* **2005**, *38*, 79 – 87.

[8] V. Percec, A. E. Dulcey, V. S. K. Balagurusamy, Y. Miura, J. Smidrkal, M. Peterca, S. Nummelin, U. Edlund, S. D. Hudson, P. A. Heiney, H. Duan, S. N. Magonov, S. A. Vinogradov, *Nature* **2004**, *430*, 764 – 768.

[9] For another excellent example of diphenylalanine assembly for the generation of peptide tubes used as templates for silver nanowire growth, see: M. Reches, E. Gazit, *Science* **2003**, *300*, 625 – 627.

[10] M. R. Ghadiri, J. R. Granja, R. A. Milligan, D. E. McRee, N. Khazanovich, *Nature* **1993**, *366*, 324 – 327.

[11] J. D. Hartgerink, T. D. Clark, M. R. Ghadiri, *Chem. Eur. J.* **1998**, *4*, 1367 – 1372.

[12] a) S. Fernandez-Lopez, H.-S. Kim, E. C. Chol, M. Delgado, J. R. Granja, A. Khasanov, K. Kraehenbuehl, G. Long, D. A. Weinberger, K. M. Wilcoxen, M. R. Ghadiri, *Nature* **2001**, *412*, 452 – 455; b) M. R. Ghadiri, J. R. Granja, L. K. Buehler, *Nature* **1994**, *369*, 301 – 304.

[13] Special Issue "Supramolecular Chemistry & Self-Assembly": *Science* **2002**, *295*, 2395 – 2421.

[14] L. Brunsveld, B. J. B. Folmer, E. W. Meijer, R. P. Sijbesma, *Chem. Rev.* **2001**, *101*, 4071 – 4097.

[15] J. Sanchez-Quesada, M. P. Isler, M. R. Ghadiri, *J. Am. Chem. Soc.* **2002**, *124*, 10004 – 10005.

[16] S. I. Stupp, V. LeBonheur, K. Walker, L. S. Li, K. E. Huggins, M. Keser, A. Amstutz, *Science* **1997**, *276*, 384 – 389.

[17] In pioneering work, Höger and co-workers used stacking phenylene ethynylene macrocycles appended with polystyrene segments to form a polymer sheath around the self-assembled tube: S. Rosselli, A.-D. Ramminger, T. Wagner, B. Silier, S. Wiegand, W. Haussler, G. Lieser, V. Scheumann, S. Höger, *Angew. Chem.* **2001**, *113*, 3233 – 3237; *Angew. Chem. Int. Ed.* **2001**, *40*, 3138 – 3141.

[18] H.-A. Klok, *J. Polym. Sci. Part A* **2005**, *43*, 1 – 17.

[19] For reviews on controlled free-radical polymerization, see about ATRP: a) K. Matyjaszewski, J. Xia, *Chem. Rev.* **2001**, *101*, 2921 – 2990; and b) M. Kamigaito, T. Ando, M. Sawamoto, *Chem. Rev.* **2001**, *101*, 3689 – 3745; NMP: c) C. J. Hawker, A. W. Bosman, E. Harth, *Chem. Rev.* **2001**, *101*, 3661 – 3688;

 © 2005 Wiley-VCH Verlag GmbH & Co. KGaA, Weinheim

RAFT: d) G. Moad, J. Chiefari, Y. K. Chong, J. Krstina, R. T. A. Mayadunne, A. Postma, E. Rizzardo, S. H. Thang, *Polym. Int.* **2000**, *49*, 993 – 1001.

[20] a) M. L. Becker, J. Liu, K. L. Wooley, *Chem. Commun.* **2003**, 180 – 181; b) H. Rettig, E. Krause, H. G. Börner, *Macromol. Rapid Commun.* **2004**, *25*, 1251 – 1256; c) Y. Mei, K. L. Beers, H. C. Michelle Byrd, D. L. van der Hart, N. R. Washburn, *J. Am. Chem. Soc.* **2004**, *126*, 3472 – 3476.

[21] J. Couet, J. D. Jeyaprakash, S. Samuel, A. Kopyshev, S. Santer, M. Biesalski, *Angew. Chem.* **2005**, *117*, 3361 – 3365; *Angew. Chem. Int. Ed.* **2005**, *44*, 3297 – 3301.

[22] a) J. M. Antos, M. B. Francis, *J. Am. Chem. Soc.* **2004**, *126*, 10256 – 10257; b) J. M. Hooker, E. W. Kovacs, M. B. Francis, *J. Am. Chem. Soc.* **2004**, *126*, 3718 – 3719; c) N. S. Joshi, L. R. Whitaker, M. B. Francis, *J. Am. Chem. Soc.* **2004**, *126*, 15942 – 15943.

[23] T. L. Schlick, Z. Ding, E. W. Kovacs, M. B. Francis, *J. Am. Chem. Soc.* **2005**, *127*, 3718 – 3723.

[24] The orthogonal ketone functionality has proven extremely versatile in bioconjugation, for example, in the selective functionalization of cell surfaces: L. K. Mahal, K. J. Yarema, C. R. Bertozzi, *Science* **1997**, *276*, 1125 – 1128.

Life's Simple Pleasures!

1328407_EU

No need to waste precious time looking for the right information – Register now for the free Wiley-VCH Alerting Service.

www.wiley-vch.de/home/pas/

It's simple – and it's fast.

WILEY-VCH

18 000 organic chemicals, 1 simple phone call !

TCI Europe, the European distribution centre in Antwerp, Belgium, guarantees a speedy delivery of all TCI products to European users, from university laboratories to corporate research facilities.

TCI 2005 Euro Catalogue

FREE

Ask your copy today!

TCI EUROPE N.V.
+800 46 73 86 67 • +32 (0)3 735 07 00
Fax +32 (0)3 735 07 01
sales@tcieurope.be • www.tcieurope.be
<Head Office> TOKYO KASEI KOGYO CO., LTD.
www.tokyokasei.co.jp

TCI has over 50 years of experience synthesizing fine organic chemicals

 © 2005 Wiley-VCH Verlag GmbH & Co. KGaA, Weinheim

Gold Catalysis

DOI: 10.1002/anie.200502735

The Catalysis Gold Rush: New Claims**

*A. Stephen K. Hashmi**

Keywords:
hydrogenation · alkenes · alkynes · gold · homogeneous catalysis

1. Introduction

Homogeneous catalysis by gold is not new: the roots reach back at least 70 years.[1] The catalysts are quite robust; an exclusion of water or oxygen in most cases is not necessary.[1,2] Nevertheless, only very few publications in this field appeared up to the end of the year 2003. In a review on homogenous gold-catalyzed reactions from that year,[1] I concluded with the sentence *"I am confident that these developments will accelerate in the near future, and that most people working in the field of homogeneous transition-metal catalysis will also give gold a chance on a regular basis"*. Obviously many investigators had the same thought: since 2004 a sharp and continuing increase of the publications on homogeneous catalysis by gold complexes can be observed. Here, I would like to "highlight" some of the exciting new "claims" in this emerging field (excluding aspects recently reviewed elsewhere).[3–5]

2. Nucleophilic Additions to Unactivated Olefins as Substrates: The Gate to Catalytic Asymmetric Synthesis

Hutchings was the first to recognize the superiority of gold catalysts for the electrophilic activation of alkynes.[6] This field has been reviewed,[3c] and further examples for that type of reaction have been reported recently.[7] In particular, the addition of water and alcohols to alkynes, which in the case of terminal alkynes cleanly delivers the Markovnikov product, has become a kind of benchmark for gold catalysts.[8] Intramolecular reactions investigated by Kozmin and Genet have proven to be useful tools for organic synthesis.[9]

In 2000 we described the formation of compound **3** from **1** and suggested the intramolecular addition of a hydroxy group to a furyl-substituted, styrene-like alkene **2** as the final step in its formation (Scheme 1).[10] This was not straightforward: Teles et al. had shown that alkynes were highly reactive,[8b] but they also claimed that alkenes do not react.[11] Our work,[10] work of Krause et al.,[12] and a beautiful application of Lee et al.[13] subsequently demonstrated that strained allenes also react.[14] But the twofold addition of alcohols to alkynes[8] indicated that even the intermediate enol ethers can be activated for the attack of a second alcohol nucleophile by the gold catalyst.

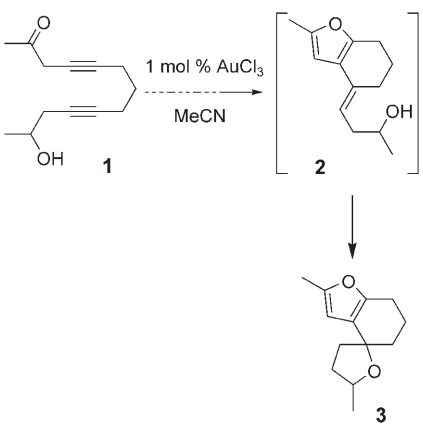

Scheme 1. Proposed pathway for the formation of **3**.

The first examples for such gold-catalyzed nucleophilic addition reactions were provided by Li et al.[15] In 2004, they successfully used 1,3-dicarbonyl compounds **4** as pronucleophiles and activated alkenes **5** (styrene derivatives; in one example also norbornene; Scheme 2). Li et al.[16] could also extend that principle to the intermolecular reaction of **4** with cyclic enol ethers **7** and cyclic 1,3-dienes **9** (Scheme 3). In these examples the authors propose that the gold catalyst might activate the C–H

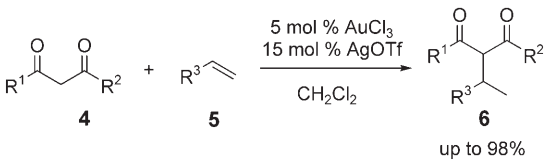

Scheme 2. Addition of pronucleophiles to activated alkenes. R^1, R^2 = alkyl, aryl; R^3 = aryl.

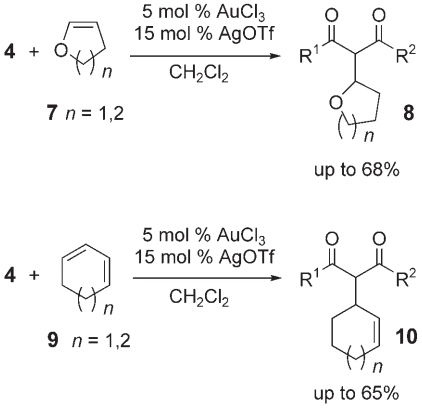

Scheme 3. Addition of pronucleophiles to enol ethers and dienes. R^1, R^2 = alkyl, aryl.

[*] Prof. Dr. A. S. K. Hashmi
Institut für Organische Chemie
Universität Stuttgart
Pfaffenwaldring 55
70569 Stuttgart (Germany)
Fax: (+49) 711-685-4321
E-mail: hashmi@hashmi.de

[**] A.S.K.H. thanks the European Union for financial support (AURICAT EU-RTN, HPRN-CT-2002-00174).

InterScience
© 2005 Wiley-VCH Verlag GmbH & Co. KGaA, Weinheim

bond of the nucleophile instead of activating the alkene for a reaction with the enol tautomer of **4**, but so far there is no experimental data to support either model.

Just recently, in a remarkable paper He et al.[17] reported that at 85 °C in toluene even unactivated alkenes **12** reacted readily with weak nucleophiles like phenols **11** or carboxylic acids **14** (Scheme 4)! All these additions follow

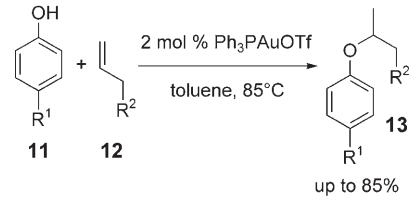

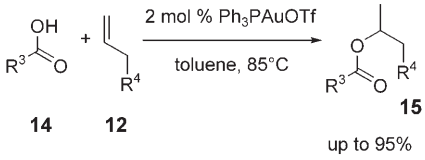

Scheme 4. Addition of weak nucleophiles to unactivated alkenes. R^1 = OMe, *t*Bu, CO_2Me, NO_2; R^2 = alkyl, aryl; R^3 = benzyl, alkyl; R^4 = alkyl, aryl.

Markovnikov's rule. This regioselectivity is, in contrast to the additions to alkynes, connected with the formation of new stereogenic centers even when terminal alkenes are the starting compounds. Now the possibility for the development of stereoselective catalysis was opened.

Ito and Hayashi[18] had provided the first example for asymmetric gold catalysts almost 20 years ago, and Echavarren et al. recently revived this aspect with the enyne cyclization catalyzed by **17** (Scheme 5).[7e] Although the *ee* values are still low, if we extrapolate from the Ito–Hayashi asymmetric aldol reaction better enantioselectivity can be expected.

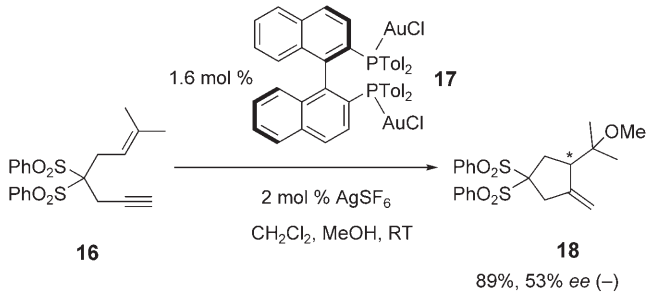

Scheme 5. Catalytic asymmetric cyclization of an enyne.

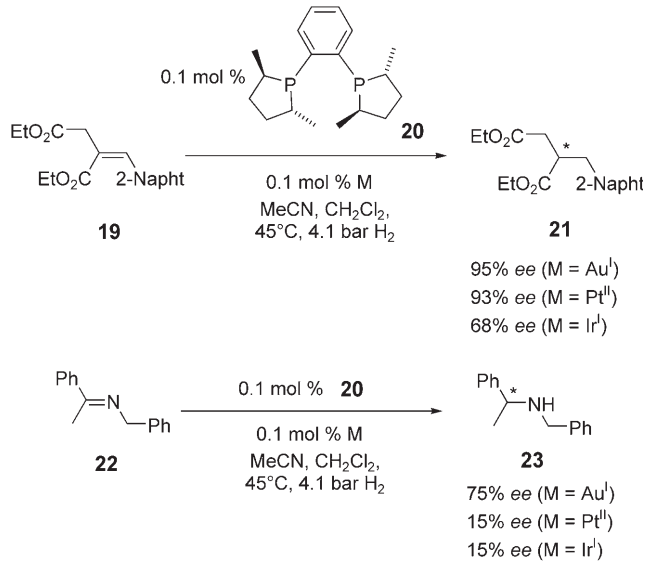

Scheme 6. Catalytic asymmetric hydrogenation. Napht = naphthyl.

One first example documenting that trend was reported by Corma et al.:[19] The [$(AuCl)_2$\{(*R*,*R*)-Me-Duphos\}] complex (Me-Duphos = 1,2-bis(2,5-dimethylphospholanyl)benzene) can be used in catalytic enantioselective hydrogenations of esters **19** and imines **22** (Scheme 6). The activities were comparable to the activities of the analoguous Pt and Ir complexes, but with gold the *ee* values were superior. Rather than a dihydride formed by oxidative addition, the authors suggest a unique gold(I) monohydride complex as an intermediate.

3. The First Auraoxetane: Model Compound for an Organometallic Intermediate in Gold-Catalyzed Reactions

Despite significant effort, so far only two intermediates of gold-catalyzed reactions have ever been proven experimentally.[20] Unfortunately, these intermediates, a 5-alkylidene-4,5-dihydrooxazole and an arene oxide, were not organometallic but merely organic compounds. Now, in a spectacular paper Cinellu et al. managed to isolate and characterize the very first auraoxetanes[21] as stable organometallic analogues of intermediates in gold-catalyzed reactions. The reaction of the bridged μ-oxo dimer **24** with norbornene **25** led to the alkene complex **26**, also a representative of a rare species, and the unique auraoxetane **27** (Scheme 7). In addition, the epoxynorbornane **28** was identified as the final product of the reaction. A related reaction of a platinum(II) compound had been reported before, but there the oxygen always coordinated to two platinum centers and the formation of oxiranes was not observed.[22]

While Teles et al.[8b] initially suggested a *syn* oxyauration for the gold(I)-catalyzed additions of alcohols to alkynes, we have proven an *anti* oxyauration for the gold(III)-catalyzed oxazole synthesis.[20a] It will be a future challenge for both theoreticians and experimentalists to verify whether Cinellu's *syn*-addition mode is a general principle or the outcome of the preferred *exo* addition at the strained norbornene. The ligand used by Cinellu et al. might also serve as a lead structure for the detection of intermediates in other gold-catalyzed reactions. The diastereoselec-

 © 2005 Wiley-VCH Verlag GmbH & Co. KGaA, Weinheim

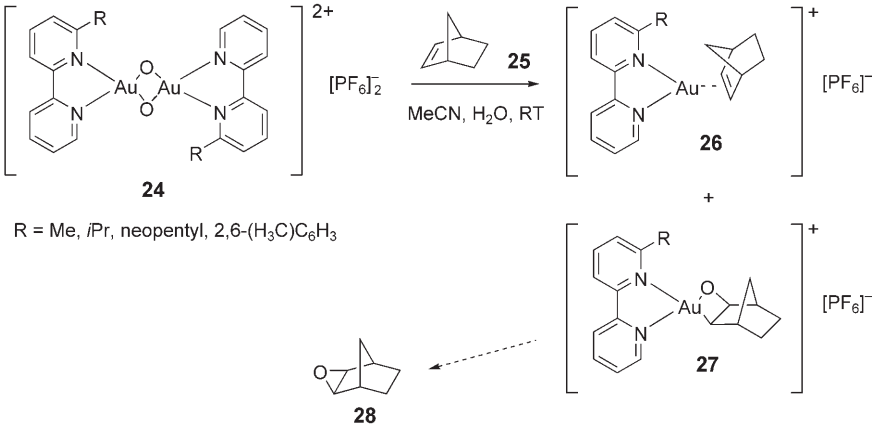

Scheme 7. Formation of auraoxetane **27**.

tivity is also of importance for asymmetric catalysis (see the end of the Section 2). The prognosis or understanding of the stereoselectivity observed is intrinsically linked to knowing whether a *syn* or an *anti* addition is occurring.

4. The Oxidation State of the Active Species: New Pieces of the Puzzle

Often the same reaction can be catalyzed by gold(I) as well as gold(III).[1] Since it is conceivable that the active species is formed in situ from the precatalyst by a change of the oxidation state (for example, either by reduction of gold(III) or by disproportionation of gold(I) to gold(III) and gold(0)), the same catalyst might be operating in both cases. Periana et al. and Straub set out to resolve this question by theoretical calculations, but they could not rule out simultaneous catalysis by gold(I) and gold(III).[23,24] Nevertheless, all gold-catalyzed reactions discussed so far probably do not involve a change in the oxidation state of the gold catalyst (classical steps like oxidative addition or reductive elimination do not occur) in the catalytic cycle.

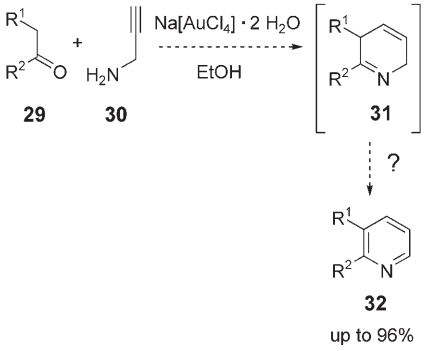

Scheme 8. Dehydrogenation as part of the gold-catalyzed synthesis of pyridine derivatives. R^1 = H, alkyl, aryl; R^2 = H, alkyl, aryl, heteroaryl.

Arcadi et al.[25] developed a synthesis of pyridines **32** from carbonyl compounds **29** and propargylamine **30** (Scheme 8). The initial isomerization product is the dihydropyridine **31**, which must be dehydrogenated somehow. Whether H_2, which potentially should reduce the catalyst, is released or a transfer hydrogenation to the alkyne occurs, was not investigated.

Corma et al. now have reported the remarkable observation that gold on supported nanocrystalline CeO_2 efficiently catalyzes the homocoupling of boronic acids (Scheme 9).[26] Since the reactivity correlates with the amount of gold(III) on the surface, it is assumed that

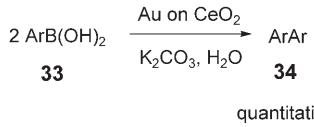

Scheme 9. Catalytic homocoupling of boronic acids.

the reaction is initiated by a twofold transmetalation from boron to gold(III) followed by reductive elimination of the biaryl compound. Now the catalytic cycle can be completed only when gold(I) is reoxidized. The reaction proceeds in the absence of oxygen, and H_2 could be detected by Raman spectroscopy. This suggests that possibly nanoparticles containing gold(I) are directly oxidized by protons. Corma et al. were also able to extend this principle to the reaction of homogeneous gold catalysts with N,O ligands and similar systems anchored in zeolites.[27] Unlike with palladium catalysts in the Suzuki coupling, cross-coupling products were not observed even in the presence of aryl iodides.

Ito, Sawamura et al.[28] discovered the chemoselective dehydrogenative silylation of alcohols (Scheme 10). The [AuCl(xantphos)] complex (**36**; xantphos = 9,9-dimethyl-4,5-bis(diphenylphosphanyl)xanthene) allows the formation of the silyl ethers from alcohols like **35** and triethylsilane in the presence of other functional groups like alkenes, alkynes, alkyl halides, tertiary alcohols, aldehydes, ketones, and carbamates. The mechanistic proposal, in analogy to Corma's asymmetric hydrogenation (see Section 2) also involves a gold monohydride.

The latest contribution addressing the oxidation state of the catalyst was delivered from Gevorgyan et al.[29] They used the haloallenyl ketones **38** in gold-catalyzed cycloisomerizations yielding furans (Scheme 11). With $AuCl_3$ they observed a preference for the product **40**, probably formed by carbonyl coordination and via a bromoirenium zwitterion intermediate, while $Au(PR_3)Cl$ exclusively delivered **42**, presumably by means of initial π coordination. This concept for the synthesis of halofurans had previously failed with Pd^{II} catalysts

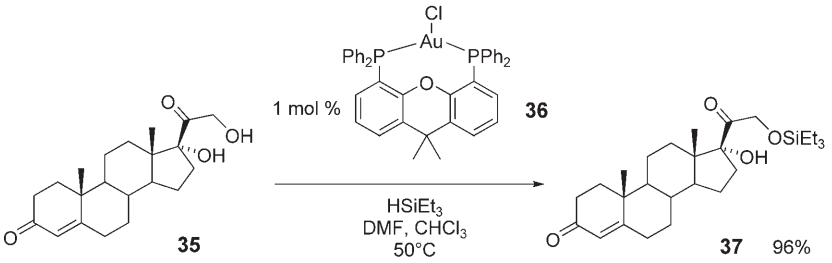

Scheme 10. Silyl ethers prepared by dehydrogenative coupling.

 © 2005 Wiley-VCH Verlag GmbH & Co. KGaA, Weinheim

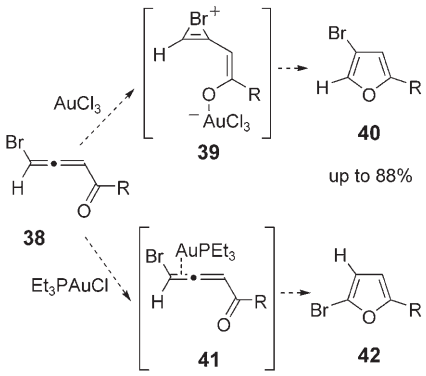

Scheme 11. Products resulting from precatalysts of different oxidation states. R = C_8H_{17}.

and a bromoallenyl compound. Only with a chloroallenyl substrate was a low yield (2%) of the corresponding 2-chlorofuran obtained.[30]

Gevorgyan et al. presents the very first example for a gold-catalyzed reaction in which different oxidation states of the precatalyst lead to different products. This is a very important contribution to the discussion of the oxidation state of the active gold species.

5. Outlook

Gold catalysis has become a hot spot in organometallic chemistry. The many examples published for transformations that were previously possible only with other reagents or catalysts, or even multistep syntheses, demonstrate the benefits of the gold catalyst, for example, higher activity, higher selectivity, and milder conditions. It is no longer sufficient to simply reinvestigate known reactions and to show that gold has some activity there. Stereoselectivity will probably be a major synthetic focus in the future. The fact that in many reactions the gold catalysts are superior to other catalysts is still not understood. Here further mechanistic insight is a challenge for experiment and theory. And the digging for new, unprecedented reactions certainly continues.

[1] A. S. K. Hashmi, *Gold Bull.* **2004**, *37*, 51 – 65.

[2] A. S. K. Hashmi, T. M. Frost, J. W. Bats, *J. Am. Chem. Soc.* **2000**, *122*, 11553 – 11554.

[3] Recent reviews: a) A. Hoffmann-Röder, N. Krause, *Org. Biomol. Chem.* **2005**, *3*, 387 – 391; b) A. Arcadi, S. Di Giuseppe, *Curr. Org. Chem.* **2004**, *8*, 795 – 812; c) A. S. K. Hashmi, *Gold Bull.* **2003**, *36*, 3 – 9.

[4] C,H activation of methane: D. E. De-Vos, B. F. Sels, *Angew. Chem.* **2005**, *117*, 30 – 32; *Angew. Chem. Int. Ed.* **2005**, *44*, 30 – 32.

[5] Involvement of carbenoids in the enyne cyclization: a) L. Hintermann, *Nachr. Chem.* **2005**, *53*, 420 – 423; b) C. Bruneau, *Angew. Chem.* **2005**, *117*, 2380 – 2386; *Angew. Chem. Int. Ed.* **2005**, *44*, 2328 – 2334.

[6] G. J. Hutchings, *J. Catal.* **1985**, *96*, 292 – 295.

[7] a) S. T. Staben, J. J. Kennedy-Smith, F. D. Toste, *Angew. Chem.* **2004**, *116*, 5464 – 5466; *Angew. Chem. Int. Ed.* **2004**, *43*, 5350 – 5352; b) T. Yao, X. Zhang, R. C. Larock, *J. Am. Chem. Soc.* **2004**, *126*, 11164 – 11165; c) A. S. K. Hashmi, P. Sinha, *Adv. Synth. Catal.* **2004**, *346*, 432 – 438; d) N. Asao, K. Sato, Meggenbateer, Y. Yamamoto, *J. Org. Chem.* **2005**, *70*, 3682 – 3685; e) M. P. Munoz, J. Adrio, J. C. Carretero, A. M. Echavarren, *Organometallics* **2005**, *24*, 1293 – 1300; f) M. Alfonsi, A. Arcadi, M. Aschi, G. Bianchi, F. Marinelli, *J. Org. Chem.* **2005**, *70*, 2265 – 2273; g) A. S. K. Hashmi, L. Grundl, *Tetrahedron* **2005**, *61*, 6231 – 6236; h) C. Nieto-Oberhuber, S. López, A. M. Echavarren, *J. Am. Chem. Soc.* **2005**, *127*, 6178 – 6179; i) J. P. Markham, S. T. Staben, F. D. Toste, *J. Am. Chem. Soc.* **2005**, *127*, 9708 – 9709.

[8] a) Y. Fukuda, K. Utimoto, *J. Org. Chem.* **1991**, *56*, 3729 – 3731; b) J. H. Teles, S. Brode, M. Chabanas, *Angew. Chem.* **1998**, *110*, 1475 – 1478; *Angew. Chem. Int. Ed.* **1998**, *37*, 1415 – 1418; c) E. Mizushima, K. Sato, T. Hayashi, M. Tanaka, *Angew. Chem.* **2002**, *114*, 4745 – 4747; *Angew. Chem. Int. Ed.* **2002**, *41*, 4563 – 4565; d) R. Casado, M. Contel, M. Laguna, P. Romero, S. Sanz, *J. Am. Chem. Soc.* **2003**, *125*, 11925 – 11935; e) P. Roembke, H. Schmidbaur, S. Cronje, H. Raubenheimer, *J. Mol. Catal. A* **2004**, *212*, 35 – 42.

[9] a) L. Zhang, S. A. Kozmin, *J. Am. Chem. Soc.* **2005**, *127*, 6962 – 6963; b) S. Antoniotti, E. Genin, V. Michelet, J.-P. Genêt, *J. Am. Chem. Soc.* **2005**, *127*, 9976 – 9977.

[10] A. S. K. Hashmi, L. Schwarz, J.-H. Choi, T. M. Frost, *Angew. Chem.* **2000**, *112*, 2382 – 2385; *Angew. Chem. Int. Ed.* **2000**, *39*, 2285 – 2288.

[11] J. H. Teles, personal communication. For this reason allenes but not alkenes were covered in a patent: J. H. Teles, M. Schulz (BASF AG), WO-AI 9721648, **1997** [*Chem. Abstr.* **1997**, *127*, 121499].

[12] a) A. Hoffmann-Röder, N. Krause, *Org. Lett.* **2001**, *3*, 2537 – 2538; b) N. Morita, N. Krause, *Org. Lett.* **2004**, *6*, 4121 – 4123.

[13] P. H. Lee, H. Kim, K. Lee, M. Kim, K. Noh, H. Kim, D. Seomoon, *Angew. Chem.* **2005**, *117*, 1874 – 1877; *Angew. Chem. Int. Ed.* **2005**, *44*, 1840 – 1843.

[14] There is one report of a gold-catalyzed propargyl Claisen rearrangement/reduction to form β-hydroxy allenes and γ-hydroxy alkynes as stable products without further intramolecular addition to the C–C multiple bonds: B. D. Sherry, F. D. Toste, *J. Am. Chem. Soc.* **2004**, *126*, 15978 – 15979.

[15] X. Yao, C.-J. Li, *J. Am. Chem. Soc.* **2004**, *126*, 6884 – 6885.

[16] R.-V. Nguyen, X.-Q. Yao, D. S. Bohle, C.-J. Li, *Org. Lett.* **2005**, *7*, 673 – 675.

[17] C.-G. Yang, C. He, *J. Am. Chem. Soc.* **2005**, *127*, 6966 – 6967.

[18] Y. Ito, M. Sawamura, T. Hayashi, *J. Am. Chem. Soc.* **1986**, *108*, 6405 – 6406.

[19] C. González-Arellano, A. Corma, M. Iglesias, F. Sánchez, *Chem. Commun.* **2005**, 3451 – 3453.

[20] a) A. S. K. Hashmi, J. P. Weyrauch, W. Frey, J. W. Bats, *Org. Lett.* **2004**, *6*, 4391 – 4394; b) A. S. K. Hashmi, M. Rudolph, J. P. Weyrauch, M. Wölfle, W. Frey, J. W. Bats, *Angew. Chem.* **2005**, *117*, 2858 – 2861; *Angew. Chem. Int. Ed.* **2005**, *44*, 2798 – 2801.

[21] M. A. Cinellu, G. Minghetti, F. Cocco, S. Stoccoro, A. Zucca, M. Manassero, *Angew. Chem.* **2005**, *117*, 7052–7055; *Angew. Chem. Int. Ed.* **2005**, *44*, 6892–6895.

[22] E. Szuromi, H. Shan, P. R. Sharp, *J. Am. Chem. Soc.* **2003**, *125*, 10522 – 10523.

[23] B. F. Straub, *Chem. Commun.* **2004**, 1726 – 1728.

[24] C. J. Jones, D. Taube, V. R. Ziatdinov, R. A. Periana, R. J. Nielsen, J. Oxgaard, W. A. Goddard III, *Angew. Chem.* **2004**, *116*, 4726 – 4729; *Angew. Chem. Int. Ed.* **2004**, *43*, 4626 – 4629.

[25] G. Abbiati, A. Arcadi, G. Bianchi, S. Di Giuseppe, F. Marinelli, E. Rossi, *J. Org. Chem.* **2003**, *68*, 6959 – 6966.

[26] S. Carretin, J. Guzman, A. Corma, *Angew. Chem.* **2005**, *117*, 2282 – 2285; *Angew. Chem. Int. Ed.* **2005**, *44*, 2242 – 2245.

[27] C. González-Arellano, A. Corma, M. Iglesias, F. Sánchez, *Chem. Commun.* **2005**, 1990 – 1992.

[28] H. Ito, K. Takagi, T. Miyahara, M. Sawamura, *Org. Lett.* **2005**, *7*, 3001 – 3004.

[29] A. W. Sromek, M. Rubina, V. Gevorgyan, *J. Am. Chem. Soc.* **2005**, *127*, 105000 – 10501.

[30] A. S. K. Hashmi, J.-H. Choi, J. W. Bats, *J. Prakt. Chem.* **1999**, *341*, 342 – 357.

© 2005 Wiley-VCH Verlag GmbH & Co. KGaA, Weinheim

Synthesis in Metal Flux

DOI: 10.1002/anie.200462170

The Metal Flux: A Preparative Tool for the Exploration of Intermetallic Compounds

Mercouri G. Kanatzidis, Rainer Pöttgen,* and Wolfgang Jeitschko**

Keywords:
exploratory synthesis · intermetallic compounds · metal fluxes · solid-state chemistry

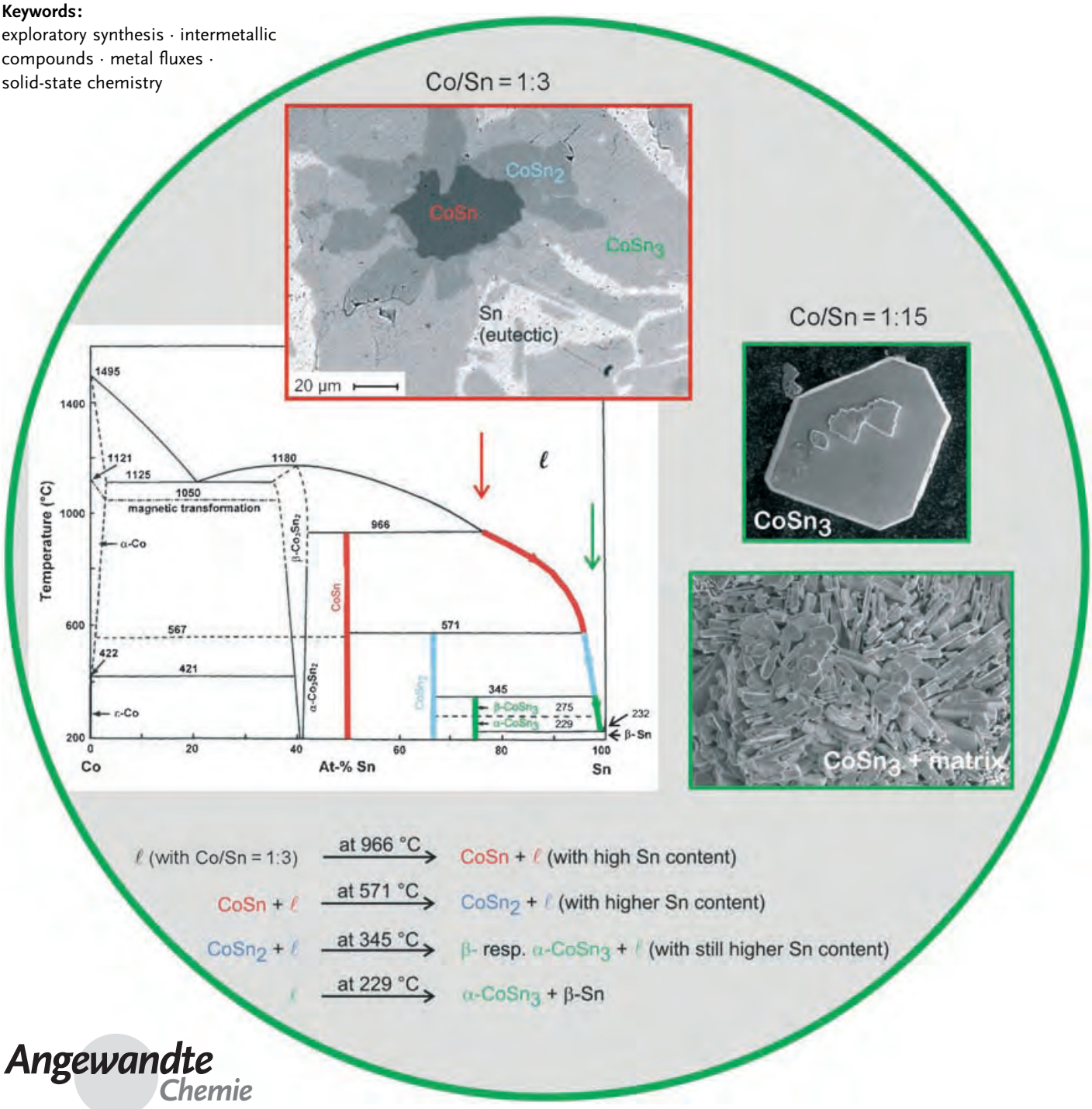

© 2005 Wiley-VCH Verlag GmbH & Co. KGaA, Weinheim

This review highlights the use and great potential of liquid metals as exotic and powerful solvents (i.e. fluxes) for the synthesis of intermetallic phases. The results presented demonstrate that considerable advances in the discovery of novel and complex phases are achievable utilizing molten metals as solvents. A wide cross-section of examples of flux-grown intermetallic phases and related solids are discussed and a brief history of the origins of flux chemistry is given. The most commonly used metal fluxes are surveyed and where possible, the underlying principal reasons that make the flux reaction work are discussed.

From the Contents

1. Introduction	6997
2. Challenges	6999
3. Metallic Fluxes	6999
4. Historical Perspective	6999
5. Peritectic Reactions and Reactive Fluxes	7000
6. Experimental Techniques	7001
7. The Tin Flux	7002
8. The Lead Flux	7007
9. Liquid Aluminum as a Flux	7008
10. Reactions in Liquid Gallium	7011
11. Indium Flux	7013
12. Lithium and Sodium Fluxes	7014
13. Miscellaneous Metallic Fluxes and Materials	7015
14. Concluding Remarks	7017

1. Introduction

1.1. Intermetallic Phases in Science and Technology

Compounds containing exclusively two or more different kinds of metal (or metalloid) atoms are defined as intermetallic compounds. The difference between an intermetallic compound and a regular metal (e.g. a metallic element) is in the way the atoms bond. In metals, the bonding electrons distribute themselves throughout the material (i.e. the electrons are more delocalized), giving rise to predominantly nondirectional bonding in the solid. Intermetallic compounds, on the other hand, maintain a slight ionic and covalent character (i.e. the electrons are localized), and the atomic bonding becomes more directional. This difference in bonding character results in differences in material behavior. Chemists have often given secondary attention to intermetallic compounds as a class of materials, compared to the more ionic materials such as oxides, ceramics, chalcogenides, or halides. This lack of appeal may have been partly due to the difficulty in understanding some very basic characteristics of intermetallic compounds such as their compositions, bonding, and assignment of oxidation states for individual atoms. As a result, the bulk of synthetic activity and innovation in solid-state chemistry has focused primarily on the ionic type of materials, whereas typically the synthesis of intermetallic compounds has been carried out in only a few laboratories and requires very high temperature conditions which are achieved by the use of induction heating and arc melting.

Some important intermetallic compounds are aluminum-based and silicon-based materials. In commercial aluminum alloys (many of which also contain silicon), rare-earth or transition metals are included to improve the properties. A result of this approach is the formation of both known as well as yet unexplored multinary intermetallic compounds within the aluminum matrix.[1] The study of possible multinary compounds formed during the alloying process is vital to understand how to optimize the bulk material. Rare-earth-element-containing binary and ternary aluminides often have complex structures and interesting magnetic and electronic behavior.[2]

Silicides are both scientifically and industrially important,[3] and have been extensively studied during the past few decades. Because of their hardness, chemical stability, and high melting point, silicides are well known as high-temperature, oxygen-resistant structural materials which are used, for example, in making high-temperature furnaces[4] and for high-temperature coatings.[5] Transition-metal silicides are highly valued as electrical and magnetic materials, in addition to several new applications such as thermoelectric energy conversion,[6] and compatible electrode materials in electronics.[7] Some silicides are low-temperature superconductors.[8] Several reviews and papers regarding their preparation, properties, and crystal chemistry,[9] thermodynamics,[10] applications in silicon technology,[11] and materials aspects of silicides for advanced technologies[12] have been published.

Silicides are usually synthesized by direct reaction of the elements heated in vacuum or in an inert atmosphere. The

[*] Prof. Dr. M. G. Kanatzidis
Department of Chemistry
Michigan State University
320 Chemistry Building, East Lansing, Michigan 48824 (USA)
Fax: (+1) 517-353-1793
E-mail: kanatzid@cem.msu.edu
Prof. Dr. R. Pöttgen, Prof. Dr. W. Jeitschko
Institut für Anorganische und Analytische Chemie
Westfälische Wilhelms-Universität Münster
Corrensstrasse 30/36, 48149 Münster (Germany)
Fax: (+49) 251-83-38002
E-mail: pottgen@uni-muenster.de
jeitsch@uni-muenster.de

© 2005 Wiley-VCH Verlag GmbH & Co. KGaA, Weinheim

required reaction temperatures are usually over 1000 °C necessitating the use of an arc welder or inductive furnace. Although single crystals sometimes can be obtained by annealing or quenching the product, in most situations only powder samples are obtained using these methods. This situation often makes crystal-structure determination difficult and limits proper characterization.

Of course there are many other important intermetallic compounds including nickel superalloys and titanium- and molybdenum-based systems which are remarkably heat and corrosion resistant, finding applications in jet engines, as coatings, as well as in the biomedical and automotive industries.[13] Many titanium-based alloys are also used in orthopedic applications owing to their good biocompatibility, appropriate mechanical properties, and excellent corrosion resistance. Advanced copper alloys are of interest for fusion-reactor applications and to aerospace engine makers (as liners for thrust cell combustion chambers and nozzle ramps).[14] A large number of intermetallic systems based on a variety of elements including Ti, Fe, Al, Ni, Ga, and Mn exhibit interesting shape-memory effects with implications in a number of important applications.[15] The remarkable compound Ti_3SiC_2 is damage tolerant, not susceptible to thermal shock, has excellent oxidation resistance, and is as readily machinable as graphite.[16] Single-crystalline samples of $MnNi_2Ga$ have been shown to produce close to 10% magnetic-field-induced strain.[17] Platinum intermetallic compounds are also of interest for use as catalysts[18] and for high-temperature applications such as inert coatings for titanium alloys.[19]

Traditionally, the study of intermetallic phases has been mainly the subject of metallurgists who have synthesized many of the known compounds. As a result, intermetallic compounds are critical as structural materials in technological applications. Many new applications, however, are emerging or envisioned, and to go forward, advances in the understanding and in the discovery of new intermetallic compounds are needed. Solid-state chemistry has a significant role to play in this regard.

1.2. The Flux Method in Solid-State Chemistry

The synthetic toolbox of the solid-state chemist contains several powerful and productive means, each with its unique capabilities, advantages, and disadvantages. For intermetallic compounds these techniques generally involve very high temperatures as for example arc-melting and radio frequency (rf or high frequency (hf)) induction heating. These methods are necessary because the starting materials employed in such reactions are usually solids themselves and very high temperatures are necessary to cause sufficient diffusion for a reaction to take place. Often even high temperatures alone are not enough to overcome these barriers and the samples need to be ground to powders several times during the synthesis to expose fresh surfaces on which reactions can occur. These high temperatures give rise to two important synthetic limitations. The reactions generally proceed to the most thermodynamically stable products; the high energies involved often leave little room for kinetic control. These thermodynamically stable products are typically the simplest of binary or ternary compounds, which because of their high structural stability can become synthetic roadblocks, and often are difficult to circumvent. In addition, the rapid cooling of reactants from high temperatures along with the repeated grinding of the samples, as mentioned above, do not create a favorable environment for crystal growth. Single crystals can sometimes form through extended annealing, and even then the growth of crystals large enough for physicochemical analysis is not always seen. Microcrystalline products can limit the proper characterization of the new material both

Wolfgang Jeitschko, born 1936 in Prague, received his Ph.D. in 1964 with H. Nowotny with a thesis on ternary carbides at the University of Vienna. After postdoctoral years in the metallurgy departments of the universities of Pennsylvania and Illinois and as lecturer at the University of Illinois he worked as a crystallographer for DuPont in Wilmington. In 1975 he became Professor of Inorganic Chemistry at the Universität Gießen, in 1978 at the Universität Dortmund, and in 1981 at the Universität Münster. His research interests extend from the preparation of new solid-state compounds and their characterization mainly by X-ray and neutron diffraction to applications of materials science.

Rainer Pöttgen was born in 1966 in Meschede, Germany, and received his Ph.D. in 1993 at the University of Münster with Wolfgang Jeitschko, followed by postdoctoral studies at the ICMCB CNRS in Bordeaux (France) with Jean Etourneau (1993) and at the Max-Planck-Institut für Festkörperforschung in Stuttgart (Germany) with Arndt Simon (1994–1995). After habilitation at the University of Münster (1997) he became Professor for Inorganic Solid State Chemistry at LMU München (2000–2001). Since autumn 2001 he has been Chair of Inorganic Chemistry at the University of Münster. His research interests include the synthesis and structure–property relations of intermetallic compounds.

Mercouri G. Kanatzidis was born in Thessaloniki, Greece in 1957. After obtaining a B.Sc. from Aristotle University in Greece he received his Ph.D. in chemistry from the University of Iowa in 1984. He was a postdoctoral research associate at the University of Michigan and Northwestern University from 1985 to 1987 and is currently a University Distinguished Professor of Chemistry at Michigan State University where he has served since 1987. His research concerns metal chalcogenide chemistry, the development of solid-state synthesis by flux methods, hydrothermal, and solvothermal techniques. He is also active in the fields of new thermoelectric materials, the synthetic design of framework solids, intermetallic phases, and nanocomposite materials.

 © 2005 Wiley-VCH Verlag GmbH & Co. KGaA, Weinheim

structurally and physically, particularly when knowledge about anisotropic effects is desired, and may even prevent the proper identification of the products in extreme cases.

Methods that permit reactions to be carried out at lower temperature are likely to produce new phases. This thesis applies to all classes of compounds including intermetallic phases.[20–22] To increase the odds for new compound formation and avoid the thermodynamic traps, the reactant diffusion must be increased so that the activation energy barrier (associated with solid–solid reactions) is lowered. Under these conditions the reaction could proceed at lower temperatures to some other outcome. High diffusion rates (from a solid-state perspective) could be achieved by simply allowing soluble starting materials to react in a solvent.

To achieve enhanced diffusion of reactants in solid-state synthesis, molten solids can be used as solvents (i.e. fluxes). Such media (predominantly salts) have been employed for well over a 100 years for high-temperature single-crystal growth. Although many salts are high-melting species, eutectic combinations of binary salts and salts of polyatomic species often have melting points well below the temperatures of classical solid-state synthesis, making possible the exploration of new chemistry at intermediate temperatures. In many instances, these liquids act not only as solvents, but also as reactants, providing species which can be incorporated into the final product. In the latter case this is analogous to solvate formation or to cases where the solvent provides atoms to the compound being formed. Such a molten solvent is called a "reactive flux". Therefore, appropriate molten metals can act in such a fashion to become bona-fide solvents for synthesis. Lessons learnt from solution synthesis could be applied in this type of solid-state synthesis with, as we will show in this review, remarkable results.

2. Challenges in the Solid-State Chemistry of Intermetallic Compounds

Because the composition of most intermetallic compounds does not yield to the type of electron counting and oxidation-number analysis typically applied to more familiar solid-state compounds such as halides, oxides, and chalcogenides, it is very difficult to predict the type of composition that would be stable in a given system of metallic elements (except for special cases, such as Zintl, Laves, or Hume–Rothery phases). For example, whereas compositions of the type K_2MoO_4, Ag_2HgI_4, FeS_2, and Fe_2SnS_4 are well understood and can be predicted and therefore can be targeted for synthesis, the compositions $FeGa_3$, $YNiGe_2$, $RhSn_4$, Sm_2NiGa_{12}, or $SmNiSi_3$ appear totally strange to the average chemist. The situation is even more complicated when considering quaternary systems such as $Sm_2NiAl_7Si_5$ or $Sm_8Ru_{12}Al_{49}Si_{21}$. For intermetallics such stoichiometries are more the norm than the exception, whereas in more polar non-intermetallic compounds it is generally the other way around. Non-intermetallic compounds display more ionic character in their bonding, extensive charge transfer between different atoms, and as a result can be explained easily to a chemistry student, whereas this is difficult for intermetallic compounds. A different type of basic understanding and intuition is required, one that goes beyond the complexity of the electronic band-structure calculations usually done to deal with these kinds of compounds. How can such compositions be predicted, so they can be targeted for exploratory synthesis? Of course, the answer today is that they cannot be. Using liquid metals as fluxes, to carry out synthetic explorations, could serve as a great way to discovering (without having to predict) a large variety of intermetallic compounds.

Herein we present the use of liquid metals as reaction media to synthesize new classes of intermetallics and other non-oxidic solids, such as carbides, nitrides, and pnictides. The emphasis is placed on the utility of the fluxes to discover new materials rather than to grow large crystals of known materials. We highlight herein how the metal-flux technique is aimed at gaining control at lower temperatures and is a critical synthetic tool in the solid-state chemist's arsenal of methods. This review is not meant to be an exhaustive account of what has transpired since the first example of metal-flux synthesis was reported. Therefore a number of worthwhile reports may not be referenced. Instead our goal is to increase awareness of this synthetic approach by drawing attention to the possibilities it offers. This article is written from a solid-state chemist's point of view and we mainly focus on the recent literature with respect to the synthesis and crystal growth of new compounds.

3. Metallic Fluxes

The use of molten metals as media for the synthesis of new materials has been limited compared to the highly successful use of molten salts. In those cases where metallic fluxes have been used, new compounds have resulted that are interesting from the structural, physicochemical, and even the practical point of view. In the vast majority of cases, however, use of molten metals has been focused primarily on growing single crystals of known compounds, not for exploratory synthesis.[23,24] The purpose of this article is to give an overview of the known chemistry associated with exploratory synthesis using metallic fluxes and to highlight the potential of this approach.

Several key characteristics must be met for a metal to be a viable flux for reaction chemistry: 1) the metal should form a flux (i.e. a melt) at reasonably low temperatures so that normal heating equipment and containers can be used, 2) the metal should have a large difference between its melting point and boiling point temperatures, 3) it should be possible to separate the metal from the products, by chemical dissolution, filtration during its liquid state, or if necessary mechanical removal, 4) the metal flux should not form highly stable binary compounds with any of the reactants. This last point is critical.

4. Historical Perspective on the Preparation and Crystal Growth from Metallic Melts

Metallic fluxes were employed early on in the preparative chemistry of solids. Henri Moissan (1852–1907) tried to obtain

© 2005 Wiley-VCH Verlag GmbH & Co. KGaA, Weinheim

diamonds in many experiments by rapidly quenching carbon containing (in homogeneous and heterogeneous form) liquid iron and other metals from high temperatures using the electric furnace that he developed.[25] In this way he had hoped to create the required high pressure within the contracting metal jacket. After dissolving the metallic matrices in acids he found tiny, very hard crystals, some with octahedral shape which burned and produced carbon dioxide. Moissan died believing that he had made diamonds. His experiments were reproduced and resulted in carborundum (SiC, with the mineral name moissanite). It is interesting that industrial diamonds were first successfully synthesized in 1954 in the laboratories of the General Electric Company at high pressure, again in the presence of liquid iron. Without the metallic flux, much higher pressure is required. Thus, this process, generally regarded only as a high-pressure synthesis, may also be quoted as a crystal growth from a metallic flux. Now it is estimated, that about one hundred tons of synthetic diamonds are produced annually by this process.[26]

At around 1900 Paul Lebeau, a co-worker of Moissan, prepared various silicides of late transition metals from a copper flux, and Jolibois of that school has to be credited for being the first to employ a tin flux to grow nickel phosphides.[27] In subsequent years such solution growth from metallic fluxes has variously been called menstruum technique, Lebeau method, auxiliary bath method (Hilfsmetallbadtechnik), and molten metal solution growth. Many borides, carbides, silicides, and nitrides of the early transition metals have been obtained this way in well-crystallized form, usually with higher purity than by direct reaction of the elemental components. Some of the early literature about metallic fluxes is cited in the introductory paragraphs of various papers reporting on the recrystallization of transition-metal borides (e.g., TiB_2, ZrB_2, VB, NbB_2, W_2B_5) using iron, copper, aluminum, tin, or lead as fluxes,[28–30] the preparation of the high-melting carbides (e.g., TiC, WC, UC) with iron, cobalt, nickel, or aluminum as fluxes,[31] and the preparation of various silicides of early transition metals (e.g., $TiSi_2$, $CrSi_2$, Mo_5Si_3, $MoSi_2$, W_5Si_3, WSi_2) employing mainly copper or tin as fluxes.[32,33] Deitch reviewed the early literature on the growth of semiconductors, e.g., Si, SiC, AlP, GaAs, ZnS, ZnTe, $ZnSiP_2$, $CdSiP_2$,[34] and Lundström summarized the literature on the preparation and crystal growth of non-oxidic refractories using molten metallic solutions.[35] The handbooks on crystal growth by Elwell and Scheel[24] and Wilke and Bohm[36] list more than 100 references on the growth of single crystals of various, mostly binary compounds from metallic fluxes.

By using a metallic flux, it is not necessary to completely dissolve the elemental components of the desired products. The flux may act as a transporting medium, which dissolves a component in one place and grows the product at another location of the sample container. Nevertheless, it is important for the flux to have reasonable solubilities for the components to avoid exceedingly long growth times. Gumiński has published a compilation of experimental solubilities of metals in liquid low-melting metallic fluxes, such as mercury, gallium, indium, tin, lead, and bismuth. He also gives some estimates for combinations of metallic elements, where no experimental data are available.[37] The solubilities of various industrially important transition-metal disilicides MSi_2 with M = Ti, V, Nb, Ta, Cr, Mo, and W in metallic fluxes have been investigated experimentally.[38] The monograph edited by Hein and Buhrig[39] gives an extensive treatment of such data both for equilibrium and non-equilibrium conditions, and also from a theoretical point of view.

5. Peritectic Reactions and Reactive Fluxes

Some terms, commonly known by metallurgists and crystal growers, may be less appreciated by preparative chemists. A compound formed by a *peritectic* reaction may be such a case. Consider the phase diagram of the binary system cobalt–tin (Figure 1).[40,41] The compound designated as β-Co_3Sn_2 melts congruently (that is, the solid and liquid have the same composition) at 1180 °C. In contrast, CoSn melts incongruently at 966 °C, forming solid β-Co_3Sn_2 and a liquid ℓ of a composition, which is indicated by the large down-pointing arrow in that phase diagram. Conversely, if a melt of that composition (with a Co:Sn ratio of approximately 1:3) is cooled, the liquidus line will be reached at 966 °C. On further cooling, the compound CoSn will crystallize until the sample reaches 571 °C. At that temperature solid CoSn will react with the liquid (by what is called a peritectic reaction) to form $CoSn_2$. The problem is, that this phase forms an envelope around the reactant CoSn. Thus, this (peritectic) reaction can now only proceed by diffusion through the solid envelope of $CoSn_2$. This diffusion process takes time and may not be finished before the sample reaches the next peritectic equilibrium temperature of 345 °C. At that temperature (the high-temperature modification) β-$CoSn_3$ is formed. The melt changes its composition continuously, following the red, then the blue, and finally the green liquidus curves. The remaining melt will solidify at the eutectic temperature of 229 °C.

A scanning electron micrograph of a sample with a slightly higher tin content (Co:Sn ratio 1:4) is shown in the lower part of Figure 1. The very light areas of the micrograph have the lowest cobalt content; they correspond to the tin-rich eutectic. Naturally it will be very difficult to isolate single crystals of (one or the other modification of) $CoSn_3$ from such a sample.

A single-phase sample of α- or β-$CoSn_3$ (depending on the relatively low annealing temperature above or below 275 °C) can be obtained from a solidified melt of that composition (1:3) only by annealing for a very long time, for example, for several weeks. However, the situation changes dramatically if a large excess of tin is used. In this case, well-developed crystals of $CoSn_3$ can be grown by slow cooling down to the eutectic temperature. The crystals of $CoSn_3$ are then embedded in a tin-rich matrix, which can be dissolved in diluted hydrochloric acid.

Herein we have described the preparation of single-phase $CoSn_3$ by using an excess of tin as—what may be called—a *reactive flux*, thus avoiding the very slowly proceeding peritectic reaction. Frequently the phase diagram is not known, and guess work or trial and error are required to find the excess of the reactive flux needed to crystallize the desired product. This of course will be the normal situation in

 © 2005 Wiley-VCH Verlag GmbH & Co. KGaA, Weinheim

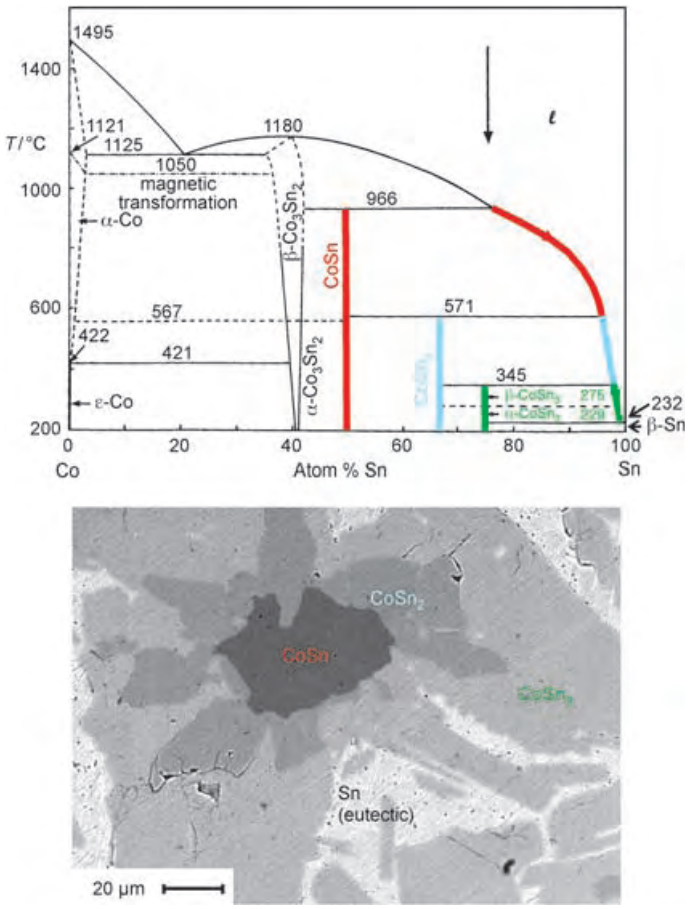

Figure 1. Peritectic reactions in the binary system Co–Sn. Top: the phase diagram of the Co–Sn system. By rapidly cooling a melt (liquidus, ℓ) of the approximate composition Co:Sn = 1:3 (large black arrow) crystals of composition CoSn are obtained first. Since these crystals have a higher Co content than the original melt, the liquid phase changes its composition on cooling along the red liquidus line. At 571 °C the crystals of CoSn start to react with the remaining melt, thereby forming a microcrystalline envelope of the compound $CoSn_2$. During this reaction, the liquid phase changes its composition along the blue line. After further cooling, at 345 °C, the melt, now with a Sn content of approximately 98 atom%, starts to react with $CoSn_2$ and forms another microcrystalline envelope this time of microcrystalline β-$CoSn_3$. Thereby the melt changes its composition along the green line. Finally, at 229 °C it solidifies, to form the eutectic, which consists of a matrix of a solid solution of Co in β-Sn with heterogeneous inclusions of α-$CoSn_3$. Bottom: A micrograph of a corresponding sample (with the slightly different overall composition Co:Sn = 1:4).[41] It is clear that well developed large crystals of α- or β-$CoSn_3$ cannot be grown by such a cascade of peritectic reactions. This sample has been cooled at the relatively slow rate of 100 °C h^{-1}. Nevertheless, it has not reached thermodynamic equilibrium. In its center it contains the remains of a primarily crystallized grain of CoSn, embedded in grains of $CoSn_2$. Before reaching equilibrium the sample had cooled to 345 °C, thus forming β-$CoSn_3$.

exploratory research, where the emphasis is on novel materials with potentially interesting properties. Such materials may contain several components and it may be impractical to work out the phase diagrams. However, it must be remembered, that the kind of the reaction product obtained will depend not only on the annealing conditions, but also on the amount of the reactive flux used.

When such transition metal stannide crystals are grown from a tin-rich flux, the solidified excess flux can be dissolved with hydrochloric acid, since the stannides are more stable than the flux. Figure 2 shows the experimental results for the preparation of $RhSn_4$ crystals. In the upper part of the Figure a partially dissolved matrix is shown, while one selected crystal is presented at the bottom.

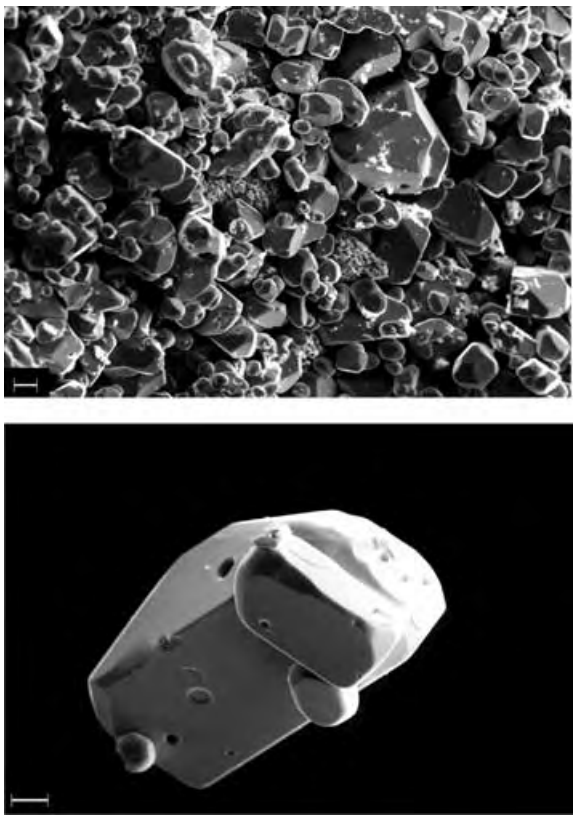

Figure 2. Single crystals of $RhSn_4$ grown in a tin flux. Top: the tin-rich matrix partially dissolved with diluted hydrochloric acid (scale bar 20 μm); bottom: a selected single crystal, with a few much smaller attached crystals (scale bar 10 μm)).

6. Experimental Techniques

To carry out exploratory reactions in a metallic flux, care must be taken to contain the liquid metal and prevent it from reacting with the container or evaporating. Therefore, the procedures and containers vary, depending on the liquid metal. Generally, liquid metals such as aluminum are highly reducing and react quickly with conventional container materials such as silica. Less reactive metals such as Sn, Ga, or In also react with silica if in contact for prolonged times and/or if the temperature is too high. A more attractive container material is alumina (Al_2O_3), which is inert to Al, Sn, or Ga. In this case alumina thimbles are used and are placed inside silica tubes, which are then sealed. Alternatively, for Sn or Ga fluxes graphite thimbles or crucibles can be used. Typically these are left open (i.e. without lid) because of the relatively low volatility of these metals at the temperatures used. Alumina and graphite, however, react with liquid alkali

© 2005 Wiley-VCH Verlag GmbH & Co. KGaA, Weinheim

metals, and therefore are unsuitable when these are used as fluxes. In some cases glassy carbon can be used as container material. Most metal fluxes do not react with this rather inert material. For reactions at higher temperatures tubes or crucibles of high-melting metals (Nb, Ta, Mo, W) may be used. Indium flux reactions have often been carried out in ZrO_2 crucibles. An extensive discussion of experimental techniques and procedures has been published by Fisk and Remeika.[42] For experimental details we refer to the original literature.

After the reaction is finished, isolation is either by recovering the solid ingot which contains the products embedded in the flux, or by immersing the entire thimble inside a flux-dissolving solution such as hydrochloric acid or aqueous sodium hydroxide. More exotic combinations can be used to dissolve the metal flux such as organic solvents containing various oxidants such as Br_2, I_2, peroxides. In the case of gallium and tin fluxes, the centrifugation technique has successfully been used for the separation of the crystals from the excess flux.[43–45] In the following sections we summarize recent results categorized by the respective flux medium.

7. The Tin Flux

The chemical and physical databases reveal a huge amount of literature dealing with the development of tin-based low-melting alloys for welding and soldering applications. We do not refer to this literature herein. In the case of tin fluxes we focus only on the preparation of new compounds.

7.1. Binary Phosphides and Polyphosphides

Elemental tin as a flux has already been used by Jolibois[27] to prepare the phosphides NiP_2 and NiP_3 in well-crystallized form. Crystal-structure investigations, carried out much later, showed that these compounds have P–P bonds. Such compounds are called polyphosphides today. Phosphides with high phosphorus content are difficult to synthesize by direct reaction of the elemental components. At relatively low temperatures (e.g. 500 °C), the reactions are too slow, and at higher temperatures polyphosphides tend to decompose into lower phosphides and phosphorus vapor. With the tin-flux technique this difficulty can be overcome as long as the desired polyphosphides are thermodynamically more stable than the corresponding stannides. Thus, phosphides and polyphosphides of the Mn, Fe, and Co group can be prepared this way, while Pd, Pt, and the coinage metals under similar conditions frequently form the corresponding transition-metal stannides (Figure 3) or ternary polyphosphides such as Cu_4SnP_{10}.[46] This limitation can be overcome to some extent by increasing the phosphorus and decreasing the tin content of the sample.

Usually, after such reactions, the tin-rich matrix of the binary or ternary transition-metal phosphides and polyphosphides can be dissolved in hydrochloric acid. The extent to which the acid attacks the phosphides and polyphosphides depends on the reactivity of the transition metal. Thus, for instance, after dissolving their tin-rich matrix, crystals of MoP_2 show rounded-off edges, whereas crystals of ReP_4 appear practically unattacked (Figure 4).

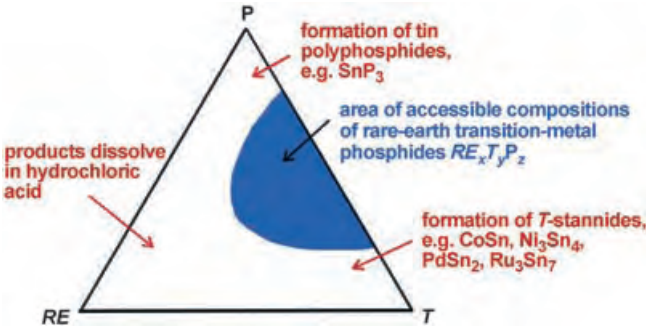

Figure 3. The use of a tin flux to prepare ternary phosphides of the type $RE_xT_yP_z$ (RE = rare-earth, T = transition-metal) Only phosphides within the blue area of the ternary phase diagram *RE*-*T*-P can be prepared well and isolated. Attempts to prepare samples with compositions which have high contents of phosphorus or with high contents of certain late transition metals may result in binary tin polyphosphides or transition-metal stannides, respectively. Ternary phosphides with a high content of rare-earth elements dissolve in hydrochloric acid and therefore are difficult to isolate from the tin-rich matrix.

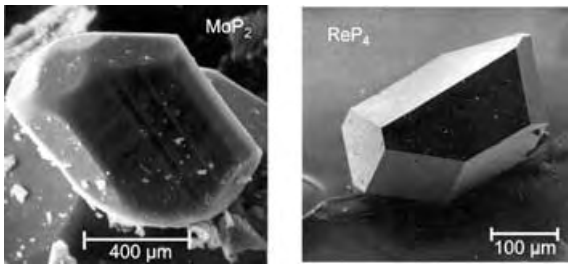

Figure 4. The appearance of the transition-metal polyphosphides MoP_2 and ReP_4 after their tin-rich matrix has been dissolved in diluted hydrochloric acid. Note that the edges of the MoP_2 crystal are rounded, while the crystal of ReP_4 has not been attacked by this acid.

Examples for binary phosphides and polyphosphides prepared in liquid tin are given in Table 1. It should be mentioned that the compounds SiP (sphalerite type),[47] *p*-SiP_2 (pyrite type),[47] CrP_4,[48] MoP_4,[48] and one modification of MnP_4[49]—subsequently called 8-MnP_4[50]—were first thought to be high-pressure compounds, because they could not be obtained by direct reaction of the elemental components at normal pressure. Their preparation by using a tin flux (for references see Table 1) showed that they must be considered as ambient-pressure compounds. In turn, the fact that these compounds could be prepared in the absence of tin, shows that they are not stabilized by small amounts of tin.

The preparation of binary rhenium phosphides and polyphosphides has been studied systematically, both using iodine as a mineralizer (somewhat similar to chemical vapor transport reactions, but over a shorter distance) or in a tin flux. As could have been expected, both preparation techni-

 © 2005 Wiley-VCH Verlag GmbH & Co. KGaA, Weinheim

Table 1: Binary phosphides and polyphosphides prepared from a tin flux.

Compound	Sample composition Atomic ratio *M*:P:Sn	Typical preparation conditions[a]	Ref.
SiP	1:1:10	1150 °C→10 °C h^{-1}→300 °C	[51]
SiP_2	1:8:12	1000 °C→10 °C h^{-1}→300 °C	[52, 53]
CrP_4	1:10:15	1 day, 800 °C→2 °C h^{-1}→ 300 °C	[54]
MoP_2	1:10:6	10 days, 850 °C	[55]
MoP_4	1:10:6	10 days, 550 °C	[55]
α-WP_2	1:10:6	14 days, 750 °C	[55]
β-WP_2	1:10:6	7 days, 950 °C	[55]
2-MnP_4	1:10:20	21 days, 550 °C	[50, 56]
6-MnP_4	1:10:6	14 days, 600 °C	[50, 56]
8-MnP_4	1:10:15	1 day, 800 °C→2 °C h^{-1}→ 100 °C	[54]
Tc_3P	3:1:18	20 days, 950 °C	[57]
Tc_2P_3	1:3:6	20 days, 950 °C	[58]
TcP_3	2:9:12	20 days, 950 °C	[59]
TcP_4	1:10:6	20 days, 950 °C	[57]
Re_2P	2:1:12	7 days, 900 °C→5 °C h^{-1}→ 300 °C	[60]
Re_3P_4	1:1:6	7 days, 800 °C	[60]
Re_6P_{13}	1:4:8	7 days, 800 °C	[60, 61]
Re_2P_5	10:33:57, 8:42:50	7 days, 850 °C; 7 days, 950 °C	[60, 62]
ReP_3	2:9:12	14 days, 750 °C	[59, 60]
ReP_4	1:5:9	7 days, 800 °C	[60, 63]
α-FeP_4	1:5:40, 1:10:40	10 days, 650 °C→5 °C h^{-1}→ 200 °C	[64, 65]
RuP_2	1:2:100	3 days, 1200 °C→ 25 °C h^{-1}→300 °C	[66]
RuP_3	1:5:4	6 h, 1000 °C→50 °C h^{-1}→ 300 °C	[67]
α-RuP_4	1:8:10	7 days, 600 °C	[68, 69]
β-RuP_4	1:10:15	30 days, 700 °C	[68, 69]
α-OsP_4	1:12:20	10 days 700 °C	[68, 69]
β-OsP_4	1:10:40	30 days, 800 °C	[68, 69]
CoP_2	not stated	not stated	[70]
CoP_3	1:8:3	1 day, 450 °C; 7 days, 675 °C	[71]
RhP_3	1:3:80	1 day, 1150 °C→5 °C h^{-1}→ 550 °C	[72]
IrP_2	1:2:100	2 days, 1200 °C→ 50 °C h^{-1}→300 °C	[66]
NiP_2	1:2:40	1 day, 1150 °C→5 °C h^{-1}→ 550 °C	[27, 72]
NiP_3	1:6:7	7 days, 700 °C	[27, 71, 73]
PtP_2	1:15:30	1 day, 1200 °C→5 °C h^{-1}→ 550 °C	[74]
CuP_2	1:2:10	1 day, 1150 °C→5 °C h^{-1}→ 550 °C	[72, 75]

[a] **Caution**: Usually the less reactive modification of red phosphorus is used. Nevertheless, even this modification reacts violently with tin. Thus, care must be taken in heating the reactive mixtures of the elements. Frequently the samples are heated to the desired temperatures at very slow rates, for example, 5 °C h^{-1}. For detailed reaction conditions the original publications should be consulted.

ques yield essentially the same sequence of phases, however, the synthesis in the tin-flux proceeds faster and thermodynamic equilibria were reached at lower temperatures than in the reactions with iodine.[60] The compound Re_2P_5 was obtained only through the tin-flux synthesis. However, neither an energy dispersive X-ray fluorescence analysis, nor the structure determination gave any indication for it being stabilized by tin.[62] Furthermore, the structure of Re_2P_5 can be completely rationalized on the basis of a two-electron model, counting two electrons for each Re–Re, Re–P, and P–P interaction. In agreement with this extremely simple model, the compound shows semiconducting behavior. In contrast, the compound Re_6P_{13} with a very similar composition, prepared the same way by the tin-flux technique, lacks electrons to fill all the bonding states required according to the two-electron bond model. And in agreement with this result, its electrical conductivity is several orders of magnitude higher and has an inverse temperature dependence, thus indicating metallic behavior.[62] This result demonstrates not only the usefulness of the two-electron model for the rationalization of the physical properties of such transition-metal phosphides, but also that only insignificant amounts of tin were incorporated during the tin-flux syntheses of these compounds.

7.2. Ternary Phosphides and Polyphosphides of Rare-Earth and Transition Metals and Related Compositions

A large number of ternary rare-earth (*RE*) transition-metal (*T*) phosphides and polyphosphides were prepared by the tin-flux method. The polyphosphides with "filled" skutterudite type structure were the first to be investigated. They derive their name from the mineral $CoAs_3$ (Co_4As_{12}). Their crystal structure was determined for $LaFe_4P_{12}$. Some twenty phosphides are known to crystallize with this structure type, where iron may be substituted by its homologues ruthenium and osmium.[71,76] They were originally prepared from the elemental components in a tin flux with the atomic ratio *RE*:*T*:P:Sn = 1:4:20:50 in sealed silica tubes by slowly heating (to avoid violent reactions!) to 800 °C, annealing at that temperature for one week, followed by slow cooling (2 °C h^{-1}) to room temperature. After dissolving the tin-rich matrix in moderately diluted hydrochloric acid, crystals with diameters up to 2 mm can be obtained by this method.[77,78] As an example, we show a crystal of $NdFe_4P_{12}$ in Figure 5. In these compounds the *RE* components are usually the early-rare-earth elements from lanthanum to gadolinium. In addition, polyphosphides with the actinoids have also been synthesized from a tin flux: $ThFe_4P_{12}$,[79] $ThRu_4P_{12}$,[79] and UFe_4P_{12}.[80,81] The preparation of such polyphosphides without a tin flux has been successful mainly at high pressure (for references see ref. [82]). One exception is the sodium-containing filled skutterudite type polyphosphide $Na_{1+x}Fe_4P_{12}$ with excess sodium ($x \approx 1$), which has been prepared hydrothermally.[83] Another, very interesting exception is the series of metastable phosphides $LnFe_4P_{12}$, where the *Ln* components are late-rare-earth elements. These were prepared by heating of multilayer precursors at the relatively low temperature of 200 °C.[84] Many of these polyphosphides with $LaFe_4P_{12}$-type structure have interesting physical properties, including superconductivity and heavy fermion behavior. The purity of such samples prepared from a tin flux can be judged from the fact, that the cerium compounds are semiconducting—clearly, all four

 © 2005 Wiley-VCH Verlag GmbH & Co. KGaA, Weinheim

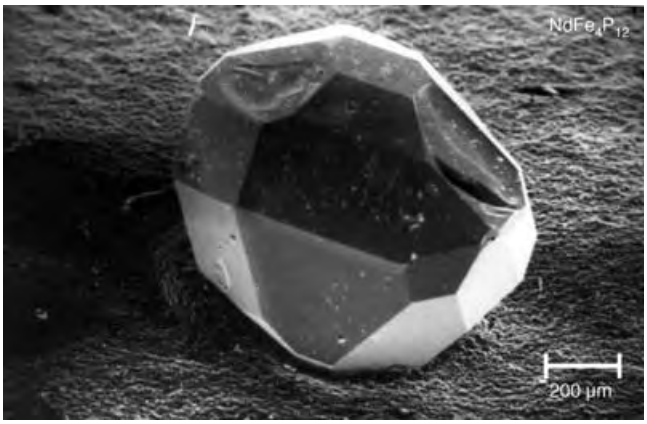

Figure 5. A crystal of $NdFe_4P_{12}$ with the cubic $LaFe_4P_{12}$ type structure grown from a tin flux.

valence electrons of the cerium atoms are involved in one way or the other in chemical bonding—whereas the skutterudite phosphides filled with the typically trivalent rare-earth elements are metallic conductors. The isostructural antimonides (RET_4Sb_{12}) have outstanding thermoelectric properties. Thus, the filled skutterudites have been studied by many research groups, details about their preparation can be found through the review articles.[82,85]

The ternary "filled" skutterudites RET_4P_{12} usually contain iron and its homologues ruthenium and osmium as the transition-metal components. When cobalt or its congeners rhodium and iridium are used as transition metals, the ternary compounds are nonstoichiometric with large defects at the *RE* positions, for example, $La_{0.2}Co_4P_{12}$ and $Ce_{0.25}Co_4P_{12}$.[86] With nickel as the transition metal the cubic compounds $Ln_6Ni_6P_{17}$ with $Ln = La$, Ce, Pr are obtained. These form by reactions of the elemental components in tin fluxes of greatly varying compositions. For example $La_6Ni_6P_{17}$ could be isolated from samples with the atomic ratios La:Ni:P:Sn = 1:1:8:20 and 3:1:6:10.[87] With analogous reaction conditions, using palladium as the transition-metal component, the low-temperature modification of the binary palladium stannide $PdSn_2$ is obtained (Figure 3), although the intended palladium compounds $La_6Pd_6P_{17}$ and $Ce_6Ni_6P_{17}$ could be prepared in microcrystalline form by direct reaction of the elemental components.[88]

Another large series of ternary phosphides frequently prepared by the tin-flux method have the composition AT_2P_2, where *A* is a lanthanoid or actinoid and *T* a late transition metal. Most of these phosphides crystallize with a body-centered tetragonal structure, variously called $BaAl_4$- and $ThCr_2Si_2$-type structures after the first binary or ternary representatives, respectively. From a crystallographic point of view, this structure type is interesting, because it is the one with the highest number of representatives, some 800. While the many silicides with this structure are usually prepared by direct reaction of the elemental components, the phosphides are best obtained by the tin-flux route, although most of these compounds have also been prepared in the absence of tin. Most phosphides of the three series AFe_2P_2, ACo_2P_2, and ANi_2P_2 (where A is practically all of the lanthanoids, including cerium, europium, and ytterbium which frequently show mixed-valent behavior in these compounds) have first been prepared from idealized starting compositions *A*:*T*:P:Sn varying between 1:2:2:3 and 1:2:2:25.[89,90a,b,91] Later, when the physical properties of these phosphides were investigated, it became important to prepare samples with higher purity and the starting compositions of the melts were optimized by trial and error. Thus, for instance the series of the nickel containing compounds ANi_2P_2 (A = Ca, La–Yb) were prepared with higher purity and yield from melts with the compositions A:Ni:P:Sn = 1.3:2:2.3:16.[92] Similar compositions have been used for the preparation of iron- and cobalt-containing phosphides with this structure.[93] Usually the mixtures of the elemental components are slowly heated (e.g. at a rate of 4 °C h^{-1}) to a temperature of between 850 and 950 °C, held at that temperature for one week, then quenched or slowly cooled to room temperature. After dissolving the tin-rich matrices, single crystals with edge lengths of up to 2 mm have been obtained from such fluxes (Figure 6).[94,95] Energy

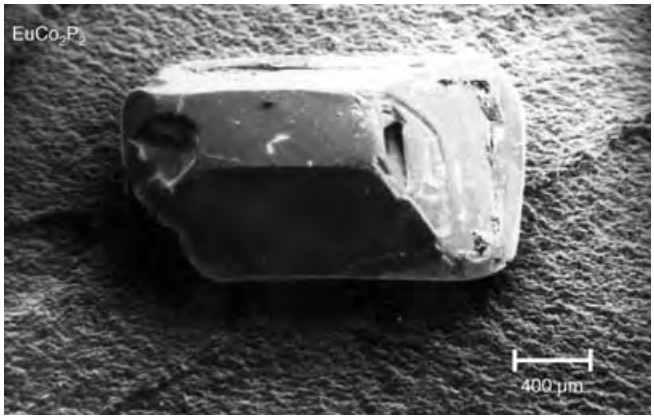

Figure 6. A 1.44 mm^3 single crystal of $EuCo_2P_2$ with the tetragonal $ThCr_2Si_2$ type structure grown from a tin flux.[95]

dispersive X-ray fluorescence analyses in scanning electron microscopes usually do not reveal any impurities such as tin or silicon (from the silica tubes) unless the reaction temperatures have been extremely high. However, heterogeneous inclusions of elemental tin have been observed in many cases, as concluded from the signals observed by difference scanning calorimetry at 232 °C, the melting point of tin.[96]

The phosphides with $ThCr_2Si_2$-type structure are known to crystallize with two different variants of this tetragonal structure with very different ratios of the unit cell dimensions *c*/*a* e.g., $EuCo_2P_2$ with $c/a = 3.01$ and $EuNi_2P_2$ with $c/a = 2.41$.[90] When the physical properties of these compounds became of interest, it was attempted to prepare samples of solid solutions between compounds with drastically different *c*/*a* ratios. Thus, the solid solutions $Ca_{1-x}Sr_xCo_2P_2$,[97] $LaCo_{2-x}Ni_xP_2$,[97] $LaFe_{2-x}Ni_xP_2$,[97] and $EuCo_{2-x}Ni_xP_2$[98] were investigated. More or less continuous changes in the *c*/*a* ratios were observed for $Ca_{1-x}Sr_xCo_2P_2$ between $x = 0.25$ and $x = 0.50$, for $LaCo_{2-x}Ni_xP_2$ between $x = 0.5$ and $x = 1.5$, and for $LaFe_{2-x}Ni_xP_2$ between $x = 1.0$ and $x = 2.0$. These samples were prepared by slowly heating powders in the ratio *A*-

 © 2005 Wiley-VCH Verlag GmbH & Co. KGaA, Weinheim

(Ca,Sr,La):*T*(Fe,Co,Ni):P:Sn = 1.1:2:2:20 at a rate of 40 °C h^{-1} to 880 °C and annealing at that temperature for 10 days. In contrast, a discontinuous change of the *c*/*a* ratio was observed for $x = 1.0$ in the pseudobinary system $EuCo_{2-x}Ni_xP_2$. The samples for this latter investigation were prepared by mixing powders of the end-members $EuCo_2P_2$ and $EuNi_2P_2$, and annealing these mixtures for two weeks at 910 °C in the presence of a relatively small amount of tin (29 mol %). This reaction was termed activated solid-state synthesis.[98]

With ruthenium as the transition-metal component the series ARu_2P_2 (A = Ca, Sr, La–Yb) with $ThCr_2Si_2$-type structure have been prepared from tin fluxes with atomic starting ratios varying between A:Ru:P:Sn = 1:2:2:5, 1:2:2:20, and 3:2:2:15. Of these products, $LaRu_2P_2$ becomes superconducting with a critical temperature of $T_c = 4.1$ K.[99] The compound $BaRu_2P_2$ has not been obtained this way, although it could be prepared by direct reaction of the elemental components.[100] Similarly, the palladium-containing phosphides of the series APd_2P_2 (A = Ca, Sr, Y, La–Er, Yb) with $ThCr_2Si_2$-type structure were obtained only by reaction of the elements.[88] The ternary actinoid phosphides $AnCo_2P_2$ (An = Th and U) crystallize with a primitive tetragonal $CaBe_2Ge_2$-type structure, which is closely related to the body-centered tetragonal structure of $ThCr_2Si_2$. These phosphides were also prepared from a tin flux using atomic ratios close to An:Co:P:Sn = 1:2:2:25.[90b,93b,93d] An entirely different orthorhombic structure, closely related to those of $BaZn_2As_2$ and $BaCu_2S_2$, was found for the phosphides $ThRu_2P_2$ and URu_2P_2. For the preparation of these phosphides with a tin flux, the binary phosphide RuP and a prereacted heterogeneous binary alloy of the overall composition "$U_{1.3}Ru_2$" were used with the starting ratios for both Th:RuP:Sn and $U_{1.3}Ru_2$:P:Sn of 1:2:10.[101a] Two modifications of $ThNi_2P_2$ with $BaCu_2S_2$-type and $CaBe_2Ge_2$-type structures, were prepared in a tin flux by annealing at 850 and 1000 °C, respectively, both with the same starting composition Th:Ni:P:Sn = 8:13:13:66.[101b] The manganese-containing compounds $EuMn_2Pn_2$ (Pn = P, As, Sb) have a simple hexagonal structure first determined for Ce_2O_2S and $CaAl_2Si_2$.[102a] For the physical characterization of the phosphide $EuMn_2P_2$ the crystal growth of this compound from a tin flux was optimized. Relatively large crystals with diameters up to 2 mm were obtained from a melt in the atomic ratio Eu:Mn:P:Sn = 14:4:11:265 ($\approx$ 90 atom % Sn). After slow heating, the sample was annealed at 1050 °C for 6 h, slow-cooled at 3 °C h^{-1} to 700 °C, and centrifuged at that temperature through silica wool into another vessel.[102b]

The uranium nickel phosphides UNi_3P_2,[103] $U_6Ni_{20}P_{13}$,[103] $U_2Ni_{12}P_7$,[103] and $U_3Ni_{3.34}P_6$[104] were prepared by reacting the elemental components in a tin flux with a tin content of 67 and 59 atom %, respectively. Two modifications of UCr_6P_4 were obtained by reactions of the binary uranium phosphide UP_2, phosphorus, and chromium in a tin flux of 70 atom %.[105]

A large family of closely related ternary rare-earth transition-metal phosphides has been found for compositions with a metal:phosphorus ratio of exactly or very close to 2:1. Most of the iron- and cobalt-containing compounds have been obtained in well-crystallized form with tin as a flux, while many of the corresponding nickel compounds were prepared in the absence of tin.[106] Nevertheless, the phosphides of the three series $RE_2Fe_{12}P_7$, $RE_2Co_{12}P_7$, and $RE_2Ni_{12}P_7$, were all prepared first using a tin flux with tin contents of between 70 and 80 atom % for the iron and cobalt containing compounds,[107] and between 25 and 35 atom % for the nickel compounds (note that the amount of tin flux tolerated for the nickel compounds is much lower, see Figure 3).[108] Needle-shaped crystals of $Tm_2Ni_{12}P_7$ with lengths of up to 2 cm were obtained by this preparation method.[109] The corresponding uranium compounds $U_2T_{12}P_7$ (T = Fe, Co, Ni) were also obtained this way.[110] Other compounds belonging to this structural family which were prepared by the tin flux technique include the two isotypic phosphides $LaNi_5P_3$ (La:Ni:P:Sn = 5:45:25:25)[91] and $EuNi_5P_3$ (Eu:Ni:P:Sn = 1:2:2:20),[111] the two isotypic series $RECo_5P_3$[112,113] and $REFe_5P_3$[107b] crystallizing with a different structure type, and the three isotypic phosphides $LaCo_8P_5$,[114,115] $PrCo_8P_5$,[115] and $EuCo_8P_5$.[115] In the case of the latter compounds the annealing was for 7 days at 880 °C, followed by controlled cooling (10 °C min^{-1}) to 600 °C and quenching. Crystals of the europium compound of up to 3 mm length and with diameters up to 1 mm were obtained this way. The barium nickel phosphide $BaNi_9P_5$ has also been prepared from a tin flux by slowly heating the components to 850 °C, and subsequent slow cooling at a rate of 2 °C h^{-1}. This resulted in equidimensional crystals with diameters of up to 3 mm.[116] The three series of phosphides $RECo_3P_2$,[113,117] $RE_5Co_{19}P_{12}$,[113,118] and $RE_6Co_{30}P_{19}$[119] were also prepared by the tin-flux technique, and they also belong to this large family of ternary structures with a metal/metalloid ratio of exactly or nearly 2:1. In this family the metalloid components are mainly silicon, phosphorus, and their homologues.[120]

The system scandium–cobalt–phosphorus contains the phosphides ScCoP, $ScCo_5P_3$, $Sc_2Co_{12}P_7$, and $Sc_5Co_{19}P_{12}$. They were all prepared using a tin flux of 80 atom %.[118] For the other ternary rare-earth–cobalt–phosphorus systems the phase equilibria, as far as they are accessible with a 75 atom % tin flux, have been investigated systematically for the sections at 850 °C. The samples were annealed for about two weeks, followed by quenching in air. Generally, between three and eight ternary phases were found in this way.[121] A remarkable result of this investigation is the fact that the sample composition required for the syntheses of certain isotypic phosphides, changes systematically with the rare-earth components. This situation is demonstrated in Figure 7 for three pairs of isotypic samarium and thulium phosphides with the three structure types first established for $Zr_2Fe_{12}P_7$,[122] YCo_5P_3,[112] and $HoCo_3P_2$.[117] It can be seen that higher phosphorus contents of the samples are needed for the synthesis of the thulium compounds than for the corresponding samarium compounds.

Ternary rare-earth and actinoid transition-metal phosphides prepared by the tin-flux technique with iron and nickel as the transition-metal components include the compounds $ScFe_4P_2$[123] and $ThFe_4P_2$,[124] which crystallize with two different structure types, $Th_5Fe_{19}P_{12}$[124] and isotypic $Yb_5Ni_{19}P_{12}$,[125] $ThFe_5P_3$,[126] $La_2Fe_{25}P_{12}$,[127] $Th_{11}Ni_{25}P_{20}$ and isotypic $U_{11}Ni_{25}P_{20}$,[128] $Yb_9Ni_{26}P_{12}$,[129] and $YbNi_5P_3$.[129] With chromium as the transition-metal component the compounds UCr_5P_3,[130] $A_2Cr_{30}P_{19}$ (A = U and Zr),[131,132] and $Zr_6Cr_{60}P_{39}$[133]

 © 2005 Wiley-VCH Verlag GmbH & Co. KGaA, Weinheim

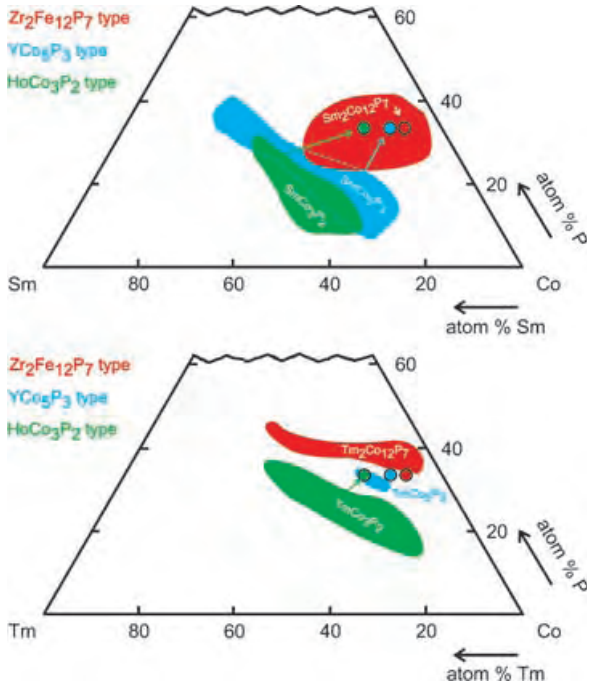

Figure 7. Sample compositions for the preparation of ternary Sm (top) and Tm (bottom) cobalt phosphides from a tin flux. All samples were prepared with 75 atom% tin as a flux. The diagrams indicate the ratio of the remaining 25% of the elements samarium, thulium, cobalt, and phosphorus. The phase diagrams contain several ternary phosphide phases. Only the sample compositions resulting in ternary phosphides with $Zr_2Fe_{12}P_7$-type,[107a] YCo_5P_3-type,[112] and $HoCo_3P_2$-type[117a] structures are shown. The compositions of the ternary phosphides are indicated by large colored dots. All samples were equilibrated for two weeks at 850°C and the tin-rich matrix was dissolved in diluted hydrochloric acid.[117b]

were prepared in well-crystallized form from a tin flux. For the syntheses of corresponding molybdenum compounds (e.g. $U_2Mo_{30}P_{19}$[131] and $U_6Mo_{60}P_{39}$[134]), however, arc-melting of prereacted pellets of the elemental components turned out to be more successful.

7.3. Ternary Transition-Metal Polyphosphides

Generally, the use of a tin flux for the preparation of phosphides containing two different kinds of transition metals has been explored less systematically than the investigations for the syntheses of ternary phosphides containing lanthanoids or actinoids as one metal component and a transition-metal element as the other. Ternary phosphides with a relatively high metal content of two different transition-metal elements can be prepared well by arc melting of the prereacted components. Only some polyphosphides, which are difficult to prepare otherwise (e.g. at high pressure), have been synthesized with a tin flux. The first examples seem to have been the isotypic diamagnetic semimetals $MoFe_2P_{12}$ and WFe_2P_{12}. For their preparation the elemental components were allowed to react in the atomic ratio Mo(W):Fe:P:Sn = 1:2:12:20. The annealing was at 970 K, with subsequent quenching in air. Annealing at lower or higher temperatures (870 and 1170 K) resulted in the binary polyphosphides MoP_2 and α-FeP_4 or MoP_2 and FeP_2, respectively.[135] The metallic conductor $TiMn_2P_{12}$ has a different structure. It could be prepared from the elemental components in the presence of iodine. For its preparation with a tin flux only a relatively small amount of tin was used: Ti:Mn:P:Sn = 1:2:30:20.[136] With similar atomic ratios the $TiMn_2P_{12}$-type compounds $NbMn_2P_{12}$ (5:2:10:17), $MoMn_2P_{12}$ (1:2:30:20), and WMn_2P_{12} (1:2:15:20) were prepared from a tin flux.[137] For the syntheses of the polyphosphides $MoNiP_8$ and $WNiP_8$ the elements were allowed to react in the ratio Mo(W):Ni:P:Sn = 1:1:40:50.[138]

The preparation of the compound Ti_2NiP_5 by reaction of the elemental components in a tin flux failed. However, this compound could be prepared by using powders of the binary alloy of the composition TiNi in a tin flux with the ratio TiNi:P:Sn = 1:20:25. After slow heating (it is important to remember the violent reactivity of phosphorus) the annealing was for one month at 650°C.[139] Apparently, when the metals Ti and Ni are used instead of the binary alloy TiNi, the binary phosphides of the transition metals are formed first. And at 650°C these react too slowly to produce the intended ternary phosphide. Similarly, powders of the binary alloys were used for the preparation of the ternary polyphosphides VNi_4P_{16}, $NbNi_4P_{16}$, and WNi_4P_{16}.[140] Three stacking variants of the binary manganese polyphosphide MnP_4 are known: 2-MnP_4,[56] 6-MnP_4,[50] and 8-MnP_4.[49] The missing stacking variant 4-MnP_4 could only be prepared in form of a solid solution with chromium: $Cr_{1-x}Mn_xP_4$ with x having values between 0.3 and 0.7. Again, for the preparation of these samples in a tin flux powders of binary Cr/Mn alloys were used.[141]

Many of the compounds listed in Table 1 are polyphosphides of the late transition metals. With copper as the transition-metal component, only CuP_2 could be prepared from a tin flux, although with Cu_2P_7 a polyphosphide with a still higher phosphorus content has been obtained in well crystallized form using iodine as a mineralizer.[142] Apparently, the presence of tin reduces the chemical activity of phosphorus to the extent that the higher polyphosphides cannot be prepared (Figure 3) and the ternary compound Cu_4SnP_{10} is formed instead.[46,142] Similarly, no silver phosphide could be obtained from a tin flux, although the compounds AgP_2[142] and Ag_3P_{11}[143] could be prepared in the presence of iodine. With the subsequent elements gold, zinc, cadmium, and mercury the presence of tin prevents the formation of binary phosphides and the ternary compounds $MSnP_{14}$ (M = Zn, Cd, Hg) and $Au_{1-x}Sn_{1+x}P_{14}$ are obtained.[144,145] Also, apparently, in trying to optimize the preparation conditions for the binary nickel polyphosphide NiP_3[27,71,73] from a tin flux, the ternary compounds Ni_2SnP[146] and $Ni_{1.17}Sn_{0.69}P_{0.31}$[147] were obtained using atomic ratios Ni:Sn:P of 2:6:1 and 4:40:1, respectively, at well defined temperatures.

7.4. Borides, Silicides, and Further Pnictides from Liquid Tin

The excellent wettability of tin enables the preparation of a large variety of compounds. Besides the numerous phos-

 © 2005 Wiley-VCH Verlag GmbH & Co. KGaA, Weinheim

phides reported in the previous sections, also some boron-rich solids such as YB_{25}[148] or the silicide boride $Er_8Si_{17}B_3$[149] have been synthesized in liquid tin. Binary silicides can be obtained in various metal fluxes. As discussed in Section 13, liquid copper has widely been used for the growth of such silicide crystals, but compounds such as V_3Si, V_5Si_3, VSi_2,[150] Mn_5Si_3, MnSi, or $Mn_{27}Si_{47}$[151] are also accessible from liquid tin.

In the case of ternaries, many compounds with two different main-group elements in ordered two- or three-dimensional networks have been synthesized. Single crystals of EuSnP[152] and Nb_5Sn_2Ga[153] can be obtained by the tin self-flux technique. The growth of larger crystals enables direction-dependent investigations of the physical properties. A larger family of compounds was observed for the silicon phosphides such as $ZnSiP_2$,[154] $Sn_{4.2}Si_9P_{16}$,[155] TSi_4P_4 (T = Fe, Ru, Os),[156] $RESi_2P_6$ (RE = La, Ce, Pr, Nd),[157] TSi_3P_3 (T = Rh, Ir),[158] $PtSi_3P_2$, and $PtSi_2P_2$.[159] Owing to the similar X-ray scattering power, the correct determination of the silicon and phosphorus sites is the main problem for this interesting class of compounds. Also some of the quaternary phosphide oxides of the series REFePO, RERuPO, and RECoPO,[160] and $Th_4Fe_{17}P_{10}O_{1-x}$[126] were first obtained from tin fluxes. Later most of these materials were been synthesized in NaCl/KCl salt fluxes. Some more recent developments are referred to in a paper on $Pr_3Cu_4P_4O_{2-x}$.[161]

Liquid tin is also a suitable flux for the higher homologues arsenic and antimony. For example, the ternary arsenide $Ba_{0.8}Hf_{12}As_{17.7}$ was synthesized in a tin flux at 950 °C.[162] With antimony, several ternary alkaline-earth, rare-earth metal, or uranium-containing compounds such as RE_3TiSb_5 (RE = La, Ce, Pr, Nd, Sm),[163] La_3ZrSb_5, La_3HfSb_5, $LaCrSb_3$,[164] $Sr_{21}Mn_4Sb_{18}$,[165] $Eu_{10}Mn_6Sb_{13}$,[166] or U_3TiSb_5 and U_3MnSb_5[167] have been obtained in well crystallized form. For instance, the latter two antimonides were obtained with the atomic starting ratios U:Ti:Sb:Sn = 1:3:2:6 and U:Mn:Sb:Sn = 1:3:2:9 in alumina crucibles. The temperature was allowed to oscillate between 600 and 700 °C for one week. After quenching, the tin matrix was dissolved in diluted hydrochloric acid, which attacked the needle-shaped hexagonal crystals of U_3TiSb_5 and U_3MnSb_5 at a much slower rate. The fact that these antimonides were also prepared without the tin flux—albeit in microcrystalline form—shows that they are not stabilized by small amounts of tin. Containing two main-group elements, the Zintl phases $Ba_2Sn_3Sb_6$,[168] $EuSn_3Sb_4$,[169] $Ba_3Sn_4As_6$,[170] and $SrSn_3Sb_4$[171] are accessible by a tin flux.

7.5. Binary and Ternary Stannides

As already discussed for some of the Zintl phases in Section 7.4, liquid tin is often used as a self-flux. As examples, we have already mentioned above the growth of the binary cobalt stannides CoSn, $CoSn_2$, and $CoSn_3$ by peritectic reactions.[41] This preparation technique has widely been used also for binary stannides of the early transition metals such as Ti_2Sn_3,[172,173] VSn_2,[174] or $MoSn_2$.[175] Stannides with even higher tin contents are formed with the noble metals. Recent examples are Os_4Sn_{17},[176] Os_3Sn_7,[177] $RhSn_3$,[177] $RhSn_4$,[177] Ir_3Sn_7,[178] and two modifications of $IrSn_4$.[177,179] Furthermore, a variety of mixed transition-metal stannides have been prepared, for example AuMnSn[180] or $Co_{1-x}Ni_xSn_2$ ($0.23 < x < 0.59$).[181]

The largest families of stannides that can be prepared from liquid tin are alkaline-earth or rare-earth transition-metal stannides. A good overview on the manifold phase relationships and the crystal chemistry of these intermetallics has been given by Skolozdra.[182] Three recent examples for crystal growth are the stannides $RE$$Mn_6Sn_6$ (RE = Tb, Ho, Er, Tm, Lu),[183] ScPtSn,[184] and $La_{4.87}Ni_{12}Sn_{24}$.[185]

8. The Lead Flux

Tin is a well known flux medium for the growth of single crystals of metal-rich phosphides and arsenides with a metal:phosphorus (arsenic) ratio close to 2:1. In some cases better crystal-growth results have been obtained using a lead flux rather than tin, especially for compounds with the platinum metals, which form very stable stannides, as already pointed out above. Recent examples for products from such reactions are $Ca_2Ir_{12}P_7$, $Ca_5T_{19}P_{12}$ (T = Rh, Ir), or $Eu_6Rh_{30}As_{19}$,[186] $AEIr_2P_2$ (AE = Ca, Sr, Ba),[187] $Sr_2Rh_7P_6$,[188] and $MgRh_6P_4$.[189] The elements can be treated with an excess of lead at 1100 °C in an alumina crucible that is sealed in a silica ampoule. A typical starting composition is approximately 60 equivalents of lead for one formula unit of the desired compound. A large advantage for crystal growth in the lead flux in these cases is the reduction of the reaction time. The conventional synthesis often requires repeated regrinding and annealing of the reaction components. The dissolution of the flux with hydrochloric acid is less suitable because lead chloride is only significantly soluble in hot water. In this case an elegant way to dissolve the flux is to use a mixture of concentrated acetic acid and H_2O_2 (30 %).

A lead flux was already used by Hittorf in 1865 for the recrystallization of elemental phosphorus. Some 50 years ago Krebs and co-workers reproduced these experiments.[190] They also used metallic fluxes, mostly lead, for the growth of polyphosphides with high phosphorus content, for example, CdP_4[191] and the compounds $MPbP_{14}$ (M = Zn, Cd, Hg).[192] Various other polyphosphides with $HgPbP_{14}$ type structure have been described later.[144,145] The polyphosphide Au_2PbP_2[193] was grown from a starting composition Au:Pb:P = 1:3:1. The sample was first heated to 400 °C within 20 min, held at that temperature for 16 h, heated to 800 °C at a rate of 5 °C h^{-1}, kept at that temperature for 100 h, and subsequently furnace-cooled.

Excellent crystals of the silicides $RE$$Mn_2Si_2$ (RE = Y, Tb–Lu) have been grown from molten lead under an argon atmosphere, Figure 8.[194,195] The rare-earth elements were mixed with manganese and lead in the ideal 1:2:2 atomic ratio and lead was added to these mixtures at a ratio of 3.8:1 in weight. This mixture was placed in a crucible of high-purity hexagonal boron nitride, annealed under argon at 1350 °C for 5 h, cooled to 800 °C at a rate of 50 °C h^{-1}, and finally quenched to room temperature. The excess lead had been dissolved in hydrogen peroxide and diluted acetic acid.

 © 2005 Wiley-VCH Verlag GmbH & Co. KGaA, Weinheim

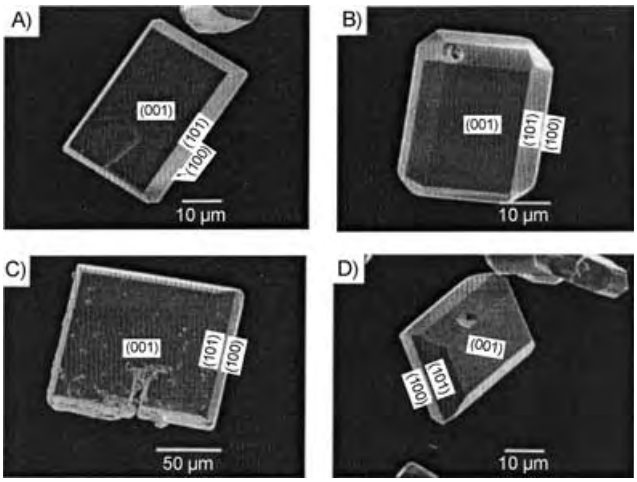

Figure 8. Scanning electron micrographs of $ErMn_2Si_2$ (A), $TmMn_2Si_2$ (B), $YbMn_2Si_2$ (C), and $LuMn_2Si_2$ (D) grown from a lead flux. From Okada et al.[195]

Lead fluxes have not had the type of extensive use in the syntheses of intermetallics as other fluxes described herein. In the examples cited, the reactions were run at rather high temperatures, many hundred degrees above lead's melting point, possibly because the solubility in lead of most elements is lower than that in tin. Nevertheless, it would be worthwhile to explore reactions in molten lead at lower temperatures as well, using longer annealing times.

9. Liquid Aluminum as a Flux

Aluminum melts at 660 °C and dissolves a large number of elements as can readily be seen from the extensive binary phase diagram information available in the literature.[40] Furthermore, it dissolves readily in non-oxidizing acids, for example, in hydrochloric acid. This property makes aluminum potentially a great flux system in which reactions can be carried out and indeed its utility as such has been demonstrated in the last few decades. A large variety of intermetallic aluminides have been prepared from liquid aluminum, many featuring fascinating new structures, and many being key components in advanced aluminum alloys.

9.1. Borides from an Aluminum Flux

Aluminum has been shown to be a useful flux in the synthesis of metal borides and ternary metal aluminides. Primarily Japanese, Swedish, and Russian groups have been active in boride synthesis using molten aluminum.[196] Some of the compounds reported include V_2B_3,[197a] Cr_3B_4, Cr_2B_3, and CrB_2,[197b] Ta_5B_6,[198a] Ta_3B_4, and TaB_2,[198b] LaB_6,[199a] LuB_4, $LuAlB_4$, and Lu_2AlB_6.[199b] Single crystals of TmB_4 and $TmAlB_{14}$ were obtained by the high-temperature aluminum-solution method using thulium powder and crystalline boron powder as starting materials. The optimum conditions required a temperature of 1500–1600 °C.[200] Crystals of the icosahedral B_{12} compounds $AlLiB_{14}$ and $AlMgB_{14}$[201] were grown from high-temperature aluminum solutions.

Also ternary transition-metal-containing borides can be prepared from liquid aluminum. MoAlB[202] and Fe_2AlB_2[203] were obtained from samples with starting compositions 1:6:1 and 35:35:30, respectively, were aluminum is used as a self-flux. These borides are stable in concentrated hydrochloric acid.

9.2. Binary and Ternary Aluminides

As is evident from the binary transition-metal–aluminum phase diagrams,[40] the aluminum self-flux technique is very useful for the preparation of binary aluminum-rich transition-metal aluminides. Some recent examples include Co_4Al_{13},[204] Re_4Al_{11}, $ReAl_6$,[205] $ReAl_{2.63}$,[206] and $IrAl_{2.75}$.[207]

Numerous ternary rare-earth– and actinoid–transition-metal aluminides have been prepared in recent years using an excess of aluminum as a reactive flux.[208a–o] Many of these have interesting magnetic properties.[208p–v] They crystallize with some ten different structure types sometimes in strange stoichiometries. For example, some 80 compounds have the compositions $A_6T_4Al_{43}$ (A = Y, La–Lu (with the exception of Eu), Th, and U; T = Ti, V, Nb, Ta, Cr, Mo, W, and Mn)[208a,b,r] and crystallize with a hexagonal structure which was determined for $Ho_6Mo_4Al_{43}$.[208a] The compounds of the series $RERe_2Al_{10}$ crystallize with four different structure types,[208i,k,n] one of which was determined some 20 years ago for $CaCr_2Al_{10}$.[209a] Some 20 isotypic aluminides have the general formula $RE_{7+x}T_{12}Al_{61+y}$ (T = Os and Re), where it could be shown for the rhenium compounds that their composition varies systematically between $Gd_{7.23}Re_{12}Al_{61.70}$ and $Lu_{7.61}Re_{12}Al_{61.02}$ depending on the size of the rare-earth atoms.[208d,n,p] Many representatives have been found for the compositions $A_2T_3Al_9$ (A = Lanthanoids and Actinoids, T = Co, Rh, Ir, and Pd),[208v] crystallizing with a structure first determined for $Y_2Co_3Ga_9$.[209b] Reactions in the systems RE–Au–excess Al (atomic ratio 1:1:10) produced low yields of $REAu_3Al_7$ with more prevalent products being $REAuAl_3$, and binary aluminides such as $REAl_3$. Increasing the amount of gold in the reaction (using a reactant ratio of 1:2:15) increased the yield of $REAu_3Al_7$.[210] Further preparation conditions of ternary aluminides grown from melts with an excess of aluminum can be found in the literature.[208]

9.3. Quaternary Compounds

The phase diagram of the binary system Al–Si shows that these elements form a eutectic system with a eutectic point at 577 °C and 12.2 mol % Si.[40] Aluminum melts dissolve some silicon, but they do not form any binary compounds. This situation is supported by the fact that silicon crystals are frequently found as by-products of reactions aimed at the synthesis and crystal growth of silicides. With rapid silicon diffusion in the melt, comes increased reactivity with the other metals which initiates phase formation. Most elements are to a certain extent soluble in aluminum and, in this sense,

 © 2005 Wiley-VCH Verlag GmbH & Co. KGaA, Weinheim

the flux reaction is not different from any conventional solvent.

There are few rare-earth aluminum silicides reported.[211] Most of them were synthesized as powders and their crystal structures have not been determined or refined. For Ho, Er, and Tm, only RE_6Al_3Si (RE = Ho, Tm)[212] and Er_4AlSi_3[213] have been reported.

In the late 1990s the first deliberate attempt was made to produce silicon intermetallics by reacting rare-earth elements with silicon in excess aluminum. Crystals of various metal–aluminum silicides grow easily in an aluminum melt below 900 °C, and a large number of such silicides has been identified. These reactions proceed rapidly; examples are the series $RE_2Al_3Si_2$ (RE = Ho, Er, Dy, Tm)[214] as well as the quaternary aluminum silicide $Sm_2Ni(Ni_xSi_{1-x})Al_4Si_6$. Crystals as long as 4 mm form readily in the aluminum flux. A crystal of $Ho_2Al_3Si_2$ grown in this fashion is shown in Figure 9. These

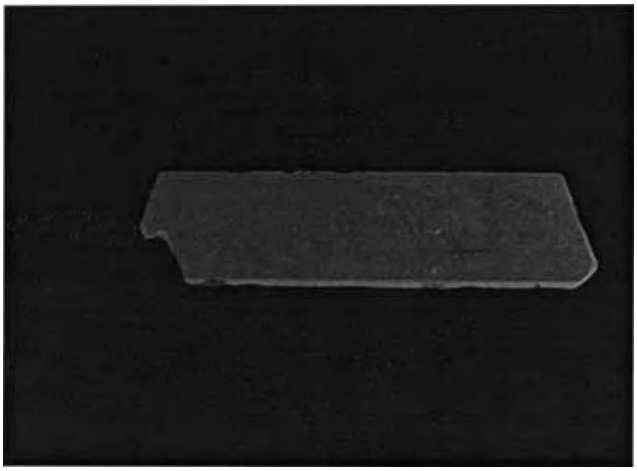

Figure 9. Scanning electron micrograph of a crystal of $Ho_2Al_3Si_2$ (length 0.5 mm).

compounds form with the late lanthanoids whereas the reactions with the mid and early lanthanoids, such as La, Ce, Nd, Sm, give REAlSi, and La, Sm, Tb, Yb give $REAl_2Si_2$. Neither of these two types of compounds has been found for Ho, Er, and Tm to date. Instead, the $RE_2Al_3Si_2$[214] and $REAl_{3-x}Si_x$[215,216] series seems to be favored. There are several old reports that claimed the production of binary silicides, such as $RESi_2$, $ThSi_2$, $MoSi_2$, and WSi_2 in molten aluminum. However, we find that most of these are in fact ternary metal aluminum silicides (e.g. REAlSi) rather than binary metal silicides.

The reaction of Sm, Ni, and Si in molten aluminum proceeds at approximately 750 °C to yield well-formed crystals of $Sm_2Ni(Ni_xSi_{1-x})Al_4Si_6$.[217] To obtain a single-phase product, it is necessary to use stoichiometric amounts of Sm, Ni, and Si with excess aluminum metal. To isolate the compound the excess aluminum metal was dissolved with NaOH (aq) because $Sm_2Ni(Ni_xSi_{1-x})Al_4Si_6$ ($x = 0.18$–0.27) decomposes in dilute hydrochloric acid and therefore its isolation in strong basic solution was important for its discovery.

The isostructural compounds $Dy_2Ni(Ni_xSi_{1-x})Al_4Si_6$, $Gd_2Ni(Ni_xSi_{1-x})Al_4Si_6$, and $Sm_{2-y}Y_yNi(Ni_xSi_{1-x})Al_4Si_6$ also form from an aluminum flux.[218] An intriguing observation in the structures of these compounds is the presence of certain crystallographic sites with mixed Ni/Si occupancy. Such mixed Ni/Si and Ni/Ge occupancies are often observed in *RE*/Ni/Si and *RE*/Ni/Ge phases. The really interesting part about these results is the complex stoichiometries of these compounds, which are unlikely to be discovered rationally by mixing these elements in direct-combination reactions. They are too difficult to guess. The flux chemistry leads to the most feasible result under the prevailing conditions of reactant ratio and concentration. In other words, it "finds" the accessible compositions regardless of complexity and this underscores the great potential of molten metals as reaction media for accessing novel multinary phases.

Many other *RE*/*T*/Al/Si phases were discovered in aluminum flux. An intriguing new compound is $Sm_5(Cu_{4.26}Si_{3.74})Al_8Si_2$,[218] which has a three-dimensional Cu/Al/Si framework with infinite zigzag silicon chains and crystallographic sites with extensive Cu/Si mixed occupancy, similar to the Si/Ni disorder described above. The zigzag silicon chains do not contain copper.

Additional examples include $RE_2NiAl_4Ge_2$,[219] $RENiAl_4Ge_2$, $RE_{1-x}T_2Al_{5-y}Si_y$, $RE_{2-x}T_2Al_4Tt_2(Al_{1-y}Tt_y)(Al_{1-z}Tt_z)_2$, ($RE$ = rare earth element; T = Ni, Co; Tt = Si, Ge)[220] $RE_4Fe_{2+x}Al_{7-x}Si_8$, and $REFe_4Al_9Si_6$. Along with the new structure types of these compounds, several isostructural analogues, such as $RENiAl_4(Si_{2-x}Ni_x)$ and $RENiAl_{6-x}Ge_{4-y}$, have also been synthesized. Explorations with 4d and 5d transition metals revealed intriguingly complex phases such as $Th_2[AuAl_2]_n(Au_xSi_{1-x})Si_2$,[221a] $Gd_{1.33}Pt_3Al_7Si$,[221b] and the series of the cubic compounds $RE_8Ru_{12}Al_{49}Si_9(Al_xSi_{12-x})$.[222] The latter feature unique $(Al/Si)_{12}$ cuboctahedral clusters. Figure 10 show several typical crystals of various compounds grown in liquid aluminum. Table 2 summarizes some of the ternary and quaternary compounds synthesized or discovered in aluminum flux.

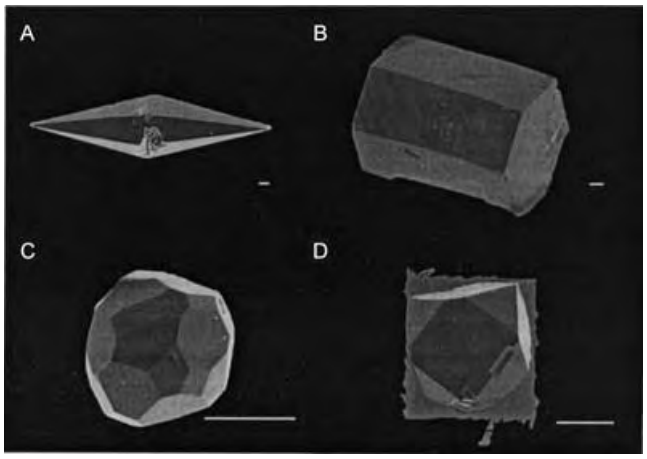

Figure 10. Typical crystals grown in liquid metals (scanning electron micrographs): A) $Sm_{2-x}Ni_2Al_4Si_2(Al_{1-y}Si_y)(Al_{1-z}Si_z)_2$, (from molten Al), B) $YNiAl_4Ge_2$, C) $CrSi_2$ (from molten In), and D) $RE_8Ru_{12}Al_{49}Si_9(Al_xSi_{12-x})$ (from molten Al). All the scale bars are 0.3 mm.

© 2005 Wiley-VCH Verlag GmbH & Co. KGaA, Weinheim

remaining product consists of $GdAl_3$ needles, but also

Table 2: Examples of ternary and quaternary compounds grown in liquid aluminum.

Compound	Composition (atomic ratio)	Typical preparation conditions [°C]	Reference
ternary			
$REAl_{3-x}Ge_x$	2:15:2	50→1000 in 15 h, 3 days at 1000, 1000→650 in 36 h, 650→RT in 10 h	[216b]
$RE_2Al_3Si_2$ (RE = Tb–Tm)	1:10:1	50→1000 in 24 h, 5 days at 1000, 1000→300 in 96 h, 300→RT in 10 h	[214]
$REAu_3Al_7$ (all RE with the exception of La and Eu)	1:2:15	50→1000 in 12 h, 15 h at 1000, 1000→860 in 24 h, 60 h at 860, 860→RT in 72 h	[210]
$Gd_{1.33}Pt_3Al_8$	1:1:12	50→1000 in 12 h, 15 h at 1000,	[221b]
$Gd_{0.67}Pt_2Al_5$	0.33:1:12	1000→860 in 24 h, 48 h at 860, 860→RT in 72 h	
quaternary			
$RE_2Ni(Ni_xSi_{1-x})Al_4Si_6$ (RE = Pr, Nd, Sm, Gd–Tb)	2:1:20:7	50→1000 in 12 h, 15 h at 1000, 1000→860 in 10 h, 96 h at 860, 860→360 in 5 h	[217]
$Sm_2Co(Co_xAl_{1-x})Al_4Ge_{6-y}$	2:1:20:7	50→1000 in 12 h, 15 h at 1000, 1000→860 in 10 h, 96 h at 860, 860→360 in 5 h	[220]
$RENiAl_4(Si_{2-x}Ni_x)$ (RE = La–Nd, Eu)	1:1:10:2	50→1000 in 12 h, 8 h at 1000,	[220]
$CeCoAl_4Si_2$		1000→860 in 10 h, 48 h at 860,	
$RECuAl_4(Si_{2-x}Cu_x)$ (RE = La, Ce, Sm)		860→260 in 36 h, 260→50 in 6 h	
$LaPdAl_4(Si_{2-x}Pd_x)$			
$RE_2NiAl_4Ge_2$ (RE = Gd–Dy, Er)	2:1:10:2	50→1000 in 24 h, 48 h at 1000,	[220]
$RE_2CoAl_4Ge_2$ (RE = Sm, Gd, Tb)	2:1:10:2	1000→500 in 48 h, 500→50 in 12 h	[220]
$RE_2NiAl_{6-x}Ge_{4-y}$ ($x \approx 0.24$, $y \approx 1.33$; RE = La–Nd, Sm)	1:1:30:1	50→850 in 20 h, 96 h at 850, 850→500 in 72 h, 500→50 in 12 h	[220]
$RENiAl_4Ge_2$ (RE = Y, Sm, Gd–Lu,)	1:1:15:5	50→800 in 20 h, 96 h at 800, 800→500 in 48 h, 500→50 in 9 h	[220]
$RE_{1-x}T_2Al_{5-y}Si_y$ (RE=Y, Nd, Sm, Tb, Tm, Yb; T = Ni, Pd)	1:2:20:2	50→1000 in 15 h, 5 h at 1000, 1000→850 in 2 h, 72 h at 850, 850→50 in 36 h	[220]
$RE_{2-x}TAl_4Tt_2(Al_{1-y}Tt_y)(Al_{1-z}Tt_z)_2$ (RE=Sm, Dy, Er; T = Ni, Co; Tt = Si, Ge)	3:4:20:6	50→1000 in 15 h, 5 h at 1000, 1000→850 in 2 h, 72 h at 850, 850→50 in 36 h	[219]
$RE_4Fe_{2+x}Al_{7-x}Si_8$ (RE = Ce–Nd, Sm)	1:2:15:4	50→850 in 20 h, 96 h at 850, 850→500 in 72 h, 500→50 in 12 h	[220]
$RE_4Mn_{2+x}Al_{7-x}Si_8$ (RE = Ce–Nd, Gd)	1:2:15:4	50→850 in 20 h, 96 h at 850, 850→500 in 72 h, 500→50 in 12 h	[220]
$REFe_4Al_9Si_6$ (RE = Gd–Er)	1:4:20:6	50→850 in 20 h, 96 h at 850, 850→500 in 72 h, 500→50 in 12 h	[220]
$RE_8Ru_{12}Al_{49}Si_9(Al_xSi_{12-x})$ (RE = Pr, Nd, Sm, Gd, Tb, Er)	6.5:10:100:8	50→1000 in 15 h, 15 h at 1000, 1000→860 in 10 h, 96 h at 860, 860→500 in 72 h	[222]
$Gd_{1.33}Pt_3Al_7Si$	1:1:10:5	50→1000 in 12 h, 15 h at 1000,	[221b]
$Gd_{0.67}Pt_2Al_4Si$	0.33:1:10:5	1000→860 in 24 h, 48 h at 860, 860→RT in 72 h	
$Th_2AuAl_2Si_3$	1:1:10:5	50→1000 in 12 h, 15 h at 1000,	[221a]
$Th_2Au_3Al_4Si_2$		1000→860 in 20 h, 48 h at 860, 860→RT in 72 h	

$Gd_{1.33}Pt_3Al_8$ was synthesized by the combination of Gd and Pt in liquid aluminum.[221b] Addition of silicon resulted in the incorporation of a small amount of this element into the material to form the isostructural compound $Gd_{1.33}Pt_3Al_7Si$. Both compounds grow as facetted hexagonal rodlike crystals (Figure 11). The rods also appear to have corrugated surfaces; the corrugation lines are perpendicular to the long direction, indicative of polysynthetic twinning. The related compounds $Gd_{0.67}Pt_2Al_5$ and $Gd_{0.67}Pt_2Al_4Si$ also form as hexagonal rods, but they are not characterized by the aforementioned uneven surfaces. These complex intermetallics only account for 10–20% of the solid isolated after removal of the flux. The contains plate-like silicon crystals and crystals of $GdAl_2Si_2$. Evidently, in this case the flux does not completely meet criterion 4 mentioned in Section 3 and reacts to form undesirable phases.

Thorium metal reacts with gold and silicon in molten aluminum to give a mixture of the two quaternaries $Th_2AuAl_2Si_3$ (comprising about 40% of the solid product after soaking in NaOH) and $Th_2Au_3Al_4Si_2$ (40%), as well as small amounts of silicon crystals (10%) and $ThSi_2$ crystals (10%). The quaternary compounds are part of a homologous series of intermetallics, with the general formula $Th_2(Au_xSi_{1-x})[AuAl_2]_nSi_2$.[221a]

 © 2005 Wiley-VCH Verlag GmbH & Co. KGaA, Weinheim

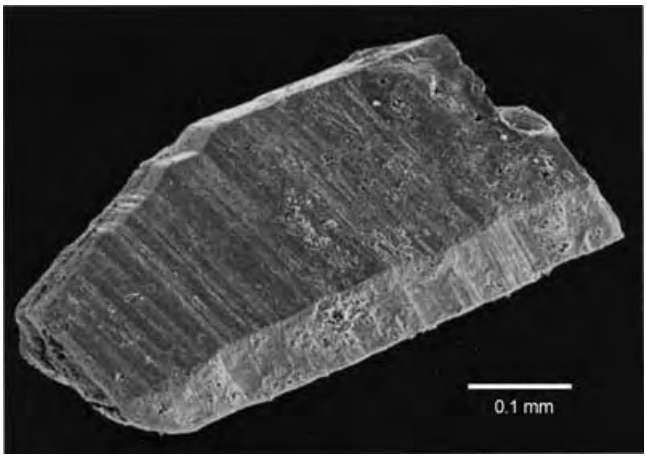

Figure 11. A representative crystal of $Gd_{1.33}Pt_3Al_7Si$, showing the typical shape of a polysynthetic twin.

10. Reactions in Liquid Gallium

Gallium has been relatively little utilized as a synthetic flux medium. The success of molten aluminum melts, however, to uncover new materials naturally stimulates inquiry into the related gallium system. The known binary and ternary compounds of gallium are numerous.[223] Most work on these systems, especially with the 3d transition metals was carried out by Grin and co-workers. Some ternary rare-earth–transition-metal gallides with ruthenium and osmium as the transition-metal components and a high content of gallium, for example, the series $RERu_2Ga_8$ or $REOsGa_4$, have recently been prepared by Schlüter and Jeitschko.[224] Reports on quaternary intermetallic phases, such as silicides and germanides, are still few. It would be interesting to assess the behavior of liquid gallium in light of that of aluminum, by performing corresponding experiments using gallium as the solvent. There are again two types of reactions, those in which gallium is incorporated into the compounds (reactive flux) and those in which it is not.

Interestingly, analogous reactions to those with aluminum that give rise to $RE_2Ni(Si_{1-x},Ni_x)Al_4Si_6$ do not yield analogous results. In the case of the quaternary system Sm/Ni/Si/Ga, phase separation results in the silicide $SmNiSi_3$,[225] and the gallide Sm_2NiGa_{12}.[226] The latter has a fascinating tetragonal structure with a three-dimensional gallium network. It is noteworthy that many *RE*/Ni/Ga phases have been known for some time[227,228] and the Sm/Ni/Ga phase diagram contains a striking number of phases: SmNiGa, $SmNiGa_2$, Sm_2Ni_2Ga, $SmNi_3Ga_2$, $Sm_3Ni_6Ga_2$, $SmNiGa_3$, Sm_2NiGa_3, $SmNiGa_4$, $Sm_{26}Ni_{11}Ga_6$, Sm_4NiGa_7, and $Sm_{17}Ni_{58}Ga_{25}$.[223] None of these materials was synthesized in a gallium flux. It is therefore rather remarkable that despite the great number of ternary compounds in this system Sm_2NiGa_{12} is a new addition. Another gallide that was discovered in this fashion was $SmNi_3Ga_9$, a hexagonal compound which adopts the $ErNi_3Al_9$ structure type.[215]

The use of molten gallium as a nonreactive solvent was demonstrated to give single crystals for the ternary silicides $RE_2Ni_{3+x}Si_{5-x}$ (RE = Sm, Gd, and Tb).[229] This allowed the structure of these compounds to be solved and refined with great accuracy. The structure is related to the $U_2Co_3Si_5$ structure type; however, the new studies suggested that the earlier crystallographic site assignments in $U_2Co_3Si_5$ were incorrect.

Table 3 summarizes some of the ternary and quaternary compounds synthesized or discovered with a gallium flux. The compounds $RE_4FeGa_{12-x}Ge_x$[230] were discovered during investigations of reactions in liquid gallium involving *RE*, *T*, and Ge, where *RE* = Y, Ce, Sm, Gd, Tb; and *T* = Fe, Co, Ni, or Cu. These systems were investigated at various metal ratios and different heating regimes. A heating regime with a shorter isothermal step was shown to favor the formation of the cubic phases $RE_4FeGa_{12-x}Ge_x$. For example, when a six-day isothermal step (T = 850 °C) was used in the system Tb/Fe/Ga/Ge, the products were Tb_4FeGe_8[231] and $Tb_2Ga_2Ge_5$,[232,239] along with the cubic phase as a minor product. Whereas a shorter isothermal step of three days at 850 °C produced the cubic phase in high yield. For *RE* = Sm, the situation was similar, as the six day isothermal heating gave rise to Sm_3Ga_9Ge as the major component, and the cubic phase, $FeGa_3$, and Ge as minor components. Reducing the time by half brought about an increase in the yield of the cubic phase. From this it can be concluded that the cubic phases are essentially a kinetic product of the reaction. Furthermore, it is clear that the time can be an important reaction parameter allowing the chemical reactivity of a system to be explored and access to kinetic and thermodynamic products. Large single crystals of $Tb_4FeGa_{12-x}Ge_x$, measuring up to 2 mm each side, could be grown from molten gallium (Figure 12). The incorporation of gallium in these phases shows that in this case the solvent is reactive. This situation is in contrast to the Sm/Ni/Ga/Si system in which the gallium-free $SmNiSi_3$ phase could be obtained.

It is interesting that isostructural phases to $RE_4FeGa_{12-x}Ge_x$ were not observed when iron was changed to Co, Ni, or Cu. Instead, a variety of other quaternary compounds arising form liquid gallium were detected.[232,235,236] In addition, the type of rare-earth metal appears to be important in phase formation. Thus, in the system *RE*/Fe/Ga/Ge, when *RE* was Y, Ce, or Gd, the RE_3Ga_9Ge phases were obtained.

Recent studies of the reactivity and phase formation in the systems *RE/T*/Ga/Ge, where *T* = Ni and Co, in liquid gallium showed that different compounds are obtained depending on the *RE*:*T* ratio. When the ratio *RE*:*T* <1 the reactions resulted in the hexagonal compounds $RE_{0.67}T_2Ga_{5-x}Tt_x$, and $RE_{0.67}T_2Ga_{6-x}Tt_x$[235] (*Tt* = Si or Ge) that form readily within a rather broad range of synthetic conditions (time and temperature). However, ratios with *RE*:*T* ≥ 1, give results that depend strongly on the nature of *RE*. For these ratios the chemistry is significantly more sensitive to the reaction conditions. For these studies the following compounds were obtained $RETGa_3Ge$, $RE_2TGa_9Ge_2$ (*RE* = Y, Sm, Tb, Gd, Er, Tm; *T* = Ni, Co), $RE_3Ni_3Ga_8Ge_3$ (*RE* = Sm, Gd), and $RE_4Ni_3Ga_6Ge_4$.[232]

There is an interesting contrast in the behavior of nickel and cobalt. When *T* = Ni the reaction of different lanthanoid elements under otherwise identical conditions results in $YNiGa_3Ge$, $Ce_2NiGa_9Ge_2$, $Gd_3Ni_3Ga_8Ge_3$, and $TbNiGa_3Ge$.

© 2005 Wiley-VCH Verlag GmbH & Co. KGaA, Weinheim

Table 3: Examples of ternary and quaternary compounds grown in liquid gallium.

Compounds (see Table 2)	Sample composition (atomic ratio)	Typical preparation conditions [°C]	Ref.
ternary			
*RE*NiSi$_3$ (*RE* = Y, Sm)	*RE*:Ni:Ga:Si 1:1:15:3	50→1000 in 4 h, 1000→850 in 5 h, 4 days at 850, 850→150 in 4 days	[225]
Sm$_2$NiGa$_{12}$	Sm:Ni:Ga 2:1:18	50→900 in 12 h, 4 days at 900, 900→150 in 72 h	[226]
Sm$_2$NiGa$_{12-x}$Si$_x$	Sm:Ni:Ga:Si 2:1:10:4	50→1000 in 15 h, 5 h at 1000, 10 days at 1000, 1000→150 in 6 days	[226]
$RE_2Ni_{3+x}Si_{5-x}$ (*RE* = Sm, Gd, Tb)	*RE*:Ni:Ga:Si 1:2:30:2	50→1000 in 15 h, 5 h at 1000, 1000→600 in 16 h, 600→50 in 5 h	[229]
$RE_4FeGa_{12-x}Ge_x$ (*RE* = Y, Ce, Sm, Gd, Tb)	*RE*:Fe:Ga:Ge 4:1:30:3	50→1000 in 15 h, 5 h at 1000, 3 days at 850, 850→200 in 10 h	[230]
Tb$_4$FeGe$_8$	Tb:Fe:Ga:Ge 4:1:30:4	50→1000 in 15 h, 5 h at 1000, 6 days at 850, 850→200 in 3 days	[231]
$RE_2Ga_2Ge_5$ (*RE* = La, Sm, Tb)	Byproducts of *RE*:Fe:Ga:Ge 4:1:30:6	50→1000 in 15 h, 5 h at 1000, 6 days at 850, 850→200 in 3 days	[232]
RE_3Ga_9Ge (*RE* = Y, Ce, Gd)	*RE*:Ga:Ge 1:15:1	50→1000 in 15 h, 5 h at 1000, 6 days at 850, 850→200 in 3 days	[233]
Yb$_3$Ga$_4$Ge$_6$	Yb:Ga:Ge 1:10:2	50→1000 in 15 h, 5 h at 1000, 3 days at 850, 850→200 in 36 h	[234]
Yb$_2$Ga$_4$Ge$_6$	Yb:Ga:Ge 1:10:3	50→1000 in 15 h, 5 h at 1000, 3 days at 750, 750→200 in 36 h	[234]
quaternary			
$RE_{0.67}T_2Ga_{5-x}Tt_x$ (*RE* = Y, Sm, Gd–Tm; *T* = Ni, Co; *Tt* = Si, Ge)	*RE*:*T*:Ga:*Tt* 1:2:30:2	50→1000 in 15 h, 5 h at 1000, 3 days at 850, 850→200 in 36 h	[235]
$RE_{0.67}T_2Ga_{6-x}Tt_x$ (*RE* = Y, Sm, Gd–Dy; *T* = Ni, Co; *Tt* = Si, Ge)	*RE*:*T*:Ga:*Tt* 1:2:30:2	50→1000 in 15 h, 5 h at 1000, 3 days at 850, 850→200 in 36 h	[235]
*RET*Ga$_3$Ge (*RE* = Y, Sm, Gd, Tb, Er, Tm; *T* = Ni, Co)	*RE*:*T*:Ga:Ge 1:1:15:1	50→1000 in 15 h, 5 h at 1000, 36 h at 850, 850→250 in 18 h	[236]
$RE_2TGa_9Ge_2$ (*RE* = Y, Sm, Gd, Tb, Er, Tm; *T* = Ni, Co)	*RE*:*T*:Ga:Ge 2:1:30:3	50→1000 in 15 h, 5 h at 1000, 6 days at 850, 850→250 in 75 h	[232]
$RE_3Ni_3Ga_8Ge_3$ (*RE* = Sm, Gd)	*RE*:*T*:Ga:Ge 1:1:15:1	50→1000 in 15 h, 5 h at 1000, 36 h at 850, 850→250 in 18 h	[236]
$RE_4Ni_3Ga_6Ge_4$ (*RE* = Y,Tb)	*RE*:*T*:Ga:Ge 1:1:15:1	50→1000 in 15 h, 5 h at 1000, 6 days at 850, 850→250 in 75 h	[232]
$Tb_{1.8}Si_8C_2(B_{12})_3$	Tb:B:Ni:Si 1:6:1:1 + a 10-fold molar excess of Ga	50→1000 in 12 h, 96 h at 1000, 1000→500 in 60 h	[237]
β-SiB$_3$	B:Si:Cu:Ga 4:1:1:20	50→1000 in 12 h, 96 h at 1000	[238a]

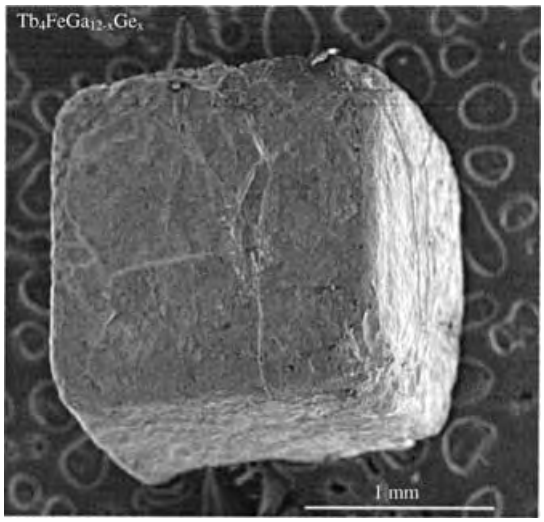

Figure 12. SEM image of a typical Ga-grown Tb$_4$FeGa$_{12-x}$Ge$_x$ crystal. The roughening of the surface is caused by an etching process during isolation.

The case is even more complicated for samarium, as up to three phases Sm$_2$NiGa$_9$Ge$_2$, SmNiGa$_3$Ge, and Sm$_3$Ni$_3$Ga$_8$Ge$_3$ could be observed. With Y and Tb, long reaction times (3–6 days) produced Y$_4$Ni$_3$Ga$_6$Ge$_4$ and Tb$_4$Ni$_3$Ga$_6$Ge$_4$, whereas shorter reaction times gave YNiGa$_3$Ge and TbNiGa$_3$Ge. Interestingly, when *T* = Co, the following phases form in quantitative yield: YCoGa$_3$Ge, Ce$_2$CoGa$_9$Ge$_2$, SmCoGa$_3$Ge, GdCoGa$_3$Ge, and ErCoGa$_5$. These phases probably have similar formation energies because they have common structural components.

The gallium flux medium works well for silicon/boron compounds probably because both silicon and boron are soluble in it and do not form binary compounds.[240] For example we have applied the gallium flux to *RE*/*T*/B/Si (borosilicides) in an attempt to produce lighter analogues of the *RE*/*T*/Al/Si compounds. We have shown that liquid gallium can provide an excellent route to complex quaternary silicon borides such as $Tb_{1.8}Si_8C_2(B_{12})_3$ that cannot be formed using high-temperature techniques such as arc melting.[237] Boron-containing solids have acquired renewed interest because of the discovery of superconducting quaternary borocarbides[241] and the binary MgB$_2$, a well-known compound with a very simple structure, but only recently recognized as a high-temperature non-oxidic superconductor.[242]

A spectacular illustration of the ability of liquid gallium to stabilize phases that are inaccessible by conventional synthetic routes is the discovery of the binary boride β-SiB$_3$.[238a] This was a surprising discovery because a phase with a similar formula, $Si_{1-x}B_{3+x}$ (α-SiB$_3$)[238b] and a rhombohedral structure has been known for decades.[243] In contrast, β-SiB$_3$ has a new structure type with very different structural features, physical and electronic properties. It is significant that the synthesis of β-SiB$_3$ requires metallic flux conditions, which permit the total bypass of the rhombohedral compound α-SiB$_3$.

 © 2005 Wiley-VCH Verlag GmbH & Co. KGaA, Weinheim

11. Indium Flux

Due to its low melting temperature of 157 °C, indium is an ideal metal for use as a reactive flux (self-flux condition). It has widely been used for the synthesis and crystal growth of indium-rich binary and ternary indides. In many cases, a slight excess of indium significantly increases the crystal growth. Good examples in the case of binary intermetallics are compounds such as $T\mathrm{In}_3$ (T = Co, Ru, Rh, Ir),[244,245] $\mathrm{Ti}_2\mathrm{In}_5$,[246] $\mathrm{Hf}_2\mathrm{In}_5$,[247] or IrIn_2.[248] In these cases, two strategies may be applied. Pure polycrystalline samples for physical-property measurements can be synthesized with the ideal starting composition, while high-quality single crystals for structure refinements can be grown from a flux with an indium excess. Indium has been exploited even less as a synthetic flux medium than aluminum and gallium. With indium there are again two types of reactions possible; those in which indium is incorporated in the products and those where it is acting strictly as a solvent. Its low melting point makes indium convenient for reaction chemistry at relatively low temperatures and facilitates its removal during isolation. Herein we will give some examples of phases crystallized in liquid indium.

11.1. Indium as a Reactive Flux

Besides the binary transition-metal–indium compounds, a large family of ternary rare-earth-metal–transition-metal indides has been synthesized in liquid indium. Several members of the compounds $\mathrm{Ce}T\mathrm{In}_5$ with HoCoGa_5-type structure and $\mathrm{Ce}_2T\mathrm{In}_8$ with $\mathrm{Ho}_2\mathrm{CoGa}_8$-type structure have been prepared in the form of relatively large single crystals for physical-property measurements.[249–252] Experimental details about the method are given in refs. [23, 24]. In a typical experiment, cerium, the transition metal, and indium are mixed in the atomic ratio 1:1:20 and placed in an alumina crucible which is sealed in a silica tube to prevent oxidation. The sample is then heated over several hours to 1100 °C, kept at that temperature for 2 h, and then slowly cooled to 700 °C at a rate of 10 °C h^{-1}. At that temperature the excess indium is decanted in a centrifuge resulting in well-shaped single crystals with volumes up to 1 cm^3. The melt-centrifugation method has also been used by Boström[43,44] for the crystal growth of manganese gallides and by Nylén et al.[45] for the crystal growth of palladium stannides.

A variety of other rare-earth-based indides has been obtained by using an excess of indium. For the growth of CeNiIn_2 crystals, an arc-melted CeNiIn_2 sample can be recrystallized using an excess of about 10 wt% indium in a ZrO_2 crucible.[253] The temperature is first raised to 1200 °C, kept at that temperature for 6 h, cooled at a rate of 5 °C h^{-1} to 600 °C, and quenched in air. Similar temperature profiles have been used for the synthesis of $\mathrm{Tb}_6\mathrm{Pt}_{12}\mathrm{In}_{23}$ and $\mathrm{Dy}_2\mathrm{Pt}_7\mathrm{In}_{16}$,[254] however in these cases, arc-melted precursor alloys TbPtIn_4 and $\mathrm{DyPt}_3\mathrm{In}_6$ were used for recrystallization from liquid indium. Selected single crystals of CeNiIn_2, $\mathrm{Tb}_6\mathrm{Pt}_{12}\mathrm{In}_{23}$, and $\mathrm{Dy}_2\mathrm{Pt}_7\mathrm{In}_{16}$ are shown in Figure 13.

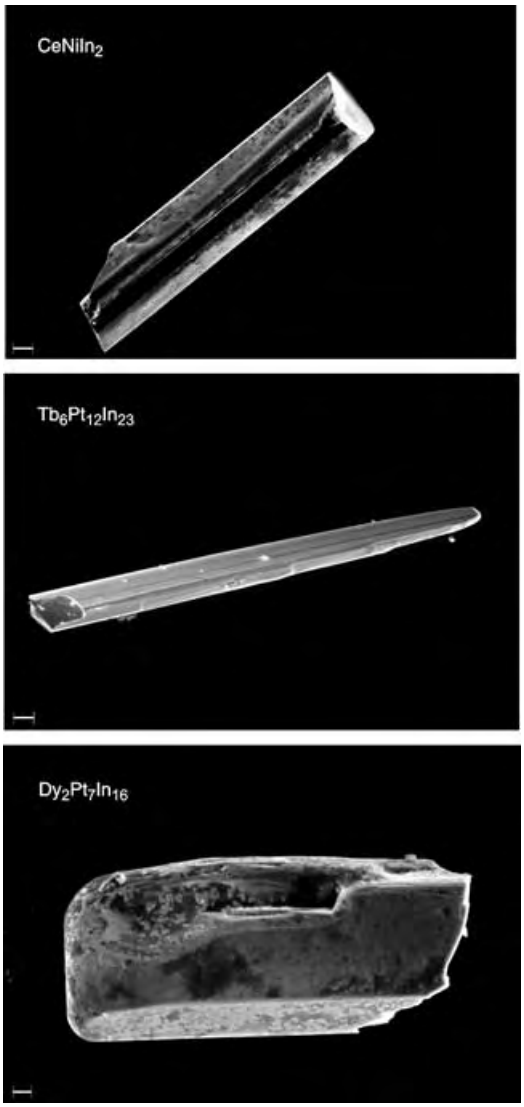

Figure 13. Scanning electron micrographs of CeNiIn_2 (scale bar 10 μm) $\mathrm{Tb}_6\mathrm{Pt}_{12}\mathrm{In}_{23}$ (scale bar 10 μm), and $\mathrm{Dy}_2\mathrm{Pt}_7\mathrm{In}_{16}$ (scale bar 3 μm) single crystals.

If only a small excess of indium is used for the self-flux technique, the melt-centrifugation technique cannot be applied. In this case it is better to dissolve the indium. This is a significant difference between indides and binary and ternary stannides, while most stannides resist 2 N hydrochloric acid, indides are often destroyed. The problem can be avoided by removing the melt with diluted acetic acid. The crystals shown in Figure 13 have been cleaned in this way. In most cases, the crystals have a thin indium coating which can easily be removed with diluted acetic acid.

The ytterbium based indides $\mathrm{Yb}T\mathrm{In}_5$ (T = Co, Rh, Ir) have been prepared from an indium flux with starting compositions Yb:T:In = 1:1:7.[255,256] Tantalum was used as crucible material and the samples were initially heated to 1050 °C, kept at that temperature for 6 h, and then cooled at a rate of 5 °C h^{-1} to 400 °C, with subsequent quenching to room temperature. A different procedure was used for YbPtIn_4.[255] An arc-melted

© 2005 Wiley-VCH Verlag GmbH & Co. KGaA, Weinheim

precursor alloy of approximate composition $YbPtIn_2$ was annealed with indium in the ideal ratio 1:2 in a molybdenum crucible. The initial step was rapid heating at 1100 °C, this temperature was maintained for 6 h, and then slow cooling at a rate of 5 °C h^{-1} to room temperature. The four ytterbium compounds were thus obtained as well-shaped crystals with edge lengths larger than 200 μm. Interestingly, the heavy-rare-earth-containing series of compounds RE_2Cu_2In (RE = Gd–Lu, except Yb) were also grown in an indium flux despite their relatively low indium content.[257]

11.2. Indium as a Nonreactive Flux

Similar to molten aluminum and gallium, indium is also attractive for its capacity to dissolve Si, Ge, and a host of lanthanoid and transition metals, which results in highly reactive forms of the elements. Further, In does not form binary compounds with Ge or Si.[258] For example, reactions of Cr, W, V, and several rare-earth elements with silicon in indium flux at 800–900 °C result in well formed single crystals of the corresponding disilicides $CrSi_2$, WSi_2, VSi_2, and $RESi_2$.[259] No indium incorporation is observed. Also single crystals of the ternary compound $CeCu_2Si_2$ were grown from indium flux. However, in this case elemental analysis showed that small amounts of indium had entered into the compound.[260]

When a transition metal such as nickel is added to the reactions with rare-earth elements and germanium in indium flux, new forms of the compounds β-$RENiGe_2$ (RE = Dy, Er, Yb, Lu) are obtained which crystallize with the $YIrGe_2$ structure type.[261] This result is intriguing because phases with the same composition (α-$RENiGe_2$) have been known for some time, but crystallize in the $CeNiSi_2$ structure type. In fact, many germanides $RETGe_2$ with RE = Y, Tb–Lu, and T = Pd, Pt, Ir with the $YIrGe_2$-type structure are known, but phases containing first-row transition metals were not known till the indium flux was used.

It is of note that the formation of β-$RENiGe_2$ occurs exclusively in liquid iridium. The yields from these reactions range from 60 to 70 % (based on the RE), with approximately 70 % purity. The main impurities were the α-phase and recrystallized Ge. When other methods, such as arc-melting or radio-frequency furnace heating, were used to synthesize $RENiGe_2$ compounds they only led to the α-form. Furthermore when the reaction times were increased from 48 to 96 h the α-phase was the dominant fraction at approximately 65 %. Likewise, if the isotherm temperature for the reaction was increased from 850 to 1000 °C a larger fraction of the reaction product, approximately 50–60 %, crystallized as the α-form. Two other experiments were also conducted where the elements Dy or Er, Ni, Ge, and In were combined in a 1:1:2:10 ratio, and then were arc-melted for 3 min, or heated with a radio frequency furnace for 1 h. Both of these methods, which employ much higher temperatures than the flux reaction, yielded practically pure α-form despite using excess indium. These results indicate that a combination of low temperature and excess indium are needed to arrive at the β-form and suggests that the α-phase is thermodynamically the more stable form, and the β-form is the kinetically stable phase.

12. Lithium and Sodium Fluxes

Among the alkali metals, lithium has the highest melting (180.5 °C) and boiling (1374 °C) point.[258] This difference in temperatures is a good prerequisite for use as a metal flux. Jung and Diessenbacher[262] reported on the growth of single crystals of the boride $Sr_2Ru_7B_8$ in a lithium flux from the starting composition Li:Sr:Ru:B = 50:2.3:7:8. A sealed tantalum tube was used as a container material and the annealing temperature was 1100 °C for 4 days.

The same technique was subsequently used for the crystal growth of various rare-earth-metal–transition-metal carbides.[263] The lithium flux is especially useful for the synthesis of ytterbium-based carbides. Owing to the low boiling temperature of ytterbium (1193 °C) a synthesis of such carbides by arc-melting always results in large weight losses. In contrast, liquid lithium served as an excellent medium for the synthesis of $YbAl_3C_3$.[264] The elements were combined in the atomic ratio Yb:Al:C:Li = 1:3:3:30, sealed in an iron ampoule (tube volume ca. 4 cm^3), annealed for one day at 800 °C, and finally cooled at a rate of 7 °C h^{-1} to room temperature. Lithium was dissolved in ethanol in an ultrasonic bath leaving silvery small hexagonal platelets. The single-phase reaction product was suitable for physical property investigations.

Iron or nickel ampoules can be used as container materials, since molten lithium reactively penetrates silica tubes. Typical tube sizes have an outer diameter of 10 mm and a wall thickness of 1 mm (100 mm length). The tubes are closed by 5-mm bolts that are sealed by arc-welding under an argon atmosphere.[265] For short reaction times (1–3 days) and moderate temperatures (< 500 °C), the metal ampoules can be annealed directly in a muffle furnace. For high-temperature annealing, the iron or nickel ampoules are sealed in silica tubes to prevent surface oxidation.

Using this experimental technique, the new carbides $Yb_2Cr_2C_3$,[266] $Yb_4Ni_2C_5$,[267] YbCoC,[268] and $Gd_{10.34}Mn_{12.66}C_{18}$[269] have been synthesized. At this point it is worth noting that an independent synthesis without lithium as flux medium is necessary to prove that lithium does not stabilize the respective structure. In all cases the carbides have independently been prepared by arc-melting, but these experiments did not result in single-phase samples.

The choice of the ampoule material is very important. Nickel, iron, and stainless steel are inexpensive, while niobium and tantalum are much more expensive. Especially iron and steel tubes contain small amounts of carbon which the liquid lithium is able to extract from the tube. Studies of recrystallizing praseodymium nickel arsenides in a lithium flux in steel tubes[270] resulted in well shaped single crystals of $PrNiC_2$.[271]

Besides lithium, the higher congener sodium has been widely used for the growth of crystals or fine powders for various industrially important nitrides such as BN, AlN, or GaN. A severe problem occurs for the production of

 © 2005 Wiley-VCH Verlag GmbH & Co. KGaA, Weinheim

aluminum nitride powder. Owing to the large heat of formation of AlN, the AlN particles already sinter and form agglomerates during the reaction. These preparative problems can easily be overcome by using a sodium flux.[272] Aluminum metal powder can be reacted with the azide NaN_3 in a sealed stainless steel ampoule. Thermal decomposition of NaN_3 at 300 °C provides pure N_2 and Na. The reaction mixture is heated to 600 °C for 12 h and then to 700 °C and 24 h. The furnace is then turned off and the tube cooled to room temperature within the furnace. The sodium metal, including the fine AlN powder, is allowed to react with isopropanol and then with ethanol. The product can be cleaned with ethanol in an ultrasonic bath and may be collected by centrifugation. Finally the products can be dipped into distilled water for 10–20 h to ensure the removal of all free sodium.

The sodium flux technique with the azide route was also used for the growth of *h*-BN and GaN crystals.[273] In these cases, at the final reaction temperature of 800 °C a nitrogen pressure of 100 atm was generated by the decomposition of sodium azide. Especially for GaN, the influence of the N_2 pressure and various Na–Ga melts as the staring flux material have been investigated in detail.[274–276]

As well as the Group III nitrides, complex alkaline-earth-metal–transition-metal nitrides and nitride oxides with peculiar new crystal structures have also been discovered. Sodium flux was used to generate new nitride compounds, such as Ba_2GeGaN and $(Ba_xSr_{1-x})_3Ge_2N_2$,[277] $Sr_3Ge_2N_2$ and Sr_2GeN_2,[278] $Ba_3Ge_2N_2$,[279] and $Ba_5Si_2N_6$.[280] Additional examples are Ba_3ZnN_2O,[281] $Sr_{39}Co_{12}N_{31}$,[282] Sr_2NiN_2,[283] or $Ba_{14}Cu_2In_4N_7$.[284] Niobium ampoules were used as a crucible material for the synthesis of Ba_3ZnN_2O and $Sr_{39}Co_{12}N_{31}$. $Ba_{14}Cu_2In_4N_7$ was prepared in a BN crucible which was placed in a stainless steel container, while the synthesis of Sr_2NiN_2 was carried out in a nickel ampoule. For all nitrides, the products within the crucibles or within the ampoules were washed with liquid ammonia using a special glass apparatus.[285] The nitrogen pressure in the ampoules was generated through decomposition of sodium azide.

Liquid sodium is also a very suitable flux for the growth of subnitride and suboxide crystals of the alkaline-earth elements.[286–288] Examples are the subnitride series $Na_xBa_{14}CaN_6$ ($x = 8,14,17,21,22$) with the new cluster type $[Ba_{14}CaN_6]$, the binary nitride Ba_3N, or the mixed oxide $NaBa_2O$, or the mixed nitride $NaBa_3N$.[286,288] The excess sodium can either be distilled away or it may be separated from the reaction product using a special press.[289]

13. Miscellaneous Metallic Fluxes and Materials

Many other fluxes have been reported for the preparation of peculiar compounds or for crystal growth starting from polycrystalline materials. It is impossible to list all the work herein. In this last section we summarize some of the most interesting results.

13.1. Copper and Cobalt Flux

Copper has been used sporadically in growing crystals of boride compounds with very interesting results. In 1973 Johnson described in detail how to grow well formed octahedral crystals of MnSi by reaction of Mn and Si in a copper flux. A mixture of Mn, Si, and excess Cu is heated to 1200 °C over a period of 12 h and then cooled to 500 °C at 10 °C h^{-1}. The copper-rich Cu-Mn-Si matrix was dissolved in 8 N HNO_3 leaving octahedral crystals of MnSi.[290] More recently, the well-known silicide Mn_5Si_3 was reported to grow from liquid copper but interestingly no other known binaries such as $Mn_{27}Si_{47}$ formed under these conditions.[151]

Crystals of Cr_3Si and Cr_5Si_3 single crystals were prepared in copper flux using Cr and Si powders as starting materials in an argon atmosphere. The conditions for obtaining these crystals as single-phase materials and of a relatively large size were established.[291] Crystals of NbB, Nb_5B_6, Nb_3B_4, Nb_2B_3 (new phase), and NbB_2 were prepared similarly using Nb and B as starting materials in an argon atmosphere.[292] Crystals of W_2B, δ-WB, and WB_2 were prepared from copper solutions using tungsten metal and crystalline boron powders as starting materials under an argon atmosphere.[293]

Multinary boride compounds have been grown as well. The first such report involved the growth of the series $RERh_4B_4$ (RE = Y, Sm, Gd–Tm, and Lu).[294] Later, Japanese workers confirmed these results and reported the additional boride series $RERh_3B_2$ (RE = Gd, Dy, Er–Lu) and $RERh_3B$ (RE = Sm, Gd, Er, Tm) as well as the two boride carbides $RERh_2B_2C$ with RE = Er and Gd.[295a] The layered compound $PrRh_{4.8}B_2$ was obtained as hexagonal plates by a molten metal-flux growth method, using copper as a flux. The X-ray photoelectron spectroscopic study and electron probe microanalysis results showed the presence of a few monolayers of copper atoms between the crystals of $PrRh_{4.8}B_2$.[295b,c] Similarly, slow cooling molten copper solutions of the systems *RE*-Rh-B and *RE*-Rh-B-C gave single crystals of the above mentioned ternary borides $RERh_4B_4$, $RERh_3B_2$, and $RERh_3B$. Crystals of $ErRh_3B_2$ grew as hexagonal objects, crystals of $ErRh_4B_4$ were obtained as rectangular objects with a tetragonal structure, and single crystals of cubic $ErRh_3B$ were extracted as cubes. Single crystals of the new tetragonal compounds $RERh_2B_2C$ have been obtained as thin plates.[295] Clearly these results give a preview of what could be accomplished with copper.

The equiatomic transition-metal boride MoCoB[296] was prepared in a cobalt flux from a sample with the starting composition Mo:Co:B = 7:70:21. The excess cobalt was dissolved in concentrated hydrochloric acid, while the ternary boride is stable under these conditions.

13.2. Quasicrystals

Flux-growth techniques have been successfully applied by Canfield et al. for the preparation of several families of quasicrystals and related approximant phases. Large (up to 1 cm^3) single-grain samples have been obtained for icosahedral *RE*-Mg-Zn (RE = Y, Gd–Er) and Al-Pd-Mn, decagonal

© 2005 Wiley-VCH Verlag GmbH & Co. KGaA, Weinheim

Al-Ni-Co, and other quasicrystals. Grown in a flux with a high content of magnesium and zinc by slowly cooling from 700 to 480 °C, the *RE*-Mg-Zn family of approximant phases (composition $\approx RE_9Mg_{34}Zn_{57}$) were the first rare-earth-containing quasicrystals that allowed the study of localized magnetic moments in a quasiperiodic environment (Figure 14).

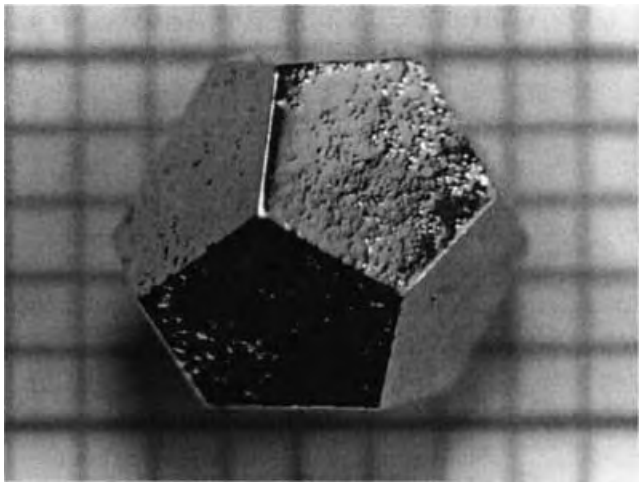

Figure 14. A well-formed Ho-Mg-Zn quasicrystal with dodecahedral morphology (mm grid) grown from a flux with a high content of magnesium and zinc.[297c]

Samples of the Al-Pd-Mn and the Al-Ga-Pd-Mn approximant phases were obtained by slowly cooling ternary (or quaternary) melts of a composition that intersects the primary solidification surface of the desired phase in the equilibrium ternary-alloy phase diagram. The metallic fluxes lead to almost strain-free quasicrystals and clearly allow the fascinating pentagonal growth habit to be revealed.[297]

13.3. Zinc Flux

Zinc is a metal with a comparatively low melting point (420 °C). Like for the preparation of binary stannides discussed in Sections 5 and 7, peritectic reactions are found also in the zinc-rich regions of the transition-metal–zinc systems.[40] Such reactions can occur when zinc coatings are used to protect iron- and steel-based materials. For this reason the Fe–Zn phase diagram has been investigated in detail.

The binary compounds Ti_3Zn_{22} and $TiZn_{16}$[298] have been prepared from samples of the starting compositions Ti:Zn 5:95 and 3:97, respectively. The 5:95 sample (silica tubes as crucible material) was first equilibrated for two days at 850 °C, then cooled at a rate of 5 °C h^{-1} to 500 °C and quenched in air from that temperature. The final annealing temperature for the 3:97 sample was 455 °C. Large crystals with edge lengths up to 4 mm were obtained after dissolution of the matrix in hydrochloric acid. With similar preparation conditions well-developed crystals of the compounds Zr_5Zn_{39} and $ZrZn_{22}$ were obtained.[299] As a by-product of these reactions $Zr_6Zn_{23}Si$[300] with a "filled" Th_6Mn_{23}-type structure was observed, where the silicon content arises from the quartz tube. Subsequently this compound was also prepared in alumina containers, where the silicon had to be added deliberately. By slow cooling of melts with very high zinc contents (98 and 99% Zn) the compounds $NbZn_3$, $NbZn_{16}$, and $MoZn_{20.44}$[301] were prepared in well-crystallized form. Also the rhodium-based compounds RhZn, Rh_2Zn_{11}, and $RhZn_{13}$ (Figure 15) are accessible in this way.[302]

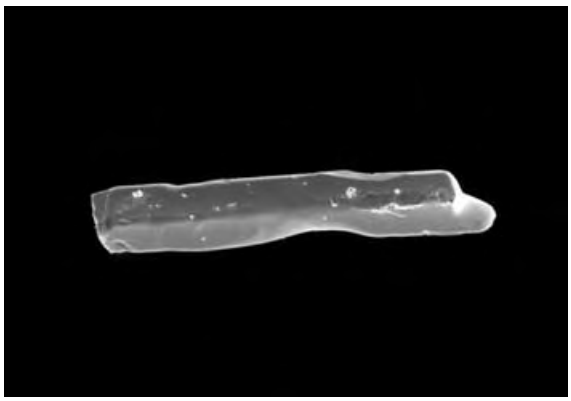

Figure 15. Scanning electron micrograph of a $RhZn_{13}$ single crystal (length ca. 0.2 mm).

Similar to the ternary aluminides reported in Section 9, ternary transition-metal–zinc compounds and rare-earth-metal–transition metal–zinc compounds can also be obtained from liquid zinc. Recent examples are the compounds RET_2Zn_{20} (T = Fe, Ru, Co, Rh, Ni),[303] TT'_2Zn_{20} (T = Zr, Hf, Nb; T' = Mn, Fe, Ru, Co, Rh, Ni),[304] or $RE_2T_3Zn_{14}$ (T = Fe, Co, Rh, Ni, Pd, Pt) with ordered Th_2Zn_{17} structure.[305] As an example a crystal of $HfRu_2Zn_{20}$ is shown in Figure 16. When carrying out reactions with zinc, care must be taken to control and handle the high vapor pressure of this metal at high temperatures.

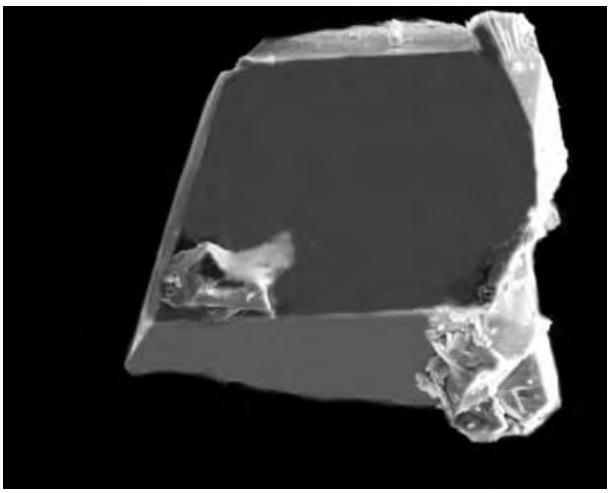

Figure 16. Scanning electron micrograph of a $HfRu_2Zn_{20}$ single crystal (length ca. 0.12 mm).

 © 2005 Wiley-VCH Verlag GmbH & Co. KGaA, Weinheim

13.4. Mixed-Metal Fluxes

Almost all reactions reported in the previous sections used an excess of only one metal as flux. Even more preparation possibilities are available through multinary mixtures. An interesting approach by Hillebrecht and Gebhardt with different Cu–Al fluxes revealed a whole series of niobium boride carbides.[306] The molar ratios Cu:Al:B:C:Nb were 20:5:2:1:4 for Nb_3B_3C, 20:5:0.2:0.1:0.2 for $Nb_4B_3C_2$, 20:5:2:1:2 for $Nb_7B_6C_3$, and 20:5:0.1:0.1:0.2 for $Nb_7B_4C_4$. Alumina was used as crucible material with the following temperature program: room temperature to 1600 °C with 400 °C h^{-1}, 24 h holding, cooling to 1500 °C at a rate of 100 °C h^{-1}, to 1100 °C at a rate of 1 °C h^{-1}, and finally to room temperature at 150 °C h^{-1}. The metal excess was dissolved in half-concentrated nitric acid.

Reactions in combined Ga:Zn fluxes revealed a large series of compounds: $MoZn_6$, $NbZn_3Ga_3$, $TaZn_3Ga_3$, $MoZn_{4.5}Ga_{4.5}$, or $Mo_7Ga_9Zn_{43}$.[307] Such intermetallics show packings of polyhedra that resemble the structures of the metallic elements. Ti/Al/Sn fluxes have been used for the preparation of ternary titanium–aluminum–carbides.[308]

14. Concluding Remarks and Prospects and Opportunities for the Future

Fluxes are solvents in almost all respects and they have recently emerged as an important synthetic tool in solid-state chemistry for both crystal-growth studies and exploratory studies of new chemical systems. Because of the huge potential for new materials discovery in the realm of intermetallics, the molten metal-flux technique is proving to be an outstanding tool for preparation. The advantages of this method lie in the enhanced diffusion of the elements facilitated by the solvent and the lower reaction temperatures that can be tolerated. The latter allow better kinetic control that gives more flexibility for novel compositions and atomic arrangements to be adopted in the structure.

For the synthesis of intermetallic tetrelide (mainly Si and Ge containing) compounds, the option of molten metal fluxes presents a promising approach, particularly with the use of low melting metals of Group 13 (Al, Ga, and In). These metals have low melting points, large solubility limits for tetrelides at moderate temperatures, do not form binary compounds with tetrelides, and are easily isolable from the final products through either chemical or physical means.

Lower temperatures also facilitate the formation of kinetically derived materials that may not be accessible by traditional high-temperature synthetic methods, such as arc melting or radio-frequency heating. Even within the flux-growth scenario, variation of the reaction time and temperature can influence the product outcome within a system just as in any conventional solution-based process.

The results presented herein indicate that considerable advances in the discovery of novel and complex phases are achievable utilizing molten metal fluxes as solvents. The flux approach to exploratory synthesis is the solid-state equivalent of conventional synthetic approach in coordination chemistry. The underlying principal reasons that make the flux reaction work, are the lower temperatures and enhanced diffusion rates that become accessible. When the benefits of flux synthesis are combined with the constant need to explore the chemistry of most elements of the periodic table, we have a powerful means with which to grasp the potential for future inquiry in solid-state chemistry. Naturally, this type of research is largely synthetic in nature, but the results could affect both basic and applied chemistry as well as physics, since in the plethora of new compounds to be discovered, exciting materials are sure to exist that have a variety of interesting phenomena and applications.

The benefits of molten metal solvents are by no means limited to the liquid metals described herein. Many other metal fluxes, such as lead, indium, and bismuth, can be explored more systematically as elemental solvents with relatively low melting points. It is also easy to imagine the use of binary or ternary compositions with low melting temperatures as solvents for similar reactions, such as various eutectic compositions of Co, Ni, or Cu with boron.

The investigations at the WWU Münster have continuously been supported by the Degussa–Hüls AG and the Heraeus Quarzschmelze through generous gifts of noble metals and silica tubes. This work was financially supported by the Fonds der Chemischen Industrie and by the Deutsche Forschungsgemeinschaft. M.G.K. thanks the Alexander von Humboldt Foundation for allowing him an extended stay in Germany where this article was written. Research at Michigan State University was supported by the Department of Energy Office of Basic Energy Sciences.

Received: September 30, 2004
Revised: March 10, 2005

[1] a) S. Suresh, A. Mortensen, A. Needleman, *Fundamentals of Metal-Matrix Composites*, Butterworths-Heinemann, Boston, **1993**; b) L. F. Mondolfo, *Aluminum Alloys: Structure and Properties*, Butterworths, Boston, **1979**; c) S. Gowri, F. H. Samuel, *Metall. Mater. Trans. A* **1994**, *25*, 437–448.

[2] a) K. H. J. Buschow, *J. Alloys Compd.* **1993**, *193*, 223–230; b) A. Szytuła, J. Leciejewicz, *CRC Handbook of Crystal Structures and Magnetic Properties of Rare Earth Intermetallics*, CRC, Boca Raton, **1994**.

[3] a) L. Miglio, F. d'Heurle, *Silicides – Fundamentals and Applications*, World Scientific, Singapore, **2000**; b) D. M. Shah, D. Berczik, D. L. Anton, R. Hecht, *Mater. Sci. Eng. A* **1992**, *155*, 45–57; c) P. J. Meschter, D. Schwartz, *JOM* **1989**, *41*, 52–55; d) H. Inui, M. Moriwaki, K. Ito, M. Yamaguchi, *Philos. Mag. A* **1998**, *77*, 375–394.

[4] E. Fitzer in *Plansee Proceedings* (Ed.: F. Benesovsky), Pergamon, London, **1956**, Chap. 7, pp. 56–79.

[5] G. H. Meier in *High-Temperature Ordered Intermetallic Alloys II* (Eds.: N. S. Stoloff, C. Koch, C. T. Liu, O. Izumi), Materials Research Society Symposium Proceedings 81, Materials Research Society, Pittsburgh, **1987**, p. 443.

[6] *CRC Handbook of Thermoelectrics* (Ed.: D. M. Rowe), CRC, Boca Raton, **1995**.

[7] a) K. Maex, *Mater. Sci. Eng. R* **1993**, *11*, 53–153; b) S. P. Murarka, *Silicides for VLSI Application*, Academic Press, New York, **1983**, and references therein.

 © 2005 Wiley-VCH Verlag GmbH & Co. KGaA, Weinheim

[8] a) B. W. Roberts, *J. Phys. Chem. Ref. Data* **1976**, *5*, 581 – 821; b) R. B. King, *Inorg. Chem.* **1990**, *29*, 2164 – 2170, and references therein.
[9] B. Aronsson, T. Lundström, S. Rundqvist, *Borides, Silicides and Phosphides*, Methuen, London, **1965**.
[10] a) M. E. Schlesinger, *Chem. Rev.* **1990**, *90*, 607 – 628; b) T. G. Chart, *A Critical Assessment of Thermochemical Data for Transition Metal-Silicon Systems*, NPL report on Chemistry 18, National Physical Laboratory, Teddington, **1972**.
[11] A. H. Reader, A. H. Vanommen, P. J. W. Weijs, R. A. M. Wolters, D. J. Oostra, *Rep. Prog. Phys.* **1993**, *56*, 1397 – 1467.
[12] K. Maex, *Appl. Surf. Sci.* **1991**, *53*, 328 – 337.
[13] a) C. Leyens, M. Schmidt, M. Peters, W. A. Kaysser, *Mater. Sci. Eng. A* **1997**, *239–240*, 680 – 688; b) J. J. Jacobs, J. L. Gilbert, R. M. Urban, *J. Bone Jt. Surg. Am. Vol.* **1998**, *80*, 268 – 273; c) H. Clemens, H. Kestler, *Adv. Eng. Mater.* **2000**, *2*, 551 – 555.
[14] G. Piatti, D. Boerman, *J. Nucl. Mater.* **1991**, *185*, 29 – 38.
[15] J. Van Humbeeck, M. Chandrasekaran, L. Delaey, *Endeavour* **1991**, *50*, 148 – 154.
[16] a) M. W. Barsoum, T. ElRaghy, *J. Am. Ceram. Soc.* **1996**, *79*, 1953 – 1956; b) M. W. Barsoum, *Prog. Solid State Chem.* **2000**, *28*, 201 – 281.
[17] a) K. Ullakko, J. K. Huang, C. Kantner, R. C. O'Handley, V. V. Kokorin, *Appl. Phys. Lett.* **1996**, *69*, 1966 – 1968; b) A. Sozinov, A. A. Likhachev, N. Lanska, K. Ullakko, *Appl. Phys. Lett.* **2002**, *80*, 1746 – 1748.
[18] a) T. Komatsu, M. Mesuda, T. Yashima, *Appl. Catal. A* **2000**, *194*, 333 – 339; b) E. Casado-Rivera, D. J. Volpe, L. Alden, C. Lind, C. Downie, T. Vazquez-Alvarez, A. C. D. Angelo, F. J. DiSalvo, H. D. Abruna, *J. Am. Chem. Soc.* **2004**, *126*, 4043 – 4049.
[19] I. Gurrappa, A. K. Gogia, *Surf. Coat. Technol.* **2001**, *139*, 216 – 221.
[20] a) A. Stein, S. W. Keller, T. E. Mallouk, *Science* **1993**, *259*, 1558 – 1564; b) M. G. Kanatzidis, A. C. Sutorik, *Prog. Inorg. Chem.* **1995**, *43*, 151 – 265.
[21] a) R. G. Blair, E. G. Gillan, N. K. B. Nguyen, D. Daurio, R. B. Kaner, *Chem. Mater.* **2003**, *15*, 3286 – 3293; b) P. R. Bonneau, R. F. Jarvis, R. B. Kaner, *Nature* **1991**, *349*, 510 – 512.
[22] a) J. C. Schön, M. Jansen, *Z. Kristallogr.* **2001**, *216*, 361 – 383; b) M. Jansen, J. C. Schön, *Nat. Mater.* **2004**, *3*, 838 – 838; c) M. A. C. Wevers, J. C. Schön, M. Jansen, *J. Solid State Chem.* **1998**, *136*, 233 – 246.
[23] a) P. C. Canfield, Z. Fisk, *Philos. Mag. B* **1992**, *65*, 1117 – 1123; b) D. T. Morelli, P. C. Canfield, P. Drymiotis, *Phys. Rev. B* **1996**, *53*, 12 896 – 12 901.
[24] D. Elwell, H. J. Scheel, *Crystal Growth from High-Temperature Solutions*, Academic Press, New York, **1975**; some of the old literature is reviewed in this book.
[25] H. Moissan, *The Electric Furnace* (translated by A. T. de Mouilpied), Arnold, London, **1904**.
[26] a) D. Elwell, *Man-Made Gemstones*, Wiley, New York, **1979**; b) R. M. Hazen, *The Diamond Makers*, Cambridge University Press, Cambridge, **1999**.
[27] P. Jolibois, *C. R. Hebd. Seances Acad. Sci.* **1910**, *150*, 106 – 108.
[28] G. Jangg, R. Kieffer, *Monatsh. Chem.* **1973**, *104*, 226 – 233.
[29] B. Champagne, S. Dallaire, A. A. Adnot, *J. Less-Common Met.* **1984**, *98*, L21 – L25.
[30] a) K. Nakano, H. Hayashi, T. Imura, *J. Cryst. Growth* **1974**, *24/25*, 679 – 682; b) I. Higashi, Y. Takahashi, T. Atoda, *J. Cryst. Growth* **1976**, *33*, 207 – 211.
[31] G. Jangg, R. Kieffer, L. Usner, *J. Less-Common Met.* **1968**, *14*, 269 – 277.
[32] G. Jangg, R. Kieffer, H. Kögler, *Z. Metallkd.* **1968**, *59*, 546 – 552.
[33] P. Peshev, M. Khristov, G. Gyurov, *J. Less-Common Met.* **1989**, *153*, 15 – 22.
[34] R. H. Deitch, *Crystal Growth* (Ed.: B. R. Pamplin), Pergamon, Oxford, **1975**, pp. 427 – 496.
[35] T. Lundström, *J. Less-Common Met.* **1984**, *100*, 215 – 228.
[36] K.-T. Wilke, J. Bohm, *Kristall-Züchtung*, 2nd ed., Harri Deutsch, Thun, Frankfurt/Main, **1988**.
[37] C. Gumiński, *Z. Metallkd.* **1990**, *81*, 105 – 110.
[38] G. Jangg, R. Kieffer, A. Blaha, T. Sultan, *Z. Metallkd.* **1972**, *63*, 670 – 676.
[39] K. Hein, E. Buhrig, *Kristallisation aus Schmelzen*, VEB Deutscher Verlag für Grundstoffindustrie, Leipzig, **1983**.
[40] a) M. Hansen, K. Anderko, *Constitution of Binary Alloys*, 2nd ed., McGraw-Hill, New York, **1958**; b) *Binary Alloy Phase Diagrams* (Ed.: T. B. Massalski), ASM, Metals Park, **1986**.
[41] A. Lang, W. Jeitschko, *Z. Metallkd.* **1996**, *87*, 759 – 764.
[42] Z. Fisk, J. P. Remeika in *Handbook on the Physics and Chemistry of Rare Earths*, Vol. *12* (Eds.: K. A. Gschneidner, Jr., L. Eyring), Elsevier, Amsterdam, **1989**, Chap. 81.
[43] M. Boström, S. Hovmöller, *J. Solid State Chem.* **2000**, *153*, 398 – 403.
[44] M. Boström, *Crystal Structures and Phase Equilibria in the Mn-Ga System*, PhD Thesis, University of Stockholm, Sweden, **2002**.
[45] J. Nylén, F. J. Garcia Garcia, B. D. Mosel, R. Pöttgen, U. Häussermann, *Solid State Sci.* **2004**, *6*, 147 – 155.
[46] W. Hönle, H. G. von Schnering, *Z. Kristallogr.* **1980**, *153*, 339 – 350.
[47] J. Osugi, R. Namikawa, Y. Tanaka, *Rev. Phys. Chem. Jpn.* **1967**, *36*, 35 – 43.
[48] W. Jeitschko, P. C. Donohue, *Acta Crystallogr. B* **1972**, *28*, 1893 – 1898.
[49] W. Jeitschko, P. C. Donohue, *Acta Crystallogr. B* **1975**, *31*, 574 – 580.
[50] R. Rühl, W. Jeitschko, *Acta Crystallogr. B* **1981**, *37*, 39 – 44.
[51] T. Wadsten, *Chem. Scr.* **1975**, *8*, 63 – 69.
[52] T. K. Chattopadhyay, H. G. von Schnering, *Z. Kristallogr.* **1984**, *167*, 1 – 12.
[53] W. Hönle, personal communication, **2003**.
[54] D. J. Braun, W. Jeitschko, *Z. Anorg. Allg. Chem.* **1978**, *445*, 157 – 166.
[55] R. Rühl, W. Jeitschko, *Monatsh. Chem.* **1983**, *114*, 817 – 828.
[56] a) W. Jeitschko, R. Rühl, U. Krieger, C. Heiden, *Mater. Res. Bull.* **1980**, *15*, 1755 – 1762; b) B. I. Noläng, L.-E. Tergenius, *Acta Chem. Scand. A* **1980**, *34*, 311 – 312.
[57] R. Rühl, W. Jeitschko, K. Schwochau, *J. Solid State Chem.* **1982**, *44*, 134 – 140.
[58] L. H. Dietrich, W. Jeitschko, *J. Solid State Chem.* **1986**, *63*, 377 – 385.
[59] R. Rühl, W. Jeitschko, *Acta Crystallogr. B* **1982**, *38*, 2784 – 2788.
[60] R. Rühl, U. Flörke, W. Jeitschko, *J. Solid State Chem.* **1984**, *53*, 55 – 63.
[61] R. Rühl, W. Jeitschko, *Z. Anorg. Allg. Chem.* **1980**, *466*, 171 – 178.
[62] R. Rühl, W. Jeitschko, *Inorg. Chem.* **1982**, *21*, 1886 – 1891.
[63] W. Jeitschko, R. Rühl, *Acta Crystallogr. B* **1979**, *35*, 1953 – 1958.
[64] W. Jeitschko, D. J. Braun, *Acta Crystallogr. B* **1978**, *34*, 3196 – 3201.
[65] F. Grandjean, A. Gerard, U. Krieger, C. Heiden, D. J. Braun, W. Jeitschko, *Solid State Commun.* **1980**, *33*, 261 – 264.
[66] R. Kaner, C. A. Castro, R. P. Gruska, A. Wold, *Mater. Res. Bull.* **1977**, *12*, 1143 – 1147.
[67] W. Hönle, R. Kremer, H. G. von Schnering, *Z. Kristallogr.* **1987**, *179*, 443 – 453.
[68] W. Jeitschko, D. J. Braun, *Z. Anorg. Allg. Chem.* **1978**, *445*, 157 – 166.
[69] U. Flörke, W. Jeitschko, *J. Less-Common Met.* **1982**, *86*, 247 – 253.

 © 2005 Wiley-VCH Verlag GmbH & Co. KGaA, Weinheim

[70] H. D. Lutz, G. Schneider, G. Kliche, *Phys. Chem. Miner.* **1983**, *9*, 109 – 114.
[71] W. Jeitschko, A. J. Foecker, D. Paschke, M. V. Dewalsky, C. B. H. Evers, B. Künnen, A. Lang, G. Kotzyba, U. C. Rodewald, M. H. Möller, *Z. Anorg. Allg. Chem.* **2000**, *626*, 1112 – 1120.
[72] J. P. Odile, S. Soled, C. A. Castro, A. Wold, *Inorg. Chem.* **1978**, *17*, 283 – 286.
[73] K. Zeppenfeld, W. Jeitschko, *J. Phys. Chem. Solids* **1993**, *54*, 1527 – 1531.
[74] A. Baghdadi, A. Finley, P. Russo, R. J. Arnott, A. Wold, *J. Less-Common Met.* **1974**, *34*, 31 – 38.
[75] N. A. Goryunova, V. M. Orlov, V. I. Sokolova, G. P. Shpenkov, E. V. Tsvetkova, *Phys. Status Solidi* **1968**, *25*, 513 – 519.
[76] W. Jeitschko, D. J. Braun, *Acta Crystallogr. B* **1977**, *33*, 3401 – 3406.
[77] M. S. Torikachvili, J. W. Chen, Y. Dalichaouch, R. P. Guertin, M. W. McElfresh, C. Rossel, M. P. Maple, G. P. Meisner, *Phys. Rev. B* **1987**, *36*, 8660 – 8664.
[78] A. Watcharapasorn, R. C. DeMattei, R. S. Feigelson, T. Caillat, A. Borshchevsky, G. J. Snyder, J.-P. Fleurial, *J. Appl. Phys.* **1999**, *86*, 6213 – 6217.
[79] D. J. Braun, W. Jeitschko, *J. Less-Common Met.* **1980**, *76*, 33 – 40.
[80] G. P. Meisner, M. S. Torikachvili, K. N. Yang, M. B. Maple, R. P. Guertin, *J. Appl. Phys.* **1985**, *57*, 3073 – 3075.
[81] C. B. H. Evers, W. Jeitschko, L. Boonk, D. J. Braun, T. Ebel, U. D. Scholz, *J. Alloys Compd.* **1995**, *224*, 184 – 189.
[82] B. C. Sales in *Handbook on the Physics and Chemistry of Rare Earths*, Vol. *33* (Eds.: K. A. Gschneidner, Jr., L. Eyring), Elsevier, Amsterdam **2003**, pp. 1 – 34.
[83] H. Liu, J. Y. Wang, X. B. Hu, F. Gu, L. Hua, C. Q. Zhang, B. Teng, D. L. Cui, J. Q. Pan, *Chem. Mater.* **2001**, *13*, 151 – 154.
[84] M. D. Hornbostel, E. J. Hyer, J. H. Edvalson, D. C. Johnson, *Inorg. Chem.* **1997**, *36*, 4270 – 4274.
[85] a) G. S. Nolas, D. T. Morelli, T. M. Tritt, *Annu. Rev. Mater. Sci.* **1999**, *29*, 89 – 116; b) C. Uher, *Semicond. Semimetals* **2001**, *69*, 139 – 253.
[86] S. Zemni, D. Tranqui, P. Chaudouet, R. Madar, J. P. Senateur, *J. Solid State Chem.* **1986**, *65*, 1 – 5.
[87] D. J. Braun, W. Jeitschko, *Acta Crystallogr. B* **1978**, *34*, 2069 – 2074.
[88] W. Jeitschko, W. K. Hofmann, *J. Less-Common Met.* **1983**, *95*, 317 – 322.
[89] R. Marchand, W. Jeitschko, *J. Solid State Chem.* **1978**, *24*, 351 – 357.
[90] a) W. Jeitschko, B. Jaberg, *J. Solid State Chem.* **1980**, *35*, 312 – 317; b) W. Jeitschko, U. Meisen, M. H. Möller, M. Reehuis, *Z. Anorg. Allg. Chem.* **1985**, *527*, 73 – 84; c) H. G. von Schnering, R. Türck, W. Hönle, K. Peters, E.-M. Peters, R. Kremer, J.-H. Chang, *Z. Anorg. Allg. Chem.* **2002**, *628*, 2772 – 2777; d) D. Schmitz, W. Bronger, *Z. Anorg. Allg. Chem.* **1987**, *553*, 248 – 260.
[91] W. K. Hofmann, W. Jeitschko, *J. Solid State Chem.* **1984**, *51*, 152 – 158.
[92] W. Jeitschko, M. Reehuis, *J. Phys. Chem. Solids* **1987**, *48*, 667 – 673.
[93] a) M. Reehuis, W. Jeitschko, *J. Phys. Chem. Solids* **1990**, *51*, 961 – 968; b) M. Reehuis, T. Vomhof, W. Jeitschko, *J. Less-Common Met.* **1991**, *169*, 139 – 145; c) M. Reehuis, P. J. Brown, W. Jeitschko, M. H. Möller, T. Vomhof, *J. Phys. Chem. Solids* **1993**, *54*, 469 – 475; d) M. Reehuis, T. Vomhof, W. Jeitschko, *J. Phys. Chem. Solids* **1994**, *55*, 625 – 630.
[94] E. Mörsen, B. D. Mosel, W. Müller-Warmuth, M. Reehuis, W. Jeitschko, *J. Phys. Chem. Solids* **1988**, *49*, 785 – 795.
[95] M. Reehuis, W. Jeitschko, M. H. Möller, P. J. Brown, *J. Phys. Chem. Solids* **1992**, *53*, 687 – 690.
[96] C. Brendel, W. Jeitschko, unpublished results.
[97] Th. Vomhof, Diplomarbeit, Universität Münster, **1988**.
[98] R. M. Bornick, A. M. Stacy, *Chem. Mater.* **1994**, *6*, 333 – 338.
[99] W. Jeitschko, R. Glaum, L. Boonk, *J. Solid State Chem.* **1987**, *69*, 93 – 100.
[100] G. Wenski, A. Mewis, *Z. Naturforsch. B* **1986**, *41*, 38 – 43.
[101] a) R. Glaum, J. H. Albering, W. Jeitschko, L. Boonk, *J. Alloys Compd.* **1992**, *185*, 301 – 309; b) J. H. Albering, W. Jeitschko, *Z. Naturforsch. B* **1994**, *49*, 1074 – 1080.
[102] a) R. Rühl, W. Jeitschko, *Mater. Res. Bull.* **1979**, *14*, 513 – 517; b) A. C. Payne, A. E. Sprauve, M. M. Olmstead, S. M. Kauzlarich, J. Y. Chan, B. A. Reisner, J. W. Lynn, *J. Solid State Chem.* **2002**, *163*, 498 – 505.
[103] T. Ebel, J. H. Albering, W. Jeitschko, *J. Alloys Compd.* **1998**, *266*, 71 – 76.
[104] T. Ebel, W. Jeitschko, *J. Solid State Chem.* **1995**, *116*, 307 – 313.
[105] W. Jeitschko, R. Brink, *Z. Naturforsch. B* **1991**, *46*, 192 – 196.
[106] Yu. B. Kuz'ma, S. I. Chikhrij in *Handbook on the Physics and Chemistry of Rare Earths*, Vol. *23* (Eds.: K. A. Gschneidner, Jr., L. Eyring), Elsevier, Amsterdam, **1996**, pp. 285 – 434.
[107] a) W. Jeitschko, D. J. Braun, R. H. Ashcraft, R. Marchand, *J. Solid State Chem.* **1978**, *25*, 309 – 313; b) W. Jeitschko, U. Meisen, U. D. Scholz, *J. Solid State Chem.* **1984**, *55*, 331 – 336; c) M. Reehuis, W. Jeitschko, *J. Phys. Chem. Solids* **1989**, *50*, 563 – 569.
[108] W. Jeitschko, B. Jaberg, *Z. Anorg. Allg. Chem.* **1980**, *467*, 95 – 104.
[109] T. P. Braun, F. J. DiSalvo, *J. Alloys Compd.* **2000**, *307*, 111 – 113.
[110] W. Jeitschko, P. G. Pollmeier, U. Meisen, *J. Alloys Compd.* **1993**, *196*, 105 – 109.
[111] J. V. Badding, A. M. Stacy, *J. Solid State Chem.* **1987**, *67*, 354 – 358.
[112] U. Meisen, W. Jeitschko, *J. Less-Common Met.* **1984**, *102*, 127 – 134.
[113] U. Jakubowski-Ripke, W. Jeitschko, *J. Less-Common Met.* **1988**, *136*, 261 – 270.
[114] U. Meisen, W. Jeitschko, *Z. Kristallogr.* **1984**, *167*, 135 – 143.
[115] M. Reehuis, W. Jeitschko, E. Mörsen, W. Müller-Warmuth, *J. Less-Common Met.* **1988**, *139*, 359 – 369.
[116] J. V. Badding, A. M. Stacy, *J. Solid State Chem.* **1990**, *87*, 10 – 14.
[117] a) W. Jeitschko, U. Jakubowski, *J. Less-Common Met.* **1985**, *110*, 339 – 348; b) U. Jakubowski-Ripke, W. Jeitschko, unpublished results.
[118] W. Jeitschko, E. J. Reinbold, *Z. Naturforsch. B* **1985**, *40*, 900 – 905.
[119] W. Jeitschko, U. Jakubowski-Ripke, *Z. Kristallogr.* **1993**, *207*, 69 – 79.
[120] a) J. Y. Pivan, R. Guérin, *J. Solid State Chem.* **1998**, *135*, 218 – 227; b) Yu. M. Prots', W. Jeitschko, *Inorg. Chem.* **1998**, *37*, 5431 – 5438, and references therein.
[121] U. Jakubowski-Ripke, *Darstellung und Charakterisierung ternärer Seltenerdmetall-Cobalt-Phosphide.* PhD Thesis, Universität Münster, **1989**.
[122] E. Ganglberger, *Monatsh. Chem.* **1968**, *99*, 557 – 565.
[123] W. Jeitschko, L. J. Terbüchte, E. J. Reinbold, P. G. Pollmeier, T. Vomhof, *J. Less-Common Met.* **1990**, *161*, 125 – 134.
[124] J. H. Albering, W. Jeitschko, *Z. Naturforsch. B* **1992**, *47*, 1521 – 1528.
[125] S. I. Chikhrij, Yu. B. Kuz'ma, V. N. Davydov, S. L. Budnyk, S. V. Orishchin, *Kristallografya* **1998**, *43*, 596 – 600.
[126] J. H. Albering, W. Jeitschko, *J. Solid State Chem.* **1995**, *117*, 80 – 87.
[127] B. I. Zimmer, W. Jeitschko, *Z. Kristallogr.* **1994**, *209*, 950 – 953.
[128] J. H. Albering, W. Jeitschko, *J. Alloys Compd.* **1996**, *241*, 44 – 50.
[129] Yu. B. Kuz'ma, S. I. Chikhrij, S. L. Budnyk, *J. Alloys Compd.* **2000**, *298*, 190 – 194.

 © 2005 Wiley-VCH Verlag GmbH & Co. KGaA, Weinheim

[130] W. Jeitschko, R. Brink, P. G. Pollmeier, *Z. Naturforsch. B* **1993**, *48*, 52 – 57.
[131] R. Brink, W. Jeitschko, *Z. Kristallogr.* **1987**, *178*, 30.
[132] C. Le Sénéchal, J. Y. Pivan, S. Députier, R. Guérin, *Mater. Res. Bull.* **1998**, *33*, 887 – 902.
[133] C. Le Sénéchal, V. Babizhets'ky, S. Députier, J. Y. Pivan, R. Guérin, *J. Solid State Chem.* **1999**, *144*, 277 – 286.
[134] R. Brink, *Strukturchemische Untersuchungen von Phosphiden des Urans mit Chrom und Molybdän*, PhD Thesis, Universität Münster, **1989**.
[135] U. Flörke, W. Jeitschko, *Inorg. Chem.* **1983**, *22*, 1736 – 1739.
[136] U. D. Scholz, W. Jeitschko, *Z. Anorg. Allg. Chem.* **1986**, *540/541*, 234 – 242.
[137] U. D. Scholz, W. Jeitschko, M. Reehuis, *J. Solid State Chem.* **1988**, *74*, 260 – 267.
[138] M. V. Dewalsky, W. Jeitschko, *Acta Chem. Scand.* **1991**, *45*, 828 – 832.
[139] M. V. Dewalsky, W. Jeitschko, U. Wortmann, *Chem. Mater.* **1991**, *3*, 316 – 319.
[140] W. Jeitschko, J. Wallinda, M. V. Dewalsky, U. Wortmann, *Z. Naturforsch. B* **1993**, *48*, 1774 – 1780.
[141] D. Paschke, J. Wallinda, W. Jeitschko, *J. Solid State Chem.* **1996**, *122*, 206 – 213.
[142] M. H. Möller, W. Jeitschko, *Z. Anorg. Allg. Chem.* **1982**, *491*, 225 – 236.
[143] M. H. Möller, W. Jeitschko, *Inorg. Chem.* **1981**, *20*, 828 – 833.
[144] U. D. Scholz, W. Jeitschko, *J. Solid State Chem.* **1987**, *67*, 271 – 277.
[145] M. Eschen, J. Wallinda, W. Jeitschko, *Z. Anorg. Allg. Chem.* **2002**, *628*, 2764 – 2771.
[146] S. Furuseth, H. Fjellvåg, *Acta Chem. Scand. A* **1985**, *39*, 537 – 544.
[147] S. Furuseth, H. Fjellvåg, *Acta Chem. Scand.* **1994**, *48*, 134 – 138.
[148] F. X. Zhang, F. F. Xu, A. Leithe-Jasper, T. Mori, T. Tanaka, A. Sato, P. Salamakha, Y. Bando, *J. Alloys Compd.* **2002**, *337*, 120 – 127.
[149] R. Jardin, V. Babizhetskyy, R. Guérin, J. Bauer, *J. Alloys Compd.* **2003**, *353*, 233 – 239.
[150] S. Okada, T. Suda, A. Kamezaki, K. Hamano, K. Kudou, K. Takagi, T. Lundström, *Mater. Sci. Eng. A* **1996**, *209*, 33 – 37.
[151] S. Okada, T. Shishido, Y. Ishizawa, M. Ogawa, K. Kudou, T. Fukuda, T. Lundström, *J. Alloys Compd.* **2001**, *317–318*, 315 – 319.
[152] A. C. Payne, A. E. Sprauve, A. P. Holm, M. M. Olmstead, S. M. Kauzlarich, P. Klavins, *J. Alloys Compd.* **2002**, *338*, 229 – 234.
[153] S. Okada, K. Kudou, T. Shishido, I. Higashi, H. Horiuchi, T. Fukada, *J. Alloys Compd.* **1998**, *281*, 160 – 162.
[154] T. A. Vanderah, R. A. Nissan, *J. Phys. Chem. Solids* **1988**, *49*, 1335 – 1338.
[155] J.-Y. Pivan, R. Guérin, J. Padiou, M. Sergent, *J. Solid State Chem.* **1988**, *76*, 26 – 32.
[156] C. Perrier, H. Vincent, P. Chadouët, B. Chenevier, R. Madar, *Mater. Res. Bull.* **1995**, *30*, 357 – 364.
[157] P. Kaiser, W. Jeitschko, *J. Solid State Chem.* **1996**, *124*, 346 – 352.
[158] a) J. Kreisel, O. Chaix-Pluchery, F. Genet, G. Lucazeau, H. Vincent, R. Madar, *J. Solid State Chem.* **1997**, *128*, 142 – 149; b) P. Kaiser, W. Jeitschko, *Z. Kristallogr.* **1996**, *Suppl. 11*, 100.
[159] C. Perrier, M. Kirschen, H. Vincent, U. Gottlieb, B. Chenevier, R. Madar, *J. Solid State Chem.* **1997**, *133*, 473 – 478.
[160] B. I. Zimmer, W. Jeitschko, J. H. Albering, R. Glaum, M. Reehuis, *J. Alloys Compd.* **1995**, *229*, 238 – 242.
[161] J. W. Kaiser, W. Jeitschko, *Z. Naturforsch. B* **2002**, *57*, 165 – 170.
[162] R. Lam, A. Mar, *Inorg. Chem.* **1998**, *37*, 5364 – 5368.
[163] S. H. D. Moore, L. Deakin, M. J. Ferguson, A. Mar, *Chem. Mater.* **2002**, *14*, 4867 – 4873.
[164] M. J. Ferguson, R. W. Hushagen, A. Mar, *J. Alloys Compd.* **1997**, *249*, 191 – 198.
[165] H. Kim, C. L. Condron, A. P. Holm, S. M. Kauzlarich, *J. Am. Chem. Soc.* **2000**, *122*, 10720 – 10721.
[166] A. P. Holm, S.-M. Park, C. L. Condron, M. M. Olmstead, H. Kim, P. Klavins, F. Grandjean, R. P. Hermann, G. J. Long, M. G. Kanatzidis, S. M. Kauzlarich, S.-J. Kim, *Inorg. Chem.* **2003**, *42*, 4660 – 4667.
[167] M. Brylak, W. Jeitschko, *Z. Naturforsch. B* **1994**, *49*, 747 – 752.
[168] R. Lam, A. Mar, *Inorg. Chem.* **1996**, *35*, 6959 – 6963.
[169] R. Lam, J. Zhang, A. Mar, *J. Solid State Chem.* **2000**, *150*, 371 – 376.
[170] R. Lam, A. Mar, *Solid State Sci.* **2001**, *3*, 503 – 512.
[171] L. Deakin, R. Lam, F. Marsiglio, A. Mar, *J. Alloys Compd.* **2002**, *338*, 69 – 72.
[172] B. Künnen, W. Jeitschko, G. Kotzyba, B. D. Mosel, *Z. Naturforsch. B* **2000**, *55*, 425 – 430; Erratum: B. Künnen, W. Jeitschko, G. Kotzyba, B. D. Mosel, *Z. Naturforsch. B* **2000**, *55*, 887.
[173] H. Kleinke, M. Waldeck, P. Gütlich, *Chem. Mater.* **2000**, *12*, 2219 – 2224.
[174] T. Wölpl, W. Jeitschko, *J. Alloys Compd.* **1994**, *210*, 185 – 190.
[175] T. Wölpl, W. Jeitschko, *Z. Anorg. Allg. Chem.* **1994**, *620*, 467 – 470.
[176] A. Lang, W. Jeitschko, *J. Mater. Chem.* **1996**, *6*, 1897 – 1903.
[177] B. Künnen, D. Niepmann, W. Jeitschko, *J. Alloys Compd.* **2000**, *309*, 1 – 9.
[178] M. Schlüter, U. Häussermann, B. Heying, R. Pöttgen, *J. Solid State Chem.* **2003**, *173*, 418 – 424.
[179] E.-L. Nordmark, O. Wallner, U. Häussermann, *J. Solid State Chem.* **2002**, *168*, 34 – 40.
[180] L. Offernes, A. Neumann Torgersen, A. Kjekshus, *J. Alloys Compd.* **2000**, *307*, 174 – 178.
[181] U. Häussermann, A. R. Landa-Cánovas, S. Lidin, *Inorg. Chem.* **1997**, *36*, 4307 – 4315.
[182] R. V. Skolozdra in *Handbook on the Physics and Chemistry of Rare Earths* (Eds.: K. A. Gschneidner, Jr., L. Eyring), Elsevier, Amsterdam, **1997**, pp. 399 – 517.
[183] D. M. Clatterbuck, K. A. Gschneidner, Jr., *J. Magn. Magn. Mater.* **1999**, *207*, 78 – 94.
[184] R. Mishra, R. Pöttgen, R.-D. Hoffmann, H. Trill, B. D. Mosel, H. Piotrowski, M. F. Zumdick, *Z. Naturforsch. B* **2001**, *56*, 589 – 597.
[185] M. A. Zhuravleva, D. Bilc, S. D. Mahanti, M. G. Kanatzidis, *Z. Anorg. Allg. Chem.* **2003**, *629*, 327 – 334.
[186] A. Löhken, C. Lux, D. Johrendt, A. Mewis, *Z. Anorg. Allg. Chem.* **2002**, *628*, 1472 – 1476.
[187] A. Wurth, A. Löhken, A. Mewis, *Z. Anorg. Allg. Chem.* **2002**, *628*, 661 – 666.
[188] A. Wurth, A. Mewis, *Z. Anorg. Allg. Chem.* **1999**, *625*, 1486 – 1488.
[189] A. Wurth, A. Mewis, *Z. Anorg. Allg. Chem.* **1999**, *625*, 449 – 452.
[190] H. Thurn, H. Krebs, *Acta Crystallogr. B* **1969**, *25*, 125-135, and references therein.
[191] H. Krebs, K. H. Müller, G. Zürn, *Z. Anorg. Allg. Chem.* **1956**, *285*, 15 – 28.
[192] H. Krebs, I. Pakulla, G. Zürn, *Z. Anorg. Allg. Chem.* **1955**, *278*, 274 – 286.
[193] M. Eschen, W. Jeitschko, *J. Solid State Chem.* **2002**, *165*, 238 – 246.
[194] S. Okada, K. Kudou, T. Mori, K. Iizumi, T. Shishido, T. Tanaka, K. Nakajima, P. Rogl, *Jpn. J. Appl. Phys.* **2002**, *41*, L555 – L558.
[195] S. Okada, K. Kudou, T. Mori, K. Iizumi, T. Shishido, T. Tanaka, P. Rogl, *J. Cryst. Growth* **2002**, *244*, 267 – 273.
[196] *Boron and Refractory Borides* (Ed.: V. I. Matkovich), Springer, Berlin, **1977**, and references therein.
[197] a) Y. Yu, L.-E. Tergenius, T. Lundström, S. Okada, *J. Alloys Compd.* **1995**, *221*, 86 – 90; b) S. Okada, K. Kudou, K. Iizumi, K. Kudaka, I. Higashi, T. Lundström, *J. Cryst. Growth* **1996**, *166*, 429 – 435.

 © 2005 Wiley-VCH Verlag GmbH & Co. KGaA, Weinheim

[198] a) S. Okada, K. Hamano, I. Higashi, T. Lundström, L.-E. Tergenius, *Bull. Chem. Soc. Jpn.* **1990**, *63*, 687 – 691; b) S. Okada, K. Kudou, I. Higashi, T. Lundström, *J. Cryst. Growth* **1993**, *128*, 1120 – 1124.

[199] a) M. M. Korsukova, T. Lundström, V. N. Gurin, L.-E. Tergenius, *Z. Kristallogr.* **1984**, *168*, 299 – 306; b) S. Okada, Y. Yu, T. Lundström, K. Kudou, T. Tanaka, *Jpn. J. Appl. Phys.* **1996**, *35*, 4718 – 4723.

[200] S. Okada, K. Kudou, Y. Yu, T. Lundström, *Jpn. J. Appl. Phys.* **1994**, *33*, 2663 – 2666.

[201] I. Higashi, M. Kobayashi, S. Okada, K. Hamano, T. Lundström, *J. Cryst. Growth* **1993**, *128*, 1113 – 1119.

[202] W. Jeitschko, *Monatsh. Chem.* **1966**, *97*, 1472 – 1476.

[203] W. Jeitschko, *Acta Crystallogr. B* **1969**, *25*, 163 – 165.

[204] J. Grin', U. Burkhardt, M. Ellner, K. Peters, *J. Alloys Compd.* **1994**, *206*, 243 – 247.

[205] S. Niemann, W. Jeitschko, *Z. Naturforsch. B.* **1993**, *48*, 1767 – 1773.

[206] K. Gotzmann, M. Ellner, Yu. Grin', *Powder Diffr.* **1997**, *12*, 248 – 251.

[207] Y. Grin', K. Peters, U. Burkhardt, K. Gotzmann, M. Ellner, *Z. Kristallogr.* **1997**, *212*, 439 – 444.

[208] a) S. Niemann, W. Jeitschko, *Z. Metallkd.* **1994**, *85*, 345 – 349; b) S. Niemann, W. Jeitschko, *J. Solid State Chem.* **1995**, *114*, 337 – 341; c) S. Niemann, W. Jeitschko, *J. Solid State Chem.* **1995**, *116*, 131 – 135; d) S. Niemann, W. Jeitschko, *J. Alloys Compd.* **1995**, *221*, 235 – 239; e) S. Niemann, W. Jeitschko, *Z. Kristallogr.* **1995**, *210*, 338 – 341; f) V. M. T. Thiede, W. Jeitschko, *Z. Naturforsch. B* **1998**, *53*, 673 – 678; g) V. M. T. Thiede, W. Jeitschko, *J. Solid State Chem.* **1999**, *143*, 198 – 201; h) V. M. T. Thiede, W. Jeitschko, *Z. Kristallogr. New Cryst. Struct.* **1999**, *214*, 149 – 150; i) B. Fehrmann, W. Jeitschko, *Inorg. Chem.* **1999**, *38*, 3344 – 3351; j) V. M. T. Thiede, B. Fehrmann, W. Jeitschko, *Z. Anorg. Allg. Chem.* **1999**, *625*, 1417 – 1425; k) B. Fehrmann, W. Jeitschko, *Z. Naturforsch. B* **1999**, *54*, 1277 – 1282; l) B. Fehrmann, W. Jeitschko, *J. Alloys Compd.* **2000**, *298*, 153 – 159; m) J. Niermann, W. Jeitschko, *Z. Anorg. Allg. Chem.* **2002**, *628*, 2549 – 2556; n) J. Niermann, W. Jeitschko, *Inorg. Chem.* **2004**, *43*, 3264 – 3270; o) J. Niermann, W. Jeitschko, *Z. Anorg. Allg. Chem.* **2004**, *630*, 361 – 368; p) V. M. T. Thiede, M. H. Gerdes, U. C. Rodewald, W. Jeitschko, *J. Alloys Compd.* **1997**, *261*, 54 – 61; q) V. M. T. Thiede, T. Ebel, W. Jeitschko, *J. Mater. Chem.* **1998**, *8*, 125 – 130; r) V. M. T. Thiede, W. Jeitschko, S. Niemann, T. Ebel, *J. Alloys Compd.* **1998**, *267*, 23 – 31; s) M. Reehuis, B. Fehrmann, M. W. Wolff, W. Jeitschko, M. Hofmann, *Phys. B* **2000**, *276–278*, 594 – 595; t) M. W. Wolff, S. Niemann, T. Ebel, W. Jeitschko, *J. Magn. Magn. Mater.* **2001**, *223*, 1 – 15; u) M. Reehuis, M. W. Wolff, A. Krimmel, E.-W. Scheidt, N. Stüsser, A. Loidl, W. Jeitschko, *J. Phys. Condens. Matter* **2003**, *15*, 1773 – 1782; v) J. Niermann, B. Fehrmann, M. W. Wolff, W. Jeitschko, *J. Solid State Chem.* **2004**, *177*, 2600 – 2609.

[209] a) G. Cordier, E. Czech, H. Ochmann, H. Schäfer, *J. Less-Common Met.* **1984**, *99*, 173 – 185; b) Yu. N. Grin', R. E. Gladyshevskii, O. M. Sichevich, V. E. Zavodnik, Ya. P. Yarmolyuk, I. V. Rozhdestvenskaya, *Sov. Phys. Crystallogr.* **1984**, *29*, 528 – 531.

[210] S. E. Latturner, D. Bilc, J. R. Ireland, C. R. Kannewurf, S. D. Mahanti, M. G. Kanatzidis, *J. Solid State Chem.* **2003**, *170*, 48 – 57.

[211] a) O. Hönigschmid, *Monatsh. Chem.* **1906**, *27*, 1069 – 1081; b) G. Brauer, A. Mitius, *Z. Anorg. Allg. Chem.* **1942**, *249*, 325 – 339; c) G. Brauer, H. Haag, *Z. Anorg. Allg. Chem.* **1952**, *267*, 198 – 212.

[212] I. S. Dubenko, A. A. Evdokimov, Yu. N. Titov, *Russ. J. Inorg. Chem.* **1985**, *30*, 1707 – 1708.

[213] A. Raman, *Inorg. Chem.* **1968**, *7*, 973 – 976.

[214] X.-Z. Chen, P. Brazis, C. R. Kannewurf, J. A. Cowen, R. Crosby, M. G. Kanatzidis, *Angew. Chem.* **1999**, *111*, 695 – 698; *Angew. Chem. Int. Ed.* **1999**, *38*, 693 – 696.

[215] P. Small, M. A. Zhuravleva, B. Sieve, M. G. Kanatzidis, unpublished results.

[216] a) T. I. Yanson, M. B. Manyakov, O. I. Bodak, R. E. Gladyshevskii, R. Cerny, K. Yvon, *Acta Crystallogr. Sect. C* **1994**, *50*, 1377 – 1379; b) M. A. Zhuravleva, K. K. Rangan, M. Lane, P. Brazis, C. R. Kannewurf, M. G. Kanatzidis, *J. Alloys Compd.* **2001**, *316*, 137 – 145.

[217] X.-Z. Chen, S. Sportouch, B. Sieve, P. Brazis, C. R. Kannewurf, J. A. Cowen, R. Patschke, M. G. Kanatzidis, *Chem. Mater.* **1998**, *10*, 3202 – 3211.

[218] B. Sieve, M. A. Zhuravleva, X.-Z. Chen, R. Henning, A. J. Schultz, P. Brazis, C. R. Kannewurf, M. G. Kanatzidis, unpublished results.

[219] B. Sieve, P. N. Trikalitis, M. G. Kanatzidis, *Z. Anorg. Allg. Chem.* **2002**, *628*, 1568 – 1574.

[220] B. Sieve, PhD Thesis , Michigan State University, **2002**.

[221] a) S. E. Latturner, D. Bilc, S. D. Mahanti, M. G. Kanatzidis, *Chem. Mater.* **2002**, *14*, 1695 – 1705; b) S. E. Latturner, M. G. Kanatzidis, *Inorg. Chem.* **2002**, *41*, 5479 – 5486.

[222] B. Sieve, X.-Z. Chen, R. Henning, P. Brazis, C. R. Kannewurf, J. A. Cowen, A. J. Schultz, M. G. Kanatzidis, *J. Am. Chem. Soc.* **2001**, *123*, 7040 – 7047.

[223] For an exhaustive review of gallium intermetallic compounds see: Yu. N. Grin', R. E. Gladyshevskii, *Gallides Handbook*, Moscow, Metallurgy, **1989** (in Russian).

[224] a) M. Schlüter, W. Jeitschko, *Z. Anorg. Allg. Chem.* **2000**, *626*, 2217 – 2222; b) M. Schlüter, W. Jeitschko, *Inorg. Chem.* **2001**, *40*, 6362 – 6368; c) M. Schlüter, W. Jeitschko, *Z. Kristallogr. New Cryst. Struct.* **2002**, *217*, 27 – 28; d) M. Schlüter, W. Jeitschko, *Z. Anorg. Allg. Chem.* **2002**, *628*, 1505 – 1510; e) M. Schlüter, W. Jeitschko, *J. Solid State Chem.* **2003**, *172*, 27 – 34.

[225] X.-Z. Chen, P. Larson, S. Sportouch, P. Brazis, S. D. Mahanti, C. R. Kannewurf, M. G. Kanatzidis, *Chem. Mater.* **1999**, *11*, 75 – 83.

[226] X.-Z. Chen, P. Small, S. Sportouch, M. A. Zhuravleva, P. Brazis, C. R. Kannewurf, M. G. Kanatzidis, *Chem. Mater.* **2000**, *12*, 2520 – 2522.

[227] Yu. N. Grin', Ya. P. Yarmolyuk, I. V. Rozhdestvenskaya, E. I. Gladyshevskii, *Krystallografya* **1982**, *27*, 693 – 969.

[228] P. Villars, L. D. Calvert, *Pearson's Handbook of Crystallographic Data for Intermetallic Phases*, ASM International, Materials Park, **1991**.

[229] M. A. Zhuravleva, M. G. Kanatzidis, *Z. Naturforsch. B* **2003**, *58*, 649 – 657.

[230] M. A. Zhuravleva, X. Wang, A. J. Schultz, T. Bakas, M. G. Kanatzidis, *Inorg. Chem.* **2002**, *41*, 6056 – 6061.

[231] M. A. Zhuravleva, D. Bilc, R. J. Pcionek, S. D. Mahanti, M. G. Kanatzidis, *Inorg. Chem.* **2005**, *44*, 2177 – 2188.

[232] M. A. Zhuravleva, PhD Thesis, Michigan State University, **2002**.

[233] M. A. Zhuravleva, M. G. Kanatzidis, *J. Solid State Chem.* **2003**, *173*, 280 – 292.

[234] M. A. Zhuravleva, J. Salvador, D. Bilc, S. D. Mahanti, J. Ireland, C. R. Kannewurf, M. G. Kanatzidis, *Chem. Eur. J.* **2004**, *10*, 3197 – 3208.

[235] M. A. Zhuravleva, X.-Z. Chen, X. Wang, A. J. Schultz, J. Ireland, C. R. Kannewurf, M. G. Kanatzidis, *Chem. Mater.* **2002**, *14*, 3066 – 3081.

[236] M. A. Zhuravleva, R. J. Pcionek, X. Wang, A. J. Schultz, M. G. Kanatzidis, *Inorg. Chem.* **2003**, *42*, 6412 – 6424.

[237] J. R. Salvador, D. Bilc, S. D. Mahanti, M. G. Kanatzidis, *Angew. Chem.* **2002**, *114*, 872 – 874; *Angew. Chem. Int. Ed.* **2002**, *41*, 844 – 846.

 © 2005 Wiley-VCH Verlag GmbH & Co. KGaA, Weinheim

[238] a) J. R. Salvador, D. Bilc, S. D. Mahanti, M. G. Kanatzidis, *Angew. Chem.* **2003**, *115*, 1973 – 1976; *Angew. Chem. Int. Ed.* **2003**, *42*, 1929 – 1932; b) The phases SiB_3 and SiB_4 are listed separately in *Pearson's Handbook*[228] and are even listed as different structure types: isotypic with B_6P and $B_{13}C_2$, respectively. In fact SiB_3 and SiB_4 have the same structure, namely that of B_6P, and the variation in stoichiometry is the result of a compositional spread ranging from $SiB_{2.89}$ up to SiB_4. This stoichiometric flexibility arises from the substitution of varying amounts of Si into the polar sites of the B_{12} cages.
[239] $Tb_2Ga_2Ge_5$ crystallizes in the Ce_2GaGe_6 structure type.
[240] T. B. Massalski, *Binary Alloy Phase Diagrams*, Vol. *1*, 2nd ed., ASM, New York, **1990**, p. 484; T. B. Massalski, *Binary Alloy Phase Diagrams*, Vol. *2*, 2nd ed., ASM, New York, **1990**, p. 1856.
[241] a) R. J. Cava, H. Takagi, B. Batlogg, H. W. Zandbergen, J. J. Krajewski, W. F. Peck, Jr., R. B. van Dover, R. J. Felder, T. Siegrist, K. Mizuhashi, J. O. Lee, H. Eisaki, S. A. Carter, S. Uchida, *Nature* **1994**, *367*, 146 – 148; b) R. Nagarajan, C. Mazumdar, Z. Hossain, S. K. Dhar, K. V. Gopalakrisnan, L. C. Gupta, C. Godart, B. D. Padalia, R. Vijayaraghavan, *Phys. Rev. Lett.* **1994**, *72*, 274 – 277.
[242] J. Nagamatsu, N. Nakagawa, T. Muranaka, Y. Zenitani, J. Akimitsu, *Nature* **2001**, *410*, 63 – 64.
[243] *Boron and Refractory Borides* (Ed.: V. I. Matkovich), Springer, New York, **1977**, pp. 100 – 101, and references therein; *Boron and Refractory Borides* (Ed.: V. I. Matkovich), Springer, New York, **1977**, pp. 321 – 326, and references therein.
[244] R. Pöttgen, *J. Alloys Compd.* **1995**, *226*, 59 – 64.
[245] R. Pöttgen, R.-D. Hoffmann, G. Kotzyba, *Z. Anorg. Allg. Chem.* **1998**, *624*, 244 – 250.
[246] R. Pöttgen, *Z. Naturforsch. B* **1995**, *50*, 1505 – 1509.
[247] R. Pöttgen, R. Dronskowski, *Chem. Eur. J.* **1996**, *2*, 800 – 804.
[248] M. F. Zumdick, G. A. Landrum, R. Dronskowski, R.-D. Hoffmann, R. Pöttgen, *J. Solid State Chem.* **2000**, *150*, 19 – 30.
[249] H. Hegger, C. Petrovic, E. G. Moshopoulou, M. F. Hundley, J. L. Sarrao, Z. Fisk, J. D. Thompson, *Phys. Rev. Lett.* **2000**, *84*, 4986 – 4989.
[250] E. G. Moshopoulou, Z. Fisk, J. L. Sarrao, J. D. Thompson, *J. Solid State Chem.* **2001**, *158*, 25 – 33.
[251] R. T. Macaluso, J. L. Sarrao, P. G. Pagliuso, N. O. Moreno, R. G. Goodrich, A. Browne, F. R. Fronczek, J. Y. Chan, *J. Solid State Chem.* **2002**, *166*, 245 – 250.
[252] R. T. Macaluso, J. L. Sarrao, N. O. Moreno, P. G. Pagliuso, J. D. Thompson, F. R. Fronczek, M. F. Hundley, A. Malinowski, J. Y. Chan, *Chem. Mater.* **2003**, *15*, 1394 – 1398.
[253] V. I. Zaremba, Ya. M. Kalychak, Yu. B. Tyvanchuk, R.-D. Hoffmann, M. H. Möller, R. Pöttgen, *Z. Naturforsch. B* **2002**, *57*, 791 – 797.
[254] V. I. Zaremba, Ya. M. Kalychak, V. P. Dubenskiy, R.-D. Hoffmann, U. Ch. Rodewald, R. Pöttgen, *J. Solid State Chem.* **2002**, *169*, 118 – 124.
[255] V. I. Zaremba, U. C. Rodewald, R.-D. Hoffmann, Ya. M. Kalychak, R. Pöttgen, *Z. Anorg. Allg. Chem.* **2003**, *629*, 1157 – 1161.
[256] V. I. Zaremba, U. C. Rodewald, R. Pöttgen, *Z. Naturforsch. B* **2003**, *58*, 805 – 808.
[257] I. R. Fisher, Z. Islam, P. C. Canfield, *J. Magn. Magn. Mater.* **1999**, *202*, 1 – 10.
[258] J. Emsley, *The Elements*, 3rd ed., Oxford University Press, **1999**.
[259] X.-Z. Chen, M. G. Kanatzidis, unpublished results.
[260] G. R. Stewart, Z. Fisk, J. O. Willis, *Phys. Rev. B* **1983**, *28*, 172 – 177.
[261] J. R. Salvador, J. R. Gour, D. Bilc, S. D. Mahanti, M. G. Kanatzidis, *Inorg. Chem.* **2004**, *43*, 1403 – 1410.
[262] W. Jung, F. Diessenbacher, *Z. Anorg. Allg. Chem.* **1991**, *594*, 57 – 65.
[263] R. Pöttgen, PhD Thesis, Universität Münster, **1993**.
[264] T.-M. Gesing, R. Pöttgen, W. Jeitschko, U. Wortmann, *J. Alloys Compd.* **1992**, *186*, 321 – 331.
[265] R. Pöttgen, T. Gulden, A. Simon, *GIT Labor-Fachz.* **1999**, *43*, 133 – 136.
[266] K. Zeppenfeld, R. Pöttgen, M. Reehuis, W. Jeitschko, R. Behrens, *J. Phys. Chem. Solids* **1993**, *54*, 257 – 261.
[267] U. E. Musanke, W. Jeitschko, M. E. Danebrock, *Z. Anorg. Allg. Chem.* **1993**, *619*, 321 – 326.
[268] M. E. Danebrock, W. Jeitschko, A. M. Witte, R. Pöttgen, *J. Phys. Chem. Solids* **1995**, *56*, 807 – 811.
[269] U. A. Böcker, W. Jeitschko, *J. Alloys Compd.* **1996**, *243*, L8 – L10.
[270] P. Quebe, W. Jeitschko, unpublished results.
[271] O. I. Bodak, E. P. Marusin, *Dopov. Akad. Nauk Ukr. RSR Ser. A* **1979**, 1048 – 1050.
[272] H. Yamane, M. Shimada, F. J. DiSalvo, *J. Mater. Sci. Lett.* **1998**, *17*, 399 – 401.
[273] M. Yano, M. Okamoto, Y. K. Yap, M. Yoshimura, Y. Mori, T. Sasaki, *Diamond Relat. Mater.* **2000**, *9*, 512 – 515.
[274] M. Aoki, H. Yamane, M. Shimada, S. Sarayama, F. J. DiSalvo, *Mater. Lett.* **2002**, *56*, 660 – 664.
[275] M. Aoki, H. Yamane, M. Shimada, S. Sarayama, F. J. DiSalvo, *J. Cryst. Growth* **2002**, *242*, 70 – 76.
[276] M. Onda, T. Iwahashi, M. Okamoto, Y. K. Yap, M. Yoshimura, Y. Mori, T. Sasaki, *J. Cryst. Growth* **2002**, *237–239*, 2112-2115.
[277] S. J. Clarke, F. J. DiSalvo, *J. Alloys Compd.* **1997**, *259*, 158 – 162.
[278] S. J. Clarke, G. R. Kowach, F. J. DiSalvo, *Inorg. Chem.* **1996**, *35*, 7009 – 7012.
[279] H. Yamane, F. J. DiSalvo, *J. Alloys Compd.* **1996**, *241*, 69 – 74.
[280] H. Yamane, F. J. DiSalvo, *J. Alloys Compd.* **1996**, *240*, 33 – 36.
[281] H. Yamane, F. J. DiSalvo, *J. Alloys Compd.* **1996**, *234*, 203 – 206.
[282] G. R. Kowach, H. Y. Lin, F. J. DiSalvo, *J. Solid State Chem.* **1998**, *141*, 1 – 9.
[283] G. R. Kowach, N. E. Brese, U. M. Bolle, C. J. Warren, F. J. DiSalvo, *J. Solid State Chem.* **2000**, *154*, 542 – 550.
[284] H. Yamane, S. Sasaki, S. Kubota, T. Kajiwara, M. Shimada, *Acta Crystallogr. Sect. C* **2002**, *58*, i50 – i52.
[285] A. L. Wayda, J. L. Dye, *J. Chem. Educ.* **1985**, *62*, 356 – 359.
[286] U. Steinbrenner, A. Simon, *Angew. Chem.* **1996**, *108*, 595 – 597; *Angew. Chem. Int. Ed. Engl.* **1996**, *35*, 552 – 554.
[287] U. Steinbrenner, A. Simon, *Z. Anorg. Allg. Chem.* **1998**, *624*, 228 – 232.
[288] G. V. Vajenine, A. Simon, *Eur. J. Inorg. Chem.* **2001**, 1189 – 1193.
[289] G. V. Vajenine, A. Simon, *Angew. Chem.* **2001**, *113*, 4348 – 4351; *Angew. Chem. Int. Ed.* **2001**, *40*, 4220 – 4222.
[290] V. Johnson, *Inorg. Synth.* **1973**, *14*, 182 – 184.
[291] S. Okada, K. Kudou, M. Miyamoto, Y. Hikichi, *Nippon Kagaku Kaishi* **1991**, *12*, 1612 – 1617.
[292] S. Okada, K. Hamano, T. Lundström, I. Higashi, *AIP Conf. Proc.* **1991**, *231*, 456 – 459.
[293] S. Okada, K. Kudou, T. Lundström, *Jpn. J. Appl. Phys.* **1995**, *34*, 226 – 231.
[294] S. Lambert, H. Zhou, J. W. Chen, M. B. Maple, *Physica B + C* **1985**, *135*, 329 – 332.
[295] a) T. Shishido, J. Ye, T. Sasaki, R. Note, K. Obara, T. Takahashi, T. Matsumoto, T. Fukuda, *J. Solid State Chem.* **1997**, *133*, 82 – 87; b) T. Shishido, M. Oku, I. Higashi, S. Okada, K. Kudou, K. Asami, H. Horiuchi, T. Fukuda, *J. Ceram. Soc. Jpn.* **1999**, *107*, 1087 – 1092; c) S. Okada, T. Shishido, K. Kudou, I. Higashi, M. Ogawa, H. Horiuchi, T. Fukuda, *J. Ceram. Soc. Jpn.* **1999**, *107*, 184 – 186.
[296] W. Jeitschko, *Acta Crystallogr. B* **1968**, *24*, 930 – 934.
[297] a) I. R. Fisher, Z. Islam, J. Zarestky, C. Stassis, M. J. Kramer, A. I. Goldman, P. C. Canfield, *J. Alloys Compd.* **2000**, *303–304*, 223 – 227; b) I. R. Fisher, M. J. Kramer, Z. Islam, T. A. Wiener,

 © 2005 Wiley-VCH Verlag GmbH & Co. KGaA, Weinheim

A. Kracher, A. R. Ross, T. A. Lograsso, A. I. Goldman, P. C. Canfield, *Mater. Sci. Eng. A* **2000**, *294*, 10 – 16; c) I. R. Fisher, O. K. Cheon, A. F. Panchula, P. C. Canfield, M. Chernikov, H. R. Ott, K. Dennis, *Phys. Rev. B* **1999**, *59*, 308 – 321; d) I. R. Fisher, Z. Islam, A. F. Panchula, K. O. Cheon, M. J. Kramer, P. C. Canfield, A. I. Goldman, *Philos. Mag. B* **1998**, *77*, 1601 – 1615.

[298] X.-A. Chen, W. Jeitschko, M. E. Danebrock, C. B. H. Evers, K. Wagner, *J. Solid State Chem.* **1995**, *118*, 219 – 226.

[299] X.-A. Chen, W. Jeitschko, *J. Solid State Chem.* **1996**, *121*, 95 – 104.

[300] X.-A. Chen, W. Jeitschko, M. H. Gerdes, *J. Alloys Compd.* **1996**, *234*, 12 – 18.

[301] T. Nasch, W. Jeitschko, *J. Solid State Chem.* **1999**, *143*, 95 – 103.

[302] N. Gross, G. Kotzyba, B. Künnen, W. Jeitschko, *Z. Anorg. Allg. Chem.* **2001**, *627*, 155 – 163.

[303] T. Nasch, W. Jeitschko, U. C. Rodewald, *Z. Naturforsch. B* **1997**, *52*, 1023 – 1030.

[304] N. Gross, T. Nasch, W. Jeitschko, *J. Solid State Chem.* **2001**, *161*, 288 – 293.

[305] N. Gross, G. Block, W. Jeitschko, *Chem. Mater.* **2002**, *14*, 2725 – 2731.

[306] H. Hillebrecht, K. Gebhardt, *Angew. Chem.* **2001**, *113*, 1492 – 1495; *Angew. Chem. Int. Ed.* **2001**, *40*, 1445 – 1447.

[307] a) R. Lux, V. Kuntze, H. Hillebrecht, *Z. Kristallogr.* **2001**, *Suppl. 18*, 107; b) H. Hillebrecht, V. Kuntze, K. Gebhardt, *Z. Kristallogr. Suppl.* **1998**, *15*, 34.

[308] H. Hillebrecht, M. Ade, *Z. Kristallogr. Suppl.* **1998**, *15*, 34.

 © 2005 Wiley-VCH Verlag GmbH & Co. KGaA, Weinheim

Communications

DOI: 10.1002/anie.200501553

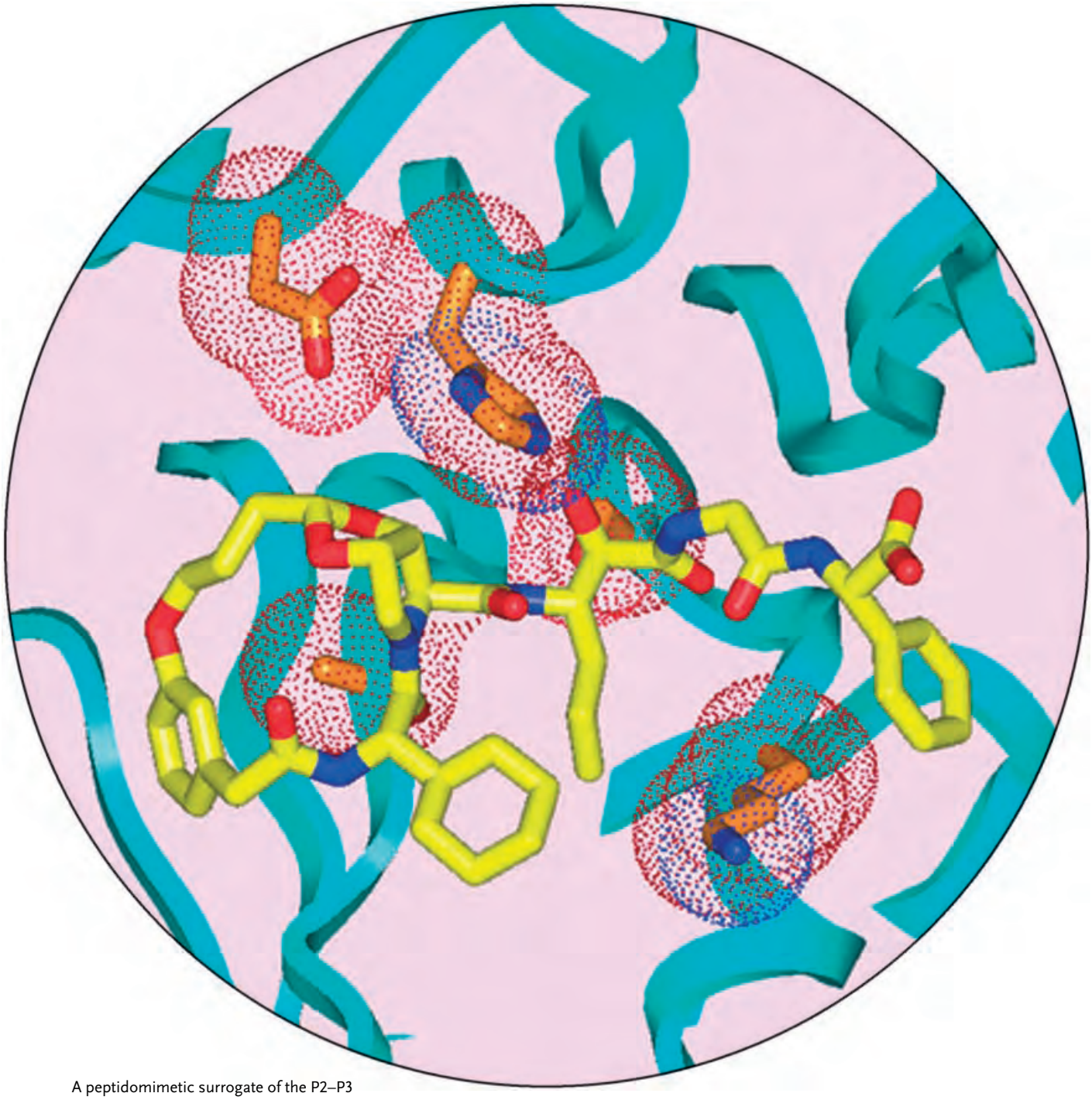

A peptidomimetic surrogate of the P2–P3 dipeptide moiety acts as a potent hepatitis C virus (HCV) inhibitor. This proline-based macrocycle binds tightly with the Ala156 methyl group of HCV NS3 protease while the P2′ phenyl and P1 *n*-propyl groups form a C-shaped clamp around the Lys136 side chain. For more information, see the Communication by K. X. Chen et al. on the following pages.

InterScience
© 2005 Wiley-VCH Verlag GmbH & Co. KGaA, Weinheim

Protease Inhibitors

DOI: 10.1002/anie.200501553

Proline-Based Macrocyclic Inhibitors of the Hepatitis C Virus: Stereoselective Synthesis and Biological Activity

Kevin X. Chen, F. George Njoroge, Bancha Vibulbhan, Andrew Prongay, John Pichardo, Vincent Madison, Alexei Buevich, and Tze-Ming Chan*

The hepatitis C virus (HCV) is the leading cause of chronic liver disease and has infected more than 170 million people worldwide. It has emerged as a major public health threat.[1] Currently, the standard treatment is α-interferon that is attached to polyethylene glycol, in combination with the antiviral agent ribavirin.[2] This therapy is effective only in approximately 50% of patients and has considerable associated side effects. Given the prevalence of HCV infections, there is an urgent need to develop more-effective, less-toxic, and orally bioavailable small-molecule antiviral agents.

HCV is a single-stranded RNA genome that encodes a polyprotein of about 3000 amino acids. The polyprotein is processed into structural and nonstructural (NS) proteins by host peptidases and virally encoded proteases. The NS3 protease, located towards the N-terminal side of the NS3 protein, is a chymotrypsin-like serine protease.[3] As a result of its essential role in HCV replication, it has been an attractive target for intensive research for new anti-HCV therapy.[4] However, the fact that the NS3 protease has a shallow and solvent-exposed substrate-binding region makes it a formidable task to develop apropriate small-molecule inhibitors.[5]

During the course of our research in potency optimization and structure depeptization of peptide-based substrates of HCV NS3 protease,[6] we were interested in the incorporation of macrocyclic structures into our target molecules. The bicyclic-acetal proline-based macrocycle **9** (Scheme 2) was designed as a peptidomimetic surrogate for the P2–P3 dipeptide moiety on the substrate. We envisioned that the additional contact of the macrocycle with the Ala156 methyl group of the enzyme backbone would enhance binding of the inhibitors. We anticipated two major challenges in the synthesis: first, the stereoselective construction of 3,4-proline cyclic acetal core 3 (Scheme 1), and second, macrocyclization to the 17-membered ring **9**. The former could be achieved through an acid-catalyzed reaction between an aldehyde (or acetal) and 3,4-dihydroxyproline, and the latter through aryl alkyl ether formation under Mitsunobu reaction conditions.[7]

The synthesis started with osmium-catalyzed dihydroxylation of commercially available *N*-Boc-3,4-dehydroproline methyl ester (**1**; Scheme 1), to give an inseparable mixture of

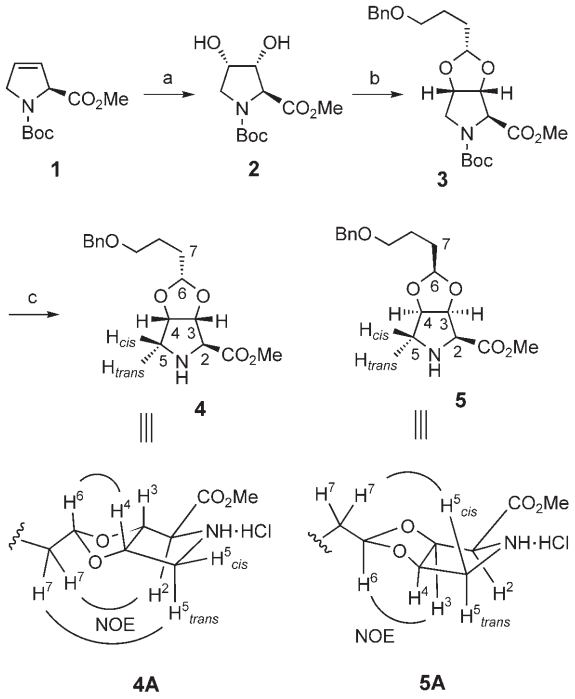

1 **2** **3** **4** **5** **4A** **5A**

Scheme 1. a) OsO_4, NMO, *t*BuOH/H_2O/acetone/THF, RT, 77%; b) $BnO(CH_2)_3CHO$, *p*-TsOH, $MgSO_4$, CH_2Cl_2, RT, 91%; c) HCl (2 M, dioxane/EtOAc, RT, quant. NMO = *N*-methylmorpholine *N*-oxide, Boc = *tert*-butyloxycarbonyl, *p*-TsOH = *p*-toluenesulfonic acid.

3*S*,4*R*-diol **2** (major) and 3*R*,4*S*-diol (minor, structure not shown).[8] Both diols were then treated with 4-benzyloxybutyraldehyde in the presence of a catalytic amount of *p*-TsOH.[9] The product **3**, and its isomer were isolated as a mixture in excellent yield (91%) when 2 equivalents of the aldehyde were used. The two isomers could be separated in a ratio of 2:1, respectively, by column chromatography. 2D ^{1}H NMR spectroscopy experiments were conducted to determine the absolute configuration of the products and the stereochemical outcome of the acetal formation. To avoid interference from rotamers in **3**, it was necessary to perform the ^{1}H NMR spectroscopic analysis on amine **4** instead. The Boc protecting group was removed selectively in the presence of acid-sensitive acetal functionality when **3** was treated with hydrochloric acid (2 M). NOSEY experiments on compound **4** revealed the presence of NOE interactions between 6-H and 4-H, 7-H and 2-H, and 7-H and 5-H_{trans}. However, there was no observed coupling between protons 2-H and 3-H, which therefore indicates a *trans* relationship. This evidence led to the structural assignment of **4**, with **4A** as its preferred conformation. On the other hand, the amine derived from the minor isomer demonstrated NOE signals between 7-H and 5-H_{cis} as well as 6-H and 3-H, but not between 7-H and 2-H. The coupling constant between 2-H and 3-H ($J = 5.2$ Hz) suggests

[*] Dr. K. X. Chen, Dr. F. G. Njoroge, B. Vibulbhan, Dr. A. Prongay, J. Pichardo, Dr. V. Madison, Dr. A. Buevich, Dr. T.-M. Chan
Schering-Plough Research Institute
2015 Galloping Hill Road, K-15-3/3545, Kenilworth, NJ 07033 (USA)
Fax: (+1) 908-740-7152
E-mail: kevin.chen@spcorp.com

Supporting information for this article is available on the WWW under http://www.angewandte.org or from the author.

 © 2005 Wiley-VCH Verlag GmbH & Co. KGaA, Weinheim

a *cis* relationship. As a result, the structure **5** and its preferred conformation **5A** was assigned. Significantly, the formation of the acetal with both 3*S*,4*R*- and 3*R*,4*S*-dihydroxyprolines led exclusively to the *endo* products.[10]

Once the stereochemistry was established, amine **4** was then coupled to *N*-Boc-cyclohexylglycine under standard conditions to give dipeptide **6** (Scheme 2). Selective removal

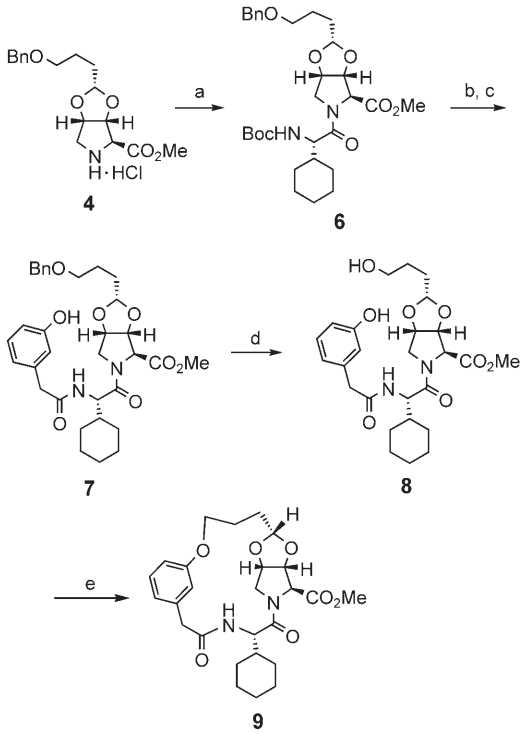

Scheme 2. a) *N*-Boc-Chg-OH, HATU, iPr$_2$NEt, CH_2Cl_2, 0 °C→RT, 76%; b) HCl (2 M), dioxane/EtOAc, RT, quant.; c) 3-OH-PhCO$_2$H, HATU, iPr$_2$NEt, CH_2Cl_2, 0 °C to RT, 98%; d) H_2, Pd C 10%, EtOH/EtOAc, RT, quant.; e) PPh_3, ADDP, CH_2Cl_2, RT, 72%. Chg-OH = cyclohexylglycine, HATU = *O*-(7-azabenzotriazol-1-yl)-*N*,*N*,*N*′*N*′-tetramethyluronium hexafluorophosphate, ADDP = 1,1′-(azodicarbonyl)dipiperidine.

of the Boc protecting group and subsequent coupling with 3-hydroxyphenylacetic acid provided compound **7**. Cleavage of the benzyl ether gave the phenol alcohol **8**, which is the substrate for the key Mitsunobu macrocyclization reaction.[11] Treatment of **8** with triphenylphosphane and 1,1′-(azodicarbonyl)dipiperidine furnished the desired macrocycle **9** in excellent yield (72%).

The "right-hand" segment (P1–P2′) of the molecule was prepared through a series of peptide couplings and deprotections, starting with α-hydroxy-β-amino acid norvaline (Nva) and norleucine (Nle) derivatives[12] (**10** and **15**, respectively; Scheme 3). The hydrochloride intermediates of the tripeptide amines **12**, **13**, **16**, and allyl amide amine **14** were obtained as mixtures of four diastereomers.

Finally, the macrocyclic "left-hand" segment and the α-hydroxyamide "right-hand" moiety were combined (Scheme 4). The methyl ester **9** was hydrolyzed to the carboxylic acid **17**, which was then coupled with amines **12**–**14** and **16**. The resulting hydroxyamides were oxidized to the

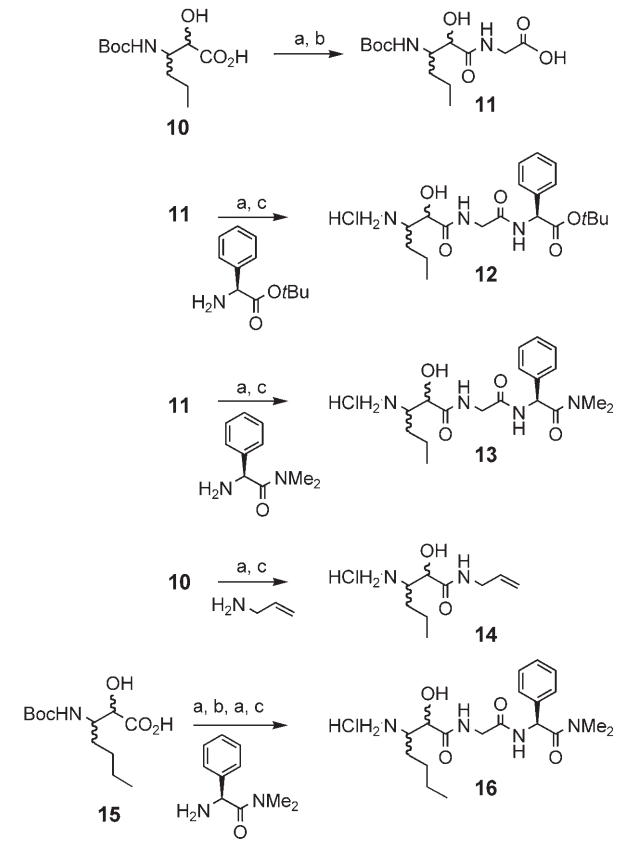

Scheme 3. a) respective amine, DhBtOH, $ClCH_2CH_2Cl$, NMM, DMF/CH_2Cl_2, −20 °C, 65–95%; b) H_2, Pd-C, EtOH, RT, 98%; c) 2 M HCl, dioxane/EtOAc, RT, quant. DhBtOH = 3,4-dihydro-3-hydroxy-4-oxo-1,2,3-benzotriazine, NMM = *N*-methylmorpholine, DMF = *N*,*N*-dimethylformamide.

corresponding α-ketoamides by using Dess–Martin periodinane.[13] The products were mixtures of two diastereomers at the P1–Nva/Nle α center. The *tert*-butyl ester isomers **18** and **21** and the dimethyl amides **20** and **23**, were separated. Treatment of **18** and **21** with TFA gave carboxylic acids **19** and **22**, respectively. The allyl amide **24** and the P1–Nle analogue **25** were an inseparable mixture of diastereomers.

All macrocyclic inhibitors **18**–**25** were tested in an HCV continuous assay[14] (Table 1). The inhibition constants (K_i^*) were determined by using NS4A-tethered single-strain NS3 serine protease.[15] The K_i^* values for compounds **18**, **19**, and **20** were 0.81, 0.36, and 0.21 μM, respectively. However, the opposite diastereomers **21**, **22**, and **23** were much more potent (K_i^* = 0.038, 0.038, and 0.044 μM, respectively). Based on the structure–activity relationship results from our acyclic peptide HCV protease inhibitors,[16] the more potent compounds **21**–**23** were assigned the *S* configuration at P1 and the less potent compounds **18**–**20** the *R* configuration. The P1–Nle analogue **25** was equally potent (0.076 μM) considering it was a mixture of two isomers, whereas the smaller tripeptide inhibitor **24** was only moderately active (3.1 μM).

The selectivity of these inhibitors against human neutrophil elastase (HNE), a structurally closely related serine protease, was also measured (Table 1). Compounds **18**–**23** were moderately selective against elastase (HNE/HCV =

 © 2005 Wiley-VCH Verlag GmbH & Co. KGaA, Weinheim

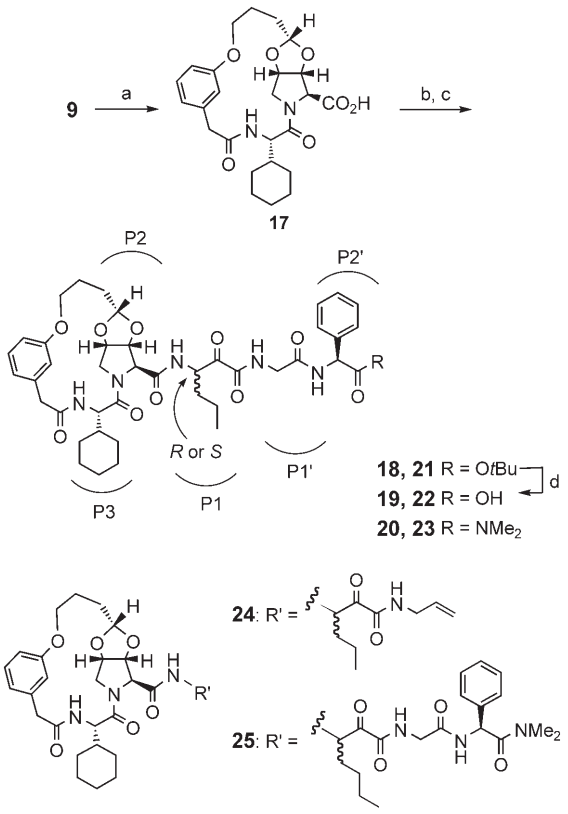

Scheme 4. a) LiOH, MeOH/THF/H_2O, RT, 93%; b) **12–14** or **16**, DhBtOH, EDC, NMM, DMF/CH_2Cl_2, −20°C, 50–85%; c) Dess–Martin periodinane, CH_2Cl_2, RT, 51–89%; d) TFA, CH_2Cl_2, RT, quant. TFA = trifluoroacetic acid

Table 1: Potency and selectivity of compounds **18–25** against HCV protease.

Compound	R	P1	K_i^*[μM]	HNE/HCV
18	O*t*Bu	(*R*)-Nva	0.81 ± 0.04	6
19	OH	(*R*)-Nva	0.36 ± 0.03	11
20	NMe_2	(*R*)-NVa	0.21 ± 0.04	32
21	O*t*Bu	(*S*)-Nva	0.038 ± 0.001	3
22	OH	(*S*)-Nva	0.038 ± 0.001	4
23	NMe_2	(*S*)-Nva	0.044 ± 0.009	5
24	–	(*R*,*S*)-Nva	3.1 ± 0.3	–
25	NMe_2	(*R*,*S*)-Nle	0.076 ± 0.006	383

3:32), whereas the P1–Nle derivative **25** was highly selective (383-fold). This indicates that the P1 residue plays an important role in selectivity. Pharmacokinetic (PK) studies in rats showed that compound **23** had a low oral AUC (area under the curve) value (0.1 μM h@3 mpk) and bioavailability (0.3%), whereas compound **24** gave a respectable AUC value (2.6 μM h). Presumably, the smaller size and fewer amide bonds of **24** contributed to the improved PK profile. The solubility of **18–23** in pH 7.4 buffer was in the range of 5–80 μM, with **19** and **20** at the higher end and **18**, **21, 22**, and **23** at the lower end.

The X-ray crystallography structure of compound **22** bound to the active site of HCV protease was obtained (Figure 1). It confirmed the absolute configurations at both

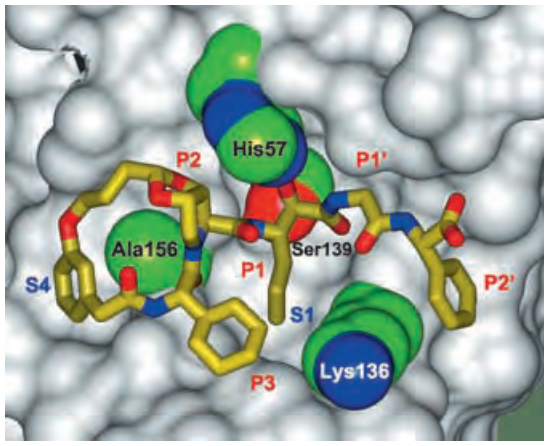

Figure 1. The X-ray crystal structure of compound **22** bound to HCV protease.

the acetal center and the P1 α center. As expected a reversible covalent-bond formation occurred between the carbonyl group of the ketone and the hydroxyl group of Ser139. Most importantly, the 17-membered macrocycle formed a perfect "donut" that surrounded the Ala156 methyl group. The P1 *n*-propyl side chain was buried in the S1 pocket and a "C"-shaped clamp was formed around the side chain of Lys136 along with the P2′ phenyl group. The P2 bicyclic praline derivitive, the P3 cyclohexyl ring and the phenyl group in the macrocycle all had hydrophobic interactions with the protein surface. Furthermore, there were several hydrogen bonds between the inhibitor peptide chain and that of the enzyme backbone. All these interactions contributed to the excellent potency of **22**.

In summary, a concise and highly stereoselective synthesis of the 17-membered macrocycle **9** was completed and the *endo* product was shown to form exclusively at the acetal center of the bicyclic proline core. The key macrocyclization provided excellent yields through a Mitsunobu protocol. The resultant macrocyclic inhibitors were active against HCV NS3 serine protease with the (*S*)-P1 isomers being the more potent. The X-ray crystal structure of compound **22** bound to the enzyme revealed that the macrocycle formed good contact with the enzyme by adopting a "donut"-shaped conformation above the methyl group of Ala156. Further evaluation of these compounds and the design of inhibitors with better potency and PK profiles are currently in progress.

Received: May 6, 2005
Revised: August 14, 2005
Published online: October 7, 2005

Keywords: antiviral agents · inhibitors · macrocycles · peptides · proteases

[1] J. Cohen, *Science* **1999**, *285*, 26.
[2] a) A. U. Neumann, N. P. Lam, H. Dahari, D. R. Gretch, T. E. Wiley, T. J. Layden, A. S. Perelson, *Science* **1998**, *282*, 103; b) A. M. Di Bisceglie, J. McHutchison, C. M. Rice, *Hepatology* **2002**, *35*, 224.
[3] A. M. Lesk, W. D. Fordham, *J. Mol. Biol.* **1996**, *258*, 501.

 © 2005 Wiley-VCH Verlag GmbH & Co. KGaA, Weinheim

[4] a) S.-L. Tan, Y. He, Y. Huang, M. Gale, Jr., *Curr. Opin. Pharmacol.* **2004**, *4*, 465; b) C. Steinkuhler, U. Koch, F. Narjes, V. G. Matassa, *Curr. Med. Chem.* **2001**, *8*, 919; c) S. Colarrusso, U. Koch, B. Gerlach, C. Steinkuhler, R. De Francesco, S. Atlamura, V. G. Matassa, F. Narjes, *J. Med. Chem.* **2003**, *46*, 345; d) M. Llinas-Brunet, M. D. Bailey, E. Ghiro, V. Gorys, T. Halmos, M. Poirier, J. Rancourt, N. Goudreau, *J. Med. Chem.* **2004**, *47*, 6584; e) Y. S. Tsantrizos, G. Bolger, P. Bonneau, D. R. Cameron, N. Gordreau, G. Kukolj, S. R. LaPlante, M. Llinas-Brunet, H. Nar, D. Lamarre, *Angew. Chem.* **2003**, *115*, 1394; *Angew. Chem. Int. Ed.* **2003**, *42*, 1355; f) E. S. Priestley, I. De Lucca, B. Ghavimi, S. Erickson-Viitanen, *Bioorg. Med. Chem. Lett.* **2002**, *12*, 3199.

[5] A. D. Kwong, J. L. Kim, G. Rao, D. Lipovsek, S. A. Raybuck, *Antiviral Res.* **1998**, *40*, 1.

[6] M. Llinas-Brunet, M. D. Bailey, G. Fazal, S. Goulet, T. Halmos, S. R. LePlante, R. Maurice, M. Poirier, M.-A. Poupart, D. Thibeault, D. Wernic, D. Lamarre, *Bioorg. Med. Chem. Lett.* **1998**, *8*, 1713.

[7] a) D. L. Hughes, *Org. React.* **1992**, *42*, 335; b) O. Mitsunobu, *Synthesis* **1981**, 1.

[8] G. Guillerm, M. Varkados, S. Auvin, F. Le Goffic, *Tetrahedron Lett.* **1987**, *28*, 535.

[9] M. H. Hopkins, L. E. Overman, G. M. Rishton, *J. Am. Chem. Soc.* **1991**, *113*, 5354.

[10] a) M. Garcia-Valverde, R. Pedrosa, M. Vincente, *Tetrahedron: Asymmetry* **1995**, *6*, 1787; b) X. Ariza, A. M. Costa, M. Faja, O. Pineda, J. Vilarrasa, *Org. Lett.* **2000**, *2*, 2809; c) P. T. Kaye, W. E. Molema, *Synth. Commun.* **1999**, *29*, 1889.

[11] K. X. Chen, F. G. Njoroge, B. Vibulbhan, A. Buevich, T.-M. Chan, V. Girijavallahan, *J. Org. Chem.* **2002**, *67*, 2730.

[12] S. L. Harbeson, S. M. Abelleira, A. Akiyama, R. Barrett, R. M. Carroll, J. A. Straub, J. N. Tkacz, C. Wu, G. F. Musso, *J. Med. Chem.* **1994**, *37*, 2918.

[13] D. B. Dess, J. C. Martin, *J. Am. Chem. Soc.* **1991**. *113*, 7277.

[14] R. Zhang, B. M. Beyer, J. Durkin, R. Ingram, F. G. Njoroge, W. T. Windsor, B. A. Malcolm, *Anal. Biochem.* **1999**, *270*, 268.

[15] S. S. Taremi, B. Beyer, M. Maher, N. Yao, W. Prosise, P. C. Weber, B. A. Malcolm, *Protein Sci.* **1998**, *7*, 2143.

[16] Unpublished results from the Schering-Plough Research Institute.

 © 2005 Wiley-VCH Verlag GmbH & Co. KGaA, Weinheim

Homochirality

DOI: 10.1002/anie.200502388

The Origin of Stereoselectivity in Primary Amino Acid Catalyzed Intermolecular Aldol Reactions**

Arianna Bassan, Weibiao Zou, Efraim Reyes, Fahmi Himo, and Armando Córdova**

The asymmetric amino acid catalyzed aldol reaction is plausibly an ancient transformation,[1] which enzymes have catalyzed for billions of years. These enzyme-catalyzed stereoselective aldol reactions involve enamine intermediates (type I aldolases) or zinc enolates (type II aldolases) as the reactive nucleophile.[2] The catalytic residue of type I aldolases is the primary amino group of a lysine moiety, which forms enamine intermediates with the help of a proton relay system by neighboring amino acids.[2c]

The ability of amino acids to catalyze the asymmetric aldol reaction was discovered in the 1970s by Hajos and Parrish[3] and Wiechert and co-workers,[4] and amino acid mediated stereoselective Robinson annulations were utilized numerous times in natural-product synthesis.[5] In 2000, List and co-workers demonstrated that proline and its derivatives can be used as catalysts for intermolecular asymmetric aldol reactions between ketones and aldehydes with moderate-to-excellent enantioselectivities.[6–7] Both the proline-catalyzed intramolecular and intermolecular aldol reactions involve an enamine mechanism, in which one proline molecule takes part in the transition state, as established by Houk, List, and co-workers.[8]

We recently found that acyclic amino acids and their derivatives are able to catalyze asymmetric intermolecular aldol reactions with high stereoselectivity.[1b,9] For example, simple natural and unnatural primary amino acid derivatives catalyzed the reaction between cyclohexanone **1** and an

[*] Prof. Dr. F. Himo
Department of Theoretical Chemistry
The Royal Institute of Technology
ALBANOVA, 10691 Stockholm (Sweden)
E-mail: himo@teochem.kth.se
Dr. W. Zou, E. Reyes, Prof. Dr. A. Córdova
Department of Organic Chemistry
Arrhenius Laboratory
Stockholm University
10691 Stockholm (Sweden)
Fax: (+46) 815-4908
E-mail: acordova1a@netscape.net
E-mail: acordova@organ.su.se
Dr. A. Bassan
Stockholm University
Department of Physics
ALBANOVA, 106 91 Stockholm (Sweden)

[**] A.C. and F.H. gratefully acknowledge the Swedish National Research Council, Lars-Hierta Foundation, and Wenner Gren-Foundations for financial support.

Supporting information for this article is available on the WWW under http://www.angewandte.org or from the author.

© 2005 Wiley-VCH Verlag GmbH & Co. KGaA, Weinheim

aldehyde in high yield and with up to >99% *ee* [Eq. (1); amino acid: (*S*)-alanine, (*S*)-aminobutyric acid, (*S*)-valine, (*S*)-asparatate, (*S*)-isoleucine, (*S*)-serine].[9]

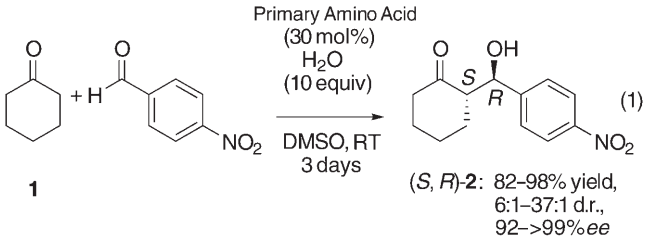

Intrigued by the enzyme-like enantioselectivity of the acyclic amino acid catalyzed asymmetric aldol reaction, we became interested in unraveling the origins of its stereoselectivity. The origin of the stereoselectivity of acyclic amino acids is of great importance in understanding the origins of biological homochirality and the evolution of the catalytic mechanism of aldolase enzymes. In addition, the information gathered can aid the development of new organocatalysts.

Herein, we present how theoretical and experimental data can be combined to understand the stereochemistry of primary amino acid catalyzed intermolecular aldol reactions that involve enamine intermediates. We show that calculations provide key insight, not yet accessible by other means, into the mechanism and accurately predict the stereochemistry of the observed product.

We initially investigated the relationship between the enantiomeric excess of aldol product **2**, derived from the aldol reaction shown in Eq. (1), and the optical purity of the simplest chiral amino acid catalyst, (*S*)-alanine. Plotting the enantiomeric excess of alanine versus that of β-hydroxy ketone **2** showed a linear correlation (Figure 1).

Our results support the supposition that only one alanine molecule takes part in the transition state of the primary amino acid catalyzed asymmetric aldol reactions. This correlation together with previous theoretical findings by Houk and co-workers for proline-catalyzed aldol reactions[8] suggests that three possible mechanisms may describe the primary amino acid catalyzed asymmetric aldol reactions: the carboxylic acid catalyzed enamine mechanism, the amino catalyzed enamine mechanism, and the enaminium catalyzed mechanism (Scheme 1).

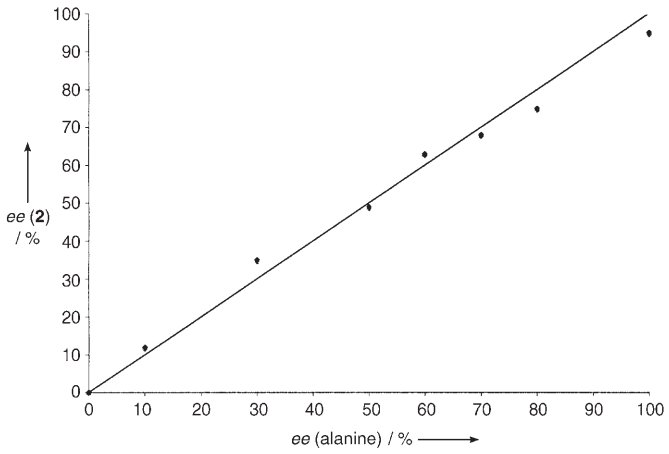

Figure 1. Relation between the enantiomeric excess of (*S*)-alanine and that of the aldol product **2** in the catalytic intermolecular asymmetric synthesis of **2**.

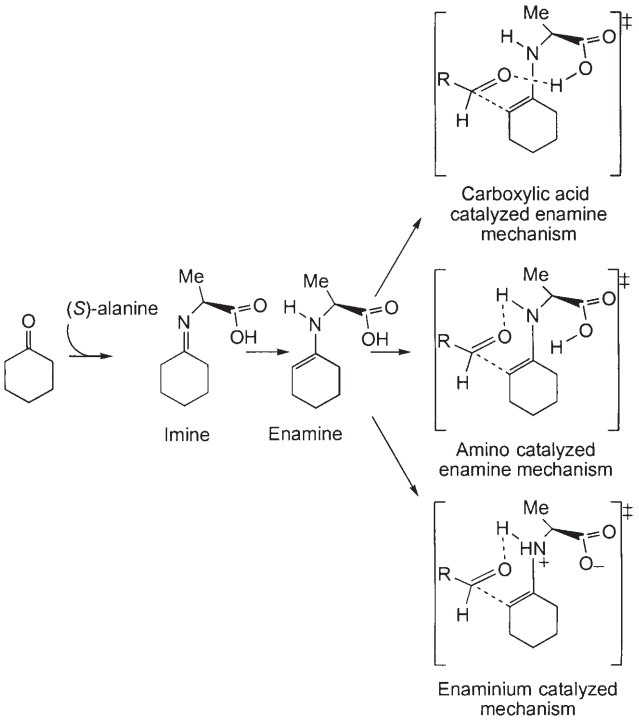

Scheme 1. The three possible mechanisms in the alanine-mediated aldol reaction which involve an enamine intermediate.

We then performed density functional theory (DFT) calculations on the alanine-catalyzed aldol reaction with **1** as the donor and benzaldehyde as the acceptor species. More specifically, we focused our attention on the nucleophilic attack of the enamine/enaminium moiety on the carbonyl group (see Scheme 1), as this step governs the configuration of the product, and located the possible transition-state structures associated with the C–C bond formation. Calculations indicate that the most accessible pathway corresponds to the enamine-catalyzed reaction, in which the C–C bond formation is coupled with proton transfer from the carboxylic group of the alanine moiety to the developing alkoxide (Scheme 1). Primary amino acids lead to an enamine intermediate that can rotate about the C_α–N bond in contrast to the corresponding proline-derived enamine intermediate, and thus more transition-state structures have to be envisioned. As shown in Scheme 2, different transition-state orientations that generate products with different configurations have been considered. For each of the eight orientations shown in Scheme 2, two possible proton-transfer arrangements have been studied together with two different conformations of the enamine ring, thus giving a total of 32 transition states. As an example, four transition-state structures that lead to the same *S*,*R* product are shown in Figure 2 (more transition-state structures are given in the Supporting Information).

Figure 3 shows the four transition-state structures that generate the four different stereoisomers with the lowest energy barriers. Among these four transition states, the one

 © 2005 Wiley-VCH Verlag GmbH & Co. KGaA, Weinheim

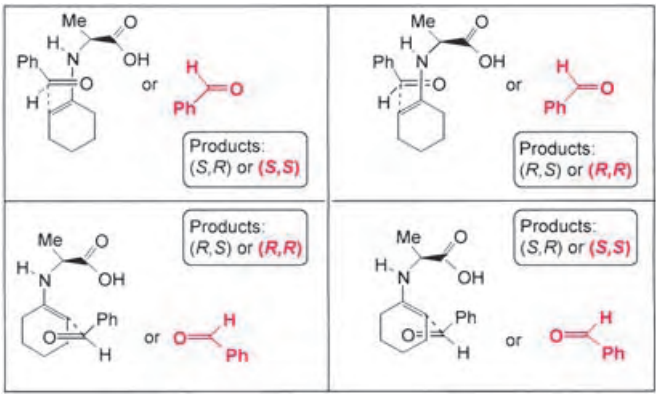

Scheme 2. Transition-state arrangements that generate different diastereoisomers in the alanine-catalyzed aldol reaction between cyclohexanone and benzaldehyde.

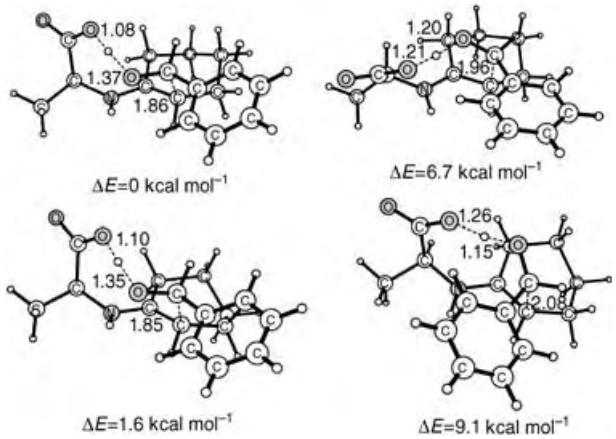

Figure 2. Four possible transition-state structures that generate the *S*,*R* product. They differ in the proton-transfer arrangement and the conformation of the enamine ring. Relative energies and relevant geometric parameters are shown (in Å).

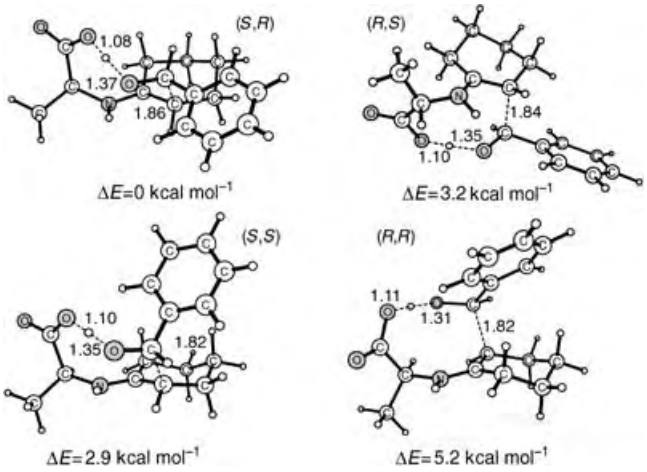

Figure 3. The energetically most accessible transition-state structures that lead to the four different diastereoisomers. Relative energies and relevant geometric parameters are shown (in Å).

that requires the lowest activation energy leads to the *S*,*R* enantiomer, which is indeed the product observed experimentally. The *R*,*S* enantiomer is formed through a transition-state structure that lies 3.2 kcal mol^{-1} higher in energy, which is in accordance with the experimental results (> 90 % *ee*).[9] The *S*,*S* enantiomer also requires a higher energy barrier (2.9 kcal mol^{-1}), thus explaining the high *anti* diastereoselectivity (d.r. > 10:1).

Scrutiny of the geometrical arrangements of the low-lying transition-state structures that lead to the different products (as shown in Figure 3) allows us to identify a few effects that contribute to the stereoselectivity of the reaction. First, it can be noticed that the electrostatic hydrogen-bonding interaction between the amino group and the developing alkoxide moiety plays an important role. The hydrogen bond (NH···O) is relatively short (about 2 Å) for the three lowest transition-state structures in Figure 3 (those that lead to the *S*,*R*-, *R*,*S*-, and *S*,*S*-enantiomeric products). This hydrogen-bonding interaction is absent in the transition-state structure that leads to the *R*,*R* product and in general in most of the transition-state structures with higher energies (see the Supporting Information). Another factor that regulates the stereoselectivity is the steric repulsion between the phenyl and cyclohexyl rings in the transition state. Accordingly, the eclipsed conformation of the phenyl and cyclohexyl rings in the transition state that leads to the *S*,*S* product results in higher energy relative to the *S*,*R* transition state, in which the two rings are in a staggered conformation instead. Finally, the methyl substituent of (*S*)-alanine interacts unfavorably with the cyclohexyl ring, thus leading to the higher energy of the *R*,*S* transition state relative to the *S*,*R* structure, in which the methyl group points away from the cyclohexyl moiety. The interplay between these effects ultimately determines the relative energies of the various transition states and, thus, drives the stereoselectivity of the primary amino acid catalyzed intermolecular aldol reaction.

The energy diagram associated with the formation of the observed product, the *S*,*R* enantiomer (see Figure 4), shows that the nucleophilic attack is slightly endothermic and, thus, reversible.

The other two mechanisms investigated herein, the enaminium- and the amino-catalyzed mechanisms, are presented in Scheme 1. In the calculations that involve zwitterionic-like structures, geometric optimizations in a dielectric

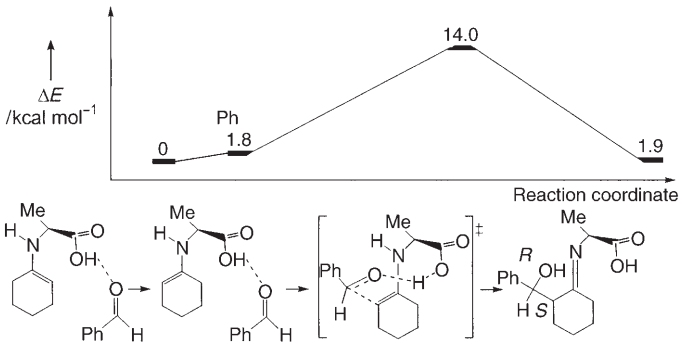

Figure 4. The energy diagram associated with the formation of the *S*,*R* product. For convenience, the neutral intermediate, and not the zwitterionic-type structure, has been optimized.

 © 2005 Wiley-VCH Verlag GmbH & Co. KGaA, Weinheim

continuum medium were necessary to fully optimize the transition-state structures (more details of the calculations are described in the Experimental Section). The two alternative mechanisms require activation energies much higher than the corresponding energies of the carboxylic acid catalyzed enamine mechanism at the same level of theory (see details in the Supporting Information). The higher energy barriers, as found by computation (higher than 15 kcal mol^{-1}, as described in the Supporting Information), allow us to safely dismiss the enaminium- as well as the amino-catalyzed mechanisms in the alanine-catalyzed aldol reaction and, by extension, for the other primary amino acids as well.

The acyclic amino acid catalyzed aldol reaction is significantly accelerated by a small amount of water.[9] We therefore performed NMR spectroscopic analysis according to List et al.[7j] to reveal the possible presence of oxazolidinone intermediates formed between the ketone donor and alanine, which would thus reduce the enamine concentration and lead to a decrease in the reaction rate (Scheme 3). The

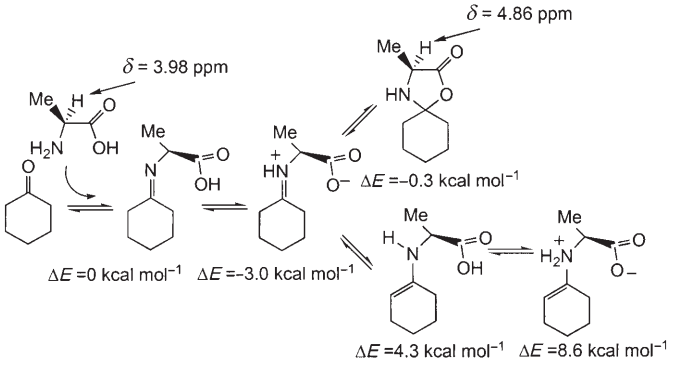

Scheme 3. Relative energies of different intermediates and of the oxazolidinone inhibitor in the alanine-mediated aldol reaction occurring by an enamine pathway.

formation of the oxazolidinone was indicated by a change in the chemical shift of the α proton of alanine from $\delta = 3.98$ to 4.86 ppm. In addition, calculations were made to shed light on the NMR spectral data. The computed relative energies of the imine, iminium, enamine, enaminium, and oxazolidinone moieties show that the formation of oxazolidinone from the imine functionality is a slightly exothermic and, thus, more favorable process (see Scheme 3). Moreover, the oxazolidinone lies lower in energy than the enamine, which is the reactive nucleophile in the aldol reaction. Hence, the competing oxazolidinone reaction may explain why the primary amino acid catalyzed aldol reactions are very slow in the absence of a few equivalents of water.[9]

In summary, our DFT calculations, supported by additional experimental data, provide a key basis for understanding primary amino acid intermolecular aldol reactions in which only one amino acid molecule is involved in the transition state. We showed for alanine that the carboxylic acid catalyzed enamine mechanism is more favorable than other mechanisms because it requires the lowest activation energy. Furthermore, the calculations demonstrate that such a mechanism accurately predicts the proper stereochemistry of the reaction.

Experimental Section

All ground-state and transition-state geometries were optimized by using hybrid density functional theory[10] and a standard double zeta plus polarization basis set (B3LYP/6-31G(d,p)) with the Gaussian03 software package.[11] Final energies for the fully optimized structures were obtained by using the larger basis set 6-311 + (2d,2p) and were corrected for zero-point effects derived from frequency analysis at the B3LYP/6-31G(d,p) level of theory. When zwitterionic-like structures were involved, geometry optimizations and frequency calculations were performed in the presence of a solvent by using the CPCM polarizable conductor calculation model ($\varepsilon = 36.5$);[12] the radii derived from the UFF force field were employed to build the cavity. This procedure was adopted in the evaluation of the energies of the imine, iminium, enamine, enaminium, and oxazolidinone moieties (Scheme 3), and in the investigation of the enaminium-catalyzed mechanism (see the Supporting Information); for comparison, it was also used for the amino-catalyzed enamine mechanism. To test the solvent effects in the carboxylic acid catalyzed enamine mechanism and to compare the energies of the three different mechanisms, three transition-state structures from the carboxylic acid catalyzed enamine mechanism (those with the lowest energy barrier) were reoptimized in the presence of the solvent. Their relative energies were not significantly affected by the different optimization procedure (see Figure 3 and the Supporting Information).

Received: July 8, 2005

Keywords: aldol reaction · amino acids · asymmetric catalysis · density functional calculations · transition states

[1] a) S. Pizzarello, A. L. Weber, *Science* **2004**, *303*, 1151; b) A. Córdova, I. Ibrahem, J. Casas, H. Sundén, M. Engqvist, E. Reyes, *Chem. Eur. J.* **2005**, *11*, 4772; c) A. Córdova, M. Engqvist, I. Ibrahem, J. Casas, H. Sundén, *Chem. Commun.* **2005**, 2047; d) J. Kofoed, M. Machuqueiro, J.-L. Reymond, T. Darbre, *Chem. Commun.* **2004**, *26*, 1540.

[2] a) W.-D. Fessner in *Stereoselective Biocatalysis*; (Ed.: R. N. Patel), Marcel Dekker, New York **2000**, p. 239; b) T. D. Machajewski, C.-H. Wong, *Angew. Chem.* **2000**, *112*, 1406; *Angew. Chem. Int. Ed.* **2000**, *39*, 1352; c) A. Heine, G. DeSantis, J. G. Luz, M. Mitchell, C.-H. Wong, I. A. Wilson, *Science* **2001**, *294*, 369.

[3] a) Z. G. Hajos, D. R. Parrish, German Patent DE 2102623, July 29, **1971**; b) Z. G. Hajos, D. R. Parrish, *J. Org. Chem.* **1974**, *39*, 1615.

[4] a) U. Eder, G. Sauer, R. Wiechert, German Patent DE 2014757, Oct. 7, **1971**; b) U. Eder, G. Sauer, R. Wiechert, *Angew. Chem.* **1971**, *83*, 492; *Angew. Chem. Int. Ed. Engl.* **1971**, *10*, 496.

[5] a) S. Danishefsky, P. Cain, *J. Am. Chem. Soc.* **1975**, *97*, 5282; b) I. Shimizu, Y. Naito, J. Tsuji, *Tetrahedron Lett.* **1980**, *21*, 4975; c) H. Hagiwara, H. Uda, *J. Org. Chem.* **1988**, *53*, 2308; d) E. J. Corey, S. C. Virgil, *J. Am. Chem. Soc.* **1990**, *112*, 6429.

[6] B. List, R. A. Lerner, C. F. Barbas III, *J. Am. Chem. Soc.* **2000**, *122*, 2395; W. Notz, B. List, *J. Am. Chem. Soc.* **2000**, *122*, 7386.

[7] For reviews, see: a) P. I. Dalko, L. Moisan, *Angew. Chem.* **2001**, *113*, 3840; *Angew. Chem. Int. Ed.* **2001**, *40*, 3726; b) B. List, *Tetrahedron* **2002**, *58*, 5573; c) P. I. Dalko, L. Moisan, *Angew. Chem.* **2004**, *116*, 5248; *Angew. Chem. Int. Ed.* **2004**, *43*, 5138; see, also; d) B. List, P. Pojarliev, C. Castello, *Org. Lett.* **2001**, *3*, 573; e) K. S. Sakthivel, W. Notz, T. Bui, C. F. Barbas III, *J. Am. Chem. Soc.* **2001**, *123*, 5260; f) A. Córdova, W. Notz, C. F. Barbas III, *Chem. Commun.* **2002**, *67*, 3034; g) A. Córdova, W. Notz, C. F. Barbas III, *J. Org. Chem.* **2002**, *67*, 301; h) A. B. Northrup, D. W. C. MacMillan, *J. Am. Chem. Soc.* **2002**, *124*, 6798; i) A. Bøgevig, N. Kumaragurubaran, K. A. Jørgensen,

 © 2005 Wiley-VCH Verlag GmbH & Co. KGaA, Weinheim

Chem. Commun. **2002**, 620; j) B. List, L. Hoang, H. J. Martin, *Proc. Natl. Acad. Sci. USA* **2004**, *101*, 5839; k) A. I. Nyberg, A. Usano, P. Pihko, *Synlett* **2004**, 1891.

[8] a) S. Bahmanyar, K. N. Houk, *J. Am. Chem. Soc.* **2001**, *123*, 12911; b) S. Bahmanyar, K. N. Houk, *J. Am. Chem. Soc.* **2001**, *123*, 11273; c) S. Bahmanyar, K. N. Houk, H. J. Martin, B. List, *J. Am. Chem. Soc.* **2003**, *125*, 2475; d) L. Hoang, S. Bahmanyar, K. N. Houk, B. List, *J. Am. Chem. Soc.* **2003**, *125*, 16; e) F. R. Clemente, K. N. Houk, *Angew. Chem.* **2004**, *116*, 5890; *Angew. Chem. Int. Ed.* **2004**, *43*, 5766; f) K. N. Rankin, J. W. Gauld, R. Boyd, *J. Phys. Chem. A* **2002**, *106*, 5155; g) C. Alleman, R. Gordillo, F. R. Clemente, P. H.-Y. Cheong, K. N. Houk, *Acc. Chem. Res.* **2004**, *37*, 558; after our submission an excellent paper appeared that includes DFT calculations of the acyclic amino acid catalyzed intramolecular aldol reaction: F. R. Clemente, K. N. Houk, *J. Am. Chem. Soc.* **2005**, *127*, 11294.

[9] A. Córdova, W. Zou, I. Ibrahem, E. Reyes, M. Engqvist, W.-W. Liao, *Chem. Commun.* **2005**, 3586.

[10] A. D. Becke, *J. Chem. Phys.* **1993**, *98*, 5648.

[11] Gaussian 03, Revision B.03, M. J. Frisch et al., Gaussian, Inc., Wallingford CT, **2004**.

[12] V. Barone, M. Cossi, *J. Phys. Chem. A* **1998**, *102*, 1995.

 © 2005 Wiley-VCH Verlag GmbH & Co. KGaA, Weinheim

Crystallography

DOI: 10.1002/anie.200501146

Polymorphism in Benzamide**

W. I. F. David, K. Shankland, C. R. Pulham, N. Blagden, R. J. Davey, and M. Song*

One of the major challenges of solid-state chemistry in the early 21st century is, without doubt, the understanding of the structural, thermodynamic, and kinetic factors associated with the crystallization of molecular compounds. Our limited ability to predict and control the appearance of desirable crystal phases of molecular materials has a major and lasting impact on both technological and commercial progress in the fields of pharmaceuticals, health care, specialty chemicals, and optoelectronics. Although there have been major advances in the field over recent years (in terms of strategies for structure prediction and nucleation control), apparently simple systems such as benzamide sometimes present seemingly intractable problems. In their seminal paper of 1832, Wöhler and Liebig[1] described how slow cooling of a "boiling hot" aqueous solution of benzamide resulted in solidification of the liquid in a white mass of silky needles (Figure 1a). They noted that the transformation of this mass gave a few well-formed rhombic crystals (Figure 1b,c) and identified this process as a phase transformation. This stable, rhombic form of benzamide has been widely studied over the years and its monoclinic crystal structure was first determined in 1959 by using single-crystal X-ray diffraction.[2–4] In contrast, the very existence of a metastable form appears to have been largely forgotten. In 1904, Mohr [5] performed some microscopic studies and Penfold and White[2] made a fleeting reference to it in 1959 but otherwise, probably as a result of its highly metastable nature,[6] it has not received any serious attention. The "plaitlike" fibrous intertwining of the birefringent, metastable crystals shown in Figure 1a, suggests a high degree of strain and structural disorder at the molecular level. Figure 1d reveals the possibility of a direct solid-state transformation between the two forms and gives an initial indication that the needle axis is related to the monoclinic *b* axis of the known stable structure.

With the availability of third-generation synchrotron sources, it is now possible to record diffraction data sufficiently quickly to determine the structures of transient species through powder-diffraction analysis, even in the presence of solvents and other crystalline phases. To this end, we performed a series of X-ray powder diffraction (XRPD) experiments on beamline ID31 at the European Synchrotron Radiation Facility in Grenoble, France. A hot aqueous solution of benzamide (0.347 M) was loaded into a glass capillary (1.5 mm), which was flame-sealed at both ends. The capillary was first warmed to ensure complete dissolution of the solid, cooled to 20 °C, and mounted on the goniometer of the diffractometer. The capillary was then rotated at 2 kHz to minimize the effects of the preferred orientation, and an incident wavelength of 0.8 Å was applied. Although the resulting XRPD pattern was dominated by the known monoclinic form, a small quantity of a new form was also observed. Through the use of a more-dilute aqueous solution of benzamide (0.173 M), cooled in situ on the diffractometer to 2 °C and then flash cooled through brief contact with a cotton bud soaked in liquid nitrogen, a substantial increase in the relative proportion of the new form was obtained; it was not possible to eliminate the known monoclinic form completely. This new form persisted for over 60 min, and the XRPD patterns collected during this period allowed the identification of just twelve diffraction peak positions that are attributable to the new form. These were indexed by using the program DICVOL91[7] to give an orthorhombic unit cell ($a = 17.4322$, $b = 14.1937$, $c = 4.9773$ Å) with excellent figures

[*] Prof. R. J. Davey, M. Song
Molecular Materials Centre
School of Chemical Engineering and Analytical Sciences
University of Manchester
PO Box 88, Manchester, M60 1QD (UK)
Fax: (+44) 161-306-4399
E-mail: roger.davey@manchester.ac.uk
Prof. W. I. F. David, Prof. K. Shankland
ISIS Facility, Rutherford Appleton Laboratory, Chilton, Oxon, OX11 0QX (UK)
C. R. Pulham
School of Chemistry, The University of Edinburgh
King's Buildings
West Mains Road, Edinburgh EH9 3JJ (UK)
N. Blagden
School of Pharmacy, University of Bradford
Bradford B7 1DP (UK)

[**] The authors gratefully acknowledge Michela Brunelli for setting up beamline ID31 for this experiment and the referees for their helpful comments.

 InterScience © 2005 Wiley-VCH Verlag GmbH & Co. KGaA, Weinheim

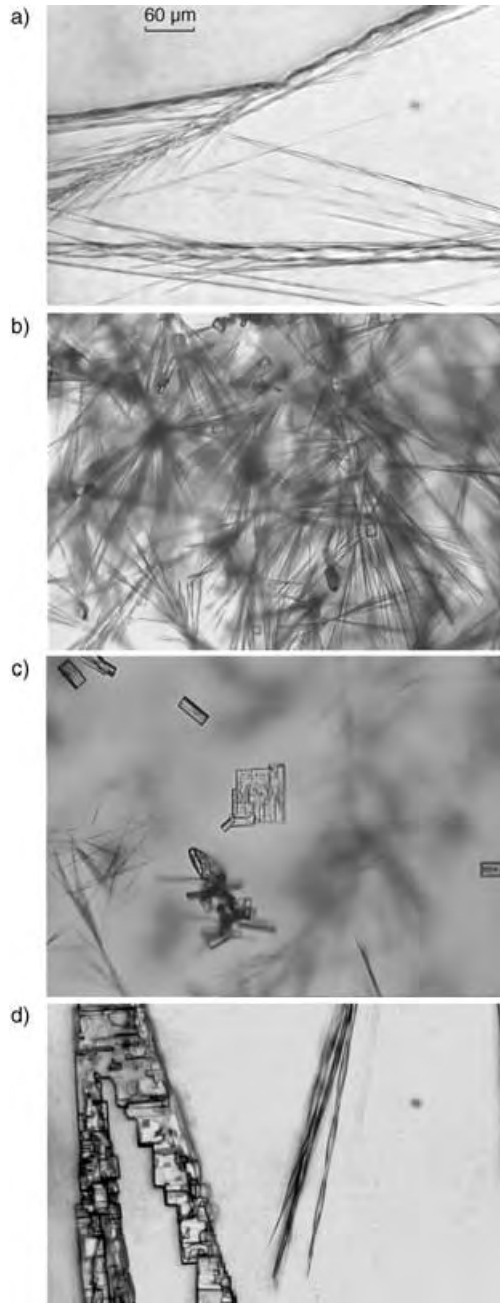

Figure 1. a) Needlelike plaits of the metastable form of benzamide in aqueous solution at room temperature. b) An aqueous suspension of needles taken 30 s after crystallization, and c) the same sample 60 s after crystallization shows the solution-mediated transformation of the needles to the stable form. d) An aggregate of stable monoclinic crystals (left) and a plait of needles (right). The individual crystals of the monoclinic aggregate are all aligned with their *b* axes along its length.[11] As this aggregate originated from the solid-state transformation of a metastable needle, it is reasonable to deduce that the directions of elongation in both forms share a common structural motif. In all photos the scale can be judged from the diameter of a needle, which (as seen from the 60-µm scale bar in a)) is about 30-µm in all cases.

of merit,[8] $M(12) = 63.6$ and $F(12) = 156.3$. The unit cell volume was 1231.52 Å^3, which is slightly less than double that of the monoclinic form (624.25 Å^3) and suggests, unusually, that the metastable form is denser than the stable form. A probabilistic analysis of the extracted reflection intensities, obtained by using the program DASH,[9] identified the most likely extinction symbol to be *Pba-* (the log-likelihood gain of *Pba-* over *P---* was 7.4), which corresponds to space group *Pba*2 or *Pbam*. The centrosymmetric space group *Pbam* was initially chosen as the most likely candidate for the crystal structure as it results in the presence of only one molecule in the asymmetric unit. Structure determination was performed by global-optimization methods by using DASH, and the molecular geometry of the benzamide molecule (excluding the torsion-angle value for the single rotation of the amide group relative to the benzene ring) was taken from the known crystal structure. However, no satisfactory solutions were found in this space group, either from the point of view of profile fitting or crystal packing. Indeed, the best Rietveld χ^2 value in *Pbam* was 254.0, which is very poor when compared with the Pawley χ^2 value of 4.0. Accordingly, structure determination was then performed in the noncentrosymmetric space group *Pba*2, which requires the use of two crystallographically independent benzamide molecules in the asymmetric unit. Ten independent global-optimization runs were conducted, and in eight of the ten attempts, the same excellent fit to the data was obtained with a Rietveld χ^2 value of 6.30, which is very close to the Pawley χ^2 value. Promisingly, the crystal structure that corresponds to these runs exhibited good packing and formation of favorable hydrogen bonds. To obtain reliable structural coordinates from the multiphase XRPD pattern, restrained refinement of the structure of the orthorhombic form was performed simultaneously with refinement of the structure of the known monoclinic form and the solvent background structure. The final Rietveld refinement of the crystal structure was performed with the program TOPAS[10] (refinement details are given in Table 1). The two independent benzamide molecules, which form a dimer in the structure, were modeled by using a constrained Z-matrix description for each molecule. Bond-length and planarity restraints were employed to maintain the dimer

Table 1: Rietveld refinement details for the XRPD data obtained at room temperature.

	Mixed-phase refinement	
	Orthorhombic component	Monoclinic component
a [Å]	17.4317(2)	5.607
b [Å]	14.1944(3)	5.0394
c [Å]	4.977(1)	22.0930
β [°]	–	90.626
V [Å^3]	1231.4(3)	624.25
space group	*Pba*2	$P2_1/c$
Z	8	4
Z′	2	1
reflections	187	151
phase fraction	17.3(2)	82.7(2)
data range 2θ [°]	2–27.97	
number of data points	8657	
R_e (background subtracted)	8.43	
R_{wp} (background subtracted)	13.24	
zero point	−0.0039	

© 2005 Wiley-VCH Verlag GmbH & Co. KGaA, Weinheim

geometry. Separate isotropic temperature factors for each molecule were required to obtain an adequate structural refinement. The final fit between the observed and calculated diffraction patterns is shown in Figure 2, and the figures of

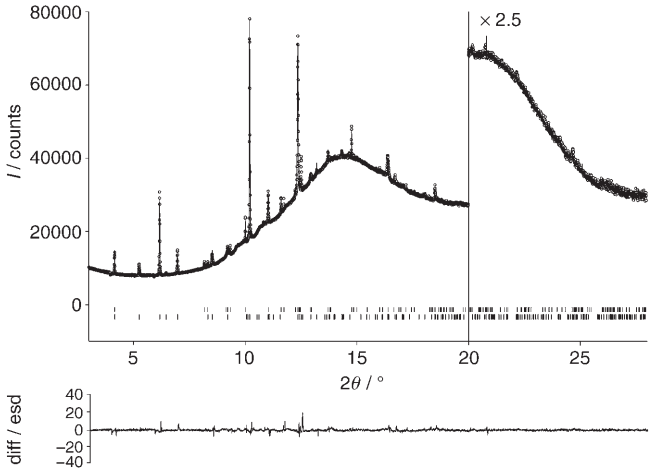

Figure 2. The powder X-ray diffraction pattern shows the excellent fit between the observed and calculated data based upon a two-phase refinement. The upper and lower tick marks indicate the positions of the Bragg reflections in the monoclinic and orthorhombic forms, respectively. The large background is a result of the water that surrounds the benzamide crystallites in the capillary. The *y* axis for the region beyond $2\theta = 20°$ is expanded by a factor of 2.5 for clarity. A difference over estimated standard deviation (esd) plot for the fit to the data is also shown.

merit ($R_{exp} = 8.4\,\%$ and $R_{wp} = 13.2\,\%$, background subtracted) confirm the excellent fit obtained. The sample was found to be comprised of approximately 20% monoclinic form and 80% orthorhombic form. A (001) projection of the resultant metastable orthorhombic crystal structure is shown in Figure 3a, with the corresponding (010) projection of the stable monoclinic form shown for comparison (Figure 3b). The intermolecular interactions perpendicular to the plane are essentially identical in both structures and confirm the evidence from optical microscopy for a common major-growth direction for both forms (Figure 1d); the needle axis of the metastable form is, therefore, along the short [001] direction, which was anticipated from basic crystal morphology arguments.[11] Anisotropic broadening of the Bragg peaks in the powder diffraction pattern also indicates that the needle axis of the metastable structure is along the *c* axis. This is indicated in Figure 4, where it can be seen that the (001) reflection is substantially broader than the other peaks at similar 2θ values. Interestingly, the 2θ dependence of the anisotropic broadening refinement indicates that the origin of the broadening is dominated not by size but rather by strain effects—the plaitlike habit is caused by strain effects that are predominantly associated with the needle direction in which the root-mean-square strain $\Delta d/d$, measured from the anomalous peak width, is approximately 0.004. Furthermore, the constrained refinement of the crystal structure revealed that the isotropic temperature factor for one of the molecules was anomalously large ($B = 12.4(3)$ Å^2, the other value being

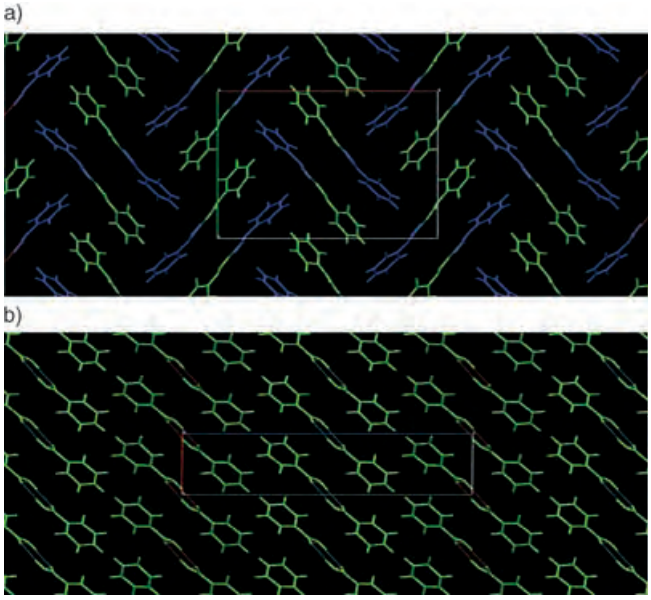

Figure 3. a) A projection of the orthorhombic needle structure looking along [001]. b) A projection of the stable monoclinic structure looking along [010]. In both cases, the views are along hydrogen-bonded ribbons that comprise molecular dimers. The transformation from one form to the other can conserve these ribbon directions and only involve the rearrangement of ribbons in the plane of the pictures. Symmetry-related molecules are shown in identical colors.

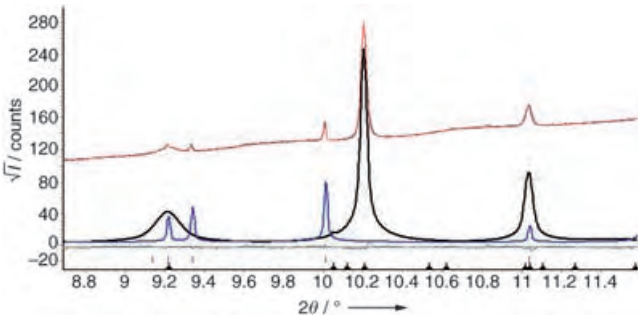

Figure 4. A section of the powder X-ray diffraction pattern that shows the excellent fit between the observed and calculated data based upon a two-phase refinement. The blue line and upper set of tick marks show the contribution of the monoclinic form to this portion of the diffraction pattern; the black line and the lower tick marks show the contribution of the orthorhombic form. The severe anisotropic line broadening in the orthorhombic form is clearly visible in the (001) reflection at just over $2\theta = 9.2°$.

4.3(3) Å^2), which is consistent with substantial structural disorder. Thus, the plaitlike morphology appears to be associated with the static disorder of only one of the molecules in the asymmetric unit. The XRPD data are of insufficient quality to allow a more-detailed characterization of the disorder beyond that of the initial observations.

The concomitant appearance of two distinct crystalline polymorphs of benzamide highlights the delicate balance that can exist between kinetics and thermodynamics in the appearance of polymorphic forms. The needlelike habit of the metastable form reflects rapid, uniaxial crystal growth with the molecular disorder possibly driving the formation of

 © 2005 Wiley-VCH Verlag GmbH & Co. KGaA, Weinheim

fibrous, plaitlike aggregates. At the same time, the complex *ab* plane packing in the metastable form leads to a smaller specific volume than that of the stable monoclinic form, which is more energetically favorable. Furthermore, the entropic factors also favor structural disorder at higher temperatures. From these morphological and thermodynamic arguments, it is not surprising that the metastable structure grows rapidly at first. The subsequent rapid interconversion from metastable to stable polymorph, although clearly facilitated by the preservation of dimer ribbons along the fast-growth axes and their facile rearrangement within the *ab* orthorhombic plane, implies that overall the monoclinic form is significantly more stable than the orthorhombic modification.

Thus, 173 years after the discovery of the first polymorphic molecular crystal, benzamide, by Wöhler and Liebig,[1] the crystal structure of the metastable form has been determined from an in situ synchrotron XRPD experiment. A comparison of the metastable and stable structures provides an explanation not only for the mechanism of transformation but also for the initial rapid crystallization of the metastable structure. The research methods outlined herein are of general applicability to the area of polymorphism and phase transformations, and offer the prospect of the determination of relationships and transformations in numerous polymorphic systems, especially in cases in which metastable states are of a transitory nature.

Received: March 31, 2005
Revised: July 6, 2005
Published online: October 12, 2005

Keywords: benzamide · polymorphism · structure elucidation · X-ray diffraction

[1] J. Liebig, F. Wöhler, *Ann. Pharm.* **1832**, *3*, 249 – 282.
[2] B. R. Penfold, J. C. B. White, *Acta Crystallogr.* **1959**, 12, 130 – 135.
[3] C. C. F. Blake, R. W. H. Small, *Acta Crystallogr.* **1959**, *12*, 417.
[4] C. C. F. Blake, R. W. H. Small, *Acta Crystallogr. Sect. B* **1972**, *28*, 2201 – 2206.
[5] E. Mohr, *J. Prakt. Chem.* **1904**, *70*, 307 – 312.
[6] J. Bernstein, R. J. Davey, J.-O. Henck, *Angew. Chem.* **1999**, *111*, 3646 – 3669; *Angew. Chem. Int. Ed.* **1999**, *38*, 3440 – 3461.
[7] A. Boultif, D. Louer, *J. Appl. Crystallogr.* **1991**, *24*, 987 – 993.
[8] IUCr Monographs on Crystallography 13 P.-E. Werner in *Structure determination from powder diffraction data* (Eds.: W. I. F. David, K. Shankland, L. B. McCusker, C. Baerlocher), Oxford University Press, Oxford, **2002**.
[9] W. I. F. David, K. Shankland, N. Shankland, *Chem. Commun.* **1998**, 931 – 932.
[10] A. A. Coelho, *TOPAS User's Manual*, *Version 3.1*, Brucker AXS GmbH, Karlsruhe, Germany, **2003**.
[11] Z. Berkovitch-Yellin, J. van Mil, L. Addadi, M. Idelson, M. Lahav, L. Lieserowitz, *J. Am. Chem. Soc.* **1985**, *107*, 3111 – 3122.

 © 2005 Wiley-VCH Verlag GmbH & Co. KGaA, Weinheim

Molecular Devices

DOI: 10.1002/anie.200501538

Structural Evidence of Mechanical Shuttling in Condensed Monolayers of Bistable Rotaxane Molecules**

*Kasper Nørgaard, Bo W. Laursen, Sune Nygaard, Kristian Kjaer, Hsian-Rong Tseng, Amar H. Flood, J. Fraser Stoddart, and Thomas Bjørnholm**

Bistable, redox-controllable [2]rotaxanes constitute a class of artificial molecular machines[1,2] in which a mobile ring is confined to move between two different recognition sites (stations) along a dumbbell-shaped component. Linear motor molecules and nanoelectromechanical actuators[3] can be constructed from such redox-controllable [2]rotaxanes. These latter compounds have also been utilized[4,5] as electromechanical switches in molecular memory devices. In this context, the possibility of relative mechanical motion occurring within such bistable [2]rotaxanes in condensed phases has been questioned[6] and disputed.[7] Such motion has been demonstrated unequivocally in solution,[8] in polymer matrices,[9] and in self-assembled monolayers on gold electrodes[10] to result in the movement of the ring from one primary station to a secondary one and then back again in a stepwise manner. One glaring deficiency, however, has been the lack of structural characterization methods for these switching processes in nanoscale systems that can be applied directly to highly condensed phases on surfaces and at interfaces.

[*] Dr. K. Nørgaard, Dr. B. W. Laursen, Prof. T. Bjørnholm
Nano-Science Center
University of Copenhagen
Universitetsparken 5, 2100 København (Denmark)
Fax: (+45) 3532-0406
E-mail: tb@nano.ku.dk

S. Nygaard
Department of Chemistry
University of Southern Denmark
Campusvej 55, 5230 Odense M (Denmark)

Dr. K. Kjaer
Materials Research Department
Risø National Laboratory
4000 Roskilde (Denmark)

Dr. H.-R. Tseng, Dr. A. H. Flood, Prof. J. F. Stoddart
California NanoSystems Institute and
Department of Chemistry and Biochemistry
University of California
405 Hilgard Avenue, Los Angeles, CA 90095-1569 (USA)

[**] This research was funded by the Danish Natural Science Research Council under the programs DANSYNC and Nanoscience. We thank HASYLAB at DESY in Hamburg for time on the beam line BW1 granted under the European Community Research Infrastructure Action under the FP6 "Structuring the European Research Area" Program (through the Integrated Infrastructure Initiative "Integrating Activity on Synchrotron and Free-Electron Laser Science").

Supporting information for this article is available on the WWW under http://www.angewandte.org or from the author.

 © 2005 Wiley-VCH Verlag GmbH & Co. KGaA, Weinheim

Herein, we describe the use of surface-sensitive synchrotron X-ray reflectometry[11] (XR) to provide the first direct structural investigation of the redox-controlled switching process in condensed monolayers of amphiphilic, bistable [2]rotaxanes at the air/water interface. We find that efficient shuttling of the ring component in such [2]rotaxanes takes place in the condensed liquidlike monolayers. The ring travels the 37 Å between the two stations of the dumbbell along a path that is largely confined to the plane of the monolayer. This movement causes insignificant changes in the overall monolayer thickness. Our study has focused on exactly the same molecules whose switching within molecular monolayers has recently been characterized,[12] albeit indirectly, by Langmuir π-A isotherms and the Langmuir–Blodgett (LB) technique in combination with X-ray photoelectron spectroscopy (XPS). By contrast, XR has previously been demonstrated to provide direct detailed information about monolayer organization in general[13] and of amphiphilic bistable rotaxanes at the air/water interface in particular.[14] The working principle of XR is illustrated schematically in Figure 1 a. The incident (α_i) and exit (α_f) grazing angles are varied simultaneously ($\alpha_f = \alpha_i$) while the intensity pattern that results from the interference of X-rays reflected from different depths of the sample is recorded. Data inversion[15] yields—on an absolute scale—the out-of-plane electron-density distribution across the water/monolayer/air interface. The density profiles are smeared by the intrinsic roughness (ca. 3 Å (rms)) of the water surface on account of capillary waves.[16] The bistable [2]rotaxanes **R1**$^{4+}$ and **R2**$^{4+}$ (Figure 1 b) consist of a tetracationic ring component (dark blue) encircling a linear dumbbell-shaped component, which contains two different stations for the ring: 1) a tetrathiafulvalene (TTF) unit (green) and 2) a 1,5-dioxynaphthalene (DNP) unit (red). The two recognition sites are separated by a rigid *p*-terphenylene spacer (black). Both molecules are terminated by a hydrophilic (light blue) and a hydrophobic (gray) stopper at opposite ends of the dumbbell component. This constitution renders the molecules amphiphilic and accordingly enables them to form monomolecular (Langmuir) layers when deposited at the air/water interface. The [2]rotaxanes **R1**$^{4+}$ and **R2**$^{4+}$ are constitutional isomers, differing only in the relative positions of the TTF and DNP units with respect to the two stoppers. The ring will therefore move in an opposite direction (up or down) when the TTF unit of **R1**$^{4+}$ and **R2**$^{4+}$ is oxidized, thus allowing critical internal comparisons to be made.

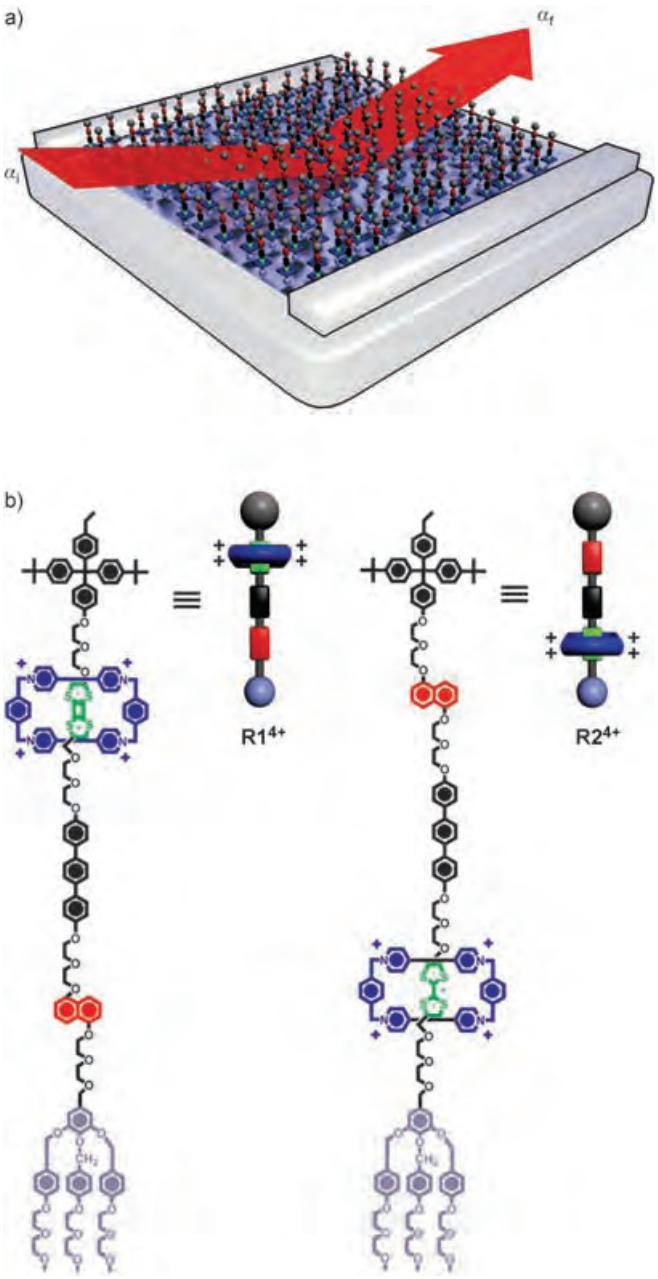

Figure 1. a) A schematic illustration of the working principle in specular X-ray reflectivity measurements of Langmuir monolayers. b) Graphical representations and structural formulas of the amphiphilic, bistable [2]rotaxanes **R1**$^{4+}$ and **R2**$^{4+}$.

Electrochemical switching of the relative position of the ring within these particular bistable [2]rotaxanes is well documented from solution-phase studies,[8,17] and for closely related bistable [2]rotaxanes across a range of different environments.[8c,9,10] In the initial states within each environment, the rotaxane exists in its ground-state co-conformation with the cyclophane encircling the TTF station preferentially by a factor of greater than 9, relative to the DNP station.[18] However, the monocationic TTF$^{\bullet+}$ or dicationic TTF^{2+} species that is produced upon oxidation repels[8–10,17] electrostatically the tetracationic cyclophane and induces the ring to move to the DNP station. In condensed media akin to the Langmuir films characterized here, this switching behavior and the two states associated with the two different locations of the ring have thus far only been observed by indirect methods of structural analysis, such as XPS[12] and electrochemistry.[10] XR investigations, on the other hand, give direct structural information about the electron distribution in thin films, and hence of the two isomeric structures associated with the location of the ring—up or down.

The experimental approach followed in this work, including oxidation of the rotaxane monolayers in situ, is illustrated schematically in Figure 2. Solutions of **R1**$^{4+}$ and **R2**$^{4+}$ in chloroform were spread onto the pure water surface of a

 © 2005 Wiley-VCH Verlag GmbH & Co. KGaA, Weinheim

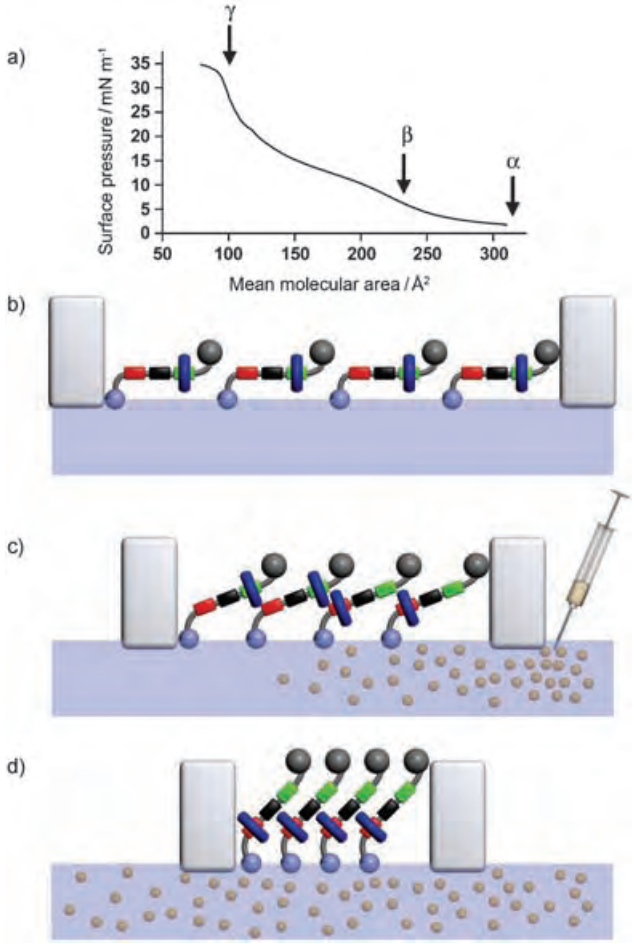

Figure 2. Illustration of the experimental procedure. a) Compression isotherm (surface pressure versus area) for $\mathbf{R2}^{4+}$. b) A schematic representation of a moderately expanded monolayer of $\mathbf{R1}^{4+}$ at the air/water interface. c) Injection of the oxidant $Fe(ClO_4)_3$ into the water subphase at various points along the isotherm (α, β, or γ). d) A densely compressed monolayer of the oxidized form of $\mathbf{R1}^{4+}$.

Langmuir trough, and the resulting monolayers were compressed at a constant rate while the surface pressure was monitored as a function of the mean molecular area (Figure 2a,b). Oxidation of the monolayers was performed[12] in situ by injecting an aqueous solution of the oxidant $Fe(ClO_4)_3$ into the water subphase beneath the Langmuir monolayer to obtain a nominal concentration of 5×10^{-4} M (Figure 2c). The oxidant was injected at decreasing mean molecular areas of 330, 230, or 100 Å^2, as indicated on the compression isotherm (Figure 2a). After injection, one hour was allowed for the oxidant to diffuse to the surface, and the monolayer was typically compressed to a mean molecular area of 100 Å^2 to maximize the electron density changes along the surface normal resulting from the reduced molecular tilting and folding (Figure 2c,d).[19] This area corresponds[12,19] to a very closely packed Langmuir monolayer (Figure 2d). All experiments were performed on a subphase containing 10^{-3}–10^{-4} M $NaClO_4$ to allow efficient ion exchange[12] of PF_6^- with ClO_4^- ions, regardless of the presence of the oxidant. This condition is the only deviation from the procedure described in the literature.[12]

The in-plane structure of the rotaxane monolayers was investigated by grazing-incidence X-ray diffraction.[11] As expected for such flexible molecules that bear a rich array of subunits capable of intra- and intermolecular interactions mediated by noncovalent forces, none of the Langmuir monolayers showed any crystallinity at any of the surface pressures investigated. XR measurements, which probe the out-of-plane structure, as described in Figure 1a, were performed on Langmuir monolayers of the unoxidized rotaxanes, as well as on the oxidized states of the monolayers at several positions (Figure 2a) along the compression isotherm. Figure 3a shows the resulting electron-density profiles for the highly compressed Langmuir monolayers of $\mathbf{R1}^{4+}$ with the ring up, measured at a mean molecular area of 100 Å^2. The green line represents the monolayer of unoxidized $\mathbf{R1}^{4+}$ and the red line corresponds to the monolayer of $\mathbf{R1}^{6+}$, oxidized in situ. The oxidation was performed on a moderately condensed monolayer with a mean molecular area of 230 Å^2 that was subsequently compressed to 100 Å^2. The areas above the horizontal dashed lines represent the total number of electrons in one molecule (including counterions). The horizontal dotted lines correspond to the approximate positions of the interfaces with bulk water and were chosen as the point on the curve where the electron density is 5% larger than that of bulk water. The discrepancy between the dashed and dotted lines in Figure 3 is caused by the inclusion of a small number of water molecules (ca. 10 per rotaxane molecule, see Supporting Information) from the subphase into the hydrophilic parts of the rotaxane monolayer. This water inclusion is less pronounced in highly compressed Langmuir monolayers than in less closely packed monolayers.[14]

Two distinct features emerge from the data analysis shown in Figure 3a: 1) The profiles of $\mathbf{R1}^{4+}$ and $\mathbf{R1}^{6+}$ contain two peaks with a vertical separation of approximately 12 Å. These peaks correspond to regions of high electron density within the Langmuir monolayer, and are therefore ascribed (see below) to the locations of the two stations along the rod segments of the dumbbell components in the two bistable [2]rotaxanes. This assignment is corroborated[20] by recent molecular dynamic simulations of similar systems.[14] 2) The relative densities of the two peaks associated with $\mathbf{R1}^{4+}$ and $\mathbf{R2}^{4+}$ change significantly upon oxidation of the monolayers. Hence, a shift of the electron distribution towards the water surface (namely, down) is observed in oxidized monolayers of $\mathbf{R1}^{6+}$ relative to the unoxidized case. This shift is in agreement with a vertical change in the position of the ring upon oxidation from the "upper" station (TTF) to the "lower" station (DNP), analogous to the movement known[8,17,18] to take place in solution. The shaded areas between the red and green curves represent the net number of electrons that change vertical position upon oxidation. Since the movement of the ring is compensated by reorganization of the local environment, the effective number of electrons changing places upon oxidation is relatively small. We notice, however, that the shift in electron density is symmetrical around the intersection point, which shows that the switching is a local

 © 2005 Wiley-VCH Verlag GmbH & Co. KGaA, Weinheim

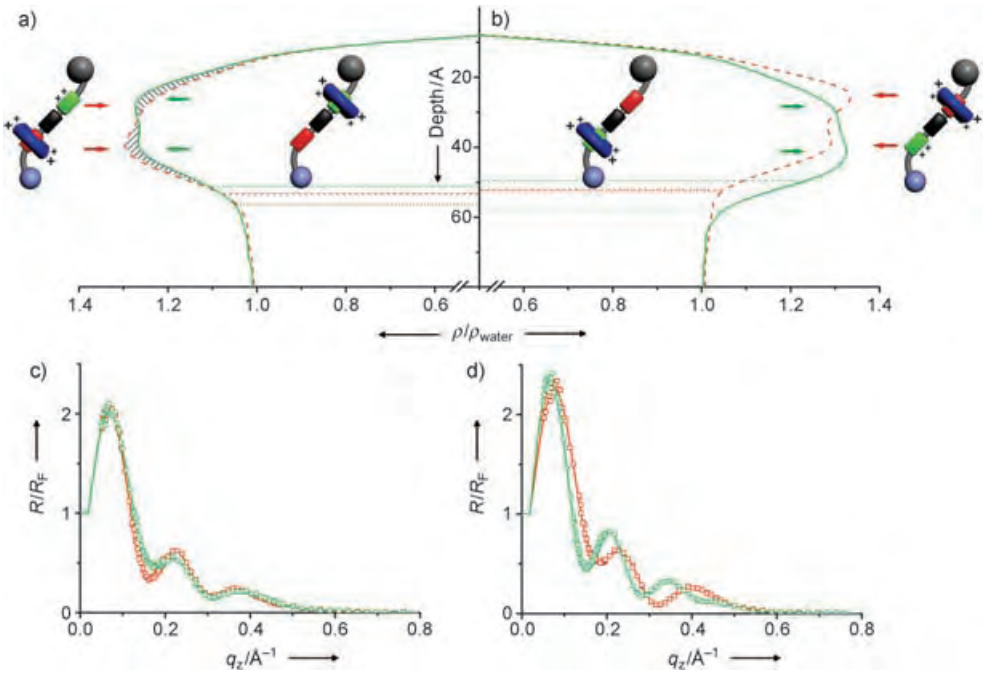

Figure 3. X-ray reflectivity measurements. a,b) Electron-density profiles for $\mathbf{R1}^{4+}$ and $\mathbf{R2}^{4+}$, respectively, inverted from the reflectivity data for the tetracationic starting compounds (green lines) and the hexacationic compounds $\mathbf{R1}^{6+}$ and $\mathbf{R2}^{6+}$ oxidized in situ (red lines). The areas above the horizontal dashed lines correspond to the numbers of electrons in one molecule, while the dotted lines represent the approximate position of the interface to bulk water. c,d) The measured reflectivities R (open circles or squares; normalized to the Fresnel reflectivity of bare water, R_F) and the best fits to the data (solid lines) corresponding to the $\rho(z)$ curves in (a) and (b) for $\mathbf{R1}^{4+}$ and $\mathbf{R2}^{4+}$, respectively. The green lines and circles correspond to the starting compounds and the red lines and squares correspond to the oxidized compounds. The data was obtained at beamline BW1 at the DESY synchrotron facility in Hamburg, Germany.

reorganization that does not change the overall hydration state of the rotaxane. If nearly all of the rings are located initially on the TTF station—as documented for solution-phase experiments[8,17,18]—then this symmetry also indicates that almost all of the rings move from the upper to the lower station upon oxidation because a fractional displacement (for example, 50%) would otherwise lead to a smearing of the two peaks, which is not observed. The 12-Å vertical shift is less than the expected distance between the two stations in a fully stretched and vertically aligned rotaxane. Molecular modeling studies[12] indicate that this distance is 37 Å. This value implies that at a mean molecular area of 100 $Å^2$ within the Langmuir monolayer, the rotaxane molecules are tilted and locally folded,[19] even in these very compressed Langmuir monolayers.[21] Similar attenuation of the distance traveled out of the plane was observed in the XPS data of Langmuir monolayers transferred onto SiO_2 substrates.[12] Consequently, the movement of the ring must have a significant component in the plane of the Langmuir film. Further evidence of folding and tilting comes from observations of the total monolayer thicknesses, which fall in the range 50–55 Å (Figure 3) and are notably smaller than the thickness (ca. 80 Å) expected for a monolayer of fully extended and nontilted rotaxanes. The electron-density profiles of $\mathbf{R1}^{4+}$, measured for both low and moderately compressed Langmuir monolayers, show that the molecules are folded and tilted to an even greater extent with respect to the normal of the water surface, as illustrated schematically in Figure 2b,c. This observation is consistent with our previous investigations[14] of similar amphiphilic, bistable [2]rotaxanes. The local folding of molecular segments along the rod can be considered to be a consequence of the large differences between the cross-sectional areas of different segments along the fully stretched rod. To fill space, the slimmer segments must fold and tilt, which, in turn, gives rise to a fluidlike, disordered local environment within the monolayer. This property allows the ring to be displaced in a fluidlike environment without any significant changes[20] in the overall thickness of the film, as is clearly illustrated by the density profiles in Figure 3a. This latter observation indicates that switching would also be possible in films sandwiched between two solid surfaces, as for example, in crossbar memory devices.[4,5]

In a control experiment, monolayers of the constitutionally isomeric $\mathbf{R2}^{4+}$ were examined by using identical experimental procedures. The monolayers of $\mathbf{R2}^{4+}$ show (Figure 3b) the opposite effect upon oxidation to that observed for $\mathbf{R1}^{4+}$, that is, the peak in the electron distribution shifts upwards. This result, therefore, supports the notion that the observed shift in electron density is caused by a net movement of the ring component relative to the dumbbell (in the case of $\mathbf{R2}^{4+/6+}$, from the lower TTF to the upper DNP station) and is not a consequence of the movement of water or counterions. It is evident from Figure 3b that the unoxidized monolayers of $\mathbf{R2}^{4+}$ contained more water molecules than was observed for $\mathbf{R1}^{4+}$. This condition may be related to the proximity of the tetracationic ring to the water surface.

Analogous XR measurements for $\mathbf{R1}^{4+}$ and $\mathbf{R2}^{4+}$ were performed at different mean molecular areas. Similar trends were observed at 230 $Å^2 mol^{-1}$ (Figure 4), albeit with less distinct changes in the electron density, presumably on account of a larger in-plane component of the movement—that is, the amphiphilic bistable rotaxanes have ample room to lie down at the interface. Attempts to perform the entire oxidation at a mean molecular area of 100 $Å^2 mol^{-1}$ did not result in any changes in the electron density profiles, an observation which indicates that the oxidant is unable to react with the TTF unit in these extremely dense monolayers, or that ring movement is inhibited.[21]

In summary, X-ray reflectivity data have provided direct structural evidence for the molecular motion of the ring

 © 2005 Wiley-VCH Verlag GmbH & Co. KGaA, Weinheim

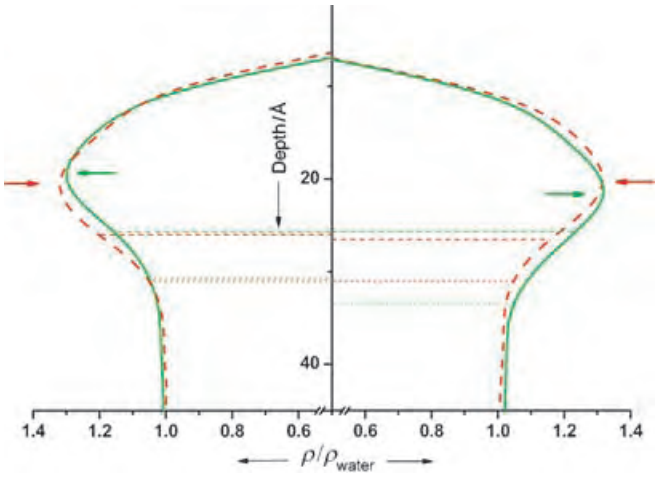

Figure 4. Electron-density profiles for $\mathbf{R1}^{4+}$ (left) and $\mathbf{R2}^{4+}$ (right), both measured at a mean molecular area of 230 Å^2. The profiles are inverted from the reflectivity data for the starting compounds (green lines) and the oxidized compounds (red lines). Oxidation was performed in situ at a mean molecular area of 230 Å^2. The areas above the horizontal dashed lines correspond to the numbers of electrons in one molecule, whereas the dotted lines represent the approximate position of the interface to bulk water. A comparison of these density profiles with the profiles measured at mean molecular area of 100 Å^2 (see Figure 3) shows that the ring motion contains a large in-plane component.

component of amphiphilic bistable [2]rotaxanes in condensed, oriented monolayers during redox-controlled switching.

Received: May 4, 2005
Revised: August 24, 2005
Published online: October 11, 2005

Keywords: Langmuir–Blodgett films · molecular devices · monolayers · rotaxanes · X-ray reflectivity

[1] a) V. Balzani, M. Gómez-López, J. F. Stoddart, *Acc. Chem. Res.* **1998**, *31*, 405–414; b) V. Balzani, A. Credi, F. M. Raymo, J. F. Stoddart, *Angew. Chem.* **2000**, *112*, 3484–3530; *Angew. Chem. Int. Ed.* **2000**, *39*, 3348–3391.

[2] V. Balzani, A. Credi, M. Venturi, *Molecular Devices and Machines—A Journey into the Nano World*, Wiley-VCH, Weinheim, **2003**.

[3] a) T. J. Huang, B. Brough, C.-M. Ho, Y. Liu, A. H. Flood, P. A. Bonvallet, H.-R. Tseng, J. F. Stoddart, M. Baller, S. Magonov, *Appl. Phys. Lett.* **2004**, *85*, 5391–5393; b) Y. Liu, A. H. Flood, P. A. Bonvallet, S. A. Vignon, H.-R. Tseng, T. J. Huang, B. Brough, M. Baller, S. Magonov, S. D. Solares, W. A. Goddard, C.-M. Ho, J. F. Stoddart, *J. Am. Chem. Soc.* **2005**, *127*, 9745–9759.

[4] Y. Luo, C. P. Collier, J. O. Jeppesen, K. A. Nielsen, E. DeIonno, G. Ho, J. Perkins, H.-R. Tseng, T. Yamamoto, J. F. Stoddart, J. R. Heath, *ChemPhysChem* **2002**, *3*, 519–525.

[5] a) A. H. Flood, R. J. A. Ramirez, W.-Q. Deng, R. P. Muller, W. A. Goddard, J. F. Stoddart, *Aust. J. Chem.* **2004**, *57*, 301–322; b) P. M. Mendes, A. H. Flood, J. F. Stoddart, *Appl. Phys. A* **2005**, *80*, 1197–1209.

[6] R. F. Service, *Science* **2003**, *302*, 556.

[7] a) J. R. Heath, J. F. Stoddart, R. S. Williams, *Science* **2006**, *303*, 1136; b) A. H. Flood, J. F. Stoddart, D. W. Steuerman, J. R. Heath, *Science* **2004**, *306*, 2055–2056.

[8] a) J. O. Jeppesen, K. A. Nielsen, J. Perkins, S. A. Vignon, A. DiFabio, R. Ballardini, M. T. Gandolfi, M. Venturi, V. Balzani, J. Becher, J. F. Stoddart, *Chem. Eur. J.* **2003**, *9*, 2982–3007; b) T. Yamamoto, H.-R. Tseng, J. F. Stoddart, V. Balzani, A. Credi, F. Marchioni, M. Venturi, *Collect. Czech. Chem. Commun.* **2003**, *68*, 1488–1514; c) A. H. Flood, A. J. Peters, S. A. Vignon, D. W. Steuerman, H.-R. Tseng, S. Kang, J. R. Heath, J. F. Stoddart, *Chem. Eur. J.* **2004**, *10*, 6558–6561.

[9] D. W. Steuerman, H.-R. Tseng, A. J. Peters, A. H. Flood, J. O. Jeppesen, K. A. Nielsen, J. F. Stoddart, J. R. Heath, *Angew. Chem. Int. Ed.* **2004**, *43*, 6486–6491.

[10] H.-R. Tseng, D. Wu, N. X. Fang, X. Zhang, J. F. Stoddart, *ChemPhysChem* **2004**, *5*, 111–116.

[11] J. Als-Nielsen, D. Jacquemain, K. Kjaer, F. Leveiller, M. Lahav, L. Leiserowitz, *Phys. Rep.* **1994**, *246*, 251–313.

[12] T. J. Huang, H.-R. Tseng, L. Sha, W. Lu, B. Brough, A. H. Flood, B. D. Yu, P. C. Celestre, J. P. Chang, J. F. Stoddart, C.-M. Ho, *Nano Lett.* **2004**, *4*, 2065–2071.

[13] K. Nørgaard, T. Bjørnholm, *Chem. Commun.* **2005**, 1812–1823.

[14] K. Nørgaard, J. O. Jeppesen, B. W. Laursen, J. B. Simonsen, M. J. Weygand, K. Kjaer, J. F. Stoddart, T. Bjørnholm, *J. Phys. Chem. B* **2005**, *109*, 1063–1066.

[15] J. S. Pedersen, I. W. Hamley, *J. Appl. Crystallogr.* **1994**, *27*, 36–49.

[16] A. Braslau, M. Deutsch, P. S. Pershan, A. H. Weiss, J. Als-Nielsen, J. Bohr, *Phys. Rev. Lett.* **1985**, *54*, 114–117.

[17] H.-R. Tseng, S. A. Vignon, P. C. Celestre, J. Perkins, J. O. Jeppesen, A. DiFabio, R. Ballardini, M. T. Gandolfi, M. Venuri, V. Balzani, J. F. Stoddart, *Chem. Eur. J.* **2004**, *10*, 155–172.

[18] Quantitative measurements of the preference of the ring for the TTF station are based on solution studies of model, degenerate rotaxanes bearing either two TTF or two DNP stations, each with the *p*-terphenylene spacer used in $\mathbf{R1}^{4+}$ and $\mathbf{R2}^{4+}$. The barriers to shuttling measured for the two degenerate rotaxanes are 17–18 kcal mol^{-1} and 15 kcal mol^{-1}, respectively. The difference of 2–3 kcal mol^{-1} is related to the energy difference between the preferences of the cyclophane for the TTF station over the DNP station, which leads to ratios of 96:4–99.3:0.7; see: S. Kang, S. A. Vignon, H.-R. Tseng; J. F. Stoddart, *Chem. Eur. J.* **2004**, *10*, 2555–2564. In order to reflect these thermodynamic differences, we have introduced the term ground-state co-conformation for the translational isomer with the cyclophane residing at the TTF station and metastable state co-conformation when it is at the DNP station; see references 8c and 9 for more details.

[19] I. C. Lee, C. W. Frank, T. Yamamoto, H.-R. Tseng, A. H. Flood, J. F. Stoddart, J. O. Jeppesen, *Langmuir* **2004**, *20*, 5809–5828.

[20] S. S. Jang, Y. H. Jang, Y.-H. Kim, W. A. Goddard, J. W. Choi, J. R. Heath, B. W. Laursen, A. H. Flood, J. F. Stoddart, K. Nørgaard, T. Bjørnholm, *J. Am. Chem. Soc.* **2005**, *127*, ASAP: DOI:10.1021/ja0531531.

[21] The XPS data recorded on LB films of $\mathbf{R1}^{4+}$ oxidized at a mean molecular area of approximately 150 Å^2 per molecule indicate, although indirectly, that oxidation and movement are still favored at these densities; see reference 12 for more details. Films at densities of approximately 150 Å^2 per molecule were also used to prepare molecular memory devices, see reference [4].

 © 2005 Wiley-VCH Verlag GmbH & Co. KGaA, Weinheim

Luminescence

DOI: 10.1002/anie.200502214

Banana-Shaped Oligo(aryleneethynylene)s: Synthesis and Light-Emitting Characteristics**

Yoshihiro Yamaguchi, Shigeya Kobayashi, Tateaki Wakamiya, Yoshio Matsubara, and Zen-ichi Yoshida**

Bent (so-called banana-shaped) molecules which consist, for example, of an aromatic unit and ester unit are currently attracting interest in the field of liquid crystals.[1] However, to the best of our knowledge, the light-emitting efficiency of banana-shaped molecules have not been reported so far, even though bent light emitters have been reported.[2] In view of the growing importance of highly efficient light-emitting materials in biological, chemical, and materials science, we report here the synthesis and light-emitting characteristics of banana-shaped oligo(arylene ethynylene)s **2**–**6** containing pyridine rings as it is not clear what influence pyridine ring(s) would have on the emission characteristics.

In regard to the banana-shaped molecules, we considered **1** (the simplest trimeric hydrocarbon system), **2** (with a pyridine ring substituting the central benzene ring of **1**), **3** (with a pyridine ring substituting both terminal benzene rings of **1**), **4** (a donor/acceptor (OMe group/pyridine C=N group) trimeric system), **5** (donor/acceptor pentameric system with a single banana structure), and **6** (a donor/acceptor pentameric system with a double banana structure).

The synthesis of **4**–**6** was achieved by using the Sonogashira C–C coupling reaction[3] as the key step (Scheme 1). Although **1**,[4] **2**,[5] and **3**[6] are known compounds, we prepared them in a similar manner to **4**, that is, in a different way from the reported methods.[4–6] The structures of **1**–**6** were confirmed by spectral data (^{1}H and ^{13}C NMR spectroscopy and HR-FAB MS, see the Supporting Information).

The emission and absorption characteristics of **1**–**6** and the rod-shaped donor/acceptor pentameric systems (**15** and **16**)[7] together with the radiative rate constants (k_r), radiationless rate constants (k_d), k_r/k_d (our measure for emissivity), and emission life times (τ) are shown in Table 1. Since the k_r and k_d values are related to the corresponding emission quantum yields and life times by $\Phi_f = k_r\tau$ and $k_r + k_d = \tau^{-1}$, it is possible to calculate the values of k_r and k_d whenever quantum yield and life time data are available.[8]

The important results contained in Table 1 are as follows: First, the Φ_f and k_r/k_d values for **1**–**3** demonstrate that the emission efficiency markedly increases when the central pyridine ring is present (Φ_f: 0.48, k_r/k_d: 0.92 for **2**), while it greatly decreases when terminal pyridine rings are present (Φ_f: 0.03, k_r/k_d: 0.03 for **3**). Second, the introduction of MeO groups into both benzene rings of **2** (construction of the donor/acceptor system) leads to a more efficient light emitter (Φ_f: 0.58, k_r/k_d: 1.38 for **4**) than **2**. The maximum emission of **4** (λ_{em}: 397 nm) appears at a longer wavelength (by 49 nm) than that of **2** (λ_{em}: 348 nm). Third, and the most remarkable finding, is that the donor/acceptor pentameric system shown in single banana structure **5** is a highly efficient violet-light emitter (Φ_f: 0.84, λ_{em}: 414 nm, k_r/k_d: 5.25), and the donor/acceptor pentameric system shown in double banana structure **6** is an excellent violet-light emitter (Φ_f: 0.91, λ_{em}: 417 nm, k_r/k_d: 10.11) despite the interruption of the π conjugation by one *meta* substitution in the former and by two *meta* substitutions in the latter. It is evident that the Φ_f values for **5** and **6** are greater than those of the rod-shaped donor/acceptor pentameric systems **15** (Φ_f: 0.75, k_r/k_d: 3.00) and **16** (Φ_f: 0.76, k_r/k_d: 3.17).

The superior emissive properties of **5** and **6** (in particular of **6**) relative to **15** and **16** is ascribed to the decrease in their k_d values compared to those of **15** and **16**, since the k_r values of **5** and **6** are similar to those of **15** and **16**. It is well known that *meta*-substituted systems are weaker light emitters than the corresponding *para* isomers, as exemplified by bis(phe-

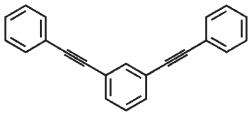

1

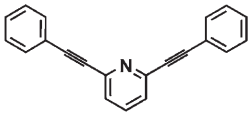

2

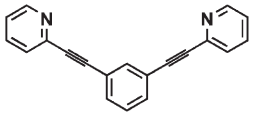

3

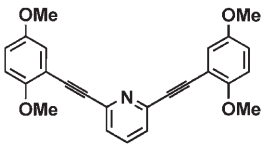

4

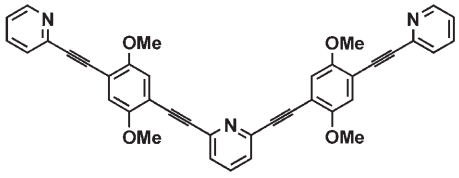

5

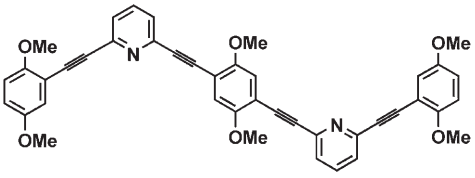

6

[*] Prof. Dr. Y. Yamaguchi, Dr. S. Kobayashi, Prof. Dr. T. Wakamiya, Prof. Dr. Y. Matsubara, Prof. Dr. Z.-i. Yoshida
Faculty of Science and Engineering
Kinki University
Higashi-Osaka, Osaka 577-8502 (Japan)
Fax: (+81) 6-6723-2721
E-mail: yamaguch@chem.kindai.ac.jp
yoshida@chem.kindai.ac.jp

[**] We thank Professor Masanori Morita (Kinki University) for MS measurements and Yoko Maeda for assistance in this study. This work was supported by a Grant-in-Aid for Creative Scientific Research (No. 16GS0209) and Scientific Research (No. 16550131) from the Ministry of Education, Science, Sports, and Culture of Japan.

Supporting information for this article is available on the WWW under http://www.angewandte.org or from the author.

InterScience
© 2005 Wiley-VCH Verlag GmbH & Co. KGaA, Weinheim

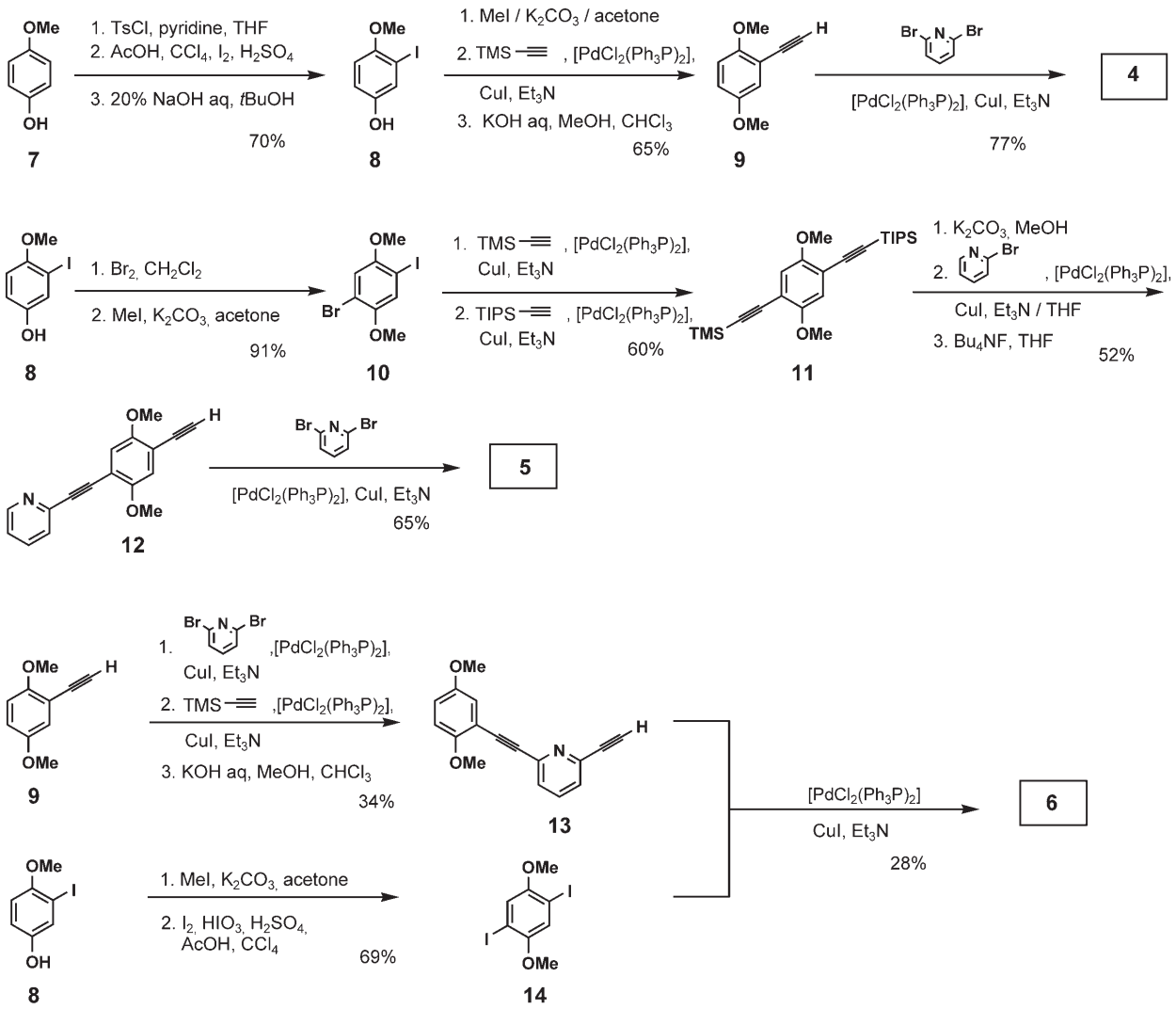

Scheme 1. Synthesis of donor/acceptor banana-shaped oligo(aryleneethynylene)s **4**, **5**, and **6**. Ts = toluene-4-sulfonyl, TMS = trimethylsilyl, TIPS = triisopropylsilyl.

Table 1: Emission and absorption characteristics of banana-shaped oligo(aryleneethynylene)s **1**–**6**, **15**, and **16** in $CHCl_3$.[a]

Compound	Φ_f[b]	λ_{em}[nm]	logε	λ_{abs}[nm]	τ[ns]	k_r[s^{-1}]	k_d[s^{-1}]	k_r/k_d
1	0.14	330	4.70	302	2.00	7.02×10^7	4.31×10^8	0.16
2	0.48	348	4.49	320	3.24	1.48×10^8	1.61×10^8	0.92
3	0.03	329	4.70	307	2.00	1.50×10^7	4.86×10^8	0.03
4	0.58	397	4.44	344	3.63	1.60×10^8	1.16×10^8	1.38
5	0.84	414	4.82	381	1.51	5.50×10^8	1.05×10^8	5.25
6	0.91	418	4.58	369	2.63	3.43×10^8	3.39×10^7	10.11
15	0.75	437	4.93	398	1.17	6.38×10^8	2.13×10^8	3.00
16	0.76	436	4.66	381	2.19	3.47×10^8	1.10×10^8	3.17

[a] All spectra were measured at 295 K. [b] Quantum yield is calculated relative to quinine ($\Phi_f = 0.55$ in 0.1 M H_2SO_4).

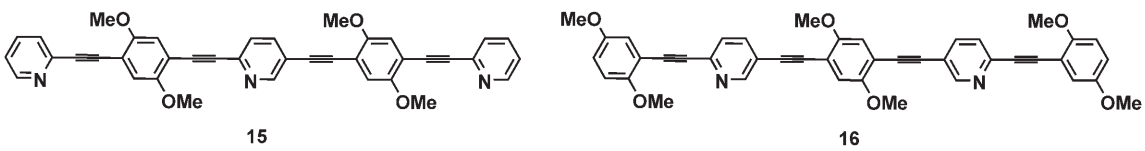

15 **16**

 © 2005 Wiley-VCH Verlag GmbH & Co. KGaA, Weinheim

nylethynyl)benzenes (Φ_f: 0.50, λ_{em}: 345 nm for the *para* isomer; Φ_f: 0.14, λ_{em}: 330 nm for the *meta* isomer), and terphenyls (Φ_f: 0.54, λ_{em}: 342 nm for the *para* isomer; Φ_f: 0.039, λ_{em}: 331 nm for the *meta* isomer).[9] We previously reported the importance of π extension and donor/acceptor groups on the emission efficiency of the rod-shaped oligo(*p*-phenyleneethynylene)s.[10] The banana-shaped molecules **5** and **6**, which consist of alternately arranged pyridine (acceptor) and dimethoxybenzene (donor) rings, have a *meta*-substituted structure in addition to a *para*-substituted (rod-shaped) structure. Since oligo(*p*-phenyleneethynylene) has an almost acetylenic structure, even in the excited singlet state,[10,11] and the excited singlet state has a dipolar structure, the higher emission efficiency (Φ_f) of **5** and **6** relative to that of **15** and **16** might be explained by assuming that the emission efficiency depends on the movability of the dipolar structure (**17**) among the structurally equivalent donor/acceptor diads

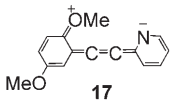

17

(dimethoxyphenylethynylpyridine units) in the excited singlet state molecules (in other words, the number of structurally equivalent dipolar diad units to **17**). The pyridine ring in the banana-shaped molecules (**5** and **6**) is able to move the dipolar structure **17** by both the half π bonds (C_2–N and C_6–N), while the pyridine ring in the rod-shaped molecules (**15** and **16**) is not able to move the dipolar structure because of the interruption of the dipolar structure.

The fluorescence spectra of **5** and **6** are relatively sharp relative to that of **4** (Figure 1).

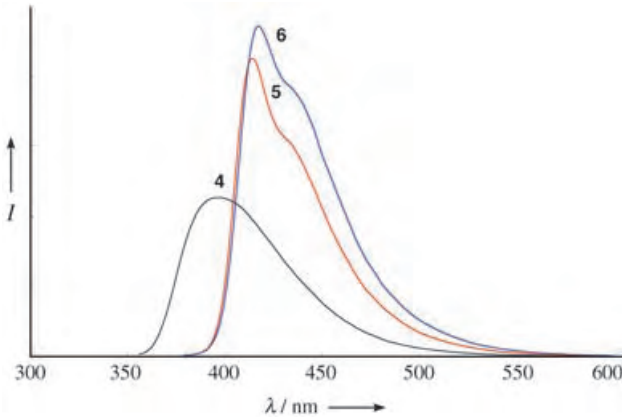

Figure 1. Fluorescence spectra of banana-shaped donor/acceptor oligo(aryleneethynylene)s **4** (black), **5** (red), and **6** (blue) in $CHCl_3$ at 295 K.

The effect of solvent on the emission efficiency of **5** and **6** is noteworthy (Table 2). Almost no solvent effect is observed for the absorption spectra of both **5** and **6**, while the fluorescence maxima of **5** and **6** are slightly shifted to longer wavelengths as the solvent polarity increases. Although the quantum yield of **5** is not similarly altered with a change in the solvent polarity, that of **6** remarkably decreases with an increase in the solvent polarity. The observed effect of the solvent on the Φ_f values of **5** and **6** can be interpreted by a change in the k_r and k_d values of **5** and **6** with a change in the solvent polarity: The k_r and k_d values for **5** are not so affected by solvent polarity. However, the k_r value of **6** decreases with an increase in solvent polarity even though the k_d value does not change, except for the cases of benzene and $CHCl_3$, where the k_d values decrease. The vastly different solvent dependency of the Φ_f values of **5** and **6** might be explained by the marked disparity between the distribution of the difference density (difference in the atomic charge in the excited state from that in the ground state) of **5** and **6**. The INDO/S difference density distribution (DDD) in the excited state of **5** and **6** is shown in Figure 2. It is evident that the marked change in the DDD in the excited state is not observed for **5**, while it is seen between the terminal regions and the central part of **6**, thus suggesting that the solvent polarity dependence of the Φ_f value should be negligible for **5**, but large for **6**.

The behavior of banana-shaped molecule **3** having pyridine rings at both termini towards metal ions should be of interest in regard to the emission characteristics of the resulting complex.[12]

We have prepared the 1:1 complex **18** (Tf = trifluoromethanesulfonyl) both by reaction of a solution of **3** in CH_2Cl_2 with $[Ti^{IV}Cl_3]^+$ freshly generated from a solution of $TiCl_4$ in

Table 2: Effect of solvent on the absorption and fluorescence characteristics of **5** and **6**.[a]

Compound	Solvent	Φ_f	λ_{em}[nm]	logε	λ_{abs}[nm]	k_r[s^{-1}]	k_d[s^{-1}]	k_r/k_d
5	C_6H_6	0.79	413	4.81	380	5.09×10^8	1.35×10^8	3.76
	$CHCl_3$	0.84	414	4.82	381	5.50×10^8	1.05×10^8	5.25
	THF	0.80	413	4.83	378	5.39×10^8	1.35×10^8	4.00
	CH_3CN	0.77	417	4.82	376	5.07×10^8	1.52×10^8	3.35
	DMF	0.82	422	4.80	379	5.18×10^8	1.14×10^8	4.56
	MeOH	0.76	425	4.84	379	5.25×10^8	1.66×10^8	3.17
6	C_6H_6	0.90	416	4.56	365	3.24×10^8	3.60×10^7	9.00
	$CHCl_3$	0.91	418	4.58	369	3.43×10^8	3.39×10^7	10.11
	THF	0.68	417	4.58	365	2.61×10^8	1.23×10^8	2.13
	CH_3CN	0.43	423	4.59	369	1.69×10^8	2.24×10^8	0.75
	DMF	0.48	427	4.56	367	1.75×10^8	1.89×10^8	0.92
	MeOH	0.42	427	4.61	371	1.71×10^8	2.36×10^8	0.72

[a] All spectra were measured at 295 K.

 © 2005 Wiley-VCH Verlag GmbH & Co. KGaA, Weinheim

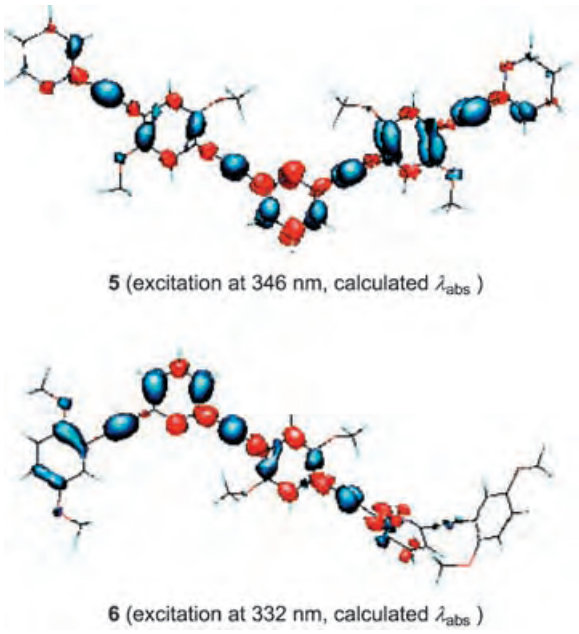

Figure 2. INDO/S difference density distribution of **5** and **6** in the excited singlet states (the red parts designate the atomic charges that are more negative in the excited state than in the ground state. The blue parts show the reverse situation. Colorless parts designate equal density in both the excited and ground states).

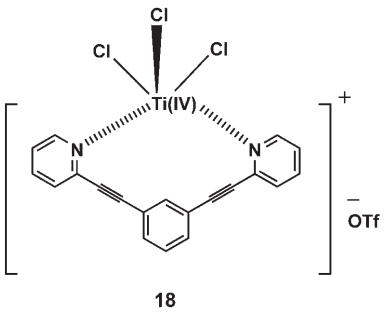

18

CH_2Cl_2 and a solution of AgOTf in benzene, and by mixing **3** (in CH_2Cl_2) first with AgOTf (in benzene) and then adding $TiCl_4$ (in CH_2Cl_2).[13] Complex **18** is stable in the solid state, and does not dissociate in solution. However, its ligand **3** can be replaced by stronger ligand(s) such as 2,2′-bipyridine.

Although X-ray diffraction analysis of **18** has not yet been accomplished, because of difficulty in growing suitable single crystals, the MM2 structure (Figure 3) of **18** is very similar to that of the 1:1 Sb^V complex (**21**) of tetrakisareneazaarenecyclyne (**20**) with respect to the ligand **3** (see the Supporting Information).[14,15] The ^{1}H NMR spectroscopic and FAB MS data (Supporting Information) support this structure.[16]

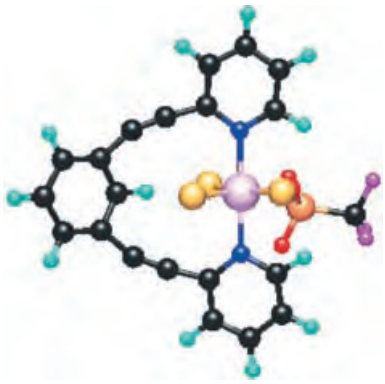

Figure 3. MM2 structure of **18**.

The absorption and fluorescence spectra of **18** are shown in Figure 4. The emission and absorption characteristics of **3** and **18**–**21** (**19:** trifluoromethanesulfonic acid salt of **3**) are summarized in Table 3.

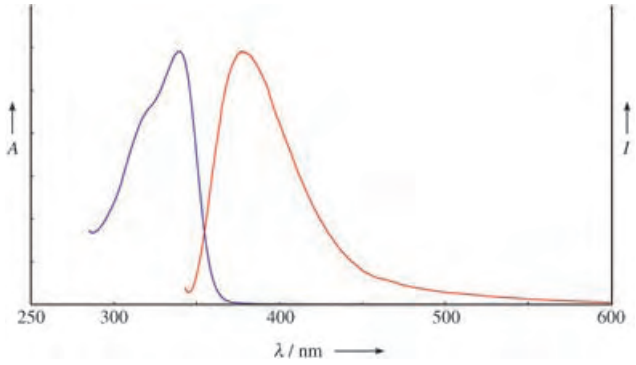

Figure 4. Absorption (blue) and fluorescence (red) spectra of **18** in CH_2Cl_2 at 295 K.

It is noted that the emission efficiency of **18** is about 60 times greater than that of **3**. An increase in the Φ_f value on formation of the metal bridge is also observed in **21**. In both cases, the k_d values decrease and the k_r values increase, thus resulting in an enhancement of the Φ_f value. Since a large increase in the Φ_f value is also seen for **19** (diprotonated **3**), the increase resulting from metal bridging is ascribed to the increase in the electron-accepting ability of the pyridine C=N groups by coordination to Ti^{IV} centers (formation of a positively charged sp^2 nitrogen atom).

In conclusion, we have created donor/acceptor banana-shaped molecules, and found that the donor/acceptor pentameric aryleneethyny-

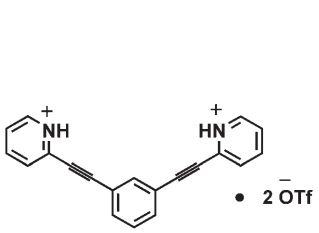

19

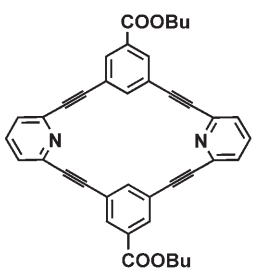

20

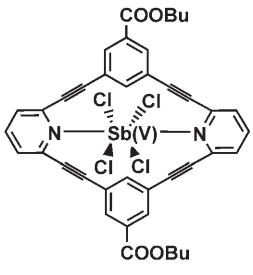

21

© 2005 Wiley-VCH Verlag GmbH & Co. KGaA, Weinheim

Table 3: Emission and absorption characteristics of **3** and **18**–**21** in CH_2Cl_2.[a]

Compound	Φ_f[b]	λ_{em}[nm]	logε	λ_{abs}[nm]	τ[ns]	k_r[s^{-1}]	k_d[s^{-1}]	k_r/k_d
3	0.01	328	4.70	306	1.98	5.06×10^6	5.01×10^8	0.01
18	0.63	378	4.79	339	1.62	3.90×10^8	2.29×10^8	1.70
19	0.60	378	4.76	340	1.75	3.45×10^8	2.28×10^8	1.52
20	0.18	355	4.62	322	2.40	7.50×10^7	3.42×10^8	0.22
21	0.41	433	4.62	355	3.47	1.18×10^8	1.70×10^8	0.70

[a] All spectra were measured at 295 K. [b] Quantum yield is calculated relative to quinine ($\Phi_f = 0.55$ in 0.1 M H_2SO_4).

lenes (**5** and **6**) with single and double banana structures are highly efficient light emitters despite the interruption of the π conjugation. The emission efficiency is interpreted in terms of k_r and k_d values. A new concept on movability of the dipolar dimethoxyphenylethynylpyridine structure (in other words, the number of dipolar diad units structurally equivalent to **17**) in the excited singlet state molecules is presented to explain the results. A quite contrasting effect of the solvent on the emission efficiency was observed for **5** and **6**, which might be explained by the marked disparity between the difference density distribution in the excited states of **5** and **6**. The emission efficiency of **3** (very weak fluorophore) was found to dramatically increase on formation of a Ti^{IV} complex. The main reason for this is ascribed to the increase in the electron-accepting ability of the pyridine C=N groups by the coordination to Ti^{IV} centers.

Received: June 24, 2005
Published online: October 11, 2005

Keywords: C–C coupling · conjugation · luminescence · solvent effects · titanium

[1] a) T. Nori, T. Sekine, J. Watanabe, T. Furukawa, H. Takezoe, *J. Mater. Chem.* **1996**, *6*, 1231–1233; b) G. Pelzl, S. Diele, W. Weissflog, *Adv. Mater.* **1999**, *11*, 707–724, and references therein; c) D. M. Walba, E. Korblova, R. Shao, J. E. Maclennan, D. R. Link, M. A. Glases, N. A. Clark, *Science* **2000**, *288*, 2181–2183; d) R. Pratibha, N. V. Madbusundana, B. K. Sadashiva, *Science* **2000**, *288*, 2184–2187; e) J. Barbera, N. Gimeno, L. Monreal, R. Pinol, B. Ros, J. L. Serrano, *J. Am. Chem. Soc.* **2004**, *126*, 7190–7191; f) N. Ginemo, M. B. Ros, J. L. Serrano, M. R. de la Fuente, *Angew. Chem.* **2004**, *116*, 5347–5350; *Angew. Chem. Int. Ed.* **2004**, *43*, 5235–5238; g) C. Keith, R. A. Reddy, U. Baumeisster, C. Tschierske, *J. Am. Chem. Soc.* **2004**, *126*, 14312–14313.

[2] a) Y. Pang, J. Li, B. Hu, F. E. Karasz, *Macromolecules* **1998**, *31*, 6730–6732; b) R. B. Pince, J. G. Saven, P. G. Wolynes, J. S. Moore, *J. Am. Chem. Soc.* **1999**, *121*, 3114–3121; c) S. Lahii, J. L. Thompson, J. S. Moore, *J. Am. Chem. Soc.* **2000**, *122*, 11315–11319; d) A. Zhu, J. Mio, J. S. Moore, H. G. Drickamer, *J. Phys. Chem. B* **2001**, *105*, 12374–12377; e) S. Anderson, *Chem. Eur. J.* **2001**, *7*, 4706–4714; f) H. Huang, K. Wang, W. Tan, D. An, X. Yang, S. Huang, Q. Zhai, L. Zhou, Y. Jin, *Angew. Chem.* **2004**, *116*, 5753–5756; *Angew. Chem. Int. Ed.* **2004**, *43*, 5635–5638; g) S. Shotwell, P. M. Windscheif, M. P. Smith, U. H. F. Bunz, *Org. Lett.* **2004**, *6*, 4151–4154; h) M. Hirohata, K. Tada, T. Kawai, M. Onoda, K. Yoshino, *Synth. Met.* **1997**, *85*, 1273–1274.

[3] K. Sonogashira in *Comprehensive Organic Synthesis, Vol. 3* (Eds.: B. M. Trost, I. Fleming), Pergamon, Oxford, **1991**, pp. 521–549.

[4] C. Songkram, K. Takaishi, K. Yamaguchi, H. Kagechika, Y. Endo, *Tetrahedron Lett.* **2001**, *42*, 6365–6368.

[5] a) M. A. Pena, I. Perez, J. P. Sestelo, L. A. Sarandeses, *Chem. Commun.* **2002**, *43*, 2246–2247; b) A. Orita, T. Nakano, T. Yokoyama, G. Babu, J. Otera, *Chem. Lett.* **2004**, *33*, 1298–1299.

[6] Y. Yamaguchi, S. Kobayashi, S. Miyamura, Y. Okamoto, T. Wakamiya, Y. Matsubara, Z. Yoshida, *Angew. Chem.* **2004**, *116*, 370–373; *Angew. Chem. Int. Ed.* **2004**, *43*, 366–369.

[7] The details of the synthesis and light-emitting characteristics of **15** and **16** will be reported elsewhere.

[8] a) J. A. Barltrop, J. D. Coyle, *Principles of photochemistry*, Wiley, New York, **1978**, p. 68; b) N. Leventis, A.-M. M. Rawashdeh, I. A. Elder, J. Yang, A. Dass, C. Sotiriou-Leventis, *Chem. Mater.* **2004**, *16*, 1493–1506.

[9] Y. Yamaguchi, T. Wakamiya, Y. Matsubara, Z. Yoshida, unpublished results.

[10] Y. Yamaguchi, T. Tanaka, S. Kobayashi, T. Wakamiya, Y. Matsubara, Z. Yoshida, *J. Am. Chem. Soc.* **2005**, *127*, 9332–9333.

[11] A. Beeby, K. S. Findlay, P. J. Low, T. B. Marder, P. Matousek, A. W. Parker, S. R. Rutter, M. Towrie, *Chem. Commun.* **2003**, 2406–2407.

[12] For example, a) J. N. Wilson, U. H. F. Bunz, *J. Am. Chem. Soc.* **2005**, *127*, 4124–4125; b) K. A. Walters, K. D. Ley, C. S. P. Cavalaheiro, S. E. Miller, D. Gosztola, M. R. Wasielewski, A. P. Bussandri, H. v. Willigen, K. S. Schange, *J. Am. Chem. Soc.* **2001**, *123*, 8329–8342; c) V. Patroniak, P. N. W. Baxter, J.-M. Lehn, Z. Hnatejko, M. Kubicki, *Eur. J. Inorg. Chem.* **2004**, 2379–2384; d) S. Höger, *Angew. Chem.* **2005**, *117*, 3872–3875; *Angew. Chem. Int. Ed.* **2005**, *44*, 3806–3808.

[13] We confirmed the formation of $[Ti^{IV}Cl_3]^+ \cdot OT_f^-$ from $TiCl_4$ and $AgOT_f$ by mass spectrometry (FAB MS; positive mode: *m*/*z* 153 ($TiCl_3^+$), negative mode: *m*/*z* 149 ($CF_3SO_3^-$)).

[14] S. Kobayashi, Y. Yamaguchi, T. Wakamiya, Y. Matsubara, K. Sugimoto, Z. Yoshida, *Tetrahedron Lett.* **2003**, *44*, 1469–1472.

[15] Y. Yamaguchi, Z. Yoshida, *Chem. Eur. J.* **2003**, *9*, 5430–5440.

[16] Other complexes such as the cyclic dimer and oligomer were not detected even by other mild MS techniques (MALDI TOF MS and ESI-LC MS).

 © 2005 Wiley-VCH Verlag GmbH & Co. KGaA, Weinheim

Biosynthesis

DOI: 10.1002/anie.200501942

Systematic Investigation of the *Escherichia coli* Metabolome for the Biosynthetic Origin of an Isocyanide Carbon Atom**

Sean F. Brady and Jon Clardy*

In vivo studies on the biosynthesis of natural products are often hampered by the inability to predictably control the metabolome of the producing organism. In contrast, when biosynthetic pathways are expressed in well-understood model organisms, the ability to predictably control metabolism through the use of mutant strains allows pathways to be examined with a rigor that cannot be achieved in the wild-type-producing organism. Recently, we have described the isolation and characterization of the isocyanide-containing antibiotic **1** along with its biosynthetic genes (*isnA* and *isnB*) from an environmental DNA (eDNA) clone.[1] The ability to control *Escherichia coli* metabolism systematically through the mutagenesis of genes that code for primary metabolic enzymes has enabled us to elucidate the biosynthetic origin of the isocyanide functional group found in **1** (Scheme 1).

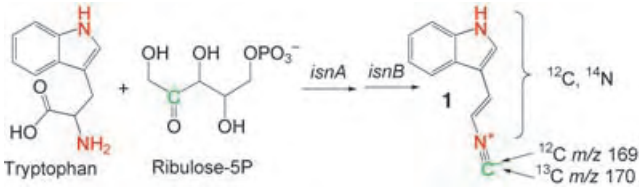

Scheme 1. Compound **1** is derived from tryptophan and C2 of ribulose-5P. Predicted *m/z* $[M+H]^+$ values for isotopically labeled **1** are shown.

Almost fifty years after the discovery of the first isocyanide-functionalized natural product, xanthocillin, no consensus view of isocyanide biosynthesis has emerged from the extensive feeding studies that use isocyanide-producing organisms.[2,3] The origin of the carbon atom of the isocyanide group found in **1** is presented herein.

In most biosynthetic studies, a hint as to the origin of a fragment can be seen in its structure, but the lone carbon atom of an isocyanide group contains no such clue. In a normal feeding study, labeled precursors are added to an unlabeled background to decipher the origin of the atoms in a molecule; however, because of the abundance of possible isocyanide precursors, we chose to use an "inverse-labeling" strategy to study the origin of the carbon atom of the isocyanide group. In this approach, ^{12}C precursors are added to a ^{13}C background, thus eliminating the need to synthesize a ^{13}C (or ^{14}C) sample of every precursor.

Feeding studies that used native-isocyanide-producing organisms have suggested that the isocyanide carbon atom might be derived from an amino acid.[2,3] To test this hypothesis, we carried out feeding studies using *isnA*/*B*, the biosynthetic pathway for **1**, expressed in *E. coli* amino acid auxotrophs.[4] Each auxotroph was grown in minimal media that contained ^{13}C-glucose, ^{12}C-tryptophan, and the appropriate ^{12}C-amino acids needed to compensate for the auxotrophies. Compound **1** isolated from these cultures always has an observed *m/z* value of 170, which is consistent with its containing ten carbon atoms from ^{12}C-tryptophan,[5] the isocyanide carbon atom from ^{13}C-glucose, and no carbon atoms from the other ^{12}C-amino acids added to the media. By using this strategy, the amino acids colored dark blue in the overview of the *E. coli* metabolome shown in Figure 1 were ruled out as precursors in the biosynthesis of the isocyanide functional group.

None of the amino acids tested labeled the isocyanide carbon atom, so we chose to examine the remainder of the *E. coli* metabolome systematically for the source of the isocyanide carbon atom. Figure 1 summarizes the differential labeling of **1** in a variety of *E. coli* strains deficient in key primary metabolic enzymes. Each strain was transformed with *isnA*/*B* and grown in an isotopically defined mixture of carbon sources such that unique regions of the metabolome were labeled in isotopically distinct manners. This approach allowed us to rapidly investigate the entire *E. coli* metabolome for the source of the isocyanide carbon atom. When the carbon flow between early and late glycolysis is blocked by a mutation in *gapA*, the *E. coli* metabolome is dissected into two distinct carbon pools (Figure 1). Compound **1** isolated from a *gapA* mutant transformed with *isnA*/*B* and grown in ^{13}C-glucose, ^{12}C-malate from the tricarboxylic acid cycle, and ^{12}C-tryptophan has an observed *m/z* value of 170. The isocyanide carbon atom is, therefore, derived from a descendant of ^{13}C-glucose before the conversion of glyceraldehyde-3P to 1,3-bis-phosphoglycerate by GAPDH. In addition to the dark-blue regions in Figure 1, the peach-colored area of the *E. coli* metabolome could now also be eliminated as a source of the isocyanide carbon atom.

The pentose phosphate pathway is central to the remaining portion of the *E. coli* metabolome from which the isocyanide carbon atom must be derived (Figure 1). We tested the major metabolic branches that arise from the pentose phosphate pathway as possible sources of the isocyanide carbon atom.[6] *E. coli* strains that contain mutations in genes that represent the metabolic entrance points into the following pentose pathway branch points were transformed with *isnA/B* (Figure 1):[6] glycerol-derived metabolites (*fba*), sugar phosphates (*manA* and *glmS*),

[*] Dr. S. F. Brady, Prof. J. Clardy
Department of Biological Chemistry and Molecular Pharmacology
Harvard Medical School
240 Longwood Avenue, Boston, MA 02115 (USA)
Fax: (+1) 617-432-3702
E-mail: sean_brady@hms.harvard.edu

[**] We thank NIH CA24487 (J.C.) and the Ellison Medical Foundation (J.C.) for support of this work. We thank the *E. coli* Genetic Stock Center (CGSC) for provision of *E. coli* strains used in the feeding experiments and Bjarne Hove-Jensen (University of Copenhagen) for the *prs* mutant.

Supporting information for this article is available on the WWW under http://www.angewandte.org or from the author.

 © 2005 Wiley-VCH Verlag GmbH & Co. KGaA, Weinheim

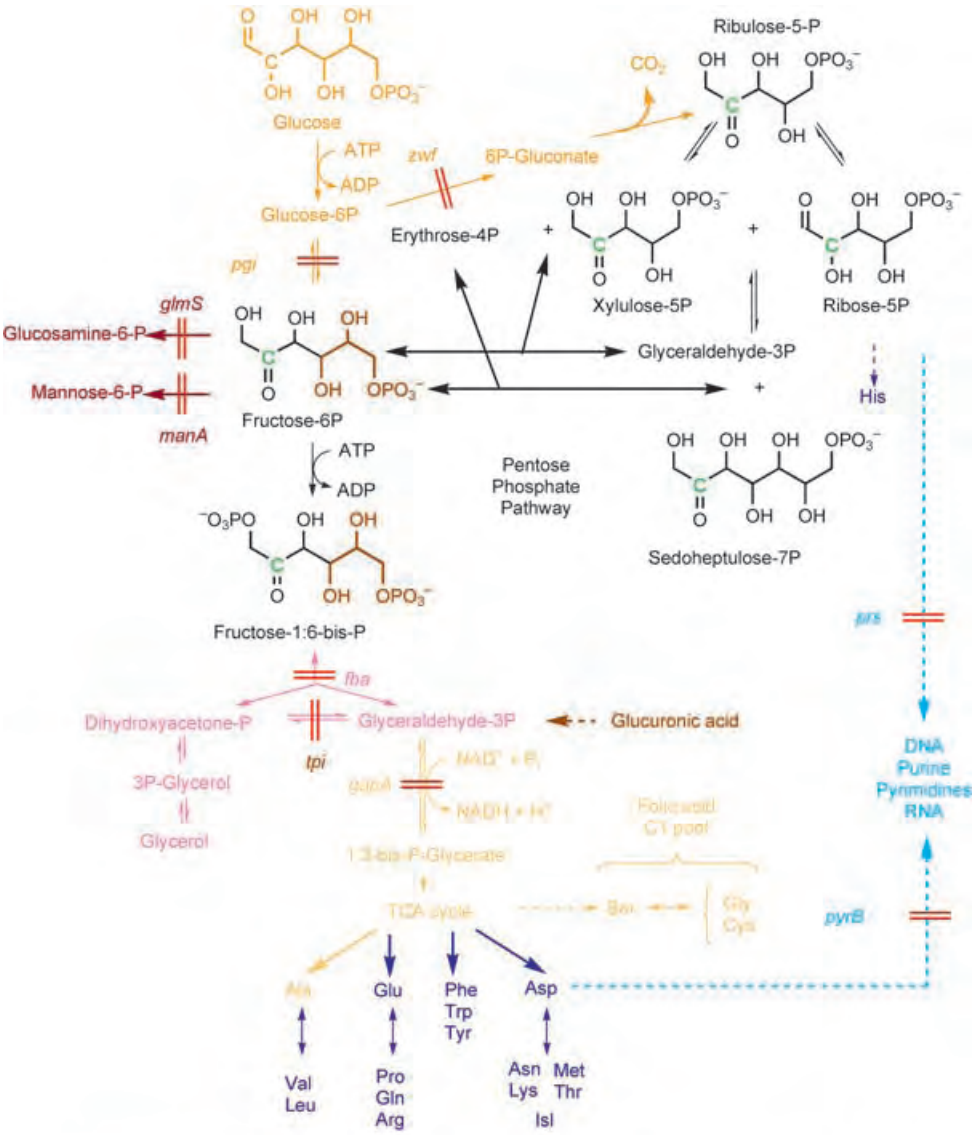

Mutation(s)	^{13}C source	^{12}C source(s)	*m/z*	^{13}C/^{12}C
a.a. auxotrophs	^{13}C-glucose	^{12}C-amino acid(s)	170	^{13}C
gapA	^{13}C-glucose	^{12}C-malate	170	^{13}C
fba	^{13}C-glucose	^{12}C-3P-glycerol	170	^{13}C
manA	^{13}C-glucose	^{12}C-mannose	170/169	^{13}C/^{12}C
glmS	^{13}C-glucose	^{12}C-glucosamine	170/169	^{13}C/^{12}C
pgi/zwf	^{13}C-glucose	^{12}C-fructose	169	^{12}C
prs or *pyrB*	^{13}C-glucose	^{12}C-multiple	170	^{13}C
tpi	^{13}C-glycerol	^{12}C-glucuronic acid	170	^{13}C
zwf	^{13}C-2C-glucose	^{12}C-1,2,4,5,6C-glucose	170	^{13}C

Figure 1. The systematic differential labeling of **1** produced by *E. coli* strains deficient in specific primary metabolic enzymes (=) indicates that the isocyanide carbon atom is derived from the C2 atom (C) of an intermediate in the pentose phosphate pathway. Color is used to designate the region of metabolism that was ruled out with feeding experiments in different *E. coli* mutants. a.a. = amino acids, *gapA* = glyceraldehyde-3P dehydrogenase (GAPDH), *fba* = fructose-1,6-bisphosphate aldolase, *manA* = mannose-6-phosphate isomerase, *glmS* = L-glutamine:D-fructose-6-phosphate aminotransferase, *prs* = ribose-phosphate diphosphokinase, *pyrB* = aspartate transcarbamylase, *pgi* = phosphoglucose isomerase, *zwf* = glucose-6-phosphate-1-dehydrogenase, ATP = adenosine triphosphate, ADP = adenosine diphosphate.

nucleic acids (*prs* and *pyrB*), and glucose-derived metabolites (*pgi* and *zwf*).[7] Each strain was grown in ^{12}C-tryptophan, ^{13}C-glucose, and a ^{12}C-carbon source(s) that would supply an isotopically distinct carbon pool to the blocked region of metabolism (Figure 1).[7] In each feeding experiment, we observed that the isocyanide carbon atom was derived from the carbon source that is able to flux into the pentose phosphate pathway and not the blocked region of metabolism. In the case of *manA* and *glmS*, each of which block the exit of metabolites from the pentose phosphate pathway but not the entrance, we detected a mixture of labeled and unlabeled isocyanide groups (Figure 1). As with the other feeding studies, this suggests that the isocyanide carbon atom must be derived from the carbon source that is able to flux into the pentose phosphate pathway and not the blocked region of metabolism. The regions colored pink (glycerol metabolites, *fba*), purple (sugar phosphates, *manA* or *glmS*), orange (glucose metabolites, *pgi*/*zwf*), and light blue (nucleic acids, *prs* or *pyrB*) in Figure 1 could, therefore, now also be excluded as sources of the isocyanide carbon atom. Taken together, these feeding studies indicate that the isocyanide carbon atom is likely to be derived from one of the eight sugars directly involved in the pentose phosphate shunt (Figure 1, black), the major region of metabolism that was not eliminated by our feeding experiments.[8]

Additional feeding experiments were performed to determine which of the carbon atoms present in early glycolytic hexose intermediates feeds directly into the isocyanide carbon atom. In a triose-phosphate isomerase (*tpi*) mutant, the C1-C2-C3 and C4-C5-C6 units of early glycolytic intermediates can be differentially labeled using glycerol and glucuronic acid. Compound **1** that has been isolated from cultures of a *tpi* knockout, transformed with *isnA*/*B*, and grown in media that contain ^{13}C-glycerol and ^{12}C-glucuronic acid (Figure 1, brown) has an observed *m*/*z* value of 170. Therefore, the isocyanide carbon atom must arise from ^{13}C-glycerol,

© 2005 Wiley-VCH Verlag GmbH & Co. KGaA, Weinheim

which corresponds to the C1-C2-C3 portion of early glycolytic hexose intermediates (Figure 1, black). The carbon atoms derived from glucuronic acid (Figure 1, brown) could, therefore, also be eliminated as possible sources of the isocyanide carbon atom.

A *zwf*-deficient strain of *E. coli,* which helps to prevent the scrambling of labeled sugars in the pentose phosphate shunt by blocking the decarboxylation of 6P-gluconate, was used to determine which of the three remaining carbon atoms is incorporated into the isocyanide functionality. The *zwf*-knockout strain grown on C1-labeled ^{13}C-glucose did not produce ^{13}C-labeled **1**, whereas cultures grown on either universally labeled or C2-labeled ^{13}C-glucose almost exclusively produced ^{13}C-labeled **1** (Figure 2). In this system, the C2 atom in glucose specifically labels only six major sugars that were not excluded as a source of the isocyanide carbon atom by our other feeding studies. The six remaining metabolites (fructose-6P, fructose-1,6-bis-P, ribulose-5P, ribose-5P, xylulose-5P, and sedoheptulose-7P) are shown in Figure 1 and the C2 position of each is highlighted in green. Five of these six sugar phosphates are commercially available and were therefore tested in in vitro reconstitution experiments.[9] The in vitro reconstitution experiments using purified IsnA, IsnB, tryptophan, α-ketoglutarate, and both ribulose-5P and ribose-5P were found to produce a compound with the same retention time and mass as the naturally occurring **1**. Other commercially available C4–C7 sugars and sugar phosphates were tested in the same reconstitution system, and only arabinose-5P was found to result in isocyanide production.[10]

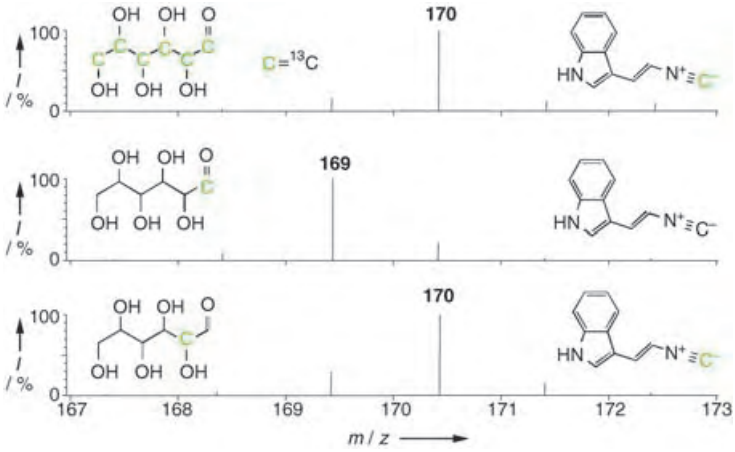

Figure 2. The *m*/*z* values observed for **1** obtained from cultures of *E. coli* transformed with *isnA*/*B* and grown in uniformly C1- and C2-labeled ^{13}C-glucose.

To investigate the source of the isocyanide carbon atom in vitro, C1- and C2-labeled ^{13}C-ribose were phosphorylated with recombinant *E. coli* ribokinase (rbsK), and each of the products was used for the in vitro biosynthesis of **1**.[11] As suggested by the in vivo feeding experiments, the C2 atom of the sugar phosphate is used in the enzymatic synthesis of **1**. C1-labeled ribose leads to the production of unlabeled **1** (*m*/*z* 169), whereas C2-labeled ribose leads to a ^{13}C-labeled isocyanide group (*m*/*z* 170). The tautomerization of ribose-5P and arabinose-5P to ribulose-5P either in solution or in an enzyme-assisted fashion could explain the use of all three sugars in the in vitro system (Scheme 2). 2-Deoxyriobose-5P, which cannot tautomerize to the equivalent keto sugar, does not serve as a substrate for the enzymatic synthesis of **1** by using this system.

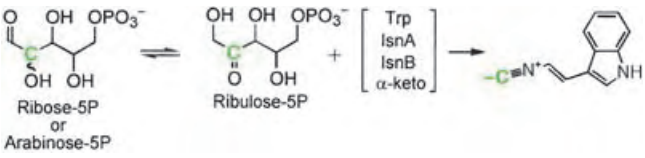

Scheme 2. The tautomerization of aldo and keto sugars may explain the use of different regio- and stereochemical sugar isomers in the enzymatic synthesis of **1**.

The ability to control *E. coli* metabolism through the systematic use of strains that carry mutations in primary metabolic pathways allowed us to identify the origin of the isocyanide carbon atom in **1** as the C2 atom of ribulose-5P, or a tautomerically equivalent sugar. As shown previously, the isocyanide nitrogen atom can be traced to the amine functionality in tryptophan.[1] The isocyanide group present in many known microbial natural products can also theoretically be traced to the free amine moiety of an amino acid.[2] The proposed biosynthetic scheme for **1** may, therefore, be general for the biosynthesis of microbial-derived isocyanides. The differential labeling of natural products produced by microorganisms that carry mutations in primary metabolic genes that lead to predictable changes in the microbial metabolome can now be carried out in a systematic fashion in many model microorganisms and could be a generally useful strategy for the study of the biosynthetic origin of individual atoms found in microbial secondary metabolites.

Received: June 4, 2005
Revised: August 4, 2005
Published online: October 11, 2005

Keywords: biosynthesis · DNA · heterologous expression · isocyanides · natural products

[1] S. F. Brady, J. Clardy, *Angew. Chem.* **2005**, *115*, 7225; *Angew. Chem. Int. Ed.* **2005**, *44*, 7063.
[2] I. Hagendorn, H. Tonjes, *Pharmazie* **1957**, *5*, 567.
[3] a) R. B. Herbert, J. Mann, *Tetrahedron Lett.* **1984**, *25*, 4263; b) R. B. Herbert, J. Mann, *J. Chem. Soc. Chem. Commun.* **1984**, 1474; c) M. S. Puar, H. Munayyer, V. Hegde, B. K. Lee, J. A. Waitz, *J. Antibiot.* **1985**, *38*, 530; d) J. E. Baldwin, H. S. Bansal, J. Chondrogianni, L. D. Field, A. A. Taha, V. Thaller, *Tetrahedron* **1985**, *41*, 1931; e) V. Bornemann, G. M. L. Patterson, R. E. Moore, *J. Am. Chem. Soc.* **1988**, *110*, 2339; f) C. W. J. Chang, P. J. Scheuer, *Comp. Biochem. Physiol. Part B* **1990**, *97*, 227; g) P. J. Scheuer, *Acc. Chem. Res.* **1992**, *25*, 433; h) K. M. Cable, R. B.

 © 2005 Wiley-VCH Verlag GmbH & Co. KGaA, Weinheim

Herbert, A. R. Knaggs, J. Mann, *J. Chem. Soc. Perkin Trans. 1* **1991**, 595.

[4] Strains used in the amino acid feeding studies are referenced as follows: strain name (*E. coli* genetic stock center (CGSC) number) reference: a) Strain AB1359 (CGSC 1359) A. L. Taylor, M. S. Thoman, *Genetics* **1964**, *50*, 659; b) Strain S1228 (CGSC 6432) A. del Campillo-Campbell, A. Campbell, *J. Bacteriol.* **1982**, *149*, 469; c) Strain DG30 (CGSC 5799) D. H. Gelfand, R. A. Steinberg, *J. Bacteriol.* **1977**, *130*, 429; d) Strain KL285 (CGSC 4310) S. J. Clarke, B. Low, W. Konigsberg, *J. Bacteriol.* **1973**, *113*, 1096.

[5] All feeding experiments were carried out in the presence of ^{12}C-tryptophan, the tryptophan portion of **1** is, therefore, always derived from a ^{12}C source; see the Supporting Information for a more detailed description of the feeding-experiment methods.

[6] G. A. Sprenger, *Arch. Microbiol.* **1995**, *164*, 324.

[7] Strains used in the differential labeling studies are referenced as follows: relevant mutation(s), strain name (CGSC number) reference: a) *gapA*, DS112 (CGSC 7563) F. D. Seta, S. Boschi-Muller, M. L. Vignais, G. Branlant, *J. Bacteriol.* **1997**, *179*, 5218; b) *fba*, JM2087 (CGSC 6806) E. O. Davis, M. C. Jones-Mortimer, P. J. Henderson, *J. Biol. Chem.* **1984**, *259*, 1520; c) *manA*, JE5511 (CGSC 5505) Y. Hirota, H. Suzuki, Y. Nishimura, S. Yasuda, *Proc. Natl. Acad. Sci. USA* **1977**, *74*, 1417; d) *manA*, F500/GMS724 (CGSC 6673) M. Novel, G. Novel, *J. Bacteriol.* **1976**, *127*, 406; e) *glmS*, E111 (CGSC 5393) H. C. Wu, T. C. Wu, *J. Bacteriol.* **1971**, *105*, 455; f) *zwf* and *pgi*, DF2000 (CGSC 4873) D. G. Fraenkel, S. Banerjee, *Genetics* **1972**, *71*, 481; g) *prs*, HO733; B. Hove-Jensen, *J. Bacteriol.* **1996**, *178*, 714; h) *pyrB*, Hfr 3000 pyr (CGSC 6851) J. R. Beckwith, A. B. Pardee, R. Austrian, F. Jacob, *J. Mol. Biol.* **1962**, *5*, 618; i) *tpi*, AA200 (CGSC 5570) A. Anderson, R. A. Cooper, *J. Gen. Microbiol.* **1970**, *62*, 329; j) *zwf*, K10-15-16 (CGSC 4848).

[8] Metabolites downstream of xylulose-5P and ribulose-5P were not ruled out in these experiments.

[9] Xylulose-5P was not tested because it was not commercially available.

[10] The following sugars were tested in reconstitution experiments: ribulose-5P, ribose-5P, arabinose-5P, erythrose-4P, ribulose, ribose, arabinose, xylose, xylulose, glucose-6P, glucosamine-6P, 6P-gluconate, fructose, fructose-6P, fructose-1:6-bis-P, mannose, mannose-6P, allose, sedoheptulose-7P, and 2-deoxyribose-5P; only a small quantity of **1** is produced in the reconstitution system; experiments are being performed to look for possible cofactor and Fe requirements (see the Supporting Information for cloning, protein-expression, and reconstitution procedures).

[11] a) J. N. Hope, A. W. Bell, M. A. Hermodson, J. M. Groarke, *J. Biol. Chem.* **1986**, *261*, 7663; b) C. E. Andersson, S. L. Mowbray, *J. Mol. Biol.* **2002**, *315*, 409.

 © 2005 Wiley-VCH Verlag GmbH & Co. KGaA, Weinheim

Hybrid Materials

DOI: 10.1002/anie.200501748

Thermolysis of a Hybrid Organic–Inorganic Supramolecular Coordination Assembly: Templating the Formation of Nanostructured Fibrous Materials and Carbon-Based Microcapsules**

Wolfgang Schmitt, Jonathan P. Hill, Sharali Malik, Cynthia A. Volkert, Izumi Ichinose, Christopher E. Anson, and Annie K. Powell**

Materials of nanosize or bearing nanoscale features represent a significant class of substance that have the potential for advanced applications because of their superior chemical and physical properties.[1] The preparation and characterization of such substances is, therefore, of interest not only from a scientific viewpoint but because of their possible uses in such diverse fields as catalysis[2] and microelectronics.[3] Currently, much attention is focused on inorganic nanotubes, organic polymers, and nanostructured inorganic oxides whose properties endow them with considerable potential.[4]

The structures and properties of nanosized hybrid organic–inorganic materials are influenced by the functionalities present in both the inorganic and organic components,[5] whereas the use of coordination compounds as templates or precursors in decomposition processes is a

[*] Dr. W. Schmitt, Dr. J. P. Hill, Dr. C. E. Anson, Prof. A. K. Powell
Institut für Anorganische Chemie
Universität Karlsruhe
Engesserstrasse Geb. 30.45, 76128 Karlsruhe (Germany)
Fax: (+49) 721-608-8142
E-mail: schmitt.wolfgang@nims.go.jp
powell@chemie.uni-karlsruhe.de

Dr. W. Schmitt, Dr. J. P. Hill
National Institute for Materials Science
International Centre for Young Scientists
Tsukuba, 1-1 Namiki, Ibaraki 305 0044 (Japan)
Fax: (+81) 29-860-4708

Dr. S. Malik
Institut für Nanotechnologie (INT)
Forschungszentrum Karlsruhe
76344 Eggenstein-Leopoldshafen (Germany)

Dr. C. A. Volkert
Institut für Materialienforschung (IMF)
Forschungszentrum Karlsruhe
76344 Eggenstein-Leopoldshafen (Germany)

Dr. I. Ichinose
Advanced Materials Laboratory
National Institute for Materials Science
1-1 Namiki, Tskuba, Ibaraki 305-0044 (Japan)

[**] This work was supported by the DFG "Center for Functional Nanostructures (CFN)" and the Special Coordination Funds for Promoting Science and Technology from MEXT, Japan through ICYS Fellowships (W.S. and J.P.H.).

Supporting information for this article is available on the WWW under http://www.angewandte.org or from the author.

InterScience
© 2005 Wiley-VCH Verlag GmbH & Co. KGaA, Weinheim

promising strategy for the synthesis of nanocomposites.[6] Supramolecular coordination compounds that contain nanosized features within their structures are ideal precursor candidates for these purposes. One aim of such investigations is to develop an understanding of how the structures of the precursor complexes influence the structure and stoichiometry of the decomposition products. Thermolysis of metal complexes is already widely used for the synthesis of superconducting, nanocrystalline mixed-metal oxides[7] and also for the incorporation of transition-metal ions into porous carriers, such as zeolites or silicates.[8] Hybrid materials themselves can have unique properties, and their synthesis on the atomic-to-mesoscopic scales can have significant impact on diverse fields of technology.[9]

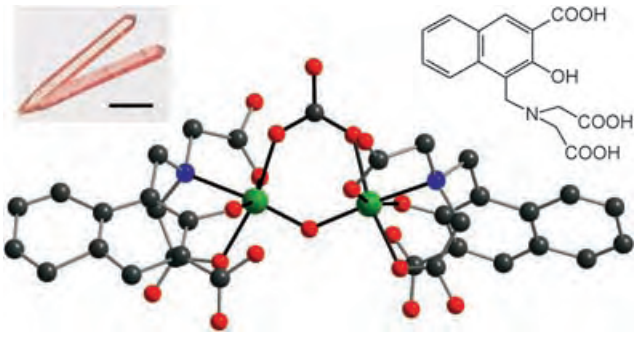

Figure 1. Structure of the dinuclear $[Fe_2(\mu\text{-}O)(\mu\text{-}CO_3)(chnida)_2]^{6-}$ unit contained in **1** (Fe: green, O: red, N: blue, C: gray). Inset: crystals of **1** (left; scale bar: 300 μm) and the organic chnida ligand (right).

Reaction systems that contain large organic hydrophobic ligands and hydrophilic ions favor the formation of cross-linked structures in which supramolecular aggregates are organized within vast areas of different polarities. We have previously described how increased steric hindrance around aromatic cycles (L) influences the topology and dimensionality of coordination chemistry networks based on $\{Fe_2(\mu\text{-}O)(\mu\text{-}CO_3)(L)_2\}$ units,[10,11] thus bringing a new dimension to the now classical isoreticular chemistry concept. Herein, we describe the pyrolysis of an example of one of these compounds. The coordination network used in these investigations, $Na_6[Fe_2(\mu\text{-}O)(\mu\text{-}CO_3)(chnida)_2]\cdot 13.5\,H_2O$ (**1**; chnida = *N*-[(3-carboxy-2-oxy-naphthyl)methylene]iminodiacetato), consists of a simple oxo/carbonato bridged diiron(III) unit coordinated by two chnida ligands. Figure 1 shows the basic diiron unit $[Fe_2(\mu\text{-}O)(\mu\text{-}CO_3)(chnida)_2]^{6-}$ within the structure of complex **1**, together with the chemical structure of the ligand and an optical micrograph of crystals of the complex. Within the dinuclear transition-metal complex, nitrogen and oxygen donors of the iminodiacetic acid moiety of the organic ligands occupy facial positions of the distorted octahedral coordination polyhedra, whereas the bridging O atom and the N-donors coordinate *trans* with respect to each other.

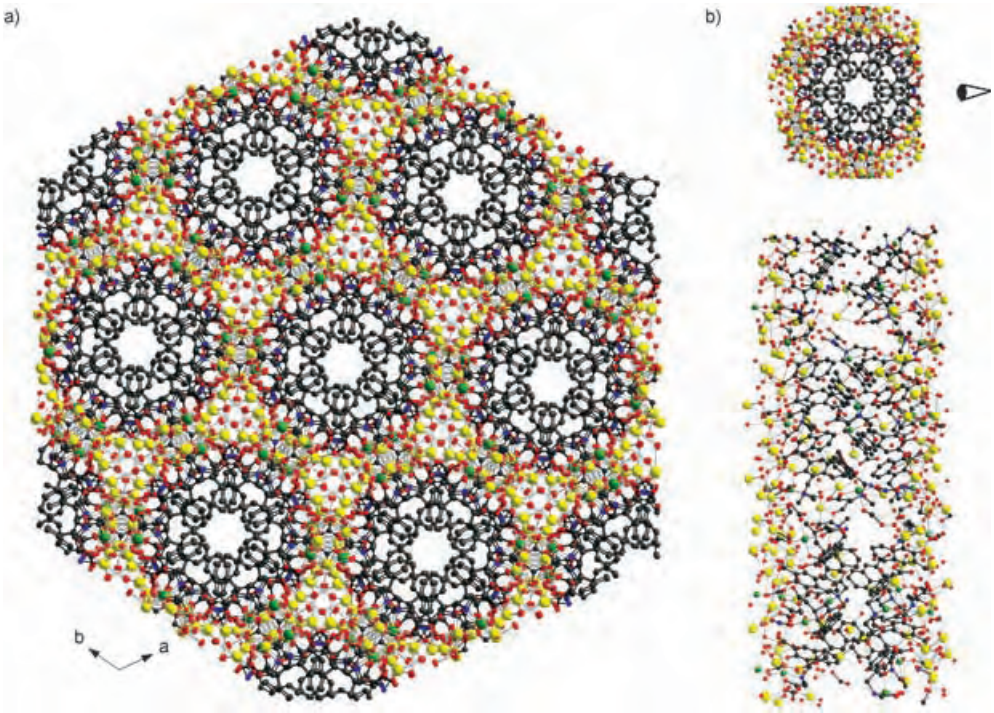

Figure 2. Supramolecular structure of **1**. a) Viewed along the *c* axis. b) Section through a channel viewed perpendicular to the *c* axis. (Fe: green, Na: yellow, O: red, N: blue, C: gray.)

Within the coordination ensemble (Figure 2), the $[Fe_2(\mu\text{-}O)(\mu\text{-}CO_3)(chnida)_2]^{6-}$ complexes are organized in such a way that the organic residues of the ligands are contained in tubular cavities that run along the long axis (crystallographic *c* axis) of the crystals. The intercavity spaces are occupied by hydrated sodium ions which are present to balance the negative charge of the diiron complex and which are linked to the complexes through oxygen donors. The hydrophobic cavities of this honeycomb-type structure have a maximum cross-sectional distance of approximately 1.2 nm. The preponderance for the hexagonal symmetry within the structure is consistent with the morphology of the compound, which crystallizes as needles with a hexagonal cross-section. Single-crystal X-ray analysis of **1** found its structure to be within the trigonal space group $R\bar{3}c$ and demonstrates that **1** is isostructural with its potassium analogue.[11,12] Further confirmation of the space-group assignment was gained from X-ray powder diffraction measurements and simulations (see the Supporting Information). The presence of clearly demarcated nanosized organic and inorganic regions organized into a honeycomb-type structure prompted us to speculate about the synthesis of materials with nanoscale features by using thermal decomposition.

Crystals of **1** are sensitive to solvent loss, and we investigated this behavior by cutting crystals, which had been stored for six weeks at room temperature, perpendicular to the *c* axis by using a focused gallium ion beam. Previously,

 © 2005 Wiley-VCH Verlag GmbH & Co. KGaA, Weinheim

we have successfully used electron microscopic techniques to identify structural patterns within crystals[11] and, in this case, the scanning electron microscopy (SEM) observation of the resulting *a*–*b* surface revealed a transformation of some regions of the crystal into fibers with a diameter of approximately 50–100 nm (Figure 3a). These fibers are coagulated into bundles. The IR and UV/VIS spectra and X-ray powder diffraction patterns of the crystals prior to and following desolvation are similar, which demonstrates that the structure of the dinuclear Fe^{III} unit is intact and that the structures of single crystals and the observed hybrid organic–inorganic fibers are closely related.

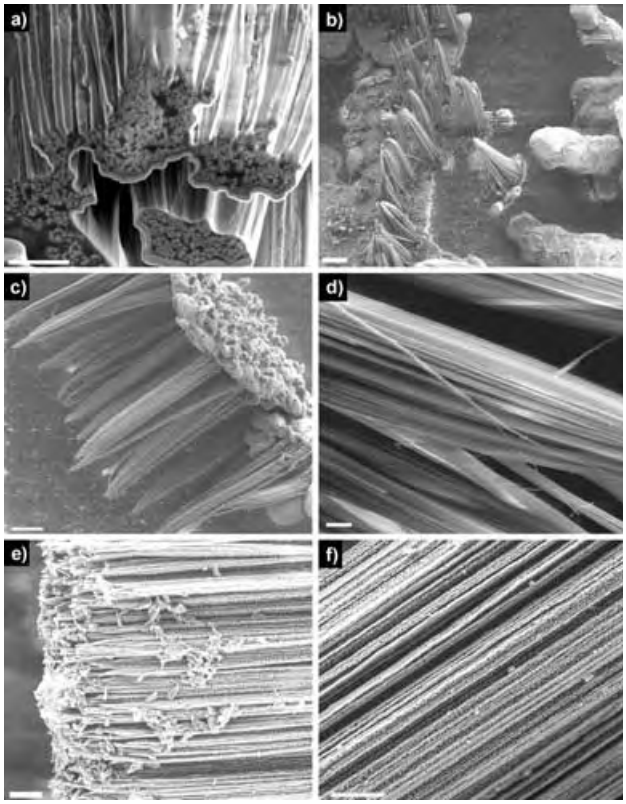

Figure 3. SEM images of **1**: a) A crystal cut perpendicular to the crystallographic *c* axis with a focused ion beam (scale bar: 2 μm). b) Crystals after thermolysis at 370 °C, thus showing fibers and burnt crystals in the same sample (scale bar: 20 μm). c) View of aggregated fibers (scale bar: 20 μm). d) Magnification showing some individual fibers (scale bar: 2 μm). e) and f) Further views of the fibrous structures (scale bars: 2 μm).

Thermolysis of crystals of **1** under nitrogen confirms fiber formation after desolvation (Figure 3b–f) and provides a means for variation of the fiber composition up to their decomposition at approximately 400 °C. Thermogravimetric analysis (TGA), in combination with TGA–MS, IR, and X-ray diffraction (XRD) analysis, provided information about the composition of the sample during thermolysis. On the basis of elemental analysis, the formula $Na_6[Fe_2(\mu\text{-}O)(\mu\text{-}CO_3)(chnida)_2]\cdot 9H_2O$ was assigned to crystalline samples of **1** used in this study. TGA events (Figure 4a) in the temperature range 25–140 °C result from solvent loss. The thermolytic destruction of the Fe^{III} complex occurs during the event between 250 and 350 °C and is accompanied by the formation of sodium carbonate, as demonstrated by FTIR and X-ray powder diffraction analysis (Figure 4b–d).[13] Samples thermolyzed at 350–370 °C were black in appearance because of deposition of amorphous carbon in the sample. This amorphous carbon was detected by TGA-MS (*m*/*z* 12 amu), and its formation is attributed to combustion of the ligand in an anoxygenic environment, such as that in the tubular channels of the crystals. This process is commonplace in the pyrolysis of organic molecules within zeolite templates in which efficient carbonization occurs at elevated temperatures.[14]

The combustion of the remnant carboniferous materials occurs between 380 and 480 °C. During this event, samples contain Na_2CO_3 and iron oxide species which further react between 480 and 600 °C with the loss of dioxide lost from the sample to form $NaFeO_2$.[15] X-ray powder diffraction patterns of samples of **1** heated to 600 °C identify the trigonal and orthorhombic phases of $NaFeO_2$ and γ-Na_2CO_3. Upon heating the sample to 1100 °C, sodium carbonate is no longer present and only the orthorhombic form of the binary sodium iron oxide can be observed (Figure 4c, d).[16]

We analyzed thermolyzed samples using scanning electron microscopy (SEM). Decomposition temperatures were selected by reference to thermogravimetric (TG) and differential thermogravimetric (*d*TG) data. Thus, the plateau between 350 and 390 °C in the *d*TG trace was selected as being of interest as it marks a borderline for the hybrid material transforming into purely inorganic product. At this point, the sample appears to be between two distinct weight losses. From the TGA–MS analysis, the first event entails loss of water, carbon dioxide, and small quantities of both benzene and naphthalene, whereas the second is dominated by loss of carbon monoxide, carbon dioxide, and water, together with benzene and other fragments from the incomplete combustion of the ligand. The SEM micrographs shown in Figures 3b–f and 5b show the result of the thermolysis of **1** at 370 °C and illustrate the formation of a highly aligned fibrous structure.

The energy dispersive X-ray analysis (EDAX) analysis confirms the presence of sodium carbonate in the fibrous material obtained at 370 °C, which is coated with a carbon-rich shell. The fibrous nature of the materials inside a thermolyzed crystal could also be observed through the carboniferous husks at several sites (see also Figure 5b). Closer observation of the fibers reveals that they have a cross-sectional thickness of 50 nm and tend to be segmented. This segmentation differs from the materials obtained at temperatures below 300 °C, in which the fibers are more homogeneous, or even microcrystalline, and contain the intact dinuclear complex.

To illustrate the structure of the product of the thermolysis of **1** at 370 °C, we have presented a scheme in Figure 5. Our observations and analysis rationalize the following thermally induced transformation process of single crystals. Components in a single crystal of **1** aggregate into fibers upon solvent loss. This process is enhanced by the morphology of the crystals and the supramolecular structure of the coordination compound, which contains nanosized channels of

 © 2005 Wiley-VCH Verlag GmbH & Co. KGaA, Weinheim

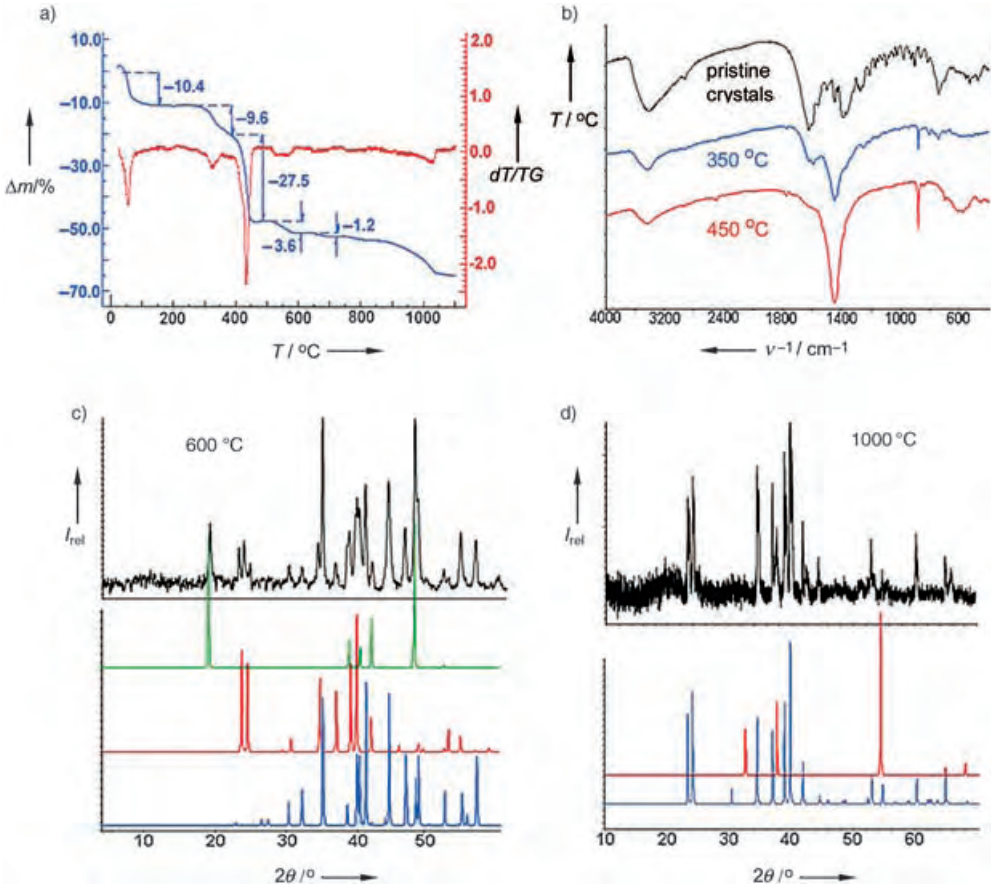

Figure 4. a) Thermogravimetric analysis of **1**. b) FTIR spectra of **1** and thermolyzed samples. c) XRD pattern of **1** thermolyzed to 600 °C; identification of the components was carried out by comparison with generated XRD patterns of trigonal $NaFeO_2$ (green), orthorhombic $NaFeO_2$ (red), and γ-Na_2CO_3. d) XRD pattern of **1** thermolyzed to 1000 °C; comparison with generated XRD patterns of orthorhombic $NaFeO_2$ (blue) and Na_2O (red).

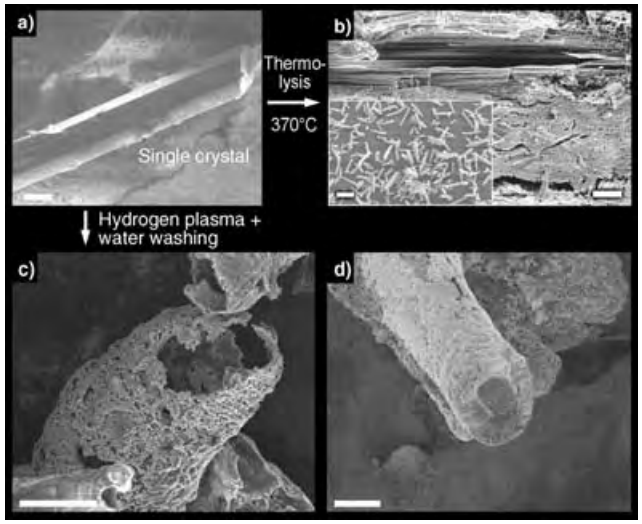

Figure 5. SEM images that illustrate microcapsular formations after crystal decomposition: a) Morphology of a single crystal (scale bar: 10 μm). b) Fibrous structure viewed through a break in the surface of a thermolyzed crystal (scale bar: 2 μm); inset: crystals thermolyzed in bulk (scale bar: 100 μm). c) Carbon microcapsule formed during plasma treatment of crystals of **1** after washing with water (scale bar: 10 μm). d) Cross-sectional view of broken carboniferous microcapsule (scale bar: 5 μm).

clearly separated polarity that run parallel to the longitudinal axis of the needlelike crystals. Heating of the resulting hybrid organic–inorganic fibers to 370 °C causes a chemical transformation in which they form sodium carbonate by decomposition of the dinuclear complex. The facile formation of sodium carbonate upon heating is dictated by the stoichiometry and the structure of the complex, which contains a large number of alkali-metal counterions that bind to carbonate and carboxylate oxygen atoms and are localized in the hydrophilic regions. Naphthoic acid derivatives are known to undergo facile decarboxylation upon heating, and the Na_2CO_3 formation is likely to be the result of this and other decomposition reactions. Further ligand decomposition at 370 °C and at higher temperatures enriches the carbon content at the outside of the burnt crystals so that sodium carbonate fibers are usually contained within capsules composed of amorphous carbon. Thus, it is relatively simple to remove the sodium carbonate by washing with water to leave the empty carbon capsule of micrometer dimensions, which is determined by the morphology of the crystalline precursor. Furthermore, it is possible to improve the formation of amorphous carbon by the application of a reductive process to the crystals of **1**, whereby the crystals are treated with a plasma of hydrogen gas at a temperature slightly higher than the decomposition temperature of 400 °C. In that case, much more robust carbon microcapsules are produced, as shown in Figure 5c,d.

High-surface-area sodium carbonates are used for the removal of SO_x, NO_x, HF, and HCl pollutants from industrial emissions.[17] The high activity of these sodium carbonates makes them the preferred substances for dry-sorbent injection processes; thus, they are used for flue-gas desulfurization and scrubbing, effectively decreasing the impact of acid rain on the environment.[17,18] Therefore, nanostructured particulates, or even better, sodium carbonate nanomaterials contained in microcapsular entities, are of substantial industrial interest. Such alkali or alkali-earth carbonates are currently used as NO_x storage/reduction catalysts for the cleansing of emissions from diesel engines.[19] Furthermore, alkali iron oxide phases also possess high activity for the reduction of

 © 2005 Wiley-VCH Verlag GmbH & Co. KGaA, Weinheim

NO_x emissions[20] and are the main active components of the industrially applied Fe_2O_3 dehydrogenation catalyst for the production of styrene from ethylbenzene.[21] It is interesting that we obtain such alkali iron oxides (e.g., the different phases $NaFeO_2$, $KFeO_2$, and $K_xFe_{22}O_{34}$ ($x = 2$–4)) in our system, albeit at elevated temperatures.

In summary, we have demonstrated that a hybrid organic–inorganic coordination complex with an extended 3D structure that contains separated organic and inorganic regions can be used as a template in thermal decomposition reactions that produce nano- and microsized products. Comparable thermolysis studies of crystals of such a hybrid compound have not been reported, and our results validate a synthetic concept for the preparation of nanostructured materials by taking advantage of a pristine crystalline coordination compound that contains the starting components from the thermolysis reaction that are prearranged in a 3D form. Thus, the molecular structure, stoichiometry, and crystal morphology of the precursor determines the 3D structure and constitution of the decomposition products: we obtained aligned nanosized hybrid organic–inorganic fibers by desolvation. Thermolysis changes the fiber composition and results in mainly fibrous sodium carbonate and a concomitant deposition of amorphous carbon at the crystal surface. If sufficient carbon is deposited, stable microcapsules can be obtained after removal of the sodium carbonate by washing with water, thus leaving the carbon microcapsules intact. The components react at higher temperatures to give different phases of sodium iron oxides. We are currently investigating the inorganic products obtained from thermolysis of **1** by transmission electron microscopy (TEM). In addition, we are preparing derivatives of **1** in which sodium ions have been substituted with a variety of metal ions and are carrying out thermolysis of these novel supramolecular transition-metal assemblies under different atmospheres.

Experimental Section

The starting materials were purchased from Aldrich Chemical Co. and used without further purification. Thermogravimetric analyses were carried out using a Netzsch STA 409C operating in the TG mode under both nitrogen and oxygen. TGA–MS measurements were performed on a similar device equipped with a quadrupole mass detector by using electron impact ionization. In that case, the analysis was done under vacuum. Scanning electron micrographs were obtained using a LEO 1530 SEM with a spatial resolution of 1 nm at 20 kV and 3 nm at 1 kV and equipped with an energy-dispersive X-ray analysis system EDX INCA 400 from Oxford Instruments. Focused ion-beam sectioning and scanning-electron micrographs of the sections were obtained using a FEI 200 × P dual beam SEM/FIB. FTIR spectra were obtained with KBr pellets of the analytes with a Perkin-Elmer Spectrum One spectrophotometer. XRD analysis was performed on a STOE Stadi *P* diffractometer (equipped with Ge monochromator) using $Co_{K\alpha}$ radiation ($\lambda = 1.78897$ Å). Sample thermolysis of **1** was performed using a Netzsch STA 409C apparatus with sample heating and cooling rates of 2 or 5 °C min^{-1}. The sample was held isothermally at the selected thermolysis temperature for 1 min.

The chnida ligand was prepared by the Mannich reaction[22] of 3-hydroxy-2-naphthoic acid: ^{1}H NMR ($D_2O + Na_2CO_3$): $\delta = 3.62$ (s, 4H), 4.35 (s, 2H), 7.42 (m, 1H), 7.65 (m, 1H), 7.86 (d, 1H, J(H,H′) = 8.0 Hz), 7.99 (d, 1H, J(H,H′) = 8.6 Hz), 8.29 ppm (s, 1H).

1: Ligand chnida (0.088 g, 2.64×10^{-4} mol) was treated with iron(III) chloride hexahydrate (0.142 g, 5.28×10^{-4} mol) in methanol (30 mL), followed by addition of 2 M aqueous sodium hydroxide (2 mL). Ethanol (20 mL) was added after dissolution of all reagents, and the solution container was covered with parafilm, which was perforated several times to allow slow evaporation of the solvent. It is vital that the solution is open to the atmosphere to allow dissolution of carbon dioxide into the reaction mixture. Small well-formed needles with a hexagonal base of **1** formed after 10 days. Yield: 0.09 g (56% based on chnida). Elemental analysis (%) calcd for ($C_{33}H_{49}Fe_2N_2Na_6O_{31.5}$): C 32.3, H 4.0, N 2.3; found C 32.6, H 4.2 N 2.4.[23]

Received: May 20, 2005
Published online: October 13, 2005

Keywords: iron · nanostructures · organic–inorganic hybrid composites · supramolecular chemistry · thermochemistry

[1] *Encyclopedia of Nanoscience and Nanotechnology, Vol. 1–10* (Ed.: H. S. Nalwa), American Scientific Publishers, CA, **2004**.
[2] a) R. Schlögl, S. B. A. Hamid, *Angew. Chem.* **2004**, *116*, 1656–1667; *Angew. Chem. Int. Ed.* **2004**, *43*, 1628–1637; b) N. Pinna, M. Willinger, K. Weiss, J. Urban, R. Schlögl, *Nano Lett.* **2003**, *3*, 1131–1134.
[3] a) D. A. Doshi, N. K. Huesing, M. Lu, H. Fan, Y. Lu, K. Simmons-Potter, B. G. Potter, A. J. Hurd, C. J. Brinker, *Nature* **2000**, *406*, 107–111; b) *Future Trends in Microelectronics* (Eds.: S. Luryi, J. Xu, A. Zaslavsky), Wiley-VCH, Weinheim, **2004**.
[4] a) M. Brorson, T.W Hansen, C. J. H. Jacobsen, *J. Am. Chem. Soc.* **2002**, *124*, 11582–11583, and references therein; b) J. Ruokalainen, G. ten Brinke, O. Ikkala, *Adv. Mater.* **1999**, *11*, 777–780; c) G. J. de A. A. Soler-Illia, C. Sanchez, B. Lebeau, J. Patarin, *Chem. Rev.* **2002**, *102*, 4093–4138; d) C. N. R. Rao, M. Nath, *Dalton Trans.* **2003**, 1–24.
[5] a) *Handbook of Organic–Inorganic Hybrid Materials and Nanocomposites, Vol. 1* (Ed.: H. S. Nalwa), American Scientific Publishers, CA, **2003**; b) O. M. Yaghi, M. O'Keeffe, N. W. Ockwig, H. K. Chae, M. Eddaoudi, J. Kim, *Nature* **2003**, *423*, 705–714; c) P. M. Forster, A. K. Cheetham, *Angew. Chem.* **2002**, *114*, 475–477; *Angew. Chem. Int. Ed.* **2002**, *41*, 457–459.
[6] C.-Y. Su, A. M. Goforth, M. D. Smith, P. J. Pellechia, *J. Am. Chem. Soc.* **2004**, *126*, 3576–3586.
[7] K. Knoth, R. Hühne, S. Oswald, L. Schultz, B. Holzapfel, *Supercond. Sci. Technol.* **2005**, *18*, 334–339.
[8] For example: a) J. Xu, M. Ekblad, S. Nishiyama, S. Tsuruya, M. Masai, *J. Chem. Soc. Faraday Trans.* **1998**, *94*, 473–479; b) T. Mishra, K. Parida, *J. Mater. Chem.* **1997**, *7*, 147–152.
[9] a) G. Ozin, *Chem. Commun.* **2000**, 419–432; b) M. Eddaoudi, J. Kim, N. Rosi, D. Vodak, J. Wachter, M. O'Keeffe, O. M. Yaghi, *Science* **2002**, *295*, 469–472; c) N. L. Rosi, J. Eckert, M. Eddaoudi, D. T. Vodak, J. Kim, M. O'Keeffe, O. M. Yaghi, *Science* **2003**, *300*, 1127–1129; d) G. Férey, M. Latroche, C. Serre, F. Millange, T. Loiseau, A. Percheron-Guégan, *Chem. Commun.* **2003**, 2976–2977.
[10] W. Schmitt, M. Murugesu, J. C. Goodwin, J. P. Hill, A. Mandel, R. Bhalla, C. E. Anson, S. L. Heath, A. K. Powell, *Polyhedron* **2001**, *20*, 1687–1697.
[11] a) W. Schmitt, J. P. Hill, M. P. Juanico, A. Caneschi, F. Costantino, C. E. Anson, A. K. Powell, *Angew. Chem.* **2005**, *117*, 4259–4264; *Angew. Chem. Int. Ed.*, **2005**, *44*, 4187–4192; b) W. Schmitt, C. E. Anson, J. P. Hill, A. K. Powell, *J. Am. Chem. Soc.* **2003**, *125*, 11142–11143.
[12] Cell dimensions of **1**: space group $R\bar{3}c$, $a = 35.301(4)$, $c = 43.356(6)$ Å, $V = 46719(9)$ Å^3, $Z = 36$; for isostructural potassium compound[11] $K_6[Fe_2(\mu\text{-}O)(\mu\text{-}CO_3)(chnida)_2]\cdot 13.5\,H_2O$

 © 2005 Wiley-VCH Verlag GmbH & Co. KGaA, Weinheim

(CCDC-262831): $C_{33}H_{49}Fe_2K_6N_2O_{31.5}$, $R\bar{3}c$, $a = 35.3692(10)$, $c = 43.3010(18)$ Å, $V = 46911(3)$ Å^3, $Z = 36$. The high-quality structural refinement of **1** was impossible as the single crystals diffracted weakly and no dataset with a satisfactory I/σ ratio was successfully obtained; however, single-crystal X-ray analysis confirms the identity of the compound. Powder diffraction patterns of **1** and generated patterns (generated on the basis of the structure given in Figure 2 and the coordinates of the isostructural K^+ analogue) agree well (see the Supporting Information). Microanalytical data for freshly-prepared crystals of **1** were also in good agreement with the formulation Na_6-$[Fe_2(\mu\text{-}O)(\mu\text{-}CO_3)(chnida)_2]\cdot 13.5\,H_2O$ analogous to the K^+ compound (see the Experimental Section).

[13] IR data: A. K. Shokanov, M. I. Bakeev, *Akad. Nauk Kaz. SSR* **1967**, *3*, 102; powder XRD data: W. v. Aalst, J. den Holander, W. J. A. M. Peterse, P. M. de Wolff, *Acta Crystallogr. Sect. B* **1976**, *32*, 47–58; comparison of the IR spectra reveals that parts of the organic ligand are still intact at 350 °C but that symmetric and antisymmetric stretching vibrations of the carboxylate group (1621 and 1395 cm^{-1}, respectively) are strongly diminished with a concurrent increase in the intensity of the band at 1447 cm^{-1} (symmetric stretching vibration of the carbonate anion) as well as the band at 880 cm^{-1} (antisymmetric deformation of CO_3^{2-}). Loss of complexity in the IR fingerprint region signifies the destruction of the ligand.

[14] a) K. Matsuoka, Y. Yamagishi, T. Yamazaki, N. Setoyama, A. Tomita, T. Kyotani, *Carbon* **2005**, *43*, 855–894; b) Z. Ma, T. Kyotani, A. Tomita, *Chem. Commun.* **2000**, 2365–2366.

[15] The synthesis of $NaFeO_2$ from Na_2CO_3 and Fe_2O_3 is well documented as it is currently being used as an active cathode material in nonaqueous electrolyte batteries: M. C. Blesa, E. Moran, C. León, J. Santamaria, J. D. Tornero, N. Menéndez, *Solid State Ionics* **1999**, *126*, 81–87, and references therein; Y. Takeda, J. Akagi, A. Edagawa, M. Inagaki, S. Naka, *Mater. Res. Bull.* **1980**, *15*, 1167–1172; batteries assembled using $NaFeO_2$ as the cathode material have high discharge capacities and long cycle lives.

[16] Sodium oxide, which must be present, could not be observed in our samples presumably because it is present in a glassy state and transparent to X-ray radiation.

[17] *Ullmann's Encyclopedia of Industrial Chemistry* (Ed.: B. Elvers, S. Hawkins), 7th ed., Wiley-VCH, Weinheim, **2004**.

[18] a) U.S. EPA/DOE/EPRI Combined Power Plant Air Pollutant Control Symposium: *The Mega Symposium*, Proceedings, August 20–23, **2001**, Chicago, Illinois, USA; b) R. Bell, US Patent 19924982672, **1992**; c) *Full-Scale Evaluation of a Multi-Pollutant Reduction Technology: SO_2, Hg, and NO_x*, E. Haddad, J. Ralston, S. Castagnero, Mobotec USA, Inc. **2003**, p. 101; d) *Solvay T-200 Use in Dry Sodium Injection for SO_2 Removal* (Ed.: L. Ninane), Central Study and Research Center, Solvay S.A., Dombasle, France, **1993**.

[19] A. F. Cheffey, P. R. Philips, US Patent, 200500116164, **2005**.

[20] S. Kureti, W. Weisweiler, K. Hizbullah, *Appl. Catal. B* **2003**, 43, 281–291.

[21] P. G. Menon, B. Delmon in *Handbook of Heterogeneous Catalysis, Vol. 1* (Eds.: G. Ertl, H. Knözinger, J. Weitkamp), VCH, Weinheim, **1997**, p. 101.

[22] V. Temkina, M. N. Rusina, G. F. Yaroschenko, M. Z. Branzburg, L. M. Timakova, N. M. Dyatlova, *Zh. Obshch. Khim.* **1975**, *45*, 1564–1570.

[23] Details of the thermogravimetric analysis, the XRD pattern of **1**, and the pattern generated on the basis of the structural model given in Figure 2; XRD, IR, and TGA–MS analysis; and further SEM images of samples thermolyzed at 510 °C and of hybrid organic–inorganic fibers in samples obtained at 250 °C are given in the Supporting Information.

 © 2005 Wiley-VCH Verlag GmbH & Co. KGaA, Weinheim

Mesoporous Polymers

DOI: 10.1002/anie.200501561

Ordered Mesoporous Polymers and Homologous Carbon Frameworks: Amphiphilic Surfactant Templating and Direct Transformation**

*Yan Meng, Dong Gu, Fuqiang Zhang, Yifeng Shi, Haifeng Yang, Zheng Li, Chengzhong Yu, Bo Tu, and Dongyuan Zhao**

Organic porous materials—a class of advanced materials—possess enormous potential for many high-tech applications, such as bioreactors,[1] dielectrics,[2] sensors,[3] microelectrophoresis,[4] thermal insulation,[5] and catalysts.[6] In general, they can be prepared by phase separation,[7] and a hard templating approach, such as those employing colloidal particles.[8] Phase separation can be derived from organic–organic phases, while the pore structures can be formed after etching, or by dissolving one block (A) from the assembled block copolymer (A–B).[9] However, most of the resulting porous polymer structures are disordered with wide pore size distributions because of the contraction and swelling from changes in volume, as well as the structured defects formed during template removal.[10] Large porosities have rarely been reported.[11] Furthermore, the resistance of the pore structure to heat and solvents is rather low because the materials are formed by weak van der Waals forces and physical twists between polymer chains, which means that the framework is not connected by covalent bonds. Recently, a procedure for cross-linking lyotropic liquid crystals (LLC) in water was introduced to prepare periodic porous organic mesostructures.[12] Unfortunately, polymerization only occurs between nearest neighboring head groups, and the mesostructured channels are fully occupied with solution.[13] Therefore, it is not surprising that porosity has yet to be reported.

Carbon materials, including nanotubes and fullerenes, have attracted considerable attention because of their remarkable properties.[14] The traditional carbonization process for active carbon and related materials can only generate

[*] Y. Meng, D. Gu, F. Q. Zhang, Y. F. Shi, Dr. H. F. Yang, Z. Li, Dr. C. Z. Yu, Dr. B. Tu, Prof. Dr. D. Y. Zhao
Department of Chemistry
Molecular Catalysis and Innovative Materials Lab
Fudan University, Shanghai 200433 (P.R. China)
Fax: (+86) 21-6564-1740
E-mail: dyzhao@fudan.edu.cn

[**] This work was supported by the NSF of China (20233030 and 20421303), the State Key Basic Research Program of PRC (G200048001, 2001CB610506), Project 863 of the Sci. & Tech Ministry of China (2002 AA321010), the Shanghai Sci. & Tech. Committee (03J14004, 02A14005, 03527001, 04JC14087), LG Company, Unilever Research China, and the Shanghai HuaYi Chemical Group. We thank Dr. T. C. Li, S. H. Xie, and Dr. Y. Wan for experimental and characterization assistance.

Supporting information for this article is available on the WWW under http://www.angewandte.org or from the author.

 © 2005 Wiley-VCH Verlag GmbH & Co. KGaA, Weinheim

porosity with a tunable pore size, but not regular pore structures. Ryoo et al. developed a nanocasting method to prepare mesoporous carbon replicas through carbonization of sucrose-filled ordered mesoporous silica, with subsequent removal of the silica frameworks by HF or NaOH.[15] The replicas obtained from these time-consuming and costly procedures are ordered arrays of carbon nanorods or nanowires with reverse structures to the parent mesoporous silica. It remains a challenge to prepare ordered mesoporous carbon materials with open frameworks which may find applications in hydrogen-storage, catalysis, adsorption, separations, electrochemical double capacitors, or even ordered carbon nanotube arrays.

The organic-templating pathway has been applied extremely successfully to the preparation of ordered mesoporous inorganic oxides.[16–18] Amphiphilic surfactants and block copolymers can be used as templates to achieve highly ordered mesoporous materials, with large surface areas and uniform pore sizes (1.5–30 nm) that are suitable for countless potential applications.[16–18] Among these periodic solids, mesoporous silica materials are the easiest to prepare and the most widely investigated as a result of their highly stable, covalently bonded frameworks.[19] Many silica mesostructures, such as 2D hexagonal (*p6m*)[17] and 3D cubic (*Ia*$\bar{3}$*d*, *Im*$\bar{3}$*m*, *Pm*$\bar{3}$*n*)[20–22] structures, have been synthesized. However, perhaps because of thermal instability resulting from noncovalently bonded frameworks, the preparation of ordered mesoporous organic materials by the amphiphilic surfactant-templating approach has seldom been reported.[23,24] Although Hillmyer and co-workers have obtained ordered epoxy resin/amphiphilic block copolymer nanocomposites, the porosity of the nanocomposites was not reported as a result of difficulties in removal of the amphiphilic block copolymer template.[23] More recently, Tanaka et al.[24] used resorcinol/formaldehyde, and triethyl orthoacetate (EOA) as the carbon co-precursor under strongly acidic conditions (5 M HCl) in a direct carbonization method to prepare ordered mesoporous carbon frameworks with channel structures. The resulting materials have a hexagonal mesostructure, mainly as a result of EOA, which might reduce the polymerization and interaction of the precursors derived from resorcinol/formaldehyde.

Herein, we report a simple and reproducible synthesis of highly ordered and stable mesoporous polymers by an amphiphilic surfactant-templating approach that is derived from examination of the successful assembly of mesoporous silica. We chose resol (phenol/formaldehyde) as a cheap precursor which can form three-connected covalently bonded zeolite-like frameworks by thermopolymerization. We also demonstrate that these polymers, with rigid networks, can be directly transformed by a careful carbonization process into well-ordered and ultrastable ($>1400\,^{\circ}C$) open mesoporous carbon frameworks. The obtained mesoporous polymers have large uniform mesopores, surface areas, and pore volumes. Moreover, the mesostructures can be readily tuned from 2D hexagonal (*p6m*), to 3D caged cubic (*Im*$\bar{3}$*m*), and lamellar frameworks by simply adjusting the mass ratio of the polymer precursors and amphiphilic surfactants. The mesoporous carbon frameworks have homologous mesostructures with high surface areas, narrow pore size distributions, and large pore volumes.

Highly ordered mesoporous polymers can be synthesized by a solvent evaporation induced self-assembly method (EISA),[25] by using amphiphilic triblock copolymers (PEO-PPO-PEO) as templates, and a soluble low-molecular weight polymer of phenol and formaldehyde (resol; $M_w = 500$–5000) as precursors, followed by a thermopolymerization process (Figure 1). The choice of resol as a precursor is key to the successful organization of organic–organic mesostructures because resol has a large number of hydroxy groups (-OH) which can interact strongly with triblock copolymers through formation of H bonds.[26] Many kinds of amphiphilic surfactants, such as triblock copolymers containing a PEO segment, cationic surfactants,[27] and nonionic alkyl PEO oligomers[28] can be used as templates. Simple thermopolymerization of resol at low temperatures (100–140 °C) around the triblock copolymer can yield a rigid zeolite-like hydrocarbon network with three-connected benzene rings through formation of covalent bonds.[29] This feature makes the polymers stable and permits direct transformation to homologous carbon frameworks by carbonization to 900–1400 °C under nitrogen. The surfactant templates can be removed by solvent extraction assisted oxidation, or calcination at 300–500 °C under nitrogen. Low-cost, nontoxic, and commercially available copolymers are highly suitable templates because they contain a large amount of oxygen and can be easily decomposed. A carbonization process with a slow heating rate ($<2\,^{\circ}C\,min^{-1}$) under nitrogen is adopted to prepare ordered mesoporous carbon frameworks. The structures of the assembled frameworks can be controlled by varying the surfactant/resol ratio or choosing different surfactants. 2D hexagonal (*p6m*) and 3D cubic (*Im*$\bar{3}$*m*) structures can be obtained by using F127 (EO106PO70 EO106) as a template, whilst a lamellar mesostructure can be prepared using P123 ($EO_{20}PO_{70}$ EO_{20}) as a template (see the Supporting Information). The ordered mesoporous carbon frameworks have the same structures as the parent polymers as well as high surface areas and uniform pores. The walls of the carbon frameworks are amorphous, very thick (ca. 7 nm), and ultrastable ($>1400\,^{\circ}C$).

The X-ray diffraction (XRD) pattern (Figure 2a) for untreated mesoporous polymer (FDU-15) shows an intense diffraction peak and two weak peaks at a 2θ range of 0.5 to 2° that can be indexed as (10), (20), (21) reflections associated with 2D hexagonal *p6m* symmetry.[17] This observation indicates that untreated FDU-15 has a high degree of hexagonal mesoscopic organization. The intense (10) peak reflects a *d*-spacing of 12.8 nm, which corresponds to a large unit-cell parameter ($a_0 = 14.8$ nm). Small-angle X-ray scattering (SAXS; see the Supporting Information) reveals four well-resolved reflections, further confirming a highly ordered hexagonal mesostructure. After calcination of the sample under nitrogen at 350 °C, the XRD pattern (Figure 2b) shows four well-resolved peaks of a hexagonal mesostructure that is similar to that of mesoporous silica SBA-15, thus suggesting that the *p6m* morphology is preserved, although the XRD peaks appear at slightly larger 2θ values with a $d(10)$-spacing of 10.5 nm ($a_0 = 12.1$ nm). These results clearly indicate that the mesostructure is thermally stable in a nitrogen atmos-

 © 2005 Wiley-VCH Verlag GmbH & Co. KGaA, Weinheim

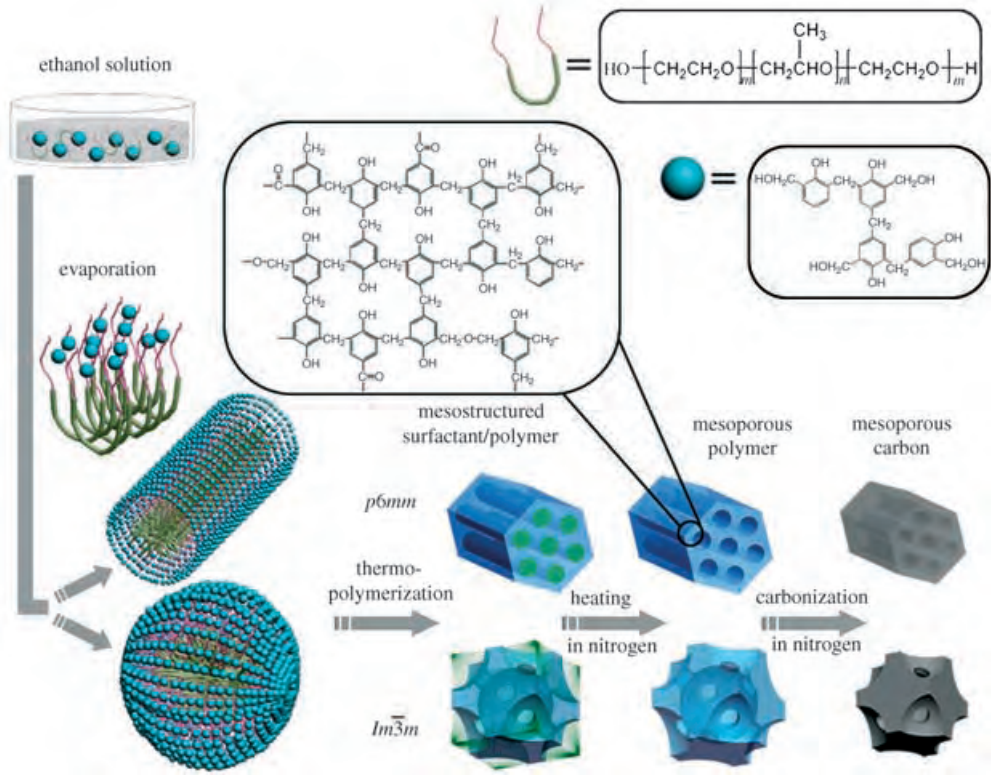

Figure 1. Schematic representation of the procedure used to prepare mesoporous polymers and carbon frameworks.

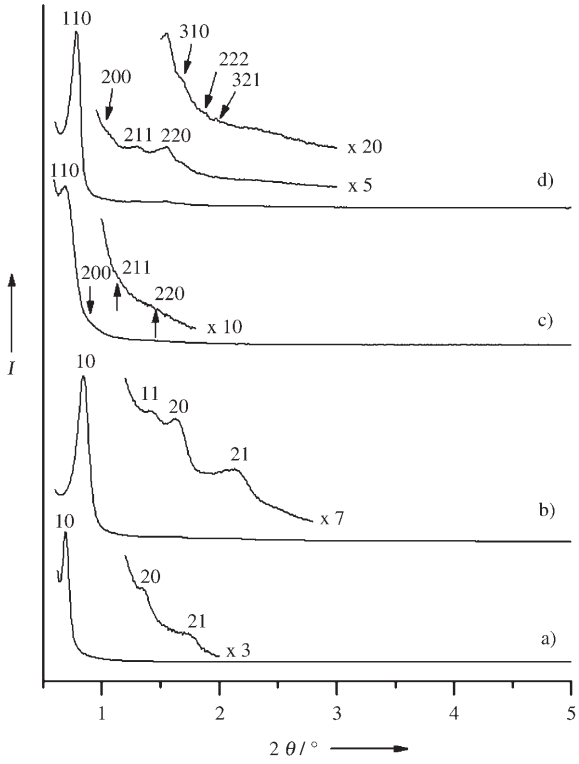

Figure 2. Powder XRD patterns of a) untreated FDU-15, b) FDU-15 calcined at 350 °C, c) untreated FDU-16, and d) FDU-16 calcined at 350 °C. The patterns were recorded on a Brucker D4 powder X-ray diffractometer using $Cu_{K\alpha}$ radiation.

phere, and the lattice of the framework shrinks by about 2.7 nm. The SAXS pattern shows three well-resolved peaks, thus providing evidence of thermal stability.

The photographic image of untreated FDU-15 (Figure 3 a) shows that it is a transparent and soft membrane, and indicates it is a homogeneous organic–organic composite. Transmission electron microscopy (TEM) images of FDU-15 calcined at 350 °C (C-FDU-15; Figure 3 b, c) show well-ordered hexagonal arrays of mesopores with 1D channels that are similar to SBA-15,[17] further confirming a 2D ordered hexagonal mesostructure. The cell parameter (a_0) estimated from the TEM images is approximately 11.5 nm, which is in agreement with the value calculated from XRD data.

The N_2 sorption isotherms (shown as circles in Figure 4 a) of FDU-15 calcined in a nitrogen atmosphere at 350 °C yield a type-IV curve with a sharp capillary condensation step at $P/P_0 = 0.6$–0.7 and an H_1-type hysteresis loop which is typical of large-pore mesoporous materials with cylindrical channels.[17] These results suggest that FDU-15 has uniform cylindrical mesoporous channels, similar to those of SBA-15.[17] The BET surface area and the total pore volume are calculated to be 652 $m^2 g^{-1}$ and 0.63 $cm^3 g^{-1}$, respectively. The pore diameter is about 6.8 nm with a narrow distribution. The wall thickness is estimated to be 5.3 nm, which indicates a thick organic network.

The ^{13}C solid-state NMR spectra (see the Supporting Information) reveal that calcination at 350 °C can decompose the triblock copolymers because they contain a large amount of oxygen, but the phenolic resin networks are preserved.

 © 2005 Wiley-VCH Verlag GmbH & Co. KGaA, Weinheim

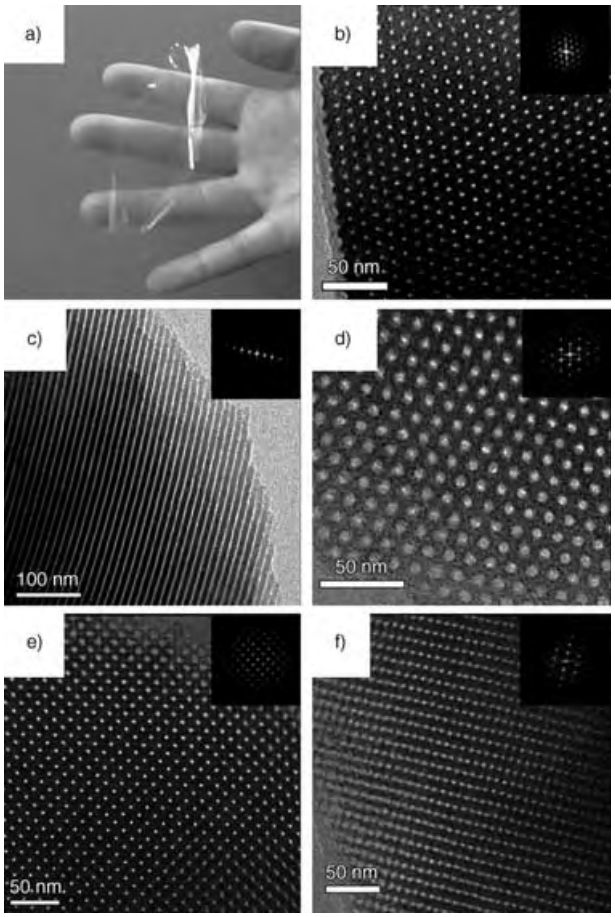

Figure 3. a) Photographic image of untreated FDU-15, b) TEM image of FDU-15 calcined at 350 °C viewed in the [001] direction, c) TEM image of FDU-15 calcined at 350 °C viewed in the [110] direction, d) TEM image of FDU-16 calcined at 350 °C viewed in the [111] direction, e) TEM image of FDU-16 calcined at 350 °C viewed in the [100] direction, and f) TEM image of FDU-16 calcined at 350 °C viewed in the [110] direction. TEM images were recorded on a JEOL 2011 microscope operated at 200 kV.

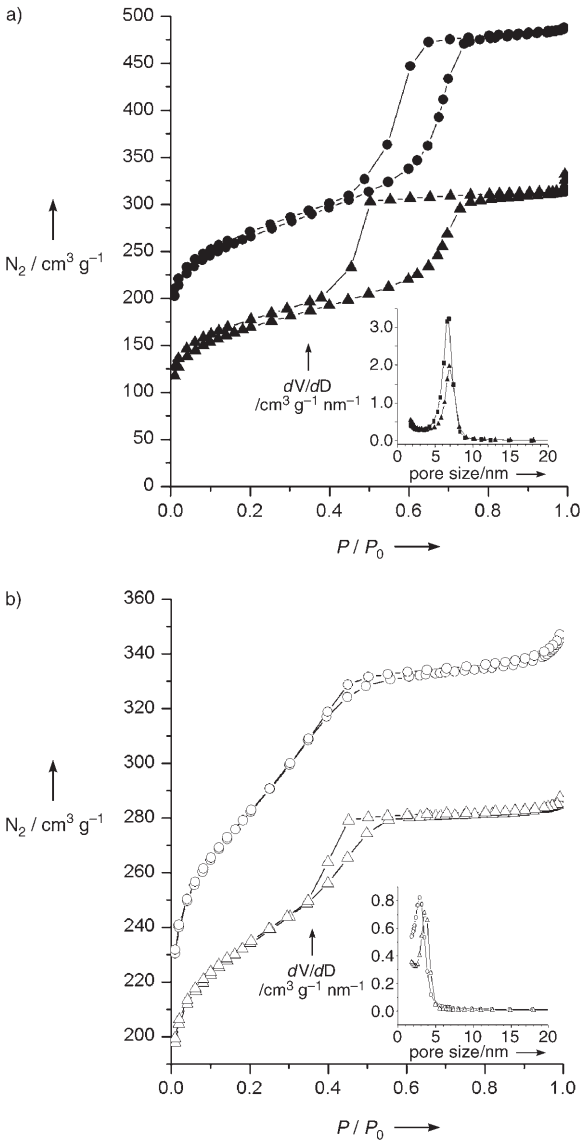

Figure 4. a) N_2 adsorption/desorption isotherms of FDU-15 (solid circles) calcined at 350 °C and FDU-16 (solid triangles) calcined at 350 °C, b) N_2 adsorption/desorption isotherms of C-FDU-15 (circles) calcined at 900 °C and C-FDU-16 (triangles) calcined at 900 °C. The pore-size distribution of FDU-15, FDU-16, C-FDU-15, and C-FDU-16 was determined by Barrett–Joyner–Halenda (BJH) analysis (inset). For clarity, the isotherms of C-FDU-15 in Figure 4a are offset along the *y* axis by 100 cm^3 g^{-1}. N_2 sorption isotherms were measured using a Micromeritics Tristar 300 analyzer at 77 K.

Elemental analysis reveals that calcined FDU-15 consists of C (77.97 %), H (5.20 %), O (16.8 %) with C/H/O molar ratio of 1:0.80:0.15, clearly suggesting a highly cross-linked phenol resin.

The 3D cubic mesoporous polymer structure (FDU-16) can be synthesized with a low F127/resol ratio. The XRD pattern for untreated FDU-16 (Figure 2c) shows one intense and three weak diffraction peaks. This result, combined with the SAXS pattern (see the Supporting Information), suggests a cubic mesostructure.[21] After calcination of the sample at 350 °C in a nitrogen atmosphere, the XRD pattern (Figure 2d) becomes more resolved, and seven diffraction peaks are observed. SAXS results (see the Supporting Information) show a well-resolved pattern. These reflection peaks can be indexed as (110), (200), (211), (220), (310), (222), and (321) of the body-centered cubic space group ($Im\bar{3}m$).[21] The lattice parameters are calculated to be 18.1 and 16.0 nm for untreated and calcined FDU-16, respectively. The lattice shrinkage is about 2.1 nm (11.6 %), which is slightly smaller than that for FDU-15 (18.2 %).

The large domain regularity of calcined FDU-16 is verified by TEM images (Figure 3d–f). These images viewed along the [111], [100], and [110] directions, together with electron diffraction data, further confirm an ordered cubic ($Im\bar{3}m$) mesostructure. The cell parameter estimated from the TEM images is approximately 15.9 nm, which is consistent with the value determined from the XRD data.

The N_2 sorption isotherms (shown as triangles in Figure 4a) of C-FDU-16 show typical type-IV curves with an H_2-type hysteresis loop which imply a 3D caged pore structure

 © 2005 Wiley-VCH Verlag GmbH & Co. KGaA, Weinheim

with a small entrance size (< 4 nm).[30] C-FDU-16 has a BET surface area of 590 $m^2 g^{-1}$, a pore volume of 0.51 $cm^3 g^{-1}$, and a narrow pore distribution at about 6.8 nm. The pore size is identical to that of FDU-16, thus suggesting there is a dependence upon the template.

The ^{13}C solid-state NMR and FT-IR spectra of FDU-16 (see the Supporting Information) indicate that the copolymers can be decomposed and result in polymer networks after calcination at 350 °C. Elemental analysis shows a composition of calcined FDU-16 with a molar ratio of C/H/O = 1:0.70:0.20 (C 75.10, H 4.36, O 20.5 %).

Thermogravimetric curves (see the Supporting Information) show that significant weight losses of about 55 and 43 % occurred from 270 to 380 °C for FDU-15 and FDU-16, respectively. This weight loss can be mainly attributed to the decomposition of copolymer F127. Slow weight losses of 25.6 and 26.5 % between 380 and 900 °C as a result of carbonization is observed for FDU-15 and FDU-16, respectively. The carbonization yield, calculated on the basis of the phenol resin, is 43.0 and 65.9 % for FDU-15 and FDU-16, respectively. Elemental analysis data indicate that carbonization (> 900 °C) is almost completely achieved, with < 5 % oxygen and hydrogen remaining, thus suggesting that a pure carbon, homologous framework is obtained.

XRD patterns (Figure 5 a) show that the ordered mesostructures are preserved during the carbonization process, even up to 1400 °C. A 2D hexagonal mesoporous carbon framework (C-FDU-15) can be obtained from polymer FDU-15 after carbonization at 900 °C. XRD patterns show that C-FDU-15 has a highly ordered hexagonal (*p6m*) mesostructure which is the same as that of FDU-15, in contrast to the mesoporous carbon replicas (CMK-3) which are made up of carbon nanorods or arrays of nanowires and have the reverse structure of the mesoporous silica template.[31] The cell parameter (a_0) is calculated from XRD data to be 8.7 nm. Comparison of this value with that of its parent shows that shrinkage is as large as 28 %. TEM images (Figure 6 a, b) show that C-FDU-15 has well-ordered hexagonal arrays with 1D channels even after calcinations at 1400 °C, thus indicating a high thermal stability.

The N_2 sorption isotherms (shown as circles in Figure 4 b) of C-FDU-15 obtained at 900 °C also show typical curves for mesoporous materials, with a sharp capillary condensation step at low relative pressures ($P/P_0 = 0.2$–0.4). A small hysteresis loop is observed, which is similar to small-pore mesoporous silica MCM-41.[16] A narrow pore size distribution at about 2.9 nm is obtained, even though the pore size shrinkage is as large as approximately 57 %. The wall thickness is calculated to be 5.8 nm, which is similar to that of FDU-15. C-FDU-15 obtained at 900 °C has a large BET surface area of 968 $m^2 g^{-1}$, and a pore volume of 0.56 $cm^3 g^{-1}$.

Our results show that the successful formation of ordered mesoporous carbon frameworks is due to the rigid resin networks and a slow carbonization process. With increasing temperature, the a_0 and pore size decrease rapidly at first then decrease more slowly after 600 °C (see the Supporting Information), thus implying that heating at low temperature (< 600 °C) may be an important step for stabilizing the carbon frameworks.

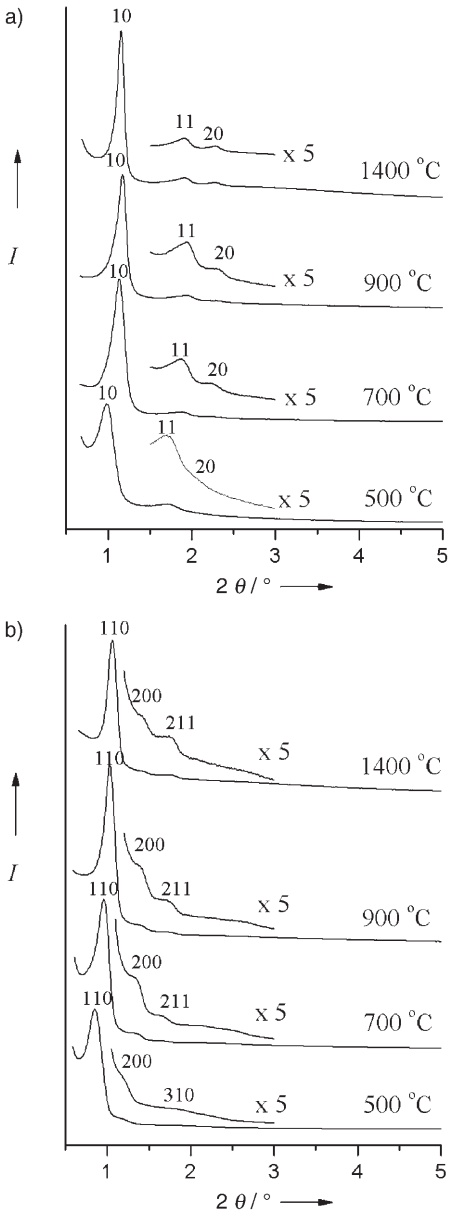

Figure 5. a) XRD patterns of C-FDU-15 calcined at temperatures ranging from 500 to 1400 °C, and b) XRD patterns of C-FDU-16 calcined at temperatures ranging from 500 to 1400 °C.

C-FDU-16 has a well-ordered cubic ($Im\bar{3}m$) mesostructure. Three well-resolved peaks can be observed in the XRD patterns (Figure 5 b). SAXS patterns (see the Supporting Information) confirm that the cubic mesostructure is retained during carbonization. The cell parameter (a_0) for the sample obtained at 900 °C is estimated to be 12.1 nm, and the shrinkage is about 24 %, which is slightly smaller than that for C-FDU-15. This observation implies that the 3D framework is more rigid than the 2D hexagonal structure. TEM images (Figure 6 c, d) show that C-FDU-16 has a large domain regularity with body-centered cubic symmetry ($Im\bar{3}m$) even after calcination at 1400 °C, which indicates ultrahigh thermal stability.

 © 2005 Wiley-VCH Verlag GmbH & Co. KGaA, Weinheim

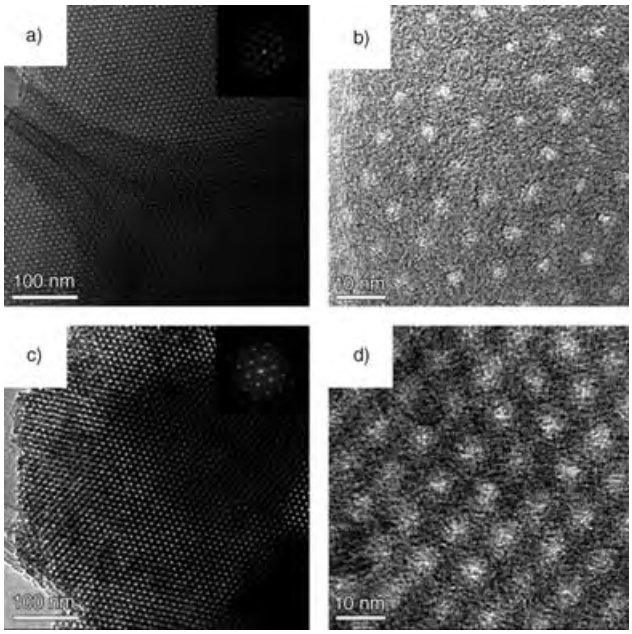

Figure 6. a) TEM image of C-FDU-15 calcined at 1400 °C, b) HRTEM image of FDU-15 calcined at 1400 °C, c) TEM image of C-FDU-16 calcined at 1400 °C, and d) HRTEM image of C-FDU-16 calcined at 1400 °C.

C-FDU-16 obtained at 900 °C also shows type-IV isotherms with a small H_2-hysteresis loop (shown as triangles in Figure 4b), thus implying small cage-like mesopores.[28] The pore size (ca. 3.7 nm), with a narrow distribution range, is smaller than that for its parent and the shrinkage (about ca. 45 %) is lower than that for C-FDU-15 which implies the cubic framework is more stable, and may be related to the 3D frameworks. C-FDU-16 obtained at 900 °C has a surface area of 778 $m^2 g^{-1}$ and a pore volume of 0.44 $cm^3 g^{-1}$.

The wide-angle XRD patterns (see the Supporting Information) for the carbon homologues are characteristic of amorphous carbon frameworks even after carbonization at 1400 °C.[32] The Raman spectra results (see the Supporting Information) also suggest an amorphous carbon framework.[32] High-resolution TEM (HRTEM) images (Figure 3d) of mesoporous carbon obtained at 1400 °C show that most of the carbon is amorphous, which suggests that graphitization is difficult.

In summary, highly ordered mesoporous polymers and carbon frameworks, with large uniform pores and surface areas, have been synthesized successfully. Two examples, FDU-15 and FDU-16, with hexagonal and cubic mesostructures, synthesized from triblock copolymers have been demonstrated. Ordered mesoporous carbon structures can be directly prepared from the polymers without defects. The resulting open carbon frameworks, connected by covalent bonds, have ultrahigh stability (> 1400 °C). The two new families of ordered mesoporous organic polymers and inorganic carbon solids, whose physical and chemical properties are quite easily distinguished from those of mesoporous silica, could have many potential applications in catalysis, separation, hydrogen storage, drug delivery, electrode materials, microdevices, and even in bioengineering.

Experimental Section

Resol precursor preparation: A soluble low-molecular-weight polymer ($M_w = 500$–5000) derived from phenol and formaldehyde (resol) was prepared by a basic polymerization method. Typical preparation procedure: Phenol (0.61 g, 6.50 mmol) was melted at 40–42 °C before 20 % NaOH (aq; 0.13 g, 0.65 mmol) was added slowly over 10 min with stirring. Formalin (37 wt %, 1.05 g) containing formaldehyde (13.0 mmol) was added dropwise, and the reaction mixture was stirred at 70 °C for 60 min. After cooling the mixture to room temperature, the pH of the reaction mixture was adjusted to neutral (7.0) using 0.6 M HCl solution. Water was then removed under vaccum below 50 °C. The final product ($M_w < 500$ measured by GPC) was redissolved in ethanol before use.

Synthesis of mesoporous polymer FDU-15 and FDU-16: Typical synthetic procedure of FDU-15: triblock copolymer poly(ethylene oxide)-*b*-poly(propylene oxide)-*b*-poly(ethylene oxide) (PEO-PPO-PEO, pluronic 127; 1.00 g) was dissolved in ethanol (20.0 g), then the ethanol solution of the above precursors containing phenol (0.61 g, 6.50 mmol) and (0.39 g, 13.0 mmol) formaldehyde was added by stirring for 10 min to form a homogeneous solution with the molar composition of F127/phenol/formaldehyde/ethanol of 0.012:1:2:67. The solution was transferred to a dish and the ethanol evaporated at room temperature over 5–8 h to produce a transparent membrane. The membrane was then heated in an oven at 100 °C for 24 h to thermopolymerize the phenolic resins. The products were calcined at 350 °C under nitrogen for 5 h with a temperature increase rate of 1 °C min^{-1} to obtain the porosity and decomposition of the amiphiphilic triblock copolymer template.

Cubic mesostructured resin polymers FDU-16 were synthesized by a procedure similar to that above, using triblock copolymer F127 (1.00 g), ethanol (15.0 g), resol precursor solution containing phenol (1.22 g, 13.0 mmol), and formaldehyde (0.78 g, 26.0 mmol). F127/phenol/formaldehyde/ethanol = 0.005–0.006:1:2:50.

Synthesis of lamellar mesostructured polymers from P123: Lamellar mesostructured polymer was prepared by using triblock copolymer pluronic P123 according to the above procedure. A homogeneous solution with the molar composition of P123/phenol/formaldehyde/ethanol = 0.022:1:1.2:50 was obtained and transferred into a dish to evaporate the ethanol. The resulting membrane was then heated in an oven at 100 °C for 24 h.

Synthesis of mesoporous carbon frameworks C-FDU-15 and C-FDU-16: Mesoporous carbon materials, C-FDU-15 and C-FDU-16, were prepared by direct transformation of the corresponding mesostructured polymers by carbonization under nitrogen. Carbonization was carried out in a tube oven under nitrogen at 700–1400 °C for 5 h. The temperature was increased at a rate of about 1 °C min^{-1} and held at 200, 350, and 500 °C for 2 h before reaching the final temperature. Elemental analysis results showed that the products contained > 90 wt % carbon, < 1.9 wt % H after carbonization at > 700 °C.

Measurements: XRD patterns were recorded on a Brucker D4 powder X-ray diffractometer by using $Cu_{K\alpha}$ radiation (40 kV, 40 mA). TEM images were obtained with a JEOL 2011 microscope operated at 200 kV. Samples for TEM measurements were suspended in ethanol and supported on a carbon-coated copper grid. N_2 adsorption isotherms were measured using a Micromeritics Tristar 3000 analyzer at 77 K. Before measurements were taken, all samples were degassed at 473 K for more than 12 h.

Received: May 7, 2005
Published online: October 12, 2005

Keywords: mesoporous materials · self-assembly · synthesis design · template synthesis

 © 2005 Wiley-VCH Verlag GmbH & Co. KGaA, Weinheim

[1] E. C. Peters, F. Svec, J. M. J. Frechet, *Adv. Mater.* **1999**, *11*, 1169 – 1181.
[2] J. L. Hedrick, R. D. Miller, C. J. Hawker, K. R. Carter, W. Volksen, D. Y. Yoon, M. Trollsas, *Adv. Mater.* **1998**, *10*, 1049 – 1053.
[3] M. Kanungo, A. Kumar, A. Q. Contractor, *J. Electroanal. Chem.* **2002**, *528*, 46 – 56.
[4] D. S. Peterson, T. Rohr, F. Svec, J. M. J. Frechet, *J. Proteome Res.* **2002**, *1*, 563 – 568.
[5] B. de Boer, U. Stalmach, H. Nijland, G. Hadziioannou, *Adv. Mater.* **2000**, *12*, 1581 – 1583.
[6] H. Deng, D. L. Gin, R. C. Smith, *J. Am. Chem. Soc.* **1998**, *120*, 3522 – 3523.
[7] S. A. Jenekhe, X. L. Chen, *Science* **1999**, *283*, 372 – 375.
[8] S. A. Johnson, P. J. Ollivier, T. E. Mallouk, *Science* **1999**, *283*, 963 – 965.
[9] A. S. Zalusky, R. Olayo-Valles, J. H. Wolf, M. A. Hillmyer, *J. Am. Chem. Soc.* **2002**, *124*, 12761 – 12773.
[10] X. X. Zhu, K. Banana, R. Yen, *Macromolecules* **1997**, *30*, 3031 – 3035.
[11] H. K. Lee, H. Y. Lee, Y. H. Ko, Y. J. Chang, N. K. Oh, W. C. Zin, K. Kim, *Angew. Chem.* **2001**, *113*, 2741 – 2743; *Angew. Chem. Int. Ed.* **2001**, *40*, 2669 – 2671.
[12] B. A. Pindzola, B. P. Hoag, D. L. Gin, *J. Am. Chem. Soc.* **2001**, *123*, 4617 – 4618.
[13] D. L. Gin, W. Q. Gu, B. A. Pindzola, W. J. Zhou, *Acc. Chem. Res.* **2001**, *34*, 973 – 980.
[14] R. H. Baughman, A. A. Zakhidov, W. A. de Heer, *Science* **2002**, *297*, 787 – 792.
[15] R. Ryoo, S. H. Joo, S. Jun, *J. Phys. Chem. B* **1999**, *103*, 7743 – 7746.
[16] C. T. Kresge, M. E. Leonowicz, W. J. Roth, J. C. Vartuli, J. S. Beck, *Nature* **1992**, *359*, 710 – 712.
[17] D. Y. Zhao, J. L. Feng, Q. S. Huo, N. Melosh, G. H. Fredrickson, B. F. Chmelka, G. D. Stucky, *Science* **1998**, *279*, 548 – 552.
[18] F. Schuth, *Chem. Mater.* **2001**, *13*, 3184 – 3195.
[19] R. Szostak, *Molecular Sieves: Principle of Synthesis and Identification*, van Nostrand Reinhold, New York, **1989**,
[20] Y. Sakamoto, T. W. Kim, R. Ryoo, O. Terasaki, *Angew. Chem.* **2004**, *116*, 5343 – 5346; *Angew. Chem. Int. Ed.* **2004**, *43*, 5231 – 5234.
[21] D. Y. Zhao, Q. S. Huo, J. L. Feng, B. F. Chmelka, G. D. Stucky, *J. Am. Chem. Soc.* **1998**, *120*, 6024 – 6036.
[22] Q. S. Huo, D. I. Margolese, U. Ciesla, P. Y. Feng, T. E. Gier, P. Sieger, R. Leon, P. M. Petroff, F. Schuth, G. D. Stucky, *Nature* **1994**, *368*, 317 – 321.
[23] P. M. Lipic, F. S. Bates, M. A. Hillmyer, *J. Am. Chem. Soc.* **1998**, *120*, 8963 – 8970.
[24] S. Tanaka, N. Nishiyama, Y. Egashira, K. Ueyama, *Chem. Commun.* **2005**, 2125 – 2127.
[25] Y. F. Lu, R. Ganguli, C. A. Drewien, M. T. Anderson, C. J. Brinker, W. L. Gong, Y. X. Guo, H. Soyez, B. Dunn, M. H. Huang, J. I. Zink, *Nature* **1997**, *389*, 364 – 368.
[26] P. P. Chu, H. D. Wu, *Polymer* **2000**, *41*, 101 – 109.
[27] K. T. Lee, S. M. Oh, *Chem. Commun.* **2002**, 2722 – 2723.
[28] J. Jang, J. Bae, *Chem. Commun.* **2005**, 1200 – 1202.
[29] H. R. Allcock, F. W. Lampe, J. E. Mark, *Contemporary Polymer Chemistry*, 3rd ed., Pearson Education, New Jersey, **2003**.
[30] J. R. Matos, M. Kruk, L. P. Mercuri, M. Jaroniec, L. Zhao, T. Kamiyama, O. Terasaki, T. J. Pinnavaia, Y. Liu, *J. Am. Chem. Soc.* **2003**, *125*, 821 – 829.
[31] R. Ryoo, S. H. Joo, M. Kruk, M. Jaroniec, *Adv. Mater.* **2001**, *13*, 677 – 681.
[32] C. D. Liang, K. L. Hong, G. A. Guiochon, J. W. Mays, S. Dai, *Angew. Chem.* **2004**, *116*, 5909 – 5913; *Angew. Chem. Int. Ed.* **2004**, *43*, 5785 – 5789.

 © 2005 Wiley-VCH Verlag GmbH & Co. KGaA, Weinheim

Crystal Engineering

DOI: 10.1002/anie.200501678

Multicomponent Organic Alloys Based on Organic Layered Crystals**

Kazuki Sada, Katsunari Inoue, Tomoyuki Tanaka, Attila Epergyes, Akira Tanaka, Norimitsu Tohnai, Akikazu Matsumoto, and Mikiji Miyata**

Inorganic mixed crystals or solid solutions such as metal alloys and intermetallic compounds are composed of two or more kinds of atoms or ions homogeneously mixed in the crystal.[1–3] They have been widely prepared and utilized as structural materials for daily life since ancient times. Formation of mixed crystals has been extensively investigated in the search for new functional materials with optical, electrical, and magnetic properties. Integration and fine-tuning of the functions have been often carried out by varying combinations of the components and the mixing ratios,[4] since the atoms and ions are easily mixed in the inorganic materials due to their spherical structures.

On the other hand, recrystallization from solution or crystallization from the melt is generally used for purification of crystalline organic compounds. Studies on organic mixed crystals have focused chiefly on well-defined molecular complexes in the crystalline state, such as inclusion crystals,[4] hydrogen-bonded cocrystals,[5] and charge-transfer complexes.[6] Less attention has been paid to formation of organic solid solutions or alloys that are composed of many kinds of organic molecules. Kitaigorodsky pointed out that similarity of molecular structures plays a crucial role in formation of organic solid solutions,[1] and some examples such as *n*-paraffins,[7] dicarboxylic acids,[8] naphthalene derivatives,[9]

[*] Dr. K. Sada
Department of Chemistry & Biochemistry
Graduate School of Engineering, Kyushu University
744 Motooka, Nishi-ku, Fukuoka 819-0395 (Japan)
Fax: (+81) 92-802-2820
E-mail: sadatcm@mbox.nc.kyushu-u.ac.jp

K. Inoue, T. Tanaka, A. Epergyes, A. Tanaka, Dr. N. Tohnai, Prof. Dr. M. Miyata
Department of Material & Life Science
Graduate School of Engineering, Osaka University, and
Handai FRC, 2-1 Yamadaoka, Suita 565-0871 (Japan)
Fax: (+81) 6-6879-7404
E-mail: miyata@mls.eng.osaka-u.ac.jp

Prof. Dr. A. Matsumoto
Department of Applied Chemistry
Graduate School of Engineering, Osaka City University
Sugimoto, Sumiyoshi-ku, Osaka 558-8585 (Japan)

[**] Financial support for this research was provided by the Ministry of Education, Culture, Sports, Science and Technology of Japan (MEXT) for K.S. and M.M., and by PRESTO-JST for A.M. A part of this work was supported by "Nanotechnology Support Project" of MEXT.

Supporting information for this article is available on the WWW under http://www.angewandte.org or from the author.

© 2005 Wiley-VCH Verlag GmbH & Co. KGaA, Weinheim

and metal complexes[10] have already been reported. However, multicomponent organic solid solutions prepared from three or more organic molecules are quite rare,[11] because their sizes and shapes are incompatible for forming homogeneous solid solutions, and they recrystallize separately to form eutectic mixtures of the pure components. No other strategy to prepare multicomponent organic solid solutions has ever been reported. Herein, we report novel organic solid solutions based on a robust layered structure and a new strategy to construct multicomponent solid solutions composed of organic molecules with different sizes and shapes. Exploration of design and control of multicomponent organic solid solutions should allow functions of the organic molecules to be accumulated by the same strategy as employed with inorganic molecules.

Carboxylate salts of amines have been widely used for screening of functional organic crystalline materials. For example, they are used for optical resolution of racemic acids or bases,[12–14] crystalline-state reactions,[15] topochemical polymerizations,[16] host–guest crystals,[17] and so on. Salt formation has some advantages for crystal engineering: easy preparation, various combinations, and strong intermolecular interactions between the ion pairs, such as hydrogen bonds and electrostatic interactions. We previously reported that 1-naphthylmethylammonium (NMA) *n*-aliphatic carboxylates from acetate (**C2**) to triacontanate (**C30**) have the same layer structure independent of the length of the alkyl group (Figure 1a).[18] This phenomenon is ubiquitous for inorganic layered structures such as zeolites and smectite clays.[19] This prompted us to prepare organic solid solutions from mixtures of two or more NMA carboxylate salts, just like inorganic substitutional alloys.

Equimolar mixtures of two or more carboxylic acids were treated with NMA in methanol (Figure 1b), and removal of the solvent by an evaporator yielded white solids. They were characterized by XRD (Figure 2a). The sample prepared from a 1:1 mixture of propanoic acid (**C3**) and butanoic acid (**C4**) had an XRD pattern similar to those of the pure crystals (**C3s** and **C4s**), but it was not identical to their sum.

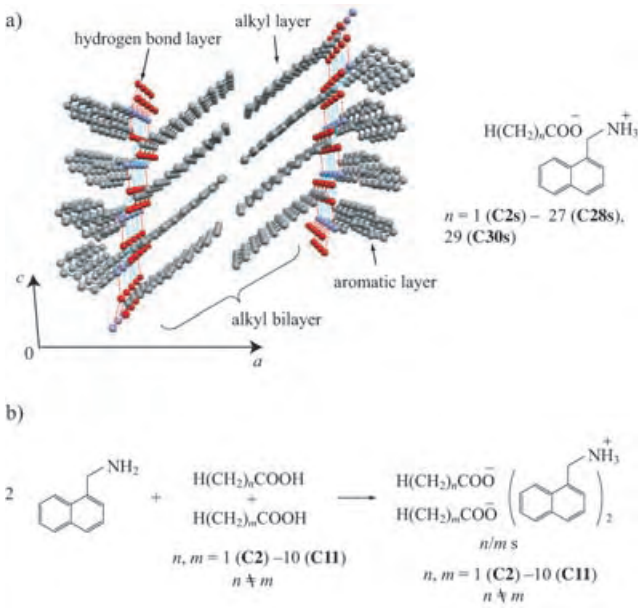

Figure 1. a) Bilayer structure in the crystalline state of **C9s**,[17] and b) the reaction scheme of the solid solutions.

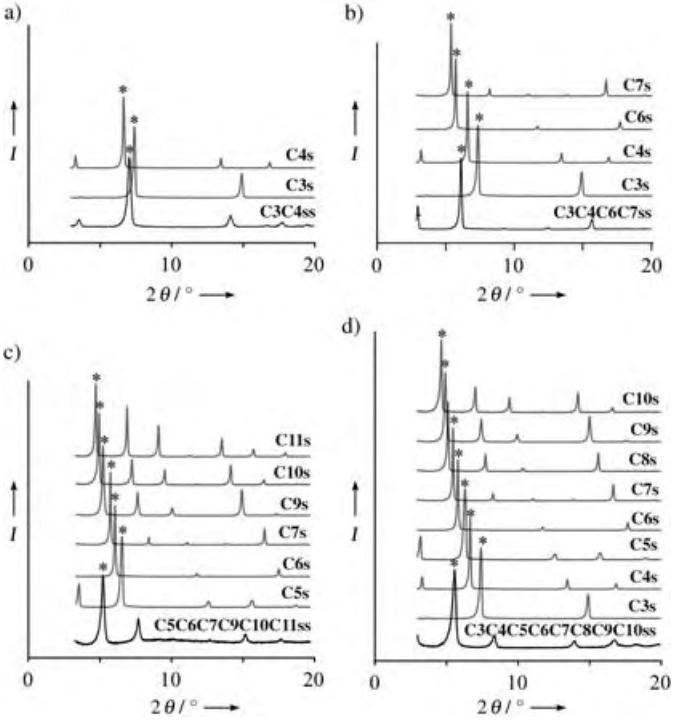

Figure 2. XRD patterns of solid solutions. a) Homogeneous solid solution from **C3** and **C4** (1:1) and the reference single-component salts **C3s** and **C4s**. b) Homogeneous solid solution from **C3**, **C4**, **C6**, and **C7** (1:1:1:1) and the reference single-component salts **C3s**, **C4s**, **C6s**, and **C7s**. c) Homogeneous solid solution from **C5**, **C6**, **C7**, **C9**, **C10**, and **C11** (1:1:1:1:1:1) and the reference single-component salts **C5s**, **C6s**, **C7s**, **C9s**, **C10s**, and **C11s**. d) Homogeneous solid solution from **C3**, **C4**, **C5**, **C6**, **C7**, **C8**, **C9**, and **C10** (1:1:1:1:1:1:1:1) and the reference single-component salts **C3s**, **C4s**, **C5s**, **C6s**, **C7s**, **C8s**, **C9s**, and **C10s**. Asterisks indicate 002 diffractions.

Differential scanning calorimetry (DSC) revealed that the melting point is 124.6 °C, which is lower than that of each pure salt (130.0 °C for **C3s** and 130.9 °C for **C4s**). From these results, we conclude that the white solid is a homogeneous solid solution of the two components (**C3C4ss**), rather than a eutectic mixture (**C3s** + **C4s**) of the individual crystals. The similarity in the XRD patterns suggested that the crystal structure of the solid solution **C3C4ss** resembles those of the pure salts. The FTIR spectrum of **C3C4ss** indicates the presence of the same hydrogen bonds as in the pure salts (carbonyl stretching bands of **C3C4ss**, **C3s**, and **C4s**: 1623, 1623, and 1623 cm^{-1}, respectively). The sharp 002 diffraction peak of the solid solution was observed at $d = 12.48$ Å, between those of **C3s** ($d = 11.87$ Å) and **C4s** ($d = 13.22$ Å). The interlayer distance of the solid solution was intermediate between those of the pure salts.[20]

Furthermore, we tried to prepare multicomponent solid solutions by mixing various carboxylate salts. We first investigated formation of a quaternary solid solution from

 © 2005 Wiley-VCH Verlag GmbH & Co. KGaA, Weinheim

C3, **C4**, **C6**, and **C7** (1:1:1:1). The XRD pattern (Figure 2b) showed a single sharp profile, and the *d* spacing was 14.20 Å, which corresponds to **C5s** ($d = 13.97$ Å). This indicates that the quaternary mixtures gave the solid solution (**C3C4C6C7ss**) of these four components, and not their eutectic mixture (**C3s** + **C4s** + **C6s** + **C7s**). Six- and eight-component solid solutions also gave similar XRD results (Figure 2c and d). The *d* spacing from the single peak of the six-component solid solution **C5C6C7C9C10C11ss** was 17.66 Å, which corresponds to **C8s** ($d = 17.18$ Å). The *d* spacing from the peak of **C3C4C5C6C7C8C9C10ss** was 15.77 Å, which corresponds to the average value of **C6s** and **C7s** ($d = 15.17$ and 16.31 Å, respectively). These results provide insight into the structure and mechanism of formation of the solid solution. Mixing the four components can give the following ten possible *d* spacings (probabilities in parentheses): **C3s** (1/16), **C3C4ss** (1/8), **C4s** (1/16), **C3C6ss** (1/8), **C3C7ss** (1/4), **C4C6ss** (1/4), **C4C7ss** (1/8), **C6s** (1/16), **C6C7ss** (1/8), and **C7s** (1/16). However, the single peak around **C5s** ($d = 13.97$ Å) indicates that the bilayer is selectively composed of two sets of the alkyl chain pairs, namely, **C3**/**C7** and **C4**/**C6**. Otherwise, the peak should be much broader or split into several peaks due to the various layer distances. Indeed, as shown in Figure 3, a mixture

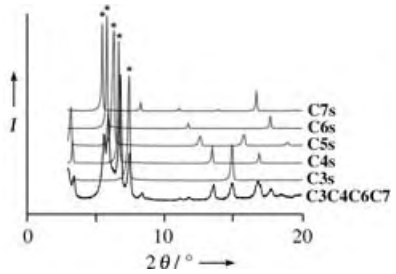

Figure 3. XRD patterns of a ground eutectic mixture of crystals of **C3s**, **C4s**, **C6s**, and **C7s** (black line), together with those of **C3s**, **C4s**, **C5s**, **C6s**, and **C7s** (grey lines). Asterisks indicate 002 diffractions.

prepared by grinding the pure salts shows corresponding peaks in each individual XRD pattern. Moreover, the six- and eight-component solid solutions have more possible *d* spacings, but they converged to averages among the mixtures. They should be composed of the following sets of alkyl-chain pairs: **C5**/**C11**, **C6**/**C10**, and **C7**/**C9** for **C5C6C7C9C10C11ss** and **C3**/**C10**, **C4**/**C9**, **C5**/**C8**, and **C6**/**C7** for **C3C4C5C6C7C8C9C10ss**. Each carboxylate anion recognized the sterically complementary partner. The sterically complementary pairs, for example, **C3**/**C7** and **C4**/**C6** for **C3C4C6C7ss**, have the same width in the alkyl bilayer structure, which provided the closest packing in the alkyl bilayer structure, and made them flat to form the two-dimensional hydrogen-bond network among the ion pairs and CH–π/π–π interactions between the naphthalene rings.[14] Furthermore, these results suggested random arrangement of the pairs. There are two hypothetical models to provide the averaged *d* spacing: a random model[20d] and a staged model[20d] (Figure 4). In staged model, a segregated layer is composed of one single carboxylate of the four carboxylates present, and the layer is paired with the specific partner.

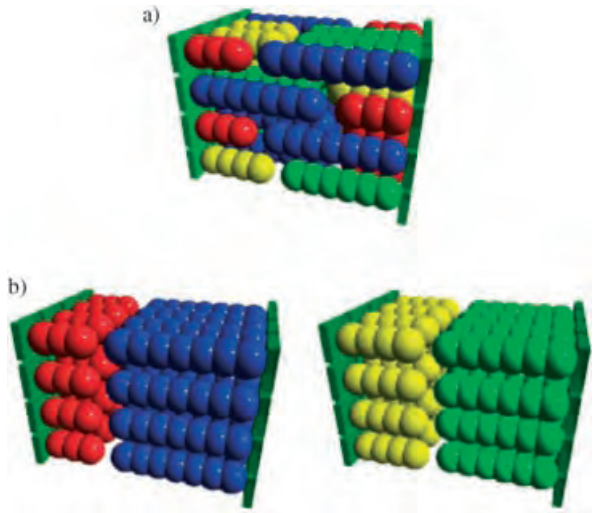

Figure 4. Schematic representations of the layer structures of the four-component homogeneous mixed salt a) with a random arrangement and b) with a staged arrangement.

There is no reason for selective stacking of these staged layers to afford layer structures with constant averaged *d* spacing. Therefore, the random layer is more likely. Thus, formation of the multicomponent solid solutions from more than two kinds of carboxylates was ascribed to specific pairing of the sterically complementary alkyl groups and their randomly disordered arrangement in the alkyl bilayer structure. During crystallization, the most probable pairs (e.g., **C3**/**C7** and **C4**/**C6** in **C3**, **C4**, **C6**, and **C7**) excluded the others by replacement of the counter alkyl group in the alkyl bilayer structure to keep the CH–π/π–π stacking and the two-dimensional hydrogen-bond networks parallel, and afforded the averaged layer distances.

The robust frameworks of NMA salts that accommodate isosteric pairs between their layers play a key role in formation of the solid solutions. These results indicate that robust structural motifs act as template for organic solid solutions and expand Kitaigorodsky's requirement for formation of binary organic solid solutions. Furthermore we could prepare the organic solid solutions from many components with different size and shape.[1] This strategy should be useful for designing wide ranges of the organic solid solutions. To our knowledge, the solid solution composed of eight organic molecules **C3C4C5C6C7C8C9C10ss** has the largest number of mixed components. Finally, introduction of functional groups into the isosteric pairs should provide integration of functions by a similar methodology to inorganic alloys.

Received: May 16, 2005
Published online: October 12, 2005

Keywords: crystal engineering · mixed crystals · organic alloys · self-assembly

[1] A. I. Kitaigorodsky, *Mixed Crystals*, Springer, Berlin, **1984**.
[2] a) R. W. Thomas, *Materials We Use, No. 4: Metals and Alloys*, Wheaton, Oxford, **1975**; b) M. Yamaguchi, J. C. Williams, *Metals*

 © 2005 Wiley-VCH Verlag GmbH & Co. KGaA, Weinheim

and Alloys, Elsevier, Oxford, **1999**. [In *Curr. Opin. Solid State Mater. Sci.* **1999**, *4*(3)].

[3] a) *Intermetallic Compounds* (Eds.: J. H. Westbrook, J. Hall), Krieger, Huntington, **1977**; b) *Intermetallics* (Ed.: G. Sauthoff), VCH, Weinheim, **1995**; c) *Intermetallic Compounds: Principles and Practice, Vol. 3* (Eds.: J. H. Westbrook, R. L. Fleischer), Krieger, Huntington, **2002**; for examples and a recent review, see d) H. Koinuma, I. Takeuchi, *Nat. Mater.* **2004**, *3*, 429.

[4] a) *Comprehensive Supramolecular Chemistry, Vol. 6* (Eds.: D. D. MacNicol, F. Toda, R. Bishop), Pergamon, Oxford, **1996**; b) *Inclusion Compounds, Vols. 1–3* (Eds.: J. L. Atwood, J. E. D. Davies, D. D. MacNichol), Academic Press, London, **1984**; c) *Inclusion Compounds, Vols. 4,5* (Eds.: J. L. Atwood, J. E. D. Davies, D. D. MacNichol), Oxford Press, Oxford, **1991**; d) F. Toda, *Supramol. Sci.* **1996**, *3*, 139; e) F. Toda, *CrystEngComm* **2002**, *4*, 215.

[5] For example, a) M. C. Etter, T. W. Panunto, *J. Am. Chem. Soc.* **1988**, *110*, 5896; b) M. C. Etter, Z. Urbanczyk-Lipkowska, M. Zia-Ebrahimi, T. W. Panunto, *J. Am. Chem. Soc.* **1990**, *112*, 8415; c) M. C. Etter, S. M. Reutzel, C. G. Choo, *J. Am. Chem. Soc.* **1993**, *115*, 4411; d) J. A. Zerkowski, C. T. Seto, D. A. Wierda, G. M. Whitesides, *J. Am. Chem. Soc.* **1990**, *112*, 9025; e) K. E. Schwiebert, D. N. Chin, J. C. MacDonald, G. M. Whitesides, *J. Am. Chem. Soc.* **1996**, *118*, 4018; f) S. Palacin, D. N. Chin, E. E. Simanek, J. C. MacDonald, G. M. Whitesides, M. T. McBride, G. T. R. Palmore, *J. Am. Chem. Soc.* **1997**, *119*, 11807.

[6] a) R. Foster, *Organic Charge-Transfer Complexes*, Academic Press, New York, **1969**; b) Z. G. Soos, *Annu. Rev. Phys. Chem.* **1974**, *25*, 121.

[7] a) Yu. V. Mnyukh, *Zh. Strukt. Khim.* **1960**, *1*, 370; b) D. L. Dorset, *Macromolecules* **1985**, *18*, 2158; c) D. L. Dorset, *Proc. Natl. Acad. Sci. USA* **1990**, *87*, 8541; d) D. L. Dorset, *Macromolecules* **1990**, *23*, 623; e) D. L. Dorset, B. K. Annis, *Macromolecules* **1996**, *29*, 2969; f) M. Maroncelli, H. L. Strauss, R. G. Snyder, *J. Phys. Chem.* **1985**, *89*, 5260; g) A. R. Gerson, S. C. Nyburg, *Acta Crystallogr. Sect. B* **1994**, *50*, 252; h) E. B. Sirota, H. E. King, Jr., H. H. Shao, D. M. Singer, *J. Phys. Chem.* **1995**, *99*, 798; i) M. Dirand, Z. Achour, B. Jouti, A. Sabour, J. C. Gachon, *Mol. Cryst. Liq. Cryst.* **1996**, *275*, 293; j) D. Mondieig, P. Espeau, L. Robles, Y. Haget, H. A. J. Oonk, M. A. Cuevas-Diarte, *J. Chem. Soc. Faraday Trans.* **1997**, *93*, 3343.

[8] a) N. B. Chanh, Y. Haget, J. Bedoin, *Bull. Soc. Fr. Mineral. Cristallogr.* **1972**, *95*, 281; b) Y. Bouillaud, N. B. Chanh, J. Bedoin, *Bull. Soc. Fr. Mineral. Cristallogr.* **1970**, *93*, 300.

[9] a) Y. Haget, N. B. Chanh, A. Corson, A. Meresse, *Mol. Cryst. Liq. Cryst.* **1975**, *31*, 93; b) F. Baumgarth, N. B. Chanh, R. Gay, J. Lascombe, *J. Chin. Phys.* **1969**, *6*, 862; c) N. B. Chanh, Y. Bouillard, P. Lencrerot, *J. Chim. Phys.* **1970**, *67*, 1206; d) Y. Haget, N. B. Chanh, A. Corson, A. Meresse, *Mol. Cryst. Liq. Cryst.* **1975**, *31*, 93; e) N. B. Chanh, Y. Haget, L. Bonpunt, A. Meresse, J. Housty, *Anal. Calorim.* **1977**, *4*, 233.

[10] a) D. Braga, D. Paolucci, G. Cojazzi, F. Grepioni, *Chem. Commun.* **2001**, *9*, 803; b) J. C. MacDonald, P. C. Dorrestein, M. M. Pilley, M. M. Foote, J. L. Lundburg, R. W. Henning, A. J. Schultz, J. L. Manson, *J. Am. Chem. Soc.* **2000**, *122*, 11692; c) S. Ferlay, W. Hosseini, *Chem. Commun.* **2004**, *7*, 788.

[11] a) D. L. Dorset, *Acta Crystallogr. Sect. B* **1995**, *51*, 1021; b) D. L. Dorset, *J. Phys. D* **1997**, *30*, 451; c) D. L. Dorset, R. G. Snyder, *J. Phys. Chem. B* **1999**, *103*, 3282; d) M. Dirand, M. Bouroukba, V. Chevallier, D. Petitjean, E. Behar, V. Ruffier-Meray, *J. Chem. Eng. Data* **2002**, *47*, 115.

[12] a) J. Jacques, A. Collet, S. H. Wilen, *Enantiomers, Racemates, and Resolutions*, Krieger, Malabar, **1981**; b) A. Collet in *Comprehensive Supramolecular Chemistry, Vol. 10* (Ed.: D. N. Reinhoudt), Pergamon, Oxford, **1996**, pp. 113–149.

[13] a) D. Kozma, G. Pokol, M. Ács, *J. Chem. Soc. Perkin Trans. 2* **1992**, *3*, 435; b) E. J. Ebbers, B. J. Plum, G. J. A. Ariaans, B. Kaptein, Q. B. Broxterman, A. Bruggink, B. Zwanenburg, *Tetrahedron: Asymmetry* **1997**, *8*, 4047; c) E. Ebbers, G. J. A. Ariaans, B. Zwanenburg, A. Bruggink, *Tetrahedron: Asymmetry* **1998**, *9*, 2745; d) T. Vries, H. Wynberg, E. van Echten, J. Koek, W. ten Hoeve, R. M. Kellogg, Q. B. Broxterman, A. Minnaard, B. Kaptein, S. van der Sluis, L. Hulshof, J. Kooistra, *Angew. Chem.* **1998**, *110*, 2491; *Angew. Chem. Int. Ed.* **1998**, *37*, 2349.

[14] a) K. Kinbara, Y. Hashimoto, M. Sukegawa, H. Nohira, K. Saigo, *J. Am. Chem. Soc.* **1996**, *118*, 3441; b) K. Kinbara, K. Sakai, Y. Hashimoto, H. Nohira, K. Saigo, *J. Chem. Soc. Perkin Trans. 2* **1996**, *12*, 2615; c) K. Kinbara, Y. Kobayashi, K. Saigo, *J. Chem. Soc. Perkin Trans. 2* **1998**, *8*, 1767; d) K. Kinbara, Y. Kobayashi, K. Saigo, *J. Chem. Soc. Perkin Trans. 2* **2000**, *1*, 111; e) K. Kinbara, Y. Harada, K. Saigo, *J. Chem. Soc. Perkin Trans. 2* **2000**, *7*, 1339; f) K. Kinbara, K. Oishi, Y. Harada, K. Saigo, *Tetrahedron* **2000**, *56*, 6651; g) K. Kinbara, Y. Tagawa, K. Saigo, *Tetrahedron: Asymmetry* **2001**, *12*, 2927; h) K. Kinbara, Y. Katsumata, K. Saigo, *Chem. Lett.* **2002**, *3*, 266; i) K. Kinbara, Y. Katsumata, K. Saigo, *Chirality* **2003**, *15*, 564; j) Y. Kobayashi, K. Kodama, K. Saigo, *Org. Lett.* **2004**, *6*, 2941; k) Y. Kobayashi, K. Kinbara, M. Sato, K. Saigo, *Chirality* **2005**, *17*, 108.

[15] a) Y. Ito, B. Borecka, J. Trotter, J. R. Scheffer, *Tetrahedron Lett.* **1995**, *36*, 6083; b) Y. Ito, B. Borecka, B. G. Olovsson, J. Trotter, J. R. Scheffer, *Tetrahedron Lett.* **1995**, *36*, 6087; c) J. N. Gamlin, R. Jones, M. Leibovitch, B. Patrick, J. R. Scheffer, J. Trotter, *Acc. Chem. Res.* **1996**, *29*, 203; d) E. Chenug, K. Rademacher, J. R. Scheffer, J. Trotter, *Tetrahedron Lett.* **1999**, *40*, 8733; e) E. Chenug, M. R. Netherton, J. R. Scheffer, J. Trotter, *J. Am. Chem. Soc.* **1999**, *121*, 2919; f) J. R. Scheffer, L. Wang, *J. Phys. Org. Chem.* **2000**, *13*, 531; g) K. C. W. Chong, J. R. Scheffer, *J. Am. Chem. Soc.* **2003**, *125*, 4040; h) W. Xia, C. Yang, B. O. Patrick, J. R. Scheffer, C. Scott, *J. Am. Chem. Soc.* **2005**, *127*, 2725; i) K. Kinbara, A. Kai, Y. Maekawa, Y. Hashimoto, S. Naruse, M. Hasegawa, K. Saigo, *J. Chem. Soc. Perkin 2* **1996**, *2*, 247; j) T. Odani, A. Matsumoto, K. Sada, M. Miyata, *Chem. Commun.* **2001**, *19*, 2004.

[16] a) A. Matsumoto, T. Odani, M. Chikada, K. Sada, M. Miyata, *J. Am. Chem. Soc.* **1999**, *121*, 11122; b) A. Matsumoto, S, Nagahama, T. Odani, *J. Am. Chem. Soc.* **2000**, *122*, 9109; c) A. Matsumoto, S. Nagahama, *J. Am. Chem. Soc.* **2001**, *123*, 12176; d) A. Matsumoto, K. Sada, K. Tashiro, M. Miyata, T. Tsubouchi, T. Tanaka, T. Odani, S. Nagahama, T. Tanaka, K. Inoue, S. Saragai, S. Nakamoto, *Angew. Chem.* **2002**, *114*, 2612; *Angew. Chem. Int. Ed.* **2002**, *41*, 2502; e) S. Nagahama, K. Inoue, K. Sada, M. Miyata, A. Matsumoto, *Cryst. Growth Des.* **2003**, *3*, 247.

[17] a) K. Sada, K. Yoshikawa, M. Miyata, *Chem. Commun.* **1998**, *16*, 1763; b) K. Sada, N. Shiomi, M. Miyata, *J. Am. Chem. Soc.* **1998**, *120*, 10543,

[18] K. Sada, K. Inoue, T. Tanaka, A. Tanaka, A. Epergyes, S. Nagahama, A. Matsumoto, M. Miyata, *J. Am. Chem. Soc.* **2004**, *126*, 1764.

[19] a) *Intercalation Chemistry* (Eds.: M. S. Whittingham, A. J. Jacobson), Academic Press, New York, **1982**; b) A. Clearfield, *Chem. Rev.* **1988**, *88*, 125; c) *Comprehensive Supramolecular Chemistry, Vol. 7* (Eds.: G. Alberti, T. Bein), Pergamon, Oxford, **1996**.

[20] Intermediate *d* spacing of inorganic layered crystals: a) G. Alberti, U. Constantino, J. Környei, M. L. Giovagnotti, *React. Polym.* **1985**, *4*, 1; b) W. R. Leenstra, J. C. Amicangelo, *Inorg. Chem.* **1998**, *37*, 5317; c) J. C. Amicangelo, G. L. Rosenthal, W. R. Leenstra, *Chem. Mater.* **2003**, *15*, 390; d) J. C. Amicangelo, W. R. Leenstra, *Inorg. Chem.* **2005**, *44*, 2067.

 © 2005 Wiley-VCH Verlag GmbH & Co. KGaA, Weinheim

Biosynthesis

DOI: 10.1002/anie.200501941

Cloning and Heterologous Expression of Isocyanide Biosynthetic Genes from Environmental DNA**

Sean F. Brady and Jon Clardy*

Cultured soil bacteria have been an important source of biologically active, naturally occurring small molecules. Uncultured soil bacteria, which outnumber their cultured counterparts by at least two orders of magnitude, are likely to be an equally important source of such molecules. In an attempt to access the biosynthetic potential of uncultured soil bacteria, we have explored an approach that involves the cloning and heterologous expression of DNA extracted directly from environmental samples (environmental DNA, eDNA) into readily cultured bacteria. Earlier, we described the identification and characterization of small-molecule antibiotics from antibacterially active eDNA clones found using a high-throughput phenotypic screen.[1] This approach directly couples the biosynthesis of each natural product that is found to a relatively small piece of cloned eDNA and therefore permits the characterization of both new natural products and their biosynthetic gene clusters simultaneously. Herein, we report the isolation and characterization of the isocyanide-containing eDNA-derived antibiotic **1**, its biosynthetic genes (*isnA* and *isnB*), the origin of the isocyanide nitrogen atom, and the general outline of the biosynthesis of **1**.

CSLG18, the eDNA clone that produces **1**, was found in a cosmid library constructed from blunt-ended gel-purified high-molecular-weight eDNA extracted directly from soil collected in Boston (MA, USA). The cosmid library was screened for antibacterially active clones by using a top agar overlay which contained *Bacillus subtilis*.[1] Clones that produced a zone of growth inhibition in the overlayed *B. subtilis* lawn were recovered from the assay plates and tested for the production of extractable organic antibacterial activities.[1]

Bioassay-guided fractionation of the antibacterially active extract in ethyl acetate from cultures of CSLG18 led to the isolation of **1**, an isocyanide-functionalized C3-substituted indole. The indole and *trans* olefin were readily inferred from standard 1D and 2D NMR spectroscopic experiments.[2] The triplet resonance observed at $\Delta\delta = 107.4$ ppm in the ^{13}C NMR spectrum suggested the presence of the isocyanide functionality as ^{13}C–^{14}N coupling between the nitrogen atom and the adjacent carbon atom of the isocyanide group results in a triplet resonance for the carbon atoms, which is a hallmark of this functional group. The proposed structure of **1** was subsequently confirmed by single-crystal X-ray diffraction (Figure 1).[3] Although the *cis* isomer of **1** has been obtained from cultured bacteria, to the best of our knowledge **1** has never been reported as a natural product.[4]

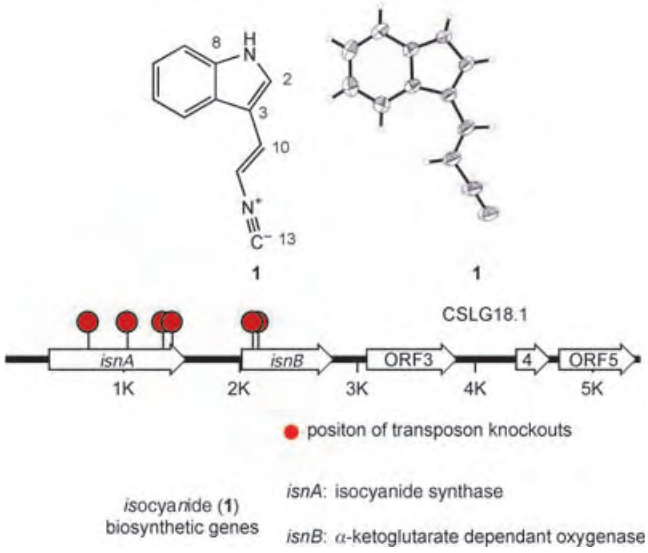

Figure 1. The natural-product antibiotic **1** was isolated from the culture broth of a 5.5-kB antibacterially active subclone of the eDNA cosmid, pCSLG18. The genes *isnA*/*B* are necessary and sufficient to confer the production of **1** to *E. coli*.

The genes responsible for the biosynthesis of **1** were sought in pCSLG18.1, a 5.5-kB antibacterially active EcoRI subclone (58.8% GC content) of the original eDNA cosmid, pCSLG18.[5] Two predicted open-reading frames (ORFs) contained in pCSLG18.1 (Figure 1) were identified by transposon mutagenesis as necessary for the production of **1** and have been given the names *isnA* and *isnB* (*is*ocya*n*ide, *iso*nitrile), respectively. The predicted translation product of *isnA* shows the highest-sequence identity to predicted proteins related to PvcA of pyoverdine chromophore biosynthesis (33%) and Dit1 of yeast-spore wall biosynthesis (21%). Neither PvcA nor Dit1 has been functionally characterized, although both are thought to be involved in the biosynthesis of C–N bonds.[6,7] The predicted translation product of *isnB* shows the highest-sequence identity to non-heme iron α-ketoglutarate dependent oxygenases, including the oxygenase from clavaminate biosynthesis and PvcB, a second enzyme thought to be involved in pyoverdine chromophore biosynthesis.[8] Three additional ORFs (>100 amino acids) were found in CSLG18.1; ORFs 4 and 5 are related to hypothetical proteins of unknown function and ORF 3 is related to prenyltransferases.

The successful expression of *isnA* and *isnB* (*isnA*/*B*), the biosynthetic genes for **1**, in *E. coli* allowed the biosynthesis of

[*] Dr. S. F. Brady, Prof. J. Clardy
Department of Biological Chemistry and Molecular Pharmacology
Harvard Medical School
240 Longwood Avenue, Boston, MA 02115 (USA)
Fax: (+1) 617-432-3702
E-mail: sean_brady@hms.harvard.edu

[**] We thank NIH CA24487 (J.C.) and the Ellison Medical Foundation (J.C.) for support of this work. We thank the *E. coli* Genetic Stock Center (CGSC) for providing the *E. coli* strains used in the feeding experiments.

Supporting information for this article is available on the WWW under http://www.angewandte.org or from the author.

 © 2005 Wiley-VCH Verlag GmbH & Co. KGaA, Weinheim

1 and, more specifically, the isocyanide functional group to be studied in detail. As with many isocyanide-containing natural products isolated from cultured bacteria and fungi, the structure of **1** suggests that the isocyanide nitrogen atom is likely to be derived from the amine of an amino acid. Feeding studies that used native-isocyanide-producing organisms have not, however, always supported this hypothesis.[9] The cloning and heterologous expression of isocyanide biosynthetic enzymes in *E. coli* allowed us to perform controlled feeding experiments which could not be carried out in less well-understood microbes and plants.

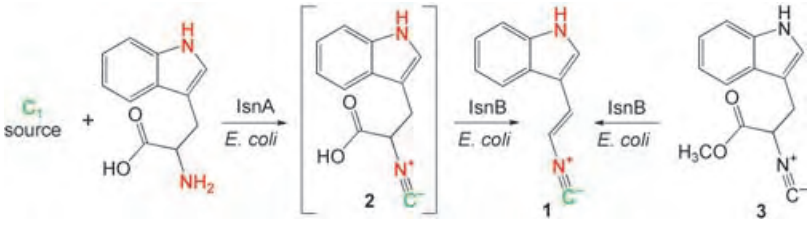

Scheme 1. Feeding experiments in *E. coli* indicate IsnA uses tryptophan in the biosynthesis of **1**. The proposed intermediate **2** is suggested by feeding experiments that use the methyl ester **3**.

The role of tryptophan in the biosynthesis of **1**, and its connection with the isocyanide nitrogen atom especially, was investigated by using *isnA*/*B* expressed in an *E. coli* host with a genetic background selected to eliminate the ambiguity seen in feeding experiments carried out in wild-type-isocyanide-producing organisms. To assess the role of tryptophan in the biosynthesis of **1**, doubly labeled ^{15}N-tryptophan was fed to a culture of a tryptophan auxotroph (*trpC*) and transaminase-deficient (*aspC*, *ilvE*, and *tyrB*) strain of *E. coli* (DL39W) transformed with *isnA*/*B*.[10] Incorporation of the ^{15}N label into **1** was determined by LCMS. The tryptophan auxotrophy ensures that the doubly labeled ^{15}N-tryptophan is the only tryptophan present in the culture, and the transaminase deficiencies ensure that the ^{15}N-labeled amine group of tryptophan is not lost during the feeding experiment. If both nitrogen atoms are incorporated into **1**, the observed *m*/*z* value $[M+H]^+$ for **1** would be 171; whereas if tryptophan is not used in the biosynthesis of **1**, no ^{15}N label will be incorporated into **1** which would result in an observed *m*/*z* value of 169. If only one of the two ^{15}N-labeled nitrogen atoms, either from the indole unit or the free amine group, is incorporated into **1** the observed *m*/*z* value for **1** would be 170.

In the presence of the doubly labeled ^{15}N-tryptophan, the general transaminase- and tryptophan-deficient strain of *E. coli* transformed with *isnA*/*B* produces **1** with *m*/*z* 171 being observed. Both the nitrogen atoms in **1**, including the isocyanide nitrogen atom, are therefore derived from tryptophan (Figure 2 and Scheme 1). Almost all of **1** obtained from a wild-type (transaminase-proficient) *E. coli*, contained a single ^{15}N label (*m*/*z* 170). Labeling studies performed in wild-type-isocyanide-producing organisms would be likely to give the same result and could explain the ambiguous feeding results obtained from these organisms previously. Many of the drawbacks traditionally associated with feeding studies can be significantly reduced or completely eliminated in model microbial systems by using mutants that create an appropriately controlled metabolic background.

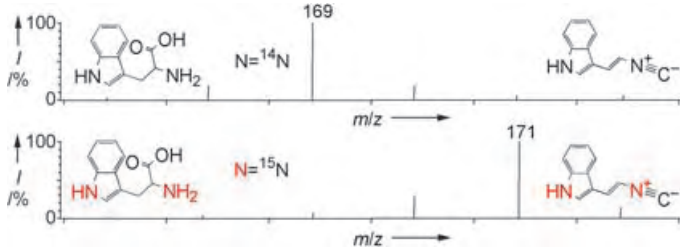

Figure 2. The *m*/*z* values observed for **1** obtained from cultures of *E. coli* transformed with *isnA*/*B* and grown in either ^{14}N-tryptophan or ^{15}N-tryptophan. A transaminase-deficient (*aspC*, *ilvE*, and *tyrB*) *E. coli* strain was used in these feeding experiments to prevent the loss of the labeled amine group.

IsnA and IsnB individually expressed as glutathione-*S*-transferase fusion proteins (IsnA-GST and IsnB-GST, respectively) were used to elucidate the overall scheme for the biosynthesis of **1** (Table 1). Cultures of *E. coli* that overexpressed either IsnA-GST or IsnB-GST individually did not accumulate **1**. However, **1** accumulated in the culture broth when these two strains were cocultured in the same flask. IsnA and IsnB are therefore necessary and sufficient to confer the production of **1** to *E. coli*, and one of the two enzymes must produce a diffusible intermediate that is converted into **1** by the other. *E. coli* that express IsnA-GST grown in media preconditioned with the growth of *E. coli* that express IsnB-GST does not lead to the accumulation of **1** in the culture broth; however, cultures of *E. coli* that express IsnB-GST grown in media preconditioned with the growth of *E. coli* that express IsnA-GST do accumulate **1** in the culture broth. The diffusible intermediate is therefore produced by IsnA and converted into **1** by IsnB (Scheme 1). All attempts to isolate this intermediate from cultures that either overexpress IsnA-GST or are transformed with *isnA*/*B* were unsuccessful.

Table 1: Results from feeding experiments used to decipher the overall biosynthetic approach to **1**.

E. coli (strain 1)	*E. coli* (strain 2)	Culturing treatment	**1**[a]
isnA + *isnB*			+
isnA–GST			–
isnB–GST			–
isnA–GST	*isnB*–GST	cocultured[b]	+
isnA–GST	*isnB*–GST	preconditioned[c]	+
isnB–GST	*isnA*–GST	preconditioned[c]	–
isnB–GST		*N*-methyl tryptophan[d]	–
isnB–GST		*N*-formyl tryptophan[d]	–
isnB–GST		*N*-methyl tryptamine[d]	–
isnB–GST		*N*-formyl tryptamine[d]	–

N-formyl and *N*-methyl compounds have been proposed as possible isocyanide intermediates in what could be a two- or three-step isocyanide biosynthetic scheme.[11] However, *N*-formyl and *N*-methyl derivatives of tryptophan and tryptamine (0.1 mg mL^{-1}) did not serve as substrates for the

© 2005 Wiley-VCH Verlag GmbH & Co. KGaA, Weinheim

production of **1** when added to cultures that overexpress IsnB-GST. It seemed plausible that IsnA might form the isocyanide function in a single enzymatic step and that the role of IsnB would be the oxidative decarboxylation of the proposed isocyanide-functionalized intermediate **2**. In our hands, the synthetic intermediate **2** was not stable and, therefore, could not be used in feeding experiments to test this hypothesis. However, we were able to synthesize the methyl ester of **2** (**3**) and thought that the slow cleavage of the methyl ester by promiscuous bacterial esterases might circumvent the instability problem.[12] The addition of **3** (0.1 mg mL^{-1}) to cultures that express IsnB-GST led to the accumulation of **1** in the culture broth, and when the cultures of CSLG18.1 were spiked with **3**, they showed increased production of **1** relative to the control cultures of CSLG18.1. Compound **1** was not detected in the extracts in ethyl acetate from the vector control cultures spiked with **3** or from IsnA-GST cultures spiked with **3**. These feeding studies suggest that the isocyanide group seen in **1** is formed in a single enzymatic step on IsnA and that the proposed isocyanide-containing intermediate **2** is oxidatively decarboxylated by IsnB to give **1** (Scheme 1). The lack of stability of **2** is likely to be responsible for our inability to isolate the proposed intermediate.

The eDNA approach, used in this study to discover antibiotic **1**, directly couples natural products with their biosynthetic gene clusters, thus providing both a means for the isolation of previously inaccessible natural products from uncultured bacteria and a direct link to their biosynthetic enzymes. Characterization of the antibacterially active eDNA clone CLSG18 led to the identification of the isocyanide-containing natural-product antibiotic **1**, and in turn to the first isocyanide synthase, IsnA. The origin of the isocyanide carbon atom is an intriguing, but unanswered question, for all naturally occurring isocyanides. This question will be addressed in due course.

Received: June 4, 2005
Published online: October 5, 2005

Keywords: biosynthesis · DNA · heterologous expression · isocyanides · natural products

[1] a) S. F. Brady, J. Clardy, *J. Am. Chem. Soc.* **2000**, *122*, 12903; b) S. F. Brady, C. J. Chao, J. Handelsman, J. Clardy, *Org. Lett.* **2001**, *3*, 1981; c) S. F. Brady, C. J. Chao, J. Clardy, *J. Am. Chem. Soc.* **2002**, *124*, 9968; d) S. F. Brady, C. J. Chao, J. Clardy, *Appl. Environ. Microbiol.* **2004**, *70*, 6865; e) S. F. Brady, J. Clardy, *J. Nat. Prod.* **2004**, *67*, 1283; see the Supporting Information for library construction and screening methods.

[2] ^{13}C NMR (125 MHz, CD_2Cl_2): $\delta = 163.9$, 137.5, 130.7, 127.3, 125.1, 123.8, 121.8, 120.3, 112.4, 111.24, 107.4 ppm (t); ^{1}H NMR (500 MHz, CD_3OD): $\delta = 8.58$ (1H, s), 7.68 (1H, d, 7.5), 7.45 (1H, d, 8), 7.39 (1H, d, 3), 7.28 (1H, m), 7.24 (1H, m), 7.16 (1H, d, 14.5), 6.37 ppm (1H, d, 14); HRMS (ESI-TOF): *m*/*z* calcd for $C_{11}H_9N_2$: 169.0766; found 169.0774 $[M+H]^+$; see the Supporting Information for a description of the isolation procedure, structure-elucidation methods, and the ^{1}H and ^{13}C NMR spectra of **1**.

[3] CCDC-273844 contains the supplementary crystallographic data for this paper. These data can be obtained free of charge from the Cambridge Crystallographic Data Centre via www.ccdc.cam.ac.uk/data_request/cif.

[4] a) J. R. Evans, E. J. Napier, P. Yates, *J. Antibiot.* **1976**, *29*, 850; b) I. Hoppe, U. Schollkopf, *Liebigs Ann. Chem.* **1984**, 600.

[5] GenBank accession number DQ084328.

[6] a) P. Briza, M. Eckerstorfer, M. Breitenbach, *Proc. Natl. Acad. Sci. USA* **1994**, *91*, 4524; b) P. Briza, H. Kalchhauser, E. Pittenauer, G. Allmaier, M. Breitenbach, *Eur. J. Biochem.* **1996**, *239*, 124.

[7] A. Stintzi, Z. Johnson, M. Stonehouse, U. Ochsner, J. M. Meyer, M. L. Vasil, K. Poole, *J. Bacteriol.* **1999**, *181*, 4118.

[8] a) E. N. Marsh, M. D. Chang, C. A. Townsend, *Biochemistry* **1992**, *31*, 12648; b) J. E. Hodgson, A. P. Fosberry, N. S. Rawlinson, H. N. Ross, R. J. Neal, J. C. Arnell, A. J. Earl, E. J. Lawlor, *Gene* **1995**, *166*, 49.

[9] a) H. Achenbach, H. Grisebach, *Z. Naturforsch B* **1965**, *20*, 137; b) V. Bornemann, G. M. L. Patterson, R. E. Moore, *J. Am. Chem. Soc.* **1988**, *110*, 2339; c) P. J. Scheuer, *Acc. Chem. Res.* **1992**, *25*, 433.

[10] D. M. LeMaster, F. M. Richards, *Biochemistry* **1988**, *27*, 142; see the Supporting Information for a detailed description of the methods used in these feeding experiments.

[11] M. S. Puar, H. Munayyer, V. Hegde, B. K. Lee, J. A. Waitz, *J. Antibiot.* **1985**, *38*, 530.

[12] a) D. H. R. Barton, G. Bringmann, W. B. Motherwell, *Synthesis* **1980**, 68; b) N. Hashimoto, T. Aoyama, T. Shioiri, *Chem. Pharm. Bull.* **1981**, *29*, 1475.

 © 2005 Wiley-VCH Verlag GmbH & Co. KGaA, Weinheim

Regioselective Reactions

DOI: 10.1002/anie.200501638

Regioselective Hypervalent-Iodine(III)-Mediated Dearomatizing Phenylation of Phenols through Direct Ligand Coupling**

*Aurélie Ozanne-Beaudenon and Stéphane Quideau**

Dearomatization of phenols often constitutes an ultimate key transformation in the biogenesis of many natural products and a powerful strategy for the rapid construction of highly

[*] A. Ozanne-Beaudenon, Dr. S. Quideau
Institut Européen de Chimie et Biologie
2 rue Robert Escarpit, 33607 Pessac Cedex (France)
Fax: (+33) 540-00-22-15
E-mail: s.quideau@iecb.u-bordeaux.fr
and
Laboratoire de Chimie Organique et Organométallique (CNRS UMR5802), Centre de Recherche en Chimie Moléculaire
Université Bordeaux 1
351 Cours de la Libération, 33405 Talence Cedex (France).

[**] We gratefully acknowledge Simafex and the Association Nationale de la Recherche Technique (CIFRE Grant N°301/2002) for their financial support and Aurélie Ozanne-Beaudenon's graduate research assistantship.

Supporting information for this article is available on the WWW under http://www.angewandte.org or from the author. It includes detailed descriptions of experimental procedures, characterization data, and ^{1}H and ^{13}C NMR spectra of all compounds.

© 2005 Wiley-VCH Verlag GmbH & Co. KGaA, Weinheim

functionalized intermediates in the elaboration of complex organic molecules.[1] One class of chemical reagents that is continuously finding new applications in this area of synthetic organic chemistry is composed of hypervalent λ^3- and λ^5-iodanes.[2] Herein we report a new phenol dearomatization process that involves the use diaryl λ^3-iodanes (i.e., Ar_2IL, L = Cl, BF_4, OTs)[3] to promote regioselective *ortho* phenylation to give 6-phenylcyclohexa-2,4-dienones. Diaryl-λ^3-iodane reagents have previously been used with success to give α-arylated ketones, esters, silyl enol ethers, and various 1,3-dicarbonyl compounds,[3–5] but the only products that were obtained when phenolic substrates were used under basic conditions were derived from an O-arylation process.[6] The reaction conditions unveiled herein permit us to direct the entry of an aryl group to a substituted position on the starting phenol and offer an alternative to stoichiometric processes that involve the use of toxic aryl–lead or aryl–bismuth reagents[7,8] and an alternative to transition-metal-catalyzed processes that only furnish diaryl products.[9]

We selected 2,3,5-trimethylphenol (**1a**, see Table 1) as a first model substrate to search for appropriate C-phenylation conditions and treated it with chlorodiphenyl-λ^3-iodane (Ph_2ICl) in dimethylformamide (DMF) in the presence of potassium *tert*-butoxide (*t*BuOK, 1.1 equiv) for 20 h at room temperature. Only the diaryl ether **2a** was isolated with a yield of 53%, but no formation of the desired cyclohexa-2,4-dienone **3a** was observed (Table 1, entry 1).[10] The first glimpse of success was obtained by changing the reaction solvent to a protic solvent with a low dielectric constant (i.e., *t*BuOH),[11] whereupon **3a** was isolated with a yield of 8% (Table 1, entry 1). It is worth noting that no diaryl product, which could have resulted from introduction of the phenyl group at the unsubstituted C6 position of the starting phenol **1a**, was observed. A small and weakly electron-donating substituent such as a methyl group at an *ortho* position thus appears sufficient to direct delivery of the phenyl unit to that substituted position. In accordance with this first observation, only diaryl ether products were obtained in good yields when starting from phenol (**1b**) or from the *meta*-substituted phenol, 3,5-dimethylphenol (**1c**; Table 1, entries 2 and 3). Moreover, the symmetrically *ortho*-substituted 2,6-di- and 2,4,6-trimethylphenols, **1d** and **1e**, gave rise to the formation of the desired cyclohexa-2,4-dienones, **3d** and **3e**, in 37% and 42% yields, respectively (Table 1, entries 4 and 5). Interestingly, the *para*-methylated phenol **1e** also afforded 4-phenylcyclohexa-2,5-dienone (**4e**) in 7% yield. Biasing the system with sterically demanding alkyl groups at the two *ortho* positions should lead to a quasi-exclusive phenylation at the *para*-alkylated position. This was indeed the case with 4-methyl-2,6-di-*tert*-butylphenol (**1f**), the use of which only furnished 4-methyl-4-phenylcyclohexa-2,5-dienone (**4f**) in an excellent yield of 94% (Table 1, entry 6). Further evidence of the role played by the methyl group in mediating transfer of a phenyl group from Ph_2ICl was then obtained by performing the same reaction with 2,6-di-*tert*-butylphenol (**1g**; not shown), in which case no phenylation product was isolated.

Having thus established the prominent role that is played by alkyl substituents in the regiocontrol of this λ^3-iodane-mediated phenylation of phenols, we turned our attention to a series of 1-naphthols, each bearing an electronically different *ortho* substituent. Experiments carried out with Ph_2ICl on 2-methyl- (**1i**), 2-methoxy- (**1j**), and 2-nitrosonaphthol (**1k**) revealed a somewhat different reactivity from that of the phenols as no diaryl ether was observed. Nevertheless, the expected dearomatization products, **3i**, **3j**, or **3k**, were isolated as the sole products in increasing yields ranging from 36 to 74% (Table 2, entries 1–3). Naphthols, as well as phenols, that bear an electron-demanding *ortho* substituent such as 2-carboxymethoxynaphthol (**1l**), 2-nitronaphthol (**1m**; see Scheme 2), 2-hydroxynaphthaldehyde, and 4-nitrophenol (**1n**, **1h**; not shown) were all found to be refractory substrates at room temperature (see below). Only the ester **1l** gave rise to the formation of the diaryl ether **2l** and the desired dearomatized phenylation product **3l**, albeit in low yields (Table 2, entry 4).

In contrast to the unsubstituted 1-naphthol (**1o**; not shown) that led to a complex product mixture, the unsubstituted 2-naphthol (**1p**) was reactive towards Ph_2ICl and underwent both O- and C-phenylation to furnish three products: the diaryl ether **2p** (9%), 1-phenyl-2-naphthol (**3p**, 18%), and the diaryl ether **4p** (22%) through trans-

Table 1: Phenylation of phenols mediated by chorodiphenyl-λ^3-iodane.[a]

Entry	Substrate	O-phenylation	Yield [%][b] *o*-C-phenylation	*p*-C-phenylation
1	**1a**	**2a** (53),[c] (63)	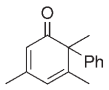 **3a** (0),[c] (8)	–
2	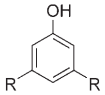 **1b**: R = H	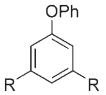 **2b** (75)	–	–
3	**1c**: R = Me	**2c** (59)	–	–
4	**1d**	**2d** (24), (35)[d]	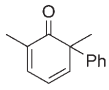 **3d** (37), (44)[c]	–
5	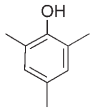 **1e**	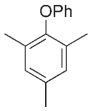 **2e** (7),[e] (63)	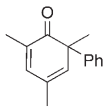 **3e** (42)[e,f]	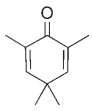 **4e** (7)[e,f]
6	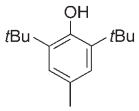 **1f**	–	–	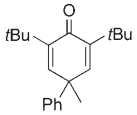 **4f** (94)

[a] Reactions were carried out by adding chlorodiphenyl-λ^3-iodane (1.3 mmol) to a stirred solution of the starting phenol in *t*BuOH (4 mL) in the presence of *t*BuOK (1.4 mmol) at room temperature. [b] Yield of isolated product. [c] This reaction was carried out with DMF. [d] This reaction was carried out in (tetrafluoroboro)diphenyl-λ^3-iodane. [e] Similar results were obtained in the presence of 1,1′-diphenylethylene (2 equiv). [f] Products **3e** and **4e** could not be cleanly separated by column chromatography on silica gel, so yields were evaluated by ^{1}H NMR spectroscopic analysis of the mixture.

 © 2005 Wiley-VCH Verlag GmbH & Co. KGaA, Weinheim

Table 2: Phenylation of naphthols mediated by chorodiphenyl-λ^3-iodane.[a]

Entry	Substrate	Yield [%][b] O-phenylation	Yield [%][b] *o*-C-phenylation
	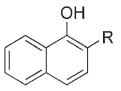		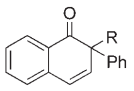
1	**1i**, R = Me	–	**3i** (36)
2	**1j**, R = OMe	–	**3j** (52)[c]
3	**1k**, R = NO	–	**3k** (74)[c]
	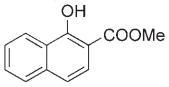	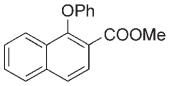	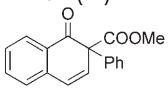
4	**1l**	**2l** (21)	**3l** (7)
	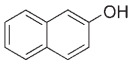	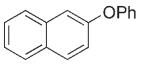	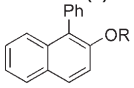
5	**1p**	**2p** (9)	**3p**: R = H (18) **4p**: R = Ph (22)

[a] Reactions were carried out by adding chlorodiphenyl-λ^3-iodane (1.3 mmol) to a stirred solution of the starting phenol in *t*BuOH (4 mL) in the presence of *t*BuOK (1.4 mmol) at room temperature. [b] Yields of isolated products. [c] Similar results were obtained in the presence of 1,1′-diphenylethylene (2 equiv).

ferring a second phenyl unit to **3p** (Table 2, entry 5). The C-phenylation course is thus globally favored over the O-phenylation alternative for this unsubstituted 2-naphthol treated under basic conditions in a protic solvent.[11] It is interesting to note that 2-naphthol (**1p**) was also the only phenol among those we used to furnish a diaryl product through phenylation at its unsubstituted C1 center. This is probably due to the more pronounced ambident character of the delocalized 2-naphthoxide anion relative to that of unsubstituted phenoxide anions[11] and to the aromaticity retained when this anion engages itself in bond formation at C1, but not at C3.

We next wondered about the mechanism that is operative in these phenylation reactions of phenols and naphthols as they constitute a novel aspect of hypervalent iodine chemistry. The first experimental observations of mechanistic relevance were that iodobenzene was formed as a by-product and that no reaction took place in the absence of a base strong enough to deprotonate the starting phenol. The delocalized phenolate nucleophile can then attack the iodine(III) center of Ph_2ICl in a ligand-exchange step, thus displacing the chloride anion ligand to furnish (aryloxy)diphenyl-λ^3-iodanes of type **A** (Scheme 1, path a) and/or their C-iodanylated cyclohexadienone variants of types **B** and **C** (Scheme 1 paths b and c) depending upon the electronic and steric demands of the substituents on the starting phenol.

Alternatively, the phenolate anion could engage itself in an aromatic nucleophilic-substitution reaction (i.e., S_NAr) and directly attack Ph_2ICl at one of its two phenyl carbon atoms bonded to the iodine(III) center. This S_NAr mechanistic path is generally proposed to rationalize the reactivity of species such as Ph_2ICl towards nucleophiles.[12] It must be recalled that these species are not tetrahedral diaryliodonium salts, as commonly thought, but 10-I-3 T-shaped pseudotrigonal bipyramidal entities, as expected for hypervalent I^{III} species.[3] To find evidence for one or the other mechanistic alternative, we revisited some of the reactions we had performed with the aim of characterizing any stable reaction intermediates. This was accomplished by isolating an intermediate from the reaction performed at room temperature with the apparently refractory substrate, 2-nitronaphthol (**1m**, see above). This intermediate was characterized as the type-**A** (2-nitronaphthoxy)diphenyl-λ^3-iodane, **5** (see Supporting Information and Scheme 2). In contrast to reactions

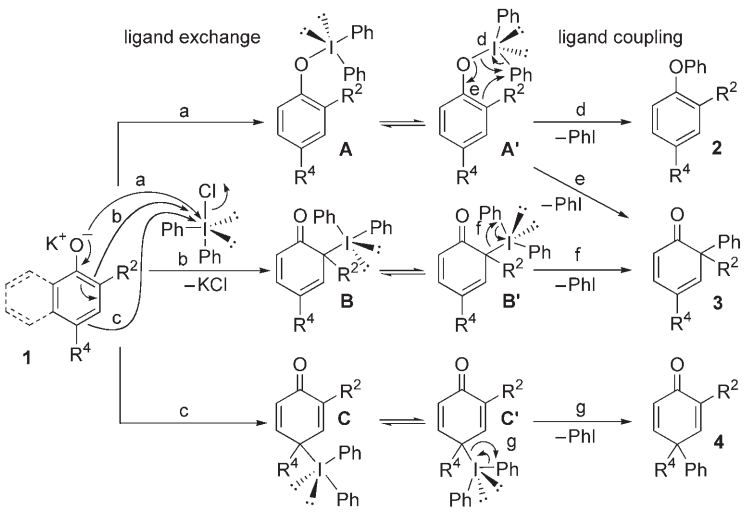

Scheme 1. Mechanistic description of the phenol phenylation reactions through direct ligand coupling. **A**, **B**, and **C**: 10-I-3 trigonal-bipyramidal intermediates; **A**′, **B**′, and **C**′: tetragonal-pyramidal intermediates. R^2, R^4: various substituents.

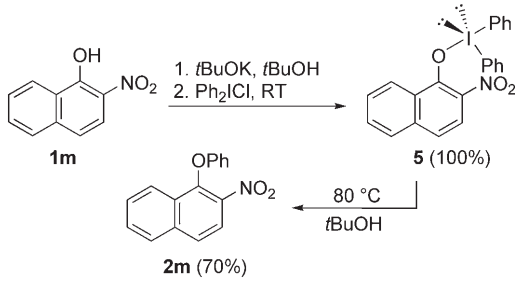

Scheme 2. Evidence of ligand exchange: isolation of type-**A** intermediate **5** and its heat-induced conversion into the diaryl ether **2m**.

carried out with phenols bearing electron-releasing *ortho* substituents, this intermediate does not further evolve at room temperature but gives the starting naphthol **1m** upon chromatography on silica gel. However, compound **5** furnishes the O-phenylated product **2m** in 70% yield when heated to reflux in *t*BuOH for 8 h (Scheme 2).

These observations are in agreement with an initial ligand-exchange step, but not with a direct S_NAr-type mechanism. Furthermore, the isolation of the 10-I-3 species **5** is particularly revealing of the mechanistic path followed in this process as the presence of a strongly electron-withdrawing *ortho* substituent on the starting phenol is usually

 © 2005 Wiley-VCH Verlag GmbH & Co. KGaA, Weinheim

associated with the stabilization of S_NAr Meisenheimer-type intermediates.[12,13]

Hence, the phenylation products observed with concomitant reductive elimination of iodobenzene can, in principle, result either from collapse of the λ^3-iodanyl intermediate into a phenyl and a phenoxy radical, which would then pair off, or from a concerted ligand coupling on the iodine(III) center itself.[4,13] To address this question, the efficient phenyl radical trapping agent, 1,1-diphenylethylene (DPE)[5g,8d,8e] was added to the reaction medium during the phenylation of **1e, 1j**, and **1k** (Table 1, entry 5 and Table 2, entries 2 and 3). The presence of DPE did not affect the outcome of the reaction, thus showing that no radical-based intermediate plays any determinant role in the process. These observations are in agreement with the proposal of an exclusive nonradical ligand-coupling mechanism. Thus, the 10-I-3 intermediates of types **A**, **B**, and **C** may evolve through coupling of their phenolate-derived ligand with one of the phenyl groups. Ligand coupling is symmetry-forbidden on these trigonal-bipyramidal structures, but bond-forming events can occur from tetragonal-pyramidal transient species of types **A′**, **B′**, and **C′** during ligand pseudorotation around the iodine(III) center (Scheme 1).[3,12,13]

Formation of diaryl ethers of type **2** would then result from intermediates of type **A′** through a nonsynchronous *ipso–ipso* coupling (path d) with a polar transition state as a consequence of the difference of polarity between the two ligands (i.e., LC_N-type coupling).[13] The formation of cyclohexa-2,4-dienone products of type **3** could either also arise from intermediates of type **A′** through an *ipso–allyl* $LC_{N'}$-type coupling (path e) or from **B′** through a quasi-synchronous *ipso–ipso* LC-type coupling (path f).[13] The fact that Ph_2ICl was also capable of transferring one of its phenyl ligands to the *para* position of 2,4,6-trimethylphenol (**1e**) and 4-methyl-2,6-di-*tert*-butylphenol (**1f**) to furnish cyclohexa-2,5-dienone products of type **4** (Table 1, entries 5 and 6) can only be rationalized in terms of a passage through intermediates of type **C′**, which then evolve through an *ipso–ipso* LC-type coupling (path g).

Semiempirical and Hartree–Fock calculations that we performed at the AM1 and 6-31G* levels to determine the electrostatic charge distribution and the relative magnitudes of the atomic coefficients of the highest occupied molecular orbital (HOMO) of the phenolate forms of **1a, d–g** illustrate the contribution of *ortho* and *para* methyl groups in controlling the regiochemical outcome of these phenylation reactions (see Supporting Information). In all cases, the negative charge is mostly localized on the oxygen atom, and the presence of a methyl group at one *ortho* position (**1a**) reinforces partial localization of the charge at the unsubstituted *ortho* and *para* positions (i.e., C6 and C4). Similarly, when comparing data for **1d** versus **1e** and **1f** versus **1g**, it can be read that the presence of a methyl group at the *para* position decreases the extent of partial localization of the charge at this locus. Hence, the O-phenylation path of the reaction may benefit from this charge distribution, but not its C-phenylation alternatives. However, the presence of a methyl group at C2 of **1a** or at C4 of **1e** and **1f** renders the relative magnitudes of the HOMO atomic coefficients at these centers larger in comparison to those at the unsubstituted *ortho* position in **1a** and at the unsubstituted *para* position in **1d** and **1g**, respectively. The dearomatizing C-phenylation path of the reaction would thus seem to be essentially under this orbital control. The results obtained with naphthols **1i–l** are in agreement with this substituent-controlled modulation of reactivity, since the more electron-releasing the substitutent at C2, the better is the yield of the dearomatizing *ortho*-phenylation reaction (Table 2, entries 1–3).

In conclusion, the work described herein presents a novel aspect of the versatility of hypervalent iodine(III) reagents in organic synthesis, which is illustrated by the use of the diaryl-λ^3-iodane Ph_2ICl to promote regioselective C-phenylation of *ortho*- and/or *para*-substituted phenols to give cyclohexadienone derivatives under basic conditions. The presence of a small electron-donating substituent at the *ortho* and/or *para* positions of the starting phenol determines the efficacy and regioselectivity of the process, which involves a nonradical coupling of the phenolate-derived and phenyl ligands directly around the iodine(III) center. Evidence of such a direct ligand-coupling mechanism is also given for the competitive O-phenylation process, which is commonly thought to follow an intermolecular aromatic nucleophilic-substitution reaction path.

Received: May 12, 2005
Revised: July 13, 2005
Published online: October 6, 2005

Keywords: aromaticity · hypervalent compounds · iodine · reaction mechanisms · regioselectivity

[1] For recent reviews on this topic, see: a) S. Quideau, L. Pouységu, *Org. Prep. Proced. Int.* **1999**, *31*, 617–680; b) S. Quideau in *Modern Arene Chemistry* (Ed.: D. Astruc), Wiley-VCH, Weinheim, **2002**, pp. 539–573; c) D. Magdziak, S. J. Meek, T. R. R. Pettus, *Chem. Rev.* **2004**, *104*, 1383–1429.

[2] a) A. Varvoglis, *Hypervalent Iodine In Organic Synthesis*, Academic Press, London, **1997**; b) T. Wirth, *Angew. Chem.* **2005**, *117*, 3722–3731; *Angew. Chem. Int. Ed.* **2005**, *44*, 3656–3665; c) V. V. Zhdankin, P. J. Stang, *Chem. Rev.* **2002**, *102*, 2523–2584.

[3] M. Ochiai, *Top. Curr. Chem.* **2003**, *224*, 5–68.

[4] a) R. M. Moriarty, R. K. Vaid, *Synthesis* **1990**, 431–447; b) R. M. Moriarty, *J. Org. Chem.* **2005**, *70*, 2893–2903.

[5] a) F. M. Beringer, P. S. Forgione, M. D. Yudis, *Tetrahedron* **1960**, 49–63; b) F. M. Beringer, S. A. Galton, S. J. Huang, *J. Am. Chem. Soc.* **1962**, *84*, 2819–2823; c) F. M. Beringer, P. S. Forgione, *J. Org. Chem.* **1963**, *28*, 714–717; d) F. M. Beringer, W. J. Daniel, S. A. Galton, G. Rubin, *J. Org. Chem.* **1966**, *31*, 4315–4318; e) K. Chen, G. F. Koser, *J. Org. Chem.* **1991**, *56*, 5764–5767; f) J. H. Ryan, P. J. Stang, *Tetrahedron Lett.* **1997**, *38*, 5061–5064; g) M. Ochiai, T. Shu, T. Nagaoka, Y. Kitagawa, *J. Org. Chem.* **1997**, *62*, 2130–2138; h) C. H. Oh, J. S. Kim, H. H. Jung, *J. Org. Chem.* **1999**, *64*, 1338–1340; i) M. Ochiai, Y. Kitagawa, N. Takayama, Y. Takaoka, M. Shiro, *J. Am. Chem. Soc.* **1999**, *121*, 9233–9234; j) M. Ochiai, Y. Kitagawa, M. Toyonari, *ARKIVOC* **2003**, 43–48.

[6] a) F. M. Beringer, E. M. Gindler, *J. Am. Chem. Soc.* **1955**, *77*, 3203–3207; b) A. Dibbo, L. Stephenson, T. Walker, W. K. Warburton, *J. Chem. Soc.* **1961**, 2645–2651; c) J. R. Crowder,

 © 2005 Wiley-VCH Verlag GmbH & Co. KGaA, Weinheim

E. E. Glover, M. F. Grundon, H. X. Kaempfen, *J. Chem. Soc.* **1963**, 4578 – 4585; d) R. A. Scherrer, H. R. Beatty, *J. Org. Chem.* **1980**, *45*, 2127 – 2131.

[7] a) H. C. Bell, G. L. May, J. T. Pinhey, S. Sternhell, *Tetrahedron Lett.* **1976**, 4303 – 4306; b) H. C. Bell, J. T. Pinhey, S. Sternhell, *Aust. J. Chem.* **1979**, *32*, 1551 – 1560; c) S. Saito, T. Kano, H. Muto, M. Nakadai, H. Yamamoto, *J. Am. Chem. Soc.* **1999**, *121*, 8943 – 8944; d) T. Kano, Y. Ohyabu, S. Saito, H. Yamamoto, *J. Am. Chem. Soc.* **2002**, *124*, 5365 – 5373.

[8] a) D. H. R. Barton, J.-C. Blazejewski, B. Charpiot, W. B. Motherwell, *J. Chem. Soc. Chem. Commun.* **1981**, 503 – 504; b) D. H. R. Barton, N. Yadav-Bhatnagar, J.-C. Blazejewski, B. Charpiot, J.-P. Finet, D. J. Lester, W. B. Motherwell, M. T. B. Papoula, S. P. Stanforth, *J. Chem. Soc. Perkin Trans. 1* **1985**, 2657 – 2665; c) D. H. R. Barton, N. Yadav-Bhatnagar, J.-P. Finet, J. Khamsi, W. B. Motherwell, S. P. Stanforth, *Tetrahedron* **1987**, *43*, 323 – 332; d) D. H. R. Barton, J.-P. Finet, C. Giannotti, F. Halley, *J. Chem. Soc. Perkin Trans. 1* **1987**, 241 – 249; e) D. H. R. Barton, J.-P. Finet, C. Giannotti, F. Halley, *Tetrahedron* **1988**, *44*, 4483 – 4494; f) A. Fedorov, S. Combes, J.-P. Finet, *Tetrahedron* **1999**, *55*, 1341 – 1352.

[9] a) R. B. Bedford, M. E. Limmert, *J. Org. Chem.* **2003**, *68*, 8669 – 8682; b) S. Oi, S.-i. Watanabe, S. Fulkita, Y. Inoue, *Tetrahedron Lett.* **2003**, *44*, 8665 – 8668; c) D. D. Hennings, S. Iwasa, V. H. Rawal, *J. Org. Chem.* **1997**, *62*, 2 – 3.

[10] S. Quideau, L. Pouységu, A. Ozanne, J. Gagnepain, *Molecules* **2005**, *10*, 201 – 216.

[11] N. Kornblum, R. Seltzer, P. Haberfield, *J. Chem. Soc.* **1963**, 85, 1148 – 1154.

[12] V. V. Grushin, *Acc. Chem. Res.* **1992**, *25*, 529 – 536.

[13] "Ligand Coupling Reaction with Heteroatomic Compounds": J.-P. Finet, *Tetrahedron Organic Chemistry Series, Vol. 18*, Pergamon, Oxford, **1998**.

 © 2005 Wiley-VCH Verlag GmbH & Co. KGaA, Weinheim

Self-Assembly

DOI: 10.1002/anie.200502539

Hydrogen-Bond-Mediated Self-Assembly of Aminopyrazolones: Macrocyclic Quartets—Single and Stacked One-Dimensional Motifs**

*Hegui Gong and Michael J. Krische**

A broad goal of modern research resides in the development of selective protocols for the organization of matter across length scales.[1] Toward this end, the self-assembly of molecular components has garnered considerable success as a procedure for the spontaneous generation of well-defined discrete and recurrent architectures.[2,3] Hydrogen-bond-mediated self-assembly has proven especially effective,[3] largely because of the design of tailored recognition elements in the form of hydrogen-bond donor–acceptor arrays, which allows the free energy and "orthogonality" of recognition events to be tuned.[3c] The utility of hydrogen-bond recognition elements is highlighted by their application to the design of oligomers (foldamers) that adopt specific secondary structures,[4,5] molecular strands that engage in specific modes of intermolecular aggregation,[6] polymers possessing non-covalent main chains[7] and side chains,[8] as well as the self-assembly of dendritic macromolecules.[9]

We recently developed duplex molecular strands based on the aminotriazine and diaminopyridazine hydrogen-bonding motifs as part of a program concerning hydrogen-bond-mediated self-assembly.[10] These systems engage in high-affinity twofold self-association, as established by isothermal titration calorimetry (ITC), ^{1}H NMR dilution studies, vapor pressure osmometry (VPO), and single-crystal X-ray diffraction analysis. With the goal of developing synthetic strands that self-assemble to form transmembrane channels,[11] we sought oligomers incorporating recognition elements that direct fourfold self-association. While quadruplexes based on guanosine and their structural relatives are commonplace,[12] other heterocyclic molecules that participate in hydrogen-bond-mediated fourfold self-association are exceptionally uncommon.[13] 3,5-Disubstituted pyrazoles are known to form dimers **A**, as well as cyclic trimers **B** and tetramers **C**, in solution and in the solid state (Scheme 1).[14] It was postulated that the hitherto unexplored aminopyrazolones **1** should preferentially engage in fourfold self-association through heteromeric aggregation (amide–amidine), as the quadruplex type arrangement is reinforced by four additional hydrogen bonds as in $\mathbf{1}_4$. However, homomeric association (amide–amide, amidine–amidine) of aminopyrazolone **1** may compete to provide 1-dimensional motif $\mathbf{1}_n$. Finally, because ditopic association is relatively weak, arrangements involving unrequited hydrogen-bond donor–acceptor sites are probable in the solid state.[15]

Aminopyrazolones **1a**–**1c** were synthesized according to a literature procedure.[16] Specifically, ethyl cyanoacetate was subjected to exhaustive alkylation followed by hydrazination to afford dibutylaminopyrazolone **1a**, didodecylaminopyrazolone **1b**, and dibenzylaminopyrazolone **1c**. Synthesis of the optically pure C_2-symmetric bis(aminopyrazolone) **1d** was achieved through the alkylation of a chirally modified cyanoacetate ester based on (1*S*,2*R*,4*R*)-10-dicyclohexylsulfamoylisoborneol (Scheme 2).[17]

Single crystals of compounds **1a**–**1d** were obtained and subjected to X-ray diffraction analysis to determine the mode of assembly in the solid state. Analysis of crystals of dibutylaminopyrazolone **1a** obtained from ethyl acetate reveal a 1-dimensional hydrogen-bonding motif involving homomeric association of the ditopic hydrogen-bond donor–acceptor sites (amide–amide, amidine–amidine; Figure 1). The N–H···N and N–H···O hydrogen bonds in the linear aggregate $(\mathbf{1a})_n$ have equal lengths of 3.07 Å. In contrast, X-

[*] H. Gong, Prof. M. J. Krische
University of Texas at Austin
Department of Chemistry and Biochemistry
1 University Station–A5300
Austin, TX 78712-1167 (USA)
Fax: (+1) 512-471-8696
E-mail: mkrische@mail.utexas.edu

[**] Acknowledgment is made to the Research Corporation Cottrell Scholar Award (CS0927), the Alfred P. Sloan Foundation, the Dreyfus Foundation, and the NSF-CAREER Program.

Supporting information for this article is available on the WWW under http://www.angewandte.org or from the author.

 © 2005 Wiley-VCH Verlag GmbH & Co. KGaA, Weinheim

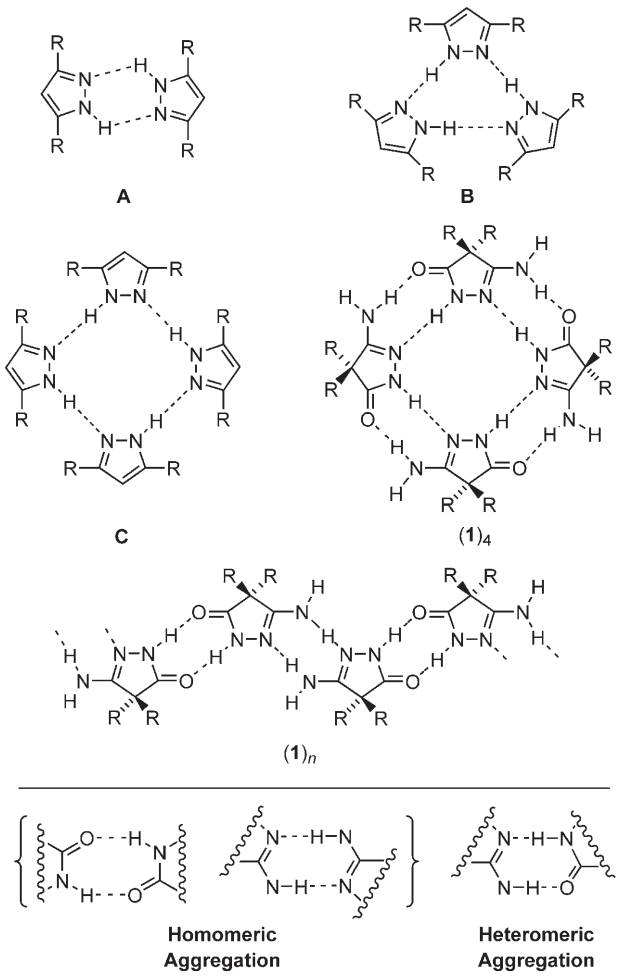

Scheme 1. Assembly modes established for 3,5-disubstituted pyrazoles and those proposed for aminopyrazolones **1**.

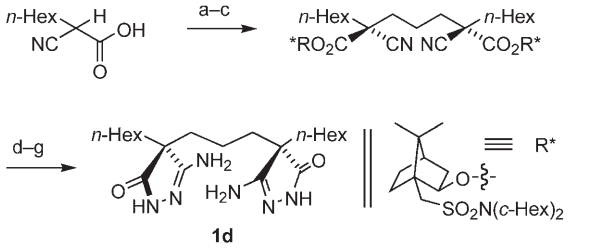

Scheme 2. Synthesis of bis(aminopyrazolone) **1d**. Reagents: a) PCl_5 (100 mol%), Et_2O (0.3 M), 25 °C. b) R*OH (50 mol%), AgCN (75 mol%), $PhCH_3$ (0.1 M), 60 °C, 70% over two steps. c) LDA (120 mol%), 1,3-diiodopropane (50 mol%), HMPA (150 mol%), THF (0.1 M), −78 °C to 25 °C, 38%. d) LiOH in MeOH (1.83 N, 1830 mol%), 25 °C, 83%. e) PCl_5 (212 mol%), Et_2O (0.1 M). f) MeOH (excess), 25 °C, 97% over two steps. g) NH_2NH_2-H_2O (1000 mol%), 105 °C, 70%. LDA = lithium diisopropylamide, HMPA = hexamethyl phosphoramide.

ray diffraction analysis of crystals of didodecylaminopyrazolone **1b** obtained from 1,2-dichloroethane reveals the desired cyclic quartet structure $(\mathbf{1b})_4$ derived through heteromeric association (amide–amidine, amide–amidine; Figure 2). The N–H···N and N–H···O hydrogen-bond lengths in the cyclic

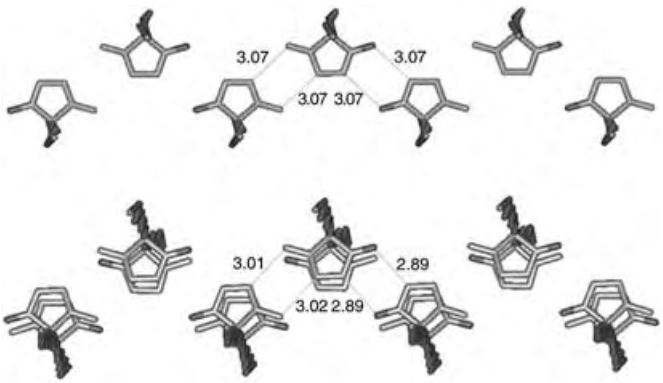

Figure 1. Top: Solid-state structure of dibutylaminopyrazolone **1a**. Bottom: Solid-state structure of C_2-symmetric bis(aminopyrazolone) **1d**. Solvent is omitted for clarity.

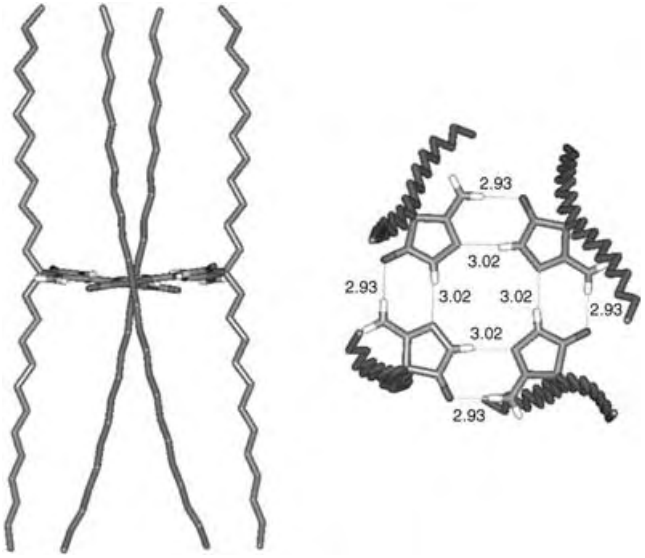

Figure 2. Solid-state structure of didodecylaminopyrazolone **1b**.

aggregate are 3.02 Å and 2.93 Å, respectively. A pore size of approximately 2.6 Å is estimated when the van der Waals radii are taken into account; hence, the pore size is sufficiently large to accommodate lithium, sodium, and potassium ions. The solid-state structure of dibenzylaminopyrazolone **1c** reveals a non-coplanar arrangement of the aminopyrazolone rings.[18] The energetic driving force represented by the packing preferences of the phenyl moieties in **1c**, appears to supercede the free energy of hydrogen-bond formation, as only one of the four hydrogen-bond donor–acceptor sites forms a contact with another aminopyridazine molecule. Finally, X-ray diffraction analysis of a crystal of C_2-symmetric bis(aminopyrazolone) **1d** obtained from 1,3-dimethyl-2-imidazolidinone reveals a stacked 1-dimensional motif. In this stacked motif, N–H···N and N–H···O hydrogen-bond lengths of 3.01/3.02 Å and 2.89 Å are observed, respectively.

In summary, initial studies on the hydrogen-bond-mediated self-assembly of aminopyrazolones have established that two primary modes of aggregation are evident for *n*-alkyl-substituted aminopyrazolones **1a**, **1b**, and **1d** in the solid

 © 2005 Wiley-VCH Verlag GmbH & Co. KGaA, Weinheim

state. Homomeric aggregation (amide–amide, amidine–amidine) of aminopyrazolones **1a** and **1d** gives rise 1-dimensional architectures $(\mathbf{1})_n$, while heteromeric aggregation (amide–amidine) generates the desired macrocyclic quartets $(\mathbf{1})_4$. The self-assembly of aminopyrazolones in solution is currently under investigation. These studies suggest that suitably tailored aminopyrazolone oligomers may spontaneously assemble to form channel-type aggregates.

Received: July 20, 2005
Published online: October 7, 2005

Keywords: donor–acceptor systems · host–guest systems · hydrogen bonds · noncovalent interactions · self-assembly

[1] For selected reviews, see: a) G. A. Ozin, *Chem. Commun.* **2000**, 419–432; b) G. M. Whitesides, J. P. Matthias, C. T. Seto, *Science* **1991**, *254*, 1312–1319; c) A. P. Alivisatos, P. F. Barbara, A. W. Castleman, J. Chang, D. A. Dixon, M. L. Klein, G. L. McLendon, J. S. Miller, M. A. Ratner, P. J. Rossky, S. I. Stupp, M. E. Thompson, *Adv. Mater.* **1998**, *10*, 1297–1336; d) Y. Xia, J. A. Rogers, K. E. Paul, G. M. Whitesides, *Chem. Rev.* **1999**, *99*, 1823–1848.

[2] For reviews on the general topic of self-assembly, see: a) D. Philp, J. F. Stoddart, *Angew. Chem.* **1996**, *108*, 1242–1286; *Angew. Chem. Int. Ed.* **1996**, *35*, 1154–1196; b) D. S. Lawrence, T. Jiang, M. Levett, *Chem. Rev.* **1995**, *95*, 2229–2260; c) S. J. Langford, J. F. Stoddart, *Pure Appl. Chem.* **1996**, *68*, 1255–1260; d) J.-H. Fuhrhop, B. Rosengarten, *Synlett* **1997**, 1015–1028; e) J. S. Lindsey, *New J. Chem.* **1991**, *15*, 153–180.

[3] For reviews on hydrogen-bond-mediated self-assembly, see: a) D. C. Sherrington, K. A. Taskinen, *Chem. Soc. Rev.* **2001**, *30*, 83–93; b) M. J. Krische, J.-M. Lehn, *Struct. Bonding* (*Berlin*) **2000**, *94*, 3–30; c) S. C. Zimmerman, P. S. Corbin, *Struct. Bonding (Berlin)* **2000**, *94*, 63–94; d) J. R. Fredericks, A. D. Hamilton in *Comprehensive Supramolecular Chemistry* (Eds.: J. L. Atwood, J. E. D. Davies, D. D. MacNicol, F. Vögtle), Elsevier, New York, **1996**, pp. 565–594; e) J. C. MacDonald, G. M. Whitesides, *Chem. Rev.* **1994**, *94*, 2383–2420; f) M. C. Etter, *Acc. Chem. Res.* **1990**, *23*, 120–126.

[4] For reviews encompassing foldamers, see: a) D. J. Hill, M. J. Mio, R. B. Prince, T. S. Hughes, J. S. Moore, *Chem. Rev.* **2001**, *101*, 3893–4011; b) S. H. Gellman, *Acc. Chem. Res.* **1998**, *31*, 173–180.

[5] For a seminal contribution to the field of foldamer chemistry, see: R. S. Lokey, B. L. Iverson, *Nature* **1995**, *375*, 303–305.

[6] For reviews encompassing duplex association of molecular strands, see: a) A. R. Sanford, K. Yamato, X. Yang, L. Yuan, Y. Han, B. Gong, *Eur. J. Biochem.* **2004**, *271*, 1416–1425; b) B. Gong, *Synlett* **2001**, 582–589; c) E. A. Archer, H. Gong, M. J. Krische, *Tetrahedron* **2001**, *57*, 1139–1159.

[7] For reviews encompassing hydrogen-bonded main-chain polymers, see: a) L. Brunsveld, B. J. B. Folmer, E. W. Meijer, R. P. Sijbesma, *Chem. Rev.* **2001**, *101*, 4071–4097; b) J. S. Moore, *Curr. Opin. Colloid Interface Sci.* **1999**, *4*, 108–116; c) N. Zimmerman, J. S. Moore, S. C. Zimmerman, *Chem. Ind.* **1998**, 604–607; d) C. T. Imrie, *Trends Polym. Sci.* **1995**, *3*, 22–29; e) C. Alexander, C. P. Jariwala, C.-M. Lee, A. Griffin, C *Macromol. Chem. Macromol. Symp.* **1994**, *77*, 283–294; f) J.-M. Lehn, *Macromol. Symp.* **1993**, *69*, 1–17.

[8] For examples of polymers possessing hydrogen-bonded side chains, see: a) L. P. Stubbs, M. Weck, *Chem. Eur. J.* **2003**, *9*, 992–999; b) B. D. Edgecombe, J. M. J. Fréchet, *Chem. Mater.* **1998**, *10*, 994–1002; c) B. D. Edgecombe, J. A. Stein, J. M. J. Fréchet, Z. Xu, E. J. Kramer, *Macromolecules* **1998**, *31*, 1292–1304; d) D. Stewart, C. T. Imrie, *Macromolecules* **1997**, *30*, 877–884; e) T. Kato, H. Kihara, S. Ujiie, T. Uryu, J. M. J. Fréchet, *Macromolecules* **1996**, *29*, 8734–8739; f) R. F. M. Lange, E. W. Meijer, *Macromol. Symp.* **1996**, *102*, 301–308; g) T. Kato, H. Kihara, T. Uryu, A. Fujishima, J. M. J. Fréchet, *Macromolecules* **1992**, *25*, 6836–6841; h) T. Kato, N. Hirota, A. Fujishima, J. M. J. Fréchet, *J. Polym. Sci. Polym. Chem. Ed.* **1996**, *34*, 57–62.

[9] For examples, see: a) B. Huang, J. R. Parquette, *J. Am. Chem. Soc.* **2001**, *123*, 2689–2690; b) J. Recker, D. J. Tomcik, J. R. Parquette, *J. Am. Chem. Soc.* **2000**, *122*, 10298–10307; c) S. C. Zimmerman, F. Zeng, D. E. C. Reichert, S. V. Kolotuchin, *Science* **1996**, *271*, 1095–1098.

[10] a) H. Gong, M. J. Krische, *J. Am. Chem. Soc.* **2005**, *127*, 1719–1725; b) E. A. Archer, M. J. Krische, *J. Am. Chem. Soc.* **2002**, *124*, 5074–5083.

[11] For reviews encompassing the self-assembly of tubular structures, see: a) G. W. Gokel, W. M. Leevy, M. E. Weber, *Chem. Rev.* **2004**, *104*, 2723–2750; b) D. T. Bong, T. D. Clark, J. R. Granja, M. R. Ghadiri, *Angew. Chem.* **2001**, *113*, 1016–1041; *Angew. Chem. Int. Ed.* **2001**, *40*, 988–1011; c) G. W. Gokel, O. Murillo, *Acc. Chem. Res.* **1996**, *29*, 425–432.

[12] For reviews encompassing G quartets and their structural relatives in molecular self-assembly, see: a) J. T. Davis, *Angew. Chem.* **2004**, *116*, 684–716; *Angew. Chem. Int. Ed.* **2004**, *43*, 668–698; b) G. Gottarelli, G. P. Spada, A. Garbesi in *Comprehensive Supramolecular Chemistry* (Eds.: J. L. Atwood, J. E. D. Davies, D. D. MacNicol, F. Vögtle), Elsevier, New York, **1996**, pp. 483–506; c) see also F. Seela, R. Kroschel, *Bioconjugate Chem.* **2001**, *12*, 1043, and references therein.

[13] To our knowledge, other than guanosines and pyrazoles, only one example of a heterocycle that engages in fourfold self-association through hydrogen-bond-mediated self-assembly has been reported: M. Mazik, D. Bläser, R. Boese, *Chem. Eur. J.* **2000**, *6*, 2865–2873.

[14] For an exhaustive account of the self-assembly of 3,5-disubstituted pyrazoles, see: O. Klein, F. Aguilar-Parilla, J. M. Lopez, N. Jagerovic, J. Elguero, H.-H. Limbach, *J. Am. Chem. Soc.* **2004**, *126*, 11718–11732, and references therein.

[15] 2-Aminopyrimidines which incorporate ditopic hydrogen-bond donor–acceptor arrays often adopt arrangements in the solid state that result in unrequited hydrogen-bond donor–acceptor sites: a) M. J. Krische, J.-M. Lehn, N. Kyritsakas, J. Fischer, *Helv. Chim. Acta* **1998**, *81*, 1909–1920; b) M. J. Krische, J.-M. Lehn, N. Kyritsakas, J. Fischer, E. K. Wegelius, M. J. Nissinen, K. Rissanen, *Helv. Chim. Acta* **1998**, *81*, 1921–1930.

[16] A. Echevarría, J. Elguero, G. I. Yranzo, E. Diez-Barra, A. Hoz, A. Moreno, M. A. García-Martín, *J. Chem. Soc. Perkin Trans. 1* **1993**, 2229–2232.

[17] N. Martin, A. Martinez-Grau, C. Seoane, J. L. Marco, A. Albert, F. H. Cano, *J. Heterocycl. Chem.* **1996**, *33*, 27–31.

[18] Detailed depictions of the solid-state structure of **1c** are provided in the Supporting Information.

 © 2005 Wiley-VCH Verlag GmbH & Co. KGaA, Weinheim

Aluminum Complexes

DOI: 10.1002/anie.200502251

Janus-Faced Aluminum: A Demonstration of Unique Lewis Acid and Lewis Base Behavior of the Aluminum Atom in $[LAlB(C_6F_5)_3]$**

Zhi Yang, Xiaoli Ma, Rainer B. Oswald, Herbert W. Roesky, Hongping Zhu, Carola Schulzke, Kerstin Starke, Marc Baldus, Hans-Georg Schmidt, and Mathias Noltemeyer*

Compounds of aluminum with a formal +3 oxidation state on aluminum, such as trihalides, trialkyls, and triaryls, show classical behavior of Lewis acids.[1] In recent years, another class of compounds containing aluminum with the +1 oxidation state has attracted great interest.[2] These compounds, which have a nonbonding lone pair of electrons at the aluminum center, are proposed to have singlet, carbene-like character and they exhibit the potential for Lewis base behavior. In 2000, Cowley and co-workers reported the first example of an aluminum(I)–boron donor–acceptor bond, in $[Cp^*Al{\rightarrow}B(C_6F_5)_3]$ ($Cp^* = C_6Me_5$),[3] and one year later a corresponding Al–Al bond in $[Cp^*Al{\rightarrow}Al(C_6F_5)_3]$.[4] In neither of these systems did an aluminum center show both Lewis acid and Lewis base behavior.

The reduction of $[I_2AlL]$ ($L = HC(CMeNAr)_2$; $Ar = 2,6\text{-}iPr_2C_6H_3$) with potassium resulted in the formation of monomeric [LAl] (**1**).[5] This was the first stable two-coordinate aluminum(I) compound to be prepared and structurally characterized in the solid state. The fascinating aspect of **1** is its dual Lewis acid and Lewis base character. Ab initio calculations[6] with analysis of the Laplacian of the electron density[7] within the plane show a geometrically active lone pair of electrons on the aluminum atom with a probable quasi-trigonal-planar orientation of orbitals. This observation clearly indicates that **1** is Lewis basic. Moreover, charge depletion close to the aluminum atom in the semiplane of the six-membered ring indicates that **1** is Lewis acidic. Herein, we report the reaction of [LAl] (**1**) with $B(C_6F_5)_3$ to yield $[LAlB(C_6F_5)_3]$ (**2**), the first aluminum compound displaying both Lewis base and Lewis acid character at the metal center.

The reaction of a 1:1 molar ratio of [LAl] (**1**) and $B(C_6F_5)_3$ in toluene between −78 °C and room temperature resulted in the formation of **2** (Scheme 1). Compound **2** was characterized by ^1H, ^{13}C, ^{11}B, ^{19}F, and ^{27}Al NMR spectroscopy, as well as EI mass spectrometry and elemental analysis. ^1H, ^{13}C, ^{11}B, and ^{19}F NMR spectroscopic analysis was carried out at room temperature in $[D_6]$benzene or $[D_8]$toluene. No resonance signals were observed in the ^{27}Al NMR spectra of **2** in C_6D_6 or C_7D_8; consequently, the measurement was carried out in the solid state. The ^{19}F NMR spectrum of **2** exhibits nine partly overlapping resonances, and therefore an unambiguous assignment is not possible. However, this pattern indicates a distorted $B(C_6F_5)_3$ group caused by an Al–F interaction. The EI mass spectrum shows the molecular ion of **2** (*m*/*z* 956). Single crystals of **2** suitable for X-ray crystallographic analysis were obtained by keeping the hexane solution at room temperature for two weeks.[8] The solid-state structure consists of individual molecules of the Lewis acid/base adduct (Figure 1). An Al–F interaction arises from close intramolecular contact between one of the *ortho* fluorine atoms and the Al atom with the formation of an $AlBC_2F$ five-membered ring (Figure 2). There is a distorted tetrahedral geometry around the aluminum atom, with an average Al–N bond length of 1.892(6) Å. This distance is considerably shorter than the Al–N bonds in **1** (av 1.957(6) Å). This observation is consistent with the partial transfer of the lone pair of electrons on the aluminum center upon formation of the donor–acceptor bond. The Al–B bond in **2** (2.183(3) Å) is slightly longer than that in $[Cp^*Al{-}B(C_6F_5)_3]$ (2.169(2) Å). Also, the geometry of the $B(C_6F_5)_3$ group changes from trigonal planar to distorted tetrahedral in **2**. The extent of the geometrical change has been taken as an indication of the strength of the donor–acceptor interaction.[9] The sum of the C-B-C angles around the boron atom in **2** (330.3(2)°) is the smallest of those (333.5(2)–342.2(2)°) reported for $B(C_6F_5)_3$ compounds.[3,10,11] Thus, **1** appears to be a stronger base than {Cp*Al}. However it must to be considered that the relatively close Al–F contact in **2** (2.156(2) Å) changes the electron density on the aluminum center. The noticeable Al–F interaction is indicated by the lengthening of the C–F bond (1.414(6) Å) relative to the remaining 14 C–F bonds (av 1.355 Å). In addition, the C(41)-B(1)-Al(1) angle is clearly smaller

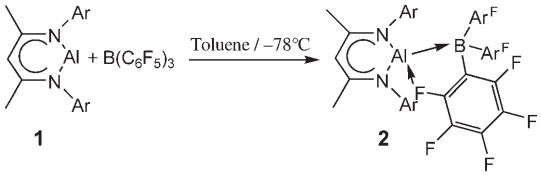

1 2

Scheme 1. Formation of **2**. $Ar = 2,6\text{-}iPr_2C_6H_3$, $Ar^F = C_6F_5$.

[*] Z. Yang, X. Ma, Prof. Dr. H. W. Roesky, H. Zhu, Dr. C. Schulzke, K. Starke, H.-G. Schmidt, M. Noltemeyer
Institut für Anorganische Chemie
Universität Göttingen
Tammannstrasse 4, 37077 Göttingen (Germany)
Fax: (+49) 551-39-3373
E-mail: hroesky@gwdg.de
Dr. R. B. Oswald
Institut für Physikalische Chemie
Universität Göttingen
Tammannstrasse 6, 37077 Göttingen (Germany)
Dr. M. Baldus
Max-Planck-Institut für Biophysikalische Chemie
Solid-State NMR
Am Fassberg 11, 37077 Göttingen (Germany)

[**] This work was supported by the Göttinger Akademie der Wissenschaften and the Fonds der Chemischen Industrie. $L = HC(CMeNAr)_2$, $Ar = 2,6\text{-}iPr_2C_6H_3$. The Roman god Janus has two faces looking in opposite directions. Herein, the aluminum is showing its two "faces" of Lewis acid and Lewis base properties.

 InterScience © 2005 Wiley-VCH Verlag GmbH & Co. KGaA, Weinheim

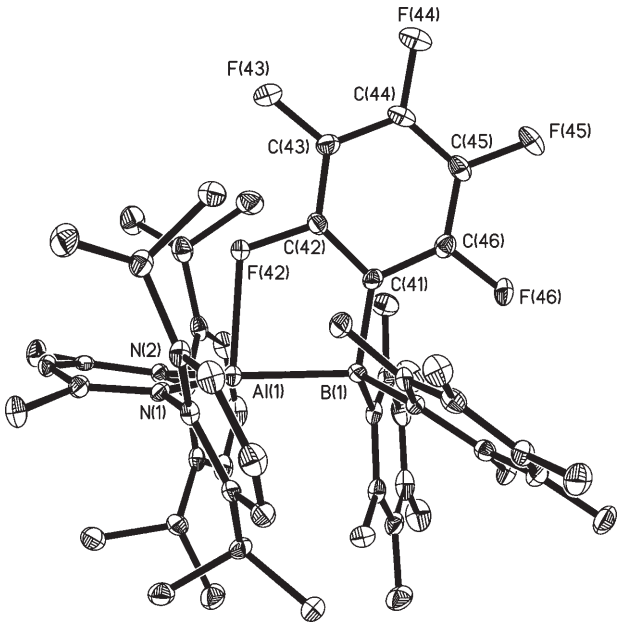

Figure 1. X-ray crystal structure of **2**. Selected bond lengths [Å] and angles [°]: Al(1)–B(1) 2.183(5), Al(1)–F(42) 2.156(3), C(42)–F(42) 1.414(4), Al(1)–N(2) 1.885(4), Al(1)–N(1) 1.900(3), C(33)–F(33) 1.371(5); C(41)-B(1)-Al(1) 100.4(3), C(51)-B(1)-Al(1) 115.1(3), C(31)-B(1)-Al(1) 110.1(3), F(42)-Al(1)-B(1) 85.99(15); $\Sigma\sphericalangle$CBC 330.3(2)°.

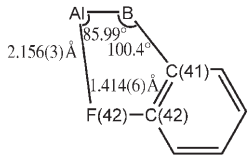

Figure 2. Depiction of Al-B-C(41)-C(42)-F(42) five-membered ring.

(100.4(3)°) than the C_{ipso}-B-Al angles (115.1(3)° and 110.1(3)°) of the two non-interacting perfluorophenyl rings. These data indicate that the lengthening of the C–F bond and the narrowing of the Al-B-C angle are due to the F→Al interaction and are consistent with a F→Al donor–acceptor behavior.

It is evident from the crystallographic data that there is a weak interaction between the aluminum and fluorine F(42) centers. To gain a better understanding of the bonding situation, **2** was examined by means of ab initio calculations. The first and crucial step in these calculations is to reproduce the crystallographic data with a reliable quantum-chemical method. Starting from this structure, the analysis of the molecular orbitals and bond order gives the most accurate picture of the electronic structure.

The calculated structural parameters (Al–F(42) 2.1626 Å, F(42)–C(42) 1.4384 Å, and F(42)-Al-B 85.236°) are in good agreement with the crystallographic data (Figure 1). The bond-order analysis reveals that the electron density of the fluorine atom is distributed between the carbon and aluminum centers with a (Al–F)/(F–C) ratio of 0.2930/0.7148, which indicates that there is a significant interaction between the fluorine and aluminum centers. The consequence of this interaction is the elongation of the C(42)–F(42) bond by 0.075 Å (calcd 1.4385 Å) relative to the other C–F bonds in the same ring (calcd range 1.3633–1.3636 Å). From natural bond order (NBO) analysis,[12] the bond between aluminum and fluorine can be described as the overlap of two hybrid orbitals of sp^n type with one located at Al (16.24% s and 83.76% p) and the other at F(42) (11.56% s and 88.44% p). The bonding orbital located on C(42) has $sp^{2.72}$ character, whereas the remaining carbon atoms in this ring have $sp^{2.22}$ character. This situation is also clearly visible in the corresponding orbital picture. Figure 3 shows the contour plots of two orbitals contributing to the formation of the Al–F bond.

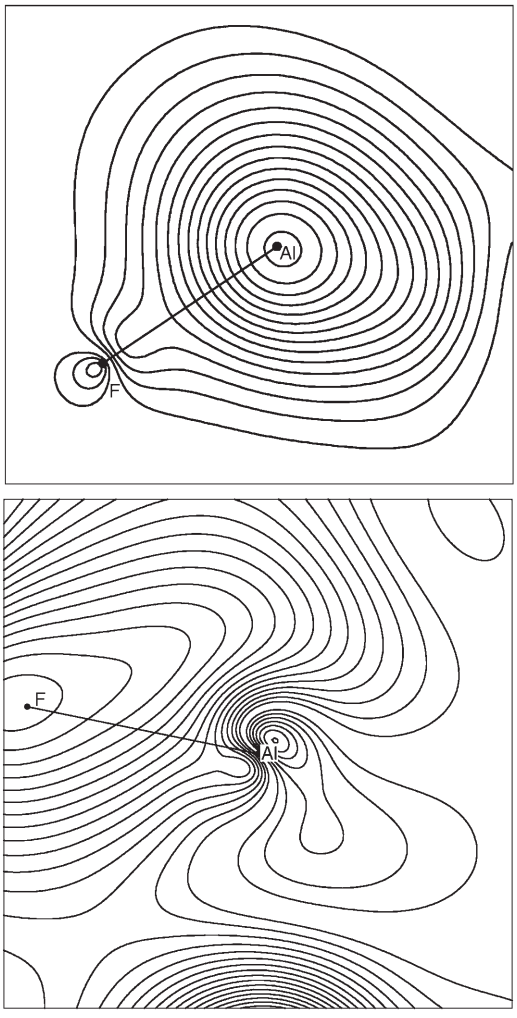

Figure 3. Schematic representation of the Al–F linkage resulting from the overlap of wave functions centered on aluminum and fluorine. The two relevant orbitals are shown here as contour plots. The clearly visible deformation in the second plot is due to the fact that there is a strong interaction with orbitals forming the Al–N bonds.

In conclusion, we have prepared $[LAlB(C_6F_5)_3]$, a unique compound of aluminum showing Lewis base and Lewis acid character at the aluminum center. There are no known precedents of this type of bonding in the literature.

 © 2005 Wiley-VCH Verlag GmbH & Co. KGaA, Weinheim

Experimental Section

All manipulations were performed under a dry, oxygen-free atmosphere (N_2 or Ar) by using Schlenk and glove-box techniques.

2: Toluene (20 mL) was added to a mixture of **1** (0.223 g, 0.5 mmol) and $B(C_6F_5)_3$ (0.256 g, 0.5 mmol) at −78 °C. The mixture was stirred and slowly warmed to room temperature. After stirring the mixture for an additional 15 h, the solvent was removed under reduced pressure, and the solution was treated with hexane (30 mL). The solution was filtered and allowed to stand for two weeks at room temperature to afford colorless crystals of **2**. Yield: 0.09 g (19 %); m.p. 208–209 °C; EI-MS: *m/z* (%) 956 (10) [M^+], 403 (100) [L−Me]; ^{1}H NMR (300.13 MHz, C_6D_6): $\delta = 6.80$–6.75 (m, 6H, Ar-H), 4.91 (s, 1H, γ-H), 2.80 (sept, $^3J_{H,H} = 6.8$ Hz, 4H, C*H*Me$_2$), 1.61 (s, 6H, Me), 1.15 (d, $^3J_{H,H} = 6.8$ Hz, 12H, CH*Me*$_2$), 0.87 ppm (d, $^3J_{H,H} = 6.8$ Hz, 12H, CH*Me*$_2$); ^{13}C NMR (75.48 MHz, C_6D_6): $\delta = 173.33$ (CN), 142.75, 139.49, 129.27, 124.76 (Ar), 150.25, 147.13, 140.75, 138.63, 137.38, 134.95 (br, C_6F_5), 102.07 (γ-C), 24.53, 25.09(CH*Me*$_2$), 22.68 (CH*Me*$_2$), 20.74 ppm (Me). ^{11}B NMR (95.29 MHz, C_6D_6): $\delta = -26.52$ ppm; ^{19}F NMR (188.28 MHz, C_7D_8) $\delta = -124.28$ (br m), −128.26 (br m), −129.97 (d), −154.41 (t), −156.49 (br m), −157.27 (t), −158.86 (br m), −160.24 (t), −160.99 ppm (t); ^{27}Al NMR (400 MHz, 16 KHz, MAS, $AlCl_3$): $\delta = 0$–50 ppm; elemental analysis (%) calcd for $C_{47}H_{41}AlBF_{15}N_2$ ($M_r = 956.61$): C 59.01, H 4.32, N 2.93; found: C 58.66, H 4.67, N 2.70.

Details of ab initio calculations: The well-established B3LYP[13,14] method was employed for all the ab initio calculations because of the size of the system. Two different basis sets were used for the computations: a small one as the 3-21G basis set, and an extended one in which the aluminum atoms are described with functions taken from the 631-G basis set including double-diffuse functions.[15,16] The Gaussian G03[17] program suite was used to optimize the structure with the 3-21G basis first, and this structure was used as the starting geometry for a further optimization with the larger basis set to give an appropriate description of the aluminum atom and its binding situation. The resulting structure was used for visualization of the orbitals. The nature of the quantum-chemical method results in a wave function that produces molecular orbitals involving nearly every atom. Therefore, this method leads to a picture that, despite being mathematically correct, is difficult to interpret. A more descriptive picture is obtained by localizing the orbitals at those atoms according to the Boys Method.[18] Quantitative data about the bond between Al and F(42) was obtained by analyzing the bond order following a proposal of I. Mayer.[19]

Received: June 27, 2005
Published online: October 11, 2005

Keywords: aluminum · boron · fluorine · Lewis acids · Lewis bases

[1] See, for example: *Chemistry of Aluminum, Gallium, Indium, Thallium* (Ed.: A. J. Downs), Chapman and Hall, New York, **1993**.
[2] For a review, see: H. W. Roesky, *Inorg. Chem.* **2004**, *43*, 7284–7293.
[3] J. D. Gorden, A. Voigt, C. L. B. Macdonald, J. S. Silverman, A. H. Cowley, *J. Am. Chem. Soc.* **2000**, *122*, 950–951.
[4] J. D. Gorden, C. L. B. Macdonald, A. H. Cowley, *Chem. Commun.* **2001**, 75–76.
[5] C. Cui, H. W. Roesky, H.-G. Schmidt, M. Noltemeyer, H. Hao, F. Cimpoesu, *Angew. Chem.* **2000**, *112*, 4444–4446; *Angew. Chem. Int. Ed.* **2000**, *39*, 4274–4276.
[6] M. W. Schmidt, K. K. Baldringe, J. A. Boatz, S. T. Edbert, M. S. Gordon, J. H. Jensen, S. Koseki, N. Matsunaga, K. A. Nguyen, S. J. Su, T. L. Windus, *J. Comput. Chem.* **1993**, *14*, 1347–1363.
[7] R. F. W. Bader, *Chem. Rev.* **1991**, *91*, 893–928.
[8] Crystal data for **2**: $C_{47}H_{41}AlBF_{15}N_2$, $M_r = 956.61$, triclinic, space group $P\bar{1}$, $a = 1168.97(12)$, $b = 1265.34(13)$, $c = 1607.85(17)$ pm, $\alpha = 74.641(8)$, $\beta = 73.606(8)$, $\gamma = 76.347(8)°$, $V = 2.1664(4)$ nm^3, $Z = 2$, $\rho_{calcd} = 1.466$ Mg m^{-3}, $F(000) = 980$, $1.69 \le \theta \le 24.66°$; of 21853 reflections collected, 7306 were independent. The *R* values are $R1 = 0.0557$ and $wR2 = 0.0750$ ($I > 2\sigma(I)$); min./max. residual electron density: 0.297/−0.305 e Å^{-3}. All non-hydrogen atoms were located by difference Fourier synthesis and refined anisotropically. All hydrogen atoms were included at geometrically calculated positions and refined by using a riding model. CCDC-273349 contains the supplementary crystallographic data for this paper. These data can be obtained free of charge from The Cambridge Crystallographic Data Centre via www.ccdc.cam.ac.uk/data_request/cif.
[9] H. Jacobsen, H. Berke, S. Döring, G. Kehr, G. Erker, H. Fröhlich, O. Meyer, *Organometallics* **1999**, *18*, 1724–1735.
[10] A. H. Cowley, *Chem. Commun.* **2004**, 2369–2375.
[11] a) R. J. Wright, A. D. Phillips, N. J. Hardman, P. P. Power, *J. Am. Chem. Soc.* **2002**, *124*, 8538–8539; b) N. J. Hardman, P. P. Power, J. D. Gorden, C. L. B. Macdonald, A. H. Cowley, *Chem. Commun.* **2001**, 1866–1867; c) N. J. Hardman, R. J. Wright, A. D. Phillips, P. P. Power, *J. Am. Chem. Soc.* **2003**, *125*, 2667–2679; d) P. Jutzi, B. Neumann, G. Reumann, L. O. Schebaum, H.-G. Stammler, *Organometallics* **2001**, *20*, 2854–2858.
[12] J. E. Carpenter, F. Weinhold, *J. Mol. Struct.* (*Theochem*) **1988**, 169, 41–62.
[13] C. Lee, W. Yang, R. G. Parr, *Phys. Rev. B* **1988**, 37, 785–789.
[14] B. Miehlich, A. Savin, H. Stoll, H. Preuss, *Chem. Phys. Lett.* **1989**, *157*, 200–206.
[15] G. A. Petersson, M. A. Al-Laham, *J. Chem. Phys.* **1991**, *94*, 6081–6090.
[16] G. A. Petersson, A. Bennett, T. G. Tensfeldt, M. A. Al-Laham, W. A. Shirley, J. Mantzaris, *J. Chem. Phys.* **1988**, *89*, 2193–2218.
[17] Gaussian 03, Revision C.02, M. J. Frisch et al., Gaussian Inc., Wallingford CT, **2004**.
[18] S. F. Boys, *Rev. Mod. Phys.* **1960**, *32*, 296–299.
[19] I. Mayer, *Chem. Phys. Lett.* **1983**, *97*, 270–274.

 © 2005 Wiley-VCH Verlag GmbH & Co. KGaA, Weinheim

Biosynthesis

DOI: 10.1002/anie.200501757

Accumulation of an *E*,*E*,*E*-Triene by the Monensin-Producing Polyketide Synthase when Oxidative Cyclization is Blocked**

*Apoorva Bhatt, Christian B. W. Stark, Barbara M. Harvey, Andrew R. Gallimore, Yuliya A. Demydchuk, Jonathan B. Spencer, James Staunton, and Peter F. Leadlay**

Monensin A (**1a**) from *Streptomyces cinnamonensis* is an antibiotic ionophore[1] widely used in veterinary medicine and in animal husbandry (Scheme 1). It is one of the most important and best-studied members of a large family of structurally related polyketide secondary metabolites, the ionophoric polyethers, which are attracting renewed interest for their activity against drug-resistant strains of malaria.[2] As with all natural polyethers, the molecule contains a multiplicity of asymmetric centers, but only one stereoisomer (out of a possible 2^{17}) is produced by *S. cinnamonensis*. The molecular basis for this exquisite stereocontrol is not known, and even the nature of the intermediates in polyether biosynthesis remains obscure. Early feeding studies established that monensin A (**1a**) is derived by a classic polyketide pathway from five acetate, one butyrate, and seven propionate units[3] and that oxygen atoms at C1, C3, C5, C7, C9, and C25 arise from the carboxylate oxygen atoms of the corresponding carboxylic acid precursor units, whereas the remaining oxygen atoms at C13, C17, C21, and C26 are derived from molecular oxygen.[4] On this basis, the "cascade" mechanism shown in Scheme 2a was proposed for the key oxidative steps.[4b] This mechanism involves the intermediacy of the linear *E*,*E*,*E*-triene **2** and of the triepoxide **3** as enzyme-free intermediates. However, it has proved difficult to obtain direct experimental support for this mechanism, and in particular, a synthetic sample of the full-length putative linear *E*,*E*,*E*-triene precursor **2** was found not to be incorporated into monensin A by *S. cinnamonensis*.[5] The configuration of the double bonds in a putative linear precursor of monensin, as well as the mode of oxidative cyclization, therefore, remained undefined, and alternative pathways for oxidative cyclization[6] that involved either a *Z*,*Z*,*Z* triene[6d,e] or a *E*,*Z*,*Z* triene[6f] have been subsequently proposed (Scheme 2b).

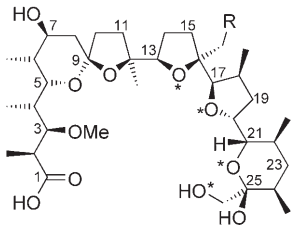

1a: R = CH_3
1b: R = H

Scheme 1. The polyether ionophores monensin A (**1a**) and monensin B (**1b**). Oxygen atoms arising from molecular oxygen are denoted by *.

The recent total sequencing of gene clusters for the biosynthesis of monensin[6f,7] and of nanchangmycin[8] revealed, in each case, large open reading frames (ORFs) encoding a modular polyketide synthase (PKS) with the anticipated number of extension modules consistent with the production of a linear "pre-polyether" polyketide chain of the requisite length. Complete deletion of the gene cluster from *S. cinnamonensis* resulted in loss of monensin production, thus confirming its role in monensin biosynthesis.[7] Each cluster contains numerous other genes, in particular four ORFs which, on the basis of database comparisons, appear to relate to the unusual oxidative cyclizations that are required to produce the polycyclic product.[6f,7] Thus, the monensin-producing cluster contains an epoxidase gene (*monCI*), a gene with apparent similarity to an epoxide-opening enzyme (*monCII*), and two mutually homologous genes (*monBI* and *monBII*) with apparent similarity to the Δ^5-3-ketosteroid isomerase of *Comamonas testosteroni* and which were considered initially to possibly function as *cis–trans* isomerases.[6f,7] Further proof that MonCI was an epoxidase was obtained when a *Streptomyces coelicolor* strain that overexpressed monCI converted the unsaturated terpene (±)-linalool into linalool oxide at levels 10–20-fold higher than a control strain.[7] Subsequently, it proved possible to interrupt polyketide-chain synthesis by genetically relocating a chain-terminating thioesterase (TE)/cyclase domain, obtained from the modular PKS that governs the biosynthesis of the macrolide erythromycin A in *Saccharopolyspora erythraea*,[9] to downstream of extension module four of the monensin PKS. In the pentaketide released by this recombi-

[*] Dr. A. Bhatt,[+] Y. A. Demydchuk, Prof. P. F. Leadlay
Department of Biochemistry
University of Cambridge
80 Tennis Court Road, Cambridge CB21GA (UK)
Fax: (+44) 1223-766-091
E-mail: pfl10@mole.bio.cam.ac.uk
Dr. C. B. W. Stark,[++] B. M. Harvey, A. R. Gallimore, Dr. J. B. Spencer, Prof. J. Staunton
University Chemical Laboratory
University of Cambridge
Lensfield Road, Cambridge CB21EW (UK)
[+] current address:
Howard Hughes Medical Institute
Albert Einstein College of Medicine
Department of Microbiology and Immunology
Bronx, NY 10461 (USA)
[++] current address:
Freie Universität Berlin
Institut für Chemie—Organische Chemie
Takustrasse 3, 14195 Berlin (Germany)

[**] This research was supported by the Biotechnology and Biological Sciences Research Council (BBSRC). We gratefully acknowledge the support of studentships from the EPSRC (to A.R.G. and B.M.H.), a grant from Roche Pharmaceuticals (Basel), and an EU Marie Curie Postdoctoral Training Fellowship (to C.B.W.S.)

Supporting information for this article is available on the WWW under http://www.angewandte.org or from the author.

 © 2005 Wiley-VCH Verlag GmbH & Co. KGaA, Weinheim

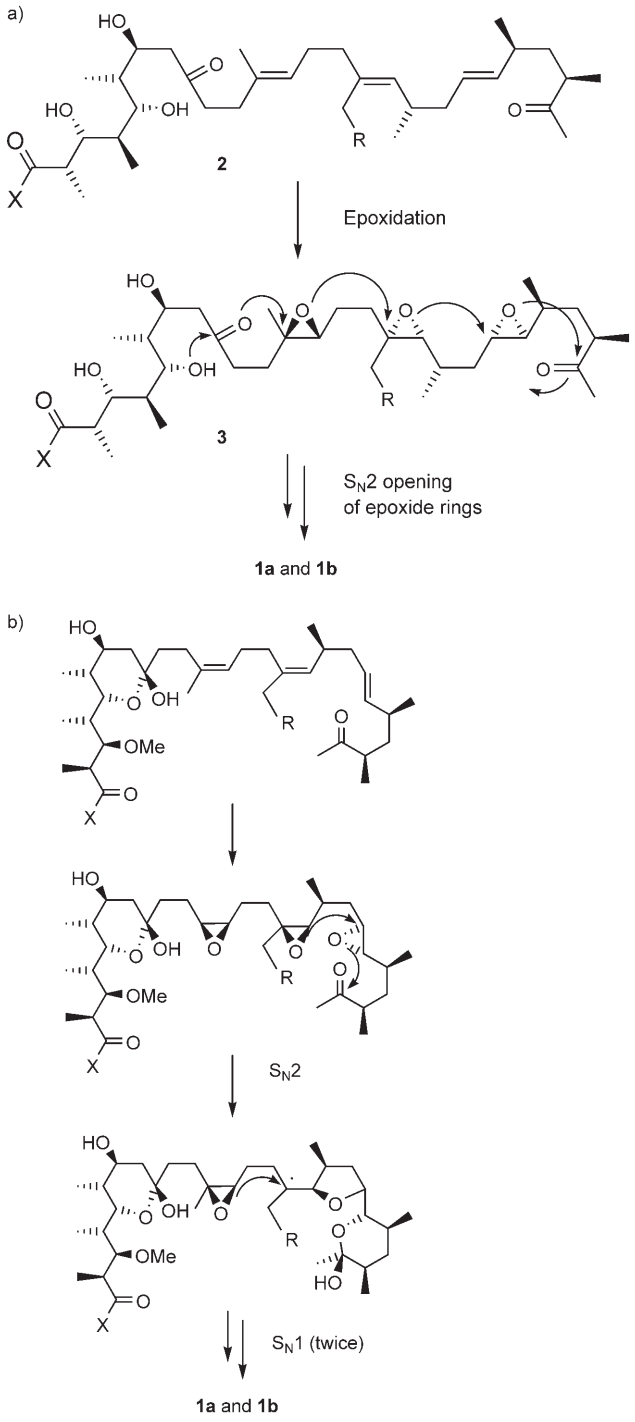

Scheme 2. Alternative mechanisms for oxidative cyclization to produce monensins A and B. a) A polyepoxide cyclization cascade that starts from an *E*,*E*,*E* triene[6b]; b) a polyepoxide cyclization cascade starting from an *E*,*Z*,*Z* triene[6f] **3**. X = OH, SCoA, or S-protein.

nant strain, the configuration of the disubstituted double bond was unequivocally shown to be *E*,[10] which weighed in favor of **2** as an intermediate[6b] or a variant of **2** in which the other bonds are *Z*,[6g] but ruled out the mechanistic proposal of Townsend and Basak.[6d] Based on these results, we reasoned that if *monCI* were indeed the sole initiator of oxidative cyclization in monensin biosynthesis then the deletion of this single gene in *S. cinnamonensis* ought to allow the accumulation of a linear molecule, such as **2** (or perhaps of a shunt product derived from such a compound) whose structural characterization might reveal the likely pathway for cyclization, thus allowing discrimination between the mechanistic proposals of Scheme 2.

Deletion of *monCI*, which encodes the putative flavin-dependent epoxidase from the monensin cluster, was accomplished by homologous recombination into wild-type *S. cinnamonensis* through two successive single crossover events, thus leading to replacement by a hygromycin resistance gene.[11a] Correct integration into the chromosome was proved for the mutant strain ABΔCI by Southern hybridization. Further confirmation of its identity was provided by complemention with the cloned gene borne on an expression plasmid (see the Supporting Information) which restored monensin production (data not shown). By further engineering of the *monCI*-deleted strain so that it also contained an in-frame deletion in *monBI*, the additional blocked mutant ABΔCIΔBI was obtained. Further mutants with insertional inactivation of both of the adjacent genes[6f,7] *monCI* and *monBII* (BHΔCIBII) and of all three genes *monCI, monBII*, and *monBI* (BHΔCIBIBII) were created in the same way as for the strain ABΔCI.

Neither monensin A (**1a**) nor monensin B (**1b**) was produced by any of these mutants, as judged by HPLC–mass-spectrometric analysis of the crude extracts.[11a] The analyte from the ABΔCI strain showed a major peak that corresponds to the predicted mass of **4a**, (Scheme 3) a triene lactone that differs only from **2** by the presence of a δ-lactone structure.[11a] A second smaller peak had the predicted mass of a similar triene lactone **4b** that lacks a methylene moiety, thus corresponding to the mass difference between **1a** and **1b**. To confirm the structure and the configuration of **4a** and **4b**, a culture of mutant ABΔCI (7 L) was grown under standard conditions,[6f,11a] and the crude extract of the supernatant was purified by column chromatography on silica gel, which yielded 1.4 mg of **4** and 1.2 mg of **5**. Detailed NMR spectroscopic analysis of these lactones[5,11] proved unequivocally that all the double bonds were *E* configured, that is, the structures of **4a** and **4b** as shown. The 1D NMR spectra collected were similar to that reported by Robinson and coworkers for the synthetic *N*-acylcysteamine thioester of a *E*,*E*,*E* triene.[5] The disubstituted double bond between H20 and H21 was assigned from the coupling constant of $J =$ 15.3 Hz for the double-bond protons, which is indicative of a *trans* double bond as confirmed by NOE interaction studies between H22 and H20 and between H21 and H19 (Scheme 4).[11a] The NOESY NMR spectrum[11a] shows an interaction between H17 of a trisubstituted double bond and H15, whereas no interactions are seen between H17 and H16′ or H16″, thus showing the double bond to be *E* configured. Similarly the NOE interaction observed for H13 with H11 but not with H12′, also confirms an *E* configuration. No evidence was obtained in these analyses for the presence of an oxidized derivative of either **4a** or **4b**, which suggests (although it does not prove) that the epoxidase encoded by *monCI* is necessary and sufficient for the epoxidation of all three double bonds in

 © 2005 Wiley-VCH Verlag GmbH & Co. KGaA, Weinheim

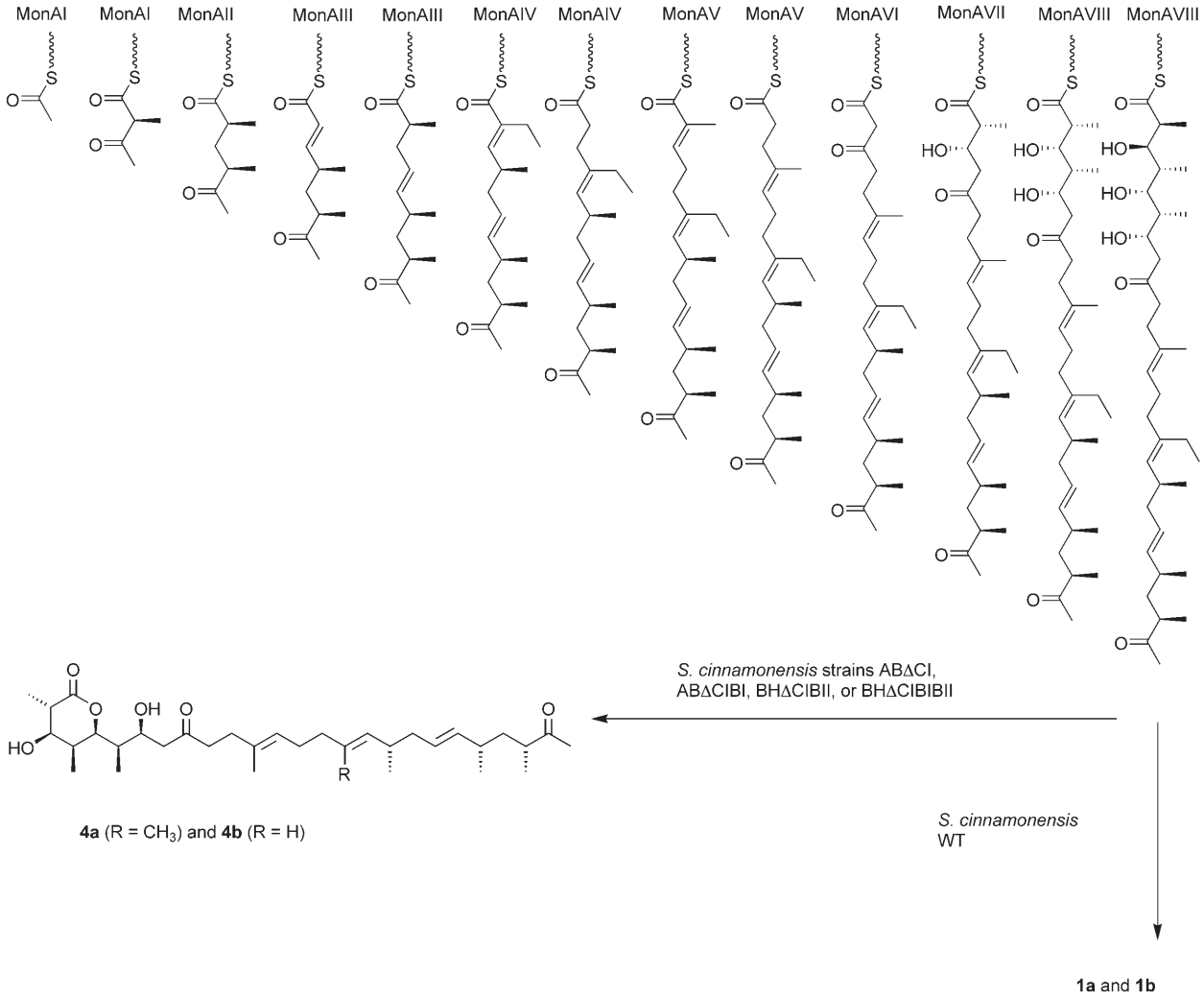

Scheme 3. The monensin PKS, which consists of a loading module and 12 extension modules distributed across eight multienzymes (MonAI–MonAVIII), produces *E*,*E*,*E*-trienes **4a** and **4b** when gene *monCI* is deleted, irrespective of whether additional genes *monBI* and *monBII* are also deleted. WT = wild type.

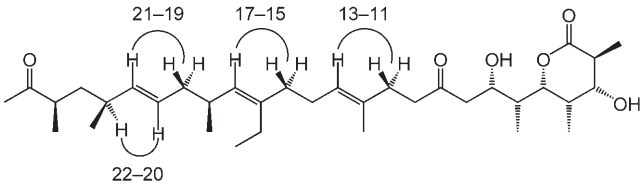

Scheme 4. The critical NOE interactions for the assignment of the double-bond geometry in lactone **4a** as the *E*,*E*,*E* isomer.

the linear intermediate to form **1**. This remarkable transformation is apparently catalyzed at all three target double bonds with complete stereoselectivity and stereospecificity. There is no effect of additional mutations in one or other or both of the *monB* genes.[11a] The MonB gene products were considered initially, given their significant sequence similarity to the δ-5(3)-ketosteroid isomerase of *C. testosteroni*,[6f,7] to be involved in the alteration of the geometry of two of the double bonds in the triene intermediate at the point during polyketide-chain growth at which they are activated by conjugation with the thioester that links the growing polyketide chain to the PKS multienzyme. As **4a** and **4b** are likely to be shunt metabolites rather than true intermediates in the biosynthetic pathway, such a role is not completely excluded, but the fact that no isomer of **4a** or **4b** with an altered geometry about the double bonds was found undermines such a hypothesis (see also below).

These results taken together confirm that *monCI* is essential for monensin biosynthesis, indicate directly that the all-*E* configuration of **4a** and **4b** is derived from intermediates in monensin biosynthesis, and that these *E* configured double bonds are the targets for the epoxidase MonCI that initiates oxidative cyclization.[6f,7] These results are more consistent with the original proposal of Cane et al.[6b] (Scheme 2a) than with the modification of this proposal in which trisubstituted double bonds are isomerized before epoxidation (Scheme 2b).[6f] Consequently, fresh questions are posed as to the true role of the MonB proteins and their

 © 2005 Wiley-VCH Verlag GmbH & Co. KGaA, Weinheim

counterparts in nanchangmycin biosynthesis, which are found fused head to tail as the product of the single gene *nanI*.[8] Evidence that they play a role in epoxide ring opening will be presented separately.[13] The stage is set for dissection of the respective contributions of these and the other "post-PKS" enzymes to the stereocontrol of polyether biosynthesis. In addition, the successful isolation of novel polyketides **4a** and **4b** underscores the potential of the targeted engineering of polyketide biosynthetic pathways to produce novel stereochemically rich molecules that profoundly differ in structure from the parent molecule. In the present case, **4a** and **4b** are not expected to have ionophoric properties; intriguingly, their structures more closely resemble δ lactones isolated from a number of marine organisms, such as the potent antitumor compounds discodermolide[13] and callystatin.[14] It may be that the elusive PKSs for such marine polyketides are actually closely related to those for ionophoric polyethers.

Received: May 21, 2005
Revised: July 6, 2005
Published online: October 11, 2005

Keywords: biosynthesis · epoxidases · natural products · polyethers · protein engineering

[1] A. Agatrap, J. W. Chamberlin, M. Pinkerton, L. Steinrauf, *J. Am. Chem. Soc.* **1967**, *89*, 5737–5748; J. W. Westley in *Antibiotics IV. Biosynthesis* (Ed.: J. W. Corcoran), Springer, New York, **1981**, pp. 41–73.

[2] C. Gumila, M. L. Ancelin, A. M. Delort, G. Jeminet, H. J. Vial, *Antimicrob. Agents Chemother.* **1997**, *41*, 523–529; K. Otoguro, A. Kohana, C. Manabe, A Ishiyama, H. Ui, K. Shiomi, H. Yamada, S. Omura, *J. Antibiot.* **2001**, *54*, 658–663; K. Otoguro, A. Ishiyama, H. Ui, M. Kobayashi, C. Manabe, G. Yan, Y. Takahashi, H. Tanaka, H. Yamada, S. Omura, *J. Antibiot.* **2002**, *55*, 832–834.

[3] L. E. Day, J. W. Chamberlin, E. Z. Gordee, S. Chen, M. Gorman, R. L. Hamill, T. Ness, R. E. Weeks, R. Stroshane, *Antimicrob. Agents Chemother.* **1973**, *4*, 410–414.

[4] a) D. E. Cane, T. C. Liang, H. Hasler, *J. Am. Chem. Soc.* **1981**, *103*, 5962–5965; b) D. E. Cane, T. C. Liang, H. Hasler, *J. Am. Chem. Soc.* **1982**, *104*, 7274–7281; c) A. A. Ajaz, J. A. Robinson, *J. Chem. Soc. Chem. Commun.* **1983**, *12*, 679–680.

[5] D. S. Holmes, J. A. Sherringham, U. C. Dyer, S. T. Russell, J. A. Robinson, *Helv. Chim. Acta* **1990**, *73*, 239–259.

[6] a) J. W. Westley, J. F. Blunt, J. R. H. Evans, A. Stepmel, J. Berger, *J. Antibiot.* **1974**, *27*, 597–604; b) D. E. Cane, W. D. Celmer, J. W. Westley, *J. Am. Chem. Soc.* **1983**, *105*, 3594–3600; c) A. A. Ajaz, J. A. Robinson, D. L. Turner, *J. Chem. Soc. Perkin Trans. 1* **1987**, 27–36; d) C. A. Townsend, A. Basak, *Tetrahedron* **1991**, *47*, 2591–2602; e) F. E. McDonald, T. B. Towne, *J. Am. Chem. Soc.* **1994**, *116*, 7921–7922; f) P. F. Leadlay, J. Staunton, M. Oliynyk, C. Bisang, J. Cortés, E. Frost, Z. A. Hughes-Thomas, M. A. Jones, S. G. Kendrew, J. B. Lester, P. F. Long, H. A. I. McArthur, E. L. McCormick, Z. Oliynyk, C. B. W. Stark, C. J. Wilkinson, *J. Ind. Microbiol. Biotechnol.* **2001**, *27*, 360–367; for a review, see: g) U. Kört, *Angew. Chem.* **1995**, *107*, 326–328; *Angew. Chem. Int. Ed. Engl.* **1995**, *34*, 298–300.

[7] M. Oliynyk, C. B. Stark, A. Bhatt, M. A. Jones, Z. A. Hughes-Thomas, C. Wilkinson, Z. Oliynyk, Y. Demydchuk, J. Staunton, P. F. Leadlay, *Mol. Microbiol.* **2003**, *49*, 1179–1190.

[8] Y. Sun, X. Zhou, H. Dong, G. Tu, M. Wang, B. Wang, Z. Deng, *Chem. Biol.* **2003**, *10*, 431–441.

[9] J. Cortés, K. E. H. Wiesmann, G. A. Roberts, M. J. B. Brown, J. Staunton, P. F. Leadlay, *Science* **1995**, *268*, 1487–1489; C. M. Kao, G. L. Luo, L. Katz, D. E. Cane, C. Khosla, *J. Am. Chem. Soc.* **1995**, *117*, 9105–9106; C. M. Kao, G. L. Luo, L. Katz, D. E. Cane, C. Khosla, *J. Am. Chem. Soc.* **1996**, *118*, 9184–9185.

[10] Z. A. Hughes-Thomas, C. B. W. Stark, I. U. Böhm, J. Staunton, P. F. Leadlay, *Angew. Chem.* **2003**, *115*, 4613–4616; *Angew. Chem. Int. Ed.* **2003**, *42*, 4475–4478.

[11] a) The construction, characterization, and fermentation of all the mutant strains of *S. cinnamonensis* described herein are given in detail in the Supporting Information, together with the details of complementation by cloned genes *in trans* to restore monensin production, the HPLC–mass-spectrometric analyses of the mutants described, and the NMR spectra; b) spectral data for the *E*,*E*,*E*-triene lactone **4a**: ^{1}H NMR (500 MHz, $CDCl_3$): $\delta = 0.89$ (d, $J = 6.6$ Hz, 3H), 0.93 (t, $J = 8.6$ Hz, 3H), 0.94 (d, $J = 7.9$ Hz, 2H), 0.96 (d, $J = 6.5$ Hz, 2H), 1.02 (d, $J = 6.9$ Hz, 3H), 1.09 (d, $J = 6.7$ Hz, 3H), 1.20 (ddd, $J = 13.6$, 8.4, 5.1 Hz, 1H), 1.39 (d, $J = 7.1$ Hz, 3H), 1.58 (ddd, $J = 13.6$, 9.6, 5.6 Hz, 1H), 1.59 (s, 3H), 1.73, (m, 1H), 1.90 (m, 2H), 1.95 (m, 2H), 1.98 (m, 2H), 2.01 (m, 2H), 2.08 (m, 1H), 2.09 (s, 3H), 2.25 (t, $J = 7.6$ Hz, 2H), 2.37 (m, 1H), 2.42–2.53 (m, 5H), 2.54, (m, 1H), 2.68 (dd, J = 18.0, 9.9 Hz, 1H), 3.83 (dd, $J = 10.3$, 4.3 Hz, 1H), 4.19 (dt, $J = 10.0$, 2.2 Hz, 1H), 4.21 (dd, $J = 9.3$, 1.9 Hz, 1H), 4.83 (d, $J = 9.59$ Hz, 1H), 5.10 (t, $J = 6.0$ Hz, 1H), 5.12 (dd, $J = 15.3$, 8.45 Hz, 1H), 5.36 ppm (dt, $J = 15.2$, 7.6 Hz, 1H); ^{13}C NMR (500 MHz, $CDCl_3$, 25 °C): $\delta = 4.8$, 9.8, 13.5, 14.5, 15.9, 16.1, 21.2, 21.7, 23.3, 26.8, 28.0, 32.4, 33.3, 35.1, 35.2, 36.2, 38.6, 39.9, 39.9, 40.7, 42.2, 45.2, 46.5, 66.1, 74.0, 81.4, 125.4, 128.3, 130.6, 132.9, 136.2, 139.0, 173.8, 212.3, 213.2 ppm.

[12] A. R. Gallimore, J. B. Spencer, B. M. Harvey, P. F. Leadlay, unpublished results.

[13] S. P. Gunasekera, M. Gunasekera, R. E. Longley, G. K. Schulte, *J. Org. Chem.* **1990**, *55*, 4912–4915.

[14] M. Kobayashi, K. Higuchi, N. Murakami, H. Tajima, S. Aoki, *Tetrahedron Lett.* **1997**, *38*, 2859–2862.

 © 2005 Wiley-VCH Verlag GmbH & Co. KGaA, Weinheim

Enzyme Reaction Mechanisms

DOI: 10.1002/anie.200501670

A Method for Trapping Intermediates of Polyketide Biosynthesis with a Nonhydrolyzable Malonyl-Coenzyme A Analogue**

*Dieter Spiteller, Claire L. Waterman, and Jonathan B. Spencer**

There are currently about 10000 natural products that have been classified as polyketides. Their structures range from simple molecules, such as 6-methylsalicylic acid,[1] to complex natural products, such as brevetoxin.[2] Polyketides are an invaluable source of bioactive compounds with many being clinically important, for example, the antibiotic erythromycin and the immunosupressant rapamycin.[3] Despite their diversity, all polyketides share a common biosynthetic pathway; a starter unit, which is normally acetyl coenzyme A (CoA), undergoes sequential condensation with an extender unit (usually malonyl or (*S*)-methylmalonyl-CoA) in a similar manner to fatty acid biosynthesis. However, unlike fatty acid biosynthesis, the carbonyl group is not always completely reduced after each condensation, which partly accounts for the huge variety of polyketide structures (Scheme 1).[3]

Experiments with labeled precursors, in combination with mechanistic considerations, have been extensively used to investigate the details of polyketide biosynthesis.[1,3] However, it has proven very difficult to isolate intermediates directly as they are covalently attached to the polyketide synthases (PKSs).[3] One approach that has been possible with the cloning and sequencing of genes for many PKSs[4] is to design mutants that halt the biosynthesis at a desired point. For instance, by genetically engineering the fusion of the thioesterase from the third subunit of the deoxyerythronolide synthase onto the first subunit, deoxyerythronolide biosynthesis was stopped after two rounds of (*S*)-methylmalonyl-CoA condensations and the intermediate removed in sufficient quantity to be fully characterized.[5] Whereas this strategy has potential with all type I modular PKSs, it is very limited when applied to type I iterative, type II, and type III PKSs, as the same catalytic activities are usually used repeatedly. For example, if a mutation is made in the ketosynthase, polyketide synthesis could not occur at all. To address this point, we sought to develop a chemical approach that used a non-hydrolyzable malonyl-CoA analogue which can potentially trap polyketide intermediates from these classes of PKSs.

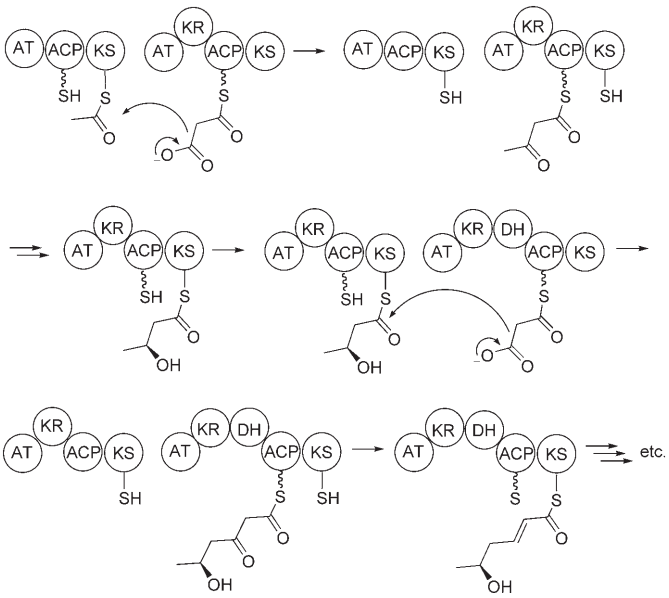

Scheme 1. Schematic diagram of the mechanism of two rounds of polyketide biosynthesis by a polyketide synthase (AT: acyl transferase, KS: ketosynthase, ACP: acyl carrier protein, DH: dehydratase, KR: ketoreductase). In type III polyketide synthases, such as the stilbene synthase from *Pinus sylvestris*, malonyl-CoA is used directly for the elongation instead of the corresponding ACPs.

Analogues of coenzyme A[6–8] have been used previously to investigate a range of enzyme reaction mechanisms, such as the condensation of acetyl-CoA with oxaloacetate catalyzed by citrate synthase[7] and the enzymic carboxylation of acetyl-CoA by acetyl-CoA carboxylase.[9] However, malonyl-CoA analogues have never been used before to investigate the biosynthesis of polyketides. In our strategy, the malonyl-CoA analogue would react with the growing polyketide chain but would not be able to undergo transesterification back onto the PKS resulting in the accumulation of polyketide intermediates attached to the analogue (Scheme 2a).

The analogue of malonyl-CoA **3** used in this study contains an additional methylene unit between the thiol of the coenzyme A and the malonate moiety. This methylene unit could possibly be detrimental to the correct positioning of the analogue at the active site of a PKS, as the malonyl moiety is displaced by one carbon atom. However, we felt that this potential disadvantage was out-weighed by the straightforward preparation of **3** in two steps. Commercially available ethyl 4-chloro-3-oxobutanoate (**1**) was treated with coenzyme A in aqueous 0.11M Li_2CO_3.[7,8] After purification with

[*] C. L. Waterman, Dr. J. B. Spencer
University Chemical Laboratory
University of Cambridge
Lensfield Road, Cambridge, CB21EW (UK)
Fax: (+44) 1223-336-362
E-mail: jbs20@cam.ac.uk
Dr. D. Spiteller
Department of Biochemistry
University of Cambridge
80 Tennis Court Road, Cambridge CB21GA (UK)

[**] We are indebted to Prof. Dr. Joachim Schröder (Institut für Biologie II, Biochemie der Pflanzen, Freiburg (Germany)) for providing the cDNA of stilbene synthase and to Prof. Dr. Fraser (University of Calgary, Canada) for the gift of a plasmid coding for the succinyl-CoA:3-ketoacid transferase. D.S. thanks the Deutschen Akademie der Naturforscher Leopoldina (Germany), for a postdoctoral fellowship (BMBF-LPD 9901/8-90). Financial support by the BBSRC is gratefully acknowledged.

Supporting information for this article is available on the WWW under http://www.angewandte.org or from the author.

 © 2005 Wiley-VCH Verlag GmbH & Co. KGaA, Weinheim

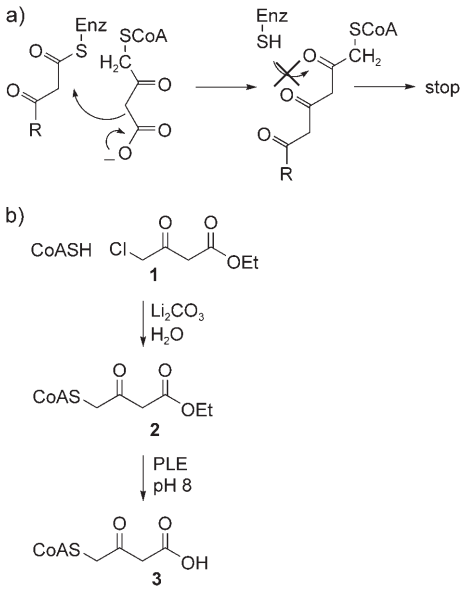

Scheme 2. a) Trapping intermediates of polyketide biosynthesis with a malonyl-CoA analogue **3**; b) synthesis of **3**. Enz = enzyme.

RP-18 HPLC, the ethyl ester **2** was hydrolyzed to **3** with pig liver esterase (PLE; Scheme 2b).[10] As anticipated, **3** was found to undergo decarboxylation more readily than malonyl-CoA (**4**) during purification, therefore it was used directly after precipitation of the PLE.

The potential of **3** to trap intermediates of polyketide biosynthesis was investigated with the type III PKS stilbene synthase (STS) from *Pinus sylvestris*[11,12] as a model system. This class of PKS is the simplest to investigate this approach with as it uses **4** directly, in contrast to type I and II PKSs that carry out condensations with malonyl acid carrier proteins (ACPs).[3] STS has a broad substrate specificity with regard to the starter unit, thus producing a number of stilbene and pyrone products.[13] If cinnamoyl-CoA (**6**) is used as the starter unit, the enzyme catalyzes its sequential condensation with three molecules of **4** to form the stilbene pinosylvin (**8**),[12] and with 4-hydroxyphenylacetyl-CoA (**5**), only two condensations with **4** occur to give the pyrone **7** (see Scheme 3).

For our initial experiments, **5** was used as a starter unit and the ratio of **3** to **4** was varied. Formation of the products was followed by LC-MS, and across a range of conditions (a ratio of 3:4 of **3**/**4** was found to give the highest yield) we observed ions at *m*/*z* 958 and 1000 that correspond to one and two condensation steps, in addition to the ion at *m*/*z* 219 for the normal pyrone product **7** (Figure 1).

Interestingly, we also observed the ions at *m*/*z* 958 and 1000 at very low levels in the control samples without the addition of the enzyme. Although not totally unexpected, to our knowledge, the non-enzymic formation of polyketides from malonyl-CoA has not been previously reported.

Several closely eluting peaks, all exhibiting *m*/*z* 1000, were observed in some LC-MS traces of **10** instead of a single one, thus suggesting the presence of isomers of **10** probably formed by enolization and/or cyclization.

The MS/MS spectrum of both intermediates that exhibit ($[M+H]^+$) peaks at *m*/*z* 958 and 1000 showed characteristic fragments for the presence of coenzyme A derivatives (see Figure 2 and the Supporting Information). In the case of the triketide intermediate **10**, the fragments at *m*/*z* 591 and 428 are characteristic for the cleavage of the phosphodiester bond of the coenzyme A unit of the molecule (Figure 2). Furthermore, a fragment at *m*/*z* 493 was also observed that corresponds to loss of the 3′-phospho adenosine diphosphate moiety from the alkyl chain. The observed fragmentation pattern for the intermediates of *m*/*z* 958 and 1000 is in agreement with a study of the MS/MS fragmentation of other coenzyme A derivatives by Burns et al.[14]

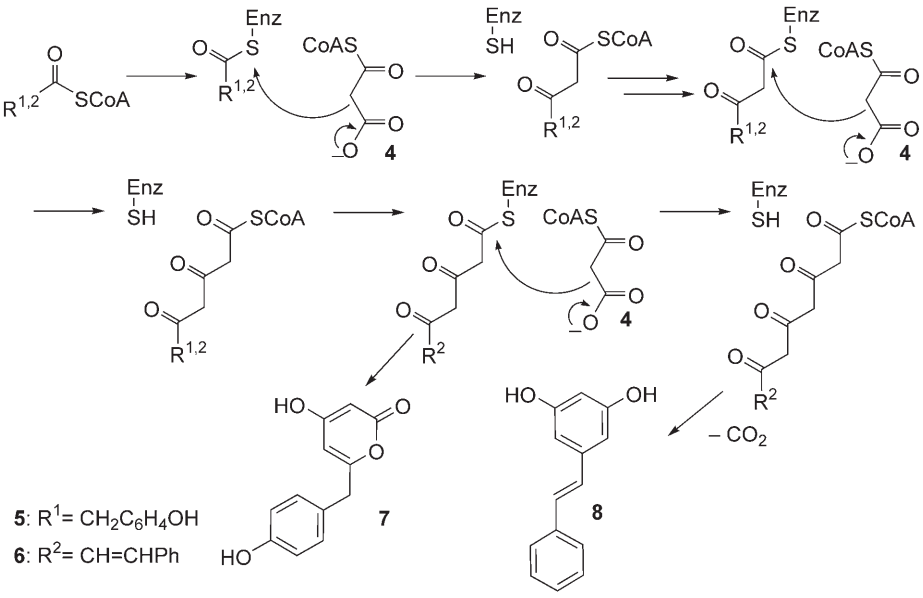

Scheme 3. Formation of the pyrone-type and stilbene-type products **7** and **8**, respectively, by stilbene synthase from *Pinus sylvestris* using either **5** or **6** as the starter unit and **4** for chain elongation.

To provide further evidence for the isolation of these intermediates, assays were carried out with [$^{13}C_3$]malonyl-CoA.[15] The incorporation of the labeled substrate should shift the mass of the $[M+H]^+$ ion to 1002 amu in the case of **10**, as one molecule of [$^{13}C_3$]malonyl-CoA is utilized in its formation. Figure 2 clearly shows that the MS/MS spectra complement and confirm the MS/MS spectra of the unlabeled assay. All signals at *m*/*z* 1002, 984, 593, 575, 495, and 477, which contain the polyketide chain in their fragments, are shifted by 2 amu, whereas the signals at *m*/*z* 428 and 410, which correspond to the 3′-phospho adenosine diphosphate moiety, remained unchanged.

 © 2005 Wiley-VCH Verlag GmbH & Co. KGaA, Weinheim

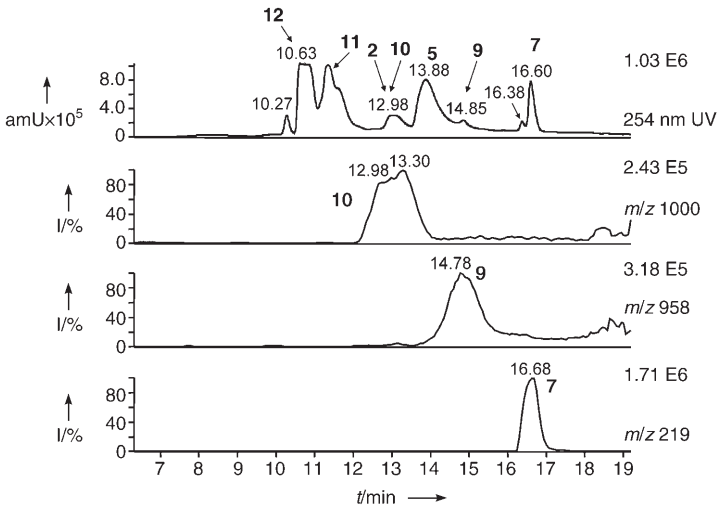

Figure 1. UV chromatogram and ion traces *m/z* 219, 958, and 1000 observed after the reaction of the stilbene synthase with **5** and **4** in presence of **3.** Peaks: Coenzyme A (**12**); decarboxylated malonyl-CoA analogue **11**; ethylmalonyl-CoA analogue **2**; STS intermediate formed from two condensations condensations **10**; 4-hydroxyphenylacetyl-CoA **5**; STS intermediate formed from one condensation **9**; 4-hydroxyphenylacetylpyrone (**7**).

These results show that the malonyl-CoA analogue **3** can be successfully used to trap the growing polyketide chain. It is also interesting that the tetraketide is not observed. This result indicates that the triketide formed from the starter unit and two malonyl-CoA molecules either rapidly cyclizes to the observed pyrone **7** or is not readily transferred back onto the STS after the final condensation.

To see if longer intermediates could be trapped, we used **6** as starter unit because the favored product in this case is the stilbene **8** formed from the tetraketide intermediate. Therefore, the addition of **3** to the assay could trap three different intermediates during the stilbene formation. However, no intermediates were detected above the background levels under a range of conditions. It is possible that the positioning of the analogue in the active site of the STS is better matched with **5** as a starter unit because it has one less carbon atom than **6** and **3** has one more carbon atom than **4**. This observation indicates that the positioning of the growing polyketide chain bound to the active-site cysteine unit is strongly influenced by the structure of the starter unit. A smaller starter unit may allow the necessary flexibility in the active site for the analogue to be able to be correctly positioned and react.

In summary, we have shown for the first time that intermediates of polyketide biosynthesis can be trapped for detailed analytical studies with a non-hydrolyzable malonyl-CoA analogue. This finding potentially opens the way to the determination of the timing of crucial events, such as cyclization of the polyketone chain. It is highly likely that the analogue can be transferred to ACPs with Sfp, a phosphopantetheinyl transferase from *Bacillus subtilis*, as this enzyme has been shown to have a wide substrate specificity.[16]

This approach should allow type I and II PKSs to be investigated. Experiments to apply this concept to other polyketide synthases and the synthesis of alternative analogues that may be better steric matches for malonyl-CoA are currently under investigation.

Received: May 14, 2005
Published online: October 6, 2005

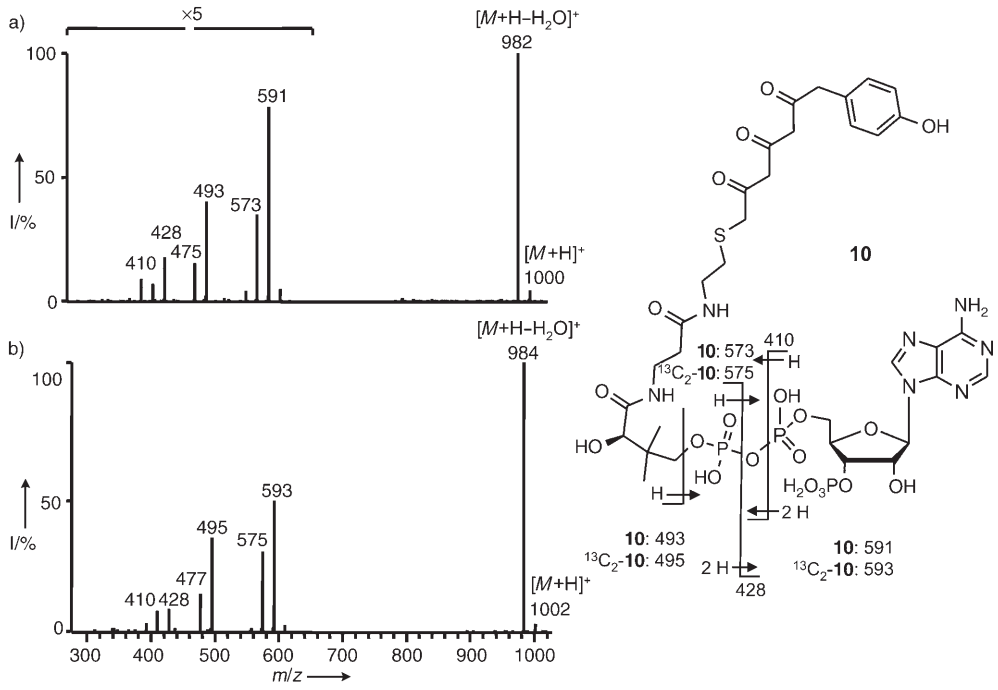

Figure 2. ESI-MS/MS of **10** formed by the stilbene synthase using **5**, **3**, and either a) **4** or b) [$^{13}C_3$]malonyl-CoA.

 © 2005 Wiley-VCH Verlag GmbH & Co. KGaA, Weinheim

Keywords: biosynthesis · coenzymes · mass spectrometry · polyketides · synthases

[1] A. J. Birch, P. A. Massy-Westropp, C. J. Moye, *Aust. J. Chem.* **1955**, *8*, 539 – 544.
[2] Y. Y. Lin, M. Risk, S. M. Ray, D. Vanengen, J. Clardy, J. Golik, J. C. James, K. Nakanishi, *J. Am. Chem. Soc.* **1981**, *103*, 6773 – 6775.
[3] J. Staunton, K. J. Weissman, *Nat. Prod. Rep.* **2001**, *18*, 380 – 416.
[4] F. H. Malpartida, D. A. Hopwood, *Nature* **1984**, *309*, 462 – 464; J. Cortes, S. F. Haydock, G. A. Roberts, D. J. Bevitt, P. F. Leadlay, *Nature* **1990**, *348*, 176 – 178; S. Donadio, M. J. Staver, J. B. McAlpine, S. J. Swanson, L. Katz, *Science* **1991**, *252*, 675 – 679.
[5] J. Cortes, K. E. H. Wiesmann, G. A. Roberts, M. J. B. Brown, J. Staunton, P. F. Leadlay, *Science* **1995**, *268*, 1487 – 1489; C. M. Kao, G. L. Luo, L. Katz, D. E. Cane, C. Khosla, *J. Am. Chem. Soc.* **1995**, *117*, 9105 – 9106.
[6] Y. M. Zhao, M. Michenfelder, J. Retey, *Can. J. Chem.* **1994**, *72*, 164 – 169; K. W. Vogel, D. G. Drueckhammer, *J. Am. Chem. Soc.* **1998**, *120*, 3275 – 3283; P. K. Mishra, D. G. Drueckhammer, *Chem. Rev.* **2000**, *100*, 3283 – 3309.
[7] T. Ciardelli, C. J. Stewart, A. Seeliger, T. Wieland, *Liebigs Ann. Chem.* **1981**, 828 – 841.
[8] L. A. Paige, G. Q. Zheng, S. A. Defrees, J. M. Cassady, R. L. Geahlen, *J. Med. Chem.* **1989**, *32*, 1665 – 1667.
[9] J. Nikawa, S. Numa, T. Shiba, C. J. Stewart, T. Wieland, *FEBS Lett.* **1978**, *91*, 144 – 148.
[10] W. Boland, C. Frössl, M. Lorenz, *Synthesis* **1991**, 1049 – 1072.
[11] J. Fliegmann, G. Schröder, S. Schanz, L. Britsch, J. Schröder, *Plant Mol. Biol.* **1992**, *18*, 489 – 503.
[12] S. Schanz, G. Schröder, J. Schröder, *FEBS Lett.* **1992**, *313*, 71 – 74.
[13] H. Morita, H. Noguchi, J. Schröder, I. Abe, *Eur. J. Biochem.* **2001**, *268*, 3759 – 3766.
[14] K. L. Burns, L. T. Gelbaum, M. C. Sullards, D. E. Bostwick, S. W. May, *J. Biol. Chem.* **2005**, *280*, 16550 – 16558.
[15] P. M. Jordan, J. B. Spencer, D. L. Corina, *J. Chem. Soc. Chem. Commun.* **1986**, 911 – 913.
[16] L. E. N. Quadri, P. H. Weinreb, M. Lei, M. M. Nakano, P. Zuber, C. T. Walsh, *Biochemistry* **1998**, *37*, 1585 – 1595.

 © 2005 Wiley-VCH Verlag GmbH & Co. KGaA, Weinheim

Diels–Alder Reactions

DOI: 10.1002/anie.200501345

Catalytic Asymmetric Nitroso-Diels–Alder Reaction with Acyclic Dienes**

*Yuhei Yamamoto and Hisashi Yamamoto**

The nitroso-Diels–Alder reaction has long been a valuable synthetic operation for multistep syntheses given that the resulting adducts serve as 1-amino-4-hydroxy-2-ene derivatives after a single step. Subsequent to earlier studies by Kresze and co-workers[1] on the use of simple nitroso derivatives, many research groups have made significant contributions to the steady improvement of this methodology.[2] Recently, we enhanced this transformation to catalytic and enantioselective methods through the use of nitrosopyridine as a dienophile in the presence of a chiral copper catalyst.[3] Unfortunately, the new asymmetric reaction did not proceed as smoothly for acyclic dienes as it did for cyclic systems, which therefore limits its range of application. Herein, we report catalytic regio-, diastereo-, and enantioselective nitroso-Diels–Alder reactions of acyclic 2-silyloxy-1,3-dienes that have a broad substrate scope. The pathway for the present catalytic enantioselective transformation is outlined in Scheme 1.

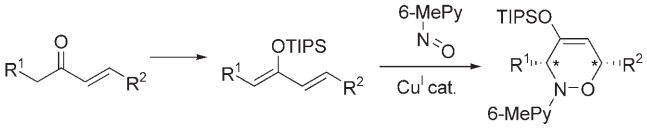

Scheme 1. The present pathway for the catalytic enantioselective transformation of acyclic 2-silyloxy-1,3-dienes. TIPS = triisopropylsilyl, Py = pyridine.

The nitroso-Diels–Alder reaction of pentadiene and 6-methyl-2-nitrosopyridine in the presence of $[Cu(MeCN)_4(segphos)]PF_6$ gave a mixture of 1- and 4-amino derivatives in a 3:1 ratio with up to 10% *ee*. The reactivity of the diene was increased, and (2*Z*,4*E*)-3-trimethylsilyloxy-2,4-hexadiene[4] (**1a**) was examined in the presence of a catalytic amount of

[*] Y. Yamamoto, Prof. Dr. H. Yamamoto
Department of Chemistry, The University of Chicago
5735 South Ellis Avenue, Chicago, IL 60637 (USA)
Fax: (+1) 773-702-0805
E-mail: yamamoto@uchicago.edu

[**] Support for this research was provided by the National Institutes of Health (NIH) (GM068433-01) and a grant from the University of Chicago. We acknowledge Dr. Ian Steele for X-ray crystallographic measurements and Dr. Antoni Jurkiewicz for technical support with NMR spectroscopy. We thank Takasago International Corporation for its generous gift of (*S*)-segphos, and the Merck Research Laboratories for their generous support. Y.Y. thanks Dr. K. Suzuki, BANYU Pharmaceutical Co. Ltd., for generous support.

Supporting information for this article is available on the WWW under http://www.angewandte.org or from the author.

InterScience
© 2005 Wiley-VCH Verlag GmbH & Co. KGaA, Weinheim

$[Cu(MeCN)_4(segphos)]PF_6$. Although this experiment gave complete regioselectivity[5] (4-silyloxy/5-silyloxy ≥ 99:1), the enantioselectivity (16% *ee* for the 4-silyloxy derivative) remained low. Surprisingly, the low enantioselectivity was improved significantly by simply increasing the size of the silyl group (**1a**γ**1b**γ**1c**): Up to 98% *ee* in the presence of Cu^I–segphos[6] and >99% *ee* with $[Cu(MeCN)_4(difluorophos)]PF_6$[7] were attained in the reaction of the triisopropylsilyl derivative **1c** (Table 1).

The applicability of this reaction was demonstrated for the functionalized dienes **1c–m** (summarized in Table 2). All of the reactions proceeded in high yields and enantioselectivities, with complete regio- and diastereoselectivities. The dialkyl-substituted dienes generally gave high enantioselectivities (Table 2, entries 1–3 and 11). Interestingly, reactions with trienes proceeded in a completely regioselective manner and provided only a single regioisomer (Table 2, entries 4 and 5).[8] Phenyl-substituted alkenes (R^2 = Ph) gave a relatively lower enantioselectivity (Table 2, entries 6 and 10), whereas methoxyphenyl derivitive **1i** and heteroaromatic **1j** gave high enantioselectivities (Table 2, entries 7, 8). Lewis basic substituents such as protected alcohols (Table 2, entry 3) and ester functional groups (Table 2, entries 10 and 11) were also used in the reaction and gave highly functionalized products enantioselectively.

Table 2: Reaction with various dienes.[a]

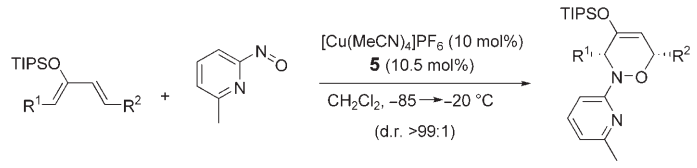

1c–1m 2 3c–3m

Entry	Product	Yield [%]	*ee* [%][b]	Entry	Product	Yield [%]	*ee* [%][b]
1	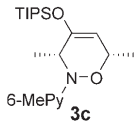 **3c**	95	99	7	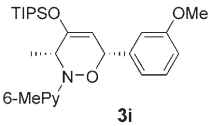 **3i**	91	99
2	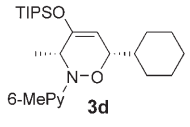 **3d**	93	91	8	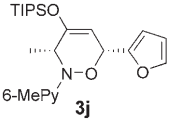 **3j**	91	95
3	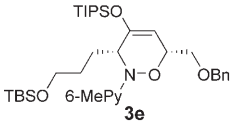 **3e**	86	95	9	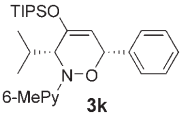 **3k**	97	95
4	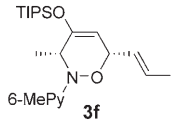 **3f**	91	96	10	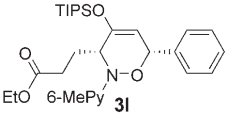 **3l**	94	88
5	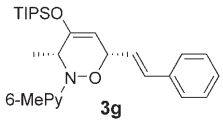 **3g**	84	85	11	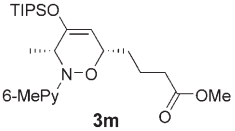 **3m**	96	93
6	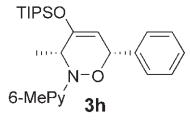 **3h**	95	81				

[a] The reaction was conducted with catalyst (10 mol%), nitrosopyridine (1 equiv), and silyloxydiene (1.2 equiv) under N_2 at −85 °C and gradually warmed to −20 °C over 5 h. [b] The *ee* values were determined by HPLC analysis (Supporting Information).

Table 1: Effect of size the of the silicon group on the enantioselectivity.[a]

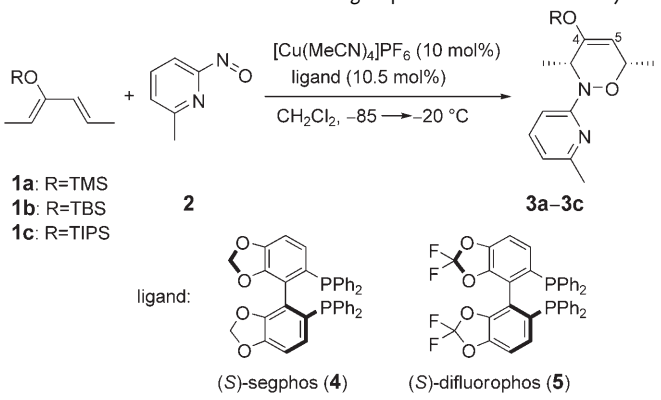

Entry	Diene	Ligand	Yield [%]	*ee* [%][b]
1	**1a**	**4**	86	16
2	**1b**	**4**	88	84
3	**1c**	**4**	93	98
4	**1c**	**5**	95	>99

[a] The reaction was conducted with catalyst (10 mol%), nitrosopyridine (1 equiv), and silyloxydiene (1.4 equiv) in a N_2 atmosphere at −85 °C and gradually warmed to −20 °C over 5 h. [b] The *ee* values were determined by HPLC (Supporting Information). TMS = trimethylsilyl.

The products **3c–m** can be cleanly converted into the respective protected amino alcohol. For example, after hydrolysis of the silyl enol ether **3c** by TBAF/AcOH, reduction of the ketone gave the corresponding alcohol **6** as a single diastereomer.[8] Further transformations then gave the protected amino alcohol with a defined configuration that is found in several important natural products (Scheme 2).[9]

The absolute and relative configurations of the nitroso-Diels–Alder adducts were assigned by X-ray crystallographic analysis. Compound **8** was prepared under the standard reaction conditions discussed above, then further transformed into the 3,5-dinitrobenzoic acid ester **9**, which was crystallized from Et_2O (Scheme 3, Figure 1).[8]

The absolute stereochemical course of the reaction was found to be in accordance with the mechanistic model we previously reported (Scheme 4).[3] This model strongly supports the importance of the pyridine moiety in the formation of a highly organized chelating intermediate during the reaction. Such an effect could not be expected for nitrosobenzene.[2i]

 © 2005 Wiley-VCH Verlag GmbH & Co. KGaA, Weinheim

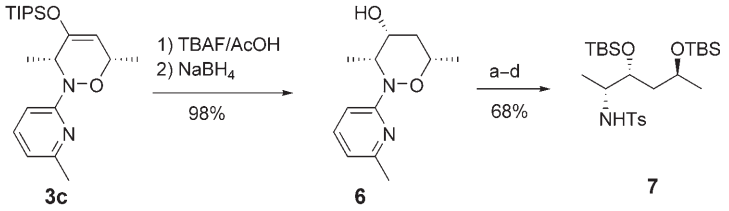

Scheme 2. Conversion of the nitroso-Diels–Alder adduct into the protected amino alcohol **7**. Reaction conditions: a) Pd/C 10%, H_2, MeOH; then 2,2-dimethoxypropane, TsOH; b) Ts_2O, diethylisopropylamine, 1,2-dichloroethane; c) TsOH, MeOH; then TBSOTf, 2,6-lutidune, CH_2Cl_2; d) MeOTf, CH_2Cl_2; then 10 N KOH, MeOH. TBAF = tetrabutylammonium fluoride, Ts = *p*-toluenesulfonyl, TBS = *tert*-butyldimethylsilyl, Tf = trifluoromethanesulfonyl.

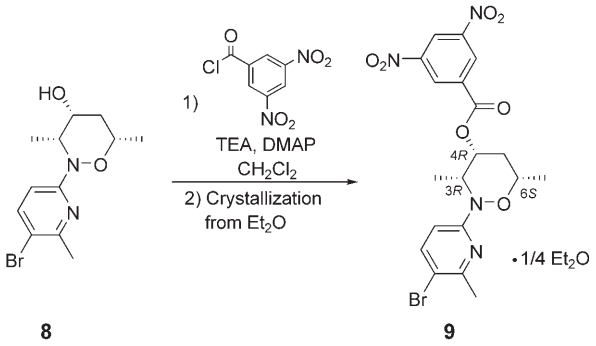

Scheme 3. Transformation of the alcohol **8** into the 3,5-dinitrobenzoic acid ester **9**. TEA = triethylamine, DMAP = 4-(dimethylamino)pyridine.

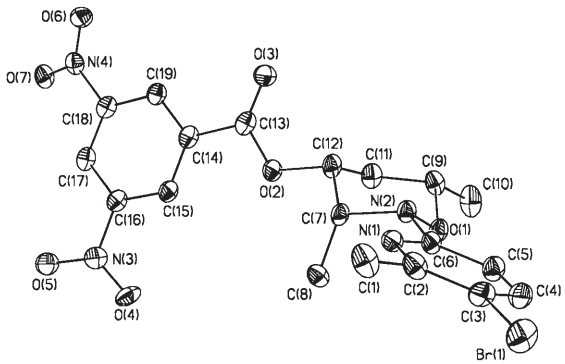

Figure 1. X-ray crystallographic structure of **9**, Et_2O is omitted for clarity. Elipsoids drawn at the 50% probability level

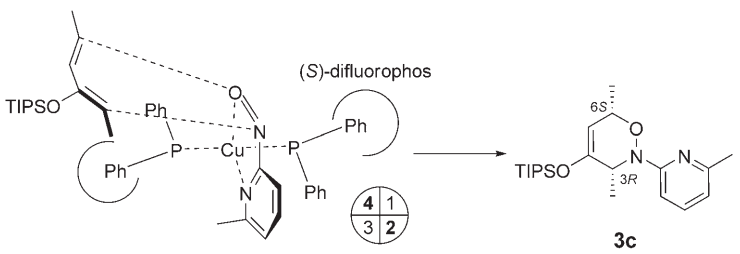

Scheme 4. Model for a plausible chelate intermediate.

The acyclic nitroso-Diels–Alder reaction proceeds exceedingly smoothly with TIPS derivatives, but rather slowly with TMS ethers, a fact that is of great mechanistic interest. 6-Methyl-2-nitrosopyridine (1 equiv) was treated with a 1:1 mixture of two silyloxydienes (1.4 equiv each) in competitive experiments with and without the use of a copper catalyst [Eq. (1)]. The OTIPS diene was clearly shown to be far more reactive than the OTMS or OTBS dienes.[10,11] A similar trend of differences in reactivity was observed for the Diels–Alder reaction of maleic anhydride with and without Lewis acid catalysis [Eq. (2)].

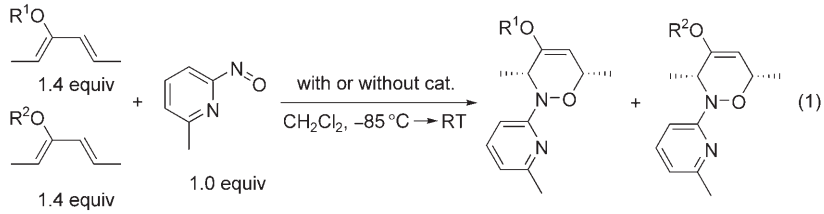

R^1 = TIPS, R^2 = TMS			
no catalysis	>99	:	<1
with $[Cu(MeCN)_4]PF_6$/difluorophos	>99 (99% *ee*)	:	<1
R^1 = TIPS, R^2 = TBS			
no catalysis	3	:	1
with $[Cu(MeCN)_4]PF_6$/difluorophos	11 (99% *ee*)	:	1

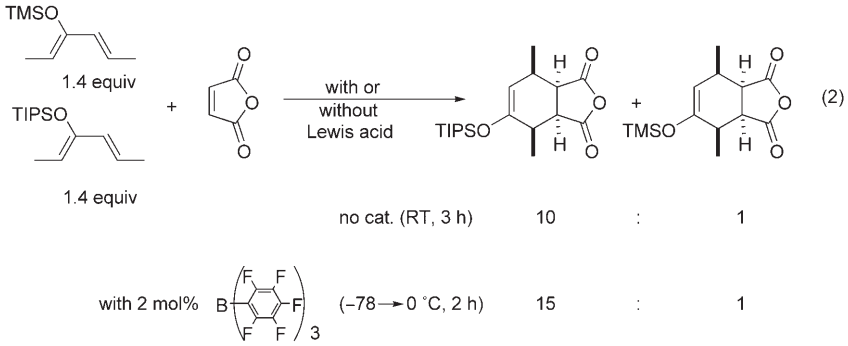

no cat. (RT, 3 h)	10	:	1
with 2 mol% (–78 → 0 °C, 2 h)	15	:	1

The above reactions provide strong evidence that the high reactivity arises from the bulk of the TIPS group, which forces the diene to adopt an *s-cis* configuration in favor of the concerted [4+2] cycloaddition reaction [Eq. (3)].[12] A large

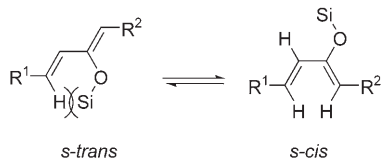

NOE interaction (10.7%) was observed between H1 and H4 of the OTIPS diene, whereas no significant NOE interaction was observed for the OTMS diene.[13] The difference in

 © 2005 Wiley-VCH Verlag GmbH & Co. KGaA, Weinheim

reactivity between Me_3Si and iPr_3Si can also be attributed to the exceedingly rapid copper-catalyzed nitroso-Diels–Alder reaction.

In summary, we have developed a highly practical and promising method for the regio-, diastereo-, and enantioselective introduction of oxygen and nitrogen groups into simple acyclic unsaturated ketones.

Received: April 18, 2005
Revised: August 18, 2005
Published online: October 13, 2005

Keywords: amino alcohols · asymmetric catalysis · cycloaddition · dienes · nitroso compounds

[1] a) G. Kresze, J. Firl, *Tetrahedron* **1968**, *24*, 1043 – 1050; b) H. Nitsch, G. Kresze, *Angew. Chem.* **1976**, *88*, 801; *Angew. Chem. Int. Ed. Engl.* **1976**, *15*, 760.

[2] For reviews, see: a) J. Streith, A. Defoin, *Synthesis* **1994**, 1107 – 1117; b) P. F. Vogt, M. J. Miller, *Tetrahedron* **1998**, *54*, 1317 – 1348; for recent reports, see: c) A. A. P. Meekel, M. Resmini, U. K. Pandit, *Bioorg. Med. Chem.* **1996**, *4*, 1051 – 1057; d) D. Zhang, C. Süling, M. J. Miller, *J. Org. Chem.* **1998**, *63*, 885 – 888; e) S. Aoyagi, R. Tanaka, M. Naruse, C. Kibayashi, *J. Org. Chem.* **1998**, *63*, 8397 – 8406; f) S. J. Gouverneur, J. McCarthy, C. Mineur, D. Belloti, G. Dive, L. Ghosez, *Tetrahedron* **1998**, *54*, 10537 – 10554; g) C. Arribas, M. C. Carreño, J. L. García-Ruano, J. F. Rodríguez, M. Santos, M. A. Sanz-Tejedor, *Org. Lett.* **2000**, *2*, 3165 – 3168; h) Y.-C. Wang, T.-M. Lu, S. Elango, C.-K. Lin, C.-T. Tsai, Y.-H. Yan, *Tetrahedron: Asymmetry* **2002**, *13*, 691 – 695; i) A. P. Lightfoot, R. G. Pritchard, H. Wan, J. E. Warren, A. Whiting, *Chem. Commun.* **2002**, 2072 – 2073; j) K. R. Flower, A. P. Lightfoot, H. Wan, A. Whiting, *J. Chem. Soc. Perkin Trans. 1* **2002**, 2058 – 2064; k) X. Ding, Y. Ukaji, S. Fujinami, K. Inomata, *Chem. Lett.* **2003**, *32*, 582 – 583; l) C. Miller, R. A. Batey, *Org. Lett.* **2003**, *5*, 699 – 702; m) Y. Yamamoto, N. Momiyama, H. Yamamoto, *J. Am. Chem. Soc.* **2004**, *126*, 5962 – 5963; n) C. Geraldine, D. Marion, B. Nicolas, K. Cyrille, *Org. Lett.* **2004**, *6*, 2449 – 2451; o) C. P. Chow, K. J. Shea, *J. Am. Chem. Soc.* **2005**, *127*, 3678 – 3679.

[3] Y. Yamamoto, H. Yamamoto, *J. Am. Chem. Soc.* **2004**, *126*, 4128 – 4129.

[4] A. G. Dossetter, T. F. Jamison, E. N. Jacobsen, *Angew. Chem.* **1999**, *111*, 2549 – 2552; *Angew. Chem. Int. Ed.* **1999**, *38*, 2398 – 2400.

[5] a) D. L. Boger, M. Patel, F. Takusagawa, *J. Org. Chem.* **1985**, *50*, 1911 – 1916; b) K. F. McClure, S. J. Danishefsky, *J. Org. Chem.* **1991**, *56*, 850 – 853; c) V. Gouverneur, L. Ghosez, *Tetrahedron: Asymmetry* **1991**, *2*, 1173 – 1176; d) I. Cabanal-Duvillard, J.-F. Berrien, L. Ghosez, H.-P. Husson, J. Royer, *Tetrahedron* **2000**, *56*, 3763 – 3769; e) A. G. Leach, K. N. Houk, *J. Org. Chem.* **2001**, *66*, 5192 – 5200.

[6] T. Saito, T. Yokozawa, T. Ishizaki, T. Moroi, N. Sayo, T. Miura, H. Kumobayashi, *Adv. Synth. Catal.* **2001**, *343*, 264 – 267.

[7] a) S. Jeulin, S. Duprat de Paule, V. Ratovelomanana-Vidal, J.-P. Gênet, N. Champion, P. Dellis, *Angew. Chem.* **2004**, *116*, 324 – 329; *Angew. Chem. Int. Ed.* **2004**, *43*, 320 – 325; b) F. Leroux, J. Gorecka, M. Schlosser, *Synthesis* **2004**, 326 – 328; c) S. Jeulin, S. Duprat de Paule, V. Ratovelomanana-Vidal, J.-P. Gênet, N. Champion, N. P. Dellis, *Proc. Natl. Acad. Sci.* **2004**, *101*, 5799 – 5804.

[8] CCDC-271386 (**3g**), -271387 (**6**), and -271388 (**9**) contain the supplementary crystallographic data for this paper. These data can be obtained free of charge from the Cambridge Crystallographic Data Centre via www.ccdc.cam.ac.uk/data_request/cif.

[9] For example, fumonisin B_2: a) Y. S. Lee, L. F. Peng, Y. Kishi, *J. Org. Chem.* **1997**, *62*, 5666 – 5667, and references therein; galantin I: b) N. Sakai, Y. Ohfune, *J. Am. Chem. Soc.* **1992**, *114*, 998 – 1010, and references therein.

[10] For a review on use of the TIPS group in organic chemistry, see: C. Rücker, *Chem. Rev.* **1995**, *95*, 1009., and references therein.

[11] For a review on π nucleophilicity, see: H. Mayr, B. Kempf, A. R. Ofial, *Acc. Chem. Res.* **2003**, *36*, 66 – 77.

[12] A similar observation of the relationship between the enantioselectivity and size of the silicon group was observed: a) E. J. Corey, A. Guzman-Perez, T.-P. Loh, *J. Am. Chem. Soc.* **1994**, *116*, 3611 – 3612; a diene that bears the OTBS group and reacts through a more pericyclic pathway than the OTMS group has been reported: b) S. Danishefsky, K.-U. Chao, G. Schulte, *J. Org. Chem.* **1985**, *50*, 4650 – 4652.

[13] The NOESY experiment was conducted with both dienes (see Supporting Information).

 © 2005 Wiley-VCH Verlag GmbH & Co. KGaA, Weinheim

Composite Films

DOI: 10.1002/anie.200501905

Nickel-Foam-Supported Reticular CoO–Li_2O Composite Anode Materials for Lithium Ion Batteries**

Yan Yu, Chun-Hua Chen, Jiang-Lan Shui, and Song Xie*

Since the early 1990s[1] people everywhere have been enjoying the great convenience brought about in daily life through the use of rechargeable lithium-ion batteries (LIBs): Modern portable consumer electronics such as laptops, cellular phones, camcorders, and MP3 players are mostly powered by LIBs. Compared with other battery systems, LIBs show the advantages of high energy density, long cycle and shelf life, and no memory effect. The search for better electrode materials has been the most dynamic motivation behind the research and development of lithium-ion batteries.[2–10] Graphite is the state-of-the-art anode material with a specific capacity of 320–340 $mA\,h\,g^{-1}$ (theoretically 372 $mA\,h\,g^{-1}$).[11,12] Transition metal oxides such as CoO and Cu_2O represent a new class of anode material with significantly higher capacities up to 800 $mA\,h\,g^{-1}$.[5,7,13–15] However, such a high capacity can only be achieved with the help of

[*] Y. Yu, Prof. C.-H. Chen, J.-L. Shui, S. Xie
Department of Materials Science and Engineering
University of Science and Technology of China
Anhui Hefei 230026 (P.R. China)
Fax: (+86) 551-360-2940
E-mail: cchchen@ustc.edu.cn

[**] This work was supported by the 100 Talents Program of the Academia Sinica and the National Science Foundation of China (grant nos. 50372064 and 20471057). We are also grateful to The Ministry of Education (SRFDP no. 20030358057).

Supporting information for this article is available on the WWW under http://www.angewandte.org or from the author.

© 2005 Wiley-VCH Verlag GmbH & Co. KGaA, Weinheim

carbon additives, and is accompanied by a large irreversible capacity loss of up to 30%. Graphite-based composite electrodes that are modified with metal oxides (for example, SnO, CuO, and NiO) have displayed increased first-cycle lithiation capacity, but with even greater capacity loss.[16–18]

Here we present a new carbon-free anode, that is, CoO–Li_2O composite films, prepared by the electrostatic spray deposition (ESD) technique.[19–21] The structure of the films is controlled as a novel reticular morphology supported on a conducting nickel-foam substrate. This new composite electrode has an initial capacity loss of only 16.4% and 13% at 0.2C and 1C cycling rates, respectively, and yet retains a very high capacity (up to 877 mA h g^{-1} at a 0.2C rate) and excellent rate capability.

The first novelty of our study is the use of a very porous nickel-foam substrate (Figure 1a) rather than a conventional dense metal foil (for example, copper) as the current

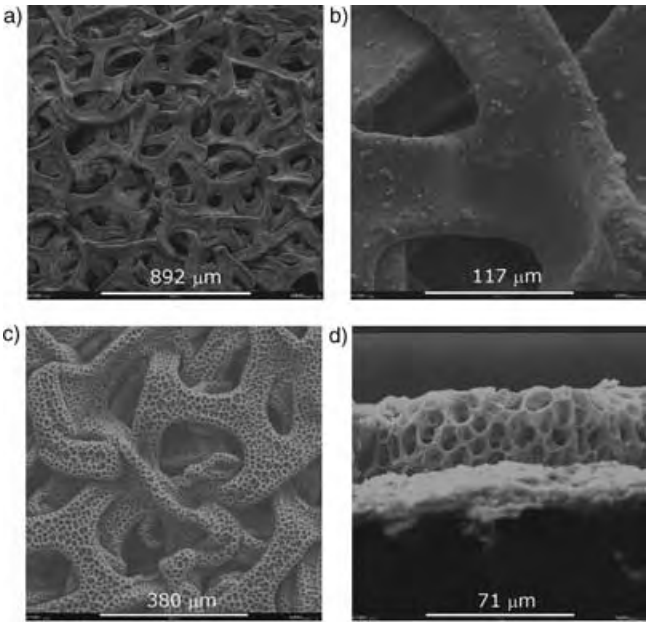

Figure 1. SEM images of the substrate and the CoO–Li_2O thin films. a) The porous nickel-foam substrate; b) surface morphology of a dense film from nitrate precursors; c) surface morphology of a reticular film from acetate precursors; d) cross-section of the reticular film from c). See the Experimental Section.

collector. This change results in maximization of the contact area between the electrode and the electrolyte. Similar to the well-established results obtained with a dense substrate,[19] depending on whether nitrates or acetates are used as the precursors, dense (Figure 1b) or reticular films (Figure 1c) are formed. The thickness of the reticular film is about 30 μm (Figure 1d). The formation of film textures that show a very high degree of conformity to the substrates represents an advantage of the ESD technique. It results from a preferential landing mechanism in ESD, that is, the charged droplets of a precursor solution may "land" preferentially on the conducting parts of a substrate and become discharged there.

Except for the diffraction peaks from the nickel substrate, no other peaks can be discerned from the X-ray diffraction patterns (not shown). However, the X-ray diffraction patterns of the as-deposited films prepared under the same conditions but on an aluminum-foil substrate (lighter than nickel) clearly show the diffraction peaks from CoO in addition to those from the aluminum substrate (Figure 2). Nevertheless, the weak and broad CoO peaks indicate that the CoO in the films

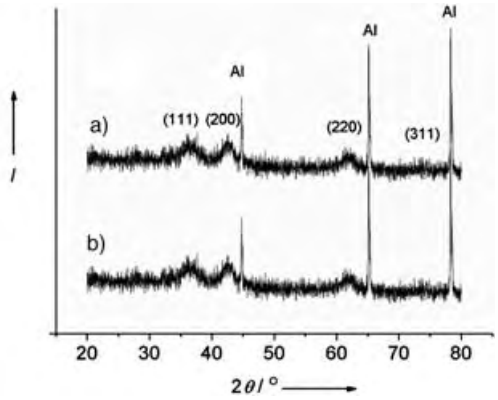

Figure 2. The X-ray diffraction patterns of the CoO–Li_2O thin films deposited on the aluminum substrate at 235 °C in air. a) Dense film; b) reticular film. The diffraction peaks from CoO are indexed in the patterns. I = intensity.

must be nanocrystalline or even amorphous. No peak is seen for any lithium compound, suggesting that the lithium product, which can be reasonably believed to be Li_2O formed at 235 °C, is amorphous. Therefore, the film is a CoO–Li_2O composite. The introduction of Li_2O, which alone is usually thought as an inactive component, in the composite is the second novelty of this work.

The voltage profiles of the electrochemical cells CoO–Li_2O/Li (Figure 3a,b) indicate that these composite electrodes have the typical characteristics of CoO electrodes, that is, a long voltage plateau at about 0.75 V followed by a sloping discharge curve down to the cut-off voltage of 0.01 V during the first discharge step.[5] After the first discharge, the 0.75 V discharge plateau does not appear anymore, suggesting a heterogeneous reaction mechanism of lithium insertion and extraction.[10,14,22] Remarkably, the first discharge step delivers a specific capacity of 900 mA h g^{-1} for the reticular CoO–Li_2O film (1:1 Co/Li molar ratio; Figure 3a) and 730 mA h g^{-1} for the dense CoO–Li_2O film (Co/Li 1:1; Figure 3b) at a current density of 0.1 mA cm^{-2}. Both values are significantly higher than the theoretical capacity (596 mA h g^{-1}) expected if only the film component CoO is active. On the other hand, the surface of the nickel substrate can be slightly oxidized at 235 °C in air. An independent measurement on an oxidized nickel substrate showed that the capacity owing to the substrate could account for about 10% of the total capacity of the reticular electrode film (see the Supporting Information). Even if the contribution from the substrate is discounted, the capacity of the electrode is still markedly higher than 596 mA h g^{-1}. Tarascon et al. have established that the extra capacity is likely due to the reversible formation and decomposition of a polymeric gel-like film on the surface of the CoO particles.[14,15] This film results from kinetically activated electrolyte degradation enabled by the active metal nanoparticles (Co). The presence of the film component Li_2O

 © 2005 Wiley-VCH Verlag GmbH & Co. KGaA, Weinheim

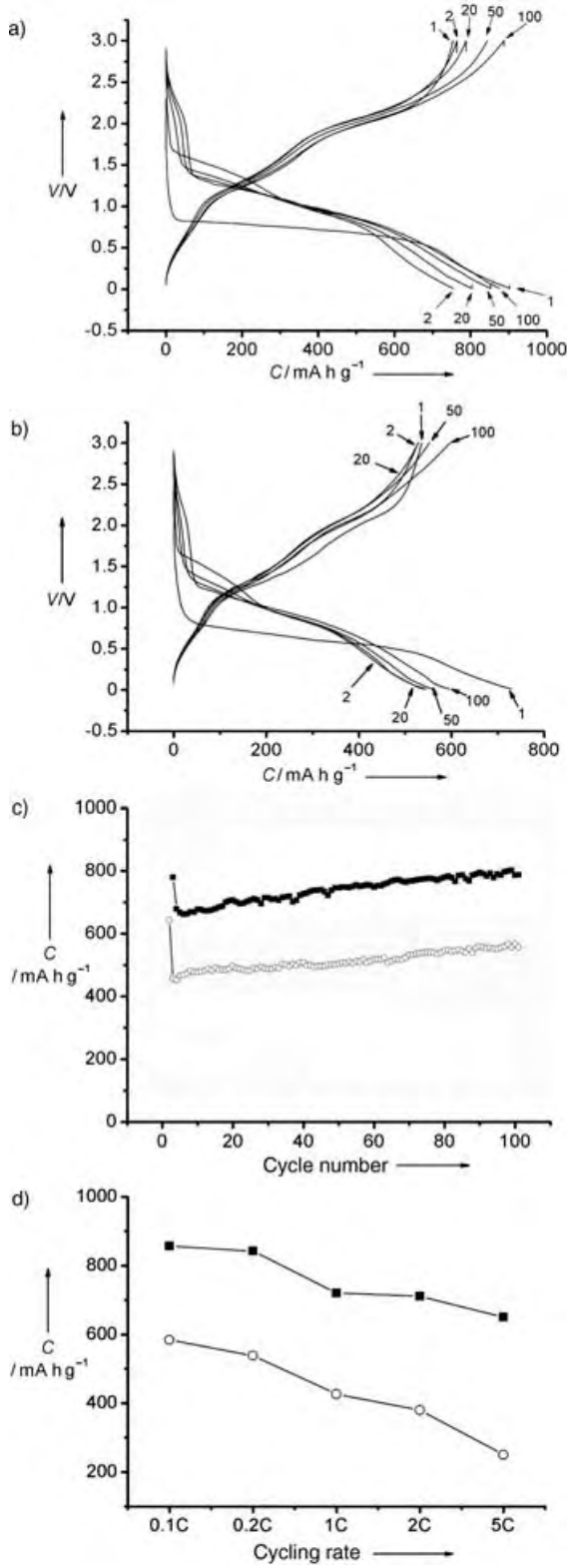

Figure 3. The electrochemical performance of the CoO–Li_2O thin-film electrodes cycled between 0.01 V and 3 V vs. Li^+/Li. a), b) Plots of the voltage–capacity curves of a reticular (a) and a dense (b) CoO–Li_2O film at a cycling rate of 0.2C (the numbers indicate the cycle number); c) the capacity–cycle-number curves of the CoO–Li_2O films at a cycling rate of 1C; d) the discharge capacity of the CoO–Li_2O films as a function of the cycling rate (0.1C–5C). ■ = reticular film, ○ = dense film; *C* = capacity, *V* = cell voltage.

may prohibit the growth of CoO particles and thus create a maximum CoO surface area. Hence, the capacity associated with the polymeric film is maximized.

The discharge capacity of the CoO–Li_2O composite films at a 0.2C cycling rate drops from 903 to 755 $mA\,h\,g^{-1}$ for the reticular morphology (Figure 3a) and from 729 to 538 $mA\,h\,g^{-1}$ for the dense morphology (Figure 3b) after the first cycle. However, the discharge capacity is gradually restored during the subsequent cycles; at the 100th cycle, it is 877 and 595 $mA\,h\,g^{-1}$ for the reticular and dense films, respectively. At a higher current density of about 1C rate, the capacity of the CoO–Li_2O composite films follows a similar trend as for a lower current density, although the values at different cycles decrease a little (Figure 3c). For the reticular CoO–Li_2O film, the specific capacity is 781 (1st cycle), 679 (2nd), 673 (10th), 695 (20th), 779 (80th), and 788 $mA\,h\,g^{-1}$ (100th). The phenomenon of an initial drop in capacity followed by a gradual increase (Figure 3c) is well documented in the literature, and is attributed to some irreversible Li_2O generated in the first discharge step.[14,23] Nonetheless, in the present study, the rise in capacity during cycling is also partly attributed to the increase in Co valence (see below). The reticular film also shows excellent rate capability; it reaches a specific capacity of 650 $mA\,h\,g^{-1}$ when cycled at a 5C rate (Figure 3d). For comparison, the 5C rate capacity is only 250 $mA\,h\,g^{-1}$ for the dense film. The difference in the rate capabilities for the two different morphologies originates from the difference in their impedance (see the Supporting Information); the reticular film leads to relatively small cell impedance. The high capacity achieved at a high cycling rate implies that this electrode can be used for high-power applications such as hybrid electric vehicles (HEV).

To investigate the effect of composite composition (that is, the Li/Co molar ratio) on the electrochemical performance, we prepared reticular films of five different Li/Co ratios ranging from 1:4 to 4:1. We found that there is an optimal composition around Li/Co = 1 for achieving a maximum specific capacity. The capacity of the cells measured at a 1C rate is shown in Figure 4. The capacity of the cells with the two extreme compositions is 545 $mA\,h\,g^{-1}$ for Li/Co = 1:4 and 267 $mA\,h\,g^{-1}$ for Li/Co = 4:1. According to the curve shape, it is expected that pure CoO must have a reasonably high capacity while pure Li_2O is electrochemically inactive. In fact, it is difficult to prepare a reticular-structured pure CoO film under similar deposition conditions. The electrochemical performance of the non-reticular CoO film is markedly worse than that of the Li_2O-containing composite films (see the Supporting Information).

As mentioned before, the Li_2O in the composite plays an important role in optimizing and even enhancing the electrochemical performance of the CoO component. Firstly, as Li_2O prohibits the particle growth of CoO, a maximized CoO surface area may be obtained so that the capacity related to the polymeric gel-like film can be enhanced. Secondly, Li_2O is an oxidant that converts CoO into Co_3O_4 or even Co_2O_3 during cycling according to the reactions (1) or (2), where the

$$Li_2O + 3\,CoO \rightarrow Co_3O_4 + 2\,Li \quad (1)$$

$$Li_2O + 2\,CoO \rightarrow Co_2O_3 + 2\,Li \quad (2)$$

 © 2005 Wiley-VCH Verlag GmbH & Co. KGaA, Weinheim

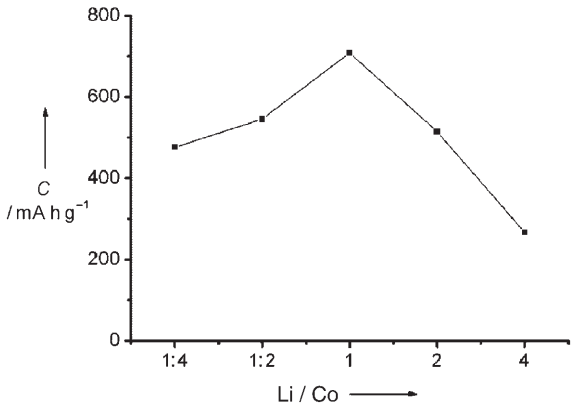

Figure 4. Plot of the discharge capacity of reticular CoO–Li_2O thin-film electrodes as a function of the Li/Co molar ratio in the precursor solutions. The cycling rate was 1C.

Li from Li_2O is transferred to the lithium metal electrode. The resulting increase in valency of the Co ions must partly account for the capacity that exceeds the theoretical value and the capacity rise of the composite films (Figure 3). The Li/Co molar ratios derived from these two reactions are 2:3 and 1:1, respectively, which are close to the optimal Li/Co ratio (Figure 4).

With a reticular CoO–Li_2O film (Li/Co 1:1) on a copper foil substrate, we confirmed the conversion of CoO into Co_3O_4 after five cycles (Figure 5). The third role of Li_2O is its

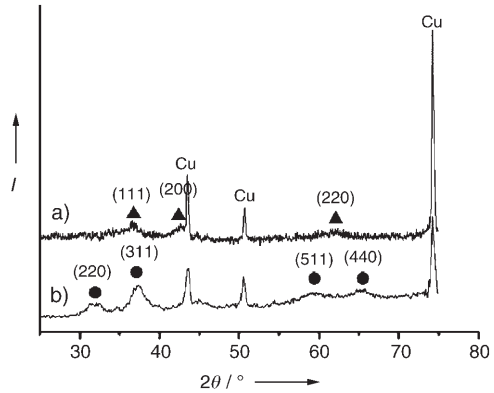

Figure 5. The X-ray diffraction patterns of CoO–Li_2O thin films (Li/Co 1:1) on a Cu foil substrate: as-deposited (a) and disassembled from a fully charged cell after five cycles (b). The diffraction peaks of CoO and Co_3O_4 are indexed in the patterns. ▲ = CoO, ● = Co_3O_4; *I* = intensity.

likely buffering effect by relieving the stress caused by the volume change during the reduction of CoO, so that the structural integrity of the electrode can be readily maintained. Notable is the absence of a carbon additive in the composite films studied in this work. The nickel-foam substrate provides an excellent electronic conduction pathway for the electrochemical processes.

In conclusion, carbon-free CoO–Li_2O composite films with a novel reticular morphology supported on a conducting nickel-foam substrate have been prepared by the ESD technique. The initial discharge capacity of a CoO–Li_2O film (Li/Co 1:1) reaches 903 mA h g^{-1} with a first-cycle capacity loss of only 16.4%. After 100 cycles, this film electrode retains a discharge capacity of 877 mA h g^{-1}. It also shows excellent rate capability with a 5C-rate capacity of up to 650 mA h g^{-1}. The Li_2O component in the composite is believed to play a threefold role: as a prohibitor for the CoO particle growth during synthesis, as an oxidizer for the conversion of Co^{2+} to Co^{3+}, and as a structural buffer. Such a composite anode opens the possibility of producing lithium-ion batteries with higher energy densities.

Experimental Section

With a precursor solution of lithium and cobalt acetates or nitrates in butyl carbitol ($CH_3(CH_2)_3OCH_2OCH_2CH_2OH$; 0.005 M), composite films of cobalt oxide and lithium oxide were deposited by the ESD technique for 2 h on a nickel-foam substrate heated at 235 °C (feeding rate 4 mL h^{-1}). A distance of 2–3 cm was kept between the needle and the substrate; the applied voltage was 11–13 kV. The composition and crystal structures of the as-deposited films were characterized by X-ray diffraction. The surface morphology was analyzed with a scanning electron microscope (Hitachi X-650).

The CoO-Li_2O films were used as the electrodes of electrochemical cells CoO–Li_2O/Li with 1 M $LiPF_6$ in ethylene carbonate and diethyl carbonate (EC/DEC 1:1 v/v) as the electrolyte. The cells were assembled in an argon-filled glove box (MBRAUN LABMASTER 130; moisture and oxygen levels less than 1 ppm) and cycled in the voltage range between 3.0 V and 0.01 V with a battery test system (NEWARE BTS-610).

To study the phase evolution of the CoO–Li_2O electrodes during cell cycling, a reticular CoO–Li_2O film (Li/Co 1:1) on a was deposited copper-foil substrate and assembled into a CoO–Li_2O/Li cell. The as-deposited film and the film disassembled from a fully charged cell after five cycles were characterized by X-ray diffraction.

Received: June 1, 2005
Revised: August 13, 2005
Published online: October 7, 2005

Keywords: batteries · cobalt · composites · electrodeposition · lithium

[1] K. Ozawa, *Solid State Ionics* **1994**, *69*, 212–221.
[2] B. Scrosati, *Nature* **1995**, *373*, 557–558.
[3] M. Thackeray, *Nat. Mater.* **2002**, *1*, 81–82.
[4] I. A. Courtney, J. R. Dahn, *J. Electrochem. Soc.* **1997**, *144*, 2045–2052.
[5] P. Poizot, S. Laruelle, S. Grugeon, L. Dupont, J. M. Tarascon, *Nature* **2000**, *407*, 496–499.
[6] J. M. Tarascon, M. Armand, *Nature* **2001**, *414*, 359–367.
[7] S. Grugeon, S. Laruelle, R. Herrera-Urbina, L. Dupont, P. Poizot, J. M. Tarascon, *J. Electrochem. Soc.* **2001**, *148*, A285–A292.
[8] E. Shembel, R. Apostolova, V. Nagirny, I. Kirsanova, Ph. Grebenkin, P. Lytvyn, *J. Solid State Electrochem.* **2005**, *9*, 96–105.
[9] V. G. Kumar, J. S. Gnanaraj, G. Salitra, A. Abramov, A. Gedanken, D. Aurbach, J. B. Soupart, J. C. Rousche, *J. Solid State Electrochem.* **2004**, *8*, 957–967.
[10] H. Li, P. Balaya, J. Maier, *J. Electrochem. Soc.* **2004**, *151*, A1878-A1885.
[11] M. Winter, G. H. Wrodnigg, J. O. Besenhard, W. Biberacher, P. Novak, *J. Electrochem. Soc.* **2000**, *147*, 2427–2431.

 © 2005 Wiley-VCH Verlag GmbH & Co. KGaA, Weinheim

[12] M. Winter, J. O. Besenhard, M. E. Spahr, P. Novak, *Adv. Mater.* **1998**, *10*, 725 – 763.
[13] Y. M. Kang, K. T. Kim, K. Y. Lee, S. J. Lee, J. H. Jung, J. Y. Lee, *J. Electrochem. Soc.* **2003**, *150*, A1538 – A1543.
[14] S. Grugeon, S. Laruelle, L. Dupont, J. M. Tarascon, *Solid State Sci.* **2003**. *5*, 895 – 904.
[15] R. Dedryvere, S. Laruelle, S. Grugeon, P. Poizot, D. Gonbeau, J. M. Tarascon, *Chem. Mater.* **2004**, *16*, 1056 – 1061.
[16] J. Y. Lee, R. F. Zhang, Z. L. Liu, *J. Power Sources* **2000**, *90*, 70 – 75.
[17] H. Huang, E. M. Kelder, J. Schoonman, *J. Power Sources* **2001**, *97–98*, 114 – 117.
[18] B. Veeraraghavan, A. Durairajan, B. Haran, B. Popov, R. Guidottib, *J. Electrochem. Soc.* **2002**, *149*, A675 – A681.
[19] C. H. Chen, E. M. Kelder, P. J. J. M. van der Put, J. Schoonman, *J. Mater. Chem.* **1996**, *6*, 765 – 771.
[20] C. H. Chen, E. M. Kelder, J. Schoonman, *J. Mater. Sci.* **1996**, *31*, 5437 – 5442.
[21] Y. Yu, J. L. Shui, S. Xie, C. H. Chen, *Aerosol Sci. Technol.* **2005**, *39*, 276 – 281.
[22] P. Poizot, S. Laruelle, S. Grugeon, J. M. Tarascon, *J. Electrochem. Soc.* **2002**, *149*, A1212 – A1217.
[23] J. S. Do, C. H. Weng, *J. Power Sources* **2005**, *146*, 482 – 486.

 © 2005 Wiley-VCH Verlag GmbH & Co. KGaA, Weinheim

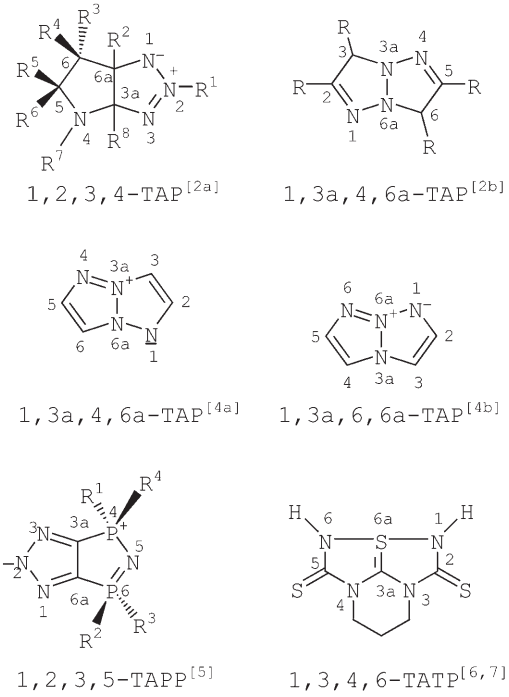

Scheme 1. The structures of tetraazapentalenes (TAPs), tetraazaphosphapentalenes (TAPPs), tetraazathiapentalenes (TATPs), and tetraazaselenapentalenes (TASPs).

Explosives

DOI: 10.1002/anie.200502342

Tetraazapentalene Chemistry: Unexpected Intramolecular Electron Rearrangement Induced by Highly Reactive ψ-Dinitroso Substituents**

My Hang V. Huynh, Michael A. Hiskey,* David E. Chavez, and Richard D. Gilardi*

Tetraazapentalenes (TAP),[1–4] tetraazaphosphapentalenes (TAPP),[5] tetraazathiapentalenes (TATP),[6–7] tetraazaselenapentalenes (TASP),[8–9] and their derivatives (Scheme 1) are of special interest owing to their unusual electronic structure and chemical behavior which is governed by the striking orientations of the heteroatoms. These heterocyclic systems promise a variety of applications including in organic synthesis, redox chemistry, and in industry, military, and space programs. Some examples of these applications include the derivatization of π-hypervalent heterocyclic TATP,[10–12] the synthesis of versatile heterocyclic compounds,[13–15] exotic metal carbene chemistry,[16–20] shaped charges for downhole penetrators,[21] and thermally stable high-energy materials.[22–26] Much attention has been focused on the preparation (precursors and methods) and properties of the heterocyclic tetraazapentalenes and their derivatives because their applications depend significantly on their thermal stability, performance, and synthetic practicality.

We are interested in the preparation of high-nitrogen-content energetic materials, heterocyclic high-density materials, and green primary explosives for a wide variety of applications through the utilization of tetrazines,[27] tetrazoles,[28] triazines,[29] furazans,[30] triazoles,[31] pyridines,[32] and azetidines.[33] Our interest in heterocyclic tetraazapentalenes was to probe the explosive performance (detonation velocity (V_D) and detonation pressure (P_{CJ})) of previously synthesized, thermally stable high-energy compounds and to

[*] Dr. M. H. V. Huynh, Dr. M. A. Hiskey, Dr. D. E. Chavez
Dynamic Experiment Division
DX-2: Materials Dynamics Group, MS C920
Los Alamos National Laboratory
Los Alamos, NM 87545 (USA)
Fax: (+1) 505-667-0500
E-mail: huynh@lanl.gov
hiskey@lanl.gov
Dr. R. D. Gilardi
Laboratory for the Structure of Matter
Naval Research Laboratory
Washington, DC 20375 (USA)

[**] This work was supported at Los Alamos by the joint program of the Department of Defense and the Department of Energy for the preparation and characterization of new energetic materials and at the Naval Research Laboratory by the Office of Naval Research, Mechanics Division.

 © 2005 Wiley-VCH Verlag GmbH & Co. KGaA, Weinheim

develop candidates with a better performance for realistic and yet practical applications.

Maquestiau et al. reported the preparation and partial physical characterization (MS: $[M^+] = 389$; IR: $\tilde{\nu} = 1530$ and 1320 cm^{-1}) of **1**, but neither crystal structure, thermal stability, sensitivity, nor explosive performance were provided.[34–35] Herein, we report an improved preparation of **1**, its full characterization, including energetic properties, and its novel reactivity through intramolecular electron rearrangement. The details of the three-step preparation are shown in Scheme 2.

The condensation reaction between benzotriazole and 2-chloro-3-nitropyridine was performed in acetonitrile in the presence of Na_2CO_3, to give regioisomer **1A**, which then underwent ring closure by treatment with $P(OEt)_3$ in refluxing xylene to yield **1B**. After its dissolution in H_2SO_4 (98%) at

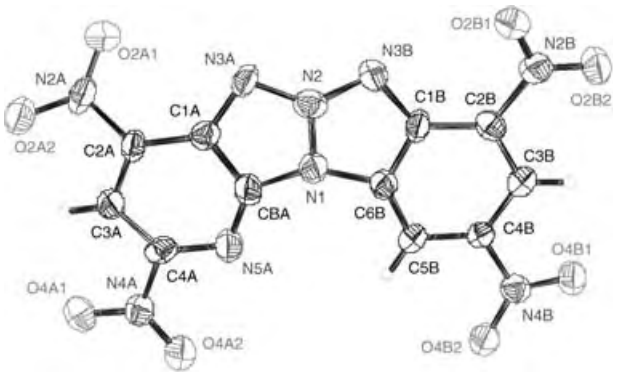

Figure 1. The ORTEP diagram (ellipsoids drawn at the 25% probability level) with labeling scheme for **1**. Selected bond lengths [Å] and angles [°]: N1-N2 1.370(14), N2-N3A 1.337(12), N2-N3B 1.330(13), N1-N2-N3A 114.2(11), N2-N1-C6A 108.3(11), N3A-C1A-C6A 111.5(12).

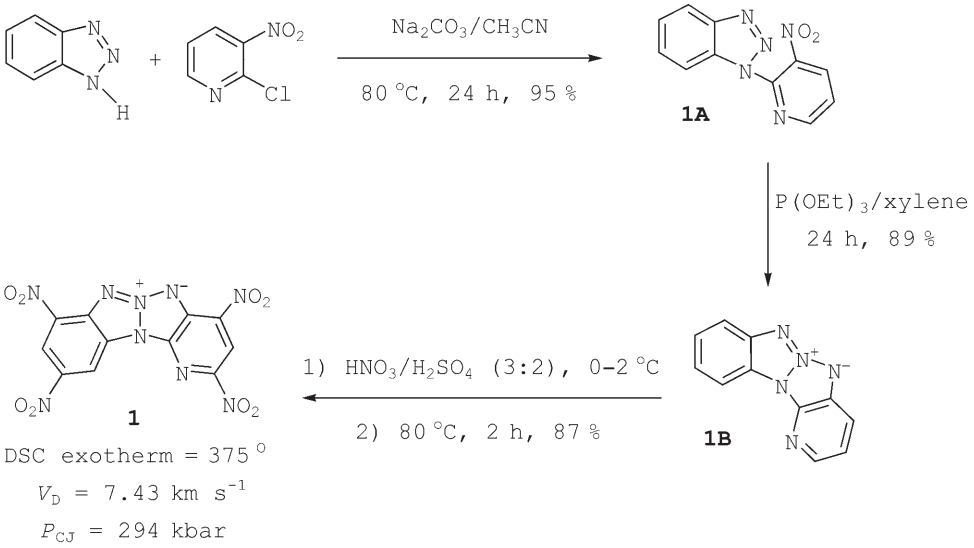

Scheme 2. Detailed preparation of **1**.

5 °C, HNO_3 (90%) was slowly added, while the temperature was maintained below 2 °C. The reaction mixture was stirred vigorously at 80 °C for 2 h, cooled to room temperature, and poured onto crushed ice. Once filtered and washed with cold water, the yellow product was triturated consecutively with a minimum amount of acetone, acetonitrile, and methanol to remove any remaining acids.[21]

Isolated **1** was characterized by X-ray crystallography,[36a] differential scanning calorimetry (DSC, exotherm of fast decomposition), heat of formation, and UV/Vis, IR, and ^1H and ^{13}C NMR spectroscopy.[37] The X-ray crystal structure of **1** (grown through the slow evaporation of a solution in nitromethane), is shown in Figure 1.

Overall, the reaction sequence shown in Scheme 2 gives **1** in 74% yield, which is two and half times greater than that reported by Maquestiau et al.[34–35] Furthermore, the duration of the nitration reaction is much shorter (2 vs 48 h), and both solvents (acetonitrile from the condensation reaction and xylenes from the ring-closure step) are subsequently distilled to allow recovery and reuse. Compound **1** has a thermal stability similar to that of the other well-known thermally stable analogues shown in Scheme 3, but exhibits the highest experimentally measured V_D and P_{CJ}. As a consequence, the combination of better reaction yield, cheaper production cost, and higher performance has made **1** attractive for use in realistic and practical applications.[21]

A stoichiometric reaction between **1** and NaN_3 in DMSO at 40 °C gave **2**. After the reaction was cooled to room temperature, water was added to precipitate the analytically pure brown product, which was filtered, washed thoroughly with water, and air-dried, [Eq. (1)].

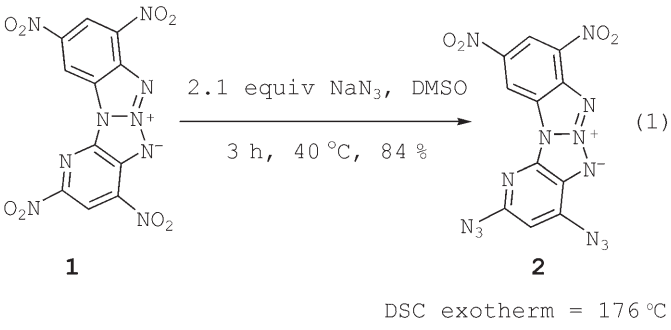

(1)

Compound **2** was characterized by DSC, elemental analysis, and UV/Vis, IR, and ^1H and ^{13}C NMR spectroscopy.[38] **Caution!** Compound **2** is very sensitive to sparks, friction, and impact,[39] hence, plastic spatulas should be used. This reaction should be performed within a fume hood fitted with a thick blast shield. Grounding straps, thick gloves, and a face shield should be worn at all times.

The reaction shown in Equation (2) exhibits the same nucleophilic disubstitution of the benzopyridotetraazapenta-

 © 2005 Wiley-VCH Verlag GmbH & Co. KGaA, Weinheim

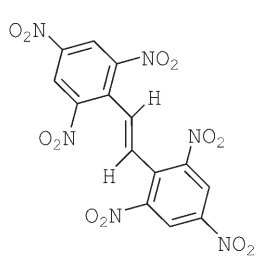

HNS

DSC exotherm = 315 °C

ρ = 1.74 g cm^{-3}

V_D = 7.00 km s^{-1}

P_{CJ} = 199 kbar

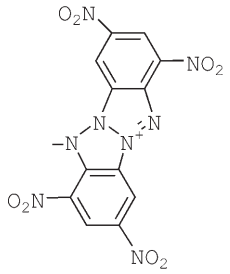

Z-shaped TACOT

DSC exotherm = 378 °C

ρ = 1.85 g cm^{-3}

V_D = 7.20 km s^{-1}

P_{CJ} = 245 kbar

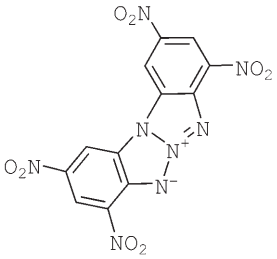

T-shaped TACOT

DSC exotherm = 400 °C

ρ = 1.84 g cm^{-3}

V_D = 7.06 km s^{-1}

P_{CJ} = 202 kbar

Scheme 3. Some common thermally stable compounds.

and (2) is unique when compared to those of the Z-shaped and T-shaped isomers of dibenzotetraazapentalene (BBTAP; **7**) and dipyridotetraazapentalene (PPTAP; **9**).[22–24] As shown in Scheme 4, substitution by the azide group occurred only *ortho* to the N bridgeheads.[22–24] Even with excess NaN_3, higher temperature, and longer reaction time, only one azide group substituted on each side of the BBTAP and PPTAP systems.

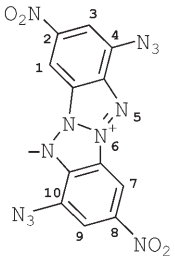

BBTAP (**7**)

DSC exotherm = 187 °C

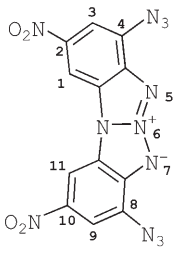

BBTAP (**8**)

DSC exotherm = 176 °C

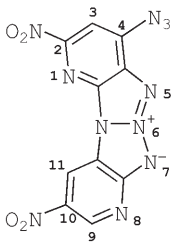

PPTAP (**9**)

DSC exotherm = 173 °C

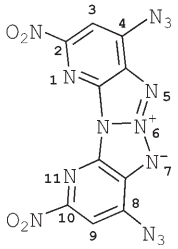

PPTAP (**10**)

DSC exotherm = 157 °C

Scheme 4. Diazido-substituted isomeric tetraazapentalenes.

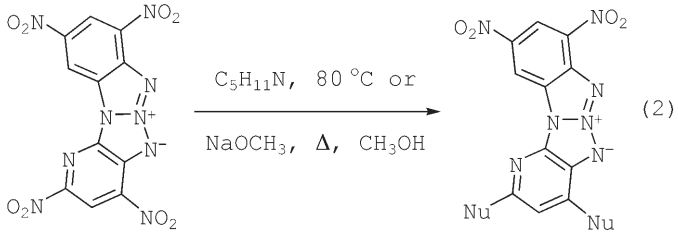

1 → **5**: Nu = OCH_3; **6**: Nu = $C_5H_{10}N$ (2)

lene (BPTAP) backbone. However, it was necessary to use a large excess of nucleophile (sodium methoxide or piperidine) in the appropriate solvent and to heat the reaction mixtures at reflux or at 80 °C. The isolated product was purified through column chromatography.

The disubstitution pattern of **2**, **5**, and **6** in Equations (1)

Based on the preparation of **12** (nitrogen atoms form a Z-shaped structure) from **7**[22] [Eq. (3)] or the analogous compound from **8** (the nitrogen atoms in a T-shaped structure),[23] we predicted that the nitration of **2**, followed by azido–nitro ring closure, would give the corresponding furoxano–tetrazolo product **13** as shown in Equation (4).

The reaction shown in Equation (4) did not form **13**, but rather took a substantially different pathway as shown in

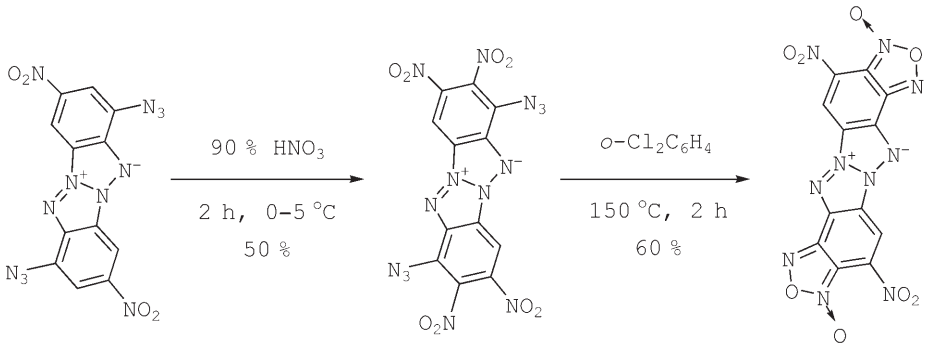

7 → **11** → **12** (3)

© 2005 Wiley-VCH Verlag GmbH & Co. KGaA, Weinheim

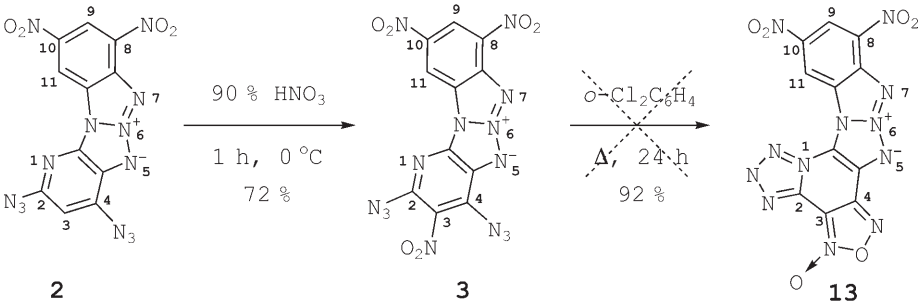

(4)

Scheme 5. The adjacent 2-azido and 3-nitro positioning provoked the elimination of molecular nitrogen followed by ring closure to form the corresponding furazan *N*-oxide compound **3A** or the resonance hybrid ψ-2,3-dinitroso compound **3B**. The presence of the ψ-3-nitroso group triggers the elimination of the second nitrogen molecule and subsequent ring closure to form **3C**, which is the valence isomer of **3D**. The ψ-4-nitroso substituent in **3D** stimulates an intramolecular electron rearrangement to open the T-shaped tetraazapentalene backbone to form **4**. This is the first example of the ring opening of the T-shaped tetraazapentalene isomer. This ring opening is unlike the ring scissions of the Z-shaped TACOT, which was attacked either by oxidation with peracetic acid,[41] reduction with lithium aluminum hydride (or copper(I) cyanide),[41] or nucleophilic substitution with sodium methoxide.[42] The unpredicted product **4** was confirmed through the X-ray crystal structure shown in Figure 2,[36b] and fully characterized by DSC, elemental analysis, and UV/Vis, IR, and ^{1}H and ^{13}C NMR spectroscopy.[43]

These results are important in demonstrating the improved preparation of **1**, which may lead to a variety of realistic and yet practical applications. Ring scission of the T-shaped tetraazapentalene isomer is novel as it occurs through an unpredicted intramolecular electron rearrangement activated by the highly reactive ψ-dinitroso substituents of **3c**.

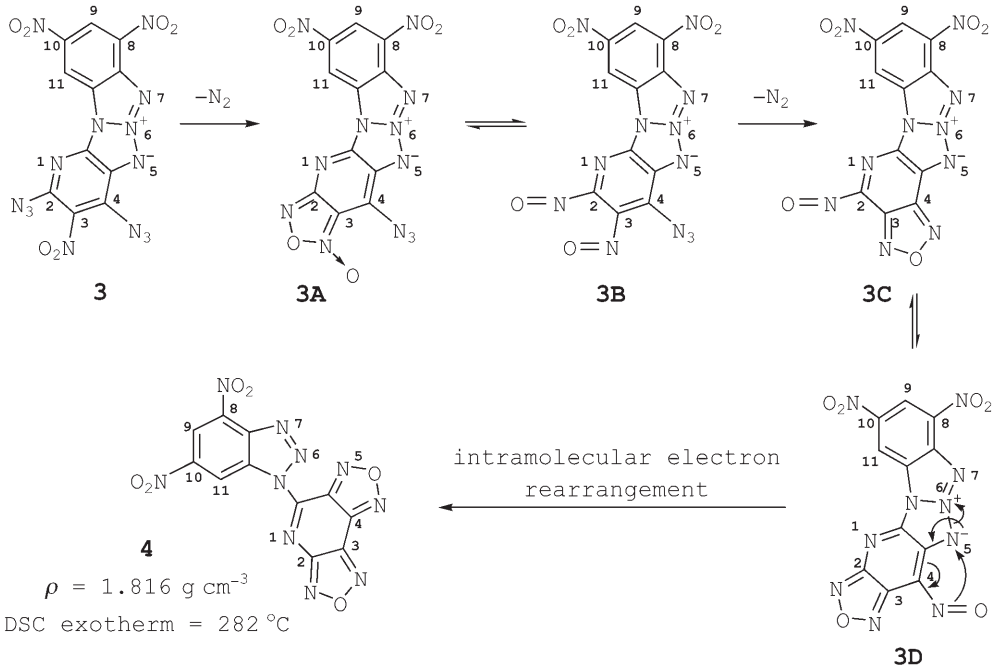

Scheme 5. Proposed reaction mechanism for the formation of **4**.

Received: July 5, 2005
Published online: October 12, 2005

Keywords: azides · nitrogen heterocycles · reactive intermediates · rearrangement · ring opening

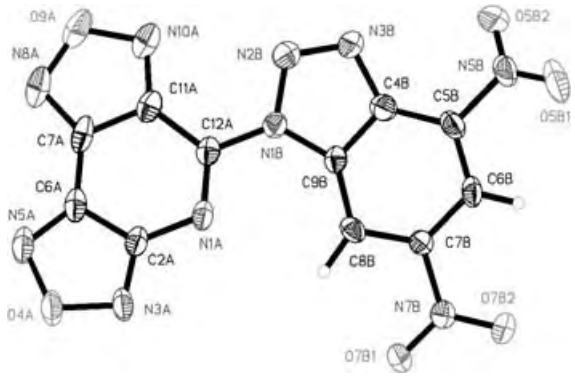

Figure 2. The ORTEP diagram (ellipsoids drawn at the 25% probability level) with labeling scheme for **4**. Selected bond lengths [Å] and angles [°]: N1B–N2B 1.375(4) N2B-N3B = 1.284(3), N1OA-C11A 1.313(4), N1B-N2B-N3B 108.8(2), N2B-N3B-C4B 108.4(3), N2B-N3B-C9B 109.7(2).

[1] a) D. Balachari, M. L. Trudell, *Tetrahedron Lett.* **1997**, *38*, 8607–8610; b) V. Galasso, D. Jones, A. Modelli, M. L. Trudell, *Chem. Phys.* **2000**, *254*, 375–384; c) M. P. Groziak, S. R. Wilson, G. L. Clauson, N. J. Leonard, *J. Am. Chem. Soc.* **1986**, *108*, 8002–8006; d) A. M. Halpern, C. J. Ruggles, X.-K. Zhang, M. P. Groziak, N. J. Leonard, *J. Phys. Chem.* **1987**, *91*, 1366–1367; e) B. Bhat, K. A. Cruickshank, N. J. Leonard, *J. Org. Chem.* **1989**, *54*, 2028–2030.

[2] a) D. Ramaiah, N. P. Rath, M. V. George, *Acta Crystallogr. Sect. C* **1998**, *54*, 872–875; b) M. Brufani, G. Casini, W. Fedeli, F. Mazza, A. Vaciago, *Gazz. Chim. Ital.* **1971**, *101*, 322–343; c) G. Subramanian, M. L. Trudell, J. H. Boyer, *Heteroat. Chem.* **1996**, *7*, 163; d) G. Subramanian, M. L. Trudell, J. H. Boyer, *Heteroat. Chem.* **1995**, *6*, 391–395; e) A. Gunasekaran, T. Jayachandran, J. H. Boyer, M. L. Trudell, *J. Heterocycl. Chem.* **1995**, *32*, 1405–1407; f) A. Gunasekaran, M. L. Trudell, J. H. Boyer, *Heteroat. Chem.* **1994**, *5*, 441–446; g) K. A. Cruickshank, K. Sumoto, N. J.

 © 2005 Wiley-VCH Verlag GmbH & Co. KGaA, Weinheim

Leonard, *Tetrahedron Lett.* **1985**, *26*, 2723–2726; h) D. E. Pereira, N. J. Leonard, *Tetrahedron Lett.* **1986**, *27*, 4129–4132.
[3] a) J. Kalinowski, P. Nantka-Namirski, I. Szczerek, *Pol. Acad. Sci.* **1977**, *34*, 9–15; b) P. Nantka-Namirski, J. Kalinowski, *Pol. Acad. Sci.* **1974**, *31*, 125–136 and P. Nantka-Namirski, J. Kalinowski, *Pol. Acad. Sci.* **1974**, *31*, 137–145; c) P. Nantka-Namirski, J. Kalinowski, *Pol. Acad. Sci.* **1971**, *28*, 219–221; d) N. Matsumura, M. Tomura, Y. Tsuchiya, S. Yoneda, M. Nakamura, *Chem. Express* **1986**, *1*, 487–490; e) M. D. Bargamova, M. Y. Antipin, L. S. German, Y. T. Struchkov, *Dokl. Akad. Nauk* **1993**, *329*, 44–47; f) K. C. V. Ramanaiah, E. D. Stevens, M. L. Trudell, *J. Heterocycl. Chem.* **2000**, *37*, 1597–1602.
[4] a) R. A. Carboni, J. E. Castle, *J. Am. Chem. Soc.* **1962**, *84*, 2453–2454; b) R. A. Carboni, J. C. Kauer, J. E. Castle, H. E. Simmons, *J. Am. Chem. Soc.* **1967**, *89*, 2618–2625; c) J. C. Kauer, R. A. Carboni, *J. Am. Chem. Soc.* **1967**, *89*, 2633–2637; d) Y. T. Chia, H. E. Simmons, *J. Am. Chem. Soc.* **1967**, *89*, 2638–2643; e) R. J. Harder, R. A. Carboni, J. E. Castle, *J. Am. Chem. Soc.* **1967**, *89*, 2643–2647; f) M. E. Grice, P. Politzer, *J. Mol. Struct.* **1995**, *358*, 63–69; g) W. Selig, B. J. Mallon, *Explosivstoffe* **1968**, *16*, 266–273; h) J. H. Hall, *J. Org. Chem.* **1971**, *36*, 217; i) A. Matsumot, J. H. Lee, M. Yoshida, O. Simamura, *Chem. Lett.* **1973**, 455–456; j) G. Norwitz, H. Gordon, *Appl. Spectrosc.* **1975**, *29*, 521–523; k) M. B. Laing, R. A. Sparks, M. J. Laing, K. N. Trueblood, *Acta Crystallogr. Sect. B* **1976**, *32*, 2518–2520.
[5] S. Trofimenko, A. L. Rheingold, C. D. Incarvito, *Angew. Chem.* **2003**, *115*, 3630–3633; *Angew. Chem. Int. Ed.* **2003**, *42*, 3506–3509.
[6] a) F. Iwasaki, K. Akiba, *Bull. Chem. Soc. Jpn.* **1984**, *57*, 2581–2583; b) M. Tomura, O. Mori, H. Chikusa, K. Inazu, A. Ito, N. Matsumura, H. Inoue, *Synthesis* **1991**, 457–459.
[7] N. Matsumura, T. Konishi, H. Hayashi, M. Yasui, F. Iwasaki, K. Mizuno, *J. Heterocycl. Chem.* **2002**, *39*, 189–202.
[8] N. Matsumura, M. Tomura, H. Inoue, *J. Heterocycl. Chem.* **1989**, *26*, 1655–1657.
[9] F. Iwasaki, H. Murakami, N. Yamazaki, M. Yasui, M. Tomura, N. Matsumura, *Acta Crystallogr. Sect. C* **1991**, *47*, 998–1003.
[10] a) N. Matsumura, O. Mori, T. Takeguchi, Y. Okumura, K. Mizuno, *J. Heterocycl. Chem.* **2004**, *41*, 873–876; b) N. Matsumura, R. Hirase, O. Mori, H. Inoue, *Chem. Lett.* **1993**, *5*, 865–868.
[11] a) G. Morel, E. Marchand, S. Sinbandhit, L. Toupet, *Heteroat. Chem.* **2003**, *14*, 95–105; b) F. Iwasaki, S. Kakuma, S. Yoshida, S. Murata, M. Yasui, *Phosphorus Sulfur Relat. Elem.* **1994**, *95–96*, 515–516.
[12] M. Tomura, O. Mori, N. Matsumura, H. Inoue, *J. Heterocycl. Chem.* **1991**, *28*, 221–224.
[13] a) N. Matsumura, A. Ito, M. Tomura, Y. Okumura, K. Mizuno, *J. Heterocycl. Chem.* **2004**, *41*, 99–102; b) L. L. Lai, D. H. Reid, R. H. Nicol, J. B. Rhodes, *Heteroat. Chem.* **1994**, *5*, 149–157.
[14] M. Tomura, N. Matsumura, O. Mori, H. Chikusa, S. Kamitani, H. Inoue, *J. Heterocycl. Chem.* **1990**, *27*, 2215–2217.
[15] G. Labbe, N. Weyns, I. Sannen, P. Delbeke, S. Toppet, *J. Heterocycl. Chem.* **1991**, *28*, 405–409.
[16] N. Matsumura, J. Kawano, N. Fukunishi, H. Inoue, M. Yasui, H. Iwasaki, *J. Am. Chem. Soc.* **1995**, *117*, 3623–3624.
[17] M. Yasui, S. Yoshida, S. Kakuma, S. Shimamoto, N. Matsumura, F. Iwasaki, *Bull. Chem. Soc. Jpn.* **1996**, *69*, 2739–2747.
[18] F. Iwasaki, N. Manabe, M. Yasui, N. Matsumura, N. Kamiya, H. Iwasaki, *Bull. Chem. Soc. Jpn.* **1996**, *69*, 2749–2757.
[19] F. Iwasaki, M. Yasui, S. Yoshida, H. Nishiyama, S. Shimamoto, N. Matsumura, *Bull. Chem. Soc. Jpn.* **1996**, *69*, 2759–2770.
[20] N. Manabe, M. Yasui, H. Nishiyama, S. Shimamoto, N. Matsumura, F. Iwasaki, *Bull. Chem. Soc. Jpn.* **1996**, *69*, 2771–2780.
[21] M. H. V. Huynh, M. A. Hiskey, *J. Energ. Mater.* **2004**, *22*, 109–115.
[22] G. Subramanian, G. Eck, J. H. Boyer, E. D. Stevens, M. L. Trudell, *J. Org. Chem.* **1996**, *61*, 5801–5803, and references therein.
[23] G. Subramanian, J. H. Boyer, D. Buzatu, E. D. Stevens, M. L. Trudell, *J. Org. Chem.* **1995**, *60*, 6110–6113, and references therein.
[24] D. Balachari, E. D. Stevens, M. L. Trudell, D. Beardall, C. A. Wight, *Propellants Explos. Pyrotech.* **2000**, *25*, 75–80, and references therein.
[25] a) J. Kerth, S. Lobbecke, *Propellants Explos. Pyrotech.* **2002**, *27*, 111–118; b) X. N. Diwu, B. Z. Lin, *Theo. Pract. Energ. Mater.* **2003**, *5*, 144–148; c) T. B. Brill, H. Ramanathan, R. W. Beal, *Combust. Energ. Mater.* **2002**, 22–30; d) Z.-X. Li, Y.-X. Ou, B.-R. Chen, *J. Beijing Inst. Technol. (Engl. Ed.)* **2001**, *10*, 322–325; e) A. Hammerl, T. M. Klapotke, H. Noth, M. Warchhold, G. Holl, M. Kaiser, U. Ticmanis, *Inorg. Chem.* **2001**, *40*, 3570–3575, and references therein; f) S. F. Son, H. L. Berghout, C. A. Bolme, D. E. Chavez, D. L. Naud, M. A. Hiskey, *Proc. Combust. Inst.* **2000**, *28*, 919–924; g) J. R. Stine, *Mater. Res. Soc. Symp. Proc.* **1993**, *296*, 3–12; h) R. Haiges, J. A. Boatz, A. Vij, M. Gerken, S. Schneider, T. Schroer, K. O. Christe, *Angew. Chem.* **2003**, *115*, 6027–6031; *Angew. Chem. Int. Ed.* **2003**, *42*, 5847–5851, and references therein.
[26] M. H. V. Huynh, M. A. Hiskey, **2004**, Patent pending.
[27] M. H. V. Huynh, M. A. Hiskey, J. G. Archuleta, E. L. Roemer, R. D. Gilardi, *Angew. Chem.* **2004**, *116*, 5776–5779; *Angew. Chem. Int. Ed.* **2004**, *43*, 5658–5661, and references therein.
[28] M. A. Hiskey, N. Goldman, J. R. Stine, *J. Energ. Mater.* **1998**, *16*, 119–127.
[29] M. H. V. Huynh, M. A. Hiskey, E. L. Hartline, D. P. Montoya, R. D. Gilardi, *Angew. Chem.* **2004**, *116*, 5032–5036; *Angew. Chem. Int. Ed.* **2004**, *43*, 4924–4928, and references therein.
[30] D. E. Chavez, L. Hill, M. A. Hiskey, S. Kinkead, *J. Energ. Mater.* **2000**, *18*, 219–236.
[31] M. H. V. Huynh, M. A. Hiskey, *J. Energ. Mater.* **2005**, *23*, 27–32.
[32] M. D. Coburn, J. L. Singleton, *J. Heterocycl. Chem.* **1972**, *9*, 1039–1044.
[33] M. A. Hiskey, M. D. Coburn, M. A. Stinecipher, M. A. Mitchell, B. C. Benicewicz, *J. Heterocycl. Chem.* **1992**, *29*, 1855–1856.
[34] A. Maquestiau, M. Flammang-Barbieux, E. Vilain, Pfister- G. Guillouzo, *Bull. Soc. Chim. Belges* **1983**, *92*, 67–75.
[35] A. Maquestiau, M. Flammang-Barbieux, E. Vilain, G. Pfister-Guillouzo, *Bull. Soc. Chim. Belges* **1986**, *95*, 1117–1122.
[36] CCDC-277008 (**1**) and -277007 (**4**) contain the supplementary crystallographic data for this paper. These data can be obtained free of charge from the Cambridge Crystallographic Data Centre at www.ccdc.cam.ac.uk/data_request/cif.
[37] Characterization of **1**: DSC: exotherm at 375 °C; heat of formation (ΔH_f): 90.4 kcal mol^{-1}; UV/Vis (DMSO): λ_{max} (ε, M^{-1}cm^{-1}) = 472 (1.55×10^4), 314 (5.86×10^3), and 258 nm (5.65×10^3); IR (nujol): $\tilde{\nu}$ = 1599 (vs), 1589 (vs), 1556 (vs), and 1537 (vs) ($\nu(NO_2)$); 1453 (vs), 1417 (vs), 1372 (vs), 1336 (vs), 1249 (vs), 1178 (vs), 1123 (vs), 1108 (vs), 1056 (vs), 938 (vs), 910 (vs), 896 (vs), 864 (vs), 837 (vs), 782 (vs), 756 (vs), 740 (vs), 727 (vs), 718 (vs), 694 (vs), 612 (vs), 550 (vs), and 481 cm^{-1} (vs) (ν(BPTAP)); ^{1}H NMR (300 MHz, [D$_6$]DMSO, 85 °C): δ = 9.27 (*s*, 1H), 9.30 (*d*, J = 2.0 Hz, 1H), 9.38 ppm (*d*, J = 2.0 Hz, 1H); and ^{13}C NMR (300 MHz, [D$_6$]DMSO, 85 °C): δ = 103.1, 111.2, 118.9, 122.8, 130.9, 132.5, 135.2, 139.6, 140.9, 153.6, 157.8 ppm.
[38] Characterization of **2**: DSC: exotherm at 176 °C; elemental analysis :calcd for $C_{11}H_3N_{13}O_4$: C 34.66, H 0.79, N 47.76; found: C 34.78, H 0.81, N 47.12; UV/Vis (DMSO): λ_{max}(ε, M^{-1}cm^{-1}) = 469 (9.55×10^3), 335 (5.17×10^3), 267 nm (1.51×10^4); IR (nujol): $\tilde{\nu}$ = 2133 (vs) and 2121 (vs) (ν (N_3)); 1586 (vs), 1533 (vs) ($\nu(NO_2)$); 1457 (vs), 1375 (vs), 1333 (vs), 1289 (vs), 1262 (vs), 1243 (vs), 1192 (vs), 1165 (vs), 1109 (vs), 1057 (vs), 938 (vs), 924 (vs), 863 (vs), 844 (vs), 776 (vs), 738 (vs), 718 (vs), 652 (vs), 576

 © 2005 Wiley-VCH Verlag GmbH & Co. KGaA, Weinheim

(vs), 535 cm^{-1} (vs) (ν(BPTAP)); ^{1}H NMR (300 MHz, [D$_6$]DMSO): $\delta = 7.26$ (*s*, 1H), 9.18 (d, $J = 2.0$ Hz, 1H), 9.06 ppm (d, $J = 2.0$ Hz, 1H); ^{13}C NMR (300 MHz, [D$_6$]DMSO, 80 °C): $\delta = 103.9$, 111.5, 119.5, 122.8, 127.6, 131.8, 136.2, 138.9, 141.4, 141.6, 152.9 ppm.

[39] For explosive sensitivity testing, see: R. T. Paine, W. Koestle, T. T. Borek, E. Duesler, M. A. Hiskey, *Inorg. Chem.* **1999**, *38*, 3738 – 3743.

[40] A. Maquestiau, M. Flammang-Barbieux, E. Vilain, G. Pfister-Guillouzo, *Bull. Soc. Chim. Belges* **1984**, *93*, 973 – 982.

[41] R. A. Carboni, J. C. Kauer, W. R. Hatchard, R. J. Harder, *J. Am. Chem. Soc.* **1967**, *89*, 2626 – 2633.

[42] K. L. Altmann, A. P. Chafin, L. H. Merwin, W. S. Wilson, R. Gilardi, *J. Org. Chem.* **1998**, *63*, 3352 – 3356.

[43] Characterization of **4**: DSC: exotherm. at 282 °C; elemental analysis: calcd for $C_{11}H_2N_{10}O_6$: C 35.69, H 0.54, N 37.84; found: C 35.73, H 0.61, N 38.1; UV/Vis (DMSO): λ_{max} (ε, $M^{-1}cm^{-1}$) = 530 (1.27×10^3), 471 (1.71×10^3), 335 nm (9.47×10^3); IR (nujol): $\tilde{\nu} =$ 1556 (vs), 1541 (vs) ($\nu(NO_2)$); 1498 (vs), 1458 (vs), 1377 (vs), 1347 (vs), 1224 (vs), 1137 (vs), 1058 (vs), 1023 (vs), 995 (vs), 945 (vs), 927 (vs), 880 (vs), 802 (vs), 746 (vs), 724 (vs), 680 (vs), 637 (vs), 611 cm^{-1} (vs) (ν(BPTAP)); ^{1}H NMR (300 MHz, [D$_6$]DMSO): $\delta = 9.16$ (d, $J = 2.0$ Hz, 1H), 9.69 ppm (d, $J =$ 2.0 Hz, 1H); ^{13}C NMR (300 MHz, [D$_6$]DMSO, 80 °C): $\delta =$ 116.7, 118.8, 132.9, 136.2, 138.6, 140.5, 143.1, 143.8, 147.2, 148.2, 157.6 ppm.

 © 2005 Wiley-VCH Verlag GmbH & Co. KGaA, Weinheim

Phospholipids

DOI: 10.1002/anie.200502362

Mass Spectrometric Profiling of Intact Biological Tissue by Using Desorption Electrospray Ionization**

Justin M. Wiseman, Satu M. Puolitaival, Zoltán Takáts, R. Graham Cooks, and Richard M. Caprioli**

Imaging mass spectrometry has emerged as a powerful technique based on time-of-flight secondary-ion mass spectrometry (TOF-SIMS)[1] and matrix-assisted laser desorption/ionization (MALDI).[2,3] However, until now, the mass-spectrometric analysis of biological tissues has been limited to techniques that require sample preparation after which the sample is confined to the high-vacuum region of the instrument, thus making this approach inaccessible to further physical or chemical manipulations. Herein, direct chemical profiling of biological tissues is achieved under ambient conditions at atmospheric pressure by desorption electrospray ionization mass spectrometry (DESI-MS),[4] which is a new and versatile method for the creation of ions from surfaces outside of the mass spectrometer. The profiling of lipids in biological tissues by using DESI-MS provides highly sensitive and chemically specific information almost instantaneously. This capability is illustrated by examples in which phospholipid profiles of mouse pancreas, rat brain, and metastatic human-liver adenocarcinoma tissues are obtained without any sample pretreatment.

Biological membranes serve as crucial mediators in cellular differentiation and proliferation; the former being important in tumor formation, the latter in tumor progression. Phospholipids play important roles in maintaining the structural integrity of the cell by forming of the characteristic bilayer of the membrane and by serving as key mediators in important cellular events, for example, cell signaling and protein sorting on so-called lipid rafts. As such, the chemical and physical properties of the cell membrane are determined by the phospholipid composition. Alterations in the phospholipid composition of tissues have been reported for certain diseases, including cancer and Alzheimer's disease.[5] Importantly, the abundance of certain phospholipids and their enzymatic by-products has been associated with malignant transformations in some tissues.[6] These findings emphasize the importance of the determination of the composition of phospholipids in biological tissues, information which may serve as prognostic variables in diseased and nondiseased tissues.

Mass spectrometry has been used extensively to investigate lipids (e.g., phospholipids),[7] although not under ambient conditions. MALDI-TOF has been used for the analysis of lipids in lens tissue[8] and has emerged as a particularly powerful technique for profiling the spatial distributions of peptides and proteins in biological tissues.[3,9] An alternative molecular imaging method, TOF-SIMS, has been applied to the investigation of the phosphocholine distribution in *Tetrahymena* mating junction by monitoring the phosphocholine head group at m/z 184.[10] In another report, TOF-SIMS imaging of lipids in mouse-brain sections was performed and various sulfatides, as well as phosphatidylinositol, phosphatidylcholine, and cholesterol, were identified and their spatial distributions determined.[11]

DESI belongs to the family of spray ionization methods, such as electrospray ionization (ESI),[12] as well as to the family of desorption ionization methods.[13] DESI allows direct and rapid analysis of surfaces without sample preparation or the need to introduce the sample into a vacuum system.[4] The methodology has been applied to the analysis of trace levels of many classes of compounds, including peptides, proteins, nucleotides, nitroaromatic compounds, and others.[14] Semiquantitative results have been obtained from

[*] J. M. Wiseman, Dr. Z. Takáts, Prof. R. G. Cooks
Purdue University
Department of Chemistry
West Lafayette, IN 47907 (USA)
Fax: (+1) 765-494-0239
E-mail: cooks@purdue.edu
S. M. Puolitaival, Prof. R. M. Caprioli
Vanderbilt University
Department of Chemistry and Department of Biochemistry
Nashville, TN 37232-0146 (USA)
E-mail: richard.m.caprioli@vanderbilt.edu

[**] This work was supported by Prosolia Inc. (Indianapolis, IN), the Office of Naval Research, and NIH/NIGMS Grant No. 5R01 GM58008-07. We gratefully acknowledge Pierre Chaurand and Hans-Rudolf Aerni for supplying the mouse pancreas and rat-brain sections and for their technical assistance. In addition, we also thank Anthony Frazier at the Vanderbilt-Ingram Cancer Center, Human Tissue Acquisition and Pathology Shared Resource laboratory for the metastatic human-liver tissue sections.

 InterScience © 2005 Wiley-VCH Verlag GmbH & Co. KGaA, Weinheim

the crude profiling of plant tissue for alkaloid content,[15] whereas a computer-controlled moving stage has been used for the direct analysis of dyes and other compounds on chromatography plates.[16] In another example, DESI was combined with an ion-mobility time-of-flight mass spectrometer to probe the conformations of proteins desorbed from an insulating surface.[17]

Herein, DESI-MS is used to investigate the lipid distributions in mouse-pancreas, rat-brain, and metastatic human-liver adenocarcinoma tissue; additional data is presented for whole tissue analysis. These experiments represent the first application of DESI to biological-tissue imaging. The secondary-ion signals in DESI-MS are affected by solvent composition, that is, polarity, pH value, salt concentration, applied voltage, backing pressure in the source, and surface chemistry, as well as other factors.[4,14] These parameters can be adjusted to enhance signals from other compound classes. Direct investigation (without tissue preparation except for microtoming) of biological tissues by using DESI-MS showed very intense peaks because of the phospholipids present. Strong ion signals from phosphatidylcholine (PC) species are consistent with the fact that these species constitute the majority of biological membranes (Figure 1 a). The mass-to-charge (m/z) range 700–900 in Figure 1 a shows the phospholipids detected in untreated mouse-pancreas tissue. The phospholipids appear as potassium adducts as a result of endogenous potassium in the tissue (Figure 1 b). Chemical assignments were confirmed by tandem mass spectrometry (Figure 1 a, inset). Similar studies on rat-brain sections were performed and gave results typified by those shown in Figure 2. As expected,[11] the rat-brain sections produced phospholipid profiles composed mainly of saturated fatty acids, specifically palimitate and stearate.

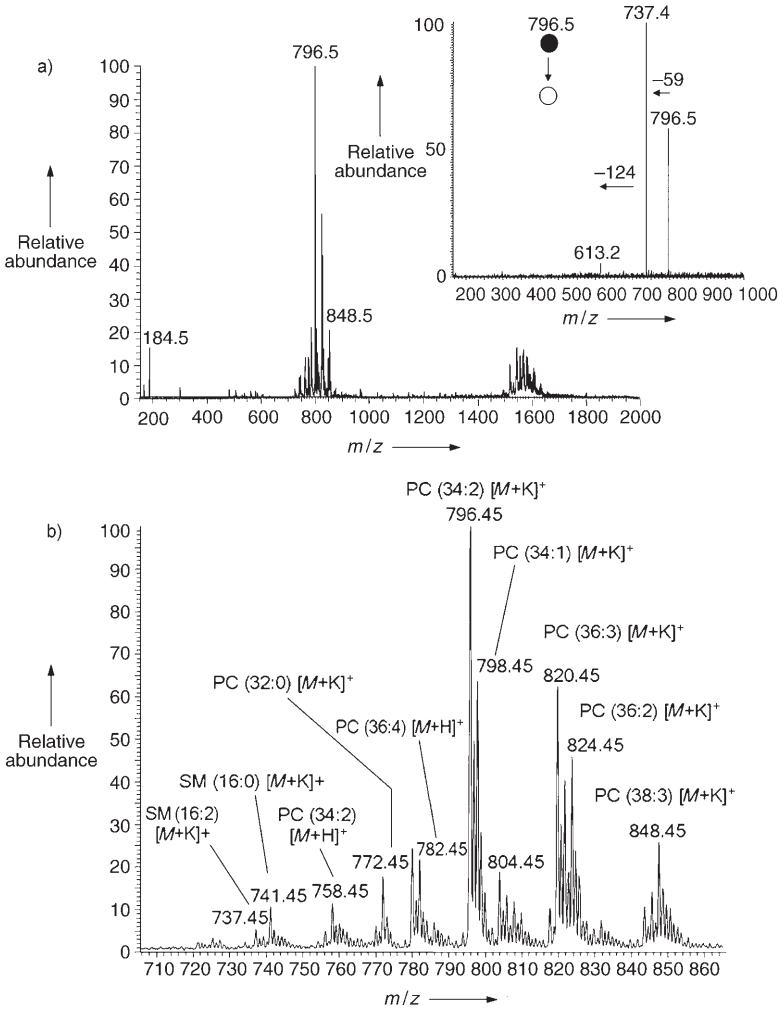

Figure 1. a) Positive-ion DESI mass spectrum recorded on mouse-pancreas tissue with methanol/water (1:1) with 1% acetic acid as the spray solvent at a flow rate of 3 μL min^{-1} and a nebulizing N_2 back pressure of 7 bar. The ions at m/z 184 represent the phosphatidylcholine (PC) head group, thus indicating the presence of free phosphocholine. The ions present at m/z 1550–1650 are phospholipid dimers. The inset shows the MS/MS spectrum of the base peak, and the characteristic neutral losses that were observed make its identification as PC (34:2; $[M+K]^+$) unequivocal. b) An expanded view between m/z 700 and 900 which shows individual phospholipid species and their potassium adducts. The ratio of number of carbon atoms/number of double bonds is given in brackets.

Because considerable information on the disease state of a tissue can be obtained by determination of the distribution of marker compounds, such as phospholipids, investigations of biological tissue utilizing DESI-MS were carried out on metastatic human-liver adenocarcinoma tissue. Lipid distributions in cancerous tissues are known to vary in composition from noncancerous tissue.[18] It has been shown in some cases that elevated levels of phosphatidylcholine species are linked to malignant transformations in cancer cells.[6] In addition, cell-signaling molecules, such as ceramides, derivatives of the sphingomyelin species, are involved in cell-signaling cascades that are directly related to tumor survival. In some cases, extracellular vesicles rich in sphingomyelin have been reported to induce angiogenesis in tumor-proliferating cells.[19] These prior findings emphasize the importance of the determination of the composition of phospholipids in biological tissues and indicate that such information may serve as a prognostic variable in diseased and nondiseased tissues.

Herein, spot sizes are less than 1 mm and the tissue is untreated and examined in the ambient environment. Approximately 50 scans (25 s) were taken on average per spot to obtain high-quality data; however, chemically specific information can be obtained in less than 5 s per spot, including the use of MS/MS.[15] Figure 3 shows a comparison of DESI mass spectra collected from two different regions of metastatic human-liver adenocarcinoma tissue. In the nontumor regions, the lipids are predominantly in the form of palmitic acid containing phospholipids (Figure 3 a). In the transition region from nontumor tissue to cancerous tissue, the lipid distribution is composed of mostly unsaturated fatty acids containing phospholipids (Figure 3 b), whereas the cancerous portions of the tissue showed elevated levels of sphingomyelin (Figure 3 c), which may be associated with a dysfunctional ceramide-mediated apoptosis pathway.[20] In the case of healthy cells, sphingomyelinase can be activated, which results in lower sphingomyelin concentrations.

 © 2005 Wiley-VCH Verlag GmbH & Co. KGaA, Weinheim

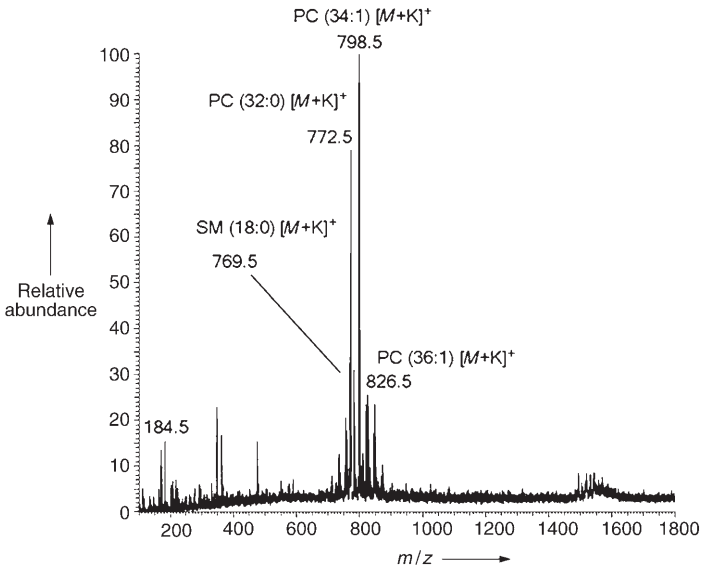

Figure 2. Positive-ion DESI mass spectrum recorded on rat-brain tissue with methanol/water (1:1) with 1% acetic acid as the spray solvent at a flow rate of 3 μL min^{-1} and a nebulizing N_2 gas back pressure of 7 bar. The base peak is identified as the potassium form of phosphatidylcholine (34:1). The ratio of number of carbon atoms/number of double bonds is given in brackets

Intact nonsectioned tissues can also be examined by DESI. Results from the analysis of adipose tissue in situ surrounding a chicken heart are presented in Figure 4. The mass spectrum indicates the presence of free fatty acids on the tissue surface, whereas other spectra collected from a freshly cut surface of chicken heart feature small peptide components, as well as constituents of hemoglobin (heme and Hb (α_a, α_d, and β chains)).

These results serve as the basis for in vivo/in situ applications to tissue under ambient conditions, a topic with implications for basic biochemistry, as well as pathology, food safety, and real-time diagnosis during surgery. In summary, DESI allows: 1) the direct and rapid analysis of intact biological tissues, including whole organs; 2) sensitive and specific molecular detection; 3) adequate secondary-ion yields for chemical confirmation by tandem mass spectrometry; 4) samples to be used that do not need to be confined under high vacuum or subjected to any other preparation procedure; 5) chemical imaging with spot sizes of less than 1 mm.

Experimental Section

All experiments were performed on a Thermo Finnigan LTQ mass spectrometer (San Jose, CA) equipped with a desorption electrospray ion source, (prototype Omni Spray Ion Source, Prosolia Inc., Indianapolis, IN) which is described elsewhere.[4,14] After dissection, the mouse-pancreas, rat-brain, and human-liver tissues were frozen in liquid nitrogen and stored at −80 °C. Prior to analysis, the tissue sections were prepared by cryosectioning with a Leica CM3050 S (Leica Microsystems, Inc., Bannockburn, IL) to a thickness of 16 μm, thaw mounted directly onto a microscope glass slide, and stored under vacuum until analyzed. No further treatment of the tissue samples was necessary. DESI-MS analysis of the tissues was carried out by directing the

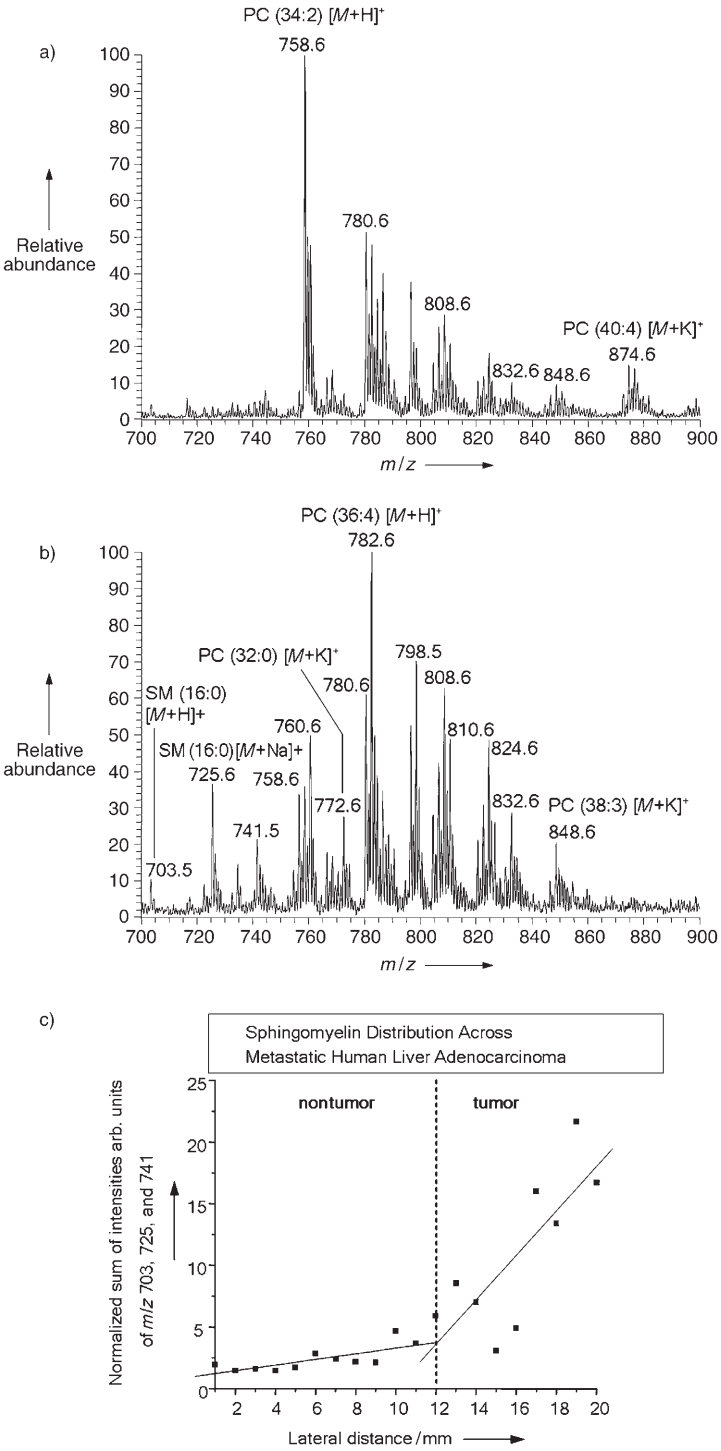

Figure 3. Positive-ion DESI mass spectra recorded on metastatic human-liver adenocarcinoma tissue. The experiment was conducted with methanol/water (1:1, v/v) with 0.1% NH_4OH added. Line scans were performed by moving the sample stage in 1 mm increments across the tissue at 50 scans step^{-1} (25 s step^{-1}). a) DESI mass spectrum representative of the nontumor region of the tissue. b) DESI mass spectrum representative of the cancerous region of the tissue. Enhanced signals from sphingomyelin species at *m/z* 703, 725, and 741 are detected in this region of the tissue. c) Ion-intensity distribution of the sum of the *m/z* values 703, 725, and 741 which correspond to the protonated, sodium, and potassium forms of sphingomyelin (16:0), respectively, versus position in the tissue. The intensities were normalized to the ion intensity at *m/z* 184, which corresponds to phosphocholine. The ratio of number of carbon atoms/number of double bonds is given in parentheses.

 © 2005 Wiley-VCH Verlag GmbH & Co. KGaA, Weinheim

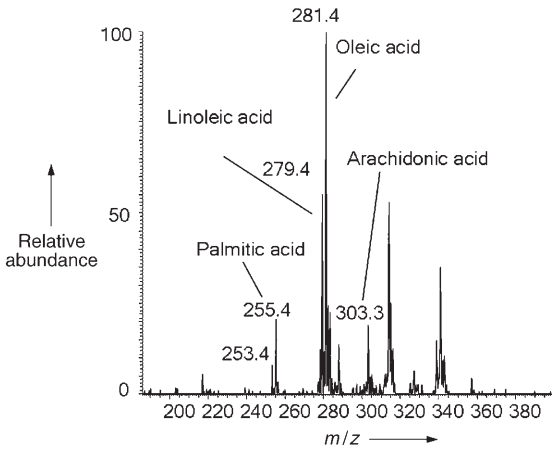

Figure 4. A negative-ion DESI mass spectrum recorded on adipose tissue that surrounds gallus heart with methanol/water (1:1) with 1% acetic acid as the spray solvent at a flow rate of 3 μL min^{-1} and a nebulizing N_2 gas back pressure of 7 bar.

electrospray (5 kV), composed of either methanol/water/acetic acid (50:49:1 v/v) or methanol/water/ammonium hydroxide (50:49.9:0.1 v/v), at an incident angle of approximately 50° toward the tissue. The volumetric flow rate and the back pressure in the source were 3 μL min^{-1} and 7 bar, respectively. Ions generated from the surface were collected using a standard heated capillary interface with an orifice diameter of 500 μm at approximately 10°.

Received: July 6, 2005

Keywords: imaging agents · ionization · mass spectrometry · phospholipids

[1] M. L. Pacholski, N. Winograd, *Chem. Rev.* **1999**, *99*, 2977.
[2] P. J. Todd, T. G. Schaaff, P. Chaurand, R. M. Caprioli, *J. Mass Spectrom.* **2001**, *36*, 355.
[3] C. R. Jimenez, K. W. Li, K. Dreisewerd, S. Spijker, R. Kingston, R. H. Bateman, A. L. Burlingame, A. B. Smit, J. van Minnen, W. P. M. Geraerts, *Biochemistry* **1998**, *37*, 2070.
[4] Z. Takats, J. M. Wiseman, B. Gologan, R. G. Cooks, *Science* **2004**, *306*, 471.
[5] T. J. Montine, M. D. Neely, J. F. Quinn, M. F. Beal, W. R. Markesberry, I. L. J. Roberts, J. D. Morrow, *Free Radical Biology Medicine* **2002**, *33*, 620; M. Athar, *Indian J. Exp. Biol.* **2002**, *40*, 656.
[6] E. O. Aboagye, Z. M. Bhujwalla, *Cancer Res.* **1999**, *59*, 80; K. Glunde, C. Jie, Z. M. Bhujwalla, *Cancer Res.* **2004**, *64*, 4270.
[7] R. C. Murphy, J. Fiedler, J. Hevko, *Chem. Rev.* **2001**, *101*, 479; Y. L. Li, M. L. Gross, F. F. Hsu, *J. Am. Soc. Mass Spectrom.* **2005**, *16*, 679; E. K. Fridriksson, P. A. Shipkova, E. D. Sheets, D. Holowka, B. Baird, F. W. Mclafferty, *Biochemistry* **1999**, *38*, 8056.
[8] M. Rujoi, R. Estrada, M. C. Yappert, *Anal. Chem.* **2004**, *76*, 1657.
[9] R. M. Caprioli, T. B. Farmer, J. Gile, *Anal. Chem.* **1997**, *69*, 4751.
[10] S. G. Ostrowski, C. T. Van Bell, N. Winograd, A. G. Ewing, *Science* **2004**, *305*, 71.
[11] P. Sjovall, J. Lausmaa, B. Johansson, *Anal. Chem.* **2004**, *76*, 4271.
[12] J. B. Fenn, M. Mann, C. K. Meng, S. F. Wong, C. M. Whitehouse, *Science* **1989**, *246*, 64; J. B. Fenn, M. Mann, C. K. Meng, S. F. Wong, C. M. Whitehouse, *Mass Spectrom. Rev.* **1990**, *9*, 37.
[13] J. Wei, J. M. Buriak, G. Siuzdak, *Nature* **1999**, *399*, 243; A. Benninghoven, F. G. Rudenauer, H. W. Werner, *Secondary Ion Mass Spectrometry: Basic Concepts, Instrumental Aspects, Applications and Trends*, Wiley, New York, **1987**; M. Karas, U. Bahr, A. Ingendoh, F. Hillenkamp, *Angew. Chem.* **1989**, *101*, 805; *Angew. Chem. Int. Ed. Engl.* **1989**, *28*, 760; M. Karas, F. Hillenkamp, *Anal. Chem.* **1988**, *60*, 2299.
[14] Z. Takats, J. M. Wiseman, R. G. Cooks, *J. Mass Spectr.* **2005**, in press.
[15] N. Talaty, Z. Takats, R. G. Cooks, *Analyst* **2005**, in press.
[16] G. J. Van Berkel, M. J. Ford, M. A. Deibel, *Anal. Chem.* **2005**, *77*, 1207.
[17] S. Myung, J. M. Wiseman, S. J. Valentine, Z. Takats, R. G. Cooks, D. E. Clemmer, unpublished results.
[18] L. D. Bergelson, *Prog. Chem. Fats Other Lipids* **1972**, *13*, 1.
[19] C. W. Kim, H. M. Lee, T. H. Lee, C. H. Kang, H. K. Kleinman, Y. S. Gho, *Cancer Res.* **2002**, *62*, 6312.
[20] L. M. Obeid, C. M. Linardic, L. A. Karolak, Y. A. Hannun, *Science* **1993**, *259*, 1769; R. N. Kolesnick, M. Kronke, *Annu. Rev. Physiol.* **1998**, *60*, 643.

 © 2005 Wiley-VCH Verlag GmbH & Co. KGaA, Weinheim

Superoxidation

DOI: 10.1002/anie.200501346

Superoxidation of Bisretinoids**

Ilyas Washington, Steffen Jockusch, Yasuhiro Itagaki, Nicholas J. Turro, and Koji Nakanishi**

In addition to their role in vision, retinoids, for example, **1a–k** and their derivatives, have been found to affect fetal development, cell differentiation, metabolism, and organ and cell regulation.[1] They also provide lead structures for various anticancer, anti-inflammatory, and antibacterial drugs. In plants and food, they act as hormones, pigments, flavors, aromas, and as defense substances.[1]

The polyenes **1a–k** react readily with singlet oxygen.[2,3] Reactions with oxygen can be initiated by light, in the presence or absence of a photosensitizer, or by autoxidation.[3] The oxidized products often show biological activity and are responsible for various aromas and tastes of food.[2,3] Identification of the oxygenated products is complicated by the fact that the initial species are reactive dioxetanes, peroxides,

[*] Dr. I. Washington, Dr. S. Jockusch, Dr. Y. Itagaki, Prof. N. J. Turro, Prof. K. Nakanishi
Department of Chemistry
Columbia University
New York, NY 10027 (USA)
Fax: (+1) 212-932-1289
E-mail: njt3@columbia.edu
kn5@columbia.edu

[**] We thank the National Institutes of Health (GM 036564 to K.N.) and the National Science Foundation (CHE 04—10655, N.J.T.) for financial support.

© 2005 Wiley-VCH Verlag GmbH & Co. KGaA, Weinheim

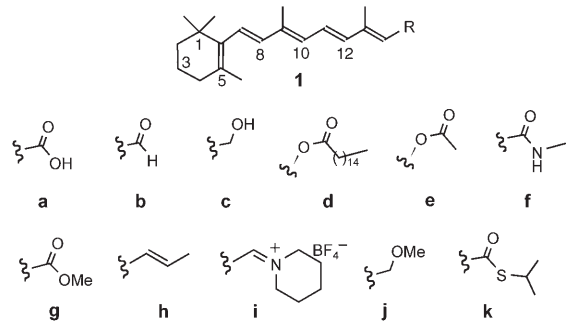

epoxides, and endoperoxides that can undergo secondary reactions and rearrangements upon chromatographic separation and identification.[2,3] Furthermore, various *cis*/*trans*, stereo-, and regioisomers are often obtained.

To date, nine different products have been reported for the reaction of retinoic acid (**1a**) with singlet oxygen (Scheme 1).[3f,g] These products include epoxide **2**, furan **3**

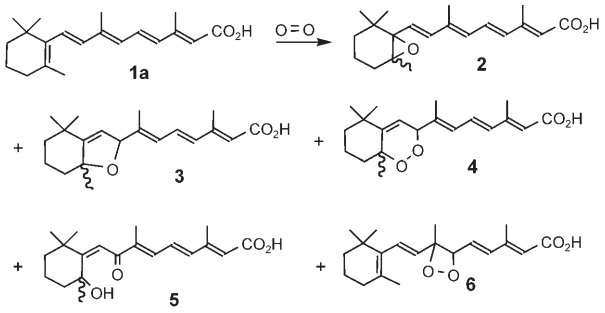

Scheme 1. The reaction of retinoic acid (**1a**) with singlet oxygen.

(through rearrangement of **2**), endoperoxide **4**, hydroxyketone **5**, dioxetane **6**, and four degradation products (products with molecular weights lower than that of the parent retinoic acid). Similar oxidation products have also been reported for the oxidation of retinal (**1b**),[3d,e] retinol (**1c**),[3a,c] and retinol palmitate (**1d**).[3a] In most cases, the oxidation is reported to stop upon the addition of two oxygen atoms, with either the major or sole initial product proposed to be 5,8-endoperoxide (similar to **4**).[3] In contrast, A2E (**7**), a bisretinoid isolated from human lipofuscin, reacts with singlet oxygen to form the polyepoxide species **8** (Scheme 2).[4a] This is in contrast to retinoids **1a**–**d**, which add two oxygen atoms. In the case of **7**,

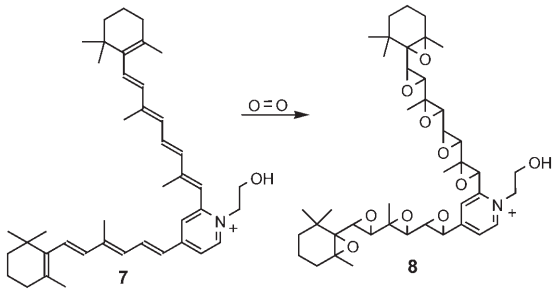

Scheme 2. The reaction of A2E (**7**) with singlet oxygen to form the polyepoxide species **8**.

a maximum of nine oxygen atoms can add to the polyene chain. The epoxides of **7** have been shown to be biologically active and are speculated to be involved in age-related macular degeneration.[4b] Polyepoxide **8** was not isolated, and its structure was proposed based on mass-spectrometric measurements.[4a]

To explain the difference between the reactivity of **7** and that of retinoids **1a**–**d** towards singlet oxygen and to explore the reactivity of singlet oxygen towards polyenes, several bisretinoids **10**–**12** (Schemes 5–7) as well as several monoretinoids **1a**–**c** and **1e**–**k** (Scheme 1) were treated with singlet oxygen. Through MS analysis of the reactant mixtures, it was concluded that the polyene chains, when held in proximity to one another, react readily with oxygen to give superoxygenated species. On the other hand, the oxidation of spatially isolated polyenes stops upon the addition of two oxygen atoms.

The photoreactions were carried out for 1–3 h at 25 °C in CH_2Cl_2 in the presence of tetraphenylporphyrin (TPP) as a photosensitizer. The irradiation was effected by a 300-W halogen lamp that was equipped with a 400-nm cut-off filter. The exposure of solutions of the reagents in acetone (in a borosilicate glass vile with a UV cut-off of 340 nm) to sunlight for 3–6 h in the absence of added sensitizer gave similar results. All samples were analyzed directly by MS without any further manipulation. Figure 1 shows the fast-atom-bombard-

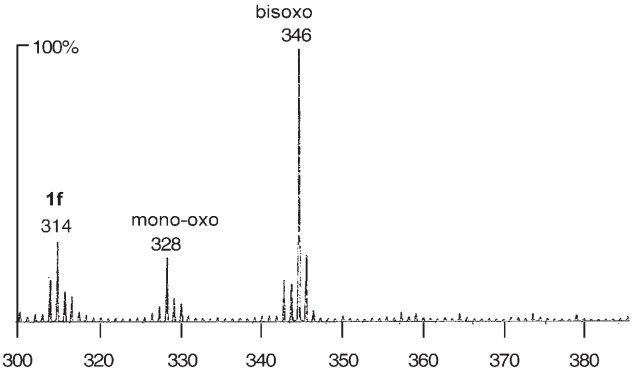

Figure 1. FAB MS of the products of **1f**, 3 h after irradiation (300 W) at 25 °C in CH_2Cl_2 in the presence of tetraphenylporphyrin as a photosensitizer. The maximum increase by m/z 32 (two oxygen atoms)

ment (FYB) mass spectrum of the products of the amide **1f** after 3 h of irradiation (Scheme 3). The peak at m/z 314 corresponds to **1f** $[M+1]$. The spectrum has a strong signal at m/z 346, which corresponds to the mass of **1f** plus two oxygen atoms $[M+1]$. The smaller peak at m/z 328 represents the mono-oxygen adduct of **1f** $[M-1]$. No peaks were found above m/z 346 which suggests that oxidation of **1f** stops cleanly after the addition of two oxygen atoms.

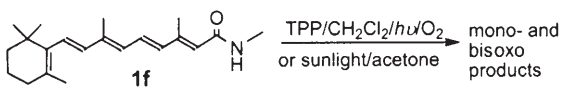

Scheme 3. The irradiation of amide **1f**. Oxidation was shown to cease after the addition of two oxygen atoms.

 © 2005 Wiley-VCH Verlag GmbH & Co. KGaA, Weinheim

Similarly, retinoids **1a–c** and **1e–k** were prepared, irradiated, and the reactant mixture analyzed by MS. All the measured spectra were similar to that shown in Figure 1, with a maximum peak at +32 Da, which corresponds to the parent ion of the retinoid plus two oxygen atoms, and a smaller peak at +16 Da, which corresponds to the addition of one oxygen atom to the parent ion. The peaks located at 16 and 32 Da are consistent with literature reports for the formation of the 5,6-epoxide and the 5,8-endoperoxide, respectively, which are two well-characterized photo-oxidation products of retinoic acid (**1a**), retinal (**1b**), retinol (**1c**), and retinol palmitate (**1d**).[3]

Beta-carotene (**9**) was also examined (Scheme 4). The mass spectrum showed a maximum mass that corresponds to

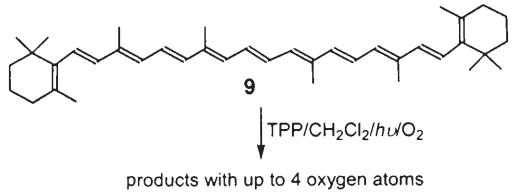

Scheme 4. The irradiation of beta-carotene (**9**), which results in the addition of up to four oxygen atoms.

an increase of 64 Da, which is double that observed for the compounds **1a–c** and **1e–k**. Furthermore, peaks that correspond to the addition of one, two, and three oxygen atoms were also observed. The mass spectrum is consistent with the previously characterized products of singlet-oxygen-mediated oxidation products of beta-carotene, which are mixtures of bis and mono 5,6-epoxides and 5,8-endoperoxides.[3h]

Figure 2 shows the electrospray ionization mass spectrum obtained after 1 h of irradiation of a solution of bisretinoid *ortho*-**10** (Scheme 5). The peak at *m*/*z* 672 corresponds to the

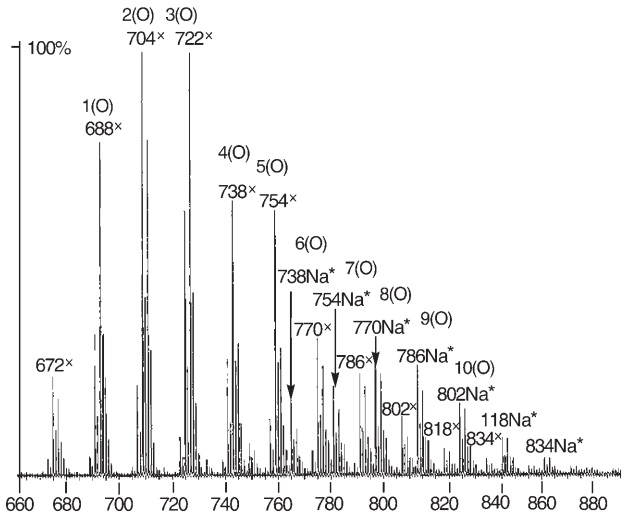

Figure 2. ESI MS of the reaction mixture of *ortho*-**10** after irradiation (300 W) for 1 h at 25 °C in CH_2Cl_2 in the presence of tetraphenylporphyrin as a photosensitizer. Labels show the consecutive increase by 16 Da and the corresponding sodium adducts, × represents the addition of an oxygen atom, * are sodium adducts (+23 Da).

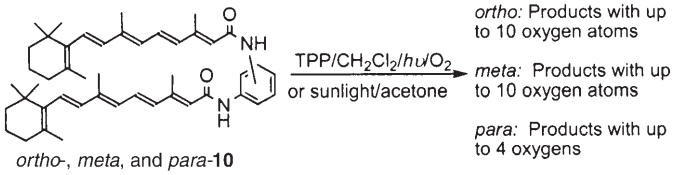

Scheme 5. The irradiation of a solution of bisretinoid *ortho*-, *meta*-, and *para*-**10**, which results in the addition of ten, ten, and four oxygen atoms, respectively.

parent mass of *ortho*-**10**. Subsequent peaks (labeled with an ×) were found at increments of 16 Da, which corresponds to the addition of one oxygen atom. The peaks labeled with an * are sodium adducts (+23 Da). The spectrum shows the maximum *m*/*z* at 834 or 856 (834+Na) which corresponds to the addition of ten oxygen atoms. The spectrum is similar to that observed after the irradiation of **7,** which was reported to yield the polyepoxide species **8**. Superoxidation was also observed by MS for the isomer *meta*-**10**. When the isomer *para*-**10** was irradiated, the mass spectrum showed a maximum peak that corresponds to the addition of only four oxygens, and was similar to that observed for beta-carotene (**9**).

For the *trans*-substituted cyclohexane derivative **11**, there is no conjugation between the two polyene chains. However, superoxidation is still observed by MS (Scheme 6). When the

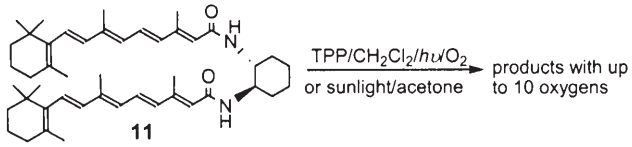

Scheme 6. Irradiation of the *trans*-substituted cyclohexane derivative **11**, despite the absence of conjugation between the two polyene chains, resulted in superoxidation.

two polyene chains are held together by a flexible linker as in **12**, oxidation was found mostly to stop upon the addition of one to four oxygen atoms (Figure 3 and Scheme 7). After the complete conversion of **12** (*m*/*z* 652) as shown by MS, only small peaks located at *m*/*z* 733 and 749, which correspond to

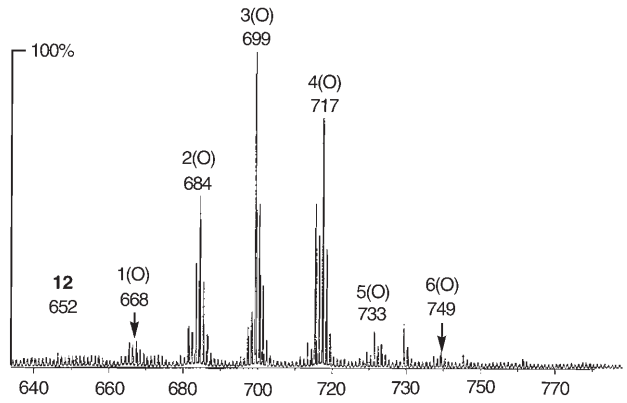

Figure 3. FAB MS of the reaction mixture of **12** after irradiation (300 W) for 3.5 h at 25 °C in CH_2Cl_2, in the presence of tetraphenylporphyrin as a photosensitizer.

© 2005 Wiley-VCH Verlag GmbH & Co. KGaA, Weinheim

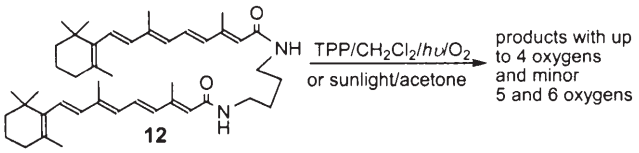

Scheme 7. The irradiation of **12**, in which the two polyene chains are held together by a flexible linker. No further oxidation occurred after the addition of one to four oxygen atoms.

the addition of five and six oxygen atoms, respectively, were found.

The λ_{max} of **11** in ethanol is blue shifted by 5 nm relative to the similar retinoids **12** and **1f**. Retinoid **11** has a fluorescence quantum yield in ethanol of 0.08 at 25 °C relative to 9,10-diphenylanthracene ($\Phi_F = 0.95$).[5] The fluorescence quantum yield of **12** and **1f** were measured to be 0.07 and 0.05, respectively. This is in accord with the reported fluorescence quantum yields for retinal, retinol, and retinal acetate, which are between 0.03 and 0.01 at 25 °C.[6] Retinoids do not stack in apolar or polar solutions.[7] A slight increase in fluorescence is expected for **11**, as the proximity of the polyene chains restricts their movement, thus a greater amount of excited energy is emitted rather then dissipated by isomerization or vibrational motion. The blue shift in the absorption spectrum and the greater fluorescence of **11** relative to **12** and **1f** suggest that the polyene chains in **11** are stacked. Similar observations have been reported for retinoids.[7]

The rate constants for the quenching of singlet oxygen by **11** and **1f** were determined through pseudo-first-order treatment of the singlet oxygen phosphorescence decays by using TPP as a sensitizer and a pulsed Nd–YAG laser (532 nm) to generate singlet oxygen.[8] Rate constants of $(2.0 \pm 0.1) \times 10^6\,M^{-1}s^{-1}$ and $(1.9 \pm 0.1) \times 10^6\,M^{-1}s^{-1}$ were determined for the quenching of singlet oxygen by **11** and **1f**, respectively. The determined values are in accord with the reported rate constants for the quenching of singlet oxygen by *trans*-retinal ($3.6 \times 10^6\,M^{-1}s^{-1}$) and retinol acetate ($7 \times 10^5\,M^{-1}s^{-1}$).[9] As the number of double bonds in bisretinoid **11** is doubled, an increased rate constant for quenching would have been expected. The observed value suggests that some of the double bonds are less accessible to singlet oxygen in the bisretinoid **11** when both retinal arms are in proximity.

The similarity between the rate constants of the quenching of singlet oxygen by **1f** and **11** and the fact that different products are obtained from the reactions of monoretinoids and bisretinoids with oxygen suggest that they are oxidized by two species: singlet oxygen and oxygen radicals or oxygen radical anions. The endoperoxide products, typically observed after light-mediated oxidation of retinoids, are the products of the [2+4] addition of singlet oxygen. The higher energy oxygen radicals or oxygen radical anions are expected to give a more complex mixture of products,[10] as seen for the oxidation of the bisretinoids. Upon irradiation, retinoids **1a–c** have been shown to produce both singlet oxygen and radical species.[11] It has also been reported that singlet oxygen plays a minor role in the oxidation of **7**.[12] Singlet oxygen chemistry often competes with or produces oxygen radicals or oxygen radical anions. In the case of the bisretinoids, the latter species may be formed to a greater extent and play a larger role in oxidation.

These data suggest that when two polyenes chains are able to communicate through space they react with oxygen upon exposure to light to give superoxidized species. Oxidation is limited, however, in the absence of such communication. The enhanced oxidative damage of bispolyenes versus monopolyenes may have implications with regard to the mechanisms of action of naturally occurring bispolyene compounds.[13]

Received: April 18, 2005
Revised: August 1, 2005
Published online: October 12, 2005

Keywords: alkenes · bisretinoids · carotenoids · photochemistry · singlet oxygen

[1] For a review on retinoids, see: "Vitamin A (retinoids)": J. L. Napoli in *Encyclopedia of Biological Chemistry, Vol. 4* (Eds.: W. J. Lennarz, M. D. Lane), Elsevier, Oxford, **2004**, pp. 354–359.
[2] For a review on the photochemistry of retinoids, see: P. P. Fu, S. H. Cheng, L. Coop, Q. Xia, S. J. Culp, W. H. Tolleson, W. G. Wamer, P. C. Howard, *J. Environ. Sci. Health Part C* **2003**, *21*, 165–196.
[3] a) G. Crank; M. S. Pardijanto, J. *Photochem. Photobiol. A* **1995**, *8*, 93–100; b) K. Suyama, T. Yeow, S. Nakai, *J. Agric. Food Chem.* **1983**, *31*, 22–26; c) M. Mousseron-Canet, *Methods Enzymol.* **1971**, *18*, 591–615; d) K. Tsujimoto, H. Hozoji, M. Ohashi, M. Watanabe, H. Hattori, *Chem. Lett.* **1984**, 1673–1676; e) M. H. Baron, M. J. Coulange, C. Coupry, D. Baron, J. Favrot, M. M. Abo-Aly, *Photochem. Photobiol.* **1989**, *49*, 736–751; f) K. B. Clark, J. A. Howard, A. J. Oyler, *J. Am. Chem. Soc.* **1997**, *119*, 9560–9561; g) A. J. Oyler, M. G. Motto, R. E. Naldi, K. L. Facchine, P. F. Hamburg, D. J. Burinsky, R, Dunphy, M. L. Cotter, *Tetrahedron* **1989**, *45*, 7679–7694; h) G. W. Burton, L. Huges, K. U. Ingold, D. A. Lindsy, D. J. Moffatt, *Tetrahedron* **1993**, *49*, 911–928.
[4] a) S. Ben-Shabat, Y. Itagaki, S. Jockusch, J. R. Sparrow, N. J. Turro, K. Nakanishi, *Angew. Chem.* **2002**, *114*, 842–845; *Angew. Chem. Int. Ed.* **2002**, *41*, 814–817; b) J. R. Sparrow, H. R. Vollmer-Snarr, J. Zhou, B. Cai, S. Jockusch, Y. Itagaki, K. Nakanishi, *J. Biol. Chem.* **2003**, *278*, 18207–18213.
[5] J. V. Morris, M. A. Mahaney, J. R. Huber, *J. Phys. Chem.* **1976**, *80*, 969–974.
[6] a) A. T. C. Tsin, P. A. Fernandez, J. M. Gallas, J. P. Chambers, *Life Sci.* **1988**, *43* 1379–1384; b) A. J. Thomson, *J. Chem. Phys.* **1969**, *51*, 4106–4116.
[7] a) K. Chihara, W. H. Waddell, *J. Am. Chem. Soc.* **1980**, *102*, 2963–2968; b) T. Takemura, K. Chihara, R. S. Becker, P. K. Das, G. L. Hug, *J. Am. Chem. Soc.* **1980**, *102*, 2604–2609.
[8] G. E. Khalil, A. Chang, M. Gouterman, J. B. Callis, L. R. Dalton, N. J. Turro, S. Jockusch, *Rev. Sci. Instrum.* 2005, 76, 054101/1–054101/8.
[9] A. A. Krasnovsky, V. E. Kagan, *FEBS Lett.* **1979**, *108*, 152–154.
[10] a) R. C. Kanner, C. S. Foote, *J. Am. Chem. Soc.* **1992**, *114*, 682–688; b) X. G. Fu, L. P. Zhang, L. Z. Wu, C. H. Tung, *J. Photosci.* **2003**, *10*, 175–180.
[11] J. Dillon, E. R. Gaillard, P. Bilski, C. F. Chignell, K. J. Reszka, *Photochem. Photobiol.* **1996**, *63*, 680–685.
[12] E. R. Gaillard, L. B. Avalle, L. M. M. Keller, Z. Wang, K. J. Reszka, J. P. Dillon, *Exp. Eye Res.* **2004**, *79*, 313–319.
[13] For a review on polyene natural products, see: C. Thirsk, A. Whiting, *J. Chem. Soc. Perkin Trans. 1* **2002**, 999–1023.

 © 2005 Wiley-VCH Verlag GmbH & Co. KGaA, Weinheim

Nitrogen Fixation

DOI: 10.1002/anie.200501371

How Many Methyl Groups in $[\{(\eta^5\text{-}C_5Me_nH_{5-n})_2Zr\}_2(\mu_2,\eta^2,\eta^2\text{-}N_2)]$ Are Needed for Dinitrogen Hydrogenation? A Theoretical Study**

Petia Bobadova-Parvanova, Qinfang Wang, Keiji Morokuma, and Djamaladdin G. Musaev**

Nitrogen fixation under mild conditions is one of the most fascinating processes of modern chemical and biochemical sciences.[1] The major fraction of all nitrogen required in human nutrition derives from biological nitrogen fixation,[1c] which uses the nitrogenase enzyme and proceeds by a protonation-and-reduction mechanism of a coordinated N_2 molecule. In industry, almost all dinitrogen fixation comes from the Haber–Bosch process, which transforms dinitrogen to ammonia through hydrogenation. In contrast to biological fixation, the Haber–Bosch process requires extreme temperatures ranging from 400 to 650 °C and pressures ranging from 200 to 400 atm. Therefore, for more than a century scientists have searched for an alternative and economically more effective hydrogen-fixation process.

It was demonstrated previously that the side-on, η^2 coordination of N_2 in transition-metal systems is required for its hydrogenation.[2] This coordination ensures significant back-donation from d orbitals of the transition metal to the π^* orbital of the N–N bond. The stronger the back-donation, the more activated the N–N bond would be. The back-donation from the metal center, M, to N_2 is considerably smaller for end-on, η^1 coordination of N_2.

The side-on coordination of N_2 to the transition-metal center could occur in multinuclear transition-metal complexes and clusters. Although it was predicted theoretically a few years ago that N_2 in binuclear zirconium–N_2 complexes could be hydrogenated and add several dihydrogen molecules,[3] it was only last year that Chirik and co-workers showed experimentally that the side-on-coordinated dinitrogen molecule in $[\{(\eta^5\text{-}C_5Me_4H)_2Zr\}_2(\mu_2,\eta^2,\eta^2\text{-}N_2)]$ (**1**) is hydrogenated under mild conditions and even produces small amount of ammonia.[4] This reaction is still not catalytic, but its importance to the field is indisputable. It is intriguing that

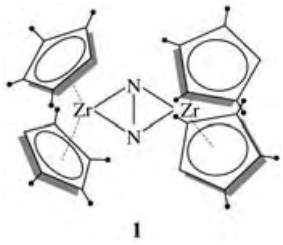

1

the same complex with a slightly different ligand, $C_5Me_5^-$ instead of $C_5Me_4H^-$, coordinates an N_2 molecule with an end-on, η^1 mode (**2**, Figure 1); the addition of H_2 follows a different path and dinitrogen is not hydrogenated.[5] Thus, replacing only one methyl group on each cyclopentadienyl ligand with a hydrogen atom significantly alters the reactivity of the complex.[6] What causes this remarkable difference?

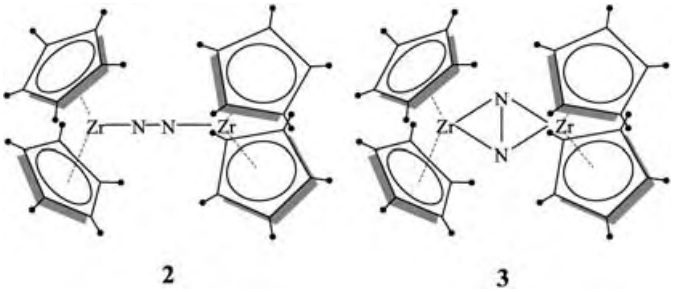

2 **3**

Figure 1. Structures of the coordination isomers $[\{(\eta^5\text{-}C_5Me_5)_2Zr\}_2(\mu_2,\eta^2,\eta^2\text{-}N_2)]$ (**2**) and $[\{(\eta^5\text{-}C_5Me_5)_2Zr\}_2(\mu_2,\eta^1,\eta^1\text{-}N_2)]$ (**3**).

To elucidate the factors controlling the N_2 coordination and to rationalize the role of the methyl substitution, we studied computationally side-on and end-on coordination of an N_2 molecule in mono- and binuclear complexes, $[(Cp')_2Zr(N_2)]$ and $[(Cp')_2Zr(N_2)Zr(Cp')_2]$, in which $Cp' = C_5H_{5-n}Me_n$, $n = 0$–5. All calculations were performed in the gas phase by using the Gaussian 03 program[7] at the B3LYP/CEP-31G level with additional d-type polarization functions on the N atom (CEP-31G(d)). Previously, this approach was shown to accurately describe the energetics and geometries of similar complexes.[3] All structures were optimized until no imaginary frequencies were found.

At first, we examined the role of the methyl groups on the coordination mode of N_2 by studying the side-on- and the end-on-coordinated mononuclear complexes $[(Cp')_2Zr(N_2)]$. The relative energies of the optimized structures (including zero-point-energy (ZPE) corrections) are shown with open squares in Figure 2. The optimized Cartesian coordinates of these and all other examined structures are given in the Supporting Information. For all values of n, the complexes with side-on coordination are more stable than those with end-on coordination. The energy difference slightly increases with the number of methyl groups, n. Thus, the presence of methyl substituents on the Cp′ ring favors side-on coordination. This effect is caused by electron donation from the methyl groups as can be seen from the data shown in Table 1. For side-on-coordinated complexes, an increase in the number of methyl

[*] Dr. P. Bobadova-Parvanova, Q. Wang, Prof. Dr. K. Morokuma, Dr. D. G. Musaev
Cherry L. Emerson Center for Scientific Computation and Department of Chemistry
Emory University, Atlanta, GA 30322 (USA)
Fax: (+1) 404-727-7412
E-mail: dmusaev@emory.edu
morokuma@emory.edu

[**] This work was supported in part by a grant (CHE-0209660) from the US National Science Foundation. We thank also the Cherry L. Emerson Center of Emory University for the use of its resources.

Supporting information for this article is available on the WWW under http://www.angewandte.org or from the author.

 © 2005 Wiley-VCH Verlag GmbH & Co. KGaA, Weinheim

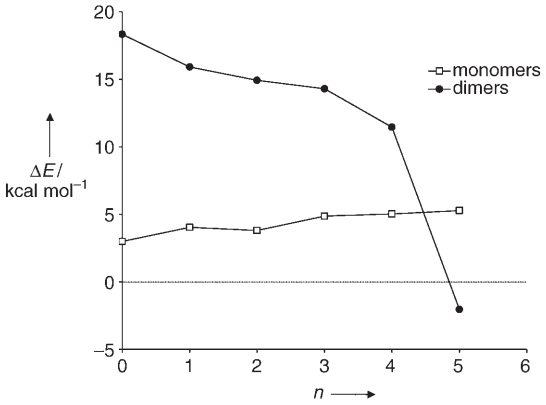

Figure 2. Energy difference, $\Delta E = (E_{\text{end-on}} + \text{ZPE}_{\text{end-on}}) - (E_{\text{side-on}} + \text{ZPE}_{\text{side-on}})$, between the end-on- and the side-on-coordinated complexes $[(Cp')_2Zr(N_2)]$ and $[(Cp')_2Zr(N_2)Zr(Cp')_2]$ as a function of the number of methyl groups, *n*.

Table 1: Nitrogen NPA[a] atomic charges (Q_N [e])[10] and N–N bond lengths (r_{NN} [Å]) of the complexes $[(Cp')_2Zr(N_2)]$ and $[(Cp')_2Zr(N_2)Zr(Cp')_2]$.

	Side-on		End-on		
n	Q_N	r_{NN}	$Q_N^{(near)}$	$Q_N^{(remote)}$	r_{NN}
			Mononuclear		
0	−0.28	1.20	−0.22	−0.03	1.16
1	−0.29	1.20	−0.22	−0.04	1.16
2	−0.31	1.21	−0.23	−0.05	1.16
3	−0.33	1.21	−0.25	−0.05	1.16
4	−0.35	1.21	−0.27	−0.07	1.16
5	−0.38	1.21	−0.29	−0.10	1.16
			Binuclear		
0	−0.72	1.42	−0.53		1.25
1	−0.74	1.41	−0.54		1.25
2	−0.78	1.41	−0.52		1.24
3	−0.82	1.42	−0.60		1.25
4	−0.82	1.40	−0.66		1.26
5	−0.84	1.41	−0.69		1.26

[a] Natural population analysis.

groups leads to an increase in negative charge on the two N atoms ($n = 0$: −0.28 e; $n = 5$: −0.38 e). In the case of end-on complexes, the trend is still valid, but the charges are much smaller in absolute terms and the negative charge on the remote N atom is negligible (see Table 1). The stronger back-donation makes the N–N bond in side-on complexes longer (1.20–1.21 Å) than in end-on complexes (1.16 Å). The electrostatic repulsion between the two negative charges also leads to a longer N–N bond in side-on-coordinated complexes. The above results suggest that the steric repulsion caused by the methyl substituents is small as they are far away from the coordinated dinitrogen ligand.

Our study of mononuclear complexes suggests that an increased number of methyl groups would favor the side-on coordination, but what happens with the binuclear complexes? We examined the full set of side-on- and end-on-coordinated binuclear complexes, $n = 0$–5. Their relative energies (ZPE corrected) are shown with closed circles in Figure 2. For $n \leq 4$ the side-on coordination is more stable than the respective end-on coordination. However, the energy difference between the two coordination modes decreases as *n* increases. Finally, for $n = 5$, the end-on-coordinated complex **2** is more stable than the side-on-coordinated complex **3** (see Figure 1); the energy difference is small, only 2.04 kcal mol^{-1}, but the trend is clear. With C_5Me_5 as the ligand, the side-on coordination is less stable than the end-on coordination. Therefore, the more stable end-on structure which cannot lead to N_2 hydrogenation is the dominant species. This is consistent with the experimental results.[5]

The results for mononuclear complexes show that the electronic effect favors side-on coordination when more methyl groups are on the Cp' ring. For binuclear complexes, the electronic effect has a similar influence (Table 1). Increasing the number of methyl groups increases the negative charge on the N atoms from −0.72 e to −0.84 e for side-on complexes, and from −0.53 e to −0.69 e for end-on complexes. However, our calculations show that for binuclear complexes the energy trend is opposite to that of the mononuclear complexes: the more methyl groups there are the less stable the side-on coordination is. What causes this opposite trend is not the electronic effect but the increasing steric repulsion with an increasing number of methyl groups. For $n = 0$ the steric repulsion is minimal and ΔE has the largest value (Figure 2). The more methyl groups we add, the stronger the steric repulsion becomes and ΔE decreases. The case of $n = 4$ represents a boundary line for which the steric repulsion is yet not strong enough and the side-on coordination is more stable than the end-on coordination. At $n = 5$, however, the steric repulsion is so strong that ΔE drops substantially (by more than 15 kcal mol^{-1}); the end-on complex is more stable and N_2 cannot be hydrogenated. This is the reason for the experimental observation that the pentamethyl complex does not activate N_2 towards hydrogenation. In principle, in all other cases N_2 can be activated. Our calculations suggest that any complex with 0–4 methyl groups may lead to N_2 hydrogenation under appropriate experimental conditions.

Our conclusion is in agreement with the experimental study of Pool et al. on the reaction of the complex $[\{(\eta^5\text{-}C_5Me_5)(\eta^5\text{-}C_5Me_4H)Zr(\eta^1\text{-}N_2)\}_2(\mu_2,\eta^1,\eta^1\text{-}N_2)]$ with dihydrogen,[8] which resulted in the liberation of dinitrogen rather than its hydrogenation. As concluded by the authors, one of the reasons for this reactivity is the steric protection provided by the ancillary ligand framework in their complex that prevents the the side-on coordination of the N_2 ligand, which is essential for dinitrogen hydrogenation.

Computational studies by Pool et al. on the electronic structure of **1** demonstrated that twisting of θ (the dihedral angle between the metallocene wedges) is essential—it prepares the side-on-coordinated N_2 molecule for hydrogenation.[8] They showed that twisting of **1** ($\theta \approx 60°$) changes the symmetry of the highest occupied molecular orbital (HOMO) and allows π bonding between Zr and N_2, thus reducing the strength of the N–N bond and activating it. The authors also examined a hypothetical untwisted ($\theta \approx 0°$) structure of $[\{(\eta^5\text{-}C_5H_5)_2Zr\}_2(\mu_2,\eta^2,\eta^2\text{-}N_2)]$ (**4**; Figure 3). In this case, the HOMO does not have the appropriate symmetry

 © 2005 Wiley-VCH Verlag GmbH & Co. KGaA, Weinheim

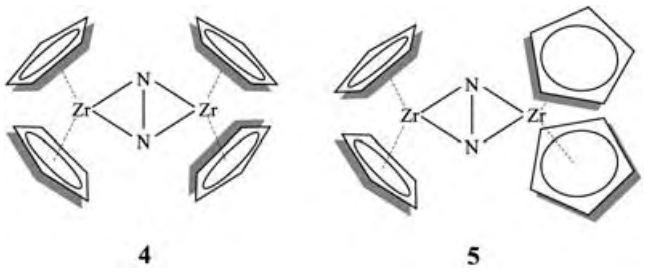

Figure 3. Untwisted (**4**) and twisted (**5**) structure of $[\{(\eta^5\text{-}C_5H_5)_2Zr\}_2(\mu_2,\eta^2,\eta^2\text{-}N_2)]$. The twisted structure ($\theta = 49°$) is more stable than the untwisted structure ($\theta = 2°$) by 6.19 kcal mol^{-1}.

to allow significant back-bonding with the N_2 ligand and the complex is not active toward hydrogenation.

We have further elaborated the role of the angle θ and found that all the optimal structures of $[\{(\eta^5\text{-}C_5Me_nH_{5-n})_2Zr\}_2(\mu_2,\eta^2,\eta^2\text{-}N_2)]$ for $n = 0$–4 (including $n = 0$) are twisted and have dihedral angle of 49°, 54°, 60°, 61°, and 63°, respectively. As a result, the HOMO orbitals of all complexes have the appropriate symmetry for significant π bonding between Zr and the N_2 ligand. Thus, we predict that all complexes with $n = 0$–4 can be used for N_2 hydrogenation.

We found that the untwisted structure **4** ($\theta = 2°$) is 6.19 kcal mol^{-1} higher in energy than the twisted conformer **5** ($\theta = 49°$, Figure 3). In addition, we scanned the potential-energy surface by fixing the twisting angle, θ, and by optimizing all other geometrical parameters. The results are shown in Figure 4. The open rhombuses correspond to

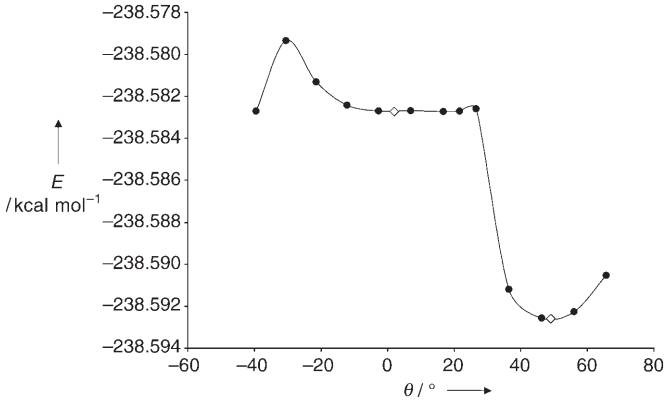

Figure 4. Total energy (E) of $[\{(\eta^5\text{-}C_5H_5)_2Zr\}_2(\mu_2,\eta^2,\eta^2\text{-}N_2)]$ as a function of the twisting angle, θ. The white rhombuses correspond to structures **4** ($\theta = 2°$) and **5** ($\theta = 49°$), respectively.

structures **4** and **5**. The potential-energy surface is very flat around $\theta = 2°$; the untwisted structure represents a flat and very shallow local minimum. There is almost no barrier (around 0.06 kcal mol^{-1}) between structures **4** and **5**. Even if structure **4** is formed it will transform into the active structure **5**.

To further prove that **5** could serve as a N_2 fixation catalyst, we examined the addition of H_2. The details of the study will be given elsewhere.[9] We found that there is no principal difference when $C_5Me_4H^-$ or $C_5H_5^-$ is used as the ligand. As previously shown,[4] the rate-determining step of such reactions is the H–H bond activation, which occurs with a barrier of 17.9 kcal mol^{-1} in the case of $C_5Me_4H^-$ and with a barrier of 18.8 kcal mol^{-1} in the case of $C_5H_5^-$. These similar barriers suggest that there is no principal difference between the two complexes, at least in the first phase of the reaction. Our theoretical study predicts that the presence of $C_5H_5^-$ gives an active twisted structure, which could be used for N_2 cleavage and hydrogenation. We encourage experimentalists to follow up our suggestion.

In summary, we examined the mono- and binuclear complexes $[(Cp')_2Zr(N_2)]$ and $[(Cp')_2Zr(N_2)Zr(Cp')_2]$ ($Cp' = C_5H_{5-n}Me_n$, $n = 0$–5). We found that the case $n = 4$ represents a boundary in the ability to activate N_2 for hydrogenation. When $n \leq 4$, the complex is active and leads to N_2 fixation. When $n = 5$ the active side-on complex is no longer stable and the inactive end-on complex is formed instead. Our results explain why the C_5Me_5 complex is inactive.

Cartesian coordinates of all optimized structures of mononuclear $[(Cp')_2Zr(N_2)]$ and binuclear $[(Cp')_2Zr(N_2)Zr(Cp')_2]$ complexes and the complete reference [7] are given in the Supporting Information.

Received: April 21, 2005
Revised: July 7, 2005
Published online: October 13, 2005

Keywords: computer chemistry · density functional calculations · homogeneous catalysis · ligand effects · nitrogen fixation

[1] a) M. D. Fryzuk, S. A. Johnson, *Coord. Chem. Rev.* **2000**, *200–202*, 379; b) *Catalytic Ammonia Synthesis* (Ed.: J. R. Jennings), Plenum, New York, **1991**; c) J. Postgate, *Nitrogen Fixation*, Cambridge University Press, Cambridge, **1998**; d) R. Schlögl, *Angew. Chem.* **2003**, *115*, 2050; *Angew. Chem. Int. Ed.* **2003**, *42*, 2004.
[2] D. G. Musaev, *J. Phys. Chem. B* **2004**, *108*, 10012.
[3] H. Basch, D. G. Musaev, K. Morokuma, *Organometallics* **2000**, *19*, 3393.
[4] J. A. Pool, E. Lobkovsky, P. J. Chirik, *Nature* **2004**, *427*, 527.
[5] J. M. Manriquez, J. E. Bercaw, *J. Am. Chem. Soc.* **1974**, *96*, 6229.
[6] M. D. Fryzuk, *Nature* **2004**, *427*, 498.
[7] Gaussian 03, Revision C.01, M. J. Frisch et al., Gaussian, Inc., Wallingford, CT, **2004**
[8] J. A. Pool, E. Lobkovsky, P. J. Chirik, *J. Am. Chem. Soc.* **2004**, *126*, 14326.
[9] P. Bobadova-Parvanova, Q. Wang, D. Quinonero-Santiago, K. Morokuma, D. G. Musaev, still unpublished.
[10] A. E. Reed, L. A. Curtiss, F. Weinhold, *Chem. Rev.* **1988**, *88*, 899.

 © 2005 Wiley-VCH Verlag GmbH & Co. KGaA, Weinheim

Epoxidation Catalysts

DOI: 10.1002/anie.200501825

A Diiron Center Stabilized by a Bis-TPA Ligand as a Model of Soluble Methane Monooxygenase: Predominant Alkene Epoxidation with H_2O_2**

Masahito Kodera, Motoharu Itoh, Koji Kano, Takuzo Funabiki, and Marius Reglier*

Models of soluble methane monooxygenase (sMMO)[1] are useful for studying peroxodiiron(III) and oxodiiron(IV) intermediates in O–O activation,[1] as well as for developing an efficient oxidation catalyst.[2] Our synthetic efforts to obtain models for dimetal biosites yielded a series of dinucleating polypyridine ligands.[3] The diiron complex of the hexapyridine ligand efficiently catalyzes the oxidation of alkanes and forms a thermally stable peroxo complex.[3d–f] Diiron complexes of tris(2-pyridylmethyl)amine (TPA) and related ligands are known as effective sMMO models.[4] However, such ligands do not stabilize the diiron core in solution,[5] and the resulting complexes display varied reactivity, depending on them being mono- or diiron complexes.[6,7] Iron complexes of TPA derivatives catalyze alkene oxidation with H_2O_2 to give the 1,2-*cis*-diol and epoxide, and Rieske dioxygenase-type monoiron active species have been proposed.[6] However, predominant epoxidation was observed with the iron complex of the ligand *N*,*N*′-dimethyl-*N*,*N*′-bis(2-pyridylmethyl)ethane-1,2-diamine (MEP), which is similar to TPA, and an sMMO-type diiron species was proposed.[7] Therefore, a TPA-containing dinucleating ligand capable of stabilizing a diiron core in solution would be useful for the development of an effective sMMO model.

We prepared 1,2-bis[2-{bis(2-pyridylmethyl)aminomethyl}-6-pyridyl]ethane (6-HPA) as a bis-TPA dinucleating ligand. Herein, we describe the synthesis, structure, and application of the diiron complex of 6-HPA as a highly useful sMMO model. The complex can catalyze epoxidation with H_2O_2 with high yields and large turnover numbers. Spectral studies showed that a peroxodiiron(III) complex is formed as an intermediate. ^{18}O-labeling studies demonstrated that the O atoms of μ-oxo and μ-peroxo groups in the peroxo intermediate were incorporated equivalently into the epoxide. Thus, the oxo- and peroxo-derived O atoms in the active species scramble one another.

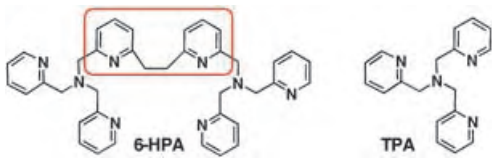

6-HPA forms the diiron complexes $[Fe_2(6\text{-HPA})(O)(OH_2)_2](ClO_4)_4$ (**1**) and $[Fe_2(6\text{-HPA})(TfO)_4]$ (**2**; TfO = triflate). The structure of **1** was revealed by X-ray structure analysis (Figure 1).[8] The distances and angles of the diiron

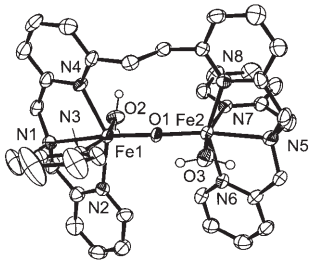

Figure 1. ORTEP view (40% probability) of the structure of the cation in **1**. Selected distances [Å] and angles [°]: Fe1···Fe2 3.607(3), Fe1-O1 1.795(2), Fe2-O1 1.812(2), Fe1-O2 2.084(7), Fe2-O3 2.059(2), Fe1-N1 2.244(1), Fe1-N2 2.151(5), Fe1-N3 2.114(1), Fe1-N4 2.187(7), Fe2-N5 2.235(5), Fe2-N6 2.152(7), Fe2-N7 2.120(9), Fe2-N8 2.196(6); Fe1-O1-Fe2 179.2.

core in **1** are almost equivalent to those in a corresponding diiron(III) complex of TPA, $[Fe_2(TPA)_2(O)(OH_2)_2](ClO_4)_3$ (**3**),[9] which indicates that 6-HPA stabilizes the diiron core without distortion. The ESI mass spectrum of **1** exhibited a major peak at *m*/*z* 1033 arising from $\{[Fe_2(6\text{-HPA})(O)(OH_2)_2](ClO_4)_3\}^+$, and the spectrum of **3** showed two major peaks at *m*/*z* 362 and 445 that resulted from the monoiron species and two minor peaks at *m*/*z* 923 and 1007 arising from the diiron species. These results clearly show that 6-HPA specifically stabilizes the diiron core of **1** in solution.

Efficient and predominant epoxidation of alkenes with H_2O_2 catalyzed by **1** was achieved, and the results are summarized in Table 1.[10] Cyclooctene was converted to the epoxide and 1,2-*cis*-diol in 75 and 2% yields, respectively. In an effort to determine the durability of **1** as a catalyst, an experiment with repeated additions of H_2O_2 was performed under similar conditions, in which the turnover number of **1** exceeded 100. For other alkenes, the epoxide was formed

Table 1: Oxygenation of alkenes with H_2O_2 catalyzed by **1** and **2**.

alkene [IP (eV)][b]	Yield[a] [%] (turnover number) epoxide/*cis*-1,2-diol **1**	**2**
cyclooctene [8.98]	75(7.5)/2(0.2)[c] 70(105)/2(3.0)[d]	42(4.2)/24(2.4)[c]
trans-β-methylstyrene [8.08]	91(9.1)/0[c]	
cis-β-methylstyrene [8.48]	79(7.9)/0[c]	
styrene [8.49]	63(6.3)/0[c]	
1-octene [9.52]	37(3.7)/0[c]	

[a] Yield based on the H_2O_2 used. [b] IP is the ionization potential of the alkene. [c] 10 equiv of H_2O_2 was added. [d] 150 equiv of H_2O_2 was added.

[*] Prof. Dr. M. Kodera, M. Itoh, Prof. Dr. K. Kano, Dr. T. Funabiki
Department of Molecular Science and Technology
Faculty of Engineering, Doshisha University
Kyotanabe, Kyoto 610-0321 (Japan)
Fax: (+81) 774-65-6848
E-mail: mkodera@mail.doshisha.ac.jp
Dr. M. Reglier
Université Paul Cezanne
Escadrille Normandie-Niemen
13397 Marseille Cedex 20 (France)

[**] This work was supported by a Grant-in-Aid for Scientific B (14340210) from the JSPS. TPA = tris(2-pyridylmethyl)amine.

InterScience
© 2005 Wiley-VCH Verlag GmbH & Co. KGaA, Weinheim

predominantly and the 1,2-*cis*-diol was not detected. The *trans*-epoxide was obtained from *trans*-β-methylstyrene in 91% yield. Given the large turnover number and high epoxide yield, it can be stated that **1** is an effective sMMO model. The epoxide yield increased with decreasing ionization potential (IP)[11] of the alkene (Table 1); *trans*-β-methylstyrene, which had the lowest IP value, gave the highest epoxide yield. Moreover, epoxidation was not stereospecific, as *cis*- and *trans*-epoxides were obtained from *cis*-β-methylstyrene with an RC value of 63%.[12] These data indicate that the first step in the epoxidation represents a one-electron oxidation of the alkene by an active species, and that the radical cation generated undergoes a *cis*-to-*trans* configuration change. As 6-HPA stabilizes the diiron core of **1** in solution, the active species generated from **1** must be a dinuclear complex relevant to sMMO.

Interestingly, when the diiron(II) complex **2**, which does not have bridging oxo or hydroxo groups, was used as a catalyst for the oxygenation of cyclooctene, the 1,2-*cis*-diol was a main product (see Table 1). When 1 equiv of H_2O_2 was added to **2**, the epoxide/*cis*-1,2-diol product ratio was 0.15:0.85. With an increase in the amount of H_2O_2 added, the yield of epoxide was increased and that of *cis*-1,2-diol was decreased according to the following epoxide/*cis*-1,2-diol ratios: 0.26:0.74, 0.53:0.47, and 0.64:0.36 for 2, 5, and 10 equiv of H_2O_2 added, respectively. These results clearly show that **2** mainly produces *cis*-1,2-diol, and **1** gradually generated by oxidation of **2** with H_2O_2 mainly produces epoxide. This finding indicates that the μ-oxo bridge in **1** plays an essential role for the sMMO-type reactivity.

Addition of 2 equiv of H_2O_2 to a solution of **1** in CH_3CN at −40 °C generated a green species **4** that exhibited absorption bands at 490 ($\varepsilon = 1130\ M^{-1}cm^{-1}$), 670 (1060), and 882 nm (sh, 370). These data are similar to those of the peroxodiiron complex $[Fe_2(O)(O_2)(6\text{-}Me_3\text{-}TPA)_2](ClO_4)_2$ (**5**; 6-Me$_3$-TPA = tris(6-methyl-2-pyridylmethyl)amine).[13] The cold-spray ionization (CSI) mass spectrum of **4** showed a parent peak at *m*/*z* 865 arising from a peroxodiiron complex, $\{[Fe_2(O)(O_2)(6\text{-}HPA)](ClO_4)\}^+$, as the strongest peak (Figure 2). The ion exhibited an isotope intensity pattern that matched the calculated one. Upon addition of $H_2{}^{18}O_2$ instead of $H_2{}^{16}O_2$, the mass of the ion increased by four units. These results indicate that **4** is best formulated as $[Fe_2(O)(O_2)(6\text{-}HPA)](ClO_4)_2$. Spontaneous decomposition of **4** in CH_3CN monitored at 680 nm obeyed first-order kinetics with $k = 1.6 \times 10^{-3}\ s^{-1}$ at 243 K (the half-life $\tau_{1/2} = 7.2$ min). This value was equivalent to that of **5** under the same conditions.[13] Compound **4** was as stable as **5** but without steric hindrance, as was the case with the Me groups of 6-Me$_3$-TPA in **5**. When *trans*-β-methylstyrene was added to the solution of **4** generated as described above at −40 °C, the decay of **4** was not accelerated at all. The mixture was analyzed after warming to room temperature; the epoxide yield was increased to almost quantitative.

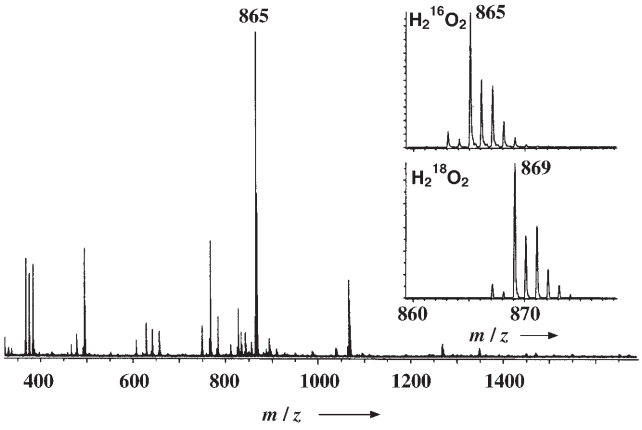

Figure 2. CSI mass spectrum of **4** obtained at −40 °C in CH_3CN. The isotope patterns assignable to $\{[Fe_2(O)(^{16}O_2)(6\text{-}HPA)](ClO_4)\}^+$ and $\{[Fe_2(O)(^{18}O_2)(6\text{-}HPA)](ClO_4)\}^+$ are shown in the insets.

Isotope-labeling experiments with *trans*-β-methylstyrene as substrate were carried out by using $H_2{}^{18}O_2$ and μ-^{18}O-**1** under argon to gain insight into the O–O activation mechanism. Upon addition of 10 equiv of $H_2{}^{18}O_2$ to **1**, ^{18}O was incorporated into 94% of the epoxide, whereas addition of 1 or 3 equiv of $H_2{}^{16}O_2$ to μ-^{18}O-**1** resulted in incorporation of ^{18}O into 31 or 17% of the epoxide, respectively. Thus, μ-^{18}O is incorporated into the epoxide in addition to $H_2{}^{18}O_2$. This finding can be explained if it is assumed that a dioxo-μ-oxodiiron(IV) moiety is generated from **4** as an active species via homolytic scission of the O–O bond, and that three O atoms in the active species scramble one another. Accordingly, with $H_2{}^{16}O_2$ (1 equiv)/μ-^{18}O-**1**, 33% of each oxo group in the active species was labeled with ^{18}O, and thus the theoretical yield of the ^{18}O-epoxide was 33% (Scheme 1).

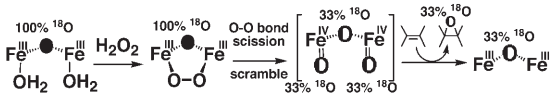

Scheme 1. Incorporation of the ^{18}O atom on labeling with μ-^{18}O-**1**.

Similarly, with $H_2{}^{16}O_2$ (3 equiv)/μ-^{18}O-**1** or $H_2{}^{18}O_2$ (10 equiv)/**1**, the yield of ^{18}O-epoxide is estimated to be 16 or 95%, respectively. The theoretical values of 33, 16, and 95% agree with the experimental results of 31, 17, and 94%, respectively.

Further experiments with an excess amount of $H_2{}^{18}O$ or under $^{18}O_2$ revealed the unique reactivity of the active species. With $H_2{}^{18}O/H_2{}^{16}O_2$/**1** (1000:10:1), only 1.5% of the epoxide was labeled with ^{18}O, which shows that O-atom exchange of the active species with H_2O was much slower than O-atom transfer to the alkene.[14] When the reaction was carried out with $H_2{}^{16}O_2$ (10 equiv)/**1** under $^{18}O_2$, 5% of the epoxide was labeled with ^{18}O. This result suggests that a one-electron oxidation of the alkene by the active species occurs to form a radical cation and a diiron(III),(IV) species, as ^{18}O labeling from $^{18}O_2$ must occur by autoxidation of the radical cation. The remaining 95% of nonlabeled epoxide could be accounted for by O-atom transfer from the resultant diiron(III),(IV) species to the radical cation. We are presently attempting to detect the diiron(III),(IV) and diiron(IV) species, which would be generated from **1** and H_2O_2 via the peroxo intermediate **4**.

 © 2005 Wiley-VCH Verlag GmbH & Co. KGaA, Weinheim

Experimental Section

6-HPA: An aqueous solution of NaOH (2.3 M, 5 mL) was added dropwise with vigorous stirring to a solution of TPA (0.77 g, 3.87 mmol) and 1,2-bis(6-bromomethyl-2-pyridyl)ethane·2 HBr (1.03 g, 1.94 mmol) in water (5 mL) at room temperature. The reaction mixture was stirred for 24 h at room temperature and then extracted with $CHCl_3$. The extracts were dried over Na_2SO_4 and the product 6-HPA was isolated as a white solid (0.71 g, 60 %). Mp.: 133.5–135.0 °C. Elemental analysis (%) calcd for $C_{38}H_{38}N_8$: C 75.22, H 6.31, N 18.34; found: C 74.99, H 6.34, N 18.34. ^{1}H NMR (Me_4Si, in $CDCl_3$): $\delta = 8.52$ (dq, 4H, py′-6), 7.65 (m, 6H, py-4 and py′-4), 7.49 (s, 4H,py′-3), 7.36 (d, 2H, py-5), 7.13 (s, 4H, py′-5), 6.96 (d, 2H, py-3), 3.89 (s, 8H, $pyCH_2N(CH_2py)_2$), 3.86 (s, 4H, $pyCH_2N(CH_2py)_2$), 3.19 ppm (s, 4H, CH_2); ^{13}C NMR (Me_4Si, in $CDCl_3$): $\delta = 160.3$, 159.3, 158.5 (py-2, py-6, py′-2), 148.8 (py′-6), 136.4, 136.2, 122.6, 121.7, 120.9, 119.9 (py-4, py′-4, py′-3, py′-5, py-5, py-3), 60.0, 59.9 (methylene), 38.0 ppm (ethylene). FAB MS: m/z 607 $[M+H]^+$.

1: 6-HPA (60.5 mg, 0.1 mmol) was dissolved in water (1 mL), a solution of $Fe(ClO_4)_3·9H_2O$ (103 mg, 0.2 mmol) in water (1 mL) was added, and the mixture was stirred overnight. **1** precipitated as a brown powder (yield 86.5 %) and was recrystallized from C_6H_6/CH_3CN to give crystals suitable for X-ray structure analysis. Elemental analysis (%) calcd for $C_{38}H_{50}N_8Cl_4O_{23}Fe_2$: C 36.80, H 4.06, N 9.03, Fe 9.00; found: C 36.62, H 4.03, N 9.04, Fe 8.73. UV/Vis absorption (in CH_3CN): $\lambda_{max} = 515$ nm^{-1} ($\varepsilon_{max} = 110$ M^{-1}cm^{-1}). IR (KBr disk): $\tilde{\nu} = 3072$, 3032 (aromatic C–H), 2959, 2924 (aliphatic C–H), 1607, 1572 (pyridine ring), 1113, 1084 (ClO_4), 810 cm^{-1} (Fe–O–Fe). ESI MS: m/z 1033 $[M-2H_2O-ClO_4]^+$, 466 $[M-2H_2O-2ClO_4]^{2+}$.

μ-^{18}O-**1:** 6-HPA (20.3 mg, 33 μmol) and $Fe(ClO_4)_3·9H_2{}^{18}O$ (35.9 mg, 67 μmol) were dissolved in $H_2{}^{18}O$ (1 mL) and the mixture was stirred overnight. μ-^{18}O-**1** precipitated as a brown powder (yield 65 %) and was recrystallized from dry C_6H_6/CH_3CN. IR (KBr disk): $\tilde{\nu} = 3069$, 3034 (aromatic C–H), 2953, 2922 (aliphatic C–H), 1607, 1572 (pyridine ring), 1092 (ClO_4), 768 cm^{-1} (Fe–O–Fe). ESI MS: m/z 1035 $[M-2H_2{}^{18}O-ClO_4]^+$, 467 $[M-2H_2{}^{18}O-2ClO_4]^{2+}$, 278 $[M-2H_2{}^{18}O-3ClO_4]^{3+}$.

2: A solution of 6-HPA (30.75 mg, 0.051 mmol) in CH_2Cl_2 (1 mL) was added to a solution of $Fe^{II}(TfO)_2·2CH_3CN$ (40.1 mg, 0.11 mmol) in THF (2 mL) and the mixture was stirred overnight under Ar. Complex **2** precipitated as a pale yellow powder, and was isolated by filtration (46.8 mg, yield 70 %) and recrystallized from CH_2Cl_2/CH_3CN/Et_2O under Ar. Elemental analysis (%) calcd for $C_{42}H_{38}N_8F_{12}S_4O_{12}Fe_2$: C 38.37, H 2.91, N 8.52, Fe 8.50; found: C 38.29, H 2.89, N 8.31, Fe 8.19. UV/Vis absorption (in CH_3CN): λ_{max} (ε_{max} M^{-1}cm^{-1}) = 355 (1600), 540 nm^{-1} (20). IR (KBr disk): $\tilde{\nu} = 3119$, 3082 (aromatic C–H), 2984, 2926 (aliphatic C–H), 1607, 1576, 1466, 1447 (pyridine ring), 1283, 1254, 1167, 1030 cm^{-1} (CF_3SO_3). ESI MS (in CH_3CN): m/z 1165 $[M-CF_3SO_3]^+$, 508 $[M-2CF_3SO_3]^{2+}$, 289 $[M-3CF_3SO_3]^{3+}$.

Isotope-labeling experiments were carried out under similar conditions in the presence of an excess amount of $H_2{}^{18}O$ or under $^{18}O_2$. The epoxidation reaction was also performed with μ-^{18}O-**1**/H_2O_2 ratios of 1:1 and 1:3 under Ar. The resultant mixtures were analyzed by GC-MS, and the rate of ^{18}O labeling was determined from the isotope-intensity pattern.

Received: May 26, 2005
Published online: October 11, 2005

Keywords: alkenes · epoxidation · iron · isotopic labeling · peroxo ligands

[1] a) M. Costas, M. P. Mehn, M. P. Jensen, L. Que, Jr., *Chem. Rev.* **2004**, *104*, 939; b) E. Y. Tshuva, S. J. Lippard, *Chem. Rev.* **2004**, *104*, 987.

[2] a) Y. Mekmouche, S. Ménage, C. Toia-Duboc, M. Fontecave, J.-B. Galey, C. Lebrun, J. Pécaut, *Angew. Chem.* **2001**, *113*, 975; *Angew. Chem. Int. Ed.* **2001**, *40*, 949; b) A. Murphy, G. Dubois, T. D. P. Stack, *J. Am. Chem. Soc.* **2003**, *125*, 5250; c) K. Kamata, K. Yonehara, Y. Sumida, K. Yamaguchi, S. Hikichi, N. Mizuno, *Science* **2003**, *300*, 964.

[3] a) M. Kodera, K. Katayama, Y. Tachi, K. Kano, S. Hirota, S. Fujinami, M. Suzuki, *J. Am. Chem. Soc.* **1999**, *121*, 11006; b) M. Kodera, Y. Kajita, Y. Tachi, K. Katayama, K. Kano, S. Hirota, S. Fujinami, M. Suzuki, *Angew. Chem.* **2004**, *116*, 338; *Angew. Chem. Int. Ed.* **2004**, *43*, 334; c) M. Itoh, J. Nakazawa, K. Maeda, K. Kano, T. Mizutani, M. Kodera, *Inorg. Chem.* **2005**, *44*, 691; d) M. Kodera, H. Shimakoshi, K. Kano, *Chem. Commun.* **1996**, 1737; e) M. Kodera, H. Shimakoshi, M. Nishimura, H. Okawa, S. Iijima, K. Kano, *Inorg. Chem.* **1996**, *35*, 4967; f) M. Kodera, Y. Taniike, M. Itoh, Y. Tanahashi, H. Shimakoshi, K. Kano, S. Hirota, S. Iijima, M. Ohba, H. Okawa, *Inorg. Chem.* **2001**, *40*, 4821.

[4] a) Y. Dong, H. Fujii, M. P. Hendrich, R. A. Leising, G. Pan, C. R. Randall, E. C. Wilkinson, Y. Zang, L. Que, Jr., B. G. Fox, K. Kauffman, E. Münck, *J. Am. Chem. Soc.* **1995**, *117*, 2778; b) C. Kim, Y. Dong, L. Que, Jr., *J. Am. Chem. Soc.* **1997**, *119*, 3635; c) Y. Dong, Y. Zang, L. Shu, E. C. Wilkinson, L. Que, Jr., *J. Am. Chem. Soc.* **1997**, *119*, 12683; d) H.-F. Hsu, Y. Dong, L. Shu, V. G. Young, Jr., L. Que, Jr., *J. Am. Chem. Soc.* **1999**, *121*, 5230.

[5] J. Kim, Y. Dong, E. Larka, L. Que, Jr., *Inorg. Chem.* **1996**, *35*, 2369.

[6] a) K. Chen, M. Costas, J. Kim, A. K. Tipton, L. Que, Jr., *J. Am. Chem. Soc.* **2002**, *124*, 3026; b) M. Costas, L. Que, Jr., *Angew. Chem.* **2002**, *114*, 2283; *Angew. Chem. Int. Ed.* **2002**, *41*, 2179; c) M. Fujita, M. Costas, L. Que, Jr., *J. Am. Chem. Soc.* **2003**, *125*, 9912.

[7] a) M. C. White, A. G. Doyle, E. N. Jacobsen, *J. Am. Chem. Soc.* **2001**, *123*, 7194; b) J. Y. Ryu, J. Kim, M. Costas, K. Chen, W. Nam, L. Que, Jr., *Chem. Commun.* **2002**, 1288.

[8] Rigaku AFC7R/CCD diffractometer, 12-kW rotating-anode generator. $C_{50}H_{54}Cl_4Fe_2N_8O_{19}$, $M_w = 1324.52$, red crystals, 0.20 × 0.30 × 0.50 mm, monoclinic, $P2_1/c$ (No. 14), $a = 13.522(3)$, $b = 18.669(3)$, $c = 24.486(5)$ Å, $\beta = 101.364(4)°$, $V = 6060.1(20)$ Å^3, $Z = 4$, $\rho_{calcd} = 1.452$ g cm^{-3}, $2\theta_{max} = 55°$, $Mo_{K\alpha}$ ($\lambda = 0.71069$), $T = -50$ °C, total number of independent reflections 61013 ($R_{int} = 0.086$), number of reflections used 32710 ($I > 3.00\sigma(I)$), $R = 10.0$, $R_w = 16.1$, GOF = 1.213, $\mu = 7.30$ cm^{-1}, full-matrix least squares on *F*. CCDC-274091 contains the supplementary crystallographic data for this paper. These data can be obtained free of charge from the Cambridge Crystallographic Data Centre via www.ccdc.cam.ac.uk/data_request/cif.

[9] B. R. Whittlesey, Z. Pang, R. A. Holwerda, *Inorg. Chim. Acta* **1999**, *284*, 124.

[10] In a typical reaction, a solution of H_2O_2 (21 μmol) in CH_3CN was added over 30 min to a solution of **1** (2.1 μmol) and cyclooctene (2.1 mmol) in CH_3CN (3.0 mL) by using a syringe pump under Ar with stirring at 25 °C. The mixture was analyzed by gas–liquid chromatography with nitrobenzene as internal standard.

[11] a) T. G. Traylor, F. Xu, *J. Am. Chem. Soc.* **1988**, *110*, 1953; b) J. M. Garrison, D. Ostovic, T. C. Bruice, *J. Am. Chem. Soc.* **1989**, *111*, 4960; c) M. S. Workentin, B. D. Wagner, J. Lusztyk, D. D. M. Wayner, *J. Am. Chem. Soc.* **1995**, *117*, 119.

[12] When the RC value is 100%, the reaction is stereospecific and when the RC value is 0%, the reaction is completely non-stereospecific. (RC) (%) of epoxide = 100 × (*cis*–*trans*)/(*cis*+*trans*); see reference [6].

[13] Y. Dong, Y. Zang, L. Shu, E. C. Wilkinson, L. Que, Jr., *J. Am. Chem. Soc.* **1997**, *119*, 12683.

[14] M. S. Seo, J.-H. In, S. O. Kim, N. Y. Oh, J. Hong, J. Kim, L. Que, Jr., W. Nam, *Angew. Chem.* **2004**, *116*, 2471; *Angew. Chem. Int. Ed.* **2004**, *43*, 2417.

 © 2005 Wiley-VCH Verlag GmbH & Co. KGaA, Weinheim

Host–Guest Systems

DOI: 10.1002/anie.200501840

A "Through-Shell" Binding Isotope Effect**

*Yong Liu and Ralf Warmuth**

Isotope effects play an important role in chemical and biological sciences.[1] In particular, kinetic isotope effects allow the probing of reaction mechanisms,[2] transition-state geometries,[3] tunneling contributions to reaction rates, and steric requirements in the rapture of mechanical bonds.[4,5] In addition, substantial differences in noncovalent interactions that underlie olfaction,[6] enzyme–cofactor binding,[7] retention on normal and reversed phase HPLC columns,[8,9] and molecular encapsulation have been observed upon deuteration.[10,11] Isotopic substitution also affects the thermodynamic properties of molecules, thus leading to changes in the vapor pressure and melting point, as well as to the phase segregation of polymers.[12–14] However, the origin of binding isotope effects (BIE) and how specific molecular interactions influence the volume, energy, and entropy of a molecule and give rise to the observed changes in properties upon isotopic substitution is not fully understood.[15] It is well established that the molar volume of a molecule decreases upon deuteration as a consequence of the smaller zero point energy (ZPE) of the C–D bond relative to the C–H bond and the anharmonicity of the potential energy surface, which leads to different equilibrium interatomic distances. For example, the difference in the mean C–H and C–D bond lengths of methane is $\Delta l = 0.004$ Å, as determined by gas-phase electron-diffraction studies.[16]

Here we introduce a novel supramolecular approach for the determination of the changes in the bond lengths and volume upon deuteration which allows determination of the differences in the C–H/C–D bond lengths of a single molecule that is isolated inside a highly polarizable medium.[17] A comparison of the apparent differences in the C–H/C–D bond lengths in different media might provide new insights into the magnitude of the intermolecular and intramolecular contributions to the observed molar volume isotope effect.[18] In our approach, a hemicarcerand serves as a sensitive "molecular ruler" that allows the precise determination of small size differences between two incarcerated guests from the chromatographic properties of both hemicarceplexes. We also provide for the first time a quantitative analysis of the chromatographic behavior of hemicarceplexes and an understanding of how the molecular information that is stored in the encapsulated guest (size, shape, chirality, electrostatic potential, and local and global dipole moment) is translated through the hemicarcerand shell into a surface–hemicarceplex interaction.[19,20] A detailed understanding of such inside–outside information transfer[19–21] might shed light on similar processes in biological systems and should be important for applications of container molecules or self-assembled capsules as molecular switches, sensors, information storage devices, or new tools in separation technology.[21a,22]

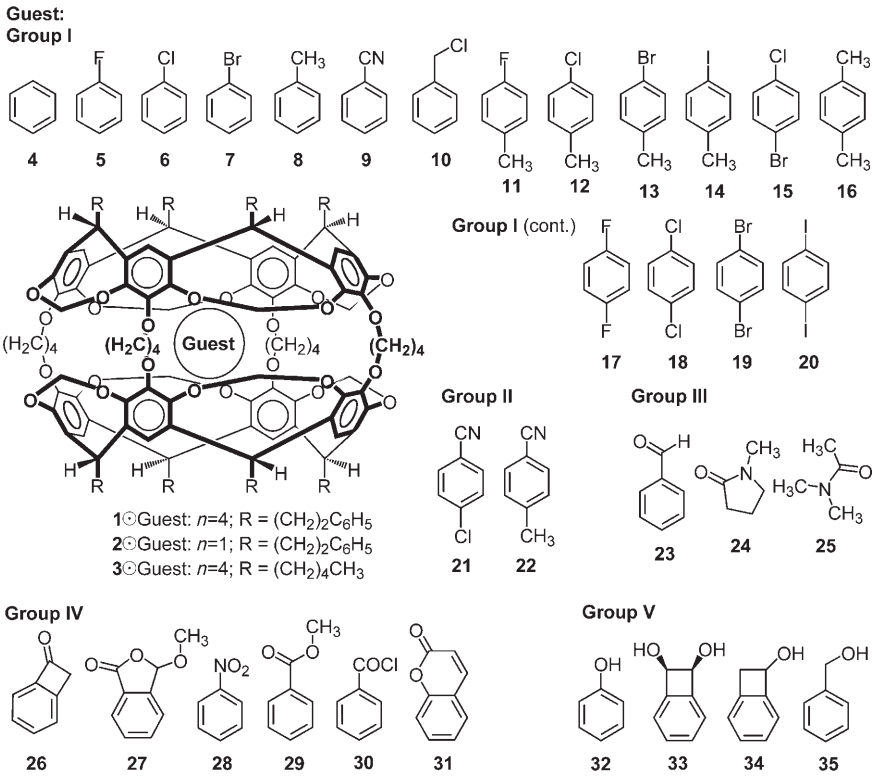

Scheme 1. Hosts and guests investigated in the study.

In an investigation that addressed how the guest of hemicarceplexes **1** ⊙ guest (guest: **4**–**35**; Scheme 1)[23–25] communicates with an external chromatographic stationary phase we noted a large increase in the HPLC retention factor $k' = (t_R - t_0)/t_0$ (t_R = solute retention time; t_0 = retention time of unretained solute; mobile phase: CH_2Cl_2/0.5% Et_2O;

[*] Y. Liu, Dr. R. Warmuth
Department of Chemistry and Chemical Biology
Rutgers, The State University of New Jersey
610 Taylor Road, Piscataway, NJ 08854 (USA)
Fax: (+1) 732-445-5312
E-mail: warmuth@rutchem.rutgers.edu
Y. Liu
Merck Research Laboratories
Department of Analytical Research
Building RY818-C220
P.O. Box 2000, Rahway, NJ 07065 (USA)

[**] We warmly thank the National Science Foundation (grant CHE-0431749) and Merck Research Laboratories for generous support of this research.

Supporting information for this article is available on the WWW under http://www.angewandte.org or from the author.

 © 2005 Wiley-VCH Verlag GmbH & Co. KGaA, Weinheim

1 mL min^{-1}) with increasing guest size. The value of k' increased 35-fold between the fastest (**1** ⊙ benzene; $k' = 1.5$) and slowest eluting hemicarceplex (**1** ⊙ 7-methoxyphthalide; $k' = 51.86$). Furthermore, retention did not correlate with guest polarity; for example, the value of k' increased in the order **1** ⊙ **4** < **1** ⊙ **5** < **1** ⊙ **6** < **1** ⊙ **9** < **1** ⊙ **8** ≈ **1** ⊙ **7** ≪ **1** ⊙ **16**. The flexible $O(CH_2)_4O$ linkers of **1** allow adaptation of the inner phase of the host to the size and shape of the guest in order to maintain an optimal space occupancy.[26] Thus, it is tempting to assume that the retention times are related to the size and shape of the hemicarceplexes: An increased outer surface should increase the surface–surface interaction. To test this hypothesis we carried out molecular dynamics simulations (MDSs) for each hemicarceplex **1** ⊙ guest (guest: **4**–**35**) and chose the distance d between the center of the two squares formed by connecting the four ether oxygen atoms of a cavitand as a measure for the change in the hemicarcerand size (Figure 1). These MDS studies (Amber*, 300 K, 10 ns) provided time-averaged values for d and

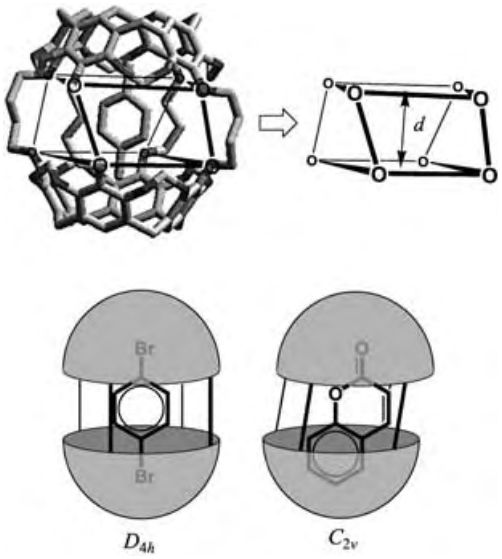

Figure 1. Definition of d for the energy-minimized structure of **1** ⊙ **16** (left) and shapes of hemicarceplexes: D_{4h}: guests **4**–**25**, **32**, **35**; C_{2v}: guests **26**–**31**, **33**, **34**.

information about the shape of the hemicarceplexes, which we categorized as D_{4h}- (guests **4**–**25**, **32**, **35**) or C_{2v}-symmetric (guests **26**–**31**, **33**, **34**) according to the relative orientation of the cavitands.[27] We were delighted to find that $\ln k'$, which is proportional to the change in free energy ΔG upon transferring a hemicarceplex from the mobile phase to the stationary phase, correlates almost linearly with the value of d for hemicarceplexes having nearly D_{4h} symmetry (group I hemicarceplexes in Scheme 1; Figure 2).

What is the physical basis behind this correlation? Further analysis of the MDS studies shows that elongation of a hemicarceplex leads to an increased outward rotation of the lone pairs of electrons on the oxygen atoms of the $O(CH_2)_4O$ linker. Since an outward pointing lone pair of electrons on an oxygen atom is able to engage in polar Si–OH···O_{host}

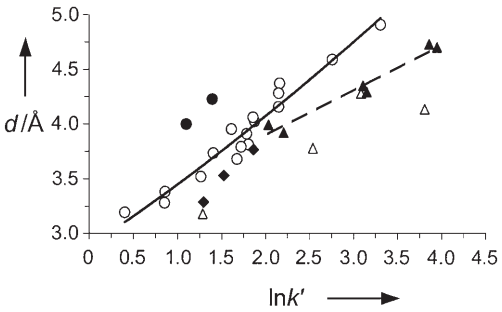

Figure 2. Semilogarithmic plot of hemicarceplex **1** ⊙ guest length (d) and retention factor ($\ln k'$): guests of group I (○); guests of group II (●); guests of group III (◆); guests of group IV (▲); guests of group V (△; see Scheme 1); and best fit for the correlation of group I guests. (CH_2Cl_2/0.5% Et_2O; 1 mL min^{-1}; Phenomenax, Luna Si (2), 15 cm × 4.6 mm, 5 μm; 22 °C).

interactions with the silica surface of the stationary phase, this will increase the retention of the hemicarceplex. In fact, a good linear correlation between $\ln k'$ and the time-averaged sum of all the C_1-O_2-C_3-C_4 dihedral angles (θ) is observed (see Scheme 2 and Supporting Information).

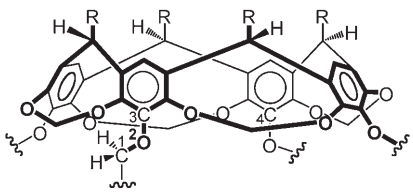

Scheme 2. Definition of C_1-O_2-C_3-C_4 dihedral angle θ. Lone pairs of electrons on the oxygen atoms are fully protected (inwards) for $\theta = 180°$ and fully exposed (outwards) for $\theta = 0°$.

Thus, differences in the retention times of the hemicarceplexes with D_{4h} symmetry are primarily controlled by the length of the hemicarcerand through the time-averaged orientation of the lone pairs of electrons on the ether oxygen atoms. However, several hemicarceplexes deviated from this behavior and showed weaker (group II, Scheme 1) and stronger retention (group III, Scheme 1) than predicted based on their length. Even though the exact reason for their different behavior is not fully understood, it might be a consequence of the particularly large dipole moment of the guest, which influences the hemicarceplex–silica interaction. In fact, Cram and co-workers explained the differences in the thin layer chromatography retention factors of hemicarceplexes **2** ⊙ DMF, **2** ⊙ *N*,*N*-dimethylacetamide, and **2** ⊙ DMSO on the basis of such modulations of carceplex–silica dipole–dipole interactions induced by the dipole of the guest.[19] In the group II hemicarceplexes the CN groups are aligned along the polar axis of the host and are "pushed" into the cavitand such that the positively charged C atom is in the same horizontal plane as the cavitand's oxygen belt. We believe that the proximity of the positive pole of the CN group leads to a slight weakening of all Si–OH···O_{host} interactions involving these oxygen atoms. A related but opposite effect could explain the retention behavior of the group III hemicarce-

 © 2005 Wiley-VCH Verlag GmbH & Co. KGaA, Weinheim

plexes: their guests possess a carbonyl group, whose negative pole is in proximity to the oxygen atom rim of a cavitand leading to a slight strengthening of local Si–OH···O_{host} and dipole–dipole silica–hemicarceplex interactions by roughly an equal amount in all three hemicarceplexes.

Hemicarceplexes whose guest induces C_{2v} symmetry of the host (group IV, Scheme 1) are retained more strongly than hemicarceplexes of group I with a comparable *d* value, but still show a linear correlation between $\ln k'$ and *d*. Because of the limited number of hemicarceplexes in this series and the fact that each guest has a polar functional group, is not fully clear whether the increased hemicarceplex–silica surface interaction is a result of the shape of the hemicarceplex or the presence of the polar functional group.

Finally, hemicarceplexes whose guest has a hydroxy group all show stronger retention, as predicted (group V, Scheme 1). A logical explanation would be through-shell guest-OH···O-silica hydrogen bonds that increase the binding interaction of the hemicarceplex with the surface.

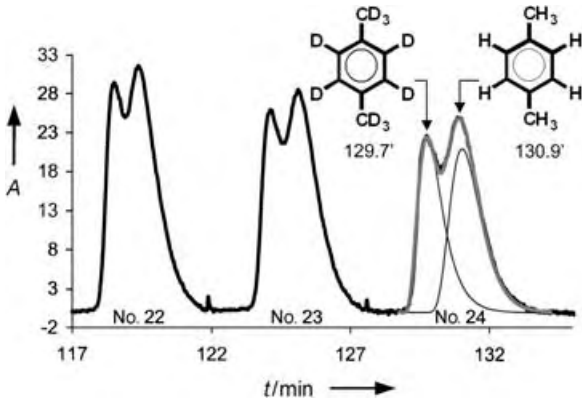

Figure 3. Normal-phase HPLC recycle chromatogram (thick blackline) of a 1:1 mixture of **3** ⊙ *p*-xylene and **3** ⊙ [D_{10}]-*p*-xylene and peak deconvolution of the 24th cycle (mobile phase: A/B, 65:35, A: 2.0 v% Et_2O in CH_2Cl_2, B: CH_2Cl_2; 1 mL min^{-1}; Phenomenax, Luna Si (2), 25 cm × 4.6 mm, 5 μm; 22 °C). Gray line: best fit of the double peak of the 24th cycle; thin black line): peak **3** ⊙ [D_{10}]-*p*-xylene and **3** ⊙ *p*-xylene.

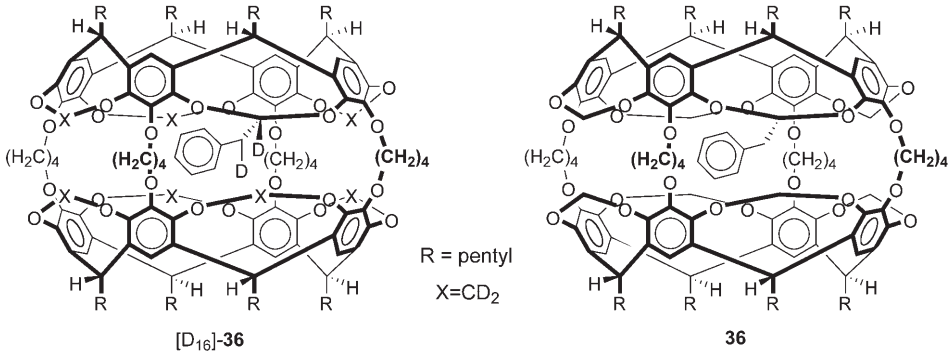

Even though the dipole moment or OH group of a tightly bound guest is able to "communicate" with the silica surface, the length of the hemicarceplex is the key factor that controls retention in all hemicarceplex groups (I–V). If this is indeed true, separation of isotopomeric hemicarceplexes that differ solely in the extent of guest deuteration might be possible. We tested this idea with the **1** ⊙ *p*-xylene/**1** ⊙ [D_{10}]-*p*-xylene pair. Initial attempts to separate both hemicarceplexes failed even with recycling chromatography because of strong tailing of the peaks. A screen of other hemicarceplexes with different appending groups showed reduced tailing for **3** ⊙ **16** and, indeed, the onset of separation of **3** ⊙ **16** and **3** ⊙ [D_{10}]-**16** was observed after 14 chromatographic cycles, with **3** ⊙ [D_{10}]-**16** eluting before **3** ⊙ **16** as predicted from the volume isotope effect of the guest (Figure 3).[28] From the difference in the retention times in the 24th cycle (Figure 3), we determined $\Delta\ln k' = \ln k'_H - \ln k'_D = 0.013(1)$ and a binding isotope effect of $k'_H/k'_D = 1.013(1)$. This binding isotope effect is conceptionally new since it depends primarily on the volume difference between the two isotopomers, which induces a small structural change in the surrounding hemicarcerand that leads to the observed change in the binding energy of $\Delta\Delta G = 7.6(6)$ cal mol^{-1}. The following observations rule out participation of the guest's C–H/D bonds in the hemicarceplex–silica interaction: 1) the isotopomeric hemicarceplexes **36** and [D_{16}]-**36**, in which the outward-pointing acetal C–H/D bonds interact with the stationary phase, show a reversed elution order;[8] 2) the absence of separation for the pair **3** ⊙ **16** and **3** ⊙ [D_4]-**16**, in which the aryl protons of the guest more exposed to the bulk phase are labeled, but partial separation for the pair **3** ⊙ **16** and **3** ⊙ [D_6]-**16**, in which the shielded methyl groups of the guest are labeled. The latter experiments also demonstrate that the partial separation of the pair **3** ⊙ **16** and **3** ⊙ [D_{10}]-**16** is a consequence of deuterating the methyl groups of the guest.

If the volume isotope effect of the guest were the sole cause of the difference in the retention time between **3** ⊙ **16** and **3** ⊙ [D_{10}]-**16**, what would be the difference in the C–H/C–D bond lengths? From the $\Delta\ln k'$ value and the slope of the $\ln k'$ versus *d* plot for hemicarceplexes **3** ⊙ guest (guest = **4**–**8**, **11**–**19**; see Supporting Information), we calculated the hemicarceplex contraction upon guest deuteration as $\Delta d = 0.0098 \pm 0.0009$ Å. MDS studies of *p*-xylene hemicarceplexes in which we systematically constrained the C–H bonds of the guest to a length between 1.0 and 1.1 Å showed that a shortening of the methyl C–H bonds by 0.01 Å decreased *d* by 0.0204 Å. Thus, the measured Δd value corresponds to a difference in the C–H/C–D bond lengths of $\Delta l = 0.0048 \pm 0.0005$ Å. Bartell and Roskos used $\Delta l = 0.005$ Å in model calculations that accurately predicted the measured volume isotope effect of benzene.[29] Likewise, Bates et al. found a good agreement between the experimentally observed and modeled differences in the unit cell dimensions of crystalline $C_{36}H_{74}$ and $C_{36}D_{74}$ by assuming $\Delta l = 0.005$ Å.[18a] The close match between these and our measured bond lengths suggest that the volume isotope effect of the guest is likely the main reason for the observed chromatographic isotope effect. However, other contributions to the observed difference in the deuteration-induced hemicarceplex length cannot be

 © 2005 Wiley-VCH Verlag GmbH & Co. KGaA, Weinheim

excluded. For example, the higher polarizability of a C–H bond relative to a C–D bond would result in stronger CH–π interactions between the host and guest and a decrease in the difference in length between **3**⊙**16** and **3**⊙[D_{10}]-**16**.[18a,b] Furthermore, Rebek and co-workers showed that a CD_3 group is more strongly attracted to the inner surface of a cavitand than is a CH_3 group.[10] This result has been explained with a blue shift of the C–H/C–D stretching frequency upon formation of a CH/CD–π interaction that leads to an increased ZPE splitting.[15] Since hemicarceplexes are fluxional in solution,[30] a tighter host–guest complex is expected for **3**⊙[D_{10}]-**16** than **3**⊙**16**, which will increase the difference in length between **3**⊙**16** and **3**⊙[D_{10}]-**16** beyond what is expected based on the different dimensions of the C–H and C–D bond.[16]

In conclusion, we have unraveled some of the mechanisms that lead to the observed large differences in the chromatographic behavior of hemicarceplexes. Our investigations show that guest size plays a crucial role in modulating the hemicarceplex–surface interactions and that even such subtle changes resulting from deuteration lead to a measurable change in the retention time. We believe that simple correlations between retention behavior and structural parameters, such as the computed length and shape of the complex also exist for other hemicarcerands and capsules. If indeed such correlations can be found for chiral hemicarceplexes,[18b] novel and powerful methodologies for chiral separation and the determination of the absolute configuration of a chiral guest molecule might become available.

Received: May 26, 2005
Published online: October 11, 2005

Keywords: encapsulation · host–guest systems · isotope effect · liquid chromatography · molecular recognition

[1] L. Melander, W. H. Saunders, Jr., *Reaction Rates of Isotopic Molecules*, Wiley, New York, **1980**.
[2] *Isotope Effects in Chemical Reactions* (Eds.: C. J. Collins, N. S. Bowman), ACS Monograph 167, Van Nostrand Reinhold, New York, **1970**.
[3] a) D. A. Singleton, A. A. Thomas, *J. Am. Chem. Soc.* **1995**, *117*, 9357; b) D. A. Singleton, M. J. Szymanski, *J. Am. Chem. Soc.* **1999**, *121*, 9455.
[4] a) A. Kohen, J. P. Klinman, *Acc. Chem. Res.* **1998**, *31*, 397; b) R. P. Bell, *The Tunneling Effect in Chemistry*, Chapman & Hall, London, **1980**; c) T. Jonsson, M. H. Glickman, S. Sun, J. P. Klinman, *J. Am. Chem. Soc.* **1996**, *118*, 10319.
[5] T. Felder, C. A. Schalley, *Angew. Chem.* **2003**, *115*, 2360; *Angew. Chem. Int. Ed.* **2003**, *42*, 2258.
[6] C. E. Meloan, V.-S. Wang, R. Scriven, C. K. Kuo, *Frontiers of Flavor, Proceedings of the 5th International Flavor Conference*, Elsevier, Amsterdam, **1988**, 29.
[7] R. D. LaReau, W. Wan, V. E. Anderson, *Biochemistry* **1989**, *28*, 3619.
[8] M. Richelle , I. Tavazzi, L. B. Fay, *J. Chromatogr. B* **2003**, *794*, 1.
[9] M. Turowski, N. Yamakawa, J. Meller, K. Kimata, T. Ikegami, K. Hosoya, N. Tanaka, E. R. Thornton, *J. Am. Chem. Soc.* **2003**, *125*, 13836.
[10] D. Rechavi, A. Scarso, J. Rebek, Jr., *J. Am. Chem. Soc.* **2004**, *126*, 7738.
[11] D. Wade, *Chem.-Biol. Interact.* **1999**, *117*, 191.
[12] F. A. Lindemann, *Philos. Mag.* **1919**, *38*, 173.
[13] a) F. C. Stehling, E. Ergos, L. Mandelkern, *Macromolecules* **1971**, *4*, 672; b) F. S. Bates, H. D. Keith, D. B. McWhan, *Macromolecules* **1987**, *20*, 3065; K. Mezghani P. J. Phillips, *Macromolecules* **1994**, *27*, 6145.
[14] a) F. S. Bates, G. D. Wignall, W. C. Koehler, *Phys. Rev. Lett.* **1985**, *55*, 2425; b) F. S. Bates, G. D. Wignall, *Phys. Rev. Lett.* **1986**, *57*, 1429; c) F. S. Bates, P. J. Wiltzius, *J. Chem. Phys.* **1989**, *91*, 3258.
[15] Y.-L. Zhao, K. N. Houk, D. Rechavi, A. Scarso, J. Rebek, Jr., *J. Am. Chem. Soc.* **2004**, *126*, 11428.
[16] a) L. S. Bartell, K. Kuchitsu, R. DeNeui, *J. Chem. Phys.* **1961**, *35*, 1211; b) K. Kuchitsu L. S. Bartell, *J. Chem. Phys.* **1962**, *36*, 2470.
[17] a) C. Marquez, W. M. Nau, *Angew. Chem.* **2001**, *113*, 4515; *Angew. Chem. Int. Ed.* **2001**, *40*, 4387; b) R. Warmuth, J.-L. Kerdelhué, S. Sánchez Carrera, K. J. Langenwalter, N. Brown, *Angew. Chem.* **2002**, *114*, 102; *Angew. Chem. Int. Ed.* **2002**, *41*, 96.
[18] a) F. S. Bates, H. D. Keith, D. B. McWhan, *Macromolecules* **1987**, *20*, 3065; b) D. J. Lacks, *J. Chem. Phys.* **1995**, *103*, 5085; c) N. L. Allan T. H. K. Barron, J. A. O. Bruno, *J. Chem. Phys.* **1996**, *105*, 8300.
[19] J. C. Sherman, C. B. Knobler, D. J. Cram, *J. Am. Chem. Soc.* **1991**, *113*, 2194.
[20] J. Yoon, D. J. Cram, *J. Am. Chem. Soc.* **1997**, *119*, 11796.
[21] For other through-shell phenomena, see: a) T. A. Robbins, D. J. Cram, *J. Am. Chem. Soc.* **1993**, *115*, 12199; b) J. Yoon, D. J. Cram, *Chem. Commun.* **1997**, 2065; c) S. Mendoza, P. D. Davidov, A. E. Kaifer, *Chem. Eur. J.* **1998**, *4*, 864; d) N. Chopra, C. Naumann, J. C. Sherman, *Angew. Chem.* **2000**, *112*, 200; *Angew. Chem. Int. Ed.* **2000**, *39*, 194; e) Z. S. Romanova, K. Deshayes, P. Piotrowiak, *J. Am. Chem. Soc.* **2001**, *123*, 11029; f) M. M. Spence, S. M. Rubin, I. E. Dimitrov, E. J. Ruiz, D. E. Wemmer, A. Pines, S. Q. Yao, F. Tian, P. G. Schultz, *Proc. Natl. Acad. Sci. USA* **2001**, *98*, 10654; g) Z. S. Romanova, K. Deshayes, P. Piotrowiak, *J. Am. Chem. Soc.* **2001**, *123*, 2444; h) C. Kemmis, R. Warmuth, *J. Supramol. Chem.* **2003**, 253; i) T. Amaya; J. Rebek, Jr., *J. Am. Chem. Soc.* **2004**, *126*, 6216; j) G. W. V. Cave, J. Antesberger, L. J. Barbour, R. M. McKinlay, J. L. Atwood, *Angew. Chem.* **2004**, *116*, 5375; *Angew. Chem. Int. Ed.* **2004**, *43*, 5263.
[22] F. Hof, S. L. Craig, C. Nuckolls, J. Rebek, Jr., *Angew. Chem.* **2002**, *114*, 1556; *Angew. Chem. Int. Ed.* **2002**, *41*, 1488.
[23] T. A. Robbins, C. B. Knobler, D. R. Bellew, D. J. Cram, *J. Am. Chem. Soc.* **1994**, *116*, 111.
[24] R. Warmuth, E. F. Maverick, C. B. Knobler, D. J. Cram, *J. Org. Chem.* **2003**, *68*, 2077.
[25] D. A. Makeiff, D. J. Pope, J. C. Sherman, *J. Am. Chem. Soc.* **2000**, *122*, 1337.
[26] S. Mecozzi, J. Rebek, Jr., *Chem. Eur. J.* **1998**, *4*, 1016.
[27] Longer simulation times (up to 40 ns) had little effect on the value of *d*.
[28] The order of elution was determined from the relative peak intensities for 3:1 and 1:2 mixtures of **3**⊙*p*-xylene and **3**⊙[D_{10}]-*p*-xylene.
[29] L. S. Bartell, R. R. Roskos, *J. Chem. Phys.* **1966**, *44*, 457.
[30] R. G. Chapman, J. C. Sherman, *J. Am. Chem. Soc.* **1999**, *121*, 1962.

 © 2005 Wiley-VCH Verlag GmbH & Co. KGaA, Weinheim

Magnetic Compounds

DOI: 10.1002/anie.200501987

Hysteretic Magnetic Bistability Based on a Molecular Azide Switch**

*Guido Leibeling, Serhiy Demeshko, Sebastian Dechert, and Franc Meyer**

Dedicated to Professor Gottfried Huttner on the occasion of his 68th birthday

Materials that exhibit hysteretic bistability at temperatures not too far from ambient conditions are expected to have great potential for future memory or sensing applications.[1] The two relatively stable states should be clearly distinguished by their physical properties, such as their magnetic or optical characteristics. Thermal magnetic hysteresis with an abrupt and rapid property change around room temperature is particularly rare for molecule-based materials,[2] with spin-crossover compounds providing the most prominent examples.[3] More recently, magnetic hysteresis has also been observed for some molecular organic radicals[4] or transition metal coordination compounds,[5,6] where switching between two states occurs through a thermal phase transition with orientational changes in the 3D crystal lattice. Herein, we report thermal hysteresis of the magnetic susceptibility for single crystals of the molecular dinickel(II) complex $[LNi_2(N_3)_3]$ (**1**), in which a $\mu_{1,3}$-azido ligand functions as an on/off switch for the intramolecular antiferromagnetic coupling between the two metal ions.

Pyrazolate-based compartmental ligands such as L^-, which bears thioether side-arms, have previously proven suitable as dinucleating scaffolds for the synthesis of preorganized azidonickel(II) complexes that can serve as modules for the assembly of oligonuclear species or 1D extended chain compounds;[7] the bimetallic complex **1** was prepared as a potential building block in this context. Single crystals of **1** were grown from acetone/hexane, and an initial X-ray crystallographic analysis was carried out at 133 K (Figure 1).[8] As anticipated, both nickel ions in the C_2-symmetric array are nested within their respective ligand compartment (with two sulfur and one nitrogen donors from the ligand side-arm) and are spanned by the bridging pyrazolate. A $\mu_{1,3}$-azido bridge is found within the bimetallic pocket, and an additional terminal azide fills the remaining site at each of the six-coordinate metal ions.

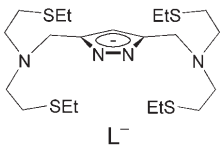

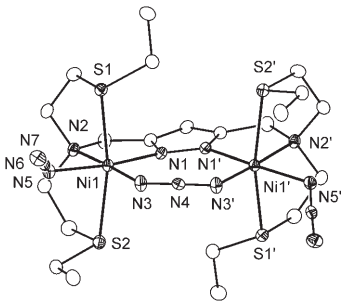

Figure 1. ORTEP plot (30% probability thermal ellipsoids) of the structure of **1** at 133 K. All hydrogen atoms have been omitted for the sake of clarity.

Since **1** did not exhibit any unusual structural features at this stage, the temperature dependence of its magnetic susceptibility was highly unexpected. The product $\chi_M T$ for a polycrystalline sample of **1** is depicted in Figure 2 for both decreasing and increasing temperature. The value of $1.82\ cm^3 K mol^{-1}$ at 300 K is somewhat lower then the spin-only value expected for two uncoupled high-spin nickel(II) ions ($2.14\ cm^3 K mol^{-1}$ for $g = 2.07$), and decreases only slightly upon lowering the temperature to 220 K. At 215 K, however, an abrupt drop of $\chi_M T$ occurs (centered at $T_\downarrow = 212$ K), followed by a much more rapid decline at lower temperatures; below 50 K $\chi_M T$ tends towards zero. The low-temperature data are indicative of strong antiferromagnetic coupling and an $S = 0$ ground state, while coupling is apparently only weak above 220 K. $\chi_M T$ shows an analogous behavior when measured as a function of increasing temperature, but exhibits thermal hysteresis with $\Delta T \approx 13$ K ($T_\uparrow$

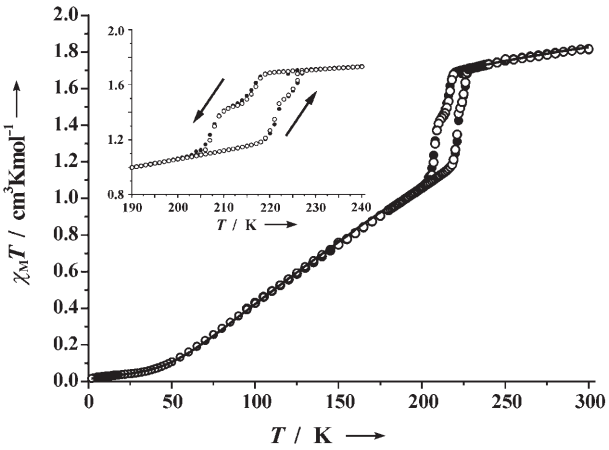

Figure 2. Plot of $\chi_M T(T)$ at two different magnetic fields (closed circles: 5000 G; open circles: 2000 G) for decreasing and increasing temperature. The solid lines represent the calculated curve fits at high and low temperature (see text). The inset shows an enlargement for the temperature region between 190 und 240 K.

[*] Dr. G. Leibeling, S. Demeshko, Dr. S. Dechert, Prof. Dr. F. Meyer
Institut für Anorganische Chemie
Georg-August-Universität Göttingen
Tammannstrasse 4, 37077 Göttingen (Germany)
Fax: (+49) 551-39-3063
E-mail: franc.meyer@chemie.uni-goettingen.de

[**] Financial support from the DFG (priority program 1137 "Molecular Magnetism") is gratefully acknowledged.

Supporting information for this article is available on the WWW under http://www.angewandte.org or from the author.

© 2005 Wiley-VCH Verlag GmbH & Co. KGaA, Weinheim

centered at 223 K). No field dependence of the magnetic data was observed. Complex **1** thus undergoes a reversible and field-independent switching of the magnitude of the magnetic exchange interaction, with hysteresis occurring not too far from room temperature.

The experimental magnetic data were modeled separately in the range from 200 to 5 K and above 230 K using Equation (1), which is deduced from the Hamiltonian $\mathscr{H} = -2J\hat{S}_1\hat{S}_2$, with additional terms accounting for residual amounts of paramagnetic impurity (ρ), and for the temperature-independent paramagnetism (TIP).

$$\chi_M = \frac{N g^2 \mu_B^2}{k T}\frac{2e^{2(J/kT)} + 10e^{6(J/kT)}}{1 + 3e^{2(J/kT)} + 5e^{6(J/kT)}}(1-\rho) + \frac{2N g^2 \mu_B^2}{3kT}\rho + \mathrm{TIP} \qquad (1)$$

Good fits were obtained with the parameters $g = 2.24 \pm 0.01$, $J = -(81 \pm 1.5)\ \mathrm{cm}^{-1}$ ($\rho = (0.6 \pm 0.1)\%$; $\mathrm{TIP} = 1.2 \times 10^{-3}$) at low temperatures and $g = 2.07 \pm 0.01$, $J = -(24 \pm 1.0)\ \mathrm{cm}^{-1}$ ($\rho = (0.8 \pm 0.1)\%$; $\mathrm{TIP} = 1.0 \times 10^{-4}$) above 230 K,[9] thereby confirming the drastic differences in the strength of the antiferromagnetic coupling for the two temperature domains, with strong or weak antiferromagnetic coupling below or above the hysteretic transition, respectively.

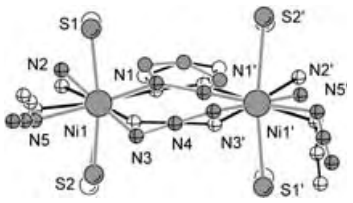

Figure 3. Overlay of the molecular structures at 253 K (grey) and 133 K (white) of **1**, showing the changes of the dihedral angles. Selected interatomic distances [Å] and angles [°] at 133 K [253 K]: Ni1-N1 2.071(3) [2.065(2)], Ni1-N2 2.139(3) [2.136(3)], Ni1-N3 2.056(3) [2.078(3)], Ni1-N5 2.079(3) [2.067(3)], Ni1-S1 2.4279(9) [2.436(1)], Ni1-S2 2.5319(9) [2.496(1)], Ni1···Ni1′ 4.5538(8) [4.5201(8)], N3-N4 1.174(3) [1.170(3)]; N1-Ni1-N5 170.6(1) [171.2(1)], N2-Ni1-N3 177.3(1) [178.4(1)], S1-Ni1-S2 167.96(3) [169.26(4)], N1-Ni1-N2 82.6(1) [82.3(1)], N2-Ni1-N5 88.7(1) [88.9(1)], N5-Ni1-N3 91.4(1) [92.7(1)], N3-Ni1-N1 97.5(1) [96.1(1)], N4-N3-Ni1 120.7(3) [116.7(3)], N3-N4-N3′ 176.4(5) [177.5(5)]. Symmetry transformation used to generate equivalent atoms (′): 1−*x*, *y*, 1.5−*z*.

Table 1: Unit-cell parameters and selected dihedral angles for **1** at different temperatures.

T [K]	*a* [Å]	*b* [Å]	*c* [Å]	*V* [Å^3]	Ni1-N1-N1′-Ni1′ [°]	Ni1-N3-N3′-Ni1′ [°]
133	15.9739(12)	8.6167(8)	22.8983(17)	3151.8(4)	23.1(6)	4.3(4)
195	16.0886(12)	8.6241(8)	22.9437(16)	3183.4(4)	20.9(7)	4.8(5)
223	16.3424(12)	8.6933(8)	22.9634(15)	3262.4(4)	−39.8(7)	−48.7(4)
253	16.3677(10)	8.7169(7)	22.9876(13)	3279.8(4)	−38.8(6)	−46.6(4)

In order to elucidate the molecular cause of this unexpected magnetic behavior and to characterize the magnetic phase transition, a single crystal of **1** was investigated crystallographically at different temperatures. The crystal was first mounted at room temperature and data sets were then collected at 253, 173, 223, and 195 K (in that order). In each case the temperature was allowed to equilibrate for one hour before data collection was started. It is apparent from the crystallographic data that the crystal stays intact upon temperature variation and repeated shuttling through the hysteresis range as the crystal system remains orthorhombic for all temperatures. Inspection of the molecular structures above and below the hysteresis temperature, however, reveals significant differences of the bimetallic scaffold. These differences can clearly be seen by overlaying the molecular structures of the central dinickel core obtained at 133 and 253 K (Figure 3).

Structural alterations are basically expressed through changes of the dihedral angle formed by the two metal centers and the outer nitrogen atoms of the bridging azide (N3 and N3′) as well as the dihedral angle formed by the metals and the pyrazolate nitrogen atoms (N1 and N1′) (Table 1). A major change is observed between 195 and 223 K, which is consistent with the abrupt drop of the magnetic susceptibility in this temperature range. Between 133 and 195 K or between 223 and 253 K, however, the dihedral angles show no significant variation, which is again in agreement with the magnetic data.

The unusual magnetic properties of **1** can be rationalized on the basis of the crystallographic findings. While some contribution to magnetic coupling from the pyrazolate is certainly present, it is likely that the azide provides the dominant intramolecular pathway.[10] Magnetostructural correlations for $\mu_{1,3}$-azido bridged dinickel(II) complexes have revealed that two geometric parameters, namely the Ni-N-N angles and the dihedral angle, ϕ, along the azide ligand, are of major importance.[11,12] For a Ni-NNN-Ni torsion angle of $\phi = 180°$, the antiferromagnetic coupling is predicted to have a maximum at Ni-N-N angles of around 108° and to decrease at larger angles. On the other hand, the maximum coupling for all Ni-N-N angles is expected for a torsion of 180° (or 0°). In the absence of any constraining ligand scaffold, Ni-N-N angles in dinuclear complexes or 1D extended systems with a single $\mu_{1,3}$-azido bridge tend to lie in the range 115–145°, with $\phi = 140$–180°, thus resulting in J values in the range −17 to $-100\ \mathrm{cm}^{-1}$.[11] A particularly strong antiferromagnetic coupling of around $-100\ \mathrm{cm}^{-1}$ has been observed for some 1D chain complexes with a *trans*-{Ni-($\mu_{1,3}$-N_3)-Ni} motif featuring acute Ni-N-N angles (120.9 or 115.6/116.8°, respectively) and a large ϕ (180 or 175.5°, respectively),[11,13] or in a dinickel(II) complex with extremely obtuse Ni-N-N angles of 109.9°.[14] Similar correlations appear also to be valid for μ_3- or μ_4-azide linkages.[7]

In the case of **1** the Ni1-N3-N4 angles are quite acute and are similar at 133 K [120.7(3)°] and 253 K [116.7(3)°], whereas the torsion Ni-NNN-Ni differs dramatically [4.3(4) versus −46.6(4)°]. Given the above-mentioned magnetostructural correlations, a large antiferromagnetic intramolecular coupling of the order of almost $-100\ \mathrm{cm}^{-1}$ can thus be anticipated for the low-temperature phase (where the torsion angle is close to 0°), while a significantly diminished coupling should result from the severe tilting of the azide bridge in the high-temperature species, in accordance with the experimental

 © 2005 Wiley-VCH Verlag GmbH & Co. KGaA, Weinheim

findings ($-(81\pm1.5)$ versus $-(24\pm1.0)\,cm^{-1}$). Hence, the bridging azide within the bimetallic pocket of the dinickel(II) scaffold of **1** can be viewed as a molecular on/off switch for the antiferromagnetic coupling between the two metal ions.

Close inspection of the crystallographic changes accompanying the phase transition reveals that the sulfur-bound ethyl groups of the ligand side arms of L^- are disordered about two positions above the hysteresis range (at 223 and 253 K), with temperature-dependent occupancy factors for S2-Et, whereas this disorder disappears below the hysteresis range. Concomitantly, an abrupt shrinkage of the crystallographic *a* axis upon cooling below the hysteresis range is observed, whereas the changes of the *b* and *c* axes are only minor (Table 1). As can be seen from the unit-cell plot (Figure S1 in the Supporting Information), the disordered ethyl group bound to S2 affects the stacking along the *a* axis. The abrupt shrinkage of this axis can thus be linked to the disappearance of the disorder, which apparently allows a more efficient packing of the molecules at low temperatures. However, it is still unclear at this stage how the appearance or disappearance of the disorder is coupled to the changes of the dihedral Ni-NNN-Ni angle within the bimetallic molecules.

Interestingly, a two-step behavior of the phase transition is discernible from the magnetic data. The DSC curve not only reflects the approximately 20-K hysteresis, but also this two-step behavior of the phase transition (Figure 4). Determination of the cause of this unusual feature and a more detailed analysis of the phase transition is currently under investigation.

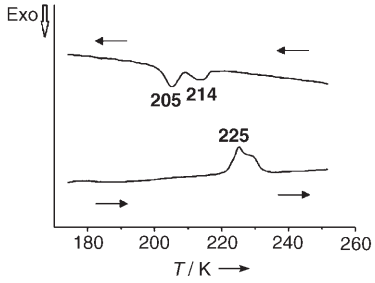

Figure 4. DSC curve for **1** showing the two-step thermal hysteresis between 205 and 230 K.

While phenomenologically reminiscent of spin-crossover behavior, the origin of the thermal magnetic bistability of **1** is fundamentally different: both metal ions retain their individual high-spin ($S=1$) state, but the bridging azide acts as a toggle switch that turns the antiferromagnetic coupling between the nickel(II) ions on or off. While phase transitions associated with small changes in magnetic properties have been observed for polymeric metal azide systems,[15] a hysteresis as distinct as that observed for **1** is unprecedented, and to the best of our knowledge this is the first case where both the high- and low-temperature phases have been characterized crystallographically to reveal the azide functioning as a well-defined molecular switch. Current work focuses on, inter alia, elucidating the cause of the two-step hysteretic behavior as well as investigating pressure effects on the magnetic bistability of **1**.

Experimental Section

Caution! Although no problems were encountered in this work, transition metal perchlorate and azide complexes are potentially explosive and should be handled with due care.

$[LNi_2(N_3)_3]$ (**1**): A solution of HL[16] (512 mg, 1.07 mmol) in methanol (65 mL) was treated with KO*t*Bu (1 equiv, 120 mg, 1.07 mmol). After stirring the mixture for 1 h at room temperature, $Ni(ClO_4)_2\cdot 6H_2O$ (2 equiv, 783 mg, 2.14 mmol) was added and the reaction mixture was stirred overnight. Any white precipitate was then removed by filtration and the resulting green solution was treated with 3.5 equiv of NaN_3 (244 mg, 3.75 mmol) and the mixture again stirred overnight. The light-green precipitate was separated by filtration and the resulting green solution was evaporated to dryness. The residue was taken up in acetone (15 mL) and layered with hexane (15 mL) to obtain green crystals of **1** (275 mg, 36%). IR (KBr): $\tilde{\nu}=$ 2965 (w), 2924 (w), 2870 (w), 2854(w), 2043 [(vs), $\nu(N_3^-)$], 1454 (w), 1418 (w), 778 (w) cm^{-1}. MS(FAB+): m/z (%) = 677 (100) $[LNi_2(N_3)_2]^+$, 635 (15) $[LNi_2(N_3)]^+$. $C_{21}H_{41}N_{13}Ni_2S_4$ (721.3): calcd.: C 34.97, H 5.73, N 25.24; found: C 35.03, H 5.75, N 24.60.

Received: June 8, 2005
Published online: October 7, 2005

Keywords: azides · bridging ligands · magnetic properties · molecular switches · nickel

[1] O. Kahn, J. P. Launay, *Chemtronics* **1988**, *3*, 140–151.
[2] J. S. Miller, *Angew. Chem.* **2003**, *115*, 27–29; *Angew. Chem. Int. Ed.* **2003**, *42*, 27–29.
[3] a) P. Gütlich, A. Hauser, H. Spiering, *Angew. Chem.* **1994**, *106*, 2109–2141; *Angew. Chem. Int. Ed. Engl.* **1994**, *33*, 2024–2054; b) O. Kahn, C. J. Martinez, *Science* **1998**, *279*, 44–48; c) O. Kahn, J. Kröber, C. Jay, *Adv. Mater.* **1992**, *4*, 718–728; d) A. Bousseksou, G. Molnár, G. Matouzenko, *Eur. J. Inorg. Chem.* **2004**, 4353–4369.
[4] a) W. Fujita, K. Awaga, *Science* **1999**, *286*, 261–262; b) W. Fujita, K. Awaga, *J. Solid State Chem.* **2001**, *159*, 451–454; c) M. E. Itkis, X. Chi, A. W. Cordes, R. C. Haddon, *Science* **2002**, *296*, 1443–1445; d) J. L. Brussom, O. P. Clements, R. C. Haddon, M. E. Itkis, A. A. Leitch, R. T. Oakley, R. W. Reed, J. F. Richardson, *J. Am. Chem. Soc.* **2004**, *126*, 14692–14693.
[5] F. L. De Panthou, D. Luneau, R. Musin, L. Öhrström, A. Grand, P. Turek, P. Rey, *Inorg. Chem.* **1996**, *35*, 3484–3491.
[6] a) J. M. Migliori, W. M. Reiff, A. M. Arif, J. S. Miller, *Inorg. Chem.* **2004**, *43*, 6875–6877; b) S. M. Humphrey, P. T. Wood, *J. Am. Chem. Soc.* **2004**, *126*, 13236–13237.
[7] a) F. Meyer, P. Kircher, H. Pritzkow, *Chem. Commun.* **2003**, 774–775; b) S. Demeshko, G. Leibeling, W. Maringgele, F. Meyer, C. Mennerich, H.-H. Klauss, H. Pritzkow, *Inorg. Chem.* **2005**, *44*, 519–528; c) F. Meyer, S. Demeshko, G. Leibeling, B. Kerstiug, E. Kaifer, H. Pritzkow, *Chem. Eur. J.* **2005**, *11*, 1518–1526.
[8] X-ray structure data: Stoe IPDS II diffractometer, ω scans, $Mo_{K\alpha}$ radiation ($\lambda=0.71093$ Å), graphite monochromator, structure solution with direct methods and refinement against F^2 (SHELX-97)[17] with anisotropic thermal parameters for all non-hydrogen atoms; for hydrogen atoms fixed isotropic thermal parameters ($U_{iso}=0.08$ Å^2) on calculated positions were used. Crystal dimensions: $0.21\times0.16\times0.12$ mm^3, orthorhombic, space group *Pbcn* (no. 60), $Z=4$, $F(000)=1512$. At 223 and 253 K the sulfur-bound ethyl groups are disordered about two positions with temperature-dependent occupancy factors (S1-Et at 253 K: 0.46(7)/0.54(7); at 223 K: 0.46(8)/0.54(8). S2-Et at 253 K: 0.766(9)/0.234(9); at 223 K: 0.836(10)/0.164(10)). For the disordered parts, DFIX restraints were applied for the S–C

 © 2005 Wiley-VCH Verlag GmbH & Co. KGaA, Weinheim

(1.81 Å) and C–C (1.51 Å) distances, with DELU and SIMU restraints for refinement with anisotropic displacement parameters. Data collection at 133 K: $a = 15.9739(12)$, $b = 8.6167(8)$, $c = 22.8983(17)$ Å, $V = 3151.8(4)$ Å^3, $\rho_{calcd} = 1.520$ kg m^{-3}, $\mu = 1.496$ mm^{-1}, $3.6 \le 2\theta \le 49.4°$, $-18 \le h \le 18$, $-10 \le k \le 9$, $-24 \le l \le 26$, 13945 data collected, 2679 unique data ($R_{int} = 0.0647$), 2123 data with $I > 2\sigma(I)$, 184 refined parameters, GOF(F^2) = 1.057, final R indices: $R1 = 0.0368$ (0.0556 all data), $wR2 = 0.0680$ (0.0731 all data), max./min. residual electron density: 0.365/−0.427 e Å^{-3}. Data collection at 195 K: $a = 16.0886(12)$, $b = 8.6241(8)$, $c = 22.9437(16)$ Å, $V = 3183.4(4)$ Å^3, $\rho_{calcd} = 1.505$ kg m^{-3}, $\mu = 1.481$ mm^{-1}, $3.6 \le 2\theta \le 49.4°$, $-18 \le h \le 18$, $-10 \le k \le 9$, $-24 \le l \le 26$, 14216 data collected, 2706 unique data ($R_{int} = 0.0745$), 2031 data with $I > 2\sigma(I)$, 184 refined parameters, GOF(F^2) = 1.092, final R indices: $R1 = 0.0422$ (0.0672 all data), $wR2 = 0.0780$ (0.0848 all data), max./min. residual electron density: 0.465/−0.280 e Å^{-3}. Data collection at 223 K: $a = 16.3424(12)$, $b = 8.6933(8)$, $c = 22.9634(15)$ Å, $V = 3262.4(4)$ Å^3, $\rho_{calcd} = 1.469$ kg m^{-3}, $\mu = 1.446$ mm^{-1}, $3.5 \le 2\theta \le 49.6°$, $-19 \le h \le 19$, $-9 \le k \le 10$, $-26 \le l \le 24$, 14688 data collected, 2784 unique data ($R_{int} = 0.0752$), 2016 data with $I > 2\sigma(I)$, 220 refined parameters, GOF(F^2) = 1.060, final R indices: $R1 = 0.0437$ (0.0728 all data), $wR2 = 0.0748$ (0.0826 all data), max./min. residual electron density: 0.344/−0.228 e Å^{-3}. Data collection at 253 K: $a = 16.3677(10)$, $b = 8.7169(7)$, $c = 22.9876(13)$ Å, $V = 3279.8(4)$ Å^3, $\rho_{calcd} = 1.461$ kg m^{-3}, $\mu = 1.438$ mm^{-1}, $3.5 \le 2\theta \le 49.7°$, $-19 \le h \le 19$, $-10 \le k \le 10$, $-24 \le l \le 27$, 19079 data collected, 2838 unique data ($R_{int} = 0.0706$), 2045 data with $I > 2\sigma(I)$, 220 refined parameters, GOF(F^2) = 1.019, final R indices: $R1 = 0.0370$ (0.0614 all data), $wR2 = 0.0729$ (0.0804 all data), max./min. residual electron density: 0.260/−0.230 e Å^{-3}. CCDC-271898 (133 K), -271899 (195 K), -271900 (223 K), and -271901 (253 K) contain the supplementary crystallographic data for this paper. These data can be obtained free of charge from the Cambridge Crystallographic Data Centre via www.ccdc.cam.ac.uk/data_request/cif.

[9] Parameters obtained for data above 230 K should be interpreted with care because of the limited temperature range available for the fitting procedure.

[10] a) M. Konrad, F. Meyer, A. Jacobi, P. Kircher, P. Rutsch, L. Zsolnai, *Inorg. Chem.* **1999**, *38*, 4559 – 4566; b) G. Leibeling, S. Demeshko, B. Bauer-Siebenlist, F. Meyer, H. Pritzkow, *Eur. J. Inorg. Chem.* **2004**, 2413 – 2420.

[11] J. Ribas, A. Escuer, M. Monfort, R. Vicente, R. Cortés, L. Lezama, T. Rojo, *Coord. Chem. Rev.* **1999**, *193–195*, 1027 – 1068, and references therein.

[12] F. Meyer, H. Kozlowski in *Comprehensive Coordination Chemistry II, Vol. 6* (Eds.: J. A. McCleverty, T. J. Meyer), Pergamon, **2004**, pp. 247 – 554.

[13] R. Vicente, A. Escuer, J. Ribas, M. S. El Fallah, X. Solans, M. Font-Bardia, *Inorg. Chem.* **1995**, *34*, 1278 – 1281.

[14] J. Hausmann, M. H. Klingele, V. Lozan, G. Steinfeld, D. Siebert, Y. Journaux, J. J. Girerd, B. Kersting, *Chem. Eur. J.* **2004**, *10*, 1716 – 1728.

[15] a) A. Escuer, R. Vicente, J. Ribas, X. Solans, *Inorg. Chem.* **1995**, *34*, 1793 – 1798; b) M. Monfort, J. Ribas, X. Solans, M. Font-Bardia, *Inorg. Chem.* **1996**, *35*, 7633 – 7638; c) F. A. Mautner, R. Cortés, L. Lezama, T. Rojo, *Angew. Chem.* **1996**, *108*, 96 – 98; *Angew. Chem. Int. Ed. Engl.* **1996**, *35*, 78 – 80.

[16] M. Konrad, F. Meyer, K. Heinze, L. Zsolnai, *J. Chem. Soc. Dalton Trans.* **1998**, 199 – 205.

[17] G. M. Sheldrick, SHELXL-97, Program for Crystal Structure Refinement, University of Göttingen, Göttingen (Germany), **1997**; G. M. Sheldrick, SHELXS-97, Program for Crystal Structure Solution, University of Göttingen, Göttingen (Germany), **1997**.

 © 2005 Wiley-VCH Verlag GmbH & Co. KGaA, Weinheim

Synthetic Methods

DOI: 10.1002/anie.200502038

Chemo-, Regio-, and Stereoselective Cobalt-Mediated [2+2+2] Cycloaddition of Alkynyl Boronates to Alkenes: 1,3- and 1,4-Diboryl-1,3-cyclohexadienes**

*Vincent Gandon, David Leboeuf, Sabine Amslinger, K. Peter C. Vollhardt, Max Malacria, and Corinne Aubert**

Alkenylboranes are useful intermediates for the preparation of a wide range of important organic compounds.[1] Specifically, mono- and diborylated 1,3-dienes have found various applications in dienylations,[2] Diels–Alder reactions,[3] and in the synthesis of α,β- or γ,δ-unsaturated ketones.[4] Their cyclic counterparts, namely boryl-1,3-cyclohexadienes, are as yet unknown. Considering that the 1,3-cyclohexadiene nucleus is a key subunit of many natural and/or biologically active compounds,[5] including those of the didehydroretinol and -carotene families,[6] borylated 1,3-cyclohexadienes constitute valuable reagents with which to introduce this synthon directly. The latter task has been accomplished in the past by using 1,3-cyclohexadienyl–metal complexes,[7] triflates,[8] or phosphates,[9] although these reagents have to be generated in several steps from enolizable cyclohexenone derivatives; this methodology has not been applied to dimetalated 1,3-cyclohexadienes.[10] We report here the preparation of 1,3- and 1,4-diboryl-1,3-cyclohexadienes by means of the cobalt-mediated [2+2+2] cocyclization of alkynyl boronates with alkenes.[11] Alkynyl boronates have recently been used as substrates in various transition-metal-mediated reactions[12] that lead to valuable building blocks, because the newly formed C_{sp^2}–B bonds can be subjected to couplings[13] and a plethora of other functional group transformations.[14] Siebert et al. have shown

[*] Dr. V. Gandon, D. Leboeuf, Prof. Dr. M. Malacria, Dr. C. Aubert
Université Pierre et Marie Curie
Institut de Chimie Moléculaire-FR2769
Laboratoire de Chimie Organique -UMR 7611
Tour 44–54, 2° étage, CC. 229, 4 place Jussieu, 75252 Paris Cedex 05 (France)
Fax: (+33) 1-4427-7360
E-mail: aubert@ccr.jussieu.fr
Dr. S. Amslinger, Prof. Dr. K. P. C. Vollhardt
Center for New Directions in Organic Synthesis
Department of Chemistry
University of California at Berkeley
and
Chemical Sciences Division
Lawrence Berkeley National Laboratory
Berkeley, CA 94720-1460 (USA)

[**] This work was supported by CNRS, MRES, and by the NSF (CHE 0451241). The Center for New Directions in Organic Synthesis is enabled by Bristol–Myers Squibb as a Sponsoring Member and Novartis as a Supporting Member.

Supporting information for this article is available on the WWW under http://www.angewandte.org or from the author.

InterScience
© 2005 Wiley-VCH Verlag GmbH & Co. KGaA, Weinheim

that catechol-substituted mono- and diborylalkynes undergo facile catalytic cyclotrimerization in the presence of cobalt(0) or cobalt(I) complexes to furnish oligoborylarenes.[12g] We have recently disclosed that alkynyl(pinacol)boronic esters add to α,ω-diynes under similar experimental conditions to assemble fused arylboronic esters.[12i]

The success of the present study was predicated on the employment of η^5-cyclopentadienylbis(ethene)cobalt (**1**),[15] which we have employed previously as an active source of CpCo in cooligomerizations of alkynes with alkenes.[11c–e] Preliminary experiments were carried out under an ethene atmosphere by treating **1** with two equivalents of alkynyl(pinacol)boronic esters **2**–**6** in THF (Table 1).[16] Under these

Table 1: CpCo-mediated cycloaddition of alkynylboronic esters to ethene.

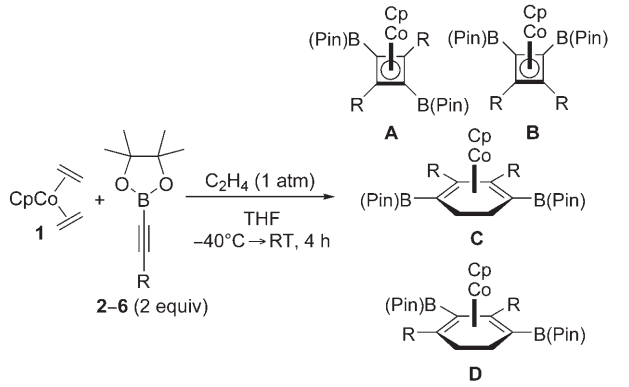

Entry	R	**A**/**B** (yield [%])[a]	**C**/**D** (yield [%])[a]
1	*t*Bu (**2**)	**7A**/**7B** 1:0 (59)	–
2	*i*Pr (**3**)	**8A**/**8B** 3.4:1 (54)[b]	**8C**/**8D** 1:0 (18)
3	C_6H_{13} (**4**)	–	**9C**/**9D** 1.5:1 (93)[c]
4	CH_2OMe (**5**)	–	**10C**/**10D** 1:9 (84)[b]
5	Ph (**6**)	–	**11C**/**11D** 1:20 (92)[b,d]

[a] Yields of product isolated after flash chromatography. [b] Unseparated mixture. [c] The yield is the sum of those for isolated **9C** (56%) and **9D** (37%). [d] The yield is that for complex **11D**, obtained pure by crystallization from the mixture in hexane. The presence of **11C** was surmised on the basis of the ^{1}H NMR spectroscopic data of the mixture.

conditions, alkyne cyclotrimerization[12g,i] was suppressed in favour of the formation of mixtures of the regioisomeric 1,2- and 1,3-diboryl(η^4-cyclobutadiene)cyclopentadienylcobalt complexes **A** and **B**, respectively, as well as the 1,4- and 1,3-diboryl(η^4-1,3-cyclohexadiene)cyclopentadienylcobalt complexes **C** and **D**, respectively. The 2,3-diboryl(η^4-1,3-cyclohexadiene) substitution pattern was notably absent.

These air-stable products were purified by flash chromatography on silica gel. As shown in Table 1 (entry 1), only the 1,3-diboryl(η^4-cyclobutadiene)cyclopentadienylcobalt complex **7A** was formed for R = *t*Bu. Its structure was confirmed unambiguously by an X-ray analysis (see Supporting Information). Changing the alkynyl substituent to the less bulky *i*Pr group (entry 2) resulted in the formation of a mixture of **8A** and **8B** in 54% yield, accompanied by 18% of the 1,4-diboryl(η^4-1,3-cyclohexadiene)cyclopentadienylcobalt complex **8C**. Following this trend, the reaction with the hexyl-substituted boronic ester **4** afforded products **9C** and **9D** in an excellent 93% yield in the ratio 1.5:1 without side products (entry 3). Similar yields (84% and 92%, respectively), but better regioselectivities for 1,3-diborylated products (9:1 and 20:1, respectively) were obtained with **5** or **6** as starting materials (entries 4 and 5). The less symmetrical structures of isomers **9D**–**11D** were readily assigned by NMR spectroscopy, and the structure of **11D** was confirmed by a single-crystal X-ray analysis (Figure 1).[17] Interestingly, boryl substitution

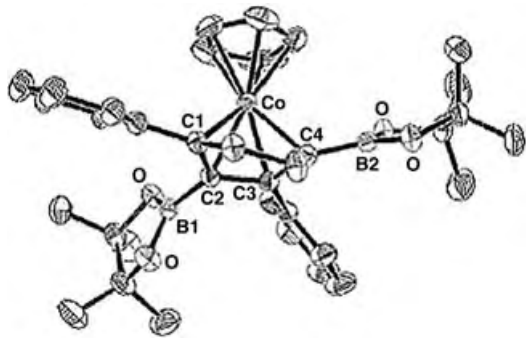

Figure 1. ORTEP view of complex **11D** in the solid state (30% probability thermal ellipsoids). Selected bond lengths [Å] and angles [°]: Co–C_{Cp} 2.05 (av), C2–B1 1.565(5), C4–B2 1.546(5), B–O 1.37 (av), C–C_{diene} 1.44 (av), Co–C1 2.062(3), Co–C2 1.996(3); C1-C2-C3-C(4) 3.9.

does not cause significant structural alteration of the CpCo(η^4-1,3-cyclohexadiene) core of the component fragments.[18] The higher symmetry of complexes **8C**–**10C** was again evident from their NMR spectra, and a distinction between the 2,3- and 1,4-diboryl substitution pattern was possible on the basis of the characteristic chemical shifts of the complexed diene carbons,[11c,e,18a] in conjunction with the effect of boron nuclear quadrupole broadening. Hence, the clearly resolved peaks at $\delta = 110.0$, 105.2, and 100.1 ppm are diagnostic of alkyl-substituted internal quaternary diene carbons in **8C**, **9C**, and **10C**, respectively, whereas the terminal carbons are either unobservable (**8C**, **10C**) or appear as a broad signal at $\delta = 46.7$ ppm (**9C**).

The results in Table 1 are consistent with the notions that steric effects dominate the chemistry of the putative intermediate CpCo(dialkyne) complexes and the resulting metallacycles, which are the relay points on route to the metalated cyclobutadiene and cyclohexadiene products.[11,19] When R is bulky, the route leading to the former is favored[19b] and the steric hindrance retards alkene incorporation to the latter; cyclohexadiene formation is dominant for less bulky R groups. Similarly, the regioselectivity appears to be controlled by the largest substituent, thus favoring the ostensibly least sterically demanding 2,4-substitution in the cobaltacyclopentadiene. When R is larger or smaller than $B(OR)_2$ such control is extensive (**7A**, **10D**, **11D**), whereas when R is comparable to $B(OR)_2$ it is not. Remarkably, an electronic influence of the boryl group is not evident.[20]

The cyclization is not restricted to ethene, and with **6** as the alkyne component and five equivalents of alkene the

 © 2005 Wiley-VCH Verlag GmbH & Co. KGaA, Weinheim

results summarized in Table 2 and Table 3 were obtained. Specifically, the alkene and **1** were stirred initially in THF at room temperature for 4 h,[21] during which ethene evolution was visible. Subsequently, **6** was added at −40 °C, followed by stirring at room temperature for 4 h. With 2,5-dihydrofuran, cyclopentene, and cyclohexene, the reactions proceeded completely regioselectively in very good overall yields, with moderate to excellent stereoselectivity and no competing ethene insertion (Table 2). Stereochemical assignments were based on the characteristic chemical shifts of the tertiary cyclohexadiene hydrogen atoms, which are shielded when located *anti* to cobalt and deshielded when located *syn*.[11c,e,18a,22] The *endo* diastereomer was favored in all cases, in agreement with the stereochemical preference of cycloadditions of some α,ω-diynes to pyrimidines[23] and indoles.[24]

Table 2: CpCo-mediated cocyclizations of **6** with cyclic alkenes.

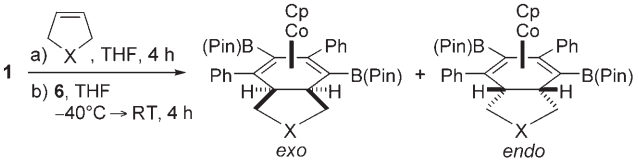

Entry	X	*exo*/*endo*[a] (yield [%])[b]
1	O	**12**/**13** 1:3.6 (88)
2	CH_2	**14**/**15** 1:1.9 (86)
3	$(CH_2)_2$	**16**/**17** 1:20 (70)

[a] The designations *exo* and *endo* refer to the configuration of the precursor cobaltacyclopentadiene(alkene) complexes and are in analogy to Diels–Alder cycloaddition terminology. [b] Yields of product isolated after flash chromatography on SiO_2. Compounds **13**–**15** could be obtained in pure form, but **12** remained contaminated by some **13**, and **17** by traces of **16.**

Table 3: CpCo-mediated cocyclizations of **6** with acyclic alkenes.

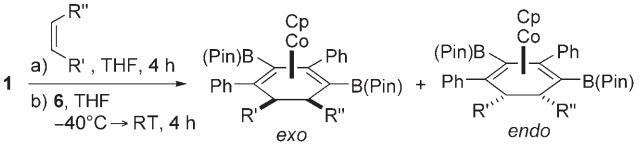

Entry	R′	R″	*exo* or *endo*[a] (yield [%])[b]
1	Ph	Ph	**18**, *endo* (25)
2	H	Ph	**19**, *endo* (50)
3	H	$SiMe_3$	**20**, *exo* (50)
	$SiMe_3$	H	**21**, *exo* (18)
4	H	$SnBu_3$	**22**, *exo* (34)
	$SnBu_3$	H	**23**, *exo* (11)

[a] The designations *exo* and *endo* refer to the configuration of the precursor cobaltacyclopentadiene(alkene) complexes and are in analogy to Diels–Alder cycloaddition terminology. Regio- and stereochemical assignments were made by chemical shift, NOE, DEPT, and 2D-NMR (COSY, HMBC) analyses. [b] Yields of product isolated after flash chromatography on SiO_2, except for **22** and **23**, for which basic alumina was used.

In the case of acyclic, particularly internal, alkenes, competition with ethene becomes an issue (Table 3). For example, *trans*-stilbene failed to undergo cycloaddition, the reaction mixture rendering only **11D** in 70% yield. On the other hand, *cis*-stilbene provided **18** as a single diastereomer, albeit in moderate yield (entry 1), diminished by the generation of **11D** (50% yield). Terminal alkenes proved more amenable and revealed interesting stereo- and regioselectivities. For instance, styrene (entry 2) yielded only the *endo*-2,4,6-triphenyl derivative **19** (50% yield). A similar, but attenuated, preference for placing the substituted ethene carbon adjacent to the boron-substituted terminus was found with vinyltrimethylsilane and vinyl(tributyl)tin (entries 3 and 4, respectively). However, in sharp contrast to styrene, the stereochemistry of addition was exclusively *exo*, an outcome that is most likely caused by steric factors.

The scope of the reaction was expanded to the cycloaddition of various α,ω-diboryldiynes to alkenes (Scheme 1). These substrates enforce the 1,4-orientation of the boryl substituents in the resulting diene and grant access to the first polycyclic 1,4-diborylcyclohexa-1,3-diene derivatives. The reactions proceed in good yield (61–80%) and, in the case of **26**, high stereoselectivity, which bodes well for synthetic application to more complex structures. The ^{13}C NMR spectroscopic data confirm the location of the boryl groups in complexes **8C**–**11C**. The structure of **27**, while showing some disorder of one of the boryl groups, was confirmed by an X-ray analysis (Figure 2).[25] Again, the effect of the boryl substituents on the remainder of the molecule appears minimal.

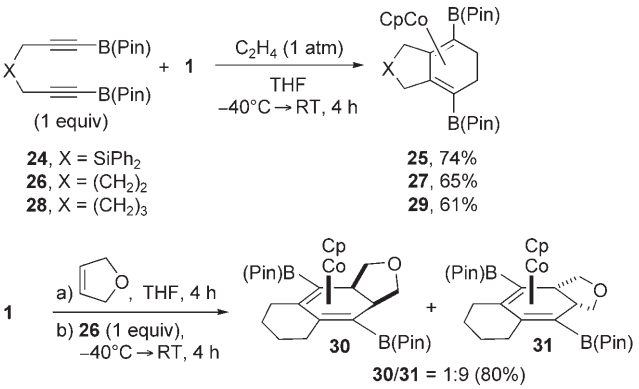

Scheme 1. CpCo-mediated cocyclizations of α,ω-diboryldiynes with alkenes leading to bicyclic and tricyclic 1,4-diborylcyclohexadiene complexes.

While the reported cyclizations furnish the desired organic products complexed to cobalt, this outcome is advantageous as it stabilizes the ligands and, at the same time, potentially activates them towards hydride abstraction and further substitution.[11,22,24,26] Nevertheless, the air- and heat-sensitive free dienes could be liberated by rapid oxidative demetalation with iron(III) chloride (1.5 equiv) in acetonitrile (Table 4, entries 1–11). As expected, the respective *endo*- and *exo*-cyclopentadienylcobalt diastereomers

 © 2005 Wiley-VCH Verlag GmbH & Co. KGaA, Weinheim

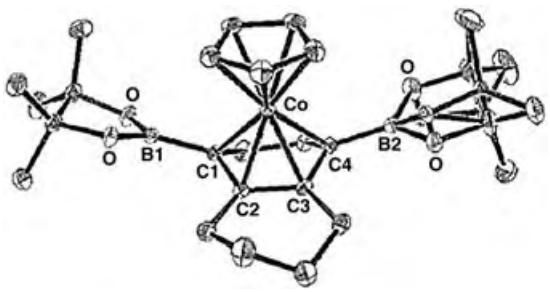

Figure 2. ORTEP view of complex **27** in the solid state (30% probability thermal ellipsoids). Selected bond lengths [Å] and angles [°]: Co–C_{Cp} 2.07 (av), C1–B1 1.547(4), C4–B2 1.543(4), B–O 1.37 (av), C–C_{diene} 1.44 (av), Co–C1 2.055(3), Co–C2 1.980(3); C1-C2-C3-C4 2.1.

Table 4: Oxidative demetalation of CpCo(cyclohexadiene) complexes with $FeCl_3 \cdot 6\,H_2O$ and demetalative aromatizations with ceric ammonium nitrate.

Entry	Substrate	Product		Yield [%][a]
		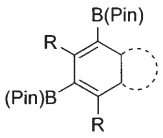	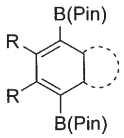	
1	**9D**	**32**		71
2	**9C**		**33**	69
3	**10D**[b]	**34**		74
4	**11D**[b]	**35**		75
5	**14/15**	**37**		79
6	**16/17**	**38**		80
7	**12/13**	**36**		69
8	**25**		**40**	69
9	**27**		**41**	76
10	**29**		**42**	80
11	**30/31**		**43**	82
12[c]	**36**	**39**[e]		45
13[d]	**30/31**		**44**[e]	49

[a] Yields of product isolated after column chromatography. [b] Reacted as a mixture with minor isomer **C**. [c] Treatment with CAN (4×0.5 equiv.) in acetone (RT, 2 h). [d] Treatment with CAN (4×0.75 equiv.) in acetone (RT, 12 h). [e]

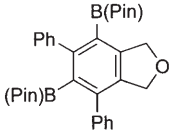

39

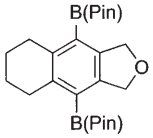

44

gave the same diborylcyclohexa-1,3-diene after cobalt removal, thus providing additional proof for the structure of the starting complexes. Aromatization was also accomplished, albeit in only moderate yields so far, using ceric ammonium nitrate (CAN), either starting from the free ligand (entry 12) or directly from the complex (entry 13).

In this work we have described the extensively chemo-, regio-, and diastereoselective assembly of mono-, bi-, and tricyclic 1,3- and 1,4-diboryl-1,3-cyclohexadienes by means of the CpCo-mediated cycloaddition of alkynyl pinacolboronates to alkenes. This method provides a rapid entry into highly functionalized 1,3-cyclohexadiene synthons of potential use in complex molecule synthesis. A mechanistic rationale for the regio- and diastereoselective outcome of this cycloaddition reaction is currently being sought by means of density functional computations.

Received: June 13, 2005
Published online: October 11, 2005

Keywords: alkenes · alkynylboronates · cobalt · cycloaddition · diene ligands

[1] a) A. Pelter, K. Amith, H. C. Brown, *Borane Reagents*, Academic Press, London, **1988**; b) B. Carboni, M. Vaultier, *Bull. Soc. Chim. Fr.* **1995**, *132*, 1003; c) A. Suzuki, *Rev. Heteroat. Chem.* **1997**, *17*, 271; d) B. Carboni, L. Monnier, *Tetrahedron* **1999**, *55*, 1197; e) M. Vaultier, G. Alcaraz, in *Science of Synthesis: Houben–Weyl Methods of Molecular Transformations*, Vol. *6* (Eds.: D. E. Kaufmann, D. S. Matteson), Thieme, Stuttgart, **2005**, pp. 721; f) K. Albrecht, D. E. Kaufmann, in *Science of Synthesis: Houben–Weyl Methods of Molecular Transformations*, Vol. *6* (Eds.: D. E. Kaufmann, D. S. Matteson), Thieme, Stuttgart, **2005**, pp. 697.

[2] For examples, see: a) A. B. Smith, G. K. Friestad, J. Barbosa, E. Bertunesque, J. J.-W. Duan, K. G. Hull, M. Iwashima, Y. Qiu, P. G. Spoors, B. A. Salvatore, *J. Am. Chem. Soc.* **1999**, *121*, 10478; b) S. A. Frank, W. R. Roush, *J. Org. Chem.* **2002**, *67*, 4316; c) G. N. Maw, C. Thirsk, J.-L. Toujas, M. Vaultier, A. Whiting, *Synlett* **2004**, 1183, and references therein.

[3] For examples, see: a) R. A. Batey, A. N. Thadani, A. J. Lough, *Chem. Commun.* **1999**, 475; b) J. Renaud, C.-D. Graf, L. Oberer, *Angew. Chem.* **2000**, *112*, 3231; *Angew. Chem. Int. Ed.* **2000**, *39*, 3101; c) M. Shimizu, T. Kurahashi, T. Hiyama, *Synlett* **2001**, 1006, and references therein.

[4] For examples, see: a) A. Hassner, J. A. Soderquist, *J. Organomet. Chem.* **1977**, *131*, C1; b) G. Zweifel, M. R. Najafi, S. Rajagopalan, *Tetrahedron Lett.* **1988**, *29*, 1895; c) G. Desurmont, S. Dalton, D. M. Giolando, M. Srebnik, *J. Org. Chem.* **1996**, *61*, 7943, and references therein.

[5] For cyclohexadiene synthesis, see: W. H. Okamura, A. R. De Lera, in *Comprehensive Organic Synthesis*, Vol. *5* (Eds.: B. M. Trost, I. Fleming), Pergamon, New York, **1991**, chap. 6.2.

[6] For representative examples, see: a) M. B. Ksebati, F. J. Schmitz, *J. Org. Chem.* **1985**, *50*, 5637; b) R. D. Dawe, J. L. C. Wright, *Tetrahedron Lett.* **1986**, *27*, 2559; c) X. Fu, E. P. Hong, F. J. Schmitz, *Tetrahedron* **2000**, *56*, 8989.

[7] a) E. Piers, H. E. Morton, *J. Org. Chem.* **1979**, *44*, 3437; b) E. J. Corey, H. Kigoshi, *Tetrahedron Lett.* **1991**, *32*, 5025; c) K. Morihira, T. Nishimori, H. Kusama, Y. Horiguchi, I. Kuwajima, T. Tsuruo, *Bioorg. Med. Chem. Lett.* **1998**, *8*, 2977; d) K. Morihira, R. Hara, S. Kawahara, T. Nishimori, N. Nakamura, H. Kusama, I. Kuwajima, *J. Am. Chem. Soc.* **1998**, *120*, 12980; e) S. Aoyagi, R. Tanaka, M. Naruse, C. Kibayashi, *J. Org. Chem.* **1998**, *63*, 8397.

[8] A. S. E. Karlström, M. Rönn, A. Thorarensen, J.-E. Bäckvall, *J. Org. Chem.* **1998**, *63*, 2517.

[9] A. S. E. Karlström, K. Itami, J.-E. Bäckvall, *J. Org. Chem.* **1999**, *64*, 1745.

[10] Mixtures of polylithiated 1,3-cyclohexadienes have been reported: J. A. Morrison, C. Chung, R. J. Lagow, *J. Am. Chem. Soc.* **1975**, *97*, 5015.

[11] For general reviews of transition-metal-mediated [2+2+2] cycloadditions of alkynes to alkenes, see: a) N. E. Schore, *Chem. Rev.* **1988**, *88*, 1081; b) D. B. Grotjahn, in *Comprehensive Organometallic Chemistry II*, Vol. *12* (Eds.: E. W. Abel, F. G. A.

 © 2005 Wiley-VCH Verlag GmbH & Co. KGaA, Weinheim

Stone, G. Wilkinson, L. Hegedus), Pergamon, Oxford, **1995**, pp. 741. For reviews of corresponding cobalt-mediated reactions, see: c) K. P. C. Vollhardt, *Angew. Chem.* **1984**, *96*, 525; *Angew. Chem. Int. Ed. Engl.* **1984**, *23*, 539; d) M. Malacria, C. Aubert, J. L. Renaud, in *Science of Synthesis: Houben–Weyl Methods of Molecular Transformations*, Vol. *1* (Eds.: M. Lautens, B. M. Trost), Thieme, Stuttgart, **2001**, p. 439; see also: e) M. J. Eichberg, R. L. Dorta, D. B. Grotjahn, K. Lamottke, M. Schmidt, K. P. C. Vollhardt, *J. Am. Chem. Soc.* **2001**, *123*, 9324, and references therein.

[12] For general information, see: a) D. E. Kaufmann, N. Öcal, in *Science of Synthesis: Houben–Weyl Methods of Molecular Transformations*, Vol. *1* (Eds.: D. E. Kaufmann, D. S. Matteson), Thieme, Stuttgart, **2005**, p. 635. Specific examples include the zirconium-mediated couplings reported in ref. [4c] and: b) N. Metzler, H. Nöth, M. Thomann, *Organometallics* **1993**, *12*, 2423; c) A. A. A. Quntar, M. Srebnik, *Org. Lett.* **2004**, *6*, 4243. Cobalt-catalyzed Diels–Alder reactions: d) G. Hilt, K. I. Smolko, *Angew. Chem.* **2003**, *115*, 2901; *Angew. Chem. Int. Ed.* **2003**, *42*, 2795; e) G. Hilt, S. Lüers, K. I. Smolko, *Org. Lett.* **2005**, *7*, 251. Chromium-mediated Dötz benzannulations: f) M. W. Davies, C. N. Johnson, J. P. A. Harrity, *J. Org. Chem.* **2001**, *66*, 3525. Cobalt-, nickel-, or ruthenium-catalyzed cyclotrimerizations: g) A. Goswami, C.-J. Maier, H. Pritzkow, W. Siebert, *Eur. J. Inorg. Chem.* **2004**, 2635; h) Y. Yamamoto, J.-i. Ishii, H. Nishiyama, K. Itoh, *J. Am. Chem. Soc.* **2004**, *126*, 3712; i) V. Gandon, D. Leca, T. Aechtner, K. P. C. Vollhardt, M. Malacria, C. Aubert, *Org. Lett.* **2004**, *6*, 3405. Ruthenium-catalyzed metathesis reactions: ref. [3b] and references therein. Ruthenium-catalyzed Alder–ene reaction: j) E. C. Hansen, D. Lee, *J. Am. Chem. Soc.* **2005**, *127*, 3252.

[13] For reviews, see : a) N. Miyaura, A. Suzuki, *Chem. Rev.* **1995**, *95*, 2457; b) N. Miyaura, *Top. Curr. Chem.* **2002**, *219*, 11; c) N. Miyaura, in *Metal-Catalyzed Cross-Coupling Reactions*, Vol. *1* (Eds.: A. de Meijere, F. Diederich), Wiley-VCH, Weinheim, **2004**, p. 41.

[14] For representative examples, see: a) C. Thiebes, G. K. Surya Prakash, N. A. Petasis, G. A. Olah, *Synlett* **1998**, 141; b) K. S. Webb, D. Levy, *Tetrahedron Lett.* **1995**, *36*, 5117; c) T. D. Quach, R. A. Batey, *Org. Lett.* **2003**, *5*, 4397.

[15] a) K. Jonas, E. Deffense, D. Habermann, *Angew. Chem.* **1983**, *95*, 729; *Angew. Chem. Int. Ed. Engl.* **1983**, *22*, 716; K. Jonas, E. Deffense, D. Habermann, *Angew. Chem.* **1983**, *Suppl.*, 1005. See also: b) J. K. Cammack, S. Jalisatgi, A. J. Matzger, A. Negron, K. P. C. Vollhardt, *J. Org. Chem.* **1996**, *61*, 4798.

[16] For some rare examples of ethene incorporation in CpCo-mediated cotrimerizations with alkynes, see: a) Y. Wakatsuki, T. Kuramitsu, H. Yamazaki, *Tetrahedron Lett.* **1974**, *15*, 4549; b) Y. Wakatsuki, H. Yamazaki, *J. Organomet. Chem.* **1977**, *139*, 169; c) R. G. Beevor, S. A. Frith, J. L. Spencer, *J. Organomet. Chem.* **1981**, *221*, C25; d) R. Benn, K. Cibura, P. Hofmann, K. Jonas, A. Rufińska, *Organometallics* **1985**, *4*, 2214; e) K. Jonas, *Angew. Chem.* **1985**, *97*, 292; *Angew. Chem. Int. Ed. Engl.* **1985**, *24*, 295; f) U. Kölle, B. Fuss, *Chem. Ber.* **1986**, *119*, 116.

[17] **11D**: $C_{35}H_{43}B_2CoO_4$, $M_r = 608.28$, crystal size $0.10 \times 0.10 \times 0.10\ mm^3$, triclinic, space group $P\bar{1}$ (no. 1), $a = 10.584(3)$, $b = 11.347(4)$, $c = 14.593(3)$ Å, $\alpha = 95.72(2)$, $\beta = 109.511(19)$, $\gamma = 94.51(2)°$, $V = 1632.0(8)$ Å^3, $Z = 2$, $\rho_{calcd} = 1.238\ g\,cm^{-3}$, scan range $4.00 < 2\theta < 50°$, $\lambda(Mo_{K\alpha}) = 0.71073$ Å, $\mu(Mo_{K\alpha}) = 0.562\ cm^{-1}$, $T = 295$ K, 5702 unique reflections, of which 3702 were taken as observed ($I > 1.50\sigma(I)$), $R = 0.051$, $R_w = 0.043$. CCDC-272959 (**11D**) contains the supplementary crystallographic data for this paper. These data can be obtained free of charge from the Cambridge Crystallographic Data Centre via www.ccdc.cam.ac.uk/data_request/cif.

[18] For pertinent examples of CpCo(diene) structures, see: a) D. W. Macomber, A. G. Verma, R. D. Rogers, *Organometallics* **1988**, *7*, 1241, and references therein. For pertinent alkenyl boronate structures, see: b) T. Sagawa, Y. Asano, F. Ozawa, *Organometallics* **2002**, *21*, 5879; c) Y. Gu, H. Pritzkow, W. Siebert, *Eur. J. Inorg. Chem.* **2001**, 373; d) R. Widmaier, J. J. Alexander, J. A. Krause Bauer, M. Srebnik, G. Desurmont, C. A. Homrighausen, *Inorg. Chim. Acta* **1999**, *290*, 159.

[19] a) Y. Wakatsuki, O. Nomura, K. Kitaura, K. Morokuma, H. Yamazaki, *J. Am. Chem. Soc.* **1983**, *105*, 1907; b) J. H. Hardesty, J. B. Koerner, T. A. Albright, G.-Y. Lee, *J. Am. Chem. Soc.* **1999**, *121*, 6055; c) K. Kirchner, M. J. Calhorda, R. Schmid, L. F. Veiros, *J. Am. Chem. Soc.* **2003**, *125*, 11721; d) L. F. Veiros, G. Dazinger, K. Kirchner, M. J. Calhorda, R. Schmid, *Chem. Eur. J.* **2004**, *10*, 5860. For a recent discussion, see also: e) K. Tanaka, K. Toyoda, A. Wada, K. Shirasaka, M. Hirano, *Chem. Eur. J.* **2005**, *11*, 1145.

[20] See, for example: a) K. T. Giju, F. M. Bickelhaupt, G. Frenking, *Inorg. Chem.* **2000**, *39*, 4776; b) W. H. Lam, S. Shimada, A. S. Batsanov, Z. Lin, T. B. Marder, J. A. Cowan, J. A. K. Howard, S. A. Mason, G. J. McIntyre, *Organometallics* **2003**, *22*, 4557; c) K. C. Lam, W. H. Lam, Z. Lin, T. B. Marder, N. C. Norman, *Inorg. Chem.* **2004**, *43*, 2541.

[21] The use of toluene or hexane led to lower yields due to competitive ethene insertion.

[22] E. D. Sternberg, K. P. C. Vollhardt, *J. Org. Chem.* **1984**, *49*, 1564.

[23] H. Pelissier, J. Rodriguez, K. P. C. Vollhardt, *Chem. Eur. J.* **1999**, *5*, 3549.

[24] R. Boese, A. P. Van Sickle, K. P. C. Vollhardt, *Synthesis* **1994**, 1374.

[25] **27**: $C_{27}H_{35}B_2CoO_4$, $M_r = 504.13$, crystal size $0.10 \times 0.10 \times 0.10\ mm^3$, triclinic, space group $P\bar{1}$ (no. 1), $a = 10.4024(7)$, $b = 12.1415(11)$, $c = 12.1749(8)$ Å, $\alpha = 100.563(6)$, $\beta = 99.681(6)$, $\gamma = 113.834(6)°$, $V = 1331.6(2)$ Å^3, $Z = 2$, $\rho_{calcd} = 1.257\ g\,cm^{-3}$, scan range $23.2 < 2\theta < 55°$, $\lambda(Mo_{K\alpha}) = 0.71073$ Å, $\mu(Mo_{K\alpha}) = 0.674\ cm^{-1}$, $T = 200$ K, 5589 unique reflections, of which 3033 were taken as observed ($I > 3.00\sigma(I)$), $R = 0.038$, $R_w = 0.043$. CCDC-272960 (**27**) contains the supplementary crystallographic data for this paper. These data can be obtained free of charge from the Cambridge Crystallographic Data Centre via www.ccdc.cam.ac.uk/data_request/cif.

[26] Y.-H. Lai, W. Tam, K. P. C. Vollhardt, *J. Organomet. Chem.* **1981**, *216*, 97.

 © 2005 Wiley-VCH Verlag GmbH & Co. KGaA, Weinheim

Gold Clusters

DOI: 10.1002/anie.200502795

Experimental and Theoretical Investigation of the Electronic and Geometrical Structures of the Au_{32} Cluster**

Min Ji, Xiao Gu, Xi Li, Xingao Gong, Jun Li,* and Lai-Sheng Wang**

Gold clusters and nanoparticles have received significant attention in cluster science because of their potential applications in nanotechnology.[1–4] The discovery of unexpected catalytic properties of nanosized gold particles supported on substrates[5] has rekindled extensive interest in the chemical and physical properties of gold clusters. The strong relativistic effects of gold[6] results in Au clusters exhibiting many unique properties that are different from the other coinage metals. For example, gold clusters assume two-dimensional (2D) structures even at relatively large sizes, whereas the corresponding Cu and Ag clusters are three-dimensional (3D).[7,8] The most recent surprise in Au cluster chemistry is the prediction of a highly stable Au_{32} cage cluster,[9,10] which was calculated to have the same icosahedral (I_h) symmetry as C_{60} and can be regarded as having one atom located on each of the 32 faces of C_{60}. Such a high symmetry structure with a hollow core is intriguing, but completely unexpected for a metal cluster. Explanations involving aromaticity and the tendency of Au to form 2D structures have been proposed to account for the stability of this unusual cluster.[9,10] Should such a Au_{32} cage be stable enough to be synthesized, it is anticipated to possess some fascinating physical and chemical properties. However, this structure has not been confirmed experimentally and it is not known how stable this structure would be in a charged state or upon ligand coordination. The stability towards ligand coordination will be particularly important if bulk quantities of Au_{32} are to be made.[11]

Although the direct experimental determination of cluster structures has been challenging, electron diffraction studies of trapped ions have recently shown considerable promise.[12] Photoelectron spectroscopy (PES) of size-selected anions in combination with quantum-mechanical calculations has been shown to be a powerful indirect approach to yield structural information for clusters.[13–15] By using this approach, we recently discovered that Au_{20} possesses a highly symmetric and compact structure,[16] which has since been confirmed in numerous studies to be the global minimum of Au_{20}.[17–19] Herein, we describe the combination of PES and density functional theory (DFT) calculations to elucidate the electronic and geometrical structures of Au_{32} and Au_{32}^-.

The experiment was performed by using a laser vaporization magnetic-bottle PES apparatus[20] similar to that used in our previous studies on Au_{20}^-.[16] The anionic Au_{32}^- clusters were produced by laser vaporization of a gold foil and their mass was analyzed by means of time-of-flight mass spectrometry. PES spectra of Au_{32}^- (Figure 1) were measured at two

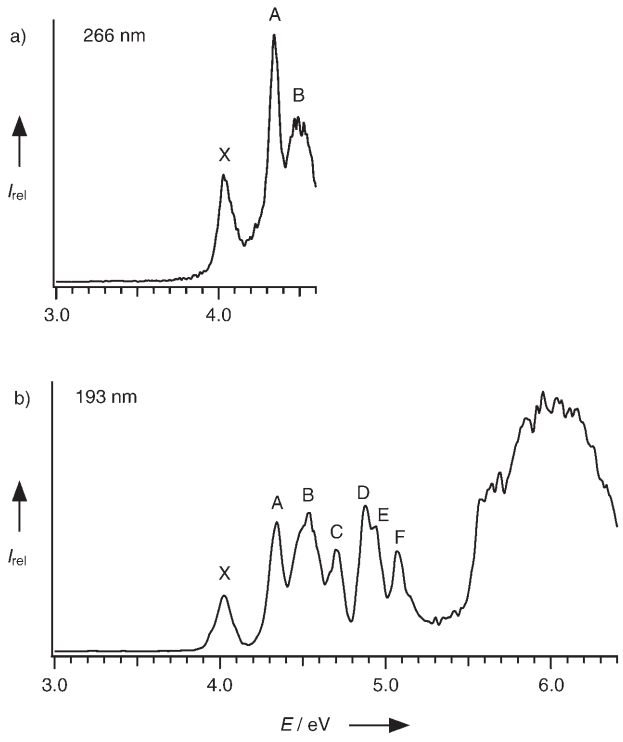

Figure 1. Photoelectron spectra of Au_{32}^- at a) 266 nm (4.661 eV) and b) 193 nm (6.424 eV).

[*] M. Ji, X. Gu, Prof. Dr. X. G. Gong
Surface Physics Laboratory and
Department of Physics
Fudan University
Shanghai 200433 (China)
Fax: (+86) 21-6510-4949
E-mail: xggong@fudan.edu.cn
Dr. J. Li
W. R. Wiley Environmental Molecular Sciences Laboratory
Pacific Northwest National Laboratory, MS K1-96
P.O. Box 999, Richland, WA 99352 (USA)
Fax: (+1) 509-376-0420
E-mail: jun.li@pnl.gov
X. Li, Prof. Dr. L.-S. Wang
Department of Physics
Washington State University
2710 University Drive
Richland, WA 99352 (USA)
and
W. R. Wiley Environmental Molecular Sciences Laboratory and
Chemical Sciences Division
Pacific Northwest National Laboratory, MS K8-88
P.O. Box 999, Richland, WA 99352 (USA)
Fax: (+1) 509-376-6066
E-mail: ls.wang@pnl.gov

[**] The experimental work was supported by the U.S. NSF (CHE-0349426) and performed at the EMSL, a national scientific user facility sponsored by the U.S. DOE Office of Biological and Environmental Research and located at PNNL, operated for the DOE by Battelle. X.G.G. is partially supported by the NSF of China and the Special Funds for Major National Basic Research Projects of China. Calculations were performed on the supercomputers at the EMSL Molecular Science Computing Facility, at the Shanghai Supercomputer Center, and the Fudan Supercomputer Center.

© 2005 Wiley-VCH Verlag GmbH & Co. KGaA, Weinheim

photon energies (266 nm (4.661 eV) and 193 nm (6.424 eV)) at an electron kinetic energy resolution of $\Delta E_k/E_k \approx 2.5\,\%$ (ca. 25 meV for 1-eV electrons). The general spectral pattern in Figure 1 agrees with a previous PES study of the coinage metal clusters,[21] but considerable fine features were resolved in the current spectra in the lower-binding-energy range: a total of seven discrete bands were resolved (labeled as X, A–F). The higher-binding-energy range (> 5.5 eV) exhibited continuous spectral features derived from the Au 5d band. The discrete, lower-binding-energy features were ascribed primarily to the Au 6s states and should be very sensitive to the structure of the cluster. The well-resolved bands in this spectral range make it possible to compare the results with theoretical calculations. The X band revealed the electron affinity of Au_{32} to be 3.96 ± 0.02 eV. The PES spectral pattern indicates that Au_{32} has a closed-shell electronic structure with a relatively small energy gap of 0.30 eV, defined by the X–A separation (Figure 1). It should also be pointed out that the observed main spectral features (X, A–F) were not dependent on the source conditions, which suggests that higher-energy isomers were not present in the beam in significant amounts.

Our calculations are based on plane-wave and Slater-basis DFT with the generalized gradient approximation (GGA) as implemented in the VASP[22] and ADF[23] codes.[24] Our previous theoretical search showed that for neutral Au_{32}, the I_h cage is the most stable structure with the nearest-energy isomer (D_{6h}) 0.94 eV higher in energy.[10] We found that the I_h cluster with a slight Jahn–Teller distortion (D_{3d}) remains the lowest energy structure for Au_{32}^- (Figure 2a and Table 1), but the closest-energy noncage isomer (C_1-I; Figure 2b) is only 0.40 eV higher in energy on the basis of the ADF calculations. Four other low-lying isomers of Au_{32}^- are also shown in Figure 2. Table 1 gives the electron configuration, relative energy, adiabatic detachment energy (ADE), and vertical detachment energy (VDE) for the six isomers of Au_{32}^-, as well as the electron configurations and the energy gaps for the corresponding neutral Au_{32} isomers. The Jahn–Teller effect meant that several lower-symmetry species had to be considered for the cage structure of Au_{32}^-. The structural distortions are all very minor and the four lower-symmetry structures are close in energy (Table 1). With the exception of the planar (C_{2v}) structure, the other low-lying isomers (C_1-I, D_{6h}, C_2, and C_1-II) of Au_{32}^- are also close in energy. The two C_1 isomers have no symmetry elements and can be characterized as being amorphous. These two structures and the C_2 isomer are three dimensional, whereas the I_h and D_{6h} structures are cages, which can be considered to be quasi-2D because they are hollow. The three low-symmetry 3D structures are more compact and can be regarded essentially as distorted cages with two to four atoms inside.

The I_h Au_{32} cluster has been shown to possess a very large

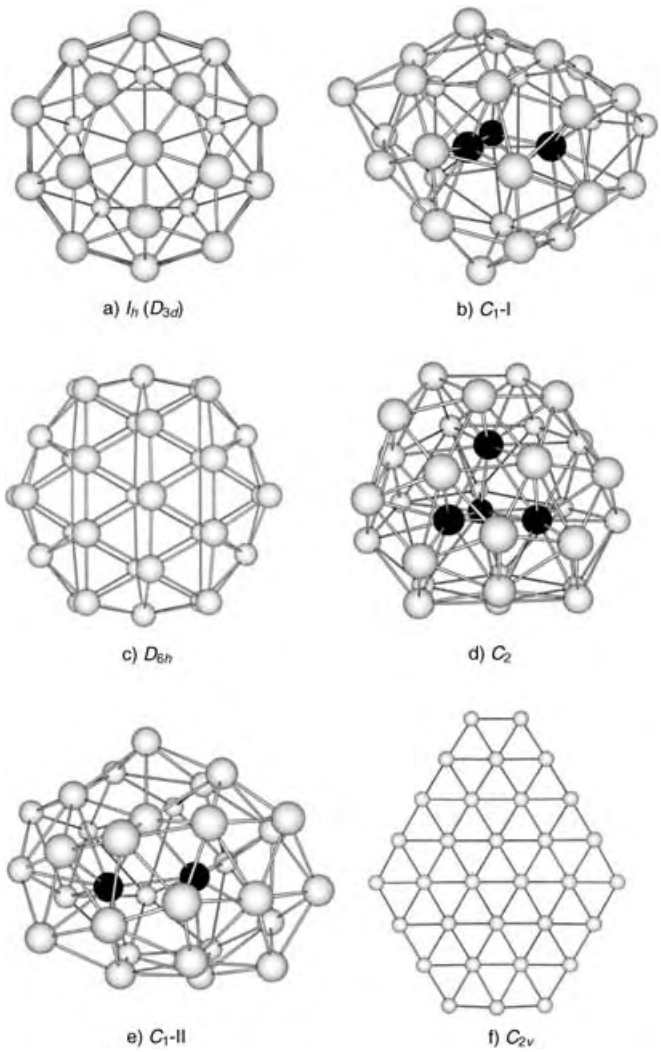

Figure 2. Selected structures of the Au_{32}^- cluster: a) the global minimum icosahedral cage structure, b) first isomer with C_1 symmetry (C_1-I), c) isomer with D_{6h} symmetry, d) isomer with C_2 symmetry, e) second isomer with C_1 symmetry (C_1-II), f) planar structure with C_{2v} symmetry.

Table 1: Optimized structures and electron configurations for Au_{32} and Au_{32}^-, HOMO–LUMO energy gaps (ΔE_{HL}) for Au_{32}, relative total energies [ΔE(tot)], and adiabatic (ADE) and vertical (VDE) detachment energies for Au_{32}^-, all calculated by the ADF PW91/TZ2P method.[a]

	neutral			anion			
Sym.	Config.	ΔE_{HL}	Sym.	Config.	ΔE(tot)	ADE	VDE
C_{2v}	$(b_2)^2(a_1)^0$	≈ 0	C_{2v}	$(b_2)^2(a_1)^1$	2.50	4.28	4.32
C_1	$(a)^2(a)^0$	0.44	C_1-II	$(a)^2(a)^1$	0.81	3.74	3.79
C_2	$(b)^2(a)^0$	0.39	C_2	$(b)^2(a)^1$	0.46	3.94	4.11
D_{6h}	$(e_{1u})^4(e_{2g})^0$	0.84	D_{2h}[b]	$(b_{3u})^2(b_{1g})^1$	0.41	3.63	3.68
C_1	$(a)^2(a)^0$	0.22	C_1-I	$(a)^2(a)^1$	0.40	3.96	4.03
I_h	$(g_u)^8(g_g)^0$	1.56	D_{5d}	$(e_{2u})^4(a_{1g})^1$	0.16	2.90	3.02
			D_{2h}	$(a_{1u})^2(a_{1g})^1$	0.02	3.05	3.10
			C_{2h}	$(b_u)^2(b_g)^1$	0.01	3.06	3.16
			D_{3d}	$(a_{1u})^2(a_{1g})^1$	0.00	3.06	3.15

[a] All energies are in eV. The HOMO–LUMO energy gaps are for the optimized neutral species. [b] The structural distortion in the anion is very small and the anion symmetry is very close to the neutral D_{6h} structure.

 © 2005 Wiley-VCH Verlag GmbH & Co. KGaA, Weinheim

HOMO–LUMO gap because of its high symmetry. Energy gaps of 1.7 and 2.5 eV were evaluated from the BP86 and PBE0 functions, respectively,[9] whereas an energy gap of 1.5 eV was given by using the VASP code.[10] These values are considerably larger than the 0.30 eV measured in our PES spectra of Au_{32}^-, which suggests that the experimentally observed Au_{32}^- cannot be the I_h cluster. To help determine the structure of Au_{32}^-, we computed the ADE and VDE of all the six low-lying isomers for comparison with the experimental PES spectra. As shown in Table 1, the calculated ADEs for the C_1-I isomer (3.96 eV) and the C_2 isomer (3.94 eV) are both in agreement with the experimental value (3.96 ± 0.02 eV), whereas that of the I_h structure is considerably smaller. The calculated ADEs of the other isomers are also in poor agreement with the experimental value. The computed VDE spectra, convoluted with Gaussian-shaped bands (0.05 eV full width at half-maximum (fwhm)) to approximately simulate the PES spectra,[16] are shown in Figure 3

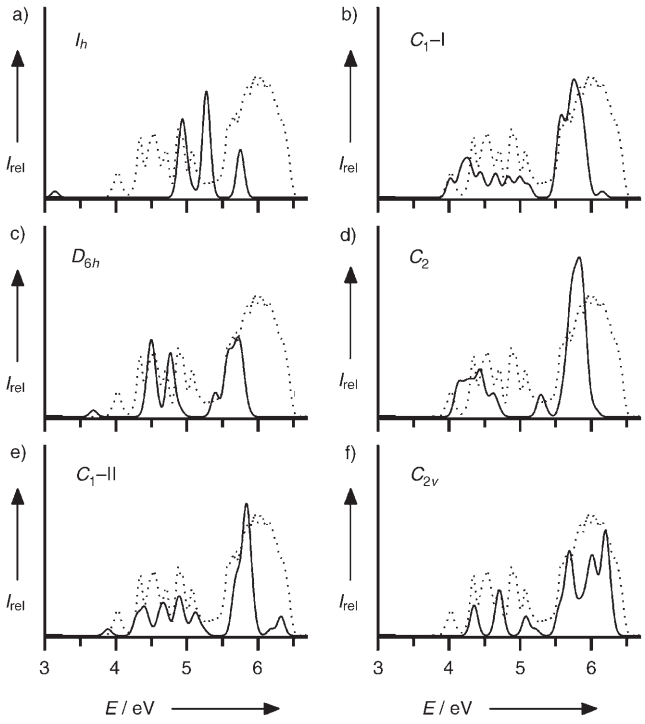

Figure 3. Simulated photoelectron spectra for the different isomers of Au_{32}^- overlaid with the experimental spectrum at 193 nm (dotted curves): a) the icosahedral cage structure, b) the C_1-I structure, c) the D_{6h} structure, d) the C_2 structure, e) the C_1-II structure, f) the planar C_{2v} structure. The simulated spectra were constructed by fitting each of the vertical detachment transitions with a Gaussian of 0.05 eV width.[16]

overlaid with the experimental PES spectrum at 193 nm. The simulated spectrum of the I_h isomer (Figure 3a) is very simple as a result of its large HOMO–LUMO gap caused by the high symmetry of this cage structure. The simulated spectra of the D_{6h} and the C_{2v} planar structures are also quite simple because of their relatively high symmetries. These spectra clearly disagree with the experimental PES data (Figure 3c and f).

The simulated spectra of the three low-symmetry structures display some similarities (Figure 3b, d, e): all have an intense band above 5.5 eV derived from the high density of states of the 5d electrons. However, the lower-binding-energy parts of the simulated spectra are highly structured and exhibit clear differences, which seem to be quite sensitive to the detailed structure of the clusters. The simulated spectrum of the C_2 structure (Figure 3d) is very congested near the threshold region between 4.0 and 4.8 eV, which is followed by a gap and another band at 5.3 eV. This simulated pattern is clearly inconsistent with the observed PES spectra shown in Figure 1. At first glance, the simulated spectrum of the C_1-II structure (Figure 3e) seemed to display some similarity to the experimental spectra. However, the calculated ADE for the first peak of this structure (3.74 eV) is considerably smaller than the experimental value (3.93 eV). The number of bands between 4.2 and 5.1 eV is also inconsistent with the experimentally observed bands. Furthermore, the total energy of the C_1-II structure is 0.81 eV higher than the ground state, which means that this structure is unlikely to be present under our experimental conditions (see below). On the other hand, the calculated ADE of the C_1-I structure (3.96 eV) is in excellent agreement with the experimental data (3.96 ± 0.02 eV), so that the first peak of the simulated spectrum of the C_1-I structure (Figure 3b) coincides with the first experimental peak. The calculated HOMO–LUMO gap (0.22 eV) for the C_1-I structure seems to be slightly smaller than the measured gap of 0.3 eV. The number of bands and their positions in the low-binding-energy part of Figure 3b (except the HOMO–LUMO gap) are in excellent agreement with the observed PES spectra for Au_{32}^-. Overall, the simulated spectrum of the C_1-I structure agrees best with the PES spectra.

Although the C_1-I isomer lies closest in energy above the I_h structure on the basis of our DFT calculations, it is still 0.4 eV higher. Why was this isomer observed experimentally, whereas the energetically more favorable Au_{32}^- cage was not? To understand this apparent paradox, we considered the relative stabilities of the various isomers as a function of temperature by taking into account the contribution of entropy, that is, by considering the free energy. We calculated the free energies of all of the six low-lying structures of Au_{32}^- by using the calculated total binding energies (E_0) from ADF at zero temperature and the harmonic vibrational entropy with Equation (1).[25]

$$F = E_0 - \frac{1}{2}\sum_i \hbar\omega_i + k_B T \sum_i \ln\left(\exp\frac{\hbar\omega_i}{k_B T} - 1\right) \quad (1)$$

In this equation, F is the free energy, E_0 is the total binding energy calculated with ADF, and the last two terms give the vibrational entropic contribution to the free energy at finite temperature by using the harmonic approximation and summing over all the vibrational degrees of freedom ($3n-6=90$ for Au_{32}^-). Figure 4 shows the computed curves for the free-energy of the six low-lying structures of Au_{32}^- relative to that of the D_{3d} cage structure as a function of temperature. We found that although the I_h cage is the most stable structure at zero temperature, the relative stability of

 © 2005 Wiley-VCH Verlag GmbH & Co. KGaA, Weinheim

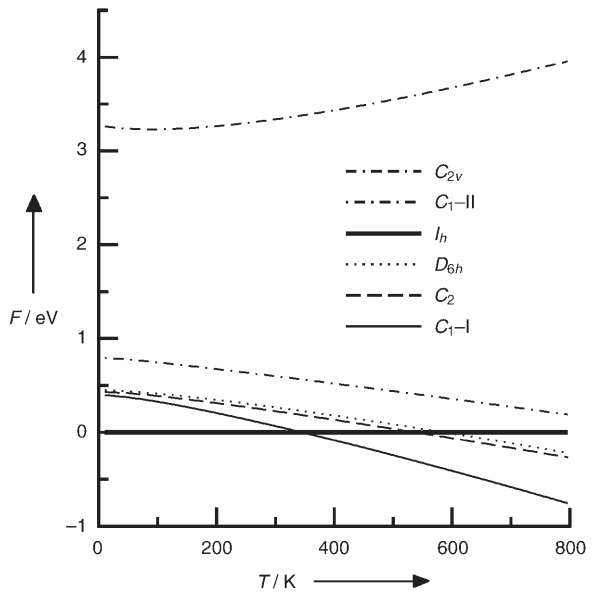

Figure 4. Free energies of the six low-lying isomers of the Au_{32}^- cluster as a function of temperature, calculated using a harmonic approximation and the ADF total binding energy at zero temperature. The free energies are plotted relative that of the D_{3d} cage structure to show more clearly that several low-symmetry isomers become more stable at high temperatures as a result of the entropic effect. Note that the C_1-I structure becomes the most stable isomer at temperatures $> \approx 300$ K.

the C_1-I isomer increases rapidly with temperature because of the contributions from vibrational entropy. Significantly, we observed that the C_1-I isomer becomes the most stable cluster above approximately 300 K. Although the actual cluster temperature in our experiment was not known, our previous experience shows that for medium-sized Al clusters, a vibrational temperature of room temperature or slightly lower can be achieved.[26] The large size of the Au_{32}^- cluster and the ineffectiveness of the supersonic cooling means our best estimate for its vibrational temperature even under our relatively cold source conditions is that it was probably around or slightly below room temperature. Considering the approximate nature of the free-energy calculations, we conclude that the formation of the amorphous C_1-I Au_{32}^- cluster in our experiment was indeed controlled by the vibrational entropy. It should be pointed out that the C_1-II isomer is higher in energy than the lowest-energy C_1-I isomer at room temperature by 0.5 eV, which makes it very unlikely that it is significantly formed under our experimental conditions. This view is reinforced by the observation that the C_2 and D_{6h} isomers, which are both more stable than the C_1-II isomer, do not seem to have any contribution to the observed spectra. Furthermore, aurophilic interactions,[6] which may not be completely accounted for in the DFT calculations, are expected to favor the 3D structures, which would bring the energy of the C_1-I structure even closer to the cage structure. All these observations lend credence to our assignment that the C_1-I structure is the dominant cluster observed in our experiment.

In a similar recent study on the B_{20}^- cluster, we found that although a 3D ring-type structure was predicted by DFT calculations to be the global minimum, only planar structures were observed experimentally because of the large entropy contributions of the planar structures at finite temperatures.[27] This recent study along with the current work suggest that vibrational entropies are important in controlling the stabilities of relatively large cluster structures when isomers are closely lying in energy. Thermal effects have to be considered when comparing experiments performed at finite temperatures with theoretical calculations.

Received: August 7, 2005
Published online: October 11, 2005

Keywords: cluster compounds · density functional calculations · gold · photoelectron spectroscopy · structure elucidation

[1] C. L. Cleveland, U. Landman, T. G. Schaaff, M. N. Shafigullin, P. W. Stephens, R. L. Whetten, *Phys. Rev. Lett.* **1997**, *79*, 187.
[2] Y. Kondo, K. Takayanagi, *Science* **2000**, *289*, 606.
[3] M. C. Daniel, D. Astruc, *Chem. Rev.* **2004**, *104*, 293.
[4] H. B. Weber, J. Reichert, F. Weigend, R. Ochs, D. Beckmann, M. Mayor, R. Ahlrichs, H. v. Löhneysen, *Chem. Phys.* **2002**, *281*, 113.
[5] M. Haruta, *Catal. Today* **1997**, *36*, 153.
[6] P. Pyykkö, *Angew. Chem.* **2004**, *116*, 4512; *Angew. Chem. Int. Ed.* **2004**, *43*, 4412.
[7] F. Furche, R. Ahlrichs, P. Weis, C. Jacob, S. Gilb, T. Bierweiler, M. M. Kappes, *J. Chem. Phys.* **2002**, *117*, 6982.
[8] H. Häkkinen, M. Moseler, U. Landman, *Phys. Rev. Lett.* **2002**, *89*, 033401.
[9] M. P. Johansson, D. Sundholm, J. Vaara, *Angew. Chem.* **2004**, *116*, 2732; *Angew. Chem. Int. Ed.* **2004**, *43*, 2678.
[10] X. Gu, M. Ji, S. H. Wei, X. G. Gong, *Phys. Rev. B* **2004**, *70*, 205401.
[11] H. F. Zhang, M. Stender, R. Zhang, C. M. Wang, J. Li, L. S. Wang, *J. Phys. Chem. B* **2004**, *108*, 12259.
[12] S. Kruckeberg, D. Schooss, M. Maier-Borst, J. H. Parks, *Phys. Rev. Lett.* **2000**, *85*, 4494.
[13] L. Kronik, R. Fromherz, E. Ko, G. Ganteför, J. R. Chelikowsky, *Nat. Mater.* **2002**, *1*, 49.
[14] C. Massobrio, A. Pasquarello, R. Car, *Phys. Rev. Lett.* **1995**, *75*, 2104.
[15] A. I. Boldyrev, L. S. Wang, *J. Phys. Chem. A* **2001**, *105*, 10759.
[16] J. Li, X. Li, H. J. Zhai, L. S. Wang, *Science* **2003**, *299*, 864.
[17] J. Wang, G. Wang, J. Zhao, *Chem. Phys. Lett.* **2003**, *380*, 716.
[18] B. Soule de Bas, M. J. Ford, M. B. Cortie, *J. Mol. Struct. (Theochem)* **2004**, *686*, 193.
[19] E. M. Fernandez, J. M. Soler, I. L. Garzon, L. C. Balbas, *Phys. Rev. B* **2004**, *70*, 165403.
[20] L. S. Wang, H. Wu in *Advances in Metal and Semiconductor Clusters. IV. Cluster Materials* (Ed.: M. A. Duncan), JAI, Greenwich, CT, **1998**, p. 299.
[21] K. J. Taylor, C. L. Pettiette-Hall, O. Cheshnovsky, R. E. Smalley, *J. Chem. Phys.* **1992**, *96*, 3319.
[22] In the VASP calculations (G. Kresse, J. Furthmuller, *Phys. Rev. B* **1996**, *54*, 11169), the $5d^{10}6s^1$ valence electrons were treated explicitly and their interactions with the ionic cores are described by the PAW potentials (G. Kresse, D. Joubert, *Phys. Rev. B* **1999**, *59*, 175) with scalar relativistic effects included. The wave functions were expanded in plane waves with an energy cutoff of approximately 230 eV. We used a simple cubic cell of 30 Å edge length with periodic boundary conditions, and the Γ point approximation for the Brillouin zone sampling. To test the accuracy of the theoretical method, we calculated the bond

 © 2005 Wiley-VCH Verlag GmbH & Co. KGaA, Weinheim

length of the Au dimer and the lattice constant of the crystalline solid. The values obtained are in agreement with experimental data to within 2%. To facilitate comparisons with the experimental results, we carried out an extensive search for the global minimum of Au_{32}^- by simulated annealing, starting with various structures previously found for neutral Au_{32},[10] as well as many other low-symmetry structures. The atomic structures were optimized by the conjugated-gradient method with a force convergence of 1.0×10^{-3} eV Å^{-1}.

[23] The Amsterdam density functional (ADF) calculations (ADF 2004, SCM, Theoretical Chemistry, Vrije Universiteit, Amsterdam, The Netherlands (http://www.scm.com)) were performed by using the GGA of Perdew–Wang 1991 (PW91; J. P. Perdew, Y. Wang, *Phys. Rev. B* **1992**, *45*, 13244) and triple-zeta Slater basis sets plus p- and f-polarization functions (TZ2P) for the valence orbitals of the Au atoms. The frozen-core approximation was applied to the $\{1s^2 4f^{14}\}$ core, and the $5s^2 5p^6 5d^{10} 6s^1$ electrons were explicitly treated variationally. The scalar and spin-orbit relativistic effects were taken into account through the zero-order-regular approach (ZORA; E. van Lenthe, E. J. Baerends, J. G. Snijders, *J. Chem. Phys.* **1993**, *99*, 4597). The simulations of the PES spectra were performed by using procedures described previously.[16]

[24] The VASP code is an efficient simulated-annealing method, which allows local minima to be readily identified. The ADF code, which has higher-quality basis sets and involves advanced relativistic treatment, is used to produce the final energy profiles for comparison with the experimental results. The good performance of ADF for Au clusters has been well tested in our previous studies in conjunction with PES data (see reference [16], for example).

[25] See, for example: K. Huang, *Statistical Mechanics*, 2nd ed., Wiley, New York, **1987**, p. 184.

[26] J. Akola, M. Manninen, H. Häkkinen, U. Landman, X. Li, L. S. Wang, *Phys. Rev. B* **1999**, *60*, R11297.

[27] B. Kiran, S. Bulusu, H. J. Zhai, S. Yoo, X. C. Zeng, L. S. Wang, *Proc. Natl. Acad. Sci. USA* **2005**, *102*, 961.

 © 2005 Wiley-VCH Verlag GmbH & Co. KGaA, Weinheim

Selective Glycosylations

DOI: 10.1002/anie.200502694

Development of an Arming Participating Group for Stereoselective Glycosylation and Chemoselective Oligosaccharide Synthesis**

*James T. Smoot, Papapida Pornsuriyasak, and Alexei V. Demchenko**

Dedicated to Professor Andras Liptak on the occasion of his 70th birthday

Carbohydrates are involved in many harmful processes such as bacterial and viral infections, development and growth of tumors, metastasis, tissue rejection, etc. Many of these processes are directly associated with deadly diseases of the 21st century including AIDS, cancer, meningitis, hepatitis, septicemia, etc.[1] Elucidation of the exact mechanisms of the carbohydrate involvement in disease pathogenesis would be significantly facilitated if we could rely on the comprehensive knowledge of the structure, conformation, and properties of the carbohydrate molecules. It is critical to make complex carbohydrates more accessible to general chemical, biochemical, and industrial audiences to keep pace with the exploding area of glycobiology.[2] One way to increase the access to carbohydrates is to develop reliable methods for stereoselective glycoside synthesis and convergent oligosaccharide assembly that would be applicable to both laboratory and industrial preparation.

Many, if not all, known convergent strategies for oligosaccharide synthesis are based on the selective activation of one leaving group (LG) over another, which allows a decrease in the number of synthetic steps.[3,4] One of the most efficient procedures, the Fraser–Reid "armed–disarmed" approach, is based on the chemoselectivity principle.[5,6] Accordingly, in the presence of a mild promoter, a benzylated (armed) glycosyl donor is chemoselectively activated in preference to an acylated (disarmed) derivative bearing the same type of leaving group (Scheme 1). At this stage, a 1,2-*cis*-linked disaccharide is obtained preferentially as a result of the necessity to use the ether-type substituent (arming nonparticipating group). The obtained disaccharide can then be used

[*] J. T. Smoot, P. Pornsuriyasak, Prof. Dr. A. V. Demchenko
Department of Chemistry and Biochemistry
University of Missouri–St. Louis
One University Boulevard, St. Louis, MO 63121 (USA)
Fax: (+1) 314-516-5342
E-mail: demchenkoa@umsl.edu

[**] The authors thank the University of Missouri–St. Louis and the ACS PRF 42397-G1 for financial support of this research; the NSF for grants to purchase an NMR spectrometer (CHE-9974801) and the mass spectrometer (CHE-9708640) used in this work, Dr. R. S. Luo for assistance with 500 MHz 2D NMR experiments, and Dr. R. E. K. Winter and Mr. J. Kramer for HRMS determinations.

Supporting information for this article is available on the WWW under http://www.angewandte.org or from the author.

© 2005 Wiley-VCH Verlag GmbH & Co. KGaA, Weinheim

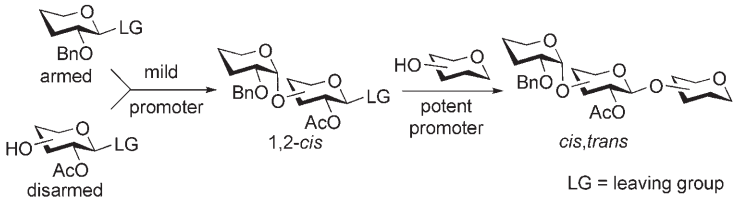

Scheme 1. The "armed–disarmed" strategy. Bn = benzyl

directly for 1,2-*trans* glycosylation (in the presence of a more potent promoter that can activate the disarmed leaving group) to afford a *cis*,*trans*-linked trisaccharide.

This concept was initially designed for *O*-pentenyl glycosides and was further explored for the chemoselective glycosidations of other glycosyl donors, including thioglycosides,[7] selenoglycosides,[8] fluorides,[9] phosphoroamidates,[10] substituted thioformimidates,[11] and S-benzoxazolyl glycosides.[12] Glycal reactivity was also found to be influenced by disarming acyl substituents.[13] Fraser-Reid et al.[14] and Ley and co-workers[15] found that torsional effects of cyclic acetal and dispiroketal protecting groups also promote anomeric deactivation. Moreover, Zhu and Boons demonstrated that thioglycosides that are protected as cyclic 2,3-carbonates are even less reactive than traditional disarmed acylated derivatives.[16] The chemoselective activation principles were summarized and expanded on by Ley and co-workers,[17] Wong and co-workers,[18–20] and other groups.[21,22] As a result, programmable multistep reactivity-based techniques, including highly efficient one-pot approaches, have become available.

S-thiazolinyl (STaz) glycosides, recently developed in our laboratory, were found to be compatible with the armed–disarmed procedure. Thus, chemoselective activation of **1**[23] over **2**[24] in the presence of either AgOTf or $Cu(OTf)_2$ afforded the disaccharide **3** as an anomeric mixture in 79–88% yield (Scheme 2). The latter was then converted into the *cis*,*trans*-linked trisaccharide **5** by treatment with the acceptor **4**.

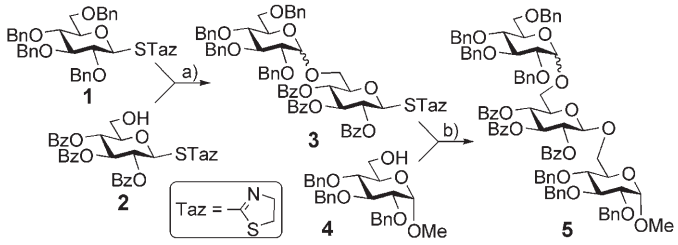

Scheme 2. Chemoselective activation of the STaz glycosides. a) 1. AgOTf, 1,2-DCE, 1 h, room temperature, 79%, $\alpha/\beta = 2:1$; or 2. $Cu(OTf)_2$, 1,2-DCE, 3.5 h, room temperature, 88%, $\alpha/\beta = 1.5:1$; b) AgOTf, 1,2-DCE, 2.5 h, room temperature, 83%. Bz = benzoyl, Tf = trifluoromethanesulfonyl, DCE = dichloroethane.

The armed–disarmed strategy thus offers an efficient tool for the synthesis of oligosaccharides with a *cis*,*trans* glycosylation pattern. Although the synthesis of *cis*,*cis*-linked derivatives is also possible,[5,6] this method is not applicable to the synthesis of *trans*,*cis*- or *trans*,*trans*-linked oligosaccharide fragments. The use of other techniques, such as orthogonal[25] or semiorthogonal synthesis[26] offer further advantages; however, these strategies require a set of at least two orthogonal leaving groups, which may not always be accessible. To address this challenge, we initiated studies of the "inverse armed–disarmed strategy", which would enable the stereoselective introduction of a 1,2-*trans* linkage prior to another 1,2-*trans* or 1,2-*cis* linkage.

Such an inverse approach would require the use of a neighboring substituent that is capable of both activation and participation (arming participating group (APG)). For this purpose we investigated a number of substituents **A**–**C** as APGs (Scheme 3). Our studies were based on STaz glycosides

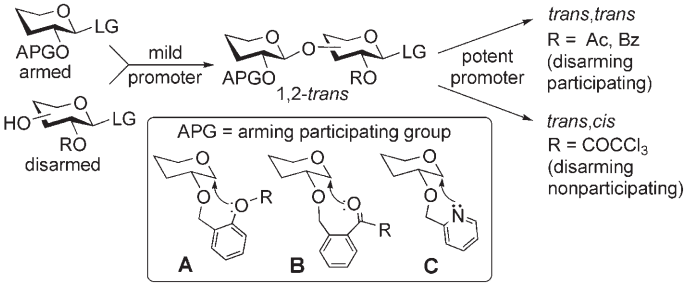

Scheme 3. Outline of an inverse armed–disarmed strategy.

owing to their superb glycosyl-donor properties.[23] The preliminary results obtained with a 2-*O*-(*o*,*o*-dimethoxybenzyl) glycosyl donor (type **A**) showed a fairly high diastereoselectivity (up to α/β 1:5), which was a significant improvement over the 2:1 α/β ratio found with perbenzylated STaz glycosyl donor **1** under the same reaction conditions. Nevertheless, it remained uncertain if the high β stereoselectivity is attributable to the anticipated participation of a seven-membered transition state (Scheme 3 or rather to the increased steric hindrance of the bottom face of the ring. The same uncertainty was anticipated for glycosyl donors of type **B**. To exclude the possibility of the increased steric hindrance, our further studies focused on the investigation of the 2-pyridylmethylpicolyl group, which is capable of a six-membered ring participation through the nitrogen atom (**C**, Scheme 3).

The glycosyl donor **8** bearing a picolyl substituent at C2 was synthesized from thioorthoester **6a**[27] (Scheme 4). Conveniently, the picolyl moiety was introduced with commercial picolyl bromide in the presence of NaH in DMF. In this

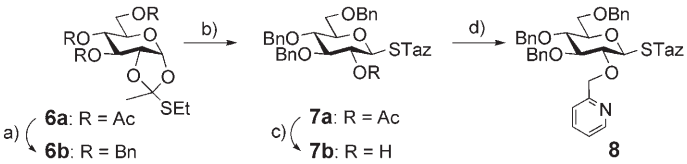

Scheme 4. Synthesis of the glycosyl donor **8**. a) 1) MeONa, MeOH, 2) BnBr, NaH, DMF, 85%; b) HSTaz/TMSOTf, CH_2Cl_2, 85%; c) MeONa, MeOH, 92%; d) PicBr, NaH, DMF, 90%. DMF = *N*,*N*-dimethylformamide, Pic = picolyl, TMS = trimethylsilyl.

 © 2005 Wiley-VCH Verlag GmbH & Co. KGaA, Weinheim

context, although an approach for the control of the anomeric stereoselectivity with a neighboring substituent that is capable of six-membered participation is relatively unexplored, a number of moieties for stereoselective glycosylation have recently been reported.[28,29]

Having synthesized the glycosyl donor **8**, we turned our attention to glycosidation studies. For this purpose, a range of differently protected glycosyl acceptors **2**, **4**, and **9**–**12** was selected. Based on our preliminary results

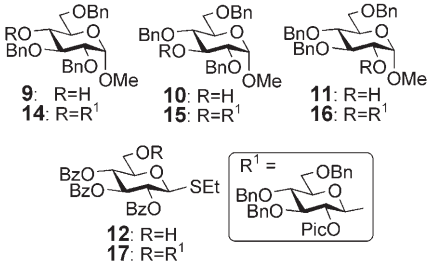

(Scheme 2), we employed $Cu(OTf)_2$ either alone, or in combination with catalytic TfOH as a promoter. All of the glycosylations summarized in Table 1 proceeded with complete 1,2-*trans* stereoselectivity.

Table 1: Synthesis of 1,2-*trans*-linked disaccharides **13**–**18**.

Entry	Acceptor	Promoter	Product	Yield [%]
1	**4**	$Cu(OTf)_2$	**13**	80
2	**9**	$Cu(OTf)_2$	**14**	84
3	**10**	$Cu(OTf)_2$/TfOH	**15**	82
4	**11**	$Cu(OTf)_2$/TfOH	**16**	80
5	**12**	$Cu(OTf)_2$	**17**	77
6	**2**	$Cu(OTf)_2$/TfOH	**18**	74

Notably, the glycosidation of **8** at room temperature required significantly more time than that of **1** (48 vs. 1–3 h, respectively). Therefore, to shorten the reaction time (12–16 h), all of the glycosylations shown in Table 1 were performed in 1,2-DCE at 50 °C. As the chemoselective activation of **8** in reference to the benzoylated acceptor **2** was also possible under these reaction conditions, the observed phenomenon could not be simply explained by the very low reactivity of **8**. In this context, perbenzoylated STaz glycosides typically require 1–20 h for glycosidation at room temperature.[23] The working hypothesis for subsequent studies was that upon departure of the promoter-assisted leaving group, the formed oxocarbenium ion is converted into a stable intermediate, such as **19**, which results from the anticipated 2-*O*-picolyl participation through a six-membered ring (Scheme 5).

To establish whether the process actually follows the anticipated pathway, the AgOTf-promoted glycosidation of **8** with methanol was monitored by ^{1}H NMR spectroscopy (synthesis of **21**, Scheme 5). It was determined that **8** is entirely consumed in approximately 1 h, regardless of whether the reaction is performed at room temperature or at 50 °C. At this stage, the ^{1}H NMR spectrum shows the

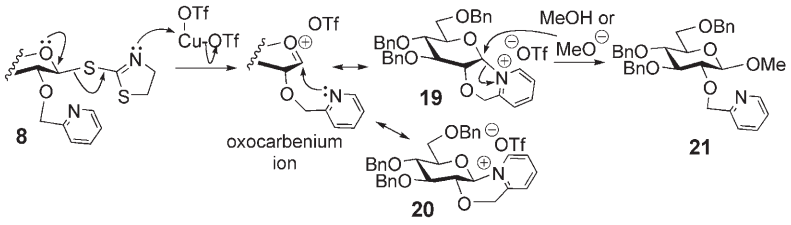

Scheme 5. Proposed reaction mechanism for the glycosidation of **8**.

presence of peaks that correspond to two compounds, presumably **19** (major) and **20** (minor) with a ratio that varied with the reaction conditions (5:1 (50 °C) to 20:1 (room temperature)). During this transition, the signal for the anomeric H atom of **8** (1-H, Figure 1 a) shifted downfield from $\delta \approx 5.30$ to ≈ 6.15 ppm for the anticipated intermediate **19** (1-β-H) and $\delta \approx 5.75$ ppm for the anticipated intermediate **20** (1-α-H, Figure 1 b), which could be an indication of the N-glycosidic linkage.

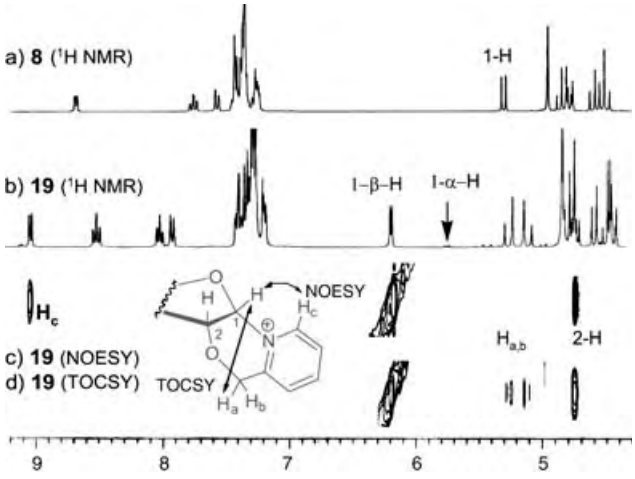

Figure 1. NMR analysis of the reaction of **8**, indicating the formation of the major intermediate **19**. a) 1H NMR spectum of **8**; b) 1H NMR spectrum of the major intermediate **19** and the minor intermediate **20**; c) NOESY spectrum of **19**; d) TOCSY spectrum of **19**.

Glycosylation experiments performed through glycosyl donor preactivation with subsequent addition of the glycosyl acceptor, provided a very similar outcome. The bicyclic intermediate **19** was isolated from the reaction of **8** with $Cu(OTf)_2$ (2 h at room temperature) and purified by column chromatography (silica gel).[30,31] The intermediate **19** was found to be reactive with potent nucleophiles such as NaOMe, even in the absence of a promoter, to afford **21** (Scheme 5). However, in all cases the β intermediate **20** remained completely inert and could typically be isolated from the reaction mixture.[32]

The 2D NMR determinations were also found to be very informative for the structural elucidation of **19**. Thus, correlations in the NOESY experiment between 1-H ($\delta =$ 6.15 ppm) and the aromatic H atom located adjacent to the picolyl nitrogen atom (H_c, $\delta = 9.00$ ppm) indicated that these

 © 2005 Wiley-VCH Verlag GmbH & Co. KGaA, Weinheim

H atoms were situated in close proximity (Figure 1c). The TOCSY data revealed that 1-H and the benzylic H atoms of the picolyl group (H_a and H_b, $\delta = 5.15$ ppm) were part of the same spin system (Figure 1d). Furthermore, long-range coupling between C1 ($\delta = 84.89$ ppm) and H_c was confirmed by the HMBC data, which indicated that C1 and H_c were three bonds apart.

Subsequently, to broaden the scope of the developed approach, we demonstrated that the 2-*O*-picolyl moiety could be removed under conventional catalytic hydrogenation conditions (Pd/C). Thus, hydrogenolysis of the *O*-picolyl moiety in **13** with concomitant removal of the benzyl protecting groups afforded **22** in 92% yield (Scheme 6). The

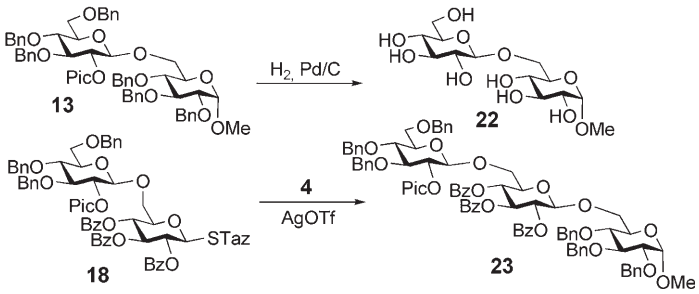

Scheme 6. Picolyl moiety removal and the synthesis of a *trans,trans*-linked trisaccharide **23**.

disaccharide **18**, obtained by the chemoselective activation of **8** in preference to **2** (Table 1), was glycosidated with **4** in the presence of AgOTf to afford *trans,trans*-linked trisaccharide **23** in 91% yield (Scheme 6). Further investigation of this approach and its application to convergent target synthesis is underway in our laboratory. We anticipated that the use of a disarming nonparticipating group for the second activation step would be required to achieve the 'inverse' *trans*, *cis*-linked oligosaccharide pattern. This type of a neighboring moiety includes, but perhaps is not limited to, halodenoacyls (trichloroacetyl, Scheme 3) or other functionalities recently reported by Crich et al.[33]

In conclusion, a new method for stereocontrolled glycosylation was developed. We demonstrated that complete 1,2-*trans* selectivity can be achieved with the use of a 2-*O*-picolyl moiety, a novel neighboring group that is capable of efficient participation through a six-membered intermediate. The 2-*O*-picolyl moiety has been shown to retain the glycosyl donor in the armed state as opposed to conventional acyl participating moieties. The application of a novel arming participating moiety to complementary chemoselective oligosaccharide synthesis also has been developed. This new armed–disarmed glycosylation strategy allows chemoselective introduction of a 1,2-*trans* glycosidic linkage prior to other linkages, in contrast to the Fraser-Reid approach. We expect that the developed technique, along with the classic armed–disarmed approach will allow convergent chemoselective synthesis of virtually any oligosaccharide sequence.

Received: August 1, 2005
Published online: October 13, 2005

Keywords: carbohydrates · glycosides · glycosylation · oligosaccharides · thioimidates

[1] Z. J. Witczak in *Carbohydrates in Drug Design* (Eds.: Z. J. Witczak, K. A. Nieforth), Marcel Dekker, New York, **1997**, p. 1.
[2] S. I. Nishimura in *Glycoscience: Chemistry and Chemical Biology, Vol. 3* (Eds.: B. Fraser-Reid, K. Tatsuta, J. Thiem), Springer, Berlin, **2001**, p. 1993.
[3] G.-J. Boons, *Tetrahedron* **1996**, *52*, 1095.
[4] A. V. Demchenko, *Lett. Org. Chem.* **2005**, *2*, 580.
[5] D. R. Mootoo, P. Konradsson, U. Udodong, B. Fraser-Reid, *J. Am. Chem. Soc.* **1988**, *110*, 5583.
[6] B. Fraser-Reid, U. E. Udodong, Z. F. Wu, H. Ottosson, J. R. Merritt, C. S. Rao, C. Roberts, R. Madsen, *Synlett* **1992**, 927.
[7] G. H. Veeneman, J. H. van Boom, *Tetrahedron Lett.* **1990**, *31*, 275.
[8] D. K. Baeschlin, A. R. Chaperon, V. Charbonneau, L. G. Green, S. V. Ley, U. Lucking, E. Walther, *Angew. Chem.* **1998**, *110*, 3609; *Angew. Chem. Int. Ed.* **1998**, *37*, 3423.
[9] M. I. Barrena, R. Echarri, S. Castillon, *Synlett* **1996**, 675.
[10] S. I. Hashimoto, H. Sakamoto, T. Honda, H. Abe, S. I. Nakamura, S. Ikegami, *Tetrahedron Lett.* **1997**, *38*, 8969.
[11] H. Chiba, S. Funasaka, K. Kiyota, T. Mukaiyama, *Chem. Lett.* **2002**, 746.
[12] M. N. Kamat, A. V. Demchenko, *Org. Lett.* **2005**, *7*, 3215.
[13] R. W. Friesen, S. J. Danishefsky, *J. Am. Chem. Soc.* **1989**, *111*, 6656.
[14] B. Fraser-Reid, Z. Wu, C. W. Andrews, E. Skowronski, *J. Am. Chem. Soc.* **1991**, *113*, 1434.
[15] G.-J. Boons, P. Grice, R. Leslie, S. V. Ley, L. L. Yeung, *Tetrahedron Lett.* **1993**, *34*, 8523.
[16] T. Zhu, G.-J. Boons, *Org. Lett.* **2001**, *3*, 4201.
[17] N. L. Douglas, S. V. Ley, U. Lucking, S. L. Warriner, *J. Chem. Soc. Perkin Trans. 1* **1998**, 51.
[18] Z. Zhang, I. R. Ollmann, X. S. Ye, R. Wischnat, T. Baasov, C. H. Wong, *J. Am. Chem. Soc.* **1999**, *121*, 734.
[19] X. S. Ye, C. H. Wong, *J. Org. Chem.* **2000**, *65*, 2410.
[20] F. Burkhart, A. Zhang, S. Wacowich-Sgarbi, C. H. Wong, *Angew. Chem.* **2001**, *113*, 1314; *Angew. Chem. Int. Ed.* **2001**, *40*, 1274.
[21] M. Fridman, D. Solomon, S. Yogev, T. Baasov, *Org. Lett.* **2002**, *4*, 281.
[22] Y. Wang, X. Huang, L. H. Zhang, X. S. Ye, *Org. Lett.* **2004**, *6*, 4415.
[23] A. V. Demchenko, P. Pornsuriyasak, C. De Meo, N. N. Malysheva, *Angew. Chem.* **2004**, *116*, 3131; *Angew. Chem. Int. Ed.* **2004**, *43*, 3069.
[24] P. Pornsuriyasak, U. B. Gangadharmath, N. P. Rath, A. V. Demchenko, *Org. Lett.* **2004**, *6*, 4515.
[25] O. Kanie, Y. Ito, T. Ogawa, *J. Am. Chem. Soc.* **1994**, *116*, 12073.
[26] A. V. Demchenko, C. De Meo, *Tetrahedron Lett.* **2002**, *43*, 8819.
[27] N. K. Kochetkov, L. V. Backinowsky, Y. E. Tsvetkov, *Tetrahedron Lett.* **1977**, 3681.
[28] J. H. Kim, H. Yang, J. Park, G. J. Boons, *J. Am. Chem. Soc.* **2005**, *127*, 12090.
[29] J. H. Kim, H. Yang, G. J. Boons, *Angew. Chem.* **2005**, *117*, 969; *Angew. Chem. Int. Ed.* **2005**, *44*, 947.
[30] Notably, the ^{1}H and ^{13}C NMR data of **19** and **20** are in good aggreement with those reported for α- and β-N-pyridinium salts: R. U. Lemieux, A. R. Morgan, *Can. J. Chem.* **1965**, *43*, 2205.
[31] K. Bock, C. Pedersen, *J. Chem. Soc. Perkin Trans. 2* **1974**, 293.
[32] One of the possible explanations for the higher stability of **20** could be the influence of the reverse anomeric effect: I. Tvaroska, T. Bleha, *Adv. Carbohydr. Chem. Biochem.* **1989**, *47*, 45.
[33] D. Crich, T. K. Hutton, A. Bangerjee, P. Jayalath, J. Picione, *Tetrahedron: Asymmetry* **2005**, *16*, 105.

 © 2005 Wiley-VCH Verlag GmbH & Co. KGaA, Weinheim

Synthetic Methods

DOI: 10.1002/anie.200502707

Synthesis, Structure, and Chemoselective Reactivity of *N*-(2-Iodylphenyl)acylamides: Hypervalent Iodine Reagents Bearing a Pseudo-Six-Membered Ring Scaffold**

Uladzimir Ladziata, Alexey Y. Koposov, Ka Y. Lo, Jeff Willging, Victor N. Nemykin, and Viktor V. Zhdankin**

During the past decade, hypervalent iodine compounds have gained significant attention as mild, selective, and environmentally benign reagents in synthetic organic chemistry.[1,2] The oxidation of sensitive and complex alcohols[2a,b] and amines,[2c] the cyclization of anilides,[2d] the introduction of α,β unsaturation into carbonyl compounds,[2e] and the aromatization of tetrahydronaphthalene-1,4-diones[2f] are among elegant synthetic transformations effected by organic iodine(v) compounds (λ^5-iodanes). However, the major reagents used for these unique protocols, Dess–Martin periodinane (DMP, **1**)[2a] and its precursor 1-hydroxy-1,2-benziodoxol-3-(1*H*)-one (IBX, **2**; see Scheme 1,[2b] suffer from a number of drawbacks, namely, DMP is highly sensitive towards moisture[3a] and unstable to prolonged storage, whereas IBX is explosive under impact or on heating to $>200\,^{\circ}C$,[3b] is nonrecyclable, and has limited solubility in most organic solvents except dimethyl sulfoxide (DMSO).

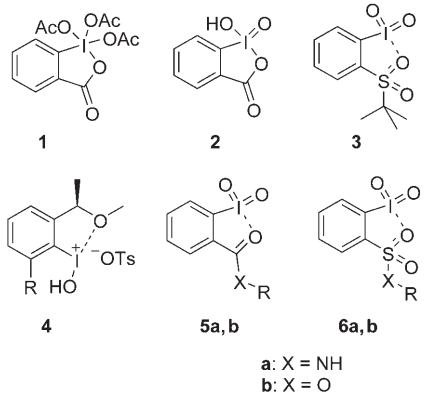

Scheme 1. Cyclic and pseudocyclic hypervalent iodine reagents.

[*] U. Ladziata, A. Y. Koposov, K. Y. Lo, J. Willging, Prof. Dr. V. N. Nemykin, Prof. Dr. V. V. Zhdankin
Department of Chemistry
University of Minnesota Duluth
Duluth, MN 55812 (USA)
Fax: (+1) 218-726-7394
E-mail: vnemykin@d.umn.edu
vzhdanki@d.umn.edu

[**] This work was supported by a research grant from the National Science Foundation (CHE 0353541) and by a NSF-MRI award (CHE 0416157).

Supporting information for this article is available on the WWW under http://www.angewandte.org or from the author.

The low solubility of **2**, which restricts its practical application, arises from strong intermolecular secondary I···O, hydrogen-bonding, and π-stacking interactions observed for IBX in the solid state.[4] Several research groups have tried to overcome this preparative limitation by performing oxidation at elevated temperatures,[5a] using an ionic liquid and water as a reaction medium,[5b] or functionalizing the IBX aromatic core.[5c] Also, a number of solid-supported reagents in which the IBX scaffold is linked to a polymer have been reported.[6] Another fruitful approach coined by Protasiewicz, Wirth, and co-workers[7a–e] involves the incorporation of an *ortho*-substituent into λ^5- and λ^3-iodanes (e.g., sulfone **3** and benzyl ether **4**), thus resulting in intramolecular secondary bonding interactions. This *ortho*-stabilization leads to a partial disruption of the polymeric network, and consequently enhances solubility. More recently, investigations from our group have resulted in a series of stable and soluble IBX analogs: IBX amides **5a**,[7f] IBX esters **5b**,[7g] as well as IBX sulfonamides **6a** and IBX sulfonate esters **6b**.[7h] A planar pseudo-benziodoxole moiety that arises from the intramolecular nonbonding iodine–oxygen interaction is a key structural feature present in this series of compounds, as shown by X-ray crystallographic analysis. The readily available hypervalent iodine reagents **5**–**6** possess reactivity similar to IBX and DMP and have proved to be useful oxidizing reagents towards alcohols[8a] and sulfides.[8b] The synthesis of polymer-supported IBX esters and amides has been reported as well.[8c]

We report herein the elaboration of the *ortho*-stabilization concept with regard to λ^5-iodanes. Our initial aim was to furnish an aryl iodyl species with a pseudo-six-membered ring unit such that the iodine(v) atom and *ortho*-sustituent donor atom were located in the 1,6-position. To obtain the required scaffold, we decided on an amide group as the *ortho* sustituent. Indeed, changing the aryl amide function in the substituted IBX amide to an aryl carbamoyl group yields *N*-(2-iodylphenyl)acylamides **7** with the required pseudo-benziodoxazine structure (Scheme 2). Assuming that an isosteric switch will not substantially change the molecular electronic parameters of the system when carried out, one can expect **7** to be close to the IBX amides in oxidative properties. Furthermore, the *ortho*-amide group offers a large variety of structural modifications, which may allow control over the reactivity profile of the title compounds.

A set of sixteen pseudo-benziodoxazines **14**–**17** was prepared to investigate the influence of the structure of the *ortho* sustituent on the oxidative activity of the target *N*-(2-iodylphenyl)acylamides and to explore the chemistry of these novel reagents (Scheme 2). Synthesis of **14**–**17** was performed by acylation of the commercially available 2-iodoaniline (**8**) with a range of acyl chlorides. Subsequent treatment of the obtained amides **9a**–**e** and **10** with NaH in dry THF, followed by alkylation with MeI and BnBr in the case of **9a**–**e**, led to pyrrolidinone **13** and substituted amides **11a**–**e** and **12a**–**e**. Oxidation of iodoarenes **11**–**13** with 3,3-dimethyldioxirane afforded **14**–**17** in good yields. All the products were isolated in the form of stable, white solids.[9]

Compounds **14**–**17** were identified by spectroscopic and ESI-mass-spectrometric analysis; single-crystal X-ray analysis

 © 2005 Wiley-VCH Verlag GmbH & Co. KGaA, Weinheim

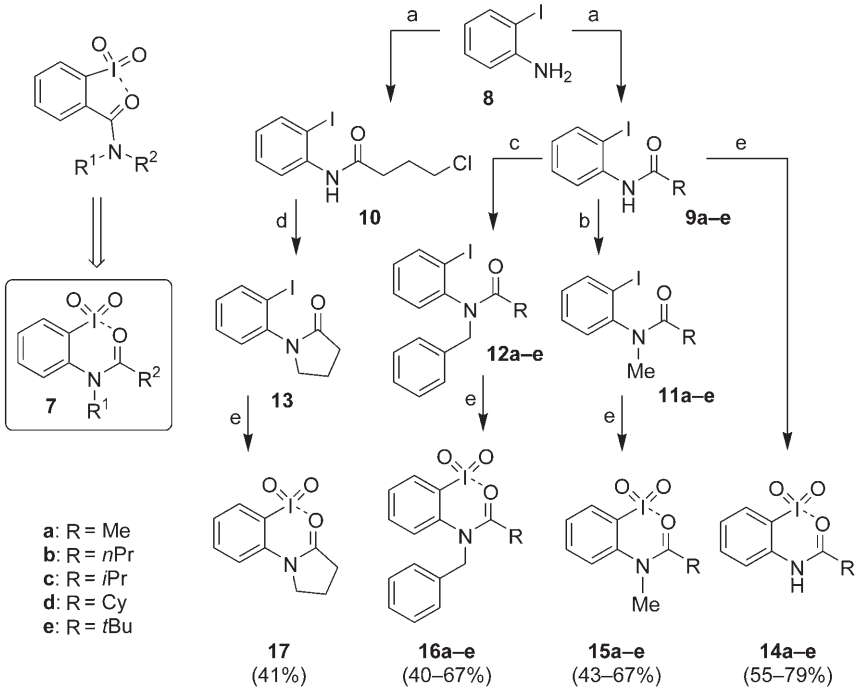

Scheme 2. Preparation of target aryl iodyl derivatives **14a–e**, **15a–e**, **16a–e**, and **17**. a) RCOCl (1.0 equiv), Et_3N (1.1 equiv), THF, 0°C→RT, 30 min; b) 1. NaH (1.1 equiv), THF, 0°C, 30 min; 2. MeI (1.3 equiv), THF, 0°C→RT, 3 h; (c) 1. NaH (1.1 equiv), THF, 0°C, 30 min; 2. BnBr (1.3 equiv), THF, 0°C→RT, 3 h; d) NaH (1.1 equiv), THF, 0°C→RT, 3 h; e) 3,3-dimethyldioxirane (3.0 equiv, 0.1 M in acetone), CH_2Cl_2, 0°C→RT, 3 h. Cy = cyclohexyl.

was also used in the case of **15e**. IR spectra of all compounds showed a strong absorption for I=O at 760–780 cm^{-1}. With a few exceptions (amides **14e**, **15c–e**, **16e**, and **17**), the expected carbonyl absorption appeared as two strong bands: the first band at 1640–1675 cm^{-1} (characteristic amide C=O stretch)[10] and the second at 1600–1620 cm^{-1} (C=N–Ar stretch).[10] Compounds **14e** and **15c–e** showed a single band at 1600–1620 cm^{-1}, whereas **16e** and **17** were characterized by a sole band at 1643 cm^{-1}. ^1H NMR analysis indicated practically no downfield shift for the proton *ortho* to the iodine atom relative to iodo derivatives **9–13**. In the ^{13}C NMR spectra of iodyl arenes **14a–e** and **17**, the signal for C–IO_2 was observed at approximately $\delta = 133$ ppm, whereas for amides **15–16** this signal emerged at $\delta = 142$ ppm. The ESI-HRMS spectra of **14–17** demonstrated strong peaks that correspond to dimers $[2M+Na]^+$, as well as weaker $[M+Na]^+$ peaks. These data will be rationalized later during the discussion of the reactivity profile of compounds **7**.

Single crystals of **15e** of X-ray-diffraction quality were obtained by slow evaporation from a methanol solution.[11] As anticipated, the structure of **15e** exhibits a strong I(1)···O(4) intramolecular interaction which affords the pseudo-benziodoxazine ring (Figure 1). The observed I(1)···O(4) distance of 2.647 Å is a typical for I^v pseudocyclic moieties.[7a–h] The resulting pseudo-benziodoxazine scaffold is not planar and a torsion angle of 41.33° was observed for the C(6)-C(11)-N(5)-C(13) fragment. This observation is rather intriguing because all known five-membered pseudocyclic iodine(v)-containing compounds have a planar geometry. Such a dramatic difference can be explained by the steric interaction between the hypervalent iodine center and the carbonyl oxygen atom. Indeed, the rotation of the C(6)-C(11)-N(5)-C(13) fragment to a zero-degree torsion angle results in a I(1)···O(4) distance of 1.86 Å, which is typical for the I=O bond, and therefore a planar geometry in the case of **15e** cannot be achieved. Another important feature of the crystal structure of **15e** is an unusual arrangement of the 3D polymeric network. As with the previously reported IBX analogues,[7a–h] molecules of **15e** form infinite polymeric chains in the bis-μ-oxo motif. This structure, however, differs from those observed earlier in two ways: First, the I(1)···O″(2) and I(1)···O′(3) distances are unusually different, with the latter close to the intramolecular I(1)···O(4) distance, whereas the former is close to the sum of the iodine and oxygen van der Waals radii (Figure 1). Second, the observed polymeric chain is spiral shaped along the principal *c* axis, whereas in previously reported IBX analogs such polymer motifs were close to a linear geometry. Overall, the formation of a six-membered pseudocycle in **15e** leads to several unique features in the solid-state structure.

The solubility of **14–17** varies appreciably depending on the nature of the substituents. Specifically, **14a–d** and pyrrolidinone **17** have very limited solubilities in polar organic solvents, such as dichloromethane, 1,2-dichloroethane (DCE), and acetonitrile. In contrast, **15a–e** and especially **16** exhibit

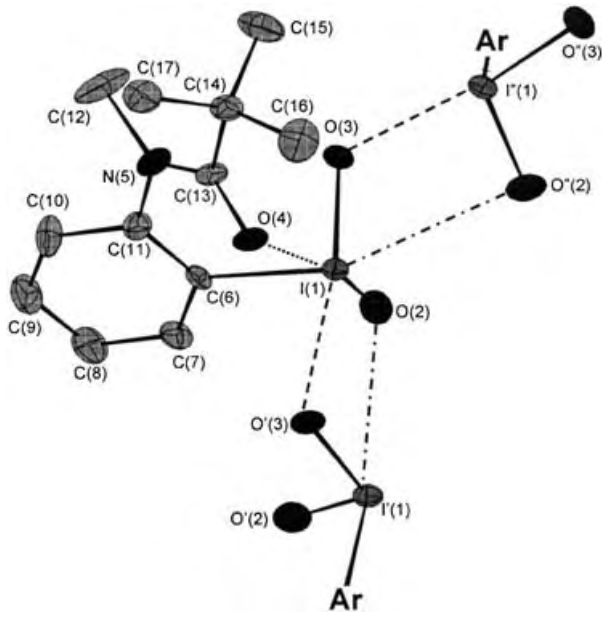

Figure 1. CAMERON drawing of a polymeric chain in the solid-state structure of **15e** at the 30% probability level (hydrogen atoms are omitted for clarity, Ar = 2-$C_6H_4NMeCOtBu$). Selected distances [Å] and angles [°]: I(1)–O(2) 1.791, I(1)–O(3) 1.832, I(1)···O″(2) 3.226, I(1)···O′(3) 2.627, I(1)–C(6) 2.115, I(1)···O(4) 2.647, N(5)–C(13) 1.349, O(4)–C(13) 1.225, O(2)-I(1)-O(3) 103.88, O(2)-I(1)-C(6) 99.01, O(3)-I(1)-C(6) 94.38, O(2)-I(1)···O(4) 166.31, C(6)-C(11)-N(5)-C(13) 41.33.

 © 2005 Wiley-VCH Verlag GmbH & Co. KGaA, Weinheim

excellent solubility in polar organic solvents, for example, the solubilities of **15d**, **15e**, and **16e** in CH_2Cl_2 are 0.97, 0.12, and 1.4 M, respectively. The plausible reason for the low solubility of **14** is the formation of intermolecular hydrogen bonds through amide hydrogen atoms which cause extra reinforcement of the polymeric network. In the case of **17**, the low solubility could be explained by the presence of a compact pyrrolidinone ring which offers minor steric demand and, thus, causes no disruption of the polymeric structure.

The oxidation activity of **14**–**17** was evaluated by studying the oxidation of benzyl alcohol and methyl *para*-tolyl sulfide. Preliminary reactivity investigations with **16d** (reagent/substrate = 1:2) showed that these oxidations proceed quantitatively at reflux within 1.5 hours and with MeCN or DCE as the optimal reaction solvents. Reaction at reflux is essential for fast conversions; for example, full conversion requires 36–48 hours at room temperature in DCE as the solvent. To compare reactivity, **14**–**17** were reacted under uniform conditions (the results are presented in Table 1).

The experimental results show that the oxidative activity of **14**–**17** depends on the nature of the *ortho*-substituent to a significant extent. On examination of the oxidative ability of **14**–**17**, a clear pattern emerges: First, unsubstituted amides **14**, with the exception of pivalamide **14e**, exhibit virtually no oxidative activity. This fact appears to arise from the negligible solubility of these compounds in MeCN. Compound **14e** renders moderate solubility and, hence, oxidizes benzyl alcohol. Interestingly, amide **14e** is not reactive towards methyl *para*-tolyl sulfide. Furthermore, series **15**, with **15d** displaying the optimal activity, also demonstrates similar selective oxidative behavior. In series **16**, the selectivity vanishes and both benzyl alcohol and methyl *para*-tolyl sulfide were oxidized effectively. In both sets of compounds, the acetamide derivatives (**15a** and **16a**) display considerable reactivity towards methyl *para*-tolyl sulfide. Finally, **17** does not oxidize alcohols, but reacts slowly with the sulfide functionality.

The character of such a structure–activity relationship can be explained by examination of the equilibrium between amide **7** and benziodoxazine **18** (Scheme 3). The cyclic form **18** apparently has decreased electrophilic reactivity because of its zwitterionic structure with the negative charge on the iodyl moiety and is, thus, not able to react with sulfides to form either intermediates **19** or **20**. On the other hand, the iodyl moiety in benziodoxazine **18** is possibly basic enough to abstract a proton from an alcohol to yield the protonated cyclic form **21**. Subsequent attack by an alkoxide leads to alkoxyiodane **23**, which undergoes decomposition to form

Table 1: Oxidative activity of **14**–**17** towards benzyl alcohol and methyl *para*-tolyl sulfide.

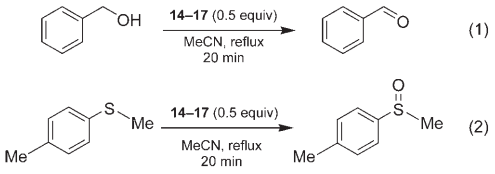

Entry	Reagent[a]	Conversion[b] in reaction (1) [%]	Conversion[c] in reaction (2) [%]
1	**14a**	0	0
2	**14b**	0	0
3	**14c**	2	0
4	**14d**	3	0
5	**14e**	36	0
6	**15a**	32	9
7	**15b**	70	6
8	**15c**	22	0
9	**15d**	72	0
10	**15e**	39	0
11	**16a**	19	95
12	**16b**	68	81
13	**16c**	36	31
14	**16d**	66	64
15	**16e**	79	96
16	**17**	0	8
17	**15d**	77[d]	89[d]

[a] The ratio of BnOH and *para*-Tol SMe to reagents **14**–**17** was 2:1. [b] Determined by GCMS; benzaldehyde and the respective iodoarenes **9** and **11**–**13** were the only reaction products detected. [c] Determined by GCMS; methyl *para*-tolyl sulfoxide and the respective iodoarenes **9** and **11**–**13** were the only reaction products detected. [d] Reaction was performed in the presence of TsOH (10 mol%).

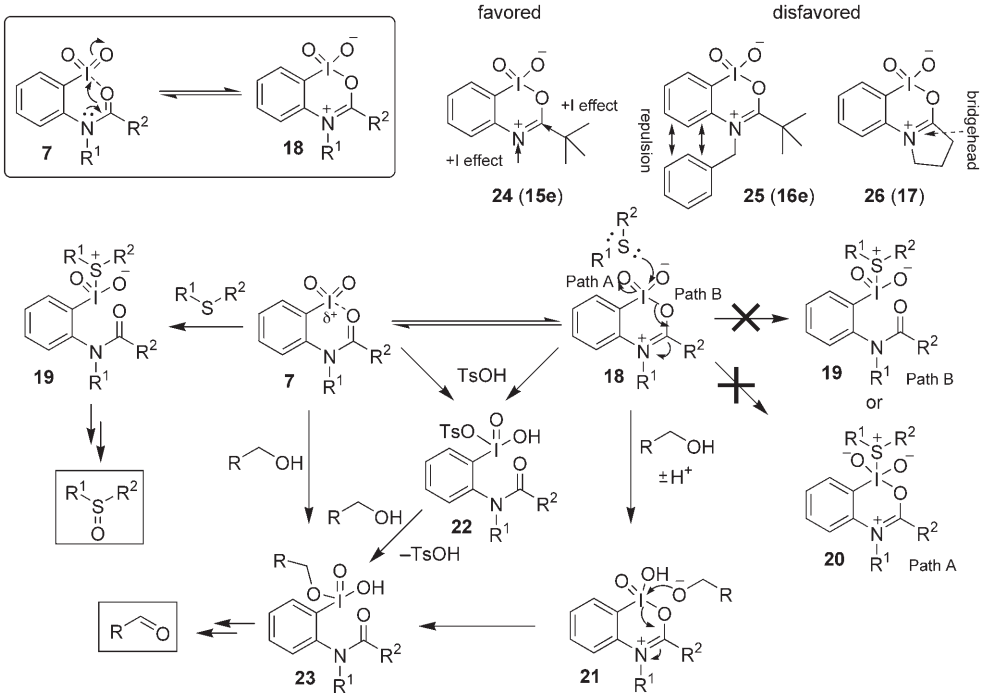

Scheme 3. Proposed mechanistic rationale for the reactivity of pseudo-benziodoxazines **14**–**17** towards alcohols and sulfides. I effect = inductive effect.

© 2005 Wiley-VCH Verlag GmbH & Co. KGaA, Weinheim

an aldehyde according to the conventional mechanism.[3a] In contrast, the open form **7** is more electrophilic and reacts unselectively with both the alcohol and sulfide groups. We can speculate that **14e** and **15c–e**, which are selective towards alcohol oxidation, have **18** as the major form in solution. The cyclic form **18** of **14e** and **15c–e** is possibly stabilized by the electron-donating effect of the R^1 group and especially the R^2 group through the decrease in the positive charge on the nitrogen atom (see **24**). In **15a**,**b**, the Me and *n*Pr substituents offer less stabilization, and minor amounts of the open form **7** is present in solution. Hence, partial oxidation of the sulfur atom is observed in **15a**,**b**. For series **16**, the cyclic form **18** is highly disfavored because of steric reasons (Scheme 3; see **25**), and no selectivity is observed. Compound **17** possesses lowered reactivity because of low solubility, and it is exclusively reactive towards the sulfide group. This behavior could be explained by the fact that the formation of benziodoxazine **26** is also highly disfavored because of the formation of a double bond at the bridgehead of a bicyclic system.

The proposed mechanism is supported by experimental and spectral data. In their IR spectra, **14e** and **15c–e** showed a single band at 1600–1620 cm^{-1}, which is a typical C=N–Ar stretch. Compounds **16e** and **17** were characterized by a single band at 1643 cm^{-1}, thus indicating an amide carbonyl function. All other compounds showed carbonyl absorptions in both of these regions. The ^{13}C NMR spectra of **15a** in [D_6]DMSO revealed pairs of close signals for C=O, C–NRCO, and C–IO_2 (Figure 2). We assume that this phenomenon results from the coexistence of forms **7** and **18** in solution. The same type of spectrum is observed for **15b** and **16a–d** in [D_6]DMSO and CD_3CN (but not in CD_3OD). Addition of MsOH (Ms = methanesulfonyl; approximately 1.0 equiv) led to upfield signals for C–NRCO and C–IO_2, whereas the upfield signal for C=O vanished, thus putatively yielding the mesylate species similar to the open form **7** (Figure 2). Indeed, no selectivity was observed when oxidations were carried out with **15d** in the presence of a catalytic amount of TsOH (Ts = *para*-toluenesulfonyl; Table 1, entry 17). Conceivably, the formation of electrophilic species **22**, which is close to **7** in reactivity, is responsible for such a major change in the oxidative behavior. The ^{13}C NMR spectra of **15e** and **16e** correspond to the cyclic and open forms of **15a**, respectively (Figure 2). The latter spectroscopic data match the reactivity profile of **15e** and **16e** perfectly but contradict the X-ray data obtained for **15e**. This data can be rationalized by the supposition that the zwitterionic cyclic form **18** exists only in solution, in which charge separation is stabilized by polar solvent molecules, and thus could not be observed in the solid state.

To validate the chemoselective reactivity of **15d**, the oxidation reactions of thioalcohols **26** and **28** were studied (Scheme 4). However, when 0.5 equivalents of oxidant in DCE at reflux were used, considerable amounts (approximately 30% by GCMS) of the respective sulfoxides were formed along with the main products **27** and **29**. Probably, the

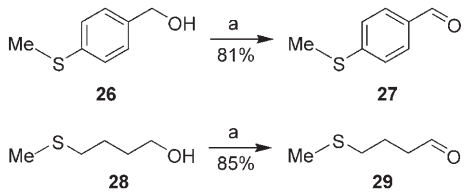

Scheme 4. Site-selective oxidation of thioalcohols **26** and **28**. a) **15d** (1.0 equiv), MeSEt (1.0 equiv), DCE, reflux, 2.5 h.

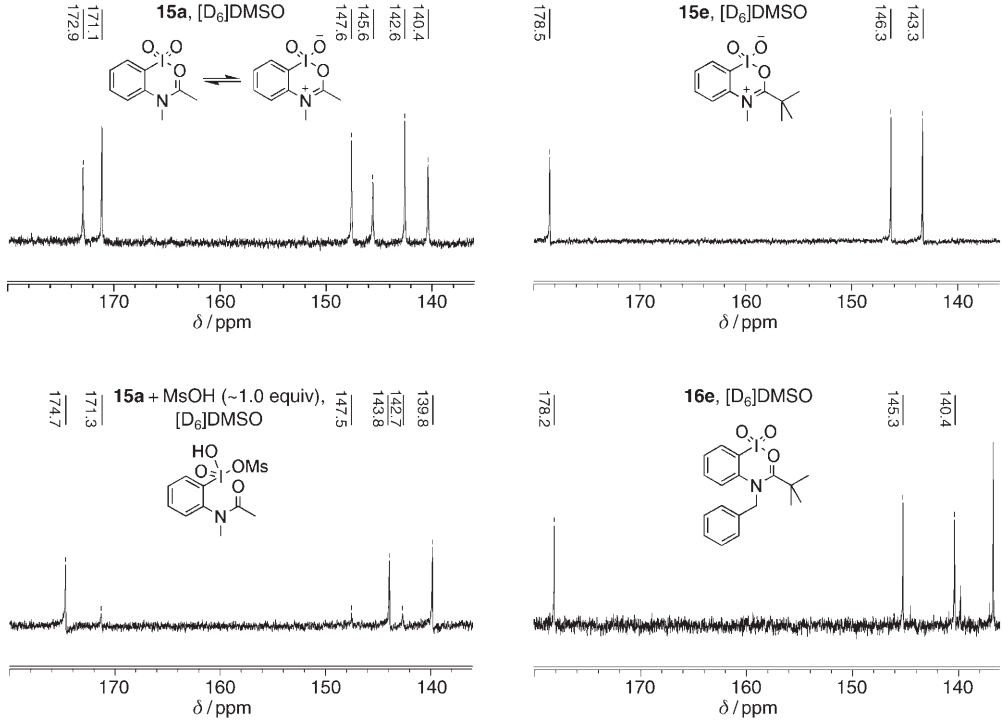

Figure 2. ^{13}C NMR spectra (δ = 136–180 ppm) of iodylarenes **15a**, **15a** + MsOH (1.0 equiv), **15e**, and **16e** in [D_6]DMSO.

 © 2005 Wiley-VCH Verlag GmbH & Co. KGaA, Weinheim

initially formed alkoxyiodane **23** can oxidize the sulfur atom to yield the sulfoxide functionality. To avoid this complication, MeSEt (1.0 equiv) was added to the reaction mixture and the quantity of **15d** was increased to 1.0 equivalent. This alteration in the protocol afforded target aldehydes **27** and **29** (sole oxidation products of **26** and **28** as determined by GCMS) in good preparative yields (Scheme 4); furthermore, small amounts of MeSOEt were also isolated. It is notable that oxidation of the thioalcohol **28** using DMP gives only 20% yield of the aldehyde **29**.[12]

In conclusion, the design, preparation, structure, and oxidative properties of novel *N*-(2-iodylphenyl)acylamides **14**–**17** have been described herein, and a mechanistic proposal that accounts for the reactivity pattern of **14**–**17** has also been sufficiently espoused. X-ray studies of **15e** revealed a unique pseudo-benziodoxazine structure, the first reported example of a six-membered pseudocyclic scaffold for iodine(v), with intramolecular secondary I···O bonding interactions. Preliminary experiments indicate that the reagents **14**–**17** can oxidize alcohols and sulfides and that the reactivity largely depends on the substitution pattern of the amide group adjacent to the iodyl moiety. This discovery suggests that the pseudo-benziodoxazine scaffold is a promising lead structure for the design of new regio- and stereoselective hypervalent iodine oxidants. Investigations into mechanistic and reactivity aspects of **14**–**17**, as well as the design of a polymer-supported derivative of the described reagents is ongoing and will be reported in due course.

Received: August 1, 2005

Keywords: alcohols · hypervalent iodine · oxidation · regioselectivity · thiols

[1] a) A. Varvoglis, *Hypervalent Iodine in Organic Synthesis*, Academic Press, London, **1997**; b) *Hypervalent Iodine Chemistry* (Ed.: T. Wirth), Springer, Berlin, **2003**; c) M. Ochiai in *Chemistry of Hypervalent Compounds* (Ed.: K. Akiba), VCH Publishers, New York, **1999**; d) H. Tohma, Y. Kita, *Adv. Synth. Catal.* **2004**, *346*, 111; e) T. Wirth, *Angew. Chem.* **2005**, *117*, 3722; *Angew. Chem. Int. Ed.* **2005**, *44*, 3656; f) P. J. Stang, *J. Org. Chem.* **2003**, *68*, 2997; g) V. V. Zhdankin, P. J. Stang, *Chem. Rev.* **2002**, *102*, 2523; h) V. V. Zhdankin, *Curr. Org. Synth.* **2005**, *2*, 121.

[2] a) D. B. Dess, J. C. Martin, *J. Org. Chem.* **1983**, *48*, 4155; b) M. Frigerio, M. Santagostino, *Tetrahedron Lett.* **1994**, *35*, 8019; c) K. C. Nicolaou, C. J. N. Mathison, J. N. Casey, T. Montagnon, *J. Am. Chem. Soc.* **2004**, *126*, 5192; d) K. C. Nicolaou, P. S. Baran, R. Kranich, Y. Zhong, K. Sugita, N. Zou, *Angew. Chem.* **2001**, *113*, 208; *Angew. Chem. Int. Ed.* **2001**, *40*, 202; e) K. C. Nicolaou, T. Montagnon, P. S. Baran, *Angew. Chem.* **2002**, *114*, 1035; *Angew. Chem. Int. Ed.* **2002**, *41*, 993; f) S. Kotha, S. Banerjee, K. Mandal, *Synlett* **2004**, 2043.

[3] a) D. B. Dess, J. C. Martin, *J. Am. Chem. Soc.* **1991**, *113*, 7277; b) M. Frigerio, M. Santagostino, S. Sputore, *J. Org. Chem.* **1999**, *64*, 4537.

[4] P. J. Stevenson, A. B. Treacy, M. Nieuwenhuyzen, *J. Chem. Soc. Perkin Trans. 2* **1997**, 589.

[5] a) J. D. More, N. S. Finney, *Org. Lett.* **2002**, *4*, 3001; b) Z. Liu, Z.-C. Chen, Q.-G. Zheng, *Org. Lett.* **2003**, *5*, 3321; c) A. P. Thottumkara, T. K. Vinod, *Tetrahedron Lett.* **2002**, *43*, 569.

[6] a) M. Mülbaier, A. Giannis, *Angew. Chem.* **2001**, *113*, 4530; *Angew. Chem. Int. Ed.* **2001**, *40*, 4393; b) G. Sorg, A. Mengel, G. Jung, J. Rademann, *Angew. Chem.* **2001**, *113*, 4532; *Angew. Chem. Int. Ed.* **2001**, *40*, 4395; c) N. N. Reed, M. Delgado, K. Hereford, B. Clapham, K. D. Janda, *Bioorg. Med. Chem. Lett.* **2002**, *12*, 2047; d) Z. Lei, C. Denecker, S. Jegasothy, D. C. Sherrington, N. K. H. Slater, A. J. Sutherland, *Tetrahedron Lett.* **2003**, *44*, 1635.

[7] a) D. Macikenas, E. Skrzypczak-Jankun, J. D. Protasiewicz, *Angew. Chem.* **2000**, *112*, 2063; *Angew. Chem. Int. Ed.* **2000**, *39*, 2007; b) B. V. Meprathu, M. W. Justik, J. D. Protasiewicz, *Tetrahedron Lett.* **2005**, *46*, 5187; c) U. H. Hirt, M. F. H. Schuster, A. N. French, O. G. Wiest, T. Wirth, *Eur. J. Org. Chem.* **2001**, 1569; d) U. H. Hirt, B. Spingler, T. Wirth, *J. Org. Chem.* **1998**, *63*, 7674; e) T. Wirth, U. H. Hirt, *Tetrahedron: Asymmetry* **1997**, *8*, 23; f) V. V Zhdankin, A. Y. Koposov, B. C. Netzel, N. V. Yashin, B. P. Rempel, M. J. Ferguson, R. R. Tykwinski, *Angew. Chem.* **2003**, *115*, 2244; *Angew. Chem. Int. Ed.* **2003**, *42*, 2194; g) V. V Zhdankin, D. N. Litvinov, A. Y. Koposov, M. J. Ferguson, R. McDonald, R. R. Tykwinski, *Chem. Commun.* **2004**, 106; h) A. Y. Koposov, D. N. Litvinov, V. V. Zhdankin, *Tetrahedron Lett.* **2004**, *45*, 2719.

[8] a) V. V. Zhdankin, A. Y. Koposov, D. N. Litvinov, M. J. Ferguson, R. McDonald, T. Luu, R. R. Tikwinski, *J. Org. Chem.* **2005**, *70*, 6484; b) A. Y. Koposov, V. V. Zhdankin, *Synthesis* **2005**, 22; c) W. J. Chung, D. K. Kim, Y. S. Lee, *Tetrahedron Lett.* **2003**, *44*, 9251.

[9] Representative procedure for the preparation of **15e**: A freshly prepared solution of 3,3-dimethyldioxirane in acetone (0.1M, 30 mL, 3.0 mmol) was added to a stirred solution of amide **11e** (0.317 g, 1.0 mmol) in CH_2Cl_2 (5 mL) at 0°C (ice bath). The reaction mixture was stirred for 1 h at 0°C, the ice bath was removed, and the solution was additionally stirred for 2 h at room temperature. The solvent was removed under reduced pressure, the remaining white solid was stirred with Et_2O (5 mL) for 15 min, filtered, washed with cold Et_2O (2 × 2.5 mL), and dried in vacuum to afford analytically pure **15e** (0.293 g, 84%) as a snow-white solid. M.p. 172°C (decomp.); ^{1}H NMR (300 MHz, CD_3OD): $\delta = 8.00$ (dd, $^3J = 8.0$ Hz, $^4J = 1.5$ Hz, 1H, Ar), 7.69 (td, $^3J = 7.7$ Hz, $^4J = 1.5$ Hz, 1H, Ar), 7.51–7.59 (m, 2H, Ar), 3.68 (s, 3H, CH_3), 1.43 ppm (s, 9H, $3CH_3$); ^{13}C NMR (75.5 MHz, CD_3OD): $\delta = 182.0$, 147.0, 144.7 (C–IO_2), 134.9, 128.4, 128.3, 127.0, 41.5, 41.0, 28.2 ppm; IR (NaCl): $\tilde{\nu} = 1602$ (C=O), 760 cm^{-1} (I=O); ESI-HRMS: *m*/*z* (%) 372.0075 (23) $[M+Na]^+$, 721.0684 (100) $[2M+Na]^+$. Refer to the Supporting Information for additional synthetic protocols and spectral data.

[10] E. Pretsch, P. Bühlmann, C. Affolter, *Structure Determination of Organic Compounds: Tables of Spectral Data*, 3rd ed., Springer, Berlin, **2001**.

[11] X-ray diffraction data were collected on Rigaku AFC-7R diffractometer using graphite-monochromated molybdenum Kα radiation ($\lambda = 0.71073$ Å) at 293 K. Psi-scan absorption corrections were applied to the data using TeXsan 10.3b program (Rigaku Inc. 1997). The structure was solved by direct methods (SIR-92) and refined by full-matrix least-squares refinement on F^2 using Crystals for Windows program. Crystal data for **15e** $C_{12}H_{16}INO_3$: $M_r = 349.17$, tetragonal, space group $I4_1$, $a = b = 14.268(2)$, $c = 12.832(3)$ Å, $\alpha = \beta = \gamma = 90°$, $V = 2612.3(7)$ Å^3, $Z = 8$, $\mu = 2.448$ mm^{-1}, 1685 reflections measured, 1568 unique ($R_{int} = 0.10$); final $R_1 = 0.040$, $R_w = 0.101$. CCDC-279792 (**15e**) contains the supplementary crystallographic data for this paper. These data can be obtained free of charge from the Cambridge Crystallographic Data Centre via www.ccdc.cam.ac.uk/data_request/cif.

[12] G. Xu, M. Micklatcher, M. A. Silvestri, T. L. Hartman, J. Burrier, M. C. Osterling, H. Wargo, J. A. Turpin, R. W. Buckheit, Jr., M. Cushman, *J. Med. Chem.* **2001**, *44*, 4092.

 © 2005 Wiley-VCH Verlag GmbH & Co. KGaA, Weinheim

Supported Au Catalysts

DOI: 10.1002/anie.200502101

Catalysis by Gold: Isolated Surface Au^{3+} Ions are Active Sites for Selective Hydrogenation of 1,3-Butadiene over Au/ZrO_2 Catalysts**

*Xin Zhang, Hui Shi, and Bo-Qing Xu**

In recent years, there has been an increasing interest in catalysis by nanosized gold catalysts,[1–5] which are active in reactions such as CO oxidation,[1–10] propylene epoxidation,[1–3] hydrogenation of unsaturated compounds,[3,12–15] vinyl chloride synthesis,[5] and others.[2,3,5,11] Despite such a diverse spectrum of reactions, efforts have been mainly devoted to elucidating the catalytically active sites in the oxidation reactions.[1–10] Little attention has been paid to the nature of active gold, especially cationic gold species,[5,11] in the other reactions such as hydrogenation of unsaturated compounds.[12–17] This is surprising, since catalytic hydrogenation is one category of the best studied and industrially most important reactions on conventional transition metal catalysts,[18,19] and Au^{3+} ions in solution can activate carbon–carbon double and triple bonds and are finding applications as efficient homogeneous catalysts in many organic reactions.[20,21] Hydrogenation of 1,3-butadiene has long been a model reaction for the study of active sites on conventional metal catalysts.[18,19] A few preliminary investigations[12,13] on the hydrogenation of 1,3-butadiene with supported gold catalysts showed that small gold nanoparticles were active in the reaction, although theoretical calculations seem to suggest that the surface of metallic gold is chemically inert for hydrogen activation.[22,23]

By using Au/ZrO_2 catalysts with very low loadings of Au ($< 0.1\,\%$), we have now discovered that isolated surface-type Au^{3+} ions are actually the active sites for the selective hydrogenation of 1,3-butadiene. The activity and selectivity of these Au^{3+} ions are comparable to those of conventional precious transition metals such as Pd and Pt. This finding that low loadings of Au^{3+} ions are more active for the hydrogenation reaction than high loadings of Au nanoparticles could raise intensive interest in exploring the potential of surface-type Au^{3+} ions in heterogeneous catalytic reactions. The use of isolated and heterogenized Au^{3+} ions in catalysis and related materials may be the key to using the noble gold in areas usually reserved for conventional precious metal catalysts, for example, to significantly improve the economics and reduce the use of other precious metals.

Figure 1 shows the effect of gold loading on 1,3-butadiene conversion over Au/ZrO_2 catalysts calcined at 200 °C. No butane (i.e., the product of complete hydrogenation) but only butenes were detected as the hydrogenation products over all catalysts used. The conversion was less than 1 % in our blank test with bare ZrO_2 support as catalyst. The activity was enhanced greatly on loading with gold, and only a slight decrease in catalyst activity was observed up to 6 h of reaction time on stream (TOS). Surprisingly, higher conversion (ca. 50 %) is obtained over 0.05 % Au/ZrO_2 than over 0.23 % Au/ZrO_2 catalyst (ca. 40 %). The 1,3-butadiene conversions are converted to show the specific mass activity of gold in the catalysts in Table 1. The catalytic turnover frequencies (TOFs) based on surface gold atoms or nonmetallic Au "atoms" are also given in the table. These catalytic rates decreased sharply when the Au loading was increased from 0.05 to 0.23 % and higher. It is noteworthy that the TOFs are very similar (ca. 0.40 s^{-1}) for the catalysts containing 0.05 and 0.01 % Au, that is, the gold "atoms" in these two samples are equally active for the selective hydrogenation reaction.

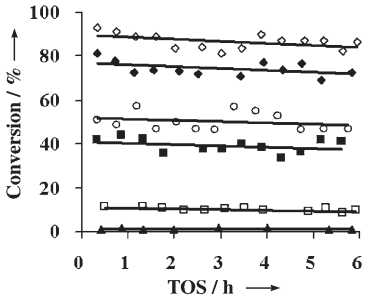

Figure 1. Conversion of 1,3-butadiene at 120 °C over Au/ZrO_2 catalysts (calcined at 200 °C) containing 0.76 (◆), 0.23 (■), 0.08 (◇), 0.05 (○), and 0.01 % Au (□). The (▲) data show the conversion over bare ZrO_2 support. TOS = reaction time on stream.

The same high TOFs of the Au/ZrO_2 catalysts containing no more than 0.05 % Au would mean that the active gold species are atomically dispersed and isolated from each other on the surface of the zirconia support. It was shown previously[11,25] that treatment of supported gold catalysts with an aqueous solution of NaCN can dissolve the gold particles and create isolated gold cations on the support surface. Using a similar procedure (Supporting Information), we treated the 0.76 % Au/ZrO_2 sample with an aqueous solution of 2 % KCN. According to measurements of the Au content by inductively coupled plasma atomic emission spectrometry (ICP-AES), such treatment removed about 90 % of the gold from the solid catalyst and gave a 0.08 % Au/ZrO_2 catalyst. The ICP-AES analysis detected no contamination by K^+ or Na^+ of the sample after treatment. The catalytic activity data of this 0.08 % Au/ZrO_2 catalyst in 1,3-butadiene conversion are included in Figure 1 for comparison

[*] X. Zhang, H. Shi, Prof. B.-Q. Xu
Innovative Catalysis Program
Key Lab of Organic Optoelectronics & Molecular Engineering
Department of Chemistry
Tsinghua University
Beijing 100084 (China)
Fax: (+86) 10-6279-2122
E-mail: bqxu@mail.tsinghua.edu.cn

[**] We gratefully acknowledge the financial support of this work by NSF of China (grants: 20443008, 20125310, and 20590360) and National Basic Research Project of China (grant: 2003CB615804). We also thank the referees for their insightful comments.

Supporting information for this article is available on the WWW under http://www.angewandte.org or from the author.

InterScience
© 2005 Wiley-VCH Verlag GmbH & Co. KGaA, Weinheim

Table 1: Average Au particle size (TEM), hydrogen consumption (TPR), and 1,3-butadiene hydrogenation rates at 120 °C over Au/ZrO_2 catalysts.

Au loading [wt%]	d_{Au}[d] [nm]	H_2 consumed [mol(H_2)/mol(Au)]	Au^{3+}/Au^0 ratio[e]	Au^{3+} [μmol g(cat.)$^{-1}$]	Reaction rate [mmol s^{-1} g(Au)$^{-1}$]	TOF [s^{-1}][d]
0.01	nd[e]	1.57	–	0.5	2.08	0.41
0.05	nd	1.49	–	2.5	2.01	0.40
0.08[a]	nd	1.50	–	4.1	2.15	0.42
0.23	2.9	0.68	0.83	5.3	0.34	0.17
0.76	4.1	0.37	0.33	9.6	0.20	0.14
0.76[b]	6.7	0.25	0.20	6.4	0.14	0.13
0.76[c]	11.7	0	0	0	0.02	0.03

[a] Sample obtained by treatment of the 0.76% Au/ZrO_2 catalyst with 2% KCN solution. [b] Sample calcined at 300 °C. [c] Sample calcined at 500 °C. [d] The average particle size of Au was determined according to the equation $d = \Sigma n_i d_i / n_i$ by randomly measuring for each sample ca. 200 particles by TEM; the TOF data were calculated on the basis of Au atoms exposed on the surface, which were obtained from the average particle sizes by assuming closed-shell Au particles of spherical shape. All of the nonmetallic Au "atoms" in the catalyst containing less than 0.1% Au were assumed to be the catalytic sites in calculating the TOF data. [e] nd: no metallic Au particle was found in the high-resolution TEM image.

with the other catalysts of different Au loadings. To our surprise, this 0.08% Au/ZrO_2 catalyst effected the highest 1,3-butadiene conversion (ca. 85%). Assuming that every gold "atom" in this 0.08% Au/ZrO_2 catalyst was active for the reaction, we obtained a TOF of 0.42 s^{-1}, which is basically the same as those of the 0.05% Au/ZrO_2 and 0.01% Au/ZrO_2 catalysts (Table 1). This is remarkable, since these rates reveal that the loaded gold "atoms" were 100% accessible for the reaction at these low loadings. According to references [11,25], the 0.08% Au/ZrO_2 sample obtained by treatment of 0.76% Au/ZrO_2 with aqueous 2% KCN solution should contain only surface-type gold cations. The unchanged TOFs of gold at such low loadings could hint that the catalytic active sites are gold cations rather than gold nanoparticles.

We then studied the effect of calcination temperature of the 0.76% Au/ZrO_2 catalyst on the selective hydrogenation reaction, since the calcination temperature appears to affect the ratio of Au^{3+}/Au^0 in oxide-supported gold catalysts.[25,26] We found that the conversion of 1,3-butadiene clearly increased with decreasing catalyst calcination temperature in the range of 200–500 °C (Figure 2). We used a combination of temperature-programmed reduction (TPR) and X-ray photoelectron spectroscopy (XPS) to quantitatively characterize the oxidation states of gold. The XPS data (Figure 3) showed that the sample calcined at 500 °C contained only metallic Au^0 showing $4f_{7/2}$ and $4f_{5/2}$ signals at 83.7 and 87.6 eV, respectively.[26] In addition to metallic Au^0, XPS spectra of samples calcined at 300 and 200 °C also contained the $4f_{7/2}$ (86.1 eV) and $4f_{5/2}$ (89.4 eV) signals from Au^{3+} ions. Thus the Au^{3+}/Au^0 ratio increases with decreasing catalyst calcination temperature.

Figure 4 shows the temperature-programmed reduction (TPR) profiles of the bare ZrO_2 support as well as 0.08% and 0.76% Au/ZrO_2 catalysts. Bare ZrO_2 showed no consumption of hydrogen up to 800 °C. The TPR profiles of the samples calcined at 200 and 300 °C feature two hydrogen consumption peaks, one at low (210–230 °C) and the other at high temperature (550–580 °C). However, only the high-temperature peak appeared for the sample calcined at 500 °C. With reference to the XPS characterization data, the low-temperature peak should be due to reduction of Au^{3+} ions, while the high-temperature peak can be assigned to partial (< 3%) reduction of surface Zr^{4+} ions of the zirconia support to Zr^{3+}.[14]

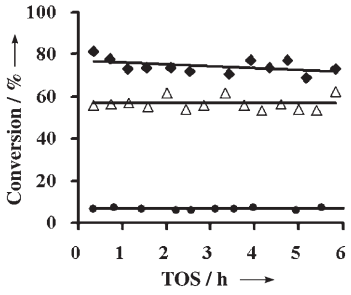

Figure 2. Effect of the catalyst (0.76% Au/ZrO_2) calcination temperature on 1,3-butadiene conversion: (◆) 200, (△) 300, and (●) 500 °C.

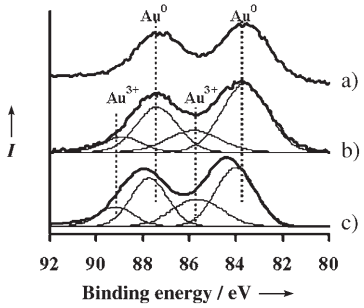

Figure 3. XPS spectra (Au 4f) of 0.76% Au/ZrO_2 catalysts calcined at different temperatures: a) 500, b) 300, and c) 200 °C.

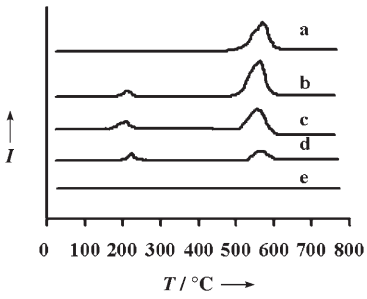

Figure 4. TPR profiles of 0.76% Au/ZrO_2 catalysts calcined at different temperatures: a) 500, b) 300, c) 200 °C. d) TPR profile for the 0.08% Au/ZrO_2 catalyst obtained by treatment of sample (c) with 2% KCN solution. e) TPR profile for bare ZrO_2 support. Intensity *I* was measured with a thermal conductivity detector.

 © 2005 Wiley-VCH Verlag GmbH & Co. KGaA, Weinheim

The samples with very low Au loadings (< 0.1 %) were also characterized by the TPR technique. The TPR profile of the 0.08 % Au/ZrO_2 sample is presented as the profile (d) in Figure 4. Calibration of the hydrogen-consumption peak showed that the number of hydrogen molecules (H_2) consumed under the low-temperature peak was just 1.5 times the molar number of gold in the 0.08 % Au/ZrO_2 sample. Since this sample should contain only gold cations after treatment with 2 % KCN solution,[11,25] such stoichiometry ($H_2/Au = 1.5$ or $H/Au = 3.0$) of the reduction proves that the gold cations in the 0.08 % Au/ZrO_2 sample are actually Au^{3+}. The TPR profiles of the samples containing 0.01 and 0.05 % Au were very similar to that of 0.08 % Au/ZrO_2 (not shown in Figure 2). Their reduction stoichiometries (Table 1) also prove that these two samples contain only Au^{3+} ions.

We then measured the Au^{3+}/Au^0 ratios in the 0.76 % Au/ZrO_2 catalysts by calibrating the reduction peaks of their Au^{3+} ions; the ratios were 0.33 and 0.20 for samples calcined at 200 and 300 °C, respectively. For 0.23 % Au/ZrO_2, the measured Au^{3+}/Au^0 ratio was 0.83.

The effects of catalyst calcination temperature and Au loading on the catalyst activity are also compared in Table 1. The 0.76 % Au/ZrO_2 catalyst calcined at 500 °C, which contains only metallic Au particles but no Au^{3+} ions, exhibited a TOF of 0.03 s^{-1}, which is comparable to those of 0.01–0.02 s^{-1} at 150 °C of the most active metallic Au nanoparticles supported on TiO_2 and Al_2O_3 in reference [13]. However, this activity of the metallic gold (0.03 s^{-1}) in the 0.76 % Au/ZrO_2 catalyst is one order of magnitude lower than that of catalysts containing only small amounts of Au^{3+} ions (0.4 s^{-1}). The specific mass activity of the supported metallic Au particles in the 0.76 % Au/ZrO_2 catalyst, as well as in the 1 % Au/TiO_2 and 1 % Au/Al_2O_3 catalysts in ref. [13], is even two orders of magnitude lower. These remarkable differences demonstrate that the surface-type Au^{3+} ions are far more active than the Au^0 atoms at the surface of metal nanoparticles. Earlier, Guzman and Gates[15,16] reported that mononuclear organo-Au^{3+} complexes supported on MgO were active in the catalytic hydrogenation of ethene, while metallic Au^0 particles were inactive. Cationic gold was also found to be responsible for the activity of Au/CeO_2 catalysts in the water-gas shift reaction involving oxygen-containing reactants ($CO + H_2O$).[11] It is noteworthy in the present study that the Au^{3+} ions "fixed" at the ZrO_2 surface are stable and active even under a completely reducing atmosphere (H_2).

The catalytic activity in terms of conversion of 1,3-butadiene (Figures 1 and 2) or mass of gold (Table 1) is apparently not in proportion with the number of Au^{3+} ions in the catalysts containing 0.23 and 0.76 % Au. The numbers of Au^{3+} ions in the 0.23 % Au/ZrO_2 (5.3 μmol g^{-1}) and 0.76 % Au/ZrO_2 (e.g., 9.6 μmol g^{-1} for the sample calcined at 200 °C) catalysts were much higher than that in the 0.08 % Au/ZrO_2 (4.1 μmol g^{-1}) catalyst, but their activities were significantly lower. This indicates that the highly active Au^{3+} ions are not those with interaction to the metallic gold particles but those independently "fixed" at specific locations of the zirconia surface. The surface density of Au^{3+} ions in the most active 0.08 % Au/ZrO_2 catalyst is 0.02 per square nanometer. This surface density of Au^{3+} ions is sufficiently low to ensure that the most active sites for the hydrogenation reaction are isolated surface-type Au^{3+} ions.

Structure sensitivity is an important issue in gold catalysis even in the case of selective hydrogenation.[14,17,27] Since the present work is intended to show the important catalytic implications of Au^{3+} cations at the zirconia surface, it is not clear whether the selective hydrogenation of 1,3-butadiene is structure sensitive or not with respect to the ZrO_2-supported Au particles. We note, however, that in work by Haruta et al.[13] the same reaction was almost insensitive to the size of the Au particles and nature of the support, while an earlier paper by Buchanan and Webb[28] suggested a strong influence of the support materials. Claus et al. found that the same reaction over metallic Au is also sensitive to the nature of the support oxide,[17] but the hydrogenation of acrolein is mainly affected by the percentage of edge/corner atoms relative to the total surface atoms.[14,27]

Due to their ability to activate carbon–carbon double and triple bonds (e.g., alkynes and allenes), Au^{3+} ions (i.e., gold salts) in solution are finding applications as efficient homogeneous catalysts in many organic reactions.[20,21] If the Au^{3+} ions can be properly heterogenized onto a solid surface while still maintaining their catalytic efficiency in the homogeneous systems, the "golden gate"[21] of catalysis by homogeneous gold would be even more useful for advanced heterogeneous catalysis. By reducing the loading of gold to very low levels (< 0.1 % Au), the present work is the first to demonstrate that high loadings of Au nanoparticles are actually not required for the hydrogenation reaction; the very low concentration of Au^{3+} ions (0.02 Au^{3+}/nm^2) heterogenized on zirconia surface from a cheap inorganic gold source ($HAuCl_4$) is enough to grant much higher catalytic activity. Moreover, the present heterogenized Au^{3+} ions were simply prepared from an inorganic gold salt in aqueous solution and were stable in ambient air, which can be very important in practical applications.

The TOF of the isolated Au^{3+} ions (0.4 s^{-1}) is comparable to that of conventional supported precious metals (e.g., ca. 0.2–1.0 s^{-1} for Pd).[18,19] Interestingly, the hydrogenation of 1,3-butadiene over the present Au/ZrO_2 catalysts has 100 % selectivity for butenes; no butane is detected even over the most active 0.08 % Au/ZrO_2 catalyst at high conversions of 1,3-butadiene (80–90 %; see Figure 1). The major component of the product butenes is 1-butene (ca. 60 %), and the *trans*/*cis* ratio of 2-butene is in the range of 0.3–1.0 over all of the Au/ZrO_2 catalysts (Figure 5). This *trans*/*cis* ratio is much lower than that obtained over supported Pd (*trans*/*cis* = 10–14) but close to that over supported Pt and other group VIII metals (*trans*/*cis* = 1.5–2.0).[18,19,29] The comparable activity (TOF) of the surface-type Au^{3+} ions to those of the group VIII precious metals and their unique selectivity in the hydrogenation reaction are of potential for many selective hydrogenations and related reactions. The isolated nature of the active Au^{3+} ions can also have important applications in improving the economics of gold catalysis.

Although this work was successful in demonstrating that the most active sites for the selective hydrogenation reaction are isolated Au^{3+} ions at the surface of zirconia, the mechanism of hydrogen activation by these surface-type

 © 2005 Wiley-VCH Verlag GmbH & Co. KGaA, Weinheim

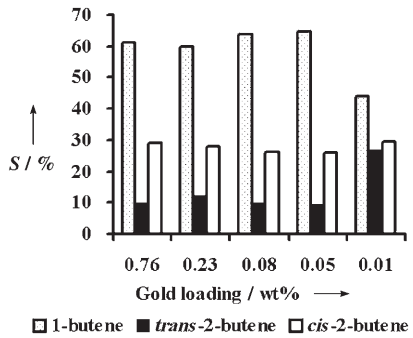

Figure 5. Product selectivity *S* of 1,3-butadiene hydrogenation over Au/ZrO_2 catalysts of different Au loadings.

Au^{3+} ions remains to be elucidated. Hydrogen chemisorption on supported gold was occasionally detected, but sometimes it has not been detectable at all.[3,27] The remarkable activity difference discovered between surface-type Au^{3+} ions and metallic Au^0 atoms could mean a different mechanism for hydrogen activation. Comprehensive in situ spectroscopic studies will be needed to understand the mechanistic aspect of the surface-type Au^{3+} cations in the hydrogen activation.

In conclusion, we have shown that isolated Au^{3+} ions on a zirconia support are obtained by loading very small amount ($< 0.1\,\%$) of gold with simple methods. These heterogenized Au^{3+} ions are highly active for the selective hydrogenation of 1,3-butadiene to butenes. Further exploration of the potential of the surface-type Au^{3+} ions in heterogeneous catalysis may be the key to using the noble metal gold in areas usually reserved for conventional precious metal catalysts such as Pt and Pd.

Experimental Section

A conventionally prepared $ZrO(OH)_2$ hydrogel was calcined at 400 °C to produce a ZrO_2 support with BET surface area of $120\ m^2\,g^{-1}$.[24] Samples of Au/ZrO_2 were prepared by loading the support with appropriate amounts of Au by the deposition–precipitation method with $HAuCl_4$ precursor,[8] the concentration of which was adjusted to yield catalysts containing 0.76, 0.23, 0.05, and 0.01 wt % Au (ICP-AES analysis). The 0.76 % Au/ZrO_2 sample was treated with an aqueous solution of KCN in a process similar to that reported by Fu et al.[11] to give 0.08 % Au/ZrO_2 catalyst. The Au/ZrO_2 catalysts were dried and calcined at 200 °C in flowing air. We also prepared 0.76 % Au/ZrO_2 catalysts at different calcination temperatures, that is, 200, 300, and 500 °C. TPR was used in combination with XPS measurements to quantitatively characterize the oxidation state of gold. TEM/HRTEM images were recorded on a JEM-2010F (200 kV) transmission electron microscope.

Hydrogenation of 1,3-butadiene was conducted at 120 °C in a fixed-bed stainless steel reactor (i.d. 4 mm) at atmospheric pressure. The reaction feed (2.15 vol % 1,3-butadiene in H_2) was introduced to the catalyst at a flow rate of $13.5\ mL\,min^{-1}$ (gas hourly space velocity (GHSV) = $8100\ mL\,h^{-1}\,(g\,cat.)^{-1}$. Before reaction all samples (ca. 80–120 mesh, 0.1 g diluted with 0.45 g quartz powder) were pretreated in situ in $30\ mL\,min^{-1}$ Ar at 200 °C for 2 h. The selected reaction conditions precluded any significant mass-transfer limitation in a series of pre-experiments at fixed space velocity (GHSV = $8100\ mL\,h^{-1}\,(g\,cat.)^{-1}$) so that the conversion of butadiene (ca. 75 %) over the 0.76 % Au/ZrO_2 catalyst (calcined at 200 °C) was not significantly affected by changing the flow rate of the reaction feed and the catalyst pellet size (40–120 mesh). The reactor effluent was analyzed in situ by gas chromatography. Experimental details and representative TEM images of the Au/ZrO_2 catalysts can be found in the Supporting Information.

Received: June 17, 2005
Published online: October 7, 2005

Keywords: gold · heterogeneous catalysis · hydrogenation · supported catalysts

[1] M. Haruta, M. Daté, *Appl. Catal. A* **2001**, *222*, 427.
[2] M. Haruta, *CATTECH* **2002**, *6*, 102.
[3] G. C. Bond, D. T. Thompson, *Catal. Rev. Sci. Eng.* **1999**, *41*, 319.
[4] G. C. Bond, D. T. Thompson, *Gold Bull.* **2000**, *33*, 41.
[5] G. J. Hutchings, *Gold Bull.* **2004**, *37*, 3.
[6] M. Valden, X. Lai, D. W. Goodman, *Science* **1998**, *281*, 1647.
[7] B. Yoon, H. Häkkinen, U. Landman, A. S. Wörz, J.-M. Antonietti, S. Abbet, K. Judai, U. Heiz, *Science* **2005**, *307*, 403.
[8] X. Zhang, H. Wang, B.-Q. Xu, *J. Phys. Chem. B* **2005**, *109*, 9678.
[9] H. H. Kung, M. C. Kung, C. K. Costello, *J. Catal.* **2003**, *216*, 425.
[10] J. Guzman, B. C. Gates, *J. Am. Chem. Soc.* **2004**, *126*, 2672.
[11] Q. Fu, H. Saltsburg, M. Flytzani-Stephanopoulos, *Science* **2003**, *301*, 935.
[12] G. C. Bond, P. A. Sermon, *Gold Bull.* **1973**, *6*, 102.
[13] M. Okumura, T. Akita, M. Haruta, *Catal. Today* **2002**, *74*, 265. We found that the TOF data in Table 1 of this paper were erroneous by one order of magnitude. We communicated with the authors (Drs. Okumura and Haruta) who confirmed that TOF ($\times 10^{-3}\ s^{-1}$) in the table was a mistyping of TOF ($\times 10^{-2}\ s^{-1}$) and kindly allowed us to make the correction herein.
[14] P. Claus, A. Brücker, C. Mohr, H. Hofmeister, *J. Am. Chem. Soc.* **2000**, *122*, 11430.
[15] J. Guzman, B. C. Gates, *Angew. Chem.* **2003**, *115*, 714; *Angew. Chem. Int. Ed.* **2003**, *42*, 690.
[16] J. Guzman, B. C. Gates, *J. Catal.* **2004**, *226*, 111.
[17] S. Schimpf, M. Lucas, P. Claus, *Proceedings of DGMK-Conference, Creating Value from Light Olefins—Production and Conversion*, Hamburg, Germany, October 10–12, **2001**, pp. 97–102.
[18] H. Arnold, F. Doebert, J. Gaube in *Handbook of Heterogeneous Catalysis, Vol. 5* (Eds.: G. Ertl, H. Knözinger, J. Weitkamp), VCH, Weinheim, **1997**, pp. 2165–2186.
[19] G. C. Bond, P. B. Wells, *Adv. Catal.* **1964**, *15*, 91.
[20] A. Stephen, K. Hashmi, *Gold Bull.* **2004**, *37*, 51.
[21] A. Hoffmann-Röder, N. Krause, *Org. Biomol. Chem.* **2005**, *3*, 387.
[22] B. Hammer, J. K. Norskov, *Nature* **1995**, *376*, 238.
[23] J. Li, X. Li, H.-J. Zhai, L.-S. Wang, *Science* **2003**, *299*, 864.
[24] B.-Q. Xu, J.-M. Wei, J.-L. Li, Q.-M. Zhu, *J. Phys. Chem. B* **2003**, *107*, 5203.
[25] J. T. Calla, R. J. Davis, *Catal. Lett.* **2005**, *99*, 21.
[26] E. D. Park, J. S. Lee, *J. Catal.* **1999**, *186*, 1.
[27] P. Claus, *Appl. Catal. A* **2005**, *291*, 222, and references therein.
[28] D. A. Buchanan, G. Webb, *J. Chem. Soc. Faraday Trans.* **1975**, *71*, 134.
[29] J. Massardier, J. C. Bertolini, A. Renouprez in *Proc. 9th Int. Cong. Catal.*, *Vol. III* (Eds.: M. J. Philips, M. Ternan), Calgary, **1988**, pp. 1222–1229.

 © 2005 Wiley-VCH Verlag GmbH & Co. KGaA, Weinheim

Helical Structures

DOI: 10.1002/anie.200502855

Stereospecific Synthesis of Hetero[7]helicenes by Pd-Catalyzed Double *N*-Arylation and Intramolecular *O*-Arylation**

*Koji Nakano, Yuko Hidehira, Keita Takahashi, Tamejiro Hiyama, and Kyoko Nozaki**

Helicenes consist of *ortho*-annulated aromatic and/or heteroaromatic rings endowed with a helical chirality.[1] Enantiopure helicenes can be isolated because of their stable and rigid helical conformation; furthermore, some of them form aggregates to give helical supramolecular architectures potentially applicable to nonlinear optics, electrooptic switches, and circularly polarized luminescent materials.[2] To expand the application of helicene molecules as functional materials, it is important to develop an efficient synthetic strategy for the production of helicenes with a variety of frameworks and substituents in enantiopure form. The classical methodology to synthesize helicenes is an oxidative photocyclization of stilbene-type precursors.[3] Several non-photochemical synthetic methods have been reported,[4] which have been applied to the syntheses of enantioenriched helicenes.[4a,f,5] Among these previous examples of helicene synthesis, however, only a few demonstrate the synthesis of azahelicenes with pyrrole rings or oxahelicenes with furan rings in spite of their potential to alter molecular properties,[5g,6,7] which prompted us to develop a new synthetic route that would produce aza- and oxahelicenes.

The key reactions in the heterohelicene syntheses are shown in Scheme 1. Carbazole derivatives can be prepared by the double N-arylation of primary amines with dihalobiphenyls or biphenylylene disulfonate **1**, as we reported recently.[8] The intramolecular O-arylation of 2′-hydroxybiphenyl-2-yl halides or sulfonates **2** is anticipated to give dibenzofuran, which we refer to as the palladium-catalyzed intermolecular diaryl ether synthesis.[9] These reactions of biphenyls were applied to biphenanthryls to form an efficient synthetic route to hetero[7]helicenes.

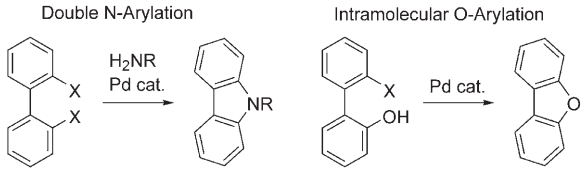

Scheme 1. Key reactions for the synthesis of heterohelicenes.

The target aza[7]helicene *rac*-**5** was obtained in 64% yield by the reaction of aniline with racemic 4,4′-biphenanthryl-3,3′-ylene ditriflate (*rac*-**4a**), which was prepared from racemic 4,4′-biphenanthryl-3,3′-diol (*rac*-**3**; Table 1, run 1). Oxa[7]helicene *rac*-**6** was produced as a by-product (10% yield) through the intramolecular O-arylation of 3′-hydroxy-4,4′-biphenanthryl-3-yl triflate (*rac*-**7a**), which was formed by

Table 1: Syntheses of aza[7]helicene and oxa[7]helicene.

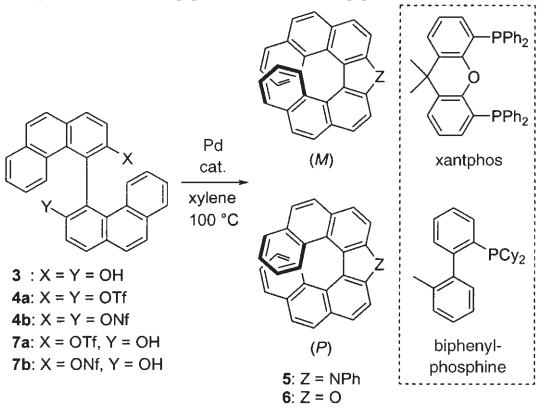

Run	Substrate	Conditions[a]	t [h]	Product	Yield [%]
1	*rac*-**4a**	A	141	*rac*-**5**	64[b]
2	*rac*-**4b**	A	123	*rac*-**5**	88
3	(*S*)-**4b**	B	123	(*P*)-**5**	94 (>99% *ee*) $[\alpha]_D^{22} = +2310$ (c=0.10, $CHCl_3$)
4	*rac*-**7a**	C	18	*rac*-**6**	45[c]
5	*rac*-**7b**	C	96	*rac*-**6**	62
6	(*S*)-**7b**	C	96	(*P*)-**6**	60 (20% *ee*)
7	(*S*)-**7b**	D	13	(*P*)-**6**	49 (94% *ee*) $[\alpha]_D^{23} = +1430$ (c=0.10, $CHCl_3$)

[a] Reaction conditions: A: H_2NPh (1.2 equiv), $[Pd_2(dba)_3]\cdot CHCl_3$ (5 mol%), xantphos (10 mol%), K_3PO_4 (2.8 equiv); B: H_2NPh (1.2 equiv), $[Pd_2(dba)_3]\cdot CHCl_3$ (10 mol%), xantphos (20 mol%), K_3PO_4 (2.8 equiv); C: $[Pd_2(dba)_3]\cdot CHCl_3$ (5 mol%), biphenylphosphine (20 mol%), K_3PO_4 (2.0 equiv); D: $[Pd_2(dba)_3]\cdot CHCl_3$ (10 mol%), biphenylphosphine (40 mol%), K_3PO_4 (2.0 equiv). [b] A 10% yield of *rac*-**6** as a by-product was obtained. [c] Consumption of the substrate was confirmed by TLC; the major by-product was diol *rac*-**3**. Cy = cyclohexyl, dba = dibenzylideneacetone.

[*] Dr. K. Nakano, Y. Hidehira, Prof. Dr. K. Nozaki
Department of Chemistry and Biotechnology
Graduate School of Engineering
The University of Tokyo
7-3-1 Hongo, Bunkyo-ku, Tokyo 113-8656 (Japan)
Fax: (+81) 3-5841-7261
E-mail: nozaki@chembio.t.u-tokyo.ac.jp
K. Takahashi, Prof. Dr. T. Hiyama
Department of Material Chemistry
Graduate School of Engineering
Kyoto University
Nishikyo-ku, Kyoto 615-8510 (Japan)

[**] We are grateful to Prof. Takuzo Aida (The University of Tokyo) for CD spectroscopic analysis and to Prof. Takayuki Kawashima and Dr. Makoto Yamashita (The University of Tokyo) for X-ray crystallographic analysis. We also thank Prof. Koji Araki, Dr. Toshiki Mutai, and Mr. Isao Yoshikawa (The University of Tokyo) for HRMS analysis. Financial support from the Yamada Science Foundation to K. Nozaki and from Konica Minolta Technology Center, Inc. to K. Nakano are gratefully acknowledged.

Supporting information for this article is available on the WWW under http://www.angewandte.org or from the author.

InterScience
© 2005 Wiley-VCH Verlag GmbH & Co. KGaA, Weinheim

the partial hydrolysis of *rac*-**4a**. The hydrolysis of the sulfonate functionality was successfully avoided by using a nonaflate (Nf) group instead of a triflate (Tf).[10] Thus, the yield was elevated to 88% (run 2) under the optimized reaction conditions (*rac*-**4b** with aniline (1.2 equiv), $[Pd_2(dba)_3]$ (5 mol%), xantphos (10 mol%), K_3PO_4 (2.8 equiv), xylene, 100°C, 123 h).

The optical resolution of *rac*-**3**[11] was investigated for the preparation of optically active heterohelicenes (Scheme 2).

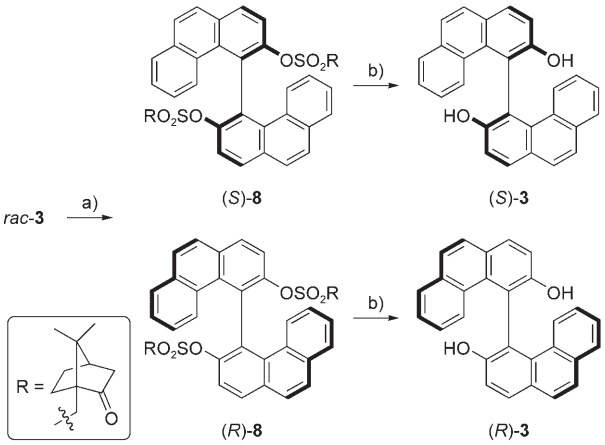

Scheme 2. Optical resolution of *rac*-**3**. a) RSO_2Cl (3.0 equiv), 4-(*N*,*N*-dimethylamino)pyridine (5.0 mol%), Et_3N, DMF, 0°C→RT, 15 h, separation by column chromatography on silica gel ((*S*)-**8**: 49% yield; (*R*)-**8**: 47% yield); b) THF, MeOH, aq. NaOH (5.0 M), reflux, 15 h ((*S*)-**3** and (*R*)-**3**: 95% yield; (*S*)-**3**: >99% *ee*; (*R*)-**3**: >99% *ee*). DMF = dimethylformamide.

The esterification of *rac*-**3** with the commercially available (1*S*)-10-camphorsulfonyl chloride gave diastereomers of disulfonate **8**, which were readily separated by column chromatography on silica gel. Hydrolysis of the obtained two single diastereomers gave (*S*)-**3** and (*R*)-**3** in enantiopure form.

A single enantiomer of **5** was readily prepared from (*S*)-**4b** by a stereospecific double N-arylation reaction; transformation of (*S*)-**4b** (>99% *ee*) gave (*P*)-**5** in 94% yield with >99% *ee* (Table 1, run 3). The absolute configuration of (*P*)-**5** was confirmed by its optical rotation ($[\alpha]_D^{22} = +2310$ ($c = 0.10$, $CHCl_3$)) and CD spectrum,[12] both of which are similar to those of the known dextrorotatory (*P*)-heterohelicenes.[5g,6a,13] Thus, the absolute configuration of (*S*)-**4b** is maintained under the reaction conditions (100°C, 123 h) in contrast to the O-arylation of (*S*)-**7b** (see below).

Oxa[7]helicene **6** was successfully synthesized through intramolecular O-arylation. The reaction of triflate *rac*-**7a** or nonaflate *rac*-**7b** using a palladium catalyst gave the desired *rac*-**6** in yields of 45 or 62%, respectively (runs 4 and 5). Unlike the double N-arylation of (*S*)-**4b** (run 3), however, the reaction of optically active (*S*)-**7b** (>99% *ee*) gave (*P*)-**6** (20% *ee*) with significant loss of enantiomeric excess (run 6; 100°C, 96 h). Racemization was suppressed effectively by shortening the reaction time (13 h) to afford (*P*)-**6** in 49% yield with high enantiopurity (94% *ee*; $[\alpha]_D^{23} = +1430$ ($c = 0.10$, $CHCl_3$); run 7). It should be noted that racemization of (*P*)-**6** takes place under the reaction conditions: treatment of optically active (*P*)-**6** (92% *ee*) in toluene at 100°C for 88 h resulted in partial racemization (42% *ee*). In contrast, none of (*S*)-**7b** (98% *ee*), (*R*)-**4b** (>99% *ee*), and (*M*)-**5** (97% *ee*) underwent racemization in toluene at 100°C. These results indicate that the stereospecific intramolecular O-arylation of (*S*)-**7b** gives (*P*)-**6** without any significant loss of enantiopurity, and the racemization takes place after the formation of (*P*)-**6**. The lower tolerance of **6** to racemization relative to **5** may be attributed to the differences in their structure. Indeed, the single-crystal X-ray analyses suggested that **6** has a less-distorted structure than **5** (Figure 1), thus indicating that the terminal two rings in **6** have weaker steric repulsions which should lead to a lower racemization barrier.[14,15]

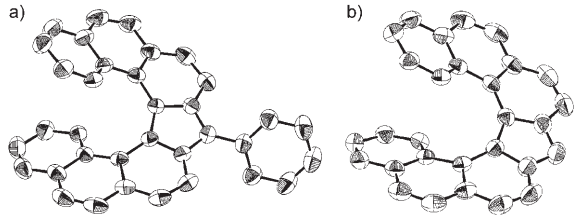

Figure 1. ORTEP drawings of a) **5** and b) **6**, with thermal ellipsoids shown at the 50% probability level. All hydrogen atoms and the $CHCl_3$ molecule are omitted for clarity.

The introduction of substituents into aza[7]helicene was investigated toward the development of hetero[7]helicenes as functional materials. Regioselective bromination was successfully achieved by the treatment of *rac*-**5** with two and four equivalents of NBS to yield di- and tetrabromoaza[7]helicenes *rac*-**9** and *rac*-**10**, respectively (Scheme 3).[16] The

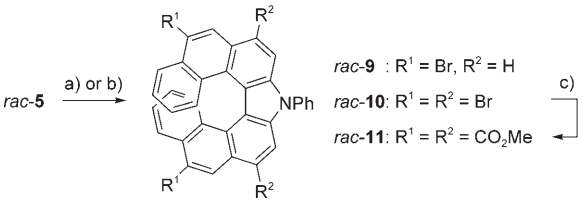

Scheme 3. Functionalization of *rac*-**5**. a) NBS (2.0 equiv), SiO_2 (2.0 g mmol^{-1} NBS), CH_2Cl_2, RT, 31 h (*rac*-**9**: 61% yield; b) NBS (4.0 equiv), SiO_2 (2.0 g mmol^{-1} NBS), CH_2Cl_2, RT, 43 h (*rac*-**10**: 84% yield); c) *t*BuLi (8.4 equiv), THF, −78°C, 4 h, then $ClCO_2Me$ (8.4 equiv), −78°C→RT, 13 h, (*rac*-**11**: 44% yield). NBS = *N*-bromosuccinimide.

substituted positions were determined by single-crystal X-ray analyses.[17] These brominated aza[7]helicenes should be useful intermediates for further functionalizations; for example, *rac*-**10** was converted into tetraester *rac*-**11** in 44% yield (Scheme 3).

In conclusion, we have reported an efficient strategy for the synthesis of aza- and oxa[7]helicenes **5** and **6** from the same precursor, 4,4′-biphenanthryl-3,3′-diol (**3**); highly enantioenriched **5** and **6** were successfully obtained in good yields. In addition, tetrabromoaza[7]helicene **10** was produced by

 © 2005 Wiley-VCH Verlag GmbH & Co. KGaA, Weinheim

the regioselective bromination of **5**. Aggregates of the aza[7]helicenes, which are potentially attractive new materials, could be synthesized by further functionalization of **10**, with the introduction, for example, of long alkyl chains.[2]

Received: August 11, 2005
Published online: October 6, 2005

Keywords: arylation · bromination · chirality · helical structures · palladium

[1] For reviews, see: a) H. Osuga, K. Tanaka, *J. Syn. Org. Chem. Jpn.* **2002**, *60*, 593; b) K. Sato, S. Arai in *Cyclophane Chemistry for the 21th Century* (Ed.: H. Takemura), Research Signpost, Kerala, **2002**, chap. 8, p. 173; c) H. Hopf, *Classics in Hydrocarbon Chemistry: Syntheses, Concepts, Perspectives*, Wiley-VCH, Weinheim, **2000**, chap. 12, p. 321; d) K. P. Meurer, F. Vögtle, *Top. Curr. Chem.* **1985**, *127*, 1; e) W. H. Laarhoven, W. J. C. Prinsen, *Top. Curr. Chem.* **1984**, *125*, 63; f) R. H. Martin, *Angew. Chem.* **1974**, *86*, 727; *Angew. Chem. Int. Ed. Engl.* **1974**, *13*, 649.

[2] a) C. Nuckolls, R. F. Shao, W. G. Jang, N. A. Clark, D. M. Walba, T. J. Katz, *Chem. Mater.* **2002**, *14*, 773; b) T. J. Katz, *Angew. Chem.* **2000**, *112*, 1997; *Angew. Chem. Int. Ed.* **2000**, *39*, 1921; c) C. Nuckolls, T. J. Katz, G. Katz, P. J. Collings, L. Castellanos, *J. Am. Chem. Soc.* **1999**, *121*, 79; d) T. Verbiest, S. Van Elshocht, M. Kauranen, L. Hellemans, J. Snauwaert, C. Nuckolls, T. J. Katz, A. Persoons, *Science* **1998**, *282*, 913; e) C. Nuckolls, T. J. Katz, *J. Am. Chem. Soc.* **1998**, *120*, 9541.

[3] a) L. Liu, B. Yang, T. J. Katz, M. K. Poindexter, *J. Org. Chem.* **1991**, *56*, 3769; b) M. Flammang-Barbieux, J. Nasielski, R. H. Martin. *Tetrahedron Lett.* **1967**, *8*, 743.

[4] a) A. Rajca, M. Miyasaka, M. Pink, H. Wang, S. Rajca, *J. Am. Chem. Soc.* **2004**, *126*, 15211; b) A. Urbano, *Angew. Chem.* **2003**, *115*, 4116; *Angew. Chem. Int. Ed.* **2003**, *42*, 3986; c) D. Peña, A. Cobas, D. Pérez, E. Guitián, L. Castedo, *Org. Lett.* **2003**, *5*, 1863; d) F. Teplý, I. G. Stará, I. Starý, A. Kollárovič, D. Šaman, L. Rulíšek, P. Fiedler, *J. Am. Chem. Soc.* **2002**, *124*, 9175; e) M. Gingras, F. Dubois, *Tetrahedron Lett.* **1999**, *40*, 1309; f) C. Nuckolls, T. J. Katz, L. Castellanos, *J. Am. Chem. Soc.* **1996**, *118*, 3767.

[5] For recent examples of the preparation of enantioenriched helicenes or helicene-like molecules, see: a) T. J. Wigglesworth, D. Sud, T. B. Norsten, V. S. Lekhi, N. R. Branda, *J. Am. Chem. Soc.* **2005**, *127*, 7272; b) I. G. Stará, Z. Alexandrová, F. Teplý, P. Sehnal, I. Starý, D. Šaman, M. Buděšínský, J. Cvačka, *Org. Lett.* **2005**, *7*, 2547; c) M. C. Carreño, M. González-López, A. Urbano, *Chem. Commun.* **2005**, 611; d) J. E. Field, G. Muller, J. P. Riehl, D. Venkataraman, *J. Am. Chem. Soc.* **2003**, *125*, 11808; e) Y. Ogawa, M. Toyama, M. Karikomi, K. Seki, K. Haga, T. Uyehara, *Tetrahedron Lett.* **2003**, *44*, 2167; f) M. C. Carreño, S. García-Cerrada, A. Urbano, *J. Am. Chem. Soc.* **2001**, *123*, 7929; g) S. D. Dreher, D. J. Weix, T. J. Katz, *J. Org. Chem.* **1999**, *64*, 3671; h) K. Tanaka, H. Suzuki, H. Osuga, *J. Org. Chem.* **1997**, *62*, 4465.

[6] a) I. Pischel, S. Grimme, S. Kotila, M. Nieger, F. Vögtle, *Tetrahedron: Asymmetry* **1996**, *7*, 109; b) H.-E. Högberg, *Acta Chem. Scand.* **1973**, *27*, 2591; c) M. B. Groen, H. Schadenberg, H. Wynberg, *J. Org. Chem.* **1971**, *36*, 2797; d) J. N. Chatterjea, K. D. Banerji, *J. Indian Chem. Soc.* **1970**, *47*, 576.

[7] For reports on the synthesis of helicenes or helicene-like molecules that contain nitrogen atom(s) in the fused-ring framework, see: a) J. E. Field, T. J. Hill, D. Venkataraman, *J. Org. Chem.* **2003**, *68*, 6071; b) E. Murguly, R. McDonald, N. R. Branda, *Org. Lett.* **2000**, *2*, 3169; c) S. Arai, T. Yafune, M. Ōkubo, M. Hida, *Tetrahedron Lett.* **1989**, *30*, 7217; d) D. E. Pereira, G. L. Clauson, N. J. Leonard, *Tetrahedron* **1987**, *43*, 4931; e) R. H. Martin, M. Deblecker, *Tetrahedron Lett.* **1969**, *10*, 3597.

[8] a) A. Kuwahara, K. Nakano, K. Nozaki, *J. Org. Chem.* **2005**, *70*, 413; b) K. Nozaki, K. Takahashi, K. Nakano, T. Hiyama, H. Z. Tang, M. Fujiki, S. Yamaguchi, K. Tamao, *Angew. Chem.* **2003**, *115*, 2097; *Angew. Chem. Int. Ed.* **2003**, *42*, 2051.

[9] A. Aranyos, D. W. Old, A. Kiyomori, J. P. Wolfe, J. P. Sadighi, S. L. Buchwald, *J. Am. Chem. Soc.* **1999**, *121*, 4369.

[10] K. W. Anderson, M. Mendez-Perez, J. Priego, S. L. Buchwald, *J. Org. Chem.* **2003**, *68*, 9563.

[11] a) N. Koike, T. Hattori, S. Miyano, *Tetrahedron: Asymmetry* **1994**, *5*, 1899; b) K. Yamamura, S. Ono, H. Ogoshi, H. Masuda, Y. Kuroda, *Synlett* **1989**, 18.

[12] See the Supporting Information.

[13] a) G. Gottarelli, G. Proni, G. P. Spada, D. Fabbri, S. Gladiali, C. Rosini, *J. Org. Chem.* **1996**, *61*, 2013; b) M. B. Groen, H. Wynberg, *J. Am. Chem. Soc.* **1971**, *93*, 2968.

[14] A discussion about structural differences between **5** and **6** is given in the Supporting Information.

[15] R. H. Martin, M. J. Marchant, *Tetrahedron* **1974**, *30*, 347.

[16] K. Smith, D. M. James, A. G. Mistry, M. R. Bye, D. J. Faulkner, *Tetrahedron* **1992**, *48*, 7479.

[17] ORTEP drawings and the X-ray crystallographic data of **9** and **10** are given in the Supporting Information; CCDC-280430–280433 (**5**·$CHCl_3$, **6**, **9**, and **10**·$CHCl_3$, respectively) contain the supplementary crystallographic data for this paper. These data can be obtained free of charge from the Cambridge Crystallographic Data Centre via www.ccdc.cam.ac.uk/data_request/cif.

 © 2005 Wiley-VCH Verlag GmbH & Co. KGaA, Weinheim

Cover Picture

Marcin Fialkowski, Kyle J. M. Bishop, Victor A. Chubukov, Christopher J. Campbell, and Bartosz A. Grzybowski*

Organic synthetic reactions are treated as a connected network so that the mechanism by which organic chemistry evolved can be studied. In their Communication on page 7263 ff., B. A. Grzybowski and co-workers analyze organic syntheses reported between 1850 and 2004, thus revealing the architecture and evolution of the synthesis of molecules, and discuss the application of this technique to the chemical industry. The cover picture shows a typical "hub" in a network of organic chemistry.

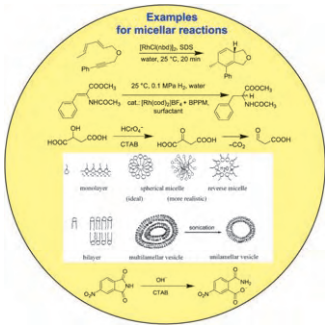

Micelles
The increased selectivities and activities achieved in catalytic organic reactions carried out in water and by using micelle-forming amphiphilic agents is described in the Review by G. Oehme and co-workers on page 7174 ff.

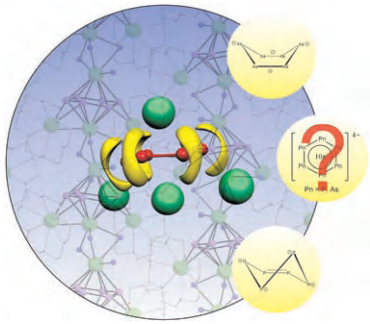

Cluster Anions
Through use of the electron-localization function, N. Korber and co-workers attempt, in their Communication on page 7200 ff, to clarify the nature of the chemical bond in the P_6^{4-} and As_6^{4-} ions.

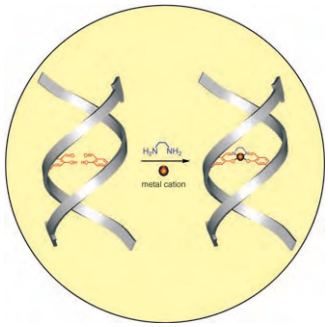

DNA Structures
Stabilization of a DNA duplex containing two salicylic acid aldehyde nucleosides results from its treatment with ethylenediamine and Cu^{2+} or Mn^{2+} ions, as described by T. Carell and co-workers in their Communication on page 7204 ff.

Contents

VIP *The following Communications have been judged by at least two referees to be "very important papers" and will be published online at www.angewandte.org soon:*

*C. Drago, L. Caggiano, R. F. W. Jackson**
Vanadium-Catalyzed Sulfur Oxidation/Kinetic Resolution in the Synthesis of Enantiomerically Pure Alkyl Aryl Sulfoxides

*Q. Qing, F. Chen, P. Li, W. Tang, Z. Wu, Z. Liu**
Finely Tuning the Metallic Nanogap Size with Electrodeposition Utilizing High-Frequency Impedance in Feedback

X. Rocquefelte, S. E. Boulfelfel, M. B. Yahia, J. Bauer, J.-Y. Saillard,* J.-F. Halet**
The Structural Preferences of Boron and Carbon within MB_2C_2 (M = Mg,Sc,Ca,Y,Ln) Phases: The "Coloring Problem" Revisited by DFT Calculations

G. C. Lloyd-Jones, R. G. Margue, J. G. de Vries*
Rate Enhancement by Ethylene in the Ru-Catalyzed Ring-Closing Metathesis of Enynes: Evidence for an "Ene-then-Yne" Pathway That Diverts through a Second Catalytic Cycle

S. Klaus, H. Neumann, A. Zapf, D. Strübing, S. Hübner, J. Almena, T. Riermeier, P. Groß, M. Sarich, W.-R. Krahnert, K. Rossen, M. Beller**
A General and Efficient Method for the Formylation of Aryl and Heteroaryl Bromides

N. Martín, Á. Martín-Domenech, S. Filippone, M. Altable, L. Echegoyen,* C. M. Cardona*
Retrocycloaddition Reactions of Pyrrolidinofullerenes

Meeting Reviews

European Conference on Solid-State Chemistry in Sheffield — *T. Sörgel, M. Schulz-Dobrick* ——— ***7160***

Books

Chemoinformatics in Drug Discovery — Tudor I. Oprea — *reviewed by T. Engel* ——— **7163**

Molecular Orbitals of Transition Metal Complexes — Yves Jean — *reviewed by E. Hey-Hawkins* ——— **7163**

Highlights

Synthetic Biology

J. W. Engels* ——— **7166 – 7169**

Gene Synthesis on Microchips

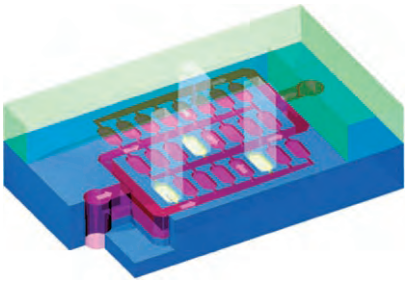

Splice of life: The error-free, rapid, and economic synthesis of genes is an important requirement for an effective functional genome. The latest developments in gene research cover the parallel synthesis of oligonucleotides on microchips (see picture), their error-free selection through hybridization, and one-step multiple gene construction by polymerases.

Organic Radicals

P. G. Wenthold* ——— **7170 – 7172**

Toward the Systematic Decomposition of Benzene

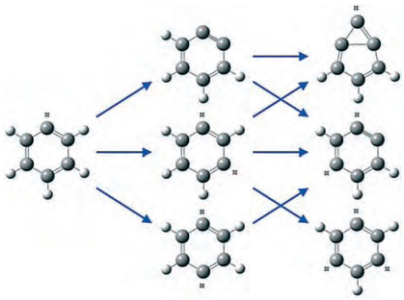

Breaking up: The detection and characterization of the 1,2,3-tridehydrobenzene triradical provides another step in the systematic decomposition of benzene. The implications of this study with regard to the electronic structure of the triradical and in light of results of previous experimental and theoretical studies are considered.

InterScience

© 2005 Wiley-VCH Verlag GmbH & Co. KGaA, Weinheim

Reviews

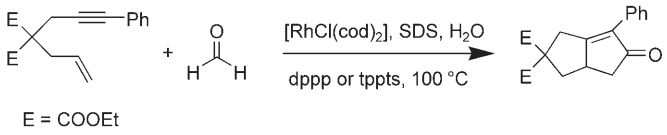

Not only clean, but fast as well: Numerous catalytic organic reactions can be realized in water with excellent activities and selectivities in the presence of micelle-forming amphiphilic agents (surfactants; see scheme). The micellar effect is part of supramolecular chemistry on the nanometer scale. cod = cycloocta-1,5-diene, SDS = sodium dodecylsulfate, dppp = diphenylphosphanylpropane, tppts = triphenylphosphanetri-*meta*-sulfonate sodium salt.

Micelles

T. Dwars, E. Paetzold, G. Oehme* ——— **7174 – 7199**

Reactions in Micellar Systems

Communications

Are the homoatomic ring anions P_6^{4-} and As_6^{4-} really planar and 10π aromatic outside of the binary alkali-metal compounds? With the crystal structure of $\{Rb[18]crown\text{-}6)\}_2Rb_2As_6 \cdot 6\,NH_3$ (see structure of the $\{Rb_4As_6\}$ core; Rb green, As red) and the electron localization function, an attempt is made to clarify the nature of the chemical bond in these pnictides.

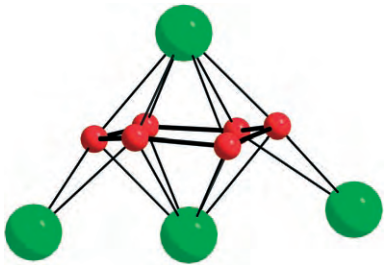

Cluster Anions

F. Kraus, T. Hanauer, N. Korber* ——— **7200 – 7204**

Chemical Bond in the Cyclic Anions P_6^{4-} and As_6^{4-}: Synthesis, Crystal Structure, and Electron Localization Function of $\{Rb[18]crown\text{-}6)\}_2Rb_2As_6 \cdot 6\,NH_3$

Stabilizing influence: When a DNA duplex containing two salicylic aldehyde nucleosides facing each other is treated with ethylenediamine and one equivalent of a Cu^{2+} or Mn^{2+} salt, a metal–salen base pair is formed within the DNA. The resulting stabilization of the DNA structure is attributed to the cross-linking of the salicylic aldehyde units with ethylenediamine.

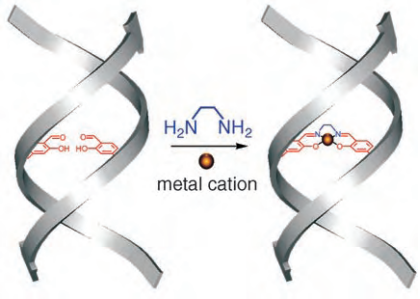

DNA Structures

G. H. Clever, K. Polborn, T. Carell* ——— **7204 – 7208**

A Highly DNA-Duplex-Stabilizing Metal–Salen Base Pair

For the USA and Canada:
ANGEWANDTE CHEMIE International Edition (ISSN 1433-7851) is published weekly by Wiley-VCH PO Box 191161, D 69451 Weinheim, Germany. Air freight and mailing in the USA by Publications Expediting Inc. 200 Meacham Ave., Elmont, NY 11003. Periodicals postage paid at Jamaica NY 11431. US POSTMASTER: send address changes to *Angewandte Chemie*, Wiley-VCH, 111 River Street, Hoboken, NJ 07030. Annual subscription price for institutions: US$ 5685/5168 (valid for print and electronic / print or electronic delivery); for individuals who are personal members of a national chemical society prices are available on request. Postage and handling charges included. All prices are subject to local VAT/sales tax.

© 2005 Wiley-VCH Verlag GmbH & Co. KGaA, Weinheim

The best in chemistry –

for more than a hundred years

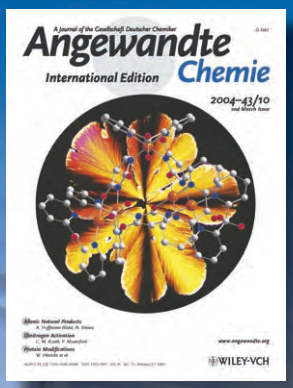

A Journal of the Gesellschaft Deutscher Chemiker

Angewandte
International Edition **Chemie**

www.angewandte.org

1888: ***The beginning of a success story***

Constant Innovations

1962: *First issue of the International Edition*
1976: *Graphical abstracts*
1979: *Cover pictures*
1988: *Centenary of Angewandte*
1989: *Routine use of color*
1991: *New section: Highlights*
1992: *Computerized editorial tracking system*
1995: *Internet service for readers*
1998: *Regular press service; full-text online*
2000: *New section: Essays; EarlyView: Communications available online ahead of the printed version*
2001: *New section: Minireviews*
2002: *Online submission of manuscripts*
2003: *Weekly publication; new section: News; new layout*
2004: *Backfiles (1962-1997); ManuscriptXpress: Online system for authors and referees*

Angewandte's advisors...

Frans C. De Schryver
Katholieke Universiteit Leuven

*» Over the years **Angewandte Chemie** has been a beacon for sound, exciting, and novel chemistry and has built its well-deserved reputation on nonsubjective, thorough, but constructive refereeing and a highly professional layout. I am sure that the new initiatives will further strengthen its leadership with the help of scientists and the outstanding staff. «*

Angewandte Chemie International Edition *is a journal of the German Chemical Society (GDCh)*

GDCh

WILEY InterScience® DISCOVER SOMETHING GREAT

WILEY-VCH

1613412_gu

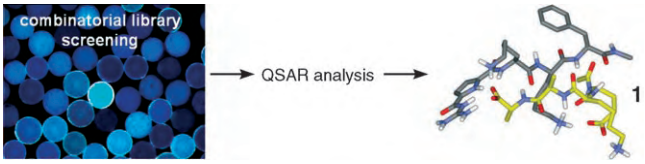

Statistical QSAR analysis (QSAR = quantitative structure–activity relationship) was applied to quantitative experimental screening data of a small, but focused, combinatorial library to identify potent receptors (**1**, see scheme). Analysis showed that no receptors with better efficiency would be expected, even if a 15-times larger library was used.

Artificial Peptide Receptors

C. Schmuck,* M. Heil, J. Scheiber, K. Baumann ——— 7208 – 7212

Charge Interactions Do the Job: A Combined Statistical and Combinatorial Approach to Finding Artificial Receptors for Binding Tetrapeptides in Water

---

Predictions confirmed: The phase $RhFe_3N$ (see unit cell), which was recently predicted by total-energy density functional calculations and proposed to have exciting magnetic properties, was synthesized for the first time. The experimental lattice parameter is in good agreement with the theoretical prediction, and the phase appears to be a semihard itinerant ferromagnet. The atomic magnetic saturation moment, μ_a^s, is 8.3 μ_B per formula unit, and the Curie temperature, T_C, is 505(25) K.

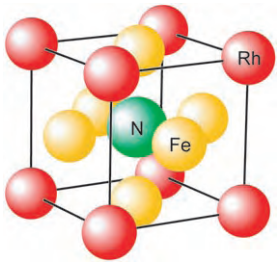

Magnetic Storage Materials

A. Houben, P. Müller, J. von Appen, H. Lueken, R. Niewa, R. Dronskowski* ——— 7212 – 7215

Synthesis, Crystal Structure, and Magnetic Properties of the Semihard Itinerant Ferromagnet $RhFe_3N$

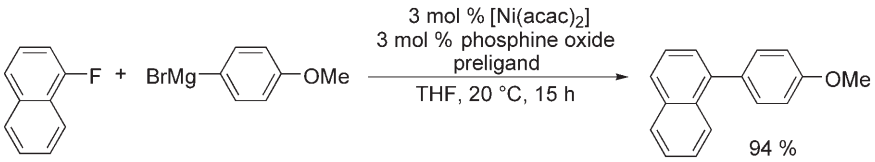

A couple of couplings: Air-stable diamino- and dioxophosphine oxides are used as preligands in the nickel-catalyzed Kumada cross-coupling reactions of aryl Grignard reagents. A sterically hindered preligand allows for highly efficient cross-coupling of aryl fluorides at ambient temperature (acac = acetylacetonate).

Cross-Coupling

L. Ackermann,* R. Born, J. H. Spatz, D. Meyer ——— 7216 – 7219

Efficient Aryl–(Hetero)Aryl Coupling by Activation of C–Cl and C–F Bonds Using Nickel Complexes of Air-Stable Phosphine Oxides

---

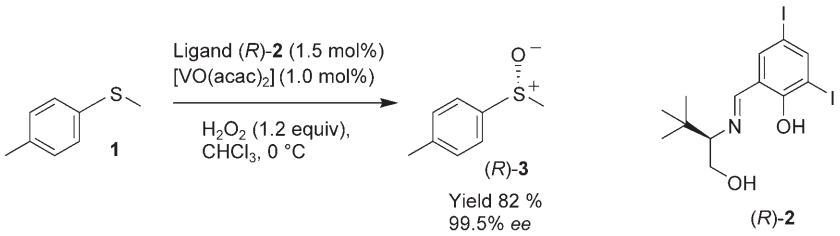

The importance of the mix: The use of chloroform as solvent, the ligand (*R*)-**2** and $[VO(acac)_2]$ as catalyst, and H_2O_2 as oxidant promotes the highly enantioselective oxidation of simple alkyl aryl sulfides **1** to give alkyl aryl sulfoxides (*R*)-**3** (see scheme). The success of this process partly derives from an efficient kinetic resolution of the product sulfoxides.

Asymmetric Catalysis

C. Drago, L. Caggiano, R. F. W. Jackson* ——— 7221 – 7223

Vanadium-Catalyzed Sulfur Oxidation/Kinetic Resolution in the Synthesis of Enantiomerically Pure Alkyl Aryl Sulfoxides

© 2005 Wiley-VCH Verlag GmbH & Co. KGaA, Weinheim

Contents

Chemistry in Space

Y. Trolez, J.-C. Guillemin* — **7224 – 7226**

Synthesis and Characterization of 2,4-Pentadiynenitrile—A Key Compound in Space Science

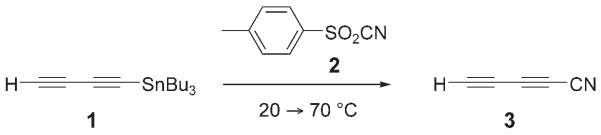

Spaced out: Cyanobutadiyne (**3**) was synthesized in pure form from 1,3-butadiynyltributylstannane (**1**) and *p*-toluenesulfonyl cyanide (**2**). Diyne **3** might be formed in the atmosphere of Titan or in the interstellar medium by photolysis of mixtures of acetylene and cyanoacetylene or dicyanoacetylene or of butadiyne and dicyanoacetylene. Only 1,6-addition is observed with nucleophiles.

Dihydrogen or Dihydride?

M. Yousufuddin, T. B. Wen, S. A. Mason, G. J. McIntyre, G. Jia,* R. Bau* — **7227 – 7230**

A Neutron Diffraction Study of $[OsClH_3(PPh_3)_3]$: A Complex Containing a Highly "Stretched" Dihydrogen Ligand

Elastic bonds: The structure of $[OsHCl(\eta^2\text{-}H_2)(PPh_3)_3]$ has been determined by neutron diffraction (see figure). The complex presents an unusual H···H contact of 1.48(2) Å and can be regarded either as a highly stretched dihydrogen complex or as a compressed dihydride complex.

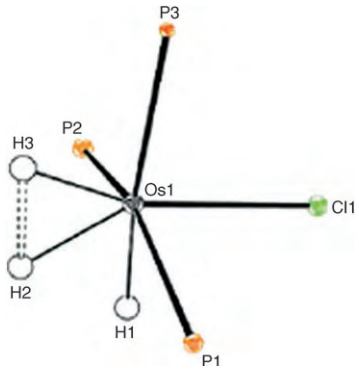

Fullerenes

J. M. Campanera, C. Bo, J. M. Poblet* — **7230 – 7233**

General Rule for the Stabilization of Fullerene Cages Encapsulating Trimetallic Nitride Templates

Ruling the cage: The bonding in trimetallic nitride template (TNT) endohedral metallofullerenes is widely described by the ionic model $Sc_3N^{6+}@C_k^{6-}$. The ability of the fullerene cage to accept six electrons determines its capacity to encapsulate the TNT unit (see picture). Only free fullerene isomers with a large (LUMO+3)–(LUMO+4) gap can capture and stabilize these four-atom units.

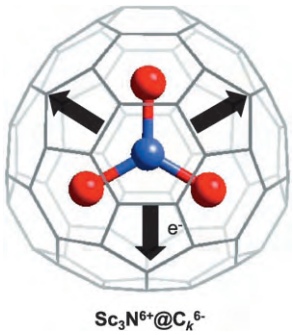

Photochemistry

H. Okada, N. Nakajima, T. Tanaka, M. Iwamoto* — **7233 – 7236**

Improvement in Photocyclization Efficiency of Diaryl Ethenes by Adjusting the Pore Size of Mesoporous Silica

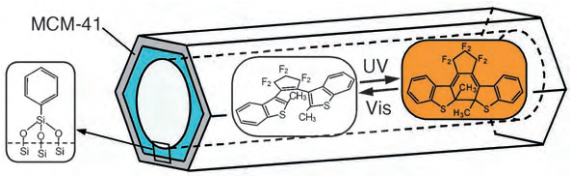

Photochromism in nanospace: Reversible photochromic reaction of a diaryl ethene (DE) takes place in the pores of MCM-41s modified with organic groups. The efficiency of the photocyclization reaction increases fourfold when the diameter of the pore is decreased to approximately the same size of the DE, which indicates that the conformation of the open-ring isomer is regulated in the confines of the pore (see picture).

© 2005 Wiley-VCH Verlag GmbH & Co. KGaA, Weinheim

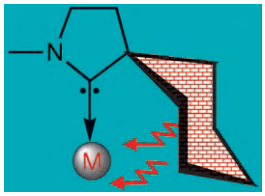

A protecting wall for low-coordinate metal centers, reinforced by agostic interactions, is provided by a rigid cyclic (alkyl)(amino)carbene ligand (CAAC), as shown by the preparation of [RhCl(CO)(CAAC)] and [Pd(All)(CAAC)]$^+BF_4^-$ complexes (All = allyl). The former is related to the active species of Wilkinson's catalyst, and the latter is the first isolated cationic, formally 14-electron Pd^{II} species.

Low-Coordinate Complexes

V. Lavallo, Y. Canac, A. DeHope, B. Donnadieu, G. Bertrand* **7236 – 7239**

A Rigid Cyclic (Alkyl)(amino)carbene Ligand Leads to Isolation of Low-Coordinate Transition-Metal Complexes

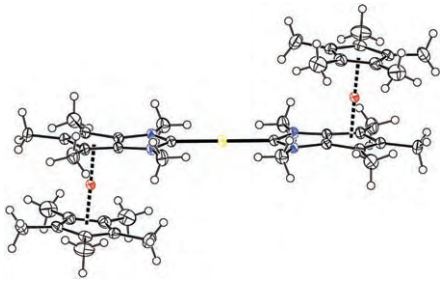

A zwitterionic ligand yields a trimetallic carbene complex (see structure), in which the metal centers are electronically coupled by a single ligand that employs both σ and π bonding. This imidazol-2-ylidene complex, derived from the imidazolium-cyclopentadienide zwitterion, reveals a carbene-ligand architecture that allows the incorporation of multiple metal and/or main-group element centers.

Carbene Ligands

A. J. Arduengo III,* D. Tapu, W. J. Marshall **7240 – 7244**

The Generation of a Metallocene-Fused Imidazol-2-ylidene and Its Mercury Complex

Current affairs: Incorporation of a 1,4-phenylene bridge into *meso* aryl-substituted decaphyrin and octaphyrin has a profound impact on the structural and electronic properties of the macrocycles. Bridged decaphyrin has two oxidation states, one of which shows a rather strong diatropic ring current. X-ray crystal structure analyses reveal bridged octaphyrin possesses a *p*-quinodimethane unit, while bridged decaphyrin has a phenylene unit (see picture).

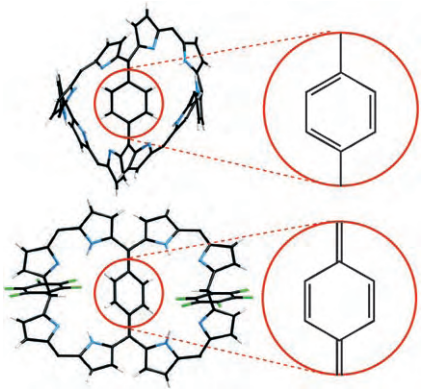

Porphyrins

V. G. Anand, S. Saito, S. Shimizu, A. Osuka* **7244 – 7248**

Internally 1,4-Phenylene-Bridged *meso* Aryl-Substituted Expanded Porphyrins: The Decaphyrin and Octaphyrin Cases

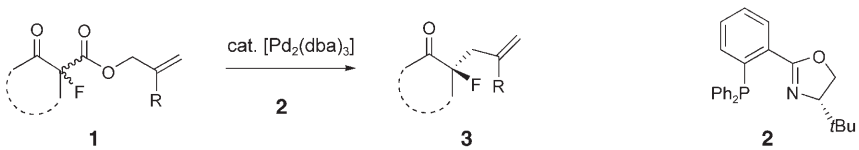

1 3 2

A conceptually new approach affords optically active α-fluoroketones **3** in high yields with up to 99% *ee* from racemic α-fluoro-β-ketoesters **1** in the presence of a chiral phosphinooxazoline ligand **2**. The palladium-catalyzed decarboxylation/allylation reaction also allows the highly enantioselective construction of an all-carbon quaternary center. dba = dibenzylideneacetone.

Organofluorine Compounds

M. Nakamura,* A. Hajra, K. Endo, E. Nakamura* **7248 – 7251**

Synthesis of Chiral α-Fluoroketones through Catalytic Enantioselective Decarboxylation

© 2005 Wiley-VCH Verlag GmbH & Co. KGaA, Weinheim

Contents

Cluster Compounds

X. Huang, H.-J. Zhai, B. Kiran, L.-S. Wang* ——— **7251 – 7254**

Observation of d-Orbital Aromaticity

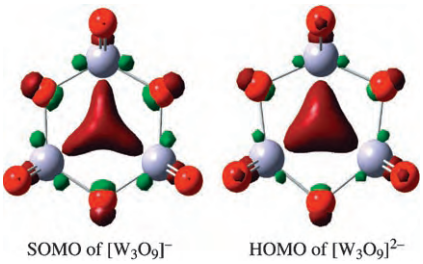

The metal oxide clusters $[W_3O_9]^-$ and $[Mo_3O_9]^-$ were studied by photoelectron spectroscopy and theoretical calculations, which show that $[W_3O_9]$ and $[Mo_3O_9]$ both have a D_{3h} structure with a low-lying unoccupied molecular orbital formed from the metal d orbitals. Occupation of this orbital by one or two electrons leads to aromatic anions (see picture) with strong three-center, one-electron and three-center, two-electron metal–metal bonds, respectively.

Micelles

M. Kunishima,* H. Imada, K. Kikuchi, K. Hioki, J. Nishida, S. Tani **7254 – 7257**

Unusual Rate Enhancement of Bimolecular Dehydrocondensation To Form Amides at the Interface of Micelles of Fatty Acid Salts

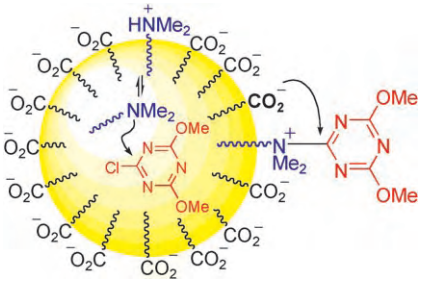

Speeding up: A micelle–water interface acts as a suitable reaction field for dehydrocondensation. The coupling reaction of fatty acid salts with a triazine-type amphiphilic dehydrocondensing agent in a micellar system (see picture) underwent up to 2000-fold acceleration. The rate enhancement can be attributed to the higher local concentration and preorientation of the reactants in the micelles.

Asymmetric Catalysts

K. Mikami,* H. Kakuno, K. Aikawa ——— **7257 – 7260**

Enantiodiscrimination and Enantiocontrol of Neutral and Cationic Pt^{II} Complexes Bearing the *Tropos* Biphep Ligand: Application to Asymmetric Lewis Acid Catalysis

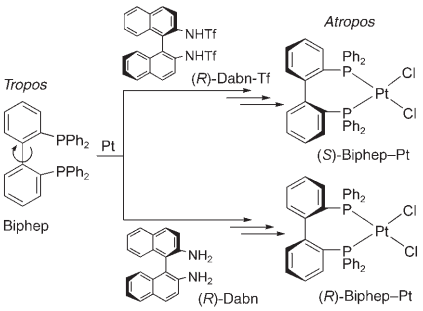

The stereochemically stable, enantiopure biphep–Pt complexes can be employed as an *atropos* asymmetric catalyst at 50 °C or below. Both enantiomeric forms of this complex can be obtained by using either the chiral diamine (*R*)-dabn or its diamide (*R*)-dabnTf followed by chirally controlled formation of the single biphep–Pt enantiomer at higher (> 60 °C) temperatures (see scheme; Tf = trifluoromethanesulfonate).

Carbocyclization

K. Tanaka,* Y. Hagiwara, K. Noguchi ——— **7260 – 7263**

Rhodium-Catalyzed Regio- and Enantioselective Intermolecular [4+2] Carbocyclization of 4-Alkynals with *N*,*N*-Dialkyl Acrylamides

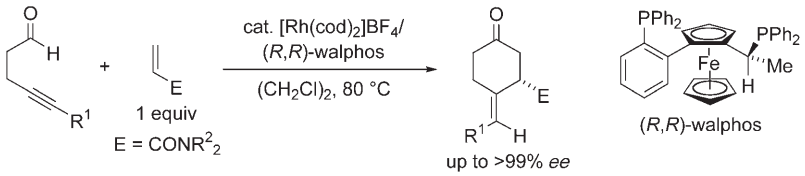

Selective rings: A cationic Rh^I–(*R*,*R*)-walphos complex catalyzes a highly regio- and enantioselective intermolecular [4+2] carbocyclization of 4-alkynals with *N*,*N*-dialkyl acrylamides to afford enantioenriched cyclohexanones (see scheme; cod = cycloocta-1,5-diene). This new route is attractive in view of the one-step access to 4-alkynals from commercially available reagents.

© 2005 Wiley-VCH Verlag GmbH & Co. KGaA, Weinheim

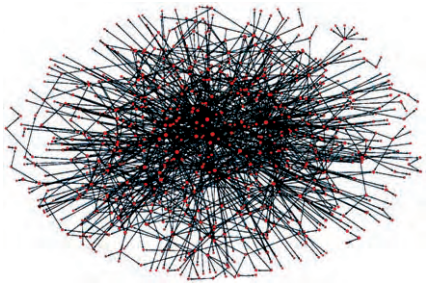

Organic syntheses reported in the literature between 1850 and 2000 are analyzed at the simplified level of a connected network (see the picture of the network for 1850). Fundamental statistical laws that govern organic syntheses are established. These laws allow the estimation of the synthetic and industrial usefulness of organic molecules.

Computational Chemistry

M. Fialkowski, K. J. M. Bishop, V. A. Chubukov, C. J. Campbell, B. A. Grzybowski* ——— **7263 – 7269**

Architecture and Evolution of Organic Chemistry

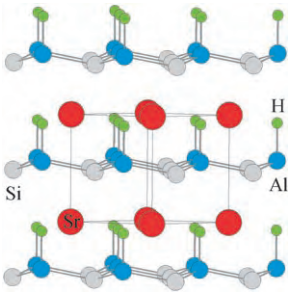

Stable and semiconducting: Polyanionic hydrides represent a new class of main-group-metal hydrides with unforeseen hydrogen-coordination environments. The hydrogen atom in SrAlSiH is attached exclusively to Al and forms part of a layered $[AlHSi]^{2-}$ polyanion (see figure). This material is the first narrow bandgap semiconductor hydride and combines the high thermal stability of saline hydrides with the air and moisture stability of interstitial transition-metal hydrides.

Semiconductor Materials

T. Björling, D. Noréus, K. Jansson, M. Andersson, E. Leonova M. Edén, U. Hålenius, U. Häussermann* ——— **7269 – 7273**

SrAlSiH: A Polyanionic Semiconductor Hydride

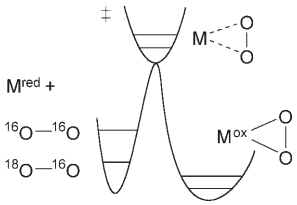

Kinetic isotope effects (KIEs) have been used to probe the mechanism of the binding of O_2 to classic inorganic compounds. The intermolecular ^{18}O KIEs decrease with increasing rate constants, and the correlation of the KIEs with the $\log k_{O_2}$ values establishes that the same oxidative addition mechanism is operative in all cases, but with marked differences in the transition-state structure (see figure).

Oxygen Activation

M. P. Lanci, D. W. Brinkley, K. L. Stone, V. V. Smirnov, J. P. Roth* ——— **7273 – 7276**

Structures of Transition States in Metal-Mediated O_2-Activation Reactions

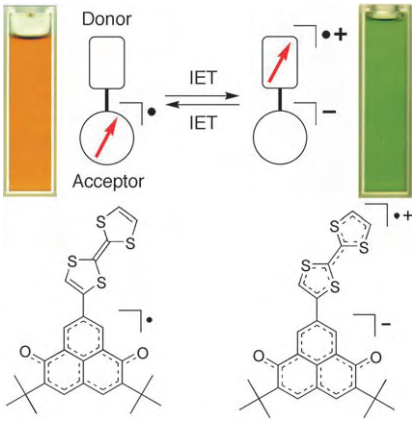

Doctoring spin: Spin transfer and solvato-/thermochromism have been observed in a purely organic open-shell system comprising electron-donor and -acceptor moieties, in which a 6-oxo-phenalenoxyl neutral radical is directly linked with tetrathiafulvalene. Intramolecular electron transfer (IET, see scheme) causes this interconversion, which can be controlled by a moderate change in the solvent environment and temperature.

Electron Transfer

S. Nishida, Y. Morita,* K. Fukui, K. Sato, D. Shiomi, T. Takui,* K. Nakasuji* ——— **7277 – 7280**

Spin Transfer and Solvato-/Thermochromism Induced by Intramolecular Electron Transfer in a Purely Organic Open-Shell System

© 2005 Wiley-VCH Verlag GmbH & Co. KGaA, Weinheim

Contents

DNA Cleavage

T. Peng, K. Nakatani* ——— **7280 – 7283**

Binding of Naphthyridine Carbamate Dimer to the $(CGG)_n$ Repeat Results in the Disruption of the G–C Base Pairing

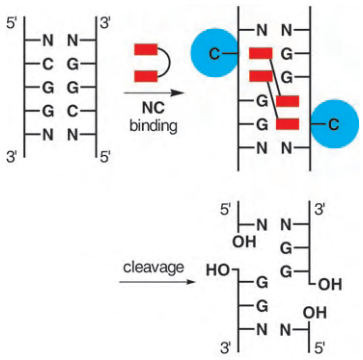

A disruptive influence: The naphthyridine carbamate dimer (**NC**) binds to the CGG/CGG triad with an exclusive 2:1 stoichiometry. A DNA oligomer is selectively cleaved at the site of cytosine in the triad upon treatment of the **NC**-bound CGG/CGG triad with hydroxylamine and hot piperidine (see picture; red: 2-amino-1,8-naphthyridine, blue: cytosine). The 2:1 **NC**-CGG/CGG complex is also produced in the $(CGG)_n$ repeat.

Nanostructures

T. Akutagawa,* K. Kakiuchi, T. Hasegawa, S.-i. Noro, T. Nakamura,* H. Hasegawa, S. Mashiko, J. Becher ——— **7283 – 7287**

Molecularly Assembled Nanostructures of a Redox-Active Organogelator

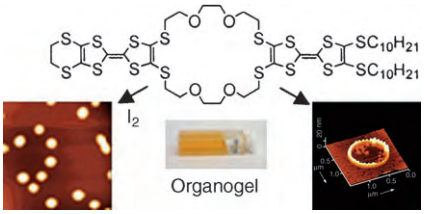

Introduction of an ethylenedithio group into an amphiphilic bis(tetrathiafulvalene) annulated macrocycle results in the formation of organogels which produce nanodot-array structures in Langmuir–Blodgett films (see picture). Chemical oxidation of the sulphur-containing π-electron system afforded size-controllable electrically conducting nanodot structures.

Reaction Mechanisms

Y. Ishibashi, Y. Bessho, M. Yoshimura, M. Tsukamoto, M. Kitamura* ——— **7287 – 7290**

Origin of the Minor Enantiomeric Product in a Noyori Asymmetric Hydrogenation: Evidence for Pathways Different to the Major Mechanism

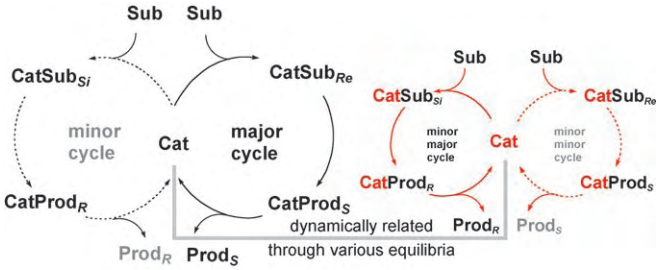

Hidden pathways: The enantiomeric products of the catalytic hydrogenation of an isotopically labeled substrate were separated. The ratios of the isotopomers revealed that the major and minor enantiomers are formed mostly through different mechanisms. Hence, when analyzing the energy profile of an asymmetric catalytic reaction with the Arrhenius equation, two competing diastereomorphic catalytic cycles should be considered (see scheme).

Nanotechnology

J. Liu, D. P. Wernette, Y. Lu* **7290 – 7293**

Proofreading and Error Removal in a Nanomaterial Assembly

We all make mistakes! The specific removal of error particles in nanomaterial assemblies is achieved by using a DNAzyme as a proofreading and error-removal unit (see picture of a DNA-templated gold nanoparticle assembly). Parallels can be drawn with the proofreading and error-removal process in biology. A and B = gold nanoparticles attached to DNA sequences; B′ = error particle.

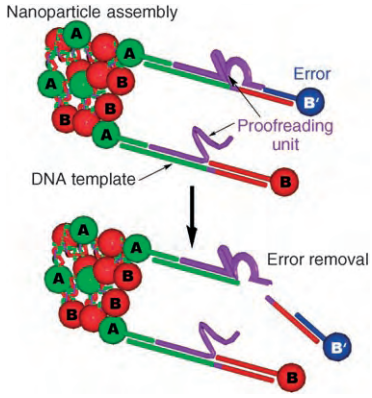

© 2005 Wiley-VCH Verlag GmbH & Co. KGaA, Weinheim

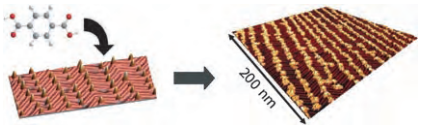

In a two-stage assembly protocol, regularly spaced transition-metal islands on a Au(111) surface are employed to steer the formation and organization of metallosupramolecular nanosystems (see picture). Following terephthalate exposure, Fe–terephthalate linkages evolve between next-neighbor Fe islands.

Supramolecular Chemistry

S. Clair, S. Pons, H. Brune, K. Kern, J. V. Barth* ——— **7294 – 7297**

Mesoscopic Metallosupramolecular Texturing by Hierarchic Assembly

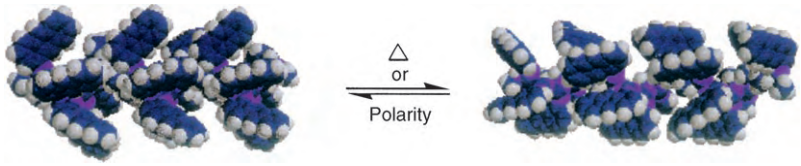

Helix-sense-selective polymerization of an achiral carbodiimide using a chiral titanium catalyst yields the regioregular, stereoregular poly[*N*-(1-anthryl)-*N*′-*n*-octadecylguanidine] (poly-**1**). A reversible thermo- and solvent-driven switching phenomena is exhibited by poly-**1** (see scheme) in electronic circular dichroism and optical rotation studies. Furthermore, the helicity of poly-**1** is assigned and the mechanism of this switching process is elucidated.

Molecular Motors

H.-Z. Tang, B. M. Novak,* J. He, P. L. Polavarapu* ——— **7298 – 7301**

A Thermal and Solvocontrollable Cylindrical Nanoshutter Based on a Single Screw-Sense Helical Polyguanidine

With a twist: When oligosilanes are mixed with polysaccharides, such as amylose and schizophyllan, novel inclusion complexes are formed (see picture). The oligosilane guests adopt a helical conformation within the chiral channel created by left- or right-handed helical wrapping with the polysaccharide host polymers.

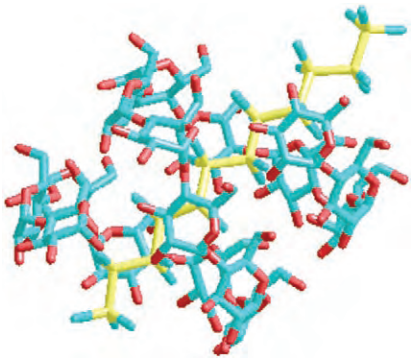

Host–Guest Systems

T. Sanji,* N. Kato, M. Kato, M. Tanaka* ——— **7301 – 7304**

Helical Folding in a Helical Channel: Chiroptical Transcription of Helical Information through Chiral Wrapping

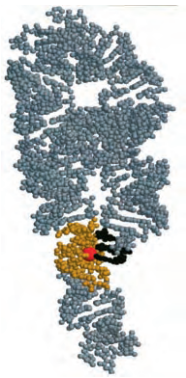

Knock it off: Individual RNA nucleotides with a caged nucleobase were incorporated, through their phosphoramidites, into a 160-mer RNA molecule that adopts a specific tertiary structure (see picture). Position-dependent local and global effects on RNA structure were observed, and photocleavage of the caging group was seen to restore the native folding.

RNA Folding

VIP

C. Höbartner, S. K. Silverman* ——— **7305 – 7309**

Modulation of RNA Tertiary Folding by Incorporation of Caged Nucleotides

© 2005 Wiley-VCH Verlag GmbH & Co. KGaA, Weinheim

Contents

WILEY InterScience®
DISCOVER SOMETHING GREAT

"Hot Papers" are chosen by the Editors for their importance in a rapidly evolving field of high current interest. A preview with the graphical abstracts of these articles can be found on the *Angewandte Chemie* homepage in Wiley InterScience at www.angewandte.org.

All articles in *Angewandte Chemie* are published online several weeks ahead of print. They are found under the "EarlyView" link on the journal's homepage in Wiley InterScience.

Service

Keywords ——— 7310

Authors ——— 7311

Preview ——— 7313

Concise Insight of 20 Years of Research

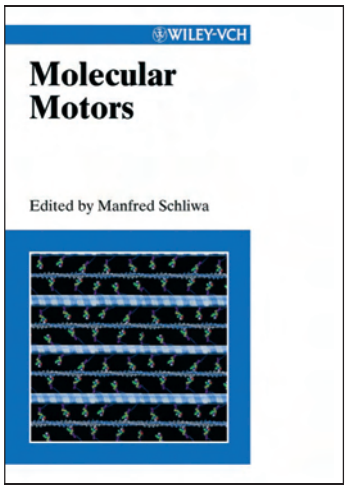

2002. XXII, 582 pages, 129 figures 48 in color, 20 tables. Hardcover. ISBN 3-527-30594-7
€ 179.- /£ 125.- /US$ 245.-

MANFRED SCHLIWA, University of Munich, Germany (Ed.)

Molecular Motors

Cell motility, virus transport and developmental asymmetry are examples of biological processes related to the function or malfunction of the minute machinery of molecular motors. This handbook brings together current knowledge on the functionality, regulation, and interactions of cytoskeletal, DNA, and rotary motors. Leading experts present principles and applications ranging from atomic structure, biochemistry, and biophysics to cell biology, developmental biology and pathology - all set to become a "classic" in the years to come.

"...essential reading for graduate students in the field of cell motility and molecular motors... recommend it enthusiastically..."
- Nature Cell Biology

22540509_kn

Register now for the free
WILEY-VCH Newsletter!
www.wiley-vch.de/home/pas

WILEY-VCH • P.O. Box 10 11 61 • D-69451 Weinheim, Germany
Fax: +49 (0) 62 01 - 60 61 84
e-mail: service@wiley-vch.de • http://www.wiley-vch.de

WILEY-VCH

© 2005 Wiley-VCH Verlag GmbH & Co. KGaA, Weinheim

European Conference on Solid-State Chemistry in Sheffield**

Timo Sörgel* and Martin Schulz-Dobrick*

The European Conference on Solid-State Chemistry rotates biennially among the major European centers for solid-state chemistry. Following Zürich, Madrid, Oslo, and Stuttgart, the community got together for the 10th meeting at the University of Sheffield, which is celebrating its centenary this year. The team around Anthony West, Derek Sinclair, and Neil Hyatt organized the conference in nine oral sessions that focused on different aspects of solid-state chemistry and one poster session of almost 140 contributions. The conference counted about 200 participants, mostly from Great Britain, Germany, Russia, France, and Spain. The scientific program was opened by Sir John Meurig Thomas (University of Cambridge, UK) with a survey of his work on catalysis. He pointed out the increasing importance of developing catalysts with shape-, size-, regio-, or enantioselectivity. One of his concepts is the immobilization of homogeneous catalysts in nanoporous silica or aluminumphosphate. He demonstrated with several examples how these additional spatial restrictions increased the already existing selectivity of a catalyst or even accessed new reaction products.[1]

[*] T. Sörgel, M. Schulz-Dobrick
Max-Planck-Institut für Festkörperforschung
Heisenbergstrasse 1
70569 Stuttgart (Germany)
E-mail: T.Soergel@fkf.mpg.de
M.Schulzd@fkf.mpg.de

[**] 10th ECSSC in Sheffield (UK), August 29–September 1, 2005.

Recently, the pioneering work of Juza in the chemistry of lithium–transition-metal nitrides has received much renewed attention, as the ternary nitrides $Li_{3-x-y}M_xN$ (M = transition metal) have been proposed as possible anode materials in lithium batteries. This aspect was elucidated in the talk given by Duncan H. Gregory (University of Nottingham, UK). Additionally, his presentation dealt with Li_3N, a well known ion-conductor. This compound undergoes reversible reactions with hydrogen and could be used as a light material for hydrogen-storage applications. Gregory's group has been able to synthesize Li_3N nanorods by a transport reaction. Due to their large surface area, they undergo a much faster reaction with hydrogen compared to the bulk material.

Antoine Maignan (CRISMAT, Caen, France) reported that a small variation in the oxygen content of $Sr_{2/3}Y_{1/3}CoO_{8/3+\delta}$ leads to a drastic change of magnetic and electric properties. For $\delta = 0.00$, the compound is an antiferromagnetic isolator, while for $\delta = 0.04$, the average oxidation state of 3.08 for cobalt leads to a semiconducting ferromagnet. This observation can be explained by the additional O^{2-} ions, which give rise to a disorder of the CoO_4 tetrahedra.

Miniaturization in the computer industry still proceeds steadily. In the sector of hard-disc technology, a data storage area density of about 100 Gb/in^2 is accessible today. Storing a bit of information requires about 100–300 grains, each having a diameter of 10–12 nm. However, this technique is limited and the search for new data-storage materials remains an important field in current research. Andrei A. Eliseev (Lomonosovoscow State University, Russia) gave an introduction to this topic. He pointed out that magnetic particles are not only required to be larger than the superparamagnetic limit but also should exhibit a sufficiently high magnetic moment in order to store the information at higher temperatures. Furthermore, it is important that neighboring domains do not influence each other. One solution could be the patterning of surfaces with highly anisotropic particles. Eliseev's approach to the fabrication of such a material consists of the growth of nanoscale iron wires by using mesoporous silica or porous alumina as a template.

Reactions between metals and gaseous nonmetal halides at temperatures above 1000 °C, for example, of Fe with $SiCl_4$ to give FeSi,[2] were the topic of the presentation by Michael Binnewies (University of Hannover, Germany). Interestingly, the shape of the starting material is preserved during the reaction and, depending on the materials, porous or dense products are formed. A potential application of this elegant transformation between solids and gases would be the production of components out of otherwise barely processable hard materials.

Yuri Grin (MPI for Chemical Physics of Solids, Dresden, Germany) presented results of a joint project between solid-state chemists and physicists which concentrates on the search for new low-temperature thermoelectrics. The focus lies on clathrate-type compounds, in which rare-earth ions are enclosed by Ga/Ge cages.

Additional lectures in the field of cluster compounds were given by Jürgen Köhler and Martin Jansen (both MPI for Solid State Research, Stuttgart, Germany). Köhler reported on the class of low-valent platinum indium fluorides, which contain, as in the case of $Pt_2In_{14}Ga_3O_8F_{15}$, low-valent In^+ ions as well as $[PtIn_6]^{10+}$ cluster ions.[3] The new silver cluster compound $Ag_{13}OsO_6$ was introduced by M. Jansen. The crystal structure can be described by a CsCl-type arrangement of $[Ag_{13}]^{4+}$ icosahedra and OsO_6^{4-} octahedra. The icosahedra are linked along their twofold axis with alternating 90° rotations. Thus, a three-dimensional network of subvalent silver with the average oxidation state 13/4 is formed. The composition of cluster units can be recognized by using atomic force microscopy; indeed, surface steps of the height of an $[Ag_{13}]^{4+}$ cluster unit were observed with this method.

John E. Greedan's (McMaster University, Hamilton, Canada) extensive work on $Nd_{1-x}TiO_3$ has led to remarkable results. An almost continuous solid solution exists in the range of $0 \le x \le 1/3$. Interestingly, two metal–insulator phase transitions occur at $x = 0.1$ and $x = 0.2$, while $NdTiO_3$ and $Nd_{2/3}TiO_3$ are a Mott–Hubbard and a charge-transfer

WILEY InterScience DISCOVER SOMETHING GREAT
© 2005 Wiley-VCH Verlag GmbH & Co. KGaA, Weinheim

insulator, respectively. Introducing holes into the conduction band causes a loss of the long-range spin order. Upon reaching a critical carrier concentration, the antiferromagnetic interaction turns into a paramagnetic short-range order.

In the session on structure–property relations in the important family of perovskite oxides, Evgeny V. Antipov (Lomonosov Moscow State University, Russia) presented investigations on $PbVO_3$.[4] The structure consists of corner-sharing VO_5 pyramids, which are formed by an exceptionally large tetragonal distortion ($c/a = 1.23$). This observation can be explained by the V^{4+} ion readily adopting a quadratic-pyramidal coordination and the stereochemical activity of the Pb^{2+} lone pair, which shifts the Pb^{2+} ion from the center of the unit cell towards one of the two $[VO_2]$ sheets (Figure 1). The semiconducting properties of $PbVO_3$ can be attributed to this two-dimensional character of the structure.

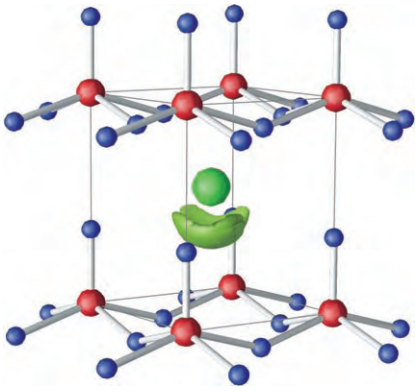

Figure 1. Visualization of the valence-ELF in the surroundings of Pb^{2+} in $PbVO_3$ ($\eta = 0.85$; Pb green, V red, O blue). The stereochemical orientation of the lone pair can clearly be seen (picture courtesy of E. V. Antipov, Moscow).

Philip Lightfoot (University of St Andrews, UK) has studied the hydrothermal synthesis of new metal fluorides and oxyfluorides with structure-directing organic ligands. The main goal is the fabrication of materials with second-harmonic generation properties in which the polarity of the building blocks is macroscopically preserved in the crystal.

The lecture by John B. Claridge (University of Liverpool, UK) pointed towards the more unusual class of transition-metal oxide hydrides. He had investigated several intermediate phases in the synthesis of $LaSrCoO_3H_{0.7}$, which exhibits antiferromagnetic order up to a temperature of 380 K. He showed that the magnetic and electronic properties strongly depend on the fraction of oxide and hydride ions.

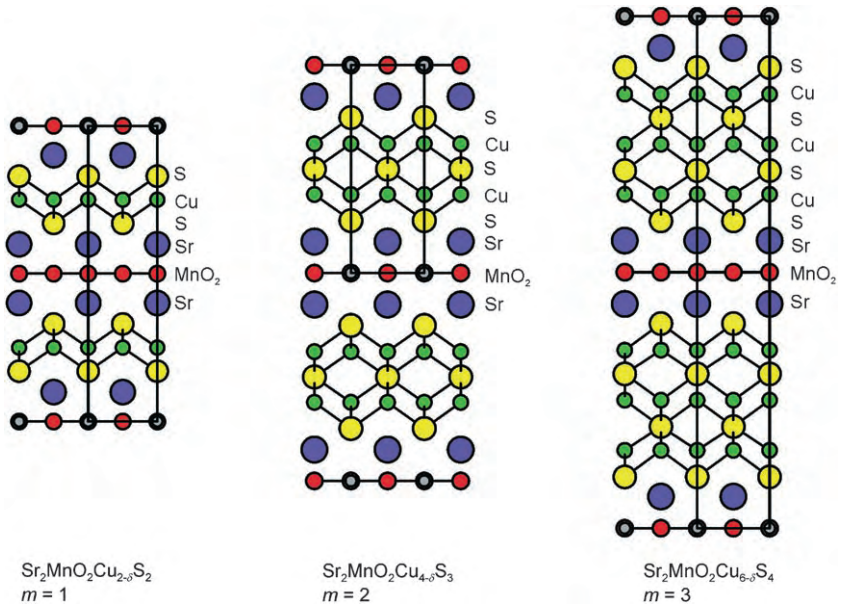

Figure 2. Homologous series $Sr_2MnO_2Cu_{2m-\delta}S_{m+1}$ with variable copper sulfide layer thicknesses ($m = 1, 2, 3$). The copper deficiency is reflected by $\delta = 0.5$ for all three compounds (picture courtesy of S. J. Clarke, Oxford).

Owing to the very different structural demands of O^{2-} and S^{2-} ions, oxysulfides often form layer-type structures, which consist of structure fragments formed by the respective oxide and sulfide. Simon J. Clarke (University of Oxford, UK) showed that the copper sulfide layer in the series of compounds $Sr_2MnO_2Cu_{2m-\delta}S_{m+1}$ ($m = 1, 2, 3$) can be varied in thickness (Figure 2). The copper position is not fully occupied, and the Cu–S distances in the CuS_4 tetrahedra are elongated as a response to the rigid Sr_2MnO_2 layers. Due to the copper deficiency, manganese is in a mixed-valent state with oxidation states of II and III which leads to interesting magnetic properties. The compounds are antiferromagnetic, while the spins on the Mn^{III} ions of consecutive layers order ferromagnetically in relatively low magnetic fields. The required field strength decreases with increasing values of m.

Welf Bronger (RWTH Aachen, Germany) outlined a comparison of atomic volume increments that were specified classically according to W. Biltz with those based on quantum chemistry according to R. F. W. Bader or the ELF (electron-localization function) method. The change in the volume of the highly polarizable hydride ion can be followed from ionic to metallic hydrides on the basis of all three concepts.[5]

Transparent, conducting main-group-metal oxides are found in many applications, such as flat-panel displays, energy-efficient window coatings, photovoltaics, and light-emitting diodes (LEDs). As not all required properties are combined in one single material, the search for new transparent conducting oxides and a fundamental understanding of their properties are of great current interest. According to Patrick M. Woodward (Ohio State University, Columbus, USA), the crucial point in such compounds is the presence of a low-lying dispersive conduction band, which is well separated from other conduction bands. Furthermore, it must be possible to dope the respective oxide to introduce charge carriers in the conduction band without essentially affecting the charge-carrier mobility. A structural feature of many of these oxides are edge-sharing octahedra in addition to a large covalent cation–anion interaction. Woodward reported that the desired

© 2005 Wiley-VCH Verlag GmbH & Co. KGaA, Weinheim

physical properties are mostly due to the highly symmetric environment of oxygen.[6]

The progressing miniaturization in the field of GHz telecommunication applications has increased the demands for dielectric ceramics. Besides a high relative permeability, a high Q value and an almost temperature-independent resonance frequency are the most important criteria. Robert Freer (University of Manchester, UK) reported on such dielectric ceramics. In different systems, he has investigated how the dielectric properties depend on the applied processing conditions and thus the grain sizes, twinning, and the presence of surface phases and point defects. Understanding these correlations plays an important role in the search for improved materials.

The social highlight was the conference dinner in the richly decorated Cutlers' Hall, built in 1832, during which host Anthony R. West thanked his organizing committee and announced that the 11th ECSSC will take place in the French city of Caen. During the conference it became clear, that solid-state chemistry is a constantly developing and fascinating field of research, where the interplay of chemistry, materials science, and physics—in experiment and theory—gains an increasingly important role.

[1] J. M. Thomas, B. F. G. Johnson, R. Raja, G. Sankar, P. A. Midgley, *Acc. Chem. Res.* **2003**, *36*, 20–30; J. M. Thomas, R. Raja, D. W. Lewis, *Angew. Chem.* **2005**, *117*, 6614–6641; *Angew. Chem. Int. Ed.* **2005**, *44*, 6456–6482.

[2] M. Binnewies, A. Meyer, M. Schütte, *Angew. Chem.* **2001**, *113*, 3801–3803; *Angew. Chem. Int. Ed.* **2001**, *40*, 3688–3690.

[3] J. Köhler, J. H. Chang, M. H. Whangbo, *J. Am. Chem. Soc.* **2005**, *127*, 2277–2284.

[4] R. V. Shpanchenko, V. V. Chernaya, A. A. Tsirlin, P. S. Chiznov, D. E. Sklovsky, E. V. Antipov, E. P. Khlybov, V. Pomjakushin, A. M. Balagurov, J. E. Medvedeva, E. E. Kaul, C. Geibel, *Chem. Mater.* **2004**, *16*, 3267–3273.

[5] W. Bronger, R. Kniep, M. Kohout, *Z. Anorg. Allg. Chem.* **2005**, *631*, 265–271.

[6] H. Mizoguchi, P. M. Woodward, *Chem. Mater.* **2004**, *16*, 5233–5248.

DOI: 10.1002/anie.200503352

Technology for industrial applications and products in our modern life

14,000 pages at a special price. Save 85 % with the softcover edition

Cahn, R.W., Haasen, P., Kramer, E.J. (Eds.)

Materials Science and Technology – A Comprehensive Treatment

The Classic Softcover Edition
ISBN 3-527-31395-8
May 2005
Approx. 14,000 pages
11 Volumes. English.
€ 599.-/ SFr 886.- / US$ 780.-

The right choice of materials is essential for satisfying the consumers and customers needs.

"Materials Science and Technology" is forming the basis for modern research in the interdisciplinary field of materials science. It encompasses all different classes of materials - metals, alloys, ceramics, composites, semiconductors and polymers – and is essential for anyone involved in production and development of new products in modern industry.

This softcover edition offers the wealth of information of the renowned series "Materials Science and Technology" in one complete set of eleven volumes.

For ordering information, please contact our customer service:

Wiley-VCH · Tel.: +49 (0) 6201 606-400
E-Mail: service@wiley-vch.de · www.wiley-vch.de

John Wiley & Sons, Inc. · Tel.: +1 877-762-2974
E-Mail: custserv@wiley.com · www.wiley.com

John Wiley & Sons, Ltd. · Tel.: +44 (0) 1243-843-294
E-Mail: cs-books@wiley.co.uk · www.wiley.com

WILEY InterScience® DISCOVER SOMETHING GREAT

WILEY-VCH WILEY

19081504_gu

 © 2005 Wiley-VCH Verlag GmbH & Co. KGaA, Weinheim

Synthetic Biology

DOI: 10.1002/anie.200501896

Gene Synthesis on Microchips**

*Joachim W. Engels**

Keywords:
chemical biology · hybridization · microchips · oligonucleotides · polymerase chain reaction

With gene synthesis we will in future be able to synthesize complete genomes. From there, we will be able to answer essential biological questions, for example, how chemical reactions proceed within a cell. The first step, genome sequencing, especially of the human genome, has created a huge amount of data. It is currently estimated that humans have about 25000 genes. Chemically speaking, genes are merely defined sequences of long DNA stretches. In the last 40 years, methods for the chemical synthesis of DNA have improved drastically.[1–3] These processes are based on the stepwise coupling of individual nucleotide building blocks to yield oligonucleotides. These in turn, arrange themselves into double-stranded DNA owing to their base complementarity. Hydrogen bonding followed by chemical or chemoenzymatic ligation of the phosphoric esters results in the stable duplexes. By exploiting this principle, Khorana and co-workers were able to synthesize the first gene in 1970, the yeast $tRNA^{Ala}$ gene.[3] Since then, synthetic methods have been refined, most noteworthy by the application of the polymerase chain reaction (PCR), and the goals have become more ambitious.[4–6] The subsequent years witnessed the syntheses of the following genes: α-interferon (1985),[7] the interleukin-2 receptor α (1987),[8] and a plasmid (1990).[9] The year 2002 saw the synthesis of a polio virus DNA[10] with around 7500 base pairs. Its biological activity was proven by its infectivity. The synthesis of the bacteriophage ΦX174 with 5386 base pairs was reported in 2003;[11a] this molecule was first sequenced by Fred Sanger with the newly developed dideoxy sequencing method.[11b] The longest recorded gene

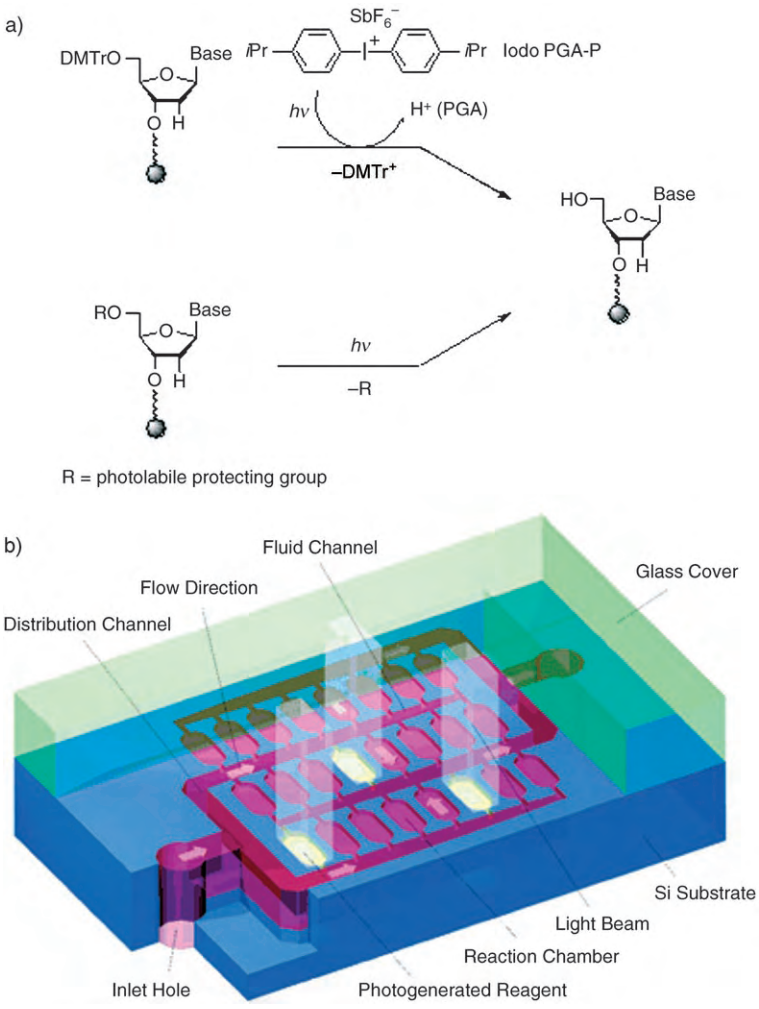

Figure 1. Phosphoramidite oligonucleotide synthesis on a chip: a) First step in the oligonucleotide synthesis, the 5′-deprotection: synthesis with photogenerated acid (PGA) or photolabile protecting groups. b) The actual chip used: PicoArray reactor for parallel oligonucleotide synthesis (University of Michigan). 128×31 (3968) individual reaction chambers with an internal volume of 270 pL (total volume 10 μL). The digital light projection shows the PGA controlled reactions. Reproduced from reference [17] with permission of Oxford University Press.

[*] Prof. Dr. J. W. Engels
Institut für Organische Chemie und Chemische Biologie
Johann Wolfgang-Goethe Universität
Marie-Curie-Strasse 11, 60439 Frankfurt am Main (Germany)
Fax: (+49) 69-798-29148
E-mail: joachim.engels@chemie.uni-frankfurt.de

[**] I thank A. Klöpffer, K. Strube, and C. Engels for technical support during 20 years of developing and teaching biological synthesis.

InterScience
© 2005 Wiley-VCH Verlag GmbH & Co. KGaA, Weinheim

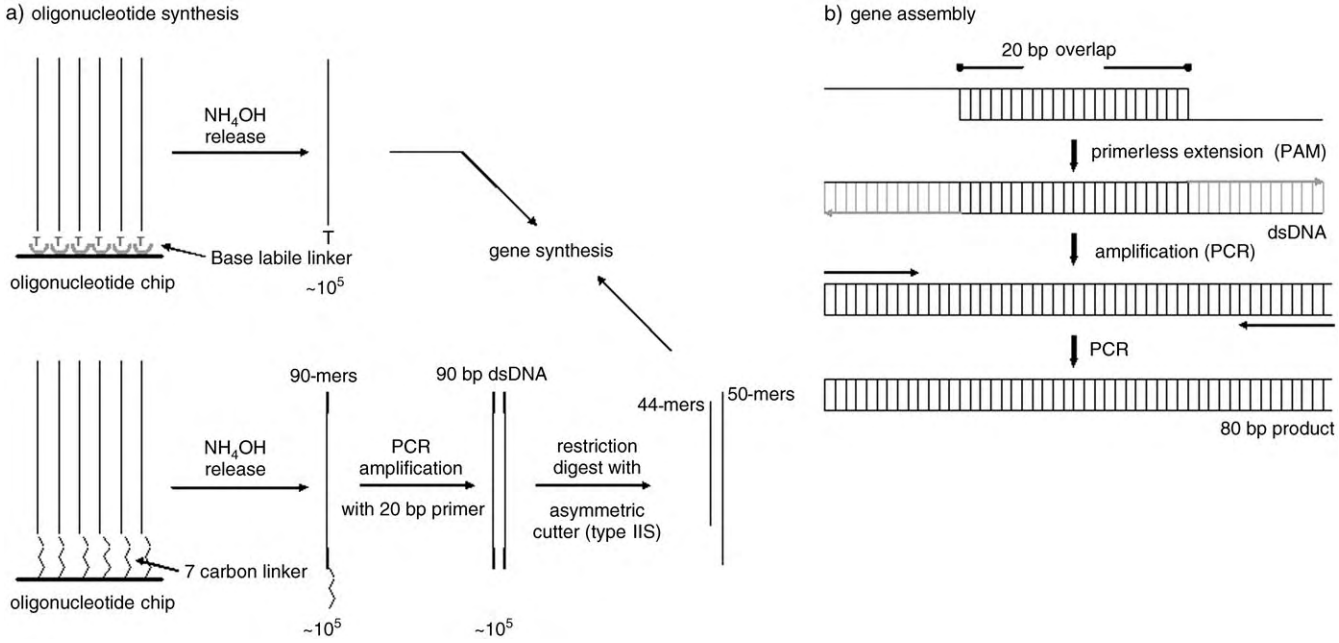

Figure 2. Oligonucleotide und gene assembly synthesis. a) On-chip oligonucleotide (50-mer) synthesis with and without PCR amplification and cleavage of the primer. b) Polymerase-assisted synthesis of genes, fill-in reaction (primerless extension), and PCR of two 50-mer oligonucleotides.

synthesized to date is the 32 000 base pair polyketide synthase gene cluster (2004).[12] This gene was also biologically active and yielded 6-deoxyerythronolide after transformation in *E. coli*.

Combinatorial or parallel syntheses yield a variety of chemical structures, whose functions can be analyzed through appropriate assays. Genes on the megabase scale (e.g. human DNA) can, in principle, be synthesized chemically or chemoenzymatically. Oligonucleotides in the range of 20 to 100 mers are now commercially available for about 0.10 euro per nucleotide and have error rates of around 1:100 to 1:400. These errors are mainly due to problems that occur during the chemical synthesis, such as incomplete reactions during coupling and deprotection and side reactions caused by the reagents used (e.g. Michael addition of acrylonitrile to thymine). High-throughput gene synthesis is limited by economic factors and error rates; cloning and sequencing raise the price about tenfold.

Consequently, parallel syntheses on microchips were introduced to reduce the costs. The yield of the oligonucleotides turned out to be problematically low (atto- and femtomolar range). These 10^5–10^9 molecules must then be amplified by PCR to 10^9–10^{12} molecules.[13] Gao, Church, and co-workers have recently showed[14] how approximately 4000 oligonucleotides can be synthesized simultaneously on light programmable microarrays (Figures 1a and b).[15–17] Photolabile protecting groups or photoliberated protons and the dimethoxytrityl (DMTr) protecting group allow on-chip synthesis according to the phosphoramidite method of Caruthers and Beaucage.[1] As mentioned above, errors appear during the chemical synthesis on chip and hence Gao, Church, and co-workers chose stringent hybridization as a cheap means of quality control, utilizing so-called quality assessment chips synthesized with the complementary oligonucleotides. Error-containing oligonucleotides, for example, oligonucleotides with the incorporation of wrong bases (point mutations) were purified by affinity chromatography on immobilized short complementary oligonucleotides. In this step it is important to synchronize the melting points (T_m values) isothermally by choosing oligonucleotides of different lengths.

An important point in gene design is the selection of the restriction enzymes to be used. Restriction enzymes of the type IIS were chosen which cut the DNA outside the recognition sequence and thus liberate internal sequences at will—in this case gene sequences (Figure 2). The authors used the enzymes BsaI with the recognition sequence 5′-GGTCTC(1/5) and a four-base 5′-overlap and BseRI with the recognition sequence 5′-GAGGAG(10/8) and a two-base 3′-overlap of undefined sequence. In addition to the gene sequences, selection oligonucleotides immobilized on streptavidin beads through a biotin linker (Figure 3) were used for separation. Only the unmodified, error-free oligonucleotides (in this case 50-mers) were selected! The exactly fitting oligonucleotides were filtered out in two steps with the help of 25-mer complementary oligonucleotides R and L (so-called capture probes). Following this purification by selection, the gene-assembly experiment is developed on microtiter plates (e.g. 96 or 384 wells) by the polymerase assembly multiplexing (PAM) reaction. In this case the dsDNA, which is held together by hydrogen-bonding interactions, is assembled into a gene by the action of polymerases, without a primer. The quality of the oligonucleotides used for gene synthesis was tested in three different formats: 1) unpurified (as synthesized), 2) purified by gel electrophoresis, and 3) purified through hybridization on affinity beads.[18] The latter method showed the lowest error rate (1:1394 bp), which is an improvement

 © 2005 Wiley-VCH Verlag GmbH & Co. KGaA, Weinheim

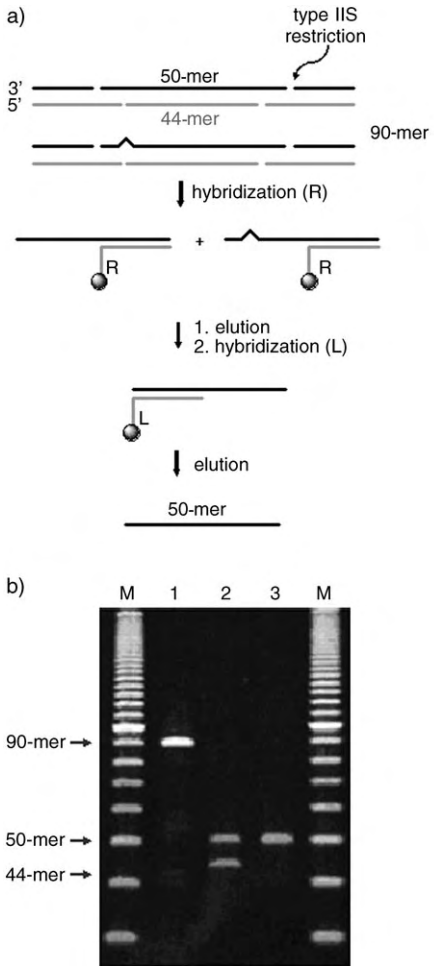

Figure 3. Selection of synthetic oligonucleotides through hybridization: a) Scheme for the hybridization of PCR-amplified 90-mers by immobilized oligonucleotides L und R. b) PAA gel, oligonucleotides (50- and 44-mers, lane 2) cut with type IIS restriction enzymes BsaI and BseRI and selected 50-mers (lane 3). Reproduced from reference [14] with permission of Nature Publishing.

(roughly by a factor of 10) over the assembly by chemical synthesis on a polymer support followed by enzymatic ligation.

As an example for the application of this method in synthetic biology, Gao, Church, and co-workers[14] synthesized codon-varied genes for 21 proteins of the small 30S ribosome subunit of *E. coli*.[19] It is known that the expression rate of these 21 proteins in vitro is low and it was hoped that the translation efficiency would be increased by choosing the appropriate codons. Secondary structures of the mRNA have been discussed as the cause of low synthetic efficiency. It was hoped that the formation of these secondary structures could be limited by decreasing the G/C content of the DNA. Thus, 50-mer oligonucleotides were chosen with PCR primer binding sites on both ends, yielding 70-mers. The experiment shows the result of a successful PAM assembly strategy, which was checked by means of a computer program to be unequivocal for finding the right oligonucleotide partner by hybridization. All 21 genes, their transcribed RNA, and the resulting proteins were successfully detected on gel. Finally, a complete operon of 14.6 kb for all 21 genes was assembled (Figure 4). The error rate for the oligonucleotides was estimated to be 1:7300 bp! This clearly proves that the error rate of synthetic oligonucleotides is the limiting step in chemoenzymatic gene synthesis and not the precision of the polymerases, which have an error rate of about 1:100000 bp.

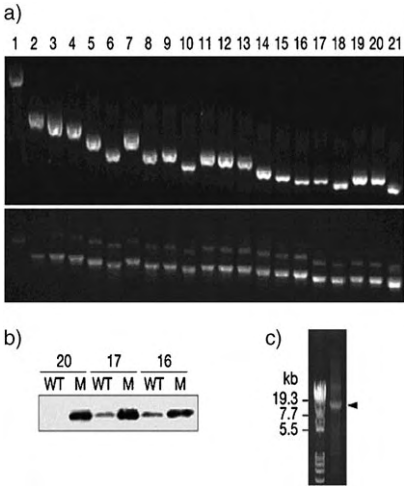

Figure 4. Gene constructs and their transcriptional (mRNA) and translational products (proteins) on polyacrylamide gels. a) Synthetic genes of 21 ribosomal proteins (upper gel) and their RNA transcribed in vitro (lower gel). b) Western blot of the selected translated genes of ribosomal proteins 16, 17, and 20 (WT = wild-type, M = synthetic variant). c) Final assembly of the 14.6-kb operon for all 21 ribosomal proteins. Reproduced from reference [14] with permission of Nature Publishing.

This experiment clearly demonstrates the potential of on-chip oligonucleotide synthesis. Given the present capacity of microchips, large-scale gene-synthesis experiments are possible. A rough calculation indicates the possibility of lowering the costs for gene synthesis from 10 bp per euro to 20 kbp per euro. This is possible by using, for example, microchips from NimbleGen (www.nimblegen.com) with an oligonucleotide density of 95000–382000, to give a final sum of 2–18 Mbp DNA.

In an effort to reduce the error rate for the synthetic gene even further, a correction of the assembled oligonucleotides or gene fragments by a protein from the DNA-repair machinery (e.g. mutS) is being pursued.[20] Thus, Jacobson and co-workers corrected a synthetic DNA with the fixed mismatch binding protein mutS from *Thermus aquaticus*. They eliminated mismatch products and obtained DNA with an error rate of around 1:10000. Another alternative to obtain completely error-free DNA is a cheap high-throughput-sequencing method in which thousands of sequences can be read simultaneously.[21]

In summary, the methods and procedures for the synthesis of genes were mostly known, but they have now been combined in a new way to allow more-efficient and economic access to error-free genes in the 10-kb range. The individual steps include (estimated times in brackets):[14]

a) Design and modeling of the appropriate oligonucleotide building blocks for the gene synthesis (2 h).
b) Oligonucleotide synthesis in microfluidic devices (8 h).
c) Amplification of the synthetic, on-chip oligonucleotides by PCR (14 h).
d) Cutting the amplified oligonucleotides by type IIS restriction enzymes to the appropriate size (50-mers).
e) Selection of the correct sequences through hybridization (30 h).
f) Assembly of the final gene by polymerase fill-in followed by PCR (4 h).
g) In vitro transcription/translation and detection of mRNAs and proteins (1 h).

As potential application one can envisage the synthesis of gene clusters for natural products such as polyketides or the resynthesis of bacterial cell genomes(e.g. mycoplasma). Thus gene synthesis will be a way to evolve new secondary metabolites such as polyketides or peptide antibiotics to obtain non-natural isomers of natural products. Gene synthesis is key to functional

 © 2005 Wiley-VCH Verlag GmbH & Co. KGaA, Weinheim

genomics and will result in the assignment of all chemical reactions within a cell. The ultimate goal of biological synthesis will be to find new arrangements of genes from a gene pool and hence to search for new solutions for new products.

[1] a) S. L. Beaucage, M. H. Caruthers, *Tetrahedron Lett.* **1981**, *22*, 1859 – 1862; b) M. H. Caruthers, *Science* **1985**, *230*, 281 – 285.

[2] J. W. Engels, E. Uhlmann, *Angew. Chem.* **1989**, *101*, 733 – 752; *Angew. Chem. Int. Ed. Engl.* **1989**, *28*, 716 – 734.

[3] K. L. Agarwal, H. Büchi, M. H. Caruthers, N. Gupta, H. G. Khorana, K. Kleppe, A. Kumar, E. Ohtsuka, U. L. Rajbhandary, J. H. Van de Sande, V. Sgaramella, H. Weber, T. Yamada, *Nature* **1970**, *227*, 27 – 34.

[4] P. J. Dillon, C. A. Rosen, *BioTechniques* **1990**, *9*, 298 – 300.

[5] W. P. C. Stemmer, A. Crameri, K. D. Ha, T. M. Brennan, H. L. Heyneker, *Gene* **1995**, *164*, 49 – 53.

[6] S. R. Casimiro, P. E. Wright, H. J. Dyson, *Structure* **1997**, *5*, 1407 – 1412.

[7] M. Edge, A. R. Greene, G. R. Heathcliffe, P. A. Meacock, W. Schuch, D. B. Scanlon, T. C. Atkinson, C. R. Newton, A. Markham, *Nature* **1981**, *292*, 756 – 762.

[8] J. Engels, W. Becker, T. Beckers, D. Hüsken, W. Wetekam, *Pure Appl. Chem.* **1987**, *59*, 437 – 444.

[9] W. Mandecki, M. A. Hayden, M. A. Shallcross, E. Stotland, *Gene* **1990**, *94*, 103 – 107.

[10] J. Cello, A. V. Paul, E. Wimmer, *Science* **2002**, *297*, 1016 – 1018.

[11] a) H. O. Smith, C. A. Hutchison, C. Pfannkoch, J. C. Venter, *Proc. Natl. Acad. Sci. USA* **2003**, *100*, 15440 – 15445; b) F. Sanger, A. R. Coulson, T. Friedmann, G. M. Air, B. G. Barrell, N. L. Brown, J. C. Fiddes, C. A. Hutchinson III, P. M. Slocombe, M. Smith, *J. Mol. Biol.* **1978**, *125*, 225 – 246.

[12] S. J. Kodumal, K. G. Patel, R. Reid, H. G. Menzella, M. Welch, D. V. Santi, *Proc. Natl. Acad. Sci. USA* **2004**, *101*, 15573 – 15578.

[13] K. E. Richmond, M.-H. Li, M. J. Rodesch, M. Patel, A. M. Lowe, C. Kim, L. L. Chu, N. Venkataramaian, S. F. Flickinger, J. Kaysen, P. J. Belshaw, M. R. Sussman, F. Cerrina, *Nucleic Acids Res.* **2004**, *32*, 5011 – 5018.

[14] J. Tian, H. Gong, N. Sheng, X. Zhou, E. Gulari, X. Gao, G. Church, *Nature* **2004**, *432*, 1050 – 1053.

[15] X. Gao, P. Yu, E. LeProust, L. Sonigo, J. P. Pellois, H. Zhang, *J. Am. Chem. Soc.* **1998**, *120*, 12698 – 12699.

[16] X. Gao, E. LeProust, H. Zhang, O. Srivannavit, E. Gulari, P. Yu, C. Nishiguchi, Q. Xiang, X. Zhou, *Nucleic Acids Res.* **2001**, *29*, 4744 – 4750.

[17] X. Zhou, S. Cai, A. Hong, Q. You, P. Yu, N. Sheng, O. Srivannavit, S. Muranjan, J. M. Rouillard, Y. Xia, X. Zhang, Q. Xiang, R. Ganesh, Q. Zhu, A. Matejko, E. Gulari, X. Gao, *Nucleic Acids Res.* **2004**, *32*, 5409 – 5417.

[18] R. G. Eason, N. Poumand, W. Tongprasit, Z. S. Herman, K. Anthony, O. Jejelowo, R. W. Davis, V. Stolc, *Proc. Natl. Acad. Sci. USA* **2004**, *101*, 11046 – 11051.

[19] G. M. Culver, H. F. Noller, *RNA* **1999**, *5*, 832 – 843.

[20] P. A. Carr, J. S. Park, Y.-J. Lee, T. Yu, S. Zhang, J. M. Jacobson, *Nucleic Acids Res.* **2004**, *32*, e162.

[21] J. Shendure, R. D. Mitra, C. Varma, G. M. Church, *Nat. Rev. Genet.* **2004**, *5*, 335 – 343.

© 2005 Wiley-VCH Verlag GmbH & Co. KGaA, Weinheim

Organic Radicals

DOI: 10.1002/anie.200502644

Toward the Systematic Decomposition of Benzene

*Paul G. Wenthold**

Keywords:
benzene · bond energy · dissociation · radicals · reactive intermediates

Open-shell organic molecules have been the subject of considerable interest ever since the first report of the triphenylmethyl radical over 100 years ago by Gomberg.[1] In the intervening century, the study of organic radicals has advanced from the controversial isolation of a stable, trivalent carbon molecule to the generation of polymeric polyradicals with 10000 unpaired electrons,[2] with many variations in between. The properties of radicals that have been considered include their thermochemical stability, molecular structure, spectroscopic characteristics, chemical reactivity, and electronic structure, such as spin density and magnetic properties.

The concept of bond dissociation underlies many of the features of organic radicals. In principle, hypovalent organic systems can be considered to arise from a bond-dissociation process. Radicals, for example, are formed by homolytic bond dissociation of closed-shell precursors. Breaking a second bond in the precursor (or breaking a bond in the radical) leads to the formation of didehydro systems, such as carbenes and diradicals. Triradicals result from breaking bonds in diradicals and dissociate to give tetraradicals, and thus the process continues.

However, a discussion of radicals in the context of bond dissociation does more than provide an idealized genesis for their formation, it also provides a basis for understanding many of their unusual characteristics. Because bond dissociation is an energetically costly process, radicals are generally high energy species and, consequently, will undergo transformations normally considered to be disfavored if the energy benefit is greater than the cost. The enhanced reactivity of hypovalent systems reflects the positive effect of stabilizing the open-shell wave function through bond formation in an addition reaction or by atom abstraction to form a more stable radical.

In molecules with more than one unpaired electron, electron–electron interactions can have a significant role in the stabilization of the system. Bond formation that results from direct orbital overlap is highly favorable and, thus, is an overriding consideration in all low-spin polyradicals, even to the extent that the system is better described as being a strained, closed-shell state as opposed to a polyradical. In cases in which bonding cannot occur, indirect interactions that are usually insignificant, such as electron exchange and spin polarization, can have significant impact.

Significant attention has been paid to the determination of thermochemical properties because of the important role that bond-dissociation energies (BDEs) play in providing a fundamental understanding of structure and reactivity. Not only do thermochemical properties help to evaluate the stability of the reactive species, but variations in BDEs provides a means to investigate the effects of their origins. In this way, it is possible to assess the influence of the geometric distortions and electronic interactions that occur in the reactants and products.

A commonly used systematic approach to the investigation of BDEs and how they are affected by structure involves measuring the energetics for the sequential decomposition of an organic molecule.[3,4] In 1990, Ellison and co-workers reported the energetics for the dissociation of ethylene into component atoms (Figure 1).[5] They were able to describe the energetics for the dissociation of ethylene by all possible pathways by measuring the thermochemical properties of the intermediates, including vinyl and acetylenic radicals and vinylidene. Similar schemes can be constructed for other simple systems, such as formaldehyde, and some larger systems, such as ketene, are also nearly completely known.[4]

The decomposition of a much larger molecule, such as benzene, becomes a much more complicated process, with many possible pathways available. However, studies of reactive molecules derived from benzene have led to insight into the initial steps that result from breaking C–H bonds. The phenyl radical, generated by breaking the first C–H bond, is well characterized spectroscopically[6] and thermochemically.[7] *Ortho*, *meta*, and *para* benzynes **1**-*o*,*m*,*p* (Scheme 1), which are generated by breaking a second bond in benzene, are also very well known. The thermochemical properties of the singlet and triplet states have been determined,[8,9] and IR spectroscopy has been carried out for the *ortho*[10] and *meta* isomers.[11] The structure of *o*-benzyne has even been investigated by using NMR spectroscopic analysis.[12] Thus, only the *para*-isomer **1**-*p* awaits detailed spectroscopic characterization, although limited spectroscopic data are available.[9]

Recent investigations[13–15] have focused on the properties of the dehydrobenzynes, which are triradicals formed by dissociation of a third bond in benzene. As indicated in Scheme 1, there are many different C–H bonds in the benzynes that can be broken, but there are only three dehydrobenzynes

[*] Prof. P. G. Wenthold
Department of Chemistry
Purdue University
West Lafayette, IN 47907 (USA)
Fax: (+1) 765-494-0475
E-mail: pgw@purdue.edu

InterScience
© 2005 Wiley-VCH Verlag GmbH & Co. KGaA, Weinheim

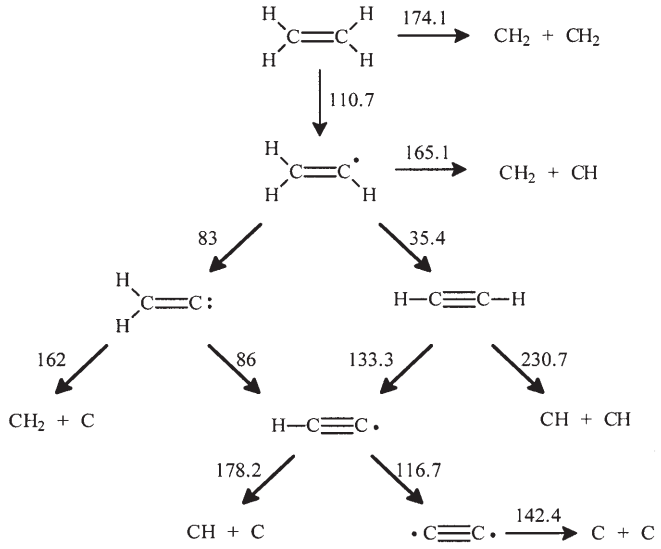

Figure 1. Bond-dissociation energies (kcal mol^{-1}) for the decomposition of ethylene.[5] Hydrogen-atom fragments have been omitted for simplicity.

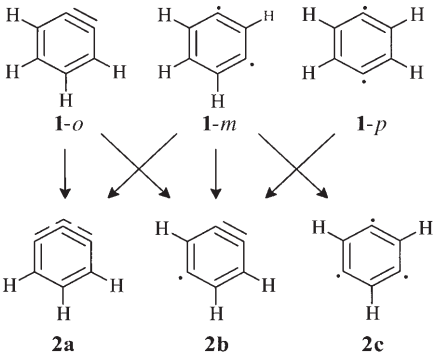

Scheme 1.

that can be formed. The first experimental study of a dehydrobenzyne was a determination of the heat of formation of the 1,3,5-tridehydrobenzene isomer **2c** by Lardin et al.[13] The measured heat of formation of **2c** reflects a BDE of 109.2 ± 5.6 kcal mol^{-1} at the 5-position of *m*-benzyne [Eq. (1)].

The similarity between the BDE in *m*-benzyne and that in benzene (112.9 ± 0.5 kcal mol^{-1})[7] indicates little interaction between the newly formed radical center and the *m*-benzyne moiety. This was explained by consideration of the electronic structure of the triradical formed. A molecular-orbital energy diagram for D_{3h}-symmetric **2c** is shown in Figure 2. In the high-symmetry structure, the system consists of one electron in a degenerate pair of e′ orbitals and, therefore, undergoes a Jahn–Teller distortion to a lower symmetry C_{2v} structure. Whereas two distortions are possible, electronic-structure calculations predict that the lower energy state is the $^2A_1$ state, in which the unpaired electron is in an orbital with an antibonding interaction with the bonding molecular orbital of the *m*-benzyne. Therefore, there is little interaction between the unpaired electron and the *m*-benzyne moiety.

Sander and co-workers[14] reported recently the formation of 1,2,3-tridehydrobenzene **2a** in a neon matrix. Their approach to the generation of the triradical involves photodissociation of 3-iodophthalic anhydride [**3**, Eq. (2)].

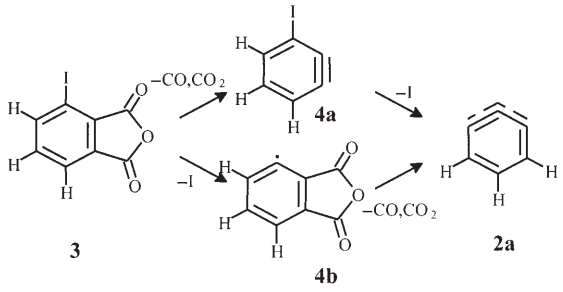

The results provide insight into the mechanism for the formation of **2a**. For example, other products formed upon the photodissociation of **3** in a neon matrix [Eq. (2)] include 3-iodobenzyne (**4a**) and the phthalic anhydride radical **4b**. However, **4a** prepared independently from 1,2,3-triiodobenzene in an argon matrix does not produce the 1,2,3-triradical, thus suggesting that 3-dehydro-*o*-benzyne is formed from **4b**, although matrix effects cannot be ruled out.

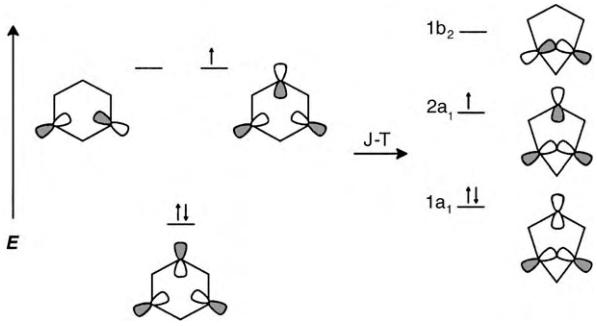

Figure 2. Orbital-energy diagram for **2c**. The orbitals on the left are for D_{3h} symmetry, and the orbitals on the right are for the C_{2v} state that results from Jahn–Teller distortion.

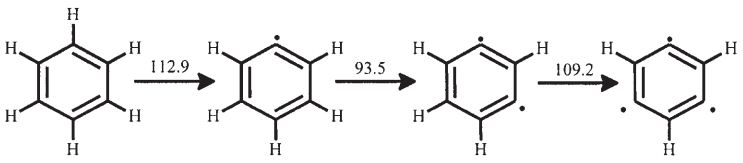

(1)

An important and surprising conclusion of the IR spectroscopic study[14] of **2a** is that the triradical has a $^2A_1$ ground state, as opposed to the $^2B_2$ state predicted in a recent computational study by Cristian et al.[15] The

© 2005 Wiley-VCH Verlag GmbH & Co. KGaA, Weinheim

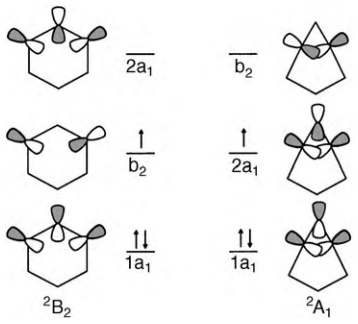

Figure 3. Electronic structures of the $^2B_2$ and $^2A_1$ states of 1,2,3-tridehydrobenzene.

difference between the states can be seen by consideration of the nonbonding molecular orbitals in Figure 3. The properties of the nonbonding molecular orbitals in **2a** are reminiscent of those in the allyl radical, with bonding ($1a_1$), nonbonding (b_2), and antibonding ($2a_1$) orbitals. Initial considerations suggest an electronic structure that consists of two electrons in the bonding orbital and single occupation of the nonbonding orbital (calculations indicate little multiconfigurational character),[14,15] similar to the allyl radical, thus creating the $^2B_2$ state. Consequently, one might expect this state to benefit from "allylic stabilization", which results from delocalization of the unpaired electron. However, whereas Cristian et al.[15] concluded that $^2B_2$ is the ground state of the system, they did not find it to be especially stable and calculated little energy difference for the three isomers of **2**.

The IR spectroscopic data reported by Sander and co-workers indicate the presence of the $^2A_1$ state.[14] In this state, the unpaired electron occupies the "antibonding" molecular orbital $2a_1$. However, the characterization of the $2a_1$ orbital as antibonding is misleading. Unlike in the allyl radical, there is a significant interaction between the terminal carbon atoms in the triradical **2a**. Thus, as shown by Sander et al.,[14] there is a significant energy dependence on the distance between the dehydrocarbons in both electronic states. The $^2B_2$ state, with the unpaired electron in a b_2 orbital that has an antibonding relationship between the dehydrocarbons, is favored at longer C–C lengths, whereas the $^2A_1$ state, with the unpaired electron in the orbital that is involved in the bonding interaction between the dehydrocarbons, prefers a short C–C length. Restricted open-shell coupled-cluster calculations reported by Sander and co-workers predict that the $^2A_1$ state has the absolute lowest energy, with a C–C bond length of 1.69 Å. Therefore, the bonding interaction in **2a** is even stronger than that in *m*-benzyne or **2c**, in which the distances between the carbon atoms are approximately 2 Å.[15,16]

Given the $^2A_1$ ground state of 1,2,3-tridehydrobenzene, the view of a triradical stabilized by a σ-allylic interaction must be refined. Instead of viewing the system as an allylic-like radical in which the electrons are delocalized through resonance, the stabilization results from delocalization of the radical through direct overlap of orbitals. At the very least, the system can be described as a *m*-benzyne compound that lacks a hydrogen atom. However, given the additional bonding interactions between the dehydrocarbons, the localized picture of bicyclic radical **5** is not unreasonable and may actually be a more accurate depiction of the interactions that are present.

5

Whereas modern theoretical methods can provide detailed descriptions of geometries and electronic structures, experimental results alone still reveal the important qualities of the bonding in a system. However, detailed experimental studies become much more challenging as the systems become more reactive. How much dissociation can occur and still produce a stable species? Remarkably, Graham and co-workers have reported the generation and isolation of the cyclic C_6 unit—benzene without hydrogen atoms.[17] Thus, it is apparently possible to strip benzene down to its simplest fragments. Undoubtedly, the exploration of the pathways that can be used to realize this species, and the intermediates accessed along the way, will continue.

[1] M. Gomberg, *J. Am. Chem. Soc.* **1900**, *12*, 757.
[2] A. Rajca, J. Wongsriratanakul, S. Rajca, *Science* **2001**, *294*, 1503.
[3] J. Berkowitz, G. B. Ellison, D. Gutman, *J. Phys. Chem.* **1994**, *98*, 2744.
[4] S. J. Blanksby, G. B. Ellison, *Acc. Chem. Res.* **2003**, *36*, 255.
[5] K. M. Ervin, S. Gronert, S. E. Barlow, M. K. Gilles, A. G. Harrison, V. M. Bierbaum, C. H. DePuy, W. C. Lineberger, G. B. Ellison, *J. Am. Chem. Soc.* **1990**, *112*, 5750.
[6] A. V. Friderichsen, J. G. Radziszewski, M. R. Nimlos, P. R. Winter, D. C. Dayton, D. E. David, G. B. Ellison, *J. Am. Chem. Soc.* **2001**, *123*, 1977.
[7] K. M. Ervin, V. F. DeTuri, *J. Phys. Chem. A* **2002**, *106*, 9947.
[8] P. G. Wenthold, R. R. Squires, *J. Am. Chem. Soc.* **1994**, *116*, 6401.
[9] P. G. Wenthold, R. R. Squires, W. C. Lineberger, *J. Am. Chem. Soc.* **1998**, *120*, 5279.
[10] J. G. Radziszewski, B. A. Hess, Jr., R. Zahradnik, *J. Am. Chem. Soc.* **1992**, *114*, 52.
[11] W. Sander, M. Exner, M. Winkler, A. Balster, A. Hjerpe, E. Kraka, D. Cremer, *J. Am. Chem. Soc.* **2002**, *124*, 13072.
[12] R. Warmuth, *Angew. Chem.* **1997**, *109*, 1406; *Angew. Chem. Int. Ed. Engl.* **1997**, *36*, 1347.
[13] H. A. Lardin, J. J. Nash, P. G. Wenthold, *J. Am. Chem. Soc.* **2002**, *124*, 12612.
[14] S. Venkataramani, M. Winkler, W. Sander, *Angew. Chem.* **2005**, *117*, 6464; *Angew. Chem. Int. Ed.* **2005**, *44*, 6306.
[15] A.-M. C. Cristian, Y. Shao, A. I. Krylov, *J. Phys. Chem. A* **2004**, *108*, 6581.
[16] M. Winkler, W. Sander, *J. Phys. Chem. A* **2001**, *105*, 10422.
[17] S. L. Wang, C. M. L. Rittby, W. R. M. Graham, *J. Chem. Phys.* **1997**, *107*, 6032.

 © 2005 Wiley-VCH Verlag GmbH & Co. KGaA, Weinheim

DOI: 10.1002/anie.200501365

Micelles

Reactions in Micellar Systems

*Torsten Dwars, Eckhard Paetzold, and Günther Oehme**

Keywords:
amphiphiles · micelles · organic reactions · polymers · tensides

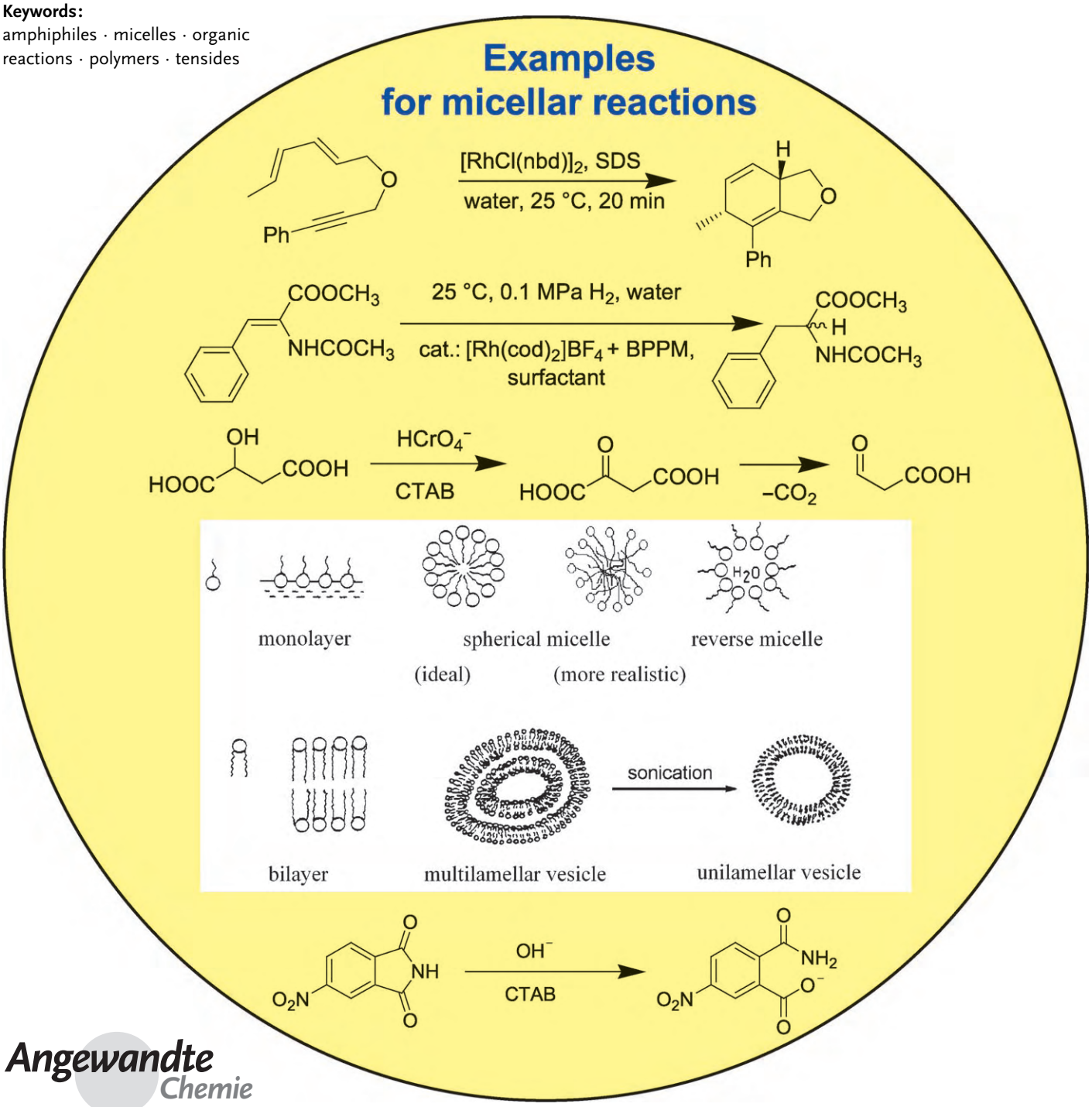

© 2005 Wiley-VCH Verlag GmbH & Co. KGaA, Weinheim

The notion of "green chemistry" has encouraged even synthetic organic chemists to include water as a solvent. Incredible selectivities and activities can be achieved through the addition of amphiphiles with a defined structure. The morphology of supramolecular assemblies or associates formed by surfactants vary according to the temperature and concentration. As a rule, reactions are typically conducted using simple spherical aggregates, that is, micelles in the nanometer range. The strong polarity gradient present between the hydrophilic surface and the hydrophobic core of the micelle means that both nonpolar and polar reagents can be solubilized. This solubilization results in reactants becoming more concentrated within the micelle than in the surrounding water phase and leads to an acceleration of the reaction and causes selective effects. The kinetic treatment of reactions in micellar systems can be accomplished by considering them as microheterogeneous two-phase systems.

From the Contents

1. Introduction and Overview 7175
2. Micelles and Related Aggregates 7175
3. Solubilization 7178
4. The Kinetics of Micellar Effects 7178
5. Reactions in Micelles 7181
6. Enantioselective Reactions 7190
7. Selected Reactions in Reverse Micelles 7191
8. Some Special Applications of Surfactants 7193
9. Summary and Conclusions 7194

1. Introduction and Overview

This Review deals with chemical reactions which take place in the presence of amphiphilic (synonym: amphipathic) compounds and are decisively affected by them under certain conditions.[1] Amphiphiles are molecules consisting of a hydrophilic head group and a hydrophobic (lipophilic) tail, and are thus able to interact with both polar and nonpolar compounds. When the hydrophobic tail reaches a certain chain length, the amphiphiles reduce the unusually high surface tension of water and are referred to as tensides (or surfactants).[2] Very practical effects are associated with this property, for example, the "detergent effect", the stabilization of emulsions and foams, and the application as an aid for dispersions. In this context we speak of detergents. These effects are caused by associates of surfactants whose form is dependent on the temperature, concentration, and molecular structure.[3] Since cohesion occurs through noncovalent forces, we speak of supramolecules or supramolecular structures.[4]

Micelles are especially simple spherical supramolecules, which are formed by amphiphiles in water or media similar to water. A micellar system appears to be homogeneous since these aggregates are of colloidal size; however, in reality the absorbed reactants are in a microheterogeneous two-phase system.[5] Micelles can cause an acceleration or inhibition of a given chemical reaction relative to the equivalent reaction in an aqueous medium. This phenomenon was recognized relatively early on and was investigated extensively, as reflected in early review articles and a monograph published in 1975.[6]

In general, the micellar effect is referred to as "micellar catalysis" when it refers to the acceleration of the rate of a reaction; this assignment is however only an approximation for a kinetic analysis.[7] It is interesting that micellar catalysis is described together with the catalysis of functionalized polymers or macromolecules in most of the older review articles. A connection with enzymatic catalysis was sought as hydrophilic and hydrophobic regions exist in both supramolecular and macromolecular structures.[8]

It is now virtually impossible to cover the entire area of catalysis in micellar systems in one review article. Work from the last 20 years in which transition metals play a catalytic role will be predominately reviewed in this article.[9] Important trends and developments will also be highlighted, and older work of fundamental importance will, however, also be included in the discussion.

2. Micelles and Related Aggregates

Some typical micelle-forming amphiphiles together with their critical micelle concentrations (CMCs) are shown in Table 1. The CMC is the lowest concentration at which spherical micelles form. The formation of micelles is characterized by an often sharp discontinuity in system properties, such as surface tension, conductivity, light scattering, self-diffusion, and the molality of dissolved compounds.[10] A prerequisite however is sufficient solubility of the amphiphile in water, the medium in which the micelles are formed. The temperature at which the concentration of the amphiphile reaches the CMC is defined as the Krafft point or Krafft

[*] Dr. T. Dwars, Dr. E. Paetzold, Prof. Dr. G. Oehme
Leibniz-Institut für Organische Katalyse (IFOK)
Universität Rostock e.V.
Albert-Einstein-Strasse 29a, 18059 Rostock (Germany)
Fax: (+49) 381-1281-5000
E-mail: guenther.oehme@gmx.de

© 2005 Wiley-VCH Verlag GmbH & Co. KGaA, Weinheim

Table 1: Typical micelle-forming surfactants and their CMC values.

Surfactant	CMC [mol L^{-1}]
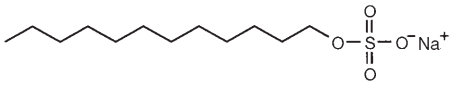	8.1×10^{-3}
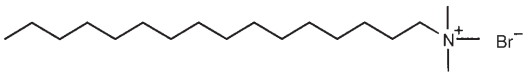	9.2×10^{-4}
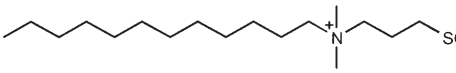	1.2×10^{-3}
	7.7×10^{-5}
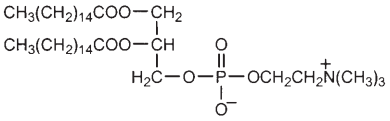	4.7×10^{-10}

temperature, and is generally associated with a sudden increase in solubility.[11]

The amphiphiles shown in Table 1 all possess a long alkyl chain, which is an important precondition for the formation of micelles. The hydrophilic head group can be cationic (tetraalkylammonium, alkyl pyridinium), anionic (alkyl sulfate, alkyl sulfonate), zwitterionic (trialkylammoniopropanesulfonate), or non-ionic (polyoxyethylenealkyl ether, alkyl glycoside). The relationship between the hydrophilic head group and the hydrophobic chain is given by the hydrophilic–lipophilic balance (HLB), which is generally calculated by increments.[12] The hydrophobic chain must have a certain length ($>C_{10}$) to enable successful micelle formation. The CMC generally drops as the chain length increases.

Amphiphiles with short alkyl chains (for example, tetrabutylammonium halides, sodium butyl sulfate) do not form micelles, but they do influence the hydrogen-bonding structure of water and are termed hydrotropes. Hydrotropes can also form associates, but these have a much smaller size than micelles.[13] An aggregation of approximately 50 monomers is typical for micelles. Perfluorinated alkyl chains represent a special type of amphiphile, which are especially hydrophobic and form micelles even with short chain lengths ($>C_8$).[14] Spherical micelles only exist in relatively dilute dispersions. The formation of "rodlike" structures occurs relatively quickly with increasing concentration, and this is then followed by hexagonal phases.[15] Some principle morphologic structures are shown in Figure 1.

A characteristic of amphiphiles with *one* long alkyl chain is that they initially form a unimolecular layer on the surface

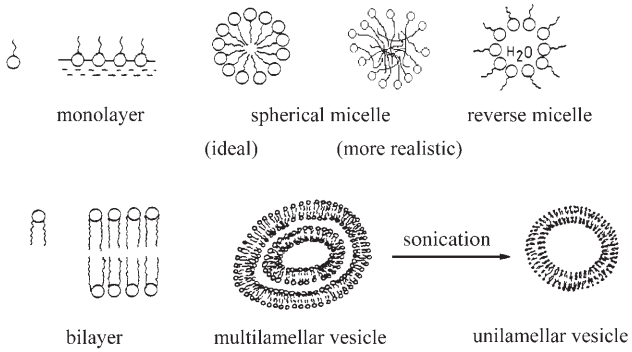

Figure 1. Schematic representation of micelles and vesicles.

of the water, that is, at the interface between water and air, through which the surface tension of the water is reduced. Micelles only form spherical aggregates upon reaching the CMC. As is to be expected, the hydrophilic head groups form the phase barrier to the water, while the hydrophobic alkyl chains orientate themselves inwards and form the core of the micelle. A frequently used representation in which the chains are arranged coaxially towards the centre of the micelle is not realistic, since this is not compatible with the geometry of the amphiphile as a whole. A more probable representation, reported by Menger,[16] is where an irregular arrangement of the chain occurs, which in principle also allows an orientation of the polarity gradient from the hydrophilic region towards the center (Figure 1).

The counterion must also be taken into account in the case of ionic surfactants. Depending on the charge density and hydrophilicity, the counterion is to be found in the immediate proximity of the micellar surface, in the so-called "Stern layer". As a rule 70–90 % of the ion pairs are located on the surface of the micelle.[17] Dissociated counterions can advance to the nearest Guy–Chapman layer. The interactions between the micelles and the counterions have been thoroughly investigated. The strongly electronegative and hydrated fluoride and hydroxide ions assume a special status as they

Torsten Dwars completed his degree in teaching mathematics and chemistry in secondary schools in 1995. He studied for his PhD between 1995 and 1999 in the research group of G. Oehme at the Institute of Organic Catalysis Research in Rostock. After spending four months in the "technical chemistry" research group of Prof. Kragl (University of Rostock), he has worked as a scientific researcher at the Institute of Organic Catalysis Research in the field of plasma polymerization of amphiphilic aggregates in aqueous media.

Eckhard Paetzold studied chemistry at the Ernst–Moritz–Arndt University of Greifswald, Germany, and obtained his PhD in 1983 under the supervision of Horst Pracejus in the former working group Complex catalysis of the Academy of Science of the GDR in Rostock. Since then he has worked as a scientific researcher at the Leibniz Institute of Organic Catalysis Research. His interests focus on C–C coupling in aqueous (micellar) phases and more recently the modification of renewable resources.

 © 2005 Wiley-VCH Verlag GmbH & Co. KGaA, Weinheim

remain in the aqueous phase. The structure and character of micelles can be influenced by exchange equilibria resulting from the addition of salts to the aqueous phase that contain ions different to those of the surfactant.

The extraordinary variety of phase behavior of amphiphiles can be found in other review articles.[18] An original proposal is contained in a monograph by Fuhrhop and Köning, in which the term "synkinone" is suggested for associative amphiphiles and the term "synkinese" is suggested for the aggregation process.[19]

Aggregations of surfactants with two long alkyl chains per head group are also shown in Figure 1. These amphiphiles form bilayers in water which unite at a given concentration to form multilamellar or unilamellar vesicles. These are bubble-like structures in which a water-containing interior is enclosed by a double-layer membrane. Such double-layer membranes are models of naturally occurring membranes in which the building blocks are lipids, and can be relatively complex structures.[20] Vesicles formed from lipids are called "liposomes".[21] The literature about the formation, structure, and application of vesicles is very extensive.[22] Knowledge about the structural requirements for the formation of vesicles has been extended considerably, especially through the introduction of so-called "bolaamphiphiles" which are alkyl chains with a head group at each end.[23] Despite their great significance for the simulation of natural processes, we will only occasionally draw comparisons to reactions in vesicles within the scope of this article. Micelles and vesicles differ not only in their structure but also in their size; while the diameter of a micelle is 3–7 nm, multilamellar vesicles have a size in the range of about 1000 nm and unilamellar vesicles in the range of about 25 nm.[24]

The formation and morphology of amphiphile aggregates in water are dependent on the balance of two opposing forces: the hydrophobic interaction between the alkyl chains and the polar repulsion between the head groups.[25] The attraction of the alkyl chains is a mainly entropic effect. Water displays a high degree of order along the alkyl chains, because more hydrogen bonds exist to neighboring water molecules than are formed in the bulk water phase. The loss of entropy is cancelled ("hydrophobic effect") through the assembly of the alkyl chains.[26] Little is known about the dispersive forces between nonbinding alkyl groups.[27] An attempt at analysis can be found in studies by Blokzijl and Engberts,[28] Evans,[29] as well as Ruelle and Kesselring.[30] The free enthalpy of formation is almost constant over a large temperature range, which shows that enthalpy–entropy compensation occurs. Associates of amphiphiles and especially micelles can be formed in solvents which have a similar polarity and hydrogen-bonding structure to water.[31]

The stability of micelles and vesicles is strongly dependent on the mobility of the alkyl chains, as shown by experiments with spirotensides and spirophospholipids.[32] The hydrated head groups, which are aligned to the interface with water, repel each other as a result of their uniform polar structure and thereby determine the curvature of the spherical micelle (Figure 2).[33]

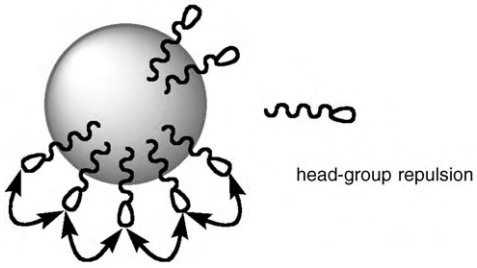

Figure 2. Principle of opposed forces during micelle formation: Repulsion between head groups and attraction between the hydrophobic chains.

The conical order of the structural units is achieved by entanglement of the alkyl chains. "Conical molecules" themselves do not exist.[19] The distance between the polar groups is larger and thus the curvature smaller in bilayers of vesicles formed from amphiphiles with two alkyl chains per head group, mainly as a consequence of compensation by polar groups on the opposite side of the bilayer.

Associates of amphiphiles are kinetically labile. Micelles are formed and decay within milliseconds, which is in general more rapid than thermally induced reactions.[34] It is thus problematic to understand the polymerization of micelles, which consist of unsaturated surfactants.[35] Vesicles containing amphiphilic bilayers are kinetically much more stable.

A wide range of new amphiphiles (surfactants) have been synthesized in recent decades to keep pace with increasing technical demands.[36] Typical aspects that have been considered include biological degradability and physiological compatibility,[37] cleavability,[38] the ability to form polymers,[39] and the photolytic formation of amphiphiles.[40] Variations were mostly incorporated into the head groups. The purity of the surfactants is often uncertain, which casts doubt on the validity of the characterization data, and extreme techniques aimed at purification have been suggested.[41]

Extensive synthetic modifications are available for vesicle-forming reagents which act as carriers for drugs and have to be recognized by certain biological targets.[42] Block copolymers of the type $(EO)_n$-$(PO)_m$-$(EO)_n$, which consist of polypropylene oxide as the hydrophobic component and polyethylene oxide as the hydrophilic component, are becoming increasingly important and are biological fairly harmless.[43] These non-ionic amphiphiles can be used for micellar

Günther Oehme studied chemistry in Köthen and Halle on the Saale and obtained his PhD with Alfred Schellenberger at the Martin-Luther University of Halle-Wittenberg in 1966. Since 1967 he has worked at the Institute of Organic Catalysis Research. He become a Professor of the Academy of Science of the GDR in 1986, and between 1987 and 1998 he was the head of the Institute in Rostock. His areas of research include asymmetric reactions in multiple-phase systems and under micellar conditions, enantiomeric analysis, photoaccelerated reactions, and C–C coupling. He received emeritus status in 2003.

© 2005 Wiley-VCH Verlag GmbH & Co. KGaA, Weinheim

reactions. In this Review, surfactants whose head group has been modified to allow them to function in a catalytic manner in a given reaction play an important role. We will discuss such "functionalized" amphiphiles individually (see Section 5).

Since both micelles and vesicles can be easily destroyed by organic solvents mixed into the water phase (lysis), the idea of stabilization through polymerization seems reasonable and would entail the transformation of a supramolecular aggregate into a macromolecule. It has been proven in numerous examples that the shape existing after polymerization is similar to that before polymerization.[44] This situation is especially true for the kinetically more stable vesicles;[45] however, encouraging results have also been obtained with micelles.[46] A further possibility is the utilization of amphiphilic polymers.[47] The systematic construction of "unimolecular" micelles (dendrimers) is synthetically time-consuming but has already yielded interesting results (see Sections 6 and 8).

3. Solubilization

Solubilization refers here to an increase in the solubility of hydrophobic compounds in water through the influence of amphiphilic molecules. We are particularly interested in solubilization in aqueous micelles, which is a prerequisite for reactions to be influenced by micelles.[48] Since a micelle possesses regions of different polarity, both polar and nonpolar reagents can be incorporated into the micelle.

This process can be described by using a pseudophase model in which water and the micelle are considered as two phases. The micelle is described in terms of the associate M of the free surfactant molecule S (Scheme 1). The additive (reactant R) can be added to this associate in a stepwise manner until the "maximum additive concentration" (MAC) of MR_m has been reached. Since the micelle as an associate is not really monodisperse, the MAC should be considered as the maximum of a Poisson distribution.[49] The MAC can rise above the CMC. The concentration of hydrophobic reactants per mole of micelle-forming surfactant increases with the chain length of the alkyl tail of the surfactant on one hand, while the MAC drops with increasing hydrophobicity of the reactant on the other hand. The CMC with non-ionic micelles of the polyoxyethylene type decreases with increasing temperature as a result of dehydration, since the surfactant becomes more hydrophobic and its solubilization capacity increases. Added salts can bring about a similar effect with ionic micelles. In this case a decrease in the CMC and an increase in micelle size occurs, since the repulsion between the head groups diminishes. A consequence of this is the expansion of the "palisade layer", the border region between the head groups and the hydrophobic chains.

$$n\,S \overset{K_n}{\rightleftharpoons} M$$

$$M + R \overset{K_1}{\rightleftharpoons} MR_1$$

$$MR_1 + R \overset{K_2}{\rightleftharpoons} MR_2$$

$$\cdots$$

$$MR_{m-1} + R \overset{K_m}{\rightleftharpoons} MR_m$$

Scheme 1. Stepwise inclusion of reactants into micelles.

The solubilizing capacity of a micelle for hydrophobic compounds can be increased by the addition of cosolvents, for example, long-chain alcohols. A microemulsion might be formed if the MAC of a component is exceeded and if a new phase comes into being. The importance of microemulsions will be covered briefly in Section 7. If the solvent effects for a given compound are known, then information about the location of the solubilized compound within the micelle can be obtained by using spectroscopic techniques. This possibility is especially true for colorants and fluorescent compounds.[50] It has been established that nonpolar compounds such as hydrocarbons are generally to be found in the hydrophobic core while semipolar and polar compounds such as alcohols, carboxylic acids, and amines are located in the palisade layer. Aromatic compounds are often found to be present in both the head-group region and the core, and can be described using equilibria.

Solubility data for gases are important for reactions with gaseous reactants. In this respect the high solubility of oxygen in fluorinated micelles is noteworthy.[51] Vesicles represent more-complex solubilizing systems than micelles since an additional water phase is present in the core, which is surrounded by a bilayer membrane and can absorb hydrophilic substances.[52] The permeability of the membrane is of great importance since vesicles (liposomes) are frequently employed as carriers of active hydrophilic substances in physiological systems. The permeability of the membrane is often increased with respect to encapsulated hydrophilic compounds by adding lipophilic compounds, through which the membranes become more fluid.[53] The encapsulation of substances in the inner water phase usually takes place during the formation of the vesicle, while solubilization of substances into the membrane from the outer water phase is possible at any time for hydrophobic or hydrophilic compounds in equilibrium. Thus, effects can be observed which are similar to those in micelles. A special role is played by vesicle membranes for separated reaction spaces, as, for example, is necessary in the simulation of photosynthesis.[54] It can also be assumed that the alkyl chains of amphiphiles in vesicle membranes are ordered in a regular fashion as in micelles, which should be advantageous for stereoselective reactions.

4. The Kinetics of Micellar Effects

Morawetz[6b] presented and discussed three typical possibilities for micellar catalysis in an earlier review:

1. A reagent is amphiphilic and forms a micelle which then changes during the reaction.
2. The interactions between reactants and the micellar surfactant influence the rate of the reaction.
3. The micelle possesses catalytically active groups and functions as a catalyst.

Almost all micellar effects can indeed be categorized into one of the above possibilities. The origin of the acceleration or inhibition of reactions in micelles will now be discussed. The feature that makes a micelle special with respect to its functioning as a micro- or nanoreactor is the proximity of extremely polar and nonpolar regions. The effect of micelles

 © 2005 Wiley-VCH Verlag GmbH & Co. KGaA, Weinheim

on reactions can, according to Brown et al.,[55] be ascribed to a combination of the following factors:

1. The dielectric constant in the micelle is lower than in water, which causes a solvent effect.
2. The transition state of the reaction can be stabilized by interaction with the polar head groups.
3. The reactants are concentrated relative to the surrounding water phase through interactions with the micelle surface or through insertion into the micelle itself, thus leading to an increased rate of bimolecular reactions. The acidity or basicity of ionic amphiphiles can be significantly higher on the surface of micelles than in the surrounding aqueous phase.

The concentration effect can be considered as dominant in many cases.

A kinetic treatment of micellar effects requires some approximations. From a purely formal approach, the Michaelis–Menten methods known from enzyme chemistry can be recognized, and many authors attempt to discern a type of enzyme mimetic. The effects observed in micelles are in general much smaller than for enzymes with respect to both the increase in reaction rate as well as the influence on reaction selectivity.

Kinetic considerations are most frequently based on the so-called pseudophase model,[56] in which the aqueous medium and the micelle are viewed as separated phases with which the substrate is in thermodynamic equilibrium [Eq. (1)]. R_W and R_M designate a reactant in the aqueous and

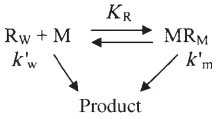

(1)

the micellar phase, respectively, M is the surfactant bound in the micelle, K_R is the equilibrium constant of the reactants between the aqueous and the micellar phases, and k'_w and k'_m are the first-order rate constants, which come from the aqueous and micellar phases and lead to product. According to the law of mass action, Equation (2) is valid for the

$$K_R = \frac{[M R_M]}{[R_M][M]} \quad (2)$$

equilibrium constant K_R. For the surfactant bound to the micelle: $[M] = [T_{total}] - CMC$. The observed rate constant can be described mathematically as Equation (3), a derivation of the Michaelis–Menten equation.

$$k_{obs.} = \frac{k'_w + k'_m K_R [M]}{1 + K_R [M]} \quad (3)$$

Kinetic measurements are usually conducted at low concentrations (ca. 10^{-4} M) to ensure the existence of only a single type of surfactant aggregate, so that the reactant does not alter the structure of the micelle. The pseudophase model only takes into account the occurrence of the reactants in two phases and gives no information about the reaction site within the micelle. Equation (3) can be used to describe so-called "spontaneous reactions" fairly convincingly. These spontaneous reactions are of first or pseudo-first order and follow condition (2), thus requiring the transport of only one reactant into the micellar phase. Examples include some decarboxylation reactions,[57] reactions in which water acts as both the reactant and catalyst,[58] and intramolecular ring-closing reactions.[59]

The distribution of the substrate between the aqueous and micellar pseudophase is strictly governed by charge and determines the micellar effects.[60] Thus, the conversion of anionic substrates into product is usually accelerated in cationic micelles, but is not influenced by anionic micelles. Hydrolysis reactions with water are frequently inhibited by micelles, as although the micelles can incorporate the substrate, the reaction takes place predominantly in the aqueous pseudophase. The acceleration of the rate of reactions by micelles is often interpreted as solvent effects.[61]

Competition of the nucleophile with the counterion of the surfactant must be taken into account in the case of a bimolecular reaction with a uncharged hydrophobic substrate and an anionic nucleophile in a cationic micelle. This is possible by the introduction of an ion-exchange equilibrium [Eq. (4); Nu^-: nucleophile, X^-: counterion]. The ionic con-

$$K_X^{Nu} = \frac{[Nu_W^-]\,[X_M^-]}{[Nu_M^-]\,[X_W^-]} \quad (4)$$

centration in the aqueous and the micellar pseudophase can be calculated using Equation (4). The underlying model is called the pseudophase ion-exchange (PIE) model.[62] An important requirement for the validity of this model is the continual coverage of the micelle surface by the counterion, which is expressed by the mole fraction β, where $\beta = 1-\alpha$ and the mole fraction α represents the free charge on the micelle surface. The value of β is dependent on both the charge and the affinity component of the counterion. A typical β value for Br^- in CTAB is for example 0.8. Comparable values are found for Cl^-, I^-, NO_3^-, and tosylate, while the extremely hydrophilic OH^- and F^- ions have β values near 0.5 and hardly compete with the ions mentioned above. A similar problem occurs with H_3O^+ and anionic micelles. A limit of the PIE model is reached here. Nucleophilic reactions conducted at low concentrations with OH^- can, however, be described satisfactorily with the model.

A formal problem encountered during the treatment of bimolecular reactions in micellar systems should be pointed out. The relationship between one of the first-order constants (k'_w or k'_m) and one of second order (k_w or k_m) can be expressed by Equation (5). The units of k_m are s^{-1}, and the units of k_w are

$$k'_w = k_w[Nu_W^-] \;\text{ or }\; k'_m = k_m \frac{[Nu_M^-]}{[M]} \quad (5)$$

$L\,mol^{-1}\,s^{-1}$ ($M^{-1}\,s^{-1}$). To achieve a comparable second-order constant for the pseudomicellar phase, the molar volume of the reaction site in the micelle V_M is introduced [Eq. (6)]. V_M

$$k_2^m = k_m V_M \quad (6)$$

© 2005 Wiley-VCH Verlag GmbH & Co. KGaA, Weinheim

has a value of between 0.14 and 0.37 $L\,mol^{-1}$.[63] The combination of Equations (3) and (5) gives an expression for bimolecular reactions [Eq. (7)]. The condition $[R] \ll [M]$ must be fulfilled. It is further assumed that a micellar reaction only takes place within one micelle and not between micelles. Only in this way is it possible to understand the typically observed dependence of k_{obs} and [M]: An increasing concentration of M in micellar accelerated reactions results in k_{obs} initially rises rapidly, going through a maximum, and then falling again, which can be interpreted as a dilution effect. In practical analyses, the values of k_{obs} are frequently based on the TON values for the productivity and TOF values for the activity of a catalyst. (see the Glossary at the end of this section).

$$k_{obs} = \frac{k_w[Nu_W^-] + k_m K_R[Nu_M^-]}{1 + K_R[M]} \quad (7)$$

The "mass action" model was developed as an alternative to the PIE model with hydrophilic ions acting as reactants.[64] The distribution of the reactive ions on the surface of the micelle is expressed by the Langmuir isotherm. As an example, Equation (8) can be generated for OH^- as a nucleophile. The counterion of the micelle can also be included in this equation. A substantial quantity of kinetic data for reactions ranging from micelle-soluble hydrophobic reactants, hydrophilic reactants bound to the surface of the micelle, to reactions run at a moderate concentration can be satisfactorily represented with the mass-action model, although a physical interpretation is hard to find.

$$K'_{Nu} = \frac{[Nu_M^-]}{[Nu_M^-]([M]-[Nu_M^-])} \quad (8)$$

A further possible description of ionic interactions is based on coulombic forces, that is, where the macro ion micelle and the counterion are considered as point charges.[65] Specific ionic interactions are initially neglected. Consideration of these specific interactions is, however, possible using a Volmer isotherm, where the spatial requirement of ions located on the micelle surface is included [Eq. (9)]. The factor f describes the mole fraction of the micelle surface that is covered by the counterion X^-, and the parameter δ contains the specific interactions between X^- and the cationic micelle surface.

$$f = \frac{\delta\exp(-f/(1-f))[X_W^-]}{1 + \delta\exp(-f/(1-f))[X_W^-]} \quad (9)$$

The coulombic interactions are described by a modified Poisson–Boltzmann expression,[66] and is thus designated a PBE model. It is assumed that micellar reactions take place within a reaction shell of diameter Δ located near the surface of the micelle. The kinetic expression obtained for the reaction of a hydrophobic reactant R with a nucleophile Nu^- is given by Equation (10). The specification of Δ is problematic, since added counterions compete with the nucleophile and thus inhibit the reaction. In contrast to the PIE model, reactions where both reactants carry charge can be described by the PBE model. However, a problem occurs if the micelle and the ionic reagent have the same charge: Although complete inhibition of the reaction might be expected, nucleophilic reactions in anionic micelles also yield a finite amount of product. An acceleration of the reaction rate is often observed when counterions are added, since free charges are no longer available on the micelle surface. This situation can be treated by using the PBE model.

$$k_{obs} = \frac{k_w[Nu_M^-] + k_2^m K_R[M][Nu_\Delta^-]}{1 + K_R[M]} \quad (10)$$

Both the PIE and PBE models describe the dependence of the rate constants on the surfactant concentration and both are only valid at high dilution. The PIE model fails to describe the situation where ions of drastically different hydrophilicity compete, while the PBE model is able to describe these situations since it is based on coulombic and specific interactions. In the PIE model the reactive volume V_M is independent of the form and size of the micelle, while in the PBE model this volume is dependent on the reaction shell diameter Δ and the micelle radius. The PBE model assumes the micelles are spherical and of uniform size.

Functional micelles containing a bound reagent (for example, the nucleophile) or a bound catalyst in the head group are of considerable interest. In this way, a high concentration of the reactant is always ensured on the surface of the micelle and a similarity to enzymatic reactions becomes apparent. This area includes metallomicelles.

It is frequently observed in bimolecular reactions that the rate constants in water and in the micelle are fairly similar, which would imply that the acceleration effect is predominantly based on concentration differences.[67] It can also be concluded that the reactions take place in the proximity of the head group, where the polarity is very similar to that of the water. It was indeed possible to achieve a small increase in the rate constants by stepwise modification of the head group from $-N^+Me_3$ to $-N^+(n\text{Bu})_3$ for a series of spontaneous reactions. Furthermore, measurement of the Hammett curve for the hydrolysis of substituted benzene sulfonates in cationic micelles led, on the basis of the ρ values, to the conclusion that the polarity in the head group can be totally different from the surrounding water.[68]

The pseudophase model can be applied to vesicles, microemulsions, and reverse micelles. Engberts and co-workers[69] found an enthalpy–entropy compensation for the decarboxylation of 6-nitrobenzeneisoxazole-3-carboxylate in micellar and vesicular media, with the highest reaction rate being observed in vesicles of low fluidity in the membrane layer (below the phase transition).

Glossary

CMC	critical micelle concentration
R_W	reactant in the aqueous phase
R_M	reactant in the micellar phase
T	tenside, surfactant
M	micelle-bound surfactant
k_{obs}	observed rate constant

 © 2005 Wiley-VCH Verlag GmbH & Co. KGaA, Weinheim

k'_w	pseudo-first-order rate constant in the aqueous phase
k'_m	pseudo-first-order rate constant in the micellar phase
K_R	equilibrium constant for reactant R between the aqueous and micellar phases
Nu^-_W	anionic nucleophile in the aqueous phase
Nu^-_M	anionic nucleophile in the micellar phase (Stern layer)
X^-_W	counterion in the aqueous phase
X^-_M	counterion in the micellar phase (Stern layer)
K^{Nu}_X	equilibrium constant for the nucleophile and counterion between the aqueous and micellar phases
k_w, k_m	second-order rate constant in the aqueous and micellar phases, respectively
k^m_2	corrected second-order rate constant for the micellar phase ($k^m_2 = k_m V_M$)
V_M	molar volume of the reaction site in the micelle
K'_{Nu}	Langmuir isotherm for a nucleophile Nu^-
f	Volmer isotherm (mole fraction of the coverage of the micelle surface by anion X^-)
δ	Volmer parameter for specific interactions between X^- and the cationic micelle surface
Δ	diameter of a reaction shell in which the micellar reaction takes place
TON	turnover number: mole conversion per mole of catalyst (measure of catalyst productivity)
TOF	turnover frequency: mole conversion per mole of catalyst per time unit (measure of catalyst activity)

5. Reactions in Micelles

In the following sections some more-recent examples of organic reactions conducted under micellar conditions are presented. Catalytic reactions have been treated preferentially. Reactions from inorganic chemistry which take place in micelles,[70] photochemical reactions in organized systems,[71] systematically constructed "artificial enzymes",[72] and the very extensive area of surfactant-influenced polymerization are not considered.[73]

5.1. Solvolyses and Metalloenzyme Models

A comprehensive summary and discussion of solvolytic reactions can be found in Ref. [63]. The solvolyses of esters and related nucleophilic reactions in micelles have been investigated extensively. Nitroaryl esters of alkane carboxylic acids and phosphoric acid, phosphonic acid, or sulfonic acid are frequently used to enable easier access to kinetic data. Selected structures of this compound class are shown in Scheme 2.

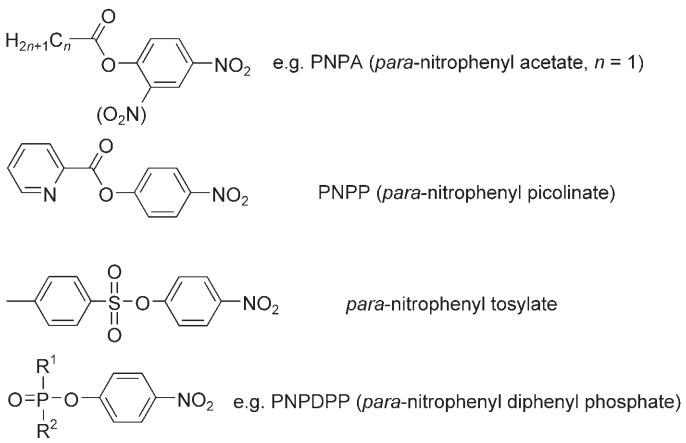

Scheme 2. Nitrophenyl esters as substrates for solvolytic reactions in a micellar medium.

Biomimetic systems, including micelles, are frequently developed to gain a more in-depth understanding of biological systems. Enzymatic and enzyme-analogous systems have a practical significance for the hydrolytic detoxification of organic compounds.[74–78] Examples of toxic organophosphorus compounds (chemical weapons) which can be detoxified by micellar systems (hydrolyzed) are shown in Scheme 3.

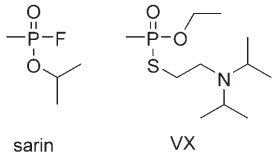

Scheme 3. Toxic organophosphonates.

Certain basic phenomena are observed time after time, although the reaction in the ionic bilayer of the aggregate, the Stern layer, competes with the reaction of the free substrate in the aqueous phase during solvolytic reactions in a micellar medium. Reactivity maxima are frequently found for substrates of a certain chain length in reactions in micellar aggregates, which leads to the conclusion that there must be an optimal reaction site for the reactions where the rate is increased the most. The proximity of the reaction partners (hydroxide ions and the carbonyl group of the ester in the case of alkaline ester hydrolysis) in the Stern layer determines the higher rate of reaction relative to that in aqueous media and thus allows the introduction of the term "micellar catalysis".[56a,63,68,79–82]

Buffers can be of great importance for solvolytic reactions in micellar systems since micelles or their constituents, surfactants, can influence the pH value at the reaction site. Buffers can also influence the CMC, number of molecules in an aggregation, or the shape of the micelle. Studies have proven that buffered aqueous micellar systems are highly complex. An exchange of the counterion for the buffer ions can occur, especially for ionic amphiphiles. The so-called "salt effect", that is, the influence of the reaction rate through the addition of an inert salt to micellar dispersions, is frequently

© 2005 Wiley-VCH Verlag GmbH & Co. KGaA, Weinheim

observed for solvolyses (hydrolyses). The salt effect is larger the lower the charge density in the palisade layer is and the more hydrophobic the ions are.[83,84]

Metal ions frequently play the role of activators in the active site of enzymes (for example, by lowering the pK_a value) for nucleophiles such as water or OH^- groups at physiological pH values. Micellar surroundings influence the complexation of the nucleophile through electrostatic effects and thus also effect the function of the nucleophile in reactions.[85] Biologically interesting metal ions display differing catalytic behavior in different micellar media. Functionalized micelles containing a bound nucleophile accelerate reactions at acyl or phosphoryl groups.[74,86–96]

In general, cationic micelles accelerate the reaction of neutral substrates with anionic reactants, for example, hydroxide ions,[46,97–101] oximate ions,[84,86,102–104] fluoride ions,[83] or thiolate ions.[105] Miller et al.[100] found that the main causes for the 16.5-fold increase in the reaction rate of the basic hydrolysis of homologous nitrophenyl esters of carboxylic acids in latices functionalized with quaternary ammonium groups was a 90000-fold increase in substrate concentration and a 10-fold increase in the hydroxide ion concentration. Boutevin et al.[46] observed a comparable effect (a 3.3-fold acceleration) with increasing degrees of polymerization in polymerized micelles formed from cationic micelle precursors.

Alkoxide ions of the type $C_{12}H_{25}O(CH_2CH_2O)_n-CH2CH2O^-$, originating from the action of hydroxide ions on non-ionic micelle precursors containing terminal hydroxy groups, accelerate the hydrolysis of phosphoryl nitrophenyl esters in non-ionic micelles and are phosphorylated. The phosphorylation is repressed in the presence of 1-chloro-2,4-dinitrobenzene, and dinitrophenyl ethers are formed (Scheme 4). Bunton and co-workers[101] asserted that the reason for this affect was the different reactivity of hydroxide and alkoxide ions to phosphoric esters at the reaction site in the palisade layer. Moreover, phosphoric nitrophenyl esters are deeply embedded in the hydrophobic region of the micelle. Chlorodinitrobenzene is, however, more hydrophilic and resides closer to the head groups in the micellar aggregate.

Work has recently been published which used micellar-accelerated ester hydrolysis to examine the influence of β-cyclodextrins on micellar systems. β-Cyclodextrin forms a complex with CTAB, but the micellar hydrolysis of esters is only influenced at high cyclodextrin concentrations.[106] Dorrego et al.[107] found during investigations into the stoichiometry of various β-cyclodextrin–surfactant complexes that micelle formation in water also does not begin after complete complexation of the cyclodextrin, but rather that normal micelle formation competes with complexation.

Some research groups investigated the effect of various metal ions on ester hydrolysis. Yu et al.[89] found, for example, that micelles formed from cationic amphiphiles inhibit metal-ion-catalyzed hydrolysis in water, while this reaction is catalyzed by anionic aggregates (for example, from SDS). The order of reactivity of $Cu^{2+} > Ni^{2+} > Zn^{2+} > Co^{2+} > La^{3+}$ in the hydrolytic reaction (Table 2) is mainly affected by the polarizability of the solvated metal ion in the micellar medium.

Table 2: Pseudo-first-order rate constants in the hydrolysis of PNPP (Scheme 2) at pH 7 and 25 °C.[89]

Amphiphile	Metal ion					
	without	Cu^{2+}	Zn^{2+}	Ni^{2+}	Co^{2+}	La^{3+}
without	0.02	16.20	0.92	1.10	0.81	0.47
CTAB	0.02	14.50	0.86	0.95	0.80	0.21
SDS	0.02	20.00	0.98	1.67	1.84	0.88
Brij 35	0.03	16.70	0.92	1.13	0.82	0.47

Huang et al.[92] observed differences in reactivity in the Cu^{2+}-catalyzed hydrolysis of PNPP and PNPA substrates (see Scheme 2) in metallomicelles, which can be explained by there being different structures. The hydrolysis of PNPA is an intermolecular reaction and the saponification of PNPP an intramolecular reaction, which can presumably be explained by the coordinative ability of the substrate to the metal ion (Cu^{2+}).

A more effective catalysis appears to be possible using metal complexes with hemilabile amphiphilic ligands (Scheme 5),[91] which promote hydrolysis by nucleophilic attack on the carboxyl group of the ester (system in Ref. [91a] (Zn^{2+}, ligand, CTAB) results in a 7000-fold acceleration). For this reason metal-ion complexes with multiple OH groups are common in hydrolytic metalloen-

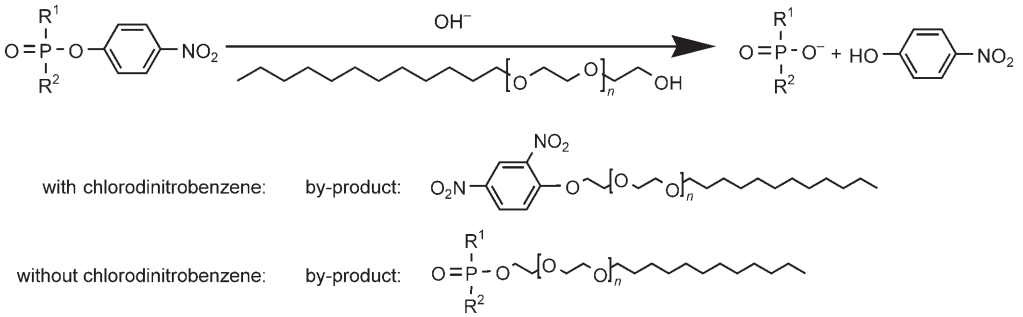

Scheme 4. Reaction of 1-chloro-2,4-dinitrobenzene and nitrophenyl esters of phosphoric acid in a basic non-ionic micellar medium.

 © 2005 Wiley-VCH Verlag GmbH & Co. KGaA, Weinheim

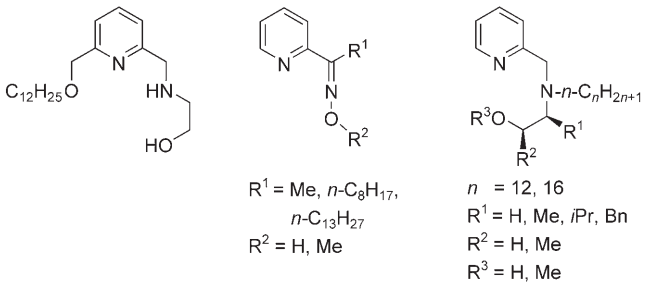

Scheme 5. Examples of hemilabile amphiphilic ligands for the formation of metallomicelles.

zyme model reactions. These groups function like metal-ion-activated nucleophiles. The positively charged Stern layer of CTAB micelles increases the electrophilicity of the metal ions with respect to the micellar-bound substrate. Furthermore, a different complexation of the metal ions in CTAB (Cu/L = 2:1) and in Brij 35 (Cu/L = 1:2) was observed (Brij 35 = polyoxyethylene(23)monolauryl ether).[93,94]

An enantioselective hydrolysis of amino acid esters has been described by You et al.[108] The highest enantioselectivity towards racemic *N*-dodecanoyl-leucine-4-nitrophenyl ester ($k_S/k_R = 3$) could be achieved with metallomicellar systems containing lipophilic L-histidinol and zinc ions.

Descriptions of solvolytic reactions in micellar systems in the literature are not just restricted to the hydrolysis of nitrophenyl esters. Khan et al. investigated the effect of salts and the addition of organic solvents on the conversion of both phthalic acid[109] (Scheme 6) and salicylic acid derivatives[110] in micelles.

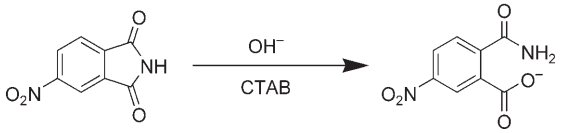

Scheme 6. Alkaline hydrolysis of phthalic acid derivatives.

An increase in the CMC and the stepwise lysis caused by the addition of organic solvents such as acetonitrile results in a reduction in the reaction rate by a factor of approximately 10. An additive (NaBr) containing the same counterion as the cationic micelle precursor (CTAB) also leads to a reduction in the rate of reaction, which can be attributed to the exchange of hydroxide ions for halide ions which cause a reduction in the concentration of the reaction partner in the Stern layer.

The maximum reaction rate was found to depend on the surfactant concentration in the reaction of dinitrochlorobenzene with hydroxide ions.[111] With increasing concentration of tetradecyltrimethylammonium bromide (TTAB), the rate of reaction also increased as a result of the solubilization of the hydrophobic substrate.

Vesicle-forming agents and their aggregates are, just like micelles, frequently utilized as models for natural membranes. The Kemp elimination depicted in Scheme 7 proceeds up to 65 times more rapidly in a vesicular bilayer of dioctadecyldimethylammonium chloride and sodium didecyl phosphate

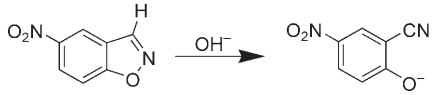

Scheme 7. Kemp elimination of 5-nitro-1,2-benzisoxazole.

than in water.[112] The maximal reaction rate observed at a particular composition is caused by the locally raised hydroxide ion concentration in the pseudophase.

The hydrolysis of benzoyl chloride and benzene sulfonyl chloride in aqueous micelles has been investigated by Bunton.[113] The micellar reactions are inhibited in anionic micelles more than in cationic micelles relative to reactions in the aqueous phase.

The acceleration in the nucleophilic substitution of nitro groups by thiols (Scheme 8) by a factor of 400000 brought about by the addition of CTAB is caused by an increased concentration of the starting material in the micelles as well as by local effects on the acid–base relationship of the nucleophilic thiolation equilibrium.[114]

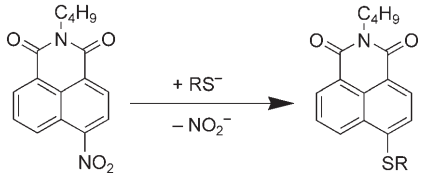

Scheme 8. Thiolytic substitution of a nitro group. R = Ph.

Iglesias[115] studied the behavior of diketones and β-keto acids in micelles in the presence of acids and bases. It was found that hydrolysis and nitrosylation compete depending on the type of surfactant used (Scheme 9). Cyclohexanone-2-

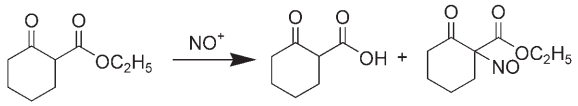

Scheme 9. Hydrolysis and nitrosylation in aqueous micelles.

carboxylic acid esters react in acidic micellar media formed from cationic (tetradecyltrimethylammonium halide, TTAX) and anionic (SDS) surfactants. While micelles of cationic surfactants inhibit the nitrosylation, this reaction is preferred to ester hydrolysis in SDS dispersions.[115,116]

The acidity of the diketo compound shown in Scheme 10 is drastically increased by stabilization of the enol form

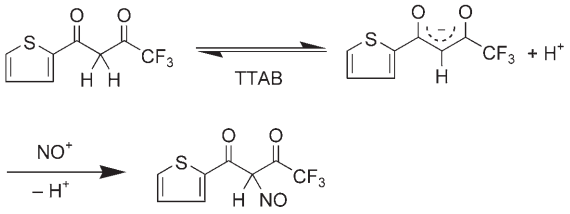

Scheme 10. Nitrosylation in a micellar medium.

 © 2005 Wiley-VCH Verlag GmbH & Co. KGaA, Weinheim

through the micellar environment, and reaction with electrophiles such as nitrosyl ions can take place up to 30 times more rapidly in the positively charged boundary layer than in water.[117]

5.2. Oxidations

Oxidations play a rather secondary role as micellar reactions. The (enzymatic) degradation of toxic organic substances in ground and drinking water is, however, of great interest,[118–120] and since organic substances normally have a low solubility in water, micellar dispersions are frequently utilized for such reactions.

In the oxidation of cyclohexane with *tert*-butylhydroperoxide in the presence of iron-containing biomimetic methane monooxygenase enzyme complexes (for example, [Fe] = $[Fe_2O(\eta^1\text{-}H_2O)(\eta^1\text{-}OAc)L_2]^{3+}$ (L = tris[(2-pyridyl)methyl]-amine),[121] the TON of the oxidation products (Scheme 11)

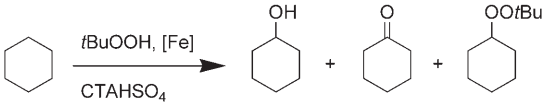

Scheme 11. Oxidation of cyclohexane in a micellar medium.

increases by a factor of 10 with increasing surfactant quantities and is directly comparable to the TON obtained in non-aqueous systems (acetonitrile as the solvent). A graph of the TON against surfactant concentration shows there is a point of inflexion after reaching the CMC of the surfactant employed.

The reaction rate of the sulfoxidation of thiols using amphiphilic hydrogen peroxycarbonate ions ($CTAHCO_4$), produced themselves through the oxidation of cetyltrimethylammonium hydrogen carbonate ions with hydrogen peroxide (Scheme 12), was increased by up to 180-fold.[122] Peroxides

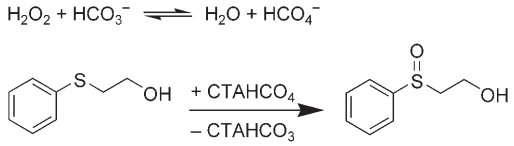

Scheme 12. Sulfoxidation with amphiphilic hydrogen peroxycarbonate ions.

produced and activated by bicarbonate in this way have been suggested for use as "green oxidants" in organic synthesis, for the decomposition of chemical weapons, and for bleaching processes.[123–125]

A different reaction behavior was observed for the sulfoxidation with water-soluble peroxomonosulfate and with the less-water-soluble *meta*-chloroperbenzoic acid (MCPBA) in water and in micellar media, respectively.[126] The increased reactivity for the oxidation of hydrophobic sulfides using hydrophobic *meta*-chloroperbenzoic acid has been accounted for by the increased concentration of the reactants in the inner region of the micelles formed from the triblock copolymer (P104) (Scheme 13). In contrast to this, the oxidation with peroxomonosulfate takes place more easily in water than in micellar systems because in micellar systems the reactants have less contact with each other because of their different solubility.

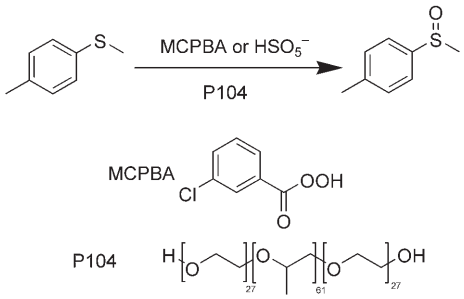

Scheme 13. Sulfoxidation with different peroxide sources.

Enzymes can also be utilized in the chemical synthesis of sulfoxides. Kadnikova and Kostic[127] found a three- to fivefold increase in the yield with enantioselectivities up to 40% for the oxidation of sulfides using hydrogen peroxide in micellar media by immobilization (encapsulation, physisorption or chemisorption, or covalent attachment to SiO_2) of microperoxidase 11.

Different catalytic activities for various micelle-forming agents could be measured in the epoxidation of styrol in micellar media using manganese porphyrinato complexes, a biomimetic system for cytochrome P450, in the presence of sodium hypochlorite as the oxidant.[128] The fact that a conversion of 90% was achieved using cetylpyridinium chloride, but only 25% with CTAB, can be explained through π interactions between the pyridinium structure and the aromatic system of the substrate in the palisade layer of the micelle. An increased aggregation number and an enhanced solubilization support this argument.

The rate of oxidation of malic acid to oxaloacetic acid or carbon dioxide and β-oxopropanoic acid with chromium or manganese catalysts (Scheme 14) could be doubled by

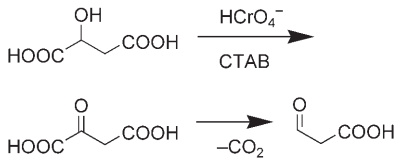

Scheme 14. Oxidation of malic acid in a micellar medium.

changing the reaction system from an aqueous to a micellar system.[129,130] Exchange of the counterion (bromide) in cationic micelle-forming agents such as CTAB for an oxidizing species such as $HCrO_4^-$ would have as a consequence a further increase in the reaction rate as a result of an increased local concentration of the anionic reactant in the Stern layer of the micelle. No such acceleration was found for anionic micelles.

 © 2005 Wiley-VCH Verlag GmbH & Co. KGaA, Weinheim

Enzymatic electron-transfer reactions are of outstanding importance in biochemistry. Comparable redox reactions conducted in micellar systems can serve as model systems for biological processes. Das et al.[131,132] found that anionic micelles accelerated and that cationic micelles formed by cetylpyridinium chloride inhibited the Cr^{VI}-catalyzed oxidation of alcohols to aldehydes, which implies the existence of a positively charged transition state.

The abstraction of an electron from phenyl hydrazine by $[Fe(CN)_6]^{3-}$ is impeded by anionic micelle-forming agents (for example, SDS).[133] The extent of the inhibition depends on the concentration of the substrate in the proximity of the micellar surface. Thus, addition of urea causes a displacement of the substrate from the Stern layer, and leads to a further retardation of the oxidation reaction.

The redox reaction of alkyl ferrocenes with glucose oxidase was investigated in different micellar environments by Ryabov et al.[134] The rate of the electron transfer is dependent on the alkyl chain of the ferrocenes and the charge of the micelle. In comparison to micelles formed from nonionic triton X-100 (octylphenoxypolyethoxyethanol), a 14-fold acceleration in the rate was observed in cationic micelles (CTAB) with *n*-butylferrocene, and a 3000-fold inhibition was observed in anionic micelles (SDS) with pentylferrocene.

Zeng and co-workers[135,136] recently described the oxidation of hydroquinone with hydrogen peroxide in a micellar system catalyzed by a transition metal (Cu, Fe, Co, and Mn). The cause of the micellar acceleration was attributed to a concentration effect as well as the electrostatic influence of the micelle-forming agent on the substrate and on the transition state.

The kinetics of the oxidation of hydroxylamine by vanadium(v) compounds has been described by Swain and Panigrahi.[137] Micelles from SDS cause a moderate acceleration in the rate of the reaction.

Polypeptides are frequently used as models for naturally occurring proteins or enzymes. The catalytic oxidation of *N*-alkyl-1,4-dihydronicotinamides was investigated in micellar media in the presence of a peptide consisting of 53 amino acids by Tomizaki et al.[138] The use of micelle-forming molecules extends the possibility of increasing the substrate concentration at the catalytic active site. The longer the alkyl chain of the surfactant, the greater the affinity for the hydrophobic substrate, through which the rate of the oxidation reaction can be increased by up to six times.

5.3. Reductions

The most commonly reported examples of reductions conducted in micellar systems include reactions of carbonyl compounds with sodium borohydride and hydrogenations of olefin double bonds with elemental hydrogen. Most of the substrates are prochiral, and thus the possibility of enantioselective reactions exists. Chirality can be induced either through optically active surfactants or through optically active hydrogenation catalysts. The classical results in optically active micelles range between two extremes. In 1978 Goldberg et al.[139] reported an induction of 1.66% *ee* for the reduction of phenyl-*n*-propylketone in micelles formed from α-phenylethyldodecyldimethylammonium bromide. In contrast, in 1988 Hui and Yang reported a spectacular enantiomeric excess of 98% for an analogous reduction of acetophenone in aqueous micelles formed from dodecyl-β-D-glucopyranoside.[140] It is conceivable that the reducing agent sodium borohydride reacts with the surfactant in an initial reaction step to form a chiral reagent, since the induction obtained with a homochiral micelle is usually small.

The low stereochemical induction might arise from the dynamic instability of the micelles. It was shown in more recent work that a considerably higher enantiomeric excess (> 50% *ee*) could be achieved for the reduction of prochiral ketones in micelle-analogous optically active dendrimers, used as models of stabilized micelles, than in corresponding supramolecular aqueous micelles or vesicles (less than 10% *ee*).[141] Cerichelli et al.[142] reduced substituted acetophenones in cationic micelles (formed from CTAB and cetyltrimethylammonizm chloride (CTAC)). Kinetic analysis of the results showed that the rate constant for the reaction in the aqueous pseudophase is considerably larger than in the micellar phase.

The regioselectivity of the reduction of α,β-unsaturated ketones with sodium borohydride was investigated by Aramini et al.[143] (Scheme 15). The authors also utilized the

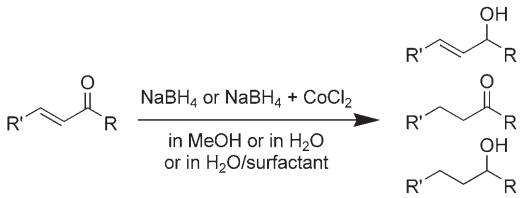

Scheme 15. Reduction of α,β-unsaturated ketones with sodium borohydride in a micellar medium.

alternative $NaBH_4 + CoCl_2$ reduction system and used MeOH, water, or water in combination with a micelle-forming surfactant. Each of the three possible products could be formed selectively depending on the choice of the system. Finally, however, only SDS and CTAB were chosen as optimal from the large number of surfactants examined. The combination of $NaBH_4 + CoCl_2$ proved to be especially favorable.

High regioselectivities were observed when α,β-unsaturated ketones were reduced in the presence of glycosidic amphiphiles. The unsaturated alcohols are formed almost exclusively with sodium borohydride. If cyclic ketones are used as starting materials, the reduction occurs amazingly stereoselectively with respect to the formation of *cis*/*trans* isomers. The enantioselectivity of the reaction was not examined.[144]

Esters have also been reduced successfully with $NaBH_4$ under cationic micellar conditions.[145] The yields were dependent on the structure of the residues R and R′ in RCOOR′ as well as on the structure of the surfactant. Especially favorable results were obtained with cetyldimethylhydroxyethylammonium bromide as the surfactant. Kinetic resolution

 © 2005 Wiley-VCH Verlag GmbH & Co. KGaA, Weinheim

was observed for racemic chiral esters when an optically active surfactant derived from L-tryptophan was employed (Scheme 16).

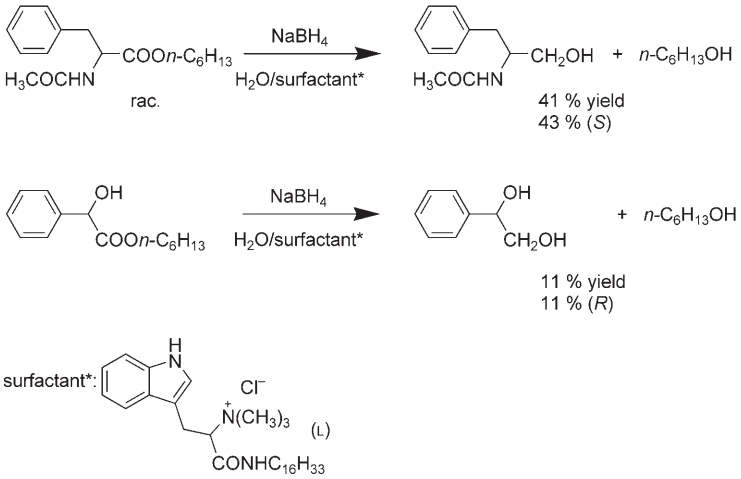

Scheme 16. Kinetic resolution using chiral surfactants.

Aqueous micelles can take on an interesting role in the homogeneous asymmetric hydrogenation of amino acid precursors. While only a stabilizing effect of the amphiphile on the catalyst system was found in earlier experiments,[146] the hydrogenation of (*Z*)-α-acetamidocinnamic acid methyl ester with an optically active rhodium–phosphane complex and in the presence of amphiphiles led to a significant increase in the activity and enantioselectivity relative to the corresponding hydrogenation conducted in pure water.[147] The effect could be observed with completely different types of surfactants, as shown in Table 3. The isolation of the product was accomplished by extraction into chloroform, while the surfactant and catalyst remained in the aqueous phase. The surfactant was present in substoichiometric quantities (20 mol%) relative to the substrate. A significant effect on the activity and enantioselectivity above the CMC implies the manifestation of a micellar effect.

Table 3: Hydrogenation of amino acid precursors in the presence of tensides.

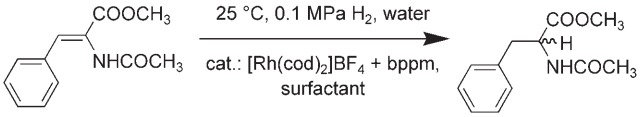

Surfactant	$t_{1/2}$ [min]	*ee* [%]
without surfactant in methanol	2	90
without surfactant in water	90	78
anionic		
sodium dodecyl sulfate (SDS)	6	94
cationic		
cetyltrimethylammonium hydrogen sulfate ($CTAHSO_4$)	5	95
zwitterionic		
N-dodecyl-*N*,*N*-dimethyl-3-ammonium-1-propanesulfonate	5	93
non-ionic		
polyoxyethylene(10)hexadecyl ether (Brij 56)	7	95

BPPM = (2*S*,4*S*)-*N*-*tert*-butyloxycarbonyl-4-diphenylphosphanyl-2-diphenylphosphanylmethylpyrrolidine.

Recycling of the catalytic system and the clean separation of the surfactant and catalyst from the product are made possible by the use of polymerized micelles,[148] amphiphilic polymers,[149] or alternatively immobilized amphiphiles.[150] Such macromolecular amphiphiles could be used in a membrane reactor.[151] Besides a series of dehydroamino acid derivatives,[152] the asymmetric hydrogenation of dehydrophosphonic acid esters[153] and dehydrophosphinic acid esters[154] could also be performed successfully. Unexpectedly high increases in the enantioselectivity were obtained in the latter cases.[155]

In the previous examples the enantioselectivity was induced by the catalyst. Only low inductions of up to 11% have been observed when nonchiral catalysts and optically active surfactants, such as derivatives of cholesterol,[156] carbohydrates,[157] and α-amino acids,[158] have been employed. The use of (D)- and (L)-prolinates as well as (D,D)-, (L,L)-, (D,L)-, and (L,D)-prolylprolinates as hydrophilic head groups have given particularly important clues about the reaction site within the micelle.[158] The transfer of chirality implies that the hydrogenation takes place in the palisade layer, that is, at the interface of the head group with the hydrophobic core.[2a] Other important hints at a intramicellar mechanism were gained from "pulsed field gradient spin echo" NMR (PGSE-NMR) measurements.[159]

The micelle-forming surfactant could be functionalized with an optically active rhodium complex at the head group. The micelles formed from this surfactant showed a rather disappointing effect at first, as the coverage of the surface with catalyst was so complete that mutual inhibition occurred. An optimal effect was only achieved in "mixed micelles", with SDS acting as an inert surfactant[160] (see also Section 6).

A CH/CD exchange occurs predominantly in the α position of the ester in the product during the hydrogenation if deuterium oxide is chosen as the medium instead of water.[161] While this exchange can be significantly increased by using a cationic micelle-forming agent, SDS acts in an inhibitory way, probably because SDS micelles are less permeable to D_2O.[162] A consequence of this is that hydrogenations in SDS micelles are less pH-dependent than hydrogenations in cationic, zwitterionic, and non-ionic micelles.[163] Mechanistically, the activation step for the hydrogenation needs to be classified differently to that of the CH/CD exchange.[164]

The kinetics of the micellar hydrogenation of (*Z*)-α-acetamidocinnamic acid methyl ester catalyzed by a rhodium complex has been investigated by Weitbrecht et al.[165] They used SDS as an anionic surfactant and marlipal O13/80 (eightfold ethoxylated C_{13} alcohol) as a non-ionic surfactant and found unambiguously that the dissociation constants of the catalyst substrate complexes under micellar conditions are considerably smaller than if methanol is used as the solvent. The insertion of hydrogen is thus clearly the rate-limiting step.

If these kinetic measurements are used to attempt to explain the previously obtained results of hydrogenations conducted in micellar media, the increase in the activity compared to the corresponding hydrogenation in water can

 © 2005 Wiley-VCH Verlag GmbH & Co. KGaA, Weinheim

be interpreted as a concentration effect: the substrate and catalyst meet in a small, confined space and form a stable initial complex. There is no reliable data about the solubility of hydrogen in micelles, but it is surely more soluble in micelles than in water. It is more difficult to interpret the sometimes spectacular micellar effects on enantioselectivity. Probably a solvent of favorable molecular order is present in the micelle.

Yonehara et al.[166] showed that a series of unsaturated substrates can be successfully hydrogenated with rhodium phosphinite complexes under micellar conditions, however the enantioselectivity was found to be strongly dependent on the structure of the substrate.

The effect of surfactants and also mixed surfactant systems on the hydride transfer of methylene blue in the leukoform to 2,5-dihydoxy-1,4-benzoquinone was studied by Zeng and co-workers.[167] Ionic micelles generally acted in an inhibitory way, while non-ionic surfactants had practically no effect, thus indicating electrostatic interactions with the charge-transfer complex.

5.4. C–C Coupling Reactions

Hydroformylation is, from an industrial viewpoint, the most important homogeneous catalyzed reaction. Over nine million tons of product are formed by hydroformylation reactions each year, from which a large portion is produced in aqueous systems.[168] Although propene can be successfully hydroformylated in an aqueous medium, this process can not be extended to higher olefins as their solubility in water is too low. Surfactants can be applied here as phase mediators and this application is discussed below.

As one of the first and stoichiometric hydroformylations in an aqueous micellar system, cyclopropene was converted in the presence of SDS and an excess of $[HMn(CO)_5]$ into approximately 90% of the corresponding aldehyde (Scheme 17).[169]

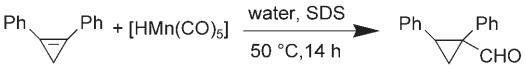

Scheme 17. Stoichiometric hydroformylation with manganese pentacarbonyl hydride.

Riisager and Hanson[170] reported the hydroformylation of 1-octene in aqueous systems where the catalyst was prepared in situ from $[Rh(CO)_2acac]$ (acac = acetylacetonate) and tris(*meta*-sulfonatophenyl)phosphane sodium salt (TPPTS) in the presence of CTAB. Intense interactions between the CTAB of the micelle and TPPTS were shown to exist by NMR experiments. Optimal concentrations were determined for the amphiphile and the ligand.

Gimenez-Pedros et al.[171] hydroformylated 1-octene and 1-decene in two-phase aqueous systems with water-soluble rhodium complexes, which contained tetrasulfonated 1,3-bis(diphenylphosphanyl)propane or 1,4-bis(diphenylphosphanyl)butane, in the presence of various surfactants. The best results were achieved with cetyltrimethylammonium hydrogen sulfate.

Li et al.[172] hydroformylated 1-dodecene with the water-soluble $[RhCl(CO)(tppts)_2]$ complex as the catalyst in the presence of various micelle-forming agents. The best results with respect to yield and regioselectivity (*n*/*iso* ratio of the aldehyde) were observed in mixed micelles from cetylpyridinium chloride with SDS, dodecyl benzenesulfonate, triton X-100, or Brij 35.

An investigation of the hydroformylation of 1-dodecene in an aqueous two-phase system in the presence of CTAB using $[RhCl(CO)(tppts)_2]$ as the catalyst precursor was conducted by Mao and co-workers.[173] They obtained impressive *n*/*iso* aldehyde selectivities (up to ca. 20:1) with moderate substrate/Rh catalyst ratios, which also showed a dependence on the speed of stirring. The authors postulated that the catalysis takes place in the phase border layer between the surface of the micelles and the water phase (Stern layer).

Li and co-workers[174] investigated the hydroformylation of 1-olefins (C_6–C_{12}) with Rh–TPPTS complexes in aqueous organic two-phase systems with CTAB as the phase mediator. Regioselectivities of 96% were achieved with respect to *n*-tridecanal at 120 °C and 20 bar CO/H_2 in the hydroformylation of 1-dodecene using [RhCl(CO)(tppts)(bisbis)] (bisbis = sodium salt of the sulfonated 2,2′-bis(diphenylphosphanylmethyl)-1,1′-biphenyl) as the catalyst in aqueous two-phase systems. The existence of larger mixed micelles is assumed and SDS was found to inhibit the reaction.

Jin and co-workers[175] investigated the hydroformylation of 1-olefins using various rhodium complexes in aqueous two-phase systems in the presence of thermoregulatable amphiphilic ligands, for example, $P[p\text{-}C_6H_4O(CH_2CH_2O)_nH]_3$. These ligands serve as catalyst-transfer reagents in organo-aqueous systems: At low temperatures (for example, room temperature) they are found in the aqueous phase, but at 120 °C they are in the organic phase. The recovery of the catalyst system is possible by cooling to room temperature. This principle was convincingly demonstrated for 1-decene, where the catalyst system was recycled 20 times without a large loss of activity or selectivity. At moderate decene/Rh ratios TONs > 19000 and TOFs of approximately 200 h^{-1} can be achieved. Initial attempts at the hydroformylation of the renewable resource oleyl alcohol resulted in internal aldehydes.[175c]

Oehme et al.[176a] found that the hydroformylation of 1-dodecene gave good conversions with rhodium complexes of the water-soluble ligands $Ph_2P(CH_2)_2S(CH_2)_2SO_3Na$ or $Ph_2P(CH_2)_2S(CH_2)_3SO_3Na$ in aqueous two-phase systems at 120 °C and 60 bar CO/H_2 with the addition of amphiphilic additives. The dodecene/Rh ratio amounted to 10000:1. For the recycling of the catalyst a TONs of approximately 50000 were found without the addition of phase-active materials and a TON of about 65000 when polyoxyalkylene triblock copolymers were used. The advantage of the triblock copolymer in comparison to low-molecular-weight surfactants is that the organic phase can be easily separated from the aqueous phase. The application of surfactants immobilized on inorganic carriers in the hydroformylation reaction was

 © 2005 Wiley-VCH Verlag GmbH & Co. KGaA, Weinheim

examined, but did not yield the activities which were hoped for.[176b]

Zarka et al.[177] prepared amphiphilic water-soluble diblock copolymers based on 2-oxazoline with *N*-heterocyclic rhodium–carbene complexes. The catalysts obtained were applied to the hydroformylation of 1-octene in aqueous two-phase systems and were able to be recycled three times, but an accompanying drastic drop in the *n*/*iso* ratio was observed. Hydroformylation in microemulsions[178] is also a possibility.

Other C–C bond-forming reactions under aqueous micellar conditions shall be discussed because of their general significance in the synthesis of organic compounds. Bassetti et al.[179] conducted Michael additions with butenone and 2,4-pentanedione in aqueous solutions in the presence of cationic surfactants. Interestingly, the two partners react in the micelles without the addition of a base.

Kobayashi et al.[180] developed water-stabile Lewis acids (for example, lanthanide triflates) as effective catalysts for aldol and related reactions in aqueous media. The conversions of numerous reactions were able to be increased by the addition of surfactants such as SDS and triton X-100 ("LASC = Lewis acid/surfactant combined catalyst"). Asymmetric aldol reactions were realized by means of various LASCs (for an example see Section 6).

An asymmetric Mukaiyama–aldol reaction in water using chiral disulfonated binapthyl dialkyl ethers (Scheme 18) with $Ga(OTf)_3$, $Sc(OTf)_3$, and $Cu(OTf)_2$ as Lewis acids which generated moderate *ee* values (< 50%) was described by Li et al.[181] The chiral amphiphile was used in an equimolar amount relative to the substrate.

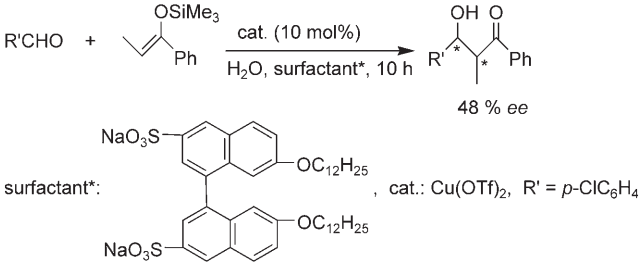

Scheme 18. Asymmetric Mukaiyama aldol synthesis by means of a chiral amphiphilic disulfonate.

The L-proline-catalyzed aldol reaction between nitrobenzaldehyde and various ketones was also investigated in aqueous anionic micelles.[182] Various micelle-forming agents were used in reactions lasting up to 120 h and SDS was found to be the most favorable detergent, which gave 87% conversion after 5 h with acetone and 40 mol% proline (Scheme 19). *Syn*/*anti* product ratios of between 93:7 and 1:1 were found when butanone, cyclopentanone, or cyclohexanone were used as the ketone. No enantiomeric excess data was given.

Otto et al.[183a] observed a millionfold increase in the rate of reaction for the Diels–Alder reactions of substituted 2-propenones with cyclopentadiene in water using a combination of Lewis acids and micellar systems. The micellar effect of SDS, CTAB, and dodecyl heptaoxyethylene ether in the

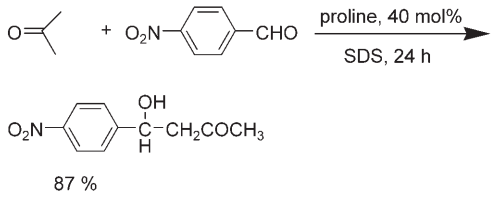

Scheme 19. Micellar aldol synthesis catalyzed by L-proline.

presence of copper and zinc bis(dodecyl sulfate) was investigated. It was shown by the same research group that these reactions take place up to 580 times more rapidly in vesicles than in micelles.[183b,c]

A phosphane-free intramolecular stereoselective [4+2] diene–yne cycloaddition in water in the presence of SDS and $[RhCl(nbd)_2]$ (nbd = norbornadiene) was reported by Motoda et al.[184] The yields were between 71 and 97% in the best cases (Scheme 20).

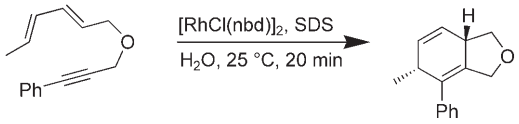

Scheme 20. Rhodium-catalyzed [4+2] diene–yne cycloaddition in SDS micelles.

Uozumi et al.[185] developed amphiphilic polysterol/polyethylene glycol resins with anchor groups for binding allylpalladium complexes. These polymer-bound amphiphilic complexes were tested in various catalytic reactions under mild conditions (room temperature) over long reaction periods (for example, Heck, Suzuki, Sonogashira, and hydroxycarbonylation reactions). Optical inductions of up to 99% *ee* were achieved in the asymmetric allyl alkylation with chiral imidazoindolphosphane anchor groups as ligands.

Three amphiphilic water-soluble diblock copolymers based on 2-oxazoline with N-heterocyclic-bound palladium carbene groups were synthesized by Nuyken and co-workers.[186] The polymer-bound complexes formed aggregates with hydrodynamic radii of 10–30 nm in water. The complexes were applied to the Heck reaction and showed TOFs of up to 570 h^{-1}. Analogously immobilized Grubbs-II metathesis catalysts were utilized for ring-forming polymerization in an aqueous medium. The catalysts could be recycled up to five times, but was accompanied by a large loss in conversion.

Oehme and co-workers[149a,176b,187] have investigated C–C coupling reactions in the presence of surfactants. The Heck, Sonogashira, and especially the Suzuki reactions between aryl halides and boronic acids were investigated with water-soluble Pd–phosphane complexes, where $[PdCl_2\{Ph_2P(CH_2)_4SO_3K\}_2]$ was employed as the catalyst precursor. Substituted iodo-, bromo-, and chloroarenes were tested as aryl halides with differently substituted boronic acids. Monomer surfactants such as CTAB and SDS are able to significantly increase the activity and selectivity of the reaction, but act as a hindrance to both the phase separation

 © 2005 Wiley-VCH Verlag GmbH & Co. KGaA, Weinheim

and product isolation. A simplification of the product separation was achieved by immobilization of the amphiphile on silica gel.[176b]

Davis and Sinou[188] have reported the ring-closing metathesis (RCM) of dienes using $[RuCl_2(PPh_3)_2(=CHPh)]$ as the catalyst in water, both with and without surfactants (Scheme 21). The substrates and catalyst were virtually

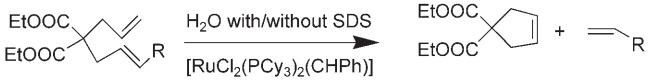

Scheme 21. Ring-closing metathesis of dienes. Cy = cyclohexyl.

insoluble in water and surfactants enabled the formation of a dispersion, with SDS being especially effective. A conversion of 51 % was obtained after one hour in the absence of an amphiphile, while the conversion was 100 % after the same time in the presence of SDS acting as an amphiphile. Surprisingly, no differences were found when R was phenyl.

Fuji et al.[189] described a Pauson–Khand reaction in a micellar system, in which the ring closure of an enyne occurs with concomitant incorporation of CO. In addition to the surfactant SDS, both tppts and diphenylphosphanylpropane (dppp) ligands are necessary in the rhodium complex to attain almost quantitative conversion (Scheme 22).

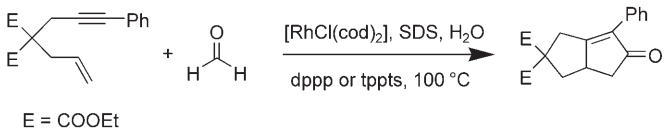

Scheme 22. Paulson–Khand reaction in a micellar system. cod = cycloocta-1,5-diene.

The asymmetric Pd-catalyzed alkylation of 1,3-diphenyl-2-propenyl acetate with C and N nucleophiles takes place in water in the presence of a surfactant, a base, and 2,2′-bis(diphenylphosphanyl)-1,1′-binaphthyl (binap) as the chiral ligand. Enantiomeric excesses of greater than 90 % were obtained when K_2CO_3 was used as the base[190] and cetyltrimethyl ammonium hydrogen sulfate as the surfactant.

The selective telomerization of 1,3-butadiene to 2,7-octadien-1-ol was investigated in micellar systems in the presence of hydrophobic and hydrophilic phosphanes as ligands for the palladium complexes (Scheme 23).[191] Activities and selectivities of the individual systems are strongly

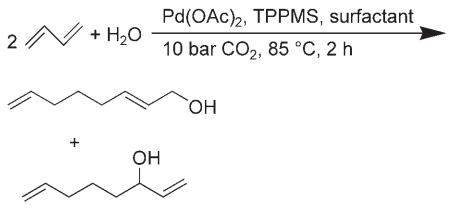

Scheme 23. Selective telomerizations in micelles.

dependent on the steric properties of the phosphane and the nature of the respective phosphane/surfactant combination. In each case the presence of CO_2 is necessary. The various phosphanes (tpp, tppms, tppts, ttpts) used in this reaction and some of the ligands cited in this Review are depicted in Scheme 24.

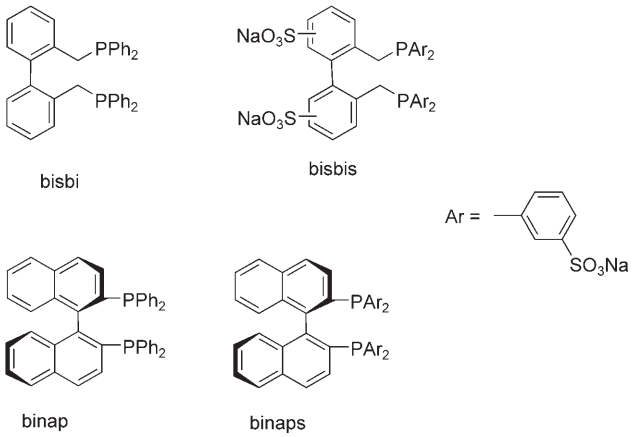

Scheme 24. Compilation of phosphanes used in complex catalysis. tpp = triphenylphosphane; dppe = diphenylphosphanylethane; dppp = diphenylphosphanylpropane; tppms = triphenylphosphane-*meta*-monosulfonate sodium salt; tppds = triphenylphosphane-di-*meta*-sulfonate sodium salt; tppts = triphenylphosphane-tri-*meta*-sulfonate sodium salt; ttpts = tri-2-tolylphosphane-tri-5-sulfonate sodium salt; dpps = diphenylphosphanylpropansulfonate sodium salt, $Ph_2P(CH_2)_3SO_3Na$; dpbs = diphenylphosphanylbutansulfonate sodium salt, $Ph_2P(CH_2)_4SO_3Na$.

5.5. Other Reactions

In a series of investigations Broxton et al.[192] examined the conversion of aryl halides into phenols in cationic micellar systems.[70] Conclusions about the CMC of the surfactant under the reaction conditions could be drawn from kinetic data. Interestingly, a variety of counterions only had a small effect. Hydroxy-functionalized surfactants of the general type $C_{16}H_{33}N^+(R_2)CH_2CH_2OH\ Br^-$ with R = Me, Et, *n*Bu[192b] proved to be particularly advantageous. Presumably the aryl halide forms an intermediary ether with the micelle, which is then cleaved by OH^- ions [Eq. (11)].

$$\begin{aligned} &C_{16}H_{33}N^+(R_2)CH_2CH_2OH\ Br^- + ArX \rightarrow \\ &C_{16}H_{33}N^+(R_2)CH_2CH_2OAr\ Br^- + OH^- \rightarrow ArOH \end{aligned} \quad (11)$$

A surprising observation was reported by Kobayashi and co-workers:[193] Typical reactions, which proceed by loss of water, for example, the formation of esters, ethers, thioethers, or dithioacetals, can be conducted with the help of 10 mol % dodecylbenzenesulfonic acid in excellent yield in water. The conversion clearly takes place in catalytic micelles formed from the sulfonic acid, from which the water formed during the reaction is lost and thus removed from the equilibrium. It can be recognized from this example that the possibility exists for "green chemistry" through the application of micellar reactions.

 © 2005 Wiley-VCH Verlag GmbH & Co. KGaA, Weinheim

The transfer of the nitroso group from *N*-methyl-*N*-nitroso-*para*-toluenesulfonamide to a series of secondary amines in various amphiphile associates (micelles, vesicles, microemulsions) was studied by Garcia-Rio et al.[194] A kinetic analysis according to the pseudophase model shows a strong dependence on the hydrophobicity of the amines and the hydrophobicity of the reaction medium. The highest activation was measured in a vesicular medium and the smallest in a micellar medium.

A stereoselective hydrosilylation of alkynes in aqueous SDS micelles was reported by Sato et al.[195] (Scheme 25). The reactions require only mild conditions (room temperature). Normally the *E* isomer is formed, but the selectivity is reversed upon addition of one equivalent of NaI and predominantly the *Z* isomer is formed.

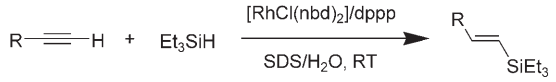

Scheme 25. Micellar hydrosilylation of alkynes.

6. Enantioselective Reactions

As has been seen during the discussion of the various reactions, enantioselective catalytic reactions can be conducted very successfully in micellar media. The stereochemical induction originates in this case from the catalyst and can be promoted by embedding it into the micelle. An interesting question is whether chirality can also be transferred from optically active surfactants in supramolecular arrays to prochiral substrates. In fact small to moderate effects have been observed for all reaction types: nucleophilic conversions, oxidations, reductions, and C–C bond-forming reactions. A summary of earlier work can be found in the reviews by Bunton and Savelli and from Kunitake and Shinkai.[67,196] Mechanistic considerations have been reported, for example, by Moss et al.[197] as well as by Ueoka et al.[198] Moss et al.[197] made the observation that alcohols formed from the nitrosation of optically active secondary amines in a micellar medium showed up to 22% retention, while inversion was predominately found for the same reaction in water—clearly water attacks the intermediate carbenium ion from various sides. The effect of the micellar medium is promoted by hydrophobic counterions such as BF_4^- or ClO_4^-, as these can occupy the back side of the carbenium ion. The problem was reinvestigated later by Brosch und Kirmse,[199] who used primary octylamine deuterated in the 1-position. Salt formation with $HClO_4$ led to a micelle-forming ammonium salt, which reacted with 90% retention in the substrate above the CMC, while 95% inversion of the configuration occurred in water.

An interesting model reaction was jointly pursued by the research groups of Ueoka[200] and Moss. As shown in Scheme 26, the *para*-nitrophenyl esters of *N*-lauroylphenylalanine were hydrolyzed under the catalytic influence of a tripeptide in aggregated amphiphiles. The hydrolysis constants for the L- and D-phenylalanine derivatives were determined separately and their ratio (k^L_{obs}/k^D_{obs}) was plotted against the mole fractions of the micelle-forming agent (CTAB or SDS or triton X-100) and the vesicle-forming agent (ditetradecyldimethylammonium bromide). Massive increases in the enantioselectivity were observed for the addition of small amounts of micelle-forming agents (for SDS 15–20 mol%). The authors ascribed this result to morphological changes in the aggregates. Thus, stepwise addition causes a transformation of the vesicular structures into a "rodlike" form. A maximum enantioselectivity was found in a pure vesicular state at a temperature above the transition point of the gel phase into the liquid-crystalline phase.

Extensive work on the hydrolysis of activated chiral amino acid esters has been conducted with so-called metallomicelles as catalysts. The head group of the surfactants contains a chiral ligand, which is coordinated with hydrolytically active metal ions such as Cu^{2+} or Zn^{2+}. The function of a metalloenzyme is thus formally approached—the enantioselectivities are, however, not yet satisfactory.[91b,201] Excellent summaries exist with respect to mechanistic considerations for the formation of intermediary diastereomeric complexes with the substrate.[61,202] In a more recent study by You et al. lipophilic L-histidinol was suggested as a ligand and complexed with a series of heavy metal ions (for example, Ni^{2+}, Co^{2+}, Mn^{2+}, Cu^{2+}, and Zn^{2+}).[108] The best activities and enantioselectivities in the hydrolysis of a *N*-lauroyl leucine-*p*-nitrophenyl ester were obtained using the zinc complex.

An amphiphilic ligand with the structure shown in Figure 3 was also developed for the hydrogenation of a prochiral dehydro-amino acid derivative.[160b] Enantioselec-

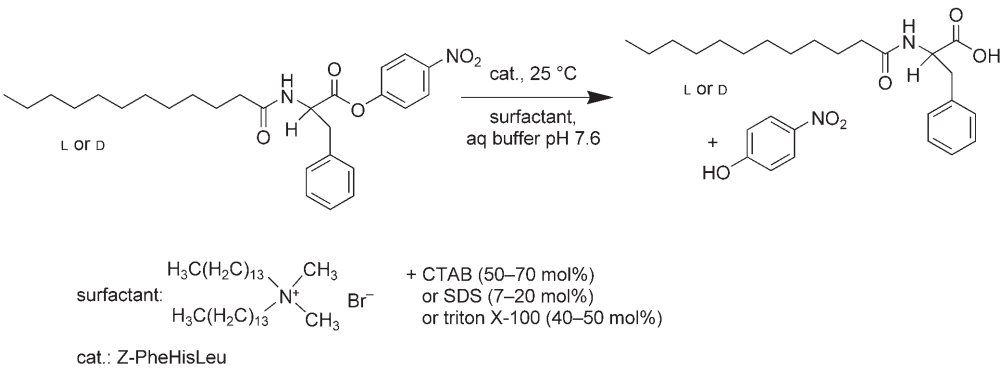

Scheme 26. Stereoselective hydrolysis of phenylalanine esters in aggregates of mixed surfactants. Z = benzyloxycarbonyl.

 © 2005 Wiley-VCH Verlag GmbH & Co. KGaA, Weinheim

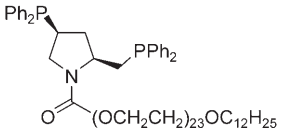

Figure 3. Chiral amphiphilic ligands for asymmetric hydrogenations.

tivities of only between 85–91 % were obtained after complexation with rhodium(I) and treatment with α-acetamidocinnamic acid methyl ester in an aqueous micellar medium. Only after addition of the SDS surfactant did the enantiomeric excess of the product increase to over 94 %.

Examples of high enantioselectivities with catalytic systems in micelles from nonfunctional surfactants were shown in Section 5.3. The micelles should be regarded here as the medium. The increase in the enantioselectivity can be dependent on the structure of the chiral rhodium complex. Thus, Selke and co-workers[159] found that seven-membered-ring chelates are considerably more effective than five- and six-membered-ring chelates. The increase in the selectivity in the transition from water to a micellar medium can be better represented by enantiomer ratio than by the enantiomeric excess *ee*.

Fundamental statements concerning the chiral induction of surfactants on enantioselective reactions were made by Rico-Lattes and co-workers.[141b] They synthesized micelle-forming and vesicle-forming surfactants with carbohydrates as optically active head groups and transferred analogous building blocks to the amino groups of third-generation dendrimers (PAMAM = poly(amidoamine)). The resulting dendrimer was morphologically similar to a micelle, but did not display their kinetic instability. While inductions of < 10 % *ee* were observed in the reaction of acetophenone with $NaBH_4$ in micelles and vesicles, 50 % *ee* was achieved in the presence of the dendrimer (unimolecular micelle), and values higher than 82 % *ee* were seen when THF was used as the solvent. It thus appears that micellar (vesicular) dynamics limit chiral induction.

Chiral inductions were also observed in C–C coupling reactions in micelles. Sinou and co-workers[190a,203] investigated the effect of various surfactants on the asymmetric alkylation of 1,3-diphenyl-2-propenyl acetate with malonic acid dimethyl ester in the presence of potassium carbonate as the base and with a palladium complex catalyst. The best results with respect to activity and selectivity (> 90 % *ee*) were attained with binap as the ligand and cetyltrimethylammonium hydrogen sulfate as the surfactant.

In an older publication, Zhang et al.[204] described the asymmetric Michael addition of nitromethane or thiophenol to chalcone (1,3-diphenylprop-2-en-1-one) in aqueous micelles of *N*-dodecyl-*N*,*N*-dimethylephedrinium bromide or *N*-hexadecyl-*N*,*N*-dimethylephedrinium bromide. The maximum enantioselectivity so obtained was 17 % *ee*.

New catalysts for the asymmetric aldol synthesis (Scheme 27) were developed by Kobayashi et al.[180b,c] by combining asymmetric-substituted Lewis acids with amphiphilic counterions. This is also a type of metallomicelle, and a principle that other authors have also adopted.[181] A short

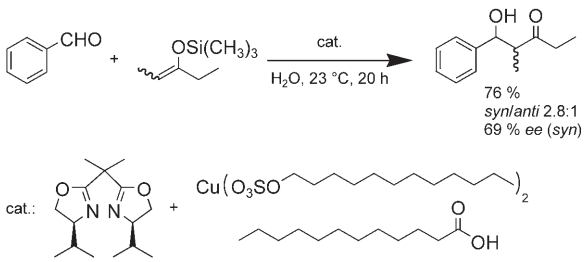

Scheme 27. Stereoselective aldol synthesis with LASC (see Section 5.4).

overview of asymmetric reactions in aqueous micelles has been written by Lindström.[205]

There are only suppositions about the mechanism of enantioselective reactions in micelles. Ueoka et al. summarized some observations, especially regarding the enantioselective cleavage of activated amino acid esters,[200] and showed that a spatial separation of the intermediate diastereomer structure should be possible, and is favored by the hydrophobicity of the medium. Since hydrogen bonds often play a role in the selection, water should, as far as possible, be excluded as a competing reagent.[206] Investigations into the structure of the chiral surfaces of micelles can be found in work by Shinitzky and Haimovitz.[207]

7. Selected Reactions in Reverse Micelles

Water is practically immiscible with nonpolar solvents under normal conditions. The addition of surfactants enables the formation of transparent dispersions, which are termed microemulsions.[208] Morphologically, they are a microheterogeneous phase distribution on a nanometer scale. Depending on the ratio of the components, a spherical ordering is observed, in which microdroplets of the nonpolar solvent are stabilized in water by the surfactant, or at the other extreme, water droplets are stabilized by surfactant molecules in nonpolar solvents. Following the formalism that is depicted in Figure 1, one speaks of a reverse micelle in the latter case, and this shall be addressed in this section.[209] Quite complicated phase relations occur between the two extremes of a spherical oil/water (o/w) and water/oil (w/o) structure which can often be modified by the addition of cosolvents. Microemulsions are very versatile solvent systems, which also play an outstanding role as reaction media. Since this is a very extensive research area, both from a physical and technical viewpoint, the reader is referred here to other review articles.[210]

Reverse micelles are complementary systems to aqueous micelles and can be divided into three phases in regard to reaction media: The aqueous core, the hydrophilic–hydrophobic interphase, and the surrounding hydrophobic medium. Water in the core displays deviating electrophilic and nucleophilic properties relative to free "bulk water" because of hydrogen bonds between the head groups of the surfactant and the counterion. Thus, the effect on reactions is often dependent on the water/surfactant (w) ratio. The surfactants

 © 2005 Wiley-VCH Verlag GmbH & Co. KGaA, Weinheim

known from the field of aqueous micelles are also in principle suited to form reverse micelles, with the sodium salt of the bis(2-ethylhexyl)ester of sulfosuccinic acid (AOT) proving to be especially suitable, probably for geometric reasons.[211] As in the case of aqueous micelles, reactions in reverse micelles are only possible at high dilution. This is not generally valid for microemulsions, which sometimes have remarkable solubilizing capacities. Examples of potential applications for reverse micelles are the decontamination of chemical weapons, as suggested by Menger and co-workers,[212] and C–C coupling with palladium catalysts, similar to those developed by Beletskaya.[213]

Typical reactions in reverse micelles include the reduction of ketones with $NaBH_4$. Zhang and Sun[214] described the reduction of a series of phenyl allyl ketones in benzene/hexanol/water systems in the presence of a chiral alkylephedrinium bromide. The highest enantioselectivity of 17.2 % *ee* was observed in the reaction shown in Scheme 28. The enantioselectivity could be increased further by the addition of D-glucose or D-fructose to the aqueous phase.

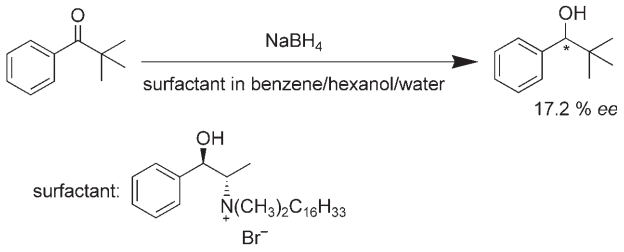

Scheme 28. Stereoselective ketone reduction in chiral reverse micelles.

The kinetics of reduction of various substituted acetophenones were investigated by Cerichelli and co-workers[215] in water/AOT/isooctane, water/AOT/toluene, water/BHDC/isooctane, and water/BHDC/toluene (BHDC = benzylhexadecyldimethylammonium chloride). While the anionic surfactant inhibits the reaction relative to free water, the cationic surfactant causes an acceleration of the reaction in the micelle. This latter result can be attributed to the interaction with the anionic reagent BH_4^-. Isooctane is a better medium than toluene. The reaction rate of the nucleophilic aromatic substitution of 2,4-dinitrofluorobenzene with piperidine, which has been conducted in water/AOT/benzene and water/BHDC/benzene in reverse micelles, was accelerated (relative to the reaction in pure benzene) only in the presence of a cationic surfactant.[216]

Ghosh and Tiwary[217] found a clear dependence of the rate constants on the ratio [water]/[AOT] (w) in the hydrolysis of salicylhydroxamic acid in water/AOT/isooctane. A maximum occurred at $w = 12.3$, which according to the authors shows that water not bound to the head groups is involved in the rate-determining step.

The solvolysis of various benzoyl halides in water/AOT/isooctane was investigated by Garcia-Rio et al.[218] With increasing values of w, a limiting value of $\log k$ was quickly reached, which was however still below that in pure water. The hydrolysis probably occurs in reverse micelles predominately through an associative mechanism (Scheme 29), which is favored by the increased nucleophilicity of the water bound to the surfactant. A high negative activation entropy supports this hypothesis.

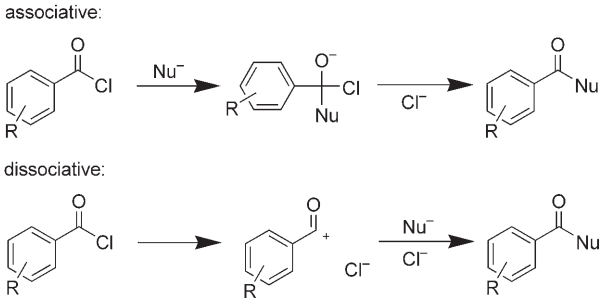

Scheme 29. Solvolysis of benzoyl halides in reverse micelles.

A clear acceleration of the imidazole-catalyzed hydrolysis of acetylsalicylic acid was found by Shervani and Ikushima[219] in a water/AOT/sc-ethane (sc = supercritical) system. The largest acceleration of the reaction rate occurred at low water contents ($w = 1$). Supercritical systems are especially suited for the isolation of products. In this way the oxidation of toluene to benzoic acid was successfully achieved in water using oxygen from the air as the oxidant and cobalt bromide as the catalyst in supercritical CO_2 and with various fluorinated surfactants; oxygen is very soluble in this reaction mixture.[220]

A kinetic analysis of the properties of water in the core of water/AOT/isooctane reverse micelles was attempted by Ruasse et al.[221] by means of the electrophilic bromination of alkenes. Water can display an increased H-donor ability of up to 65 times in the core of the micelles, relative to normal water, as a consequence of interactions with the surfactant. This makes the removal of the bromide ion easier, as shown by the transition state in Figure 4.

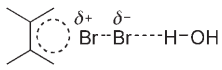

Figure 4. Probable transition state during the bromination of alkenes in reverse micelles.

Water catalysis in reverse micelles is much more intensive than in water itself. Some of the best results in reverse micelles were obtained by Elsevier and co-workers[222] for regioselective C–H activation by means of a sodium tetrachloroplatinate catalyst in a D_2O/AOT/methylcyclohexane or D_2O/AOT/*n*-heptane system. CH/CD exchange was found only in the methyl group of the nonpolar solvent under mild conditions (80 °C).

An example of enantioselective sulfoxidation in reverse micelles was described by Tohma et al.[223] Quantitative yields and enantioselectivities up to 72 % *ee* were possible using iodoxybenzene as the oxidizing agent and a tartaric acid derivative as the source of chirality in a water/CTAB/toluene system without the presence of metal.

Reverse micelles have an important significance in the preparation of monodisperse organic latices as well as in the preparation of other nanomaterials. Dadyburjor et al.[224] described the synthesis of an iron sulfide catalyst for coal

 © 2005 Wiley-VCH Verlag GmbH & Co. KGaA, Weinheim

hydrogenation, and Hong et al.[225] reported TiO_2/SiO_2 nanoparticles having an increased photoactivity with respect to the decomposition of *para*-nitrophenol.

It is possible to disperse a series of enzymes in a predominantly organic medium by using reverse micelles, thus enabling substrates not soluble in water to be used.[226] New types of reactions are favored by the special structure of the water within the micelle,[227] which can lead to acidity and basicity gradients located close together.

Two introductory review articles by Sanchez-Ferrer and Garcia-Carmona[228] and by Holmberg[229] should be cited from the extensive literature. In the first review, reverse micelles are compared with reverse vesicles, which were uniquely described for the first time in 1991.[230] The application of reverse micelles in biocatalysis is limited by their capacity. The enzymatic esterification using a lipase in a "microaqueous" two-phase and a reverse micellar media were compared in a "strategic study" by Borzeix et al.[231] and shows that the solubilization ability of the micelle appears to be too small.

While aqueous micelles form and dissociate very rapidly, the dynamics of reverse micelles are total different: Collisions, fusions, and subsequent separations can occur.[228] A reverse micelle stabilized by polymerization was reported relatively recently, although the formation and dissociation takes place more slowly than with aqueous micelles.[232] A certain permeability for small molecules evidently remains, so that application to catalytic reactions appears to be possible.

8. Some Special Applications of Surfactants

The term micellar autocatalysis can be traced back to the observation that nonlinear behavior occurs in the two-phase basic hydrolysis of ethyl octanoate: The reaction proceeds very slowly at first and then suddenly approaches completion at a high rate.[233] Since the alkali-metal octanoate is a micelle-forming agent and the increase in the reaction rate only takes place above the CMC, it is postulated that the two-phase saponification is displaced by an intramicellar reaction. An argument against this postulate is that the OH^- ions required as reactants can hardly penetrate the anionic surface of the micelle. Micheau and co-workers[234] developed a mechanism in which the octanoate micelles assume a phase-transfer function and transport ester molecules into the aqueous phase. The mechanistic work is discussed in a review.[235] A comparable effect was noticed in the hydrolysis of benzoic acid esters. It is known that alkali-metal benzoates form layer associations with benzoic acid esters and that they are able to assume a transport function.[236] A further self-replicating micellar system, the autocatalytic formation of dodecyl dimethylamine-*N*-oxide, was reported by Kust and Rathman.[237]

Battal and Rathman also investigated two-phase systems, for example, the alkylation of phenolate with *n*-bromobutane. The conversion into product in this reaction was considerably increased by the addition of a cationic surfactant (CTAB), with the reaction taking on the character of a micellar reaction. The addition of a typical phase-transfer reagent (tetrabutylammonium bromide) resulted in the rate of the reaction increasing still further and the reaction progression becoming nonlinear.[238] The authors interpret the acceleration as being based on facilitated transport of the reactants into the micelle and speak of a micellar phase-transfer catalysis (MPTC). No explanation has yet been found for the nonlinear course of the reaction.

Micelle-forming surfactants have proven to be considerably better as phase-transfer reagents than the more usual short-chain amphiphiles in some two-phase systems. This observation has been interpreted in terms of the transfer function of the surfactant *and* a micelle reaction.[182a,239] The effect is a lot smaller with polymerized micelles, since transport from the organic phase into the micelle is inhibited.

In addition to micelles, vesicles, and microemulsions, other associates of amphiphiles can exert an influence on reactions. As the simplest model, monolayers or bilayers of amphiphiles should be mentioned here. These are formed on the surface of water and are strictly ordered by their alignment (head group aligned to the water, hydrophobic chain aligned to the air). The order and pressure can be influenced through compression of the film. Such Langmuir films have been transferred to glass surfaces and have been employed as Langmuir–Blodgett films for reactions.[240]

Only a few selected studies will be cited here, which are however representative of a larger number of investigations. Miyasaka et al.[241] found that amphiphilic amino acid esters spontaneously condense to give a polypeptide monolayer in a Langmuir film. Mingotaud and co-workers[242] reported that the epoxidation of (*E*)-cinnamic alcohol in a Langmuir film of an amphiphilic manganese–salen complex was strongly dependent on the pressure applied to the film. Milstein and co-workers[243] prepared a Langmuir–Blodgett film from an amphiphilic rhodium–2,2′-dipyridyl complex, and found considerably higher conversions in the hydrogenation of ketones and aldehydes were achieved than is possible in homogeneous media.

Amphiphile layers can be immobilized onto organic or inorganic polymers under certain conditions to give fixed micelle membranes. In the simplest case, surfactants can be adsorbed on Al_2O_3 or SiO_2 surfaces to give "admicelles", which have been successfully applied as reaction media.[244] Moreover, there is a series of proposals of how to bind thin, unimolecular surfactant layers on carriers.[55,150a,b,176b,245] Some of these proposals are outlined in Scheme 30.

These immobilized surfactants can successfully take on the function of micelles in hydrogenation reactions with hydrogen, in oxidations with oxygen, and even in Suzuki reactions, and then can be simply recycled by filtration. In the case of hydrogenation, for example, the optically active rhodium catalyst remained solubilized in the surfactant layer. After 10 cycles the enantioselectivities were still high, but the activity clearly diminished.[150a,b]

The stabilization of micelles formed from unsaturated surfactants by polymerization has already been mentioned several times. In addition to conventional polymerization methods, a polymerization by exposure to low-temperature plasma was suggested.[246] An important addition are "unimolecular micelles", which are systematically constructed

 © 2005 Wiley-VCH Verlag GmbH & Co. KGaA, Weinheim

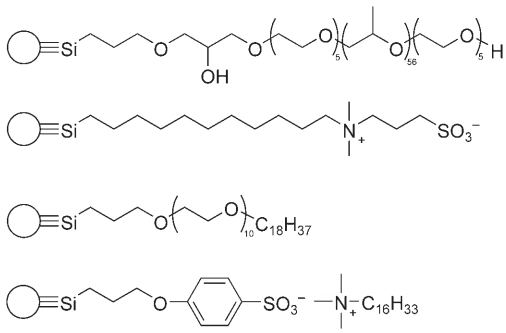

Scheme 30. Examples of immobilized amphiphiles.

dendrimers with hydrophilic interfaces.[247] Micelle-analogous dendrimer micelles and polymerized micelles might be superior because of their dynamic stability and internal regularity. A prerequisite for stereoselectivity has already been mentioned in Section 6. The work from the research group of van Koten[248] should be mentioned here because of its high potential in catalysis.

Dendrimer chemistry is extremely versatile and also plays an important role in the preparation of nanomaterials, but in comparison to micellar chemistry is elaborate and synthetically time consuming.[249] A comparable role is played by amphiphilic star-shaped polymers, which are used in the field of nanomaterials.[250] The application of amphiphilic polymers in micellar chemistry is becoming ever more significant, in that macromolecules are used as carriers for reactions in membrane reactors and colloids for the preparation of nanomaterials. The use in catalysis has been pointed out at various places in this Review. A more recent study by Zarka et al.[251] in which a new type of block copolymer was used in the asymmetric hydrogenation of an amino acid precursors is cited here as a representative example. The preparation of an oxidation catalyst through the combination of a functionalized amphiphilic polymer with an inorganic carrier also appears to be of interest.[252] A recent review article covers the synthesis and micellar properties of block polymers.[253]

The development of the field of nanoparticles has resulted in amphiphilic and dendrimetric systems becoming of outstanding significance, both in terms of their synthesis and application. In the simplest case, monomeric surfactants are used as aggregates.[254] Of increasing significance are micelles formed from polymers, whose hydrophilic core is removable and whose spherical shape is stabilized by polymerization ("shell cross-linked micelles").[255]

As examples of catalysis with metal nanoparticles stabilized by amphiphiles, polymeric micelles, or dendrimers are arene hydrogenation,[256] alkene hydrogenation,[257] as well as dehalogenation[258] and C–C coupling.[259]

Finally it should be pointed out that surfactants, surfactant polymers, and dendrimers as templates are of great significance for modern mesoporous materials.[260] A review about the template synthesis of porous organic polymers has been written by Hentze and Antonietti.[261]

9. Summary and Conclusions

The present Review should demonstrate that surfactant associates considerably extend organic chemistry in water and lead to notable effects on the rate of reaction and the selectivity of reactions. In general, this is only true for high dilution and low concentrations, but there are examples where surfactants can be used in substoichiometric quantities with respect to the substrate, for example, in enantioselective hydrogenation or in aldol condensations. Despite the original results, "micellar catalysis" is only occasionally employed above a laboratory scale. It does, however, have a firm place in kinetic analytical processes.[262] Likewise, there are uses in medical diagnostics and in cosmetics,[263] and surfactants play a large technical role in emulsion polymerization.[264] The combination of surfactants with classical phase-transfer reagents might extend the field of phase-transfer reactions and micellar reactions.

The limited applicability to organic chemistry has its origin in the problematic work-up of the reactions, since separation of the aqueous and organic phases is difficult. New perspectives are emerging from the development of polymers and polymer-bound amphiphiles. Attempts at immobilizing surfactants have stimulated three-phase catalysis, as described by Regen.[265] Above all, amphiphilic block copolymers—which have been prepared in many variations—should be highlighted.[266] Functionalization of such macromolecules opens the way to their use as catalysts in membrane reactors. Competing with this, however, is the use of dendrimers possessing an amphiphilic structure (unimolecular micelles).

The significance of aggregated surfactants in photochemistry and for the solubilization of enzymes in organic media should also be pointed out. It can also be expected that the use of surfactants will in some way be inevitable in such technically important reactions as the hydroformylation of higher olefins in aqueous systems.

We would like to thank Professor Matthias Beller for both stimulating and supporting our work. We also thank our coworkers cited in this Review.

Received: April 20, 2005
Translated by Dr. Martin Hateley

[1] S. Taşcioğlu, *Tetrahedron* **1996**, *52*, 11113.
[2] a) M. J. Rosen, *Surfactants and Interfacial Phenomena*, Wiley, New York, 2nd ed., **1989**; b) D. F. Evans, H. Wennerström, *The Colloidal Domain. Where Physics, Chemistry, Biology, and Technology Meet*, VCH, New York, **1994**.
[3] a) U. Pfüller, *Mizellen, Vesikel, Mikroemulsionen*, VEB Volk und Gesundheit, Berlin, **1986**; b) F. M. Menger, *Angew. Chem.* **1991**, *103*, 1104; *Angew. Chem. Int. Ed. Engl.* **1991**, *30*, 1086.
[4] a) F. Vögtle, *Supramolekulare Chemie*, Teubner, Stuttgart, **1992**; b) J.-M. Lehn, *Supramolecular Chemistry*, VCH, Weinheim, **1995**.
[5] *Kinetics and Catalysis in Microheterogeneous Systems*, (Eds.: M. Grätzel, K. Kalyanasundaram), Marcel Dekker, New York, **1991**.

 © 2005 Wiley-VCH Verlag GmbH & Co. KGaA, Weinheim

[6] a) J. H. Fendler, E. J. Fendler, *Catalysis in Micellar and Macromolecular Systems*, Academic Press, New York, **1975**; b) H. Morawetz, *Adv. Catal.* **1969**, *20*, 341.
[7] P. Scrimin, P. Tecilla, U. Tonellato, C. A. Bunton, *Colloids Surf. A* **1998**, *144*, 71.
[8] a) H. Ringsdorf, B. Schlarb, J. Venzmer, *Angew. Chem.* **1988**, *100*, 117; *Angew. Chem. Int. Ed. Engl.* **1988**, *27*, 113; b) B. Jönsson, B. Lindman, K. Holmberg, B. Kronberg, *Surfactants and Polymers in Aqueous Solution*, Wiley, Chichester, **1999**.
[9] G. Oehme in *Aqueous-Phase Organometallic Catalysis*, (Eds.: B. Cornils, W. A. Herrmann), 2nd ed., Wiley-VCH, Weinheim, **2004**, p. 256.
[10] N. M. van Os, J. R. Haak, L. A. M. Rupert, *Physico-Chemical Properties of Selected Anionic, Cationic, and Nonionic Surfactants*, Elsevier, Amsterdam, **1993**.
[11] J. H. Clint, *Surfactant Aggregation*, Blackie, Glasgow, **1992**, p. 148.
[12] D. Myers, *Surfactant Science and Technology*, 2nd ed., VCH, Weinheim, **1992**, p. 233.
[13] N. J. Buurma, M. J. Blandamer, J. B. F. N. Engberts, *Adv. Synth. Catal.* **2002**, *344*, 413.
[14] a) O. J. Rojas, L. Macakova, E. Blomberg, A. Emmer, P. M. Claesson, *Langmuir* **2002**, *18*, 8085; b) E. Kissa, *Fluorinated Surfactants: Synthesis, Properties Applications*, Marcel Dekker, New York, **1994**.
[15] Y. Moroi, *Micelles. Theoretical and Applied Aspects*, Plenum, New York, **1992**, p. 66.
[16] F. M. Menger, *Acc. Chem. Res.* **1979**, *12*, 111.
[17] C. A. Bunton, F. Nome, F. H. Quina, L. S. Romsted, *Acc. Chem. Res.* **1991**, *24*, 357.
[18] T. Kunitake, *Angew. Chem.* **1992**, *104*, 692; *Angew. Chem. Int. Ed. Engl.* **1992**, *31*, 709.
[19] J.-H. Fuhrhop, J. Köning, *Membranes and Molecular Assemblies: The Synkinetic Approach*, The Royal Society of Chemistry, Cambridge, **1994**.
[20] J.-H. Fuhrhop, *Bio-organische Chemie*, Thieme, Stuttgart, **1982**, p. 181.
[21] a) D. Arndt, I. Fichtner, *Liposomen. Darstellung-Eigenschaften-Anwendung*, Akademie-Verlag, Berlin, **1986**; *Handbook of Nonmedical Applications of Liposomes, Model for Biological Phenomena, Vol. II* (Eds.: B. Yechezkel, D. D. Lasic), CRC, Boca Raton, **1996**.
[22] J. H. Fendler, *Membrane Mimetic Chemistry*, Wiley, New York, **1982**, Chap. 6.
[23] a) R. Nagarajan, *Chem. Eng. Commun.* **1987**, *55*, 251; b) J.-H. Fuhrhop, J. Mathieu, *Angew. Chem.* **1984**, *96*, 124; *Angew. Chem. Int. Ed. Engl.* **1984**, *23*, 100.
[24] U. Pfüller, *Mizellen, Vesikel, Mikroemulsionen*, VEB Volk und Gesundheit, Berlin, **1986**, p. 57, 64.
[25] J. N. Israelachvili, *Intermolecular and Surface Forces*, 2nd ed., Academic Press, London, **1992**, Chap. 17.
[26] C. Tanford, *The Hydrophobic Effect: Formation of Micelles and Biological Membranes*, 2nd ed., Wiley, New York, **1980**.
[27] J. N. Israelachvih, *Intermolecular and Surface Forces*, 2nd ed., Academic Press, London, **1992**, Chap. 18.
[28] W. Blokzijl, J. B. F. N. Engberts, *Angew. Chem.* **1993**, *105*, 1610; *Angew. Chem. Int. Ed. Engl.* **1993**, *32*, 1545.
[29] D. F. Evans, *Langmuir* **1998**, *14*, 3.
[30] P. Ruelle, U. W. Kesselring, *J. Pharm. Sci.* **1998**, *87*, 987.
[31] a) M. S. Akhter, S. M. Alawi, *Colloids Surf. A* **2003**, *219*, 281; b) M. S. Akhter, S. M. Alawi, *Colloids Surf. A* **2000**, *173*, 95; c) M. S. Akhter, *Colloids Surf. A* **1999**, *150*, 25.
[32] F. M. Menger, J. Ding, *Angew. Chem.* **1996**, *108*, 2266; *Angew. Chem. Int. Ed. Engl.* **1996**, *35*, 2137.
[33] J. N. Israelachvili, *Intermolecular and Surface Forces*, 2nd ed., Academic Press, London, **1992**, p. 368.
[34] J. H. Fendler, *Membrane Mimetic Chemistry*, Wiley, New York, **1982**, p. 25.
[35] a) S. Hamid, D. Sherrington, *J. Chem. Soc. Chem. Commun.* **1986**, 937; b) K. Nagai, H.-G. Elias, *Macromol. Chem.* **1987**, *188*, 1095.
[36] *Novel Surfactants. Preparation, Applications, Biodegradability* (Ed.: K. Holmberg), Marcel Dekker, New York, **1998**.
[37] a) D. W. P. M. Löwik, J. C. M. van Hest, *Chem. Soc. Rev.* **2004**, *33*, 234; b) W. von Rybinski, K. Hill in *Novel Surfactants. Preparation, Applications, Biodegradability* (Ed.: K. Holmberg), Marcel Dekker, New York, **1998**, p. 32; c) M. Svensson in *Novel Surfactants. Preparation, Applications, Biodegradability* (Ed.: K. Holmberg), Marcel Dekker, New York, **1998**, p. 180; d) R. Infante, L. Pérez, A. Pinazo in *Novel Surfactants. Preparation, Applications, Biodegradability* (Ed.: K. Holmberg), Marcel Dekker, New York, **1998**, p. 90; e) R. Miethchen, D. Peters, *Wiss. Z. Wilhelm-Pieck-Univ. Rostock, Naturwiss. Reihe* **1987**, *37*, 55.
[38] K. Holmberg in *Novel Surfactants. Preparation, Applications, Biodegradability* (Ed.: K. Holmberg), Marcel Dekker, New York, **1998**, p. 333.
[39] A. Guyot in *Novel Surfactants. Preparation, Applications, Biodegradability* (Ed.: K. Holmberg), Marcel Dekker, New York, **1998**, p. 301.
[40] A. Veronese, N. Berclaz, P. L. Luisi, *J. Phys. Chem. B* **1998**, *102*, 7078.
[41] K. Lunkenheimer, G. Wienskol, A. J. Prosser, *Langmuir* **2004**, *20*, 5738.
[42] See Ref. [8a], p. 121.
[43] a) *Nonionic Surfactants. Polyoxyalkylene Block Copolymers* (Ed.: V. M. Nace), Marcel Dekker, New York, **1996**; b) P. Alexandridis, *Curr. Opin. Colloid Interface Sci.* **1996**, *1*, 490.
[44] a) H. Bader, K. Dorn, B. Hupfer, H. Ringsdorf, *Adv. Polym. Sci.* **1985**, *64*, 1; b) *Polymerization in Organized Media* (Ed.: C. M. Paleos), Gordon and Breach, Philadelphia, **1992**.
[45] A. Singh, J. M. Schnur in *Phospholipids Handbook* (Ed.: G. Cevc), Marcel Dekker, New York, **1993**, p. 233.
[46] B. Boutevin, J.-J. Robin, B. Boyer, G. Lamaty, A. Leydet, J.-P. Roque, O. Senhaji, *New J. Chem.* **1996**, *20*, 137.
[47] A. Laschewsky, *Adv. Polym. Sci.* **1995**, *124*, 2.
[48] *Solubilization in Surfactant Aggregates* (Eds.: S. D. Christian, J. E. Scamehorn), Marcel Dekker, New York, **1995**.
[49] Y. Moroi, *Micelles. Theoretical and Applied Aspects*, Plenum, New York, **1992**, p. 167.
[50] M. J. Rosen, *Surfactants and Interfacial Phenomena*, Wiley, New York, 2nd ed., **1989**, p. 172.
[51] A. D. King, Jr. in *Solubilization in Surfactant Aggregates* (Eds.: S. D. Christian, J. E. Scamehorn), Marcel Dekker, New York, **1995**, p. 35.
[52] M. Abe, H. Yamauchi, K. Ogino in *Solubilization in Surfactant Aggregates* (Eds.: S. D. Christian, J. E. Scamehorn), Marcel Dekker, New York, **1995**, p. 333.
[53] M. Abe, Y. Takao, T. Yamamoto, K. O. Kwon, H. Yamauchi, K. Ogino, *J. Jpn. Oil Chem. Soc.* **1992**, *41*, 404.
[54] J. H. Fendler, *Chem. Rev.* **1987**, *87*, 877.
[55] J. M. Brown, S. K. Baker, A. Colens, J. R. Darwent in *Enzymic and Non-enzymic Catalysis* (Eds.: P. Dunnill, A. Wiseman, N. Blakebrough), Horwood, Chichester, **1980**, p. 111.
[56] a) F. M. Menger, C. E. Portnoy, *J. Am. Chem. Soc.* **1967**, *89*, 4698; b) E. J. Fendler, J. H. Fendler, *Adv. Phys. Org. Chem.* **1970**, *8*, 271.
[57] a) D. S. Paul, K. G. Kemp, *J. Am. Chem. Soc.* **1975**, *97*, 7305; b) R. Germani, P. P. Ponti, T. Romeo, G. Savelli, N. Spredi, G. Cerichelli, L. Luchetti, G. Mancini, C. A. Bunton, *J. Phys. Org. Chem.* **1989**, *2*, 553.
[58] a) F. Del Rosso, A. Bartoletti, P. Di Profio, R. Germani, G. Savelli, A. Blaskó, C. A. Bunton, *J. Chem. Soc. Perkin Trans. 2*

 © 2005 Wiley-VCH Verlag GmbH & Co. KGaA, Weinheim

1995, 673; b) C. A. Bunton, E. L. Dorwin, G. Savelli, V. C. Si, *Recl. Trav. Chim. Pays-Bas* **1990**, *109*, 64.
[59] G. Cerichelli, L. Luchetti, G. Manchini, M. N. Muzzioli, R. Germani, P. P. Ponti, N. Spreti, G. Savelli, *J. Chem. Soc. Perkin Trans. 2* **1989**, 1081.
[60] C. A. Bunton in *Kinetics and Catalysis in Microheterogeneous Systems* (Eds.: M. Grätzel, K. Kalanasundaram), Marcel Dekker, New York, **1991**, p. 13, particularly p. 18.
[61] P. Scrimin in *Supramolecular Control of Structure and Reactivity, Vol. III* (Ed.: A. D. Hamilton), Wiley, Chichester, **1996**, p. 101, particularly, p. 111.
[62] M. N. Khan, E. Ismail, *J. Chem. Soc. Perkin 2* **2001**, 1346.
[63] G. Savelli, R. Germani, L. Brinchi in *Reactions and Synthesis in Surfactant Systems* (Ed.: J. Texter), Marcel Dekker, New York, **2001**, p. 175, particularly p. 184.
[64] C. A. Bunton, L.-H. Gran, J. R. Moffat, L. S. Romsted, G. Savelli, *J. Phys. Chem.* **1981**, *85*, 4118.
[65] a) M. R. Mille, G. Vanderkooi, *J. Colloid Interface Sci.* **1977**, *59*, 211; b) G. Gunnarsson, B. Jonsson, H. Wennerström, *J. Phys. Chem.* **1980**, *84*, 3114.
[66] C. A. Bunton in *Surfactants in Solution, Vol. 11* (Eds.: K. L. Mittal, D. O. Shah), Plenum, New York, **1991**, p. 17.
[67] C. A. Bunton, G. Savelli, *Adv. Phys. Org. Chem.* **1986**, *22*, 213–309, spez. p. 254.
[68] L. Brinchi, P. Di Profio, R. Germani, G. Savelli, N. Spreti, C. A. Bunton, *Eur. J. Org. Chem.* **2000**, 3849.
[69] M. S. Patel, K. Bijma, J. B. F. N. Engberts, *Langmuir* **1994**, *10*, 2491.
[70] a) A. D. James, B. H. Robinson, *J. Chem. Soc. Faraday Trans. 1* **1978**, *74*, 10; b) J. Burgess, *Pure Appl. Chem.* **1991**, *63*, 1677; c) J. Burgess, E. Pelizzetti, *Prog. React. Kinet.* **1992**, *17*, 1.
[71] a) V. Balzani, F. Scandola, *Supramolecular Photochemistry*, Ellis Horwood, New York, **1991**; b) *Photochemistry in Organized & Constrained Media*, (Ed.: V. Ramamurthy), VCH, New York, **1991**.
[72] a) Y. Murakami, J. Kikuchi, Y. Hiseada, O. Hayashida, *Chem. Rev.* **1996**, *96*, 721; b) M. C. Feiters, R. J. M. K. Gebbink, A. B. H. J. Schenning, G. P. F. van Strijdonck, C. F. Martens, R. J. M. Nolte, *Pure Appl. Chem.* **1996**, *68*, 2163.
[73] a) K. Tauer in *Reactions and Synthesis in Surfactant Systems* (Ed.: J. Texter), Marcel Dekker, New York, **2001**, p. 429; b) J. P. Claverie, R. Soula, *Prog. Polym. Sci.* **2003**, *28*, 619.
[74] T. B. Körner, R. S. Brown, *Can. J. Chem.* **2002**, *80*, 183.
[75] J. Emsley, D. Hall, *The Chemistry of Phosphorus*, Wiley, New York, **1976**.
[76] M. A. Sogorb, E. Vinalova, *Toxicol. Lett.* **2000**, *128*, 215.
[77] N. B. Munro, K. R. Ambrose, A. P. Watson, *Environ. Health Perspect.* **1994**, *102*, 18.
[78] S. M. Ahmed, *Orient. J. Chem.* **2003**, *19*, 519.
[79] E. Rodenas, C. Dolcet, M. Valiente, E. C. Valeron, *Langmuir* **1994**, *10*, 2088.
[80] C. A. Bunton, *Catal. Rev. Sci. Eng.* **1979**, *83*, 680.
[81] K. M. Martinek, A. K. Yatimirski, A. P. Osipov, I. V. Berezin, *Tetrahedron* **1973**, *29*, 962.
[82] X. Yu, J. You, Y. Xiao, Z. Lan, R. Xie, *Huaxue Yanjiu Yu Yingyong* **1997**, *9*, 219.
[83] E. B. Tada, N. Ouarti, P. L. Silva, I. B. Blagoeva, O. A. El Seoud, M.-F. Ruasse, *Langmuir* **2003**, *19*, 10666.
[84] N. Ouarti, I. B. Blagoeva, O. A. El Seoud, M.-F. Ruasse, *J. Phys. Org. Chem.* **2001**, *14*, 823.
[85] F. Mancin, P. Tecilla, U. Tonellato, *Langmuir* **2000**, *16*, 227.
[86] Y. S. Simanenko, E. A. Karpichev, T. M. Prokop'eva, B. V. Panchenko, C. A. Bunton, *Langmuir* **2001**, *17*, 581.
[87] P. Scrimin, P. Tecilla, U. Tonellato, *J. Org. Chem.* **1991**, *56*, 161.
[88] L. Pasquato, F. Rancan, P. Scrimin, F. Mancin, C. Frigeri, *Chem. Commun.* **2000**, 2253.
[89] X. Yu, B. Jiang, S. Cheng, Z. Huang, X. Zeng, *J. Dispersion Sci. Technol.* **2003**, *24*, 761.
[90] X. Jiaging, C. Siqing, D. Juan, Z. Xiancheng, *J. Dispersion Sci. Technol.* **2001**, *22*, 337.
[91] a) D. Juan, J. Bingying, K. Xingming, Z. Xiancheng, X. Qingxian, *J. Colloid Interface Sci.* **2002**, *256*, 428; b) P. Scrimin, P. Tecilla, U. Tonellato, *J. Org. Chem.* **1994**, *59*, 4194; c) J. Budka, F. Hampl, F. Liska, P. Scrimin, P. Tecilla, U. Tonellato, *J. Mol. Catal. A* **1996**, *104*, L201.
[92] Z. Huang, S. Cheng, X. Zeng, *J. Dispersion Sci. Technol.* **2003**, *24*, 213.
[93] F. Jiang, J. Bingying, C. Yong, Y. Xiaoqi, Z. Xiangcheng, *J. Mol. Catal. A* **2004**, *210*, 9.
[94] F. Jiang, B. Jiang, Y. Cao, X. Meng, X. Yu, X. Zeng, *Colloids Surf. A* **2005**, *254*, 91.
[95] S. Bhattacharya, K. Suehalatha, V. P. Kumar, *J. Org. Chem.* **2003**, *68*, 2741.
[96] A. G. Meier, L. Dai, Q. Chen, C. J. Easton, L. Xia, *New J. Chem.* **2001**, *25*, 887.
[97] R. F. Bakeeva, L. A. Kudryavtseva, G. Eme (Oehme), E. M. Kosacheva, V. E. Bel'skii, D. B. Kudryavtsev, R. R. Shagidullin, V. F. Sopin, *Russ. Chem. Bull.* **1998**, *47*, 1454.
[98] F. G. Valeeva, A. V. Zakharov, M. A. Voronin, L. Y. Zakharova, L. A. Kudryavtseva, O. G. Isaikina, A. A. Kalinin, V. A. Mamedov, *Russ. Chem. Bull.* **2004**, *53*, 1563.
[99] U. Costas-Costas, C. Bravo-Diaz, H. Chaimovich, I. M. Cuccovia, *Colloids Surf. A* **2004**, *250*, 385.
[100] P. D. Miller, H. O. Spivey, S. L. Copeland, R. Sanders, A. Woodruff, D. Gearhart, W. T. Ford, *Langmuir* **2000**, *16*, 108.
[101] H. J. Foroudian, N. D. Gillitt, C. A. Bunton, *J. Colloid Interface Sci.* **2002**, *250*, 230.
[102] Y. S. Simanenko, A. F. Popov, E. A. Karpichev, T. M. Prokop'eva, V. A. Savelova, C. A. Bunton, *Russ. J. Org. Chem.* **2002**, *38*, 1314.
[103] V. P. Kumar, B. Ganguly, S. Bhattacharya, *J. Org. Chem.* **2004**, *69*, 8634.
[104] K. K. Ghosh, D. Sinha, M. Lal Satnami, *J. Surf. Sci. Technol.* **2003**, *19*, 159.
[105] O. S. Tee, O. J. Yazbeck, *Can. J. Chem.* **2000**, *78*, 1100.
[106] J. Xie, Y. Zhang, J. Du, X.-C. Zeng, Y.-J. Liu, Y. Shunzo, S. Yoshimi, *J. Dispersion Sci. Technol.* **2003**, *24*, 97.
[107] A. B. Dorrego, L. Garcia-Rio, P. Herves, J. R. Leis, J. C. Mejuto, J. Perez-Juste, *Angew. Chem.* **2000**, *112*, 3060; *Angew. Chem. Int. Ed.* **2000**, *39*, 2945.
[108] J.-S. You, X.-Q. Yu, X.-Y. Su, T. Wang, Q.-X. Xiang, M. Yang, R.-G. Xie, *J. Mol. Catal. A* **2003**, *202*, 17.
[109] M. N. Khan, R. Musa, *J. Mol. Catal. A* **2002**, *179*, 143.
[110] M. N. Khan, Z. Arifin, E. Ismail, S. F. M. Ali, *J. Org. Chem.* **2000**, *65*, 1331.
[111] M. del Mar Graciani, A. Rodriguez, M. Munoz, M. L. Moya, *React. Kinet. Catal. Lett.* **2003**, *78*, 113.
[112] J. E. Klijn, J. B. F. N. Engberts, *J. Am. Chem. Soc.* **2003**, *125*, 1825.
[113] C. A. Bunton, *J. Phys. Org. Chem.* **2005**, *18*, 115.
[114] E. R. Triboni, M. J. Politi, I. M. Cuccovia, H. Chaimovich, P. B. Filho, *J. Phys. Org. Chem.* **2003**, *16*, 311.
[115] E. Iglesias, *J. Phys. Chem. B* **2001**, *105*, 10295.
[116] E. Iglesias, *J. Phys. Chem. B* **2001**, *105*, 10287.
[117] E. Iglesias, *Langmuir* **2001**, *17*, 6871.
[118] P. H. Pritchard, C. F. Costa, *Environ. Sci. Technol.* **1991**, *25*, 372.
[119] J. Green, H. J. Dalton, *Biol. Chem.* **1989**, *264*, 17698.
[120] B. G. Fox, J. G. Borneman, L. P. Wacket, J. D. Lipscomp, *Biochemistry* **1990**, *29*, 6419.
[121] A. Rabion, R. M. Buchanan, J.-L. Seris, R. H. Fish, *J. Mol. Catal. A* **1997**, *116*, 43.
[122] H. Yao, D. E. Richardson, *J. Am. Chem. Soc.* **2003**, *125*, 6211.
[123] R. A. Sheldon, *Top. Curr. Chem.* **1993**, *164*, 21.

 © 2005 Wiley-VCH Verlag GmbH & Co. KGaA, Weinheim

[124] Y.-C. Yang, J. A. Baker, J. R. Ward, *Chem. Rev.* **1992**, *92*, 1729.
[125] K. M. Thompson, W. P. Griffith, M. Spiro, *J. Chem. Soc. Chem. Commun.* **1992**, 1600.
[126] D. M. Davies, E. L. Stringer, *Langmuir* **2003**, *19*, 1927.
[127] E. N. Kadnikova, N. M. Kostic, *J. Org. Chem.* **2003**, *68*, 2600.
[128] D. Monti, A. Pastorini, G. Mancini, S. Borocci, P. Tagliatesta, *J. Mol. Catal. A* **2002**, *179*, 125.
[129] K. -ud-Din, K. Hartani, Z. Khan, *Indian J. Chem. Sect. B* **2002**, *41*, 2614.
[130] K. -ud-Din, A. M. A. Morshed, Z. Khan, *Indian J. Chem. Sect. B* **2004**, *43*, 2178.
[131] A. K. Das, A. Roy, S. K. Mondal, G. Mukherjee, *React. Kinet. Catal. Lett.* **2001**, *73*, 257.
[132] B. Saha, M. Das, R. K. Mohanty, A. K. Das, *J. Chin. Chem. Soc.* **2004**, *51*, 399.
[133] J. K. J. Salem, R. M. Baraka, T. M. Haboush, A. A. S. El Khaldy, *Tenside Surfactants Deterg.* **2002**, *39*, 23.
[134] A. D. Ryabov, E. S. Ryabova, M. D. Reshetova, *J. Organomet. Chem.* **2001**, *637–639*, 469.
[135] X.-G. Meng, Y. Guo, C.-W. Hu, X.-C. Zeng, *J. Inorg. Biochem.* **2004**, *98*, 2107.
[136] W. Jiang, F. Feng, J. Xie, X. Meng, X. Zeng, *Sichuan Daxue Xuebao* **2003**, *40*, 926.
[137] R. Swain, G. P. Panigrahi, *Indian J. Chem. Sect. A* **2001**, *40*, 1191.
[138] K. Tomizaki, Y. Tsunekawa, H. Akisada, H. Mihara, N. Nishino, *J. Chem. Soc. Perkin Trans. 2* **2000**, 813.
[139] S. I. Goldberg, N. Baba, R. L. Green, R. Pandian, J. Stowes, R. L. Dunlap, *J. Am. Chem. Soc.* **1978**, *100*, 6768.
[140] Y. Hui, C. Yang, *Huaxue Xuebao* **1988**, *46*, 239.
[141] a) A. Schmitzer, E. Perez, I. Rico-Lattes, A. Lattes, *Tetrahedron Lett.* **1999**, *40*, 2947; b) I. Rico-Lattes, A. Schmitzer, E. Prez, A. Lattes, *Chirality* **2001**, *13*, 24.
[142] G. Cerichelli, M. Coreno, G. Manchini, *J. Colloid Interface Sci.* **1993**, *158*, 33.
[143] A. Aramini, L. Brinchi, R. Germani, G. Savelli, *Eur. J. Org. Chem.* **2000**, 1793.
[144] C. Denis, B. Laignel, D. Plusquellec, J.-Y. Le Marouille, A. Botrel, *Tetrahedron Lett.* **1996**, *37*, 53.
[145] D. Das, S. Roy, P. K. Das, *Org. Lett.* **2004**, *6*, 4133.
[146] a) Y. Dror, J. Manassen, *J. Mol Catal.* **1977**, *2*, 219; b) D. L. Reger, A. Gabrielli, *J. Mol. Catal.* **1981**, *12*, 173; c) P. J. Quinn, C. E. Taylor, *J. Mol. Catal.* **1981**, *13*, 389; d) R. G. Nuzzo, S. L. Haynie, M. L. Wilson, G. M. Whitesides, *J. Org. Chem.* **1981**, *46*, 2861; e) K. Ohkubo, T. Kawabe, K. Yamashita, S. Sakaki, *J. Mol. Catal.* **1984**, *24*, 83.
[147] a) G. Oehme, E. Paetzold, R. Selke, *J. Mol. Catal.* **1992**, *71*, L1; b) I. Grassert, E. Paetzold, G. Oehme, *Tetrahedron* **1993**, *49*, 6605; c) F. Joó, E. Papp, A. Kathó, *Top. Catal.* **1998**, *5*, 113.
[148] G. Oehme, I. Grassert, E. Paetzold, R. Meisel, K. Drexler, H. Fuhrmann, *Coord. Chem. Rev.* **1999**, *185–186*, 585.
[149] a) K. Drexler, R. Meisel, I. Grassert, E. Paetzold, H. Fuhrmann, G. Oehme, *Macromol. Chem. Phys.* **2000**, *201*, 1436; b) H. Fuhrmann, I. Grassert, T. Schareina, G. Holzhüter, G. Oehme, *Macromol. Chem. Phys.* **2001**, *202*, 426; c) H. Fuhrmann, I. Grassert, G. Holzhüter, C. Grüttner, G. Oehme, *New J. Chem.* **2002**, *26*, 1675.
[150] a) H. N. Flach, I. Grassert, G. Oehme, *Macromol. Chem. Phys.* **1994**, *195*, 3289; b) H. N. Flach, I. Grassert, G. Oehme, M. Capka, *Colloid Polym. Sci.* **1996**, *274*, 261.
[151] a) T. Dwars, J. Haberland, I. Grassert, G. Oehme, U. Kragl, *J. Mol. Catal. A* **2001**, *168*, 81; b) H. Fuhrmann, T. Dwars, D. Michalik, G. Holzhüter, C. Grüttner, U. Kragl, G. Oehme, *Adv. Synth. Catal.* **2003**, *345*, 202.
[152] A. Kumar, G. Oehme, J. P. Roque, M. Schwarze, R. Selke, *Angew. Chem.* **1994**, *106*, 2272; *Angew. Chem. Int. Ed. Engl.* **1994**, *33*, 2197.
[153] I. Grassert, U. Schmidt, S. Ziegler, C. Fischer, G. Oehme, *Tetrahedron: Asymmetry* **1998**, *9*, 4193.
[154] a) T. Dwars, U. Schmidt, C. Fischer, I. Grassert, R. Kempe, R. Fröhlich, K. Drauz, G. Oehme, *Angew. Chem.* **1998**, *110*, 3033; *Angew. Chem. Int. Ed.* **1998**, *37*, 2851; b) T. Dwars, U. Schmidt, C. Fischer, I. Grassert, H.-W. Krause, M. Michalik, G. Oehme, *Phosphorus Sulfur Silicon Relat. Elem.* **2000**, *158*, 209.
[155] a) R. Selke, J. Holz, A. Riepe, A. Börner, *Chem. Eur. J.* **1998**, *4*, 769; b) F. Robert, G. Oehme, I. Grassert, D. Sinou, *J. Mol. Catal. A* **2000**, *156*, 127.
[156] a) D. Meißner, T. Schareina, I. Grassert, G. Oehme, G. Holzhüter, *J. Prakt. Chem.* **1996**, *338*, 614; b) D. Meißner, I. Grassert, G. Oehme, G. Holzhüter, V. Vill, *Colloid Polym. Sci.* **2000**, *278*, 364.
[157] a) I. Grassert, V. Vill, G. Oehme, *J. Mol. Catal. A* **1997**, *116*, 231; b) V. Fehring, R. Kadyrov, M. Ludwig, J. Holz, K. Haage, R. Selke, *J. Organomet. Chem.* **2001**, *621*, 120.
[158] I. Grassert, K. Schinkowski, D. Vollhardt, G. Oehme, *Chirality* **1998**, *10*, 754.
[159] M. Ludwig, R. Kadyrov, H. Fiedler, K. Haage, R. Selke, *Chem. Eur. J.* **2001**, *7*, 3298.
[160] a) S. Ziegler, Dissertation, University Rostock, **1997**; b) G. Oehme, I. Grassert, S. Ziegler, R. Meisel, H. Fuhrmann, *Catal. Today* **1998**, *42*, 459.
[161] E. Papp, I. Banyai, F. Joó, *React. Kinet. Catal. Lett.* **2000**, *69*, 23.
[162] I. Grassert, G. Oehme, *J. Organomet. Chem.* **2001**, *621*, 158.
[163] I. Grassert, J. Kovacs, H. Fuhrmann, G. Oehme, *Adv. Synth. Catal.* **2002**, *344*, 312.
[164] A. Arrieta, G. Oehme, unpublished results.
[165] N. Weitbrecht, M. Kratzat, S. Santoso, R. Schomäcker, *Catal. Today* **2003**, *79–80*, 401.
[166] K. Yonehara, K. Ohe, S. Uemura, *J. Org. Chem.* **1999**, *64*, 9381.
[167] a) X. Zeng, S. Cheng, *J. Dispersion Sci. Technol* **2001**, *22*, 535; b) B. Jiang, S. Cheng, X. Zeng, Y. Liu, S. Yamamoto, Y. Sueishi, *J. Dispersion Sci. Technol.* **2003**, *24*, 691.
[168] B. Cornils, E. G. Kuntz in *Aqueous-Phase Organometallic Catalysis* (Eds.: B. Cornils, W. A. Herrmann), 2nd ed., Wiley-VCH, Weinheim, **2004**, p. 351.
[169] Y. Matsui, M. Orchin, *J. Organomet. Chem.* **1983**, *244*, 369.
[170] A. Riisager, B. E. Hanson, *J. Mol. Catal. A* **2002**, *189*, 195.
[171] M. Gimenez-Petros, A. Aghmiz, C. Claver, A. M. Masdeu-Bulto, D. Sinou, *J. Mol. Catal. A* **2003**, *203*, 157.
[172] M. Li, Y. Z. Li, H. Chen, Y. E. He, X. J. Li, *J. Mol. Catal. A* **2003**, *194*, 13.
[173] a) Y. Zang, Z.-S. Mao, J. Chen, *Catal. Today* **2002**, *74*, 23; b) C. Yang, X. Bi, Z.-S. Mao, *J. Mol. Catal. A* **2002**, *187*, 35.
[174] a) H. Chen, Y. Li, R. Li, P. Cheng, X. Li, *J. Mol. Catal. A* **2003**, *198*, 1; b) H. Chen, Y. Li, J. Cheng, P. Cheng, X. Li, *Catal. Today* **2002**, *74*, 131; c) L. Wang, H. Cheng, Y. Li, M. Li, X. Li, *Appl. Catal. A* **2003**, *242*, 85.
[175] a) Y. Wang, J. Jiang, F. Cheng, Z. Jin, *J. Mol. Catal. A* **2002**, *188*, 79; b) X.-Z. Liu, F. Kong, X. Zheng, Z. Jin, *Catal. Commun.* **2003**, *4*, 129; c) C. Liu, J. Jiang, Y. Wang, F. Cheng, Z. Jin, *J. Mol. Catal. A* **2003**, *198*, 23.
[176] a) G. Oehme, E. Paetzold, C. Fischer, M. Frank, *J. Mol. Catal. A* **2003**, *200*, 95; b) E. Paetzold, I. Jovel, G. Oehme, *J. Mol. Catal. A* **2004**, *214*, 241.
[177] M. T. Zarka, M. Bortenschlager, K. Wurst, O. Nuyken, R. Weberskirch, *Organometallics* **2004**, *23*, 4817.
[178] a) M. Haumann, H. Koch, P. Hugo, R. Schomäcker, *Appl. Catal. A* **2002**, *225*, 239; b) M. Haumann, H. Koch, R. Schomäcker, *Catal. Today* **2003**, *79*, 43; c) W. Tic, I. Miesiac, J. Szymanowski, *J. Colloid Interface Sci.* **2001**, *244*, 423.
[179] M. Bassetti, G. Cerichelli, B. Floris, *Gazz. Chim. Ital.* **1991**, *121*, 527.
[180] a) S. Kobayashi in *Aqueous-Phase Organometallic Catalysis* (Eds.: B. Cornils, W. A. Herrmann), 2nd ed., Wiley-VCH,

 © 2005 Wiley-VCH Verlag GmbH & Co. KGaA, Weinheim

Weinheim, **2004**, p. 88; b) S. Kobayashi, K. Manabe, *Acc. Chem. Res.* **2002**, *35*, 209; c) S. Kobayashi, K. Manabe, *Pure Appl. Chem.* **2000**, *72*, 1373; d) S. Kobayashi, T. Hamada, S. Nagayama, K. Manabe, *J. Braz. Chem. Soc.* **2001**, *12*, 627.
[181] H. J. Li, H. Y. Tian, Y. J. Chen, D. Wang, C. J. Li, *J. Chem. Res.* **2003**, 153.
[182] Y.-Y. Peng, Q.-P. Ding, Z. Li, P. G. Wang, J.-P. Cheng, *Tetrahedron Lett.* **2003**, *44*, 3871.
[183] a) S. Otto, J. B. F. N. Engberts, J. C. T. Kwak, *J. Am. Chem. Soc.* **1998**, *120*, 9517; b) T. Rispens, J. B. F. N. Engberts, *J. Org. Chem.* **2002**, *67*, 7369; c) J. Perez-Juste, F. Hollfelder, A. Kirby, J. B. F. N. Engberts, *Org. Lett.* **2000**, *2*, 127.
[184] D. Motoda, H. Kinoshita, H. Shinokubo, K. Oshima, *Angew. Chem.* **2004**, *116*, 1896; *Angew. Chem. Int. Ed.* **2004**, *43*, 1860.
[185] a) Y. Uozumi, T. Kimura, *Synlett* **2002**, 2045; b) Y. Uozumi, *Synth. Org. Chem. Jpn.* **2002**, *60*, 1063; c) Y. Uozumi, Y. Kobayashi, *Heterocycles* **2003**, *59*, 71.
[186] a) D. Schönfelder, K. Fischer, M. Schmidt, O. Nuyken, R. Weberskirch, *Organometallics* **2004**, *23*, 4817; b) J. O. Krause, M. T. Zarka, U. Anders, R. Weberskirch, O. Nuyken, M. R. Buchmeiser, *Angew. Chem.* **2003**, *115*, 6147; *Angew. Chem. Int. Ed.* **2003**, *42*, 5965; c) T. Zarka, O. Nuyken, R. Weberskirch, *Macromol. Rapid Commun.* **2004**, *25*, 858.
[187] G. Oehme, E. Paetzold, *J. Mol. Catal. A* **2000**, *152*, 69.
[188] K. J. Davis, D. Sinou, *J. Mol. Catal. A* **2002**, *177*, 173.
[189] K. Fuji, T. Morimoto, K. Tsutsumi, K. Kakiuchi, *Angew. Chem.* **2003**, *115*, 2511; *Angew. Chem. Int. Ed.* **2003**, *42*, 2409.
[190] a) C. Rabeyrin, D. Sinou, *Tetrahedron Lett.* **2000**, *41*, 7461; b) C. Rabeyrin, D. Sinou, *Tetrahedron: Asymmetry* **2003**, *14*, 3891.
[191] a) E. Monflier, P. Bourdauducq, J.-L. Couturier, J. Kervennal, A. Mortreux, *Appl. Catal. A* **1995**, *131*, 167; b) E. Monflier, P. Bourdauducq, J.-L. Couturier, J. Kervennal, I. Suisse, A. Mortreux, *Catal. Lett.* **1995**, *34*, 201.
[192] a) T. J. Broxton, J. R. Christie, A. J. Dole, *J. Phys. Org. Chem.* **1994**, *7*, 437; b) T. J. Broxton, M. Lucas, *J. Phys. Org. Chem.* **1994**, *7*, 442.
[193] K. Manabe, S. Iimura, X.-M. Sun, S. Kobayashi, *J. Am. Chem. Soc.* **2002**, *124*, 11971.
[194] L. Garcia-Rio, P. Hervés, J. C. Mejuto, J. Pérez-Juste, P. Rodriguez-Dafonte, *New J. Chem.* **2003**, *27*, 372.
[195] A. Sato, H. Kinoshita, H. Shinokubo, K. Oshima, *Org. Lett.* **2004**, *6*, 2217.
[196] T. Kunitake, S. Shinkai, *Adv. Phys. Org. Chem.* **1980**, *17*, 435.
[197] R. A. Moss, C. J. Takowski, D. W. Reger, C. E. Powell, *J. Am. Chem. Soc.* **1973**, *95*, 5215.
[198] a) R. Ueoka, Y. Matsumoto, T. Yoshino, N. Watanabe, K. Omura, Y. Murakami, *Chem. Lett.* **1986**, 1743; b) R. Ueoka, Y. Matsumoto, N. Matsuo, T. Taguchi, S. Ubata, *Nippon Kagaku Kaishi* **1989**, *2*, 181.
[199] D. Brosch, W. Kirmse, *J. Org. Chem.* **1993**, *58*, 1118.
[200] R. Ueoka, Y. Matsumoto, R. A. Moss, S. Swarup, A. Sugii, K. Harada, J. Kikuchi, Y. Murakami, *J. Am. Chem. Soc.* **1988**, *110*, 1588.
[201] J. G. J. Weijnen, A. Koudija, J. F. J. Engbersen, *J. Org. Chem.* **1992**, *57*, 7258.
[202] U. Tonellato, *Pure Appl. Chem.* **1998**, *70*, 1961.
[203] D. Sinou, C. Rabeyrin, C. Nguefack, *Adv. Synth. Catal.* **2003**, *345*, 357.
[204] Y.-M. Zhang, X.-H. Fang, S.-Q. Wang, *Youji Huaxue* **1992**, *12*, 488.
[205] U. M. Lindström, *Chem. Rev.* **2002**, *102*, 2751.
[206] B. S. Jursic, *Tetrahedron Lett.* **1993**, *34*, 963.
[207] M. Shinitzky, R. Haimovitz, *J. Am. Chem. Soc.* **1993**, *115*, 12545.
[208] J. S. Clint, *Surfactant Aggregation*, Blackie, Glasgow, **1992**, p. 222.
[209] D. F. Evans, H. Wennerström, *The Colloidal Domain. Where Physics, Chemistry, Biology, and Technology Meet*, VCH Publishers, New York, **1994**, p. 462.
[210] a) K. Holmberg, *Curr. Opin. Colloid Interface Sci.* **2003**, *8*, 187; b) H.-J. Schwuger, K. Stickdorn, R. Schomäcker, *Chem. Rev.* **1995**, *95*, 849; c) *Structure and Reactivity in Reverse Micelles* (Ed.: M. L. Pileni), Elsevier, Amsterdam, **1989**.
[211] P. L. Luisi in *Kinetics and Catalysis in Microheterogeneous Systems* (Eds.: M. Grätzel, K. Kalyanasundaram), Marcel Dekker, New York, **1991**, p. 115.
[212] a) F. M. Menger, A. R. Elrington, *J. Am. Chem. Soc.* **1991**, *113*, 9621; b) F. M. Menger, H. Park, *Recl. Trav. Chim. Pays-Bas* **1994**, *113*, 176.
[213] I. P. Beletskaya, *Pure Appl. Chem.* **1997**, *69*, 471.
[214] Y. Zhang, P. Sun, *Tetrahedron: Asymmetry* **1996**, *7*, 3055.
[215] a) N. M. Correa, D. H. Zorzan, M. Chiarini, G. Cerichelli, *J. Org. Chem.* **2004**, *69*, 8224; b) N. M. Correa, D. H. Zorzan, L. D'Anteo, E. Lasta, M. Chiarini, G. Cerichelli, *J. Org. Chem.* **2004**, *69*, 8231.
[216] N. M. Correa, E. N. Durantini, J. J. Silber, *J. Org. Chem.* **2000**, *65*, 6427.
[217] K. K. Ghosh, L. K. Tiwary, *J. Mol. Liq.* **2003**, *102*, 183.
[218] a) L. Garcia-Rio, J. R. Leis, J. C. Mejuto, *Langmuir* **2003**, *19*, 3190; b) E. Fernández, L. Garcia-Rio, A. Godoy, J. R. Leis, *New J. Chem.* **2003**, *27*, 1207; c) L. Garcia-Rio, J. R. Leis, J. A. Moreira, *J. Am. Chem. Soc.* **2000**, *122*, 10325; d) L. Garcia-Rio, J. R. Leis, *Chem. Commun.* **2000**, 455.
[219] a) Z. Shervani, Y. Ikushima, *Chem. Lett.* **2002**, 178; b) Z. Shervani, Y. Ikushima, *New J. Chem.* **2002**, *26*, 1257.
[220] J. Zhu, S. C. Tsang, *Catal. Today* **2003**, *81*, 673.
[221] M.-F. Ruasse, I. B. Blagoeva, R. Ciri, L. Garcia-Rio, J. R. Leis, A. Marques, J. Mejuto, E. Monnier, *Pure Appl. Chem.* **1997**, *69*, 1923.
[222] S. Gaemers, K. Keune, A. M. Kluwer, C. J. Elsevier, *Eur. J. Inorg. Chem.* **2000**, 1139.
[223] H. Tohma, S. Takizawa, H. Watanabe, Y. Fukuoka, T. Maegawa, Y. Kita, *J. Org. Chem.* **1999**, *64*, 3519.
[224] D. B. Dadyburjor, T. E. Fout, J. W. Zondlo, *Catal. Today* **2000**, *63*, 33.
[225] S.-S. Hong, M. S. Lee, S. S. Park, G.-D. Lee, *Catal. Today* **2003**, *87*, 99.
[226] N. L. Klyachko, A. V. Levashov, A. V. Kabanov, Y. L. Khmelnitzky, K. Martinek in *Kinetics and Catalysis in Microheterogeneous Systems* (Eds.: M. Grätzel, K. Kalyanasundaram), Marcel Dekker, New York, **1991**, p. 135.
[227] C. J. O'Connor, P. M. Wiggins, *Biocatalysis* **1988**, *1*, 249.
[228] A. Sanchez-Ferrer, F. Garcia-Carmona, *Enzyme Microb. Technol.* **1994**, *15*, 409.
[229] K. Holmberg, *Adv. Colloid Interface Sci.* **1994**, *51*, 137.
[230] H. Kunieda, K. Nakamura, D. F. Evans, *J. Am. Chem. Soc.* **1991**, *113*, 1051.
[231] F. Borzeix, F. Monot, J.-P. Vandecasteele, *Enzyme Microb. Technol.* **1992**, *14*, 791.
[232] H. M. Jung, K. E. Price, D. T. McQuade, *J. Am. Chem. Soc.* **2003**, *125*, 5351.
[233] P. A. Bachmann, P. L. Luisi, J. Lang, *Nature* **1992**, *357*, 57.
[234] T. Buhse, R. Nagarajan, D. Lavabre, J.-C. Micheau, *J. Phys. Chem. A* **1997**, *101*, 3910.
[235] J.-C. Micheau, R. Nagarajan in *Reactions and Synthesis in Surfactant Systems* (Ed.: J. Texter), Marcel Dekker, New York, **2001**, p. 413.
[236] X. Chen, J.-C. Micheau, *J. Colloid Interface Sci.* **2002**, *249*, 172.
[237] P. R. Kust, J. F. Rathman, *Langmuir* **1995**, *11*, 3007.
[238] a) T. Battal, J. F. Rathman in *Reactions and Synthesis in Surfactant Systems* (Ed.: J. Texter), Marcel Dekker, New York, **2001**, p. 359; b) J. F. Rathman, *Curr. Opin. Colloid Interface Sci.* **1996**, *1*, 514.

 © 2005 Wiley-VCH Verlag GmbH & Co. KGaA, Weinheim

[239] a) B. Boyer, J.-F. Betzer, G. Lamaty, A. Leydet, J.-P. Roque, *New J. Chem.* **1995**, *19*, 807; b) G. S. Simonyan, N. M. Beileryan, *Kinet. Catal. (Engl. Transl.)* **2002**, *43*, 337; G. S. Simonyan, N. M. Beileryan, *Kinet. Katal.* **2002**, *43*, 367.

[240] D. Andelman, F. Brochard, C. Knobler, F. Rondelez in *Micelles, Membranes, Microemulsions, and Monolayers* (Eds.: W. M. Gelbart, A. Ben-Shaul, D. Roux), Springer, New York, **1994**, p.. 559.

[241] T. Miyasaka, N. Nishikawa, M. Ono, *Thin Solid Films* **1992**, *210–211*, 393.

[242] A. Pasc-Banu, C. Sugisaki, T. Gharsa, J.-D. Marty, I. Gascon, G. Pozzi, S. Quici, I. Rico-Lattes, C. Mingotaud, *Angew. Chem.* **2004**, *116*, 3600; *Angew. Chem. Int. Ed.* **2004**, *43*, 6174.

[243] K. Töllner, R. Popovitz-Biro, M. Lahav, D. Milstein, *Science* **1997**, *278*, 2100.

[244] C.-C. Yu, L. L. Lobban in *Surfactant Adsorption and Surface Solubilization* (Ed.: R. Sharma), ACS Symposium Series 615, Washington DC, **1995**, p. 67.

[245] a) J. M. Brown, J. A. Jenkins, *J. Chem. Soc. Chem. Commun.* **1976**, 458; b) S. C. Tsang, K. M. K. Yu, A. M. Steele, J. Zhu, Q. J. Fu, *Catal. Today* **2003**, *81*, 573.

[246] T. Dwars, H. Fuhrmann, J. Ehlbeck, M. Maaß, G. Oehme, *Surf. Coat. Technol.* **2003**, *174–175*, 597.

[247] G. R. Newkome, C. N. Moorefield, G. R. Baker, M. J. Saunders, S. H. Grossman, *Angew. Chem.* **1991**, *103*, 1207; *Angew. Chem. Int. Ed. Engl.* **1991**, *30*, 1178.

[248] M. Q. Slagt, S.-A. Stiriba, H. Kautz, R. J. M. K. Gebbink, H. Frey, G. van Koten, *Organometallics* **2004**, *23*, 1525.

[249] G. R. Newkome, C. N. Moorefield, F. Vögtle, *Dendrimers and Dendrons: Concepts, Syntheses, Perspectives*, Wiley-VCH, Weinheim, **2001**.

[250] E. F. Connor, L. K. Sundberg, H.-C. Kim, J. J. Cornelissen, T. Magbitang, P. M. Rice, V. I. Lee, C. J, Hawker, W. Volksen, J. L. Hedrick, R. D. Miller, *Angew. Chem.* **2003**, *115*, 3915; *Angew. Chem. Int. Ed.* **2003**, *42*, 3785.

[251] M. T. Zarka, O. Nuyken, R. Weberskirch, *Chem. Eur. J.* **2003**, *9*, 3228.

[252] Y. M. A. Yamada, H. Tabata, M. Ichinohe, H. Takahashi, S. Ikegami, *Tetrahedron* **2004**, *60*, 4087.

[253] G. Riess, *Prog. Polym. Sci.* **2003**, *28*, 1107.

[254] a) H. Bönnemann, W. Brijoux, R. Brinkmann, E. Dinjus, T. Joußen, B. Korall, *Angew. Chem.* **1991**, *103*, 1344; *Angew. Chem. Int. Ed. Engl.* **1991**, *30*, 1312; b) D.-H. Chen, C.-H. Hsieh, *J. Mater. Chem.* **2002**, *12*, 2412.

[255] a) F. Caruso, R. Caruso, H. Möhwald, *Science* **1998**, *282*, 1111; b) Q. Zhang, E. E. Remsen, K. L. Wooley, *J. Am. Chem. Soc.* **2000**, *122*, 3642; c) S. Liu, J. V. M. Weaver, M. Save, S. P. Armes, *Langmuir* **2002**, *18*, 8350; d) S. Liu, S. P. Armes, *J. Am. Chem. Soc.* **2001**, *123*, 9910.

[256] A. Roucoux, J. Schulz, H. Patin, *Adv. Synth. Catal.* **2003**, *345*, 222.

[257] N. V. Semagina, A. V. Bykov, E. M. Sulman, V. G. Matveeva, S. N. Sidorov, L. V. Dubrovina, P. M. Valetsky, O. I. Kiselyova, A. R. Khokhlov, B. Stein, L. M. Bronstein, *J. Mol. Catal. A* **2004**, *208*, 273.

[258] R. Nakao, H. Rhee, Y. Uozumi, *Org. Lett.* **2005**, *7*, 163.

[259] a) T. Sanji, Y. Ogawa, Y. Nakatsuka, M. Tanaka, H. Sakurai, *Chem. Lett.* **2003**, *32*, 980; b) Y. Li, M. A. El Sayed, *J. Phys. Chem. B* **2001**, *105*, 8938; c) L. K. Yeung, R. M. Crooks, *Nano Lett.* **2001**, *1*, 14.

[260] a) S. Förster, *Top. Curr. Chem.* **2003**, *226*, 1; b) F. Schüth, *Angew. Chem.* **2003**, *115*, 3731; *Angew. Chem. Int. Ed.* **2003**, *42*, 3604; c) M. O. Coppens, J. Sun, T. Maschmeyer, *Catal. Today* **2001**, *69*, 331.

[261] H.-P. Hentze, M. Antonietti, *Curr. Opin. Solid State Mater. Sci.* **2001**, *6*, 343.

[262] M. López Carreto, D. Rubio, D. Pérez-Bendito, *Analyst* **1996**, *121*, 33R.

[263] U. Pfüller, *Mizellen, Vesikel, Mikroemulsionen*, VEB Volk und Gesundheit, Berlin, **1986**, p. 184.

[264] J. P. Claverie, R. Soula, *Prog. Polym. Sci.* **2003**, *28*, 619.

[265] S. L. Regen, *Angew. Chem.* **1979**, *91*, 464; *Angew. Chem. Int. Ed. Engl.* **1979**, *18*, 421.

[266] a) *Solvents and Self-Organization of Polymers* (Eds.: S. E. Webber, P. Munk, Z. Tuzar), Nato ACS Series, Kluwer, Dordrecht, **1996**; b) *Amphiphilic Block Copolymers* (Eds.: P. Alexandridis, B. Lindman), Elsevier, Amsterdam, **2000**.

© 2005 Wiley-VCH Verlag GmbH & Co. KGaA, Weinheim

Communications

DOI: 10.1002/anie.200502535

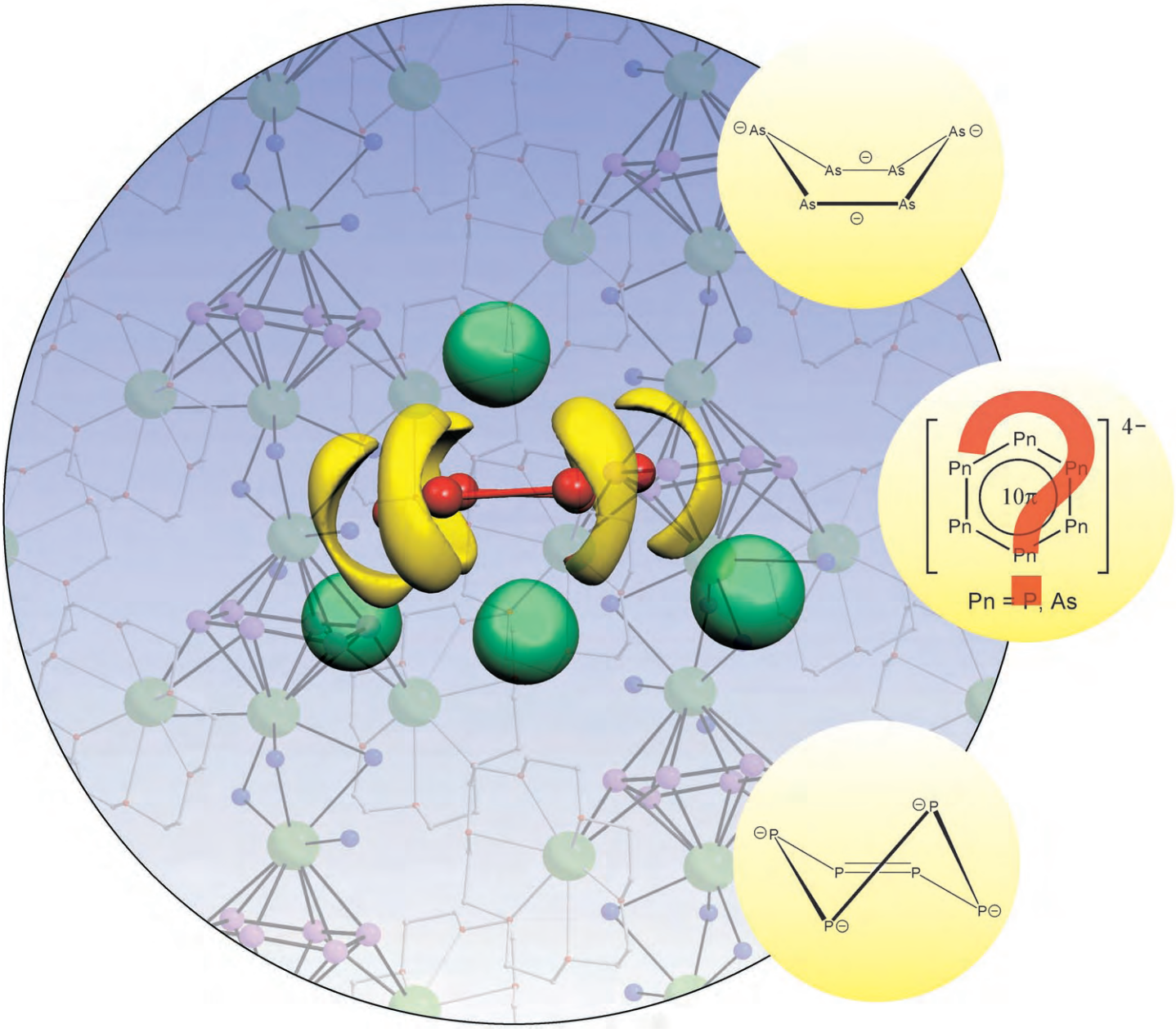

The bonding in the As_6^{4-} ion is studied in the unusually low-coordination environment provided by the compound $\{Rb[18]crown\text{-}6)\}_2Rb_2As_6 \cdot 6\,NH_3$. Theoretical analysis of the related P_6^{4-} ion indicates an unusual P=P bond which contains major contributions from the lone pairs. Outside a highly coordinating environment, these Pn_6^{4-} (Pn = P, As) species do not seem to be planar, 10π aromatic, or lone-pair aromatic. For details, see the Communication by N. Korber and co-workers on the following pages.

WILEY InterScience DISCOVER SOMETHING GREAT
© 2005 Wiley-VCH Verlag GmbH & Co. KGaA, Weinheim

Cluster Anions

DOI: 10.1002/anie.200502535

Chemical Bond in the Cyclic Anions P_6^{4-} and As_6^{4-}: Synthesis, Crystal Structure, and Electron Localization Function of $\{Rb[18]crown\text{-}6)\}_2$-$Rb_2As_6{\cdot}6NH_3$**

*Florian Kraus, Tobias Hanauer, and Nikolaus Korber**

Dedicated to Professor Henri Brunner on the occasion of his 70th birthday

The cyclohexaphosphide anion P_6^{4-} is only encountered in the very air and moisture sensitive binary compounds M_4P_6 (M = K, Rb, Cs)[1–3] in the solid state or as a ligand in organometallic complexes. In both cases the P_6^{4-} ion has a molecular shape close to D_{6h} symmetry.[4–8] Solvation of the binary compounds M_4P_6 in ethylenediammine or liquid ammonia, does not yield stable solutions of P_6^{4-} ions (according to NMR spectroscopy) because these react to form a variety of compounds such as the lone pair aromatic cyclotetraphosphide anion P_4^{2-}[9] and the cyclopentaphosphide anion P_5^-,[10] the heptaphosphanorticyclane anion P_7^{3-} and also the undecaphosphatrishomocubane anion P_{11}^{3-}.[11] Thus, the isolation of the P_6^{4-} ion in solvate crystals, in crystals containing it as an isolated anion without metal contacts, or as an ion complex has not been possible, and to date, attempts to detect it in liquid ammonia solution have also failed. A previous report on the existence of P_6^{4-} in an ethylenediammine solution has been shown to be in error, in this case a singlet in the ^{31}P NMR spectra was falsely assigned to P_6^{4-} instead to P_4^{2-}.[2,9]

Arsenic, the heavier congener of phosphorus, forms the compounds M_4As_6 (M = Rb, Cs),[12] which are isotypic to the hexaphosphides. Upon solvation in liquid ammonia, these hexaarsenides form heptaarsenide As_7^{3-},[13] tetradecaarsenide $[(As_7)_2]^{4-}$,[14] and the lone pair aromatic cyclotetraarsenide As_4^{2-} as crystalline products.[15,16] However, in contrast to the hexaphosphide anion, the hexaarsenide anion seems to be moderately stable in liquid ammonia solutions, and we have now been able to dissolve Rb_4As_6 congruently in it. We isolated the As_6^{4-} ion as an ion complex in which only four rubidium cations coordinate to it instead of fourteen as in the solid-state compound Rb_4As_6.

Herein we report the structure of the ammoniate $\{Rb([18]crown\text{-}6)\}_2Rb_2As_6{\cdot}6NH_3$ (**1**) which was obtained as a single crystal. As the compound crystallizes in the polar space group $P2_1$, all the six arsenic atoms of the cyclohexaarsenide anion As_6^{4-} are crystallographically not equivalent. The As_6^{4-} ring has a chair conformation with As–As bond lengths in the range 2.399(4) to 2.415(3) Å and bond angles close to 120° (Figure 1a). The arsenic atoms As1 and As4 are located, respectively, 0.421(3) Å above and 0.266(3) Å below an averaged plane defined by the arsenic atoms As2, As3, As5, and As6 (torsion angle As2-As3-As5-As6 2.4(2)°). The anion is coordinated by the rubidium cations Rb1 and Rb2 which are, respectively, 2.624(3) Å above and 2.693(3) Å below the aforementioned plane with Rb–As bond lengths in the range 3.434(3) to 3.718(3) Å. Additionally, the rubidium cation Rb3 coordinates to As3 and As4 with bond lengths of 3.638(3), 3.659(3) Å and Rb4 coordinates to As1 and As6 (bond lengths 3.581(3), 3.687(3) Å). In addition to this η^2-like coordination to the As_6^{4-} ion, the rubidium cations Rb3 and Rb4 are each sequestered by a molecule of [18]crown-6, which leads to a coordination number of eight. This unit may be considered as a $[\{Rb([18]crown\text{-}6)\}_2As_6]^{2-}$ entity. Additional to the η^6-like coordination of the rubidium ions Rb1 and Rb2 by the As_6^{4-} ring, these rubidium ions each coordinate to four molecules of ammonia. Three of these ammonia molecules form bridges between the two rubidium cations above and below neighboring As_6^{4-} rings, resulting in a dicationic $[NH_3(Rb(\mu\text{-}NH_3)_3Rb)NH_3]^{2+}$ unit (Figure 1b). Through the η^6-like coordination of the $[\{Rb([18]crown\text{-}6)\}_2As_6]^{2-}$ units to these symmetry equivalent dicationic $[Rb_2(NH_3)_5]^{2+}$ fragments, one-dimensional infinite strands of $^1_\infty[Rb_2(NH_3)_5(As_6)\text{-}\{Rb[18]crown\text{-}6\}_2]$ are formed, which run parallel to the crystallographic *b*-axis (Figure 1b).

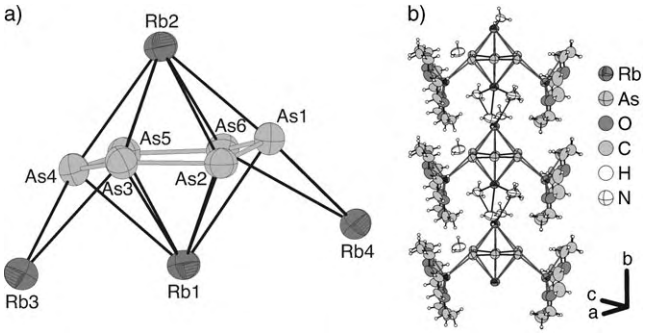

Figure 1. Structure of **1** in the solid state: a) coordination of the As_6^{4-} ion by the rubidium cations. b) A section of the $^1_\infty[Rb_2(NH_3)_5(As_6)\text{-}\{Rb([18]crown\text{-}6\}_2]$ strand. Thermal ellipsoids are drawn at the 70% probability level. Selected bond lengths [Å] and angles [°]: As1–As2 2.399(4), As1–As6 2.415(3), As2–As3 2.420(4), As3–As4 2.414(4), As4–As5 2.407(4), As5–As6 2.395(4); As2-As1-As6 118.4(1), As1-As2-As3 118.4(1), As4-As3-As2 119.2(1), As5-As4-As3 119.4(1), As6-As5-As4 119.1(1), As5-As6-As1 119.8(1).

With ab initio calculations and a topological analysis of the electron localization function (ELF),[17–23] we examined the bonds and lone pairs of the arsenic atoms of the As_6^{4-} species. Several energy minima of the free As_6^{4-} ion show that the boat conformation (C_{2v}) is a frequently encountered ground state—the point groups D_{3d}, D_{6h}, and C_2 correspond to

[*] F. Kraus, T. Hanauer, Prof. Dr. N. Korber
Institut für Anorganische Chemie der Universität Regensburg
Universitätsstrasse 31
93053 Regensburg (Germany)
Fax: (+49) 941-943-1812
E-mail: nikolaus.korber@chemie.uni-regensburg.de

[**] This work was supported by the Deutsche Forschungsgemeinschaft and the Fonds der Chemischen Industrie. F.K. thanks the Studienstiftung des Deutschen Volkes and the Fonds der Chemischen Industrie for a fellowship.

 © 2005 Wiley-VCH Verlag GmbH & Co. KGaA, Weinheim

transition states and to date we have not encountered other ground states. For the base of the boat conformer, the calculated As–As bond lengths (Figure 2a) are only 2.258 Å, which is quite short for As–As bonds. The bonds of the four arsenic atoms of the base to the two arsenic atoms forming the bow (As_{bow}) are 2.413 Å long. This finding suggests the localization of two double bonds and is also confirmed by the ELF calculations. Figure 2b shows the short basal As–As bonds each consist of two localization domains, their population, however, does not add up to four electrons (Table 1). The variance in these basins is quite high which indicates the delocalization of electrons. Looking at the lone pairs, that is, the monosynaptic valence basins of these arsenic atoms, three electrons with a very high variance are found in each which again shows the delocalization in the system. A calculation of the covariance for one of these monosynaptic valence basins clarifies the delocalization: The arsenic core basin C(As) contributes 18.2%, the disynaptic valence basin V(As–As_{bow}) 6.9%, and the disynaptic valence basin V(As–As) 5.6% to the population, but the neighboring V(As) contributes 4.3% whereas the two V(As_{bow}) only contribute 2.4% in total to the population. Consequently, these As=As bonds cannot be described properly within the Lewis model, since a large contribution to the double bond is made by the lone pairs. It might be possible to isolate this conformational isomer if noncoordinating, or weakly coordinating, counterions were present.

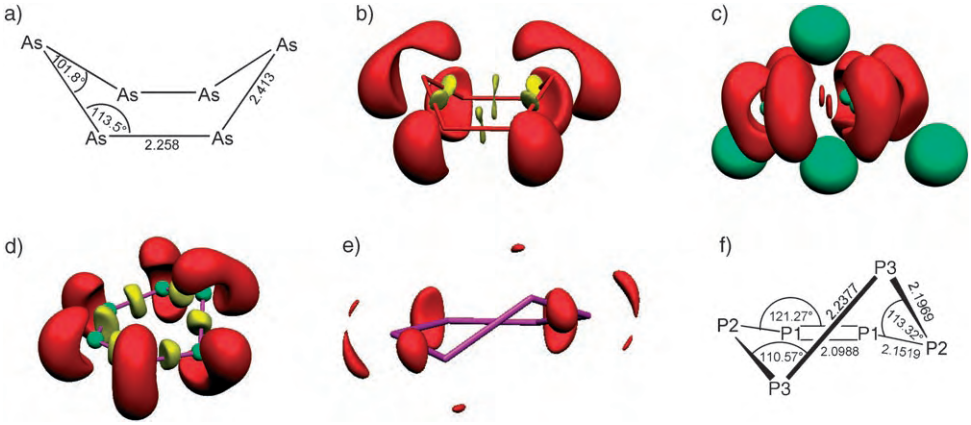

Figure 2. Calculated structures and electron localization functions of As_6^{4-} and P_6^{4-}: a) calculated structure of the free As_6^{4-} ion. b) ELF of the boat conformer of As_6^{4-} with $\eta(r) = 0.81$. c) ELF of $\{Rb_4As_6\}$ in the geometry found in the crystal structure of **1** $\eta(r) = 0.70$. d),e) ELF of P_6^{4-} in C_2 symmetry with $\eta(r) = 0.82$ (d) and $\eta(r) = 0.948$ (e; at this high value for the ELF, the localization of the negative formal charges becomes evident since the atoms P2 and P3 have two monosynaptic valence basins each). f) Calculated structure of the free P_6^{4-} ion. Green: core basins, red: monosynaptic valence basins, yellow: the disynaptic valence basins.

The topological analysis of the $\{Rb_4As_6\}$ unit found in the crystal structure (Figure 2c, Table 1) shows all the arsenic–arsenic bonds to have a similar population of about 1.45 electrons with a rather low variance of 1.00. Twelve monosynaptic valence basins are found, that is, for each arsenic atom there are two lone pairs with a population of 2.31 and a variance of 1.32, and the covariance matrix shows no distinctive contributions of neighboring lone pairs to the delocalization. Thus, the arsenic–arsenic bonds in the $\{Rb_4As_6\}$ ion complex are better described as depopulated single bonds. In contrast to As_4^{2-},[15] no lone pair aromaticity seems to be present in As_6^{4-}, which also means that this anion should not be 10π aromatic.

The isolation of an As_6^{4-} ion that is less coordinated than that in the binary solid also suggests that it might be possible to obtain the P_6^{4-} ion in a similar solvate crystal. Since we do not have further experimental evidence for the possible existence of the P_6^{4-} ion outside of the compound types mentioned above, we used ab initio calculations to look for ground states for the free P_6^{4-} ion. Several different starting geometries, such as D_{6h}, D_{3d}, D_{3h}, and C_{2v}, yielded only transition states, with geometries close to the D_{6h} case. The D_{2h} symmetric P_6^{4-} ion in the crystal structures of α-K_4P_6, Rb_4P_6, and Cs_4P_6 (space group *Fmmm*) is not a ground state of the free anion. However, a structure in point group C_2 yields a ground state (Figure 2d–f). This result is surprising since the P_6^{4-} ring was once thought to be a 10π aromatic ground state system in Hückel and Hartree Fock (HF) calculations.[2,24,25]

These results are not verified by ab initio calculations at the HF[15,26] or B3LYP[15] level of theory which include the evaluation of the Hesse matrix. The topological analysis of the ELF[17–23] of the P_6^{4-} ion indicates a localized P=P double bond (Figure 2d,e). As can be seen from Figure 2d–f and Table 1, the four formal negative charges are localized on the phosphorus atoms P2 and P3, because these atoms have two monosynaptic valence basins (two lone pairs), each with a population close to two electrons. The phosphorus atoms P1 each

Table 1: Compilation of the basin populations and variances of As_6^{4-}, $\{Rb_4As_6\}$ in **1**, and P_6^{4-}.

As_6^{4-} (boat conformation) basin	population [e] (variance)	$\{Rb_4As_6\}$ crystal geometry basin	population [e] (variance)	P_6^{4-} (C_2 symmetry) basin	population [e] (variance)
V(As_{bow})	1.93 (1.13)	V(As)[a]	2.31 (1.32)	V(P1)	3.04 (1.31)
	2.51 (1.34)			V(P2)	1.98 (1.02)
					1.70 (0.98)
V(As)	3.03 (1.53)			V(P3)	2.09 (1.01)
					1.91 (1.03)
V(As-As_{bow})	2.00 (1.22)	V(As-As)[a]	1.45 (1.00)	V(P1,P1)	2.46 (1.27)
				V(P1,P2)	2.19 (1.17)
V(As-As)	1.45 (1.00)			V(P2,P3)	1.99 (1.09)
	1.45 (1.00)			V(P3,P3)	1.81 (1.04)

[a] Average values.

© 2005 Wiley-VCH Verlag GmbH & Co. KGaA, Weinheim

have only one monosynaptic valence basin with a high population of 3.04 electrons and a very high variance of 1.31 which shows a high degree of electron delocalization. The P–P bonds shorten along the series P3–P3 (2.2377 Å) to P2–P3 to P1–P1 (2.0988 Å). The population of the long bond is 1.81 electrons with a variance of 1.04, whereas the population of the short bond is very high with 2.46 electrons and a high variance of 1.27, which again indicates the delocalization of the electrons. The covariance matrix shows a value of −0.13 (4.3 %) for the exchange between the monosynaptic basins on the two P1 atoms, but only −0.06 (2 %) for the delocalization between the monosynaptic valence basins of P1 and P2. The covariance is even lower for the exchange between P2 and P3 or from P3 and P3. Additionally, the covariance is high, with a value of −0.34 (11.2 %), between V(P1) and V(P1,P1). There is also some delocalization between V(P1) and V(P1,P2) which explains the higher population of the latter. So, the bond between the phosphorus atoms P1 is not a double bond in the sense of the C=C double bond, since a large contribution to the bonding is made by the lone pairs on the P1 phosphorus atoms. Furthermore, the system seems neither to be 10π aromatic nor lone pair aromatic.

It is gratifying to see that the ELF model of the P_6^{4-} ion corresponds closely to the simplest Lewis formula for this anion; even the C_2 symmetry may be predicted using VSEPR considerations. On the other hand, our results show that the Pn=Pn (Pn = P, As) double bonds differ markedly from the traditional hybridization model, since major contributions to the double bonds are made by the lone pairs. Another model describing such bonds in terms of the hybridization defect concept is extensively discussed by Kutzelnigg.[27] As was evidenced by the isolation of **1** and confirmed by ab initio calculations, the Pn_6^{4-} species seem not to be planar outside a highly coordinating environment and do not seem to be 10π or lone pair aromatic either.

Experimental Section

All procedures were carried out under an atmosphere of purified argon and by excluding moisture and air. Liquid ammonia was dried and stored over sodium metal. [18]Crown-6 was purified by sublimation. Rb_4As_6 was synthesized from the elements,[12] $AsPh_3$ (97 %) was obtained commercially from Aldrich. The crystal structure was recorded at 123 K on a Stoe & Cie GmbH Imaging Plate Diffraction System I with graphite-monochromatized $Mo_{K\alpha}$ radiation (λ = 0.71073 Å), the crystal was mounted on a nylon loop in perfluorinated polyether oil.

1 was synthesized from Rb_4As_6 (134 mg, 0.17 mmol), $AsPh_3$ (77 mg, 0.51 mmol), [18]crown-6 (89 mg, 0.34 mmol), through the addition of liquid ammonia (approximately 20 mL) at −78 °C. Without the $AsPh_3$, the As_7^{3-} ion was formed as the major product. After storage for one month at −40 °C, green needle-shaped crystals of **1** had formed.

Single crystal X-ray diffraction analysis of **1**: $C_{24}H_{66}As_6N_6O_{12}Rb_4$, M_r = 1422.23 g mol^{-1}, crystal size 0.3 × 0.02 × 0.02 mm^3, monoclinic, space group $P2_1$, a = 11.492(1), b = 9.2227(7), c = 23.888(2) Å, β = 99.03(1)°, V = 2500.4(4) Å^3, Z = 2, ρ_{calcd} = 1.889 Mg m^{-3}, $F(000)$ = 1387, $\mu(Mo_{K\alpha})$ = 7.882 mm^{-1}, θ = 2.11–21.49°, measured/independent/observed ($I > 2\sigma(I)$) reflections 9169/5720/3908, R_{int} = 0.1107, *hkl* range −11 to 11, −9 to 9, −24 to 23, $R(F)$ (all data) = 0.0781, $wR(F^2)$ (all data) = 0.1388, S (all data) = 0.886, data/parameter/restraints 5720/501/1, Flack parameter x = −0.07(2), $(\Delta/\sigma)_{max}$ = 0.001, max./min. residual electron density: 0.834/−0.713 e Å^{-3}. The structure was solved in space group $P2_1$ using direct methods (SHELXS-97).[28] After all non-hydrogen atoms were located and refined anistropically (SHELXL-97)[29] an absorption correction using DELrefABS of the PLATON suite was applied.[30] Hydrogen atoms were located and refined isotropically using a riding model or with Fourier cycling methods. CCDC-276490 contains the supplementary crystallographic data for this paper. These data can be obtained free of charge from the Cambridge Crystallographic Data Centre via www.ccdc.cam.ac.uk/data_request/cif.

Theoretical Procedures: All energy minimizations were carried out with the Gaussian03[31] package at the HF level of theory and 6-311++G(3df)[32–35] was applied as a basis set for phosphorus, 6-311G[36] for arsenic. For rubidium the 3-21G[37–39] basis was used. To assure the usage of ground-state geometries in all calculations, the Hesse matrix was checked for the absence of imaginary entries. The electron localization functions and basin populations were calculated with the ToPMoD package from the Gaussian HF wavefunctions, a resolution of at least 0.1 Å was used throughout the calculations.[40,41] For visualization, Molekel4.0[42] and Molden[43] were used.

Received: July 20, 2005
Published online: October 20, 2005

Keywords: arsenic · cluster compounds · ELF (electron localization function) · rubidium · structure elucidation

[1] W. Schmettow, A. Lipka, H. G. von Schnering, *Angew. Chem.* **1974**, *86*, 379–380; *Angew. Chem. Int. Ed. Engl.* **1974**, *13*, 345.
[2] H. G. von Schnering, T. Meyer, W. Hönle, W. Schmettow, U. Hinze, W. Bauhofer, G. Kliche, *Z. Anorg. Allg. Chem.* **1987**, *553*, 261–279.
[3] H. P. Abicht, W. Hönle, H. G. von Schnering, *Z. Anorg. Allg. Chem.* **1984**, *519*, 7–23.
[4] O. J. Scherer, H. Sitzmann, G. Wolmershäuser, *Angew. Chem.* **1985**, *97*, 358–359; *Angew. Chem. Int. Ed. Engl.* **1985**, *24*, 351–353.
[5] O. J. Scherer, J. Schwalb, M. Swarowsky, G. Wolmershäuser, W. Kaim, R. Groß, *Chem. Ber.* **1988**, *121*, 443–449.
[6] P. Jutzi, R. Kroos, *Chem. Ber.* **1988**, *121*, 1399–1401.
[7] O. J. Scherer, *Acc. Chem. Res.* **1999**, *32*, 751–762.
[8] O. J. Scherer, *Angew. Chem.* **2000**, *112*, 1069–1071; *Angew. Chem. Int. Ed.* **2000**, *39*, 1029–1030.
[9] F. Kraus, J. C. Aschenbrenner, N. Korber, *Angew. Chem.* **2003**, *115*, 4162–4165; *Angew. Chem. Int. Ed.* **2003**, *42*, 4030–4033.
[10] M. Baudler, S. Akpapoglou, D. Ouzounis, F. Wasgestian, B. Meinigke, H. Budzikiewicz, H. Münster, *Angew. Chem.* **1988**, *100*, 288–289; *Angew. Chem. Int. Ed. Engl.* **1988**, *27*, 280–281.
[11] F. Kraus, N. Korber, *Chem.Eur. J.* **2005**, *11*, 5945–5959.
[12] W. Hönle, G. Krogull, K. Peters, H. G. von Schnering, *Z. Kristallogr. New Cryst. Struct.* **1999**, *214*, 17–18.
[13] T. Hanauer, M. Grothe, M. Reil, N. Korber, *Helv. Chim. Acta* **2005**, *88*, 950–961.
[14] T. Hanauer, N. Korber, **2005**, unpublished results.
[15] F. Kraus, T. Hanauer, N. Korber, *Inorg. Chem.* **2005**, submitted.
[16] T. Hanauer, F. Kraus, N. Korber, *Monatsh. Chem.* **2005**, in press.
[17] A. D. Becke, K. E. J. Edgecombe, *J. Chem. Phys.* **1990**, *92*, 5397–5403.
[18] A. Savin, A. D. Becke, J. Flad, R. Nesper, H. Preuss, H. G. von Schnering, *Angew. Chem.* **1991**, *103*, 421–424; *Angew. Chem. Int. Ed. Engl.* **1991**, *30*, 409–412.
[19] B. Silvi, A. Savin, *Nature* **1994**, *371*, 683–686.
[20] A. Savin, R. Nesper, S. Wengert, T. Fässler, *Angew. Chem.* **1997**, *109*,1892–1918; *Angew. Chem. Int. Ed. Engl.* **1997**, *36*, 1808–1832.
[21] D. B. Chesnut, L. J. Bartolotti, *Chem. Phys.* **2000**, *253*, 1–11.

 © 2005 Wiley-VCH Verlag GmbH & Co. KGaA, Weinheim

[22] B. Silvi, *Phys. Chem. Chem. Phys.* **2004**, *6* 256 – 260.
[23] B. Silvi, I. Fourré, M. E. Alikhani, *Monatsh. Chem.* **2005**, *136*, 855 – 879.
[24] R. C. Burns, R. J. Gillespie, J. A. Barnes, M. J. McGlinchey, *Inorg. Chem.* **1982**, *21*, 799 – 807.
[25] J. Li, C.-W. Liu, J.-X. Lu, *THEOCHEM* **1993**, *280*, 223 – 231.
[26] M. Ystenes, *THEOCHEM* **1996**, *369*, 23 – 28.
[27] W. Kutzelnigg, *Angew. Chem.* **1984**, *96*, 262 – 286; *Angew. Chem. Int. Ed. Engl.* **1984**, *23*, 272 – 295.
[28] G. M. Sheldrick, *SHELXS-97*, Universiy of Göttingen, Germany, **1997**.
[29] G. M. Sheldrick, *SHELXL-97*, University of Göttingen, Germany, **1997**.
[30] A. L. Spek, PLATON—A Multipurpose Crystallographic Tool, Utrecht University, Utrecht, The Netherlands, **2003**.
[31] Gaussian 03 (Revision C.02), M. J. Frisch, G. W. Trucks, H. B. Schlegel, G. E. Scuseria, M. A. Robb, J. R. Cheeseman, J. A. Montgomery, Jr., T. Vreven, K. N. Kudin, J. C. Burant, J. M. Millam, S. S. Iyengar, J. Tomasi, V. Barone, B. Mennucci, M. Cossi, G. Scalmani, N. Rega, G. A. Petersson, H. Nakatsuji, M. Hada, M. Ehara, K. Toyota, R. Fukuda, J. Hasegawa, M. Ishida, T. Nakajima, Y. Honda, O. Kitao, H. Nakai, M. Klene, X. Li, J. E. Knox, H. P. Hratchian, J. B. Cross, C. Adamo, J. Jaramillo, R. Gomperts, R. E. Stratmann, O. Yazyev, A. J. Austin, R. Cammi, C. Pomelli, J. W. Ochterski, P. Y. Ayala, K. Morokuma, G. A. Voth, P. Salvador, J. J. Dannenberg, V. G. Zakrzewski, S. Dapprich, A. D. Daniels, M. C. Strain, O. Farkas, D. K. Malick, A. D. Rabuck, K. Raghavachari, J. B. Foresman, J. V. Ortiz, Q. Cui, A. G. Baboul, S. Clifford, J. Cioslowski, B. B. Stefanov, G. Liu, A. Liashenko, P. Piskorz, I. Komaromi, R. L. Martin, D. J. Fox, T. Keith, M. A. Al-Laham, C. Y. Peng, A. Nanayakkara, M. Challacombe, P. M. W. Gill, B. Johnson, W. Chen, M. W. Wong, C. Gonzalez, J. A. Pople, Gaussian, Inc., Pittsburgh, PA, **2004**.
[32] R. Krishnan, J. S. Binkley, R. Seeger, J. A. Pople, *J. Chem. Phys.* **1980**, *72*, 650 – 654.
[33] A. D. McLean, G. S. Chandler, *J. Chem. Phys.* **1980**, *72*, 5639 – 5648.
[34] T. Clark, J. Chandrasekhar, G. W. Spitznagel, P. von R. Schleyer, *J. Comput. Chem.* **1983**, *4*, 294 – 301.
[35] M. J. Frisch, J. A. Pople, J. S. Binkley, *J. Chem. Phys.* **1984**, *80*, 3265 – 3269.
[36] L. A. Curtiss, M. P. McGrath, J.-P. Blandeau, N. E. Davis, R. C. Binning, L. Radom, *J. Chem. Phys.* **1995**, *103*, 6104 – 6113.
[37] K. D. Dobbs, W. J. Hehre, *J. Comput. Chem.* **1986**, *7*, 359 – 378.
[38] K. D. Dobbs, W. J. Hehre, *J. Comput. Chem.* **1987**, *8*, 880 – 893.
[39] E. D. Glenning, D. Feller, *J. Phys. Chem.* **1995**, *99*, 3060 – 3067.
[40] S. Noury, X. Krokidis, F. Fuster, B. Silvi, ToPMoD, Laboratoire de Chimie Théorique (UMR-CNRS 7616) Université Pierre et Marie Curie, 75252 Paris cédex, France, **1997**.
[41] S. Noury, X. Krokidis, F. Fuster, B. Silvi, *Comput. Chem.* **1999**, *23*, 597 – 604.
[42] P. Flükinger, H. P. Lüthi, S. Portmann, J. Weber, MOLEKEL 4.0, Swiss Center for Scientific Computing, Manno, Switzerland, **2000**.
[43] G. Schaftenaar, J. H. Noordik, *J. Comput.-Aided Mol. Des.* **2000**, *14*, 123 – 134.

 © 2005 Wiley-VCH Verlag GmbH & Co. KGaA, Weinheim

DNA Structures

DOI: 10.1002/anie.200501589

A Highly DNA-Duplex-Stabilizing Metal–Salen Base Pair**

*Guido H. Clever, Kurt Polborn, and Thomas Carell**

The incorporation of one or multiple metal ions into nucleic acids in a defined fashion is currently of great interest for the development of alternative base pairs and the generation of DNA and RNA with novel catalytic and electronic properties.[1] The general idea regarding catalysis is that the metal ion provides a unique catalytic property, while the nucleic acids surrounding it serve as a chiral ligand amenable to evolutionary optimization.[2,3] Recently, the groups led by Leumann,[4] Meggers,[5] Schultz,[6] Shionoya,[7] Switzer,[8] and Tor[9] presented metal-coordinating nucleic acids, so-called ligandosides, which are able to hold a metal ion inside the double helix.

Regarding electronic application, Shionoya et al. achieved the incorporation of five consecutive metal–base pairs, thereby creating a double helix in which five copper ions are presumably stacked on top of each other.[1] On the way to the goal of creating metal-based catalytic nucleic acids, it would be desirable to create new metal–base pairs in DNA or RNA from chemical entities known to be "privileged ligands" for the construction of powerful catalysts.[10] We therefore decided to develop a DNA metal–base pair based on the *N*,*N*′-bis(salicylidene)ethylenediamine (salen) ligand,[11] which is today one of the most versatile ligands used for the generation of metal catalysts. Metal–salen complexes are able to accelerate a wide range of reactions such as cyclopropanations, epoxidations,[12] and oxidations[13] and are applicable for kinetic resolutions.[14]

The development of our metal–base pair is based on earlier studies of Sheppard and Gothelf et al., who assembled intrastrand salen complexes from phosphate-bound salicylic aldehydes.[15] To create a salen-based metal–base pair that fits optimally into the double-helix structure, we decided to connect the salicylic aldehyde at the C4 atom to the C1′ position of 2′-deoxyribose. Based on molecular modeling we

[*] Dipl.-Chem. G. H. Clever, Dr. K. Polborn, Prof. Dr. T. Carell
Department of Chemistry and Biochemistry
Ludwig-Maximilians University Munich
Butenandtstrasse 5–13, Haus F, 81377 München (Germany)
Fax: (+49) 89-2180-77756
E-mail: thomas.carell@cup.uni-muenchen.de

[**] This research was supported by the Volkswagen Foundation and the Deutsche Forschungsgemeinschaft (research group: Hybrid Compounds) and by the Stiftung Stipendien-Fonds des Verbandes der Chemischen Industrie e.V. (Kekulé fellowship to G.C.). We thank Prof. P. Klüfers for helpful discussions and Heather Burks, Tanja Köpping, Kirsten Schwekendiek, and Michaela Vedecnik for assistance in synthesis.

Supporting information for this article is available on the WWW under http://www.angewandte.org or from the author.

 InterScience © 2005 Wiley-VCH Verlag GmbH & Co. KGaA, Weinheim

envisioned that two such ligands facing each other in a duplex structure may assemble in the presence of a suitable metal ion and ethylenediamine to give a metal–salen complex (Figure 1). This complex was envisioned to stack inside the duplex structure, presenting the metal in the minor groove. In contrast to the metal–base pairs investigated so far, the salen–base pair requires both the metal and ethylenediamine for assembly. The inclusion of ethylenediamine gives the resulting complex cross-linking character, although in water imine formation is generally highly reversible.[16]

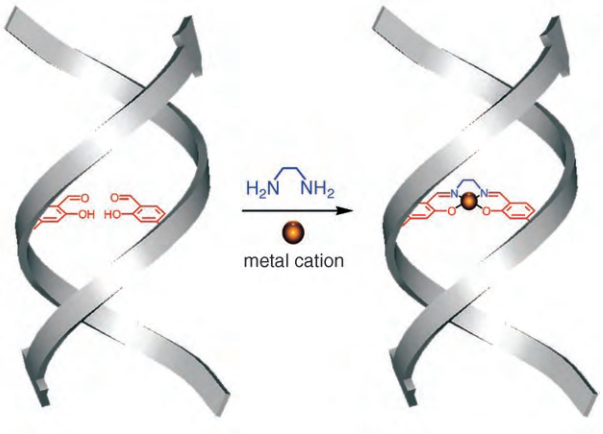

Figure 1. Depiction of the salicylic aldehyde base pair (LL) and assembly of the metal–salen complex inside the duplex.

The protecting groups on the ligand were chosen to comply with ligandoside synthesis and DNA chemistry. The triisopropylsilyl (TIPS) protecting group for the phenol is cleavable under the conditions used to remove the synthesized DNA from the solid support. The aldehyde functionality was protected as an acetal, cleavable with 2% dichloroacetic acid in wet dichloromethane. This reagent is also used for the cleavage of the 5′-DMT protecting groups during DNA synthesis.

The preparation of the protected salicylic aldehyde nucleobase was achieved as depicted in Scheme 1 by ortho-formylation of 3-bromophenol (**1**) with paraformaldehyde in the presence of $MgCl_2$ and triethylamine.[17] The formylation was followed by first an acetalization according to a special procedure for salicylic aldehydes[18] and second by TIPS protection to yield the protected ligand **2**. The C-glycosidation[19] was achieved after lithium–bromine exchange with *tert*-butyllithium, transmetalation, and reaction of the resulting aryl copper species with α-2′-deoxyribosylchloride **3**, which was prepared in two steps from 2′-deoxyribose.[20] After separation of the α and β anomers of nucleoside **4** by column chromatography (the configuration at C1′ of both anomers was assigned by evaluation of the NOESY contacts between the hydrogen atoms C1′-H, C2′-H, and C3′-H), we depro-

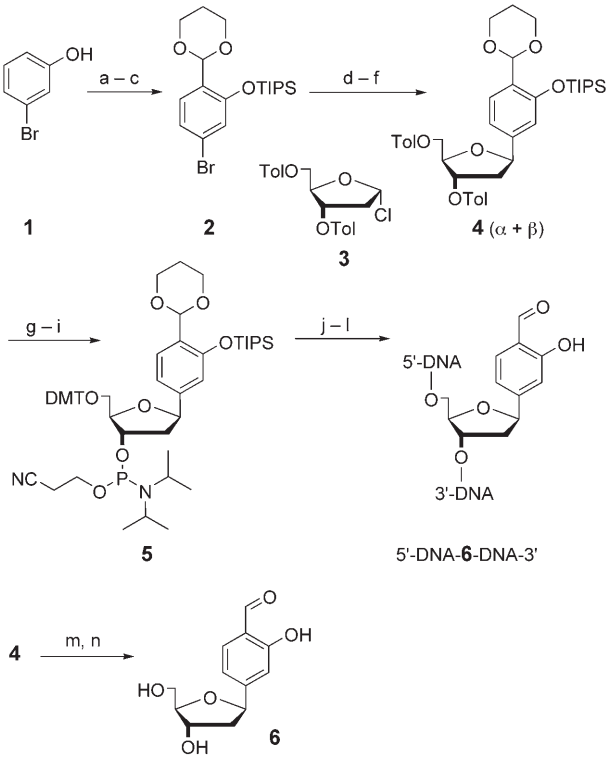

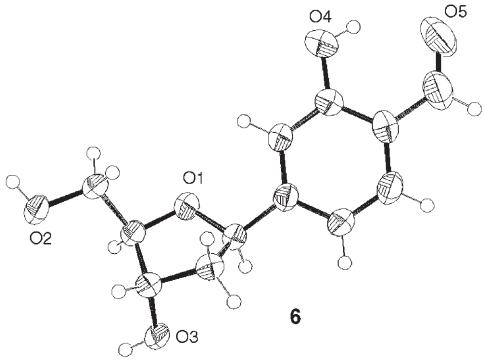

8-L-a = 5′-CACATTA**L**TGTTGTA-3′
8-L-b = 3′-GTGTAAT**L**ACAACAT-5′
7-L = 5′-GTA**L**AGTTTTCT**L**TAC-3′
L = ligand **6**

Scheme 1. Synthesis of the salen ligandoside **6** and its phosphoramidite together with the crystal structure of **6** and the sequences of the DNA strands prepared for this study. a) $(CH_2O)_n$, NEt_3, $MgCl_2$, toluene, 100 °C, 10 h, 49%; b) 1,3-propanediol, $HC(OEt)_3$, $N(nBu)_4Br_3$, RT, 24 h, 86%; c) TIPS-OTf, $NEt(iPr)_2$, CH_2Cl_2, RT, 12 h, 87%; d) 2 equiv *t*BuLi, Et_2O, −78 °C, 2 h; e) CuBr·SMe_2, −78 → −30 °C, 20 min; f) **3**, CH_2Cl_2, 12 h, −78 °C → RT, 78% (α/β = 3:2); g) K_2CO_3, MeOH, RT, 2 h, 72%; h) DMT-Cl, pyridine, 3 h, 67%; i) CED-Cl, $NEt(iPr)_2$, THF, RT, 2 h, 78%; j) automated DNA synthesis; k) deprotection of aldehydes with wet 2% $CHCl_2COOH$ in CH_2Cl_2; l) cleavage from solid support and cleavage of TIPS with $NH_{3(aq)}$/EtOH = 3:1; m) $N(nBu)_4F$, THF; n) 2% $CHCl_2COOH$, CH_2Cl_2. CED-Cl = (2-cyanoethyl)-*N*,*N*-diisopropylphosphorimidochloridite, DMT = 4,4′-dimethoxytrityl, Tf = trifluoromethanesulfonyl, TIPS = triisopropylsilyl, Tol = tolyl. X-ray structure: Ligandoside **6** crystallized from EtOAc.[24]

 © 2005 Wiley-VCH Verlag GmbH & Co. KGaA, Weinheim

tected the sugar hydroxy groups under Zémplen conditions[21] and protected the 5′-OH group with DMT-Cl followed by the synthesis of phosphoramidite **5**. In order to establish the configuration at C1′ unambiguously, **4** was treated with tetrabutylammonium fluoride and dichloroacetic acid to yield the fully unprotected C-nucleoside **6** for crystallization. The crystal structure of the salicylic aldehyde **6** finally confirmed the desired β configuration (Scheme 1).

DNA synthesis was performed using a standard phosphoramidite protocol on an Expedite DNA synthesizer with prolonged coupling times for the incorporation of the salicylic aldehyde phosphoramidite. After additional treatment of the assembled DNA with wet dichloroacetic acid in CH_2Cl_2 and final cleavage from the solid support with saturated ammonia in water/ethanol, the oligonucleotides **7**, **8-a**, and **8-b** containing the salicylic aldehyde nucleobase were purified by reversed-phase high-performance liquid chromatography (RP-HPLC) and analyzed by MALDI-TOF mass spectrometry. The presence of the aldehyde was additionally proven by reaction of the obtained DNA with an amine; the resulting yellow color was indicative for the formation of salicylic aldimines. In addition, reaction of the DNA with *O*-benzylhydroxylamine and reductive amination using different primary amines and sodium cyanoborohydride gave quantitatively the corresponding *O*-benzyloximes and amines, respectively, as shown by mass spectrometric analysis.

All the prepared DNA duplexes and DNA hairpins together with their measured melting temperatures are listed in Table 1. In one sequence, replacement of an AT base pair (entry 1) with the salicylic aldehyde base pair (LL, entry 7) was found to decrease the melting temperature by 9.0 K. Addition of an excess of ethylenediamine (en) to a solution containing the DNA duplex caused an increase of the melting temperature by 4.8 K (Table 1, entries 4 and 5) accompanied by changes in the fluorescence and emission spectra indicative for the formation of salicylic aldimines. More important, however, is our observation that the careful titration of a solution of divalent metal ions to the ethylenediamine-containing DNA solution resulted in systematically increasing duplex stabilization (Figure 2a,b) accompanied by changes of the CD spectra (Figure 3a,b). One equivalent of Cu^{2+} induced a shift of the melting temperature to 82.4 °C (Table 1, entry 3), a shift of more than 30 K with respect to a normal AT base pair (+42.5 K with respect to the duplex containing the LL "base pair", Table 1, entry 2 and Figure 2a). Additional Cu^{2+} had no further effect. To the best of our knowledge, this is the most dramatic increase in duplex stabilization ever observed with a metal–base pair. Addition of one equivalent of Mn^{2+} (which is known to be oxidized to Mn^{3+} upon complexation by salen ligands)[22] increased the T_M by 28.1 K to 68.8 °C (Table 1, entries 4 and 6; Figure 2b).

Table 1: Melting-temperature experiments with oligonucleotides **7** and **8**.

Entry	Strands [a]	Additive(s)	T_M [°C]
1	**8-A-a/-T-b**	[d]	50.1
2	**8-L-a/b**	[b]	39.9
3	**8-L-a/b**	100 μM en 3 μM Cu^{2+} [b]	82.4
4	**8-L-a/b**	[c]	40.7
5	**8-L-a/b**	100 μM en [c]	45.5
6	**8-L-a/b**	100 μM en 3 μM Mn^{2+} [c]	68.8[e]
7	**8-L-a/b**	[d]	41.1
8	**8-L-a/b**	100 μM en 400 μM Zn^{2+} [d]	48.8[e]
9	**8-L-a/b**	100 μM en 400 μM Ni^{2+} [d]	36.5
10	**8-L-a/b**	200 μM $MeNH_2$ 4 μM Cu^{2+} [b]	52.3
11	**8-L-a/b**	4 μM Cu^{2+} [b]	54.9
12	**8-L-a/b**	6 μM Mn^{2+} [c]	40.7
13	**7-L**	[b]	19.9
14	**7-L**	100 μM en 6 μM Cu^{2+} [b]	65.2
15	**7-L**	[c]	22.1
16	**7-L**	100 μM en 4 μM Mn^{2+} [c]	[f]
17	**7-T/A**		46.5

[a] For sequences see Scheme 1. In **8-A-a** and **8-T-b** the salicylic aldehyde is replaced by A and T, respectively. All samples contained 3 μM DNA (duplex or hairpin) and 150 mM NaCl. Melting profiles were measured from 0 °C to 85 °C (for Cu^{2+}: 95 °C) with a rate of 0.5 K min^{-1}. Further details are given in the Supporting Information. [b] All experiments using Cu^{2+} and corresponding controls were carried out in 10 mM Ches (*N*-cyclohexyl-2-aminoethanesulfonic acid) buffer at pH 9.0. [c] All experiments using Mn^{2+} and corresponding controls were carried out in 10 mM Hepes (*N*-(2-hydroxyethyl)piperazine-*N*′-(2-ethanesulfonic acid)) buffer at pH 9.0. [d] Measured in 10 mM Tris(2-amino-2-(hydroxymethyl)propane-1,3-diol) buffer at pH 7.4. [e] Reproducible differences in de- and renaturing profiles due to thermal instability of the complex (see the Supporting Information). [f] No T_M determined (see the Supporting Information).

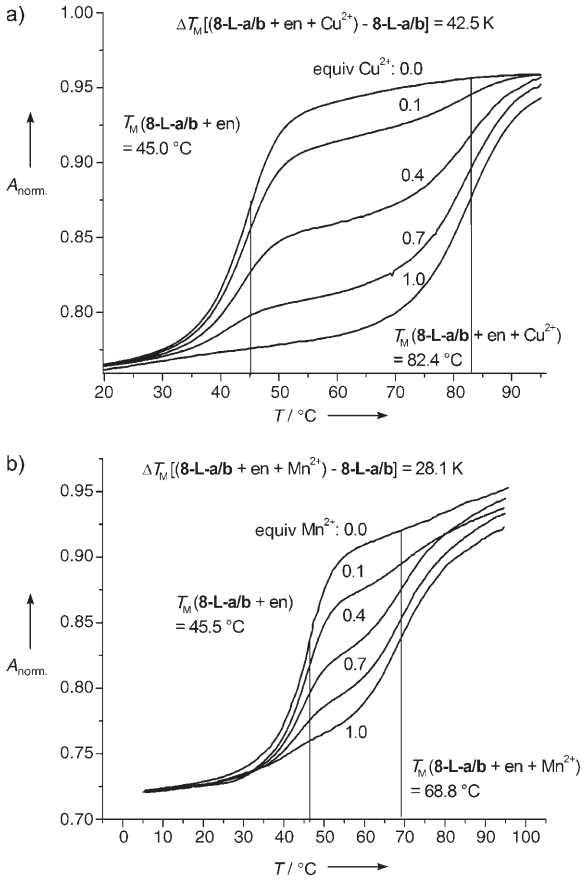

Figure 2. Melting profiles of 3 μM **8-L-a/b** with 100 μM ethylenediamine (en) in the presence of various amounts of a) Cu^{2+} (0–1 equiv) and b) Mn^{2+} (0–1 equiv). The samples contained 150 mM NaCl and 10 mM buffer (Ches pH 9 for Cu^{2+}, Hepes pH 9 for Mn^{2+}).

 © 2005 Wiley-VCH Verlag GmbH & Co. KGaA, Weinheim

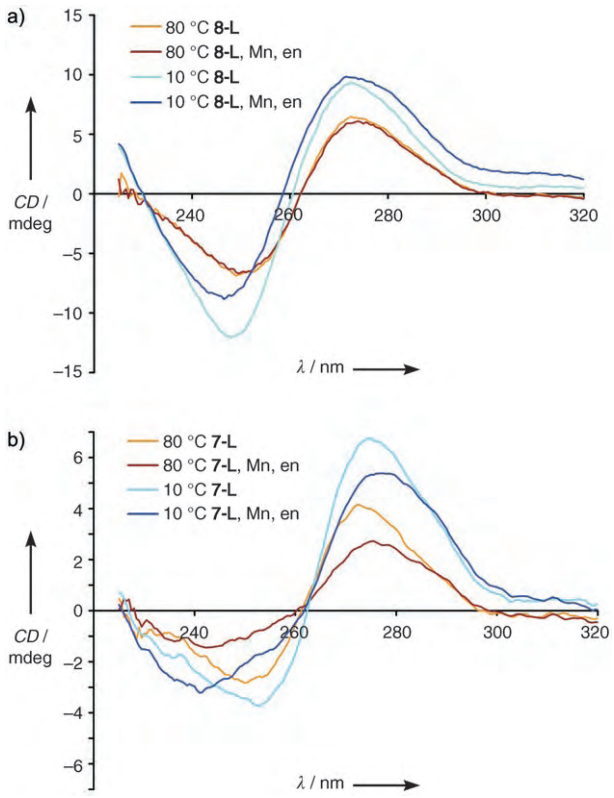

Figure 3. Comparison of CD spectra at 10 °C and 80 °C of a) **8-L-a/b** and b) **7-L** in the absence and presence of ethylenediamine and Mn^{2+}.

Again, additional Mn^{2+} did not further increase the melting temperature. Addition of Zn^{2+} gave an increase of T_M by 7.7 K (Table 1, entries 7 and 8). Interestingly, addition of Ni^{2+} caused reproducibly a decrease of the melting temperature by 4.6 K (Table 1, entries 7 and 9; see the Supporting Information). For Zn and Ni, however, high concentrations of the metal salts were required. When ethylenediamine was replaced by propylenediamine, only Cu^{2+} was able to shift the melting point (addition of butylenediamine had no effect). Addition of Cu^{2+} and not ethylenediamine resulted in an increase of T_M by 15.0 K relative to the melting temperature of the duplex with the pure LL "base pair" (Table 1, entries 2 and 11). In contrast, Mn^{2+} did not cause a shift in melting temperature when ethylenediamine was absent. No changes in the melting temperatures were observed in the absence of either one or both salicylic aldehyde nucleobases, showing that formation of the salen complex inside the duplex is indeed responsible for these dramatic shifts. Formation of the salen complex could be completely reversed by addition of an excess of EDTA to the DNA solution. In order to estimate the effect of the cross-linking, we added to the LL-containing duplex **8-L-a/b** first Cu^{2+} and then methylamine. In this case, a much smaller stabilization of only 12 K was observed (Table 1, entry 10).

Formation of the salen complex inside the duplex was further confirmed by CD spectroscopy of the DNA duplex **8-L-a/b** and the DNA hairpin **7-L** measured with and without metal and ethylenediamine (Figure 3). The CD spectra measured between 80 °C and 10 °C show clearly formation of B-type DNA structures in all cases (see the Supporting Information).[23] Addition of ethylenediamine and either Mn^{2+} or Cu^{2+} resulted in changes of the CD spectra below the individual melting temperatures, indicating formation of the salen complex (only the spectra with Mn^{2+} are shown). Above the melting temperatures the obtained CD spectra of the duplex are undistinguishable from those of DNA strands without the metal. However, the CD spectrum of the hairpin **7-L** at 80 °C in the presence of Mn^{2+} is clearly different from that without the metal. This indicates that the salen complex may stay intact to some extent in the hairpin even at rather high temperatures. (Analogous results were obtained for samples with Cu^{2+}).

In conclusion, we have described the synthesis of a salen-based metal–base pair inside a DNA duplex, in which the metal is located inside the duplex structure. We believe that the extreme increase of the melting temperature by more than 40 KC is induced by the reversible cross-linking of the ligand with ethylenediamine and additionally maybe by axial coordination of the metal with heteroatoms present in the base pairs below and above the metal–base pair.

Received: May 10, 2005
Revised: July 4, 2005
Published online: October 18, 2005

Keywords: DNA · DNA structures · metal–base pairs · nucleobases

[1] K. Tanaka, A. Tengeiji, T. Kato, N. Toyama, M. Shionoya, *Science* **2003**, *299*, 1212.
[2] a) S. Klug, M. Famulok, *Mol. Biol. Rep.* **1994**, *20*, 97; b) D. Zha, A. Eipper, M. T. Reetz, *ChemBioChem* **2003**, *4*, 34.
[3] G. Roelfes, B. L. Feringa, *Angew. Chem.* **2005**, *117*, 3294 – 3296; *Angew. Chem. Int. Ed. Engl.* **2005**, *44*, 3230 – 3232.
[4] C. Brotschi, C. J. Leumann, *Nucleosides Nucleotides Nucleic Acids* **2003**, *22*, 1195.
[5] L. Zhang, E. Meggers, *J. Am. Chem. Soc.* **2005**, *127*, 74.
[6] a) N. Zimmerman, E. Meggers, P. G. Schultz, *J. Am. Chem. Soc.* **2002**, *124*, 13684; b) E. Meggers, P. L. Holland, W. B. Tolman, F. E. Romesberg, P. G. Schultz, *J. Am. Chem. Soc.* **2000**, *122*, 10714.
[7] a) T. Tanaka, A. Tengeiji, T. Kato, N. Toyama, M. Shiro, M. Shionoya, *J. Am. Chem. Soc.* **2002**, *124*, 12494; b) K. Tanaka, Y. Yamada, M. Shionoya, *J. Am. Chem. Soc.* **2002**, *124*, 8802.
[8] a) C. Switzer, S. Sinha, P. H. Kim, B. D. Heuberger, *Angew. Chem.* **2005**, *117*, 1553; *Angew. Chem. Int. Ed.* **2005**, *44*, 1529; b) C. Switzer, D. Shin, *Chem. Commun.* **2005**, 1342.
[9] H. Weizman, Y. Tor, *J. Am. Chem. Soc.* **2001**, *123*, 3375.
[10] T. P. Yoon, E. N. Jacobsen, *Science* **2003**, *299*, 1691.
[11] a) J. F. Larrow, E. N. Jacobsen, *Top. Organomet. Chem.* **2004**, *6*, 123; b) T. Katsuki, *Chem. Soc. Rev.* **2004**, *33*, 437.
[12] T. Katsuki, *Adv. Synth. Catal.* **2002**, *344*, 131.
[13] T. Katsuki, *Coord. Chem. Rev.* **1995**, *140*, 189.
[14] a) M. Tokunaga, J. F. Larrow, F. Kakiuchi, E. N. Jacobsen, *Science* **1997**, *277*, 936; b) W. Sun, H. Wang, C. Xia, J. Li, P. Zhao, *Angew. Chem.* **2003**, *115*, 1072; *Angew. Chem. Int. Ed.* **2003**, *42*, 1042.
[15] a) J. L. Czlapinski, T. L. Sheppard, *J. Am. Chem. Soc.* **2001**, *123*, 8618; b) J. L. Czlapinski, T. L. Sheppard, *ChemBioChem* **2004**, *5*, 127; c) M. Nielsen, A. H. Thomsen, E. Cló, F. Kirpekar, K. V. Gothelf, *J. Org. Chem.* **2004**, *69*, 2240; d) K. V. Gothelf, A.

 © 2005 Wiley-VCH Verlag GmbH & Co. KGaA, Weinheim

Thomsen, M. Nielsen, E. Cló, R. S. Brown, *J. Am. Chem. Soc.* **2004**, *126*, 1044.
[16] S. Akine, T. Taniguchi, T. Nabeshima, *Chem. Lett.* **2001**, *7*, 682.
[17] N. U. Hofsløkken, L. Skattebøl, *Acta Chem. Scand.* **1999**, *53*, 258.
[18] R. Gopinath, S. J. Haque, B. K. Patel, *J. Org. Chem.* **2002**, *67*, 5842.
[19] R. Bihovsky, C. Selick, I. Guisti, *J. Org. Chem.* **1988**, *53*, 4026.
[20] a) M. Hoffer, *Chem. Ber.* **1960**, *93*, 2777; b) I. Singh, W. Hecker, A. K. Prasad, V. S. Parmar, O. Seitz, *Chem. Commun.* **2002**, 500.
[21] G. Zemplén, E. Pascu, *Ber. Dtsch. Chem. Ges.* **1929**, *62*, 1613.
[22] J. F. Larrow, E. N. Jacobsen, *J. Org. Chem.* **1994**, *59*, 1939.
[23] G. M. Segers-Nolten, N. M. Sijtsema, C. Otto, *Biochemistry* **1997**, *36*, 13241.
[24] CCDC 271234 contains the supplementary crystallographic data for this paper. These data can be obtained free of charge from The Cambridge Crystallographic Data Centre via www.ccdc.cam.ac.uk/data_request/cif.

 © 2005 Wiley-VCH Verlag GmbH & Co. KGaA, Weinheim

Artificial Peptide Receptors

DOI: 10.1002/anie.200501812

Charge Interactions Do the Job: A Combined Statistical and Combinatorial Approach to Finding Artificial Receptors for Binding Tetrapeptides in Water**

Carsten Schmuck, Martin Heil, Josef Scheiber, and Knut Baumann*

Intermolecular interactions involving oligopeptides or protein fragments are important supramolecular events responsible for a variety of biochemical and medicinal processes. Therefore, artificial peptide receptors are not only interesting as model systems for studying the principles of the underlying supramolecular recognition event but also as starting points for the development of sensors or drug candidates.[1] For this purpose strong complexation of the given target peptide by the artificial host under physiological conditions (in water) is necessary. This is, however, quite challenging.[2,3] On the one hand, hydrophobic interactions, which are especially important in water, are rather nonspecific, making the design of selective host molecules difficult.[4] On the other hand, electrostatic interactions such as ion pairs and H bonds, which as a result of their specificity and in the case of H bonds also directionality[5] are quite useful for imposing selectivity in the formation of supramolecular complexes,[6] are significantly weakened because of competitive solvation by the polar water molecules.[7] To the best of our knowledge no artificial oligopeptide receptor has been reported up to now that is capable of binding its substrate in water solely based on H bonds in combination with ion pairing. All known receptors for larger oligopeptides require additional hydrophobic,[8] aromatic,[1b,9] and/or the much stronger metal–ligand interactions[10] for efficient substrate binding.

We could recently show, for example, that one-armed tripeptide-based cationic guanidiniocarbonyl pyrrole receptors strongly bind the anionic tetrapeptide *N*-Ac-L-Val-L-Val-L-Ile-L-Ala-OH,[2b] a model for the C terminus of the amyloid β-peptide Aβ (1–42) and even interfere with fibril formation of the native Aβ (1–42) in vitro.[11] Complex formation in this case is, however, critically dependent on hydrophobic interactions with the alkyl side chains. Similar observations were also made by Kilburn et al., who screened a library of guanidinium-based flexible tweezer receptors for tripeptide binding.[2d] In aqueous solvent, efficient binding of the dye-labeled anionic tripeptide Glu(O*t*Bu)-Ser(O*t*Bu)-Val was observed ($K = 8 \times 10^4\,\text{M}^{-1}$). But the deprotected substrate was not bound at all. This indicates again that complex formation is mainly driven by hydrophobic interactions (probably with the bulky *t*Bu protecting groups). Ellman et al. described a synthetic vancomycin analogue, a rigidified tripeptide composed of nonnatural hydrophobic amino acids attached to vancomycin's carboxylate binding site; this receptor relies heavily on hydrophobic interactions for substrate binding.[2e]

Here, in a quantitative experimental screening of a medium-sized but focused combinatorial receptor library **1** in combination with a statistical QSAR analysis (QSAR = quantitative structure–activity relationship), we show that the binding of a nonhydrophobic tetrapeptide **2** in water by an artificial receptor **1** is possible without additional hydrophobic or metal–ligand interactions. To our knowledge this is the first example of tetrapeptide binding in water based on a combination of H bonds and ion pairing, and our study underlines the power of this combined experimental and theoretical approach for the identification of supramolecular receptors.

The general design of the receptor library **1** is shown in Figure 1. An efficient carboxylate binding site for the C terminus of the tetrapeptide[12,13] is attached to a linear tripeptide unit, allowing for the formation of a hydrogen-bonded β sheet with tetrapeptide substrate **2**. Interactions between the amino acid side chains both in the substrate and the receptor further stabilize the complex and provide the necessary substrate selectivity. Based on this receptor design (abbreviated CBS-AA^1-AA^2-AA^3) facile and fast solid-phase peptide synthesis can be used. By using a combinatorial variation of the amino acids in the tripeptide unit, structural diversity can be introduced.[14]

[*] Prof. Dr. C. Schmuck, Dr. M. Heil
Universität Würzburg
Institut für Organische Chemie
Am Hubland, 97074 Würzburg (Germany)
Fax: (+49) 931-888-4626
E-mail: schmuck@chemie.uni-wuerzburg.de
J. Scheiber, Dr. K. Baumann
Universität Würzburg
Institut für Pharmazie und Lebensmittelchemie
Am Hubland, 97074 Würzburg (Germany)

[**] Financial support from the Fonds der Chemischen Industrie and the Deutsche Forschungsgemeinschaft (SFB 630) is gratefully acknowledged.

Supporting information for this article is available on the WWW under http://www.angewandte.org or from the author.

InterScience
© 2005 Wiley-VCH Verlag GmbH & Co. KGaA, Weinheim

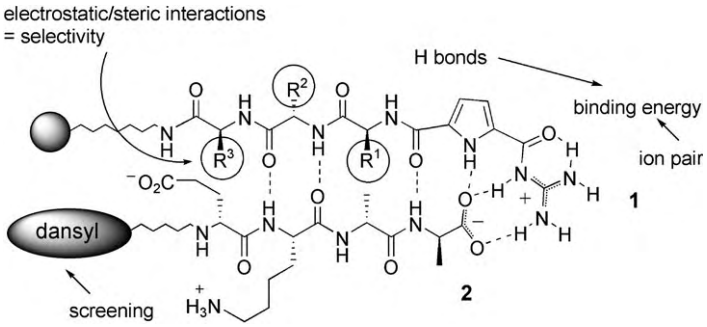

Figure 1. Schematic representation of complex formation between the receptor library **1** and the dansylated tetrapeptide substrate **2**. Dansyl = (dimethylamino)naphthalene-1-sulfonyl.

Table 1: Selected association constants K_{ass} for the complexation of the dansylated tetrapeptide **2** (EKAA) by receptors of type **1** (CBS-AA^1-AA^2-AA^3-resin).[a]

Entry	Receptor	K_{ass} [M^{-1}]
1	CBS-KKF	17100
2	CBS-KKL	15400
3	CBS-KKE	15300
4	CBS-KLF	8800
5	CBS-FKK	6200
6	CBS-KYK	5900
7	CBS-FEK	1600
8	CBS-VFF	660
9	CBS-VYV	360
10	CBS-KEE	100

[a] Obtained from quantitative screening of the library in buffered water (experimental errors of K are estimated to be ±20%).

We synthesized a combinatorial receptor library **1** on Amino-TentaGel as the solid support according to a standard Fmoc protocol using the split-mix approach[15] in combination with the IRORI radio-frequency tagging technology.[16] In each of the three coupling steps the same eight amino acids were used: Lys(Boc), Tyr(*t*Bu), Ser(*t*Bu), Glu(OBzl), Phe, Val, Leu, and Trp. The resulting library had 512 members. These specific amino acids used were chosen among the twenty proteinogenic amino acids to provide a representative range of varying polar, charged, and hydrophobic residues within the final receptor library. The side chains in the final library were deprotected on-bead using HBr (25%) in acetic acid to provide the receptors as charged species. As a first target for this library the polar tetrapeptide D-Glu-L-Lys-D-Ala-D-Ala-OH (EKAA) was chosen. This substrate is not only challenging because of its highly flexible and polar character but also biologically relevant as it plays a critical role in bacterial cell wall maturation.[17] To assess the binding properties of the 512 combinatorial receptors in aqueous solvents, a fluorescent and water-soluble derivative **2** of this tetrapeptide EKAA was synthesized on Wang resin as a solid support again using a standard Fmoc protocol. Full experimental details on the synthesis of the labeled substrate are provided in the Supporting Information.

In a first experiment a qualitative on-bead binding assay in water (incubation of the library with a 5 μM solution of the labeled tetrapeptide **2** in 20 μM bis-tris buffer, pH 6.0; bis-tris = 2,2-bis(hydroxyethyl)iminotris(hydroxymethyl)methane) indicated that receptors of the general structure **1** are indeed capable of binding the tetrapeptide substrate **2** under these conditions. We then determined the binding affinities of all of the 512 receptors in the library using an on-bead quantitative fluorescence assay in 200 μM bis-tris buffer at pH 6.0 in combination with a high-throughput microtiter-plate reader.[2b,18] According to this assay, the binding affinities for tetrapeptide **2** within the library vary from $K_{ass} = 17100\,M^{-1}$ (best receptor) to $K_{ass} < 20\,M^{-1}$ (worst receptor; Table 1). This amounts to a difference in activity of more than two orders of magnitude!

To validate the binding data obtained from the solid-phase screening, we performed complexation studies in solution for the selected receptors **3** and **4**, which were resynthesized on Rink-amide resin using standard Fmoc protocol. (Experimental details on the syntheses can be found in the Supporting Information.) Receptor **3** (CBS-KKF) was the most efficient in the on-bead screening (entry 1, Table 1), whereas **4** (CBS-KYK) showed a medium affinity (entry 6). UV-titration experiments[19] (Figure 2) confirmed that these two receptors form stable complexes with the unlabeled tetrapeptide *N*-Ac-EKAA-OH also in solution. Furthermore, the calculated binding constants obtained from the nonlinear regression analysis of the binding isotherms ($K_{ass} = 15400\,M^{-1}$ for **3** and $6200\,M^{-1}$ for **4**) are in good agreement with the values obtained from the quantitative on-bead screening assay ($K_{ass} = 17100\,M^{-1}$ and $5900\,M^{-1}$, respectively).

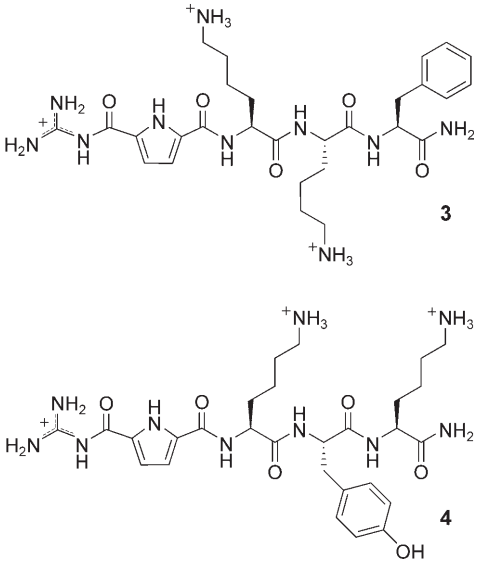

Hence, the on-bead screening results indeed represent the situation in free solution. An inspection of the relative binding affinities within the library (Table 1) reveals that complex formation is strongly correlated with the positive charge of the receptors. Those receptors containing two lysine residues next to the guanidinium cation form the strongest complexes with binding affinities $K_{ass} > 10^4\,M^{-1}$ (e.g. entries 1–3 in Table 1), whereas overall neutral or anionic receptors do not bind the substrate efficiently. For example, the binding

 © 2005 Wiley-VCH Verlag GmbH & Co. KGaA, Weinheim

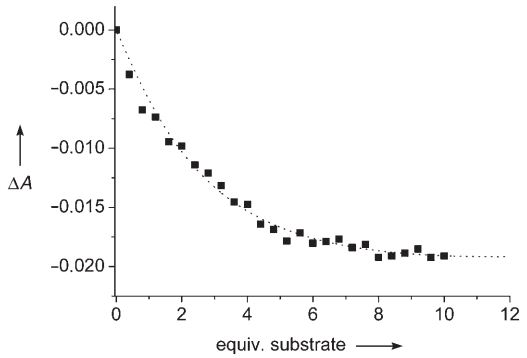

Figure 2. Binding isotherm for the complexation of tetrapeptide *N*-Ac-EKAA-OH by receptor **3** as obtained from a UV titration experiment corrected for absorption changes due to dilution. The dotted line represents the curve fitting for 1:1 complexation.

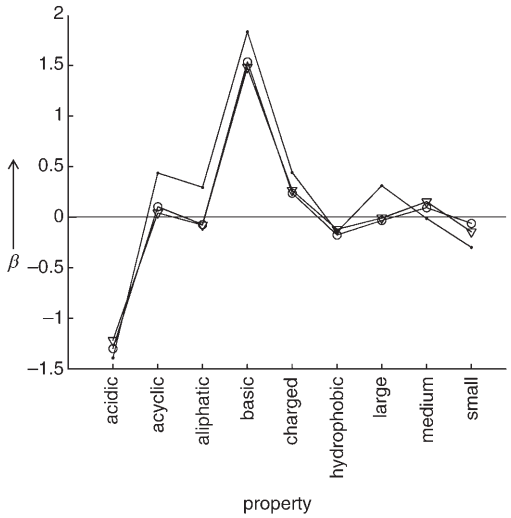

Figure 3. Comparison of the regression coefficients (β) for the binary descriptors. The charge of the amino acid (AA) strongly affects complex stability. For basic AAs (positive charge under physiological conditions) K_{ass} is greater (positive sign for β); for acidic AAs K_{ass} is less. All other descriptors such as hydrophobicity have hardly any influence. In general, the AA in the first position is more important than the other two (increased magnitude of β). –•–• first AA, ○ second AA, ▽ third AA.

affinity drops from $K_{ass} = 15300\,M^{-1}$ for CBS-KKE (entry 3) to $K_{ass} \approx 100\,M^{-1}$ for CBS-KEE (entry 10). This correspond to a change in affinity by two orders of magnitude for a single amino acid substitution, an exchange that transforms an overall dicationic receptor into a neutral one. Hydrophobic interactions are not important for substrate binding. Receptors with just hydrophobic side chains (e.g. entry 8 or 9) have only modest affinities ($K \leq 1000\,M^{-1}$).

These qualitative trends for the binding affinities of our flexible receptors **1** for the tetrapeptide EKAA (**2**) were then quantified using a statistical QSAR analysis. To get a rough impression of the most important structural features determining efficient binding, a simple binary structure descriptor was used first. The following nine different properties of the amino acids constituting the receptor were encoded in binary fashion: acidic (= negatively charged under physiological conditions), acyclic, aliphatic, basic (= positively charged), charged (= either acidic or basic), hydrophobic, large, medium, and small.[20] Figure 3 shows the regression coefficients for these nine binary variables and each of the three amino acids within the receptor as obtained from the statistical analysis. It can be seen that the property basicity (= positively charged side chain), in particular of the first amino acid next to the carboxylate binding site, has a strong positive effect on $\lg K_{ass}$, while the property acidity (= negatively charged side chain) has a negative effect, and other properties, for example, hydrophobicity have hardly any effect at all. This clearly shows that complex formation between receptor **1** and the tetrapeptide **2** is strongly dependent on charge interactions.

Next, a quantitative mathematical QSAR model was used to predict the binding affinity of receptors that were not part of our initial library used for the screening. To improve the quality of the mathematical model for this purpose we first extended the initial rough set of nine descriptors, which for example, do not allow to distinguish between basic amino acids such as lysine or histidine, to a set of 49 selected physicochemical, energetic, and conformational properties.[21] This model allows an individual description of all 20 proteinogenic amino acids. This descriptor set is a subset of the amino acid index[22] that resulted from a cluster analysis conducted by Tomii and Kanehisa.[21,22] A plot of the experimental $\lg K_{ass}$ values versus the cross-validated predictions of $\lg K_{ass}$ is shown in Figure 4.[23]

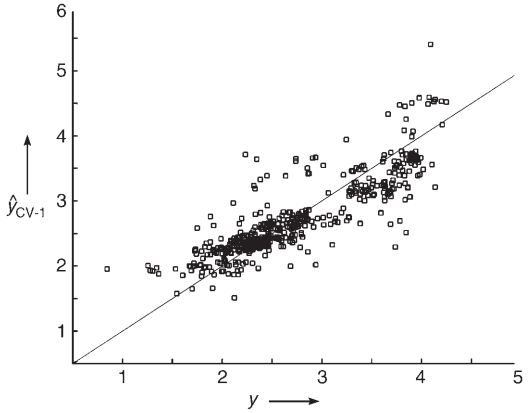

Figure 4. Experimental (*y*) vs. predicted values of $\lg K_{ass}$ ($\hat{y}_{CV\text{-}1}$).

A quantitative inspection of this elaborated mathematical model using a variable-selection routine[24,25] again confirmed that tetrapeptide binding is based solely on charge interactions.[26] The descriptors encoding hydrophobicity, aromatic character, and van der Waals interactions hardly affect the quality of the model.

Finally, the full model (i.e. all $3 \times 49 = 147$ variables) was used to predict the binding affinities of a virtual combinatorial library containing all possible tripeptide sequences in the receptor that can be obtained from the common 20 proteinogenic amino acids (library size $n = 8000$ members). This virtual library is 15 times larger than the initial experimental

 © 2005 Wiley-VCH Verlag GmbH & Co. KGaA, Weinheim

receptor library **1** used for the screening (512 members). But even out of the 7488 virtual receptors not yet synthesized, no receptors with significantly improved binding properties for tetrapeptide **2** are expected based on the QSAR analysis. The most efficient receptor in this much larger virtual library, CBS-KKR, is predicted to be only less than three times better than the best hit (CBS-KKF) in our initial library ($K = 50\,000\,\text{M}^{-1}$ vs. $17\,100\,\text{M}^{-1}$, respectively). Hence, the additional investment of time and money for the synthesis and screening of this 15-times larger virtual library based on the full set of all 20 proteinogenic amino acids instead of just the focused library based on the preselected subset of eight amino acids used here would not have paid off.[27]

In summary, quantitative combinatorial library screening in combination with the statistical QSAR analysis reveals three important points: 1) Fully flexible one-armed artificical receptors **1** efficiently bind polar tetrapeptides such as EKAA in water. 2) For this substrate, ion-pair formation in combination with H bonds is the main driving force for complex formation. Hence, additional hydrophobic or aromatic interactions are not necessarily required to achieve strong peptide binding under physiological conditions. 3) Small but carefully designed libraries ("focused libraries") are sufficient to explore the features of even much larger ensembles. Hence, the size of a combinatorial library alone is not decisive as long as the library contains the correct range of diversity for the given problem.[28] Currently, we are exploring the potential of such peptide receptors as identified here for the design of selective peptide sensors.

Received: May 25, 2005
Published online: October 18, 2005

Keywords: combinatorial chemistry · receptors · structure–activity relationships · supramolecular chemistry

[1] a) H.-J. Böhm, G. Klebe, *Angew. Chem.* **1996**, *108*, 2750 – 2778; *Angew. Chem. Int. Ed. Engl.* **1996**, *35*, 2588 – 2614; b) E. A. Meyer, R. K. Castellano, F. Diederich, *Angew. Chem.* **2003**, *115*, 1244 – 1287; *Angew. Chem. Int. Ed.* **2003**, *42*, 1210 – 1250.

[2] For selected examples of artifical peptide receptors see: a) C. Schmuck, L. Geiger, *J. Am. Chem. Soc.* **2004**, *126*, 8898 – 8899; b) C. Schmuck, M. Heil, *ChemBioChem* **2003**, *4*, 1232 – 1238; c) S. Rensing, T. Schrader, *Org. Lett.* **2002**, *4*, 2161 – 2164; d) K. Jensen, T. M. Braxmeier, M. Demarcus, J. G. Frey, J. D. Kilburn, *Chem. Eur. J.* **2002**, *8*, 1300 – 1309; e) R. Xuo, G. Greiveldinger, L. E. Marenus, A. Cooper, J. A. Ellman, *J. Am. Chem. Soc.* **1999**, *121*, 4898 – 4899; f) M. Sirish, H.-J. Schneider, *Chem. Commun.* **1999**, *10*, 907 – 908; g) M. Davies, M. Bonnat, F. Guillier, J. D. Kilburn, M. Bradley, *J. Org. Chem.* **1998**, *63*, 8696 – 8703; h) A. Hossain, H. J. Schneider, *J. Am. Chem. Soc.* **1998**, *120*, 11 208 – 11 209; i) R. Breslow, Z. Yang, R. Ching, G. Trojandt, F. Odobel, *J. Am. Chem. Soc.* **1998**, *120*, 3536 – 3537; j) J. S. Albert, M. W. Peczuh, A. D. Hamilton, *Bioorg. Med. Chem.* **1997**, *5*, 1455 – 1467.

[3] For review articles on artificial peptide receptors see: a) M. W. Peczuh, A. D. Hamilton, *Chem. Rev.* **2000**, *100*, 2479 – 2494; b) H.-J. Schneider, *Adv. Supramol. Chem.* **2000**, *6*, 185 – 216; c) H.-J. Schneider, *Angew. Chem.* **1993**, *105*, 890 – 892; *Angew. Chem. Int. Ed. Engl.* **1993**, *32*, 848 – 850; d) T. H. Webb, C. S. Wilcox, *Chem. Soc. Rev.* **1993**, *22*, 383 – 395.

[4] For reviews on hydrophobic interactions see: a) B. Widom, P. Bhimalapuram, K. Koga, *Phys. Chem. Chem. Phys.* **2003**, *5*, 3085 – 3093; b) L. R. Pratt, A. Pohorille, *Chem. Rev.* **2002**, *102*, 2671 – 2691; c) N. T. Southall, K. A. Dill, A. D. J. Haymet, *J. Phys. Chem. B* **2002**, *106*, 521 – 533.

[5] J. P. Glusker, *Top. Curr. Chem.* **1998**, *198*, 1 – 56.

[6] L.-J. Prins, D. N. Reinhoudt, P. Timmerman, *Angew. Chem.* **2001**, *113*, 2446 – 2492; *Angew. Chem. Int. Ed.* **2001**, *40*, 2383 – 2426.

[7] a) M. Meot-Ner, *Chem. Rev.* **2005**, *105*, 213 – 284; b) G. A. Jeffrey, *An Introduction to Hydrogen Bonding*, Oxford University Press, New York, **1997**; c) J. Israelachvili, *Intermolecular & Surface Forces*, 2nd ed., Academic Press, London, **1992**.

[8] The importance of hydrophobic interactions for peptide-peptide interactions within model systems ("hydrophobic cluster formation") was for example demonstrated by Kelly in his work on β-sheet nucleators: a) P. Chitnumsub, W. R. Fiori, H. A. Lashuel, H. Diaz, J. W. Kelly, *Bioorg. Med. Chem.* **1999**, *7*, 39 – 59; b) K. Y. Tsang, H. Diaz, N. Graciana, J. W. Kelly, *J. Am. Chem. Soc.* **1994**, *116*, 3988 – 4005; c) J. P. Schneider, J. W. Kelly, *Chem. Rev.* **1995**, *95*, 2169 – 2187.

[9] For reviews on aromatic interactions within peptides and in supramolecular model systems see: a) M. L. Waters, *Biopolymers* **2004**, *76*, 435 – 445; b) M. L. Waters, *Curr. Opin. Chem. Biol.* **2002**, *6*, 736 – 741; c) C. A. Hunter, K. R. Lawson, J. Perkins, C. J. Urch, *J. Chem. Soc. Perkin Trans. 2* **2001**, 651 – 669.

[10] Some recent example of metal-based peptide binding: a) A. Buryak, K. Severin, *Angew. Chem.* **2004**, *116*, 4875 – 4878; *Angew. Chem. Int. Ed.* **2004**, *43*, 4771 – 4774; b) H. Imai, H. Munakata, Y. Uemori, N. Sakura, *Inorg. Chem.* **2004**, *43*, 1211 – 1213; c) A. T. Wright, E. V. Anslyn, *Org. Lett.* **2004**, *6*, 1341 – 1344; d) M. Sirish, V. Chertkov, H.-J. Schneider, *Chem. Eur. J.* **2002**, *8*, 1181 – 1188; e) H. Ogoshi, T. Mizutani, *Acc. Chem. Res.* **1998**, *31*, 81 – 89.

[11] C. Schmuck, P. Frey, M. Heil, *ChemBioChem* **2005**, *6*, 628 – 631.

[12] a) C. Schmuck, V. Bickert, *Org. Lett.* **2003**, *5*, 4579 – 4581; b) C. Schmuck, L. Geiger, *Curr. Org. Chem.* **2003**, *7*, 1485 – 1502; c) C. Schmuck, *Chem. Eur. J.* **2000**, *6*, 709 – 718.

[13] For comprehensive reviews of anion recognition see the following: a) K. A. Schug, W. Lindner, *Chem. Rev.* **2005**, *105*, 67 – 113; b) M. D. Best, S. L. Tobey, E. V. Anslyn, *Coord. Chem. Rev.* **2003**, *240*, 3 – 15; c) P. A. Gale, *Coord. Chem. Rev.* **2003**, *240*, 191 – 221; d) R. J. Fitzmaurice, G. M. Kyne, D. Douheret, J. D. Kilburn, *J. Chem. Soc. Perkin Trans. 1* **2002**, 841 – 864; e) T. S. Snowden, E. V. Anslyn, *Curr. Opin. Chem. Biol.* **1999**, *3*, 740 – 746; f) P. D. Beer, P. Schmitt, *Curr. Opin. Chem. Biol.* **1997**, *1*, 475 – 482; g) A. Bianchi, K. Bowman-James, E. Garcia-España, *Supramolecular Chemistry of Anions*, Wiley-VCH, New York, **1997**; h) F. P. Schmidtchen, M. Berger, *Chem. Rev.* **1997**, *97*, 1609 – 1646; i) C. Seel, A. Galán, J. deMendoza, *Top. Curr. Chem.* **1995**, *175*, 101 – 132.

[14] For review articels on the use of combinatorial receptor libraries see: a) N. Srinivasan, J. D. Kilburn, *Curr. Opin. Chem. Biol.* **2004**, *8*, 305 – 310; b) B. Linton, A. D. Hamilton, *Curr. Opin. Chem. Biol.* **1999**, *3*, 307 – 312; c) Y. R. DeMiguel, J. M. K. Sanders, *Curr. Opin. Chem. Biol.* **1998**, *2*, 417 – 421; d) W. C. Still, *Acc. Chem. Res.* **1996**, *29*, 155 – 163.

[15] K. S. Lam, M. Lebl, V. Krchnak, *Chem. Rev.* **1997**, *97*, 411 – 448.

[16] A. W. Czarnik, *Curr. Opin. Chem. Biol.* **1997**, *1*, 60 – 66.

[17] a) R. D. Süssmuth, *ChemBioChem* **2002**, *3*, 295 – 298; b) K. C. Nicolaou, C. N. Boddy, S. Bräse, N. Wissinger, *Angew. Chem.* **1999**, *111*, 2230 – 2287; *Angew. Chem. Int. Ed.* **1999**, *38*, 2096 – 2152; c) D. H. Williams, B. Bardsley, *Angew. Chem.* **1999**, *111*, 1264 – 1286; *Angew. Chem. Int. Ed.* **1999**, *38*, 1173 – 1193; d) C. T. Walsh, S. L. Fisher, I.-S. Park, M. Prahalad, Z. Wu, *Chem. Biol.* **1996**, *3*, 21 – 28.

[18] a) P. W. Smith, G. Chang, W. C. Still, *J. Org. Chem.* **1988**, *53*, 1587 – 1590; b) S. S. Yoon, W. C. Still, *Tetrahedron* **1995**, *51*, 567 –

 © 2005 Wiley-VCH Verlag GmbH & Co. KGaA, Weinheim

578; c) Y. Cheng, T. Suenaga, W. C. Still, *J. Am. Chem. Soc.* **1996**, *118*, 1813 – 1814; d) R. Arienzo, J. D. Kilburn, *Tetrahedron* **2002**, *58*, 711 – 719.

[19] a) C. S. Wilcox in *Frontiers in Supramolecular Chemistry and Photochemistry* (Eds.: H.-J. Schneider, H. Dürr), VCH, Weinheim, **1990**, pp. 123 – 144; b) K. Hirose, *J. Inclusion Phenom. Macrocyclic Chem.* **2001**, *39*, 193 – 209; c) K. A. Connors, *Binding Constants*, Wiley, New York, **1987**; d) L. Fielding, *Tetrahedron* **2000**, *56*, 6151 – 6170.

[20] Even for these simple binary descriptors the quality of the cross-validated model was quite satisfactory given the limited accuracy of the experimental screening data. 72 % of the variation in the data could be explained ($R^2_{\text{CV-1}} = 0.72$, $RMSEP_{\text{CV-1}} = 0.87$, $n = 476$). The figures of merit for test set prediction (average over 100 splits) were virtually identical to those of the cross-validation ($R^2_{\text{Test,Avg}} = 0.72$, $RMSEP_{\text{Test,Avg}} = 0.87$, $\theta = 3$) underlining the stability of the model.

[21] a) M. M. Gromiha, M. Oobatake, A. Sarai, *Biophys. Chem.* **1999**, *82*, 51 – 67; b) M. M. Gromiha, *J. Chem. Inf. Comput. Sci.* **2003**, *43*, 1481 – 1485.

[22] K. Tomii, M. Kanehisa, *Protein Eng.* **1996**, *9*, 27 – 36.

[23] Since these 49 indices were measured on different scales (e.g. molecular weight vs. isoelectric point), the variables were autoscaled prior to analysis (i.e. subtraction of the mean and division by the standard deviation of the variable). The resulting model using these 49 diverse descriptors for each amino acid ($m = 147$) yielded a model quality similar to the simple binary model ($R^2_{\text{CV-1}} = 0.71$, $RMSEP_{\text{CV-1}} = 0.88$, $\theta = 3$, $n = 476$; $R^2_{\text{Test,Avg}} = 0.73$, $RMSEP_{\text{Test,Avg}} = 0.85$) but now allows to dinstinguish between all 20 proteinogenic amino acids.

[24] a) K. Baumann, H. Albert, M. von Korff, *J. Chemom.* **2002**, *16*, 339 – 350; b) K. Baumann, M. von Korff, H. Albert, *J. Chemom.* **2002**,*16*, 351 – 360.

[25] M. Stone, *J. Roy. Statist. Soc. Ser. B* **1974**, *36*, 111 – 147.

[26] The isoelectric point of the amino acid side chain alone is sufficient to predict the binding affinity of the receptors. Using only this one variable for each of the three amino acids alone results in only a slightly decreased model quality as compared to the full set of 49 descriptors ($R^2_{\text{CV-1}} = 0.69$, $RMSEP_{\text{CV-1}} = 0.91$, $\theta = 1$, $n = 476$; $R^2_{\text{Test,Avg}} = 0.69$, $RMSEP_{\text{Test,Avg}} = 0.91$).

[27] For a critical comment on library size in the context of drug-development see: R. Breinbauer, I. R. Vetter, H. Waldmann, H. *Angew. Chem.* **2002**, *114*, 3002 – 3015; *Angew. Chem. Int. Ed.* **2002**, *41*, 2878 – 2890.

[28] A lot of effort is nowadays directed to find this correct diversity in designing combinatorial libraries. See for example : a) G. Chen, S. Zheng, X. Luo, J. Shen, W. Zhu, H. Liu, C. Gui, J. Zhang, M. Zheng, C. M. Puah, K. Chen, H. Jang, *J. Comb. Chem.* **2005**, *7*, 398 – 406; b) B. K. Shoichet, *Nature* **2004**, *432*, 862 – 865; c) S. L. Schreiber, *Chem. Eng. News* **2003**, *81*, 51 – 61.

 © 2005 Wiley-VCH Verlag GmbH & Co. KGaA, Weinheim

Magnetic Storage Materials

DOI: 10.1002/anie.200502579

Synthesis, Crystal Structure, and Magnetic Properties of the Semihard Itinerant Ferromagnet $RhFe_3N$**

*Andreas Houben, Paul Müller, Jörg von Appen, Heiko Lueken, Rainer Niewa, and Richard Dronskowski**

Since the invention of magnetic data recording by Poulsen more than a century ago and the development of the first magnetic hard disc by the IBM company,[1] there has always been a persistent demand for magnetic storage devices. At present, the capacity of hard discs doubles every year and, fortunately enough, this expansion outpaces the performance enhancement of computer chips predicted by Moore's law.[2] If data storage should continue to keep ahead of data production, intense research for new materials needed in high-performance magnetic recording devices will remain a challenge for solid-state chemistry.[3] But this is merely the logical continuation of the impressive history of solid-state magnetochemistry, as demonstrated by well-known example of the maghemite phase.[4]

Within the realm of nitrogen-containing materials, the binary nitride γ′-Fe_4N has been studied intensively both by experimental[5–7] and also theoretical[8,9] methods. In addition to its remarkable chemical inertness, the phase exhibits fascinating magnetic properties that make γ′-Fe_4N a possible material for high-performance magnetic recording heads. In particular, the very large specific saturation magnetization of $\sigma^s = 208\ A\,m^2\,kg^{-1}$ (which is close to that of α-Fe, $\sigma^s = 218\ A\,m^2\,kg^{-1}$) and also the low coercive field of $H_C = 460\ A\,m^{-1}$ have attracted major attention.[6] γ′-Fe_4N adopts a perovskite-like crystal structure (Figure 1) with the space group $Pm\bar{3}m$ and the lattice parameter $a = 3.7900(6)$ Å.[7]

It was realized some time ago that the magnetic properties of γ′-Fe_4N may be influenced by replacing the iron atoms on Wyckoff positions 1*a* and/or 3*c*. The newly introduced atoms mainly control the crystal growth, yielding magnetic particles with a pronounced anisotropic shape and a high coercive field which makes them suitable for high-density storage materi-

[*] Dipl.-Chem. A. Houben, Dr. P. Müller, Dipl.-Chem. J. von Appen, Prof. Dr. H. Lueken, Prof. Dr. R. Dronskowski
Institut für Anorganische Chemie
Rheinisch-Westfälische Technische Hochschule Aachen
Landoltweg 1, 52056 Aachen (Germany)
Fax: (+49) 241-80-92642
E-mail: drons@HAL9000.ac.rwth-aachen.de
Dr. R. Niewa
Max-Planck-Institut für Chemische Physik fester Stoffe
Nöthnitzer Strasse 40, 01187 Dresden (Germany)

[**] We thank Klaus Kruse for measurement of the magnetization data, Dipl.-Chem. Manfred Speldrich for competent help with their graphical representation, and Dr. Roland Winde (Umicore, Wolfgang-Hanau) for the kind supply of metallic rhodium.

InterScience
© 2005 Wiley-VCH Verlag GmbH & Co. KGaA, Weinheim

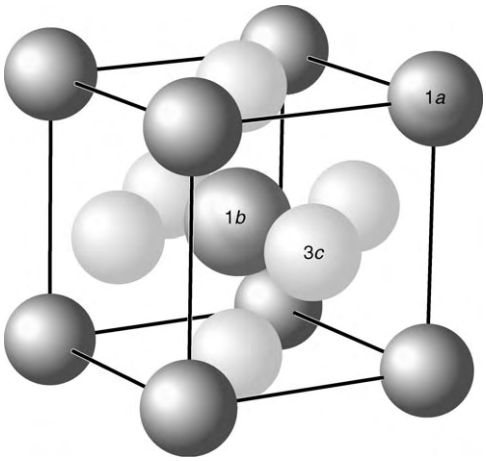

Figure 1. The crystal structure of γ′-Fe_4N in space group $Pm\bar{3}m$ ($a = 3.7900(6)$ Å).[7] The large nitrogen atom (gray) occupies the very center (Wyckoff position 1*b*), and the iron atoms (dark and light gray) are found at the corners (1*a*) and face centers (3*c*). In $RhFe_3N$, the 1*a* position is completely substituted by Rh.

als.[10–12] We know—without claiming completeness—of a couple of reports dealing with berthollide ternary nitrides of the general form $M_xFe_{4-x}N$ with M = Ru,[10] Os,[10] Co,[11] Ir,[10] Cu,[13] Ag,[14] and Zn[15] ($x \ll 1$) as well as Sn ($0 \le x \le 1.2$),[16–18] Mn,[12] and Ni[5,19–21] ($0 \le x \le 4$). In contrast, replacing Fe with Pd,[22] Pt,[5] Au,[14] or In[15] leads to daltonide ternary nitrides MFe_3N of the simple perovskite type.

There have been early attempts to relate preference for substitution at the Wyckoff positions 1*a* and 3*c*[23] to the relative affinities of Fe and M atoms to the nitrogen atom and, even more importantly, the relative sizes of the metal-atom radii. Only if the radius of the substituting M atom is smaller than that of the Fe atom ($r_{Fe} = 1.24$ Å), are both Wyckoff positions statistically occupied. This is found for Mn with $r_{Mn} = 1.17$ Å. Otherwise, the larger atoms clearly prefer position 1*a* because the coordination sphere of the 1*a*-centered cuboctahedron in γ′-Fe_4N is much larger than that of the 3*c* position. This is easily rationalized by the fact that the ^{1a}Fe–^{3c}Fe distance (2.68 Å) is longer than the ^{3c}Fe–^{1b}N distance (1.90 Å) or, alternatively, by the fact that the 1*a* position does not have nearest nitrogen neighbors but is subject to an fcc-like environment of Fe atoms.

These classical ideas have been corroborated recently and quantified by quantum-mechanical total-energy calculations from first principles, and the Aachen group has also predicted, by means of parameter-free enthalpy calculations, the existence of an enthalpically stable and also ferromagnetic ternary nitride phase, namely $RhFe_3N$. Based on density-functional theory and the GGA exchange-correlation functional,[24] the plausible chemical reaction [Eq. (1)] will be

$$FeRh + Fe + FeN \rightarrow RhFe_3N \qquad (1)$$

exothermic with an energy (enthalpy at 0 K) gain of about $\Delta E = -7$ kJ mol^{-1} and a larger −23 kJ mol^{-1} when the starting materials are Rh, Fe, and FeN. Also, the GGA lattice parameter of $RhFe_3N$ in space group $Pm\bar{3}m$ is predicted to be $a = 3.87$ Å, but one has to keep in mind that the GGA is known to overestimate this value by ca. 1%. In addition, the calculations clearly predict that only the 1*a* position of $RhFe_3N$ will be occupied by the rhodium atom, fully and exclusively. In other words, $RhFe_3N$, yet to be made, must be a daltonide phase. Its magnetic saturation moment μ_A^s is predicted to be 9.2 μ_B per formula unit, with local moments of 0.96 and 2.76 μ_B for Rh and Fe, respectively.[24]

We have now succeeded in preparing $RhFe_3N$ for the first time, and there are at least two synthetic routes. In the first approach elemental Rh and Fe or ε-Fe_3N are mixed in a planetary ball mill under Ar atmosphere for 40 h until the products are nearly X-ray amorphous. Subsequent nitridation in flowing ammonia at temperatures above 600 °C leads to two-phase samples containing $RhFe_3N$ and FeRh. Although the percentage of FeRh decreases upon increasing Fe/Rh molar ratio, the relative intensities of the ternary nitride and its unit cell parameter remain practically unaltered, thereby indicating the absence of a significant homogeneity range in the sense of $(Rh_{1-x}Fe_x)Fe_3N$.

Alternatively, one may follow the coupled-reduction route[25,26] developed by Klemm and co-workers, in which the reduction of a metal oxide is accompanied by the simultaneous formation of an intermetallic alloy. Ternary nitrides such as $RhFe_3N$ are accessible by this method starting with an NH_3/H_2 ammonolysis (1:1 ratio) of iron(III) oxide, Fe_2O_3, and elemental rhodium; in fact, the best results are achieved upon using these starting materials. Nonetheless, other iron oxides may also be utilized in combination with rhodium, and even a solid mixture of iron/rhodium oxides eventually leads to $RhFe_3N$ but with slightly lower yields. We also note that the coupled-reduction principle also explains, in retrospect, the early existence of $NiFe_3N$, $PdFe_3N$, and $PtFe_3N$ by the original thermodynamic considerations made four decades ago.[25,26]

Probably because of the minute enthalpy of formation (see above) of $RhFe_3N$, its synthesis is always accompanied by the formation of competing phases. At high temperatures the second phase FeRh ($Pm\bar{3}m$; $a = 2.9825(3)$ Å) is observed, whereas at lower reaction temperatures different iron nitrides come into play, mainly ε-Fe_3N ($P6_322$; $a = 4.699(2)$ Å, $c = 4.382(4)$ Å). The above-mentioned ammonolysis of oxide/element precursors results in the highest $RhFe_3N$ yield (85 wt.% or 75 mol%) at 1100 °C, whereas at around 1000 °C, the yield decreases to approximately 70 wt.%. Neverthess, we believe that it should be possible to obtain pure $RhFe_3N$ samples by non-equilibrium synthetic techniques.

The phase and structure determination is based on high-resolution X-ray powder diffraction. An aluminum foil was inserted into the X-ray beam line to reduce the effect of Fe fluorescence radiation that results from the $Cu_{K\alpha 1}$ radiation. A typical diffraction pattern including the Rietveld refinement[27] is shown in Figure 2.[28]

Although γ′-Fe_4N and $RhFe_3N$ have very similar lattice parameters, the intensities of the 100 and 110 Bragg reflections help to easily discriminate between the two phases. Both reflections are quite weak for the binary nitride but of medium intensity for the ternary nitride. Also, the 100

 © 2005 Wiley-VCH Verlag GmbH & Co. KGaA, Weinheim

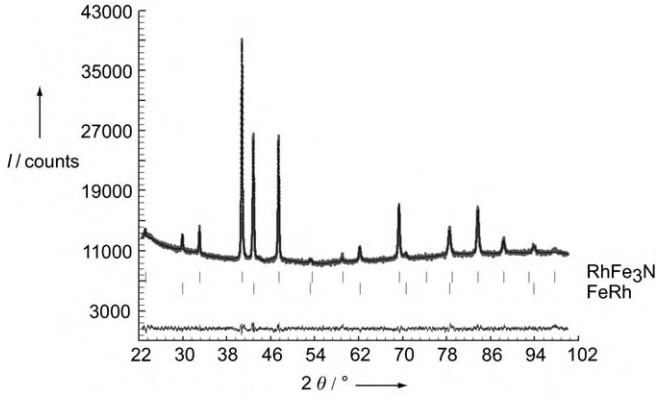

Figure 2. Diffraction pattern and Rietveld refinement of $RhFe_3N$ (first phase: $Pm\bar{3}m$; $a = 3.8292(2)$ Å) and FeRh (second phase: $Pm\bar{3}m$; $a = 2.9825(3)$ Å). The vertical bars designate the positions of the Bragg reflections.

intensity is almost twice as large as the 110 intensity for the case of γ′-Fe_4N. But, on the other hand, the 100 intensity is only about one-third as strong as the 110 intensity for $RhFe_3N$. As predicted from the theoretical calculations, the refinement clearly indicates that among the two possible Wyckoff positions (1*a* and 3*c*) only the 1*a* site is taken by the Rh atom, and no substitution of Fe by Rh is found for position 3*c*. In addition, position 1*a* is fully occupied by rhodium. Thus, $RhFe_3N$ is indeed a daltonide compound.

In accord with the larger radius of rhodium ($r_{Rh} = 1.34$ Å) compared to that of iron ($r_{Fe} = 1.24$ Å), the lattice parameter of $RhFe_3N$ ($a = 3.8292(2)$ Å) is also slightly larger (by about 1%) than that of γ′-Fe_4N. The theoretical prediction by the GGA method ($a = 3.87$ Å) overestimates the lattice parameter by 1%, which is characteristic of the GGA method.[24,29]

The magnetic properties of $RhFe_3N$ samples, which are unavoidably admixed with ca. 15 wt.% FeRh, were determined by SQUID magnetometry (MPMS-5S, Quantum Design) in the temperature range 300–650 K at an applied field of $B_0 = 0.01$ T. At a temperature of 5 K, a hysteresis loop was recorded in the field range ± 5 T. To allow for the magnetic contribution of FeRh, a corresponding pure sample of FeRh was also prepared and magnetically characterized under the same conditions, and its signal was subtracted from the original susceptibility data. Diamagnetic corrections and contributions from conduction electrons cancel to a large extent and have therefore been neglected.

The results of the magnetization measurements before and after subtraction of the magnetic FeRh contribution are presented in Figure 3 in a plot of the atomic magnetic moment μ_a per formula unit as a function of the temperature. On heating $RhFe_3N$ above 400 K one finds behavior typical of a ferromagnetic compound, and T_C is estimated to be 505(25) K. (T_C is given by the intersection of the linear fit of the steepest part of the magnetization curve with the T axis.[30]) The accuracy is somewhat limited not only because of the uncertainty of the amount of FeRh in the sample but also because of the annealing effects of the latter phase.[31] The hysteresis loop at 5 K is given in Figure 4. Its evaluation results in a coercive field H_C approximately one order of

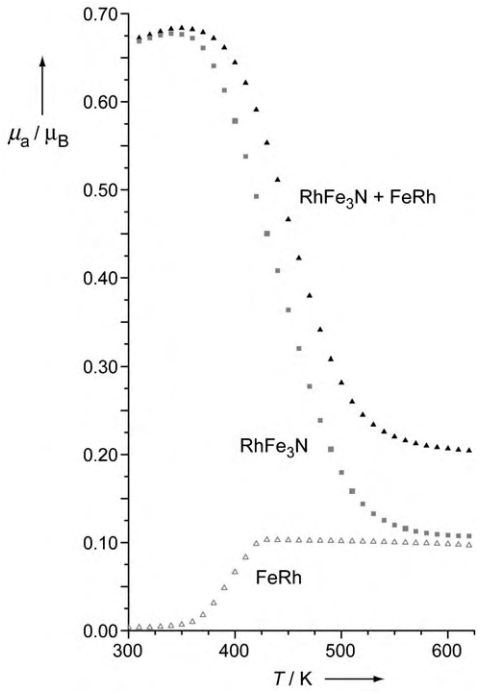

Figure 3. Variation of the magnetic moment μ_a per formula unit $RhFe_3N$ at a field of $B_0 = 0.01$ T as a function of the temperature, with actual measured data (▲), the FeRh contribution (△), and the $RhFe_3N$ contribution (■).

magnitude larger than that of γ′-Fe_4N. This finding in combination with a remanence of $\mu_0 M_R = 0.52(1)$ T allows us to categorize $RhFe_3N$ as a semihard ferromagnetic material.[32] At $B_0 = 5$ T the specific saturation magnetization reaches $\sigma^s = 163(2)$ A m^2 kg^{-1}, corresponding to $\mu_a^s = 8.3(1)$ μ_B per formula unit. Why H_C of $RhFe_3N$ is enhanced relative to that of γ′-Fe_4N is unknown as yet, and the 11% discrepancy between the experimental value for μ_a^s (8.3 μ_B) and the theoretical (9.2 μ_B) is probably a result of a theoretically overestimated (GGA) local moment of the Rh atom. Neutron diffraction measurements are needed to fully answer that question, and corresponding experimental studies are underway.

The density-functional (GGA) prediction of the bulk modulus K_0 (which serves as a simple measure of the phase's mechanical hardness) of the binary γ′-Fe_4N results in the theoretical value of 172 GPa, which compares satisfactorily with the recently determined experimental value[33] of 155(3) GPa; the small theoretical overestimation must be considered quite acceptable for the GGA functional. Interestingly, the bulk modulus of $RhFe_3N$ is predicted even to be larger, namely 187 GPa. Consequently, the ternary phase is not only a magnetically semihard ferromagnet, but it is also mechanically harder than γ′-Fe_4N itself; this is a truly promising combination of physical properties for recording heads.

In summary, the new ternary iron rhodium nitride $RhFe_3N$ was synthesized and structurally characterized. $RhFe_3N$ is a daltonide phase in which exclusively Rh occupies the 1*a* position, just as predicted by density-functional theory. The

 © 2005 Wiley-VCH Verlag GmbH & Co. KGaA, Weinheim

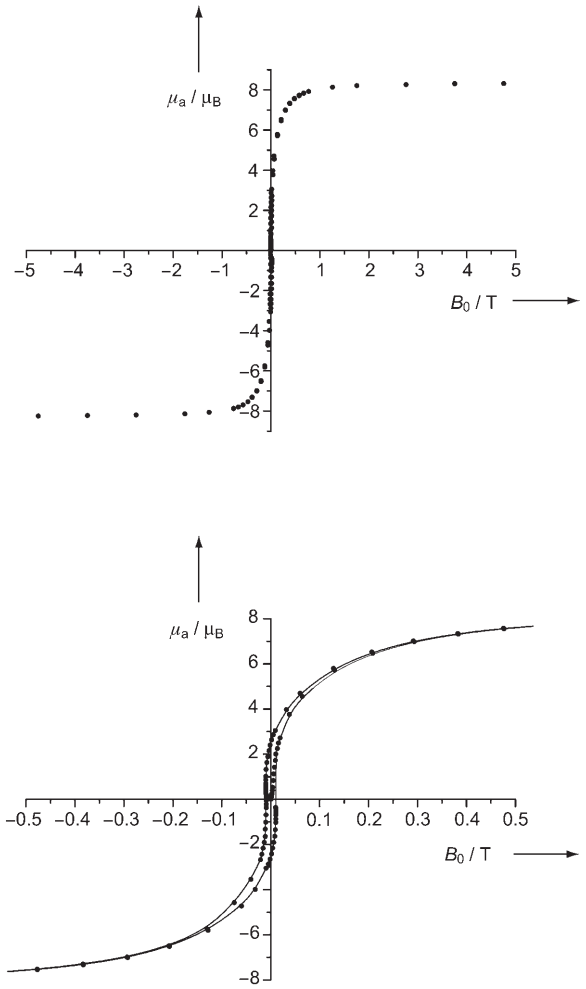

Figure 4. Hysteresis loop of $RhFe_3N$ at 5 K (top) and part of the loop showing remanent magnetization and coercive field (bottom). In the bottom part, the solid lines only serve to guide the eye.

magnetic properties indicate that the new phase is a semihard itinerant ferromagnet with a saturation moment of 8.3 μ_B per formula unit and a Curie ordering temperature of $T_C \approx 505$ K.

Received: July 22, 2005
Published online: October 18, 2005

Keywords: ferromagnetism · rhodium · solid-state synthesis · structure elucidation · ternary nitrides

[1] A. S. Hoagland, *IEEE Trans. Magn.* **2003**, *39*, 1871.
[2] G. E. Moore, *Electronics* **1965**, *38*, 114.
[3] M. Albrecht, J.-U. Thiele, A. Moser, *Phys. J.* **2003**, *2*, 25.
[4] R. Dronskowski, *Adv. Funct. Mater.* **2001**, *11*, 27.
[5] G. W. Wiener, J. A. Berger, *J. Met.* **1955**, *7*, 360.
[6] S. K. Chen, S. Jin, T. H. Tiefel, Y. F. Hsieh, E. M. Gyorgy, D. W. Jonson, Jr., *J. Appl. Phys.* **1991**, *70*, 6247.
[7] H. Jacobs, D. Rechenbach, U. Zachwieja, *J. Alloys Compd.* **1995**, *227*, 10.
[8] S. Matar, P. Mohn, G. Demazeau, B. Siberchicot, *J. Phys. Fr.* **1988**, *49*, 1761.
[9] C. A. Kuhnen, R. S. De Figueiredo, V. Drago, E. Z. da Silva, *J. Magn. Magn. Mater.* **1992**, *111*, 95.
[10] D. Andriamandroso, S. Matar, G. Demazeau, L. Fournès, *IEEE Trans. Magn.* **1993**, *29*, 2.
[11] S. Matar, L. Fournès, S. Chérubin-Jeannette, G. Demazeau, *Eur. J. Solid State Inorg. Chem.* **1993**, *30*, 871.
[12] B. Siberchicot, S. F. Matar, L. Fournès, G. Demazeau, P. Hagenmuller, *J. Solid State Chem.* **1990**, *84*, 10.
[13] R. S. de Figueiredo, J. Foct, A. V. dos Santos, C. A. Kuhnen, *J. Alloys Compd.* **2001**, *315*, 42.
[14] R. S. De Figueiredo, C. A. Kuhnen, A. V. dos Santos, *J. Magn. Magn. Mater.* **1997**, *173*, 141.
[15] C. A. Kuhnen, R. S. De Figueiredo, A. V. dos Santos, *J. Magn. Magn. Mater.* **2000**, *219*, 58.
[16] D. Andriamandroso, L. Fefilatiev, G. Demazeau, L. Fournès, M. Pouchard, *Mater. Res. Bull.* **1984**, *19*, 1187.
[17] Z. J. Zhao, D. S. Xue, F. S. Li, *J. Magn. Magn. Mater.* **2001**, *232*, 155.
[18] Z. Zhao, D. Xue, Z. Chen, F. Li, *Phys. Status Solidi A* **1999**, *174*, 249.
[19] F. Li, J. Yang, D. Xue, R. Zhou, *Appl. Phys. Lett.* **1995**, *66*, 2343.
[20] P. Rochegude, J. Foct, *Ann. Chim.* **1983**, *8*, 533.
[21] G. Shirane, W. J. Takei, S. L. Ruby, *Phys. Rev.* **1962**, *126*, 49.
[22] H. H. Stadelmaier, A. C. Fraker, *Trans. Metall. Soc. AIME* **1960**, *218*, 571.
[23] C. Cordier-Robert, J. Foct, *Eur. J. Solid State Inorg. Chem.* **1992**, *29*, 39.
[24] J. von Appen, R. Dronskowski, *Angew. Chem.* **2005**, *117*, 1230; *Angew. Chem. Int. Ed.* **2005**, *44*, 1205.
[25] W. Bronger, W. Klemm, *Z. Anorg. Allg. Chem.* **1962**, *319*, 58.
[26] H. Schulz, K. Ritapal, W. Bronger, W. Klemm, *Z. Anorg. Allg. Chem.* **1968**, *357*, 299.
[27] J. Rodriguez-Carvajal, FULLPROF *Version 2.8*, July 2004, ILL, unpublished.
[28] X-ray diffraction at room temperature was measured by using a calibrated Huber G670 Image plate powder diffractometer with $Cu_{K\alpha 1}$ radiation ($\lambda = 1.54059$ Å; flat sample; $5° \le 2\theta \le 100°$; step rate 0.005° in 2θ). The Rietveld refinement was carried out with the program FullProf[27] and a pseudo-Voigt profile function with a Gaussian/Lorentz η mixing parameter of 0.48(2). The residual values for $RhFe_3N$ are $R_p = 0.0114$ and $R_B = 0.0790$ for 14 Bragg reflections (19001 data points) and 11 refined parameters. The positions are 1*a* for Rh, 1*b* for N, and 3*c* for Fe (space group $Pm\bar{3}m$). The formula weight is $M = 284.45\ g\,mol^{-1}$ with a cell volume of $V = 56.147(3)$ Å^3. The X-ray density is $\rho = 8.41\ g\,cm^{-3}$.
[29] J. P. Perdew in *Electronic Structure of Solids '91* (Eds.: P. Ziesche, H. Eschrig), Akademie Verlag, Berlin, **1991**.
[30] R. Andrés, M. Brissard, M. Gruselle, C. Train, J. Vaissermann, B. Malézieux, J.-P. Jamet, M. Verdaguer, *Inorg. Chem.* **2001**, *40*, 4633.
[31] J. M. Lommel, J. S. Kouvel, *J. Appl. Phys.* **1967**, *38*, 1263.
[32] S. Chikazumi, *Physics of Ferromagnetism*, Clarendon Press, Oxford, **1997**.
[33] J. F. Adler, Q. Williams, *J. Geophys. Res. B* **2005**, *110*, 1203.

 © 2005 Wiley-VCH Verlag GmbH & Co. KGaA, Weinheim

Cross-Coupling

DOI: 10.1002/anie.200501860

Efficient Aryl–(Hetero)Aryl Coupling by Activation of C–Cl and C–F Bonds Using Nickel Complexes of Air-Stable Phosphine Oxides**

Lutz Ackermann, Robert Born, Julia H. Spatz, and Daniel Meyer*

Transition-metal-catalyzed cross-coupling reactions of organomagnesium compounds[1–4] are useful tools for the synthesis of unsymmetrically substituted biaryls, which are valuable building blocks for the synthesis of natural products, liquid crystals, polymers, and ligands.[5] Predominantly aryl iodides and bromides, and more recently aryl chlorides,[6] are employed as electrophiles. In contrast, the catalytic activation of unreactive C–F bonds remains extremely challenging because of the inherent strength of the C–F bond.[7,8] The activation of C–F bonds in general is of utmost importance because this transformation contributes to the fundamental understanding of the reactivity of very stable bonds, and because the selective synthesis of partially fluorinated compounds is still a challenge.

Herrmann showed elegantly that efficient nickel-catalyzed[9] cross-couplings between electronically nonactivated aryl fluorides and aryl Grignard reagents[10] can be accomplished at ambient temperature,[11] if appropriate stabilizing ligands are employed.[12,13] Recently, we employed modular air-stable dioxo- and diaminophosphine oxides in palladium-catalyzed Suzuki cross-coupling reactions between aryl chlorides and boronic acids.[14] Herein, we report the use of air-stable phosphine oxide preligands[15] for the activation of C–Cl and C–F bonds[16] in cross-coupling reactions.

The catalytic activity of different preligands was first evaluated in the Kumada cross-coupling reaction of electronically deactivated 4-chloroanisole (**1a**) with phenyl magnesium chloride (**2a**) at ambient temperature (Table 1 and the Supporting Information).[17] Diaminophosphine oxide **7** gave rise to more efficient catalysis than the corresponding diaminophosphine chloride **6**[14] (Table 1, entries 1 and 2). However, significant amounts of the undesired homocoupling product **5a** were also generated. Similar results were obtained with dioxophosphine oxides **8** and **9** (Table 1, entries 3 and 4). A more selective reaction was achieved with sterically hindered phosphine oxide **10** and particularly **11**, which bear aromatic substituents on nitrogen (Table 1, entries 5 and 6). Again, the corresponding phosphine chloride **12** gave rise to less efficient and less selective catalysis (Table 1, entry 7).

Recently, Dankwardt showed that a sterically encumbered phosphite facilitates efficient nickel-catalyzed Kumada cross-coupling reactions at elevated temperature.[11] However, neither the corresponding phosphite **13** (Table 1,

Table 1: Ligand optimization studies.[a]

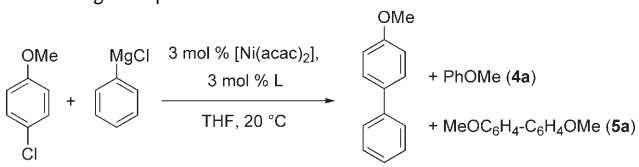

Entry	Ligand (L)		t [h]	1a/3a/4a/5a
1	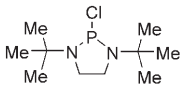	**6**	24	16:**76**:1:6
2	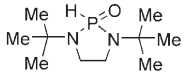	**7**	1	4:**85**:1:10
3	$(EtO)_2PHO$	**8**	1	/:**89**:1:10
4	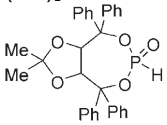	**9**	1	/:**91**:1:7
5	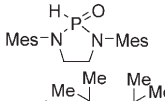	**10**	1	/:**96**:/:4
6	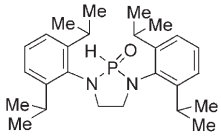	**11**	1	/:**97**:/:3
7	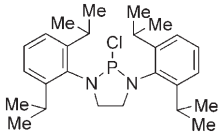	**12**	1	41:**45**:9:5
8	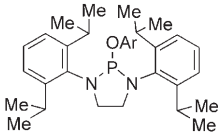	**13**	1	65:**22**:10:3
9	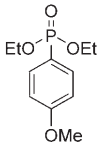	**14**	1	66:**29**:2:2
10	Ph_2PHO	**15**	1	/:**89**:1:9
11	tBu_2PHO	**16**	1	/:**97**:/:3
12	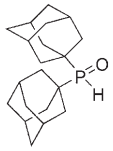	**17**	1	/:**99**:/:1

[a] Reaction conditions: **1a** (1.00 mmol), **2a** (1.50 mmol), $[Ni(acac)_2]$ (3 mol%), L (3 mol%), THF (2 mL); GC yield; Ar = 4-$MeOC_6H_4$.

[*] Dr. L. Ackermann, R. Born, J. H. Spatz, D. Meyer
Ludwig-Maximilians-Universität München
Department Chemie und Biochemie
Butenandtstrasse 5–13, Haus F, 81377 München (Germany)
Fax: (+49) 89-218-077-425
E-mail: Lutz.Ackermann@cup.uni-muenchen.de

[**] This research was supported by Prof. Paul Knochel, the DFG (Emmy Noether-Programm), the Fonds der Chemischen Industrie, and the Ludwig-Maximilians-Universität.

Supporting information for this article is available on the WWW under http://www.angewandte.org or from the author.

InterScience
© 2005 Wiley-VCH Verlag GmbH & Co. KGaA, Weinheim

entry 8) nor arylphosphonate **14**[18] (Table 1, entry 9) exhibited reactivity comparable to that observed with phosphine oxide **11**. In contrast, alkyl-substituted secondary phosphine oxides yielded quantitative conversion of electrophile **1a** (Table 1, entries 11 and 12). In particular, the sterically hindered 1-adamantyl-substituted derivative **17**[19] gave rise to selective catalysis (Table 1, entry 12).[20] The high catalytic activity achieved with secondary phosphine oxides is most likely a result of the generation and subsequent deprotonation of phosphinous acid nickel complexes featuring anionic electron-rich P-bound ligands.[21]

The catalyst derived from phosphine oxide **11** facilitated efficient conversion of a representative set of electron-rich aryl chlorides at ambient temperature (Table 2). Also the functionalization of pyridyl chlorides (Table 2, entries 8–10) proceeded in high yields.

With optimized catalytic systems in hand, we tested the air-stable phosphine oxides **11**, **16**, and **17** as preligands in the cross-coupling of aryl fluoride **18a** (Table 3, entries 1–3). Interestingly, diaminophosphine oxide **11** exhibited superior catalytic activity in the activation of C–F bonds (Table 3, entry 1). Highly efficient catalysis was achieved with this preligand even at ambient temperature with different Grignard reagents (Table 3, entries 1, 4, and 5). These results suggest an improved reactivity compared to that in known protocols for nickel-catalyzed cross-coupling of aryl fluorides at ambient temperature.[12] Heteroarenes (Table 3, entries 7–10) gave rise to the corresponding products in high yields.[13a] Also the synthesis of terphenyl derivatives (Table 3, entries 11 and 12) and an amino-substituted biaryl (Table 3, entry 13), as well as the conversion of sterically more hindered naphtha-

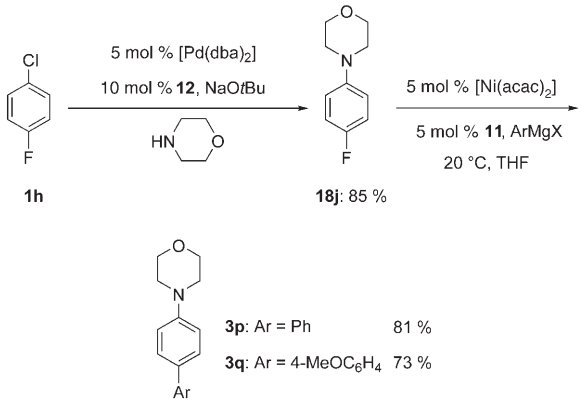

Scheme 1. Selective functionalization of arene **1h**; dba = *trans,trans*-dibenzylideneacetone.

Table 2: Kumada cross-coupling of aryl chlorides at ambient temperature.[a]

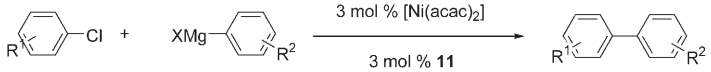

Entry	Aryl chloride		Grignard reagent		Product		Yield [%]
1	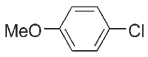	**1a**	ClMgPh	**2a**	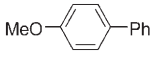	**3a**	97
2[b]	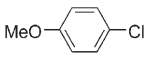	**1a**	ClMgPh	**2a**	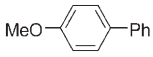	**3a**	99
3	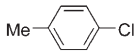	**1b**	ClMgPh	**2a**	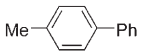	**3b**	92
4	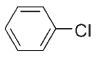	**1c**	4-BrMgC$_6$H$_4$OMe	**2b**	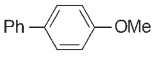	**3a**	97
5	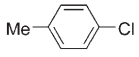	**1b**	4-BrMgC$_6$H$_4$OMe	**2b**	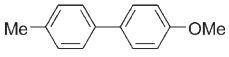	**3c**	97
6	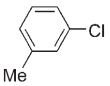	**1d**	4-BrMgC$_6$H$_4$OMe	**2b**	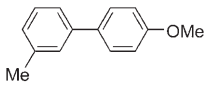	**3d**	99
7		**1e**	4-BrMgC$_6$H$_4$OMe	**2b**	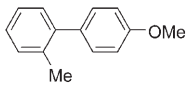	**3e**	89
8		**1f**	4-BrMgC$_6$H$_4$OMe	**2b**	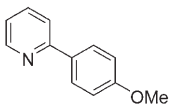	**3f**	87
9		**1g**	ClMgPh	**2a**		**3g**	85
10		**1g**	4-BrMgC$_6$H$_4$OMe	**2b**	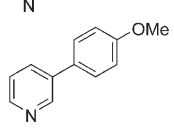	**3h**	85

[a] Reaction conditions: **1** (1.00 mmol), **2** (1.50 mmol), [Ni(acac)$_2$] (3 mol%), **11** (3 mol%), THF (2 mL), 20°C; yield of isolated product. [b] **17** (3 mol%) instead of **11**.

 © 2005 Wiley-VCH Verlag GmbH & Co. KGaA, Weinheim

Table 3: Kumada cross-coupling with aryl fluorides.[a]

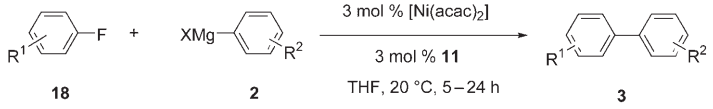

18 2 3

Entry	Aryl fluoride		Grignard reagent		Product		Yield [%]
1	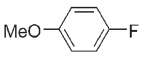	**18a**	ClMgPh	**2a**	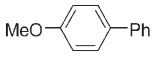	**3a**	80
2[b]	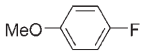	**18a**	ClMgPh	**2a**	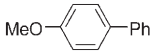	**3a**	55
3[c]	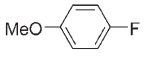	**18a**	ClMgPh	**2a**	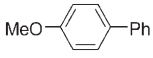	**3a**	64
4		**18b**	4-BrMgC$_6$H$_4$OMe	**2b**	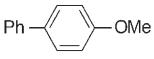	**3a**	88
5[d]	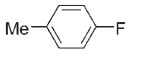	**18c**	4-BrMgC$_6$H$_4$OMe	**2b**	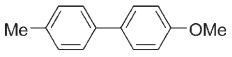	**3c**	88
6[c]	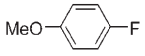	**18b**	4-BrMgMes	**2c**	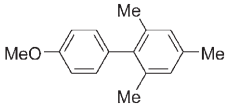	**3i**	88
7		**18d**	4-BrMgC$_6$H$_4$OMe	**2b**	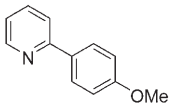	**3f**	90
8		**18d**	ClMgPh	**2a**	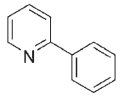	**3j**	63
9		**18e**	ClMgPh	**2a**		**3g**	72
10		**18e**	4-BrMgC$_6$H$_4$OMe	**2b**	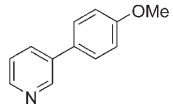	**3h**	95
11	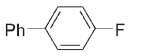	**18f**	4-BrMgC$_6$H$_4$OMe	**2b**	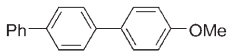	**3k**	88
12	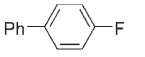	**18f**	ClMgPh	**2a**	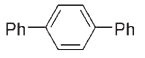	**3l**	89
13[e]	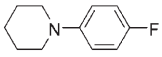	**18g**	ClMgPh	**2a**	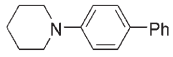	**3m**	61
14	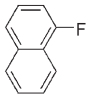	**18h**	ClMgPh	**2a**	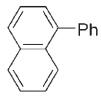	**3n**	84
15		**18h**	4-BrMgC$_6$H$_4$OMe	**2b**	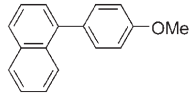	**3o**	94
16	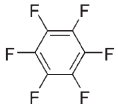	**18i**	4-BrMgC$_6$H$_4$OMe	**2b**	–	–	–

[a] Reaction conditions: **18** (1.00 mmol), **2** (1.50 mmol), [Ni(acac)$_2$] (3 mol%), **11** (3 mol%), THF (2 mL), 20°C; yield of isolated product; Mes = 2,4,6-Me$_3$C$_6$H$_2$. [b] **16** (3 mol%) instead of **11**. [c] **17** (3 mol%) instead of **11**. [d] [Ni(acac)$_2$] (5 mol%), **11** (5 mol%). [e] [Ni(acac)$_2$] (8 mol%), **11** (8 mol%).

lene fluoride **18h** (entries 14 and 15), was feasible with phosphine oxide **11**. However, electron-poor polyfluorinated **18i** was not converted.

Finally, a combination of a palladium-catalyzed amination[14] and a nickel-catalyzed Kumada cross-coupling of the resulting electron-rich aryl fluoride **18j** was used for the regioselective functionalization of fluorobenzene **1h** (Scheme 1).

In summary, we reported the first use of air-stable secondary phosphine oxides for the activation of C–F bonds in aryl fluorides. In particular, a complex derived from the sterically congested preligand **11** showed activity superior to that of known protocols for the nickel-catalyzed cross-coupling reactions of aryl Grignard reagents at ambient temperature.

Experimental Section

Representative procedure for nickel-catalyzed cross-coupling reactions of aryl fluorides (Table 3, entry 15): A solution of [Ni(acac)$_2$] (7 mg, 0.03 mmol, 3 mol%) and **11** (13 mg, 0.03 mmol, 3 mol%) in dry THF (0.5 mL) was stirred for 10 min at ambient temperature under N_2. 1-Fluoronaphthalene (**18h**) (148 mg, 1.01 mmol) was added, and the solution was stirred for 5 min. Thereafter, **2b** (0.5 M in THF, 3.0 mL, 1.50 mmol) was added. The resulting dark solution was stirred at ambient temperature for 15 h. Et_2O (75 mL) and H_2O (75 mL) were added to the reaction mixture. The separated aqueous phase was extracted with Et_2O (2 × 75 mL). The combined organic layers were dried over $MgSO_4$ and concentrated in vacuo. The remaining residue was purified by column chromatography on silica gel (*n*-pentane/Et_2O, 300:1→200:1→150:1→100:1) to yield **3o** as a pale yellow solid (223 mg, 94%).

Received: May 29, 2005
Published online: October 17, 2005

Keywords: C–C coupling · C–F activation · Grignard reaction · nickel · phosphine oxides

[1] K. Tamao, K. Sumitani, M. Kumada, *J. Am. Chem. Soc.* **1972**, *94*, 4374–4376.
[2] R. J. P. Corriu, J. P. Masse, *J. Chem. Soc. Chem. Commun.* **1972**, 144.
[3] K. Tamao, *J. Organomet. Chem.* **2002**, *653*, 23–26.
[4] P. Knochel, I. Sapountzis, N. Gommermann, in *Metal-Catalyzed Cross-Coupling Reactions*, 2nd ed. (Eds.: A. de Meijere, F. Diederich), Wiley-VCH, Weinheim, **2004**, pp. 671–698.
[5] A. de Meijere, F. Diederich, *Metal-Catalyzed Cross-Coupling Reactions*, 2nd ed., Wiley-VCH, Weinheim, **2004**.
[6] A. F. Littke, G. C. Fu, *Angew. Chem.* **2002**, *114*, 4350–4386; *Angew. Chem. Int. Ed.* **2002**, *41*, 4176–4211.
[7] T. G. Richmond, *Angew. Chem.* **2000**, *112*, 3378–3380; *Angew. Chem. Int. Ed.* **2000**, *39*, 3241–3244.
[8] T. Braun, R. N. Perutz, *Chem. Commun.* **2002**, 2749–2757.
[9] T. Takahashi, K. Kanno in *Modern Organonickel Chemistry* (Ed.: Y. Tamaru), Wiley-VCH, Weinheim, **2005**, pp. 41–55.

 © 2005 Wiley-VCH Verlag GmbH & Co. KGaA, Weinheim

[10] For an unselective coupling with an alkyl Grignard reagent, see: Y. Kiso, K. Tamao, M. Kumada, *J. Organomet. Chem.* **1973**, *50*, C12 – C14.
[11] For a recent study on thermal and microwave-mediated reactions, see: J. W. Dankwardt, *J. Organomet. Chem.* **2005**, *690*, 932 – 938.
[12] V. P. W. Böhm, C. W. K. Gstöttmayr, T. Weskamp, W. A. Herrmann, *Angew. Chem.* **2001**, *113*, 3500 – 3503; *Angew. Chem. Int. Ed.* **2001**, *40*, 3387 – 3389.
[13] See also: a) F. Mongin, L. Mojovic, B. Guillamet, F. Trecourt, G. Quéguiner, *J. Org. Chem.* **2002**, *67*, 8991 – 8994; b) K. Lamm, M. Stollenz, M. Meier, H. Görls, B. Walther, *J. Organomet. Chem.* **2003**, *681*, 24 – 36.
[14] L. Ackermann, R. Born, *Angew. Chem.* **2005**, *117*, 2497 – 2500; *Angew. Chem. Int. Ed.* **2005**, *44*, 2444 – 2447.
[15] N. V. Dubrovina, A. Börner, *Angew. Chem.* **2004**, *116*, 6007 – 6010; *Angew. Chem. Int. Ed.* **2004**, *43*, 5883 – 5886.
[16] For the use of alkyl-substituted phosphine oxides in nickel-catalyzed cross-couplings with aryl chlorides, see: a) G. Y. Li, *Angew. Chem.* **2001**, *113*, 1561 – 1564; *Angew. Chem. Int. Ed.* **2001**, *40*, 1513 – 1516; b) G. Y. Li, W. J. Marshall, *Organometallics* **2002**, *21*, 590 – 591.
[17] For a thorough evaluation of a variety of preligands, see the Supporting Information in: V. P. W. Böhm, T. Weskamp, C. W. K. Gstöttmayr, W. A. Herrmann, *Angew. Chem.* **2000**, *112*, 1672 – 1674; *Angew. Chem. Int. Ed.* **2000**, *39*, 1602 – 1604.
[18] The corresponding arylphosphonate derived from phosphine oxide **11** could not be obtained by standard synthetic procedures; this underscores the steric demand of preligand **11**. A practical protocol for the synthesis of arylphosphonates: L. J. Gooßen, M. K. Dezfuli, *Synlett* **2005**, 445 – 448, and references therein.
[19] J. R. Goerlich, A. Fischer, P. G. Jonas, R. Schmutzler, *Z. Naturforsch. B* **1994**, *49*, 801 – 811, and references therein.
[20] For use in C–H bond functionalization reactions with aryl chlorides, see: L. Ackermann, *Org. Lett.* **2005**, *7*, 3123 – 3125.
[21] For the synthesis of a phosphinous acid nickel complex, starting from $[Ni(acac)_2]$ and phosphine oxide **15**, see: B. Walther, H. Hartung, M. Maschmeier, U. Baumeister, B. Messbauer, *Z. Anorg. Allg. Chem.* **1988**, *566*, 121 – 130.

 © 2005 Wiley-VCH Verlag GmbH & Co. KGaA, Weinheim

Asymmetric Catalysis

DOI: 10.1002/anie.200503046

Vanadium-Catalyzed Sulfur Oxidation/Kinetic Resolution in the Synthesis of Enantiomerically Pure Alkyl Aryl Sulfoxides**

*Carmelo Drago, Lorenzo Caggiano, and Richard F. W. Jackson**

Chiral sulfoxides are an important class of compounds that find increasing use as chiral auxiliaries in asymmetric synthesis.[1,2] Current interest also reflects the existence of products with biological properties containing a sulfinyl group with a defined configuration.[3]

Several methods for the asymmetric oxidation of prochiral sulfides have been reported, including the use of chiral oxidants, such as chiral oxaziridines,[4] chiral hydroperoxides,[5] and enzymes.[6,7] The majority of investigations have concentrated on the use of chiral metal complexes[1,3,8–11] following the initial reports by Kagan and co-workers[12,13] and Modena and co-workers[14] on the use of variously modified Sharpless reagents for this reaction.

One of the most widely studied metal-based systems has been that discovered by Bolm and Bienewald,[15,16] who employed a combination of Schiff bases **1** derived from chiral amino alcohols and $[VO(acac)_2]$ (1.0 mol%; acac = acetylacetanoate), with aqueous hydrogen peroxide as the oxidant, in a two-phase system using dichloromethane as the solvent at 20°C (Scheme 1). The advantages of the system developed by Bolm et al. include high activity, the very simple reaction conditions, and the use of hydrogen peroxide as the oxidant. The only drawback associated with the initial ligands tested was that the levels of enantiomeric excess were good, rather than excellent. Other research groups sought to optimize the system, by variation of the aromatic aldehyde,[17–19] the amino alcohol,[20] and the manner of addition of hydrogen peroxide,[21] and in many cases it is striking that the best outcome was usually obtained when the reaction was conducted in dichloromethane at 0°C. A very nice application of the system developed by Bolm et al. was the asymmetric oxidation of di-*tert*-butyl disulfide, reported by Ellman and co-workers,[22] who have since reported the results of spectroscopic studies

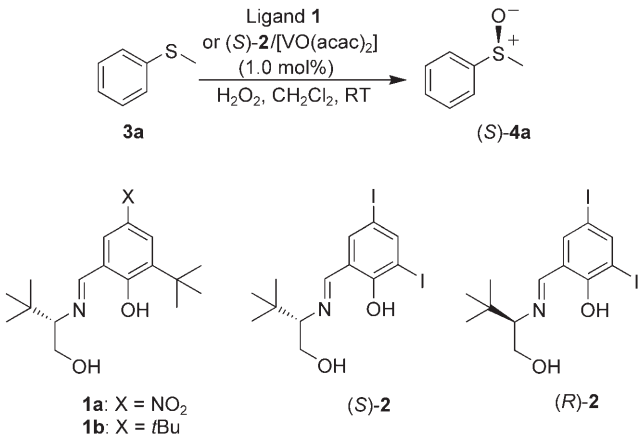

Scheme 1. Vanadium-catalyzed asymmetric oxidation of alkyl aryl sulfides.

with a view to understanding the nature of the active catalytic species better.[23] The nature of the active species is still not completely established, but while spectroscopic studies indicate the presence of a vanadium(v)oxomonoperoxo species,[24] recent calculations suggest that the active species may be a vanadium(v)oxohydroperoxide.[25] Recently, the use of analogous salan ligands has been reported to give high levels of enantioselectivity (95% *ee*) in the oxidation of methyl phenyl sulfide, but lower levels of enantioselectivity were observed with other substrates.[26]

Anson and co-workers screened a variety of chiral Schiff base ligands, and found that the 3,5-diiodo ligand (*S*)-**2**, in combination with $[VO(acac)_2]$ gave excellent results in the catalytic asymmetric sulfoxidation of alkyl aryl sulfides with hydrogen peroxide, again in dichloromethane at 0°C.[27] For example, methyl phenyl sulfide was oxidized to (*S*)-methyl phenyl sulfoxide (81%, 90% *ee*). Recently, Bolm and co-workers reported that a combination of this ligand with iron is also very effective for the asymmetric oxidation of prochiral sulfides,[28,29] especially in the presence of substituted benzoic acids and with the corresponding lithium salts as additives.[30,31]

In all asymmetric oxidations of prochiral sulfides to sulfoxides, the possibility of subsequent kinetic resolution of the product sulfoxide by oxidation to the corresponding sulfone exists. Uemura and co-workers had demonstrated the viability of this process as long ago as 1993; they observed stereoselectivity factors of 7.4–8.5 for kinetic resolutions[32] using a catalyst prepared from $Ti(OiPr)_4$, 2,2′-dihydroxy-1,1′-binaphthyl (binol), and H_2O.[33] A more recent example makes use of a catalyst derived from WO_3 and cinchona alkaloids for the kinetic resolution of alkyl aryl sulfoxides using hydrogen peroxide.[34] The process developed by Uemura and co-workers[33,35] has been exploited by Scettri and co-workers (using furyl hydroperoxides as the oxidant)[36] and more recently by Chan and co-workers (using *tert*-butylhydroperoxide as the oxidant).[37] Specifically, Chan and co-workers described a process in which an initial oxidation at 0°C (at which temperature the enantioselectivity is optimum) and then at 25°C (where the kinetic resolution is most efficient) allowed the isolation of sulfoxides in reasonable

[*] C. Drago, Dr. L. Caggiano, Prof. Dr. R. F. W. Jackson
Department of Chemistry
Dainton Building
University of Sheffield
Sheffield, S3 7HF (UK)
Fax: (+44) 114-273-8673
E-mail: r.f.w.jackson@shef.ac.uk

[**] This work was supported by the Commission of the European Union (IHP Network HPRN-CT-2000-00014) through a studentship (to C.D.), supported by GSK. We thank Dr. Chiara Monti for preliminary studies on the kinetic resolution of alkyl aryl sulfoxides, Dr. M. S. Anson and Dr. S. J. F. Macdonald for helpful discussions, and Degussa AG (Dr. D. Reichert and Dr. Krahnert) for a generous gift of (*R*)-*tert*-leucinol.

 © 2005 Wiley-VCH Verlag GmbH & Co. KGaA, Weinheim

yields and excellent *ee* values (65% and 99.9% *ee* in the case of methyl *para*-tolyl sulfoxide, the best so far published).[37] However, it appears that no significant kinetic resolution in the oxidation of sulfoxides has so far been reported in studies in which chiral vanadium(IV)–Schiff base complexes were used. Nevertheless, such an effect has been reported in the case of vanadium–salan systems (selectivity factor $S = 7.3$ for the resolution of methyl phenyl sulfoxide) when larger amounts of catalyst (5 mol%) were used.[26]

In an initial experiment it was confirmed that there was no significant kinetic resolution in the oxidation of racemic methyl phenyl sulfoxide using 3,5-diiodo ligand (*R*)-**2** (prepared from (*R*)-*tert*-leucinol, which has recently become commercially available) in combination with $[VO(acac)_2]$ and hydrogen peroxide in dichloromethane at 0°C ($S = 1.1$). However, a significant effect was observed ($S = 5.8$) when the kinetic resolution was carried out at 20°C. A tandem catalytic approach to the asymmetric oxidation of methyl phenyl sulfoxide using a combination of (*R*)-**2** with $[VO(acac)_2]$ in dichloromethane was developed: an initial oxidation step at 0°C followed by the addition of further oxidant to the same reaction vessel and warming to 20°C allowed the isolation of (*R*)-methyl phenyl sulfoxide (44%, 97.3% *ee*; Scheme 2). While this was an interesting result, the modest yield meant that it was not ideal from a preparative perspective.

Given the striking effect of temperature on the efficiency of the kinetic resolution, it seemed appropriate to explore the influence of the solvent. After substantial solvent screening in the oxidation of racemic methyl phenyl sulfoxide (**4a**) using (*R*)-**2** and $[VO(acac)_2]$ as the catalyst, and hydrogen peroxide as oxidant (0.5 equiv), it was found that the use of chloroform as the solvent[38] resulted in an improved kinetic resolution effect at 20°C ($S = 7.7$). No other solvent that was screened gave comparable results. The kinetic resolution in chloroform was more efficient at 0°C ($S = 11.6$). The highest value so far reported ($S = 28$) was obtained when the kinetic resolution of

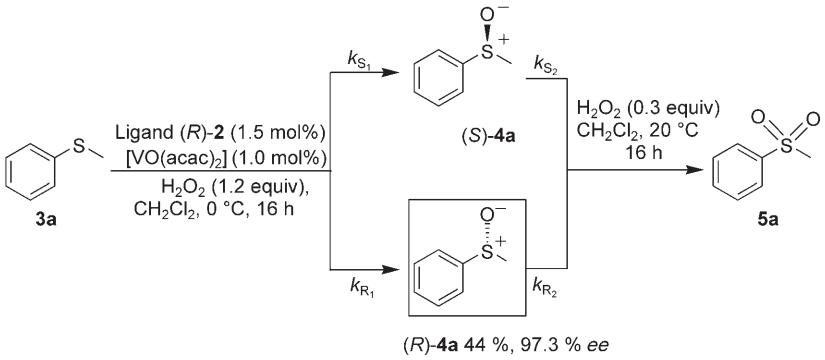

Scheme 2. Oxidation/kinetic resolution process for the preparation of (*R*)-methyl phenyl sulfoxide (**4a**).

racemic methyl *para*-tolyl sulfoxide (**4b**) at 0°C was investigated (Scettri and co-workers reported $S = 23$ by using a stoichiometric process).[36] This kinetic resolution could be adapted for preparative use (with 0.6 equiv of hydrogen peroxide), which allowed the isolation of (*R*)-methyl *para*-tolyl sulfoxide (**4b**, 41% of a maximum of 50%, 98.0% *ee*), as well as sulfone **5b** (Scheme 3).

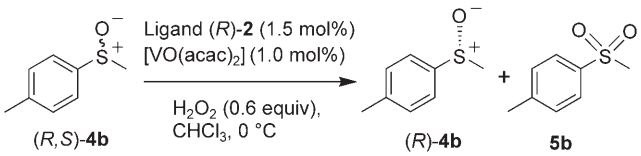

Scheme 3. Kinetic resolution of methyl *para*-tolyl sulfoxide.

The observation that the optimum temperature for the kinetic resolution of racemic sulfoxides with the catalyst derived from (*R*)-**2** and $[VO(acac)_2]$ in chloroform was 0°C (the optimum temperature for most previous asymmetric oxidations of prochiral sulfides using chiral vanadium(IV)–Schiff base complexes) suggested that these conditions might also be extremely effective for the enantioselective preparation of alkyl aryl sulfoxides. This indeed proved to be the case, and Table 1 shows results from the oxidation of a range of alkyl aryl sulfides to give the (*R*)-alkyl aryl sulfoxides (Scheme 4). In each case, the corresponding sulfone **5** was also observed, thus indicating that, as expected, some kinetic resolution had taken place. The only unsatisfactory result was the oxidation of methyl *para*-nitrophenyl sulfide (**3d**), which gave the product **4d** in only 86.9% *ee*.

Table 1: Asymmetric oxidation of alkyl aryl sulfides **3** in chloroform using ligand (*R*)-**2** with $[VO(acac)_2]$ and H_2O_2 (1.2 equiv).

Ar	R	Product	Yield [%][a]	*ee* [%][b]
Ph	Me	(*R*)-**4a**	70	96.7
4-MeC_6H_4	Me	(*R*)-**4b**	70	>99.5
2-naphthyl	Me	(*R*)-**4c**	73	>99.5
4-$NO_2C_6H_4$	Me	(*R*)-**4d**	88	86.9
4-ClC_6H_4	Me	(*R*)-**4e**	72	96.9
4-$MeOC_6H_4$	Me	(*R*)-**4f**	71	99.5
4-BrC_6H_4	Me	(*R*)-**4g**	79	95.5
Ph	Pr	(*R*)-**4h**	86	98.3
Ph	Et	(*R*)-**4i**	76	97.4

[a] Yield of isolated product. Reactions were conducted on a 1.5 mmol scale. [b] Determined by HPLC of the purified products on a chiral stationary phase using a DAICEL Chiralpak AS column.

These encouraging results on a small scale prompted an investigation into scaling the reaction up. Oxidation of methyl phenyl sulfide (**3a**) with 60.0 mmol of substrate under the same reaction conditions (albeit with an increase in the reaction time from 16 h to 48 h) allowed the isolation of (*R*)-

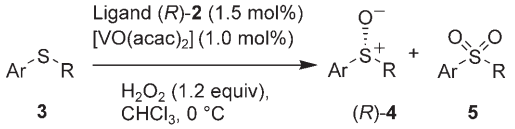

Scheme 4. Optimized asymmetric oxidation of alkyl aryl sulfides.

 © 2005 Wiley-VCH Verlag GmbH & Co. KGaA, Weinheim

methyl phenyl sulfoxide (**4a**; 87%, 93% *ee*). The oxidation was also performed on the same scale using methyl *para*-tolyl sulfide (**3b**), to give (*R*)-methyl *para*-tolyl sulfoxide (**4b**; 82%, >99.5% *ee* after one recrystallization from Et_2O/hexane), and methyl *para*-bromophenyl sulfide (**3g**), to give (*R*)-methyl *para*-bromophenyl sulfoxide (**4g**; 77%, >99.5% *ee* after one recrystallization from Et_2O/hexane). In these latter two cases, the efficiency of the process was even higher than that observed on a small scale.

The combination of very high *ee* values with high yield, the consequence of an efficient initial asymmetric oxidation followed by an efficient kinetic resolution process, makes this system very practical for the catalytic asymmetric oxidation of simple alkyl aryl sulfides. Both enantiomers of ligand **2** are easily prepared on a multigram scale from commercially available precursors, and the ligands may be stored at room temperature on the open bench without any special precautions.

Experimental Section

Typical large-scale asymmetric oxidation procedure for the preparation of (*R*)-**4b**: A solution of [VO(acac)$_2$] (159.0 mg, 0.60 mmol) in chloroform (15 mL) was added to a solution of (*R*)-**2** (425.8 mg, 0.90 mmol) in chloroform (15 mL) and the reaction mixture was stirred for 2 h. A solution of **3b** (8.29 g, 60.0 mmol) in chloroform (30 mL) was added and the reaction mixture stirred for 30 min at room temperature before cooling it to 0 °C. After 30 min, 30% H_2O_2 (7.36 mL, 72.0 mmol) was added to the reaction mixture, which was stirred vigorously at 0 °C for 48 h. Samples (1–2 μL) were then removed at different times and diluted with 20% isopropanol/heptane for analysis by HPLC. The reaction was quenched with 10% $Na_2S_2O_3$ solution (200 mL) and the mixture extracted with chloroform (3 × 100 mL). The extracts were combined, washed with brine (3 × 100 mL), and dried ($MgSO_4$). Finally, the solvent was removed under reduced pressure. The crude product was purified by flash chromatography (EtOAc/petroleum ether 50:50). The purified product was dissolved in the minimum amount of hot diethyl ether, and hexane was added until the solution became turbid. The solution was then gently warmed to give a clear solution, which was allowed to cool to room temperature and then kept at −15 °C overnight to give the product sulfoxide as needles. The crystalline solid was then filtered and washed with cooled (−15 °C) hexane to (*R*)-**4b** (7.60 g, 82%), *ee* > 99.5% (determined by HPLC on a Daicel Chiralpak AS column, with 15% isopropanol in heptane, and a flow rate of 1.0 mL min^{-1}), $[\alpha]_D^{20} = 151$ ($c = 1.0$, acetone); [(Lit.[39] (*R*)-**4b**; *ee* 95%); $[\alpha]_D^{20} = 142$ ($c = 1.5$, acetone)].

Received: August 26, 2005
Published online: October 17, 2005

Keywords: asymmetric catalysis · kinetic resolution · oxidation · sulfoxides · vanadium

[1] I. Fernández, N. Khiar, *Chem. Rev.* **2003**, *103*, 3651–3705.
[2] M. C. Carreño, *Chem. Rev.* **1995**, *95*, 1717–1760.
[3] J. Legros, J. R. Dehli, C. Bolm, *Adv. Synth. Catal.* **2005**, *347*, 19–31.
[4] F. A. Davis, R. T. Reddy, W. Han, P. J. Carroll, *J. Am. Chem. Soc.* **1992**, *114*, 1428–1437.
[5] W. Adam, M. N. Korb, K. J. Roschmann, C. R. Saha-Möller, *J. Org. Chem.* **1998**, *63*, 3423–3428.
[6] E. G. Mata, *Phosphorus Sulfur Relat. Elem.* **1996**, *117*, 231–286.
[7] D. R. Boyd, N. D. Sharma, S. A. Haughey, M. A. Kennedy, B. T. McMurray, G. N. Sheldrake, C. C. R. Allen, H. Dalton, K. Sproule, *J. Chem. Soc. Perkin Trans. 1* **1998**, 1929–1933.
[8] K. Kaczorowska, Z. Kolarska, K. Mitka, P. Kowalski, *Tetrahedron* **2005**, *61*, 8315–8327.
[9] H. B. Kagan, T. O. Luukas, in *Transition Metals for Organic Synthesis, Vol. 2*, 2nd ed. (Eds.: M. Beller, C. Bolm), Wiley-VCH, Weinheim, **2004**, pp. 479–495.
[10] K. P. Volcho, N. F. Salakhutdinov, A. G. Tolstikov, *Russ. J. Org. Chem.* **2003**, *39*, 1537–1552.
[11] C. Bolm, *Coord. Chem. Rev.* **2003**, *237*, 245–256.
[12] P. Pitchen, E. Duñach, M. N. Deshmukh, H. B. Kagan, *J. Am. Chem. Soc.* **1984**, *106*, 8188–8193.
[13] P. Pitchen, H. B. Kagan, *Tetrahedron Lett.* **1984**, *25*, 1049–1052.
[14] F. DiFuria, G. Modena, R. Seraglia, *Synthesis* **1984**, 325–326.
[15] C. Bolm, F. Bienewald, *Angew. Chem.* **1995**, *107*, 2883–2885; *Angew. Chem. Int. Ed. Engl.* **1995**, *34*, 2640–2642.
[16] C. Bolm, G. Schlingloff, F. Bienewald, *J. Mol. Catal. A* **1997**, *117*, 347–350.
[17] A. H. Vetter, A. Berkessel, *Tetrahedron Lett.* **1998**, *39*, 1741–1744.
[18] J. Skarzewski, E. Ostrycharz, R. Siedlecka, *Tetrahedron: Asymmetry* **1999**, *10*, 3457–3461.
[19] Y. C. Jeong, S. Choi, Y. D. Hwang, K. H. Ahn, *Tetrahedron Lett.* **2004**, *45*, 9249–9252.
[20] C. Ohta, T. Katsuki, *Tetrahedron Lett.* **2001**, *42*, 3885–3888.
[21] N. N. Karpyshev, O. D. Yakovleva, E. P. Talsi, K. P. Bryliakov, O. V. Tolstikova, A. G. Tolstikov, *J. Mol. Catal. A* **2000**, *157*, 91–95.
[22] D. A. Cogan, G. C. Liu, K. J. Kim, B. J. Backes, J. A. Ellman, *J. Am. Chem. Soc.* **1998**, *120*, 8011–8019.
[23] S. A. Blum, R. G. Bergman, J. A. Ellman, *J. Org. Chem.* **2003**, *68*, 150–155.
[24] K. P. Bryliakov, N. N. Karpyshev, S. A. Fominsky, A. G. Tolstikov, E. P. Talsi, *J. Mol. Catal. A* **2001**, *171*, 73–80.
[25] D. Balcells, F. Maseras, G. Ujaque, *J. Am. Chem. Soc.* **2005**, *127*, 3624–3634.
[26] J. T. Sun, C. J. Zhu, Z. Y. Dai, M. H. Yang, Y. Pan, H. W. Hu, *J. Org. Chem.* **2004**, *69*, 8500–8503.
[27] B. Pelotier, M. S. Anson, I. B. Campbell, S. J. F. Macdonald, G. Priem, R. F. W. Jackson, *Synlett* **2002**, 1055–1060.
[28] J. Legros, C. Bolm, *Angew. Chem.* **2003**, *115*, 5645–5647; *Angew. Chem. Int. Ed.* **2003**, *42*, 5487–5489.
[29] A. Korte, J. Legros, C. Bolm, *Synlett* **2004**, 2397–2399.
[30] J. Legros, C. Bolm, *Angew. Chem.* **2004**, *116*, 4321–4324; *Angew. Chem. Int. Ed.* **2004**, *43*, 4225–4228.
[31] J. Legros, C. Bolm, *Chem. Eur. J.* **2005**, *11*, 1086–1092.
[32] All stereoselectivity factors were calculated using the equation developed by Kagan and Fiaud.[40]
[33] N. Komatsu, M. Hashizume, T. Sugita, S. Uemura, *J. Org. Chem.* **1993**, *58*, 7624–7626.
[34] V. V. Thakur, A. Sudalai, *Tetrahedron: Asymmetry* **2003**, *14*, 407–410.
[35] N. Komatsu, M. Hashizume, T. Sugita, S. Uemura, *J. Org. Chem.* **1993**, *58*, 4529–4533.
[36] A. Massa, F. R. Siniscalchi, V. Bugatti, A. Lattanzi, A. Scettri, *Tetrahedron: Asymmetry* **2002**, *13*, 1277–1283.
[37] X. Jia, X. Li, L. Xu, Y. Li, Q. Shi, T. Au-Yeung, C. Yip, X. Yao, A. Chan, *Adv. Synth. Catal.* **2004**, *346*, 723–726.
[38] Chloroform had been used by Ellman and co-workers in the oxidation of di-*tert*-butyl disulfide,[22] and by Zhu and co-workers[26] in oxidations of alkyl aryl sulfides catalyzed by vanadium–salan complexes.
[39] A. Lattanzi, F. Bonadies, A. Senatore, A. Soriente, A. Scettri, *Tetrahedron: Asymmetry* **1997**, *8*, 2473–2478.
[40] H. B. Kagan, J. C. Fiaud, *Top. Stereochem.* **1988**, *18*, 249.

 © 2005 Wiley-VCH Verlag GmbH & Co. KGaA, Weinheim

Chemistry in Space

DOI: 10.1002/anie.200502122

Synthesis and Characterization of 2,4-Pentadiynenitrile—A Key Compound in Space Science**

*Yann Trolez and Jean-Claude Guillemin**

Many molecules have been detected in the interstellar medium, around the stars, in comets, and in the atmospheres of the planets or satellites of the solar system.[1,2] Several of these molecules were probably also present on primitive Earth. Among the satellites, Titan, the largest moon of Saturn, is considered as a frozen model of early Earth. Many compounds were observed in the atmosphere of Titan, and assessments by astrobiologists have revealed that it could have similar atmospheric components and pressure conditions as Earth had four billion years ago. It is generally believed that the first chemical steps that led to life might have taken place in the atmosphere of Titan, and that the products were kept by freezing.[3]

The family of compounds that associates one or several C–C triple bonds and only one carbonitrile substituent (H−(C≡C)$_n$−C≡N) plays an important role in astrobiology.[4] As an example, the largest molecule detected in the interstellar medium is $HC_{11}N$ ($n=5$). The first member of this family, cyanoacetylene (HC≡C−C≡N (**1**)), has been observed in the atmosphere of Titan,[3] in the interstellar medium,[1] in comets,[2] and in numerous laboratory simulations of planetary atmospheres.[5] It was often proposed as a key compound because it reacts readily with many nucleophiles,[6,7] and that could be the starting point of a rich organic chemistry in these media and particularly on primitive Earth.[8] Cyanobutadiyne (2,4-pentadiynenitrile, HC≡C−C≡C−C≡N (**2**)) is the second member of this family. It has been detected in the interstellar medium,[1] in comets,[2] and appears in numerous laboratory simulations of Titan's atmosphere.[5]

To confirm (or to disprove) models that foresee the presence of cyanobutadiyne on Titan, it is essential to have this molecule at hand. An infrared spectrum of the pure product would allow an estimation of the partial pressure of this molecule on Titan, provided it is detected there. The reaction of this compound with many reagents is of great interest in itself and by comparison with cyanoacetylene and cyanopropyne.[6,7] Moreover, the synthesis of pure cyanopolyynes with the formula H−(C≡C)$_n$−C≡N is the key to a better knowledge of this family of compounds.

However, although the preparation of cyanoacetylene was reported long ago,[9] cyanobutadiyne has never been prepared in a pure form. The most important approaches are the desilylation of the corresponding trimethylsilylcyanobutadiyne[10] and a direct-current discharge in a mixture of cyanoacetylene and acetylene.[11] The recent detection of HC_5N in the pyrolysis of pyridine at 1200 °C in the presence of PCl_3[12] shows, once again, how challenging the preparation of this species is. In these approaches, the analysis was performed in the gas phase by microwave or infrared spectroscopy, but cyanobutadiyne has never been characterized in the condensed phase (by NMR spectroscopy, for example).

We now report the first isolation of cyanobutadiyne, its characterization by ^{1}H and ^{13}C NMR spectroscopy and by HRMS. We also described photochemical studies to propose syntheses of this compound in the interstellar medium or on planetary atmospheres, and some chemical reactions (the addition of Me_2NH, NH_3, and *t*BuSH) to study its reactivity with nucleophiles.

In 1993, Knochel and co-workers reported the synthesis of cyanooctyne by the reaction of commercially available *para*-toluenesulfonyl cyanide (**3**) with an octynylzinc derivative.[13] Some other organometallic compounds have also been used in such cyanation reactions.[14] Most of these compounds were prepared in low-boiling-point solvents (mainly ethers) and were not easily isolated in pure form. Hence, even if the reaction of alkynyl metal compounds with **3** could give the expected product, the extraction of a kinetically unstable product from the reaction mixture and its purification would be a very difficult problem. Other heterocompounds, such as silicon derivatives, can only be obtained by heating the reaction mixture for long periods of time, and these methods cannot be used to prepare kinetically unstable compounds in a facile manner.[15] However, tin derivatives with various functional groups are easily prepared, can be isolated in pure form, and are often reasonably reactive. For instance, 1,3-butadiynyltributylstannane (**4**), a potential precursor for cyanobutadiyne, has already been synthesized.[16] Thus, we sought an approach starting from **4** that would allow the continuous extraction of cyanobutadiyne from the reaction mixture as it is formed.[17]

The reaction of **4** with excess cyanide **3** led to the cyanobutadiyne **2**, which was selectively trapped at −80 °C to remove low-boiling-point impurities [Eq. (1)]. The high-boiling-point impurities were removed in the first trap cooled at −30 °C. The compound was obtained in pure form but in only 15 % yield. About 300 mg of cyanobutadiyne (**2**) has been prepared in one experiment through this approach. The

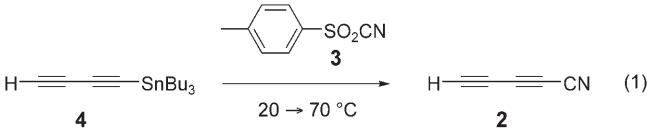

(1)

[*] Y. Trolez, Dr. J.-C. Guillemin
Laboratoire de Synthèse et Activation de Biomolécules
UMR CNRS 6052, ENSCR
Institut de Chimie de Rennes
35 700 Rennes (France)
Fax: (+33) 2-2323-8108
E-mail: jean-claude.guillemin@ensc-rennes.fr

[**] We acknowledge the PCMI (INSU-CNRS), the CNES, and the GDR CNRS Exobiology for financial support. We thank Professor James P. Ferris (RPI, USA) and Professor François Raulin (LISA, France) for helpful suggestions.

Supporting information for this article (synthesis of **8**–**10** and photochemical studies) is available on the WWW under http://www.angewandte.org or from the author.

InterScience
© 2005 Wiley-VCH Verlag GmbH & Co. KGaA, Weinheim

dilution of the reagents in a solvent (DMSO, dichlorobenzene, tetraethyleneglycol dimethyl ether, BMI-PF6 (an ionic liquid)) gave the product in similar or lower yields. The ^{1}H NMR signal was observed at $\delta = 2.41$ ppm, slightly upfield of the chemical shift for cyanoacetylene ($\delta = 2.51$ ppm). In the ^{13}C NMR spectra, the five signals for H-C5≡C4-C3≡C2-C1≡N were easily assigned by the decrease in the coupling constants between 5-H and the five carbon atoms. The molecular ion was detected by HRMS. Pure cyanobutadiyne can be kept indefinitely in dry ice, but decomposes slowly at −40 °C in pure form or at room temperature in $CDCl_3$.

This reaction between an unsaturated stannane and **3** can be extended to the preparation of cyanopropyne (85 % yield) or cyanoacetylene (37 % yield). Crotylstannane and allenylstannane reacted with a partial allylic transposition (crotyl/1-methallyl cyanide = 3:2, 43 % yield; allenyl/propargyl cyanide = 2:3, 72 % yield respectively).

The formation of cyanobutadiyne in the interstellar medium or in planetary atmospheres could occur photochemically.[18] Our synthesis of **2** allows traces of this molecule to be detected easily by ^{1}H NMR spectroscopy in various mixtures of compounds. Its presence can be confirmed by the addition of small amounts of an authentic sample to the NMR sample solutions and the observation of only one signal at $\delta_H = 2.41$ ppm. Thus we tried to determine which mixtures of gases would allow the photochemical formation of cyanobutadiyne. We irradiated gas mixtures with a mercury lamp ($\lambda =$ 185 and 254 nm or $\lambda = 254$ nm) with mercury UV lamps. We studied the photolysis of cyanoacetylene by itself, of cyanoacetylene with acetylene or butadiyne (**5**), and of dicyanoacetylene (**6**) with acetylene or butadiyne. All these compounds have been observed in the interstellar medium and the atmosphere of Titan. Several compounds were formed during the irradiations,[19] but we only discuss cyanobutadiyne.

We did not detect cyanobutadiyne in the photolysis of cyanoacetylene (50 mbar) by itself at 254 nm or at 185 and 254 nm. However, traces were detected in the photolysis of cyanoacetylene (50 mbar) with acetylene (50 mbar) at 185 and 254 nm. The best results were obtained when cyanoacetylene (3 equiv) absorbed most of the light (80 %).[19] Cyanobutadiyne was not observed in the same experiment with the 254-nm lamp. These results allow us to propose a reaction pathway that accounts for the fact that the breaking of the H–C bond of cyanoacetylene [Eq. (2)] and acetylene [Eq. (3)]

$$HC{\equiv}C{-}C{\equiv}N\ (\mathbf{1}) \xrightarrow{h\nu} H^{\cdot} + {}^{\cdot}C{\equiv}C{-}CN \tag{2}$$

$$H{-}C{\equiv}C{-}H \xrightarrow{h\nu} {}^{\cdot}C{\equiv}C{-}H + H^{\cdot} \tag{3}$$

does not occur at 254 nm irradiation.[20,21] A radical recombination of ethynyl and cyanoethynyl radicals could lead to the formation of **2** on a third body [Eq. (4)]. However, the

$${}^{\cdot}C{\equiv}C{-}H + {}^{\cdot}C{\equiv}C{-}CN \xrightarrow{M} \mathbf{2} \tag{4}$$

amounts of both radicals are probably too low to allow them to come close enough to each other to react. Consequently, the addition of the cyanoethynyl radical to acetylene [Eq. (5)]

$${}^{\cdot}C{\equiv}C{-}CN + H{-}C{\equiv}C{-}H \rightarrow \mathbf{2} + H^{\cdot} \tag{5}$$

or of the ethynyl radical to **1** [Eq. (6)] with concomitant

$${}^{\cdot}C{\equiv}C{-}H + \mathbf{1} \rightarrow \mathbf{2} + H^{\cdot} \tag{6}$$

elimination of a hydrogen radical is a more likely reaction pathway. On the basis of previous studies[18,22] and by comparison with the addition of cyanide to acetylene,[23] the reaction pathway corresponding to Equations (2) and (5) seems to be the most favourable.

A mixture of **1** (50 mbar) and **5** (50 mbar) was irradiated at 254 or at 185 and 254 nm. In both cases, cyanobutadiyne (**2**) was not detected. A mixture of dicyanoacetylene (**6**) (50 mbar) and acetylene (50 mbar) was also irradiated. Traces of **2** were detected in the sample irradiated at 254 or at 185 and 254 nm. In this case, the absorption coefficients of each reactant gas are quite similar at 185 nm but only **6** absorbs light at 254 nm.[19] Compound **2** could possibly be formed by the breaking of an NC–C bond of **6** [Eq. (7)] and

$$NC{-}C{\equiv}C{-}CN\ (\mathbf{6}) \xrightarrow{h\nu} N{\equiv}C^{\cdot} + {}^{\cdot}C{\equiv}C{-}CN \tag{7}$$

then by addition of cyanoethynyl radical to acetylene [Eq. (5)]. On the other hand the formation of cyanoacetylene (**1**) in these reactions can be attributed to the addition of the cyanide radical to acetylene.[23]

Under irradiation at 254 or at 185 and 254 nm, the photolysis of mixtures of **5** (50 mbar) and **6** (50 mbar) led to small amounts of **2**. The addition of the cyanide radical to **5** [Eq. (8)] gives a simple explanation of these results.[24]

$$N{\equiv}C^{\cdot} + H{-}C{\equiv}C{-}C{\equiv}C{-}H\ (\mathbf{5}) \rightarrow \mathbf{2} + H^{\cdot} \tag{8}$$

It also seems possible that cyanohexatriyne (HC≡C–C≡C–C≡C–C≡N (**7**)) is formed by the addition of the cyanoethynyl radical to butadiyne. Similarly, **7** might be formed in the photolysis of mixtures of **1** and **5** reported above. In both cases, without an authentic sample of **7**, we were not able to confirm its presence on the sole basis of the signal observed at $\delta_H = 2.38$ ppm. For the moment we have demonstrated that cyanobutadiyne (**2**) is easily formed in the photolysis of several mixtures of gases. More sophisticated experiments will be necessary to quantify its formation.

Cyanoacetylene reacts readily with nucleophiles such as ammonia, primary or secondary amines, and thiols to give the corresponding adduct.[6,7,25,26] In the same way, we investigated the reactivity of cyanobutadiyne, particularly with nucleophiles, and determined the products formed. Cyanobutadiyne can potentially undergo 1,4- or 1,6-addition. In this preliminary study, we carried out the addition to cyanobutadiyne in a solvent of Me_2NH, NH_3, and *t*BuSH.

N,*N*-Dimethylamine reacts with cyanobutadiyne (**2**) to give the corresponding 1,6-adduct. The 5-(dimethylamino)-4-penten-2-ynenitrile (**8**) was analyzed by HRMS and by ^{1}H and ^{13}C NMR spectroscopy [Eq. (9)]. Compound **8** decomposes upon standing at room temperature. Similarly, ammonia

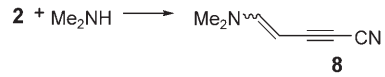

(9)

8

 © 2005 Wiley-VCH Verlag GmbH & Co. KGaA, Weinheim

reacts with cyanobutadiyne to give 5-amino-4-penten-2-ynenitrile (**9**), which is kinetically unstable at room temperature, even when diluted in $CDCl_3$ ($\tau_{1/2} = 1$ h) [Eq. (10)]. A

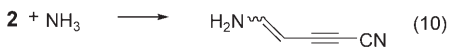

(10)

9

stable adduct, 5-[(1,1-dimethylethyl)thio]-4-penten-2-ynenitrile (**10**) was obtained by the addition of *t*BuSH to **2** in the presence of a catalytic amount of triethylamine [Eq. (11)]. In all cases, only the product corresponding to the 1,6-addition reaction was observed.

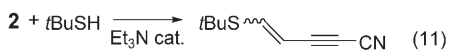

(11)

10

In conclusion, cyanobutadiyne (**2**) was synthesized in pure form by the reaction of the 1,3-butadiynyltributylstannane with *p*-toluenesulfonyl cyanide. This approach paves the way to the synthesis of other cyanopolyynes and the corresponding isotopomers. According to our study, cyanobutadiyne can possibly be formed on Titan or in the interstellar medium by photolysis of mixtures of acetylene and cyanoacetylene or dicyanoacetylene or mixtures of dicyanoacetylene and butadiyne. Compound **2** only undergoes 1,6-addition with nucleophiles. The measurement of the gas-phase IR spectrum of a pure sample of **2**, the study of its photochemistry, and the extension of this approach to other cyanopolyynes are currently underway in our laboratory.

Experimental Section

2: Two traps equipped with stopcocks were attached to a vacuum line. 1,3-Butadiynyltri-*n*-butylstannane (**4**; 0.54 g, 1.6 mmol) and *p*-toluenesulfonyl cyanide (**3**; 0.90 g, 5.0 mmol) were introduced into a flask equipped with a stirrer bar and the flask was attached to the vacuum line. The flask was immersed in a bath and slowly warmed to 70 °C over 1 h. The cyanobutadiyne (**2**) formed was continuously removed by distillation in vacuo from the reaction mixture. The first trap, cooled at −30 °C, selectively removed the less-volatile products, and **2** (18 mg, 0.24 mmol, 15 %) was selectively condensed in the second trap cooled at −80 °C. IR (gas phase): $\tilde{\nu} = 642$, 1272, 2190 ($\nu_{C\equiv C}$), 2253 ($\nu_{C\equiv N}$), 3328 cm^{-1} ($\nu_{C\text{-}H}$); ^1H NMR ($CDCl_3$, 400 MHz, 298 K): $\delta =$ 2.41 ppm; ^{13}C NMR ($CDCl_3$, 100 MHz, 298 K): $\delta = 48.9$ ($^4J_{C,H} <$ 1 Hz; C2), 66.0 ($^2J_{C,H} = 52.2$ Hz; C4), 66.9 ($^3J_{C,H} = 6.4$ Hz; C3), 71.7 ($^1J_{C,H} = 265.0$ Hz; C5), 104.8 ppm (C1); HRMS: calcd for HC_5N: 75.01090; found: 75.0109; MS: *m/z* (%): 76 (3.6), 75 (100), 74 (11.2), 50 (3.4), 49 (6.8).

Received: June 18, 2005
Published online: October 17, 2005

Keywords: alkynes · cyanides · diynes · nucleophilic addition · photochemistry

[1] S. Charmley, P. Ehrenfreund, Y.-J. Kuan, *Phys. World* **2003**, *16*, 35 – 38; P. Ehrenfreund, S. Charmley, *Annu. Rev. Astron. Astrophys.* **2000**, *38*, 427 – 483.
[2] W. F. Huebner, *Earth Moon Planets* **2002**, *89*, 179 – 195.
[3] V. G. Kunde, A. C. Aikin, R. A. Hanel, D. E. Jennings, W. C. Maguire, R. E. Samuelson, *Nature* **1981**, *292*, 686 – 688; A. Coustenis, T. Encrenaz, B. Bézard, B. Bjoraker, G. Graner, G. Dang-Nhu, E. Arié, *Icarus* **1993**, *102*, 240 – 260.
[4] H. W. Kroto, *Angew. Chem.* **1992**, *104*, 113 – 131; *Angew. Chem. Int. Ed. Engl.* **1992**, *31*, 111 – 129.
[5] P. Coll, D. Coscia, N. Smith, M.-C. Gazeau, S. I. Ramirez, G. Cernagora, G. Israel, F. Raulin, *Planet. Space Sci.* **1999**, 47, 1331 – 1340; E. de Vanssay, M.-C. Gazeau, J.-C. Guillemin, F. Raulin, *Planet. Space Sci.* **1995**, 43, 25 – 31.
[6] R. A. Sanchez, J. P. Ferris, L. E. Orgel, *Science* **1966**, *154*, 784 – 785; J. P. Ferris, R. A. Sanchez, L. E. Orgel, *J. Mol. Biol.* **1968**, *33*, 693 – 704; Y.-B. Xiang, S. Drenkard, K. Baumann, D. Hickey, A. Eschenmoser, *Helv. Chim. Acta* **1994**, *77*, 2209 – 2250.
[7] a) J.-C. Guillemin, C. M. Breneman, J. C. Josepha, J. P. Ferris, *Chem. Eur. J.* **1998**, *4*, 1074 – 1082; b) A. Benidar, J.-C. Guillemin, O. Mo, M. Yanez, *J. Phys. Chem. A* **2005**, *109*, 4705 – 4712.
[8] L. E. Orgel, *Origins Life Evol. Biosphere* **2002**, *32*, 279 – 281, and references therein.
[9] C. Moureu, J. C. Bongrand, *C. R. Hebd. Seances Acad. Sci.* **1910**, 151.
[10] A. J. Alexander, H. W. Kroto, D. R. M. Walton, *J. Mol. Spectrosc.* **1976**, *62*, 175 – 180.
[11] S. Haas, G. Winnewisser, K. M. T. Yamada, *Can. J. Phys.* **1994**, *72*, 1165 – 1178.
[12] L. Bizzocchi, C. Degli Esposti, P. Botschwina, *J. Mol. Spectrosc.* **2004**, *225*, 145 – 151.
[13] I. Klement, K. Lennick, C. E. Tucker, P. Knochel, *Tetrahedron Lett.* **1993**, *34*, 4623 – 4626; I. Klement, M. Rottlaender, C. E. Tucker, T. N. Majid, P. Knochel, *Tetrahedron* **1996**, *52*, 7201 – 7220.
[14] L. Berillon, A. Lepretre, A. Turck, N. Ple, G. Queguiner, G. Cahiez, P. Knochel, *Synlett* **1998**, 1359 – 1360; M. Rottlaender, L. Boymond, G. Cahiez, P. Knochel, *J. Org. Chem.* **1999**, *64*, 1080 – 1081.
[15] I. Nagasaki, Y. Suzuri, K.-i. Iwamoto, T. Higashino, A. Miyashita, *Heterocycles* **1997**, *46*, 443 – 450.
[16] M. I. Bruce, P. J. Low, A. Werth, B. W. Skelton, A. H. White, *J. Chem. Soc. Dalton Trans.* **1996**, 1551 – 1566.
[17] The formation of cyanoalkynes by reaction of an alkynyl stannane with a $ClCN–AlCl_3$ complex in dichloromethane has already been reported.[10] However, purification with aqueous HCl followed by flash chromatography is inappropriate for kinetically unstable compounds.
[18] I. Cherchneff, A. E. Glassgold, G. A. Mamon, *Astrophys. J.* **1993**, *410*, 188 – 201.
[19] J. P. Ferris, J.-C. Guillemin, *J. Org. Chem.* **1990**, *55*, 5601 – 5606.
[20] The breaking of the H–C bond of cyanoacetylene does not occur upon irradiation at wavelengths longer than 240 nm: D. W. Clarke, J. P. Ferris, *Icarus* **1995**, *115*, 119 – 125.
[21] C. K. Ingold, G. W. King, *J. Chem. Soc.* **1953**, 2704 – 2707; H. Okabe, *J. Chem. Phys.* **1983**, *78*, 1312 – 1317.
[22] D. Toublanc, J. P. Parisot, J. Brillet, D. Gautier, F. Raulin, C. P. McKay, *Icarus* **1995**, *113*, 2 – 26; S. Lebonnois, D. Toublanc, F. Hourdin, P. Rannou, *Icarus* **2001**, *152*, 384 – 406; S. Lebonnois, E. L. O. Bakes, C. P. McKay, *Icarus* **2002**, *159*, 505 – 517.
[23] D. L. Yang, T. Yu, N. S. Wang, M. C. Lin, *Chem. Phys.* **1992**, *160*, 317 – 325.
[24] K. Seki, M. Yagi, M. He, J. B. Halpern, H. Okabe, *Chem. Phys. Lett.* **1996**, *258*, 657 – 662.
[25] M. Prochazka, A. Zaruba, *Collect. Czech. Chem. Commun.* **1983**, 48, 89 – 95.
[26] For a review on the chemistry of cyanoacetylenes, see: "Functionalized acetylenes in organic synthesis. The case of the 1-cyano- and the 1-haloacetylenes" H. Hopf, B. Witulski in *Modern Acetylene Chemistry* (Eds: P. J. Stang, F. Diederich), VCH, Weinheim, **1995**, pp. 33 – 66.

 © 2005 Wiley-VCH Verlag GmbH & Co. KGaA, Weinheim

Dihydrogen or Dihydride?

DOI: 10.1002/anie.200502297

A Neutron Diffraction Study of $[OsClH_3(PPh_3)_3]$: A Complex Containing a Highly "Stretched" Dihydrogen Ligand**

Muhammed Yousufuddin, Ting Bin Wen, Sax A. Mason, Garry J. McIntyre, Guochen Jia, and Robert Bau**

Oxidative addition of dihydrogen to a transition metal is one of the most important steps in many catalytic processes.[1] Some years ago, Kubas and co-workers[2] used neutron diffraction to show for the first time that H_2 could bind to a metal in a sideways fashion as η^2-H_2, now called the nonclassical dihydrogen ligand (**I**). Further insertion of the metal into the dihydrogen ligand, upon continuation of the oxidative addition process, weakens the H–H bond causing it to lengthen (**II**) and finally cleave to form two terminal hydride ligands (**III**). The weakening of the H–H bond (**II**) is considered to be an intermediate step along the pathway, and it is this step that has garnered a considerable amount of interest.[3–5]

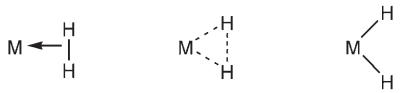

I **II** **III**

Structural studies[5] in this area have thus far provided significant information regarding the metal–dihydrogen interaction along the reaction pathway. The side-on, or nonclassical dihydrogen complexes **I**, have an H–H bond length of the order of 0.8–1.0 Å (not much longer than the H–H distance of 0.74 Å in H_2 itself[6]) while classical dihydride complexes **III** (with essentially no H···H interactions) generally have H···H distances greater than 1.7 Å. The intermediate, or stretched dihydrogen complexes **II** (also called "compressed dihydride" complexes[3a,f,g]) have H–H distances in the range 1.1–1.5 Å.[4] Although a moderate number of stretched dihydrogen complexes have been reported, the H–H distances in these complexes have mainly been obtained from NMR spectroscopic data (T_1 and $J_{H,D}$ measurements) or from X-ray data, which are not very sensitive to H positions.[3]

The most reliable technique to determine H–H distances in hydride complexes is neutron diffraction. However, only a few examples of molecules exhibiting the intermediate stage **II** have been structurally characterized by this technique.[4,5] Intramolecular "reaction trajectories" have been mapped out before in a classical series of studies of organic molecules by Bürgi and Dunitz using X-ray crystallography.[7a] In addition, Crabtree et al.[7b] have used a series of X-ray and some neutron structures to map the lengthening of a C–H bond during metal insertion, although the variation in those C–H distances (±0.1 Å) is much less pronounced than the large distributions of H···H distances we will discuss later in Table 1. Several authors have pointed out[3a,h,i] that the energy barrier for moving the H···H distance from 1.00 to 1.60 Å is only about 4 kcal mol^{-1}, which suggests that the ligand environment around the metal atom should have a significant effect.[3c] Clearly, a more complete set of stretched dihydrogen ligands is needed to obtain a clearer understanding of this intriguing interaction. In this regard, we report herein a new example of the stretched dihydrogen phenomenon in the complex $[OsClH_3(PPh_3)_3]$ (**1**).

The title complex was prepared by the reaction of $[OsCl_2(PPh_3)_3]$[8a] with H_2 in the presence of NEt_3, as described by Caulton and co-workers.[8b] The compound **1** was first made about 30 years ago, but was wrongly formulated as $[OsClH(PPh_3)_3]$.[8c] However, a careful analysis of the ^{1}H NMR spectroscopic data by Caulton et al. showed that the complex **1** was actually $[OsClH_3(PPh_3)_3]$ with a nonclassical dihydrogen ligand, as suggested by the short relaxation time ($T_1 = 26$ ms) of the hydride at −40 °C and 300 MHz. However, a minimum T_1 value could not be determined due to the low solubility of the Os complex at low temperatures, nor was it possible to conclude from the NMR study if the suspected dihydrogen ligand was *trans* to a chloride or a phosphane ligand.[8b] It was also difficult to determine the $J_{H,D}$ coupling constant for the isotopolog $[OsClHD_2(PPh_3)_3]$ due to the broadness of the hydride signal. Thus, it was impossible to estimate the H–D distance in the complex. In the present study, the structure has been unequivocally determined by a single-crystal neutron diffraction analysis.

The sample was initially characterized by X-ray diffraction[9] in order to determine the atomic coordinates used for neutron diffraction data analysis. The neutron data analysis was carried out both at room temperature and at 5 K on a crystal measuring $1.2 \times 0.8 \times 0.3$ mm^3 using the VIVALDI diffractometer at the Institut Laue–Langevin in Grenoble.[10] Full-matrix least-squares refinement of atomic positions yielded the following agreement factors for the low-temperature data set: $R(F) = 0.0831$ for 3560 independent reflections ($I > 2\sigma(I)$).[11]

Figure 1 shows the molecular sructure of **1** and its core at 5 K. Our results reveal the presence of a dihydrogen ligand

[*] M. Yousufuddin, Prof. Dr. R. Bau
Department of Chemistry
University of Southern California
Los Angeles, CA 90089 (USA)
Fax: (+1) 213-740-0930
E-mail: bau@usc.edu
Dr. T. B. Wen, Prof. Dr. G. Jia
Department of Chemistry
Hong Kong University of Science and Technology
Clear Water Bay (Hong Kong)
Fax: (+852) 2352 1594
E-mail: chjiag@ust.hk
Dr. S. A. Mason, Dr. G. J. McIntyre
Institut Laue–Langevin
6, rue Jules Howowitz, BP 156
38042 Grenoble Cedex (France)

[**] This work was funded by the American Chemical Society (grant PRF-40715-AC3) and by the Hong Kong Research Grant Council (project no. 601804).

 © 2005 Wiley-VCH Verlag GmbH & Co. KGaA, Weinheim

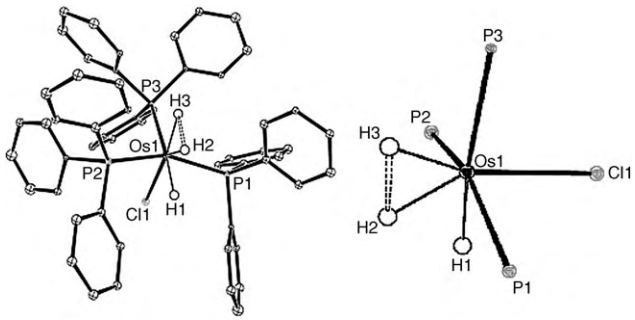

Figure 1. Molecular structure of $[OsClH_3(PPh_3)_3]$ (**1**, left) and its core (right). The H2–H3 distance is 1.48(2) Å and the H1···H2 distance is 1.67(2) Å, as determined from this neutron study. Other notable bond distances include: Os–H2 = 1.59(2) and Os–H3 1.61(1) Å.

(H2···H3), although not of the nonclassical type originally envisioned,[8b] but of the "stretched" variety (**II**), with an H···H bond distance of 1.48(2) Å. In addition, one terminal hydride ligand (H1) was located, plus one chloride and three phosphane ligands. The Os–H1 distance to the terminal hydride ligand (1.62(2) Å) is similar to other Os–H distances reported in literature,[12] and this terminal hydride ligand H1 is positioned 1.67(2) Å from the H2 atom of the dihydrogen ligand, a distance which is in the range of slightly nonbonding interactions.[5] It should be noted that, within experimental error, we found a barely significant increase in geometry between the neutron structures refined at 5 K and at 295 K,[13a] which is somewhat consistent with a theoretical study which suggests that the H···H distance in a stretched dihydrogen ligand could be temperature dependent.[13b]

The molecule is substantially distorted from an ideal octahedral geometry. The terminal hydride is located *trans* to a phosphane ligand (H1-Os1-P3 172.5(6)°) while the dihydrogen ligand sits essentially *trans* to the chloride ligand (X-Os1-Cl1 171.4(3)°, where X represents the center of the dihydrogen ligand). The dihydrogen, hydride, and chloride ligands lie in the same plane (Figure 1), which is similar to the atomic arrangement in $[IrCl_2H(H\cdots H)(PiPr_3)_2]$.[4e] Two other stretched dihydrogen moieties previously studied by neutron diffraction, in which the dihydrogen ligands were also located *trans* to negatively charged ligands, were also found in six-coordinate osmium complexes.[4b,c]

Speculation can be made as to the role of the chloride ligand in influencing the geometry of complex **1**. Some years ago we reported the results of a neutron diffraction analysis of $[OsH_4(PMe_2Ph)_3]$, which contains four terminal hydrides with an average Os–H bond distance of 1.659(3) Å.[12a] The only apparent difference between that complex and the present complex **1** (besides the difference in phosphane ligands) is the substitution of a chloride ligand for a hydride ligand. Perhaps the presence of the *trans* chloride ligand, which is more electronegative than hydride, promotes closer H···H interactions,[3h] and this could be the driving force for formation of the stretched dihydrogen ligand.

The main point of our communication is shown in Table 1, which summarizes experimental data, from which a crude approximation of a "reaction profile" can be derived, for the specific process of oxidative addition of a metal atom into an H–H bond. In this table, we have included all neutron diffraction data on H–H complexes that were available to us, with the exception of the last category at the bottom of the table ("classical" hydride complexes, in which there are no H···H bonding interactions), for which neutron results are too numerous to be listed in full.

Table 1: A selection of H···H distances [Å] and H-M-H angles [°] determined by neutron diffraction.[a]

	Compound	1 H–H	2 H-M-H	3 Av. M–H	4 "Adjusted" av. M–H[b]	5 M–X[c]	6 "Adjusted" M–X[b,c]
Nonclassical Complexes (with "almost unstretched" H···H distances)	$[Mo(CO)(\eta^2\text{-}H_2)(dppe)_2]$	0.80–0.85[14e]	24.0–25.6	1.922(15)	1.79	1.886(15)	1.76
	$[Fe(H)(\eta^2\text{-}H_2)(dppe)_2]^+$	0.816(16)[14a]	29.3(5)	1.616(10)	1.62	1.616(10)	1.62
	$[W(CO)_3(\eta^2\text{-}H_2)(PiPr_3)_2]$	0.82(1)[14b]	25.1	1.89(1)	1.76	1.89(1)	1.76
	$[FeH_2(\eta^2\text{-}H_2)(PPh_2Et)_3]$	0.821(10)[14d]	29.9(4)	1.592(8)	1.59	1.538(8)	1.54
	$[Ir(H)_2(I)(\eta^2\text{-}H_2)(PiPr_3)_2]$	0.856(9)[14c]	28.2(3)	1.756(7)	1.66	1.703(7)	1.60
Slightly Stretched H···H distances	$[(C_5Me_5)OsH_2(\eta^2\text{-}H_2)(PPh_3)]^+$	1.014(11)[4g]	35.4(4)	1.669(9)	1.58	1.589(9)	1.50
	$[(C_5Me_5)Ru(\eta^2\text{-}H_2)(dppm)]^+$	1.10(2)[4d]	38(1)	1.67(2)	1.59	1.58(2)	1.50
	$[IrCl_2H(\eta^2\text{-}H_2)(PiPr_3)_2]$	1.11(3)[4e]	42.3(9)	1.444(18)	1.34	1.347(18)	1.25
Significantly Stretched H···H distances	$[OsCl(\eta^2\text{-}H_2)(dppe)_2]^+$	1.22(3)[4c]	42.6(12)	1.58(2)	1.49	1.47(2)	1.38
	$[Os(CH_3CO_2)(\eta^2\text{-}H_2)(en)_2]^+$	1.34(2)[4b]	49.6(6)	1.60(1)	1.51	1.45(1)	1.36
	$[ReH_7\{P(p\text{-tolyl})_3\}_2]$	1.357(7)[4a]	47.6(2)	1.681(4)	1.57	1.538(4)	1.43
	$[OsClH_3(PPh_3)_3]$	1.48(2)[d]	55.1(8)	1.60(2)	1.51	1.42(2)	1.33
	$[OsH_5(PMe_2Ph)_3]^+$	1.49(4)[4f]	54.1(1)	1.64(2)	1.55	1.46(2)	1.37
Classical Complexes (no H···H bonding)	$[OsH_4(PMe_2Ph)_3]$	1.840(6)[12a]	67.9(2)	1.646(3)	1.56	–[e]	–[e]
	$[ReH_5(PMePh_2)_3]$	1.845(7)[15a]	66.8(3)	1.677(5)	1.57	–[e]	–[e]
	$[FeH_2(CO)_2\{P(OPh)_3\}_2]$	2.011(3)[15b]	82.5(1)	1.525(2)	1.53	–[e]	–[e]

[a] Abbreviations: dppe = 1,2-bis(diphenylphosphanyl)ethane; dppm = 1,2-bis(diphenylphosphanyl)methane; en = ethylenediamine. [b] The "adjusted" M–H and M–X distances were corrected for the differences in the atomic radii of the metal atoms; the correction term for Fe was arbitrarily set to be zero. Atomic radii data from Ref. [16]. [c] M–X distances involved with the H_2 ligand; X is the center of the H···H bond. [d] Present work. [e] The position of "X" (the mid-point of the H···H bond) is not meaningful for classical hydrides, in which there are no H···H interactions.

 © 2005 Wiley-VCH Verlag GmbH & Co. KGaA, Weinheim

Columns 1, 2, and 3 list the experimental H–H distances, H-M-H angles, and M–H distances, respectively, sorted in the order of increasing H–H distance. One can discern a very crude general trend of longer H–H distances coupled with shorter M–H distances. However, one has to account for differences in atomic radii of the metal atoms, and so in column 4 we list "adjusted" M–H distances in which the differences in atomic radii are used as "correction factors", with the atomic radius of iron selected arbitrarily as a "standard". One can see that column 4 is somewhat "smoother" than column 3. Finally, recognizing that one should rather consider metal–ligand distances instead of metal–hydrogen distances, we have provided two extra columns in which M–X distances are tabulated (X is the midpoint of the H–H bond). Once again, we give "unadjusted" and "adjusted" values (columns 5 and 6, respectively), in which column 6 contains the values "corrected" for differences in atomic radii. The differences between M–H distances (column 3) and metal–ligand distances (column 5) are not large for true nonclassical H_2 complexes (top portion of Table 1), but the differences become more apparent where "slightly stretched" and "significantly stretched" dihydrogen complexes are concerned (middle portion of Table 1).

Perhaps the most meaningful comparison is between column 1 (or column 2) and column 6. Although there is obviously some scatter in the data, one can discern a definite trend in which an increasing H–H distance appears to be correlated with a decreasing metal–ligand distance. In other words, this is experimental evidence for the reaction pathway **I**→**II**→**III**. A somewhat similar conclusion for metal insertion into a C–H bond has appeared earlier,[7b] but in that case only a small spread of C–H distances was observed, much more subtle than the large spread in H–H distances listed in Table 1. One can conclude from this comparison that the process of oxidative addition into an H–H bond is intrinsically different to oxidative addition into a C–H bond.

Received: June 30, 2005
Revised: August 22, 2005
Published online: October 17, 2005

Keywords: hydride ligands · hydrogen · neutron diffraction · osmium · oxidative addition

[1] a) G. Kubas, *Metal Dihydrogen and σ-Bond Complexes: Structure, Theory, and Reactivity*, Kluwer, New York, **2001**; b) M. Peruzzini, R. Poli, *Recent Advances in Hydride Chemistry*, Elsevier, Amsterdam, **2001**.

[2] G. J. Kubas, R. R. Ryan, B. I. Swanson, P. J. Vergamini, H. J. Wasserman, *J. Am. Chem. Soc.* **1985**, *107*, 451.

[3] Examples of recent work: a) D. M. Heinekey, A. Lledos, J. M. Lluch, *Chem. Soc. Rev.* **2004**, *33*, 175; b) D. G. Gusev, *J. Am. Chem. Soc.* **2004**, *126*, 14249; c) R. Gelabert, M. Moreno, J. M. Lluch, A. Lledos, V. Pons, D. M. Heinekey, *J. Am. Chem. Soc.* **2004**, *126*, 8813; d) P. Barrio, M. A. Esteruelas, A. Lledos, E. Onate, J. Tomas, *Organometallics* **2004**, *23*, 3008; e) B. Eguillor, M. A. Esteruelas, M. Olivan, E. Onate, O *rganometallics* **2005**, *24*, 1428; f) M. Vogt, V. Pons, D. M. Heinekey, *Organometallics* **2005**, *24*, 1832; g) R. Gelabert, M. Moreno, J. M. Lluch, A. Lledos, D. M. Heinekey, *J. Am. Chem. Soc.* **2005**, *127*, 5632; h) G. Barea, M. A. Esteruelas, A. Lledos, A. M. Lopez, E. Onate, J. I. Tolosa, *Organometallics* **1998**, *17*, 4065; i) F. Maseras, A. Lledos, E. Clot, O. Eisenstein, *Chem. Rev.* **2000**, *100*, 601.

[4] a) L. Brammer, J. A. K. Howard, O. Johnson, T. F. Koetzle, J. L. Spencer, A. M. Stringer, *J. Chem. Soc. Chem. Commun.* **1991**, 241; b) T. Hasegawa, Z. Li, S. Parkin, H. Hope, R. K. McMullan, T. F. Koetzle, H. Taube, *J. Am. Chem. Soc.* **1994**, *116*, 4352; c) P. A. Maltby, M. Schlaf, M. Steinbeck, A. J. Lough, R. H. Morris, W. T. Klooster, T. F. Koetzle, R. C. Srivastava, *J. Am. Chem. Soc.* **1996**, *118*, 5396; d) W. T. Klooster, T. F. Koetzle, G. Jia, T. P. Fong, R. H. Morris, A. Albinati, *J. Am. Chem. Soc.* **1994**, *116*, 7677; e) A. Albinati, V. I. Bakhmutov, K. G. Caulton, E. Clot, J. Eckert, O. Eisenstein, D. G. Gusev, V. V. Grushin, B. E. Hauger, W. T. Klooster, T. F. Koetzle, R. K. McMullan, T. J. O'Loughlin, M. Pelissier, J. S. Ricci, M. P. Sigalas, A. B. Vymenits, *J. Am. Chem. Soc.* **1993**, *115*, 7300; f) T. J. Johnson, A. Albinati, T. F. Koetzle, J. Ricci, O. Eisenstein, J. C. Huffman, K. G. Caulton, *Inorg. Chem.* **1994**, *33*, 4966; g) C. L. Gross, D. M. Young, A. J. Schultz, G. S. Girolami, *J. Chem. Soc. Dalton Trans.* **1997**, 3081.

[5] R. Bau, M. H. Drabnis, *Inorg. Chim. Acta* **1997**, *259*, 27, and references therein.

[6] *CRC Handbook of Chemistry and Physics* (Ed.: D. R. Lide), 75th ed., CRC, Ann Arbor, MI, **1994**, p. 9.

[7] a) H. B. Bürgi, J. D. Dunitz, *Acc. Chem. Res.* **1983**, *16*, 153; b) R. H. Crabtree, E. M. Holt, M. Lavin, S. M. Morehouse, *Inorg. Chem.* **1985**, *24*, 1986.

[8] a) P. R. Hoffman, K. G. Caulton, *J. Am. Chem. Soc.* **1975**, *97*, 4221; b) G. Ferrando, K. G. Caulton, *Inorg. Chem.* **1999**, *38*, 4168; c) A. Oudeman, F. Van Rantwijk, H. J. Van Bekkum, *J. Coord. Chem.* **1974**, *4*, 1.

[9] T. B. Wen, G. Jia, unpublished results.

[10] C. Wilkinson, J. A. Cowan, D. A. A. Myles, F. Cipriani, G. J. McIntyre, *Neutron News* **2002**, *13*, 37.

[11] Crystals suitable for neutron-diffraction studies were grown by layering a minimum amount of hexane over a dichloromethane solution of the compound under an atmosphere of hydrogen. A triangular prismatic single crystal with a volume of less than 0.5 mm^3 was wrapped in aluminum foil in a helium-filled glove bag and glued to a vanadium pin. The crystal was then mounted in a He cryostat on the Very-Intense Vertical-Axis Laue Diffractometer ("VIVALDI") at the Institut Laue–Langevin in Grenoble, France. Initially, data collection proceeded at room temperature until a sufficient number of unique reflections was obtained for structure refinement. This was a precautionary step taken just in case the crystal cracked during the subsequent cooling procedure. The crystal was then cooled to 5 K and data collection repeated. Crystal data for **1** (unit cell dimensions from the X-ray analysis[9]): $C_{54}H_{48}ClOsP_3$, $M_r = 834$, approximate crystal dimensions $1.2 \times 0.8 \times 0.3$ mm^3; orthorhombic, space group $Pca2_1$, $a = 19.258(1)$, $b = 12.949(1)$, $c = 17.836(1)$ Å, $V = 4448(1)$ $Å^3$, $F(000) = 862$, $Z = 4$, $\rho_{calcd} = 1.245$ $g\,cm^{-3}$, $\mu = 0.310$ mm^{-1}. $\theta = 4$–$72°$, completeness = 72%, resolution d-(min) = 0.92 Å, white beam neutron source ($\lambda = 0.9$–2.7 Å), $T = 5$ K, 25311 measured data (VIVALDI instrument with cylindrical area detector made from Gd_2O_3-doped BAFBR:Eu^{2+} image plates), of which 4552 ($R_{int} = 0.2856$) were unique. Intensities were indexed and processed using LAUEGEN, reflections were integrated and the background removed using INTEGRATE+, reflections were normalized to a constant incident wavelength using LAUENORM, and neutron data were phased using the atomic coordinates determined from the X-ray structure. For a full description of data collection and treatment using VIVALDI, see: E. Ding, B. Du, E. A. Meyers, S. G. Shore, M. Yousufuddin, R. Bau, G. J. McIntyre, *Inorg. Chem.* **2005**, *44*, 2459. Full-matrix least-squares refinement on F^2, data to parameters ratio: 10.6:1, final R indices ($I > 2\sigma(I)$):

 © 2005 Wiley-VCH Verlag GmbH & Co. KGaA, Weinheim

$R1 = 0.0831$, $wR2 = 0.1812$; $R1 = 0.1205$, $wR2 = 0.1984$ for all data, GOF on $F^2 = 1.037$. CCDC-275803 contains the supplementary crystallographic data for this paper. These data can be obtained free of charge from The Cambridge Crystallographic Data Center via www.ccdc.cam.ac.uk/data_request/cif.

[12] a) D. W. Hart, R. Bau, T. F. Koetzle, *J. Am. Chem. Soc.* **1977**, *99*, 7557; b) J. A. K. Howard, O. Johnson, T. F. Koetzle, J. L. Spencer, *Inorg. Chem.* **1987**, *26*, 2930.

[13] a) For data at 295 K, we obtained the following results: H1–H2 1.71(4) and H2–H3 1.56(4) Å, $R(F) = 0.1403$ for 2818 independent reflections ($I > 2\sigma(I)$); b) R. Gelabert, M. Moreno, J. M. Lluch, A. Lledos, *J. Am. Chem. Soc.* **1997**, *119*, 9840.

[14] a) J. S. Ricci, T. F. Koetzle, M. T. Bautista, T. M. Hofstede, R. H. Morris, J. F. Sawyer, *J. Am. Chem. Soc.* **1989**, *111*, 8823; b) G. J. Kubas, R. R. Ryan, B. I. Swanson, P. J. Vergamini, H. J. Wasserman, *J. Am. Chem. Soc.* **1984**, *106*, 451; c) J. Eckert, C. M. Jensen, T. F. Koetzle, T. L. Husebo, J. Nicol, P. Wu, *J. Am. Chem. Soc.* **1995**, *117*, 7271; d) L. S. van der Sluys, J. Eckert, O. Eisenstein, J. H. Hall, J. C. Huffman, S. A. Jackson, T. F. Koetzle, G. J. Kubas, P. J. Vergamini, K. G. Caulton, *J. Am. Chem. Soc.* **1990**, *112*, 4831; e) G. J. Kubas, C. J. Burns, J. Eckert, S. W. Johnson, A. C. Larson, P. J. Vergamini, C. J. Unkefer, G. R. K. Khalsa, S. A. Jackson, O. Eisenstein, *J. Am. Chem. Soc.* **1993**, *115*, 569.

[15] a) T. J. Emge, T. F. Koetzle, J. W. Bruno, K. G. Caulton, *Inorg. Chem.* **1984**, *23*, 4012; b) N. N. Ho, R. Bau, S. A. Mason, *J. Organomet. Chem.* **2003**, *676*, 85.

[16] J. McMurray, R. C. Fay, *Chemistry*, *2nd ed.*, Prentice Hall, New Jersey, **1998**.

 © 2005 Wiley-VCH Verlag GmbH & Co. KGaA, Weinheim

Fullerenes

DOI: 10.1002/anie.200501791

General Rule for the Stabilization of Fullerene Cages Encapsulating Trimetallic Nitride Templates**

*Josep M. Campanera, Carles Bo, and Josep M. Poblet**

Fullerenes containing a trimetallic nitride template (TNT) within the cage are a particularly interesting class of endohedral metallofullerenes. Not only are the cage properties modified by the presence of the incarcerated group but, almost uniquely among endohedral metallofullerenes, they are quite stable. Furthermore, they can be produced in multimilligram quantities, and these amounts should increase in the future. The electronic effect of the TNT is such that some fullerenes of sizes and symmetry that are otherwise relatively unstable become available for investigation.[1] The general formula of these TNT endohedral metallofullerenes is $A_{3-n}B_nN@C_k$ ($n=0$–3; A,B = group III, IV, and rare-earth metals; $k=68$, 78, and 80) with the archetypal examples of: $Sc_3N@C_{80}$,[2,3] $Sc_3N@C_{68}$,[4] and $Sc_3N@C_{78}$.[5] The structures of $Sc_3N@C_{78}$, $Sc_3N@C_{80}$, and $Sc_3N@C_{68}$ are displayed in Figure 1.

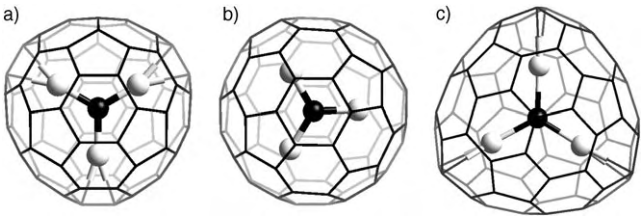

Figure 1. Optimized structures of the archetypal TNT endohedral metallofullerenes: a) D_{3h}-$Sc_3N@C_{78}$, b) C_s-$Sc_3N@C_{80}$ (I_h-C_{80}:**7**), and c) D_3-$Sc_3N@C_{68}$.

Special attention has been paid to lutetium-based TNT endohedral metallofullerenes, $Lu_{3-n}A_nN@C_{80}$ ($n=0$–2; A = Gd, Ga, and Ho), because they may prove useful as multifunctional contrast agents for X-ray, magnetic resonance imaging, and radiopharmaceuticals.[6] The aim of this research is to use methods based on density functional theory (DFT) to answer the questions: How can the stability of the TNT endohedral metallofullerenes be predicted? Which fullerene cages between C_{60} and C_{84} will be capable of encapsulating TNTs? Aihara and co-workers proposed the bond resonance energy (BRE)[7] to be an indicator of the particular stabilization of free fullerene cages when they encapsulate metal units.[8] However, this method was not a predictive tool because it could not answer whether or not new cages will be capable of encapsulating TNTs.

Up to now, only four carbon cages have been capable of encapsulating TNT units: D_3-C_{68}:**6140**, D_{3h}-C_{78}:**5**, D_{5h}-C_{80}:**6** and I_h-C_{80}:**7**. All these cages, except C_{68}, satisfy the isolated-pentagon rule (IPR). But it is interesting to see that in all cases the empty IPR fullerene isomers isolated so far are different from the carbon cages found in isolable TNT endohedral metallofullerenes. The incorporation of a TNT into the fullerene results in an electron transfer from the metal atoms to the carbon cage, in other words, the formation of a stable ion pair. It should be noted that these fullerene cages are produced only when they are negatively charged by the encapsulated species. Theoretical calculations indicated that the thermodynamic stability of a fullerene molecule depends heavily on the negative charge that resides on it.[9] The bond between the nitride and the cage is markedly defined by the ionic model $Sc_3N^{6+}@C_k^{6-}$ ($k=68$, 78, and 80).[10] From the geometric point of view, although the free Sc_3N molecule is pyramidal, this fragment has a planar structure inside the fullerene cage. When the Sc_3N unit is

[*] Prof. J. M. Poblet
Departament de Química Física i Inorgànica
Universitat Rovira i Virgili
c/Marcel lí Domingo, s/n
Campus Sescelades
43007 Tarragona Catalonia (Spain)
Fax: (+34) 977-559-563
E-mail: josepmaria.poblet@urv.net
Dr. J. M. Campanera, Dr. C. Bo
ICIQ–Institute of Chemical Research of Catalonia
Avda. Països Catalans, 16
43007 Tarragona Catalonia (Spain)

[**] This work was supported by the Spanish Ministry of Science and Technology (BQU2002-04110-C02-02), by the DURSI of the Generalitat de Catalunya (SGR01-00315), and by the Institute of Chemical Research of Catalonia Foundation.

InterScience
© 2005 Wiley-VCH Verlag GmbH & Co. KGaA, Weinheim

encapsulated, there is a significant local distortion in the fullerene cage. This distortion results in the outward movement of the carbon atoms closest to the scandium ions, which gives rise to an increase in the tendency of the carbon structure to form a pyramid and an increase in the radius of the fullerene cage.

The first ^{13}C NMR spectroscopic analysis of $Sc_3N@C_{80}$ revealed that the Sc_3N moiety rotates freely in the highly symmetric I_h-C_{80}:**7** isomer.[2] Thus, several different orientations of the TNT were found for the slightly different TNT endohedral metallofullerenes of I_h-C_{80}:**7**—$Lu_3N@C_{80}$,[11] $ErSc_2N@C_{80}$,[12] $Sc_3N@C_{80}$,[2] and $Sc_3N@C_{80}$-$C_8H_6(OCH_3)_2$.[13] DFT calculations corroborated that the differences among the most stable isomers are rather small, <0.10 eV.[10,14] Later, a minor new isomer of $Sc_3N@C_{80}$, which corresponds to the Sc_3N fragment encapsulated by the D_{5h}-C_{80}:**6** isomer, was also isolated and characterized.[3] We focus our study only on the TNT endohedral metallofullerenes of I_h-C_{80}:**7** isomer. Neither of these C_{80} isomers have been isolated as empty fullerenes and are not even the most stable isomers among the seven distinct isomers that satisfy the IPR:[15] D_{5d}-C_{80}:**1**, D_2-C_{80}:**2**, C_{2v}-C_{80}:**3**, D_3-C_{80}:**4**, $C_{2v'}$-C_{80}:**5**, D_{5h}-C_{80}:**6**, and I_h-C_{80}:**7**.[16] Two empty-cage isomers, D_2-C_{80}:**2** and D_{5d}-C_{80}:**1**, have been isolated,[17] and theoretical calculations have shown that the I_h-C_{80}:**7** structure is the less-stable isomer overall.[18] However, electronic-structure calculations showed that the stability of the I_h-C_{80}:**7** isomer increases markedly when six electrons are added to the cage.[19] In the case of $Sc_3N@C_{78}$, the $D_{3h'}$-C_{78}:**5** isomer has not been calculated as the most stable nor has ever been isolated as an empty cage. There are five IPR isomers for the empty C_{78} cage with the following relative stability order: $C_{2v'}$-C_{78}:**3** > C_{2v}-C_{78}:**2** > D_3-C_{78}:**1** > $D_{3h'}$-C_{78}:**5** > D_{3h}-C_{78}:**4**.[20] Unlike in $Sc_3N@C_{80}$, in $Sc_3N@C_{78}$ the metal atoms reside over three pyracylene 6:6 C–C bonds. The fourth fullerene cage, which is capable of incarcerating four atoms, is the non-IPR D_3-C_{68}:**6140**. Other non-IPR structures have also been investigated for $Ca@C_{72}$,[21,22] $La_2@C_{72}$,[23] $Ca@C_{74}$,[21] $Sc_2@C_{74}$,[21,24] and $Sc_2@C_{66}$.[25] It is interesting to note that the only known violations of the IPR rule occur in endohedral metallofullerenes. For the C_{68} stoichiometry, the carbon surface of which consists solely of pentagons and hexagons, there are 6332 possible isomers. Nevertheless, the detailed structural characterization of $Sc_3N@C_{68}$ showed that the carbon cage is the 6140 isomer.[4] Although the cage radius of D_3-C_{68}:**6140** is not only considerably smaller but also distorted, the TNT guest can be encapsulated in a plane in which scandium atoms are directly connected to 5:5 ring junctions.[26]

Formally, a total of six electrons go from the highest occupied nitride orbitals to the lowest unoccupied cage orbitals. This formal electron transfer is accompanied by a large binding energy for the encapsulation process. These were calculated to be -173, -224, and -268 kcal mol^{-1} for $Sc_3N@C_k$ when $k=68$, 78, and 80, respectively.[10] The $D_{3h'}$-C_{78}:**5** isomer has a closed-shell ground state with three low unoccupied orbitals of symmetries a_2' (-5.15 eV) and e′ (-4.88 eV) that are π-antibonding orbitals basically centered in the set of pyracylene 6:6 C–C bond type. These unoccupied orbitals can receive six electrons from the three highest occupied orbitals of the TNT, which are very high in energy: a_1' (-4.44 eV) and e′(-3.51 eV), see Figure 2. For the I_h-C_{80}:**7** isomer, previous theoretical calculations have shown that it has the open-shell configuration $(t_{1g}+h_u)^{16}(g_g)^2(a_g+h_g)^0$.

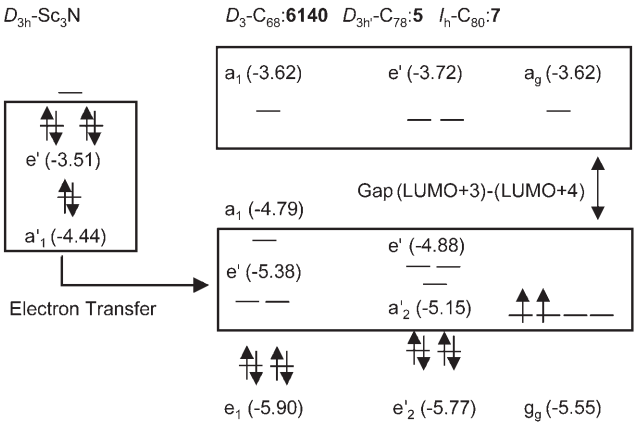

Figure 2. Representation of the ionic bond between the trimetallic nitride template (TNT) and the fullerene cages D_3-C_{68}:**6140**, $D_{3h'}$-C_{78}:**5**, and I_h-C_{80}:**7**. There is a formal transfer of six electrons from the three highest occupied orbitals of the TNT unit to the three lowest unoccupied orbitals of the fullerene cages. Consequently, the $M_3N@C_k$ ($k=68$, 78, and 80) complexes are described as $Sc_3N^{6+}@C_k^{6-}$ with a relatively large HOMO–LUMO gap nearly equal to the (LUMO+3)–(LUMO+4) found in the free cages: The (LUMO+3)–(LUMO+4) rule.

Moreover, I_h-C_{80}:**7** may deform to lower symmetries by Jahn–Teller distortion.[27] It represents an electronic configuration with only two electrons in four low-lying degenerate orbitals, -5.55 eV, which can easily accept six electrons. As a consequence of this electron-charge transfer, the resulting endohedral has a closed-shell configuration. D_3-C_{68}:**6140** has a closed-shell ground state with a HOMO–LUMO gap of 0.52 eV and with three low unoccupied orbitals of symmetries e′ (-5.38 eV) and a_1 (-4.79 eV), which can easily accept six electrons as the other two fullerenes do. Indeed, after the electron-charge transfer, the cage is stabilized as the final endohedral complex has a HOMO–LUMO gap of 1.27 eV. A similar gap was found for the TNT endohedral complexes of $D_{3h'}$-C_{78}:**5** and I_h-C_{80}:**7** with 1.24 and 1.18 eV, respectively. These electronic considerations are the key to rationalizing why only some cages can encapsulate TNTs.

On the one hand, the three cages studied here—D_3-C_{68}:**6140**, $D_{3h'}$-C_{78}:**5**, and I_h-C_{80}:**7**—have three very low-lying LUMOs accompanied with a large energy separation between the LUMO+3 and LUMO+4 (see Figure 2). On the other hand, the TNT has three HOMOs that are relatively high in energy. Consequently, the cage orbitals can easily accommodate six electrons that stem from the three destabilized orbitals. Moreover, the electronic structure of the empty fullerenes suggests that it acquires, presumably, a considerable HOMO–LUMO gap after a transfer of six electrons, thus giving stability to the final complex. The final HOMO–LUMO gap of the TNT endohedral metallofullerenes can be estimated from the gap between LUMO+3 and LUMO+4

 © 2005 Wiley-VCH Verlag GmbH & Co. KGaA, Weinheim

of the free cages. The calculated and estimated values are 1.27/1.17 eV for $Sc_3N@C_{68}$, 1.24/1.16 eV for $Sc_3N@C_{78}$, and 1.18/1.93 eV for $Sc_3N@C_{80}$. The main conclusion that can be drawn from this observation is that we can predict HOMO–LUMO gaps by simply checking the molecular-orbital energies of the free fullerene cage. In principle, only the free isomers with a large (LUMO + 3)–(LUMO + 4) gap will be predisposed to encapsulate TNTs. To check whether this statement can be generalized, we calculated (LUMO + 3)–(LUMO + 4) gaps for all the IPR isomers from C_{60} to C_{84}. There are 51 IPR isomers: 1 of C_{60}, C_{70}, C_{72}, and C_{74}; 2 of C_{76}; 5 of C_{78}; 7 of C_{80}; 9 of C_{82}; 24 for C_{84}.[16] The result is quite surprising and conclusive: the (LUMO + 3)–(LUMO + 4) gap for all IPR cages is smaller than 1 eV, except for C_{60}, D_{3h}-C_{78}:**5**, D_{5h}-C_{80}:**6**, and I_h-C_{80}:**7** isomers, see Figure 3. C_{60} can be

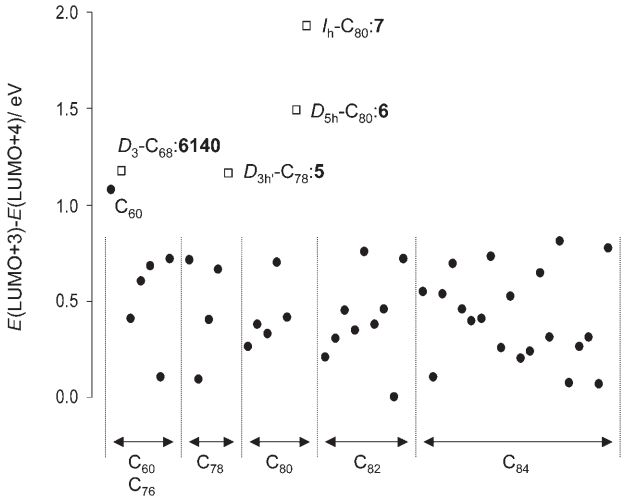

Figure 3. The (LUMO + 3)–(LUMO + 4) gap for all IPR isomers from C_{60} to C_{84} and also the non-IPR D_3-C_{68}:**6140**. Only isomers with the gap larger than 1 eV have been capable of encapsulating TNT units.

rejected because its cavity measured through the cage radius, 3.551 Å, is not big enough to encapsulate a four-atom unit. In the rest of fullerene cages the cavity is not a limitation for the encapsulation. Apart from the well-known TNT endohedral metallofullerenes we have encapsulated Sc_3N into D_{3h}-C_{78}:**4** and C_s-C_{84}:**3** isomers as a test case to corroborate our predictions. D_{3h}-C_{78}:**4** isomer is the least-stable isomer among all IPR C_{78} isomers and is 0.99 eV less stable than the $D_{3h'}$-C_{78}:**5** isomer. The cage seems to be suitable for the TNT encapsulation as the scandium atoms can be also oriented to the reactive 6:6 C–C bonds as occurs in $D_{3h'}$-C_{78}:**5**. However, the electronic configuration of the free cage does not seem to be favorable for the encapsulation due to a small (LUMO + 3)–(LUMO + 4) gap of 0.66 eV, which, according to the rule, prevents the maximum stabilization required for the formation. The final TNT endohedral complex of D_{3h}-C_{78}:**4** is 4.89 eV less stable than the TNT encapsulation inside $D_{3h'}$-C_{78}:**5**. Up to now, none of the C_{84} isomers has encapsulated TNTs although from the geometric point of view these cages have a big enough cavity. However, no C_{84} isomer has a (LUMO + 3)–(LUMO + 4) gap larger than 1 eV. For instance, C_s-C_{84}:**3** isomer has a (LUMO + 3)–(LUMO + 4) of 0.53 eV, which is a good prediction of the final HOMO–LUMO gap for the $Sc_3N@C_{84}$ complex, 0.48 eV.

In summary, we propose an easy way of determining which fullerene cages will be capable of encapsulating TNTs based on the electronic structure of the free fullerene cages. All TNT endohedral metallofullerenes are formed by the encapsulation of a metallic nitride template inside one of the following cages: D_3-C_{68}:**6140**; $D_{3h'}$-C_{78}:**5**; D_{5h}-C_{80}:**6**; I_h-C_{80}:**7**. None of these cages has ever been isolated or detected experimentally. $Sc_3N@C_k$ ($k = 68$, 78, 80) complexes may be formally described by the ionic model $Sc_3N^{6+}@C_k^{6-}$. A total of six electrons formally transfer from the three highest occupied TNT orbitals to three low-lying unoccupied cage orbitals. The resulting endohedral complex has a relatively large HOMO–LUMO gap, which gives it stability. We have shown that the final HOMO–LUMO gap of these TNT endohedral metallofullerenes can be estimated from the (LUMO + 3)–(LUMO + 4) gap found in the free cages, which corresponds to the hypothetical anion when six additional electrons are added to the free cage, C_k^{6-}. The search for large (LUMO + 3)–(LUMO + 4) gaps (> 1 eV) in the 51 IPR fullerene isomers from C_{60} to C_{84} revealed that only C_{60}, D_{3h}-C_{78}:**5**, D_{5h}-C_{80}:**6**, and I_h-C_{80}:**7** provide a suitable electronic structure for encapsulating the TNTs. From the geometrical point of view, C_{60} is the only fullerene cage limited by having a cavity too small to encapsulate a four-atom unit. Furthermore, on principle we can predict that no other IPR fullerene cages between C_{60} and C_{84} will be capable of encapsulating a TNT. At least, they will not be as stable as the TNT complexes already known now. The non-IPR D_3-C_{68}:**6140** cage also obeys the (LUMO + 3)–(LUMO + 4) rule. Therefore, the search for new fullerene cages that encapsulate TNTs must be focused on non-IPR fullerenes only.

Experimental Section

Methods: The calculations were carried out by using DFT methodology with the ADF2000 program.[28] The local-density approximation (LDA) characterized by the electron-gas exchange together with the Vosko–Wilk–Nusair (VWN) parameterization[29] for correlation were used. Gradients were corrected by means of the Becke[30] and Perdew[31] non-local corrections to the exchange and correlation energy, respectively. First-order Pauli scalar relativistic corrections were added in variation to the total energy for all systems. Triple-ζ polarization Slater basis sets were employed to describe the valence electrons of C, Sc, and N atoms.[32] The geometries of all fullerene cages have been extracted from the Fullerene Structure Library constructed by Mitsuho Yoshida.[33] Single-point calculations were used for all empty cages except for the free cages D_3-C_{68}:**6140**, $D_{3h'}$-C_{78}:**5**, I_h-C_{80}:**7**, and the TNT endohedral complexes, which were fully optimized.

Received: May 24, 2005
Published online: October 13, 2005

Keywords: density functional calculations · electron transfer · electronic structure · fullerenes · host–guest systems

 © 2005 Wiley-VCH Verlag GmbH & Co. KGaA, Weinheim

[1] "Endofullerenes: A New Family of Carbon Clusters": T. Akasaka, S. Nagase, *Developments in Fullerene Science*, Kluwer, Dordrecht, **2002**, chap. 4 and 5.

[2] S. Stevenson, G. Rice, T. Glass, K. Harich, F. Cromer, M. R. Jordan, J. Craft, E. Hadju, R. Bible, M. M. Olmstead, K. Maltra, A. J. Fisher, A. L. Balch, H. C. Dorn, *Nature* **1999**, *401*, 55.

[3] J. C. Duchamp, A. Demortier, K. R. Fletcher, D. Dorn, E. B. Iezzi, T. Glass, H. C. Dorn, *Chem. Phys. Lett.* **2003**, *375*, 655.

[4] S. Stevenson, P. W. Fowler, T. Heine, J. C. Duchamp, G. Rice, T. Glass, K. Harich, E. Hajdu, R. Bible, H. C. Dorn, *Nature* **2000**, *408*, 428.

[5] M. M. Olmstead, A. Bettencourt-Dias, J. C. Duchamp, S. Stevenson, D. Marciu, H. C. Dorn, A. L. Balch, *Angew. Chem.* **2001**, *113*, 1263; *Angew. Chem. Int. Ed.* **2001**, *40*, 1223.

[6] a) E. B. Iezzi, J. C. Duchamp, K. R. Fletcher, T. E. Glass, H. C. Dorn, *Nano Lett.* **2002**, *2*, 1187; b) S. Stevenson, J. P. Phillips, J. E. Reid, M. M. Olmstead, S. P. Rath, A. L. Balch, *Chem. Commun.* **2004**, *24*, 2814.

[7] a) J. Aihara, *J. Am. Chem. Soc.* **1995**, *117*, 4130; b) J. Aihara, *J. Phys. Chem.* **1995**, *99*, 12739; c) J. Aihara, S. Oe, M. Yoshida, E. Osawa, *J. Comput. Chem.* **1996**, *17*, 1387; d) J. Aihara, *Bull. Chem. Soc. Jpn.* **1999**, *72*, 7; e) J. Aihara, *Phys. Chem.* **2001**, *3*, 1427; f) J. Aihara, *Chem. Phys. Lett.* **2001**, *343*, 465.

[8] J. Aihara, *J. Phys. Chem. A* **2002**, *106*, 11371.

[9] E. G. Gillan, C. Yeretzian, K. S. Min, M. M. Alvarez, R. L. Whetten, R. B. Kaner, *J. Phys. Chem.* **1992**, *96*, 6869.

[10] J. M. Campanera, C. Bo, M. M. Olmstead, A. L. Balch, J. M. Poblet, *J. Phys. Chem. A* **2002**, *106*, 12356.

[11] S. Stevenson, H. M. Lee, M. M. Olmstead, C. Kozikowski, P. Stevenson, A. L. Balch, *Chem. Eur. J.* **2002**, *8*, 4528.

[12] M. M. Olmstead, A. Bettencourt-Dias, J. C. Duchamp, S. Stevenson, H. C. Dorn, A. L. Balch, *J. Am. Chem. Soc.* **2000**, *122*, 12220.

[13] E. B. Iezzi, J. C. Duchamp, K. Harich, T. E. Glass, H. M. Lee, M. M. Olmstead, A. L. Balch, H. C. Dorn, *J. Am. Chem. Soc.* **2002**, *124*, 524.

[14] The most stable overall isomer, which is displayed in Figure 1b, is $Sc_3N@C_{80}$:**11** in ref. [10].

[15] a) H. Kroto, *Nature* **1987**, *329*, 529; b) T. G. Schmalz, W. A. Seitz, D. J. Klein, G. E. Hite, *J. Am. Chem. Soc.* **1988**, *110*, 1113.

[16] P. W. Fowler, D. E. Manoloupoulus, *An Atlas of Fullerenes*, Oxford University Press, Oxford, **1995**.

[17] a) F. H. Hennrich, R. H. Michel, A. Fischer, S. Richard-Schneider, S. Gilb, M. M. Kappes, D. Fuchs, M. Bürk, K. Kobayashi, S. Nagase, *Angew. Chem.* **1996**, *108*, 1839; *Angew. Chem. Int. Ed. Engl.* **1996**, *35*, 1732; b) C. R. Wang, T. Sugai, T. Kai, T. Tomiyama, H. Shinohara, *Chem. Commun.* **2000**, 557.

[18] K. Kobayashi, S. Nagase, T. Akasaka, *Chem. Phys. Lett.* **1995**, *245*, 230.

[19] P. W. Fowler, F. Zerbetto, *Chem. Phys. Lett.* **1995**, *243*, 36.

[20] a) B. L. Zhang, C. Z. Wang, K. M. Ho, *Chem. Phys. Lett.* **1992**, *193*, 225; b) Z. Slanina, J. P. Francois, D. Bakowies, W. Thiel, *THEOCHEM* **1993**, *279*, 213; c) M. Bühl, C. van Wüllen, *Chem. Phys. Lett.* **1995**, *247*, 63; d) E. Osawa, H. Ueno, M. Yoshida, Z. Slanina, X. Zhao, M. Nishiyama, H. Saito, *J. Chem. Soc. Perkin Trans. 2* **1998**, 943; e) G. Sun, M. Kertesz, *J. Phys. Chem. A* **2000**, *104*, 7398; f) T. Heine, G. Seifert, P. W. Fowler, F. Zerbetto, *J. Phys. Chem. A* **1999**, *103*, 8738.

[21] S. Nagase, K. Kobayashi, T. Akasaka, *THEOCHEM* **1999**, *461*, 97.

[22] a) K. Kobayashi, S. Nagase, M. Yoshida, E. Osawa, *J. Am. Chem. Soc.* **1997**, *119*, 12693; b) Z. Slanina, K. Ishimura, K. Kobayashi, S. Nagase, *Chem. Phys. Lett.* **2004**, *384*, 114.

[23] H. Kato, A. Taninaka, T. Sugai, H. Shinohara, *J. Am. Chem. Soc.* **2003**, *125*, 7782.

[24] S. Nagase, K. Kobayashi, *Chem. Phys. Lett.* **1997**, *276*, 55.

[25] C. Wang, T. Kai, T. Tomiyama, T. Yoshida, Y. Kobayashi, E. Nishibori, M. Takata, M. Sakata, H. Shinohara, *Nature* **2000**, *408*, 426.

[26] M. M. Olmstead, H. M. Lee, J. C. Duchamp, S. Stevenson, D. Marciu, H. C. Dorn, A. L. Balch, *Angew. Chem.* **2003**, *115*, 928; *Angew. Chem. Int. Ed.* **2003**, *42*, 900.

[27] S. L. Lee, M. L. Sun, Z. Slanina, *Int. J. Quantum Chem.* **1996**, *60*, 355.

[28] a) ADF 2000.01, Department of Theoretical Chemistry, Vrije Universitei, Amsterdam (http://www.scm.com); b) E. J. Baerends, D. E. Ellis, P. Ros, *Chem. Phys.* **1973**, *2*, 41; c) L. Versluis, T. Ziegler, *J. Chem. Phys.* **1988**, *88*, 322; d) G. te Velde, E. J. Baerends, *J. Comput. Phys.* **1992**, *99*, 84; e) C. F. Guerra, J. G. Snijders, G. te Velde, E. J. Baerends, *Theor. Chem. Acc.* **1998**, *99*, 391.

[29] S. H. Vosko, L. Wilk, M. Nusair, *Can. J. Phys.* **1980**, *58*, 1200.

[30] a) A. D. Becke, *J. Chem. Phys.* **1986**, *84*, 4524; b) A. D. Becke, *Phys. Rev.* A **1988**, *38*, 3098.

[31] a) J. P. Perdew, *Phys. Rev.* **1986**, *84*, 4524; b) J. P. Perdew, *Phys. Rev. A* **1986**, *34*, 7406.

[32] a) J. G. Snijders, E. J. Baerends, P. Vernooijs, *At. Data Nucl. Data Tables* **1982**, *26*, 483; b) P. Vernooijs, J. G. Snijders, E. J. Baerends, *Slater Type Basis Functions for the Whole Periodic System*, Internal Report, Free University of Amsterdam, The Netherlands, **1981**.

[33] http://www.cochem2.tutkie.tut.ac.jp/Fuller/Fuller.html

 © 2005 Wiley-VCH Verlag GmbH & Co. KGaA, Weinheim

Photochemistry

DOI: 10.1002/anie.200501992

Improvement in Photocyclization Efficiency of Diaryl Ethenes by Adjusting the Pore Size of Mesoporous Silica**

*Haruki Okada, Nozomi Nakajima, Toshihiro Tanaka, and Masakazu Iwamoto**

Photochromic compounds have attracted much attention because of their potential application in photonic devices such as optical memories and optical switches. Diaryl ethenes (DE) are known to show excellent thermal stability and resistance to fatigue,[1] and they are one of the most promising family of compounds for such applications. The two isomers, open-ring and closed-ring, undergo reversible cyclization/

[*] H. Okada, N. Nakajima, Dr. T. Tanaka, Prof. Dr. M. Iwamoto
Chemical Resources Laboratory
Tokyo Institute of Technology
4259-R1-5 Nagatsuta, Midori-ku, Yokohama, 226-8503 (Japan)
Fax: (+81) 45-924-5228
E-mail: iwamoto@res.titech.ac.jp

[**] This work was supported in part by Grants-in-Aid from the Ministry of Education, Culture, Sports, Science, and Technology of Japan and CREST of JST. We thank Prof. Dr. Masahiro Irie, Graduate School of Engineering, Kyushu University, for his helpful discussion.

Supporting information for this article is available on the WWW under http://www.angewandte.org or from the author.

© 2005 Wiley-VCH Verlag GmbH & Co. KGaA, Weinheim

cycloreversion upon irradiation with UV and visible light (Scheme 1). There are two conformations, parallel and antiparallel, in the open-ring isomer. Since only the antiparallel conformation participates in the photocyclization, the quantum yield of photocyclization is usually lower than 0.5.[1] Effort has been made to increase the fraction of the antiparallel conformation by, for example, encapsulation of DE into the cylindrical framework of a cyclodextrin host,[2a] introduction of bulky substituents to the reactive carbon atoms of DE,[2b] incorporation of DE into the main chain of a polymer,[2c] and photochromic ractions in the crystalline phase.[2d–e]

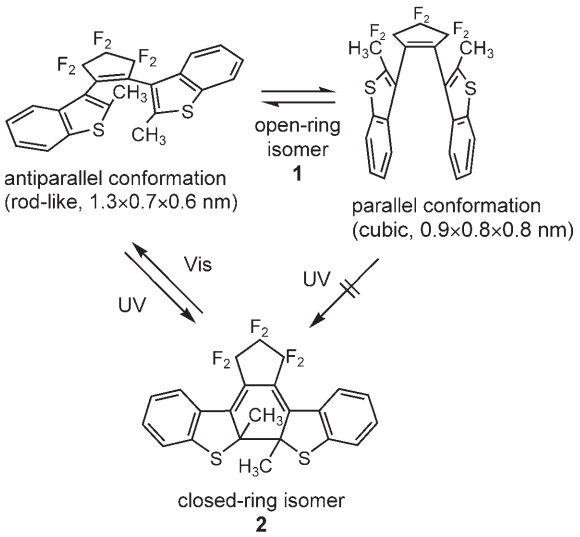

Scheme 1. Photochromic reactions of **1**. Values for molecule size are given in nm, as in the text.

Mesoporous silica materials such as MCM-41 (M41) and FSM-16 have regular pore structures and uniform pore diameters. [3,4] The pore diameter can be adjusted by changing the carbon number—the number of carbon atoms in the backbone of the alkyl chain—of the surfactant micelles in the hydrothermal synthesis,[3,5,6] by adding swelling agents to the synthesis gels,[3] or by modifying the surface of the silica with organic silylating reagents.[3,7,8] Although the photochromism of azobenzene and spiropyran on mesoporous materials has already been studied,[9] no attention has been paid to the correlation between the pore diameter and the quantum yield of photoisomerization. This subject is dealt with here: the photocyclization rate constants were greatly dependent on the pore diameters of M41. In addition, reversible photochromism was observed in substrates with limited functional groups. Our findings establish a new technique to control photochromism by tuning the pore size.

M41 materials with different pore diameters were prepared by using surfactants with carbon numbers of 10, 12, 14, 16, and 22.[6] The M41 sample obtained with a dodecyltrimethylammonium salt, for example, is abbreviated as M41–12. Various organic groups (phenyl, methyl, 3-aminopropyl, 3-sulfanylpropyl, and 4-hydroxyphenyl) were planted on M41 and the resulting products are designated R-M41s (R = organic group). The DE 1,2-Bis[2-methyl-benzo[b]thiophen-3-yl]-3,3,4,4,5,5- hexafluoro-1-cyclopentene (**1**, Scheme 1) was used as a model photochromic compound. The diffuse-reflectance UV/Vis absorption spectrum of Ph-M41 was almost the same as that of $PhSi(OEt)_3$ itself (see Supporting Information). The observation of characteristic vibrational structures of the phenyl group reveals that there is no exciton coupling between the phenyl groups and no interaction between the phenyl groups and the silica surface; therefore, each phenyl ring is isolated on the M41 wall. The pore diameters measured by N_2 or Ar adsorption/desorption measurements are summarized in Table 1. The decrements in the pore diameters on modification were 0.9–1.3 nm on Ph-M41 and 0.4–0.5 on Me-M41; these values are very close to twice the lengths of Si–Ph (0.55 nm) and Si–Me units (0.22 nm), respectively, which indicates that each organic group is bonded upright on the surface.

Reversible and irreversible photoisomerization of **1** were observed, which were dependent on the surface states of the pore wall. The UV/Vis spectra for a typical example of the former are shown in Figure 1. The absorption bands at 358 and 525 nm, which are assignable to the closed-ring isomer **2**, increased with UV irradiation and decreased with visible-light irradiation. The diffuse-reflectance spectra are plotted in Figure 2 as a function of the alternating irradiation with UV and visible light: A reversible change in the UV/Vis bands was obtained on Ph-M41 (Figure 2a). The Me-, 3-aminopropyl-, or 3-sulfanylpropyl-modified M41 also provided this reversible, fatigue-resistant reaction (see Supporting Information). In contrast, the change that occurred on irradiating **1** loaded on unmodified M41 was irreversible (Figure 2b). After several UV/Vis irradiations, a new UV band at 388 nm emerged which could not be assigned (see Supporting

Table 1: Properties of unmodified M41 and M41s modified with organic groups.[a]

	Unmodified M41	Ph-M41			Me-M41		
	d [nm][c]	Organic groups per nm^2	*d* [nm][c]	Δd [nm][d]	Organic groups per nm^2	*d* [nm][c]	Δd [nm][d]
M41-12	2.27	0.99	1.35[b]	0.92	2.3	1.84[b]	0.43
M41-16	3.00	0.88	1.80	1.20	2.7	2.51	0.49
M41-22	4.04	1.1	2.74	1.30	3.6	3.50	0.54

[a] The amounts of organic groups were determined by the elemental analysis and the pore diameters by the Barrett–Joiner–Halenda (BJH) method with N_2 desorption isotherms. [b] Determined by the HKSF (Horvath–Kawazoe–Saito–Foley) method with Ar desorption isotherms. [c] Pore diameter. [d] Decrements of pore diameter upon modification of the organic group.

 © 2005 Wiley-VCH Verlag GmbH & Co. KGaA, Weinheim

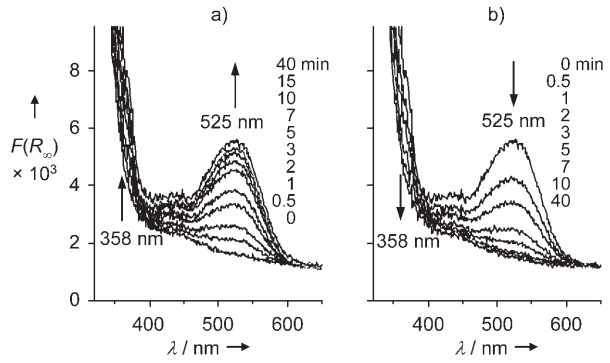

Figure 1. Changes in the diffuse-reflectance UV/Vis absorption spectra of Ph-M41-12 loaded with **1** during a) UV and b) visible-light irradiation. The amount of loaded **1** was 0.56 μmol g^{-1}. *F* is Kubelka–Munk function, R_∞ is the absolute reflectance.

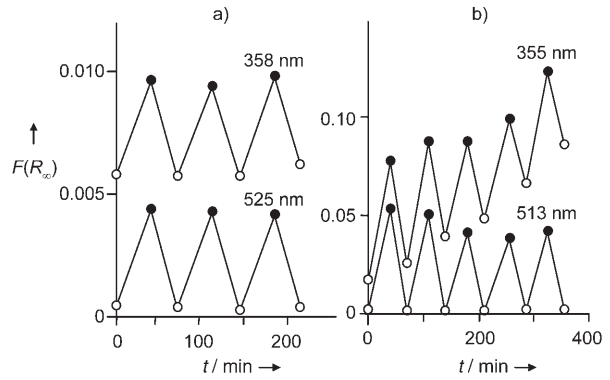

Figure 2. Changes in the intensities of diffuse-reflectance UV/Vis spectra of **1** loaded on a) Ph-M41-12 and b) M41-12 during alternate UV (●) and visible-light (○) irradiation. The amounts of **1** loaded on Ph-M41-12 and M41-12 were 0.56 and 1.57 μmol g^{-1}, respectively.

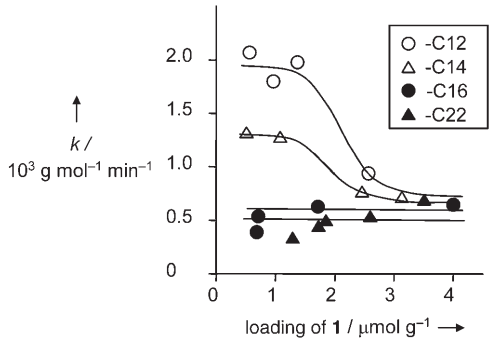

Figure 3. The *k* values for the photochromic reaction of **1** in Ph-M41 at different pore diameters and the loadings of **1**.

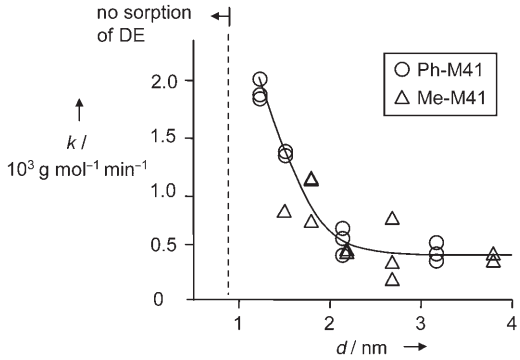

Figure 4. Dependence of *k* on the pore diameter of Ph-M41 and Me-M41.

Information). A similar phenomenon was also observed on 4-hydroxyphenyl-M41. The degradation mechanism is likely to be associated with the hydroxy groups on the surface of the M41.

The dependence of the coloration rate constant (*k*) of **1** on the pore diameter was studied on Ph-M41 and Me-M41 as the quantum yield was very difficult to determined in the present solid sample system. The *k* values were calculated from the changes in UV/Vis spectra (Figure 1) on the assumption of a pseudo-first-order reversible reaction and used to compare the efficiencies of photocyclization.[10] The dependence of the value of *k* on the amount of **1** loaded onto M41 was measured (Figure 3). Note that the *k* values were calculated per mole of supported **1**. The values were remarkably dependent on the amount of **1** in the cases of Ph-M41-12 and Ph-M41-14. Too high loadings of **1** gave incorrect *k* values due to insufficient irradiation of UV light so that *k* values should be determined only for loadings of **1** below 1.5 μmol g^{-1}.

As shown in Figure 4, the *k* value depended greatly on the pore diameter of the M41 samples. Two interesting findings are revealed: 1) The *k* value was 0.4–0.5 10^3 g mol^{-1} min^{-1} for pore diameters of 2.5–3.8 nm and it increased to about 2.0 10^3 g mol^{-1} min^{-1} when the pore diameter decreased to around 2.5 to 1.2 nm. When the pore size was below 0.9 nm, no molecules of **1** could be incorporated into the pore, which is reasonable in light of the molecular size of **1** (see Scheme 1). 2) There was no difference in the *k* values on Ph-M41 and Me-M41. Clearly, the *k* value is controlled only by the pore diameter and is independent of the organic groups on the surface of M41.

In conclusion, reversible photochromic reaction of **1** occurred without any deactivation in the pores of M41 modified with organic groups. The efficiency of the reaction increased with shrinking pore diameter in the range 1.2–3.8 nm, which results from how well the rod-like antiparallel form fits into the pore structure. The materials described here would be useful for high-density optical memory.

Experimental Section

The parent M41s were prepared by using colloidal silica or water glass according to a previously described method.[5,6] The modification of M41 was carried out as follows: M41 (1 g) was suspended in a solution (6 mmol) of R-Si$(OEt)_3$ in *n*-heptane (20 mL) and stirred for 24 h at 353 K. The resulting samples were filtered, washed with *n*-heptane and acetone, then dried at 323 K in air. The M41 samples were simply stirred with the *n*-heptane solution (1 mM) of **1**[11] for 6 h at room temperature. After the samples were isolated by filtration and washed with *n*-heptane, they were dried at 323 K in air.[12] The amount of loaded **1** was determined by measuring the difference between the concentrations of **1** in solution before and after the loading procedure.

 © 2005 Wiley-VCH Verlag GmbH & Co. KGaA, Weinheim

UV and visible light came from a superhigh-pressure Hg lamp (USHIO, 500 W) with one or two filter papers and an optical filter UV-D33S or L-39 (Asahi technoglass). Diffuse-reflectance UV/Vis spectra were measured by using a Perkin Elmer Lambda 19 spectrometer with barium sulfate as a reference. The obtained spectra were converted into absorption spectra through the Kubelka–Munk function.

Received: June 9, 2005
Revised: August 19, 2005
Published online: October 17, 2005

Keywords: alkenes · isomerization · mesoporous materials · nanostructures · photochemistry

[1] a) M. Irie, K. Uchida, *Bull. Chem. Soc. Jpn.* **1998**, *71*, 985–996; b) M. Irie, *Chem. Rev.* **2000**, *100*, 1685–1716, and references therein.
[2] a) K. Uchida, E. Tsuchida, Y. Aoi, S. Nakamura, M. Irie, *Chem. Lett.* **1999**, 63–64; b) M. Takeshita, C.-N. Choi, M. Irie, *Chem. Commun.* **1997**, 2265–2266; c) F. Stellacci, C. Bertarelli, F. Toscano, M. C. Gallazzi, G. Zotti, G. Zerbi, *Adv. Mater.* **1999**, *11*, 292–295; d) S. Kobatake, T. Yamada, M. Irie, *J. Am. Chem. Soc.* **1999**, *121*, 2380–2386; e) S. Kobatake, Y. Matsumoto, M. Irie, *Angew. Chem.* **2005**, *117*, 2186–2189; *Angew. Chem. Int. Ed.* **2005**, *44*, 2148–2151.
[3] a) C. T. Kresge, M. E. Leonowicz, W. J. Roth, J. C. Vartuli, J. S. Beck, *Nature* **1992**, *359*, 710–712; b) J. S. Beck, J. C. Vartuli, W. J. Roth, M. E. Leonowicz, C. T. Kresge, K. D. Schmitt, C. T-W. Chu, D. H. Olson, E. W. Sheppard, S. B. McCullen, J. B. Higgins, J. L. Schlenker, *J. Am. Chem. Soc.* **1992**, *114*, 10834–10843.
[4] a) T. Yanagisawa, T. Shimizu, K. Kuroda, C. Kato, *Bull. Chem. Soc. Jpn.* **1990**, *63*, 988–992; b) S. Inagaki, Y. Fukushima, K. Kuroda, *J. Chem. Soc. Chem. Commun.* **1993**, 680–681.
[5] a) T. Abe, Y. Tachibana, T. Uematsu, M. Iwamoto, *J. Chem. Soc. Chem. Commun.* **1995**, 1617–1618; b) M. Iwamoto, T. Abe, Y. Tachibana, *J. Mol. Catal. A* **2000**, *155*, 143–153.
[6] S. Namba, A. Mochizuki, M. Kito, *Chem. Lett.* **1998**, 569–570.
[7] a) N. Nakajima, H. Aritani, S. Namba, M. Irie, M. Iwamoto, *Shokubai* **2000**, *42*, 160–162 (in Japanese); b) T. Kimura, S. Saeki, Y. Sugahara, K. Kuroda, *Langmuir* **1999**, *15*, 2794–2798.
[8] a) A. Stein, B. J. Medle, R. C. Schroden, *Adv. Mater.* **2000**, *12*, 1403–1419; b) A. P. Wight, M. E. Davis, *Chem. Rev.* **2002**, *102*, 3589–3613, and references therein.
[9] a) M. Ogawa, K. Kuroda, J. Mori, *Chem. Commun.* **2000**, 2441–2442; b) K. Hoffmann, U. Resch-Genger, F. Marlow, *Microporous Mesoporous Mater.* **2000**, *41*, 99–106; c) C. Schomburg, M. Wark, Y. Rohlfing, G. Schulz-Ekloff, D. Wöhrle, *J. Mater. Chem.* **2001**, *11*, 2014–2021.
[10] The k values were calculated by using the following equation.

$$\frac{x_e}{a_0}\ln\frac{x_e}{x_e-x}=kt$$

in which x is the $F(R_\infty)$ value of the Kubelka–Munk calculation at time t, x_e the value at the steady state under UV irradiation, and a_0 the amount of **1** loaded in M41 ($mol\,g^{-1}$).
[11] Compound **1** was purchased from Tokyo Chemical Industry Co., Japan, and used without further purification. No impurity was observed by ^1H NMR spectroscopy.
[12] The inclusion materials obtained were stable in air during our experiments; no change in the spectra or photochromic behavior was observed.

 © 2005 Wiley-VCH Verlag GmbH & Co. KGaA, Weinheim

Low-Coordinate Complexes

DOI: 10.1002/anie.200502566

A Rigid Cyclic (Alkyl)(amino)carbene Ligand Leads to Isolation of Low-Coordinate Transition-Metal Complexes**

*Vincent Lavallo, Yves Canac, Alan DeHope, Bruno Donnadieu, and Guy Bertrand**

In the last decade the use of diamino N-heterocyclic carbenes (NHCs) **A** as ancillary ligands for transition-metal catalysts and as organic catalysts on their own has proven very fruitful.[1] The efficiency of NHCs is attributed to their strong σ-donor properties and sterically demanding structure.[1,2] Not only have NHCs yielded improved transition metal catalysts, but they have also lead to the isolation of unusual low-coordinate metal complexes,[2] which often play a key role in catalytic processes. Recently, we reported the synthesis of stable cyclic (alkyl)(amino)carbenes (CAACs) **B**[3] and demonstrated that CAACs can be even stronger σ donors than NHCs, and lead to highly efficient palladium catalysts for the α-arylation of ketones and aldehydes. Here we report that the peculiar steric and electronic properties of rigid CAAC ligands allow the preparation of low-coordinate metal complexes, hitherto not isolable with any other ligands.

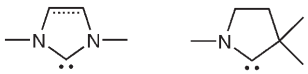

A B

To further evaluate the electronic properties of rigid CAAC **B1**, we attempted to prepare the [RhCl(CO)$_2$(**B1**)] complex, since the CO stretching frequencies of this type of rhodium complexes are recognized as an excellent measure of the σ-donor ability of the ligand L, and a large amount of data is available for comparison.[4] Reaction of carbene **B1** with half an equivalent of [{RhCl(cod)$_2$}$_2$] (cod = 1,5-cyclooctadiene) afforded complex **1**, which after purification by column chromatography on silica gel was obtained as orange crystals in 79% yield (Scheme 1). The structure of **1** was unambiguously determined by single-crystal X-ray diffraction.[5] Following the classical procedure, a solution of **1** in chloroform was treated with an excess of CO. Surprisingly, the ^{13}C NMR spectrum of the product (95% yield) showed only

[*] V. Lavallo, Dr. Y. Canac, A. DeHope, B. Donnadieu, Prof. Dr. G. Bertrand
UCR-CNRS Joint Research Chemistry Laboratory (UMR 2282)
Department of Chemistry
University of California
Riverside, CA 92521-0403 (USA)
Fax: (+1) 951-827-2725
E-mail: gbertran@mail.ucr.edu

[**] We are grateful to the NIH (R01 GM 68825) and RHODIA for financial support of this work.

InterScience
© 2005 Wiley-VCH Verlag GmbH & Co. KGaA, Weinheim

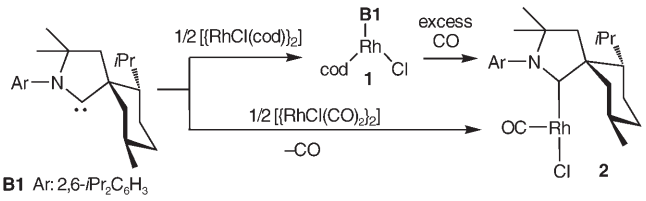

Scheme 1. Synthesis of [RhCl(CO)(**B1**)] complex **2**.

one CO signal, with a large coupling constant ($J_{Rh,C} = 134$ Hz), and not two signals with smaller J values ($J_{Rh,C} = 33$–82 Hz), as observed for $[RhCl(CO)_2(L)]$ complexes.[4] It is known that when bulky ligands L are present $[RhCl(CO)_2L]$ complexes can readily lose one CO ligand to give a chloro-bridged dimer.[6] However, single-crystal X-ray diffraction[5] revealed that even in the solid state complex **2** is formally a 14-electron [RhCl(CO)L] monomer (Figure 1).

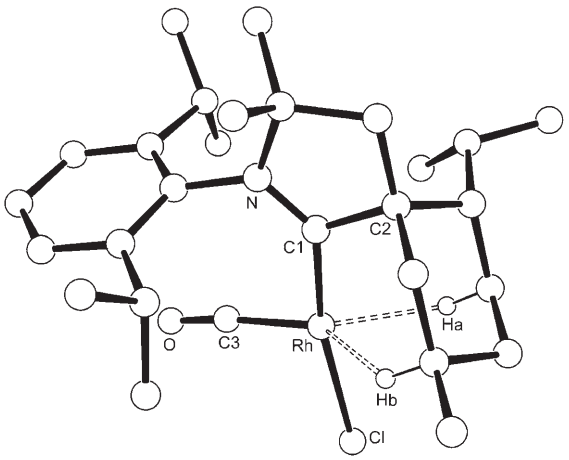

Figure 1. Molecular structure of **2** in the solid state. Selected bond lengths [Å] and angles [°]: N–C1 1.3174(14), C1–C2 1.5368(15), C1–Rh 1.9399(10) Rh–Cl 2.3740 (3), Rh–C3 1.7955(11), C3–O 1.1433(14), Rh–Ha 2.183(17), Rh–Hb 2.231(17); N-C1-C2 108.70(9), C1-Rh-C3 97.99(5), C3-Rh-Cl 94.55(4), C1-Rh-Cl 167.35(3), Rh-C3-O 173.46(10).

Interestingly, **2** can also be synthesized in 80% yield by reaction of one equivalent of carbene **B1** with half an equivalent of $[\{RhCl(CO)_2\}_2]$. The extreme hindrance provided by the menthyl ring of CAAC **B1**, which is locked in the most sterically demanding conformation with respect to the metal center, explains in part why dimerization does not occur. Moreover, the short Rh–Ha (2.183 Å) and Rh–Hb (2.231 Å) distances suggest the existence of agostic interactions, which bring additional stabilization to the metal center. In solution, an agostic interaction is also apparent in the ^{1}H NMR spectrum, which shows a broad multiplet (1H) at 0.08 ppm. Complex **2** is indefinitely stable at room temperature in air. Related $[RhClL_2]$ complexes, exemplified by the active species of Wilkinson's catalyst $[RhCl(PPh_3)_2]$, are known only as transient species.[7] They have only been generated in situ by ligand dissociation[8] or by hapticity changes;[9] otherwise they readily form chloro-bridged dimers, even when two very bulky ligands L are present.[6] Although other neutral T-shaped formally 14-electron Rh^I complexes have been isolated, they are still very rare, and none of them have a bridging-capable halide ligand like complex **2**.[10,11]

The isolation of this low-coordinate Rh^I complex **2** made us confident that other low-ligated transition-metal complexes could be stabilized by rigid CAAC **B1**. After close scrutiny of the literature, it came to our attention that other ligands, particularly NHCs, have consistently failed to allow the isolation of cationic 14-electron $[Pd(All)(L)]^+$ complexes (Scheme 2, All = allyl).[12] In 2003, Nolan et al.[12a] were able

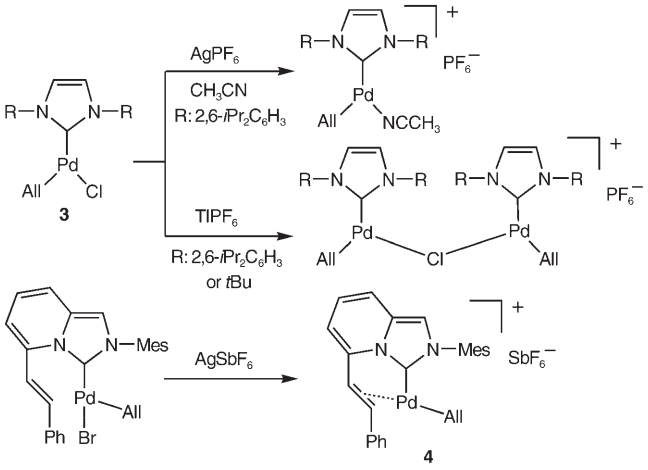

Scheme 2. Previous attempts to prepare cationic 14-electron $[Pd(All)(L)]^+$ complexes.

to abstract chloride from complex **3**, but the cationic complex generated was either unstable and decomposed upon workup or isolated and structurally characterized as an acetonitrile adduct. In 2005, Porschke et al.[12b] reported that chloride abstraction with thallium salts from NHC complexes **3** led to ionic binuclear compounds, which result from combination of the transiently formed desired cationic species with the starting neutral complex. Most recently, Glorius et al.[12c] generated cationic complex **4**, which, despite intramolecular stabilization by double-bond complexation, appeared to be rather unstable and was only characterized by ^{1}H NMR spectroscopy.

In marked contrast, chloride abstraction from [PdCl(All)(**B1**)] (**5**)[3] with a stoichiometric amount of $AgBF_4$ produced the elusive cationic palladium complex **6** as yellow crystals (88% yield, Scheme 3). The structure of **6** was unambiguously established by single-crystal X-ray diffraction (Figure 2).[5] As expected, **6** has a T-shaped geometry with no interaction between the metal atom and tetrafluoro-

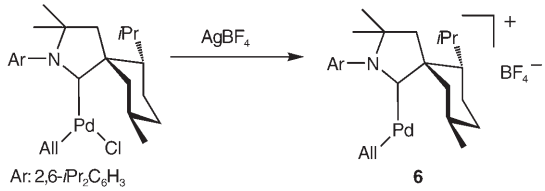

Scheme 3. Synthesis of $[Pd(All)(B1)]^+$ complex **6**.

© 2005 Wiley-VCH Verlag GmbH & Co. KGaA, Weinheim

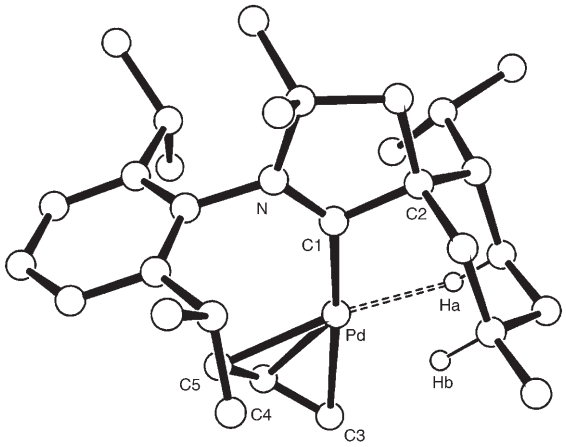

Figure 2. Structure of the cation of **6** in the solid state. Selected bond lengths [Å] and angles [°]: N–C1 1.293(3), C1–C2 1.519(3), C1–Pd 2.038(3), Pd–Ha 2.048, Pd–Hb 2.509, Pd–C3 2.272(13), Pd–C4 2.148(4), Pd–C5 2.126(9); N-C1-C2 109.4(2), N-C1-Pd 133.96(18), C2-C1-Pd 116.64(15).

borate anion (shortest Pd–F distance 3.88 Å). Similar to the above-mentioned Rh^I complex **2**, at least one of the axial H atoms of the menthyl ring provides a stabilizing agostic interaction (Pd–Ha 2.048, Pd–Hb 2.509 Å). This interaction is also apparent from the ^{1}H NMR spectrum, which shows a broad multiplet (1H) at −0.17 ppm. This is the first example of a stable, formally 14-electron, Pd^{II} cation.[13]

To further demonstrate the increased stabilization of metal centers provided by the rigid menthyl moiety of carbene **B1**, we attempted to prepare complexes analogous to **2** and **6**, using the CAAC **B2**, featuring the unlocked and therefore flexible cyclohexyl ring.[3,14] Treatment of [{RhCl(CO)$_2$}$_2$] with two equivalents of carbene **B2** afforded exclusively the classical dicarbonyl complex **7**, while treatment of **8**[3] with $AgBF_4$ led to rapid formation of palladium black (Scheme 4). Clearly, in contrast to **B1**, the cyclohexane ring of CAAC **B2** can flip to the less sterically demanding conformation, in which no H atoms are available for strong agostic interactions with the metal center.

The isolation of complexes **2** and **6** clearly demonstrates the advantages of rigid CAACs over classical ligands. By manipulating the quaternary carbon atom adjacent to the carbene center it is possible to design ligands with an electronically active wall of protection for the metal center. We are currently exploring the possibility that CAAC ligands will stabilize even lower coordinate metal complexes.

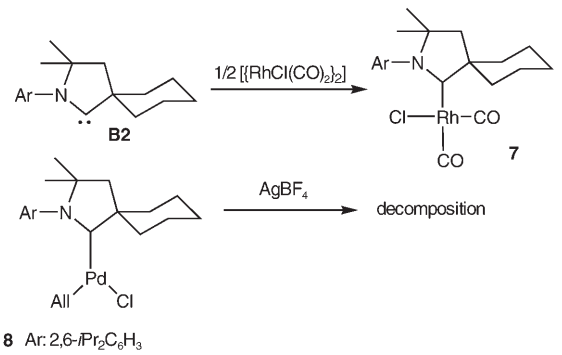

Scheme 4. Synthesis of [RhCl(CO)$_2$(**B2**)] complex **7**, and attempted chloride abstraction from [PdCl(All)(**B2**)] complex **8**.

Experimental Section

All manipulations were performed under an inert atmosphere of argon by using standard Schlenk techniques. Dry, oxygen-free solvents were employed. ^{1}H and ^{13}C NMR spectra were recorded on Varian Inova 300, 500 and Bruker Avance 300 spectrometers.

1: A solution of carbene **B1**[3] (0.45 g, 1.18 mmol) in THF (10 mL) was added at −78 °C to a stirred solution of [{RhCl(cod)$_2$}$_2$] (0.26 g, 0.53 mmol) in THF (5 mL). The solution was warmed to room temperature and stirred for 3 h. After evaporation of the solvent under vacuum, washing with hexane (15 mL), and purification by column chromatography on silica gel with diethyl ether as eluant, complex **1** was obtained as an orange powder (0.52 g, 79 %). Recrystallization from diethyl ether/pentane at −20 °C afforded **1** as orange crystals (m.p. 184–186 °C). $[\alpha]_D^{23} = +189°$ ($CHCl_3$). ^{1}H NMR ($CDCl_3$, 25 °C, 300 MHz): δ = 7.41–7.54 (m, 2H, H_{ar}), 7.17–7.20 (m, 1H, H_{ar}), 5.44 (m, 1H, CH_{cod}), 4.65 (m, 1H, CH_{cod}), 4.21 (m, 1H, CH_{cod}), 3.06–3.23 (m, 5H), 2.68 (m, 2H), 2.51 (d, 1H, J = 12.9 Hz), 1.99–2.13 (m, 4H), 1.77 (d, 3H, CHCH_3, J = 6.0 Hz), 1.45–1.71 (m, 10H), 1.29 (d, 3H, CHCH_3, J = 6.6 Hz), 1.24 (d, 3H, CHCH_3, J = 6.6), 1.20 (s, 6H), 1.11 (d, 3H, CHCH_3, J = 6.3 Hz), 1.04 (d, 3H, CHCH_3, J = 6.3 Hz), 0.97 (d, 3H, CHCH_3, J = 6.6 Hz), 0.92 ppm (d, 3H, CHCH_3, J = 6.3 Hz). ^{13}C NMR ($CDCl_3$, 25 °C, 75 MHz): δ = 278.26 (d, J = 44.5 Hz), 148.76, 146.13, 138.42, 128.94, 127.28, 124.30, 100.03 (d, J = 6.0 Hz), 99.72 (d, J = 5.3 Hz), 76.62, 72.44 (d, J = 16.2 Hz), 70.69, 60.43 (d, J = 14.5 Hz), 54.96, 51.34, 49.81, 36.42, 35.53, 33.69, 32.93, 31.63, 29.63, 29.34, 29.13, 29.03, 28.48, 27.97, 27.70, 26.71, 25.78, 25.59, 24.90, 22.35, 22.27 ppm.

2: Carbon monoxide was bubbled (60 min) through a solution of complex **1** (0.58 g, 0.92 mmol) in chloroform (15 mL). After evaporation of the solvent under vacuum and washing with hexane (10 mL), complex **2** was obtained as an orange powder (0.48 g, 95 %). Alternatively, a solution of carbene **B1** (0.40 g, 1.04 mmol) in THF (5 mL) was added at −78 °C to a stirred solution of [{RhCl(CO)$_2$}$_2$] (0.18 g, 0.47 mmol) in THF (5 mL). The solution was warmed to room temperature and stirred for 2 h. After evaporation of the solvent under vacuum and washing with hexane (20 mL), a solid residue was obtained (0.41 g, 80 %). Recrystallization from chloroform by slow evaporation at room temperature afforded **2** as orange crystals (m.p. 251 °C decomp). $[\alpha]_D^{23} = -0.1°$ ($CHCl_3$). ^{1}H NMR ($CDCl_3$, 25 °C, 300 MHz): δ = 7.45 (m, 1H, H_{ar}), 7.28 (m, 2H, H_{ar}), 2.83 (sept, 2H, CHCH$_3$, J = 6.6 Hz), 2.60 (m, 1H), 2.47 (d, 1H, J = 13.5 Hz), 2.27 (m, 1H), 1.89–2.12 (m, 5H), 1.61 (d, 3H, CHCH_3, J = 6.6 Hz), 1.24–1.44 (m, 20H), 1.13 (d, 3H, CHCH_3, J = 5.7), 1.06 (d, 3H, CHCH_3, J = 6.9), 0.08 ppm (m, 1H, H_{agos}). ^{13}C NMR ($CDCl_3$, 25 °C, 75 MHz): δ = 248.47 (d, J = 48.8 Hz), 181.21 (d, J = 134.3 Hz), 146.20, 145.72, 136.90, 130.28, 125.82, 125.70, 77.67, 71.85, 51.85, 50.39, 46.26, 40.60, 35.13, 34.78, 30.58, 30.38, 29.13, 27.11, 26.43, 26.26, 24.29, 24.16, 22.63, 20.19 ppm. IR (CH_2Cl_2): $\tilde{\nu}$(CO) = 1989 cm^{-1}.

6: A 1:1 mixture of carbene complex **5**[3] (0.50 g, 0.9 mmol) and silver tetrafluoroborate was cooled to −40 °C and 5 mL of fluorobenzene was added. The suspension was warmed to room temperature and stirred for 30 min. After filtration, evaporation of the solvent under vacuum, and washing with hexane (10 mL), a solid residue was obtained (0.48 g, 88 %). Recrystallization from toluene/fluorobenzene at −20 °C afforded **6** as yellow crystals (m.p. 157–159 °C decomp). $[\alpha]_D^{23} = -6°$ (C_6H_5F). ^{1}H NMR (C_6D_5F, 25 °C, 300 MHz): δ = 6.78–7.15 (m, 3H, H_{ar}), 5.00 (m, 1H, H_{allyl}), 3.34–3.48 (m, 2H, H_{allyl}), 2.90 (m, 2H), 2.59 (m, 2H), 2.36–2.41 (m, 1H), 1.91–2.17 (m, 3H), 1.65–1.82 (m, 3H), 1.13–1.22 (m, 12H), 1.06 (d, 3H, CHCH_3, J = 6.3 Hz), 1.05 (d, 3H, CHCH_3, J = 6.9 Hz), 0.99 (d, 3H, CHCH_3, J = 6.9 Hz), 0.98 (s, 3H, CH_3), 0.88 (d, 3H, CHCH_3, J =

 © 2005 Wiley-VCH Verlag GmbH & Co. KGaA, Weinheim

6.9 Hz), 0.73 (d, 3H, $CHCH_3$, $J = 6.9$ Hz), −0.17 ppm (m, 1H, H_{agos}). ^{13}C NMR (C_6D_5F, 25 °C, 75 MHz): $\delta = 251.46$, 145.54, 145.33, 133.42, 130.92, 126.33, 126.17, 118.76, 81.45, 70.74, 51.49, 50.60, 45.86, 40.19, 35.20, 33.95, 29.87, 29.17, 28.93, 26.86, 26.16, 25.44, 23.88, 23.60, 22.94, 22.55, 18.58 ppm.

7: A solution of carbene **B2** (0.56 g, 1.72 mmol) in THF (10 mL) was added at −78 °C to a stirred solution of $[\{RhCl(CO)_2\}_2]$ (0.30 g, 0.77 mmol) in THF (10 mL). The solution was warmed to room temperature and stirred for 3 h. After evaporation of the solvent under vacuum, washing with hexane (20 mL), and extraction with chloroform (20 mL), a gray solid residue was obtained (0.67 g, 84 %). ^1H NMR ($CDCl_3$, 25 °C, 300 MHz): $\delta = 7.42$–7.47 (m, 1H, H_{ar}), 7.28–7.34 (m, 2H, H_{ar}), 3.02 (sept, 2H, $CHCH_3$, $J = 6.6$ Hz), 2.58 (m, 2H, CH_2), 2.09 (s, 2H, CH_2), 1.39–1.90 (m, 8H, CH_2), 1.34 (d, 6H, $CHCH_3$, $J = 6.6$ Hz), 1.33 (d, 6H, $CHCH_3$, $J = 6.6$), 1.32 ppm (s, 6H, CH_3). ^{13}C NMR ($CDCl_3$, 25 °C, 100.5 MHz): $\delta = 259.82$ (d, $J = 38.4$ Hz), 185.95 (d, $J = 50.7$ Hz), 184.61 (d, $J = 77.3$ Hz), 146.41, 134.15, 129.56, 125.49, 81.81, 62.93, 45.27, 38.34, 30.47, 29.12, 28.78, 25.35, 24.94, 22.48 ppm. IR (CH_2Cl_2): $\tilde{\nu}(CO) = 1994$, 2077 cm^{-1}.

Received: July 22, 2005
Published online: October 17, 2005

Keywords: agostic interactions · carbene ligands · low-coordinate complexes · palladium · rhodium

[1] Recent reviews: a) E. Peris, R. H. Crabtree, *Coord. Chem. Rev.* **2004**, *248*, 2239; b) C. M. Crudden, D. P. Allen, *Coord. Chem. Rev.* **2004**, *248*, 2247; c) V. César, S. Bellemin-Laponnaz, L. H. Gade, *Chem. Soc. Rev.* **2004**, *33*, 619; d) D. Enders, T. Balensiefer, *Acc. Chem. Res.* **2004**, *37*, 534; e) W. Kirmse, *Angew. Chem.* **2004**, *116*, 1799; *Angew. Chem. Int. Ed.* **2004**, *43*, 1767; f) R. W. Alder, M. E. Blake, M. E. Chaker, J. N. Harvey, F. Paolini, J. Schütz, *Angew. Chem.* **2004**, *116*, 6020; *Angew. Chem. Int. Ed.* **2004**, *43*, 5896; g) Y. Canac, M. Soleilhavoup, S. Conejero, G. Bertrand, *J. Organomet. Chem.* **2004**, *689*, 3857; h) M. C. Perry, K. Burgess, *Tetrahedron: Asymmetry* **2003**, *14*, 951; i) W. A. Herrmann, *Angew. Chem.* **2002**, *114*, 1342; *Angew. Chem. Int. Ed.* **2002**, *41*, 1290; k) L. Jafarpour, S. P. Nolan, *Adv. Organomet. Chem.* **2001**, *46*, 181; j) D. Enders, H. Gielen, *J. Organomet. Chem.* **2001**, *617–618*, 70.

[2] Recent review: N. M. Scott, S. P. Nolan, *Eur. J. Inorg. Chem.* **2005**, 1815.

[3] V. Lavallo, Y. Canac, C. Prasang, B. Donnadieu, G. Bertrand, *Angew. Chem.* **2005**, *117*, 5851; *Angew. Chem. Int. Ed.* **2005**, *44*, 5705.

[4] a) M. Alcarazo, S. J. Roseblade, A. R. Cowley, R. Fernandez, J. M. Brown, J. M. Lassaletta, *J. Am. Chem. Soc.* **2005**, *127*, 3290; b) D. Martin, A. Baceiredo, H. Gornitzka, W. W. Schoeller, G. Bertrand, *Angew. Chem.* **2005**, *117*, 1728; *Angew. Chem. Int. Ed.* **2005**, *44*, 1700; c) Y. Canac, S. Conejero, B. Donnadieu, W. W. Schoeller, G. Bertrand, *J. Am. Chem. Soc.* **2005**, *127*, 7312; d) A. M. Magill, K. J. Cavell, B. F. Yates, *J. Am. Chem. Soc.* **2004**, *126*, 8717; e) V. Lavallo, J. Mafhouz, Y. Canac, B. Donnadieu, W. W. Schoeller, G. Bertrand, *J. Am. Chem. Soc.* **2004**, *126*, 8670; f) M. Mayr, K. Wurst, K.-H. Ongania, M. Buchmeiser, *Chem. Eur. J.* **2004**, *10*, 1256; g) W. A. Herrmann, K. Öfele, D. von Preysing, E. Herdtweck, *J. Organomet. Chem.* **2003**, *684*, 235; h) K. Denk, P. Sirsch, W. A. Herrmann, *J. Organomet. Chem.* **2002**, *649*, 219; i) D. Enders, H. Gielen, J. Runsink, K. Breuer, S. Brode, K. Boehn, *Eur. J. Inorg. Chem.* **1998**, 913; j) W. A. Herrmann, M. Elison, J. Fischer, C. Köcher, G. R. J. Artus, *Chem. Eur. J.* **1996**, *2*, 772; k) A. W. Coleman, P. B. Hitchcock, M. F. Lappert, R. K. Maskell, J. H. Müller, *J. Organomet. Chem.* **1985**, *296*, 173.

[5] CCDC-278744 (**1**), -269951 (**2**), and -265857 (**6**) contain the supplementary crystallographic data for this paper. These data can be obtained free of charge from the Cambridge Crystallographic Data Centre via www.ccdc.cam.ac.uk/data_request/cif.

[6] a) G. Canepa, C. D. Brandt, H. Werner, *Organometallics* **2004**, *23*, 1140; b) G. Canepa, C. D. Brandt, H. Werner, *J. Am. Chem. Soc.* **2002**, *124*, 9666.

[7] *Principles and Applications of Organotransition Metal Chemistry* (Eds.: J. P. Collman, L. S. Hegedus, J. R. Norton, R. G. Finke), University Science Books, Mill Valley, CA, **1987**.

[8] a) P. C. Ford, T. L. Netzel, C. T. Spillett, D. B. Pourreau, *Pure Appl. Chem.* **1990**, *62*, 1091; b) J. A. Maguire, W. T. Boese, M. E. Goldman, A. S. Goldman, *Coord. Chem. Rev.* **1990**, *97*, 179; c) A. Vigalok, Y. Ben-David, D. Milstein, *Organometallics* **1996**, *15*, 1839.

[9] a) P. Hofmann, C. Meier, W. Hiller, M. Heckel, J. Riede, M. U. Schmidt, *J. Organomet. Chem.* **1995**, *490*, 51; b) H. Werner, M. Schäfer, O. Nürnberg, J. Wolf, *Chem. Ber.* **1994**, *127*, 27; c) M. Schäfer, N. Mahr, J. Wolf, H. Werner, *Angew. Chem.* **1993**, *105*, 1377; *Angew. Chem. Int. Ed. Engl.* **1993**, *32*, 1315; d) R. T. Price, R. A. Anderson, E. L. Muetterties, *J. Organomet. Chem.* **1984**, *267*, 407; e) M. D. Fryzuk, D. H. McConville, S. J. Rettig, *J. Organomet. Chem.* **1993**, *445*, 245.

[10] a) H. Urtel, C. Meier, F. Eisenträger, F. Rominger, J. P. Joschek, P. Hofmann, *Angew. Chem.* **2001**, *113*, 803; *Angew. Chem. Int. Ed.* **2001**, *40*, 781; b) P. H. M. Budzelaar, N. N. P. Moonen, R. de Gelder, J. M. M. Smith, A. W. Gal, *Eur. J. Inorg. Chem.* **2000**, 753.

[11] A cationic 14-electron Rh^I species has been isolated: Y. W. Yared, S. L. Miles, R. Bau, C. A. Reed, *J. Am. Chem. Soc.* **1977**, *99*, 7076.

[12] a) M. S. Viciu, F. K. Zinn, E. D. Stevens, S. P. Nolan, *Organometallics* **2003**, *22*, 3175; b) Y. Ding, R. Goddard, K. R. Pörschke, *Organometallics* **2005**, *24*, 439; c) C. Burstein, C. W. Lehmann, F. Glorius, *Tetrahedron* **2005**, *61*, 6207.

[13] Neutral, three-coordinate, T-shaped d^8 palladium(II) complexes have recently been isolated: M. Yamashita, J. F. Hartwig, *J. Am. Chem. Soc.* **2004**, *126*, 5344.

[14] a) G. Altenhoff, R. Goddard, C. W. Lehmann, F. Glorius, *J. Am. Chem. Soc.* **2004**, *126*, 15195; b) G. Altenhoff, R. Goddard, C. W. Lehmann, F. Glorius, *Angew. Chem.* **2003**, *115*, 3818; *Angew. Chem. Int. Ed.* **2003**, *42*, 3690.

 © 2005 Wiley-VCH Verlag GmbH & Co. KGaA, Weinheim

Carbene Ligands

DOI: 10.1002/anie.200502814

The Generation of a Metallocene-Fused Imidazol-2-ylidene and Its Mercury Complex**

Anthony J. Arduengo III, Daniela Tapu, and William J. Marshall*

Imidazolium salts and imidazol-2-thiones have been widely used as precursors for the synthesis of stable imidazol-2-ylidene.[1] We recently reported successful methodologies for the synthesis of the first directly annulated imidazolium cyclopentadienide zwitterion (**1**) and its ferrocenyl bis-(thione) derivative (**2**).[2] These structures provide an entry

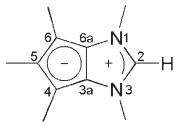

1

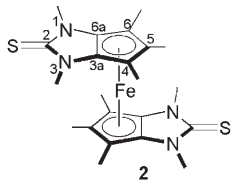

2

into a new class of metallocene-fused imidazole-2-ylidenes. This new architecture for carbenes allows the incorporation of two or more metal centers into a molecule through a combination of σ and π bonding that is tightly coupled through the annulated ligand.

The ruthenocene **3**, a yellow solid that melts at 240–242 °C, was produced in 91 % yield from **1** and $[Cp^*Ru(CH_3CN)_3][CF_3SO_3]$ (Cp^* = pentamethyl cyclopentadienyl;[3] Scheme 1). A single crystal of **3** suitable

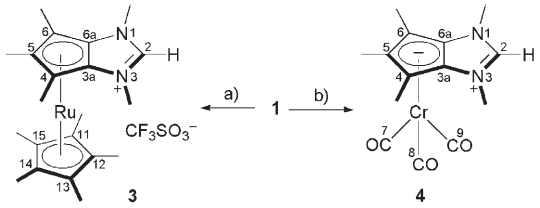

3 **4**

Scheme 1. Reactions of **1**. a) $[Cp^*Ru(CH_3CN)_3][CF_3SO_3]$; b) $[Cr(CH_3CN)_3(CO)_3]$.

[*] Prof. Dr. A. J. Arduengo III, D. Tapu
Department of Chemistry
The University of Alabama
Box 870306, Tuscaloosa, AL 35487-0336 (USA)
Fax: (+1) 205-348-4704
E-mail: ajarduengo@worldnet.att.net
W. J. Marshall
DuPont Central Research
Experimental Station
Wilmington, DE 19880-0228 (USA)

[**] This work was supported by Atotech USA (fellowship to D.T.), E.I. Du Pont de Nemours and Co., and the National Science Foundation (CHE-0413521 and CHE-0115760). A.J.A. gratefully acknowledges The Saxon Endowment of the University of Alabama.

for X-ray crystallographic measurements was grown by recrystallization from THF (selected bond lengths and angles are given in Table 1). The 3D structure of **3** is depicted by the KANVAS[4] drawing in Figure 1. Ruthenocene **3** crystallizes in the triclinic space group $P\bar{1}$, and the two π-ligands (**1** and Cp*) are bound to the ruthenium center in a η^5-fashion. The planes of the two cyclopentadienyl ligands are essentially parallel ($\phi = 1.13°$) and adopt an eclipsed conformation. The average Ru–C(ring) length of 219.78(4) pm in **1** is slightly longer than the average Ru–Cp*(ring) length of 218.08(4) pm. This small difference is consistent with the more extensive π delocalization of the zwitterion. The N1-C2-N3 angle of 112.7(3)° is 2.33° greater than that found in **1** and also larger than those found in typical imidazolium ions.[5]

Metalation of **1** with chromium can be accomplished by treatment of **1** with tris(acetonitrile)tricarbonylchromium(0). The half-sandwich chromium complex **4** was obtained in almost quantitative yield (Scheme 1) as an orange solid which melts at 286–288 °C. Complex **4** is not soluble in nonpolar or halogenated solvents, but it is sparingly soluble in acetonitrile and readily soluble in dimethyl sulfoxide (DMSO).

The molecular structure of **4** was determined by X-ray crystallographic studies. Quality crystals were grown by slow diffusion of petroleum ether into a saturated solution of **4** in acetonitrile. The X-ray crystal structure of **4** is illustrated by the KANVAS[4] drawing in Figure 2, and selected bond lengths and angles in **4** are presented in Table 1. Compound **4** crystallizes in the monoclinic space group $P2_1/n$. The chromium atom is η^5-coordinated to the cyclopentadienyl ring with an average Cr–C(ring) length of 221.84 pm. The average Cr–CO and C–O lengths are 181.5 and 117.3 pm, respectively.

Generation of the free, stable carbenes in solution by deprotonation of **3** or **4** has proved problematic. These carbenes may be too electron-rich (nucleophilic) to allow easy isolation, or alternatively the in situ generated carbene is capable of reaction with the other electrophilic centers in the complex (e.g., ruthenium, chromium, or carbonyl centers). Carbene generation in the presence of electrophiles (metals or main-group elements) has, however, allowed the isolation of various carbene adducts.

A benchmark reaction[6] of the imidazol-2-ylidene with sulfur produced imidazole-2-thione **5** in almost quantitative yield (Scheme 2). The ruthenocene-substituted thione was isolated as an air-stable colorless solid that melts at 282–284 °C. An analogous reaction allowed a clean conversion of imidazolium salt **4** to thione **6**, which was characterized by NMR spectroscopy of the reaction mixture (Scheme 2).

Cooling a saturated solution of **5** in THF/petroleum ether allowed crystals suitable for X-ray structure determination to be grown. Thione **5** crystallizes in the monoclinic space group $P2_1/n$, and the asymmetric unit contains two unique molecules. The crystal structure is depicted as a KANVAS[4] drawing in Figure 3, and selected bond lengths and angles are presented in Table 1. The Cp* rings exhibit large axial positional variance. (A second position for the Cp* ring could not be refined rotationally along the metal–Cp* centroid, but prolate thermal ellipsoids (with the longest axis tangential to the Cp–ring) provided the best model. No hydrogen atoms

 InterScience © 2005 Wiley-VCH Verlag GmbH & Co. KGaA, Weinheim

Table 1: Selected bond lengths [pm] and angles [°] for **1**–**5** and **7**.

Property	**1**	**2**	**3**	**4**	**5**	**7**
r(C2–N1(3))	133.6(3)	136.9(2)	133.3(5)	132.7(3)	136.9(5)	135.3(3)
	134.0(3)	136.9(2)	132.4(5)	133.3(3)	137.5(4)	134.9(3)
r(N1(3)–C6a(3a))	139.6(3)	140.2(2)	140.9(5)	139.9(2)	139.8(4)	140.5(3)
	140.3(3)	140.2(2)	141.0(5)	140.0(2)	139.2(4)	140.3(3)
r(C3a–C6a)	140.3(3)	140.3(3)	141.4(5)	139.7(3)	139.1(5)	141.1(4)
r(C3a(6a)–C4(6))	140.7(3)	142.7(2)	142.7(5)	142.8(3)	143.5(4)	143.6(3)
	140.9(3)	142.7(3)	142.7(5)	142.0(3)	143.9(5)	143.8(3)
r(C4(6)–C5)	141.9(3)	145.0(3)	144.7(5)	144.0(3)	143.7(5)	145.2(4)
	141.6(3)	144.9(3)	145.4(6)	143.9(3)	145.0(5)	145.4(4)
r_{av}(C–C)Cp*	–	–	144.92	–	136.92	143.44
r_{av}(M–C3a–6a)	–	205.8	219.78	221.84	214.8	219.86
r_{av}(M–CCp*)	–	–	218.08	–	218.86	217.72
r_{av}(M–CO)	–	–	–	181.5	–	–
r_{av}(C–O)	–	–	–	117.3	–	–
r(C2–E) (E = S, Hg)	–	167.7(19)	–	–	167.3(3)	208.5(2)
θ(N1-C2-N3)	110.37(19)	108.25(16)	112.7(3)	111.59(18)	107.9(3)	109.4(2)
θ(C2-N1(3)-C6a(3a))	108.53(19)	108.96(15)	107.2(3)	107.59(16)	108.8(3)	108.7(2)
	108.11(18)	108.92(15)	107.2(3)	107.50(16)	108.6(3)	109.0(2)
θ(N1(3)-C6a(3a)-C3a(6a))	106.52(19)	106.89(15)	106.3(3)	106.73(16)	107.0(3)	106.5(2)
	106.45(18)	106.96(15)	106.6(3)	106.58(16)	107.5(3)	106.4(2)
θ(C3a(6a)-C6a(3a)-C6(4))	109.67(18)	109.79(16)	110.6(3)	110.20(17)	110.0(3)	109.8(2)
	109.95(19)	110.14(15)	109.6(3)	110.18(17)	109.9(3)	110.1(2)
θ(C3a(6a)-C4(6)-C5)	103.84(19)	104.83(16)	104.6(3)	103.82(17)	105.1(3)	104.7(2)
	104.04(18)	105.04(16)	103.8(3)	104.19(17)	104.5(3)	104.7(2)
θ(C4-C5-C6)	112.50(18)	110.18(16)	111.3(3)	111.55(17)	110.5(3)	110.6(2)
θ_{av}(C-C-C)^{Cp*}	–	–	108	–	107.98	108.02

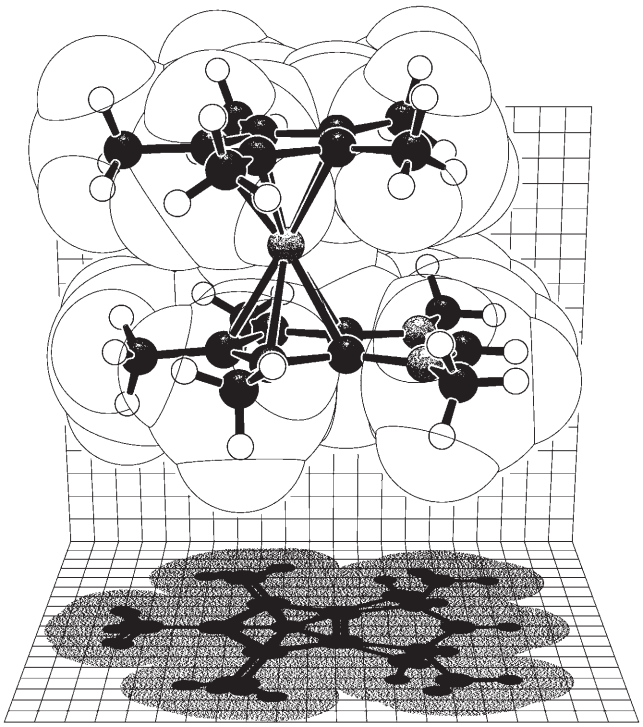

Figure 1. KANVAS[4] drawing of the X-ray structure of **3**.

were affixed to these atoms because of the large thermal motions. The C=S bond of 167.3(3) pm is comparable to that in our previously reported bis(thione) substituted ferrocene **2** (167.7(19) pm.)[2a]

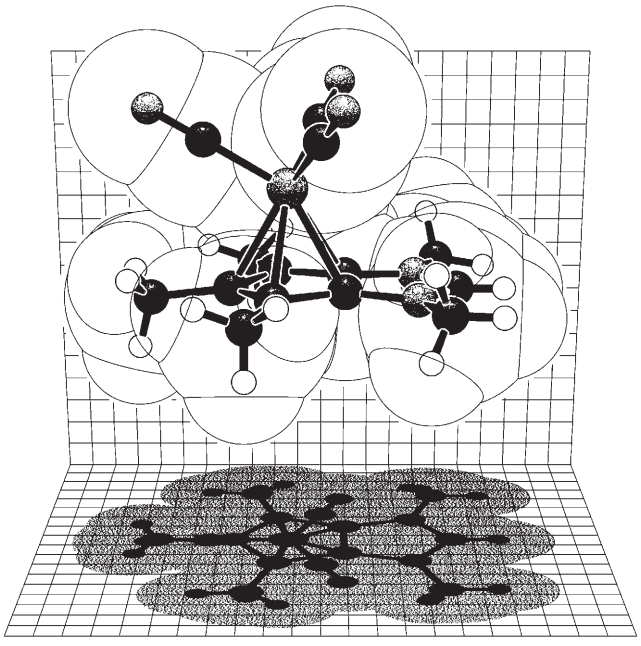

Figure 2. KANVAS[4] drawing of **4**.

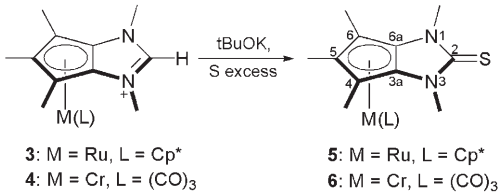

3: M = Ru, L = Cp*
4: M = Cr, L = $(CO)_3$

5: M = Ru, L = Cp*
6: M = Cr, L = $(CO)_3$

Scheme 2. The synthesis of **5** and **6**.

 © 2005 Wiley-VCH Verlag GmbH & Co. KGaA, Weinheim

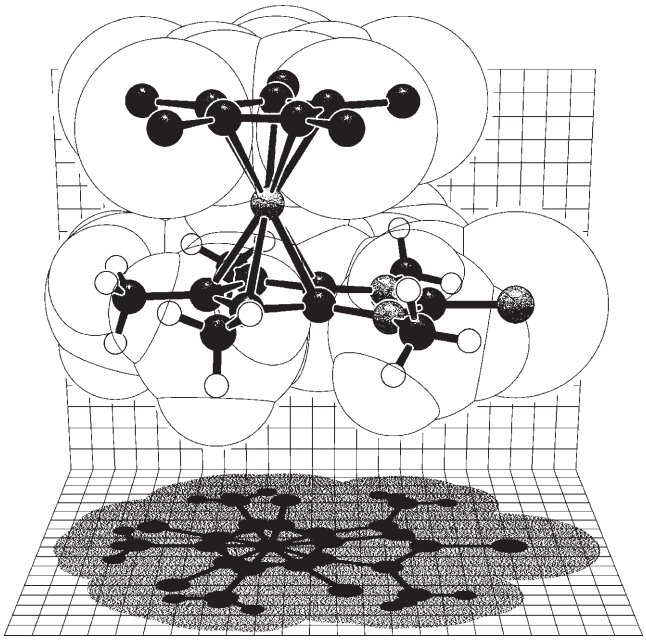

Figure 3. KANVAS[4] drawing of **5**.

The first example of metalation of the carbene center in **3** was accomplished by mercuration. The imidazolium salt **3** reacted slowly with mercury acetate in different stoichiometries. When 0.5 equivalents of mercury acetate were employed in the reaction, after 20 days of stirring at 60 °C, 38 % conversion into the disubstituted mercury complex **7** was observed. No further conversion was observed after longer reaction times. A 1:1 stoichiometry led to a mixture of the mono- and disubstituted mercury complexes **8** and **7**. When a large excess of mercury acetate was used, the monosubstituted mercury complex **8** could be isolated as the only product of the reaction after 2 days at 60 °C (Scheme 3).

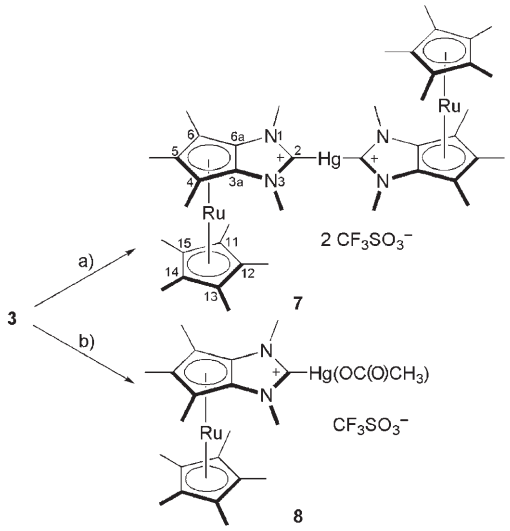

Scheme 3. Reactions of **3**. Reagents: a) 0.5 equivalents of $Hg(OAc)_2$, b) excess of $Hg(OAc)_2$.

Mercury bis(carbene) complex **7** is a yellow crystalline solid that is poorly soluble in most organic solvents except acetonitrile and DMSO. Crystals of **7** of suitable quality for X-ray crystallographic studies were obtained by recrystallization from acetonitrile. Figure 4 shows a KANVAS[4] drawing, and selected bond lengths and angles are given in Table 1.

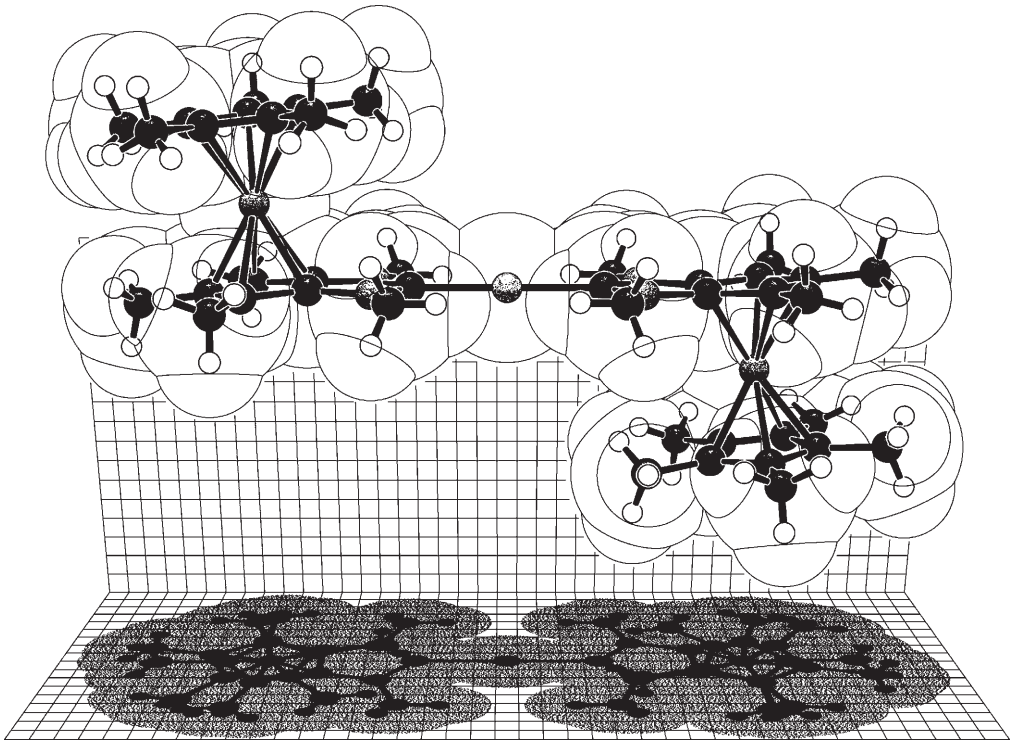

Figure 4. KANVAS[4] drawing of the X-ray structure of **7** (the triflate counterions are omitted for clarity).

 © 2005 Wiley-VCH Verlag GmbH & Co. KGaA, Weinheim

Complex **7** crystallizes in the triclinic space group $P\bar{1}$, with an asymmetric unit that contains half of a molecule, a triflate counterion, and an acetonitrile molecule. The ruthenocene fragments are oriented in an antiperiplanar conformation with a C2-Hg-C22 bond angle of 180°. The internal ring angle at the carbene center of 109.4(2)° is larger than that in typical imidazol-2-ylidene/mercury complexes.[7] The larger angle might be the result of strain that arises from fusion of the two five-membered rings.

A comparative analysis of the bond lengths and angles for the zwitterion fragments in all of the studied compounds reveals certain trends among this new class of organometallic compound. The lengths of the C2–N1(3) bonds are greater for thiones **2** and **5** and mercury complex **7** than those found in imidazolium salts **1**, **3**, and **4**. The N-C-N angle is smaller in **2**, **5**, and **7** relative to the corresponding angle in **1**, **3**, and **4**. These changes suggest diminished π delocalization in **2**, **5**, and **7** relative to the imidazolium salts and may reflect a tendency of π-bond fixation when the substituent at C2 is capable of p–π or d–π backdonation.

In summary, a new carbene (imidazol-2-ylidene) architecture has been realized that allows the incorporation of multiple metal and/or main-group element centers in a combination of σ- and π-bonding motifs. Zwitterion **1** combines these two major bonding concepts in organometallic chemistry in a single ligand, in which there is tight electronic coupling between the ligated centers. This investigation has reported the first bi- and trimetallic complexes of this ligand. Future reports will detail electronic interactions in these systems and their influence on structure, chemistry, and catalysis.

Experimental Section

The reactions were carried out in an atmosphere of dry nitrogen using Schlenk techniques or a dry box. Solvents were dried by using standard procedures.[8] The NMR spectra were recorded on a Bruker AMX 360 spectrometer. Melting points were obtained on a MEL-TEMP II apparatus (Laboratory Devices, USA) and were not corrected. Elemental analysis was performed by Atlantic Microlab, Inc., GA. The ruthenium-transfer reagent was prepared according to a reported procedure.[3] All other chemicals were purchased from commercial sources and used as received.

3: A solution of **1**[2b] (0.090 g, 0.51 mmol) in THF (5 mL) was added dropwise to a solution of pentamethylcyclopentadienylruthenium(tris(acetonitrile)) triflate (0.259 g, 0.51 mmol) in THF (25 mL). The reaction mixture was stirred overnight. After evaporation of volatiles, the resulting yellow solid was dissolved in dichloromethane (1 mL) and reprecipitated with diethyl ether (20 mL). After filtration and drying, a yellow product was obtained (0.259 g, 91% yield). M.p. 240–242 °C; ^{1}H NMR (360 MHz, $CDCl_3$): $\delta = 9.26$ (s, 1H), 3.79 (s, 6H), 2.02(s, 6H), 1.67(s, 15H), 1.63 ppm (s, 3H); ^{13}C NMR (90 MHz, $CDCl_3$) $\delta = 147.89$, 101.18, 88.16, 85.31, 67.44, 34.24, 10.43, 10.35, 9.52 ppm; elemental analysis (%) calcd for $C_{22}H_{31}N_2RuF_3SO_3$: C 47.05, H 5.56, N 4.99; found: C 46.96, H 5.53, N 5.09.

4: A solution of **1** (0.100 g, 0.56 mmol) in THF (5 mL) was added dropwise to a solution of tris(acetonitrile)tricarbonylchromium(0) (0.147 g, 0.56 mmol) in THF (10 mL), on which a yellow precipitate formed immediately. After stirring of the reaction mixture overnight, the volatiles were evaporated to obtain a yellow product (0.176 g, 99.4% yield). Crystals of suitable quality for X-ray crystallographic studies were obtained by slow diffusion of diethyl ether into a saturated solution of **4** in acetonitrile. M.p. 286–288 °C; ^{1}H NMR (360 MHz, [D$_6$]DMSO): $\delta = 8.57$ (s, 1H), 3.82 (s, 6H), 2.19(s, 6H), 1.77 ppm (s, 3H); ^{13}C NMR (90 MHz, [D$_6$]DMSO): $\delta = 222.25$, 144.77, 108.37, 99.42, 74.20, 33.92, 11.45, 10.23 ppm; elemental analysis (%) calcd for $C_{14}H_{16}N_2CrO_3$: C 53.85, H 5.16, N 8.97; found: C 53.76, H 5.13, N 8.88.

5: A 50-mL round-bottomed flask was charged with **3** (95.7 mg, 0.17 mmol), sulfur (18 mg, 0.56 mmol), and THF (10 mL), and a solution of potassium *tert*-butoxide (20 mg, 0.17 mmol) in THF (6 mL) was added dropwise. The reaction mixture was stirred for 40 min and then the volatiles were evaporated. The resulting residue was extracted with toluene (40 mL), and after filtration and evaporation of toluene, the product as obtained as a white solid (73 mg, 97% yield). Crystals of suitable quality for X-ray crystallographic studies were obtained by cooling a solution of **5** in THF/petroleum ether. M.p. 282–284 °C (decomp); ^{1}H NMR (360 MHz, $CDCl_3$): $\delta = 3.56$ (s, 6H), 1.96 (s, 6H), 1.70(s, 15H), 1.57 ppm (s, 3H); ^{13}C NMR (90 MHz, $CDCl_3$): $\delta = 175.23$, 100.57, 84.85, 82.55, 64.99, 32.49, 11.11, 10.39, 9.91 ppm; elemental analysis (%) calcd for $C_{21}H_{30}N_2RuS$: C 56.86, H 6.82, N 6.31; found: C 56.88, H 6.85, N 6.34.

6: A solution of potassium *tert*-butoxide (15 mg, 0.128 mmol) in THF (1 mL) was added to a mixture of **4** (40 mg, 0.128 mmol), sulfur (10 mg, 0.25 mmol), and THF (12 mL). The reaction mixture was stirred for 3 h and then concentrated under vacuum. ^{1}H NMR (360 MHz, [D$_6$]DMSO): $\delta = 3.35$ (s, 6H), 2.18 (s, 6H), 1.85 ppm (s, 3H); ^{13}C NMR (90 MHz, [D$_6$]DMSO): $\delta = 200.59$, 173.43, 112.21, 94.10, 76.53, 32.18, 25.03, 11.09 ppm.

7: A sealed bomb was charged with **3** (150 mg, 0.267 mmol), $Hg(OAc)_2$ (43 mg, 0.135 mmol) and DMSO (2 mL). The reaction mixture was stirred at 60 °C for 20 days. The volatiles were evaporated, and the crude reaction mixture was dissolved in acetonitrile (2 mL) and filtered through celite. This solution was allowed to stand overnight at −22 °C to induce crystallization. The crystalline product was collected by filtration and dried under vacuum to afford the product (68 mg, 39%; the mother liquor contained starting material). M.p. 325–326 °C decomp; ^{1}H NMR (360 MHz, CD_3CN): $\delta = 3.83$ (s, 6H), 2.06 (s, 6H), 1.69(s, 15H), 1.65 ppm (s, 3H; ^{13}C NMR (90 MHz, CD_3CN) $\delta = 186.97$, 104.55, 89.21, 85.59, 68.20, 37.44, 10.62, 10.42, 9.64 ppm; ^{19}F NMR: $\delta = -78.73$ ppm; elemental analysis (%) calcd for $C_{44}H_{60}N_4Ru_2HgF_6S_2O_6$: C 39.98, H 4.57, N 4.23; found: C 39.79, H 4.65, N 4.24.

8: A sealed bomb was charged with **3** (159 mg, 0.283 mmol), $Hg(OAc)_2$ (210 mg, 0.658 mmol), and DMSO (5 mL). The reaction mixture was stirred at 60 °C for 48 h. The volatiles were evaporated and the resulting brown oil contained only the desired complex **8** and excess mercury acetate. The crude reaction mixture was dissolved in $CHCl_3$ and filtered through celite. Further purification of the product was difficult because the monosubstituted complex converts into the disubstituted complex over time. ^{1}H NMR (360 MHz, CD_3Cl): $\delta =$ 3.88 (s, 6H), 2.06 (s, 3H), 2.01 (s, 6H) 1.64 (s, 15H), 1.62 ppm (s, 3H); ^{13}C NMR (90 MHz, CD_3CN): $\delta = 177.60$, 174.06, 104.11, 89.08, 85.57, 68.38, 36.92, 22.08, 10.58, 10.32, 9.58 ppm; ^{19}F NMR: $\delta = -78.73$ ppm; elemental analysis (%) calcd for $C_{24}H_{33}N_2RuHgF_3SO_5$: C 35.14, H 4.06, N 3.42; found: C 33.74, H 3.77, N 3.36.

Received: August 8, 2005
Published online: October 17, 2005

Keywords: azolium salts · carbene ligands · metallocenes · thiones · zwitterions

[1] a) A. J. Arduengo III, R. L. Harlow, M. Kline, *J. Am. Chem. Soc.* **1991**, *113*, 361; b) A. J. Arduengo III, H. V. R. Dias, R. L. Harlow, M. Kline, *J. Am. Chem. Soc.* **1992**, *114*, 5530; c) N. Kuhn, T. Kratz, *Synthesis* **1993**, 561; d) W. A. Herrmann, C. Kocher, L. Goossen, G. R. J. Artus, *Chem. Eur. J.* **1996**, *2*, 1627; e) A. J. Arduengo III,

 © 2005 Wiley-VCH Verlag GmbH & Co. KGaA, Weinheim

H. A. Craig, J. R. Goerlich, R. Krafczyk, W. J. Marshall, R. Schmutzler, M. Unverzagt, *Tetrahedron* **1999**, *55*, 14523.
[2] a) A. J. Arduengo III, T. P. Bannenberg, D. Tapu, W. J. Marshall, *Chem. Lett.* **2005**, *34*, 1010; b) A. J. Arduengo III, T. P. Bannenberg, D. Tapu, W. J. Marshall, *Tetrahedron Lett.* **2005**, *46*, 6847.
[3] P. J. Fagan, M. D. Ward, J. C. Calabrese, *J. Am. Chem. Soc.* **1998**, *120*, 1698.
[4] This drawing was made with the KANVAS computer graphics program, which is based on the program SCHAKAL of E. Keller (Kristallographisches Institute der Universität Freiburg, Germany) and was modified by A. J. Arduengo III (The University of Alabama) to produce the back and shadowed planes. The planes bear a 50-pm grid, and the lighting source is at infinity so that shadow size is meaningful. CCDC-280394–280396 contain the supplementary crystallographic data for this paper. These data can be obtained free of charge from the Cambridge Crystallographic Data Centre via www.ccdc.cam.ac.uk/data_request/cif.
[5] a) V. Langer, K. Huml, G. Reck, *Acta Crystallogr. Sect. B* **1982**, *38*, 298; b) P. Luger, G. Ruban, *Z. Kristallogr.* **1975**, *142*, 177; c) A. K. Abdul-Sada, A. M. Greenway, P. B. Hitchcock, T. J. Mohammed, K. R. Seddon, J. A. Zora, *J. Chem. Soc. Chem. Commun.* **1986**, 1753.
[6] A. J. Arduengo III, R. Krafczyk, *Chem. Unserer Zeit* **1998**, *32*, 6.
[7] A. J. Arduengo III, R. L. Harlow, W. J. Marshall, T. K. Prakasha, W. J. Marshall, *Heteroat. Chem.* **1996**, *7*, 421.
[8] D. D. Perrin, W. L. F. Armarengo, *Purification of Laboratory Chemicals*, Pergamon Press, Oxford, **1988**.

 © 2005 Wiley-VCH Verlag GmbH & Co. KGaA, Weinheim

Porphyrins

DOI: 10.1002/anie.200502769

Internally 1,4-Phenylene-Bridged *meso* Aryl-Substituted Expanded Porphyrins: The Decaphyrin and Octaphyrin Cases**

*Venkataramanarao G. Anand, Shohei Saito, Soji Shimizu, and Atsuhiro Osuka**

The chemistry of expanded porphyrins is the current focus of intensive research because of their unique properties.[1,2] Among their many expected properties, extensive aromaticity is realized in expanded porphyrins such as sapphyrins,[3] rubyrins,[1d,4] and hexaphyrins.[5] However, such aromaticity becomes increasingly difficult to obtain with larger expanded porphyrins, particularly for systems larger than octapyrroles, mainly because of intrinsic conformational distortion from planarity.[2c,d,6] Rare examples are the 34π-electron core-modified octaphyrin[1d,7] and 30π-electron cyclo[8]pyrrole,[8] both of which exhibit planar conformations and strong aromaticity, thus underscoring the influence of the conformation of the expanded porphyrins upon their electronic structures.

Several years ago we found that a series of *meso* aryl-substituted expanded porphyrins could be prepared by a simple one-pot reaction by using modified Rothemund–Lindsey conditions.[5c,9] These *meso* aryl expanded porphyrins can be regarded as real homologues of porphyrins in terms of regular alternate arrangements of pyrrole rings and methine carbon atoms. These molecules become more twisted with increasing number of pyrrolic subunits. It then occurred to us that suppression of this intrinsic twisting attribute may be a promising means to tune their conformational and electronic properties to generate large aromatic ring systems. We now report the influence of an internal 1,4-phenylene bridge that bisects large *meso* aryl-substituted expanded porphyrins—particularly the cases of decaphyrin and octaphyrin—on their structural and electronic properties.

A solution of one equivalent of 1,4-phenylene-bridged bis(dipyrromethane) **1a**[10] and two equivalents of tripyrrane diol **2** in dichloromethane was stirred in the presence of *p*-toluenesulfonic acid for 1 h, followed by oxidation with 2,3-dichloro-5,6-dicyano-1,4-benzoquinone (DDQ) (2.6 equivalents relative to **1a**) for an additional 1 h. Separation of the products by column chromatography on silica gel gave internally 1,4-phenylene-bridged [46]decaphyrin **4a** as a major product with a green metallic luster in 7% yield. Neither the 1,4-phenylene-bridged pentaphyrin dimer nor its derived products[11] were detected in the reaction mixture. Treatment of **4a** with 10 equivalents of DDQ resulted in its quantitative conversion into [44]decaphyrin **5a**, with a color change from dark red to dark green. [44]Decaphyrin **5a** was in turn quantitatively reduced to **4a** with $NaBH_4$, thus indicating a reversible redox interconversion. Electrospray ionization mass spectrometry revealed a parent ion peak for **4a** at *m*/*z* 2179.2163 (calcd for $C_{104}H_{31}F_{40}N_{10}$ $[M+H]^+$, *m*/*z* 2179.2100) and that for **5a** at *m*/*z* 2177.2032 (calcd for $C_{104}H_{29}F_{40}N_{10}$ $[M+H]^+$, *m*/*z* 2177.1943).

The structures of both **4a** and **5a** have been confirmed by X-ray diffraction analyses. Decaphyrin **4a** exhibits a C_2-symmetric nonplanar, but not a "figure-eight", structure (Figure 1),[12a] in which the two twisted pentapyrrolic subunits are interconnected by the central 1,4-phenylene bridge. Each pentapyrrolic arm consists of a dipyrromethene unit (pyrrole rings A and B or F and G) and a tripyrrodimethene unit (pyrrole rings C, D, and E or H, I, and J), both of which are roughly planar but almost opposite each other. The central 1,4-phenylene unit (ring K) is tilted relative to the neighboring pyrrole rings A and J as well as E and F, with dihedral angles of 60.1° and 59.8°, respectively, hence allowing its deconjugation from the rest of the conjugated network.

[*] Dr. V. G. Anand, S. Saito, S. Shimizu, Prof. Dr. A. Osuka
Department of Chemistry
Graduate School of Science
Kyoto University
Sakyo-ku, Kyoto 606-8502 (Japan)
Fax: (+81) 75-753-3970
E-mail: osuka@kuchem.kyoto-u.ac.jp

[**] This work was supported by Core Research for Evolutional Science and Technology (CREST), Japan Science and Technology Agency (JST). We thank Shinetsu Igarashi and Kenji Yoza, Bruker Japan, for X-ray data. V.G.A. and S.S. thank the JSPS for a postdoctoral fellowship and for a Research Fellowship for Young Scientists, respectively.

Supporting information for this article is available on the WWW under http://www.angewandte.org or from the author.

InterScience
© 2005 Wiley-VCH Verlag GmbH & Co. KGaA, Weinheim

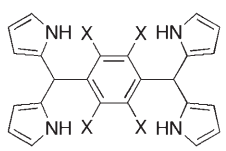

1a: X = H
1b: X = D

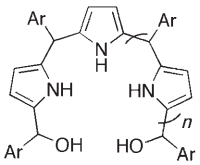

2: *n* = 1
3: *n* = 0

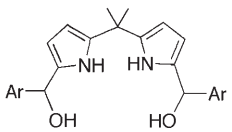

8

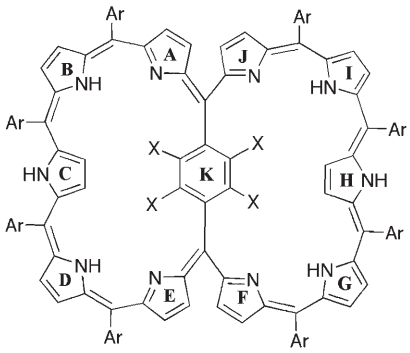

4a: X = H
4b: X = D

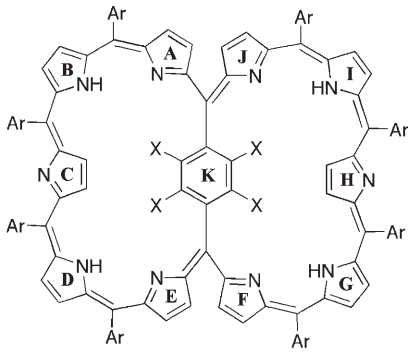

5a: X = H
5b: X = D

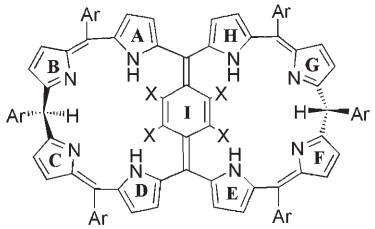

6a: X = H
6b: X = D

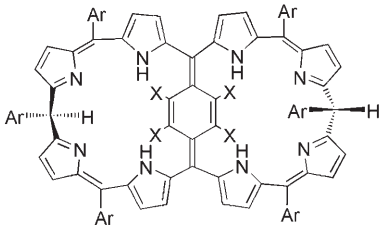

7a: X = H
7b: X = D

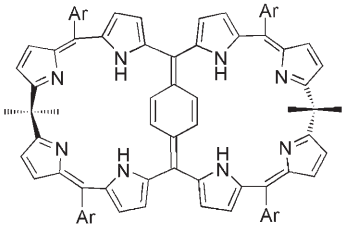

9

Ar = pentafluorophenyl

Interestingly, the two C(pyrrole-α)–C(*meso*) bond lengths at the bridging positions are quite similar, thus suggesting effective conjugation over the overall macrocycle and in line with the 46π electronic circuit. The ^{1}H NMR spectrum of **4a** was quite broad at room temperature, indicative of fast conformational dynamics in solution relative to the NMR time scale. However, the spectrum became well resolved at 233 K with distinct differences in chemical shifts evident between the outer and inner protons of the macrocycle: the outer two NH protons at $\delta = 9.01$ ppm versus the inner four NH protons at $\delta = 5.84$ ppm; the outer β protons as two sets of mutually coupled doublets at $\delta = 7.36$ and 6.84 ppm and $\delta = 7.31$ and 7.19 ppm versus the inner β protons as a singlet at $\delta = 1.2$ ppm. The protons of the 1,4-phenylene bridge, assigned by comparison of the spectrum with that of the corresponding deuterated decaphyrin **4b**, appear as a sharp singlet at $\delta = 3.78$ ppm. These data support a diatropic ring current in **4**.

On the other hand, [44]decaphyrin **5a** shows a D_2-symmetric framework that is distinctly different from that of **4a** (Figure 2).[12b] Pairs of neighboring pyrrole rings (A and B, D and E, F and G, and I and J) constitute planar dipyrromethene units, and the pyrrole rings C and H are completely inverted, with the pyrrolic nitrogen atoms pointing outward. Each pentapyrrolic arm adopts a twisted but relatively planar structure, which constitutes a so-called benzihexaphyrin macrocycle. The arms are connected by the central 1,4-phenylene spacer in an almost perpendicular arrangement. Decaphyrin **5a** exhibits a well-resolved ^{1}H NMR spectrum at room temperature, with the inner four NH protons as a singlet at $\delta = 13.6$ ppm; the outer β protons as doublets at $\delta =$ 6.82 and 6.30 ppm and a multiplet at $\delta = 6.36$ ppm; the inverted pyrrole β protons as a singlet at $\delta =$ 7.78 ppm, and the bridging 1,4-phenylene protons as a singlet at $\delta =$ 8.98 ppm. The protons of the 1,4-phenylene bridge were assigned by comparison with the ^{1}H NMR spectrum of **5b**. There is no distinct difference between the chemical shifts of the inner and outer protons in **5a**, which is indicative of its non-aromatic character, and in line with its 44π electronic circuit and solid-state structure. The absorption spectrum of **4a** shows a Soret-like band at 505 nm and strong Q-like split bands at 800 and 856 nm, while that of **5a** exhibits broad bands at 454 and 619 nm (Figure 3). Interestingly, protonation of **4a** with trifluoroacetic acid (TFA) led to an intense and sharp Soret-like band at 846 nm and a Q-like band at 1221 nm.

We then examined the reaction of **1a** with dipyrromethane diol **3**. A solution of **1a** and **3** in dichloromethane and THF (3:1) was treated with methanesulfonic acid for 1 h and the resulting solution was oxidized with *p*-chloranil for 2 h. Together with the expected 1,4-phenylene-linked porphyrin dimer[14] (1–2% yield) which appeared as a red band by TLC analysis of the reaction mixture, two violet bands were observed and the products were isolated in yields of 0.6 and 0.5%. Despite the low yields, the formation of these products is quite reproducible when *p*-chloranil is used as the oxidant and the reaction time of the secondary oxidation step is maintained at 2 h. High-resolution electrospray ionization mass spectrometry revealed the parent ion peak at *m*/*z*

 © 2005 Wiley-VCH Verlag GmbH & Co. KGaA, Weinheim

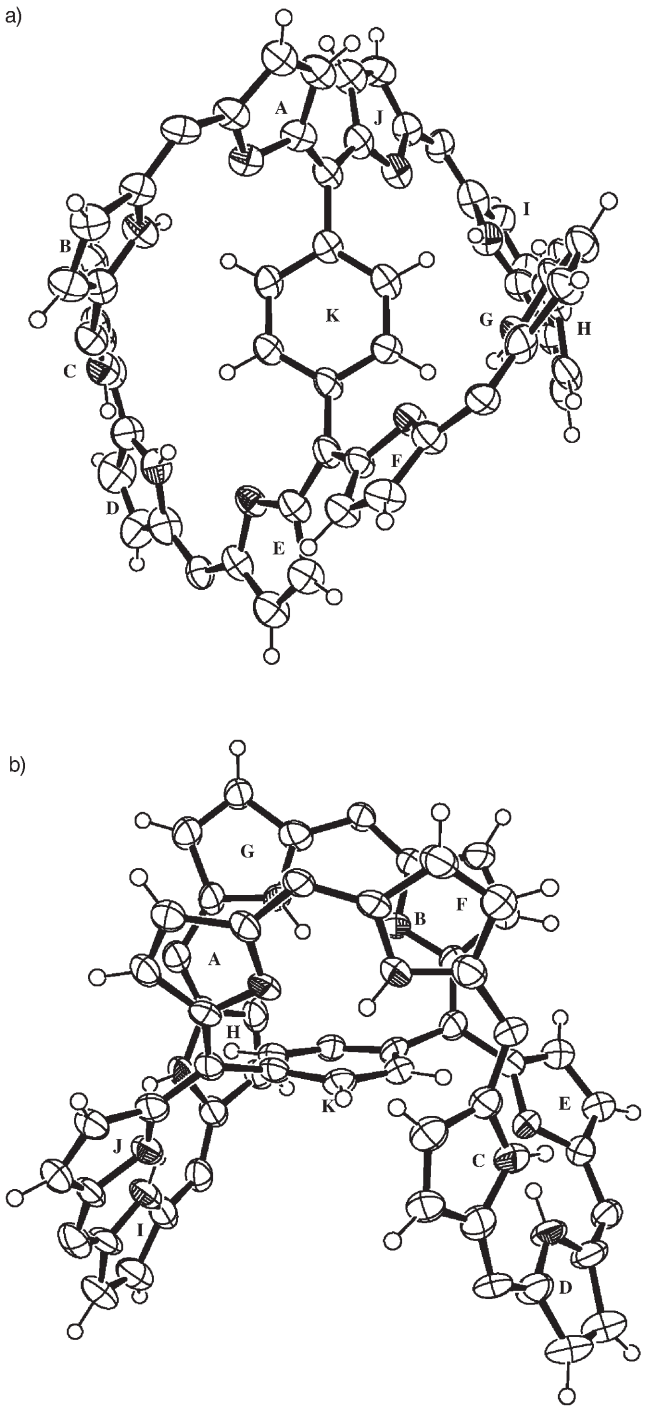

Figure 1. X-ray crystal structure of **4a**: a) top view and b) side view. Solvent molecules and *meso*-pentafluorophenyl groups are omitted for clarity.

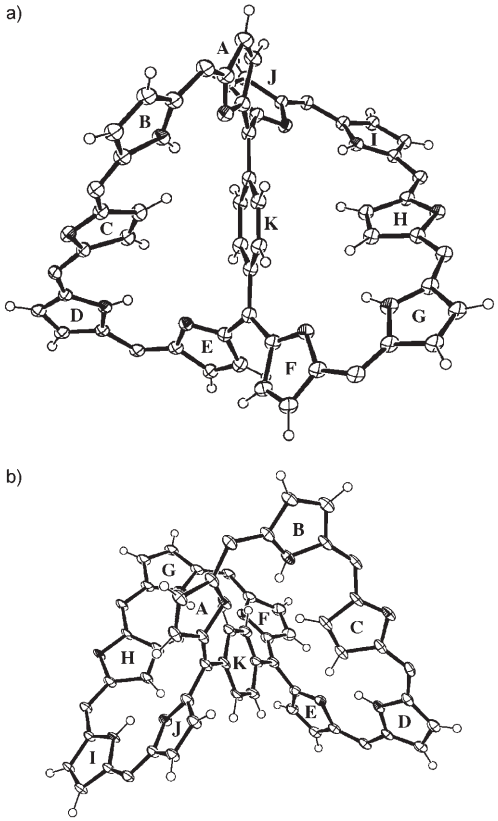

Figure 2. X-ray crystal structure of **5a**: a) top view and b) side view. Solvent molecules and *meso*-pentafluorophenyl groups are omitted for clarity.

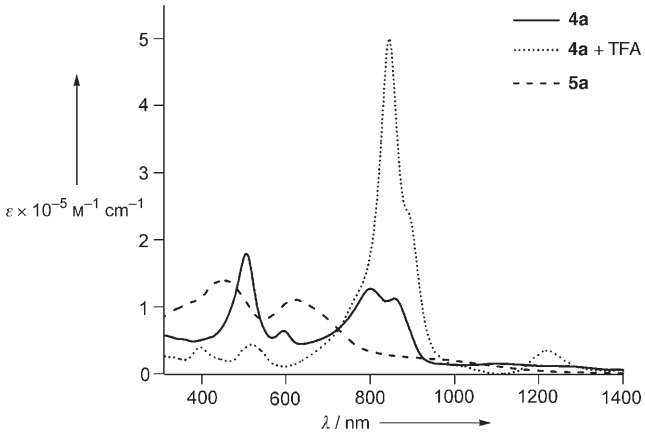

Figure 3. Absorption spectra of **4a**, **4a** + TFA, and **5a** in dichloromethane.

1693.1920 for **6a** (calcd for $C_{82}H_{27}F_{30}N_8$ $[M+H]^+$, m/z 1693.1874) and 1693.1915 for **7a** (calcd for $C_{82}H_{27}F_{30}N_8$ $[M+H]^+$, m/z 1693.1874). The absorption spectra of **6a** and **7a** are also quite similar to each other, with bands at 394, 593, and 895 nm, and 392, 593, and 898 nm, respectively. The structure of **6a** has been unambiguously revealed by X-ray diffraction analysis to be a *p*-quinodimethane-bridged calixoctaphyrin with two sp^3 meso carbon atoms at the diagonal positions and overall C_{2h} symmetry (Figure 4).[13] The bicyclic macrocycle adopts a saddle conformation consisting of four planar dipyrromethene units rather than a non-figure-eight structure. The quinodimethane structure is evident from a distinctly shorter C(22)–C(23) bond (1.367(4) Å) relative to that of C(21)–C(22) (1.430(4) Å). The angle C(23)*-C(21)-C(22) is 115.6(2)°, which is distinctly smaller than that of C(21)-C(22)-C(23) (122.7(3)°) and C(22)-C(23)-C(21)*

 © 2005 Wiley-VCH Verlag GmbH & Co. KGaA, Weinheim

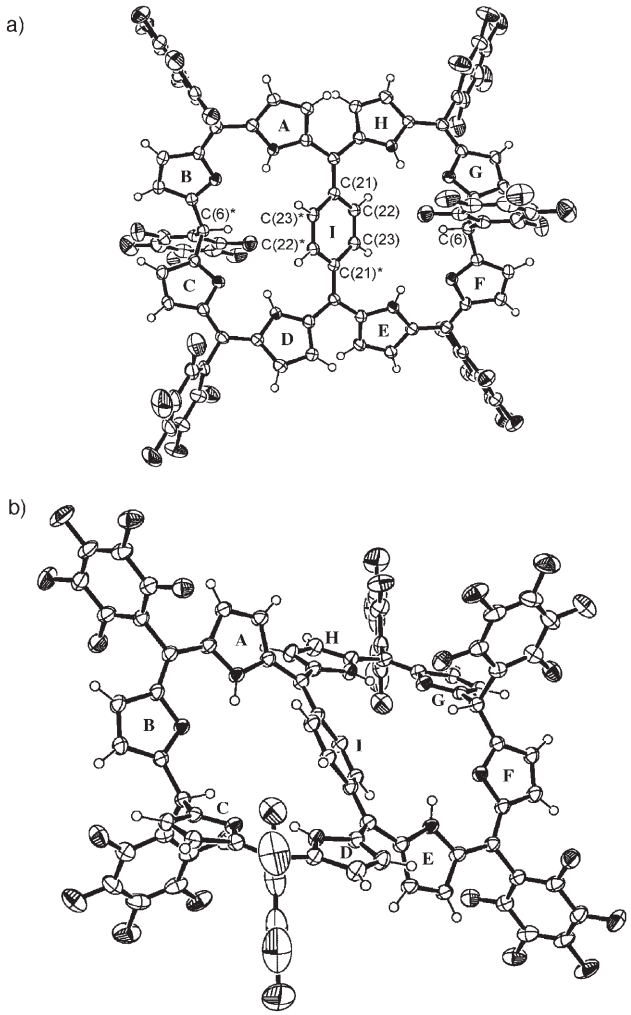

Figure 4. X-ray crystal structure of **6a**: a) top view and b) side view. Solvent molecules are omitted for clarity.

(121.7(3)°). The exo-methylene moieties in the quinodimethane unit are tilted by 18.1° relative to the six-membered ring. The dipyrromethene units are all maintained planar by hydrogen bonding, and thus all the pyrrolic nitrogen atoms point inward. The dipyrromethene units A, B and C, D are arranged with a dihedral angle of 60.9°, which are tilted relative to the central quinodimethane unit by 46.0 and 49.4°, respectively. The two pentafluorophenyl substituents at C(6) take anti and exo positions. The symmetric structure of **6a** is supported by its simple ^{1}H NMR spectrum, in which the central quinodimethane protons appear as a singlet at $\delta =$ 5.09 ppm and the meso protons appear as a singlet at $\delta =$ 2.71 ppm. The structure of **7a** has been revealed by a preliminary X-ray diffraction analysis to be almost the same as that of **6a** except for the positions of the pentafluorophenyl groups at C(6), which are both anti but not identical, each exo and endo (Supporting Information). The nonsymmetric structure of **7a** is in good agreement with the NMR data, with the central quinodimethane protons appearing as two singlets at $\delta = 5.21$ and 4.85 ppm and the *meso* protons appearing as two singlets at $\delta = 6.42$ and 2.45 ppm.

The reaction of **1** with dipyrromethane diol **8** afforded calixoctaphyrin **9** as a single major product as a violet solid in 3% yield. In the ^{1}H NMR spectrum of **9** the internal *p*-quinodimethane protons appear as a singlet at $\delta = 4.65$ ppm and the *gem*-dimethyl protons as two singlets at $\delta = 1.39$ and -1.03 ppm. The high chemical shifts of one of the dimethyl groups can be ascribed to its positioning just above the central bridge. Therefore, a *p*-quinodimethane structure may be considered to be a general concequence when a 1,4-phenylene bridge is incorporated in *meso* aryl-substituted calixoctaphyrins. In sharp contrast to **6a** and **7a** the calixoctaphyrin **9** is quite stable under oxidizing conditions.

This study shows that the incorporation of a 1,4-phenylene bridge into *meso* aryl-substituted expanded porphyrins has a profound impact on the structural and electronic properties of the macrocycles. Such modifications lead to suppression of the intrinsic property to take a twisting conformation and result in planar conformations. The structural modification result in diatropic ring current in the decaphyrin case, and forces a macrocycle to become calixoctaphyrin with an internal *p*-quinodimethane bridge in the octaphyrin case. Lastly, it is interesting to note that [46]decaphyrin is, to the best of our knowledge, the largest macrocycle that exhibits a diatropic ring current.

Received: August 5, 2005
Published online: October 17, 2005

Keywords: aromaticity · macrocycles · porphyrins · structure elucidation

[1] a) A. Jasat, D. Dolphin, *Chem. Rev.* **1997**, *97*, 2267; b) T. D. Lash, *Angew. Chem.* **2000**, *112*, 1833; *Angew. Chem. Int. Ed.* **2000**, *39*, 1763; c) H. Furuta, H. Maeda, A. Osuka, *Chem. Commun.* **2002**, 1795; d) T. K. Chandrashekar, S. Venkatraman, *Acc. Chem. Res.* **2003**, *36*, 676; e) J. L. Sessler, D. Seidel, *Angew. Chem.* **2003**, *115*, 5292; *Angew. Chem. Int. Ed.* **2003**, *42*, 5134; f) A. Ghosh, *Angew. Chem.* **2004**, *116*, 1952; *Angew. Chem. Int. Ed.* **2004**, *43*, 1918.

[2] a) B. Franck, A. Nonn, *Angew. Chem.* **1995**, *107*, 1941; *Angew. Chem. Int. Ed. Engl.* **1995**, *34*, 1795; b) A. Werner, M. Michels, L. Zander, J. Lex, E. Vogel, *Angew. Chem.* **1999**, *111*, 3866; *Angew. Chem. Int. Ed.* **1999**, *38*, 3650; c) J. Setsune, Y. Katakami, N. Iizuna, *J. Am. Chem. Soc.* **1999**, *121*, 8957; d) N. Sprutta, L. Latos-Grazynski, *Chem. Eur. J.* **2001**, *7*, 5099.

[3] a) V. J. Bauer, D. L. J. Clive, D. Dolphin, J. B. Paine III, F. L. Harris, M. M. King, J. Loder, S.-W. C. Wang, R. B. Woodward, *J. Am. Chem. Soc.* **1983**, *105*, 6429; b) J. L. Sessler, M. J. Cyr, V. Lynch, E. McGhee, J. A. Ibers, *J. Am. Chem. Soc.* **1990**, *112*, 2810; c) J. L. Sessler, J. M. Davis, *Acc. Chem. Res.* **2001**, *34*, 989.

[4] a) J. L. Sessler, T. Morishima, V. Lynch, *Angew. Chem.* **1991**, *103*, 1018; *Angew. Chem. Int. Ed. Engl.* **1991**, *30*, 977; b) S. Shimizu, R. Taniguchi, A. Osuka, *Angew. Chem.* **2005**, *117*, 2265; *Angew. Chem. Int. Ed.* **2005**, *44*, 2225.

[5] a) R. Charriere, T. A. Jenny, H. Rexhausen, A. Gossauer, *Heterocycles* **1993**, *36*, 1561; b) M. G. P. M. S. Neves, R. M. Martins, A. C. Tomé, A. J. D. Silvestre, A. M. S. Silva, V. Félix, M. G. B. Drew, J. A. S. Cavaleiro, *Chem. Commun.* **1999**, 385; c) J.-Y. Shin, H. Furuta, K. Yoza, S. Igarashi, A. Osuka, *J. Am. Chem. Soc.* **2001**, *123*, 7190.

[6] a) J. L. Sessler, S. J. Weghorn, V. Lynch, M. R. Johnson, *Angew. Chem.* **1994**, *106*, 1572; *Angew. Chem. Int. Ed. Engl.* **1994**, *33*, 1509; b) E. Vogel, M. Bröring, J. Fink, D. Rosen, H. Schmickler,

 © 2005 Wiley-VCH Verlag GmbH & Co. KGaA, Weinheim

J. Lex, K. W. K. Chan, Y.-D. Wu, D. A. Plattner, M. Nendel, K. N. Houk, *Angew. Chem.* **1995**, *107*, 2705; *Angew. Chem. Int. Ed. Engl.* **1995**, *34*, 2511; c) M. Bröring, J. Jendrny, L. Zander, H. Schmickler, J. Lex, Y.-D. Wu, M. Nendel, J. Chen, D. A. Plattner, K. N. Houk, E. Vogel, *Angew. Chem.* **1995**, *107*, 2709; *Angew. Chem. Int. Ed. Engl.* **1995**, *34*, 2515.

[7] V. G. Anand, S. K. Pushpan, S. Venkatraman, A. Dey, T. K. Chandrashekar, B. S. Joshi, R. Roy, W. Teng, K. R. Senge, *J. Am. Chem. Soc.* **2001**, *123*, 8620.

[8] D. Seidel, V. Lynch, J. L. Sessler, *Angew. Chem.* **2002**, *114*, 1480; *Angew. Chem. Int. Ed.* **2002**, *41*, 1422.

[9] S. Shimizu, J.-Y. Shin, H. Furuta, R. Ismael, A. Osuka, *Angew. Chem.* **2003**, *115*, 82; *Angew. Chem. Int. Ed.* **2003**, *42*, 78.

[10] C.-H. Lee, J. S. Lindsey, *Tetrahedron* **1994**, *50*, 11427.

[11] a) H. Rexhausen, A. Gossauer, *J. Chem. Soc. Chem. Commun.* **1983**, *275*; b) J.-Y. Shin, H. Furuta, A. Osuka, *Angew. Chem.* **2001**, *113*, 639; *Angew. Chem. Int. Ed.* **2001**, *40*, 619; c) S. Mori, J.-Y. Shin, S. Shimizu, F. Ishikawa, H. Furuta, A. Osuka, *Chem. Eur. J.* **2005**, *11*, 2417.

[12] a) Crystallographic data for **4a**: $C_{113}H_{50}Cl_4F_{40}N_{10}O_6$, $M_r = 2545.43$, triclinic, space group $P\bar{1}$ (No. 2), $a = 17.897(2)$, $b = 18.824(2)$, $c = 19.929(3)$ Å, $\alpha = 62.486(3)$, $\beta = 78.326(3)$, $\gamma = 62.418(3)°$, $V = 5277.3(11)$ Å^3, $\rho_{calcd} = 1.602\ mg\,mm^{-3}$, $Z = 2$, $R_1 = 0.1069$, R_w (all data) $= 0.3199$, GOF $= 1.044$ ($I > 2.0\sigma(I)$); b) crystallographic data for **5a**: $C_{254}H_{160}Cl_8F_{80}N_{20}$, $M_r = 5343.62$, monoclinic, space group Cc (No. 9), $a = 32.0109(8)$, $b = 21.9539(5)$, $c = 37.7303(10)$ Å, $\beta = 111.0570(10)°$, $V = 24744.9(11)$ Å^3, $\rho_{calcd} = 1.434\ mg\,mm^{-3}$, $Z = 4$, $R_1 = 0.0956$, R_w (all data) $= 0.2966$, GOF $= 1.028$ ($I > 2.0\sigma(I)$).

[13] Crystallographic data for **6a**: $C_{86}H_{26}F_{30}N_{10}$, $M_r = 1769.17$, triclinic, space group $P\bar{1}$ (No. 2), $a = 11.002(5)$, $b = 11.829(5)$, $c = 16.816(10)$ Å, $\alpha = 77.742(18)$, $\beta = 80.313(19)$, $\gamma = 62.352(14)°$, $V = 1888.3(16)$ Å^3, $\rho_{calcd} = 1.556\ mg\,mm^{-3}$, $Z = 1$, $R_1 = 0.0678$, R_w (all data) $= 0.1726$, GOF $= 1.063$ ($I > 2.0\sigma(I)$). CCDC-280276–280278 contain the supplementary crystallographic data for this paper. These data can be obtained free of charge from the Cambridge Crystallographic Data Centre via www.ccdc.cam.ac.uk/data_request/cif.

[14] S. I. Yang, R. K. Lammi, J. Seth, J. A. Riggs, T. Arai, D. Kim, D. F. Bocian, D. Holten, J. S. Lindsey, *J. Phys. Chem. B* **1998**, *102*, 9426.

 © 2005 Wiley-VCH Verlag GmbH & Co. KGaA, Weinheim

Organofluorine Compounds

DOI: 10.1002/anie.200502703

Synthesis of Chiral α-Fluoroketones through Catalytic Enantioselective Decarboxylation**

Masaharu Nakamura, Alakananda Hajra, Kohei Endo, and Eiichi Nakamura**

A number of biologically active compounds bear secondary stereogenic centers next to a carbonyl group as a key structural feature, which are often susceptible to racemization during manipulation, storage, synthesis, or under physiological conditions under which they are expected to exhibit useful functions. Optically active α-fluoroketones could serve as nonracemizable surrogates of these compounds and have received much attention in medicinal chemistry.[1,2] Interest in their synthesis therefore resulted in several recent reports on the enantioselective synthesis of α-fluorinated carbonyl compounds from the corresponding α-protio precursors,[3] but the scope of the known fluorination methods is still limited.[4] We report herein a new alternative synthetic strategy in which racemic α-fluoroketones are converted into optically active ketones through enantioselective C–C bond reorganization.

A racemic α-fluoro-β-ketoester **1** was converted into the corresponding optically active α-fluoroketone **2** by palladium-catalyzed extrusion of carbon dioxide (Table 1). On the basis of the original Tsuji reaction mechanism, we surmised that the reaction possibly proceeds first through the formation of a palladium enolate, through which the new chirality is introduced under the influence of a chiral ligand.[5] This palladium enolate, which is tetrasubstituted and bears a fluorine substituent *cis* to the carbonyl oxygen atom,[5b] is probably related to that generated by palladium-catalyzed decarboxylation of the corresponding enol allyl carbonate reported recently by the groups of Stoltz and Trost.[6]

Investigation of the reaction conditions by using [Pd_2-$(dba)_3$] as a catalyst precursor and a variety of chiral ligands

[*] Prof. Dr. M. Nakamura, Dr. A. Hajra, K. Endo, Prof. Dr. E. Nakamura
Department of Chemistry
The University of Tokyo
Hongo, Bunkyo-ku, Tokyo (Japan)
Fax: (+81) 3-3812-8099
E-mail: masaharu@chem.s.u-tokyo.ac.jp
nakamura@chem.s.u-tokyo.ac.jp
Prof. Dr. M. Nakamura
PRESTO, Japan Science and Technology Agency
Kawaguchi, Saitama (Japan)

[**] This work was supported in part by the Japan Science and Technology Agency (JST) and the Ministry of Education, Culture, Sports, Science, and Technology of Japan through a Grant-in-Aid for Exploratory Research and for the 21st Century COE Program for Frontiers in Fundamental Chemistry. A.H. is grateful to the Japan Society for the Promotion of Science for a postdoctoral fellowship.

Supporting information for this article is available on the WWW under http://www.angewandte.org or from the author.

© 2005 Wiley-VCH Verlag GmbH & Co. KGaA, Weinheim

(1.25 equiv relative to Pd) gave us some insight into the nature of the catalytic process. A comparison of entry 1 of Table 1 with the remaining entries shows that the reaction is vastly accelerated by the phosphine ligands **3**–**7**. After screening of a variety of ligands[7] including binap (**3**),[8] which gave low selectivity (Table 1, entry 2), we found that chiral phosphinooxazolines **4**–**6**[9] were suitable for the reaction. The enantioselectivity is very sensitive to the substituent on the oxazoline ring: phenyl-substituted ligand **4** led to only 11% *ee*, whereas the selectivities improved greatly with the isopropyl- **5** (83% *ee*) and the *tert*-butyl-substituted **6** analogues (96% *ee*) (Table 1, entries 3–5). The catalyst loading can be decreased to 1 mol% at the expense of reaction rate, but without erosion of yield and selectivity (Table 1, entries 5–7). The choice of solvent is very important, as seen in the significant decrease in the selectivity when the reaction was carried out in dichloromethane (25% *ee*; Table 1, entry 9) instead of in THF or diethyl ether (96% *ee*; Table 1, entry 8). A decrease in the reaction temperature from 25 to 0°C did not change the performance of the reaction (Table 1, entry 10). The chiral bisphosphine ligand **7**, which gave good results in the related decarboxylative allylation reaction of allyl enol carbonates,[6b] was ineffective in the present reaction (Table 1, entry 11).

Table 1: Enantioselective decarboxylative allylation of tetralone **1**.[a]

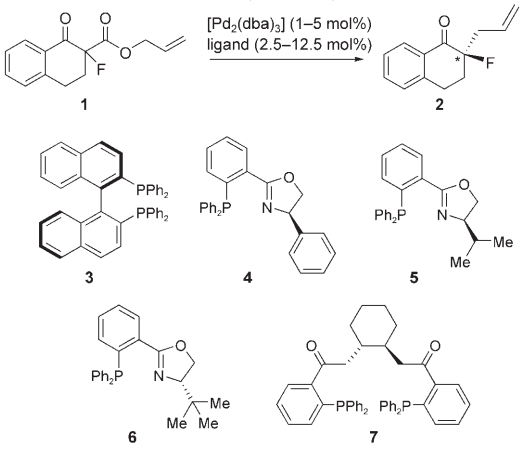

Entry	Ligand	*t* [h]	Solvent	[$Pd_2(dba)_3$][b] [mol%]	Yield [%][c]	*ee* [%][d]
1	none	24	THF	5	0	–
2	**3**	5	THF	5	83	11
3	**4**	3	THF	5	91	11
4	**5**	3	THF	5	94	83
5	**6**	3	THF	5	95	96
6	**6**	4	THF	2.5	95	96
7	**6**	10	THF	1	93	94[e]
8	**6**	4	Et_2O	5	93	96
9	**6**	5	CH_2Cl_2	5	89	25
10	**6**	4	THF	2.5	94	96[f]
11	**7**	10	THF	5	9	n.d.[g]

[a] All reactions were performed on a 0.5-mmol scale at a 0.05 M substrate concentration at ambient temperature (22–25°C), unless otherwise noted. [b] dba = dibenzylideneacetone. [c] Yields of isolated product. [d] The enantiomeric excess was determined by chiral HPLC analysis on a Daicel Chiralcel OJ-H column. The antipode of **2** is the major product in entries 2, 3, and 4. [e] The reaction was conducted on a 1-mmol scale. [f] The reaction was performed at 0°C. [g] The *ee* value was not determined, and the yield is based on the ratio of areas of the uncalibrated GC peaks for **1** and **2**.

The scope of the reaction was examined and representative results are shown in Table 2. The α-fluorinated ketoester starting materials were readily obtained from the corresponding α-protio compounds in quantitative yields through standard methods.[11] Results obtained with α-alkyl- and α-alkenyl-β-ketoesters instead of α-fluoro compounds are also included (Table 2, entries 10–12).

The decarboxylation reaction of a methallyl tetralone compound (Table 2, entry 3) gave almost the same level of selectivity as the allyl analogue. The selectivity improved to 99% *ee* when the catalyst loading was doubled (Table 2, entries 2 and 3), which suggests that there are ligand-independent racemic pathways operating along with the desired enantioselective catalytic process. Methoxy substitution on the aromatic ring of tetralone that may exert certain conjugation electronic effects on the reaction did not affect the selectivity (Table 2, entry 4). Modification of the saturated ring of the tetralone structure affects the enantioselectivity (Table 2, entries 5 and 6), which suggests that the steric environment has larger impact on the selectivity. The aromatic moiety of the tetralone is not required for high enantioselectivity, as can be seen in the example of the cyclopentane analogue (Table 2, entry 7). However, the selectivity was slightly lower. This example shows that the decarboxylative mechanism dictates the regioselective formation of the more-substituted α-fluoro ketone. The reaction can also be applied to acyclic ketones but the selectivity is moderate (Table 2, entries 8 and 9). This seems reasonable because an *E*/*Z* mixture of the palladium enolate may form in situ and lead to lower selectivity. This issue is related to the reaction mechanism and needs further studies.

The reaction could be a viable method for the creation of nonracemic all-carbon quaternary centers (Table 2, entries 10 and 11).[12] This reaction seems to be related to that reported recently by the Trost and Stoltz groups,[6] but is different in practice as the method creates a quaternary carbon center from synthetically more-readily accessible β-ketoesters rather than from allyl enol carbonates. A few characteristics are noteworthy: The new chirality is also generated at a palladium enolate. The putative tetrasubstituted enolate intermediate bears three alkyl groups and one oxygen atom rather than a fluorine substituent, but the enantioselectivity was still found to be high (Table 2, entry 10). However, the selectivity decreases when the ketone is part of a five-membered ring (Table 2, entry 11) and when the substrate bears an α-alkenyl group (Table 2, entry 12).[13] The intermediate in this case is a conjugated dienolate of palladium instead of a simple palladium enolate. The undesirable effect of the conjugation is apparent, in contrast to the slightly positive effect of the highly electron withdrawing fluorine atom (Table 2, entries 3 and 10). Interestingly, the reaction still results in C–C bond formation at the α-carbon atom

 © 2005 Wiley-VCH Verlag GmbH & Co. KGaA, Weinheim

Table 2: Enantioselective synthesis of chiral α,α-disubstituted ketones from racemic substrates.[a]

Entry	Substrate	Product	Yield [%][b]	*ee* [%][c]
1	**1**	**2**	95	96
2[d]	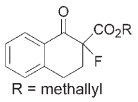	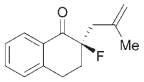	96	99
3	R = methallyl		95	97
4	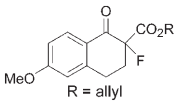 R = allyl	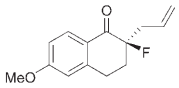	92	96
5	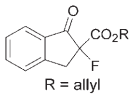 R = allyl	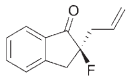	94	91
6	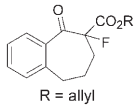 R = allyl	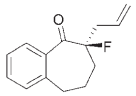	94	93
7	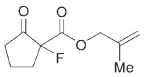	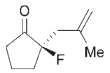	82[e]	85
8	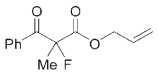	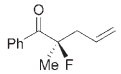	89	51
9	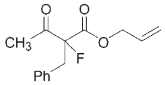	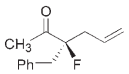	91	55
10	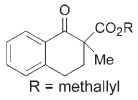 R = methallyl	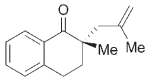	94	95
11	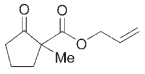		87[e]	84
12	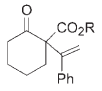		89	39

[a] All reactions were performed on a 1.0-mmol scale with a 0.05 M substrate concentration in THF for 4–10 h at 22–25 °C in the presence of $[Pd_2(dba)_3]$ (2.5 mol%) and ligand **6** (6.25 mol%), unless otherwise noted. [b] Yields of isolated product. [c] The enantiomeric excess was determined by chiral HPLC analysis, except in entries 7 and 11 for which it was determined by GC analysis (see Supporting Information). The absolute configuration of the major enantiomers was inferred from the sign of their circular dichroism spectra identical to those observed for the compounds in entries 10 and 11,[10] whose stereochemistry was determined by comparison of their optical rotation with that of the known compounds.[6] [d] The reaction was carried out with $[Pd_2(dba)_3]$ (5 mol%) and **6** (12.5 mol%). [e] The yield suffered from evaporative loss owing to the low boiling point of the product.

rather than at the distal carbon atom (which would produce a more-stable α,β-unsaturated ketone product).

In summary, we have developed a new class of enantioselective C–C bond-forming reactions that is useful for regio- and enantioselective synthesis of α-allyl-α-fluoro ketones as well as ketones that bear an α-quaternary center. The reaction is mechanistically different to the recently reported enantioselective synthesis of α-fluoro carbonyl compounds and appears to involve intriguing mechanistic details that are as yet to be explored by theory and experiments.

Experimental Section

A 50-mL two-necked round-bottomed flask equipped with a magnetic stirrer bar was flame dried in vacuo, cooled to room temperature, and charged with $[Pd_2(dba)_3]$ (22.9 mg, 0.025 mmol, 0.025 equiv) and ligand **6** (24.2 mg, 0.0625 mmol, 0.0625 equiv) under argon. The system was evacuated slowly and flushed with argon three times. THF (20 mL) was added. The mixture was stirred for 30 min, and ketoester **1** (248 mg, 1.0 mmol, 1.0 equiv) was added dropwise through a syringe to the reaction mixture. The resulting solution was stirred for 4 h at 25 °C (full conversion checked by TLC and GC), and the solvent was then evaporated in vacuo. Purification by column chromatography on silica gel (eluent: Et_2O/hexane 5:95) gave the fluoroketone **2** (193.9 mg, 95% yield) as a colorless oil.

Received: August 1, 2005
Published online: October 17, 2005

Keywords: allylation · asymmetric synthesis · decarboxylation · enantioselectivity · fluoroketones

[1] a) *Biomedical Frontiers of Fluorine Chemistry* (Eds.: I. Ojima, J. R. McCarthy, J. T. Welch), ACS Symposium Series 639, American Chemical Society, Washington, **1996**; b) *Asymmmetric Fluoroorganic Chemistry*; *Synthesis, Application and Future Directions* (Eds.: P. V. Ramachandran), ACS Symposium series 746, American Chemical Society, Washington, **2000**; Synthetic chemistry of α-fluorocarbonyl compounds see: c) S. Rozen, R. Filler, *Tetrahedron* **1985**, *41*, 1111.

[2] a) K. Nagai, T. A. Davies, L. M. Ednie, A. Bryskier, E. Palavecino, M. R. Jacobs, P. C. Appelbaum, *Antimicrob. Agents Chemother.* **2001**, *45*, 3242; b) L. Zoute, C. Audouard, J.-C. Plaquevent, D. Cahard, *Org. Biomol. Chem.* **2003**, *1*, 1833.

[3] a) L. Hintermann, A. Togni, *Angew. Chem.* **2000**, *112*, 4530; *Angew. Chem. Int. Ed.* **2000**, *39*, 4359; b) Y. Hamashima, D. Hotta, M. Sodeoka, *J. Am. Chem. Soc.* **2002**, *124*, 11240; c) D. Y. Kim, E. J. Park, *Org. Lett.* **2002**, *4*, 545; d) N. Shibata, J. Kohno, K. Takai, T. Ishimaru, S. Nakamura, T. Toru, S. Kanemasa, *Angew. Chem.* **2005**, *117*, 4276; *Angew. Chem. Int. Ed.* **2005**, *44*, 4204; e) D. Enders, M. R. M. Hüttl, *Synlett* **2005**, 991; f) D. D. Steiner, N. Mase, C. F. Barbas III, *Angew. Chem.* **2005**, *117*, 3772; *Angew. Chem. Int. Ed.* **2005**, *44*, 3706; g) M. Marigo, D. Fielenbach, A. Braunton, A. Kjaersgaard, K. A. Jørgensen, *Angew. Chem.* **2005**, *117*, 3769; *Angew. Chem. Int. Ed.* **2005**, *44*, 3703; h) T. D. Beeson, D. W. C. MacMillan, *J. Am. Chem. Soc.* **2005**, *127*, 8826; i) Y. Hamashima, T. Suzuki, H. Takano, Y. Shimura, M. Sodeoka, *J. Am. Chem. Soc.* **2005**, *127*, 10164; j) S. M. Kim, H. R. Kim, D. Y. Kim, *Org. Lett.* **2005**, *7*, 2309.

[4] a) K. Muñiz, *Angew. Chem.* **2001**, *113*, 1701; *Angew. Chem. Int. Ed.* **2001**, *40*, 1653; b) H. Ibrahim, A. Togni, *Chem. Commun.*

 © 2005 Wiley-VCH Verlag GmbH & Co. KGaA, Weinheim

2004, 1147; c) J.-A. Ma, D. Cahard, *Chem. Rev.* **2004**, *104*, 6119; d) K. Mikami, Y. Itoh, M. Yamanaka, *Chem. Rev.* **2004**, *104*, 1; e) J.-A. Ma, D. Cahard, *Tetrahedron: Asymmetry* **2004**, *15*, 1007; f) S. France, A. Weatherwax, T. Lectka, *Eur. J. Org. Chem.* **2005**, *3*, 475.

[5] a) I. Shimizu, T. Yamada, J. Tsuji, *Tetrahedron Lett.* **1980**, *21*, 3199; b) I. Shimizu, H. Ishii, *Tetrahedron* **1994**, *50*, 487; c) J.-F. Detalle, A. Riahi, V. Steinmetz, F. Hénin, J. Muzart, *J. Org. Chem.* **2004**, *69*, 6528; a Pd-catalyzed asymmetric decarboxylation/allylation was reported recently for certain α-amino-β-carbonyl compounds: d) R. Kuwano, N. Ishida, M. Murakami, *Chem. Commun.* **2005**, 3951.

[6] a) D. C. Behenna, B. M. Stoltz, *J. Am. Chem. Soc.* **2004**, *126*, 15044; b) B. M. Trost, J. Xu, *J. Am. Chem. Soc.* **2005**, *127*, 2846.

[7] a) B. M. Trost, C. Lee, *Catalytic Asymmetric Synthesis*, 2nd ed. (Eds.: I. Ojima), Wiley, New York, **2000**, pp. 593–649; b) A. Pfaltz, M. Lautens in *Comprehensive Asymmetric Catalysis, Vol. 2* (Eds.: E. N. Jacobsen, A. Pfaltz, H. Yamamoto), Springer, New York, **1999**, pp. 833–884; c) G. Helmchen, *J. Organomet. Chem.* **1999**, *576*, 203; d) B. M. Trost, D. L. V. Vranken, *Chem. Rev.* **1996**, *96*, 395; e) J. M. J. Williams, *Synlett* **1996**, 705.

[8] A. Miyashita, A. Yasuda, H. Takaya, K. Toriumi, T. Ito, T. Souchi, R. Noyori, *J. Am. Chem. Soc.* **1980**, *102*, 7932.

[9] P. von Matt, A. Pfaltz, *Angew. Chem.* **1993**, *105*, 614; *Angew. Chem. Int. Ed. Engl.* **1993**, *32*, 566.

[10] J. T. Welch, K. W. Seper, *J. Org. Chem.* **1988**, *53*, 2991.

[11] F. A. Davis, W. Han, C. K. Murphy, *J. Org. Chem.* **1995**, *60*, 4730, and references therein.

[12] a) C. J. Douglas, L. E. Overman, *Proc. Natl. Acad. Sci. USA* **2004**, *101*, 5363; b) J. Christoffers, A. Baro, *Angew. Chem.* **2003**, *115*, 1726; *Angew. Chem. Int. Ed.* **2003**, *42*, 1688; c) E. J. Corey, A. Guzman-Perez, *Angew. Chem.* **1998**, *110*, 402; *Angew. Chem. Int. Ed.* **1998**, *37*, 388.

[13] a) M. Nakamura, K. Endo, E. Nakamura, *J. Am. Chem. Soc.* **2003**, *125*, 13002; b) M. Nakamura, K. Endo, E. Nakamura, *Org. Lett.* **2005**, *7*, 3279; c) M. Nakamura, K. Endo, E. Nakamura, *Adv. Synth. Cat.* **2005**, 347, in press.

 © 2005 Wiley-VCH Verlag GmbH & Co. KGaA, Weinheim

Cluster Compounds

DOI: 10.1002/anie.200502678

Observation of d-Orbital Aromaticity**

*Xin Huang, Hua-Jin Zhai, Boggavarapu Kiran, and Lai-Sheng Wang**

Aromaticity is one of the most important concepts in chemistry and refers to planar cyclic hydrocarbon molecules that exhibit delocalized π-bonds and unusual stability, such as benzene. This concept has been extended to metal-substituted organic molecules,[1,2] as well as main group organometallic complexes.[3–6] The recent discovery of aromaticity in all-metal clusters, for instance $[Al_4]^{2-}$ in $[MAl_4]^-$ (M = Cu, Li, Na),[7] has led to a flurry of research activities[8–16] and predictions of new aromatic metal clusters,[17–23] among which is a class of interesting cyclic species containing Cu.[20,23]

While main group clusters can give rise to σ- and π-aromaticity, transition-metal-containing clusters can exhibit d-orbital aromaticity or, more interestingly, δ-aromaticity due to δ bonding interactions. However, d-orbital aromaticity requires significant d–d bonding interactions. Unlike valent s or p orbitals, d orbitals are spatially more contracted, and their tendency to participate in chemical bonding depends strongly on the position of the transition metals in the periodic table and their coordination environments. The predicted aromaticity in the cyclic Cu-containing species,[20,23] for example, has not been verified experimentally. More promisingly, d-orbital aromaticity is expected to be found in early or 4d/5d transition metal systems, where strong d–d interactions are known. Here, we report experimental and theoretical evidence of d-orbital aromaticity in two early 4d and 5d transition metal oxide clusters, namely $[M_3O_9]^-$ and $[M_3O_9]^{2-}$ (M = W, Mo).

[*] Dr. X. Huang, Dr. H.-J. Zhai, Dr. B. Kiran, Prof. Dr. L.-S. Wang
Department of Physics
Washington State University
2710 University Drive, Richland, WA 99354 (USA)
and
W. R. Wiley Environmental Molecular Sciences Laboratory and
Chemical Sciences Division
Pacific Northwest National Laboratory
P.O. Box 999, Richland, WA 99352 (USA)
Fax: (+1) 509-376-6066
E-mail: ls.wang@pnl.gov

[**] We thank Prof. A. I. Boldyrev, Dr. Jun Li, and Dr. Tom Waters for valuable discussions. This work was supported by the Chemical Sciences, Geosciences, and Biosciences Division of the Office of Basic Energy Sciences, U.S. Department of Energy (DOE) under grant number DE-FG02-03ER15481 (catalysis center program) and was performed at the W. R. Wiley Environmental Molecular Sciences Laboratory (EMSL), a national scientific user facility sponsored by DOE's Office of Biological and Environmental Research and located at Pacific Northwest National Laboratory, operated for DOE by Battelle. Calculations were performed at the EMSL Molecular Science Computing Facility.

Supporting information for this article is available on the WWW under http://www.angewandte.org or from the author.

 © 2005 Wiley-VCH Verlag GmbH & Co. KGaA, Weinheim

Early transition metal oxide clusters have recently gained experimental and theoretical attention due to their importance in catalysis.[24–26] We investigated the structure and bonding of early transition metal oxide clusters using a combined photoelectron spectroscopy (PES) and theoretical approach with the aim of discovering specific structures or clusters that may mimic a catalytic site.[27,28] Our experiment was carried out with a magnetic-bottle PES apparatus with a laser vaporization cluster source. A pure metal target (W or Mo) was used in the laser vaporization with a helium carrier gas containing 0.5% O_2. $[M_xO_y]^-$-type clusters with various stoichiometry were produced from reactions between the laser-induced plasma and O_2 in the carrier gas and were separated in a time-of-flight mass spectrometer. The $[M_3O_9]^-$ clusters (M = W, Mo) of interest were selected and decelerated before being intercepted by a 157-nm laser beam from an F_2 excimer laser. Photoemitted electrons were collected by a magnetic bottle with nearly 100% efficiency and analyzed in a 3.5-m-long electron flight tube. The photoelectron spectra were calibrated against the known spectrum of Rh^- and the apparatus had an electron energy resolution of $\Delta E_k/E_k \approx 2.5\%$, i.e., approximately 25 meV for 1-eV electrons.

Figure 1 displays the 157-nm spectra of $[W_3O_9]^-$ and $[Mo_3O_9]^-$, which are similar, each with a weak and broad threshold band (X) followed by a large energy gap and more features at very high electron-binding energies. The X band in both spectra yields a similar threshold detachment energy of about 3.5 eV for $[W_3O_9]^-$ and $[Mo_3O_9]^-$, and vertical detachment energies (VDEs) of 4.2 and 4.0 eV, respectively. The neutral $[M_3O_9]$ clusters are stoichiometric species in which W and Mo assume their highest oxidation state, M^{6+}. Thus, the threshold band (X) should correspond to detachment of the extra electron in the anions that occupies an d-type orbital that is empty in the neutral species, whereas the higher detachment features should all derive from detachment from O 2p-type orbitals. Interestingly, the observed energy gaps in the photoelectron spectra (Figure 1) of about 3.3 eV (3.2 eV) for $[W_3O_9]^-$ ($[Mo_3O_9]^-$), are already very close to that for the corresponding bulk MO_3 oxides. The threshold band (X) in both spectra is extremely broad, in particular in the spectrum of $[W_3O_9]^-$, thus suggesting that there is a large difference in geometry between the anion and neutral ground state of the $[M_3O_9]$ clusters.

To understand the structures and bonding in the $[M_3O_9]$ and $[M_3O_9]^-$ clusters, we carried out density functional theory (DFT) calculations.[29] Figure 2 displays the ground-state structures for $[M_3O_9]$ and $[M_3O_9]^-$. The structures of neutral $[W_3O_9]$ and $[Mo_3O_9]$ are nearly identical, with D_{3h} symmetry, and each metal atom is bonded to two bridging O atoms and two terminal O atoms. The $[W_3O_9]^-$ and $[Mo_3O_9]^-$ anions also display D_{3h} symmetry, but the M–M distance is significantly reduced by 0.29 Å in $[W_3O_9]^-$ and 0.25 Å in $[Mo_3O_9]^-$ relative to the neutral structures, and this is accompanied by a large increase in the OMO angle and a large decrease in the MOM angle that makes the M_3O_3 ring almost a perfect hexagon in $[M_3O_9]^-$ (Figures 2b and 2e). These geometrical changes are consistent with the broad ground-state PES band for the two clusters (Figure 1). Our calculated VDEs of 4.39 and 4.11 eV agree well with the measured values of 4.2 and 4.0 eV for $[W_3O_9]^-$ and $[Mo_3O_9]^-$, respectively, and our calculated adiabatic detachment energies (ADEs) for the two anions are 3.0 eV, which is smaller than the experimental threshold value of 3.5 eV. The large differences between the calculated ADEs and VDEs are consistent with the large difference in geometry between the anion and neutral ground-states. The smaller value of the calculated ADE relative to the experimental threshold value suggests that the 0–0 transition from the ground state of the anion to that of the neutral clusters may have negligible Franck–Condon factors due to the large difference in geometry, and the measured threshold detach-

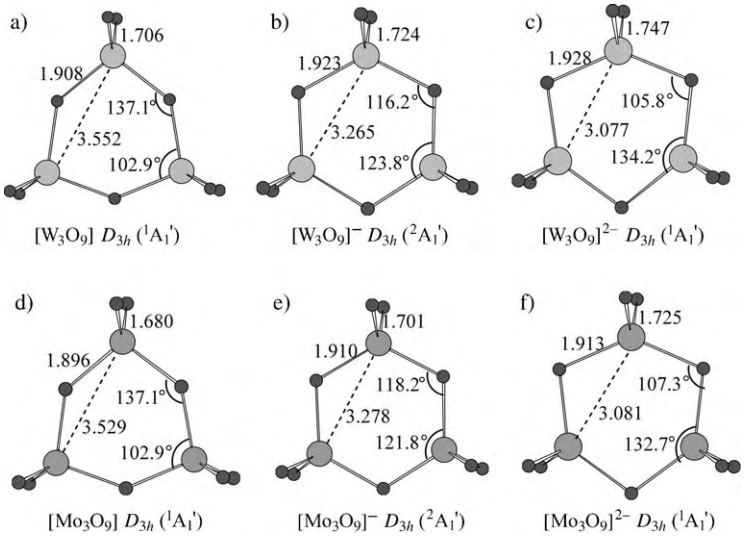

Figure 2. Optimized structures for $[M_3O_9]$, $[M_3O_9]^-$, and $[M_3O_9]^{2-}$ (M = W and Mo).

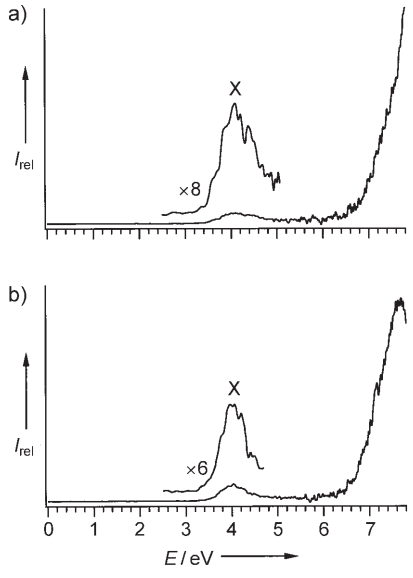

Figure 1. Photoelectron spectra of $[W_3O_9]^-$ (a) and $[Mo_3O_9]^-$ (b) at 157 nm (7.866 eV).

 © 2005 Wiley-VCH Verlag GmbH & Co. KGaA, Weinheim

ment energy can only serve as an upper limit for the true adiabatic value.

The surprisingly large geometry change induced by addition of a single electron to $[M_3O_9]$ suggests that the molecular orbital that the extra electron occupies in the anion must involve strong metal–metal bonding. Figures 3a and 3b

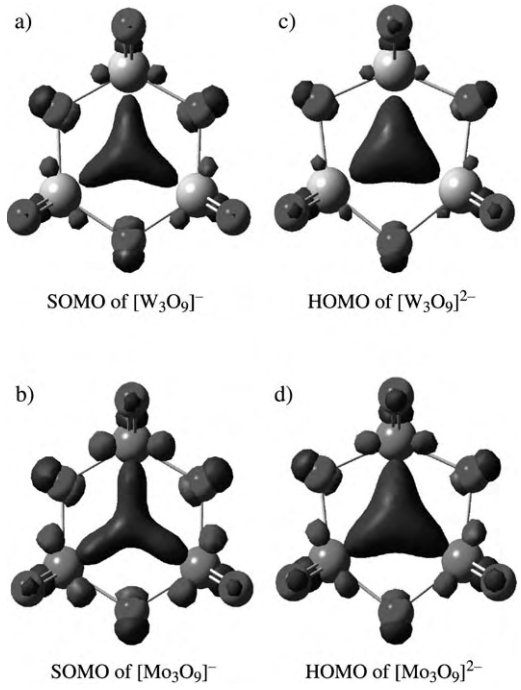

Figure 3. The singly occupied molecular orbital (SOMO) for $[W_3O_9]^-$ (a) and $[Mo_3O_9]^-$ (b) and the highest occupied molecular orbital (HOMO) of $[W_3O_9]^{2-}$ (c) and $[Mo_3O_9]^{2-}$ (d).

show the singly occupied molecular orbitals (SOMOs) for $[M_3O_9]^-$, which indeed describe nearly pure three-center M–M σ-bonding interactions with very little contribution from the O atoms. Judging by the huge M–M distance change induced by the single electron, these SOMOs must depict two strong three-center, one-electron (3c–1e) metal–metal bonds. The SOMO of $[M_3O_9]^-$ is a nondegenerate a_1' orbital. Addition of a second electron to this a_1' orbital gives rise to closed-shell $[M_3O_9]^{2-}$ dianions, which also display D_{3h} symmetry (Figure 2c, f) and a three-center, two-electron (3c–2e) bond (Figures 3c and 3d). Our calculations show that the dianions are also unusually stable despite the strong intramolecular coulomb repulsion. In fact, $[W_3O_9]^{2-}$ is predicted to be a stable gas-phase dianion with a calculated electron binding energy of 0.03 eV relative to $[W_3O_9]^-$. The $[Mo_3O_9]^{2-}$ dianion is predicted to be slightly unstable, with a small negative electron binding energy of −0.14 eV. More significantly, we found that the addition of a second electron to $[M_3O_9]^-$ also induces a considerable shortening of the M–M bond length of 0.19 Å (0.20 Å) for $[W_3O_9]^{2-}$ ($[Mo_3O_9]^{2-}$) relative to $[M_3O_9]^-$.

To gain further insight into the 3c–1e and 3c–2e bonds in $[M_3O_9]^-$ and $[M_3O_9]^{2-}$, we estimated their resonance energies (see Supporting Information).[30] Two isodesmic equations were used for $[W_3O_9]^{2-}$ to eliminate the potential influence of the different electrostatic interactions in the doubly charged anions. When the intramolecular coulomb interactions of the dianions involved are balanced by the K^+ cation a very large resonance energy of 1.05 eV is obtained, which is, in fact, comparable to the value estimated for benzene.[30] This large resonance energy suggests that the $[M_3O_9]^{2-}$ species may be viewed as highly aromatic. We further calculated their nucleus independent chemical shifts (NICS), which have been suggested as a magnetic criterion for aromaticity.[31] We obtained NICS values of −21.5 and −20.5 at the ring center for $[W_3O_9]^{2-}$ and $[Mo_3O_9]^{2-}$, respectively (see Supporting Information), that are much higher than those predicted for the cyclic Cu-containing clusters[20,23] and are comparable to the multiply aromatic $[Al_4]^{2-}$. The large resonance energies, the equal M–M bond lengths, and the large negative NICS values all suggest that $[W_3O_9]^{2-}$ and $[Mo_3O_9]^{2-}$ are highly aromatic species. More interestingly, we also obtained a sizable resonance energy for $[W_3O_9]^-$ (0.33 eV, see Supporting Information) even though it only contains a single delocalized electron, which suggests it may also be considered as aromatic; this was corroborated by the NICS values.

Trinuclear clusters of W and Mo have been studied extensively.[32,33] However, all these cluster complexes involve M^{4+} metal centers, typified by the $[M_3O_4]^{4+}$ core, whose metal–metal bonding can be described by three classical 2c–2e metal–metal bonds; they are therefore not expected to exhibit aromaticity. Quasi-aromaticity has been invoked to explain the strong M–O interactions in the $[M_3O_4]^{4+}$-type complexes,[34,35] but that is very different from the d-orbital aromaticity in the $[M_3O_9]^-$ and $[M_3O_9]^{2-}$ clusters discussed here. Aromaticity has also been considered in trinuclear Pt_3 and Os_3 metal complexes solely on the basis of molecular orbital topologies,[36,37] but it has not been verified using other criteria for aromaticity.

The $[M_3O_9]^-$ and $[M_3O_9]^{2-}$ clusters described here are unique in that they involve a single, fully delocalized metal–metal bond and may be considered as a new class of d-orbital aromatic molecules. The oxidation state of M can be considered to be fractional— +17/3 in $[M_3O_9]^-$ and +16/3 in $[M_3O_9]^{2-}$. Polyoxometalate clusters involving W and Mo are also well known.[38] The high stability of the $[M_3O_9]^-$ and $[M_3O_9]^{2-}$ clusters suggest that they may also be synthesized in the condensed phase. With the extra delocalized d-electrons, these clusters may exhibit novel chemical, electrochemical, and catalytic properties.

Received: July 29, 2005
Published online: October 17, 2005

Keywords: aromaticity · cluster compounds · density functional calculations · metal–metal interactions · photoelectron spectroscopy

[1] J. R. Bleeke, *Chem. Rev.* **2001**, *101*, 1205.
[2] B. E. Bursten, R. F. Fenske, *Inorg. Chem.* **1979**, *18*, 1760.
[3] X. W. Li, W. T. Pennington, G. H. Robinson, *J. Am. Chem. Soc.* **1995**, *117*, 7578.
[4] Y. Xie, P. R. Schreiner, H. F. Schaefer III, X. W. Li, G. H. Robinson, *J. Am. Chem. Soc.* **1996**, *118*, 10635.

 © 2005 Wiley-VCH Verlag GmbH & Co. KGaA, Weinheim

[5] A. E. Kuznetsov, A. I. Boldyrev, X. Li, L. S. Wang, *J. Am. Chem. Soc.* **2001**, *123*, 8825.
[6] A. D. Phillips, P. P. Power, *J. Cluster Sci.* **2002**, *13*, 569.
[7] X. Li, A. E. Kuznetsov, H. F. Zhang, A. I. Boldyrev, L. S. Wang, *Science* **2001**, *291*, 859.
[8] P. W. Fowler, R. W. A. Havenoth, E. Steiner, *Chem. Phys. Lett.* **2001**, *342*, 85.
[9] X. Li, H. F. Zhang, L. S. Wang, A. E. Kuznetsov, N. A. Cannon, A. I. Boldyrev, *Angew. Chem.* **2001**, *113*, 1919; *Angew. Chem. Int. Ed.* **2001**, *40*, 1867.
[10] A. E. Kuznetsov, J. D. Corbett, L. S. Wang, A. I. Boldyrev, *Angew. Chem.* **2001**, *113*, 3473; *Angew. Chem. Int. Ed.* **2001**, *40*, 3369.
[11] A. I. Boldyrev, A. E. Kuznetsov, *Inorg. Chem.* **2002**, *41*, 532.
[12] C. G. Zhan, F. Zheng, D. A. Dixon, *J. Am. Chem. Soc.* **2002**, *124*, 14795.
[13] P. W. Fowler, R. W. A. Havenoth, E. Steiner, *Chem. Phys. Lett.* **2002**, *359*, 530.
[14] A. E. Kuznetsov, H. J. Zhai, L. S. Wang, A. I. Boldyrev, *Inorg. Chem.* **2002**, *41*, 6062.
[15] H. Tanaka, S. Neukemans, E. Janssens, R. E. Silverans, P. Lievens, *J. Am. Chem. Soc.* **2003**, *125*, 2862.
[16] J. C. Santos, W. Tiznado, R. Contreras, P. Fuentealba, *J. Chem. Phys.* **2004**, *120*, 1670.
[17] J. Juselius, M. Straka, D. Sundholm, *J. Phys. Chem. A* **2001**, *105*, 9939.
[18] X. X. Chi, X. H. Li, X. J. Chen, Z. S. Yuang, *J. Mol. Struct. (Theochem)* **2004**, *677*, 21.
[19] A. E. Kuznetsov, A. I. Boldyrev, *Struct. Chem.* **2002**, *12*, 141.
[20] A. C. Tsipis, C. A. Tsipis, *J. Am. Chem. Soc.* **2003**, *125*, 1136.
[21] J. M. Mercero, J. M. Ugalde, *J. Am. Chem. Soc.* **2004**, *126*, 3380.
[22] Q. Kong, M. Chen, J. Dong, Z. Li, K. Fan, M. Zhou, *J. Phys. Chem. A* **2002**, *106*, 11709.
[23] C. S. Wannere, C. Corminboeuf, Z. X. Wang, M. D. Wodrich, R. B. King, P. von R. Schleyer, *J. Am. Chem. Soc.* **2005**, *127*, 5701.
[24] H. T. Deng, K. P. Kerns, A. W. Castleman, Jr., *J. Phys. Chem.* **1996**, *100*, 13385.
[25] Q. Sun, B. K. Rao, P. Jena, D. Stolcic, Y. D. Kim, G. Gantefor, A. W. Castleman, Jr., *J. Chem. Phys.* **2004**, *121*, 9417.
[26] B. L. Yoder, J. T. Maze, K. Raghavachari, C. C. Jarrold, *J. Chem. Phys.* **2005**, *122*, 094313.
[27] H. J. Zhai, B. Kiran, L. F. Cui, X. Li, D. A. Dixon, L. S. Wang, *J. Am. Chem. Soc.* **2004**, *126*, 16134.
[28] H. J. Zhai, X. Huang, L. F. Cui, X. Li, J. Li, L. S. Wang, *J. Phys. Chem. A* **2005**, *109*, 6019.
[29] The theoretical calculations were performed at the DFT level using the B3LYP hybrid functional (A. D. Becke, *J. Chem. Phys.* **1993**, *98*, 1372). A number of possible structures were evaluated, and the search for the global minima and vibrational frequency calculations were performed using analytical gradients with the Stuttgart 14-valence-electron pseudo-potentials and the valence basis sets (D. Andrae, U. Haeussermann, M. Dolg, H. Stoll, H. Preuss, *Theor. Chim. Acta* **1990**, *77*, 123) augmented with two f-type and one g-type polarization functions for W ($\zeta(f)=0.256$, 0.825; $\zeta(g)=0.627$) for Mo and ($\zeta(f)=0.338$, 1.223; $\zeta(g)=$ 0.744), as recommended by Martin and Sundermann (J. M. L. Martin, A. Sundermann, *J. Chem. Phys.* **2001**, *114*, 3408), and the aug-cc-pVTZ basis set for oxygen (R. A. Kendall, T. H. Dunning, Jr., R. J. Harrison, *J. Chem. Phys.* **1992**, *96*, 6796). Scalar relativistic effects, i.e., the mass-velocity and Darwin effects, were taken into account by using the quasi-relativistic pseudopotentials. Vertical electron detachment energies (VDEs) were calculated using the generalized Koopman's theorem (D. J. Tozer, N. C. Handy, *J. Chem. Phys.* **1998**, *109*, 10180). The extra-fine integration grid was used to obtain accurate DFT results. The geometry optimizations and vibrational frequency analysis were accomplished with the NWChem 4.6 program (*NWChem, A Computational Chemistry Package for Parallel Computers, Version 4.6*: E. Aprà et al., see Supporting Information) and the Molecular Science Computing Facility located at the Environmental Molecular Sciences Laboratory. GaussView 3.0 was used to generate the three-dimensional contours of the calculated Kohn–Sham orbitals. Nucleus-independent chemical shifts (in ppm) were computed at the centers of the optimized structures using the GIAO-B3LYP (SDD for W and Mo, 6-31+G* for O) method with the Gaussian03 program (Gaussian03 (Revision B.04): M. J. Frisch et al., see Supporting Information).
[30] P. von R. Schleyer, H. Jiao, *Pure Appl. Chem.* **1996**, *68*, 209.
[31] P. von R. Schleyer, C. Maerker, A. Dransfeld, H. Jiao, N. J. R. van Eikema Hommes, *J. Am. Chem. Soc.* **1996**, *118*, 6317.
[32] A. Müller, R. Jostes, F. A. Cotton, *Angew. Chem.* **1980**, *92*, 921; *Angew. Chem. Int. Ed. Engl.* **1980**, *19*, 875.
[33] B. E. Bursten, F. A. Cotton, M. B. Hall, R. C. Najjar, *Inorg. Chem.* **1982**, *21*, 302.
[34] J. Li, C. W. Liu, J. X. Lu, *Polyhedron* **1994**, *13*, 1841.
[35] J. X. Lu, Z. D. Chen, *Int. Rev. Phys. Chem.* **1994**, *13*, 85.
[36] R. B. King, *Inorg. Chim. Acta* **2003**, *350*, 126.
[37] F. F. de Biani, A. Ienco, F. Laschi, P. Leoni, F. Marchetti, L. Marchetti, C. Mealli, P. Zanello, *J. Am. Chem. Soc.* **2005**, *127*, 3076.
[38] M. T. Pope, *Heteropoly and Isopoly Oxometalates*, Springer, Berlin, **1983**.

 © 2005 Wiley-VCH Verlag GmbH & Co. KGaA, Weinheim

Micelles

DOI: 10.1002/anie.200502594

Unusual Rate Enhancement of Bimolecular Dehydrocondensation To Form Amides at the Interface of Micelles of Fatty Acid Salts**

Munetaka Kunishima, Hiroko Imada, Kanako Kikuchi, Kazuhito Hioki, Jin Nishida, and Shohei Tani*

Nature has long succeeded in utilizing the interface of membranes as a reaction field for a variety of biological chemical transformations in which bimolecular reactions between reactants of very low concentrations can be effec-

[*] Prof. Dr. M. Kunishima, H. Imada, K. Kikuchi, Dr. K. Hioki, Prof. Dr. S. Tani
Faculty of Pharmaceutical Sciences
Kobe Gakuin University
Nishi-ku, Kobe 651-2180 (Japan)
Fax: (+81) 78-974-5689
E-mail: kunisima@pharm.kobegakuin.ac.jp
Prof. Dr. M. Kunishima, Dr. J. Nishida
PRESTO, JST
Nishi-ku, Kobe 651-2180 (Japan)

[**] We thank Dr. Keisuke Matsuoka, Showa Pharmaceutical University, for a useful discussion on critical micelle concentration. This work was supported partially by a Grant-in-Aid for Science Research (No. 14572025) from the Ministry of Education, Science, Sports, and Culture, Japan.

Supporting information for this article is available on the WWW under http://www.angewandte.org or from the author.

WILEY InterScience DISCOVER SOMETHING GREAT
© 2005 Wiley-VCH Verlag GmbH & Co. KGaA, Weinheim

tively accelerated. In contrast, mankind has not yet succeeded in the practical application of either membrane–water or micelle–water interfaces as a reaction field. To enhance the rate of reactions in the micellar phase, the reactions must proceed in water, and all the compounds (reactants and intermediates) involved in the rate-determining step must be incorporated in the micelles to increase their local concentration. Furthermore, the molecules must be oriented appropriately for the reaction to take place. The fact that very few organic reactions (e.g. hydrolysis) meet these requirements makes it difficult to utilize micelles as a reaction field.

We believe that dehydrocondensation is most ideally suited for such rate enhancement in micelles, because all reactants that bear long hydrophobic alkyl chains, whether carboxylic acids, amines, or alcohols, are capable of forming micelles by themselves or can be incorporated in micelles formed by surfactants. Furthermore, the reacting moieties involved in the condensation (carboxy, ammonium, and hydroxy groups) are polar, and thus are located in close proximity to one another at the micellar interface. However, it has been very difficult to verify such a rate enhancement because of two major problems: 1) dehydrocondensations generally require dry conditions because many reagents and activated intermediates derived from carboxylic acids are susceptible to hydrolysis, and 2) hydrolysis reactions, the reverse reaction of dehydrocondensation, are originally promoted at the interface of micelles.[1]

In contrast to the numerous studies of unimolecular hydrolysis reactions with micelles,[1–3] successful studies on bimolecular dehydrocondensation in micelles, which involves the activation of carboxylic acids in micelles formed in an aqueous medium, are very limited. Both lactonization with a carbodiimide[4] and lactamization in the presence of an amphiphilic Mukaiyama reagent[5] at a reverse micelle proceeded in low yields under dry conditions. Peptide synthesis at a reverse micellar interface in the presence of water proceeded in moderate yields.[6,7] As no significant rate acceleration was observed with these reactions, the micellar effect mentioned above would seem to be inadequate. More recently, Kobayashi and co-workers realized a 60-fold rate enhancement in acid-catalyzed esterification, which proceeded in the hydrophobic interior of emulsion droplets formed in water.[8,9]

In the course of our studies on 1,3,5-triazine-based dehydrocondensing agents that are available in an aqueous solvent,[10–12] we found that the reaction of the carboxylate **1** with the dehydrocondensing agent **3** to form acyloxytriazine **4** was the rate-determining step, because the reaction rate depended on the concentration of **1** [Eq. (1)]. Since both the reactants **1** and **3** have ionic structures, they should be aligned at the interface of micelles when a hydrophobic alkyl group is introduced into their structure. In the studies discussed herein, we employed amphiphilic dehydrocondensing agents based on 1,3,5-triazine to demonstrate that a large rate enhancement of bimolecular dehydrocondensation occurs in micelles as a result of both the proximity and the preorientational effects.

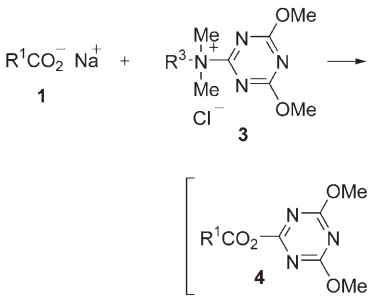

(1)

To simplify the reaction system, we employed the sodium salt **1** of a fatty acid which can serve both as a substrate and a surfactant. The reaction is illustrated in Scheme 1. Both hydrophobic 2-chloro-4,6-dimethoxy-1,3,5-triazine (DMT-Cl) and an amphiphilic tertiary amine **2** are incorporated in the micelles consisting of **1**. Nonionized amine **2** is buried in the micelle and then couples with DMT-Cl (step 1). This step can occur either in the outer core or in the palisade layer of the micelle[3] and can be accelerated by increasing the local concentration of the reactants. Amine **2** acts as a catalyst for the activation of DMT-Cl toward **1** through the formation of **3** (step 2). The resulting quaternary ammonium group of the amphiphilic agent **3** will be located at the interface of the

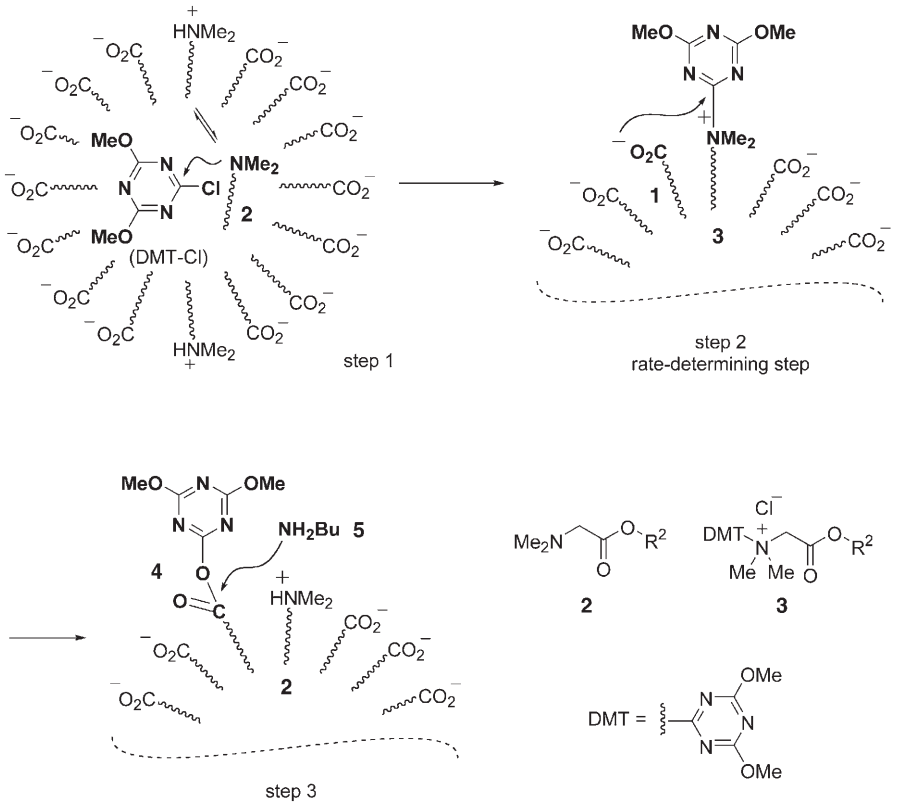

Scheme 1. Micellar effects on the catalytic dehydrocondensation.

 © 2005 Wiley-VCH Verlag GmbH & Co. KGaA, Weinheim

micelle, thus forming an ion pair with **1**. Therefore, as **1** is closely concentrated around **3**, it can readily attack the triazinyl group of **3** with concomitant liberation of **2**, which can be recycled to step 1. Step 2 is accelerated by the preorientational effect as well as the local concentration effect of the reactants at the micellar interface. The resulting activated triazinyl ester **4** undergoes aminolysis with butylamine (**5**), which is expected to be partitioned mainly in the aqueous phase, to form the amide **6** (step 3). As this step is known to be much faster than hydrolysis in water,[10] it is not rate-limiting and thus it appeared to be unimportant to ensure that it occurs in the micelle rather than at the aqueous phase.

We employed four sodium carboxylates **1A–D** with alkyl chains of different lengths. On the basis of the critical micelle concentration and Kraft points of these compounds, **1A** and **1B** should form a simple molecular dispersion phase in which these electrolytes are homogeneously dissolved in a dissociated form, whereas **1C** and **1D** should form a micellar phase at a concentration of 15 mM (25 °C).[13,14] If the bimolecular reaction rate constants between carboxylates **1** and **3** are assumed to be independent of their chain length, the observed change in reaction rate can be attributed to the micellar effect.

First, we examined the reaction of carboxylates **1A–D** with condensing agents **3a–d**[15] to estimate the acceleration of the rate-determining step (step 2) in the micelle. The reaction should be close to first-order with respect to **3**. The reaction was conducted using **1** (15 mM), **5** (as hydrochloride, 20 mM), and **3** (1.5 mM) in phosphate buffer (pH 8, 20 mM) containing MeOH (3 %)[16] at 25 °C (Table 1). The pseudo-first-order rate

Table 1: Relative rates for the stoichiometric reaction of **1** and **3**.[a]

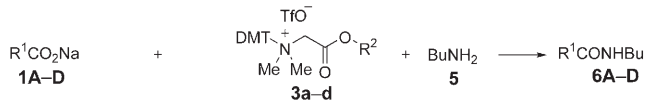

A: $R^1 = C_3H_9$ **a**: $R^2 = C_2H_5$
B: $R^1 = C_7H_{15}$ **b**: $R^2 = C_8H_{17}$
C: $R^1 = C_{11}H_{23}$ **c**: $R^2 = C_{12}H_{25}$
D: $R^1 = C_8H_{17}CH{=}CHC_7H_{14}$ **d**: $R^2 = C_{16}H_{33}$

3	1A	1B	1C	1D
3a	1.0[a]	1.1	56	63
3b	0.7	3.0	1200	830
3c	21	280	860	840
3d	30	340	1400	690

[a] Pseudo-first-order rate constant: $k = 1.0 \times 10^{-3}$ min^{-1}.

constants for the reaction with respect to **3** were calculated based on the amount of the amide **6** produced. The relative rates were normalized to the reaction rate of **3a** with **1A** (rate defined as 1). In the reactions of **3a**, which has a short alkyl chain (ethyl group), no rate acceleration was observed in the reaction with octanoate **1B**, which has an alkyl chain that is four carbon atoms longer than that of butyrate **1A**, whereas the reaction with laurate **1C**, whose alkyl chain is elongated by an additional four carbon atoms, was accelerated by a factor of 56. In a series of reactions with **1C**, the reaction rate increased up to 1400 times by elongation of the ester alkyl chain of **3**. Interestingly, the reaction rates appeared to plateau with the **1C** series; reactions were not accelerated further when a longer acyl chain was used (see series **1D**).

As **1C** and **1D** form micelles under these reaction conditions, the large rate enhancements observed with these two carboxylates are attributable to the micellar effect (Scheme 1, step 2). Dehydrocondensing agents **3b–d** have alkyl chains with eight carbon atoms or more, which puts them on the borderline in their ability to be incorporated in micelles. Moderate accelerations in the reactions of **1B** with **3c** or **3d** do not arise from micelle formation but rather from a disordered aggregation owing to the hydrophobic effect. This explanation is based on the fact that **3c**, which is poorly soluble in water, does not form micelles under the reaction conditions. In fact, a white turbidity appeared upon addition of **3c** or **3d** to initiate the reaction with **1B**, whereas no turbidity was observed with **1C** and **1D**, presumably as a result of mixed micelle formation.

The substrate concentration dependence of the reaction rate in the micellar system when using **3b** was also examined. The reaction rate was found to be independent of the concentration of **1C** (15, 30, and 60 mM) whereas the reaction rate showed a linear relationship to the concentration of butylamine **5** (5, 10, 15, and 20 mM). The results indicate that step 3 becomes the rate-determining step in the micellar system instead of step 2.[17] The rate of aminolysis of the triazinyl ester with **5** dissolved in the aqueous phase is independent of the length of the acyl chain. Thus, in the micellar system, there was no significant difference between **1C** and **1D**, despite the difference in chain length (six carbon atoms).

Competitive reactions between **1A** and **1B** with either **3a** or **3b** afforded amides **6A** and **6B** (42:58 or 25:75, respectively) after the reaction mixture was stirred for 4 h at room temperature (Table 2). In contrast, the competitive reaction

Table 2: Substrate selectivity in the competitive reaction between two carboxylates in the stoichiometric system.

Carboxylates	3	*t* [h]	Yield [%]	Ratio
1A vs. **1B**	**3a**	4	16	**6A**/**6B** 42:58
1A vs. **1B**	**3b**	4	24	**6A**/**6B** 25:75
1A vs. **1C**	**3b**	1	88	**6A**/**6C** 0.4:99.6

between **1A** and **1C** with **3b** proceeded within 1 h in both good yield (88 %) and high selectivity (0.4:99.6). These selectivities are in good agreement with the relative reaction rates shown in Table 1.

Finally, the catalytic reaction of *N*,*N*-dimethylglycine alkyl esters **2** and DMT-Cl, which generate condensing agent **3** in situ, was also found to be accelerated by a factor of 140 in micelles (Table 3). The moderate acceleration in the catalytic system relative to the stoichiometric system may be attributed to the generation of **3** (step 1) which may become the rate-determining step after acceleration of step 2. This catalytic system can be considered as an acyl transferase model for preparing lipid molecules.

The amide-forming reaction in the cyclodextrin-based artificial enzyme was accelerated by a factor of 13 because of

 © 2005 Wiley-VCH Verlag GmbH & Co. KGaA, Weinheim

Table 3: Relative rates for the catalytic reaction of tertiary amines **2** with carboxylates **1B** and **1C**.

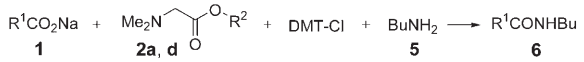

2	1B	1C
2a ($R^2 = C_2H_5$)	1.0[a]	33
2d ($R^2 = C_{16}H_{33}$)	11	140

[a] Pseudo-first-order rate constant: $k = 8.5 \times 10^{-5}$ min^{-1}.

a proximity effect resulting from the formation of an inclusion complex.[12] By comparison, the large rate enhancement of the present system should be ascribed to the micellar effect (preorientational effect and local concentration effect) illustrated in Scheme 1. Micelles of quaternary ammonium surfactants are known to promote the hydrolysis of both activated esters and condensing agents because the hydroxide ion with a negative charge opposite to that of the surfactant is concentrated at the interface.[1–7] As the present system employs carboxylate anions as surfactants, the hydroxide ion (with the same charge) does not concentrate at the micellar interface, and the hydrolysis of **3** and **4** does not become a serious side reaction. Thus, we have succeeded in demonstrating that amphiphilic dehydrocondensing agents based on 1,3,5-triazine offer the micellar interface as a superior reaction field for dehydrocondensation.

Experimental Section

General procedure: **3** (3 μmol) in aqueous methanol (40%; 0.15 mL) was added to a stirred aqueous solution (1.85 mL) of **1** (30 μmol) and **5**·HCl (40 μmol) in sodium phosphate buffer (pH 8) at 25°C. The initial concentration of reactants in the resulting solution were as follows: **1**: 15 mM; **5**: 20 mM; **3**: 1.5 mM; NaPi: 20 mM; and MeOH: 3%. The mixture was stirred at 25°C, and HCl (5M; 0.3 mL) was added at a specific time. The resulting mixture was applied to Extrelut NT (Merck, 2 g) and eluted with AcOEt. The product **6** was quantified by GC (silicone SE-30 for **6A**, silicone OV-17 for **6B**–**D**). The pseudo-first-order rate constants were determined from the slopes of liner plots of $\ln([\mathbf{3}]_t/[\mathbf{3}]_0)$ versus time (min).

Received: July 25, 2005
Published online: October 17, 2005

Keywords: amides · condensation · kinetics · micelles · triazines

[1] J. H. Fendler, E. J. Fendler, *Catalysis in Micellar and Macromolecular Systems*, Academic Press, New York, **1975**.
[2] J. H. Fendler, *Membrane Mimetic Chemistry*, Wiley, New York, **1982**.
[3] S. Tascioglu, *Tetrahedron* **1996**, *52*, 11113 – 11152.
[4] D. A. Jaeger, J. T. Ippoliti, *J. Org. Chem.* **1981**, *46*, 4964 – 4968.
[5] I. Rico, K. Halvorsen, C. Dubrule, A. Lattes, *J. Org. Chem.* **1994**, *59*, 415 – 420.
[6] D. Ranganathan, G. P. Singh, S. Ranganathan, *J. Am. Chem. Soc.* **1989**, *111*, 1144 – 1145.
[7] D. Ranganathan, S. Ranganathan, *Tetrahedron Lett.* **1993**, *34*, 525 – 528.
[8] K. Manabe, X.-M. Sun, S. Kobayashi, *J. Am. Chem. Soc.* **2001**, *123*, 10101 – 10102.
[9] K. Manabe, S. Iimura, X.-M. Sun, S. Kobayashi, *J. Am. Chem. Soc.* **2002**, *124*, 11971 – 11978.
[10] M. Kunishima, C. Kawachi, K. Hioki, K. Terao, S. Tani, *Tetrahedron* **2001**, *57*, 1551 – 1558.
[11] M. Kunishima, C. Kawachi, J. Morita, K. Terao, F. Iwasaki, S. Tani, *Tetrahedron* **1999**, *55*, 13159 – 13170.
[12] M. Kunishima, K. Yoshimura, H. Morigaki, R. Kawamata, K. Terao, S. Tani, *J. Am. Chem. Soc.* **2001**, *123*, 10760 – 10761.
[13] The critical micellar concentration of **1B**, **1C**, and **1D** under the reaction conditions (in the absence of **3**) were determined as 330, 4.5, and 0.2 mM, respectively.[14]
[14] Y. Moroi, *Micelles: Theoretical and Applied Aspects*, Plenum, New York, **1992**, pp. 211 ff.
[15] M. Kunishima, K. Hioki, A. Wada, H. Kobayashi, S. Tani, *Tetrahedron Lett.* **2002**, *43*, 3323 – 3326.
[16] MeOH was required to dissolve **3**.
[17] The second-order rate constant of aminolysis was calculated to be 58 min^{-1}M^{-1}.

 © 2005 Wiley-VCH Verlag GmbH & Co. KGaA, Weinheim

Asymmetric Catalysts

DOI: 10.1002/anie.200502682

Enantiodiscrimination and Enantiocontrol of Neutral and Cationic Pt^{II} Complexes Bearing the *Tropos* Biphep Ligand: Application to Asymmetric Lewis Acid Catalysis**

Koichi Mikami, Hitomi Kakuno, and Kohsuke Aikawa*

The development of asymmetric catalysts for organic reactions is one of the most challenging subjects in modern science and technology.[1] These catalysts are generally metal complexes that bear chiral and atropisomeric ligands, which require the enantioresolution and synthetic transformation of a chiral pool (atropisomeric is from the Greek *atropos*, *a* meaning not and *tropos* meaning turn).[2] However, we have already demonstrated that chirally flexible (*tropos*) 2,2′-bis(diphenylphosphanyl)biphenyl (biphep)[3] can act as a chiral ligand for Ru,[4] Rh,[5] and Pd[6] complexes through axial chirality control by chiral diamines. Therefore, the biphep complexes of Ru, Rh, and Pd can provide high levels of enantioselectivity in asymmetric hydrogenation, ene-type cyclization, and hetero-Diels–Alder reactions, respectively. Similarly, in the neutral biphep–Pt complex the chirality

[*] Prof. Dr. K. Mikami, H. Kakuno, Dr. K. Aikawa
Department of Applied Chemistry
Graduate School of Science and Engineering
Tokyo Institute of Technology
Ookayama, Meguro-ku, Tokyo 152-8552 (Japan)
Fax: (+81) 3-5734-2776
E-mail: kmikami@o.cc.titech.ac.jp

[**] Biphep is 2,2′-bis(diphenylphosphanyl)biphenyl.

Supporting information for this article is available on the WWW under http://www.angewandte.org or from the author.

© 2005 Wiley-VCH Verlag GmbH & Co. KGaA, Weinheim

control of the biphep moiety by chiral 1,1'-binaphthalene-2,2'-diol (binol) was reported not high enough (95:5) and hence recrystallization was essential to obtain the single biphep–Pt diastereomer and enantiomer.[7a,b]

Herein, we report the complete chirality control of both neutral and cationic biphep–Pt complexes without the need for recrystallization and the application of this complex to asymmetric Lewis acid catalysis (Scheme 1). Interestingly, both enantiopure (*S*)- and (*R*)-biphep–Pt complexes can be obtained quantitatively through enantiodiscrimination by using (*R*)-2,2′-bis(trifluoromethanesulfonylamino)-1,1′-binaphthyl (dabnTf) and (*R*)-2,2′-diamino-1,1′-binapthyl (dabn) with the same absolute configuration.

The highly effective enantiodiscriminating agent dabnTf was first used for enantiomer-selective complexation[8] of the neutral racemic biphep-$PtCO_3$ complex **1** (Figure 1)[7a] with complete enantiomer discrimination. Complexation of racemic complex **1** and (*R*)-dabnTf at a specified temperature was monitored by NMR spectroscopy until product (*S*)/(*R*)-**2** was precipitated. A combination of racemic complex **1** with 1.0 equivalent of (*R*)-dabnTf in [D_8]toluene gave the single diastereomer (*S*,*R*)-**2** along with the remaining (*R*)-**1** and (*R*)-dabnTf (0.5 equiv), which form a hydrogen bond between the proton of the diamide and oxygen atom of the carbonate complex (*R*)-**1**. In fact, treatment of [{(*S*)-binap}$PtCO_3$] with (*R*)-dabnTf (1.0 equiv) gave the (*S*,*R*) diastereomer complex, but the combination of [{(*R*)-binap}$PtCO_3$] with (*R*)-dabnTf (1.0 equiv) did not.[8] There was no isomerization of the remaining (*R*)-**1** enantiomer, which did not form a complex with (*R*)-dabnTf even at 50 °C after 120 h (Figure 1). Therefore, these results imply that complex **1** is *atropos* below 50 °C. At higher temperatures, isomerization of complex (*R*)-**1** followed by complexation with remaining (*R*)-dabnTf was observed. These results indicate that complex **1** is *tropos* at higher (> 60 °C) temperatures.

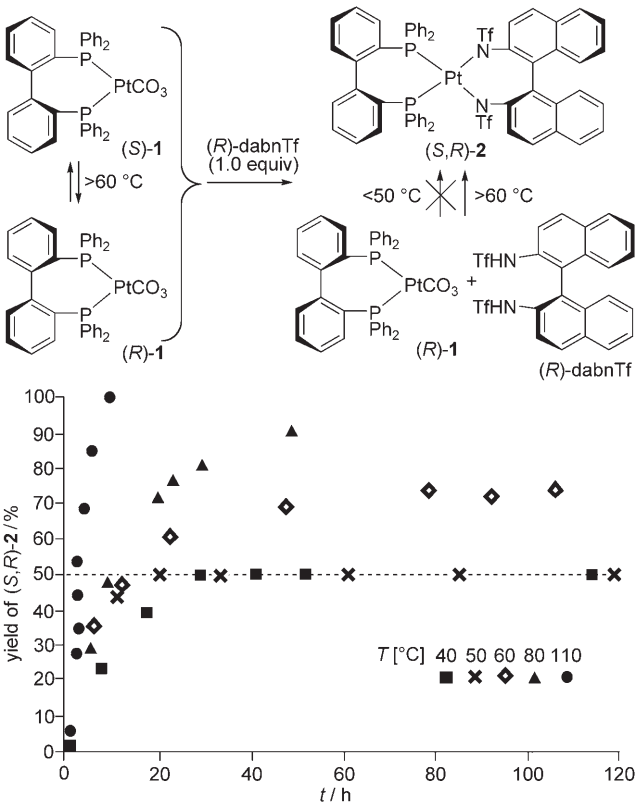

Figure 1. Temperature dependence of the isomerization of complex **1**.

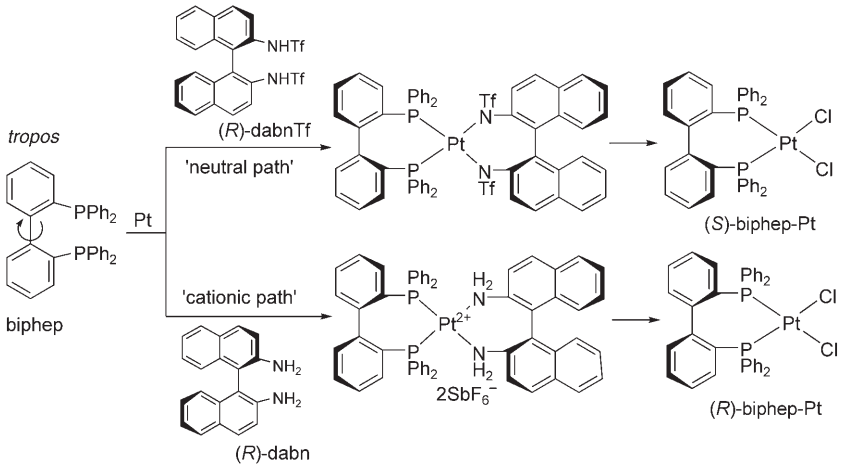

Scheme 1. Complete chirality control of both neutral and cationic biphep–Pt complexes.

After proving the *atropos* nature of biphep–Pt species even at 50 °C, we tried to isolate the enantiopure biphep–$PtCl_2$ complex **3** without epimerization. Upon addition of concentrated HCl in dichloromethane at room temperature, complex (*S*,*R*)-**2** provided the enantiopure (*S*)-**3** (> 99 % *ee*) quantitatively (Scheme 2).[7b] Pure dabnTf could also be recovered quantitatively. The enantiomeric excess (% *ee*) of (*S*)-**3** was determined by ^{1}H and ^{31}P NMR spectroscopies after complexation with enantiopure (*S*,*S*)-diphenylethylenediamine (dpen) and upon addition of 2.0 equivalents of $AgSbF_6$. In sharp contrast to the Pt complex, the Pd complex was protonated with concentrated HCl in dichloromethane even at 0 °C and the biphep moiety was epimerized (24 % *ee*) as biphep–Pd is stereochemically less stable through decomplexation of the sterically demanding dabnTf. These results show that the Pt center coordinates to the biphep diphosphine ligand more strongly than the Pd center.

We also clarified the *atropos* nature of cationic biphep–Pt complexes at room temperature. Chiral diamine

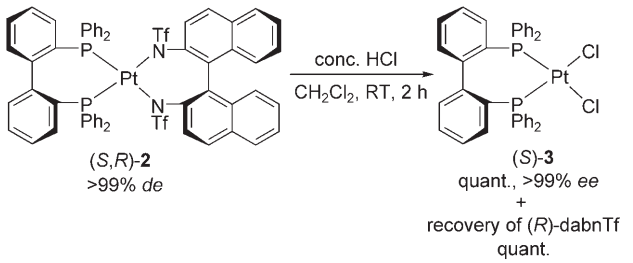

Scheme 2. Quantitative isolation of enantiopure (*S*)-**3**.

 © 2005 Wiley-VCH Verlag GmbH & Co. KGaA, Weinheim

dabn was used for nonselective complexation and axial chirality control of the racemic cationic complex **4** (Scheme 3).[6b] With 1.0 equivalent of (*R*)-dabn, complexation of both enantiomers took place to afford a 1:1 ratio of a

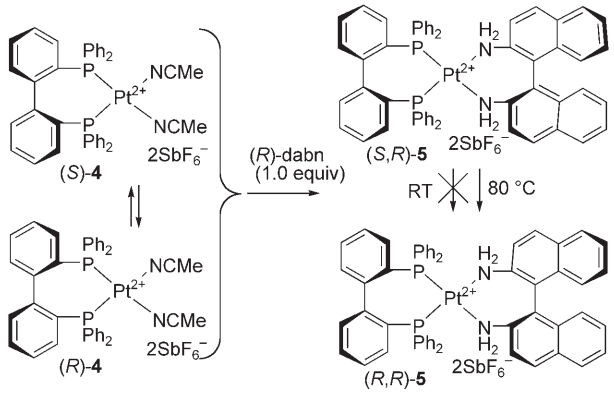

Scheme 3. Complete chirality control of cationic biphep–Pt complex **4**.

diastereomer mixture of (*R*,*R*)-**5** and (*S*,*R*)-**5** complexes. The complex **5** bearing (*R*)-dabn did not isomerize at room temperature over 3 days but did isomerize at 80 °C after 30 h to afford exclusively the favorable (*R*,*R*)-**5** (> 99 % *de*). In the Pd complex, the favorable (*R*,*R*) complex is obtained exclusively after an even shorter period.[6b]

The complex (*R*,*R*)-**5** provided enantiopure (*R*)-**3** (> 99 % *ee*) quantitatively upon addition of aqueous HCl at room temperature (Scheme 4); dabn could also be recovered

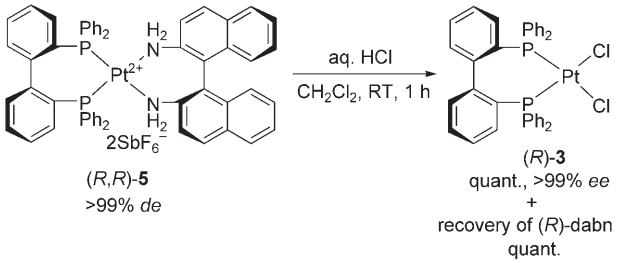

Scheme 4. Quantitative isolation of the enantiopure (*R*)-**3**.

quantitatively. The enantiomer excess of (*R*)-**3** was determined by addition of enantiopure dpen under the same conditions as those shown in Scheme 2. The opposite axial chirality to that controlled by its amide (*R*)-dabnTf can be controlled by (*R*)-dabn with the same absolute configuration.

The structure of racemic complex **3** was determined by X-ray crystal structure analysis of a single crystal obtained from dichloromethane/hexane solution.[9] Indeed, the orientations of axial and equatorial phenyl groups in biphep portion were quite similar to those of biphep–Pd complexes.[6,10] In the enantiodiscrimination of the neutral (*R*,*R*)-**2** complex, there is strong steric repulsion between equatorial phenyl group of biphep and the trifluoromethanesulfonyl substituent (Tf) of chiral amide dabnTf (Figure 2a). In contrast, there is no steric repulsion in complex (*S*,*R*)-**2**. As a result, (*R*)-dabnTf could complex only with the single enantiomer (*S*)-**1** after isomer-

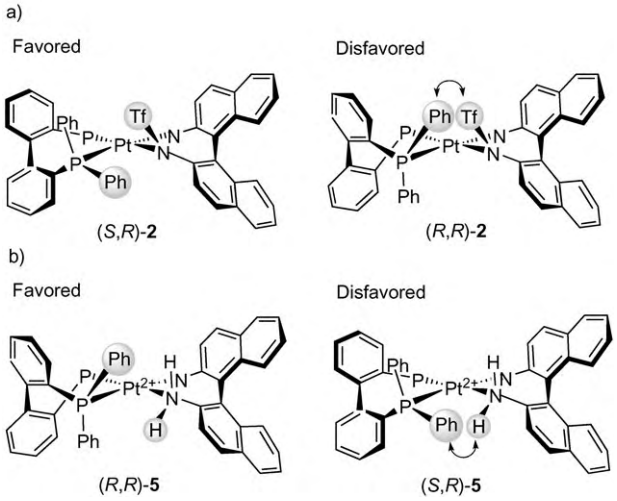

Figure 2. Enantiomer discrimination of (*R*)-dabnTf and (*R*)-dabn.

ization of the opposite enantiomer (*R*)-**1**. In the cationic (*S*,*R*)-**5** complex, there is strong repulsion between equatorial phenyl group of biphep and hydrogen atom of chiral diamine dabn. In contrast, there is no steric repulsion in the complex (*R*,*R*)-**5** (Figure 2b).

The enantiopure complex **3** thus obtained can be employed as an *atropos* asymmetric catalyst (Scheme 5).[5–7]

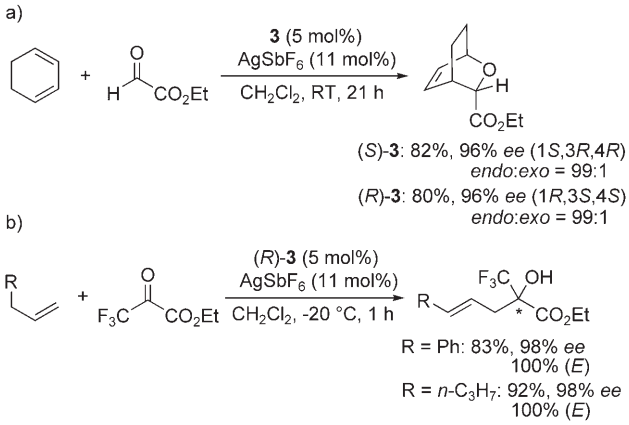

Scheme 5. Enantiopure **3** as an *atropos* asymmetric Lewis acid catalyst.

Indeed, the hetero-Diels–Alder reaction of 1,3-cyclohexadiene with glyoxylate[11] was catalyzed by enantiopure (*S*)-**3** (5 mol %) and $AgSbF_6$ (11 mol %) as a highly efficient Lewis acid catalyst. The hetero-Diels–Alder product was obtained with high enantioselectivity (96 % *ee*, *endo*:*exo* = 99:1) even at room temperature (Scheme 5a). Use of enantiopure (*R*)-**3** gave the hetero-Diels–Alder product with opposite absolute configuration in equally high selectivity. The complex (*S*)-**3** was obtained with (*R*)-dabnTf, and (*R*)-**3** was obtained with (*R*)-dabn. It was confirmed by addition of enantiopure dpen that racemization of the biphep moiety did not occur during the course of reaction. Additionally, enantiopure dicationic complex **3** gave high chemical yields and high levels of enantio- and *E*-selectivity in carbonyl-ene reactions with

 © 2005 Wiley-VCH Verlag GmbH & Co. KGaA, Weinheim

trifluoropyruvate and with less reactive monosubstituted olefins (Scheme 5b).[12]

In summary, we have proven that the racemic Pt complexes even with *tropos* biphep ligands can be resolved as the *atropos* complex even at 50 °C but converted at higher temperatures into either enantiopure complex just by exchanging (*R*)-dabn and (*R*)-dabnTf with identical absolute configuration. In carbon–carbon bond-forming reactions, the enantiopure biphep–Pt complexes thus obtained can be used as the *atropos* catalysts to give high enantioselectivity.

Received: July 30, 2005
Published online: October 18, 2005

Keywords: chirality · Diels–Alder reaction · enantioselectivity · ene reaction · platinum

[1] a) E. N. Jacobsen, A. Pfaltz, H. Yamamoto, *Comprehensive Asymmetric Catalysis, Vol. 1–3*, Springer, Berlin, **1999**; b) *Transition Metals for Organic Synthesis* (Eds.: M. Beller, C. Bolm), VCH, Weinheim, **1998**; c) R. Noyori, *Asymmetric Catalysis in Organic Synthesis*, Wiley, New York, **1994**; d) H. Brunner, W. Zettlmeier, *Handbook of Enantioselective Catalysis*, VCH, Weinheim, **1993**; e) *Catalytic Asymmetric Synthesis, Vol. I and II* (Ed.: I. Ojima), VCH, New York, **1993**, **2000**.

[2] K. Mikami, K. Aikawa, Y. Yusa, J. J. Jodry, M. Yamanaka, *Synlett* **2002**, *10*, 1561.

[3] The activation barrier to axial torsion in selectively deuterated biphep is measured to be only (22 ± 1) kcal, which suggests that axial rotation takes place at room temperature or above: O. Desponds, M. Schlosser, *Tetrahedron Lett.* **1996**, *37*, 47.

[4] a) K. Mikami, T. Korenaga, M. Terada, T. Ohkuma, T. Pham, R. Noyori, *Angew. Chem.* **1999**, *111*, 517; *Angew. Chem. Int. Ed.* **1999**, *38*, 495; b) K. Mikami, K. Aikawa, T. Korenaga, *Org. Lett.* **2001**, *3*, 243; c) T. Korenaga, K. Aikawa, M. Terada, S. Kawauchi, K. Mikami, *Adv. Synth. Catal.* **2001**, *3*, 284.

[5] K. Mikami, S. Kataoka, Y. Yusa, K. Aikawa, *Org. Lett.* **2004**, *6*, 3699.

[6] a) K. Mikami, K. Aikawa, Y. Yusa, M. Hatano, *Org. Lett.* **2002**, *4*, 91; b) K. Mikami, K. Aikawa, Y. Yusa, *Org. Lett.* **2002**, *4*, 95.

[7] For biphep-Pt complex: a) M. D. Tudor, J. J. Becker, P. S. White, M. R. Gagné, *Organometallics* **2000**, *19*, 4376; b) J. J. Becker, P. S. White, M. R. Gagné, *J. Am. Chem. Soc.* **2001**, *123*, 9478. Use of different chirally flexible (*tropos*) nuphos ligands: c) S. Doherty, C. R. Newman, R. K. Rath, H. Luo, M. Nieuwenhuyzen, J. G. Knight, *Org. Lett.* **2003**, *5*, 3863; d) S. Doherty, J. K. Knight, C. Hardacre, H. Lou, C. R. Newman, R. K. Rath, S. Campbell, M. Nieuwenhuyzen, *Organometallics* **2004**, *23*, 6127.

[8] K. Mikami, Y. Yusa, K. Aikawa, M. Hatano, *Chirality* **2003**, *15*, 105.

[9] Crystal data for **3**: formula $C_{36}H_{28}Cl_2P_2Pt{\cdot}CH_2Cl_2$, monoclinic, space group $P2_1/n$, $a = 10.406(4)$, $b = 17.887(6)$, $c = 18.695(7)$ Å, $\beta = 94.096(5)°$, $V = 3470.8(21)$ Å^3, $Z = 4$, $D = 1.672$ g cm^{-3}, and $\mu = 44.52$ cm^{-1}. All measurements were made on a Rigaku Saturn CCD area detector with graphite monochromated $Mo_{K\alpha}$ radiation ($\lambda = 0.71070$ Å) at 193 K and the structure was solved by direct methods (SIR92). Of the 32323 reflections that were collected, 9997 were unique ($R_{int} = 0.082$). $R = 0.080$, $Rw = 0.171$, goodness of fit = 0.993, and shift/error = 0.008. CCDC 277173 contains the supplementary crystallographic data for this paper. These data can be obtained free of charge from The Cambridge Crystallographic Data Centre via www.ccdc.cam.ac.uk/data_request/cif.

[10] M. Ogasawara, K. Yoshida, T. Hayashi, *Organometallics* **2000**, *19*, 1567.

[11] a) M. Johannsen, K. A. Jørgensen, *J. Org. Chem.* **1995**, *60*, 5757; b) M. Johannsen, K. A. Jørgensen, *Tetrahedron* **1996**, *52*, 7321; c) S. Oi, K. Kashiwagi, E. Terada, K. Ohuchi, Y Inoue, *Tetrahedron Lett.* **1996**, *37*, 6351; d) S. Oi, E. Terada, K. Ohuchi, T. Kato, Y. Tachibana, Y. Inoue, *J. Org. Chem.* **1999**, *64*, 8660.

[12] a) K. Aikawa, S. Kainuma, M. Hatano, K. Mikami, *Tetrahedron Lett.* **2004**, *45*, 183; b) K. Mikami, K. Aikawa, S. Kainuma, Y. Kawakami, T. Saito, N. Sayo, H. Kumobayashi, *Tetrahedron: Asymmetry* **2004**, *15*, 3885.

 © 2005 Wiley-VCH Verlag GmbH & Co. KGaA, Weinheim

Carbocyclization

DOI: 10.1002/anie.200502380

Rhodium-Catalyzed Regio- and Enantioselective Intermolecular [4+2] Carbocyclization of 4-Alkynals with *N*,*N*-Dialkyl Acrylamides**

Ken Tanaka, Yuji Hagiwara, and Keiichi Noguchi*

Transition-metal-catalyzed cycloaddition is a powerful synthetic method for the construction of cyclic frameworks.[1] In particular, [4+2] cycloadditions of dienes or enynes with alkynes or alkenes have been widely examined for the construction of six-membered-ring systems.[2–4] However, [4+2] cycloadditions via cyclic acyl metal intermediates to give six-membered carbonyl compounds are rare.[5] Furthermore, although some transition-metal-catalyzed enantioselective intramolecular [4+2] cycloadditions have been reported,[3] enantioselective intermolecular [4+2] cycloaddition has not been established.

A recent report described the rhodium-catalyzed [4+2] carbocyclization of 4-alkynals with alkynes to afford cyclo-

[*] Prof. Dr. K. Tanaka, Y. Hagiwara
Department of Applied Chemistry
Graduate School of Engineering
Tokyo University of Agriculture and Technology
Koganei, Tokyo 184-8588 (Japan)
Fax: (+81) 42-388-7037
E-mail: tanaka-k@cc.tuat.ac.jp
Prof. Dr. K. Noguchi
Instrumentation Analysis Center
Tokyo University of Agriculture and Technology
Koganei, Tokyo 184-8588 (Japan)

[**] We thank Solvias AG for a gift of chiral ligands **5**, **6**, and **7** under their University Ligand Kit program. We also thank Dr. Masayuki Watanabe (JASCO Corp.) for his circular dichroism exciton chirality analysis and Professor Gregory C. Fu (Massachusetts Institute of Technology) for his helpful encouragement.

Supporting information for this article (full procedures and characterization data) is available on the WWW under http://www.angewandte.org or from the author.

WILEY InterScience DISCOVER SOMETHING GREAT
© 2005 Wiley-VCH Verlag GmbH & Co. KGaA, Weinheim

hexenones via five-membered acyl rhodium intermediates **A**, formed through the intramolecular hydroacylation of alkynes.[6] Murakami et al. also reported that similar five-membered acyl rhodium intermediates, formed by insertion of rhodium between the carbonyl carbon atom and the α-carbon atom of cyclobutanones, undergoes intramolecular reaction with alkenes to afford bicyclic cyclohexanones.[7] Herein we reveal that a cationic rhodium(I) complex of (*R*,*R*)-walphos (*R*,*R*-**7**)[8] catalyzes a highly regio- and enantioselective intermolecular [4+2] carbocyclization of 4-alkynals with *N*,*N*-dialkyl acrylamides to give enantioenriched cyclohexanones(Scheme 1).

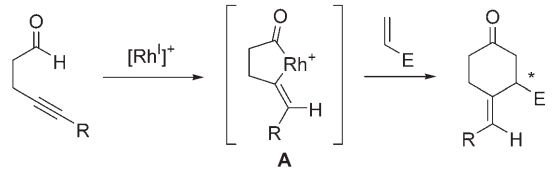

Scheme 1. Regio- and enantioselective intermolecular [4+2] carbocyclization of 4-alkynals with alkenes.

We first examined the [4+2] carbocyclization of 5-phenyl-4-pentynal (**1a**) with alkenes. After screening various alkenes and rhodium(I) complexes, we found that the reaction of **1a** with *N*,*N*-dimethylacrylamide (**2a**) in the presence of catalytic [Rh(cod)$_2$]BF$_4$/dppb furnished cyclohexanone **3aa** in low yield along with alkynyl ketone **4** (Scheme 2). On the other hand, the use of dppe as a ligand did not furnished cyclohexanone **3aa** at all.

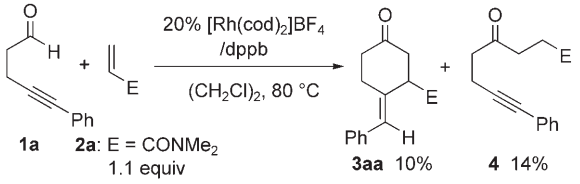

Scheme 2. [4+2] Carbocyclization of 5-phenyl-4-pentynal (**1a**) with *N*,*N*-dimethylacrylamide (**2a**).

The enantioselective [4+2] carbocyclization of **1a** with **2a** was examined with various chiral bidentate phosphine ligands (Table 1), which have large P-M-P natural bite angles to facilitate the reductive elimination step. The study revealed that the use of ligand (*R*,*R*)-**7** dramatically increased the yield and *ee* value of **3aa** (Table 1, entry 5). Although lower yield and *ee* were observed, the reaction can be carried out with a low catalyst loading of 5% (Table 1, entry 7). The reaction did not proceed at all in the presence of (*R*,*R*)-**6**, which bears a coordinating dimethylamino group (Table 1, entry 4).

A series of 5-substituted-4-pentynals **1a**–**f** was subjected to the above optimized reaction conditions (Table 2). The reactions of aryl- (Table 2, entries 1–4), alkenyl- (Table 2, entry 6), and alkyl- (Table 2, entry 7) substituted 4-pentynals with **2a** afforded the corresponding cyclohexanones in good yield with high enantioselectivity. The absolute configuration

Table 1: Screening of ligands **5**–**7** in the rhodium-catalyzed enantioselective [4+2] carbocyclization of **1a** with **2a** to give **3aa**.

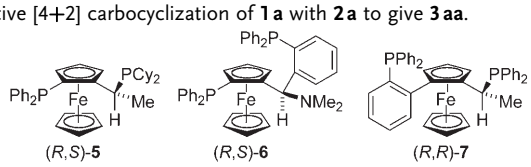

Entry	Ligand	Catalyst [%]	Yield [%]	*ee* [%]
1	(*S*,*S*)-diop	20	10[a]	37
2	(*R*)-Tol-binap	20	9[a]	2
3	(*R*,*S*)-**5**	20	15[a]	20
4	(*R*,*S*)-**6**	20	0[a]	
5	(*R*,*R*)-**7**	20	72[b]	>99
6	(*R*,*R*)-**7**	10	57[b]	>99
7	(*R*,*R*)-**7**	5	52[b]	98

[a] Yield determined by NMR spectroscopy. [b] Yields of isolated products.

Table 2: Rhodium-catalyzed enantioselective [4+2] carbocyclization of 5-substituted-4-pentynals with *N*,*N*-dialkylacrylamides.[a]

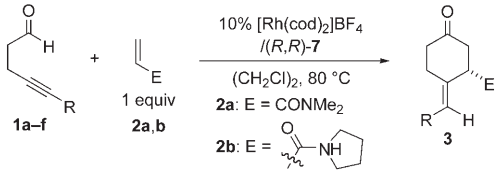

Entry	**1** (R)	Alkene	Product	Yield [%][b]	*ee* [%]
1	**a** (Ph)	**2a**	(+)-**3aa**	57	>99
2	**b** (4-MeOC$_6$H$_4$)	**2a**	(+)-**3ba**	58	>99
3	**c** (4-F$_3$CC$_6$H$_4$)	**2a**	(+)-**3ca**	51	94
4	**d** (4-ClC$_6$H$_4$)	**2a**	(+)-(*S*)-**3da**	68	>99
5	**d** (4-ClC$_6$H$_4$)	**2b**	(+)-**3db**	77	>99
6[c]	**e** (1-cyclohexenyl)	**2a**	(+)-**3ea**	50	97
7[c,d]	**f** (*n*Bu)	**2a**	(+)-(*S*)-**3fa**	77	>99

[a] No signals for other regioisomers were observed in the ^{1}H NMR spectra. The *ee* values were determined by chiral HPLC and GC analysis. [b] Yields of isolated products. [c] Catalyst: 20%. [d] Temperature: 40°C.

of (+)-**3da** was determined to be *S* by an anomalous dispersion method (Figure 1),[9] and that of (+)-**3fa** was determined to be *S* by the circular dichroism exciton chirality method.

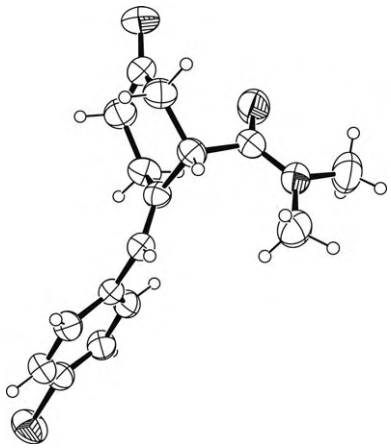

Figure 1. ORTEP diagram of (*S*)-(+)-**3da**. Ellipsoids drawn at the 50% probability level.

 © 2005 Wiley-VCH Verlag GmbH & Co. KGaA, Weinheim

The enantioselective [4+2] carbocyclization of 2-alkynyl benzaldehydes **1g–k** with **2a** was investigated next (Table 3). Aryl- (Table 3, entries 1 and 3), alkenyl- (Table 3, entry 4), and alkyl- (Table 3, entries 5 and 6) substituted 2-ethynyl-

Table 3: Rhodium-catalyzed enantioselective [4+2] carbocyclization of 2-alkynylbenzaldehydes with *N*,*N*-dialkylacrylamides.[a]

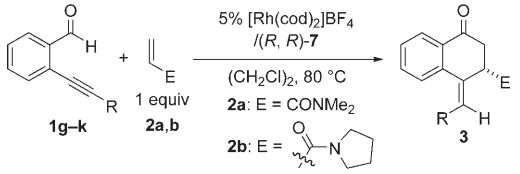

Entry	**1** (R)	Alkene	Product	Yield [%][b]	*ee* [%]
1	**g** (Ph)	**2a**	(+)-**3ga**	80	97
2	**g** (Ph)	**2b**	(+)-**3gb**	80	97
3	**h** (2-ClC_6H_4)	**2a**	(+)-**3ha**	94	90
4	**i** (1-cyclohexenyl)	**2a**	(+)-**3ia**	56	99
5	**j** (*n*Bu)	**2a**	(+)-**3ja**	56	>99
6	**k** ($Cl(CH_2)_3$)	**2a**	(+)-**3ka**	81	97

[a] No signals for other regioisomers were observed in the ^{1}H NMR spectra. The *ee* values were determined by chiral HPLC analysis. [b] Yields of isolated products.

benzaldehydes afforded the corresponding cyclohexanones in good yield with high enantioselectivity. Not only *N*,*N*-dimethylacrylamide (**2a**), but also *N*-acryloylpyrrolidine (**2b**) can be employed (Table 2, entry 5 and Table 3, entry 2).[10] In general, the reactions of 2-alkynylbenzaldehydes **1g–k** are more facile than those of 5-substituted-4-pentynals **1a–f**, which allows a lower catalyst loading. Because the [4+2] carbocyclization of 2-alkynyl benzaldehydes with alkynes did not proceed at all, this successful [4+2] carbocyclization of 2-alkynyl benzaldehydes with *N*,*N*-dialkylacrylamides is noteworthy. Importantly, these [4+2] carbocyclizations of 4-alkynals **1a–k** with **2a**,**b** are highly regioselective and no regioisomers were detected in the crude reaction mixtures.[11]

Scheme 3 shows a plausible mechanism for this carbocyclization. We infer that the rhodium catalyst oxidatively inserts into the aldehyde C–H bond to afford a rhodium acyl hydride **B**. The *cis* addition of the rhodium hydride species to the metal-bound alkyne then provides the five-membered acyl rhodium intermediate **A**.[12] Complexation of the alkene is followed by insertion to form metallacycle **C**. Reductive elimination furnishes the cyclohexanone **3** and regenerates the Rh catalyst. On the other hand, β-hydride elimination from metallacycle **C** can furnish the alkynyl ketone **4**. Alternatively, carbometalation of intermediate **B** with the alkene prior to hydrometalation can also furnish **4**.

In conclusion, we have developed a rhodium-catalyzed regio- and enantioselective intermolecular [4+2] carbocyclization of 4-alkynals with *N*,*N*-dialkylacrylamides. This method serves as an attractive new route to enantioenriched cyclohexanones in view of the one-step access to 4-alkynals from readily available terminal alkynes (1,4-addition to acrolein or Sonogashira coupling with 2-bromobenzaldehyde).

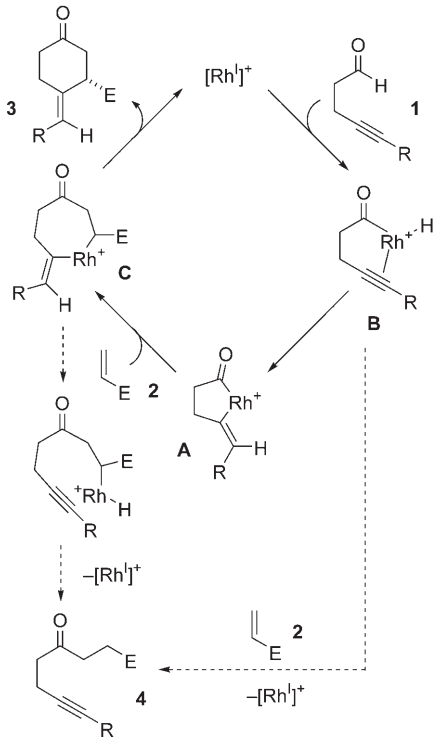

Scheme 3. Plausible mechanism for the rhodium-catalyzed [4+2] carbocyclization of 4-alkynals with *N*,*N*-dialkylacrylamides.

Experimental Section

Representative procedure (Table 3, entry 1): Under an Ar atmosphere, a solution of (*R*,*R*)-**7** (9.9 mg, 0.015 mmol) in CH_2Cl_2 (1.0 mL) was added to a solution of $[Rh(cod)_2]BF_4$ (6.6 mg, 0.015 mmol) in CH_2Cl_2 (1.0 mL) at room temperature, and the mixture was stirred for 5 min. H_2 was introduced to the resulting solution in a Schlenk tube. The mixture was stirred at room temperature for 0.5 h, and the resulting solution was concentrated to dryness. Benzaldehyde **1g** (61.9 mg, 0.300 mmol) and **2a** (29.7 mg, 0.300 mmol) were added to the residue by using $(CH_2Cl)_2$ (1.5 mL). The mixture was stirred at 80 °C for 20 h. The resulting solution was concentrated and purified by preparative TLC (hexane/EtOAc 1:4) to furnish (+)-**3ga** (73.3 mg, 0.240 mmol, 80 % yield, 97 % *ee*) as an orange solid. M.p. 56–58 °C; $[\alpha]_D^{25}$ +201.0° (acetone, *c* 1.534; 97 % *ee*); IR (neat): $\tilde{\nu}$ = 2930, 1680, 1630, 1600, 1445, 1400, 1282, 1240, 1142, 772, 758, 730, 700 cm^{-1}; ^{1}H NMR ($CDCl_3$, 300 MHz) δ = 8.12–8.02 (m, 1H), 7.37–7.28 (m, 1H), 7.27–7.07 (m, 7H), 6.67 (s, 1H), 4.04 (dd, *J* = 6.9 and 4.5 Hz, 1H), 3.25 (dd, *J* = 17.4 and 6.9 Hz, 1H), 3.20 (s, 3H), 2.94 (s, 3H), 2.87 ppm (dd, *J* = 17.4 and 4.5 Hz, 1H); ^{13}C NMR ($CDCl_3$, 75 MHz) δ = 196.2, 170.2, 137.5, 136.1, 134.1, 133.2, 132.2, 129.1, 128.9, 128.7, 128.5, 128.3, 127.5, 126.7, 48.7, 43.1, 37.6, 36.0 ppm; HRMS (EI): calcd for $C_{17}H_{13}O$ [*M*–$CONMe_2$]$^+$: 233.0967; found; 233.0984; HPLC: t_R = 18.3 min (major isomer) and 22.7 min (minor isomer) (CHIRALPAK AD, hexane/*i*PrOH 90:10, 1.0 mL min^{-1})

Received: July 8, 2005
Revised: September 7, 2005
Published online: October 18, 2005

Keywords: aldehydes · alkynes · asymmetric catalysis · carbocyclization · cyclohexanones · rhodium

 © 2005 Wiley-VCH Verlag GmbH & Co. KGaA, Weinheim

[1] For reviews of transition-metal-catalyzed cycloadditions, see: a) I. Ojima, M. Tzamarioudaki, Z. Li, R. J. Donovan, *Chem. Rev.* **1996**, *96*, 635 – 662; b) M. Lautens, W. Klute, W. Tam, *Chem. Rev.* **1996**, *96*, 49 – 92; c) J. E. Robinson in *Modern Rhodium-Catalyzed Organic Reactions* (Ed.: P. A. Evans), Wiley-VCH, **2005**, p. 241.

[2] For transition-metal-catalyzed intramolecular [4+2] cycloadditions, see: Rh: a) D. Motoda, H. Kinoshita, H. Shinokubo, K. Oshima, *Angew. Chem.* **2004**, *116*, 1896 – 1898; *Angew. Chem. Int. Ed.* **2004**, *43*, 1860 – 1862; b) B. Wang, P. Cao, X. Zhang, *Tetrahedron Lett.* **2000**, *41*, 8041 – 8044; c) S. R. Gilbertson, G. S. Hoge, *Tetrahedron Lett.* **1998**, *39*, 2075 – 2078; d) P. A. Wender, T. E. Jenkins, S. Suzuki, *J. Am. Chem. Soc.* **1995**, *117*, 1843 – 1844; e) R. S. Jolly, G. Luedtke, D. Sheehan, T. Livinghouse, *J. Am. Chem. Soc.* **1990**, *112*, 4965 – 4966; Ni: f) P. A. Wender, T. E. Smith, *J. Org. Chem.* **1996**, *61*, 824 – 825; g) P. A. Wender, T. E. Smith, *J. Org. Chem.* **1995**, *60*, 2962 – 2963; h) P. A. Wender, T. E. Jenkins, *J. Am. Chem. Soc.* **1989**, *111*, 6432 – 6434; Pd: i) J. R. Dunetz, R. L. Danheiser, *J. Am. Chem. Soc.* **2005**, *127*, 5776 – 5777; j) L. J. van Boxtel, S. Körbe, M. Noltemeyer, A. de Meijere, *Eur. J. Org. Chem.* **2001**, 2283 – 2292; k) K. Kumar, R. Jolly, *Tetrahedron Lett.* **1998**, *39*, 3047 – 3048; l) M. Murakami, K. Itami, Y. Ito, *J. Am. Chem. Soc.* **1997**, *119*, 7163 – 7164; m) T. Mandai, S. Suzuki, A. Ikawa, T. Murakami, M. Kawada, J. Tsuji, *Tetrahedron Lett.* **1991**, *32*, 7687 – 7688.

[3] For transition-metal-catalyzed enantioselective intramolecular [4+2] cycloadditions, see: a) T. Shibata, K. Takasaku, Y. Takesue, N. Hirata, K. Takagi, *Synlett* **2002**, 1681 – 1682; b) H. Heath, B. Wolfe, T. Livinghouse, S. K. Bae, *Synthesis* **2001**, 2341 – 2347; c) S. R. Gilbertson, G. S. Hoge, D. G. Genov, *J. Org. Chem.* **1998**, *63*, 10077 – 10080; d) D. J. R. O'Mahony, D. B. Belanger, T. Livinghouse, *Synlett* **1998**, 443 – 445; e) L. Mckinstry, T. Livinghouse, *Tetrahedron* **1994**, *50*, 6145 – 6154.

[4] For transition-metal-catalyzed intermolecular [4+2] cycloadditions, see: a) S.-J. Paik, S. U. Son, Y. K. Chung, *Org. Lett.* **1999**, *1*, 2045 – 2047; b) I. Matsuda, M. Shibata, S. Sato, Y. Izumi, *Tetrahedron Lett.* **1987**, *28*, 3361 – 3362; c) K. Mach, H. Antropiusovä, L. Petrusovä, F. Turecek, V. Hanus, *J. Organomet. Chem.* **1985**, *289*, 331 – 339; d) H. tom Dieck, R. Diercks, *Angew. Chem.* **1983**, *95*, 801 – 802; *Angew. Chem. Int. Ed. Engl.* **1983**, *22*, 778 – 779.

[5] For the synthesis of quinones through the reactions of maleoyl cobalt complexes with alkynes, see: a) S. Iyer, L. S. Liebeskind, *J. Am. Chem. Soc.* **1987**, *109*, 2759 – 2770; b) L. S. Liebeskind, S. L. Baysdon, V. Goedken, R. Chidambaram, *Organometallics* **1986**, *5*, 1086 – 1092; c) L. S. Liebeskind, J. P. Leeds, S. L. Baysdon, S. Iyer, *J. Am. Chem. Soc.* **1984**, *106*, 6451 – 6453.

[6] K. Tanaka, G. C. Fu, *Org. Lett.* **2002**, *4*, 933 – 935.

[7] M. Murakami, T. Itahashi, Y. Ito, *J. Am. Chem. Soc.* **2002**, *124*, 13976 – 13977.

[8] T. Sturm, W. Weissensteiner, F. Spindler, *Adv. Synth. Catal.* **2003**, *345*, 160 – 164.

[9] CCDC-277585 (**3da**) contains the supplementary crystallographic data for this paper. These data can be obtained free of charge from The Cambridge Crystallographic Data Centre via www.ccdc.cam.ac.uk/data_request/cif.

[10] The use of substituted *N*,*N*-dialkyl acrylamides (*N*,*N*-dimethylmethacrylamide, 1-pyrrolidinylpropenone, *N*-methylmaleimide) did not afford the desired carbocyclization products.

[11] In the case of the reactions of **1a–k** with Rh^{I}–(*R*,*R*)-walphos, no vinyl protons other than those for the desired cyclohexanones **3** were observed by ^{1}H NMR spectroscopic analysis of the crude reaction mixtures. Although we examined a wide variety of phosphine ligands, the other regioisomer derived from **1a** and **2a** was not obtained at all. On the other hand, the other regioisomer derived from **1g** and **2a** was isolated in trace amounts when using Rh^{I}–dppb. The desired major regioisomer **3ga** and the minor regioisomer can easily be distinguished by the ^{1}H NMR chemical shifts of their vinyl protons (major isomer: $\delta =$ 6.68 ppm (s), minor isomer: $\delta = 6.78$ ppm (d, $J = 1.2$ Hz)).

[12] K. Tanaka, G. C. Fu, *Angew. Chem.* **2002**, *114*, 1677 – 1679; *Angew. Chem. Int. Ed.* **2002**, *41*, 1607 – 1609.

 © 2005 Wiley-VCH Verlag GmbH & Co. KGaA, Weinheim

Computational Chemistry

DOI: 10.1002/anie.200502272

Architecture and Evolution of Organic Chemistry**

*Marcin Fialkowski, Kyle J. M. Bishop, Victor A. Chubukov, Christopher J. Campbell, and Bartosz A. Grzybowski**

For almost two centuries, chemists all over the world have applied their expertise and creativity[1–5] to the synthesis of new molecules. Since each individual chemist—or a collaborating group of chemists—tries to select unique synthetic targets[6–9] and come up with a maximally original and/or efficient method of making them, it might appear that the activities of such independent "agents" should be largely uncorrelated, and that no generalizations about the evolution of chemistry *en large* could be made. As we show here, however, there exist several statistical laws that describe how molecules are made and interconverted. We analyze organic synthesis at the level of an abstract network representation whereby molecules correspond to nodes characterized by molecular masses, and reactions to directed edges connecting these nodes (Figure 1a). We show, among others, that the connections between the nodes form a time-evolving scale free network[10–14] of structure similar to that of the world wide web (WWW),[12,15,16] and that masses of molecules in this network are governed by a single stochastic process.[17,18] Aside from fundamental interest, the trends we identify allow making predictions of potential economical impact for the chemical industry, for example, how many molecules will be synthesized in the future, molecules of which molecular

[*] Dr. M. Fialkowski, K. J. M. Bishop, V. A. Chubukov, C. J. Campbell, Prof. Dr. B. A. Grzybowski
Department of Chemical and Biological Engineering and Northwestern Institute of Complexity
Northwestern University
2145 Sheridan Road, Evanston, IL 60208 (USA)
Fax: (+1) 847-491-3728
E-mail: grzybor@northwestern.edu

[**] B.A.G. gratefully acknowledges financial support from the Camille and Henry Dreyfus New Faculty Awards Program. K.J.M.B. and C.J.C. were supported in part by the NSF-IGERT program "Dynamics of Complex Systems in Science and Engineering" (DGE-9987577).

Supporting information for this article is available on the WWW under http://www.angewandte.org or from the author.

© 2005 Wiley-VCH Verlag GmbH & Co. KGaA, Weinheim

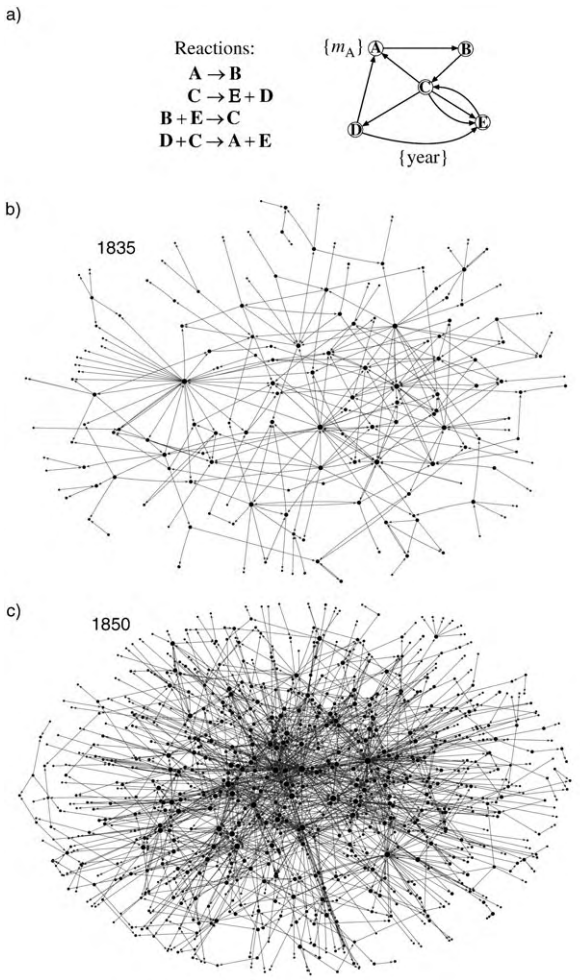

Figure 1. a) Illustration of the conversion of a collection of chemical reactions into a directed-graph (network) representation. Chemical compounds **A**–**E** correspond to the nodes of the network characterized by molecular masses, *m*. Directed edges are assigned for a given reaction by connecting all reactants to all products. The connectivity of each node is described by the number of incoming arrows, k_{in} (e.g., $k_{in}(C) = 2$), and the number of outgoing arrows, k_{out} (e.g., $k_{out}(C) = 4$). The edges are characterized by the earliest publication date of the corresponding reaction. Note that multiple edges—of the same or different directions—can connect two nodes if these nodes are involved in more than one chemical reaction (e.g., **C** and **E** above). b) Visual representation of the giant connected component (GCC)—that is, the largest subset of nodes that are connected to each other—of the organic-chemistry network in 1835. This network contains only 176 compounds; the size of a node corresponds to its total connectivity. Note the scale-free architecture in which most nodes connect to others through highly connected "hub" molecules. c) The GCC in 1850 contains 867 compounds. While the scale-free architecture remains unchanged, the complexity of the network has increased substantially within the elapsed 15 years. One can only imagine the network of organic chemistry in 2004, which contains approximately six million compounds! (The graphs were created using Pajek, a freely available software package for the visualization of large networks.)

masses are more likely to be made or used as substrates, how the network connectivities can be used to assess a molecule's industrial importance, and how the equation describing evolution of masses could help in designing fragment libraries for combinatorial chemistry.

Analysis was performed on data stored in the Beilstein database (BD),[19] which is the largest repository of organic reactions, containing (up to April 2004) 9550398 chemical substances and 9293250 reactions in which these substances participate. In choosing BD, we adopted its well-established criterion for the classification of chemical substances as "organic" and its comprehensive coverage of the chemical literature dating back to 1779 (see the Supporting Information and reference [19] for details of BD). Although we stress that BD is not without omissions, it provides the single, most-complete description of organic chemistry and its evolution. Therefore, it seems reasonable to assume that statistical laws derived from data described therein are indeed representative of organic chemistry in general, and we present them as such.

In the translation of organic synthesis into a network of chemical connectivity, each node represented a chemical compound characterized by its molecular mass (99.7% of the compounds had mass data). Substances that participated in no reactions or acted only as catalysts or solvents were excluded from the network, thereby decreasing the number of "active" nodes to 5957807. Reactions between these chemicals were used to assign directed edges, each characterized by the year in which the reaction was published (99.7% of the reactions had date information). Duplicate reactions—that is, reactions with identical reactants and products—were considered only once and characterized by the date of the earliest reaction. Reactions that lacked either reactants or products (that is, "half reactions") were not included in the network. Stoichiometry and reaction yields were not considered, as they were reported for only a few percent of database entries. After parsing, the total number of reactions was decreased to 6539158. In the conversion of the set of chemical reactions into a directed network, all reactants were connected to all products by directed edges, as illustrated in Figure 1a (see Supporting Information).

The starting point of our analysis was 1850, and since then both the numbers of molecules and the numbers of chemical reactions have increased exponentially. The corresponding growth rates were constant within time periods up to the beginning of the twentieth century ($r_m = 0.083\ \text{year}^{-1}$ for molecules and $r_r = 0.087\ \text{year}^{-1}$ for reactions) and afterwards ($r_m = 0.044\ \text{year}^{-1}$ and $r_r = 0.038\ \text{year}^{-1}$; Figure 2a). At the same time, the average connectivity between molecules (Figure 2b)—defined as the number of edges divided by the number of nodes—initially increased, reached a maximum by about 1885, and then steadily decreased to the value of approximately 2 in 2004. It appears that the early days of chemistry were dominated by "wiring" existing molecules (presumably, to perfect/optimize known synthetic methodologies); when these methodologies matured, exploration of unknown structural space became a dominant activity.

To establish the topological characteristics of the expanding network of chemical reactions, we analyzed distributions of the numbers of connections outgoing from a given node, k_{out} (i.e., the number of times a given molecule was used as a reaction substrate), and the number of connections incoming to a given node, k_{in} (i.e., the number of times a molecule was obtained as a reaction product). As shown in Figure 2c, the distributions of both $p(k_{out})$ and $p(k_{in})$ decay algebraically

 © 2005 Wiley-VCH Verlag GmbH & Co. KGaA, Weinheim

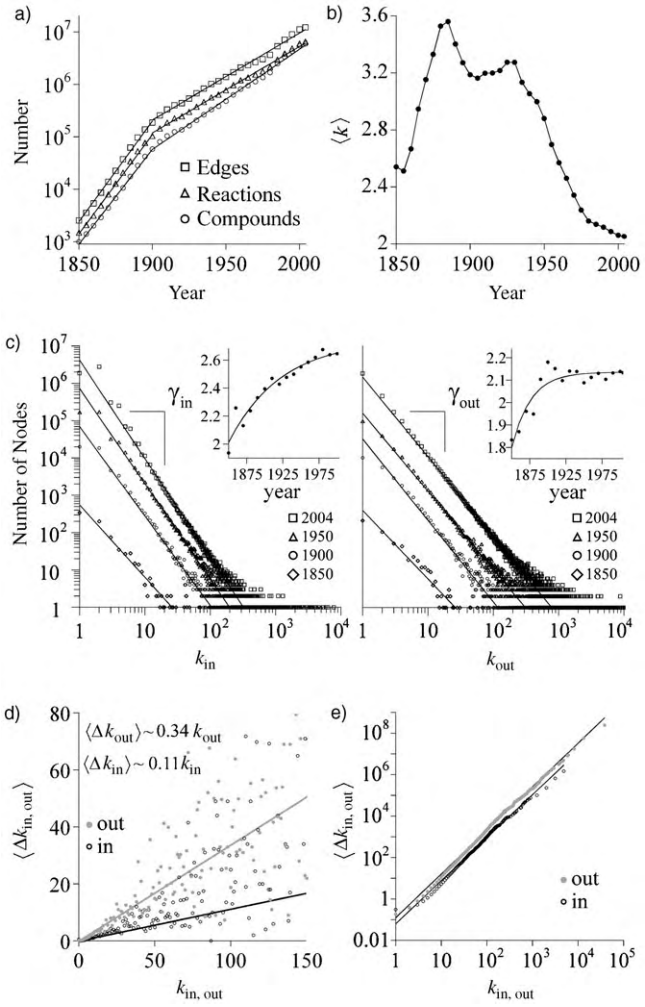

Figure 2. a) The number of chemical compounds, reactions, and graph edges as a function of time. Although all three grow exponentially with time, the rate of growth changes near the turn of the twentieth century. b) Average connectivity (degree)—defined as the number of edges divided by the number of nodes—as a function of time. In the nineteenth century, chemistry focused on "rewiring" existing compounds, whereas in the twentieth century, it has been dominated by the synthesis of new compounds. c) In- and out-degree distributions of molecules that comprise the chemistry network obey a power law $p(k) = k^{-\gamma}$ characteristic of scale-free networks. From 1850 to 2004, the power-law exponents γ_{in} and γ_{out} (inserts) have been steadily growing and approach constant values of approximately 2.7 and 2.1, respectively. d) Evolution of the chemistry network is governed by a "two-way" (i.e., both "in" and "out") mechanism of preferential attachment. The plots show the average increase in connectivities of one million random nodes from 1990 to 2000. The "strength" of preferential attachment (measured by the slope of the linear fit, $d\langle\Delta k\rangle/dk$) is approximately three times greater for out than for in connectivities. This helps to explain why the power-law exponent γ_{out} is smaller than γ_{in} and indicates that highly connected substrates are more likely to be found than highly connected products. e) The corresponding cumulative distribution for preferential attachment defined as $\kappa(k) = \sum_{k_i=0}^{k} \langle\Delta k_i\rangle$. The distribution follows a power law $\kappa(k) = k^{\sigma}$, where $\sigma \approx 2.1$ for both the in and out distributions, which implies that the preferential attachment distribution plotted in (e) is indeed linear ($\langle\Delta k\rangle \propto k^{\sigma-1} \approx k$).

with the number of connections, $p(k) \sim k^{-\gamma}$, and the γ exponents for both in and out distributions increase with time (measured in years) approximately as $\gamma_{in}(t) = 2.67[1-\exp(-(t-1780)/52.4)]$ and $\gamma_{out}(t) = 2.14[1-\exp(-(t-1780)/36.2)]$. Interestingly, the values these exponents asymptotically approach ($\gamma_{in} = 2.67$ and $\gamma_{out} = 2.14$) are similar to those that characterize the directed network of the WWW (2.71 and 2.1, respectively), thus suggesting that the network of chemistry and the WWW have similar topologies (although the latter is more highly connected; $\langle k\rangle = 7.5$ for the WWW in 2000 vs $\langle k\rangle = 2.1$ for chemistry in the same year).[16]

The observed power-law dependencies indicate that organic reactions—like the WWW,[12,15,16] the internet,[20] metabolic networks,[21] and even societies[22,23]—form a scale-free network,[10] whose architecture is distinguished by the presence of highly connected "hubs." These hub molecules of organic chemistry are directly analogous to those found in the scale-free network of the airline system in which they facilitate transportation from one poorly connected airport to another. Likewise, the synthesis of one molecule in organic chemistry from another by a series of chemical transformations will likely utilize one of these versatile hub compounds as an intermediate (as we shall see later, this also has an added economic advantage, since hub compounds are significantly less expensive than poorly connected ones).

The presence of a scale-free topology also provides evidence as to the mechanism by which the network evolves over time. Specifically, the connectivities of organic molecules evolve according to a two-way mechanism of preferential attachment (i.e., both in and out connections), which stipulates that well-connected substances are more likely to participate in new reactions than poorly connected compounds. We verified this mechanism directly, by analyzing how the connectivities of one million randomly chosen nodes changed over time. We found that the average increase in both in or out connectivities over a given time period was proportional to their values at the beginning of this period ($\langle\Delta k_{in,out}\rangle \propto k_{in,out}$; see Figure 2d,e). This result means that 1) the more times a molecule has been used as a synthetic substrate (i.e., large k_{out} value), the higher the chances that it will be used again in the future; 2) conversely, the higher its k_{in} value, the more likely that chemists will try to make it by a new reaction. Interestingly, this mechanism also implies that the evolution of a molecule's usefulness—measured by its participation in new reactions—increases exponentially over time. Therefore, highly connected compounds create exponential "explosions," thus leading to the formation of preferred substrates and target molecules (the "hubs") in organic chemistry.

The fact that the exponent characterizing outgoing connections, γ_{out}, is smaller than that characterizing incoming ones, γ_{in}, indicates (see Figure 2c) that the most connected hubs of the chemistry network have on average more outgoing than incoming connections—the most-connected molecules are usually used as synthetic substrates. At the same time, as chemistry develops, the degree of correlation between in and out connectivities of the molecules increases from $R(k_{out},k_{in}) = 0.327$ in 1850 to 0.571 in 2004 (see Support-

 © 2005 Wiley-VCH Verlag GmbH & Co. KGaA, Weinheim

ing Information). The rationale for this trend is that the more useful a compound is as a synthetic substrate, the more ways are designed to prepare it (presumably, in an effort to maximize yields and minimize reaction costs); conversely, the more synthetic recipes exist for making a compound, the more available it becomes and can be used for further syntheses.

Information about the molecular masses (henceforth, simply "masses" or m) of the network's nodes (i.e., molecules) provides an additional source of information about its evolution. While mass is the simplest of the possible molecular descriptors, it was chosen because it was readily available from the database and because it correlated with several other scalar descriptors (e.g., molecular volume[24,25] or structural complexity factor[26,27] of organic molecules).

Figure 3a,b shows the frequency distribution of masses that were used as substrates ($g_{out}(m,t)$; left) and products ($g_{in}(m,t)$; right) in reactions reported between 1850 and 2004. The most commonly used substrates are those near $m = 150\,g\,mol^{-1}$ and the most common products near $m = 250\,g\,mol^{-1}$. Importantly, the shapes of both distributions and the locations of their maxima do not change with time but only shift upwards according to $g_{in,out}(m,t) = \theta_{in,out}(t)\,g^{*}_{in,out}(m)$, where $g^{*}_{in,out}(m)$ are "master" distributions (here, in 1850) and $\theta_{in,out}(t) = N_0^{in,out}\exp((t-t_0)/\tau_{in,out})$ are the propagating/scaling functions ($t_0 = 1850$, $N_0^{in} = 5910.1$, $N_0^{out} = 4869.0$, $\tau_{in} = 19.34$, $\tau_{out} = 19.07$)). These results show that the masses of the most popular substrates and products have not significantly changed for 150 years; moreover, these masses *will remain* the most popular in the future, as they correspond to the most rapidly connecting nodes of the network.

Abundances of molecules depend on their masses. Figure 3c shows the $M(m,t{=}2004)$ mass distribution of all nodes in the network. Aside from an obvious overall trend (few very small and very large molecules), the curve exhibits pronounced "high-frequency" oscillations. The Fourier spectrum of the distribution (Figure 3c, insert) shows a dominant, sharp peak at 2 and a broader peak centered at 14–15. The former indicates that there are significantly more molecules (indeed, by $\approx 48\,\%$) of even than of odd masses; the latter corresponds to the masses of the most common chemical "building blocks" (e.g., CH_2, CH_3, OH, NH_2, etc.) from which molecules are made.

More detailed, time-dependent analysis of $M(m,t)$ distributions (Figure 3d) reveals that chemists create molecules according to a single stochastic process. When plotted on a log–log scale (Figure 3e), the $M(m,t)$ curves for $t = 1850$–2004: 1) are log-normal for the majority ($> 90\,\%$) of masses around the peak; 2) decay algebraically, $M(m,t) \sim m^{-\beta}$ with the exponent $\beta \approx 4$, for $m > 800$; and 3) exhibit a characteristic "shoulder" for $m < 50$. Since 1850, the average mass increased from 200 to 350 (2004)

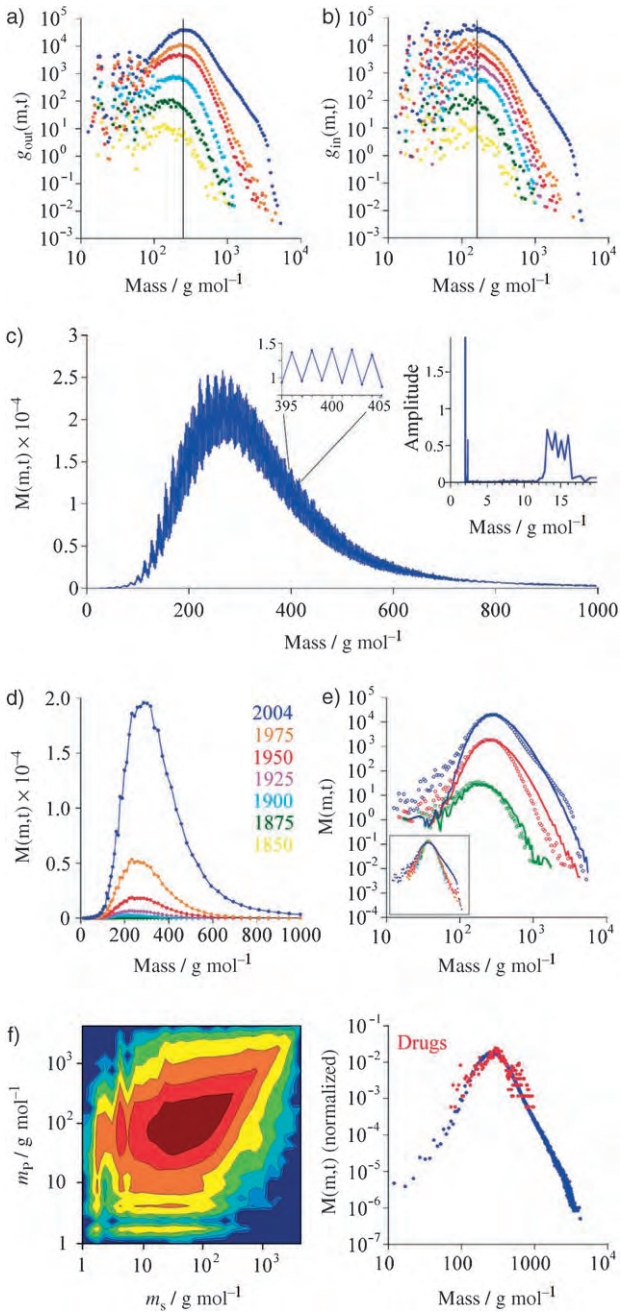

Figure 3. Frequency distributions of masses that were used as a) substrates ($g_{out}(m,t)$) and b) products ($g_{in}(m,t)$) in reactions reported in 25-year intervals between 1850 and 2004. Specifically, the substrate- and product-mass distributions were found by calculating the statistics of all masses weighted by k_{out} and k_{in}, respectively. c) Distribution of masses, $M(m,t)$, of all molecules in the chemistry network as of 2004. The zoom-in illustrates periodic variation in the abundances of molecules with even and odd masses. The insert is a Fourier spectrum of the $M(m,t)$ distribution. d) Evolution of mass distributions with time. All $M(m,t)$ curves are plotted against masses binned into $m = 2$ intervals; this binning removes high-frequency oscillations and simplifies calculations but does not, as we verified, affect the generality of the results. e) The lines in this log–log plot correspond to the theoretical mass distributions for 1875 (green), 1950 (red), and 2004 (blue) propagated from the initial distribution in 1850 according to the master equation; these simulated curves agree with the Beilstein data (points). The characteristic shape of the distributions indicates that molecules are created by a stochastic Kesten process. Insert: Mass distributions overlap when rescaled[20] with respect to the location of the peak and the total number of molecules. f) Correlation between masses of substrates m_S and products m_P based on all reactions stored in the database. g) Log–log plot of normalized mass distributions of all compounds stored in Beilstein (blue) and 1382 most important drugs (red). The two distributions are nearly identical with the goodness-of-fit $R^2 = 0.779$ (for which the Beilstein data is taken as the reference distribution).

 © 2005 Wiley-VCH Verlag GmbH & Co. KGaA, Weinheim

according to $\langle m(t)\rangle = m_{fin}[1-\exp((t-1780)/\tau)]$, where $m_{fin} = 356.55\ g\,mol^{-1}$ and $\tau = 94.7$, and, as mentioned previously, the total number of masses (i.e., of molecules) increased exponentially with time. Importantly, when the $M(m,t)$ distributions for different times were rescaled,[28] they collapsed onto a single master curve (Figure 3e, insert).

The shapes and scaling properties of the mass distributions indicate that they evolve according to a Kesten-type mechanism,[17,18,29] in which new masses are created according to the multiplicative-additive master equation $m_{t+1} = \lambda_t m_t + \alpha_t$, where index t has a meaning of time. Briefly, at each update (i.e., time step), every molecule from a currently existing distribution $M(m,t)$ is used with equal, constant probability p_0 to generate a new molecule whose mass is prescribed by the master equation. The value of p_0 is determined by the "experimental" growth rate of the total number of molecules—$p_0 = \ln(N(2004)/N(1850))/n$, where n is the number of distribution updates simulated between 1850 and 2004—and sets the relationship between t and the real time. The number of updates, T, that correspond to one year is $T = 154/n$. After the update, both the "old" and the newly created masses are retained in a distribution $M(m,t+1)$, thus accounting for the increase in the number of molecules with time.[30] When stochastic (i.e., random) variables λ and α were sampled from uniform distributions (whose bounds—$\lambda_{min} = 0.9$, $\lambda_{max} = 1.091$ and $\alpha_{min} = 0$, $\alpha_{max} = 5.0$—were determined by fitting the mass distribution in year 2004), the master equation propagated experimental mass distributions faithfully; at every instant of time, these distributions were given by $M(m,t) = M(m,0)/(1+p_0)^t + p_0 \sum_{i=0}^{t-1} (1+p_0)^{i-t}\,\delta(m,i)$, where $M(m,0)$ is the initial mass distribution and $\delta(m,i)$ denotes the distribution of masses derived from $M(m,i-1)$ in the ith update.

Although the identified stochastic process reflects the fundamental statistical dependence between the masses of the substrates m_s and the products m_p in the network $m_p = a m_s + b$ (Figure 3f),[31] its practical significance goes well beyond this simple correlation. Because molecular masses evolve according to the master equation from the very inception of modern chemistry—irrespective of any prevalent "trends of the day" and constant progress in synthetic methodologies—this equation can be extrapolated into the future. In other words, it can be used to *predict* what masses (and with what probabilities) will be obtained in any reaction or set of reactions to be carried out.

Two important generalizations follow: First, the master equation indicates that very large and very small molecules are hard to make.[32] When large substrates are used, the multiplicative term dominates to give a product of a smaller mass; conversely, for small substrates, the additive term increases the mass. Beyond this common-sense result, the master equation provides quantitative information in the form of probabilities, which give an estimate of *how difficult* it is to make a molecule of a given mass. We stress that these observations should be understood only in a statistical sense and by no means exclude the possibility of the preparation of any particular small/large molecules. Second, the knowledge of the stochastic process that governs the generation of masses can be used to predict the outcomes of parallel (combinatorial) syntheses. Making a reasonable assumption that such syntheses are based on standard chemical transformations (i.e., likely described in BD), it is expected that the masses of the initial collections of fragments should evolve according to the master equation. This property could be used in designing fragment libraries[33,34] that would evolve into a desirable, final distribution of masses after a specified (and, hopefully, minimal) number of synthetic steps. An example of such an analysis for three potential libraries is illustrated in Figure 4a and further discussed in the Supporting Information.

One of the most prominent areas in which such desirable mass distributions are sought is in drug design—where it is widely believed that masses of druggable substances differ statistically from those of random ones.[35–37] Our analysis, however, reveals (Figure 3g) that this belief is unfounded and that most important drugs[38] have a mass distribution virtually identical to that of all chemicals stored in Beilstein. Whether this is a result of drugs being discovered by random sampling from the pool of existing substances or of synthetic limitations imposed by the master equation (see below) eventually leading to a log-normal distribution is an interesting, albeit speculative, question.

Unlike molecular mass, the network connectivity of a chemical is a valuable descriptor of its pharmacological or economic importance. As we have already suggested, it is reasonable to expect that for the most useful compounds, the number of ways in which they can be used should correlate with the number of ways in which they can be prepared. Indeed, for the 1382 most important drugs[38] and the top 300 most important industrial chemicals,[39] the correlations between k_{in} and k_{out} values are not only higher ($R \approx 0.6$) than for randomly chosen compounds, but are also historically persistent, as illustrated in Figure 4a, which shows time "trajectories" of these important substances in the $\ln(k_{in})$ versus $\ln(k_{out})$ plane. Their trajectories are long, highly focused, and linear—in sharp contradistinction to short and curvilinear paths traced by randomly chosen compounds. In other words, by looking at a historical evolution of the connectivity of a substance, one can make inferences about its industrial significance. In practice, this significance is often measured in monetary terms, and the prices of chemicals should be dictated by their uniqueness (here, measured by k_{in}, the known ways of preparing a chemical) and by the existing demand (measured by k_{out}, the number of reactions/chemists that use them). As expected, the prices per mole of the top 300 chemicals correlate well (Figure 4b) with these economic indicators and obey a power law of the form $\text{Cost} \propto k_{in,out}^{-\nu}$; the price of a chemical rapidly decreases with both k_{in} and k_{out}.

Of course, this and other trends we identified are only the first attempt to explore the richness of information contained in the history of chemistry. Although additional theoretical analyses can be envisioned with the Beilstein repository (e.g., network's centrality, diameter, shortest paths, aspects of molecular chirality and other structural descriptors, etc.), the unraveling of more economy-oriented trends will likely require the use of databases that report reaction stoichiometries, yields, and costs. Also, it would be interesting to see what

 © 2005 Wiley-VCH Verlag GmbH & Co. KGaA, Weinheim

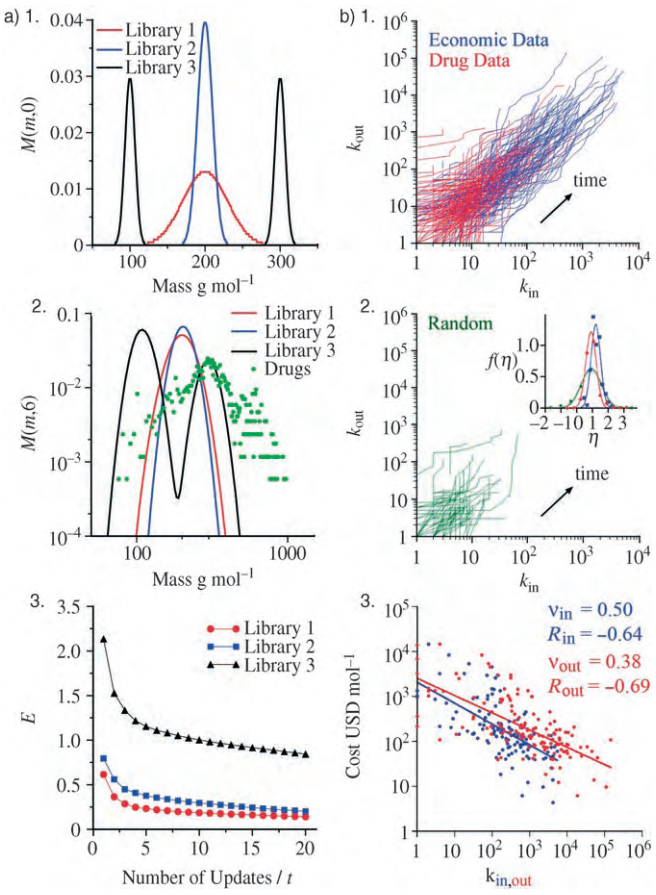

Figure 4. a) 1. Evolution of three initial "fragment libraries" in the realistic range of $m = 100$–300 simulated by the master equation. Libraries 1 and 2 represent normal distributions of masses centered at $m = 200\ g\,mol^{-1}$, and characterized by dispersions $\sigma_M = 30$ and $\sigma_M = 10\ g\,mol^{-1}$, respectively. The third library is a sum of two normal distributions of masses centered at $m = 100$ and $300\ g\,mol^{-1}$ and characterized by the same dispersion $\sigma_M = 7\ g\,mol^{-1}$. 2. Distributions obtained from the three initial "fragment libraries" after 6 updates. The target distribution of masses of 1382 most important drugs is also shown. 3. The average error coefficient, E, which measures similarity between the distributions ($E = 0$ if they are identical) obtained from Libraries 1, 2, and 3 and the target distribution of drugs plotted as a function of synthetic generations (i.e., the number of updates). The broadly distributed Library 1 converges most rapidly. b) Time trajectories of important (1382 drugs and the top 300 economically relevant chemicals and 2. 2000 randomly chosen molecules (right) plotted in the $\ln k_{in}$–$\ln k_{out}$ plane. The trajectories of the important chemicals are long and linear (i.e., $k_{out} \propto (k_{in})^{\eta}$ where $\eta \approx 1$), whereas those of "random" ones are short and of varying curvatures (with η between approximately -1.5 and 3). The insert shows probability distributions of the trajectory exponents η; the curves are best Gaussian fits to the data. Standard deviation of η is higher (0.64) for randomly chosen compounds than for economically relevant chemicals (0.30) and drugs (0.33). 3. Cost (per kmol) as a function of in and out connectivities of the top 300 economically relevant compounds. The power-law dependence indicates that more highly connected compounds are significantly less expensive. USD = US dollar.

trends could be established for particular branches of chemistry (e.g., the rapidly growing carbohydrate and lipid research, fluorine chemistry, etc.) and whether these trends would differ from the "mainstream" trends discussed herein.

On a fundamental level, our results provide yet another demonstration of how seemingly independent/uncorrelated activities of individual agents[40–44] fall into a larger scheme and obey—or, as proponents of emergence[11] would argue, "give rise to"—unifying statistical rules.[45]

Received: June 29, 2005
Revised: August 31, 2005
Please note: Minor changes have been made to this manuscript since its publication in *Angewandte Chemie* Early View. The Editor.

Keywords: combinatorial chemistry · master equations · networks · organic reactions · stochastic modeling

[1] K. C. Nicolaou, E. J. Sorensen, *Classics in Total Synthesis: Targets Strategies, Methods*, Weinheim, New York, **1996**.
[2] N. Anand, J. S. Bindra, S. Randanathan, *Art in Organic Synthesis*, Holden-Day, San Francisco, **1970**.
[3] E. J. Corey, A. K. Long, S. D. Rubenstein, *Science* **1985**, *228*, 408.
[4] S. L. Schreiber, *Science* **2000**, *287*, 1964.
[5] K. C. Nicolaou, D. Vourloumis, N. Winssinger, P. S. Baran, *Angew. Chem.* **2000**, *112*, 46; *Angew. Chem. Int. Ed.* **2000**, *39*, 44.
[6] M. D. Burke, S. L. Schreiber, *Angew. Chem.* **2004**, *116*, 48; *Angew. Chem. Int. Ed.* **2004**, *43*, 46.
[7] E. J. Corey, X.-M. Cheng, *The Logic of Chemical Synthesis*, Wiley, New York, **1989**.
[8] M. R. Spaller, M. T. Burger, M. Fardis, P. A. Bartlett, *Curr. Opin. Chem. Biol.* **1997**, *1*, 47.
[9] C. Lipinski, A. Hopkins, *Nature* **2004**, *432*, 855.
[10] R. Albert, A. L. Barabasi, *Rev. Mod. Phys.* **2002**, 74, 47.
[11] A. L. Barabasi, R. Albert, *Science* **1999**, *286*, 509.
[12] L. A. N. Amaral, J. M. Ottino, *Eur. Phys. J. B* **2004**, *38*, 147.
[13] L. A. N. Amaral, A. Scala, M. Barthelemy, H. E. Stanley, *Proc. Natl. Acad. Sci. USA* **2000**, *97*, 11149.
[14] C. M. Song, S. Havlin, H. A. Makse, *Nature* **2005**, *433*, 392.
[15] R. Albert, H. Jeong, A. L. Barabasi, *Nature* **1999**, *401*, 130.
[16] A. Broder, R. Kumar, F. Maghoul, P. Raghavan, S. Rajagopalan, R. Stata, A. Tomkins, J. Wiener, *Comput. Networking* **2000**, *33*, 309.
[17] D. Sornette, R. Cont, *J. Phys. I* **1997**, *7*, 431.
[18] L. Dehaan, R. L. Karandikar, *Stoch. Process. Their Appl.* **1989**, *32*, 225.
[19] MDL Crossfire Beilstein database; we stress that although Beilstein has data on numerous man-made polymers, it is not a comprehensive repository of biological polymers (proteins, DNA).
[20] M. Faloutsos, P. Faloutsos, C. Faloutsos, *Comput. Commun. Rev.* **1999**, *29*, 251.
[21] H. Jeong, B. Tombor, R. Albert, Z. N. Oltval, A. L. Barabasi, *Nature* **2000**, *407*, 651.
[22] S. Redner, *Eur. Phys. J. B* **1998**, *4*, 131.
[23] F. Liljeros, C. R. Edling, L. A. N. Amaral, H. E. Stanley, Y. Aberg, *Nature* **2001**, *411*, 907.
[24] C. G. Screttas, G. A. Heropoulos, *THEOCHEM* **1994**, *309*, 149.
[25] C. Wandrey, A. Bartkowiak, D. Hunkeler, *Langmuir* **1999**, *15*, 4062.
[26] J. B. Hendrickson, P. Huang, A. G. Toczko, *J. Chem. Inf. Comput. Sci.* **1987**, *27*, 63; we wrote a computer program based on the Hendrickson algorithm, which was used to calculate complexity factors of 1000 randomly chosen organic molecules from the BD. We found that the values of the factors correlated with molecular masses with the correlation coefficient $R = 0.72$. The executable of the program along with instructions can be downloaded free of charge from our web page (http://www.dysa.northwestern.edu).

 © 2005 Wiley-VCH Verlag GmbH & Co. KGaA, Weinheim

[27] T. K. Allu, T. I. Oprea, *J. Chem. Info. Model.* **2005**, *45*, 1237.
[28] The rescaling procedure consisted of: 1) multiplying the distribution $M(m,t)$ by the ratio $N(t{=}2004)/N(t{=}1850)$, where $N(t)$ stands for the total number of molecules at time t, and 2) translation by $\Delta M = M_{max}(2004) - M_{max}(t)$, where M_{max} corresponds to the distribution maximum.
[29] In its original version, the Kesten process describes the transformation of an arbitrary distribution of variable x according to a multiplicative-additive equation $x_j = \lambda_j x_j + \alpha_j$, where j stands for the iteration number and λ_j and α_j are independent, positive stochastic variables. In the limit of large j, this procedure generates a log-normal distribution $w_K(x)$ with a characteristic "algebraic" tail $w_K(x) \sim x^{-(1+\mu)}$ in which the exponent is determined by the condition $\langle \lambda^\mu \rangle = 1$.
[30] This is unlike the pure Kesten process, in which the old distribution is discarded after each iteration.
[31] The values of the effective multiplicative ($a = 0.67$) and additive ($b = 179.94$) coefficients are commensurate with those derived from the stochastic master equation, $a = \langle \prod_{i=1}^{i=T} \lambda_i \rangle = 0.91$ and $b = \langle \sum_{j=1}^{j=T} \alpha_j \prod_{i=j+i}^{T} \lambda_i \rangle = 47.7$.
[32] These observations can also be understood in terms of combinatorial considerations and reflect the fact that 1) on one hand, there are relatively few combinations of atoms that give rise to structures of low molecular mass. It can be readily estimated that the possible numbers of molecules of mass m increase roughly exponentially with m. 2) On the other hand, when two large molecules are "stitched" together, there are many possible combinations (orientations) of doing so and achieving a selective, high-yield synthesis is problematic.
[33] D. C. Rees, M. Congreve, C. W. Murray, R. Carr, *Nat. Rev. Drug Discovery* **2004**, *3*, 660.
[34] E. J. Martin, R. E. Critchlow, *J. Comb. Chem.* **1999**, *1*, 32.
[35] A. K. Ghose, V. N. Viswanadhan, J. J. Wendoloski, *J. Comb. Chem.* **1999**, *1*, 55.
[36] T. I. Oprea, *J. Comput.-Aided Mater. Des.* **2000**, *14*, 251; therein a comparison is made between the mass distributions of the Available Chemical Directory (ADC) and MACCS II Drug Data Report (MDDR) (we note that the ADC is not necessarily representative of "random" substances).
[37] J. Xu, J. Stevenson, *J. Chem. Inf. Comput. Sci.* **2000**, *40*, 1177.
[38] Medical Essential Drug Database http://lsb.sbs.auckland.ac.nz/classic/medbase.
[39] Chemical Prices, *Chemical Market Reporter*, March 7, **2005** http://www.chemicalmarketreporter.com.
[40] S. Camazine, *Behav. Ecol. Sociobiol.* **1991**, *28*, 61.
[41] S. Camazine, J.-L. Deneubourg, N. R. Franks, J. Sneyd, G. Theraulaz, E. Bonabeau, *Self-Organization in Biological Systems*, Princeton University Press, Princeton, **2001**.
[42] D. J. Watts, S. H. Strogatz, *Nature* **1998**, *393*, 440.
[43] R. V. Sole, J. M. Montoya, *Proc. R. Soc. London Ser. B* **2001**, *268*, 2039.
[44] A. Sih, G. Englund, D. Wooster, *Trends Ecol. Evol.* **1998**, *13*, 350.
[45] Details of an example for combinatorial chemistry, a discussion of the network wiring scheme, and details of the Beilstein Database are given in the Supporting Information.

 © 2005 Wiley-VCH Verlag GmbH & Co. KGaA, Weinheim

Semiconductor Materials

DOI: 10.1002/anie.200502090

SrAlSiH: A Polyanionic Semiconductor Hydride**

*Thomas Björling, Dag Noréus, Kjell Jansson, Magnus Andersson, Ekaterina Leonova, Mattias Edén, Ulf Hålenius, and Ulrich Häussermann**

In 2000 Gingl et al. reported the synthesis and structural characterization of the novel compound $SrAl_2H_2$.[1] Contrary to the alanates $A_mAe_nAl_oH_{m+2n+3o}$ (A, Ae = alkali and alkaline-earth metal, respectively), this aluminum hydride is not fully hydrogenated and was described as a "Zintl phase hydride". It features a two-dimensional $[Al_2H_2]^{2-}$ polyanion in which the Al atoms are arranged as a puckered graphitic layer with three nearest neighbors. The vacant coordination site is taken by hydrogen and the compound appears to be charge-balanced (Figure 1a). A structural entity with both Al–Al and Al–H bonds had not been observed before and is indeed remarkable.

Herein we report the synthesis of SrAlSiH, which is a further example of a polyanionic hydride that is structurally closely related to $SrAl_2H_2$. However, it displays striking differences in its properties. In contrast to metallic, thermally labile $SrAl_2H_2$, isoelectronic SrAlSiH is an air- and moisture-stable semiconductor with a thermal decomposition temperature that is among the highest known for hydride compounds. Additionally, SrAlSiH displays a peculiar electronic structure that suggests interesting transport properties. The combination of properties of SrAlSiH is unexpected for a

[*] Dr. K. Jansson, Dr. U. Häussermann
Inorganic Chemistry, Stockholm University
10691 Stockholm (Sweden)
Fax: (+46) 8-152-187
E-mail: ulrich@inorg.su.se

T. Björling, Prof. D. Noréus
Structural Chemistry, Stockholm University
10691 Stockholm (Sweden)

E. Leonova, Dr. M. Edén
Physical Chemistry, Stockholm University
10691 Stockholm (Sweden)

Prof. U. Hålenius
Department of Mineralogy, Swedish Museum of Natural History
10405 Stockholm (Sweden)

Dr. M. Andersson
Solid State Physics
IMIT, Royal Institute of Technology
KTH Electrum 229
16440 Kista (Sweden)

[**] This work was supported by the Swedish Research Council (VR) and the Henrik Granholm foundation. The European Union is also acknowledged for financial support through the European Project HYSTORY (contract number ENK6-CT-2002-00600). We thank Zheng Weng for instrumental NMR support.

Supporting information for this article is available on the WWW under http://www.angewandte.org or from the author.

© 2005 Wiley-VCH Verlag GmbH & Co. KGaA, Weinheim

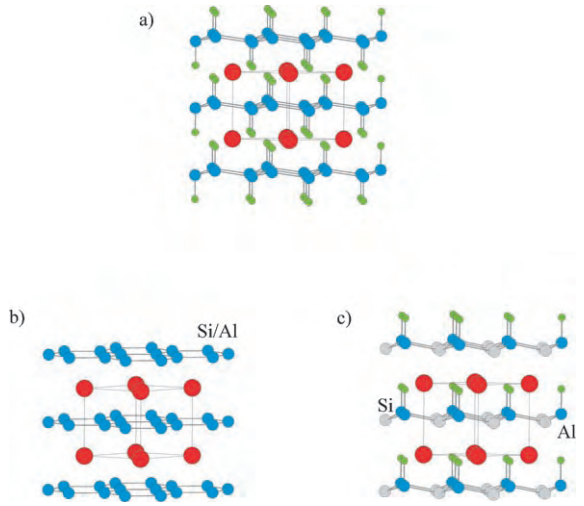

Figure 1. Crystal structures of $SrAl_2H_2$ (a), SrAlSi (b), and SrAlSiH (c) viewed along [110]. Red, blue, gray, and green circles denote Sr, Al (Al/Si), Si, and H atoms, respectively.

hydride and prompts an important issue: Polyanionic ("Zintl phase") hydrides provide novel coordination environments for H atoms and possess a huge compositional potential that is virtually unexplored. If physical properties inherent to hydrides and Zintl phases can be combined in these materials unexpected prospects are opened, thereby extending hydride materials' research beyond the traditional quest for hydrogen storage materials.[2]

SrAlSiH is obtained by hydrogenation of the alloy SrAlSi. This alloy is part of the solid solution $SrAl_{2-x}Si_x$ ($0.6 < x < 1.2$), which crystallizes in the hexagonal AlB_2 structure.[3] It is assumed that the Al and Si atoms in SrAlSi are more or less randomly distributed on the AlB_2 majority site, defining graphitic nets (Figure 1b). At a hydrogen pressure of 50 bar complete hydrogenation is typically obtained at temperatures between 600 and 700 °C and reaction times of 48 h. The refined lattice parameters of the final product are $a = 4.2139(3)$ and $c = 4.9550(6)$ Å. The c lattice parameter of the hydrogenated product is 5% larger than that of the starting material SrAlSi ($a = 4.2367(7)$, $c = 4.7442(9)$ Å), whereas the a lattice parameters are very similar. SrAlSiH possesses a gray and is air and moisture stable. This is remarkable in view of the sensitivity of other main group metal hydrides containing aluminium (e.g., alanates, $SrAl_2H_2$), which rapidly decompose when exposed to air and moisture. Another interesting observation is that when SrAlSi is employed in a compacted form for hydrogenation reactions (e.g. as a pellet or ingot), the shape of the starting material sample is completely preserved in the reaction product. In particular, single crystals of SrAlSi are transformed into identically shaped crystals of the hydrogenated product. Again, this is a remarkable feature because solid-state hydrogenations typically yield finely powdered products.

The structure of SrAlSiH (Figure 1c) was determined unambiguously by the refinement of neutron powder diffraction data of a deuterated sample (SrAlSiD) and by solid-state NMR investigations. It displays slightly puckered hexagon nets in which Si and Al atoms are arranged strictly alternately. H is exclusively attached to Al, and the Al–D distance in the deuteride is 1.77 Å. These puckered nets are stacked on top of each other, with the same orientation, and sandwich Sr atoms. Thus, compared with the starting material SrAlSi, the hydride experiences only small structural changes, which explains why single crystals of SrAlSi undergo hydrogenation into SrSiAlH without deterioration. In particular, the planar hexagon nets in SrAlSi become puckered in the hydride, and at the same time the interatomic distances within the nets increase from 2.46 to 2.50 Å. This leaves the a lattice parameter of both compounds about the same, whereas the c parameter is increased in the hydride.

Figure 2 shows magic-angle spinning (MAS) ^{27}Al (a), ^{29}Si (b), and ^{2}H NMR spectra (c) of a powder of SrSiAlD. Each spectrum is characteristic of a single site, as expected for a perfectly ordered structure consisting of hexagon nets of alternating Al and Si atoms, with ^{2}H exclusively attached to Al. As this sample displays comparatively long T_1 relaxation times for each of the nuclei involved, the absence of addi-

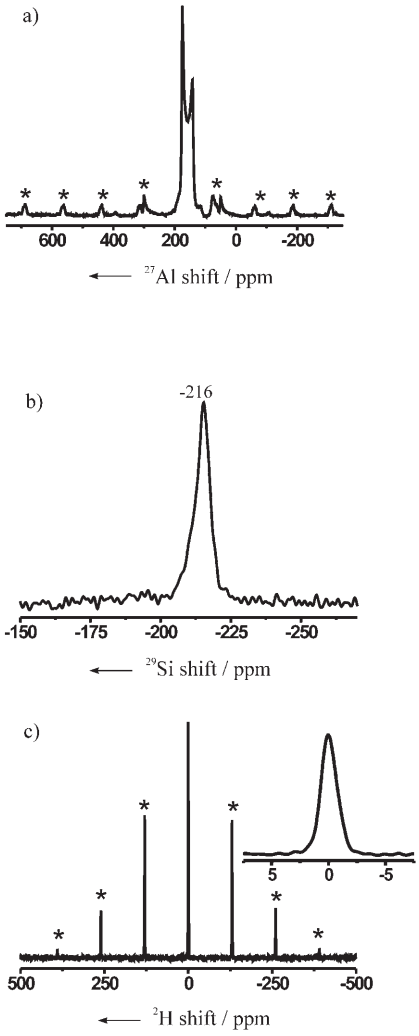

Figure 2. Magic-angle-spinning NMR spectra of SrSiAlD at 9.4 T. a) ^{27}Al spectrum recorded at 13.0 kHz spinning frequency. Asterisks indicate spinning sidebands. b) ^{29}Si spectrum at 8.0 kHz spinning frequency. c) ^{2}H spectrum at 8.0 kHz. The inset spectrum is a zoom around the centerband region.

 © 2005 Wiley-VCH Verlag GmbH & Co. KGaA, Weinheim

tional spectral components was verified by saturation-recovery experiments. The ^{27}Al NMR spectrum displays a characteristic second-order powder line-shape of a well crystalline compound.[4] In conjunction with 3QMAS data[5] and numerical simulations (not shown), we estimated the isotropic chemical shift and quadrupolar parameters as follows: $\delta_{iso} = 185.5 \pm 1.5$ ppm, $C_Q = e^2 q Q/h = 7.5 \pm 0.2$ MHz, and $\eta < 0.1$.[6] As expected from the proposed structure, the local symmetry around Al is associated with an axially symmetric electric field gradient tensor. The ^{2}H spectrum corresponds to a main resonance at $\delta = 0$ ppm flanked by a set of spinning sidebands generated from the quadrupolar interaction and associated with a small quadrupolar coupling constant, $C_Q = 26 \pm 3$ kHz.

The structure of SrAlSiH is very similar to that of $SrAl_2H_2$ (see Figure 1): half of the Al–H entities in the 2D polyanionic layer of $SrAl_2H_2$ are replaced by isoelectronic Si. This replacement occurs in a completely ordered way, that is, each Si atom is surrounded by three Al–H entities and vice versa. The center of inversion present in $SrAl_2H_2$ is lost in SrSiAlH and the space-group symmetry is reduced to $P3m1$. The interatomic distances and angles of $SrAl_2H_2$ and SrAlSiH are given as Supporting Information. The most conspicuous difference between the two structures is that the Sr atom in SrAlSiH is only coordinated by three H atoms. The Sr–H distance in SrAlSiH is considerably smaller than in $SrAl_2H_2$ (2.48 vs 2.65 Å) and the Al–H distance significantly larger (1.77 vs. 1.71 Å). Both compounds possess electron-precise polyanions—$[Al_2H_2]^{2-}$ and $[AlHSi]^{2-}$—with structures in accordance with the Zintl concept.

Despite their great structural similarity the thermal behavior of $SrAl_2H_2$ and SrAlSiH is strikingly different. Figure 3 displays heat-effect curves for both compounds at atmospheric pressure. Hydrogen desorption starts at 300 °C for $SrAl_2H_2$, whereas SrAlSiH only starts to decompose at temperatures above 600 °C. Higher decomposition temperatures are only known for some saline alkali and alkaline-earth metal hydrides.[7] Furthermore, hydrogen release of $SrAl_2H_2$ produces a mixture of the intermetallic compounds $SrAl_2$ and $SrAl_4$, whereas in the case of SrAlSiH the starting material SrAlSi is quantitatively regained. This means that although the Al–H distance in SrAlSiH is longer than in $SrAl_2H_2$, hydrogen is more tightly bound in SrAlSiH. This is easily explained by the higher positively charged environment that H experiences in SrAlSiH. Firstly, Al—to which H is attached—is positively polarized by the surrounding Si atoms in the polyanion, and secondly the Sr–H distance in SrAlSiH is considerably smaller. As a matter of fact, the Sr–H distance in SrAlSiH corresponds very well to the smallest Sr–H distances in saline SrH_2 (2.43–2.48 Å).[8]

Figure 4 compares the electronic density of states (DOS) of $SrAl_2H_2$ and SrAlSiH in their computationally relaxed equilibrium structures. The Fermi level for $SrAl_2H_2$ is situated at a pseudo gap. The metallic behavior of this compound is due to Al p bands crossing the Fermi level. In contrast, a real bandgap of about 0.65 eV is opened at the Fermi level for SrAlSiH and the compound is a semiconductor. The contribution of Sr atoms to the occupied states is rather low for both compounds, but rises sharply above the Fermi level (see Supporting Information). This is a typical feature of polar intermetallic and Zintl phases. The contribution of H is mainly into the intermediate energy regions of the DOS (between −6.5 and −2 eV), which are the parts where Al s and p bands mix strongly. The DOS of SrAlSiH is characterized by a pronounced singularity below the Fermi level. As can be seen in the band structure (Figure 4c), this singularity originates from a flat band corresponding to the Si p_z (lone pair) orbitals. These orbitals are virtually isolated in SrAlSiH and the arising band displays a very small dispersion. As a consequence, this compound attains a peculiar electronic structure in which a narrow bandgap is combined with a flat band exactly below the Fermi level.

According to the calculated band structure the bandgap is of indirect nature; the valence band maximum is located at Γ and the conduction band minimum at M. Optical absorption spectra obtained from diffuse reflectance measurements

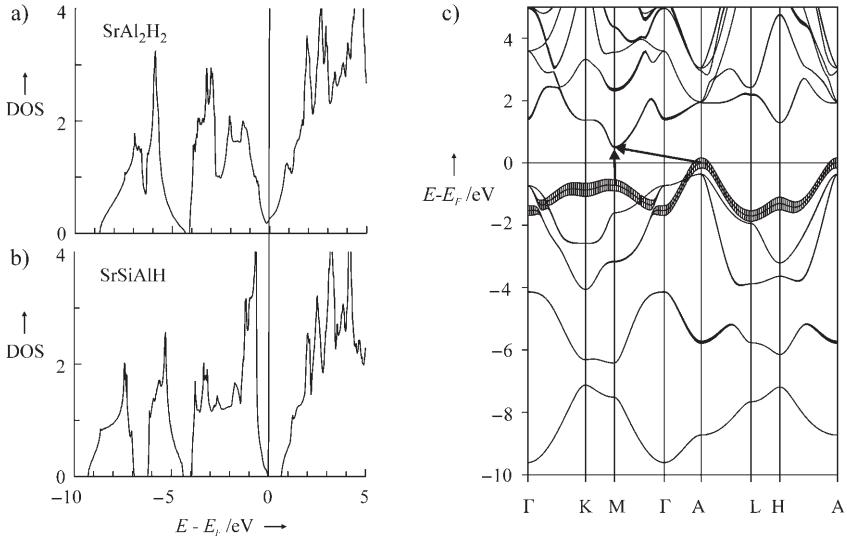

Figure 4. Electronic density of states, DOS (states $eV^{-1}Z^{-1}$), for $SrAl_2H_2$ (a) and SrAlSiH (b). The Fermi level is indicated by a vertical line. c) Band structure of SrAlSiH. The Si p_z orbital contribution is shown as broad-band representation. The lowest energy transition A→M, which is indirect, and the direct transition with lowest energy are indicated as arrows.

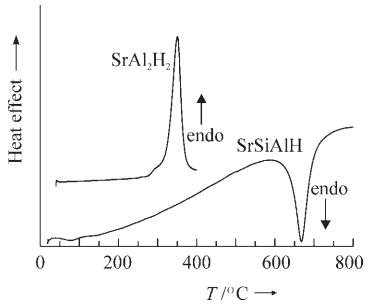

Figure 3. Heat-effect curves for $SrAl_2H_2$ (DSC) and SrAlSiH (DTA).

 © 2005 Wiley-VCH Verlag GmbH & Co. KGaA, Weinheim

confirmed the presence of the bandgap. The experimental value of 0.63 eV is, coincidentally, in close agreement with the calculated one. The room-temperature resistivity of SrAlSiH is about 110 Ω cm, which can be compared to the intrinsic room-temperature resistivity of Ge (46 Ω cm) with a bandgap of 0.73 eV. The thermopower of SrAlSiH is around $-90\ \mu V\,K^{-1}$ at room temperature, and the negative sign of the Seebeck coefficient implies that electrons are the charge carriers in this material (see Supporting Information for further details).

In conclusion, we have reported on the novel semiconductor hydride SrAlSiH. Several aspects make this compound remarkable: 1) SrAlSiH is, after $SrAl_2H_2$, the second example of a "Zintl phase hydride" where H is part of a polyanion. The two-dimensional polyanion of SrAlSiH is composed of isolectronic, three-bonded $[Al{-}H]^-$ and Si^- entities and is charge balanced by Sr^{2+}. 2) SrAlSiH is a semiconductor with an indirect bandgap of about 0.65 eV. Metal hydrides with narrow bandgap (0.2–1.2 eV) semiconductor properties are unprecedented; fully hydrogenated main group metal systems are typically insulators. The wide homogeneity range of underlying AlB_2-type $SrAl_{2-x}Si_x$ ($0.6 < x < 1.2$) may allow triggering of a transition to a metallic $SrAl_{2-x}Si_xH_{2-x}$ for low values of x. In this case, the Fermi level would cut the singularity in the DOS which may give rise to superconductivity. On the other hand, for $x > 1$ a widening of the bandgap is expected. 3) The NMR investigation of SrAlSiD has provided the first ^{27}Al and ^{29}Si data for a structure involving direct Al–Si contacts and where spectral resolution is not limited by fast T_2-relaxation, which is observed in metallic compounds because of the conducting electrons.[9] The ^{29}Si chemical shift ($\delta_{Si} = -216$ ppm) implies large diamagnetic contributions due to the localized negative charge of a lone electron pair at Si. This shift is somewhat more shielded than observed for the ^{29}Si site in antifluorite-type Mg_2Si ($\delta_{Si} = -177$ ppm), where formally Si^{4-} is cubically surrounded by eight strongly polarizing Mg^{2+} ions.[10] The large paramagnetic contribution to the isotropic ^{27}Al chemical shift ($\delta_{Al} = 185.5$ ppm) arises from a high degree of charge asymmetry at the Al nucleus due to bonding to two different ligands, Si and D (also reflected in the relatively high quadrupolar coupling constant).[11] 4) Al and Si are strictly ordered in SrAlSiH. This is in contrast to the starting material SrAlSi, where Al and Si are distributed more or less randomly. It is known that conventional (disordered) SrAlSi is a superconductor with a T_c of 5.1 K.[3] However, the nature of the superconducting properties remains unclear.[12] Hydrogen desorption of SrAlSiH provides an elegant way to obtain ordered SrAlSi. The study of the ordered material could provide some deeper understanding of the superconducting properties of SrAlSi.

Experimental Section

Synthesis: All steps of the synthesis and sample preparation for diffraction experiments were carried out under dry argon. The starting materials $SrAl_2$ and SrSiAl were prepared by arc-melting stoichiometric mixtures of the pure elements. For hydrogenation, the starting materials were loaded in corundum crucibles, which were placed in stainless steel autoclaves. Reactions were carried out at 50–60 bar hydrogen pressure and temperatures of 200 °C and 700 °C for $SrAl_2$ and SrAlSi, respectively. SrAlSiD was prepared analogously. Starting materials and hydrides were characterized by Guinier powder patterns ($CuK\alpha_1$; Si standard) and EDX (energy-disperse X-ray) analysis in a JEOL 820 scanning electron microscope. SrAlSiH can be exposed to air and moisture without decomposition.

Structural characterization: Lattice constants of SrAlSi, SrAlSiH, and SrAlSiD were obtained from least-squares refinement of measured and indexed lines of the corresponding Guinier powder diffractograms.[13] Atomic positions of SrAlSiD were determined from a Rietveld refinement of neutron powder diffraction data[14] collected at the Studsvik Neutron Research Laboratory, Sweden (room temperature, $\lambda = 1.47$ Å, data resolution $\Delta d/d = 2 \times 10^{-3}$). SrAlSiD: space group $P3m1$ (no. 156); cell parameters (X-rays): $a = 4.2113(3)$, $c = 4.9518(5)$ Å, $V = 76.05$ Å^3, $Z = 1$; $R_B = 1.87\%$, $R_P = 9.49\%$, $R_{wp} = 9.44\%$, $\chi^2 = 1.44$ for 85 reflections (positional parameters are provided as Supporting Information).

NMR spectroscopy: MAS NMR experiments were carried out at room temperature on a Varian/Chemagnetics Infinity-400 spectrometer operating at 9.4 T, giving the Larmor frequencies −61.43, −104.28, and 79.50 MHz and for ^2H (spin 1), ^{27}Al (spin 5/2), and ^{29}Si (spin 1/2), respectively. Powders of SrSiAlD (99% enriched with respect to ^2H) were filled in zirconia rotors of outer diameters 3.2, 4, and 6 mm, and spun at 8.0 (for ^2H acquisitions), 13.0 (^{27}Al), and 8.0 kHz (^{29}Si), respectively. 48 ^2H signal transients were recorded with 90° pulses (76 kHz nutation frequency) and 120 s relaxation delays. The ^{29}Si spectrum was recorded using 30° pulses and 188 accumulated transients with 600 s relaxation delays. ^{27}Al acquisitions resulted from 840 transients, 60 s relaxation delays, and 11° pulses (86 kHz nutation frequency, measured with respect to Al^{3+}(aq)). No additional line-broadening was applied in the spectral processing. Chemical shifts are reported in deshielding (δ) units of ppm, referenced externally to D_2O (^2H), Al^{3+}(aq) (^{27}Al), and TMS (^{29}Si).

Thermal investigations: The thermal behavior of powdered samples of $SrAl_2H_2$ and SrAlSiH was investigated by differential thermal analysis (DTA-TG, Setaram Labsys 1600) and differential scanning calorimetry (Perkin Elmer DSC 7), respectively. $SrAl_2H_2$ was placed in a steel container, which was sealed with gold foil to prevent exposure to air and moisture, and the temperature was raised from 40 to 400 °C. SrAlSiH was placed in an open corundum crucible and the temperature was raised from 40 to 800 °C. Both experiments were performed under a flow of dry argon and with a temperature-increase rate of $5\ K\,min^{-1}$.

Diffuse reflectance measurements: Optical diffuse reflectance measurements were made on finely ground samples of SrAlSiH and SrAlSiD at room temperature. The spectrum was recorded in the region 3200–10500 cm^{-1} with a Bruker Equinox 55 FT-IR spectrometer equipped with a diffuse reflectance accessory (Harrick). The measurement of diffuse reflectivity can be used to determine bandgaps. For this, absorption data (α/S) were extracted from the reflectance data by using the Kubelka–Munk function.[15]

Resistivity and thermopower measurements: Resistivity measurements were performed using a four-point in-line contact arrangement on a $2 \times 3.3 \times 6$ mm^3 bar of SrAlSiH. This bar was obtained by polishing an ingot of SrAlSi and subsequent hydrogenation. The thermoelectric voltage, U, was measured for different temperature gradients ΔT between two sides of the bar. A straight line was fitted to $U(\Delta T)$, which has the slope $dU/d(\Delta T) = S_w - S_s$, where S_s is the thermopower of the sample and S_w is the thermopower of the connecting wires.

Electronic structure calculations: Total energy calculations for $SrAl_2H_2$ and SrAlSiH were performed in the framework of the frozen core all-electron Projected Augmented Wave (PAW) method,[16] as implemented in the program VASP.[17] The energy cut-off was set to 500 eV. Exchange and correlation effects were treated by the generalized gradient approximation (GGA), usually referred to as

 © 2005 Wiley-VCH Verlag GmbH & Co. KGaA, Weinheim

PW91.[18] The integration over the Brillouin zone was done on special *k*-points determined according to the Monkhorst–Pack scheme.[19] Total energies were converged to at least 1 meV per atom. Structural parameters were relaxed until forces had converged to less than 0.01 eV Å^{-1}.

Received: June 16, 2005
Revised: August 31, 2005
Published online: October 18, 2005

Keywords: aluminum · hydrides · NMR spectroscopy · semiconductors · zintl phases

[1] F. Gingl, T. Vogt, E. Akiba, *J. Alloys Compd.* **2000**, *306*, 127.
[2] A. M. Seayad, D. M. Antonelli, *Adv. Mater.* **2004**, *16*, 765.
[3] B. Lorenz, J. Lenzi, J. Cmaidalka, R. L. Meng, Y. Y. Sun, Y. Y. Xue, C. W. Chu, *Phys. C* **2002**, *383*, 191.
[4] K. J. D. McKenzie, M. E. Smith, *Multinuclear Solid-State NMR of Inorganic Materials* (Pergamon Materials Series 6), Elsevier, Amsterdam, **2002**.
[5] L. Frydman, J. S. Harwood, *J. Am. Chem. Soc.* **1995**, *117*, 5367.
[6] The asymmetry parameter of the electric-field gradient tensor is defined as $\eta = (V_{yy} - V_{xx})/V_{zz}$ $(0 \le \eta \le 1)$, with the principal values, V_{ii}, ordered according to $|V_{yy}| \le |V_{xx}| \le |V_{zz}|$.
[7] W. Grochala, P. P. Edwards, *Chem. Rev.* **2004**, *104*, 1283.
[8] N. E. Brese, M. O'Keeffe, R. B. von Dreele, *J. Solid State Chem.* **1990**, *88*, 571.
[9] However, as the ^{29}Si peak (Figure 2b) is rather broad and slightly asymmetric, we believe its width is primarily dictated by unresolved splittings from scalar couplings to its ^{27}Al neighbors. Broadening may also stem from "residual" ^{27}Al–^{29}Si dipolar couplings, unaveraged by MAS due to the ^{27}Al quadrupolar interaction [R. K. Harris, A. Olivieri, *Prog. Nucl. Magn. Reson. Spectrosc.* **1992**, *24*, 435], as observed even across Si–O–Al linkages in minerals at low magnetic fields [J. S. Hartman, B. L. Sheriff, *J. Phys. Chem.* **1991**, *95*, 7575].
[10] E. Ratai, M. P. Augustine, S. M. Kauzlarich, *J. Phys. Chem. B* **2003**, *107*, 12573.
[11] For comparison, the chemical shifts of the tetrahedral ^{27}Al site in the III–V semiconductors AlP and AlAs are $\delta = 142$ and 130 ppm, respectively [O. H. Han, H. K. C. Timken, E. Oldfield, *J. Chem. Phys.* **1988**, *89*, 6046].
[12] I. I. Mazin, D. A. Papaconstantopoulos, *Phys. Rev. B* **2004**, *69*, 180512.
[13] P.-E. Werner, *Ark. Kemi* **1969**, *31*, 513.
[14] J. Rodriguez-Carvajal, *FULLPROF: A Program for Rietveld Refinement and Pattern Matching Analysis*, Abstracts of the Satellite Meeting on Powder Diffraction of the XV Congress of the IUCr, Toulouse, France, **1990**, p. 127.
[15] G. Kotiim, *Reflectance Spectroscopy*, Springer, New York, **1969**.
[16] a) P. E. Blöchl, *Phys. Rev. B* **1994**, *50*, 17953; b) G. Kresse, J. Joubert, *Phys. Rev. B* **1999**, *59*, 1758.
[17] a) G. Kresse, J. Hafner, *Phys. Rev. B* **1993**, *47*, 558; b) G. Kresse, J. Furthmüller, *Phys. Rev. B* **1996**, *54*, 11169.
[18] J. P. Perdew, Y. Wang, *Phys. Rev. B* **1992**, *45*, 13244.
[19] H. J. Monkhorst, J. D. Pack, *Phys. Rev. B* **1972**, *13*, 5188.

 © 2005 Wiley-VCH Verlag GmbH & Co. KGaA, Weinheim

Oxygen Activation

DOI: 10.1002/anie.200502096

Structures of Transition States in Metal-Mediated O_2-Activation Reactions**

*Michael P. Lanci, David W. Brinkley, Kristie L. Stone, Valeriy V. Smirnov, and Justine P. Roth**

Enrichment of heavy oxygen (^{18}O) from its level at natural abundance is widely used to probe O_2-dependent processes in the atmospheric and biological sciences.[1–4] Here we describe the first application of this technique to O_2-binding reactions of classic inorganic compounds. Competitive ^{18}O kinetic isotope effects (KIEs)[5–7] reflecting the ratio of second-order rate constants for the formation of η^2-peroxide compounds from $^{16,16}O_2$ and $^{18,16}O_2$ ($k_{16,16}/k_{18,16}$) have been determined (Scheme 1). Related measurements on enzymatic

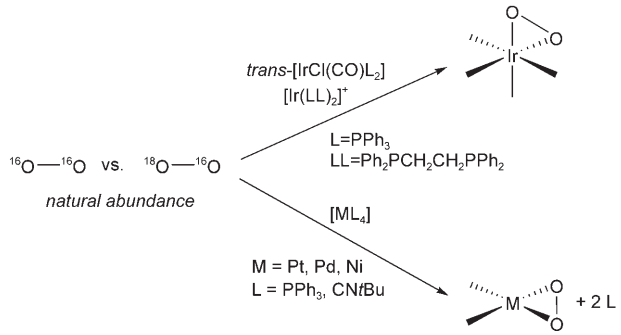

Scheme 1. Competitive ^{18}O isotope effect on the formation of η^2-peroxo complexes.

reactions[4,8–11] have been interpreted on the basis of equilibrium isotope effects (EIEs) and simple models that neglect variations in the transition-state structure. The present studies suggest that the proposed enzyme mechanisms may need to be reevaluated in light of the sensitivity of ^{18}O KIEs to changes in the height of the free-energy barrier for reactions involving the formation of a metal–O_2 bond.

Oxygenation of solutions prepared from *trans*-[IrCl(CO)-$(PPh_3)_2$], $[Ir(dppe)_2]Cl$, $[Pt(PPh_3)_4]$, $[Pd(PPh_3)_4]$, $[Ni(PPh_3)_4]$, and $[Ni(CNtBu)_4]$ (PPh_3 = triphenylphosphine, dppe = 1,2-bis(diphenylphosphino)ethane, $CNtBu$ = *tert-n*-butylisocya-

[*] M. P. Lanci, Dr. D. W. Brinkley, K. L. Stone, Dr. V. V. Smirnov, Prof. J. P. Roth
Department of Chemistry
The Johns Hopkins University
3400 North Charles Street, Baltimore, MD 21218 (USA)
Fax: (+1) 410-516-8420
E-mail: jproth@jhu.edu

[**] We are grateful for support from NSF CAREER award CHE-0449900.

Supporting information (experimental details and isotope-effect calculations) for this article is available on the WWW under http://www.angewandte.org or from the author.

© 2005 Wiley-VCH Verlag GmbH & Co. KGaA, Weinheim

nide) affords the corresponding η^2-peroxides [IrCl(CO)O_2-(PPh_3)$_2$], [IrO_2(dppe)$_2$]Cl, [PtO_2(PPh_3)$_2$], [PdO_2(PPh_3)$_2$], [NiO_2(PPh_3)$_2$], and [NiO_2(CN*t*Bu)$_2$].[12–16] On the basis of early studies on *trans*-[IrCl(CO)(PPh_3)$_2$] and [Pt(PPh_3)$_4$],[13,14] concerted oxidative-addition mechanisms have been proposed in which two electrons transfer to O_2 at the same time that two metal–oxygen bonds form.[17,18]

This work describes O_2-binding mechanisms for a series of compounds in "anhydrous" *N*,*N*-dimethylformamide (DMF) and dimethylsulfoxide (DMSO).[19] In most cases, high yields of stable products were obtained, as revealed by $^{31}P\{^1H\}$ and ^1H NMR as well as UV/Vis spectroscopy.[20] Kinetics studies were performed by monitoring the disappearance of the reduced compound (0.05–0.35 mM) upon reaction with a greater than tenfold excess of O_2, either by conventional or stopped-flow UV/Vis spectrophotometry. The irreversible formation of η^2-peroxide products on the time scale of the experiments is reported in terms of the rate constant for O_2 binding (k_{O_2}) in DMF at 25 ± 2 °C unless noted.

Depending on the stability of the reduced compounds in Scheme 1, the reaction mechanisms range from simple to complex, thus making it a challenge to probe the relative energy barriers to O_2 activation. Bimolecular kinetics observed for *trans*-[IrCl(CO)(PPh_3)$_2$][21] and [Ir(dppe)$_2$]Cl indicate $k_{O_2} = 0.17 \pm 0.02\ M^{-1}s^{-1}$ and $2.8 \pm 0.4\ M^{-1}s^{-1}$, respectively. The slowest reacting complex, *trans*-[IrCl(CO)-(PPh_3)$_2$], has the lowest O_2 affinity ($\Delta G_{298K} = -5.6 \pm 0.2$ kcal mol^{-1} in DMF). No sign of reversible O_2 loss could be detected for any of the other peroxide compounds examined.[22] [Pt(PPh_3)$_4$], [Pd(PPh_3)$_4$], [Ni(PPh_3)$_4$], and [Ni-(CN*t*Bu)$_4$] dissociate in solution to two- and three-coordinate species[14,16,23] which are oxidized 10^2–10^5 times faster than *trans*-[IrCl(CO)(PPh_3)$_2$]. In the simplest case involving a d^{10} metal, disappearance of [Pt(PPh_3)$_4$] is first order in O_2 and the derived rate constant ($k_{O_2} = 32 \pm 8\ M^{-1}s^{-1}$) is independent of the PPh_3 concentration. This behavior is consistent with [Pt(PPh_3)$_3$] being the primary reactive species.[14]

The oxidation of [Pd(PPh_3)$_4$] is more than 10^3 times faster than that of [Pt(PPh_3)$_4$] and exhibits more complex kinetics. The reactions are first order with respect to O_2, yet the rate constant ($k_{O_2} = 41\,100 \pm 300\ M^{-1}s^{-1}$) decreases in response to added PPh_3 until a limiting k_{O_2} value of $2480 \pm 130\ M^{-1}s^{-1}$ is reached at a PPh_3 concentration of 0.025–0.08 M. This behavior is consistent with a two-term rate law and competitive binding of O_2 to [Pd(PPh_3)$_2$] and [Pd(PPh_3)$_3$] (Scheme 2). The first term in the rate law simplifies to k_{O_2} for [Pd(PPh_3)$_2$] when the reduced species are present in rapid equilibrium and $k_{-1}[L] \gg k_2[O_2]$, whereas the second term gives k_{O_2} for [Pd(PPh_3)$_3$] at high PPh_3 concentration.

Reactions of [Ni(PPh_3)$_4$] and [Ni(CN*t*Bu)$_4$] can also be understood in terms of Scheme 2. In the absence of added

$$[ML_3] \underset{k_{-1}}{\overset{k_1}{\rightleftharpoons}} [ML_2] + L + O_2 \xrightarrow{k_2} [MO_2L_2]$$

$$[ML_3] + O_2 \xrightarrow{k_3} [MO_2L_2] + L$$

$$-\frac{d[ML_3]}{dt} = \frac{k_1 k_2 [O_2][ML_3]}{k_{-1}[L] + k_2[O_2]} + k_3[O_2][ML_3]$$

Scheme 2. Kinetic scheme for O_2 binding.

PPh_3, the disappearance of [Ni(PPh_3)$_4$] depends only slightly on the concentration of O_2. This behavior is consistent with dissociation of [Ni(PPh_3)$_3$] in a kinetically irreversible manner caused by fast trapping of [Ni(PPh_3)$_2$] by O_2. The addition of PPh_3 (0.15–0.34 M) causes ligand association to compete with O_2 binding and allows the determination of k_{O_2} ($230 \pm 10\ M^{-1}s^{-1}$) for [Ni(PPh_3)$_3$]. Spectroscopic evidence suggests that [Ni(PPh_3)$_2$(DMSO)] is the reactive species in DMSO (see Supporting Information), where the reaction is first order in O_2 without added PPh_3, and $k_{O_2} = 3300 \pm 80\ M^{-1}s^{-1}$. The kinetics of the oxygenation reaction of [Ni(CN*t*Bu)$_4$] give a linear first-order plot with a nonzero *y*-intercept, which suggests that the rates of ligand dissociation and O_2 binding are comparable, that is, $k_1 \approx k_3[O_2]$. Addition of CN*t*Bu causes the intercept to approach zero but the slope, which corresponds to $k_{O_2} = 3300 \pm 150\ M^{-1}s^{-1}$, remains unchanged; this is consistent with [Ni(CN*t*Bu)$_3$] being the reactive species.

The ^{18}O KIEs for the O_2-binding reactions were determined by a method in which stable-isotope mass spectrometry is used.[1,4] Experiments were performed under conditions of intermolecular competition by introducing a substoichiometric amount of metal compound into a sealed reaction vessel containing natural-abundance O_2. Subsequent to the reaction, isolation and analysis of the O_2 remaining in solution revealed ^{18}O enrichment as a result of a faster consumption of $^{16,16}O_2$ than $^{18,16}O_2$. Data were collected at varying concentrations of metal complex to determine $k_{16,16}/k_{18,16}$ (Figure 1). The ^{18}O

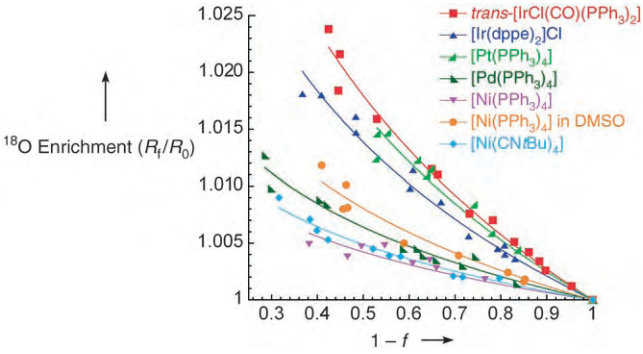

Figure 1. ^{18}O enrichment plot. Data are fitted to the equation: $R_f/R_0 = (1-f)^{((1/(k_{16,16}/k_{18,16}))-1)}$; R_0 and R_f are the $^{18}O/^{16}O$ ratios prior to reaction and at a fractional conversion (f), respectively.

KIEs are independent of both the fractional O_2 consumption and the ratio of O_2 consumed per mole of reduced compound. This ratio was 1:1 in most cases but as high as 1.6 ± 0.4:1 for [Pt(PPh_3)$_4$] and 2.3 ± 0.8:1 for [Ni(PPh_3)$_4$] because of the catalytic oxidation of PPh_3.[15,24] The $k_{16,16}/k_{18,16}$ ratio is a competitive effect and serves as a probe of all the steps from the encounter of the metal complex with O_2 to the first kinetically irreversible step. Thus, the KIEs in this work reflect O_2 binding concomitant with reduction to peroxide (O_2^{2-}) and are independent of ligand dissociation and subsequent ligand oxidation.

The formation of η^2-peroxide compounds is characterized by $k_{16,16}/k_{18,16}$ values from 1.0069 to 1.0268 (Table 1). The ^{18}O

 © 2005 Wiley-VCH Verlag GmbH & Co. KGaA, Weinheim

Table 1: Rate constants for O_2 binding and ^{18}O isotope effects ($\pm 2\sigma$) at 25 ± 2 °C.[a]

Product	k_{O_2} [$M^{-1}s^{-1}$]	$k_{16,16}/k_{18,16}$	ν_{O-O}, sym ν_{M-O}, asym ν_{M-O} ($^{16,16}\nu - ^{18,16}\nu$) [$cm^{-1}$][f]	$(K_{16,16}/K_{18,16})_{calcd}$
trans-[IrCl(CO)O_2(PPh_3)$_2$]	0.17 ± 0.02	1.0268(37)[e]	858(24), 581(9), 595(9) [g]	1.028
[IrO_2(dppe)$_2$]Cl	2.8 ± 0.4	1.0205(36)[e]	843(25), 547(9), 533(9) [g]	1.028
[PtO_2(PPh_3)$_2$]	32 ± 7	1.0251(51)	827(23), 470(10) 488(10)	1.031
[NiO_2(PPh_3)$_2$]	> 230[c]	1.0071(14)	–	1.028[h]
[NiO_2(PPh_3)$_2$][b]	3000 ± 80[b]	1.0113(27)[b]	–	1.028[h]
[NiO_2(CN*t*Bu)$_2$]	3300 ± 150[d]	1.0069(16)[d,e]	897(25), 560(10), 523(10)	1.026
[PdO_2(PPh_3)$_2$]	$41\,100 \pm 300$	1.0093(29)[e]	877(23), 496 (10), 487(10)	1.030

[a] In DMF unless noted. [b] In DMSO. [c] k_{O_2} is a lower limit in the absence of added PPh_3 (see text). [d] [CN*t*Bu] = 0–0.088 M. [e] In DMF and DMSO. [f] Refs. [27–29]. [g] $\Delta\nu_{M-O}$ for [RhCl(CN*t*Bu)O_2(PPh_3)$_2$] in Ref. [28]. [h] Average of $(K_{16,16}/K_{18,16})_{calcd}$ for [PdO_2(PPh_3)$_2$] and [Ni (CN*t*Bu)$_2O_2$].

KIEs are larger for the O_2-binding reactions with third-row metals than for the faster reactions with first- and second-row metals. This range of values is larger than that determined for iron-, copper-, and flavin-containing enzymes, which react with O_2 according to diverse mechanisms.[4] The formation of η^2-peroxide compounds is characterized by ^{18}O KIEs that are less than the EIEs ($K_{16,16}/K_{18,16}$) calculated from Bigeleisen's formalism[25] using normal mode stretching frequencies.[26–29] Although the products are structurally quite different, they exhibit similar shifts of oxygen-isotope-dependent stretching frequencies resulting in a narrow range of $(K_{16,16}/K_{18,16})_{calcd}$ values (1.026 to 1.031; see Table 1 and Supporting Information). The average value is three times greater than that reported for the reduction of O_2 to H_2O_2 (1.0089) and previously used as a benchmark to identify metal–peroxide intermediates in enzymes and O_2-carrier proteins.[4,8–10,26]

Heavy-atom KIEs are conventionally interpreted with transition state theory and the equation, $k_{16,16}/k_{18,16} = (\nu^{\ddagger}_{16,16}/\nu^{\ddagger}_{18,16})(K^{TS}_{16,16}/K^{TS}_{18,16})$, which includes contributions from the reaction-coordinate frequency ($\nu^{\ddagger}$) and the equilibrium constant for the formation of the transition state (K^{TS}).[6] The transition states for η^2-O_2 binding are visualized in terms of structures that are intermediate between the reactant and product states, in which the O–O bond is partially weakened and two new metal–O bonds are partially formed. The results reported here support an assumption that is commonly made when interpreting mechanisms based on ^{18}O KIEs: that $\nu^{\ddagger}_{16,16}/\nu^{\ddagger}_{18,16}$ is approximately 1 and that $K_{16,16}/K_{18,16}$ is the upper limit to $K^{TS}_{16,16}/K^{TS}_{18,16}$ and therefore to $k_{16,16}/k_{18,16}$.[4–7]

For inner-sphere electron transfer (ET), in which new bonds are formed during the redox reaction, the productlike character of the transition state can be defined in terms of the ratio of the ^{18}O KIE to the EIE. The parameter $[(k_{16,16}/k_{18,16})-1]/[(K_{16,16}/K_{18,16})_{calcd}-1]$ is expected to correlate with the barrier height ($\Delta G^{\ddagger} \propto \log k_{O_2}$) when the reaction coordinate includes the reorganization of bonds involving oxygen nuclei.[5] This is precisely the behavior observed in Figure 2, which supports the proposal that the reactions examined occur by oxidative addition of O_2. Alternative mechanisms, such as those involving η^1-superoxide intermediates, are unlikely in view of a) the absence of optically detectable intermediates in the kinetics experiments and b) ^{18}O KIEs that are significantly larger than the EIEs of 1.005 reported for η^1-binding of O_2 to metalloproteins.[4,26] Although the $k_{16,16}/k_{18,16}$ ratio for *trans*-[IrCl(CO)(PPh_3)$_2$] is very close to

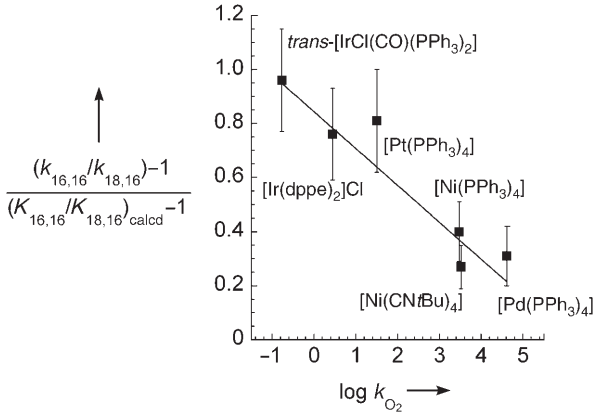

Figure 2. Isotope effects reflecting variation in transition-state structures for O_2 binding.

that reported for outer-sphere ET,[30] this mechanism can be ruled out because the value of $\Delta G°$ (44.7 kcal mol^{-1}) estimated from one-electron redox potentials[31,32] greatly exceeds the observed $\Delta G^{\ddagger}$ value (18.7 kcal mol^{-1}).

These studies show that ^{18}O KIEs are sensitive probes of transition-state structure in reactions where O_2 binds to a transition-metal center. Consistent with a productlike transition state, a value of $[(k_{16,16}/k_{18,16})-1]/[(K_{16,16}/K_{18,16})_{calcd}-1]$ close to 1 is obtained for *trans*-[IrCl(CO)(PPh_3)$_2$], the compound which exhibits the slowest and least thermodynamically favorable reaction with O_2. This parameter decreases for the other reactions as the transition state becomes more reactant-like. These reactions are ostensibly more exothermic as k_{O_2} increases systematically over five orders of magnitude. The trend can be explained in the context of the Marcus theory of electron transfer, in which the ^{18}O KIE arises from oxygen nuclear reorganization (λ).[30] As $\Delta G°$ becomes increasingly favorable, the contribution of this term to $\Delta G^{\ddagger}$ decreases as shown in Figure 3.

In summary, competitive ^{18}O KIEs have been used for the first time to probe the binding of O_2 to inorganic compounds. All KIEs are less than the theoretical EIEs calculated from the stretching frequencies of O_2 and the structurally defined η^2-peroxo products. The ^{18}O KIEs decrease as O_2-binding rate constants increase by over five orders of magnitude. This trend indicates that all the reactions occur by the same

 © 2005 Wiley-VCH Verlag GmbH & Co. KGaA, Weinheim

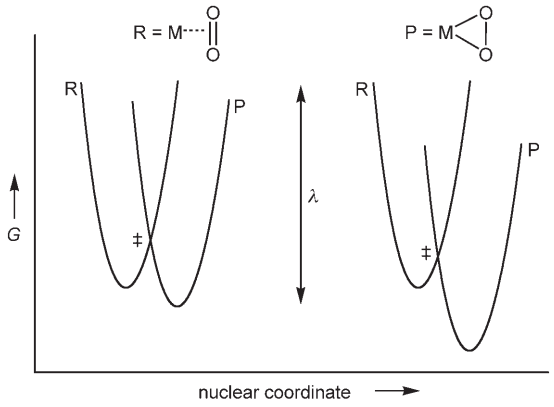

Figure 3. Model for the contribution of λ to the reaction barrier (designated ‡).

mechanism, albeit with measurable differences in the transition-state structure. The correlation of the product-like character of the transition state with the barrier height can be explained in terms of Marcus theory, where an increasingly favorable $\Delta G°$ value decreases the contribution of isotope-dependent nuclear reorganization to $\Delta G^{\ddagger}$. This property appears to differentiate reactions involving inner-sphere ET to O_2 from reactions proceeding by outer-sphere ET, in which ^{18}O KIEs appear to be relatively insensitive to the value of $\Delta G°$.[30] The highly variable ^{18}O KIEs determined in this work for a single class of metal-mediated oxidation reactions underscores the need for benchmarks and relevant models to interpret such measurements upon O_2-activation reactions of metalloenzymes.

Received: June 17, 2005
Published online: October 13, 2005

Keywords: electron transfer · enzymes · isotope effects · O–O activation · transition states

[1] R. D. Guy, M. L. Fogel, J. A. Berry, *Plant Physiol.* **1993**, *101*, 37.
[2] B. Luz, E. Barkan, M. L. Bender, M. H. Thiemens, K. A. Boering, *Nature* **1999**, *400*, 547.
[3] Y. Q. Gao, R. A. Marcus, *Science* **2001**, *293*, 259.
[4] J. P. Roth, J. P. Klinman in *Isotope Effects in Chemistry and Biology* (Eds.: A. Kohen, H. Limbach), CRC, Boca Raton, **2005**.
[5] W. P. Huskey in *Enzyme Mechanism from Isotope Effects* (Ed.: P. F. Cook), CRC, Boca Raton, **1991**.
[6] L. Melander, W. H. J. Saunders, *Reaction Rates of Isotopic Molecules*, Wiley, New York, **1980**.
[7] J. Bigeleisen, M. Wolfsberg, *Adv. Chem. Phys.* **1958**, *1*, 15.
[8] S. A. Mills, Y. Goto, Q. Su, J. Plastino, J. P. Klinman, *Biochemistry* **2002**, *41*, 10577.
[9] S. S. Stahl, W. A. Francisco, M. Merkx, J. P. Klinman, S. J. Lippard, *J. Biol. Chem.* **2001**, *276*, 4549.
[10] W. A. Francisco, G. Tian, P. F. Fitzpatrick, J. P. Klinman, *J. Am. Chem. Soc.* **1998**, *120*, 4057.
[11] G. Tian, J. A. Berry, J. P. Klinman, *Biochemistry* **1994**, *33*, 226.
[12] L. Vaska, L. S. Chen, C. V. Senoff, *Science* **1971**, *174*, 587.
[13] J. A. McGinnety, J. A. Ibers, *Chem. Commun.* **1968**, 235.
[14] J. P. Birk, J. Halpern, A. L. Pickard, *J. Am. Chem. Soc.* **1968**, *90*, 4491.
[15] G. Wilke, H. Schott, P. Heimbach, *Angew. Chem.* **1967**, *79*, 62; *Angew. Chem. Int. Ed. Engl.* **1967**, *6*, 92.
[16] S. Otsuka, T. Yoshida, Y. Tatsuno, *J. Am. Chem. Soc.* **1971**, *93*, 6462.
[17] J. P. Collman, L. S. Hegedus, J. R. Norton, R. G. Finke, *Principles and Applications of Transition Metal Chemistry*, University Science, Mill Valley, **1987**.
[18] R. H. Crabtree, *Organometallic Chemistry of the Transition Metals*, Wiley, New York, **2001**.
[19] Burdick & Jackson "Anhydrous" brand solvents were used as received.
[20] Yields: *trans*-$[IrCl(CO)O_2(PPh_3)_2]$ $96\pm7\%$, $[IrO_2(dppe)_2]Cl$ $97\pm5\%$, $[PtO_2(PPh_3)_2]$ $107\pm7\%$, $[PdO_2(PPh_3)_4]$ $91\pm9\%$, and $[NiO_2(CNtBu)_2]$ $103\pm10\%$. $[NiO_2(PPh_3)_2]$ decomposes affording PPh_3 $44\pm10\%$ and $PPh_3(O)$ $48\pm9\%$.
[21] P. B. Chock, J. Halpern, *J. Am. Chem. Soc.* **1966**, *88*, 3511.
[22] No O_2 was released upon sparging solutions with He at 2 Torr for up to 2 h.
[23] C. A. Tolman, W. C. Seidel, D. H. Gerlach, *J. Am. Chem. Soc.* **1972**, *94*, 2669.
[24] A. Sen, J. Halpern, *J. Am. Chem. Soc.* **1977**, *99*, 8337.
[25] J. Bigeleisen, M. G. Mayer, *J. Chem. Phys.* **1947**, *15*, 261.
[26] G. Tian, J. P. Klinman, *J. Am. Chem. Soc.* **1993**, *115*, 8891.
[27] R. W. Horn, E. Weissberger, J. P. Collman, *Inorg. Chem.* **1970**, *9*, 2367.
[28] A. Nakamura, Y. Tatsuno, M. Yamamoto, S. Otsuka, *J. Am. Chem. Soc.* **1971**, *93*, 6052.
[29] P. J. Hayward, D. M. Blake, G. Wilkinson, C. J. Nyman, *J. Am. Chem. Soc.* **1970**, *92*, 5873.
[30] J. P. Roth, R. Wincek, G. Nodet, D. E. Edmondson, W. S. McIntire, J. P. Klinman, *J. Am. Chem. Soc.* **2004**, *126*, 15120.
[31] $E°'(Ir^{I}/Ir^{II}) = 1.32$ V vs the normal hydrogen electrode (NHE): K. Y. Jun, K. M. Ok, C. S. Chin, W. Shin, *Bull. Korean Chem. Soc.* **1998**, *19*, 23.
[32] $E°'(O_2^{0}/O_2^{-}) = -0.62$ vs NHE: D. T. Sawyer, A. Sobkowiak, J. L. J. Roberts, *Electrochemistry for Chemists*, Wiley, New York, **1995**.

 © 2005 Wiley-VCH Verlag GmbH & Co. KGaA, Weinheim

Electron Transfer

DOI: 10.1002/anie.200502180

Spin Transfer and Solvato-/Thermochromism Induced by Intramolecular Electron Transfer in a Purely Organic Open-Shell System**

Shinsuke Nishida, Yasushi Morita, Kozo Fukui, Kazunobu Sato, Daisuke Shiomi, Takeji Takui,* and Kazuhiro Nakasuji**

In search of organic functional materials, investigators have focused much attention on the switching of physical properties by using appropriate perturbation or stimuli. The integration of multiple controllable properties into a single-component system has been the subject of growing interest. Among such examples are the photoswitching of magnetic interaction by using a photochromic reaction[1] and thermal bistability in electric, magnetic, and optical properties of a crystalline neutral radical.[2] To realize spin-mediated new responsive materials, we are interested in reversible intramolecular electron transfer (IET), which can cause a complete transformation of magnetic and electronic properties in a purely organic system.[3] In an attempt to embody this concept, we have examined a stable neutral radical comprising electron-donor and -acceptor moieties, both of which can have spin before and after IET.

Taking advantage of the high electron-accepting ability of 2,5-di-*tert*-butyl-6-oxophenalenoxyl (6OP) stable neutral radical,[4] we have designed a diad system, **1**, in which 6OP radical is directly linked with a tetrathiafulvalene (TTF) molecule as an electron donor (Scheme 1).[5] In addition to the expected molecular spin, the diad **1** also meets the design criteria for organomagnetic materials,[6–8] single-component organic conductors,[2,9] and other potential applications.[10,11] Prior to the detailed characterization of its solid-state properties, we report herein the IET-induced transfer of spin that accompanies solvato-/thermochromism of **1** as a new molecular-scale function in solution, which is controlled by moderate change in the solvent environment and temperature.

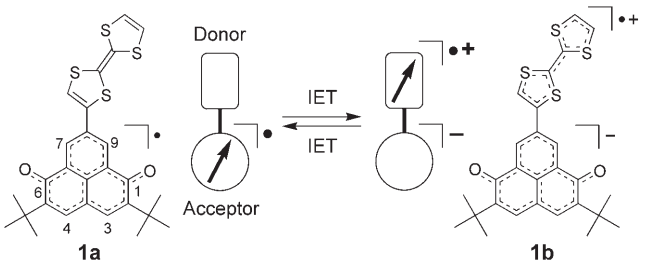

Scheme 1.

The neutral radical **1** was synthesized from 2,7-dimethoxyphenalanone derivative **2**[4a] in five steps (Scheme 2). Iodophenalenone **3** was prepared by treating **2** with iodine and cerium(IV) ammonium nitrate (CAN). TTF was introduced into phenalenone skeleton by the Stille reaction of **3** with the tributyltin derivative **4**. Reduction and demethylation of the coupling product **5** afforded the 6-hydroxyphenalenone derivative **6**.[12] Oxidation of **6** with PbO_2 in toluene gave neutral radical **1** as a black powder,[13] which is reasonably stable in air at room temperature for weeks. The radical is very stable in degassed solutions.

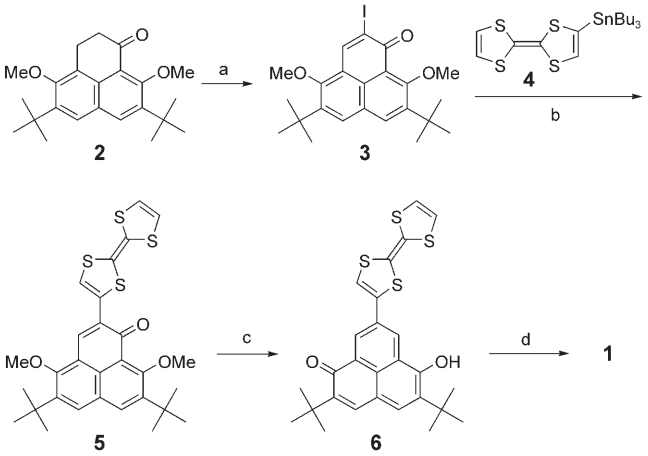

Scheme 2. Synthesis of neutral radical **1**: a) I_2 (2.5 equiv), CAN (2.5 equiv), $AcOH/H_2O$, 50 °C, 91 %; b) **3**, $[Pd(PPh_3)_4]$ (2 mol %), CuI (10 mol %), THF, 80 °C, 76 %; c) $NaBH_4$ (40 equiv), EtOH/THF (3:1); then LiI (20 equiv), *N*,*N*-dimethylacetamide, 170 °C, 34 %; d) PbO_2 (5 equiv), toluene, RT, 87 %.

The cyclic voltammogram of **1** in PhCN solution showed three fully reversible redox waves (Figure 1a). The observed redox potentials are close to those of the two constituent molecules (Table 1), which suggests that **1** is reduced and oxidized in a stepwise manner, with each step occurring independently at each moiety. The potential difference ΔE ($= E_{1/2}^{ox1} - E_{1/2}^{red}$) can, in principle, be related to the likelihood of IET of **1**; a smaller ΔE could lead to easier IET. The use of a $PhCN/CF_3CH_2OH$ solvent mixture significantly changed the first reduction potential ($E_{1/2}^{red}$) of **1**, depending on the mixing ratio (Figure 1b and c), without affecting the oxidation

[*] Dr. S. Nishida, Prof. Dr. Y. Morita, Prof. Dr. K. Nakasuji
Department of Chemistry, Graduate School of Science
Osaka University
Toyonaka, Osaka 560-0043 (Japan)
Fax: (+81) 6-6850-5395
E-mail: morita@chem.sci.osaka-u.ac.jp

Prof. Dr. K. Sato, Prof. Dr. D. Shiomi, Prof. Dr. T. Takui
Departments of Chemistry and Materials Science
Graduate School of Science, Osaka City University
Sumiyoshi-ku, Osaka 558-8585 (Japan)
E-mail: takui@sci.osaka-cu.ac.jp

Prof. Dr. Y. Morita, Dr. K. Fukui
PRESTO, Japan Science and Technology Agency (JST) (Japan)

[**] This work was supported by PRESTO-JST, Grant-in-Aid for Scientific Research (No. 769) from Ministry of Education, Culture, Sports, Science and Technology, Japan, and 21COE program "Creation of Integrated EcoChemistry of Osaka University".

Supporting information for this article is available on the WWW under http://www.angewandte.org or from the author.

 © 2005 Wiley-VCH Verlag GmbH & Co. KGaA, Weinheim

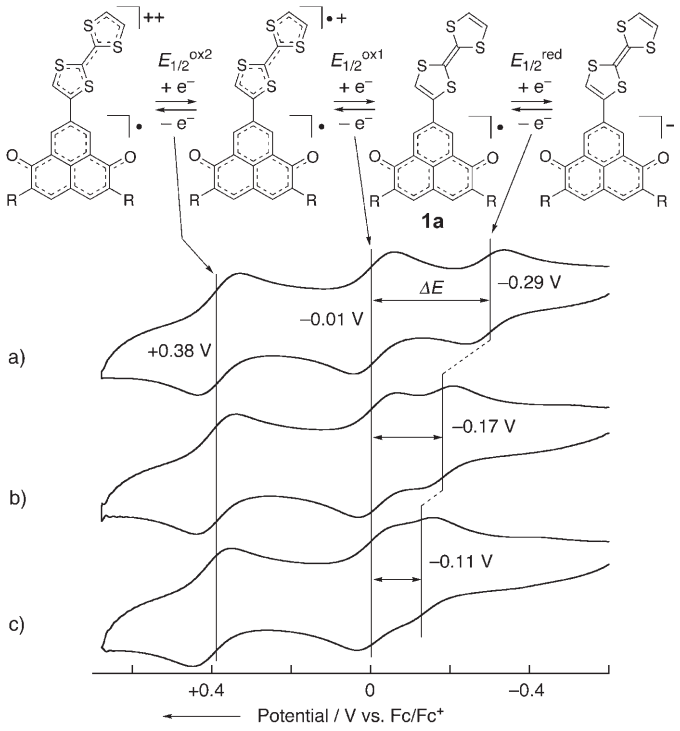

Figure 1. Cyclic voltammograms of solutions of **1** in PhCN/CF_3CH_2OH (1.0 mM) with the solvent ratio of a) 1:0, b) 9:1, and c) 4:1 measured at 293 K. Final potentials were calibrated with the ferrocene/ferrocenium (Fc/Fc^+) couple. R = *t*Bu.

Table 1: Redox potentials[a] of **1**, TTF, and 6OP.

	$E^{ox2}_{1/2}$	$E^{ox1}_{1/2}$	$E^{red}_{1/2}$
1	+0.38	−0.01	−0.29
TTF	+0.36[b]	−0.09	–
6OP	–	–	−0.36

[a] Potentials [V] vs. Fc/Fc^+ in PhCN at 293 K. Details are given in the Supporting Information. [b] Oxidation peak potential.

potentials for the TTF moiety ($E^{ox1}_{1/2}$, $E^{ox2}_{1/2}$). These results are interpreted as a marked effect of protonation or hydrogen-bonding interactions of a protic solvent to carbonyl groups, which stabilizes the anionic R-O^- structure.[14,15] This electrochemical study suggests that the IET of **1** can be controlled by the solvent environment.

The UV/Vis spectrum of a solution of **1** in CH_2Cl_2 (Figure 2a) showed a sharp absorption band at 414 nm, typical of the 6OP radical,[4a] which indicates the presence of the neutral radical **1a**. In addition, a weak broad absorption centered at 1315 nm was observed, which can safely be assigned to an IET band, not an intermolecular band, as proven by dilution studies (between 1.2×10^{-5} and 1.2×10^{-3} M). In contrast, a solution of **1** in CF_3CH_2OH did not show the sharp peak at 414 nm or the broad IET band while a new absorption at 605 nm appeared (Figure 2b). These changes are explained by assuming the zwitterionic structure **1b** with a TTF radical cation and 6OP anion moiety; all the spectral features can be reproduced by superimposition of the component spectra (see Supporting Information). Interestingly, the diad **1** shows solvatochromism depending on the IET states, as is evident from the different absorption wavelengths of **1a** and **1b** (Figure 2).

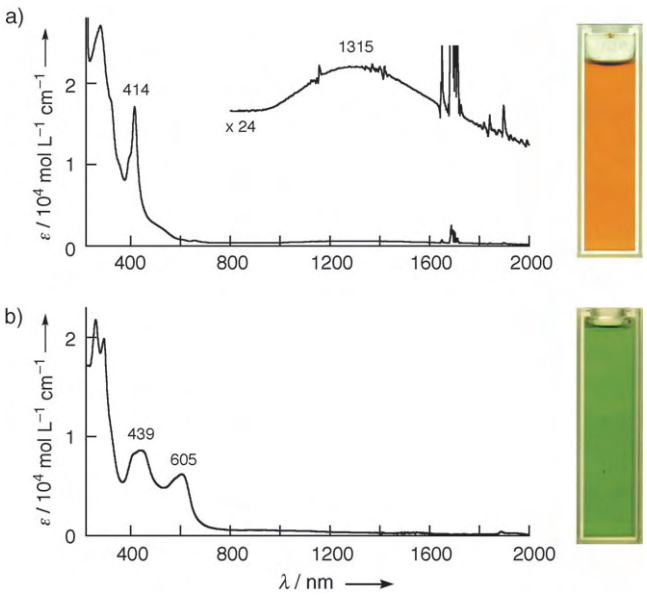

Figure 2. UV/Vis spectra and color of **1** in a) CH_2Cl_2 (1.2×10^{-4} M) and b) CF_3CH_2OH (7.6×10^{-5} M) solutions at 293 K.

To confirm the electronic structures of the two IET states, we have recorded the ESR spectra of **1** in aprotic and protic media. In a degassed toluene solution (1.0×10^{-4} M), radical **1** showed well-resolved hyperfine structures at 290 K with a *g* value of 2.0047 (Figure 3a). Electron-nuclear multiple resonance spectroscopy (^{1}H ENDOR/TRIPLE) unequivocally determined the hyperfine coupling constants (hfccs) of protons and their relative signs (Table 2). The obtained hfccs and *g* value are typical of 6OP radicals,[4a] which is clear evidence of the neutral radical structure **1a**. Although a small amount of spin density is delocalized into the TTF moiety, the spin structure virtually holds the 6OP-type distribution (Figure 4a).

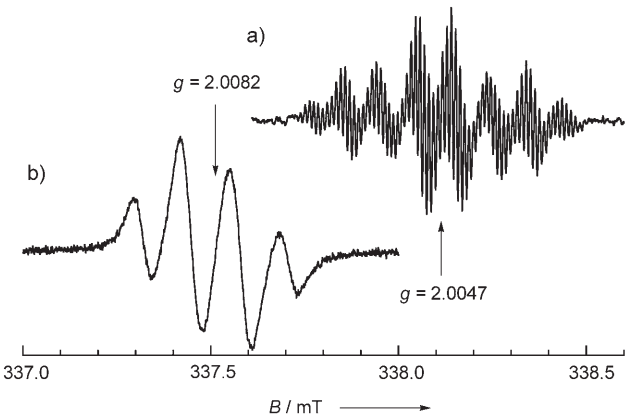

Figure 3. Liquid-phase ESR spectra of **1** in a) toluene (1.0×10^{-4} M) and b) CF_3CH_2OH (3.0×10^{-5} M) at 290 K. The microwave frequency used was 9.487717 GHz.

 © 2005 Wiley-VCH Verlag GmbH & Co. KGaA, Weinheim

Table 2: Proton hyperfine coupling constants [mT] and *g* values of **1a**, 6OP neutral radical, **1b**, and TTF radical cation.

	3, 4	7, 9	2,5-*t*Bu	TTF	*g* value
1a[a]	+0.199	+0.082	+0.011	−0.096	2.0047
6OP[a,b]	+0.206	+0.078	+0.012	–	2.0046
1b[c]	–	–	–	−0.126	2.0082
$TTF^{\bullet+}$[d]	–	–	–	−0.126	2.0084

[a] In toluene. [b] See ref. [4a]. [c] In CF_3CH_2OH. [d] In CH_2Cl_2. See reference [18].

In contrast, an ESR spectrum of **1** in a degassed CF_3CH_2OH solution (3.0×10^{-5} M) at 290 K gave a more downfield absorption ($g = 2.0082$) with three nearly equivalent ^1H couplings (Figure 3b). The observed hfccs and *g* value (Table 2) identified this species as the zwitterionic radical **1b** in which the TTF radical cation moiety is the spin-bearing center (Figure 4b). The localization of the spin densities at the TTF moiety may be associated with a possible twisted structure of **1b** induced by charge separation due to IET.[16]

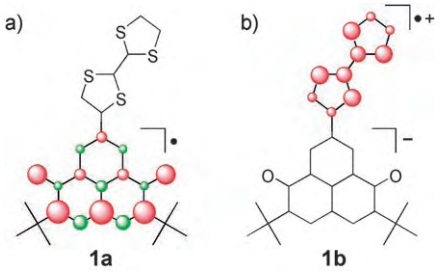

Figure 4. Postulated spin structures of a) **1a** and b) **1b**, assuming dominant contributions from 6OP neutral radical and TTF radical cation, respectively. Spin densities are calculated for the constituent molecules at the UBLYP/6-31G(d) level. Red and green denote positive and negative signs, respectively. Only the σ skeletons of **1a** and **1b** are depicted.

It is of interest to explore the possibility of the interconversion between the two states of **1** in a more controllable manner. By changing the solvent mixing ratio, we found an intermediate experimental condition that gave a mixture of **1a** and **1b**, which may be sensitive to additional perturbation or stimuli. A solution in CH_2Cl_2/CF_3CH_2OH (199:1) gave such an intermediate state at 263 K, the ESR spectrum of which is the superimposition of the spectra of **1a** and **1b** (Figure 5c). Furthermore, we observed a smooth transition from the **1b**-only pattern at 243 K to the **1a**-only pattern at 293 K in the ESR spectra (Figure 5). This process that accompanies themochromism is reversible, which suggests a temperature-dependent equilibrium between **1a** and **1b**. The mechanism of this interconversion needs to be studied further by considering quantitative analysis and solvent effects.[17]

In summary, we have described a purely organic open-shell donor–acceptor diad system, **1**, which exhibits an IET-induced spin transfer by solvatochromism, depending on the nature of solvent. Both the neutral radical, **1a**, and zwitterionic radical, **1b**, have been unequivocally characterized by

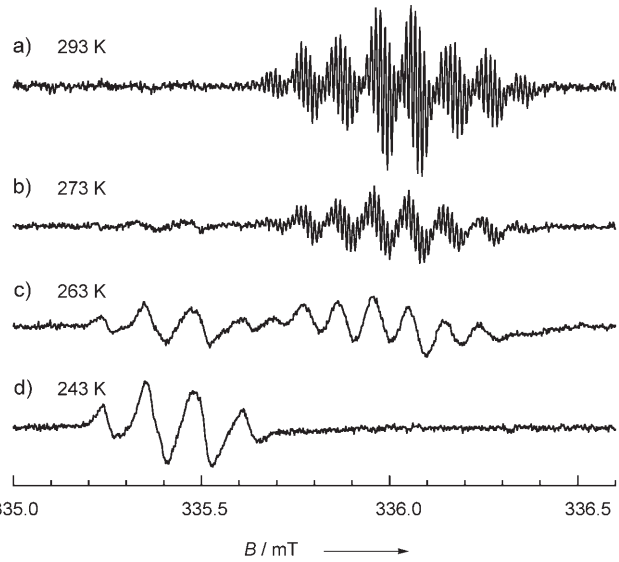

Figure 5. Temperature dependence of the liquid-phase ESR spectra of **1** in a CH_2Cl_2/CF_3CH_2OH (199:1) solution (7.7×10^{-5} M) at a) 293 K, b) 273 K, c) 263 K, and d) 243 K. The microwave frequency used was 9.4283 GHz.

UV/Vis and ESR spectroscopies in aprotic and protic media, respectively. The thermochromic interconversion between the two IET states of **1** has also been realized in a mixed solvent system. A possible switching of these combined properties by applying external stimuli such as an electrostatic field is of particular interest for molecular functionality, as well as for the characterization of its solid-state properties.

Received: June 22, 2005
Revised: August 24, 2005
Published online: October 13, 2005

Keywords: electron transfer · EPR spectroscopy · radicals · solvatochromism · thermochromism

[1] a) K. Matsuda, *Bull. Chem. Soc. Jpn.* **2005**, *78*, 383–392; b) S. Nakatsuji, *Chem. Soc. Rev.* **2004**, *33*, 348–353.
[2] M. E. Itkis, X. Chi, A. E. Cordes, R. C. Haddon, *Science* **2002**, *296*, 1443–1445.
[3] As for transition-metal complexes, such an interconversion is known as valence tautomerism, see: a) R. M. Buchanan, C. G. Pierpont, *J. Am. Chem. Soc.* **1980**, *102*, 4951–4957; b) P. Gütlich, A. Dei, *Angew. Chem.* **1997**, *109*, 2852–2857; *Angew. Chem. Int. Ed. Engl.* **1997**, *36*, 2734–2736; c) D. A. Shultz in *Magnetism: Molecule to Materials, Vol. II* (Eds.: J. S. Miller, M. Drillon), Wiley-VCH, Weinheim, **2001**, chap. 8, pp. 281–306; d) I. Ratera, D. Ruiz-Molina, F. Renz, J. Ensling, K. Wurst, C. Rovira, P. Gütlich, J. Veciana, *J. Am. Chem. Soc.* **2003**, *125*, 1462–1463; e) A. Dei, D. Gatteschi, C. Sangregorio, L. Sorace, *Acc. Chem. Res.* **2004**, *37*, 827–835.
[4] a) Y. Morita, T. Ohba, N. Haneda, S. Maki, J. Kawai, K. Hatanaka, K. Sato, D. Shiomi, T. Takui, K. Nakasuji, *J. Am. Chem. Soc.* **2000**, *122*, 4825–4826; b) Y. Morita, S. Maki, K. Fukui, T. Ohba, J. Kawai, K. Sato, D. Shiomi, T. Takui, K. Nakasuji, *Org. Lett.* **2001**, *3*, 3099–3102; c) Y. Morita, S. Nishida, J. Kawai, K. Fukui, S. Nakazawa, K. Sato, D. Shiomi, T. Takui, K. Nakasuji, *Org. Lett.* **2002**, *4*, 1985–1988; d) Y. Morita, J. Kawai,

 © 2005 Wiley-VCH Verlag GmbH & Co. KGaA, Weinheim

S. Nishida, N. Haneda, K. Fukui, K. Sato, D. Shiomi, T. Takui, K. Nakasuji, *Synth. Met.* **2003**, *137*, 1217 – 1218.
[5] *TTF Chemistry: Fundamentals and Applications of Tetrathiafulvalene* (Eds.: J. Yamada, T. Sugimoto), Kodansha & Springer, Heidelberg, **2004**.
[6] a) K. Yamaguchi, H. Namimoto, T. Fueno, T. Nogami, Y. Shirota, *Chem. Phys. Lett.* **1990**, *166*, 408 – 414; b) K. Yamaguchi, M. Okumura, T. Fueno, K. Nakasuji, *Synth. Met.* **1991**, *41–43*, 3631 – 3634.
[7] K. Maekawa, D. Shiomi, T. Ise, K. Sato, T. Takui, *J. Phys. Chem. B* **2005**, *109*, 9299 – 9304, and references therein.
[8] a) *Molecular Magnetism* (Eds.: K. Itoh, M. Kinoshita), Kodansha & Gordon and Breach, Tokyo, **2000**; b) *Magnetic Properties of Organic Materials* (Ed.: P. M. Lahti), Dekker, New York, **1999**.
[9] For zwitterionic radicals as single-component conductors, see: a) Y. Tsubata, T. Suzuki, T. Miyashi, Y. Yamashita, *J. Org. Chem.* **1992**, *57*, 6749 – 6755; b) K. Balodis, S. Khasanov, C. Chong, M. Maesato, H. Yamochi, G. Saito, O. Neilands, *Synth. Met.* **2003**, *133–134*, 353 – 355; c) T. Suzuki, S. Miyanari, H. Kawai, K. Fujiwara, T. Fukushima, T. Miyashi, Y. Yamashita, *Tetrahedron* **2004**, *60*, 1997 – 2003; See also: d) D. F. Perepichka, M. R. Bryce, C. Pearson, M. C. Petty, E. J. L. McInnes, J. P. Zhao, *Angew. Chem.* **2003**, *115*, 4784 – 4787; *Angew. Chem. Int. Ed.* **2003**, *42*, 4636 – 4639.
[10] For nonlinear optical materials, see: a) S. R. Marder, B. Kippelen, A. K.-Y. Jen, N. Peyghambarian, *Nature* **1997**, *388*, 845 – 851; b) S. Houbrechts, E. Hendrickx, T. Verbiest, K. Clays, A. Persoons in *Electron Transfer in Chemistry, Vol. 5* (Ed.: V. Balzani), Wiley-VCH, Weinheim, **2001**, chap. 8, pp. 241 – 281.
[11] For a unimolecular rectifier, see: R. M. Metzger, *Chem. Rev.* **2003**, *103*, 3803 – 3834.
[12] Selected physical data for **6**: m.p. 230–232 °C (decomp); thin layer chromatography (TLC) $R_f = 0.46$ (silica, hexane/ethyl acetate 2:1); C,H,N analysis (%)calcd for $C_{27}H_{26}O_2S_4$: C 63.49, H 5.13, N 0.00; found: C 63.34, H 5.23, N 0.00.
[13] Selected physical data for **1**: m.p. 166–168 °C (decomp); elemental analysis (%) calcd for $C_{27}H_{25}O_2S_4 \cdot H_2O \cdot 0.5\,C_6H_5CH_3$: C 63.84, H 5.45, N 0.00, S 22.35; found: C 63.67, H 5.22, N 0.00, S 22.25.
[14] N. Gupta, H. Linschitz, *J. Am. Chem. Soc.* **1997**, *119*, 6384 – 6391.
[15] a) Influence from solvent polarity on this effect seems to be negligible because the relative permittivity (ε) in the mixed solvents was kept constant ($\varepsilon \approx 26$), and the use of higher ε aprotic solvent does not cause this effect; b) In a mixed solvent, ε is given by $1/\varepsilon = \varphi_A/\varepsilon_A + \varphi_B/\varepsilon_B$, in which φ_A and ε_A are volume fraction and ε of solvent A, respectively; $\varepsilon_A(PhCN) = 25.30$, $\varepsilon_B(CF_3CH_2OH) = 26.67$. Y. Marcus, *Ion Solvation*, Wiley, New York, **1985**, chap. 7.
[16] Structural changes accompanying IET have been discussed: Z. R. Grabowski, K. Rotkiewicz, W. Rettig, *Chem. Rev.* **2003**, *103*, 3899 – 4031.
[17] S. V. Rosokha, D.-L. Sun, J. K. Kochi, *J. Phys. Chem. A* **2002**, *106*, 2283 – 2292.
[18] A. Terahara, H. Ohya-Nishiguchi, N. Hirota, H. Awaji, T. Kawase, S. Yoneda, T. Sugimoto, Z. Yoshida, *Bull. Chem. Soc. Jpn.* **1984**, *57*, 1760 – 1765.

 © 2005 Wiley-VCH Verlag GmbH & Co. KGaA, Weinheim

DNA Cleavage

DOI: 10.1002/anie.200502282

Binding of Naphthyridine Carbamate Dimer to the $(CGG)_n$ Repeat Results in the Disruption of the G–C Base Pairing

*Tao Peng and Kazuhiko Nakatani**

The expansion of the $(CGG)_n$ trinucleotide repeat in the FMR1 gene causes the neurological disorder fragile X syndrome.[1–3] The molecular basis for the $(CGG)_n$ expansion involves the formation of a metastable hairpin structure[4–6] consisting of continued 5′-CGG-3′/5′-CGG-3′ triads, in which a G–G mismatch is flanked by two G–C base pairs. We recently reported the remarkable binding of naphthyridine azaquinolone (**NA**) to the 5′-CAG-3′/5′-CAG-3′ triad in the hairpin form of the $(CAG)_n$ repeat, where the A–A mismatch was flanked by G–C base pairs. The ligand-bound structure was intriguing because 1) two **NA** molecules were bound to a single CAG/CAG triad which 2) induced the cytosine—which was hydrogen-bonded to the guanine—to flip out from the base stack (Figure 1).[7] The **NA**-immobilized sensor was useful for the rapid diagnosis of the $(CAG)_n$ repeat length. We have reported a series of ligands binding to a G–G mismatch,[8–10] and therefore the remarkable structure of **NA** bound to the CAG/CAG triad prompted us to investigate the mode of ligand binding to the CGG/CGG triad and, hence, the possibility of the cytosine flipping out in the ligand-bound complex. Herein, we report that naphthyridine carbamate dimer (**NC**)[11] binds to a single CGG/CGG triad with exclusively 2:1 **NC**/triad stoichiometry. The binding of **NC** to the CGG/CGG triad induced the disruption of the guanine–cytosine base pairing in the triad, and made the cytosine susceptible to the subsequent chemical cleavage reaction initiated by addition of hydroxylamine.

Among the ligands that we synthesized for binding to the G–G mismatch, **NC** showed a marked preference in binding to the CGG/CGG triad. The binding of **NC** to the CGG/CGG triad in the 13-mer duplex increased the melting temperature (T_m) by 23.1 °C, whereas the increase in T_m (ΔT_m) was only 6.7 °C for the GGC/GGC triad (Table 1). A survey of the effect of the flanking sequence suggested that the strong and selective **NC** binding to the CGG/CGG triad is most likely a consequence of the interaction of **NC** not only with the G–G mismatch, but also with the cytosine on the 5′ side and/or the guanine on the 3′ side.

[*] T. Peng, Prof. K. Nakatani
The Institute of Scientific and Industrial Research
Osaka University
Ibaraki 567-0047 (Japan)
Fax: (+81) 6-6879-8459
E-mail: nakatani@sanken.osaka-u.ac.jp

Supporting information for this article is available on the WWW under http://www.angewandte.org or from the author.

WILEY InterScience DISCOVER SOMETHING GREAT
© 2005 Wiley-VCH Verlag GmbH & Co. KGaA, Weinheim

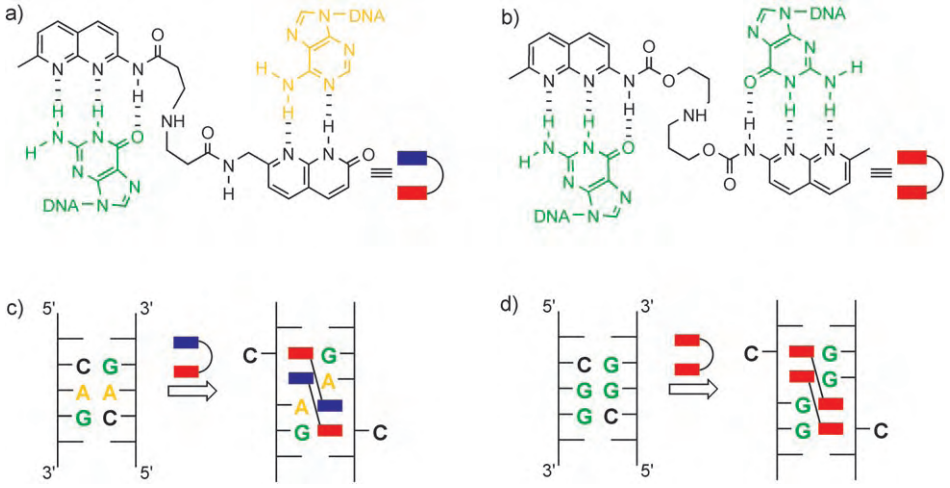

Figure 1. Hydrogen-bonding between a) **NA** and the G–A mismatch and b) **NC** and the G–G mismatch. Schematic illustrations of c) the NMR-confirmed **NA**-CAG/CAG triad complex and d) the proposed **NC** binding to the CGG/CGG triad. Red rectangles: 2-amino-1,8-naphthyridine; blue rectangles: 8-azaquinolone.

Table 1: ΔT_m [°C] and ΔT_m values [°C] for the 13-mer duplexes containing a G–G mismatch in a different flanking sequence.[a]

5′-GCTAA XGZ AATGA-3′
3′-CGATT YGW TTACT-5′

5′-XGZ-3′/5′-WGY-3′	$T_m(-)$[b]	$T_m(+)$[c]	ΔT_m[d]
CGG/CGG	34.1 (0.9)	57.2 (0.4)	23.1 (0.4)
CGC/GGG	38.6 (0.1)	49.3 (0.8)	10.7 (0.8)
GGC/GGC	40.4 (0.3)	47.1 (1.4)	6.7 (1.4)
CGA/TGG	31.8 (0.2)	44.4 (0.3)	12.6 (0.3)
CGT/AGG	33.6 (0.2)	44.0 (0.5)	10.4 (0.5)
GGA/TGC	34.2 (0.3)	43.4 (0.4)	9.2 (0.4)
AGT/AGT	28.7 (0.4)	41.9 (1.0)	13.2 (1.0)
AGG/CGT	31.8 (0.6)	39.9 (0.8)	8.1 (0.8)
GGT/AGC	33.7 (0.4)	39.3 (0.3)	5.6 (0.3)
TGA/TGA	17.8 (0.4)	35.9 (1.0)	18.1 (1.0)

[a] The UV melting curve was measured for a duplex (4.5 μM) in a sodium cacodylate buffer (10 mM, pH 7.0) containing NaCl (100 mM). The temperature was increased at a rate of 1 K min^{-1}. All measurements were made three times, and standard deviations are shown in parentheses. [b] T_m values of oligomers. [c] T_m values of oligomers in the presence of **NC** (100 μM). [d] ΔT_m was calculated as the difference between $T_m(+)$ and $T_m(-)$.

To determine the stoichiometry of the **NC**-CGG/CGG complex, cold-spray ionization time-of-flight mass spectrometry (CSI-TOF MS)[12] of the 11-mer self-complementary duplex containing the CGG/CGG triad was carried out (Figure 2). In the absence of **NC**, three ions derived from the oligomer were observed. One ion corresponded to the 3− ion of a single-stranded form ($[ss]^{3-}$; m/z: found 1118.13, calcd 1117.19). Duplexes were detected as a 5− ion ($[G–G]^{5-}$; m/z: found 1342.32, calcd 1340.83) and a 4− ion ($[G–G]^{4-}$; m/z: found 1678.07, calcd 1676.29). Upon addition of **NC** to the duplex with a 1:1 molar ratio, the intensity of the ions corresponding to $[ss]^{3-}$, $[G–G]^{5-}$, and $[G–G]^{4-}$ became weak, with the concomitant appearance of a new ion corresponding to the 5− ion of a 2:1 complex of **NC** and the duplex ($[G–G+2\mathbf{NC}]^{5-}$; m/z: found 1544.13, calcd 1542.13). A 1:1 complex was not detected. In the presence of two equivalents of **NC**, ions derived from the free duplex disappeared and only $[G–G+2\mathbf{NC}]^{5-}$ was detected. At an increased concentration of **NC**, the ion corresponding to $[G–G+2\mathbf{NC}]^{5-}$ was still predominant. These results clearly show that the binding of **NC** to the duplex containing the CGG/CGG triad proceeded exclusively with a 2:1 stoichiometry. The binding of **NC** to the CGG/CGG triad was further characterized by UV absorption titration experiments (see the Supporting Information). The crossover point of the Job's plot obtained from the titration was at 66%, which confirmed that the binding stoichiometry of **NC** to the CGG/CGG triad was 2:1, as determined by CSI-TOF MS (see the Supporting Information).

The high sequence preference and the 2:1 stoichiometry for **NC** binding are the same characteristic features that we observed for the binding of **NA** to the CAG/CAG triad.[7] Encouraged by these facts, we investigated whether the

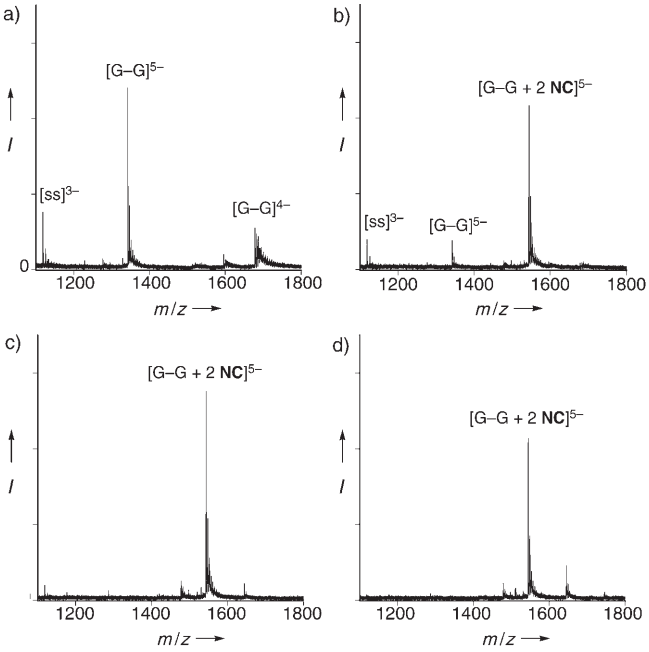

Figure 2. CSI-TOF MS of 11-mer self-complementary duplex 5′-d(TCAA CGG TTGA)-3′/5′-d(TCAA CGG TTGA)-3′ containing the CGG/CGG triad. Samples contained 20 μM duplex in 50% aqueous methanol and 100 mM ammonium acetate. The sample solution was cooled at −10°C during injection at a flow rate of 0.5 mL h^{-1}. a) Duplex only; b)–d) duplex with 20, 40, and 60 μM **NC**, respectively.

 © 2005 Wiley-VCH Verlag GmbH & Co. KGaA, Weinheim

cytosine in the CGG/CGG triad was free from the G–C base pairing upon **NC** binding. We examined the reaction of **NC**-bound CGG/CGG triad with hydroxylamine. Cytosines in the single-stranded regions and in the mismatched base pairs efficiently reacted with two molecules of hydroxylamine at the C4 and C6 positions, whereas those in the G–C base pair in a duplex were not susceptible to the addition of hydroxylamine. The cytosine modified with hydroxylamine underwent degradation on heating with piperidine, eventually leading to strand cleavage.[13]

The reaction of 11-mer self-complementary 5′-d(TCAA CGG TTGA)-3′ (**1**) with hydroxylamine was monitored by reversed-phase HPLC (Figure 3). The duplex of **1** (13 μM) was not reactive toward hydroxylamine (2.8 M, pH 6.0) at 0 °C for 12 h, whereas a new product **2** was produced in the presence of **NC** (40 μM). A prolonged reaction time (≈24 h) resulted in 70% consumption of **1** without the formation of any major by-products (see the Supporting Information), which suggests that both strands of **1** duplex reacted with hydroxylamine and produced **2**. MALDI-TOF MS showed that product **2** was the adduct of **1** with two molecules of hydroxylamine (*m*/*z*: found 3406.06, calcd 3403.62; see Scheme 1 and the Supporting Information).[13] After isolation by HPLC, product **2** was treated with piperidine at 90 °C for 30 min to give products **3** and **4**. The

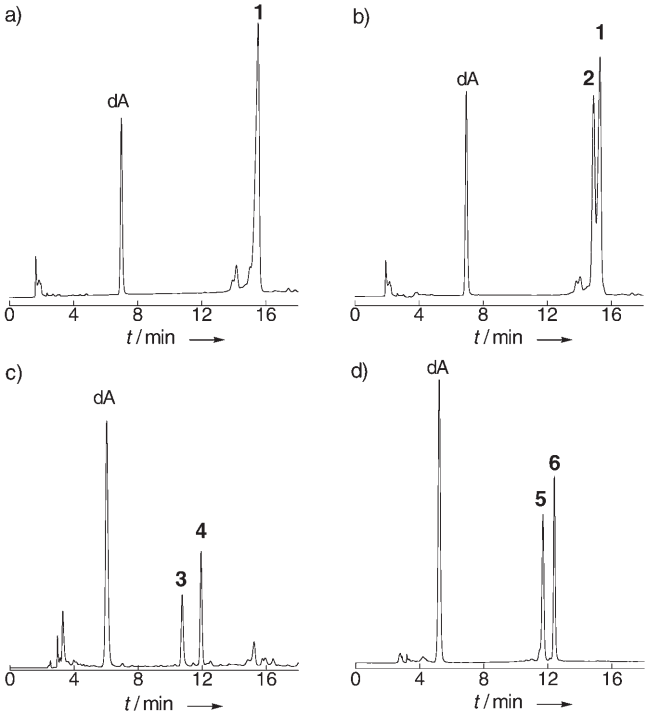

Figure 3. HPLC profiles for the hydroxylamine-induced cleavage at the cytosine moiety in the CGG/CGG triad. The 11-mer self-complementary oligomer 5′-d(TCAA CGG TTGA)-3′ (**1**) (13 μM as a duplex) in NaCl (100 mM) was treated with hydroxylamine (2.8 M, pH 6.0) in the a) absence and b) presence of **NC** (40 μM) at 0 °C for 12 h. c) Product **2** was isolated and treated with piperidine at 90 °C for 30 min. d) Products **3** and **4** were treated with alkaline phosphatase at 37 °C for 2 h. Deoxyadenosine (dA) was added as an internal standard.

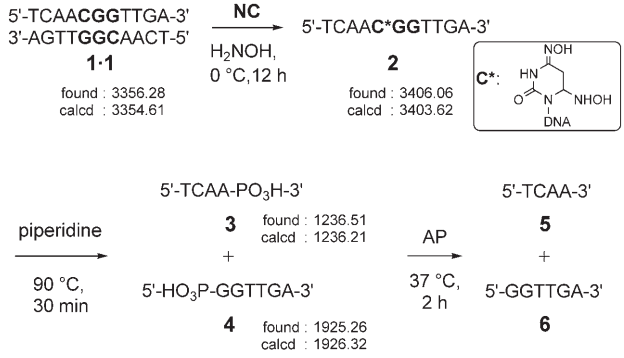

Scheme 1. Hydroxylamine-induced cleavage at cytosine in the **NC**-bound CGG/CGG triad. AP = alkaline phosphatase.

MALDI-TOF mass spectra showed that **3** was the oligomer 5′-d(TCAA)-PO_3H-3′ (*m*/*z*: found 1236.51, calcd 1236.21), whereas **4** was the oligomer 5′-HO_3P-d(GGTTGA)-3′ (*m*/*z*: found 1925.26, calcd 1926.32). The phosphorylated termini of **3** and **4** were removed by treatment with alkaline phosphatase to give 5′-d(TCAA)-3′ (**5**) and 5′-d(GGTTGA)-3′ (**6**), respectively. The oligomers **5** and **6** showed the same retention times as authentic oligomers, as observed by co-injection in reversed-phase HPLC. These HPLC analyses clarified that the cytosine in the CGG/CGG triad in **1** duplex became susceptible to the hydroxylamine upon binding with **NC**. The **1** duplex contained two kinds of cytosine, one in the CGG/CGG triad and the other in 5′-TCA-3′/5′-TGA-3′. The cytosine in the latter sequence was insensitive to hydroxylamine, regardless of the presence of **NC**. These results showed that the binding of **NC** to the CGG/CGG triad made the cytosine free from the base pairing to the guanine moiety in the opposite strand.

CSI-TOF MS measurements suggested that the 2:1 **NC**-CGG/CGG complex, which was confirmed for an oligomer duplex, was also produced in the $(CGG)_n$ repeat. CSI-TOF MS of $d(CGG)_{10}$ with **NC** showed the ions corresponding to $[d(CGG)_{10}+6\mathbf{NC}]^{6-}$ and $[d(CGG)_{10}+6\mathbf{NC}]^{7-}$, which suggests the formation of the 2:1 **NC**-CGG/CGG triad complex in the $d(CGG)_{10}$ repeat (see the Supporting Information). In addition, a large conformational change of $d(CGG)_{10}$ was observed in CD measurements upon binding with **NC** (see the Supporting Information), which supports the formation of a hairpin structure, as observed in the binding of **NA** to $d(CAG)_{10}$.[7]

In summary, the data presented herein have shown that 1) **NC** is the first molecule to bind to the CGG/CGG triad, and 2) the cytosine in the triad is free from hydrogen bonding to the guanine moiety upon **NC** binding. It is suggested that the 2:1 **NC**-CGG/CGG complex is produced in the hairpin structure of the $d(CGG)_n$ repeat, which is proposed to form in the replication leading to the repeat expansion. From the structural viewpoint, the **NC**-bound CGG repeats are particularly interesting. Base flipping as a result of the disruption of base pairing is one of the mechanisms for the repair enzyme to recognize the damaged bases and mismatched base pairs.[14–17] Therefore, **NC** could be a useful molecule for studying not only the repeat expansion mechanism, but also

 © 2005 Wiley-VCH Verlag GmbH & Co. KGaA, Weinheim

the nucleobase–ligand interactions on the biologically important repeat sequence.

Received: June 30, 2005
Revised: August 20, 2005
Published online: October 17, 2005

Keywords: DNA cleavage · mass spectrometry · nucleotides

[1] S. T. Warren, C. T. Ashley, *Annu. Rev. Neurosci.* **1995**, *18*, 77 – 99.
[2] R. D. Wells, S. T. Warren, *Genetic Instabilities and Hereditary Neurological Diseases*, Academic Press, New York, **1998**.
[3] A. Brussino, C. Gellera, A. Saluto, C. Mariotti, C. Arduino, B. Castellotti, M. Camerlingo, V. de Angelis, L. Orsi, P. Tosca, N. Migone, F. Taroni, A. Brusco, *Neurology* **2005**, *64*, 145 – 147.
[4] A. M. Gacy, G. Goellner, N. Juranic, S. Macura, C. T. McMurray, *Cell* **1995**, *81*, 533 – 540.
[5] K. Ohshima, R. D. Wells, *J. Biol. Chem.* **1997**, *272*, 16798 – 16806.
[6] A. M. Paiva, R. D. Sheardy, *J. Am. Chem. Soc.* **2005**, *127*, 5581 – 5585.
[7] K. Nakatani, S. Hagihara, Y. Goto, A. Kobori, M. Hagihara, G. Hayashi, M. Kyo, M. Nomura, M. Mishima, C. Kojima, *Nat. Chem. Biol.* **2005**, *1*, 39 – 43.
[8] K. Nakatani, S. Sando, I. Saito, *Nat. Biotechnol.* **2001**, *19*, 51 – 55.
[9] K. Nakatani, S. Sando, H. Kumasawa, J. Kikuchi, I. Saito, *J. Am. Chem. Soc.* **2001**, *123*, 12650 – 12657.
[10] K. Nakatani, S. Sando, I. Saito, *Bioorg. Med. Chem.* **2001**, *9*, 2381 – 2385.
[11] T. Peng, T. Murase, Y. Goto, A. Kobori, K. Nakatani, *Bioorg. Med. Chem. Lett.* **2005**, *15*, 259 – 262.
[12] K. Yamaguchi, *J. Mass Spectrom.* **2003**, *38*, 473 – 490.
[13] B. H. Johnston, *Methods Enzymol.* **1992**, *212*, 180 – 194.
[14] R. J. Roberts, X. Chen, *Annu. Rev. Biochem.* **1998**, *67*, 181 – 198.
[15] E. Seibert, J. B. A. Ross, R. Osman, *J. Mol. Biol.* **2003**, *330*, 687 – 703.
[16] D. S. Daniels, T. T. Woo, K. X. Luu, D. M. Noll, N. D. Clarke, A. E. Pegg, J. A. Tainer, *Nat. Struct. Mol. Biol.* **2004**, *11*, 714 – 720.
[17] C. Cao, Y. L. Jiang, J. T. Stivers, F. Song, *Nat. Struct. Mol. Biol.* **2004**, *11*, 1230 – 1236.

 © 2005 Wiley-VCH Verlag GmbH & Co. KGaA, Weinheim

DOI: 10.1002/anie.200502336

Molecularly Assembled Nanostructures of a Redox-Active Organogelator**

Tomoyuki Akutagawa, Keiko Kakiuchi, Tatsuo Hasegawa, Sin-ichiro Noro, Takayoshi Nakamura,* Hiroyuki Hasegawa, Sinro Mashiko, and Jan Becher*

Amphiphilic molecules in solution can form a variety of molecularly assembled structures, composed, for example, of gels, micelles, vesicles, tubes, or lamellas, in a variety of dimensions, shapes, and sizes.[1–3] Several types of low-molecular-weight molecules can form organogels that generate macroscopic phase-separated molecularly assembled structures in organic solvents.[4–7] Each molecule is assembled through specific intermolecular interactions and becomes part of a fibrous structure, which is entangled to form a three-dimensional (3D) pore structure.[4–7] In general, the most important type of intermolecular interaction in an organogel is hydrogen bonding. Therefore, the molecular structure of organogelators has been limited to about 30 kinds of molecules, such as fatty acids and their monovalent salts, steroids, anthryls, amino acids, and organometallic derivatives having hydrogen-bonding sites, such as hydroxy, carboxylic, amino, and carbonyl groups.[4–7] With the exception of 2,3-bis-*n*-decyloxyanthracene,[8] organogelators have been designed

[*] Prof. T. Akutagawa, Prof. T. Hasegawa, Dr. S.-i. Noro, Prof. T. Nakamura
Research Institute for Electronic Science
Hokkaido University
Sapporo 060-0812 (Japan)
Fax: (+81) 11-706-4972
E-mail: takuta@imd.es.hokudai.ac.jp
tnaka@imd.es.hokudai.ac.jp

Prof. T. Akutagawa, K. Kakiuchi, Prof. T. Hasegawa, Dr. S.-i. Noro, Prof. T. Nakamura
Graduate Schools of Environmental and Earth Science
Hokkaido University
Sapporo 060-0810 (Japan)

Prof. T. Akutagawa, Prof. T. Nakamura
CREST, Japan Science and Technology Agency (JST)
Kawaguchi 332-0012 (Japan)

Dr. H. Hasegawa, Dr. S. Mashiko
Kansai Advanced Research Center
Communication Research Laboratory
Incorporated Administrative Agency
Kobe 651-2492 (Japan)

Prof. J. Becher
University of Southern Denmark
Campusvej 55, 5230, Odense M (Denmark)

[**] This work was partly supported by a Grant-in-Aid for Science Research from the Ministry of Education, Culture, Sports, Science, and Technology of Japan.

Supporting information for this article is available on the WWW under http://www.angewandte.org or from the author.

© 2005 Wiley-VCH Verlag GmbH & Co. KGaA, Weinheim
InterScience

on the basis of their ability to participate in hydrogen-bonding interactions.

Organogelators have a tendency to form fibrous structures, which can be used to construct electrically active low-dimensional nanostructures even though most organogelators do not possess an electrically active π-electron system.[4–7] Electrically and optically active molecules, such as phthalocyanine, porphyrin, and thiophene, have been used to construct organogels through hydrogen-bonding interactions.[6,9–11] Sulfur-containing π-electron systems are useful building blocks for constructing highly electrically conducting molecularly assembled structures. For example, a variety of molecular metals and superconductors have been developed by incorporating the radical ions of tetrathiafulvalene (TTF) derivatives.[12] Organogelators incorporating S-containing π-electron systems have been reported, namely amphiphilic thiophene and TTF derivatives with hydrogen-bonding sites, which exhibit a capacity to gelate despite the absence of π–π interactions. To the best of our knowledge, the electronic properties of these organogelators have not yet been characterized. New organogelators with S-containing π-electron systems capable of self-assembling into fibrous structures through strong intermolecular S–S and π–π interactions have the potential to form electron-conducting pathways through the formation of a π-band structure. Thus, the π-stacking interaction is intrinsically a prerequisite for the formation of electrically active organogels.

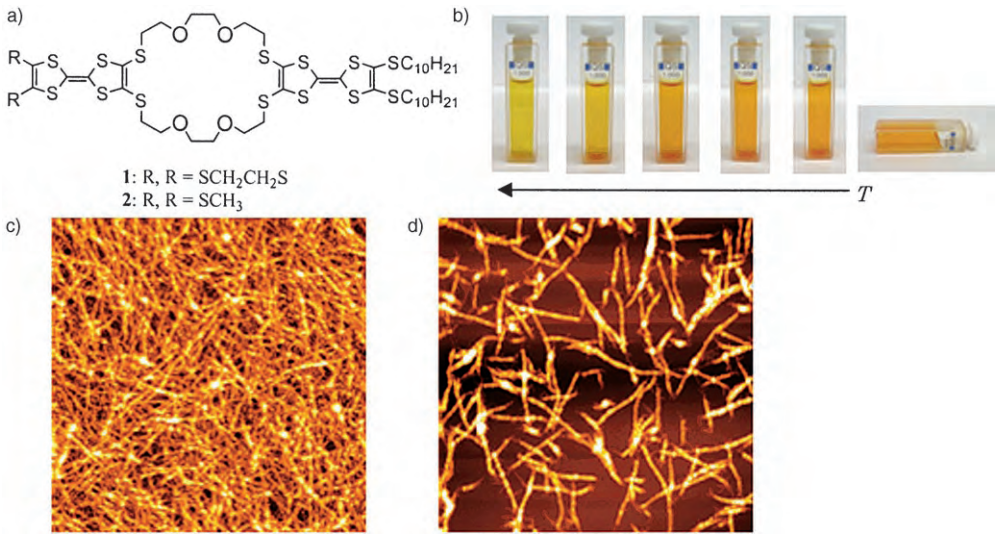

Figure 1. a) Molecular structure of amphiphilic bis-TTF annulated macrocyclic derivatives. b) Temperature-dependent organogelation of **1**. A 1 mM solution of **1** in $CHCl_3/CH_3CN$ (6/4) at 333 K was slowly cooled to 298 K. Organogelation was accompanied by a color change from yellow ($T = 333$ K) to orange ($T = 298$ K). c) Surface structure of the cast film of dried organogels on mica. d) Surface structure of a spin-coated film of dried organogels on mica. The rotational speed of the spinner was fixed at 4000 rpm. AFM images were recorded in a $10 \times 10\ \mu m^2$ scanning area.

We have constructed nanowires based on charge-transfer (CT) complexes of amphiphilic bis(tetrathiafulvalene) (bis-TTF) annulated macrocycles by molecular assembly as examples of electrically conducting nanostructures.[13,14] Formation of molecularly assembled nanowires with a typical dimension of $2.5 \times 50 \times \approx 1000\ nm^3$ has been achieved with a charge-transfer complex of a methylthio-substituted bis-TTF annulated macrocycle derivative.[2] Herein, we report a new amphiphilic bis-TTF annulated macrocycle derivative **1**, which can form redox-active organogels as well as electrically active nanostructures, such as nanowires and size-controllable nanodots (Figure 1 a).

Molecule **1** was synthesized to increase the magnitude of the intermolecular interactions: a terminal ethylenedithio group ($-SCH_2CH_2S-$) effectively enhances the intermolecular interactions through lateral S–S contacts in the molecularly assembled structures compared to those in **2**, which contains methylthio groups ($-SCH_3$).[13, 14] Molecule **1** was soluble in CH_2Cl_2, $CHCl_3$, toluene, 1,2-dichloroethane, but less-soluble in CH_3CN, acetone, CH_3OH, C_2H_5OH, and *n*-hexane. Slow cooling of a solution of **1** (1 mM) in $CHCl_3/CH_3CN$ (6/4) from 333 K resulted in the generation of organogels at 293 K (Figure 1 b). The yellow solution of **1** changed to an orange organogel upon cooling. The formation of organogels depended on the volume fraction of CH_3CN in the $CHCl_3/CH_3CN$ mixed solvent system. No organogels formed at room temperature at volume fractions of CH_3CN less than 40%. Other mixed-solvent systems such as $CHCl_3/CH_3OH$ (4/6), C_6H_6/CH_3CN (4/6), and $ClCH_2CH_2Cl/CH_3CN$ (4/6) also yielded organogels. However, the mixed-solvent systems of $CHCl_3/CH_3COCH_3$, $CHCl_3/C_2H_5OH$, and $CHCl_3/C_2H_5CN$ prevented formation of organogels.

Multiple hydrogen-bonding sites are the functional units that lead to one-dimensional fibrous structures in most organogelators. Although **1** possesses no hydrogen-bonding sites, the strong intermolecular π–π interactions enabled formation of an organogel. Organogelation of **1** results from replacing the terminal functional group by the ethylenedithio group since the bis(methylthio)-substituted bis-TTF annulated macrocycle **2** is incapable of forming organogels. It is known that a terminal ethylenedithio group sufficiently increases the dimensionality of intermolecular interactions through lateral interatomic S–S contacts along the peripheral direction in the π stacks.[12] Together with the π–π interaction, these intermolecular S–S interactions provide a two-dimensional electronic structure for a stable metallic and superconducting state in certain ion-radical salts of bis(ethylenedithio)-TTF.[12] Intermolecular S–S contacts of the terminal ethylenedithio group in **1** play an important role in increasing the intermolecular interaction to form fibrous structures in the organogel. The intermolecular interactions between

 © 2005 Wiley-VCH Verlag GmbH & Co. KGaA, Weinheim

electrically active TTF units, which lead to a π-band structure in the solid state, are important for obtaining electrically conducting nanoscale materials.

Figure 1c,d shows organogel structures fabricated as a dried gel by cast and spin-coating techniques (1 mM $CHCl_3$/CH_3CN (6/4)), respectively, on mica. In the case of the cast film, the fibers were entangled to form a 3D structure. The film surface morphology was characteristic of an organogel:[16] introduction of organic solvents into the 3D pore yielded an organogel. By contrast, isolated fibrous structures were observed in the case of the spin-coated film. The average width and height of the fibers were 50 and 8 nm, respectively, as revealed by AFM measurements.

The fibrous shape of the organogels is conducive to constructing novel low-dimensional nanostructures. We employed the Langmuir–Blodgett (LB) technique to obtain nanostructures from organogelator **1**. Transfer of the film from the Langmuir layer on an aqueous 0.01M KCl subphase onto mica resulted in the formation of fibrous structures with an average dimension of $7 \times 70 \times$ ca. 10000 nm^3. A 2.2-nm-thick two-dimensional monolayer underlays the fibers and covers 90% of the surface area (Figure 2a). The fibers were distributed randomly on the monolayer. Although a uniform Langmuir layer was observed in the film transferred from pure water, no fiberlike domains were formed, thus suggesting that the addition of ions into the subphase contributed to the formation of the fibrous structures of donor **1** in the LB film. The addition of electrolytes, such as NaCl, NaBr, and KCl, to water decreases the surface tension of amphiphilic molecules at the air–water interface[15] as a result of the stronger adsorption of the molecules on the electrolyte-containing interface than on pure water. The decrease in the surface tension of donor **1** on the 0.01M KCl aqueous subphase accelerates the formation of micellelike molecularly assembled structures.

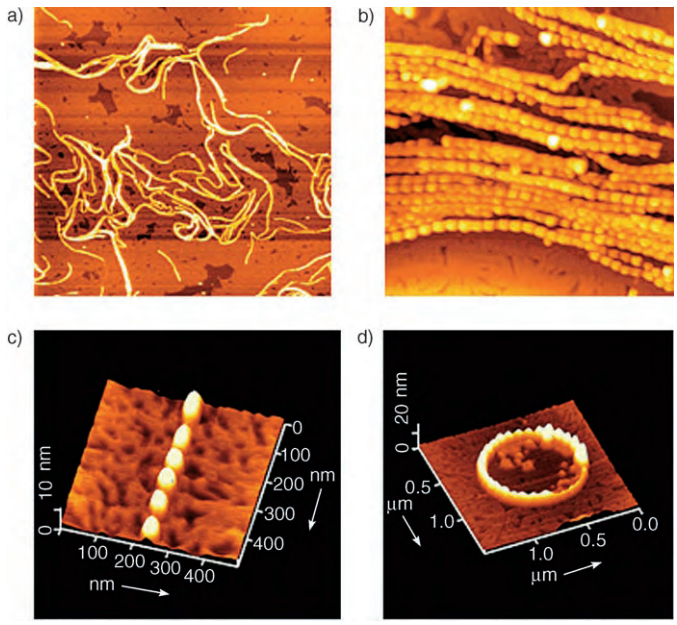

Figure 2. Surface structure of Langmuir–Blodgett films of **1** on mica. The films were fabricated by using a standard Langmuir trough at 291 K with a subphase containing 0.01 M KCl. The spreading solvent was a 0.5 mM solution of **1** in $CHCl_3$/CH_3CN (6/4) and the barrier speed was 50 $mm^2 min^{-1}$. Films were deposited by the vertical-dipping method at a constant surface pressure of 5 $mN m^{-1}$. a, b) The AFM images were recorded over an area of 10×10 and 2×2 μm^2. c, d) Expanded AFM images of a nanodot array. The nanodot-array structure has a connection of six nanodots (500×500 nm^2 image) and nanodot-ring structure is composed of about 40 nanodots (1.5×1.5 μm^2).

Each fiber was composed of a one-dimensional nanodot array (Figure 2b). The average diameter and height of the nanodots were 70 and 7 nm, respectively. The nanodots in the films often formed a regular array and ring structures (Figure 2c,d). The diameter of a nanodot ring consisting of about 40 nanodots was roughly 500 nm. The circumference of the nanodot ring (ca. 3 μm) was almost consistent with the sum of the average diameter of 40 nanodots (40×70 nm^2).

Although **1** forms nanofibers of nanodot arrays, these nanostructures are not expected to have a high electrical conductivity because of the closed-shell electronic structure. Molecule **1** shows a two-step redox behavior, with the first and second oxidation potentials at $E^1_{1/2} = 0.60$ and $E^2_{1/2} = 0.94$ V in CH_2Cl_2 (versus the saturated calomel electrode (SCE)), respectively, each of which corresponds to a two-electron ($2e^-$) oxidation reaction. The high electron-donating capacity of **1** enabled us to apply chemical oxidation by dissolving two equivalents of iodine (I_2) in a 0.5 mM solution of **1** in $CHCl_3$/CH_3CN (8/2).

The obtained CT complex of donor **1** with an open-shell electronic structure was subjected to spin coating using a drop (ca. 1 μL) of a 0.5 mM solution of **1**/$(I_2)_2$ in $CHCl_3$/CH_3CN on freshly cleaved mica. The rotational speed of the spinner was varied between 500 and 6000 rpm. Isolated nanodots were observed in spin-coated films (Figure 3a–d). No organogel was formed in the case of the 0.5 mM solution of **1**/$(I_2)_2$, thus indicating that the ability of **1** to form a fibrous structure was poor in the oxidized state. The diameter and height of the nanodots clearly depended on the rotational speed of the spinner (Figure 3e), with the nanodot diameter decreasing with increasing rotational speed. For example, the average diameter and height of the nanodots at a rotational speed of 6000 rpm were 200 and 20 nm, respectively, while those at 500 rpm were 800 and 400 nm, respectively. The diameters of the nanodots increased exponentially as the rotational speed decreases. The diameters of the nanodots can be varied from 200 to 1000 nm by adjusting the rotational speed of the spinner between 6000 and 500 rpm. The size of the nanodots can also be controlled by changing the experimental conditions, for example, the concentration of the CT complex and wetting angle of the substrate. Much smaller nanodots with a diameter of approximately 150 nm and a height of 13 nm were obtained in a diluted solution of the CT complex (0.1 mM) at a rotational speed of 4000 rpm. Small nanodots with a typical diameter of 20 nm and a height of 1.2 nm were often observed on the same spin-coated film.

The conductance of single nanodots fabricated on highly ordered pyrolytic graphite (HOPG) substrates was measured by conducting AFM (C-AFM).[16] The Pt-coated AFM tip directly contacted a single nanodot, thus forming an HOPG/nanodot/Pt sandwich. The red circles in Figure 4a at points I

 © 2005 Wiley-VCH Verlag GmbH & Co. KGaA, Weinheim

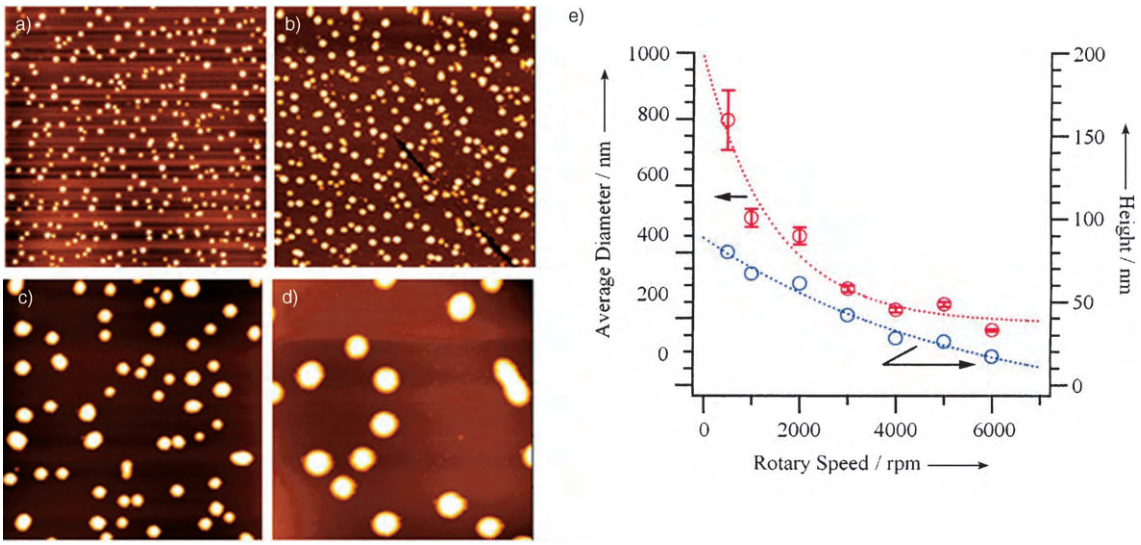

Figure 3. a–d) AFM images of size-controllable nanodots of the **1**/$(I_2)_2$ complex with an open-shell electronic structure on mica. The rotation speed of the substrate on the spinner was 6000, 4000, 2000, and 500 rpm for (a)–(d), respectively. The scale of all AFM images is $10\times10\ \mu m^2$. e) Rotational-speed dependence of the average diameter and height of the nanodots on mica. The average diameter and height of the nanodots were obtained by statistical analysis of the AFM images ($10\times10\ \mu m^2$).

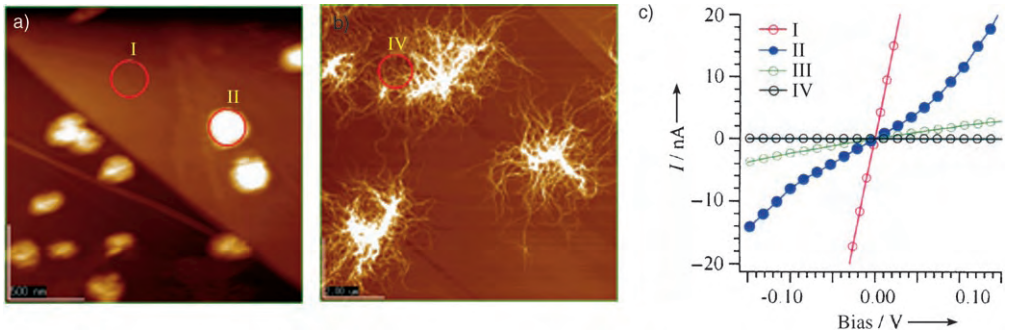

Figure 4. a) AFM image of nanodots of **1**/$(I_2)_2$ on HOPG for conducting-AFM (C-AFM) measurements ($2\times2\ \mu m^2$). After measurement of the topological image, the Pt-coated AFM tip contacted the bare HOPG surface (point I) and a single nanodot (point II) to measure their *I–V* characteristics. The nanodot structures were retained after the conductivity measurement, as confirmed by AFM measurement. b) AFM image of fibrous structures of **1** on HOPG ($10\times10\ \mu m^2$) prepared by spin casting of a 1 mM solution ($CHCl_3/CH_3CN$ 6:4). A Pt-coated AFM tip contacted a bundle of fibers with a height of about 2 nm (point IV). c) *I–V* characteristics at points I (HOPG), II (single nanodot in air), III (single nanodot in vacuum at 5×10^{-3} Pa), and IV (bundle of fibers). DC bias was applied from −0.2 to 0.2 V.

(bare HOPG) and II (single nanodot with a diameter of 200 nm and a height of 23 nm) correspond to the contact area of the C-AFM tip during *I–V* measurements. The conductance of bare HOPG and a single nanodot were obtained from the slope of the *I–V* curve to be 730 and 20 nS, respectively, at 5×10^{-3} Pa. The conductance of the nanodot increased to 86 nS under ambient conditions because of the effects of oxygen and/or water. The fibrous structure of **1** was formed on HOPG by spin coating using a 1 mM solution of **1** in $CHCl_3/CH_3CN$ (6/4). The surface morphology shows a neuronlike network structure (Figure 4b), with the bundles of fibers randomly distributed on the HOPG. The conductance of a fiber bundle with a height of about 2 nm (point IV in Figure 4b) was about 0.03 nS, which is four to five orders of magnitude smaller than that of a single nanodot with an open-shell electronic structure. The high conductance of single nanodots of the CT complex reflect the high concentration of the conduction carriers.

In conclusion, a new organogelator consisting of an amphiphilic bis-TTF annulated macrocyclic derivative was synthesized. The terminal ethylenedithio group increased the intermolecular interactions through lateral S–S contacts, in addition to the π–π interaction, which was responsible for organogelation. A three-dimensional entangled structure of fibers was confirmed in the dried organogel. The organogelator produced nanodot-array structures in Langmuir–Blodgett films. The chemically oxidized organogelator formed size-controllable isolated nanodot structures, which were simply fabricated by the spin-coating technique. The size of the nanodots depended on the rotational speed of the substrate, and was thus controllable. The conductance of a single nanodot with an open-shell electronic structure was four to five orders of magnitude higher than that of fibers of **1** with a closed-shell electronic structure. Nanostructures of molecular conductors can potentially be used in molecular electronic devices as electrically active units.

 © 2005 Wiley-VCH Verlag GmbH & Co. KGaA, Weinheim

Experimental Section

1: Donor **1** was synthesized by a stepwise protection/deprotection protocol of the cyanoethylene groups. 2-Iodoethoxyethane was introduced into ethylenedithiolo-bis(2-cyanoethylthio)TTF by deprotection of a cyanoethylene group, then treated under high-dilution conditions in DMF. The [24]crown-8 macrocycle was formed by addition of two equivalents of CsOH to the bis(TTF) compound, which yielded the amphiphilic bis(TTF) annulated macrocycle **1**. The **1**/$(I_2)_2$ complex was prepared in situ by mixing donor **1** and two equivalents of I_2 in $CHCl_3/CH_3CN$ (8/2, v/v). The concentration of the CT complex solution was fixed at 0.5 mM with respect to **1**/$(I_2)_2$.

The spin-coated films were produced on a mica surface ($10 \times 10\ mm^2$) by adjusting the rotational speed from 500 to 6000 rpm. About 1 μL of the CT complex solution was dropped onto the rotating mica surface, which was rotated for a further 60 s. The floating monolayers were left for 30 min after spreading of the CT complex (NIMA633 D2/D1). The LB monolayers were transferred onto freshly cleaved mica surfaces at a fixed surface pressure of $10\ mN\,m^{-1}$ by a single up-stroke.

Dynamic mode AFM images were recorded on a Seiko SPA 400 with an SPI 3800 probe station and JEOL JSPM-5200. Commercially available Si cantilevers with a force constant of $13\ N\,m^{-1}$ were used. *I–V* characteristics of the nanodots were measured by direct contact of the Pt-coated AFM tip with single nanodots on the HOPG surface.

Received: July 5, 2005
Published online: October 17, 2005

Keywords: conducting materials · gels · molecular electronics · nanostructures · thin films

[1] J. N. Israelachvili, *Intermolecular and Surface Forces*, Academic Press, London, **1992**.
[2] G. William, O. Leonard, J. Barbour, J. L. Atwood, *Science* **1999**, *285*, 1049 – 1052.
[3] S. I. Stupp, V. LeBonheur, K. Walker, L. S. Li, K. E. Huggins, M. Keser, A. Amstutz, *Science* **1997**, *276*, 384 – 389.
[4] P. Terech, R. G. Weiss, *Chem. Rev.* **1997**, *97*, 3133 – 3159.
[5] L. A. Estroff, A. D. Hamilton, *Chem. Rev.* **2004**, *104*, 1201 – 1218.
[6] D. J. Abdallah, R. G. Weiss, *Adv. Mater.* **2000**, *12*, 1237 – 1247.
[7] O. Gronwald, E. Snip, S. Shinkai, *Curr. Opin. Colloid Interface Sci.* **2002**, *7*, 148 – 156.
[8] F. Placin, M. Colomès, J.-P. Desvergne, *Tetrhadron Lett.* **1997**, *38*, 2665 – 2668.
[9] a) M. Jörgensen, K. Bechgaard, T. Björnholm, P. Sommer-Larsen, L. G. Hansen, K. Schaumburg, *J. Org. Chem.* **1994**, *59*, 5877 – 5882; b) T. L. Gall, C. Pearson, M. R. Bryce, M. C. Petty, H. Dahlgaard, J. Becher, *Eur. J. Org. Chem.* **2003**, 3562 – 3568.
[10] C. F. van Nostrum, S. J. Picken, A.-J. Schouten, R. J. M. Nolte, *J. Am. Chem. Soc.* **1995**, *117*, 9957 – 9965.
[11] F. S. Schoonbeek, J. H. van Esch, B. Wegewijs, D. B. A. Rep, M. P. de Haas, T. M. Klapwijk, R. M. Kellogg, B. L. Feringa, *Angew. Chem.* **1999**, *111*, 1486 – 1490; *Angew. Chem. Int. Ed.* **1999**, *38*, 1393 – 1397.
[12] T. Ishiguro, K. Yamaji, G. Saito, *Organic Superconductors*, Springer, New York, **1998**.
[13] T. Akutagawa, T. Ohta, T. Hasegawa, T. Nakamura, C. A. Christensen, J. Becher, *Proc. Natl. Acad. Sci. USA* **2002**, *99*, 5028 – 5033.
[14] T. Akutagawa, K. Kakiuchi, T. Hasegawa, T. Nakamura, C. A. Christensen, J. Becher, *Langmuir* **2004**, *20*, 4187 – 4195.
[15] P. Mukerjee, *J. Phys. Chem.* **1965**, *69*, 4038 – 4040.
[16] T. W. Kelley, E. L. Granstrom, C. D. Frisbie, *Adv. Mater.* **1999**, *11*, 261 – 264.

 © 2005 Wiley-VCH Verlag GmbH & Co. KGaA, Weinheim

DOI: 10.1002/anie.200502463

Origin of the Minor Enantiomeric Product in a Noyori Asymmetric Hydrogenation: Evidence for Pathways Different to the Major Mechanism**

*Yoshitaka Ishibashi, Yuhki Bessho, Masahiro Yoshimura, Masaki Tsukamoto, and Masato Kitamura**

In a typical asymmetric catalytic process, a prochiral substrate (Sub) is converted into a major ($Prod_S$) and a minor ($Prod_R$) enantiomeric product via diastereomeric catalyst–substrate (CatSub) and catalyst–product (CatProd) complexes (Scheme 1). The two cycles are diastereomorphic to each

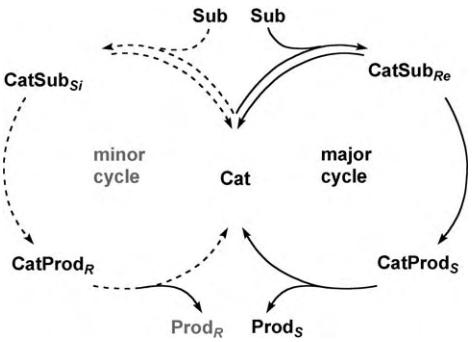

Scheme 1. Competition between diastereomorphic catalytic cycles.

other, but they take place through a single mechanism. As such, the Arrhenius equation can be applied confidently to correlate the $Prod_S/Prod_R$ ratio to the relative stabilities of the diastereomeric transition states at the first irreversible step from CatSub to CatProd.[1] The energy profile thus obtained can be utilized to estimate the structural difference between the two transition states. In most cases, however, this premise of a single mechanism has not been confirmed.[2] We have long suspected that in some cases $Prod_S$ and $Prod_R$ may be

[*] Y. Ishibashi, Y. Bessho, M. Yoshimura, M. Tsukamoto, Prof. Dr. M. Kitamura
Research Center for Materials Science and Department of Chemistry, Nagoya University
Chikusa, Nagoya 464–8602 (Japan)
Fax: (+81) 52-789-2261
E-mail: kitamura@os.rcms.nagoya-u.ac.jp

[**] This work was supported by a Grant-in-Aid for Scientific Research (No. 14078121) from the Ministry of Education, Science, Sports, and Culture, Japan. We are grateful to Professor R. Noyori for valuable discussions and to T. Noda, K. Oyama, and Y. Maeda for their technical support with reaction vessel production and measurements of NMR spectra.

Supporting information for this article (asymmetric hydrogenation and isotope-labeling experiments) is available on the WWW under http://www.angewandte.org or from the author.

 © 2005 Wiley-VCH Verlag GmbH & Co. KGaA, Weinheim InterScience

generated through entirely different catalytic cycles in which several chain carriers produced in a given reaction system convert the same substrate but with different reactivities and enantioselectivities. In such a catalytic process, various reaction parameters dynamically link the species, and therefore the observed enantioselectivity becomes the average contribution of the mechanistically different cycles.[3] Herein, we report for the first time a clear example of asymmetric catalysis that yields $Prod_S$ and $Prod_R$ from the same substrate but through different mechanisms.

This new case was identified in the hydrogenation of (*Z*)-3-phenyl-2-butenoic acid ((*Z*)-**2**) in the presence of [Ru-$(CH_3CO_2)_2$\{(*R*)-binap\}] ((*R*)-**1**).[4] Under standard conditions ((*R*)-**1** (0.5 mM), (*Z*)-**2** (100 mM), Sub/Cat = 200:1, methanol, 30 °C, 1–4 atm), (*S*)-3-phenylbutanoic acid ((*S*)-**3**) was obtained with 94 % ee when a pressure of 1–4 atm was applied. The value decreased to 92 % *ee* at 50 atm and to 88 % *ee* at 100 atm,[5] whereas the reaction rate was enhanced when the pressure of the hydrogen was increased.[6] The substrate (*Z*)-**2** is stable and undergoes neither *Z*/*E* geometrical nor α,β/β,γ (C2–C3/C3–C4) positional isomerization during the course of the hydrogenation.[5,7] To improve the accuracy of the isotope-labeling experiments, the ^{13}C-labeled substrate (*Z*)-[3-^{13}C]**2** was used, and the (*R*)-**1**-catalyzed hydrogenations were carried out in CH_3OD by changing the hydrogen pressure and the ratio of H_2 and D_2. All the reactions were stopped at low conversions to minimize complications caused by gas–solvent and gas–gas isotope exchange.[2,5] The enantiomeric products, (*S*)-**3** (major) and (*R*)-**3** (minor), were separated by chiral HPLC (CHIRALCEL OD (20 mm × 25 cm); eluent: hexane/2-PrOH/AcOH 1000:1:3),[5] and the ratio of the eight isotopomers (3*S*)-2H,3H-[3-^{13}C]**3**, (3*S*)-2H,3D-[3-^{13}C]**3**, (2*R*,3*S*)-2D,3H-[3-^{13}C]**3**,[9] (2*R*,3*S*)-2D,3D-[3-^{13}C]**3**,[9] (3*R*)-2H,3H-[3-^{13}C]**3**, (3*R*)-2H,3D-[3-^{13}C]**3**, (2*S*,3*R*)-2D,3H-[3-^{13}C]**3**,[9] and (2*S*,3*R*)-2D,3D-[3-^{13}C]**3**[9] was determined by $^{13}C\{^1H,^2H\}$ NMR spectroscopic analysis of the *S* and *R* products (Scheme 2).[5,10]

Figure 1 represents the change in the distribution pattern of the major and minor enantiomeric products in going from the H_2 to H_2/D_2 conditions. When the reaction was carried out in CH_3OD under a pressure of 4 atm of H_2, a mixture of (*S*)-**3** and (*R*)-**3** was obtained in a ratio of 97:3. The major *S* product consisted of 2H,3H, 2H,3D, 2D,3H, and 2D,3D isotopomers (10:89:0:1). Under an atmosphere of H_2/D_2 (1:1) in CH_3OD, the ratio shifted to 3:46:3:48. This change in distribution can be understood simply in terms of the Ru monohydride mechanism proposed in the Ru–binap-catalyzed hydrogenation of tiglic acid[11,12] or α-(acylamino)acrylic esters.[2,13] In short, a RuH species, generated from (*R*)-**1** and H_2, delivers hydride to the *Si* face at C2 of (*Z*)-**2** to form the (3*R*)-C3–Ru intermediate. Cleavage of the C–Ru bond utilizes both H_2 gas (the RuH/C3–Ru/H_2 route) and CH_3OD (the RuH/C3–Ru/H^+ route), and leads to a mixture of (3*S*)-2H,3H and (3*S*)-2H,3D (10:89).[14,15] Under a 1:1 mixture of H_2/D_2 gas, the RuH/C3–Ru/H_2 route should produce the four isotopomers in a 1:1:1:1 ratio (blue line) and the RuH/C3–Ru/H^+ route should produce 2H,3D and 2D,3D in a 1:1 ratio (green line); therefore, a relative proportion of ≈3 each for the (3*S*)-2H,3H, (3*S*)-2H,3D, (3*S*)-2D,3H, and (3*S*)-2D,3D isotopomers will be derived from the 10 part, and ≈44 for the (3*S*)-2H,3D and (3*S*)-2D,3D isotopomers from the 89 part. Simple calculation estimates the ratio to be 3:47:3:47, which is consistent with the observed ratio.

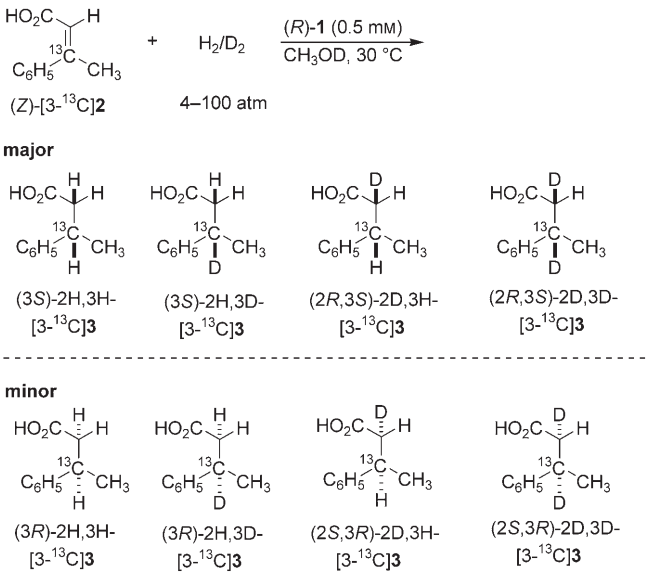

Scheme 2. Structures of the eight possible isotopomers from the reduction of (*Z*)-[3-^{13}C]**2** in CH_3OD under H_2/D_2 mixtures at different pressures.

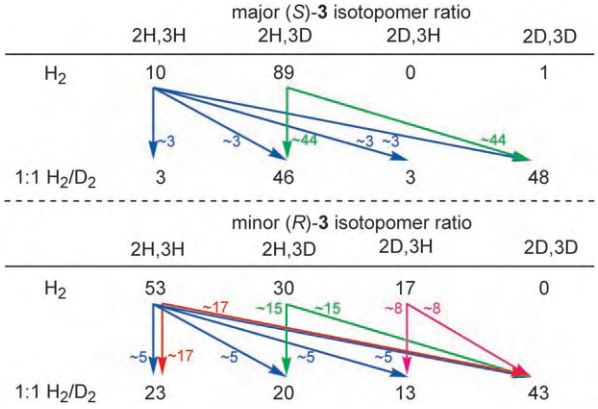

Figure 1. Change of the isotopomer ratios in the (*R*)-binap–Ru-catalyzed hydrogenation of (*Z*)-[3-^{13}C]**2** in CH_3OD under 4 atm of H_2 or H_2/D_2 (1:1). Top: (*S*)-[3-^{13}C]**3** obtained as the major product (97 %). Bottom: (*R*)-[3-^{13}C]**3** obtained as the minor product (3 %). The colored arrows indicate the reaction pathways and the estimated distribution of the isotopomers when the conditions are switched from H_2 to H_2/D_2 (1:1). → RuH/C3–Ru/H_2 and/or RuH/C2–Ru/H_2 (RuH/H_2); → RuH/C3–Ru/H^+; → RuH_2; → RuH/C2–Ru/H^+.

In contrast, the minor *R* enantiomer contained largely the (3*R*)-2H,3H (53 %) together with the (3*R*)-2H,3D (30 %) and (3*R*)-2D,3H (17 %) isotopomers. More gaseous hydrogen appears to be consumed in the formation of the minor product than in that of the major *S* enantiomer, and formation of the 2D,3H isotopomer is characteristic of the minor product. The reaction carried out in CH_3OD under a mixture of H_2/D_2 (1:1) generated a 23:20:13:43 mixture of the four 3*R* isotopomers. The ambiguous isotope-labeling patterns, which

 © 2005 Wiley-VCH Verlag GmbH & Co. KGaA, Weinheim

are totally different from those of the major enantiomer, can be explained by assuming that the RuH_2 route[5] (red line) and the RuH/C2–Ru/H^+ route (purple line) are involved as well as the above two reaction pathways (blue and green lines) (Figure 1, minor). The two hydrides on RuH_2 are delivered from the same *Re*,*Si* face of (*Z*)-**2** to C2 and C3 in a pairwise manner.[16] In the RuH/C2–Ru route, a conjugate-type addition of the hydride of a RuH species onto the *Si* face of C3 generates a (2*R*,3*S*)-C2–Ru intermediate,[17] which then undergoes hydrogenolysis (RuH/C2–Ru/H_2) or protonolysis (RuH/C2–Ru/H^+). Thus, the 2H,3H, the 2H,3D, and the 2D,3H isotopomers in the H_2/CH_3OD reaction are produced through the pathways RuH_2 and RuH/H_2,[18] the RuH/C3–Ru/H^+ route, and the RuH/C2–Ru/H^+ route, respectively. In light of the 2H,3H:2H,3D:2D,3H:2D,3D distribution coefficients (1:1:1:1 for RuH/C3–Ru/H_2 and RuH/C2–Ru/H_2 (blue line), 0:1:0:1 for RuH/C3–Ru/H^+ (green line), 1:0:0:1 for RuH_2 (red line), and 0:0:1:1 for RuH/C2–Ru/H^+ (purple line)), the isotopomer ratio obtained by the replacement of H_2 with a 1:1 mixture of H_2/D_2 gas is calculated to be 22:20:13:45. Figure 2a shows the good agreement between the values estimated from the H_2/CH_3OD results (colored bars) and the experimental values (gray bars). The colors correspond to those of the reaction pathways shown in Figure 1.

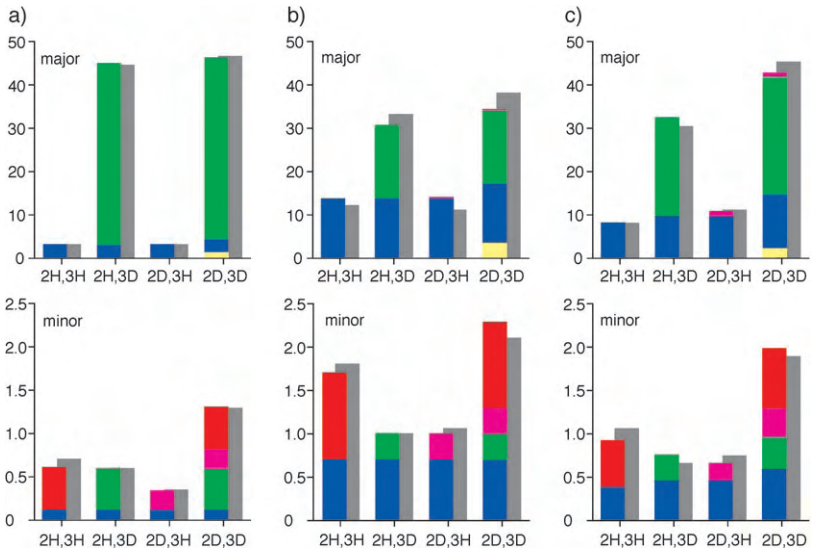

Figure 2. Observed (gray) and estimated (colored) isotopomer ratios of the major *S* and minor *R* products in the (*R*)-binap–Ru-catalyzed hydrogenation of (*Z*)-[3-^{13}C]**2** in CH_3OD under: a) 4 atm of H_2/D_2 (1:1), b) 100 atm of H_2/D_2 (1:1), and c) 50 atm of H_2/D_2 (44:56). Colored values are estimated from the experimental results of 4, 50, and 100 atm H_2/CH_3OD conditions. ■ RuH/C3–Ru/H^+; ■ RuH/C3–Ru/H_2 and/or RuH/C2–Ru/H_2; ■ RuH_2; ■ RuH/C2–Ru/H^+; ■ unknown mechanisms; *x* axis: isotopomers of **3**; *y* axis: yield [%].

This tendency is also seen with changes in the pressure of the hydrogen gas and the H_2/D_2 ratio (Figure 2b,c).[19] An increase in hydrogen pressure from 4 to 100 atm in CH_3OD approximately tripled the formation of the minor enantiomer (Figure 2a, minor vs. Figure 2b, minor), and enhanced the contribution of gaseous hydrogen to both the major and minor product pathways. The amount of major product formed by the RuH/H_2 pathway (blue bars) increased approximately five times and was coupled with a significant decrease in the involvement of the RuH/C3–Ru/H^+ route (green bars), whereas the contribution of the RuH_2 pathway (red bars) to the formation of the minor product doubled. In the case of the reaction carried out in CH_3OD under H_2/D_2 gas (44:56) at 50 atm, the *S* and *R* products (96:4) consisted of the eight isotopomers in a 9:31:11:45:1.0:0.6:0.7:1.7 ratio, as indicated by the gray bars in Figure 2c. A reasonable agreement with the estimation from the results obtained from the reaction in CH_3OD under 50 atm of H_2 was observed after a 0.44/0.56 correction to the above distribution coefficients.

Each asymmetric catalytic cycle proceeding through the RuH/C3–Ru/H_2, RuH/C3–Ru/H^+, RuH/C2–Ru/H_2, RuH/C2–Ru/H^+, or RuH_2 routes, or other possible reaction pathways, has its own energy diagram, according to which the overall rate as well as the stereochemistry is determined.[20] Neither the details of the kinetics nor the structures of the intermediates are known at present, but a series of isotope-labeling experiments indicated that this Ru–binap-catalyzed asymmetric hydrogenation of an α,β-unsaturated carboxylic acid involves several catalytic species and that a significant amount of the minor *R* enantiomer is formed through the RuH/C2–Ru/H^+ and RuH_2 pathways, which are hardly involved in the formation of the major product (Scheme 3). Asymmetric catalytic reactions convert a prochiral substrate

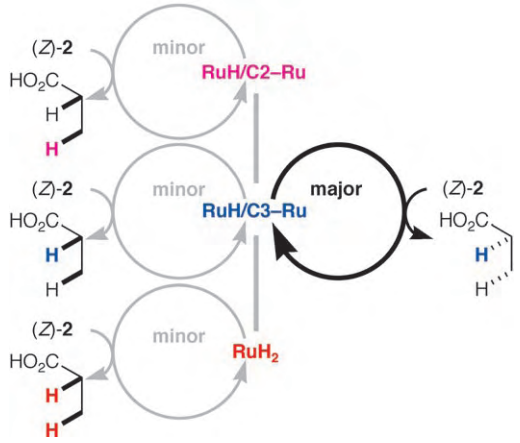

Scheme 3. Possible catalytic cycles producing the major *S* and minor *R* enantiomers from the same (*Z*)-**2** substrate through different chain carriers. C3 substituents of (*Z*)-**2** and products have been omitted for clarity.

into an enantiomer-enriched chiral product. The observed enantioselectivity has generally been interpreted to result from competing diastereomorphic catalytic cycles caused by a single chiral catalyst. However, this supposition has not been substantiated. Together with earlier examples,[2,11,12] our study calls into question such a generalized treatment.

Received: July 14, 2005
Published online: October 18, 2005

 © 2005 Wiley-VCH Verlag GmbH & Co. KGaA, Weinheim

Keywords: enantioselectivity · homogeneous catalysis · hydrogenation · isotopic labeling · reaction mechanisms

[1] S. Arrhenius, *Z. Phys. Chem.* **1889**, *4*, 226 – 248.

[2] For the first report of the confirmation of the involvement of the two diastereomeric cycles, see: M. Kitamura, M. Tsukamoto, Y. Bessho, M. Yoshimura, U. Kobs, M. Widhalm, R. Noyori, *J. Am. Chem. Soc.* **2002**, *124*, 6649 – 6667.

[3] For examples of the different pathways through initial isomerization of substrates, see: a) Y. Sun, C. LeBlond, J. Wang, D. G. Blackmond, J. Laquidara, J. R. Sowa, Jr., *J. Am. Chem. Soc.* **1995**, *117*, 12647 – 12648; b) C. Detellier, G. Gelbard, H. B. Kagan, *J. Am. Chem. Soc.* **1978**, *100*, 7556 – 7561; c) K. E. Koenig, W. S. Knowles, *J. Am. Chem. Soc.* **1978**, *100*, 7561 – 7564; d) C. A. Willoughby, S. L. Buchwald, *J. Am. Chem. Soc.* **1994**, *116*, 11703 – 11714; e) D.-R. Hou, J. Reibenspies, T. J. Colacot, K. Burgess, *Chem. Eur. J.* **2001**, *7*, 5391 – 5400; for a concept of different pathways with the same chain carrier, see: f) M. Sawamura, R. Kuwano, Y. Ito, *J. Am. Chem. Soc.* **1995**, *117*, 9602 – 9603.

[4] Binap = 2,2′-bis(diphenylphosphanyl)-1,1′-binaphthyl.

[5] For details, see Supporting Information.

[6] For an opposite effect, see: M. Kitamura, M. Yoshimura, M. Tsukamoto, R. Noyori, *Enantiomer* **1996**, *1*, 281 – 303.

[7] T. Ohta, H. Takaya, M. Kitamura, K. Nagai, R. Noyori, *J. Org. Chem.* **1987**, *52*, 3174 – 3176; hydrogenation of (*E*)-**2** in methanol at 4 atm and 10–25 °C for 25 h gave (*R*)-**3** in 97 % yield with 5 % *ee*; notably, the *E* isomer readily isomerizes to β,γ-unsaturated carboxylic acid, which was hydrogenated with (*R*)-**1** in methanol under similar conditions (S/C = 200:1, 1.5 atm, 10–25 °C, 2 h) to afford (*S*)-**3** with 74 % *ee*.[8]

[8] T. Uemura, X. Zhang, K. Matsumura, N. Sayo, H. Kumobayashi, T. Ohta, K. Nozaki, H. Takaya, *J. Org. Chem.* **1996**, *61*, 5510 – 5516.

[9] The absolute configurations, 2*R*,3*S* and 2*S*,3*R*, are altered to 2*S*,3*S* and 2*R*,3*R* with ^{13}C-unlabeled 2D,3H-**3** and 2D,3D-**3**.

[10] The authentic (2*R**,3*S**)-2D,3H-**3** and (2*S**,3*S**)-2D,3H-**3** were prepared by diimide reduction of (*Z*)-2D-**2** and (*E*)-2D-**2**, respectively.[9] The isotope stability of the product was confirmed.[5]

[11] M. T. Ashby, J. Halpern, *J. Am. Chem. Soc.* **1991**, *113*, 589 – 594.

[12] T. Ohta, H. Takaya, R. Noyori, *Tetrahedron Lett.* **1990**, *31*, 7189 – 7192.

[13] a) J. A. Wiles, S. H. Bergens, *Organometallics* **1998**, *17*, 2228 – 2240; b) J. A. Wiles, S. H. Bergens, *Organometallics* **1999**, *18*, 3709 – 3714.

[14] The hydrogenation proceeded with overall *cis* addition.[5]

[15] The mechanism for the generation of (*S*)-2D,3D in 1 % yield is unknown.

[16] R. Eisenberg, *Acc. Chem. Res.* **1991**, *24*, 110 – 116.

[17] D. W. Lubell, M. Kitamura, R. Noyori, *Tetrahedron: Asymmetry* **1991**, *2*, 543 – 554.

[18] In this experiment, RuH/C3–Ru/H_2 and RuH/C2–Ru/H_2 cannot be discriminated.

[19] Some deviations from expectations are probably due to the gas/gas and gas/solvent isotope exchange and to the isotope effect. For the mechanism of the H/D exchange between RuH and CH_3OD and between RuH and D_2, see: P. G. Jessop, R. H. Morris, *Coord. Chem. Rev.* **1992**, *92*, 155 – 284.

[20] a) R. Noyori, M. Kitamura in *Modern Synthetic Methods* (Ed.: R. Scheffold), Springer, Berlin, **1989**, pp. 115 – 198; b) R. Noyori in *Asymmetric Catalysis in Organic Synthesis*, Wiley, New York, **1994**, chap. 2.

 © 2005 Wiley-VCH Verlag GmbH & Co. KGaA, Weinheim

Nanotechnology

DOI: 10.1002/anie.200501815

Proofreading and Error Removal in a Nanomaterial Assembly**

*Juewen Liu, Daryl P. Wernette, and Yi Lu**

Recent progress in the self-assembly of nanomaterials promises to revolutionalize a number of science and engineering fields such as molecular electronics, photonics, and computation.[1–7] A key hurdle to realizing such a potential is the presence of imperfect structures or errors in the assembly process. To overcome this problem, major efforts have been focused on optimizing the assembly process to minimize errors or to design devices that can tolerate errors.[8–11] We argue that it could be equally valuable to investigate proofreading and error removal during and after assembly, as demonstrated beautifully in a number of processes in biology, such as in mRNA-templated protein synthesis (Figure 1 a).[12] Herein, we provide the first experimental demonstration of proofreading and error removal in nanomaterial assembly by using DNAzymes to specifically locate and remove errors in DNA-templated gold nanoparticle assemblies (Figure 1 b). The concept demonstrated here can be applied to the assembly of other nanomaterials using other bio- or biomimetic molecules.

We chose to demonstrate the proofreading and error-removal process in a DNA-templated nanoparticle assembly because remarkable progress has been made in the field, which has resulted in both nanostructures with high resolution, controllability, and versatility[1–3,13–15] and nanomaterials with potential for practical applications such as colorimetric sensing.[16–19] For a design strategy, we searched biological processes for guiding principles. As shown in Figure 1 a, errors could occur in protein synthesis on an mRNA template where an incorrect amino acid might be incorporated. To prevent such a process, proofreading units (such as GTPase elongation factor-Tu) are employed to identify such an error and remove the wrong amino acid.[12] Similarly, errors could occur in a DNA-templated gold nanoparticle assembly, where each nanoparticle is coded by DNA molecules with a unique sequence, just as each amino acid is coded by a transfer RNA (tRNA) molecule. Among the three kinds of nanoparticles in the system, two (A and B) are defined as "correct" particles to be assembled on the template, while the remaining one (B′) is

[*] J. Liu, D. P. Wernette, Dr. Y. Lu
Department of Chemistry
Beckman Institute for Advanced Science and Technology
University of Illinois at Urbana-Champaign
Urbana, IL 61801 (USA)
Fax: (+1) 217-333-2685
E-mail: yi-lu@uiuc.edu

[**] This material is based upon work supported by the U. S. Army Research Laboratory and the U. S. Army Research Office under grant number DAAD19-03-1-0227, and the U. S. National Science Foundation under grant number DMR-0117792.

WILEY InterScience DISCOVER SOMETHING GREAT
© 2005 Wiley-VCH Verlag GmbH & Co. KGaA, Weinheim

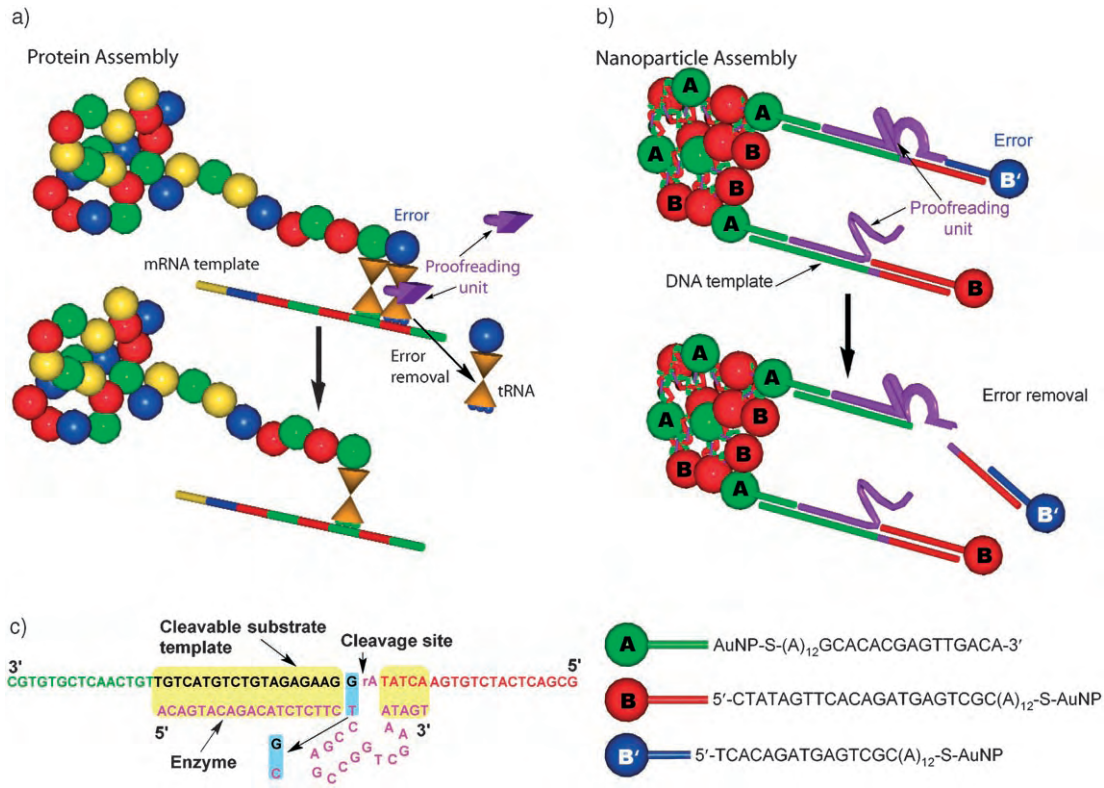

Figure 1. Proofreading and error removal in biology (a) and in materials science (b). a) The last tRNA moiety and its amino acid do not match the mRNA template (coded by colors) and are removed by the proofreading unit. b) The error-removal process is triggered by adding Pb^{2+} ions. c) Secondary structure of the DNAzyme used for proofreading and error removal in DNA-functionalized gold nanoparticle assemblies. The DNA sequences attached to gold nanoparticles (AuNP) are also shown. $(A)_{12}$ denotes a polyadenine spacer containing 12 A bases.

defined as an "error" particle (Figure 1b). Nanoparticle A can bind to the 3′ arm of the DNA template, while nanoparticle B binds to the 5′ arm of the template, both through sequence-specific hybridization. The error particle B′ can also bind to the 5′ arm of the template. However, the DNA attached to B′ is seven bases shorter than that attached to nanoparticle B. As a result, the affinity of B′ to the template is less than that of B, similar to the decreased affinity between an error tRNA and the mRNA template.

Instead of using protein enzymes for proofreading and error removal in protein synthesis, we chose to use a DNAzyme (DNA with catalytic activity), because it has the advantage of performing both structural roles to assemble nanoparticles and functional roles for proofreading and error removal.[20–22] The DNAzyme contains a substrate strand and an enzyme strand that form two duplex regions (Figure 1c, highlighted in yellow). In the presence of Pb^{2+} ions, the substrate is cleaved into two pieces at the rA position by the enzyme. The two duplex regions are designed to be asymmetrical, with one side containing 19 base pairs while the other side contains only five base pairs. Therefore, the cleaved fragment with the shorter binding arm can be easily released. To allow the DNAzyme substrate to be a template for nanoparticle assembly, the two overhangs on the substrate strand are complementary to the DNA attached to the nanoparticles. If a correct particle B is incorporated, binding of the longer arm of the enzyme to the DNA template is permitted while binding of the shorter arm to the DNA template is inhibited so that the active structure of the DNAzyme cannot form. As a result, the template is not cleaved and particle B is incorporated. When a B′ error particle is incorporated, the enzyme can bind both its arms to the substrate template and form an active structure to cleave the substrate and remove the B′ particle. This process is summarized in Figure 1b.

To demonstrate the specific removal of B′ particles from the assembly, a series of nanoparticle assemblies were prepared in such a way that the number of A particles equaled the sum of B and B′ particles. First, two extreme scenarios, 100% B (no B′) and 100% B′ (no B), were tested. The UV/Vis spectra of the two samples before and after error removal by Pb^{2+} addition are presented in Figure 2a and b, respectively. The sample with 100% B particles had only a slight increase of extinction at the 522-nm peak after error removal, which suggests that the assembly did not undergo significant changes (Figure 2a). However, for the sample with 100% B′ particles, the extinction at 522 nm increased whereas the extinction in the 700-nm region decreased significantly, thus resulting in a higher 522 to 700 nm extinction ratio. This finding suggests that nanoparticles in the A/B′ system were in the disassembled state (Figure 2b).[18,19] To test the effectiveness of proofreading and error removal in between the two extreme conditions, samples with various percentages of B′ particles were prepared and the 522 to 700 nm extinction

 © 2005 Wiley-VCH Verlag GmbH & Co. KGaA, Weinheim

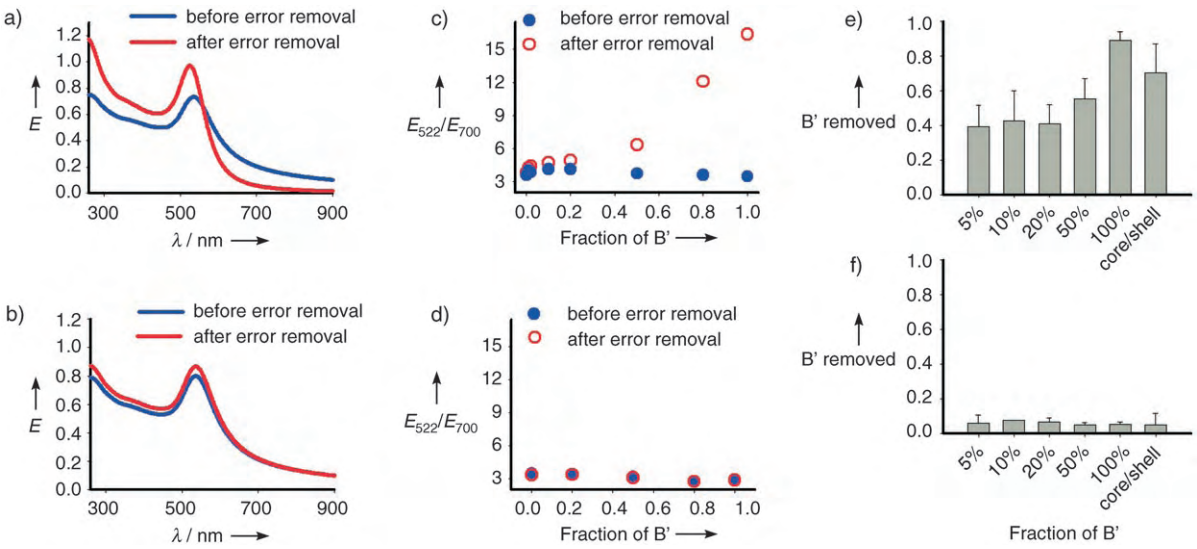

Figure 2. UV/Vis spectra of the nanoparticle assemblies made of particles A/B′ (a) or A/B (b) before and after proofreading and error removal. Extinction (*E*) ratios of the samples with various fractions of B′ particles before and after error removal with the native active enzyme (c) or mutated inactive enzyme (d). Fluorescence-based quantification of B′ particles removed from nanoparticle assemblies with the native active enzyme (e) or mutated inactive enzyme (f).

ratios before and after error removal were plotted against the fraction of B′ particles (Figure 2c). The extinction ratio increased with an increase of B′ particles, which suggests successful removal of the B′ particles from the assembly. To confirm that the change in the extinction ratio was a result of the error-removal mechanism, a control experiment was performed by replacing the enzyme strand with an inactive mutant. The mutated enzyme differs by only one base from the native enzyme (the T base highlighted in blue in Figure 1c was mutated to a C base.[23]) No change in the extinction ratio was observed by error removal with the mutated enzyme (Figure 2d). This control experiment strongly suggests that the DNAzyme is the key element in the proofreading and error-removal process.

To further investigate the extent of error removal, fluorescein-labeled DNA was used to functionalize the B′ particles in addition to the original fluorescein-free DNA. After addition of Pb^{2+} ions, the samples were centrifuged at 2000 rpm for 2 min. At such a speed, the nanoparticle assemblies were forced to the bottom, while dispersed particles remained in the supernatant. The isolated precipitate was redispersed and recentrifuged twice to completely separate the assembled nanoparticles from the dispersed nanoparticles. The fluorescein-labeled DNA was then displaced into solution by adding a high concentration of β-mercaptopropionic acid.[24] The percentage of B′ particles released from the assembled nanoparticles was calculated by comparing the fluorescence intensity from the assembled nanoparticles to that of the supernatant. As shown in Figure 2e, the percentage of B′ particles removed increased with the B′ particle percentage present in the assembled nanoparticles, from ca. 40% removal at a low percentage of B′ particles to almost complete removal at the 100% level. The incomplete removal of B′ particles at a low percentage in the assemblies is attributable to the fact that B′ particles embedded inside the assembled nanoparticles may not be released, even if the DNA template is cleaved. To support this hypothesis, assemblies of A and B particles were first prepared as a core, and then B′ particles were added as a shell to ensure that they were exposed on the surface of the assembly. Indeed, at a similarly low percentage of B′ particles, the percentage removal increased from ca. 40 to 70% for the core–shell structures. In addition, nonspecific release of nanoparticles in the process may contribute to the calculated percentage of error removal. This possibility was investigated by using the inactive enzyme mutant where the T base highlighted in Figure 1b was mutated to a C base (Figure 2f). Less than 10% of the B′ nanoparticles were released in the process of washing and handling. Therefore, nonspecific dissociations cannot account for the observed error removal.

The specific error-removal process was also confirmed by transmission electron microscopy (TEM). Instead of using 13-nm particles in all cases, 5-nm particles were used as the B′ error particles to differentiate them from the 13-nm correct particles (A and B). Typical TEM images of nanoparticle assemblies before and after error removal are presented in Figures 3a and b, respectively. The images indicate clearly that the number of 5-nm error particles in Figure 3a decreased significantly after error removal.

In summary, we have designed an experimental system for studying proofreading and error removal in a nanomaterial assembly. We showed that error particles can be specifically removed from the system. In addition, the error-correction process is controlled by a chemical stimulus (in this, case Pb^{2+} ions). By replacing the lead-specific DNAzyme with DNAzymes sensitive to other analytes, chemically controlled error removal can also be realized.[20,22,25,26] Finally, the concept presented here can be extended to other biomolecules, for example, to protein enzymes or biomimetic compounds such as chemical nucleases, for controlling the assembly not only of

 © 2005 Wiley-VCH Verlag GmbH & Co. KGaA, Weinheim

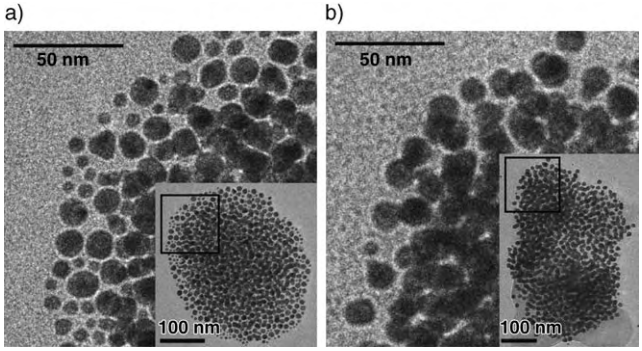

Figure 3. TEM images (acquired with a Philips CM200 TEM) of a nanoparticle assembly before (a) and after (b) proofreading and error removal. The complete nanoparticle assemblies are shown in the insets and the magnified regions are highlighted by squares. There are two kinds of nanoparticles in the images, with average diameters of 13 and 5 nm. The number of 5-nm error particles decreased significantly after the proofreading and error-removal process.

nanoparticles with defined size, shape, or composition, but also of other nanomaterials such as nanotubes or nanowires.

Experimental Section

Gold nanoparticles of 13- and 5-nm diameter were prepared by the citrate reduction[27] and $NaBH_4$ reduction[28] methods, respectively. Thiol-labeled DNA molecules were attached to gold nanoparticles by methods described in the literature.[27] The nanoparticles were purified twice by centrifugation, removal of the supernatant, and replacement with new buffer (100 mM NaCl, 25 mM Tris acetate, pH 8.2). To prepare fluorescein-labeled B′ particles, 5′-FAM-$(A)_{12}$-SH-3′ (20%) was also added in addition to the original DNA (80%).

Nanoparticles A, B, and/or B′ were mixed at designated ratios with a final extinction at 522 nm of ≈ 2. The system also contained substrate (100 nM), the enzyme strand (or the mutated enzyme, 200 nM), NaCl (300 mM), and Tris acetate buffer (25 mM, pH 8.2). The assembled nanoparticles were prepared by heating the sample at 65 °C for 1 min in a water bath (containing 60 mL water), and subsequently cooling to room temperature for 1 h. The sample was then centrifuged at 2000 rpm for 1 min. The supernatant was removed and the assembled nanoparticles were redispersed in NaCl (100 mM) and Tris acetate (25 mM, pH 8.2). To prepare samples for the TEM experiment, the 5-nm B′ particles were added later to form a core–shell (A/B–B′) structure, so that the B′ particles were mostly on the surface of the assembled nanoparticles, thus facilitating their release and observation.

Typically, two aliquots were taken from the prepared nanoparticle assemblies. Pb^{2+} ions (final concentration 20 μM) were added to one of the aliquots to initiate the error-correction process (reaction time 30 min), and the other aliquot was used for comparison.

Received: May 25, 2005
Published online: October 17, 2005

Keywords: DNA · enzymes · gold · materials science · nanotechnology

[1] N. C. Seeman, *Nature* **2003**, *421*, 427.
[2] C. A. Mirkin, R. L. Letsinger, R. C. Mucic, J. J. Storhoff, *Nature* **1996**, *382*, 607.
[3] A. P. Alivisatos, K. P. Johnsson, X. Peng, T. E. Wilson, C. J. Loweth, M. P. Bruchez, Jr., P. G. Schultz, *Nature* **1996**, *382*, 609.
[4] A. Van Blaaderen, R. Rue, P. Wiltzius, *Nature* **1997**, *385*, 321.
[5] G. C. L. Wong, J. X. Tang, A. Lin, Y. Li, P. A. Janmey, C. R. Safinya, *Science* **2000**, *288*, 2035.
[6] C. M. Niemeyer, *Angew. Chem.* **2001**, *113*, 4254; *Angew. Chem. Int. Ed.* **2001**, *40*, 4128.
[7] E. Katz, I. Willner, *Angew. Chem.* **2004**, *116*, 6166; *Angew. Chem. Int. Ed.* **2004**, *43*, 6042.
[8] H. Fan, K. Yang, D. M. Boye, T. Sigmon, K. J. Malloy, H. Xu, G. P. Lopez, C. J. Brinker, *Science* **2004**, *304*, 567.
[9] J. R. Heath, P. J. Kuekes, G. S. Snider, R. S. Williams, *Science* **1998**, *280*, 1716.
[10] J. H. Reif, T. H. LaBean, S. Sahu, H. Yan, P. Yin, *Lect. Notes Comput. Sci.* **2005**, 173, *3566*.
[11] S. Roweis, E. Winfree, *J. Comput. Biol.* **1999**, *6*, 65.
[12] S. C. Blanchard, R. L. Gonzalez, H. D. Kim, S. Chu, J. D. Puglisi, *Nat. Struct. Mol. Biol.* **2004**, *11*, 1008.
[13] E. Winfree, F. Liu, L. A. Wenzler, N. C. Seeman, *Nature* **1998**, *394*, 539.
[14] H. Yan, S. H. Park, G. Finkelstein, J. H. Reif, T. H. LaBean, *Science* **2003**, *301*, 1882.
[15] W. M. Shih, J. D. Quispe, G. F. Joyce, *Nature* **2004**, *427*, 618.
[16] R. Elghanian, J. J. Storhoff, R. C. Mucic, R. L. Letsinger, C. A. Mirkin, *Science* **1997**, *277*, 1078.
[17] N. L. Rosi, C. A. Mirkin, *Chem. Rev.* **2005**, *105*, 1547.
[18] J. Liu, Y. Lu, *J. Am. Chem. Soc.* **2003**, *125*, 6642.
[19] J. Liu, Y. Lu, *J. Am. Chem. Soc.* **2004**, *126*, 12298.
[20] G. F. Joyce, *Annu. Rev. Biochem.* **2004**, *73*, 791.
[21] S. W. Santoro, G. F. Joyce, *Proc. Natl. Acad. Sci. USA* **1997**, *94*, 4262.
[22] a) Y. Lu, *Chem. Euro. J.* **2002**, *8*, 4588; b) J. Li, W. Zheng, A. H. Kwon, Y. Lu, *Nucleic Acids Res.* **2000**, *28*, 481.
[23] A. K. Brown, J. Li, C. M. B. Pavot, Y. Lu, *Biochemistry* **2003**, *42*, 7152.
[24] L. M. Demers, C. A. Mirkin, R. C. Mucic, R. A. Reynolds III, R. L. Letsinger, R. Elghanian, G. Viswanadham, *Anal. Chem.* **2000**, *72*, 5535.
[25] G. A. Soukup, R. R. Breaker, *Curr. Opin. Struct. Biol.* **2000**, *10*, 318.
[26] J. C. Achenbach, W. Chiuman, R. P. G. Cruz, Y. Li, *Curr. Pharm. Biotechnol.* **2004**, *5*, 312.
[27] J. J. Storhoff, R. Elghanian, R. C. Mucic, C. A. Mirkin, R. L. Letsinger, *J. Am. Chem. Soc.* **1998**, *120*, 1959.
[28] D. A. Handley, in *Colloidal Gold: Principles, Methods, and Applications, Vol. 1* (Ed.: M. A. Hayat), Academic Press, San Diego, **1995**, pp. 13–32.

 © 2005 Wiley-VCH Verlag GmbH & Co. KGaA, Weinheim

Supramolecular Chemistry

DOI: 10.1002/anie.200501906

Mesoscopic Metallosupramolecular Texturing by Hierarchic Assembly**

*Sylvain Clair, Stéphane Pons, Harald Brune, Klaus Kern, and Johannes V. Barth**

Currently, there is a strong interest in improving the fabrication and mesoscopic integration of functional nanosystems at surfaces. In particular, new pathways need to be developed to provide methodologies for the synthesis and embedding of nanostructures across multiple length scales.[1–4] Herein, we introduce the combination of nanopatterning and controlled metal–organic assembly to process prestructured metallic templates and generate arrangements at a higher hierarchical level. We present results of scanning tunneling microscopy (STM) on the metal-directed assembly and mesoscopic organization of supramolecular architectures by using a textured metal substrate, that is, an Au(111) surface decorated with Fe or Co nanodot arrays. By tuning the local reaction conditions with co-deposited dicarboxylate linker molecules, distinct low-dimensional metallosupramolecular systems have been synthesized, which include regularly spaced iron terephthalate ribbons that form a grating whose extension is only limited by the substrate terrace morphology. These findings indicate that hierarchic assembly protocols blending physical nanopatterning[5–9] and supramolecular engineering[10–13] on surfaces are generally useful for fabricating nanomaterials with control of features at the mesoscopic level.

Metal-directed self-assembly of functional molecules provides a versatile strategy towards highly organized supramolecular systems.[14–17] Recent findings reveal that similar processes can be conducted at surfaces, where notably a series of metal–carboxylate architectures were generated, including mononuclear arrays, ladder structures, and nanoporous 2D metal–organic coordination networks.[13,18–21] However, until now these systems have been constructed on homogeneous substrates on which typically organic layers were exposed to a flux of metal atoms. To control the spatial distribution of surface coordination architectures, it is promising to explore prestructured surfaces, which—due to their intrinsic anisotropy, local concentration of reactants and site reactivity—allow us to direct and confine the assembly. This control is not possible with homogeneous substrates. Herein we present a temperature-controlled STM investigation of the steering of metallosupramolecular reticulation by using nanopatterned templates. This approach is a model for a two-stage assembly that combines self-organized metal-on-metal growth followed by chemical processing. This methodology may allow the fabrication of low-dimensional functional nanosystems, steer the formation of (metallo-) supramolecular assemblies, enable the study and control of metal–molecule interfacing, or structure template layers in the 100 nm regime for handling nanoscale objects.

Specifically, we employed regular lattices of transition metal dots by depositing small amounts of cobalt or iron on Au(111) at room temperature. Due to preferred nucleation of metal islands at the elbow sites of a reconstructed surface,[22] Fe or Co nanoarrays are readily obtained.[23,24] Islands of monoatomic height evolve as a consequence of Fe deposition, whereas bilayer dots are encountered with Co deposition. In agreement with earlier findings, the STM data confirm that the Au(111) reconstruction is maintained as demonstrated in the exemplary results in Figure 1. The superstructure is equivalent for the two elements. The lattice unit cell is nearly rectangular and ca. 15 nm × 7 nm in size. However, on smaller terraces and in the vicinity of defects substantial variations can occur. Typically 0.1 ML of Co or Fe atoms produces islands of about 140 atoms (one ML of metal atoms refers to a hypothetical perfect commensurate monatomic layer on the gold surface). As we will show, these islands act as nanoreservoirs for the metal-directed assembly of co-deposited terephthalic acid molecules (TPA, 1,4-benzenedicarboxylic acid).

While the TPA molecules are entirely preserved on the bare Au(111) substrate, where they form hydrogen-bonded sheets,[25] they readily react with an available Co or Fe atom at room temperature or at slightly elevated temperatures to form metal–organic nanostructures. The respective complexation is a reaction between the carboxyl groups of the molecules and one or more transition metal adatoms (M), which eventually can be extracted from the islands. This implies deprotonation of the carboxyl group, that is, an M–carboxylate evolves and leads to the formation of reticulated planar metal–organic arrangements. The resulting hydrogen atoms are expected to recombine to form molecular hydrogen, which is known to thermally desorb from noble-metal substrates under the conditions employed.[26] The complexation reaction is therefore irreversible and can be represented formally by the following net equation [Eq.(1)]:

$$2\,\mathrm{RCOOH} + \mathrm{M} \rightarrow (\mathrm{RCOO})_2 \cdots \mathrm{M} + \mathrm{H_2}(\uparrow) \qquad (1)$$

Since the diffusivity of the complexes is limited and the metal–organic bond has appreciable strength, the connection between building blocks can be kept localized in the vicinity of the originally deposited metal dots. In contrast, the high

[*] Dr. S. Clair, Dr. S. Pons, Prof. H. Brune, Prof. K. Kern, Prof. J. V. Barth
Institut de Physique des Nanostructures
Ecole Polytechnique Fédérale de Lausanne
1015 Lausanne (Switzerland)
E-mail: jvb@chem.ubc.ca
Prof. K. Kern
Max-Planck-Institut für Festkörperforschung
Heisenbergstrasse 1, 70569 Stuttgart (Germany)
Prof. J. V. Barth
Departments of Chemistry and Physics & Astronomy
The University of British Columbia
Vancouver, B.C. V6T1Z4 (Canada)

[**] This work was supported by the Swiss National Science Foundation (as part of the European Science Foundation EUROCORES Programme SONS) and the EC Sixth Framework Programme (as part of the STREP BioMACH).

 InterScience © 2005 Wiley-VCH Verlag GmbH & Co. KGaA, Weinheim

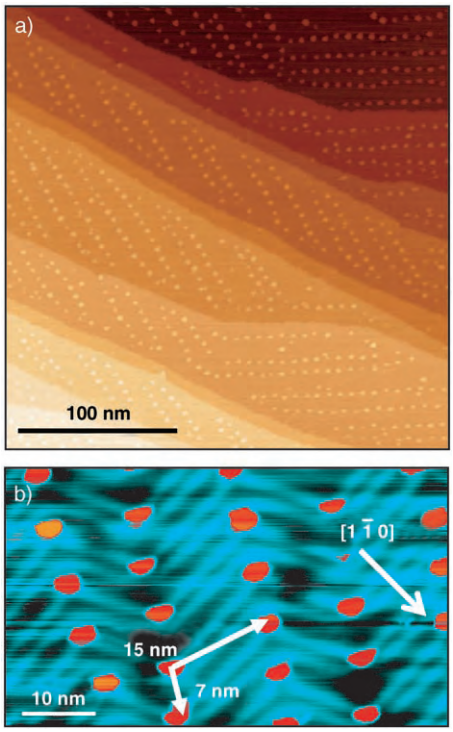

Figure 1. STM images of the Au(111) template with its chevron reconstruction dislocation pattern decorated with transition-metal arrays, which reflect preferential nucleation at elbow sites. a) Bilayer cobalt islands form regular lattices on several terraces (0.14 ML Co deposited at room temperature; image size 280×280 nm^2, $V=-25$ mV, $I=0.8$ nA, recorded at room temperature). b) Monolayer high Fe dots (red spots) on a single terrace with the characteristic double lines of the reconstruction simultaneously resolved. The unit cell of the regular lattice is ca. 15 nm×7 nm in size. (0.1 ML Fe deposited at room temperature; image size 60×35 nm^2, $V=20$ mV, $I=1$ nA, recorded at 5 K).

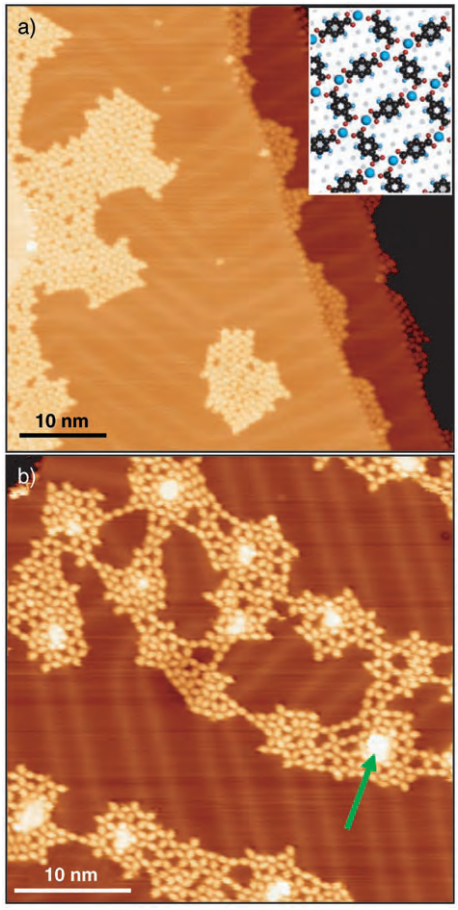

Figure 2. Controlling the Fe–TPA complexation reaction. a) Complete dissolution of Fe islands for a Fe–TPA stoichiometry of ca. 1:1 following deposition of TPA on the Fe nanoarrays at 355 K. Fe–carboxylate islands preferentially decorate step edges (image size 51×51 nm^2, $V=-2.5$ V, $I=0.5$ nA, recorded at 5 K). The inset shows a tentative model for an ideal Fe–TPA nanogrid where at each diiron center the endgroups of four molecular linkers come together. b) Localized reaction with TPA deposition at 325 K and 10 min post-deposition annealing at 330 K. The Fe islands are only partially consumed in the complexation reaction. The resulting nanogrid structure reflects selective growth of metal–organic islands at residual Fe dots (Fe island indicated by arrow; 0.1 ML Fe, 0.25 ML TPA; image size 38×38 nm^2, $V=1.5$ V, $I=0.2$ nA, recorded at 5 K).

mobility of TPA on bare Au(111) provides the necessary easy transport of the incoming molecule flux to the rims of the reactive metal islands.

Careful tuning of the conditions for molecular deposition has been used to steer the formation of various metal–carboxylate arrangements. In particular we have obtained architectures comprising regularly spaced nanoporous islands, extended metallosupramolecular ribbons, or one-dimensional systems. In general we observed that use of cobalt gives rise to better-ordered structures at the molecular scale than iron, while the latter allows easier steering at the mesoscopic level. The set of parameters that we optimized to obtain well-ordered architectures are the dosage (experiments were performed in the sub-monolayer range), the relative stoichiometry of M:TPA, the thermal energy of the adspecies tuned by the temperature of the substrate during deposition, and postdeposition annealing. With adequate temperature control, it is possible to obtain surface nanostructures comprising a) exclusively M–TPA compounds (M:TPA < 1) or b) coexisting residual metal nanodots and reticulated M–TPA compounds (M:TPA > 1).

Figure 2a shows an STM image of an Fe nanoarray on Au(111) after exposure to TPA with a stoichiometry of about one Fe atom per TPA molecule; the sample was maintained at $T=355$ K during the molecular deposition. This procedure resulted in the complete dissolution of the Fe dots and the formation of irregular islands that coexist with the unperturbed chevron pattern of the Au(111) substrate. While the presence of the latter clearly indicates that surface alloying between Fe and the substrate does not occur in the terraces, the irregular islands are clearly distinct from the extended close-packed quasi-hexagonal domains of hydrogen-bonded molecules that is characteristic of the adsorption of pure TPA.[25] The islands have open networks, which are reminiscent of the ordering found in nanoporous iron–carboxylate layers with TPA and related ditopic linear linkers on a square Cu(100) substrate.[13,18,28] Thus we conclude that these islands consist of iron–diterephthalate arrangements stabilized by metal–organic reticulation. The size of the characteristic open

 © 2005 Wiley-VCH Verlag GmbH & Co. KGaA, Weinheim

nanogrids is about $1 \times 1.2\ nm^2$; their relation to the metal–organic networks on Cu(100) suggests that, similarly, the network nodes consist of diiron centers surrounded by four molecules.[13,18,28] This analogy is illustrated in the tentative model for an ideal Fe–TPA nanogrid with 1:1 stoichiometry depicted in the inset in Figure 2a. However, in contrast to the square Cu(100) substrate, the metal centers are not directly resolved by STM and the quasi-hexagonal lattice of Au(111) offers no match with an overlayer structure composed of rectangular motifs. As a consequence the Fe–TPA islands do not exceed 10 to 15 nm in size and present frequent distortions and misorientations. Indeed, we found that it is impossible to create extended regular nanogrid domains despite the smoothness of the substrate, which indicates that while the strength of the metal–ligand interactions is appreciable, it is not sufficient to dictate the entire overlayer structure. In contrast with Co/Au(111) nanotemplates, the Fe–TPA system is more sensitive to stoichiometry and temperature and is harder to control. While Co–TPA complexes organize in locally regular porous islands for the deposition parameters described above, Fe–TPA complex islands are rather disordered and give rise to a mixture of regular metal–organic grids and complicated irregular phases. Finally, the decoration of Au step edges is associated with local intermixing or coupling of Au and Fe, which is in agreement with findings for a pure Fe/Au(111) system,[29] and implies that Fe atoms can transport under these reaction conditions either directly by evaporation from the Fe dots or indirectly by release in the form of TPA–Fe complexes. In general, for Fe–TPA assemblies with 1:1 stoichiometry (see for example Figure 2a), step decoration occurs preferentially at the bottom edges.

By lowering the annealing or deposition temperature and reducing the TPA concentration, we succeeded in confining the complexation reaction. This confinement is demonstrated in the STM image of Figure 2b, which shows the result of a TPA dosage too small to form networks with all of the Fe atoms available on the surface. Consequently, there is merely a partial dissolution of Fe islands and the cores of the metal islands remain at the Au(111) elbow sites. These residual Fe dots act as anchoring sites for reticulated metal–organic assemblies. All Fe islands are decorated by nanoporous irregular islands and chainlike features where the endgroups of the rodlike molecules are connected. The formation of these open structures again is in direct contrast with the compact packing in hydrogen-bonded pure TPA layers.[25] Consequently these arrangements must be stabilized by the incorporation of metal centers and reflect the limited surface mass transport of the reactants under the conditions employed. Thus the Fe–TPA nanogrid structure is poorly developed but the metal–organic islands coalesce and local bridges have evolved between them.

The connection between the localized complex islands is favored along the symmetry axis of the chevron pattern along the elbows. Two aspects can explain this growth anisotropy. First, along this direction is the shortest distance between two metallic dots and, indeed, we observed that the closer two metal–organic islands are, the more likely they are to coalesce. Second, the substrate reconstruction pattern with its substantial lattice distortions at the elbows may induce directional molecular transport and orientations. By carefully controlling the molecular surface concentration, extended metallosupramolecular ribbons with regular residual Fe anchoring sites can be fabricated. This point is illustrated in the STM image of Figure 3, which shows the mesoscopic ordering of Fe–TPA ribbons induced by the chevron structure. The widths of the stripes in this architecture are usually around 5 to 10 nm, while their lengths can reach hundreds of nanometers, that is, they span entire terraces until they terminate at the Au step edges. Therefore, the aspect ratios of the ribbons frequently exceeds 40 and by using vicinal transition-metal decorated Au(111) substrates with parallel step edges,[7] macroscopically elongated metal–organic ribbons are expected to form.

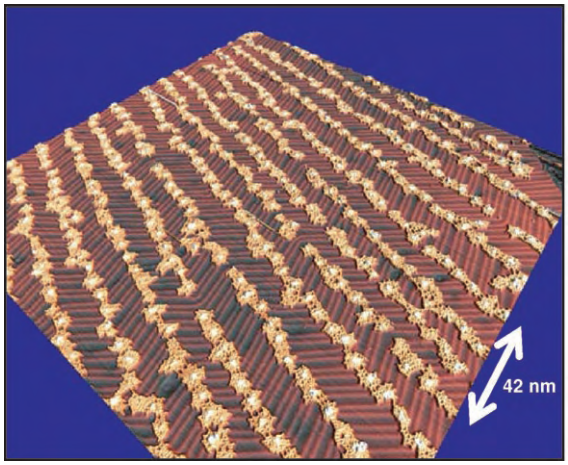

Figure 3. Mesoscopic ordering of metallosupramolecular ribbons. Fe–terephthalate linkages evolve between next-neighbor Fe islands following TPA exposure. The residual Fe dots at the elbow sites of the reconstruction anchor the pattern, that is, the spatial distribution of the Fe dots steers the organization. The length of the metal–organic ribbons is around several hundred nm, with typical widths of 5–10 nm. The respective aspect ratio of the stripes is commonly greater than 20 to 40 (image size $220 \times 220\ nm^2$, $V = -1.5$ V, $I = 0.8$ nA, recorded at 5 K; 0.1 ML Fe exposed to 0.25 ML TPA at 325 K, i.e., fourfold Fe excess with respect to ideal 1:1 nanogrid stoichiometry).

By further fine tuning the deposition parameters, we assembled monomolecular chains in the Co–TPA system on Au(111) as shown in Figure 4. Such metal–organic wires form at reduced molecular coverages but with limited success, and these 1D structures coexist with nanogrid patches (not shown). The wires establish a connection between two adjacent dots and therefore do not exceed 10 nm in length. The exact internal structure and stoichiometry of these chains composed of M–terephthalate segments could not be determined. However, the distance between the molecular building blocks in the chain increases by about 10% with respect to that in the hydrogen-bonded assemblies, which corroborates that it arises from a complexation of TPA and Co atoms, where distances of 0.2 nm between metal center and carboxylate oxygen atoms are expected. Moreover, the 1D Co–TPA chains anchored by the Co dots are stable at room temperature, which reflects the appreciable strength of metal–ligand

 © 2005 Wiley-VCH Verlag GmbH & Co. KGaA, Weinheim

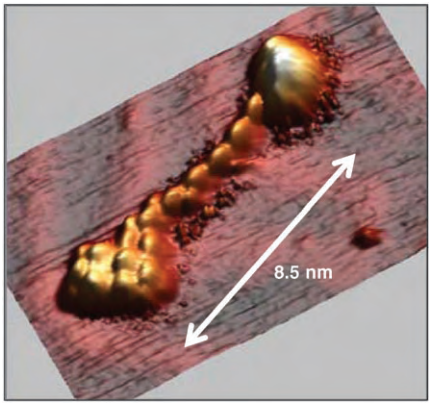

Figure 4. Monomolecular Co–TPA "wire" linking two cobalt nanodots. The rims of the Co islands are also decorated with molecules. This 1D structure coexists on the surface with regions covered by nanogrids (doses: 0.2 ML Co, 0.2 ML TPA; sample kept at 360 K during TPA deposition; image size 15×8 nm^2, $V=-700$ mV, $I=0.6$ nA, recorded at room temperature).

interactions that exceed hydrogen-bonding interactions of 1D TPA polymers. Accordingly, monomolecular hydrogen-bonded chains can neither be obtained by molecular self-assembly at room temperature[25] nor are they encountered under cryogenic conditions.

In conclusion we have demonstrated that substrates patterned with transition-metal nanoarrays can be processed by tuning and spatially confining their reaction with functional molecular species. Methodologies that use such hierarchic assembly protocols are conceivable for a great variety of systems and can be applied at substrates with different symmetries, physical, and chemical properties. Thus, they are a promising route for the metallo-supramolecular engineering of patterned templates by using linker molecules with specific functionalities. We expect that these findings will contribute to an improved control of matter at the nanoscale, the mesoscopic organization of template structures, and the design of supramolecular functional systems.

Experimental Section

Experiments were performed in a ultrahigh vacuum system (base pressure $<3\times10^{-10}$ mbar) comprising a home-built STM working at variable temperature (400–5 K) as previously described.[27] Data were recorded in constant-current mode; indicated voltages refer to the sample bias. The Au(111) substrate was prepared by repeated cycles of room-temperature Ar bombardment (≈5 μA cm^{-2} at 800 eV) then annealing at 900 K. Terraces larger than 100 nm were commonly observed. Iron and cobalt were evaporated at low deposition rates ($<{}^1/_3$ ML per minute). TPA molecules (FLUKA, purity $>99\,\%$) were evaporated with an organic molecular beam deposition (OMBD) source, by heating a crucible to 150 °C—the pertaining evaporation rate was ≈1 ML (i.e., a complete monomolecular layer) per minute.[27] A metal-to-TPA stoichiometry of 1:1 corresponds to a coverage ratio of ≈9:1.

Received: June 2, 2005
Revised: August 24, 2005
Published online: October 17, 2005

Keywords: coordination modes · nanotechnology · scanning probe microscopy · self-assembly · supramolecular chemistry

[1] T. Ogino, H. Hibino, T. Homma, Y. Kobayashi, K. Prabhakaran, K. Sumitomo, H. Omi, *Acc. Chem. Res.* **1999**, *32*, 447.
[2] Y. N. Xia, J. A. Rogers, K. E. Paul, G. M. Whitesides, *Chem. Rev.* **1999**, *99*, 1823.
[3] H. Cölfen, S. Mann, *Angew. Chem.* **2003**, *115*, 2452; *Angew. Chem. Int. Ed.* **2003**, *42*, 2350.
[4] C. Lin, C. R. Kagan, *J. Am. Chem. Soc.* **2003**, *125*, 336.
[5] K. Kern, H. Niehus, A. Schatz, P. Zeppenfeld, J. George, G. Comsa, *Phys. Rev. Lett.* **1991**, *67*, 855.
[6] H. Brune, M. Giovannini, K. Bromann, K. Kern, *Nature* **1998**, *394*, 451.
[7] V. Repain, G. Baudot, H. Ellmer, S. Rousset, *Europhys. Lett.* **2002**, *58*, 730.
[8] M. Corso, W. Auwärter, M. Muntwiler, A. Tamai, T. Greber, J. Osterwalder, *Science* **2004**, *303*, 217.
[9] R. Otero, Y. Naitoh, F. Rosei, P. Jiang, P. Thostrup, A. Gourdon, E. Laegsgaard, I. Stensgaard, C. Joachim, F. Besenbacher, *Angew. Chem.* **2004**, *116*, 2144; *Angew. Chem. Int. Ed.* **2004**, *43*, 2092.
[10] J. V. Barth, J. Weckesser, C. Cai, P. Günter, L. Bürgi, O. Jeandupeux, K. Kern, *Angew. Chem.* **2000**, *112*, 1285; *Angew. Chem. Int. Ed.* **2000**, *39*, 1230.
[11] J. A. Theobald, N. S. Oxtoby, M. A. Phillips, N. R. Champness, P. H. Beton, *Nature* **2003**, *424*, 1029.
[12] T. Yokoyama, S. Yokoyama, T. Kamikado, Y. Okuno, S. Mashiko, *Nature* **2001**, *413*, 619.
[13] S. Stepanow, M. Lingenfelder, A. Dmitriev, H. Spillmann, E. Delvigne, N. Lin, X. Deng, C. Cai, J. V. Barth, K. Kern, *Nat. Mater.* **2004**, *3*, 229.
[14] D. Philp, J. F. Stoddart, *Angew. Chem.* **1996**, *108*, 1242; *Angew. Chem. Int. Ed. Engl.* **1996**, *35*, 1154.
[15] S. Leininger, B. Olenyuk, P. J. Stang, *Chem. Rev.* **2000**, *100*, 853.
[16] J. M. Lehn, *Proc. Natl. Acad. Sci. USA* **2002**, *99*, 4763.
[17] B. J. Holliday, C. A. Mirkin, *Angew. Chem.* **2001**, *113*, 2076; *Angew. Chem. Int. Ed.* **2001**, *40*, 2022.
[18] A. Dmitriev, H. Spillmann, N. Lin, J. V. Barth, K. Kern, *Angew. Chem.* **2003**, *115*, 2774; *Angew. Chem. Int. Ed.* **2003**, *42*, 2670.
[19] J. V. Barth, J. Weckesser, N. Lin, S. Dmitriev, K. Kern, *Appl. Phys. A* **2003**, *76*, 645.
[20] H. Spillmann, A. Dmitriev, N. Lin, P. Messina, J. V. Barth, K. Kern, *J. Am. Chem. Soc.* **2003**, *125*, 10725.
[21] A. Dmitriev, H. Spillmann, M. Lingenfelder, N. Lin, J. V. Barth, K. Kern, *Langmuir* **2004**, *41*, 4799.
[22] J. V. Barth, H. Brune, G. Ertl, R. J. Behm, *Phys. Rev. B* **1990**, *42*, 9307.
[23] B. Voigtländer, G. Meyer, N. M. Amer, *Phys. Rev. B* **1991**, *44*, 10354.
[24] J. A. Stroscio, D. T. Pierce, R. A. Dragoset, P. N. First, *J. Vac. Sci. Technol. A* **1992**, *10*, 1981.
[25] S. Clair, S. Pons, A. P. Seitsonen, H. Brune, K. Kern, J. V. Barth, *J. Phys. Chem. B* **2004**, *108*, 14585.
[26] X.-L. Zhou, J. M. White, B. E. Koel, *Surf. Sci.* **1989**, *218*, 201.
[27] S. Clair, PhD thesis, EPF (Lausanne), **2004**.
[28] M. A. Lingenfelder, H. Spillmann, A. Dmitriev, S. Stepanov, N. Lin, J. V. Barth, K. Kern, *Chem. Eur. J.* **2004**, *10*, 1913.
[29] S. Shiraki, H. Fujisawa, M. Nantoh, M. Kawai, *J. Electron Spectrosc. Relat. Phenom.* **2004**, *137–140*, 177.

 © 2005 Wiley-VCH Verlag GmbH & Co. KGaA, Weinheim

Molecular Motors

DOI: 10.1002/anie.200501977

A Thermal and Solvocontrollable Cylindrical Nanoshutter Based on a Single Screw-Sense Helical Polyguanidine**

Hong-Zhi Tang, Bruce M. Novak, Jiangtao He, and Prasad L. Polavarapu**

Controlling and switching the chiroptical properties, for example, electronic circular dichroism (ECD) and optical rotation, of helical polymers continues to attract great interest because of potential applications in sensor data storage, optical devices, and liquid crystalline displays.[1] Thermo-driven and/or solvent-driven switching helical polymers in particular have been studied extensively; examples include poly(L-aspartate β-esters),[2] polyisocyanates,[3] polysilanes,[1d,4] and polyacetylenes.[5] These helical polymers possess chiral moieties, which are introduced from chiral monomers, into the polymer backbones or side chains. These switching phenomena are generally interpreted to date as helical inversions that occur in the polymer backbones and which are driven by thermal or solvent-polarity changes.

We recently reported a novel thermal and solvocontrollable switching polyguanidine (poly-**1**, Figure 1), which was synthesized by helix-sense-selective polymerization of an achiral monomer.[6] Three possible mechanisms were proposed to explain this interesting switching phenomenon: helix inversions φ,[2–5] imine inversions ω,[7] and/or rotations around the N–$C_{anthracene}$ bonds θ[8] (Scheme 1). The switching phenomenon was further studied by using vibrational circular dichroism (VCD)[9] and computational modeling techniques to determine the specific mechanism. We herein report that the switching phenomenon arises from large-amplitude ordered synchronous wagging of the anthracene units without helical and imine inversions. This system is a new model for a nano molecular motor:[10] a cylindrical nanoshutter that transforms the low-input energy of thermal and/or solvent-polarity changes to mechanical output (work) through the synchronous wag of the aligned anthracene units. We also assigned the helicity of poly-**1** as *P* by means of density functional theory (DFT) calculations[11] and showed that it remains fixed during the reversible shuttering phenomenon.

Regioregular, stereoregular poly-**1** ($M_w = 16000$, $M_w/M_n = 2.7$) was obtained by helix-sense-selective polymerization of an achiral carbodiimide of **1** using chiral catalyst R–Ti.[6a] The chirality of this macromolecule is because of 1) its single-handed screw sense and 2) the stereoregular registry of both the anthracene units and the projection angle of the imine groups.

Full racemization requires transition through a symmetric intermediate which involves inversion of the helix sense φ and at least one or both of the molecular motions: free rotations around N–$C_{anthracene}$ θ and imine inversion ω. The complete racemization of poly-**1** in toluene requires high temperatures of nearly 80 °C for reaction times longer than 100 hours.

However, the ECD and UV/Vis spectra of poly-**1** are reversibly switched when a solution of poly-**1** in toluene is heated and cooled cyclically between 25 and 60 °C (Figure 2 A). Poly-**1** shows a positive Cotton effect of $\Delta\varepsilon = +2.0\,\text{M}^{-1}\,\text{cm}^{-1}$ at 382.0 nm and 25 °C, but a negative one of $\Delta\varepsilon = -2.6\,\text{M}^{-1}\,\text{cm}^{-1}$ at 382.0 nm and 60 °C. Poly-**1** shows an intense absorption of $\varepsilon = 5400\,\text{M}^{-1}\,\text{cm}^{-1}$ at $\lambda_{max} = 384.4$ nm and 25 °C, but a less intense absorption of $\varepsilon = 4700\,\text{M}^{-1}\,\text{cm}^{-1}$ at $\lambda_{max} = 382.4$ nm and 60 °C, thus corresponding to the ECD switching. It is of note that the wavelengths of the absorption maxima undergo a slight blue/red shift along with the heating–cooling cycles. Very large changes in the optical-rotation values are also observed between 31 and 40 °C (e.g., +297–−77°). The optical-rotation data indicate that the switching temperature is 38.5 °C. This switching phenomenon also can be observed when the polarity of the solvent is changed (Figure 2 B). For example, the ECD spectra of poly-**1** exhibit a negative Cotton effect in the polar solvents THF (dipole moment $\mu = 1.75$ D, dielectric constant $\varepsilon' = 7.5$) and $CHCl_3$ ($\mu = 1.15$ D, $\varepsilon' = 4.8$) at 25 °C, thus resembling that observed in toluene ($\mu = 0.31$ D, $\varepsilon' = 2.4$) at the higher temperature of 60 °C. The switching point occurs at 10 vol % of toluene in a mixed solvent system of THF/toluene.

Of the three possible mechanisms to explain this interesting switching phenomenon, that is, helix inversion, imine inversion, and/or rotation around the N–$C_{anthracene}$ bonds, partial rotation (reorientation) around the N–$C_{anthracene}$ bonds is the lowest-energy process. Notably, the free rotation around N–$C_{anthracene}$ is prohibited because the distance between two anthracene units is less than the length of one anthracene unit. Reversible switching occurs quickly (within seconds) in both the thermo-driven process at the lower temperature of 38.5 °C in toluene and in the solvent-driven process relative to the time-consuming (100 hours) and energy-demanding (80 °C) full-racemization process. This increase implies that the imine configuration inversion and the helix inversion in poly-**1** are not involved in the reversible switching process.

The barrier of imine inversion in small molecules is in the range 20–26 kcal mol^{-1} (coalescence temperatures are in the range 50–180 °C).[7] The required temperature is much higher than the switching temperature of 38.5 °C, which is hence further indication that the imine inversion is unlikely in the observed switching process.

[*] Dr. H.-Z. Tang, Prof. Dr. B. M. Novak
Department of Chemistry
North Carolina State University
Raleigh, NC 27695 (USA)
Fax: (+1) 919-513-2828
E-mail: novak@chemdept.chem.ncsu.edu
Dr. J. He, Prof. Dr. P. L. Polavarapu
Department of Chemistry
Vanderbilt University
Nashville, TN 37235 (USA)
Fax: (+1) 615-322-4936
E-mail: prasad.l.polavarapu@vanderbilt.edu

[**] This work was supported by grants from the NSF (CHE0092922) and National Computational Science Alliance (CHE040009N utilizing the IBM P690 (University of Illinois)).

Supporting information for this article is available on the WWW under http://www.angewandte.org or from the author.

WILEY InterScience DISCOVER SOMETHING GREAT
© 2005 Wiley-VCH Verlag GmbH & Co. KGaA, Weinheim

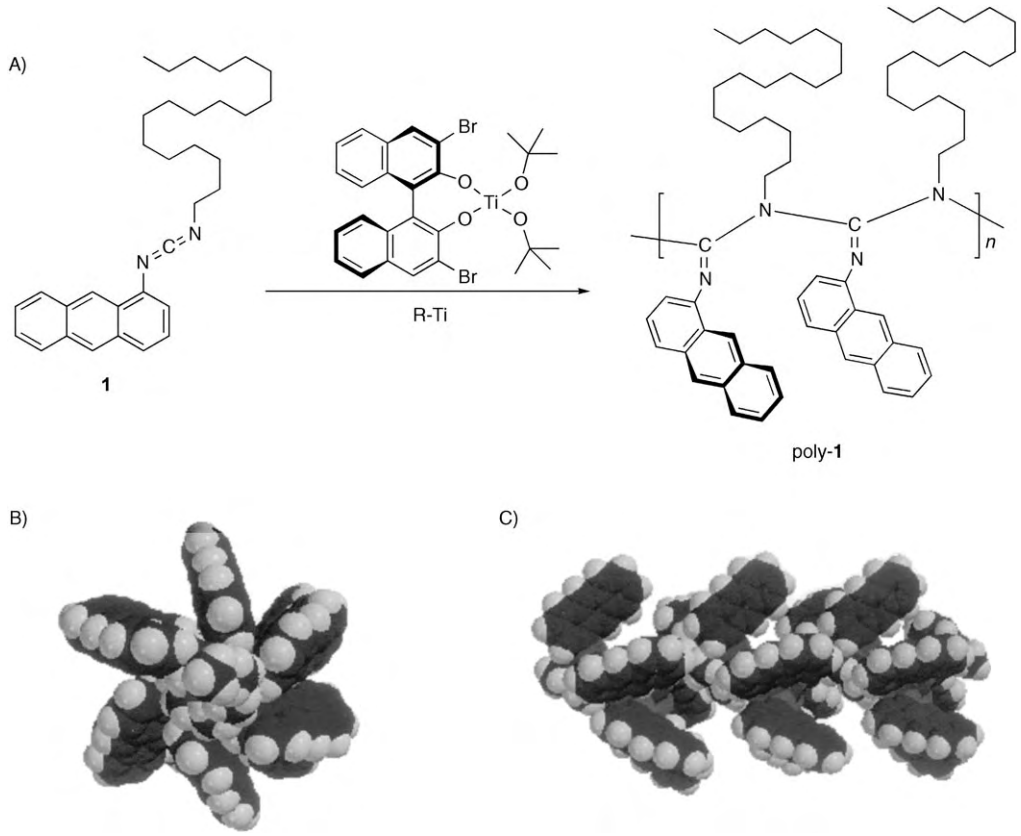

Figure 1. A) Synthesis of regioregular, stereoregular poly-**1**. B) Top view and C) side view of the 6_1-helical structure of poly-**1** (18-mer). Methyl groups replace *n*-octadecyl groups in poly-**1** to clarify the orientation of the anthracene units.

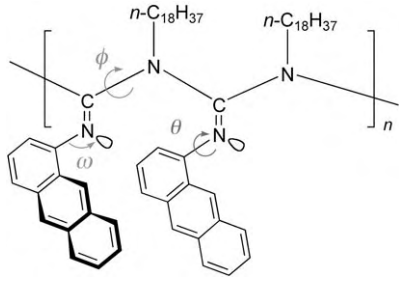

Scheme 1. Three possible molecular motions in the helical poly-**1**.

Standard variable-temperature (VT) ^{1}H and ^{13}C NMR spectroscopic experiments to elucidate the origin of the switching process were attempted (see the Supporting Information). However, these studies proved inconclusive because of signal broadening. VCD studies were then carried out in the polar solvent $CHCl_3$ and the less-polar solvent toluene at various temperatures to clarify the nature of the switching phenomenon in poly-**1** (as observed from the ECD and optical-rotation studies). To our surprise, the VCD spectra of poly-**1** remained unchanged except for a slight variation in intensity, unlike the ECD spectra. Typical VCD spectra of poly-**1** in $CHCl_3$ and toluene at 25 °C are shown in Figure 3 B, C in which a large bisignate couplet at 1641 cm^{-1} is exhibited that matches the vibrational absorbance of imine groups in the polyguanidine backbone (Figure 3 A). The concentrations used for the measurement of VCD are significantly greater than those for ECD. The ECD was measured at the concentrations used for the VCD studies to determine whether concentration may have had an influence. We found, however, that ECD spectra at higher concentrations have the similar ECD values as those at lower concentrations. These VCD data strongly support that the chirality of the helical polyguanidine backbone does not change during the reversible switching of the observed ECD and optical-rotation properties. The extremely slight change in the VCD intensity also implies that there is no change in the helical pitch during this switching process.

These two contradictory observations, namely, switching of the ECD and optical-rotation properties with temperature and solvent polarity and the lack of such switching of VCD, can only be reconciled if the anthracene units are considered to wag synchronously around the $N-C_{anthracene}$ bonds (thereby acting like a shutter). In that event, the orientation of the anthracene units relative to the position of the lone-pair electrons on the nitrogen atoms changes, which in turn changes the lone-pair/π-electron interactions, and hence the ECD and optical-rotation properties, but the chirality sensed by the vibrations of C=N bonds is not effected.

The blue/red shifts in the UV/Vis absorption and ECD bands above and below the switching temperature (Figure 2), also suggest that the orientation of the anthracene units cooperatively switch relative to the helix director (namely, wagging around $N-C_{anthracene}$ θ). Further computational mod-

 © 2005 Wiley-VCH Verlag GmbH & Co. KGaA, Weinheim

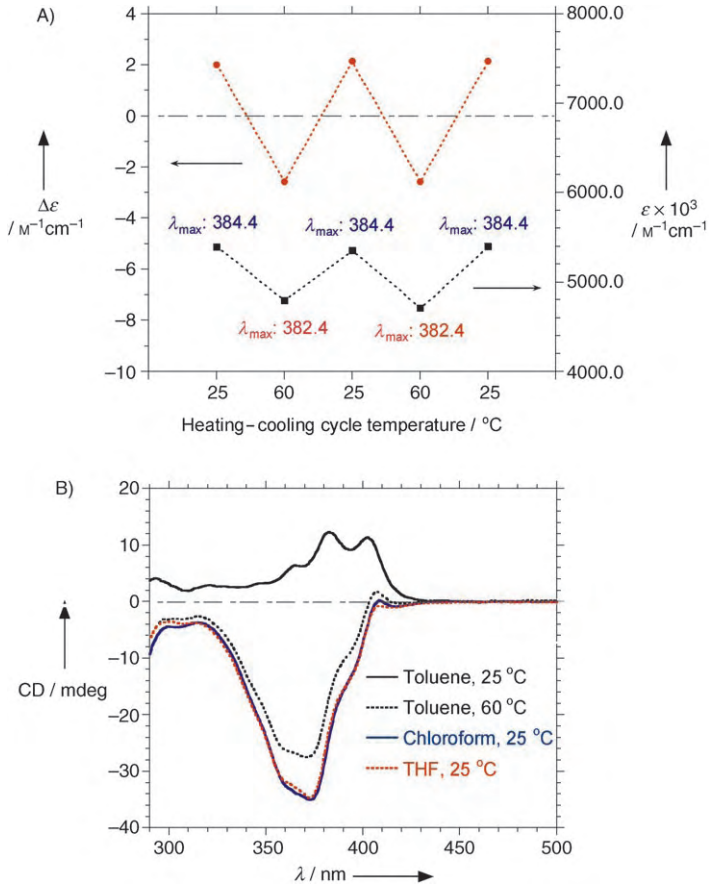

Figure 2. A) Heating–cooling thermal cycles of poly-**1** in toluene ($c = 2.1 \times 10^{-4}$ M, path length = 10 mm); wavelength for $\Delta\varepsilon$ is 382.0 nm. B) ECD spectra of poly-**1** in toluene at 25 and 60 °C, in $CHCl_3$ at 25 °C, and in THF at 25 °C; the intensities of the corresponding UV/Vis absorption maxima are normalized to 1.0. Very slight changes were observed in the ECD spectra of poly-**1** in THF and $CHCl_3$ when the solutions were heated to 50 °C. The ECD spectra of poly-**1** are independent of concentration in the range 2.1×10^{-4}–5.3×10^{-2} M. Dihedral angles [°] of **2**: C1-N2-C3-N4 −150, C1′-N2′-C3′-N4′ −153, N2-C3-N4-C5 −166, N2′-C3′-N4′-C5′ −168, C3-N4-C5-C6 63, C3′-N4′-C5′-C6′ 66, N2-C3-N2′-C3′ −103.

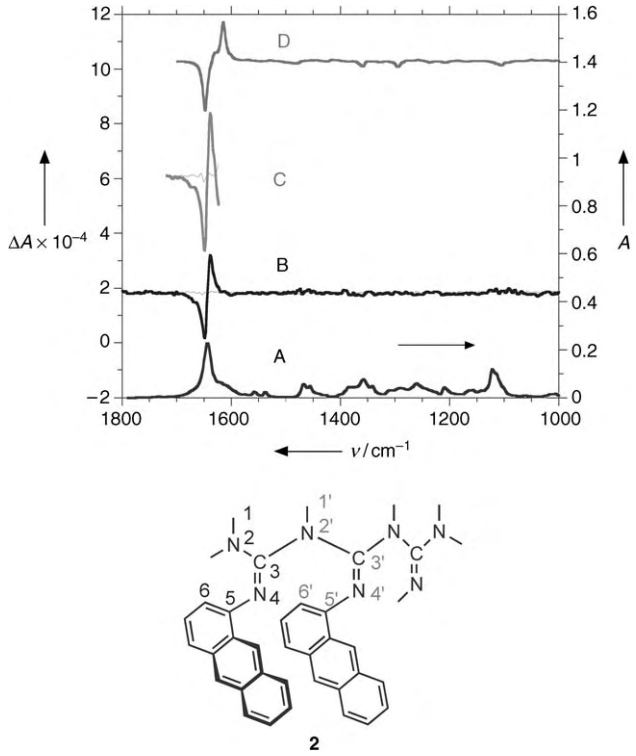

Figure 3. A) The experimental vibrational absorbance and B) VCD spectra of poly-**1** in $CDCl_3$ at 25 °C ($c = 10.0$ mg mL^{-1}, path length = 300 μm). c) VCD spectrum of poly-**1** in toluene at 25 °C ($c = 20.1$ mg mL^{-1}, path length = 200 μm) is also shown. The solvent absorption and VCD values were subtracted from the corresponding experimental spectra. The flat thin lines represent the noise level in the VCD spectra. D) The optimized *P* model **2** and its VCD spectrum calculated by density functional theory using B3LYP functional and 6-31G(d) basis sets. The calculated frequencies were scaled with 0.9613.

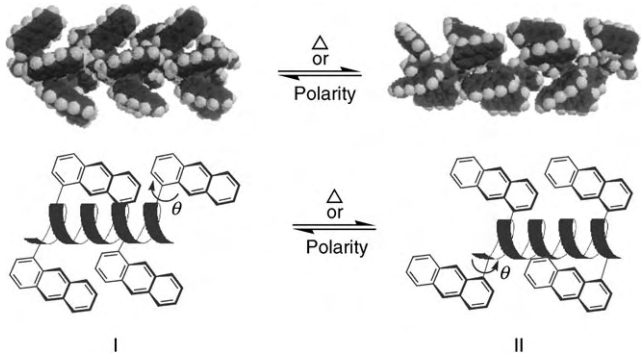

Figure 4. Theoretical models of the two states which result from the shutter-like motions of the anthracene unit. The geometries of these two states were determined by optimization of the repeat unit at the semiempirical level (AM1)[12] and then optimization of the 18-mer at the molecular-mechanics level (MMFF94).[13]

eling on this system was carried out to confirm these suggestions. Our working model (Figure 4) consists of a lower-energy state (**I**, $\mu_I = 6.9$ D), which has the dipole moments of the flipping ends of the anthracene aligned opposing the helix director, and a higher-energy state (**II**, $\mu_{II} = 7.7$ D), which has the dipole moments of the anthracenes aligned with the helix director; the polar solvents stabilize the more polar second state. In this reversible cooperative switching process, the chirality, the imine configuration, and the helical pitches remain unchanged.

It is a challenge to assign the chirality of poly-**1**. We built and initially optimized model compound **2** (Figure 3) with molecular mechanics MMFF94,[13] and optimized its *P* structure by DFT at the B3LYP/6-31G(d) level[14] with the Gaussian98 program. The VCD spectrum, calculated at this optimized geometry, is in excellent agreement with the experimentally observed VCD spectra of poly-**1** (Figure 3D), thus indicating that poly-**1** is a *P* structure.

We have clarified the mechanism of the unusually large reversible thermo- and solvent-driven shuttering phenomenon of poly-**1**. We have also successfully assigned the helicity of poly-**1** as *P* and showed that it remains fixed during the reversible shuttering phenomenon. This anthracene-containing polyguanidine nanoshutter underwent large-amplitude

 © 2005 Wiley-VCH Verlag GmbH & Co. KGaA, Weinheim

ordered synchronous wagging of anthracene units relative to the helix director when actuated by a change in energy caused by temperature or solvent polarity, and exhibited two important criteria for the bottom-up construction of a nanomachine. Further modification and applications (e.g., display technology) are currently under investigation.

Received: August 25, 2005
Published online: October 13, 2005

Keywords: circular dichroism · helical structures · molecular devices · polyguanidine · switching

[1] Typical reviews: a) J. J. L. M. Cornelissen, A. E. Rowan, R. J. M. Nolte, N. A. J. M. Sommerdijk, *Chem. Rev.* **2001**, *101*, 4039 – 4070; b) D. J. Hill, M. J. Mio, R. B. Prince, T. S. Hughes, J. S. Moore, *Chem. Rev.* **2001**, *101*, 3893 – 4012; c) Y. Okamoto, T. Nakano, *Chem. Rev.* **1994**, *94*, 349 – 372; d) M. Fujiki, *J. Organomet. Chem.* **2003**, *685*, 15 – 34; e) Y. Kawakami, H.-Z. Tang, *Des. Monomers Polym.* **2000**, *3*, 1 – 16.

[2] a) E. M. Bradbury, B. G. Carpenter, H. Goldman, *Biopolymers* **1968**, *6*, 837 – 850; b) J. Watanabe, S. Okamoto, K. Satoh, K. Sakajiri, H. Furuya, A. Abe, *Macromolecules* **1996**, *29*, 7084 – 7088; c) C. Toniolo, M. L. Falxa, M. Goodman, *Biopolymers* **1968**, *6*, 1579 – 1603.

[3] a) K. Maeda, Y. Okamoto, *Macromolecules* **1999**, *32*, 974 – 980; b) K. Tang, M. M. Green, K. S. Choen, J. V. Selinger, B. A. Garetz, *J. Am. Chem. Soc.* **2003**, *125*, 7313 – 7323.

[4] a) M. Fujiki, H.-Z. Tang, M. Motonaga, K. Torimitsu, J. R. Koe, J. Watanabe, T. Sato, A. Teramoto, *Silicon Chem.* **2002**, *1*, 67 – 72; b) A. Teramoto, K. Terao, Y. Terao, H. Nakashima, T. Sato, M. Fujiki, *J. Am. Chem. Soc.* **2001**, *123*, 12303 – 12310.

[5] a) J. Tabei, R. Nomura, F. Sanda, T. Masuda, *Macromolecules* **2004**, *37*, 1175 – 1179; b) K. K. L. Cheuk, J. W. Y. Lam, L. M. Lai, Y. Dong, B. Z. Tang, *Macromolecules* **2003**, *36*, 9752 – 9762; c) E. Yashima, K. Maeda, O. Sato, *J. Am. Chem. Soc.* **2001**, *123*, 8159 – 8160.

[6] a) H.-Z. Tang, P. D. Boyle, B. M. Novak, *J. Am. Chem. Soc.* **2005**, *127*, 2136 – 2142; b) H.-Z. Tang, Y. Lu, G. Tian, M. D. Capracotta, B. M. Novak, *J. Am. Chem. Soc.* **2004**, *126*, 3722 – 3723; c) G. Gong, Y. Lu, B. M. Novak, *J. Am. Chem. Soc.* **2004**, *126*, 4082 – 4083.

[7] W. B. Jennings, D. R. Boyd, *J. Am. Chem. Soc.* **1972**, *94*, 7187 – 7188.

[8] I. Tinoco Jr., *J. Chim. Phys.* **1968**, *65*, 91 – 97.

[9] a) P. L. Polavarapu, J. He, *Anal. Chem.* **2004**, *76*, 61A – 67A; b) H. Izumi, S. Yamagami, S. Futamura, L. A. Nafie, R. K. Dukor, *J. Am. Chem. Soc.* **2004**, *126*, 194 – 198; c) M. Urbanova, V. Setnicka, F. J. Devlin, P. J. Stephens, *J. Am. Chem. Soc.* **2005**, *127*, 6700 – 6711; d) T. B. Freedman, X. Cao, R. K. Dukor, L. A. Nafie, *Chirality* **2003**, *15*, 743 – 758; e) P. J. Stephens, F. J. Devlin, *Chirality* **2000**, *12*, 172 – 179.

[10] Typical review of nanomachines and therein: V. Balzani, A. Credi, F. M. Raymo, J. F. Stoddart, *Angew. Chem.* **2000**, *112*, 3484 – 3530; *Angew. Chem. Int. Ed.* **2000**, *39*, 3348 – 3391.

[11] W. Koch, M. C. Holthausen, *A Chemists Guide to Density Functional Theory*, 2nd ed., Wiley-VCH, Weinheim, **2001**.

[12] M. J. S. Dewar, E. G. Zoebisch, E. F. Healy, J. J. P. Stewart, *J. Am. Chem. Soc.* **1985**, *107*, 3902 – 3909.

[13] T. A. Halgren, *J. Comput. Chem.* **1996**, *17*, 490 – 519.

[14] W. J. Hehre, L. Radom, P. V. R. Schleyer, J. A. Pople, *Ab initio Molecular Orbital Theory*, Wiley, New York, **1986**.

 © 2005 Wiley-VCH Verlag GmbH & Co. KGaA, Weinheim

Host–Guest Systems

DOI: 10.1002/anie.200502073

Helical Folding in a Helical Channel: Chiroptical Transcription of Helical Information through Chiral Wrapping**

Takanobu Sanji, Nobu Kato, Masako Kato, and Masato Tanaka**

The helical structure is one of the most significant motifs in macromolecules. In nature, helical structures are often found in biomacromolecules and appear to play a critical role in biological phenomena such as molecular recognition and information storage. This is exemplified by the double helix of DNA and the α helix of proteins,[1] and some synthetic polymers also adopt a helical conformation.[2] Recently, the design and synthesis of macromolecules with a helical structure has attracted a great deal of interest as a result of their relationship to life sciences as well as their potential applications in materials science.[3] Herein, we show that linear oligosilanes acting as axle guest molecules within the internal helical channel of a polymer can be induced to form a preferential helical conformation. The helical sense of the guest molecules is then controlled by wrapping with either the left-handed or the right-handed helical conformation of the host polymer. The system presented herein offers a new approach in the field of helical expression in molecular and macromolecular systems.[4]

To explore the possibility of "helix-in-helix" supramolecular architecture, we have chosen host–guest combinations of linear polysaccharides and oligosilanes (Figure 1). One of the polysaccharides used is amylose, which is composed of α-1,4-linkages between D-glucopyranose residues. Amylose adopts a left-handed helical conformation and forms inclusion complexes as a result of hydrophobic interactions with guest molecules confined within the helical cavity.[5] The helical dimensions of amylose can be adjusted according to the size of the guest. The other polysaccharide examined was schizophyllan (SPG), which is composed of β-1,3-linkages between glucose units (β-1,3-glucan) and adopts a right-

[*] Dr. T. Sanji, N. Kato, Prof. M. Tanaka
Chemical Resources Laboratory
Tokyo Institute of Technology
4259 Nagatsuta, Midori-ku, Yokohama 226-8503 (Japan)
Fax: (+81) 45-924-5279
E-mail: sanji@res.titech.ac.jp
m.tanaka@res.titech.ac.jp

M. Kato
Department of Pure and Applied Chemistry
Tokyo University of Science
Noda 278-8510 (Japan)

[**] We thank Dr. Y. Nakamura for the NMR spectroscopic measurements. This work is supported by the Ministry of Education, Culture, Sports, Science, and Technology of Japan (No. 16685004).

Supporting information for this article is available on the WWW under http://www.angewandte.org or from the author.

© 2005 Wiley-VCH Verlag GmbH & Co. KGaA, Weinheim

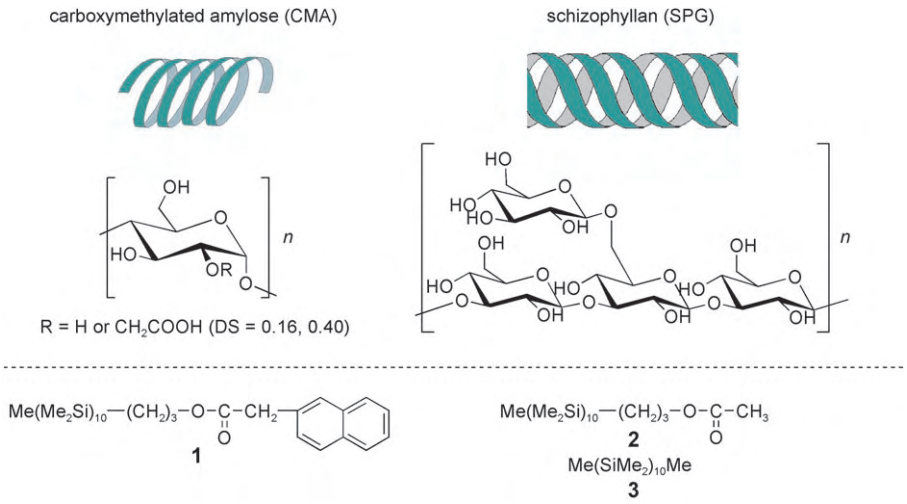

Figure 1. Combinations of host–guest complexation for linear polysaccharides and oligosilanes.

handed triple helix in nature.[6] On the other hand, oligosilanes **1**–**3**, used as the axle guests, are unique molecules that exhibit absorption in the UV region as a result of σ conjugation along the main chain. The absorption behavior of σ-conjugated systems is extremely sensitive to the conformation.[7] This sensitivity is exemplified by the behavior of helical poly- or oligosilanes in response to the chiral stimulus of their optically active substituents.[8] This allowed us to study photophysical properties that are dependent on the conformation of the main chain. Several reports have addressed control of the conformation of oligosilanes,[9] for example, by inclusion of a macrocyclic molecule (with α-1,4-glucopyranose units) into cyclodextrins.[10] Recently, we found the induction of a preferential helical-sense conformation in oligosilanes that are located within the internal cavity of cyclodextrins.[11]

Molecular mechanics was used to study models of the complexes at hand.[12] The minimum-energy structure of the simple model complex formed by the interaction between permethyldodecasilane and an amylose fragment that contains 16 repeating α-1,4-D-glucopyranose units is illustrated in Figure 2. The amylose fragment is shown to adopt a left-handed helical conformation by wrapping around the oligosilane axle. In the helical cavity created by the amylose wrapping, the oligosilane main chain assumes a helical conformation with a Si–Si torsion angle of about 165°.

In our experiments, we used partially carboxymethylated amylose (CMA), with DS = 0.16 or 0.40 (DS = the degree of carboxymethyl substitution) to increase the solubility of the resulting inclusion complex in water. In a typical preparation of the inclusion complex, a mixture of decasilane **1** (30 mg, 3.7×10^{-2} mmol) and CMA (DS = 0.16, 150 mg, 8.5×10^{-1} mmol glucose unit) in water (20 mL) was dispersed ultrasonically for 5 min and then stirred at room temperature for 8 days. The precipitate was collected by centrifugation and dried under vacuum to give the **1**–CMA complex (32 mg, 18%), which was slightly soluble in water (up to concentrations of $\approx 10^{-4}$ M).[13] In agreement with the model structure, the **1**–CMA inclusion complex exhibited CP MAS (cross-polarization magic-angle spinning) ^{13}C NMR and the MASGHD (magic-angle spinning gate ^{1}H decoupled) ^{29}Si NMR signals that arose from CMA and the incorporated oligosilane chain.[14] A powder X-ray diffraction study demonstrated that the reflection pattern was very similar to that reported for a complex of γ-cyclodextrin (a macrocyclic molecule consisting of eight α-1,4-glucopyranose units), which exhibits a channel-type structure.[11,15] These studies suggest that the amylose is probably adopts a 8_1-helical structure (eight α-D-glucopyranose resides per turn) with a cross-section diameter of 8.5–9 Å to fit to the sequential size of the dimethylsilylene units of **1** (≈6 Å).

As was envisioned, and reinforced by the molecular mechanics calculations, decasilane **1** is indeed located in a helical channel and confined by CMA wrapping. The absorption and CD spectra provided information on the conformation of the oligosilane main chain within the channel (Figure 3). Thus, the absorption spectrum of a **1**–CMA complex (DS = 0.40) in water, at room temperature, exhibits an absorption maximum at 280 nm owing to the conjugated Si backbone σ–σ* transition ($\varepsilon = 1.1\times10^{4}\,\text{M}^{-1}\,\text{cm}^{-1}$).[16,17] In the CD spectrum, the complex displays an intense positive CD signal in the absorption region of the oligosilane ($\Delta\varepsilon = 2.56\ \text{mol}^{-1}\,\text{dm}^{3}\,\text{cm}^{-1}$ at 275 nm). Decasilane **1** does not give rise to any CD signals because of an equal mixture of enantiomeric twisted or helical conformers. However, in the helical channel of CMA, the decasilane **1** is induced to adopt a preferential helical conformation as a result of diastereoselective complexation with the chiral host. In this case, the main chain assumes a predominantly transoid conformation with a Si–Si torsion angle of 160–175° (15/7 helix).[18,19] The dissymmetry ratio, g_{abs} ($=\Delta\varepsilon/\varepsilon$), is usually used to characterize helical structures, such as right- and left-handed helix populations. The dissymmetry ratio for the **1**–CMA complex, $g_{abs} = 2.3\times10^{-4}$, is of the same order of magnitude ($1\text{–}2\times10^{-4}$) as that observed for a range of polysilanes with optically pure substituents that adopt a preferential screw sense.[20]

SPG also acts as a helical host polymer.[21] Decasilane **1**, in the presence of SPG, exhibits an absorption maximum at 284 nm ($\varepsilon = 1.1\times10^{4}\,\text{M}^{-1}\,\text{cm}^{-1}$) that is attributable to the σ–σ* transitions of the oligosilane main chain (Figure 3). In the CD spectrum, an induced CD signal is observed in the same region ($\Delta\varepsilon = -2.88\ \text{mol}^{-1}\,\text{dm}^{3}\,\text{cm}^{-1}$ at 282 nm). This signal is indicative of **1** being induced to assume a preferential helical conformation by complexation with SPG. The CD signal of the **1**–SPG complex is slightly red shifted relative to that of the **1**–CMA (DS = 0.40) complex. This shift is presumably associated with the pitch of the helical conformation of **1**. Such a pitch is induced when **1** is confined by the helices of the polysaccharide host molecules, as the pitch and the diameter of the host helices are different.[22,23] Interestingly, complexation of **1** with SPG, which conforms to a right-handed helix in water, induces a negative CD signal, whereas complexation

 © 2005 Wiley-VCH Verlag GmbH & Co. KGaA, Weinheim

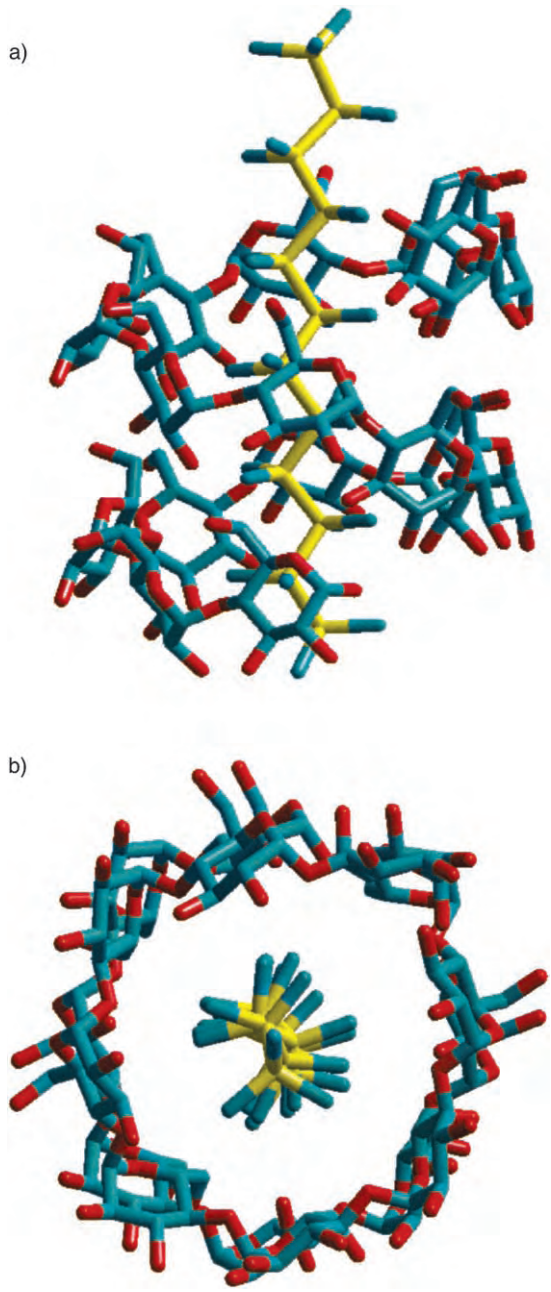

Figure 2. Energy-minimized models based on the AMBER force field for an inclusion complex of $Me(SiMe_2)_{12}Me$ with an amylose fragment containing 16 repeating α-1,4-D-glucopyranose residues: a) side view and b) top view. Carbon, oxygen, and silicon atoms are shown in blue, red, and yellow, respectively. The hydrogen atoms have been omitted for clarity.

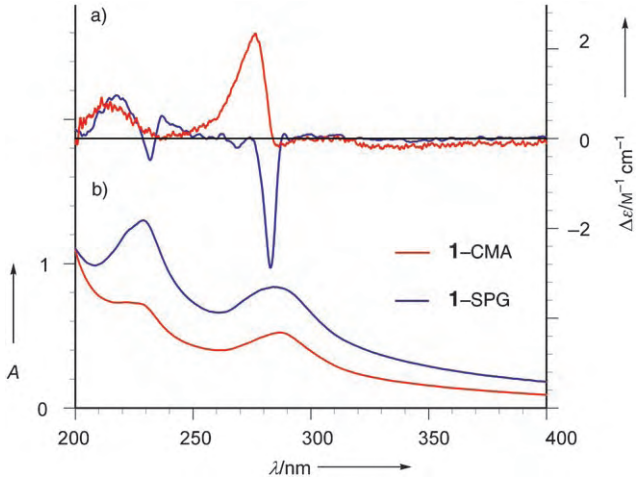

Figure 3. a) CD and b) absorption spectra of **1**–CMA (red line) and **1**–SPG (blue line) in water.

with CMA adopts a left-handed helical conformation in water and induces a positive CD signal (see above). Thus, the helical sense of the guest molecule is dependent on, and can be controlled by, the helical sense of the host polymer.

The time course of the absorption and CD spectra of a mixture of **1** and CMA revealed the progress of the folding process. The inclusion complex, generated in situ by mixing **1** and CMA in water for 40 h, showed an absorption maximum at 279 nm and a positive Cotton effect. However, the absorption undergoes a bathochromic shift to 293 nm over a period of a month without a change in the sign of the Cotton effect.[24,25] This can be attributed to changes in the helical pitch of the oligosilane to accommodate the dimensions of the helical channel. However, as **1** is confined by amylose wrapping, progress is slow as a result of the steric constraint. The fluorescence spectrum of the **1**–CMA complex discloses the more detailed structure of **1** in the channel. Thus, the **1**–CMA (DS = 0.40) complex, when excited at 298 nm, exhibits a local emission at 330 nm from both the naphthyl group and the oligosilane chain and an emission for the dimer at 400 nm from the naphthyl groups.[26] Accordingly, oligosilane **1**, within the complex, is envisioned to have aligned in a head-to-head fashion with the stacking of the naphthyl groups within the helical amylose.

Finally, a similar wrapping with CMA (DS = 0.16) has also been found to proceed with **2** and **3** as the guest molecules (Figure 1). The resultant complexes exhibit a positive Cotton effect; however, the intensities of the signals are weak. We presume that further to the hydrophobic interactions between the guest molecules and the helical cavity as the major driving force for complex formation, hydrogen bonding and/or π–π interactions within the channel also play an important role in the formation or stabilization of the complex.

In summary, we have demonstrated helical induction of oligosilane by using peripheral wrapping with amylose and schizophyllan. This system is the basis for a new and simple concept of helical expression in molecular and macromolecular systems.

Received: June 16, 2005
Revised: August 25, 2005
Published online: October 17, 2005

Keywords: chirality · helical structures · host–guest systems · molecular recognition · supramolecular chemistry

 © 2005 Wiley-VCH Verlag GmbH & Co. KGaA, Weinheim

[1] W. Saenger, *Principles of Nucleic Acid Structure*, Springer, New York, **1984**; G. E. Schulz, R. H. Schimer, *Principles of Protein Structure*, Springer, New York, **1979**, chap. 5; P. H. Pain, *Mechanism of Protein Folding*, 2nd ed. Oxford University Press, Oxford, **2000**.

[2] T. Nakano, Y. Okamoto, *Chem. Rev.* **2001**, *101*, 4013 – 4038; D. J. Hill, M. J. Mio, R. B. Prince, T. S. Hughes, J. S. Moore, *Chem. Rev.* **2001**, *101*, 3893 – 4011; M. M. Green, N. C. Peterson, T. Sato, A. Teramoto, R. Cook, S. Lifson, *Science* **1995**, *268*, 1860 – 1866.

[3] E. Yashima, K. Maeda, Y. Okamoto, *Nature* **1999**, *399*, 449 – 451; V. Berl, I. Huc, R. G. Khoury, M. J. Krische, J.-M. Lehn, *Nature* **2000**, *407*, 720 – 723; A. Tanatani, M. J. Mio, J. S. Moore, *J. Am. Chem. Soc.* **2001**, *123*, 1792 – 1793; S. H. Gellman, *Acc. Chem. Res.* **1998**, *31*, 173 – 180; Y.-M. Guo, H. Oike, T. Aida, *J. Am. Chem. Soc.* **2004**, *126*, 716 – 717.

[4] Helical folding of alkanes in a hydrophobic cavitand has been reported: L. Trembleau, J. Rebek, Jr., *Science* **2003**, *301*, 1219 – 1220; A. Scarso, L. Trembleau, J. Rebek, Jr., *Angew. Chem.* **2003**, *115*, 5657 – 5660; *Angew. Chem. Int. Ed.* **2003**, *42*, 5499 – 5502.

[5] W. Hinrichs, G. Büttner, M. Steifa, C. Betzel, V. Zabel, B. Pfannemüller, W. Saenger, *Science* **1987**, *235*, 205 – 208; G. Wulff, S. Kubik, *Makromol. Chem.* **1992**, *193*, 1071 – 1080; O. Nimz, K. Gessler, I. Usón, G. M. Sheldrick, W. Saenger, *Carbohydr. Res.* **2004**, *339*, 1427 – 1437; A. Star, D. W. Steuerman, J. R. Heath, J. F. Stoddart, *Angew. Chem.* **2002**, *114*, 2618 – 2622; *Angew. Chem. Int. Ed.* **2002**, *41*, 2508 – 2512; J. Kadokawa, Y. Kaneko, A. Nakaya, H. Tagaya, *Macromolecules* **2001**, *34*, 6536 – 6538.

[6] T. M. McIntire, D. A. Brant, *J. Am. Chem. Soc.* **1998**, *120*, 6909 – 6919; K. Sakurai, S. Shinkai, *J. Am. Chem. Soc.* **2000**, *122*, 4520 – 4521.

[7] R. D. Miller, J. Michl, *Chem. Rev.* **1989**, *89*, 1359 – 1410; H. Tsuji, M. Terada, A. Toshimitsu, K. Tamao, *J. Am. Chem. Soc.* **2003**, *125*, 7486 – 7487.

[8] M. Fujiki, *J. Am. Chem. Soc.* **1994**, *116*, 11 976 – 11 977.

[9] S. Maziéres, M. K. Raymond, P. A. Raabe, J. Michl, *J. Am. Chem. Soc.* **1997**, *119*, 6682 – 6683; K. Tamao, H. Tsuji, M. Terada, M. Asahara, S. Yamaguchi, *Angew. Chem.* **2000**, *112*, 3425 – 3428; *Angew. Chem. Int. Ed.* **2000**, *39*, 3287 – 3290; I. El-Sayed, Y. Hatanaka, S. Onozawa, M. Tanaka, *J. Am. Chem. Soc.* **2001**, *123*, 3597 – 3598.

[10] H. Okumura, Y. Kawaguchi, A. Harada, *Macromol. Rapid Commun.* **2002**, *23*, 781 – 785; H. Okumura, Y. Kawaguchi, A. Harada, *Macromolecules* **2003**, *36*, 6422 – 6429; K. Sakamoto, T. Naruoka, M. Kira, M. *Chem. Lett.* **2003**, *32*, 380 – 381.

[11] T. Sanji, A. Yoshiwara, H. Sakurai, M. Tanaka, *Chem. Commun.* **2003**, 1506 – 1507; T. Sanji, M. Kato, M. Tanaka, *Macromolecules* **2005**, *38*, 4034 – 4037.

[12] Monte Carlo searches for minimum-energy conformations were performed by using the HyperChem 7.5 and the AMBER force field.

[13] The NMR spectroscopic measurement was not possible because of the solubility of **1**–CMA in H_2O. A detailed description of the structure of the complex by, for example, X-ray single-crystal analysis or SPM observation requires further study.

[14] See Supporting Information.

[15] T. Oguchi, H. Yamasato, S. Limmatvapirat, E. Yonemochi, K. Yamamoto, *J. Chem. Soc. Faraday Trans.* **1998**, *94*, 923 – 927.

[16] K. Obata, M. Kira, *Organometallics* **1999**, *18*, 2216 – 2222.

[17] Although the absorption overlapped with that of the naphthyl group chromophore, the molar extinction coefficient of the permethyldecasilane was much higher than that of naphthylacetic acid ($\varepsilon = 500\,\text{M}^{-1}\,\text{cm}^{-1}$ at 273 nm). The absorption of **1**, which occurs at around 290 nm, was ascribed to the oligosilane.

[18] J. Michl, R. West, *Acc. Chem. Res.* **2000**, *33*, 821 – 823.

[19] The band widths of the absorption and the CD at 280 nm look somewhat different, probably due to incomplete inclusion of the oligosilane into the cavity or incomplete induction of the helical sense in the cavity. The other conformation of the oligosilane in the complex may also induce a Cotton signal.

[20] M. Fujiki, *Macromol. Rapid Commun.* **2001**, *22*, 539 – 563; S. Toyoda, M. Fujiki, *Macromolecules* **2001**, *34*, 640 – 644.

[21] Very recently, Shinkai and co-workers reported on a supramolecular chiral complex with SPG and polythiophene, see; C. Li, M. Numata, A.-H. Bae, K. Sakurai, S. Shinkai, *J. Am. Chem. Soc.* **2005**, *127*, 4548 – 4549.

[22] The helical CMA composed of α-1,4-D-glucopyranose residues assumes a 6/1–8/1 helical pitch (0.8 nm) with a 0.5–0.8 nm inner diameter, whereas the helical SPG composed of β-1,3-glucose residues assumes a 6/1 helical pitch (1.8 nm) with 1.75 nm inner diameter.

[23] Very recently, we found the supramolecular complex forms between a triple helix of SPG and two molecules of oligosilane **1**; for the detailed structure of the **1**–SPG complex, see: T. Sanji, N. Kato, M. Tanaka, *Chem. Lett.* **2005**, *34*, 1144 – 1145.

[24] The degree of carboxymethyl substitution on the amylose (DS) affects the helix formation of the amylose, the complexation ability between guest molecules and amylose, as well as the solubility in water. We found that complex formation between CMA and the oligosilanes depends on the DS. In the case of CMA (DS = 0.16), the complex, which was monitored with UV and CD measurements, was formed in a few hours after ultrasonic dispersion. In the case of CMA (DS = 0.40), complex formation was quite slow. Once the complex was formed, however, it was stable for more than a few months without alteration in the UV absorption intensity or the sign of the CD signal. We also examined the pH dependence of the complex formation under buffered conditions. In the neutral (pH 7.0) and the basic (pH 9.2) buffer solution, the situation of complex formation was almost the same. In the acid buffer solution (pH 5.0), however, complex formation was hardly observed. Furthermore, the thermostability of the complex was examined. At 80 °C no Cotton effect was observed, thus indicating that the complex was not stable at high temperature. We thank a referee for valuable suggestions.

[25] The material partially precipitates during complexation.

[26] A. Ueno, K. Takahashi, T. Osa, *J. Chem. Soc. Chem. Commun.* **1980**, 921 – 922.

 © 2005 Wiley-VCH Verlag GmbH & Co. KGaA, Weinheim

RNA Folding

DOI: 10.1002/anie.200502928

Modulation of RNA Tertiary Folding by Incorporation of Caged Nucleotides**

*Claudia Höbartner and Scott K. Silverman**

Photochemical caging groups[1] are often used to study biomolecular interactions, such as those between cofactors and enzymes or between neurotransmitters and their receptors.[2] In a caging experiment, a functionally important part of a molecule is modified by the strategic introduction of a non-natural moiety that disrupts key contacts or interferes with a critical reaction step. When the non-natural moiety is removed by photolysis, the native biomolecular interactions are restored. Photochemical caging has been used to study protein folding,[3] RNA catalysis,[4] secondary structure changes in RNA,[5] and other RNA-related phenomena,[6] but not higher-order tertiary folding of RNA.[7] When a caging group is appended at any specific nucleotide position, the effect on RNA tertiary folding is difficult to predict. This is unlike the situation of RNA catalysis (for which caging of an active-site hydroxy-group nucleophile is certain to disrupt reactivity) or of RNA secondary structure changes (for which reliable Watson–Crick interactions provide a strong predictive tool). Herein we report how an RNA molecule with a well-defined tertiary structure responds to the introduction of individual caging groups. Our results, which demonstrate varying local and global structural effects, have several implications for ongoing efforts to understand RNA folding.

We appended the photochemically removable (*S*)-1-(2-nitrophenyl)ethyl (NPE) group onto the nucleobase of each of the four standard RNA nucleotides (Figure 1).[8] The four corresponding phosphoramidites (NPE-U, NPE-C, NPE-A, and NPE-G) were prepared for conventional solid-phase RNA synthesis by using the 2′-*O*-triisopropylsilyloxymethyl (TOM) methodology.[9] The preparative route for the caged guanosine phosphoramidite was based on a recent report,[5] and the routes for the other three phosphoramidites are detailed in the Supporting Information. For each of the four phosphoramidites, solid-phase synthesis was used to prepare

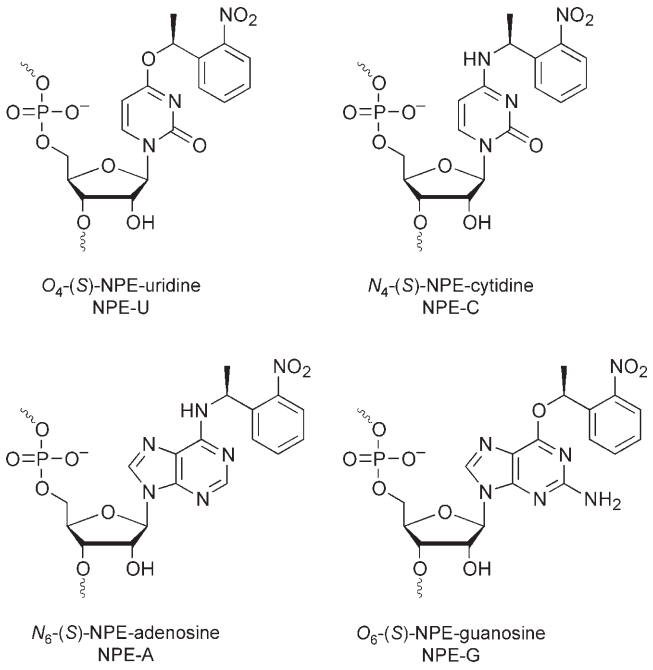

Figure 1. Structures of the (*S*)-NPE-caged RNA nucleotides.

15-mer and 24-mer RNA oligonucleotides, each of which incorporate a single caged RNA nucleotide at a specific internal position. In all cases, denaturing polyacrylamide gel electrophoresis (PAGE), anion-exchange HPLC analysis, and ESI mass spectrometry revealed that decaging proceeds to completion in less than 10 min by using a 300-W Xe-arc-lamp source (300–400 nm; Figure 2) or in approximately 30–60 min by using a handheld UV illuminator (365 nm; data not shown).[10]

We then placed individual caged nucleotides within a large RNA molecule, P4–P6. The 160-nucleotide P4–P6 domain of the *Tetrahymena* group I intron RNA adopts a characteristic tertiary structure in the presence of millimolar concentrations of Mg^{2+}.[11,12] As revealed by X-ray crystallography, the folded domain adopts a three-dimensional structure that resembles a candy cane (Figure 3).[13,14] The two largely helical domains of the RNA are held together, in part, by a key tertiary interaction between the GAAA tetraloop and its 11-nucleotide receptor.[15] Nucleotide and functional-group alterations within this tetraloop–receptor interaction have deleterious effects on the P4–P6 thermodynamic stability.[11,12,15–17]

We sought to probe the effects on P4-P6 folding of caging specific nucleotides with the NPE group. For this purpose, we synthesized modified P4–P6 variants by using a ligation strategy that joins a caged 15-mer or 24-mer oligonucleotide with an unmodified 145-mer or 136-mer T7 RNA polymerase transcript (see Supporting Information). We prepared 14 caged P4–P6 derivatives in this fashion. The caging sites were distributed throughout the RNA and were chosen on the basis of the X-ray crystal structure (Figure 3a). Caging sites were placed in positions where the NPE group was anticipated to have a combination of three effects: 1) alteration of the hydrogen-bonding interactions within either secondary- or

[*] Dr. C. Höbartner, Prof. S. K. Silverman
Department of Chemistry
University of Illinois at Urbana-Champaign
600 South Mathews Avenue, Urbana, IL 61801 (USA)
Fax: (+1) 217-244-8024
E-mail: scott@scs.uiuc.edu

[**] This research was supported by an Erwin Schrödinger fellowship from the Austrian Science Fund to C.H. and by the UIUC Department of Chemistry. S.K.S. is a Fellow of The David and Lucile Packard Foundation. We thank Prof. Ronald Micura (Innsbruck) for use of the HPLC system, Mary Smalley and Chandra Miduturu for assistance with RNA transcriptions, and Kimberly Peterson for preliminary synthetic experiments.

Supporting information for this article is available on the WWW under http://www.angewandte.org or from the author.

© 2005 Wiley-VCH Verlag GmbH & Co. KGaA, Weinheim

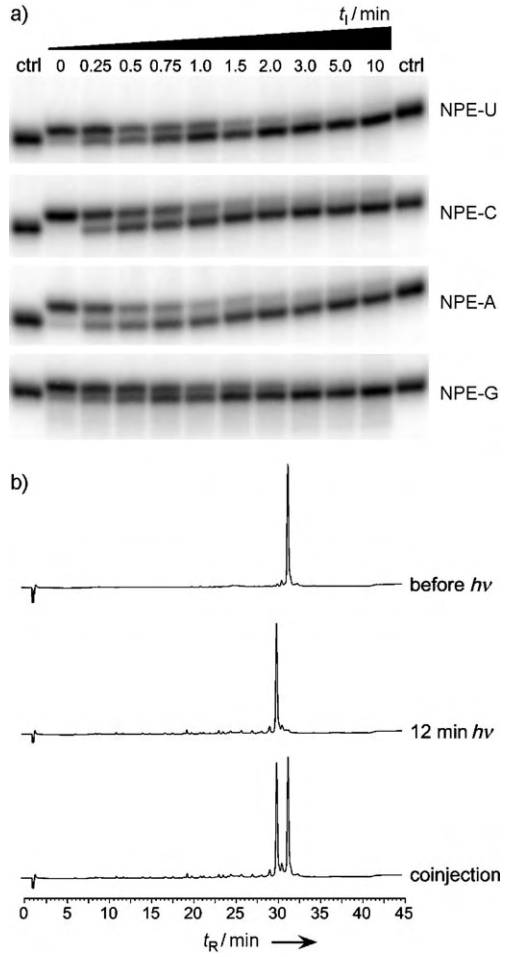

Figure 2. Photodeprotection of caged RNA oligoribonucleotides. a) Denaturing PAGE (20%) shows the photolysis time course for each of four caged 15-mer oligonucleotides (5′-GGAAUUGCGGGAAAG-3′, the underlined positions were individually caged with the NPE group). Control (ctrl) = oligonucleotide of the same sequence without the NPE group. b) Representative anion-exchange HPLC traces for the oligonucleotide with NPE-caged adenosine. Photolysis was carried out with a 300-W Xe arc lamp. (Traces for the other three caged oligonucleotides are shown in the Supporting Information, along with ESIMS data before and after photolysis for all four caged oligonucleotides.)

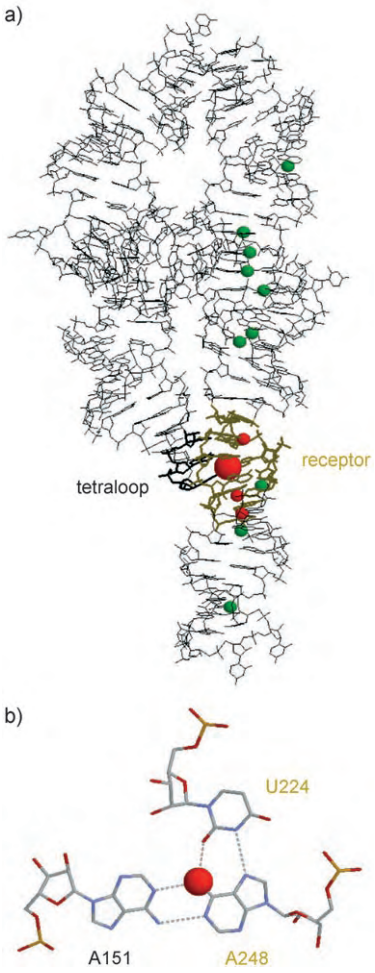

Figure 3. The 160-nucleotide P4–P6 RNA and sites of caging. a) X-ray crystal structure[13] with caging sites marked. Spheres are centered on the nucleobase atoms that bear the NPE caging groups and are colored red or green as in the data plots. The sphere marking the N6 atom of A248 is larger than the other spheres. Adenosine nucleotides A151, A152, and A153 of the GAAA tetraloop are thickened for emphasis. See Supporting Information for a picture of secondary structure. b) The base triple involving A248.

tertiary-structure elements; 2) disruption of base-stacking interactions; and 3) introduction of steric clashes (see Supporting Information for detailed images). In the NPE-A248 P4–P6 derivative, for example, the NPE caging group is placed on an adenine N6 group that is located in a densely packed region of RNA structure and at the interface between the GAAA tetraloop and the tetraloop receptor (Figure 3a). Because A248 is the central nucleotide of a base triple (Figure 3b) and because there appears to be no room to accommodate the bulky NPE group, NPE caging of A248 is expected to disrupt several hydrogen bonds and introduce a steric clash directly within the key tetraloop–receptor tertiary interaction. The determination of the consequences of such disruptions on RNA tertiary folding was a main experimental goal of this study.

The effects of individual caged nucleotides on P4–P6 folding were analyzed by nondenaturing (native) PAGE, which reports on global folding (Figure 4a).[17] The P4–P6 domain has a Mg^{2+}-dependent mobility on native PAGE; that is, when the RNA folds at higher Mg^{2+} concentrations, it adopts a more compact structure and thus migrates faster through the gel. Thermodynamic disruptions to the P4–P6 structure result in an increased Mg^{2+} requirement for folding, as quantified by the Mg^{2+} midpoint ($[Mg^{2+}]_{1/2}$ value) of a mobility versus $[Mg^{2+}]$ titration curve.[15,17,18] Our data allowed all 14 of the caged P4–P6 derivatives to be classified readily into just two types (Figure 4b): 1) those in which the caging group has a substantially destabilizing thermodynamic impact on tertiary folding (red), and 2) those in which the thermodynamic impact is small (green). Regardless of the effect of the caging group, its photolytic removal before analysis by native PAGE restored the RNA folding to that of the unmodified wild-type P4–P6 (Figure 4).

When the differential effects of caging the various nucleotides are considered in the context of their locations

 © 2005 Wiley-VCH Verlag GmbH & Co. KGaA, Weinheim

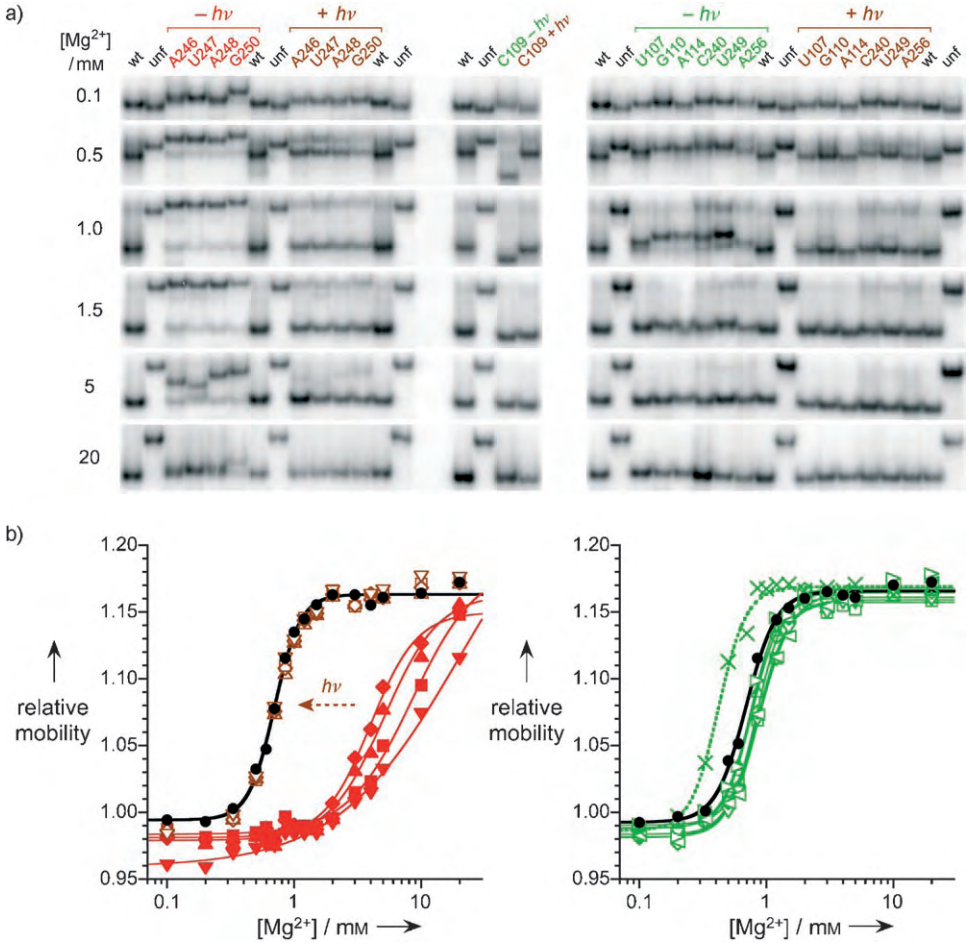

Figure 4. Native PAGE analysis of caged P4–P6 RNAs. a) Representative gel images. wt = unmodified wild-type P4–P6; unf = unfolded control that cannot fold even at high $[Mg^{2+}]$.[11,17,23] b) Mg^{2+} dependence of native gel mobility, computed for each caged derivative relative to the unfolded control. The wild-type P4–P6 is in black (●). Data in red represent positions where an unambiguous thermodynamic disruption is observed (▲ A246; ◆ U247; ■ A248; ▼ G250). Data in green represent positions where little effect is observed (× C109; the remaining symbols represent other positions from panel (a)). Photolysis of samples before native PAGE restored folding to that equivalent to the wild-type P4–P6 (brown). See the Supporting Information for experimental details.

within P4–P6, a clear pattern emerges. Caging of a nucleotide far from the tetraloop–receptor interaction has little effect on global folding. In sharp contrast, caging of a nucleotide that is located within (or very close to) the tetraloop–receptor interaction, such as A248, introduces a distinct thermodynamic destabilization. Nevertheless, native PAGE indicates that each of the latter derivatives eventually adopts the native global tertiary structure when the Mg^{2+} concentration is increased sufficiently (≥ 20 mM). For the NPE-caged A248 derivative, this finding is surprising because the tetraloop–receptor interaction must distort considerably to accommodate the NPE group, although the precise nature of the distortion cannot be discerned from these data. The only exception to the clear pattern is that the NPE-caged U249 derivative is not destabilized even though it is located within the receptor. Significantly, U249 is a bulged nucleotide in which the nucleobase does not form any tertiary hydrogen bonds, and inspection of the X-ray crystal structure suggests that the NPE caging group should be accommodated without causing a steric clash.

To provide an assessment of RNA folding that is independent of the native gel experiments, chemical probing with dimethyl sulfate was also performed. This reagent methylates either N1 of adenine or N3 of cytosine but only if the nucleobase is locally accessible to the reagent.[11,12,19] Tertiary folding of the RNA molecule buries some of the nucleobase functional groups within its interior;[20] this renders these functional groups inaccessible to dimethyl sulfate and thus protects them from methylation. Because the functional groups methylated by dimethyl sulfate are located on the Watson–Crick faces of the nucleobases, methylation inhibits primer extension by reverse transcriptase and leads to an abort band when the RTase reaction assay is examined by denaturing PAGE. The adenosine nucleotides of the GAAA tetraloop in unfolded P4–P6 (for example, P4–P6 in the absence of Mg^{2+}) are methylated readily by dimethyl sulfate. These nucleotides, however, are substantially protected from methylation when P4–P6 is folded properly owing to their sequestration in the tetraloop–receptor interaction.[11,12]

For several of the caged P4–P6 RNAs, dimethyl sulfate probing was performed at varying Mg^{2+} concentrations, and the accessibility of the GAAA tetraloop was monitored (Figure 5a). These experiments provide information on local structure that cannot be determined with native PAGE. Depending on the caging site, the dimethyl sulfate probing results revealed a difference in the accessibilities of the GAAA tetraloop at high Mg^{2+} concentrations (Figure 5b). The tested caging sites that are remote from the tetraloop–receptor interaction (U107, C109) had essentially no effect on Mg^{2+}-dependent accessibility of the tetraloop. In contrast, caging of nucleotides within or near the receptor (A246, U247, A248, and G250) significantly suppressed protection of the tetraloop from dimethyl sulfate modification upon an increase in the Mg^{2+} concentration. As with the native gel assays, U249 located within the receptor provides a predict-

 © 2005 Wiley-VCH Verlag GmbH & Co. KGaA, Weinheim

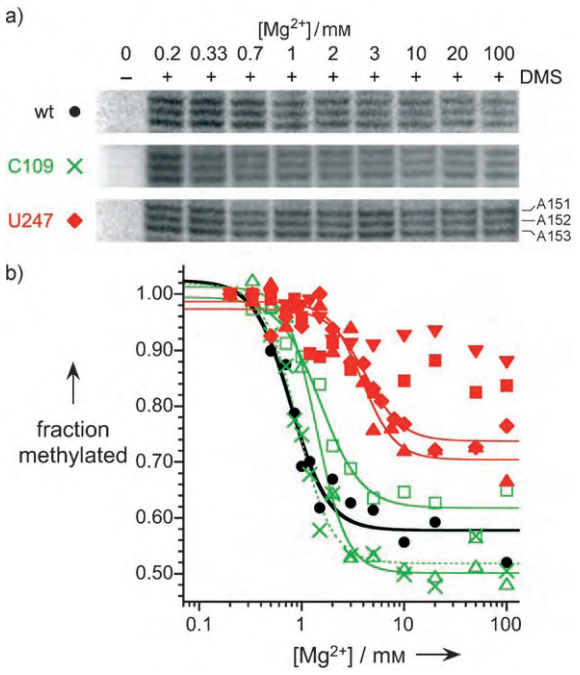

Figure 5. Chemical probing experiments with dimethyl sulfate of caged P4–P6 RNAs. a) Representative gel images for reverse transcriptase (RTase) assays of caged P4–P6 treated with dimethyl sulfate. The presence of an RTase abort band indicates methylation of the corresponding nucleobase with dimethyl sulfate, which must have been accessible to the reagent. The GAAA tetraloop includes nucleotides A151–A153. b) Mg^{2+} dependence of fraction methylated for the tetraloop adenosine nucleotides when various nucleotides are caged (● wild-type RNA; △ U107, × C109; □ U249; ▲ A246; ◆ U247; ■ A248; ▼ G250). A high fraction methylated implies high accessibility of the tetraloop to dimethyl sulfate. Photolysis of the samples before dimethyl sulfate probing restored protection from methylation (see Supporting Information).

able exception in this regard. These data show that the tetraloop–receptor interaction can be substantially perturbed on the local structural level, even when the global structure is essentially native. This conspicuous difference between local and global structural effects due to caging of specific nucleotides increases our understanding of how 'key interactions' contribute to RNA tertiary structure. Our results may also relate to the concept of compact, misfolded RNA states.[21] Some of the caged P4–P6 derivatives such as NPE-caged A248 adopt globally compact structures (as revealed by native PAGE) that nevertheless lack at least one native tertiary interaction (as indicated by dimethyl sulfate probing).

In summary, we have shown herein that nucleotides with caged nucleobases are readily incorporated into large RNA molecules that have complex tertiary structures, and the effects of the caged nucleotides are assessable with appropriate biochemical assays. From our results, we drew two conclusions that relate to the control of RNA folding by using caged nucleotides. First, incorporation of a bulky caging group can thermodynamically disrupt global RNA tertiary structure, but in all tested cases the disruption is relatively modest because it can be overcome by a sufficient increase in the Mg^{2+} concentration. This indicates that even 'key' tertiary contacts, such as the tetraloop–receptor interaction, are not strictly required for RNA tertiary folding. It also suggests that a chemically more sophisticated strategy (e.g., one that involves the attachment of a covalent tether at more than one position) is required to induce qualitative changes in global RNA structure that cannot be recovered simply by an increase in the Mg^{2+} concentration.[22] Second, comparisons of the native PAGE and dimethyl sulfate probing data indicate a clear differentiation between local and global structural effects upon the introduction of a chemical perturbation. This relates to the ability of individual caging groups to induce misfolded RNA states. A future direction for these studies will be to combine individual caging groups or photocleavable covalent tethers with time-resolved decaging to monitor RNA tertiary-folding processes in real time.

Received: August 18, 2005
Published online: October 17, 2005

Keywords: caging · nucleobases · oligonucleotides · photolysis · RNA structures

[1] J. H. Kaplan, B. Forbush III, J. F. Hoffman, *Biochemistry* **1978**, *17*, 1929–1935.
[2] a) H. A. Lester, J. M. Nerbonne, *Annu. Rev. Biophys. Bioeng.* **1982**, *11*, 151–175; b) A. M. Gurney, H. A. Lester, *Physiol. Rev.* **1987**, *67*, 583–617; c) J. A. McCray, D. R. Trentham, *Annu. Rev. Biophys. Biophys. Chem.* **1989**, *18*, 239–270; d) S. R. Adams, R. Y. Tsien, *Annu. Rev. Physiol.* **1993**, *55*, 755–784; e) B. E. Cohen, B. L. Stoddard, D. E. Koshland, Jr., *Biochemistry* **1997**, *36*, 9035–9044; f) J. C. Miller, S. K. Silverman, P. M. England, D. A. Dougherty, H. A. Lester, *Neuron* **1998**, *20*, 619–624; g) K. Curley, D. S. Lawrence, *Curr. Opin. Chem. Biol.* **1999**, *3*, 84–88; h) A. P. Pelliccioli, J. Wirz, *Photochem. Photobiol. Sci.* **2002**, *1*, 441–458; i) J. E. T. Corrie in *Dynamic Studies in Biology* (Eds.: M. Goeldner, R. Givens), Wiley-VCH, Weinheim, **2005**, pp. 1–28.
[3] a) H. S. M. Lu, M. Volk, Y. Kholodenko, E. Gooding, R. M. Hochstrasser, W. F. DeGrado, *J. Am. Chem. Soc.* **1997**, *119*, 7173–7180; b) K. C. Hansen, R. S. Rock, R. W. Larsen, S. I. Chan, *J. Am. Chem. Soc.* **2000**, *122*, 11567–11568.
[4] a) S. G. Chaulk, A. M. MacMillan, *Nucleic Acids Res.* **1998**, *26*, 3173–3178; b) S. G. Chaulk, A. M. MacMillan, *Angew. Chem.* **2001**, *113*, 2207–2210; *Angew. Chem. Int. Ed.* **2001**, *40*, 2149–2152.
[5] P. Wenter, B. Fürtig, A. Hainard, H. Schwalbe, S. Pitsch, *Angew. Chem.* **2005**, *117*, 2656–2659; *Angew. Chem. Int. Ed.* **2005**, *44*, 2600–2603.
[6] a) L. Kröck, A. Heckel, *Angew. Chem.* **2005**, *117*, 475–477; *Angew. Chem. Int. Ed.* **2005**, *44*, 471–473; b) S. Shah, S. Rangarajan, S. H. Friedman, *Angew. Chem.* **2005**, *117*, 1352–1356; *Angew. Chem. Int. Ed.* **2005**, *44*, 1328–1332.
[7] a) P. Brion, E. Westhof, *Annu. Rev. Biophys. Biomol. Struct.* **1997**, *26*, 113–137; b) I. Tinoco, Jr., C. Bustamante, *J. Mol. Biol.* **1999**, *293*, 271–281.
[8] The *S* isomer of the NPE group was chosen to be consistent with the report of Wenter et al.[5]
[9] a) S. Pitsch, P. A. Weiss, L. Jenny, A. Stutz, X. Wu, *Helv. Chim. Acta* **2001**, *84*, 3773–3795; b) R. Micura, *Angew. Chem.* **2002**, *114*, 2369–2373; *Angew. Chem. Int. Ed.* **2002**, *41*, 2265–2269.
[10] The caged uridine derivative with the NPE group at N3 instead of at O4 was also prepared. However, its photocleavage is inefficient (only ≈50% deprotection in 10 min with the arc

 © 2005 Wiley-VCH Verlag GmbH & Co. KGaA, Weinheim

lamp) and results in a mixture of two cleavage products, only one of which has an unmodified uracil nucleobase. Therefore, we did not pursue the N_3-NPE-caged uridine derivative any further. See Supporting Information for details.

[11] F. L. Murphy, T. R. Cech, *Biochemistry* **1993**, *32*, 5291 – 5300.
[12] F. L. Murphy, T. R. Cech, *J. Mol. Biol.* **1994**, *236*, 49 – 63.
[13] J. H. Cate, A. R. Gooding, E. Podell, K. Zhou, B. L. Golden, C. E. Kundrot, T. R. Cech, J. A. Doudna, *Science* **1996**, *273*, 1678 – 1685.
[14] K. Juneau, E. Podell, D. J. Harrington, T. R. Cech, *Structure* **2001**, *9*, 221 – 231.
[15] B. T. Young, S. K. Silverman, *Biochemistry* **2002**, *41*, 12271 – 12276.
[16] D. L. Abramovitz, A. M. Pyle, *J. Mol. Biol.* **1997**, *266*, 493 – 506.
[17] S. K. Silverman, T. R. Cech, *Biochemistry* **1999**, *38*, 8691 – 8702.
[18] a) S. K. Silverman, T. R. Cech, *Biochemistry* **1999**, *38*, 14224 – 14237; b) S. K. Silverman, M. Zheng, M. Wu, I. Tinoco, Jr., T. R. Cech, *RNA* **1999**, *5*, 1665 – 1674; c) S. K. Silverman, M. L. Deras, S. A. Woodson, S. A. Scaringe, T. R. Cech, *Biochemistry* **2000**, *39*, 12465 – 12475; d) S. K. Silverman, T. R. Cech, *RNA* **2001**, *7*, 161 – 166; e) E. A. Doherty, R. T. Batey, B. Masquida, J. A. Doudna, *Nat. Struct. Biol.* **2001**, *8*, 339 – 343; f) S. Matsumura, Y. Ikawa, T. Inoue, *Nucleic Acids Res.* **2003**, *31*, 5544 – 5551.
[19] D. A. Peattie, *Proc. Natl. Acad. Sci. USA* **1979**, *76*, 1760 – 1764.
[20] D. W. Celander, T. R. Cech, *Science* **1991**, *251*, 401 – 407.
[21] a) S. A. Woodson, *Nat. Struct. Biol.* **2000**, *7*, 349 – 352; b) K. L. Buchmueller, A. E. Webb, D. A. Richardson, K. M. Weeks, *Nat. Struct. Biol.* **2000**, *7*, 362 – 366; c) R. Russell, I. S. Millett, S. Doniach, D. Herschlag, *Nat. Struct. Biol.* **2000**, *7*, 367 – 370; d) R. Russell, I. S. Millett, M. W. Tate, L. W. Kwok, B. Nakatani, S. M. Gruner, S. G. Mochrie, V. Pande, S. Doniach, D. Herschlag, L. Pollack, *Proc. Natl. Acad. Sci. USA* **2002**, *99*, 4266 – 4271; e) X. W. Fang, P. Thiyagarajan, T. R. Sosnick, T. Pan, *Proc. Natl. Acad. Sci. USA* **2002**, *99*, 8518 – 8523; f) K. Takamoto, Q. He, S. Morris, M. R. Chance, M. Brenowitz, *Nat. Struct. Biol.* **2002**, *9*, 928 – 933; g) K. L. Buchmueller, K. M. Weeks, *Biochemistry* **2003**, *42*, 13869 – 13878; h) K. Takamoto, R. Das, Q. He, S. Doniach, M. Brenowitz, D. Herschlag, M. R. Chance, *J. Mol. Biol.* **2004**, *343*, 1195 – 1206.
[22] a) C. R. Allerson, G. L. Verdine, *Chem. Biol.* **1995**, *2*, 667 – 675; b) G. D. Glick, *Biopolymers* **1998**, *48*, 83 – 96; c) S. B. Cohen, T. R. Cech, *J. Am. Chem. Soc.* **1997**, *119*, 6259 – 6268.
[23] A. A. Szewczak, T. R. Cech, *RNA* **1997**, *3*, 838 – 849.

 © 2005 Wiley-VCH Verlag GmbH & Co. KGaA, Weinheim

Cover Picture

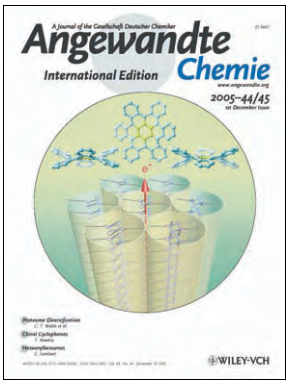

Shengxiong Xiao, Matthew Myers, Qian Miao, Sébastien Sanaur, Keliang Pang, Michael L. Steigerwald, and Colin Nuckolls*

Nonplanar aromatic cores are used for the design of molecule-based electronic materials. In their Communication on page 7390 ff., C. Nuckolls and co-workers discuss the preparation of materials that can be applied to field-effect transistors as an active layer owing to their high carrier mobilities, low turn-on voltages, and high on/off current ratios. The cover picture shows the molecular structure of a new class of hexabenzocoronenes in which the core is severely distorted out of planarity.

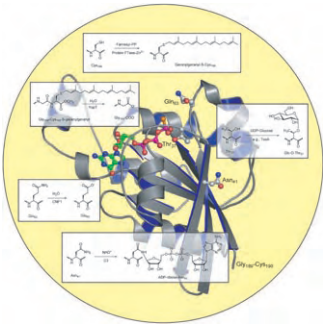

Proteome Chemistry
The proteome encompasses far more proteins than predicted from the coding capabilities of DNA. The reasons for this diversity are directed posttranslational modifications, of which the main types and mechanisms are discussed by C. T. Walsh et al. in their Review on page 7342 ff.

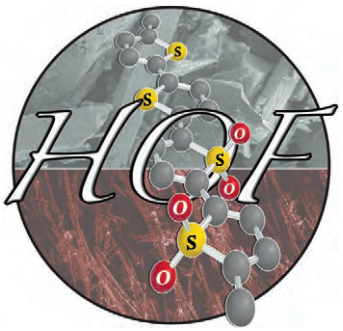

Hypofluorous Acid
E. Amir and S. Rozen describe in their Communication on page 7374 ff. the use of $HOF{\cdot}CH_3CN$ in the synthesis of *S*,*S*-dioxide oligothiophene derivatives, which show significantly different properties compared to nonoxidized oligothiophenes.

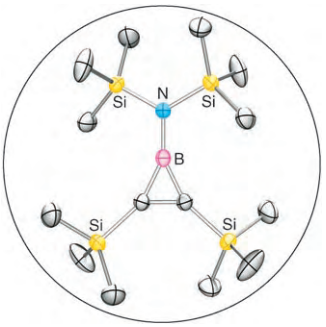

Aromaticity
In their Communication on page 7461 ff., H. Braunschweig et al. report on borylene transfer to alkynes at room temperature to give boracyclopropenes (borirenes) and discuss the experimental evidence for the theoretically predicted aromaticity of this class of compounds.

Contents

VIP *The following Communications have been judged by at least two referees to be "very important papers" and will be published online at www.angewandte.org soon:*

*S. J. Dalgarno, G. W. V. Cave, J. L. Atwood**
Toward the Isolation of Functional Organic Nanotubes

*Y. Nakajima, H. Kameo, H. Suzuki**
Cleavage of the Nitrogen-Hydrogen Bond of Ammonia Induced by Triruthenium Polyhydrido Clusters

N. Lu, H. P. S. Kumar, J. L. Fye, J. S. Blanks, J. S. Thrasher,* H. Willner, H. Oberhammer*
The Initial Synthesis of the Long Sought After Compound Pentafluoronitrosulfane, SF_5NO_2

*G. I. Elliott, J. Velcicky, H. Ishikawa, YongKai Li, D. L. Boger**
Total Synthesis of (−)- and ent-(+)-Vindorosine: Tandem Intramolecular Diels-Alder/1,3-Dipolar Cycloaddition of 1,3,4-Oxadiazoles

*G. Krebs, L. Hugonet, J. D. Sutherland**
Substrate Ambiguity and Catalytic Promiscuity Within a Bacterial Proteome Probed by an Easy Phenotypic Screen for Aldehydes

E. Álvarez, M. Paneque, M. L. Poveda,* N. Rendón*
Formation of Iridabenzenes by Coupling of Iridacyclopentadienes and Alkenes

News

Combinatorial Chemistry: P. Seeberger Recognized ____ **7330**

Medicinal Chemistry: R. Metternich on Board ____ **7330**

Pharmaceutical Chemistry: G. Wess Directs GSF ____ **7330**

Books

Practical Interpretation of P-31 NMR Spectra and Computer Assisted Structure Verification — Louis D. Quin, Antony J. Williams — *reviewed by H.-F. Klein* ____ **7331**

The Elements of Murder — John Emsley — *reviewed by V. Jacob* ____ **7331**

Highlights

Cyclophanes

T. Kawase* ____ **7334 – 7336**

Allenophane and Allenoacetylenic Macrocycles: A New Class of Chiral Cyclophanes

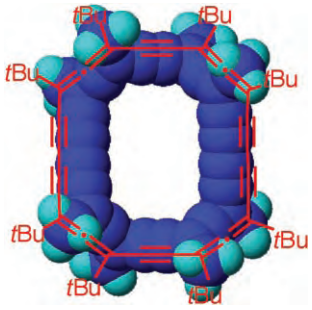

Building bridges: Allenophanes, cyclophanes that bear allene bridges, are attractive targets owing to their unique structural features and reactivity. Recently, chiral acetylenic allenophanes and allenoacetylenic macrocycles (see structure) were prepared.

Delocalization

C. Lambert* ____ **7337 – 7339**

Hexaarylbenzenes—Prospects for Toroidal Delocalization of Charge and Energy

The radical cation of substituted hexaphenylbenzene derivatives displays toroidal delocalization (see picture). Owing to the face-to-face orientation of six aryl groups, the hole is (almost) completely delocalized over these π systems, as has been proved by the deconvolution and analysis of the Vis/NIR absorption bands.

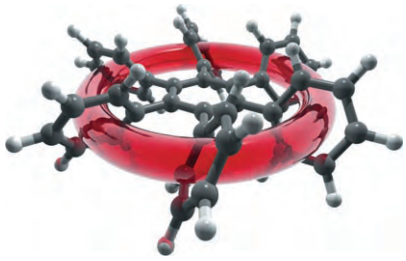

WILEY InterScience DISCOVER SOMETHING GREAT
© 2005 Wiley-VCH Verlag GmbH & Co. KGaA, Weinheim

Reviews

A variety of covalent alterations to the side chains and backbone atoms of proteins expand the diversity of proteomes beyond the number predicted by natural genome sequences. The predominant posttranslational modifications are described with an emphasis on the mechanisms of formation and reversal. The picture shows ADP ribosylation of a modified histidine residue of elongation factor eEF-2 catalyed by diphtheria toxin.

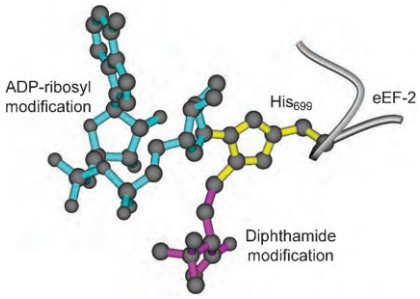

Protein Chemistry

C. T. Walsh,* S. Garneau-Tsodikova, G. J. Gatto, Jr. ——— 7342 – 7372

Protein Posttranslational Modifications: The Chemistry of Proteome Diversifications

Communications

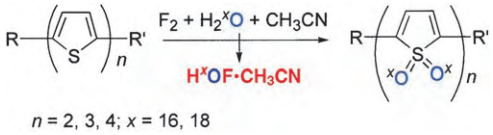

Nonaromatic stable polyenes are obtained by dioxygenation of oligothiophenes using $HOF{\cdot}CH_3CN$ prepared in situ by passing F_2 through aqueous acetonitrile (see scheme). These fully *S*,*S*-dioxygenated derivatives have a considerably smaller HOMO–LUMO gap than the parent compounds; furthermore, in the solid state they tend to form favorable π–π stacking interactions, unlike most non-oxidized oligothiophenes which adopt the "herringbone" motif.

Oligomers

E. Amir, S. Rozen* ——— 7374 – 7378

Synthesis of [all]-*S*,*S*-Dioxide Oligothiophenes Using $HOF{\cdot}CH_3CN$

A triolefin and a tripeptide were prepared in a single solution (see scheme) by ordered multistep synthesis. Temperature-sensitive variations in DNA secondary structure were used to orchestrate a series of effective molarity changes among four reactants of comparable intrinsic reactivity, resulting predominantly in one ordered product out of many possibilities. This approach mimics the selective control of effective molarity at precise moments during biosynthesis.

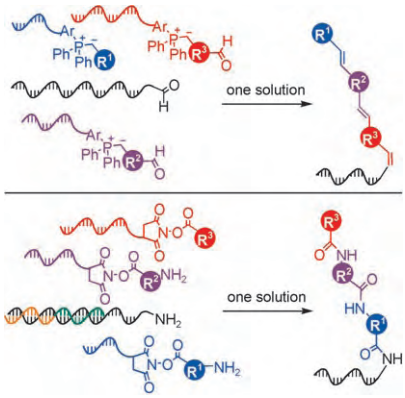

Synthetic Methods

T. M. Snyder, D. R. Liu* ——— 7379 – 7382

Ordered Multistep Synthesis in a Single Solution Directed by DNA Templates

For the USA and Canada:
ANGEWANDTE CHEMIE International Edition (ISSN 1433-7851) is published weekly by Wiley-VCH PO Box 191161, D 69451 Weinheim, Germany. Air freight and mailing in the USA by Publications Expediting Inc. 200 Meacham Ave., Elmont, NY 11003. Periodicals postage paid at Jamaica NY 11431. US POSTMASTER: send address changes to *Angewandte Chemie*, Wiley-VCH, 111 River Street, Hoboken, NJ 07030. Annual subscription price for institutions: US$ 5685/5168 (valid for print and electronic / print or electronic delivery); for individuals who are personal members of a national chemical society prices are available on request. Postage and handling charges included. All prices are subject to local VAT/sales tax.

© 2005 Wiley-VCH Verlag GmbH & Co. KGaA, Weinheim

The best in chemistry –

for more than a hundred years

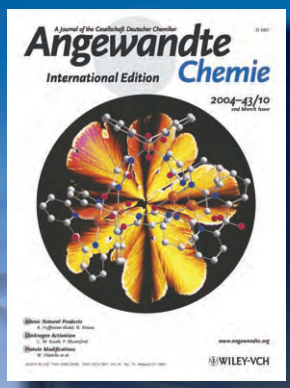

A Journal of the Gesellschaft Deutscher Chemiker

Angewandte
International Edition **Chemie**

www.angewandte.org

1888: ***The beginning of a success story***

Constant Innovations

1962: *First issue of the International Edition*
1976: *Graphical abstracts*
1979: *Cover pictures*
1988: *Centenary of Angewandte*
1989: *Routine use of color*
1991: *New section: Highlights*
1992: *Computerized editorial tracking system*
1995: *Internet service for readers*
1998: *Regular press service; full-text online*
2000: *New section: Essays; EarlyView: Communications available online ahead of the printed version*
2001: *New section: Minireviews*
2002: *Online submission of manuscripts*
2003: *Weekly publication; new section: News; new layout*
2004: *Backfiles (1962-1997); ManuscriptXpress: Online system for authors and referees*

Angewandte's advisors...

Ryoji Noyori
Nagoya University and RIKEN (Tokyo)

*»**Angewandte Chemie** is the best scientific arena for both players and audience. This international journal has taken a leading role in raising the potential of chemistry to the current high standard.«*

***Angewandte Chemie International Edition** is a journal of the German Chemical Society (GDCh)*

GDCh

WILEY InterScience® DISCOVER SOMETHING GREAT

WILEY-VCH

1871404_gu

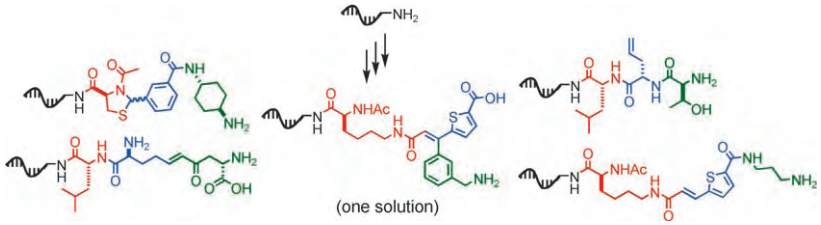

Combinatorial Chemistry

C. T. Calderone, D. R. Liu* _ 7383 – 7386

Small-Molecule Diversification from Iterated Branching Reaction Pathways Enabled by DNA-Templated Synthesis

Two unique features of DNA-templated synthesis were integrated to prepare complex small molecules by using iterated branching reaction pathways: the direction of multiple, otherwise "incompatible", reaction types in one reaction vessel and the direction of sequence-programmed subsets of reaction intermediates to appropriate reagents.

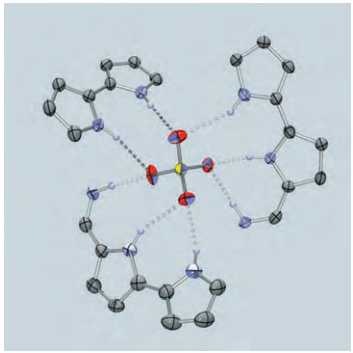

Host–Guest Chemistry

E. A. Katayev, G. D. Pantos, M. D. Reshetova, V. N. Khrustalev, V. M. Lynch, Y. A. Ustynyuk, J. L. Sessler* _____ 7386 – 7390

Anion-Induced Synthesis and Combinatorial Selection of Polypyrrolic Macrocycles

Stimulating reactions: The anion-induced synthesis of a new class of 2,6-diamidopyridine–bipyrrole macrocyclic receptors that undergo combinatorial selection as a result of their interaction with anionic guests has been demonstrated (see picture of the interaction of bipyrrole fragments with a sulfate ion). The outcome of this stimulus-driven reaction bears analogy to recent macrocycle-forming strategies based on dynamic combinatorial processes.

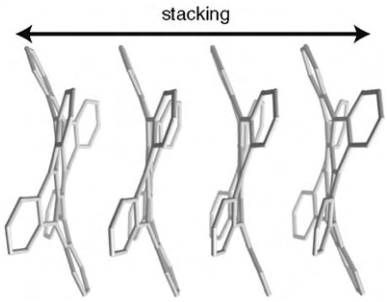

Self-Assembly

S. Xiao, M. Myers, Q. Miao, S. Sanaur, K. Pang, M. L. Steigerwald, C. Nuckolls* _____ 7390 – 7394

Molecular Wires from Contorted Aromatic Compounds

In a twist: A design strategy for molecule-based electronic materials using aromatic compounds with a nonplanar core is presented. A new class of hexabenzocoronene is put forth that has its core severely distorted out of planarity into a corrugated structure. When substituted with four alkoxy side chains, this material self-assembles into infinitely long columns through stacking (see picture) and acts as an active layer in field-effect transistors.

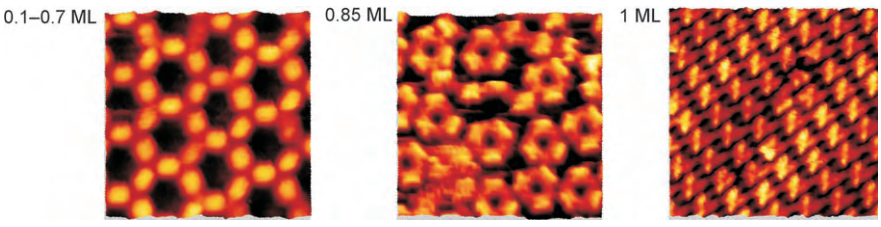

Surface Chemistry

M. Stöhr,* M. Wahl, C. H. Galka, T. Riehm, T. A. Jung, L. H. Gade* ____ 7394 – 7398

Controlling Molecular Assembly in Two Dimensions: The Concentration Dependence of Thermally Induced 2D Aggregation of Molecules on a Metal Surface

Dilution principle in two dimensions: One building block yields three forms of aggregation on variation of the surface concentration of the molecular precursor (see picture; ML = monolayer coverage). Upon annealing at 300 °C, highly robust 2D aggregates are obtained on metal surfaces which lend themselves to the construction of hierarchic systems of higher complexity.

© 2005 Wiley-VCH Verlag GmbH & Co. KGaA, Weinheim

Contents

Polyolefins

C. Ornelas, D. Méry, J.-C. Blais, E. Cloutet, J. Ruiz Aranzaes, D. Astruc* **7399 – 7404**

Efficient Mono- and Bifunctionalization of Polyolefin Dendrimers by Olefin Metathesis

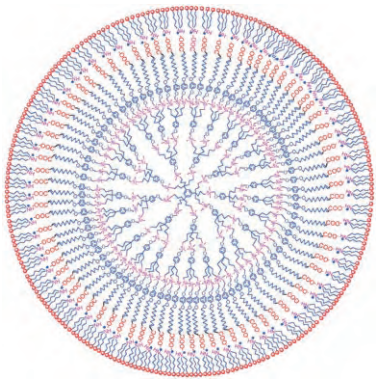

Star- and dendritic-shaped polyolefins can be cleanly and stereospecifically mono- or bifunctionalized by catalytic cross olefin metathesis. Furthermore, this approach provides a rapid overall synthesis of water-soluble dendrimers (see picture) from simple polymethylbenzenes, such as mesitylene and hexamethylbenzene.

Synthetic Methods

B. Xu, G. B. Hammond* **7404 – 7407**

Difluoroallenyl Bromide as a Wide-Ranging Difluoromethylene Cation Equivalent: S_N2 Substitution of Difluoropropargyl Bromide through Sequential S_E2' and S_N2' Reactions

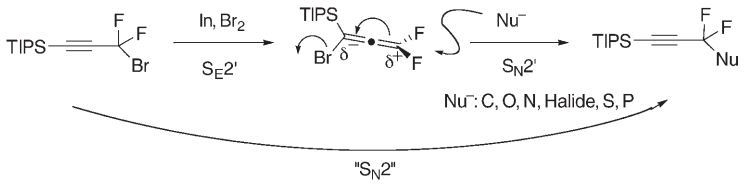

A synthetic challenge: a two-step conversion of RCF_2Br into RCF_2Nu has been achieved (see scheme; Nu = nucleophile). Nucleophilic substitution at a difluoromethylene carbon atom is carried out by using a functionalized difluoroallene as a CF_2 cation equivalent. The resulting product contains a triisopropylsilyl (TIPS)–acetylenic linkage suitable for further functionalization.

Synthetic Methods

K. Moonen, E. Van Meenen, A. Verwée, C. V. Stevens* **7407 – 7411**

One-Pot Tandem 1,4–1,2-Addition of Phosphites to α,β-Unsaturated Imines for the Synthesis of Glutamic Acid Analogues

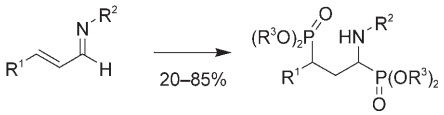

Evidently so: New mechanistic findings indicate that addition of dialkyl trimethylsilyl phosphites to α,β-unsaturated imines has been incorrectly reported as an exclusive 1,2-addition. When α,β-unsaturated imines are used as substrates, 1-alkylamino 3-phosphonyl phosphonates are formed in high yields in the presence of a suitable proton source through a sequential 1,4- and 1,2-addition.

Ceria Nanostructures

T. Yu, J. Joo, Y. I. Park, T. Hyeon* **7411 – 7414**

Large-Scale Nonhydrolytic Sol–Gel Synthesis of Uniform-Sized Ceria Nanocrystals with Spherical, Wire, and Tadpole Shapes

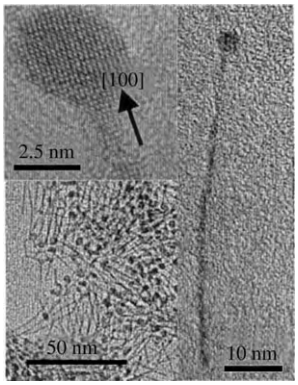

Spawning nanostructures: Uniform-sized ceria nanocrystals with sphere, wire, and tadpole shapes were synthesized from the nonhydrolytic sol–gel reaction of cerium(III) nitrate and diphenyl ether in the presence of appropriate surfactants. The picture shows a TEM image of a batch of tadpole-shaped nanowires (bottom left) and low-magnification and high-resolution TEM images of a single tadpole-shaped nanowire (right and top left, respectively).

© 2005 Wiley-VCH Verlag GmbH & Co. KGaA, Weinheim

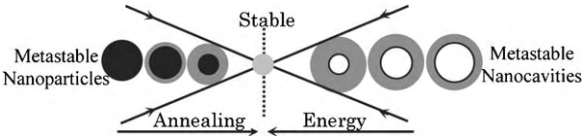

Nanodiamond Stability

C. X. Wang, J. Chen, G. W. Yang,* N. S. Xu* ——— 7414 – 7418

Thermodynamic Stability and Ultrasmall-Size Effect of Nanodiamonds

Below 3 nm, nanodiamonds were experimentally verified to be more stable than graphite. Experimental and theoretical studies reveal that the nanometer-sized curvature of nanodiamonds is the physical origin of their stability. A similar nanosize effect was reported for the shrinkage of nanocavities on ion-beam irradiation (see schematic diagram).

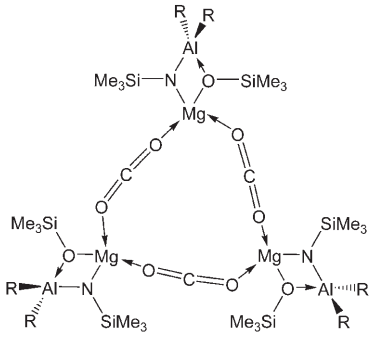

Carbon Dioxide Complexes

C.-C. Chang,* M.-C. Liao, T.-H. Chang, S.-M. Peng, G.-H. Lee ——— 7418 – 7420

Aluminum–Magnesium Complexes with Linearly Bridging Carbon Dioxide

The linear μ(O,O′) bonding mode of CO_2 has been found for the first time in the magnesium–aluminum compounds $[\{R_2Al(\mu\text{-}NSiMe_3)(\mu\text{-}OSiMe_3)Mg(thf)_2(\mu\text{-}O_2C)\}_3]$ (**1** (R = Me) and **2** (R = Et); THF ligands omitted), which were obtained by bubbling CO_2 through a mixture of AlR_3 and $Mg[N(SiMe_3)_2]_2$ in THF.

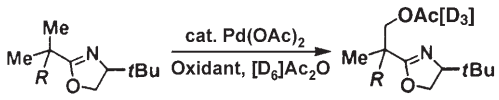

Asymmetric Catalysis

R. Giri, J. Liang, J.-G. Lei, J.-J. Li, D.-H. Wang, X. Chen, I. C. Naggar, C. Guo, B. M. Foxman, J.-Q. Yu* ——— 7420 – 7424

Pd-Catalyzed Stereoselective Oxidation of Methyl Groups by Inexpensive Oxidants under Mild Conditions: A Dual Role for Carboxylic Anhydrides in Catalytic C–H Bond Oxidation

Unactivated CH_3 groups in 2-oxazolines are oxidized by inexpensive oxidants, such as *tert*-butyl peroxyacetate and lauroyl peroxide, in the presence of a catalytic amount of $Pd(OAc)_2$. Carboxylic anhydrides are essential for both the oxidation of the Pd–C bonds and regeneration of $Pd(OAc)_2$. The use of $[D_6]Ac_2O$ as the solvent shows that the acetyl group incorporated into the product is from acetic anhydride rather than the oxidant (see scheme).

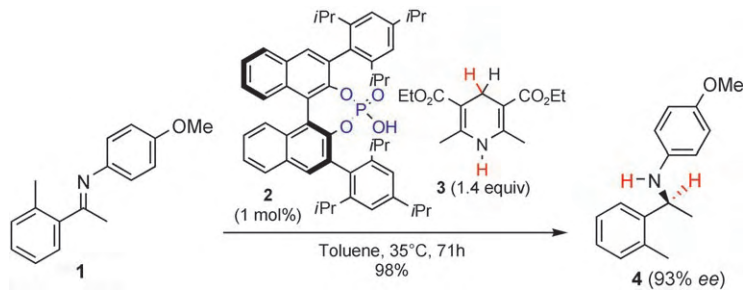

Asymmetric Catalysis

S. Hoffmann, A. M. Seayad, B. List* ——— 7424 – 7427

A Powerful Brønsted Acid Catalyst for the Organocatalytic Asymmetric Transfer Hydrogenation of Imines

A little goes a long way: A 1 mol% loading of the chiral phosphoric acid catalyst **2** converts aromatic and aliphatic imines such as **1** into the corresponding amines (**4**) in high yields and enantioselectivities if treated with Hantzsch dihydropyridine **3**.

© 2005 Wiley-VCH Verlag GmbH & Co. KGaA, Weinheim

Contents

Bioelectrochemistry

J. Lee, D. Lee, E. Oh, J. Kim, Y.-P. Kim, S. Jin, H.-S. Kim,* Y. Hwang, J. H. Kwak, J.-G. Park, C.-H. Shin, J. Kim,* T. Hyeon* ——— **7427 – 7432**

Preparation of a Magnetically Switchable Bio-electrocatalytic System Employing Cross-Linked Enzyme Aggregates in Magnetic Mesocellular Carbon Foam

Glucose oxidase (GOx) was immobilized in magnetic mesocellular carbon foam by cross-linking with glutaraldehyde. This material has been utilized to construct a magnetically switchable bio-electrocatalytic system in which the catalytic oxidation of glucose could be switched on and off by the positioning of an external magnet near and away from the electrode (see scheme).

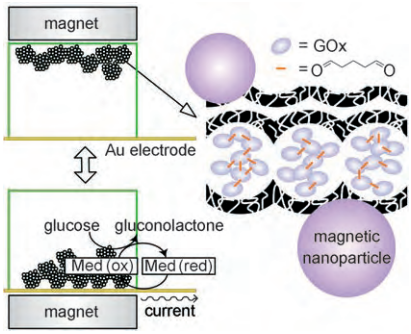

Mechanical Properties

L. Itzhaki, E. Altus, H. Basch, S. Hoz* ——— **7432 – 7435**

Harder than Diamond: Determining the Cross-Sectional Area and Young's Modulus of Molecular Rods

Hard and straight: Diamond is the hardest material known, yet polyyne—a molecular rod comprised of C≡C units—resists longitudinal compression with a Young's Modulus 40 times larger than diamond, whereas [*n*]staffanes have a Young's Modulus close to that of diamond. Mechanical engineering provides the connection between the point at which a rod buckles under longitudinal load and its cross-sectional area.

Chiral Molecules

G. Borsato,* M. Crisma, O. De Lucchi, V. Lucchini,* A. Zambon ——— **7435 – 7439**

"Hexacarboxytrindanes": Benzene Rings with Homotopic Faces as Scaffolds for the Construction of D_3 Chiral Architectures

Thermodynamically driven epimerization at the trindane benzylic positions of "hexacarboxytrindanes" generates benzene rings with D_3 symmetry and with *R* or *S* homotopic faces. Almost total resolution towards *S* trindanes was achieved by epimerization and transesterification with lithium (−)-mentholate. These structures are attractive cores for the construction of macromolecules in which asymmetry is induced by the center of the molecule.

Nanoparticle Assemblies

J. Lee, A. O. Govorov, N. A. Kotov* ——— **7439 – 7442**

Nanoparticle Assemblies with Molecular Springs: A Nanoscale Thermometer

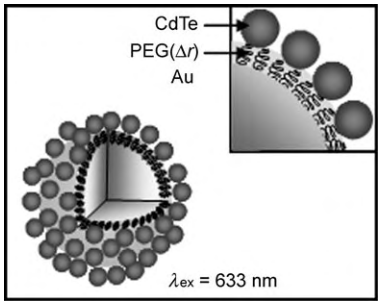

A temperature-dependent emission is observed for CdTe nanoparticles connected to Au nanoparticles by a flexible poly(ethyleneglycol) (PEG) link acting as a molecular spring (see picture). The extension of the PEG springs varies depending on the temperature, which causes variations in CdTe emission caused by plasmon–exciton interactions. A theoretical model of plasmon–exciton coupling explains the optical and thermal effects.

© 2005 Wiley-VCH Verlag GmbH & Co. KGaA, Weinheim

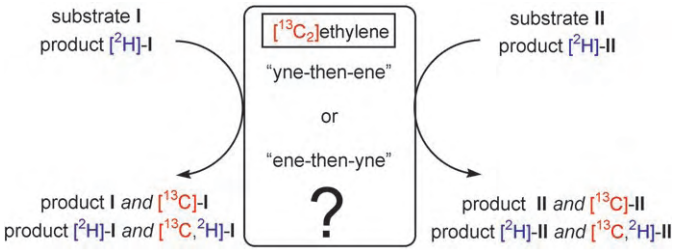

Mixing it: A dual-substrate/dual isotopic labeling strategy has shown that the accelerating effect of ethylene in intermolecular ring-closing metathesis of enynes is best explained by an ene-then-yne mechanism rather than the commonly proposed yne-then-ene mechanism (see picture).

Reaction Mechanisms

G. C. Lloyd-Jones,* R. G. Margue, J. G. de Vries ——— 7442 – 7447

Rate Enhancement by Ethylene in the Ru-Catalyzed Ring-Closing Metathesis of Enynes: Evidence for an "Ene-then-Yne" Pathway that Diverts through a Second Catalytic Cycle

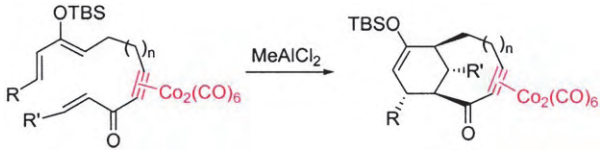

The characteristic structural features of [(alkyne)$Co_2(CO)_6$] complexes were used to achieve bridged-type intramolecular [4+2] cycloaddition reactions. The reaction of such complexes bearing a siloxydiene and an electron-deficient dienophile moiety on opposite ends decreases steric congestion and allows formation of a bridged-type adduct. Reaction of these complexes with $MeAlCl_2$ in the presence of 2,6-di-*tert*-butylpyridine in CH_2Cl_2 provides the novel [4+2] cycloadducts as single stereoisomers in good yields (see reaction).

Cycloadditions

N. Iwasawa,* K. Inaba, S. Nakayama, M. Aoki ——— 7447 – 7450

Complexation-Initiated Intramolecular [4+2] Cycloaddition: Construction of Bridged-Type Cycloadducts

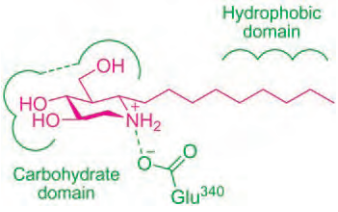

Highly potent human β-glucocerebrosidase inhibitors have been synthesized that appear to recognize both carbohydrate and hydrophobic binding sites. The most potent inhibitor, 6-nonyl isofagomine (see formula), shows an IC_{50} value at subnanomolar concentrations. These compounds are potential candidates for the development of small-molecule drugs for the treatment of Gaucher disease.

Drug Design

X. Zhu, K. A. Sheth, S. Li, H.-H. Chang, J.-Q. Fan* ——— 7450 – 7453

Rational Design and Synthesis of Highly Potent β-Glucocerebrosidase Inhibitors

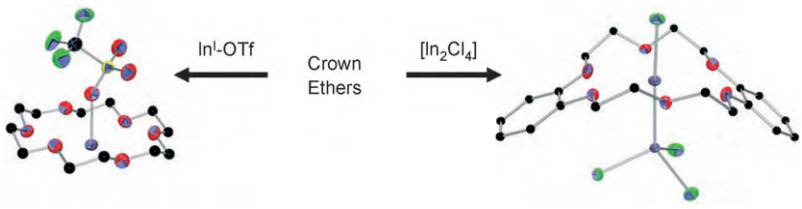

A crowning achievement: Appropriately sized crown ethers can stabilize or enable In^{I} compounds to be generated without decomposition or disproportionation (see scheme). The resulting coordination compounds include the only example of a donor group complexed to a monomeric, univalent Group 13 center and the first example of a homoleptic Group 13–Group 13 donor–acceptor complex.

Coordination Chemistry

C. G. Andrews, C. L. B. Macdonald* ——— 7453 – 7456

Crown Ether Ligation: An Approach to Low-Oxidation-State Indium Compounds

© 2005 Wiley-VCH Verlag GmbH & Co. KGaA, Weinheim

Contents

M=B Metathesis

D. L. Kays (née Coombs), J. K. Day, L.-L. Ooi, S. Aldridge* ——— **7457 – 7460**

Cationic Terminal Borylene Complexes: A Synthetic and Mechanistic Investigation of M=B Metathesis Chemistry

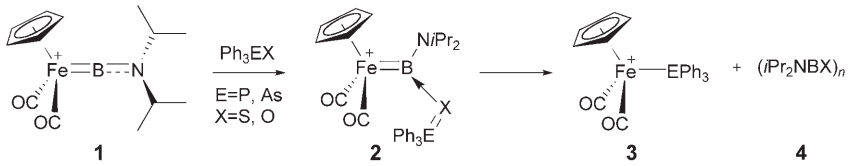

Halide abstraction chemistry has been exploited to generate the cationic terminal borylene complex **1**, which reacts with $Ph_3P{=}S$ or $Ph_3As{=}O$ to form **3** and **4**. In the case of the corresponding reaction with $Ph_3P{=}O$, the intermediate **2** can be isolated, which provides evidence for a two-step addition/substitution mechanism for the overall metathesis reaction.

Boracycles

H. Braunschweig,* T. Herbst, D. Rais, F. Seeler ——— **7461 – 7463**

Synthesis of Borirenes by Photochemical Borylene Transfer from $[(OC)_5M{=}BN(SiMe_3)_2]$ (M = Cr, Mo) to Alkynes

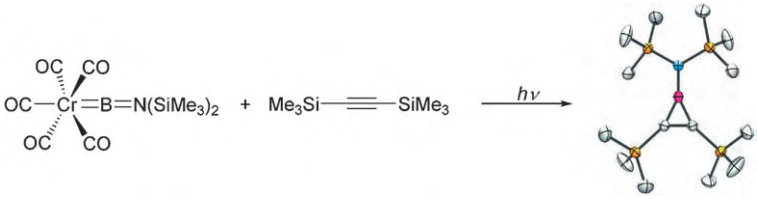

Light movements: Irradiation of terminal borylene complexes $[(OC)_5M{=}BN(SiMe_3)_2]$ (M = Cr, Mo) at room temperature in the presence of alkynes allows access to various substituted borirenes—an unprecedented borylene transfer to main-group-element substrates (see scheme; B red, C white, N blue, Si yellow).

Nanoporous Materials

J. M. Macak, H. Tsuchiya, L. Taveira, S. Aldabergerova, P. Schmuki* ——— **7463 – 7465**

Smooth Anodic TiO_2 Nanotubes

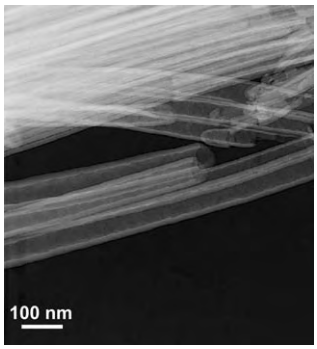

Smooth results with glycerol: A highly viscous glycerol electrolyte suppresses local concentration fluctuations and changes in pH during the anodization of titanium. This leads to layers of smooth TiO_2 nanotubes up to 7 μm thick and with an average pore diameter of 40 nm (see transmission electron micrograph).

Asymmetric Organocatalysis

A. Berkessel,* F. Cleemann, S. Mukherjee ——— **7466 – 7469**

Kinetic Resolution of Oxazinones: An Organocatalytic Approach to Enantiomerically Pure β-Amino Acids

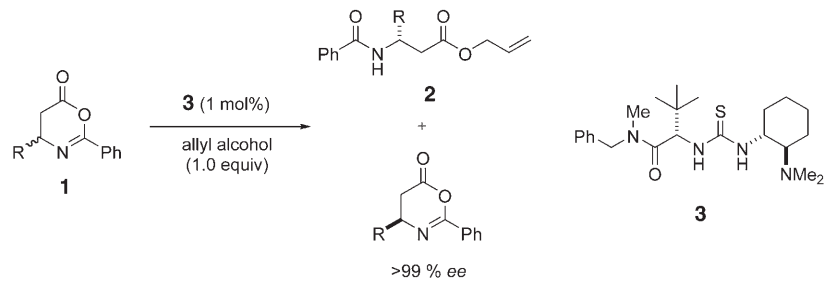

A profitable split: An organocatalytic resolution converts readily available racemic oxazinones **1** into valuable enantiomerically pure β-amino acid derivatives **2** (>99% *ee* of the remaining **1** at 53% conversion; 88% *ee* of the ester **2**). This catalytic ring-opening reaction requires as little as 1 mol% of the modular and readily accessible thiourea organocatalyst **3**.

© 2005 Wiley-VCH Verlag GmbH & Co. KGaA, Weinheim

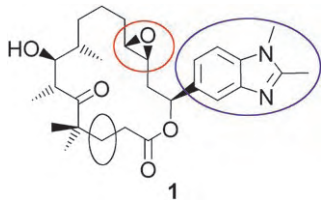

The microtubule-stabilizing agent 1 was obtained through extensive modification (colored circles) of the structure of natural epothilone. Despite these structural differences, the biological potency of **1** is comparable with that of epothilone A and taxol!

Epothilones

F. Cachoux, T. Isarno, M. Wartmann, K.-H. Altmann* ——— **7469 – 7473**

Scaffolds for Microtubule Inhibition through Extensive Modification of the Epothilone Template

Models get choosey: Structurally characterized mono- and dicationic yttrium methyl complexes (**3** and **4**) are accessible by protonolysis of the hexamethylate complexes (**1** and **2**) and function as models for the homogeneous catalysts for 1,4-*cis*-selective polymerization of 1,3-dienes by the industrially applied multicomponent catalyst.

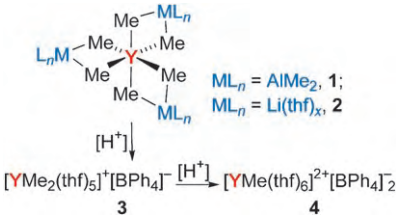

Polymerization Catalysts

S. Arndt, K. Beckerle, P. M. Zeimentz, T. P. Spaniol, J. Okuda* ——— **7473 – 7477**

Cationic Yttrium Methyl Complexes as Functional Models for Polymerization Catalysts of 1,3-Dienes

The issues for November 2005 appeared online on the following dates
Issue 41: October 14 · Issue 42: October 25 · Issue 43: October 31 · Issue 44: November 8

Sources

Product and Company Directory

You can start the entry for your company in "Sources" in any issue of *Angewandte Chemie*.

If you would like more information, please do not hesitate to contact us.

Wiley-VCH Verlag – Advertising Department
Tel.: 0 62 01 - 60 65 65
Fax: 0 62 01 - 60 65 50
E-Mail: MSchulz@wiley-vch.de

Service

Keywords ——— *7478*

Authors ——— *7479*

Angewandte's Sister Journals ——— *7480 – 7481*

Preview ——— *7483*

Corrigendum

The authors acknowledge the crucial contributions of Dr. Paultheo von Zezschwitz in the preliminary stages of this project.

Highly Enantioselective Thiourea-Catalyzed Nitro-Mannich Reactions

T. P. Yoon, E. N. Jacobsen* ——— **466–468**

Angew. Chem. Int. Ed. **2005**, *44*

DOI 10.1002/anie.200461814

© 2005 Wiley-VCH Verlag GmbH & Co. KGaA, Weinheim

P. Seeberger Receives ESCS Award

Peter H. Seeberger (ETH Zürich) received the European Society of Combinatorial Sciences (ESCS) Award for his outstanding contribution to combinatorial carbohydrate chemistry. He presented his award lecture on "Automated Synthesis of Oligosaccharides: From Carbohydrate Arrays to Vaccines" at the Eurocombi-3 Conference.

P. Seeberger

Seeberger studied chemistry at the Universität Erlangen-Nürnberg and received his doctorate under the guidance of M. Caruthers (University of Colorado) in 1995. After a postdoctoral stay in the group of S. Danishefsky at the Sloan–Kettering Institute in New York, he began his independent research at the Massachussets Institute of Technology, where he became professor in 2002. A year later, he accepted a chair as professor of organic chemistry (successor to Dieter Seebach) at the ETH Zürich. Seeberger's research interest lies at the interface between chemistry and biology, with particular regard to glycoproteins and glycolipids. He recently reported in *Angewandte Chemie* on an anthrax tetrasaccharide antigen as a candidate vaccine against anthrax.[1] Seeberger is a member of the editorial board for *QSAR & Combinatorial Science*.

R. Metternich Takes On Responsibility for Schering Research

From January 1, 2006, Rainer Metternich will join the board of Schering AG and be responsible for the research division. In 2000, he joined Schering AG in Berlin as director of medicinal chemistry, and since 2001 he has led the European Research Center there. Between 1986 and 1997 he moved up the ranks in pharmaceutical research at Sandoz AG in Basel from laboratory to division leader. From 1997 to 2000 he worked as a senior chemistry expert and member of the global research management committee at Novartis.

R. Metternich

Metternich studied chemical engineering in Jülich (Germany), then chemistry at the Universität Marburg, where he completed his PhD in 1985 with R. W. Hoffmann on topics including the configurational stability of chiral organometallic reagents.[2] During a postdoctoral stay with D. A. Evans at Harvard University in Cambridge, MA (USA), he worked on stereoselective synthesis and the total synthesis of natural products. In 2001, he was named Honorary Professor of Organic Chemistry at the Technische Universität Berlin (Germany). Since 2004, Metternich has been a board member of the German Chemical Society (GDCh) as well as an editorial board member for *Angewandte Chemie*.

G. Wess Directs GSF Center

Günther Wess (formerly at Sanofi-Aventis, Frankfurt/M) succeeds E.-G. Afting as Scientific and Technical Director at the GSF – National Research Center for Environment and Health in Neuherberg (near Munich) from November 1, 2005. The Company for Radiation Research (Gesellschaft für Strahlenforschung, GSF) is a member of the Helmholtz Association of German Research Centers and is funded by the Federal Republic of Germany as well as the State of Bavaria.

Wess studied at the Universität Frankfurt (Germany) and earned his habilitation in pharmaceutical chemistry from the Universität Mainz in 1999. Since 2000, he has been Honorary Professor at the Johann-Wolfgang-Goethe-Universität, Frankfurt. Wess began his career in 1982 at Hoeschst AG. After a research stay with E. J. Corey (Harvard University), he went on to become leader of the medicinal development division at Hoechst Marion Roussel (Germany) in 1998 and its successor company Aventis, which merged into Sanofi–Aventis in 2004. Wess is a member of the editorial board for *ChemBioChem* and was co-editor of three special issues of this journal: "Systems Biology & Chemistry" (10/2004), "RNA Targeting" (10/2003), and "G-Protein-Coupled Receptors" (10/2002). He also highlighted the prospects and challenges in medicinal chemistry in an essay that appeared in *Angewandte Chemie* in 2001.[3]

G. Wess

[1] D. B. Werz, P. H. Seeberger, *Angew. Chem.* **2005**, *117*, 6474; *Angew. Chem. Int. Ed.* **2005**, *44*, 6315.

[2] R. W. Hoffmann, J. Lanz, R. Metternich, G. Tarara, D. Hoppe, *Angew. Chem.* **1987**, *99*, 1196; *Angew. Chem. Int. Ed. Engl.* **1987**, *26*, 1145.

[3] G. Wess, M. Urmann, B. Sickenberger, *Angew. Chem.* **2001**, *113*, 3443; *Angew. Chem. Int. Ed.* **2001**, *40*, 3341.

DOI: 10.1002/anie.200503723

InterScience
© 2005 Wiley-VCH Verlag GmbH & Co. KGaA, Weinheim

Cyclophanes

DOI: 10.1002/anie.200502474

Allenophane and Allenoacetylenic Macrocycles: A New Class of Chiral Cyclophanes

*Takeshi Kawase**

Keywords:
allenes · chirality · cyclophanes · hydrocarbons · macrocycles

The determination of the relationship between molecular structure and physical properties is a major goal in organic chemistry. Cyclophane chemistry has continuously advanced and expanded over the years and has attracted the curiosity of organic chemists in pursuit of this goal. Researchers of this field have designed and created new cyclophanes with a variety of structures.[1,2] Recently, macrocyclic cyclophanes bearing acetylene bridges have received much attention. These cyclophanes with conformationally rigid and shape-persistent structures can also be regarded as dehydroannulenes.[3] The fruitful combination of cyclophane and annulene chemistry has furnished many new compounds; these substances exhibit unique molecular functions, such as aggregation behavior, host–guest complexation, and novel electronic properties.[1b,4]

In contrast, cyclophanes bearing allene (1,2-propadiene) bridges, termed allenophanes, have not been studied extensively, probably due to the difficulty of their synthesis and the high reactivity of allene moieties.[5] In 1875 van't Hoff predicted that the four substituents in allene must be arranged in two perpendicular planes.[6a] The proposal implied that suitably substituted allenes are axially chiral. The prediction was confirmed 60 years later.[6b] Thus, the incorporation of an allene skeleton in a compound leads to a three-dimensional structure and imparts chirality to the molecule. In 1961 the cyclic bisallene cyclodeca-1,2,6,7-tetraene (**1**) was synthesized from 1,5-cyclooctadiene by bisdibromocarbene addition and ring opening with methyllithium.[7] X-ray crystallographic analysis proved it to be a *meso* diastereomer. The corresponding *d*,*l*-**1** was not formed, probably due to its inherent strain. Strained cyclic allenes, including **1**, have been investigated theoretically and experimentally from the viewpoints of molecular strain and Möbius aromaticity.[5,8] However, the molecular structures have not been studied in detail because of their lability.

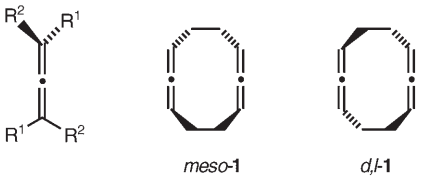

meso-**1** *d*,*l*-**1**

On the other hand, a number of natural products that bear an allene moiety have been isolated. Synthetic organic chemists have established synthetic procedures for the preparation of chiral allenes[9] that may pave the way for the synthesis of allenophanes. The first synthesis of a "true" allenophane, **2**, was presented by Thorand, Vögtle, and Krause in 1999.[10] The cyclophane consists of four 1,4-phenylene and four 1,3-dimethylallene moieties and exists as a mixture of four diastereomers with different topologies. The intramolecular cyclization, a key step of the synthesis, was effected by addition of the acyclic precursors **3** to a dilute solution of $KN(SiMe_3)_2$ in THF to form macrocyclic propargyl alcohol **4**. Further manipulation of **4** culminated in the construction of the fourth allene bridge through the action of a methyl cuprate species (Scheme 1). However, the synthesis was not stereoselective. In fact, the precursor **3** was synthesized and em-

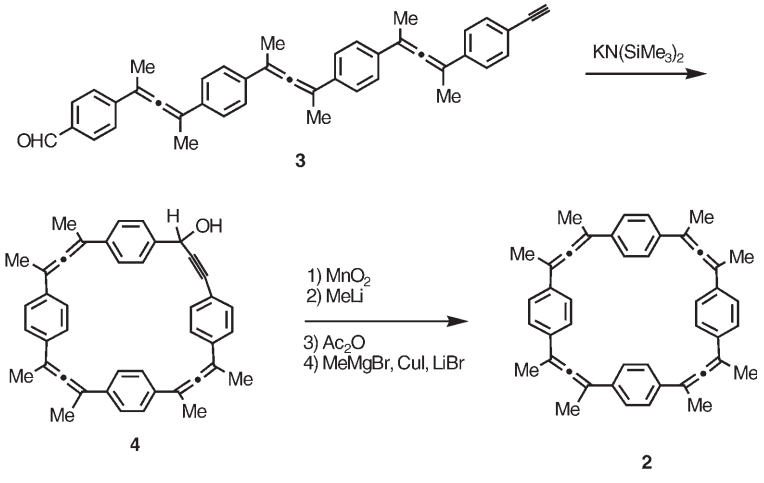

Scheme 1. The synthesis of **2** by Thorand, Vögtle, and Krause.[10]

[*] Prof. Dr. T. Kawase
Department of Chemistry
Graduate School of Science
Osaka University
Toyonaka, Osaka 560-0043 (Japan)
Fax: (+81) 6-6850-5387
E-mail: tkawase@chem.sci.osaka-u.ac.jp

InterScience
© 2005 Wiley-VCH Verlag GmbH & Co. KGaA, Weinheim

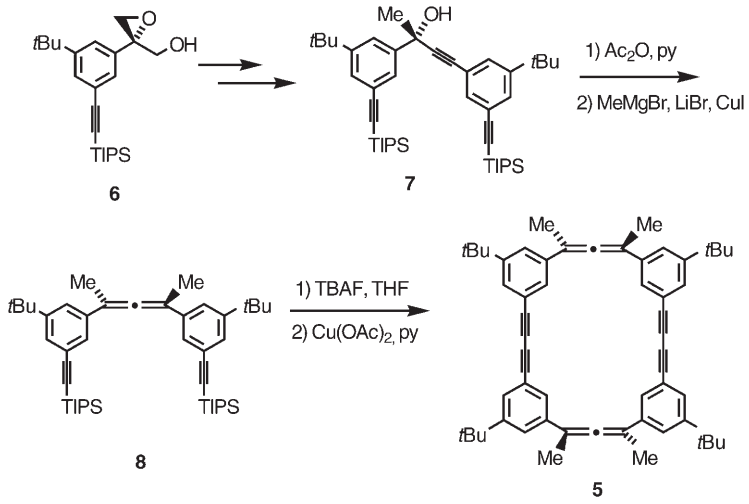

Scheme 2. The synthesis of **5** by Clay and Fallis.[11] TIPS = triisopropylsilyl.

ployed as a mixture of four diastereomers and afforded **2** as a mixture of diastereomers as expected. These isomers could not be separated by HPLC, and therefore the physical and chiroptical properties were not discussed.

Recently, some research groups have reported the synthesis of racemic and enantiomerically pure acetylenic allenophanes. Clay and Fallis reported the first synthesis of enantiomerically pure acetylenic allenophane **5**.[11] The synthesis started from the chiral epoxide **6** (88% *ee*), which was prepared by a Sharpless asymmetric epoxidation. The tertiary propargyl alcohol **7** (derived from **6**) led to chiral *S* allene **8** after a sequence of steps, including the addition of a methyl cuprate species (Scheme 2). Oxidative coupling of **8** afforded the *S*,*S* allenophane **5** in moderate yield. The molecular structure was not determined experimentally, theoretical calculations however revealed a helical structure for the molecule. The CD spectrum exhibits large bands at 263 and 270 nm owing to intramolecular interactions between the phenylene units of **5**.

Diederich and co-workers have carried out extensive studies on π-conjugated systems consisting of acetylene and cumulene bonds for the construction of three-dimensional all-carbon networks and all-carbon backbone polymers and oligomers with novel physical and physicochemical properties.[12] In the course of their studies, they aimed to synthesize chiral acetylenic allenophanes that do not bear aromatic rings, which have become challenging and fascinating targets in this field.[13]

(±)-1,3-Diethynylallenes **10** are promising intermediates and were prepared by palladium-catalyzed cross-coupling of bispropargylic esters **9** and alkynes (Scheme 3). However, the labile

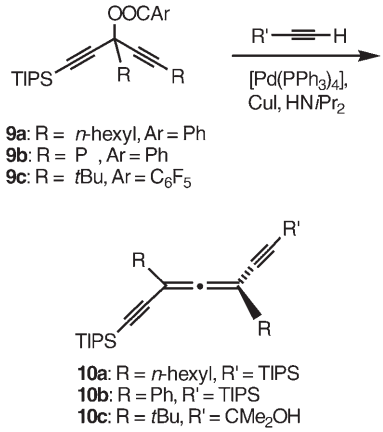

Scheme 3. The synthesis of (±)-1,3-diethynylallenes **10** by Diederich and co-workers.[15]

phenyl and *n*-hexyl derivatives **10a** and **10b** dimerize, even at low temperatures.[14] The relatively stable *tert*-butyl-substituted **10c** was obtained in high yield when pentafluorobenzoate was used as the leaving group. The bulky substituents of **10c** play an important role in the high stability of the molecule. The racemic allene **10c** was converted into an isomeric mixture of acyclic precursors **11**. Eglinton–Galbraith coupling of **11** under high-dilution conditions afforded cyclic tetraallene **12** in 80% yield.[15] Compound **12** was obtained as a mixture of five diastereomers

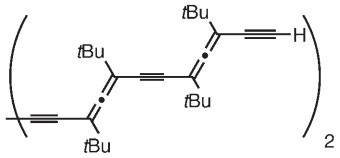

11

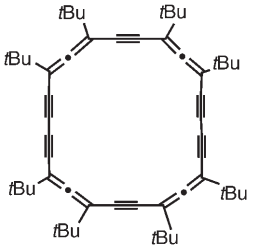

12

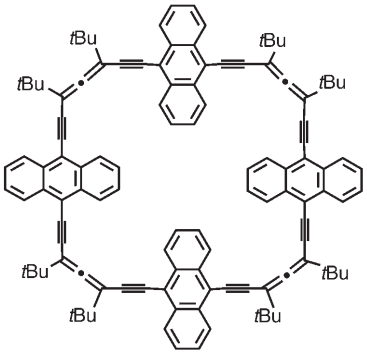

13

involving two enantiomers. The ratio of these diastereomers (1:1:4:1:1) corresponds roughly to the statistically controlled ring closure. These isomers were successfully separated with a combination of two different HPLC techniques. The major component of **12** was determined to be the C_1 isomer by NMR spectroscopy on the basis of the low symmetry. The formation of racemic C_1-symmetric **12** is expected to be favored over the formation of the other isomers. Moreover, an allenophane **13** that bears anthracene units was prepared from **10c**. All four isomers were also separated, the structures were characterized spectroscopically, and the structure of the D_4 isomer was confirmed by X-ray crystal-structure analysis. The isomers of **12** are colorless solids and those of **13** are brown. All compounds are stable under air at room temperature when

 © 2005 Wiley-VCH Verlag GmbH & Co. KGaA, Weinheim

protected from light. Whereas **12** remains unchanged after irradiation from a xenon lamp, **13** undergoes photoisomerization to form a photostationary state ($C_2/C_{2h}/D_4/D_{2d} = 10:5:1:5$). The anthracene units in **13** may act as intramolecular sensitizers. To explore the chiroptical properties, the synthesis of an enantiomerically pure compound is the next step of this study.

Recently, chiral cyclophanes, particularly those with helical chirality, have received much attention,[16] because these compounds should provide insight into the relationship between structure and chiroptical properties. Moreover, these compounds should exhibit interesting properties as chiral ligands/hosts for metal ions and small guest molecules. The synthesis described herein is an important advance in cyclophane chemistry.

Published online: October 18, 2005

[1] a) F. Diederich, *Cyclophanes, Monographs in Supramolecular Chemistry, Vol. 2* (Ed.: J. F. Stoddart), Royal Society of Chemistry, Cambridge, **1991**; b) F. Vögtle, *Cyclophane Chemistry*, Wiley, New York, **1993**; c) Modern Cyclophane Chemistry (Eds.: R. Gleiter, H. Hopf), Wiley-VCH, Weinheim, **2004**.

[2] G. J. Bodwell, T. Sato, *Angew. Chem.* **2002**, *114*, 4175 – 4177; *Angew. Chem. Int. Ed.* **2002**, *41*, 4003 – 4005; A. Urbano, *Angew. Chem.* **2003**, *115*, 4116 – 4119; *Angew. Chem. Int. Ed.* **2003**, *42*, 3986 – 3989.

[3] For pioneering work in this area, see: H. A. Staab, F. Graf, *Tetrahedron Lett.* **1966**, 751 – 757.

[4] a) M. M. Haley, *Top. Curr. Chem.* **1999**, *201*, 81 – 130; b) U. H. Bunz, Y. Rubin, Y. Tobe, *Chem. Soc. Rev.* **1999**, *28*, 107 – 119; c) C. Grave, A. D. Schlüter, *Eur. J. Org. Chem.* **2002**, 3075 – 3098; d) D. Zhao, J. S. Moore, *Chem. Commun.* **2003**, 807; e) J. A. Marsden, G. J. Palmer, M. M. Haley, *Eur. J. Org. Chem.* **2003**, 2355 – 2369; f) S. Höger, *Chem. Eur. J.* **2004**, *10*, 1320 – 1329.

[5] H. Hopf, *Classics in Hydrocarbon Chemistry*, Wiley-VCH, Weinheim, **2000**, pp. 171 – 196.

[6] a) J. H. van't Hoff, *La Chimie dans L'Espace*, Bazendijk, Rotterdam, **1875**; J. H. van't Hoff, *Die Lagerung der Atome im Raume*, Vieweg, Braunschweig, **1877**; b) P. Maitland, W. H. Mills, *Nature* **1935**, *135*, 994.

[7] a) L. Skatteböl, *Tetrahedron Lett.* **1961**, 167 – 172; b) H. Irngartinger, H.-U. Jäger, *Tetrahedron Lett.* **1976**, 3595 – 3596.

[8] a) D. Ajami, O. Oeckler, A. Simon, R. Herges, *Nature* **2003**, *426*, 819 – 821; b) T. Kawase, M. Oda, *Angew. Chem.* **2004**, *116*, 4496 – 4498; *Angew. Chem. Int. Ed.* **2004**, *43*, 4396 – 4398.

[9] a) A. Hoffmann-Röder, N. Krause, *Angew. Chem.* **2002**, *114*, 3057 – 3059; *Angew. Chem. Int. Ed.* **2002**, *41*, 2933 – 2935; b) A. Hoffmann-Röder, N. Krause, *Angew. Chem.* **2004**, *116*, 1216 – 1236; *Angew. Chem. Int. Ed.* **2004**, *43*, 1196 – 1216; c) *Modern Allene Chemistry* (Eds: N. Krause, A. S. K. Hashmi), Wiley-VCH, Weinheim, **2004**.

[10] S. Thorand, F. Vögtle, N. Krause, *Angew. Chem.* **1999**, *111*, 3929 – 3931; *Angew. Chem. Int. Ed.* **1999**, *38*, 3721 – 3723.

[11] M. D. Clay, A. G. Fallis, *Angew. Chem.* **2005**, *117*, 4107 – 4110; *Angew. Chem. Int. Ed.* **2005**, *44*, 4039 – 4042.

[12] F. Diederich, L. Gobbi, *Top. Curr. Chem.* **1999**, *201*, 43 – 79; F. Diederich, *Chem. Commun.* **2001**, 219 – 227.

[13] In contrast to allenes, some acetylenic butatriene macrocycles, Sworski-type dehydroannulenes, were successfully synthesized: Y. Kuwatani, N. Watanabe, I. Ueda, *Tetrahedron Lett.* **1995**, *36*, 119 – 122; Y. Kuwatani, I. Ueda, *Angew. Chem.* **1995**, *107*, 2017 – 2019; *Angew. Chem. Int. Ed. Engl.* **1995**, *34*, 1892 – 1894.

[14] R. C. Livingston, L. R. Cox, V. Gramlich, F. Diederich, *Angew. Chem.* **2001**, *113*, 2396 – 2399; *Angew. Chem. Int. Ed.* **2001**, *40*, 2334 – 2337; R. Livingston, L. R. Cox, S. Odermatt, F. Diederich, *Helv. Chim. Acta* **2002**, *85*, 3052 – 3065.

[15] S. Odermatt, J. L. Alonso-Gomez, P. Seiler, M. M. Cid, F. Diederich, *Angew. Chem.* **2005**, *117*, 5203 – 5207; *Angew. Chem. Int. Ed.* **2005**, *44*, 5074 – 5078.

[16] a) R. C. Helgeson, J.-P. Mazaleyrat, D. J. Cram, *J. Am. Chem. Soc.* **1981**, *103*, 3929 – 3931; b) S. Anderson, U. Neidlein, V. Gramlich, F. Diederich, *Angew. Chem.* **1995**, *107*, 1722 – 1724; *Angew. Chem. Int. Ed. Engl.* **1995**, *34*, 1596 – 1600; c) U. Neidlein, F. Diederich, *Chem. Commun.* **1996**, 1493 – 1494; d) S. Grimme, J. Harren, A. Sobanski, F. Vögtle, *Eur. J. Org. Chem.* **1998**, 1491 – 1509; e) A. Bähr, A. S. Droz, M. Püntener, U. Neidlein, S. Anderson, P. Seiler, F. Diederich, *Helv. Chim. Acta* **1998**, *81*, 1931 – 1963; f) A. S. Droz, U. Neidlein, S. Anderson, P. Seiler, F. Diederich, *Helv. Chim. Acta* **2001**, *84*, 2243 – 2289; g) L. L. Schafer, T. D. Tilley, *J. Am. Chem. Soc.* **2001**, *123*, 2683 – 2684; h) L. An, T. Nakano, A. Orita, J. Otera, *Angew. Chem.* **2002**, *114*, 179 – 181; *Angew. Chem. Int. Ed.* **2002**, *41*, 171 – 173; i) K. Campbell, C. A. Johnson, II, R. McDonald, M. J. Ferguson, M. M. Haley, R. R. Tykwinski, *Angew. Chem.* **2004**, *116*, 6093 – 6097; *Angew. Chem. Int. Ed.* **2004**, *43*, 5967 – 5971.

 © 2005 Wiley-VCH Verlag GmbH & Co. KGaA, Weinheim

Delocalization

DOI: 10.1002/anie.200502105

Hexaarylbenzenes—Prospects for Toroidal Delocalization of Charge and Energy

*Christoph Lambert**

Keywords:
amines · aromaticity · charge transfer · energy transfer · pi systems

Interactions between organic π systems govern to a large extent the electronic and functional properties of many microscopic and macroscopic photonic, electronic, and optoelectronic devices.[1] Prominent examples from nature are the light-harvesting complexes LH-I and LH-II in purple bacteria, where several dozen bacteriochlorophyll *a* molecules form a highly symmetrical ring that collects sunlight energy, which is ultimately transferred to a photosynthetic reaction center.[2] Delocalization of the excited state over many chromophore units (exciton delocalization) plays an important role in these systems. Examples of man-made systems are, for example, organic field effect transistors (OFETs), where a high charge (hole or electron) mobility is required which, up to date, can be achieved only in highly organized arrangements of π systems in thin-film transistors.[3] In this context, a detailed understanding of the interactions of π systems is required, and small model systems will help to elucidate the basic mechanisms that act on electron- and energy-transfer processes between π-system subunits.

For both processes one can distinguish between *delocalized* systems (charge or exciton delocalization) and *localized* systems (charge or exciton localization). While in the former case, either charge or energy is stabilized by resonance between two diabatic (formally noninteracting) states [Eq. (1a) and (1b)], in the latter case either charge

$$M^+/M \overset{\text{charge resonance}}{\leftrightarrow} M/M^+ \quad (1a)$$

$$M^*/M \overset{\text{exciton delocalization}}{\leftrightarrow} M/M^* \quad (1b)$$

or energy is transferred between different sites [Eq. (2a) and (2b)]. Whether

$$M^*/M \overset{\text{charge transfer}}{\rightleftharpoons} M/M^* \quad (2a)$$

$$M^*/M \overset{\text{energy transfer}}{\rightleftharpoons} M/M^* \quad (2b)$$

charge or energy is either localized or delocalized depends on the electronic coupling between the diabatic states relative to the reorganization energy for the considered process. Generally, if the coupling is much larger than the reorganization energy, delocalization occurs.

Hexaarylbenzene derivatives may serve as model compounds to investigate these processes between a number of π systems, because the six arene units can assume a ringlike arrangement in which the local C_2 axes of the aryl faces form 60° angles with each other. In addition, the arene planes are tilted (ca. 60°) rather than perpendicular to the central benzene ring (see Figure 1). The individual motion of the six arene moieties in this paddlewheel-like arrangement is to some extent correlated at low temperature due to steric interlinkage.

In a recent communication in *Angewandte Chemie* Kochi et al.[4] used the hexaarylbenzene motif to investigate the hole-transfer properties of radical cation **1**$^{\bullet+}$, in which all six benzene substituents are further substituted by dialkylamino redox centers in *para* position. Unlike hexakis(4-dianisylaminophenyl)benzene,[5] compound **1** shows partially resolved redox waves in the cyclic voltammogram which allowed the preparation and isolation of the salt of radical cation **1**$^{\bullet+}$ by either controlled coulometry or stoichometric chemical oxidation. This lucky circumstance is due to the relatively strong electronic

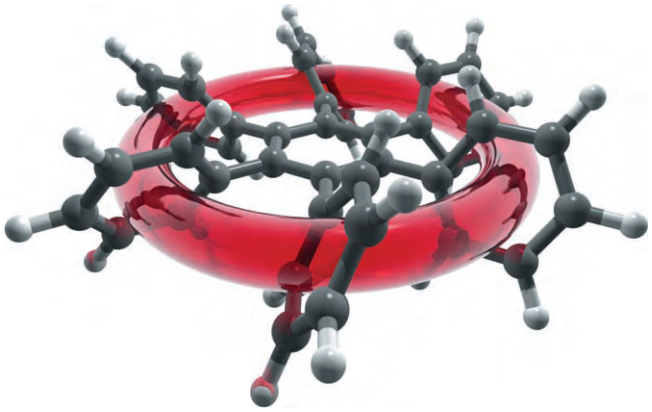

Figure 1. Toroidal delocalization of charge in hexaphenylbenzene radical cation (schematic representation).

[*] Prof. Dr. C. Lambert
Institut für Organische Chemie
Bayerische Julius-Maximilians-Universität Würzburg
Am Hubland, 97074 Würzburg (Germany)
Fax: (+49) 931-888-4606
E-mail: lambert@chemie.uni-wuerzburg.de

© 2005 Wiley-VCH Verlag GmbH & Co. KGaA, Weinheim

interaction between the dialkylaniline groups which separates the redox potential for **1**/**1**$^{\bullet+}$ from those of higher charged species.

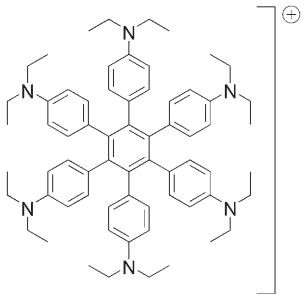

1$^{\bullet+}$

Kochi et al. were able to record the whole Vis/NIR spectral region down to $\tilde{\nu} \approx 2000\ cm^{-1}$ by combining the data from two separate Vis/NIR and FTIR measurements. The absorption spectrum of **1**$^{\bullet+}$ shows a structured signal between $\lambda \approx 900$ and ca. 5000 nm which was assigned to several optically induced hole-transition processes from an oxidized dialkylaniline group to five higher lying excited states. These observed absorption bands can be interpreted as intervalence charge-transfer processes (IV-CT). Adopting a methodology outlined by us a few years ago,[6] Kochi et al. described the adiabatic ground state and the five excited states by mixing of six diabatic states. The solution of an adequate secular determinant yielded the eigenvalues and eigenfunctions of the ground state and the five excited states. Kochi et al. used these eigenvalues together with estimated coupling energies and reorganization energies to deconvolute the experimental absorption bands into five Gaussian subbands by a repetitive fitting procedure. This fitting procedure also leads to optimized electronic couplings and reorganization energies without the effective electron-transfer distance being known. The latter is usually required for calculating the electronic coupling and is difficult to estimate.[7] The energies and intensities of these experimental transitions are in remarkable agreement with theoretical values based on the above-mentioned eigenvalues and evaluated by Mulliken–Hush theory.

Owing to the relatively strong electronic coupling and the weak reorganization energy, the thermal hole-transfer barrier between different redox sites is very small, if at all present. These results indicate that the hole is (almost) delocalized over all the six redox centers in a toroidal fashion (see Figure 1) because of the geometrical arrangement of the redox sites whose π-orbital planes point face to face. This leads to a partial overlap of the π orbitals of the *ipso* carbon atoms (the atoms attached to the central benzene ring) of adjacent aniline groups.

Somewhat earlier Rathore et al.[8] investigated an analogous hexakis[(triphenylethenyl)phenyl]benzene radical cation **2**$^{\bullet+}$, for which the authors observed a broad and unresolved IV-CT band in the NIR. However, although spectra deconvolution yields a IV-CT band at 1450 cm^{-1} a further analysis that would allow the quantification of the associated hole-transfer processes was not described. The authors also suggest a toroidal hopping mechanism operating between the six equivalent redox sites. The fact that the IV-CT band is broad and featureless indicates a much weaker electronic interaction in **2**$^{\bullet+}$ than in **1**$^{\bullet+}$.

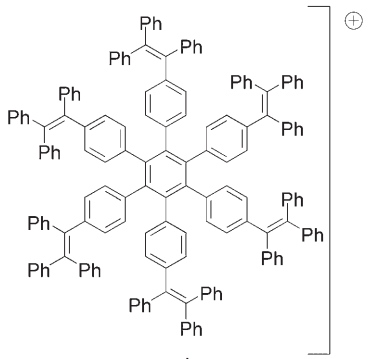

2$^{\bullet+}$

Our own studies on the trication of 1,3,5-tris[(4-dianisylamino)phenyl]-2,4,6-tris[(4-ditolylamino)phenyl]benzene (**3**$^{3+}$) stand in contrast to the results of Kochi et al. and of Rathore et al.[6] In this molecule it was possible to generate the trication owing to the significant difference in redox potential between the tolyl- and the anisyl-substituted amino groups. This trication **3**$^{3+}$ also shows a broad IV-CT band in the NIR. Deconvolution of this band indicated that the trication has a *localized* structure and that there is a significant barrier for the superexchange hole transfer from site to site.

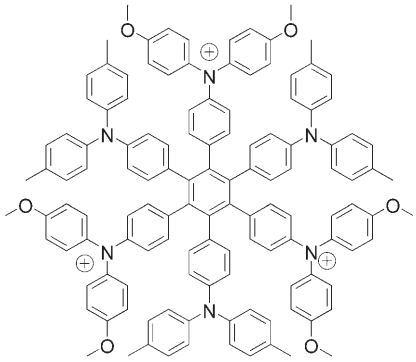

3^{3+}

What is the reason for this difference between **1**$^{\bullet+}$ and **3**$^{3+}$? For toroidal delocalization it is necessary that the charge-bearing units are as close as possible. The closest contact between adjacent aniline groups in **1**$^{\bullet+}$ is 2.9 Å (C_{ipso}–C_{ipso}) and the greatest separation is 7.1 Å (N–N). If we assume that the charge in **1**$^{\bullet+}$ is delocalized within the aniline group with the center of charge distribution being somewhere between the nitrogen and the center of the aniline ring, there might be sufficient overlap of the C_{ipso} π orbitals to provide toroidal delocalization. In contrast, in **3**$^{3+}$ the individual charges are delocalized within the three (dianisylamino)phenyl moieties with the respective center of charge being likely even beyond the location of the nitrogen atom. Therefore, the partial charge at the C_{ipso} atoms in **3**$^{3+}$ is much less than that in **1**$^{\bullet+}$ which results in a much weaker interaction between the aryl groups and a localized electronic structure. From this interpretation I conclude that in order to gain perfect toroidal delocalization in hexaarylbenzenes one possible strategy would be to move the center of charge towards the C_{ipso} atoms by, for example, electron-withdrawing substituents rather than electron-donating substituents. This hypothesis is supported by the observation of Rathore et al.[9] that in hexakis[(4-methyl-2,5-dimethoxy)biphenyl]benzene radical cations there is no significant interaction between the aryl branches because the center of charge is even much farther away from the C_{ipso} atoms than in **3**$^{3+}$.

All of these studies were preceded by the work of Sagl and Martin.[10] In

 © 2005 Wiley-VCH Verlag GmbH & Co. KGaA, Weinheim

1988 they analyzed the electronic structure of hexaiodobenzene dication by NMR spectroscopy and extended Hückel calculations and presented evidence for its σ aromaticity resulting from the overlap of iodine p orbitals and carbon orbitals in the molecular plane. Although I do not want to start a discussion of σ aromaticity at this point, it is worth noting that the delocalization in $\mathbf{1}^+$ results from the face-to-face overlap of π orbitals in a toroidal, that is, three-dimensional fashion rather than solely in a σ framework. Clearly, further theoretical work is necessary to establish the electronic interactions in hexaarylbenzenes and in hexaiodobenzene dication.

To some extent, energy-transfer processes are akin to electron-transfer processes. Some years ago Warman et al.[11] reported on the energy migration between carbazole chromophores in hexakis(carbazolyl)benzene **4**. The carbazole units show significant interaction in their absorption and fluorescence spectra compared to the monomeric analogue *N*-phenylcarbazole. Using time-resolved microwave conductivity methods, the authors showed that **4** exhibits a rapid rotary diffusion of the excimeric state which is initially localized at two neighboring carbazole moieties with a relaxation time of 3 ps. This means that within the 5-ns lifetime of the excited state, the excitation undergoes more than 1000 round-trips. Also from the viewpoint of hole-transfer processes, **4** would be an interesting candidate to examine.

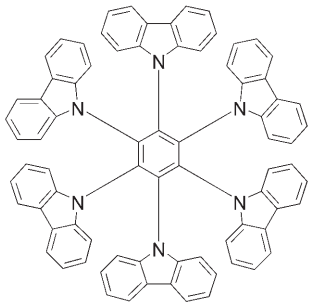

4

Warman et al. described **4** as a "storage-ring". Not only this term is attractive, but this concept is also appealing because it points to new possible molecular properties of both toroidal energy- and charge-delocalized systems. Time will tell if such systems can be used to "store" (= stabilize) charges or energy more efficiently than other species of similar size.

Published online: October 5, 2005

[1] J.-L. Bredas, D. Beljonne, V. Coropceanu, J. Cornil, *Chem. Rev.* **2004**, *104*, 4971.
[2] X. Hu, K. Schulten, *Phys. Today* **1997**, *50*, 28.
[3] Y. Sun, Y. Liu, D. Zhu, *J. Mater. Chem.* **2005**, *15*, 53.
[4] D. Sun, S. V. Rosokha, J. K. Kochi, *Angew. Chem.* **2005**, *117*, 5263; *Angew. Chem. Int. Ed.* **2005**, *44*, 5133.
[5] C. Lambert, G. Nöll, *Angew. Chem.* **1998**, *110*, 2239; *Angew. Chem. Int. Ed.* **1998**, *37*, 2107.
[6] C. Lambert, G. Nöll, *Chem. Eur. J.* **2002**, *8*, 3467.
[7] A. Heckmann, C. Lambert, M. Goebel, R. Wortmann, *Angew. Chem.* **2004**, *116*, 5976; *Angew. Chem. Int. Ed.* **2004**, *43*, 5851.
[8] R. B. Rathore, L. Carrie, S. A. Abdelwahed, *Org. Lett.* **2004**, *6*, 1689.
[9] R. Rathore, C. L. Burns, M. I. Deselnicu, *Org. Lett.* **2001**, *3*, 2887.
[10] D. J. Sagl, J. C. Martin, *J. Am. Chem. Soc.* **1988**, *110*, 5827.
[11] J. J. Piet, H. A. M. Biemans, J. M. Warman, E. W. Meijer, *Chem. Phys. Lett.* **1998**, *289*, 13.

© 2005 Wiley-VCH Verlag GmbH & Co. KGaA, Weinheim

Protein Chemistry

DOI: 10.1002/anie.200501023

Protein Posttranslational Modifications: The Chemistry of Proteome Diversifications

Christopher T. Walsh, Sylvie Garneau-Tsodikova, and Gregory J. Gatto, Jr.*

Keywords:
amino acids · enzymes · protein modifications · proteomics

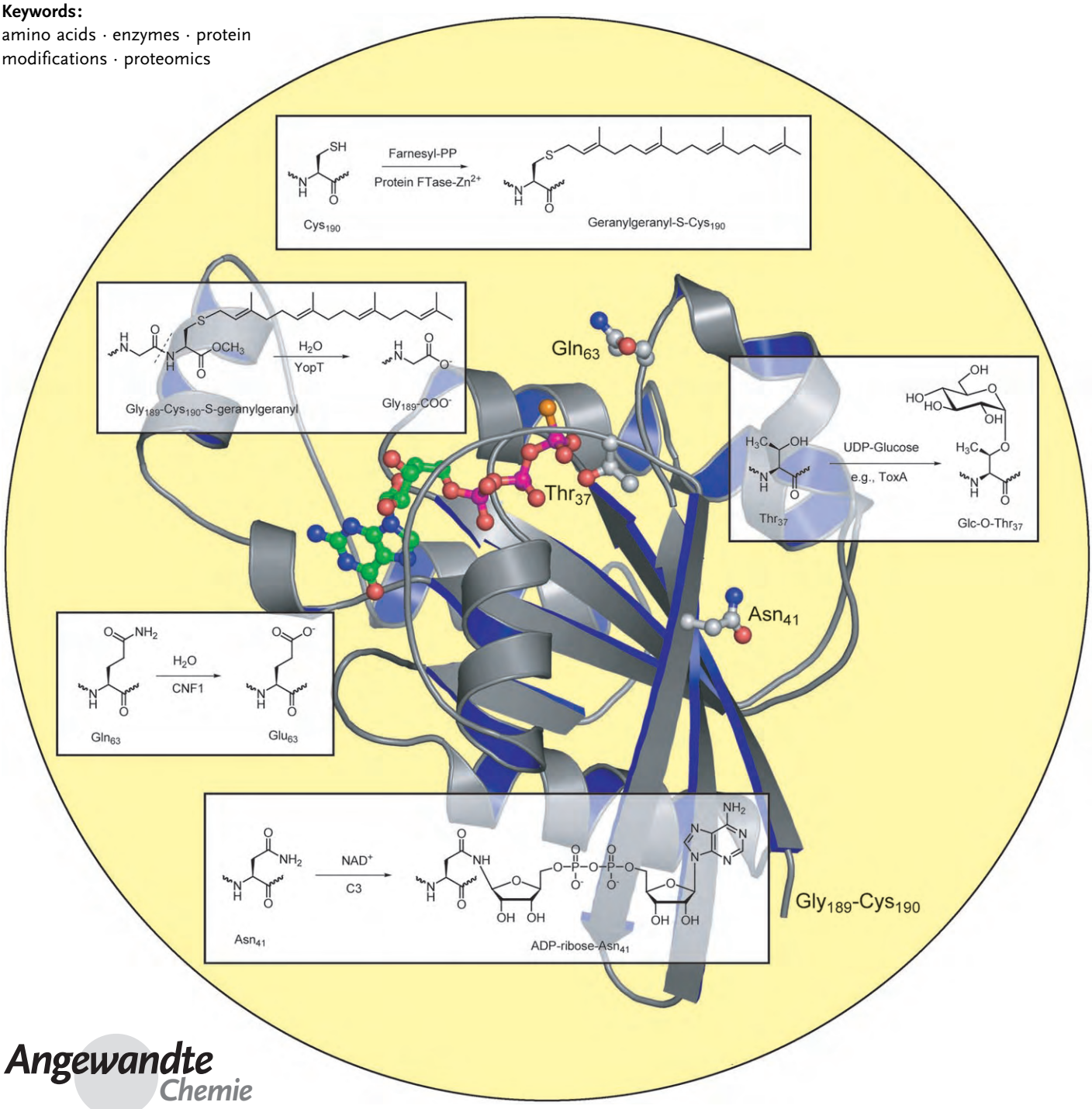

© 2005 Wiley-VCH Verlag GmbH & Co. KGaA, Weinheim

The diversity of distinct covalent forms of proteins (the proteome) greatly exceeds the number of proteins predicted by DNA coding capacities owing to directed posttranslational modifications. Enzymes dedicated to such protein modifications include 500 human protein kinases, 150 protein phosphatases, and 500 proteases. The major types of protein covalent modifications, such as phosphorylation, acetylation, glycosylation, methylation, and ubiquitylation, can be classified according to the type of amino acid side chain modified, the category of the modifying enzyme, and the extent of reversibility. Chemical events such as protein splicing, green fluorescent protein maturation, and proteasome autoactivations also represent posttranslational modifications. An understanding of the scope and pattern of the many posttranslational modifications in eukaryotic cells provides insight into the function and dynamics of proteome compositions.

From the Contents

1. Introduction	7343
2. Covalent Addition: The Main Acts	7345
3. Covalent Addition: The Supporting Cast	7354
4. Cataloguing the Posttranslational Modification	7360
5. Multiple and Tandem Posttranslational Modification of Proteins	7361
6. Reversible versus Irreversible Posttranslational Modification	7362
7. Controlled Proteolysis	7364
8. Autocleavage and Peptide-Bond Rearrangement	7365
9. Peptide Bond Rearrangement without Autocleavage	7368
10. Conclusions	7369

1. Introduction

There are two major mechanisms for expanding the coding capacity of the 6000 (yeast) to 30,000 (human) genes in eukaryotic genomes to generate diversity in the corresponding proteomes, the inventory of all proteins in a cell or organism. Proteomes may be two to three orders of magnitude more complex (>1000000 molecular species of proteins) than the encoding genomes would predict. The first route of diversification of proteins is at the transcriptional level, by mRNA splicing, including tissue-specific alternate splicing.[1,2] This is a central topic in RNA metabolism in eukaryotic biology.

The second route to proteome expansion is the focus of this Review: covalent posttranslational modification (PTM) of proteins at one or more sites.[3] As the name implies, these are covalent modifications that occur after DNA has been transcribed into RNA and translated into proteins. The nascent or folded proteins, which are stable under physiological conditions, are then subjected to a battery of specific enzyme-catalyzed modifications on the side chains or backbones. Proteome diversification by covalent modification occurs in prokaryotes but is much more extensively encountered in nucleated cells, both in terms of types of modifications and frequency of occurrence. About 5% of the genomes of higher eukaryotes can be dedicated to enzymes that carry out posttranslational modifications of the proteomes.

Two broad categories of protein PTM occur (Scheme 1). The first subsumes all enzyme-catalyzed covalent additions of some chemical group, usually an electrophilic fragment of a cosubstrate, to a side chain residue in a protein. The side chain modified is usually electron rich, acting as a nucleophile in the transfer. The second category of PTM is covalent cleavage of peptide backbones in proteins either by action of proteases or, less commonly, by autocatalytic cleavage. Limited proteolysis to control location, activity, and lifetime of each protein in intracellular and extracellular milieus is a central strategy for the regulation of the composition and function of proteomes.

Protein covalent modifications can be sorted along several axes. One is by the identity of the protein side chain modified; 15 of the 20 common proteinogenic amino acid side chains

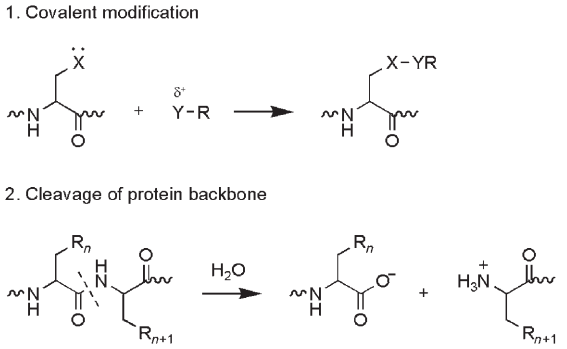

Scheme 1. Two categories of posttranslational modifications of proteins: 1) covalent modification of a nucleophilic amino acid side chain by an electrophilic fragment of a cosubstrate; 2) cleavage of a protein backbone at a specific peptide bond.

[*] Prof. C. T. Walsh, Dr. S. Garneau-Tsodikova, Dr. G. J. Gatto, Jr.
Department of Biological Chemistry and Molecular Pharmacology
Harvard Medical School
Boston, MA 02115 (USA)
Fax: (+1) 617-432-0348
E-mail: Christopher_walsh@hms.harvard.edu

© 2005 Wiley-VCH Verlag GmbH & Co. KGaA, Weinheim

undergo such diversification (Table 1). Another classification is that by the fragment of cosubstrate or coenzyme that is enzymatically coupled to the protein and the concomitant chemical nature of the protein modification. This catalogue includes *S*-adenosylmethionine (SAM)-dependent methylation, ATP-dependent phosphorylation, acetyl CoA dependent acetylation, NAD-dependent ADP ribosylation, CoASH-dependent phosphopantetheinylation, and phosphoadenosinephosphosulfate (PAPS)-dependent sulfurylation. A third axis of categorization of PTM is by the new function enabled by the covalent addition. These include gain in catalytic function of enzymes that have acquired tethered biotinyl, lipoyl, and phosphopantetheinyl groups, changes of subcellular address for proteins undergoing various lipid modifications (prenylation, palmitoylation, glycosyl phosphatidylinositol (GPI) anchor attachment), and targeting of the modified protein for proteolytic destruction by ubiquitylation to mark transport to lysosomes or proteasomes.

Christpher T. Walsh, born in 1944, majored in biology at Harvard and completed his PhD in biochemistry in the lab of Fritz Lipmann at the Rockefeller Institute of Medical Research. He was on the MIT faculty (1972–1987), and since 1987 has been at Harvard Medical School. He served as Chair of the Dept. of Chemistry at MIT (1982–1987) and of the Dept. of Biological Chemistry and Molecular Pharmacology at Harvard Medical School (1987–1995). His research interests lie in enzyme and inhibitor mechanisms and in the biosynthesis of non-ribosomal peptide antibiotics.

Sylvie Garneau, born in Québec, Canada, received her BSc (1995) and MSc (1997) in chemistry from the Université Laval, where she worked under the supervision of Robert Chênevert and Perséphone Canonne. She completed her PhD in chemistry in January 2003 at the University of Alberta with John C. Vederas on the studies of new antimicrobial agents acting on bacterial cell walls. She is currently a postdoctoral fellow with Christopher T. Walsh at Harvard Medical School, studying halogenation and pyrrole formation various of natural products.

Gregory J. Gatto, Jr., born in 1972, majored in chemistry at Princeton University, where he worked under the direction of Martin Semmelhack. In 2003, he received his MD and PhD degrees from the Johns Hopkins University School of Medicine. There, he worked in the lab of Jeremy Berg on the structural biology of peroxisomal targeting signal recognition. He is currently an NIH postdoctoral fellow in the lab of Christopher T. Walsh at Harvard Medical School, studying the biosynthesis of the macrolide immunosuppressants.

Table 1: Posttranslational protein modifications at the side chains.[a]

Residue	Reaction	Example
Asp	phosphorylation	protein tyrosine phosphatases; response regulators in two-component systems
	isomerization to isoAsp	
Glu	methylation	chemotaxis receptor proteins
	carboxylation	Gla residues in blood coagulation
	polyglycination	tubulin
	polyglutamylation	tubulin
Ser	phosphorylation	protein serine kinases and phosphatases
	O-glycosylation	notch O-glycosylation
	phosphopantetheinylation	fatty acid synthase
	autocleavages	pyruvamidyl enzyme formation
Thr	phosphorylation	protein threonine kinases/phosphatases
	O-glycosylation	
Tyr	phosphorylation	tyrosine kinases/phosphatases
	sulfation	CCR5 receptor maturation
	ortho-nitration	inflammatory responses
	TOPA quinone	amine oxidase maturation
His	phosphorylation	sensor protein kinases in two-component regulatory systems
	aminocarboxypropylation	diphthamide formation
	N-methylation	methyl CoM reductase
Lys	N-methylation	histone methylation
	N-acylation by acetyl, biotinyl, lipoyl, ubiquityl groups	histone acetylation; swinging-arm prosthetic groups; ubiquitin; SUMO (small ubiquitin-like modifier) tagging of proteins
	C-hydroxylation	collagen maturation
Cys	S-hydroxylation (S-OH)	sulfenate intermediates
	disulfide bond formation	protein in oxidizing environments
	phosphorylation	PTPases
	S-acylation	Ras
	S-prenylation	Ras
	protein splicing	intein excisions
Met	oxidation to sulfoxide	Met sulfoxide reductase
Arg	N-methylation	histones
	N-ADP-ribosylation	$G_{s\alpha}$
Asn	N-glycosylation	N-glycoproteins
	N-ADP-ribosylation	eEF-2
	protein splicing	intein excision step
Gln	transglutamination	protein cross-linking
Trp	C-mannosylation	plasma-membrane proteins
Pro	C-hydroxylation	collagen; HIF-1α
Gly	C-hydroxylation	C-terminal amide formation

[a] No modifications of Leu, Ile, Val, Ala, Phe side chains are known. A more extensive list can be found in reference [3].

 © 2005 Wiley-VCH Verlag GmbH & Co. KGaA, Weinheim

2. Covalent Addition: The Main Acts

The five most common types of covalent additions to proteins are phosphorylation, acylation, alkylation, glycosylation, and oxidation, which are catalyzed by dedicated PTM enzymes (Scheme 2). The protein products obtained in this manner make up subsets of the proteome of an organism: the phosphoproteome, the acyl proteome, the alkyl proteome, the glycoproteome, and the oxidized proteome. In turn, each of these subproteomes can contain substantial diversity.

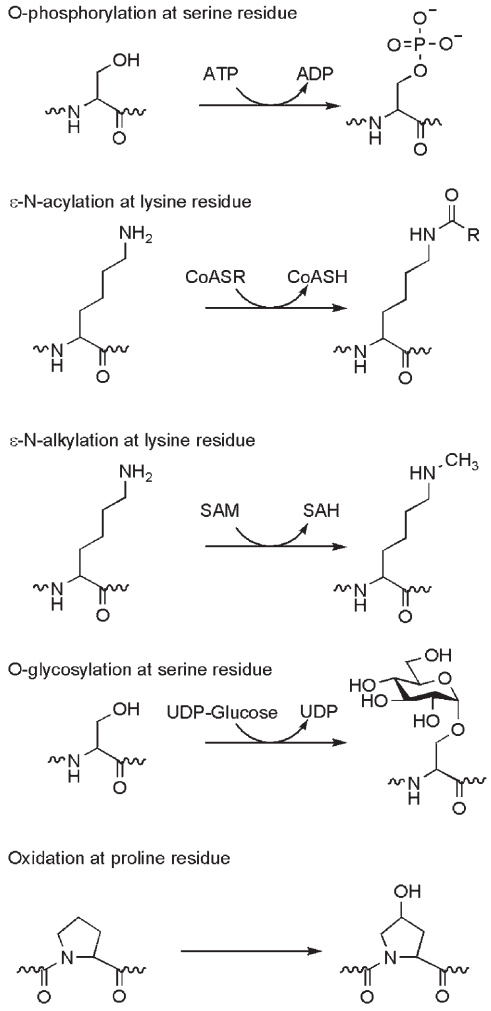

Scheme 2. Five major types of covalent additions to protein side chains: phosphorylation, acylation, alkylation, glycosylation, oxidation.

2.1. Protein Phosphorylation

The mammalian phosphoproteomes have phosphoSer (pS), phosphoThr (pT) and phosphoTyr (pY) residues with a split of about 90:10 (pS, pT/pY; Figure 1).[4] Bacterial and fungal phosphoproteomes will also have phosphoHis and phosphoAsp residues derived from proteins in two-component signal-transduction cascades.[5] The pathogenic bacterium *Pseudomonas aeruginosa* exhibits more than 60 such pathways.[6]

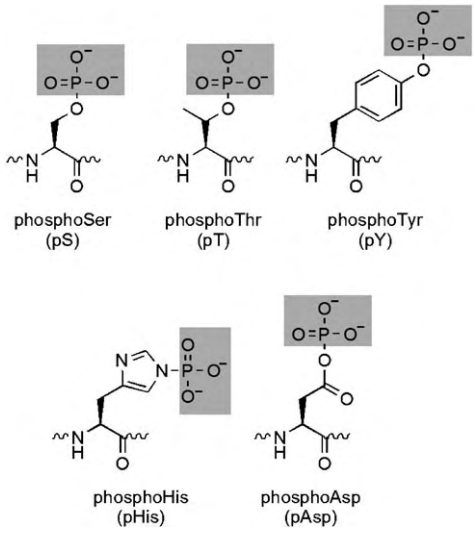

Figure 1. Phosphorylated forms of amino acid side chains in proteins: phosphoSer (pS); phosphoThr (pT); phosphoTyr (pY); phosphoHis (pHis); phosphoAsp (pAsp).

The enzymes dedicated to protein phosphorylation are among the largest class of PTM enzymes. This superfamily of protein kinases have been termed the kinome, with over 500 members in the human kinome.[7] If these acted on average on only 20 different protein substrates, or different residues within a smaller subset of proteins, 10000 distinct molecular forms of phosphorylated proteins would be produced. This is most probably a substantial underestimate of the true size of phosphoproteomes of higher eukaryotes, in which phosphorylation sites can be predicted but, as yet, cannot be completely measured. For example, the enzymatic activity of Abl protein kinase is modulated by phosphorylation at up to 11 distinct residues (Tyr, Thr, Ser; Figure 2).

Introduction of the charged, dianionic tetrahedral phosphate group induces altered conformations in local protein microenvironments[8] and is often paired with cationic arginine side chains (Figure 3). These local reorganizations of protein domains often create the architectural impetus for signal initiation, for example, in the four parallel MAP kinase pathways in eukaryotes and in the activation of many membrane receptor tyrosine kinases during autophosphorylation. The enzymatic conversion of a neutral OH side chain to dianionic phosphate has proven to be such a useful conformation switch in protein-domain restructuring that it has evolved into a major recurring theme in eukaryotic proteome diversity.

2.2. Protein Acylation

The most common acyl chains found in proteins that have undergone posttranslational modifications are C_2 (acetyl, e.g. histone tail acetylations),[9] C_{14} (myristoylation at glycine N termini),[10] and C_{16} (palmitoylated-*S*-Cys residues).[11] The 8-kDa chain of the small protein ubiquitin[12] (and congeners)

 © 2005 Wiley-VCH Verlag GmbH & Co. KGaA, Weinheim

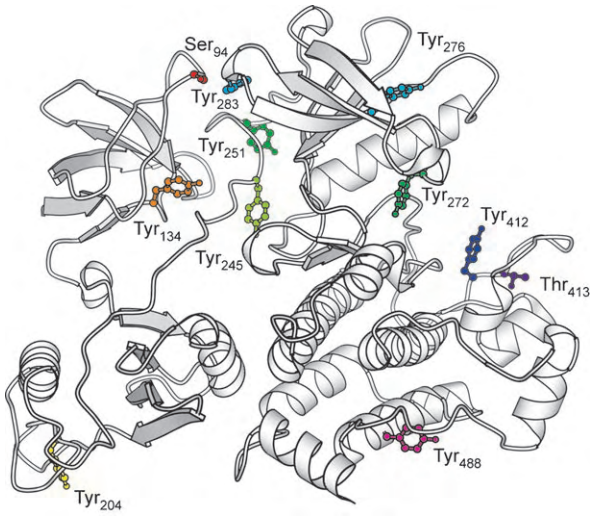

Figure 2. Eleven phosphorylation sites in the tyrosine kinase Abl, including Ser, Thr, and Tyr residues, color coded from red near the N terminus to purple near the C terminus. This figure and all other three-dimensional structural representations in this Review were generated with MolScript.[122]

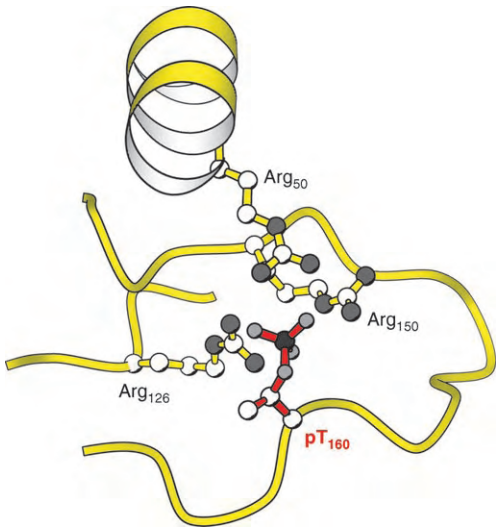

Figure 3. Conversion of a neutral OH side chain to a dianionic PO_3^{2-} side chain recruits cationic Arg side chains to make bifurcated charge-pairing interactions that can restructure the microenvironment of a protein region, induce a conformational change, and thereby initiate or propagate signaling information to partner proteins or small molecules. Shown is the interaction in Cdk2 of $pThr_{160}$ with the guanidinium side chains of Arg_{50}, Arg_{126}, and Arg_{150}.

is enzymatically transferred as an acyl moiety by ubiquityl ligases and chemically falls into this group of PTMs. The biological consequences of the acylation of a given protein with C_2, C_{14}, C_{16}, or 8-kDa chains are vastly different.

2.2.1. *ε-N-Acetylation of Lysine*

Acetylations of multiple lysine residues in histone N-terminal tails or at the C-terminus of the p53 transcription factor[13] are viewed as an integral part of the epigenetic code that controls selective gene transcription. The acetyl-group donor is the primary metabolite acetyl CoA, and dedicated histone acetyltransferase (HAT) isoenzymes select distinct combinations of the ε-NH_2 groups of Lys side chains in the N-terminal tails of histones: two Lys residues on histone H2A, four on H2B, four on H3, and four on H4 (Figure 4). Given

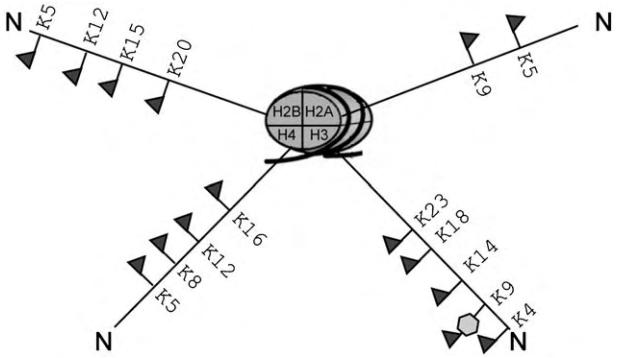

Figure 4. There are 15 Lys residues in the N-terminal tails of H2A, H2B, H3, and H4 that are sites for possible enzymatic acetylation. The dark gray flags represent sites of acetylation on the indicated lysine (K) residues.

two copies of each histone per octamer core in nucleosomes, there are $14 \times 2 = 28$ potential Lys side chains available for acetylation. Yeast histones with up to 13 acetylations have been reported,[14] which reflects almost 50% posttranslational modification. The combinatorial possibilities for differentially acetylated histone tails in nucleosomes become astronomically large.

The acetyl groups on Lys side chains convert potentially cationic side chains into groups, thus altering the charge distribution. The *N*-acetyl Lys group is also specifically recognized by discrete protein domains, termed bromodomains (Figure 5), which are embedded in transcription factors and associated proteins. Thus, the acetylation state of histone tails can regulate the recruitment of transcription factor machinery that controls the initiation of transcription of the genes in the region of chromatin covered by those nucleosomes.[14] In Section 5, we describe how five Lys residues at the C terminus of the transcription factor p53 can either be acetylated or ubiquitylated. Acetylation blocks the Lys side chains from ubiquitylation and prolongs the half-life of the p53 protein molecule.

2.2.2. *N-Myristoylation and S-Palmitoylation*

Myristoylation of eukaryotic proteins at an N-terminal glycine residue is catalyzed by the PTM enzyme protein N-myristoyltransferase, which utilizes the C_{14} myristoyl CoA as the donor substrate.[15] As protein synthesis is initiated with N-terminal methionine residues, cotranslational hydrolysis of the Met_1–Gly_2 bond by methionine aminopeptidase is a prerequisite to myristoylation (Scheme 3). The newly generated free amino group of the now N-terminal Gly is the nucleophile in the acylation reaction. The introduced hydrophobic C_{14} fatty acyl group can be a membrane-directing

 © 2005 Wiley-VCH Verlag GmbH & Co. KGaA, Weinheim

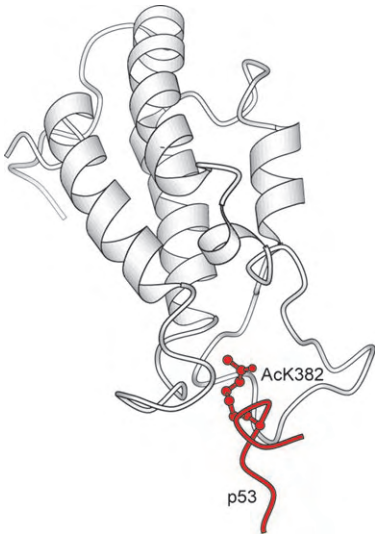

Figure 5. The acetylation status of the histone N-terminal tail can recruit partner proteins to control transcriptional activity on a nucleosome. The interaction of an acetyl-ε-NH-Lys side chain on a peptide fragment of histone H3 with a bromodomain of coactivator protein is redrawn from reference [32].

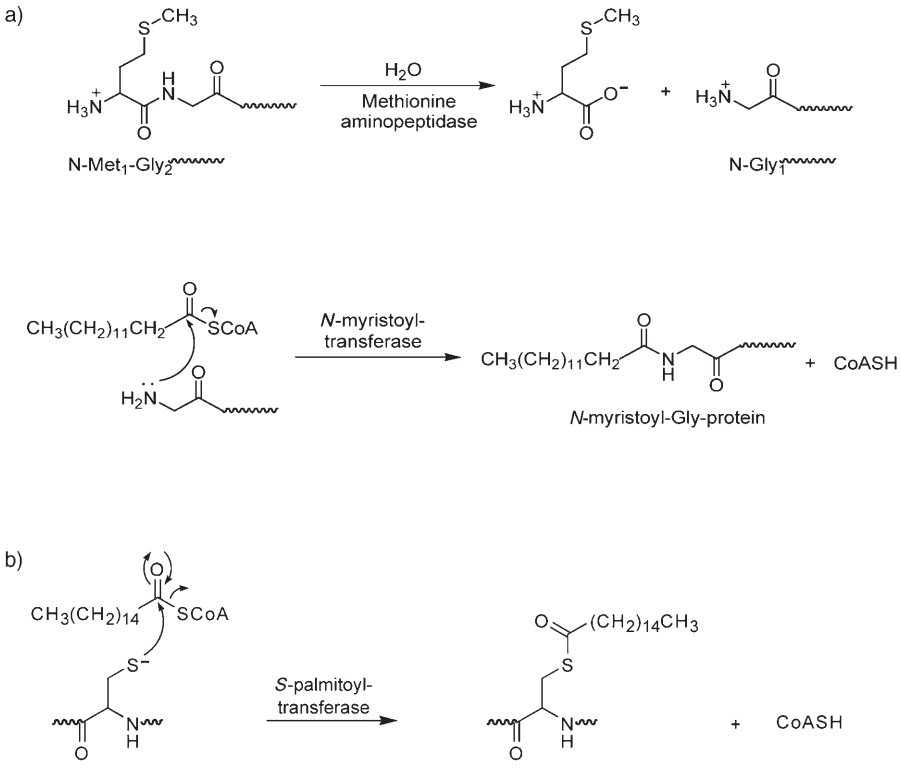

Scheme 3. a) Prior cleavage of the Met_1–Gly_2 peptide bond by methionine aminopeptidase liberates the NH_2 of the Gly residue for N-myristoylation by N-myristoyltransferase with myristoyl CoA as donor. b) The thiolate side chain of a Cys residue as nucleophile towards palmitoyl CoA, catalyzed by palmitoyl-*S*-protein transferases.

group to move proteins to membrane interfaces.[10] Additionally the myristoyl tail can switch from being buried in a cleft within the protein in one state to being available for membrane insertion in another conformational state.[16]

Examples of N-myristoylated proteins include HIV Gag protein and protein kinase A.[17]

Palmitoylation of proteins requires the C_{16} fatty acyl CoA as donor for the PTM acyltransferases, but the acyl group is typically transferred to the sulfhydryl side chains of Cys residues rather than to N-termini of proteins (Scheme 3).[11] Among the most-well-studied examples are S-palmitoylation of cysteines in the C-terminal regions of proteins such as the Ras GTPase. The lipidation of these nucleophilic thiolate side chains is consequential for partitioning Ras from the cytoplasm to membrane interfaces to meet up with its signaling partner proteins.[10] As explained in Section 5, the S-palmitoylation of Ras isoforms is part of a cascade of reversible posttranslational modifications involved in maturation and membrane anchoring of modified forms of Ras.[18] Protein substrates for S-palmitoylation can be transmembrane receptors such as the CD8α chain and the CCR chemokine receptor or cytoplasmic proteins such as the protein tyrosine kinase Lck.[11]

2.2.3. *Mono- and Polyubiquitylation of Proteins*

An extension of the logic of posttranslational transfer of low-molecular-weight (C_2, C_{14}, C_{16}) acyl chains to proteins is the acylation on lysine ε-amino groups by the carboxy terminus of the 8-kDa protein ubiquitin. In analogy to acyl CoA donors of the electrophilic acetyl, myristoyl, and palmitoyl acyl groups, the C-terminal carboxy group of the 76-residue ubiquitin must be preactivated for acyl transfer. The activation principle is the same as that of the acyl thioester system, but eukaryotic cells make use of ubiquityl-S-protein as donors instead of ubiquityl CoA.[19,20] The enzymatic activation machinery involves an enzyme 1 to make ubiquityl-AMP and a set of about a dozen thiol-containing enzymes 2 (Scheme 4) that provide the active-site nucleophile to capture the ubiquityl group as a set of ubiquityl-S-enzyme 2 family members. In general a third set of proteins, known collectively as enzyme 3 variants, are then required to catalyze the efficient transfer of the activated ubiquityl protein tag to Lys side chains of client proteins. Some of the enzyme 3 subclasses are multicomponent catalysts, with up to four subunits, which provide selectivity for a given protein target.[21] There are several hundred isoforms of such E3 ubiquityl ligases in higher eukaryotes, which allow subtle discrimination among many target proteins selected for ubiquitylation.[22]

© 2005 Wiley-VCH Verlag GmbH & Co. KGaA, Weinheim

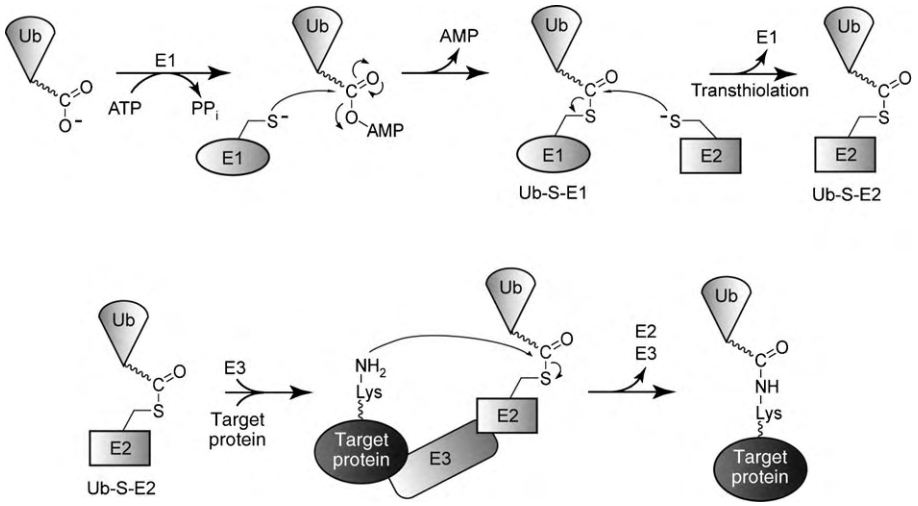

Scheme 4. Activation of the C-terminus of ubiquitin (at residue Gly_{76}) by enzyme 1 to make Ub-AMP, followed by transfer to a Cys thiolate in the active site of enzymes 2 to yield Ub-S-E2. Enzymes 3 can act as chaperones and recruiters of specific proteins for ubiquitylation at Lys side chains.

Unlike the small-molecule acyl groups described in Section 2.2.2., the ubiquityl acyl moiety provides an information-rich architectural scaffold (Figure 6) that can be read by particular partner proteins that control the downstream biological response. Two types of protein ubiquitylation can be distinguished according to the number of ubiquitins added: monoubiquitylation and polyubiquitylation. Polyubiquitylation specifically refers to the enzymatic construction of chains of ubiquitin molecules. As shown in Figure 6a, ubiquitin has Lys side chains on different surfaces and tandem attachment could go from any Lys unit on one ubiquitin monomer to the C-terminal Gly_{76} on the preceding monomer. It appears that polyubiquitin chains are built up most often through Lys_{48} side chains, although chains tethered through Lys_{63} are also well-known.[23] The X-ray structure of a Ub_4 chain is shown in Figure 6b. It is not clear how E3 ligases act processively to build up Ub_n chains (up to Ub_{20}) tethered to proteins in cells.

Monoubiquitylation and polyubiquitylation consign proteins to relocation in cells, most often with the net consequence of proteolytic degradation, albeit by quite different mechanisms. Protein monoubiquitylation at a Lys-ε-NH_2 group by an E3 ubiquitin ligase can initiate relocation of transmembrane receptor proteins from the plasma membrane to the trans Golgi network sorting compartments.[24–26] The covalent Ub tag is information-rich and recruits various partner proteins that contain one or more of several variants of Ub-binding domains. The partner proteins can act as chaperones for internalization of the ubiquitylated receptor, import into early endosomes, and transit to lysosomes in which lysosomal proteases can cause hydrolytic degradation (Scheme 5).[23] These pathways are part of the homeostatic regulation of receptor density and lifetimes at plasma membranes.

In contrast to the sorting fate of monoubiquitylated proteins, polyubiquitylation sends modified proteins to the chambered proteases that constitute the proteasome. Tandem attachment of four or more ubiquitin molecules to such a lysine side chain constitutes an architectural signal that recruits protein chaperones with ubiquitin-binding domains. The chaperone complexes then escort the marked protein to the proteasomes,[27] where the chaperones dissociate, and the polyubiquitin chain is removed hydrolytically, perhaps during ATP-driven unfolding of the targeted protein (Scheme 6). The unfolded protein is then threaded

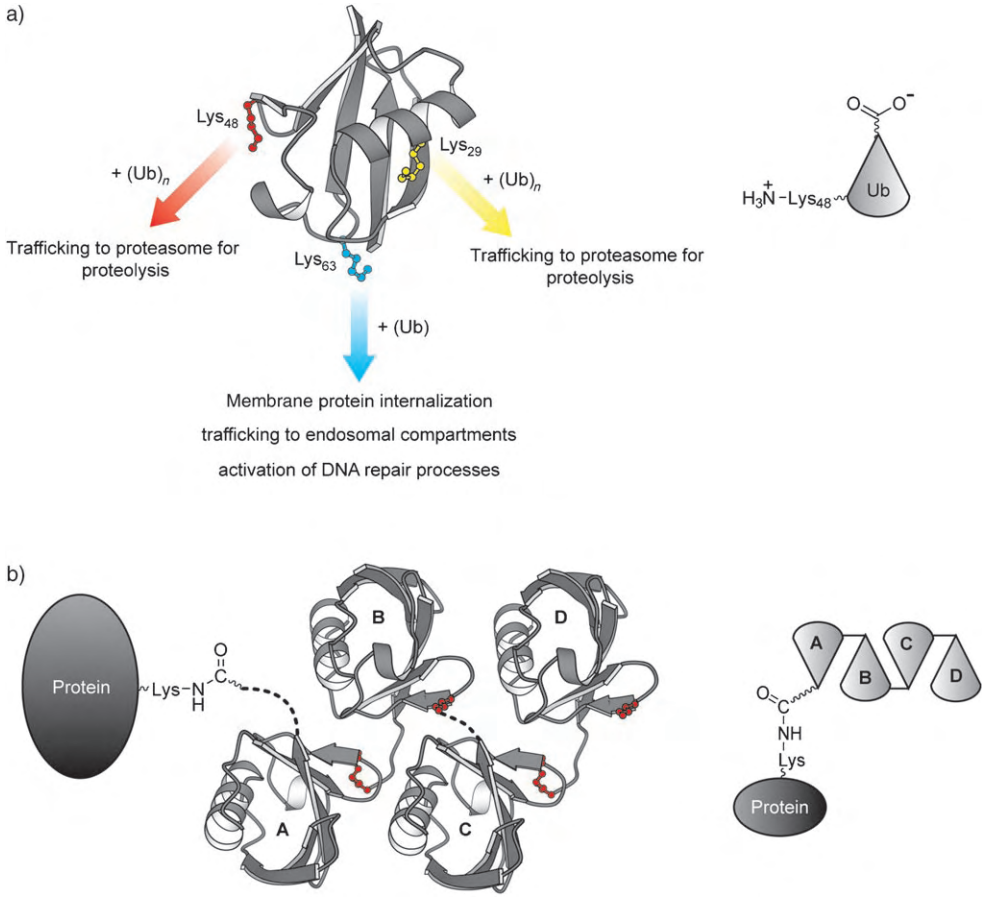

Figure 6. a) 3D trace of the 76-residue ubiquitin: $Lys_{29,48,63}$ side chains on different faces of ubiquitin offer different surfaces for tandem conjugation of growing polyubiquityl chains; b) structure of a tetraubiquityl unit, the minimum chain length to direct polyubiquitylated proteins to the proteasome.

 © 2005 Wiley-VCH Verlag GmbH & Co. KGaA, Weinheim

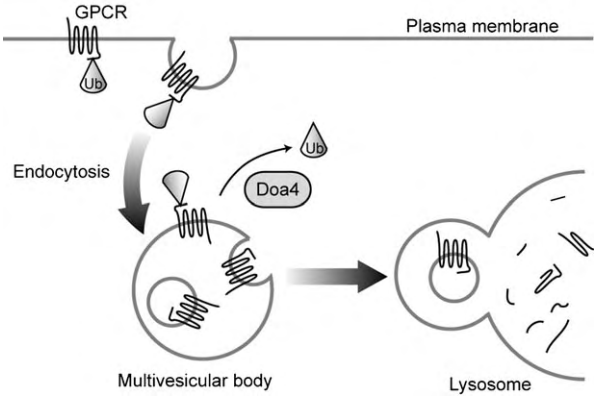

Scheme 5. Recognition of the Ub architecture in a monoubiquitin-tagged protein by partner proteins/chaperones that have one or more ubiquitin-recognition domains for transit to the secretory system.

into the chamber of the proteasome where the active sites of the protease subunits degrade it to small peptides. The characteristic temporal control of proteins destroyed during the cell cycle, such as the cyclin subunits of cyclin-dependent protein kinases,[28,29] is effected by the E1–E2–E3 ubiquitin ligase machinery. The activity of various multisubunit E3 ligases can be controlled by posttranslational states of the catalysts or of the target proteins, such as phosphorylation of particular Ser and Thr residues.

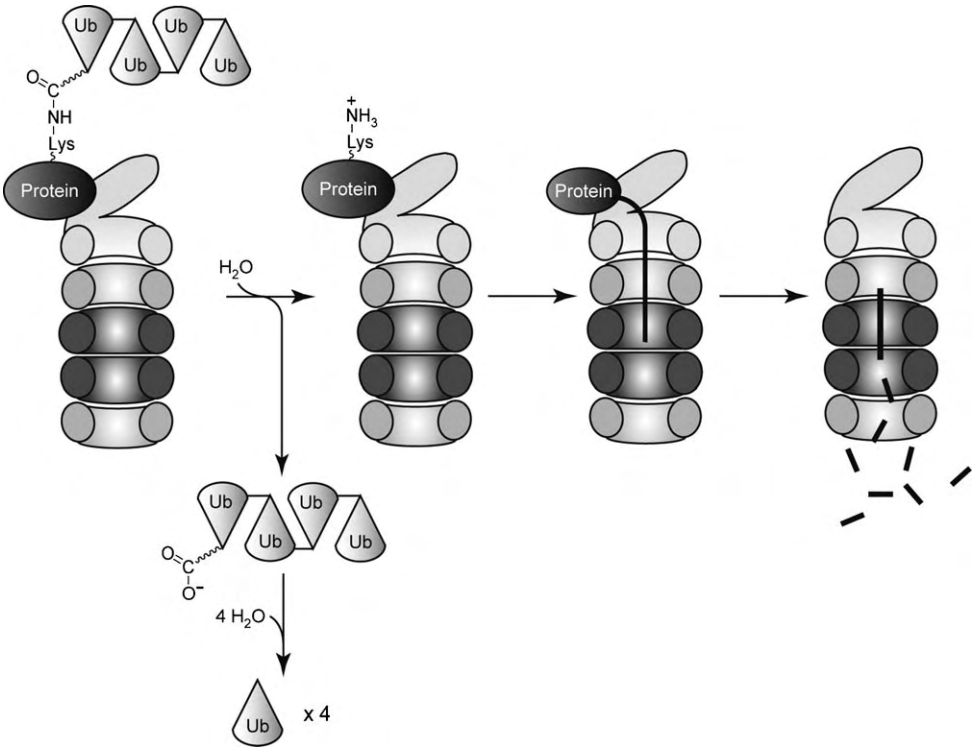

Scheme 6. Recognition of Ub_n-tagged protein for chaperoning to proteasomes where the Ub_n tag is retrieved by hydrolysis of the isopeptide link to the target protein; the target protein is unfolded and threaded into the chamber of the proteasome.

2.3. Protein Alkylation

Alkyl substituents are attached regiospecifically to proteins by posttranslational modification enzymes. The three common alkyl groups transferred are the methyl (C_1), for example, in histone methylations of Lys and Arg side chains,[30] or the C_{15} and C_{20} isoprenyl (farnesyl and geranylgeranyl) groups (Scheme 7).[31] The small C_1 and the large

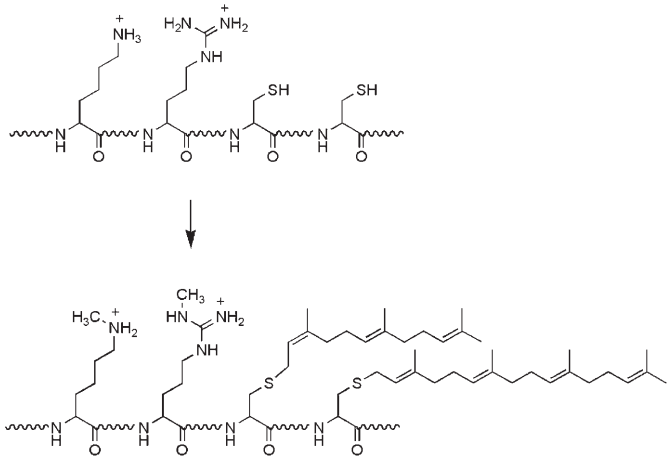

Scheme 7. Alkyl groups transferred to protein side chains: the methyl group from *S*-adenosylmethionine (SAM) is transferred most often to Lys and Arg side chains (although O-, S-, and C-methylations of protein side chains are known); the two isoprenyl units transferred by protein prenyltransferases to Cys side chains are the C_{15} (farnesyl) and the C_{20} (geranylgeranyl) groups from the corresponding prenyl diphosphate substrates.

hydrophobic C_{15} and C_{20} groups each serve to introduce hydrophobicity but they do so to very different degrees.

2.3.1. N-Methylations

Whereas C-, O-, and S-methylations of protein side chains are known,[3] the reactions of most contemporary interest are the N-methylations of Lys and Arg side chains, particularly on the same histone tails that are acetylated. Indeed, covalent posttranslational N-methylation of histone tails complements acetylation as the second main part of writing and reading the histone code (Figure 7). For example, 7 of the first 36 residues, $Arg_{2,17,26}$ and $Lys_{4,9,27,36}$ of histone H3 are known to be methylated

 © 2005 Wiley-VCH Verlag GmbH & Co. KGaA, Weinheim

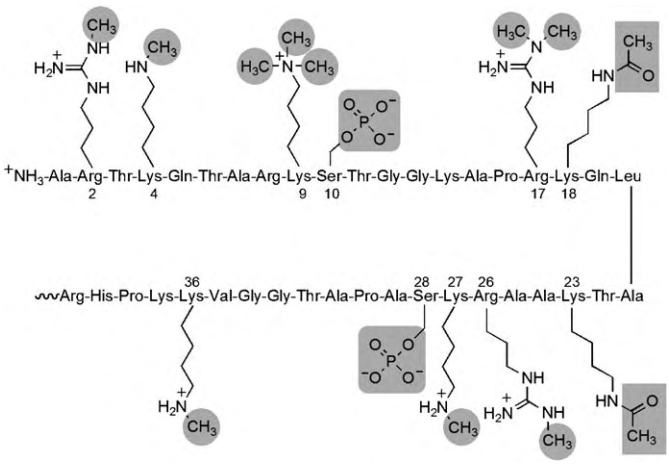

Figure 7. N-methylations can occur at $Arg_{2,17,26}$ and $Lys_{4,9,27,36}$ of histone H3. Lys_{18} and Lys_{27} can be acetylated and Ser_{10} and Ser_{28} phosphorylated.

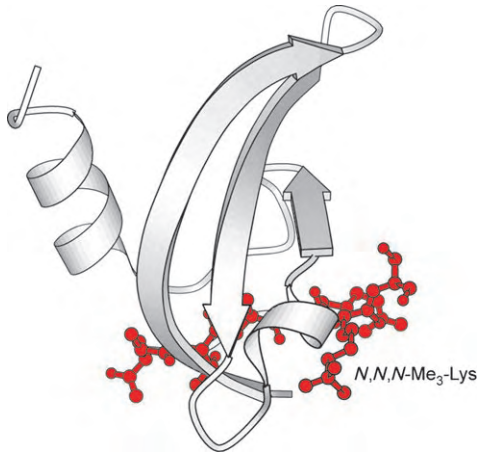

Figure 8. *N*,*N*,*N*-Trimethyl-Lys_9 of histone H3 as a ligand to recruit protein HP1 through its chromo domain.

by a family of histone methyltransferases,[32] several of which are residue-specific. An additional layer of information content and combinatoric complexity is enabled by the fact that Lys-ε-NH_2 groups can be progressivly mono-, di-, or trimethylated, again with distinct distributions shown by different methyltransferases. Analogously both monomethyl- and dimethylArg residues are observed (Scheme 8). The size and hydrophobicity differences between monomethyl- and trimethyl substituents on Lys side chains enable selective recruitment of proteins involved in transcriptional control. For example, trimethyl-Lys_9 in H3 recruits partner protein HP1 by binding to its chromodomain (Figure 8) as part of transcription factor and coactivator protein complex assemblies.[14,32]

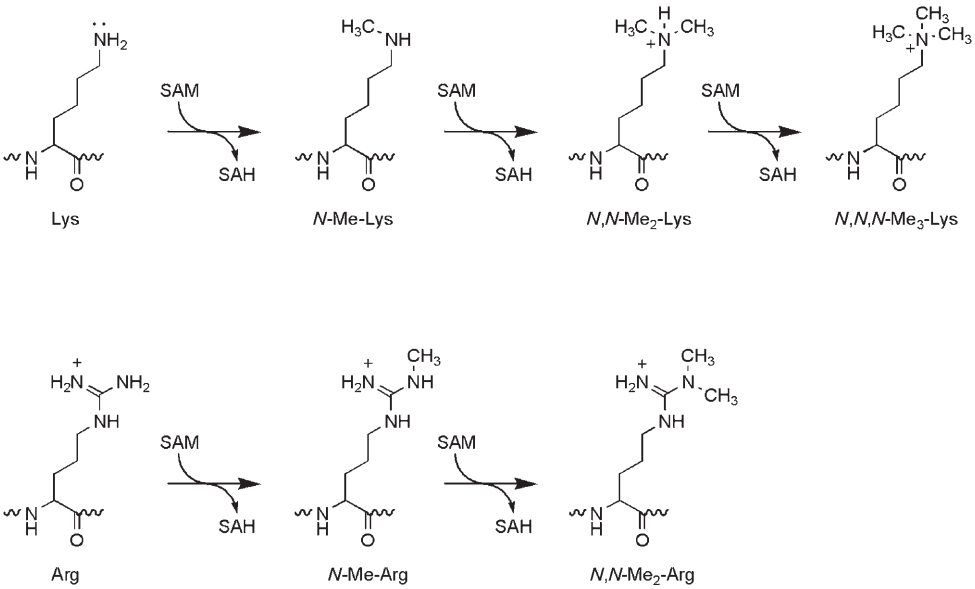

Scheme 8. Progressive mono-, di-, and trimethylation of Lys side chains and mono- and dimethylation of Arg side chains in histone N-terminal tail regions. SAH = *S*-adenosylhomocysteine.

N-Acetylations and N-methylations of side chains in histone tails can have opposite effects on gene transcriptional silencing and activation. Histone H3 is just one of the four histones, each present as a dimer, in the nucleosome core. The balance of the four acetylations and seven methylations on the tail of histone H3 give, on this subunit alone, $11 \times 2 = 22$ sites for titration of transcriptional coactivator and corepressor complexes.

2.3.2. *Protein S-Prenylation*

The C_{15} farnesyl and C_{20} geranylgeranyl lipid groups are built up from C_5 isoprenyl diphosphate primary metabolites by iterative alkyl extension by action of C–C bond-forming enzymes.[33] The farnesyl and geranylgeranyl-PP molecules can be used for further isoprene elongation (e.g. C_{15} dimerization to squalene in the cholesterol biosynthetic pathway) or they can be utilized as electrophilic alkyl donors in posttranslational protein prenylation (Scheme 9).[34] There are protein farnesyltransferases and protein geranylgeranyltransferases, which are αβ heterodimers that share a common α subunit. The Ras GTPase superfamily have members that can be prenylated on Cys thiolate side chains, some with the C_{15} and some with the C_{20} prenyl chain. Typically, Ras family proteins that have a CaaX motif at the C terminus are farnesylated, when X is a small amino acid such as Ala or Ser. When X is Leu as in both Rac and RhoA GTPases, then the cysteine residue (C) is geranylgeranylated (Scheme 10a). The Rab subfamily of GTPases, over 60 in number, have two cysteine residues at or near the C terminus, for example, in a CCXX arrangement. Both cysteine groups undergo posttranslational gera-

 © 2005 Wiley-VCH Verlag GmbH & Co. KGaA, Weinheim

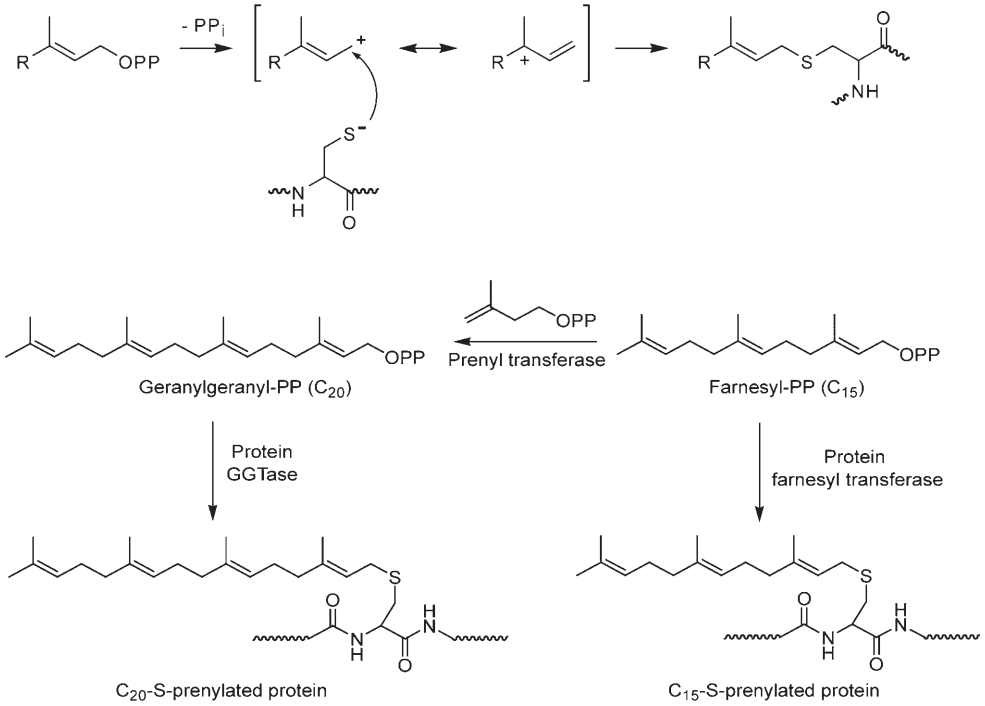

Scheme 9. Mechanism for Cys S-isoprenylation by protein prenyltransferases.

nylgeranylation (Scheme 10b), thus introducing two C_{20} lipid anchors.[35] Rab proteins cycle between membrane vesicles in the secretory system; escort proteins are used to control location and cycling.[36,37]

Some proteins undergo both N- and S-acylation and some combination of S-prenylation. All of these lipid anchors drive the modified proteins to partition more to membranes, thus controlling subcellular localizations.

2.4. Protein Glycosylation

Covalent glycosylation of proteins is relatively rare in prokaryotes and quite common in eukaryotes. C-glycosylation, O-glycosylation, and N-glycosylation of proteins are known, but C-glycosylation, specifically mannosylation of C2 of the indole ring of tryptophan residues,[38] is quite rare.

2.4.1. N-Glycosylation

N-glycoproteins are both more common and typically more complex in structure and architecture than O-glycoproteins in eukaryotes.[39] The branching glycan unit in N-glycoproteins is preassembled on a lipid diphosphate scaffold by a series of membrane-associated glycosyltransferases in the endoplasmic reticulum.[40] The assembled N-glycan unit that serves as a substrate for the multisubunit oligosaccharyltransferase is a tetradecasaccharyl-PP-dolichol substrate

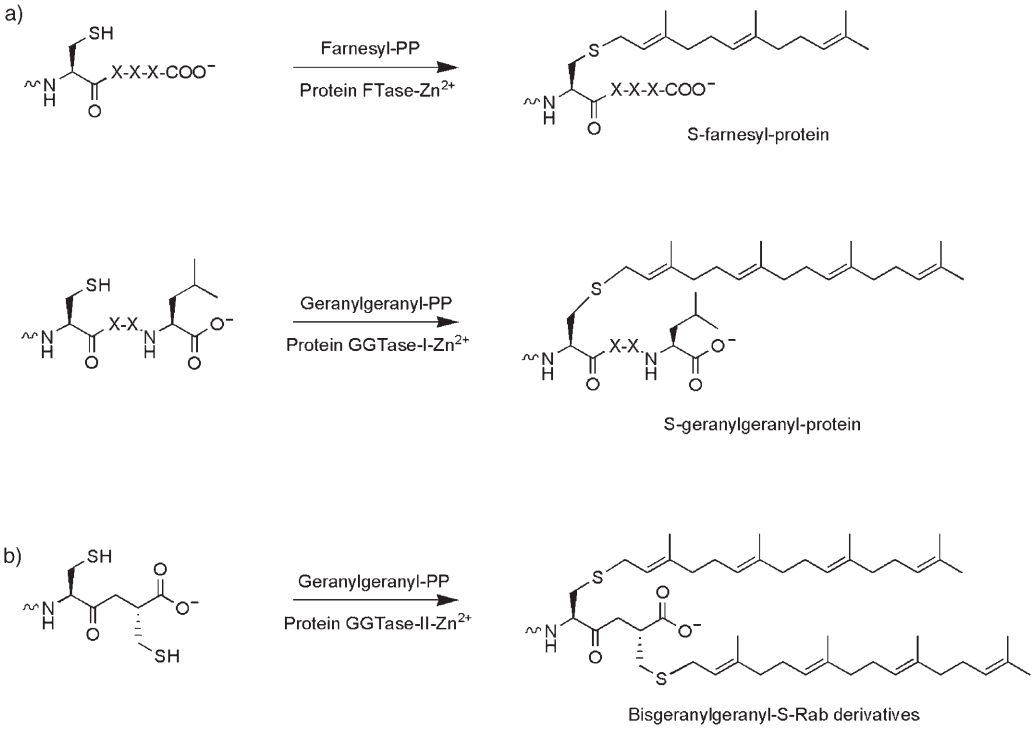

Scheme 10. Prenylation reactions at the C termini of the Ras protein superfamily: a) farnesylation of the C terminus of Ras at CaaX (X = Ala, Ser). Geranylgeranylation of Rac at CaaX (X = Leu); b) double geranylgeranylation of the CC carboxy terminus of Rab proteins.

 © 2005 Wiley-VCH Verlag GmbH & Co. KGaA, Weinheim

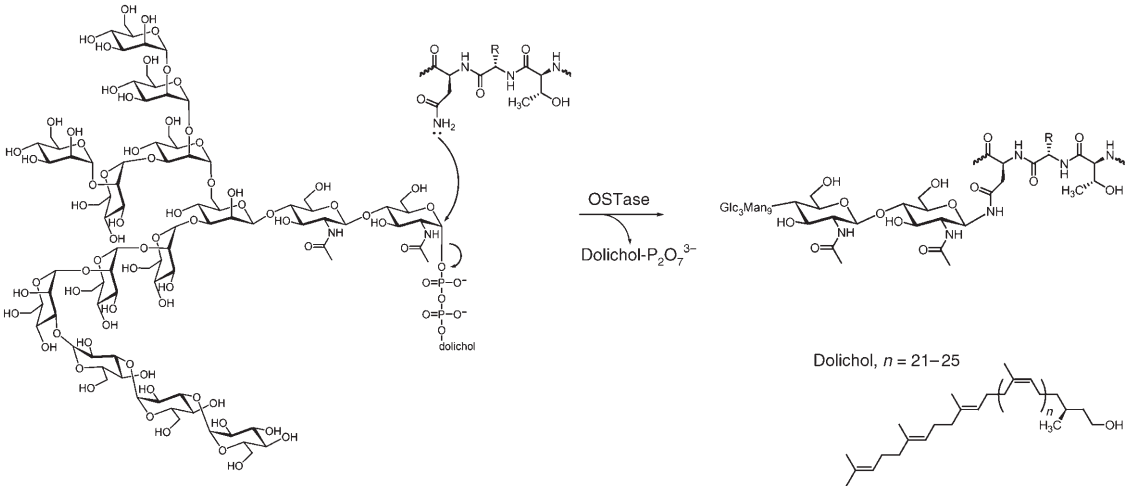

Scheme 11. The branched tetradecasaccharyl-PP substrate is the donor substrate in the Asn N-glycosylation reaction catalyzed by the oligosaccharyltransferase that initiates N-glycoprotein modifications.

(Scheme 11).[41] The side-chain atoms that are modified in N-glycoprotein biogenesis are the carboxamide nitrogen atoms of asparagine groups, almost always in the sequence Ser/Thr-X-Asn. The low nucleophilicity of the Asn $CONH_2$ is thought to be enhanced by hydrogen bonding to the Ser/Thr-OH side chain but the initial glycan transfer step is still poorly understood.

The initial tetradecasaccharyl chain $Glc_3Man_9(GlcNAc)_2$ then undergoes a remarkable enzymatic hydrolytic trimming and refashioning of the identity and linkages of the N-glycan chains (Scheme 12). The first hydrolytic tailoring enzymes are

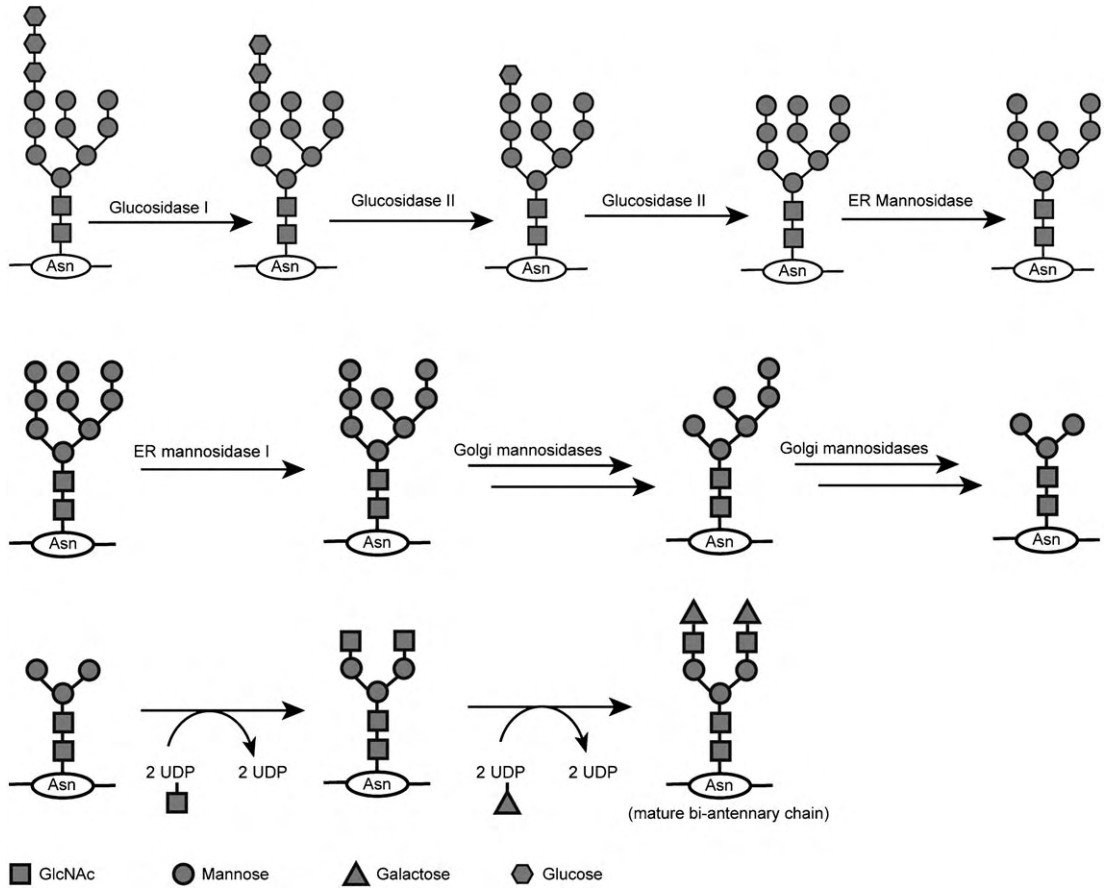

Scheme 12. Progressive trimming of the initial N-linked $Glc_3Man_9(GlcNAc)_2$ glycan chain to $Man_9(GlcNAc)_2$ in the ER and then to the core pentasaccharide $Man_3(GlcNAc)_2$ in the Golgi complex before being built back up to mature N-glycan chains found on N-glycoproteins that have transited the secretory system.

 © 2005 Wiley-VCH Verlag GmbH & Co. KGaA, Weinheim

two glucosidases in the ER lumen which generate the dodecasaccharyl $GlcMan_9(GlcNAc)_2$ N-linked proteins. These are ligands for calnexin and calreticulin, protein chaperones that recognize the dodecasaccharyl chain and help refold the nascent glycoproteins as they are extruded through the ER membrane into the lumen. As the remaining Glc is hydrolyzed by the ER glucosidase, the chaperones lose affinity for the undecasaccharyl-N-protein products. A UDP-glucose glycoprotein glucosyltransferase[42] puts the Glc residue back on the undecasaccharide unit to give the calreticulin and calnexin chaperones another round of assisted refolding. Thus, this is a refolding/protein-quality-control way station during glycoprotein secretion. If the glycoprotein cannot be refolded after several cycles of deglucosylation/reglucosylation, it is targeted for export back to the cytoplasm. There it undergoes polyubiquitylation, and proteasome-mediated degradation of the unfolded protein by a glycoprotein-targeting E3 ligase as part of the ER-accelerated degradation (ERAD) quality-control pathway (Scheme 13).[42]

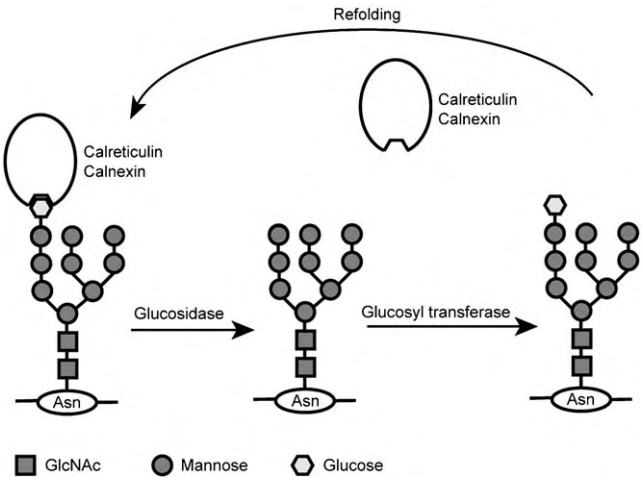

Scheme 13. Cycling of the oligosaccharyl chain between $GlcMan_9(GlcNAc)_2$-Asn and $Man_9(GlcNAc)_2$-Asn in the ER from opposing action of glucosidase and UDP-glucose glycoprotein glucosyltransferase. The Glc-containing oligosaccharyl chain is recognized by the chaperone proteins calreticulin and calnexin to help refold the nascent N-glycoproteins that have been glycosylated and extruded cotranslationally into the ER lumen. The glucosylation cycle is part of the protein quality-control system for proteins secreted into the endoplasmic reticulum.

For $Man_9(GlcNAc)_2$–N-glycoproteins that have refolded and passed into the Golgi compartment, six of the mannose residues are then trimmed hydrolytically by mannosidases to yield the $Man_3(GlcNAc)_2$ pentasaccharyl core found in all mature N-glycoproteins. At this point the branched oligosaccharide core is rebuilt back up to biantennary and triantennary oligosaccharides characteristic of mature N-glycoproteins present on the cell surface.[43] The multiplicity of glycosyltransferases in the Golgi can create enormous diversity in the mature N-glycan chains.

Multiple Asn side chains can be glycosylated in a given protein, and the identity of the glycan chains at each Asn residue can vary depending on stochastic encounters with at least 10 trimming and rebuilding enzymes during passage through the ER and Golgi compartments.[41,43] It has been estimated that about a third of all proteins that enter secretory pathways in eukaryotic cells may be N-glycosylated, and so tens of thousands of glycoprotein variants may coexist in eukaryotic cells. For example, 52 glyco forms of the prion protein have been reported.[44,45]

2.4.2. *O-Glycosylation*

O-glycosyl chains in eukaryotic proteins are generally shorter and less complex than those in N-glycoproteins. Many proteins contain the monosaccharide GlcNAc[46] that is put on by a specific O-GlcNAc transferase and removed by a corresponding hydrolase. Other proteins such as the signaling protein Notch contain tri- and tetrasaccharides in the EGF repeat domains (Figure 9).[47,48] O-glycosylation is a crucial

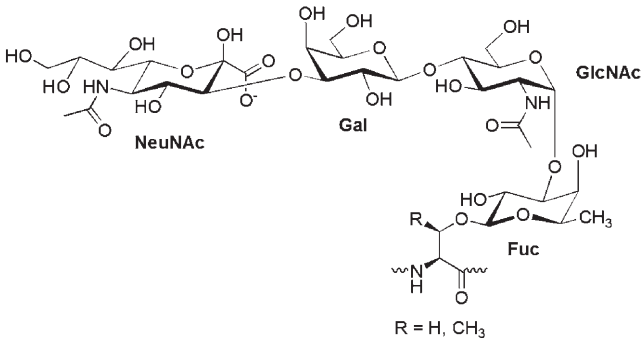

Figure 9. The O-linked tetrasaccharide sialyl-α-2,3-Gal-x-1,4-GlcNAc-β-1,3-fucosyl-Ser attached to the protein Notch during its transit through the secretory pathway on the way to the cell surface.

part of the maturation of Notch during its transit through the secretory pathway to the cell surface. The short O-linked sugar chains are important in a variety of functional contexts, from modulating transcription factor activity,[49] to acting as essential recognition elements in signaling by Notch at cell surfaces.[50,51]

2.5. *S–S Bond Formation*

Two main types of linkages serve to cross-link proteins, or portions of proteins, covalently. By far the more common are disulfide links from oxidation of cysteinyl residue thiolate side chains.[52,53] The cytoplasmic and nuclear compartments in eukaryotic cells are reducing microenvironments, as reflected in the 100:1 ratio of the redox-active tripeptide glutathione in reduced (GSH) to oxidized (GSSG) state.[54] The high reducing ratio is maintained by the high levels of NAD(P)H and enzymes, such as glutathione reductase and thioredoxin reductase[3] that use the reduction potential of NAD(P)H to re-reduce disulfides in proteins that have become oxidized (Scheme 14a). As proteins pass through the secretory pathway in eukaryotic cells, the levels of total glutathione and reduced nicotinamide coenzyme fall, compartments become

© 2005 Wiley-VCH Verlag GmbH & Co. KGaA, Weinheim

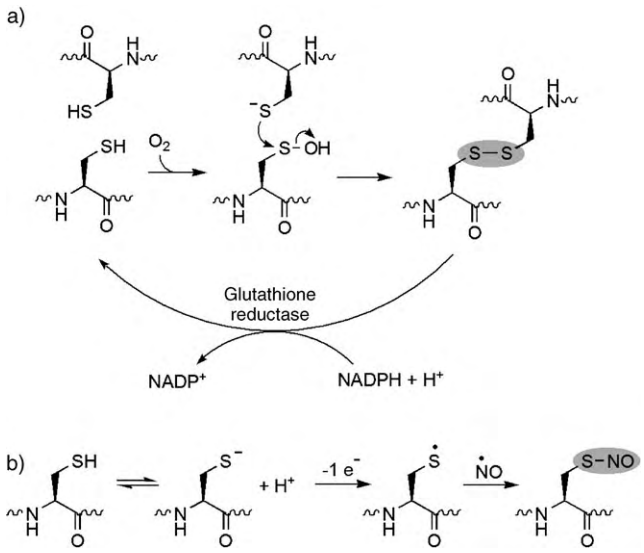

Scheme 14. Oxidation of thiolate side chains of cysteine residues: a) oxidation of dithiols to disulfides (for example via sulfenic acid intermediates) and reversible reduction back to dithiols by glutathione reductase action; b) oxidation of Cys-S^- side chain to S-nitrosyl-Cys by nitric oxide (·NO).

more oxidizing, and disulfide links predominate. The disulfide bonds may stabilize protein architectures as proteins reach cell outer surfaces or are excreted into extracellular spaces. The formation of disulfide bonds in zymogen forms of pancreatic protease as they are packaged into the oxidizing microenvironment of zymogen granules is a prototypical case.

The mechanism for oxidation of protein dithiols to disulfides typically involves oxidation of the electron-rich thiolate side chains of Cys residues. One-electron oxidation would yield thiyl radicals that could dimerize to the disulfides. Alternatively, thiolate side chains can be oxygenated by a variety of oxygen-derived oxidants (peroxide, hydroxyl radical) to generate sulfenic acid (-SOH) side chains. Capture of the sulfenate by a neighboring Cys-S^- generates disulfides. Regeneration of the dithiol forms is mediated by thiol–disulfide interchange using reduced glutathione or the low-molecular-weight dithiol protein thioredoxin (TSH). The oxidized GSSG or TSST are recycled at the expense of NADPH oxidation by thioredoxin reductase and glutathione reductases.

The electron-rich thiolates and the thiyl radicals can be captured by other oxidants and radicals, including ·NO. Such S-nitrosylation of thiolate side chains of cysteine residues is documented in many proteins by radical species derived from nitric oxide (Scheme 14b). These Cys-SNO moieties have been proposed to be widespread in oxidative signaling events.[55]

The second PTM cross-link strategy is nonoxidative and involves transglutaminase catalysis in which glutamine side chains in protein substrates are deaminated via acyl-S-transaminase intermediates, which are captured by Lys-ε-NH_2 groups to effect net transamidations (Scheme 15).[56,57]

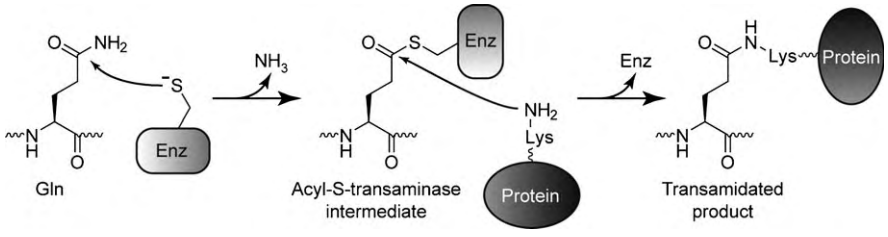

Scheme 15. Nonoxidative cross-links introduced by transglutaminases; the amide bond in Gln side chains is replaced by the ε-NH of Lys to create Glu-ε-Lys isopeptide cross-links.

3. Covalent Addition: The Supporting Cast

While the five chemical types of posttranslational modifications discussed in Section 2 are abundant and well-characterized in cells, there are many additional classes of purposeful enzymatic modification of proteins that expand the metabolic and signaling capacities of organisms.

3.1. Protein Hydroxylation

One additional category of protein posttranslational oxidation is enzyme-mediated hydroxylation. Hydroxylations occur at nonnucleophilic sites in aminoacyl side chains to generate 3-OH-Pro, 4-OH-Pro, and 5-OH-Lys (Figure 10) in collagen at Pro-Gly and Lys-Gly sites. These hydroxylations are key modifications for proper maturation of collagen fibers.[58] Some of the 5-OH-Lys residues are then subsequently tandemly glycosylated on the newly introduced OH group to create an O-disaccharide linkage. 4-Hydroxyproline modifications, about tenfold more abundant than the hydroxylations at C3 of Pro residues, are involved in the triple helical strands of collagen, with the 4-OH pointing away from the helix.

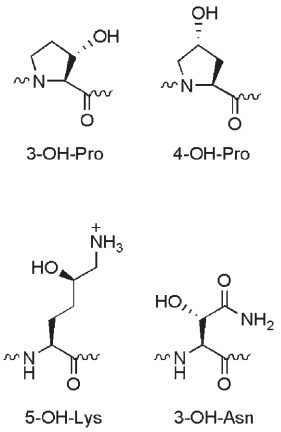

Figure 10. Hydroxylated amino acid residues generated by posttranslational Fe^{II}-dependent monooxygenases: 3-OH-Pro, 4-OH-Pro, 5-OH-Lys, 3-OH-Asn.

A third side chain in which a CH_2 group is converted into CH-OH is

 © 2005 Wiley-VCH Verlag GmbH & Co. KGaA, Weinheim

Asn (to 3-OH-Asn, Figure 10) in a small number of proteins, including the transcription factor HIF (hypoxia inducible factor).[59] HIF transcription is initiated at low partial pressures of O_2 and induces the transcription of hundreds of genes, including the gene that encodes erythropoietin to make more red cells that can carry more O_2 to hypoxic tissues.

The HIF-1α subunit in the HIFαβ heterodimer is post-translationally hydroxylated by hydroxylases, one specifically acting at two Pro residues to create 4-OH-Pro[60] and the other acting at a particular Asn residue to generate 3-OH-Asn.[61] These are determinative changes in the oxygen-sensing cascade in mammalian tissues (Scheme 16).[62] The lifetime of the HIF-1α subunit in cells is controlled by proteolysis in the ubiquitylation pathway, which involves chaperoned escort to the proteasome, unfolding, and threading into the proteasome chamber for proteolysis to limit peptides. The polyubiquitylation of HIF-1α is carried out by a particular E3 ligase, the von Hippel-Lindau (VHL) protein.[63,64] The hydroxylation status of Pro_{402} and Pro_{564} in HIF-1α controls the affinity for the VHL E3 ligase.[60] At low pO_2 in cells the Pro hydroxylase is not saturated with its substrate O_2 and has low activity. At high pO_2 the hydroxylase is active and converts the two Pro residues into 4-OH-Pro residues. The hydroxy side chain in $HO\text{-}Pro_{564}$ provides about a 1000-fold tighter binding of modified HIF-1α over unmodified HIF-1α for the VHL ubiquityl ligase.[60] This is the mechanism for selective polyubiquitylation of the hydroxylated forms of HIF-1α, which leads to its proteasome-mediated destruction at high pO_2 levels but its persistence at low pO_2. Persistence means a longer lifetime for the heterodimeric HIF-1αβ and the longer gene-transcriptional-activation response characteristic of hypoxia.

The protein hydroxylases that catalyze the side-chain hydroxylations noted in this section belong to the family of non-heme Fe^{II} monooxygenases that have two His and one Asp side chains to provide three of the six coordination sites to the Fe^{II} (Scheme 17).[65] Two additional coordination sites are filled by cosubstrate α-ketoglutarate and the sixth by O_2. When both O_2 and α-KG are bound, the organic diacid is oxidatively decarboxylated to succinate. O_2 is cleaved in such a way that one atom ends up in succinate and the other is coordinated to the iron as a high-valent $Fe^{IV}=O$. This high-valent oxoiron complex is a sufficiently powerful oxidant to cleave the unactivated C–H bonds at C3 and C4 of Pro residues, C5 of Lys residues, and C3 of Asn residues to generate transient ·CH radicals and Fe^{III}-OH. OH· transfer from the Fe^{III}-OH to the carbon-centered radical yields the hydroxylated protein side chains. The polarity of these side-chain hydroxylations is quite distinct from the bulk of the other posttranslational modifications considered in this Review. The amino acid side chains undergoing modification are not electron rich or nucleophilic. Instead, the iron-based modifying enzyme generates a powerful oxidant and leads to homolytic cleavage of unactivated C–H bonds with regio- and stereospecificity.

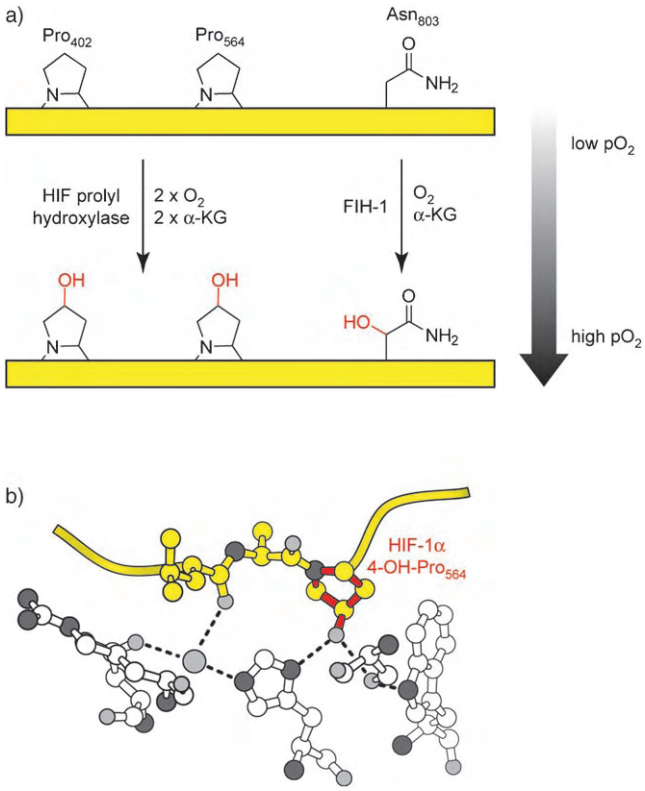

Scheme 16. a) Hydroxylation of Pro and Asn residues in the HIF-1α subunit; b) interaction of the $HO\text{-}Pro_{564}$ residue of HIF with the E3 ligase that will catalyze polyubiquitylation of HIF.

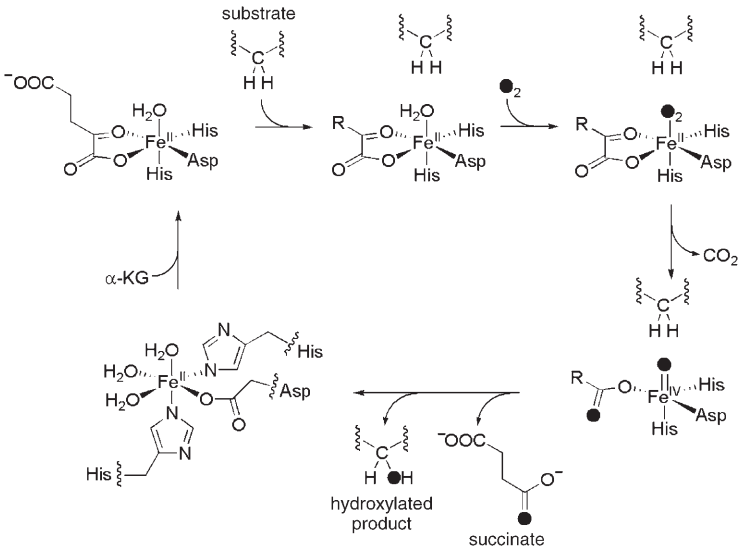

Scheme 17. Mechanism of protein hydroxylation by the nonheme Fe^{II} monooxygenases. The active site iron(II) is coordinated by three residues from within the protein (two His, one Asp). Subsequent coordination by α-ketoglutarate and O_2 results in the cleavage of dioxygen and formation of a high-valent $Fe^{IV}=O$ species. This iron complex cleaves the unactivated C–H bond of the substrate, yielding hydroxylated product and succinate.

© 2005 Wiley-VCH Verlag GmbH & Co. KGaA, Weinheim

3.2. Protein Sulfur Transfer

Phosphoryl groups are not the only inorganic moieties transferred to protein side chains. The SO_3^- group is also transferred from phosphoadenosine phosphosulfate (PAPS) to tyrosine side chains in proteins.[66] PAPS is the biological reagent for transfer of activated sulfuryl (SO_3^-) groups to nucleophiles in both small molecules (e.g. oligosaccharides such as heparin[67]) as well as proteins and proteoglycans. Enzymatic sulfation of four tyrosine residues occur in the Golgi complex at the N-terminus of the CCR5 receptor (Scheme 18) during its transit to the plasma membrane[68] where the N-terminus is displayed at the extracellular surface. This cluster of anionic Tyr-OSO_3^- modifications is important for recognition by the CCR5 chemokine ligand.

Once sulfated molecules are internalized, the sulfate ester bond is hydrolyzed enzymatically by sulfatases in the secretory compartment, predominantly in lysosomes.[69–71] The set of sulfatases known to degrade aryl sulfate ester substrates are themselves in inactive proenzyme forms until they undergo posttranslational activation. This involves oxidative conversion of an active-site cysteine residue into an aldehyde in the form of formylglycine (Fgly).[70] This conversion of a thiolate nucleophile into an electrophilic carbonyl is followed by a hydration equilibrium to distribute the Fgly between the aldehyde and the *gem* diol, the aldehyde hydrate (Scheme 19). It is the hydrated form of the aldehyde group in the formylglycine side chain that initiates covalent attack on sulfated protein substrates bound in the sulfatase active sites[72] with resultant O–SO_3^- bond cleavage.

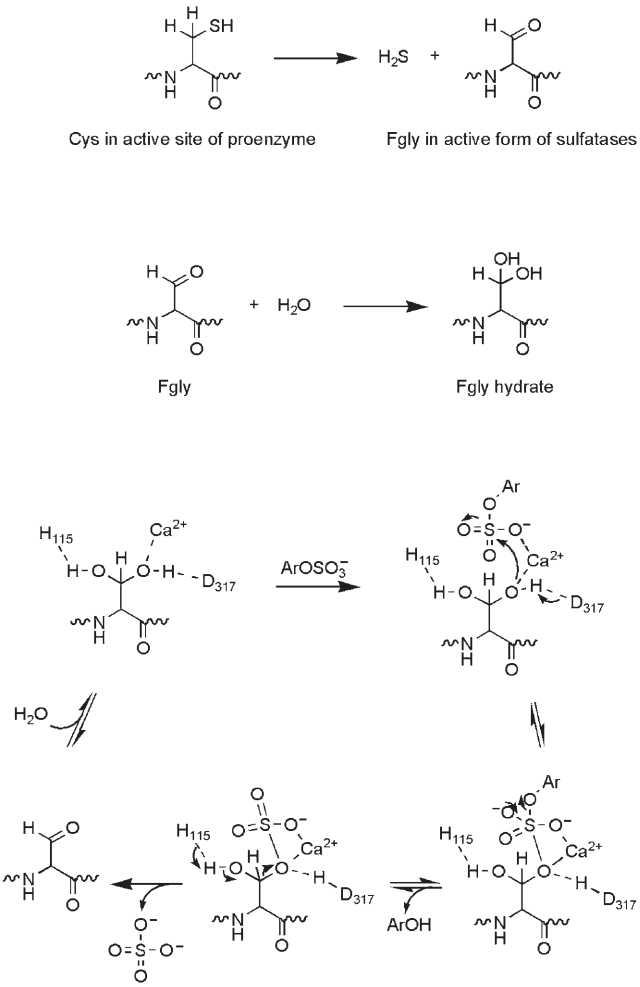

Scheme 19. Oxidative conversion of an active site Cys-S^- to the aldehyde of formylGly (Fgly) converts inactive precursors of sulfatases to active catalysts. Hydration of the Fgly side chain generates a *gem* diol, which is the active nucleophile that attacks the Ar-OSO_3^- substrate on sulfur to initiate the O-SO_3^- bond cleavage.

3.3. Protein Modification by Bacterial Toxins

Bacteria that invade eukaryotic cells secrete a complement of proteins into the host cell to neutralize its defense mechanisms. Among these virulence factors are three types of enzymes that act as posttranslational modification catalysts for ADP ribosylation, glucosylation, and deamidation of host target proteins.[3]

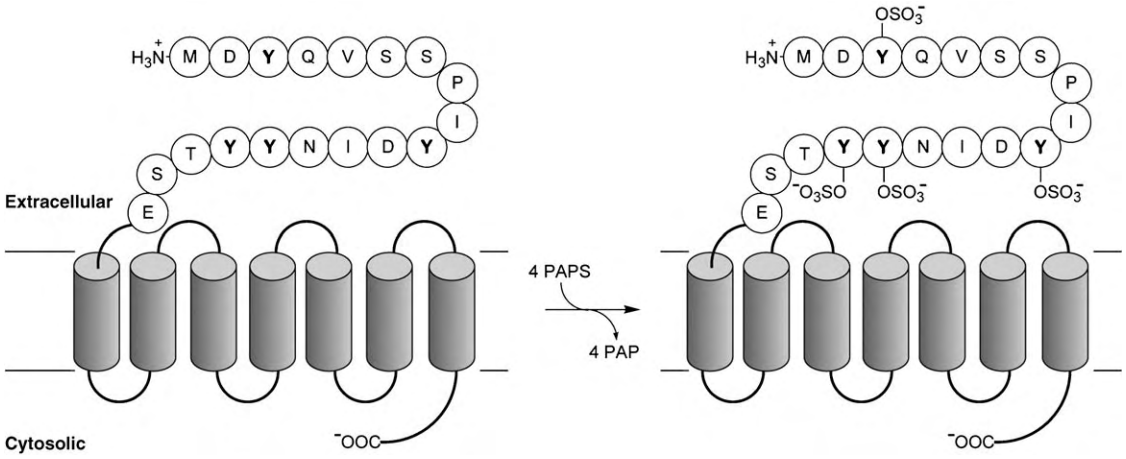

Scheme 18. Transfer of four SO_3^- groups from PAPS to the phenolate oxygen atoms of four side chains of Tyr residues at the N-terminal region of the CCR5 receptor during its passage through the secretory compartments to the cell surface.

 © 2005 Wiley-VCH Verlag GmbH & Co. KGaA, Weinheim

3.3.1. ADP Ribosylation

Several famous bacterial exotoxins, including the cholera toxin, the diphtheria toxin, the pertussis toxin, and the botulinum C3 toxin,[73] are ADP ribosyltransferases. The donor substrate of the ADP ribosyl moiety is the readily available coenzyme NAD. The positively charged nicotinamide group departs in a transition state involving the ribaoxacarbenium ion of the transferring ADP ribosyl group (Scheme 20a). This ion can be captured by robust nucleophiles in protein cosubstrates in the active site of the toxin, such as thiolate side chains of Cys, for example when pertussis toxin modifies the α subunit of the inhibitory GTPase G_i that regulates cyclic AMP production. The transferring ribaoxacarbenium ion can also be captured by weak nucleophiles such as the guanidino group of Arg in the α subunits of the G_s GTPase by the cholera toxin. Another example of the capture of the potent electrophilic form of the ADP ribosyl moiety is the modification of the weakly nucleophilic Asn_{41} in the Rho subfamily of small GTPases by the C3 toxin from *Clostridium botulinum*, ultimately leading to a net depolymerization of the actin mesh work in the host cell.

A fourth example of bacterial toxin ADP ribosyltransferase activity on a specific host protein with deleterious consequence is the action of the diphtheria toxin on His_{715} in the protein synthesis factor eukaryotic elongation factor 2 (eEF-2). That histidine in mature eEF-2 has already undergone a preparatory set of posttranslational modifications involving the aminocarboxypropyl transfer from cosubstrate *S*-adenosylmethionine (SAM), N,N,N-trimethylation by three additional SAM molecules, and glutamine-mediated amidation to convert His_{715} into a diphthamide residue. This is the molecular form of eEF-2 that undergoes ADP ribosylation by the diphtheria toxin (Scheme 20b) and rendered inactive in its essential elongation functions, bringing host protein synthesis to a halt in the infected cell.[73]

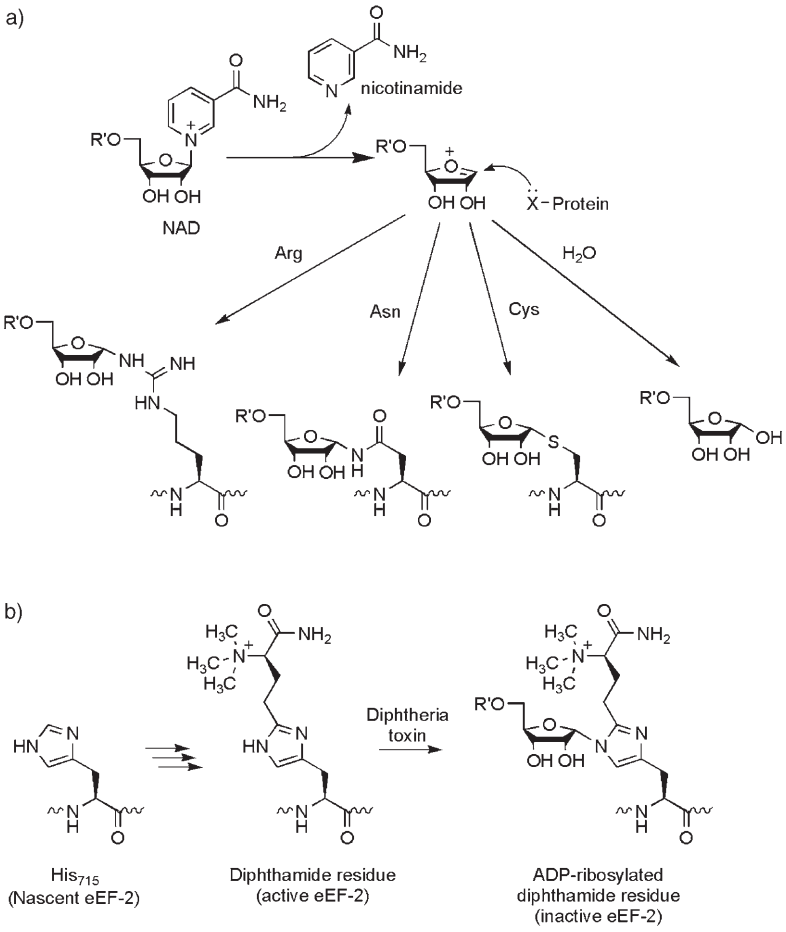

Scheme 20. ADP ribosylation of protein substrates by bacterial toxins: a) Cleavage of NAD releases nicotinamide and generates a stabilized ribaoxacarbenium ion in the active site. This can be captured by a range of cosubstrate nucleophiles, from the robust Cys-S^- in pertussis toxin catalysis to the weak Asn and Arg side chains in botulinum and cholera toxins. Water is a natural nucleophile and leads to NAD glycohydrolase side reactions; b) diphtheria toxin catalyzes ADP ribosylation of a modified histidine residue in the eukaryotic host cell protein synthesis elongation factor eEF-2. The residue, His_{715} in the nascent eEF-2 undergoes five posttranslational steps of transfer of the methionyl moiety from SAM, N,N,N-trimethylation, and amidation to yield the diphthamide residue at position 715. This is the residue targeted for ADP ribosylation on N_3 of the imidazole ring by the diphtheria toxin.

3.3.2. Other Modification Activities of Bacterial Toxins

The Ras and Rho GTPase families are also targets of additional bacterial toxin enzymes that inactivate the GTPases by chemical modifications distinct from ADP ribosylation. One is the lethal toxin protein from *Clostridium sordelli* which also is a protein glycosyltransferase. In this case it is not transfer of the ADP ribosyl moiety from NAD but instead the transfer of a glucosyl group from UDP-glucose that is catalyzed by the protein toxin. The target nucleophile is the β-OH of Thr_{35} in Ras. This O-glucosylation blocks the catalytic activity of Ras.[74,75]

A distinct type of posttranslational modification strategy is deamidation of Gln_{61} in Rho by the cytotoxic necrotizing protein from pathogenic strains of *E. coli*.[76] This Gln carboxamide side chain is in the GTPase active site and its hydrolysis to the γ-COO^- of Glu_{61} disrupts the active-site machinery. Altogether, the small GTPase families, because they act as thermodynamic switches at so many cellular intersections of signaling and metabolism, are subjected to a diverse set of programmed chemical modifications. The covalent modifications alter localization and control function both in normal maturation and in pathogen interceptions.

3.4. Installation of Swinging-Arm Cofactors

Several enzymes central to primary metabolism are nonfunctional until posttranslation-

© 2005 Wiley-VCH Verlag GmbH & Co. KGaA, Weinheim

ally primed with prosthetic groups that provide key functional groups to enable acyl- and carboxyl-transfer chemistry. The acyl-transfer coenzymes are lipoic acid and phosphopantetheine. The carboxyl-transfer prosthetic group is biotin (Scheme 21). All three cofactors are covalently attached to side chains of target apo proteins by dedicated activating/loading enzymes. Biotin and lipoate can be activated as the acyl AMP species and captured by the ε-NH_2 of lysine side chains presented in folded 100-residue domains of the target proteins to create the biotinylamide and lipoamide linkages. The full reach of the Lys biotin and Lys lipoate chains is about 20 Å, leading to the historical connotation as swinging-arm prosthetic groups that can visit different domains in multienzyme complexes.[77] In analogous logic the phosphopantetheinyl moiety of CoASH as donor substrate can be captured by the β-OH side chain of a specific Ser side chain in a 80–100-residue acyl-carrier protein domain, again to create a tethered prosthetic group on a 20-Å pivot. In this case the chemical bond is not an amide linkage but a phosphodiester.

The tethered biotinyl cofactor is used for the transfer of C_1 groups in the form of CO_2. In carboxylases that fix HCO_3^- into acetyl CoA and propionyl CoA, to yield malonyl and methylmalonyl CoA products, there are multiple subsites or distinct subunits with different chemical functions. In the biotin carboxylase subunit, ATP is used as cosubstrate with HCO_3^- to generate a transient carboxyphosphate mixed anhydride that is captured by the biotinyl-Lys on the N_1 ureido nitrogen atom to produce N_1-carboxybiotinyl-Lys-enzyme (Scheme 22). This form of fixed CO_2 is shuttled to the active site where the C_2 carbanion on the acetyl moiety of acetyl CoA is generated and used to attack the N-carboxybiotinyl tether. This action leads to C–C bond formation as acetyl CoA is carboxylated to malonyl CoA, one of the key building blocks for fatty acid biosynthesis in cells.

The other two tethered coenzymes, lipoamide and pantetheinyl-phosphate, are used to ferry substrate-derived acyl groups between active sites of multidomain enzymatic assembly lines.[77,78] The lipoamide prosthetic group is found in all α-keto acid dehydrogenase complexes that carry out oxidative decarboxylation, for example, of pyruvate at the end of glycolysis and of α-ketoglutarate in the citric acid cycle. For example, in pyruvate dehydrogenation the disulfide form of the lipoamide cofactor is the electron sink for ring-opening capture by the C_2 carbanion of hydroxyethylthiamine-PP (Scheme 23). The transferring two-carbon fragment has been oxidized from the acetaldehyde to the acetate oxidation state and captured as an activated acetyl-*S*-lipoamide thioester as the disulfide link of oxidized lipoamide is reduced. This is the prototypic redox/energy-capture role for the lipoamide prosthetic group. In the second half-reaction, the acetyl-*S*-lipoamide arm moves to a separate active site and docks next to a CoASH molecule, thus allowing acetyl transfer to the thiolate of $CoAS^-$, an isoenergetic transfer that now releases the oxidized acetyl moiety as the diffusible cellular energy currency acetyl CoA.

A third example of cofactor tethering, the pantetheinyl moiety on acyl-carrier protein domains (ACPs), also offers a terminal nucleophilic thiolate for capture of acyl groups. Its central role in primary metabolism is in fatty acid biosynthesis in which acyl chains are built up by two carbon atoms at a time by cycles of Claisen condensation followed by redox tailoring to convert

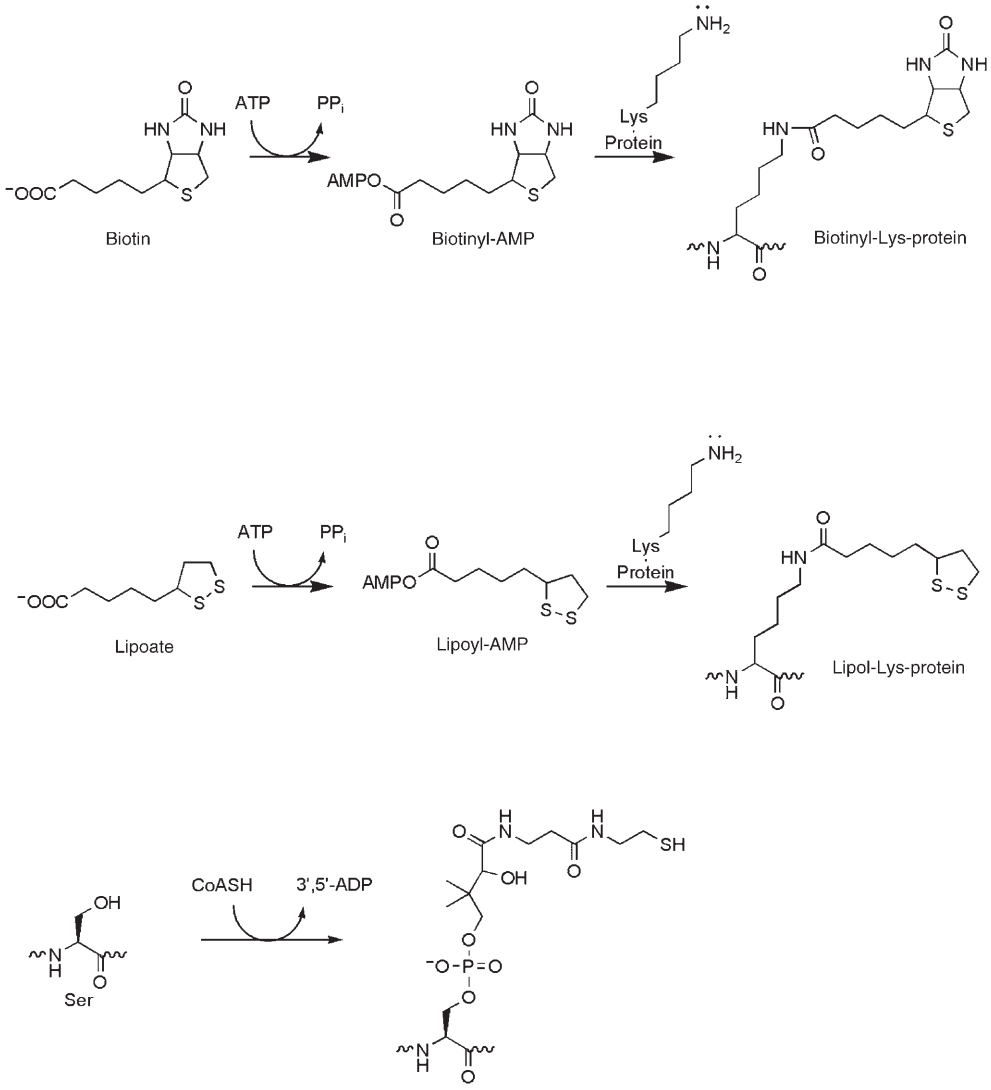

Scheme 21. Coenzymes that are tethered in the active sites of enzymes to act as swinging-arm prosthetic groups, carrying CO_2 or acyl groups between active sites: biotin and the resultant biotinylamide-Lys; lipoate and the resultant lipoamide-Lys; CoASH and the resultant pantetheinyl-OPO_3-Ser linkages.

 © 2005 Wiley-VCH Verlag GmbH & Co. KGaA, Weinheim

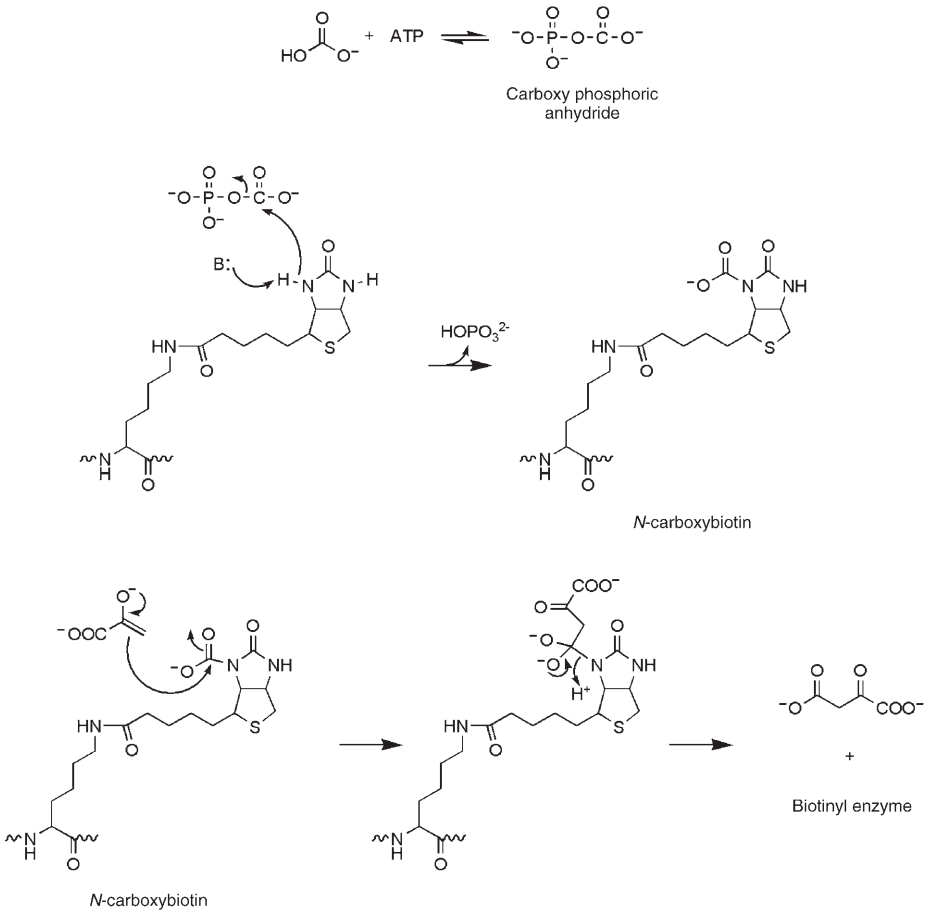

Scheme 22. N-carboxylation of biotinylamide by ATP and HCO_3^- in the biotin carboxylase active site followed by ferrying of the tethered CO_2 to the acetyl CoA carboxylation active site for C–C bond formation as malonyl CoA is produced.

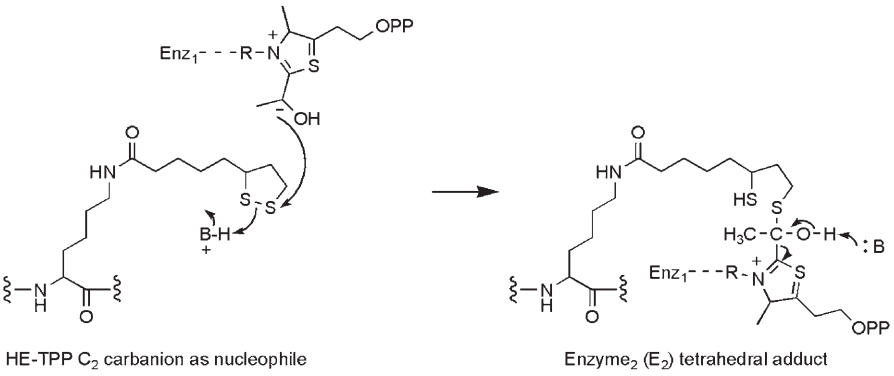

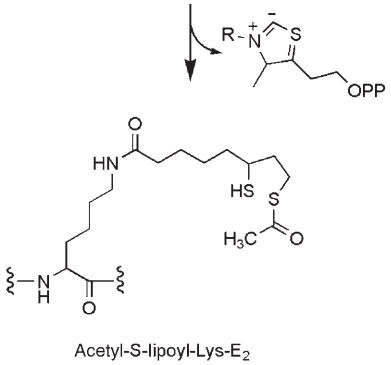

Scheme 23. The oxidized disulfide form of lipoamide is the electron sink for capture by the C_2 carbanion of hydroxyethylthiamine pyrophosphate (HE-TPP), resulting in release of the TPP thiazole carbanion and generation of acetyl-S-lipoamide. The transferring two-carbon-atom fragment has undergone oxidation, the lipoamide disulfide has undergone reduction, and energy has been captured in the acetyl thioester linkage, which is maintained in subsequent transfer of the acetyl moiety to $CoAS^-$.

elongated beta keto acyl-*S*-ACP intermediate into the beta methylene acyl-*S*-ACPs for the next round of C_2-unit elongation (Scheme 24).[78] The acyl groups are proposed to visit ketosynthase, ketoreductase, dehydratase, and enoyl reductase active sites sequentially while tethered to the flexible phosphopantetheinyl arm.

It would appear that Nature has invented the coenzyme covalent tethering strategy in these three cases to fix small-molecule acyl fragments or CO_2 and ferry them to distinct sites on multienzyme complexes and assembly lines. There are other examples in which cofactors are tethered to lysine side chains of proteins, through hydrolyzable imine links between the Lys-NH_2 and an aldehyde carbon atom in the cofactor. This is true for the aldehyde form of vitamin B6, pyridoxal phosphate, in all pyridoxal phosphate dependent enzymes, and in the visual pigment proteins, the rhodopsins, in which vitamin A aldehyde (retinal) is the aldehydic chromophore.

3.5. Posttranslational Carboxylation of Glutamyl Residues for Bidentate Calcium Binding

A family of proteins involved in blood coagulation in mammals undergoes posttranslational modifications at sets of closely spaced glutamate residues during passage through secretory compartments on their way to the extracellular space. These modifications involve fixation of CO_2 to the γ-methylene carbon atoms of Glu residues, thus creating malonyl-type side chains, known as γ-carboxy Glu (Gla). The Gla side chains provide the possibility for bidentate chelation of divalent cations, of which interaction with Ca^{2+} ions is most significant. The proteins that undergo tandem γ-Glu carboxylation include the proenzyme forms of proteases such as prothrombin, proFac-

© 2005 Wiley-VCH Verlag GmbH & Co. KGaA, Weinheim

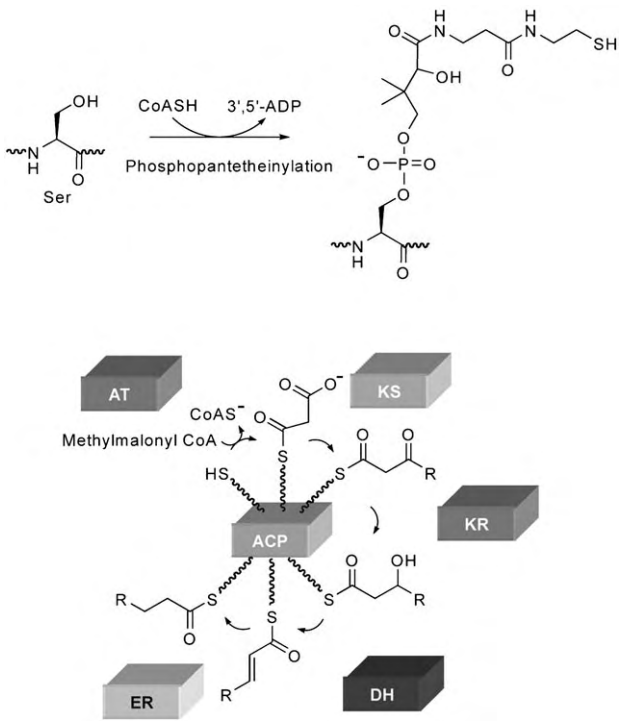

Scheme 24. The terminal thiolate of the phosphopantetheinyl prosthetic group is the nucleophile that captures the starting acyl fragment in fatty acid biosynthesis and serves as the platform on which the acyl chain is elongated by two carbon atoms in each subsequent cycle. The pantetheinyl arm carries the growing acyl chain between the active sites of ketosynthase, ketoreductase, dehydratase, and enoyl reductase in each cycle, converting the β-ketone into the four-electron-reduced β-methylene oxidation state.

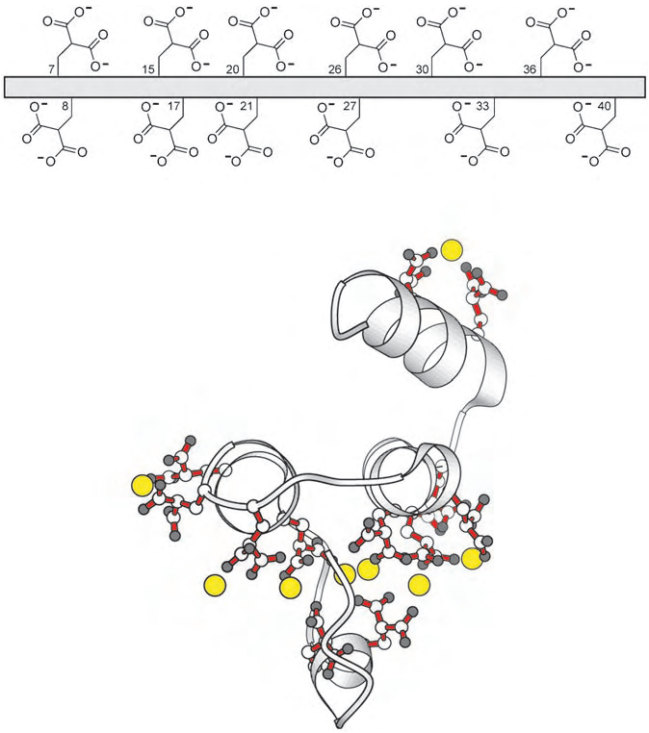

Figure 11. Twelve closely spaced Glu residues in the carboxylation domain of the pro form of the coagulation protease factor IX are modified to γ-carboxy-Glu (Gla) residues and provide a high local concentration of bidentate malonyl side chains for Ca^{2+} coordination. The 3D fold of dodecaGla region complexed to eight calcium ions (yellow spheres) emphasizes the divalent metal-ion-dependent structuring of this region of the protein.

tor IX, and proFactor X.[79] The carboxylation of 10–12 glutamate side chains to γ-carboxy-Glu residues in a 40-residue stretch of the proenzyme forms of proteases creates a local high density of bidentate chelators for Ca^{2+} ions (Figure 11). The conformations of the Gla domains are altered in the presence of Ca^{2+} and drive the association of the proteases on platelet surfaces, leading to the formation of protein complexes and the activation of neighboring proteases to initiate and propagate blood coagulation cascades.[79]

Unlike the carboxylation reactions discussed in Section 3.4, which use tethered biotin as the CO_2 carrier between the active sites of the enzymes, the Gla-forming carboxylations of glutamyl residue side chains do not use biotinyl amide dependent enzymes. Instead, the naphthoquinone vitamin K, in its only well-defined role in mammalian metabolism, is the requisite cofactor for CO_2 fixation in the Gla modifications. In fact it is the dihydro-naphthoquinol form of vitamin K, that is the active form for the vitamin K dependent protein carboxylase. O_2 is also a required cosubstrate and the mechanism of the carboxylase (Scheme 25) is proposed to involve formation of the K-OOH peroxy adduct. Cyclization of this quinone hydroperoxide to the alkoxide anion of the 2,3-epoxide of vitamin K generates the strong base required to abstract a proton from the glutamyl-γ CH_2 side chains. The carbanion generated is required to attack CO_2 and form the new C–C bond of the malonyl side chains of Gla residues in the product.

4. Cataloguing the Posttranslational Modification

Consideration of major and minor categories of posttranslational modifications above leads to at least hundreds of thousands, perhaps millions, of possible molecular variants of proteins in eukaryotic cells. The analytical problem is immense, and the challenge to integrate across the subproteomes and decipher connections for a systems biology perspective even greater. Much of the contemporary effort in PTM research involves the development of methodologies to evaluate such inventories. Mass-spectrometric approaches are dominant owing to issues such as femtomolar sensitivity of detection and simultaneous identification of many peptide fragments bearing a particular type of chemical modification.[80] Notable recent studies include the detection of hundreds of pS and pT peptides from the phosphoproteome of yeast[81] and the isolation of His-tagged ubiquitylated proteins of yeast. The latter method allows the identification of more than 100 ubiquitylated proteins that contain polyubiquityl chains connected through different Lys residues in the ubiquitin monomers.[82]

At any moment in time, sampling of the proteome in a given organism or cell provides only a snapshot of a highly dynamic process, confounding the analytical problem and ultimately arguing for time-resolved inventories. Heterogeneity can arise in several ways. Because posttranslational modification enzymes do not work off templates, the mod-

 © 2005 Wiley-VCH Verlag GmbH & Co. KGaA, Weinheim

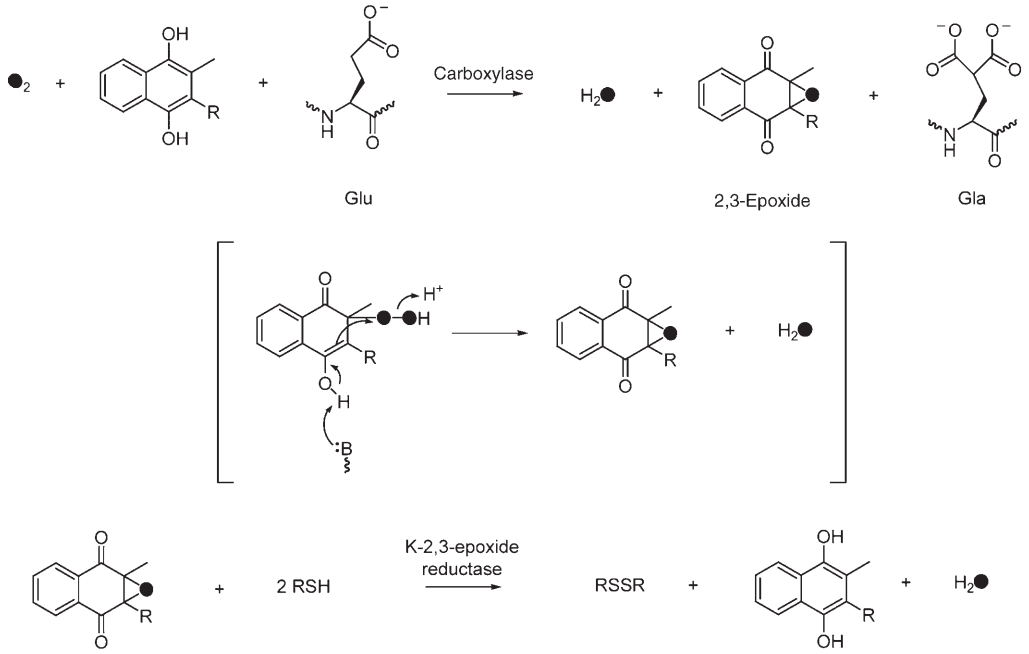

Scheme 25. Proposed mechanism for the function of the dihydro form of vitamin K (KH_2) as cosubstrate in the Glu to Gla posttranslational protein carboxylations. KH_2 reacts with cosubstrate O_2 to produce a hydroperoxy vitamin K intermediate, which can proceed to the 2,3-epoxy-vitamin K alkoxide. The alkoxide is argued to be a strong enough base to abstract one of the Glu γ-CH_2 hydrogen atoms as a proton, transiently generating the γ-carbanion required to attack CO_2 to produce the new C–C bond in the Gla product residue.

ifications are stochastic and likely to be incomplete across a target protein population. The fractional efficiency of modification of a site, for example, N-glycosylation of a particular Asn residue in an Asn-X-Ser sequence favorable for modification, may depend on the amount of time the protein region bearing that Asn is unfolded during passage across the ER membrane. The accessibility of the carboxamido nitrogen atom may be fleeting. The concentration of oligosaccharyl-N-transferase in the microenvironment may be limiting such that the dwell time of protein substrate and enzyme catalyst is too short to ensure complete modification at 100% of that site in the protein population. In the multistep maturation of N-glycan $Man_3(GlcNAc)_2$ core in glycoproteins there are up to a dozen such substrate–catalyst encounters. A 90% yield at each step would produce the kind of complex and heterogeneous glycoprotein mixtures that are often detected. As noted earlier, the prion protein has been shown to exist in some 52 glycoforms.[45]

5. Multiple and Tandem Posttranslational Modification of Proteins

Posttranslational modifications often occur at multiple sites or in tandem cascades that are crucial for function. Thus, the Abl tyrosine kinase is found phosphorylated at 11 different sites, (nine tyrosines, one serine, one threonine) spread over the different catalytic and regulatory domains of the protein[83] (see Figure 2). In principle, $11! = 40\,420\,800$ distinct phosphorylated isoforms are possible just for this one protein alone. Fractional occupancy is likely at the distinct sites, making for a large nested array of different phospho forms of this one protein.

Multiple lysine acetylations and methylations, one serine phosphorylation, and one N-terminal ubiquitylation are typical for the tails of the histone octamers in nucleosomes so that modifications at 28 sites are possible as described in Sections 2.2 and 2.3. (Surely not all of the 28! possibilities will have been explored in Nature.) Kelleher and co-workers[84] recently devised bioinformatic methods coupled with high-resolution mass spectrometry to predict, search for, and identify particular histone variants. For example, they detected one particular hexamodifed form of the N-terminus of histone H3 with an [M+238] mass signature (Figure 12) to address such a functional covalent diversity of protein isoforms. (This is the equivalent of finding one needle in a haystack. The systems approach to PTMs would be to assess how many such needles altogether are in the "haystack" of proteins.) The multiple modifications of histone tails are

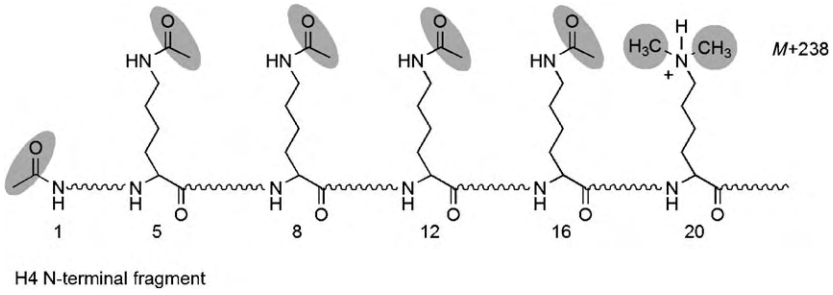

Figure 12. Tandem enzymatic posttranslational tailoring of the N-terminal tail of histone H4 generates a heptamodified protein in which the N-terminal residue is acetylated, $lysines_{5,8,12,16}$ are acetylated, and $lysine_{20}$ is N,N-dimethylated.

 © 2005 Wiley-VCH Verlag GmbH & Co. KGaA, Weinheim

presumed to be written and read by enzymatic machinery in specific temporal patterns for selective recruitment of transcriptional repressors and activator complexes.

Tandem posttranslational modifications are known in many other proteins and comprise the multilayered informational content driving the molecular logic of posttranslational modifications. The consecutive four-step modification of the C-termini of Ras proteins—1) S-prenylation, 2) S-palmitoylation of neighboring cysteine residues, 3) specific endoproteolytic cleavage to reveal one of the cysteines as the new C-terminus, and 4) methylation of that new C-terminal carboxylate—comprise the integrated maturation process that moves modified Ras to membranes to dock with its upstream protein kinase partners (Scheme 26).[35] We have noted above in Section 3.3 that the related RhoA family of GTPases can undergo ADP-ribosylation, O-glucosylation, and deamidation of the active-site Gln. Adding in this sequence of prenylation, proteolysis, and C-terminal carboxymethylation for Rho brings the total to seven specific steps of posttranslational modification. The mature RhoA can also be cleaved by the YopT protease from *Yersinia pestis* as that pathogen executes part of its virulence program.[85]

The threshold nature of tandem posttranslational modifications to provoke a biological signal is illustrated clearly in the successive addition of a minimum of four ubiquitin 8-kDa tags to a target protein to set off the cascade of events leading to proteolysis. A polyubiquitin moiety of length at least four ubiquitin units appears to be the threshold for recognition by protein chaperones to send the tagged proteins to proteasomes.[27]

Finally, there is good evidence for competition between posttranslational modifications, with opposing functional consequences for the target proteins. Two such examples involving competition between ubiquitylation and acetylation are 1) SMAD7 protein in TGFβ signal transduction pathway[86] and 2) five lysine side chains near the C-terminus of the transcription factor p53. The Lys ε-NH_2 residues can be acetylated or ubiquitylated (Scheme 27) and then extended to polyubiquitin chains, leading to proteolytic removal of p53 or SMADs. The acetylations block ubiquitylations and consequently lengthen the lifetime of the proteins in cells.[13]

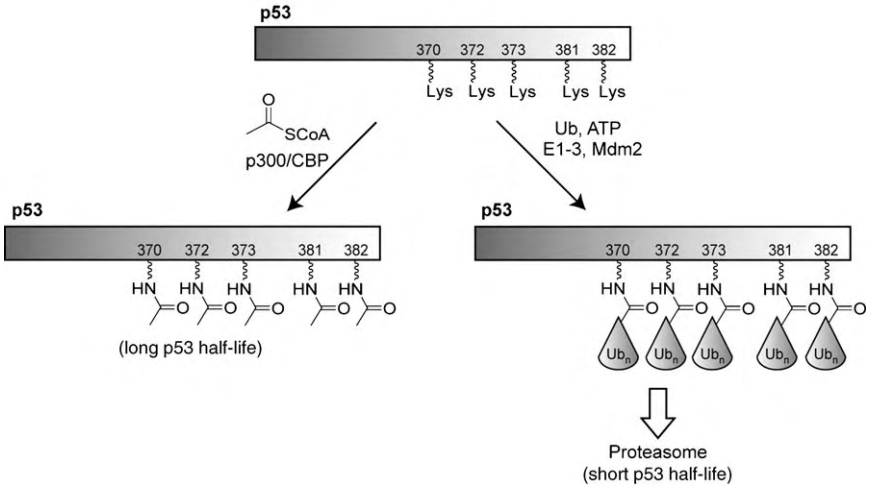

Scheme 27. Competition between acetylation and ubiquitylation at the ε-NH of $Lys_{370,372,373,381,382}$ near the C terminus of the transcription factor p53.

6. Reversible versus Irreversible Posttranslational Modification

Depending on the biological purpose of a particular covalent modification of a protein, reversibility may or may not be an important parameter to control. The prototype of reversible modification is protein phosphorylation, consistent with its evolution to the dominant role in protein-based signaling in eukaryotes. Of the five major categories of PTMs noted in Section 2 (phosphorylation, acylation, glycosylation, thiol-disulfide chemistry, and alkylation), all but alkylation have dedicated enzymes, often large enzyme families, that catalyze the removal of the covalent modifications. The enzymes that reverse phosphorylation, acylation, and glycosylation are, by and large, specific hydrolases, whereas disulfide bonds are cleaved by reductases. We note below that an oxidative enzymatic route has now been discovered for alkylation that involves removal of N-methyl substituents from the histone tails.

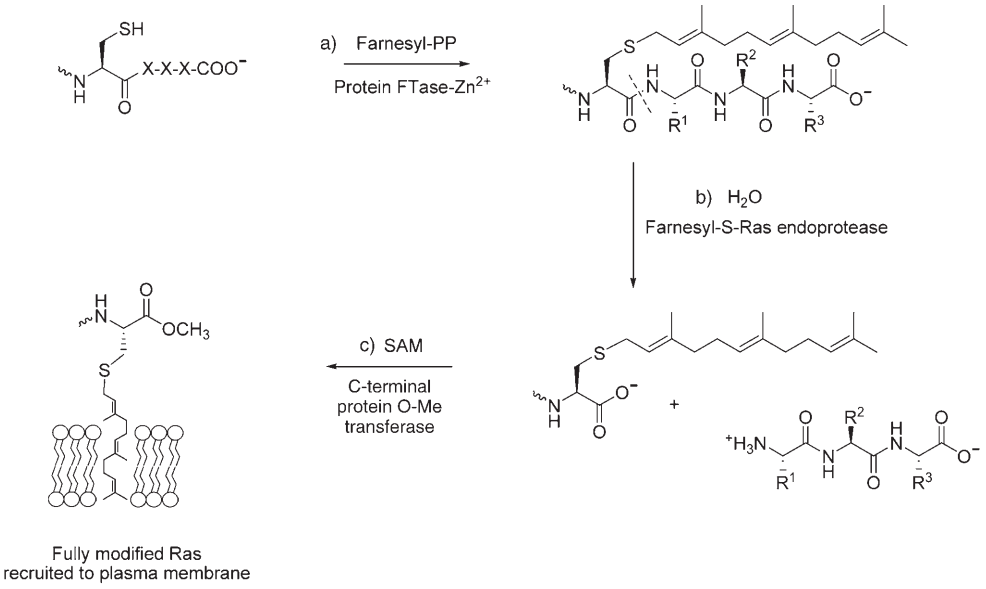

Scheme 26. Multistep modification of the Ras GTPase involves a) S-prenylation, b) endoproteolysis, and c) C-terminal O-methylation.

 © 2005 Wiley-VCH Verlag GmbH & Co. KGaA, Weinheim

Protein kinases usually occur as low-activity "off" forms in basal states in the absence of a specific stimulus. When a signal is propagated and the kinases activated, often involving covalent autophosphorylation of Thr residues to pT or TXY sequons to doubly phosphorylated pTXpY loci in MAP kinases, the activated protein kinases modify their partner target proteins with much higher catalytic efficiency.[8] The cyclic AMP activated protein kinase A, for example, phosphorylates over 100 proteins[87] on Ser and Thr residues to propagate signals.

To control the duration and intensity of phosphoprotein signaling, the signals need to be turned off. Termination is accomplished by hydrolytic removal of the PO_3^{2-} group by phosphoprotein phosphatases (Scheme 28a). There are about 150 protein phosphatases encoded in the human genome, including pS-, pT-selective phosphatases, pY phosphatases, and dual-specificity (pS and pY) phosphatases.[88] Of these, 107 are pY protein phosphatases.[89] The much smaller number of pS/pT phosphatases is balanced by the presence of many regulatory subunits that control subcellular location and substrate recognition for the pS/pT hydrolytic enzymes.

One practical consequence of PTM enzyme-mediated reversibility is that the phosphoproteome content in any cell at any given time represents the balance of activity of the 500 protein kinases/150 protein phosphatases towards their diverse protein substrates, allowing an almost infinite number of set points to a cell and true complexity for phosphoproteomicists.[90,91]

Protein acetylation, protein ubiquitylation, and protein-S-palmitoylation are three other classes of covalent modifications that are readily reversed (Scheme 28b), and so qualify for regulation and signaling roles. Histone acetyltransferases (HATs) are opposed functionally by a family of histone deacetylases (HDACs).[92,93] Some HDACs are catalytic domains embedded in multimodular proteins dynamically recruited to acetylated and methylated lysine tails of histones. A separate family of NAD-cleaving histone deacetylases, the sirtuins, are involved in gene silencing functions and couple energy metabolism with transcriptional regulation.[94,95]

Histone Lys-N-methylation, unlike Lys-acetylation, is not susceptible to enzymatic or non-enzymatic hydrolytic reversal because there is no obvious path for hydrolytic cleavage of the N-alkyl bonds. Thus, in terms of writing and rewriting the histone code, it has been assumed that acetylation can be readily erased, but not methylation. However, the recent discovery of FAD-dependent methyl-Lys deaminases provides an oxidative route for counteracting the action of histone methyltransferases.[96] Oxidative enzymatic conversion of an N-methyl-Lys into the $CH_2{=}NH$-Lys product linkage (Scheme 29) now creates a product imine labile to hydrolysis to yield the unmodified H_2N-Lys residue and 1 equivalent of formaldehyde.

The dozens/hundreds of protein ubiquitin ligases create ubiquityl-ε-NH-Lys-protein isopeptide bonds in tagged proteins. These linkages are resistant to normal proteases but the isopeptide bonds are cleaved by a family of several dozen deubiquitylases (DUBs),[97,98] presumably selective for subsets of ubiquitylated proteins at different parts of the cell at different times and rescuing those from proteasome destruction.

Palmitoylated cysteine residues involve covalent thioester linkages. They can hydrolyze non-enzymatically, but this can be slow in membranes and there are specific palmitoyl

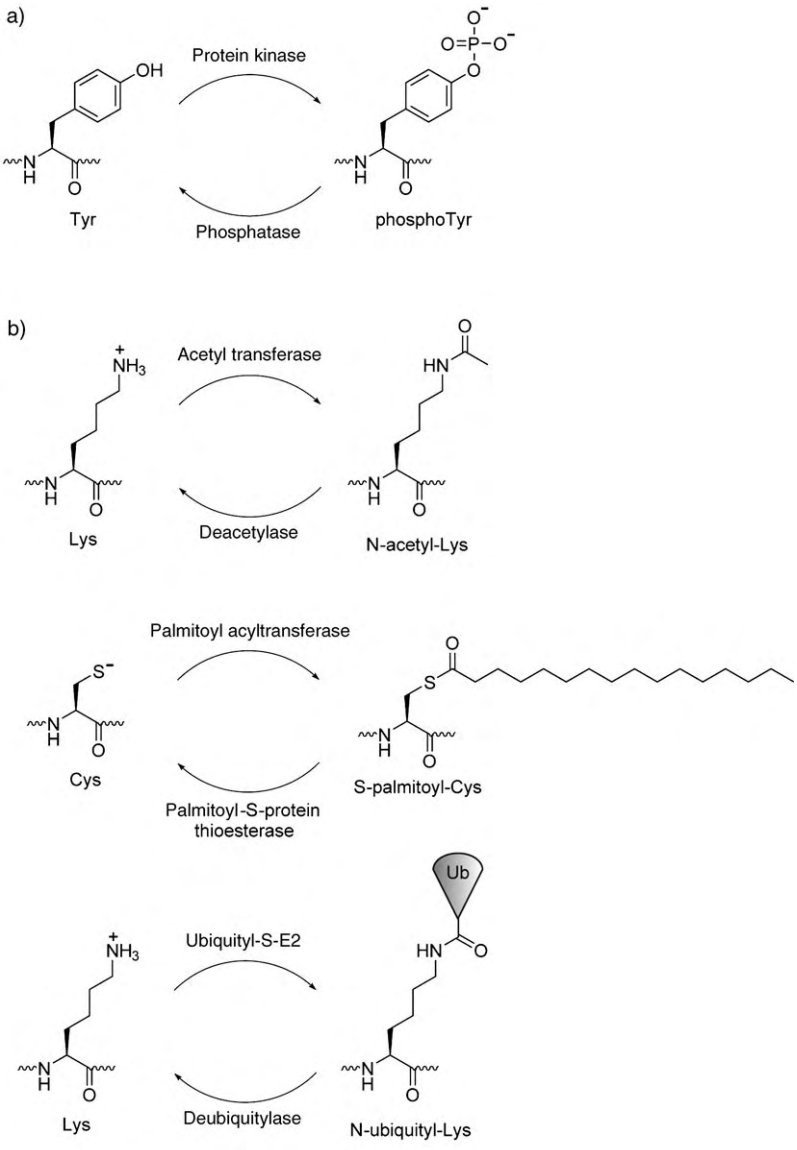

Scheme 28. Reversibility of covalent modifications in proteins; a) Phosphoprotein phosphatases oppose the effects of protein kinases; b) protein acetylations, S-palmitoylations, and ubiquitylations are reversed by deacetylases, palmitoyl-S-protein thioesterases, and deubiquitylases.

 © 2005 Wiley-VCH Verlag GmbH & Co. KGaA, Weinheim

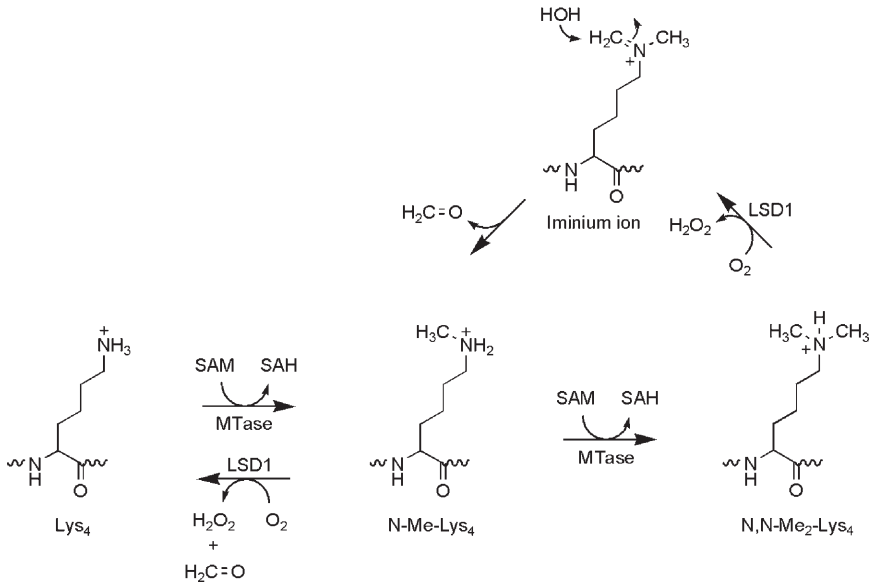

Scheme 29. Reversal of lysine ε-N-methylation occurs by oxidation (not hydrolysis) by action of a flavoprotein to generate the hydrolytically labile imine product.

protein thioesterases[11] to control lifetime and consequent localization of the protein at membrane interfaces.

In contrast to the above reversible categories of post-translational modifications are sets that are functionally irreversible. Cys-S-prenylations are thioether linkages, and in contrast to the Cys-S-palmitoyl thioester linkages are not hydrolytically reversible. (Again, oxidative routes are known but probably occur during prenylated protein degradation in lysosomes.) Thus the enzymatic strategy for attaching the two common lipid anchors for proteins, palmitoylation or prenylation, provides reversible or irreversible modification of proteins targeted to membranes. The C-carboxylation of Glu residues to Gla residues is irreversible as is side-chain hydroxylation, for example, of Pro and Asn residues on HIF-1α in oxygen sensing.

The quintessentially irreversible posttranslational modification is the second major category of covalent change to proteins: the proteolytic cleavage of peptide bonds.

7. Controlled Proteolysis

The life cycle of every protein in intracellular and extracellular compartments in an organism is controlled by homeostatic functioning of proteases, which cleave the covalent peptide backbones to release the constituent amino acids back into the monomer pool. Large subsets of proteins within eukaryotic cells may undergo consecutive limited proteolytic clipping as part of the normal temporal and spatial maturation process. These controlled proteolytic cuts at specific peptide sequences within a given set of protein substrates are effected by proteases that do not degrade but rather are involved in protein-substrate maturation and tailoring processes.

Essentially every protein that enters the endoplasmic reticulum in eukaryotic cells undergoes cleavage of the N-terminal 25–30 amino acids, the signal sequence that specified transit into the ER, by signal peptidases.[99] This first step in protein maturation can be followed by action of proprotein convertases later in the Golgi and *trans* Golgi network[100,101] of the secretory compartment. A prototypical example is the cleavage of proinsulin to insulin, whose two chains are connected by disulfide bonds. The hormone cholecystokinin undergoes six–eight cleavages and trimming proteolytic maturations to convert the 115 residue initial translational product into the eight-residue sulfated mature hormone.[102]

The maturation of the O-glycoprotein Notch by limited proteolysis occurs in four spatially and temporally distinct steps (Scheme 30): 1) signal peptide cleavage in the ER; 2) cleavage by proprotein convertases into two subunits that remain associated in the *trans* Golgi network on the way to the cell surface; 3) removal of the extracellular domain at the plasma membrane by action of sheddase-type proteolytic activity, triggered upon engagement of protein ligands; 4) regulated intramembrane proteolysis (RIP) of the truncated Notch as the fourth maturation event.[99,103,104] The cytoplasmic stub of Notch, now with only a few remaining

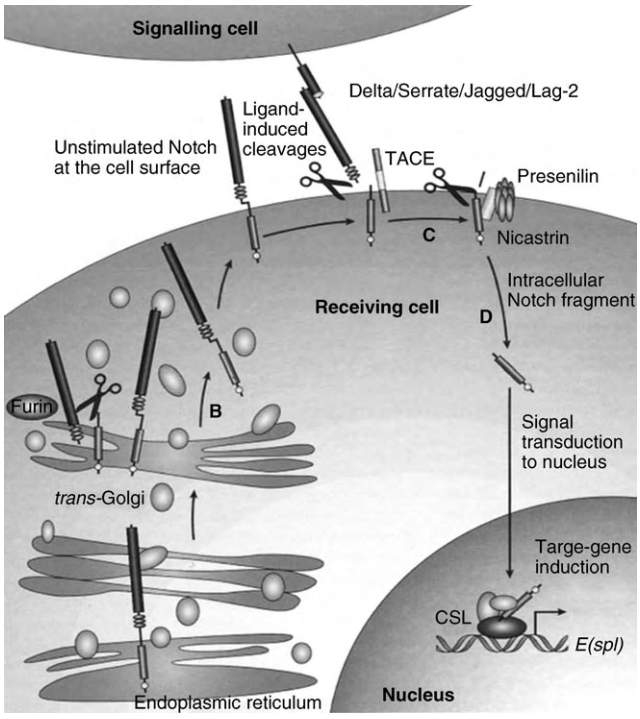

Scheme 30. Maturation of the Notch protein by four sequential proteolytic cleavages at specific sites and specific places in a eukaryotic cell: a) Cleavage of the N-terminal signal peptide upon secretion into the endoplasmic reticulum (not shown in figure); b) hydrolytic clip by proprotein convertases during passage through the *trans* Golgi network; c) hydrolytic clip by a protein sheddase at the cell surface; d) regulated intermembrane proteolysis releases the cytoplasmic stub of Notch to go to the nucleus and act as transcription factor. Reproduced with permission from reference [121].

 © 2005 Wiley-VCH Verlag GmbH & Co. KGaA, Weinheim

amino acids in the vesicle membranes, can then partition back to the cytoplasm, enter the nucleus, associate with partner proteins, and act as a selective transcriptional activator. The sequence of four limited proteolytic steps, separated in time and space, control the location and activity of Notch. It can be directed through the ER and the Golgi complex to the cell surface, function as a cell surface receptor, and then be liberated back into the cytoplasm as a transcriptionally activating fragment that can target the nucleus. Doubtless there are many other examples of multistep action of proteases to direct the location and function of client proteins and control their lifetimes in cells.

A variant of controlled proteolysis occurs when a short C-terminal peptide is excised from protein substrates by protease-like catalysts that generate transient covalent proteinyl-S-Cys-enzyme intermediates (Scheme 31). In the coupling of GPI lipid anchors to eukaryotic proteins, the transferring protein acyl group is specifically captured by an ethanolamine group in the cosubstrate GPI anchor,[105] a net switching of the C-terminal peptide of the initial translation product by the GPI anchor. In the action of bacterial sortases,[106] the incoming amine nucleophile that captures the staphylococcal proteins to be displayed as antigens at the bacterial cell surface is a Gly or Ala-NH_2 terminus from cross-bridges in the peptidoglycan layer of the cell walls. Both of these C-terminal modifications are net transamidations, in which the incoming nucleophile is an amine to give an aminolytic product rather than water in hydrolysis.

8. Autocleavage and Peptide-Bond Rearrangement

There is a set of autocatalytic processes that leads folded proteins to catalyze rearrangements of the backbone connectivity at one or more specific peptide bonds in the folded proteins. Most often these rearrangements lead to cleavage of

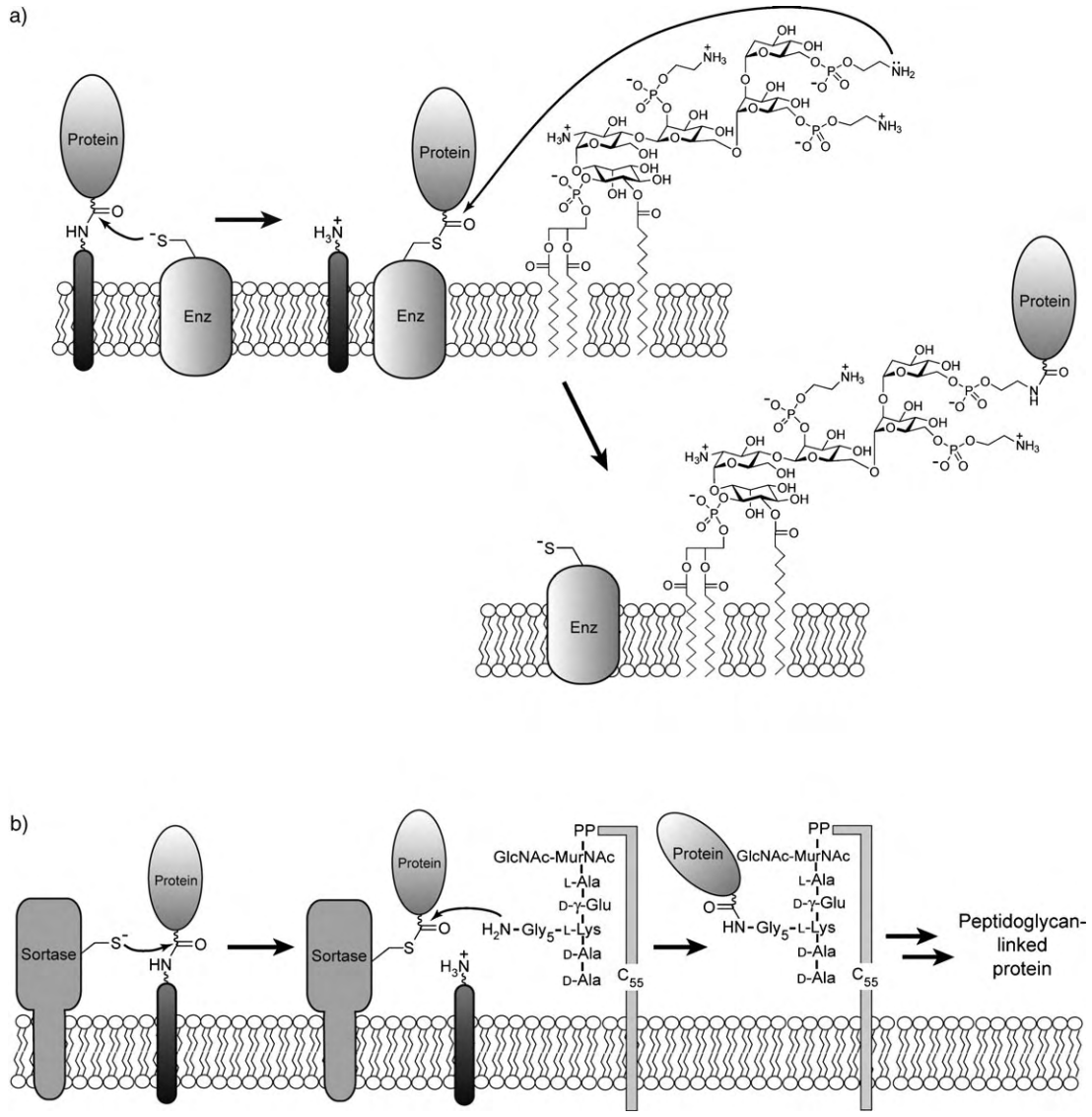

Scheme 31. Protease-like catalysts use active-site Cys nucleophiles to transfer protein-substrate-derived acyl fragments to nonprotein amine acceptors via acyl-S-Cys enzyme intermediates: a) GPI anchor attachment through enzymatic transamidation; b) cross-linking and display of proteins to the peptidoglycan cross-bridges in *Staphylococcus aureus* cell wall assembly by transamidation by the enzyme sortase.

© 2005 Wiley-VCH Verlag GmbH & Co. KGaA, Weinheim

those specific peptide bonds. The fate of the acyl fragment of the autocleaving peptide can vary depending on the capturing nucleophile. Water as cosubstrate results in hydrolysis. An alcohol as cosubstrate generates an ester product, as in the capture of the N-terminal fragment of Hedgehog protein by cholesterol. Capture by an amine, when the amine is downstream in the same protein, is the essence of protein splicing, although the amine capture is indirect as we shall note. A common type of intermediate is observed for all three such capture processes.

A second major variant of autocatalytic peptide backbone rearrangements occurs in two contexts (Section 9). One is the autoconversion of a tripeptide moiety into the highly conjugated aromatic fluorophore of the green fluorescent proteins and its relatives. The second is a related rearrangement of a tripeptide in the active site of the pro forms of phenylalanine and histidine deaminases to create the imidazolone cofactors that serve as essential electron sinks in deaminase catalysis.

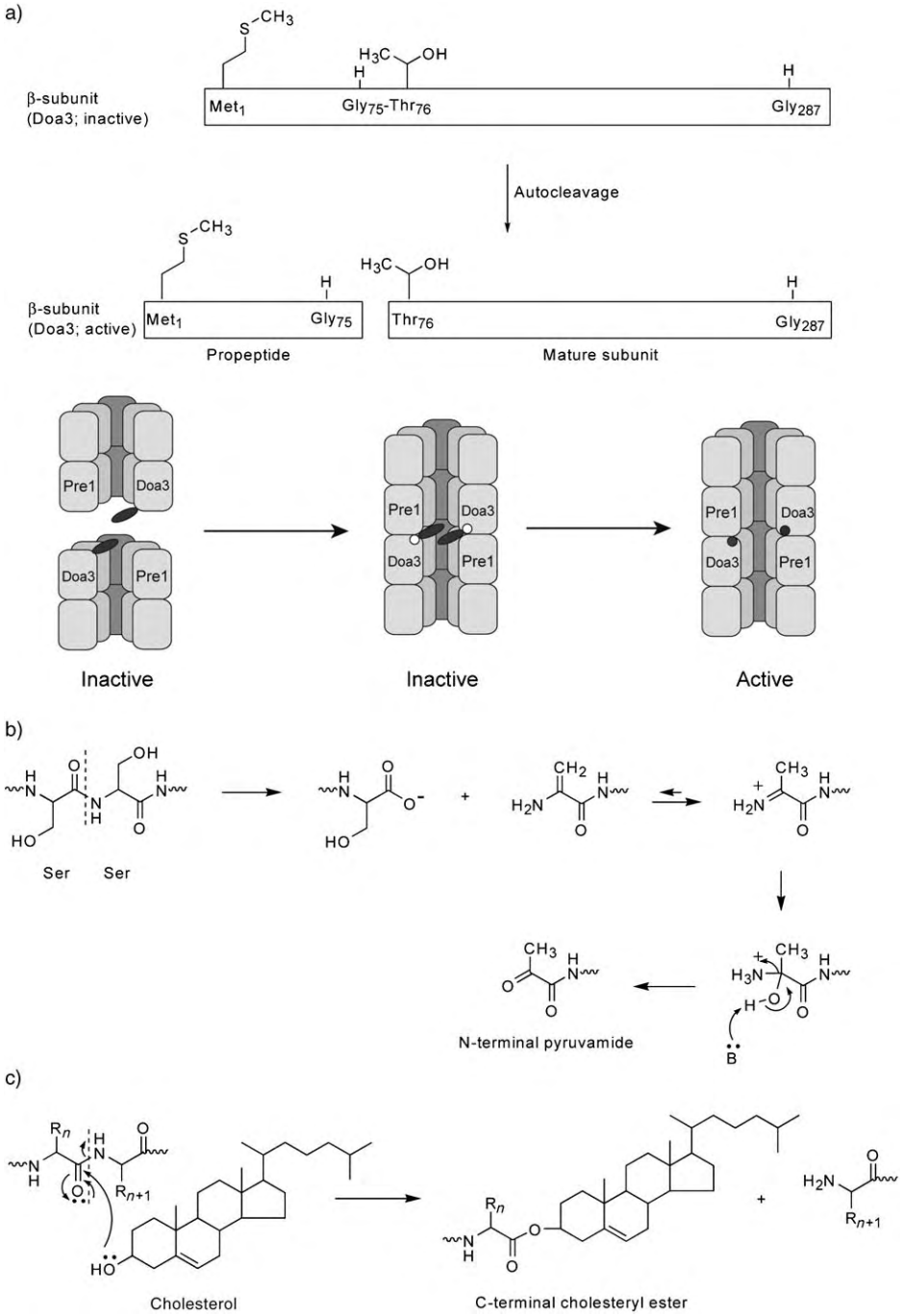

Scheme 32. Autoproteolysis at specific peptide linkages to create the active forms of enzymes in the fragmented protein products; a) autocleavage of the precursor forms of the β subunits of proteasomes to liberate the catalytic Thr nucleophile; b) autocleavage of the precursor form of aspartate decarboxylase generates the N-terminal pyruvamide electron sink; c) autocleavage of the Hedgehog precursor and capture by the 3-OH of cholesterol generates the active N-terminal fragment as a membrane-tethered cholesterol ester.

8.1. Autocleavage of Specific Peptide Bonds in Proteins During Precursor Activation

A relatively small subset of folded proteins have the capacity to convert themselves from a single-chain inactive precursor form into an active two-chain form by hydrolysis of a specific peptide bond in the precursor (Scheme 32). Three examples of variants of autoproteolytic activation are: 1) cleavage of the precursor single chain forms of the β-subunits of proteasomes; 2) cleavage and uncovering of an N-terminal pyruvamide group in aspartate α-decarboxylase; 3) cleavage and activation of Hedgehog family proteins resulting in alcoholysis of the peptide bond by cholesterol. All three enzymes use the side chain of a Ser, Thr, or Cys residue to attack the immediately adjacent upstream peptide carbonyl to generate a five-membered tetrahedral adduct (Scheme 33). If that adduct is protonated on nitrogen and reopens with cleavage of the C–N bond, then the peptide bond has been cleaved. The two parts of the protein chain are still held together, by an O-ester (Ser, Thr) or an S-thioester (Cys) linkage. This is the common thread of all three examples. The O-ester or S-thioester linkage is now labile to capture by even relatively weak nucleophiles such as water,

 © 2005 Wiley-VCH Verlag GmbH & Co. KGaA, Weinheim

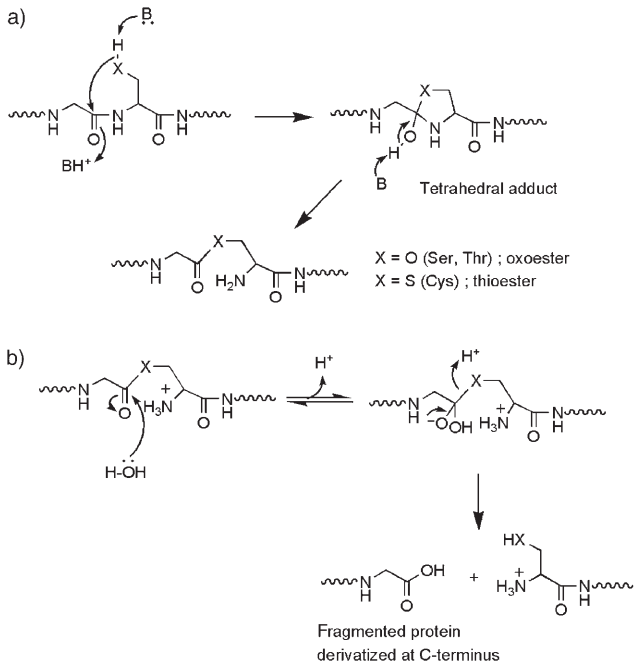

Scheme 33. Peptide-bond autocleavage mechanism proceeds via a) a tetrahedral cyclic adduct arising from attack of a nucleophilic side chain on the immediate upstream peptide bond; resolution of the adduct proceeds through C–N bond cleavage, breaking the original peptide bond and generating an oxo/thioester connectivity; b) the ester can be captured by a range of nucleophiles, including water.

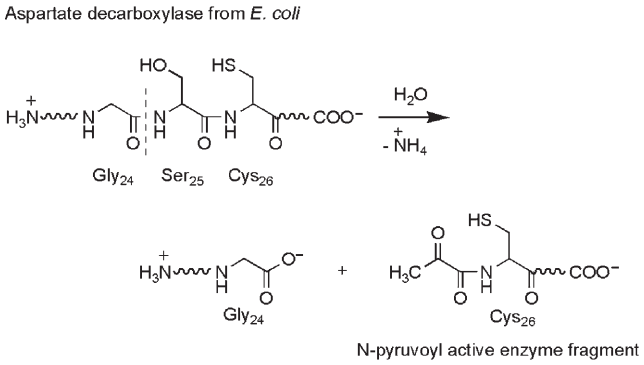

Scheme 34. Peptide autocleavage at an X-Ser linkage can be followed by elimination of the Ser-β-OH and tautomerization to an N-terminal pyruvamide group. This is an electron sink that can engage in imine formation with amino acid substrates to facilitate kinetically accessible substrate carbanions, in this case for net decarboxylation of Asp.

the alcohol group of cholesterol, or downstream Ser and Cys side chains.

The proteasome is organized in an $\alpha_7\beta_7\beta_7\alpha_7$ four-layered cylinder.[107] In yeast, three of the seven β subunits in each heptad ring are active, arising by autocleavage of the precursor β chains at Gly_{75}–Thr_{76}, releasing the Thr as the new N-terminus of the cleaved β subunit.[108–110] Cleavage occurs when the side chain of Thr_{76} attacks the adjacent peptide carbonyl to intiate cleavage. The liberated amino group of this new Thr_1 is the nucleophile in catalysis as protein substrates are cleaved, explaining why the precursor is inactive.[111] The proteasomal β subunit is one of several proenzymes that autocleave and liberate the N-terminal nucleophile as the catalytic residue.[109]

A related class of precursor forms of enzymes uses the side chain CH_2OH of a specific serine residue to initiate cleavage in the folded precursor on the adjacent upstream peptide carbonyl. As noted above, the tetrahedral adduct decomposes to an O-ester, cleaving the original C–N linkage of the peptide bond. Elimination of the RO group from this ester yields an N-terminal dehydroalanyl residue at the downstream chain of the two-chain product (Scheme 34).[109] The N-terminal dehydroalanyl moiety hydrates and ketonizes to accumulate as a pyruvamide group at the N terminus of the active enzyme. This directed autoproteolytic process has uncovered a ketone moiety, an N-terminal electrophile rather than the N-terminal nucleophile above, which acts as an active-site electron sink for the substrate aspartate. Decarboxylation of the aspartyl imino enzyme followed by hydrolysis of the bound product imine yields β-alanine, a required intermediate in CoASH biosynthesis.[112]

The third variant of precursor protein autoproteolysis is represented by the maturation of the protein Hedgehog that signals at plasma membranes of eukaryotic cells after two-dimensional diffusion in the plane of the membrane. The protein is tethered to the membrane by a C-terminal covalent lipid anchor, in this case by esterification of a cholesterol moiety with the C-terminal carboxylate.[113] This arises from the autocleavage intermediate common to the above two cases in which rearrangement of a peptide bond in the precursor to an oxoester occurs by an identical mechanism. Now, rather than capture of the acyl fragment of the precursor protein by water for net hydrolysis, there is a specific binding site for cholesterol. Its 3′-OH is the kinetically competent nucleophile, yielding the peptidyl cholesterol ester as the cholesterolysis product that is biologically active (see Scheme 32).

These three variations of folded protein-precursor autocleavage in Scheme 32 yield either a) two normal peptide fragments, b) a downstream fragment with an N-terminal pyruvamide, or c) an upstream fragment with a C-terminal cholesterol ester. This shows the versatility of this autocatalyzed peptide bond route by selective control of the fate of the common rearranged ester intermediate. In all three cases the peptide bond fragmentations are irreversible.

8.2. Autocleavage and Religation: Protein Splicing

In the final variant of autocleavage of protein precursors the ester intermediate (or thioester intermediate when a Cys thiolate attacks the adjacent upstream peptide bond) is captured by an intramolecular nucleophile rather than an external one such as HOH or ROH. The internal nucleophile is a side chain Ser, Thr, or Cys in a folded downstream domain of the precursor protein. This is the essence of protein splicing, autocleavage, and peptide-bond religation, practiced by over a hundred bacterial and yeast proteins,[109,114] including DNA polymerases and ATPases. The first peptide bond is

 © 2005 Wiley-VCH Verlag GmbH & Co. KGaA, Weinheim

cleaved at the junction of upstream extein and intein. The internal nucleophile capturing the extein 1-intein-O-ester intermediate is at the boundary of the same intein and extein 2 (Scheme 35). The new intermediate has a lariat structure. Excision of the intein is completed with participation of an Asn side chain at the downstream boundary of the intein. This yields a second ester (thioester) intermediate as the lariat is resolved. Re-formation of the peptide bond joining extein 1–extein 2 is driven by thermodynamically favored acyl-O or acyl-S to N shifts and completes an in-frame ligation.

This is ancient protein biochemistry in an evolutionary sense (found in archaeal proteins) and may be the harbinger of the other autocleavage reactions noted in the above section. The net reversibility of such peptide-bond cleavage is the remarkable outcome and is controlled by structural features in the folded intermediates to keep water from being a competent, interfering nucleophile to the intramolecular acyl transfers within the self-splicing proteins. To the extent that this is ancient protein chemistry, it emphasizes that acyl oxoester and acyl thioester intermediates were primordial species in protein reactions; they are still intermediates in many posttranslational reactions in contemporary protein maturations. Furthermore, protein splicing has many practical applications in modifications of recombinant proteins with synthetic peptides by protein ligation.[109,115]

9. Peptide Bond Rearrangement without Autocleavage

9.1. Fluorophore Formation in Green Fluorescent Protein

An additional spectacular class of autocatalyzed PTM rearrangement of the peptide backbone in folded proteins is the maturation of chromoproteins of the green fluorescent protein (GFP) and red fluorescent protein families (Scheme 36a).[116] The precursor protein folds into a β cyclinder structure and the native conformation is required for the subsequent chromophore generation. A tripepetide loop of $Ser_{65}Tyr_{66}Gly_{67}$ in the folded colorless GFP precursor is sterically compressed, populating a conformer that allows attack of the Gly_{67} amide N-H on the adjacent peptide carbonyl to generate a five-membered tetrahedral adduct reminiscent of the initial steps in the rearrangements described in Section 8. This adduct is dehydrated, and the resultant stable cyclic species is slowly autoxidized to create a double bond in conjugation with the phenol ring of Tyr_{66}. This oxidative last step generates the chromophore with absorption maximum at 506 nm and the green fluorescence useful to the producing coelenterate for energy-harvesting functions. A variant with QYG in the starting tripeptide is found in related coelenterates and yields the DsRed fluorophore after rearrangement and oxidative maturation (Scheme 36b).[117] Fluo-

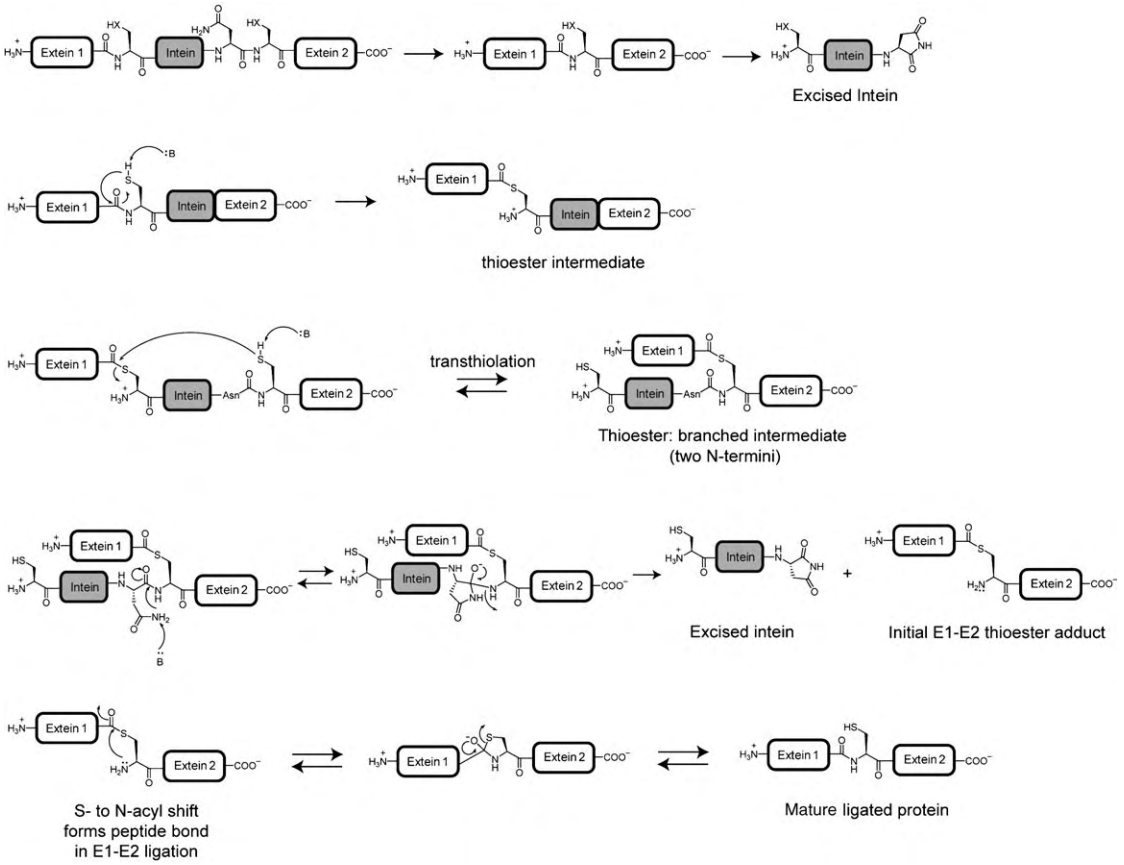

Scheme 35. Autocleavage, intein excision, and peptide religation during protein splicing: thioester formation during peptide bond autocleavage, followed by transthiolation to the cysteine at the intein–extein$_2$ boundary creates a lariat intermediate, that resolves by participation of the Asn at the C terminus of the intein. The resultant thioester reforms the extein$_1$–extein$_2$ peptide bond by acyl S to N shift.

 © 2005 Wiley-VCH Verlag GmbH & Co. KGaA, Weinheim

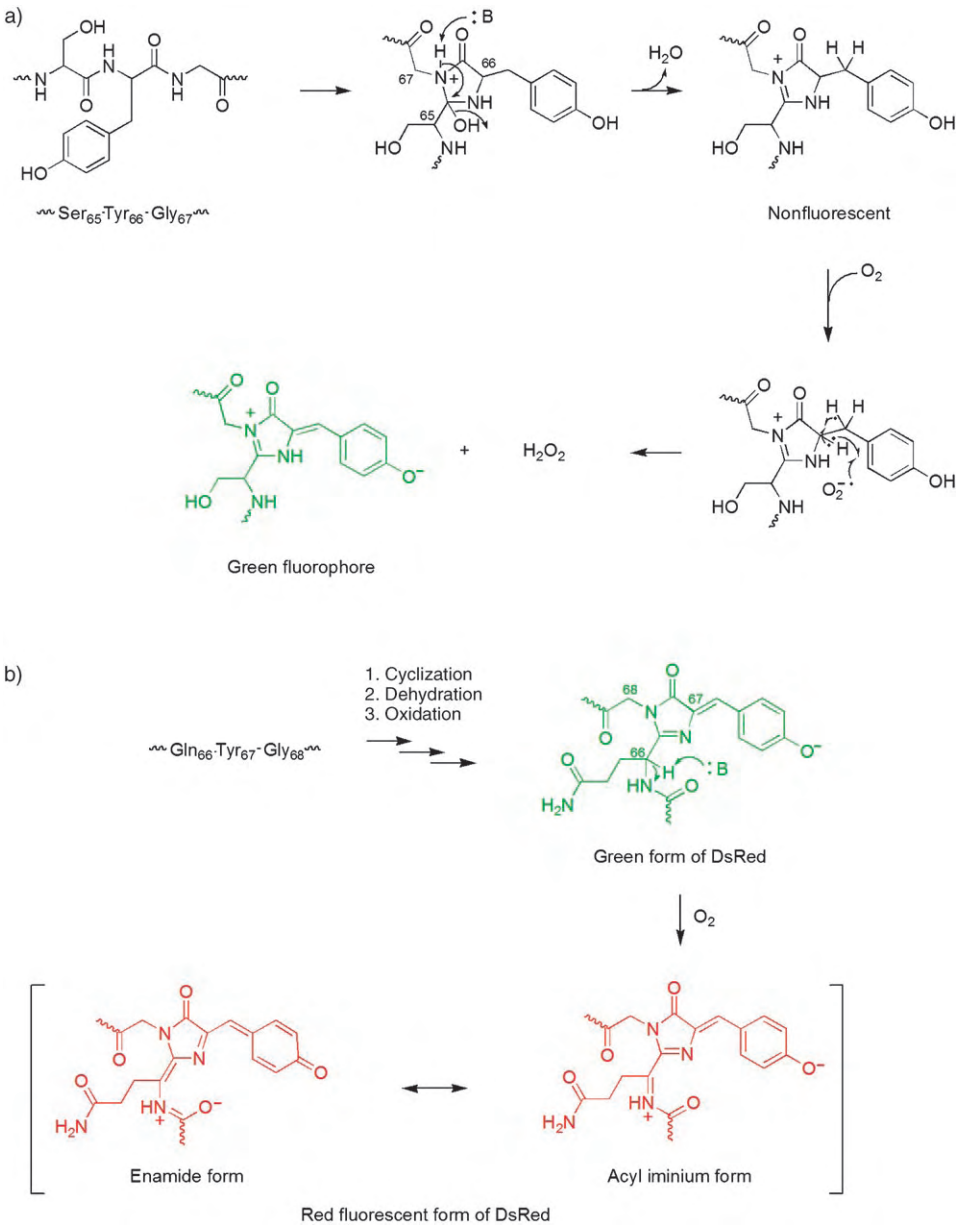

Scheme 36. a) Autoconversion of $Ser_{65}Tyr_{66}Gly_{67}$ in the precursor of green fluorescent protein (GFP) to the green fluorescent form: formation of a cyclic tetrahedral adduct followed by dehydration generates the heterocycle that is not yet fluorescent. Extension of the conjugated system is a slow, oxygen-dependent oxidation that brings the Tyr chromophore into conjugation and completes fluorophore formation. b) A related protein with a $Gln_{66}Tyr_{67}Gly_{68}$ tripeptide instead of the SerTyrGly sequence is the fluorophore in the DsRed protein from coral. It proceeds through a green intermediate on the way to the final red form.

rophores with altered colors, including cyan and gold, have been generated by protein engineering and evolution approaches, allowing many fluorescence-energy-transfer studies between pairs of variant GFPs.

9.2. The Methyleneimidazolone Chromophore

Related rearrangements of a tripeptide sequon in a loop of the folded proenzyme forms of phenylalanine and histidine deaminases produce a related cyclic imidazolone group that then functions as the active-site electrophile for substrate amine deamination (Scheme 37a).[118,119] In the *Pseudomonas* histidine deaminase, $Ala_{142}Ser_{143}Gly_{144}$ in a loop region autoconverts to a compact heterocycle in which the Gly_{144} amide nitrogen is proposed to attack the carbonyl of Ala_{142}. The cyclic tetrahedral adduct can lose water and form the C=N of the imidazolone. Loss of the -OH from the Ser_{143} side chain forms the new double bond in conjugation to produce the 4-methylene-5-imidazolone (MIO) prosthetic group. This set of transformations fashions an electrophilic heterocyclic cofactor from the tripeptide loop to generate the active enzyme. The MIO heterocycle in the mature, active enzyme could be attacked by the substrate amino group. An elimination reaction initiated by β-H removal would then generate urocanate and the amino moiety still attached to the cofactor (Scheme 37b). Release of NH_3 regenerates the starting MIO cofactor for the next catalytic cycle.[120]

10. Conclusions

This summary of posttranslational modifications of proteins has not attempted exhaustive coverage of the more than 200 known covalent modifications (see reference [3] for more complete coverage). Rather, emphasis has been on how the addition of chemical groups from common cofactors and coenzymes to side chains of 15 of the 20 amino acids found in proteins expands the proteome structurally and functionally. The dramatic enhancement of the capabilities of the limited scaffold of genetically encoded protein backbones creates new functional capacities. The modified proteins now have expanded opportunities for catalysis, initiation and termination of signal cascades, integration of information at many metabolic intersections, and alteration of cellular addresses. The posttranslational diversification of the proteome illuminates the underlying molecular logic for epigenetic acquisition of new protein functions.

© 2005 Wiley-VCH Verlag GmbH & Co. KGaA, Weinheim

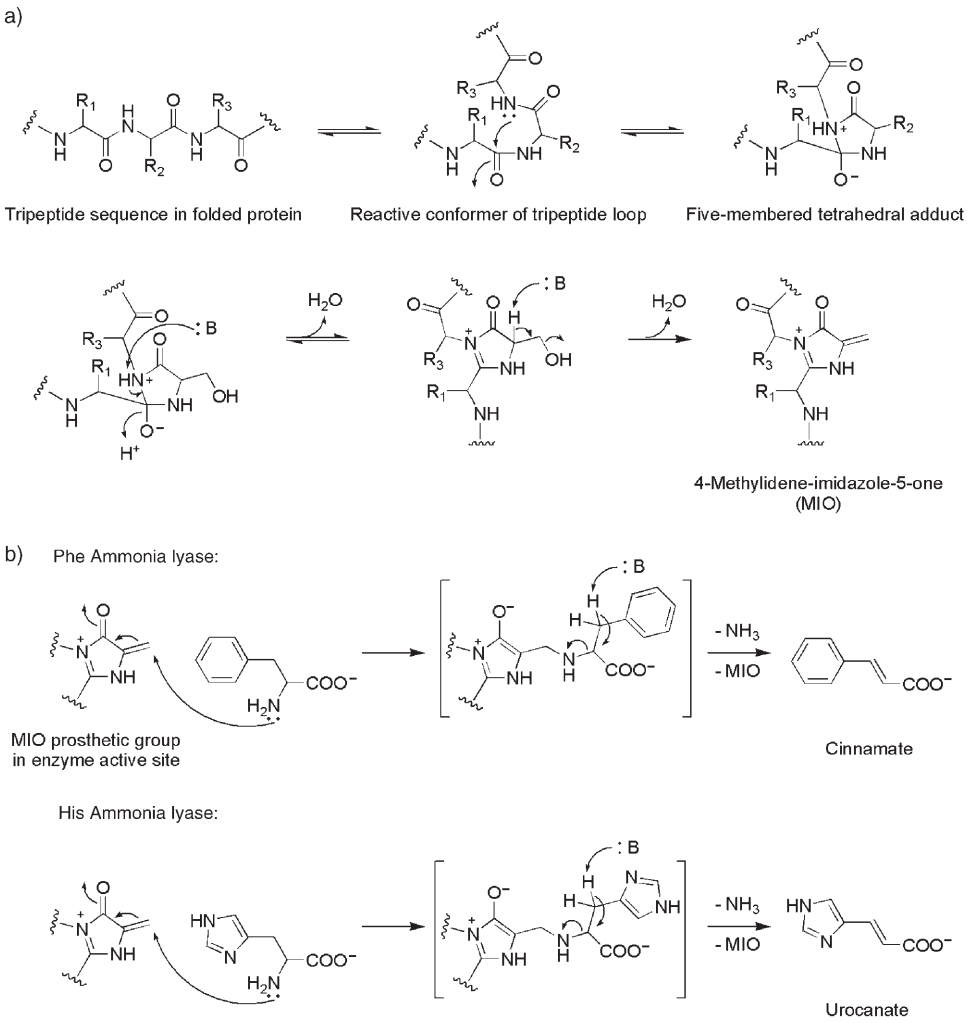

Scheme 37. a) A rearrangement of a tripeptide loop, analogous to that in GFP maturation, occurs in autoactivation of histidine and phenylalanine ammonia lyases. $Ala_{142}Ser_{143}Gly_{144}$ is converted into a compact heterocycle termed MIO (4-methylene-5-imdiazolone). b) The MIO is an electrophilic cofactor that can be attacked by the amino groups of Phe or His to set up net α,β-elimination of NH_2 and H to produce ammonia and the olefinic, deaminated acids urocanate and cinnamate.

The controlled cleavage of specific peptide bonds in particular protein substrates, especially those transiting eukaryotic secretory pathways, shows explicitly that proteases need not be blunt instruments in cellular control inventories. The life cycles of proteins secreted to the cell surface, engaged by ligands, and then retrieved to the nucleus by consecutive rounds of limited proteolysis show ingenious and sophisticated use of the molecular logic of proteolytic trimming of precursors.

Proteins can clearly help themselves for posttranslational creation of new functional groups. Folded protein precursor forms exhibit remarkable properties for autocatalytic conversion of peptide loops into cyclic derivatives for catalysis or light-energy harvesting. Controlled autocatalytic cleavages, presumably vestigial capacities of proteins during evolution, set up N-terminal nucleophiles, N-terminal electrophiles (pyruvamides), and C-terminal cholesterol esters by routing common intermediates down different decomposition pathways. The apotheosis of these autocleavages are the error-free religations in protein splicing reactions in which inteins are excised and exteins self-splice in frame to convert inactive precursors into mature proteins. Splicing may have been an important route to shuffling domains within proteins as a part of multidomain protein evolution pathways.

A given protein can be posttranslationally modified at many residues with the same group, for example, eleven phosphorylations of Abl, five acetylations at the C terminus of p53. Or a protein can be subjected to tandem modifications by several kinds of covalently introduced groups, as exemplified by the two lipidations of Ras followed by regiospecific proteolysis and C-terminal O-methylation, or the multiple modifications of Rho by bacterial protein toxins that disrupt eukaryotic cell cytoskeletal apparatus. The coordinated orchestration of acetylations, methylations, phosphorylations and ubiquitylations of histone tails on nucleosomes give insight into the finely tuned molecular logic of protein posttranslational modifications for gene-expression control.

With the advent of many variations of high-resolution mass spectrometry it is possible to detect and localize covalent changes in proteins beyond the genetically encoded sequence. Cataloguing the protein variants in various subproteomes (such as the phosphoproteome, the ubiquitylated proteome, the molecular variants of histone modifications in nucleosomes of differing transcriptional activity) will continue to be important parameters to allow a full description of the protein composition of proteomes. This information will be a necessary preamble to understanding how the diverse molecular forms of proteins carry out their integrated functions.

We thank M. Fischbach for assistance with the production of the frontispiece.

Received: March 21, 2005
Published online: November 3, 2005

[1] D. L. Black, *Annu. Rev. Biochem.* **2003**, *72*, 291 – 336.
[2] T. Maniatis, B. Tasic, *Nature* **2002**, *418*, 236 – 243.
[3] C. Walsh, *Postranslational Modification of Proteins: Expanding Nature's Inventory*, B. Roberts, Colorado, **2005**.
[4] M. Mann, S. E. Ong, M. Gronborg, H. Steen, O. N. Jensen, A. Pandey, *Trends Biotechnol.* **2002**, *20*, 261 – 268.
[5] J. A. Hoch, T. J. Silhavy, *Two Component Signal Transduction*, ASM, Washington, **1995**.

 © 2005 Wiley-VCH Verlag GmbH & Co. KGaA, Weinheim

[6] A. Rodrigue, Y. Quentin, A. Lazdunski, V. Mejean, M. Foglino, *Trends Microbiol.* **2000**, *8*, 498 – 504.
[7] G. Manning, D. B. Whyte, R. Martinez, T. Hunter, S. Sudarsanam, *Science* **2002**, *298*, 1912 – 1934.
[8] L. N. Johnson, R. J. Lewis, *Chem. Rev.* **2001**, *101*, 2209 – 2242.
[9] K. Zhang, K. E. Williams, L. Huang, P. Yau, J. S. Siino, E. M. Bradbury, P. R. Jones, M. J. Minch, A. L. Burlingame, *Mol. Cell. Proteomics* **2002**, *1*, 500 – 508.
[10] M. D. Resh, *Biochim. Biophys. Acta* **1999**, *1451*, 1 – 16.
[11] M. J. Bijlmakers, M. Marsh, *Trends Cell Biol.* **2003**, *13*, 32 – 42.
[12] C. L. Brooks, W. Gu, *Curr. Opin. Cell Biol.* **2003**, *15*, 164 – 171.
[13] M. Li, J. Luo, C. L. Brooks, W. Gu, *J. Biol. Chem.* **2002**, *277*, 50607 – 50611.
[14] B. M. Turner, *Cell* **2002**, *111*, 285 – 291.
[15] D. R. Johnson, R. S. Bhatnagar, L. J. Knoll, J. I. Gordon, *Annu. Rev. Biochem.* **1994**, *63*, 869 – 914.
[16] S. McLaughlin, A. Aderem, *Trends Biochem. Sci.* **1995**, *20*, 272 – 276.
[17] D. A. Johnson, P. Akamine, E. Radzio-Andzelm, M. Madhusudan, S. S. Taylor, *Chem. Rev.* **2001**, *101*, 2243 – 2270.
[18] O. Rocks, A. Peyker, M. Kahms, P. J. Verveer, C. Koerner, M. Lumbierres, J. Kuhlmann, H. Waldmann, A. Wittinghofer, P. I. Bastiaens, *Science* **2005**, *307*, 1746 – 1752.
[19] C. M. Pickart, *Annu. Rev. Biochem.* **2001**, *70*, 503 – 533.
[20] C. M. Pickart, R. E. Cohen, *Nat. Rev. Mol. Cell Biol.* **2004**, *5*, 177 – 187.
[21] N. Zheng, B. A. Schulman, L. Song, J. J. Miller, P. D. Jeffrey, P. Wang, C. Chu, D. M. Koepp, S. J. Elledge, M. Pagano, R. C. Conaway, J. W. Conaway, J. W. Harper, N. P. Pavletich, *Nature* **2002**, *416*, 703 – 709.
[22] T. Cardozo, M. Pagano, *Nat. Rev. Mol. Cell Biol.* **2004**, *5*, 739 – 751.
[23] J. D. Schnell, L. Hicke, *J. Biol. Chem.* **2003**, *278*, 35857 – 35860.
[24] J. S. Bonifacino, L. M. Traub, *Annu. Rev. Biochem.* **2003**, *72*, 395 – 447.
[25] L. Hicke, *Nat. Rev. Mol. Cell Biol.* **2001**, *2*, 195 – 201.
[26] D. J. Katzmann, G. Odorizzi, S. D. Emr, *Nat. Rev. Mol. Cell Biol.* **2002**, *3*, 893 – 905.
[27] A. Hershko, A. Ciechanover, *Annu. Rev. Biochem.* **1998**, *67*, 425 – 479.
[28] S. I. Reed, *Nat. Rev. Mol. Cell Biol.* **2003**, *4*, 855 – 864.
[29] A. W. Murray, *Cell* **2004**, *116*, 221 – 234.
[30] R. Marmorstein, *Nat. Rev. Mol. Cell Biol.* **2003**, *303*, 1 – 7.
[31] R. Roskoski, Jr., *Biochem. Biophys. Res. Commun.* **2003**, *303*, 1 – 7.
[32] S. Khorasanizadeh, *Cell* **2004**, *116*, 259 – 272.
[33] C. Walsh, *Enzymatic Reaction Mechanisms*, Freeman, San Francisco, **1979**.
[34] J. A. Glomset, M. H. Gelb, C. C. Farnsworth, *Trends Biochem. Sci.* **1990**, *15*, 139 – 142.
[35] F. L. Zhang, P. J. Casey, *Annu. Rev. Biochem.* **1996**, *65*, 241 – 269.
[36] O. Pylypenko, A. Rak, R. Reents, A. Niculae, V. Sidorovitch, M. D. Cioaca, E. Bessolitsyna, N. H. Thoma, H. Waldmann, I. Schlichting, R. S. Goody, K. Alexandrov, *Mol. Cell* **2003**, *11*, 483 – 494.
[37] A. Rak, O. Pylypenko, T. Durek, A. Watzke, S. Kushnir, L. Brunsveld, H. Waldmann, R. S. Goody, K. Alexandrov, *Science* **2003**, *302*, 646 – 650.
[38] A. Furmanek, J. Hofsteenge, *Acta Biochim. Pol.* **2000**, *47*, 781 – 789.
[39] Y. Mechref, M. V. Novotny, *Chem. Rev.* **2002**, *102*, 321 – 369.
[40] A. Helenius, M. Aebi, *Annu. Rev. Biochem.* **2004**, *73*, 1019 – 1049.
[41] E. S. Trombetta, A. J. Parodi, *Adv. Protein Chem.* **2001**, *54*, 303 – 344.
[42] J. Roth, *Chem. Rev.* **2002**, *102*, 285 – 303.
[43] E. S. Trombetta, A. J. Parodi, *Annu. Rev. Cell Dev. Biol.* **2003**, *19*, 649 – 676.
[44] P. M. Rudd, T. Endo, C. Colominas, D. Groth, S. F. Wheeler, D. J. Harvey, M. R. Wormald, H. Serban, S. B. Prusiner, A. Kobata, R. A. Dwek, *Proc. Natl. Acad. Sci. USA* **1999**, *96*, 13044 – 13049.
[45] P. M. Rudd, A. H. Merry, M. R. Wormald, R. A. Dwek, *Curr. Opin. Struct. Biol.* **2002**, *12*, 578 – 586.
[46] K. Vosseller, K. Sakabe, L. Wells, G. W. Hart, *Curr. Opin. Chem. Biol.* **2002**, *6*, 851 – 857.
[47] D. J. Moloney, L. H. Shair, F. M. Lu, J. Xia, R. Locke, K. L. Matta, R. S. Haltiwanger, *J. Biol. Chem.* **2000**, *275*, 9604 – 9611.
[48] D. J. Moloney, V. M. Panin, S. H. Johnston, J. Chen, L. Shao, R. Wilson, Y. Wang, P. Stanley, K. D. Irvine, R. S. Haltiwanger, T. F. Vogt, *Nature* **2000**, *406*, 369 – 375.
[49] L. Wells, S. A. Whalen, G. W. Hart, *Biochem. Biophys. Res. Commun.* **2003**, *302*, 435 – 441.
[50] N. Haines, K. D. Irvine, *Nat. Rev. Mol. Cell Biol.* **2003**, *4*, 786 – 797.
[51] T. Okajima, A. Xu, K. D. Irvine, *J. Biol. Chem.* **2003**, *278*, 42340 – 42345.
[52] N. M. Giles, A. B. Watts, G. I. Giles, F. H. Fry, J. A. Littlechild, C. Jacob, *Chem. Biol.* **2003**, *10*, 677 – 693.
[53] C. Jacob, G. I. Giles, N. M. Giles, H. Sies, *Angew. Chem.* **2003**, *115*, 4890 – 4907; *Angew. Chem. Int. Ed.* **2003**, *42*, 4742 – 4758.
[54] P. T. L. Chivers, M. R. Raines, *Protein Disulfide Isomerase: Cellular Enzymology of the CXXC Motif*, Marcel Dekker, New York, **1998**, pp. 487 – 505.
[55] J. S. Stamler, S. Lamas, F. C. Fang, *Cell* **2001**, *106*, 675 – 683.
[56] M. Griffin, R. Casadio, C. M. Bergamini, *Biochem. J.* **2002**, *368*, 377 – 396.
[57] L. Lorand, R. M. Graham, *Nat. Rev. Mol. Cell Biol.* **2003**, *4*, 140 – 156.
[58] J. A. Vranka, L. Y. Sakai, H. P. Bachinger, *J. Biol. Chem.* **2004**, *279*, 23615 – 23621.
[59] C. W. Pugh, P. J. Ratcliffe, *Nat. Med.* **2003**, *9*, 677 – 684.
[60] W. C. Hon, M. I. Wilson, K. Harlos, T. D. Claridge, C. J. Schofield, C. W. Pugh, P. H. Maxwell, P. J. Ratcliffe, D. I. Stuart, E. Y. Jones, *Nature* **2002**, *417*, 975 – 978.
[61] L. A. McNeill, K. S. Hewitson, T. D. Claridge, J. F. Seibel, L. E. Horsfall, C. J. Schofield, *Biochem. J.* **2002**, *367*, 571 – 575.
[62] C. J. Schofield, P. J. Ratcliffe, *Nat. Rev. Mol. Cell Biol.* **2004**, *5*, 343 – 354.
[63] P. H. Maxwell, M. S. Wiesener, G. W. Chang, S. C. Clifford, E. C. Vaux, M. E. Cockman, C. C. Wykoff, C. W. Pugh, E. R. Maher, P. J. Ratcliffe, *Nature* **1999**, *399*, 271 – 275.
[64] M. Ohh, C. W. Park, M. Ivan, M. A. Hoffman, T. Y. Kim, L. E. Huang, N. Pavletich, V. Chau, W. G. Kaelin, *Nat. Cell Biol.* **2000**, *2*, 423 – 427.
[65] M. J. Ryle, R. P. Hausinger, *Curr. Opin. Chem. Biol.* **2002**, *6*, 193 – 201.
[66] E. Chapman, M. D. Best, S. R. Hanson, C.-H. Wong, *Angew. Chem.* **2004**, *116*, 3610 – 3632; *Angew. Chem. Int. Ed.* **2004**, *43*, 3526 – 3548.
[67] I. Capila, R. J. Linhardt, *Angew. Chem.* **2002**, *114*, 426 – 450; *Angew. Chem. Int. Ed.* **2002**, *41*, 391 – 412.
[68] M. Farzan, T. Mirzabekov, P. Kolchinsky, R. Wyatt, M. Cayabyab, N. P. Gerard, C. Gerard, J. Sodroski, H. Choe, *Cell* **1999**, *96*, 667 – 676.
[69] K. von Figura, A. Hasilik, *Annu. Rev. Biochem.* **1986**, *55*, 167 – 193.
[70] K. von Figura, B. Schmidt, T. Selmer, T. Dierks, *Bioessays* **1998**, *20*, 505 – 510.
[71] S. R. Hanson, M. D. Best, C.-H. Wong, *Angew. Chem.* **2004**, *116*, 5858 – 5886; *Angew. Chem. Int. Ed.* **2004**, *43*, 5736 – 5763.
[72] R. von Bulow, B. Schmidt, T. Dierks, K. von Figura, I. Uson, *J. Mol. Biol.* **2001**, *305*, 269 – 277.

© 2005 Wiley-VCH Verlag GmbH & Co. KGaA, Weinheim

[73] *Bacterial Protein Toxins* (Eds.: K. Aktories, I. Just), Springer, Berlin, **2000**.
[74] I. R. Vetter, F. Hofmann, S. Wohlgemuth, C. Herrmann, I. Just, *J. Mol. Biol.* **2000**, *301*, 1091 – 1095.
[75] M. Geyer, C. Wilde, J. Selzer, K. Aktories, H. R. Kalbitzer, *Biochemistry* **2003**, *42*, 11951 – 11959.
[76] G. Schmidt, P. Sehr, M. Wilm, J. Selzer, M. Mann, K. Aktories, *Nature* **1997**, *387*, 725 – 729.
[77] R. N. Perham, *Annu. Rev. Biochem.* **2000**, *69*, 961 – 1004.
[78] C. T. Walsh, *Antibiotics: Actions, Origins, Resistance*, ASM, Washington, **2003**.
[79] B. Furie, B. A. Bouchard, B. C. Furie, *Blood* **1999**, *93*, 1798 – 1808.
[80] C. Shang, T. Shibahara, K. Hanada, Y. Iwafune, H. Hirano, *Biochemistry* **2004**, *43*, 6281 – 6292.
[81] S. B. Ficarro, M. L. McCleland, P. T. Stukenberg, D. J. Burke, M. M. Ross, J. Shabanowitz, D. F. Hunt, F. M. White, *Nat. Biotechnol.* **2002**, *20*, 301 – 305.
[82] J. Peng, D. Schwartz, J. E. Elias, C. C. Thoreen, D. Cheng, G. Marsischky, J. Roelofs, D. Finley, S. P. Gygi, *Nat. Biotechnol.* **2003**, *21*, 921 – 926.
[83] H. Steen, M. Fernandez, S. Ghaffari, A. Pandey, M. Mann, *Mol. Cell. Proteomics* **2003**, *2*, 138 – 145.
[84] J. J. Pesavento, Y.-B. Kim , G. K. Taylor, N. L. Kelleher, *J. Am. Chem. Soc.* **2004**, *126*, 3386 – 3387.
[85] F. Shao, J. E. Dixon, *Adv. Exp. Med. Biol.* **2003**, *529*, 79 – 84.
[86] L. Izzi, L. Attisano, *Oncogene* **2004**, *23*, 2071 – 2078.
[87] J. B. Shabb, *Chem. Rev.* **2001**, *101*, 2381 – 2411.
[88] M. D. Jackson, J. M. Denu, *Chem. Rev.* **2001**, *101*, 2313 – 2340.
[89] A. Alonso, J. Sasin, N. Bottini, I. Friedberg, A. Osterman, A. Godzik, T. Hunter, J. Dixon, T. Mustelin, *Cell* **2004**, *117*, 699 – 711.
[90] M. Mann, R. C. Hendrickson, A. Pandey, *Annu. Rev. Biochem.* **2001**, *70*, 437 – 473.
[91] M. Mann, O. N. Jensen, *Nat. Biotechnol.* **2003**, *21*, 255 – 261.
[92] H. H. Ng, A. Bird, *Trends Biochem. Sci.* **2000**, *25*, 121 – 126.
[93] C. M. Grozinger, S. L. Schreiber, *Chem. Biol.* **2002**, *9*, 3 – 16.
[94] A. A. Sauve, I. Celic, J. Avalos, H. Deng, J. D. Boeke, V. L. Schramm, *Biochemistry* **2001**, *40*, 15456 – 15463.
[95] A. A. Sauve, V. L. Schramm, *Biochemistry* **2003**, *42*, 9249 – 9256.
[96] Y. Shi, F. Lan, C. Matson, P. Mulligan, J. R. Whetstine, P. A. Cole, R. A. Casero, *Cell* **2004**, *119*, 941 – 953.
[97] K. D. Wilkinson, *Semin. Cell Dev. Biol.* **2000**, *11*, 141 – 148.
[98] T. Gan-Erdene, K. Nagamalleswari, L. Yin, K. Wu, Z. Q. Pan, K. D. Wilkinson, *J. Biol. Chem.* **2003**, *278*, 28892 – 28900.
[99] M. Paetzel, A. Karla, N. C. J. Strynadka, R. E. Dalbey, *Chem. Rev.* **2002**, *102*, 4549 – 4579.
[100] S. S. Molloy, E. D. Anderson, F. Jean, G. Thomas, *Trends Cell Biol.* **1999**, *9*, 28 – 35.
[101] N. C. Rockwell, D. J. Krysan, T. Komiyama, R. S. Fuller, *Chem. Rev.* **2002**, *102*, 4525 – 4548.
[102] G. A. Eberlein, V. E. Eysselein, M. T. Davis, T. D. Lee, J. E. Shively, D. Grandt, W. Niebel, R. Williams, J. Moessner, J. Zeeh, H. E. Meyer, H. Goebell, J. R. Reeve, Jr., *J. Biol. Chem.* **1992**, *267*, 1517 – 1521.
[103] J. Arribas, A. Borroto, *Chem. Rev.* **2002**, *102*, 4627 – 4638.
[104] Y. Ye, M. E. Fortini, *Semin. Cell Dev. Biol.* **2000**, *11*, 211 – 221.
[105] K. Ohishi, N. Inoue, Y. Maeda, J. Takeda, H. Riezman, T. Kinoshita, *Mol. Biol. Cell* **2000**, *11*, 1523 – 1533.
[106] S. K. Mazmanian, H. Ton-That, O. Schneewind, *Mol. Microbiol.* **2001**, *40*, 1049 – 1057.
[107] D. Stock, P. M. Nederlof, E. Seemuller, W. Baumeister, R. Huber, J. Lowe, *Curr. Opin. Biotechnol.* **1996**, *7*, 376 – 385.
[108] E. Seemuller, A. Lupas, W. Baumeister, *Nature* **1996**, *382*, 468 – 471.
[109] H. Paulus, *Annu. Rev. Biochem.* **2000**, *69*, 447 – 496.
[110] M. Groll, M. Bochtler, H. Brandstetter, T. Clausen, R. Huber, *ChemBioChem* **2005**, *6*, 222 – 256.
[111] Y. D. Kwon, I. Nagy, P. D. Adams, W. Baumeister, B. K. Jap, *J. Mol. Biol.* **2004**, *335*, 233 – 245.
[112] A. Albert, V. Dhanaraj, U. Genschel, G. Khan, M. K. Ramjee, R. Pulido, B. L. Sibanda, F. von Delft, M. Witty, T. L. Blundell, A. G. Smith, C. Abell, *Nat. Struct. Biol.* **1998**, *5*, 289 – 293.
[113] J. A. Porter, S. C. Ekker, W. J. Park, D. P. von Kessler, K. E. Young, C. H. Chen, Y. Ma, A. S. Woods, R. J. Cotter, E. V. Koonin, P. A. Beachy, *Cell* **1996**, *86*, 21 – 34.
[114] C. J. Noren, J. Wang, F. B. Perler, *Angew. Chem.* **2000**, *112*, 458 – 476; *Angew. Chem. Int. Ed.* **2000**, *39*, 450 – 466.
[115] T. W. Muir, D. Sondhi, P. A. Cole, *Proc. Natl. Acad. Sci. USA* **1998**, *95*, 6705 – 6710.
[116] R. Y. Tsien, *Annu. Rev. Biochem.* **1998**, *67*, 509 – 544.
[117] D. Yarbrough, R. M. Wachter, K. Kallio, M. V. Matz, S. J. Remington, *Proc. Natl. Acad. Sci. USA* **2001**, *98*, 462 – 467.
[118] M. Baedeker, G. E. Schulz, *Structure* **2002**, *10*, 61 – 67.
[119] T. F. Schwede, J. Retey, G. E. Schulz, *Biochemistry* **1999**, *38*, 5355 – 5361.
[120] J. C. Calabrese, D. B. Jordan, A. Boodhoo, S. Sariaslani, T. Vannelli, *Biochemistry* **2004**, *43*, 11403 – 11416.
[121] M. E. Fortini, *Nat. Rev. Mol. Cell Biol.* **2002**, *3*, 673 – 684.
[122] P. J. Kraulis, *J. Appl. Crystallogr.* **1991**, *24*, 946 – 950.

 © 2005 Wiley-VCH Verlag GmbH & Co. KGaA, Weinheim

Communications

DOI: 10.1002/anie.200501681

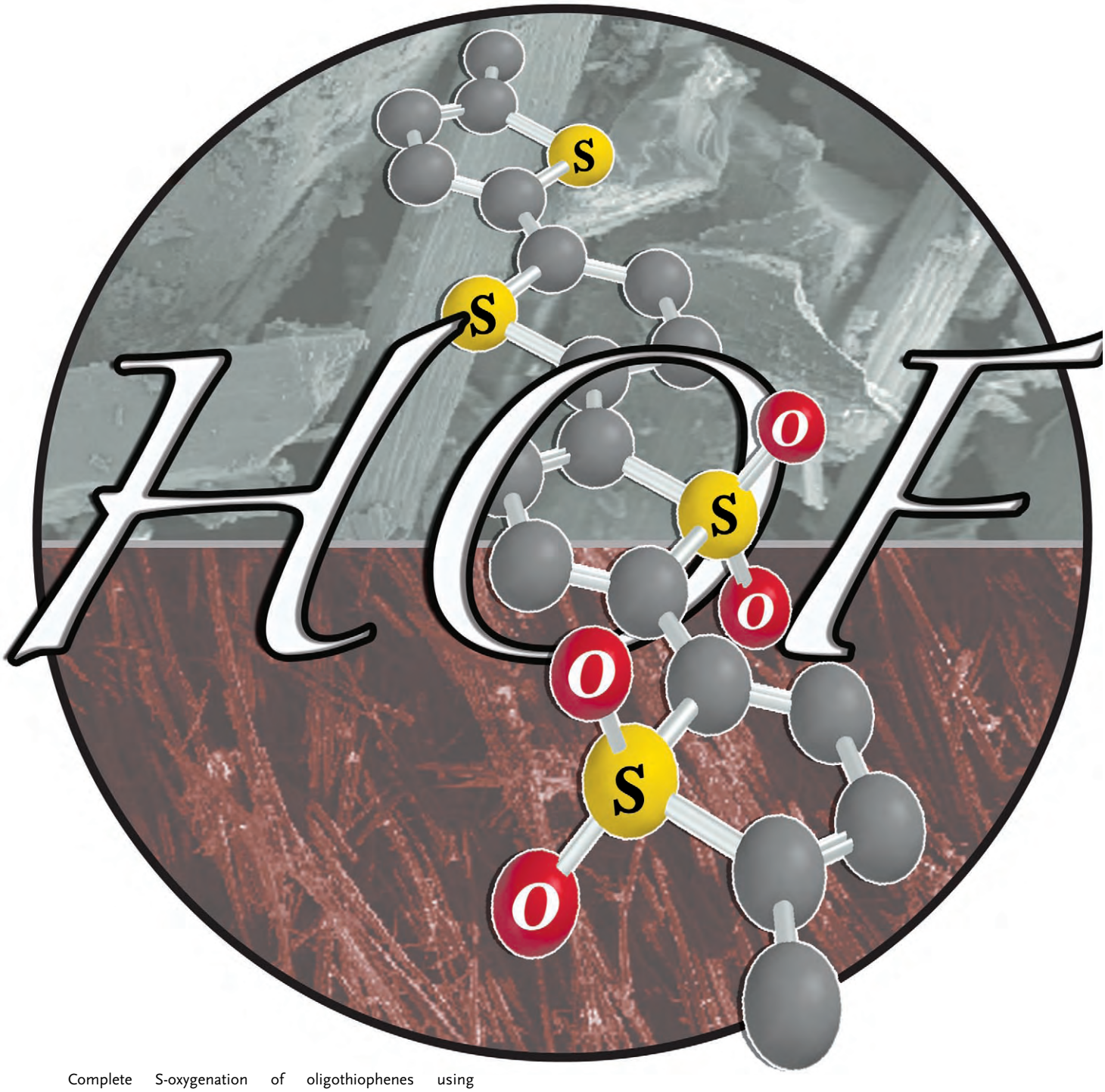

Complete S-oxygenation of oligothiophenes using HOF·CH_3CN yielded *S*,*S*-dioxide oligothiophene derivatives. In the background, scanning-electron microscopy images of the starting oligothiophenes (top) and the better-organized clusters of the products (bottom) are shown. Details of these studies can be found in the Communication by E. Amir and S. Rozen on the following pages.

WILEY InterScience DISCOVER SOMETHING GREAT
© 2005 Wiley-VCH Verlag GmbH & Co. KGaA, Weinheim

Oligomers

DOI: 10.1002/anie.200501681

Synthesis of [all]-*S*,*S*-Dioxide Oligothiophenes Using HOF·CH_3CN**

*Elizabeta Amir and Shlomo Rozen**

The last decade witnessed an exponential growth in the number of reports devoted to the development of electronic devices based on organic materials. The main synthetic effort is centered on oligothiophenes (OTs) and their many derivatives, such as thienylenvinylenes,[1] alkyl fluoride oligothiophenes,[2] ethylenedioxidethiophenes,[3] or thiazolothiazol thiophenes,[4] to mention just a few. A short search in the *Chemical Abstracts* resulted in thousands of reports concerning this subject from the last five years alone.

The channeling of such huge research efforts started in the late 1980s when Garnier and co-workers had shown for the first time that short conjugated thiophene oligomers could serve as efficient active layers in field-effect transistors (FETs).[5] Since then, the will to develop such organic semiconductors for light-emitting diodes (LEDs), molecular wires, and many other optoelectronic devices[6] has become an irresistible driving force for many chemists to continue the exploration of the possibilities offered by various types of oligothiophenes.

The major goals of the numerous OT modifications are to lower the highest-occupied molecular orbital (HOMO)–lowest-unoccupied molecular orbital (LUMO) gap and obtain highly ordered semiconducting films, as both features are responsible for the efficiency of n-type semiconductors. One of most obvious and promising modifications had already been suggested in 1989: A theoretical prediction had been made that the corresponding *S*,*S*-dioxides of OT would be better materials than OTs themselves, as the HOMO–LUMO gap should be significantly smaller.[7] Chemists tried to test this hypothesis, but the use of orthodox oxygen-transfer agents was the main reason for a complete synthetic failure of making [all]-*S*,*S*-dioxide OTs longer than bithiophene. Each time such an attempt was undertaken, only a low yield of partially oxygenated thiophene rings was achieved, even after prolonged reaction times.[8] Another approach toward the synthesis of partially oxygenated *S*,*S*-dioxide OTs was taken by Barbarella et al. who coupled 2-(dimethyl-*tert*-butylsilyl)-5-bromothiophene-*S*,*S*-dioxide with the corresponding oxygen-free derivatives, thus obtaining alternately oxygenated OTs.[9]

Some years ago, we developed a new type of oxygen-transfer agent, HOF·CH_3CN, which was unique in the sense of that it possessed a truly electrophilic oxygen center.[10] After some time, this complex was dubbed the best oxygen-transfer agent offered in organic chemistry and was instrumental in the first synthesis of 1,10-*N*,*N*-phenanthroline dioxides,[11] the first oxidation of geminal diamines[12] and azides,[13] the epoxidation of electron-depleted olefins,[14] and many other firsts or difficult transformations.[15] Among these reactions was also the mild oxidation of various thiophenes to their corresponding *S*,*S*-dioxides[16]—not an easy task considering the harsh conditions usually required to overcome the aromatic stabilization—thus possibly leading to Diels–Alder reactions and/or SO_2 eliminations. The successful preparation of these monothiophene *S*,*S*-dioxides with HOF·CH_3CN prompted us to explore the possibilities of making the long sought after oligothiophene *S*,*S*-dioxides (OTDOs). This reagent, prepared from diluted elemental fluorine and aqueous acetonitrile, was indeed able to transfer as many oxygen atoms as needed to construct the oligothiophene [all]-*S*,*S*-dioxides investigated. We report herein the synthesis and certain characteristics of some of these OTDO compounds. It is worth mentioning that previous attempts to fully oxidize 5,5′-dihexyl-2,2-bithiophene (**1e**) with *m*-chloroperoxybenzoic acid (MCPBA) were unsuccessful and only 5,5′-bis(dimethyl-*tert*-butylsilyl)-[2,2′]bithiophene (**1f**) could be oxidized to the tetraoxide **2f** in 47% yield after 12 h.[8,9] So far, this reaction was the only example of a preparation of a fully oxygenated *S*,*S*-dioxide OT; however, HOF·CH_3CN has changed this situation.

5,5′-Dimethyl-[2,2′]bithiophene (**1a**)[17] was cooled to −10 °C and treated with a slight excess of the acetonitrile complex of hypofluorous acid.[18] The corresponding, previously unknown, bis(*S*,*S*-dioxide) **2a** was obtained in about 10 s and in 85% yield. No partly oxidized regioisomers or other by-products, usually associated with long reaction times and high temperatures, were observed. Replacing the methyl groups with the bulky *tert*-butyl groups, as in **1b**,[17] did not change the outcome, and the as-yet unknown bis(*S*,*S*-dioxide) **2b** was obtained in a short reaction time at 0 °C in 83% yield. Replacing one or even both of the electron-donating alkyl groups at the 5,5′ positions with the electron-withdrawing bromine atom(s), as in 5-bromo-5′-hexyl-[2,2′]bithiophene (**1c**)[19] or 5,5′-dibromo-[2,2′]bithiophene (**1d**),[20] did not have a negative effect on the reaction and **2c** and **2d** were obtained after 5 min in 87 and 66% yield, respectively (Scheme 1).

Longer OTs were also treated successfully. It took only one minute for HOF·CH_3CN to transfer six oxygen atoms to all three sulfur atoms of the 5,5″-di-*tert*-butyl-[2,2′,5′,2″]terthiophene (**3b**),[21] thus affording the tris(*S*,*S*-dioxide) **4b** in 82% yield. This reaction is the first example of a fully oxygenated terthiophene compound. For comparison, treatment of terthiophene with MCPBA for 48 h resulted in the transfer of oxygen atoms to only the terminal rings.[8] Again, leaving two electron-withdrawing groups for future synthetic manipulation, as in 5,5″-dibromo-[2,2′,5′,2″]terthiophene

[*] E. Amir, Prof. S. Rozen
School of Chemistry
Raymond and Beverly Sackler Faculty of Exact Sciences
Tel-Aviv University
Tel-Aviv 69978 (Israel)
Fax: (+972) 3-640-9293
E-mail: rozens@post.tau.ac.il

[**] This work was supported by the Israel Science Foundation (Jerusalem, Israel).

Supporting information for this article is available on the WWW under http://www.angewandte.org or from the author.

 © 2005 Wiley-VCH Verlag GmbH & Co. KGaA, Weinheim

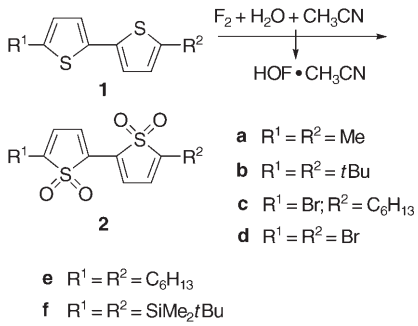

Scheme 1. Oxygenation of dithiophenes.

(**3d**),[20] did not prevent the oxygen-transfer process that forms tris(*S*,*S*-dioxide) **4d** in 60% yield. One of the advantages of HOF·CH_3CN is the origin of its electrophilic oxygen atom from water, which is the most convenient source for all oxygen isotopes; therefore, an opportunity to prepare **4b** with all six oxygen atoms being the expected ^{18}O isotope (EI MS: *m*/*z* 468.1 [M^+]) was presented.

The derivative with four thienyl rings, 5,5‴-di-*tert*-butyl-[2,2′,5′,2″,5″,2‴]quaterthiophene (**5b**),[21] was also subjected to oxygenation with the HOF·CH_3CN complex. In this case, a twofold excess (16 molar equivalent) of the oxidant and reaction times of up to 40 minutes at room temperature were required, but the main product was the tetra-*S*,*S*-dioxide **6b** in 52% yield (Scheme 2). It seems that the somewhat smaller

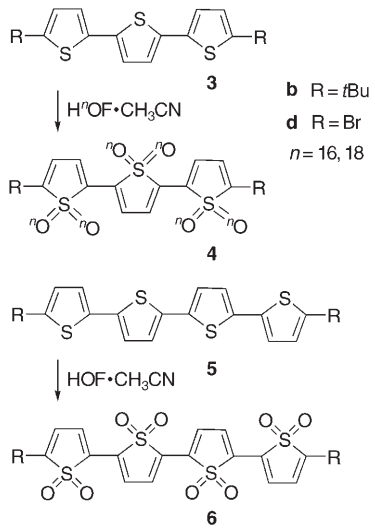

Scheme 2. Oxygenation of oligothiophenes.

yield in this case is caused by solubility problems, and we are working now on the preparation of some more soluble derivatives.

These results enabled us to test some of the theoretical predictions about the OTDOs prepared so far. Table 1 lists the UV/Vis data for both starting materials and the *S*,*S*-dioxo oligomers. There are two well-defined differences between the spectra of the two groups. Whereas in the starting materials, as well as in the partially oxygenated *S*,*S*-dioxides,

Table 1: UV/Vis spectroscopic data and the derived HOMO–LUMO energy gaps[a].

Compound	$\lambda_{1-3,max}$ [nm][b]	Energy gaps [eV]			
		ΔE_g[c]	ΔE_g[d]	$\Delta\Delta E_g$[e]	$\Delta\Delta E_g$[f]
1a	317	3.91			
2a	351, 369, 387	3.20		0.71	
1b	317	3.91	4.22		
2b	359, 374, 392	3.16	3.34	0.75	0.88
1c	320	3.87			
2c	365, 383, 401	3.09		0.78	
1d	320	3.87	3.96		
2d	370, 388, 412	3.01	3.13	0.86	0.83
3b	365	3.40	3.41		
4b	410, 434, 461	2.69	2.66	0.71	0.75
3d	364	3.41	3.34		
4d	414, 441, 468	2.65	2.56	0.76	0.78
5b	398	3.12	3.13		
6b	448, 480, 512	2.42	2.26	0.70	0.87

[a] HOMO–LUMO energy gap was derived from the UV/Vis spectroscopic data and DFT calculations. [b] These spectra consist of an underlined maximum and corresponding vibronic splitting. [c] HOMO–LUMO gap from the low-energy band of the UV/Vis spectrum. [d] These calculations obtained from DFT computations are in very good agreement with the UV measurements (for comparison purpose, see reference [9]). [e,f] Lowering the HOMO–LUMO gap following the oxygen-transfer reaction ([e] from spectral data, [f] from DFT calculations).

the reported spectrum presents a single absorption maximum, the corresponding [all]-*S*,*S*-dioxides display three major peaks because of the rigidification of the OTDO backbone.[9] A constant interval in the order of 18–32 nm between the high-energy band ($\lambda_{1,max}$), main absorption ($\lambda_{2,max}$), and low-energy transition ($\lambda_{3,max}$) was observed in all products. This energy spacing can be attributed to the stretching mode of the conjugated double bonds of the oxidized OT core. As reported previously,[22] the bathochromic shift between an OT and the same compound with one oxygenated thiophene ring is about 60 nm, whereas a second *S*,*S*-dioxide unit adds an additional shift of about 20 nm. This trend of additivity is fully expressed in the completely *S*,*S*-oxygenated derivatives. As a result, dearomatized oligothiophenes show a maximal bathochromic shift that indicates a considerable narrowing of the HOMO–LUMO gap (ΔEg), as reflected by the low-energy transition ($\lambda_{3,max}$) absorptions of the products[22] (Table 1).

To obtain a good estimation of the frontier molecular orbitals, we performed ab initio DFT/B3PW91 computations using 6-311G** and 6-31G* bases sets for the bromo and *t*Bu derivatives, respectively. The results indicated that the energies of both the HOMO and LUMO were indeed considerably lower for the oxygenated compounds, with the LUMO values dropping almost twice as much as those of the HOMO. Consequently, this lowering leads to derivatives with a significantly higher electron affinities. Table 1 reveals quite a good agreement between the computed energy-gap values and those obtained from the UV/Vis measurements concerning the narrowing of the HOMO–LUMO gap between the starting materials and the products.

Cyclic-voltammetric measurements for the pairs **1b** and **2b** and **3b** and **4b** (starting materials and products, respec-

 © 2005 Wiley-VCH Verlag GmbH & Co. KGaA, Weinheim

tively) were carried out on Pt electrodes (1.44 cm^2) in CH_3CN/Et_4NBF_4 (0.1M) and with 1×10^{-3}M substrate at 20 $mV\,s^{-1}$. The voltage was measured versus a Ag/AgCl electrode. The obtained oxidation ($E_{Ip,a}$) and reduction ($E_{Ip,c}$) peak potentials are presented in Table 2 and Figure 1.

Table 2: Oxidation ($E_{Ip,a}$) and reduction ($E_{Ip,c}$) peak potentials.

Compound	$E_{Ip,a}$ [V]	$E_{Ip,c}$ [V]
1b	1.21	−1.22
2b	2.24	−0.93
3b	1.06	−1.40
4b	2.14	−0.44

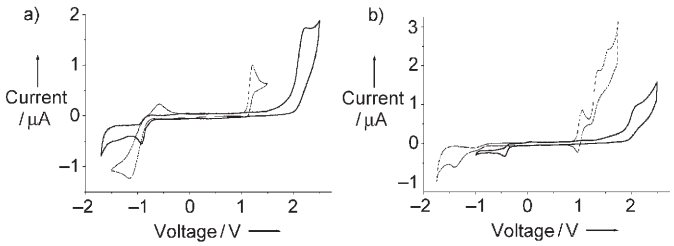

Figure 1. Cyclic voltammograms: a) dashed line: **1b**, solid line: **2b**; b) dashed line: **3b**, solid line: **4b**.

These results indicate that the reduction potential of **2b** is shifted toward the more positive value relative to its fully aromatic precursor **1b**, and the shift for the tris(*S*,*S*-dioxide) (transformation of **3b** into **4b**) is even more conspicuous. It should be emphasized, however, that although the trend is clear, it is difficult to address quantitatively the actual oxidation–reduction potentials from the above peak potentials as no reversible redox couple is observed and the addition of one electron to the oligomer alters its dimensions. What is more, caution should be exercised in the comparison of the electrochemical results of OTs that possess different chemical and regiochemical substitution because rules for such permutations have not yet been formalized.[2] The above observations, however, clearly indicate that full *S*,*S*-oxygenation of OTs leads to materials that are better electron acceptors, a trend that is strongly enhanced when the length of the oligomer is increased. As the reduction potentials are related to the LUMO energies, the conclusion is that the longer the fully *S*,*S*-oxygenated OTs are, the lower their LUMO values. This feature is of course desirable when the issue is the acceptance of electrons from an outside source. The very high oxidation peak potentials, relative to other partially oxygenated OTs,[23] points to yet another advantage, namely, a greater stability of the fully oxygenated OTs toward air and damaging oxidation processes. In addition, indirect indication of the stability of these compounds can be deduced from their melting points. All OTDOs tested were thermally stable up to 250–300 °C and beyond; they tend to blacken at these temperatures, but in some cases do not melt even at 350 °C (see the Supporting Information).

X-ray structural analysis was performed on **4d**,[24] which showed that it crystallizes in a monoclinic system with a *C*2/*c* space group and has four molecules in the unit cell. The thienyl rings of each molecule exhibit an all-*anti,* nearly planar conformation, and the torsion angles between the mean planes of the rings are 3–9° (Figure 2a), which are in a

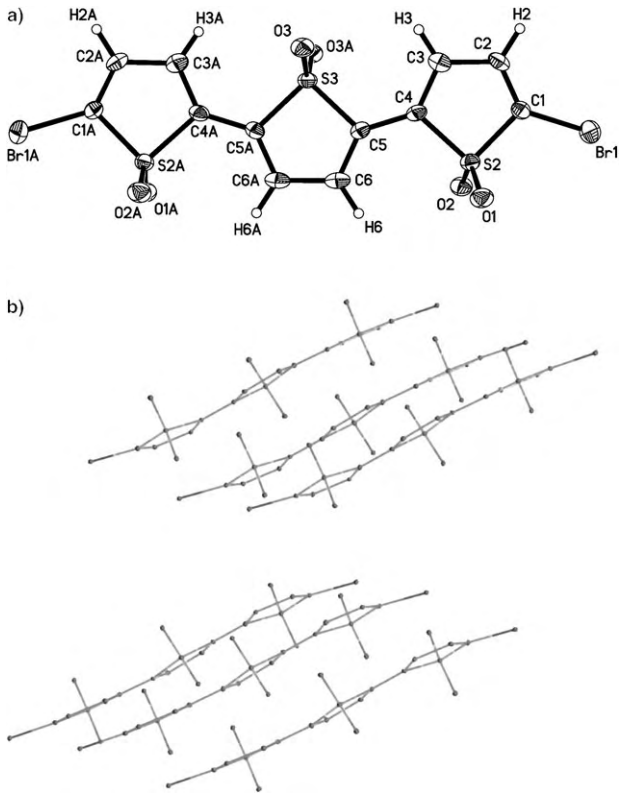

Figure 2. a) X-ray structure of **4d** and b) molecular structure and crystal packing of the unit cell of **4d**.

good agreement with the values reported for the unsubstituted α-3T.[25] The most promising feature of **4d**, however, is found in the molecular packing. It has been shown previously that, with a few exceptions,[3,26] most OTs studied so far have a typical "herringbone" (HB) arrangement with angles of 40–70° between the mean planes of the adjacent molecules. This packing is probably the best way for those molecules to decrease the intermolecular repulsion between the π orbitals, but it may also be responsible for their decreased transport properties in the direction of the long molecular axis.[27] In contrast, **4d** overcomes such repulsion and adopts an important π–π stacking arrangement of the molecular chains with an angle of 0° between the mean planes of the adjacent molecules (Figure 2b).

This favorable solid-state organization of the molecular chains may have an influence on the molecular nanoscale packing of the oligothiophene *S*,*S*-dioxides relative to the starting materials. Although not much can be said in this stage on the images obtained by scanning electron microscopy (SEM) for the OT **3b** and the product OTDO **4b**, there are some obvious differences in size and spatial distribution of the corresponding clusters. Under identical conditions, **3b** is rougher and has obvious discontinuities at grain boundaries. The *S*,*S*-dioxide **4b** displays many more clusters per a given

 © 2005 Wiley-VCH Verlag GmbH & Co. KGaA, Weinheim

area that are about ten times smaller in width, thus hinting at a greater cohesion between its crystals (Figure 3).

In conclusion, contrary to a long-held belief, working with dilute fluorine is not problematic. HOF·CH_3CN generated

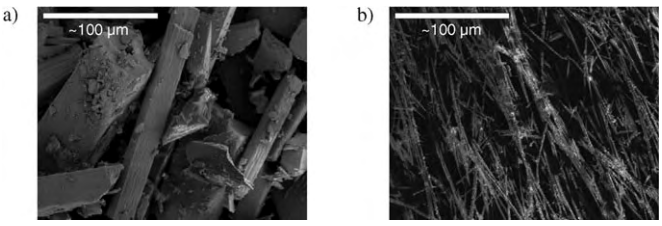

Figure 3. SEM images of a) OT **3b** and b) OTDO **4b**. Enlargement: 500× (≈100 μm).

in situ easily from F_2 and H_2O seems indeed to be the best oxygen-transfer agent offered in chemistry. Its strongly electrophilic oxygen atom opens up the only route so far that leads to the synthesis of the long sought after oligothiophene [all]-*S*,*S*-dioxides, whose initial characteristics are promising for use as field-effect transistors and other optoelectronic devices.

Experimental Section

A detailed procedure of how to work with F_2 and prepare HOF·CH_3CN can be found in reference [18]. We present a typical experiment for making the hexaoxide of the terthiophene **4b**. For full characterization of all the oxygenated compounds, see the Supporting Information.

4b: Terthiophene **3b**[21] was dissolved in CH_2Cl_2 at 0 °C. A solution of HOF·CH_3CN, kept at a similar or lower temperature, was added in one portion to the reaction mixture and the reaction was stopped after 1 min by addition of $NaHCO_3$. The organic material was extracted with CH_2Cl_2, washed with water, and dried over $MgSO_4$. The product was purified by vacuum flash chromatography on silica gel 60-H (Merck) and recrystallized from $CHCl_3$. Yield: 82%. M.p. 290–292 °C (turning black; from $CHCl_3$); ^{1}H NMR (200 MHz, $CDCl_3$): 7.28 (2H, s), 7.13 (2H, d, $J = 5$ Hz), 6.61 (2H, d, $J = 5$ Hz), 1.42 ppm (18H, s); ^{13}C NMR(50.2 MHz, $CDCl_3$): 155.3, 130.6, 129.3, 124.2, 123.9, 121.9, 35.0, 29.0 ppm; EI MS *m*/*z* (%): 456.1 ([M^+]); elemental analysis (%) calcd for $C_{20}H_{24}O_6S_3$: C 52.61, H 5.30, S 21.07; found: C 52.82, H 5.45, S 20.92.

Received: May 16, 2005
Published online: October 27, 2005

Keywords: fluorine · hypofluorous acid · oligomers · oxygenation · thiophenes

[1] E. H. Elandaloussi, P. Frere, P. Richomme, J. Orduna, J. Garin, J. Roncali, *J. Am. Chem. Soc.* **1997**, *119*, 10774.
[2] A. Facchetti, M. H. Yoon, C. L. Stern, G. R. Hutchison, M. A. Ratner, T. J. Marks, *J. Am. Chem. Soc.* **2004**, *126*, 13480.
[3] M. Turbiez, P. Frere, M. Allain, C. Videlot, J. Ackermann, J. Roncali, *Chem. Eur. J.* **2005**, *11*, 3742.
[4] S. Ando, J. Nishida, H. Tada, Y. Inoue, S. Tokito, Y. Yamashita, *J. Am. Chem. Soc.* **2005**, *127*, 5336.
[5] a) G. Horowitz, D. Fichou, X. Peng, Z. Xu, F. Garnier, *Solid State Commun.* **1989**, *72*, 381; b) F. Garnier, G. Horowitz, X. Peng, D. Fichou, *Adv. Mater.* **1990**, *2*, 592.
[6] See, for example: a) H. Shirakawa, *Chem. Commun.* **2003**, 1; b) H. E. Katz, Z. Bao, S. L. Gilat, *Acc. Chem. Res.* **2001**, *34*, 359; c) B. Crone, A. Dodabalapur, Y. Llin, R. W. Filas, Z. Bao, A. Laduca, R. Sarpeshkar, H. E. Katz, *Nature*, **2000**, *403*, 521; d) J. M. Tour, *Acc. Chem. Res.* **2000**, *33*, 791.
[7] K. Tanaka, S. Wang, T. Yamabe, *Synth. Met.* **1989**, *30*, 57.
[8] G. Barbarella, O. Pudova, C. Arbizzani, M. Mastragostino, A. Bongini, *J. Org. Chem.* **1998**, *63*, 1742.
[9] G. Barbarella, L. Favaretto, G. Sotgiu, M. Zambianchi, L. Antolini, O. Pudova, A. Bongini, *J. Org. Chem.* **1998**, *63*, 5497.
[10] S. Rozen, M. Brand, *Angew. Chem.* **1986**, *98*, 565; *Angew. Chem. Int. Ed. Engl.* **1986**, *25*, 554.
[11] a) S. Rozen, S. Dayan, *Angew. Chem.* **1999**, *111*, 3680; *Angew. Chem. Int. Ed.* **1999**, *38*, 3471; b) M. Carmeli, S. Rozen, *J. Org. Chem.* **2005**, *70*, 2131.
[12] E. Golan, S. Rozen, *J. Org. Chem.* **2003**, *68*, 9170.
[13] a) S. Rozen, M. Carmeli, *J. Am. Chem. Soc.* **2003**, *125*, 8118; b) G. K. S. Prakash, M. Etzkorn, *Angew. Chem.* **2004**, *116*, 26; *Angew. Chem. Int. Ed.* **2004**, *43*, 26.
[14] a) S. Rozen, E. Golan, *Eur. J. Org. Chem.* **2003**, 1915; b) E. Golan, A. Hagooly, S. Rozen, *Tetrahedron Lett.* **2004**, *45*, 3397.
[15] For the latest review on HOF·CH_3CN, see: S. Rozen, *Eur. J. Org. Chem.* **2005**, 2419.
[16] a) S. Rozen, Y. Bareket, *J. Chem. Soc. Chem. Commun.* **1994**, 1959; b) S. Rozen, Y. Bareket, *J. Org. Chem.* **1997**, *62*, 1457.
[17] C. Aleman, E. Brillas, A. G. Davies, L. Fajari, D. Giro, L. Julia, J. J. Perez, J. Rius, *J. Org. Chem.* **1993**, *58*, 3091.
[18] For the detailed procedure of the easy preparation of HOF·CH_3CN, see: S. Dayan, Y. Bareket, S. Rozen, *Tetrahedron* **1999**, *55*, 3657.
[19] Y. Nicolas, P. Blanchard, E. Levillain, M. Allain, N. Mercier, J. Roncali, *Org. Lett.* **2004**, *6*, 273.
[20] P. Bauerle, F. Wurthner, G. Gotz, F. Effenberger, *Synthesis* **1993**, 1099.
[21] A. Mac Eachern, C. Soucy, L. C. Leitch, J. T. Arnason, P. Morand, *Tetrahedron* **1988**, *44*, 2403.
[22] a) C. Arbizzani, G. Barbarella, A. Bongini, L. Favaretto, M. Mastragostino, P. Ostoja, O. Pudova, M. Zambianchi, *Opt. Mater.* **1998**, *9*, 43; b) G. Barbarella, L. Favaretto, M. Zambianchi, O. Pudova, C. Arbizzani, A. Bongini, M. Mastragostino, *Adv. Mater.* **1998**, *10*, 551.
[23] In several works on OT, this gap was determined from the very onset of absorption as no other alternative was to be found. This procedure can lead to rather large uncertainties and artificially high values. As the OTDO present distinguished low energy λ_{max}, we felt more comfortable and used that value for calculating the HOMO–LUMO gaps.
[24] CCDC 267228 contains the supplementary crystallographic data for this paper. These data can be obtain free of charge from the Cambridge Crystallography Data Centre via www.ccdc.cam.ac.uk/data request/cif.
[25] F. Van Bolhuis, H. Wynberg, E. E. Havinga, E. W. Meijer, E. G. J. Staring, *Synth. Met.* **1989**, *30*, 381.
[26] L. Antolini, E. Tedesco, G. Barbarella, L. Favaretto, G. Sotgiu, M. Zambianchi, D. Casarini, G. Gigli, R. Cingolani, *J. Am. Chem. Soc.* **2000**, *122*, 9006.
[27] D. Fichou, *J. Mater. Chem.* **2000**, *10*, 571.

 © 2005 Wiley-VCH Verlag GmbH & Co. KGaA, Weinheim

Synthetic Methods

DOI: 10.1002/anie.200502879

Ordered Multistep Synthesis in a Single Solution Directed by DNA Templates**

*Thomas M. Snyder and David R. Liu**

The use of DNA templates to direct chemical reactions enables the principles of biological evolution to be applied to the discovery of synthetic molecules and new chemical reactions.[1] In addition, the use of DNA hybridization to modulate the effective molarity of DNA-linked reactants allows synthetic molecules to be manipulated in ways that cannot be accessed using traditional synthetic methods.[2] For example, many oligomeric natural products, including proteins, nonribosomal peptides, and polyketides, are biosynthesized in a strictly ordered manner even though all of their constituent building blocks are simultaneously present in the cellular milieu.[3] Nature achieves single-solution ordered multistep synthesis by increasing the effective molarity of specific sets of reactants at precise moments during biosynthesis. Compared to the strategy most frequently used by chemists to execute ordered multistep synthesis—dividing the construction of a molecule into a sequence of isolated reaction steps—nature's single-solution approach is not only remarkably elegant and efficient but also sufficiently selective to obviate the need for protecting groups.

In the absence of enzymes, ordered multistep synthesis in a single solution has proven to be a challenge. The ordered oligomerization of nucleotides on nucleic acid templates[1a,4] has been achieved, but these methods have not allowed the synthesis of non-nucleic acid structures. Tamura and Schimmel[5] have used RNA-templated synthesis to direct peptide-bond formation in an order determined by intrinsic differences in substrate reactivity. Relying on substrate reactivity differences, however, imposes significant constraints on the order of building blocks within the possible products. Even with precisely tuned reactivities, multistep syntheses generally still require sequential additions of reactants to form ordered products. Herein, we report the ordered multistep syntheses of both a triolefin and a tripeptide using DNA-linked substrates of comparable intrinsic reactivity that are simultaneously present in one solution. In both cases, temperature-sensitive variations in DNA secondary structure orchestrate a series of effective molarity changes among four reactants to primarily generate one ordered product out of many possibilities. These results represent two strategies for ordered synthesis in a single solution without the structural constraints imposed by enzymes and can significantly enhance the efficiency and selectivity of multistep DNA-templated synthesis.[6]

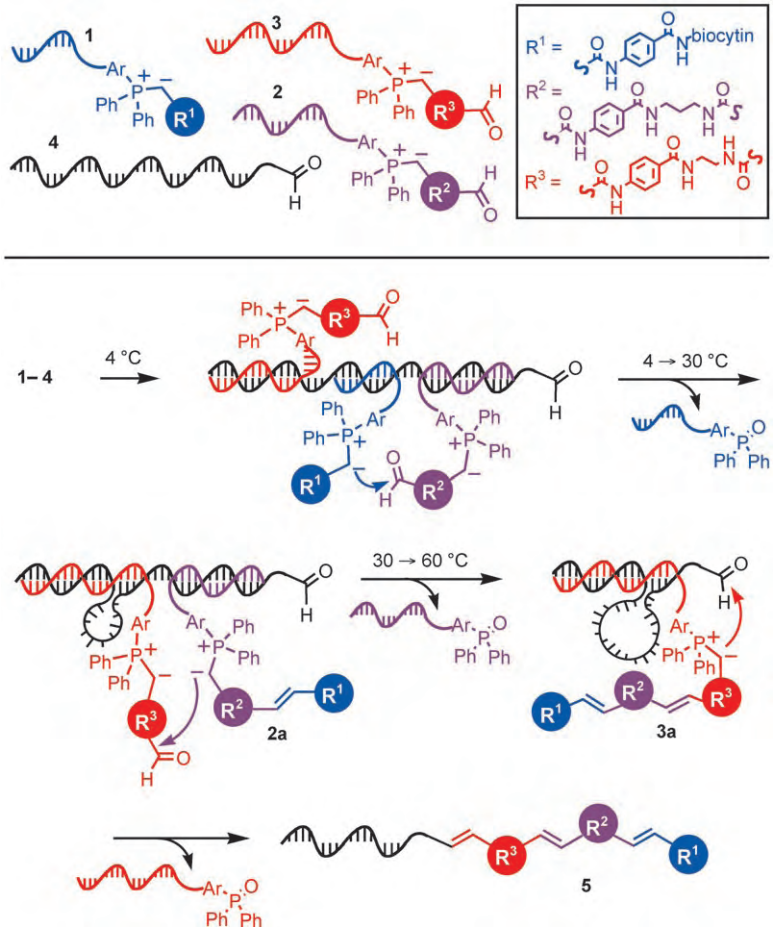

Figure 1. Strategy for the single-solution synthesis of an ordered triolefin. Building blocks are transferred sequentially among phosphorane reagents **1**–**3** before addition to an aldehyde-linked template **4**. The rigidity of double-stranded DNA enforces Wittig olefination regioselectivity. As the reaction temperature is elevated, the DNA secondary structure undergoes sequence-programmed changes that enables the desired Wittig olefination to take place selectively.

The first strategy (Figure 1) passes synthetic intermediates from site to site on a template in a manner controlled by changes in the DNA secondary structure. Three Wittig olefination substrates (**1**–**3**, with **1** containing a biotin group),[7] each linked to DNA oligonucleotides of varying melting temperature (T_m), were prepared and hybridized to an aldehyde-terminated DNA template **4** at 4 °C. If these substrates were combined at the high concentrations (mM–M) typical of organic synthesis, a complex mixture of many

[*] T. M. Snyder, Prof. D. R. Liu
Harvard University
Department of Chemistry and Chemical Biology
12 Oxford Street, Cambridge, MA 02138 (USA)
Fax (+1) 617-496-5688
E-mail: drliu@fas.harvard.edu

[**] Funding was generously provided by the NIH/NIGMS (R01 M065865), the Office of Naval Research (N00014-03-1-0749), and an NSF Graduate Research Fellowship to T.M.S.

Supporting information for this article is available on the WWW under http://www.angewandte.org or from the author.

© 2005 Wiley-VCH Verlag GmbH & Co. KGaA, Weinheim

products would result from their random reaction. At a concentration of 100 nM each, however, only substrates juxtaposed in a productive way by DNA hybridization react at a significant rate.[8] Upon phosphonium deprotonation, seven intermolecular Wittig olefinations were in principle possible among these four reactants. At the lowest temperature (4 °C), however, six of the seven possible Wittig reactions are precluded because their reactants are separated by double-stranded DNA. As we previously demonstrated, the rigidity of double-stranded DNA can enforce the separation of substrates that flank duplex DNA, thus preventing their reaction.[8] At 4 °C, the only phosphorane–aldehyde pair not separated by the duplex DNA was **1** and **2**, which reacted to generate DNA-linked monoolefin **2a**.

As the temperature was elevated to 30 °C, the species with the lowest T_m value (the phosphine oxide of **1**) dissociated from the template, thus allowing reactants **2a** and **3** to react to form diolefin **3a**. When the temperature was increased to 60 °C, the phosphine oxide of **2** dissociated, which enabled the final reaction to take place between **4** and **3a** to generate ordered triolefin **5** (Figure 1).

Following the capture of R^1-linked products with immobilized streptavidin, we obtained triolefin **5** in 24% overall yield (Figure 2a, lanes C and D). As expected, captured products lacking the R^1 group were not detected. Truncated products represented less than 10% of the isolated material, as analyzed by denaturing polyacrylamide gel electrophoresis (PAGE) analysis. To confirm the order of the building blocks in the products, control reactions were performed with reactants lacking aldehyde groups. Removing the aldehyde group from **2** prevented the reaction of **1** with **2** and resulted in a diolefin template-R^3-$R^{2\prime}$ product (Figure 2a, lane B). Removing the aldehyde group from both **3** and **2** prevented all reactions except for the reaction of **3** with template **4** to generate the monoolefin template–$R^{3\prime}$ (Figure 2a, lane A). MALDI-TOF mass-spectroscopic analysis was consistent with the expected product structures (Figure 2b).

We repeated the ordered triolefin synthesis and control reactions using reagents in which the R^2 and R^3 groups were interchanged on **2** and **3**. The resulting products contained the expected R^2-R^3-R^1 building-block order (Figure 2c). Consistent with our reactivity model, control reactions using sequence-mismatched reagents **1c**, **2c**, or **3c** resulted in either no transfer of the biotinylated R^1 group to **4** (using **1c** or **3c**) or in the direct reaction of **1** and **4** (using **2c**; see the Supporting Information). Collectively, these results demonstrate that the order of Wittig olefination in this system is tightly controlled by sequence-programmed changes in the DNA secondary structure and is not determined by intrinsic reactivity differences among the substrates.

Our second target was the synthesis of an ordered tripeptide from a single solution containing three *N*-hydroxysuccinimidyl (NHS) ester activated amino acids. Because the DNA-linked NHS by-product of amine acylation is capable of transesterification with NHS esters (see the Supporting Information), the transfer of building blocks between

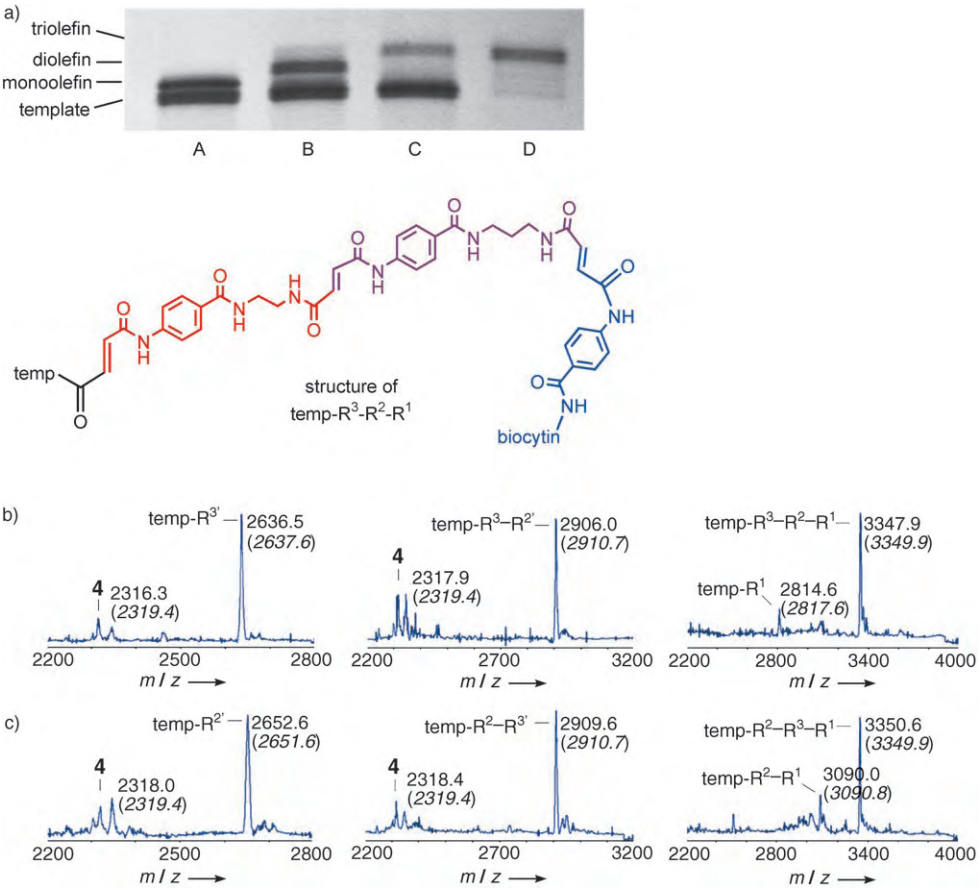

Figure 2. a) Denaturing PAGE analysis of the ordered triolefin synthesis. Conditions: 100 nM of **1**–**4** were hybridized in aqueous 50 mM NaOAc (pH 5.0), 1 M NaCl; treated with 0.1 M *N*-tris(hydroxymethyl)methyl-3-aminopropanesulfonic acid (TAPS; pH 8.0), and 1 M NaCl; and incubated for 1 h at 4 °C, 1 h at 30 °C, and 2 h at 60 °C. The crude reaction mixture is shown in lane C with the streptavidin-captured product in lane D. Control reactions lacking an aldehyde group on both **2** and **3** (lane A) or on **2** only (lane B) were performed under identical conditions to produce either a monoolefin or diolefin, respectively. b) MALDI-TOF mass-spectroscopic data of products from reactions shown in (a). The three spectra correspond, from left to right, to lanes A, B, and D from (a), respectively. c) MALDI-TOF mass-spectroscopic data for the reactions using swapped building blocks (R^3 attached to **2**, and R^2 attached to **3**). Expected masses for (b) and (c) are listed in parentheses; the expected error is ±6 Da. The prime designation ($R^{2\prime}$ and $R^{3\prime}$) in (b) and (c) refers to the forms of these building blocks lacking aldehyde groups (see the text). temp = template **4**.

© 2005 Wiley-VCH Verlag GmbH & Co. KGaA, Weinheim

reagents as in Figure 1 is not possible without significant loss of the desired product through capture by DNA-linked NHS groups. Instead, a different strategy is required that allows three consecutive transfers from three NHS ester reagents to a growing template-linked molecule. We hypothesized that oligonucleotide masks designed to selectively block the hybridization of DNA-linked reagents at certain temperatures could be used to achieve this goal (Figure 3a). Indeed,

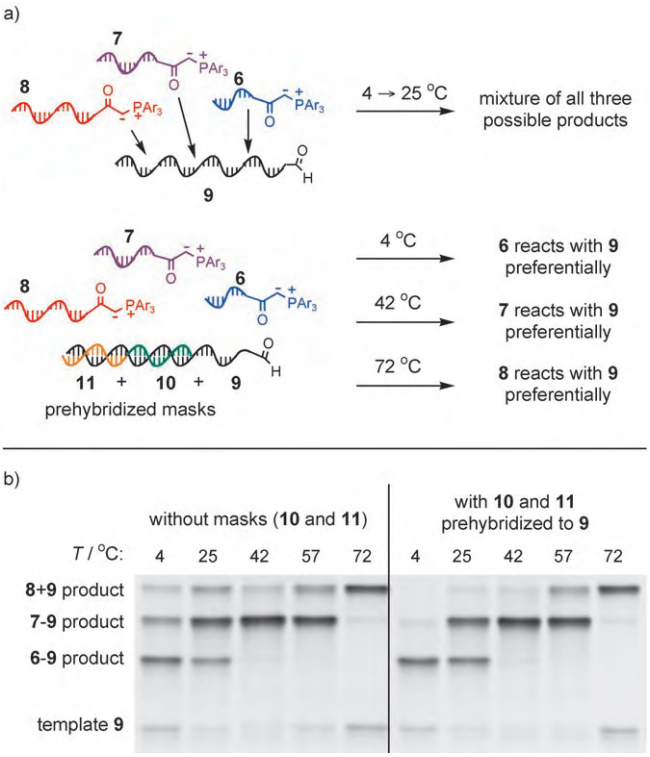

Figure 3. a) Strategy for using oligonucleotide masks **10** and **11** to order the reaction of three reagents **6**–**8** with a template (**9**). When all masks are hybridized (4 °C), only **6** can react. At an intermediate temperature (42 °C), mask **10** is melted from the template allowing **7** to react exclusively. At a high temperature (72 °C), only **8** can react. b) Denaturing PAGE analysis of the reactions in (a). Conditions: 150 nM of **9** (with or without masks **10** and **11** at 225 nM) was incubated at the indicated temperature. Reagents **6**–**8** were added simultaneously to 200 nM each and the reaction was incubated 1 h before analysis.

although a mixture of all possible products was formed when DNA-linked phosphoranes **6**–**8** were added simultaneously to aldehyde-linked template **9**, when masks **10** and **11** were prehybridized to the template before the addition of **6**–**8**, reactivity became strongly dependent on the reaction temperature approaching or exceeding the T_m value of each mask (25–30 °C for **10** and 60–65 °C for **11**; Figure 3b).

Using this approach, we performed a single-solution ordered tripeptide synthesis (Figure 4a). An amine-terminated template **12** was prehybridized with masks **10** and **11** at 4 °C. When NHS ester linked reagents **13**–**15** were combined with the masked template **10** + **11** + **12** at 4 °C for 20 min, only **13** could hybridize to the template and react to generate a monopeptide. As the solution was heated to 37 °C for 20 min, both the expended first reagent and the first mask **10** dissociated from the template, thus exposing the binding site for the second reagent **14**, which then hybridized and reacted to generate a template-linked dipeptide. At the highest temperature (62 °C for 2 h), all masks and expended reagents were melted except for **15**, which reacted to form the ordered tripeptide **16**. Unlike the first strategy in which incomplete reactivity reduces overall yield but does not generate truncated biotinylated by-products, this strategy requires each step to proceed in high yield to generate the tripeptide (and not truncated mono- or dipeptides) as the major product.

Aliquots of the reaction mixture taken after incubations at 4 and 37 °C were quenched with 1M tris(hydroxymethyl)aminomethane (Tris). Analysis by MALDI-TOF-MS (Figure 4b) revealed that **13** reacts exclusively with the template at 4 °C, followed by the reaction of **14** at 37 °C. Biotinylated templates that arise from the reaction of **15** were isolated using streptavidin-linked beads in 45% yield, as determined by denaturing PAGE, and analyzed by MALDI-TOF-MS (Figure 4b). The strongest signal in the purified product mixture is the desired tripeptide **16** with the most significant side product being the dipeptide R^1–R^3 which results from the lack of reaction with **14**. Sequence-mismatched reagents **13b** or **14b** were unable to react in place of **13** or **14** (see the Supporting Information).

When the oligonucleotides linked to the R^1 and R^2 groups were swapped, the order of building-block addition was also switched (R^2 added first at 4 °C, then R^1 added at 37 °C; see the Supporting Information). The biotinylated products of this reaction sequence, including the ordered tripeptide **12**-R^2-R^1-R^3, were isolated in 38% yield after streptavidin purification. For this reaction, the desired tripeptide and truncated side products were resolvable by denaturing PAGE (unlike in the case of **16**), revealing that 55% of the isolated material (21% total overall yield) is the ordered tripeptide (see the Supporting Information). Taken together, these findings indicate that the use of temperature-controlled template masking enables substrates that would normally form a vast mixture of oligomeric products to react in a predominantly ordered manner.

These results represent single-solution ordered multistep syntheses using comparably reactive substrates in the absence of enzymes with only a temperature gradient needed to coordinate the timing of three successive reactions. Both strategies offer faster, higher-yielding routes to multistep DNA-linked products constructed from autocleaving reagents[6] than past examples (indeed, a previous DNA-templated tripeptide synthesis using three discrete steps proceeded in 3% overall yield).[6] In addition to enabling a mode of chemical reactivity that is not possible in a conventional synthesis format, these concepts may also facilitate the design of additional systems that mimic the efficiency and selectivity of organic synthesis in the cell without the structural constraints imposed by enzymes.

Received: August 12, 2005
Published online: October 11, 2005

 © 2005 Wiley-VCH Verlag GmbH & Co. KGaA, Weinheim

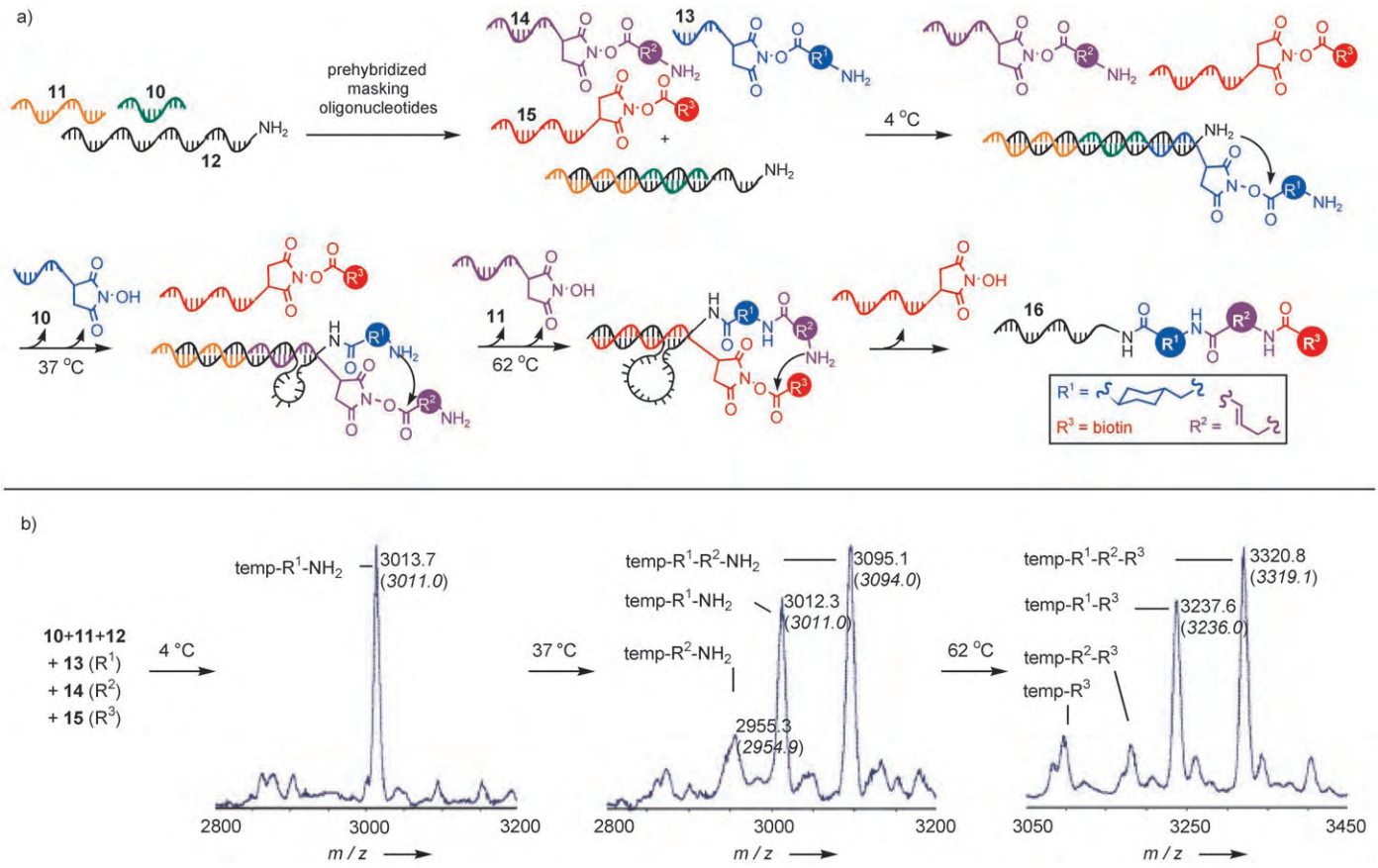

Figure 4. a) Strategy for the single-solution synthesis of an ordered tripeptide using oligonucleotide masks. b) MALDI-TOF mass spectroscopy of each stage of the reaction in (a). Conditions: 200 nM **12** was prehybridized to 1.5 equivalents each of **10** and **11** in 0.2 M 3-(*N*-morpholino)-propanesulfonic acid (MOPS, pH 7.0), 2 M NaCl at 4 °C. Simultaneously, 1.05 equivalents of **13** and **14** and 3.0 equivalents of **15** were added to **10**+**11**+**12**. After dilution caused by the addition of the reagents, the final concentration of solutes in this reaction mixture was 0.1 M MOPS (pH 7.0), 1 M NaCl with 100 nM template **12**. The reaction mixture was incubated at 20 min at 4 °C, 20 min at 37 °C, and 2 h at 62 °C. Reactions were quenched with Tris (after either of the first two steps) or purified with streptavidin-linked beads (after the third step) before analysis. Expected masses for (b) are listed in parentheses; the expected error is ±6 Da. temp = template **12**.

Keywords: biomimetic synthesis · DNA · regioselectivity · synthetic methods · template synthesis

[1] a) X. Li, D. R. Liu, *Angew. Chem.* **2004**, *116*, 4956–4979; *Angew. Chem. Int. Ed.* **2004**, *43*, 4848–4870; b) Z. J. Gartner, B. N. Tse, R. Grubina, J. B. Doyon, T. M. Snyder, D. R. Liu, *Science* **2004**, *305*, 1601–1605; c) M. W. Kanan, M. M. Rozenman, K. Sakurai, T. M. Snyder, D. R. Liu, *Nature* **2004**, *431*, 545–549.

[2] C. T. Calderone, J. W. Puckett, Z. J. Gartner, D. R. Liu, *Angew. Chem.* **2002**, *114*, 4278–4282; *Angew. Chem. Int. Ed.* **2002**, *41*, 4104–4108.

[3] C. T. Walsh, *Science* **2004**, *303*, 1805–1810.

[4] a) I. A. Kozlov, B. De Bouvere, A. V. Aerschot, P. Herdewijn, L. E. Orgel, *J. Am. Chem. Soc.* **1999**, *121*, 5856–5859; b) I. A. Kozlov, L. E. Orgel, *Mol. Biol.* **2000**, 781–789; c) X. Li, Z. J. Zhan, R. Knipe, D. G. Lynn, *J. Am. Chem. Soc.* **2002**, *124*, 746–747; d) D. M. Rosenbaum, D. R. Liu, *J. Am. Chem. Soc.* **2003**, *125*, 13924–13925.

[5] K. Tamura, P. Schimmel, *Proc. Natl. Acad. Sci. USA* **2003**, *100*, 8666–8669.

[6] Z. J. Gartner, M. W. Kanan, D. R. Liu, *J. Am. Chem. Soc.* **2002**, *124*, 10304–10306.

[7] a) Z. J. Gartner, M. W. Kanan, D. R. Liu, *Angew. Chem.* **2002**, *114*, 1874–1878; *Angew. Chem. Int. Ed.* **2002**, *41*, 1796–1800; b) Z. J. Gartner, R. Grubina, C. T. Calderone, D. R. Liu, *Angew. Chem.* **2003**, *115*, 1408–1413; *Angew. Chem. Int. Ed.* **2003**, *42*, 1370–1375.

[8] Z. J. Gartner, D. R. Liu, *J. Am. Chem. Soc.* **2001**, *123*, 6961–6963.

 © 2005 Wiley-VCH Verlag GmbH & Co. KGaA, Weinheim

Combinatorial Chemistry

DOI: 10.1002/anie.200502899

Small-Molecule Diversification from Iterated Branching Reaction Pathways Enabled by DNA-Templated Synthesis**

*Christopher T. Calderone and David R. Liu**

As synthetic small molecules continue to interface with an increasingly large swath of biology,[1,2] researchers have sought new approaches to rapidly create collections of highly diverse small molecules.[3] Early small-molecule libraries generally contained a single core scaffold decorated by different chemical groups.[4] Later efforts introduced modest structural variation in the central scaffold.[5] More recently, researchers have introduced libraries based on "folding pathways", in which library intermediates undergo diverse rearrangements, and "differentiation pathways", in which intermediates are treated with different reagents to yield different scaffolds.[3] Incorporating such branching reaction pathways into library syntheses is a promising strategy for the creation of small-molecule diversity beyond what can be accessed by using nonbranched synthetic routes.[6]

The vast majority of current library synthesis efforts are based on solid-phase, split-pool methodologies.[7,8] Although these methods offer technical advantages, they also limit the diversity of structures that can be created. With relatively few exceptions,[5,9–11] it is generally not possible to direct a specific subset within a mixture of beads (for example, those beads containing molecules with a primary amine group) to one of several possible subsequent reaction conditions (for example, exposure to an acylating agent). As a result, every intermediate in a split-pool library synthesis must be reactive toward any reactant it may encounter in a subsequent step. Moreover, it is usually not possible to purify unreacted support-bound starting material away from desired products after each library synthesis step, so only highly efficient reactions can be used. As a result, the diversification of scaffolds during library synthesis has thus far been limited to a single (predominantly terminal) step.[12–15]

We recently demonstrated the ability of DNA-templated organic synthesis (DTS) to direct multiple, otherwise incompatible reactions in a single vessel.[16] We speculated that this feature and other properties of DTS,[17] such as the ability to purify library intermediates away from starting materials independent of product structure in a single manipulation,[18,19] would enable DTS-driven library synthesis to exploit branching reaction pathways at multiple steps, thus creating a network of reaction sequences that generates highly diverse families of molecules within a single library.[16] To implement the concept of iterated branching reaction pathways in a DNA-templated format, we set out to transform a single solution containing five DNA templates into five diverse types of product structures, each arising from a unique sequence of reactions. We designed a synthetic route (Scheme 1) that combines base-labile sulfone[18] and thioester[20] linkers, previously developed for multistep DTS, together with amine acylation,[21] aldehyde thiazolidination, Wittig olefination,[21] carboxylate amidation, and palladium-catalyzed cross-coupling chemistries.[21,22]

In previous DNA-templated libraries,[19] split-pool oligonucleotide synthesis was used to generate starting-template pools in which every combination of reagent annealing sequence ("codons") was represented. In the case of libraries constructed from branching reaction pathways, however, only a fraction of such a collection of templates would encode productive reaction sequences. For example, only 36% of the possible templates of the format (reaction 1 codon)–(reaction 2 codon)–(reaction 3 codon) encode three-step products in the branching library synthesis shown in Scheme 1. To address this problem, we developed a cassette ligation strategy to generate starting-template pools. In this strategy, single-stranded DNA overhangs at the ends of each cassette were designed such that ligation is only possible between adjacent cassettes that encode productive reaction sequences (see the Supporting Information).

To validate each three-step pathway, we optimized the five syntheses individually such that all step-1 reactions, all step-2 reactions, and all step-3 reactions are carried out under reaction conditions (a), (b), or (c), respectively (Figure 1). Each pathway was then individually executed starting with amine-terminated oligonucleotide **1**. After each step, the reaction mixture was captured on immobilized streptavidin and washed to remove any starting material template. The desired template-linked product eluted from the beads upon base-induced linker cleavage.[18]

All five pathways begin with amine acylation (step 1). In step 2—the first branching step—the step-1 products participate in one of three reactions (acylation, thiazolidine formation, or Wittig olefination) dictated by the identity of the previous reaction partner of each molecule. For example, the step-1 products containing phosphorane groups exclusively participate in step-2 Wittig olefination reactions. Step 3 represents a second branch point, in which each reaction type is dictated by the structure established in step 2.

Pathway I consists of amine acylation followed by thiazolidine formation and amidation. Disulfide-protected L-cysteine was sequence-specifically delivered to the template **1** upon addition of 1-ethyl-3-(3-dimethylaminopropyl)carbodiimide (EDC) and *N*-hydroxysulfosuccinimide (*s*-NHS) in 26% yield of isolated product. After disulfide reduction,

[*] C. T. Calderone, Prof. D. R. Liu
Harvard University
Department of Chemistry and Chemical Biology
12 Oxford Street, Cambridge, MA 02138 (USA)
Fax: (+1) 617-496-5688
E-mail: drliu@fas.harvard.edu

[**] This work was supported by the NIH/NIGMS (R01GM065865), the Office of Naval Research (No. N00014-03-1-0749), and an ACS Division of Organic Chemistry Graduate Research Fellowship to C.T.C. We thank Thomas M. Snyder for assistance with codon design.

Supporting information for this article is available on the WWW under http://www.angewandte.org or from the author.

 © 2005 Wiley-VCH Verlag GmbH & Co. KGaA, Weinheim

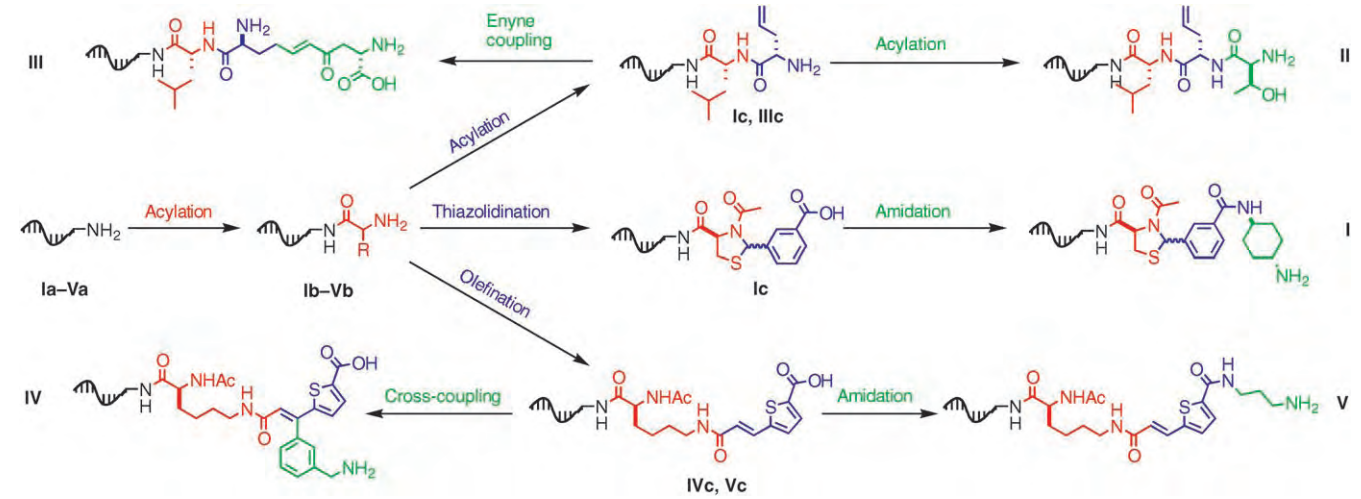

Scheme 1. Synthetic strategy for iterated branching reaction pathways.

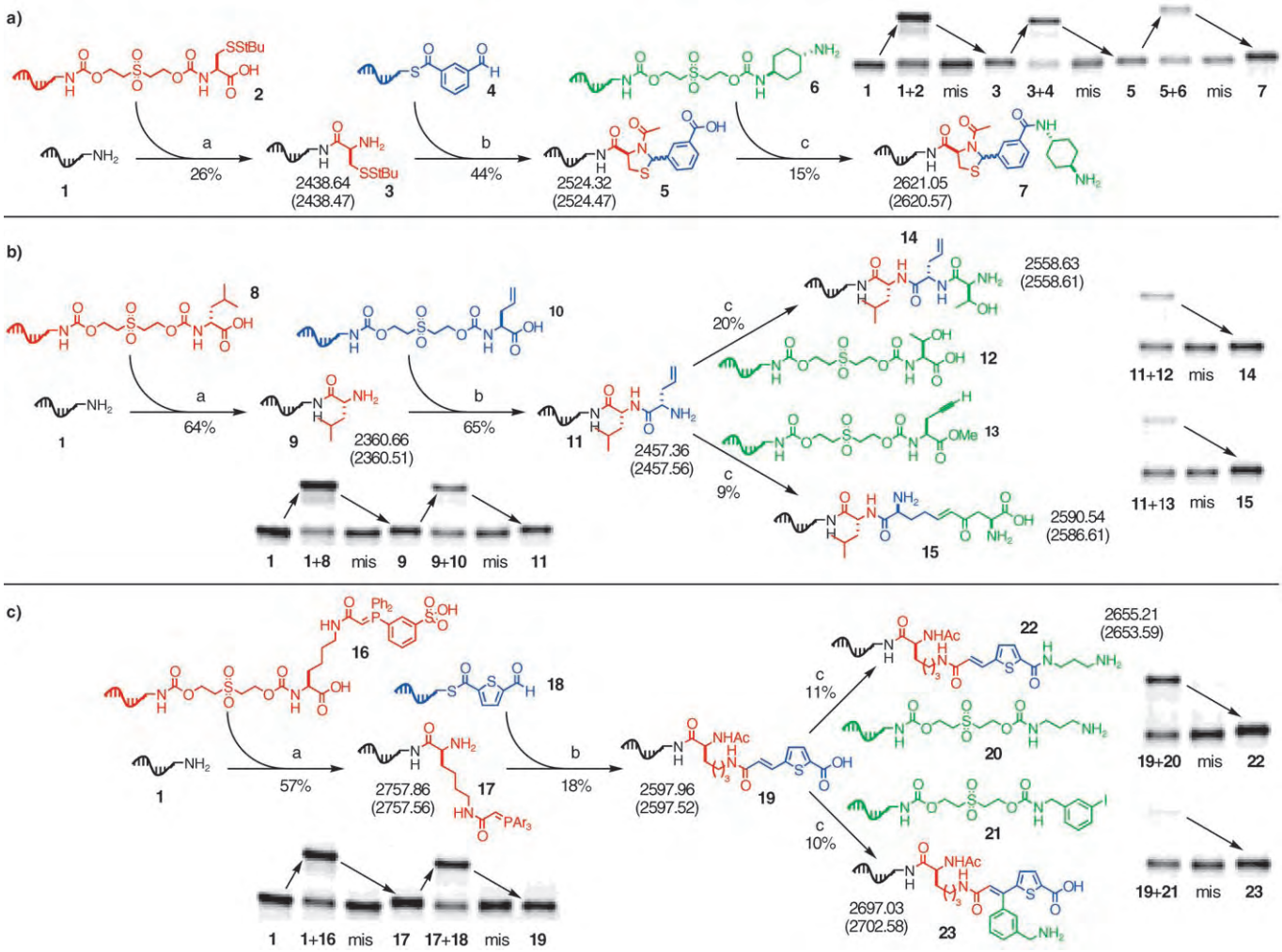

Figure 1. Individual validation of the five reaction pathways. Template amine **1** was separately treated with the specified oligonucleotide-linked reagents to yield **7**, **14**, **15**, **22**, and **23**. In each denaturing polyacrylamide gel electrophoresis (PAGE) image, lower bands represent template **1** or functionalized derivatives thereof, and upper bands represent covalently linked template–reagent pairs. Each cleaved intermediate was digested with *Eco*RI and subjected to mass-spectrometric analysis as shown, with calculated masses given in parentheses. To verify sequence specificity of each DNA-templated reaction, a sample of each template intermediate was treated with a reagent oligonucleotide containing a scrambled DNA sequence ("mis"). Reaction conditions: a) 20 mM EDC, 15 mM *s*-NHS, pH 6.0, 12 h, 23 °C, then pH 10.0 buffer, 2 h, 37 °C; b) 25 mM 1,4-dithiothreitol (DTT), pH 8.5, 1 h, 37 °C, then pH 7.0 buffer, 90 min, then 20 mM EDC, 15 mM *s*-NHS, 12 h, 23 °C, then 1:200 volume Ac_2O, 1 h, then pH 12.0 buffer, 10 mM 2-mercaptoethanol, 1 h, 37 °C; c) 1 M NaBr, 50 μM $Na_2[PdCl_4]$, pH 6.0, 4 h, 37 °C, then 25 mM DTT, 10 min, 85 °C, then 20 mM EDC, 15 mM *s*-NHS, pH 6.0, 12 h, 23 °C, then pH 12.0 buffer, 30 min, 23 °C.

© 2005 Wiley-VCH Verlag GmbH & Co. KGaA, Weinheim

treatment with a complementary DNA-linked thiol bearing 3-formylbenzoic acid for 90 min before the addition of EDC/*s*-NHS and acetylation yielded thiazolidine **5** in 44% yield. Treatment with Pd^{II} at 37°C for 4 h and addition of EDC/*s*-NHS yielded product **7** in 15% yield (2% overall yield of isolated product over three steps, Figure 1a).

Pathways II and III use identical reaction conditions as pathway I but effect two consecutive amine acylations in steps 1 and 2. The third step of pathway II consists of a final amine acylation to yield a tripeptide, whereas the third step of pathway III uses a palladium-catalyzed alkene–alkyne coupling to generate an enone.[22] To validate these pathways, D-leucine and L-allylglycine were sequentially added to template **1** (steps 1 and 2) in 64 and 65% yields of the isolated products, respectively, to form **11**. In step 3, the allylglycine was either acylated with L-threonine to yield tripeptide **14** in 20% yield (pathway III, 8.3% yield of the isolated product over three steps) or was cross-coupled[22] with the alkyne group in L-propargylglycine to yield enone **15** in 8% yield (pathway IV, 3.6% yield of the isolated product over three steps; Figure 1b).

Finally, pathways IV and V begin with amine acylation followed by Wittig olefination. The third step of pathway IV is carboxylate amidation, whereas the third step in pathway V is a palladium-catalyzed Heck reaction. Thus, a lysine derivative bearing a side-chain phosphorane **16** was coupled to **1** (step 1) in 57% yield of the isolated product followed by incubation with the DNA thioester of formylthiophene carboxylic acid (step 2) to yield **19** in 18% yield of isolated product. In the third step, treatment with amine **20** yielded disubstituted olefin **22** in 11% yield of isolated product (1.7% yield over three steps), whereas the Heck coupling with aryl iodide **21** yielded trisubstituted olefin **23** in 10% yield of isolated product (0.8% yield over three steps; Figure 1c). All five pathways were monitored by gel electrophoresis and MALDI-TOF mass-spectrometric analysis. Each pathway yielded intermediates and final products whose electrophoretic behavior and mass-spectrometric characterization were consistent with the desired structures. The reaction sequences resulted in product yields similar to those reported for previous three-step DNA-templated synthetic sequences, despite requiring compromises among the different optimal reaction conditions in steps 2 and 3.[18–20]

Having developed each of the pathways individually, we next performed the simultaneous synthesis of **I**–**V** in a single solution per step (Figure 2). The ligated and gel-purified pool of templates was treated with 1.5 equivalents of each functionalized-reagent DNA per step and was incubated under the same conditions used to verify each pathway individually. After each step, we observed only the presence of desired products by nuclease digestion followed by MALDI-TOF-MS. To evaluate the sequence specificity of each reaction, each step was repeated using reagents linked to noncomplementary (mismatched) oligonucleotides. No significant product formation (< 5%) was observed (Figure 2). Because not all five templates yield step-1 and -2 products that are distinguishable by mass, we also treated an aliquot of material at each step with a reactive oligonucleotide uniquely complementary to each template (**I′**–**V′**), thus converting a portion of each pool into a higher-molecular-weight species

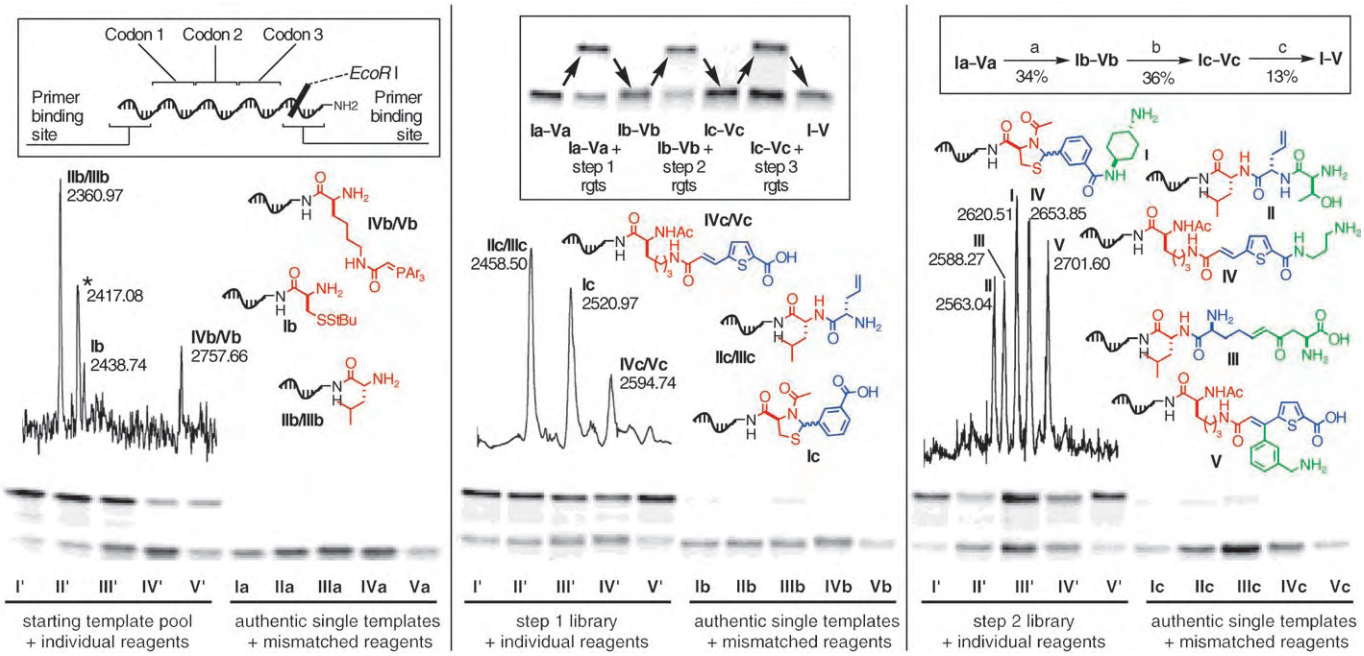

Figure 2. Characterization of the single solution per step (pooled) synthesis of **I**–**V**. PAGE analysis of the three pooled steps is shown in the upper gel image. In the mass spectrum of step 1, the peak denoted with an asterisk arises from the decomposition of **IVb** and **Vb** during mass-spectrometric analysis (see the Supporting Information). In each of the lower gels, the five lanes furthest on the left show the reaction of the starting-template pool, step-1 product pool, or step-2 product pool with each of the reagents **I′**–**V′**, which are reactive with and uniquely complementary to templates **Ia**–**Va**, respectively. The five lanes furthest on the right of each lower gel image show the reaction of individual starting materials for each step under conditions identical to those of the actual library synthesis (see Figure 1), but with sequence-mismatched reagents.

 © 2005 Wiley-VCH Verlag GmbH & Co. KGaA, Weinheim

and confirming that all five templates were present at every step of the pooled synthesis (see the Supporting Information).

From 8 nmol of template, we obtained 125 pmol of **I**–**V** which corresponds to an average overall yield of 1.6% of isolated product. This quantity of material, even if hypothetically divided among thousands of library members, is sufficient for >1000 in vitro selections and PCR-based amplifications needed to identify library members with desired properties.[19,23] Our initial use of iterated branching reaction pathways demonstrates the promise of such an approach in the synthesis of diverse small-molecule libraries that would be challenging to create by using current library synthesis methods. The structures created in this work also include several of the most complex synthetic small-molecule products translated from DNA to date.

Received: August 15, 2005
Published online: October 20, 2005

Keywords: bioorganic chemistry · combinatorial chemistry · diversity-oriented synthesis · DNA · template synthesis

[1] B. R. Stockwell, *Nature* **2004**, *432*, 846.
[2] S. L. Schreiber, *Bioorg. Med. Chem.* **1998**, *6*, 1127.
[3] M. D. Burke, S. L. Schreiber, *Angew. Chem.* **2004**, *116*, 48; *Angew. Chem. Int. Ed.* **2004**, *43*, 46.
[4] B. A. Bunin, M. J. Plunkett, J. A. Ellman, *Proc. Natl. Acad. Sci. USA* **1994**, *91*, 4708.
[5] S. Ding, N. S. Gray, X. Wu, Q. Ding, P. G. Schultz, *J. Am. Chem. Soc.* **2002**, *124*, 1594.
[6] G. C. Micalizio, S. L. Schreiber, *Angew. Chem.* **2002**, *114*, 3406; *Angew. Chem. Int. Ed.* **2002**, *41*, 3272.
[7] A. Furka, F. Sebestyen, M. Asgedom, G. Dibo, *Int. J. Pept. Protein Res.* **1991**, *37*, 487.
[8] R. B. Merrifield, *J. Am. Chem. Soc.* **1963**, *85*, 2149.
[9] K. C. Nicolaou, J. A. Pfefferkorn, S. Barluenga, H. J. Mitchell, A. J. Roecker, G. Q. Cao, *J. Am. Chem. Soc.* **2000**, *122*, 9968.
[10] K. C. Nicolaou, J. A. Pfefferkorn, H. J. Mitchell, A. J. Roecker, S. Barluenga, G. Q. Cao, R. L. Affleck, J. E. Lillig, *J. Am. Chem. Soc.* **2000**, *122*, 9954.
[11] K. C. Nicolaou, J. A. Pfefferkorn, A. J. Roecker, G. Q. Cao, S. Barluenga, H. J. Mitchell, *J. Am. Chem. Soc.* **2000**, *122*, 9939.
[12] M. D. Burke, E. M. Berger, S. L. Schreiber, *Science* **2003**, *302*, 613.
[13] M. D. Burke, E. M. Berger, S. L. Schreiber, *J. Am. Chem. Soc.* **2004**, *126*, 14095.
[14] H. Oguri, S. L. Schreiber, *Org. Lett.* **2005**, *7*, 47.
[15] S. J. Taylor, A. M. Taylor, S. L. Schreiber, *Angew. Chem.* **2004**, *116*, 1713; *Angew. Chem. Int. Ed.* **2004**, *43*, 1681.
[16] C. T. Calderone, J. W. Puckett, Z. J. Gartner, D. R. Liu, *Angew. Chem.* **2002**, *114*, 4278; *Angew. Chem. Int. Ed.* **2002**, *41*, 4104.
[17] Z. J. Gartner, D. R. Liu, *J. Am. Chem. Soc.* **2001**, *123*, 6961.
[18] Z. J. Gartner, M. W. Kanan, D. R. Liu, *J. Am. Chem. Soc.* **2002**, *124*, 10304.
[19] Z. J. Gartner, B. N. Tse, R. Grubina, J. B. Doyon, T. M. Snyder, D. R. Liu, *Science* **2004**, *305*, 1601.
[20] X. Y. Li, Z. J. Gartner, B. N. Tse, D. R. Liu, *J. Am. Chem. Soc.* **2004**, *126*, 5090.
[21] Z. J. Gartner, M. W. Kanan, D. R. Liu, *Angew. Chem.* **2002**, *114*, 1874; *Angew. Chem. Int. Ed.* **2002**, *41*, 1796.
[22] M. W. Kanan, M. M. Rozenman, K. Sakurai, T. M. Snyder, D. R. Liu, *Nature* **2004**, *431*, 545.
[23] J. B. Doyon, T. M. Snyder, D. R. Liu, *J. Am. Chem. Soc.* **2003**, *125*, 12372.

 © 2005 Wiley-VCH Verlag GmbH & Co. KGaA, Weinheim

Host–Guest Chemistry

DOI: 10.1002/anie.200502393

Anion-Induced Synthesis and Combinatorial Selection of Polypyrrolic Macrocycles**

*Evgeny A. Katayev, G. Dan Pantos, Marina D. Reshetova, Victor N. Khrustalev, Vincent M. Lynch, Yuri A. Ustynyuk, and Jonathan L. Sessler**

One of the current challenges in the area of supramolecular chemistry involves the preparation of anion receptors with high selectivity for specifically targeted anionic guests.[1] Such systems could have an important role to play in a variety of applications, including sensing, analysis, waste remediation, and drug development. One approach for designing highly efficient anion receptors is to use anion-templated strategies to produce macrocyclic systems whose geometry is complementary to that of the targeted guests.[2] Although this concept has yet to be extensively exploited in the case of pyrrole-based systems, recently we prepared cyclo[*n*]pyrroles through self-coupling of bipyrroles under oxidative conditions in the presence of suitable anionic templates. In earlier work, we found that bipyrrole-amide-derived catenanes[3] and the Schiff base expanded porphyrin **1** ("USAphyrin")[4] could be synthesized using anion-templated processes. Finally, in the case of the 2,6-diamidopyridine-containing system **2**, we noted that improved yields were seen when the initial macrocycle-forming reaction was carried out in the presence

[*] E. A. Katayev, G. D. Pantos, Dr. V. M. Lynch, Prof. J. L. Sessler
Dept. of Chemistry and Biochemistry
University of Texas at Austin
1 University Station, A5300, Austin, TX 78712-0165 (USA)
Fax: (+1) 512-471-7550
E-mail: sessler@mail.utexas.edu

E. A. Katayev, M. D. Reshetova, Prof. Y. A. Ustynyuk
Dept. of Chemistry
M.V. Lomonosov Moscow State University
Leninskie Gory, 119899 Moscow (Russian Federation)

Dr. V. N. Khrustalev
A. N. Nesmeyanov Institute of Organoelement Compounds
Russian Academy of Sciences
28, Vavilov Street, 119991 Moscow (Russian Federation)

[**] Financial support from the U.S. Department of Energy Office of Science (grant no. DE-FG02-04ER63741 to J.L.S.), the National Science Foundation (CHE-0515670 to J.L.S.), and the Russian Foundation for Basic Research (grant nos. 05-03-32684 and 05-03-08017 to Y.A.U.) is acknowledged. This project is part of an ongoing collaboration involving the groups of Dr. Bruce Moyer at the Oak Ridge National Laboratory and Prof. Kristin Bowman-James at the University of Kansas.

Supporting information for this article (general methods and materials, synthetic experimental details, representative Job plots, UV/Vis titrations, corresponding binding isotherms, and details of affinity constant determinations, as well as X-ray crystallographic information, including CIF files) is available on the WWW under http://www.angewandte.org or from the author.

InterScience
© 2005 Wiley-VCH Verlag GmbH & Co. KGaA, Weinheim

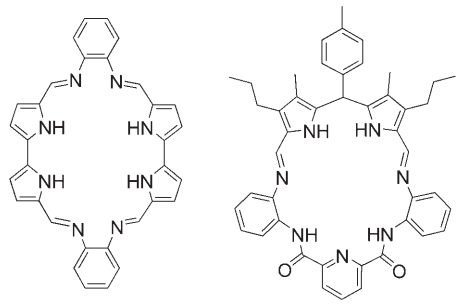

1 2

of sulfuric acid or trifluoroacetic acid.[5] Given these results, we sought to explore the effects of such putative anion-template effects in the case of other 2,6-diamidopyridine pyrrolic macrocycles. Herein, we report the anion-induced synthesis of a new class of 2,6-diamidopyridine-bipyrrole macrocyclic receptors that undergo combinatorial selection as the result of their interaction with anionic guests. This stimulus-driven reaction outcome bears analogy, and provides an interesting complement, to recent macrocycle-forming strategies based on dynamic combinatorial processes.[6]

The incorporation of 2,6-diamidopyridine subunits into appropriately designed macrocycles has been shown by us[5,7] and others[8] to result in systems that display selectivity for tetrahedral over trigonal-planar anions. A different structural motif, namely, bipyrrole, has also been used extensively by our groups to produce anion receptors, including several that display selectivity towards sulfate and other tetrahedral anions.[9,10] Thus, we were keen to explore whether macrocycles containing these two key subunits could be readily prepared and, if so, whether the reactions leading to their formation could be mediated by anion templation. To this end, the diformylbipyrrole **4**[11] was treated with diamine **3** in methanol under acidic conditions (Scheme 1). This led to the formation of Schiff base containing macrocycles along with linear oligomeric species. The choice of the acid used to promote these reactions (HCl, HBr, CH_3CO_2H, CF_3CO_2H, H_3PO_4, H_2SO_4, HNO_3) plays a critical role in defining the product distribution. In most cases, the products precipitated as the corresponding acid salts. These precipitates and the reaction mixtures themselves were analyzed by ESI and MALDI-TOF mass spectrometry. For instance, the use of hydrochloric and hydrobromic acids led to the formation of oligomers with high molecular weights ($m/z > 3000$) as the major products, with only small amounts of the [1+1] macrocycle being produced under these conditions. This latter product displayed low stability and appeared to undergo decomposition during the workup and purification stages. The use of acetic, trifluoroacetic, and phosphoric acids led to the formation of the [2+2] macrocycle **5**, which was contaminated with appreciable quantities of uncharacterized oligomers. When nitric acid was employed, only oligomeric species with high molecular weights were formed. In contrast, the use of sulfuric acid produced the [2+2] macrocycle **5**, nearly free of other side products. The resulting salt, $\mathbf{5}\cdot 2\,H_2SO_4$, was then suspended in CH_2Cl_2 and treated with triethylamine to give the free macrocycle **5** in 75% isolated yield based on **4**.

A single-crystal X-ray diffraction analysis of **5** (Figure 1) provided proof for the proposed structure and revealed that

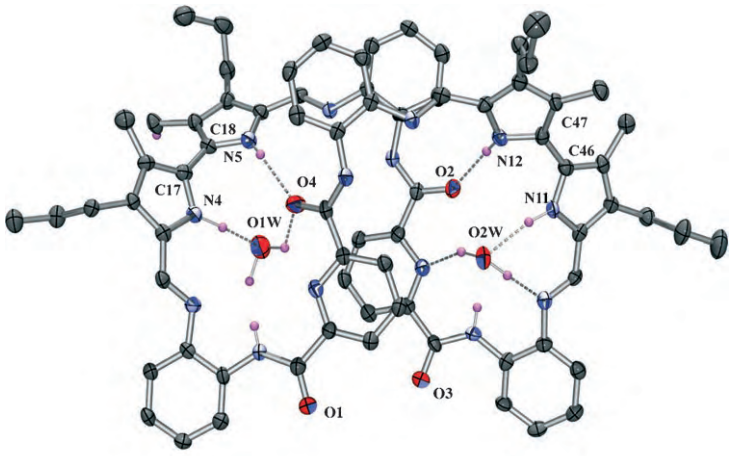

Figure 1. ORTEP-rendered view of **5** showing the two bound solvent water molecules. Three dichloromethane molecules and most hydrogen atoms have been omitted for clarity. Thermal ellipsoids are scaled to the 50% probability level. C gray, N blue, O red, H pink; dashed lines indicate hydrogen-bonding interactions. Key bond parameters: N5-H···O4 (N···O 3.109(4), H···O 2.29(4) Å, N-H···O 169(3)°); N12-H···O2 (N···O 3.013(4), H···O 2.18(4) Å, N-H···O 177(3)°).

the macrocycle adopts a figure-of-eight conformation in the solid state.[12] This three-dimensional structure is stabilized by a pair of intramolecular hydrogen bonds between the pyrrole NH protons and the amide oxygen atoms O2 and O4 that point towards the interior of the cavity. The bipyrrole fragments are twisted in both bipyrrole units, displaying dihedral angles N4-C17-C18-N5 and N11-C46-C47-N12 of 50.5(6)° and 34.4(6)°, respectively. The 2,6-diamidopyridine fragments are in a *trans*

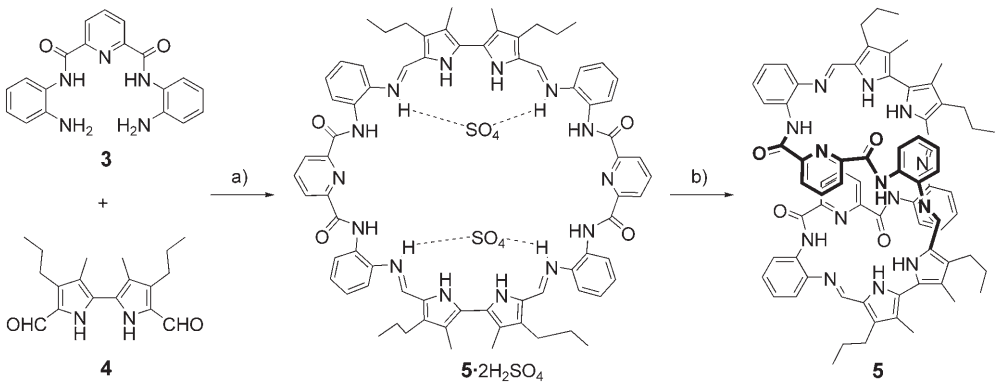

Scheme 1. a) Conc. H_2SO_4 (2.2 equiv), 48 h, room temperature; b) Et_3N (excess), $MeOH/CH_2Cl_2$.

© 2005 Wiley-VCH Verlag GmbH & Co. KGaA, Weinheim

orientation, and the amide oxygen atoms O1 and O3 that point towards the exterior of the cavity are hydrogen bonded to one dichloromethane molecule and one water (O1W) molecule, respectively. These latter intermolecular interactions presumably account for the dimerization of **5** observed in the solid state (see Supporting Information). One water molecule (O1W) is partially constrained within the macrocycle, while a second water molecule (O2W) is entirely trapped within the macrocycle. The hydrogen-bonding interactions that stabilize these species are described in the Supporting Information.

The ^{1}H NMR spectrum of **5** in $CDCl_3$ at room temperature reveals a nonequivalence for all the methyl and methylene signals, as well as a complex patterns in the aromatic region that is most readily interpreted in terms of the retention of the figure-of-eight conformation of **5** in this nonpolar solvent. At 60 °C the spectrum simplifies dramatically. Such a simplification is also observed in polar solvents (e.g. pyridine, THF) at room temperature. Presumably, this reflects the fact that in both cases the intramolecular hydrogen bonds that stabilize the figure-of-eight conformation in $CDCl_3$ at room temperature are weakened or destroyed.

The presence of bound water molecules in the solid-state structure of **5** (see Figure 1), along with the presence of what appears to be two well-defined binding pockets, led to the consideration that **5**, like its congener **2**, might act as an effective receptor for anions. Anion-binding studies were thus performed using UV/Vis spectroscopic titrations. To maintain consistency with previously reported results,[5,7] these studies were carried out in CH_3CN at 23 °C using various tetrabutylammonium (TBA) salts. Where appropriate, binding stoichiometries were determined using Job plots. On this basis it was found that macrocycle **5** interacts strongly with the tetrahedral anions HSO_4^- (1:1; $K_a = 63\,500 \pm 3000\,\text{M}^{-1}$) and $H_2PO_4^-$ (2:1; $K_{a1} = 191\,000 \pm 15\,400\,\text{M}^{-1}$; $K_{a2} = 60\,200 \pm 6000\,\text{M}^{-1}$; $K_a = 107\,000 \pm 9600\,\text{M}^{-1}$ where $K_a = (K_{a1} \times K_{a2})^{0.5}$), weakly with acetate (1:1, $K_a = 26\,000 \pm 2400\,\text{M}^{-1}$), and essentially not at all with the other anions tested, namely chloride, bromide, and nitrate (K_a values were below the detection limits in all cases). Such findings are not surprising in light of the fact that the initial "synthetic selection" in favor of macrocycle **5** was performed using a tetrahedral anion (HSO_4^-) as the template.

Interestingly, of the two tetrahedral anions subject to study, namely HSO_4^- and $H_2PO_4^-$, dihydrogen phosphate is bound more strongly and by a stepwise 2:1, as opposed to 1:1, guest/host binding process (see the K_a values given above). This result is in accord with our previous finding[5] that the related flexible macrocyclic receptor **1** also binds dihydrogen phosphate more strongly than sulfate ions and likewise displays a 2:1 guest/host binding stoichiometry.

While macrocycle **5** proved quite stable under most laboratory conditions, when dissolved in acetonitrile and allowed to stand for 5 days in the presence of dihydrogen phosphate and hydrogen sulfate (tetrabutylammonium salts) it was found to undergo rearrangement to give the corresponding [3+3] analogue **6** in quantitative and 47% yield, respectively (Scheme 2).[13] The use of chlorinated solvents during this transformation did not produce **6** but rather

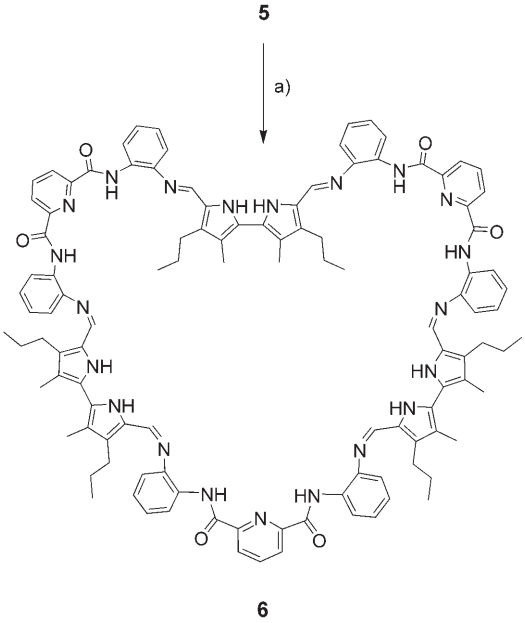

Scheme 2. a) $TBAHSO_4$, acetonitrile, 5 days, room temperature without stirring, followed by Et_3N; or $TBAH_2PO_4$, acetonitrile, 5 days, room temperature without stirring.

yielded traces of the [1+1] macrocycle (as inferred from mass spectrometric studies) along with a wide variety of soluble compounds, which as yet have not been characterized. This behavior was observed whether the reactions were performed at room temperature or at reflux. However, the ring-expanded product was formed only in traces when the reaction mixture was subject to stirring for 2 days in the presence of $TBAHSO_4$; in this case, a precipitate of $\mathbf{5}\cdot 4\,H_2SO_4$ was observed to form, along with soluble oligomeric compounds. The isolated yield for $\mathbf{5}\cdot 4\,H_2SO_4$ following this latter procedure was 30%. The salt $\mathbf{5}\cdot 4\,H_2SO_4$ (characterized by elemental analysis) differs from $\mathbf{5}\cdot 2\,H_2SO_4$ in its chemical properties and displays, for instance, different solubility in organic solvents. Pure free base **5** may be obtained in quantitative yield by treating solutions of $\mathbf{5}\cdot 4\,H_2SO_4$ in methylene chloride with triethylamine. Also note that there is no evidence that the ring-expanded product **6**, in either its neutral or acid salt form, is generated during the initial anion-induced synthesis of **5**.

From these observations we postulate that the kinetics and thermodynamics of product formation are a subtle function of the reaction conditions. In particular, we suggest that when the reaction mixture is subject to stirring, the salt $\mathbf{5}\cdot 4\,H_2SO_4$ is formed quickly (kinetic product) and under conditions that favor its precipitation, a follow-up process that also serves to affect the thermodynamics of the reaction. By contrast, in the absence of stirring, the precipitation of $\mathbf{5}\cdot 4\,H_2SO_4$ is slow and allows the isolation of **6** as the thermodynamic product. Further tests that are designed to confirm or refute such mechanistic rationalizations are currently underway.

While macrocycle **6** proved to be relatively stable in acetonitrile, both as the free base and as its H_2SO_4 salt, it was found to undergo decomposition, often rapidly, in other

 © 2005 Wiley-VCH Verlag GmbH & Co. KGaA, Weinheim

solvent systems. Decomposition was also induced upon the addition of anions other than sulfate or phosphate, a finding that served to underscore the special, anion-specific conditions that lead to its formation.

Proof for the structure of **6**, came from a single-crystal analysis of its hydrogensulfate salt, **6**·H_2SO_4 (Figure 2[14]).

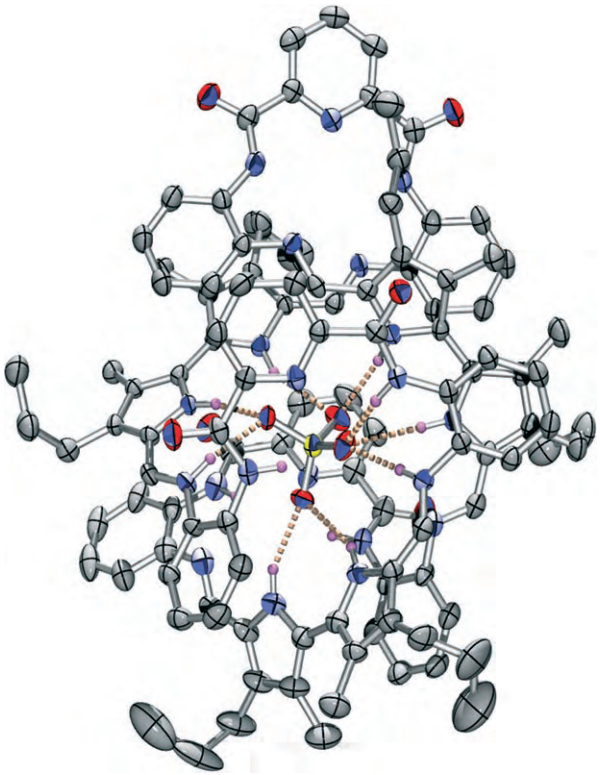

Figure 2. View of the macrocyclic complex **6**·H_2SO_4. Displacement ellipsoids are scaled to the 50% probability level. Solvent molecules (2×CH_3CN and 1×pentane), as well as hydrogen atoms, have been removed for clarity. C gray, N blue, O red, H pink; dashed lines indicate hydrogen-bonding interactions.

Although complicated, the resulting structure clearly reveals a doubly twisted, diprotonated macrocyclic dication that encapsulates a sulfate dianion. This dianion is coordinated through an intricate network of hydrogen bonds (see Supporting Information). The hydrogen-bond donors in this network consist of the NH protons from the three bipyrrole subunits, three NH protons from two 2,6-diamidopyridine subunits, and two NH protons from two protonated imine fragments. Several of these key interactions are highlighted in Figure 3. All the 2,6-diamidopyridine subunits are in their respective *cis* orientations.

The present findings provide evidence for an anion-templated reaction between diamine **3** and bipyrrole dialdehyde **4**, as well as the anion-triggered combinatorial selection of a given macrocyclic product under a particular set of experimental conditions. The present reorganization reaction differs from dynamic combinatorial libraries in that selection from a true equilibrium mixture does not occur. Instead, the choice of the anion template serves to drive the reaction towards the formation of the most stable species under the

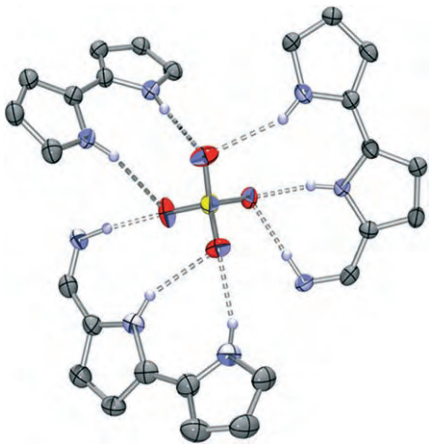

Figure 3. ORTEP–Povray-rendered view of bipyrrole and tethered protonated imine fragments forming hydrogen bonds with the sulfate ion. All other parts of the molecule have been omitted for clarity. Displacement ellipsoids are scaled to the 50% probability level. C gray, N blue ellipsoids, O red, H pale blue spheres; dashed lines indicate hydrogen-bonding interactions.

specific reaction conditions involved. In other words, the modifications used to obtain **6** from **5** (i.e. addition of the appropriate anion) serve to change the fundamental thermodynamic conditions of the system as a whole. As a consequence, a stable molecule (e.g. **5**) undergoes partial or complete decomposition only to be reassembled into a more stable homologue (**6**). Under the most favorable of conditions, an impressive degree of selectivity is observed which leads us to suggest that this strategy could provide a new concept for the design and synthesis of novel receptor systems. Work designed to explore this intriguing possibility is currently in progress.

Received: July 9, 2005
Published online: October 24, 2005

Keywords: combinatorial chemistry · host–guest systems · nitrogen heterocycles · supramolecular chemistry · template synthesis

[1] B. Dietrich, M. W. Hosseini in *Supramolecular Chemistry of Anions* (Eds.: A. Bianchi, K. Bowman-James, E. García-España), Wiley-VCH, New York, **1997**.
[2] a) D. Philp, J. F. Stoddart, *Angew. Chem.* **1996**, *108*, 1242–1286; *Angew. Chem. Int. Ed. Engl.* **1996**, *35*, 1154–1196; b) J. A. Wisner, P. D. Beer, M. G. B. Drew, *Angew. Chem.* **2001**, *113*, 3718–3721; *Angew. Chem. Int. Ed.* **2001**, *40*, 3606–3609; c) J. A. Wisner, P. D. Beer, M. G. B. Drew, M. R. Sambrook, *J. Am. Chem. Soc.* **2002**, *124*, 12469–12476.
[3] A. Andrievsky, F. Ahuis, J. L. Sessler, F. Vögtle, D. Gudat, M. Moini, *J. Am. Chem. Soc.* **1998**, *120*, 9712–9713.
[4] J. L. Sessler, T. D. Mody, V. Lynch, *J. Am. Chem. Soc.* **1993**, *115*, 3346–3347.
[5] J. L. Sessler, E. Katayev, G. D. Pantos, Yu. A. Ustynyuk, *Chem. Commun.* **2004**, 1276–1277.
[6] a) P. A. Brady, R. P. Bonar-Law, S. J. Rowan, C. J. Suckling, J. K. M. Sanders, *Chem. Commun.* **1996**, 319–320; b) J.-M. Lehn, A. V. Eliseev, *Science* **2001**, *291*, 2331–2332; c) S. J.

 © 2005 Wiley-VCH Verlag GmbH & Co. KGaA, Weinheim

Rowan, S. J. Cantrill, G. R. L. Cousins, J. K. M. Sanders, J. F. Stoddart, *Angew. Chem.* **2002**, *114*, 938 – 993; *Angew. Chem. Int. Ed.* **2002**, *41*, 898 – 952; Erratum: S. J. Rowan, S. J. Cantrill, G. R. L. Cousins, J. K. M. Sanders, J. F. Stoddart, *Angew. Chem.* **2002**, *114*, 1460; *Angew. Chem. Int. Ed.* **2002**, *41*, 1528; d) R. T. S. Lam, A. Belenguer, S. L. Roberts, C. Naumann, T. Jarrosson, S. Otto, J. K. M. Sanders, *Science* **2005**, *308*, 667 – 669.

[7] J. L. Sessler, E. Katayev, G. D. Pantos, P. Scherbakov, M. D. Reshetova, V. N. Khrustalev, V. M. Lynch, Yu. A. Ustynyuk, *J. Am. Chem. Soc.* **2005**, *127*, 11442 – 11446.

[8] a) Md. A. Hossain, J. M. Llinares, D. Powell, K. Bowman-James, *Inorg. Chem.* **2001**, *40*, 2936 – 2937; b) T. Clifford, A. Danby, J. M. Llinares, S. Mason, N. W. Alcock, D. Powell, J. A. Aguilar, E. Garcia-España, K. Bowman-James, *Inorg. Chem.* **2001**, *40*, 4710 – 4720; c) S. O. Kang, J. M. Llinares, D. Powell, D. VanderVelde, K. Bowman-James, *J. Am. Chem. Soc.* **2003**, *125*, 10152 – 10153; d) Md. A. Hossain, S. O. Kang, D. Powell, K. Bowman-James, *Inorg. Chem.* **2003**, *42*, 1397 – 1399; e) Md. A. Hossain, S. O. Kang, J. M. Llinares, D. Powell, K. Bowman-James, *Inorg. Chem.* **2003**, *42*, 5043 – 5045; f) S. O. Kang, Md. A. Hossain, D. Powell, K. Bowman-James, *Chem. Commun.* **2005**, 328 – 329.

[9] J. L. Sessler, D. Seidel, V. Lynch, *J. Am. Chem. Soc.* **1999**, *121*, 11257 – 11258.

[10] D. Seidel, J. L. Sessler, V. Lynch, *Angew. Chem.* **2002**, *114*, 1480 – 1483; *Angew. Chem. Int. Ed.* **2002**, *41*, 1422 – 1425.

[11] J. L. Sessler, D. Seidel, A. Gebauer, V. Lynch, K. A. Abboud, *J. Heterocycl. Chem.* **2001**, *38*, 1419 – 1424.

[12] Crystal data for **5**·2 H_2O·2.25 CH_2Cl_2: $C_{74}H_{74}N_{14}O_4$·2 H_2O·2.25 CH_2Cl_2, $M_r = 1450.59$, crystal size $0.21 \times 0.18 \times 0.12\ mm^3$, $Z = 2$, triclinic, space group $P\bar{1}$, $a = 13.615(2)$, $b = 16.254(3)$, $c = 19.020(3)$ Å, $\alpha = 74.731(3)$, $\beta = 87.513(4)$, $\gamma = 65.815(3)°$, $V = 3694.1(10)$ $Å^3$, $\rho_{calcd} = 1.304\ mg\,cm^{-3}$, $T = 120(2)$ K, $\theta_{min} = 2.60$, $\theta_{max} = 26.06°$, $\lambda = 0.71073$; $Mo_{K\alpha}$ radiation, data collected on a Bruker three-circle diffractometer equipped with a SMART 1000 CCD detector and corrected for absorption. The structure was solved by direct methods and refined by full-matrix least-squares technique with anisotropic thermal parameters for non-hydrogen atoms, $\mu(Mo_{K\alpha}) = 0.241\ mm^{-1}$, $T_{min} = 0.951$, $T_{max} = 0.972$. All calculations were carried out using the SHELXTL PLUS program (PC Version 5.10). Final $R1 = 0.0703$ (for 6068 reflections with $I > 2\sigma(I)$ and $wR2(F^2) = 0.1708$ (all data)).

[13] Examples of metal-induced Schiff base rearrangements are known; for instance, see: M. R. Bermejo, A. Garcia Deibe, M. Rey, J. Sanmartha, A. Sousa, N. Aurangteb, C. E. Hulme, C. A. McAuliffe, R. G. Pritchard, M. Watkinson, M. Helliwell, *J. Chem. Soc. Dalton Trans.* **1994**, 1265 – 1269.

[14] Crystal data for $(\mathbf{6}H_2)^{2+}$·SO_4^{2-}·2 CH_3CN·C_5H_{12}: $M_r = 2087.54$, crystal size $0.51 \times 0.36 \times 0.20\ mm^3$, $Z = 4$, triclinic, space group $P\bar{1}$, $a = 18.8891(2)$, $b = 23.7914(3)$, $c = 25.5253(4)$ Å, $\alpha = 77.983(1)$, $\beta = 84.781(1)$, $\gamma = 84.019(1)°$, $V = 11130.2(3)$ $Å^3$, $\rho_{calc} = 1.246\ mg\,cm^{-3}$, $T = 153(2)$ K, $\theta_{min} = 2.91$, $\theta_{max} = 25.05°$, $\lambda = 0.71073$; $Mo_{K\alpha}$ radiation, data collected on a Nonius Kappa CCD diffractometer. A total of 530 frames of data were collected using ω scans, with a scan range of 0.9° and a counting time of 131 seconds per frame. Final $R1 = 0.0715$ (for 18372 reflections with $I > 2\sigma(I)$ and $wR2(F^2) = 0.1365$ (all data)). Data reductions were performed using DENZO-SMN. The structure was solved by direct methods using SIR97 and refined by full-matrix least-squares on F^2 with anisotropic displacement parameters for the non-hydrogen atoms using SHELXL-97. CCDC 275698 (**5**) and 275834 (**6**) contain the supplementary crystallographic data for this paper. These data can be obtained free of charge from the Cambridge Crystallographic Data Centre via www.ccdc.cam.ac.uk/data_request/cif.

 © 2005 Wiley-VCH Verlag GmbH & Co. KGaA, Weinheim

Self-Assembly

DOI: 10.1002/anie.200502142

Molecular Wires from Contorted Aromatic Compounds**

*Shengxiong Xiao, Matthew Myers, Qian Miao, Sébastien Sanaur, Keliang Pang, Michael L. Steigerwald, and Colin Nuckolls**

Dedicated to Professor Thomas J. Katz

The use of planar molecules is one unifying design feature in essentially all the molecules that have been tested to date in organic field-effect transistors.[1–7] The concept explored herein is whether a nonplanar aromatic core could yield efficacious electronic materials. One significant aspect of using a nonplanar core is that the aromatic rings would be forced to adopt new and unusual intermolecular contacts that are typically unavailable to flat molecules. Moreover, these informationally rich subunits could form the basis for self-assembled and self-healing electronic materials if the core could be bent into a shape that was self-complementary.

Herein, we detail the first studies of the self-assembly and electrical properties of a new type of hexabenzocoronene (HBC) **1**, whose aromatic core is distorted away from planarity by steric congestion in its proximal carbon atoms. We became interested in this class of compound because it combines structural elements of linear acenes, which are well-

[*] S. Xiao, M. Myers, Q. Miao, K. Pang, M. L. Steigerwald, Prof. C. Nuckolls
Department of Chemistry
The Nanoscience Center, Columbia University
New York, NY 10027 (USA)
Fax: (+1) 212-932-1289
E-mail: cn37@columbia.edu

S. Sanaur
Ecole Nationale Supérieure des Mines de Saint Etienne
Centre Microélectronique de Provence—Georges Charpak
Département Packaging et Supports Souples
Avenue des Anémones, Quartier Saint Pierre
13541 Gardanne (France)

[**] We acknowledge primary financial support from the Nanoscale Science and Engineering Initiative of the National Science Foundation (NSF Award Number CHE-0117752); the New York State Office of Science, Technology, and Academic Research (NYSTAR); and the Department of Energy, Nanoscience Initiative (NSET 04ER46118). C.N. thanks the US National Science Foundation (CAREER award DMR-02-37860), the American Chemical Society (PRF type G 39263-G7), the Camille Dreyfus Teacher Scholar Program (2004), and the Alfred P. Sloan Fellowship Program (2004). We thank the MRSEC Program of the National Science Foundation (Award Number DMR-0213574) and the New York State Office of Science, Technology, and Academic Research (NYSTAR) for financial support for M.L.S. and the shared instrument facility. S.S. acknowledges financial support from the Centre Microélectronique de Provence—Georges Charpak.

Supporting information for this article is available on the WWW under http://www.angewandte.org or from the author.

WILEY InterScience DISCOVER SOMETHING GREAT
© 2005 Wiley-VCH Verlag GmbH & Co. KGaA, Weinheim

known electronic materials,[2,5,8–11] with a disk-shaped and potentially columnar liquid-crystalline core.[12–20] Methods for the synthesis and derivatization of **1** are essentially unknown.[21] Our important finding is that some derivatives of this new class of compound self-organize into liquid-crystalline phases composed of molecular stacks that orient themselves parallel to the surface. Field-effect transistors based on these materials show high charge-carrier mobilities, high on/off ratios, and low turn-on voltages.

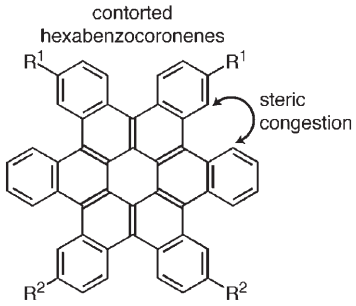

1a: $R^1 = R^2 = H$
1b: $R^1 = H$, $R^2 = OC_{12}H_{25}$
1c: $R^1 = R^2 = OC_{12}H_{25}$

Compounds **1a–c**[22] are yellow-orange solids that are readily soluble in a number of common organic solvents; for example, more than 200 mg of **1c** can be dissolved in 1 mL of $CHCl_3$. Furthermore, these solutions have an intense optical emission in the visible region. The thermal and oxidative stabilities of these compounds are also remarkable, as no loss of color is observed when oxygen is bubbled through solutions of **1a–c** over a period of a few hours under ambient light. Under identical conditions, solutions of pentacene lose their color within a few minutes through photooxidation.[23] Differential scanning calorimetry (DSC) showed no decomposition of **1a–c** up to temperatures well above 320 °C. Uniform films (approximately 100-nm thick) could be formed by spin-casting **1c** from 1,2-dichloroethane or $CHCl_3$. In contrast, films formed from **1a** and **1b** were granular in appearance and of a low quality. The ability to form good films of **1c** is a harbinger of the electrical properties described below.

Field-effect transistors were fabricated on spin-cast films of **1a–c** (Figure 1a shows the structure of the resulting devices). Transistors fabricated from **1c** have good electrical characteristics, whereas those prepared from **1a** and **1b** showed no useful properties. We deposited Au source and drain electrodes by thermal evaporation onto the spin-cast films through a metal-shadow mask. The channel length was 75 μm and the electrode width was 2 mm, and the transconductance and transistor output are shown in Figure 1b,c. The mobility (0.02 $cm^2 V^{-1} s^{-1}$) shown is calculated from the linear portion of the data in Figure 1b[24] and uses a capacitance of 11.3 $nF cm^{-2}$ for the gate dielectric layer (300 nm of SiO_2 and a monolayer of octadecyltrichlorosilane).[11] The gate dielectric capacitance comes from measurements made over a range of frequencies[11] and is as expected for a 300-nm-thick layer of silicon oxide with few defects.[25] Other critical parameters, such as the threshold voltage for the device to turn on (as low as −3 V for some

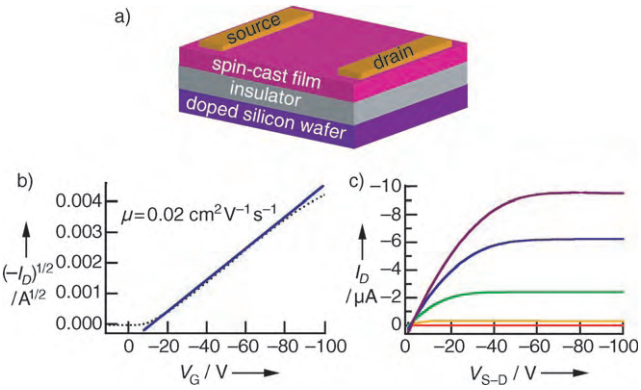

Figure 1. a) Schematic diagram of a field-effect transistor that was fabricated by evaporating source and drain electrodes onto a spin-cast film of **1c**. b) Transconductance: the blue line is a fit of the linear portion of the data points (the source–drain voltage V_{S-D} was held at −60 V). c) Transistor output for thin-film transistors from **1c**.

devices prepared from **1c**) and the on/off current ratios in the device (10^6:1), are also very good. These values are the best field-effect transistor properties achieved for a columnar discotic material[16,17,26,27] (see below) and are good for spin-cast films in general.[8,28–34] These results are even more impressive because it is likely that these properties could be improved by adjustment of critical parameters such as grain size, deposition conditions, and direction of column growth.

Encouraging electrical properties are only developed in the more substituted derivatives of **1**, thus indicating self-organization. One of the hallmarks of many self-assembled systems is the presence of liquid-crystalline phases. Each of these compounds were investigated by DSC, polarized light microscopy, and X-ray diffraction to determine whether mesophases are present (the DSC trace for **1c** is shown in Figure 2a). An extra transition that indicates the presence of an intermediate phase can be seen from both the heating and cooling cycles for **1c**. The microscopy and X-ray diffraction studies of **1c** (see below) indicate that it is a liquid-crystalline phase between 91 and 285 °C, whereas above these temperatures it melts to form an isotropic liquid. The enthalpy values, particularly going from the liquid-crystalline phase to the isotropic liquid phase, are larger than those typically observed for discotic liquid crystals.[12] This difference implies that **1c** associates strongly in this intermediate phase, possibly because it is not a flat disk.[35] DSC studies do not show any evidence for a liquid-crystalline phase for **1a** and **1b**; they simply melt, **1a** at 516 °C[21] and **1b** at 220 °C. The appearance of a mesophase correlates with **1c** having good electrical properties and indicates the potential of self-organized materials for electronic applications.

The structure of this phase was probed by powder X-ray diffraction studies and was found to be a hexagonally ordered columnar liquid-crystalline phase for **1c**. In the X-ray diffraction studies, **1c** was heated (in a Lindemann capillary tube) to an isotropic liquid (295 °C) and cooled into its mesophase. The data shown in Figure 2b were collected upon cooling to 120 °C. The diffractogram is dominated by an intense reflection characteristic of $d \approx 26$ Å. The only other discernible features of the diffractogram are two very weak,

 © 2005 Wiley-VCH Verlag GmbH & Co. KGaA, Weinheim

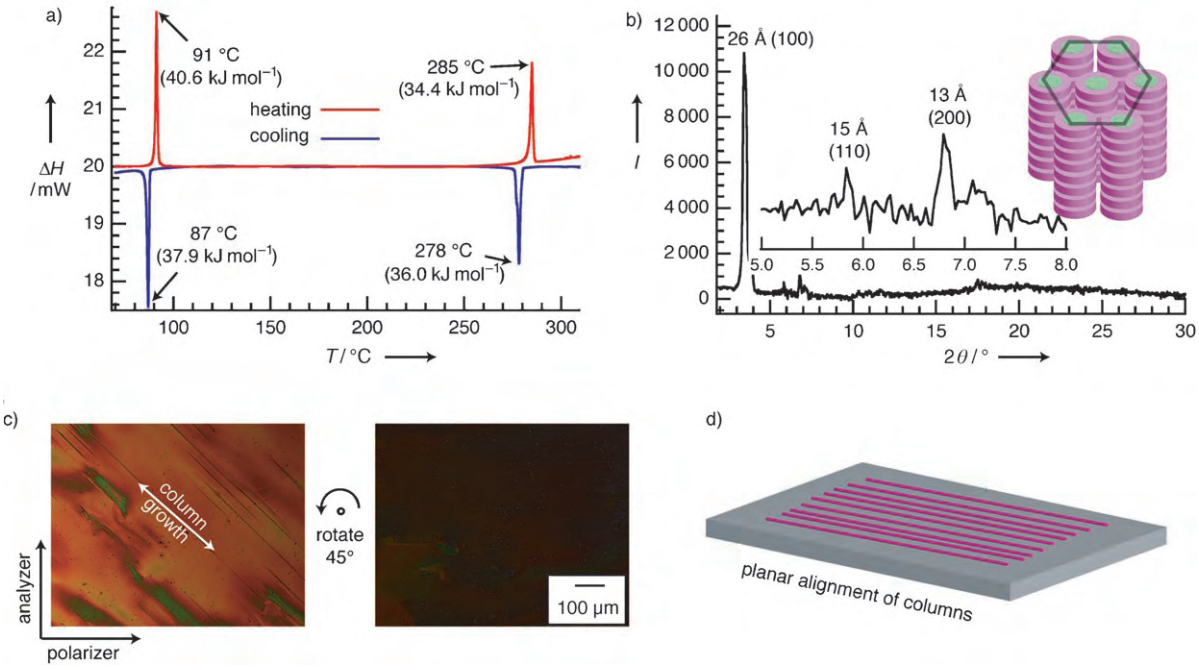

Figure 2. a) DSC trace of **1c** (scan rate = 5 °C min^{-1}) showing a mesophase. b) X-ray diffraction studies of **1c** cooled into its mesophase from 295 to 120 °C and a hexagonal lattice of columns. c) Polarized light micrograph of **1c** cooled into its mesophase which shows a planar alignment of columns that are extinguished when aligned with the polarizer or analyzer axes. The cooling rate was 5 °C min^{-1}, and the exposure time was the same for each picture. d) Schematic diagram of columns aligned parallel to the surface.

higher-order reflections ($d = 15$ and 13 Å) that allow the lattice to be indexed to a hexagonal arrangement of columns. The lack of intensity in these higher-order reflections indicates that the columns are not well correlated with each other, which is likely to be a result of the subunits not having a perfect disk shape, as is implied by the molecular model in Figure 3. The fourfold substitution would signal that at some level there is a competition between rectangular and hexagonal lattice formation.

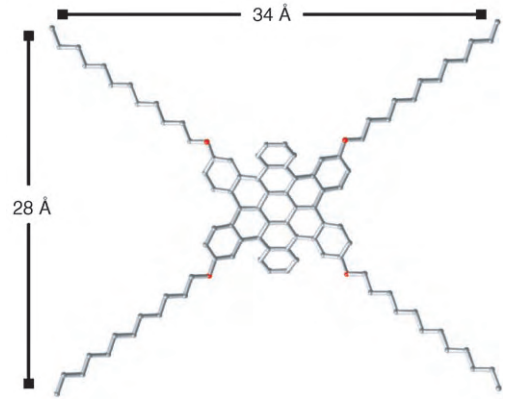

Figure 3. Molecular model of **1c** with its side chains fully extended.

Polarized light microscopy revealed that these materials tend to orient their columns parallel to the surface. The micrograph of a sample cooled to just below 278 °C and captured as the mesophase formed is shown in Figure 2c. The birefringence of the domains is extinguished when the column axes are aligned with the polarizer or analyzer (Figure 2c) and is maximally bright when the stage is rotated by 45°. The micrograph is characteristic of a planar arrangement[36] of columns in a discotic mesophase (shown schematically in Figure 2d). This arrangement of columns is important because the current flow in thin-film transistors is parallel to the surface and, in this case, runs along the column axis.

Strong aggregation of **1c** occurs in solution, thus further indicating its tendency to self-associate. NMR, UV/Vis, and fluorescence spectroscopic techniques were used to monitor this aggregation in solution. All the resonances from the protons of the aromatic ring shifted upfield as the solutions of **1c** were concentrated. For example, the ring protons of **1c** shift upfield by approximately $\Delta\delta = 0.13$ ppm in $CDCl_3$ as the concentration is increased from 6.3 to 126 mg mL^{-1}. This shift is a result of shielding from the ring current of neighboring aromatic compounds within a cofacial stack.[37–39] This face-to-face association of molecules can be further probed by UV/Vis absorption and fluorescence emission spectroscopy. In both cases, the maxima are red-shifted as the solutions become more concentrated. This behavior is not unique as there are many discotic materials that also aggregate in solution to form isolated molecular columns which show similar shifts in their UV/Vis and fluorescence spectra.[40–43] The formation of the columns from the interlocking of gearlike molecular subunits is the model that develops from these spectroscopic data.

When films of these materials are spin-cast onto transparent substrates, birefringent domains form that have the same extinction as that described for the bulk films in

 © 2005 Wiley-VCH Verlag GmbH & Co. KGaA, Weinheim

Figure 2c, thus indicating that the films also have their columns aligned parallel to the substrate. Aggregation in solution that causes the formation of columns, which can then be deposited by spin-casting, is likely to be responsible for the good electrical properties of **1c**.

Crystals of the parent HBC **1a** were grown to investigate the underlying molecular structure of the HBCs.[44] The crystals were grown from 1,2,4-trichlorobenzene and shown to include two disordered solvent molecules oriented over the coronene core. The molecular structure of this HBC moiety is shown in Figure 4a–d. The three intersecting pentacene

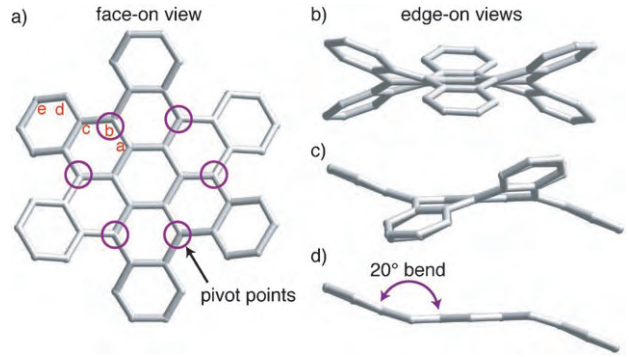

Figure 4. Crystal structure of **1a** grown from 1,2,4-trichlorobenzene. Hydrogen atoms have been removed for clarity. a) Face-on view with marked pivot points (magenta circles). The C_a–C_b bond is relatively short and the C_b–C_c bond is relatively long. Side views are given in (b) and (c). d) Side view of one of the acene segments extracted from the crystal structure. The other atoms of the HBC are hidden from view.

subunits contort into a zigzag conformation. This bending of the acene core is visualized most clearly in Figure 4d, in which portions of the structure have been suppressed to show only one pentacene subunit of the HBC. Essentially all of the bending is concentrated in pairs of carbon atoms that act as pivot points (these are highlighted with magenta circles in Figure 4a). A comparison of some of the bond lengths in this HBC with those from the pentacene crystal structure[45] is given in Table 1. One of the most interesting features is that the C_a–C_b bond is short in the HBC relative to the pentacene,

Table 1: Comparison of C–C bond lengths between **1a** and pentacene.

	C–C bond length [Å]	
	1a[a]	Pentacene[b]
C_a–$C_{a'}$	–	1.44
C_a–C_a	1.43	1.46
C_a–C_b	1.40	1.42
C_b–C_c	1.45	1.38
C_c–C_c	1.42	1.45
C_c–C_d	1.42	1.43
C_d–C_e	1.38	1.35
C_e–C_e	1.42	1.43

[a] The atom labeling scheme is shown in Figure 4a. [b] The atom labeling scheme of the pentacene skeleton is shown below.

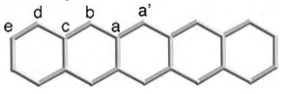

whereas the C_b–C_c bond is relatively long. A strong contribution from the radialene resonance would explain these unusual bond lengths.

In summary, this study puts forth a new design strategy for molecule-based electronic materials in which a nonplanar rigid core is used. We prepared a new class of hexabenzocoronene that is readily substituted to form columnar liquid-crystalline phases, and these columnar materials have good electrical properties in thin-film transistors. Structures with nonplanar aromatic units, such as **1**, may be able to achieve much higher mobilities than those available to flat hydrocarbons because the π surfaces of contorted molecules can approach each other and arrange themselves in very different ways. Moreover, these molecules make interesting starting materials for the synthesis of other topologically interesting hydrocarbons by oxidative closure of the proximal carbon atoms to form five-membered rings.

Received: June 20, 2005
Published online: September 20, 2005

Keywords: liquid crystals · molecular electronics · nanostructures · self-assembly

[1] C. D. Dimitrakopoulos, P. R. L. Malenfant, *Adv. Mater.* **2002**, *14*, 99.
[2] M. Bendikov, F. Wudl, D. F. Perepichka, *Chem. Rev.* **2004**, *104*, 4891.
[3] F. Garnier, *Chem. Phys.* **1998**, *227*, 253.
[4] G. Horowitz, *J. Mater. Chem.* **1999**, *9*, 2021.
[5] H. E. Katz, Z. Bao, S. L. Gilat, *Acc. Chem. Res.* **2001**, *34*, 359.
[6] D. J. Gundlach, Y. Y. Lin, T. N. Jackson, D. G. Schlom, *Appl. Phys. Lett.* **1997**, *71*, 3853.
[7] C. Reese, M. Roberts, M.-m. Ling, Z. Bao, *Mater. Today* **2004**, *7*, 20.
[8] M. M. Payne, S. R. Parkin, J. E. Anthony, C.-C. Kuo, T. N. Jackson, *J. Am. Chem. Soc.* **2005**, *127*, 4986.
[9] C. D. Sheraw, T. N. Jackson, D. L. Eaton, J. E. Anthony, *Adv. Mater.* **2003**, *15*, 2009.
[10] H. Meng, M. Bendikov, G. Mitchell, R. Helgeson, F. Wudl, Z. Bao, T. Siegrist, C. Kloc, C.-H. Chen, *Adv. Mater.* **2003**, *15*, 1090.
[11] Q. Miao, M. Lefenfeld, T.-Q. Nguyen, T. Siegrist, C. Kloc, C. Nuckolls, *Adv. Mater.* **2005**, *17*, 407.
[12] S. Chandrasekhar, *Handb. Liq. Cryst.* **1998**, *2B*, 749.
[13] S. Chandrasekhar, S. K. Prasad, *Contemp. Phys.* **1999**, *40*, 237.
[14] D. Guillon, *Struct. Bonding (Berlin)* **1999**, *95*, 41.
[15] V. S. Iyer, M. Wehmeier, J. D. Brand, M. A. Keegstra, K. Müllen, *Angew. Chem.* **1997**, *109*, 1676; *Angew. Chem. Int. Ed. Engl.* **1997**, *36*, 1604.
[16] W. Pisula, A. Menon, M. Stepputat, I. Lieberwirth, U. Kolb, A. Tracz, H. Sirringhaus, T. Pakula, K. Müllen, *Adv. Mater.* **2005**, *17*, 684.
[17] A. M. van de Craats, N. Stutzmann, O. Bunk, M. M. Nielsen, M. Watson, K. Müllen, H. D. Chanzy, H. Sirringhaus, R. H. Friend, *Adv. Mater.* **2003**, *15*, 495.
[18] A. M. van de Craats, M. P. de Haas, J. M. Warman, *Synth. Met.* **1997**, *86*, 2125.
[19] N. Boden, R. J. Bushby, J. Clements, B. Movaghar, *J. Mater. Chem.* **1999**, *9*, 2081.
[20] Z. Wang, F. Dötz, V. Enkelmann, K. Müllen, *Angew. Chem. Int. Ed.* **2005**, *44*, 1247.
[21] E. Clar, J. F. Stephen, *Tetrahedron* **1965**, *21*, 467.

© 2005 Wiley-VCH Verlag GmbH & Co. KGaA, Weinheim

[22] Details for the synthesis of **1a–c** are contained in the Supporting Information.
[23] A. Maliakal, K. Raghavachari, H. Katz, E. Chandross, T. Siegrist, *Chem. Mater.* **2004**, *16*, 4980.
[24] The mobility is calculated by plotting $|I_{DS}|^{1/2}$ with $|V_G|$ and using the equation: $I_{DS} = (\mu W C_i/2L)(V_G - V_0)^2$ with W = electrode width and L = channel length; the source–drain voltage is set at −60 V, which is in the saturated region of the current–voltage curves shown in Figure 1c.
[25] S. M. Sze, *Physics of Semiconductor Devices*, Wiley-Interscience, New York, **1969**.
[26] N. Boden, B. Movaghar, *Handb. Liq. Cryst.* **1998**, *2B*, 781.
[27] N. Boden, R. J. Bushby, O. R. Lozman, Z. Lu, A. McNeill, B. Movaghar, K. Donovan, T. Kreouzis, *Mol. Cryst. Liq. Cryst.* **2004**, *410*, 541.
[28] M. Mushrush, A. Facchetti, M. Lefenfeld, H. E. Katz, T. J. Marks, *J. Am. Chem. Soc.* **2003**, *125*, 9414.
[29] A. Facchetti, J. Letizia, M. H. Yoon, M. Mushrush, H. E. Katz, T. J. Marks, *Chem. Mater.* **2004**, *16*, 4715.
[30] A. R. Murphy, J. M. J. Frechet, P. Chang, J. Lee, V. Subramanian, *J. Am. Chem. Soc.* **2004**, *126*, 1596.
[31] H. E. Katz, W. Li, A. J. Lovinger, J. Laquindanum, *Synth. Met.* **1999**, *102*, 897.
[32] J. G. Laquindanum, H. E. Katz, A. J. Lovinger, *J. Am. Chem. Soc.* **1998**, *120*, 664.
[33] P. T. Herwig, K. Müllen, *Adv. Mater.* **1999**, *11*, 480.
[34] M. Mas-Torrent, P. Hadley, S. T. Bromley, X. Ribas, J. Tarres, M. Mas, E. Molins, J. Veciana, C. Rovira, *J. Am. Chem. Soc.* **2004**, *126*, 8546.
[35] A. M. Van de Craats, J. M. Warman, K. Müllen, Y. Geerts, J. D. Brand, *Adv. Mater.* **1998**, *10*, 36.
[36] "Low Molecular Weight Liquid Crystals II": D. Demus, J. Goodby, G. W. Gray, H. W. Spiess, V. Vill, *Handb. Liq. Cryst.* **1998**, *2B*.
[37] R. J. Abraham, S. C. M. Fell, K. M. Smith, *Org. Magn. Resonance* **1977**, *9*, 367.
[38] Y. Hamuro, S. J. Geib, A. D. Hamilton, *J. Am. Chem. Soc.* **1997**, *119*, 10587.
[39] A. S. Shetty, J. Zhang, J. S. Moore, *J. Am. Chem. Soc.* **1996**, *118*, 1019.
[40] T.-Q. Nguyen, R. Martel, P. Avouris, M. L. Bushey, L. Brus, C. Nuckolls, *J. Am. Chem. Soc.* **2004**, *126*, 5234.
[41] O. Braitbart, R. Sasson, A. Weinreb, *Mol. Cryst. Liq. Cryst.* **1988**, *159*, 233.
[42] C. Nuckolls, T. J. Katz, L. Castellanos, *J. Am. Chem. Soc.* **1996**, *118*, 3767.
[43] U. Rohr, P. Schilichting, A. Böhm, M. Gross, K. Meerholz, C. Bräuchle, K. Müllen, *Angew. Chem.* **1998**, *110*, 1463; *Angew. Chem. Int. Ed.* **1998**, *37*, 1434.
[44] CCDC-275657 contains the supplementary crystallographic data for this paper. These data can be obtained free of charge from the Cambridge Crystallographic Data Centre via www.ccdc.cam.ac.uk/data_request/cif.
[45] C. C. Mattheus, A. B. Dros, J. Baas, A. Meetsma, J. L. de Boer, T. T. M. Palstra, *Acta Crystallogr. Sect. C* **2001**, *57*, 939.

 © 2005 Wiley-VCH Verlag GmbH & Co. KGaA, Weinheim

Surface Chemistry

DOI: 10.1002/anie.200502316

Controlling Molecular Assembly in Two Dimensions: The Concentration Dependence of Thermally Induced 2D Aggregation of Molecules on a Metal Surface**

Meike Stöhr, Markus Wahl, Christian H. Galka, Till Riehm, Thomas A. Jung, and Lutz H. Gade**

The "bottom-up" construction of functional structures relies on the sophisticated interplay between individual structural units.[1–3] In most cases, the assembly of these building blocks is based on noncovalent interactions that shape extended supramolecular entities in variable dimensions.[4–6] Herein, well-ordered molecular patterns on surfaces are created from highly mobile precursor molecules which are transformed subsequent to their deposition and form autocomplementary species in the process. The end groups of the mobile precursors are activated by a thermally induced surface-assisted reaction to enable intermolecular hydrogen-bonding interactions which then lead to the formation of highly ordered structures. We demonstrate control over the 2D pattern of the assembly and over the dimensionality of the aggregate by variation of the surface concentration of the precursor prior to its transformation. Furthermore, we show that the combination of resonance-assisted hydrogen-bonding[7] and the interaction of the rectangular-shaped molecules with the metal surface leads to highly robust supramolecular networks which may serve as templates for the incorporation or trapping of guest molecules.

[*] Dr. M. Stöhr,[+] M. Wahl[+]
NCCR Nanoscale Science and Institute of Physics
University of Basel
Klingelbergstrasse 82, 4056 Basel (Switzerland)
Fax: (+41) 61-267-3784
E-mail: meike.stoehr@unibas.ch

Dr. C. H. Galka, T. Riehm, Prof. Dr. L. H. Gade
Anorganisch-Chemisches Institut
Universität Heidelberg
Im Neuenheimer Feld 270, 69120 Heidelberg (Germany)
Fax: (+49) 6221-545-609
E-mail: lutz.gade@uni-hd.de

Dr. T. A. Jung
Laboratory for Micro- and Nanostructures
Paul-Scherrer-Institute
5232 Villigen (Switzerland)

[+] These authors contributed equally to this work.

[**] Financial Support from the Swiss National Science Foundation and the National Center of Competence in Research (NCCR) "Nanoscale Science" as well as from the Fonds der Chemischen Industrie (Germany) is gratefully acknowledged. M.S. acknowledges support from the German Academy of Natural Scientists Leopoldina under the grant number BMBF-LPD 9901/8-86.

Supporting information for this article is available on the WWW under http://www.angewandte.org or from the author.

InterScience
© 2005 Wiley-VCH Verlag GmbH & Co. KGaA, Weinheim

As the starting material for the surface studies, we chose a perylene derivative, 4,9-diaminoperylene-quinone-3,10-diimine (DPDI; **1**), which is readily obtained by oxidative coupling of two 1,8-diaminonaphthalene molecules[8] and displays a particularly rich redox chemistry.[9] The most stable form of this compound corresponds to the semiquinoidal structure displayed in Scheme 1, which on the one hand can

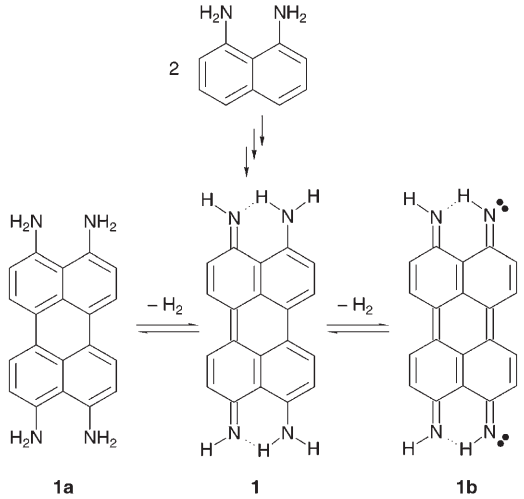

Scheme 1. The formation of DPDI (**1**) by oxidative coupling of two 1,8-diaminonaphthalene molecules, and its redox conversion into **1a** and **1b**.

be reversibly converted into the perylene **1a** by a two-electron reduction,[9] as previously shown for derivatives bearing bulky *N*-silyl groups, whereas a two-electron oxidation gives rise to the quinoidal redox state **1b**.[10] Because of this redox convertibility, **1** lends itself to chemical modification subsequent to its controlled deposition on metal surfaces and, thus, to significant changes in its intermolecular interactions.

Thin layers of **1** that range from submonolayer to monolayer (ML) coverage were prepared by thermal deposition onto a Cu(111) crystal and by subsequent annealing at 300 °C under ultra high vacuum (UHV) conditions (one monolayer of DPDI corresponds to the amount of molecules that is needed to cover the complete Cu surface and corresponds to 0.84 molecules nm^{-2}). The structures of the organic layers were characterized in UHV with room-temperature scanning tunneling microscopy (STM) and low-energy electron diffraction (LEED) before and after annealing. Before the annealing of submonolayer coverages of **1**, only a mobile phase and no ordered arrangement is found. The full monolayer assembles in an ordered aggregate with the monomers aligned in a rectangular unit cell of the size 0.92 nm × 1.3 nm,[11] an arrangement which is controlled by the molecular shape of **1**. The high mobility of **1** on the metal surface is unsurprising as there is no possibility of intermolecular hydrogen-bonding interactions in two dimensions, as the nitrogen functions are exclusively hydrogen-bond donors and there are no appropriate acceptor functionalities. As a result of the annealing process at 300 °C, the deposited molecules of **1** are chemically modified, as is reflected in the comparison of X-ray photoelectron spectroscopy (XPS) data before and after the thermolysis.[12] For surface coverages below 0.7 ML, the mobile monomers aggregate to give a well-ordered 2D honeycomb network (Figure 1 a, b). Based on the

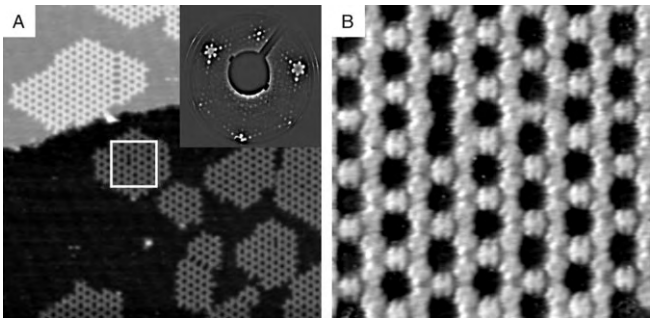

Figure 1. Self-assembly of 0.3 ML of DPDI on Cu(111) annealed at 300 °C. a) A large-scale STM image (100 nm × 100 nm, $I = 25$ pA, $U = -1.5$ V) of several DPDI islands that exhibit a honeycomb structure. Inset: LEED pattern that corresponds to this overlayer, as obtained at 52 eV primary energy representing a Cu(111)–p(10×10) DPDI lattice registry of the monomeric components. b) A high-resolution STM image (15 nm × 15 nm, $I = 25$ pA, $U = -2$ V) of the marked region, thus exhibiting the honeycomb network in detail and showing a vacancy defect.

STM data and the information obtained from the LEED pattern shown in the inset of Figure 1 a, a commensurate arrangement with regard to the Cu substrate of the DPDI monomers in a p(10×10) superlattice with a lattice constant of 2.55 nm is determined.

The assembly of these honeycomb networks can be readily explained by dehydrogenation of the DPDI monomers on the copper surface to provide the autocomplementary compound **1b**, in which the now-modified nitrogen functions may act as both hydrogen-bond acceptors and donors. The molecules, thus, link up through hydrogen-bonding interactions with each DPDI monomer binding to a total of four neighboring monomers to form the honeycomb network (Scheme 2). Hydrogen-bonding interactions between the nitrogen functions is consistent with the structural data from the STM and LEED experiments, from which a N···N distance between adjacent molecules of about 3.1 Å is derived.

The network itself exhibits an extraordinary stability, as is reflected by its inertness towards manipulation of individual monomers with the STM tip. Moreover, in LEED experiments performed while annealing the sample, the diffraction pattern of the overlayer persisted up to a temperature of 450 °C. Further increase in the temperature resulted in an irreversible destruction of the hexagonal perylene network. The considerable stability of this hexagonal network together with its commensurability with the Cu surface may be attributed to a combination of resonance-assisted hydrogen bonding[7,13] and a strong interaction with the Cu support. A similar case for a commensurate overlayer is reported for perylene tetracarboxdianhydride (PTCDA) adsorbed on a Ag(111) surface.[14]

 © 2005 Wiley-VCH Verlag GmbH & Co. KGaA, Weinheim

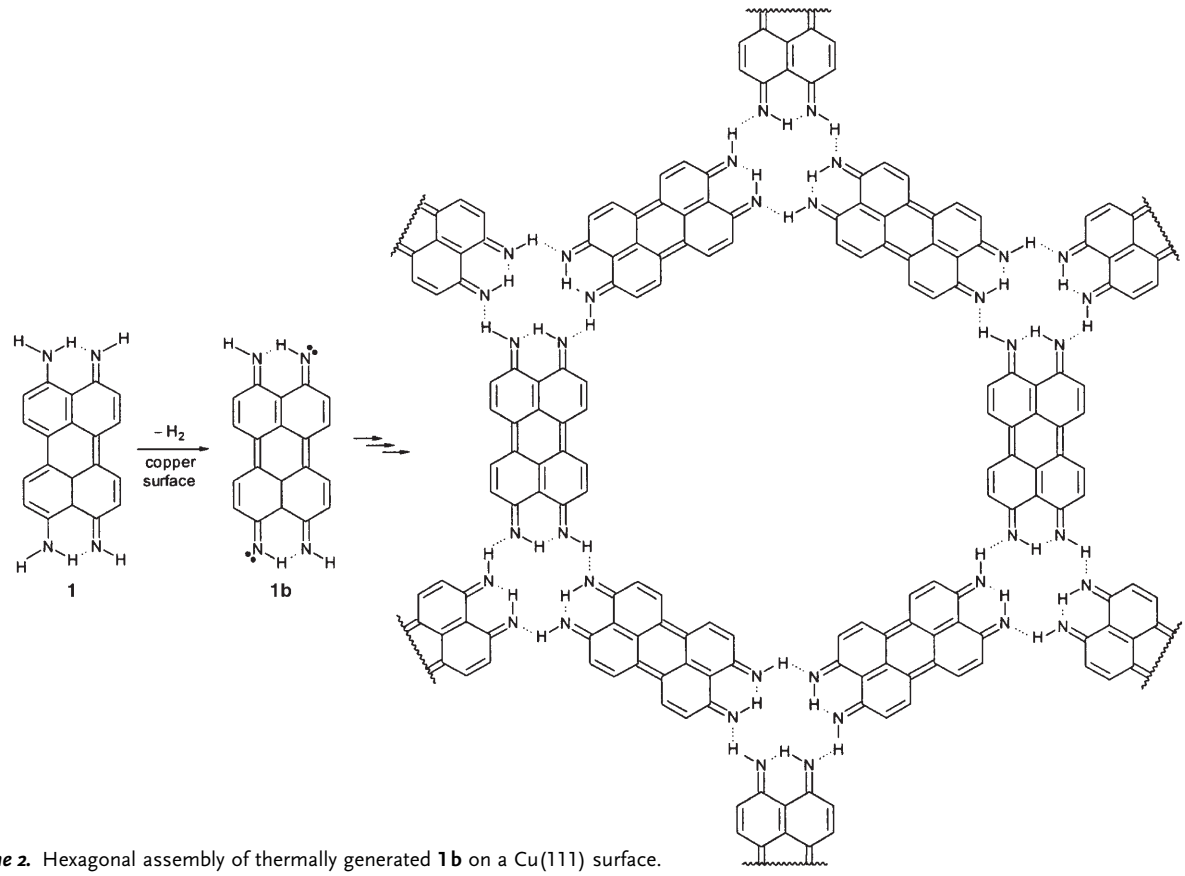

Scheme 2. Hexagonal assembly of thermally generated **1b** on a Cu(111) surface.

A key requirement for the formation of this highly ordered structure appears to be the free mobility of **1**, and subsequently **1b**, on the Cu(111) surface to attain the appropriate molecular arrangement and also the rather low molecular coverage on the metal support to accommodate the large hexagonal cavities in the 2D network. Thus, for geometrical reasons, the honeycomb structure corresponds to a maximum coverage of 0.7 ML. It was, therefore, of interest to assess if and how the polymer structure changed upon going to higher surface coverage.

Upon annealing a sample with a coverage of approximately 0.85 ML DPDI at 300 °C, trimeric structures in the form of rings are found (Figure 2

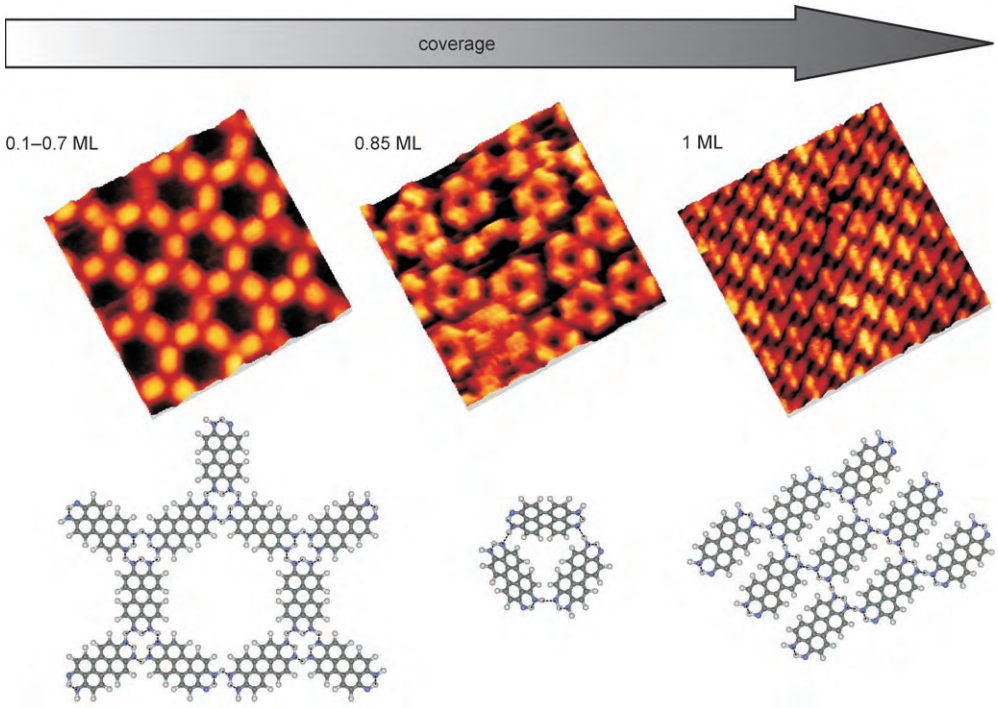

Figure 2. STM images (9 nm × 9 nm) and the corresponding chemical structures of the surface aggregates at variable coverage of **1**. All the polymeric islands were obtained by annealing the samples at 300 °C. For 0.1–0.7 ML of DPDI, an extended 2D honeycomb network is formed (left). Increasing the coverage to 0.85 ML yields a 0D trimeric structure (center), whereas at monolayer coverage a chain structure (right) is produced.

© 2005 Wiley-VCH Verlag GmbH & Co. KGaA, Weinheim

center), which are packed more densely on the surface than the honeycomb network discussed above. The formation of these trimers may be explained by the same dehydrogenation reaction as proposed for the honeycomb network that yields **1b**. This compound, activated for hydrogen-bond formation, then forms the observed cyclic hydrogen-bonded structure in a self-assembly process which is modified by a characteristic change of the diffusion length at the higher 2D molecular density. For the steric, repulsive interactions between the inwards-pointing hydrogen atoms of the perylene trimer, the overall structure is expected to deviate from a strictly planar arrangement and is expected to adopt an overall bowl-shaped form, a notion which is also supported by the STM images. Because of this steric interaction and because of the fact that each monomer is only hydrogen bonded to two neighboring monomers, a less robust structure of lower binding energy is expected in this case. This is evidenced by the observation of a dynamical equilibrium of "open" and "closed" structures (trimers, chains, and individual molecules) upon subsequent scanning of the same sample area at room temperature.[15] Furthermore, it was observed that only two preferred orientations of the trimers relative to the substrate exist, thus indicating that the structure of the Cu surface potentially contributes to the stabilization of the cyclic trimer.

For the final step of probing the concentration dependence of the polymerization pattern, we prepared full monolayers of DPDI on a Cu(111) surface. In contrast to the mobile submonolayer phases of the monomer, there is little room for molecular reorientation upon annealing of such a densely packed and highly ordered molecular array. The result of the thermal annealing of a DPDI monolayer on Cu(111) at 300 °C is displayed in Figure 2 on the right. STM analysis reveals a zigzag chain structure of the polymer with the chains packing one alongside the other. These chains derive from the regular monolayer structure of the monomer by an apparently concerted "shearing" movement, which is accompanied by shortening of the distance between adjacent molecular rows along the long molecular axis by approximately 1 Å. The same dehydrogenation reaction as for submonolayer coverage is thought to take place, thus resulting in each monomer being linked through hydrogen bonds to four adjacent monomers. The Moiré pattern in the STM images, as well as the LEED patterns, indicate that the molecular arrangement obtained in this annealing process is not commensurate to the underlying lattice of the Cu substrate.

Direct evidence for the importance of the conversion of **1** into **1b**, and thus for the formation of a monomer capable of the formation of 2D hydrogen-bonded networks, was obtained by deposition of the equivalent of approximately 0.15 ML of additional DPDI onto the previously prepared honeycomb network (Figure 3). These additional monomers in their initial, non-dehydrogenated form are not assembled into the existing honeycomb network at room temperature.[17] Instead, the additional monomer molecules are mobile on the metal surface, as found for submonolayer coverage prior to thermal treatment, and additional DPDI molecules are trapped in the hexagonal cavities of the honeycomb network, in which they are still mobile as can be deduced from their blurred appearance in the STM images. Extension of the honeycomb structure only occurs after a second annealing process. These findings indicate that the highly robust honeycomb network can be used as a template to arrange or trap molecules that are even larger than the DPDI monomers.

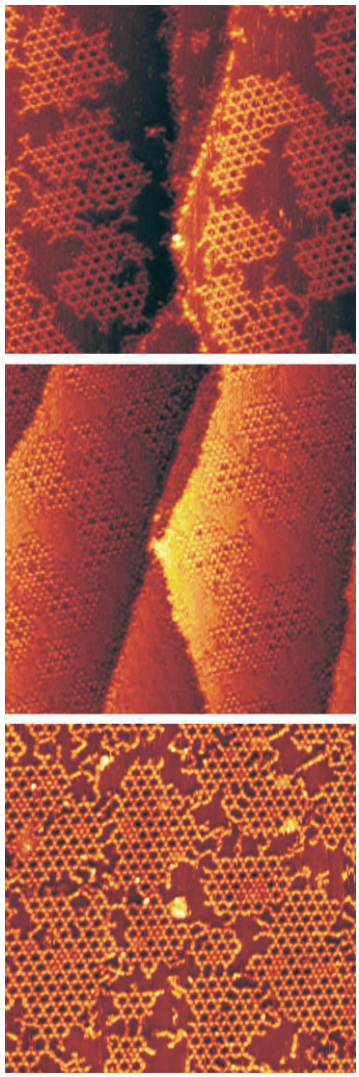

Figure 3. STM images (70 nm × 70 nm) of the same sample at different phases of sample preparation. First, the honeycomb network was prepared (top) and subsequently 0.15 ML DPDI were deposited (center). The additional DPDI molecules form a mobile phase on the bare Cu substrate and some are trapped in the pores of the honeycomb network. Annealing this sample at 300 °C converts the mobile phase into a solid phase because of dehydrogenation of DPDI, thus resulting in an enlargement of the honeycomb network (bottom). Individual molecules remain trapped within the network. However, the characteristic confined mobility disappears after annealing.

In conclusion, the deposition of 4,9-diaminoperylenequinone-3,10-diimine (**1**) on a metal surface provides highly mobile submonolayer phases because of the impossibility of significant intermolecular interactions in two dimensions. However, thermally activated dehydrogenation leads to **1b**, which is autocomplementary and serves both as an hydrogen-bond donor and acceptor. This behavior leads to well-defined polymeric structures that can be controlled by the typical diffusion length between the activation of the precursor and

 © 2005 Wiley-VCH Verlag GmbH & Co. KGaA, Weinheim

its "polymerization", which in turn is controlled through different amounts of initial monomer coverage. This reactive self-assembly represents a "surface dilution principle" akin to the dilution principle in chemical synthesis.[18] The connectivity and the resulting dimensionality of the aggregates may be varied between 0D for the trimers and 2D for the hexagonal network. Once formed, these molecular surface assemblies are highly robust and, therefore, suitable for the construction of hierarchic structures by self-organization of subsequently deposited material at lower temperatures; such investigations are currently under way.

Experimental Section

The experiments were conducted in a UHV system composed of different chambers for sample preparation and characterization (base pressure: 10^{-10} mbar). The Cu(111) substrate was prepared by subsequent cycles of sputtering with Ar^+ ions and annealing at 870 K. Thermal evaporation from a homemade crucible at a rate of about 0.5 ML min^{-1} was used to prepare thin films of DPDI on the Cu(111) surface while the substrate was kept at RT. Annealing of the DPDI films was performed by radiative heating. The investigation of the samples was carried out with a homebuilt STM operated at room temperature, by LEED and by XPS.

Received: July 3, 2005
Published online: October 17, 2005

Keywords: dilution principle · hydrogen bonds · molecular aggregation · scanning probe microscopy · surface chemistry

[1] a) J.-M. Lehn, *Supramolecular Chemistry: Concepts and Perspectives*, VCH, Weinheim, **1995**.
[2] For a collection of recent overviews of the principles of molecular self-assembly, see the whole volume of *Science* **2002**, *295*.
[3] a) J.-M. Lehn, *Science* **2002**, *295*, 2400; b) O. Ikkala, G. ten Brinke, *Science* **2002**, *295*, 2407; c) D. N. Reinhoudt, M. Crego-Calama, *Science* **2002**, *295*, 2403; d) G. M. Whitesides, B. Grzybowski, *Science* **2002**, *295*, 2418; e) M. D. Hollingsworth, *Science* **2002**, *295*, 2410; f) T. Kato, *Science* **2002**, *295*, 2414.
[4] Surface engineering of multidimensional assemblies: a) S. De Feyter, F. C. De Schryver, *Chem. Soc. Rev.* **2003**, *32*, 139; for important contributions that concern weak interactions which govern the self-assembly at surfaces as determined by STM, see: b) T. Yokoyama, S. Yokoyama, Y. Okuno, S. Mashiko, *Nature* **2001**, *413*, 619; c) S. Ito, M. Wehmeier, J. D. Brand, C. Kubel, R. Epsch, J. P. Rabe, K. Müllen, *Chem. Eur. J.* **2000**, *6*, 4327.
[5] a) J. Weckesser, A. De Vita, J. V. Barth, C. Cai, K. Kern, *Phys. Rev. Lett.* **2001**, *87*, 096101; b) A. Dmitriev, N. Lin, J. Weckesser, J. V. Barth, K. Kern, *J. Phys. Chem. B* **2002**, *106*, 6907; c) M. de Wild, S. Berner, H. Suzuki, H. Yanagi, D. Schlettwein, S. Ivan, A. Baratoff, H.-J. Güntherodt, T. A. Jung, *ChemPhysChem* **2002**, *3*, 881; d) S. De Feyter, M. Larsson, N. Schuurmans, B. Verkuijl, G. Zoriniants, A. Gesquiere, M. M. Abdel-Mottaleb, J. van Esch, B. L. Feringa, J. van Stam, F. De Schryver, *Chem. Eur. J.* **2003**, *9*, 1198; e) D. Bonifazi, H. Spillmann, A. Kiebele, M. de Wild, P. Seiler, F. Cheng, H.-J. Güntherodt, T. Jung, F. Diederich, *Angew. Chem.* **2004**, *116*, 4863; *Angew. Chem. Int. Ed.* **2004**, *43*, 4759; review: f) L. Brunsveld, B. J. B. Folmer, E. W. Meijer, R. P. Sijbesma, *Chem. Rev.* **2001**, *101*, 4071.
[6] J. A. Theobald, N. S. Oxtoby, M. A. Phillips, N. R. Champness, P. H. Beton, *Nature* **2003**, *424*, 1029.
[7] a) G. Gilli, F. Bellici, V. Ferretti, V. Bertolasi, *J. Am. Chem. Soc.* **1989**, *111*, 1023; b) P. Gilli, V. Bertolasi, V. Ferretti, G. Gilli, *J. Am. Chem. Soc.* **1994**, *116*, 909; c) P. Gilli, V. Bertolasi, L. Pretto, V. Ferretti, G. Gilli, *J. Am. Chem. Soc.* **2004**, *126*, 3845.
[8] K. W. Hellmann, C. H. Galka, I. Rüdenauer, L. H. Gade, I. J. Scowen, M. McPartlin, *Angew. Chem.* **1998**, *110*, 2053; *Angew. Chem. Int. Ed.* **1998**, *37*, 1948.
[9] L. H. Gade, C. H. Galka, K. W. Hellmann, R. M. Williams, L. de Cola, I. J. Scowen, M. McPartlin, *Chem. Eur. J.* **2002**, *8*, 3732.
[10] The reversible oxidation of 4,9-bis(triisopropylsilylamino)perylenequinone-3,10-bis(triisopropylsilylimine) which gives the bisquinoidal system is observed in the cyclic voltammogram: the half-wave potential of the first oxidation step is at +0.69 V and the second at +1.12 V (in CH_2Cl_2 at 4 °C, 10 mV s^{-1}, vs calomel electrode): T. Riehm, Diplomarbeit, Universität Heidelberg **2005**. Derivatives of the oxidized form **1b** do not appear to be stable as bulk materials.
[11] An STM image of a monolayer of DPDI molecules on a Cu(111) surface prior to the annealing step is provided in the Supporting Information.
[12] The XPS spectrum of the sample prior to annealing exhibits two individually resolved nitrogen peaks at 399.8 and 397.9 eV binding energy, thus corresponding to the imine and amine groups, whereas only the peak at 399.8 eV remains after annealing at 300 °C; this observation is attributed to the "symmetrization" of all the imine nitrogen atoms, which is consistent with the transformation of **1** into **1b**.
[13] An example for resonance-assisted hydrogen-bonding interactions on surfaces is provided by the formation of guanidine quartets stabilized by cooperative hydrogen bonds: a) R. Otero, M. Schöck, L. M. Molina, E. Laegsgaard, I. Stensgaard, B. Hammer, F. Besenbacher, *Angew. Chem.* **2005**, *44*, 2310; *Angew. Chem. Int. Ed.* **2005**, *44*, 2270; theoretical analysis: b) G. Louit, A. Hocquet, M. Ghomi, M. Meyer, J. Sühnel, *PhysChemComm* **2002**, *5*, 94.
[14] M. Eremtchenko, J. A. Schaefer, F. S. Tautz, *Nature* **2003**, *425*, 602; the electron-withdrawing functional groups in PTCDA enhance the π bonding to the metal support, thus locking the molecules into specific sites and orientations.
[15] Based on a time-lapse series (see the Supporting Information), an approximate value for the diffusion barrier and for the condensation energy can be deduced. According to the procedure described in reference [16], a value of 0.6 eV for the diffusion energy and 0.3 eV for the condensation energy are derived. Mainly, these values should only reflect the energy range for diffusion and condensation as they are obtained in a semi-quantitative way.
[16] S. Berner, M. Brunner, L. Ramoino, H. Suzuki, H.-J. Güntherodt, T. A. Jung, *Chem. Phys. Lett.* **2001**, *348*, 175.
[17] This conclusion is deduced through comparison of the surface area which is covered by the network before and after the second evaporation.
[18] a) K. Ziegler, *Methoden der Anorganischen Chemie, Houben-Weyl, Vol. IV(2)*, **1955**, p. 729; b) A. Lüttringhaus, H. Simon, *Justus Liebigs Ann. Chem.* **1947**, *557*, 120; the concept was first formulated in: c) P. Rüggli, *Justus Liebigs Ann. Chem.* **1912**, *392*, 92.

 © 2005 Wiley-VCH Verlag GmbH & Co. KGaA, Weinheim

Polyolefins

DOI: 10.1002/anie.200502848

Efficient Mono- and Bifunctionalization of Polyolefin Dendrimers by Olefin Metathesis**

*Cátia Ornelas, Denise Méry, Jean-Claude Blais, Eric Cloutet, Jaime Ruiz Aranzaes, and Didier Astruc**

Olefin metathesis has recently transformed the way molecular chemists think about synthetic strategies.[1] Remarkable examples can be found in transition-metal architectures, such as ring-closing metathesis (RCM) of olefin-terminated ligands.[2,3] van Koten and Newkome have used stars for the nanofabrication of giant ring structures by using RCM,[4] and Zimmerman and co-workers have shown that RCM successfully allows molecular imprinting inside dendrimers and can be applied to the fabrication of nanotubes.[5] Indeed, RCM and ring-opening-metathesis polymerization (ROMP) are probably the most popular facets of olefin metathesis because of their considerable impact on the synthesis of biologically important cyclic compounds and polymers, respectively.[1] At first sight, cross metathesis (CM) is marred by the thermodynamic equilibrium that produces a mixture of compounds, but Blechert and co-workers showed that the excess of one olefin together with the Schrock Mo catalyst[1b] favors the formation of the cross product, whereas steric factors favor *E* stereoselectivity.[6] Grubbs and co-workers have shown that when a terminal olefin is metathesized with the second-generation Ru catalyst **A** (Cy = cyclohexyl) in the presence of another olefin bearing a strongly electron-withdrawing substituent, the stereoselectivity leads to high yields of the *E*-functionalized cross olefin.[7]

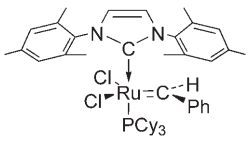

A

Despite the usefulness of this property in organic synthesis,[7] it has not been used in dendrimer chemistry.[8] Dendrimer functionalization is considerably more challenging than that of mono-olefin molecules, because it requires a clean and quantitative reaction to avoid the formation of mixtures among the branch termini.[8]

The $CpFe^+$-induced (Cp = cyclopentadienyl) activation of polymethylbenzenes under ambient or near-ambient conditions is known to efficiently produce polyolefin star and dendritic cores by reaction of such arene complexes with excess KOH and alkenyl halides in THF.[9] The reaction was extended to aryl ether complexes to yield to the phenol dendron p-$HOC_6H_4C(allyl)_3$ (**1**),[10a] which served as a brick for further dendrimer construction; for example, hydrosilylation of the polyolefin core with $HSiMe_2CH_2Cl$ followed by reaction of **1** yielded dendrimers with 3^n allyl branches ($n = 2$–10) starting from mesitylene.[10b] We now report that these star- and dendritic-shaped polyolefin dendrimers can be cleanly and stereospecifically mono- or bifunctionalized by CM or a combination of RCM + CM, respectively, using catalyst **A**. A quick, overall synthesis of water-soluble dendrimers from simple polymethylbenzenes, such as mesitylene and hexamethylbenzene, is therefore provided.

The reaction of $[CpFe(C_6Me_6)][PF_6]$ (**2**) with KOH + allyl bromide or 1-undecenyl iodide in THF, followed by visible-light irradiation in MeCN gives nearly quantitative yields of the known hexaolefin stars **4**[11a] and **5**,[11b] which give high yields of the new hexafunctionalized *trans* olefins **7** and **8** as the only reaction products upon reaction with $CH_2{=}CHCO_2R$ (R = H or Me) in the presence of 5 mol% of **A** (Scheme 1). The iron complex $[CpFe\{C_6(CH_2CH_2CH{=}CH_2)_6\}][PF_6]$ (**3**), the precursor of **4**, also gives hexafunctionalized iron complex **6a** upon metathesis with $CH_2{=}CHCO_2H$ using **A**, although partial decomplexation leads to reduced yields of the complexes.

In the case of mesitylene, complexation by the $CpFe^+$ species, reaction with KOH and allyl bromide in THF under ambient conditions, and decomplexation gives the known dendritic core $C_6H_3[C(CH_2CH{=}CH_2)_3]_3$ (**10**; generation 0 (G0)),[11c] whose metathetic reaction with $CH_2{=}CHCO_2R$ using **A** gives the new hetero-bifunctional compound **11**. This RCM + CM series of reactions inhibits the formation of the known capsule **12** formed from **10** in the absence of $CH_2{=}CHCO_2R$ with the same catalyst **A** (Scheme 2).[11d] As the tris-homofunctionalization of the triallylmethyl tripod is much less favored than RCM as an approach to form the cyclopentenyl group, we lengthened the dendritic tethers to prevent RCM. This lengthening of the tether was achieved by hydrosilylation of **10** with $HSiMe_2CH_2Cl$ followed by reaction with p-$OHC_6H_4O(CH_2)_9CH{=}CH_2$, thus giving the nonaolefin **13**. Contrary to **10**, the metathesis reaction of **13** with $CH_2{=}CHCO_2R$ only gives the CM product **14** (only *trans* isomers) which results from terminal-olefin functionalization (Scheme 2). Likewise, the tethers of the known 27- and 81-allyl dendrimers **15** and **18** (G1 and G2), which result from sequential hydrosilylation of **10** with $HSiMe_2CH_2Cl$,

[*] C. Ornelas, D. Méry, Dr. J. Ruiz Aranzaes, Prof. D. Astruc
Nanosciences and Catalysis Group
LCOO, UMR CNRS No. 5802
University Bordeaux I
33405 Talence Cedex (France)
Fax: (+33) 5-4000-6646
E-mail: d.astruc@lcoo.u-bordeaux1.fr
Dr. J.-C. Blais
LCSOB, UMR CNRS No. 7613
Université Paris 6
75252 Paris Cedex (France)
E. Cloutet
LCPO, UMR CNRS No. 5629
University Bordeaux I
33405 Talence Cedex (France)

[**] We are grateful to the Institut Universitaire de France (IUF; D.A.), Fundaçao para a Ciência e a Tecnologia (FCT), Portugal (PhD grant to C.O.), MRT (PhD grant to D.M.), CNRS, University Bordeaux I, and University Paris VI for financial support.

Supporting information for this article is available on the WWW under http://www.angewandte.org or from the author.

 © 2005 Wiley-VCH Verlag GmbH & Co. KGaA, Weinheim

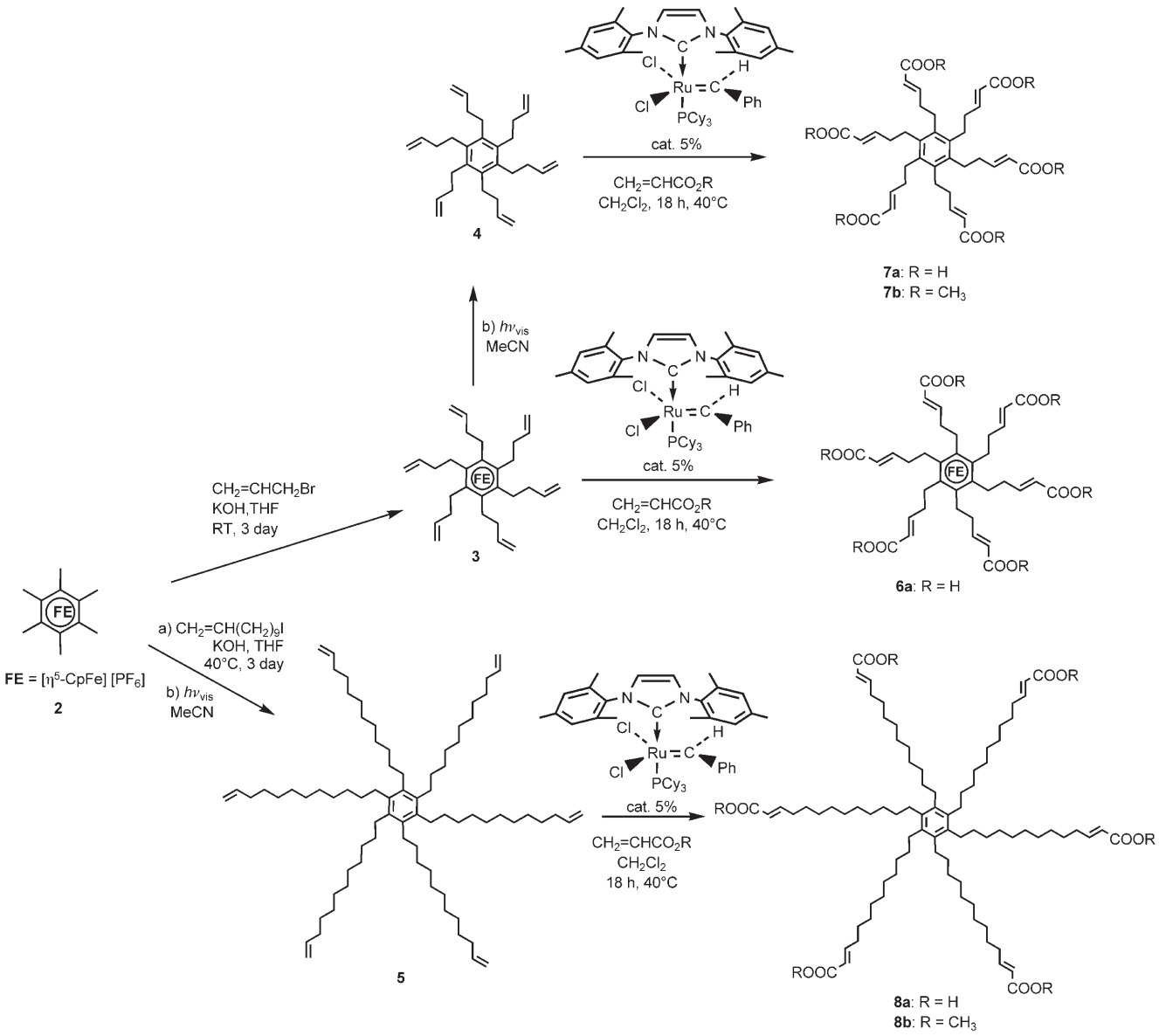

Scheme 1. Synthesis of hexafunctionalized *trans* olefins **7** and **8**.

reaction with NaI, and treatment with p-$HOC_6H_4C(allyl)_3$, were lengthened in the same way to give the new 27- and 81-olefin dendrimers **16** and **19**; their metathesis with CH_2=$CHCO_2R$ proceeded analogously with **A** to give the polyfunctional dendrimers **17** and **20** (Schemes 3 and 4). All the polyfunctionalized dendrimers were characterized by ^1H, ^{13}C, and ^{29}Si NMR spectroscopy and elemental analysis. In addition, the MALDI-TOF mass spectra of **8a**, **8b**, **14a**, and **14b** only show the molecular peaks (see the Supporting Information), and size-exclusion chromatography (SEC) showing Gaussian-type distributions (Figure 1) confirm the monodispersities of the three generations of polyallyl and polyester dendrimers.

The poly(carboxylic acid) dendrimers give water- or methanol-soluble sodium carboxylate salts upon contact with aqueous NaOH or NaOH in methanol. Water-soluble dendrimers are used for applications such as molecular micelles and cation binding and transport.[12] The poly(carboxylic acid) dendrimers are also very useful for their reactions with various amines, a further functionalization procedure. For example, reaction of the new amine dendron $N[(CH_2)_4Fc]_3$ (Fc = ferrocenyl; **21**) with **20a** quantitatively yields the 243-ferrocenyl dendrimer **22** (Scheme 4) that shows a single wave in cyclic-voltammetric studies (see the Supporting Information), which is a key feature for redox sensing—the large dendrimer size also being favorable for electrode modification.[13] The formation of the 81 ammonium carboxylate linkages is shown by the change in solubility, from **20a** that is insoluble in CH_2Cl_2 (but soluble in acetone) to **22** that becomes soluble in CH_2Cl_2. Moreover, the ^1H and ^{13}C NMR signals of the methylene groups attached to the carboxylate and amine groups, respectively, are strongly shifted as expected in **22** relative to the precursors **20a** and **21** (see the Supporting Information).

 © 2005 Wiley-VCH Verlag GmbH & Co. KGaA, Weinheim

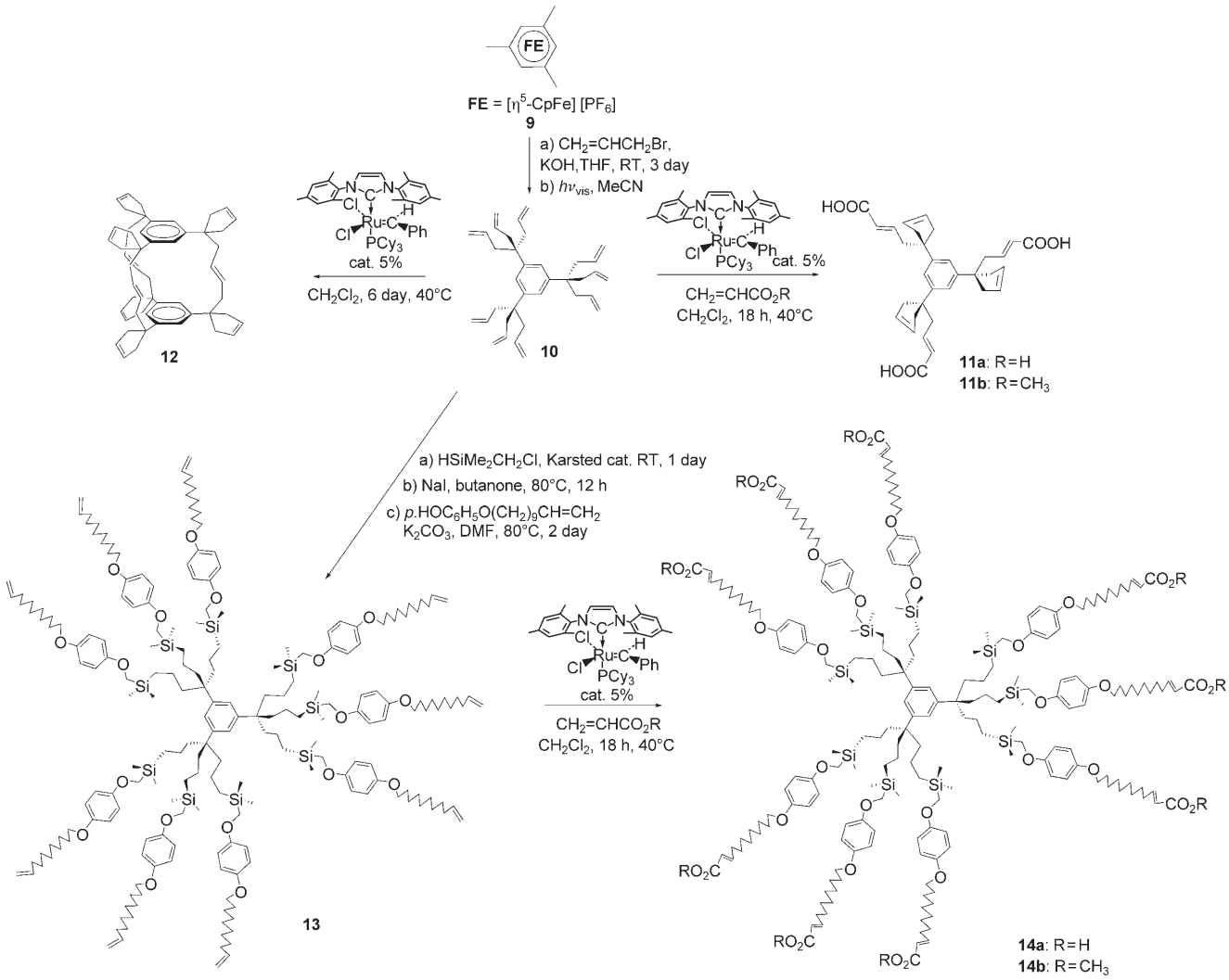

Scheme 2. Synthesis of the CM product **14**.

In conclusion, the finding of this remarkable quantitative chemio-, regio-, and stereoselective cross olefin metathesis with dendrimers using catalyst **A** provides a unique way to functionalize polyolefin-terminated dendrimers and to solubilize them in water and methanol. This reaction makes such useful dendrimers readily accessible on large scales from simple polymethylbenzenes in a few steps.[14]

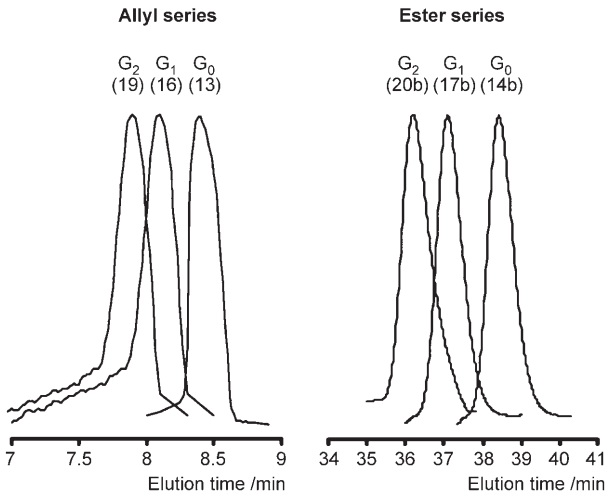

Figure 1. Size-exclusion chromatograms of the three generations of dendrimers (9, 27, and 81 tethers, respectively) before (left) and after (right) functionalization by cross metathesis with methylacrylate. The polydispersity indices obtained from these chromatograms have values between 1.00 and 1.02. Apparent molar masses of the dendrimers were determined by using two different size-exclusion chromatographic apparatus, both equipped with a refractive index (RI; Jasco) and UV/Vis (Varian 2550, $l = 254$ nm) detectors. The columns used were four TSK-gel columns (7.8×300 mm, G 2000, G 3000, G 4000, G 5000 with particle sizes of 5, 6, 6, and 9 mm, respectively) and one PL Poly Pore column (7.5×300 mm, particle size = 5 mm). The eluent was THF (0.7 mL min^{-1}) at 25 °C and calibration was carried out using linear polystyrene standards.

 © 2005 Wiley-VCH Verlag GmbH & Co. KGaA, Weinheim

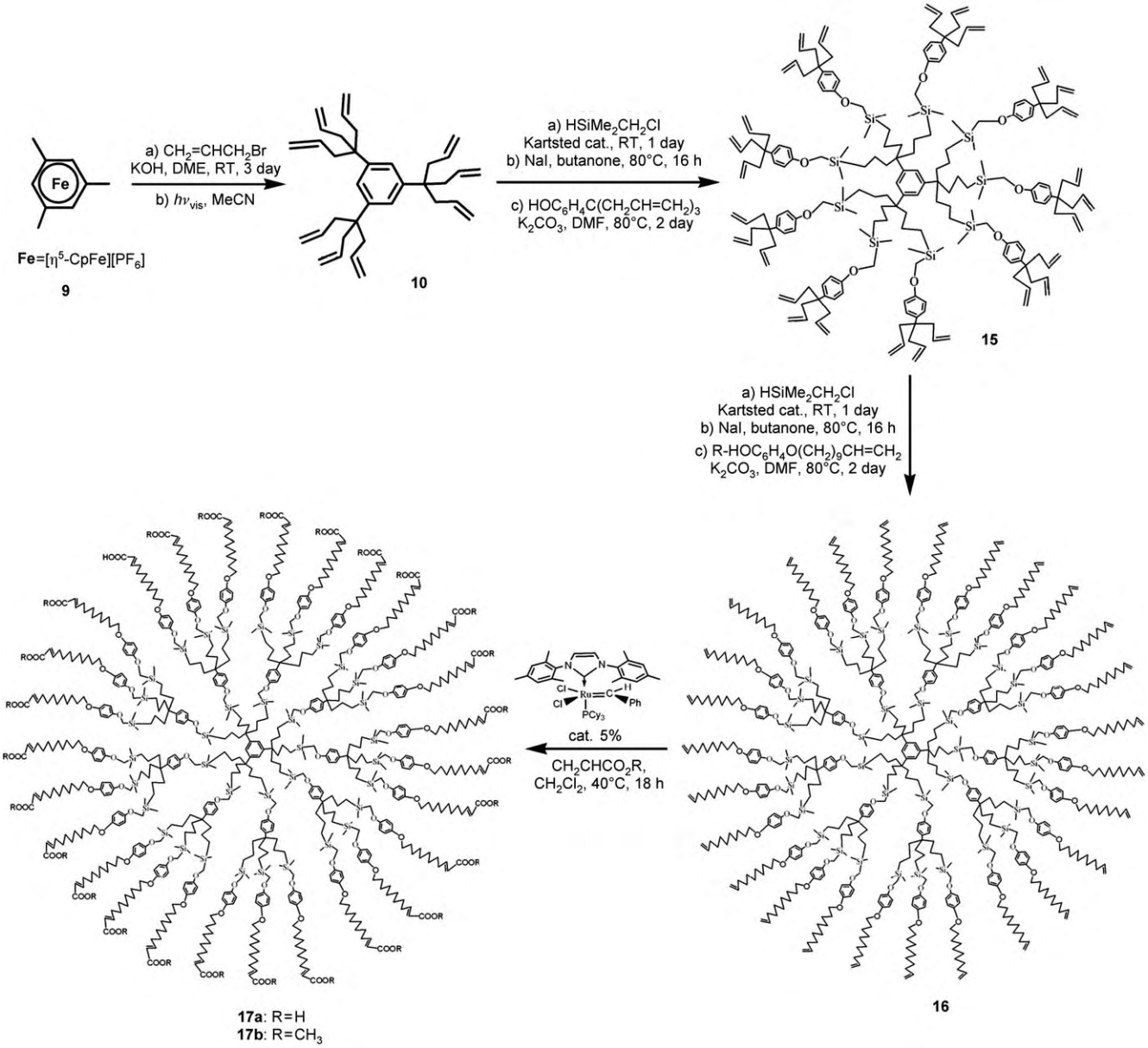

Scheme 3. Synthesis of the polyfunctional dendrimer **17**.

Experimental Section

General metathesis experiments: the polyolefin dendrimer (0.0418 mmol/n dendritic tethers), dry CH_2Cl_2 (10–50 mL), methyl acrylate or acrylic acid (0.221 mmol), and catalyst **A** (5 mol% equivalents per dendritic branch, 0.0114 g, 0.0134 mmol) were successively introduced into a Schlenk flask in an inert atmosphere. The reaction solution was warmed to 40 °C for 18 h. After removal of the solvent under vacuum, the product was washed with methanol and precipitated by addition of a tenfold excess of methanol to a solution of the polyester dendrimers in CH_2Cl_2 or to a solution of the polycarboxylic acid dendrimers in THF. The colorless waxy organic dendrimers were usually obtained in 95–99% yield and were characterized by ^1H, ^{13}C, and ^{29}Si NMR spectroscopy; MALDI-TOF-MS of **8a**, **8b**, **14a**, **14b**, **16**, **17a**, **17b**, and **21** (observation of the molecular peak and absence of other peaks); elemental analysis; and size-exclusion chromatography (SEC, Figure 1).

Received: August 10, 2005
Published online: October 25, 2005

Keywords: dendrimers · ferrocenes · iron · metathesis · organometallic reagents

[1] a) *Handbook of Metathesis, Vols. 1–3* (Ed.: R. H. Grubbs), Wiley-VCH, Weinheim, **2003**; b) R. R. Schrock, A. H. Hoveyda, *Angew. Chem.* **2003**, *115*, 4703; *Angew. Chem. Int. Ed.* **2003**, *42*, 4592; c) A. Fürstner, *Angew. Chem.* **2000**, *112*, 3140; *Angew. Chem. Int. Ed.* **2000**, *39*, 3012; d) for a recent historical perspective, see: D. Astruc, *New J. Chem.* **2005**, *29*, 42; see, also http://nobelprize.org/chemistry/laureates/2005/chemreading.html.

[2] A. M. Martin-Alvarez, F. Hampel, A. M. Arif, J. A. Gladysz, *Organometallics* **1999**, *18*, 955; E. B. Bauer, J. Ruwwe, F. A. Hampel, S. Szafert, J. A. Gladysz, *Chem. Commun.* **2000**, *22*, 2261; C. R. Horn, J. M. Martin-Alvarez, J. A. Gladysz, *Organometallics* **2002**, *21*, 5386; E. B. Bauer, F. Hampel, J. A. Gladysz, *Organometallics*, **2003**, *22*, 5567; T. Shima, E. B. Bauer, F. Hampel, J. A. Gladysz, *Dalton Trans.* **2004**, *7*, 1012; T. Shima,

 © 2005 Wiley-VCH Verlag GmbH & Co. KGaA, Weinheim

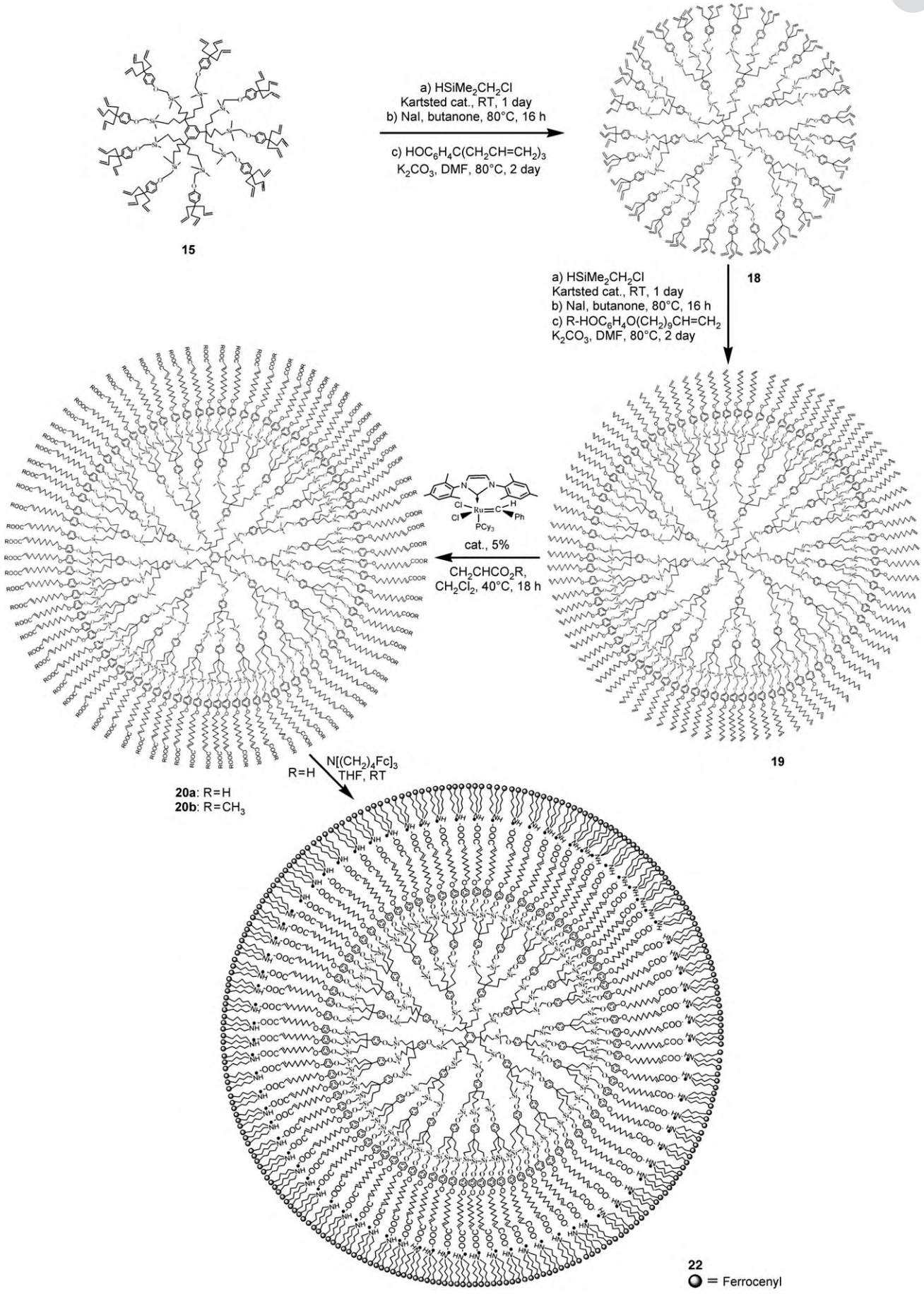

Scheme 4. Synthesis of the polyfunctional dendrimer **22**.

 © 2005 Wiley-VCH Verlag GmbH & Co. KGaA, Weinheim

F. Hampel, J. A. Gladysz, *Angew. Chem.* **2004**, *116*, 5653; *Angew. Chem. Int. Ed.* **2004**, *43*, 5537.

[3] a) C. Dietrich-Bucherer, G. Rapenne, J.-P. Sauvage, *Chem. Commun.* **1997**, 2053; b) M. Weck, B. Mohr, J.-P. Sauvage, R.-H. Grubbs, *J. Org. Chem.* **1999**, *64*, 5463; c) G. Rapenne, C. Dietrich-Bucherer, J.-P. Sauvage, *J. Am. Chem. Soc.* **1999**, *121*, 994.

[4] a) A. V. Chuchryukin, H. P. Dijkstra, B. M. J. M. Suijkerbuijk, R. J. M. Klein Gebbink, G. P. M. van Klink, A. M. Mills, A. L. Spek, G. van Koten, *Angew. Chem.* **2003**, *115*, 238; *Angew. Chem. Int. Ed.* **2003**, *42*, 228; b) P. Wang, C. N. Moorefield, G. R. Newkome, *Angew. Chem.* **2005**, *117*, 1707; *Angew. Chem. Int. Ed.* **2005**, *44*, 1679.

[5] a) M. S. Wendland, S. C. Zimmerman, *J. Am. Chem. Soc.* **1999**, *121*, 1389; b) S. C. Zimmerman, I. Zharov, M. S. Wendland, N. A. Rakow, K. S. Suslick, *J. Am. Chem. Soc.* **2003**, *125*, 13504; c) Y. Kim, M. F. Mayer, S. C. Zimmerman, *Angew. Chem.* **2003**, *115*, 1153; *Angew. Chem. Int. Ed.* **2003**, *42*, 1121; d) N. G. Lemcoff, T. A. Spurlin, A. A. Gewirth, S. C. Zimmerman, J. B. Beil, S. L. Elmer, H. G. Vandeveer, *J. Am. Chem. Soc.* **2004**, *126*, 11420; e) J. Beil, N. G. Lemcoff, S. C. Zimmerman, *J. Am. Chem. Soc.* **2004**, *126*, 13576.

[6] O. Brümmer, A. Rückert, S. Blechert, *Chem. Eur. J.* **1997**, *3*, 441; M. Schuster, S. Blechert, *Angew. Chem.* **1997**, *109*, 2124; *Angew. Chem. Int. Ed. Engl.* **1997**, *36*, 2036; S. J. Connor, S. Blechert, *Angew. Chem.* **2003**, *115*, 1944; *Angew. Chem. Int. Ed.* **2003**, *42*, 1900.

[7] A. K. Chatterjee, J. P. Morgan, M. Scholl, R. H. Grubbs, *J. Am. Chem. Soc.* **2000**, *122*, 3783; A. K. Chatterjee, T.-L. Choi, D. P. Sanders, R. H. Grubbs, *J. Am. Chem. Soc.* **2003**, *125*, 11360; A. K. Chatterjee in reference [1a], *Vol. 2*, chap. 2.8, p. 246; for catalyst **A**, see also, for example: R. H. Grubbs, *Acc. Chem. Res.* **2001**, *34*, 18.

[8] a) G. R. Newkome, C. N. Moorefield, F. Vögtle, *Dendrons and Dendrimers. Concepts, Synthesis and Applications*, Wiley-VCH, Weinheim, **2001**; b) *Dendrimers and other Dendritic Polymers* (Eds.: D. Tomalia, J. M. J. Fréchet), Wiley-VCH, New York, **2002**; c) *Dendrimers and Nanosciences* (Ed.: D. Astruc), *C. R. Chimie*, **2003**, *6*, p. 709.

[9] D. Astruc, S. Nlate, J. Ruiz in *Modern Arene Chemistry* (Ed.: D. Astruc), Wiley-VCH, Weinheim, **2003**, p. 400.

[10] a) V. Sartor, J.-L. Fillaut, L. Djakovitch, F. Moulines, V. Marvaud, F. Neveu, J.-C. Blais, D. Astruc, *J. Am. Chem. Soc.* **1999**, *121*, 2929; b) J. Ruiz, G. Lafuente, S. Marcen, C. Ornelas, S. Lazarre, J.-C. Blais, E. Cloutet, D. Astruc, *J. Am. Chem. Soc.* **2003**, *125*, 7250.

[11] a) F. Moulines, D. Astruc, *Angew. Chem.* **1988**, *100*, 1394; *Angew. Chem. Int. Ed. Engl.* **1988**, *27*, 1347; b) F. Moulines, L. Djakovitch, R. Boese, B. Gloaguen, W. Thiel, J.-L. Fillaut, M.-H. Delville, D. Astruc, *Angew. Chem.* **1993**, *105*, 1132; *Angew. Chem. Int. Ed. Engl.* **1993**, *32*, 1075; c) J.-L. Fillaut, J. Linares, D. Astruc, *Angew. Chem.* **1994**, *106*, 2540; *Angew. Chem. Int. Ed. Engl.* **1994**, *33*, 2460; d) V. Martinez, J.-C. Blais, D. Astruc, *Angew. Chem.* **2003**, *115*, 4502; *Angew. Chem. Int. Ed.* **2003**, *42*, 4366; e) L. Plault, A. Hauseler, S. Nlate, D. Astruc, S. Gatard, R. Neumann, *Angew. Chem.* **2004**, *116*, 2984; *Angew. Chem. Int. Ed.* **2004**, *43*, 2924.

[12] a) G. R. Newkome, C. N. Moorefield, G. R. Baker, M. J. Saunders, S. H. Grossman, *Angew. Chem.* **1991**, *103*, 1207; *Angew. Chem. Int. Ed. Engl.* **1991**, *30*, 1178; b) G. R. Newkome, *Pure Appl. Chem.* **1988**, *60*, 2337; c) K. R. Gopidas, A. R. Leheny, G. Caminati, N. J. Turro, D. A. Tomalia, *J. Am. Chem. Soc.* **1991**, *113*, 7335; d) J. F. G. A. Jansen, E. M. M. de Brabander-van-den Berg, E. W. Meijers, *Science* **1994**, 1226; e) V. Balzani, P. Ceroni, S. Gestermann, M. Gorka, C. Kauffmann, F. Vögtle, *Tetrahedron* **2002**, *58*, 629.

[13] For a comprehensive review on ferrocene dendrimers and their electrochemistry, see for example: C. M. Casado, M. Moran, B. Alonso, B. Garcia, J. Gonzales, J. Losada, *Coord. Chem. Rev.* **1999**, *185/186*, 53.

[14] For other appealing hexafunctionalizations of arenes, see for example: a) R. Boese, J. R. Green, J. Ittendorf, D. L. Mohler, K. P. C. Volhardt, *Angew. Chem.* **1992**, *104*, 1643; *Angew. Chem. Int. Ed. Engl.* **1992**, *31*, 1643; b) P. Prinz, A. Lansky, B. Knieriem, A. de Meijere, T. Haumann, R. Boese, M. Noltemeyer, *Angew. Chem.* **1997**, *109*, 1343; *Angew. Chem. Int. Ed. Engl.* **1997**, *36*, 1289.

 © 2005 Wiley-VCH Verlag GmbH & Co. KGaA, Weinheim

Synthetic Methods

DOI: 10.1002/anie.200502807

Difluoroallenyl Bromide as a Wide-Ranging Difluoromethylene Cation Equivalent: S_N2 Substitution of Difluoropropargyl Bromide through Sequential S_E2' and S_N2' Reactions**

*Bo Xu and Gerald B. Hammond**

Dedicated to Professor Chang N. Wu on the occasion of his 72nd birthday

Unlike the other halogens, the small size of fluorine, the strong bond it forms with carbon, and its high electronegativity make it an ideal substituent to produce compounds with unique stereoelectronic and biological properties.[1] In this regard, *gem*-difluoromethylene-containing compounds have been sought after because of their inhibition of HIV protease,[2] and protein tyrosine phosphatase,[3] together with their ability to mimic phosphate,[4] carbonyl,[5] and retropeptide[6] units. In addition, the anomeric effects of heteroatom substituents, such as α-fluorinated ethers, α-fluorinated thioethers, and α-fluorinated amines, have sparked a flurry of new applications.[7] Overall, the significance of the incorporation of fluorine in organic molecules has spurred the development of novel synthetic strategies.[8] Despite these advances, a fundamental synthetic challenge persists, namely, the S_N2 synthesis of RCF_2Nu from RCF_2X

[*] B. Xu, Prof. G. B. Hammond
Department of Chemistry
University of Louisville
Louisville, KY 40292 (USA)
Fax: (+1) 502-852-3899
E-mail: gb.hammond@louisville.edu

[**] Support of our work by the National Science Foundation (CHE-0513483) is gratefully acknowledged. The authors are also grateful to Professor Richard W. Fitch (Indiana State University) for his helpful advice on nitrogen nucleophiles and to the University of Kentucky for the use of its supercomputing facilities.

Supporting information for this article is available on the WWW under http://www.angewandte.org or from the author.

WILEY InterScience DISCOVER SOMETHING GREAT
© 2005 Wiley-VCH Verlag GmbH & Co. KGaA, Weinheim

(Scheme 1a). Whereas potent methodologies exist for S_E2-type electrophilic substitution using either difluoromethylene mono-[9] or dianion equivalents,[10] the shielding of the carbon atom by the surrounding fluorine atoms impedes substitution by a nucleophile (Nu), except under exceptional circumstances.[11] In some cases, nucleophilic substitution has been shown to proceed through a radical anion radical ($S_{RN}1$) process triggered by single electron-transfer, rather than S_N2 displacement.[12] In principle, RCF_2Nu could be synthesized by a nucleophilic reaction on *gem*-difluoroolefins (Scheme 1b), thus taking advantage of the preferential attack of nucleophiles at the terminal sp^2 difluoromethylene carbon atom. However, this approach usually yields addition–elimination products that arise from the facile β-elimination of a fluoride ion. In a couple of examples, this problem has been circumvented by using either 1,1-difluoro-2-halo-1-alken-3-ols[13] or 3,4-epoxy-1,1-difluorobutenes[14] for the synthesis of polyfluorinated pyrethroids or allylic alcohols, respectively (Scheme 1c). We now report what is in effect a widely applicable two-step S_N2 conversion of RCF_2Br into RCF_2Nu, whereby an indium-mediated S_E2' bromide substitution converts **1a** into **2a**, which in turn reacts with a nucleophile in a S_N2' fashion to produce **3** in high yield (Scheme 2). An added advantage of this strategy is that the resulting product **3** is equipped with a triisopropylsilyl (TIPS)–acetylenic linkage suitable for further synthetic manipulation.

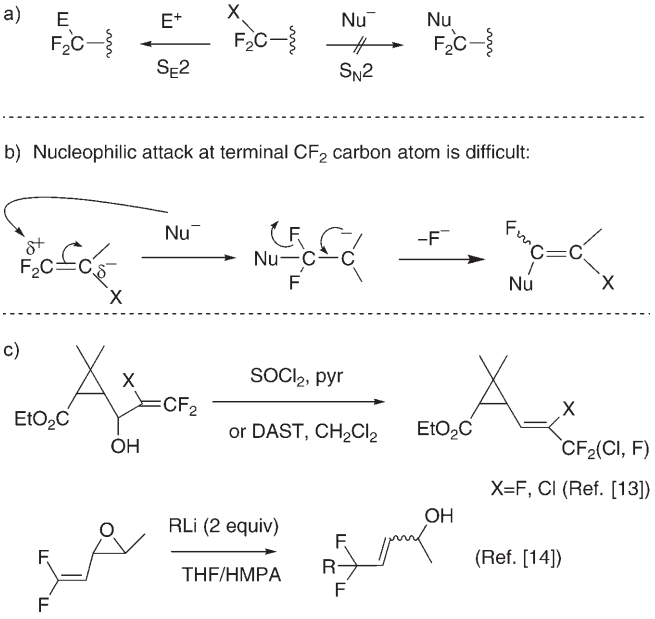

Scheme 1. a) S_N2 and S_E2 reactions; b) nucleophilic substitution on a sp^2 fluorinated carbon atom; c) synthesis of polyfluorinated pyrethroids and propargyl alcohols using nucleophiles. Nu = nucleophile, pyr = pyridine, DAST = diethylaminosulfur trifluoride, HMPA = hexamethylphosphoramide.

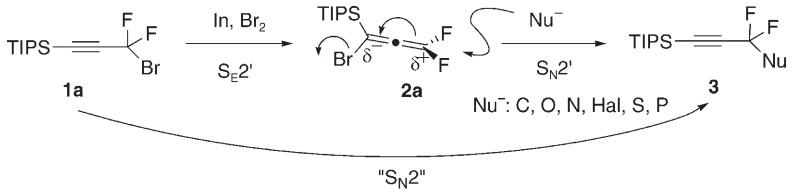

Scheme 2. Planned strategy for the synthesis of **3** from **1a** using a S_N2 substitution. Hal = halide.

targets.[15] We have recently shown that fluorine substitution imparts profound changes to the chemistry of allenes.[16] On the basis of ab initio calculations,[17] we postulated that a vinylogous *gem*-difluoro-olefin, such as fluoroallene **2a** (Figure 1), would be ideally suited to acting as a difluoromethylene-cation equivalent because of the opposite NBO charges in **2a** (+0.765 on C1 and −0.449 on C3). This charge distribution would favor a S_N2' nucleophilic attack at C1, with concomitant bromide elimination at C3; the isomerization of the allene to a propargyl group is favorable and acts as a driving force. Conversely, its non-fluorinated counterpart **2b** has the electronic charge concentrated on the carbon termini, which is a deterrent towards nucleophilic attack. The synthesis of **1a** was carried out by using our previously reported procedure[18] on a multigram scale (92% yield). We treated **1a** with both hard and soft nucleophiles, including sodium 2-methyl malonate, Grignard reagents, triphenylphosphine, or sodium ethoxide, to demonstrate the lack of reactivity of the $-CF_2Br$ moiety towards nucleophilic substitution. In all cases, we obtained either starting material or intractable, defluorinated mixtures.

Prior to the present work, γ-bromodifluoroallenes were unknown.[19] We had reported earlier that the preformed indium propargyl complex **4**[20] yielded fluoroallenyl alcohol **5** when treated with a reactive electrophile, such as aqueous formaldehyde (Scheme 3).[21] Less reactive electrophiles, such as benzaldehyde or imines, produced homopropargyl alcohol or amines. If this premise is correct, then the reaction between **4** and a reactive electrophile, such as Br_2, should produce the γ-bromodifluoroallene **2a**. To our satisfaction, the S_E2' reaction of **4** and bromine proceeded quite readily at −78 °C in THF to yield the desired **2a** in 81% yield. This compound can be stored neat for months at −5 °C without any noticeable decomposition; in solution, it reverted to **1a** most

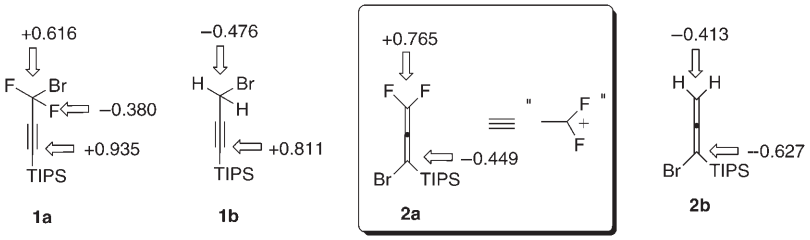

Figure 1. Ab initio calculation of *gem*-difluorinated propargyl and allenyl **1a** and **2a** and their non-fluorinated counterparts; the natural bond order (NBO) charge densities are given.

 © 2005 Wiley-VCH Verlag GmbH & Co. KGaA, Weinheim

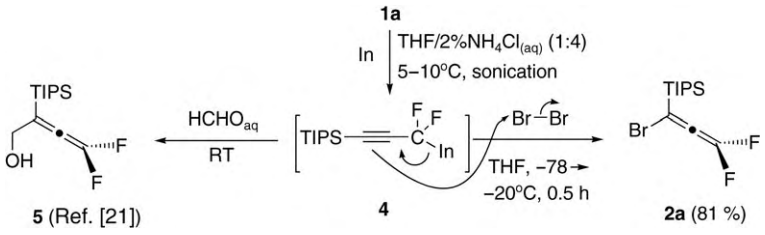

Scheme 3. Indium-mediated synthesis of **2a** via difluoropropargyl complex **4**.

likely through a S_N2' bromine displacement catalyzed by trace amounts of bromide. This proposition was later confirmed with the result obtained in entry **3g** in Table 1.

With a high-yielding synthesis of **2a** in hand, we proceeded to investigate its reactivity towards both soft and hard nucleophiles following the strategy depicted in Scheme 2. To our satisfaction, **2a** reacted readily with a wide range of weak and strong nucleophiles (P, O, S, C, N, and Br), in a S_N2' sense, thus furnishing **3** in good-to-excellent yields (Table 1). Aliphatic and aromatic amines produced complex mixtures. However, this problem was bypassed by using sodium azide as a nitrogen nucleophile, which produced a stable propargyl difluoroazide in almost 70% yield (entry **3h**). Notably, our new methodology also allowed the synthesis of hydrofluoroether **3c** in 68% yield by using trifluoroethanol as the nucleophile under very mild conditions. Prior to our disclosure, the synthesis of hydrofluoroethers could only be achieved under strongly basic conditions, which led to vinyl ether by-products, or through the very recently reported Pd^0-catalyzed hydroalkoxylation of hexafluoropropene.[22] In addition to the alkyne functionality present in **3**, the TIPS group is also a useful synthetic handle. It can be cleaved in excellent yield without loss of fluorine to yield **6a** by using TBAF. Alternatively, it can be further functionalized by using an electrophilic trap, such as *p*-chlorobenzaldehyde, to produce **6b** (see Scheme 4).

In conclusion, we have achieved a wide-ranging conversion of RCF_2Br into RCF_2Nu through a novel bromodifluoroallene **2a**, which is the synthetic equivalent of a difluoromethylene cation. We are currently exploring the use of other substituents appended to the γ-carbon atom and probing the synthetic usefulness of the diverse repertoire of $-CF_2Nu$ synthons which have been obtained through this novel reaction.

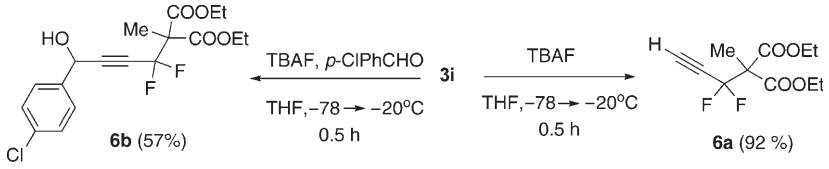

Scheme 4. Deprotection and functionalization of **3i** using tetrabutylammonium fluoride (TBAF).

Table 1: S_N2' synthesis of difluoropropynes **3** from difluoroallene **2a**.

Nucleophile/conditions		Entry (yield [%])[a]	Nucleophile/conditions		Entry (yield [%])[a]
MeOH, K_2CO_3, 0°C, 3 h	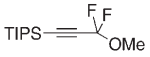	**3a** (61)	PPh_3, diethyl ether, RT, 12 h	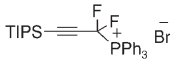	**3f** (92)
K_2CO_3, 0°C, 4 h	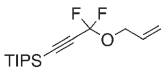	**3b** (70)	NaBr, DMF, RT, 12 h		**3g** (78)
K_2CO_3, 0°C, 4 h	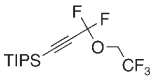	**3c** (68)	NaN_3, CH_3CN, RT, 12 h		**3h** (68)
AcOH/AgOAc, RT, 12 h	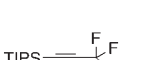	**3d** (70)	THF, NaH, 0°C 4 h	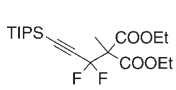	**3i** (70)
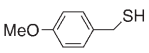 *n*BuLi, THF, −78→0°C	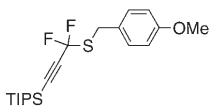	**3e** (53)	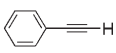 *n*BuLi, THF, −78→0°C	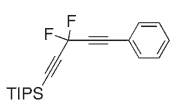	**3j** (55)

[a] Yield of the isolated products. All new compounds gave satisfactory spectral and analytical data. DMF = dimethylformamide.

Received: August 8, 2005
Published online: October 20, 2005

Keywords: allenes · cations · fluorine · nitrogen nucleophiles · nucleophilic substitution

[1] a) R. D. Chambers, *Fluorine in Organic Chemistry*, Blackwell Publishing Ltd./CRC, Boca Raton, FL, **2004**; b) P. Kirsch, *Modern Fluoroorganic Chemistry*, Wiley-VCH, Weinheim, **2004**; c) T. Hiyama, *Organofluorine Compounds. Chemistry and Applications*, Springer, Berlin, **2000**; d) M. Schlosser, *Angew. Chem.* **1998**, *110*, 1538; *Angew. Chem. Int. Ed.* **1998**, *37*, 1496; e) B. E. Smart, *J. Fluorine Chem.* **2001**, *109*, 3.

[2] a) E. Specker, J. Bottcher, H. Lilie, A. Heine, A. Schoop, G. Muller, N. Griebenow, G. Klebe, *Angew. Chem.* **2005**, *117*, 3200; *Angew. Chem. Int. Ed.* **2005**, *44*, 3140; b) A. G. Myers, J. K. Barbay, B. Zhong, *J. Am. Chem. Soc.* **2001**, *123*, 7207.

[3] L. Bialy, H. Waldmann, *Angew. Chem.* **2005**, *117*, 3880; *Angew. Chem. Int. Ed.* **2005**, *44*, 2.

[4] D. O'Hagan, H. S. Rzepa, *Chem. Commun.* **1997**, 645.

[5] C. Leriche, X. He, C. Chang, H. Liu, *J. Am. Chem. Soc.* **2003**, *125*, 6348.

[6] M. Sani, L. Bruche, G. Chiva, S. Fustero, J. Piera, A. Volonterio, M. Zanda, *Angew. Chem.* **2003**, *115*, 2106; *Angew. Chem. Int. Ed.* **2003**, *42*, 2060.

 © 2005 Wiley-VCH Verlag GmbH & Co. KGaA, Weinheim

[7] F. Leroux, P. Jeschke, M. Schlosser, *Chem. Rev.* **2005**, *105*, 827.
[8] a) For leading general references: *Fluorine-Containing Synthons*, ACS Symposium Series 911 (Ed.: V. A. Soloshonok), Oxford University Press/American Chemical Society, Washington, DC, **2005**; for leading references on asymmetric fluorination: b) T. D. Beeson, D. W. C. MacMillan, *J. Am. Chem. Soc.* **2005**, *127*, 8826; c) M. Marigo, D. Fielenbach, A. Braunton, A. Kjaersgaard, K. A. Jorgensen, *Angew. Chem.* **2005**, *117*, 3769; *Angew. Chem. Int. Ed.* **2005**, *44*, 3703; d) D. D. Steiner, N. Mase, C. F. Barbas III, *Angew. Chem.* **2005**, *117*, 3772; *Angew. Chem. Int. Ed.* **2005**, *44*, 3706.
[9] a) M. Mae, J. A. Hong, K. Uneyama, G. B. Hammond, *Tetrahedron Lett.* **2005**, *46*, 1787; b) T. Kobayashi, T. Nakagawa, H. Amii, K. Uneyama, *Org. Lett.* **2003**, *5*, 4297; D. J. Burton, L. Lu, *Top. Curr. Chem.* **1997**, *193*, 45, and references therein.
[10] G. K. S. Prakash, J. Hu, T. Mathew, G. A. Olah, *Angew. Chem.* **2003**, *115*, 5374; *Angew. Chem. Int. Ed.* **2003**, *42*, 5216, and references therein.
[11] A case in point is the substitution of R-C≡C-CF_2Br with I: a) P.-Y. Kwok, F. W. Muellner, C.-K. Chen, J. Fried, *J. Am. Chem. Soc.* **1987**, *109*, 3684; b) M. G. Barlow, S. Tajammal, A. E. Tipping, *J. Fluorine Chem.* **1993**, *64*, 61; another example is the Arbuzov reaction of CF_2Br_2 with $P(OEt)_3$.
[12] V. N. Boiko, G. M. Shchupak, *J. Fluorine Chem.* **1994**, *69*, 207.
[13] M. Fujita, T. Hiyama, *Tetrahedron Lett.* **1986**, *27*, 3659.
[14] H. Ueki, T. Chiba, T. Yamazaki, T. Kitazume, *J. Org. Chem.* **2004**, *69*, 7616.
[15] For a comprehensive coverage, see: a) *Modern Allene Chemistry, Vol. 1–2* (Eds.: N. Krause, A. S. K. Hashmi) Wiley-VCH, Weinheim, **2004**; b) A. Hoffmann-Roder, N. Krause, *Angew. Chem.* **2004**, *116*, 1216; *Angew. Chem. Int. Ed.* **2004**, *43*, 1196.
[16] Q. L. Shen, G. B. Hammond, *J. Am. Chem. Soc.* **2002**, *124*, 6534, and references therein.
[17] Computational analysis was carried out using Gaussian 03, Revision C.02 at the HF/6-311++g level of theory; Gaussian 03, Revision C.01, M. J. Frisch et al., Gaussian, Inc., Wallingford, CT, **2004**.
[18] Z. Wang, G. B. Hammond, *Chem. Commun.* **1999**, 2545.
[19] The synthesis and chemistry of bromoallenes has been recently reported: H. Ohno, H. Hamaguchi, M. Ohata, T. Tanaka, *Angew. Chem.* **2003**, *115*, 1791; *Angew. Chem. Int. Ed.* **2003**, *42*, 1749.
[20] Preliminary results from our ongoing investigation on the nature of the indium complex support the propargyl nature of **4**: B. Xu, G. B. Hammond, unpublished results.
[21] Z. G. Wang, G. B. Hammond, *J. Org. Chem.* **2000**, *65*, 6547.
[22] Y. Matsukawa, J. Mizukado, H. Quan, M. Tamura, A. Sekiya, *Angew. Chem.* **2005**, *117*, 1152; *Angew. Chem. Int. Ed.* **2005**, *44*, 1128.

 © 2005 Wiley-VCH Verlag GmbH & Co. KGaA, Weinheim

Synthetic Methods

DOI: 10.1002/anie.200501830

One-Pot Tandem 1,4–1,2-Addition of Phosphites to α,β-Unsaturated Imines for the Synthesis of Glutamic Acid Analogues**

*Kristof Moonen, Ellen Van Meenen, Annelies Verwée, and Christian V. Stevens**

Amino phosphonates and their corresponding amino phosphonic acids are known as amino acid mimetics and, therefore, affect the physiological activity of the cell.[1] The synthesis of 1-alkylamino phosphonates by a reaction of a dialkyl phosphite and an imine under thermal conditions had been described in the early 1950s.[2] However, dialkyl phosphites are generally considered to be poor nucleophiles because they exist predominantly in a $\sigma_4\lambda_5$ configuration.[3] Dialkyl trimethylsilyl phosphites were presented by Afarinkia et al. as excellent mild phosphonylation agents because the more nucleophilic $\sigma_3\lambda_3$ form of the dialkyl phosphite reagent could be obtained by O-silylation with trimethylsilyl chloride (TMSCl) in dichloromethane and triethylamine as the base.[4] Furthermore, exclusive 1,2-addition to α,β-unsaturated imines containing a phenyl group was reported by the same authors using diethyl trimethylsilyl phosphite.[5] During our research into azaheterocyclic phosphonates,[6] we planned to use this phosphonylation reaction with α,β-unsaturated imines **5a–d** derived from cinnamaldehyde. The diethyl trimethylsilyl phosphite was prepared in situ, as described previously.[4] The reaction mixture consisted mainly of the 1,2-adduct **9a** (^{31}P NMR: $\delta = 24.44$ ppm) and residual starting material after 24 h of reaction with the imine **5a**. However, several small ^{31}P NMR signals were present and became more abundant upon prolonged reaction times. The minor peaks appeared as two doublets ($J = 9.7$ Hz) next to two singlets and could be assigned to be the double-addition product **6a** (two diastereomers, ratio: 27:73) after its isolation in very low yield by column chromatography. The same type of product was obtained using imines **5b–d** in increasing amounts proportional to the steric bulk of the *N*-substituent, which also explains the decreasing yields of 1,2-adducts when more sterically demanding *N*-substituents were used in the original

[*] K. Moonen,[+] E. Van Meenen, A. Verwée, Prof. Dr. C. V. Stevens
Research Group SynBioC
Department of Organic Chemistry
Faculty of Bioscience Engineering
Ghent University, Coupure links 653, 9000 Ghent (Belgium)
Fax: (+32) 9-264-6243
E-mail: chris.stevens@ugent.be

[+] K.M. is aspirant of the Fund for Scientific Research (FWO Vlaanderen).

[**] We thank the Fund for Scientific Research Flanders and Ghent University for financial support of this research.

Supporting information for this article is available on the WWW under http://www.angewandte.org or from the author.

© 2005 Wiley-VCH Verlag GmbH & Co. KGaA, Weinheim

report.[5] With a *N*-phenyl substituent, however, only 1,2-addition was observed.

The obtained diphosphonates can be of major importance because of their high similarity to glutamic acid. (*S*)-Glutamic acid (Glu) is the main excitatory neurotransmitter in the central nervous system (CNS) and operates through two main heterogeneous classes of receptors: ionotropic and metabotropic Glu receptors (iGluRs and mGluRs, respectively). Both classes are further subdivided into several subclasses, but the number of functional receptors in the CNS is not known. Selective Glu agonists and antagonists are not only important for the characterization of different Glu receptor subtypes, but also for the treatment of CNS diseases, such as epilepsy, Huntington's disease, Parkinson's disease, dementia, chronic pain, and so forth. Therefore, the Glu receptor field has been, and continues to be, in a state of almost explosive development.[7] A number of phosphonic acid Glu analogues are known as potent selective Glu antagonists or agonists (Scheme 1). Substitution of the carboxylate group by a

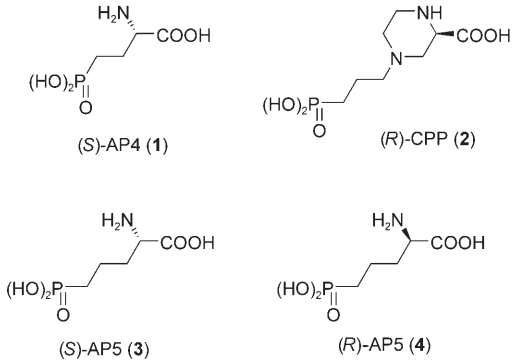

Scheme 1. Selected examples of phosphonic acid Glu analogues with GluR-agonist or -antagonist activity.

bioisosteric phosphonic acid group is known to increase receptor selectivity. For example, (*S*)-AP4 (**1**) is shown as a group III mGluR agonist, some tenfold more potent than Glu.[9] (*S*)-AP5 (**3**) activates the same group III receptors, but with markedly lower potency and selectivity. (*R*)-AP5 (**4**) on the other hand can not be shown to interact with mGluRs, but is a potent and selective competitive *N*-methyl D-aspartate (NMDA; iGluR) antagonist.[8] The diphosphonic acid derivative of AP4 has been tested several times as a Glu analogue without any activity so far.[10] However, further research into new bioisosteres has been indicated as a fruitful path to new subtype-selective mGluR ligands.[7]

The previous results prompted us to look for appropriate reaction conditions to achieve higher yields of the desired Glu bioisosteres. When the imine **5b** was added to two equivalents of diethyl trimethylsilyl phosphite, prepared in situ, complete conversion of the imine into the 3-phosphonyl 1-alkylamino phosphonate (PAP) **6c** was achieved after 72 h at reflux. However, when the diethyl trimethylsilyl phosphite was filtered first to remove the triethylammonium salts, no reaction occurred at all when the imine was added. Also no reaction was observed on addition of LiCl or TMSCl, even though the latter was said to act as a catalyst in the reaction mechanism proposed by Afarinkia et al.[4] Addition of NH_4Cl led to approximately the same result as obtained before (complete conversion in 72 h) and acidification of the reaction medium was observed. Therefore, $(NH_4)_2SO_4$ was selected as a more acidic salt to replace the triethylammonium salts after filtration, thus leading to a remarkable acceleration of the reaction rate (complete conversion after 3 h of reflux). Moreover, when diethyl trimethylsilyl phosphite was mixed with an imine in dry dichloromethane, the reaction proceeded violently upon addition of one equivalent of concentrated sulfuric acid to yield **6c** as a single product in 30 minutes at room temperature. Also with other α,β-unsaturated imines, complete conversion into the corresponding PAP was observed.[11] Diastereomeric ratios were determined from ^{31}P and ^{1}H NMR integration measurements (see Table 1).

As the reaction of imine **5b** with diethyl trimethylsilyl phosphite catalyzed by sulfuric acid proceeds too rapidly to detect any reaction intermediates, triethylammonium chloride was selected as a less potent catalyst to monitor the reaction as a function of time. Rapid disappearance of **5b** was observed, whereas the amount of the 1,2-adduct grew accordingly to a maximum. The PAP **6c** was formed more slowly, however, finally becoming the only end product of the reaction (see Figure 1). This kind of behavior suggests that the imine is protonated first by the acid and becomes activated towards nucleophilic attack of the dialkyl trimethylsilyl phosphite (Scheme 2). 1,2-Addition is clearly the fastest reaction pathway and the *N*-trimethylsilyl 1-alkylaminophosphonate **9** is formed after nucleophilic attack of the nitrogen atom at the trimethylsilyl group of phosphonium salt **8**. These three steps all occur in an equilibrium which was demonstrated in a separate experiment (Scheme 3). When dimethyl (1-amino-1-phenylmethyl)phosphonate (**14**) was N-silylated using TMSCl and subsequently treated with a large excess of diethyl trimethylsilyl phosphite, diethyl phosphonate **15** was mainly recovered along with small amounts of **14**. When the same experiment was repeated without silylation and using diethyl phosphite, no exchange at all occurred. This clearly demonstrated the reversibility (**8**⇌**9**) of the reaction and the leaving-group capacity of the intermediate positively charged phosphonium group.

The initial equilibrium allows two possible routes to the PAP **6** (Scheme 2). The first (pathway A) is complete reversion into the iminium salt **7** followed by a slow 1,4-addition, whereas the second (pathway B) starts with an S_N'-like substitution of the phosphonium group. Both routes yield the same intermediate enamine **10**, which subsequently isomerizes to the imine **11**. A final 1,2-addition then yields PAP **6**, which only shows phosphonyl exchange at the 1 position.

However, enamine **10** or imine **11**, the suggested intermediates in this reaction mechanism (Scheme 2), were never observed. Furthermore, the proposed reaction mechanisms require an external proton source, as one equivalent of protons is incorporated in the final product **6**. Therefore, an experiment was performed using only 0.1 equivalents of sulfuric acid together with 2.0 equivalents of $P(OEt)_2OTMS$.

 © 2005 Wiley-VCH Verlag GmbH & Co. KGaA, Weinheim

Table 1: Conversion of imines **5** to PAP **6** using $P(OR)_2OTMS$ (2 equiv) and H_2SO_4 (1 equiv).

	Imine	Product		Yield[a] [%]	d.r. [%]
5a	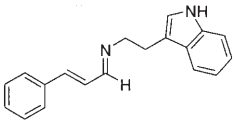	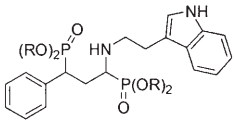	**6a** (R = Et)	82	29:71
5b	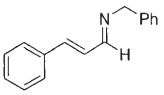	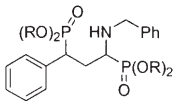	**6b** (R = Me) **6c** (R = Et)	70 80	19:81 29:71
5c	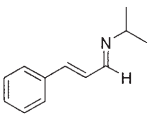	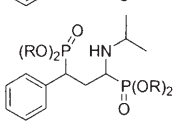	**6d** (R = Me) **6e** (R = Et)	77 78	32:68 33:67
5d	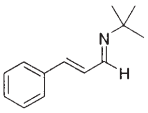	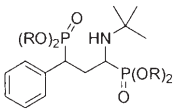	**6f** (R = Me) **6g** (R = Et)	82 85	49:51 36:64
5e	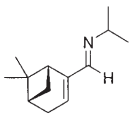	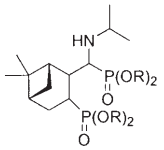	**6h** (R = Me)	46	22:78
5f	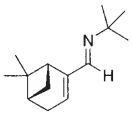	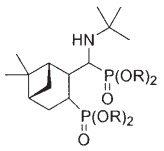	**6i** (R = Me)	20	12:88
5g	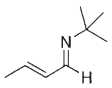	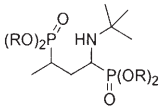	**6j** (R = Me)	74	36:64
5h	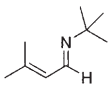	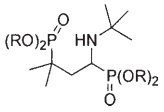	**6k** (R = Me)	60	–

[a] Yield after column chromatography or acid–base extraction.

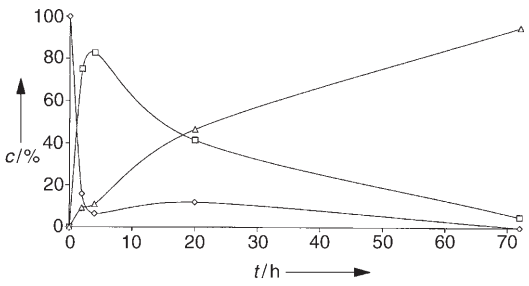

Figure 1. Composition (*c*) of the reaction mixture during the reaction of **5b** (◇) with $P(OEt)_2OTMS$ in the presence of $HNEt_3Cl$, measured by NMR spectroscopy. 1,2-Adduct **9** (□) appears as an intermediate in the reaction, whereas PAP **6c** (△) seems to be the final product.

The reaction proceeded very sluggishly under these conditions, and the formation of **6** was stopped completely after 3–4 h as expected. From that point, the concentration of **10** started to increase (^{31}P NMR: $\delta = \pm 27$ ppm in the reaction medium), while the rest of the imine **7** was slowly consumed (Figure 2). However, addition of water for the work-up led to the conversion of **10** into **6** and some of the imine **7** into the 1,2-adduct using the remaining phosphite in the reaction mixture. This result shows that water can also act as a proton source for this reaction. The structure of intermediate imine **11** was confirmed in a separate experiment (Scheme 4) using subequivalent amounts of sulfuric acid or the non-protic Lewis acid $AlCl_3$ as an activator, together with a limiting amount of diethyl trimethylsilyl phosphite (0.9 equivalents). Under these conditions, there was no free phosphite in the work-up and the intermediate 1,4-adduct **16** was obtained in a mixture of **6** and starting material **5**. The structure of **16** was confirmed after hydrolysis to the corresponding aldehyde **17** and comparison with literature data.[12]

From the evolution of the reaction intermediates as a function of the reaction time (Figure 2), it is clear that the 1,2-adduct **9** is not a real intermediate of the PAP formation. After the initial 1,2-adduct formation (which can also be noticed in Figure 1), the 1,2-addition is also blocked by the absence of protons. Furthermore, the observation that a considerably higher reaction rate results for imines bearing more sterically demanding *N*-substituents (tBu > iPr > Bn ≫ Ph) is in favor of the tandem addition, as the 1,2-addition should be slowed down by the steric bulk. One case of a

 © 2005 Wiley-VCH Verlag GmbH & Co. KGaA, Weinheim

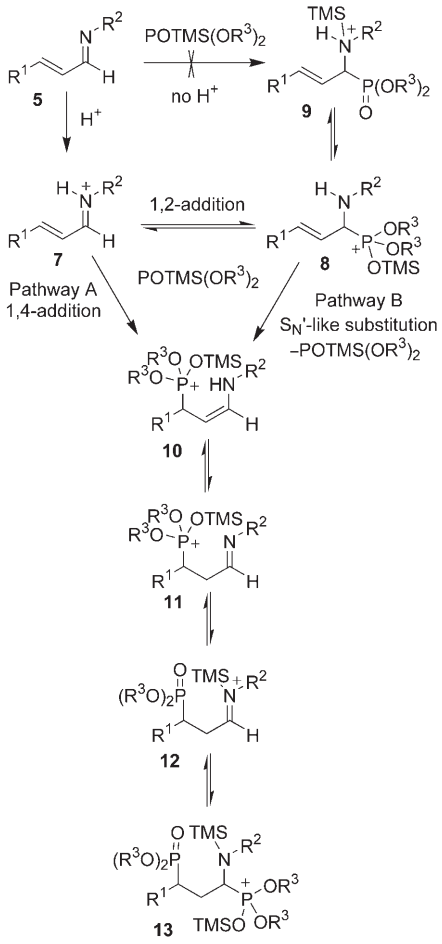

Scheme 2. Suggested reaction mechanisms.

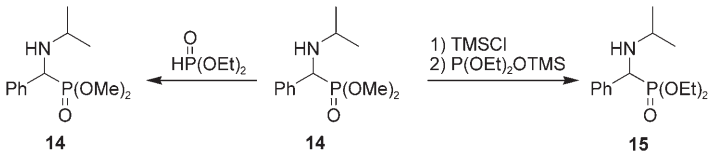

Scheme 3. Phosphonyl exchange reactions.

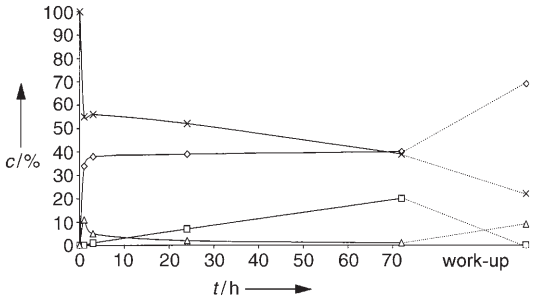

Figure 2. Composition (*c*) of the reaction mixture during the reaction of **5c** (×) with $P(OEt)_2OTMS$ in the presence of 0.1 equivalents of H_2SO_4, measured by NMR spectroscopy. Only a small amount of 1,2-adduct **9** (△) is formed, whereas PAP **6c** (◇) is formed initially very quickly. When the reaction stops because of a lack of protons, the concentration of intermediate enamine **10** (□) starts to increase.

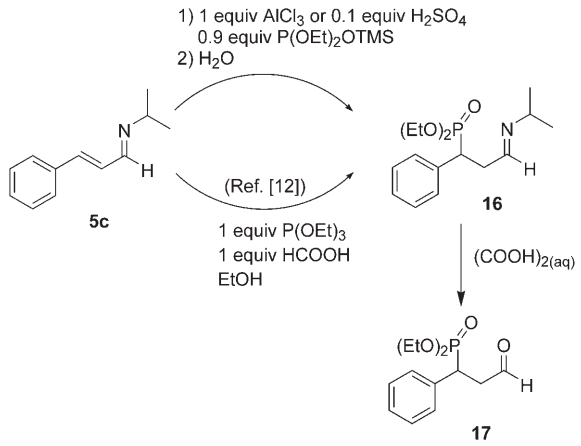

Scheme 4. Isolation and identification of the intermediate 1,4-adduct.

double addition of ketene silyl acetals to α,β-unsaturated imines has been reported, which also proceeded in a 1,4–1,2-tandem fashion.[14]

In summary, our observations in this field lead to a new insight regarding the use of dialkyl trimethylsilyl phosphite which contradicts earlier research:[5] when this reagent is present in its apparently most nucleophilic form, dialkyl trimethylsilyl phosphite fails to react either in a 1,2- or a 1,4-addition in the absence of a protic acid. Furthermore, it has been demonstrated that dialkyl phosphite itself is able to convert imines into the corresponding 1-aminoalkyl phosphonates with complete 1,2-regioselectivity.[2,13] However, in a sufficiently acidic medium, dialkyl trimethylsilyl phosphite is able to convert α,β-unsaturated imines **5** into diphosphonates **6** in one step through a sequential tandem 1,4–1,2-addition (pathway A of Scheme 2).[15] As the free phosphonic acids of diphosphonates[16] are potential Glu agonists or antagonists, our future research will be directed towards the synthesis of enantiopure PAP derivatives.[17]

Received: May 26, 2005
Published online: October 20, 2005

Keywords: amino acids · Michael addition · phosphorylation · reaction mechanisms · regioselectivity

[1] a) P. Kafarski, B. Lejczak, *Phosphorus Sulfur Silicon Relat. Elem.* **1991**, *63*, 193; b) K. Moonen, I. Laureyn, C. V. Stevens, *Chem. Rev.* **2004**, *104*, 6177.
[2] E. K. Fields, *J. Am. Chem. Soc.* **1952**, *74*, 1528.
[3] J. P. Guthrie, *Can. J. Chem.* **1979**, *57*, 236.
[4] K. Afarinkia, C. W. Rees, J. I. G. Cadogan, *Tetrahedron* **1990**, *46*, 7175.
[5] K. Afarinkia, J. I. G. Cadogan, C. W. Rees, *Synlett* **1992**, 123.
[6] a) B. Vanderhoydonck, C. V. Stevens, *Synthesis* **2004**, 722; b) F. Ghelfi, C. V. Stevens, I. Laureyn, E. Van Meenen, T. M. Rogge, L. De Buyck, K. V. Nikitin, R. Grandi, E. Libertini, U. M. Pagnoni, L. Schenetti, *Tetrahedron* **2003**, *59*, 1147; c) C. V. Stevens, W. Vekemans, K. Moonen, T. Rammeloo, *Tetrahedron Lett.* **2003**, *44*, 1619.

 © 2005 Wiley-VCH Verlag GmbH & Co. KGaA, Weinheim

[7] For an excellent review on ligands for glutamate receptors, see: H. Bräuner-Osborne, J. Egebjerg, E. Ø. Nielsen, U. Madsen, P. Krogsgaard-Larsen, *J. Med. Chem.* **2000**, *43*, 2609.
[8] a) H. Bräuner-Osborne, P. Krogsgaard-Larsen, *Br. J. Pharmacol.* **1998**, *123*, 269; b) P. A. Johansen, L. A. Chase, A. D. Sinor, J. F. Koerner, R. L. Johnson, M. B. Robinson, *Mol. Pharmacol.* **1995**, *48*, 140.
[9] a) Y. Tanabe, A. Nomura, M. Masu, R. Shigemoto, N. Mizuno, S. Nakanishi, *J. Neurosci.* **1993**, *13*, 1372; b) Y. Nakajima, H. Iwakabe, C. Akazawa, H. Nawa, R. Shigemoto, N. Mizuno, S. Nakanishi, *J. Biol. Chem.* **1993**, *268*, 11868; c) N. Okamoto, S. Hori, C. Akazawa, Y. Hayashi, R. Shigemoto, N. Mizuno, S. Nakanishi, *J. Biol. Chem.* **1994**, *269*, 1231.
[10] a) H. J. Olverman, A. W. Jones, K. N. Mewett, J. C. Watkins, *Neuroscience* **1988**, *26*, 17; b) M. Darriet, M.-J. Basurko, A. Casseigne, *Biochem. Soc. Trans.* **1988**, *16*, 611; c) M. Marche, M. -J. Basurko, A. Cassaigne, *Biochimie* **1987**, *69*, 461; d) E. Bakuniak, I. Bakuniak, B. Borucka, J. Ostrowski, *J. Environ. Sci. Health Part B* **1983**, *18*, 485; e) E. De Tinguy-Moreaud, B. Bioulac, E. Neuzil, *Biochem. Soc. Trans.* **1981**, *9*, 246.
[11] A typical procedure and spectral data of all products are available in the Supporting Information.
[12] M.-P. Teulade, P. Savignac, *Synthesis* **1987**, 1037.
[13] A. A. Sobanov, A. V. Zolotukhin, V. I. Galkin, R. A. Cherkasov, A. N. Pudovik, *Russ. J. Gen. Chem.* **2002**, *72*, 1067.
[14] M. Shimizu, A. Morita, T. Kaga, *Tetrahedron Lett.* **1999**, *40*, 8401.
[15] Only a few synthetic pathways similar to that of the PAPs are known; all consist of multiple reaction steps: a) E. Öhler, S. Kanzler, *Liebigs Ann. Chem.* **1994**, 867; b) Z. Kudzin, A. Kotynski, G. Andrijewski, *J. Organomet. Chem.* **1994**, *479*, 199; c) U. Groth, L. Richter, U. Schöllkopf, *Tetrahedron* **1992**, *48*, 117; d) G. Sturtz, J. Guervenou, *Synthesis* **1991**, 661; e) K. Issleib, K. -P. Döpfer, A. Balszuweit, *Phosphorus Sulfur Relat. Elem.* **1983**, *14*, 171.
[16] PAPs **6** can be dealkylated using TMSBr, see: C. E. McKenna, M. T. Higa, N. H. Cheung, M. C. McKenna, *Tetrahedron Lett.* **1977**, 155; an example with a general experimental procedure is included in the Supporting Information.
[17] Spectral data, general procedures, sample spectra, and additional mechanistic evidence are available in the Supporting Information.

 © 2005 Wiley-VCH Verlag GmbH & Co. KGaA, Weinheim

Ceria Nanostructures

DOI: 10.1002/anie.200500992

Large-Scale Nonhydrolytic Sol–Gel Synthesis of Uniform-Sized Ceria Nanocrystals with Spherical, Wire, and Tadpole Shapes**

*Taekyung Yu, Jin Joo, Yong Il Park, and Taeghwan Hyeon**

In the last decade, nanocrystals have been intensively studied, not only for their fundamental scientific interest owing to their size-dependent properties, but also for their many technological applications.[1] Cerium oxide (ceria, CeO_2) is a rare earth oxide that has attracted a great deal of interest owing to its unique properties, including high mechanical strength, oxygen ion conductivity, and oxygen storage capacity. Because of these characteristics, ceria has been widely used as an oxygen ion conductor in solid oxide fuel cells, oxygen pumps, and amperometric oxygen monitors.[2] Ceria has also been used as a polishing agent for the chemical mechanical planarization (CMP) process, as a gate oxide in metal oxide semiconductor devices, and as a catalytic material for three-way catalysis (TWC) of exhaust gas from automobiles and fluid catalytic cracking (FCC).[3] Several methods have been employed to synthesize ceria nanoparticles. Deshpande et al. synthesized nanoparticles of CeO_2, ZrO_2, and $Ce_{1-x}Zr_xO_2$ by hydroxide coprecipitation of a precursor solution composed of cerium ammonium nitrate and zirconyl chloride.[4] Inoue et al. obtained a colloidal solution of 2 nm ceria particles by the solvothermal process.[5] Adachi and co-workers fabricated 2.6 and 4.1 nm ceria particles using reverse micelles.[6] Gedanken and co-workers synthesized 3.3 nm ceria nanoparticles using sonochemical treatment.[7] Zhu and co-workers also prepared 2.8 nm ceria nanoparticles by the sonochemical and microwave-assisted heating methods.[8] However, the ceria nanoparticles synthesized by these methods are often highly aggregated, and a very small quantity is usually produced. Recently, Yan and co-workers synthesized nanocrystals of ceria and other rare earth oxides with various shapes from the thermolysis of metal benzoylacetonate complexes in a solvent mixture composed of oleic acid and oleylamine.[9]

Nonhydrolytic sol–gel processes have been employed to synthesize various oxide materials.[10] Recently, they were

[*] T. Yu, J. Joo, Y. I. Park, Prof. Dr. T. Hyeon
National Creative Research Initiative Center for Oxide Nanocrystalline Materials and
School of Chemical and Biological Engineering
Seoul National University, Seoul 151-744 (Korea)
Fax: (+82) 2-886-8457
E-mail: thyeon@plaza.snu.ac.kr

[**] This work was supported by the National Creative Research Initiative Program of the Korean Ministry of Science and Technology.

Supporting information for this article is available on the WWW under http://www.angewandte.org or from the author.

© 2005 Wiley-VCH Verlag GmbH & Co. KGaA, Weinheim

successfully applied to the synthesis of various nanocrystals of transition metal oxides. For example, Colvin and co-workers[11] synthesized TiO_2 nanocrystals by a nonhydrolytic alkyl halide elimination reaction. We employed a similar procedure[12] to produce uniform-sized tetragonal ZrO_2 nanocrystals on the multigram scale by high-temperature reaction of zirconium halides and zirconium isopropoxide. Recently, Brus and co-workers[13] further extended these synthetic methods to produce nanocrystals of HfO_2 and $Hf_xZr_{1-x}O_2$. Stucky and co-workers reported the synthesis of nanocrystals of various metal oxides from the reaction of metal chlorides and benzyl alcohol,[14] and Niederberger and co-workers developed a halide-free approach to synthesize nanocrystals of various oxides from the reaction of metal alkoxides and benzyl alcohol.[15]

One-dimensional (1D) nanocrystalline materials such as nanorods and nanowires have been intensively studied because of their unique properties, which are derived from their low dimensionality and possible quantum-confinement effects.[16] For extensive application of nanocrystals, an economical mass production method for the synthesis of uniform-sized nanocrystals must be developed. Recently, we reported the ultra-large-scale synthesis of monodisperse nanocrystals of many transition metal oxides and sulfides by thermolysis of metal–surfactant complexes.[17] Here we report on the large-scale synthesis of uniform-sized ceria nanocrystals with sphere, wire, and tadpole shapes by the nonhydrolytic sol–gel reaction of cerium(III) nitrate and diphenyl ether in the presence of appropriate surfactants. All of the ceria nanocrystals were produced on a scale of more than 10 g in a single reaction. In particular, we were able to synthesize ceria nanowires with the ultrasmall diameter of 1.2 nm on a multigram scale. The size and shape of the ceria nanocrystals were controlled by adjusting the experimental conditions such as the molar ratio of the surfactants, and the reaction time.

Spherical ceria nanocrystals with an average diameter of 3.5 nm were synthesized from the reaction of cerium(III) nitrate and diphenyl ether in oleylamine at 320 °C. A low-magnification transmission electron microscopy (TEM) image revealed uniform particles with an average size of 3.5 nm and a quasispherical shape (Figure 1 a). A high-resolution TEM (HRTEM) image of the ceria nanocrystals showed a cross-lattice pattern, which demonstrates their highly crystalline nature (Figure 1 a). The powder X-ray diffraction (XRD) pattern (Supporting Information) of the nanocrystals revealed that they have a cubic fluorite structure ($Fm3m$, $a = 5.41134$ Å, JCPDS Card No. 34-0394). The size of the ceria nanocrystals, calculated by using the Scherrer formula, was 3.65 nm, which matched very well with the TEM data. Larger ceria nanocrystals were synthesized by adding tri-*n*-octylamine (TOA) as a cosurfactant in addition to oleylamine. The TEM image showed that uniform quasispherical ceria nanocrystals with an average particle size of 5.2 nm were produced in this case (Figure 1 b). Under optimized synthetic conditions, we were able to synthesize both of these quasispherical ceria nanocrystals on a scale of more than 10 g in a single reaction in 200 mL of solvent (Supporting Information). The UV/Vis absorption spectrum of the 3.5 nm nanocrystals was significantly blue-shifted compared to that of the 5.2 nm nanocrystals (Supporting Information).

Recently, various anisotropic nanocrystals, including nanorods and nanowires, were synthesized by using two different kinds of surfactants.[18] In our synthesis, adding oleic acid as a cosurfactant in addition to oleylamine led to production of anisotropic wire- and tadpole-shaped ceria nanocrystals. When cerium nitrate (1.7 g, 4 mmol) dissolved in a mixture of oleic acid (3.39 g, 12 mmol) and oleylamine (20 mL, 60 mmol, 16.26 g) was treated with diphenyl ether and the resulting solution slowly heated and aged at 320 °C for 2 h, a mixture of ceria nanowires (1.2 nm in diameter and 71 nm in length) with 3.7 nm quasispherical nanocrystals was produced. The diameter of these nanowires is very similar to that of single-wall carbon nanotubes[19] and is among the thinnest of reported nanowires. Although nanowires with diameters of about 1 nm or less have been reported, they were generally produced in extremely small quantities.[20] The TEM image showed that the product was composed of about 70 % nanowires and about 30 % nanospheres (Figure 2). More careful investigation of the TEM images revealed that some nanowires were attached to nanospheres in a tadpolelike structure. The XRD pattern (Supporting Information) showed that the product had a cubic fluorite structure. The HRTEM image showed the {111} faces of a cubic fluorite structure of ceria grown along the [100] direction (Figure 2). By increasing the amount of oleic acid, while keeping the other experimental conditions unchanged, we were able to

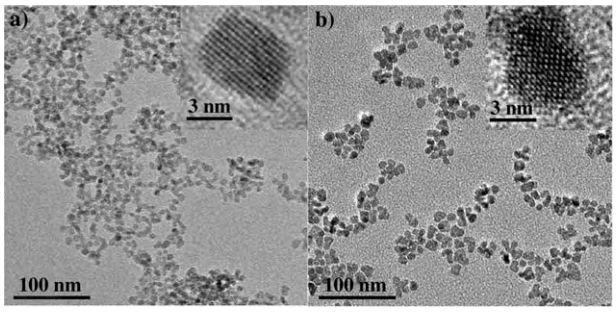

Figure 1. TEM images of a) 3.5 nm spherical ceria nanocrystals and b) 5.2 nm spherical ceria nanocrystals. Insets are their HRTEM images.

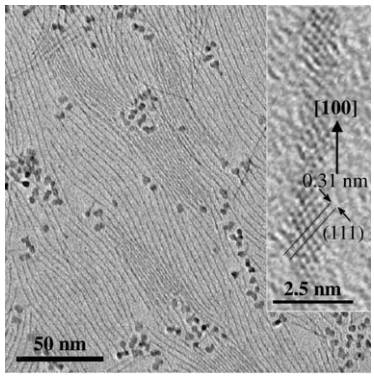

Figure 2. TEM images of 1.2 × 71 nm wire-shaped ceria nanocrystals. The inset is the HRTEM image of a wire-shaped nanocrystal.

 © 2005 Wiley-VCH Verlag GmbH & Co. KGaA, Weinheim

synthesize longer nanowires without changing the diameter. By using different amounts of oleic acid, nanowires of various lengths with a nearly constant diameter of 1.2 nm were produced (Supporting Information). We were able to synthesize the nanowires in large quantities (> 10 g) in a single reaction in 200 mL of solvent (Supporting Information).

During a shape-evolution experiment with a relatively large amount of oleylamine, we determined the optimum conditions for predominant formation of the tadpole-shaped nanowires. Tadpole-shaped nanowires consist of a spherical head with a diameter of 3.5 nm and a wire-shaped tail with a diameter of 1.2 nm and length of 27 nm. The low-magnification TEM image revealed that most of these nanocrystals were tadpole-shaped and uniform in size (Figure 3). Recently,

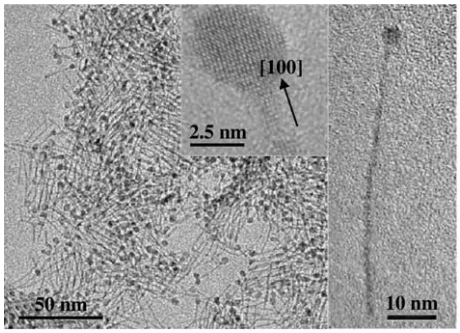

Figure 3. TEM images of the tadpole-shaped ceria nanocrystals. The inset is the HRTEM image of a tadpole shaped nanocrystal.

tadpole-shaped gold nanocrystals were produced.[21] The (HRTEM) image (Figure 3; see Supporting Information for further images) of a single tadpole-shaped ceria nanocrystal revealed that the spherical head and the wire-shaped tail grew epitaxially along the (200) planes with an interplanar distance of 0.27 nm. The XRD pattern showed that the tadpole-shaped ceria nanowires have a cubic fluorite structure (Figure 4).

In conclusion, uniform-sized ceria nanocrystals with quasispherical, wire, and tadpole shapes were synthesized from the nonhydrolytic sol–gel reaction of cerium(III) nitrate and diphenyl ether in the presence of appropriate surfactants. The synthetic procedures described in this study offer several important advantages for the production of ceria nanocrystals. First, this process allows uniform-sized nanocrystals to be obtained on a scale of tens of grams in a single reaction without the need for a further size-sorting process. When reactors are set up in parallel, several kilograms of monodisperse nanocrystals can be readily obtained. Second, ceria nanocrystals with various shapes can be produced simply by changing the experimental conditions. In particular, novel tadpole-shaped nanowires with an extremely small diameter of 1.2 nm were produced.

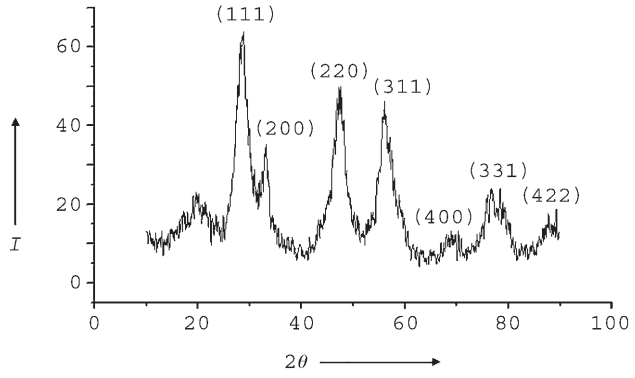

Figure 4. XRD pattern of the tadpole-shaped ceria nanocrystals.

Experimental Section

Synthesis of quasispherical ceria nanocrystals: Cerium(III) nitrate hexahydrate (1.7 g, 4 mmol) was added to oleylamine (technical grade, 20 mL, 16.26 g, 60 mmol) or a mixture of olyelamine (technical grade, 3.21 g, 12 mmol) and tri-*n*-octylamine (20 mL, 16.18 g, 45 mmol) at room temperature. The resulting solution was heated to 90 °C under vacuum, and a homogeneous, clear, black solution formed. Diphenyl ether (2 mL, 2.1 g, 12 mmol) was injected into the solution at 90 °C, and the observed increase in solution temperature to 120 °C demonstrated that the reaction between cerium nitrate and diphenyl ether did indeed occur. The resulting mixture was heated to 320 °C and aged at that temperature for 2 h to give a black colloidal solution. Ethanol (100 mL) was added to precipitate the CeO_2 nanocrystals. The precipitate was retrieved by centrifugation to give white-brown CeO_2 nanocrystals. The nanocrystals were dispersible in many organic solvents, such as toluene, hexane, and octane.

Synthesis of ceria nanowires: Cerium (III) nitrate hexahydrate (4 mmol, 1.7 g) was added to a mixture of oleylamine (technical grade, 20 mL, 16.26 g, 60 mmol) and oleic acid (3.39 g, 12 mmol) at 90 °C. The rest of the synthetic procedure was similar to that used for the synthesis of the spherical nanocrystals. Using 1.7, 3.39, 5.08, and 6.78 g (6, 12, 18, and 24 mmol) of oleic acid in the synthesis gave ceria nanowires with a uniform diameter of 1.2 nm and average lengths of 27.8, 71.1, 115.5, and 164.5 nm, respectively.

Synthesis of tadpole-shaped ceria nanowires: The synthetic procedure for the tadpole-shaped ceria nanowires was very similar to that used for the synthesis of the ceria nanowires. A reaction mixture composed of cerium (III) nitrate (0.85 g, 2 mmol), oleylamine (technical grade, 20 mL, 16.26 g, 60 mmol), of oleic acid (1.69 g, 6 mmol), and diphenyl ether (1 mL, 1.07 g, 6 mmol) was aged at 320 °C for 1 h.

UV/Vis spectra of 3.5 and 5.2 nm spherical nanocrystals, XRD patterns of 3.5 and 5.2 nm spherical nanocrystals and nanowires, TEM images of ceria nanowires of various lengths, and photographs of ceria nanocrystalline powders can be found in the Supporting Infomation.

Received: March 18, 2005
Published online: October 25, 2005
Publication delayed at author's request.

Keywords: cerium · nanocrystals · nanostructures · sol–gel processes

[1] a) G. Schmid, *Nanoparticles: From Theory to Application*, Wiley-VCH, Weinheim, **2004**; b) K. J. Klabunde, *Nanoscale Materials in Chemistry*, Wiley-Interscience, New York, **2001**; c) J. H. Fendler, *Nanoparticles and Nanostructured Films*, Wiley-VCH, Weinheim, **1998**; d) J. Z. Zhang, Z.-L. Wang, J. Liu, S. Chen, G. Y. Liu, *Self-Assembled Nanostructures*, Kluwer Academic/Plenum Publishers, New York, **2003**; e) A. L. Rogach, D. V. Talapin, E. V. Shevchenko, A. Kornowski, M. Haase, H. Weller, *Adv. Funct. Mater.* **2002**, *12*, 653; f) A. P. Alivisatos, *Science* **1996**, *271*, 933; g) T. Hyeon, *Chem. Commun.* **2003**, 927;

 © 2005 Wiley-VCH Verlag GmbH & Co. KGaA, Weinheim

h) C. B. Murray, S. Sun, W. Gaschler, H. Doyle, T. A. Betley, C. R. Kagan, *IBM J. Res. Dev.* **2001**, *45*, 47.
[2] a) S. D. Park, J. M. Vohs, R. J. Gorte, *Nature* **2000**, *404*, 265; b) G. Panzera, V. Modafferi, S. Candamano, A. Donato, F. Frusteri, P. L. Antonucci, *J. Power Sources* **2004**, *135*, 177; c) A. Trovarelli, C. de Lietenburg, M. Boaro, G. Dolcetti, *Catal. Today* **1999**, *50*, 353; d) B. C. H. Steele, *Solid State Ionics* **2000**, *129*, 95; e) V. V. Kharton, F. M. Figueiredo, L. Navarro, E. N. Naumovich, A. V. Kovalevsky, A. A. Yaremchenko, A. P. Viskup, A. Carneiro, F. M. B. Marques, J. R. Frade, *J. Mater. Sci.* **2001**, *36*, 1105; f) T. S. Stefanik, H. L. Tuller, *J. Eur. Ceram. Soc.* **2001**, *21*, 1967; g) S. K. Tadokoro, T. C. Porfirio, R. Muccillo, E. N. S. Muccillo, *J. Power Sources* **2004**, *130*, 15.
[3] a) A. Trovarelli, C. de Leitenburg, M. Boaro, and G. Dolcetti, *Catal. Today* **1999**, *50*, 353; b) S.-K. Kim, P.-W. Yoon, U. Paik, T. Katoh, J.-G. Park, *Jpn. J. Appl. Phys.* **2004**, *43*, 7427; c) H.-G. Kang, T. Katoh, M.-Y. Lee, H.-S. Park, U. Paik, J.-G. Park, *Jpn. J. Appl. Phys.* **2004**, *43*, L1060; d) H.-G. Kang, T. Katoh, W.-M. Lee, U. Paik, J.-G. Park, *Jpn. J. Appl. Phys.* **2004**, *43*, L1; e) P. Suphantharida, K. Osseo-Asare, *J. Electrochem. Soc.* **2004**, *151*, G658.
[4] A. S. Deshpande, N. Pinna, P. Beato, M. Antonietti, M. Niederberger, *Chem. Mater.* **2004**, *16*, 2599.
[5] M. Inoue, M. Kimura, T. Inui, *Chem. Commun.* **1999**, 957.
[6] T. Masui, K. Fujiwara, K. I. Machida, G. Y. Adachi, *Chem. Mater.* **1997**, *9*, 2197.
[7] L. X. Yin, Y. Q. Wang, G. S. Pang, Y. Koltypin, A. Gedanken, *J. Colloid Interface Sci.* **2002**, *246*, 78.
[8] H. Wang, J. J. Zhu, J. M. Zhu, X. H. Liao, S. Xu, T. Ding, H. Y. Chen, *Phys. Chem. Chem. Phys.* **2002**, *4*, 3794.
[9] R. Si, Y.-W. Zhang, L.-P. You, C.-H. Yan, *Angew. Chem.* **2005**, *117*, 3320; *Angew. Chem. Int. Ed.* **2005**, *44*, 3256.
[10] A. Vioux, *Chem. Mater.* **1997**, *9*, 2292.
[11] T. J. Trentler, T. E. Denler, J. F. Bertone, A. Agrwal, V. L. Colvin, *J. Am. Chem. Soc.* **1999**, *121*, 1613.
[12] J. Joo, T. Yu, Y. W. Kim, H. M. Park, F. Wu, J. Zhang, T. Hyeon, *J. Am. Chem. Soc.* **2003**, *125*, 6553.
[13] J. Tang, J. Fabbri, R. D. Robinson, Y. Zhu, I. P. Herman, M. L. Steigerwald, L. E. Brus, *Chem. Mater.* **2004**, *16*, 1336.
[14] a) M. Niederberger, M. H. Bartl, G. D. Stucky, *J. Am. Chem. Soc.* **2002**, *124*, 13642; b) M. Niederberger, M. H. Bartl, G. D. Stucky, *Chem. Mater.* **2002**, *14*, 4364.
[15] a) M. Niederberger, N. Pinna, J. Polleux, M. Antonietti, *Angew. Chem.* **2004**, *116*, 2320; *Angew. Chem. Int. Ed.* **2004**, *43*, 2270; b) N. Pinna, G. Neri, M. Antonietti, M. Niederberger, *Angew. Chem.* **2004**, *116*, 4445; *Angew. Chem. Int. Ed.* **2004**, *43*, 4345; c) M. Niederberger, G. Garnweitner, N. Pinna, M. Antonietti, *J. Am. Chem. Soc.* **2004**, *126*, 9120; d) N. Pinna, G. Garnweiter, M. Antonietti, M. Niederberger, *J. Am. Chem. Soc.* **2005**, *127*, 5608; e) N. Pinna, G. Garnweiter, M. Antonietti, M. Nederberger, *Adv. Mater.* **2004**, *16*, 2196; f) G. Garnweiter, M. Antonietti, M. Nederberger, *Chem. Commum.* **2005**, 397; g) N. Pinna, M. Antonietti, M. Nederberger, *Colloids Surf. A* **2004**, *250*, 211.
[16] a) Y. Xia, P. Yang, Y. Sun, Y. Wu, B. Mayers, B. Gates, Y. Yin, F. Kim, H. Yan, *Adv. Mater.* **2003**, *15*, 353, and references therein; b) J. T. Hu, T. W. Odom, C. M. Lieber, *Acc. Chem. Res.* **1999**, *32*, 435; c) S. M. Lee, S. N. Cho, J. Cheon, *Adv. Mater.* **2003**, *15*, 441; d) D. Holmes, R. C. Doty, K. P. Johnston, B. A. Korgel, *Science* **2000**, *287*, 1471; e) C. J. Murphy, N. R. Jana, *Adv. Mater.* **2002**, *14*, 80; f) F. Dumestre, B. Chaudret, C. Amiens, M. Respaud, P. Fejes, P. Renaud, P. Zurcher, *Angew. Chem.* **2003**, *115*, 5371; *Angew. Chem. Int. Ed.* **2003**, *42*, 5213; g) F. Dumestre, B. Chaudret, C. Amiens, M.-C. Fromen, M.-J. Casanove, M. Respaud, P. Zurcher, *Angew. Chem.* **2002**, *114*, 4462; *Angew. Chem. Int. Ed.* **2002**, *41*, 4286; h) Z. Tang, N. A. Kotov, M. Giersig, *Science* **2002**, *297*, 237; i) T. Hanrath, B. A. Korgel, *J. Am. Chem. Soc.* **2002**, *124*, 1424; j) T. K. Sau, C. J. Murphy, *J. Am. Chem. Soc.* **2004**, *126*, 8648; k) B. D. Busbee, S. O. Obare, C. J. Murphy, *Adv. Mater.* **2003**, *15*, 414.
[17] a) J. Park, K. An, Y. Hwang, J.-G. Park, H.-J. Noh, J.-Y. Kim, J.-H. Park, N.-M. Hwang, T. Hyeon, *Nat. Mater.* **2004**, *3*, 891; b) J. Joo, H. B. Na, T. Yu, J. H. Yu, Y. W. Kim, F. Wu, J. Zhang, T. Hyeon, *J. Am. Chem. Soc.* **2003**, *125*, 11100.
[18] a) V. F. Puntes, K. M. Krishnan, A. P. Alivisatos, *Science* **2001**, *291*, 2115; b) X. Peng, L. Manna, W. Yang, J. Wickham, E. Scher, A. Kadavanich, A. P. Alivisatos, *Nature* **2000**, *404*, 59; c) J. Park, B. Koo, Y. Hwang, C. Bae, K. An, J. G. Park, H. M. Park, T. Hyeon, *Angew. Chem.* **2004**, *116*, 2332; *Angew. Chem. Int. Ed.* **2004**, *43*, 2282.
[19] a) A. Hirch, *Angew. Chem.* **2002**, *114*, 1933; *Angew. Chem. Int. Ed.* **2002**, *41*, 1853; b) A. Ismach, L. Segev, E. Wachtel, E. Joselevich, *Angew. Chem.* **2004**, *116*, 6266; *Angew. Chem. Int. Ed.* **2004**, *43*, 6140; c) L. An, J. M. Owens, L. E. Mcneil, J. Liu, *J. Am. Chem. Soc.* **2002**, *124*, 13688; d) S. Huang, X. Cai, J. Liu, *J. Am. Chem. Soc.* **2003**, *125*, 5636; e) Y. Li, W. Kim, Y. Zhang, M. Rolandi, D. Wang, H. Dai, *J. Phys. Chem. B* **2001**, *105*, 11424; f) H. C. Choi, W. Kim, D. Wang, H. Dai, *J. Phys. Chem. B* **2002**, *106*, 12361; g) S. Han, T. Yu, J. Park, B. Koo, J. Joo, T. Hyeon, *J. Phys. Chem. B* **2004**, *108*, 8091.
[20] a) B. H. Hong, S. C. Bae, C.-W. Lee, S. Jeong, K. S. Kim, *Science* **2001**, *294*, 348; b) D. D. D. Ma, C. S. Lee, F. C. K. Au, S. Y. Tong, S. T. Lee, *Science* **2003**, *299*, 1894; c) A. I. Yanson, G. Rubio Bollinger, H. E. van den Brom, N. Agrait, J. M. van Ruitenbeek, *Nature* **1998**, *395*, 783; d) Y. Kondo, K. Takayanagi, *Science* **2000**, *289*, 606.
[21] J. Hu, Y. Zhang, B. Liu, J. Liu, H. Zhou, Y. Xu, Y. Jiang, Z. Yang, Z.-Q. Tian, *J. Am. Chem. Soc.* **2004**, *126*, 9470.

 © 2005 Wiley-VCH Verlag GmbH & Co. KGaA, Weinheim

Nanodiamond Stability

DOI: 10.1002/anie.200501495

Thermodynamic Stability and Ultrasmall-Size Effect of Nanodiamonds**

Chengxin Wang, Jian Chen, Guowei Yang, and Ningsheng Xu**

Nano- and ultra-nanodiamonds have emerged as promising materials for various applications,[1–4] although their stabilization is still unclear.[5] Compared with graphite, diamond is a

[*] Dr. C. X. Wang, Prof. J. Chen, Prof. G. W. Yang, Prof. N. S. Xu
State Key Laboratory of Optoelectronic Materials and Technologies
School of Physics Science & Engineering
Zhongshan University
Guangzhou 510275 (P. R. China)
Fax: (+86) 8411-3692
E-mail: stsygw@zsu.edu.cn
stsxns@zsu.edu.cn

[**] We gratefully acknowledge support by the National Science Foundation of China (NSFC) under Grants No.50072022 & 10474140 and the National Natural Science Foundation of China (the Distinguished Creative Group Project).

Supporting information for this article is available on the WWW under http://www.angewandte.org or from the author.

WILEY InterScience DISCOVER SOMETHING GREAT
© 2005 Wiley-VCH Verlag GmbH & Co. KGaA, Weinheim

metastable phase under atmospheric pressure according to the thermodynamic equilibrium phase diagram of carbon. However, it has been verified by experiments,[5–15] calculations,[16–19] and theory[20,21] that nanodiamonds with diameters of less than 5 nm are more stable than their graphitic counterparts. By calculating the structural energies (formation energies) of graphite, diamond, and fullerene on the basis of density functional theory, Barnard et al.[22] reported that the relative stability is dependent on the size of carbon clusters. For instance, diamond could be the stable phase of carbon clusters when the size is in the range of 1.9–5.2 nm. Thus, from the above studies, we conclude that a better understanding is required for two fundamental issues: 1) what relationship exists between size distribution and stability of nanodiamonds, and 2) what is the physical origin of the stability of nanodiamonds.

We have now studied the graphitization of nanodiamonds experimentally and theoretically. Interestingly, we found size-dependent graphitization of nanodiamonds, that is, the stability of nanodiamonds depends on size, and this implies that a nanosize effect is operative, remarkably similar to that of nanocavities.[23] Meanwhile, we established a thermodynamic model for the size effect on the basis of nanothermodynamic analysis.[20,24]

Commercial diamond nanoparticles with sizes of 5–6 nm and over 90% phase purity were annealed under a flow of Ar (purity $>99.99\%$) at atmospheric pressure and given temperatures. Annealing temperatures were in the range from room temperature (RT) to 1423 K, and annealing was performed for 2 h at each temperature. Transmission electron microscopy (TEM), selected-area electron diffraction (SAD), X-ray diffraction (XRD), Raman spectroscopy, and differential scanning calorimetry (DSC) were used to identify the graphitization of diamonds (for detailed analysis, see Supporting Information). The linewidth of the Raman spectrum as a function of nanodiamond size was calculated from the phonon-confinement model (Figure 1).[25] The inset to Figure 1 shows that the size of the residual nanodiamonds decreases from 5.5 to approximately 2.5 nm when the annealing temperature is elevated from RT to 1423 K. Figure 2a shows the bright-field TEM pattern of nanodiamonds annealed at 1423 K for 2 h. The size of the residual nanodiamonds is about 2.5 nm, and diamond nuclei are surrounded by an amorphous ring (see magnified view, top left in Figure 2a). These results indicate that graphitization starts at the surface region, on the basis of experiments by Enoki,[11] which are in good agreement with the above analysis. These experimental results reveal that the graphitization of nanodiamonds is size-dependent, and nanodiamonds smaller than 3 nm are more stable than graphite in graphitization at moderate temperature, that is, the phase stability of nanodiamonds is verified experimentally from the viewpoint of diamond-to-graphite transformation. This new size effect differs distinctly from the widely accepted nanosize and quantum-size effects that occur when the size confining a condensed-matter system is so small that it becomes comparable to the lattice distance.[26] A similar nanosize effect was reported for the shrinkage of nanocavities upon ion-beam irradiation.[23] A general symmetry relationship between nanoparticles and nanocavities can thus be established, as illustrated schematically in Figure 2b.

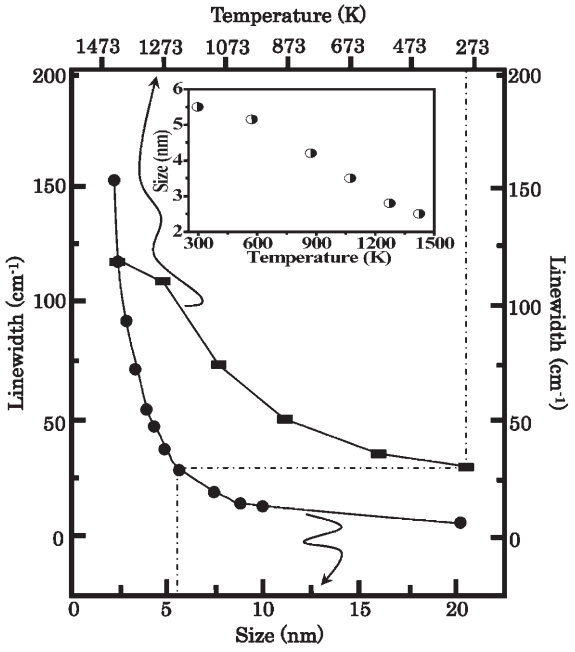

Figure 1. F_{2g} mode linewidth of Raman spectra versus annealing temperature (experimental values, ■) and variation of linewidth with particle sizes of 2.3, 2.5, 3.0, 3.5, 4.0, 4.5, 5.0, 5.7, 7.5, 8.8, 10.0, and 20.0 nm, based on the phonon-confinement model (calculated values, ●). The dash-dot line indicates the determination of particle size. The inset shows a plot of particle size versus annealing temperature.

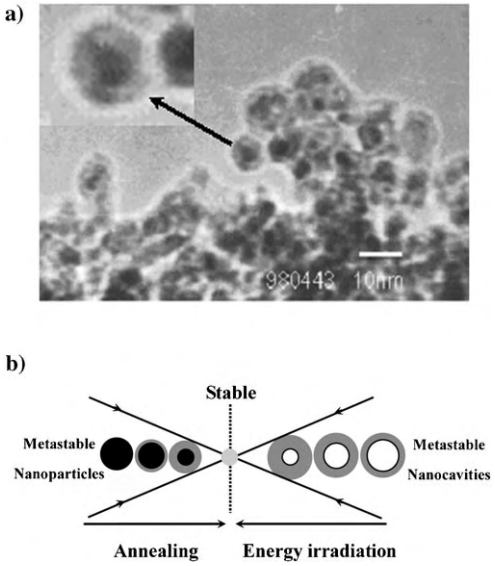

Figure 2. a) TEM images of 5–6 nm nanodiamonds after annealing at 1423 K for 2 h show that the size of the residual nanodiamonds is about 2.5 nm. b) The symmetry relationship between nanoparticles (left) and nanocavities (right) reveals that a similar nanosize effect operates in condensed-matter systems at the nanometer scale.

To provide a better understanding of the size effect in terms of thermodynamics, based on the equilibrium phase diagram of carbon[26] and thermodynamic analysis at the

 © 2005 Wiley-VCH Verlag GmbH & Co. KGaA, Weinheim

nanometer scale,[20,24] we performed a thermodynamic study, taking into account the capillary effect of the nanometer-sized curvature of diamond and graphite nanoparticles by the Laplace–Young equation. Under these assumptions of spherical and quasi-isotropic nanocrystals, the nanosize-curvature-induced interior pressure of the nanodiamonds, ΔP, is expressed by the Laplace–Young equation as $\Delta P = 4\gamma/d$, where γ and d are the surface tension and the diameter of spherical nanodiamonds, respectively. In view of the thermodynamic phase diagram of carbon,[27] the phase-equilibrium-line function $P(T)$ of the diamond–graphite phase transition in the bulk is approximately expressed by Equation (1).[20]

$$P^{be}(T)\ (\text{in Pa}) = 2.01 \times 10^6\, T + 2.02 \times 10^9 \quad (1)$$

$P^{be}(T)$ denotes the phase-equilibrium-line pressure (external pressure) in the bulk. On the basis of the liquid-drop model, the phase equilibrium line on the nanometer scale must be scaled taking into account the radius of curvature. This dependence is universal for all elements in the periodic table. Naturally, the phase equilibrium line on the nanometer scale is a function of temperature, pressure, and nanocrystal radius. The phase-equilibrium-line equation is expressed by Equation (2).[20]

$$P^{ne}(T,d)\ (\text{in Pa}) = 2.01 \times 10^6 T + 2.02 \times 10^9 - \frac{4\gamma}{d} \quad (2)$$

$P^{ne}(T,d)$ is the phase-equilibrium-line pressure (external pressure) under consideration of the radius of curvature of the nanodiamonds. In our case (under atmospheric pressure), if nanodiamonds are the stable phase, the functional relationship must fulfil the condition $4\gamma/d + 10^5 \geq 2.01 \times 10^6 T + 2.02 \times 10^9$. Thus, when $4\gamma/d + 10^5 = 2.01 \times 10^6 T + 2.02 \times 10^9$, we attain a new phase-equilibrium line for the size–temperature relationship, as shown in Figure 3a. These theoretical predictions of the nanodiamond stability are in good agreement with our experimental results. Furthermore, we calculated the Gibbs free energy of the graphitization of nanodiamonds by considering the nanosize-induced interior pressure. The Gibbs free energy is expressed as a function of radius r_g, pressure P, and temperature T [Eq. (3)].[20]

$$\Delta G(r_g,P,T)\ (\text{in J}) = \left(\frac{4}{3}\pi {r_g}^3\, \Delta g/V_{mg} + 4\pi {r_g}^2 \gamma_g\right) f(\theta) \quad (3)$$

V_{mg}, γ_g, and θ are the molar volume of graphite ($5.187 \times 10^{-6}\ m^3$), the surface energy of graphite ($0.55\ J\,m^{-2}$),[21a] and a contact angle,[20] respectively. Here, $f(\theta)$ is the so-called heterogeneous factor (in the range from 0 to 1) and can be expressed by $(1-\cos\theta)^2(2+\cos\theta)/4$, and Δg is the molar-volume Gibbs free energy, which is relative to dimension according to Equation (4), when the phase transition takes place near the phase-equilibrium line.

$$\Delta g\ (\text{in J}) = \Delta V\left(2.01 \times 10^6 T + 2.02 \times 10^9 - \frac{4\gamma}{d} - 1 \times 10^5\right) \quad (4)$$

ΔV ($1.77\ m^3\,mol^{-1}$)[20] is the molar volume difference between diamond and graphite. When $\frac{\partial \Delta G(r)}{\partial r} = 0$, the critical size of graphitization nuclei is obtained [Eq. (5)].

$$r_g^*\ (\text{in m}) = \frac{2\gamma}{\left(\frac{4\gamma}{d} + 1 \times 10^5 - 2.01 \times 10^6 T - 2.02 \times 10^9\right)\frac{V_{mg}}{\Delta V}} \quad (5)$$

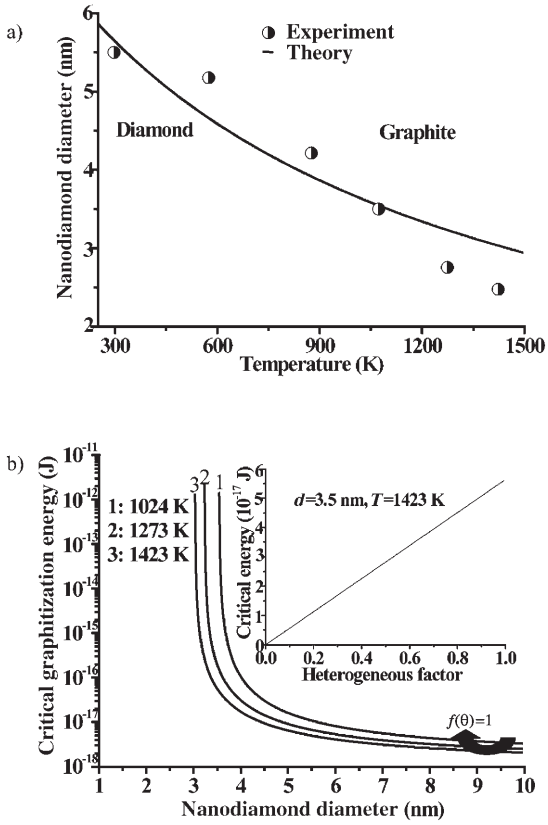

Figure 3. a) Phase-equilibrium line of diamond–graphite size–temperature relationship, which suggests that the stability of residual nanodiamonds is a function of size at a certain temperature. b) Relative curves of the diameters of nanodiamonds and the Gibbs free energy of the nanodiamond graphitization for various annealing temperatures and a given heterogeneous factor, which reveals that a definite threshold size exists for the graphitization of nanodiamonds at a given annealing temperature. The inset shows the relationship between the heterogeneous factor and the critical energy of graphitization.

Accordingly, we attain the relationship curve between size of the residual crystalline nanodiamond nuclei and the Gibbs free energy of graphitization for various annealing temperatures and heterogeneous factors (Figure 3b). Clearly, the Gibbs free energy of graphitization increases with decreasing nanodiamond size at a given temperature. For various annealing temperatures, there are corresponding thresholds of the size of residual nanodiamonds in graphitization, and this suggests that only the surface region of the nanodiamond particles is graphitized at a given temperature, and then graphitization proceeds inward on further elevation of annealing temperature at the expense of nanodiamond phase, as proved by the appearance of bands for graphitic structures in the Raman spectrum and X-ray diffraction (see Supporting Information). Thus, graphitization would display a staircase behavior with increasing annealing temperature,

 © 2005 Wiley-VCH Verlag GmbH & Co. KGaA, Weinheim

due to the surface-curvature effect of the diamond and graphite nanoparticles. For example, the threshold diameters of the residual nanodiamonds are about 3.5 and 3 nm at annealing temperatures of 1073 and 1423 K. Therefore, graphitization hardly proceeds further when the size of the residual nanodiamonds reaches 3.5 and 3 nm at annealing temperatures of 1073 and 1423 K, respectively, which are consistent with our experiments. For comparison, the relationship curve between the graphitization energy and heterogeneous factor is shown as inset in Figure 3b. Similarly, we calculated the relationship curve between the annealing temperature and the probability of diamond-to-graphite transition. According to the general expression of the phase transformation probability,[28] the probability of graphitization is expressed as $f_g = \exp[-(E_a/RT)] - \exp[-(E_a - \Delta g)/RT]$, where R and E_a are the gas constant and the activation energy (212 kJ mol^{-1}),[29] respectively, and Δg is relative to dimension and defined by Equation (4). The resulting relationship curves between annealing temperature and graphitization probability are shown in Figure 4. Apparently, threshold

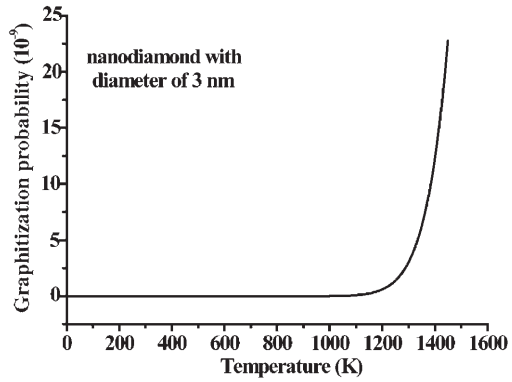

Figure 4. Dependence of the nanodiamond graphitization on annealing temperature for nanodiamonds of a given size. The transition from diamond to graphite almost stops for nanodiamonds with diameters of 3 nm at an annealing temperature of 1300 K.

temperatures exist for the graphitization of nanodiamonds of various sizes. For instance, graphitization of residual nanodiamonds with a size of 3 nm stops when the threshold temperature is about 1300 K. These theoretical results therefore indicate that the surface tension induced by the nanosized curvature of nanodiamonds is the physical origin of their stability and the size effect in nanodiamond graphitization. Accordingly, a thermodynamic approach on the nanoscale also seems applicable to the shrinkage of nanocavities.

In summary, nanodiamonds smaller than 3 nm were experimentally verified to be more stable than graphite from the viewpoint of nanodiamond graphitization. The relationship between the size of residual nanodiamonds and the critical energy of graphitization at given temperatures was studied theoretically on the basis of the size–temperature phase diagram, by taking into account the capillary effect of nanodiamonds, and revealed the dependence of graphitization on nanodiamond diameter and annealing temperature. Both experiment and theory suggested that the nanometer-sized curvature of nanodiamonds is the physical origin of the stability of nanodiamonds.

Received: April 30, 2005
Revised: August 26, 2005
Published online: October 24, 2005

Keywords: carbon · graphitization · nanostructures · phase diagrams · thermodynamics

[1] N. R. Greiner, D. S. Phillips, J. D. Johnson, F. Volk, *Nature* **1988**, *333*, 440–442.
[2] W. B. Choi, J. Liu, M. T. McClure, A. F. Myers, V. V. Zhirnov, J. J. Cuomo, J. J. Hren, *J. Vac. Sci. Technol. B* **1996**, *14*, 2050–2055.
[3] W. B. Choi, J. J. Cuomo, V. V. Zhirnov, A. F. Myers, J. J. Hren, *Appl. Phys. Lett.* **1996**, *68*, 720–722.
[4] E. I. Givargizov, V. V. Zhirnov, A. N. Stepanova, E. V. Rakova, A. N. Kiselev, P. S. Plekhanov, *Appl. Surf. Sci.* **1995**, *87*/88, 24–30.
[5] N. S. Xu, J. Chen, S. Z. Deng, *Diamond Relat. Mater.* **2002**, *11*, 249–256.
[6] P. W. Chen, Y. S. Ding, Q. Chen, F. L. Huang, S. R. Yun, *Diamond Relat. Mater.* **2000**, *9*, 1722–1725.
[7] S. Jiao, A. Sumant, M. A. Kirk, D. M. Gruen, A. R. Krauss, O. Auciello, *J. Appl. Phys.* **2001**, *90*, 118–122.
[8] S. T. Lee, H. Y. Peng, X. T. Zhou, N. Wang, C. S. Lee, I. Bello, Y. Lifshitz, *Science* **2002**, *297*, 104–106.
[9] Y. Gogotsi, S. Welz, D. A. Ersoy, M. J. McNallan, *Nature* **2001**, *411*, 283–287.
[10] Yu. V. Butenko, V. L. Kuznetsov, A. L. Chuvilin, V. N. Kolomiichuk, S. V. Stankus, R. A. Khairulin, B. Segall, *J. Appl. Phys.* **2000**, *88*, 4380–4388.
[11] T. Enoki, *Phys. Solid State* **2004**, *46*, 651–656.
[12] B. L. V. Prasad, H. Sato, T. Enoki, *Phys. Rev. B* **2000**, *62*, 11209–11218.
[13] A. E. Aleksenskiĭ, M. V. Baĭdakova, A. Ya. Vul', V. Yu. Davydov, Yu. A. Pevtsova, *Phys. Solid State* **1997**, *39*, 1007–1015.
[14] J. W. Ager III, D. K. Veirs, G. M. Rosenblatt, *Phys. Rev. B* **1991**, *43*, 6491–6499.
[15] S. Prawer, J. L. Peng, J. O. Orwa, J. C. McCallum, D. N. Jamieson, L. A. Bursill, *Phys. Rev. B* **2000**, *62*, 16360–16363.
[16] P. Badziag, W. S. Verwoerd, W. P. Ellis, N. R. Greiner, *Nature* **1990**, *343*, 244–245.
[17] N. W. Winter, F. H. Ree, *J. Comput.-Aided Mater. Des.* **1998**, *5*, 279–294.
[18] J. Y. Raty, G. Galli, *Nat. Mater.* **2003**, *2*, 792–795.
[19] H. R. Francis, N. W. Winter, J. N. Glosli, J. A. Viecelli, *Physica B* **1999**, *265*, 223–229.
[20] C. X. Wang, Y. H. Yang, N. S. Xu, G. W. Yang, *J. Am. Chem. Soc.* **2004**, *126*, 11303–11306; C. X. Wang, Y. H. Yang, G. W. Yang, *J. Appl. Phys.* **2005**, *97*, 066104–066106; Y. C. Zhang, C. X. Wang, G. W. Yang, *J. Phys. Chem. B* **2004**, *108*, 2589–2593.
[21] a) D. S. Zhao, M. Zhao, Q. Jiang, *Diamond Relat. Mater.* **2002**, *11*, 234–236; b) Q. Jiang, J. C. Li, G. Wilde, *J. Phys. Condens. Matter* **2000**, *12*, 5623–5627.
[22] A. S. Barnard, S. P. Russo, I. K. Snook, *J. Chem. Phys.* **2003**, *118*, 5094–5097.
[23] X. F. Zhu, *J. Phys. Condens. Matter* **2003**, *15*, L253–L261.
[24] C. X. Wang, Y. H. Yang, Q. X. Liu, G. W. Yang, *J. Phys. Chem. B* **2004**, *108*, 728–731; C. X. Wang, Q. X. Liu, G. W. Yang, *Chem. Vap. Deposition* **2004**, *10*, 280–283; C. X. Wang, Y. H. Yang, G. W. Yang, *Appl. Phys. Lett.* **2004**, *84*, 3034–3036.
[25] H. Richter, Z. P. Wang, L. Ley, *Solid State Commun.* **1981**, *39*, 625–629; J. Chen, S. Z. Deng, J. Chen, Z. X. Yu, N. S. Xu, *Appl. Phys. Lett.* **1999**, *74*, 3651–3653.

 © 2005 Wiley-VCH Verlag GmbH & Co. KGaA, Weinheim

[26] G. Bertsch, *Science* **1997**, *277*, 1619 – 1619.
[27] F. P. Bundy, W. A. Bassett, M. S. Weathers, R. J. Hemley, H. U. Mao, A. F. Goncharov, *Carbon* **1996**, *34*, 141 – 153.
[28] J. B. Wang, G. W. Yang, *J. Phys. Condens. Matter* **1999**, *11*, 7089 – 7094.
[29] V. L. Solozhenko, V. Z. Turkevich, O. O. Kurakevych, *J. Phys. Chem. B* **2002**, *106*, 6634 – 6637.

 © 2005 Wiley-VCH Verlag GmbH & Co. KGaA, Weinheim

Carbon Dioxide Complexes

DOI: 10.1002/anie.200502400

Aluminum–Magnesium Complexes with Linearly Bridging Carbon Dioxide**

Chung-Cheng Chang, Min-Chun Liao, Tsu-Hsin Chang, Shie-Ming Peng, and Gene-Hsiang Lee*

Earlier, we found that an oxygen atom of carbon dioxide bonds to a metal atom when carbon dioxide is fixed by the Al–Mg mixed-metal compounds $[Me_2Al(\mu\text{-}NR_2)_2Mg(\mu\text{-}Me)]_n$ (R = *i*Pr, $n = 4$; R = Et, $n = 2$). Subsequently, the amino leaving group migrates from the attacked metal atom to the carbon atom of the carbon dioxide to form Al–Mg carbamato complexes.[1] The CO_2-ligated Mg compounds show a variety of bonding modes.[2] However, to date the linear $\mu(O,O')$-CO_2 coordination mode of carbon dioxide has not been observed, either in main group or in transition metal compounds.[3]

In accordance with earlier work by Sita et al.,[4] we presume that the reaction of $Mg[N(SiMe_3)_2]_2$ with carbon dioxide could also generate an oxo-transfer product, namely, $Mg(N(SiMe_3)_2)(OSiMe_3)$, and the expected $O{=}C{=}N(SiMe_3)$, instead of generating a carbamato complex.[5] In light of our previous experience with trialkylaluminum reagents and taking advantage of the oxo-transfer compound $Mg[N(SiMe_3)_2](OSiMe_3)$, we proposed a process for studying CO_2 fixation in a mixture of $Mg[N(SiMe_3)_2]_2$ and trialkylaluminum.

One equivalent of AlR_3 (R = Me, Et) was added to a solution of $Mg[N(SiMe_3)_2]_2$ in THF at room temperature, and an excess of carbon dioxide was bubbled through the stirred, ice-cooled mixture to yield compounds **1** (R = Me) and **2** (R = Et) [Eq. (1), Scheme 1].

$$Mg[N(SiMe_3)_2]_2 + AlR_3 + CO_2 \xrightarrow[0\,^{\circ}C]{THF} [\{R_2Al(\mu\text{-}NSiMe_3)(\mu\text{-}OSiMe_3)Mg(thf)_2(\mu\text{-}O_2C)\}_3]\ (\mathbf{1}, \mathbf{2}) \quad (1)$$

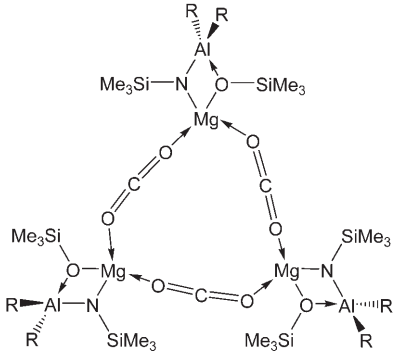

1 R=Me
2 R=Et

Scheme 1. Schematic representation of **1** and **2**. Coordinated THF omitted for clarity.

Presumably, carbon dioxide reacted with $Mg[N(SiMe_3)_2]_2$ to give oxo-transfer product $Mg[N(SiMe_3)_2](OSiMe_3)$, which is assumed to form a bridged Al–Mg intermediate with AlR_3 (R = Me, Et); this subsequently loses a ligand from the magnesium center and is attacked by a second molecule of carbon dioxide with the oxygen atom as a weak electron donor (Scheme 2). Finally, the carbon dioxide acts as a

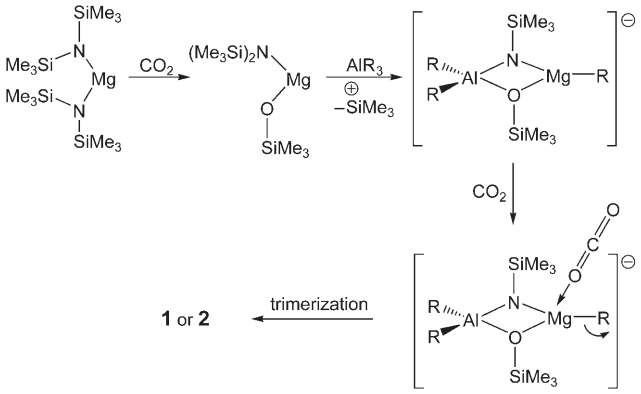

Scheme 2. Proposed reaction path for the formation of **1** and **2**.

bridging ligand to form a trimer. The products were characterized by elemental analysis, FTIR spectroscopy, and X-ray analysis. The single-crystal X-ray diffraction data confirmed the molecular structures (Figures 1 and 2).[6] The skeletons of **1** and **2** have a C_3 symmetry axis and can be viewed as composed of three equivalent motifs, each of which has a

[*] Prof. Dr. C.-C. Chang, M.-C. Liao, Prof. Dr. T.-H. Chang
Department of Chemistry
National Sun Yat-Sen University
Kaohsiung, 804 (Taiwan)
Fax: (+886) 7525-2009
E-mail: ccccc@mail.nsysu.edu.tw
Prof. Dr. S.-M. Peng, G.-H. Lee
Department of Chemistry
National Taiwan University
Taipei, 117 (Taiwan)

[**] This work was supported by the National Science Council of Taiwan (NSC 93-2113M-110-005 to C.C.C.). We are greatly indebted to Analytische Laboratorien Prof. Dr. H. Malissa und G. Reuter GmbH (Germany) for elemental analysis, and to Prof. Dr. Michael Y. Chiang at the National Sun Yat-Sen University for constructive discussions.

Supporting information for this article is available on the WWW under http://www.angewandte.org or from the author.

InterScience
© 2005 Wiley-VCH Verlag GmbH & Co. KGaA, Weinheim

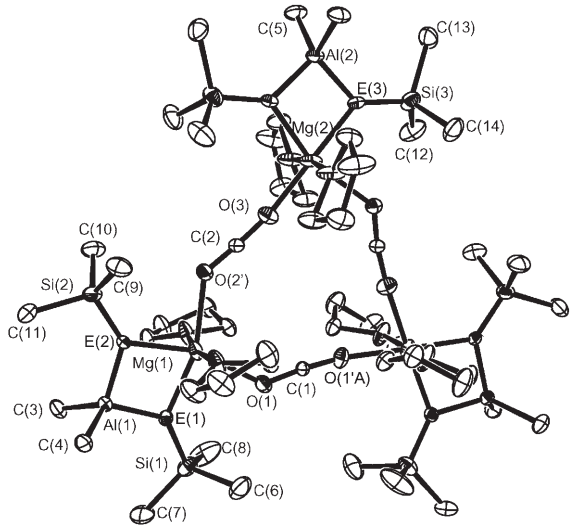

Figure 1. ORTEP view of **1** in the solid state. Thermal ellipsoids are drawn at the 20% probability level. Selected bond lengths [Å] and angles [°]: Mg(1)–O(1) 2.211(11), Mg(1)–O(2′) 2.232(12), Mg(2)–O(3) 1.944(10), O(1)–C(1) 1.208(10), O(2′)–C(2) 1.166(13), O(3)–C(2) 1.223(10); O(1′A)-C(1)-O(1) 173.6(10), O(2′)-C(2)-O(3) 175.3(8), C(1)-O(1)-Mg(1) 133.2(6), C(2)-O(2′)-Mg(1) 134.1(6), C(2′)-O(3)-Mg(2) 171.1(8), E(1)-Mg(1)-E(2) 75.53(12) E(1)-Mg(1)-O(1) 85.9(2) E(2)-Mg(1)-O(2′) 86.8(3), O(1)-Mg(1)-O(2′) 111.8(3). Atoms E(1), E(2), and E(3) were refined as mixed atoms (50% O and 50% N).

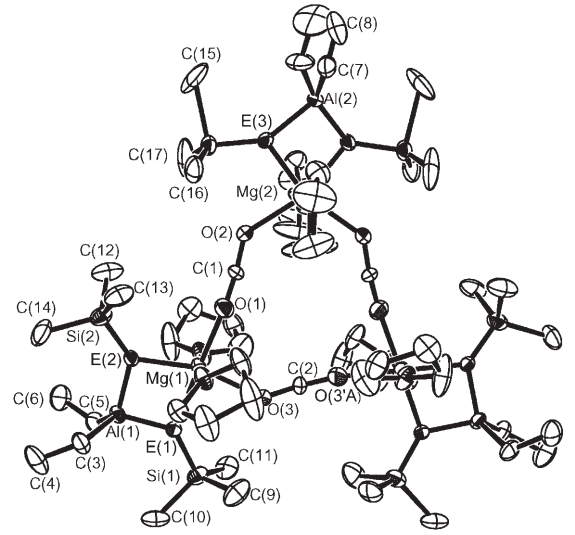

Figure 2. ORTEP view of **2** in the solid state. Thermal ellipsoids are drawn at the 20% probability level. Selected bond lengths [Å] and angles [°]: Mg(1)–O(1) 2.004(16), Mg(1)–O(3) 2.184(11), Mg(2)–O(2) 2.181(10), O(1)–C(1) 1.149(15), O(2)–C(1) 1.222(11), O(3)–C(2) 1.201(10); O(1)-C(1)-O(2) 173.3(9), O(3′A)-C(2)-O(3) 169.6(10), C(1)-O(1)-Mg(1) 171.3(11), C(1)-O(2)-Mg(2) 134.9(7), C(2)-O(3)-Mg(1) 136.9(7), O(1)-Mg(1)-E(2) 104.6(4), E(1)-Mg(1)-E(2) 76.03(13), O(1)-Mg(1)-O(3) 92.3(4), E(1)-Mg(1)-O(3) 86.9(3). Atoms E(1), E(2), and E(3) were refined as mixed atoms (50% O and 50% N).

bridged Al–Mg structure. The six-coordinate magnesium atom is linked to a four-coordinate aluminum atom by bridging $OSiMe_3$ and $NSiMe_3$ groups. Two alkyl groups are retained on each aluminum atom to attain a coordination number of four. The magnesium atoms of the three motifs are joined through three approximately linear carbon dioxide bridges to form a twelve-membered ring.

Atoms O(4)–O(6) of **1** and N(1)–N(3) of **2** were refined as mixed atoms (50% O and 50% N) due to their disorder in the $OSiMe_3$ and $NSiMe_3$ groups. The requirement for charge balance in the molecule and elemental analysis supported the assignment of these atoms. Compounds **1** and **2** have very similar skeletons.

In **1** and **2**, the Mg–O bond lengths of 1.944(10)–2.232(12) and 2.004(16)–2.184(11) Å, respectively, in the $MgCO_2$ moiety are within the range expected for such bonds (Mg←O (monodentate O donor ligand): 2.012–2.236 Å).[7] These bond lengths indicate that each oxygen atom donates a lone pair of electrons to the vacant p_z orbital of the electropositive magnesium atom in a dative bond. In other words, each carbon dioxide molecule links two magnesium atoms in a linear μ(O,O′) bonding mode. The C–O bond lengths of 1.166(13)–1.233(10) and 1.149(15)–1.222(11) Å, respectively, are very close to that of free carbon dioxide[8] and $Mn(HCOO)_3 \cdot {}^1/_2\,CO_2 \cdot {}^1/_4\,HCOOH \cdot {}^2/_3\,H_2O$,[9] and thus suggest the presence of C=O bonds. The O-C-O bond angles of 173.6(10)–175.3(8) and 169.6(10)–173.3(9)°, respectively, are close to 180° and suggest sp-hybridized C atoms. The Mg←O=C=O→Mg moieties show some disorder, with a shape like an hourglass.

The ^1H and ^{13}C NMR and IR spectroscopic data and the elemental analysis further characterized **1** and **2**.[10] The ^{13}C NMR spectra of **1** and **2** show peaks for the carbon atom of CO_2 at 120.87 and 120.76 ppm, respectively, shifted slightly upfield relative to free carbon dioxide.[11]

The IR spectra provided further strong evidence for the introduction of carbon dioxide into **1** and **2**. Compounds **1** and **2** showed strong absorption at 2267 and 2275 cm^{-1}, respectively, originating from stretching vibration of the bridging carbon dioxide. In comparison to free linear carbon dioxide (ν_{asym} 2348 cm^{-1})[12] and $Mn(HCOO)_3 \cdot {}^1/_2\,CO_2 \cdot {}^1/_4\,HCOOH \cdot {}^2/_3\,H_2O$,[9] the values are only slightly red-shifted. Decreasing CO_2 stretching frequency is an accepted measure of increasing negative charge on the Mg atom. Hence, the coordinated CO_2 molecules in **1** and **2** donate a small amount of electron density to the more electropositive Mg atoms.

In summary, we have reported a straightforward, one-pot synthetic pathway that leads to novel aluminum–magnesium complexes containing carbon dioxide in the heretofore-unknown linear μ(O,O′) bonding mode. The formation of **1** and **2** shows that interesting products can predictably be obtained when $Mg[N(SiMe_3)_2]_2$ and AlR_3 (R = Me, Et) are reacted with carbon dioxide. Investigations of the electronic and steric effects of substituents on the trialkylaluminum on the reaction with $Mg[N(SiMe_3)_2]_2$ and carbon dioxide under the same conditions are in progress.

Experimental Section

All experiments were carried out in an N_2-flushed glove bag, in a dry box, or under vacuum by using standard Schlenk techniques. All solvents were distilled and degassed prior to use. All ^1H and ^{13}C NMR spectra were measured on a Varian-500 spectrometer. Chemical shifts

 © 2005 Wiley-VCH Verlag GmbH & Co. KGaA, Weinheim

are referenced to C_6D_6 (^1H, $\delta = 7.15$ ppm; $^{13}C\{^1H\}$, $\delta = 128.00$ ppm). FTIR spectra were obtained with a Bio-Rad model FTS-155 FTIR spectrometer.

1: $AlMe_3$ (2.0 M in toluene, 12 mL, 2.38 mmol) was added to a solution of $Mg[N(SiMe_3)_2]_2$ (8.21 g, 2.38 mmol) in THF (60 mL). The mixture was cooled in an ice bath, and an excess of carbon dioxide was bubbled through the stirred mixture for 2 h. An intermediate exothermic reaction ensued. The resultant solution was cooled in a freezer to give crystals of **1**. The preparation of complex **2** was similar to that of complex **1**.

1: Yield: 20%. M.p. > 112 °C (decomp). ^1H NMR (500 MHz, C_6D_6): $\delta = -0.36$ (s, 18H, $AlCH_3$), 0.34 ppm (m, 54H, $NSi(CH_3)_3$, $OSi(CH_3)_3$). $^{13}C\{^1H\}$ NMR (C_6D_6): $\delta = -5.75$ ($AlCH_3$), 3.24 ($NSi(CH_3)_3$; $OSi(CH_3)_3$), 120.87 ppm (CO_2). IR (Nujol): $\tilde{\nu} = 2267$(s), 1252(m), 1040(m), 890(s), 841(s) cm^{-1}.

2: Yield: 53%. M.p. > 116 °C (decomp). ^1H NMR (500 MHz, C_6D_6): $\delta = 0.24$ (q, 12H, $AlCH_2$), 0.35 (m, 54H, $NSi(CH_3)_3$, $OSi(CH_3)_3$), 1.43 ppm (t, 18H, $AlCH_2CH_3$). $^{13}C\{^1H\}$ NMR (C_6D_6): $\delta = 3.12$ ($AlCH_2$, $NSi(CH_3)_3$, $OSi(CH_3)_3$), 10.42 ($AlCH_2CH_3$), 120.76 ppm (CO_2). IR (Nujol): $\tilde{\nu} = 2275$(s), 1255(m), 1041(m), 889(s), 842(s) cm^{-1}.

Received: July 11, 2005
Published online: October 25, 2005

Keywords: aluminum · carbon dioxide fixation · coordination modes · magnesium

[1] a) D. Walther, M. Ruben, S. Rau, *Coord. Chem. Rev.* **1999**, *182*, 67; b) C. C. Chang, B. Srinivas, M. L. Wu, W. H. Chiang, M. Y. Chiang, C. S. Hsiung, *Organometallics* **1995**, *14*, 5150; c) C. C. Chang, M. S. Ameerunisha, *Coord. Chem. Rev.* **1999**, *189*, 199.

[2] a) K. C. Yang, C. C. Chang, C. S. Yeh, G. H. Lee, S. M. Peng, *Organometallics* **2001**, *20*, 126; b) K. C. Yang, C. C. Chang, C. S. Yeh, G. H. Lee, Y. Wang, *Organometallics* **2002**, *21*, 1296.

[3] a) A. Behr, *Angew. Chem.* **1988**, *100*, 681; *Angew. Chem. Int. Ed. Engl.* **1988**, *27*, 661; b) D. H. Gibson, *Chem. Rev.* **1996**, *96*, 2063.

[4] L. R. Sita, J. R. Babcock, R. Xi, *J. Am. Chem. Soc.* **1996**, *118*, 10912.

[5] a) M. T. Caudle, J. W. Kampf, *Inorg. Chem.* **1999**, *38*, 5474; b) D. B. Dell'Amico, F. Calderazzo, L. Labella, F. Marchetti, G. Pampaloni, *Chem. Rev.* **2003**, *103*, 3857; c) Y. Tang, L. N. Zakharov, A. L. Rheingold, R. A. Kemp, *Organometallics* **2004**, *23*, 4788; d) D. B. Dell'Amico, F. Calderazzo, U. Englert, L. Labella, F. Marchetti, M. Specos, *Eur. J. Inorg. Chem.* **2004**, 3938; e) E. García-España, P. Gaviña, J. Latorre, C. Soriano, B. Verdejo, *J. Am. Chem. Soc.* **2004**, *126*, 5082; f) Y. Tang, W. S. Kassel, L. N. Zakharov, A. L. Rheingold, R. A. Kemp, *Inorg. Chem.* **2005**, *44*, 359.

[6] Crystal data for **1**·2THF: $C_{59}H_{136}Al_3Mg_3N_3O_{17}Si_6$, $M_r = 1482.12$, orthorhombic, space group *Pbcn*, $a = 12.4718(6)$, $b = 25.4146(11)$, $c = 28.0272(12)$ Å, $V = 8883.7(7)$ Å^3, $Z = 4$, $\rho_{calcd} = 1.108$ g cm^{-3}, $\mu = 0.199$ mm^{-1}, $\lambda = 0.71073$ Å, transmission range 0.9520–0.9247, crystal size $0.40 \times 0.40 \times 0.25$ mm^3. A total of 29148 unique reflections were collected on a Nonius KappaCCD diffractometer at 150 K in the θ range 1.45–25.00°. Full-matrix least-squares refinement on F^2 converged to $R1 = 0.1225$ (all data), 0.0783 ($I > 2\sigma(I)$); $wR2 = 0.2401$ (all data), 0.2011 ($I > 2\sigma(I)$). Atoms O(1), O(2), O(3), C(18), C(22), C(23), O(1′), O(2′), O(3′), C(18′), C(22′) and C(23′) all had half occupancies. Crystal data for **2**·THF: $C_{61}H_{140}Al_3Mg_3N_3O_{16}Si_6$, $M_r = 1494.17$, monoclinic, space group *C*2/*c*, $a = 30.5742(6)$, $b = 17.5555(3)$, $c = 21.1478(4)$ Å, $\beta = 127.6215(9)$°, $V = 8990.7(3)$ Å^3, $Z = 4$, $\rho_{calcd} = 1.104$ g cm^{-3}, $\mu = 0.196$ mm^{-1}, $\lambda = 0.71073$ Å, transmission range 0.963–0.883, crystal size $0.25 \times 0.25 \times 0.22$ mm^3. A total of 52985 unique reflections were collected on a Nonius KappaCCD diffractometer at 150 K in the θ range 1.43–25.00°. Full-matrix least-squares refinement on F^2 converged to $R1 = 0.1423$ (all data), 0.1006 ($I > 2\sigma(I)$); $wR2 = 0.3135$ (all data), 0.2731 ($I > 2\sigma(I)$). One molecule of THF was disordered. Atoms Al(2), Si(3), Si(3′), C(7), C(8), C(7′), C(8′), O(7), C(30), and C(32) all had half occupancies. All calculations were performed with the SHELXTL-97 package. CCDC-277386 (**1**) and -277385 (**2**) contain the supplementary crystallographic data for this paper. These data can be obtained free of charge from the Cambridge Crystallographic Data Centre via www.ccdc.cam.ac.uk/data_request/cif.

[7] C. E. Holloway, M. Melnik, *J. Organomet. Chem.* **1994**, *465*, 1.

[8] a) K. K. Pandey, *Coord. Chem. Rev.* **1995**, *140*, 37; b) X. Yin, J. R. Moss, *Coord. Chem. Rev.* **1999**, *181*, 27.

[9] A. Cornia, A. Caneschi, P. Dapporto, A. C. Fabretti, D. Gatteschi, W. Malavasi, C. Sangregorio, R. Sessoli, *Angew. Chem.* **1999**, *111*, 1897; *Angew. Chem. Int. Ed.* **1999**, *38*, 1780.

[10] Elemental analysis (%) calcd for **1** ($C_{51}H_{120}Al_3Mg_3N_3O_{15}Si_6$): C 45.84, H 9.05, N 3.14, Mg 5.45; found: C 45.39, H 8.83, N 3.21, Mg, 5.31. Deviations from calculated values are attributed to the extremely air sensitive and hygroscopic nature of this compound.

[11] a) N. E. Schlörer, S. Berger, *Organometallics* **2001**, *20*, 1703; b) C. S. McCowan, T. L. Groy, M. T. Caudle, *Inorg. Chem.* **2002**, *41*, 1120.

[12] A. K. Brisdon, *Inorganic Spectroscopic Methods*, Oxford, New York, **1998**, chap. 2, p. 23.

 © 2005 Wiley-VCH Verlag GmbH & Co. KGaA, Weinheim

Asymmetric Catalysis

DOI: 10.1002/anie.200502767

Pd-Catalyzed Stereoselective Oxidation of Methyl Groups by Inexpensive Oxidants under Mild Conditions: A Dual Role for Carboxylic Anhydrides in Catalytic C–H Bond Oxidation**

*Ramesh Giri, Jue Liang, Jian-Guang Lei, Jiao-Jie Li, Dong-Hui Wang, Xiao Chen, Isaac Clement Naggar, Chengyun Guo, Bruce M. Foxman, and Jin-Quan Yu**

The selective oxidation of unactivated C–H bonds is a significant research goal because of its importance in synthesis and the chemical industry.[1] In the past few years, the development of stoichiometric σ-chelation directed C–H activation processes in catalytic reactions has met with remarkable success.[2] This approach has also yielded fruitful

[*] R. Giri, J. Liang, Dr. J.-G. Lei, J.-J. Li, D.-H. Wang, Dr. X. Chen, I. C. Naggar, C. Guo, Prof. Dr. B. M. Foxman, Prof. Dr. J.-Q. Yu
Department of Chemistry
Brandeis University
Waltham, MA 02454-9110 (USA)
Fax: (+1) 781-736-2516
E-mail: yu200@brandeis.edu

[**] We wish to thank Brandeis University for financial support and the Camille and Henry Dreyfus Foundation for a New Faculty Award.

Supporting information for this article is available on the WWW under http://www.angewandte.org or from the author.

WILEY InterScience DISCOVER SOMETHING GREAT
© 2005 Wiley-VCH Verlag GmbH & Co. KGaA, Weinheim

results in the oxidation of methyl groups catalyzed by transition-metal species.[3–5] Despite this significant progress, the development of practical catalytic methods to oxidize methyl groups using inexpensive oxidants under mild conditions remains an important task.

We have recently reported the use of a chiral oxazoline as the chelating group to iodinate prochiral sp^3 and sp^2 C–H bonds diastereoselectively.[6] The importance of the direct oxidation of methyl groups in synthesis turned our attention to the development of a catalytic system using inexpensive oxidants.[7] Pyridine and *O*-methyl oxime directed palladium-catalyzed acetoxylation has been recently reported using $PhI(OAc)_2$ as an oxidant.[8] Herein, we disclose a Pd-catalyzed oxidation of unactivated methyl groups using the peroxyester MeCOOO*t*Bu as the stoichiometric oxidant and Ac_2O as a crucial promoter [Eq. (1)]. Preliminary results on the diastereoselective oxidation of methyl groups using lauroyl or benzoyl peroxide as the stoichiometric oxidant are also described.

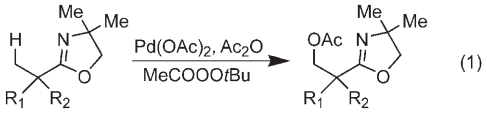

Our efforts began with the characterization of a Pd–alkyl complex formed from oxazoline directed C–H activation. The reaction of substrate **1** with 1.5 equivalents of $Pd(OAc)_2$ in CH_2Cl_2 at 24 °C for 36 h afforded a mixture of *anti* and *syn* trinuclear C(sp^3)–Pd complexes in a 3:2 ratio (Scheme 1).

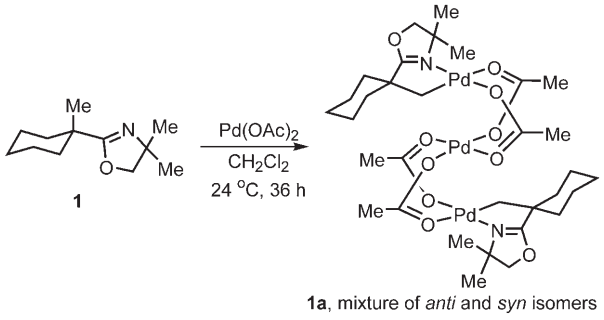

Scheme 1. Formation of trinuclear C(sp^3)–Pd complex **1a**.

The molecular structure of the *anti* isomer **1a** determined by X-ray diffraction is related to a recently obtained C(sp^2)–Pd ferrocene derivative[9] and confirms earlier proposals based on ^1H NMR spectroscopic analysis (Figure 1).[6,10]

We envisioned that *tert*-butyl hydroperoxide (TBHP) would oxidize the Pd–C(sp^3) bond in **1a** to give Pd–OR complex **1b**, as TBHP/[$VO(acac)_2$] (acac = acetylacetonate) is known to insert an oxygen atom into the Pd–C(sp^2) bond of dimeric Pd–aryl complexes (Scheme 2).[11] We found that the reaction of **1a** with five equivalents of TBHP in CH_2Cl_2 at 24 °C for 36 h, followed by reduction with NH_2NH_2, afforded the hydroxylated product **1c** in 35% yield of isolated product (Scheme 2).

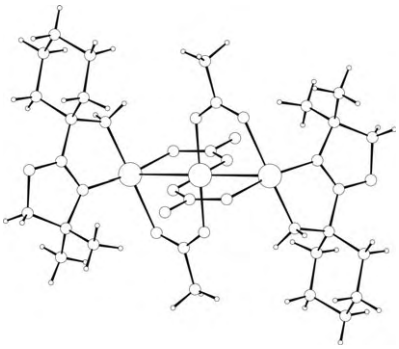

Figure 1. X-ray crystal structure of **1a**.

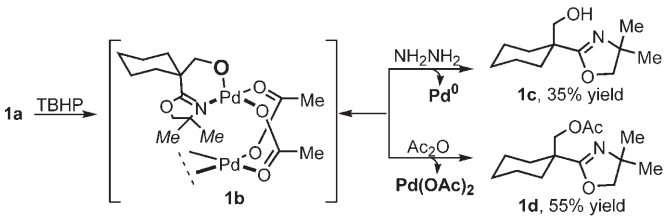

Scheme 2. Stoichiometric acetoxylation of methyl groups.

We further hypothesized that Ac_2O would acetylate the Pd–OR complex **1b** and regenerate $Pd(OAc)_2$, thereby rendering this reaction catalytic. Following the treatment of **1a** with TBHP in CH_2Cl_2 , addition of Ac_2O to the reaction mixture was found to give the product in the form of acetate **1d** and regenerate $Pd(OAc)_2$ (Scheme 2).

Carrying out this reaction with only a catalytic amount of $Pd(OAc)_2$ led us to discover that peroxyester MeCOOO*t*Bu, generated from the reaction of TBHP with Ac_2O, is an efficient oxidant for the oxidation of methyl groups. A combination of $Pd(OAc)_2$ (5 mol%) and MeCOOO*t*Bu (2 equiv) in Ac_2O was able to yield acetoxylate **1** in 71% yield.[12] A wide range of substrates are oxidized in good yields (Table 1): polar functional groups, such as ketals, imides, esters, and chlorides, are tolerated. Substrate **9** was used directly without protection of the hydroxy group, which was acetylated in the reaction. This oxidation protocol is potentially useful in the laboratory as MeCOOO*t*Bu is a cheap oxidant (TBHP: 5–6 M in hydrocarbon, $\$154\,mol^{-1}$; MeCOOO*t*Bu, 5–6 M in hydrocarbon, $\$14\,mol^{-1}$).[13]

Next, we attempted to extend this protocol to diastereoselective oxidation using a chiral oxazoline. MeCOOO*t*Bu is not compatible with a chiral oxazoline containing a hydrogen atom α to the nitrogen atom, as this hydrogen atom is readily oxidized, thus leading to the formation of an oxazole. We were delighted to find that this side reaction can be prevented by using inexpensive benzoyl or lauroyl peroxide as the oxidants (Table 2). Moderate diastereoselectivity (12–82% *de*) was observed with substrates containing prochiral methyl groups.

A chiral trinuclear C(sp^3)–Pd complex **16a** has also been obtained and characterized by X-ray studies (Figure 2). In sharp contrast to the 2:3 mixture of *syn* and *anti* complexes formed from nonchiral oxazoline **1** (Scheme 1), only the

 © 2005 Wiley-VCH Verlag GmbH & Co. KGaA, Weinheim

Table 1: $Pd(OAc)_2$-catalyzed oxidation of methyl groups by MeCOOO*t*Bu.[a]

Entry	Substrate	Product	Yield [%]
1	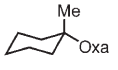 **1**	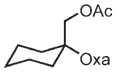 **1d**	71
2	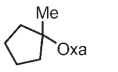 **2**	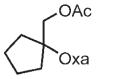 **2a**	62
3	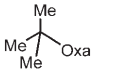 **3**	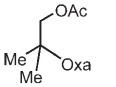 **3a**	69
4	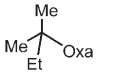 **4**	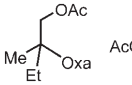 **4a** 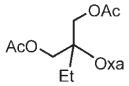 **4b**	89
5	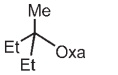 **5**	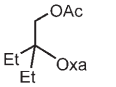 **5a**	90
6	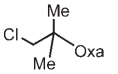 **6**	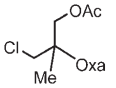 **6a**	68
7	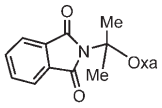 **7**	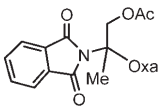 **7a**	50
8	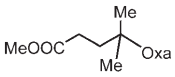 **8**	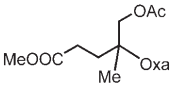 **8a**	70
9	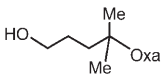 **9**	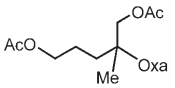 **9a**	50

[a] Oxa = 2-substituted 4,4-dimethyloxazoline. Reaction conditions: entries 1–5, $Pd(OAc)_2$ (5 mol%), Ac_2O, MeCOOO*t*Bu (2 equiv), 65°C, 48–72 h; entries 6–9, $Pd(OAc)_2$ (10 mol%). In the absence of air or pure O_2, the reaction stopped at 30–40% conversion and the precipitation of Pd^0 was observed. [b] **4a**/**4b** = 1:1.

Table 2: $Pd(OAc)_2$-catalyzed diastereoselective oxidation of methyl groups by lauroyl peroxides.[a]

Entry	Substrate	Product	Yield [%]	*de* [%]
1	**10**	**10a**	67	18
2	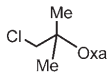 **11**	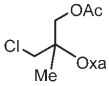 **11a**	66	38
3	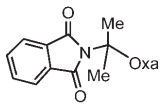 **12**	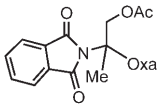 **12a**	38	12
4	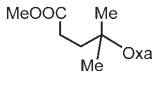 **13**	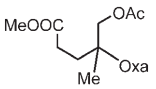 **13a**	73	24
5	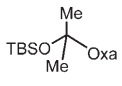 **14**	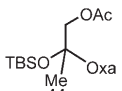 **14a**	43	62
6	**15**	**15a**	49	82

[a] Oxa = 2-substituted 4-*tert*-butyloxazoline. Reaction conditions: $Pd(OAc)_2$ (5 mol%), Ac_2O, lauroyl peroxide (2 equiv), 50°C, 48 h. The presence of air or pure O_2 increases the conversion rate.

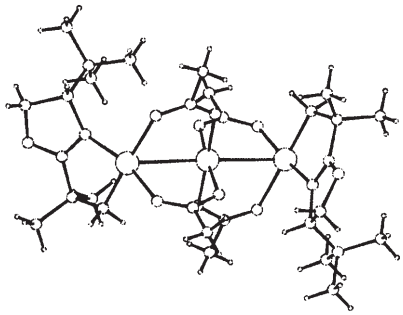

Figure 2. X-ray crystal structure of **16a**.

anti isomer was obtained from the chiral substrate **16** (Scheme 3). This result suggests that the asymmetric center on the oxazoline is crucial in the control of the geometry of the trinuclear complex. The exclusive formation of the *anti* isomer could be important for the rationalization of the observed stereoselectivity in the C–H activation step, as the *syn* isomer has a different symmetry and steric environment and could generate asymmetric centers of the opposite configuration in the C–H activation step. In future work, the crystal structures of $C(sp^3)$–Pd complexes derived from prochiral substrates, such as **15**, will be obtained and will shed further light on the stereoselectivity of the C–H activation step.

As reported previously, a mixture of $AcOH/Ac_2O$ has been used as the reaction media for Pd^{II}-catalyzed C–H activation reactions.[8,14] To the best of our knowledge, the role

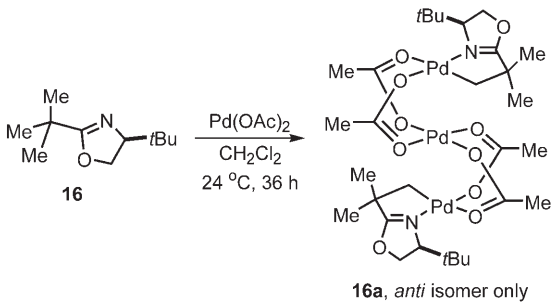

16a, *anti* isomer only

Scheme 3. Formation of chiral trinuclear $C(sp^3)$–Pd complex **16a**.

 © 2005 Wiley-VCH Verlag GmbH & Co. KGaA, Weinheim

of Ac_2O remains obscure in C–H bond oxidation reactions. Isolation of the complex **1f** prompted us to investigate the influence of Ac_2O on the elementary steps of the reaction. Although no compelling evidence for the involvement of a Pd^{IV} species has been obtained in our experiments, previous characterization of a Pd^{IV} species formed upon the oxidative addition of benzoyl peroxide or aryl transfer from diphenyliodonium triflate to 2,2′-bipyridine-coordinated Pd^{II} and Pt^{II} centers allows the proposal of a plausible pathway (Scheme 4).[15] The formation of **1f** in CH_2Cl_2 was monitored

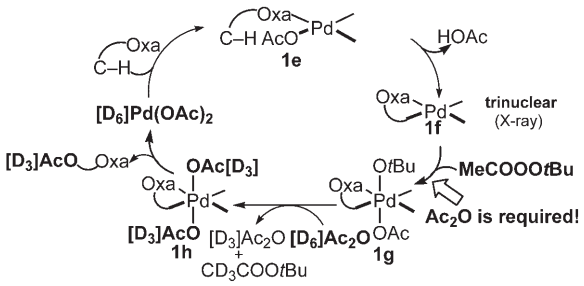

Scheme 4. Proposed catalytic cycle.

by ^1H NMR spectroscopy in the absence and presence of various amounts of Ac_2O (see the Supporting Information). The results showed that the rate was not affected by Ac_2O. The oxidative-addition step, however, was shown to require Ac_2O as no reaction of **1f** with MeCOOO*t*Bu was observed in CH_2Cl_2 at 50 °C. However, it is also possible that **1g** is in equilibrium with **1f**, largely in favor of the latter, and Ac_2O could scavenge $tBuO^-$ ions in **1g** to form **1h**, which undergoes reductive elimination.

We have also made a number of other observations that may be relevant to the mechanistic understanding of this catalytic reaction. The bridging acetate in complex **1f** undergoes rapid degenerate acetate exchange with $[D_6]Ac_2O$. The exchange process requires breaking of the μ-acetate bridge in the trinuclear complex **1f**, which could be related to the acceleration of the oxidative addition. The use of $[D_6]Ac_2O$ as a solvent also shows that the acetate or acetyl group from acetic anhydride, rather than from the oxidant, is incorporated predominantly into the product. The use of other anhydrides, such as propionic and isobutyric anhydrides, consistently affords the corresponding carboxylates [Eq. (2)].

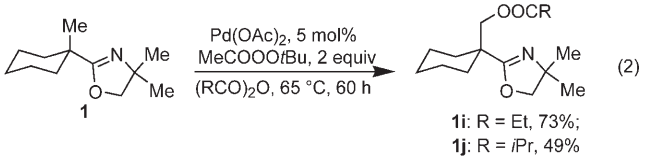

(2)

This result further suggests that the acetate ligand at the apical position of the octahedral Pd^{IV} complex **1g** also rapidly exchanges with carboxylic anhydrides to give **1i** or **1j** prior to reductive elimination. Interestingly, when PhCOOO*t*Bu is used as an oxidant, the ether product **1k** was formed predominantly [Eq. (3)], which could be explained by assuming that the $PhCOO^-$ ion is less labile than the $tBuO^-$ ion in the octahedral intermediate analogous to **1g**.

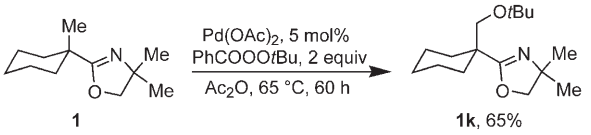

(3)

The use of lauroyl peroxide or benzoyl peroxide as the oxidant has led us to identify a second role for Ac_2O. The reaction of **1f** with both peroxides proceeds to give the acetoxylated products in the absence of Ac_2O. However, the presence of Ac_2O is essential for the catalytic turnover. Measurement of the reaction rate by GC using 20 mol% $Pd(OAc)_2$ shows that the reaction in the first 10% conversion is not influenced by the addition of Ac_2O, but does not proceed further after 15% conversion in the absence of Ac_2O. This result suggests that Ac_2O is crucial for the regeneration of the reactive $Pd(OAc)_2$, as shown in Scheme 4.

In summary, the inexpensive oxidant MeCOOO*t*Bu is shown to oxidize unactivated methyl groups in the presence of a catalytic amount of $Pd(OAc)_2$ under mild conditions. The diastereoselective oxidation of methyl groups is also achieved in moderate diastereoselective excess (*de*) by using lauroyl or benzoyl peroxide as the oxidant. Investigations into the reactivity of the characterized trinuclear Pd–alkyl complex indicated a crucial dual role for anhydrides in C–H bond oxidation. Further efforts are being directed towards the characterization of crystal structures of $C(sp^3)$–Pd complexes derived from prochiral substrates to explain the stereoselectivity shown.

Received: August 5, 2005
Published online: October 25, 2005

Keywords: asymmetric catalysis · C–H activation · oxidation · palladium · peroxides

[1] a) R. H. Crabtree, *J. Chem. Soc. Dalton Trans.* **2001**, 2437; b) "Activation and Functionalization of C–H Bonds": K. I. Goldberg, A. S. Goldman, *ACS Symp. Ser.* **2004**, *885*.
[2] For reviews on σ-chelation directed C–H activation reactions, see: a) F. Kakiuchi, S. Murai, *Acc. Chem. Res.* **2002**, *35*, 826; b) G. Dyker, *Angew. Chem.* **1999**, *111*, 1808; *Angew. Chem. Int. Ed.* **1999**, *38*, 1699.
[3] For oxidation of methyl groups using a stoichiometric amount of $Pd(OAc)_2$, see: a) K. Carr, J. K. Sutherland, *J. Chem. Soc. Chem. Commun.* **1984**, 1227; b) J. E. Baldwin, R. H. Jones, C. Najera, M. Yus, *Tetrahedron* **1985**, *41*, 699.
[4] B. D. Dangel, J. A. Johnson, D. Sames, *J. Am. Chem. Soc.* **2001**, *123*, 8149.
[5] For other C–H bond functionalization methods, see: a) J. T. Groves, P. Viski, *J. Am. Chem. Soc.* **1989**, *111*, 8537; b) R. Breslow, A. B. Brown, R. D. Mccullough, P. W. White, *J. Am. Chem. Soc.* **1989**, *111*, 4517; c) M. P. Doyle, A. B. Dyatkin, G. H. P. Roos, F. Canas, D. A. Pierson, A. V. Basten, *J. Am. Chem. Soc.* **1994**, *116*, 4507; d) C. G. Espino, P. M. Wehn, J.

 © 2005 Wiley-VCH Verlag GmbH & Co. KGaA, Weinheim

Chow, J. Du Bois, *J. Am. Chem. Soc.* **2001**, *123*, 6935; e) H. M. L. Davies, R. E. J. Beckwith, *Chem. Rev.* **2003**, *103*, 2861; f) P. Muller, C. Fruit, *Chem. Rev.* **2003**, *103*, 2905; g) A. G. Wong-Foy, G. Bhalla, X. Y. Liu, R. A. Periana, *J. Am. Chem. Soc.* **2003**, *125*, 14292; h) J. D. Lawrence, M. Takahashi, C. Bae, J. F. Hartwig, *J. Am. Chem. Soc.* **2004**, *126*, 15334; i) B. C. Bales, P. Brown, A. Dehestani, J. M. Mayer, *J. Am. Chem. Soc.* **2005**, *127*, 2832.

[6] R. Giri, X. Chen, J. Q. Yu, *Angew. Chem.* **2005**, *117*, 2150; *Angew. Chem. Int. Ed.* **2005**, *44*, 2112.

[7] For the synthetic application of the direct oxidation of unactivated methyl groups, see: a) E. J. Corey, W. R. Hertler, *J. Am. Chem. Soc.* **1958**, *80*, 2903; b) S. Lee, P. L. Fuchs, *J. Am. Chem. Soc.* **2002**, *124*, 13978.

[8] a) A. R. Dick, K. L. Hull, M. S. Sanford, *J. Am. Chem. Soc.* **2004**, *126*, 2300; b) L. V. Desai, K. L. Hull, M. S. Sanford, *J. Am. Chem. Soc.* **2004**, *126*, 9542.

[9] For the first X-ray crystal structure of a trinuclear $C(sp^2)$–Pd complex, see: A. Moyano, M. Rosol, R. M. Moreno, C. Lopez, M. A. Maestro, *Angew. Chem.* **2005**, *117*, 1899; *Angew. Chem. Int. Ed.* **2005**, *44*, 1865.

[10] The predominant formation of a dimeric complex by refluxing $Pd(OAc)_2$ and 2-*tert*-butyl-4,5-dihydro-4,4-dimethyloxazole in AcOH was previously reported; a mixture of *syn* and *anti* trinuclear Pd–alkyl species in a 2:3 ratio were also observed as minor products by ^{1}H NMR spectroscopy; see: G. Balavoine, J. C. Clinet, *J. Organomet. Chem.* **1990**, *390*, C84.

[11] P. L. Alsters, H. T. Teunissen, J. Boersma, A. L. Spek, G. V. Koten, *Organometallics* **1993**, *12*, 4691.

[12] The use of one equivalent of MeCOOO*t*Bu gives a similar yield over a prolonged time (72 h); the use of five equivalents of MeCOOO*t*Bu shortens the reaction time to 36 hours.

[13] The use of peroxyester carbonate *i*PrOCOOO*t*Bu also gives the acetoxylated products in similar yields (see the Supporting Information).

[14] For a Pd^{II}-catalyzed radical chain oxidation of methane, see: a) L. C. Kao, A. C. Hutson, A. Sen, *J. Am. Chem. Soc.* **1991**, *113*, 700; b) G. Ingrosso, N. Midollini, *J. Mol. Catal. A* **2003**, *204*, 425; for the activation of aryl C–H bonds, see: C. Jia, W. Lu, T. Kitamura, Y. Fujiwara, *Org. Lett.* **1999**, *1*, 2097.

[15] a) A. J. Canty, M. Denney, B. W. Skelton, A. H. White, *Organometallics* **2004**, *23*, 1122; b) A. Bayler, A. J. Canty, J. H. Ryan, B. W. Skelton, A. H. White, *Inorg. Chem. Commun.* **2000**, *3*, 575; c) for the first characterization of an organopalladium(IV) complex, $[PdIMe_3(bpy)]$ (bpy = 4,4′-bipyridine), see: P. K. Byers, A. J. Canty, B. W. Skelton, A. H. White, *J. Chem. Soc. Chem. Commun.* **1986**, 1722.

 © 2005 Wiley-VCH Verlag GmbH & Co. KGaA, Weinheim

Asymmetric Catalysis

DOI: 10.1002/anie.200503062

A Powerful Brønsted Acid Catalyst for the Organocatalytic Asymmetric Transfer Hydrogenation of Imines**

*Sebastian Hoffmann, Abdul Majeed Seayad, and Benjamin List**

The catalytic hydrogenation of alkenes, ketones, and imines is arguably one of the most important transformations in chemistry. Powerful asymmetric versions have been realized that require metal catalysts or the use of a stoichiometric amount of metal hydrides [Eq. (1)].[1]

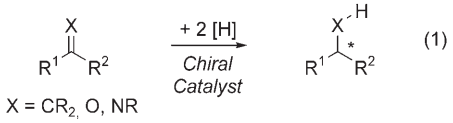

Although effective and industrially relevant catalytic asymmetric hydrogenations and transfer hydrogenations of olefins and ketones have been developed, the corresponding imine reductions, although potentially highly useful for the synthesis of enantiomerically pure amines, are less advanced.[2] Living organisms employ organic dihydropyridine cofactors such as nicotinamide adenine dinucleotide (NADH) in combination with enzyme catalysts for the reduction of imines.[3] Chemical transition metal catalyzed asymmetric imine reductions have also been developed,[4] and are used, in at least one case, on an industrial scale.[5] However, with the exception of interesting Lewis base catalyzed asymmetric imine hydrosilylations,[6] organocatalytic and metal-free variants were not known. Recently, we and MacMillan and co-workers developed an asymmetric transfer hydrogenation of α,β-unsaturated aldehydes catalyzed by a chiral ammonium salt by using Hantzsch esters as a biomimetic hydrogen source.[7] Rueping et al.[8] very recently reported the development of a novel and elegant approach using Hantzsch esters as the reducing reagent for the catalytic asymmetric reduction of imines using a chiral Brønsted acid catalyst previously developed by Akiyama et al.[9,10] We now report parallel and independent studies from our laboratory

[*] Dipl.-Chem. S. Hoffmann, Dr. A. M. Seayad, Prof. Dr. B. List
Max-Planck-Institut für Kohlenforschung
Kaiser-Wilhelm-Platz 1, 45470 Mülheim an der Ruhr (Germany)
Fax: (+49) 208-306-2999
E-mail: list@mpi-muelheim.mpg.de

[**] Generous support by the DFG (Priority Program 1179, *Organocatalysis*) is gratefully acknowledged. We thank Jayasree Seayad and Sonja Mayer for catalyst preparations.

Supporting information for this article is available on the WWW under http://www.angewandte.org or from the author.

WILEY InterScience DISCOVER SOMETHING GREAT
© 2005 Wiley-VCH Verlag GmbH & Co. KGaA, Weinheim

on the same reaction that resulted in the development of a significantly improved new catalyst for the highly efficient and enantioselective transfer hydrogenation of ketimines catalyzed by Brønsted acids.[11]

In pioneering studies, the research groups of Akiyama[10] and Terada[11] recently introduced relatively strong chiral phosphoric acid catalysts for asymmetric addition reactions to aldimines as a new strategy for organic catalysis.[12,13] Inspired by these studies, and the recent observation that imines are reduced with Hantzsch esters in the presence of achiral Lewis or Brønsted acid catalysts,[14] we envisioned a catalytic cycle which is initiated by protonation of ketimine **1** from a chiral Brønsted acid catalyst **2** [Eq. (2)]. The resulting iminium ion pair, which may be stabilized by hydrogen bonding, is chiral and its reaction with the Hantzsch dihydropyridine **3** could give an enantiomerically enriched amine **4** and pyridine **5**.

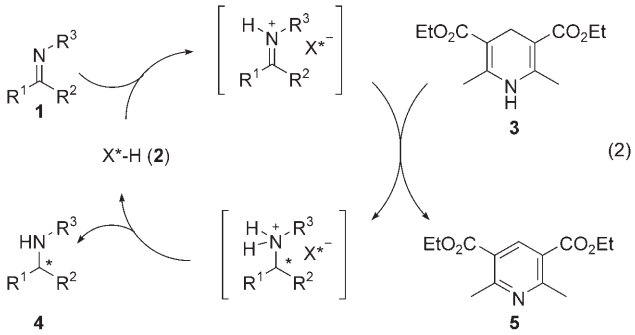

(2)

With this idea in mind, we synthesized and screened a variety of chiral phosphoric acid catalysts for the reduction of imine **1a** in the presence of Hantzsch ester **3** [Eq. (3), Table 1].[15]

Although the commercially available phosphoric acid **2a** clearly showed turnover, the enantioselectivity was low (entry 1). Increasing the steric bulk of the catalyst by adding aromatic substituents at the 3,3′-positions of the binaphthol core significantly increased the enatioselectivity but generally reduced the turnover (entries 2–9). The highest *ee* value (81%) was achieved with the new sterically congested phosphoric acid catalyst **2i**. Although the yield of **4a** was low (10% after 20 h), the only remaining material was the starting imine **1a**.

After further optimization of the reaction, which included changing the solvent from dichloromethane to toluene, increasing the temperature from RT to 35°C, and lowering the catalyst loading from 10 mol% to only 1 mol%, the *ee* value of the product **4a** could be further improved to 88% and with an excellent yield of 96% [Table 2, entry 1]. These conditions have been applied to several substituted aromatic ketimines **1a–j** and one aliphatic imine **1k** with good to excellent results [Eq. (4), Table 2].

Remarkably high yields were achieved in all cases, while the *ee* values were generally very good (80–93%). The highest yield was achieved with *p*-methyl-substituted imine **1f**, which provided amine **4f** in 98% yield (entry 6). *o*-Methyl-substituted imine **1h** gave the highest enantioselectivity and furnished amine **4h** with 93% *ee* (entry 8). Functional

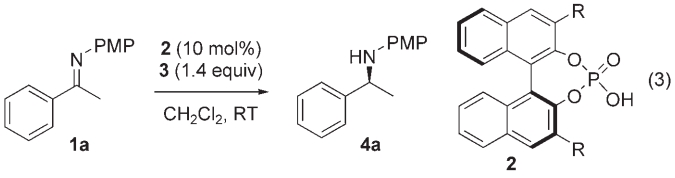

(3)

Table 1: Catalyst screening for the asymmetric transfer hydrogenation of imine **1a**.

Entry	R		Conversion [%] (*t*)	*ee* [%]
1	H	**2a**	58 (6 h)	6
2		**2b**	59 (17 h)	40
3	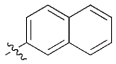	**2c**	34 (17 h)	44
4	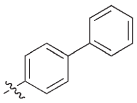	**2d**	80 (17 h)	51
5	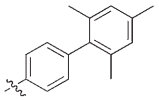	**2e**	10 (20 h)	32
6	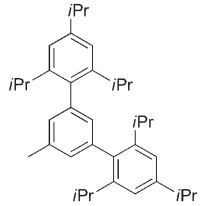	**2f**	7 (20 h)	30
7		**2g**	28 (17 h)	65
8		**2h**	4 (22 h)	n.d.[a]
9	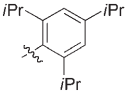	**2i**	10 (20 h)	81

[a] n.d. = not determined.

groups (-NO_2, -F, -CN, -OMe) are tolerated well, although the full scope of the reaction has yet to be established. Remarkably, even an aliphatic imine (**1k**) could be used to give amine **4k** with high enantioselectivity (90% *ee*).

A similar study by Rueping's research group using Akiyama's phosphoric acid catalyst appeared during the preparation of this manuscript.[8,10b] However, our reaction times are generally shorter (42–71 h versus 72 h), our temperature is lower (35°C versus 60°C), our yields (80–98% versus 46–91%) and *ee* values (80–93% versus 68–84%) are higher, and most importantly our catalyst loading is much lower (1 mol% versus 20 mol%). Moreover, we can also reduce aliphatic ketimines highly enantioselectively while Rueping et al. only provided aromatic examples.

Imine generation and its reduction can also be performed in situ in the presence of molecular sieves. The *ee*-conserving

 © 2005 Wiley-VCH Verlag GmbH & Co. KGaA, Weinheim

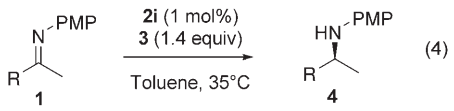

(4)

Table 2: Preliminary substrate scope of the asymmetric transfer hydrogenation of imines.

Entry	R		*t* [h]	Yield [%]	*ee* [%]
1		**a**	45	96	88
2	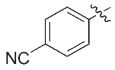	**b**	42	87	80
3	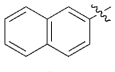	**c**	42	85	84
4		**d**	45	95	85
5	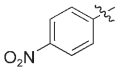	**e**	42	96	80
6		**f**	42	98	88
7	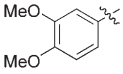	**g**	45	84	89
8		**h**	71	91	93
9		**i**	45	92	80
10		**j**	71	88	92
11		**k**	60	80	90

oxidative removal of the *p*-methoxyphenyl (PMP) group to give amine **6a** is well established [Eq. (5); CAN = cerium(IV) ammonium nitrate].[4i]

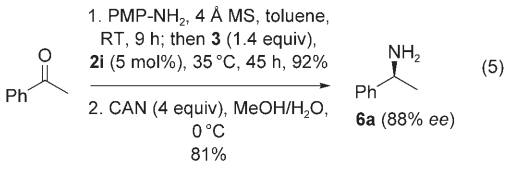

(5)

In summary we have developed an efficient organocatalytic asymmetric ketimine reduction using chiral phosphoric acid derivative **2i** in the presence of the commercially available Hantzsch ester **3**. Remarkable features of our process include a) its high yields and enantioselectivities, b) its scope, including both aliphatic and aromatic amines, c) its simplicity and practicability (in situ generation and reduction of imines), and d) the remarkably low catalyst loading, which so far is unprecedented in asymmetric Brønsted acid catalysis. Further extension of this methodology is ongoing and will be reported shortly.

Experimental Section

General procedure for the asymmetric transfer hydrogenation reaction**:** A mixture of imine **1** (0.4 mmol), Hantzsch ester **3** (142 mg, 0.56 mmol, 1.4 equiv), and phosphoric acid **2i** (3 mg, 0.004 mmol) in toluene (4 mL) was stirred at 35 °C in an argon atmosphere for 42–71 h. The solvent was evaporated at reduced pressure and the products were isolated by flash chromatography (SiO_2, ethyl acetate/hexane) to give pure amines **4**. The *ee* values were determined by using established HPLC techniques with chiral stationary phases.

Received: August 28, 2005
Revised: October 4, 2005
Published online: October 21, 2005

Keywords: asymmetric catalysis · chiral amines · rhomogeneous catalysis · hydrogenation · imines

[1] a) R. Noyori, *Angew. Chem.* **2002**, *114*, 2108–2123; *Angew. Chem. Int. Ed.* **2002**, *41*, 2008–2022; b) W. S. Knowles, *Angew. Chem.* **2002**, *114*, 2096–2107; *Angew. Chem. Int. Ed.* **2002**, *41*, 1998–2007.

[2] For reviews, see: a) V. I. Taratov, A. Börner, *Synlett* **2005**, 203–211; b) T. Ohkuma, M. Kitamura, R. Noyori in *Catalytic Asymmetric Synthesis*, 2nd ed. (Ed.: I. Ojima), Wiley-VCH, New York, **2000**, chap. 1; c) T. Ohkuma, R. Noyori in *Comprehensive Asymmetric Catalysis*, *Suppl. 1* (Eds.: E. N. Jacobsen, A. Pfaltz, H. Yamamoto), Springer, New York, **2004**, p. 43; d) H. Nishiyama, K. Itoh in *Catalytic Asymmetric Synthesis*, 2nd ed. (Ed.: I. Ojima), Wiley-VCH, New York, **2000**, chap. 2.

[3] a) B. D. Sanwal, M. W. Zink, *Arch. Biochem. Biophys.* **1961**, *94*, 430–435; b) M.-R. Kula, C. Wandrey, *Methods Enzymol.* **1988**, *136*, 34–45.

[4] For examples, see: a) N. Langlois, T. P. Dang, H. B. Kagan, *Tetrahedron Lett.* **1973**, 4865; b) R. Becker, H. Brunner, S. Mahboobi, W. Wiegrebe, *Angew. Chem.* **1985**, *97*, 969–970; *Angew. Chem. Int. Ed. Engl.* **1985**, *24*, 995–996; c) X. Verdaguer, U. E. W. Lange, M. T. Reding, S. L. Buchwald *J. Am. Chem. Soc.* **1996**, *118*, 6784; d) X. Verdaguer, U. E. W. Lange, S. L. Buchwald, *Angew. Chem.* **1998**, *110*, 1174–1178; *Angew. Chem. Int. Ed.* **1998**, *37*, 1103–1107; e) Y. Nishibayshi, I. Takei, S. Uemura, M. Hidai, *Organometallics* **1998**, *17*, 3420; f) M. C. Hansen, S. L. Buchwald, *Org. Lett.* **2000**, *2*, 713; g) D. Xiao, X. Zhang, *Angew. Chem.* **2001**, *113*, 3533–3536; *Angew. Chem. Int. Ed.* **2001**, *40*, 3425–3428; h) J. F. Carpentier, V. Bette, *Curr. Org. Chem.* **2002**, *6*, 913; i) Y. Chi, Y.-G. Zhou, X. Zhang *J. Org. Chem.* **2003**, *68*, 4120–4122; j) R. Kadyrov, T. H. Riermeier, *Angew. Chem.* **2003**, *115*, 5630–5632; *Angew. Chem. Int. Ed.* **2003**, *42*, 5472–5474; k) B. H. Lipshutz, H. Shimizu, *Angew. Chem.* **2004**, *116*, 2278–2280; *Angew. Chem. Int. Ed.* **2004**, *43*, 2228–2230; l) O. Riant, N. Mostefai, J. Courmarcel, *Synthesis* **2004**, 2943–2958; m) K. A. Nolin, R. W. Ahn, F. D. Toste, *J. Am. Chem. Soc.* **2005**, ASAP.

[5] a) H.-U. Blaser, H.-P. Buser, H.-P. Jalett, B. Pugin, F. Spindler, *Synlett* **1999**, 867–868; b) H.-U. Blaser, H.-P. Buser, K. Coers, R. Hanreich, H.-P. Jalett, E. Jelsch, B. Pugin, H. D. Schneider, F. Spindler, A. Wegmann, *Chimia* **1999**, *53*, 275–280; c) H.-U. Blaser, C. Malan, B. Pugin, F. Spindler, H. Steiner, M. Studer, *Adv. Synth. Catal.* **2003**, *345*, 103–151.

[6] a) A. V. Malkov, A. Mariani, K. N. MacDougall, P. Kocovsky, *Org. Lett.* **2004**, *6*, 2253–2256; b) F. Iwasaki, O. Omonura, K.

 © 2005 Wiley-VCH Verlag GmbH & Co. KGaA, Weinheim

Mishima, T. Kanematsu, T. Maki, Y. Matsumura, *Tetrahedron Lett.* **2001**, *42*, 2525 – 2527.
[7] a) J. W. Yang, M. T. Hechavarria Fonseca, B. List, *Angew. Chem.* **2004**, *116*, 6829 – 6832; *Angew. Chem. Int. Ed.* **2004**, *43*, 6660 – 6662; b) J. W. Yang, M. T. Hechavarria Fonseca, N. Vignola, B. List, *Angew. Chem.* **2005**, *117*, 110 – 112; *Angew. Chem. Int. Ed.* **2005**, *44*, 108 – 110; for an independent study on the same reaction, see: c) S. G. Ouellet, J. B. Tuttle, D. W. C. MacMillan, *J. Am. Chem. Soc.* **2005**, *127*, 32 – 33.
[8] a) M. Rueping, E. Sugiono, C. Azap, T. Theissmann, M. Bolte, *Org. Lett.* **2005**, *7*, 3781 – 3783; this research group also reported an effective non-asymmetric variant: b) M. Rueping, C. Azap, E. Sugiono, T. Theissmann, *Synlett* **2005**, asap.
[9] We made the first proposal of reducing imines with Hantzsch esters in the presence of a chiral Brønsted acid catalyst at a DFG proposal workshop in Bonn, Germany on December 6th 2004.
[10] Mannich reaction: a) T. Akiyama, J. Itoh, K. Yokota, K. Fuchibe, *Angew. Chem.* **2004**, *116*, 1592 – 1594; *Angew. Chem. Int. Ed.* **2004**, *43*, 1566 – 1568; imine hydrophosphonylation: b) T. Akiyama, H. Morita, J. Itoh, K. Fuchibe, *Org. Lett.* **2005**, *7*, 2583 – 2585; see also: T. Akiyama, PCT Int. Appl. WO 200409675, **2004**.
[11] Mannich reaction: a) D. Uraguchi, M. Terada, *J. Am. Chem. Soc.* **2004**, *126*, 5356 – 5357; furan aminoalkylation: b) D. Uraguchi, K. Sorimachi, M. Terada, *J. Am. Chem. Soc.* **2004**, *126*, 11804 – 11805; alkylation of α-diazo esters: c) D. Uraguchi, K. Sorimachi, M. Terada, *J. Am. Chem. Soc.* **2005**, *127*, 9360 – 9361; see also: d) M. Terada, D. Uraguchi, K. Sorimachi, H. Shimizu, PCT Int. Appl. WO 2005070875, **2005**.
[12] For excellent reviews on Brønsted acid organocatalysis, see: a) P. M. Pihko, *Angew. Chem.* **2004**, *116*, 2110 – 2113; *Angew. Chem. Int. Ed.* **2004**, *43*, 2062 – 2064; b) P. Schreiner, *Chem. Soc. Rev.* **2003**, *32*, 289 – 296; see also: J. Seayad, B. List, *Org. Biomol. Chem.* **2005**, *3*, 719 – 724.
[13] For selected recent examples of asymmetric general Brønsted acid organocatalysis, see: a) M. S. Sigman, P. Vachal, E. N. Jacobsen, *Angew. Chem.* **2000**, *112*, 1336 – 1338; *Angew. Chem. Int. Ed.* **2000**, *39*, 1279 – 1281; b) T. Okino, Y. Hoashi, Y. Takemoto, *J. Am. Chem. Soc.* **2003**, *125*, 12672 – 12673; c) B. M. Nugent, R. A. Yoder, J. N. Johnston, *J. Am. Chem. Soc.* **2004**, *126*, 3418 – 3419; d) Y. Huang, A. K. Unni, A. N. Thadani, V. H. Rawal, *Nature* **2003**, *424*, 146; e) N. T. McDougal, S. E. Schaus, *J. Am. Chem. Soc.* **2003**, *125*, 12094 – 12095; f) T. Schuster, M. Bauch, G. Duerner, M. W. Goebel, *Org. Lett.* **2000**, *2*, 179 – 181.
[14] T. Itoh, K. Nagata, M. Miyazaki, H. Ishikawa, A. Kurihara, A. Ohsawa, *Tetrahedron* **2004**, *60*, 6649 – 6655.
[15] Phosphoric acids **2** were prepared according or in analogy to the reported procedures; see references [10, 11].

 © 2005 Wiley-VCH Verlag GmbH & Co. KGaA, Weinheim

Bioelectrochemistry

DOI: 10.1002/anie.200502995

Preparation of a Magnetically Switchable Bioelectrocatalytic System Employing Cross-linked Enzyme Aggregates in Magnetic Mesocellular Carbon Foam**

Jinwoo Lee, Dohoon Lee, Eunkeu Oh, Jaeyun Kim, Young-Pil Kim, Sunmi Jin, Hak-Sung Kim, Yosun Hwang, Ja Hun Kwak, Je-Geun Park, Chae-Ho Shin, Jungbae Kim,* and Taeghwan Hyeon**

Nanostructured magnetic materials (NMMs)[1] have attracted much attention recently because of their broad biotechnological applications including support matrices for enzyme immobilization,[2] immunoassays,[3] drug delivery,[4] and biosensors.[5] Specifically, the easy separation and controlled placement of NMMs by means of an external magnetic field

[*] D. Lee,[+] E. Oh, Y.-P. Kim, Prof. H.-S. Kim
Department of Biological Sciences
Korea Advanced Institute of Science and Technology
373-1, Kusong-dong, Yusong-gu, Taejon 305-701 (Korea)
Fax: (+82) 42-869-2610
E-mail: hskim76@kaist.ac.kr

Dr. J. H. Kwak, Dr. J. Kim
Pacific Northwest National Laboratory
902 Battelle Boulevard, P.O. Box 999, Richland, WA 99352 (USA)
Fax: (+1) 509-376-5106
E-mail: Jungbae.Kim@pnl.gov

Dr. J. Lee,[+] J. Kim, S. Jin, Prof. T. Hyeon
National Creative Research Initiative Center for
Oxide Nanocrystalline Materials and
School of Chemical and Biological Engineering
Seoul National University
Seoul 151-744 (Korea)
Fax: (+82) 2-888-1604
E-mail: thyeon@plaza.snu.ac.kr

Y. Hwang, Prof. J.-G. Park
Department of Physics
Sungkyunkwan University
Suwon 440-746 (Korea)

Prof. Dr. C.-H. Shin
Department of Chemical Engineering
Chungbuk National University
Cheongju, Chungbuk 360-763 (Korea)

[+] These authors contributed equally to this work.

[**] T.H. thanks the Korean Ministry of Science and Technology for financial support through the National Creative Research Initiative Program. H.K. thanks the Nano Measurement Technology Project of the Ministry of Science and Technology and the BK21 Program of the Ministry of Education for financial support. J.K. thanks the US Department of Energy (DOE) LDRD for funds administered by the Pacific Northwest National Laboratory, the DOE Office of Biological and Environmental Research under the Environmental Management Science Program, and the Microsystems Technology Office of the US.

Supporting information for this article is available on the WWW under http://www.angewandte.org or from the author.

© 2005 Wiley-VCH Verlag GmbH & Co. KGaA, Weinheim

enables their application in the development of immobilized enzyme processes[2] and the construction of magnetically controllable bio-electrocatalytic systems.[5,6] Herein, we demonstrate the use of immobilized enzymes in NMMs for magnetically switchable bio-electrocatalysis.

Magnetic mesoporous carbons, in which magnetic nanoparticles (MNPs) are incorporated into the mesoporous carbon matrix, have many desirable characteristics for preparation of immobilized enzymes for magneto-bio-electrocatalysis: large pore size and volume, the ability to be positioned with a magnet, and good electron conductivity. Herein, we synthesized magnetic mesocellular carbon foam by a simplified approach based on the in situ generation of MNPs during the synthesis of the mesocellular carbon. The resulting material, designated Mag-MCF-C, was found to possess large interconnected pores and well-dispersed MNPs. Glucose oxidase (GOx) was immobilized within the large cellular pores of Mag-MCF-C, and the resulting material was used for the construction of a magnetically switchable bio-electrocatalytic system.

The operating principle of magnetically switchable bio-electrocatalysis is illustrated in Figure 1a.[6a] When the enzymes in the Mag-MCF-C particles in a solution containing substrate (glucose) were brought into contact with the electrode by means of a magnet placed below the electrode, an anodic current was generated by electron transport from the enzyme reaction to the working electrode (switched "on"). Conversely, when positioned above the electrochemical cell, the magnet attracted the Mag-MCF-C particles away from the electrode, and the electron-transfer efficiency was significantly lowered, and the current decreased to the background level (switched "off"). By alternate positioning of an external magnet, the bio-electrocatalytic signal could be reversibly switched back and forth between the on and off states.

Various nanoporous carbon materials have been prepared using nanostructured silica materials[7] as sacrificial templates.[8] The typical synthetic procedure for Mag-MCF-C is based on a template approach and is presented schematically in Figure 2a. MCF silica[9] was used as a template, and its surface area and pore volume were estimated by the BET method to be 574 $m^2 g^{-1}$ and 1.86 $cm^3 g^{-1}$, respectively. The cellular and window (percolation-path) pore sizes determined from the adsorption and desorption branch were 24.0 and 12.3 nm, respectively (see Supporting Information). After the polymerization of divinylbenzene (DVB), the main cellular pores of the MCF silica were partially filled by a poly(DVB) coating.[10] The BET surface area of the MCF/poly(DVB) composite was reduced to 138 $m^2 g^{-1}$, which indicates that complementary micropores in the walls of the MCF silica were filled with poly(DVB).[11] Also, the decreased cell size of 19.1 nm (see Supporting Information) indicates that poly(DVB) coatings of approximately 2.5 nm thickness were formed in the main cells of the MCF silica. The next step was impregnation of $Fe(NO_3)_3 \cdot 9H_2O$ dissolved in ethanol into the pores of the MCF/poly(DVB) composite. The Fe^{3+} ions present on the poly(DVB) surface were converted into magnetic nanoparticles during the carbonization at 800 °C. Finally, the dissolution of the MCF template in 1 M NaOH at

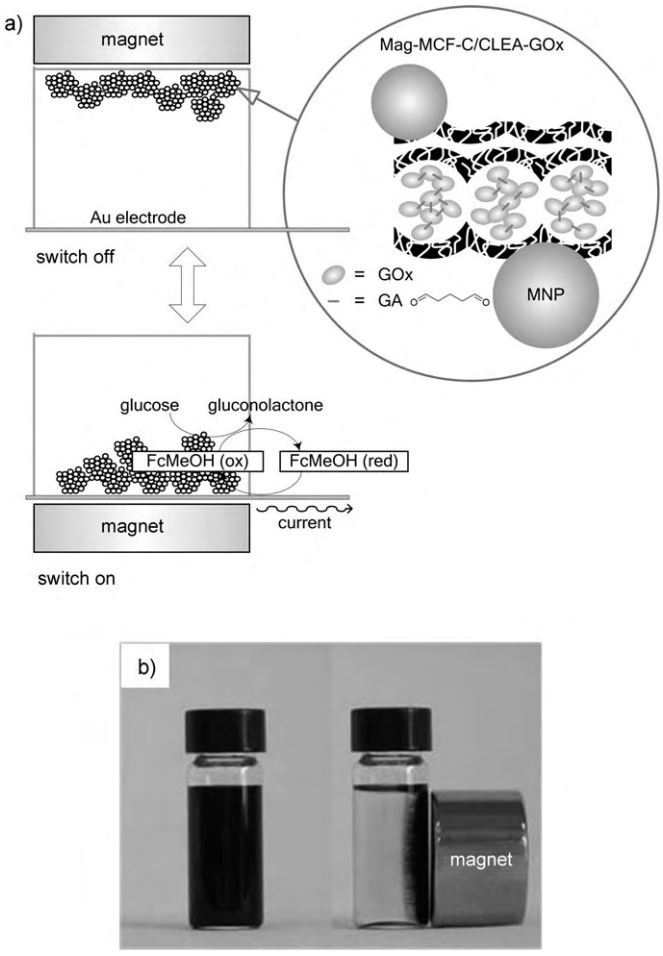

Figure 1. a) Working principle of the magnetically switchable bio-electrocatalytic oxidation of glucose by GOx immobilized in Mag-MCF-C. b) The separation of Mag-MCF-C/CELA-GOx particles by an applied magnetic field. The image shows a well-mixed suspension of Mag-MCF-C/CLEA-GOx in 0.1 M sodium phosphate buffer (ca. 10 mg mL^{-1}) before (left) and after (right) the application of a magnetic field.

100 °C yielded the magnetic mesocellular carbon foam Mag-MCF-C. The simplification of the synthetic procedure for Mag-MCF-C was attributed to the solid-state conversion of the impregnated iron salt into MNPs during the carbonization.[12] This method is in contrast with the recently reported multistep synthetic route to magnetic CMK-3 requiring separate steps for synthesis and postsynthetic deposition of the MNPs onto the carbon, and an additional carbonization step to cap the MNPs to prevent leaching.[13]

The field-emission scanning electron microscopy (SEM) image showed that the Mag-MCF-C particles had many large mesopores (see Figure 2b) open to the exterior, which was favorable for the quick incorporation of large biomolecules. The cellular mesopores were also observed in the transmission electron microscopy (TEM) image of Mag-MCF-C (Figure 2c). The cell sizes estimated from the adsorption branch of the argon isotherm were centered at 16.6 nm (Figure 3c). The window (percolation-path) sizes determined from the desorption branch were centered at 10.1 nm. The BET surface area and the single-point total pore volume were

 © 2005 Wiley-VCH Verlag GmbH & Co. KGaA, Weinheim

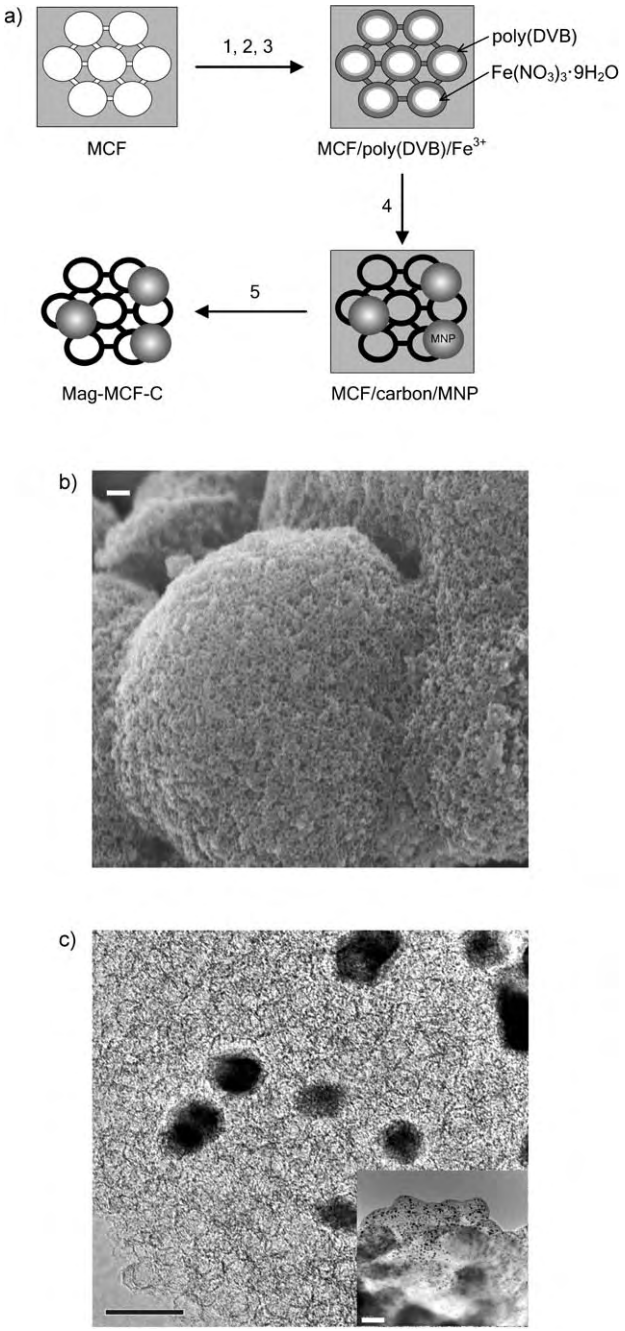

Figure 2. a) Schematic representation of the synthetic procedure for Mag-MCF-C: impregnation of DVB/AIBN (1); polymerization(2); impregnation of $Fe(NO_3)_3 \cdot 9H_2O$ (3); carbonization (4); removal of silica template (5). b) SEM image of Mag-MCF-C (scale bar: 200 nm). c) TEM image of Mag-MCF-C (scale bar: 50 nm); inset: low-magnification TEM image of Mag-MCF-C (scale bar: 500 nm). AIBN = azobisisobutyronitrile.

revealed to be 865 $m^2 g^{-1}$ and 1.43 $cm^3 g^{-1}$, respectively. The MNPs formed in situ were found to be well dispersed over the Mag-MCF-C surface (see inset of Figure 2c). The TEM (Figure 2c) and SEM images at high magnification (Supporting Information) showed clearly that the magnetic nanoparticles were formed on the external surface of the MCF-C. The iron content of the Mag-MCF-C measured by inductively coupled plasma atomic-emission spectroscopy (ICP-AES) was 26.9 wt%. The X-ray diffraction (XRD) pattern of Mag-MCF-C showed that body-centered-cubic (bcc) iron (α-Fe) nanoparticles with an average diameter of 30 nm, estimated by using the Debye–Scherer equation, were well dispersed in the mesocellular carbon foam matrix (see Supporting Information). The XRD pattern also showed small peaks attributable to magnetite, which demonstrates that the iron was partially oxidized during the NaOH etching process. Further characterization by means of TEM, convergent-beam electron diffraction (CBED), and energy-dispersive X-ray spectroscopy (EDX) showed that the nanoparticles had an Fe/Fe_3O_4 core/shell structure. The formation of large, 30-nm sized particles, which are larger than the cell diameter of MCF-C, seems to be due to sintering of the initially synthesized small nanoparticles on the surface of the mesocellular carbon foam during the carbonization at high temperature.

The magnetization curves (see Supporting Information) exhibited hysteresis over the complete temperature range of the measurements from 325 K down to 2 K, which demonstrates the ferromagnetic character of Mag-MCF-C at room temperature. The zero-field cooled and field-cooled magnetization data measured in an applied field of 100 Oe also revealed that Mag-MCF-C is ferromagnetic at room temperature (Supporting Information). This ferromagnetic property, derived from the large size of the magnetic nanoparticles, turned out to be very important to the facile and fast migration of the nanoparticles to a desired position by means of an external magnetic field (see below). The saturation magnetization value was 8.5 emu g^{-1} at 300 K, which was sufficient for magnetic separation. Furthermore, the remnant magnetization was low (< 1 emu g^{-1}), which was important for the easy redispersion of the Mag-MCF-C particles when the magnet was removed.

To demonstrate the utility of Mag-MCF-C in the construction of a magnetically switchable bio-electrocatalytic system, glucose oxidase (GOx), which is a well-studied redox enzyme, was immobilized within the Mag-MCF-C particles. A schematic representation of Mag-MCF-C with immobilized and cross-linked GOx in the large mesocellular pores is presented in Figure 3a. From the molecular dimensions of GOx ($6.0 \times 5.2 \times 7.7$ nm^3),[14] it was expected that the enzyme molecules would easily enter the large cellular pores (16.6 nm) of Mag-MCF-C through the connecting windows (10.1 nm). In fact, the amount of argon adsorbed in Mag-MCF-C was found to be significantly decreased after loading with GOx (Figure 3b), which indicates that most of the GOx molecules were incorporated into the pores of Mag-MCF-C, especially into its large cellular pores (Figure 3c). The adsorption isotherm of GOx-immobilized Mag-MCF-C (see Supporting Information) shows a maximum loading of about 53% (w/w carbon). Equilibrium was reached after a 5 h incubation period (see Supporting Information). Notably, the isotherm obtained did not conform to the Langmuir-type with an almost-linear increase in loading with initial increase in enzyme concentration. The results suggest that the immobilization mechanism involves the entrapment of enzymes in the mesocellular pores of the Mag-MCF-C particles rather

 © 2005 Wiley-VCH Verlag GmbH & Co. KGaA, Weinheim

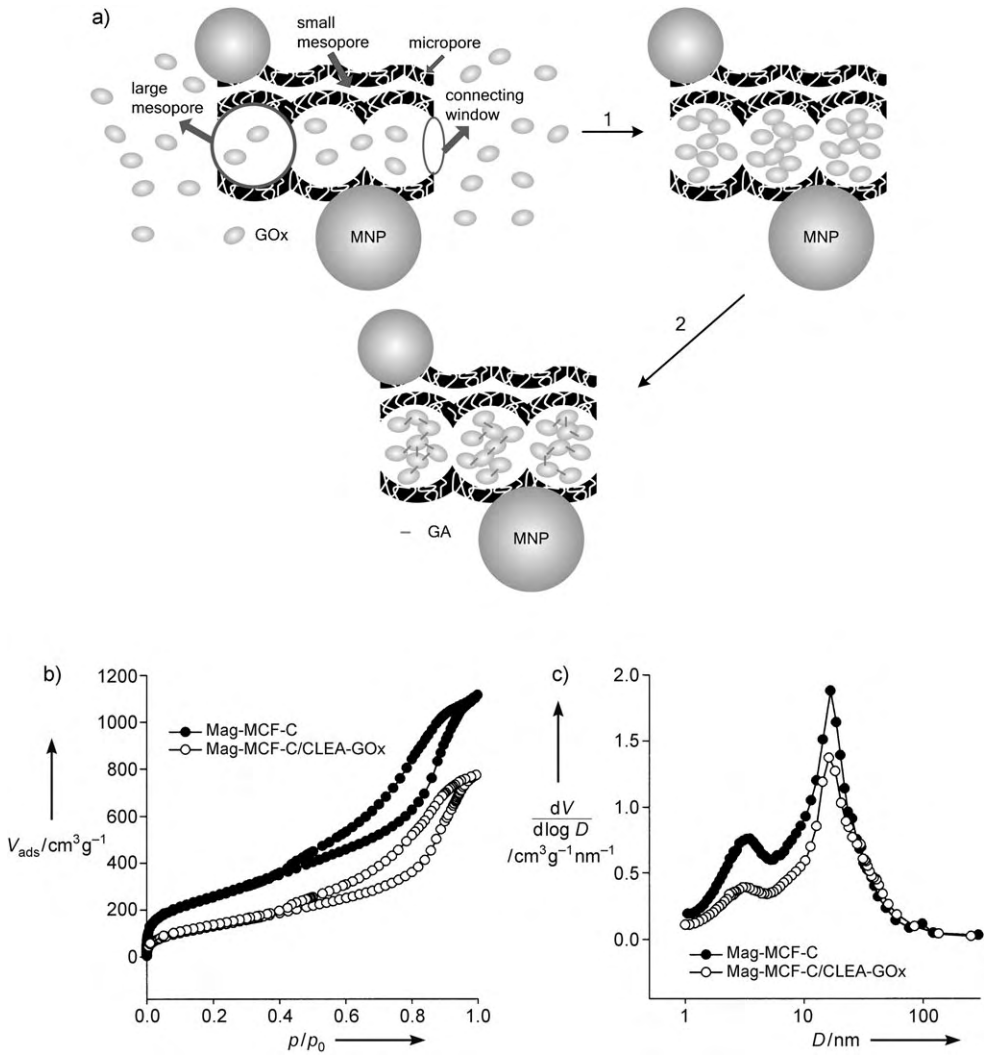

Figure 3. a) Schematic representation of Mag-MCF-C with immobilized and cross-linked GOx in large mesocellular pores. Also depicted are the incorporated MNPs and the small pores: adsorption of GOx in the mesocellular pores of Mag-MCF-C (1); cross-linking of GOx using glutaraldehyde to make enzyme aggregates (2). b) Argon-adsorption-desorption isotherms and c) pore-size distributions (PSDs) of Mag-MCF-C and Mag-MCF-C/CLEA-GOx. The PSDs were calculated from Ar adsorption data by using the Barrett–Joyner–Halenda (BJH) method. The amount of adsorbed argon was significantly reduced after loading of GOx.

than the adsorption of enzymes on the carbon surface. It was observed that the migration of the GOx-immobilized Mag-MCF-C (Mag-MCF-C/GOx) under the same strength of external magnetic field slowed down somewhat as the GOx loading increased. Consequently, Mag-MCF-C/GOx with a GOx loading of approximately 30% was used in this study to take into account the migration of Mag-MCF-C/GOx by a magnet.

The enzymes in the pores were stabilized through cross-linking with glutaraldehyde (GA).[15] As Mag-MCF-C consisted of 17-nm mesocellular pores connected with 10-nm window pores, we anticipated that the smaller size of the window pores would prevent the leaching of the cross-linked enzyme aggregates (CLEAs) and result in high enzyme loading and good enzyme retention (see Figure 3a).[15] As a result of the cross-linking, Mag-MCF-C/CLEA-GOx maintained more than 90% of its initial activity after 12 washings as well as after continuous incubation with vigorous shaking for 22 days, whereas only approximately 50% activity was retained for GOx immobilized in Mag-MCF-C without cross-linking after shaking for 22 days (see Supporting Information for experimental details). This observation suggests that the cross-linking of the enzyme was effective in improving its operational stability by preventing leaching of the enzyme from the Mag-MCF-C composite. On the basis of these results, cross-linked Mag-MCF-C/CLEA-GOx was used for the following experiments.

The specific activity of CLEA-GOx within Mag-MCF-C (45.8 ± 7.5 U per mg GOx) was estimated to be 29% of that of free GOx in buffer (155.5 ± 12.5 U per mg GOx). This 29% recovery of activity was quite impressive when the high concentration of GOx in the pores (384 mg mL^{-1}, see Supporting Information for the detailed calculation) and possible enzyme inactivation during cross-linking by GA is considered.

It was expected that the unique pore structure of the host Mag-MCF-C could relieve the mass-transport resistance: MCF-C had a variety of pore interconnections that facilitated the transport of substrate and products as shown schematically in Figure 3a. The small mesopores (diameters around 3.0 nm), which were generated by dissolution of the silica template, were too small to accommodate GOx but large enough to accommodate small molecules such as the substrate and products and thus provide "substrate transport channels". Micropores with an average diameter of around 0.7 nm (see Supporting Information) present throughout the carbon framework[16] might also provide a route for the transport of small molecules by connecting the small and the large mesopores.

Suspended Mag-MCF-C/CLEA-GOx particles were quickly attracted in the direction from which the external magnetic field was applied (see Figure 1b), which confirmed the utility of Mag-MCF-C in magnetically controllable sensing systems such as the one presented in Figure 1a. The heavily loaded, active, and stable Mag-MCF-C/CLEA-GOx composite was used for magnetically switchable bio-electrocatalysis (see Figure 1a). Figure 4a shows cyclic voltammograms obtained when the magnet was placed in the "up"

 © 2005 Wiley-VCH Verlag GmbH & Co. KGaA, Weinheim

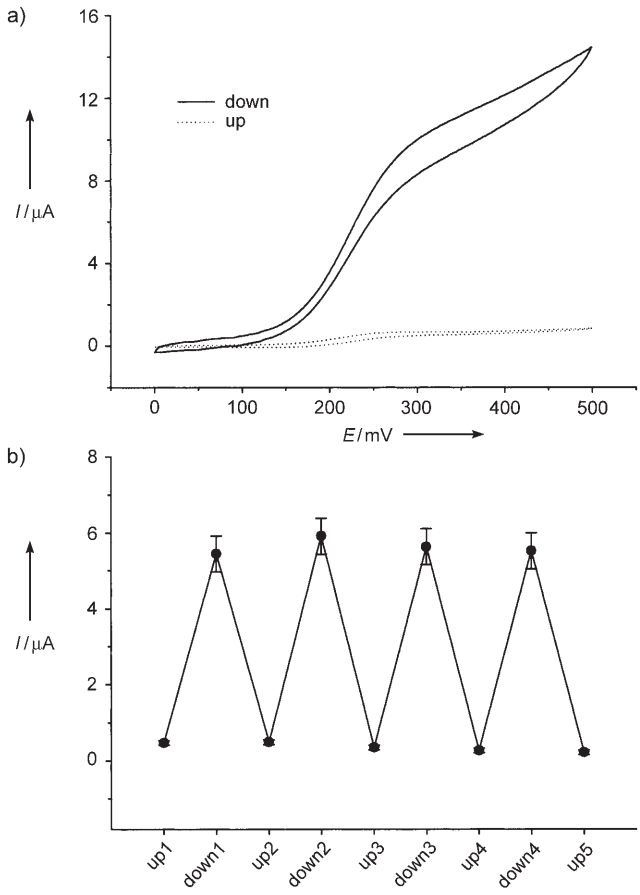

Figure 4. a) Cyclic voltammograms measured with the magnet in the "down" (Mag-MCF-C/CLEA-GOx near the electrode surface) and "up" (Mag-MCF-C/CLEA-GOx away from the electrode surface) positions. The voltammetry was performed in an electrochemical cell (4 mL) containing deoxygenated 0.1 M sodium phosphate buffer (pH 7.4) with 0.1 mM ferrocenemethanol and 5 mg of Mag-MCF-C/CLEA-GOx in the presence of 20 mM glucose. All the measurements were performed at room temperature with a scan rate of 5 $mV s^{-1}$. b) Current switching during the shuttling of the magnet between the "up" and "down" positions. The experimental conditions were the same as those described in (a).

(above the electrochemical cell) and "down" (below the electrode) positions, respectively, in the presence of 20 mM glucose. As expected, a significant increase in anodic current was observed when the Mag-MCF-C/CLEA-GOx particles were brought into contact with the electrode by a magnetic field. No such current was observed after the Mag-MCF-C/CLEA-GOx particles were pulled up by the magnet, even in the presence of glucose.

To check the reusability of Mag-MCF-C/CLEA-GOx and the reversibility of the current switching, bio-electrocatalytic oxidation of glucose was alternately repeated in the on and off states by cyclic placement of the magnet below and above the electrochemical cell. As shown in Figure 4b, anodic currents could be reversibly switched between the on and off states, and a constant signal was maintained in the on state. The magnetic capturing was also very quick; the positioning of most of the Mag-MCF-C/CLEA-GOx particles could be generally completed within 30 seconds. No catalytic current was observed even after the magnet was placed in the "up" position (off state) for several hours, which confirms that GOx was effectively retained within the Mag-MCF-C particles and leaching of the immobilized GOx was negligible, as observed earlier. The exceptional stability of the Mag-MCF-C/CLEA-GOx particles and the ability to easily control their placement by an external magnetic field allowed the construction of a highly effective magnetically switchable bio-electrocatalytic system showing a constant signal upon iterative switching.

In conclusion, we have demonstrated that the magnetic mesocellular carbon foam Mag-MCF-C can be synthesized through a simple synthetic method and used for the fabrication of a magnetically switchable bio-electrocatalytic system. The cross-linked GOx in the mesocellular pores of the Mag-MCF-C particles exhibited a high enzyme loading capacity and exceptional stability. Such advantageous characteristics of Mag-MCF-C/CLEA-GOx together with controlled positioning by an applied magnetic field were successfully utilized in the development of this system. From these results, it is anticipated that our approach will find various applications, such as bioconversion, reversible amperometric immunosensors, regeneration of enzyme electrodes, switchable biofuel cells, and site-specific immobilization of sensing elements in microsized sensing devices.

Received: August 23, 2005
Published online: October 20, 2005

Keywords: carbon · electrochemistry · enzyme catalysis · mesoporous materials · nanotechnology

[1] a) T. Hyeon, *Chem. Commun.* **2003**, 927; b) S. Sun, C. B. Murray, D. Weller, L. Folks, A. Moser, *Science* **2000**, *287*, 1989; c) F. Dumestre, B. Chaudret, C. Amiens, M. Respaud, P. Fejes, P. Renaud, P. Zurcher, *Angew. Chem.* **2003**, *115*, 5371; *Angew. Chem. Int. Ed.* **2003**, *42*, 5213; d) F. Dumestre, B. Chaudret, C. Amiens, P. Renaud, P. Fejes, *Science* **2004**, *303*, 821; e) C. Garcia, Y. Zhang, F. DiSalvo, U. Wiesner, *Angew. Chem.* **2003**, *115*, 1564; *Angew. Chem. Int. Ed.* **2003**, *42*, 1526; f) C. Garcia, Y. Zhang, S. Mahajan, F. DiSalvo, U. Wiesner, *J. Am. Chem. Soc.* **2003**. *125*, 13310; g) J. Lee, S. Jin, Y. Hwang, J.-G. Park, H. M. Park, T. Hyeon, *Carbon* **2005**, *43*, 2536.

[2] A. Dyal, K. Loos, M. Noto, S. W. Chang, C. Spagnoli, K. V. P. M. Shafi, A. Ulman, M. Cowman, R. A. Gross, *J. Am. Chem. Soc.* **2003**, *125*, 1684.

[3] J. M. Perez, L. Josephson, T. O'Loughlin, D. Högemann, R. Weissleder, *Nat. Biotechnol.* **2002**, *20*, 816.

[4] T.-J. Yoon, J. S. Kim, B. G. Kim, K. N. Yu, M.-H. Cho, J.-K. Lee, *Angew. Chem.* **2005**, *117*, 1092; *Angew. Chem. Int. Ed.* **2005**, *44*, 1068.

[5] I. Willner, E. Katz, *Angew. Chem.* **2003**, *115*, 4724; *Angew. Chem. Int. Ed.* **2003**, *42*, 4576.

[6] a) R. Hirsch, E. Katz, I. Willner, *J. Am. Chem. Soc.* **2000**, *122*, 12053; b) E. Katz, I. Willner, *Angew. Chem.* **2005**, *117*, 4869; *Angew. Chem. Int. Ed.* **2005**, *44*, 4791; c) E. Katz, I. Willner, *J. Am. Chem. Soc.* **2002**, *124*, 10290.

[7] a) J. Y. Ying, C. P. Mehnert, M. S. Wong, *Angew. Chem.* **1999**, *111*, 58; *Angew. Chem. Int. Ed.* **1999**, *38*, 56; b) X. Feng, G. E. Fryxell, L. Q. Wang, A. Y. Kim, J. Liu, K. M. Kemner, *Science* **1997**, *276*, 923; c) Y. S. Shin, J. Liu, L. Q. Wang, Z. M. Nie, W. D.

 © 2005 Wiley-VCH Verlag GmbH & Co. KGaA, Weinheim

Samuels, G. E. Fryxell, G. J. Exarhos, *Angew. Chem.* **2000**, *112*, 2814; *Angew. Chem. Int. Ed.* **2000**, *39*, 2702; d) C. Lei, Y. Shin, J. Liu, E. J. Ackerman, *J. Am. Chem. Soc.* **2002**, *124*, 11242; e) F. Schüth, *Angew. Chem.* **2003**, *115*, 3730; *Angew. Chem. Int. Ed.* **2003**, *42*, 3604.

[8] a) J. Lee, S. Han, T. Hyeon, *J. Mater. Chem.* **2004**, *14*, 478; b) J. Lee, K. Sohn, T. Hyeon, *J. Am. Chem. Soc.* **2001**, *123*, 5646; c) Z. Li, M. Jaroniec, *J. Phys. Chem. B* **2004**, *108*, 824; d) Z. X. Ma, T. Kyotani, Z. Liu, O. Terasaki, A. Tomita, *Chem. Mater.* **2001**, *13*, 4413; e) T. Kyotani, L. Tsai, A. Tomita, *Chem. Mater.* **1996**, *8*, 2109; f) Z. Li, M. Jaroniec, *J. Am. Chem. Soc.* **2001**, *123*, 9208; g) R. Ryoo, S. H. Joo, M. Kruk, M. Jaroniec, *Adv. Mater.* **2001**, *13*, 677; h) J. Lee, K. Sohn, T. Hyeon, *Chem. Commun.* **2002**, 2674; i) S. Che, A. E. Garcia-Bennett, X. Liu, R. P. Hodgkins, P. A. Wright, D. Zhao, O. Terasaki, T. Tatsumi, *Angew. Chem.* **2003**, *115*, 4060; *Angew. Chem. Int. Ed.* **2003**, *42*, 3930.

[9] a) P. Schmidt-Winkel, W. W. Lukens, D. Zhao, P. Yang, B. F. Chmelka, G. D. Stucky, *J. Am. Chem. Soc.* **1999**, *121*, 254, 356; b) P. Schmidt-Winkel, W. W. Lukens, P. Yang, D. L. Margolese, J. S. Lettow, J. Y. Ying, G. D. Stucky, *Chem. Mater.* **2000**, *12*, 686.

[10] J. Lee, J. Kim, S.-W. Kim, C.-H. Shin, T. Hyeon. *Chem. Commun.* **2004**, 562.

[11] a) M. Kruk, M. Jaroniec, C. H. Ko, R. Ryoo, *Chem. Mater.* **2000**, *12*, 1961; b) M. Impéror-Clerc, P. Davidson, A. J. Davidson, *J. Am. Chem. Soc.* **2000**, *122*, 11925.

[12] J. Geng, D. A. Jefferson, B. F. G. Johnson, *Chem. Commun.* **2004**, 2442.

[13] A.-H. Lu, W. Schmidt, N. Matoussevitch, H. Bönnemann, B. Spliethoff, B. Tesche, E. Bill, W. Kiefer, F. Schüth, *Angew. Chem.* **2004**, *116*, 4403; *Angew. Chem. Int. Ed.* **2004**, *43*, 4303.

[14] H. J. Hecht, H. M. Kalisz, J. Hendle, R. D. Schmid, D. Schomburg, *J. Mol. Biol.* **1993**, *229*, 153.

[15] J. Lee, J. B. Kim, J. Kim, H. Jia, M. I. Kim, J. H. Kwak, S. Jin, A. Dohnalkova, H. G. Park, H. N. Chang, P. Wang, J. W. Grate, T. Hyeon, *Small* **2005**, *1*, 744.

[16] a) J. Lee, S. Yoon, S. M. Oh, C.-H. Shin, T. Hyeon, *Adv. Mater.* **2000**, *12*, 359; b) R. Ryoo, S. H. Joo, S. Jun, *J. Phys. Chem. B* **1999**, *103*, 7743.

 © 2005 Wiley-VCH Verlag GmbH & Co. KGaA, Weinheim

Mechanical Properties

DOI: 10.1002/anie.200502448

Harder than Diamond: Determining the Cross-Sectional Area and Young's Modulus of Molecular Rods

*Lior Itzhaki, Eli Altus, Harold Basch, and Shmaryahu Hoz**

The rapidly growing area of nanotechnology has provoked much interest in the various moduli of elementary building blocks at the nano/molecular level. Among these moduli, the most frequently discussed is probably Young's modulus, and we describe here the derivation of Young's modulus for two molecular rods, namely polyynes (**1**) and [*n*]staffanes (**2**, poly-1.1.1-propellanes; see Figure 1)[1].

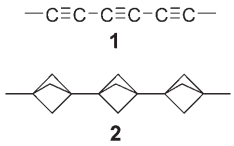

Figure 1. Sections from polyyne (**1**) and [*n*]staffane (**2**).

Given the force applied to a structure, Young's modulus (Y) can be calculated provided the area (A) to which force is applied is known. This, of course, is in addition to the deformation (ΔL) in the length (L) according to Equation (1).[2]

$$\frac{F}{A} = \frac{Y\,\Delta L}{L} \tag{1}$$

In the case of longitudinal compression of a solid homogeneous rod, the effective cross-sectional area (CSA) is the physical cross-sectional area of the rod. However, in the case of a unidimensional molecular rod such as polyyne, the effective cross-sectional area is not easily defined. The definition must rest heavily on our understanding of the nature of matter. In most cases, matter is associated with mass, therefore if the force is exerted on the mass, then the relevant dimension would be the cross-sectional area of the carbon nucleus. On the other hand, since any physical contact, including a punch thrown in a boxing ring, is in fact an interaction between electron clouds, one should consider the CSA of the electron cloud. It is, however, "already apparent from the nature of the wavefunction for atoms and ions that

[*] L. Itzhaki, Prof. H. Basch, Prof. S. Hoz
Department of Chemistry
Bar-Ilan University
Ramat-Gan 52900 (Israel)
Fax: (+972) 3-535-1250
E-mail: shoz@mail.biu.ac.il
Prof. E. Altus
Faculty of Mechanical Engineering
Technion
Israel Institute of Technology
Haifa, 32000 (Israel)

Supporting information for this article is available on the WWW under http://www.angewandte.org or from the author.

WILEY InterScience DISCOVER SOMETHING GREAT
© 2005 Wiley-VCH Verlag GmbH & Co. KGaA, Weinheim

they have no definite size."[3] Thus, the radius, like the partial atomic charge in polar molecules, although intuitively a very appealing concept, is not physically observable. Moreover, it is difficult to justify the use of any of the commonly applied radii such as the ionic, covalent, or the van der Waals radii for the electronic cloud in this context.

In the present work we have succeeded in calculating the effective cross-sectional area and the Young's modulus of a polyyne molecular rod using a combination of quantum mechanical and classical mechanical engineering tools. Our approach is based on the fact that longitudinal compression of a rod will eventually lead to its buckling. As we know that the larger the cross-sectional area of the rod the more it will resist buckling, there must be a correlation between the critical point of the collapse (buckling) and the surface area of the rod. This investigation was performed using the following procedure: In the first step, the structure and the energy of a given polyyne was calculated using the Gaussian 03 program at the B3LYP/6-31G level.[4] Next, the fixed distance between the two terminal carbon atoms was gradually reduced and the energy was optimized at each step with respect to the other structural parameters. These data were inserted into Equation (1), where F is the derivative of the energy (E) with respect to L (the distance between the two terminal carbons in the unconstrained system), and ΔL is the change of this distance upon going to the constrained structure, to give YA. This is the analog to a unidirectional loading of a rod in mechanical engineering terminology.

Further compression of the rod leads to buckling. At the onset of buckling we have the Euler relation [Eq. (2)],[5] which is the solution for a simply supported column under compression.

$$F = \frac{\pi^2 Y I}{L^2} \tag{2}$$

In this equation, I is the minimal static moment of inertia. YI can be calculated from this equation. The square root of the ratio YI/YA ($=I/A$) is equal to the radius of gyration, ρ, which in turn is equivalent to half of the radius, r, of the rod. r, Y, and I are given for a series of polyyne molecular rods in Table 1.

It should be pointed out that the values in Table 1 are not exact since they contain the approximations assumed in the mechanical engineering equations and the approximations used in the various definitions, in addition to the fact that the structure optimization was done using the default parameters of the Gaussian program. Regarding the definitions used, the buckling point was defined as the point at which one of the CCC angles decreased below 179°, and the energy before the critical point for Equation (1) was taken uniformly to be 0.1 % of the original length of the rod. The energy after the buckling was taken at a compression of 0.1 Å from this point. A change in these definitions, such as taking the buckling point as the geometry at which one of the CCC angles crossed the 178° value, rather than 179°, or varying the distances mentioned above by 50 %, changed the final value of the radius by less than 4 %. The direction of the buckling is governed by minor differences in the significant figures of the forces in the perpendicular directions.

It should be noted that the sensitivity to the basis set is rather low. The radius of the C_{10} polyyne was also calculated after addition of diffuse functions or d orbitals and the values obtained were 0.34 and 0.36 Å, respectively, instead of 0.35 Å.

An alternative method to calculate YI is by replacing the "buckling method" (first method in Table 1) with one based on a bending mode (Figure 2). Here, the two terminal carbons

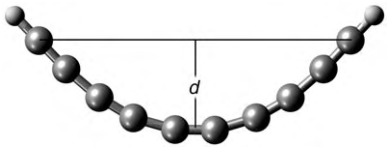

Figure 2. Bending mode for a C_{10} polyyne rod.

are restricted to a given axis and the center of the rod is forced to a point below this axis. The relation between YI and d for a small deformation is given by Equation (3)[6].

$$YI = \frac{F L^3}{48\, d} \tag{3}$$

Again, the aforementioned combination of YI and YA yields the effective radius of the rod. The data obtained using this procedure are also given in Table 1 (second method). The close resemblance of the two sets of values, in spite of the approximations involved in the mechanical engineering equations, is highly encouraging.

Thus, a physical parameter that was previously considered unobservable is quantitatively determined here. It is worth noting that we have obtained the cross-sectional area of the rod by interweaving two entirely different methodologies, none of which contains, either implicitly or explicitly, any value related to the effective radius of the rod. It is left for future studies to see how this value relates to the various π and σ components of the electronic wavefunctions.

An immediate outcome of this result is, of course, that if the cross-sectional area of a carbon atom in a nanotube, for example, is anywhere near that of our molecular rod the Young's modulus calculation for nanotubes[7] should be corrected accordingly.

Table 1: Radius, Young's modulus, and the static moment of inertia for polyyne rods (HC_mH, $m = 4$–20) calculated by the two methods.

	First method			Second method		
m	Radius [Å]	$Y\times10^{-13}$ [N m^{-2}]	$I\times10^{42}$ [m^4]	Radius [Å]	$Y\times10^{-13}$ [N m^{-2}]	$I\times10^{42}$ [m^4]
4	0.35	4.37	1.24	0.31	5.72	0.72
6	0.36	3.95	1.32	0.36	4.05	1.25
8	0.35	3.95	1.23	0.34	4.33	1.03
10	0.36	3.73	1.30	0.33	4.36	0.95
12	0.34	4.38	1.10	0.32	5.20	0.78
14	0.35	4.09	1.19	0.32	4.87	0.84
20	0.35	3.91	1.25	0.33	4.55	0.92
Av.	0.35 ± 0.005	4.0 ± 0.2	1.23 ± 0.07	0.33 ± 0.02	4.7 ± 0.6	0.9 ± 0.2

 © 2005 Wiley-VCH Verlag GmbH & Co. KGaA, Weinheim

Another interesting outcome of this study is the actual value of the Young's modulus of the acetylenic rod (Table 1). It turns out that our calculated Y is around 40 times larger than that of the hardest known material—diamond—whose Young's modulus is 1063 GPa ($Pa = N\,m^{-2}$).[8] The observed Young's modulus of a material is usually a result of the Young's modulus of the molecules of which it is comprised, their relative alignment, and the intermolecular voids. Since diamond can be viewed as a single molecule, having results for these two molecules provides, for the first time, an opportunity to examine the connection between Young's modulus and basic molecular parameters. A major difference between diamond and polyyne is the strength of the bonds involved. While the bonds in the latter are sp fortified by π bonding, the carbon atoms in diamond are interconnected by a series of much weaker sp^3-hybridized bonds. Although the issue is somewhat controversial, it seems that polyyne enjoys further strengthening due to conjugation, which is absent in diamond.[9] The hardness of the acetylenic rod stems, therefore, from the steeper potential functions of the bond, where a small compressional motion along its longitudinal axis results in a sharp rise in energy, namely higher resistance to a change in the position of the nuclei.

Since diamond has a three-dimensional network of bonds it is difficult to carve a unidirectional rod from it. One would like to simulate a rod of diamond in the sense of having a core repeating unit of the rod consisting of sp^3-hybridized carbon atoms, and [*n*]staffanes **2** seem to serve as a close model for this purpose. All carbons in the 1.1.1-bicyclopentane unit have a hybridization ranging from $sp^{3.3}$ to $sp^{2.5}$ for the internal C–C bonds, whereas the hybridization of the external bond has a somewhat lower p character ($sp^{2.1}$). Like in diamond, all four bonds of the carbon atoms along the axis of the rod participate in resisting deformation. The degree of flexibility that is acquired by bond-angle deformation in the bridges can also be found in diamond. Consequently, we have calculated the effective radius, Y, and I, using the compression/buckling method, for rods consisting of three and four bicyclopentane units, assuming that they will display a hardness similar to that of diamond.

Table 2: Radius, Young's modulus, and the static moment of inertia for [*n*]staffane rods.

n	Radius [Å]	$Y \times 10^{-12}$ [$N\,m^{-2}$]	$I \times 10^{41}$ [m^4]
3	0.78	4.9	2.9
4	0.73	5.6	2.3
Av.	0.76 ± 0.02	5.3 ± 0.3	2.6 ± 0.3

The data presented in Table 2 show, as expected, that the [*n*]staffanes' Young's modulus is close to that of diamond (around five times larger) and that its effective radius (approximating it to be a cylindrical rod) is, as expected, larger than that of a rod comprised of acetylene units.

As regards Young's modulus, one can conclude that, since among the sp-, sp^2-, and sp^3-hybridized bonds the sp^3 bond of diamond is the weakest one, some organic compounds may display a rigidity higher than that of diamond, although only along a single axis. The uniqueness of diamond stems from the fact that it displays the same strength in all directions. On the other hand, the uniqueness of polyyne is explained by the fact that it consists of the strongest bonds among the three groups of hybridization and therefore we expect that it will be very difficult to break its record in hardness, at least within the realm of carbon-based rods.

In light of the fact that no material significantly stronger than diamond has been synthesized up to now,[10] a very interesting option in three dimensions is a diamond in which two carbon atoms are connected not by a σ (sp^3) bond but by an acetylenic unit.[11] The building block of such a structure—triethynylmethane $C(C{\equiv}CH)_4$—was successfully synthesized[12] and studied computationally.[13] Although it is likely that the large voids in the "yne diamond" will take their toll on the overall hardness, it is possible that the large difference in the nature of the constituent bonds will more than overcome this deficiency. Although the hybridization of the corner carbon atoms remains sp^3, the sp^3–sp bond is significantly stronger than the sp^3–sp^3 bond and, as was shown recently by Schleyer and Houk,[9a] this bond is further stabilized by the neighboring triple bond. The internal radius of the adamantane cavity in the yne-diamond is about 2.16 Å (3.86 Å less the van der Waals radius of carbon). Chelation of an inert gas atom of the right size in this cavity will no doubt overcome the aforementioned problem of the internal voids. Based on its van der Waals radius, Xe ($r = 2.16$ Å) seems to be the element of choice (Figure 3). The synthesis of the yne-diamond is, however, an immense task to fulfill, and filling its yne-adamantane cavities with Xe, which will significantly increase its stiffness,[14] is also a colossal challenge.[15]

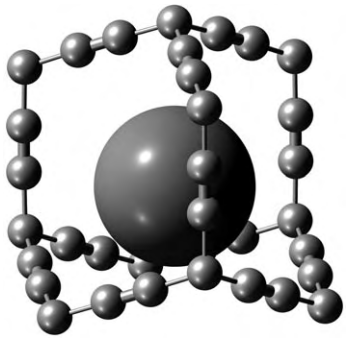

Figure 3. Yne-adamantane unit of yne-diamond containing a Xe atom. The size of the carbon atoms has been reduced to enable a better view.

Received: July 13, 2005
Published online: October 20, 2005

Keywords: ab initio calculations · materials science · mechanical properties · nanostructures · polyynes

[1] a) P. Kaszynski, J. Michl, *Advances in Strain in Organic Chemistry*, *Vol. 4*, **1995**, p. 283; b) P. F. H. Schwab, M. D. Levin, J. Michl, *Chem. Rev.* **1999**, *99*, 1863.

 © 2005 Wiley-VCH Verlag GmbH & Co. KGaA, Weinheim

[2] E. P. Popov, T. A. Balan, *Engineering Mechanics of Solids*, 2nd ed., Prentice Hall, Englewood Cliffs, NJ, **1999**, p. 67.
[3] F. A. Cotton, G. Wilkinson, *Advanced Inorganic Chemistry*, 2nd ed., Interscience, New York, **1966**, p. 44.
[4] Gaussian 03 (Revision B.04), M. J. Frisch, G. W. Trucks, H. B. Schlegel, G. E. Scuseria, M. A. Robb, J. R. Cheeseman, J. A. Montgomery, Jr., T. Vreven, K. N. Kudin, J. C. Burant, J. M. Millam, S. S. Iyengar, J. Tomasi, V. Barone, B. Mennucci, M. Cossi, G. Scalmani, N. Rega, G. A. Petersson, H. Nakatsuji, M. Hada, M. Ehara, K. Toyota, R. Fukuda, J. Hasegawa, M. Ishida, T. Nakajima, Y. Honda, O. Kitao, H. Nakai, M. Klene, X. Li, J. E. Knox, H. P. Hratchian, J. B. Cross, C. Adamo, J. Jaramillo, R. Gomperts, R. E. Stratmann, O. Yazyev, A. J. Austin, R. Cammi, C. Pomelli, J. W. Ochterski, P. Y. Ayala, K. Morokuma, G. A. Voth, P. Salvador, J. J. Dannenberg, V. G. Zakrzewski, S. Dapprich, A. D. Daniels, M. C. Strain, O. Farkas, D. K. Malick, A. D. Rabuck, K. Raghavachari, J. B. Foresman, J. V. Ortiz, Q. Cui, A. G. Baboul, S. Clifford, J. Cioslowski, B. B. Stefanov, G. Liu, A. Liashenko, P. Piskorz, I. Komaromi, R. L. Martin, D. J. Fox, T. Keith, M. A. Al-Laham, C. Y. Peng, A. Nanayakkara, M. Challacombe, P. M. W. Gill, B. Johnson, W. Chen, M. W. Wong, C. Gonzalez, J. A. Pople, Gaussian, Inc., Pittsburgh, PA, **2003**.
[5] E. P. Popov, T. A. Balan, *Engineering Mechanics of Solids*, 2nd ed., Prentice Hall, Englewood Cliffs, NJ, **1999**, p. 679.
[6] E. P. Popov, T. A. Balan, *Engineering Mechanics of Solids*, 2nd ed., Prentice Hall, Englewood Cliffs, NJ, **1999**, p. 853.
[7] G. V. Lier, C. V. Alsenoy, V. V. Doren, P. Geerlings, *Chem. Phys. Lett.* **2000**, *326*, 181.
[8] J. B. Huntington, in *Solid State Physics, Vol. 7* (Eds.: F. Seitz, D. Turnbull), Academic, New York, **1958**.
[9] a) P. D. Jarowski, M. D. Wodrich, C. S. Wannere, P. von R. Schleyer, K. N. Houk, *J. Am. Chem. Soc.* **2004**, *126*, 15036–15037; b) D. Cappel, S. Tüllmann, A. Krapp, G. Frenking, *Angew. Chem.* **2005**, *117*, 3683–3686; *Angew. Chem. Int. Ed.* **2005**, *44*, 2–5; c) D. W. Rogers, N. Matsunaga, A. A. Zavitsas, F. J. McLafferty, J. F. Liebman, *Org. Lett.* **2003**, *5*, 2373–2375; d) D. W. Rogers, N. Matsunaga, F. J. McLafferty, A. A. Zavitsas, J. F. Liebman, *J. Org. Chem.* **2004**, *69*, 7143–7147.
[10] M. M. Chaudhri, Y. Y. Lim, *Nat. Mater.* **2005**, *4*, 4.
[11] K. S. Feldman, C. M. Kaerbel, *J. Am. Chem. Soc.* **1993**, *115*, 3846.
[12] For examples of expansion of polycyclic molecules by acetylene units, see: a) P. D. Jarowski, F. Diederich, K. N. Houk, *J. Org. Chem.* **2005**, *70*, 1671; b) S. M. Bachrach, *J. Phys. Chem. A* **2003**, *107*, 4957.
[13] J. F. Capitani, *J. Mol. Struct.* **1995**, *332*, 21.
[14] Young's modulus is, in fact, the measure of stiffness that is commonly referred to as hardness. However, in materials science, hardness is measured as the deformation caused by the indenting tip. Yet, hardness and Young's modulus are closely related, and diamond has the highest known Young's modulus.
[15] Computational data are given in the Supporting Information.

 © 2005 Wiley-VCH Verlag GmbH & Co. KGaA, Weinheim

Chiral Molecules

DOI: 10.1002/anie.200502262

"Hexacarboxytrindanes": Benzene Rings with Homotopic Faces as Scaffolds for the Construction of D_3 Chiral Architectures**

Giuseppe Borsato, Marco Crisma, Ottorino De Lucchi, Vittorio Lucchini,* and Alfonso Zambon*

The advantages offered by high-symmetry chiral molecules are largely recognized in asymmetric synthesis[1] and can be readily applied in several other fields (e.g., material science, liquid crystal technology, and nanoscience). For example, in asymmetric synthesis high symmetry can enhance chiral recognition because of the reduction in the number of the possible diastereomorphic transition states, the equivalence of the functionalities, and the improvement of the ratio between the functional groups and the chiral framework.[2] Other advantages are offered by the opportunities for metal multi-coordination or high metal loading, the simplification of the spectral features, high crystallinity, and so forth. These features can benefit the design of highly efficient catalysts.

Although C_2-symmetrically chiral molecules, exemplified by binaphthol and its derivatives,[3] are quite popular, and chiral structures that possess C_3 symmetry do not attract a lot of attention but are nevertheless numerous,[4] chiral compounds with D_3 or higher symmetry are less common. Within the field of organic chemistry, the following classes of D_3 chiral structures have been reported: perhydrotriphenylenes,[5] trishomocubanes,[6] cyclotriveratrylenes,[7] macrocyclic alkanes, polyethers and polyesters with three groups of strategically positioned substituents,[8] and fullerenes.[9] Other high-symmetry chiral molecules are represented by benzene rings joined (through at least three bonds) with six homotopic centers.[10] The symmetry of these molecules is C_6 or D_6 (from dynamic averaging).

We present herein the first examples of D_3 benzene rings with six directly bound homotopic groups. The homotopicity is attained exactly because of the proximity and the reciprocal steric interaction of the groups. The common structure is that

[*] Dr. G. Borsato, Prof. V. Lucchini, Dr. A. Zambon
Dipartimento di Scienze Ambientali
Università Ca' Foscari di Venezia
Dorsoduro 2137, 30123 Venezia (Italy)
Fax: (+39) 412-348-584
E-mail: gborsato@unive.it
lucchini@unive.it

Dr. M. Crisma
Istituto di Chimica Biomolecolare, CNR
via Marzolo 1, 35131 Padova (Italy)

Prof. O. De Lucchi
Dipartimento di Chimica
Università Ca' Foscari di Venezia
Dorsoduro 2137, 30123 Venezia (Italy)

[**] This work was cofounded by MURST within the national project "Stereoselezione in Sintesi Organica: Metodologie e Applicazioni".

© 2005 Wiley-VCH Verlag GmbH & Co. KGaA, Weinheim

of 2,3,4,5,6,7,8,9-octahydro-1*H*-trindene-1,3,4,6,7,9-hexacarboxylic acid or ester ("hexacarboxytrindane"), which also, at variance from other D_3 molecules, is functionalized and thus amenable to further synthetic elaborations.

The access to these high-symmetry chiral molecules is described in Scheme 1 and Table 1 and originates from the recently synthesized cyclotrimers *syn*-**1** and *anti*-**1**, which are functionalized with three dichlorovinylene moieties on the edge.[11] These substrates could be obtained on multigram scales by cyclotrimerization of bromotrimethylstannylnorbornadiene (**2**) in the presence of copper(I) 2-thiophenecarboxylate (CuTC; Scheme 1). The oxidative cleavage of the three vinyl bonds of a mixture of *syn*-**1** and *anti*-**1** was carried out using $RuCl_3 \cdot 3H_2O/NaIO_4$,[12] thus leading to the quantitative and stereospecific formation of two isomeric trindane molecules *syn*-**3** and *anti*-**3**, in which the sets of the carboxylic groups reflect the same C_{3v} and C_s symmetries of the starting materials.

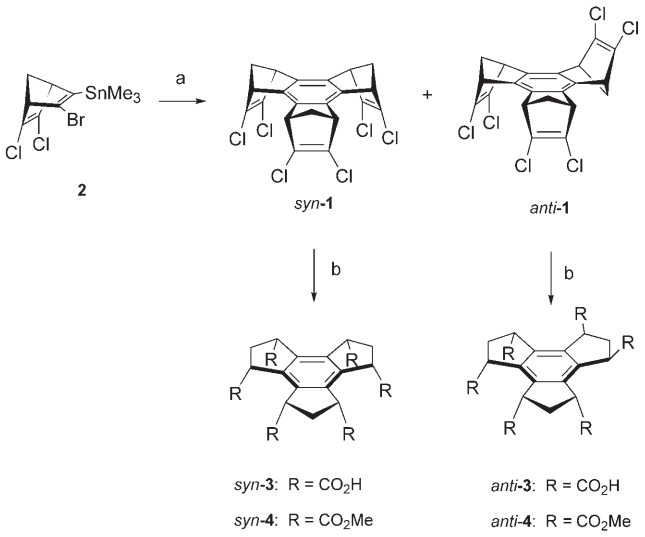

Scheme 1. Reagents and conditions: a) CuTC, NMP, −15 °C, 2 h, (>90%). b) 1. $RuCl_3 \cdot 3H_2O/NaIO_4$, CCl_4, CH_3CN, H_2O, 0 °C, 3 h, (**3**: 99%); 2. O_3/MeOH, RT, 1 h, (**4**: >95%); 3. **3**, PTSA, MeOH, reflux, 3 days (**4**: 10%). NMP = *N*-methylpyrrolidone, PTSA = *para*-toluenesulfonic acid.

Table 1: Epimerization, transesterification, and cleavage reactions

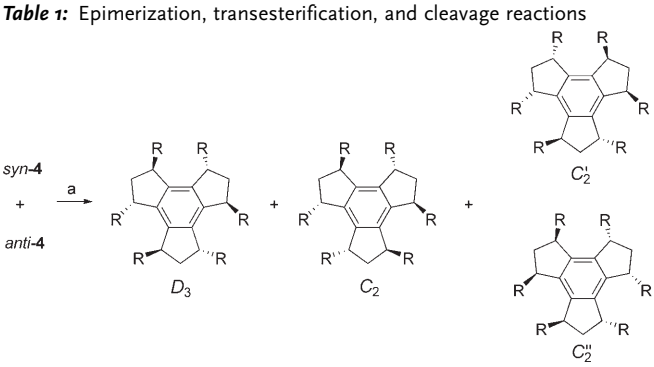

R	D_3	C_2	C_2''	D_3:C_2	Yield [%]
CO_2Me	D_3-(*R*,*S*)-**4**	C_2-**4**		1:2.1	70[a]
CO_2*i*Pr	D_3-(*R*,*S*)-**5**	C_2-**5**		1:1.2	60[a]
CO_2(−)ment	D_3-(*S*)-**6**		C_2''-**6** or C_2'-**6**	3:1	45[b]
CO_2H[c]	D_3-(*S*)-**3**			–	90
CO_2Cl[d]	D_3-(*S*)-**7**			–	>90
CO_2Me[e]	D_3-(*S*)-**4**			–	>90

[a] Yield determined spectroscopically. [b] Yield after flash-chromatographic purification. [c] Formed from CO_2(−)ment under conditions (b). [d] Formed from CO_2H under conditions (c). [e] Formed from CO_2Cl under conditions (d). Reagents and conditions: a) **4**: MeOLi, THF; **5**: *i*PrOLi, THF; **6**: (−)mentOLi, THF; b) Me_3SiI, CCl_4; c) $(COCl)_2$/DMF, CH_2Cl_2; d) MeOH. DMF = dimethylformamide, ment = menthyl.

The hexamethyl esters *syn*-**4** and *anti*-**4** can be obtained by two different synthetic approaches: oxidation by $RuCl_3$ to the corresponding acids *syn*-**3** and *anti*-**3**,[12] followed by esterification or direct oxidation of *syn*-**1** and *anti*-**1** by using ozone in methanol.[13] The first approach gives the hexaacids quantitatively, but Fischer esterification affords the esters in poor yield. As the second approach gives *syn*-**4** and *anti*-**4** directly in quantitative yield, we did not investigate any alternative to Fischer esterification.

The two base sensitive positions in *syn*-**4** and *anti*-**4**, that is, the benzylic proton and the carboxylic group, can be exploited in transesterification and epimerization processes.[14] The epimerization process may be governed by the steric hindrance between groups on the same five-membered ring or between facing groups on different rings.

The addition of MeOLi to a solution of either pure *syn*-**4** or *anti*-**4** in THF (Table 1) leads to only two out of the ten possible diastereomers, that is, D_3-(*R*,*S*)-**4** and C_2-**4**,[15] obtained in ratios of 1:2.0 (from *syn*-**4**) and 1:2.1 (from *anti*-**4**) in 70% overall yield. These results imply that the mixture of cyclotrimers, *syn*-**1** and *anti*-**1**, can be oxidized without previous separation and used in the rearrangement process. The ratios, measured from the integrated signals in the NMR spectra of the crude reaction mixture, are equal within the measurement error. When corrected for the statistical factor of 1:3, the ratio of D_3-(*R*,*S*)-**4**/C_2-**4** becomes 1:0.68, which is a thermodynamic ratio, as no change was observed from prolonged action of the base. Thus, D_3-(*R*,*S*)-**4** is somewhat more stable than C_2-**4**.

The effect of the steric hindrance of different esters was evaluated by changing the alcohol. A mixture of the isopropyl esters D_3-(*R*,*S*)-**5** and C_2-**5** was obtained from a mixture of *syn*-**4** and *anti*-**4** esters using *i*PrOLi as the base in 60% yield and in a ratio of 1:1.2, thus corresponding to a ratio of 1:0.40 after correction. The main steric hindrance is between ester groups located on the same five-membered ring, but also the steric hindrance between facing groups on different five-membered rings plays a role, which increases with the bulk of the group, thus favoring the D_3 structure.

The homotopicity of the six benzylic groups in the D_3 esters **4** and **5** allows recognition of the D_3-*R* and D_3-*S* enantiomeric forms in which the faces of the benzene ring are also homotopic.

Transesterification with a chiral alcohol allows the diastereomeric isolation of the pure enantiomers. Reaction of the mixture of *syn*-**4** and *anti*-**4** esters with lithium (−)-mentholate gives two isomers of **6** in a ratio of 3:1 and in 45% yield after flash-chromatographic purification.

The indane protons in D_3-(*S*)-**6** are represented by a unique AA′XX′ system, in the form of two pseudo triplets.

 © 2005 Wiley-VCH Verlag GmbH & Co. KGaA, Weinheim

The detection of weak transitions at the triplet sides allowed second-order spin analysis.[15] The verification of three equivalent AA′XX′ spin systems provides a rigorous argument for D_3 symmetry. The diastereomeric purity of D_3-(*S*)-**6** can be determined by careful analysis of the ^{13}C NMR spectrum (Figure 1), in which only the signals of a single compound were detected. The dipolar interactions measured by NOESY or differential NOE spectroscopy allowed, together with HMQC spectroscopy, the unequivocal assignment of ^{1}H and ^{13}C NMR resonances.

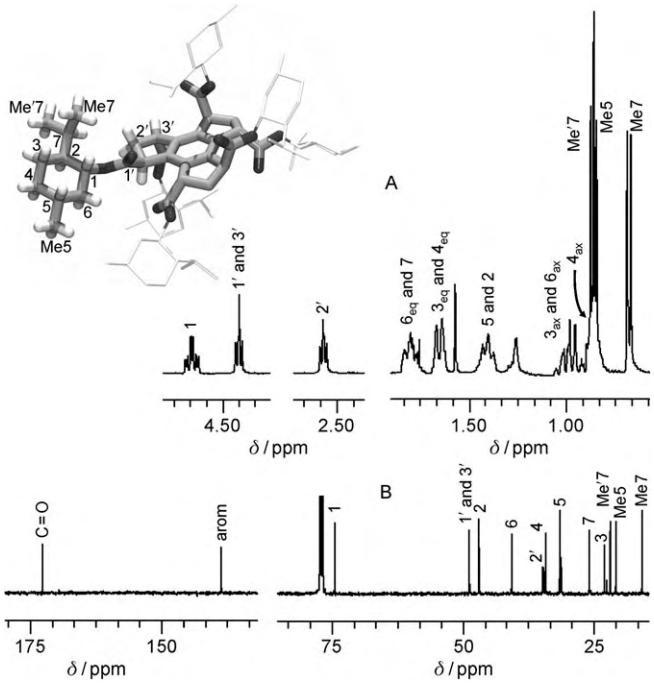

Figure 1. Complete assignment of NMR signals of D_3-(*S*)-**6** (only the relevant parts are shown). A) ^{1}H NMR (400 MHz), B) ^{13}C NMR (100 MHz) spectra.

The *S* configuration of the homotopic benzylic carbons in D_3-(*S*)-**6** was established unambiguously by single-crystal X-ray diffraction analysis[16] on the basis of the known 1*R*,2*S*,5*R* configuration of the menthyl ester units (Figure 2).

We could not find any indication of the formation of the D_3-(*R*)-**6** isomer. The isolated minor isomer displays the four protons of one five-membered ring in the form of two pseudo triplets, which is indicative of *trans* substitution, whereas the eight protons of the other rings present patterns similar to those of *syn*-**4** and *anti*-**4**, which is, therefore, indicative of *cis* substitution. Both the two C_2 structures, C_2'-**6** (more probable) or C_2''-**6**, can accommodate these features, and so we could not make an assignment.

It is appropriate to develop derivatization processes that will preserve the most valuable characteristics of the described hexaesters, particularly the up/down alternating substituents in D_3-**4**, D_3-**5**, and D_3-**6** and the enantiomeric purity of D_3-(*S*)-**6.** This possibility was verified by cleavage and esterification reactions.

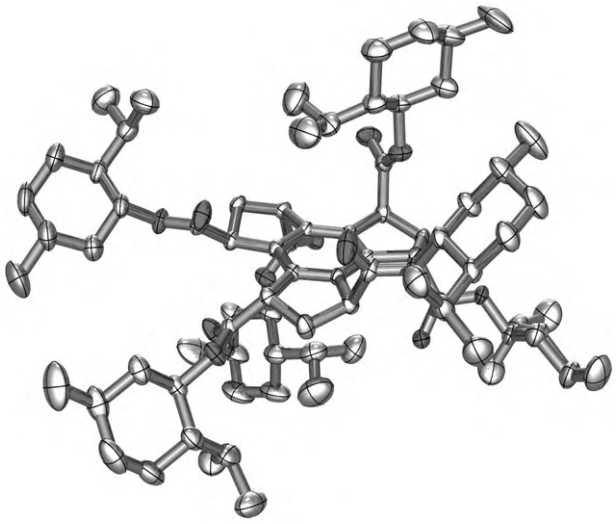

Figure 2. Structure of hexamenthyl ester D_3-(*S*)-**6** obtained by X-ray diffraction studies. Hydrogen atoms have been omitted for clarity. Ellipsoids drawn at 20% probability.

The removal of the chiral auxiliary in D_3-(*S*)-**6** gives the enantiopure hexaacid D_3-(*S*)-**3** ($[\alpha]_D^{20} = +18.16$, $c = 0.49$, dimethyl sulfoxide (DMSO)) in quantitative yield (Table 1). The cleavage reaction was carried out under neutral conditions using Me_3SiI in CCl_4.[17] The hexaacid D_3-(*S*)-**3** can be converted into the acid chloride D_3-(*S*)-**7** by using $(COCl)_2$/DMF,[17] and then esterified with MeOH giving D_3-(*S*)-**4** ($[\alpha]_D^{20} = +3.9$, $c = 0.23$, CH_2Cl_2). Compounds D_3-(*S*)-**3** and D_3-(*S*)-**4** are enantiopure, that is, the reactions occur with no rearrangement at the benzylic carbon atoms, as verified in the ^{1}H NMR spectra of the crude reaction mixture, in which no signal from the C_2 isomers could be detected.

Our approach suggests the following requirement for the generation of chiral D_3 molecules built around a benzene ring: a reversible epimerization process that will ensure the most stable configuration of the six substituents. However, in an open situation this process will lead to the alternation of *R* and *S* topicities in a molecule with C_3 symmetry (Figure 3 A). However, when the substituents with equal priority are forced toward each other by ring closures, a D_3 chiral molecule with six homotopic groups is produced (Figure 3 B).

The trindane framework with homotopic faces is the first example of an enantiopure D_3 molecule with six reactive units

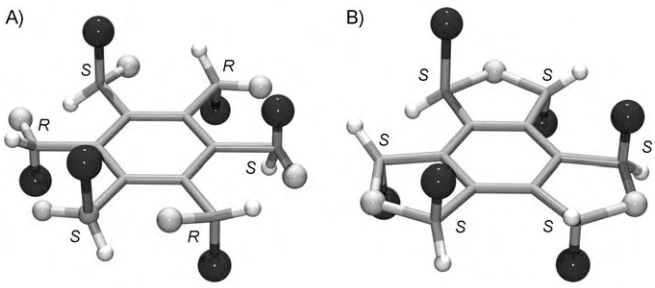

Figure 3. The effects of thermodynamic epimerization on A) open and B) ring-closed ("trindane") benzene structures.

 © 2005 Wiley-VCH Verlag GmbH & Co. KGaA, Weinheim

joined directly in a rigid structure. This feature makes D_3-(*S*)-**7** an attractive core for the construction of new macromolecules, such as dendrimers,[18] liquid crystals,[19] supramolecular polymers,[10d,20] and molecular receptors,[21] in which asymmetric induction is not driven by the periphery of the molecule but by the center.

Experimental Section

D_3-(*S*)-**6**: A solution of *n*BuLi in hexanes (2.5 M, 24 mL, 59 mmol) was added dropwise to a solution of (−)-menthol (9.27 g, 59 mmol) in dry THF (80 mL) at room temperature under argon. A solution of *syn*-**4** and *anti*-**4** (3.24 g, 5.9 mmol) was added after 10 min at −78 °C. The dark solution was quenched after 2 days with saturated NaCl solution (100 mL), extracted with Et_2O (3 × 100 mL), the organic layers dried over $MgSO_4$, and concentrated in vacuo. The crude reaction mixture was purified by flash chromatography (CH_2Cl_2/hexane 1:1) to give the white solid D_3-(*S*)-**6** (2.5 g, 33 %; m.p. 78.8 °C) as the first product and C_2'-**6** or C_2''-**6** (0.89 g, 11 %; m.p. 101.7 °C) as the second product. D_3-(*S*)-**6** was recrystallized from CH_3CN/CH_2Cl_2 by slow solvent evaporation. 1H NMR ($CDCl_3$, 400 MHz): $\delta = 4.66$ (6H, H1, td, $J =$ 10.8, 4.2 Hz), 4.42 (6H, H1′ and H3′, pseudo t), 2.57 (6H, H2′, pseudo t), 1.82 (6H, $H6_{eq}$, m), 1.79 (6H, H7, m). 1.65 (12H, $H3_{eq}$ and $H4_{eq}$, m), 1.42 (6H, H5, m), 1.40 (6H, H2, m), 1.00 (6H, $H3_{ax}$, m), 0.89 (6H, $H4_{ax}$, m), 0.87 (18H, Me7, d, $J = 6.4$ Hz), 0.85 (18H, Me5, d, $J =$ 6.8 Hz), 0.68 ppm (18H, Me7, d, $J = 6.9$ Hz); 13C NMR ($CDCl_3$, 100 MHz): $\delta = 172.79$ (6C, carboxyl), 138.66 (6C, aromatic), 74.41 (6C, C1), 48.81 (6C, C1′ and C3′), 47.06 (6C, C2), 40.73 (6C, C6), 34.71 (3C, C2′), 34.27 (6C, C4), 31.42 (6C, C5), 25.93 (6C, C7), 23.13 (6C, C3), 22.01 (6C, Me′7), 20.94 (6C, Me5), 15.88 ppm (6C, Me7).

X-ray diffraction: The data were collected on a Philips PW1100 four-circle diffractometer. Single crystals suitable for X-ray diffraction analysis were grown by slow evaporation from a solution of CH_3CN/CH_2Cl_2.[16]

Received: June 28, 2005
Published online: October 20, 2005

Keywords: chirality · epimerization · homotopy · NMR spectroscopy · symmetry

[1] E. L. Eliel, S. H. Wilen, *Stereochemistry of Organic Compounds*, Wiley, New York, **1994**.
[2] J. K. Whitesell, *Chem. Rev.* **1989**, *89*, 1581.
[3] a) R. Noyori, *Angew. Chem.* **2002**, *114*, 2108; *Angew. Chem. Int. Ed.* **2002**, *41*, 2008; b) R. Noyori, *Asymmetric Catalysis in Organic Synthesis*, Wiley, New York, **1994**.
[4] C. Moberg, *Angew. Chem.* **1998**, *110*, 260; *Angew. Chem. Int. Ed.* **1998**, *37*, 248.
[5] a) M. Farina, *Tetrahedron Lett.* **1963**, *4*, 2097; b) M. Farina, G. Audisio, *Tetrahedron* **1967**, 1285; c) M. Farina, G. Audisio, *Tetrahedron Lett.* **1970**, 1827; d) M. Farina, G. Audisio, *Tetrahedron* **1970**, 1839.
[6] a) G. R. Underwood, B. Ramamoorthy, *Tetrahedron Lett.* **1970**, 4125; b) G. Helmchen, G. Staiger, *Angew. Chem.* **1977**, *89*, 119; *Angew. Chem. Int. Ed. Engl.* **1977**, *16*, 116; c) P. E. Eaton, B. Leipzig, *J. Org. Chem.* **1978**, *43*, 2483; d) M. Nakazaki, K. Naemura, N. Arashiba, *J. Org. Chem.* **1978**, *43*, 689.
[7] a) J. Cancelli, A. Collet, G. Gottarelli, P. Palmieri, *J. Am. Chem. Soc.* **1987**, *109*, 6454; b) D. J. Cram, M. E. Tanner, S. J. Keipert, C. B. Knobler, *J. Am. Chem. Soc.* **1991**, *113*, 8909; c) D. J. Cram, *Nature* **1992**, *356*, 29.
[8] a) E. P. Kyba, G. W. Gokel, F. de Jong, K. Konga, L. R. Sousa, M. G. Siegel, L. Kaplan, G. D. Y. Sogah, D. J. Cram, *J. Org. Chem.* **1977**, *42*, 4173; b) J. M. Lehn, P. Vierling, R. C. Hayward, *J. Chem. Soc. Chem. Commun.* **1979**, 296; c) H. Löhr, F. Vögtle, *Acc. Chem. Res.* **1985**, *18*, 65; d) J. Crosby, J. F. Stoddart, X. Sun, M. R. W. Venner, *Synthesis* **1993**, 141; e) A. Gypser, D. Michel, D. S. Nirschl, K. B. Sharpless, *J. Org. Chem.* **1998**, *63*, 7322; f) M. Ricci, D. Pasini, *Org. Biomol. Chem.* **2003**, *1*, 3261.
[9] a) G. Schick, M. Levitus, L. Kvetko, B. A. Johnson, I. Lamparth, R. Lunkwitz, B. Ma, S. I. Kahn, M. A. Garcia-Garibay, Y. Rubin, *J. Am. Chem. Soc.* **1999**, *121*, 3246; b) A. A. Goryunkov, V. Y. Marcov, I. N. Ioffe, R. D. Bolskar, M. D. Diener, I. V. Kovyuchko, S. H. Strauss, O. V. Boltalina, *Angew. Chem.* **2004**, *116*, 1015; *Angew. Chem. Int. Ed.* **2004**, *43*, 997.
[10] a) A. Freer, C. J. Gilmore, D. D. MacNicol, S. Swanson, *Tetrahedron Lett.* **1980**, *21*, 205; b) R. J. Kaufman, R. S. Sidhu, *J. Org. Chem.* **1982**, *47*, 4941; c) N. Yamasaki, Y. Inoue, T. Yokoyama, A. Tai. A. Ishida, S. Takamuku, *J. Am. Chem. Soc.* **1991**, *113*, 1933; d) A. J. Wilson, M. Masuda, R. P. Sijbesma, E. W. Meijer, *Angew. Chem.* **2005**, *117*, 2315; *Angew. Chem. Int. Ed.* **2005**, *44*, 2275.
[11] G. Borsato, S. Brussolo, M. Crisma, O. De Lucchi, V. Lucchini, A. Zambon, *Synlett* **2005**, 1125.
[12] a) P. H. J. Carlsen, T. Katsuki, K. B. Sharpless, *J. Org. Chem.* **1981**, *46*, 3936; b) F. A. Khan, B. Prabhudas, J. Dash, N. Sahu, *J. Am. Chem. Soc.* **2000**, *122*, 9558.
[13] G. Nagendrappa, H. Griesbaum, *J. Agric. Food Chem.* **1978**, *26*, 581.
[14] a) K. Somekawa, M. Nomura, S. Aoki, S. Noma, T. Shimo, *Org. Prep. Proced. Int.* **1993**, *25*, 449; b) I. Michieletto, F. Fabris, O. De Lucchi, *Tetrahedron: Asymmetry* **1999**, *10*, 2505.
[15] The protons of the indane rings in D_3-(*R*,*S*)-**4** give rise to one AA′XX′ spin system, whereas the protons of C_2-**4** to give rise to one AA′XX′ and two ABXY systems, which are a good approximation of AA′XX′ systems. Each AA′XX′ system is in the form of two deceptively simple pseudo triplets. A rigorous second-order analysis was performed on the AA′XX′ spectrum of D_3-(*S*)-**6**: A (H2′) = 1027.8 ± 0.1 Hz (at 400 MHz), X (H1′ and H3′) = 1766.7 ± 0.1 Hz, J(AA′) = −12.5 ± 0.1 Hz, J(XX′) = 0 Hz, J(AX) = J(A′X′) = 7.6 ± 0.2 Hz, J(AX′) = J(A′X) = 6.3 ± 0.2 Hz. LAOCOON program: A. A. Bothner-by, S. Castellano, *J. Chem. Phys.* **1964**, *41*, 3863.
[16] Crystal-structure determination of D_3-(*S*)-**6** ($C_{81}H_{126}O_{12}$): crystal dimensions 0.45 × 0.40 × 0.40 mm^3; orthorhombic, space group $C222_1$; $a = 19.469(3)$, $b = 21.761(3)$, $c = 38.254(5)$ Å; $V =$ 16207(4) Å^3; $\rho_{calcd} = 1.059$ Mg m^{-3}; $2\theta_{max} = 120 =$; $Cu_{K\alpha}$ radiation ($\lambda = 1.54178$ Å), θ–2θ scan mode, $T = 293$ K; 6504 independent reflections collected; h,k,l limits: $0 \le h \le 21$, $0 \le k \le 24$, $0 \le l \le 42$. Intensities were corrected for Lorentz and polarization effects, not for absorption ($\mu = 0.544$ mm^{-1}) The structure was solved ab initio by using the SIR 2004 program and anisotropically refined by full-matrix block least-squares on F^2 by application of the SHELXL 97 program. Data/restraints/parameters: 6504/0/839. Hydrogen atoms were calculated at idealized positions and refined as riding. $R1 = 0.056$ (on $F \ge 4\sigma(F)$); $wR2 = 0.159$ (on F^2, all data). Max./min. residual electron density peaks: +0.201/−0.212 e Å^{-3}. CCDC-272639 contains the supplementary crystallographic data for this paper. These data can be obtained free of charge from the Cambridge Crystallographic Data Centre via www.ccdc.cam.ac.uk/data_request/cif. SIR 2004 program: M. C. Burla, R. Caliandro, M. Camalli, B. Carrozzini, G. L. Cascarano, L. De Caro, C. Giacovazzo, G. Polidori, R. Spagna, *J. Appl. Crystallogr.* **2005**, *38*, 381; SHELXL 97 program: G. M. Sheldrick et al., *SHELXL 97*, *Program for Crystal Structure Refinement*, University of Göttingen, Göttingen, **1997**.
[17] P. C. Meltzer, P. Wang, P. Blundell, B. K. Madras, *J. Med. Chem.* **2003**, *46*, 1538.
[18] S. M. Grayson, J. M. J. Fréchet, *Chem. Rev.* **2001**, *101*, 3819.

 © 2005 Wiley-VCH Verlag GmbH & Co. KGaA, Weinheim

[19] C. Nuckolls, *Angew. Chem.* **2004**, *116*, 5562; *Angew. Chem. Int. Ed.* **2004**, *43*, 5456.
[20] a) L. Brunsveld, B. J. B. Folmer, E. W. Meijer, R. P. Sijbesma, *Chem. Rev.* **2001**, *101*, 4071; b) J. van Gestel, A. R. A. Palmans, B. Titulaer, J. A. J. M. Vekemans, E. W. Meijer, *J. Am. Chem. Soc.* **2005**, *127*, 5490.
[21] H. Choi, Y. S. Park, S. H. Yun, H. Kim, C. S. Cho, K. Ko, K. H. Ahn, *Org. Lett.* **2002**, *4*, 795.

 © 2005 Wiley-VCH Verlag GmbH & Co. KGaA, Weinheim

Nanoparticle Assemblies

DOI: 10.1002/anie.200501264

Nanoparticle Assemblies with Molecular Springs: A Nanoscale Thermometer**

*Jaebeom Lee, Alexander O. Govorov, and Nicholas A. Kotov**

Nanoparticle (NP) superstructures are important in the creation of smart materials with new functionalities. Most of the current examples of complex NP systems, such as bioconjugates[1–4] or hybrid nanocolloids[5] and their lattices,[6,7] are typically static: They show a limited response to environmental parameters and do not exhibit smooth reversible transitions of their three-dimensional organization or geometry in response to external stimuli. Dynamic NP superstructures with gradual structural adaptation to common physical parameters may reveal interesting analogies to biological entities of similar scale.[8,9] Additionally, such systems can find technological applications as optical devices. Herein we describe a reversible nanothermometer built from two types of NPs connected by a polymer acting as a molecular spring. The underlying microscopic mechanism of the nanothermometer involves plasmon resonance and exciton–plasmon interaction.

Poly(ethyleneglycol) (PEG) derivatives with *tert*-butoxycarbonyl (Boc) and *N*-hydroxysulfosuccinimide (NHS) groups at the terminal ends of the linear macromolecule (molecular weight 3400 Da, see *Experimental Section*) allow the sequential conjugation of one end to 20-nm Au NPs and of the other end to 3.7-nm CdTe NPs. This results in the superstructure depicted in the insert of Figure 1. The high-resolution transmittance electron microscopy (TEM) images of the product (Figure 2) confirm the formation of corona-like superstructures, although the density of the CdTe satellite particles distributed around the central gold core is lower than expected, probably owing to structural alterations during sample preparation. The CdTe colloid can be identified by the lattice plane spacing d of 0.352 ± 0.3 nm, which is typical for cubic CdTe.[10,11] The Au NPs show a d value of 0.23 ± 0.008 nm, which corresponds to the (111) planes of the Au crystal (see Supporting Information).

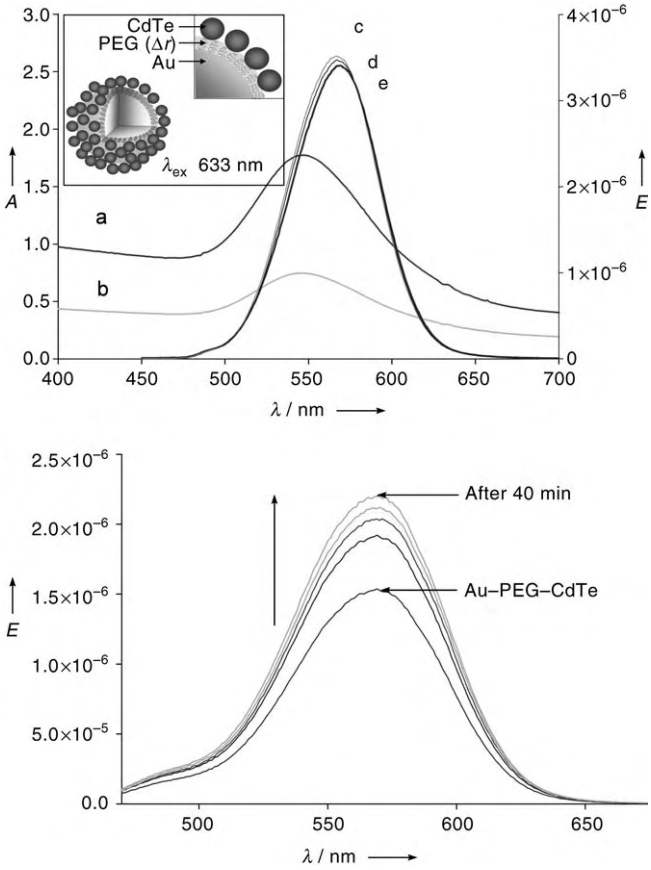

Figure 1. Top: Absorbance spectra of the PEG-conjugated Au NPs before (a) and after (b) removal of the Boc protecting groups; emission spectra of CdTe NPs after addition of EDC/NHS (c), after conjugation with Au–PEG (d), and of CdTe alone (e). Inset: Schematic drawing of the superstructure. Bottom: PL enhancement of the CdTe–PEG–Au superstructure after 40 min. A = absorbance, E = emission intensity.

The superstructure was excited with a He:Ne laser at 633 nm (20 mW, Uniphase, USA). The red light quanta result in efficient excitation of CdTe NPs, although these quanta are below the energy of the absorption threshold. This process is not as common as photoluminescence (PL) stimulated by light quanta with higher energy than the light emitted from

[*] Dr. J. Lee, Prof. Dr. N. A. Kotov
Department of Chemical Engineering
Department of Materials Science and Engineering and
Department of Biomedical Engineering
University of Michigan
Ann Arbor, MI 48109 (USA)
Fax: (+1) 734-764-7454
E-mail: kotov@umich.edu
Prof. Dr. A. O. Govorov
Department of Physics and Astronomy
Ohio University
Athens, OH 45701 (USA)

[**] This work was supported in part by an NSF-CAREER award (N.A.K.), NSF-Biophotonics (N.A.K.), AFOSR (N.A.K.), the University of Michigan (N.A.K.), and Ohio University (A.O.G.).

Supporting information for this article is available on the WWW under http://www.angewandte.org or from the author.

© 2005 Wiley-VCH Verlag GmbH & Co. KGaA, Weinheim

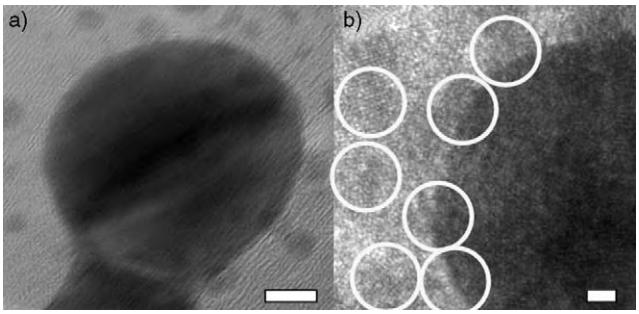

Figure 2. TEM images of the superstructure formed by conjugation of the CdTe NPs with the Au NPs: a) 5×10^5, and b) 10^6 magnification (in each case the bar represents 5 nm). The circles indicate the areas in which characteristic lattice fringes of 0.352 nm for the cubic zinc blende structure of CdTe can be seen after conjugation with PEG.

the NP, but it is well-documented for CdTe.[12,13] The mechanism of the excitation may include two-photon absorption as well as one-photon promotion of the charge carriers from thermally excited levels, yielding a complex curve with both second- and first-order dependence on the intensity of the incident light.[28] Regardless of the excitation pathway, luminescence induced by light below the absorption threshold is very useful for analytical applications because it allows effective elimination of the scattered light from the excitation source.

The similarity of the energies of the Au NP plasmon (549 nm) and the CdTe NP exciton (568 nm) results in resonance conditions in the superstructure (Figure 1). Once the exciton in the CdTe NP is generated, it induces oscillations of the electron density in the Au NP, that is, the plasmon. The resonance between them has two effects on the emission of CdTe: 1) It results in the enhancement of the luminescence intensity of the NPs at 568 nm, when the gap between the particles closes. In contrast to earlier reports on the fluorescence quenching of semiconductor colloids by gold particles,[14,15] we consistently observe a strong enhancement of the CdTe luminescence upon attachment of Au NPs, as long as certain geometrical rules are observed and the diameters selected match the resonance conditions.[16] The reasons behind this difference in observations can be understood from the theoretical description below. 2) The resonance conditions make the luminescence intensity very sensitive to the interparticle distance,[16] which is a convenient feature for analytical applications.[29,30] This complements the high signal-to-noise ratio that could result with two-photon emission. For a different geometrical arrangement—for instance, when a gold NP is attached to a CdTe nanowire, as described in our previous study[16]—a single Au NP may not produce any enhancement effect at all because of diffusion of the exciton along the nanowire. In this case, only the collective action of many NPs can provide a substantial enhancement of the emission.[16] Furthermore, the diameter of the Au NP also makes a substantial difference and, depending on the absorption peak of the Au colloid, one may not see any enhancement effect and even observe quenching of the semiconductor emission.

The temperature of the CdTe–PEG–Au dispersion was varied between 20 and 60 °C by a heating/cooling circulator (NESLAB, EX-111, USA). The conformation of the PEG can be altered as a response to the thermodynamic energy in the media. Despite the fact that PEG and PEO (poly(ethylene oxide)) have high critical temperatures, an increase in the temperature from 20 to 50 °C results in swelling of the PEG molecule and an increase in its diameter.[17,18] This alters the distance between the particles, which should produce a concomitant change in the luminescence output. Indeed, the superstructure shows a clear temperature dependence for the PL intensity. A high concentration of PEG segments attached to the Au surface can introduce additional differences compared to the classical case of diluted solutions of PEG.

A higher temperature leads to a decrease in the luminescence due to the more extended conformation of the PEG chain, and vice versa (Figure 3a, b). The non-PEG bonded system did not display any temperature dependence (see Supporting Information). Importantly, the process is totally reversible, showing less than 10% photodegradation with every temperature cycle (1500 s).

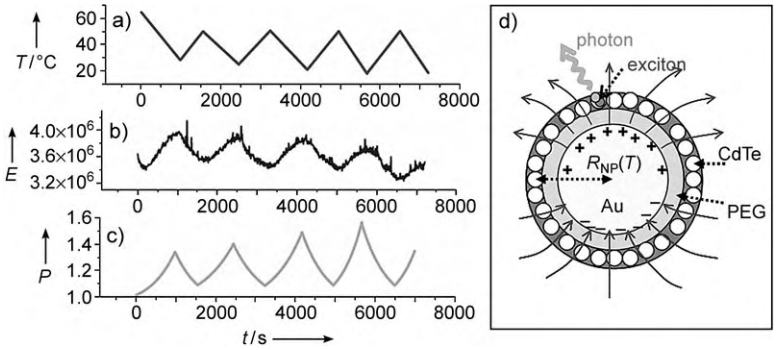

Figure 3. Variation in the PL intensity E (b) of the PEG-tethered Au and CdTe NPs depending on the temperature T (a); c) calculated photon-field enhancement factor P of the CdTe NPs as a function of time. d) Schematic representation of the dielectric model used for calculating the curve in (c) as well as the plasmon excitation with associated field lines; the plasmon excitation inside an Au nanosphere interacts with excitons in the CdTe NPs through electric fields. The distance $R_{NP}(T)$ varies with the temperature. The curve in (c) also represents a theoretical dielectric model of the NP assembly in which the CdTe NPs form a continuous spherical shell around the Au NP.

Calculations demonstrate that the change in the PEG-controlled distance between the NPs is the cause of the observed modulations in emission intensity. The photon-field enhancement factor P inside the CdTe NPs determines the probability of photon emission by an exciton trapped in a CdTe NP. Therefore, the emission intensity is proportional to the factor P [Eq. (1); where E_0 is the external electric field

$$P(\omega,R_{NP}) = \langle E^2\rangle_\Omega / E_0^2 \qquad (1)$$

inside a CdTe NP without the Au subsystem, E is the electric field in the presence of an Au NP averaged over the solid

 © 2005 Wiley-VCH Verlag GmbH & Co. KGaA, Weinheim

angle Ω, R_{NP} is the position of the CdTe NPs with respect to the center of the superstructure (Figure 3d), and ω is the laser frequency].

We use here a simplified model which approximates a granular, molecular spring superstructure (Figures 1 and 2) as an Au sphere surrounded by polymer molecules and the CdTe shell (Figure 3d). We see no evidence of clustering of Au particles in the TEM images, which also supports the suggested theoretical model. Mathematical treatment of all CdTe NPs individually could be useful, but requires sophisticated numerical simulations. At the same time, a simple shell model reveals the physical essence of the phenomenon, which is important for the further development of similar superstructures. Note that the majority of Au NPs are faceted (see Supporting Information). While being mindful of the potential electric field aberrations caused by face edges, we consider them to be secondary effects in comparison to the model approximation.

Thus, treating an Au NP as a sphere and a collection of CdTe NPs as a spherical shell, we can analytically calculate the electric fields induced around the Au NP by matching the electrical boundary conditions and involving the first spherical harmonics.[19] After averaging over Ω, we obtain Equation (2), where B and C are complicated functions of the

$$P(\omega,R_{NP}) = \frac{|B| + 2|C^2|/R_{NP}^6}{E_0^2} \quad (2)$$

dielectric constants of the metal ($\varepsilon_m(\omega)$), PEG (ε_0), and CdTe ($\varepsilon_{CdTe} = 7.2$; see Supporting Information). In addition, the coefficients B and C are dependent on the radii of the spherical shells in our model. The function $\varepsilon_m(\omega)$ for the Au NPs was taken from reference [20]. Since the UV/Vis absorption of the Au NPs is dependent on the dielectric constant of the environment, the effective value of ε_0 of the surrounding media was taken as the dielectric constant of PEG (2.3).[21] Yun et al.[29] reported a $1/R^4$ dependence of fluorescence quenching by small Au NPs. The geometry of our system seems to be an even better match for $1/R^4$ distance dependence than that in reference [29], because the diameter of the Au NPs is large, and therefore the NP may behave like a surface. Nevertheless, Equation (2) (with $1/R^6$) was used because 1) a resonance process is better described by a dipole–dipole rather than a dipole–surface model, 2) it is a more general description, which could be applied for a variety of similar systems, and 3) expressions for corresponding coefficients are known, as opposed to those in the equation with $1/R^4$. R_{NP} was determined by the radius of gyration of PEG, R_{PEG}. On the basis of literature data,[22,23] R_{PEG} of PEG with a molecular weight of 3400 Da is 2–4 nm. The temperature-induced changes in the 20–60 °C range constitute 20–30 % of the polymer globule volume ratio, that is, changes in R_{PEG} of 0.6–1.2 nm.[24] In view of the fairly small change in the overall diameter of the Au–PEG–CdTe superstructure (ca. 26 ± 1.5 nm) caused by the conformational changes in PEG, the difference between the equations with $1/R^4$ and $1/R^6$ is not that essential here, except for the fact that a $1/R^6$ dependence should give stronger optical effects, which seems to be the case. Also note that light scattering plays a small role in the observed effect of luminescence enhancement. Assuming a linear dependence of $R_{PEG}(T) = 3\,\text{nm} + 1\,\text{nm}\,(T - 30\,°\text{C})/30\,°\text{C}$, one arrives at Equation (3). The high sensitivity of the NP

$$R_{NP}(T) = 11.8\,\text{nm} + R_{PEG}(T) = 14.8\,\text{nm} + (T - 30\,^o\text{C})/30\,^o\text{C} \quad (3)$$

emission to temperature in our superstructures arises from two factors: 1) The value of P rapidly decreases with Au–CdTe distance (approximately as R_{NP}^6), and 2) the exciton energy is very close to the plasmon resonance, which leads to a plasmon enhancement of emission. Equation (2) for the emission-enhancement factor has rather a complicated distance dependence caused by the multiple-shell structure. For $R_{NP} = 15$–16 nm, the plasmon-enhanced electric field and corresponding enhancement factor rapidly decrease with distance.

Compared with other approaches to sensing with nanocolloids,[4] the expansion and contraction of molecular springs represents a very sensitive transduction mechanism for chemical detection: Any change in the dimensions of the superstructure results in a shift of the plasmon resonance with respect to the exciton energy and subsequently in a reduction of the enhancement factor. Our theoretical analysis shows that, depending on the resonance conditions, the presence of Au can either increase or decrease the fluorescence of CdTe. For example, if the plasmon peak moves towards the exciton resonance with constriction of PEG, we may obtain the enhancement effect. If the plasmon peak is shifted away from the exciton energy, the fluorescence intensity can decrease. Substitution of $R_{NP}(T)$ into the equation for $P(\omega,R_{NP})$ for $\hbar\omega = 2.2$ eV, corresponding to a resonance wavelength of 568 nm, provides an analogue of the experimental $I(T)$ curve calculated in terms of photon-field enhancement factors (Figure 3c). The amplitude of the temperature zig-zag for $P(\omega,R_{NP})$ is about 30 %. This correlates very well with the variation of the emission intensity in our experiments (Figure 3a, b). The slightly lower amplitude registered in the experiment can be attributed to steric hindrance in the CdTe corona around the Au NP, preventing formation of the perfect CdTe NP shell assumed for our model. The linearity of the temperature response (Figure 3a) can be deceptive, because all the processes here are highly nonlinear. This becomes visible in the calculated results shown in Figure 3c.

Thus, the CdTe–PEG–Au system is an example of a nanoscale superstructure that undergoes a reversible structural change in response to the environmental conditions. The combination of this property with plasmon–exciton interactions that display a high sensitivity of the optical output on the distance modulations represents the foundation of a new family of sensing and optoelectronic devices.

Experimental Section

The CdTe NPs (3.7 nm in diameter with an emission at 568 nm) were synthesized according to the literature.[25] They were conjugated to the flexible spacer PEG and then linked to Au NPs (20 nm in diameter with a surface plasmon peak at 549 nm) to form molecular spring-type structures. The level of structural control necessary to produce molecular spring assemblies from NPs as shown in the insert

 © 2005 Wiley-VCH Verlag GmbH & Co. KGaA, Weinheim

of Figure 1, rather than disorganized aggregates, was possible because the PEG oligomer had two different functional groups at the ends of the chain, NHS and Boc (Boc–NH–PEG–COO–NHS; molecular weight 3400 Da, Nektar, AL). The stabilizer, cetyltrimethylammonium bromide (CTAB, Aldrich, Milwaukee, WI) of the Au NPs was substituted with L-cysteine (Aldrich, Milwaukee, WI) in order to obtain the NH_2 functional group. The PEG (10 mg) was dissolved in deionized water (560 μL) and dimethyl sulfoxide (DMSO, 140 μL). This solution (700 μL) was mixed with the solution of the Au NPs (700 μL), and gently stirred at room temperature for 12 h. This procedure resulted in conjugation of the NHS terminus with NH_2 group of the NP stabilizer through a covalent amide linkage. Then the Boc protecting group was removed by treatment with trifluoroacetic acid (TFA, 5 μL) for 20 min.[26] The regenerated NH_2 terminus of PEG can be conjugated to a CdTe NP by standard conjugation techniques, that is, EDC/sulfo-NHS cross-linking,[16,27] resulting in covalent attachment of CdTe to the PEG chain on the end opposite to the Au NP.

Received: April 11, 2005
Revised: July 22, 2005
Published online: October 18, 2005

Keywords: excited states · luminescence · nanoparticles · poly(ethylene glycol) · thermal expansion

[1] M. Bruchez, Jr., M. Moronne, P. Gin, S. Weiss, A. P. Alivisatos, *Science* **1998**, *281*, 2013 – 2016.
[2] R. Levy, N. T. K. Thanh, R. C. Doty, I. Hussain, R. J. Nichols, D. J. Schiffrin, M. Brust, D. G. Fernig, *J. Am. Chem. Soc.* **2004**, *126*, 10076 – 10084.
[3] C. A. Mirkin, R. L. Letsinger, R. C. Mucic, J. J. Storhoff, *Nature* **1996**, *382*, 607 – 609.
[4] C. M. Niemeyer, *Biochem. Soc. Trans.* **2004**, *32*, 51 – 53.
[5] T. Mokari, E. Rothenberg, I. Popov, R. Costi, U. Banin, *Science* **2004**, *304*, 1787 – 1790.
[6] D. V. Talapin, E. V. Shevchenko, C. B. Murray, A. Kornowski, S. Foerster, H. Weller, *J. Am. Chem. Soc.* **2004**, *126*, 12984 – 12988.
[7] A. L. Rogach, *Angew. Chem.* **2004**, *116*, 150 – 151; *Angew. Chem. Int. Ed.* **2004**, *43*, 148 – 149.
[8] F. R. Aussenegg, H. Brunner, A. Leitner, C. Lobmaier, T. Schalkhammer, F. Pittner, *Sens. Actuators B* **1995**, *29*, 204 – 209.
[9] T. Schalkhammer, C. Lobmaier, F. Pittner, A. Leitner, H. Brunner, F. R. Aussenegg, *Sens. Actuators B* **1995**, *24*, 166 – 172.
[10] N. Gaponik, D. V. Talapin, A. L. Rogach, K. Hoppe, E. V. Shevchenko, A. Kornowski, A. Eychmueller, H. Weller, *J. Phys. Chem. B* **2002**, *106*, 7177 – 7185.
[11] Z. Tang, N. A. Kotov, M. Giersig, *Science* **2002**, *297*, 237 – 240.
[12] M. Goppert-Mayer, *Ann. Phys.* **1931**, *9*, 273 – 294.
[13] A. G. Joly, W. Chen, D. E. McCready, J. O. Malm, J. O. Bovin, *Phys. Rev. B* **2005**, *71*, 165304.
[14] S. Chen, K. Kimura, *Chem. Lett.* **1999**, 233 – 234.
[15] Z. Gueroui, A. Libchaber, *Phys. Rev. Lett.* **2004**, *93*, 166108.
[16] J. Lee, A. O. Govorov, J. Dulka, N. A. Kotov, *Nano Lett.* **2004**, *4*, 2323 – 2330.
[17] C. Branca, A. Faraone, S. Magazu, G. Maisano, P. Migliardo, V. Villari, *J. Mol. Struct.* **1999**, *482–483*, 503 – 507.
[18] C. Branca, S. Magazu, G. Maisano, P. Migliardo, V. Villari, *J. Phys. Condens. Matter* **1998**, *10*, 10141 – 10157.
[19] L. D. Landau, E. M. Lifshitz, *Electrodynamics of Continuous Media*, Pergamon, New York, **1960**, p. 413.
[20] M. Quinten, *Z. Phys. B* **1996**, *101*, 211 – 217.
[21] U. Raviv, J. Frey, R. Sak, P. Laurat, R. Tadmor, J. Klein, *Langmuir* **2002**, *18*, 7482 – 7495.
[22] J. D. Ferry, *Viscoelastic Properties of Polymers*, 3rd ed., Wiley, New York, **1980**.
[23] A. F. M. Barton, *CRC Handbook of Polymer–Liquid Interaction Parameters*, CRC, Boca Raton, FL, **1990**.
[24] J. C. Munro, C. W. Frank, *Langmuir* **2004**, *20*, 3339 – 3349.
[25] A. L. Rogach, D. V. Talapin, H. Weller in *Colloids and Colloidal Assembly* (Ed.: F. Caruso), Wiley-VCH, Weinheim, **2004**, pp. 52 – 95.
[26] S. Westenhoff, N. A. Kotov, *J. Am. Chem. Soc.* **2002**, *124*, 2448 – 2449.
[27] G. T. Hermanson, *Bioconjugate Techniques*, Academic Press, San Diego, **1995**, p. 786.
[28] B. Ozturk, J. Lee, N. A. Kotov, unpublished results.
[29] C. S. Yun, A. Javier, T. Jennings, M. Fisher, S. Hira, S. Peterson, B. Hopkins, N. O. Reich, G. F. Strouse, *J. Am. Chem. Soc.* **2005**, *127*, 3115 – 3119.
[30] C. Sönnichsen, B. M. Reinhard, J. Liphardt, A. P. Alivisatos, *Nature Biotechnol.* **2005**, *23*,741 – 745.

 © 2005 Wiley-VCH Verlag GmbH & Co. KGaA, Weinheim

Reaction Mechanisms

DOI: 10.1002/anie.200502243

Rate Enhancement by Ethylene in the Ru-Catalyzed Ring-Closing Metathesis of Enynes: Evidence for an "Ene-then-Yne" Pathway that Diverts through a Second Catalytic Cycle**

Guy C. Lloyd-Jones, Robert G. Margue, and Johannes G. de Vries*

The ring-closing metathesis (RCM) of enynes [**1**→**2**, Eq. (1)] was first reported by Katz and Sivavec in 1985.[1]

1 **2** (1)

A tungsten–alkylidene precatalyst was employed and, on the basis of mechanistic studies on alkene/alkyne metathesis copolymerization, a Chauvin-type[2] mechanism involving an "yne-then-ene" sequence was proposed (Scheme 1, cycle A).

[*] Prof. Dr. G. C. Lloyd-Jones, R. G. Margue
School of Chemistry
University of Bristol
Cantock's Close, Bristol BS8 1TS (UK)
Fax: (+44) 117-929-8611
E-mail: guy.lloyd-jones@bris.ac.uk
Prof. Dr. J. G. de Vries
DSM Research
Life Sciences-Advanced Synthesis
Catalysis & Development
PO Box 18, 6160 MD Geleen (The Netherlands)

[**] We thank C. Henry, M. D. Weller, and Dr. N. S. Hodnett for expert technical assistance in the early phases of this work and DSM Research, Life Sciences-Advanced Synthesis, Catalysis & Development for generous funding.

 InterScience © 2005 Wiley-VCH Verlag GmbH & Co. KGaA, Weinheim

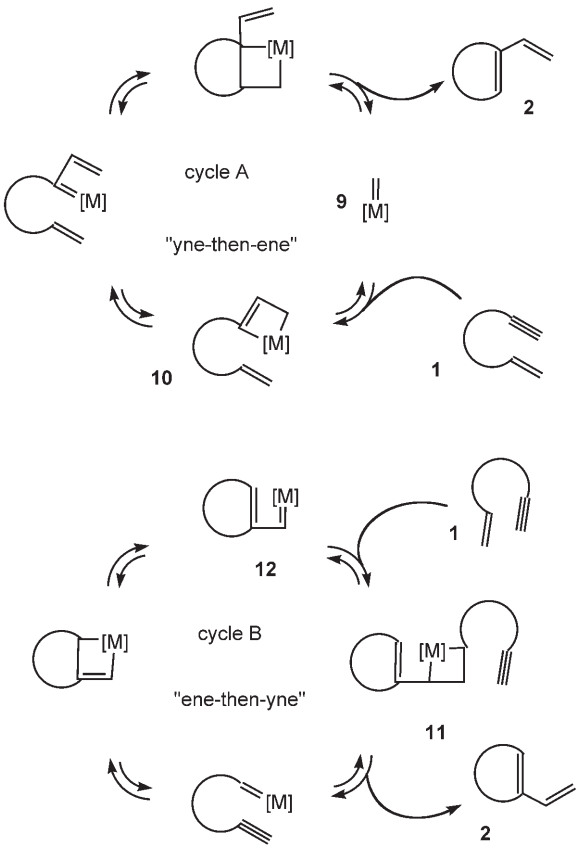

Scheme 1. The "yne-then-ene" (A) and "ene-then-yne" (B) mechanisms for RCM of enyne **1** proceeding intermolecularly via metal alkylidene intermediates.

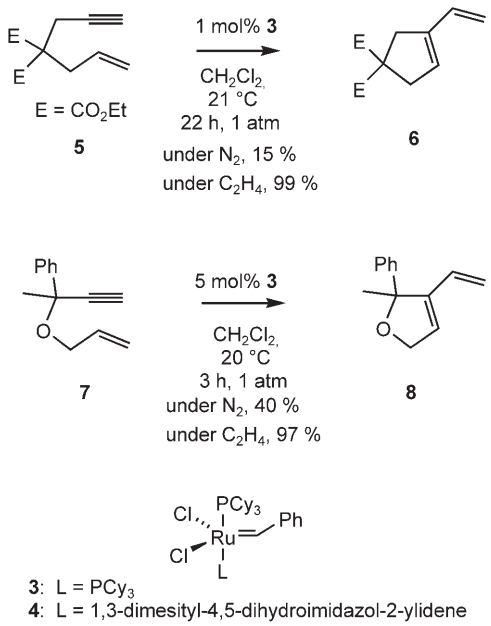

Scheme 2. The effect of ethylene ("Mori's conditions"[10]) on the Ru-catalyzed RCM of enynes **5** and **7**.

Subsequent reports by Hoye and co-workers[3] and by Mori and co-workers[4] on analogous Mo- and Cr-based carbene precatalysts also invoked mechanism A, which neatly accounted for a number of side products, for example, vinyl cyclopropanes, by reductive elimination in the metallacyclobutane intermediate.

With the advent of Ru-based alkylidene precatalysts (for example, **3**[5] and **4**,[6] Scheme 2), both enyne RCM and alkene/alkyne co-metathesis have enjoyed rapidly increasing application.[7] Possibly as a legacy from the earlier work with catalysts based on Group VI elements,[1,3,4] the "yne-then-ene" mechanism (A) is commonly postulated for the Ru-catalyzed enyne RCM reaction.[8,9]

In 1998, Mori et al. reported that ethylene can have a dramatic effect on the yield of Ru-catalyzed enyne RCM reactions, for example, in the conversion of enyne **5** into diene **6** (Scheme 2).[10] We have recently been investigating the RCM of allyl propargyl ethers,[11] for example, **7**→**8**, which also improves under ethylene (Scheme 2). It is of note that the rate of RCM of **5** is increased by ethylene more than that of **7**.

The beneficial effect of ethylene on some RCM reactions has led to "Mori's conditions"[10] being widely adopted[7a,12] to increase yields and inhibit side reactions such as epimerization,[12d] and substrate homo-cross-metathesis.[12c,g] The origin of the ethylene effect has been ascribed to the attenuation of unproductive resting states in equilibrium with the ruthenium methylidene **9** in cycle A.[10] However, such a "protective effect"[7a] would be expected to increase catalyst longevity rather than increase the reaction rate. Moreover, the effect should be operative across the full range of enynes,[12i–k] and it should extend to the RCM of the corresponding dienes.[13] An alternative explanation would be that ethylene acts as an initiator, which converts the precatalyst, for example, **3**, into the active intermediate **9** in cycle A by cross-metathesis. To test this supposition, we alternated the atmosphere above a RCM of enyne **5** (5 mol% **3**, CH_2Cl_2, 21°C) between N_2 (1 atm) and ethylene (1 atm) during the reaction. Irrespective of the extent of conversion of the substrate, catalysis always accelerated on switching to an ethylene atmosphere, and decelerated on returning to N_2, which refutes an initiation effect and emphasises that ethylene accelerates a net catalytic turnover.

An alternative mechanism for enyne RCM under standard conditions has also been proposed.[14] However, this "ene-then-yne" sequence (Scheme 1, cycle B) is seldom considered, despite a growing body of evidence.[14,15] Herein, we present ^{2}H- and ^{13}C-labeling strategies that probe the origin of the ethylene acceleration and its relationship to the mechanistic dichotomy (cycles A versus B) in Ru-catalyzed enyne RCM.

Starting with reactions conducted in the absence of ethylene, we focused on the steps in mechanisms A and B that generate the vinyl terminus (the methylene group) in the RCM product **2**. In cycle A this involves ring opening of ruthenacyclobutene **10** in which there are no C-based stereogenic centers in the ring. In cycle B, this involves ring opening of ruthenacyclobutane **11** in which there are two C-based stereogenic centers, and thus two diasteroisomeric forms. We have been able to probe for diastereoselectivity in this transient species[16] by use of stereospecifically labeled enyne substrate ((*E*)- and (*Z*)-[^{2}H]-**1**).[17]

 © 2005 Wiley-VCH Verlag GmbH & Co. KGaA, Weinheim

As illustrated for (*E*)-[^{2}H]-**1** in Scheme 3, pathway A is predicted to generate [^{2}H]-**2** with no *E*/*Z* selectivity at the CH=C(D)H group.[17] In contrast, in pathway B, any net diastereoselectivity in the formation and breakdown of [^{2}H]-**11**, will translate into *E*/*Z* selectivity, as the relative configuration of the CHD and CHR′ centers in **11** are determined by the geometry of the alkene substrate. Thus, isomeric substrate (*Z*)-[^{2}H]-**1** should give the opposite isomer of product [^{2}H]-**2**.

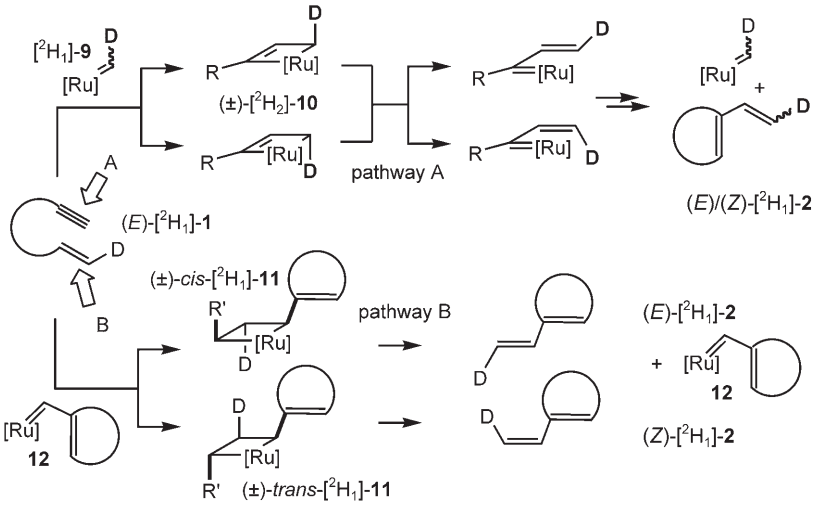

Scheme 3. The stereochemical outcome of RCM of stereospecifically labeled enyne ((*E*)-[^{2}H$_1$]-**1**) by mechanisms A and B. Note that the ruthenacyclobutane ring in **11** may well adopt a cyclobutane-like puckered structure. The deuterium atoms are marked in bold when they are derived from the alkylidene to differentiate them from those that are derived from the alkene.

Ru-catalyzed RCM reactions of enynes (*E*)-[^{2}H$_1$]-**7** and (*Z*)-[^{2}H$_2$]-**7** gave (*Z*)-[^{2}H$_1$]-**8** and (*E*)-[^{2}H$_2$]-**8**, respectively, with 68–69% selectivity irrespective of the precatalyst (Scheme 4). These results are consistent with pathway B operating in which the major flux is via the *trans* diastereomer of **11**.[18] Identical selectivities were found with the Fürstner–Ackermann catalyst system,[19] and also with an achiral analogue of (*Z*)-[1,7-^{2}H$_2$]-**7** in which the Me and Ph groups were replaced by a pentane-1,5-diyl system. The slower-reacting malonate substrate **5**, which has similar steric hindrance at the allylic and propargylic positions, proceeded with lower but analogous selectivity: (*Z*)-[^{2}H$_1$]-**5** gave (*E*)-[^{2}H$_1$]-**6** (55% (*E*)).

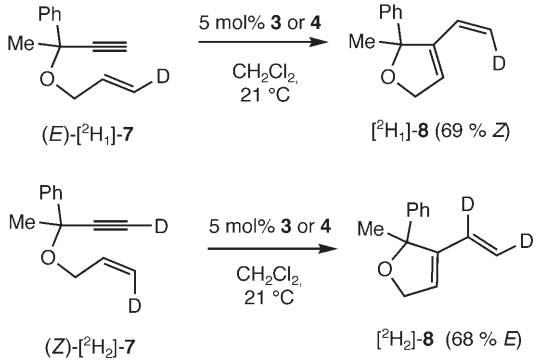

Scheme 4. Ru-catalyzed RCM of stereospecifically ^{2}H-labeled enynes. Note that the alkynyl ^{2}H label in (*Z*)-[^{2}H$_2$]-**7** arises from the synthesis and is present only as a spectator label.

The ene-then-yne sequence (cycle B) also provides a simple mechanistic rationale for the effect of ethylene (Scheme 5). The vinylalkylidene[20] complex **12**, which reacts with substrate **1** to liberate **2** via **11** on the primary cycle (B1), can also react with ethylene, as a surrogate alkene for **1**,[15] to liberate RCM product **2** via complex **13** (upper section of Scheme 5). The resulting ruthenium–methylidene complex **9**, which is identical to that found in the yne-then-ene sequence (cycle A), can rejoin the *primary* catalytic cycle (B1) by reacting with the substrate (**1**) and releasing ethylene, thereby creating a secondary cycle that is *catalyzed* by ethylene.

To investigate the possibility of turnover through a secondary cycle, we conducted RCM reactions under an atmosphere of [^{13}C$_2$]ethylene. In cycle A, cross-metathesis equilibration of [^{13}C$_2$]ethylene with Ru–methylidene **9** will lead to [^{13}C$_n$]-**9** ($n=0$ or 1). This labeled methylidene compound can then generate [^{13}C$_1$]-**2** and **9** by RCM, with the ^{13}C/^{12}C ratio in the terminal alkene of **2** being determined by the **9**/[^{13}C$_1$]-**9** ratio. In mechanism B, the primary cycle (B1) will generate unlabeled **2**, and the secondary cycle B2 will generate [^{13}C$_1$]-**2** (via [^{13}C$_2$]-**13**; see the filled circles in Scheme 5), with the ^{13}C/^{12}C ratio then being determined by B1/B2 partitioning. In addition, three more processes that can affect the ^{13}C/^{12}C ratio in **2** must be considered. Firstly, cross-metathesis of labeled methylidene [^{13}C$_1$]-**9** with the terminal alkene in **1** will generate [^{13}C$_1$]-**1**, which on RCM by pathway B1 will generate [^{13}C$_1$]-**2**. Secondly, cross-metathesis of product (**2**) with [^{13}C$_1$]-**9** will generate [^{13}C$_1$]-**2** by a non-RCM pathway. Finally, insufficiently rapid exchange of solution-phase ethylene with the bulk gaseous phase will result in temporary depletion of [^{13}C$_2$]ethylene, and enrichment of [^{13}C$_n$]ethylene ($n=0$, 1), in the solution phase. From the above analysis it is thus clear that the extent of ^{13}C incorporation in **2** cannot alone be used to distinguish mechanisms A and B.

To address this issue, we have designed a dual-substrate, dual-labeling strategy. The experiment involves RCM of a 1/1 mixture of two enynes (**5** and **7**) for which the accelerating effect of ethylene is different: the rate of RCM for the slower-reacting enyne **5** is increased 2.8 times over that of the faster-reacting enyne **7**.[21] This differential acceleration results in similar rates of RCM for **5** and **7** under ethylene (8.3×10^{-4} and 9.7×10^{-4} s^{-1}, respectively).

Conducting the reaction under [^{13}C$_2$]ethylene (1 atm, 930 mol%) gives [^{13}C$_1$]-**6**/**6** and [^{13}C$_1$]-**8**/**8.** As controls for the experiment, the reaction mixture also included 10 mol% of [D$_7$]-**6**/[D$_5$]-**8**, to allow estimation of the extent of ^{13}C$_1$ incorporation into **6** and **8** by non-RCM pathways, as well as any reversibility of the reaction (Scheme 6).

Samples taken over the entire course of the reaction were analyzed by GC and GCMS. The resulting incorporations of ^{13}C (%) in substrates **5** and **7**, products **6** and **8**, and reference products [D$_7$]-**6** and [D$_5$]-**8** as a function of conversion are shown in Figure 1.

 © 2005 Wiley-VCH Verlag GmbH & Co. KGaA, Weinheim

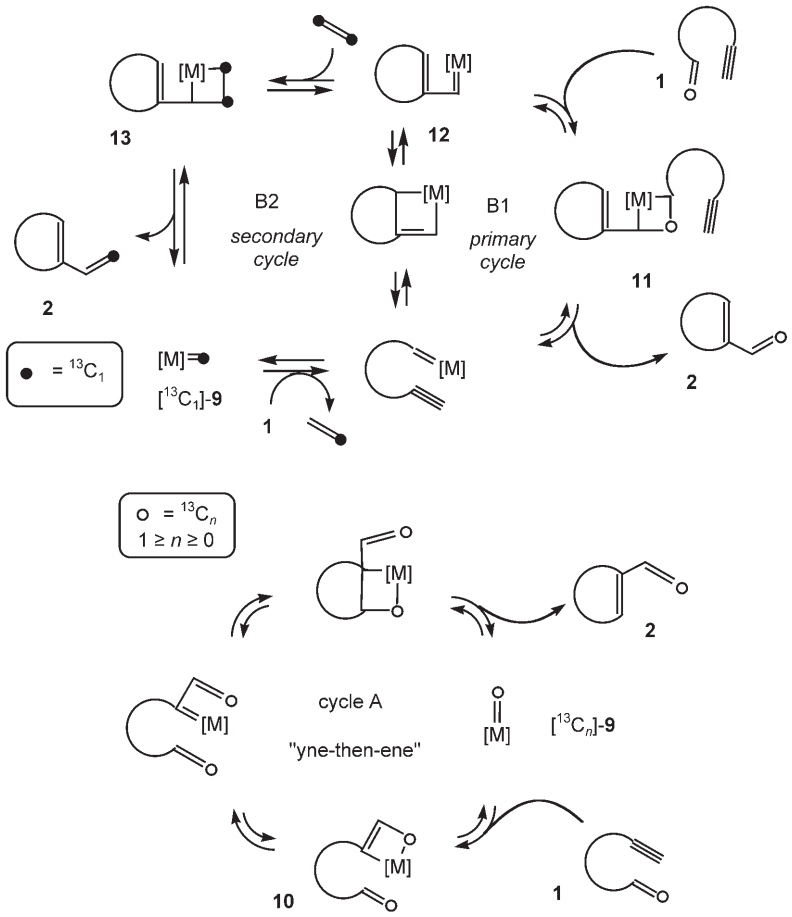

Scheme 5. Adaptation of Scheme 1, to include a secondary cycle (B2) that is catalyzed by ethylene, as well as the ^{13}C-labeling patterns predicted for cycles A and B when reaction is conducted under [$^{13}C_2$]ethylene. Partial ^{13}C incorporation at the alkene terminus of enyne **1** arising from degenerate metathesis with [$^{13}C_n$]-**9** ($1 \geq n \geq 0$) is also shown.

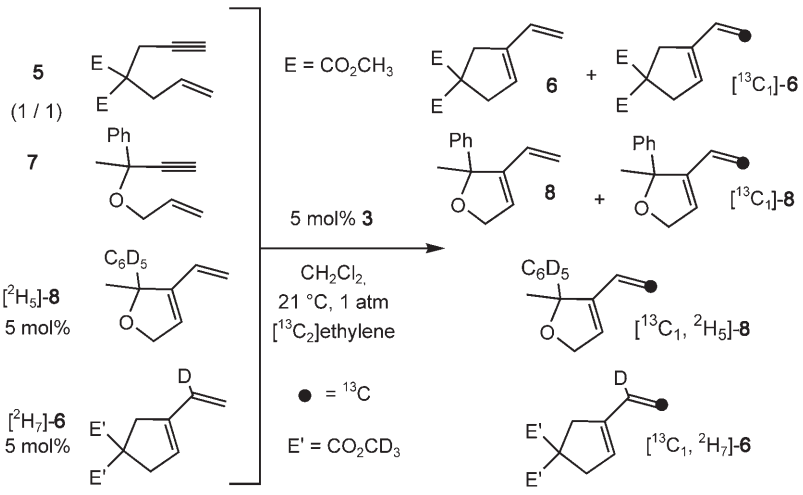

Scheme 6. A dual-substrate/dual-labeling strategy for detection of preturnover/postturnover ^{13}C-label incorporation and distinction of enyne RCM through mechanisms A and B. $[\mathbf{5}]_0 + [\mathbf{7}]_0 = 0.08$ M.

The analysis demonstrates that non-RCM incorporation of ^{13}C into both the substrates and the products becomes increasingly competitive as the reaction evolves. Moreover, further control experiments showed that the rate of equilibration of [$^{13}C_n$]ethylene between the gas and solution phases under the reaction conditions ($t_{0.5} = 83 \pm 4$ s)[22] is only one order of magnitude faster than catalyst turnover, and thus all three factors outlined above affect the $^{13}C/^{12}C$ incorporation. Nonetheless, the dual-substrate, dual-labeling approach allows the distinction of mechanisms A and B as follows. In mechanism A, although the RCM reactions of **5** and **7** have been accelerated to different extents, the $^{13}C/^{12}C$ incorporation into **6** and **8** at any time in the reaction will be determined by the **9**/[$^{13}C_1$]-**9** ratio, and will thus be *equal*. In mechanism B, enyne **5**, whose RCM is accelerated by the ethylene more than **7**, will partition more through pathway B2, thus giving rise to a greater level of ^{13}C incorporation. The ratio of $^{13}C/^{12}C$ incorporation in **6** versus **8** should thus reflect the 2.8-fold difference in acceleration by ethylene for **5** versus **7**.

In the first half of the reaction an approximately linear relationship is found between the $^{13}C/^{12}C$ ratio at the vinyl terminus in **6** and **8** and the extent of the reaction (Figure 2). The steeper gradient observed for **6**, relative to that for **8**, arises from the more rapid non-RCM incorporation of ^{13}C, as revealed by the analyses in Figure 1. Extrapolating the two relationships in Figure 2 to 0% conversion, gives the initial ratio of $^{13}C/^{12}C$ incorporations for **6** and **8** as 2.3 ± 0.6:1, which is in good agreement with the ratio of 2.8:1 predicted by mechanism B,[23] and significantly greater than the ratio of 1.0:1 predicted by mechanism A. It can thus be concluded that the reaction of enyne **7** (→**8**) under ethylene does *not* proceed predominantly through pathway A. Moreover, the differential $^{13}C/^{12}C$ incorporation data strongly supports the proposal that both processes (**5**→**6** and **7**→**8**) proceed predominantly through pathway B2 under ethylene.[24]

In summary, isotopic labeling experiments (^2H and ^{13}C) of Ru-catalyzed enyne ring-closing metathesis reactions involving enynes **5** and **7** give results that are not compatible with the commonly proposed yne-then-ene mechanism (cycle A).[23] The results are however explained by the alternative ene-then-yne mechanism (cycle B) for which ethylene can *catalyze* the reaction by diversion of the vinylalkylidene intermediate **12** on the primary cycle B1[14] onto a *second cycle* B2.[15] The use of "Mori's conditions" (conducting Ru-catalyzed enyne RCM reactions under ethylene) is wide-

 © 2005 Wiley-VCH Verlag GmbH & Co. KGaA, Weinheim

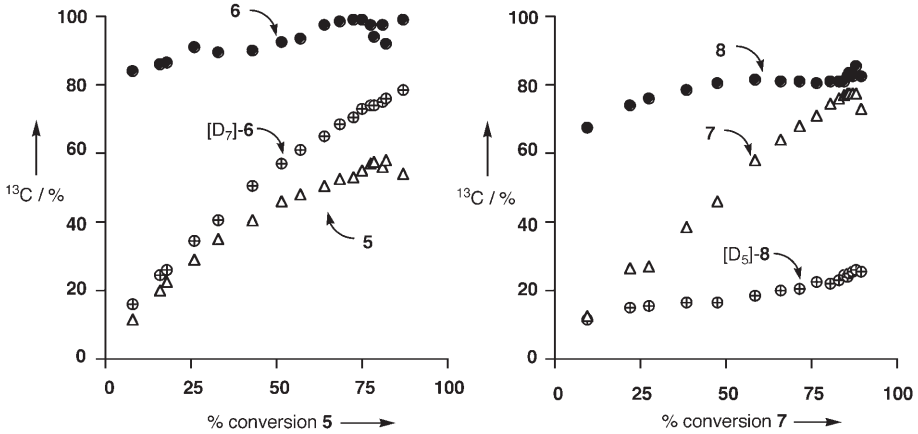

Figure 1. Relationships between ^{13}C incorporation (%) at the vinyl terminus (*y* axis) in substrates and products as a function of conversion (*x* axis) for the co-reaction of **5**, [D$_7$]-**6**, **7**, and [D$_5$]-**8** as shown in Scheme 6.

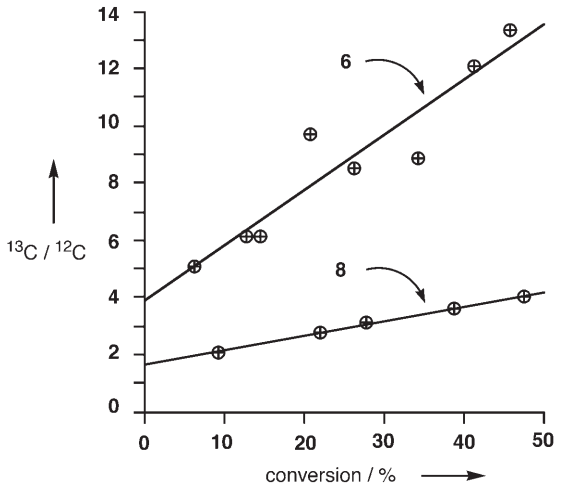

Figure 2. The ^{13}C/^{12}C ratio at the vinyl terminus (*y* axis) in **6** and **8** as a function of conversion (*c*, %, *x* axis) of **5** and **7**. The linear regressions are: $^{13}C/^{12}C = 0.19 \pm 0.03\,c + 3.86 \pm 0.82$ and $^{13}C/^{12}C = 0.05 \pm 0.002\,c + 1.65 \pm 0.05$, respectively.

spread, and thus mechanism B may apply to a broader range of substrates than previously considered.

Received: June 25, 2005
Published online: October 20, 2005

Keywords: carbenes · isotopic labeling · metathesis · reaction mechanisms · ruthenium

[1] T. J. Katz, T. M. Sivavec, *J. Am. Chem. Soc.* **1985**, *107*, 737–738.
[2] J.-L. Hérisson, Y. Chauvin, *Makromol. Chem.* **1971**, *141*, 161–176.
[3] P. F. Korkowski, T. R. Hoye, D. B. Rydberg, *J. Am. Chem. Soc.* **1988**, *110*, 2676–2678.
[4] S. Watanuki, N. Ochifuji, M. Mori, *Organometallics* **1994**, *13*, 4129–4130.
[5] E. L. Dias, S. T. Nguyen, R. H. Grubbs, *J. Am. Chem. Soc.* **1997**, *119*, 3887–3897.
[6] a) J. Huang, E. D. Stevens, S. P. Nolan, J. L. Peterson, *J. Am. Chem. Soc.* **1999** *121*, 2674–2678; b) T. Weskamp, F. J. Kohl, W. Hieringer, D. Gleich, W. A. Herrmann, *Angew. Chem.* **1999**, *111*, 2573–2576; *Angew. Chem. Int. Ed.* **1999**, *38*, 2416–2419; c) M. Scholl, S. Ding, C. W. Lee, R. H. Grubbs, *Org. Lett.* **1999**, *1*, 953–956.
[7] For recent reviews of this area see: a) S. T. Diver, A. J. Giessert, *Chem. Rev.* **2004**, *104*, 1317–1382; b) C. Aubert, O. Buisine, and M. Malacria, *Chem. Rev.* **2002**, *102*, 813–834.
[8] The discussion herein is limited to enyne RCM proceeding *intermolecularly* via alkylidene intermediates.
[9] Detailed kinetic investigations on Ru-catalyzed alkene/alkyne co-metathesis have demonstrated that the rate-limiting interaction can involve either the alkene or the alkyne, depending on the substitution patterns: B. R. Galan, A. J. Giessert, J. B. Keister, S. T. Diver, *J. Am. Chem. Soc.* **2005**, *127*, 5762–5763.
[10] a) M. Mori, N. Sakakibara, A. Kinoshita, *J. Org. Chem.* **1998**, *63*, 6082–6083; b) T. Kitamura, Y. Sato, M. Mori, *Adv. Synth. Catal.* **2002**, *344*, 678–693.
[11] G. C. Lloyd-Jones, R. G. Margue, unpublished results.
[12] For additional examples of successful application of "Mori's conditions" see: a) J. S. Clark, R. J. Townsend, A. J. Blake, S. J. Teat, A. Johns, *Tetrahedron Lett.* **2001**, *42*, 3235–3238; b) Q. Yao, *Org. Lett.* **2001**, *3*, 2069–2072; c) C. S. Poulsen, R. Madsen, *J. Org. Chem.* **2002**, *67*, 4441–4449; d) H. Guo, R. J. Madhushaw, F.-M. Shen, R.-S. Liu, *Tetrahedron* **2002**, *58*, 5627–5637; e) M. E. Layton, C. A. Morales, M. D. Shair, *J. Am. Chem. Soc.* **2002**, *124*, 773–775; f) E. C. Hansen, D. Lee, *J. Am. Chem. Soc.* **2003**, *125*, 9582–9583; g) F. Dolhem, C. Lièvre, G. Demailly, *Eur. J. Org. Chem.* **2003**, 2336–2342; h) B. Kang, D.-H. Kim, Y. Do, S. Chang, *Org. Lett.* **2003**, *5*, 3041–3043; for examples of RCM of enynes where "Mori's conditions" are not effective, see: i) M. A. Leeuwenburgh, C. M. M. Appeldoorn, P. A. V. van Hooft, H. S. Overkleeft, G. A. van der Marel, J. H. van Boom, *Eur. J. Org. Chem.* **2000**, 873–877; j) M. Mori, T. Kitamura, N. Sakakibara, Y. Sato, *Org. Lett.* **2000**, *2*, 543–545; k) N. Saito, Y. Sato, M. Mori, *Org. Lett.* **2002**, *4*, 803–805.
[13] The rate of RCM of dimethyl diallyl malonate (cf. dimethyl allyl propargyl malonate **5**) catalyzed by **3** in CH_2Cl_2 was found to be identical under N_2 (1 atm) and ethylene (1 atm), throughout the entire course of the reaction.
[14] Strong supporting evidence for the "ene-then-yne" sequence (cycle B), including NMR spectroscopic observation and isolation of Ru–alkylidenes that are plausible intermediates, has been reported, see: a) T. R. Hoye, S. M. Donaldson, T. J. Vos, *Org. Lett.* **1999**, *1*, 277–279; b) M. P. Schramm, D. S. Reddy, S. A. Kozmin, *Angew. Chem.* **2001**, *113*, 4404–4407; *Angew. Chem. Int. Ed.* **2001**, *40*, 4274–4277; c) E. C. Hansen, D. Lee, *J. Am. Chem. Soc.* **2003**, *125*, 9582–9583; however, to the best of our knowledge, a conclusive method for distinguishing *turnover* by mechanism A versus B has yet to be presented; d) The ene-yne-ene mechanism was suggested for the tandem RCM of a dieneyne: S. H. Kim, N. Bowden and R. H. Grubbs, *J. Am. Chem. Soc.* **1994**, *116*, 10801–10802.
[15] For earlier suggestions that pathway B2 provides a simple explanation for ethylene acceleration see: a) G. C. Lloyd-Jones, *Org. Biomol. Chem.* **2003**, *1*, 215–236; b) C. S. Poulsen, R. Madsen, *Synthesis* **2003**, 1–18; c) J. J. Lippstreu, B. F. Straub, *J. Am. Chem. Soc.* **2005**, *127*, 7444-7457.
[16] Although intermediates such as **11** have not yet been observed under the conditions of catalysis, a ruthenacyclobutane complex

 © 2005 Wiley-VCH Verlag GmbH & Co. KGaA, Weinheim

of the type [LRu(Cl_2)(η^2-$CHCH_2CH$)], where L = 1,3-dimesityl-4,5-dihydroimidazol-2-ylidene) has recently been observed by NMR spectroscopy at low temperatures: P. E. Romero, W. E. Piers, *J. Am. Chem. Soc.* **2005**, *127*, 5032 – 5033.

[17] The "low grade" -CH(D)- stereocenters are expected to exert negligible influence on the direction of ring opening, as evidenced by the complimentarity of the results obtained with (*E*)-[7-$^2H_1$]-**7** and (*Z*)-[1,7-$^2H_2$]-**7**. The magnitude of the selectivity is in vast excess over that expected from any secondary kinetic isotope effect in the addition of [^{2}H]-**9** to [^{2}H]-**1**.

[18] It should be noted that the observed 68.5 % (average) stereoselectivity for [^{2}H]-**7**→[^{2}H]-**8** is that at the end of reaction, during which control experiments indicate progressive scrambling of the *E*/*Z* stereochemistry in the [^{2}H]-**7** (ca. 20 % stereorandomization at 96 % conversion). The selectivity is thus consistent with the maximum range 63/37 to 0/100 A/B with 100 % to 68.5 % diastereoselectivity, respectively. For [^{2}H]-**5**, there is no scrambling during the reaction. The observed selectivity of 55 % is consistent with the range 90/10 to 0/100 A/B with 100 % to 55 % diastereoselectivity, respectively.

[19] A Fürstner, L. Ackermann, *Chem. Commun.* **1999**, 95 – 96.

[20] An η^3-coordination mode in vinylalkylidene complexes has been reported to attenuate the rate of metathesis: see T. M. Trnka, M. W. Day, R. H. Grubbs, *Organometallics* **2001**, *20*, 3845 – 3847.

[21] Reactions displayed reproducible pseudo-first-order kinetics. For **5** and **7**: under N_2: $k_{obs} = 1.1 \times 10^{-4}$ and $3.0 \times 10^{-3}\ s^{-1}$, under ethylene: $k_{obs} = 8.3 \times 10^{-4}$ and $9.7 \times 10^{-4}\ s^{-1}$; where k_{obs} was derived from a simulation of the parallel processes: 1) **1** + [Ru]→**2** + [Ru] (k), 2) [Ru]→inactive (k_{decomp}), where [Ru] = [**3**]$_0$ = 0.004 M and [**1**]$_0$ = [**5**]$_0$ or [**7**]$_0$ = 0.08 M and $k_{obs} = k \times$ [Ru]. For reactions under ethylene $k_{decomp} = 0$, for reactions under N_2, $k_{decomp} = 2 \times 10^{-4}\ s^{-1}$. Although bimolecular catalyst decomposition is probable, the model did not require this level of sophistication for satisfactory fit. The relative rate differential under ethylene = $[((k_{obs}^{5,C_2H_4} - k_{obs}^{5,N_2})/(k_{obs}^{5,N_2}))/((k_{obs}^{7,C_2H_4} - k_{obs}^{7,N_2})/(k_{obs}^{7,N_2}))] = 2.8$.

[22] After completion of the reaction, the liquid phase was replaced with an identical volume of CD_2Cl_2 and allowed to saturate with stirring in the [$^{13}C_n$]ethylene atmosphere. The CD_2Cl_2 was then transferred to an identical vessel containing [$^{12}C_2$]ethylene and the CD_2Cl_2 phase analyzed by ^{1}H NMR spectroscopy every 60 s until equilibrium was established (ca. 600 s). A plot of $-\ln([^{13}C_2]_t]/[^{13}C_2]_{eqm}])$ against t was linear, with the gradient = $(k_f + k_b) = 8.4(\pm 0.3) \times 10^{-3}\ s^{-1}$. The nonstatistical mixture of [$^{13}C_n$]ethylene (94.5 % $n = 2$, 4.9 % $n = 1$, 0.6 % $n = 0$) obtained at the end of co-RCM of **5** and **7** is qualitatively consistent with incomplete equilibration of the gas–solution phases during catalytic turnover.

[23] The $^{13}C/^{12}C$ ratios in **5** and **7** of 3.9:1 and 1.7:1 at "0 % conversion" (Figure 2) are ca. 63 % and 76 % of the predicted $^{13}C/^{12}C$ B2/B1 partitioning, which suggests that there may be an additional ethylene accelerating effect, for example, by ethylene acting as a spectator ligand, that increases the rate of pathway A or B1 slightly (for computational analysis of such effects see reference [15c]).

[24] It should be noted that in the absence of ethylene, cycles A or B may be dominant and either or both may be operative as nondominant pathways when the reaction is conducted under ethylene. However, with 1/1 mixtures of **5** and **7**, pseudo-first-order rate constants were identical under ethylene (1 atm) to those in the reactions of single components. Inconsistent with the yne-then-ene mechanism (A), the rate constant for reaction of **5**, but not of **7**, was somewhat attenuated under N_2 when mixed (1/1). Since the rate of reaction of **5** with **12**, will depend on whether **12** is derived from **7** or **5**, this further supports turnover by the primary ene-then-yne (B1) mechanism in the absence of ethylene.

 © 2005 Wiley-VCH Verlag GmbH & Co. KGaA, Weinheim

Cycloadditions

DOI: 10.1002/anie.200502313

Complexation-Initiated Intramolecular [4+2] Cycloaddition: Construction of Bridged-Type Cycloadducts**

Nobuharu Iwasawa, Kennichi Inaba, Satoko Nakayama, and Masao Aoki*

Intramolecular cycloaddition reactions of linear substrates generally give fused-type adducts selectively, owing to the favorable straight alignment of the two reacting sites (Scheme 1). There have been many examples of fused-type

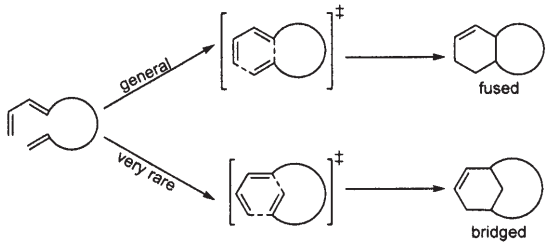

Scheme 1. The regioselectivity in the intramolecular [4+2] cycloaddition reaction.

intramolecular Diels–Alder reactions, but very few are known for the corresponding bridged-type Diels–Alder reaction.[1,2] Even in these cases, the bridged-type adducts were obtained as minor products along with the major fused-type products.[3,4]

We previously reported that alkynes bearing a furan diene and a dienophile unit on opposite ends, when complexed with $[Co_2(CO)_8]$, shift from a straight structure to a bent one (that is, the angle changes from 180° to around 140°). A subsequent intramolecular Diels–Alder reaction provides a mixture of the starting alkyne–$Co_2(CO)_6$ complex and the desired cyclized alkyne–$Co_2(CO)_6$ complex in equilibrium.[5] The important feature of this reaction is the ready formation of a seven-membered ring by the carbon tether. This is probably due to the rigid and planar structure of the alkyne–$Co_2(CO)_6$ moiety, compelling the two substituents at the alkyne to form an angle of about 140°,[6] which facilitates formation of the seven-membered ring.[7] We expected that this structural

[*] Prof. Dr. N. Iwasawa, K. Inaba, S. Nakayama, Dr. M. Aoki
Department of Chemistry
Tokyo Institute of Technology
2-12-1 E1-2, O-okayama, Meguro-ku, Tokyo 152-8551 (Japan)
Fax: (+81) 3-5734-2931
E-mail: niwasawa@chem.titech.ac.jp

[**] This research was partly supported by a Grant-in-Aid for Scientific Research from the Ministry of Education, Culture, Sports, Science, and Technology of Japan. We are grateful to the Tosoh Finechem Corporation for a generous gift of $MeAlCl_2$.

Supporting information for this article is available on the WWW under http://www.angewandte.org or from the author.

© 2005 Wiley-VCH Verlag GmbH & Co. KGaA, Weinheim

feature of the alkyne–$Co_2(CO)_6$ moiety—namely, the wider angle of alkyne substituents compared to alkene substituents—might lessen the steric congestion in the transition state and allow formation of the bridged-type adduct. Thus, by the appropriate design of substrates in which orbital or electronic control favors the formation of bridged-type products, we could carry out a bridged-type cycloaddition reaction selectively, even with simple linear substrates. Here we describe the successful development of this novel bridged-type [4+2] cycloaddition reaction of silyloxydiene derivatives[8] utilizing alkyne–$Co_2(CO)_6$ complex formation.

First, the reaction was examined using the alkyne–$Co_2(CO)_6$ complex **1**, which contains a silyloxydiene and an electron-deficient dienophile [Eq. (1); TBS = *tert*-butyldimethylsilyl]. When the reaction was carried out in the presence of 2 equivalents of $BF_3{\cdot}OEt_2$ in CH_2Cl_2 at −78 °C, the desired [4+2]-cycloadduct was not obtained; instead **4**, the hydrolyzed product of the starting material, was isolated in 34 % yield (Table 1, entry 1). In contrast, when $AlCl_3$ was employed as a Lewis acid, the starting material disappeared at −78 °C, and the cycloadduct was isolated in 34 % yield along with the Michael-type adduct **3** and the hydrolyzed ketone **4** in 12 % and 26 % yields, respectively (entry 2). Among several aluminum-containing Lewis acids examined, $MeAlCl_2$ gave the best results (entry 4).[9]

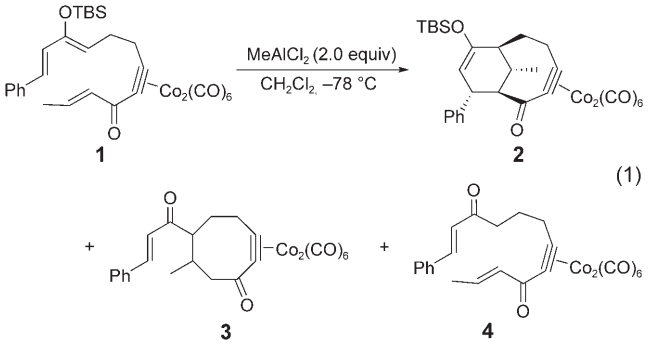

Table 1: Results of the intramolecular [4+2]-cycloaddition reaction in the presence of a Lewis acid [see Eq. (1)].

Entry	Lewis acid	*t* [h]	**2** [%]	**3** [%]	**4** [%]
1	$BF_3{\cdot}OEt_2$	0.5	0	0	34
2[a]	$AlCl_3$	25	34	12	26
3	Et_2AlCl	3.5	27	0	0
4[a]	$MeAlCl_2$	3.0	40	30	17
5[a,b]	$MeAlCl_2$	0.33	75	1	2

[a] Products **3** and **4** were obtained as an inseparable mixture. The yields were determined by ^{1}H NMR spectroscopy. [b] For this reaction 0.1 equivalent of DTBP was added.

Analysis of the NMR spectra of the cycloadduct obtained demonstrated that the product was not a normal fused-type adduct, but rather the bridged-type adduct **2** having a bicyclo[5.3.1]undec-3-yn-2-one skeleton. The product was isolated as a single stereoisomer, and the structure of the adduct was confirmed by X-ray crystal structure analysis of the corresponding hydrolyzed ketone.[10] This result proves that the cycloaddition is not a concerted Diels–Alder reaction, but a stepwise, double-Michael-type reaction giving the bridged-type [4+2]-cycloadduct.[11]

To prevent hydrolysis, we further examined the reaction in the presence of 2,6-di-*tert*-butylpyridine (DTBP), which is a well-known proton scavenger.[12] When the reaction was carried out employing 2 equivalents of $MeAlCl_2$ in the presence of 0.1 equivalents of DTBP in CH_2Cl_2 at −78 °C, formation of the hydrolyzed products was efficiently suppressed and the desired product **2** was obtained in 75 % yield (Table 1, entry 5).

We then extended the scope of the reaction using several substrates. As shown in Equation (2), the same type of substrates **5** and **6** gave the corresponding bridged-type [4+2] cycloadducts in good yield as a single stereoisomer when the reaction was carried with 2 equivalents of $MeAlCl_2$ in the presence of 0.1–0.3 equivalents of DTBP in CH_2Cl_2 at −78 °C. For the reaction with substrate **6**, the [4+2]-cycloadduct **8** was accompanied by a small amount of its hydrolyzed cycloadduct **9**. The configuration of the products were determined based on the analogy of the coupling pattern of their ^{1}H NMR spectra with that of **2**.

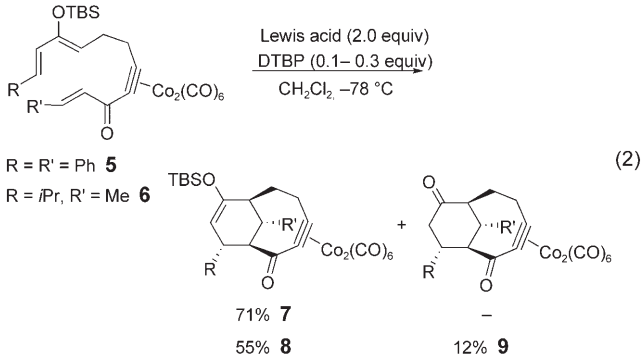

The reaction of substrate **10**, having an additional carbon atom in the tether, also gave the desired bridged-type adduct **11** with a bicyclo[6.3.1]dodec-3-yn-2-one skeleton as a single stereoisomer in reasonable yield [Eq. (3)]. The structure was again confirmed by X-ray crystal structure analysis of the corresponding hydrolyzed ketone.[10] Furthermore, the reac-

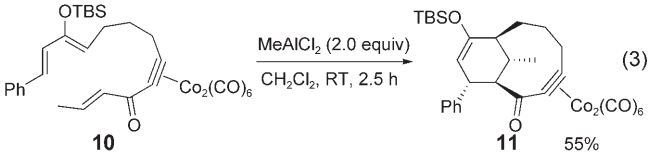

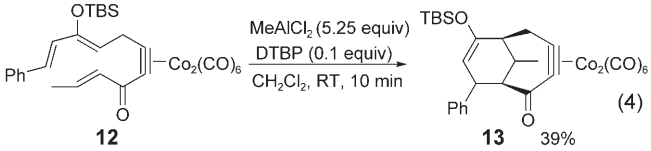

 © 2005 Wiley-VCH Verlag GmbH & Co. KGaA, Weinheim

tion of substrate **12**, which has one less carbon atom in the tether than **1**, also proceeded albeit in moderate yield, probably due to the severe strain of the system. The desired adduct **13**, with the bicyclo[4.3.1]dec-3-yn-2-one skeleton, was obtained in 39% yield by carrying out the reaction with 5.25 equivalents of $MeAlCl_2$ in CH_2Cl_2 at room temperature [Eq. (4)].[13] Thus, this bridged-type [4+2] cycloaddition reaction shows reasonable generality with respect to the substituents and the number of carbon atoms in the tether.

We then examined the reaction of the corresponding olefinic substrate **14** to confirm the importance of the alkyne–$Co_2(CO)_6$ moiety for the formation of the bridged-type products. The vinylsilane substrate **14** was obtained in 63% yield by reduction of **5** with triethylsilane.[14] Treatment of **14** under several typical cycloaddition reaction conditions did not give the corresponding bridged-type cycloadduct, but instead the monocyclic Michael addition products **15** and **16** in high yield [Eq. (5), Table 2]. We believe that the wider bent angle of the alkyne–$Co_2(CO)_6$ complexes releases the steric congestion of the transition state and enables the smooth formation of the bridged-type cycloadduct. However, further examination is necessary to clarify the exact role of the alkyne–$Co_2(CO)_6$ moiety.

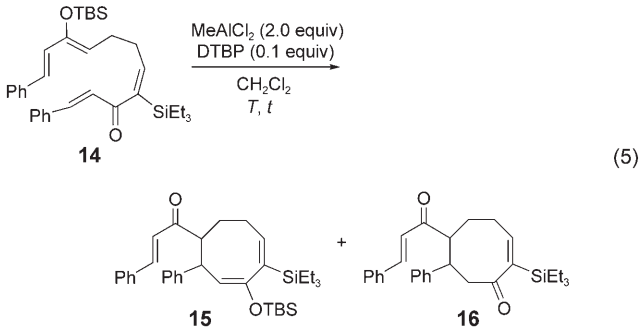

(5)

Table 2: Results of the reactions with the olefinic substrate **14** [see Eq. (5)].

Entry	*T*	*t* [min]	**15** [%]	**16** [%]
1	−78 °C	115	65	33
2[a]	−78 °C	50	45	44
3	RT	10	trace	80

[a] DTBP was not added.

Finally, we investigated the decomplexation of the alkyne–$Co_2(CO)_6$ moiety from the bridged-type cycloadducts (Table 3). The cycloadduct **2** and its hydrolyzed ketone **17** both underwent smooth hydrosilylation of the alkyne–$Co_2(CO)_6$ moiety to give vinylsilanes **18a** and **19a** in good yields upon heating of the complexes in the presence of triethylsilane (entries 1 and 2).[15] Furthermore, the reaction of **17** with sodium hypophosphite[16] proceeded smoothly to give enone **19b** (entry 3), while the same reaction using silyl enol ether **2** resulted in a complex mixture of products. To our surprise, simple heating of complex **2** in toluene/H_2O (5/1) with vigorous stirring gave the desired decomplexed enone **18b** in good yield without hydrolyzing the silyl enol ether moiety (entry 4). Although details of this demetalation reaction remain to be explored, this method affords a simple conversion of alkyne–$Co_2(CO)_6$ complexes into the corresponding alkenes.[17]

Table 3: Results of the demetalation reaction of bridged-type alkyne–$Co_2(CO)_6$ cycloadducts.[a]

Entry	Substrate	Reaction conditions	Product	Yield [%]
1	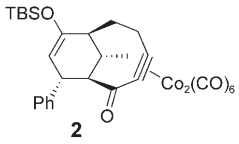 **2**	Et_3SiH, BTMSA, DCE, 65 °C, 6.5 h	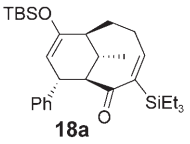 **18a**	68
2	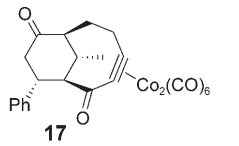 **17**	Et_3SiH, BTMSA, DCE, 65 °C, 24 h	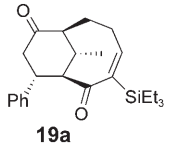 **19a**	77
3	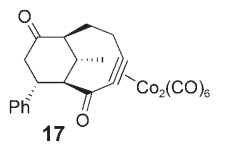 **17**	$NaH_2PO_2 \cdot H_2O$, 2-methoxyethanol, 65 °C, 2 h	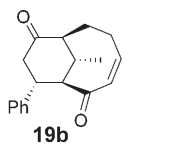 **19b**	72
4	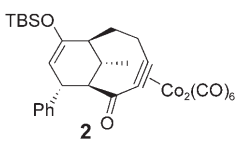 **2**	H_2O, toluene, reflux, 2 h	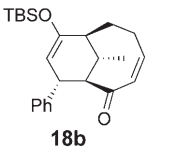 **18b**	66

[a] BTMSA = bis(trimethylsilyl)acetylene, DCE = 1,2-dichloroethane.

In conclusion, we have developed a method for the preparation of bridged-type [4+2]-cycloadducts utilizing alkyne–$Co_2(CO)_6$ complex formation. Synthetically useful bicyclo[*n*.3.1] skeletons with multiple functionalities could be prepared stereoselectively by this procedure.

Experimental Section

Cyclization of **1**: The alkyne–cobalt complex **1** was purified by PTLC (hexane/CH_2Cl_2 1/1) just before use. 2,6-Di-*tert*-butylpyridine (4.20 μL, 18.4 μmol) was added to a solution of **1** (125 mg, 0.187 mmol) in CH_2Cl_2 (19 mL) at −78 °C. After 5 min a solution of $MeAlCl_2$ (0.370 mL, 0.370 mmol) in hexane (1.0 M) was added, and the mixture was stirred for 20 min at −78 °C. Then the reaction was quenched with saturate aqueous $NaHCO_3$, and the product was extracted with ethyl acetate three times. The combined organic extracts were washed with brine, dried over anhydrous sodium sulfate, filtered, and concentrated under reduced pressure. The residue was purified by PTLC (hexane/CH_2Cl_2 1/1) to give **2** (93.0 mg, 0.140 mmol) in 75% yield as a dark red oil. Compounds **3**

 © 2005 Wiley-VCH Verlag GmbH & Co. KGaA, Weinheim

and **4** were obtained as an inseparable mixture in a 1:2 ratio (3.10 mg, 5.60 μmol) in 3% yield as a dark red oil.

Received: July 2, 2005
Published online: October 20, 2005

Keywords: alkyne ligands · cobalt · cycloaddition · demetalation

[1] a) E. Ciganek, *Org. React.* **1984**, *19*, 1; b) L. A. Paquette, *Comprehensive Organic Synthesis, Vol. 5*, Pergamon, Oxford, **1991**; c) F. Fringuelli, A. Taticchi, *The Diels–Alder Reaction: Selected Practical Methods*, Wiley, New York, **2002**.
[2] For type II intramolecular Diels–Alder reactions, see B. R. Bear, S. M. Sparks, K. J. Shea, *Angew. Chem.* **2001**, *113*, 864–894; *Angew. Chem. Int. Ed.* **2001**, *40*, 820–849.
[3] Examples for the bridged-type intramolecular Diels–Alder reaction were reported using cyclohexadienone as a dienophile unit. The *Z*-configuration of the diene part facilitates a suitable transition state for the bridged-type reaction. a) H. Greuter, G. Fráter, H. Schmid, *Helv. Chim. Acta* **1972**, *55*, 526–531; b) H. Greuter, H. Schmid, *Helv. Chim. Acta* **1972**, *55*, 2382–2400; c) G. Fráter, *Helv. Chim. Acta* **1974**, *57*, 172–179; d) H. Greuter, H. Schmid, G. Fráter, *Helv. Chim. Acta* **1977**, *60*, 1701–1729; see also G. Fráter, J. Wenger, *Helv. Chim. Acta* **1984**, *67*, 1702–1706.
[4] For the formation of the bridged-type Diels–Alder product as a minor product, see a) E. J. Corey, M. Petrzilka, *Tetrahedron Lett.* **1975**, 2537–2540; b) S. J. Bailey, E. J. Thomas, *J. Chem. Soc. Chem. Commun.* **1978**, 474–475; c) B. B. Snider, J. V. Dunćia, *J. Org. Chem.* **1980**, *45*, 3461–3464; d) A. Deagostino, J. Maddaluno, C. Prandi, P. Venturello, *J. Org. Chem.* **1996**, *61*, 7597–7599; e) D. Craig, M. J. Ford, R. S. Gordon, J. A. Stones, A. J. P. White, D. J. Williams, *Tetrahedron* **1999**, *55*, 15045–15066.
[5] N. Iwasawa, F. Sakurada, M. Iwamoto, *Org. Lett.* **2000**, *2*, 871–873.
[6] W. G. Sly, *J. Am. Chem. Soc.* **1959**, *81*, 18–20.
[7] For example, see a) N. Iwasawa, H. Satoh, *J. Am. Chem. Soc.* **1999**, *121*, 7951–7952; b) K. Tanino, F. Kondo, T. Shimizu, M. Miyashita, *Org. Lett.* **2002**, *4*, 2217–2219; c) D. G. J. Young, J. A. Burlison, U. Peters, *J. Org. Chem.* **2003**, *68*, 3494–3497; d) T. Baba, S. Takai, N. Sawada, M. Isobe, *Synlett* **2004**, 603–608.
[8] A related intramolecular Diels–Alder reaction of a siloxydiene derivative, which gave a fused-type product selectively in spite of its electronic bias, was reported: K. Takasu, S. Mizutani, M. Ihara, *J. Org. Chem.* **2002**, *67*, 2881–2884.
[9] C. Rogers, B. A. Keay, *Can. J. Chem.* **1992**, *70*, 2929–2947.
[10] CCDC-276360 (for adduct **2**) and CCDC-276361 (for adduct **11**) contain the supplementary crystallographic data for this paper. These data can be obtained free of charge from The Cambridge Crystallographic Data Centre via www.ccdc.cam.ac.uk/data_request/cif.
[11] There have been no reports on bridged-type intramolecular [4+2]-cycloaddition reactions of silyloxydiene derivatives.[8] For examples of fused-type cycloadditions, see a) M. Ihara, K. Makita, K. Takasu, *J. Org. Chem.* **1999**, *64*, 1259–1264; b) M. Ihara, K. Fukumoto, *Angew. Chem.* **1993**, *105*, 1059–1071; *Angew. Chem. Int. Ed. Engl.* **1993**, *32*, 1010–1022, and references therein.
[12] P. V. Bonnesen, C. L. Puckett, R. V. Honeychuck, W. H. Hersh, *J. Am. Chem. Soc.* **1989**, *111*, 6070–6081.
[13] Product **13** was obtained as a single stereoisomer; the relative configuration has not yet been determined.
[14] S. Hosokawa, M. Isobe, *Tetrahedron Lett.* **1998**, *39*, 2609–2612.
[15] S. Tojo, M. Isobe, *Tetrahedron Lett.* **2005**, *46*, 381–384.
[16] S. Takai, P. Ploypradith, A. Hamajima, K. Kira, M. Isobe, *Synlett* **2002**, 588–592.
[17] This demetalation reaction is general for medium-sized cyclic alkynone–$Co_2(CO)_6$ complexes. A $[HCo(CO)_3(L)]$ species, generated by decomposition of the alkyne–$Co_2(CO)_6$ complex, might be acting as a reductant; see R. W. Goetz, M. Orchin, *J. Org. Chem.* **1962**, *27*, 3698.

 © 2005 Wiley-VCH Verlag GmbH & Co. KGaA, Weinheim

Drug Design

DOI: 10.1002/anie.200502662

Rational Design and Synthesis of Highly Potent β-Glucocerebrosidase Inhibitors

*Xiaoxiang Zhu, Kamlesh A. Sheth, Shihong Li, Hui-Hwa Chang, and Jian-Qiang Fan**

β-Glucocerebrosidase (GCase or acid β-glucosidase) is a lysosomal hydrolase that catalyzes the hydrolytic cleavage of glucose from glucosylceramide.[1] A deficiency in GCase activity results in the progressive accumulation of glucosylceramide, a normal intermediate in the catabolism of globosides and gangliosides, in the lysosomes of macrophages. This deficiency leads to Gaucher disease, the most common lysosomal storage disorder.[2] The disease severity is based mainly on the level of the residual enzyme activity in the tissues of the affected patients.[3] Enzyme-replacement therapy is effective for type 1 Gaucher disease, the non-neuronopathic form; however, this therapy is not available for types 2 and 3 of Gaucher disease, the acute/subacute neuronopathic forms, because of the difficulty in delivering the replacement enzyme to the central nervous system.

We have reported that the residual enzyme activity can be increased in lymphoblasts from patients with Fabry disease, another lysosomal storage disease, when the cells were incubated with potent inhibitors of the mutant enzyme at subinhibitory concentrations.[4] The potent inhibitors serve as active-site specific chaperones (ASSCs) to assist the efficient folding process in the endoplasmic reticulum, thus accelerating the biosynthesis, processing, and maturation of the mutated protein.[5] A correlation demonstrated that the more potent inhibitors are the more effective ASSCs, because they retain high affinity with the catalytic domain of the

[*] Dr. J.-Q. Fan
Department of Human Genetics
Mount Sinai School of Medicine
5th Avenue at 100th street, New York, NY 10029 (USA)
Fax: (+1) 212-849-2508
E-mail: jian-qiang.fan@mssm.edu
Dr. X. Zhu, Dr. K. A. Sheth, Dr. S. Li, H.-H. Chang, Dr. J.-Q. Fan
Amicus Therapeutics, Inc.
Cranbury, NJ 08512 (USA)

Supporting information for this article is available on the WWW under http://www.angewandte.org or from the author.

WILEY InterScience DISCOVER SOMETHING GREAT
© 2005 Wiley-VCH Verlag GmbH & Co. KGaA, Weinheim

enzyme.[6] Sawkar et al. reported that the addition of an inhibitor of GCase to the culture medium of fibroblasts from patients with Gaucher disease led to a twofold increase in the activity of N370S GCase, which suggests that a potent inhibitor of GCase could be of therapeutic interest.[7] Therefore, an approach to the design and synthesis of potent inhibitors of GCase was undertaken.

The natural substrates for GCase are *N*-acylsphingosyl-1-*O*-β-D-glucosides, which have different fatty acid acyl and sphingosyl moieties depending upon the tissue source.[2] It is, therefore, reasonable to postulate that GCase may contain two substrate-binding sites in the catalytic domain: one that recognizes the glucosyl residue and the other that recognizes the hydrophobic ceramide moiety. Transition-state mimics are frequently potent inhibitors of the enzyme. Thus, our strategy to design potent GCase inhibitors focused on molecules that not only closely resemble both glucose and ceramide, but also mimic the transition state of enzymatic glycosidic cleavage. It is established that GCase cleaves the β-glycosidic bond to release glucose with the retention of the anomeric configuration via a covalent glucosyl enzyme intermediate with Glu340 acting as the nucleophile and Glu235 as the acidic/basic species.[8] Known as a potent inhibitor of sweet-almond β-glucosidase ($K_i = 110$ nM), isofagomine (IFG, **1**) closely resembles glucose with a nitrogen atom in the pseudo-anomeric position, thus presumably acting as a mimic of the glycosyl-enzyme intermediate.[9] The X-ray crystal structure of GCase indicated the existence of an annulus of hydrophobic residues around the entrance to the glucose binding site,[10] which could serve as a hydrophobic bind site. On the basis of these findings, derivatization of IFG with a hydrophobic group may lead to a highly potent inhibitor. We decided to synthesize a series of novel IFG analogues **2**–**6** with a hydrophobic alkyl group at C6 and IFG analogues **7**–**8** with an alkyl group at N1 in an attempt to demonstrate this concept and discover novel GCase inhibitors.

Numerous syntheses of IFG and its derivatives have been reported,[11] but the synthesis of 6-alkyl IFGs remains unexplored. As previously described,[11c] the synthesis of **1** was difficult because of the lack of a suitably branched carbohydrate precursor. In this regard, 6-alkyl IFGs with an additional chiral center might yet be more difficult to synthesize in a straightforward fashion. We envisaged a concise synthetic route for the preparation of **2**–**6** and disclose herein the success of our strategy with the stereocontrolled introduction of the 6-alkyl group by the addition of a Grignard reagent to the nitrile group.

Compounds **2**–**6** were synthesized from benzyl α-L-xylopyranoside (Scheme 1). Benzyl α-L-xylopyranoside was treated with 2-methoxypropene and *para*-toluenesulfonic acid (TsOH) in THF to afford **10** in 53% yield. Triflation of the free 4-hydroxy group of **10** and subsequent treatment with KCN in dimethylformamide (DMF) in the presence of [18]crown-6 led to nitrile **11** in 80% yield (two steps from **10**). The addition of *n*-C_4H_9MgCl to **11**, followed by reduction with $NaBH_4$, stereoselectively afforded a single stereoisomer **12** in 74% yield.[12] The same procedure was used for the synthesis of **13**–**16**, and the yield ranged from 65 to 74%. Catalytic hydrogenation of amine **12** in the presence of HCl

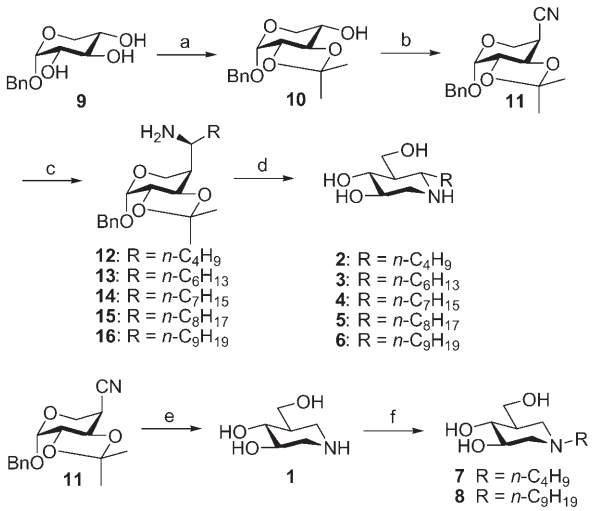

Scheme 1. Synthesis of IFG (**1**) and IFG derivatives **2**–**8**. a) CH_2=C(OMe)Me, TsOH·H_2O, THF, 1.5 h, 0°C (53%); b) Tf_2O, pyridine, CH_2Cl_2, 2 h, −78→0°C; then KCN, 18[crown]-6, DMF, 16 h, RT (80%); c) RMgX, Et_2O, 2 h, RT; then $NaBH_4$, overnight, RT (65–74%); d) H_2, 20% $Pd(OH)_2$/C, AcOH, MeOH, 50 psi, overnight, RT; then 1 N HCl (52–81%); e) H_2, 20% $Pd(OH)_2$/C, HCl (conc.), MeOH, RT (81%); f) aldehyde, $NaBH_3CN$, MeOH (79–83%). Tf=trifluoromethanesulfonyl.

over 20% $Pd(OH)_2$ on charcoal at atmospheric pressure gave **2** in 52% yield. Alternatively, amine **16** was hydrogenated in the presence of AcOH over 20% $Pd(OH)_2$ on charcoal under 50 psi, followed by acid hydrolysis of the protective group to afford **6** in 81% yield. The same procedure was successfully applied to **13**–**15** to give **3**–**5**. The hydrogenation of **11** over 20% $Pd(OH)_2$ on charcoal led to debenzylation, intramolecular cyclization, and concurrent deacetonation in one step to give **1** in 81% yield. In synopsis, although a number of methods have been reported for the synthesis of **1**,[11] the present method provides an efficient and short synthetic route for the synthesis of **1** in a total of four steps and an overall yield of 34%. In addition, *N*-alkyl IFGs **7** and **8** were prepared according to the previously reported procedure.[13]

The configuration of the newly formed stereogenic center in **12** was established based on 6-butyl IFG (**2**), whose stereochemistry was determined by 2D NMR spectroscopic analyses. The NOESY spectrum of **2** showed significant correlations of H6 with both H4 and H2a, and the coupling constant $J(5,6)$ was observed to be 10.5 Hz, thus confirming that H6 is situated at an axial orientation. Thus, the configuration of the new asymmetric center in **12** can be assigned as *S* (see the Supporting Information for the COSY, TOCSY, and NOESY spectra of **2**). Analysis of the ^{1}H NMR spectra of **2**–**6** indicates that they all possess the same configuration at the asymmetric C6 position.

The high stereoselectivity observed above can be explained by a chelation mechanism (Scheme 2). After addition of the Grignard reagent to the nitrile moiety, the magnesium atom of the magnesioimine could be chelated to the oxygen atom on the pyranose ring, thus resulting in the formation of a six-membered cyclic intermediate **17**. Further

 © 2005 Wiley-VCH Verlag GmbH & Co. KGaA, Weinheim

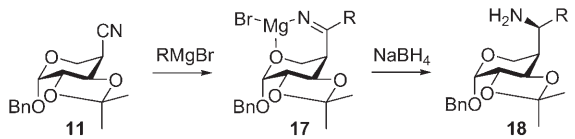

Scheme 2. Proposed mechanism for the stereoselective formation of amine **18**.

reduction of the ketimine function with $NaBH_4$ prefers an attack at the *Re* face to yield amine **18** with a *S* configuration.

The inhibitory activities of all compounds against human GCase was determined with 4-methylumbelliferyl β-glucoside (4MU-β-Glc) and are summarized in Table 1. To determine

Table 1: Inhibitory activity of **1** and derivatives **2**–**8** against GCase.

Inhibitors	IC_{50} [nM][a]	K_i [nM]
IFG (**1**)	56	25[b]
6-butyl IFG (**2**)	160	120[b]
6-hexyl IFG (**3**)	4.2	[c]
6-heptyl IFG (**4**)	1.8	[c]
6-octyl IFG (**5**)	0.8	[c]
6-nonyl IFG (**6**)	0.6	[c]
N-butyl IFG (**7**)	44000	n.d.
N-nonyl IFG (**8**)	>100000	n.d.

[a] All inhibitory activities were determined with 4MU-β-Glc at 3 mM. [b] The kinetic data were fit to a double-reciprocal plot and replotted to K_{mapp} versus [I]. [c] Data do not fit to a competitive-inhibition model by using lineal and nonlineal models (Prism GraphPad). n.d. = not determined.

the K_i values, a Lineweaver–Burk plot was used to calculate the K_{mapp} in the presence of an inhibitor at various concentrations and replotted against the concentrations of inhibitor (Figure 1). IFG (**1**) was a potent inhibitor against GCase with IC_{50} and K_i values of 56 and 25 nM, respectively. In contrast, modification of the imino group by a hydrophobic group

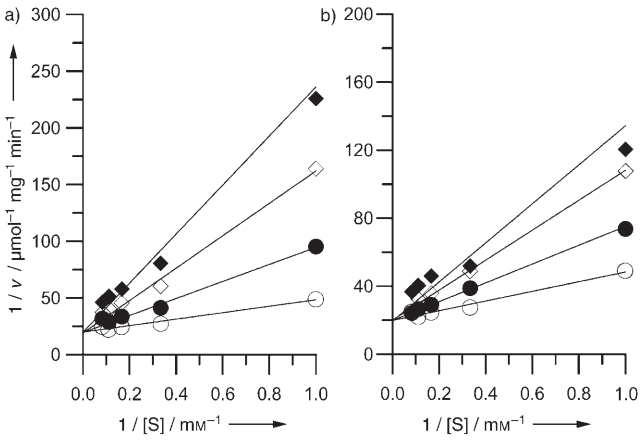

Figure 1. Lineweaver–Burk plots of **1** and 6-butyl IFG (**2**) for the inhibition of human GCase. The increasing concentrations of substrate were used to determine the K_{mapp} and K_i values and the data were plotted as $1/v$ versus 1/[S]. a) Concentrations of **1** were 0 (○), 20 (●), 50 (◇), and 150 nM (◆). b) Concentrations of **2** were 0 (○), 100 (●), 200 (◇), and 400 nM (◆).

greatly decreased the inhibitory activity ($IC_{50} \geq 44$ μM for **7** and **8**, respectively). The potent inhibitory activity of IFG is most likely attributed to the salt bridge between protonated **1** and the catalytic carboxylate of GCase.[9] The alkyl group attached to N1 might interfere with the formation of the salt bridge, thus resulting in less potent inhibitors. Incorporation of the 6-butyl group into **1** generated 6-butyl IFG (**2**), which did not exhibit a better inhibitory activity on GCase than **1**. However, 6-hexyl IFG (**3**) was apparently more potent than **1** with a 13-fold increase in potency. Further extension of the length of the alkyl chain improved the potency accordingly (**4**–**6**). The most potent inhibitor 6-nonyl IFG (**6**) displayed a remarkable IC_{50} value of 0.6 nM, which is 93-fold more potent relative to **1**. These data clearly indicate that a long alkyl chain (greater than four carbon atoms) is required to improve potency and a longer chain provides a higher potency, thus suggesting that there is a hydrophobic interaction between the alkyl group and enzyme and that an appropriate alkyl chain length is needed to bind the hydrophobic domain. In recent years, despite many efforts being directed towards the synthesis and study of IFG analogues, only weaker inhibitors have resulted from these investigations.[9,11] Based on the concept we have proposed and the x-ray crystal structure of GCase, we discovered highly potent GCase inhibitors **3**–**6**, which are between 13- and 93-fold more potent than the parent inhibitor **1**. The proposed binding of **6** with GCase is shown in Figure 2. The structural features of the potent inhibitors as described above can be applied further to find potent and selective inhibitors of GCase with an improved biopharmaceutical profile.

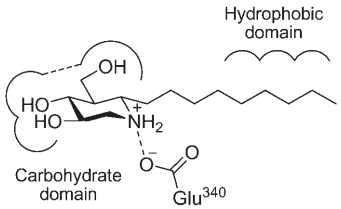

Figure 2. Proposed binding of **6** with human GCase.

The inhibition mode for **1** and **2** is competitive, with K_i values of 25 and 120 nM, respectively, using 4MU-β-Glc as the variable substrate (Table 1). The inhibition mode for the 6-alkyl IFG derivatives with longer chains was more complicated than being purely competitive but showed characteristics of a mixed-type inhibition. This difference may be explained on the basis that these inhibitors bind the enzyme through two distant binding sites: a carbohydrate binding site and a hydrophobic binding site (Figure 2). Whereas both inhibitory binding sites are likely to be competitive, the strong combination of both acts in a manner to provide a non-competitive-like inhibitory mechanism in some of the most potent 6-alkyl IFGs.

In conclusion, we have demonstrated an efficient and straightforward methodology for the synthesis of 6-alkyl IFGs, which represent a new class of highly potent inhibitors of human GCase. These inhibitors appear to utilize recog-

 © 2005 Wiley-VCH Verlag GmbH & Co. KGaA, Weinheim

nition domains for both a carbohydrate and a hydrophobic binding site. As a result, the most potent GCase inhibitor 6-nonyl IFG (**6**) shows an IC_{50} value at subnanomolar concentrations. We have used these compounds as ASSCs for the rescue of misfolded mutant GCase in cells from Gaucher patients (results to be published elsewhere). As a consequence, they may be ideal candidates for further development as small-molecule drugs for the treatment of Gaucher disease, in particular for the neuronopathic disease form.

Received: July 29, 2005
Published online: October 18, 2005

Keywords: biological activity · drug design · enzymes · inhibitors · natural products

[1] R. O. Brady, J. N. Kanfer, D. Shapiro, *Biochem. Biophys. Res. Commun.* **1965**, 18, 221 – 225.
[2] E. Beutler, G. A. Grabowski in *The Metabolic and Molecular Bases of Inherited Disease*, 8th ed. (Eds.: C. R. Scriver, A. L. Beaudet, W. S. Sly, D. Valle), McGraw-Hill, New York, **2001**, p. 3635.
[3] G. A. Grabowski in *Adv. Hum. Genet., Vol. 21* (Eds.: H. Harris, K. Hirschhorn), Plenum, New York, **1993**, p. 377.
[4] J.-Q. Fan, S. Ishii, N. Asano, Y. Suzuki, *Nat. Med.* **1999**, *5*, 112 – 115.
[5] J.-Q. Fan, *Trends Pharmacol. Sci.* **2003**, *24*, 355 – 360.
[6] N. Asano, S. Ishii, H. Kizu, K. Ikeda, K. K. Yasuda, A. Kato, O. R. Martin, J.-Q. Fan, *Eur. J. Biochem.* **2000**, *267*, 4179 – 4186.
[7] a) A. R. Sawkar, W.-C. Cheng, E. Beutler, C.-H. Wong, W. E. Balch, J. W. Kelly, *Proc. Natl. Acad. Sci. USA* **2002**, *99*, 15428 – 15433; b) H. Lin, Y. Sugimoto, Y. Ohsaki, H. Ninomiya, A. Oka, M. Taniguchi, H. Ida, Y. Eto, S. Ogawa, Y. Matsuzaki, M. Sawa, T. Inoue, K. Higaki, E. Nanba, K. Ohno, Y. Suzuki, *Biochim. Biophys. Acta* **2004**, *1689*, 219 – 228; c) S. Ogawa, Y. Kobayashi, K. Kabayama, M. Jimbo, J. Inokuchi, *Bioorg. Med. Chem.* **1998**, *6*, 1955 – 1962.
[8] a) S. Fabrega, P. Durand, P. Codogno, C. Bauvy, C. Delomenie, B. Henrissat, B. M. Martin, C. McKinney, E. I. Ginns, J. P. Mornon, P. Lehn, *Glycobiology* **2000**, *10*, 1217 – 1224; b) S. Fabrega, P. Durand, J. P. Mornon, P. Lehn, *J. Soc. Biol.* **2002**, *196*, 151 – 160; c) G. Davies, B. Henrissat, *Structure* **1995**, *3*, 853 – 859.
[9] V. H. Lillelund, H. H. Jensen, X. Liang, M. Bols, *Chem. Rev.* **2002**, *102*, 515 – 553, and references therein.
[10] H. Dvir, M. Harel, A. A. McCarthy, L. Toker, I. Silman, A. H. Futerman, *EMBO Rep.* **2003**, *4*, 1 – 6.
[11] a) T. M. Jespersen, W. Dong, M. R. Sierks, T. Skrydstrup, I. Jundt, M. Bols, *Angew. Chem.* **1994**, *106*, 1858 – 1861; *Angew. Chem. Int. Ed. Engl.* **1994**, *33*, 1778 – 1779; b) Y. Ichikawa, Y. Igarashi, M. Ichikawa, Y. Suhara, *J. Am. Chem. Soc.* **1998**, *120*, 3007 – 3018; c) J. Andersch, M. Bols, *Chem. Eur. J.* **2001**, *7*, 3744 – 3747, and references therein; d) P. Jakobsen, J. M. Lundbeck, M. Kristiansen, J. Breinholt, H. Demuth, J. Pawlas, M. Torres, B. Anderson, N. Westergaard, K. Lundgren, N. Asano, *Bioorg. Med. Chem.* **2001**, *9*, 733 – 744; e) W. M. Best, J. M. Macdonald, B. W. Skelton, R. V. Stick, D. M. Tilbrook, A. H. White, *Can. J. Chem.* **2002**, *80*, 857 – 865.
[12] HPLC and TLC analysis from the crude mixture and purified sample detected the formation of **12**; the presence of its diastereoisomer was not observed.
[13] H. R. Mellor, J. Nolan, L. Pickering, M. R. Wormald, F. M. Platt, R. A. Dwek, G. W. J. Fleet, T. D. Butters, *Biochem. J.* **2002**, *366*, 225 – 233.

 © 2005 Wiley-VCH Verlag GmbH & Co. KGaA, Weinheim

Coordination Chemistry

DOI: 10.1002/anie.200502901

Crown Ether Ligation: An Approach to Low-Oxidation-State Indium Compounds**

*Christopher G. Andrews and Charles L. B. Macdonald**

In memory of Dennis G. Tuck

The chemistry of Group 13 elements in oxidation states lower than +3 has been a subject of increasing importance in main-group chemistry over the last 20 years. Particular attention has focused on the chemistry of compounds containing Group 13 elements in the +1 oxidation state (E^I) for both fundamental and practical purposes.[1–3] The presence of the "lone pair" of electrons on E^I (Scheme 1a) often makes the

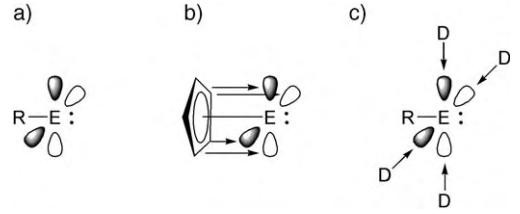

Scheme 1. a) The "lone pair" of electrons on E^I. b) Electron donation to the formally vacant p orbitals on the E^I center resulting in stabalization. The postulated use of an appropriately shaped auxiliary donor to stabilize the vacant orbitals.

normally Lewis acidic Group 13 center behave as a Lewis base instead. Such altered reactivity means that compounds containing E^I centers can be used as ligands for main-group[4] and transition-metal acceptors;[5,6] some of the coordination complexes thus obtained have proven to be useful precursors for the formation of intermetallic and other materials.[6]

Although sterically demanding substituents such as terphenyl[7,8] and β-diketiminate[9–13] ligands have been used to obtain some examples, the vast majority of stable monomeric compounds containing E^I centers (apart from thallium[14]) have the Group 13 element bound to either a cyclopentadienyl (Cp) substituent[15] or to an isolobal tris(pyrazolyl)borate group.[16] These σ- and π-donating substituents stabilize

[*] C. G. Andrews, Prof. Dr. C. L. B. Macdonald
Dept. of Chemistry and Biochemistry
University of Windsor
Windsor, Ontario, N9B 3P4 (Canada)
Fax: (+1) 519-973-7098
E-mail: cmacd@uwindsor.ca

[**] Funding of this work by the Natural Sciences and Engineering Research Council (Canada), the Canada Foundation for Innovation, the Ontario Innovation Trust, and the Ontario Research and Development Challenge Fund (University of Windsor Centre for Catalysis and Materials Research) is gratefully acknowledged.

Supporting information for this article is available on the WWW under http://www.angewandte.org or from the author.

© 2005 Wiley-VCH Verlag GmbH & Co. KGaA, Weinheim

the low-oxidation-state center by providing sufficient electron density to fill the formally vacant p orbitals on the E^I center, as illustrated for a Cp group in Scheme 1b. We postulated that monomeric E^I species containing nonbulky, poorly or non-π-donating ligands could be stabilized by using an appropriately shaped auxiliary donor to stabilize the vacant orbitals (Scheme 1c). The shape and properties of the polydentate donor ligand are important in this context because, although coordination to E^I centers may appear to be trivial in theory, all previous attempts to coordinate donors to potentially monomeric E^I centers have resulted in the disproportionation of the Group 13 compound and the isolation of higher-oxidation-state products.[17–19]

Herein, we demonstrate that properly sized crown ethers are suitable ligands for this task; this approach has allowed us to isolate the first example of a monomeric adduct of a true $R–E^I$ compound with a Lewis base. Furthermore, the presence of the crown ether modifies the reactivity of the $R–E^I$ species. Lastly, we show that appropriate crown ethers can even be used to favor the formation of an $R–E^I$ environment from higher-oxidation-state precursors.

Recently, we reported syntheses for the salt $InSO_3CF_3$ (InOTf, **1**),[20] which is unusually soluble for an inorganic In^I salt. The solubility of this reagent in organic and particularly aromatic solvents has allowed us to conduct experiments using homogeneous solutions and to avoid the heterogeneous conditions often caused by the insolubility of In^I halides. Thus the reaction of **1** with 1,4,7,10,13,16-hexaoxacyclooctadecane ([18]crown-6; compounds labeled **a**) or 2,3,11,12-dibenzo-1,4,7,10,13,16-hexaoxacyclooctadecane (dibenzo[18]crown-6; compounds labeled **b**) in toluene resulted in the formation of a colorless solution. Concentration of the solution produced crystals of the 1:1 coordination complex **2a** or **2b**, as confirmed by spectroscopic and analytical methods. The colorless crystals of **2a** were subjected to a single-crystal X-ray diffraction experiment;[21] the molecular structure of **2a** is depicted in Figure 1, and there are no unusually short intermolecular contacts. There are

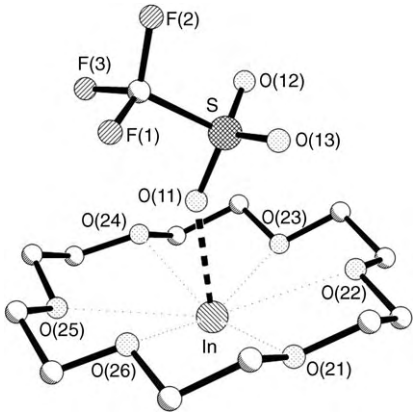

Figure 1. Molecular structure of **2a**. Hydrogen atoms are omitted for clarity. Selected bond lengths [Å] and angles [°]: O(11)-S 1.435(2), O(11)-In 2.370(2), O(12)-S 1.431(2), O(13)-S 1.426(2), O(21)-In 2.8690(18), O(22)-In 2.8492(18), O(23)-In 2.8299(18), O(24)-In 2.8513(18), O(25)-In 2.9292(18), O(26)-In 2.9167(19); S-O(11)-In 151.39(13).

three important features in the structure of **2a**. Most noticeably, the complex still contains an In^I center, and **2a** is thus the only example of an intact monomeric In^I compound acting as a Lewis acid; every previous attempt to ligate bases to In^I salts has resulted in the disproportionation of the In^I compound.[18,19] Secondly, the In atom is situated essentially on the centroid of the O_6 ring, in marked contrast to the cationic In^{III} center in $[InI_2([18]crown-6)][InI_4]$.[22] Of further note is the relatively short In–O(11) distance of 2.370(2) Å, which is considerably shorter than the shortest distance of 2.579(6) Å found in **1**. Moreover, the crystallographic equivalence of the S–O bond lengths (1.435(2), 1.432(2), and 1.426(2) Å) is consistent with an ionic trifluoromethansulfonate (triflate) anion, thus, the data suggest that **2a** is best considered as an isolated contact ion pair in the solid state. Such an interpretation is also consistent with the ionic radii suggested for In^I (1.04 Å) and O^{2-} ions (1.40 Å).[23] All other metrical parameters are as one would predict, given the components of the adduct, and require no further comment.

Perhaps surprisingly, the analogous reactions of indium(I) chloride with [18]crown-6 or dibenzo[18]crown-6 result in the immediate deposition of In metal and the formation of products with In in a higher oxidation state. The disproportionation of In^ICl clearly contrasts with the behavior of **1** and suggests that the triflate anion confers benefits other than merely increased solubility to such low-oxidation-state reagents.

As well as providing monomeric compounds, the crown ethers appear to alter the reactivity of **1**. In particular, **1** is soluble in dichloromethane and chloroform but does not appear to react with the solvents at an appreciable rate. In contrast, **2a** and **2b** react rapidly with such chlorinated solvents through formal oxidative insertions into C–Cl bonds to form the compounds **3a** and **3b**, respectively, as outlined in Scheme 2. In the case of **3b**, crystalline material suitable for

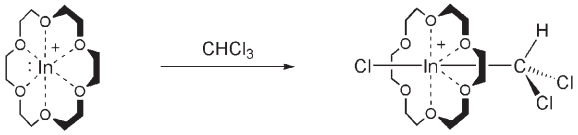

Scheme 2. Oxidative addition of a C–Cl bond in chloroform to the In^I cation in **2** to produce the cation in **3**. Note: the crown ether is [18]crown-6 for **a** and dibenzo[18]crown-6 for **b**.

analysis by X-ray diffraction was obtained and the molecular structure obtained from the experiment is displayed in Figure 2.

The molecular structure of **3b** consists of distinct cations of the form $[In(CHCl_2)Cl(dibenzo[18]crown-6)]^+$ and triflate anions. There are no unusually short interionic distances and the metrical parameters of the anion are consistent with it being noncoordinating and ionic. The structural features of the cation, although unique, are predictable. For example, the smaller In^{III} ion is offset from the center of the O_6 ring to allow for four shorter In–O contacts (2.517(5) to 2.550(5) Å) and thus leaves two much longer In···O contacts (2.738(5) and 2.756(5) Å). The In–Cl bond length of 2.304(2) Å is one of the

 © 2005 Wiley-VCH Verlag GmbH & Co. KGaA, Weinheim

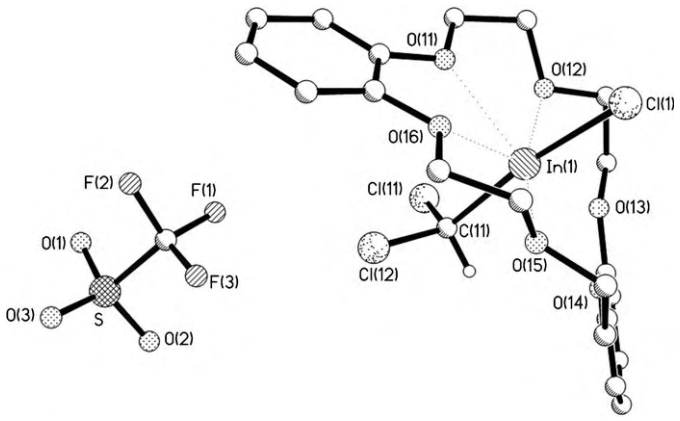

Figure 2. Molecular structure of **3b**. Most of the hydrogen atoms are omitted for clarity and two additional molecules of chloroform are not shown. Selected bond lengths [Å] and angles [°]: C(11)-In(1) 2.174(7), Cl(1)-In(1) 2.304(2), C(11)-Cl(11) 1.717(8), C(11)-Cl(12) 1.747(7), O(11)-In(1) 2.528(5), O(12)-In(1) 2.517(5), O(13)···In(1) 2.738(5), O(14)···In(1) 2.756(5), O(15)-In(1) 2.533(5), O(16)-In(1) 2.550(5), O(1)-S 1.438(6), O(2)-S 1.424(7), O(3)-S 1.425(7); C(11)-In(1)-Cl(1) 171.81(19).

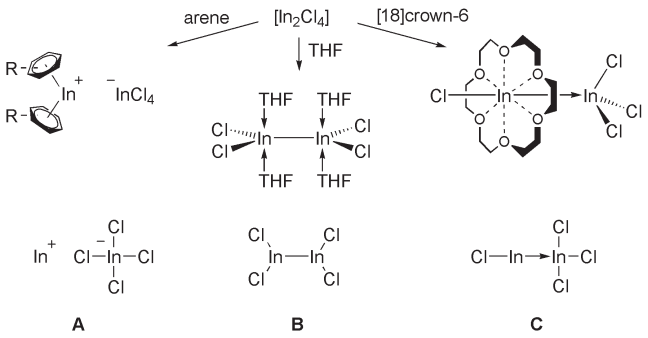

Scheme 3. Valence isomers of $[In_2Cl_4]$ (postulated or observed structures above and parent structure below): **A** is the mixed-valent ionic form (In^{I}/In^{III}); **B** is the isovalent, covalent form (In^{II}–In^{II}); and **C** is the mixed-valent donor–acceptor form (In^{I}–In^{III}) adopted by **4b**.

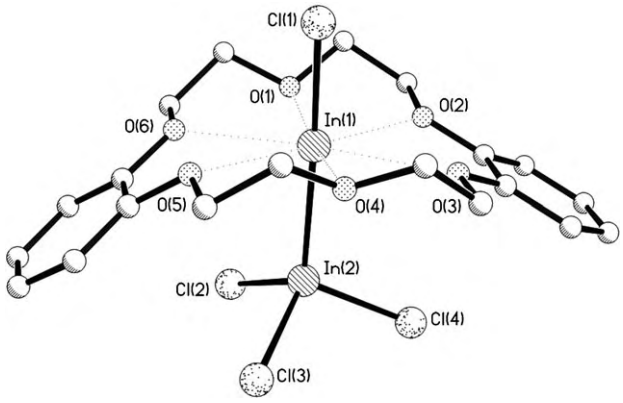

Figure 3. Molecular structure of **4b**. Hydrogen atoms are omitted for clarity. Selected bond lengths [Å] and angles [°]: In(1)-In(2) 2.7020(12), Cl(1)-In(1) 2.324(3), Cl(2)-In(2) 2.408(3), Cl(3)-In(2) 2.372(3), Cl(4)-In(2) 2.377(3), In(1)-O(1) 2.548(8), In(1)-O(2) 2.652(8), In(1)-O(3) 2.691(8), In(1)-O(4) 2.650(9), In(1)-O(5) 2.754(8), In(1)-O(6) 2.696(8); Cl(1)-In(1)-In(2) 177.12(9), Cl(3)-In(2)-Cl(4) 104.82(14), Cl(3)-In(2)-Cl(2) 102.52(12), Cl(4)-In(2)-Cl(2) 103.19(13), Cl(3)-In(2)-In(1) 116.77(9), Cl(4)-In(2)-In(1) 113.50(9), Cl(2)-In(2)-In(1) 114.47(9).

shortest such distances so far reported;[24] however, the In–C bond length of 2.174(7) Å is typical of such bonds[25,26] reported in the Cambridge Structural Database (CSD).[27] The minor deviation of the Cl-In-C angle from linearity (171.82(19)°) is consistent with the asymmetric ligation of the In center by the crown ether. All the other bond lengths and angles are typical and require no further comment.

Whereas the structural details of **3b** are unambiguous, the mechanism through which the oxidative addition occurs remains to be elucidated. Overall, we postulate that the enhanced reactivity of **2** with chlorocarbons relative to **1** may be attributable to the crown ether limiting the degree of agglomeration of **1** in solution. In this context, ligation of In^{I} species by crown ethers may possibly be used to significantly alter the reactivity of this important class of catalysts for certain organic transformations.[28]

Finally, crown ethers have provided us with a new method to generate In^{I} centers from In^{II} reagents. It is well-known that $[In_2Cl_4]$ disproportionates to form the In^{I}/In^{III} salt $[In][InCl_4]$ in the presence of certain arenes (Scheme 3, **A**);[29,30] however, the reactions of such salts with ethers or other donors yield complexes containing In^{II} (Scheme 3, **B**).[31] In contrast, the reaction of $[In_2Cl_4]$ with dibenzo[18]-crown-6 produces the In^{I}/In^{III} donor–acceptor complex **4b** (Scheme 3, **C**).[32]

Crystals of **4b** were obtained by slowly concentrating a solution of the reaction mixture in toluene; the molecular structure of the adduct is depicted in Figure 3. The structure of **4b** consists of a mixed-valent dinuclear indium core of the form Cl–In–$InCl_3$ that is symmetrically coordinated about the In^{I} center by the crown ether. Predictably, the In–In bond length of 2.7020(12) Å lies at the short end of the range of In–In bond lengths[33] compiled in the CSD and is shorter than the distance of 2.748(4) Å observed in the only other In–In donor–acceptor complex reported.[34] The In^{I}–Cl bond length of 2.324(3) Å is somewhat shorter than the In^{III}–Cl bond but still falls within the range typical for terminal bonds.[35] As observed in the structure of **2a**, the In^{I} center sits essentially at the centroid of the O_6 ring and the Cl-In^{I}-In^{III} angle of 177.12(9)° is consistent with the expected linear geometry.

We believe that the adoption of the donor–acceptor structure **4b** over the more common valence isomers (**A** and **B** depicted in Scheme 3) must be attributable to the size and shape of the crown ether. Overall, the crown ether alters the thermodynamic preference for the covalent In^{II}–In^{II} form[36] and has allowed us to isolate a homoleptic donor–acceptor isomer for the first time. Although the reaction of $[In_2Cl_4]$ with [18]crown-6 likely produces the analogous compound **4a**, we have not yet been able to obtain material suitable for single-crystal experiments.

In conclusion, we have discovered that crown ether ligation is a new, convenient, and mild method for the preparation and stabilization of In^{I} compounds. This approach has allowed for the first observation of two unprecedented structural types, and it is our hope that the stabilization or activation of low-oxidation-state centers by

 © 2005 Wiley-VCH Verlag GmbH & Co. KGaA, Weinheim

cyclic, polydentate donors will increase the availability and practicality of such reagents for use by the larger chemical community. We are currently investigating the application of compounds such as **2** as ligands for main-group and transition-metal complexes and we are examining the use of the methods outlined herein to gain access to analogous compounds containing the lighter Group 13 elements.[37]

Received: August 15, 2005
Published online: October 18, 2005

Keywords: crown compounds · indium · main-group elements · oxidation · subvalent compounds

[1] A. Schnepf, H. Schnockel, *Angew. Chem.* **2002**, *114*, 3682; *Angew. Chem. Int. Ed.* **2002**, *41*, 3533.
[2] H. Schnockel, A. Schnepf, *Adv. Organomet. Chem.* **2001**, *47*, 235.
[3] R. J. Baker, C. Jones, *Coord. Chem. Rev.* **2005**, *249*, 1857.
[4] A. H. Cowley, *Chem. Commun.* **2004**, 2369.
[5] C. Gemel, T. Steinke, M. Cokoja, A. Kempter, R. A. Fischer, *Eur. J. Inorg. Chem.* **2004**, 4161.
[6] R. A. Fischer, J. Weiss, *Angew. Chem.* **1999**, *111*, 3002; *Angew. Chem. Int. Ed.* **1999**, *38*, 2831.
[7] M. Niemeyer, P. P. Power, *Angew. Chem.* **1998**, *110*, 1291; *Angew. Chem. Int. Ed.* **1998**, *37*, 1277.
[8] S. T. Haubrich, P. P. Power, *J. Am. Chem. Soc.* **1998**, *120*, 2202.
[9] M. S. Hill, P. B. Hitchcock, R. Pongtavornpinyo, *Dalton Trans.* **2005**, 273.
[10] M. S. Hill, P. B. Hitchcock, R. Pongtavornpinyo, *Angew. Chem.* **2005**, *117*, 4303; *Angew. Chem. Int. Ed.* **2005**, *44*, 4231.
[11] M. S. Hill, P. B. Hitchcock, *Chem. Commun.* **2004**, 1818.
[12] N. J. Hardman, B. E. Eichler, P. P. Power, *Chem. Commun.* **2000**, 1991.
[13] C. M. Cui, H. W. Roesky, H. G. Schmidt, M. Noltemeyer, H. J. Hao, F. Cimpoesu, *Angew. Chem.* **2000**, *112*, 4444; *Angew. Chem. Int. Ed.* **2000**, *39*, 4274.
[14] The +1 oxidation state is generally more stable than the +3 oxidation state for Tl, and thus E refers only to B, Al, Ga, and In in this work.
[15] P. Jutzi, N. Burford, *Chem. Rev.* **1999**, *99*, 969.
[16] D. L. Reger, *Coord. Chem. Rev.* **1996**, *147*, 571.
[17] R. J. Baker, C. Jones, *Dalton Trans.* **2005**, 1341.
[18] R. J. Baker, H. Bettentrup, C. Jones, *Eur. J. Inorg. Chem.* **2003**, 2446.
[19] R. J. Baker, C. Jones, M. Kloth, D. P. Mills, *New J. Chem.* **2004**, *28*, 207.
[20] C. L. B. Macdonald, A. M. Corrente, C. G. Andrews, A. Taylor, B. D. Ellis, *Chem. Commun.* **2004**, 250.
[21] Crystallographic data: Each crystal was covered in nujol and placed rapidly into the cold N_2 stream of a Kryo-Flex low-temperature device. The data were collected on a Bruker APEX CCD diffractometer employing a graphite monochromator with MoKα radiation ($\lambda = 0.71073$ Å). A hemisphere of data was collected by using a counting time of 30 s per frame. The data were collected at −100 or −150 °C. Details of crystal data, data collection, and structure refinement are listed below. Data reductions were performed by using the SAINT software and the data were corrected for absorption with SADABS. The structures were solved by direct methods by using SIR97 and refined by full-matrix least-squares on F^2 with anisotropic displacement parameters for the non-H atoms by using SHELXL-97. **2a**: $C_{13}H_{24}F_3InO_9S$, monoclinic, space group $P2_1/n$, $a = 9.3622(5)$, $b = 11.9469(7)$, $c = 18.4097(10)$ Å, $\beta = 101.8380(10)°$, $V = 2015.32(19)$ Å^3, $Z = 4$, $\rho_{calcd} = 1.741$ g cm^{-3}, $\mu = 1.344$ mm^{-1}, $F(000) = 1064$, crystal size $0.5 \times 0.5 \times 0.3$ mm^3. A total of 17568 reflections ($2.05 \le \theta \le 27.54°$) were collected of which 4631 were unique ($R(\text{int}) = 0.0250$); 256 parameters; $R1 = 0.0287$; $wR2 = 0.0677$; GOF = 1.218. **3b**: $C_{24}H_{27}Cl_9F_3InO_9S$, monoclinic, space group $P2_1/n$, $a = 8.8651(13)$, $b = 17.844(3)$, $c = 23.039(3)$ Å, $\beta = 90.327(2)°$, $V = 3644.5(9)$ Å^3, $Z = 4$, $\rho_{calcd} = 1.790$ g cm^{-3}, $\mu = 1.427$ mm^{-1}, $F(000) = 1952$, crystal size $0.8 \times 0.3 \times 0.1$ mm^3. A total of 33811 reflections ($1.44 \le \theta \le 25.00°$) were collected of which 6424 were unique ($R(\text{int}) = 0.0808$); $R1 = 0.0826$; $wR2 = 0.1948$; GOF = 1.156. **4b**: $C_{20}H_{24}Cl_4In_2O_6$, monoclinic, space group $P2_1/c$, $a = 10.3560(15)$, $b = 15.261(2)$, $c = 16.348(2)$ Å, $\beta = 104.234(2)°$, $V = 2504.5(6)$ Å^3, $Z = 4$, $\rho_{calcd} = 1.941$ g cm^{-3}, $\mu = 2.302$ mm^{-1}, $F(000) = 1432$, crystal size $0.8 \times 0.3 \times 0.3$ mm^3. A total of 23053 reflections ($1.85 \le \theta \le 25.00°$) were collected of which 4413 were unique ($R(\text{int}) = 0.0699$); $R1 = 0.0930$; $wR2 = 0.1704$; GOF = 1.385; CCDC-280061–280063 contains the supplementary crystallographic data for this paper. These data can be obtained free of charge from the Cambridge Crystallographic Data Centre via www.ccdc.cam.ac.uk/data_request/cif.
[22] L. A. Kloo, M. J. Taylor, *J. Chem. Soc. Dalton Trans.* **1997**, 2693.
[23] http://www.webelements.com.
[24] CSD range for terminal In–Cl bonds: 2.266–2.893 Å, average 2.428 Å.
[25] C. Peppe, D. G. Tuck, F. M. de Andrade, J. A. Nobrega, M. A. Brown, R. A. Burrow, *J. Organomet. Chem.* **2005**, *690*, 925.
[26] CSD range for nonbridging In–C σ bonds: 2.044–2.453 Å, average 2.177 Å.
[27] F. H. Allen, *Acta Crystallogr. Sect. B* **2002**, *58*, 380.
[28] J. Podlech, T. C. Maier, *Synthesis* **2003**, 633.
[29] H. Schmidbaur, *Angew. Chem.* **1985**, *97*, 893; *Angew. Chem. Int. Ed. Engl.* **1985**, *24*, 893.
[30] D. G. Tuck, *Chem. Soc. Rev.* **1993**, *22*, 269.
[31] F. P. Gabbai, A. Schier, J. Riede, H. Schmidbaur, *Inorg. Chem.* **1995**, *34*, 3855.
[32] It should be noted that compounds such as **4** can also be considered as zwitterionic molecules consisting of a cationic In^{II} center ligated by the crown ether and bonded to an anionic four-coordinate In^{II} center.
[33] Not including In clusters or bridged In atoms, the In–In bond lengths range from 2.654–2.979 Å with an average of 2.795 Å.
[34] A. Frazer, P. Hodge, B. Piggott, *Chem. Commun.* **1996**, 1727.
[35] CSD range for terminal In–Cl bonds: 2.266–2.893 Å, average 2.428 Å.
[36] A. Y. Timoshkin, G. Frenking, *J. Am. Chem. Soc.* **2002**, *124*, 7240.
[37] Details of the synthesis and characterization of the products presented in this work are located in the Supporting Information.

 © 2005 Wiley-VCH Verlag GmbH & Co. KGaA, Weinheim

M=B Metathesis

DOI: 10.1002/anie.200502343

Cationic Terminal Borylene Complexes: A Synthetic and Mechanistic Investigation of M=B Metathesis Chemistry**

*Deborah L. Kays (née Coombs), Joanna K. Day, Li-Ling Ooi, and Simon Aldridge**

Metathesis reactions constitute a key component of modern synthetic chemistry; olefin metathesis, for example, provides a versatile and widely exploited carbon–carbon bond-forming methodology.[1] Such reactions are typically catalyzed by organometallic complexes that contain M=C bonds.[2] The synthesis of analogous complexes that contain M=Si bonds, for example, has led to an in-depth investigation of their reactivity towards unsaturated substrates.[3]

Synthetic approaches that lead to the isolation of related systems with M=B bonds have been developed only recently:[4–7] for example, halide-abstraction chemistry gives access to cationic terminal borylene complexes, $[L_nM{=}BX]^+$.[7] Consequently, reports of the fundamental chemistry of M=B bonds are somewhat limited (predominantly to metal–metal transfer reactions and addition/substitution reactivity towards nucleophiles).[4,6,7] Thus, the chemistry of $[Cp^*Fe(CO)_2(BMes)]^+$ (Mes = mesityl = 2,4,6-$Me_3C_6H_2$, Cp* = pentamethylcyclopentadienyl), for example, is dominated by the electrophilic character at both the Fe and B centers.[7] In an attempt to tune the reactivity of these highly unsaturated complexes we investigated the synthesis of cationic aminoborylene systems, $[L_nM{=}BNR_2]^+$.[5] Chloride abstraction from $[CpFe(CO)_2\{B(N{i}Pr_2)Cl\}]$ (**2**) (Cp = cyclopentadienyl) by $Na(BAr^f{}_4)$ (Ar^f = 3,5-$(CF_3)_2C_6H_3$) affords the thermally robust cationic B/N vinylidene analogue $[CpFe(CO)_2(BN{i}Pr_2)]^+$, which undergoes, with E=O and E=S bonds (E = P, As), the first reported examples of M=B metathesis chemistry.

The synthesis of $[CpFe(CO)_2(BN{i}Pr_2)]^+(BAr^f{}_4)^-$ (**3**) is outlined in Scheme 1. The key precursor **2** was synthesized by the selective substitution of a chloride substituent in iPr_2NBCl_2 (**1**) by $[CpFe(CO)_2]^-$. The steric bulk of the amino substituents is a key point: the use of the smaller NMe_2 group results in the formation of a thermally fragile borylene product in the subsequent halide-abstraction step,[7b,8] whereas $[CpFe(CO)_2\{B(tmp)Cl\}]$ (tmp = tetramethylpiperamino) was inaccessible from $tmpBCl_2$. Compound **2** is a pale yellow sublimable crystalline solid, which was characterized by multinuclear NMR and IR spectroscopy, mass spectrometry, and X-ray crystallographic analysis (Figure 1).

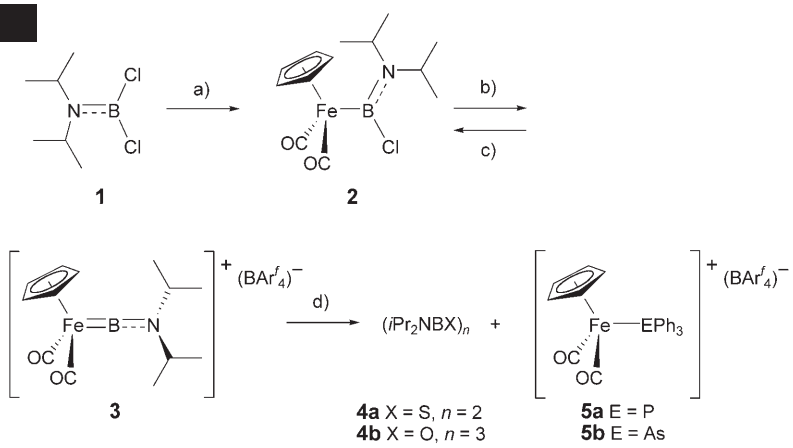

Scheme 1. Synthesis and reactions of **3**. a) Na[CpFe(CO)$_2$] (1 equiv), toluene, 20 °C, 20 h.; b) Na(BAr$^f{}_4$), (1 equiv), dichloromethane, −78→20 °C, 30 min.; c) ppnCl (1.67 equiv), dichloromethane, 20 °C, 30 min.; d) $Ph_3P{=}S$ or $Ph_3As{=}O$ (1 equiv), dichloromethane, 20 °C, 30 min. ppn = bis(triphenylphosphoranylidene)ammonium.

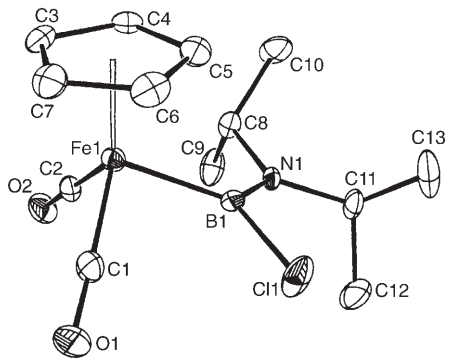

Figure 1. Structure of **2** (50% ellipsoids; H atoms omitted for clarity). Selected bond lengths [Å] and angles [°]: Fe(1)-B(1) 2.054(4), B(1)-Cl(1) 1.841(4), B(1)-N(1) 1.389(5); centroid-Fe(1)-B(1)-N(1) 83.7(4).

The reaction of **2** with Na(BAr$^f{}_4$) in dichloromethane results in a quantitative conversion (determined by ^{1}H and ^{11}B NMR spectroscopy) into **3**. The latter product (along with the C_5H_4Me analogue) is a colourless oil at (or close to) room temperature, but its formulation can be definitively established from spectroscopic and reactivity data. The measured ^{11}B chemical shift for **3** (δ_B = 93.5 ppm) is very close to that reported by Braunschweig et al. for neutral terminal-aminoborylene systems of the type $L_nM{=}BN(SiMe_3)_2$ (δ_B = 86.6–98.3 ppm).[5] The downfield shift upon chloride abstraction ($\Delta\delta_B$ = 38.1 between **2** and **3**) mirrors that found for $[Cp^*Fe(CO)_2\{B(Mes)Cl\}]/[Cp^*Fe(CO)_2(BMes)]^+$ (δ_B = 112.1 and 145.0 ppm, respectively) and for $[Cp^*Fe(CO)_2\{B(NMe_2)Cl\}]/[Cp^*Fe(CO)_2(BNMe_2)]^+$ (δ_B = 58.6 and 88.0 ppm, respectively).[7,8] The ^{1}H and ^{13}C NMR data are

[*] Dr. D. L. Kays (née Coombs), J. K. Day, Dr. L.-L. Ooi, Dr. S. Aldridge
Centre for Fundamental and Applied Main Group Chemistry
School of Chemistry, Cardiff University
Main Building, Park Place, Cardiff, CF10 3AT (UK)
Fax: (+44) 2920-874-030
E-mail: aldridges@cardiff.ac.uk

[**] We thank the EPSRC for funding and access to the National Mass Spectrometry facility and Prof. C. Jones (Cardiff) for help in modeling crystallographic disorder.

Supporting information for this article (crystal structure data for **2** and **6**, and data for **4a**, **4b**, **5a**, and **5b**) are available on the WWW under http://www.angewandte.org or from the author.

© 2005 Wiley-VCH Verlag GmbH & Co. KGaA, Weinheim

consistent with the presence of Cp, N*i*Pr$_2$, and $(BAr^f_4)^-$ moieties in a 1:1:1 ratio, and the ES+ mass spectrum shows the presence of the $[CpFe(CO)_2(BN{\it i}Pr_2)]^+$ cation. The observation of equivalent *i*Pr substituents is consistent with the structure of the related neutral system $[CpV(CO)_3{=}BN(SiMe_3)_2]$[5c] and agrees with the results of DFT calculations for the model compounds $[(\eta^5\text{-}C_5R_5)Fe(CO)_2(BNMe_2)]^+$ (R = H, Me), for which a minimum-energy structure close to C_s symmetry [< centroid-Fe-N-C ≈ 90° (84.6° for R = Me)] and a low barrier to rotation about the Fe-B-N axis (≈ 2.2 kcal mol^{-1}) have been calculated.[7b,c] Furthermore, the IR spectrum of **3** shows carbonyl stretching frequencies ($\tilde{\nu}$ = 2070, 2028 cm^{-1}) that are significantly blue shifted with respect to **2** ($\tilde{\nu}$ = 2001, 1941 cm^{-1}) ($\Delta\tilde{\nu} \approx 50$ cm^{-1} for $[Cp^*Fe(CO)_2\{B(Mes)Cl\}]/[Cp^*Fe(CO)_2(BMes)]^+$) and are very similar to those reported for the archetypal Fischer carbene systems such as $[CpFe(CO)_2{=}CH(SPh)]^+(PF_6)^-$ ($\tilde{\nu}$ = 2073, 2034 cm^{-1}).[9] Further evidence for the nature of **3** was obtained: 1) from the reaction of **3** with ppnCl (see Supporting Information), which like the analogous reaction for structurally characterized cationic derivatives,[6b,7] generates a haloboryl complex (in this case **2**) by the addition of a halide at boron and 2) from the reaction of **3** with $Ph_3P{=}O$, which proceeds via the structurally characterized adduct $[CpFe(CO)_2\{B(N{\it i}Pr_2)(OPPh_3)\}]^+(BAr^f_4)^-$ (see below).

Although the reactivity of cationic aminoborylene complex **3** towards Cl^- is indicative of electrophilic character, its reactivity towards unsaturated substrates suggests a broader scope for its chemistry. Thus, the reaction of **3** with $Ph_3P{=}S$ in dichloromethane at room temperature leads to the formation of $[{\it i}Pr_2NB(\mu\text{-}S)_2BN{\it i}Pr_2]$ (**4a**) and $[CpFe(CO)_2(PPh_3)]^+(BAr^f_4)^-$ (**5a**) with a conversion of > 95% (as determined by ^{1}H, ^{11}B and ^{31}P NMR spectroscopy). The identities of the isolated products **4a** and **5a** were confirmed by comparison of NMR (^{1}H, ^{11}B, ^{13}C, ^{19}F, and ^{31}P) and IR spectra and mass spectrometry data with those reported for authentic samples.[10a–c] The similar reactivity of **3** towards $Ph_3As{=}O$ led to the isolation of $({\it i}Pr_2NBO)_3$ (**4b**) and $[CpFe(CO)_2(AsPh_3)]^+(BAr^f_4)^-$ (**5b**).[10c,d]

The reactions of **3** with $Ph_3P{=}S$ and $Ph_3As{=}O$ therefore represent, to our knowledge, the first examples of net metathesis reactions for a terminal borylene complex.[11] Although metathesis chemistry has been reported for isoelectronic vinylidene systems $[CpM(CO)_2{=}C{=}CH_2]$ (M = Mn, Re),[12] no such reactivity has been reported for neutral aminoborylene complexes.[5,6] The origins of the different reactivity of **3** and an idea of the likely mechanism can be gauged by examining of the analogous reaction with $Ph_3P{=}O$. This reaction proceeds at a significantly slower rate than those of $Ph_3P{=}S$ or $Ph_3As{=}O$ which presumably reflects the greater strength of the P=O bond. In this case, however, it is possible to identify a reaction intermediate, which was characterized by NMR signals at δ_B = 48.9 ppm and δ_P = 48.3 ppm. The former resonance is consistent with values previously reported for base-stabilized terminal borylene complexes (e.g. δ_B = 51.7–53.2 ppm for N-donor adducts of osmium aminoborylenes),[4b,c] whereas the ^{31}P chemical shift is as expected for donor/acceptor adducts of Ph_3PO with boron-centered Lewis acids (δ_P = 43.6–46.7 ppm).[13] Furthermore, the observations of inequivalent *i*Pr groups by ^{1}H and ^{13}C NMR and of significantly lower carbonyl stretching frequencies ($\tilde{\nu}$ = 2004, 1949 cm^{-1}) are consistent with the formation of a trigonal-planar boron center by coordination of a Lewis base. Confirmation that the intermediate species is indeed the B-bound Ph_3PO adduct $[CpFe(CO)_2\{B(N{\it i}Pr_2)(OPPh_3)\}]^+(BAr^f_4)^-$(**6**) was obtained by X-ray crystallographic analysis (Figure 2). Consistent with related complexes,[4b,c,14] the Fe–B bond length for **6** [2.057(4) Å] is more akin to that expected for a single bond than a double bond (2.054(4) and 1.792(8) Å for **2** and $[Cp^*Fe(CO)_2(BMes)]^+$, respectively).[7] Such a phenomenon has previously been ascribed to significant contributions from resonance forms that incorporate a formal M–B bond (Scheme 2),[4b,c] and a description of **6** as an amino(oxy)boryl species that features a pendant cationic phosphorus centre is probably most apt. Consistent with this, the P–O distance within **6** is significantly longer than that found in free Ph_3PO (1.540(2) vs. 1.493 Å (mean)).[15]

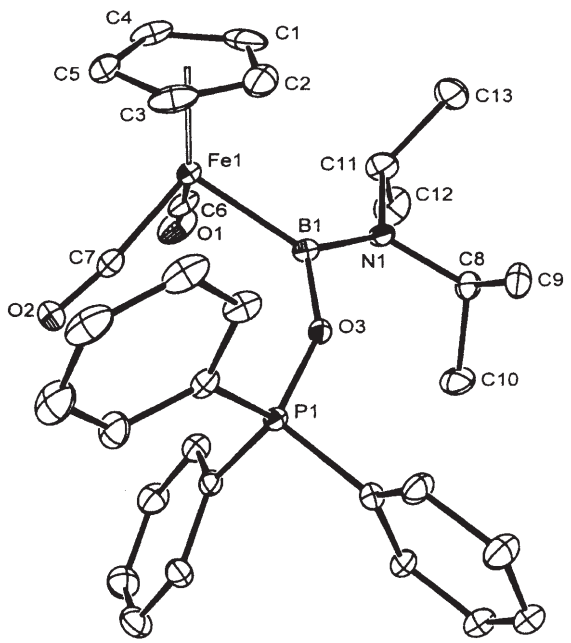

Figure 2. Structure of the cationic component of **6** (50% ellipsoids; H atoms omitted for clarity). Selected bond lengths [Å] and angles [°]: Fe(1)-B(1) 2.057(4), B(1)-O(3) 1.469(4), B(1)-N(1) 1.397(5), P(1)-O(3) 1.540(2); P(1)-O(1)-B(1) 148.0(2), centroid-Fe(1)-B(1)-N(1) 72.5(5).

Given the isolation of **6**, it is plausible that the first step in the reaction mechanism involves coordination of $Ph_3E{=}X$

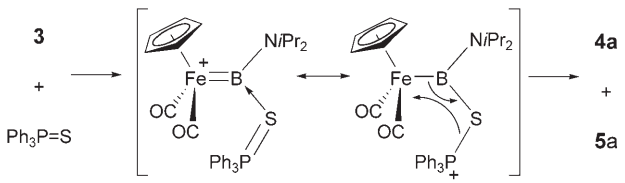

Scheme 2. Proposed addition/substitution pathway for the metathesis reaction of **3** (exemplified by $Ph_3P{=}S$).

 © 2005 Wiley-VCH Verlag GmbH & Co. KGaA, Weinheim

(E = P, As; X = O, S) at boron, and that the overall metathesis chemistry of **3** therefore occurs through a combined addition/substitution pathway (Scheme 2). Further studies aimed at better understanding the reactivity of M = B bonds towards unsaturated substrates (including C = E multiple bonds) will be reported in a full account.[17]

Experimental Section

2: Reaction of **1** (1.199 g, 6.6 mmol) with Na[CpFe(CO)$_2$] (1.318 g, 6.6 mmol) in toluene (40 cm^3) at room temperature for 20 h, followed by filtration, removal of volatile compounds in vacuo, and extraction with hexanes ($\approx$40 cm^3) yielded crude **2** as an oily brown solid. Yellow crystals suitable for X-ray diffraction were obtained by sublimation under high vacuum (40 °C at 10^{-4} Torr). Yield (of sublimed material): 0.259 g, 12 %. ^{1}H NMR (400 MHz, C_6D_6): δ = 1.11 (d, J = 6.7 Hz, 6H; CH(CH_3)$_2$ of *i*Pr), 1.39 (d, J = 6.7 Hz, 6H; CH(CH_3)$_2$), 3.40 (sept, J = 6.7 Hz, 1H; CH(CH$_3$)$_2$), 4.44 (sept, J = 6.7 Hz, 1H; CH(CH$_3$)$_2$), 4.69 ppm (s, 5H; Cp-H); ^{13}C NMR (76 MHz, C_6D_6): δ = 21.2 (CH(*C*H$_3$)$_2$), 23.9 (CH(*C*H$_3$)$_2$), 47.8 (*C*H(CH$_3$)$_2$), 55.2 (*C*H(CH$_3$)$_2$), 88.2 (Cp), 215.6 ppm (CO); ^{11}B NMR (96 MHz, C_6D_6): δ = 55.4 ppm. IR (C_6D_6 soln); $\tilde{\nu}$ = 2001, 1941 cm^{-1} νCO; MS (EI): *m*/*z* (%): 295 (65) [*M*−CO]$^+$, 288 (weak) [*M*−Cl], 267 (10) [*M*−2CO]$^+$, 223 (100) [*M*−N*i*Pr$_2$]$^+$, *M*$^+$ not observed; MS: calcd for [*M*−CO]$^+$: 295.0592; found: 295.0595; calcd for [*M*−Cl]$^+$: 288.0853; found 288.0856. Crystal data: $C_{13}H_{19}BClFeNO_2$, orthorhombic, *Pbca*, a = 11.7410(4), b = 13.9170(4), c = 19.0830(7) Å, V = 3118.15(18) Å^3, Z = 8, ρ_{calcd} = 1.378 Mg m^{-3}, M_r = 323.40, T = 150(2) K. 22231 reflections collected, 3175 independent (R(int) = 0.1524), which were used in all calculations. R_1 = 0.0572, wR_2 = 0.1157 for observed unique reflections ($F^2 > 2\sigma(F^2)$) and R_1 = 0.1048, wR_2 = 0.1338 for all unique reflections. Max./min. residual electron densities 0.505/−0.537 e Å^{-3}.[16]

3: Reaction of **2** (0.259 g, 0.80 mmol) and Na(BAr$^f_4$) (0.710 g, 0.80 mmol) in dichloromethane (15 cm^3) from −78→20 °C over 30 min leads to a quantitative conversion (determined by ^{11}B NMR) of **2** (δ_B = 55.4 ppm) to **3** (δ_B = 93.5 ppm). Filtration, and recrystallization from dichloromethane/hexanes (or fluorobenzene/hexanes) at −30 °C leads to the isolation of **3** as a spectroscopically pure colourless oil. Yield of isolated material: 0.465 g, 50 %. ^{1}H NMR (400 MHz, CD_2Cl_2): δ = 1.39 (d, J = 6.6 Hz, 12H; CH(CH_3)$_2$), 3.32 (sept, J = 6.6 Hz, 2H; CH(CH$_3$)$_2$), 5.33 (s, 5H, Cp-H), 7.55 (s, 4H; BAr$^f_4{}^-$-H$_p$), 7.70 ppm (s, 8H; BAr$^f_4{}^-$-H$_o$); ^{13}C NMR (76 MHz, CD_2Cl_2): δ = 24.4 (CH(*C*H$_3$)$_2$), 51.0 (*C*H(CH$_3$)$_2$), 87.1 (C(Cp)), 117.6 (BAr$^f_4{}^-$-CH$_p$), 124.6 (q, $^1J_{CF}$ = 272 Hz, BAr$^f_4{}^-$-CF$_3$), 128.8 (q, $^2J_{CF}$ = 34 Hz, BAr$^f_4{}^-$-CH$_m$), 134.8 (BAr$^f_4{}^-$-CH$_o$), 161.8 (q, $^1J_{CB}$ = 49 Hz, BAr$^f_4{}^-$-C$_{ipso}$), 205.6 ppm (CO); ^{11}B NMR (96 MHz, CD_2Cl_2): δ = −7.7 (BAr$^f_4{}^-$), 93.5 ppm (b, fwhm $\approx$ 615 Hz, BN*i*Pr$_2$); ^{19}F NMR (283 MHz, CD_2Cl_2): δ = −62.6 ppm (CF$_3$); IR (CD_2Cl_2 soln): $\tilde{\nu}$ = 2070, 2028 cm^{-1} νCO; MS (ES): *m*/*z* (%): *M*$^+$ 288.1 (10).

Typical reaction: **3** (0.068 g, 0.06 mmol) and Ph$_3$P=S (1.0 equiv) were stirred together in dichloromethane for 30 min, after which the reaction was judged to be complete by ^{11}B and ^{31}P NMR (conversion of signals at δ_B = 93.5 ppm and δ_P = 43.7 ppm to δ_B = 35.6 ppm and δ_P = 60.8 ppm, respectively). Removal of volatile components in vacuo and extraction into hexanes gave *i*Pr$_2$NB(μ-S)$_2$BN*i*Pr$_2$ (**4a**), which was identified by comparison of ^{1}H, ^{13}C, and ^{11}B NMR spectroscopic and mass spectrometry data with those reported previously.[10a,b] ^{1}H, ^{13}C, ^{11}B, ^{19}F, and ^{31}P NMR and IR spectra of the hexane-insoluble product confirmed it to be [CpFe(CO)$_2$(PPh$_3$)]$^+$(BAr$^f_4$)$^-$ (**5a**).[10c] A similar procedure was adopted for the reaction of **3** with Ph$_3$As = O.[10c,d]

6: Reaction of **3** (0.199 g, 0.17 mmol) and Ph$_3$PO (0.048 g, 0.17 mmol) in dichloromethane (5 cm^3) at room temperature over a period of 30 min, followed by filtration and recrystallization from dichloromethane/hexanes at −30 °C led to the isolation of **6** as pale yellow crystals. Yield of isolated product: 0.105 g, 43 %. ^{1}H NMR (400 MHz, CD_2Cl_2): δ = 1.06 (d, J = 6 Hz, 6H; CH(CH_3)$_2$), 1.20 (d, J = 6 Hz, 6H; CH(CH_3)$_2$), 3.25 (sept, J = 6 Hz, 1H; CH(CH$_3$)$_2$), 4.10 (sept, J = 6 Hz; CH(CH$_3$)$_2$), 4.50 (s, 5H; Cp-H), 7.38–7.48 (m, 9H; Ph$_3$PO-CH_o and Ph$_3$PO-CH_p), 7.55 (s, 4H; BAr$^f_4{}^-$-H$_p$), 7.60–7.78 (m, 6H; Ph$_3$PO-H$_m$), 7.73 ppm (s, 8H; BAr$^f_4{}^-$-H$_o$); ^{13}C NMR (76 MHz, C_6D_6): δ = 22.4, 23.9 (CH(*C*H$_3$)$_2$), 47.2 (*C*H(CH$_3$)$_2$), 84.4 (C(Cp)), 117.5 (BAr$^f_4{}^-$-CH$_p$), 122.6 (Ph$_3$PO-C$_{ipso}$), 124.6 (q, $^1J_{CF}$ = 272 Hz; BAr$^f_4{}^-$-CF$_3$), 128.9 (q, $^2J_{CF}$ = 34 Hz; BAr$^f_4{}^-$-C$_m$), 130.1 (Ph$_3$PO-CH$_m$), 133.5 (Ph$_3$PO-C$_o$), 134.9 (BAr$^f_4{}^-$-CH$_o$), 135.9 (Ph$_3$PO-C$_p$), 161.8 (q, $^1J_{CB}$ = 49 Hz; BAr$^f_4{}^-$-C$_{ioso}$), 214.7 ppm (CO); ^{11}B NMR (96 MHz, CD_2Cl_2): δ = −7.7 (BAr$^f_4{}^-$), 48.9 ppm (b, fwhm $\approx$ 480 Hz, B-(OPPh$_3$)N*i*Pr$_2$); ^{19}F NMR (283 MHz, CD_2Cl_2): δ = −62.7 ppm (CF$_3$); ^{31}P NMR (121 MHz, CD_2Cl_2): δ = 48.3 ppm (Ph$_3$PO); IR (CD_2Cl_2 soln): $\tilde{\nu}$ = 2004, 1949 cm^{-1} ν(CO). Crystal data: $C_{63}H_{46}B_2F_{24}FeNO_3P$, triclinic, *P*$\bar{1}$, a = 13.0324(2), b = 13.9949(2), c = 19.1002(3) Å, α = 68.7080(10), β = 83.7430(10), γ = 87.4800(10)°, V = 3226.47(8) Å^3, Z = 2, ρ_{calcd} = 1.471 Mg m^{-3}, M_r = 1429.45, T = 150(2) K. 51247 reflections collected, 14704 independent (R(int) = 0.1118) which were used in all calculations. R_1 = 0.0718, wR_2 = 1791 for observed unique reflections ($F^2 > 2\sigma(F^2)$) and R_1 = 0.1223, wR_2 = 0.1992 for all unique reflections. Max./min. residual electron densities 1.086/−0.608 e Å^{-3}.[16]

Received: July 5, 2005
Published online: October 17, 2005

Keywords: boron · borylenes · halide abstraction · metathesis · vinylidene ligands

[1] T. M. Trnka, R. H. Grubbs, *Acc. Chem. Res.* **2002**, *35*, 18–29.
[2] a) W. A. Nugent, J. M. Mayer, *Metal Ligand Multiple Bonds*, Wiley Interscience, New York, 1988; b) J. W. Hendon, *Coord. Chem. Rev.* **2003**, *243*, 3–81.
[3] G. P. Mitchell, T. D. Tilley, *J. Am. Chem. Soc.* **1997**, *119*, 11236–11243.
[4] a) H. Braunschweig, M. Colling, C. Kollann, K. Merz, K. Radacki, *Angew. Chem.* **2001**, *113*, 4327–4329; *Angew. Chem. Int. Ed.* **2001**, *40*, 4198–4200; b) G. J. Irvine, C. E. F. Rickard, W. R. Roper, A. Williamson, L. J. Wright, *Angew. Chem.* **2000**, *112*, 978–980; *Angew. Chem. Int. Ed.* **2000**, *39*, 948–950; c) C. E. F. Rickard, W. R. Roper, A. Williamson, L. J. Wright, *Organometallics* **2002**, *21*, 4862–4872; d) H. Braunschweig, K. Radacki, D. Scheschkewitz, G. R. Whittell, *Angew. Chem.* **2005**, *117*, 1685–1688; *Angew. Chem. Int. Ed.* **2005**, *44*, 1658–1661;.
[5] For neutral aminoborylene complexes, see: a) H. Braunschweig, C. Kollann, U. Englert, *Angew. Chem.* **1998**, *110*, 3355–3357; *Angew. Chem. Int. Ed.* **1998**, *37*, 3179–3180; b) H. Braunschweig, M. Colling, C. Kollann, H. G. Stammler, B. Neumann, *Angew. Chem.* **2001**, *113*, 2359–2361; *Angew. Chem. Int. Ed.* **2001**, *40*, 2298–2300; c) H. Braunschweig, M. Colling, C. Hu, K. Radacki, *Angew. Chem.* **2003**, *115*, 215–218; *Angew. Chem. Int. Ed.* **2003**, *42*, 205–208.
[6] For recent reviews of borylene chemistry, see: a) H. Braunschweig, M. Colling, *Eur. J. Inorg. Chem.* **2003**, 393–403; b) S. Aldridge, D. L. Coombs, *Coord. Chem. Rev.* **2004**, *248*, 535–559; c) H. Braunschweig, *Adv. Organomet. Chem.* **2004**, *51*, 163–192.
[7] a) D. L. Coombs, S. Aldridge, C. Jones, D. J. Willock, *J. Am. Chem. Soc.* **2003**, *125*, 6356–6357; b) D. L. Coombs, S. Aldridge, A. Rossin, C. Jones, D. J. Willock, *Organometallics* **2004**, *23*, 2911–2926; c) S. Aldridge, A. Rossin, D. L. Coombs, D. J. Willock, *Dalton Trans.* **2004**, 2649–2654.
[8] H. Braunschweig, C. Kollann, U. Englert, *Eur. J. Inorg. Chem.* **1998**, 465–468.
[9] C. Knors, G.-H. Kuo, J, W, Lauher, C. Eigenbrot, P. Helquist, *Organometallics* **1987**, *6*, 988–995.

 © 2005 Wiley-VCH Verlag GmbH & Co. KGaA, Weinheim

[10] a) H. Nöth, W. Rattay, *J. Organomet. Chem.* **1986**, *312*, 139–148; b) W. Maringgele, A. Meller, *Z. Anorg. Allg. Chem.* **1989**, *572*, 140–144; c) H. Schumann, L. Eguren, *J. Organomet. Chem.* **1991**, *403*, 183–193; d) W. Maringgele, M. Noltemeyer, A. Meller, *Organometallics* **1997**, *16*, 2276–2284.
[11] Metathesis chemistry has been reported for C=B bonds, for example see: P. Paetzold, U. Englert, R. Finger, T. Schmitz, A. Tapper, *Z. Anorg. Allg. Chem.* **2004**, *630*, 508–518.
[12] See, for example: M. R. Terry, L. A. Mercando, C. Kelley, G. L. Geoffroy, P. Nombel, N. Lugan, R. Mathieu, R. L. Ostrander, B. E. Owens-Waltermire, A. L. Rheingold, *Organometallics* **1994**, *13*, 843–865.
[13] a) N. Burford, B. W. Royan, R. E. v. H. Spence, T. S. Cameron, A. Linden, R. D. Rogers, *J. Chem. Soc. Dalton Trans.* **1990**, 1521–1528; b) G. J. P. Britovsek, J. Ugolotti, A. J. P. White, *Organometallics* **2005**, *24*, 1685–1691.
[14] H. Braunschweig, D. Rais, K. Uttinger, *Angew. Chem.* **2005**, *117*, 3829–3832; *Angew. Chem. Int. Ed.* **2005**, *44*, 3763–3766; .
[15] C. P. Brock, W. B. Schweizer, J. D. Dunitz, *J. Am. Chem. Soc.* **1985**, *107*, 6964–6970.
[16] Further details of the crystal structures investigation may be obtained from the Fachinformationszentrum, Karlsruhe, D-76344 Eggenstein-Leopoldshafen, Germany (fax: (+49) 7247-808-666; e-mail: crysdata@fiz-karlsruhe.de) on quoting the depository number CSD-277456 (**2**) and CSD-277457 (**6**), the manes of the authors, and the journal citation.
[17] For a related article, see the following Communication in this issue: H. Braunschweig, T. Herbst, D. Rais, F. Seeler, *Angew. Chem.* **2005**, *117*, 7627–7629; *Angew. Chem. Int. Ed.* **2005**, *44*, 7461–7463 (DOI: 10-1002/anie.200502524).

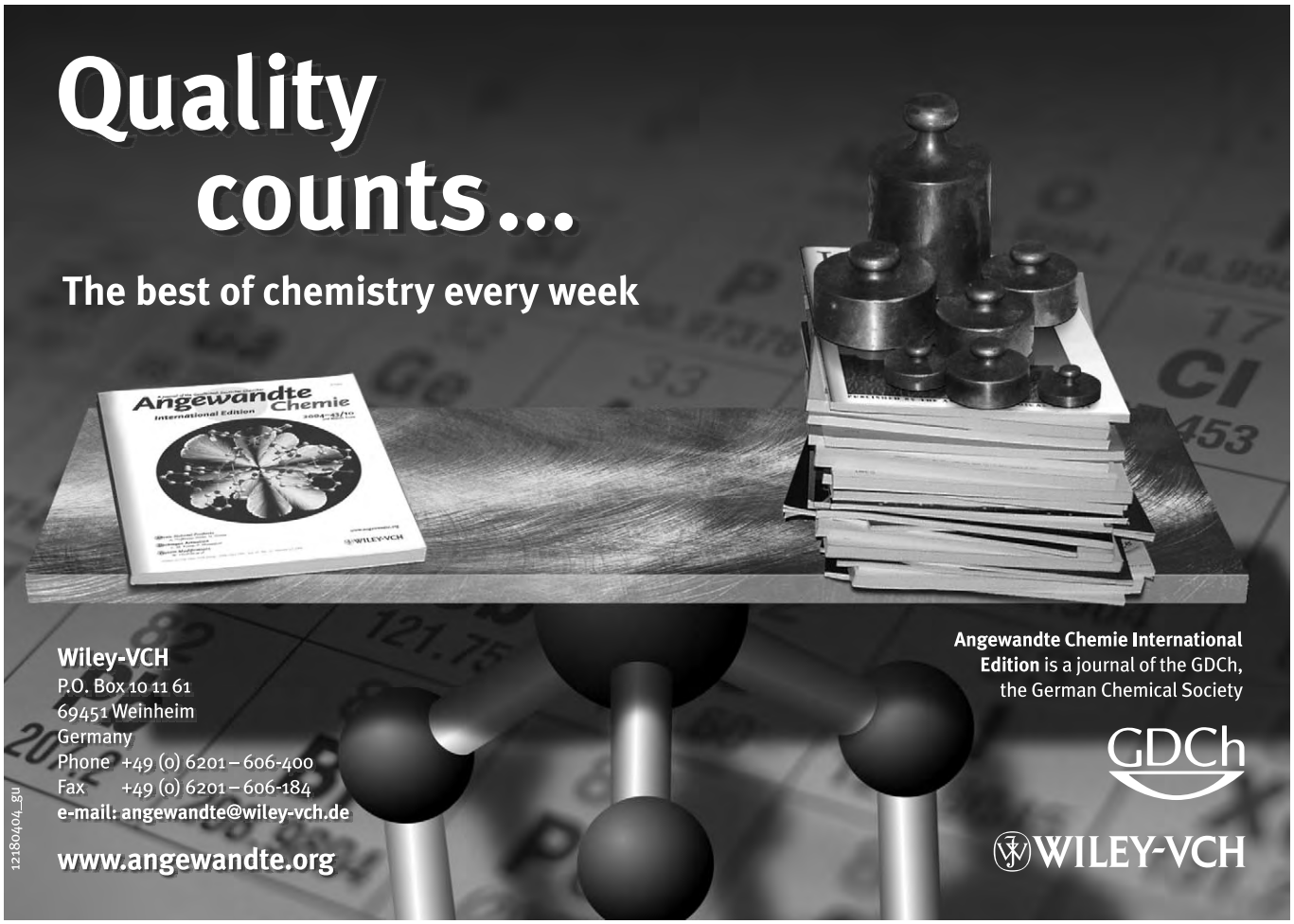

 © 2005 Wiley-VCH Verlag GmbH & Co. KGaA, Weinheim

Boracycles

DOI: 10.1002/anie.200502524

Synthesis of Borirenes by Photochemical Borylene Transfer from $[(OC)_5M{=}BN(SiMe_3)_2]$ (M = Cr, Mo) to Alkynes**

Holger Braunschweig, Thomas Herbst, Daniela Rais, and Fabian Seeler*

Boracyclopropene, or borirene, is isoelectronic with the cyclopropenylium cation and, as such, represents the simplest boron-containing cyclic system that might exhibit 2π aromatic stabilization.[1] A limited number of synthetic routes have been successfully applied to the generation of the borirene nucleus.[2–5] Among these, only two methods, although restricted in scope, yielded satisfactory amounts of the desired compounds: 1) the reaction reported by Pues and Berndt[3] of trimethylstannylalkynes with 1,2-di-*tert*-butyl-1,2-dichlorodiborane(4) which affords 1-*tert*-butylborirenes, and 2) the photoisomerization of diaryl(arylethynyl)boranes reported by Eisch et al.[5] The latter method, in particular, allowed the isolation and structural characterization of 2-(2,6-dimethylphenyl)-1,3-dimesitylborirene (**1**), thus providing experimental evidence for the theoretically predicted aromaticity of this class of compounds.

In 1984 Pachaly and West reported the formation of 1-triphenylsilyl-2,3-bis(trimethylsilyl)borirene upon reaction of the photochemically generated triphenylsilylborylene, B–$SiPh_3$, at −196 °C with bis(trimethylsilyl)ethyne. The compound was characterized by ^{1}H NMR and IR spectroscopy as well as mass spectrometry.[4] We recently demonstrated that the Group VI terminal borylene complexes $[(OC)_5M{=}B{-}N(SiMe_3)_2]$ (M = Cr, W)[6] are convenient sources of the borylene moiety $BN(SiMe_3)_2$, which can be efficiently transferred to different transition metals upon photolysis.[7] Following these important results, we turned our attention to the analogous borylene transfer to main-group-element compounds. Herein we report preliminary results of borylene transfer to alkynes which leads to borirenes in high yields.

Borirenes **4**–**6** were obtained upon photolysis of pale yellow solutions of $[(OC)_5M{=}BN(SiMe_3)_2]$ (M = Cr, **2**; M = Mo,[8] **3**) in the presence of the appropriate alkyne for 2–4 h at room temperature (Scheme 1). The reaction was monitored by multinuclear NMR spectroscopy, which revealed gradual consumption of the starting materials and quantitative formation of a new boron-containing compound, as indicated

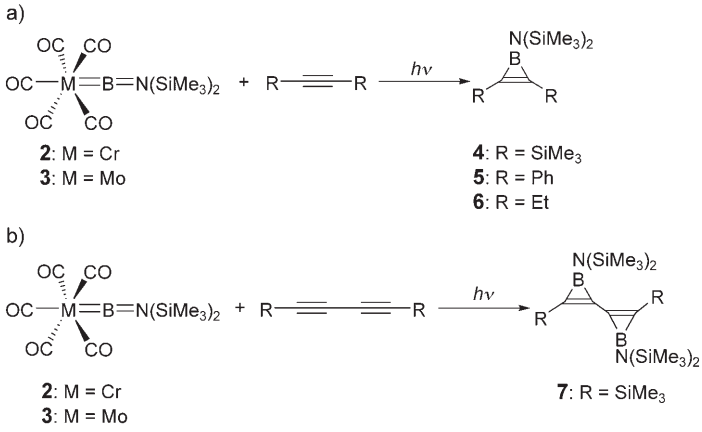

Scheme 1. Synthesis of borirenes **4**–**6** (a) and **7** (b) by photochemically induced borylene transfer to alkynes and diynes.

by the presence of a singlet resonance in the $^{11}B\{^1H\}$ NMR spectrum at $\delta = 33.2$ ppm for **4** and $\delta = 25.0$ ppm for **5** and **6**. These values are in good agreement with those reported by Habben and Meller for a series of 1-bis(trimethylsilyl)aminoborirenes ($\delta = 26.5$–27.7 ppm), which were synthesized, albeit in very low yield (2–7%), by high-vacuum pyrolysis of an uncharacterized oligomeric product stemming from the reduction of suitable 1,2-dithia-3-bis(trimethylsilyl)aminoboroles with sodium.[2]

The trimethylsilyl derivative **4** was isolated in the form of pale yellow crystals by filtration of the reaction mixture and subsequent crystallization from hexane at −60 °C. The result of the X-ray crystal-structure analysis[9] on borirene **4** is displayed in Figure 1.

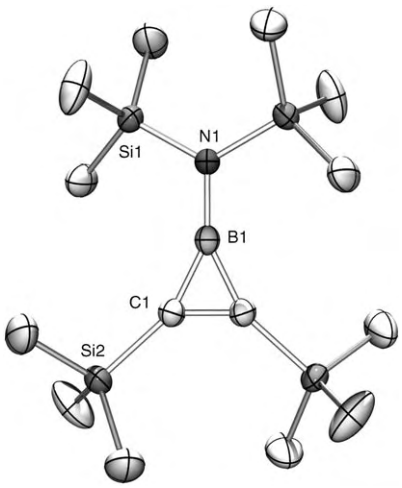

Figure 1. Molecular structure of **4**. Hydrogen atoms have been omitted for clarity. Selected bond lengths [Å] and angles [°]: N1-B1 1.421(4), C1-B1 1.485(3), C1-C1 1.376(4), C1-B1-N1-Si1 22.24(16). Ellipsoids drawn at the 50% probability level.

The C1–B1 bond length (1.485(3) Å) in **4** is comparable to those reported for 2-(2,6-dimethylphenyl)-1,3-dimesitylborirene (**1**, 1.450(10) and 1.464(11) Å)[5a] and so is the C–C bond length within the ring (**4**, 1.376(4) Å; **1**, 1.380(9) Å). In **1** such values were interpreted as indicative of extensive delocaliza-

[*] Prof. Dr. H. Braunschweig, T. Herbst, Dr. D. Rais, F. Seeler
Institut für Anorganische Chemie
Bayerische Julius-Maximilians-Universität Würzburg
Am Hubland, 97074 Würzburg (Germany)
Fax: (+49) 931-888-4623
E-mail: h.braunschweig@mail.uni-wuerzburg.de

[**] This work was supported by the Deutsche Forschungsgemeinschaft. D.R. thanks the Alexander von Humboldt Foundation for a postdoctoral fellowship.

© 2005 Wiley-VCH Verlag GmbH & Co. KGaA, Weinheim

tion of the two π electrons over a three-center bonding molecular orbital from the p atomic orbitals of boron and carbon.[5a] In **4**, such delocalization is likely to be attenuated by the presence of the amino substituent, which generally engages in a π-type interaction with the empty p orbital of boron. Interestingly, however, a tilt of the plane of the amino substituent with respect to the plane containing the boracyclopropene ring (C1-B1-N1-Si1 = 22.24(16)°) and a consequently elongated B1–N1 bond (1.421(4) Å) are observed in the molecular structure of **4**, possibly indicating a weaker π interaction between the boron and nitrogen centers as a result of the aromatic character of the boracyclopropene ring.

The versatility of the synthetic method was further probed in the reaction of $[(OC)_5Mo{=}BN(SiMe_3)_2]$ (**3**) with 1,4-bis(trimethylsilyl)-buta-1,3-diyne. Under analogous conditions to those applied for the synthesis of compounds **4**–**6**, complete consumption of the two starting materials was observed upon irradiation of the reaction mixture for 4 h, and clean formation of the unprecedented diborirene species **7** was confirmed by multinuclear and 2D NMR spectroscopy. A singlet is observed at $\delta = 28.0$ ppm in the $^{11}B\{^1H\}$ NMR spectrum of **7**. The ^1H NMR spectrum is characterized by the presence of only two singlets for the trimethylsilyl groups at $\delta = 0.29$ (36H) and 0.27 ppm (18H), implying free rotation around the B–N bond at room temperature. Cooling to −90 °C is necessary to observe two separate signals for the nitrogen-bound trimethylsilyl groups at $\delta = 0.36$ and 0.33 ppm. Most importantly, these results suggest a weak double bond character of the B–N bond in the room temperature structure of **7**, as a likely consequence of the strong conjugation of the boron atoms with the butadienyl unit.

In conclusion, the photochemical borylene transfer from $[(OC)_5M{=}BN(SiMe_3)_2]$ (M = Cr, Mo) to alkynes and diynes allows high-yielding, straightforward access to otherwise synthetically challenging borirene compounds. Furthermore, the ability of compounds **2** and **3** to act as convenient sources of the borylene moiety under standard conditions was demonstrated. Studies targeting the synthesis of polyborirene systems and the transfer of the borylene unit to different main-group-element compounds are currently underway.[10]

Experimental Section

NMR spectroscopic experiments were performed in quartz NMR tubes. The light source was a Hg/Xe arc lamp (400–550 W) equipped with IR filters, irradiating at 210–600 nm. Large-scale experiments were performed in a 150-mL Schlenk flask equipped with a quartz cooling jacket into which a Hg lamp (125 W) was inserted vertically.

4: A pale yellow solution of **2** (0.500 g, 1.38 mmol) and 1,2-bis(trimethylsilyl)ethyne (0.295 g, 1.73 mmol) in toluene (15 mL) was irradiated for 3.5 h at room temperature. After this time, the volatile components were removed under vacuum, and the remaining dark brown residue was extracted with hexane (2 × 10 mL). The orange-red filtrate was cooled to −60 °C overnight to yield pale yellow crystals of **4**. Evaporation of the filtrate afforded a second crop of analytically pure crystalline material (0.385 g, 82%). ^1H NMR (500 MHz, C_6D_6, 25 °C, TMS): $\delta = 0.32$ (s, 18H; $SiMe_3$), 0.30 ppm (s, 18H; $SiMe_3$); $^{13}C\{^1H\}$ NMR (125.8 MHz, C_6D_6, 25 °C): $\delta = 199.0$ (br s; =*C*-$SiMe_3$), 3.8 (s; $SiMe_3$), 0.7 ppm (s; $SiMe_3$); $^{11}B\{^1H\}$ (160.5 MHz, C_6D_6, 25 °C): $\delta = 33.2$ ppm (s); EI MS: *m*/*z*: 341 [M^+], 268 [$M-SiMe_3$]$^+$.

5: A pale yellow solution of **3** (0.070 g, 0.17 mmol) and 1,2-diphenylethyne (0.031 g, 0.17 mmol) in C_6D_6 (0.5 mL) was irradiated for 2 h at room temperature. After this time, the mixture was filtered over glass-fiber filter paper, and the filtrate was evaporated. The dark brown residue was taken up in hexane (5 mL). The hexane solution was stored at −30 °C for 2 weeks and yielded yellow crystals of **5** (0.051 g, 88%). ^1H NMR (500 MHz, C_6D_6, 25 °C, TMS): $\delta = 7.61$–7.59 (m, 4H; Ph), 7.16–7.13 (m, 4H; Ph), 7.07–7.04 (m, 2H; Ph), 0.36 ppm (s, 18H; $SiMe_3$); $^{13}C\{^1H\}$ NMR (125.8 MHz, C_6D_6, 25 °C): $\delta = 161.1$ (br s; Ph-*C*=), 135.0 (s; Ph), 132.4 (s; Ph), 129.3 (s; Ph), 129.3 (s; Ph), 3.7 ppm (s; $SiMe_3$); $^{11}B\{^1H\}$ (160.5 MHz, C_6D_6, 25 °C): $\delta = 25.0$ ppm (s); EI MS: *m*/*z*: 349 [M^+].

6: A pale yellow solution of **3** (0.046 g, 0.11 mmol) and 3-hexyne (0.016 g, 0.19 mmol) in C_6D_6 (0.5 mL) was irradiated for 3.5 h at room temperature. After this time, the reaction was judged to be complete by NMR spectroscopy, with quantitative formation of **6**, as ascertained by comparison of the NMR data with those reported in the literature.[2]

7: A pale yellow solution of **3** (0.160 g, 0.39 mmol) and 1,4-bis(trimethylsilyl)buta-1,3-diyne (0.067 g, 0.34 mmol) in C_6D_6 (0.5 mL) was irradiated for 4 h at room temperature. After this time, the reaction was judged to be complete by multinuclear NMR spectroscopy, with quantitative formation of **7** (>95% purity). The volatile components were then removed under vacuum, and the resulting brown residue was extracted with hexane (2 × 3 mL). The light brown filtrate was evaporated to yield crude **7** as a brown oil (>95% pure by multinuclear NMR spectroscopy). Sublimation at 100 °C/10^{-5} bar yielded **7** as an analytically pure colorless solid (0.020 g, 11%). ^1H NMR (500 MHz, [D_8]toluene, 25 °C, TMS): $\delta = 0.29$ (s, 36H; N-$SiMe_3$), 0.27 ppm (s, 18H; =C-$SiMe_3$); ^1H NMR (500 MHz, [D_8]toluene, −90 °C, TMS): $\delta = 0.37$ (s, 18H; =C-$SiMe_3$), 0.36 (s, 18H; N-$SiMe_3$), 0.33 ppm (s, 18H; N-$SiMe_3$); $^{13}C\{^1H\}$ NMR (125.8 MHz, [D_8]toluene, 25 °C): $\delta = 186.3$ (s, =*C*-$SiMe_3$), 156.1 (s, =*C*-C), 3.0 (s, N-$SiMe_3$), −0.3 ppm (s, =C-Si*Me*$_3$); $^{13}C\{^1H\}$ NMR (125.8 MHz, [D_8]toluene, −90 °C): $\delta = 186.5$ (s, =*C*-$SiMe_3$), 154.8 (s, =*C*-C), 2.8 (s, N-$SiMe_3$), 2.7 (s, N-$SiMe_3$), −0.4 ppm (s, =C-Si*Me*$_3$); $^{11}B\{^1H\}$ (160.5 MHz, C_6D_6, 25 °C): $\delta = 28.0$ ppm (s); EI MS: *m*/*z*: 536 [M^+].

Received: July 19, 2005
Published online: October 18, 2005

Keywords: alkynes · borirenes · boron · borylene complexes · photochemistry

[1] a) M. E. Volpin, Y. D. Koreshkov, V. G. Dulova, D. N. Kursanov, *Tetrahedron* **1962**, *18*, 107–122; for INDO calculations, see: b) C. U. Pittman, A. Kress, T. B. Patterson, P. Walton, L. D. Kispert, *J. Org. Chem.* **1974**, *39*, 373–378; c) N. L. Allinger, J. H. Siefert, *J. Am. Chem. Soc.* **1975**, *97*, 752–760; for ab initio calculations, see: K. Krogh-Jespersen, D. Cremer, J. D. Dill, J. A. Pople, P. von R. Schleyer, *J. Am. Chem. Soc.* **1981**, *103*, 2589–2594.

[2] C. Habben, A. Meller, *Chem. Ber.* **1984**, *117*, 2531–2537.

[3] C. Pues, A. Berndt, *Angew. Chem.* **1984**, *96*, 306–307; *Angew. Chem. Int. Ed. Engl.* **1984**, *23*, 313–314.

[4] B. Pachaly, R. West, *Angew. Chem.* **1984**, *96*, 444–445; *Angew. Chem. Int. Ed. Engl.* **1984**, *23*, 454–455.

[5] a) J. J. Eisch, B. Shafii, J. D. Odom, A. L. Rheingold, *J. Am. Chem. Soc.* **1990**, *112*, 1847–1853; b) the same authors previously reported the structural characterization of the related 1,2,3-trimesitylborirene, whose threefold disorder in the crystal lattice, however, did not allow an accurate evaluation of the structural parameters: J. J. Eisch, B. Shafii, A. L. Rheingold, *J. Am. Chem. Soc.* **1987**, *109*, 2526–2528.

 © 2005 Wiley-VCH Verlag GmbH & Co. KGaA, Weinheim

[6] a) H. Braunschweig, *Angew. Chem.* **1998**, *110*, 1882 – 1898; *Angew. Chem. Int. Ed.* **1998**, *37*, 1786 – 1801; b) H. Braunschweig, C. Kollann, U. Englert, *Angew. Chem.* **1998**, *110*, 3355 – 3357; *Angew. Chem. Int. Ed.* **1998**, *37*, 3179 – 3180; c) H. Braunschweig, M. Colling, *Eur. J. Inorg. Chem.* **2003**, 393 – 403; d) H. Braunschweig, *Adv. Organomet. Chem.* **2004**, *51*, 163 – 192.

[7] a) H. Braunschweig, M. Colling, C. Kollann, H. G. Stammler, B. Neumann, *Angew. Chem.* **2001**, *113*, 2359 – 2361; *Angew. Chem. Int. Ed.* **2001**, *40*, 2298 – 2300; b) H. Braunschweig, M. Colling, C. Hu, K. Radacki, *Angew. Chem.* **2003**, *115*, 215 – 218; *Angew. Chem. Int. Ed.* **2003**, *42*, 205 – 208.

[8] B. Blank, H. Braunschweig, C. Kollann, K. Radacki, D. Rais, G. R. Whittell, unpublished results.

[9] Crystal data for **4**: $C_{14}H_{36}BNSi_4$, yellow block, $0.16 \times 0.17 \times 0.19\ mm^3$, monoclinic, space group $C2/c$, $a = 17.777(3)$, $b = 11.0366(16)$, $c = 12.4602(19)$ Å, $\beta = 111.429(3)°$, $V = 2275.7(6)$ Å^3, $Z = 4$, $\rho_{calcd} = 0.997\ g\,cm^{-3}$, $T = 173(2)$ K; Bruker Apex platform with CCD detector, graphite-monochromated $Mo_{K\alpha}$ radiation, $2\theta_{max} = 52.12°$; 12540 reflections, 2249 independent ($R_{int} = 0.0371$), direct methods, absorption correction SADABS ($\mu = 0.255\ cm^{-1}$). All non-hydrogen atoms were refined anisotropically. Hydrogen atoms were refined on idealized positions. $R_1 = 0.0537$ ($I > 2\sigma$), $wR_2 = 0.1173$ (all data), GoF = 1.178, restrained GoF = 1.178, max./min. residual electron density: $0.446/-0.184 \times 10^{30}\ e\,m^{-3}$. CCDC-278418 (**4**) contains the supplementary crystallographic data for this paper. These data can be obtained free of charge from the Cambridge Crystallographic Data Centre via www.ccdc.cam.ac.uk/data_request/cif.

[10] For a related article, see the preceding Communication in this issue: D. L. Kays (née Coombs), J. K. Day, L.-L. Ooi, S. Aldridge, *Angew. Chem.* **2005**, *117*, 7623 – 7626; *Angew. Chem. Int. Ed.* **2005**, *44*, 7457 – 7460.

 © 2005 Wiley-VCH Verlag GmbH & Co. KGaA, Weinheim

Nanoporous Materials

DOI: 10.1002/anie.200502781

Smooth Anodic TiO_2 Nanotubes**

*Jan M. Macak, Hiroaki Tsuchiya, Luciano Taveira, Saule Aldabergerova, and Patrik Schmuki**

In 1999 Zwilling et al. reported on the electrochemical formation of self-assembled TiO_2 nanotubes (π-TiO_2) by the anodization of Ti,[1] and other reports followed soon thereafter.[2,3] A factor limiting the application of this first generation of nanotubes was their production in hydrofluoric acid based electrolytes. As a result of the high rate of chemical dissolution of TiO_2 in these solutions, the nanotubes could be grown only up to a length of 500 nm. Recently, we have shown[4–7] and explained[4] how a second generation of nanotubes with lengths up to several micrometers and aspect ratios up to 50 can be formed by adjusting the pH gradient within the growing nanotube. Common to all these anodic approaches is that the side walls of the tubes show strong irregularities, that is, the side-wall profiles show considerable thickness variations (ripples) as shown in Figure 1a. In the present work we demonstrate how TiO_2 nanotubes with extremely smooth homogenous walls and aspect ratios up to 175 can be grown (as shown in Figure 1b). This third generation of nanotubes is formed by suppressing local concentration fluctuations and pH bursts during anodization by using highly viscous glycerol electrolytes.

In previous work it has been established that the length of the nanotubes is essentially the result of a steady-state situation between electrochemical formation of TiO_2 at the pore tip and the chemical dissolution of formed TiO_2 by fluorides from the electrolyte.[3,5] We showed how the pH at the pore tip is lowered by the hydrolysis reactions of the Ti^{4+} ions formed during anodization. As the Ti^{4+} flux can be controlled by the applied current, it was possible to adjust conditions that keep the pore tip sufficiently acidic while the pore walls dissolve much more slowly.[4] As a result, the nanotubes could be grown up to 2.5 μm in length, in contrast to the previous length of 500 nm (Figure 1a). Some other reports on these micrometer-length tubes[8,9] describe nanotubes with aspect ratios up to 44[8] and 58.[9] In all these reports it is apparent that relatively regular variations of the walls' thickness occur (Figure 1a).

To explain these variations one may examine the current transients of the electrochemical anodization of Ti (Figure 2). It is apparent that relatively regular current oscillations occur during anodization, for example in sulphate electrolytes. When the frequency of the current oscillations is converted into a length scale, it compares well to the distance between ridges on the side walls. Thus, the current transients are correlated with the variations in the wall thickness. This can be explained by the fact that every current transient is accompanied by a pH burst at the pore tip. This local acidification leads to a temporarily increased dissolution rate. Since diffusion is the main effect balancing local acidification,[4] a straightforward remedy to suppress pH bursts is to damp the fluctuations by decreasing the diffusion constant in the electrolyte. This can be achieved, for example, by using highly viscous electrolytes such as glycerol-based solutions. Clearly the current–time transient in a fluoride-containing glycerol electrolyte (Figure 2) shows much lower current densities than that in the purely aqueous electrolyte. This is in line with a diffusion-controlled process (considering the Stokes–Einstein relation, where the diffusion constant, D, is proportional to $1/\eta$, where η is the solution viscosity). But even more important than the lowering of the current by glycerol is that the curves in Figure 2 do not exhibit any detectable current fluctuations.

As a result, the tubes formed under these electrochemical conditions (Figure 1b) are entirely smooth over their entire

[*] J. M. Macak, Dr. H. Tsuchiya, Dr. L. Taveira, Dr. S. Aldabergerova, Prof. Dr. P. Schmuki
Department of Materials Science, WW4-LKO
University of Erlangen-Nuremberg
Martensstrasse 7, 91058 Erlangen (Germany)
Fax: (+49) 9131-852-7582
E-mail: schmuki@ww.uni-erlangen.de

[**] We thank A. Friedrich and H. Hildebrand for SEM investigations and Hans Rollig and Martin Kolacyak for valuable technical help with the experiments.

© 2005 Wiley-VCH Verlag GmbH & Co. KGaA, Weinheim

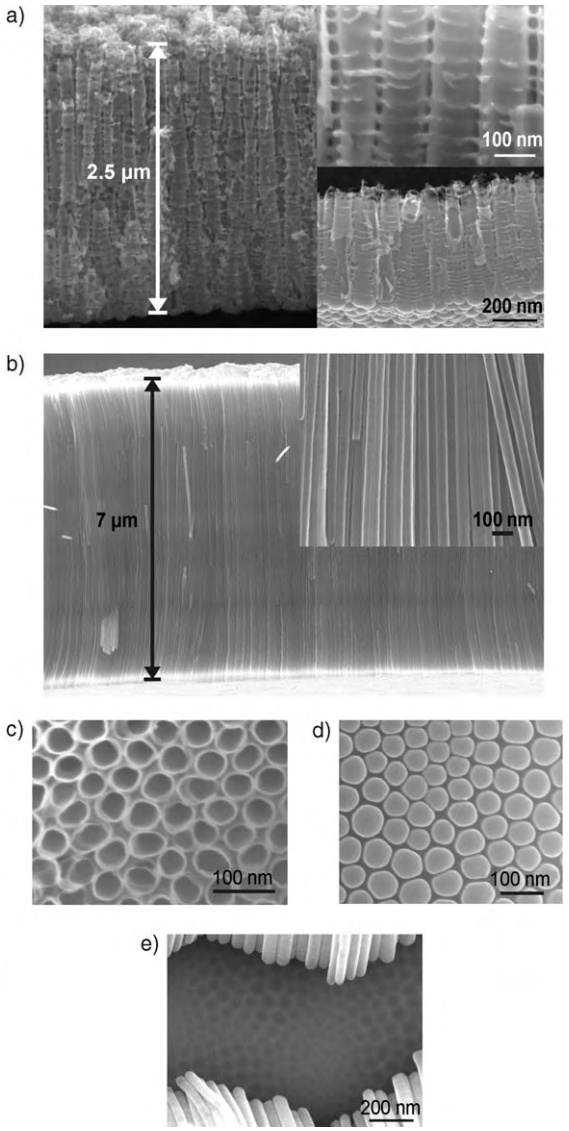

Figure 1. a) SEM images of conventional anodic TiO_2 nanotubes with marked inhomogeneities (from Ref. [4]). The insets show a magnification of the structure (top) and an example of ripples on short tubes formed in 1 M H_2SO_4 with 0.15 wt% HF (bottom). b) Smooth TiO_2 nanotubes 7-µm long produced in glycerol electrolyte with 0.5 wt% NH_4F. The inset shows the walls of the nanotubes in more detail. c)–e) SEM images of smooth TiO_2 nanotubes 7-µm long produced in glycerol electrolyte: c) top view; d) bottom view. The average nanotube diameter is approximately 40 nm and the average pore spacing is approximately 60 nm. e) Top view of an anodized sample after removal of some arrays of nanotubes. The lower part of the tubes and part of the Ti substrate surface are visible. Clearly the convex shape of the nanotube bottoms is reflected in the surface of the Ti substrate.

length. Additionally as a result of the change in the diffusion coefficients and the improved confinement of the acidic area at the pore tip, the tubes grow now to a length of 7 µm. The tubes are arranged in very tight bundles and are not connected with another; this is in contrast to all previous descriptions (Figure 1a). Figure 1c and d show scanning electron micrographic (SEM) images of self-assembled TiO_2 nanotubes from the top and bottom, respectively. It is apparent that the tubes are open on the top and closed with

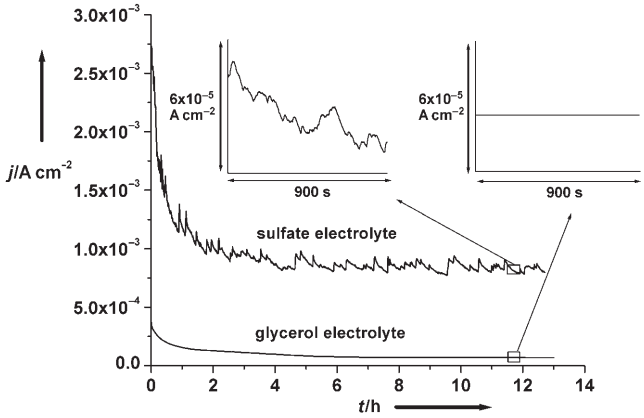

Figure 2. Current–time behavior during anodization of Ti samples at 20 V for 13 h. The samples were anodized in glycerol or in 1 M $(NH_4)_2SO_4$, in both cases with 0.5 wt% NH_4F. The insets show details of the current transients. Current fluctuations can be observed for the anodization in aqueous solution, while they are completely suppressed using the glycerol electrolyte.

a TiO_2 layer on the bottom of the layer of nanotubes. The inner diameters of the nanotubes are mostly around 40 nm; however, some tubes with diameters in the range between 30 and 60 nm can be found. In other words, tubes with aspect ratios between 233 and 117 are obtained. Figure 1e shows an SEM image of the lower part of the tubes and the interface between the TiO_2 nanotubes and the underlying Ti substrate. This image reveals that the convex shape of the closed ends of the nanotubes is reflected in the morphology of the surface of the Ti substrate. We reached a similar conclusion in our earlier work on the formation of nanotubular structures by anodization in aqueous fluoride-containing electrolytes:[4,5] We believe that the interface of the convex (nanotubes) and concave (Ti substrate) units plays a significant role for the good adhesion of both adjacent parts.

Figure 3 shows a transmission electron microscopic (TEM) image of several nanotubes (a), the TEM diffraction pattern (b), and a high-resolution TEM image of the single nanotube bottom (c). These TEM images confirm that the walls of the nanotubes are very smooth and straight over their entire length. The thickness of the walls is 12 nm, the thickness of the convex barrier oxide is 16 nm. If TEM

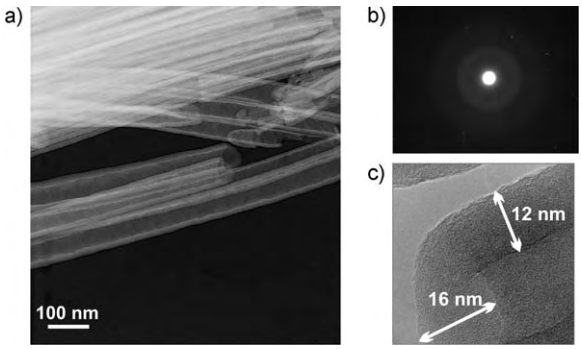

Figure 3. Smooth TiO_2 nanotubes produced in the glycerol electrolyte: a) TEM image of several TiO_2 nanotubes; b) TEM diffraction pattern of a nanotube wall; c) HRTEM image of a single nanotube.

 © 2005 Wiley-VCH Verlag GmbH & Co. KGaA, Weinheim

pictures from the side wall close to the pore bottom are compared to pictures close to the pore mouth, only minimal variations in thickness, (12 ± 2) nm, can be determined. This is also a clear improvement over previous syntheses, in which considerable thinning of the walls at the pore mouth was typically observed. The TEM diffraction pattern in Figure 3b was taken from the nanotube wall and shows clearly that the TiO_2 structure is amorphous. The high-resolution TEM image in Figure 3c additionally confirms the amorphous structure in the side wall and at the bottom of the tubes.

In summary, TiO_2 nanotubes prepared in glycerol solutions show an unprecedented degree of regularity and homogenity in comparison to the nanotubes described in earlier reports, in which thinning of the tube wall towards the mouth and ripples on the tube walls were observed.[1–9] In addition, the pore diameter is strongly affected by the electrolyte: in aqueous electrolytes it is about 100 nm, in glycerol it is about 40 nm. Besides the high aspect ratio, the smoothness of the nanotubes plays a crucial role in the improvement of various properties of the layers of self-assembled TiO_2 nanotubes. For instance, uniform depth profiles and flatter interfaces are essential from the point of view of optical devices, for example, waveguides and photonic crystals, where the light transmission is severely reduced by diffuse scattering at morphological inhomogeneities. Because of the high refractive index of TiO_2 (2.6), self-assembled nanotubular TiO_2 structures are viable candidates for applications in photonic crystals[10] and waveguides.[11]

We also note that layers of nanotubes with a tube length of 7 μm may be suitable for application in highly efficient dye-sensitized solar cells,[12] since the desired light absorption depth, nanoparticulate TiO_2 films with a thickness in the range of 5 to 10 μm yield optimum efficiency. In addition to dye sensitization,[13] several other applications have already been reported for the self-assembled TiO_2 nanotubes, for example, as a catalyst support for Pt/Ru nanoparticles for the electrooxidation of methanol[14] and as structures that can be modified with self-assembled monolayers of organic molecules to tailor surface wettability.[15]

Other potential applications of self-assembled TiO_2 nanotubular structures may be based on exploiting the specific properties of TiO_2, such as its catalytic properties,[16] self-cleaning,[17] and semiconductor properties.[18] The nanotubular structure could be also used to improve biocompatibility in biomedical applications.[19] Our results provide greatly improved nanotubular TiO_2 substrates for all these applications and represent a significant advancement towards the "ideal" tubular shape.

Experimental Section

Surface treatment: Ti samples (0.1-mm thick foils, 99.6% purity, Goodfellow, England) were degreased by sonicating in acetone, 2-propanol, and methanol, followed by rinsing with deionized water and drying in a nitrogen stream.

Electrochemical treatment: Titanium samples were contacted with a Cu plate and then pressed against an O-ring in an electrochemical cell, such that 1 cm^2 was exposed to the electrolyte. The setup consisted of a conventional three-electrode configuration with a platinum gauze as a counterelectrode and a Haber–Luggin capillary with Ag/AgCl (1M KCl) electrode as a reference electrode. Electrochemical experiments were carried out using a high-voltage potentiostat Jaissle IMP 88. Electrolytes were 0.5 wt% NH_4F in glycerol (1,2,3-propanetriol) with a dynamic viscosity of 1350 mPa s at 20 °C or in 1M $(NH_4)_2SO_4$. The electrolytes were prepared from reagent-grade chemicals. The electrochemical treatment consisted of a potential ramp from the open-circuit potential (OCP) to 20 V with a sweep rate of 1 $V s^{-1}$, after which the applied potential was held at 20 V for 13 h. The same treatment was used for reference samples produced in aqueous electrolytes. An estimate of the IR drop during experiments in glycerol electrolyte results in an error of less than 1 V on the effective potential. After the electrochemical treatment the samples were soaked with deionized water and dried in a nitrogen stream.

Surface characterization: Scanning electron microscopy (Hitachi FE-SEM S4800) was employed for the morphological characterization of the TiO_2 nanotubes. To gain information on thickness of the nanotubular layer, direct SEM cross-sectional thickness measurements were carried out on mechanically bent and cracked samples. This technique was also carried out to achieve bottom-view images of the nanotube layers. Transmission electron microscope Philips CM 30 T/STEM and high-resolution TEM Philips CM 300 UT were used for the morphological and structural characterization of the TiO_2 nanotubes.

Received: August 5, 2005
Published online: October 25, 2005

Keywords: electrochemistry · nanoporous materials · nanotubes · self-assembly · titanium oxide

[1] V. Zwilling, M. Aucouturier, E. Darque-Ceretti, *Electrochim. Acta* **1999**, *44*, 921.
[2] D. Gong, C. A. Grimes, O. K. Varghese, W. Hu, R. S. Singh, Z. Chen, E. C. Dickey, *J. Mater. Res.* **2001**, *16*, 3331.
[3] R. Beranek, H. Hildebrand, P. Schmuki, *Electrochem. Solid-State Lett.* **2003**, *6*, B12.
[4] J. M. Macak, H. Tsuchiya, P. Schmuki, *Angew. Chem.* **2005**, *117*, 2136; *Angew. Chem. Int. Ed.* **2005**, *44*, 2100.
[5] J. M. Macak, K. Sirotna, P. Schmuki, *Electrochim. Acta* **2005**, *50*, 3679.
[6] L. V. Taveira, J. M. Macak, H. Tsuchiya, L. F. P. Dick, P. Schmuki, *J. Electrochem. Soc.* **2005**, *152*, B405.
[7] A. Ghicov, H. Tsuchiya, J. M. Macak, P. Schmuki, *Electrochem. Commun.* **2005**, *7*, 505.
[8] Q. Cai, M. Paulose, O. K. Varghese, C. A. Grimes, *J. Mater. Res.* **2005**, *20*, 230.
[9] O. K. Varghese, M. Paulose, K. Shankar, G. K. Mor, C. A. Grimes, *J. Nanosci. Nanotechnol.* **2005**, *5*, 1158.
[10] A. Birner, R. Wehrspohn, U. Gösele, K. Busch, *Adv. Mater.* **2001**, *13*, 377.
[11] C. Haginoya, M. Ishibashi, K. Koike, *Appl. Phys. Lett.* **1997**, *71*, 2934.
[12] B. O'Regan, M. Grätzel, *Nature* **1991**, *353*, 737.
[13] J. M. Macak, H. Tsuchiya, A. Ghicov, P. Schmuki, *Electrochem. Commun.*, **2005**, *7*, 1138.
[14] J. M. Macak, P. Barczuk, H. Tsuchiya, S. Bauer, P. Kulesza, P. Schmuki, *Electrochem. Commun.*, in press.
[15] E. Balaur, J. M. Macak, L. Taviera, H. Tsuchiya, P. Schmuki, *Electrochem. Commun.* **2005**, *7*, 1066.
[16] N. Serpone, E. Pelizzetti, *Photocatalysis—Fundamentals and Applications*, Wiley, New York, **1989** and references therein.
[17] A. Fujishima, K. Honda, *Nature* **1972**, *238*, 37.
[18] M. Grätzel, *J. Photochem. Photobiol. C* **2003**, *4*, 145.
[19] Y. T. Sul, C. B. Johansson, S. Petronis, A. Krozer, Y. Jeong, A. Wennerberg, T. Albrektsson, *Biomaterials* **2002**, *23*, 491.

 © 2005 Wiley-VCH Verlag GmbH & Co. KGaA, Weinheim

Asymmetric Organocatalysis

DOI: 10.1002/anie.200502003

Kinetic Resolution of Oxazinones: An Organocatalytic Approach to Enantiomerically Pure β-Amino Acids**

Albrecht Berkessel, Felix Cleemann, and Santanu Mukherjee*

The development of new methods for the enantioselective synthesis of β-amino acids has been of considerable interest during the last years.[1–4] Owing to their unique pharmacological properties in the free form,[5] as cyclized β-lactams,[6] and as structural elements of naturally occurring compounds such as taxol[7] and the dolastatins,[8] there is a high demand in both academia and industry for enantiopure β-amino acids.[9] Besides chiral-auxiliary-based strategies[4] and catalytic asymmetric synthesis[1,10–13] the kinetic resolution of racemates is a well-established method for obtaining β-amino acids with high enantiomeric purity. The latter methodology is divided into "classical" chemical resolution processes, in which chiral resolving agents are used in stoichiometric amounts,[14] and enzymatic resolutions, which require acylases, amidases, or lipases.[15,16] Although the selectivity of enzymatic processes is in most cases excellent, the narrow substrate scope and thus the need for time-consuming enzyme engineering present a major drawback. To overcome these difficulties, we envisaged that the application of readily available modular organocatalysts[17] could greatly enhance the scope of these processes. Motivated by our success in the organocatalytic dynamic kinetic resolution (DKR) of azlactones *rac*-**A**, we set out to expand this methodology beyond the synthesis of (non-natural) α- to the even more challenging β-amino acids (Scheme 1).[18,19]

Azlactones **A** racemize readily and can be converted into the enantiomerically enriched N,C doubly protected α-amino acid derivatives **B**. By formally inserting a methylene group between the carbonyl group and the α-C atom of the azlactone, the nitrogen atom moves to the β position. The resulting compounds are known as 4,5-dihydro-1,3-oxazin-6-ones **C**, which are—in contrast to azlactones—configurationally stable. Although achiral and enantiomerically pure oxazinones **C** were utilized in peptide chemistry for coupling to amino acid esters,[20] no catalytic ring-opening reaction

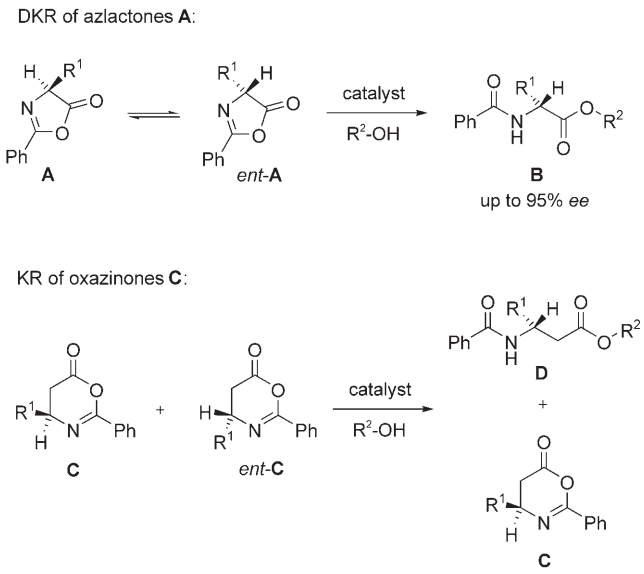

Scheme 1. Alcoholytic DKR of azlactones (**A**, *ent*-**A**;top) and KR of oxazinones (**C**, *ent*-**C**; bottom).

appears to have been reported so far.[21] We considered these compounds to be promising substrates for organocatalytic asymmetric ring opening. It was hoped that the bifunctional thiourea catalysts **2a** and **2b** (Table 1), which proved to be highly effective in the alcoholytic DKR of azlactones,[19] would effect a kinetic resolution (KR) of racemic oxazinones.[22,23] If the selectivity of the catalyst is sufficiently high, a KR process will be of practical significance, provided that the racemate is obtained in an easy and cost-effective manner and that both the remaining and the converted substrate enantiomers are valuable compounds.[24] Oxazinones can be synthesized in a way similar to azlactones by cyclodehydration of the corresponding *N*-benzoyl amino acids **3** (Scheme 2).[25] We decided to use the one-step protocol of Tan and Weaver for the synthesis of racemic β-amino acids **4** from inexpensive aldehydes, malonic acid, and ammonium acetate (Scheme 2).[26]

The crude amino acids **4a–f** were converted directly into the *N*-benzoyl derivatives **3a–f** without the need for preceding purification. Condensation to give oxazinones **1a–f** was best effected by isobutyl chloroformate. Preliminary experi-

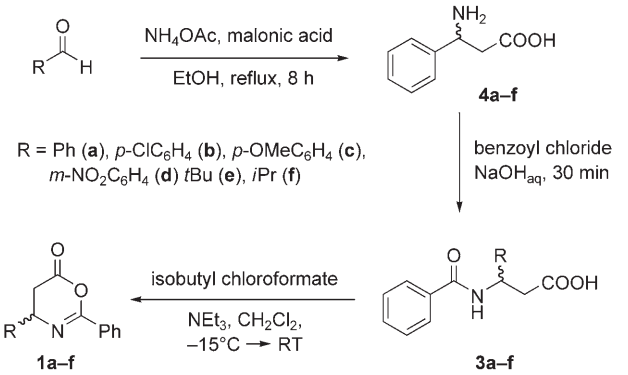

Scheme 2. Synthesis of the racemic oxazinones *rac*-**1a–f**.

[*] Prof. Dr. A. Berkessel, Dipl.-Chem. F. Cleemann, MSc S. Mukherjee
Institut für Organische Chemie
Universität zu Köln
Greinstrasse 4, 50939 Köln (Germany)
Fax: (+49) 221-470-5102
E-mail: berkessel@uni-koeln.de

[**] This work was supported by the Fonds der Chemischen Industrie, particularly through a doctoral fellowship to F.C. The authors thank Degussa AG, Hanau, for generous gifts of amino acids.

Supporting information for this article is available on the WWW under http://www.angewandte.org or from the author.

InterScience
© 2005 Wiley-VCH Verlag GmbH & Co. KGaA, Weinheim

ments indicate that **1** can also be obtained directly in a single step from β-amino acids **4** by treatment with excess benzoyl chloride. The first experiments with 4,5-dihydro-2,4-diphenyl-1,3-oxazin-6-one (*rac*-**1a**) as substrate and allyl alcohol as nucleophile in the presence of the bifunctional thiourea **2a** (5 mol%) already showed the potential of this process. As expected for a kinetic resolution, the enantiopurity of the remaining oxazinone **1a** and the product ester **5a** is a function of the conversion (Figure 1).

At 57% conversion, the *S* enantiomer of the oxazinone substrate *rac*-**1a** is completely consumed (99% *ee* in favor of the remaining *R* enantiomer), and the enantiomeric excess of the product ester (*S*)-**5a** is 86% (Table 1, entry 3). Calculated from these kinetic data, the selectivity factor *S* of the reaction is 68. At a conversion lower than 45%, the ester is produced with more than 94% *ee* (Figure 1 and Table 1, entries 1 and 2). Slightly lower selectivity and activity were observed when using 5 mol% of the cyclohexyl-substituted catalyst **2b** (Table 1, entry 4). As a consequence we chose catalyst **2a** for all further experiments. Because

Table 1: Optimization of the reaction conditions

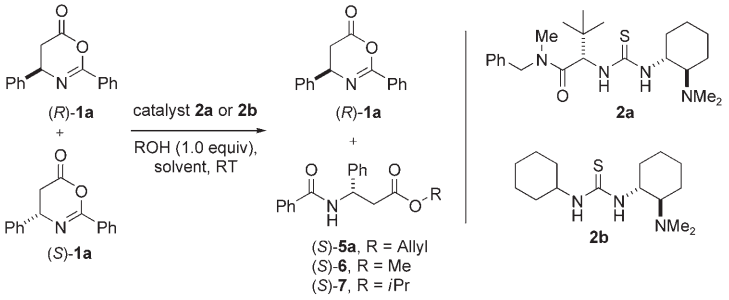

Entry	Catalyst loading [mol%]	Cat.	Solvent	Alcohol (R)	*t* [h]	Conv. [%][a]	*ee* (**1a**) [%][a]	*ee* (**5a–7**) [%][a]
1	5	**2a**	toluene	allyl	0.5	26	25	96
2	5	**2a**	toluene	allyl	1.5	45	58	94
3	5	**2a**	toluene	allyl	6.5	57	99	86
4	5	**2b**	toluene	allyl	12	59	97	81
5	10	**2a**	toluene	allyl	4.5	57	>99	84
6	2.5	**2a**	toluene	allyl	26	61	98	87
7[b]	1	**2a**	toluene	allyl	10	61	98	85
8	5	**2a**	THF	allyl	126	58	84	81
9	5	**2a**	DCM	allyl	24	66	>99	62
10	5	**2a**	CH_3CN	allyl	24	28	18	69
11	5	**2a**	toluene	Me	24	63	>99	71
12	5	**2a**	toluene	*i*Pr	24	4	<2	23

[a] Conversions and enantiomeric excesses were determined by chiral HPLC. [b] This reaction was carried out with a substrate concentration of 0.5 M; 0.1 M concentration in other reactions.

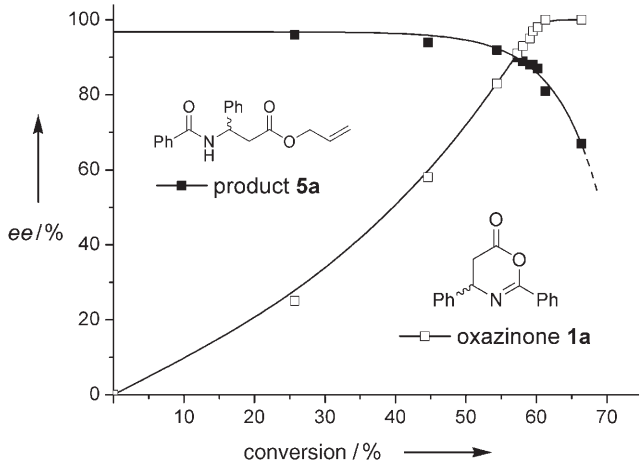

Figure 1. Time course of the kinetic resolution of *rac*-**1a** with allyl alcohol (1.0 equiv) and catalyst **2a** (5 mol% relative to *rac*-**1a**).

of the inherent difficulty in the accurate determination of selectivity factors when $S > 50$, we decided to characterize the quality of the kinetic resolution described herein solely in terms of conversion and *ee* values of the substrate and product, respectively (Table 1).[27]

The remaining oxazinone **1a** can be separated from the converted product ester **5a** by treating the reaction mixture with dilute aqueous HCl (Scheme 3; see Supporting Information for details). This hydrolytic procedure quantitatively converts the remaining oxazinone (*R*)-**1a** into the insoluble *N*-benzoyl β-amino acid (*R*)-**3a**. There is virtually no loss in

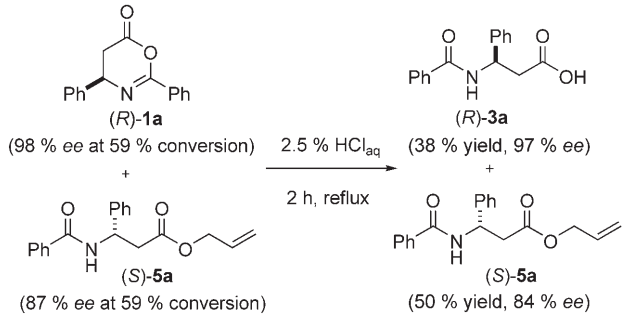

Scheme 3. Hydrolytic work-up procedure for the separation of the resolved oxazinone (*R*)-**1a** from the product ester (*S*)-**5a**.

enantiomeric purity during this hydrolysis reaction (Scheme 3). The filtrate contains the pure ester product (*S*)-**5a**.

An increase in the catalyst loading to 10 mol% decreased the reaction time to 4.5 h, without affecting the selectivity (Table 1, entry 5). At a catalyst loading of 2.5 mol%, the reaction time is longer but the selectivity remains virtually unaffected (Table 1, entry 6). This decrease in the reaction rate could be compensated for by raising the concentration of the substrates from 0.1 to 0.5 M. Under these conditions, a catalyst loading of only 1 mol% was sufficient to catalyze the reaction effectively (Table 1, entry 7). Comparison with authentic samples prepared from enantiomerically pure (*S*)-3-amino-3-phenylpropanoic acid allowed us to determine the absolute configuration of both the oxazinone **1a** and the ester product **5a** by chiral HPLC.

 © 2005 Wiley-VCH Verlag GmbH & Co. KGaA, Weinheim

An increase in the solvent polarity, for example, by changing from toluene to THF or acetonitrile, retarded the reaction quite significantly (Table 1, entries 8 and 10). Based on the assumption that hydrogen bonds between the catalyst and the substrate are crucial for the activation of the latter, this effect can be rationalized by the ability of THF to act as a competing hydrogen-bond acceptor. In the case of acetonitrile, hydrogen bonds are weakened by dipolar interaction with the solvent. In dichloromethane (DCM) the reaction proceeded with a satisfying rate, but the selectivity was somewhat lower (Table 1, entry 9). Prolonged reaction times resulted from the variation of the alcohol nucleophile to methanol or 2-propanol (Table 1, entries 11 and 12). In the case of methanol, the reaction was still practically useful, although the selectivity was somewhat lower. In contrast, the sterically more demanding 2-propanol reacts much more slowly. Only 4% conversion was observed after 24 h (Table 1, entry 12).

To demonstrate the broad substrate scope of our KR process, we chose the electron-poor *p*-chlorophenyl- and *m*-nitrophenyl-substituted oxazinones **1b** and **1d** as well as the electron-rich *p*-methoxyphenyl-substituted oxazinone **1c** as substrates (Table 2, entries 2, 4, and 3). Furthermore, to show

Table 2: Asymmetric alcoholytic ring opening of oxazinones

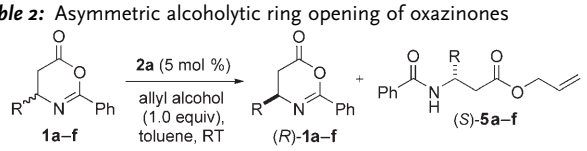

Entry	Substrate (R)	*t* [h]	Conv. [%][a]	*ee* (**1**) [%][a,b]	*ee* (**5**) [%][a]
1	**1a** (Ph)	6.5	57	99	86
2	**1b** (*p*-ClC_6H_4)	15	59	99	83
3	**1c** (*p*-$OMeC_6H_4$)	10.5	57	98	87
4	**1d** (*m*-$NO_2C_6H_4$)	3.0	64	99	81
5	**1e** (*t*Bu)	48	54	97	82
6	**1f** (*i*Pr)	48	53	98	88

[a] Conversions were determined by chiral HPLC, the enantiomeric excesses either by chiral HPLC or chiral GC. [b] The absolute configurations of the products **1b–f** were assigned by analogy to **1a**.

that the method is not limited to oxazinones with aromatic substituents, we also included the *tert*-butyl derivative **1e** and the isopropyl derivative **1f** (Table 2, entries 5 and 6) in our study. We were pleased to see that all substrates were resolved with a high degree of enantioselectivity. In the presence of catalyst **2a** (5 mol%), the oxazinones **1a–f** were generally obtained with excellent enantiomeric excess (Table 2), whereas the esters were still produced with 80–90% *ee*.

Comparison of **1a** with the *p*-chlorophenyl-substituted oxazinone **1b** and the *p*-methoxy-substituted oxazinone **1c** reveals that the enantioselectivity is not significantly affected by the substituent on the aromatic ring (Table 2, entries 1–3). The same holds for the oxazinone **1d**, which bears a nitro substituent in the *meta* position (Table 2, entry 4). With the latter substrate, the reaction is complete within only 3 h. The sterically more-demanding *tert*-butyl residue and the isopropyl group of oxazinones **1e** and **1f** are also tolerated at reaction times of 48 h (Table 2, entries 5 and 6). The latter two examples demonstrate that the procedure is not limited to β-amino acids with aromatic substituents but can also be used equally well for the enantioselective synthesis of alkyl-substituted derivatives.

In summary, we have described a novel and practical organocatalytic method for the synthesis of enantiomerically pure β-amino acids. To the best of our knowledge, this is the first time that oxazinones were applied in a catalytic ring-opening reaction. The resolutions are carried out at ambient temperature; the applied catalyst is modular, readily available, and can be used at loadings as low as 1 mol%. This process provides efficient access to highly valuable protected β-amino acids from inexpensive bulk chemicals. The resolved starting material and the product can be separated by filtration in a simple workup procedure. It is particularly noteworthy that the remaining enantiomerically pure oxazinones are activated β-amino acid derivatives that can, in principle, be applied directly in coupling reactions, for example, in the synthesis of β-peptides. The scope of this novel resolution process and its mechanism are currently under investigation.

Experimental Section

All commercially available chemicals were used without further purification. (*S*)-3-Amino-3-phenylpropionic acid was a gift from Degussa AG, Hanau. Solvents were distilled prior to use and dried, if necessary, by using standard techniques. HPLC analysis was performed on Merck–Hitachi HPLC equipment with HPLC-grade solvents from Fisher Scientific. GC analysis was performed on Hewlett-Packard equipment. Catalysis runs were carried out under inert atmosphere.

Resolution of oxazinones: The alcohol nucleophile (1.00 equiv) was added to a solution of the catalysts **2a** or **2b** (8.33 μmol, 0.05 equiv) in absolute toluene (670 μL). After the addition of a solution of the oxazinone **1a–f** (167 μmol, 1.00 equiv) in absolute toluene (1.00 mL), the homogeneous reaction mixture was stirred at ambient temperature. For analysis, 50-μL samples were withdrawn and diluted with acetonitrile (450 μL). The conversion and enantiomeric excess were determined immediately by HPLC or GC (see Supporting Information). Quantification was based on UV detection at $\lambda = 230$ nm. The conversion was determined by comparison with the peak areas of stock solutions of the oxazinones **1** and the corresponding *N*-benzoyl amino acid esters **5–7** in dichloromethane.

Received: June 10, 2005
Published online: October 24, 2005

Keywords: beta amino acids · kinetic resolution · organocatalysis · oxazinones · thiourea

[1] J.-A. Ma, *Angew. Chem.* **2003**, *115*, 4426–4435; *Angew. Chem. Int. Ed.* **2003**, *42*, 4290–4299.
[2] E. Juaristi, H. Lopez-Ruiz, *Curr. Med. Chem.* **1999**, *6*, 983–1004.
[3] A. F. Abdel-Magid, J. A. Cohen, C. A. Maryanoff, *Curr. Med. Chem.* **1999**, *6*, 955–970.
[4] E. Juaristi, *Enantioselective Synthesis of* β-*Amino Acids*, Wiley, New York, **2005**.
[5] S. Shinagawa, T. Kanamaru, S. Harada, M. Asai, H. Okazaki, *J. Med. Chem.* **1987**, *30*, 1458–1463.
[6] G. I. Georg, *The Organic Chemistry of* β-*Lactams*, VCH, New York, **1993**.

 © 2005 Wiley-VCH Verlag GmbH & Co. KGaA, Weinheim

[7] I. Ojima, S. Lin, T. Wang, *Curr. Med. Chem.* **1999**, *6*, 927 – 953.
[8] R. B. Bates, K. G. Brusoe, J. J. Burns, S. Caldera, W. Cui, S. Gangwar, M. R. Gramme, K. J. McClure, G. P. Rouen, H. Schadow, C. C. Stessman, S. R. Taylor, V. H. Vu, G. V. Yarick, J. Zhang, G. R. Pettit, R. Bontems, *J. Am. Chem. Soc.* **1997**, *119*, 2111 – 2113.
[9] D. Seebach, S. Abele, K. Gademann, G. Guichard, T. Hintermann, B. Jaun, J. L. Matthews, J. V. Schreiber, *Helv. Chim. Acta* **1998**, *81*, 932 – 982.
[10] S. Kobayashi, H. Ishitani, *Chem. Rev.* **1999**, *99*, 1069 – 1094.
[11] H. Ishitani, M. Ueno, S. Kobayashi, *J. Am. Chem. Soc.* **1997**, *119*, 7153 – 7154.
[12] M. P. Sibi, J. J. Shay, M. Liu, C. P. Jasperse, *J. Am. Chem. Soc.* **1998**, *120*, 6615 – 6616.
[13] a) J. K. Myers, E. N. Jacobsen, *J. Am. Chem. Soc.* **1999**, *121*, 8959 – 8960; b) A. G. Wenzel, E. N. Jacobsen, *J. Am. Chem. Soc.* **2002**, *124*, 12964 – 12965.
[14] J. A. Zablocki, J. G. Rico, R. B. Garland, T. E. Rogers, K. Williams, L. A. Schretzman, S. A. Rao, P. R. Bovy, F. S. Tjoeng, R. J. Lindmark, M. V. Toth, M. E. Zupec, D. E. McMackins, S. P. Adams, M. Miyano, C. S. Markos, M. N. Milton, S. Paulson, M. Herin, P. Jacqmin, N. S. Nicholson, S. G. Panzer-Knodle, N. F. Haas, J. D. Page, J. A. Szalony, B. B. Taite, A. K. Salyers, L. W. King, J. G. Campion, L. P. Feigen, *J. Med. Chem.* **1995**, *38*, 2378 – 2394.
[15] P. Flores-Sanchez, J. Escalante, E. Castillo, *Tetrahedron: Asymmetry* **2005**, *16*, 629 – 634.
[16] V. A. Soloshonok, N. A. Fokina, A. V. Rybakova, I. P. Shishkina, S. V. Galushko, A. E. Sorochinsky, V. P. Kukhar, M. V. Savchenko, V. K. Svedas, *Tetrahedron: Asymmetry* **1995**, *6*, 1601 – 1610.
[17] A. Berkessel, H. Gröger, *Asymmetric Organocatalysis*, Wiley-VCH, Weinheim, **2005**.
[18] A. Berkessel, F. Cleemann, S. Mukherjee, T. N. Müller, J. Lex, *Angew. Chem.* **2005**, *117*, 817 – 821; *Angew. Chem. Int. Ed.* **2005**, *44*, 807 – 811.
[19] A. Berkessel, S. Mukherjee, F. Cleemann, T. N. Müller, J. Lex, *Chem. Commun.* **2005**, 1898 – 1900.
[20] a) C. N. C. Drey, J. Lowbridge, R. J. Ridge, *J. Chem. Soc. Perkin Trans. 1* **1973**, 2001 – 2006; b) C. M. C. Drey, E. Mtetwa, *J. Chem. Soc. Perkin Trans. 1* **1982**, 1587 – 1592.
[21] For a report on ring-opening polymerization of oxazinones, see: S. Kobayashi, Y. Tsukamoto, T. Saegusa, *Macromolecules* **1990**, *23*, 2609 – 2612.
[22] The *tert*-leucine amide motif was employed before in the design of chiral organocatalysts: a) D. E. Fuerst, E. N. Jacobsen, *J. Am. Chem. Soc.* **2005**, *127*, 8964 – 8965; b) T. P. Yoon, E. N. Jacobsen, *Angew. Chem.* **2005**, *117*, 470 – 472; *Angew. Chem. Int. Ed.* **2005**, *44*, 466 – 468; c) M. S. Taylor, E. N. Jacobsen, *J. Am. Chem. Soc.* **2004**, *126*, 10558 – 10559; d) G. D. Joly, E. N. Jacobsen, *J. Am. Chem. Soc.* **2004**, *126*, 4102 – 4103; e) P. Vachal, E. N. Jacobsen, *J. Am. Chem. Soc.* **2002**, *124*, 10012 – 10014; f) A. G. Wenzel, M. P. Lalonde, E. N. Jacobsen, *Synlett* **2003**, 1919 – 1922.
[23] Catalysts of the thiourea-*tert*-amine type were applied before for asymmetric Michael additions and aza-Henry reactions: a) T. Okino, Y. Hoashi, Y. Takemoto, *Angew. Chem.* **2005**, *117*, 4100 – 4103; *Angew. Chem. Int. Ed.* **2005**, *44*, 4032 – 4035; b) T. Okino, T. Furukawa, X. Xu, Y. Takemoto, *J. Am. Chem. Soc.* **2005**, *127*, 119 – 125; c) T. Okino, S. Nakamura, T. Furukawa, Y. Takemoto, *Org. Lett.* **2004**, *6*, 625 – 627; d) T. Okino, Y. Hoashi, Y. Takemoto, *J. Am. Chem. Soc.* **2003**, *125*, 12672 – 12673.
[24] J. M. Keith, J. F. Larrow, E. N. Jacobsen, *Adv. Synth. Catal.* **2001**, *343*, 5 – 26.
[25] W. Baker, W. Ollis, *J. Chem. Soc.* **1949**, 345 – 349.
[26] C. Y. K. Tan, D. F. Weaver, *Tetrahedron* **2002**, *58*, 7449 – 7461.
[27] C. S. Chen, Y. Fujimoto, G. Girdaukas, C. J. Sih, *J. Am. Chem. Soc.* **1982**, *104*, 7294 – 7299.

 © 2005 Wiley-VCH Verlag GmbH & Co. KGaA, Weinheim

Epothilones

DOI: 10.1002/anie.200501760

Scaffolds for Microtubule Inhibition through Extensive Modification of the Epothilone Template**

*Frédéric Cachoux, Thomas Isarno, Markus Wartmann, and Karl-Heinz Altmann**

Cellular microtubules are important targets for the development of anticancer drugs, and a variety of microtubule-interacting agents are currently in clinical use for the treatment of human cancer.[1] Agents interfering with microtubule functionality may either stabilize or destabilize microtubules;[2] the most prominent examples of microtubule stabilizers are the clinical anticancer drugs taxol (paclitaxel) and docetaxel (taxotere).[3] While taxol and related compounds had long been the only structures known to stabilize microtubules and promote tubulin polymerization, a variety of other natural products have been recognized over the last ten years to exert their antiproliferative activity through a mechanism of action similar to that of taxol. These compounds include, for example, epothilones A and B (Epo A and B), discodermolide, laulimalide, and peloruside.[4]

Natural products have been the most productive source of potent microtubule stabilizers by far,[4] and the systematic screening of natural-product-based libraries (or perhaps libraries based on natural-product-like compounds) is likely to reveal additional templates for microtubule stabilization in the future.[5] Alternatively, such templates may be developed from existing microtubule stabilizers through extensive structural modification (and perhaps simplification), provided such modifications do not produce an unacceptable loss in the desired biological activity.

[*] Dr. F. Cachoux,[+] Dr. T. Isarno,[++] Prof. Dr. K.-H. Altmann
ETH Zürich
Department of Chemistry and Applied Biosciences
Institute of Pharmaceutical Sciences
ETH Hönggerberg, HCI H 405
Wolfgang-Pauli-Strasse 10, 8093 Zürich (Switzerland)
Fax: (+41) 44-633-1360
E-mail: karl-heinz.altmann@pharma.ethz.ch
Dr. M. Wartmann
Oncology DA
Novartis Institute for Biomedical Research
Basel (Switzerland)
[+] Current address:
Prestwick Chemical, Illkirch (France)
[++] Current address:
Carbogen AG, Aarau (Switzerland)

[**] This research was supported by Novartis Pharma AG (postdoctoral fellowships to F.C. and T.I.). We also thank Dr. Peter Ertl, Novartis Institute for Biomedical Research, Basel, for calculating the Tanimoto coefficients.

Supporting information for this article is available on the WWW under http://www.angewandte.org or from the author.

© 2005 Wiley-VCH Verlag GmbH & Co. KGaA, Weinheim

Of the various newly discovered microtubule-stabilizing agents mentioned above, the most extensively studied is Epo B,[6] for which numerous synthetic and semisynthetic variants have been prepared and subjected to biological profiling.[7] These efforts have produced an extensive database on structure–activity relationships (SAR) for epothilones and, most significantly, they have also led to the discovery of at least five analogues that are currently undergoing clinical evaluation in humans (in addition to Epo B).[7a] While the structures of these analogues are not significantly different from the original natural product lead, their biochemical and pharmacological properties appear to be distinct from that of Epo B, thus indicating that structural analogues closely related to Epo B may embody significant improvements in preclinical profile. Perhaps the most impressive examples are the 9,10-didehydro derivatives of Epo D,[8] which were recently described by the Danishefsky laboratory (and one of which has recently started phase I clinical trials).[9]

Notwithstanding these findings, it is still important to explore more extensive structural modifications of the epothilone scaffold that may lead to analogues with only limited or even no obvious structural resemblance to the starting natural product. Such analogues (if sufficiently potent) could be considered new templates for microtubule inhibition (in the same way a newly discovered natural product would be; vide supra). Here we provide a preliminary account of our synthetic and SAR work on a series of new epothilone analogues, which illustrates how iterative changes of the epothilone scaffold can lead to greatly modified ("hypermodified") structures that are still associated with potent tubulin-polymerizing and antiproliferative activity.

One of the strategic starting points for our development of hypermodified potent epothilone analogues was the removal of the hydroxy group in the 3-position of the epothilone scaffold. Rather surprisingly, the consequences of this simple modification have not been investigated explicitly to date, although other modifications at the 3-position have been described. Thus, formal dehydration at C2 and C3 (leading to 3-deoxy-2,3-didehydro derivatives) is well tolerated,[10] which is in agreement with an *anti*-periplanar conformation of the C2–C3 bond in the proposed bioactive conformation of Epo A.[11] Activity is also largely retained upon replacement of the (3*S*)-hydroxy group by a (3*S*)-cyano group,[10a] while inversion of configuration at C3 leads to a profound loss in biological potency (for both Epo A and Epo B[7d] as well as for the corresponding 3-deoxy-3-cyano analogues[10a]). Given the absence of biological information about simple 3-deoxy analogues of epothilones (with a single bond between C2 and C3), we have prepared 3-deoxy-Epo B (**1**) and assessed the biological activity of this compound. Scheme 1 summarizes our synthesis of **1**, which follows strategic principles similar to those we previously employed for the preparation of other types of epothilone analogues.[12]

Key steps are the aldol reaction between ketone **5** and aldehyde **6** (which proceeded with ca. 2.5:1 selectivity in favor of the desired aldol product **7** and was not optimized), the *B*-alkyl Suzuki coupling of **9** with vinyl iodide **10**, Yamaguchi macrolactonization, and finally epoxidation of the C12–C13 double bond in the deprotected macrolactone **12**. Unexpectedly, macrolactonization was accompanied by partial epimerization at C15 (!), which later necessitated purification of **12** by preparative HPLC.

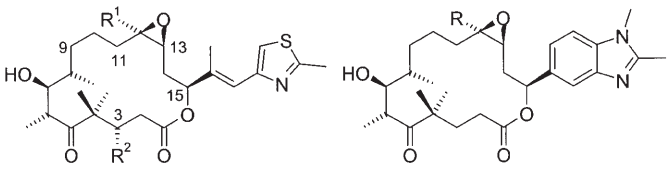

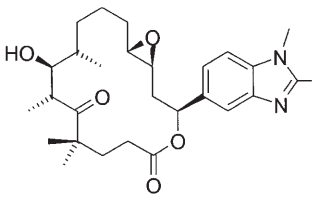

4

The data summarized in Table 1 indicate that **1** exhibits potent tubulin-polymerizing and antiproliferative activity, such that its cellular activity against the human epidermoid cancer cell line KB-31 is only ca. 25 times lower than that of

Table 1: Tubulin-polymerizing and antiproliferative activity of 3-deoxyepothilone analogues.

Cmpd.[a]	% Tubulin polymerization[b]	IC_{50}(KB-31)[c] [nM]	IC_{50}(KB-8511)[c] [nM]
Epo A	62.6 (n.d.)	2.15 ± 0.07	1.91 ± 0.07
Epo B	95.8 (73.7)	0.29 ± 0.05	0.22 ± 0.05
Epo C[a]	n.d.	24.9[d]	9.9[d]
Epo D[a]	81.0 (n.d.)	2.70 ± 1.31	1.44 ± 0.78
taxol	53.7 (n.d.)	3.68 ± 0.68	805 ± 144
1	92.2 (68.0)	7.4 ± 2.2	4.0 ± 1.6
2	91.9 (67.5)	7.4 ± 0.7	37.6 ± 1.4
3	n.d.	0.58[e]	1.89[e]
4	82.0 (71.9)	3.16 ± 0.55	7.60 ± 2.44
12	78.7 (68.7)	114 ± 7	74 ± 3
16	86.4 (66.5)	58.7 ± 3.6	58.6 ± 7.1
17	n.d.	4.99 ± 2.15	5.75 ± 3.24
18	92.2 (65.5)	39.9 ± 1.8[f]	47.3 ± 4.8[f]

[a] All compounds tested were pure stereoisomers (HPLC, NMR). Epo C = 12,13-deoxyepothilone A. [b] Induction of polymerization of pure bovine brain tubulin (Cytoskeleton; catalog no. TL238) by 5 μM (2 μM) of test compound relative to the effect of 25 μM of Epo B, which gave maximal polymerization (100%). Tubulin polymerization was determined using a modified version of the centrifugation assay described in ref. [18]. n.d. = not determined. [c] IC_{50} values for growth inhibition of the human epidermoid carcinoma cell lines KB-31 and KB-8511, respectively. KB-8511 is a P-glycoprotein 170 (P-gp170)-overexpressing multidrug-resistant subline of the KB-31 parental line. Cells were exposed to compounds for 72 h. Cell numbers were estimated by quantification of protein content of fixed cells by staining with methylene blue.[19a] For further experimental details see ref. [19b]. Values represent the means of at least three independent experiments (± standard deviation). [d] Single determination. [e] Average values for two determinations. Individuals values are 0.54/0.62 (KB-31) and 1.61/2.16 (KB-8511). [f] The corresponding values for *trans*-Epo C are 96.2 nM and 36.8 nM, respectively.

 © 2005 Wiley-VCH Verlag GmbH & Co. KGaA, Weinheim

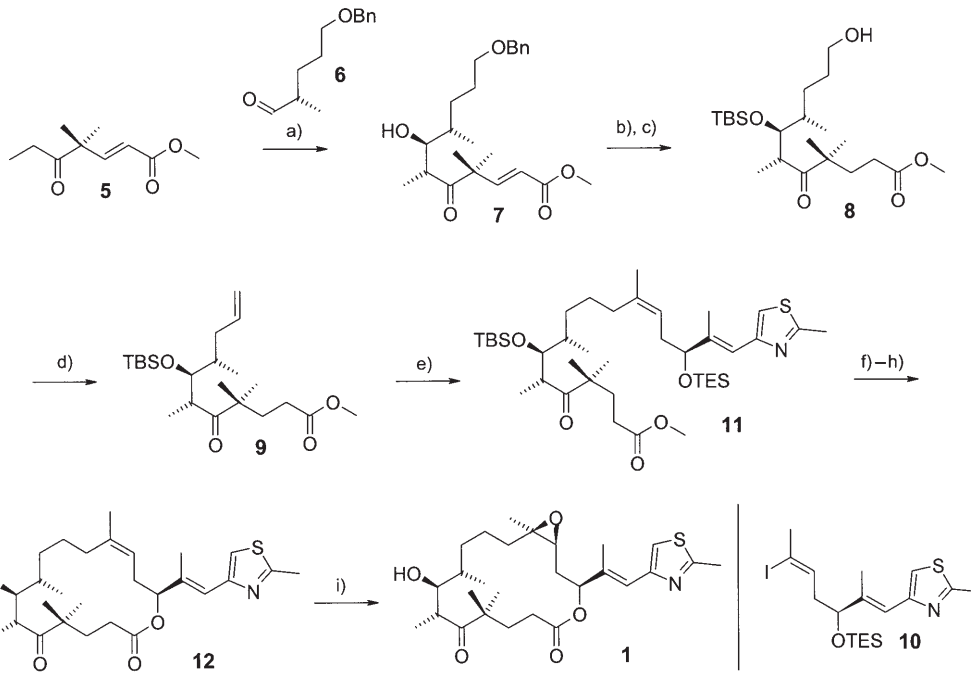

Scheme 1. a) LDA, −78 °C, 2 h, 58% (d.r. 2.5:1); b) TBSOTf, 2,6-lutidine, −10 °C, 1 h, 82%; c) H_2/Pd-C, MeOH, 1 h, 97%; d) *o*-$NO_2PhSeCN$, Bu_3P, $NaHCO_3$, H_2O_2, RT, 2 h, 69%; e) 9-BBN, THF, RT, 2 h, then added to mixture of Cs_2CO_3 (2 equiv), $[PdCl_2(dppf)_2]$ (0.2 equiv), Ph_3As (0.2 equiv.), vinyl iodide **10**, DMF, −10 °C→RT, 16 h, 55%; f) LiOH (6 equiv), *i*PrOH/H_2O 4:1, 60 °C, 3 h, 98%; g) 2,4,6-$Cl_3C_6H_2C(O)Cl$, Et_3N, THF, 0 °C, 15 min, then diluted with toluene and added to a solution of DMAP in toluene, RT, 1 h, 80% (2:1 mixture of epimers); h) HF·pyridine, THF, RT, 6 h, 90% (2:1 mixture of isomers; pure **12** obtained through purification by preparative HPLC); i) $MeReO_3$, H_2O_2/pyridine/H_2O, RT, 90 min, 72% (9:1 mixture of epoxide isomers; pure **1** obtained through purification by preparative HPLC). 9-BBN = 9-borabicyclo[3.3.1]nonane, Bn = benzyl, DMAP = 4-dimethylaminopyridine, dppf = 1,1′-bis(diphenylphosphanyl)ferrocene, LDA = lithium diisopropylamide, TBSOTf = *tert*-butyldimethylsilyl triflate, TES = triethylsilyl.

Epo B. The cellular potency of **1** is comparable with that of taxol, Epo A, and also 3-deoxy-2,3-didehydro-Epo B (data not shown), but in contrast to taxol the compound retains activity also against multidrug-resistant KB-8511 cells. The reduction in antiproliferative activity is somewhat larger at the level of deoxy compound **12**, which is roughly 40 times less potent than Epo D (12/13-deoxyEpo B).[8]

In the next step we asked whether at least some of the activity loss incurred by the removal of the 3-hydroxy group in Epo B could be recovered through additional and compensatory structural modifications. Based on our previous studies on potency-enhancing side-chain modifications,[12b] we designed compounds **2** and **3**, whose synthesis is summarized in Scheme 2. Starting from olefin **9**, Pd^0-catalyzed *B*-alkyl

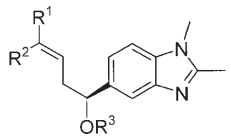

13: R^1 = H, R^2 = I, R^3 = H
14: R^1 = CH_3, R^2 = I, R^3 = TES
15: R^1 = I, R^2 = H, R^3 = TES

Suzuki coupling with *cis*-vinyl iodides **13** (free OH group) and **14**[13] was followed by ester saponification, selective removal of the TES protecting group from O–C15 (only in the synthesis of **3**), Yamaguchi macrolactonization, and deprotection of O–C7 to produce 12/13-deoxy intermediates **16** and **17**, respectively (Scheme 2).

Again, macrolactonization produced two isomers (which we presume to be epimers at C15), but in both cases the major isomer was obtained in pure form at the stage of the 12/13-deoxy compound (i.e. after removal of the TBS group from O–C7). Epoxidation of **16** and **17** with H_2O_2/pyridine in CH_2Cl_2 and catalytic $MeReO_3$[14] gave the desired analogues of Epo A and B, compounds **2** and **3**, respectively, but profound differences in epoxidation selectivity were observed between the two substrates. Thus, epoxidation of **16** proceeded with only 2:1 selectivity (in favor of the desired epoxide isomer); in addition, the epoxidation products were difficult to separate and **2** could be obtained in only 16% yield after purification by preparative TLC. In contrast, epoxidation of **17** gave the desired isomer with >10:1 selectivity (85% yield for the mixture of isomers), and pure **3** was obtained in 54% yield after purification by preparative HPLC.

As can be seen in Table 1, the presence of the benzimidazole side chain in **3** leads to a significant potency increase over **1** against the drug-sensitive KB-31 cell line, while a smaller difference is observed for the multidrug-resistant KB-8511 line. In fact, compound **3** shows a small (three- to fourfold) but clearly detectable activity differential between the sensitive and the resistant cell line, indicating that it may be a weak substrate for the P-gp efflux pump. We have previously observed a similar decrease in activity against KB-8511 cells for the corresponding benzimidazole-based ana-

 © 2005 Wiley-VCH Verlag GmbH & Co. KGaA, Weinheim

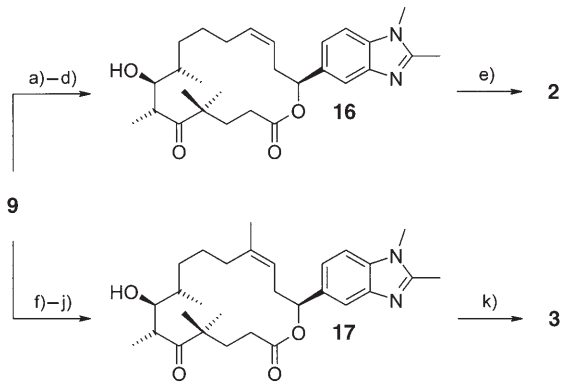

Scheme 2. a) 9-BBN (0.8 equiv), THF, RT, 100 min, then added to a mixture of Cs_2CO_3 (1.5 equiv), $[PdCl_2(dppf)_2]$ (0.2 equiv), Ph_3As (0.2 equiv), vinyl iodide **13**, DMF, 0 °C→RT, 75 min, 65%; b) LiOH (6 equiv), *i*PrOH/H_2O 4:1, 60 °C, 45 min, 87%; c) 2,4,6-$Cl_3C_6H_2C(O)Cl$, Et_3N, THF, 0 °C→RT, 30 min, then diluted with toluene and added to a solution of DMAP in toluene, RT, 2 h, 85% (4:1 mixture of epimers); d) HF·pyridine, CH_3CN, RT, 3 h, 68% (single isomer); e) $MeReO_3$, H_2O_2, pyridine, CH_2Cl_2, RT, 5 h, 16% (preparative TLC); f) 9-BBN, THF, RT, 2 h, then added to a mixture of Cs_2CO_3 (2 equiv), $[PdCl_2(dppf)_2]$ (0.2 equiv), Ph_3As (0.2 equiv), vinyl iodide **14** (1 equiv), DMF, 0 °C→RT, 2 h, 77%; g) LiOH (6 equiv), *i*PrOH/H_2O 4:1, 60 °C, 3 h, 90%; h) TBAF, THF, RT, 24 h, 75%; i) 2,4,6-$Cl_3C_6H_2C(O)Cl$, Et_3N, THF, 0 °C, 15 min, then diluted with toluene and added to a solution of DMAP in toluene, RT, 1 h, 85% (10:1 mixture of epimers); j) HF·pyridine, CH_3CN, RT, 3 h, 54% (single isomer; 87% for mixture of epimers); k) $MeReO_3$, H_2O_2/pyridine/H_2O, RT, 30 min, 64% (10:1 mixture of epoxide isomers). TBAF = tetrabutylammonium fluoride.

logue of Epo B.[12b] Moreover, we have repeatedly noted reduced activity against multidrug-resistant cells for structurally unrelated analogues, when they were more polar (reduced clogP) than the corresponding parent epothilone.[15] It is worth noting, however, that the activity of **3** against the KB-31 line is comparable with that of Epo B. Likewise, analogue **2** exhibits antiproliferative activity similar to that of Epo A and taxol, indicating that the presence of the dimethylbenzimidazole side chain can compensate for the removal of the 3-hydroxy group also in the epothilone A series. Similar conclusions can be derived from the data for 12/13-deoxy analogues **16** and **17**, which are only two times less potent antiproliferative agents than Epo C and D, respectively (Table 1; data for Epo C not shown).[8]

While the structures of compounds **2** and **3** deviate from those of Epo A and B, respectively, with regard to the core macrocycle as well as the heterocycle-bearing side chain, they are still characterized by a *cis*-configurated epoxide moiety at positions 12/13, which is a major structural hallmark of the natural products. However, we have previously shown that (12*S*,13*S*)-*trans* Epo A (but not the corresponding (12*R*,13*R*) isomer) is as potent as Epo A in terms of inducing tubulin polymerization and inhibiting cancer cell growth.[12a,16] In light of the potent biological activity of analogues **2** and **3**, the modification of (12*S*,13*S*)-*trans*-Epo A through removal of the hydroxy group at C3 and concomitant replacement of the natural side chain by a dimethylbenzimidazole moiety thus emerged as a promising approach for the creation of hypermodified but still potent epothilone analogues. These structural premises were realized in compound **4**, which was obtained from **9** by *B*-alkyl Suzuki coupling with vinyl iodide **15**,[13] elaboration of the coupling product into deoxy analogue **18**, and final epoxidation (Scheme 3).

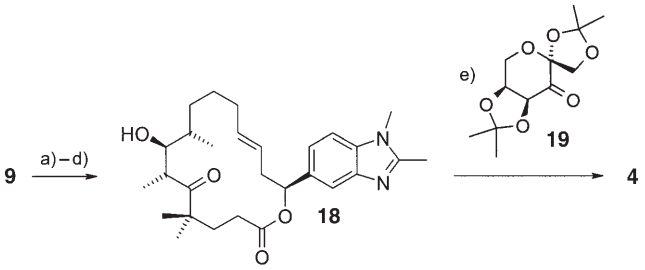

Scheme 3. a) 9-BBN (0.8 equiv), THF, RT, 2 h, then added to a mixture of Cs_2CO_3 (1.5 equiv), $[PdCl_2(dppf)_2]$ (0.1 equiv), Ph_3As (0.2 equiv), vinyl iodide **15** (1 equiv), DMF, −10 °C→RT, 16 h, 58%; b) LiOH (6 equiv), THF/H_2O 7:1, RT, 24 h, 76%; c) 2,4,6-$Cl_3C_6H_2C(O)Cl$, Et_3N, THF, 0 °C, 15 min, then diluted with toluene and added to a solution of DMAP in toluene, RT, 1 h, 71%; d) HF·pyridine, THF, RT, 6 h, 94%; e) Oxone, ketone **19** (0.8 equiv), $Bu_4N(HSO_4)$ (cat.), K_2CO_3, MeCN/DME/0.05 M $Na_2B_4O_7\times10H_2O$ in 4×10^{-4} M Na_2EDTA 1:1:1.3, 0 °C, 3 h, 65% (86% based on recovered starting material; single isomer). DME = dimethoxyethane.

For the epoxidation of **18** to give **4**, the fructose-derived epoxidation catalyst **19** was employed,[17] and pure **4** was obtained in 65% yield after simple flash chromatography. This outcome represents a major advance over the epoxidation of *trans*-deoxyEpo A under similar conditions, which proceeded less efficiently (similar selectivity, but lower conversion); in addition, isolation of pure (12*S*,13*S*)-*trans*-Epo A required purification by preparative HPLC and provided the isolated target compound in only 13% yield.[12a]

Quite remarkably, compound **4** exhibits potent biological activity in spite of major structural differences to the native epothilone scaffold (Table 1). Thus, the tubulin-polymerizing and antiproliferative activity of **4** is virtually identical to that of Epo A and taxol. As for **2** and **3**, the growth inhibitory activity of **4** is slightly lower against the multidrug-resistant KB-8511 cell line than against the taxol-sensitive KB-31 line. However, given the high levels of P-gp expression by the KB-8511 line, this small difference in cellular potency would seem unlikely to be pharmacologically relevant in a clinical setting. I n fact, this minor shortcoming might even be correctable through the incorporation of other types of fused heteroaromatic side chains.[12b]

In summary, by employing an iterative approach for the modification of a natural-product structural scaffold, we have derived a new microtubule-stabilizing agent, which we consider to represent a novel structural scaffold for microtubule inhibition. As such, **4** and related compounds may offer the same potential for pharmacological differentiation from the original epothilone leads as various newly discovered natural-product microtubule inhibitors with macrolactone structure, such as laulimalide, peloruside, and dictyostatin.[4] This view is supported by preliminary data from similarity analyses, which indicate that **4** is as structurally dissimilar to Epo A or B as laulimalide and peloruside are.[20] Future work will focus on

 © 2005 Wiley-VCH Verlag GmbH & Co. KGaA, Weinheim

synthesis scale-up and the extensive biological profiling of **4** and related structures in vitro and in vivo, in order to establish whether these compounds are in fact pharmacologically distinct from Epo A and Epo B. At the same time we will assess the effects of further structural modifications of **4** in the C8–C11 region and at the 2-position of the benzimidazole nucleus, which may or may not mirror the effects observed for analogous modifications of Epo A and Epo B.

Received: May 21, 2005
Published online: October 20, 2005

Keywords: antitumor agents · drug design · epothilones · microtubule stabilizers · natural products · total synthesis

[1] M. C. Lu in *Cancer Chemotherapeutic Agents* (Ed.: W. O. Foye), American Chemical Society, Washington, DC, **1995**, pp. 345–368.
[2] E. Hamel, *Med. Res. Rev.* **1996**, *16*, 207–231.
[3] E. K. Rowinsky, *Annu. Rev. Med.* **1997**, *48*, 353–374.
[4] For recent reviews, see, for example: a) K.-H. Altmann, *Curr. Opin. Chem. Biol.* **2001**, *5*, 424–431; b) D. C. Myles, *Annu. Rep. Med. Chem.* **2002**, *37*, 125–132.
[5] For general reviews on the potential of natural-product-based libraries in lead discovery, see: a) R. Breinbauer, I. R. Vetter, H. Waldmann, *Angew. Chem.* **2002**, *114*, 3002–3015; *Angew. Chem. Int. Ed.* **2002**, *41*, 2878–2890; b) M. A. Koch, H. Waldmann, *Drug Discovery Today* **2005**, *10*, 471–483.
[6] a) G. Höfle, N. Bedorf, K. Gerth, H. Reichenbach, German patent disclosure DE 4138042, May 5, **1993** (Priority Nov. 19, 1991); b) K. Gerth, N. Bedorf, G. Höfle, H. Irschik, H. Reichenbach, *J. Antibiot.* **1996**, *49*, 560–564.
[7] For reviews, see, for example: a) K.-H. Altmann, *Curr. Pharm. Des.* **2005**, *11*, 1595–1613; b) K.-H. Altmann, *Org. Biomol. Chem.* **2004**, *2*, 2137–2152; c) C. R. Harris, S. J. Danishefsky, *J. Org. Chem.* **1999**, *64*, 8434–8456; d) K. C. Nicolaou, F. Roschangar, D. Vourloumis, *Angew. Chem.* **1998**, *110*, 2120–2153; *Angew. Chem. Int. Ed.* **1998**, *37*, 2014–2045.
[8] Epo C and Epo D are 12/13-deoxy derivatives of Epo A and Epo B, respectively; i.e., they incorporate a *cis* double bond between C12 and C13 instead of an epoxide moiety.
[9] a) A. Rivkin, T.-C. Chou, S. J. Danishefsky, *Angew. Chem.* **2005**, *117*, 2898–2910; *Angew. Chem. Int. Ed.* **2005**, *44*, 2838–2850; b) A. Rivkin, F. Yoshimura, G. Fumihiko, A. E. Gabarda, Y. S. Cho, T.-C. Chou, H. Dong, S. J. Danishefsky, *J. Am. Chem. Soc.* **2004**, *126*, 10913–10922.
[10] a) A. Regueiro-Ren, K. Leavitt, S.-H. Kim, G. Höfle, M. Kiffe, J. Z. Gougoutas, J. DiMarco, F. Y. F. Lee, C. R. Fairchild, B. H. Long, G. D. Vite, *Org. Lett.* **2002**, *4*, 3815–3818; b) K.-H. Altmann, M. Wartmann, T. O'Reilly, *Biochim. Biophys. Acta* **2000**, *1470*, M79–M91.
[11] T. Carlomagno, M. J. J. Blommers, J. Meiler, W. Jahnke, T. Schupp, F. Petersen, D. Schinzer, K.-H. Altmann, C. Griesinger, *Angew. Chem.* **2003**, *115*, 2619–2621; *Angew. Chem. Int. Ed.* **2003**, *42*, 2511–2515.
[12] a) K.-H. Altmann, G. Bold, G. Caravatti, D. Denni, A. Flörsheimer, A. Schmidt, G. Rihs, M. Wartmann, *Helv. Chim. Acta* **2002**, *85*, 4086–4110; b) K.-H. Altmann, G. Bold, G. Caravatti, A. Flörsheimer, V. Guagnano, M. Wartmann, *Bioorg. Med. Chem. Lett.* **2000**, *10*, 2765–2768.
[13] For the synthesis of **14**, see ref. [12b]. The syntheses of **13** and **15** will be described elsewhere.
[14] J. Rudolph, K. L. Reddy, J. P. Chang, K. B. Sharpless, *J. Am. Chem. Soc.* **1997**, *119*, 6189–6190.
[15] M. Wartmann, K.-H. Altmann, A. Flörsheimer, unpublished data.
[16] See also: a) K. C. Nicolaou, K. Namoto, A. Ritzen, T. Ulven, M. Shoji, J. Li, G. D'Amico, D. Liotta, C. T. French, M. Wartmann, K.-H. Altmann, P. Giannakakou, *J. Am. Chem. Soc.* **2001**, *123*, 9313–9323; b) K. C. Nicolaou, N. Winssinger, J. Pastor, S. Ninkovic, F. Sarabia, Y. He, D. Vourloumis, Z. Yang, T. Li, P. Giannakakou, E. Hamel, *Nature* **1997**, *387*, 268–272.
[17] Z.-X. Wang, Y. Tu, M. Frohn, J.-R. Zhang, Y. Shi, *J. Am. Chem. Soc.* **1997**, *119*, 11224–11235.
[18] C. M. Lin, Y. Q. Jiang, A. G. Chaudhary, J. M. Rimoldi, D. G. Kingston, E. Hamel, *Cancer Chemother. Pharmacol.* **1996**, *38*, 136–140.
[19] a) T. Meyer, U. Regenass, D. Fabbro, E. Alteri, J. Rösel, M. Müller, G. Caravatti, A. Matter, *Int. J. Cancer* **1989**, *43*, 851–856; b) K. C. Nicolaou, R. Scarpelli, B. Bollbuck, B. Werschkun, M. M. Pereira, M. Wartmann, K.-H. Altmann, D. Zaharevitz, R. Gussio, P. Giannakakou, *Chem. Biol.* **2000**, *7*, 593–599.
[20] Structural similarity was assessed on the basis of Tanimoto coefficients (i.e., by a simple 2D fragment-based approach; see, for example: X. Chen, C. H. Reynolds, *J. Chem. Inf. Comput. Sci.* **2002**, *42*, 1407–1014). Similarity analyses using other approaches are currently underway, and the results of these studies will be published elsewhere.

 © 2005 Wiley-VCH Verlag GmbH & Co. KGaA, Weinheim

Polymerization Catalysts

DOI: 10.1002/anie.200502915

Cationic Yttrium Methyl Complexes as Functional Models for Polymerization Catalysts of 1,3-Dienes**

*Stefan Arndt, Klaus Beckerle, Peter M. Zeimentz, Thomas P. Spaniol, and Jun Okuda**

As structurally defined catalyst precursors, isolated rare-earth-metal complexes allow the examination of factors that influence the activity and stereoselectivity associated with the polymerization of conjugated dienes.[1] Metallocenes of the lanthanides, for example, form living stereospecific polymerization catalysts.[2] Although Ziegler-type catalysts based on neodymium carboxylate/ethylaluminum chloride have long been employed in industry for stereospecific 1,3-diene polymerization,[3] it has been shown only recently that alkyl

[*] Dr. S. Arndt, Dr. K. Beckerle, Dipl.-Chem. P. M. Zeimentz, Dr. T. P. Spaniol, Prof. Dr. J. Okuda
Institut für Anorganische Chemie
RWTH Aachen
Landoltweg 1, 52074 Aachen (Germany)
Fax: (+49) 241-80-92644
E-mail: jun.okuda@ac.rwth-aachen.de

[**] This work was supported by the Deutsche Forschungsgemeinschaft and the Fonds der Chemischen Industrie. We thank Prof. Dr. U. Englert for recording the crystallographic data.

Supporting information for this article is available on the WWW under http://www.angewandte.org or from the author.

© 2005 Wiley-VCH Verlag GmbH & Co. KGaA, Weinheim
InterScience

species of the rare-earth metals play a pivotal role in this catalysis.[4a–c] The presence of chloride additives in these neodymium-based catalysts had been assumed to be essential for the generation of 1,4-*cis*-configured polymers.[4d] Taube et al., however, argued that rare-earth-metal allyl dications $[Ln(allyl)]^{2+}$ (Ln = La, Nd) should be considered as the active species during the 1,4-*cis*-selective polymerization of 1,3-butadiene.[5]

We report herein on cationic yttrium alkyl complexes $[YMe_{2-n}(solv)_x]^{n+1}$ ($n = 0$, 1), available from easily accessible precursors, that can be used as functional models for the industrially applied catalysts for the polymerization of 1,3-dienes. Yttrium complex cations are particularly amenable to being isolated with the tetraphenylborate counterion, and because of yttrium's diamagnetism and nuclear spin of $I = {}^1/_2$, can be characterized in solution by NMR spectroscopy. With the perfluorinated tetraphenylborate ion they catalyze the polymerization of 1,3-butadiene and isoprene.[6] These results support the hypothesis that the 1,4-*cis*-selective polymerization of 1,3-butadiene proceeds with allyl rare-earth metal dications $[Ln(allyl)]^{2+}$.

We recently reported on $[YMe(thf)_6]^{2+}[BPh_4]^-_2$ (**4**), prepared by protonolysis of the aluminate $[Y\{(\mu\text{-}Me_2)_2(AlMe_2)\}_3]$ (**1**) by $[NEt_3H][BPh_4]$ (Scheme 1), and characterized by single-crystal structure analysis.[6b] The laboriousness of the preparation of the aluminate motivated us to turn instead to the hexamethyl trianion $[LnMe_6]^{3-}$, which has been described with the $[Li(tmeda)]^+$ counterion by Schumann et al. (tmeda = N,N,N′,N′-tetramethyl-1,2-ethanediamine).[7] YCl_3 reacts with six equivalents of LiMe to form a series of equilibrating methyl species. A THF complex with the composition $[Li_3YMe_6(thf)]$ (**2**) could be isolated as a thermally stable solid. This compound was protonolyzed with five equivalents of $[NEt_3H][BPh_4]$ to give the methyl dication **4** in 65% yield (Scheme 1). Methyl dications $[LnMe(thf)_x]^{2+}[BPh_4]^-_2$ (**9**, Ln = Sc, $x = 5$; **10**, Ln = Lu, $x = 6$; **11**, Ln = Yb, $x = 6$; **12**, Ln = Ho, $x = 6$) were prepared similarly from the hexamethyl complexes $[Li_3LnMe_6(thf)]$ (**5**, Ln = Sc; **6**, Ln = Lu; **7**, Ln = Yb; **8**, Ln = Ho). The NMR spectroscopic data of the diamagnetic scandium and lutetium complexes **9** and **10** are consistent with the proposed structures. A crystal-structure analysis showed the holmium derivative **12** to be similar to yttrium complex **4**.[8]

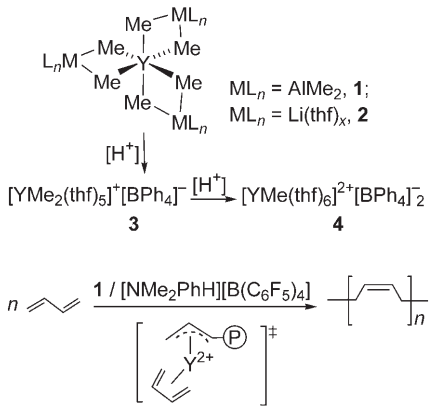

Scheme 1. Synthesis of the mono- and dicationic yttrium methyl complexes **3** and **4** from yttrium aluminate **1** or hexamethylyttrium **2**, and polymerization of 1,3-butadiene by in situ generated methyl cations. Ⓟ polymer chain.

Dimethyl monocation $[YMe_2(thf)_x]^+$ that formed from **2** could not be isolated, owing to the difficulty in separating it from the $LiBPh_4$ generated in the reaction. However, the addition of [12]crown-4 allowed the isolation of the crown-ether adduct $[YMe_2([12]crown\text{-}4)(thf)_2]^+[BPh_4]^-$ (**3′**) as thermally robust colorless crystals in 80% yield. Protonolysis of the aluminate **1** in THF with one equivalent $[NEt_3H][BPh_4]$ gave the THF adduct $[YMe_2(thf)_5]^+[BPh_4]^-$ (**3**) in moderate yield.[9]

The coordinated THF in **3** is readily displaced by pyridine, as shown by NMR spectra recorded in $[D_5]$pyridine. In the ^1H NMR spectrum, the YMe group appears as a doublet at $\delta = 0.01$ ppm ($^2J(Y,H) = 1.2$ Hz); the ^{13}C NMR spectrum contained a doublet at $\delta = 17.7$ ppm ($^1J(Y,C) = 39.3$ Hz). The coordinated crown ether of **3′** is indicated in the ^1H NMR spectrum in $[D_5]$pyridine recorded at −20 °C as a broad resonance at $\delta = 3.75$ ppm in addition to the resonances arising from $[YMe_2([D_5]pyridine)_x]^+[BPh_4]^-$ and free [12]crown-4.[10] These results are consistent with a labile coordination of the crown ether of **3′** in pyridine.

The crystal-structure analysis of **3** revealed a pentagonal-bipyramidal coordination geometry around the yttrium center with *trans*-disposed methyl groups (Figure 1), whereas the ligands around the eight-coordinate metal center in **3′** adopt an square-antiprismatic arrangement with *cis* methyl groups.[8a] The yttrium–carbon bond lengths ranging between 2.508(2) and 2.526(2) Å in **3** are slightly longer than in the dication **4**,[6b] whereas the yttrium–oxygen bond lengths are similar to those in other cationic yttrium complexes.[6b,11]

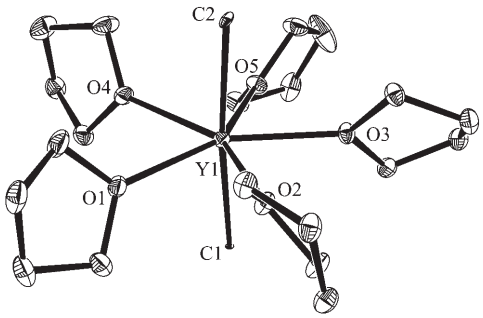

Figure 1. Molecular structure of the cation of **3**. Only one of the two crystallographic independent molecules is shown. Thermal ellipsoids are set at 30% probability, and hydrogen atoms are not shown for clarity. Selected bond lengths [Å] and angles [°]: Y1–C1 2.526(2), Y1–C2 2.508(2), Y1–O1 2.397(2), Y1–O2 2.399(2), Y1–O3 2.406(2), Y1–O4 2.395(2), Y1–O5 2.418(2); C1-Y1-C2 174.03(8).

Upon activation with $[PhNHMe_2][B(C_6F_5)_4]$, the precursors **1** and **2** both catalyzed the polymerization of 1,3-dienes (Table 1), whereas no polymerization was observed when activation of **1** and **2** was attempted with $[PhNHMe_2][BPh_4]$.[12] The in situ generated dication $[YMe(solv)_x]^{2+}$(**4a**, solv = toluene) gave 1,4-*cis*-polybutadiene in up to 97% selectivity at 100% conversion after 14 h (run 7). The in situ

 © 2005 Wiley-VCH Verlag GmbH & Co. KGaA, Weinheim

Table 1: 1,3-Diene polymerization by **1** activated by $[PhNHMe_2][B(C_6F_5)_4]$.[a]

Run	B:Y		*t* [min]	Conversion [%]	Selectivity[b]	M_n[c]	M_w/M_n
			1,3-Butadiene polymerization				
1[d]	1:1		30	< 5			
2[e]	1:1		240	73		186	4.4
3	1:1	Al*i*Bu$_3$	840	100	90:8:2	50	2.6
4	2:1		30	26	95:3:2	140	2.0
5[e]	2:1		240	93		312	2.6
6	2:1	Al*i*Bu$_3$	30	18	95:3:2	61	1.7
7	2:1	Al*i*Bu$_3$	840	100	97:2:1	100	2.1
			Isoprene polymerization				
8	1:1		10	56	60:26:14	117	1.6
9	1:1	Al*i*Bu$_3$	10	86	89:0:11	315	2.1
10	2:1		10	65	67:13:20	260	1.5
11	2:1	Al*i*Bu$_3$	10	78	90:0:10	133	2.9

[a] Conditions: 5 μmol Y; $T = 25\,^{\circ}C$. 1,3-Butadiene polymerization: $V_{butadiene} = 7.5$ mL (14 wt% in toluene); $V_{total} = 30$ mL. Isoprene polymerization: $V_{isoprene} = 1$ mL; $V_{total} = 30$ mL. [b] Ratio *cis*:*trans*:1,2 for 1,3-butadiene; ratio *cis*:*trans*:3,4 for isoprene. [c] $\times 10^3$ [g mol^{-1}]. [d] Molecular weight and microstructure not determined because of low conversion. [e] Microstructure not determined because of cross-linking; molecular weight determined for the soluble fraction.

generated monocation $[YMe_2(solv)_x]^+$ (**3a**, run 3) produced 1,4-*cis*-polybutadiene in only 90% selectivity and had a significantly lower polymerization activity (no polybutadiene was obtained after 30 min (run 2)) than the dications (18–26% conversion (runs 4 and 6)). These results show that the in situ generated monocation $[YMe_2(solv)_x]^+$ and the dication $[YMe(solv)_x]^{2+}$ have different activities and produce polybutadienes with different microstructures. The dication (Table 1, run 7) produced a polybutadiene with a molecular weight (M_n) twice as high as that obtained with the monocation (run 3). This result is consistent with an insertion mechanism assuming that the active species consists of, depending on the experimental conditions, either a dication with one growing chain or a monocation with two growing chains.[3b,13] In the absence of Al*i*Bu$_3$, cross-linked polybutadiene is isolated (runs 1, 2, and 5).

The in situ formed monocation $[YMe_2(solv)_x]^+$ polymerizes isoprene to 1,4-*cis*-enriched polyisoprene (Table 1, runs 8 and 9). In polymerization experiments with activated yttrium-aluminate **1** (run 9) as well as with the activated hexamethylyttrate **2**, polyisoprene with the same microstructure and similar molecular weight is obtained.[12b] Both catalyst precursors must therefore form the same THF-free monocationic species $[YMe_2(solv)_x]^+$.[12,14]

In the absence of Al*i*Bu$_3$, the dication forms (Table 1, run 10) polyisoprene with a molecular weight M_n that is twice as high as that formed with the monocation (run 8), analogous to the polymerization of 1,3-butadiene. In this case, however, a significant influence of the aluminum alkyl is seen. In the presence of Al*i*Bu$_3$, the dication (run 11) provides polyisoprene with a molecular weight significantly lower than that formed with the monocation (run 9). In both cases, the addition of Al*i*Bu$_3$ leads to a higher *cis*-selectivity. We are currently continuing our investigations into these effects in the polymerization of isoprene.

According to ^{1}H NMR spectra of the yttrium methyl cations in [D$_8$]THF, the cations with perfluorinated anions **3a** and **4a** are identical to the isolated model compounds **3** and **4** (see Supporting Information). The differences between the polymerization activities of the model compounds and the active compounds can be accounted for, on the one hand, by the different anions and, on the other hand, the presence of THF. Although, in principle, THF inhibits the polymerization, it can, in some cases, be trapped by Al*i*Bu$_3$.[6b,12b] The crystal structures of THF-free cationic lanthanide metallocenes with tetraphenylborate as the counterion typically show strong η^6-coordination of at least one of the phenyl groups to the metal center.[15] This bonding also occurs when these compounds are dissolved in aromatic solvents to give contact pairs, and is only removed by strong Lewis bases, such as THF, to give solvent-separated ions.[15b] From this result it may be concluded that tetraphenylborate complexes **3** and **4** form inactive contact pairs in toluene.[16] Cations with perfluorinated anions coordinate, in contrast, only very weakly,[17] and therefore form solvent-separated ion pairs in aromatic hydrocarbon solvents; as a result, in contrast to the tetraphenylborate complexes, they catalyze 1,3-diene polymerization.[16,18]

We could show that it is possible to specifically prepare the cationic yttrium methyl complexes $[YMe_2(solv)_x]^+$ and $[YMe(solv)_x]^{2+}$, which depending on the anion, could catalyze the homogeneous polymerization of 1,3-butadiene and isoprene. Further research into the systematic determination of the structure–activity relationship of this catalytic system and the polymerization behavior of the cationic methyl complexes is underway.

Experimental Section

4 and $[YMe([D_5]pyridine)_x]^{2+}[BPh_4]^-_2$: THF (150 mL) was added to a mixture of **2** (1.50 g, 5.51 mmol) and $[NEt_3H][BPh_4]$ (11.6 g, 27.6 mmol) at 25 °C; this resulted in the generation of gas. After the colorless suspension had been stirred at 25 °C for 30 min, the supernatant solution was removed by decantation. Drying in vacuo gave colorless microcrystals of **4** (4.24 g, 65%). ^{1}H NMR (200 MHz, [D$_5$]pyridine, 25 °C): $\delta = 0.67$ (d, $^2J(Y,H) = 2.0$ Hz, 3H, YCH_3), 1.61 (m, 6 × 4H, β-CH_2, THF), 3.65 (m, 6 × 4H, α-CH_2, THF), 7.08 (t, $^3J(H,H) = 7.0$ Hz, 2 × 4H, Ph-4), 7.25 (t, $^3J(H,H) = 7.4$ Hz, 2 × 8H, Ph-3), 8.02 ppm (br, 2 × 8H, Ph-2).

Polymerization of 1,3-butadiene with the in situ generated dication $[YMe(solv)_x]^{2+}$: A toluene solution of **1** (1 mL; 5 mmol L^{-1}) and a solution of $[PhNHMe_2][B(C_6F_5)_4]$ (2 mL; 5 mmol L^{-1}) were added to a 50-mL Schlenk tube containing toluene (19.5 mL; and, where appropriate, Al*i*Bu$_3$ (125 μL, 0.5 mmol)) under constant stirring. After the mixture had stirred at 25 °C for 10 min, 1,3-butadiene (7.5 mL of a 14 wt% solution in toluene) was added and the yellow reaction mixture was stirred for 30 min. The polymerization was subsequently terminated by the addition of methanol, and the reaction solution was poured into a mixture of 2,6-di-*tert*-

 © 2005 Wiley-VCH Verlag GmbH & Co. KGaA, Weinheim

butylphenol and acidified methanol (300 mL). After filtration, the polymer was washed with methanol and dried in vacuo at 25 °C until it reached a constant weight.

Received: August 16, 2005
Published online: October 25, 2005

Keywords: cations · coordination modes · polymerization · rare-earth metals · yttrium

[1] a) Z. Hou, Y. Wakatsuki, *Coord. Chem. Rev.* **2002**, *231*, 1–22; b) A. Fischbach, M. G. Klimpel, M. Widenmeyer, E. Herdtweck, W. Scherer, R. Anwander, *Angew. Chem.* **2004**, *116*, 2284–2289; *Angew. Chem. Int. Ed.* **2004**, *43*, 2234–2239; c) J. Gromada, J. F. Carpentier, A. Mortreux, *Coord. Chem. Rev.* **2004**, *248*, 397–410; d) Y. Nakayama, H. Yasuda, *J. Organomet. Chem.* **2004**, *689*, 4489–4498; e) W. J. Evans, T. M. Champagne, D. G. Giarikos, J. W. Ziller, *Organometallics* **2005**, *24*, 570–579; f) S. Arndt, J. Okuda, *Adv. Synth. Catal.* **2005**, *347*, 339–354.

[2] a) S. Kaita, Z. Hou, Y. Wakatsuki, *Macromolecules* **1999**, *32*, 9078–9079; b) S. Kaita, Z. Hou, M. Nishiura, Y. Doi, J. Kurazumi, A. C. Horiuchi, Y. Wakatsuki, *Macromol. Rapid Commun.* **2003**, *24*, 179–184; c) S. Kaita, N. Koga, Z. Hou, Y. Doi, Y. Wakatsuki, *Organometallics* **2003**, *22*, 3077–3082; d) S. Kaita, Y. Doi, K. Kaneko, A. C. Horiuchi, Y. Wakatsuki, *Macromolecules* **2004**, *37*, 5860–5862.

[3] a) A. Porri, A. Giarusso in *Comprehensive Polymer Science, Vol. 4, Part II* (Eds.: G. C. Eastmond, A. Ledwith, S. Russo, B. Sigwalt), Pergamon, Oxford, **1989**, pp. 53–108; b) R. Taube, G. Sylvester in *Applied Homogeneous Catalysis, Vol. 1* (Eds.: B. Cornils, W. A. Herrmann), VCH, Weinheim, **1996**, pp. 280–318.

[4] a) A. Fischbach, F. Perdih, P. Sirsch, W. Scherer, R. Anwander, *Organometallics* **2002**, *21*, 4569–4571; b) J. Gromada, A. Mortreux, T. Chenal, J. W. Ziller, F. Leising, J. F. Carpentier, *Chem. Eur. J.* **2002**, *8*, 3773–3788; c) J. Gromada, A. Mortreux, G. Nowogrocki, F. Leising, T. Mathivet, J. F. Carpentier, *Eur. J. Inorg. Chem.* **2004**, 3247–3253; d) see refs. [1b], [1e], and [3a], and references therein.

[5] R. Taube in *Metalorganic Catalysts for Synthesis and Polymerization* (Ed.: W. Kaminsky), Springer, Berlin, **1999**, pp. 531–547.

[6] a) We could show that alkyl dications $[LnR(solv)_x]^{2+}$ and dialkyl monocations $[LnR_2(solv)_x]^+$ participate in homogeneous ethylene polymerization (Ln = Lu, Tm, Er, Y, Ho, Dy, Tb; R = CH_2SiMe_3), see ref. [6b]; b) S. Arndt, T. P. Spaniol, J. Okuda, *Angew. Chem.* **2003**, *115*, 5229–5233; *Angew. Chem. Int. Ed.* **2003**, *42*, 5075–5079; c) Recently, Gade et al. reported the isospecific polymerization of 1-hexene by [Sc(*i*Pr-trisox)-$(CH_2SiMe_3)_3$] upon activation with 2 equivalents $[Ph_3C]$-$[B(C_6F_5)_4]$, see ref. [6d]; d) B. D. Ward, S. Bellemin-Laponnaz, L. H. Gade, *Angew. Chem.* **2005**, *117*, 1696–1699; *Angew. Chem. Int. Ed.* **2005**, *44*, 1668–1671; e) Attempts at isolating analogous cationic allyl complexes were unsuccessful, although a cationic complex $[Y(allyl)_2(thf)_x]^+[BPh_4]^-$ could be shown by ^{1}H NMR spectroscopy to form upon the protonolysis of the complex $[Mg(thf)_6]^{2+}[Y(allyl)_4]^-_2$ with $[NEt_3H][BPh_4]$: J. Okuda, S. Arndt, and Y. Sato, unpublished results.

[7] a) H. Schumann, J. Müller, *Angew. Chem.* **1978**, *90*, 307–308; *Angew. Chem. Int. Ed. Engl.* **1978**, *17*, 276; b) H. Schumann, J. Pickardt, N. Bruncks, *Angew. Chem.* **1981**, *93*, 127–128; *Angew. Chem. Int. Ed. Engl.* **1981**, *20*, 120–121; c) H. Schumann, J. Müller, N. Bruncks, H. Lauke, J. Pickardt, H. Schwarz, K. Eckart, *Organometallics* **1984**, *3*, 69–74; d) H. Schumann, H. Lauke, E. Hahn, J. Pickardt, *J. Organomet. Chem.* **1984**, *263*, 29–35.

[8] a) CCDC-268899, -268900, -268901, and -268902 contain the supplementary crystallographic data for this paper. These data can be obtained free of charge from The Cambridge Crystallographic Data Centre via www.ccdc.cam.ac.uk/data_request/cif; b) $[NdMe(thf)_7]^{2+}[BPh_4]^-_2$ was obtained as thermally robust, greenish microcrystals from the aluminate $[Nd\{(\mu\text{-}Me)_2(AlMe)_2\}_3]$ and 2 equivalents $[NEt_3H][BPh_4]$ in THF (see Supporting Information).

[9] a) The protonation of $[Nd\{(\mu\text{-}Me)_2(AlMe_2)\}_3]$ with 1 equivalent $[NEt_3H][BPh_4]$ gave a dicationic compound $[Nd\{O(CH_2)_4Me\}(thf)_6]^{2+}[BPh_4]^-_2$, which contains a ring-opened THF group according to an X-ray crystallographic determination. For similar reactions, see ref. [9b]; b) W. J. Evans, T. A. Ulibarri, L. R. Chamberlain, J. W. Ziller, D. Alvarez, Jr., *Organometallics* **1990**, *9*, 2124–2130.

[10] A singlet at $\delta = 0.02$ ppm in the ^{1}H NMR spectrum and a doublet at $\delta = 17.2$ ppm ($^1J(Y,C) = 38.9$ Hz) in the ^{13}C NMR spectrum were also observed for the YMe group of $[YMe_2(thf)_5]^+[BPh_4]^-$ in $[D_5]$pyridine (see Supporting Information).

[11] a) W. J. Evans, J. M. Olofson, J. W. Ziller, *J. Am. Chem. Soc.* **1990**, *112*, 2308–2314; b) P. Sobota, J. Utko, S. Szafert, *Inorg. Chem.* **1994**, *33*, 5203–5206; c) K. Y. Chiu, Z. Y. Zhang, T. C. W. Mak, Z. W. Xie, *J. Organomet. Chem.* **2000**, *614*, 107–112.

[12] a) "Activation" of **4** with Al*i*Bu$_3$ did not lead to 1,3-diene polymerization. b) Butadiene polymerization with **2** activated by $[PhNHMe_2][B(C_6F_5)_4]$; Conditions: 5 μmol Y; B:Y:Al = 4:1:100; $T = 25$ °C; $t = 840$ min; $V_{butadiene} = 7.5$ mL 15.8 wt % solution in toluene; $V_{total} = 30$ mL; conversion = 30 %; $M_n = 39 \times 10^3$ g mol^{-1}; $M_w/M_n = 2.4$. Isoprene polymerization by **2** activated by $[PhNHMe_2][B(C_6F_5)_4]$; Conditions: 5 μmol Y; B:Y:Al = 4:1:100; $T = 25$ °C; $t = 10$ min; $V_{isoprene} = 1$ mL; $V_{total} = 30$ mL; conversion = 15 %; *cis*:*trans*:3,4 = 90:0:10; $M_n = 323 \times 10^3$ g mol^{-1}; $M_w/M_n = 2.4$; Al*i*Bu$_3$ (probably needed as scavenger for THF). See Supporting Information for experimental details.

[13] a) Up to three growing chains per metal center have been reported for neutral allyl rare-earth complexes, see refs. [3b] and [13b]; b) R. Taube, S. Maiwald, J. Sieler, *J. Organomet. Chem.* **2001**, *621*, 327–336.

[14] a) Under conditions analogous to those of runs 8–11 in Table 1, the neodymium system $[Nd\{(\eta\text{-}Me)_2(AlMe)_2\}_3]$/$[PhNHMe_2][B(C_6F_5)_4]$ does not catalyze the polymerization of isoprene. The yellow color of the reaction mixture indicates the formation of an allylic species as a result of CH activation of toluene; b) Whereas $[LnCp^*_2(\eta^3\text{-}C_3H_5)]$ does not participate in CH activation, $[LnCp^*_2Me]_x$ reacts with $SiMe_4$, benzene, toluene, see ref. [14c] and references therein; c) W. J. Evans, J. M. Perotti, J. W. Ziller, *J. Am. Chem. Soc.* **2005**, *127*, 3894–3909.

[15] a) For examples of the η^6-coordination of phenyl groups of the borate counterion to cationic lanthanide complexes, see refs. [15b–e], and references therein; b) J. Schaverien, *Organometallics* **1992**, *11*, 3476–3478; c) W. J. Evans, C. A. Seibel, J. W. Ziller, *J. Am. Chem. Soc.* **1998**, *120*, 6745–6752; d) L. W. M. Lee, W. E. Piers, M. R. J. Elsegood, W. Clegg, M. Parvez, *Organometallics* **1999**, *18*, 2947–2949; e) W. J. Evans, J. M. Perotti, S. A. Kozimor, T. M. Champagne, B. L. Davis, G. W. Nyce, C. H. Fujimoto, R. D. Clark, M. A. Johnston, J. W. Ziller, *Organometallics* **2005**, *24*, 3916–3931.

[16] a) Polymerization-active contact ion pairs are unknown in lanthanide chemistry, the presence of non- or weakly coordinating anions is generally regarded as a decisive factor in the polymerization activity, see refs. [16b,c]; b) E. Y.-X. Chen, T. J. Marks, *Chem. Rev.* **2000**, *100*, 1391–1434; c) A. Macchioni, *Chem. Rev.* **2005**, *105*, 2039–2071.

[17] a) For Ln-F interactions in cationic lanthanide compounds with perfluorinated borate counterions, see, for example, refs. [2b] and [17b–c], and references therein; b) X. J. Song, M. Thornton-Pett, M. Bochmann, *Organometallics* **1998**, *17*, 1004–1006; c) P. G. Hayes, W. E. Piers, R. McDonald, *J. Am. Chem. Soc.* **2002**, *124*, 2132–2133; d) for η^6-coordination of the solvent to

 © 2005 Wiley-VCH Verlag GmbH & Co. KGaA, Weinheim

cationic scandium complexes, see ref. [18e]; e) P. G. Hayes, W. E. Piers, M. Parvez, *J. Am. Chem. Soc.* **2003**, *125*, 5622 – 5623.

[18] a) In cationic alkylchromium complexes, similar reactivity differences between complexes with protonated and perfluorinated counterions are seen, see ref. [18b]; b) L. A. MacAdams, G. P. Buffone, C. D. Incarvito, A. L. Rheingold, K. H. Theopold, *J. Am. Chem. Soc.* **2005**, *127*, 1082 – 1083; c) Attempts at investigating the active catalysts in [D_8]toluene by NMR spectroscopy were unsuccessful, because of the formation of easily decomposable, oily, two-phase systems as a result of the relatively high concentrations required; d) For the sake of solubility, we used THF as solvent for the isolation of the model compounds. In THF we observed a reaction analogous to the reaction described by Hou et al. of cationic metallocenic lanthanide aluminate complexes in toluene with [Ph_3C]-[$B(C_6F_5)_4$], for which the resulting cationic complex was examined by X-ray crystallography, see ref. [2b].

Unique – Comprehensive – Fascinating

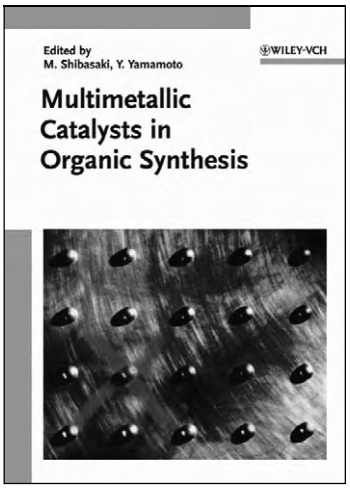

2004. XV, 295 pages, 173 figures, 66 tables. Hardcover. ISBN 3-527-30828-8 € 129.- /£ 90.- /US$ 194.-

MASAKATSU SHIBASAKI and YOSHINORI YAMAMOTO, (Eds.)

Multimetallic Catalysts in Organic Synthesis

This first book to comprehensively cover this hot topic presents the information hitherto scattered throughout smaller reviews or single book chapters to provide an introduction to this rapidly expanding field.
In ten chapters, the international team of expert authors treats asymmetric syntheses, new transformations, and organometallic reactions using homo- and hetero-bimetallic catalysts. Written for advanced researchers, this very timely publication is of significant benefit to organic and organometallic chemists in both academia and industry.

22531509_kn

Register now for the free
WILEY-VCH Newsletter!
www.wiley-vch.de/home/pas

WILEY-VCH • P.O. Box 10 11 61 • D-69451 Weinheim, Germany
Fax: +49 (0) 62 01 - 60 61 84
e-mail: service@wiley-vch.de • http://www.wiley-vch.de

WILEY-VCH

© 2005 Wiley-VCH Verlag GmbH & Co. KGaA, Weinheim

Cover Picture

Neil B. McKeown,* Saad Makhseed, Kadhum J. Msayib, Li-Ling Ooi, Madeleine Helliwell, and John E. Warren

Ein Clathrat aus einem Zinkphthalocyanin hat eine ungewöhnliche Kristallstruktur mit großen solvensgefüllten Hohlräumen ($>8\ nm^3$). Der aufgefaltete Würfel auf dem Titelbild zeigt, wie sechs Phthalocyaninmoleküle einen Nanohohlraum aufbauen. Solvensmoleküle, auch Wasser, werden zwischen den Hohlräumen ausgetauscht, und die auf den Flächen befindlichen Metallzentren lassen katalytische Wirkungen erhoffen. Einzelheiten finden sich in der Zuschrift von N. B. McKeown et al. auf S. 7718 ff.

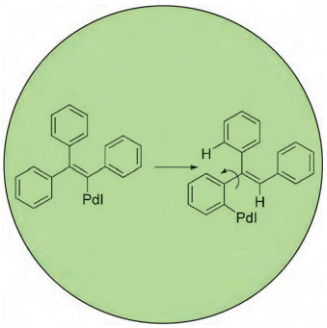

Katalysemechanismen
Bei manchen rhodium- und palladiumkatalysierten Reaktionen tritt als entscheidender Schritt eine 1,4-Wanderung des Metallzentrums auf. S. Ma und Z. Gu präsentieren einige Beispiele hierfür im Kurzaufsatz auf S. 7680 ff.

Atmosphärenforschung
Aerosole sind von zentraler Bedeutung für die Chemie und Physik der Atmosphäre, beeinflussen außerdem das Klima und können Erkrankungen auslösen. Im Aufsatz auf S. 7690 ff. fasst U. Pöschl den aktuellen Wissensstand zusammen.

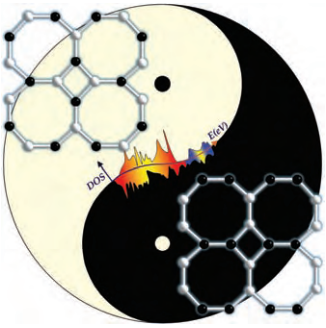

Metallborcarbidphasen
Mithilfe von DFT-Rechnungen wurde das “Coloring-Problem” in MB_2C_2-Phasen gelöst. Einzelheiten dazu finden sich in der Zuschrift von X. Rocquefelte, J.-Y. Saillard, J.-F. Halet et al. auf S. 7714 ff.

Contents

VIP *The following Communications have been judged by at least two referees to be "very important papers" and will be published online at www.angewandte.org soon:*

*S. J. Dalgarno, G. W. V. Cave, J. L. Atwood**
Toward the Isolation of Functional Organic Nanotubes

*Y. Nakajima, H. Kameo, H. Suzuki**
Cleavage of the Nitrogen-Hydrogen Bond of Ammonia Induced by Triruthenium Polyhydrido Clusters

N. Lu, H. P. S. Kumar, J. L. Fye, J. S. Blanks, J. S. Thrasher,* H. Willner, H. Oberhammer*
The Initial Synthesis of the Long Sought After Compound Pentafluoronitrosulfane, SF_5NO_2

*G. I. Elliott, J. Velcicky, H. Ishikawa, YongKai Li, D. L. Boger**
Total Synthesis of (−)- and *ent*-(+)-Vindorosine: Tandem Intramolecular Diels-Alder/1,3-Dipolar Cycloaddition of 1,3,4-Oxadiazoles

*G. Krebs, L. Hugonet, J. D. Sutherland**
Substrate Ambiguity and Catalytic Promiscuity Within a Bacterial Proteome Probed by an Easy Phenotypic Screen for Aldehydes

E. Álvarez, M. Paneque, M. L. Poveda,* N. Rendón*
Formation of Iridabenzenes by Coupling of Iridacyclopentadienes and Alkenes

Meeting Reviews

Macromolecular Metal Complexes: Materials for Various Applications — *D. Wöhrle* — **7500**

Books

The Maillard Reaction — Harry Nursten — *reviewed by H. Steinhart* — **7503**

Highlights

Organocatalysis

K. Zeitler* — **7506 – 7510**

Extending Mechanistic Routes in Heterazolium Catalysis—Promising Concepts for Versatile Synthetic Methods

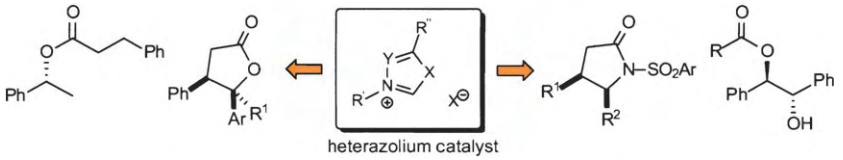

A broad spectrum of valuable cyclic and acyclic products are available in diastereo- and/or enantioselective form by sustainable, organocatalytic processes like the heterazolium-catalyzed transformations shown in the scheme. The carbene-mediated generation of activated carboxylate intermediates provides new possibilities for the straightforward synthesis of multifunctionalized compounds.

Minireviews

Reaction Mechanisms

S. Ma,* Z. Gu — **7512 – 7517**

1,4-Migration of Rhodium and Palladium in Catalytic Organometallic Reactions

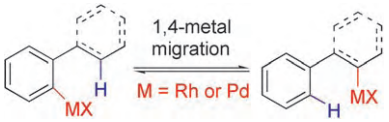

A key mechanistic step in a number of rhodium- and palladium-catalyzed reactions is the 1,4-migration of the metal center, which can be understood as the oxidative addition of the metal into a C–H or C–X bond followed by reductive elimination. Although concrete evidence for the transition state is lacking, the synthetic applications are numerous.

InterScience
© 2005 Wiley-VCH Verlag GmbH & Co. KGaA, Weinheim

Reviews

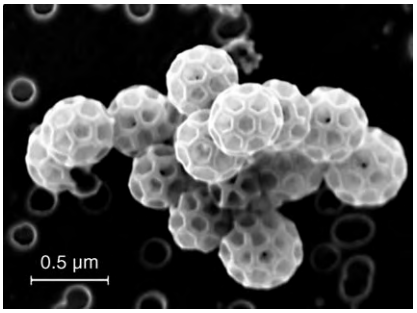

An esthetic example of the wide variety of biological aerosol particles found in the atmosphere are the pictured brochosomes, which are released by insects. Atmospheric chemistry and physics, the biosphere, the hydrological cycle, climate, and human health are all strongly influenced by natural and anthropogenic particles in the nanometer to micrometer size range.

Atmospheric Chemistry

U. Pöschl* _____ **7520 – 7540**

Atmospheric Aerosols: Composition, Transformation, Climate and Health Effects

Communications

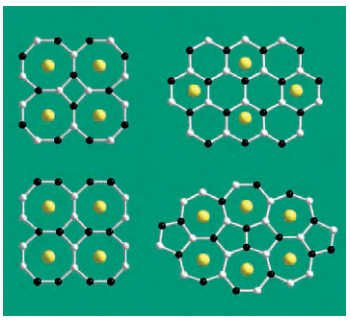

The question of coloring: Calculations present a definite solution to the "coloring problem" in the MB_2C_2 phases (M = Mg, Sc, Ca, Y, Ln; see picture of the four structure types). Electric-field gradient tensor components from NMR spectroscopy readily allow differentiation between the different B/C topologies and give support to the theoretical results.

Inclusion Compounds VIP

X. Rocquefelte,* S. E. Boulfelfel, M. Ben Yahia, J. Bauer, J.-Y. Saillard,* J.-F. Halet* _____ **7542 – 7545**

Structural Preference versus Metal within the MB_2C_2 (M = Mg, Sc, Ca, Y, Ln) Phases: The Coloring Problem Revisited by DFT Calculations

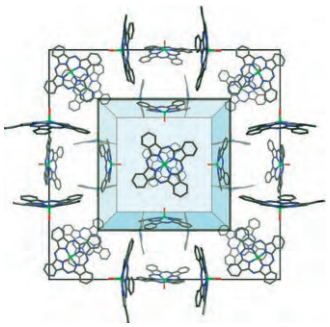

A void apart! A clathrate based on zinc octa(2,6-diisopropylphenoxy)phthalocyanine contains solvent-filled voids of exceptionally large volume (> 8 nm^3; see picture for the packing arrangement). Each nanovoid is enclosed by a cubic assembly of six phthalocyanine molecules and contains 18 molecules of water and an estimated 65 molecules of acetone, which may be exchanged for methanol or water molecules without loss of order.

Crystal Engineering

N. B. McKeown,* S. Makhseed, K. J. Msayib, L.-L. Ooi, M. Helliwell, J. E. Warren _____ **7546 – 7549**

A Phthalocyanine Clathrate of Cubic Symmetry Containing Interconnected Solvent-Filled Voids of Nanometer Dimensions

For the USA and Canada:
ANGEWANDTE CHEMIE International Edition (ISSN 1433-7851) is published weekly by Wiley-VCH PO Box 191161, D 69451 Weinheim, Germany. Air freight and mailing in the USA by Publications Expediting Inc. 200 Meacham Ave., Elmont, NY 11003. Periodicals postage paid at Jamaica NY 11431. US POSTMASTER: send address changes to *Angewandte Chemie*, Wiley-VCH, 111 River Street, Hoboken, NJ 07030. Annual subscription price for institutions: US$ 5685/5168 (valid for print and electronic / print or electronic delivery); for individuals who are personal members of a national chemical society prices are available on request. Postage and handling charges included. All prices are subject to local VAT/sales tax.

© 2005 Wiley-VCH Verlag GmbH & Co. KGaA, Weinheim

The best in chemistry –

for more than a hundred years

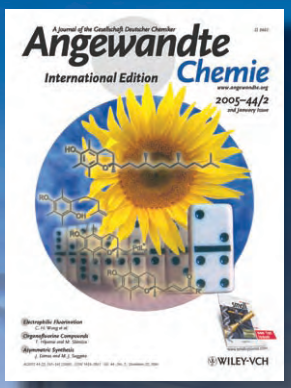

A Journal of the Gesellschaft Deutscher Chemiker

Angewandte
International Edition **Chemie**

www.angewandte.org

1888: ***The beginning of a success story***

Constant Innovations

1962: *First issue of the International Edition*
1976: *Graphical abstracts*
1979: *Cover pictures*
1988: *Centenary of Angewandte*
1989: *Routine use of color*
1991: *New section: Highlights*
1992: *Computerized editorial tracking system*
1995: *Internet service for readers*
1998: *Regular press service; full-text online*
2000: *New section: Essays; EarlyView: Communications available online ahead of the printed version*
2001: *New section: Minireviews*
2002: *Online submission of manuscripts*
2003: *Weekly publication; new section: News; new layout*
2004: *Backfiles (1962-1997); ManuscriptXpress: Online system for authors and referees*

Angewandte's advisors...

Rainer Metternich
Schering AG, Berlin

»***Angewandte Chemie*** *keeps me up to date on the top new developments in chemistry. I am engaged in drug discovery, and this high-quality journal covering breakthrough discoveries in interdisciplinary research, particularly in bioorganic chemistry, is of the highest relevance to me. Each issue of Angewandte provides an outstanding source for innovations.*«

Angewandte Chemie International Edition *is a journal of the German Chemical Society (GDCh)*

GDCh

WILEY InterScience® DISCOVER SOMETHING GREAT

WILEY-VCH

1804502_gu

It's not how short you make it, it's how you make it short! A diverse collection of compounds with short C–C single bonds whose lengths range from 1.32 Å to 1.46 Å have been theoretically designed (see structure of a "spiderane"). The strategies for squeezing the C–C bonds (encapsulation, strapping back, and stiffening) allow shorter bonds than hybridization and conjugative effects alone.

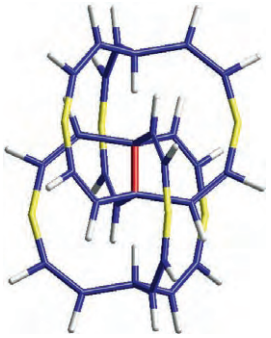

Carbon–Carbon Bonds

D. R. Huntley,* G. Markopoulos, P. M. Donovan, L. T. Scott, R. Hoffmann* ——— **7549 – 7553**

Squeezing C–C Bonds

A true convert: The carboxylesterase enzyme R.34 (see picture) can be converted into a triacylglycerol lipase without modification of the shape, size, or hydrophobicity of the substrate binding site. The substitution of Asn33 by Asp results in a salt bridge between the Asp33 and Arg49, which causes a distortion of the enzyme structure that makes the catalytic site more accessible to larger substrates but also more labile.

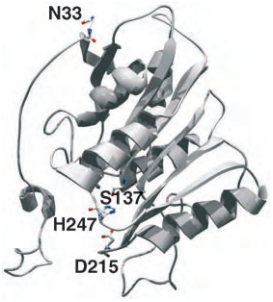

Enzyme Mutation

D. Reyes-Duarte, J. Polaina, N. López-Cortés, M. Alcalde, F. J. Plou, K. Elborough, A. Ballesteros, K. N. Timmis, P. N. Golyshin, M. Ferrer* ——— **7553 – 7557**

Conversion of a Carboxylesterase into a Triacylglycerol Lipase by a Random Mutation

---

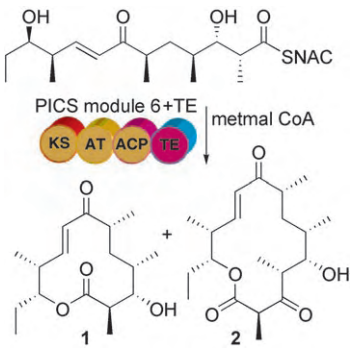

Dual action: An analogue of a natural hexaketide thioester substrate is incubated with recombinant picromycin/methymycin synthase (PICS) module 6 with its attached thioesterase (TE). A mixture of 12- and 14-membered-ring macrolactones 10-deoxymethynolide (**1**) and narbonolide (**2**) are generated (see scheme) by competing chain elongation and direct lactonization of the substrate. KS = ketosynthase, AT = methylmalonyl transferase, ACP = acyl carrier protein, metmal CoA = methylmalonyl coenzyme A.

Biosynthesis

J. Wu, W. He, C. Khosla, D. E. Cane* ——— **7557 – 7560**

Chain Elongation, Macrolactonization, and Hydrolysis of Natural and Reduced Hexaketide Substrates by the Picromycin/Methymycin Polyketide Synthase

---

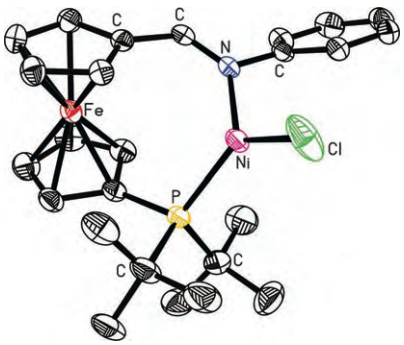

Three modes: An iminoferrocenylphosphane ligand stabilizes low-coordinate and low-valent nickel in [{[η-C_5H_4CH=N-(C_6H_5)]Fe[η-$C_5H_4P(t\mathrm{Bu})_2$]-*N*,*P*}$Ni^{I}Cl$] (see figure) and similar complexes. The coordination environment is hemilabile as exemplified by three different coordination modes: P,N(σ)-chelate, P,CN(π)-chelate, and P unidentate. These complexes are catalytically active towards ethylene oligomerization.

Nickel-Catalyzed Oligomerization

Z. Weng, S. Teo, L. L. Koh, T. S. A. Hor* ——— **7560 – 7564**

Ethylene Oligomerization at Coordinatively and Electronically Unsaturated Low-Valent Nickel

© 2005 Wiley-VCH Verlag GmbH & Co. KGaA, Weinheim

Contents

Asymmetric Hydrogenations

C. Moessner, C. Bolm* ____ **7564 – 7567**

Diphenylphosphanylsulfoximines as Ligands in Iridium-Catalyzed Asymmetric Imine Hydrogenations

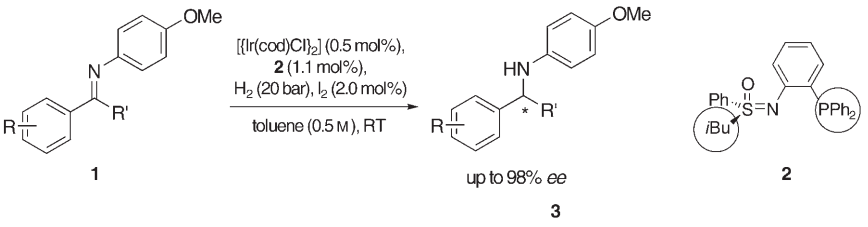

Easily accessible phosphine-substituted sulfoximines **2** have been applied in Ir-catalyzed asymmetric hydrogenations of acylic *N*-arylated imines **1**. The amines **3** are formed under mild conditions in high yields with excellent *ee* values.

Heterocycles

H. Nikawa, T. Nakahodo, T. Tsuchiya, T. Wakahara, G. M. A. Rahman, T. Akasaka,* Y. Maeda, M. T. H. Liu, A. Meguro, S. Kyushin, H. Matsumoto,* N. Mizorogi, S. Nagase* ____ **7567 – 7570**

S-Heterocyclic Carbene with a Disilane Backbone

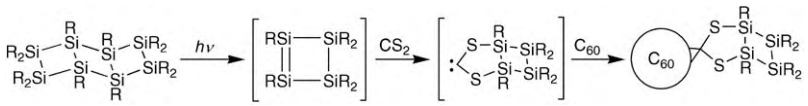

Caught in a trap! An S-heterocyclic carbene (SHC) with a cyclotetrasilane backbone is generated by a [2+3] cycloaddition of cyclotetrasilene with CS_2 and trapped with C_{60} as a chemical probe. It is demonstrated that photolysis of *anti*-dodecaisopropyltricyclo[4.2.0.0^{2,5}]octasilane and CS_2 in the presence of C_{60} affords a methanofullerene (see scheme).

Multicomponent Reactions

H. A. Dondas, C. W. G. Fishwick, X. Gai, R. Grigg,* C. Kilner, N. Dumrongchai, B. Kongkathip, N. Kongkathip, C. Polysuk, V. Sridharan ____ **7570 – 7574**

Stereoselective Palladium-Catalyzed Four-Component Cascade Synthesis of Pyrrolidinyl-, Pyrazolidinyl-, and Isoxazolidinyl Isoquinolines

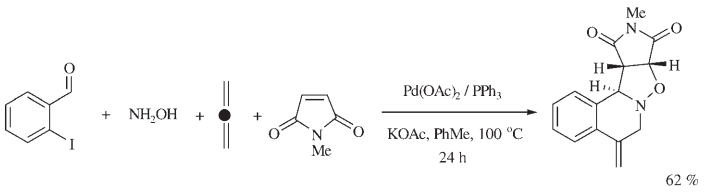

Two paths diverge: Four-component cascades that involve the cycloaddition of azomethine ylides, azomethine imines, or nitrones generated in situ, coupled with allene incorporation, give rise to five new bonds, two rings, and two to four stereocenters through two possible pathways (see picture for an example).

Template Synthesis

T. Magbitang, V. Y. Lee, J. N. Cha, H.-L. Wang, W. R. Chung, R. D. Miller, G. Dubois, W. Volksen, H.-C. Kim,* J. L. Hedrick* ____ **7574 – 7580**

Oriented Nanoporous Lamellar Organosilicates Templated from Topologically Unsymmetrical Dendritic-Linear Block Copolymers

Dendrimers between the sheets: Environmentally responsive dendritic-linear block copolymers, based on poly(ethylene oxide) and a dendron derived from 2,2′-bis(hydroxymethyl)propionic acid (see structure), were used to organize organosilicate vitrificates into nanostructured lamellar morphologies. Upon thermolysis of the template, a perforated porous lamellar structure (4 nm) between organosilicate sheets (6–9 nm) was obtained.

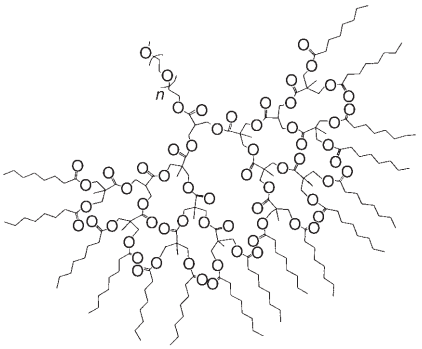

© 2005 Wiley-VCH Verlag GmbH & Co. KGaA, Weinheim

Sugar on a stick: A DNA template can bind two complementary oligonucleotides, one derivatized with glyceraldehyde (blue) and the other with glycolaldehyde (red), resulting in a cross-aldol reaction that forms pentose sugars. This reaction system serves as a model for the RNA-catalyzed synthesis of ribose, which is

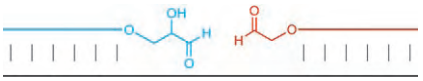

relevant to a presumed RNA-based metabolism during the early history of life on Earth.

Origin of Life

M. Oberhuber, G. F. Joyce* . **7580 – 7583**

A DNA-Templated Aldol Reaction as a Model for the Formation of Pentose Sugars in the RNA World

---

Negative beats positive: A channel composed of oligoether chains attached by amine groups to β-cyclodextrin mediates the transport of halides across a phospholipid bilayer (see scheme) at faster rates than those observed for monovalent cations. Protonation of the amine linkages likely explains the preferential anion transport.

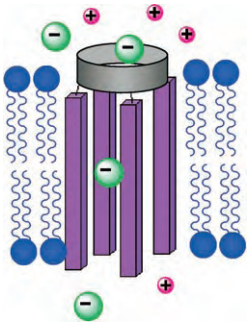

Ion Selectivity

N. Madhavan, E. C. Robert, M. S. Gin* **7584 – 7587**

A Highly Active Anion-Selective Aminocyclodextrin Ion Channel

---

Hot spots: The surprising, apparently catalytic effect of H_2 in the dehydrogenation of **1** in supercritical CO_2 is the result of thermal hot spots (see thermal image of reactor) generated in the catalyst bed by an initial exothermic hydrogenation. The localized heating forces the dehydrogenation reaction which also gives the diene **2** by a route that is potentially much simpler than the established procedure.

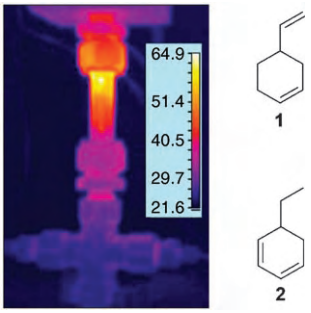

Heterogeneous Catalysis

J. R. Hyde,* B. Walsh, M. Poliakoff* **7588 – 7591**

"Hydrogen-Catalyzed" Dehydrogenation: A Supercritical Conundrum

---

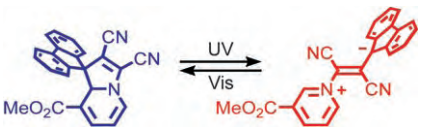

Very ANDy: A photochromic molecular switch has been found to act as an AND Boolean logic gate. The switch takes as input both UV light, which causes photoisomerization of a dihydroindolizine to an open, dipolar form, and an electric field, which aligns this isomer in solution (see scheme). The output of the gate is read as the electric linear dichroism response of the open isomer. The gate can be reset with visible light.

Molecular Electronics

J. Andréasson,* Y. Terazono, B. Albinsson, T. A. Moore,* A. L. Moore,* D. Gust* **7591 – 7594**

Molecular AND Logic Gate Based on Electric Dichroism of a Photochromic Dihydroindolizine

---

© 2005 Wiley-VCH Verlag GmbH & Co. KGaA, Weinheim

Contents

Coordination Chemistry

N. Chatterton, Y. Bretonnière, J. Pécaut, M. Mazzanti* _____ 7595 – 7598

An Efficient Design for the Rigid Assembly of Four Bidentate Chromophores in Water-Stable Highly Luminescent Lanthanide Complexes

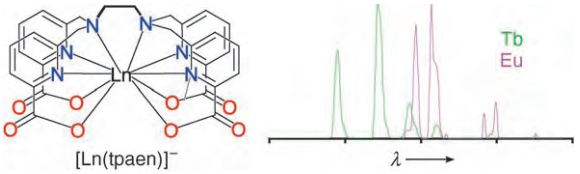

A simple bridge solves a difficult architectural problem. Ligand H_4tpaen, with an ethylenediamine backbone that has ten donor atoms, yields ten-coordinate lanthanide complexes, thus providing highly effective protection of the metal center from interaction with the solvent molecules. As a result, the Eu^{III} and Tb^{III} complexes of $(tpaen)^{4-}$ show a bright and long-lived luminescence in H_2O combined with high solubility and stability.

Ring Expansion

T. Miura, M. Shimada, M. Murakami* _____ 7598 – 7600

Acyl 1,3-Migration in Rhodium-Catalyzed Reactions of Acetylenic β-Ketoesters with Aryl Boronic Acids: Application to Two-Carbon-Atom Ring Expansions

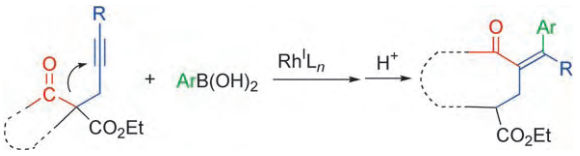

Expanding rings: An intermediate organorhodium(I) species formed in the Rh^I-catalyzed reaction of acetylenic β-ketoesters and β-diketones with aryl boronic acids undergoes intramolecular nucleophilic addition to a ketone carbonyl group. The ensuing ring-opening reaction of the resulting cyclobutanols results in acyl 1,3-migration leading to the development of a two-carbon-atom ring-expansion reaction.

Surface Chemistry

T. Schalow, M. Laurin, B. Brandt, S. Schauermann, S. Guimond, H. Kuhlenbeck, D. E. Starr, S. K. Shaikhutdinov, J. Libuda,* H.-J. Freund _____ 7601 – 7605

Oxygen Storage at the Metal/Oxide Interface of Catalyst Nanoparticles

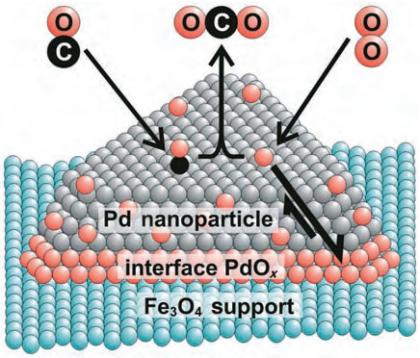

Holding its breath: Small Pd particles on an Fe_3O_4 support reversibly store large quantities of oxygen in the form of a thin Pd oxide layer at the particle/support interface. Oxygen from this reservoir can be released during oxidation reactions, as shown by a combination of molecular beam methods, scanning tunneling microscopy, and photoelectron spectroscopy.

Carbohydrate Synthesis

M. S. M. Timmer, A. Adibekian, P. H. Seeberger* _____ 7605 – 7607

Short De Novo Synthesis of Fully Functionalized Uronic Acid Monosaccharides

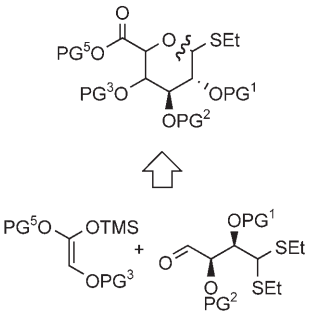

Short and Sweet: A convergent route leads to orthogonally protected D-glucuronic and L-iduronic acid thioglycoside building blocks, commonly used in heparin oligosaccharide assembly (see scheme). Rapid access to substantial quantities of these key intermediates feeds the growing need for monosaccharide building blocks for use in the assembly of bioactive oligosaccharides. PG = protecting group.

© 2005 Wiley-VCH Verlag GmbH & Co. KGaA, Weinheim

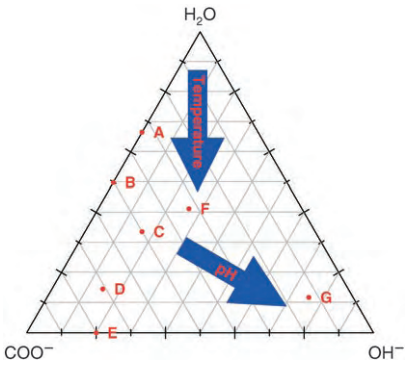

Four reaction parameters and their effects on the formation of cobalt succinate phases were studied by high-throughput methods. In addition to identifying two new phases, we show that higher reaction temperatures lead to products containing less water, more basic conditions favor increasingly condensed M-O-M networks (see phase diagram), and depending on the reaction time the products are formed under either kinetic or thermodynamic control.

High-Throughput Methods

P. M. Forster, N. Stock,*
A. K. Cheetham* ——— **7608 – 7611**

A High-Throughput Investigation of the Role of pH, Temperature, Concentration, and Time on the Synthesis of Hybrid Inorganic–Organic Materials

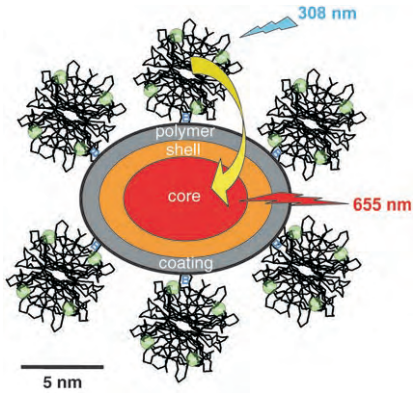

On the dot: Efficient energy transfer from Tb complexes to quantum dots with an extremely large Förster radius of 81 Å is achieved by formation of a streptavidin–biotin coupled donor–acceptor complex. The long luminescence lifetime of the Tb donor and the high absorption of the quantum dots make this couple a powerful tool for analyzing biological and biochemical interactions.

Bioanalysis

N. Hildebrandt,* L. J. Charbonnière,*
M. Beck, R. F. Ziessel,
H.-G. Löhmannsröben ——— **7612 – 7615**

Quantum Dots as Efficient Energy Acceptors in a Time-Resolved Fluoroimmunoassay

A new form of P: The crystal structure of a fibrous type of red phosphorus was solved using single-crystal X-ray diffraction methods and transmission electron microscopy. It consists of double tubes (see picture) and is closely related to the structure of Hittorf's phosphorus. Density functional calculations confirm the experimental results.

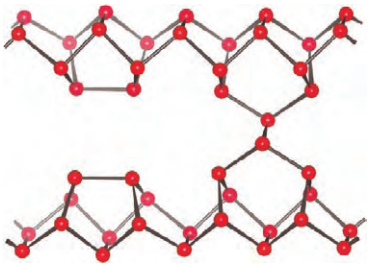

Solid-State Structures

M. Ruck,* D. Hoppe, B. Wahl, P. Simon,
Y. Wang, G. Seifert ——— **7616 – 7619**

Fibrous Red Phosphorus

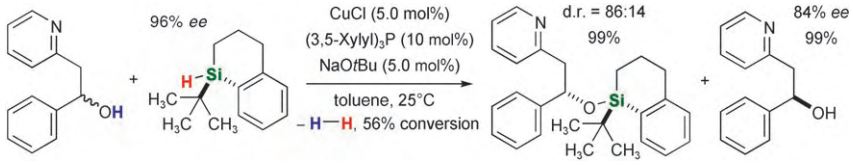

Fishing for enantiomers: A novel kinetic resolution of racemic alcohols capable of two-point binding makes use of silanes with silicon-centered chirality. This strategy is based on a diastereoselective dehydrogenative silicon–oxygen coupling under copper catalysis (see scheme). The resolving silane is completely recovered without erosion of stereochemical information at silicon.

Kinetic Resolution

S. Rendler, G. Auer,
M. Oestreich* ——— **7620 – 7624**

Kinetic Resolution of Chiral Secondary Alcohols by Dehydrogenative Coupling with Recyclable Silicon-Stereogenic Silanes

© 2005 Wiley-VCH Verlag GmbH & Co. KGaA, Weinheim

Contents

Antitumor Agents

S. Dziadek, D. Kowalczyk, H. Kunz* ——— **7624 – 7630**

Synthetic Vaccines Consisting of Tumor-Associated MUC1 Glycopeptide Antigens and Bovine Serum Albumin

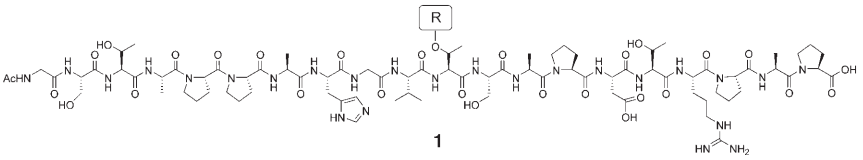

1

Sweet medicine: The mucin MUC1 is highly overexpressed on epithelial tumor cells. Glycopeptides **1** (from the repeating unit of MUC1) carrying various important sialylated tumor-associated carbohydrate antigens R were synthesized and coupled to bovine serum albumin (to generate anticancer vaccines) and to microtiter plates (to test the selectivity of the immune response).

Antitumor Agents

S. Dziadek, A. Hobel, E. Schmitt, H. Kunz* ——— **7630 – 7635**

A Fully Synthetic Vaccine Consisting of a Tumor-Associated Glycopeptide Antigen and a T-Cell Epitope for the Induction of a Highly Specific Humoral Immune Response

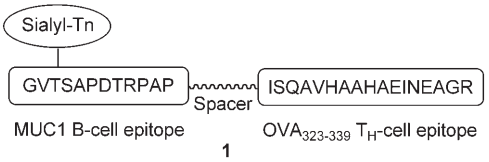

1

On target: With the fully synthetic vaccine **1** consisting of a tumor-associated sialyl-Tn glycopeptide antigen from the epithelial mucin MUC1 and a T-cell epitope from ovalbumin, a strong, highly specific immune response (IgG) directed against the glycopeptide antigen was induced in a mouse thereby realizing the most important requirement for the development of synthetic vaccines for the initiation of the body's own immune defense against tumors.

Bioanalysis

C. F. W. Becker,* R. Wacker, W. Bouschen, R. Seidel, B. Kolaric, P. Lang, H. Schroeder, O. Müller, C. M. Niemeyer, B. Spengler, R. S. Goody, M. Engelhard* ——— **7635 – 7639**

Direct Readout of Protein–Protein Interactions by Mass Spectrometry from Protein–DNA Microarrays

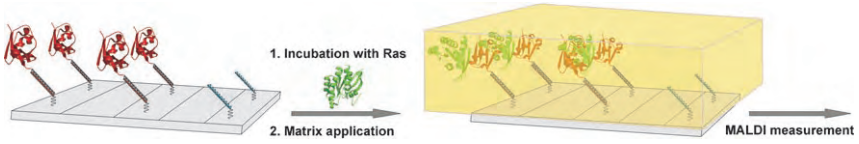

Catching proteins: Proteins from a protein–DNA microarray can be directly detected by using MALDI mass spectrometry. Capture proteins are attached to silicon chips in a highly selective and reversible way by DNA-directed immobilization (see picture). The analyte proteins bound specifically to their partners on the microarray can be detected from cell lysates.

Cluster Compounds

A. Karpov, M. Jansen* ——— **7639 – 7643**

$[Tl_8]^{6-}$ in Cs_8Tl_8O: A Naked Eight-Vertex *closo*-Deltaeder as a Cluster Anion

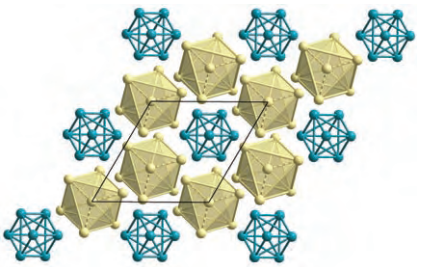

Structures to count on: The title compound crystallizes in a unique crystal-structure type which can be regarded as a rock-salt derivative composed of a suboxide group $[OCs_{6+2}]^{6+}$ (yellow) and a novel thallium cluster $[Tl_8]^{6-}$ (blue). The valence electron count of the eight-vertex cluster obeys the Wade–Mingos condensation rules when considering it as a condensation of an octahedron with two tetrahedra.

© 2005 Wiley-VCH Verlag GmbH & Co. KGaA, Weinheim

Looking for outstanding employees?

Do you need another expert for your excellent team?
...Chemists, PhD Students, Managers, Professors, Sales Representatives...

Place an advert in the printed version and have it made available online for 1 month, free of charge!

Angewandte Chemie International Edition
Advertising Sales Department: Marion Schulz
Phone: 0 62 01 - 60 65 65
Fax: 0 62 01 - 60 65 50
E-Mail: MSchulz@wiley-vch.de

Service

Keywords ____ *7644*

Authors ____ *7645*

Angewandte's Sister Journals ____ *7646*

Preview ____ *7647*

Concise Insight of 20 Years of Research

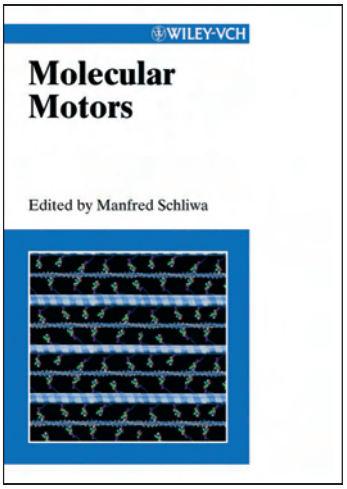

2002. XXII, 582 pages, 129 figures 48 in color, 20 tables. Hardcover. ISBN 3-527-30594-7
€ 179.- /£ 125.- /US$ 245.-

MANFRED SCHLIWA, University of Munich, Germany (Ed.)

Molecular Motors

Cell motility, virus transport and developmental asymmetry are examples of biological processes related to the function or malfunction of the minute machinery of molecular motors. This handbook brings together current knowledge on the functionality, regulation, and interactions of cytoskeletal, DNA, and rotary motors. Leading experts present principles and applications ranging from atomic structure, biochemistry, and biophysics to cell biology, developmental biology and pathology - all set to become a "classic" in the years to come.

"...essential reading for graduate students in the field of cell motility and molecular motors... recommend it enthusiastically..."
- Nature Cell Biology

22540509_kn

Register now for the free
WILEY-VCH Newsletter!
www.wiley-vch.de/home/pas

WILEY-VCH • P.O. Box 10 11 61 • D-69451 Weinheim, Germany
Fax: +49 (0) 62 01 - 60 61 84
e-mail: service@wiley-vch.de • http://www.wiley-vch.de

WILEY-VCH

© 2005 Wiley-VCH Verlag GmbH & Co. KGaA, Weinheim

Macromolecular Metal Complexes: Materials for Various Applications**

Dieter Wöhrle*

The variety of metals used by biological systems is very large and ranges from the alkali metals to the transition metals. They play an essential role in living systems, both in growth and metabolism. Examples include hemes as oxygen-carrier systems, chlorophylls as energy-conversion systems in photosynthesis, and metalloenzymes for various catalytic reactions. In living systems, metal ions can coordinate, or metal clusters are stabilized by a variety of biopolymers through covalent, ionic, or coordinative interactions. Nature shows how complicated it is to construct metal-containing macromolecules that are not only active but also selective with respect to a specific property. Therefore it is of great interest to synthesize artificial combinations of metal atoms/ions, ligands, and macromolecules with the aim to obtain new materials that exhibit a variety of properties. The first results on thermally stable polymer complexes and chelate-forming resins were published in the 1960s, while more intensive research began to stem from this towards the late 1970s/early 1980s. The first International Symposium on Macromolecule–Metal Complexes was held in 1985. In September 2005, the 11th IUPAC International Symposium organized by F. Ciardelli (University of Pisa) took place in Tirrenia (Pisa, Italy). Around 170 participants from 30 countries demonstrated the increasing interest and progress in this field, with contributions that focused on the different kinds of combinations of metal atoms/ions with organic or inorganic macromolecules.

As a result of the increasing number of new macromolecular metal complexes reported, a clear and simple classification is necessary.[1] Type I complexes consider the covalent, coordinative, or ionic binding of metal ions or complexes to linear or cross-linked macromolecules. In type II and type III complexes, the ligand or the metal, respectively, are integrated into a linear or cross-linked macromolecule thus giving the macromolecular backbone. Complexes of type IV include the physical incorporation of metal complexes or metal nanoparticles in macromolecules.

The groups of E. Tsuchida and H. Nishide (Tokyo, Japan) discussed the interaction of oxygen from air with metal porphyrins in macromolecules. Human serum albumin (HSA)—the plasma protein in our bloodstream—was modified by a proximal histidine in a subdomain, and then synthetic heme derivatives were incorporated. Dimeric and tetrameric clusters of this modified HSA can include 32 heme molecules. Tsuchida and T. Komatsu showed that this artificial hemoprotein binds and release O_2 in similar fashion to hemoglobin. This O_2-carrying plasma albumin is of importance not only for red-cell substitutes but also for O_2 therapeutic reagents (Figure 1).[2] Also, cobalt(II) porphyrin derivatives were coordinatively bound to poly(octyl methacrylate-co-vinylimidazole) or incorporated into Nafion (fluorinated sulfonic acid copolymers). Nishide demonstrated that membranes of these polymers containing the Co porphyrin act as oxygen carriers, transport oxygen through the membrane, and therefore can be used to separate O_2 from air. With one separation, O_2 in air was enriched from 21% to over 90%.[1]

The use of macromolecular metal complexes not only for binding of small molecules but also for their activation in catalytic reactions is of great industrial interest.[1] One of the promising trends in catalyst design is the use of water-soluble macromolecular metal complexes, as this allows the catalytic reaction to be carried out in a two-phase system, with the macromolecular catalyst in the aqueous phase and the reagents and reaction products in an organic phase. This process gives rise to catalytic activities that are similar to those observed in a homogeneous phase, with the added advantages of facile separation of reaction products and easy reuse of the aqueous solution of the catalyst. E. A. Karakhanov and A. Maksimov (Moscow, Russia) showed that water-soluble block copolymers of ethylene oxide–propylene oxide, dendrimers, or cyclodextrins are suitable carriers for transition-metal catalysts, as used successfully in oxidation, hydroxylation, hydrogenation, hydroformylation, and carbonylation reactions.[1] An interesting development is the use of natural macromolecules as carriers for artificial catalysts. One example is the cationic *meso*-tetrakis(4-*N*-methylpyridyl)porphyrin and its analogues, which are known to bind to DNA. H. Yamaguchi and A. Harada (Osaka, Japan) bound the Fe^{II} complex of this porphyrin to the monoclonal antibody 12E11G. This macromolecular metal complex displays remarkable activity in the oxidation of catechol, guajacol, and pyrogallol in the presence of H_2O_2 (Figure 2),[3] and exhibits a peroxidase activity that lies in the same order as that of horseradish peroxidase while

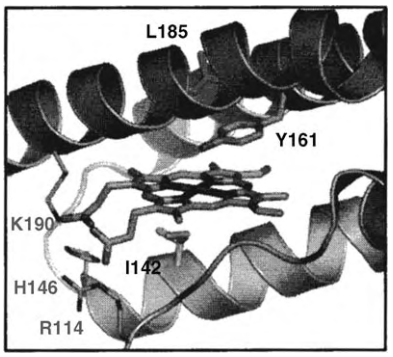

Figure 1. Synthetic heme group complexed within the heme pocket in the subdomain of an rHSA mutant (from crystal structure analysis).

[*] Prof. Dr. D. Wöhrle
Universität Bremen
Institut für Organische und Makromolekulare Chemie
P.O. Box 330404
28334 Bremen (Germany)
Fax (+49) 218-4935
E-mail: woehrle@chemie.uni-bremen.de

[**] 11th IUPAC "International Symposium on Macromolecule–Metal Complexes", Tirrenia/Pisa (Italy), September 10–13, 2005.

WILEY InterScience DISCOVER SOMETHING GREAT
© 2005 Wiley-VCH Verlag GmbH & Co. KGaA, Weinheim

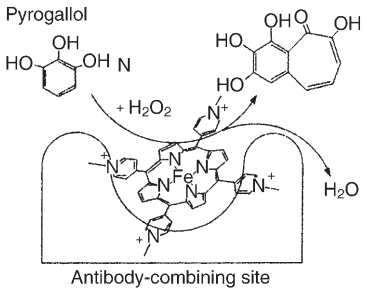

Figure 2. The complex between an antibody and a cationic Fe^{II} porphyrin, and its catalytic activity in the oxidation of pyrogallol.

showing a better stability than the natural system.

A more classical field of practical application is the binding of transition-metal ions to macromolecules for the cleaning of waste water, soils, and so on.[1] Several contributions pointed out improvements in the selectivity of metal-ion separation by using new ligands and better technologies for metal-ion binding. E. Rosenberg (Missoula, USA) optimized silica–polyamine composites by silylation of silica gel and subsequent reaction with polyamines. The average pore size of silica is critical for good performances of the gel, while the structure and the molecular weight of the polymer have a greater influence on the metal selectivity. Elsewhere, A. Kaledkowski (Wroclaw, Poland) introduced a calix[4]pyrrole[2]thiophene ligand. After binding the ligand to cross-linked polystyrene, the obtained resin shows distribution coefficients for noble-metal ions (Pt, Ag, Au) of two to four orders of magnitude greater than those observed for cations of other transition-metal ions. One of the most promising techniques for the removal of metal ions from waste water is by membrane ultrafiltration in a method known as liquid-phase polymer-based retention (LPR). Water-soluble polymers with different chelating groups of high affinity for transition-metal ions have been investigated by the LPR technique (B. L. Rivas, Concepcion, Chile; R. Molinari, Rende, Italy).[4]

With regards to type II macromolecular metal complexes, C. Lo Sterzo and co-workers (Teramo, Italy) have developed a multistep one-pot Pd-promoted synthetic strategy for the synthesis of poly(aryleneethynylene) copolymers of the general structure $[-C{\equiv}C-A-C{\equiv}C-B-]_n$, with A = 2,5-dialkoxy-substituted 1,4-phenylenes and B = substituted thiophenes, porphyrins, phenanthrolines, etc. Block A is in charge of the mechanical stability and processability, whereas block B is responsible for functional properties of the materials. Through appropriate choice of block B, functional materials that are interesting for sensoric and electronic applications have been obtained.[5]

Self-assembly to obtain type III polymers with one-dimensional architectures is a promising bottom-up strategy for nanocircuits. N. Kimizuka (Fukuoka, Japan) described supramolecular lipid Pt^{II}/Pt^{IV} complexes that spontaneously self-assemble in solution into 1D nanowires.[6] Also, the lipophilic triazole complexes $[M^{II}(\mathbf{1})_3](BF_4^-)_2$ (M = Fe, Co; **1** = azobenzene-substituted triazole moiety) self-assemble in solution in chloroform (Figure 3) and give heat-set gel-like networks. Nanofibers of the Fe complex have a width of 6 nm (the diameter of one chain) and a length of approximately 100 nm. Upon UV irradiation, reversible *trans* to *cis* isomerization of the azo group occurs and the fibrous nanostructures are transformed to irregular grains. This nanoswitching is interesting for the dynamic control of electromagnetic properties. S. Higuchi (Tsukuba, Japan) reported the self-assembly of polymers prepared from 1,4-bis(terpyridyl)benzene and Fe^{II} or Co^{II} to give metallosupramolecular polyelectrolytes, which are interesting for their reversible color change by oxidation/re-reduction processes.

Type IV polymers are used in bilayer photoreptor devices of laser printers, in which titanyl phthalocyanine clusters in polymers act as photoconductors (> 90% quantum yield of photocurrent). D. Wöhrle (Bremen, Germany) reported the preparation of thin films of polymers that contain carefully designed and monomolecular-distributed phthalocyanines. These metal complexes are among the most active known compounds for optical limiting (OL), which is a third-order nonlinear optical (NLO) property.[7] The transmission of light for an optical limiter is high at normal light intensities and low for intense beams which is interesting for the protection of eyes, optical elements, and optical sensors from intense laser pulses. It was recently found that the OL properties of phthalocyanines in multilayer films of PMMA and PVC are, in most cases, better than in solution. A field of increasing interest is metal nanoparticles in polymers, and progress in this area is described in recently published books.[8] P. A. G. Cormack (Glasgow, UK) described the synthesis of multicomponent particles in which dyes are first adsorbed onto silver colloidal nanoparticles. These modified particles are then encapsulated into cross-linked polystyrene beads followed by modification at the surface of the beads (diameter ≈ 1 μm) with functional groups (Figure 4).[9] After the binding of target oligonucleotides, a complementary DNA can interact with the modified surface. Surface-enhanced resonance Raman scattering (SERRS), which is a more sensitive technique than fluorescence by approximately three orders of magnitude, allows analysis of the DNA.

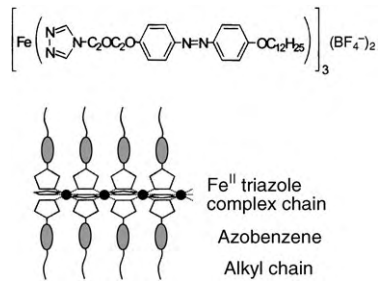

Figure 3. 1D chain of the photoresponsive iron(II) 1,2,4-triazole complex with azobenzene chromophores in the lipophilic chains.

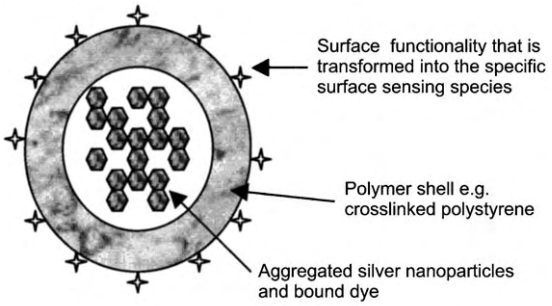

Figure 4. The encapsulation of dye-labeled Ag nanoparticles within a functionalized polymer core that allow detection by SERRS.

© 2005 Wiley-VCH Verlag GmbH & Co. KGaA, Weinheim

The reports at the conference showed impressively the rapid development of this interdisciplinary field of material science. On the one hand, more classical applications such as metal-ion binding and catalysis have been further improved. On the other hand, new supramolecular structures that include the metal and display interesting properties are obtained by self-assembly. The main contributions of this conference will be published in a special volume of *Macromolecular Symposia* (Wiley-VCH) in 2006.

[1] D. Wöhrle, A. D. Pomogailo, *Metal Complexes and Metals in Macromolecules*, Wiley-VCH, Weinheim, **2003**.

[2] T. Komatsu, N. Ohmichi, P. A. Zunszain, S. Curry, E. Tsuchida, *J. Am. Chem. Soc.* **2004**, *126*, 14304.

[3] H. Yamaguchi, K. Tsubouchi, K. Kawaguchi, E. Horita, A. Harada, *Chem. Eur. J.* **2004**, *10*, 6179.

[4] a) B. L. Rivas, E. D. Pereira, I. Moreno, *Prog. Polym. Sci.* **2003**, *28*, 173; b) R. Molinari, S. Gallo, P. Augurio, *Water Res.* **2004**, *38*, 593.

[5] A. Micozzi, M. Ottaviani, C. Lo Sterzo, *Adv. Synth. Catal.* **2005**, *347*, 143.

[6] K. Kuroiwa, T. Shibata, A. Takada, N. Nemoto, N. Kimizuka, *J. Am. Chem. Soc.* **2004**, *126*, 2016.

[7] S. M. O'Flaherty, S. V. Hold, M. J. Cook, T. Torres, Y. Chen, M. Hanack, W. J. Blau, *Adv. Mater.* **2003**, *15*, 19.

[8] a) A. D. Pomogailo, V. N. Kestelmann, *Metallopolymer Nanocomposites*, Springer, Berlin, **2005**; b) L. Nicolais, G. Carotenuto, *Metal–Polymer Nanocomposites*, Wiley, New York, **2005**.

[9] A. F. McCabe, C. Eliasson, R. A. Prasath, A. Hernandet-Santana, I. Apple, P. A. G. Cormack, *Faraday Discuss.* **2005**, *132*, in press.

DOI: 10.1002/anie.200503544

2005

Highlights 2005:

- Now 18 issues
- 4700 pages
- **Online Manuscript Submission Service**
- EarlyView® online publication
- Supplementary material (e.g. extensive tables) published online
- Indexed in Medline, ISI and other databases
- **Topical Special Issues**

For ordering information please contact:

Wiley-VCH
E-MAIL: service@wiley-vch.de
INTERNET: www.wiley-vch.de

John Wiley & Sons, Inc.
E-MAIL: subinfo@wiley.com
INTERNET: www.wiley.com

John Wiley & Sons, Ltd
E-MAIL: cs-journals@wiley.co.uk
INTERNET: www.wiley.com

WILEY InterScience® DISCOVER SOMETHING GREAT

15292410_vo

Dominating the Field of Proteomics

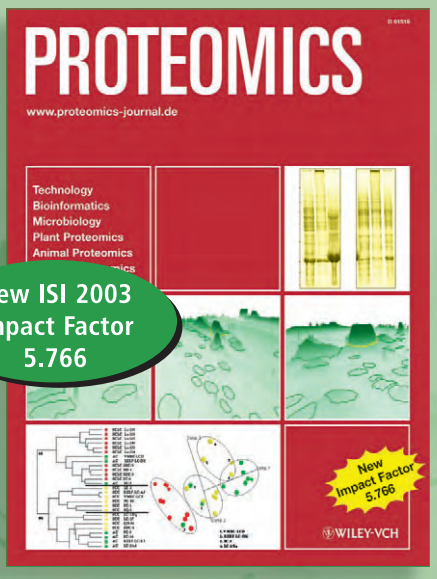

New ISI 2003 Impact Factor 5.766

2005 Volume 5 18 issues
ISSN Print 1615-9853
ISSN Electronic 1615-9861

PROTEOMICS is the premier international source for information on all aspects of applications and technologies in proteomics.

For more information, or access to an online sample copy, please visit
www.proteomics-journal.de

WILEY-VCH

WILEY

© 2005 Wiley-VCH Verlag GmbH & Co. KGaA, Weinheim

Organocatalysis

DOI: 10.1002/anie.200502617

Extending Mechanistic Routes in Heterazolium Catalysis–Promising Concepts for Versatile Synthetic Methods**

*Kirsten Zeitler**

Keywords:
aldehydes · carbenes · nitrogen heterocycles · stereoselective catalysis · umpolung

In the development of sustainable chemical transformations, the discovery of new, efficient synthetic methods, especially for carbon–carbon bond formation, remains a great challenge. Organocatalytic processes mediated by small nucleophilic molecules have gained in importance enormously over the last few years.[1] Their benefits include not only atom economy and operational simplicity, but also the possibility of nontraditional retrosynthetic bond disconnections. A powerful example for such a strategy is the inversion of reactivity of functional groups (umpolung).[2] The catalytic version of this concept was first discovered in the context of benzoin reactions[3] and has led together with the extention to the Stetter reaction to highly valuable asymmetric methods, even for the construction of quaternary stereocenters.[4,5]

The use of functionalized aldehydes as donor substrates in N-heterocyclic carbene (NHC)-catalyzed umpolung reactions opens new mechanistic pathways and gives rise to new synthetic strategies (Scheme 1). Alkenes and other reducible functional groups have been employed successfully so far to generate subsequent electrophilic character at the previously umpoled carbonyl carbon.

The covalent activation of aldehydes and α-keto acids[6] as acyl anion equivalents through addition of nucleophilic, heterazolium-derived carbene **2** leads to the so-called Breslow intermediate **5** (Scheme 2).[3b,7] Depending on the kind of electrophile applied, benzoins or 1,4-dicarbonyls **15** (Stetter reaction) are formed (cycle **A**).[8]

Based on mechanistic considerations starting from the nucleophilic alkene **5**, the scope and utility of this umpolung can be extended by the use of further functionalized donor substrates that allow the subsequent formation of an acyl

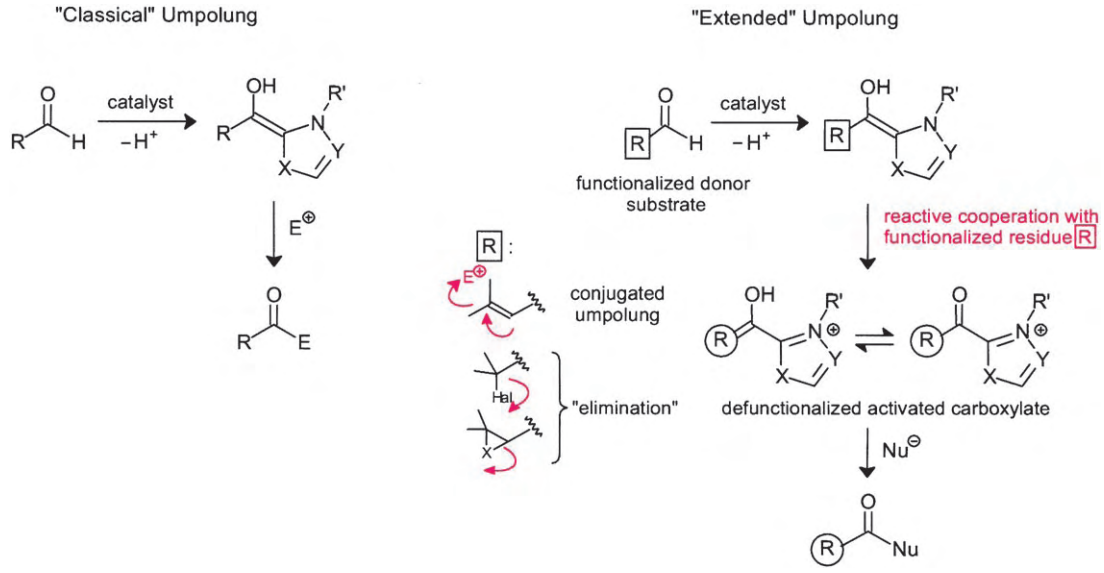

Scheme 1. Comparison of classical versus extended heterazolium catalysis.

[*] Dr. K. Zeitler
Institut für Organische Chemie
Universität Regensburg
Universitätsstrasse 31
93053 Regensburg (Germany)
Fax: (+49) 941-943-4121
E-mail:
kirsten.zeitler@chemie.uni-regensburg.de

[**] The author is indebted to the Fonds der Chemischen Industrie for a Liebig fellowship.

InterScience
© 2005 Wiley-VCH Verlag GmbH & Co. KGaA, Weinheim

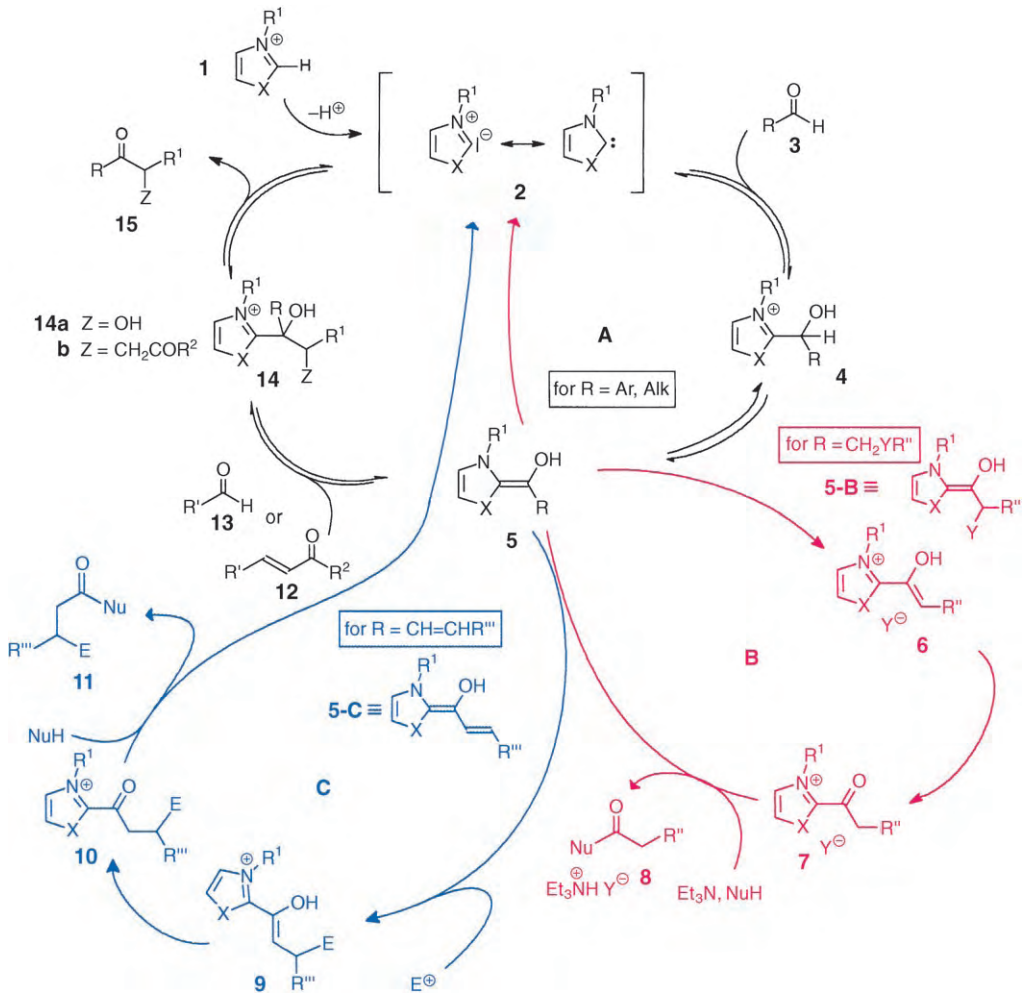

Scheme 2. Mechanistic considerations for extended reaction pathways.

azolium species, i.e. activated carboxylates **7** and **10**. This key intermediate can be formed by means of an internal redox reaction (cycle **B**) from α-heteroatomic aldehydes, such as α-halo aldehydes[11] and α,β-epoxy aldehydes[12] **5-B** by elimination of the leaving group Y through enol **6** followed by isomerization to give the corresponding acyl azolium tautomer **7**. Alternatively, the acyl azolium species arises from α,β-unsaturated aldehydes via a conjugated ("vinylogous") acyl anion equivalent **5-C** (cycle **C**).[11] This homoenolate **5-C** can undergo electrophilic trapping with subsequent tautomerization to form the pivotal catalyst-bound activated ester **10**. Reaction with appropriate nucleophiles (inter- or intramolecular) yields carboxylic acid derivatives **8** or **11**, and regenerates the catalyst **2**.

Bode et al. recently developed a direct stereoselective, catalytic method for the generation of *anti*-β-hydroxy esters from epoxy aldehydes using thiazolium precatalysts.[12] Aromatic and aliphatic epoxy aldehydes **16** react with alcohols to provide the desired esters **18** in good yield and stereoselectivity under mild conditions (Scheme 3). If one considers reaction pathway **B** (Scheme 2), the activated carboxylate **7** is formed by an epoxide-opening step from intermediate **5-B**. The synthesis of *N*-tosyl-β-amino esters from α,β-aziridinyl-aldehydes under similar conditions greatly extends the scope of this esterification approach.

Concurrently, Rovis et al. found that secondary and tertiary α-halo aldehydes provide access to dehalogenated acyl azolium species **7** (Scheme 2, pathway **B**) catalyzed by thiazolium- or triazolium-derived nucleophilic carbenes.[11] The possible nucleophiles for the interception of these acylation agents range from primary and secondary alcohols

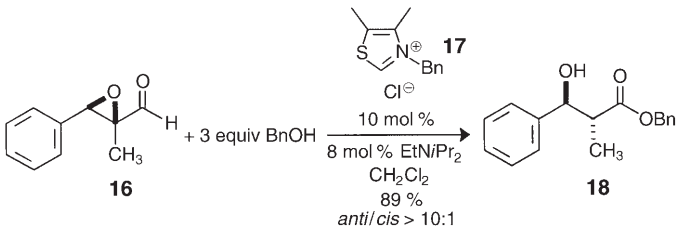

Scheme 3. Stereoselective synthesis of β-hydroxy esters from epoxy aldehydes. Bn = benzyl.

© 2005 Wiley-VCH Verlag GmbH & Co. KGaA, Weinheim

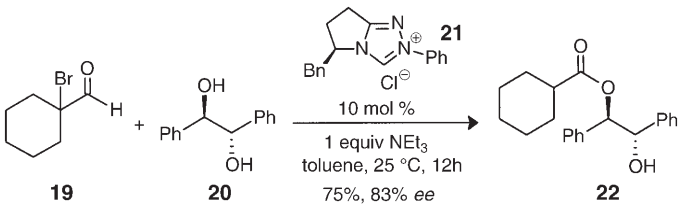

Scheme 4. Desymmetrization of *meso* diols.

(with tolerance of epimerizable stereocenters) to phenols and anilines. The use of chiral triazolium catalyst **21** allows the desymmetrization of *meso* diols **20** (Scheme 4). Interestingly, although they used reaction conditions similar to those for benzoin reactions, neither Bode nor Rovis could observe the formation of significant amounts of the corresponding benzoin or acyloin products.

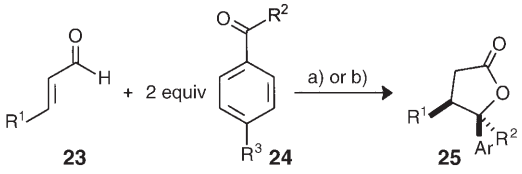

Scheme 5. Organocatalyzed conjugate umpolung for the synthesis of γ-butyrolactones. Reaction conditions: a) R^1 = Ph; R^2 = H; R^3 = Br, CO_2Me; 8 mol% IMes·HCl, 7 mol% DBU, THF/*t*BuOH 10:1, >79%, d.r. >4:1. b) R^1 = Ph; R^2 = CF_3; R^3 = H. 5 mol% IMes·HCl, 10 mol% KO*t*Bu, THF, 84%, d.r. 2:1. Mes = 2,4,6-trimethylphenyl, DBU = 1,8-diazabicyclo[5.4.0]undec-7-ene.

The synthetic utility of the conjugated umpolung (Scheme 2, cycle **C**) as an alternative pathway in heterazolium catalysis was illustrated by Bode et al.[13a] and Glorius et al.,[13b] who independently developed a direct, organocatalytic annulation of enals **23** with aldehydes **24**. Under remarkably mild conditions the stereoselective synthesis of γ-butyrolactones **25** was achieved in a flexible one-step process via homoenolate intermediates generated by sterically demanding imidazolium ylides as catalysts (Scheme 5). The conjugated acyl anion equivalent **5-C** couples with an aldehyde to yield an alkoxide intermediate, which is trapped intramolecularly by the catalyst-bound activated ester. A survey of different catalysts showed the high preference for imidazolium salts; thiazolium precursors proved to be inefficient. Whereas a wide range of enals can be used as the nucleophile, the electrophilic partner has been limited to aromatic aldehydes and trifluoromethylaryl ketones. The configuration of the product is preferrably *cis* (d.r. up to 5:1), but the stereochemical outcome is influenced by substrate, reaction conditions, and catalyst structure. The generation of quaternary stereocenters from ketone electrophiles was catalyzed by a tricyclic imidazolium-derived NHC to give a diastereomeric ratio of 3:1 (like/unlike) with 12% and 25% *ee*.[13b]

The scope of the nucleophile-catalyzed generation of homoenolates from α,β-unsaturated aldehydes was only recently extended by Bode et al.[14] In a mechanistically similar process using imines as the electrophilic partner, the direct annulation of enals **23** with *N*-4-methoxybenzenesulfonylimines **26** followed by cyclization led to disubstituted γ-lactams **27** in good yield and good to moderate diastereomeric ratios (Scheme 6). It has to be noted that there is only a narrow range of suitable imine substrates (e.g. electron-rich *N*-sulfonyl imines) as they compete to react with nucleophilic catalyst. This one-pot procedure provides a fast access to the important class of γ-butyrolactams, and by nucleophilic ring-opening with alkoxides γ-amino acid derivatives are readily available.

Scheidt et al. have shown that the reactivity of these NHC-generated homoenolates is not restricted to the coupling with aldehydes and imines as electrophiles and the subsequent intramolecular nucleophilic attack of the resulting heteroanions (alkoxides and amides, respectively) on the acyl azolium species.[13c] The electrophilic and nucleophilic partners could be decoupled by using phenol derivatives as the proton source in combination with DBU and imidazolium salts in the presence of a second alcohol as nucleophile. In this context, Bode et al. only very recently reported on the product-determining effect of the base for the subsequent reactions of catalytically generated homoenolates **5-C**.[13d] While strong bases such as KO*t*Bu predominately lead to carbon–carbon bond formation, the use of weaker bases acting as a catalytic proton shuttle promotes in situ protonation of the homoenolate without an additional proton source (Scheme 7). Application of substoichiometric amounts of the triazolium precatalyst **28**, which is more readily deprotonated than other NHC precursors, leads to the catalytic, atom-economical redox esterification of a wide variety of enals **23** with alcohols R^2OH as nucleophiles in good to high yields (Scheme 7; optimized conditions).

Whereas the use of classical nitrogen-based nucleophiles (e.g. sulfonamides, azides, anilines) under Scheidt's conditions seems to be difficult in the complex balance of acid and base in this process, the use of chiral imidazolium salts allows enantiodiscrimination. With the participation of a chiral activated ester as a possible intermediate, the organocatalytic kinetic resolution of racemic 1-phenylethanol (**31**) was achieved with cinnamaldehyde (**32**) (Scheme 8).

In situ generated N-heterocyclic carbenes are also potent catalysts for trans-

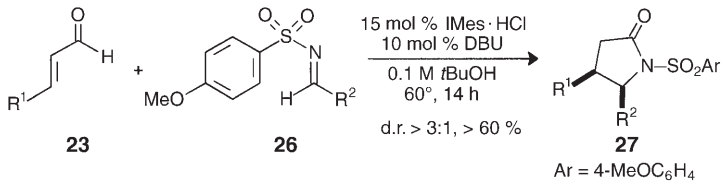

Scheme 6. Organocatalytic direct annulation to give γ-lactams. R^1 = Ph, Ar; R^2 = Ar, alkenyl.

 © 2005 Wiley-VCH Verlag GmbH & Co. KGaA, Weinheim

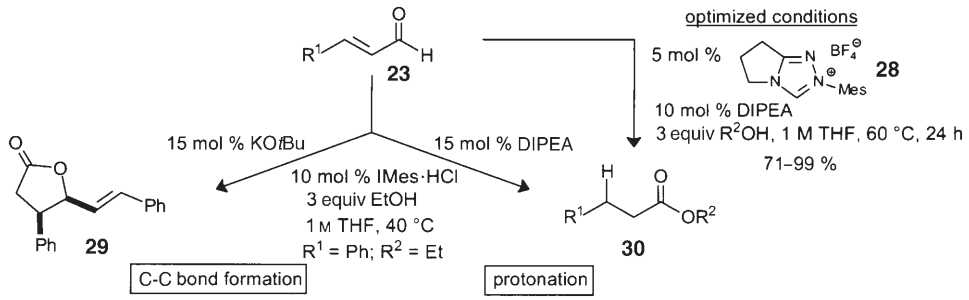

Scheme 7. Product-determining role of the base in the catalytic redox esterification.

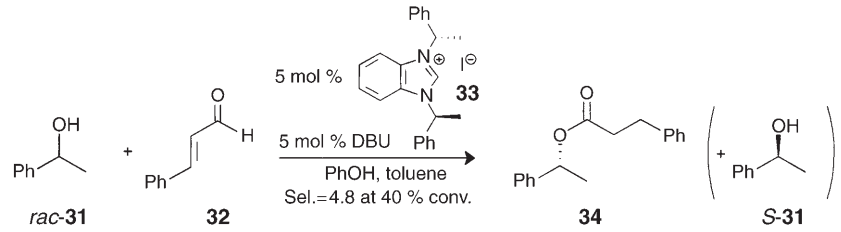

Scheme 8. Kinetic resolution of secondary alcohols by a discriminating homoenolate intermediate.

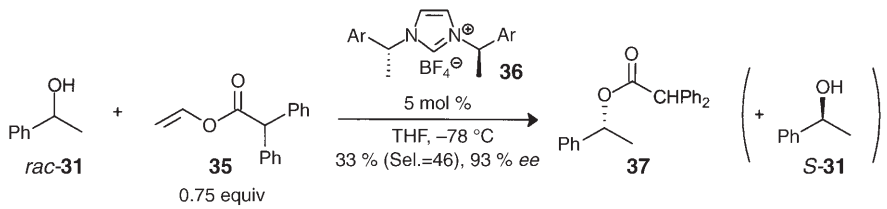

Scheme 9. Enantioselective acylation of secondary alcohols with N-heterocyclic carbenes.

esterifications[15] and ring-opening polymerization reactions. In these related processes, similarily activated carboxylates, formed from NHCs and ester or lactone precursors, are thought to be the pivotal intermediates.[16] An application of this concept to a nonenzymatic kinetic resolution has been published recently.[17,18] Chiral imidazolylidene catalysts **36** mediate a highly enantioselective transesterification of racemic secondary alcohols with vinyl esters without required stoichiometric amounts of base (Scheme 9).[18]

Not only the synthetic utility of the accessible products, but also the unique reactivity of these catalytically generated nucleophilic precursors and their subsequent electrophilic character should motivate chemists for further novel developments on this versatile mechanistic platform. Deeper insights into the mechanism and the possible combinations of electrophiles and nucleophiles should smooth the way for useful applications and further innovations in carbene-catalyzed reactions. These versatile concepts and the ample scope of possible substrates may lead to the catalytic, enantioselective, and sustainable synthesis of highly valuable, multifunctionalized molecules.

[1] a) P. I. Dalko, L. Moisan, *Angew. Chem.* **2001**, *113*, 3840–3864; *Angew. Chem. Int. Ed.* **2001**, *40*, 3726–3748; b) P. I. Dalko, L. Moisan, *Angew. Chem.* **2004**, *116*, 5248–5286; *Angew. Chem. Int. Ed.* **2004**, *43*, 5138–5175; c) J. Seayad, B. List, *Org. Biomol. Chem.* **2005**, *3*, 719–724; d) A. Berkessel, H. Gröger, *Asymmetric Organocatalysis*, Wiley-VCH, Weinheim, **2005**.

[2] D. Seebach, *Angew. Chem.* **1979**, *91*, 259–278; *Angew. Chem. Int. Ed. Engl.* **1979**, *18*, 239–258.

[3] a) T. Ukai, R. Tanaka, T. Dokawa, *J. Pharm. Soc. Jpn.* **1943**, *63*, 296–304; b) R. Breslow, *J. Am. Chem. Soc.* **1958**, *80*, 3719–3725.

[4] a) D. Enders, T. Balensiefer, *Acc. Chem. Res.* **2004**, *37*, 534–541. For general references on NHCs as ligands and reagents see: b) A. J. Arduengo III, R. Krafczyk, R. Schmutzler, H. A. Craig, J. R. Goerlich, W. J. Marshall, M. Unverzagt, *Tetrahedron* **1999**, *55*, 14523–14534; c) V. César, S. Bellemin-Laponnaz, L. H. Gade, *Chem. Soc. Rev.* **2004**, *33*, 619–636; d) V. Nair, S. Bindu, V. Sreekumar, *Angew. Chem.* **2004**, *116*, 5240–5245; *Angew. Chem. Int. Ed.* **2004**, *43*, 5130–5135.

[5] M. Christmann, *Angew. Chem.* **2005**, *117*, 2688–2690; *Angew. Chem. Int. Ed.* **2005**, *44*, 2632–2634.

[6] H. Stetter, G. Lorenz, *Chem. Ber.* **1985**, *115*, 1115–1125.

[7] R. Breslow, C. Schmuck, *Tetrahedron Lett.* **1996**, *37*, 8241–8242.

[8] Less common electrophiles are acylimines,[9] which were successfully employed recently in an asymmetric variation of this reaction mediated by a peptide-derived catalyst,[9c] and also electron-poor arenes that undergo S_NAr reactions.[10]

[9] a) J. A. Murry, D. E. Frantz, A. Soheili, R. Tillyer, E. J. J. Grabowski, P. J. Reider, *J. Am. Chem. Soc.* **2001**, *123*, 9696–9697; b) D. E. Frantz, L. Morency, A. Soheili, J. A. Murry, E. J. J. Grabowski, R. D. Tillyer, *Org. Lett.* **2003**, *5*, 843–846; c) S. M. Mennen, J. D. Gipson, Y. R. Kim, S. J. Miller, *J. Am. Chem. Soc.* **2005**, *127*, 1654–1655.

[10] A. Suzuki, T. Toyota, F. Imada, S. Masayuki, A. Miyashita, *Chem. Commun.* **2003**, 1314–1315.

[11] N. T. Reynolds, J. Read de Alaniz, T. Rovis, *J. Am. Chem. Soc.* **2004**, *126*, 9518–9519.

[12] K. Y.-K. Chow, J. W. Bode, *J. Am. Chem. Soc.* **2004**, *126*, 8126–8127.

[13] a) S. S. Sohn, E. L. Rosen, J. W. Bode, *J. Am. Chem. Soc.* **2004**, *126*, 14370–14371; b) F. Glorius, C. Burstein, *Angew. Chem.* **2004**, *116*, 6331–6334; *Angew. Chem. Int. Ed.* **2004**, *43*, 6205–

 © 2005 Wiley-VCH Verlag GmbH & Co. KGaA, Weinheim

6208; c) A. Chan, K. A. Scheidt, *Org. Lett.* **2005**, *7*, 905–908; d) S. S. Sohn, J. W. Bode, *Org. Lett.* **2005**, *7*, 3873–3876.

[14] M. He, J. W. Bode, *Org. Lett.* **2005**, *7*, 3131–3134.

[15] a) G. W. Nyce, J. A. Lamboy, E. F. Connor, R. M. Waymouth, J. L. Hedrick, *Org. Lett.* **2002**, *4*, 3587–3590; b) G. A. Grasa, R. M. Kissling, S. P. Nolan, *Org. Lett.* **2002**, *4*, 3583–3586; c) G. A. Grasa, R. Singh, S. P. Nolan, *Synthesis* **2004**, 971–985; d) R. Singh, R. M. Kissling, M.-A. Letellier, S. P. Nolan, *J. Org. Chem.* **2004**, *69*, 209–212; e) S. Csihony, D. A. Culkin, A. C. Sentman, A. P. Dove, R. M. Waymouth, J. L. Hedrick, *J. Am. Chem. Soc.* **2005**, *127*, 9079–9084; f) O. Coulembier, A. P. Dove, R. C. Pratt, A. C. Sentman, D. A. Culkin, L. Mespouille, P. Dubois, R. M. Waymouth, J. L. Hedrick, *Angew. Chem.* **2005**, *117*, 5044–5048; *Angew. Chem. Int. Ed.* **2005**, *44*, 4964–4968.

[16] a) Movassaghi et al. only recently reported on the development of a carbene-catalyzed amidation reaction of unactivated esters with amino alcohols. In contrast, based on preliminary mechanistic studies an alternative, uncharged mechanistic mode of catalysis via a carbene–alcohol intermediate followed by rapid $O \rightarrow N$ acyl transfer is suggested: M. Movassaghi, M. A. Schmidt, *Org. Lett.* **2005**, *7*, 2453–2456; b) A NHC-mediated transesterification is supposed to be part of the formation of γ-butyrolactones from benzoins with methyl acrylate in a tandem reaction: W. Ye, G. Cai, Z. Zhuang, X. Jia, H. Zhai, *Org. Lett.* **2005**, *7*, 3769–3771.

[17] Y. Suzuki, K. Yamauchi, K. Muramatsu, M. Sato, *Chem. Commun.* **2004**, 2770–2771.

[18] T. Kano, K. Sasaki, K. Maruoka, *Org. Lett.* **2005**, *7*, 1347–1349.

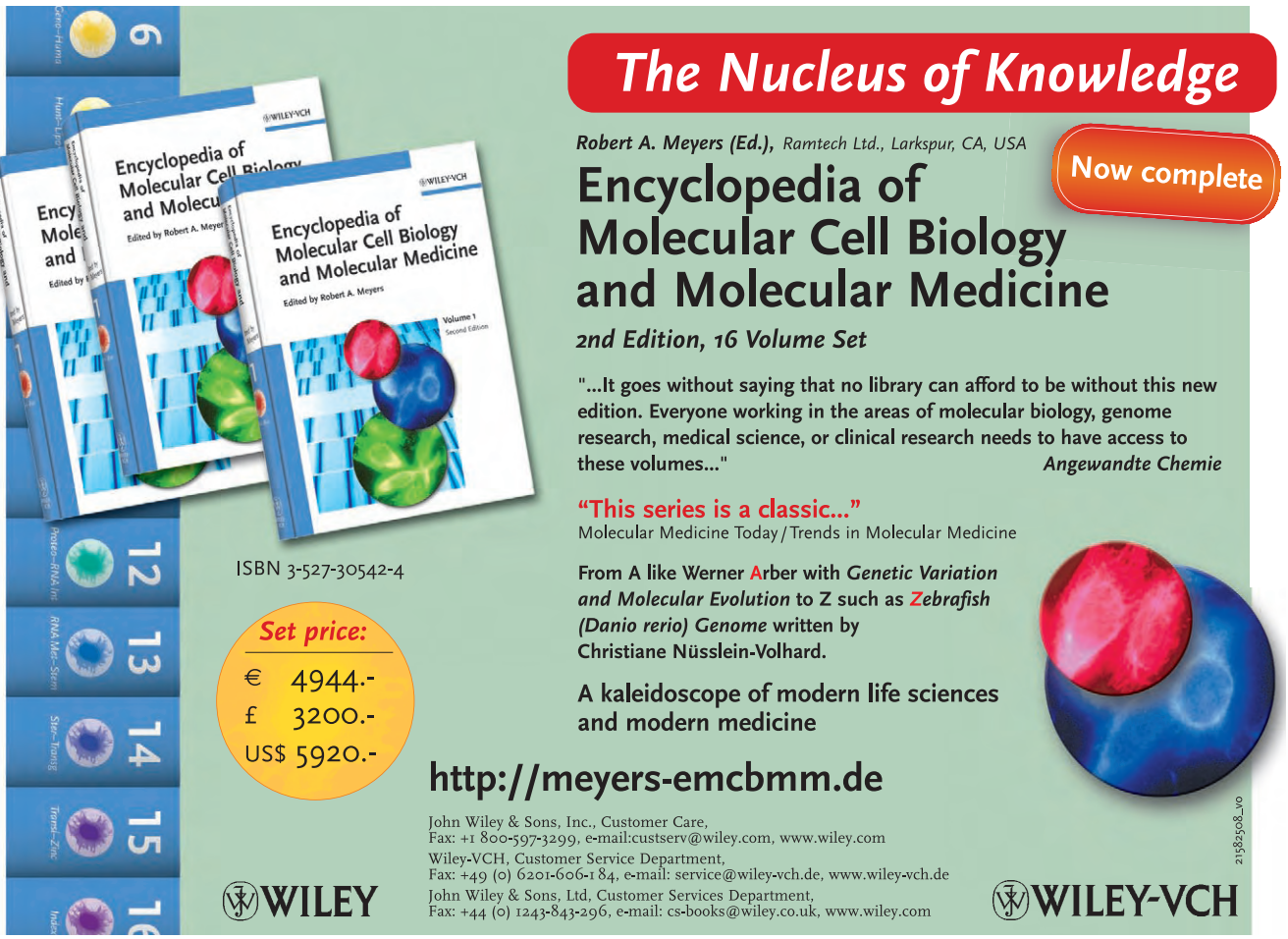

 © 2005 Wiley-VCH Verlag GmbH & Co. KGaA, Weinheim

Reaction Mechanisms

DOI: 10.1002/anie.200501298

1,4-Migration of Rhodium and Palladium in Catalytic Organometallic Reactions

Shengming Ma and Zhenhua Gu*

Keywords:
1,4-migration · C–H activation · palladium · reaction mechanisms · rhodium

Mechanisms based on the 1,4-migration of metal centers have been proposed to explain some interesting transition-metal-catalyzed organic transformations. Despite the lack of solid evidence for the real nature of this process, the 1,4-metal migration reaction is proposed to proceed by the reductive elimination of trivalent intermediates for the Rh-involved reactions and of tetravalent intermediates for the Pd-catalyzed processes. These high-valent organometallic species would be formed by the oxidative addition to C–H and C–X bonds. This minireview summarizes the results in this area.

Introduction

Transition-metal-catalyzed reactions are among the most powerful tools in organic synthesis.[1] Four fundamental reactions of the transition-metal complexes—ligand substitution, oxidative addition/reductive elimination, insertion/elimination (retro-insertion), and nucleophilic/electrophilic attacks on coordinated ligands—are proposed to explain and predict these transition-metal-mediated or -catalyzed reactions.[2] Recently, several groups reported the 1,4-migration of palladium and rhodium in transition-metal-catalyzed multistep transformations. Some of the leading reports are summarized here.

The 1,4-Rhodium Migration

Miura and co-workers demonstrated that phenylboronic acid (**1**) and a strained alkene such as 2-norbornene (**2**), in the presence of a rhodium(I) catalyst, can afford the 1:4 product **3d** in 80% selectivity along with minor amounts of the 1:2 product **3b** and the 1:3 product **3c** (Scheme 1).[3] The authors give a plausible mechanism for the formation these 1:*n* (*n* = 2–4) products. The strained alkene is important to this reaction.

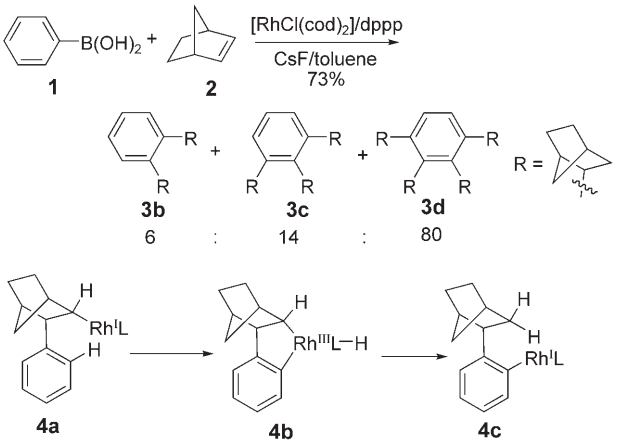

Scheme 1. Rhodium-catalyzed alkylation on an aromatic ring. cod = cycloocta-1,5-diene, dppp = 1,3-bis(diphenylphosphanyl)propane.

The key step is the intramolecular oxidative addition of the C–Rh bond in **4a** with the *ortho* C–H bond of the phenyl group to form the rhodium(III) intermediate **4b**,[4] which yields **4c** by means of reductive elimination.

Hayashi and co-workers reported the 1,4-migration of rhodium in the hydroarylation of alkynes, which was supported by two experimental observations.[5] The olefinic carbon atom in product **7a** does not have the deuterium label (Scheme 2). Instead, 98% incorporation of deuterium was found at the *ortho* position of the phenyl group. When **5** was treated with the pentadeuterated phenylboronic acid **6b**, 93% D-incorporation was found at the olefinic position.

[*] Prof. Dr. S. Ma, Z. Gu
State Key Laboratory of Organometallic Chemistry
Shanghai Institute of Organic Chemistry
Chinese Academy of Sciences
354 Fenglin Lu, Shanghai 200032 (P.R. China)
Fax: (+86) 21-6416-7510
E-mail: masm@mail.sioc.ac.cn

InterScience

© 2005 Wiley-VCH Verlag GmbH & Co. KGaA, Weinheim

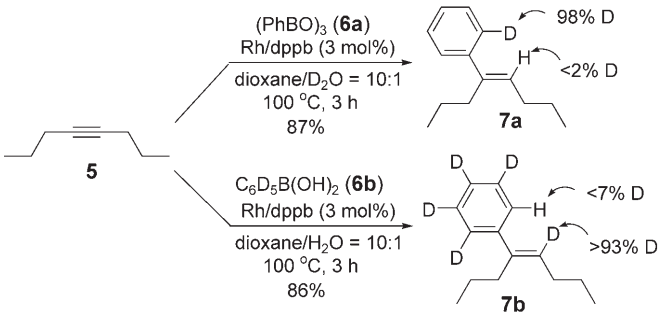

Scheme 2. Rhodium-catalyzed coupling reaction between an alkyne and boronic acid reagents. dppb = 1,4-bis(diphenylphosphanyl)butane.

A rhodium-catalyzed acylation reaction to form the bicyclic ketone **10** was reported by Murakami et al. (Scheme 3).[6] The *syn* phenylrhodation of the C–C triple bond in **8** was proposed to give the intermediate **9a**, which underwent 1,4-rhodium migration to afford **9b**. Subsequent

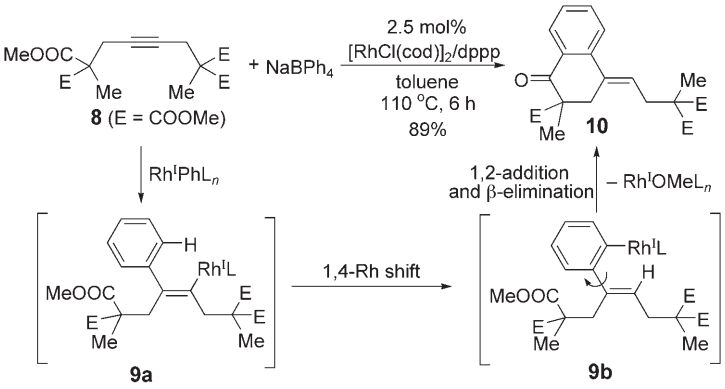

Scheme 3. Intramolecular acylation of organorhodium(I) with ester.

intramolecular acylation of the C–Rh bond in **9b** with the ester group afforded the bicyclic product **10**.

Recently, the groups led by Hayashi and Iwasawa independently reported the rhodium-catalyzed isomerization of 1-arylpropargylic alcohols almost at the same time

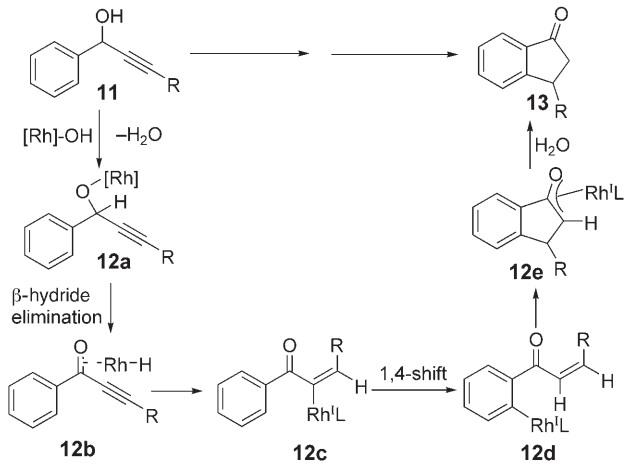

Scheme 4. Rhodium(I)-catalyzed isomerization of 1-arylpropargylic alcohols.

(Scheme 4).[7] The alkoxyrhodium species **12a**, which was formed by ligand exchange between [Rh]-OH and propargylic alcohol **11**, generated the rhodium complex **12b** by means of β-hydride elimination. Then **12b** underwent a hydrorhodation of the conjugated C–C triple bond to form the vinylic rhodium intermediate **12c**. The 1,4-rhodium migration of **12c** affording the arylrhodium intermediate **12d** is the rate-determining step ($k_H/k_D = 2.8$). Subsequent intramolecular 1,4-addition and hydrolysis provide the benzocyclopentanone product **13**. The silyl substituent of the carbon–carbon triple bond is necessary for this isomerization reaction in most cases.

The 1,4-Palladium Migration and Its Application to Organic Synthesis

A similar 1,4-migration of palladium forming arylpalladium species from 2-phenyl-substituted alkenylpalladium was

Shengming Ma is originally from Zhejiang Province, China. He received a BS degree in Chemistry from Hangzhou University (1986), and an MS (1990) and a PhD degree (1990) from Shanghai Institute of Organic Chemistry, Chinese Academy of Sciences. After postdoctoral research at the ETH in Switzerland and Purdue University in USA, he joined the faculty of Shanghai Institute of Organic Chemistry (1997), where he is currently a Professor of Chemistry and the Director of the State Key Laboratory of Organometallic Chemistry. In February 2003 he received an additional appointment by the Department of Chemistry, Zhejiang University, as a Professor of the Cheung Kong Scholars Programme.

Zhenhua Gu was born in Jiangsu Province, China. He received a BS degree in Chemistry from Nanjing University (2002). He is currently conducting PhD research in the group of Prof. Shengming Ma at Shanghai Institute of Organic Chemistry, Chinese Academy of Sciences.

© 2005 Wiley-VCH Verlag GmbH & Co. KGaA, Weinheim

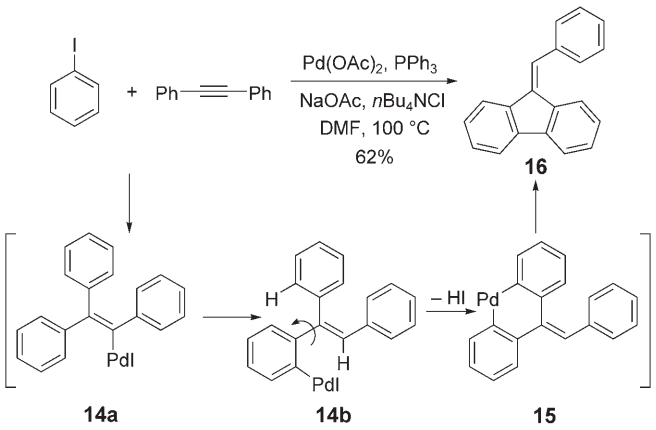

Scheme 5. Palladium-catalyzed synthesis of 9*H*-fluorene **16** from PhI and 1,2-diphenylacetylene.

reported by Larock et al. in the palladium-catalyzed synthesis of 9-alkylidene-substituted 9*H*-fluorene **16** (Scheme 5).[8] The reaction was also explained by a novel 1,4-palladium migration in alkenylpalladium intermediate **14a** to form the arylpalladium species **14b**. HI elimination afforded the palladacycle **15**, which underwent subsequent reductive elimination to afford the fluorene product **16** and regenerate the Pd^0 species.

Such a 1,4-palladium migration was also observed by Gallagher et al.[9] and Larock et al. [10] in the palladium-catalyzed reaction of *ortho*-halobiaryls (Scheme 6). The migration is increasingly favored when electron-deficient arenes are involved.[9] Furthermore, the 1,4-palladium migration can be switched by manipulating the reaction conditions.[10] Under the classical reaction conditions described by Jeffery et al.,[11] the normal product **18a** was obtained exclusively in quantitative yield, while with PPh_3 or bis(diphenylphosphanyl)methane (dppm) as the ligand the reaction afforded **18a** and **18b** in a 1:1 ratio (Scheme 7). The author successfully applied this type of 1,4-palladium migration to the synthesis of the fused polycycles **19** and **20** (Scheme 8).[12]

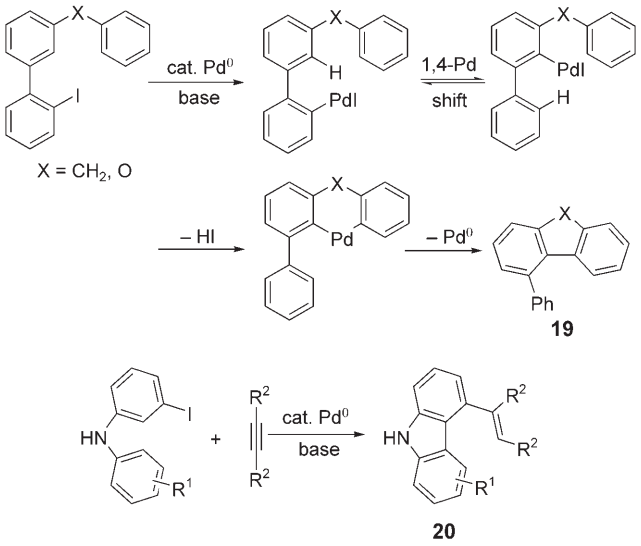

Scheme 8.

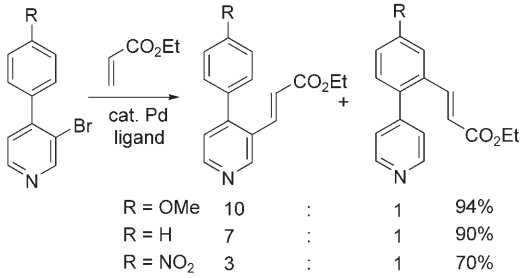

Scheme 6.

Besides the 1,4-palladium migration from an sp^2-hybridized carbon atom (vinylic, aryl) to an aryl carbon atom, Cámpora et al. reported a new palladium migration of an alkylpalladium intermediate to form an arylpalladium complex via palladacycles.[4,13] The π arene complex **21** was proposed to be the important intermediate, and it was further established by X-ray diffraction studies of the similarly structured **25**, in which the Pd–C1 distance is 2.39(1) Å (Scheme 9). The intramolecular oxidative addition of the aryl C–H bond in **21** would form **22**, which would undergo reductive elimination to afford **24**.

Larock and co-workers described a novel alkyl to aryl type 1,4-Pd migration in the successful synthesis of fused polycycles (Scheme 10).[14] Interestingly, the formed arylpalladium intermediate can also undergo standard organopalladium chemistry.[14] When aryl halide **32** was reacted with ethyl acrylate **33**, the chromene derivative **36** was generated in 62 % yield. The key step is the 1,4-palladium migration in the transformation of **35a** to **35c** (Scheme 11).

Larock et al. also reported an aryl to allyl type 1,4-palladium mi-

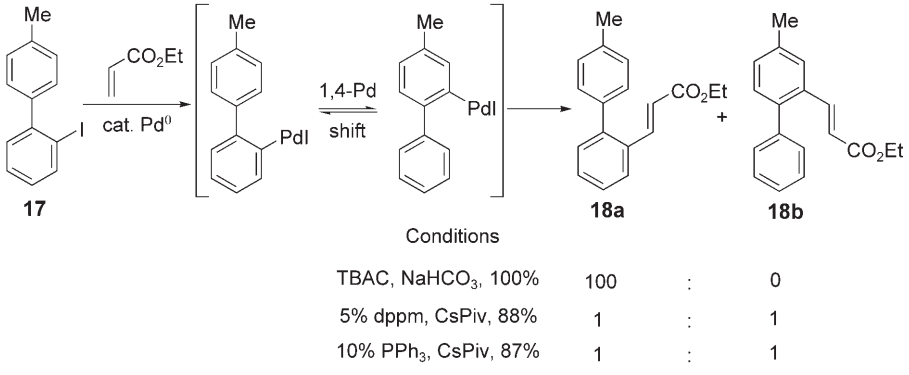

Scheme 7. Switched regioselectivity in the 1,4-palladium migration. TBAC = tetrabutylammonium chloride, Piv = Pivaloyl.

© 2005 Wiley-VCH Verlag GmbH & Co. KGaA, Weinheim

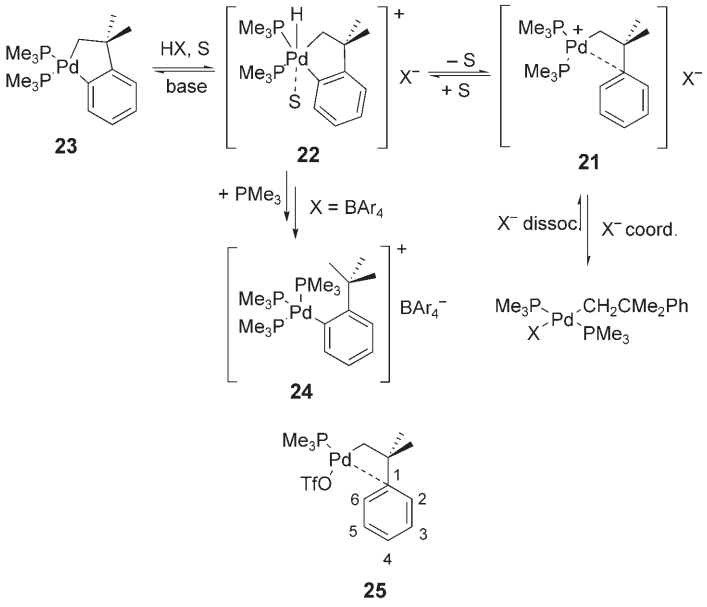

Scheme 9.

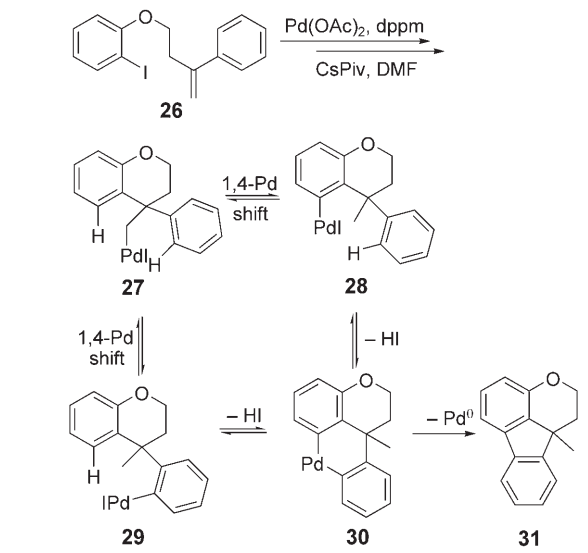

Scheme 10.

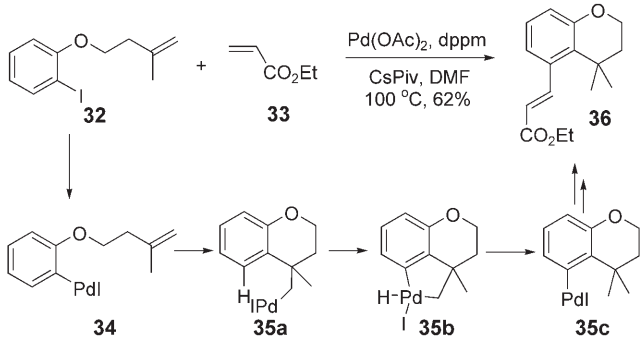

Scheme 11.

gration in the Pd^0-catalyzed coupling reaction of aryl halides with nonterminal alkynes.[15] The reaction proceeded by a double 1,4-palladium migration: 1) the isomerization of intermediate **41a** to the arylpalladium intermediate **41c**, and 2) the isomerization of intermediate **41d** to the allylic palladium intermediate **41f** via intermediate **41e** (Scheme 12).

Buchwald and co-workers reported that when the sterically hindered halide **42** was coupled with arylboronic acid **44**, a novel 1,4-palladium migration of arylpalladium intermediate **43a** was observed. The alkylpalladium intermediate **43c** formed would couple with **44** to afford product **46** (Scheme 13).[16]

Dyker proposed a similar mechanism for the 1,4-palladium migration of aryl intermediate **50a**. The reaction may proceed by the direct C–H activation of **50a** forming **50b**, which may undergo oxidative addition with **47** to afford intermediate **50c**. Subsequent reductive elimination would lead to the formation of **50d**, which would undergo HI elimination to afford **50e**.

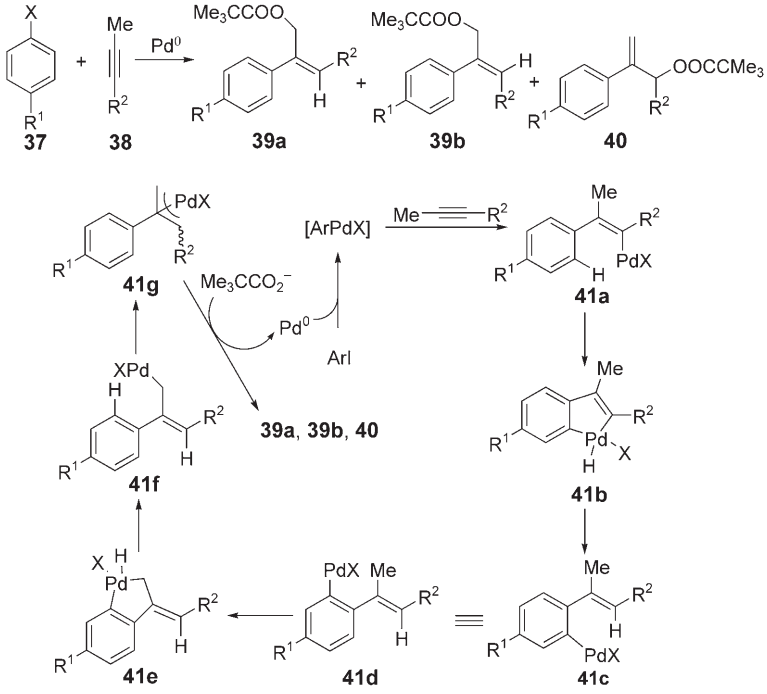

Scheme 12.

Product **48** may be formed by reductive elimination of **50e**. The formation of compound **49** by the reductive elimination of **50b** was not observed (Scheme 14).[17]

Dyker also reported a similar 1,4-palladium migration of intermediate **54a**.[18] An aryl oxapalladacyclic intermediate **54b** was formed by direct C–H activation of the *ortho*-methoxy group of **54a**. Then **54b** may react with vinylbromide **52** to afford the palladium(IV) intermediate **54c**, which would form the palladium intermediate **54d**. Intramolecular carbopalladation and β-hydride elimination would form **53a**, which upon isomerization produces **53b** (Scheme 15).[18a]

 © 2005 Wiley-VCH Verlag GmbH & Co. KGaA, Weinheim

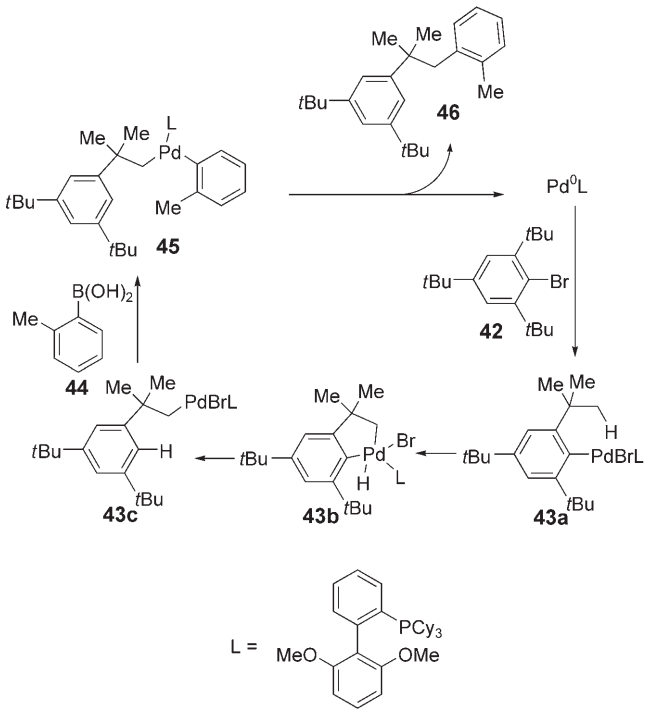

Scheme 13.

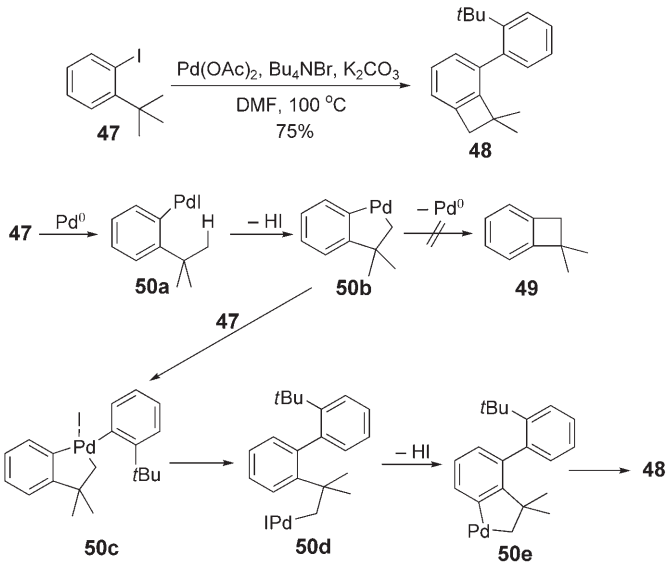

Scheme 14.

Conclusion and Outlook

In contrast to these successful experimental results, which may be explained by the 1,4-metal migration, there is currently no evidence for the exact transition state of these migrations.[19,20] The 1,4-migration of rhodium and palladium has been observed and applied in organic synthesis. The reaction may proceed by oxidative addition of a C–H bond or C–X bond followed by reductive elimination to furnish the 1,4-metal migration. Although the transition states of the migration have not been clearly known, these recent developments may open a new entry in the area of organometallic chemistry, providing powerful and efficient tools in transition-metal-catalyzed reactions.

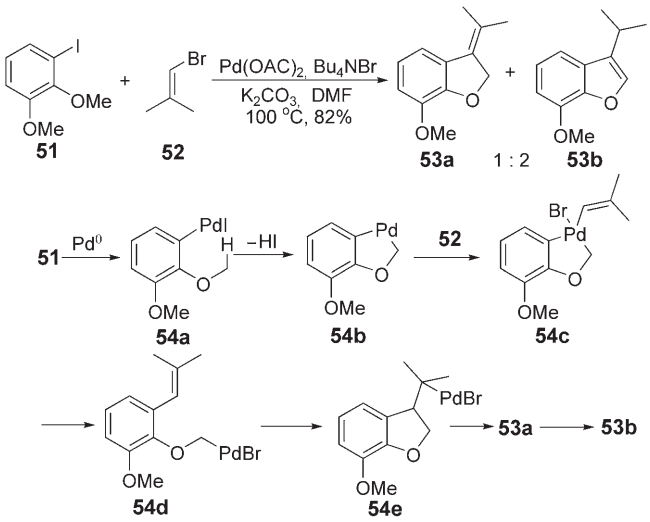

Scheme 15.

Received: April 13, 2005
Published online: November 7, 2005

[1] For a review see: *Metal-Catalyzed Cross-Coupling Reactions*, 2nd ed. (Eds.: A. de Meijere, F. Diederich), Wiley-VCH, Weinheim, **2004**.
[2] a) J. K. Kochi, *Organometallic Mechanisms and Catalysis*, Academic Press, New York, **1978**; b) F. A. Cotton, G. Wilkinson, *Advanced Inorganic Chemistry*, 4th ed., Wiley, New York, **1980**; c) A. Yamamoto, *Organotransition Metal Chemistry*, Wiley, New York, **1986**; d) F. J. McQuillin, D. G. Parker, G. R. Stephenson, *Transition Metal Organometallics for Organic Synthesis*, Cambridge University Press, Cambridge, **1991**; e) C. Amatore, A. Jutand, *J. Organomet. Chem.* **1999**, *576*, 254; f) R. Uma, C. Crévisy, R. Grée, *Chem. Rev.* **2003**, *103*, 27; g) *Palladium Reagents and Catalysts: New Perspectives for the 21th Century* (Ed.: J. Tsuji), Wiley, New York, **2004**.
[3] K. Oguma, M. Miura, T. Satoh, M. Nomura, *J. Am. Chem. Soc.* **2000**, *122*, 10464.
[4] G. Dyker, *Angew. Chem.* **1999**, *111*, 1808; *Angew. Chem. Int. Ed.* **1999**, *38*, 1698.
[5] T. Hayashi, K. Inoue, N. Taniguchi, M. Ogasawara, *J. Am. Chem. Soc.* **2001**, *123*, 9918.
[6] T. Miura, T. Sasaki, H. Nakazawa, M. Murakami, *J. Am. Chem. Soc.* **2005**, *127*, 1390.
[7] a) R. Shintani, K. Okamoto, T. Hayashi, *J. Am. Chem. Soc.* **2005**, *127*, 2872; b) H. Yamabe, A. Mizuno, H. Kusama, N. Iwasawa, *J. Am. Chem. Soc.* **2005**, *127*, 3248.
[8] a) Q. Tian, R. C. Larock, *Org. Lett.* **2000**, *2*, 3329; b) R. C. Larock, Q. Tian, *J. Org. Chem.* **2001**, *66*, 7372.
[9] G. Karig, M.-T. Moon, N. Thasana, T. Gallagher, *Org. Lett.* **2002**, *4*, 3115.
[10] a) M. A. Campo, R. C. Larock, *J. Am. Chem. Soc.* **2002**, *124*, 14326; b) Q. Huang, M. A. Campo, T. Yao, Q. Tian, R. C. Larock, *J. Org. Chem.* **2004**, *69*, 8251.
[11] T. Jeffery, *J. Chem. Soc. Chem. Commum.* **1984**, 1287.

© 2005 Wiley-VCH Verlag GmbH & Co. KGaA, Weinheim

[12] a) M. A. Campo, Q. Huang, T. Yao, Q. Tian, R. C. Larock, *J. Am. Chem. Soc.* **2003**, *125*, 11506; b) J. Zhao, R. C. Larock, *Org. Lett.* **2005**, *7*, 701.
[13] J. Cámpora, J. A. López, P. Palma, P. Valerga, E. Spillner, E. Carmona, *Angew. Chem.* **1999**, *111*, 199; *Angew. Chem. Int. Ed.* **1999**, *38*, 147.
[14] Q. Huang, A. Fazio, G. Dai, M. A. Campo, R. C. Larock, *J. Am. Chem. Soc.* **2004**, *126*, 7460.
[15] J. Jian, M. Campo, R. C. Larock, *Angew. Chem.* **2005**, *117*, 1907; *Angew. Chem. Int. Ed.* **2005**, *44*, 1873.
[16] T. E. Barder, S. D. Walker, J. R. Martinelli, S. L. Buchwald, *J. Am. Chem. Soc.* **2005**, *127*, 4685.
[17] G. Dyker, *Angew. Chem.* **1994**, *106*, 117; *Angew. Chem. Int. Ed. Engl.* **1994**, *33*, 103.
[18] a) G. Dyker, *J. Org. Chem.* **1993**, *58*, 6426; b) G. Dyker, *Angew. Chem.* **1992**, *104*, 1079; *Angew. Chem. Int. Ed. Engl.* **1992**, *31*, 1023; c) G. Dyker, *Chem. Ber.* **1994**, *127*, 739.
[19] For reports on palladacycles with Pd^{II}, see: D. J. Cárdenas, C. Mateo, A. M. Echavarren, *Angew. Chem.* **1994**, *106*, 2529; *Angew. Chem. Int. Ed. Engl.* **1994**, *33*, 2445.
[20] For reports on palladacycles with Pd^{IV}, see: a) M. Catellani, F. Frignani, A. Rangoni, *Angew. Chem.* **1997**, *109*, 142; *Angew. Chem. Int. Ed. Engl.* **1997**, *36*, 119; b) M. Lautens, S. Piguel, *Angew. Chem.* **2000**, *112*, 1087; *Angew. Chem. Int. Ed.* **2000**, *39*, 1045; c) M. Catellani, *Synlett* **2003**, 298.

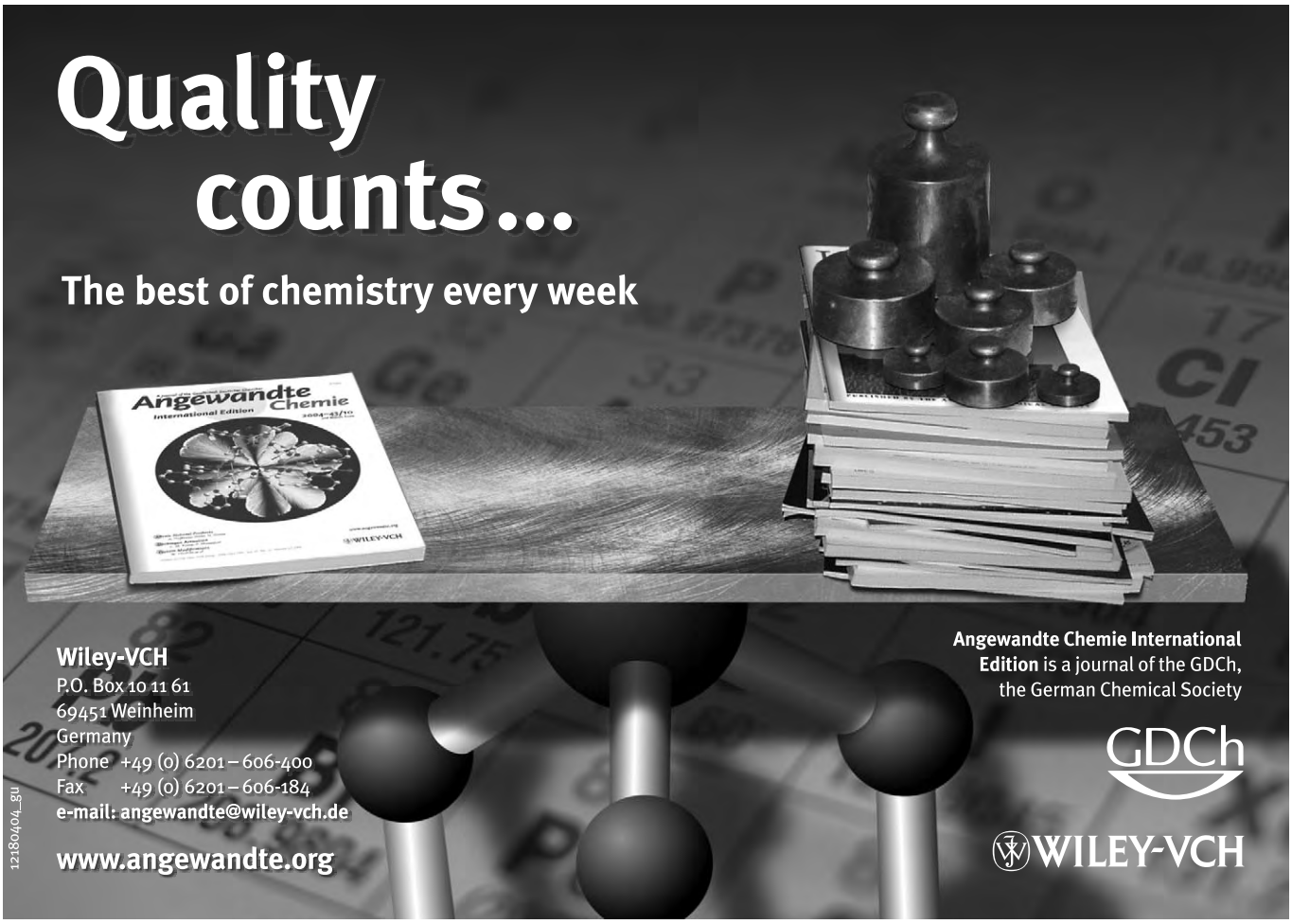

© 2005 Wiley-VCH Verlag GmbH & Co. KGaA, Weinheim

DOI: 10.1002/anie.200501122

Atmospheric Chemistry

Atmospheric Aerosols: Composition, Transformation, Climate and Health Effects

*Ulrich Pöschl**

Keywords:
aerosol particles · atmospheric chemistry · carbon · reaction mechanisms · water

© 2005 Wiley-VCH Verlag GmbH & Co. KGaA, Weinheim

Aerosols are of central importance for atmospheric chemistry and physics, the biosphere, climate, and public health. The airborne solid and liquid particles in the nanometer to micrometer size range influence the energy balance of the Earth, the hydrological cycle, atmospheric circulation, and the abundance of greenhouse and reactive trace gases. Moreover, they play important roles in the reproduction of biological organisms and can cause or enhance diseases. The primary parameters that determine the environmental and health effects of aerosol particles are their concentration, size, structure, and chemical composition. These parameters, however, are spatially and temporally highly variable. The quantification and identification of biological particles and carbonaceous components of fine particulate matter in the air (organic compounds and black or elemental carbon, respectively) represent demanding analytical challenges. This Review outlines the current state of knowledge, major open questions, and research perspectives on the properties and interactions of atmospheric aerosols and their effects on climate and human health.

From the Contents

1. Introduction	7521
2. Composition and Analysis	7523
3. Chemical Reactivity and Water Interactions	7527
4. Climate and Health Effects	7532
5. Summary and Outlook	7535
6. Appendix	7536

1. Introduction

The effects of aerosols on the atmosphere, climate, and public health are among the central topics in current environmental research. Aerosol particles scatter and absorb solar and terrestrial radiation, they are involved in the formation of clouds and precipitation as cloud condensation and ice nuclei, and they affect the abundance and distribution of atmospheric trace gases by heterogeneous chemical reactions and other multiphase processes.[1–4] Moreover, airborne particles play an important role in the spreading of biological organisms, reproductive materials, and pathogens (pollen, bacteria, spores, viruses, etc.), and they can cause or enhance respiratory, cardiovascular, infectious, and allergic diseases.[1,5–7]

An aerosol is generally defined as a suspension of liquid or solid particles in a gas, with particle diameters in the range of 10^{-9}–10^{-4} m (lower limit: molecules and molecular clusters; upper limit: rapid sedimentation).[4,7] The most evident examples of aerosols in the atmosphere are clouds, which consist primarily of condensed water with particle diameters on the order of approximately 10 μm. In atmospheric science, however, the term aerosol traditionally refers to suspended particles that contain a large proportion of condensed matter other than water, whereas clouds are considered as separate phenomena.[8]

Atmospheric aerosol particles originate from a wide variety of natural and anthropogenic sources. Primary particles are directly emitted as liquids or solids from sources such as biomass burning, incomplete combustion of fossil fuels, volcanic eruptions, and wind-driven or traffic-related suspension of road, soil, and mineral dust, sea salt, and biological materials (plant fragments, microorganisms, pollen, etc.). Secondary particles, on the other hand, are formed by gas-to-particle conversion in the atmosphere (new particle formation by nucleation and condensation of gaseous precursors). As illustrated in Figure 1, airborne particles undergo various physical and chemical interactions and transformations (atmospheric aging), that is, changes of particle size, structure, and composition (coagulation, restructuring, gas uptake, chemical reaction). Particularly efficient particle aging occurs in clouds, which are formed by condensation of water vapor on preexisting aerosol particles (cloud condensation and ice nuclei, CCN and IN[+]). Most clouds reevaporate, and modified aerosol particles are again released from

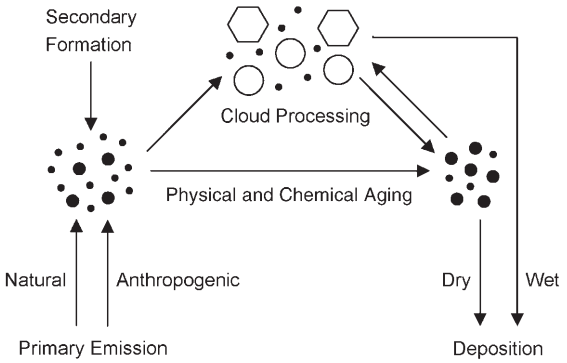

Figure 1. Atmospheric cycling of aerosols.

[*] Dr. U. Pöschl[+]
Technical University of Munich
Institute of Hydrochemistry
81377 München (Germany)
E-mail: poeschl@mpch-mainz.mpg.de

[+] Current address:
Max Planck Institute for Chemistry
Biogeochemistry Department
55128 Mainz (Germany)
Fax: (+49) 6131-305-487

[+] A list of abbreviations can be found at the end of the Review.

© 2005 Wiley-VCH Verlag GmbH & Co. KGaA, Weinheim

the evaporating cloud droplets or ice crystals (cloud processing). If, however, the cloud particles form precipitation which reaches the Earth's surface, not only the condensation nuclei but also other aerosol particles are scavenged on the way to the surface and removed from the atmosphere. This process, termed "wet deposition", is actually the main sink of atmospheric aerosol particles. Particle deposition without precipitation of hydrometeors (airborne water particles)—that is, "dry deposition" by convective transport, diffusion, and adhesion to the Earth's surface—is less important on a global scale, but is highly relevant with respect to local air quality, health effects (inhalation and deposition in the human respiratory tract), and the soiling of buildings and cultural monuments. Depending on aerosol properties and meteorological conditions, the characteristic residence times (lifetimes) of aerosol particles in the atmosphere range from hours to weeks.[9,10]

The concentration, composition, and size distribution of atmospheric aerosol particles are temporally and spatially highly variable. In the lower atmosphere (troposphere) the total particle number and mass concentrations typically vary in the range of about 10^2–10^5 cm^{-3} and 1–100 $\mu g\,m^{-3}$, respectively.[9–12] In general, the predominant chemical components of air particulate matter (PM) are sulfate, nitrate, ammonium, sea salt, mineral dust, organic compounds, and black or elemental carbon, each of which typically contribute about 10–30 % of the overall mass load. At different locations, times, meteorological conditions, and particle size fractions, however, the relative abundance of different chemical components can vary by an order of magnitude or more.[1,4,9,13] In atmospheric research the term "fine air particulate matter" is usually restricted to particles with aerodynamic diameters ≤ 1 μm (PM1) or ≤ 2.5 μm (PM2.5). In air pollution control it sometimes also includes larger particles up to 10 μm (PM10).

Characteristic examples of particle number concentration, size distribution, and chemical composition of fine particulate matter in urban and high alpine air are illustrated in Figure 2. The displayed particle number size distributions (particle number concentration per logarithmic decade of particle diameter, $dN/d(\log d_p)$ plotted against particle diameter) were observed in the city of Munich (500 m above sea level; December 8–14, 2002) and at the Schneefernerhaus research station on Mount Zugspitze (2600 m above sea level; November 6, 2002) in Southern Germany. They correspond to total particle number concentrations of about 10^2 cm^{-3} in alpine air and 10^4 cm^{-3} in urban air, and to particle mass concentrations of about 1 $\mu g\,m^{-3}$ and 10 $\mu g\,m^{-3}$, respectively. The measurements were performed with a couple of complementary techniques, an electrical low-pressure impactor (ELPI, 10 nm–10 μm, flow rate 30 $L\,min^{-1}$, measurement interval 1 min) and a scanning mobility particle sizer (SMPS, 10–300 nm, flow rate 1 $L\,min^{-1}$, measurement interval 30 min).[14,15] The deviations at very low particle size can be attributed to wall losses by diffusion in the SMPS system. The dotted lines indicate characteristic particle size modes, which can be attributed to different sources, sinks, and aging processes of atmospheric particles: nucleation (Aitken), accumulation, and coarse modes.[4,7] In corresponding mass size distributions, which are obtained by multiplication with particle volume ($d_p^3\pi/6$) and density (typically around 2 $g\,cm^{-3}$), the nucleation mode is usually negligible whereas accommodation and coarse particle modes are of comparable magnitude. The composition pie charts are based on chemical analyses of PM2.5 filter samples from the same locations and literature data for urban and remote continental background air.[1,4,9,13,16–19]

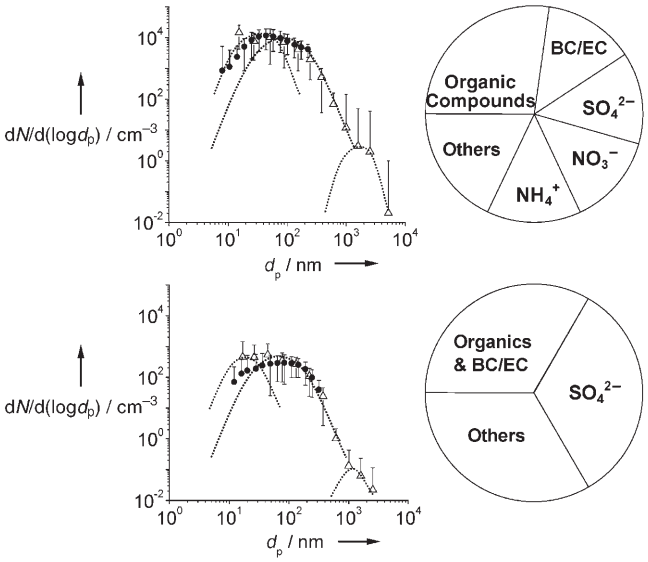

Figure 2. Characteristic examples of aerosol particle-size distribution and chemical composition in urban (top) and high alpine air (bottom). Graphs (left): number size distribution function $dN/d(\log d_p)$ (symbols and error bars: arithmetic mean values and standard deviations, △ ELPI, ● SMPS, ••••• characteristic particle size modes). Pie charts (right): typical mass proportions of main components.

Figure 3 illustrates the interdependence of composition, composition-dependent properties, atmospheric interactions and transformation, climate and health effects, and aerosol sources. The resulting feedback loops are of central importance in the science and policy of environmental pollution and global change. Thus a comprehensive characterization (climatology) and mechanistic understanding of particle sources, properties, and transformation is required for the quantitative assessment, reliable prediction, and efficient control of

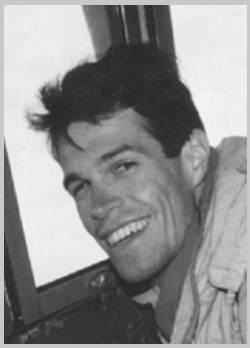

Ulrich Pöschl heads a research group at the MPI for Chemistry in Mainz (Biogeochemistry Dept., M. O. Andreae). He obtained his diploma and PhD at the TU Graz (1996) and then worked at MIT (M. J. Molina), at the MPI in Mainz (P. J. Crutzen), and at the TU Munich (R. Niessner). His research is focused on the properties and interactions of aerosols and their effects on the atmosphere, biosphere, climate, and public health. He initiated and is editor of the open-access journal Atmospheric Chemistry and Physics and is president of the Atmospheric Sciences Division of the European Geosciences Union.

 © 2005 Wiley-VCH Verlag GmbH & Co. KGaA, Weinheim

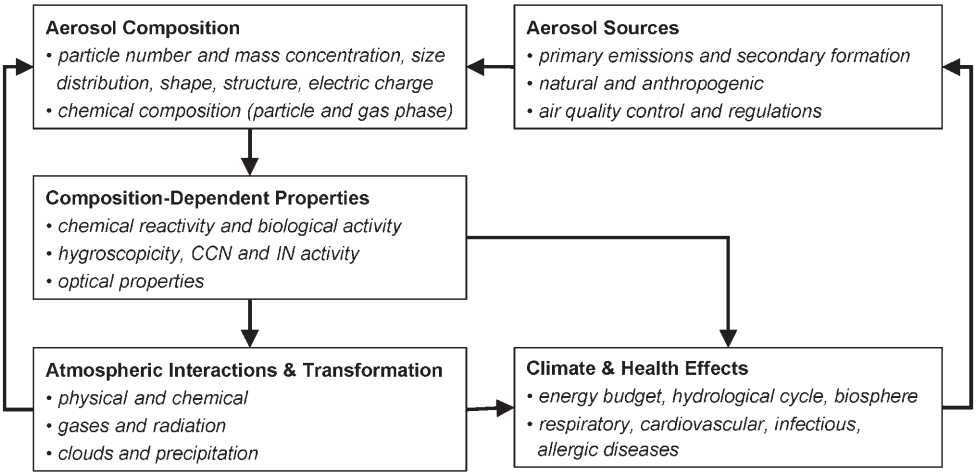

Figure 3. Interdependence and feedback between atmospheric aerosol composition, properties, interactions and transformation, climate and health effects, and sources.

natural and anthropogenic aerosol effects on climate and public health.

2. Composition and Analysis

A wide range of methods can be and have been applied for the physical and chemical analysis of aerosol particles and components.[1,20–22] Major analytical procedures and measurement techniques are outlined in Figure 4. In practice, the selection and combination of analytical methods depend on the sample type and target parameters (single particles or particle ensembles, suspended or deposited particles, physical properties or chemical composition, etc.) and requires a trade-off between sensitivity and selectivity, time and size resolution, and equipment and labor expenses.

The techniques most frequently applied for the physical characterization of atmospheric aerosol particles are: differential mobility analysis (DMA), inertial separation (impaction, time-of-flight), scanning and transmission electron microscopy (SEM, TEM), and light scattering (Mie) for particle size, structure, and density; β-ray attenuation, gravimetry, and oscillation of deposition substrates for particulate mass; spectrophotometry, photoacoustic spectroscopy, and nephelometry for absorption and scattering coefficients. Some advanced methods for the determination of physical and chemical aerosol properties involve multiple iterative steps of particle conditioning and sizing as indicated by the arrows in Figure 4. Examples are volatility and hygroscopicity tandem differential mobility analysis (V- and H-TDMA) or the online coupling of particle sizing, vaporization, and mass spectrometry with electron-impact (EI) or laser-desorption ionization (LDI). Detailed descriptions and explanations of these and related techniques can be found in recent monographs, reviews, and research articles.[1,20,22–28]

Accurate determination of the chemical composition of air particulate matter is a formidable analytical task. Minute sample amounts are usually composed of several main constituents and hundreds of minor and trace constituents. Moreover, the composition of the individual particles can be fairly uniform (internally mixed aerosols) or very different from the ensemble composition (externally mixed aerosols), depending on the particle sources and atmospheric aging processes involved (coagulation, gas–particle partitioning, chemical reactions). Especially in populated environments, air particulate matter can be pictured as the result of an "exploded pharmacy", comprising just about any non- or semivolatile chemical compound occurring in the biosphere, hydrosphere, and lithosphere, or released by human activity. Besides primary chemical components, which are directly emitted by natural and anthropogenic sources, air particulate matter mostly also contains secondary chemical components, which are formed by gas-phase reactions and subsequent gas-to-particle conversion or by chemical transformation of primary particle components in the atmosphere.

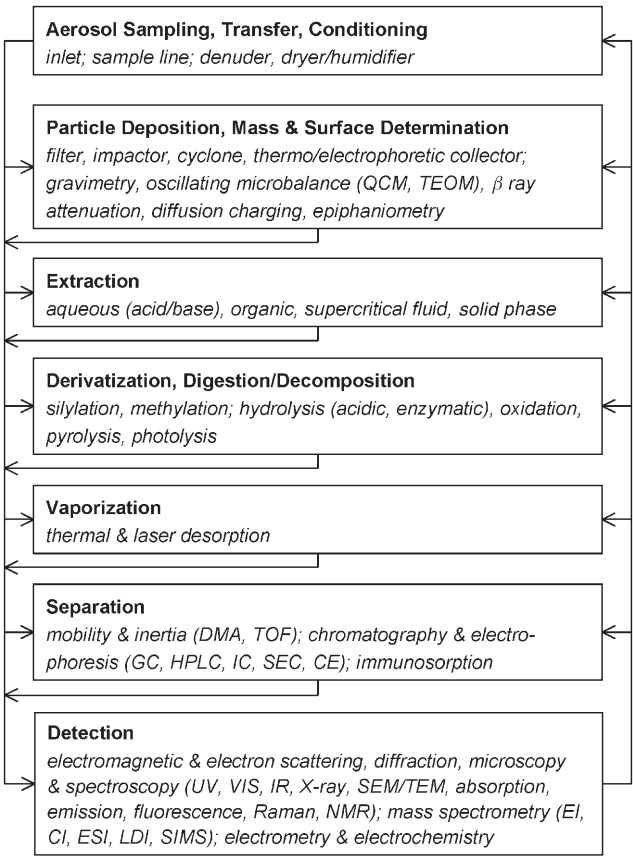

Figure 4. Major analytical procedures and techniques for the physical and chemical characterization of aerosol particles and components: arrows illustrate flexible combination and iterative application of individual steps and methods; acronyms are defined in the appendix.

 © 2005 Wiley-VCH Verlag GmbH & Co. KGaA, Weinheim

By definition, an aerosol is composed of particulate and gas-phase components, that is, the term aerosol component can refer to chemical compounds in condensed as well as in the gaseous state. In practice and in the remainder of this manuscript, however, the term aerosol component usually refers to semi- and nonvolatile particle components but not to volatile compounds residing almost exclusively in the gas phase.

Most traditional methods for the sampling and chemical analysis of air particulate matter are "offline" and involve the collection of the investigated particles on solid deposition substrates (membrane or fiber filters, inertial impaction plates, thermal or electrostatic precipitation plates) or in a liquid (wetted wall cyclone, impinger, or washing bottle) and intermediate steps of sample storage, transport, and preparation before chemical analysis.[1,20,22] These methods are prone to analytical artifacts caused by evaporation of particle components, adsorption or absorption of additional gas-phase components, and chemical reaction during sample collection, storage, transport, and preparation. The potential for measurement artifacts is particularly high for reactive and semivolatile organic aerosol components, and elaborate sampling techniques combining parallel or consecutive trains of denuders, filters, and adsorbent cartridges have been developed to minimize or at least quantify the effects outlined above.[1,19,20,29,30]

Besides the problem of sampling artifacts, offline techniques hardly allow the resolution of the high spatial and temporal variability of atmospheric aerosols. Over the past few years, however, substantial progress has been made in the development of aerosol mass spectrometers for real-time measurements of size-selected (single) particles. As the methods of vaporization, ionization, calibration, and data analysis are improved, these instruments promise reliable quantitative analyses, especially for chemical elements and inorganic species. Some of them also allow differentiation between surface and bulk composition, but the influence of matrix effects on vaporization and ionization efficiencies and thus on the interpretation of the measurement data still remains to be sorted out reliably. Advances in this rapidly moving field have been reported in a growing number of research and review articles.[20,25–28,31–40]

A particularly challenging application of aerosol mass spectrometry with high relevance for public health and security is the identification of biological particles and pathogens (bacteria, viruses, spores, etc.).[25,41,42] Alternative concepts for online monitoring of bioaerosols are based on aerodynamic sizing and fluorescence spectroscopy,[43] whereas most other applicable techniques are offline and highly labor intensive (cultivation, staining, fluorescence and electron microscopy, enzyme and immunoassays, DNA analysis, etc.).[18,44–52]

2.1. Carbonaceous Aerosol Components

Carbonaceous aerosol components (organic compounds and black or elemental carbon) account for a large fraction of air particulate matter, exhibit a wide range of molecular structures, and have a strong influence on the physicochemical, biological, climate- and health-related properties, and effects of atmospheric aerosols.[1,4,19,53–56]

Traditionally the total carbon (TC) content of air particulate matter is defined as the sum of all carbon contained in the particles, except in the form of inorganic carbonates. TC is usually determined by thermochemical oxidation and evolved gas analysis (CO_2 detection), and divided into an organic carbon (OC) fraction and a black carbon (BC) or elemental carbon (EC) fraction. Measurements of BC and EC are generally based on optical and thermochemical techniques, and OC is operationally defined as the difference between TC and BC or EC (TC = BC + OC or TC = EC + OC).[19] As illustrated in Figure 5, however, there is no real sharp

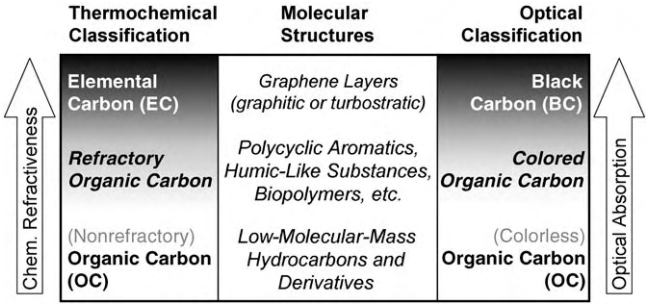

Figure 5. Optical and thermochemical classification and molecular structures of black carbon (BC), elemental carbon (EC), and organic carbon (OC = TC − BC or TC − EC).[57] Depending on the method of analysis, different amounts of carbon from refractory and colored organic compounds are included in OC and BC or EC.

boundary but a continuous decrease of thermochemical refractiveness and specific optical absorption going from graphite-like structures to nonrefractive and colorless organic compounds, respectively.[57] Both BC and EC consist of the carbon content of the graphite-like material usually contained in soot (technically defined as the black product of incomplete hydrocarbon combustion or pyrolysis) and other combustion aerosol particles, which can be pictured as more or less disordered stacks of graphene layers or large polycyclic aromatics.[58,59] Depending on the applied optical or thermochemical methods (absorption wavelength, temperature gradient, etc.), however, BC and EC measurements also include the carbon content of colored and refractory organic compounds, which can lead to substantially different results and strongly limits the comparability and suitability of BC, EC, and OC data for the determination of mass balances and physicochemical properties of air particulate matter.

Nevertheless, most information available on the abundance, properties, and effects of carbonaceous aerosol components so far is based on measurement data of TC, OC, and BC or EC.[19,56] These data are now increasingly complemented by measurements of water-soluble organic carbon (WSOC), its macromolecular fraction (MWSOC), and individual organic compounds as detailed in Section 2.2. Moreover, the combination of thermochemical oxidation with ^{14}C isotope analysis (radiocarbon determination in evolved

 © 2005 Wiley-VCH Verlag GmbH & Co. KGaA, Weinheim

CO_2 by accelerator mass spectrometry) allows a differentiation between fossil-fuel combustion and other sources of carbonaceous aerosol components. Recent results confirm that the EC is dominated by fossil-fuel combustion and indicate highly variable anthropogenic and biogenic sources and proportions of OC.[60]

Characteristic mass concentrations and concentration ratios of fine air particulate matter (PM2.5) and carbonaceous fractions in urban, rural, and alpine air in central Europe are summarized in Table 1. The reported data have been obtained on an altitude transect through Southern Germany, from the city of Munich (500 m above sea level), via the meteorological observatory Hohenpeissenberg (1000 m above sea level), to the environmental research station Schneefernerhaus on Mount Zugspitze (2600 m above sea level) during 2001–2003. The sampling locations and measurement procedures have been described in detail elsewhere,[61,62] and the results are consistent with those of other studies performed at comparable locations.[9,11,13,16–19]

Table 1: Characteristic aerosol data for urban, rural, and high alpine air in central Europe.[a]

	Urban (Munich)	Rural (Hohenpeissenberg)	Alpine (Zugspitze)
PM2.5 [$\mu g\,m^{-3}$]	20 ± 10	10 ± 5	4 ± 2
TC in PM2.5 [%]	40 ± 20	30 ± 10	20 ± 10
EC in TC [%]	50 ± 20	30 ± 10	30 ± 10
OC in TC [%]	40 ± 20	70 ± 10	70 ± 10
WSOC in TC [%]	20 ± 10	40 ± 20	60 ± 20
MWSOC in WSOC [%]	30 ± 10	50 ± 20	40 ± 20

[a] Rounded arithmetic mean values ± standard deviation determined from about 30 filter samples collected at each location during 2001–2003.

On average, the total PM2.5 mass concentration decreases by about a factor of 2 from urban to rural and from rural to alpine air, whereas the TC mass fraction decreases from around 40% to 20%. The EC/TC ratios in PM2.5 are as high as 50% in the urban air samples taken close to a major traffic junction and on the order of approximately 30% in rural and high alpine air, demonstrating the strong impact of diesel soot and other fossil-fuel combustion or biomass-burning emissions on the atmospheric aerosol burden and composition. The water-soluble fraction of organic carbon (WSOC in OC), on the other hand, exhibits a pronounced increase from urban ($\approx$20%) to rural ($\approx$40%) and high alpine ($\approx$60%) samples of air particulate matter. This observation can be attributed to different aerosol sources (e.g. water-insoluble combustion particle components versus water-soluble biogenic and secondary organic particle components) but also to chemical aging and oxidative transformation of organic aerosol components, which generally increases the number of functional groups and thus the water solubility of organic molecules (Section 3).

Figure 6 illustrates a characteristic example of the size distribution of TC in air particulate matter sampled at the meteorological observatory Hohenpeissenberg. It exhibits an absolute maximum for particles with aerodynamic diameters on the order of approximately 300 nm, which is likely due to combustion and secondary organic aerosol (SOA) particles and another local maximum at 2.5 μm, which may be due to primary biological particles or soil dust.

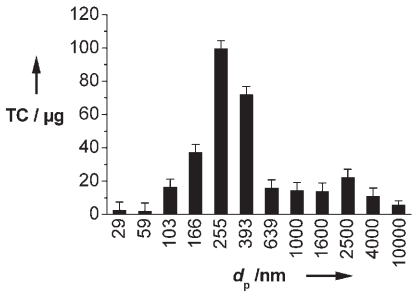

Figure 6. Total carbon content of a size-separated sample of rural air particulate matter plotted against the lower limits of the particle size classes (cut-off diameter of the impaction stages) of the applied electrical low-pressure impactor (ELPI, Hohenpeissenberg, May 27–June 6, 2002; error bars indicate TC measurement uncertainty).

Black or elemental carbon accounts for most of the light absorption by atmospheric aerosols and is therefore of crucial importance for the direct radiative effect of aerosols on climate.[63–65] Despite a long tradition of soot and aerosol research, however, there is still no universally accepted and applied operational definition of BC and EC. Several studies have compared the different optical and thermal methods applied by atmospheric research groups to measure BC and EC. Depending on techniques and measurement locations, fair agreement has been found in some cases, but mostly the results deviated considerably (up to 100% and more).[66–68]

Optical methods for the detection of BC are usually nondestructive and allow (near-)real-time operation, but on the other hand they are particularly prone to misinterpretation. They generally rely on the assumptions that BC is the dominant absorber and exhibits a uniform mass-specific absorption coefficient or cross-section. Although these assumptions may be justified under certain conditions, they are highly questionable in the context of detailed chemical characterization of aerosol particles ("How black is black carbon?").[57] Besides different types of graphite-like material, there are at least two classes of organic compounds that can contribute to the absorption of visible light by air particulate matter ("light-absorbing yellow or brown carbon"):[19] polycyclic aromatics and humic-like substances. Therefore, optically determined BC values must be considered as mass-equivalent values but not as absolute mass or concentration values. Moreover, most conventional optical methods such as aethalometry, integrating-sphere methods, and integrating-plate methods are based on the measurement of light extinction rather than absorption. As a consequence these methods require aerosol-composition-dependent calibrations or additional sample work-up processes to compensate for or minimize the influence of scattering aerosol components such as inorganic salts and acids on the measurement signal.[67,69,70] Alternatively, photoacoustic spectroscopy allows direct measurements of light absorption by airborne aerosol particles, and during the past years several photoacoustic spectrometers have been developed and applied for the measurement of aerosol absorption coefficients and BC equivalent concentrations.[71–73]

© 2005 Wiley-VCH Verlag GmbH & Co. KGaA, Weinheim

Among the few methods available for the characterization of the molecular and crystalline structures of BC and EC (graphite-like carbon proportion and degree of order) are high-resolution electron microscopy, X-ray diffraction, and Raman spectroscopy.[59,74] These measurement techniques have revealed that the microstructure and spectroscopic properties of flame soot, diesel soot, and related carbonaceous materials depend on the processes and conditions of particle formation and aging. So far, however, these methods have been too labor-intensive for routine investigations of atmospheric aerosol samples, and their application in quantitative analyses remains to be proven.[59] Nevertheless, recently developed measurement systems show promise for the quantification of graphite-like carbon and soot in aerosol filter samples by Raman spectroscopy.[75,76]

2.2. Primary and Secondary Organic Aerosol Components

The total mass of organic air particulate matter (OPM), that is, the sum of organic aerosol (OA) components, is usually estimated by multiplication of OC with a factor of about 1.5–2, depending on the assumed average molecular composition and accounting for the contribution of elements other than carbon contained in organic substances (H, O, N, S, etc.).[19,77] The only way, however, to determine the overall mass, molecular composition, physicochemical properties, and potential toxicity of OPM accurately is the identification and quantification of all relevant chemical components. Also trace substances can be hazardous to human health, and potential interferences of refractive and colored organic components in the determination of BC or EC can be assessed only to the extent to which the actual chemical composition of OPM is known.[57,78]

Depending on their origin, OA components can be classified as primary or secondary. Primary organic aerosol (POA) components are directly emitted in the condensed phase (liquid or solid particles) or as semivolatile vapors, which are condensable under atmospheric conditions. The main sources of POA particles and components are natural and anthropogenic biomass burning (forest fires, slashing and burning, domestic heating), fossil-fuel combustion (domestic, industrial, traffic), and wind-driven or traffic-related suspension of soil and road dust, biological materials (plant and animal debris, microorganisms, pollen, spores, etc.), sea spray, and spray from other surface waters with dissolved organic compounds.

Secondary organic aerosol (SOA) components are formed by chemical reaction and gas-to-particle conversion of volatile organic compounds (VOCs) in the atmosphere, which may proceed through different pathways:

a) new particle formation: formation of semivolatile organic compounds (SVOCs) by gas-phase reactions and participation of the SVOCs in the nucleation and growth of new aerosol particles;
b) gas–particle partitioning: formation of SVOCs by gas-phase reactions and uptake (adsorption or absorption) by preexisting aerosol or cloud particles;
c) heterogeneous or multiphase reactions: formation of low-volatility or nonvolatile organic compounds (LVOCs, NVOCs) by chemical reaction of VOCs or SVOCs at the surface or in the bulk of aerosol or cloud particles.

The formation of new aerosol particles from the gas phase generally proceeds through the nucleation of nanometer-sized molecular clusters and subsequent growth by condensation of condensable vapor molecules. Experimental evidence from field measurements and model simulations suggests that new particle formation in the atmosphere is most likely dominated by ternary nucleation of H_2SO_4–H_2O–NH_3 and subsequent condensation of SVOCs.[79–81] Laboratory experiments and quantum chemical calculations indicate, however, that SVOCs might also play a role in the nucleation process (H_2SO_4–SVOC complex formation).[82] The actual importance of different mechanisms of particle nucleation and growth in the atmosphere has not yet been fully unraveled and quantified. In any case, the formation of new particles exhibits a strong and nonlinear dependence on atmospheric composition and meteorological conditions, may be influenced by ions and electric-charge effects, and competes with gas–particle partitioning and heterogeneous or multiphase reactions.[83] Among the principal parameters governing secondary particle formation are temperature, relative humidity, and the concentrations of organic and inorganic nucleating and condensing vapors, which depend on atmospheric transport as well as local sources and sinks such as photochemistry and preexisting aerosol or cloud particles.[54,56,79,80] The rate and equilibrium of SVOC uptake by aerosol particles depend on the SVOC-accommodation coefficients and on the particle surface area, bulk volume, and chemical composition (kinetics and thermodynamics of gas–particle partitioning).[84]

Most earlier studies of SOA formation were focused on pathways a and b. Several recent studies indicate, however, that heterogeneous and multiphase reactions may also play an important role and contribute substantially to the overall atmospheric burden of OPM.[19,85–88] The term "heterogeneous reaction" generally refers to reactions of gases at the particle surface, whereas the term "multiphase reaction" refers to reactions in the particle bulk involving species from the gas phase.

A variety of different reversible and irreversible mechanisms of acid-catalyzed condensation and radical-initiated oligo- or polymerization reactions involving organic and inorganic acids and photooxidants can lead to secondary formation of LVOCs and NVOCs of high molecular mass (SOA oligomers/polymers; Table 2). The actual atmospheric relevance and contributions of the different SOA formation pathways and involved chemical reaction mechanisms, however, still remain to be clarified.[19,56]

Depending on local sources, meteorological conditions, and atmospheric transport and thus on location, season, and time of day, the composition of OPM can be dominated by POA or by SOA components. Recent studies indicate high abundance of POA in tropical air masses owing to intense biomass burning, whereas SOA from biogenic and anthropogenic emissions of precursor VOCs seems to dominate in

 © 2005 Wiley-VCH Verlag GmbH & Co. KGaA, Weinheim

Table 2: Prominent organic aerosol components.

Substance Classes	Proportions[a]	Sources
aliphatic hydrocarbons	10^{-2}	biomass, fossil-fuel combustion
aliphatic alcohols and carbonyls	10^{-2}	biomass, SOA/aging
levoglucosan	10^{-1}	biomass burning
fatty acids and other alkanoic acids	10^{-1}	biomass, SOA/aging
aliphatic dicarboxylic acids	10^{-1}	SOA/aging
aromatic (poly-)carboxylic acids	10^{-1}	SOA/aging, soil/dust
multifunctional aliphatic and aromatic compounds (OH, CO, COOH)	10^{-1}	SOA/aging, soil/dust
polycyclic aromatic hydrocarbons (PAHs)	10^{-3}	fossil-fuel combustion, biomass burning
nitro- and oxy-PAHs	10^{-3}	fossil-fuel combustion, biomass burning, SOA/aging
proteins and other amino compounds	10^{-1}	biomass
cellulose and other carbohydrates	10^{-2}	biomass
secondary organic oligomers/polymers and humic-like substances	10^{-1}	SOA/aging, soil/dust

[a] Characteristic magnitudes of the mass proportion in fine OPM.

mid-latitude air masses. On a global scale, the formation of SOA appears to be dominated by oxidation of biogenic VOCs (mostly by ozonolysis of terpenes)[89] and to amount to at least 50% of POA emissions.[56,90] In the atmosphere, POA and SOA components are mixed with each other, with BC/EC, and with inorganic aerosol components (externally and internally mixed aerosols).[91] Moreover, both POA and SOA components can be efficiently transformed upon interaction with reactive trace gases and solar radiation (chemical aging, Section 3).

Hundreds of organic compounds have been detected in air particulate matter. Even in the most comprehensive investigations, however, only 10–40% of the OPM content estimated from OC measurements have been unambiguously identified on a molecular level. Prominent organic substance classes, characteristic magnitudes of their proportion in fine OPM (approximate upper limit of mass fraction), and their main sources are summarized in Table 2.[1,4,19,29,56,92–96]

Several studies have shown that macromolecules such as cellulose and proteins (molecular mass $\geqslant 1$ kDa) and other compounds with relatively high molecular mass ($\geqslant 100$ Da) such as humic-like substances (HULIS) account for large proportions of OPM and WSOC.[19,62,97–101] Evidently, biopolymers and humic substances are emitted as POA components (soil and road dust, sea spray, biological particles), which may be modified by chemical aging and transformation in the atmosphere (e.g. formation of HULIS by oxidative degradation of biopolymers). On the other hand, organic compounds with high molecular mass can also originate from SOA formation by heterogeneous and multiphase reactions at the surface and in the bulk of atmospheric particles as outlined above (SOA oligomers/polymers).

For the identification and quantification of individual organic compounds, filter and impactor samples are usually extracted with appropriate solvents, and the extracts are analyzed by advanced instrumental or bioanalytical methods of separation and detection: gas and liquid chromatography; capillary electrophoresis; absorption and fluorescence spectroscopy; mass spectrometry; immunosorbent, enzyme, and dye assays; etc.[29,57,62,92,95,102–105] Alternatively, deposited or suspended particles can be partially or fully vaporized by thermal or laser desorption and directly introduced into a gas chromatograph or spectrometer.[1,20,25,26,32]

In recent studies nuclear magnetic resonance,[16] Fourier-transform infrared spectroscopy,[77] scanning transmission X-ray microscopy,[106] and aerosol mass spectrometry[107] were applied for efficient characterization and quantification of functional groups in OPM (alkyl, carbonyl, carboxyl, and hydroxy groups; C–C double bonds and aromatic rings). These methods give valuable insight into the overall chemical composition, oxidation state, and reactivity of OPM, but they provide only limited information about the actual identity of the individual compounds, which are present in the complex mixture. The molecular mass and structure of organic compounds, however, are crucial parameters for their physicochemical and biological properties and thus for their climate and health effects (volatility, solubility, hygroscopicity, CCN and IN activity, bioavailability, toxicity, allergenicity; see Sections 3 and 4).

3. Chemical Reactivity and Water Interactions

Chemical reactions proceed at the surface and in the bulk of solid and liquid aerosol particles and can influence atmospheric gas-phase chemistry as well as the properties of atmospheric particles and their effects on climate and human health.[1,4,84,108–116,117]

For example, aerosol chemistry leads to the formation of reactive halogen species, changes to reactive nitrogen compounds, and depletion of ozone—especially in the stratosphere, upper troposphere, and marine boundary layer.[118–128] On the other hand, chemical aging of aerosol particles generally changes their composition, decreases their reactivity, increases their hygroscopicity and cloud condensation activity, and can change their optical properties.[19,114,115,129–134]

Because of their high surface-to-volume ratio, fine aerosol particles can be very efficiently transformed upon interaction with solar radiation (photolysis) and reactive trace gases (oxidation, nitration, acid–base reactions, hydrolysis, condensation or radical-initiated oligomerization, etc.). For example, oxidation and nitration reactions lead to the formation or degradation of hazardous aerosol components,[6,61,78,101] they cause artifacts upon collection and analysis of air particulate matter,[1,19,30] and they play a major role in technical processes and devices for the control of combustion aerosol emissions.[74,135–137] Moreover, the interaction with water can lead to structural rearrangements of solid aerosol particles, to the

© 2005 Wiley-VCH Verlag GmbH & Co. KGaA, Weinheim

formation of highly concentrated aqueous solution droplets (hygroscopic growth), and to the formation of cloud droplets and ice crystals (Section 3.2).

Atmospheric aerosol transformations and gas–particle interactions generally involve multiple physicochemical processes such as mass transport, phase transition, and chemical reactions at the interface or in the bulk of gas, liquid and solid phases, as illustrated in Figure 7. These multiphase processes are pivotal for the aerosol and cloud interactions and feedback loops outlined in Figures 1 and 3, and thus for the climate and health effects of atmospheric aerosols detailed below (Section 4).

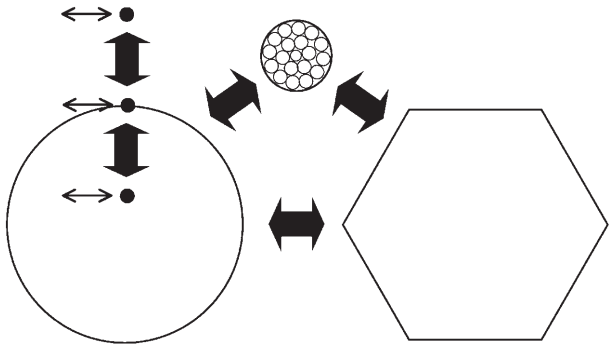

Figure 7. Schematic illustration of multiphase aerosol and cloud processes: mass transport and phase transitions of (semi-)volatile molecules between gas phase, aerosol particles, cloud droplets, and ice crystals (bold arrows); chemical reactions in the gas phase, at the particle surface, and in the particle bulk (thin arrows).

Efficient investigation, elucidation, and description of the interactions between multiple phases and chemical components of aerosols and clouds by laboratory experiments, field measurements, remote sensing, and model studies require consistent terminologies and universally applicable mathematical formalisms and physical parameters. However, the current understanding of the mechanisms and kinetics of mass transport, phase transitions, and chemical reactions in atmospheric aerosols and clouds is very limited. Besides a lack of experimental data, one of the limitations is that the formalisms applied in different studies have mostly been restricted to specific systems and boundary conditions: liquid water, ice, acid hydrates, soot, or mineral dust; fresh or aged surfaces; low or high reactant concentration levels, transient or (quasi-) steady-state conditions; limited selection of chemical species and reactions.[84] The different and sometimes inconsistent rate equations, parameters, and terminologies make it hard to compare, extrapolate, and integrate the results of different studies over the wide range of reaction conditions relevant for the atmosphere, laboratory experiments, technical processes, and emission control.

A comprehensive kinetic model framework for aerosol and cloud surface chemistry and gas–particle interactions was recently proposed by Pöschl, Rudich, and Ammann (PRA).[84] It allows the description of mass transport and chemical reactions at the gas–particle interface and the linking of surface processes with gas-phase and particle bulk processes in aerosol and cloud systems with unlimited numbers of chemical components and physicochemical processes. The key elements and essential aspects of the PRA framework are:

a) a simple and descriptive double-layer surface model (sorption layer and quasi-static layer);
b) straightforward and additive flux-based mass balance and rate equations;
c) clear separation of mass transport and chemical reactions;
d) well-defined rate parameters (uptake and accommodation coefficients, reaction- and transport-rate coefficients);
e) clear distinction between different elementary and multi-step transport processes (surface and bulk accommodation, etc.);
f) clear distinction between different elementary and multi-step heterogeneous and multiphase reactions (Langmuir–Hinshelwood and Eley–Rideal mechanisms, etc.);
g) mechanistic description of complex concentration and time dependence;
h) flexible inclusion or omission of chemical species and physicochemical processes;
i) flexible convolution or deconvolution of species and processes;
j) full compatibility with traditional resistor model formulations.

Figure 8 illustrates the PRA model compartments and elementary processes at the gas–particle interface. The individual steps of mass transport are indicated by bold

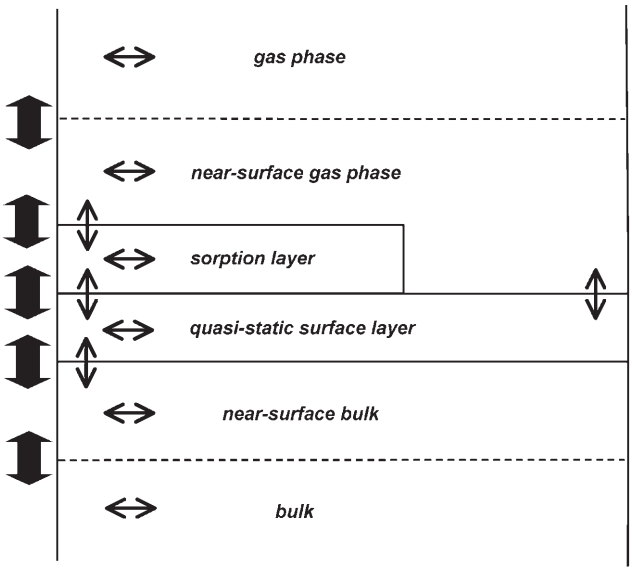

Figure 8. PRA framework model compartments, transport processes, and chemical reactions at the gas–particle interface (double-layer surface model): fluxes of diffusion in the gas phase and particle bulk, adsorption and desorption, transfer between sorption layer and quasi-static surface layer and between quasi-static surface layer and near-surface particle bulk indicated by vertical bold arrows on the left side; elementary chemical reactions between species in the same or in different model compartments indicated by horizontal and vertical thin arrows, respectively.[84]

 © 2005 Wiley-VCH Verlag GmbH & Co. KGaA, Weinheim

arrows beside the model compartments: gas-phase diffusion; reversible adsorption; mass transfer between sorption layer, quasi-static surface layer, and near-surface particle bulk; diffusion in the particle bulk. The thin arrows inside the model compartments represent different types of chemical reactions: gas-phase reactions; gas-surface reactions; surface-layer reactions; surface-bulk reactions; particle-bulk reactions.[84] Exemplary practical applications and model calculations demonstrating the relevance of these aspects were presented in a companion paper.[138]

The PRA framework is meant to serve as a common basis for experimental and theoretical studies to investigate and describe atmospheric-aerosol and cloud-surface chemistry and gas–particle interactions. In particular, it should support the following research activities: planning and design of laboratory experiments for the elucidation and determination of elementary processes and rate parameters; the establishment, evaluation, and quality assurance of comprehensive and self-consistent collections of kinetic parameters; and the development of detailed master mechanisms for process models and the derivation of simplified but yet realistic parameterizations for atmospheric and climate models in analogy to atmospheric gas-phase chemistry.[89,139–143]

3.1. Chemical Transformation of Carbonaceous Aerosol Components

Organic aerosol components as well as the surface layers of BC or EC can react with atmospheric photooxidants (OH, O_3, NO_3, NO_2, etc.), acids (HNO_3, H_2SO_4, etc.), water, and UV radiation. The chemical aging of OA components essentially follows the generic reaction pathways outlined in Figure 9 and tends to increase the oxidation state and water solubility of OC. In analogy to atmospheric gas-phase photochemistry of VOCs (methane, isoprene, terpenes, etc.),[89,140,141] oxidation, nitration, hydrolysis, and photolysis transform hydrocarbons and derivatives with one or few functional groups into multifunctional hydrocarbon derivatives. The cleavage of organic molecules and release of SVOCs, VOCs, CO, or CO_2 can also lead to volatilization of OPM. On the other hand, oxidative modification and degradation of biopolymers may convert these into HULIS (analogous to the formation of humic substances in soil, surface water, and groundwater processes). Moreover, condensation reactions and radical-initiated oligo- or polymerization can decrease the volatility of OA components and promote the formation of SOA particulate matter (SOA oligomers or HULIS; Table 2; Section 2.2).

The actual reaction mechanisms and kinetics, however, have been elucidated and fully characterized only for a small number of model reaction systems and components. So far, most progress has been made in the kinetic investigation and modeling of chemical reactions in cloud droplets.[144,145] For the reasons outlined above, very few reliable and widely applicable kinetic parameters are available for organic reactions at the surface and in the bulk of liquid and solid aerosol particles.[19,27,84,114,146,147]

Several studies have shown that surface reactions of organic molecules and black or elemental carbon with gaseous photooxidants such as ozone or nitrogen dioxide tend to exhibit nonlinear concentration dependence and competitive coadsorption of different gas-phase components, which can be described by Langmuir–Hinshelwood reaction mechanisms and rate equations.[84,109,114,138,148]

An example of such reactions is the degradation of benzo[*a*]pyrene (BaP) on soot by ozone. BaP, a prominent air pollutant, is a polycyclic aromatic hydrocarbon (PAH) with the chemical formula $C_{20}H_{12}$ and consists of five six-membered aromatic rings. It is one of the most hazardous carcinogens and mutagens among the 16 priority PAH pollutants defined by the US Environmental Protection Agency (EPA). The main source of BaP in the atmosphere are combustion aerosols, and it resides to a large extent at the surface of soot particles.[30,78,115]

Figure 10 shows pseudo-first-order rate coefficients for the degradation of BaP on soot by ozone at gas-phase mole fractions or volume mixing ratios (VMR) up to 1 ppm under dry conditions and in the presence of water vapor (relative humidity (RH) 25 %, 296 K, 1 atm). These and complementary results of aerosol flow tube experiments and model calculations indicate reversible and competitive adsorption of O_3 and H_2O, followed by a slower, rate-limiting surface reaction between adsorbed O_3 and BaP on the soot surface. The kinetic parameters determined from the displayed non-

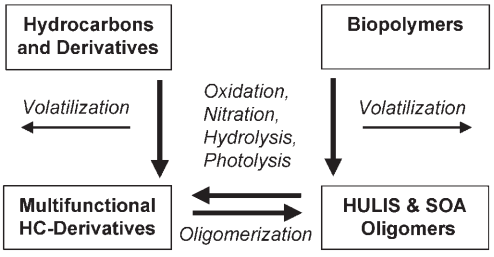

Figure 9. Generic reaction pathways for the atmospheric transformation (chemical aging) of organic aerosol components (left side: low molecular mass; right side: high molecular mass).

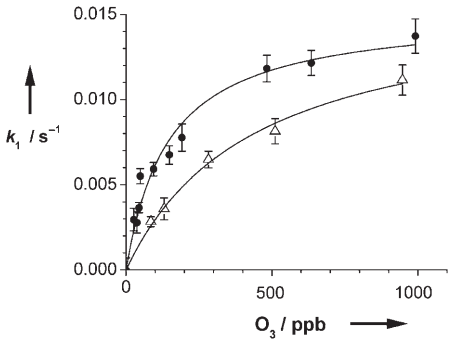

Figure 10. Pseudo-first-order rate coefficients (k_1) for the degradation of benzo[*a*]pyrene (BaP) on soot by ozone: measurement data from aerosol flow tube experiments under dry and humid conditions (symbols and error bars: arithmetic mean ± standard deviation; full circles: RH < 1 %; open triangles: RH ≈ 25 %) and nonlinear least-squares-fit lines based on Langmuir–Hinshelwood rate equation.[115]

© 2005 Wiley-VCH Verlag GmbH & Co. KGaA, Weinheim

linear least squares fits (maximum pseudo-first-order rate coefficients and effective Langmuir adsorption equilibrium constants) allow the prediction of the half-life (50% decay time) of BaP on the surface of soot particles in the atmosphere. At typical ambient ozone VMR of about 30 ppb it would be only around 5 min under dry conditions and 15 min at 25% RH.

Figure 11 illustrates the recovery ratio (RR) of BaP from fine air particulate matter (PM2.5) collected with a regular

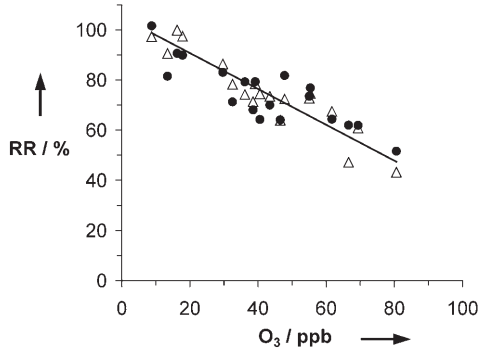

Figure 11. Recovery ratio for benzo[*a*]pyrene, BaP (full circles), and the sum of all particle-bound five- and six-ring US EPA priority PAH pollutants, PAH(5,6) (△), plotted against ambient ozone volume mixing ratio upon filter sampling of urban air particulate matter: measurement data points and linear least-squares fit.[30]

filter sampling system from urban air at ambient ozone VMRs of up to 80 ppb (Munich, 2001/2002). The plotted recovery ratios refer to filter samples collected in parallel with a system that removes ozone and other photooxidants from the sample air flow by means of an activated carbon diffusion denuder.[30] Thus deviations from unity represent the fraction of BaP degraded by reaction with ozone and other photooxidants from the sampled air during the sampling process, that is, the BaP loss by filter reaction sampling artifacts. The BaP recovery ratio is nearly identical to the recovery ratio of the sum of all particle-bound five- and six-ring US EPA priority PAH pollutants, PAH(5,6), and exhibits a negative linear correlation with ambient ozone. It decreases from 100% at low ozone levels to 50% at 80 ppb O_3, which is a characteristic concentration level for polluted urban air in summer. Similar correlations have been observed in experiments performed at different locations and with different filter sampling and denuder systems.[30]

With regard to chemical kinetics, the linear correlation between PAH recovery ratio and O_3 VMR can be attributed to the near-linear dependence of the PAH degradation rate coefficient on O_3 at low VRMs (VMR $\ll$ inverse of effective adsorption equilibrium constant; Figure 10).[84,109,115,138] Moreover, it indicates efficient protection and shielding of the PAH on deposited particles from further decay by coverage with subsequently collected particulate matter (build-up of "filter cake") on time scales similar to the half-life of PAH at the surface. Otherwise, the PAH recovery should be even lower and the ozone concentration dependence should be less pronounced.

In any case, the sampling artifacts observed by Schauer et al. (2003) and illustrated in Figure 11 imply that the real concentrations of particle-bound PAH in urban air are up to 100% higher than the measurement values obtained with simple filter-sampling systems (without activated carbon diffusion denuder or equivalent equipment) as applied for most atmospheric research and air-pollution-monitoring purposes.[30,78,115] Clearly also other OA components with similar or higher reactivity towards atmospheric oxidants (e.g. alkenes) are prone to similar or even stronger sampling artifacts, which have to be avoided or at least minimized and quantified for accurate and reliable determination of atmospheric aerosol composition and properties. These and other potential sampling and analytical artifacts caused by reactive transformation of fine air particulate matter have to be taken into account not only in atmospheric and climate research activities, but also in air-pollution control. In particular, the control and enforcement of emission limits and ambient threshold level values for OA components which pose a threat to human health (Section 4.2) require the development, careful characterization and validation, and correct application of robust analytical techniques and procedures.[78]

As far as atmospheric aerosol cycling and feedback loops are concerned (Figures 1 and 3), chemical aging and oxidative degradation of organic compounds present on the surface and in the bulk generally makes aerosol particles more hydrophilic or hygroscopic and enhances their ability to act as CCN. Besides their contribution to the water-soluble fraction of particulate matter, partially oxidized organics can act as surfactants and influence the hygroscopic growth, CCN, and IN activation of aerosol particles (Section 3.2).

The chemical reactivity of carbonaceous aerosol components also plays an important role in technical applications for the control of combustion aerosol emissions. For example, the lowering of emission limits for soot and related diesel exhaust particulate matter (DPM) necessitates the development and implementation of efficient exhaust-treatment technologies such as diesel particulate filters or particle traps with open deposition structures. These systems generally require regeneration by oxidation and gasification of the soot deposits in the filter or catalyst structures. Usually the regeneration is based on discontinuous oxidation by O_2 at high temperatures ($>500\,^{\circ}C$) or continuous oxidation by NO_2 at moderate exhaust temperatures (200–500 °C).[74,135–137,149] Efficient optimization of the design and operating conditions of such exhaust-treatment systems requires comprehensive kinetic characterization and mechanistic understanding of the chemical reactions and transport processes involved. Recent investigations have shown that the oxidation and gasification of diesel soot by NO_2 at elevated concentrations and temperatures (up to 800 ppm NO_2 and 500 °C) follow a similar Langmuir–Hinshelwood reaction mechanism as the oxidation of BaP on soot by O_3 at ambient concentrations and temperature (up to 1 ppm O_3 and 30 °C).[115,148,149]

 © 2005 Wiley-VCH Verlag GmbH & Co. KGaA, Weinheim

3.2. Restructuring, Phase Transitions, Hygroscopic Growth, and CCN/IN Activation of Aerosol Particles upon Interaction with Water Vapor

When water vapor molecules interact with aerosol particles, they can be adsorbed to the surface of the particles or absorbed into the bulk of the particles. For particles consisting of water-soluble material, the uptake of water vapor can lead to aqueous solution droplet formation and a substantial increase in the particle diameter (hygroscopic growth) even at low relative humidities (RH < 100 %; atmospheric gas phase water partial pressure < equilibrium vapor pressure of pure liquid water).[8]

At water vapor supersaturation (RH > 100 %) aerosol particles can act as nuclei for the formation of liquid cloud droplets (cloud condensation nuclei, CCN). For the formation of water droplets from a homogenous gas phase devoid of aerosol particles supersaturations of up to several hundred percent would be required (thermodynamic barrier for the homogenous nucleation of a new phase). In the atmosphere, however, water vapor supersaturations with respect to liquid water generally remain below 10 % and mostly even below 1 %, because aerosol particles induce heterogeneous nucleation, condensation, and cloud formation. At low temperatures or high altitudes clouds consist of mixtures of liquid water droplets and ice crystals, or entirely of ice crystals. The formation of ice crystals is also induced by preexisting aerosol particles, so-called ice nuclei (IN), as detailed below. Ice nucleation in clouds usually requires temperatures well below 0 °C, which can lead to high water vapor supersaturations with respect to ice.[8,150–155]

The minimum supersaturation at which aerosol particles can be effectively activated as CCN or IN, respectively, is called critical supersaturation. It is determined by the physical structure and chemical composition of the particles and generally decreases with increasing particle size. For insoluble CCN the critical supersaturation depends on the wettability of the surface (contact angle of liquid water), and for partially or fully soluble CCN it depends on the mass fraction, hygroscopicity, and surfactant activity of the water-soluble particulate matter.[8,53,55,156,157]

The nucleation of ice crystals on atmospheric aerosol particles can proceed through different pathways or modes. In the deposition mode, water vapor is adsorbed and immediately converted into ice on the surface of the IN (deposition or sorption nuclei). In the condensation freezing mode the aerosol particles act first as CCN and induce the formation of supercooled aqueous droplets, which freeze later on (condensation freezing nuclei). In the immersion mode the IN are incorporated into preexisting aqueous droplets and induce ice formation upon cooling (immersion nuclei). In the contact mode, freezing of a supercooled droplet is initiated upon contact with the surface of the IN (contact nuclei). Obviously, the IN activity of aerosol particles depends primarily on their surface composition and structure, but condensation and immersion freezing can also be governed by water-soluble bulk material.[8,154,158–164]

Most water-soluble aerosol components are hygroscopic and absorb water to form aqueous solutions at RH < 100 %. The phase transition of dry particle material into a saturated aqueous solution is called deliquescence and occurs when a substance-specific RH threshold value (deliquescence relative humidity, DRH) is exceeded. The reverse transition and its RH threshold value are called efflorescence and efflorescence relative humidity (ERH), respectively. The hygroscopic growth and CCN activation of aqueous solution droplets can be described by the so-called Köhler theory, which combines Raoult's law or alternative formulations for the activity of water in aqueous solutions and the Kelvin equation for the dependence of vapor pressure on the curvature and surface tension of a liquid droplet.[8,24,53,55,156,165–169]

Figure 12a shows a typical example of the hygroscopic growth of water-soluble inorganic salts contained in air particulate matter: the hygroscopic growth curve (humidogram) of pure NaCl aerosol particles with dry particle diameters of 100 nm measured in a hygroscopicity tandem differential mobility analyzer (H-TDMA) experiment at relative humidities of up to 95 %. Upon hydration (increase of RH) the crystalline NaCl particles undergo a deliquescence transition at DRH ≈ 75 %. The water uptake and dependence of the aqueous solution droplet diameter on RH agree very well with Köhler theory calculations, which are based on a semiempirical ion interaction parameterization of water activity and account for the effects of particle-shape transformation (cubic crystals and spherical droplets, mobility and mass equivalent diameters).[24] The hysteresis branch measured upon dehydration (decrease of RH) is due to the existence of solution droplets in a metastable state of NaCl supersaturation (ERH < RH < DRH). The efflorescence transition, that is, the formation of salt crystals and evaporation of the liquid water, occurs at ERH ≈ 40 %.

Figure 12b displays the hygroscopic growth curve of aerosol particles composed of pure bovine serum albumin (BSA) as a model for globular proteins and similar organic macromolecules. The hygroscopic growth is much less pronounced than for inorganic salts but still significant, with deliquescence and efflorescence transitions at DRH ≈ ERH ≈ 40 % (conversion of dry protein particles into saturated aqueous solution or gel-like droplets, v.v.) and no significant deviations between hydration and dehydration (no hysteresis effect). The dependence of the deliquesced particle diameter on RH is in good agreement with Köhler theory calculations based on a simple osmotic pressure parameterization of water activity, which has been derived under the assumption that the dissolved protein macromolecules behave like inert solid spheres.[24]

Figure 12c shows the hygroscopic growth curve of internally mixed NaCl–BSA particles (mass ratio 1:1) with dry particle diameters of approximately 100 nm. The mixed aerosol particles have been generated in full analogy to the pure NaCl and pure BSA particles (nebulization of an aqueous solution). Upon hydration, however, the particles exhibit a significant decrease of the measured (mobility equivalent) diameter as the relative humidity approaches the deliquescence threshold (DRH ≈ 75 %). The observed minimum diameter is about 10 % smaller than the initial diameter, indicating high initial porosity of the particles (envelope void

© 2005 Wiley-VCH Verlag GmbH & Co. KGaA, Weinheim

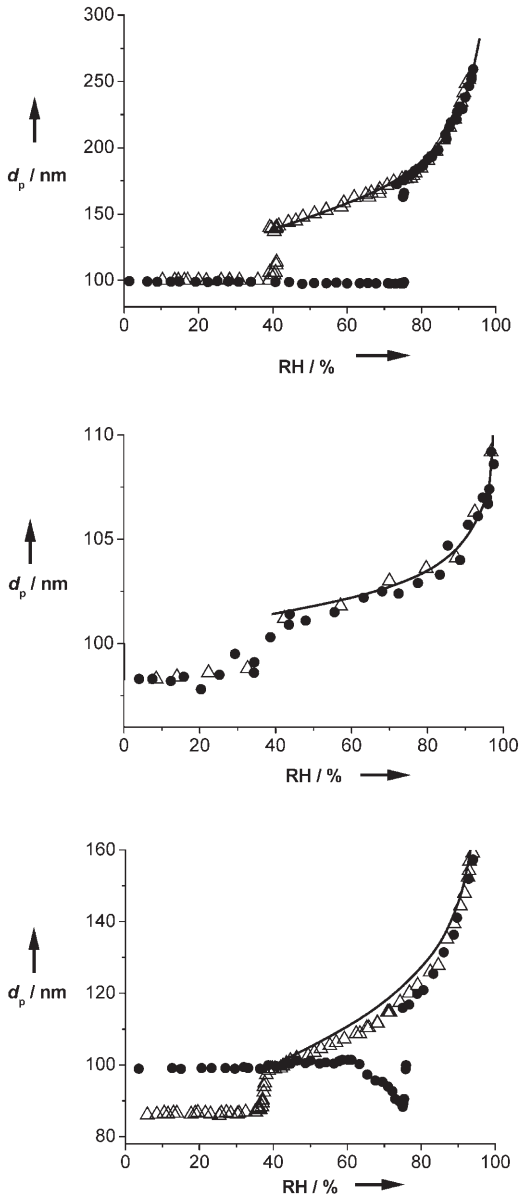

Figure 12. Hygroscopic growth curves for a) pure NaCl salt particles, b) pure BSA protein particles, and c) internally mixed BSA–NaCl protein–salt particles: data points measured upon hydration (●) and dehydration (△) in H-TDMA aerosol experiments; solid lines represent Köhler theory calculations based on NaCl ion interaction and BSA osmotic pressure parameterizations for water activity.[24]

fraction ≈30%) and strong restructuring upon humidification. Upon dehydration the efflorescence threshold is lower than for pure NaCl (ERH ≈37% vs. 40%), indicating that the protein macromolecules inhibit the formation of salt crystals and enhance the stability of supersaturated salt solution droplets. The particle diameters observed after efflorescence essentially equal the minimum diameter observed prior to deliquescence. The hygroscopic growth of the deliquesced particles (aqueous solution droplets) is in fair agreement with Köhler theory calculations based on the observed minimum diameter rather than the initial diameter and on the assumption of simple solute additivity (linear combination of NaCl ion interaction and BSA osmotic pressure parameterizations of water activity).[24] These and complementary measurement and modeling results can be explained by the formation of porous agglomerates due to ion–protein interactions and electric charge effects on the one hand, and by compaction of the agglomerate structure due to capillary condensation and surface tension effects on the other.

Depending on their origin and conditioning, aerosol particles containing inorganic salts and organic (macro-) molecules can have complex and highly porous microstructures, which are influenced by electric charge effects and interactions with water vapor. Proteins and other surfactants tend to be enriched at the particle surface and form an envelope that can inhibit the access of water vapor to the particle core and lead to kinetic limitations of hygroscopic growth, phase transitions, and CCN and IN activation. Formation and effects of organic surfactant films on sea salt particles have recently been discussed by O'Dowd et al.[170] These and other effects of (nonlinear) interactions between organic and inorganic aerosol components have to be elucidated further and considered for consistent analysis of measurement data from laboratory experiments and field measurements and for reliable modeling of atmospheric aerosol processes (Figures 1 and 3).

Structural rearrangements, hygroscopic growth, phase transitions, and CCN and IN activation of aerosol particles interacting with water vapor are not only important for the formation and properties of clouds and precipitation (number density and size of cloud droplets and ice particles; temporal and spatial distribution and intensity of precipitation). They influence also the chemical reactivity and aging of atmospheric particles (accessibility of particle components to reactive trace gases and radiation), their optical properties (absorption and scattering cross-sections), and their health effects upon inhalation into the human respiratory tract (deposition efficiency and bioavailability). Therefore, the water interactions of particles with complex chemical composition are widely and intensely studied in current aerosol, atmospheric, and climate research. So far, however, their mechanistic and quantitative understanding is still rather limited, especially with regard to carbonaceous components.[3,8,19,55,56,154,169,171–176]

4. Climate and Health Effects

Anthropogenic emissions are major sources of atmospheric aerosols. In particular, the emissions of particles and precursor gases from biomass burning and fossil-fuel combustion have massively increased since preindustrial times and account for a major fraction of fine air particulate matter in polluted urban environments as well as in the global atmosphere (carbonaceous components, sulfates, etc.).[1,2,4,9,177–183] Numerous studies have shown that both natural and anthropogenic aerosols have a strong impact on climate and human health. Due to the limited knowledge of aerosol sources, composition, properties, and processes outlined above, however, the actual effects of aerosols on climate and health are still far from being fully understood and

 © 2005 Wiley-VCH Verlag GmbH & Co. KGaA, Weinheim

quantified. Some of the most important aspects and recent developments will be addressed in the following sections.

4.1. Direct and Indirect Aerosol Effects on Climate

Aerosol effects on climate are generally classified as direct or indirect with respect to radiative forcing of the climate system. Radiative forcings are changes in the energy fluxes of solar radiation (maximum intensity in the spectral range of visible light) and terrestrial radiation (maximum intensity in the infrared spectral range) in the atmosphere, induced by anthropogenic or natural changes in atmospheric composition, Earth surface properties, or solar activity. Negative forcings such as the scattering and reflection of solar radiation by aerosols and clouds tend to cool the Earth's surface, whereas positive forcings such as the absorption of terrestrial radiation by greenhouse gases and clouds tend to warm it (greenhouse effect).[2] Figure 13 illustrates the distinction between direct and indirect aerosol effects and some major feedback loops in the climate system. Direct effects result from the scattering and absorption of radiation by aerosol particles, whereas indirect effects result from their CCN and IN activity (influence on clouds and precipitation), or from their chemical and biological activity (influence on aerosol and trace gas emissions and transformation).

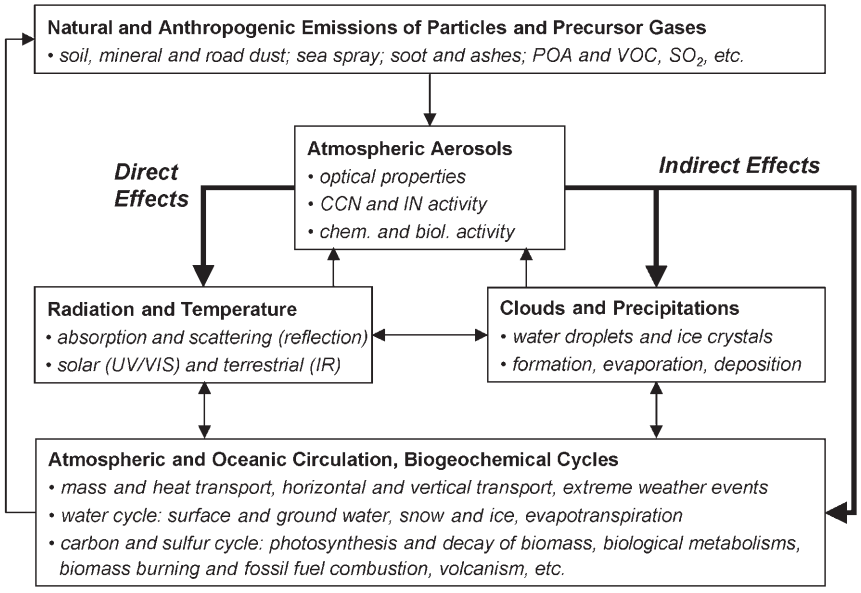

Figure 13. Direct and indirect aerosol effects and major feedback loops in the climate system.

The optical properties relevant for the direct effects (scattering and absorption coefficient or extinction cross-section and single scattering albedo, etc.) as well as the CCN, IN, chemical and biological activities relevant for indirect effects are determined by aerosol particle size, structure, and chemical composition. Thus they are strongly influenced by the atmospheric processes outlined above (coagulation, chemical transformation, water interactions).

The climate feedback loops illustrated in Figure 13 involve the interaction of atmospheric aerosols with solar and terrestrial radiation, clouds and precipitation, general circulation and hydrological cycle, and with natural and anthropogenic aerosol and trace gas sources on global and regional scales. On microscopic and molecular scales, each of the interactions outlined in Figure 13 comprises a multitude of physicochemical processes that depend on atmospheric composition and meteorological conditions and are largely not quantitatively characterized. Thus the actual climate system responses and feedback to natural or anthropogenic perturbations such as industrial and traffic-related greenhouse gas and aerosol emissions, volcanic eruptions, etc. are highly uncertain. In many cases, even the sign or direction of the feedback effect is unknown, that is, it is not clear whether a perturbation will be reinforced (positive feedback) or dampened (negative feedback).

For example, enhanced deposition and uptake of aerosol particles and trace gases on vegetation, soil, or surface water can lead to an increase or decrease in biogenic POA and SOA precursor emissions, depending on the fertilizing, toxic, or reproductive biological activity of the aerosol and trace gas components. The increase in atmospheric CO_2 and global warming is expected to enhance photosynthesis, biogenic emissions of VOC, and the formation of SOA particles, which may act as CCN, increase cloudiness, and lead to a cooling effect (negative feedback).[54] On the other hand, the negative feedback mechanism could be counteracted by temperature-related biological stress and eutrophication effects which may lead to a decrease in photosynthesis, biomass production, VOC emissions, SOA formation, and cloudiness, and further enhance global warming (positive feedback). In any case, feedback effects of this kind and the influence of SOA formation on CCN and IN concentration are determined not only by VOC emissions but also by the photochemical transformation of VOCs into SVOCs and LVOCs/NVOCs, respectively, and their contribution to the growth of preexisting particles or to the formation of new particles. As outlined above, these processes strongly depend on atmospheric composition and meteorological conditions.

An increase in atmospheric CCN and IN concentrations in the atmosphere can have different effects on the formation and properties of liquid water, ice, and mixed-phase clouds and precipitation. Among them are the so-called cloud albedo or Twomey effect (more-numerous and smaller cloud particles reflect more solar radiation), cloud lifetime effect (smaller cloud particles decrease the precipitation efficiency), thermodynamic effect (smaller cloud droplets delay the onset of freezing), and glaciation effect (more IN increase the precipitation efficiency). These and related effects of aerosol, cloud, precipitation, and radiation interactions influence the regional and global radiative energy balance and hydrological cycle as well as the temperature, dynamics, and general

 © 2005 Wiley-VCH Verlag GmbH & Co. KGaA, Weinheim

circulation of the atmosphere and oceans.[2,184–187] Moreover, they can promote extreme weather events (intense rain, hail, and thunderstorms).[188] A recent review article by Lohmann and Feichter (2005)[3] provides an overview of indirect aerosol effects, their estimated magnitude, and climatic implications.

Overall, the current aerosol radiative forcing relative to that in preindustrial times is estimated to be around -1 to $-2\ \mathrm{W\,m^{-2}}$, as opposed to a greenhouse gas forcing of about $+2.4\ \mathrm{W\,m^{-2}}$.[2,3,187] Owing to the limited understanding of the underlying physicochemical processes, however, it is still unclear if clouds provide a positive or negative feedback to an increase in atmospheric carbon dioxide and other greenhouse gases. The uncertainties of aerosol, cloud, and precipitation interactions and feedback effects are among the main reasons for the high uncertainty of climate sensitivities and for the projected global mean surface temperature increase over the next century (1–6 °C or more).[2,3,56]

4.2. Aerosol Health Effects and Air Quality

Numerous epidemiological studies show that fine air particulate matter and traffic-related air pollution are correlated with severe health effects, including enhanced mortality, cardiovascular, respiratory, and allergic diseases.[5,189–192] Moreover, toxicological investigations in vivo and in vitro have demonstrated substantial pulmonary toxicity of model and real environmental aerosol particles, but the biochemical mechanisms and molecular processes that cause the toxicological effects such as oxidative stress and inflammatory response have not yet been resolved. Among the parameters and components potentially relevant for aerosol health effects are the specific surface, transition metals, and organic compounds.[5,193–195] Some of the possible mechanisms by which air particulate matter and other pollutants may affect human health are summarized in Table 3.

Table 3: Possible mechanisms by which aerosol particles and other air pollutants may cause adverse health effects.[5]

pulmonary inflammation induced by PM or O_3
free radical and oxidative stress generated by transition metals or organic compounds (e.g. PAHs)
covalent modification of key intracellular proteins (e.g. enzymes)
inflammation and innate immune effects induced by biological compounds such as endotoxins and glucans
stimulation of nocioreceptor and autonomic nervous system activity regulating heart-rate variability and airway reactivity
adjuvant effects in the immune system (e.g. DPM and transition metals enhancing responses to common environmental allergens)
procoagulant activity by ultrafine particle accessing the systemic circulation
suppression of normal defense mechanisms (e.g. suppression of alveolar macrophage functions)

Ultrafine particles ($d_p < 100$ nm) are suspected to be particularly hazardous to human health, because they are sufficiently small to penetrate the membranes of the respiratory tract and enter the blood circulation or be transported along olfactory nerves into the brain.[196–198] Neither for ultrafine nor for larger aerosol particles, however, it is clear which physical and chemical properties actually determine their adverse health effects (particle size, structure, number, mass concentration, solubility, chemical composition, and individual components, etc.).

Particularly little is known about the relations between allergic diseases and air quality. Nevertheless, traffic-related air pollution with high concentration levels of fine air particulate matter, nitrogen oxides, and ozone is one of the prime suspects besides non-natural nutrition and excessive hygiene practices, which may be responsible for the strong increase of allergies in industrialized countries over the past decades.[5,199–201] The most prominent group of airborne allergens are protein molecules, which account for up to 5% of urban air particulate matter. They are not only contained in coarse biological particles such as pollen grains (diameter $>10\ \mu$m) but also in the fine fraction of air particulate matter, which can be explained by fine fragments of pollen, microorganisms, or plant debris and by mixing of proteins dissolved in rain water with fine soil and road dust particles.[98,101,202]

A molecular rationale for the promotion of allergies by traffic-related air pollution has been proposed by Franze et al. (2003; 2005),[101,102] who found that proteins including birch pollen allergen Bet v1 are efficiently nitrated by polluted urban air. The nitration reaction converts the natural aromatic amino acid tyrosine into nitrotyrosine and proceeds particularly fast at elevated concentrations of NO_2 and O_3 (so-called photosmog or summer smog conditions), most likely involving nitrate radicals (NO_3) as reactive intermediates. From biomedical and immunological research it is known that protein nitration occurs upon inflammation of biological tissue, where it may serve to mark foreign proteins and guide the immune system. Moreover, conjugates of proteins and peptides with nitroaromatic compounds were found to evade immune tolerance and boost immune responses, and post-translational modifications generally appear to enhance the allergenicity of proteins.[101] Thus the inhalation of aerosols containing nitrated proteins or nitrating reagents is likely to trigger immune reactions, promote the genesis of allergies, and enhance the intensity of allergic diseases and airway inflammations. This hypothesis is supported by first results of ongoing biochemical experiments with nitrated proteins.[203]

By means of newly developed enzyme immunoassays, nitrated proteins have been detected in urban road and window dust as well as in fine air particulate matter, exhibiting degrees of nitration of up to 0.1%. Upon exposure of birch pollen extract to heavily polluted air at a major urban traffic junction and to synthetic gas mixtures containing NO_2 and O_3 at concentration levels characteristic for intense summer smog, the degrees of nitration increased up to 20%. The experimental results indicate that Bet v1 is more easily nitrated than other proteins, which might be an explanation why it is a particularly strong allergen.[101] If the ongoing

 © 2005 Wiley-VCH Verlag GmbH & Co. KGaA, Weinheim

biochemical experiments and further studies confirm that protein nitration by nitrogen oxides and ozone is indeed an important link between air pollution, airway inflammations, and allergies, the spread and enhancement of these diseases could be counteracted by an improvement in the air quality and a decrease in emission limits for nitrogen oxides and other traffic-related air pollutants. Moreover, it might be possible to develop pharmaceuticals against the adverse health effects of nitrated proteins.

Efficient control of air quality and related health effects requires a comprehensive understanding of the identity, sources, atmospheric interactions, and sinks of hazardous pollutants. Without this understanding, the introduction of new laws, regulations, and technical devices for environmental protection runs the risk of being ineffective or even of causing more harm than good through unwanted side effects.

For example, epidemiological evidence for adverse health effects of fine and ultrafine particles has led to a lowering of present and future emission limits for soot and related DPM.[137,198,204–206] For compliance with these emission limits, different particle filter or trapping and exhaust-treatment technologies have been developed and are currently being introduced into diesel vehicles. Depending on the design of the particle filter or trap and catalytic converter systems, their operation can lead to substantial excess NO_2 emissions.[148] If, however, elevated NO_2 concentrations and the nitration of proteins indeed promote allergies, such systems could reduce respiratory and cardiovascular diseases related to soot particles but at the same time enhance allergic diseases. Moreover, elevated NO_2 concentrations and incomplete oxidation of soot in exhaust filter systems could also increase the emissions of volatile or semivolatile hazardous aerosol components such as nitrated PAH derivatives.[61,78] Thus an effective mitigation of the adverse health effects of diesel engine exhaust may require the introduction of advanced catalytic converter systems that minimize the emissions of both particulate and gaseous pollutants (soot, PAH and PAH derivatives, nitrogen oxides, etc.) rather than simple particle filters.

In any case, comprehensive investigations, understanding, and control of aerosol health effects need to consider both the particulate and gaseous components of aerosols as well as their chemical reactivity and aging.[78]

5. Summary and Outlook

Scientific investigations and reports of atmospheric aerosols date back as far as the 18th century, and since then it has become increasingly clear that aerosol particles are of major importance for atmospheric chemistry and physics, the hydrological cycle, climate, and human health.[207] Motivated by global change and adverse health effects of traffic-related air pollution, aerosol research has been intensified increasingly over the past couple of decades.

These activities have led to a fairly comprehensive conceptual understanding of atmospheric aerosol sources, composition, properties, interactions, and effects on climate. The parameters required for a quantitative description of the underlying physicochemical processes, however, are generally still uncertain by factors of two or more, which implies uncertainties of an order of magnitude for most effects involving multiple competitive or sequential processes.

In some cases (e.g. particle nucleation and reactive gas uptake), even the basic parameters are uncertain by orders of magnitude. Consequently, model calculations of atmospheric aerosol effects on future climate have to be regarded as sensitivity studies with more or less reliable qualitative and semiquantitative results and implications, rather than reliable quantitative predictions. In particular, interactions and feedback responses between aerosols and clouds, the hydrological cycle, and the biosphere are difficult to quantify with the currently available information. Regardless of the rapid increase in numerical simulation capacities, this situation can hardly change before the basic physicochemical processes and properties of atmospheric aerosol particles have been elucidated to an extent comparable to the present state of knowledge of atmospheric gas-phase chemistry (universally applicable and validated master mechanisms, rate coefficients, structure–reactivity relationships, etc.).

Outstanding open questions and research aims for the elucidation of aerosol effects relevant to the science and policy of global change have been outlined in several recent monographs, reviews, and research articles.[2,3,54,79,80,84] Among these are the quantification, mechanistic elucidation, and kinetic characterization of the following processes: formation of new particles and secondary organic aerosols; emission of primary organic aerosol components and black or elemental carbon; aging and deposition of aerosol particles; activation of cloud condensation and ice nuclei. As far as chemical transformations, heterogeneous and multiphase reactions, and gas–particle interactions of aerosols and clouds are concerned, one of the most important prerequisites for efficient further investigation and scientific progress is the establishment of a common basis of consistent, unambiguous, and universally applicable terminologies, model formalisms, and kinetic and thermodynamic parameters.

With regard to atmospheric aerosol effects on human health not only the quantitative but also the qualitative and conceptual understanding is very limited. Epidemiological and toxicological studies indicate strong adverse health effects of fine and ultrafine aerosol particles as well as gaseous air pollutants, but the causative relations and mechanisms are hardly known.[5,192] Their elucidation, however, is required for the development of efficient strategies for air-quality control and medical treatment of related diseases that will enable the minimization of adverse aerosol health effects at minimum social and economic costs.

Particularly little is known about the relationship between allergic diseases and air pollution and the interactions between natural aeroallergens and traffic-related pollutants. Several studies have shown synergistic and adjuvant effects of diesel particulate matter, O_3, NO_2, and allergenic pollen proteins, but the specific chemical reactions and molecular processes responsible for these effects have not yet been clearly identified. Recent investigations indicate that the nitration of allergenic proteins by polluted air may play an important role. Nitrated proteins are known to stimulate

© 2005 Wiley-VCH Verlag GmbH & Co. KGaA, Weinheim

immune responses, and they could promote the genesis of allergies, enhance allergic reactions, and influence inflammatory processes, which is confirmed by the results of ongoing biochemical investigations.[101,203]

For efficient elucidation and abatement of adverse aerosol health effects, the knowledge of atmospheric and biomedical aerosol research should be integrated to formulate plausible hypotheses that specify potentially hazardous chemical substances and reactions on a molecular level. These hypotheses have to be tested in appropriate biochemical and medical studies to identify the most relevant species and mechanisms of interaction and to establish the corresponding dose-response relationships. Ultimately, the identification and characterization of hazardous aerosol components and their sources and sinks (emission, transformation, deposition) should allow the optimization of air-pollution control and medical treatment of aerosol effects on human health.

6. Appendix

List of Abbreviations, Acronyms, and Symbols

BaP	benzo[*a*]pyrene
BC	black carbon
BSA	bovine serum albumin
CCN	cloud condensation nucleus
CE	capillary electrophoresis
CI	chemical ionization
d_p	particle diameter
$dN/d(\log d_p)$	particle number size distribution function
DMA	differential mobility analyzer
DPM	diesel exhaust particulate matter
DRH	deliquescence relative humidity
EC	elemental carbon
EI	electron impact ionization
ELPI	electrical low-pressure impactor
EPA	Environmental Protection Agency
ERH	efflorescence relative humidity
ESI	electrospray ionization
HC	hydrocarbon
H-TDMA	hygroscopicity tandem differential mobility analyzer
HULIS	humic-like substances
IC	ion chromatography
IN	ice nucleus
k_1	(pseudo-)first-order rate coefficient
LDI	laser desorption ionization
LVOC	low-volatility organic compound
MWSOC	macromolecular water-soluble organic carbon
NVOC	nonvolatile organic compound
OA	organic aerosol
OC	organic carbon
OPM	organic particulate matter
PAH	polycyclic aromatic hydrocarbon
PAH(5,6)	polycyclic aromatic hydrocarbons consisting of five or six aromatic rings
PM	particulate matter
PM2.5 (1 or 10)	particulate matter of particles with aerodynamic diameters ≤ 2.5 μm (1 or 10 μm)
POA	primary organic aerosol
PRA	Pöschl, Rudich, Ammann (2005)
QCM	quartz crystal microbalance
RH	relative humidity
RR	recovery ratio
SEC	size exclusion chromatography
SEM	scanning electron microscopy
SIMS	secondary ion mass spectrometry
SMPS	scanning mobility particle sizer
SOA	secondary organic aerosol
SPE	solid-phase extraction
SVOC	semivolatile organic compound
TC	total carbon
TEM	transmission electron microscopy
TEOM	tapered element oscillating microbalance
VMR	volume mixing ratio
VOC	volatile organic compound
WSOC	water-soluble organic carbon

I thank my colleagues at the Technical University of Munich, Institute of Hydrochemistry, and my research partners for personal and scientific collaboration, discussions, and good times—in particular M. Ammann, S. Bhowmik, A. Duschl, T. Fehrenbach, T. Franze, C. Huber, L. Krämer, R. Leube, T. Letzel, S. Mahler, A. Messerer, U. McKeon, E. Mikhailov, R. Niessner, D. Rothe, Y. Rudich, A. Sadezky, C. Schauer, M. Weller, and A. Zerrath. The German Federal Ministry of Education and Research (BMBF, AFO2000 young scientist group CARBAERO), the Bavarian Research Foundation (BFS, project PM-Kat), and the Bavarian State Ministry for Regional Development and Environmental Affairs (BayStMLU, project SCAVEX) are gratefully acknowledged for financial support. Moreover, I thank my mentors, partners, and supporting organizations of earlier and other scientific activities for encouragement, insight, and cheerful experiences, in particular P. Crutzen, J. Jayne, D. Worsnop, M. Molina, T. Koop, K. Carslaw, R. Sander, B. Sturges, A. Richter, the Austrian Science Foundation (FWF), the Max Planck Society (MPG), and the European Geosciences Union (EGU). J. Huth, B. Graham, and G. Helas are gratefully acknowledged for electron micrographs. Last but not least I thank my family and personal friends for sharing my life, interests, and pleasures.

Received: March 30, 2005

[1] B. J. Finlayson-Pitts, J. N. Pitts, *Chemistry of the Upper and Lower Atmosphere*, Academic Press, San Diego, **2000**.
[2] J. T. Houghton, Y. Ding, D. J. Griggs, M. Noguer, P. J. van der Linden, X. Dai, K. Maskell, C. A. Johnson, *Climate Change 2001: The Scientific Basis (Contribution of Working Group I to the Third Assessment Report of the Intergovernmental Panel on Climate Change)*, Cambridge University Press, Cambridge, **2001**.
[3] U. Lohmann, J. Feichter, *Atmos. Chem. Phys.* **2005**, *5*, 715.
[4] J. H. Seinfeld, S. N. Pandis, *Atmospheric Chemistry and Physics*, Wiley, New York, **1998**.

 © 2005 Wiley-VCH Verlag GmbH & Co. KGaA, Weinheim

[5] J. A. Bernstein, N. Alexis, C. Barnes, I. L. Bernstein, A. Nel, D. Peden, D. Diaz-Sanchez, S. M. Tarlo, P. B. Williams, *J. Allergy Clin. Immunol.* **2004**, *114*, 1116.
[6] B. J. Finlayson-Pitts, J. N. Pitts, *Science* **1997**, *276*, 1045.
[7] W. C. Hinds, *Aerosol Technology*, Wiley, New York, **1999**.
[8] H. R. Pruppacher, J. D. Klett, *Microphysics of clouds and precipitation*, Kluwer, Dordrecht, **1997**.
[9] F. Raes, R. Van Dingenen, E. Vignati, J. Wilson, J. P. Putaud, J. H. Seinfeld, P. Adams, *Atmos. Environ.* **2000**, *34*, 4215.
[10] J. Williams, M. de Reus, R. Krejci, H. Fischer, J. Ström, *Atmos. Chem. Phys.* **2002**, *2*, 133.
[11] R. Van Dingenen, F. Raes, J.-P. Putaud, U. Baltensperger, A. Charron, M.-C. Facchini, S. Decesari, S. Fuzzi, R. Gehrig, H.-C. Hansson, R. M. Harrison, C. Hüglin, A. M. Jones, P. Laj, G. Lorbeer, W. Maenhaut, F. Palmgren, X. Querol, S. Rodriguez, J. Schneider, H. ten Brink, P. Tunved, K. Torseth, B. Wehner, E. Weingartner, A. Wiedensohler, P. Wahlin, *Atmos. Environ.* **2004**, *38*, 2561.
[12] R. Krejci, J. Ström, M. de Reus, J. Williams, H. Fischer, M. O. Andreae, H.-C. Hansson, *Atmos. Chem. Phys.* **2005**, *5*, 1527.
[13] J.-P. Putaud, F. Raes, R. Van Dingenen, E. Brüggemann, M.-C. Facchini, S. Decesari, S. Fuzzi, R. Gehrig, C. Hüglin, P. Laj, G. Lorbeer, W. Maenhaut, N. Mihalopoulos, K. Müller, X. Querol, S. Rodriguez, J. Schneider, G. Spindler, H. ten Brink, K. Torseth, A. Wiedensohler, *Atmos. Environ.* **2004**, *38*, 2579.
[14] A. Zerrath, R. Niessner, U. Pöschl, *J. Aerosol. Sci.* **2003**, *34*, S649.
[15] A. Zerrath, *Analytik von Cellulose und Glucose in atmosphärischen Aerosolproben und physikalische Aerosol-Charakterisierung mit einem elektrischen Niederdruckimpaktor*, PhD Thesis, Technical University München, **2005**.
[16] E. Matta, M. C. Facchini, S. Decesari, M. Mircea, F. Cavalli, S. Fuzzi, J. P. Putaud, A. Dell'Acqua, *Atmos. Chem. Phys.* **2003**, *3*, 623.
[17] J. P. Putaud, R. Van Dingenen, A. Dell'Acqua, F. Raes, E. Matta, S. Decesari, M. C. Facchini, S. Fuzzi, *Atmos. Chem. Phys.* **2004**, *4*, 889.
[18] M. Ebert, S. Weinbruch, P. Hoffmann, H. M. Ortner, *Atmos. Environ.* **2004**, *38*, 6531.
[19] A. Gelencser, *Carbonaceous Aerosol*, Springer, Dordrecht, **2004**.
[20] P. H. McMurry, *Atmos. Environ.* **2000**, *34*, 1959.
[21] R. Niessner, *Angew. Chem.* **1991**, *103*, 542; *Angew. Chem. Int. Ed. Engl.* **1991**, *30*, 466.
[22] P. A. Baron, K. Willeke, *Aerosol Measurement*, Wiley, New York, **2001**.
[23] J. Joutsensaari, P. Vaattovaara, M. Vesterinen, K. Hameri, A. Laaksonen, *Atmos. Chem. Phys.* **2001**, *1*, 51.
[24] E. Mikhailov, S. Vlasenko, R. Niessner, U. Pöschl, *Atmos. Chem. Phys.* **2004**, *4*, 323.
[25] C. A. Noble, K. A. Prather, *Mass Spectrom. Rev.* **2000**, *19*, 248.
[26] D. Y. H. Pui, R. C. Flagan, S. L. Kaufman, A. D. Maynard, J. F. de la Mora, S. V. Hering, J. L. Jimenez, K. A. Prather, A. S. Wexler, P. J. Ziemann, *J. Nanopart. Res.* **2004**, *6*, 314.
[27] Y. Katrib, S. T. Martin, Y. Rudich, P. Davidovits, J. T. Jayne, D. R. Worsnop, *Atmos. Chem. Phys.* **2005**, *5*, 275.
[28] J. N. Smith, K. F. Moore, P. H. McMurry, F. L. Eisele, *Aerosol Sci. Technol.* **2004**, *38*, 100.
[29] M. C. Jacobson, H. C. Hansson, K. J. Noone, R. J. Charlson, *Rev. Geophys.* **2000**, *38*, 267.
[30] C. Schauer, R. Niessner, U. Pöschl, *Environ. Sci. Technol.* **2003**, *37*, 2861.
[31] K. P. Hinz, R. Kaufmann, B. Spengler, *Anal. Chem.* **1994**, *66*, 2071.
[32] H. J. Tobias, P. M. Kooiman, K. S. Docherty, P. J. Ziemann, *Aerosol Sci. Technol.* **2000**, *33*, 170.
[33] J. Schneider, S. Borrmann, A. G. Wollny, M. Blasner, N. Mihalopoulos, K. Oikonomou, J. Sciare, A. Teller, Z. Levin, D. R. Worsnop, *Atmos. Chem. Phys.* **2004**, *4*, 65.
[34] J. T. Jayne, D. C. Leard, X. F. Zhang, P. Davidovits, K. A. Smith, C. E. Kolb, D. R. Worsnop, *Aerosol Sci. Technol.* **2000**, *33*, 49.
[35] D. M. Murphy, D. S. Thomson, T. M. J. Mahoney, *Science* **1998**, *282*, 1664.
[36] A. M. Middlebrook, D. M. Murphy, S. H. Lee, D. S. Thomson, K. A. Prather, R. J. Wenzel, D. Y. Liu, D. J. Phares, K. P. Rhoads, A. S. Wexler, M. V. Johnston, J. L. Jimenez, J. T. Jayne, D. R. Worsnop, I. Yourshaw, J. H. Seinfeld, R. C. Flagan, *J. Geophys. Res.* **2003**, *108*.
[37] M. F. Sipin, S. A. Guazzotti, K. A. Prather, *Anal. Chem.* **2003**, *75*, 2929.
[38] F. Drewnick, J. J. Schwab, J. T. Jayne, M. Canagaratna, D. R. Worsnop, K. L. Demerjian, *Aerosol Sci. Technol.* **2004**, *38*, 92.
[39] F. Drewnick, J. T. Jayne, M. Canagaratna, D. R. Worsnop, K. L. Demerjian, *Aerosol Sci. Technol.* **2004**, *38*, 104.
[40] Q. Zhang, M. R. Canagaratna, J. T. Jayne, D. R. Worsnop, J. L. Jimenez, *J. Geophys. Res.* **2005**, *110*.
[41] A. L. van Wuijckhuijse, M. A. Stowers, W. A. Kleefsman, B. L. M. van Baar, C. E. Kientz, J. C. M. Marijnissen, *J. Aerosol Sci.* **2005**, *36*, 677.
[42] D. P. Fergenson, M. E. Pitesky, H. J. Tobias, P. T. Steele, G. A. Czerwieniec, S. C. Russell, C. B. Lebrilla, J. M. Horn, K. R. Coffee, A. Srivastava, S. P. Pillai, M. T. P. Shih, H. L. Hall, A. J. Ramponi, J. T. Chang, R. G. Langlois, P. L. Estacio, R. T. Hadley, M. Frank, E. E. Gard, *Anal. Chem.* **2004**, *76*, 373.
[43] J. Ho, *Anal. Chim. Acta* **2002**, *457*, 125.
[44] C. S. Cox, C. M. Wathes, *Bioaerosols handbook*, Lewis, Boca Raton, **1995**.
[45] S. A. Grinshpun, J. M. Clark, *J. Aerosol Sci.* **2005**, *36*, 553.
[46] P.-A. Maron, D. P. H. Lejon, E. Carvalho, K. Bizet, P. Lemanceau, L. Ranjard, C. Mougel, *Atmos. Environ.* **2005**, *39*, 3687.
[47] S. Matthias-Maser, R. Jaenicke, *Atmos. Res.* **1995**, *39*, 279.
[48] S. Matthias-Maser, R. Jaenicke, *J. Aerosol Sci.* **1994**, *25*, 1605.
[49] H. Bauer, A. Kasper-Giebl, M. Loflund, H. Giebl, R. Hitzenberger, F. Zibuschka, H. Puxbaum, *Atmos. Res.* **2002**, *64*, 109.
[50] H. Bauer, A. Kasper-Giebl, F. Zibuschka, R. Hitzenberger, G. F. Kraus, H. Puxbaum, *Anal. Chem.* **2002**, *74*, 91.
[51] H. Bauer, H. Giebl, R. Hitzenberger, A. Kasper-Giebl, G. Reischl, F. Zibuschka, H. Puxbaum, *J. Geophys. Res.* **2003**, *108*.
[52] P. Amato, M. Menagera, M. Sancelmea, P. Laj, G. Mailhot, A.-M. Delorta, *Atmos. Environ.* **2005**, *39*, 4143–4153.
[53] S. Henning, T. Rosenorn, B. D'Anna, A. A. Gola, B. Svenningsson, M. Bilde, *Atmos. Chem. Phys.* **2005**, *5*, 575.
[54] M. Kulmala, T. Suni, K. E. J. Lehtinen, M. Dal Maso, M. Boy, A. Reissell, U. Rannik, P. Aalto, P. Keronen, H. Hakola, J. B. Back, T. Hoffmann, T. Vesala, P. Hari, *Atmos. Chem. Phys.* **2004**, *4*, 557.
[55] R. Sorjamaa, B. Svenningsson, T. Raatikainen, S. Henning, M. Bilde, A. Laaksonen, *Atmos. Chem. Phys.* **2004**, *4*, 2107.
[56] M. Kanakidou, J. H. Seinfeld, S. N. Pandis, I. Barnes, F. J. Dentener, M. C. Facchini, R. Van Dingenen, B. Ervens, A. Nenes, C. J. Nielsen, E. Swietlicki, J. P. Putaud, Y. Balkanski, S. Fuzzi, J. Horth, G. K. Moortgat, R. Winterhalter, C. E. L. Myhre, K. Tsigaridis, E. Vignati, E. G. Stephanou, J. Wilson, *Atmos. Chem. Phys.* **2005**, *5*, 1053.
[57] U. Pöschl, *Anal. Bioanal. Chem.* **2003**, *375*, 30.
[58] K. H. Homann, *Angew. Chem.* **1998**, *110*, 2572; *Angew. Chem. Int. Ed.* **1998**, *37*, 2435.
[59] A. Sadezky, H. Muckenhuber, H. Grothe, R. Niessner, U. Pöschl, *Carbon* **2005**, *43*, 1731.
[60] S. Szidat, T. M. Jenk, H. W. Gaggeler, H. A. Synal, R. Fisseha, U. Baltensperger, M. Kalberer, V. Samburova, L. Wacker, M. Saurer, M. Schwikowski, I. Hajdas, *Radiocarbon* **2004**, *46*, 475.

 © 2005 Wiley-VCH Verlag GmbH & Co. KGaA, Weinheim

[61] C. Schauer, R. Niessner, U. Pöschl, *Anal. Bioanal. Chem.* **2004**, *378*, 725.
[62] T. Franze, *Analyse und Reaktivität von Proteinen in atmosphärischen Aerosolen und Enwicklung neuer Immunoassays zur Messung von Nitroproteinen*, PhD Thesis, Technical University München, **2004**.
[63] J. Hendricks, B. Kärcher, A. Dopelheuer, J. Feichter, U. Lohmann, D. Baumgardner, *Atmos. Chem. Phys.* **2004**, *4*, 2521.
[64] A. Kirkevag, T. Iversen, A. Dahlback, *Atmos. Environ.* **1999**, *33*, 2621.
[65] M. Z. Jacobson, *J. Geophys. Res.* **2002**, *107*, 4410.
[66] H. Schmid, L. Laskus, H. J. Abraham, U. Baltensperger, V. Lavanchy, M. Bizjak, P. Burba, H. Cachier, D. Crow, J. Chow, T. Gnauk, A. Even, H. M. ten Brink, K. P. Giesen, R. Hitzenberger, E. Hueglin, W. Maenhaut, C. Pio, A. Carvalho, J. P. Putaud, D. Toom-Sauntry, H. Puxbaum, *Atmos. Environ.* **2001**, *35*, 2111.
[67] R. Hitzenberger, S. G. Jennings, S. M. Larson, A. Dillner, H. Cachier, Z. Galambos, A. Rouc, T. G. Spain, *Atmos. Environ.* **1999**, *33*, 2823.
[68] K. Wittmaack, *Atmos. Chem. Phys.* **2005**, *5*, 1905.
[69] A. Petzold, H. Schloesser, P. J. Sheridan, W. P. Arnott, J. A. Ogren, A. Virkkula, *Aerosol Sci. Technol.* **2005**, *39*, 40.
[70] V. M. H. Lavanchy, H. W. Gaggeler, S. Nyeki, U. Baltensperger, *Atmos. Environ.* **1999**, *33*, 2759.
[71] H. Saathoff, K. H. Naumann, M. Schnaiter, W. Schock, E. Weingartner, U. Baltensperger, L. Kramer, Z. Bozoki, U. Pöschl, R. Niessner, U. Schurath, *J. Aerosol Sci.* **2003**, *34*, 1399.
[72] W. P. Arnott, H. Moosmüller, C. F. Rogers, T. F. Jin, R. Bruch, *Atmos. Environ.* **1999**, *33*, 2845.
[73] P. J. Sheridan, W. P. Arnott, J. A. Ogren, E. Andrews, D. B. Atkinson, D. S. Covert, H. Moosmüller, A. Petzold, B. Schmid, A. W. Strawa, R. Varma, A. Virkkula, *Aerosol Sci. Technol.* **2005**, *39*, 1.
[74] D. S. Su, R. E. Jentoft, J. O. Müller, D. Rothe, E. Jacob, C. D. Simpson, Z. Tomovic, K. Müllen, A. Messerer, U. Pöschl, R. Niessner, R. Schlögl, *Catal. Today* **2004**, *90*, 127.
[75] S. Mertes, B. Dippel, A. Schwarzenböck, *J. Aerosol Sci.* **2004**, *35*, 347.
[76] A. Stratmann, G. Schweiger, *J. Aerosol Sci.* **2005**, submitted.
[77] L. M. Russell, *Environ. Sci. Technol.* **2003**, *37*, 2982.
[78] U. Pöschl, *J. Aerosol Med.* **2002**, *15*, 203.
[79] M. Kulmala, L. Laakso, K. E. J. Lehtinen, I. Riipinen, M. Dal Maso, T. Anttila, V. M. Kerminen, U. Horrak, M. Vana, H. Tammet, *Atmos. Chem. Phys.* **2004**, *4*, 2553.
[80] M. Kulmala, H. Vehkamaki, T. Petajda, M. Dal Maso, A. Lauri, V. M. Kerminen, W. Birmili, P. H. McMurry, *J. Aerosol Sci.* **2004**, *35*, 143.
[81] T. Anttila, V. M. Kerminen, M. Kulmala, A. Laaksonen, C. D. O'Dowd, *Atmos. Chem. Phys.* **2004**, *4*, 1071.
[82] R. Y. Zhang, I. Suh, J. Zhao, D. Zhang, E. C. Fortner, X. X. Tie, L. T. Molina, M. J. Molina, *Science* **2004**, *304*, 1487.
[83] L. Laakso, T. Anttila, K. E. J. Lehtinen, P. P. Aalto, M. Kulmala, U. Horrak, J. Paatero, M. Hanke, F. Arnold, *Atmos. Chem. Phys.* **2004**, *4*, 2353.
[84] U. Pöschl, Y. Rudich, M. Ammann, *Atmos. Chem. Phys. Discuss.* **2005**, *5*, 2111, and references therein.
[85] M. P. Tolocka, M. Jang, J. M. Ginter, F. J. Cox, R. M. Kamens, M. V. Johnston, *Environ. Sci. Technol.* **2004**, *38*, 1428.
[86] M. S. Jang, N. M. Czoschke, S. Lee, R. M. Kamens, *Science* **2002**, *298*, 814.
[87] M. Kalberer, D. Paulsen, M. Sax, M. Steinbacher, J. Dommen, A. S. H. Prevot, R. Fisseha, E. Weingartner, V. Frankevich, R. Zenobi, U. Baltensperger, *Science* **2004**, *303*, 1659.
[88] A. Limbeck, M. Kulmala, H. Puxbaum, *Geophys. Res. Lett.* **2003**, *30*, 1996.
[89] M. E. Jenkin, *Atmos. Chem. Phys.* **2004**, *4*, 1741.
[90] K. Tsigaridis, M. Kanakidou, *Atmos. Chem. Phys.* **2003**, *3*, 1849.
[91] C. Marcolli, B. P. Luo, T. Peter, F. G. Wienhold, *Atmos. Chem. Phys.* **2004**, *4*, 2593.
[92] A. H. Falkovich, E. R. Graber, G. Schkolnik, Y. Rudich, W. Maenhaut, P. Artaxo, *Atmos. Chem. Phys.* **2005**, *5*, 781.
[93] B. Graham, O. L. Mayol-Bracero, P. Guyon, G. C. Roberts, S. Decesari, M. C. Facchini, P. Artaxo, W. Maenhaut, P. Koll, M. O. Andreae, *J. Geophys. Res.* **2002**, *107*.
[94] O. L. Mayol-Bracero, P. Guyon, B. Graham, G. Roberts, M. O. Andreae, S. Decesari, M. C. Facchini, S. Fuzzi, P. Artaxo, *J. Geophys. Res.* **2002**, *107*.
[95] J. F. Hamilton, P. J. Webb, A. C. Lewis, J. R. Hopkins, S. Smith, P. Davy, *Atmos. Chem. Phys.* **2004**, *4*, 1279.
[96] M. Claeys, B. Graham, G. Vas, W. Wang, R. Vermeylen, V. Pashynska, J. Cafmeyer, P. Guyon, M. O. Andreae, P. Artaxo, W. Maenhaut, *Science* **2004**, *303*, 1173.
[97] S. Zappoli, A. Andracchio, S. Fuzzi, M. C. Facchini, A. Gelencser, G. Kiss, Z. Krivacsy, A. Molnar, E. Meszaros, H. C. Hansson, K. Rosman, Y. Zebuhr, *Atmos. Environ.* **1999**, *33*, 2733.
[98] Q. Zhang, C. Anastasio, *Atmos. Environ.* **2003**, *37*, 2247.
[99] H. Puxbaum, M. Tenze-Kunit, *Atmos. Environ.* **2003**, *37*, 3693.
[100] N. Havers, P. Burba, J. Lambert, D. Klockow, *J. Atmos. Chem.* **1998**, *29*, 45.
[101] T. Franze, M. G. Weller, R. Niessner, U. Pöschl, *Environ. Sci. Technol.* **2005**, *39*, 1673.
[102] T. Franze, M. G. Weller, R. Niessner, U. Pöschl, *Analyst* **2003**, *128*, 824.
[103] T. Franze, M. G. Weller, R. Niessner, U. Pöschl, *Analyst* **2004**, *129*, 589.
[104] W. Walcher, T. Franze, M. G. Weller, U. Pöschl, C. G. Huber, *J. Proteome Res.* **2003**, *2*, 534.
[105] G. Schkolnik, A. H. Falkovich, Y. Rudich, W. Maenhaut, P. Artaxo, *Environ. Sci. Technol.* **2005**, *39*, 2744.
[106] S. F. Maria, L. M. Russell, M. K. Gilles, S. C. B. Myneni, *Science* **2004**, *306*, 1921.
[107] M. R. Alfarra, H. Coe, J. D. Allan, K. N. Bower, H. Boudries, M. R. Canagaratna, J. L. Jimenez, J. T. Jayne, A. A. Garforth, S. M. Li, D. R. Worsnop, *Atmos. Environ.* **2004**, *38*, 5745.
[108] R. Atkinson, D. L. Baulch, R. A. Cox, R. F. Hampson, J. A. Kerr, M. J. Rossi, J. Troe, *J. Phys. Chem. Ref. Data* **1997**, *26*, 1329.
[109] M. Ammann, U. Pöschl, Y. Rudich, *Phys. Chem. Chem. Phys.* **2003**, *5*, 351.
[110] J. T. Jayne, U. Pöschl, Y. M. Chen, D. Dai, L. T. Molina, D. R. Worsnop, C. E. Kolb, M. J. Molina, *J. Phys. Chem. A* **1997**, *101*, 10000.
[111] U. Pöschl, M. Canagaratna, J. T. Jayne, L. T. Molina, D. R. Worsnop, C. E. Kolb, M. J. Molina, *J. Phys. Chem. A* **1998**, *102*, 10082.
[112] A. R. Ravishankara, *Science* **1997**, *276*, 1058.
[113] J. P. Reid, R. M. Sayer, *Chem. Soc. Rev.* **2003**, *32*, 70.
[114] Y. Rudich, *Chem. Rev.* **2003**, *103*, 5097.
[115] U. Pöschl, T. Letzel, C. Schauer, R. Niessner, *J. Phys. Chem. A* **2001**, *105*, 4029.
[116] R. Sander, *Surv. Geophys.* **1999**, *20*, 1.
[117] S. P. Sander, B. J. Finlayson-Pitts, R. R. Friedl, D. M. Golden, R. E. Huie, C. E. Kolb, M. J. Kurylo, M. J. Molina, G. K. Moortgat, V. L. Orkin, A. R. Ravishankara, *Chemical kinetics and photochemical data for use in atmospheric studies, Evaluation number 14, Vol. JPL Publication 02–25*, Jet Propulsion Laboratory, Pasadena, **2002**.
[118] A. E. Waibel, T. Peter, K. S. Carslaw, H. Oelhaf, G. Wetzel, P. J. Crutzen, U. Pöschl, A. Tsias, E. Reimer, H. Fischer, *Science* **1999**, *283*, 2064.
[119] D. J. Stewart, P. T. Griffiths, R. A. Cox, *Atmos. Chem. Phys.* **2004**, *4*, 1381.

 © 2005 Wiley-VCH Verlag GmbH & Co. KGaA, Weinheim

[120] J. Austin, D. Shindell, S. R. Beagley, C. Bruhl, M. Dameris, E. Manzini, T. Nagashima, P. Newman, S. Pawson, G. Pitari, E. Rozanov, C. Schnadt, T. G. Shepherd, *Atmos. Chem. Phys.* **2003**, *3*, 1.
[121] S. K. Meilinger, B. Kärcher, T. Peter, *Atmos. Chem. Phys.* **2002**, *2*, 307.
[122] S. K. Meilinger, B. Kärcher, T. Peter, *Atmos. Chem. Phys.* **2005**, *5*, 533.
[123] M. O. Andreae, P. J. Crutzen, *Science* **1997**, *276*, 1052.
[124] R. Sander, W. C. Keene, A. A. P. Pszenny, R. Arimoto, G. P. Ayers, E. Baboukas, J. M. Cainey, P. J. Crutzen, R. A. Duce, G. Honninger, B. J. Huebert, W. Maenhaut, N. Mihalopoulos, V. C. Turekian, R. Van Dingenen, *Atmos. Chem. Phys.* **2003**, *3*, 1301.
[125] A. A. P. Pszenny, J. Moldanov, W. C. Keene, R. Sander, J. R. Maben, M. Martinez, P. J. Crutzen, D. Perner, R. G. Prinn, *Atmos. Chem. Phys.* **2004**, *4*, 147.
[126] R. C. Sullivan, T. Thornberry, J. P. D. Abbatt, *Atmos. Chem. Phys.* **2004**, *4*, 1301.
[127] S. Tilmes, R. Müller, J. U. Grooss, J. M. Russell, *Atmos. Chem. Phys.* **2004**, *4*, 2181.
[128] J.-U. Grooß, G. Günther, R. Müller, P. Konopka, S. Bausch, H. Schlager, C. Voigt, C. M. Volk, G. C. Toon, *Atmos. Chem. Phys.* **2005**, *5*, 1437.
[129] K. Broekhuizen, P. P. Kumar, J. P. D. Abbatt, *Geophys. Res. Lett.* **2004**, *31*, 1107.
[130] A. Asad, B. T. Mmereki, D. J. Donaldson, *Atmos. Chem. Phys.* **2004**, *4*, 2083.
[131] A. Gelencser, A. Hoffer, G. Kiss, E. Tombacz, R. Kurdi, L. Bencze, *J. Atmos. Chem.* **2003**, *45*, 25.
[132] P. P. Kumar, K. Broekhuizen, J. P. D. Abbatt, *Atmos. Chem. Phys.* **2003**, *3*, 509.
[133] T. Moise, Y. Rudich, *J. Phys. Chem. A* **2002**, *106*, 6469.
[134] N. O. A. Kwamena, J. A. Thornton, J. P. D. Abbatt, *J. Phys. Chem. A* **2004**, *108*, 11626.
[135] A. Messerer, R. Niessner, U. Pöschl, *J. Aerosol Sci.* **2003**, *34*, 1009.
[136] A. Messerer, H. J. Schmid, C. Knab, U. Pöschl, R. Niessner, *Chem. Ing. Tech.* **2004**, *76*, 1092.
[137] A. Messerer, D. Rothe, U. Pöschl, R. Niessner, *Top. Catal.* **2004**, *30–31*, 247.
[138] M. Ammann, U. Pöschl, *Atmos. Chem. Phys. Discuss.* **2005**, *5*, 2193.
[139] R. Atkinson, D. L. Baulch, R. A. Cox, J. N. Crowley, R. F. Hampson, R. G. Hynes, M. E. Jenkin, M. J. Rossi, J. Troe, *Atmos. Chem. Phys.* **2004**, *4*, 1461.
[140] M. E. Jenkin, S. M. Saunders, V. Wagner, M. J. Pilling, *Atmos. Chem. Phys.* **2003**, *3*, 181.
[141] S. M. Saunders, M. E. Jenkin, R. G. Derwent, M. J. Pilling, *Atmos. Chem. Phys.* **2003**, *3*, 161.
[142] U. Pöschl, R. von Kuhlmann, N. Poisson, P. J. Crutzen, *J. Atmos. Chem.* **2000**, *37*, 29.
[143] R. von Kuhlmann, M. G. Lawrence, U. Pöschl, P. J. Crutzen, *Atmos. Chem. Phys.* **2004**, *4*, 1.
[144] B. Ervens, C. George, J. E. Williams, G. V. Buxton, G. A. Salmon, M. Bydder, F. Wilkinson, F. Dentener, P. Mirabel, R. Wolke, H. Herrmann, *J. Geophys. Res.* **2003**, *108*.
[145] R. Sander, A. Kerkweg, P. Jockel, J. Lelieveld, *Atmos. Chem. Phys.* **2005**, *5*, 445.
[146] M. J. Molina, A. V. Ivanov, S. Trakhtenberg, L. T. Molina, *Geophys. Res. Lett.* **2004**, *31*.
[147] Y. Katrib, S. T. Martin, H. M. Hung, Y. Rudich, H. Z. Zhang, J. G. Slowik, P. Davidovits, J. T. Jayne, D. R. Worsnop, *J. Phys. Chem. A* **2004**, *108*, 6686.
[148] A. Messerer, R. Niessner, U. Pöschl, *Carbon* **2005**, in press (DOI: 10.1016/j.carbon.2005.07.017).
[149] A. Messerer, D. Rothe, R. Niessner, U. Pöschl, *Chem. Ing. Tech.* **2005**, *77*, 881.
[150] P. Spichtinger, K. Gierens, H. G. J. Smit, J. Ovarlez, J. F. Gayet, *Atmos. Chem. Phys.* **2004**, *4*, 639.
[151] P. Spichtinger, K. Gierens, H. Wernli, *Atmos. Chem. Phys.* **2005**, *5*, 973.
[152] P. Spichtinger, K. Gierens, A. Dornbrack, *Atmos. Chem. Phys.* **2005**, *5*, 1243.
[153] E. J. Jensen, J. B. Smith, L. Pfister, J. V. Pittman, E. M. Weinstock, D. S. Sayres, R. L. Herman, R. F. Troy, K. Rosenlof, T. L. Thompson, A. M. Fridlind, P. K. Hudson, D. J. Cziczo, A. J. Heymsfield, C. Schmitt, J. C. Wilson, *Atmos. Chem. Phys.* **2005**, *5*, 851.
[154] B. Kärcher, T. Koop, *Atmos. Chem. Phys.* **2005**, *5*, 703.
[155] K. Gierens, *Atmos. Chem. Phys.* **2003**, *3*, 437.
[156] B. Svenningsson, J. Rissler, E. Swietlicki, M. Mircea, M. Bilde, M. C. Facchini, S. Decesari, S. Fuzzi, J. Zhou, J. Mønster, T. Rosenørn, *Atmos. Chem. Phys. Discuss.* **2005**, *5*, 2833.
[157] A. M. L. Ekman, C. Wang, J. Wilson, J. Ström, *Atmos. Chem. Phys.* **2004**, *4*, 773.
[158] T. J. Fortin, K. Drdla, L. T. Iraci, M. A. Tolbert, *Atmos. Chem. Phys.* **2003**, *3*, 987.
[159] C. M. Archuleta, P. J. DeMott, S. M. Kreidenweis, *Atmos. Chem. Phys. Discuss.* **2005**, *5*, 3391.
[160] C. H. Twohy, M. R. Poellot, *Atmos. Chem. Phys. Discuss.* **2005**, *5*, 3723.
[161] M. Seifert, J. Ström, R. Krejci, A. Minikin, A. Petzold, J. F. Gayet, U. Schumann, J. Ovarlez, *Atmos. Chem. Phys.* **2003**, *3*, 1037.
[162] J. Ström, M. Seifert, B. Kärcher, J. Ovarlez, A. Minikin, J. F. Gayet, R. Krejci, A. Petzold, F. Auriol, W. Haag, R. Busen, U. Schumann, H. C. Hansson, *Atmos. Chem. Phys.* **2003**, *3*, 1807.
[163] M. Seifert, J. Ström, R. Krejci, A. Minikin, A. Petzold, J. F. Gayet, H. Schlager, H. Ziereis, U. Schumann, J. Ovarlez, *Atmos. Chem. Phys.* **2004**, *4*, 1343.
[164] M. Seifert, J. Ström, R. Krejci, A. Minikin, A. Petzold, J. F. Gayet, H. Schlager, H. Ziereis, U. Schumann, J. Ovarlez, *Atmos. Chem. Phys.* **2004**, *4*, 293.
[165] S. M. Kreidenweis, K. Koehler, P. J. DeMott, A. J. Prenni, C. Carrico, B. Ervens, *Atmos. Chem. Phys.* **2005**, *5*, 1357.
[166] D. O. Topping, G. B. McFiggans, H. Coe, *Atmos. Chem. Phys.* **2005**, *5*, 1205.
[167] D. O. Topping, G. B. McFiggans, H. Coe, *Atmos. Chem. Phys.* **2005**, *5*, 1223.
[168] C. Marcolli, T. Peter, *Atmos. Chem. Phys.* **2005**, *5*, 1545.
[169] T. Raatikainen, A. Laaksonen, *Atmos. Chem. Phys. Discuss.* **2005**, *5*, 3641.
[170] C. D. O'Dowd, M. C. Facchini, F. Cavalli, D. Ceburnis, M. Mircea, S. Decesari, S. Fuzzi, Y. J. Yoon, J. P. Putaud, *Nature* **2004**, *431*, 676.
[171] S. T. Martin, H. M. Hung, R. J. Park, D. J. Jacob, R. J. D. Spurr, K. V. Chance, M. Chin, *Atmos. Chem. Phys.* **2004**, *4*, 183.
[172] M. Gysel, E. Weingartner, S. Nyeki, D. Paulsen, U. Baltensperger, I. Galambos, G. Kiss, *Atmos. Chem. Phys.* **2004**, *4*, 35.
[173] D. V. Spracklen, K. J. Pringle, K. S. Carslaw, M. P. Chipperfield, G. W. Mann, *Atmos. Chem. Phys. Discuss.* **2005**, *5*, 179.
[174] D. V. Spracklen, K. J. Pringle, K. S. Carslaw, M. P. Chipperfield, G. W. Mann, *Atmos. Chem. Phys. Discuss.* **2005**, *5*, 3437.
[175] C. E. L. Myhre, C. J. Nielsen, *Atmos. Chem. Phys.* **2004**, *4*, 1759.
[176] A. Maßling, A. Wiedensohler, B. Busch, C. Neusüß, P. Quinn, T. Bates, D. Covert, *Atmos. Chem. Phys.* **2003**, *3*, 1377.
[177] J. S. Reid, R. Koppmann, T. F. Eck, D. P. Eleuterio, *Atmos. Chem. Phys.* **2005**, *5*, 799.
[178] J. S. Reid, T. F. Eck, S. A. Christopher, R. Koppmann, O. Dubovik, D. P. Eleuterio, B. N. Holben, E. A. Reid, J. Zhang, *Atmos. Chem. Phys.* **2005**, *5*, 827.
[179] C. Michel, C. Liousse, J. M. Gregoire, K. Tansey, G. R. Carmichael, J. H. Woo, *J. Geophys. Res.* **2005**, *110*.

 © 2005 Wiley-VCH Verlag GmbH & Co. KGaA, Weinheim

[180] F. Cousin, C. Liousse, H. Cachier, B. Bessagnet, B. Guillaume, R. Rosset, *Atmos. Environ.* **2005**, *39*, 1539.
[181] M. Z. Jacobson, *J. Geophys. Res.* **2004**, *109*.
[182] D. G. Streets, T. C. Bond, T. Lee, C. Jang, *J. Geophys. Res.* **2004**, *109*.
[183] T. C. Bond, D. G. Streets, K. F. Yarber, S. M. Nelson, J. H. Woo, Z. Klimont, *J. Geophys. Res.* **2004**, *109*.
[184] Y. Rudich, O. Khersonsky, D. Rosenfeld, *Geophys. Res. Lett.* **2002**, *29*.
[185] D. Rosenfeld, R. Lahav, A. Khain, M. Pinsky, *Science* **2002**, *297*, 1667.
[186] V. Ramanathan, P. J. Crutzen, J. T. Kiehl, D. Rosenfeld, *Science* **2001**, *294*, 2119.
[187] M. O. Andreae, C. D. Jones, P. M. Cox, *Nature* **2005**, *435*, 1187.
[188] M. O. Andreae, D. Rosenfeld, P. Artaxo, A. A. Costa, G. P. Frank, K. M. Longo, M. A. F. Silva-Dias, *Science* **2004**, *303*, 1337.
[189] W. J. Gauderman, E. Avol, F. Gilliland, H. Vora, D. Thomas, K. Berhane, R. McConnell, N. Kuenzli, F. Lurmann, E. Rappaport, H. Margolis, D. Bates, J. Peters, *N. Engl. J. Med.* **2004**, *351*, 1057.
[190] K. Katsouyanni, G. Touloumi, E. Samoli, A. Gryparis, A. Le Tertre, Y. Monopolis, G. Rossi, D. Zmirou, F. Ballester, A. Boumghar, H. R. Anderson, B. Wojtyniak, A. Paldy, R. Braunstein, J. Pekkanen, C. Schindler, J. Schwartz, *Epidemiology* **2001**, *12*, 521.
[191] C. A. Pope, R. T. Burnett, G. D. Thurston, M. J. Thun, E. E. Calle, D. Krewski, J. J. Godleski, *Circulation* **2004**, *109*, 71.
[192] J. Samet, R. Wassel, K. J. Holmes, E. Abt, K. Bakshi, *Environ. Sci. Technol.* **2005**, *39*, 209A.
[193] H. Bömmel, M. Haake, P. Luft, J. Horejs-Hoeck, H. Hein, J. Bartels, C. Schauer, U. Pöschl, M. Kracht, A. Duschl, *Int. Immunopharmacol.* **2003**, *3*, 1371.
[194] K. Donaldson, V. Stone, P. J. A. Borm, L. A. Jimenez, P. S. Gilmour, R. P. F. Schins, A. M. Knaapen, I. Rahman, S. P. Faux, D. M. Brown, W. MacNee, *Free Radical Biol. Med.* **2003**, *34*, 1369.
[195] R. P. F. Schins, J. H. Lightbody, P. J. A. Borm, T. M. Shi, K. Donaldson, V. Stone, *Toxicol. Appl. Pharmacol.* **2004**, *195*, 1.
[196] G. Oberdörster, Z. Sharp, V. Atudorei, A. Elder, R. Gelein, W. Kreyling, C. Cox, *Inhalation Toxicol.* **2004**, *16*, 437.
[197] A. Nemmar, P. H. M. Hoet, B. Vanquickenborne, D. Dinsdale, M. Thomeer, M. F. Hoylaerts, H. Vanbilloen, L. Mortelmans, B. Nemery, *Circulation* **2002**, *105*, 411.
[198] G. Oberdörster, E. Oberdörster, J. Oberdörster, *Environ. Health Perspect.* **2005**, *113*, 823.
[199] B. Brunekreef, J. Sunyer, *Eur. Respir. J.* **2003**, *21*, 913.
[200] J. Ring, U. Krämer, T. Schäfer, H. Behrendt, *Curr. Opin. Immunol.* **2001**, *13*, 701.
[201] J. Ring, B. Eberlein-Koenig, H. Behrendt, *Ann. Allergy Asthma Immunol.* **2001**, *87*, 2.
[202] A. G. Miguel, G. R. Cass, M. M. Glovsky, J. Weiss, *Environ. Sci. Technol.* **1999**, *33*, 4159.
[203] Y. K. Gruijthuijsen, I. Grieshuber, U. Tischler, T. Fehrenbach, M. G. Weller, U. Pöschl, A. Duschl, *Int. Arch. Allergy Immunol.* **2005**, submitted.
[204] A. Ibald-Mulli, H. E. Wichmann, W. Kreyling, A. Peters, *J. Aerosol Med.* **2002**, *15*, 189.
[205] A. Peters, H. E. Wichmann, T. Tuch, J. Heinrich, J. Heyder, *Am. J. Respir. Crit. Care Med.* **1997**, *155*, 1376.
[206] D. Rothe, F. I. Zuther, E. Jacob, A. Messerer, U. Pöschl, R. Niessner, C. Knab, M. Mangold, C. Mangold, *SAE Tech. Pap. Ser.* **2004**, 2004.
[207] O. Preining, J. E. Davis, *History of Aerosol Science*, Österreichische Akademie der Wissenschaften, Vienna, **2000**.

 © 2005 Wiley-VCH Verlag GmbH & Co. KGaA, Weinheim

Communications

DOI: 10.1002/anie.200503080

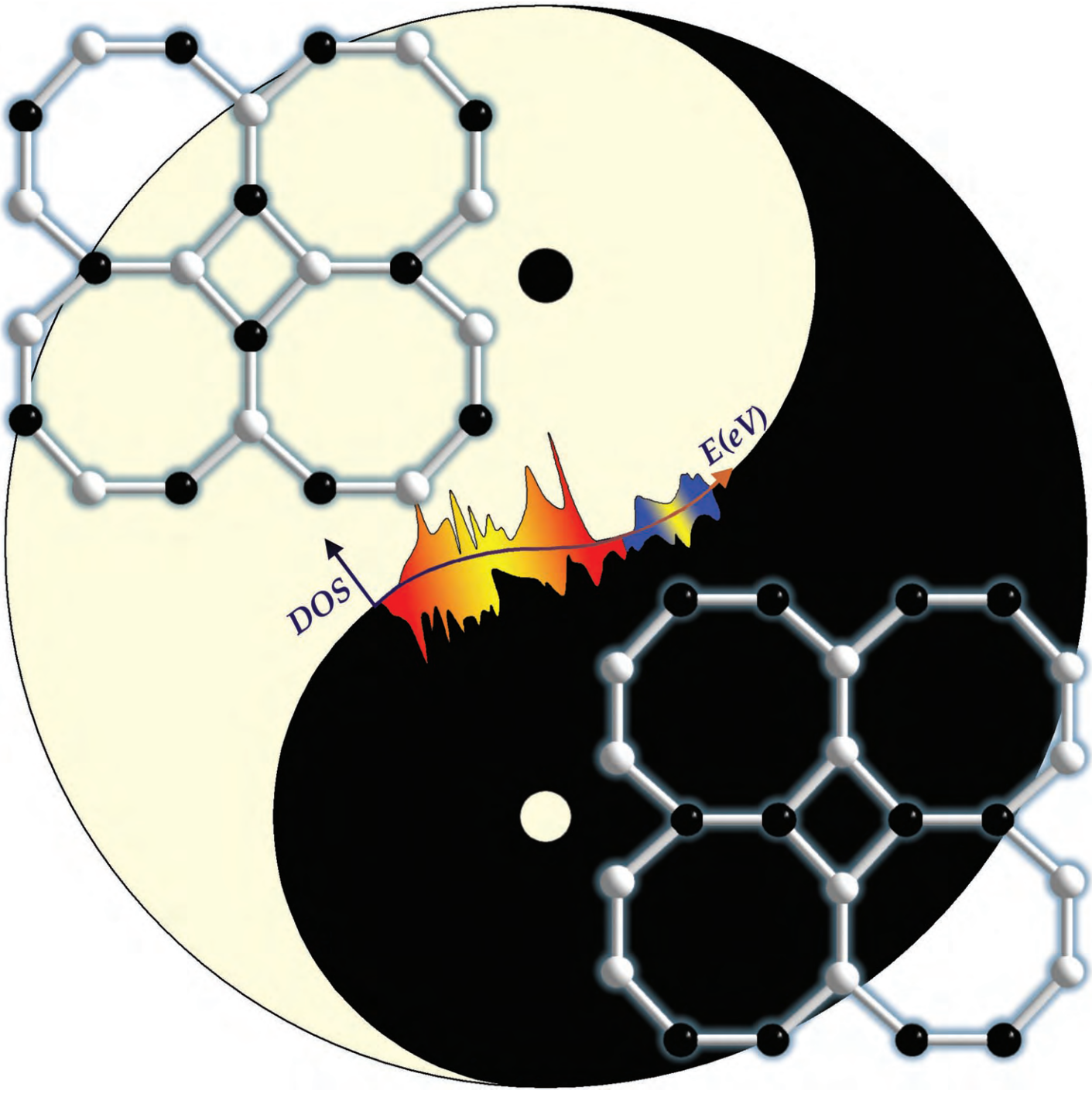

Full geometric optimizations have been applied to metal boron carbide (MB_2C_2) phases. The respective positions of the B and C atoms (the so-called "coloring problem") have been definitely solved for trivalent metals by using DFT calculations. For further details, see the Communication by J.-Y. Saillard, J.-F. Halet, X. Rocquefelte, and co-workers on the following pages.

WILEY InterScience DISCOVER SOMETHING GREAT
© 2005 Wiley-VCH Verlag GmbH & Co. KGaA, Weinheim

Inclusion Compounds

DOI: 10.1002/anie.200503080

Structural Preference versus Metal within the MB_2C_2 (M = Mg, Sc, Ca, Y, Ln) Phases: The Coloring Problem Revisited by DFT Calculations**

Xavier Rocquefelte, Salah Eddine Boulfelfel, Mouna Ben Yahia, Josef Bauer, Jean-Yves Saillard,* and Jean-François Halet**

The chemistry of boron-containing compounds is particularly rich and offers an extremely broad variety of topologies.[1] In the case of the MB_2C_2 phases (M = alkaline-earth or rare-earth metal), for instance, the recent discovery of various potentially interesting properties has revived the interest of the scientific community. For example, CeB_2C_2 is known to exhibit antiferromagnetic ordering at low temperature,[2] and antiferroquadrupolar transitions have been measured for DyB_2C_2[3] and HoB_2C_2.[4] Akimitsu et al. reported that CaB_2C_2 is a high-temperature ferromagnet,[5] although it was shown later by Mori and Otani that this ferromagnetism is due to the presence of an iron impurity.[6,7] Superconductivity at low temperature has also been reported for YB_2C_2, LuB_2C_2, and doped MgB_2C_2.[8] Although the properties of this family of compounds have been widely investigated, some of their structures are still debated, especially with respect to the position of B atoms versus C atoms (the so-called "coloring problem"[9]). Indeed, when the metal is a heavy element, it is not easy to differentiate between these two atoms, either by using X-ray or neutron-diffraction techniques.[10] Indeed, all the known MB_2C_2 structures consist of the stacking of two-dimensional (2D) B/C layers, with metal atoms in between. Four different 2D B/C topologies have been reported so far: fused six-membered rings in the 6^3 net of MgB_2C_2[11] (Figure 1a), fused five- and seven-membered rings in the 57^2 net of ScB_2C_2[12] (Figure 1b) and two different colorings of fused four- and eight-membered rings in the 48^2 net (Figure 1c,d). LaB_2C_2 (Figure 1c) has been proposed by Bauer and Bars[13] to adopt coloring I (BBCC), thus contradicting an earlier study of Smith et al. who suggested coloring II (BCBC; Figure 1d). More recently, neutron-diffraction structures of various lanthanide derivatives were solved assuming the model of Smith et al.[14] On the other hand, Albert et al.[10,15,16] have shown that CaB_2C_2 also adopts coloring II, but with a different stacking of the 2D layers (Figure 1d). Thus, among the 48^2 nets three B/C orderings with two different in-plane colorings have been proposed so far, thereby leading to controversial reports concerning these structures.[17,18]

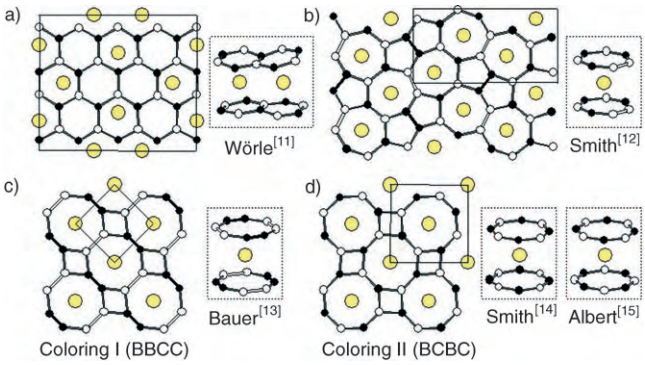

Figure 1. Schematic representation of the MB_2C_2 structure types. a) 6^3 net of MgB_2C_2 (*Cmca*) and b) 57^2 net of ScB_2C_2 (*Pbam*). Three models corresponding to the 48^2 net: c) Bauer model ($P4_2/mmc$) and d) Smith ($P4/mbm$) and Albert ($I4/mcm$) models. The insets show the corresponding stackings.

About 20 years ago, a very elegant theoretical tight-binding investigation of the 2D $B_2C_2^{2-}$ network by Burdett et al.[19] led to the conclusion that coloring II is more stable than coloring I for this formal dianionic charge. Indeed, coloring II allows a band gap at the Fermi level to open, whereas coloring I does not. This prediction was experimentally confirmed later for CaB_2C_2 (formally $[Ca^{2+}, B_2C_2^{2-}]$) by Albert et al.[10,15,16] However, the question of the coloring remains open with one more electron per formula unit (f.u.), that is, when the metal is a trivalent metal. Indeed, the presence of an extra electron occupying antibonding states is expected to destabilize coloring II.

We report herein the first quantitative theoretical analysis of the structural preference of MB_2C_2 (M = Mg, Ca, Sc, Y, La, Ce, and Lu) phases, including the answer to the coloring question for trivalent metals. Full geometric optimizations of the five structure types shown in Figure 1 were carried out for each metal at the DFT level.[20] The cohesive energies estimated from the optimized structures are given in Table 1. The stability of MgB_2C_2 and ScB_2C_2 in their experimentally characterized structures is well reproduced. This result supports our theoretical approach to estimating the relative stability of the models based on the 48^2 nets. Regardless of the metal, coloring II is significantly more stable than coloring I. CaB_2C_2 is found to be more stable in its experimental structure.[15] In the case of the trivalent metals (Y, Ce, and La), coloring II is also found to be the most stable B/C arrangement, with little energy difference between the Albert and Smith models, as observed with Ca. The Smith and

[*] Dr. X. Rocquefelte, S. E. Boulfelfel,[+] M. Ben Yahia, Dr. J. Bauer, Prof. J.-Y. Saillard, Dr. J.-F. Halet
Laboratoire de Chimie du Solide et Inorganique Moléculaire
UMR 6511 CNRS-Université de Rennes 1
Institut de Chimie de Rennes, 35042 Rennes (France)
Fax: (+33) 2-2323-6840
E-mail: xavier.rocquefelte@cnrs.imn.fr
saillard@univ-rennes1.fr
halet@univ-rennes1.fr

[+] present address:
Max-Planck-Institut Dresden
Nöthnitzer Strasse 40
01187 Dresden (Germany)

[**] The authors thank the CCIPL (Nantes), PCIO (Rennes), and IDRIS (Orsay) computing centers for computational facilities.

Supporting information for this article is available on the WWW under http://www.angewandte.org or from the author.

 © 2005 Wiley-VCH Verlag GmbH & Co. KGaA, Weinheim

Table 1: Relative cohesive energies for different optimized MB_2C_2 structures (meV f.u.$^{-1}$).

M	Ionic radius [Å][29]	Structure type				
		MgB_2C_2 6^3	ScB_2C_2 57^2	Coloring I 48^2 [a]	Coloring II 48^2 [b]	Coloring II 48^2 [c]
Mg^{2+}	0.78	0	370	1665	732	876
S^{+}	0.83	133	0	1202	486	399
Lu^{3+}	0.85	281	0	940	263	170
Y^{3+}	1.06	303	94	722	57	0
Ca^{2+}	1.06	169	316	722	0	89
Ce^{3+}	1.07	339	308	577	30	0
La^{3+}	1.22	437	592	625	0	6

[a] Bauer model. [b] Albert model. [c] Smith model.

Albert models differ only by long-distance interactions between the B/C planes and so are expected to be very close in energy. This result suggests the possibility of defaults in the stacking of the 2D B/C nets, which should render the differentiation between B and C by diffraction techniques even more difficult. On the other hand, the ScB_2C_2 structure type is found to be preferred when M = Lu,[25] thus indicating that the B/C topology is related to the ionic size of the metal. Although the structure of LuB_2C_2 in the 48^2 net was recently reported,[18e] it appears from the present calculations that it should also be possible to stabilize this metal in the 57^2 network as well.

The agreement between the most stable computed structure and the corresponding experimentally characterized structure is excellent. Interatomic distances, for example, differ by less than 0.3, 1.3, and 1.5 % in the cases of M = Mg,[11] Ca,[15] and Ce,[18c] respectively. For M = Sc, they differ by less than 1.2 %, except for the B–B distance, which is 5.8 % longer than in the rather inaccurate X-ray structure.[12]

The density of states of CaB_2C_2 is shown in Figure 2 with both coloring I and II (Smith) structure types. As initially qualitatively predicted by Burdett et al.[19] and confirmed recently by Albert et al.,[15] coloring II allows the opening of a energy band gap at the Fermi level. This gap disappears in the case of the less stable coloring I. A rather similar situation occurs for LaB_2C_2, but with one more electron per f.u. In the case of coloring II, this electron occupies the conduction band above the pseudo band gap. Our results (Table 1) show clearly that this extra electron does not destabilize coloring II with respect to coloring I. From this point of view, it is noteworthy that identical B–C distances (short: 1.525 Å; long: 1.603 Å) are computed for CaB_2C_2 and YB_2C_2 in the Smith model despite of their different electron counts.

None of the trivalent metals led to the opening of an energy gap at the Fermi level in any structure type. Band gaps were found only with divalent metals and for the MgB_2C_2 structure type (1.31[26] and 0.41 eV for Mg and Ca, respectively) and the Albert CaB_2C_2 structure type (1.13 and 0.58 eV[26] for Mg and Ca, respectively).

Magishi et al.[28] recently deduced the components of the electric-field gradient (EFG) tensor of CeB_2C_2 from ^{11}B NMR spectroscopic experiments to elucidate its magnetic properties. Such measurements combined with calculated EFG data can also be used to characterize the local environment of the probed atoms. This approach is exemplified by the ^{11}B and ^{139}La EFGs computed for different MB_2C_2 phases using the WIEN2k code[24] (Table 2). A very good agreement between the experimental data of CeB_2C_2 and the calculated data for coloring II is obtained. However, this agreement is not the case for coloring I. Note that, the EFGs are nearly the same in the Albert and Smith models. Such a result is expected because of the similar local environments of the boron atoms in these two models. For the other metals, calculations show that the EFG values, as in the case of Ce, allows differentiation between the two different colorings I and II but not between the Smith and Bauer models.

These calculations provide a clear theoretical answer to the coloring problem in these MB_2C_2 phases. As this problem is experimentally difficult to solve unambiguously by using diffraction techniques (particularly with heavy metals), we suggested EFG measurements from NMR spectroscopy instead. Indeed, our calculations show that EFGs are very sensitive to atomic local environment, and therefore should easily discriminate between colorings I and II.[31]

Received: August 30, 2005
Published online: November 7, 2005

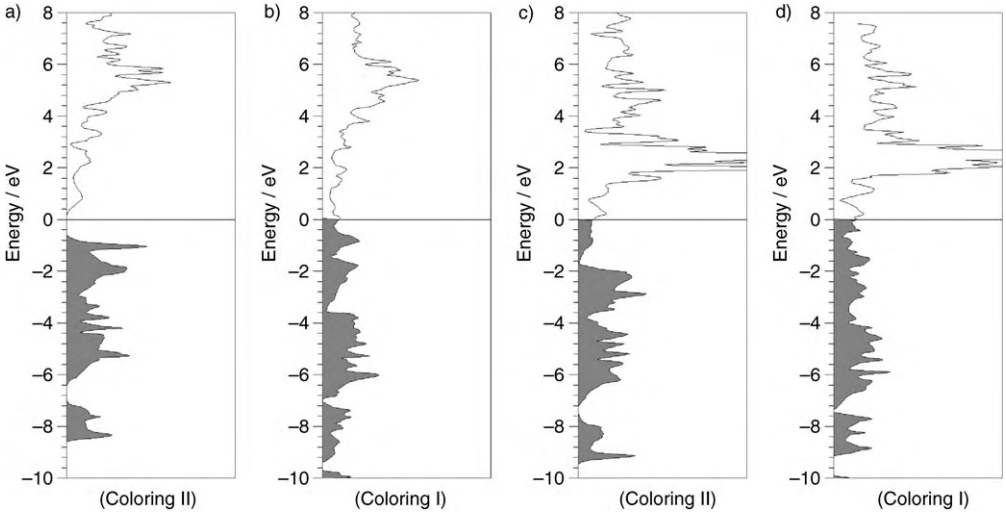

Figure 2. Total densities of states of CaB_2C_2 (a, b) and LaB_2C_2 (c, d). Colorings I and II correspond to the Bauer and Albert models, respectively.

 © 2005 Wiley-VCH Verlag GmbH & Co. KGaA, Weinheim

Table 2: Calculated components of the EFG (in MHz using $Q(^{11}B) = 0.04059$ and $Q(^{139}La) = 0.200$)[29] for different optimized MB_2C_2 structures.

	$Lu^{11}B_2C_2$			$Y^{11}B_2C_2$			$Ca^{11}B_2C_2$		
Coloring	I		II	I		II	I		II
Model	Bauer	Albert	Smith	Bauer	Albert	Smith	Bauer	Albert	Smith
v_{ZZ}	0.59	0.66	0.75	0.61	0.71	0.81	0.79	1.37	1.33
v_{YY}	−0.54	−0.45	−0.48	−0.54	−0.47	−0.50	−0.41	−0.78	−0.78
v_{XX}	−0.04	−0.21	−0.26	−0.07	−0.25	−0.30	−0.38	−0.59	−0.55
η[a]	0.85	0.36	0.29	0.77	0.31	0.25	0.03	0.13	0.17

	$Ce^{11}B_2C_2$				$L^{11}B_2C_2$			$^{139}LaB_2C_2$		
Coloring	I		II		I		II	I		II
Model	Bauer	Albert	Smith	Exp.[28]	Bauer	Albert	Smith	Bauer	Albert	Smith
v_{ZZ}	0.24	0.78	0.78	0.77	0.64	0.80	0.82	−3.64	−6.95	−6.82
v_{YY}	−0.23	−0.50	−0.50	0.47	−0.51	−0.50	−0.51	1.82	3.47	3.41
v_{XX}	−0.01	−0.29	−0.28	0.30	−0.13	−0.30	−0.31	1.82	3.47	3.41
η[a]	0.89	0.27	0.29	0.22	0.60	0.25	0.24	0.00	0.00	0.00

[a] $\eta = (|v_{XX}| - |v_{YY}|)/|v_{ZZ}|$.

Keywords: boron carbides · density functional calculations · electronic properties · inclusion compounds · structural arrangements

[1] a) N. N. Greenwood, A. Earnshaw, *Chemistry of the Elements*, Pergamon, Oxford, **1984**; b) G.-Y. Adachi, N. Imakana, Z. Fuzhong in *Handbook on the Physics and Chemistry of Rare Earths* (Eds.: K. A. Gschneidner, Jr., L. Eyring), Elsevier Amsterdam, **1991**, p. 62; c) A. I. Gusev, *Russ. Chem. Rev.* **1996**, *65*, 379–419; d) A. L. Ivanovskii, *Russ. Chem. Rev.* **1997**, *66*, 459–482; e) J. Bauer, J.-F. Halet, J.-Y. Saillard, *J. Coord. Chem.* **1998**, *178–179*, 723–753.

[2] K. Suzuki, M. Kato, R. Watanuki, T. Terashima, *J. Alloys Compd.* **2001**, *317–318*, 301–305.

[3] H. Yamauchi, H. Onodera, K. Ohoyama, T. Onimaru, M. Kosaka, M. Ohashi, Y. Yamaguchi, *J. Phys. Soc. Jpn.* **1999**, *68*, 2057–2066.

[4] K. Ohoyama, H. Yamauchi, A. Tobo, H. Onodera, H. Kadowaki, Y. Yamaguchi, *J. Phys. Soc. Jpn.* **2000**, *69*, 3401–3407.

[5] J. Akimitsu, K. Takenawa, K. Suzuki, H. Harima, Y. Kuramoto, *Science* **2001**, *293*, 1125–1127.

[6] T. Mori, S. Otani, *J. Phys. Soc. Jpn.* **2002**, *71*, 1789–1790.

[7] S. Otani, T. Mori, *J. Phys. Soc. Jpn.* **2002**, *71*, 1791–1792.

[8] a) T. Sakai, G. Adachi, J. Shiokawa, *J. Less-Common Met.* **1981**, *84*, 107–114; b) A. K. Verma, P. Modak, D. M. Gaitonde, R. S. Rao, B. K. Godwal, L. C. Gupta, *Europhys. Lett.* **2003**, *63*, 743–749; c) T. Mori, E. Takayama-Muromachi, *Curr. Appl. Phys.* **2004**, *4*, 276–279.

[9] For the definition of the coloring problem, see: J. K. Burdett, S. Lee, T. J. McLarnan, *J. Am. Chem. Soc.* **1985**, *107*, 3083–3089.

[10] K. Hofmann, B. Albert, *ChemPhysChem* **2002**, *3*, 896–898.

[11] M. Wörle, R. Nesper, *J. Alloys Compd.* **1994**, *216*, 75–83.

[12] G. S. Smith, Q. Johnson, P. C. Nordine, *Acta Crystallogr.* **1965**, *19*, 668–673.

[13] J. Bauer, O. Bars, *Acta Crystallogr. Sect. B* **1980**, *36*, 1540–1544.

[14] a) P. K. Smith, PhD Thesis, University of Kansas, **1964**; b) P. K. Smith, P. W. Gilles, *J. Inorg. Nucl. Chem.* **1967**, *29*, 375–382.

[15] B. Albert, K. Schmitt, *Inorg. Chem.* **1999**, *38*, 6159–6163.

[16] K. Hofmann, R. Gruehn, B. Albert, *Z. Anorg. Allg. Chem.* **2002**, *628*, 2691–2696.

[17] a) J. Bauer, H. Nowotny, *Monatsh. Chem.* **1971**, *102*, 1129–1145; b) R. Pöttgen, **1996**, unpublished results; c) T. Bréant, D. Pensec, J. Bauer, J. Debuigne, *C. R. Hebd. Seances Acad. Sci. Ser. 2* **1978**, *287*, 261–264.

[18] a) T. Onimaru, H. Onodera, K. Ohoyama, H. Yamauchi, Y. Yamaguchi, *J. Phys. Soc. Jpn.* **1999**, *68*, 2287–2291; b) T. Onimaru, H. Onodera, K. Ohoyama, H. Yamauchi, M. Ohashi, Y. Yamaguchi, *J. Phys. Chem. Solids* **1999**, *60*, 1435–1438; c) J. van Duijn, K. Suzuki, J. P. Attfield, *Angew. Chem.* **2000**, *112*, 373–374; *Angew. Chem. Int. Ed.* **2000**, *39*, 365–366; d) K. Kaneko, K. Ohoyama, H. Onodera, Y. Yamaguchi, *J. Phys. Soc. Jpn.* **2000**, *69*, 3762–3763; e) K. Ohoyama, K. Kaneko, K. Indoh, H. Yamauchi, A. Tobo, H. Onodera, Y. Yamaguchi, *J. Phys. Soc. Jpn.* **2001**, *70*, 3291–3295.

[19] a) J. K. Burdett, E. Canadell, T. Hughbanks, *J. Am. Chem. Soc.* **1986**, *108*, 3971–3976; b) J. M. Olivia, M. Llunell, P. Alemany, E. Canadell, *J. Solid State Chem.* **2003**, *176*, 375–389.

[20] Full optimizations of the atomic positions and cell parameters were carried out using the VASP code[20] with PAW[21] potentials; PBE generalized gradient approximation[22] was employed for the exchange and correlation energy term; similar results were obtained with the Wien2k code.[24]

[21] G. Kresse, J. Hafner, VASP program, version 4.6, Institut für Materialphysik, Universität Wien, **2000**.

[22] P. E. Blöchl, *Phys. Rev. B* **1994**, *50*, 17953–17979.

[23] J. P. Perdew, S. Burke, M. Ernzerhof, *Phys. Rev. Lett.* **1996**, *77*, 3865–3868.

[24] P. Blaha, K. Schwarz, G. K. H. Madsen, D. Kvasnicka, L. Luitz, *WIEN2k: An Augmented Plane Wave + Local Orbitals Program for Calculating Crystal Properties*, Technische Universität Wien, Wien, **2001**.

[25] This is consistent with the fact that LuB_2C exhibits the same structure type as ScB_2C, whereas different MB_2C phases are found with the other lanthanides.[1e]

[26] These results are in agreement with previous calculations on MgB_2C_2[25] and CaB_2C_2.[19]

[27] P. Ravindran, P. Vajeeston, R. Vidya, A. Kjekshus, H. Fjellvag, *Phys. Rev. B* **2001**, *64*, 224509.

[28] K. Magishi, K. Koyama, T. Saito, K. Mizuno, R. Watanuki, K. Suzuki, *Physica B* **2003**, *329–333*, 649–650.

[29] J. Emsley, *The Elements*, Clarendon, Oxford, **1989**.

[30] P. Pyykkö, *Mol. Phys.* **2001**, *99*, 1617–1629.

[31] Tables of optimized cell volumes and bond lengths are given in the Supporting Information.

 © 2005 Wiley-VCH Verlag GmbH & Co. KGaA, Weinheim

Crystal Engineering

DOI: 10.1002/anie.200502668

A Phthalocyanine Clathrate of Cubic Symmetry Containing Interconnected Solvent-Filled Voids of Nanometer Dimensions**

Neil B. McKeown, Saad Makhseed, Kadhum J. Msayib, Li-Ling Ooi, Madeleine Helliwell, and John E. Warren*

Dedicated to Professor Clifford C. Leznoff

Since the middle of the last century, the crystal structures of a vast number of organic inclusion compounds (namely, clathrates) have been determined.[1] In most cases, only one or two guest molecules reside at well-defined sites within the unit cell of the crystal; however, for a number of structures, such as those derived from urea,[2] thiourea,[2] or tris(*o*-phenylenedioxy)cyclotriphosphazene,[3] extended channels are formed within which the guest molecules, usually the solvent of recrystallization, are contained. Recent extensive research that involves rigid and extended organic components linked through hydrogen-bonding interactions[4] or by coordination to metal ions (namely, metal–organic frameworks (MOFs))[5] has resulted in structures in which solvent-filled channels occupy over 70% of the total volume of the crystal. Furthermore, there are now numerous examples of MOFs for which the removal of the included solvent does not result in loss of crystalline order, but instead gives microporous materials that resemble zeolites.[5,6] However, to offer practical advantages over conventional microporous materials, such as the zeolites and activated carbons, it is desirable that these organic-based microporous materials possess in-built functionalities for selective heterogeneous catalysis, adsorption, and separations. In this context, numerous crystalline porphyrin-based clathrates[7,8] and nanoporous coordination network polymers[8,9] have been reported which may ultimately allow the exploitation of the well-established homogeneous catalytic activity of metal-containing porphyrins in well-defined heterogeneous systems.[10]

Following on from the preparation of amorphous phthalocyanine-based microporous polymers,[11] we have become interested in the possibility of using the highly functional phthalocyanine macrocycle as a building block for the assembly of crystalline nanoporous materials. In analogy to the porphyrins, suitable transition-metal ions held in the central cavity of a phthalocyanine unit can induce catalytic behavior. Unlike porphyrins, for which large-scale production is unfeasible, the structurally related phthalocyanines are made routinely and cheaply by industry for use as stable blue colorants, photoconductors in xerography, and IR dyes, as well as for application to homogeneous oxidation catalysis in the removal of sulfurous compounds from crude petrochemicals (the Merox process).[12] Unfortunately, the extended planar shape of the phthalocyanine unit results in a strong tendency to form densely packed cofacial aggregates (e.g., stacked crystals,[13] columnar liquid crystals,[14] etc.), and this behavior must be prohibited to engineer open nanoporous structures that allow access to such active metal centers.

Our general strategy to avoid cofacial self-association involves the use of substituents that can introduce severe steric crowding adjacent to the phthalocyanine core.[15] Molecular modeling helped to identify that 2,6-diisophenoxy groups placed on the peripheral positions of the phthalocyanine ring would be perfectly suited for this purpose. Hence, a novel zinc 2,3,9,10,16,17,23,24-octa(2′,6′-diisopropylphenoxy)phthalocyanine (**1**) compound was prepared by using a simple two-step high-yielding synthesis from the commercially available 4,5-dichlorophthalonitrile and 2,6-diisopropylphenol via 4,5-di(2′,6′-disopropylphenoxy)phthalonitrile (**2**) by following a literature procedure (Scheme 1).[16]

Slow recrystallization by the diffusion of acetone into a solution of **1** in $CHCl_3$ gives large crystals (up to 1 mm^3) with a cubic morphology, for which a surprising molecular packing arrangement was revealed by single-crystal X-ray diffraction (XRD) analysis (Figure 1). The crystal structure is cubic and belongs to the exceptionally rare space group $Pn\bar{3}n$,[17] with 12 phthalocyanine molecules in the unit cell ($a = 3.77$ nm). The phthalocyanine core of **1** is a shallow cone-shape with the central Zn^{2+} ion and the oxygen atom of its axial ligand protruding from the molecular plane (probably from a water ligand as the acetone used for the recrystallization was not anhydrous). As predicted, the 2,6-diisopropylphenoxy substituents lie out of the plane of the macrocycle and thereby prohibit the formation of columnar stacks. Instead, the molecules pack to form cubes, with an equivalent of two per unit cell and a molecule of phthalocyanine comprises each of the six faces. The macrocycles are arranged so that their Zn^{2+} ion and its axial ligand point towards the center of the cube. Based upon the distance between the protruding Zn^{2+} ions on opposite sides of the cube, the minimum diameter of the cube is 2.33 nm, which gives a cavity volume of at least 8 nm^3, even if the width, calculated from the sum of the van der Waals radii, of the phthalocyanine unit (0.33 nm) is taken into account. In addition to the axial water ligand attached to the Zn^{2+} center of **1**, there are a further

[*] Prof. N. B. McKeown, Dr. K. J. Msayib, Dr. L.-L. Ooi
School of Chemistry
Cardiff University
Cardiff, CF10 3AT (UK)
Fax: (+44) 29-2087-4030
E-mail: mckeownnb@cardiff.ac.uk
Dr. S. Makhseed
Department of Chemistry
University of Kuwait
PO Box 5969, Safat-13060 (Kuwait)
Dr. M. Helliwell
School of Chemistry
University of Manchester
Manchester, M13 9PL (UK)
Dr. J. E. Warren
CCLRC Daresbury Laboratory
Daresbury, Warrington
Cheshire, WA4 4AD (UK)

[**] This work was funded by the EPSRC and Kuwait University (project no. SC06/04).

 InterScience © 2005 Wiley-VCH Verlag GmbH & Co. KGaA, Weinheim

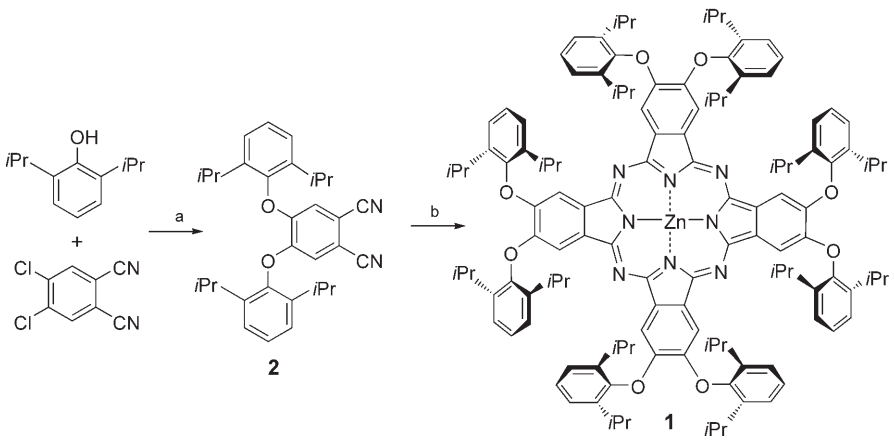

Scheme 1. The synthesis of phthalocyanine **1**. Reagents and conditions: a) K_2CO_3, DMF, 70 °C; b) $Zn(OAc)_2$, NMP, 150 °C. DMF = dimethylformamide, NMP = *N*-methylpyrrolidone.

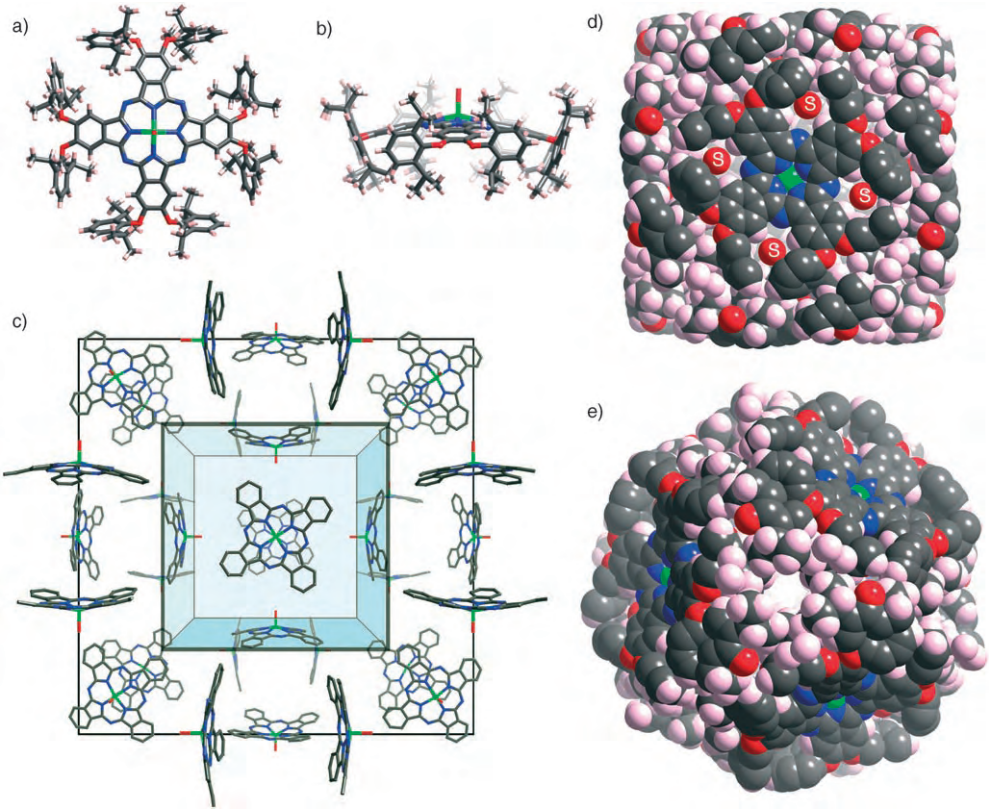

Figure 1. The molecular and crystal structure of **1**. a) Face-on and b) edge-on molecular views of **1** which show the orthogonal and square conformation of the eight peripheral 2′,6′-diisopropylphenoxy substituents relative to the phthalocyanine core, which prohibits cofacial molecular self-association. c) The cubic packing arrangement of **1** shown with the phenoxy substituents removed for clarity. The outer cube represents the unit cell, with dimensions of 3.77 nm, which contains 12 molecules of **1**. The inner cube represents one of the two voids of volume 8 nm^3 found in each unit cell. In this view, the second nanovoid is distributed at each corner of the unit cell in 8×1 nm^3 portions. d) Side-view of a space-filling representation of the central cubic subunit showing the location of the oxygen atoms (S) of the solvent (water or methanol) hydrogen bonded to the *meso* nitrogen atoms of the phthalocyanine unit. e) Corner view of the cubic subunit showing one of the 0.4-nm cylindrical openings, which interconnect the 8-nm^3 voids contained within the cubes.

24 water molecules per unit cell that appear to be associated through hydrogen-bonding interactions to the *meso* nitrogen atoms of the phthalocyanine ring (Figure 1d). No further solvent could be located within the crystal structure.

The calculated density of the crystal of **1** is only 0.75 $g\,mL^{-3}$, which when compared to that of the densely packed crystal of its phthalonitrile precursor **2** (approximately 1.15 $g\,mL^{-3}$), suggests a total void volume of 35% (namely, approximately 18 nm^3 per unit cell). Calculations with the PLATON program[18] indicate a solvent-accessible void volume of 20.5 nm^3 per unit cell (namely, 38.2% of the total volume). Thermal analysis of a freshly recrystallized sample of **1** with thermogravimetric analysis (TGA) shows a mass loss of 25.5% on heating up to 120 °C, for which the water of solvation observed in the crystal structure can account for only 1.6%. Assuming that the additional loss of mass observed by TGA is because of included, but disordered, solvent of recrystallization, it can be estimated that there is a molar ratio of **1**/acetone/H_2O of approximately 1:11:3. ^1H NMR spectroscopic analysis based on the peak integration for the clathrate dissolved in $CDCl_3$ provides a very similar molar ratio. This result is consistent with filling both of the two 8-nm^3 void spaces within the unit cell with approximately 132 molecules of acetone at a density of 0.77 $g\,mL^{-3}$ (density of acetone at 20 °C = 0.79 $g\,mL^{-3}$).

The crystal is not stable on removal from the crystallization solvent because of solvent loss, as indicated by XRD analysis, although the macroscopic appearance of the crystals is unchanged. Over half of the included solvent is lost within one hour (12% by mass remains, as determined by TGA) when placed in a dry stream of nitrogen at room temperature. A close inspection of the structure of each cubic subunit reveals that the void space appears almost fully

 © 2005 Wiley-VCH Verlag GmbH & Co. KGaA, Weinheim

enclosed by the six phthalocyanine units and their 2,6-diisopropylphenoxy substituents (Figure 1d). The largest apertures are situated at each corner of the cube, and these provide narrow cylindrical channels (approximately 0.4 nm in diameter) that connect the voids (Figure 1e). Preliminary solvent-exchange experiments were performed by submergence of the clathrate crystals in [D_6]acetone, followed by NMR spectroscopic analysis of the crystals dissolved in $CDCl_3$. These experiments show that nearly all of the included acetone (approximately 98%) is exchanged within two hours. A similar experiment using methanol indicates that all of the included acetone can be replaced to give a crystal that contains a molar ratio of **1**/MeOH/H_2O of 1:20:2, thus giving approximately 120 molecules of methanol in each void at a calculated density of 0.8 g mL^{-3} (density of methanol at 20 °C = 0.79 g mL^{-3}). XRD analysis shows that the solvent exchange does not alter the basic crystal structure, although the water molecules hydrogen bonded to the *meso* nitrogen atoms of **1** (Figure 1d) are replaced by methanol, and several other localized, but highly disordered, methanol molecules can be tentatively assigned within the crystal structure.

Remarkably, even water can be used to achieve almost complete exchange of acetone without loss of crystalline order. NMR spectroscopic analysis of the dissolved clathrate which had been previously submerged in water gives a molar ratio of **1**/acetone/H_2O of 1:0.5:30, which indicates each void is filled with approximately 180 water molecules at a calculated density of 0.65 g mL^{-3}. The apparent low density of the included water may be related to the predominately hydrophobic nature of the voids. It has been recognized that a narrow depletion layer, composed of water in the vapor phase, forms at the interface between a hydrophobic surface and water because of the disruption of hydrogen-bonding interactions.[19] At first sight, it seems surprising that water can gain access to the voids through the narrow interconnecting channels, which are lined with isopropyl groups (Figure 1e). However, the recent observation of water transport through the extended hydrophobic channel of a carbon nanotube of similar diameter provides a close analogy.[20]

The cubic packing of **1** is clearly related to the fourfold symmetry of the phthalocyanine molecule and allows the number of weak intermolecular interactions to be maximized by the interleaved phenoxy substituents along each of the 12 vertices of the cubic subunit. Relative to reported hydrogen-bonded clathrate structures, the proportion of included solvent within the crystal structure of **1** is unremarkable; however, its distribution into such large well-defined cavities is unprecedented. Molecular enclosure on the subnanoscale may be achieved within the voids of discrete molecular cages,[21] crystalline clathrates,[4] and network coordination polymers;[22] however, only a few examples approach,[23] and fewer exceed,[24] an enclosed volume of 1 nm^3. Of interest, is the potential for the exploitation of the functionalities present in the phthalocyanine unit to provide catalytic sites that would be embedded in the wall of the cavities and accessible only through the narrow size-selective channels. Hence, we envisage a clathrate that exhibits similar size and shape selectivity to that of the channel inclusion complexes (e.g., urea) but with intrinsic catalytic activity. Studies on the preparation of similar clathrates that contain catalytically active transition-metal ions (e.g., Co^{2+}, Fe^{3+}, etc.) are in progress, as are attempts to stabilize the structure through the placement of polar and hydrogen-bonding substituents on the 2,6-diisopropylphenoxyl units. Furthermore, the unique crystal structure of **1** suggests an approach to novel inorganic or organic nanoparticles by their assembly within the enclosed voids.[25]

Experimental Section

1: A mixture of 4,5-di(2,6-diisopropylphenoxy)phthalonitrile (0.5 g, 1.04 mmol; prepared by using an adapted literature procedure)[16] and an excess of anhydrous zinc acetate (20 mg) in dry NMP (6 mL) was stirred at 150 °C under nitrogen for 24 h. The reaction mixture was added to stirred distilled water (200 mL) on cooling, and the solid product was collected by filtration and washed with water and MeOH. The crude product was purified by column chromatography on silica gel with dichloromethane as the eluent and recrystallized from acetone to afford a bright green crystalline solid. Yield: 0.32 g (65%). M.p. 286 °C, elemental analysis (%) calcd for $C_{128}H_{144}O_8N_8Zn$: C 77.33, H 7.30, N 5.63; found: C 76.98, H 7.14, N 5.44; ^{1}H NMR (300 MHz, $CDCl_3$, 25 °C): δ = 1.35 (96H, br s), 3.48 (16H, sept), 7.51 (16H, d), 7.62 (8H, t), 8.20 ppm (8H, s); IR (KBr disc): λ_{max} (CH_2Cl_2, nm): 680, 362, 280 cm^{-1}; MALDI-MS (*m*/*z*) 1988 ([M^++H$^+$]).

X-ray structural analysis: Data were collected at 150 K using synchrotron radiation at Daresbury SRS, UK (Station 9.8) with a Bruker-Nonius APEX11 CCD diffractometer (λ = 0.6934 Å), and the structure was solved by direct methods. All calculations were carried out using the SHELXTL package.

Crystal data for **1**·3H_2O·11C_3H_6O: crystal size 0.7 × 0.4 × 0.4 mm^3, cubic, space group $Pn\bar{3}n$, $a = b = c$ = 3.76973(2) nm, V = 53.571.1(5) nm^3, Z = 12, R_1 = 0.0915. The asymmetric unit contains a quarter of **1** together with half a water molecule. A number of the carbon atoms were disordered over two sites, whose occupancies were constrained to sum to unity. The components of the disordered phenyl group were constrained to be regular hexagons. Non-hydrogen atoms were refined anisotropically, with restraints on the thermal motion of the carbon atoms, except those that were disordered. Hydrogen atoms were included in calculated positions, except those bonded to the axial oxygen atoms, which were omitted. CCDC-279644 contains the supplementary crystallographic data for this paper. These data can be obtained free of charge from the Cambridge Crystallographic Data Centre via www.ccdc.cam.ac.uk/data_request/cif.

Received: July 29, 2005
Published online: October 5, 2005

Keywords: clathrates · crystal engineering · microporous materials · nanostructures · phthalocyanines

[1] J. L. Atwood, J. E. D. Davies, D. D. MacNichol, *Inclusion Compounds, Vol. 1–5*, Academic Press, London, **1984/1991**.
[2] J. S. Rutherford, *Cryst. Eng.* **2001**, *4*, 269–281.
[3] H. R. Allcock, A. P. Primrose, N. J. Sunderland, A. L. Rheingold, I. A. Guzei, M. Parvez, *Chem. Mater.* **1999**, *11*, 1243–1252.
[4] J.-H. Journier, T. Maris, J. D. Wuest, *J. Org. Chem.* **2004**, *69*, 1762–1775.
[5] O. M. Yaghi, M. O'Keefe, N. W. Ockwig, H. K. Chae, M. Eddaoudi, J. Kim, *Nature* **2003**, *423*, 705–714; M. J. Rosseinsky, *Microporous Mesoporous Mater.* **2004**, *73*, 15–30; S. Kitagawa, R. Kitaura, S.-I. Noro, *Angew. Chem.* **2004**, *116*, 2388–2430; *Angew. Chem. Int. Ed.* **2004**, *43*, 2334–2375.

 © 2005 Wiley-VCH Verlag GmbH & Co. KGaA, Weinheim

[6] M. Eddaoudi, J. Kim, N. Rosi, D. Vodak, J. Wachter, M. O'Keefe, O. M. Yaghi, *Science* **2002**, *295*, 469 – 472; M. Eddaoudi, H. L. Li, O. M. Yaghi, *J. Am. Chem. Soc.* **2000**, *122*, 1391 – 1397.
[7] M. P. Byrn, C. J. Curtis, I. Goldberg, Y. Hsiou, S. I. Khan, P. A. Sawin, S. K. Tendick, C. E. Strouse, *J. Am. Chem. Soc.* **1991**, *113*, 6549 – 6557.
[8] I. Goldberg, *Chem. Eur. J.* **2000**, *6*, 3863 – 3870.
[9] B. F. Abrahams, B. F. Hoskins, D. M. Michail, R. Robson, *Nature* **1994**, *369*, 727 – 729; D. W. Smithenry, S. R. Wilson, K. S. Suslick, *Inorg. Chem.* **2003**, *42*, 7719 – 7721; M. E. Kosal, J.-H. Chou, S. R. Wilson, K. S. Suslick, *Nat. Mater.* **2002**, *1*, 119 – 121; K.-J. Lin, *Angew. Chem.* **1999**, *111*, 2894 – 2897; *Angew. Chem. Int. Ed.* **1999**, *38*, 2730 – 2732.
[10] M. C. Feiters, A. E. Rowan, R. J. M. Nolte, *Chem. Soc. Rev.* **2000**, *29*, 375 – 384.
[11] N. B. McKeown, S. Makhseed, P. M. Budd, *Chem. Commun.* **2002**, 2780 – 2781; N. B. McKeown, P. M. Budd, K. J. Msayib, B. S. Ghanem, H. J. Kingston, C. E. Tattershall, S. Makhseed, K. J. Reynolds, D. Fritsch, *Chem. Eur. J.* **2005**, *11*, 2610 – 2620.
[12] N. B. McKeown, *Phthalocyanine Materials: Synthesis, Structure and Function*, CUP, Cambridge, **1998**.
[13] M. K. Engel in *The Porphyrin Handbook, Vol. 20* (Eds.: K. M. Kadish, K. M. Smith, R. Guilard), Academic Press, New York, **2003**, pp. 1 – 243.
[14] C. Piechocki, J. Simon, A. Skoulios, D. Guillon, P. Weber, *J. Am. Chem. Soc.* **1982**, *104*, 5245 – 5247.
[15] B. M. Hassan, H. Li, N. B. McKeown, *J. Mater. Chem.* **2000**, *10*, 39 – 45.
[16] D. Wöhrle, M. Eskes, K. Shigehara, A. Yamada, *Synthesis* **1993**, 194 – 196.
[17] A search of the Cambridge Structural Database resulted in only one crystal structure (BALNIM; CCDC-179393), with the cubic $Pn\bar{3}n$ space group ($a = 2.975$ nm, $Z = 24$); this structure was obtained from 3,3′,4,4′-tetrakis((trimethylsilyl)ethynyl)biphenyl and is also of low calculated density (0.8 g mL^{-3}), but in this case the void structure is composed of interconnected channels of 0.7 nm in diameter that run parallel to the three axes of the cube; see K. Prasanna, U. Perera, M. Krawiec, D. W. Smith, *Tetrahedron* **2002**, *58*, 10197 – 10203 for the molecular structure only. We thank Jenny Field of the CCDC for informing us of this structure.
[18] A. L. Spek, *J. Appl. Crystallogr.* **2003**, *36*, 7 – 13.
[19] K. Lum, D. Chandler, J. D. Weeks, *J. Phys. Chem. B* **1999**, *103*, 4570 – 4577; S. I. Mamatkulov, P. K. Khabibullaev, R. R. Netz, *Langmuir* **2004**, *20*, 4756 – 4763.
[20] G. Hummer, J. C. Rasaiah, J. P. Noworyta, *Nature* **2001**, *414*, 188 – 190.
[21] D. J. Cram, J. M. Cram, *Container Molecules and their Guests*, RSC, Cambridge, **1994**; D. J. Cram, *Nature* **1992**, *356*, 29 – 36; S. R. Seidel, P. J. Stang, *Acc. Chem. Res.* **2002**, *35*, 972 – 983.
[22] R. Robson, *J. Chem. Soc. Dalton Trans.* **2000**, 3735 – 3744.
[23] U. Lucking, F. C. Tucci, D. M. Rudkevich, J. Rebek, *J. Am. Chem. Soc.* **2000**, *122*, 8880 – 8889; S. Aoki, M. Shiro, E. Kimura, *Chem. Eur. J.* **2002**, *8*, 929 – 939; B. F. Abrahams, S. J. Egan, R. Robson, *J. Am. Chem. Soc.* **1999**, *121*, 7172 – 7172.
[24] S. R. Batten, B. F. Hoskins, R. Robson, *J. Am. Chem. Soc.* **1995**, *117*, 5385 – 5386; L. R. MacGillivray, J. L. Atwood, *Nature* **1997**, *389*, 469 – 472.
[25] D. G. Shchukin, G. B. Sukhorukov, *Adv. Mater.* **2004**, *16*, 671 – 682.

 © 2005 Wiley-VCH Verlag GmbH & Co. KGaA, Weinheim

Carbon–Carbon Bonds

DOI: 10.1002/anie.200502721

Squeezing C–C Bonds**

Deborah R. Huntley, Georgios Markopoulos, Patrick M. Donovan, Lawrence T. Scott, and Roald Hoffmann**

Making C–C bonds long is a going enterprise; dozens of bonds that are 0.10–0.15 Å longer than a normal 1.54 Å C–C bond are known. It is possible to weaken a bond through electronic effects, but strain is the major factor. What about short C–C bonds? Single bonds between two- and three-coordinate carbon atoms (e.g., the central C–C bonds in 1,3-butadiyne and 1,3-butadiene) are certainly short—a phenomenon usually interpreted in terms of hybridization. However, short single bonds between two four-coordinate carbon atoms are rare. Two examples that have caught the attention of the community are the π-acceptor-substituent-influenced bond in a bridged bicyclobutane **1**, with a C–C bond length of 1.41 Å,[1] and the external bonds between two bicyclobutane bridgeheads in **2** and **3** with lengths of near 1.44 Å.[2] An interesting theoretical discussion of these and the related bonds in the bitetrahedryl and bicubyl molecules, **4** and **5**,[3a] has appeared.[3b–g] Recently, Tanaka and Sekiguchi published the synthesis and structure of the hexakis(trimethylsilyl) derivative of **4**, which contains a very short exocyclic C–C bond (1.436 Å).[4]

[*] Prof. D. R. Huntley
Department of Chemistry
Saginaw Valley State University
University Center, MI 48710-0001 (USA)
Fax: (+1) 989-964-2796
E-mail: huntley@svsu.edu

G. Markopoulos, Prof. R. Hoffmann
Department of Chemistry and Chemical Biology
Baker Laboratory
Cornell University
Ithaca, NY 14853-1301 (USA)
Fax: (+1) 607-255-5709
E-mail: rh34@cornell.edu

P. M. Donovan, Prof. L. T. Scott
Department of Chemistry
Merkert Chemistry Center
Boston College
Chestnut Hill, MA 02467-3860 (USA)

[**] This study was supported by the National Science Foundation through Research Grant CHE-0204841 at Cornell University and Research Grant CHE-0414066 at Boston College. We are grateful to the Heidelberg–Cornell Exchange Fellowship for making possible Georgios Markopoulos' stay at Cornell University and to the Office of Academic Affairs at Saginaw Valley State University. G.M.'s permanent address is Organisch-Chemisches Institut, Universität Heidelberg, Germany.

Supporting information for this article is available on the WWW under http://www.angewandte.org or from the author.

© 2005 Wiley-VCH Verlag GmbH & Co. KGaA, Weinheim

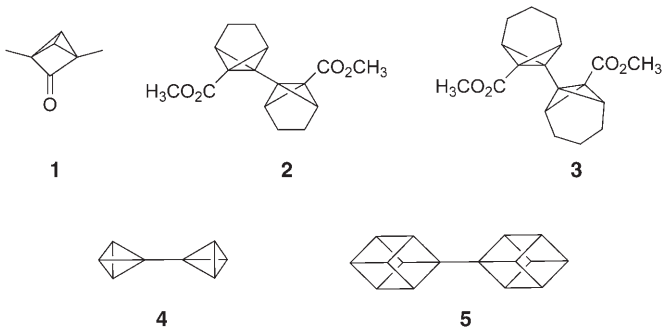

1 2 3

4 5

One might think that the normal shape of a molecular potential argues against a short C–C single bond: Aren't all such potentials anharmonic, with elongation less costly energetically than contraction? For "small" deviations (ca. 0.05 Å) it really doesn't matter that much. Single-point calculations on D_{3d} ethane (Figure 1) are indicative: it takes 2.8 kJ mol^{-1} to stretch the C–C bond by 0.05 Å from its equilibrium value and only 3.5 kJ mol^{-1} to squeeze it by the same amount; on the other hand, stretching and squeezing by 0.15 Å requires 21.9 and 37.7 kJ mol^{-1}, respectively.[5]

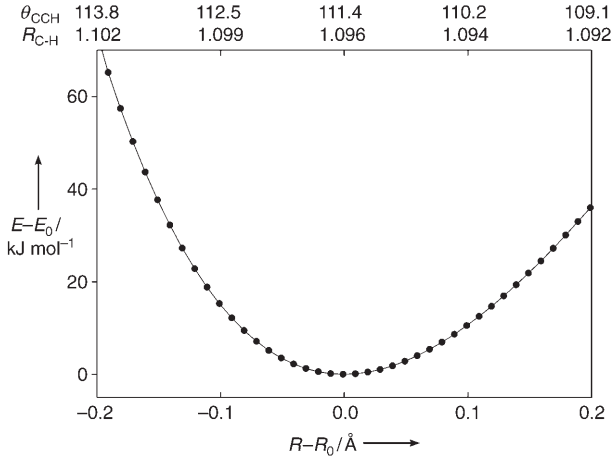

Figure 1. Computed potential-energy curve for ethane showing the energetic cost of bond stretching ($R-R_0 > 0.0$) and compression ($R-R_0 < 0.0$). At each fixed distance, the C–H bond length (R) and C-C-H angle (θ), as shown at the top of the graph, were optimized within a D_{3d} constraint.

So why do we see so few shortened C–C bonds? We think it is because strain dissipates in a multitude of ways. It is not easy to concentrate stress into a specific bond or in a single phase of the stretching motion. Herein, we report our attempts to design such squeezed C–C single bonds, making use of the reliability of contemporary computational methods to monitor how well we do. In doing so, we are responding to a question raised 29 years ago by Henning Hopf.[6] He asked "*Wie kurz kann eine Einfachbindung werden? Wie stark lässt sie sich stauchen?*" (How short can a single bond be? How strongly can it be compressed?)

We constrained ourselves (arbitrarily) to C–C bonds in which the carbon atoms involved are tetracoordinate. Also, for the initial moves in the game,[7] we did not allow substitution at either of the tetracoordinate carbon atoms by atoms other than hydrogen or carbon. Also, to rely on well-understood electronic effects (as are operative in **1**) was deemed "unsporting."

Computational Methods

Structures were optimized with the B3LYP hybrid functional and the 6-31G(d) basis set as implemented in the Gaussian 03 program.[8] This functional has been shown to be reliable for the determination of normal and anomalous C–C bond lengths using both 6-31G(d) and 6-31G(d,p) basis sets above.[3g,9] In a few cases (indicated in footnotes), a smaller basis set (6-31G) was used. Frequency calculations were performed to confirm that every structure represents a true energy minimum. Many of the structures were also optimized using the BLYP functional and triple-zeta Slater orbital basis set (TZ2P) with the Amsterdam Density Functional Program,[10] and effectively identical results were obtained. Our structures are color-coded as follows: C atoms blue; N atoms green; O atoms yellow; H atoms white; and Si atoms cyan (one exception will be specified later); the shortened bonds are highlighted in red.

Caging

The simplest strategy for applying pressure to one C–C single bond (or a group of such) is to encapsulate it in a reasonably inert cage, a game that is easier to play theoretically than experimentally. In the examples pictured here, **6** puts a molecule of neopentane inside C_{60}, **7** puts ethane in silsesquioxane $(SiH)_8O_{12}$, and **8** puts a molecule of ethane into a

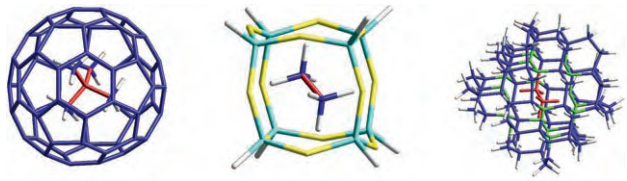

6 7 8

"diamond skin." (This last structure requires further explanation: Begin with an extended cubic diamond structure. Discard from it a C_2 unit as well as the six attached carbon atoms. Place C_2H_6 inside that space, then sculpt the outside to form a thin diamondoid layer around the molecule of ethane, and "heal" the inside cavity by replacing the 18 carbon atoms that face the ethane by nitrogen atoms. The outside of the diamond skin is passivated with hydrogen atoms.[11]) This kind of brute-force pressure leads to optimized C–C bond lengths of 1.36 Å in **6**,[12] 1.40 Å in **7**, and 1.46 Å in **8**.[13,14]

Capsule and encapsulated entities can also be combined in a single molecule. Cyclophane **9** presses a methyl group towards the aromatic ring, in a similar manner to the "iron maidens" recently reviewed by Pascal.[15] The steric congestion at the center of this molecule leads to a shortened bond length of 1.43 Å.[16] Song, Ho, and Pascal recently synthesized related in-cyclophanes with short C–Me bonds of 1.475 and 1.495 Å.[17] Tightening the cage around such an in-methyl

 © 2005 Wiley-VCH Verlag GmbH & Co. KGaA, Weinheim

group, as in **10**, leads to a corresponding C–C bond length of just 1.41 Å.

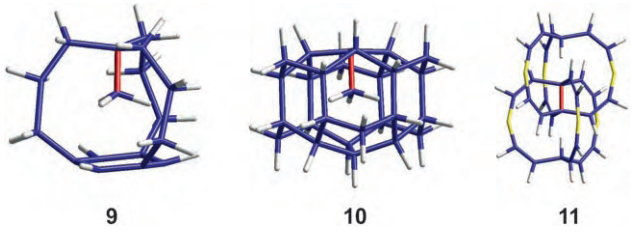

9 **10** **11**

The Spiderane

A unique topology (a spiderane) is demonstrated by **11**,[12] in which the above principle is applied twice. This "back-strapped" structure with two intertwined cages has a central C–C bond length of 1.44 Å. The hydrogen atoms pointing towards the short C–C bond are essential; replacing the CH groups with nitrogen atoms leads to a more typical bond length of 1.51 Å.

Shortening a Bond without Pushing on It

Though the spiderane **11** is sui generis, van der Waals repulsion has been crucial in our strategy so far. Many other variations are possible in which shortened bonds are achieved solely by covalent means. For example, **12** forces a carbon

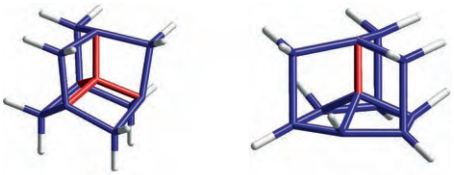

12 **13**

atom into the adamantane framework, removing the bridgehead hydrogen atoms along the way. A set of four equally shortened C–C bonds (1.44 Å) arises as a result of the small covalent cage. Next, we replaced the six bridging methylene groups with NH groups, resulting in a more compressed structure that has a central bond length of 1.39 Å.[18]

Rotation around one of the eclipsed C–C bonds in **12** and reconnection of the "bridges" in a staggered manner leads to the closely related structure **13** (bridging group $X = CH_2$). Here, we observed that one bond becomes even shorter (1.38 Å), while the three basal C–C bonds relax to a normal C–C bond length (1.54 Å). Still, the squeeze comes at a cost: the surrounding bond angles are very distorted, and the bonds to the methylene carbon atoms (1.70 and 1.84 Å) are very elongated. The use of longer bridges ($X = C_2H_2$, C_2H_4, C_3H_4, C_3H_6) reduces the distortions but also leads to a gradual lengthening of the short bond to 1.48 Å for the trimethylene species ($X = C_3H_6$).

Stiffened and Strapped, Eclipsed and Staggered

A different look at **12** opens the door to another variation: the lower part of the molecule is comprised of three fused cyclobutane rings. This connectivity provides a highly strained but rigid framework at one end of an eclipsed ethane unit. If that fused-ring system were repeated at the other end, we would have molecules that are reminiscent of bicubyl or bis(bicyclo[1.1.1]pentyl), which are known to have short central bonds.[3] Those bonds should get even shorter if we impose further geometric constraints. Implementing this idea, with three bridging methylene groups, leads to a central bond of length of 1.37 Å in **14**.

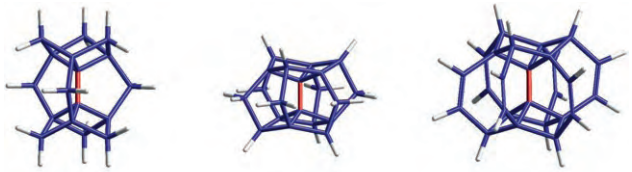

14 **15a** **15b**

Application of this concept to the "staggered" system **13** allows six bridging methylene units and leads to the shortest carbon–carbon single bond observed in the course of this study: 1.32 Å in **15a**. Although this molecule is highly congested and very, very strained, a single-bond distance in the regime of double-bond lengths is quite remarkable. The other C–C bonds in the molecule all fall in the range of 1.60–1.64 Å. Replacement of the methylene bridges in **15a** with ethyleno groups (C_2H_2) results in slight elongation of the central C–C bond to 1.35 Å (**15b**).

Tied-Up Bicycloalkanes

Clearly, stiffening both ends of an ethane unit and tying them together is a promising approach to obtain short bonds. Other examples include interior propellanes formed by strapping bicyclo[*n.n.n*]alkane units together. Many variations in the bridges are possible; herein, we show only the use of *exo* double bonds (1.37 Å in **16a**) and ethano bridges

16a **16b** **17**

(1.39 Å in **16b**). The triply methylene-bridged analogue of **16a** has a central C–C bond of 1.35 Å, but some external bonds are quite long (1.74 Å).[19] Merging the strategies of **15** (hexuple straps) and **16b** (linking bicylic units) leads to **17**, which has a central C–C bond length of 1.34 Å, again with some long C–C bonds in the bicyclic systems (1.74 Å).

Less-strained frameworks, which might be more easily synthesized, were also tested and still show significantly shortened bonds. System **18a** has a shortened bond of 1.46 Å.

© 2005 Wiley-VCH Verlag GmbH & Co. KGaA, Weinheim

Introduction of heteroatoms leads to a stronger squeeze, as shown for **18b** (1.41 Å).

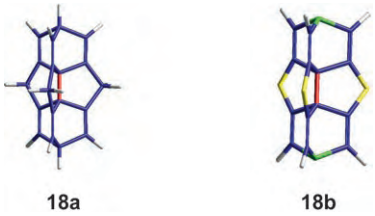

Not Just s Character

In the course of this stroll into the largely neglected land of short bonds, we have developed a menagerie of molecules that are predicted to have very short bonds between coupled four-coordinate carbon atoms. Is it simple hybridization that drives this bond shortening, as others have rather convincingly argued for bicubyl **5**, the bicyclobutane dimers **2** and **3**, bitetrahedryl **4**, and Tanaka's derivative?[3,4] We don't think so. In Figure 2, we have used natural bond orbital (NBO)

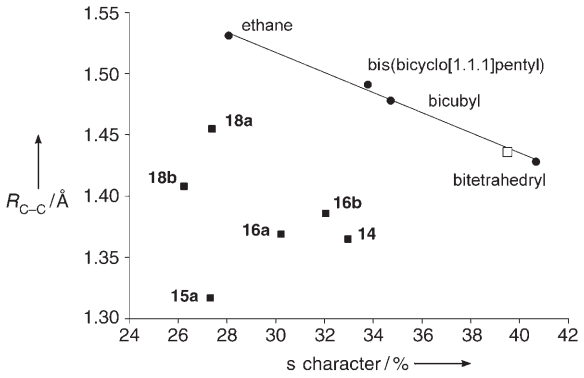

Figure 2. Percentage s orbital character (from an NBO analysis) and optimized C–C bond lengths for some selected molecules. The open square corresponds to Tanaka and Sekiguchi's hexakis(trimethylsilyl)bitetrahedryl. The squeezed bonds in the molecules proposed by us are shorter by approximately 0.1 Å or more than the lengths expected on the basis of hybridization arguments.

analysis[20] to determine the hybridization in our short bonds. The C–C bond lengths are plotted as a function of the percentage s orbital character in the bond for selected[21] molecules discussed herein as well as for some of the dimers previously studied. It is clear from Figure 2 that our molecules have C–C single bonds that are shorter by approximately 0.1 Å or more than what would be expected from hybridization alone. The additional strain caused by the threefold symmetric geometry constraints is responsible for this effect. Our short bonds simply cannot achieve "typical" lengths without wreaking havoc elsewhere in the molecule.

Received: August 2, 2005
Published online: October 31, 2005

Keywords: bond theory · C–C bonds · density functional calculations · electronic structure · strained molecules

[1] H. Irngartinger, K. L. Lukas, *Angew. Chem.* **1979**, *91*, 750; *Angew. Chem. Int. Ed. Engl.* **1979**, *18*, 694–695.
[2] O. Ermer, P. Bell, J. Schäfer, G. Szeimies, *Angew. Chem.* **1989**, *101*, 503–506; *Angew. Chem. Int. Ed. Engl.* **1989**, *28*, 473–476.
[3] a) Bicubyls have been synthesized—the observed intercubyl distances in two examples are 1.458 and 1.474 Å; see: R. Gilardi, M. Maggini, P. E. Eaton, *J. Am. Chem: Soc.* **1988**, *110*, 7232–7234; b) P. von R. Schleyer, M. Bremer, *Angew. Chem.* ***1989***, *101*, 1264–1266; *Angew. Chem. Int. Ed. Engl.* **1989**, *28*, 1226–1228; c) Y. Xie, H. F. Schaefer, III, *Chem. Phys. Lett.* **1989**, *161*, 516–518; d) Y. Xie, H. F. Schaefer, III, *Chem. Phys. Lett.* **1990**, *168*, 249–252; e) Y. Xie, H. F. Schaefer, III, P. Aped, K. Chen, N. L. Allinger, *Int. J. Quantum Chem.* **1992**, *42*, 953–963; f) M.-J. Huang, N. Bodor, *Chem. Phys. Lett.* **1992**, *190*, 25–28; g) V. Gallasso, I. Carmichael, *J. Phys. Chem. A* **2000**, *104*, 6271–6276.
[4] M. Tanaka, A. Sekiguchi, *Angew. Chem.* **2005**, *117*, 5971–5973; *Angew. Chem. Int. Ed.* **2005**, *44*, 5821–5823.
[5] In D_{3d} or D_{3h} ethane, there are three structural parameters that may be chosen as the C–C and C–H bond lengths, and a C-C-H (or H-C-H) angle. In Figure 1, the energy is plotted as a function of the C–C bond length, with the other structural parameters optimized. Schleyer and Bremer[3b] performed a similar optimization, in which the C–C bond length was plotted versus the C-C-H angle in the optimized geometries.
[6] H. Hopf, *Chem. Unserer Zeit* **1976**, *10*, 114–120.
[7] Indeed, this work began as a competition between the research groups.
[8] Gaussian 03 (Revision B.04): M. J. Frisch, G. W. Trucks, H. B. Schlegel, G. E. Scuseria, M. A. Robb, J. R. Cheeseman, J. A. Montgomery, Jr., T. Vreven, K. N. Kudin, J. C. Burant, J. M. Millam, S. S. Iyengar, J. Tomasi, V. Barone, B. Mennucci, M. Cossi, G. Scalmani, N. Rega, G. A. Petersson, H. Nakatsuji, M. Hada, M. Ehara, K. Toyota, R. Fukuda, J. Hasegawa, M. Ishida, T. Nakajima, Y. Honda, O. Kitao, H. Nakai, M. Klene, X. Li, J. E. Knox, H. P. Hratchian, J. B. Cross, C. Adamo, J. Jaramillo, R. Gomperts, R. E. Stratmann, O. Yazyev, A. J. Austin, R. Cammi, C. Pomelli, J. W. Ochterski, P. Y. Ayala, K. Morokuma, G. A. Voth, P. Salvador, J. J. Dannenberg, V. G. Zakrzewski, S. Dapprich, A. D. Daniels, M. C. Strain, O. Farkas, D. K. Malick, A. D. Rabuck, K. Raghavachari, J. B. Foresman, J. V. Ortiz, Q. Cui, A. G. Baboul, S. Clifford, J. Cioslowski, B. B. Stefanov, G. Liu, A. Liashenko, P. Piskorz, I. Komaromi, R. L. Martin, D. J. Fox, T. Keith, M. A. Al-Laham, C. Y. Peng, A. Nanayakkara, M. Challacombe, P. M. W. Gill, B. Johnson, W. Chen, M. W. Wong, C. Gonzalez, J. A. Pople, Gaussian Inc., Pittsburgh PA, **2003**.
[9] C. H. Choi, M. Kertesz, *Chem. Commun.* **1997**, *22*, 2199–2200.
[10] ADF2004.01, SCM, Theoretical Chemistry, Vrije Universiteit, Amsterdam, The Netherlands, http://www.scm.com.
[11] A cutaway image of this unusual structure is included in the Supporting Information.
[12] Calculations performed at the B3LYP/6-31G level.
[13] In this structure, the red highlighting shows the entire central ethane unit that contains the short bond. The calculation was performed using the ONIOM method, with the ethane treated at the B3LYP/6-31G* level and the diamond cage treated with AM1.
[14] For some cautionary considerations on calculations of encapsulation, see: H. Dodziuk, *Chem. Phys. Lett.* **2004**, *410*, 39–41.
[15] R. A. Pascal, Jr., *Eur. J. Org. Chem.* **2004**, 3763–3771.
[16] From here on, red indicates only the strained C–C bond.
[17] Q. Song, D. M. Ho, R. A. Pascal, Jr, *J. Am. Chem. Soc.* **2005**, *127*, 11246–11247.
[18] Replacement of the bridges with oxygen atoms gives a structure that is unstable with respect to dissociation into CO and CO_2. However, replacement of only the three bridging methylene groups associated with one inverted carbon center with nitrogen

 © 2005 Wiley-VCH Verlag GmbH & Co. KGaA, Weinheim

(or oxygen) results in stable structures with two inequivalent bond lengths, one very short bond of 1.39 (1.38) Å and a set of three less-shortened bonds of 1.43 (1.45) Å.

[19] Recent calculation suggest that C–C bonds of 1.74 Å are right on the edge of stability; see: A. A. Zavitsas, *J. Phys. Chem. A* **2003**, *107*, 897–898 for a general discussion and T. Vreven, K. Morokuma, *J. Phys. Chem. A* **2002**, *106*, 6167–6170 for detailed calculations on hexaphenylethane.

[20] A. E. Reed, L. A. Curtiss, F. Weinhold, *Chem. Rev.* **1988**, *88*, 899–926.

[21] Only those molecules in which the short-bonded carbon atoms are symmetrically equivalent were used. For some of our molecules, the NBO C–C bonding molecular orbitals have somewhat low occupancies, for instance, 1.916 in **15a**.

 © 2005 Wiley-VCH Verlag GmbH & Co. KGaA, Weinheim

Enzyme Mutation

DOI: 10.1002/anie.200502461

Conversion of a Carboxylesterase into a Triacylglycerol Lipase by a Random Mutation**

*Dolores Reyes-Duarte, Julio Polaina, Nieves López-Cortés, Miguel Alcalde, Francisco J. Plou, Kieran Elborough, Antonio Ballesteros, Kenneth N. Timmis, Peter N. Golyshin, and Manuel Ferrer**

Lipases and esterases are enzymes of increasing importance for classical and new industrial applications.[1,2] The most significant properties of these enzymes are that they are very stable and active, especially in organic solvents, and they possess regio- and stereospecificity.[2] Esterases (also called carboxylesterases, EC 3.1.1.1) preferentially hydrolyze water-soluble "simple" esters and usually only triglycerides bearing fatty acids shorter than C_6, whereas lipases (also known as triacylglycerol lipases, EC 3.1.1.3) prefer water-insoluble substrates, typically triglycerides composed of long-chain fatty acids.[1] Despite their close relationship in sequence and structure, these enzymes differ in their profile for chain-length specificity. In fact, substrate specificity is the only completely valid criterion for distinguishing between carboxylesterases and lipases, because several exceptions exist for the other criteria used previously: the existence of a *lid*, interfacial activation, and hydrophobicity of the scissile acyl-binding site of the substrate.[1,3,4]

Lipases and esterases have already been improved by methods such as medium engineering, immobilization on suitable supports, and rational protein design. Moreover, it has been demonstrated that directed evolution can lead to enzymes with thermal stability[5] and inverted or improved enantioselectivity.[6] A few examples also showed that the chain-length specificity of lipases can be achieved.[7] Notably, in all cases the original lipase showed activity toward long-chain fatty acid esters, and laboratory evolution was used to improve and thereby modify its hydrolytic activity. Clearly, the transformation of a "true carboxylesterase" into a "true lipase" seems to be difficult, as no examples of this change have been reported. Two hypotheses may explain the supposed difficulty: 1) the active center in esterases is smaller than that in lipases, so it can only accommodate short-chain fatty acid esters;[8] or 2) the esterase requires a hydrophobic mobile *lid* to facilitate its interfacial activation, and that has only been found in lipases.[9] Whatever the case, both situations seem to be critical for a high-performance lipase. Herein, we describe the conversion of a "true esterase" into a triacylglycerol lipase by directed evolution; the significance of this study is also discussed. Enzyme R.34, retrieved from the metagenome library of bovine rumen microflora,[10] was chosen as the test enzyme.

The data in Figure 1 a and b support the notion that R.34 is a true carboxylesterase, which acts preferentially on *p*-nitrophenyl (*p*-NP) esters and the triacylglycerol of short-chain fatty acids ($\leq C_4$), and is optimal for C_3 acids (up to 240 units mg^{-1}). One round of error-prone PCR was used to create a mutant with higher activity toward long-chain fatty acid esters.[12a] Potential improved variants were identified on agar plates by using α-naphthyl laurate (αNL) and an azo dye (Fast Blue RR) that reacts with the released 2-naphthol to generate an insoluble brown product.[13] Under these conditions, *Escherichia coli* colonies expressing wild-type R.34 did not produce brown halos on αNL plates, but did produce them on α-naphthyl acetate (αNA) plates.[12b] Approximately 8200 colonies were screened in the first round, and only one clone (EL1) was identified. Such a low frequency of improvement was surprising, and may reflect the fact that long-chain esters are very inefficient substrates for R.34. Both R.34 and EL1 were produced as a fusion with a hexahistidine (His_6) tag at the C terminus,[12a] and their biochemical properties were investigated. Although the optimal pH, temperature, and

[*] Dr. D. Reyes-Duarte, N. López-Cortés, Dr. M. Alcalde, Dr. F. J. Plou, Prof. A. Ballesteros, Dr. M. Ferrer
Institute of Catalysis, CSIC
Cantoblanco, 28049 Madrid (Spain)
Fax: (+34) 91-5854760
E-mail: mferrer@icp.csic.es
Dr. J. Polaina
Instituto de Agroquímica y Tecnología de Alimentos, CSIC
Paterna, 46980 Valencia (Spain)
Dr. K. Elborough
ViaLactia Biosciences Limited
PO Box 109 185, Newmarket, Auckland (New Zealand)
Prof. K. N. Timmis, Dr. P. N. Golyshin
Division of Microbiology
GBF—German Research Center for Biotechnology
38124 Braunschweig (Germany)

[**] This research was supported by EC Project MERG-CT-2004-505242 "BIOMELI", Spanish CICYT Projects BIO2002-00337 and BIO2004-03773-C04-02, and the BMBF "GenoMik" initiative. M.F. thanks the European Commission for a Marie Curie postdoctoral fellowship and the Spanish Ministerio de Ciencia y Tecnología. The authors also thank ViaLactia Biosciences Ltd. (New Zealand) for financial support. K.N.T. gratefully acknowledges the generous support by the Fonds der Chemischen Industrie.

Supporting information for this article is available on the WWW under http://www.angewandte.org or from the author.

 © 2005 Wiley-VCH Verlag GmbH & Co. KGaA, Weinheim

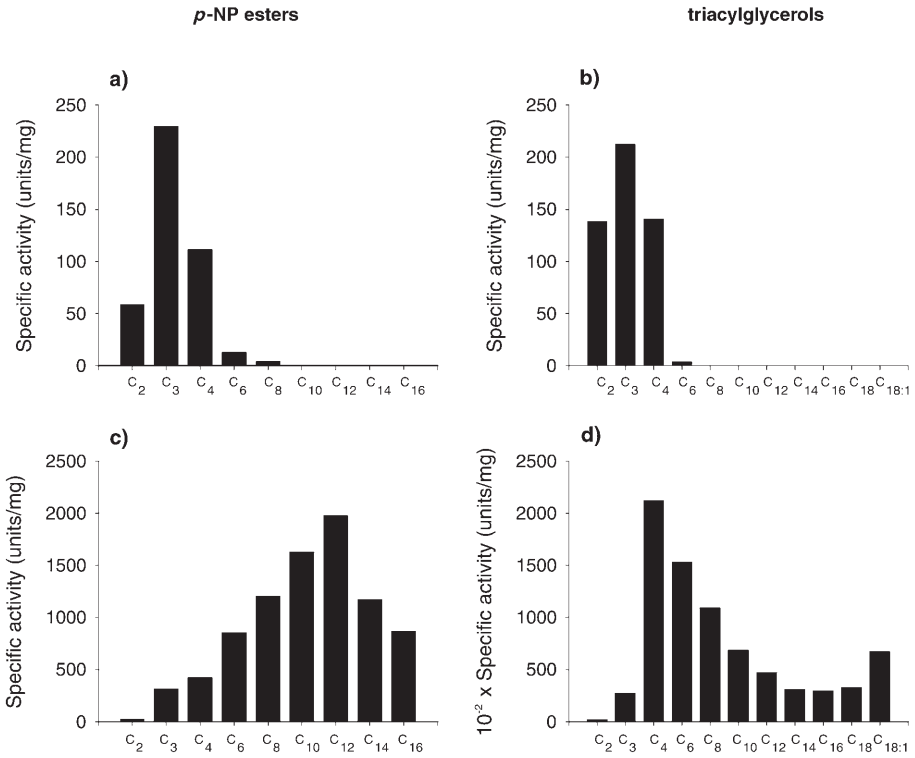

Figure 1. Relative activity of the wild-type R.34 esterase (top) and EL1 mutant (bottom) to *p*-NP esters (a and c) and triacylglycerols (b and d). Specific activities are given in units mg^{-1} pure protein. R.34 and EL1 enzymes were purified by using a Ni-Sepharose column after expression with a carboxyl-terminated His_6 tag.[12a] To exclude any influence of the His_6 tag on activity, the R.34 protein was expressed in and purified from *E. coli* XLOLR cells harboring pBKR.34 plasmid.[10] The enzyme obtained by this method did not show relevant differences in substrate specificity.

subunit composition were essentially the same for both proteins,[12c] several significant differences were found (see below).

First, the optimal acyl chain for *p*-NP esters switched to *p*-NP laurate (C_{12}) with a nearly one order of magnitude increase in specific activity ($\approx$2000 units mg^{-1}; Figure 1c). Interestingly, the specificity switched >1000-fold toward short-chain triacylglycerols (Figure 1d). Tributyrin (C_4) was the optimal substrate for EL1 (214000 units mg^{-1}), but the enzyme was also able to efficiently hydrolyze typical lipase substrates such as trilaurin, tripalmitin, and triolein (>67000 units mg^{-1}).

Encouraged by this finding, we assessed the susceptibility of EL1 to several fatty acid sulfonyl fluorides (SFs), which are potent serine-specific inhibitors. As shown in Figure 2a, R.34 was strongly inhibited by phenyl methyl sulfonyl fluoride (PMSF); however, it was partially inhibited by capryl sulfonyl fluoride (C_6SF), and was not affected by the longer lauroyl (C_{12}SF) and palmitoyl (C_{16}SF) derivatives. On the other hand, EL1 mutant was equally inhibited by all the SFs tested, which suggests that the serine residue at the active site is more accessible in this mutant compared with the wild-type enzyme.

Next, we examined the susceptibility of the EL1 variant to detergents and solvents. As illustrated in Figure 2b, the stability of the mutant was very similar to that of the wild-type enzyme upon addition of acetonitrile. This result suggests that solvent-exposed residues were, most likely, not changed by the mutation and that they were similarly exposed in both variants. However, when both enzymes were incubated at different concentrations of the ionic detergent Triton X-100, we observed that the EL1 variant was more affected than the wild-type enzyme (Figure 2c). Thus, R.34 showed maximal activity at 0.6% (w/v) detergent and retained more than 50% of the maximum activity at a 5% (w/v) concentration, whereas the EL1 mutant was strongly inhibited above 0.06% (w/v). The mutation may have induced a conformational change, whereas the catalytic residues became exposed to the large detergent micelles.

We further analyzed the secondary structure content, and found that the CD spectra for R.34 and EL1 mutant measured at 25°C were similar, with minima at 208 and 222 nm (Figure 3a), which is consistent with an α-helical protein. The thermal unfolding of each protein was determined by fitting the ellipticity at 222 nm (θ_{222}) versus temperature. As shown in Figure 3b, the melting temperature (T_m) shifted from 63.7°C (for R.34) to 51.3°C (for EL1). This result was somewhat unexpected, and indicates a lower stability for the EL1 mutant.

The creation of a lipase (EL1) prompted us to examine its positional specificity. The transesterification of the structured lipid 1,3-dipalmitoyl-2-oleoyl glycerol (POP) with ethanol[12a] was used to unambiguously identify the regiospecificity and to minimize acyl migration artifacts. When using lipase EL1 immobilized on Sepabeds EC-EP3, 2-methyl-2-butanol, and a water activity (a_w) of 0.22 (predetermined to be optimal), the reaction reached a conversion of $\approx$98% after 4 h at 30°C (Figure 4). EL1 showed a preference for the sn2 position, as deduced from the significantly higher concentrations of ethyl oleate and 1,3-dipalmitoyl glycerol over those of ethyl palmitate (Figure 4) and 1-*O*-palmitoyl- and 1(3)-palmitoyl-2-oleoyl glycerol,[12d] respectively.

The sequence analysis of EL1 mutant revealed a single amino acid substitution, N33D. The question that arises from this finding is, why does this single amino acid substitution in the EL1 mutant have such a profound effect on the substrate specificity? To understand the significant differences observed in the substrate specificity profile mediated by this substitution, we produced a three-dimensional model of the R.34 structure (Figure 5a), in which the esterase sequence was aligned with that of *Alicyclobacillus acidocaldarius*.[14]

 © 2005 Wiley-VCH Verlag GmbH & Co. KGaA, Weinheim

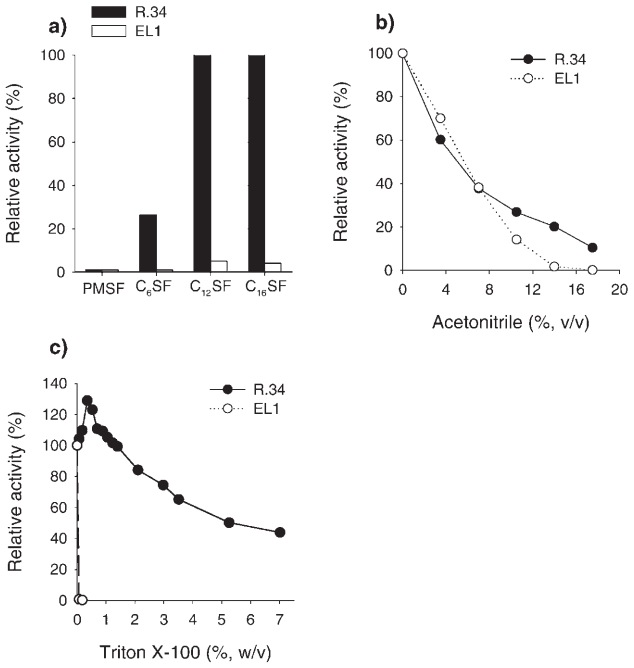

Figure 2. Parameters affecting the activities of R.34 and EL1. a) Inactivation by irreversible active-site inhibitors. Purified enzymes were incubated with 1 mM PMSF, C_6SF, C_{12}SF, and C_{16}SF. After incubation for 20 min, an aliquot was withdrawn and the hydrolytic activity was monitored. b) Effect of acetonitrile on esterase activity. c) Effect of Triton X-100 on esterase activity. Hydrolytic activity was monitored spectrophotometrically by following the increase in absorbance at 410 nm as a result of hydrolysis of *p*-NP propionate at 40 °C in HEPES buffer (100 mM, pH 7.5). The relative activity is normalized as 1.

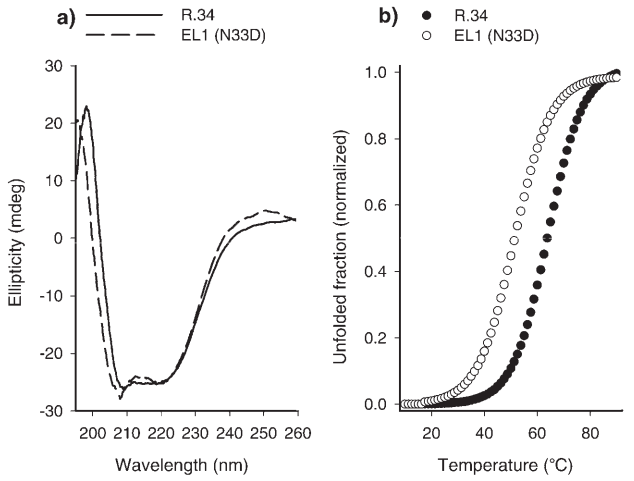

Figure 3. Circular dichroism studies. a) Far-UV CD spectra of R.34 and the EL1 mutant. b) Unfolding profiles of proteins. The samples were heated from 15 to 90 °C at 1 °C min^{-1} and the ellipticity was recorded at 222 nm. The T_m values were calculated by a nonlinear least-squares fit of the transition temperatures.

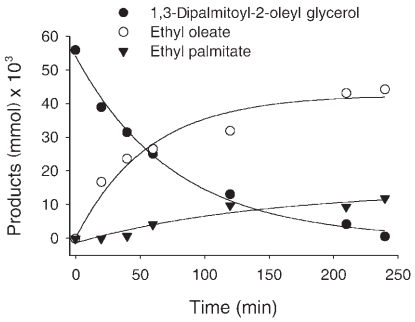

Figure 4. Time course of the transesterification reaction of POP with ethanol in 2-methyl-2-butanol using immobilized EL1 lipase (as determined by GC).[12a] Initial conditions: POP (0.056 mmol), ethanol (0.58 mmol), immobilized EL1 lipase (a_w = 0.22, 5 mg), 30 °C, 2-methyl-2-butanol (a_w = 0.22, 1 mL). Conditions as described in Ref. [12a]. The data are not fitted to any model; each point represents the mean of three experiments.

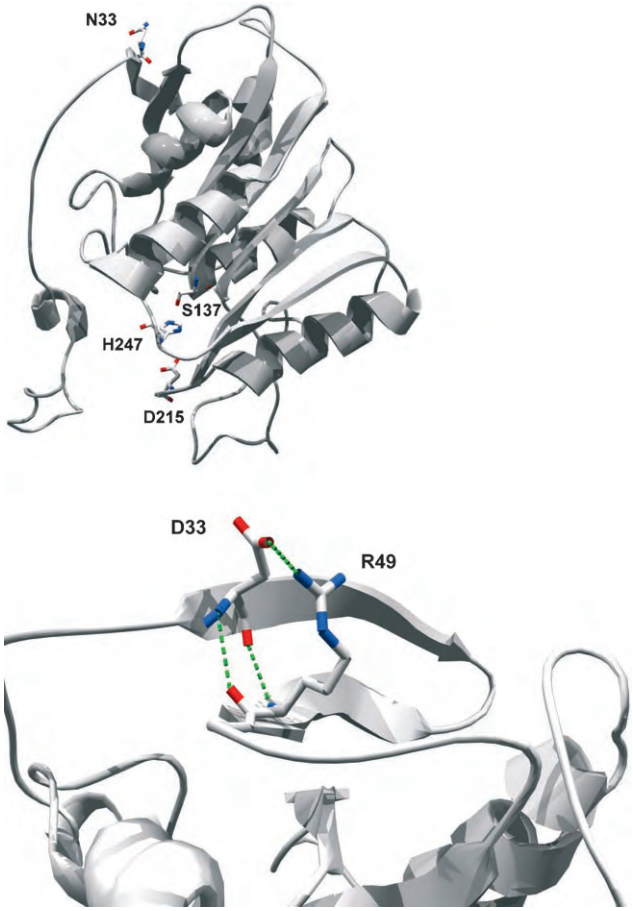

Figure 5. a) Overall three-dimensional structure of R.34, as obtained by homology modeling. Residues belonging to the catalytic triad and N33 are explicitly shown. b) Schematic representation of the putative salt-bridge binding residues D33 and R49 in the EL1 mutant.

The analysis of the *A. acidocaldarius* EST2 esterase structure indicates the existence of an ion pair between the two residues (Glu and Arg) present at positions equivalent to those of Asn33 and Arg49 in the R.34 sequence. This finding prompted us to suggest that the substitution of Asn33 by Asp leads to the formation of a salt bridge between the newly introduced Asp33 and Arg49 (Figure 5b). Most likely, this may cause a distortion of the enzyme structure (proof of which awaits 3D structure determination), which would make

 © 2005 Wiley-VCH Verlag GmbH & Co. KGaA, Weinheim

the catalytic site more accessible to larger substrates, but also more labile. This argument was supported experimentally by the analysis of the substrate-specificity profile (Figure 1), in which it was clear that the active site accommodated longer fatty acid esters, and by the higher susceptibility of EL1 to chemical inactivation and denaturation (Figure 2). In addition, the midpoint of unfolding was 12 °C lower. To prove the supposed interaction between D33 and R49, and the fact that this interaction affects the catalytic activity of the mutant enzyme toward triacylglycerols, single R49D and R49N mutant variants of the enzyme were generated by site-directed mutagenesis. Mutations at R49 produced variants with no activity on αNL plates, but they did hydrolyze αNA.[12e] Furthermore, we also introduced a reversed mutation N33R-R49D in R.34 and obtained the lipase phenotype in both αNL[12f] and rhodamine–triolein plates.[12g] These results unambiguously confirm that the interaction between residues 33 and 49 exists, and that it is essential for the substrate preference of the R.34 enzyme.

In summary, we have provided clear proof that the substrate specificity of a true carboxylesterase can be modified toward insoluble substrates, that is, turned into a true triacylglycerol lipase, without modification of the shape, size, or hydrophobicity of the substrate-binding sites that are considered to be essential for chain-length specificity.[1,7,8] Moreover, minimal changes in the structure are sufficient for enhancing the acyl chain-length preference of esterases. More significantly, compared with other lipases,[17,18] the EL1 mutant may constitute an important step toward the synthesis of structured lipids[19] and may have other lipase applications, which are under investigation.

Received: July 14, 2005
Revised: September 26, 2005
Published online: October 27, 2005

Keywords: enzymes · esterases · lipases · mutagenesis · regiospecificity

[1] U. T. Bornscheuer, *FEMS Microbiol. Rev.* **2002**, *26*, 73 – 81.
[2] K.-E. Jaeger, T. Eggert, *Curr. Opin. Biotechnol.* **2002**, *13*, 390 – 397.
[3] K.-E. Jaeger, B. W. Dijstra, M. T. Reetz, *Annu. Rev. Microbiol.* **1999**, *53*, 315 – 351.
[4] P. Fojan, P. H. Jonson, M. T. N. Petersen, S. B. Petersen, *Biochimie*, **2000**, *82*, 1033 – 1041.
[5] For examples, see: a) N. Zhang, W. C. Suen, W. Windsor, L. Xiao, V. Madison, A. Zaks, *Protein Eng.* **2003**, *16*, 599 – 605; b) P. Acharya, E. Rajakumara, R. Sankaranarayanan, N. M. Rao, *J. Mol. Biol.* **2004**, *341*, 1271 – 1281; c) G. Santarossa, P. G. Lafranconi, C. Alquati, L. DeGioia, L. Alberghina, P. Fantucci, M. Lotti, *FEBS Lett.* **2005**, *579*, 2383 – 2386.
[6] For examples, see: a) U. T. Bornscheuer, J. Altenbuchner, H. H. Meyer, *Biotechnol. Bioeng.* **1998**, *58*, 554 – 559; b) N. Krebsfänger, K. Schierholz, U. T. Bornscheuer, *J. Biotechnol.* **1998**, *60*, 105 – 111; c) N. Krebsfänger, F. Zocher, J. Altenbuchner, U. T. Bornscheuer, *Enzyme Microb. Technol.* **1998**, *22*, 641 – 646; d) E. Henke, U. T. Bornscheuer, *Biol. Chem.* **1999**, *380*, 1029 – 1033; e) K. Liebeton, A. Zonta, K. Schimossek, M. Nardini, D. Lang, B. W. Dijstra, M. T. Reetz, K.-E. Jaeger, *Chem. Biol.* **2000**, *7*, 709 – 718; f) K.-E. Jaeger, T. Eggert, A. Eipper, M. T. Reetz, *Appl. Microbiol. Biotechnol.* **2001**, *55*, 519 – 530; g) M. T. Reetz, *Methods Enzymol.* **2004**, *388*, 238 – 256; h) S. Park, K. L. Morley, G. P. Horsman, M. Holmquist, K. Hult, R. J. Kazlauskas, *Chem. Biol.* **2005**, *12*, 45 – 54.
[7] For examples, see: a) R. D. Joerger, M. J. Hass, *Lipids* **1994**, *29*, 377 – 384; b) H. Atomi, U. Bornscheuer, M. M. Soumanou, H. D. Beer, G. Wohlfahrt, R. D. Schmid, *Microbial Lipases: From Screening to Design, Vol. 1*, Barnes, Bridgwater, **1996**, pp. 49 – 50; c) R. R. Klein, G. King, R. A. Moreau, M. J. Haas, *Lipids* **1997**, *32*, 123 – 130; d) T. Eggert, G. Pencreac'h, I. Douchet, R. Verger, K.-E Jaeger, *Eur. J. Biochem.* **2000**, *267*, 6459 – 6469; e) I. Kauffmann, C. Schmidt-Dannert, *Protein Eng.* **2001**, *14*, 919 – 928; f) J. Yang, Y. Koga, H. Nakano, T. Yamane, *Protein Eng.* **2002**, *15*, 147 – 152.
[8] J. Pleiss, M. Fischer, R. D. Schmid, *Chem. Phys. Lipids* **1998**, *93*, 67 – 80.
[9] R. Verger, *Trends Biotechnol.* **1997**, *15*, 32 – 38.
[10] Wild-type esterase was retrieved from the bacteriophage lambda-based expression library created from DNA extracted from bovine rumen fluid, after screening in NZY soft agar containing α-naphthyl acetate (αNA), and expressed from the pBK-CMV phagemid pBKR.34 in *E. coli* XLOLR. Sequence analysis of R.34 is consistent with a 273 amino acid protein of $M_r = 34\,173.99$ Da and an isoelectric point of 5.03. It belongs to the ester hydrolase of family II of the Arpigny and Jaeger classification,[11] according to the conserved motif GDS(L); the catalytic triad was deduced to be formed by Ser137, Asp215, and His247. For details, see: M. Ferrer, O. V. Golyshina, T. N. Chernikova, A. N. Khachane, D. Reyes-Duarte, V. A. P. Martins Dos Santos, C. Strömpl, K. Elborough, G. Jarvis, A. Neef, M. M. Yakimov, K. N. Timmis, P. N. Golyshin, *Environ. Microbiol.* **2005**, in press.
[11] J. L. Arpigny, K.-E. Jaeger, *Biochem. J.* **1999**, *343*, 177 – 183.
[12] a) Detailed experimental procedures are available in the Supporting Information; b) The esterase–lipase phenotype of the EL1 improved variant and wild-type R.34 is shown in the Supporting Information; c) The optimal pH (7.5), temperature (50 °C), and subunit composition (monomer of ≈ 34 kDa) were essentially the same for both R.34 and EL1 enzymes (see the Supporting Information); d) HPLC chromatograms of the reaction products (from mono- to triglycerides) are shown in the Supporting Information; e) The esterase–lipase phenotype of EL1 variants containing R49N and R49D mutations is shown in the Supporting Information; f) The esterase–lipase phenotype of R.34 variant containing a reverse mutation N33R-R49D is shown in the Supporting Information; g) The lipase phenotype of R.34, EL1, and mutant variants on rhodamine–triolein plates is shown in the Supporting Information.[15]
[13] V. Khalameyzer, I. Fischer, U. T. Bornscheuer, J. Altenbuchner, *Appl. Environ. Microbiol.* **1999**, *65*, 477 – 482.
[14] a) Sequence alignment of R.34 esterase and other xylanases and esterases is shown in the Supporting Information; b) The structure of esterase EST2 from *A. acidocaldarius* (PDB Acc. number 1EVQA) was chosen as the most suitable template to generate a model for R.34. See G. De Simone, S. Galdiero, G. Manco, D. Lang, M. Rossi, C. Pedone, *J. Mol. Biol.* **2000**, *303*, 761 – 771. The degree of sequence identity between these two proteins is 19%. Ramachandran plots of both model and template proteins (see the Supporting Information) were obtained to assess the overall stereochemical quality of the model. The model is not reliable at the N-terminal part of the structure (first 32 residues of esterase R.34), where the sequence similarity between the model and template is very low. However, the results of threading[16] indicate a consistent structural similarity in the region starting at residue 33.
[15] G. Kouker, K.-E. Jaeger, *Appl. Environ. Microbiol.* **1987**, *53*, 211 – 213.

 © 2005 Wiley-VCH Verlag GmbH & Co. KGaA, Weinheim

[16] D. T. Jones, *J. Mol. Biol.* **1999**, *287*, 797 – 815.
[17] The mutant reported here exhibits preference for the sn2 position toward triacylglycerols. There are few examples of lipases specific for this position, and thus the experiments were performed under conditions in which acyl migration may occur. See: a) E. Rogalska, C. Cudrey, F. S. Ferrato, R. Verger, *Chirality* **1993**, *5*, 24 – 30; b) D. Briand, E. Dubreucq, P. Galzy, *Eur. J. Biochem.* **1995**, *228*, 169 – 175.
[18] For an extensive study on lipase regio- and stereoselectivity toward triacylglycerols, see: I. Douchet, G. de Hass, R. Verger, *Chirality* **2003**, *15*, 220 – 226, and references therein.
[19] For an extensive review, see: R. D. Schmid, R. Verger, *Angew. Chem.* **1998**, *110*, 1694 – 1720; *Angew. Chem. Int. Ed.* **1998**, *37*, 1608 – 1633.

 © 2005 Wiley-VCH Verlag GmbH & Co. KGaA, Weinheim

Biosynthesis

DOI: 10.1002/anie.200502246

Chain Elongation, Macrolactonization, and Hydrolysis of Natural and Reduced Hexaketide Substrates by the Picromycin/Methymycin Polyketide Synthase**

*Jiaquan Wu, Weiguo He, Chaitan Khosla, and David E. Cane**

Macrolide polyketides are a structurally diverse group of natural products, widely used for their pharmaceutically important antimicrobial, antitumor, and immunosuppressant properties.[1] The picromycin/methymycin synthase (PICS) of *Streptomyces venezuelae*, which is responsible for the formation of the 12- and 14-membered-ring antibiotics methymycin and picromycin,[2,3] is a typical modular polyketide synthase (PKS), in which each module is responsible for a single round of polyketide-chain elongation and functional-group modification.[4–6] Each module is in turn made up of a specific combination of fatty acid synthase-like domains that catalyze the individual biochemical steps of polyketide biosynthesis.

[*] Dr. J. Wu, W. He, Prof. Dr. D. E. Cane
Department of Chemistry
Box H, Brown University
Providence, RI 02912-9108 (USA)
Fax: (+1) 401-863-9368
E-mail: david_cane@brown.edu
Prof. Dr. C. Khosla
Departments of Chemical Engineering
Chemistry and Biochemistry
Stanford University
Stanford, CA 94305 (USA)

[**] This research was supported by NIH Grants GM22172 (D.E.C) and CA66736 (C.K.).

Supporting information for this article is available on the WWW under http://www.angewandte.org or from the author.

PICS module 6, a homodimer of subunit $M_w = 142$ kDa encoded by *pikAIV*, is organizationally one of the simplest known PKS modules, as it only consists of a ketosynthase (KS), a methylmalonyl transferase (AT), and an acyl carrier protein (ACP) domain as well as a C-terminal thioesterase (TE; Scheme 1). In spite of this apparent structural simplicity, PICS module 6(+TE) is one of the catalytically most intriguing PKS modules, on the basis of its demonstrated role in the formation of both 10-deoxymethynolide (**1**)[7] and narbonolide (**2**), the parent macrolide agylcones of methymycin and picromycin, respectively.[4,6,8–10]

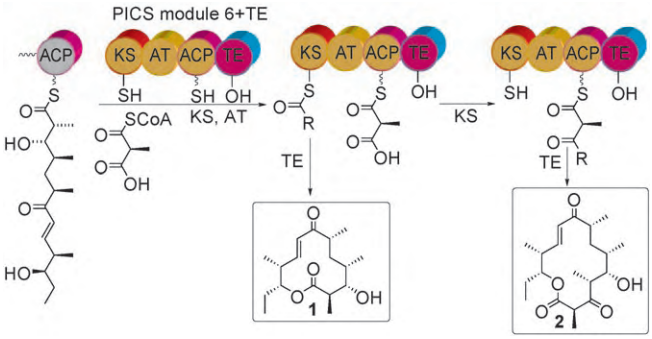

Scheme 1. Conversion of hexaketide into 10-deoxymethynolide (**1**) and narbonolide (**2**) by PICS module 6+TE.

We have reported the expression and purification of recombinant PICS module 6+TE from *Escherichia coli* and have investigated its relative substrate specificity by using *N*-acetylcysteamine (SNAC) thioesters of 2-methyl-3-hydroxypentanoic acid as diketide analogues of the natural hexaketide chain-elongation substrate.[11] It was found that PICS module 6+TE processed both *syn*-diketide diastereomers (2*S*,3*R*)-**3** and (2*R*,3*S*)-**4** with a modest 2.5:1 preference in k_{cat}/K_m for **4**, but did not process either of the two *anti* diketides (Scheme 2). Similar findings were reported independently by Sherman and co-workers,[9] who also described extensive in vivo and in vitro investigations of the biochemical basis for the competition between elongation of the natural hexaketide substrate by PICS module 6 to give **2** and direct cyclization to **1**, with the final macrolactonization being controlled in both cases by the C-terminal TE domain.[8,12] Although active KS6, AT6, and ACP6 domains were found to be essential for the formation of **1**, the precise role of these

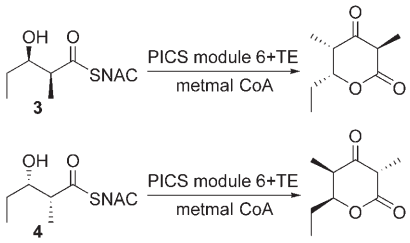

Scheme 2. Conversion of diketide-SNAC analogues into triketide ketolactones by PICS module 6+TE. metmal CoA = methylmalonyl coenzyme A.

© 2005 Wiley-VCH Verlag GmbH & Co. KGaA, Weinheim

domains in the delivery of the hexaketide substrate to the active site of the TE domain remains to be established. Investigations, both by us and Sherman and co-workers, have recently established that recombinant PICS TE alone can efficiently catalyze the macrolactonization of synthetic *seco*-hexaketide acyl SNAC **5** to **1** while catalyzing the exclusive hydrolysis of the corresponding 7-dihydro-*seco*-SNAC thioester **6**.[13,14] Most recently, Sherman also reported that PICS module 6+TE can convert the *seco*-SNAC thioester **5** and methylmalonyl coenzyme A (CoA) into **2**, although they did not monitor the competing direct lactonization to **1** and reported only a
k_{cat}/K_m value for the chain elongation and the lactonization reaction.[15] We now report that in the presence of the cosubstrate methylmalonyl CoA PICS module 6+TE catalyzes competing macrolactonization and chain elongation of **5**, which is converted into a 4:1 mixture of **1** and **2** (Scheme 3).

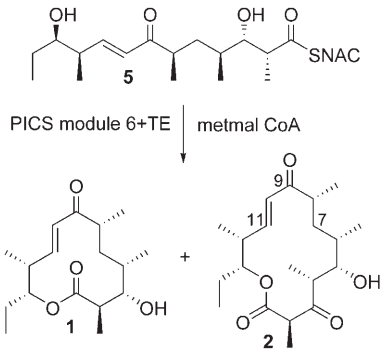

Scheme 3. Conversion of hexaketide *seco*-SNAC thioester **5** into **1** and **2** by PICS module 6+TE.

PICS module 6+TE is also shown to convert **6** and methylmalonyl CoA into a mixture of the direct hydrolysis product **7** and the isomeric chain-extended heptaketide lactones **8** and **9** (Scheme 4).

The requisite substrates **5** and **6** were each prepared by degradation and semisynthesis from **1**, as previously described.[13] The *seco*-SNAC thioester **5** is in equilibrium with approximately 50–60% of the corresponding 3,7-hemiacetal

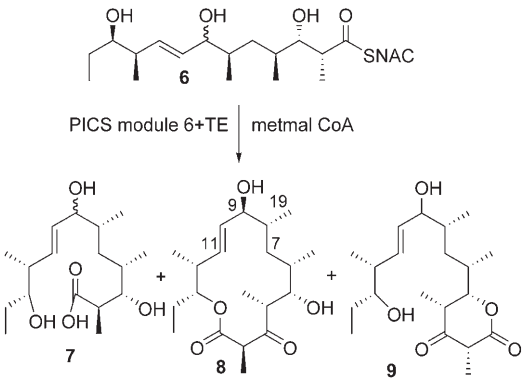

Scheme 4. Hydrolysis and lactonization of 7-dihydro-*seco*-SNAC-thioester **6** by PICS module 6+TE.

in $CDCl_3$.[13,15] Incubation of **5** with recombinant PICS module 6+TE and [2-^{14}C]methylmalonyl CoA produced a 4:1 mixture of **1** and **2**, as monitored by RP-HPLC with concatenated inline UV/Vis and flow-scintillation detection (Scheme 3). The identities of the enzymatic reaction products were confirmed by carrying out a preparative-scale reaction over 0.5 hours with **5** (2 mM) and methylmalonyl CoA (2 mM) in the presence of PICS module 6+TE (13.2 μM).[16] The resulting macrolide aglycones, purified by preparative RP-HPLC, displayed ^{1}H NMR and HR-ESI mass spectra that were identical to authentic samples of **1** as well as literature values for **1** and **2**.[17] The steady-state kinetic parameters for the formation of both **1** and **2** were determined by carrying out a series of incubations at concentrations of **5** that ranged from 0.5 to 4.0 mM, with the yields of **1** and **2** determined by HPLC/diode-array UV (230 nm) and phosphorimaging with TLC, respectively. The corresponding k_{cat} and K_m values were calculated by direct fitting of the plots of v versus [S] to the Michaelis–Menten equation (Table 1).[17] The relative values

Table 1: Steady-state kinetic parameters for PICS module 6+TE.

Substrate	Product	k_{cat} [min^{-1}]	K_M [mM]	k_{cat}/K_M [M^{-1} s^{-1}]
5	**1**	17.9±1.0	3.3±0.3	91.5±10.6
		43.0±5.2[a]	3.2±0.7[a]	223.3±56.7[a]
	2	4.4±0.7	5.2±1.5	14.1±4.7
6	**7**	6.9±0.7	2.1±0.5	64.7±14.3
	8	1.2±0.1	2.1±0.4	9.5±2.0
	9	6.8±1.2	2.6±0.9	43.6±17.3

[a] Formation of **1** in the absence of methylmalonyl CoA.

of k_{cat} showed the expected 4:1 preference for the formation of the macrolactonization product **1** over chain extension and cyclization to **2**. The observed K_m values were not corrected for the presence of the corresponding hemiacetal form of **5**, as the concentration of this species in the reaction buffer was not determined and all of the substrate was consumed in the preparative-scale reaction. Interestingly, incubation of **5** with PICS module 6+TE under identical conditions but in the absence of methylmalonyl CoA gave exclusively **1**, but with approximate 2.2-fold increases in both k_{cat} and k_{cat}/K_m values relative to the cyclization to **1** in the presence of the methylmalonyl CoA cosubstrate.

We previously reported that incubation of **6** (7*S*/7*R* 3:1) with the recombinant PICS TE alone results exclusively in hydrolysis to the corresponding diastereomeric mixture of *seco* acids **7**.[13,14] By contrast, preparative-scale incubation of **6** (2 mM) and methylmalonyl CoA (1 mM) with PICS module 6+TE (10 μM) gave **7**, **8**, and **9** in a 6:3:4 mixture that could be readily separated by flash chromatography (Scheme 4). The NMR spectroscopic and chromatographic properties of **7** were identical to those previously determined.[13] The structure and stereochemistry of **8** and **9** were determined by ^{1}H and ^{13}C NMR spectroscopy, including HMQC and NOESY analysis.[17] Both compounds exhibited HR-ESI mass spectra consistent with the molecular composition $C_{20}H_{34}O_5$ expected for the isomeric lactones. The

 © 2005 Wiley-VCH Verlag GmbH & Co. KGaA, Weinheim

^{1}H NMR spectrum of **8** closely resembled that of **2**, with several key differences. Thus, the two olefinic protons exhibited the expected upfield shift and change in multiplicity relative to the enone double bond of **2**: H10 ($\delta = 5.34$ ppm, dd, $J = 15.4$, 7.8 Hz) coupled to H11 ($\delta = 5.42$ ppm, dd, $J = 15.4$, 7.7 Hz), with similar changes in the ^{13}C NMR spectrum (C10 $\delta = 134.1$; C11 133.6 ppm). The presence of only a single resonance for allylic H9 in both the ^{1}H NMR ($\delta = 3.47$ ppm, t, $J = 8.5$ Hz—correlated to both H10 and H8 in the ^{1}H COSY spectrum) and ^{13}C NMR spectra ($\delta = 78.8$ ppm) is consistent with the formation of a single diastereomer of **8**. The configuration of **8** was readily assigned as the 9*S* isomer, as based on the NOESY spectrum, which showed crosspeaks between H9 and the H19 methyl protons ($\delta = 1.03$ ppm) as well as between H9 and both the olefinic H11 proton ($\delta = 5.42$ ppm) and one of the H7 methylene protons ($\delta = 0.74$ ppm), but not with either H8 or H10 (Figure 1). Compound **9** was assigned the isomeric δ-lactone structure based on comparison with the spectra of **8**. Thus, the ^{13}C NMR resonance for the lactonic C5 ($\delta = 82.4$ ppm) appeared downfield of the corresponding signal for C5 in **8** ($\delta = 71.7$ ppm), with the expected differences in the attached H5 protons as well (**9**: $\delta = 4.32$ ppm, dd, $J = 9.8$, 2.0 Hz; **8**: $\delta = 4.02$ ppm, dd, $J = 5.4$, 2.4 Hz). The signals for C13 (**9**: $\delta = 76.8$; **8**: 80.1 ppm) and H13 (**9**: $\delta = 3.44$ ppm, td, $J = 8.4$, 3.5 Hz; **8**: $\delta = 4.77$ ppm, td, $J = 10.3$, 3.1 Hz) also showed the expected complementary changes in chemical shift. Although **9** is most likely a single diastereomer (H9 $\delta = 3.44$ ppm, t, $J = 5.1$ Hz; C9 $\delta = 75.9$ ppm), the configuration at C9 was not assigned. The steady-state kinetic parameters for the formation of **8** and **9** (lactonization) as well as **7** (hydrolysis) were also determined (Table 1).

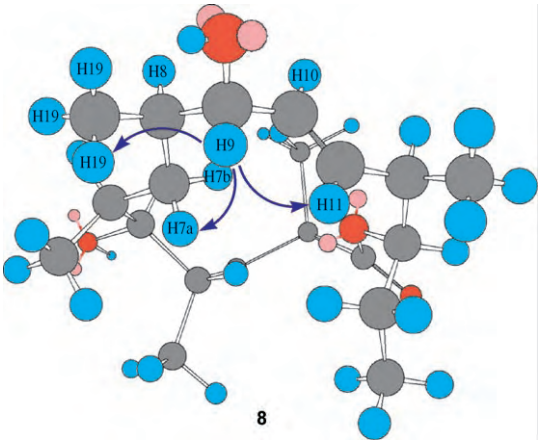

Figure 1. Key NOESY correlations for (9*S*)-9-dihydronarbonolide (**8**). (Energy-minimized conformation calculated by using the MM2 module of Chem3D.)

The observed k_{cat} and k_{cat}/K_m values for chain-elongation/cyclization of **5** to **2** (Table 1) are nearly two orders of magnitude greater than the corresponding steady-state parameters previously determined for the diketide analogue (2*R*,3*S*)-**4** ($k_{cat} = 0.057 \pm 0.003$ min^{-1} and $k_{cat}/K_m = 0.027$ M^{-1} s^{-1}); some of the difference in the k_{cat}/K_m values rises from an approximate tenfold decrease in the K_m value relative to (2*R*,3*S*)-**4** (35 ± 4 mM).[9,11] It would be expected that the natural hexaketide intermediate, which is delivered to PICS module 6 as the corresponding acyl thioester bound to the ACP of PICS module 5, would have an even lower native K_m value.[18] Although both the KS6 or ACP6 domains have been reported to be essential for in vivo macrolactonization of the hexaketide produced by PICS module 5,[8] it is not clear whether the observed dominant macrolactonization of **5** by PICS module 6 + TE involves mandatory transfer to the TE domain by way of transient covalent attachment to either the KS6 or ACP6 domains. Irreversible formation of the acyl-KS species has been shown to be the sole determinant of the k_{cat}/K_m value for the processing of substrates by PKS modules.[19] The fact that the k_{cat}/K_m values measured for lactonization and for chain-elongation of **5** are different may suggest that these two reactions do not involve partitioning of a common hexaketide KS intermediate. Indeed, recombinant PICS TE alone catalyzes the efficient conversion of **5** into **1**.[13,14] Interestingly, the observed steady-state kinetic parameters for the conversion of **5** into **1** by PICS module 6 + TE in the absence of methylmalonyl CoA are effectively the same as those that we previously determined for the macrolactonization of **5** by recombinant PICS TE ($k_{cat} = 54.4 \pm 5.8$ min^{-1}, $K_m = 4.1 \pm 0.8$ mM, $k_{cat}/K_m = 221 \pm 50$ M^{-1} s^{-1}).[13] The k_{cat} value for the formation of **1** by PICS module 6 + TE in the absence of methylmalonyl CoA is larger than the combined k_{cat} value for both the lactonization and chain elongation by the PICS module 6 + TE in the presence of methylmalonyl CoA, thus suggesting that the presence of a methylmalonyl thioester attached to the ACP of module 6 may inhibit access of the hexaketide substrate to the active site of the downstream TE domain. Alternatively, it may reflect slower cyclization of the heptaketide substrate than of the hexaketide substrate by the TE domain.

The chain elongation/lactonization of **6** into **8** and **9** by PICS module 6 + TE also takes place at rates comparable to those observed for the processing of **5**, the analogue of the natural hexaketide substrate. Interestingly, although a mixture of isomeric lactones is observed, chain elongation appears to be diastereoselective. The formation of the two lactones from **6** is in contrast to the exclusive hydrolysis of the same substrate by recombinant PICS TE alone,[13,14] thus indicating that both the PICS KS6 domain and the TE domain can process reduced hexaketide and heptaketide subtrates, respectively.

In summary, we have shown that recombinant PICS module 6 + TE is capable of mediating both chain elongation and lactonization as well as competing lactonization or hydrolysis of both the natural hexaketide substrate **5** and the reduced 7-dihydro analogue **6** and have established the full set of steady-state kinetic parameters for both sets of reactions. The observed 4:1 ratio of lactonization to chain elongation for the processing of **5** may represent the intrinsic ratio of these two processes that leads to the characteristic formation of 12- and 14-membered-ring macrolides, thereby definitively excluding the necessity for N-terminal truncation

 © 2005 Wiley-VCH Verlag GmbH & Co. KGaA, Weinheim

of PICS module 6 for formation of the hexaketide macrolactonization product 10-deoxymethynolide (**1**), as has been suggested at one time.[12]

Received: June 26, 2005
Published online: October 25, 2005

Keywords: antibiotics · biosynthesis · lyases · polyketides · synthases

[1] D. O'Hagan, *The Polyketide Metabolites*, E. Norwood, New York, **1991**.
[2] S. Omura, H. Takeshima, A. Nakagawa, J. Miyazawa, *J. Antibiot.* **1976**, *29*, 316–317.
[3] T. Hori, I. Maezawa, N. Nagahama, M. Suzuki, *J. Chem. Soc. Chem. Commun.* **1971**, 304–305.
[4] Y. Xue, L. Zhao, H.-W. Liu, D. H. Sherman, *Proc. Natl. Acad. Sci. USA* **1998**, *95*, 12111–12116.
[5] Y. Xue, D. Wilson, D. H. Sherman, *Gene* **2000**, *245*, 203–211.
[6] L. Tang, H. Fu, M. C. Betlach, R. McDaniel, *Chem. Biol.* **1999**, *6*, 553–558.
[7] R. H. Lambalot, D. E. Cane, *J. Antibiot.* **1992**, *45*, 1981–1982.
[8] B. J. Beck, Y. J. Yoon, K. A. Reynolds, D. H. Sherman, *Chem. Biol.* **2002**, *9*, 575–583.
[9] B. J. Beck, C. C. Aldrich, R. A. Fecik, K. A. Reynolds, D. H. Sherman, *J. Am. Chem. Soc.* **2003**, *125*, 12551–12557.
[10] B. J. Beck, C. C. Aldrich, R. A. Fecik, K. A. Reynolds, D. H. Sherman, *J. Am. Chem. Soc.* **2003**, *125*, 4682–4683.
[11] Y. Yin, H. Lu, C. Khosla, D. E. Cane, *J. Am. Chem. Soc.* **2003**, *125*, 5671–5676.
[12] Y. Xue, D. H. Sherman, *Nature* **2000**, *403*, 571–575.
[13] W. He, J. Wu, C. Khosla, D. E. Cane, *Bioorg. Med. Chem. Lett.*, DOI:10.1016/j.bmcl.2005.09.077.
[14] C. C. Aldrich, L. Venkatraman, D. H. Sherman, R. A. Fecik, *J. Am. Chem. Soc.* **2005**, *127*, 8910–8911.
[15] C. C. Aldrich, B. J. Beck, R. A. Fecik, D. H. Sherman, *J. Am. Chem. Soc.* **2005**, *127*, 8441–8452.
[16] Incubation for more than 1 h with >15 μM PICS module 6 + TE resulted in competing hydrolysis of the accumulated narbonolide (**2**) apparently to the corresponding *seco* acid.
[17] See the Supporting Information for details of preparative and kinetic experiments, as well as complete spectroscopic data for new compounds.
[18] N. Wu, S. Y. Tsuji, D. E. Cane, C. Khosla, *J. Am. Chem. Soc.* **2001**, *123*, 6465–6474.
[19] J. Wu, K. Kinoshita, C. Khosla, D. E. Cane, *Biochemistry* **2004**, *43*, 16301–16310.
[20] H. Lu, S. C. Tsai, C. Khosla, D. E. Cane, *Biochemistry* **2002**, *41*, 12590–12597.

 © 2005 Wiley-VCH Verlag GmbH & Co. KGaA, Weinheim

Nickel-Catalyzed Oligomerization

DOI: 10.1002/anie.200502532

Ethylene Oligomerization at Coordinatively and Electronically Unsaturated Low-Valent Nickel**

*Zhiqiang Weng, Shihui Teo, Lip Lin Koh, and T. S. Andy Hor**

Research in nickel-catalyzed olefin oligomerization and polymerization continues to progress at an accelerating pace.[1] With the synthesis of new Ni^{II} catalysts that are highly tolerant towards polar substrates and are less oxophilic,[2] we are now able to target specific functional products. This advancement has brought along a host of new ligands, catalysts,[3] and mechanistic data.[4] It has also spilled over into scientific breakthroughs in new nickel chemistry, among which the recent isolation of low-valent coordinatively unsaturated Ni^{I} is particularly noteworthy.[5,6] This immediately gave rise to some pertinent questions, such as how Ni^{I} compares to the classical Ni^{II} and the sensitive Ni^{0} in catalytic performance or whether a coordinatively and electronically unsaturated Ni^{I} center might exhibit enhanced activity.

To address some of these questions, we need to design, prepare, and isolate close counterparts for direct structural and catalytic comparisons. We herein report our preliminary findings in using a ferrocenediyl iminophosphane supporting ligand. The flexibility of the ferrocenyl backbone,[7,8] coupled with the hemilability of the donors,[9] allows the metal to "pick and choose" its donors, and tune its receptivity to the substrates. It also raises our chances of isolating catalytically important intermediates for structural verification. The use of iminophosphanes as ligands for late transition metals for olefin polymerization has been demonstrated.[10]

$NiCl_2$(DME) (DME = dimethoxyethane) reacts with [{η-$C_5H_4CH{=}N(C_6H_5)$}Fe{η-$C_5H_4P(t\mathrm{Bu})_2$}] to give the Ni^{II} complex [{[η-$C_5H_4CH{=}N(C_6H_5)$]Fe[η-$C_5H_4P(t\mathrm{Bu})_2$]}$NiCl_2$] (**1**). Addition of one equivalent of MeLi to **1** in THF at −30 °C resulted in a one-electron reduction to [{[η-$C_5H_4CH{=}N(C_6H_5)$]Fe[η-$C_5H_4P(t\mathrm{Bu})_2$]}$Ni^{I}Cl$] (**2**; Scheme 1), with no evidence of methylnickel(I/II) products similar to the result from bis(imino)pyridylcobalt(II) with methylaluminoxane (MAO).[11] Ligand replacement of [$Ni(cod)_2$] (cod = 1,5-cyclooctadiene) with [{η-$C_5H_4CH{=}N(C_6H_5)$}Fe{η-

[*] Dr. L. L. Koh, Prof. Dr. T. S. A. Hor
Department of Chemistry
National University of Singapore
3 Science Drive 3, Kent Ridge, Singapore 117543 (Singapore)
Fax: (+65) 6874-2663
E-mail: andyhor@nus.edu.sg
Dr. Z. Weng, S. Teo
Institute of Chemical and Engineering Sciences
No. 1, Pesek Road, Jurong Island, Singapore, 627833 (Singapore)

[**] We are grateful to the Agency for Science, Technology & Research (Singapore), the Institute of Chemical and Engineering Sciences (Singapore; grant 012-101-0035), and the National University of Singapore for support.

WILEY InterScience DISCOVER SOMETHING GREAT
© 2005 Wiley-VCH Verlag GmbH & Co. KGaA, Weinheim

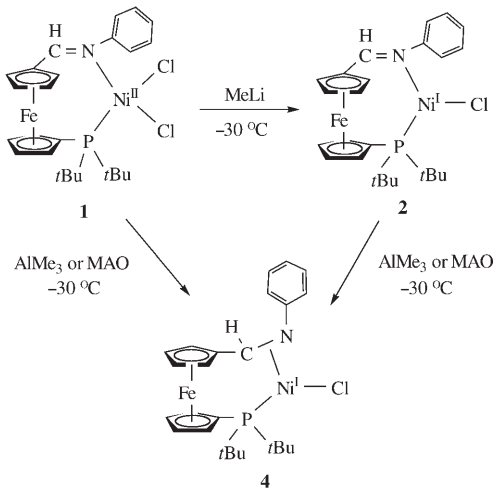

Scheme 1.

$C_5H_4P(tBu)_2$}] and [{η-$C_5H_4CH{=}N(C_6F_5)$}Fe{η-$C_5H_4PPh_2$}], in the presence of CN*t*Bu in hexane, yields dark-red solids of [{[η-$C_5H_4CH{=}N(C_6H_5)$]Fe[η-$C_5H_4P(tBu)_2$]}$Ni^0(CNtBu)_3$] (**3a**) and [{[$C_5H_4CH{=}N(C_6F_5)$]Fe[η-$C_5H_4PPh_2$]}$Ni^0(CNtBu)_3$] (**3b**), respectively (Scheme 2). All the products were isolated and characterized spectroscopically.

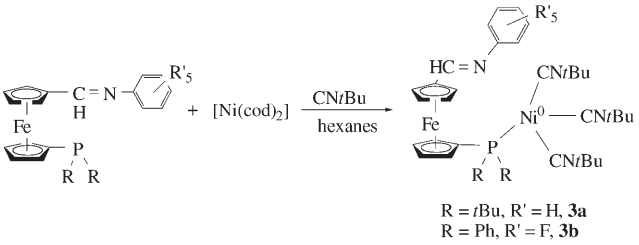

Scheme 2.

Single-crystal X-ray diffraction[12] revealed that **2** crystallizes with two independent molecules (A and B) per unit cell (molecule A is shown in Figure 1). It shows a trigonal planar (mean plane deviation 0.0045 Å) Ni^I center with three heteroatom donors, namely N, P, and Cl. There is no evidence of significant intermolecular contacts. This 15-electron, three-coordinate Ni^I is thus an unusual coordinatively exposed and electronically unsaturated paramagnetic complex. Despite the apparent electronic deficiency and coordinative exposure, there is no evidence of any electron donation by obvious means, such as dimerization, hydride formation, agostic Ni···H (Fc or Bu) interactions, π–imine coordination, or Fe→Ni dative bonding. This type of low-coordinate, low-valent Ni^I complex is rare but not unprecedented (e.g. β-diketiminatonickel(I)[5] and diphosphane-supported alkylnickel(I) complexes[6]). The Ni–N bond length (1.995(2) Å) is between that to Ni^I (1.876(1) Å)[5a] and the iminophosphanenickel(II) (2.043(6) Å),[10c] whereas the Ni–P bond (2.2251(8) Å) is also intermediate between the P,N-bound Ni^0 complex [$(iPr)_2PCH_2CH_2NMe_2$)Ni(PhC≡CPh)] (2.1565(10) Å)[13] and a Ni^{II} complex (2.338(2) Å).[10c] The Ni–Cl bond (2.1929(9) Å) is similar to those in a P,N-chelating tetrahedral Ni^{II} complex (2.191(1) and

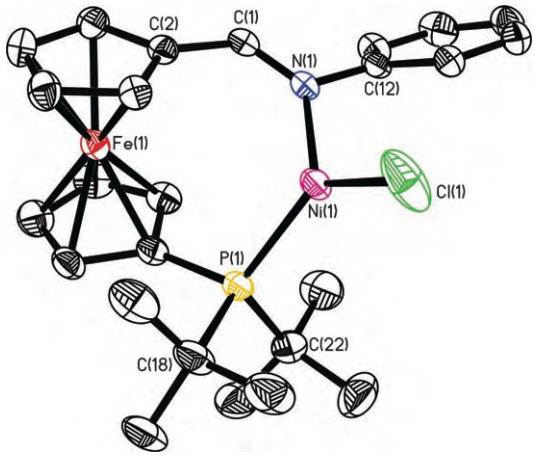

Figure 1. ORTEP representation of the X-ray structure of molecule A in **2**. Hydrogen atoms have been omitted for clarity. Thermal ellipsoids are drawn at 40% probability. Selected bond lengths [Å] and angles [°]: Ni(1)–N(1) 1.995(2), Ni(1)–P(1) 2.2251(8), Ni(1)–Cl(1) 2.1929(9), C(1)–N(1) 1.288(3); N(1)–Ni(1)–Cl(1) 119.23(7), N(1)–Ni(1)–P(1) 112.34(6), Cl(1)–Ni(1)–P(1) 128.43(4).

2.217(1) Å).[14a] To stabilize the low coordination, the chelating ligand needs to expand its spatial protection by stretching the bite angle to 112.34(6)° (compared to 98.4(1)° and 110.94(8)° in related Pd^{II} and Pd^0 complexes)[9] in order to be more compatible with a trigonal planar geometry.

The solid-state structure of **3b** reveals a tetrahedral Ni^0 complex supported by three isocyanide ligands, with the iminophosphane in an unexpected unidentate mode (Figure 2). This demonstrates that an electron-rich metal

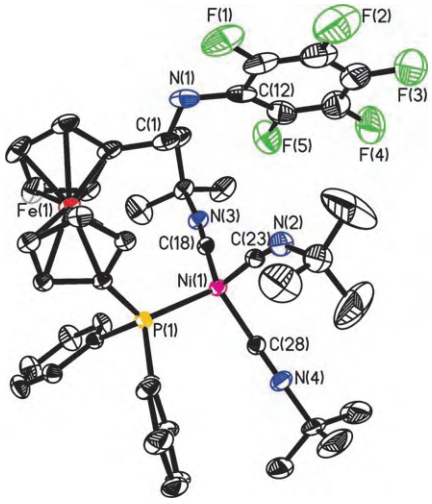

Figure 2. ORTEP representation of the X-ray structures of **3b**. Hydrogen atoms have been omitted for clarity. Thermal ellipsoids are drawn at 40% probability. Selected bond lengths [Å] and angles [°]: Ni(1)–P(1) 2.2001(10), Ni(1)–C(18) 1.843(4), Ni(1)–C(23) 1.821(4), Ni(1)–C(28) 1.842(4), C(1)–N(1) 1.282(6), C(18)–N(3) 1.161(4), C(23)–N(2) 1.168(5), C(28)–N(4) 1.159(5); C(23)–Ni(1)–C(28) 103.74(17), C(23)–Ni(1)–C(18) 116.59(17), C(18)–Ni(1)–P(1) 112.17(11), C(28)–Ni(1)–P(1) 104.52(12), C(23)–N(2)–C(24) 148.7(4), C(18)–N(3)–C(19) 173.7(4), C(28)–N(4)–C(29) 171.6(4).

© 2005 Wiley-VCH Verlag GmbH & Co. KGaA, Weinheim

opts for the stronger π-accepting environment provided by isonitrile, especially in its angular mode [C(23)–N(2)–C(24) = 148.7(4)°]. This is facilitated by the lability of the imine donor and the ability of the ferrocenyl ligand to sustain a unidentate mode with a dangling functional entity. The Ni–P bond (2.2001(10) Å) is slightly shorter than that of **2** (2.2251(8) Å). The Ni–C bond of bent isocyanide (1.821(4) Å) is slightly stronger than that of the other two Ni–C bonds (1.843(4) and 1.842(4) Å), with the latter being similar to that of the ethylene polymerization active Ni^{II}–isocyanide complex $[NiBr_2(CNAr)_2]$ (1.846(2) Å)[15] and the Ni^0–isocyanide complex $[Ni(C_6H_5N{=}NC_6H_5)(CN\textit{t}Bu)_2]$ (1.841(5) Å).[16]

Isolation of **1**–**3** pointed to some valuable features of iminophosphane as a ligand. It supports a metal (Ni) in its normal, intermediate, and low valency, it is sensitive to the coordinative change of the metal, and it uses its hemilability to adjust the electronic donation. These are essential qualities that could raise the catalytic performance and enable us to isolate catalytically important intermediates. It also enables us to directly compare the activity of Ni^{II}, Ni^{I}, and Ni^0 in ethylene oligomerization through the use of **1**, **2**, **3a**, and **3b**. Some preliminary results under ambient conditions are summarized in Table 1. Using MAO as the cocatalyst with an Al/Ni ratio of 1000, the ethylene oligomerization activity (TOF) decreases in the order $\mathbf{2} \gg \mathbf{3a} > \mathbf{1}$ which reflects the activity order of $Ni^{I} \gg Ni^0 > Ni^{II}$ (entries 1–3). The 1-butene selectivity for Ni^{II} is, however, higher. All of them give insignificant amounts of high molecular weight polymeric products. We should add, however, that the electronic effect of the iminophosphane ligand could override the metal effect. This is best exemplified in the higher TOF of **3b** (75000), which contains a pentafluorophenyl imine and phenylphosphane, compared to **3a** (10667) (entries 3 and 4, respectively). These residues raise the electrophilicity of the central metal, thus promoting substrate attack.[17]

We have also studied the effect of cocatalyst, temperature, and pressure using **3b** as the catalyst. $EtAlCl_2$ performs better than MAO (entries 5–8), possibly due to facile formation of alkylnickel species in situ, which leads to active nickel hydrides by β-elimination, consistent with the observations of Braunstein and co-workers.[14] A TOF of 119400 (entry 6) is achieved at 30 °C. There is no clear advantage from using a higher temperature (compare entries 5 and 7) or pressure (compare entries 6 and 8). The oligomerization performance depends more on catalyst design and cocatalyst support. With a metal that can attract ethylene efficiently and promote detachment through a β-hydride elimination, one would expect a good yield at ambient conditions with reasonable selectivity. Complex **2** and the reported $(N,N)Ni^{I}$ complex[5c] are both three-coordinate but they present two different assemblies in catalyst design, namely, the use of an anionic chelating ligand (diketiminato) with a terminal neutral ligand (phosphane) and a neutral ferrocenediyl iminophosphane with an anionic halide. The former relies on the lability of the phosphane, whereas the latter relies on anion (e.g. Cl→R, to give alkylnickel(I) species[6a]) or hydride exchange (Cl→H) for activation.

Complex **1** (Ni^{II}) would not survive under the reducing (and basic) conditions generated by excess MeLi. Could it, however, be active and persistent in a catalytic mixture that contains $AlMe_3$ or MAO? Experiments on the reaction of **1** with two equivalents of $AlMe_3$ or MAO at room temperature led to the isolation of the Ni^{I} complex $[\{[\eta\text{-}C_5H_4CH{=}N\text{-}(C_6H_5)]Fe[\eta\text{-}C_5H_4P(\textit{t}Bu)_2]\text{-}\textit{CN},\textit{P}\}Ni^{I}Cl]$ (**4**) (Scheme 1), which can also be independently prepared from **2** and $AlMe_3$ or MAO (1:2). Single-crystal X-ray diffraction analysis[12] revealed that **4** is related to **2** but, significantly, coordination at the N site has slipped to C=N, thus activating the π functionality, while maintaining a planar Ni^{I} (mean plane deviation 0.0147 Å; Figure 3). This lengthens and weakens the C–N bond from 1.288(3) in **2** to 1.435(9) Å in **4**. Accordingly, the Ni–P bond is shorter and presumably stronger (2.169(2) Å) than that in **2** (2.2251(8) Å), while the Ni–Cl bond is correspondingly weaker (2.231(2) Å) than that in **2** (2.1929(9) Å). The fragility of the Ni–Cl bond and the strengthening of the other protective ligands appear to support and "prepare" the metal for its catalytic function. Oligomerization experiments using **4** as the catalyst demonstrate that it is active. Upon activation with excess MAO (1000-fold), it gives a TOF of 14666 in ethylene oligomerization.

We have shown that a hemilabile iminophosphanylferrocene ligand can stabilize catalytically active low-valent nickel and the resulting complexes can be used directly to catalyze ethylene oligomerization. This highlights the potential use of Ni^0 and Ni^{I} rather than the more popular Ni^{II} in similar catalysis.[18] In Ziegler–Natta-type polymerization, the cata-

Table 1: Oligomerization of ethylene.[a,b]

Entry	Cat.	Activator	T [°C]	P [psi]	Al/Ni	t [h]	TOF[c]	Oligomer		
								$C_4/\Sigma C$ [%]	$C_6/\Sigma C$ [%]	α-olefin [%] (C_4)
1	**1**	MAO	30	300	1000	3	8000	87.3	12.7	84.6
2	**2**	MAO	30	300	1000	3	21000	70.3	29.7	72.7
3	**3a**	MAO	30	300	1000	3	10667	76.2	23.8	60.1
4	**3b**	MAO	30	300	1000	3	75000	87.1	12.9	16.5
5	**3b**	$EtAlCl_2$	30	300	146	3	91600	69.9	30.1	45.9
6	**3b**	$EtAlCl_2$	30	300	1000	2	119400	79.2	20.8	41.2
7	**3b**	$EtAlCl_2$	60	300	146	1	96000	59.0	41.0	28.5
8	**3b**	$EtAlCl_2$	30	450	1000	2	120600	70.5	29.5	53.8

[a] Optimized with the Endeavor Catalyst Screening System. [b] Conditions: 0.25 μmol of catalyst, 4 mL of toluene. [c] TOF = mol of ethylene consumed/mol of Ni h^{-1}.

 © 2005 Wiley-VCH Verlag GmbH & Co. KGaA, Weinheim

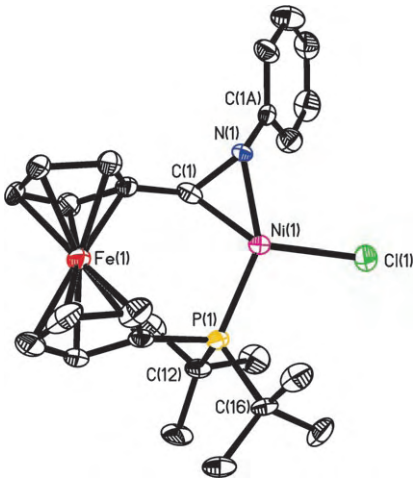

Figure 3. ORTEP representation of the X-ray structure of **4**. Hydrogen atoms have been omitted for clarity. Thermal ellipsoids are drawn at 40% probability. Selected bond lengths [Å] and angles [°]: Ni(1)–C(1) 1.887(8), Ni(1)–N(1) 1.963(6), Ni(1)–P(1) 2.169(2), Ni(1)–Cl(1) 2.231(2), C(1)–N(1) 1.435(9); C(1)–Ni(1)–N(1) 43.7(3), C(1)–Ni(1)–P(1) 103.9(2), N(1)–Ni(1)–P(1) 145.91(18), N(1)–Ni(1)–Cl(1) 107.77(7), Cl(1)–Ni(1)–P(1) 106.12(8).

lytically active species is widely believed to be a cationic alkyl–metal complex L_nMR^+.[19] Olefin oligomerization by Ni^{II} is also widely acknowledged to proceed via L_nNiR^+, which readily gives $L_nNi^{II}(H)(alkene)^+$ as a key intermediate.[20] Use of Ni^I complexes, such as **2** and **4**, or Ni^0 complexes, such as **3a** and **3b**, suggests that we can enter the catalytic cycle with non-alkyls and electronically neutral species. The key here is the use of a coordinatively exposed metal in a low oxidation state and a hemilabile ligand. These are features that are usually advantageous to catalytic pathways, such as Suzuki coupling, that hinge on the complementary oxidative addition and reductive elimination, but not olefin oligomerization. They offer new opportunities in catalyst design for polymerization, but they also pose some pertinent questions. For example, does this necessarily require a different mechanistic pathway? Do Ni^I and Ni^0 offer a better prospect in olefin oligomerization? Does the use of mononuclear paramagnetic Ni^I necessarily demand a free radical pathway, such as the one shown in other four-coordinate Ni^I complexes?[21] Our ongoing experiments are driven by these curiosities.

Received: July 20, 2005
Published online: October 27, 2005

Keywords: coordination modes · homogeneous catalysis · N,P ligands · nickel · oligomerization

[1] See, for example: a) L. K. Johnson, C. M. Killian, M. Brookhart, *J. Am. Chem. Soc.* **1995**, *117*, 6414; b) S. Mecking, *Angew. Chem.* **2001**, *113*, 550; *Angew. Chem. Int. Ed.* **2001**, *40*, 534.
[2] V. C. Gibson, S. K. Spitzmesser, *Chem. Rev.* **2003**, *103*, 283.
[3] J. M. Malinoski, M. Brookhart, *Organometallics* **2003**, *22*, 5324.
[4] J. C. Jenkins, M. Brookhart, *J. Am. Chem. Soc.* **2004**, *126*, 5827.
[5] a) P. L. Holland, T. R. Cundari, L. L. Perez, N. A. Eckert, R. J. Lachicotte, *J. Am. Chem. Soc.* **2002**, *124*, 14416; b) S. Puiu, T. H. Warren, *Organometallics* **2003**, *22*, 3974; c) D. Zhang, G.-X. Jin, L.-H. Weng, F. Wang, *Organometallics* **2004**, *23*, 3270.
[6] a) K. D. Kitiachvili, D. J. Mindiola, G. L. Hillhouse, *J. Am. Chem. Soc.* **2004**, *126*, 10554; b) D. J. Mindiola, G. L. Hillhouse, *J. Am. Chem. Soc.* **2001**, *123*, 4623.
[7] R. C. J. Atkinson, V. C. Gibson, N. J. Long, *Chem. Soc. Rev.* **2004**, *33*, 313.
[8] K.-S. Gan, T. S. A. Hor in *Ferrocenes* (Eds.: A. Togni, T. Hayashi), VCH, Weinheim, **1995**, chap. 1.
[9] Z. Weng, S. Teo, L. L. Koh, T. S. A. Hor, *Organometallics* **2004**, *23*, 4342.
[10] a) C. M. Killian, J. P. McDevitt, P. B. Mackenzie, L. S. Moody, J. A. Ponasik, Jr., WO 9840420, **1998**; b) Z. Guan, WO 0059956, **2000**; c) Z. Guan, W. J. Marshall, *Organometallics* **2002**, *21*, 3580; d) O. Daugulis, M. Brookhart, *Organometallics* **2002**, *21*, 5926.
[11] a) W. Steffen, T. Blömker, N. Kleigrewe, G. Kehr, R. Fröhlich, G. Erker, *Chem. Commun.* **2004**, 1188; b) T. M. Kooistra, Q. Knijnenburg, J. M. M. Smits, A. D. Horton, P. H. M. Budzelaar, A. W. Gal, *Angew. Chem.* **2001**, *113*, 4855; *Angew. Chem. Int. Ed.* **2001**, *40*, 4719; c) V. C. Gibson, M. J. Humphries, K. P. Tellmann, D. F. Wass, A. J. P. White, D. J. Williams, *Chem. Commun.* **2001**, 2252.
[12] Crystal data for **2**·1/2 C_7H_8: $M_r = 550.28$, triclinic, space group $P\bar{1}$, $a = 12.1887(15)$, $b = 14.1652(17)$, $c = 16.2034(19)$ Å, $\alpha = 89.038(2)°$, $\beta = 80.354(2)°$, $\gamma = 69.237(2)°$, $V = 2576.2(5)$ Å^3, $Z = 4$, $\rho = 1.419$ Mg m^{-3}, $F(000) = 1149$, $\lambda(Mo_{K\alpha}) = 0.71073$ Å, $\mu = 1.474$ mm^{-1}, $T = 233(2)$ K, crystal dimensions: $0.60 \times 0.24 \times 0.20$ mm^3. Siemens SMART diffractometer, equipped with a CCD detector. Of 33678 reflections measured, 11817 unique reflections were used in refinement. Final $R = 0.0466$, ($R_w = 0.1033$). Crystal data for **3b**: $M_r = 871.38$, monoclinic, space group $P2_1/c$, $a = 12.6330(8)$, $b = 26.9142(17)$, $c = 12.5259(7)$ Å, $\alpha = 90°$, $\beta = 91.409(2)°$, $\gamma = 90°$, $V = 4257.6(4)$ Å^3, $Z = 4$, $\rho = 1.359$ Mg m^{-3}, $F(000) = 1808$, $\lambda(Mo_{K\alpha}) = 0.71073$ Å, $\mu = 0.878$ mm^{-1}, $T = 223(2)$ K, crystal dimensions: $0.20 \times 0.10 \times 0.06$ mm^3. Siemens SMART diffractometer, equipped with a CCD detector. Of 30212 reflections measured, 9776 unique reflections were used in refinement. Final $R = 0.0656$, ($R_w = 0.1373$). Crystal data for **4**: $M_r = 527.50$, monoclinic, space group $C2/c$, $a = 15.8825(8)$, $b = 12.4015(7)$, $c = 24.0762(13)$ Å, $\alpha = 90°$, $\beta = 90.031(2)°$, $\gamma = 90°$, $V = 4742.2(4)$ Å^3, $Z = 8$, $\rho = 1.478$ Mg m^{-3}, $F(000) = 2200$, $\lambda(Mo_{K\alpha}) = 0.71073$ Å, $\mu = 1.598$ mm^{-1}, $T = 223(2)$ K, crystal dimensions: $0.12 \times 0.08 \times 0.06$ mm^3. Siemens SMART diffractometer, equipped with a CCD detector. Of 13522 reflections measured, 4157 unique reflections were used in refinement. Final $R = 0.0764$, ($R_w = 0.1569$). CCDC-266586 (**2**), -266587 (**3b**), and -278325 (**4**) contain the supplementary crystallographic data for this paper. These data can be obtained free of charge from the Cambridge Crystallographic Data Centre via www.ccdc.cam.ac.uk/data_request/cif.
[13] C. Müller, R. J. Lachicotte, W. D. Jones, *Organometallics* **2002**, *21*, 1975.
[14] a) F. Speiser, P. Braunstein, L. Saussine, R. Welter, *Organometallics* **2004**, *23*, 2613; b) F. Speiser, P. Braunstein, L. Saussine, *Organometallics* **2004**, *23*, 2625.
[15] M. Tanabiki, K. Tsuchiya, Y. Kumanomido, K. Matsubara, Y. Motoyama, H. Nagashima, *Organometallics* **2004**, *23*, 3976.
[16] R. S. Dickson, J. A. Ibers, *J. Am. Chem. Soc.* **1972**, *94*, 2988.
[17] M. S. W. Chan, L. Q. Deng, T. Ziegler, *Organometallics* **2000**, *19*, 2741.
[18] a) M. D. Leatherman, S. A. Svejda, L. K. Johnson, M. Brookhart, *J. Am. Chem. Soc.* **2003**, *125*, 3068; b) E. Kogut, A. Zeller, T. H. Warren, T. Strassner, *J. Am. Chem. Soc.* **2004**, *126*, 11984; c) E. V. Salo, Z. B. Guan, *Organometallics* **2003**, *22*, 5033;

 © 2005 Wiley-VCH Verlag GmbH & Co. KGaA, Weinheim

d) H. P. Chen, Y. H. Liu, S. M. Peng, S. T. Liu, *Organometallics* **2003**, *22*, 4893; e) C. B. Shim, Y. H. Kim, B. Y. Lee, Y. Dong, H. Yun, *Organometallics* **2003**, *22*, 4272; f) X. Wang, S. Liu, G.-X. Jin, *Organometallics* **2004**, *23*, 6002; g) F. Speiser, P. Braunstein, *Inorg. Chem.* **2004**, *43*, 4243; h) A. G. Avent, P. B. Hitchcock, M. F. Lappert, R. Sablong, J. R. Severn, *Organometallics* **2004**, *23*, 2591.

[19] X. Yang, C. L. Stern, T. J. Marks, *J. Am. Chem. Soc.* **1994**, *116*, 10015.

[20] R. F. de Souza, K. Bernardo-Gusmão, G. A. Cunha, C. Loup, F. Leca, R. Réau, *J. Catal.* **2004**, *226*, 235.

[21] T. J. Anderson, G. D. Jones, D. A. Vicic, *J. Am. Chem. Soc.* **2004**, *126*, 8100.

 © 2005 Wiley-VCH Verlag GmbH & Co. KGaA, Weinheim

Asymmetric Hydrogenations

DOI: 10.1002/anie.200502482

Diphenylphosphanylsulfoximines as Ligands in Iridium-Catalyzed Asymmetric Imine Hydrogenations**

*Christian Moessner and Carsten Bolm**

Chiral amines are ubiquitous in natural products and drugs, and their synthesis by asymmetric hydrogenation of carbon–nitrogen double bonds has attracted much attention.[1] However, the search for and development of efficient catalysts for enantioselective C–N double bond hydrogenations with high enantioselectivity at a reasonable catalyst loading proved much more difficult than for the reduction of C=C and C=O groups.[2–5] Furthermore, most of those catalysts are only suitable for asymmetric hydrogenations of cyclic substrates, whereas acyclic imines still represent challenging compounds.[6] In this case, one of the major problems for achieving a high enantiomeric excess is the equilibrium between the *E* and *Z* isomer of the imine,[7] which makes it difficult for the catalyst to convert all stereoisomers in a uniform and selective manner. Consequently, the first successful chiral catalysts for this important transformation have only recently been described. Among them, homogenous Ir complexes with chiral P,P- or P,N-ligands, which are structurally analogous to Crabtree's catalyst,[8] have attracted particular attention. For example, Zhang and co-workers reported enantioselective hydrogenations of *N*-aryl imines (with up to >99% *ee*) by applying an iridium catalyst bearing a chiral 1,1′-bisphosphanylferrocene (f-binaphane).[9] Phosphanyloxazoline complexes with noncoordinating anions have been used by several group to afford products with up to 90% *ee*.[10] Industrially relevant in this context is the asymmetric hydrogenation of an acyclic *N*-aryl imine as key step in the synthesis of the herbicide (*S*)-metolachlor by Syngenta.[11] Although only moderate enantioselectivities are achieved, the exceptionally high turnover numbers (TON) and turnover frequencies (TOF) of the iridium-ferrocenylphosphine catalyst allowed this imine reduction to become one of the largest catalytic enantioselective industrial processes to date.

Chiral sulfoximines are versatile ligands for asymmetric catalysis,[12] and highly enantioselective hetero-Diels–Alder reactions,[13] Mukaiyama-type aldol,[14] and carbonyl-ene reactions[15] with sulfoximine-based catalysts have recently been described. In all these catalytic reactions, dinitrogen chelates such as **1** or **2** with sulfoximine units linked to quinoline or aniline moieties were applied. We thus focused our attention on the synthesis and use of phosphine-substituted sulfoximines **3**, which on the basis of conclusions from solution and solid-state studies[13c,16] were expected to be good metal binders through their P and N donor sites.

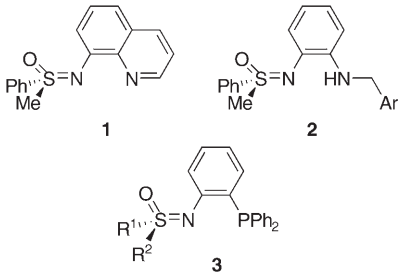

For the preparation of diphenylphosphanyl sulfoximines **3**, phosphine oxide **4**, which can be obtained by palladium-catalyzed cross-coupling of 2-bromo-1-iodobenzene with diphenylphosphane, served as starting material.[17] Application of the newly developed copper-mediated *N*-arylation reaction[18] afforded products **6a–f** from **4** and sulfoximines **5a–f**, respectively, in moderate to good yields (Scheme 1). Reductive deoxygenation of **6** with trichlorosilane gave diphenylphosphanylsulfoximines **3** as solid, air-stable products in 55–81% yield.

Guided by the successful applications of other P,N-ligands as effective hydrogenation catalysts,[3–5,19] the novel sulfoximine derivatives **3** were tested in Ir-catalyzed asymmetric imine hydrogenations. For the initial screening and optimizing process, acetophenone-derived imine **7a** was selected as substrate. To our delight we found that the catalyst generated by mixing [{Ir(cod)Cl}$_2$] (0.5 mol%) with sulfoximine **3a** (1.1 mol%) followed by the addition of iodine (2.0 mol%) led to full conversion of **7a** under H_2 into **8a** with rather encouraging 79% *ee* (Scheme 2).

[*] Dipl.-Chem. C. Moessner, Prof. Dr. C. Bolm
Institut für Organische Chemie
Rheinisch-Westfälische Technische Hochschule Aachen
Landoltweg 1, 52056 Aachen (Germany)
Fax: (+49) 241-809-2391
E-mail: carsten.bolm@oc.rwth-aachen.de

[**] We are grateful to the Fonds der Chemischen Industrie and to the Deutsche Forschungsgemeinschaft (DFG) within the SFB 380 "Asymmetric Synthesis by Chemical and Biological Methods" for financial support.

Supporting information for this article is available on the WWW under http://www.angewandte.org or from the author.

InterScience
© 2005 Wiley-VCH Verlag GmbH & Co. KGaA, Weinheim

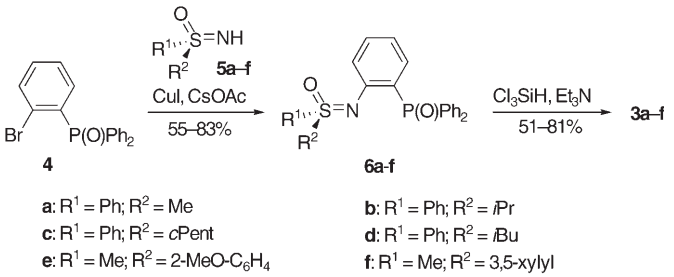

Scheme 1. Synthesis of the diphenylphosphanylsulfoximines **3**.

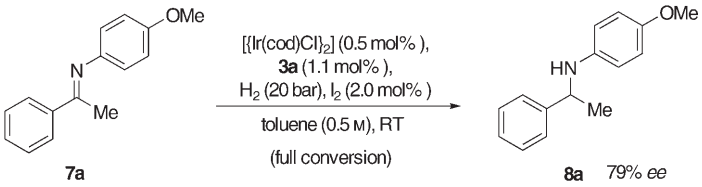

Scheme 2. Ir-catalyzed asymmetric imine hydrogenation.

Subsequent experiments revealed that no reaction occurred in the absence of iodine, which indicated that the Ir^I complex formed in situ was only a precatalyst, which most likely was further oxidized by iodine.[20] Hydrogenations of analogous substrates showed that the aryl group on the imine nitrogen atom had a strong effect on the reactivity and selectivity of the catalyst. The best result was achieved with the imine bearing the *N*-(*p*-methoxy)phenyl (PMP) group, which can easily be removed by oxidative methods. Use of the *N*-(*o*-methoxy)phenyl-protected substrate **9a** led to lower reactivity and enantioselectivity (58% *ee* after 20 h). No reaction occurred with imine **10a** bearing the *N*-mesityl group.

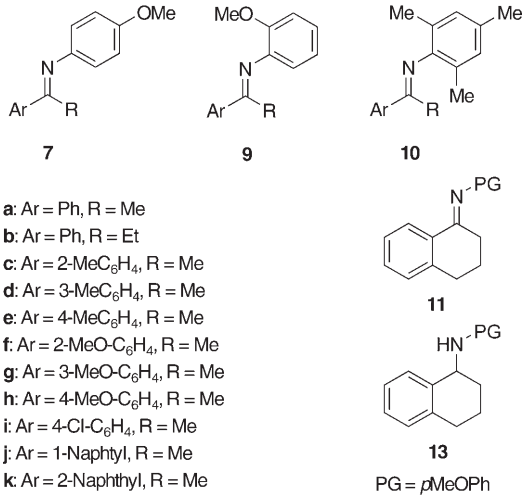

Next, the influence of the ligand structure on the catalyst performance in the test reaction depicted in Scheme 2 was studied. Increasing the steric bulk of the alkyl substituent of the sulfoximine α to the sulfur atom drastically lowered both the activity and the enantioselectivity of the resulting catalysts. Thus, use of **3b** and **3c** bearing *S*-isopropyl or *S*-cyclopentyl groups resulted in low conversions of **7a** (<40%), even after extended reaction times, to give **8a** with 66 and 10% *ee*, respectively (Table 1, entries 2 and 3). Surprisingly, however, the effect of branching at the β position of the sulfoximine alkyl group was opposite, and the catalyst efficiency increased remarkably! Thus, with isobutyl-substituted sulfoximine **3d** an excellent conversion of **7a** was achieved after only 4 h, and the enantioselectivity of the resulting amine **8a** reached an unprecedented 96% *ee* (Table 1, entry 4). Sulfoximines **3e** and **3f**, which have modified *S*-aryl groups, led to active catalysts as well (99% conversion after 12 h; Table 1, entries 5 and 6), but in these cases the enantioselectivities were lower (50 and 88% *ee*, respectively) than those attained with **3d**.

As the Ir catalyst with sulfoximine ligand **3d** performed exceptional well in the test reaction (Scheme 2), we briefly studied its catalytic behavior under modified reaction conditions. A decrease in the catalyst loading to 0.5 mol% did not result in any change in the enantioselectivity. With 0.1 mol% of catalyst, the hydrogen pressure had to be increased to 50 bar to achieve full conversion.[21] Toluene was the solvent of choice, and lowering the reaction temperature led to a slight increase in enantioselectivity (97% *ee* at 0°C).[22]

Table 1: Influence of the ligand structure on the asymmetric hydrogenation of imine **7a**.[a]

Entry	Sulfoximine	*t* [h]	Conv. [%][b]	*ee* [%][c]
1	(*S*)-**3a**	4	99	79 (−)
2	(*S*)-**3b**	8	40	66 (−)
3	(*S*)-**3c**	20	<20	10 (−)
4	(*S*)-**3d**	4	99	96 (−)
5	(*R*)-**3e**	12	99	50 (+)
6	(*R*)-**3f**	12	99	88 (+)

[a] Reaction conditions: imine **7a** (0.5 mmol), [{Ir(cod)Cl}$_2$] (0.0025 mmol), sulfoximine **3** (0.0055 mmol), iodine (0.01 mmol), H_2 (20 bar), toluene (0.5 M), room temperature. [b] Determined by ^{1}H NMR spectroscopy. [c] The enantiomer ratios were determined by HPLC by using a column with a chiral stationary phase (Chiralcel OD-H). The direction of the optical rotation of **8a** is given in parenthesis.

To explore the scope of the Ir-catalyzed asymmetric hydrogenation with the catalyst based on sulfoximine **3d**, a series of imines with 4-methoxyphenyl groups on the imine nitrogen atom were reduced under the optimized reaction conditions (Table 2).

The data can be summarized as follows: Substrates with *meta*- or *para*-substituents on the arene (e.g. **7d**, **7e**, **7g–i**) reacted equally well as unsubstituted **7a** to afford the corresponding aryl-protected amines with enantioselectivities in the range 93–96% *ee* (Table 2, entries 4, 5, 7–9). Although *ortho*-substituted imines **7c**, **7f**, and **7j** were applied as mixtures of double-bond isomers, they also gave products with excellent enantioselectivities (90–98% *ee*; Table 2, entries 3, 6, and 10). Imine **7b**, which was derived from propiophenone (and isolated as a 7:1 mixture of *E*/*Z* isomers),

 © 2005 Wiley-VCH Verlag GmbH & Co. KGaA, Weinheim

Table 2: Ir-catalyzed asymmetric hydrogenations of imines **7**.[a]

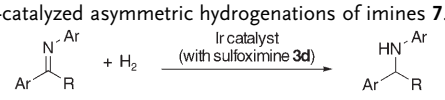

7a–k, 9i, 11 → **8a–k, 12, 13**

Entry	Imine	*t* [h]	*ee* [%][b]
1	**7a**	4	96 (−)
2	**7b**[c]	4	92 (−)
3	**7c**[c]	6	94 (+)
4	**7d**	4	93 (−)
5	**7e**	4	96 (−)
6	**7f**[c]	6	90 (+)
7	**7g**	4	96 (−)
8	**7h**	4	94 (−)
9	**7i**	4	95 (−)
10	**7j**[c]	6	98 (+)
11	**7k**	4	69 (−)
12	**9i**	12	75 (+)
13	**11**	4	91 (−)

[a] Reaction conditions: imine **7** (0.5 mmol), $[\{Ir(cod)Cl\}_2]$ (0.0025 mmol), sulfoximine **3d** (0.0055 mmol), iodine (0.01 mmol), H_2 (20 bar), toluene (0.5 M), room temperature. In all cases, full conversion was achieved. [b] The enantiomer ratios were determined by HPLC using a column with a chiral stationary phase (Chiralcel OD-H). The directions of the optical rotations of amines **8** are given in parentheses. [c] Mixture of isomers; for details see the Supporting Information.

was hydrogenated to the corresponding amine with 92% *ee* (Table 2, entry 2). Interestingly, the two isomeric naphthyl-substituted imines **7j** and **7k** afforded products with very different enantiomeric excesses. Whereas the first led to the corresponding amine with 98% *ee*, the latter gave the product with only 69% *ee* (Table 2, entries 10 and 11). Even when the alkyl group was incorporated into a cyclic structure, a high enantioselectivity was attained, as illustrated by the asymmetric hydrogenation of tetralone-derived imine **11** (91% *ee*; Table 2, entry 13). Also with the catalyst bearing sulfoximine **3d** as ligand, switching the substituent at the imine nitrogen atom from the *para*- to the *ortho*-substituted arene led to a significant lower enantioselectivity (Table 2, entry 12).

In conclusion, we introduced a novel class of C_1-symmetric sulfoximines, which can effectively be used in Ir-catalyzed asymmetric hydrogenations of acyclic *N*-aryl imines. Under optimized reaction conditions, high enantioselectivities and reaction rates have been attained for a variety of *N*-(4-methoxy)phenyl imines. Currently, the application of these novel sulfoximines in other catalytic asymmetric processes is under investigation.

Experimental Section

3d: In an oven-dried Schlenk flask under an argon atmosphere sulfoximine **6d** (446 mg, 0.94 mmol) was dissolved in toluene (3 mL). The solution was cooled to 0 °C, and NEt_3 (655 μL, 4.70 mmol) and trichlorosilane (470 μL, 4.70 mmol) were added. The heterogenous mixture was stirred for 12 h at 105 °C. The reaction mixture was then cooled to room temperature, and degassed water (3 mL) was added. The solid was filtered through a small plug of celite and thoroughly rinsed with ethyl acetate. The organic phase was dried ($MgSO_4$) and evaporated to dryness. The pure product was obtained as a colorless solid (344 mg, 81%) after flash chromatography (SiO_2; pentane/acetone 10:1). For analytical data, see the Supporting Information.

General procedure: Under an argon atmosphere $[\{Ir(cod)Cl\}_2]$ (1.7 mg, 0.0025 mmol) and sulfoximine **3d** (2.5 mg, 0.0055 mmol) were placed in a 10-mL test tube equipped with a stirrer bar. After the addition of dry toluene (0.5 mL), the yellow solution was stirred for 30 min. Iodine (2.5 mg, 0.010 mmol) was then added, and the solution turned red within 30 min. To this catalyst solution was added the imine (0.5 mmol) and additional toluene (0.5 mL). The test tube was placed in an argon-filled steel autoclave, which was purged three times with hydrogen (5 bar) and finally pressurized to 20 bar. The reaction mixture was stirred for the indicated period of time. Then, the hydrogen gas was released and the reaction quenched by addition of pentane (3 mL). The product was filtered through a short plug of silica (3 cm) and eluted with pentane/acetone (20:1).

The conversions were determined by ^1H NMR spectroscopy, and the enantiomer ratio analyzed with analytical HPLC by using chiral columns. For details, see the Supporting Information.

Received: July 16, 2005
Published online: October 10, 2005

Keywords: amines · asymmetric catalysis · hydrogenation · imines · sulfoximines

[1] a) F. Spindler, H.-U. Blaser in *Transition Metals for Organic Synthesis, 2nd ed.*, *Vol. 2* (Eds.: M. Beller, C. Bolm), Wiley-VCH, Weinheim, **2004**, pp. 113–123; b) H.-U. Blaser, F. Spindler in *Comprehensive Asymmetric Catalysis, Vol. 1* (Eds.: E. N. Jacobsen, A. Pfaltz, H. Yamamoto), Springer, Berlin, **1999**, pp. 247–265; c) H.-U. Blaser, C. Malan, B. Pugin, F. Spindler, H. Steiner, M. Studer, *Adv. Synth. Catal.* **2003**, *345*, 103–151; d) M. J. Palmer, M. Wills, *Tetrahedron: Asymmetry* **1999**, *10*, 2045–2061; e) H.-U. Blaser, F. Spindler in *Handbook of Homogeneous Hydrogenation* (Eds.: J. G. de Vries, C. J. Elsevier), Wiley-VCH, Weinheim, to appear in 2006.

[2] Titanium catalysis: a) C. A. Willoughby, S. L. Buchwald, *J. Am. Chem. Soc.* **1992**, *114*, 7562–7564; b) C. A. Willoughby, S. L. Buchwald, *J. Am. Chem. Soc.* **1994**, *116*, 8952–8965; c) X. Verdaguer, U. E. W. Lange, S. L. Buchwald, *Angew. Chem.* **1998**, *110*, 1174–1178; *Angew. Chem. Int. Ed.* **1998**, *37*, 1103–1108; for a highly enantioselective hydrosilylation of *N*-aryl imines, see: d) M. C. Hansen, S. L. Buchwald, *Org. Lett.* **2000**, *2*, 713–715.

[3] Ruthenium catalysis: a) W. Oppolzer, M. Wills, M. Starkemann, G. Bernardinelli, *Tetrahedron Lett.* **1990**, *31*, 4117–4120; b) N. Uematsu, A. Fujii, S. Hashiguchi, T. Ikariya, R. Noyori, *J. Am. Chem. Soc.* **1996**, *118*, 4916–4917; c) C. J. Cobley, J. P. Henschke, *Adv. Synth. Catal.* **2003**, *345*, 195–201.

[4] Rhodium catalysis: a) A. G. Becalski, W. R. Cullen, M. D. Fryzuk, B. R. James, G.-J. Kang, S. R. Rettig, *Inorg. Chem.* **1991**, *30*, 5002–5008; b) J. Mao, D. C. Baker, *Org. Lett.* **1999**, *1*, 841–843.

[5] Iridium catalysis: a) R. Sablong, J. A. Osborn, *Tetrahedron: Asymmetry* **1996**, *7*, 3059–3062; b) R. Sablong, J. A. Osborn, *Tetrahedron Lett.* **1996**, *37*, 4937–4940; c) G. Zhu, X. Zhang, *Tetrahedron: Asymmetry* **1998**, *9*, 2415–2418; d) C. Bianchini, P. Barbaro, G. Scapacchi, E. Farnetti, M. Graziani, *Organometallics* **1998**, *17*, 3308–3310.

[6] T. Ohkuma, M. Kitamura, R. Noyori in *Catalytic Asymmetric Synthesis, 2nd ed.* (Ed.: I. Ojima), Wiley-VCH, New York, **2000**, pp. 1–110.

[7] C. G. McCarty in *Chemistry of the Carbon-Nitrogen Double Bond* (Ed.: S. Patai), Wiley-Interscience, London, **1970**, pp. 363–464.

[8] R. H. Crabtree, *Acc. Chem. Res.* **1979**, *12*, 331–337.

 © 2005 Wiley-VCH Verlag GmbH & Co. KGaA, Weinheim

[9] a) D. Xiao, X. Zhang, *Angew. Chem.* **2001**, *113*, 3533 – 3536; *Angew. Chem. Int. Ed.* **2001**, *40*, 3425 – 3428; b) Y. Chi, Y.-G. Zhou, X. Zhang, *J. Org. Chem.* **2003**, *68*, 4120 – 4122.
[10] a) P. Schnider, G. Koch, R. Prétôt, G. Wang, F. M. Bohnen, C. Krüger, A. Pfaltz, *Chem. Eur. J.* **1997**, *3*, 887 – 892; b) S. Kainz, A. Brinkmann, W. Leitner, A. Pfaltz, *J. Am. Chem. Soc.* **1999**, *121*, 6421 – 6429; c) F. Menges, A. Pfaltz, *Adv. Synth. Catal.* **2002**, *344*, 40 – 44; d) P. G. Cozzi, F. Menges, S. Kaiser, *Synlett* **2003**, 833 – 836; e) A. Trifonova, J. S. Diesen, C. J. Chapman, P. G. Andersson, *Org. Lett.* **2004**, *6*, 3825 – 3827; f) M. Solinas, A. Pfaltz, P. G. Cozzi, W. Leitner, *J. Am. Chem. Soc.* **2004**, *126*, 16142 – 16147.
[11] a) F. Spindler, H.-U. Blaser, *Adv. Synth. Catal.* **2001**, *343*, 68 – 70; b) H.-U. Blaser, H.-P. Buser, R. Häusel, H.-P. Jalett, F. Spindler, *J. Organomet. Chem.* **2001**, *621*, 34 – 38; c) H.-U. Blaser, H.-P. Buser, H.-P. Jalett, B. Pugin, F. Spindler, *Synlett* **1999**, 867 – 868; d) H.-U. Blaser, H.-P. Buser, K. Coers, R. Hanreich, H.-P. Jalett, E. Jelsch, B. Pugin, H. D. Schneider, F. Spindler, A. Wegmann, *Chimia* **1999**, *53*, 275 – 280; e) H.-U. Blaser, F. Spindler in *Comprehensive Asymmetric Catalysis, Vol. 3* (Eds.: E. N. Jacobsen, A. Pfaltz, H. Yamamoto), Springer, Berlin, **1999**, pp. 1427 – 1437.
[12] a) M. Harmata, *Chemtracts* **2003**, *16*, 660 – 666; b) H. Okamura, C. Bolm, *Chem. Lett.* **2004**, *33*, 482 – 487; c) for a recent general review on sulfoximines, see: M. Reggelin, C. Zur, *Synthesis* **2000**, 1 – 64.
[13] a) C. Bolm, O. Simic, *J. Am. Chem. Soc.* **2001**, *123*, 3830 – 3831; b) C. Bolm, M. Martin, O. Simic, M. Verrucci, *Org. Lett.* **2003**, *5*, 427 – 429; c) C. Bolm, M. Verrucci, O. Simic, P. G. Cozzi, G. Raabe, H. Okamura, *Chem. Commun.* **2003**, 2826 – 2827.
[14] M. Langner, C. Bolm, *Angew. Chem.* **2004**, *116*, 6110 – 6113; *Angew. Chem. Int. Ed.* **2004**, *43*, 5984 – 5987.
[15] M. Langner, C. Bolm, P. Rémy, *Synlett* **2005**, 781 – 784.
[16] a) C. Bolm, M. Martin, C. Palivan, D. Neshchadin, H. Bertagnolli, M. P. Feth, A. Schweiger, G. Mitrikas, J. Harmer, *J. Am. Chem. Soc.* **2003**, *125*, 6222 – 6227; b) C. Moessner, C. Bolm, unpublished results.
[17] a) O. Herd, A. Hessler, M. Hingst, M. Trepper, O. Stelzer, *J. Organomet. Chem.* **1996**, *522*, 69 – 76; b) D. J. Brauer, M. Hingst, K. W. Kottsieper, C. Liek, T. Nickel, M. Tepper, O. Stelzer, W. S. Sheldrick, *J. Organomet. Chem.* **2002**, *645*, 14 – 26.
[18] a) G. Y. Cho, P. Rémy, J. Jansson, C. Moessner, C. Bolm, *Org. Lett.* **2004**, *6*, 3293 – 3296; b) for a catalytic variant of this process, see: J. Sedelmeier, C. Bolm, *J. Org. Chem.* **2005**, *70*, 6904 – 6906.
[19] a) A. Pfaltz, J. Blankenstein, R. Hilgraf, E. Hörmann, S. McIntyre, F. Menges, M. Schönleber, S. P. Smidt, B. Wüstenberg, N. Zimmermann, *Adv. Synth. Catal.* **2003**, *345*, 33 – 43; b) W. J. Drury III, N. Zimmermann, M. Keenan, M. Hayashi, S. Kaiser, R. Goddard, A. Pfaltz, *Angew. Chem.* **2004**, *116*, 72 – 76; *Angew. Chem. Int. Ed.* **2004**, *43*, 70 – 74.
[20] a) E. M. Vogl, H. Gröger, M. Shibasaki, *Angew. Chem.* **1999**, *111*, 1672 – 1680; *Angew. Chem. Int. Ed.* **1999**, *38*, 1570 – 1577; b) Y. N. C. Chan, J. A. Osborn, *J. Am. Chem. Soc.* **1990**, *112*, 9400 – 9401.
[21] With 0.5 mol% of the catalyst at 20 bar of H_2 pressure, the conversion of **7a** was > 99% after 4 h, and **8a** was obtained with 95% *ee*. Use of 0.1 mol% of the catalyst required 50 bar of H_2 pressure for full conversion after 4 h to obtain **8a** with 95% *ee*.
[22] For details, see the Supporting Information.

 © 2005 Wiley-VCH Verlag GmbH & Co. KGaA, Weinheim

Heterocycles

DOI: 10.1002/anie.200502971

S-Heterocyclic Carbene with a Disilane Backbone**

Hidefumi Nikawa, Tsukasa Nakahodo, Takahiro Tsuchiya, Takatsugu Wakahara, G. M. Aminur Rahman, Takeshi Akasaka, Yutaka Maeda, Michael T. H. Liu, Akira Meguro, Soichiro Kyushin, Hideyuki Matsumoto,* Naomi Mizorogi, and Shigeru Nagase**

Recently, Wiberg and co-workers reported the preparation of tetrathiofulvalene (TTF) analogue **1** with a disilane backbone (see Scheme 1), obtained from the reaction of the isolable disilene **2** with carbon disulfide.[1] Compound **1**, with a Si–Si bond instead of a C=C bond in the TTF ring, may be potentially useful as a new electron donor because of the intriguing electronic properties of the silicon σ-conjugate system (Si–Si), which resembles the carbon π-conjugate system (C=C). Apparently, **1** was formed by the dimerization of the S-heterocyclic carbene (SHC) **3** as the proposed

[*] H. Nikawa, Dr. T. Nakahodo, Dr. T. Tsuchiya, Dr. T. Wakahara, Dr. G. M. A. Rahman, Prof. Dr. T. Akasaka
Center for Tsukuba Advanced Research Alliance
University of Tsukuba
Tsukuba, Ibaraki 305-8577 (Japan)
Fax: (+81) 29-853-6409
E-mail: akasaka@tara.tsukuba.ac.jp

Dr. A. Meguro, Dr. S. Kyushin, Prof. Dr. H. Matsumoto
Department of Applied Chemistry
Faculty of Engineering
Gunma University
Kiryu, Gunma 376-8515 (Japan)
Fax: (+81) 27-730-1291
E-mail: matumoto@chem.gunma-u.ac.jp

N. Mizorogi, Prof. Dr. S. Nagase
Department of Theoretical Molecular Science
Institute for Molecular Science
Okazaki, Aichi 444-8585 (Japan)
Fax: (+81) 56-453-4660
E-mail: nagase@ims.ac.jp

Dr. Y. Maeda
Department of Chemistry
Tokyo Gakugei University
Koganei, Tokyo 184-8501 (Japan)

Prof. Dr. M. T. H. Liu
Department of Chemistry
University of Prince Edward Island
Charlottetown, Prince Edward Island, C1A4P3 (Canada)

[**] This work was supported in part by a Grant-in-Aid, the 21st Century COE Program, Nanotechnology Support Project, and NAREGI Nanoscience Project from the Ministry of Education, Culture, Sports, Science, and Technology of Japan. This work was also partly supported by a grant from the Kurata Memorial Hitachi Science and Technology Foundation.

Supporting information for this article is available on the WWW under http://www.angewandte.org or from the author.

© 2005 Wiley-VCH Verlag GmbH & Co. KGaA, Weinheim

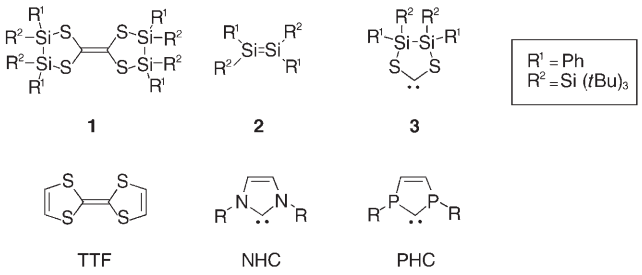

Scheme 1. TTF analogue **1** and S-heterocyclic carbene **3** with a disilane backbone.

intermediate. Meanwhile, since the discovery of the first stable carbenes by Arduengo and co-workers,[2] heterocyclic carbenes have attracted special attention as ligands, catalysts, and spin sources because of their unique coordination properties based on good σ-donor and poor π-acceptor properties.[3] A large variety of stable N-heterocyclic carbenes (NHC) have been reported so far which have various substitution patterns,[4] ring sizes that vary from four to six,[5] and inorganic backbones;[6] furthermore, a P-heterocyclic carbene (PHC) has also been reported.[7] To the best of our knowledge, only theoretical investigations into the formation of SHCs by a [2+3] cycloaddition of an alkyne with CS_2 and subsequent dimerization have been reported.[8] In this context, the generation of a carbene by the reaction of disilene with CS_2 would be a new synthetic approach to SHCs. The reactivity of a SHC with a disilane backbone and the properties of a TTF analogue with a disilane backbone prompted us to investigate the reaction of the disilene with CS_2. We have reported the photochemical generation of cyclotetrasilene **4** (see Scheme 2), which has a higher reactivity than **2**,[9] and the use of C_{60} as a probe, which is a nonspectroscopic method to confirm the formation of a carbene.[10,11] We report herein the generation of SHC **6** with a cyclotetrasilane backbone by a [2+3] cycloaddition of cyclotetrasilene, prepared by the photolysis of *anti*-dodecaisopropyltricyclo[4.2.0.0^{2,5}]octasilane[12] (**5**), with CS_2. Carbene **6** then reacts with C_{60} to result in the formation of methanofullerene **7** (Scheme 2).

Irradiation of a solution of *anti*-dodecaisopropyltricyclo[4.2.0.0^{2,5}]octasilane **5** in toluene in the presence of C_{60} and CS_2 in a degassed sealed tube at room temperature using a high-pressure mercury arc lamp resulted in the formation of the corresponding adduct $C_{60}(C_{19}H_{42}S_2Si_4)$ (**7**) in 20% yield. Compound **7** was then purified by preparative HPLC. The MALDI-TOF mass spectrum of **7** exhibits a molecular ion peak at *m*/*z* 1172–1166 and a peak at *m*/*z* 723–720 (C_{60}) because of the loss of the substituent $C_{19}H_{42}S_2Si_4$ (**8**). The UV/Vis absorption peak of **7** appears at 433 nm, which is indicative of the formation of a 6,6-adduct of C_{60}.[13]

The ^{13}C NMR spectrum of **7** shows 32 signals for the C_{60} cage, of which four peaks are at half intensity and 28 peaks are at full intensity. These results are consistent with the appropriate number and ratio of peak intensities for the C_{60} adduct with C_s symmetry. The signals at $\delta = 83.36$ and 80.63 ppm, assigned to the sp^3 carbon atom on the fullerene cage, indicate a methanofullerene structure.[13] The signal at $\delta = 58.54$ ppm is assigned to the sp^3 carbon atom on the spiro ring system. The carbon atoms in the isopropyl group on cyclotetrasilane may be observed at $\delta = 23$–14 ppm. The ^{29}Si NMR spectrum of **7** shows two signals at $\delta = 20.36$ and 0.31 ppm.

X-ray crystallographic analysis[14] unambiguously confirms the structure of **7** (Figure 1) as having a *cis*-fused bicyclic structure and a spiro ring system, which has C_1 symmetry in the crystalline state. The dithiadisilolane ring possesses a half-chair structure, and the cyclotetrasilane ring has a moderately holded structure with hold angles of 18.9 and 19.2°. (The Si–Si bond lengths range from 2.358(3) to 2.407(3) Å with an average of 2.378 Å.) As the Si(3)–Si(4) bond is within the bicycle ring, its length (2.358(3) Å) is the shortest among the others (2.362(3)–2.407(3) Å). The

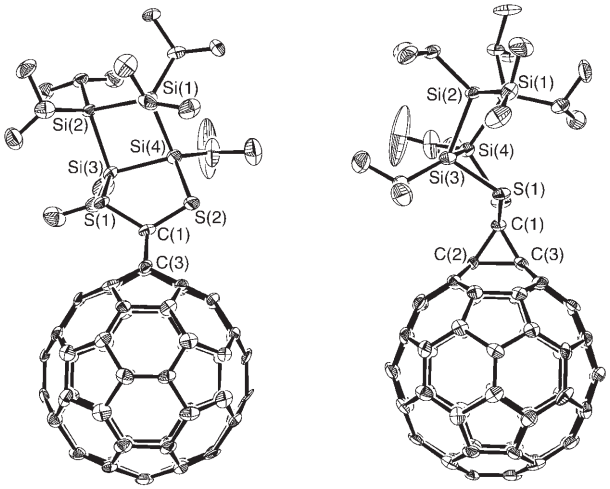

Figure 1. ORTEP drawing of $C_{60}(C_{19}H_{42}S_2Si_4)$ **7** showing thermal ellipsoids at the 30% probability level. The CS_2 molecules are omitted for clarity. Selected bond lengths [Å] and angles [°]: Si(1)–Si(2) 2.385(3), Si(2)–Si(3) 2.362(3), Si(3)–Si(4) 2.358(3), Si(1)–Si(4) 2.407(3), Si(3)–S(5) 2.182(3), Si(4)–S(6) 2.188(3), C(1)–S(5) 1.822(7), C(1)–S(6) 1.774(7), C(1)–C(2) 1.553(10), C(1)–C(3) 1.518(10), C(2)–C(3) 1.634(10), Si(1)-Si(2)-Si(3) 88.66(11), Si(2)-Si(1)-Si(4) 89.10(11), Si(2)-Si(3)-Si(4)/S(1) 90.83(11)/99.32(12), Si(1)-Si(4)-Si(3)/S(2) 88.23(11)/113.42(12), S(1)-Si(3)-Si(4) 91.52(12), Si(3)-Si(4)-S(2) 102.65(12), Si(4)-S(2)-C(1) 99.1(2), S(1)-C(1)-S(2) 117.5(4), C(1)-S(1)-Si(3) 98.2(2), C(1)-C(2)-C(3) 56.8(4), C(2)-C(3)-C(1) 58.9(4), C(2)-C(1)-C(3) 64.3(4).

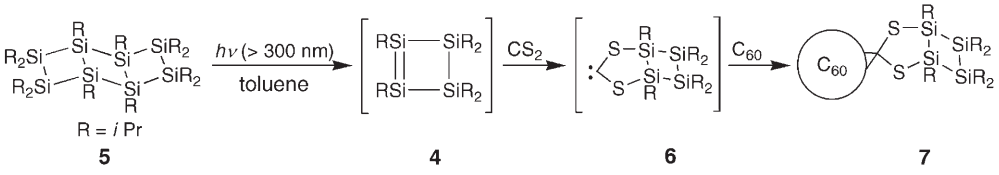

Scheme 2. Synthesis and trapping of S-heterocyclic carbene **6**.

 © 2005 Wiley-VCH Verlag GmbH & Co. KGaA, Weinheim

Si-Si-Si bond angles of the {Si_4} rings range from 88.2(11) to 90.8(11)°, with an average of 89.2°.

Table 1 shows the redox potentials of **7** and C_{60},[15] together with the 6,6-adduct of C_{60}-adamantylidene (6,6-C_{60}-Ad)[10] as a reference compound. Compound **7** exhibits three

Table 1: Redox potentials[a] (V) of $C_{60}(C_{42}H_{18}Si_4)$, 6,6-C_{60}-Ad,[10] and C_{60}[15].

Compound	oxE_1	redE_1	redE_2	redE_3
$C_{60}(C_{42}H_{18}Si_4)$	+1.04[d,e]	−1.16	−1.52	−2.01
6,6-C_{60}-Ad	+1.07[d,e]	−1.21	−1.58	−2.06
C_{60}	+1.21[d,e]	−1.12	−1.50	−1.95

[a] Versus Fc/Fc^+ in 1,2-dichlorobenzene with 0.1 M $(n\text{Bu})_4NPF_6$ at a Pt working electrode; scan rate = 20 mV s^{-1}. [b] Irreversible. [c] Values were obtained by differential pulse voltammetry: pulse amplitude = 50 mV; scan rate 20 mV s^{-1}.

one-electron reversible reduction waves and one irreversible oxidation wave, as observed for C_{60} and 6,6-C_{60}-Ad. The salient feature is that the redox potentials of **7** are cathodically shifted, thus indicating that the introduction of substituent **8** results in a decrease in the electron-acceptor property.

To characterize carbene **6**, generated by a [2+3] cycloaddition of cyclotetrasilene with CS_2, theoretical calculations were carried out.[16] The singlet state of **6** was calculated to be 23.4 kcal mol^{-1} more stable than the triplet state. The dithiadisilolane ring of **6** in the singlet state has an envelope structure with a dihedral angle of 1.6°, and the cyclotetrasilane ring has a moderately holded structure with hold angles of 8.8 and 8.9°. The carbon–sulfur bond lengths are 1.678 and 1.679 Å, which are considerably shorter than typical C–S single bond lengths (1.758–1.854 Å).[17] These bond lengths are ascribed to the conjugative donation of the lone-pair electrons on the sulfur atoms into the vacant p_π orbital at the carbene center (Scheme 3). Because of its dipolar character, **6** has a high nucleophilicity; therefore, it is not surprising that **6** reacts readily with the electrophilic C_{60}, as in the reaction of the dimethoxy carbene[18] and C_{60}.[19]

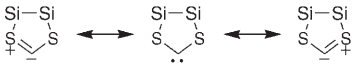

Scheme 3. Resonance structure of S-heterocyclic carbene **6**.

We have demonstrated that carbene **6** can be generated by the [2+3] cycloaddition of cyclotetrasilene **4** with CS_2 by trapping **6** with C_{60} as a chemical probe. NMR spectroscopic measurements and X-ray crystallographic analysis verify that **7** is a methanofullerene (a 6,6-adduct of C_{60}). Theoretical calculations show that **6** has a high nucleophilicity in the singlet ground state. This method to generate SHC **6** may be applied to prepare novel compounds, such as TTF analogue **1**.

Experimental Section

Irradiation of a solution of *anti*-dodecaisopropyltricyclo[4.2.0.$0^{2,5}$]octasilane (**5**; 5.1 mg, 6.9×10^{-3} mmol) in toluene in the presence of C_{60} (5.0 mg, 6.9×10^{-3} mmol) and CS_2 (0.4 mL, 6.9×10^{-3} mol) in a degassed sealed tube at room temperature using a high-pressure mercury arc lamp (cut off < 300 nm) resulted in the formation of the adduct $C_{60}(C_{20}H_{42}Si_4S_2)$ (**7**) as a dark-brown solid in 20% yield, which was purified by preparative HPLC with a Buckyprep column (ϕ20 × 250 mm; Cosmosil, Nacalai Tesque Inc.). A MALDI-TOF mass spectrum was measured on a BIFLEX III (Bruker, Germany) with 1,1,4,4-tetraphenyl-1,3-butadiene as a matrix. UV/Vis–NIR spectra were measured on a UV 3150 instrument (Shimadzu, Japan) in toluene. ^1H, ^{13}C, and ^{29}Si NMR and 2D NMR (HMQC and HMBC) spectra were recorded on Bruker AVANCE 500 spectrometer with a CryoProbe system and Bruker AVANCE 300 spectrometer in CS_2 and $CDCl_3$ (3:1). Cyclic voltammograms were measured on a potentiostat/galvanostat (BAS CW-50) in *o*-dichlorobenzene with 0.1 M $(n\text{Bu})_4NPF_6$ at a Pt working electrode.

Spectra data of **7**: ^1H NMR (500 MHz Cyroprobe, $CS_2/CDCl_3$ (3:1), 20 °C) δ = (sep, J = 7.4 Hz, 2H; CH), 1.75 (sep, J = 7.5 Hz, 2H; CH), 1.69 (sep, 2H, J = 7.4 Hz, 2H; CH), 1.38 (d, J = 7.3 Hz, 6H; CH_3), 1.36 (d, J = 7.4 Hz, 12H; CH_3), 1.35 (d, J = 7.4 Hz, 12H; CH_3), 1.31 ppm (d, J = 7.5 Hz, 6H; CH_3); ^{13}C NMR (125 MHz Cyroprobe, $CS_2/CDCl_3$ (3:1), 20 °C) δ = 148.2 (s, 2C; C_{60}), 147.6 (s, 2C; C_{60}), 145.3 (s, 2C; C_{60}), 144.9 (s, 2C; C_{60}), 144.9 (s, 2C; C_{60}), 144.8 (s, 2C; C_{60}), 144.8 (s, 2C; C_{60}), 144.7 (s, 2C; C_{60}), 144.5 (s, 2C; C_{60}), 144.4 (s, 4C; C_{60}), 144.3 (s, 1C; C_{60}), 144.3 (s, 1C; C_{60}), 144.2 (s, 2C; C_{60}), 143.8 (s, 2C; C_{60}), 143.6 (s, 4C; C_{60}), 142.9 (s, 2C; C_{60}), 142.8 (s, 2C; C_{60}), 142.7 (s, 2C; C_{60}), 142.7 (s, 2C; C_{60}), 142.6 (s, 2C; C_{60}), 141.9 (s, 4C; C_{60}), 141.9 (s, 4C; C_{60}), 140.6 (s, 4C; C_{60}), 138.5 (s, 2C; C_{60}), 138.3 (s, 2C; C_{60}), 83.3 (s, 1C; CC_{spiro}), 80.6 (s, 1C; CC_{spiro}), 58.5 (s, 1C; C_{spiro}), 22.4 (q, 3C; CH_3), 22.2(q, 3C; CH_3), 22.2(q, 3C; CH_3), 21.2 (q, 3C; CH_3), 21.1 (q, 3C; CH_3), 20.7 (q, 3C; CH_3), 17.0 (d, 3C; CH), 15.4 (d, 3C; CH), 14.5 ppm (d, 3C; CH); ^{29}Si NMR (59.6 MHz, $CS_2/CDCl_3$ (3:1), 20 °C) δ = 20.4, 0.3 ppm; MALDI-TOF mass (negative mode, matrix: 1,1,4,4-tetraphenyl-1,3-butadiene): *m/z* 1166(M), 720(C_{60}); MALDI-TOF mass (positive mode, matrix: 1,1,4,4-tetraphenyl-1,3-butadiene): *m/z* 1166[*M*], 1123; UV/Vis–NIR (toluene) $\lambda_{max}(\varepsilon)$ 694 (190), 478 (1400), 433 (2100), 330 (35000) cm^{-1}.

Received: August 21, 2005
Published online: October 27, 2005

Keywords: carbenes · cycloaddition · fullerenes · heterocycles · silanes

[1] N. Wiberg, W. Niedermayer, K. Polborn, P. Mayer, *Chem. Eur. J.* **2002**, *8*, 2730.
[2] A. J. Arduengo, III, R. L. Harlow, M. Kline, *J. Am. Chem. Soc.* **1991**, *113*, 361.
[3] a) D. Bourissou, O. Guerret, F. P. Gabbaï, G. Bertrand, *Chem. Rev.* **2000**, *100*, 39; b) L. Jafarpour, S. P. Nolan, *Adv. Organomet. Chem.* **2001**, *46*, 181; c) D. Enders, H. Gielen, *J. Organomet. Chem.* **2001**, *617*; d) A. C. Hillier, G. A. Grasa, M. S. Viciu, H. M. Lee, C. Yang, S. P. Nolan, *J. Organomet. Chem.* **2002**, *653*, 69; e) M. C. Perry, K. Burgess, *Tetrahedron: Asymmetry* **2003**, *14*, 951; f) W. A. Herrmann, *Angew. Chem.* **2002**, *114*, 1342; *Angew. Chem. Int. Ed.* **2002**, *41*, 1290.
[4] a) A. J. Arduengo, III, J. R. Goerlich, W. J. Marshall, *J. Am. Chem. Soc.* **1995**, *117*, 11027; b) F. E. Hahn, L. Wittenbecher, D. L. Van, R. Fröhlich, *Angew. Chem.* **2000**, *112*, 551; *Angew. Chem. Int. Ed.* **2000**, *39*, 541; c) M. Alcarazo, S. J. Roselade, E. Alonso, R. Fernández, E. Alvarez, F. J. Lahoz, J. M. Lassaletta, *J. Am. Chem. Soc.* **2004**, *126*, 13242.
[5] a) E. Despagnet-Ayoub, R. H. Grubbs, *J. Am. Chem. Soc.* **2004**, *126*, 10198; b) E. Despagnet-Ayoub, R. H. Grubbs, *Organometallics* **2005**, *24*, 338; c) R. W. Alder, M. E. Blake, C. Bortolotti, S. Bufali, C. P. Butts, E. Linehan, J. M. Oliva, A. G. Orpen, M. J. Quayle, *Chem. Commun.* **1999**, 241; d) P. Bazinet,

 © 2005 Wiley-VCH Verlag GmbH & Co. KGaA, Weinheim

G. P. A. Yap, D. S. Richeson, *J. Am. Chem. Soc.* **2003**, *125*, 13314; e) M. Otto, S. Conejero, Y. Canac, V. D. Romanenko, V. Rudzevitch, G. Bertrand, *J. Am. Chem. Soc.* **2004**, *126*, 1016.

[6] K. E. Krahulic, G. D. Enright, M. Parvez, R. Roesler, *J. Am. Chem. Soc.* **2005**, *127*, 4142.

[7] a) D. Martin, A. Baceiredo, H. Gornitzka, W. W. Schoeller, G. Bertrand, *Angew. Chem.* **2005**, *117*, 1728; *Angew. Chem. Int. Ed.* **2005**, *44*, 1700; b) Á. Fekete, L. Nyulászi, *J. Organomet. Chem.* **2002**, *643*, 278.

[8] a) J. Fabian, A. Krebs, D. Schönemann, W. Schaefer, *J. Org. Chem.* **2000**, *65*, 8940; b) D. C. Graham, K. J. Cavell, B. F. Yates, *J. Phys. Org. Chem.* **2005**, *18*, 298.

[9] S. Kyushin, A. Meguro, M. Unno, H. Matsumoto, *Chem. Lett.* **2000**, 494.

[10] T. Akasaka, M. T. H. Liu, Y. Niino, Y. Maeda, T. Wakahara, M. Okamura, K. Kobayashi, S. Nagase, *J. Am. Chem. Soc.* **2000**, *122*, 7134.

[11] a) T. Wakahara, Y. Niino, T. Kato, Y. Maeda, T. Akasaka, M. T. H. Liu, K. Kobayashi, S. Nagase, *J. Am. Chem. Soc.* **2002**, *124*, 9465; b) M. T. H. Liu, Y.-K. Choe, M. Kimura, K. Kobayashi, S. Nagase, T. Wakahara, Y. Niino, M. O. Ishitsuka, Y. Maeda, T. Akasaka, *J. Org. Chem.* **2003**, *68*, 7471; c) M. O. Ishitsuka, Y. Niino, T. Wakahara, T. Akasaka, M. T. H. Liu, K. Kobayashi, S. Nagase, *Tetrahedron Lett.* **2004**, *45*, 6321.

[12] a) S. Kyushin, M. Kawabata, Y. Yagihashi, H. Matsumoto, M. Goto, *Chem. Lett.* **1994**, 997; b) S. Kyushin, Y. Yagihashi, H. Matsumoto, *J. Organomet. Chem.* **1996**, *521*, 413; c) H. Matsumoto, S. Kyushin, M. Unno, R. Tanaka, *J. Organomet. Chem.* **2000**, *611*, 52.

[13] A. Hirsch, T. Grösser, A. Skiebe, A. Soi, *Chem. Ber.* **1993**, *126*, 1061.

[14] Crystal data of **7**: $C_{81}H_{42}Si_4S_6$, $M_r = 1166.18$, black crystals, $0.25 \times 0.25 \times 0.25\ mm^3$, monoclinic, space group *Cc* (no. 9), $a = 15.660(2)$, $b = 12.887(2)$, $c = 29.559(6)$ Å, $\beta = 96.606(8)°$, $V = 5925(1)$ Å^3, $Z = 4$, $\rho_{calcd} = 1.479\ g\,cm^{-3}$, $2\theta_{max} = 55.0°$, $\mu(Mo_{K\alpha}) = 3.636\ cm^{-1}$; an empirical absorption correction ($0.689 \le T \le 0.913$); $\lambda = 0.71069$ Å, ω scans, $T = 293$ K, 22393 reflections that were collected, 21327 were unique ($R_{int} = 0.124$) and 6994 refractions ($I > 3.6\ \sigma(I)$); 863 refined parameters, $R = 0.062$, $R_w = 0.104$, GOF = 1.186. The maximum and minimum residual electron density is equal to 0.65 and $-0.75\ e Å^{-3}$, respectively. Hydrogen atoms were refined using the riding model. All measurements were made on a Rigaku RAXIS RAPID imaging plate area detector with graphite monochromated $Mo_{K\alpha}$ radiation. All calculations were performed using the Crystal Structure crystallographic software package. The structure was solved by direct methods (SIR92) and expanded using Fourier techniques (DIRDIF99). The structure was refined by CRYSTALS. CCDC 281589 contains the supplementary crystallographic data for this paper. These data can be obtained free of charge from The Cambridge Crystallographic Data Centre via www.ccdc.cam.ac.uk/data_request/cif.

[15] T. Akasaka, Y. Maeda, T. Wakahara, M. Okamura, M. Fujitsuka, O. Ito, K. Kobayashi, S. Nagase, K. Kato, Y. Nakadaira, E. Horn, *Org. Lett.* **1999**, *1*, 1509.

[16] All calculations were carried out using the Gaussian 03 program. Geometries were optimized with hybrid density functional theory at the B3LYP level (A. D. Becke, *Phys. Rev. A* **1988**, *38*, 3098; A. D. Becke, *J. Chem. Phys.* **1993**, *98*, 5648; C. Lee, W. Yang, R. G. Parr, *Phys. Rev. B* **1988**, *37*, 785) with the 3-21G* basis set (W. J. Pietro, M. M. Francl, W. J. Hehre, D. J. DeFrees, J. A. Pople, J. S. Binkley, *J. Am. Chem. Soc.* **1982**, *104*, 5039); for energies, the B3LYP optimization was followed by single-point calculations using the 6-31G(d) basis set (M. M. Francl, W. J. Pietro, W. J. Hehre, J. S. Binkley, M. S. Gordon, D. J. DeFrees, J. A. Pople, *J. Chem. Phys.* **1982**, *77*, 3654).

[17] T. Hoz, H. Basch in *Supplement S: The Chemistry of Sulphur-Containing Functional Groups* (Eds.: S. Patai, Z. Rappoport), Wiley, New York, **1993**, pp. 1–174.

[18] a) R. A. Moss, *Acc. Chem. Res.* **1980**, *13*, 58; b) R. A. Moss, S. S. Wlostosky, K. Krogh-Jespersen, A. Matro, *J. Am. Chem. Soc.* **1988**, *110*, 4443.

[19] W. W. Win, M. Kao, M. Eiermann, J. J. McNamara, F. Wudl, *J. Org. Chem.* **1994**, *59*, 5817.

 © 2005 Wiley-VCH Verlag GmbH & Co. KGaA, Weinheim

Multicomponent Reactions

DOI: 10.1002/anie.200502066

Stereoselective Palladium-Catalyzed Four-Component Cascade Synthesis of Pyrrolidinyl-, Pyrazolidinyl-, and Isoxazolidinyl Isoquinolines**

H. Ali Dondas, Colin W. G. Fishwick, Xinjie Gai, Ronald Grigg, Colin Kilner, Nuethip Dumrongchai, Boonsong Kongkathip, Ngampong Kongkathip, Chatchwan Polysuk, and Visuvanathar Sridharan*

One-pot multicomponent reactions (MCRs) provide a rapid and elegant means for the preparation of complex molecular architectures from readily available building blocks.[1–5] Among the advantages of MCRs are yields that are higher than almost any sequential synthesis of the same target, a single purification step, and easy adaptation to combinatorial synthesis.

In recent years, allenes have become useful building blocks in palladium catalyzed processes.[6,7] We have demonstrated that carbon monoxide and allenes are powerful relay switches in palladium-catalyzed cyclization–anion-capture

[*] Dr. H. A. Dondas, Dr. C. W. G. Fishwick, Dr. X. Gai, Prof. R. Grigg, C. Kilner, N. Dumrongchai, C. Polysuk, Dr. V. Sridharan
Molecular Innovation, Diversity and Automated Synthesis (MIDAS) Centre
School of Chemistry, Leeds University
Leeds LS2 9JT (UK)
Fax: (+44) 113-343-6501
E-mail: r.grigg@leeds.ac.uk

Dr. B. Kongkathip, Dr. N. Kongkathip
Department of Chemistry
Faculty of Science, Kasetsart University
Bangkok (Thailand)

Dr. H. A. Dondas
Department of Chemistry
Faculty of Pharmacy, Mersin University
Yenisehir, 33342, Mersin (Turkey)

[**] We thank Leeds University and the Thailand Research Fund, under the Royal Golden Jubilee PhD program, for support.

Supporting information for this article, including general experimental procedures and selected examples, is available on the WWW under http://www.angewandte.org or from the author.

WILEY InterScience DISCOVER SOMETHING GREAT
© 2005 Wiley-VCH Verlag GmbH & Co. KGaA, Weinheim

cascades.[1,6,7] As part of our ongoing interest in the design of palladium-catalyzed allenylation processes in a tactical combination with core reactions, we have explored combinations that have 1,3-dipolar cycloaddition processes as the key step in the synthesis of heterocycles.[8] Herein we report four-component cascades with 2-iodoaryl aldehyde **1a** or 2-bromoaryl aldehyde **2b** (Scheme 1) that generate azomethine ylides, azomethine imines, and nitrones as integral parts of the cascade.

Aldehydes **1a** and **b** react, through path a or path b, with an allene, an α-amino acid methyl ester, and *N*-methyl maleimide (NMM) in the presence of Pd^0 to afford **7** (Scheme 1). Path a involves the formation of imine **2**, which undergoes 1,3-dipolar cycloaddition via azomethine ylide **3a** or **3b** (*endo* transition state) to give **4**.[9] Successive palladium-catalyzed allene/nucleophile incorporations then afford **7**. Path b proceeds by initial palladium-catalyzed allene/nucleophile incorporation to generate azomethine ylide **5**, which then undergoes 1,3-dipolar cycloaddition to afford **7**. Azomethine ylide **5** could arise through the precursors **2**, **8**, or **9**.

Our hope was that, if successful, the configuration of the product could be used to distinguish between paths a and b (Scheme 1) as the cycloaddition of *N*-alkylated azomethine ylides **5**/**6** has a different stereochemical outcome to those of **3a**/**3b**.[9]

2-Iodoaldehyde **1a** or 2-bromoaldehyde **1b** (1 mmol) were treated with allene (1 bar), alanine methyl ester hydrochloride (1.2 mmol), NMM (1 mmol), $[Pd_2(dba)_3]$ (2.5 mol%), tris(2-furyl)phosphane (TFP) (10 mol%), and Cs_2CO_3 (4 equiv) in toluene at 100°C for 24 h (48 h for **1b**) to afford **10a** and **10b** in 69% and 57% yield, respectively (Table 1, entry 1). The configuration of **10a**, **b** was established by NOE studies. Phenylalanine methyl ester, aspartic acid

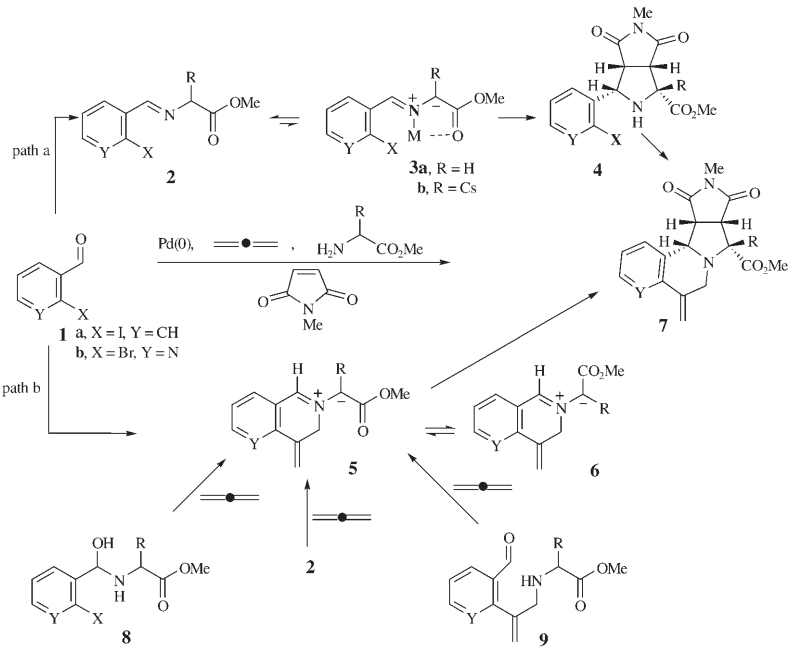

Scheme 1. Four-component cascade that begins with 2-iodoaryl aldehyde **1a** or 2-bromoaryl aldehyde **2b** and generates azomethine ylides, azomethine imines, and nitrones as integral parts of the cascade.

Table 1: Four-component azomethine ylide cycloaddition/allene insertion/nucleophile incorporation cascades with α-amino acid methyl esters.[a]

Entry	α Amino acid methyl ester	*t* [h]	Product	Yield [%]
1	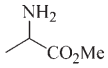	24	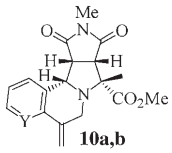 **10a,b**	69 (**10a**, Y = CH) 57[b] (**10b**, Y = N)
2	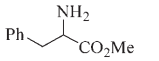	24	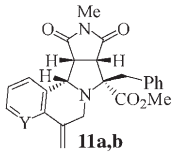 **11a,b**	54 (**11a** Y = CH) 59[b] (**11a**, Y = N)
3	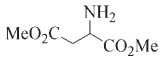	24	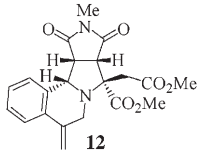 **12**	57
4	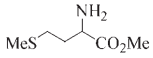	24	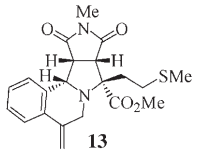 **13**	57
5	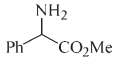	24	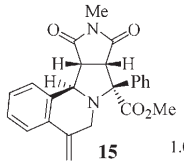 **15** 1.0 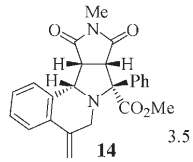 **14** 3.5	64
6	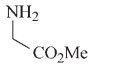	24	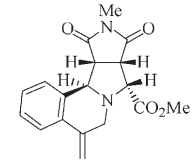 **16** : **17** 1 : 1	53

[a] All reactions were carried out in toluene at 100°C. [b] Reaction time 48 h.

methyl ester, and methionine methyl ester were successfully employed in the cascade reaction to give **11**–**13** in 54–57% yield (Table 1, entries 2–4). Interestingly phenylglycine methyl ester, under the same conditions, afforded **14**/**15** as a 3.5:1 mixture in 64% yield (Table 1, entry 5). The configuration of **14** and **15** was established by NOE studies and, in the case of the major isomer **15**, by an X-ray crystal structure (Figure 1). When the reaction was carried out at 100°C for 12 h, the crude product comprised a 12:12:1 mixture of cycloadducts **4** (R = Ph, X = I, Y = CH), **14**, and **15**. This indicates that **15** might

 © 2005 Wiley-VCH Verlag GmbH & Co. KGaA, Weinheim

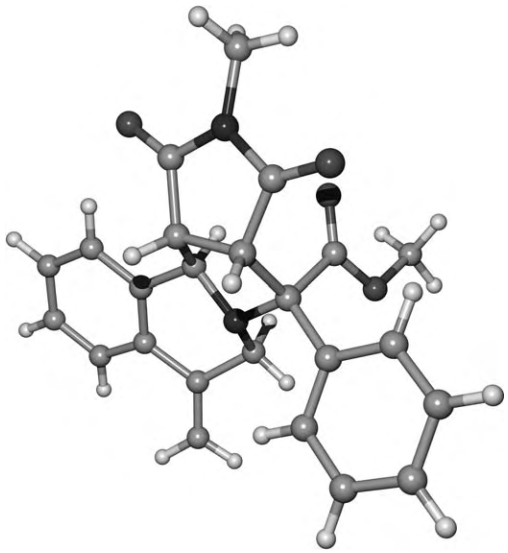

Figure 1. X-ray crystal structure of **15**.[15]

arise through epimerization of **14**, or alternatively, that **14** might undergo a slow retro-1,3-dipolar cycloaddition reaction to generate a new *syn* azomethine ylide **5** (R = Ph, Y = CH) in which the isoquinoline ring is present. The *syn* **5** ylide then equilibrates with *anti* azomethine ylide **6** (R = PH, Y = CH) followed by a 1,3-dipolar cycloaddition reaction through an *exo* transition state to give **15**. Similar results were obtained when the glycine methyl ester was employed in the above cascade (Table 1, entry 6). After 24 h, **16** and **17** were obtained as a 1:1 mixture. Further studies are clearly required to delineate the precise order and nature of the steps involved in this four-component cascade. Current evidence favors path a, which passes through compound **4**, as the configuration of the product conforms to that expected for processes that proceed via **3a**/**3b**.

In seeking to extend the cascade to azomethine imines, through the utilization of hydrazines in place of α-amino esters, we were cognizant of the fact that 1,2-prototropy in hydrazones generally requires temperatures of 120–150 °C.[10] We therefore evaluated a strategy that utilized intramolecular hydrogen bonding to proximal fluorides to stabilize the azomethine imine **18** (Scheme 2). Such hydrogen bonding appears to be weak (ca. 0.2 kcal mol^{-1}),[11] but might be enhanced by electrostatic effects.

Initially we surveyed the reactions of 2,5-difluorophenyl hydrazine and 2-fluorophenylhydrazine with **1**, NMM, and allene in toluene in the presence of a catalyst system that comprises $Pd(OAc)_2$ (10 mol%), PPh_3 (20 mol%), and Cs_2CO_3 (2 equiv). The four-component cascade products **21a** and **b** were obtained in 68 and 72% yield, respectively (Table 2, entries 1 and 2), but their configuration signaled that an *exo* transition state was involved. Azomethine imines impart an imperfect memory of dipole stereochemistry to the product owing to the absence of a fixed configuration at N2 in **21**. A similar pattern was displayed by 2-trifluoromethylphenyl hydrazine which afforded **21c** in 70% yield (Table 2, entry 3). In this case, hydrogen bonding would involve a seven-membered ring in **18**. Evaluation of other hydrazines (Table 2, entries 4–8) showed that the cascade proceeded in the absence of a proximal halogen (Table 2, entries 4 and 7) and that phenyl vinyl sulfone gave the four-component cascade product **21h** both regio- and stereoselectively (Table 2, entry 8). The structure of **21h** was unequivocally determined by X-ray crystallography (Figure 2). The phenyl and the 2,5-difluorophenyl rings are essentially parallel and approximately 3.5 Å apart, which suggests π stacking. AM 1 calculations of the activation energies for the cycloadditions of **18**, **19**, **23**, and **24** show that *exo* cycloadducts via **18** and **23** are favored, with the latter ($E_a = 19.11$ kcal mol^{-1}) favored over the former ($E_a = 22.75$ kcal mol^{-1}).[12] Hydrazones ArCH=N-NH-EWG (EWG = CO_2R, SO_2R) do not give four-component cascade products under our conditions, nor do we observe the formation of indazoles by cyclization of the palladium complex **25** to **26**.[13]

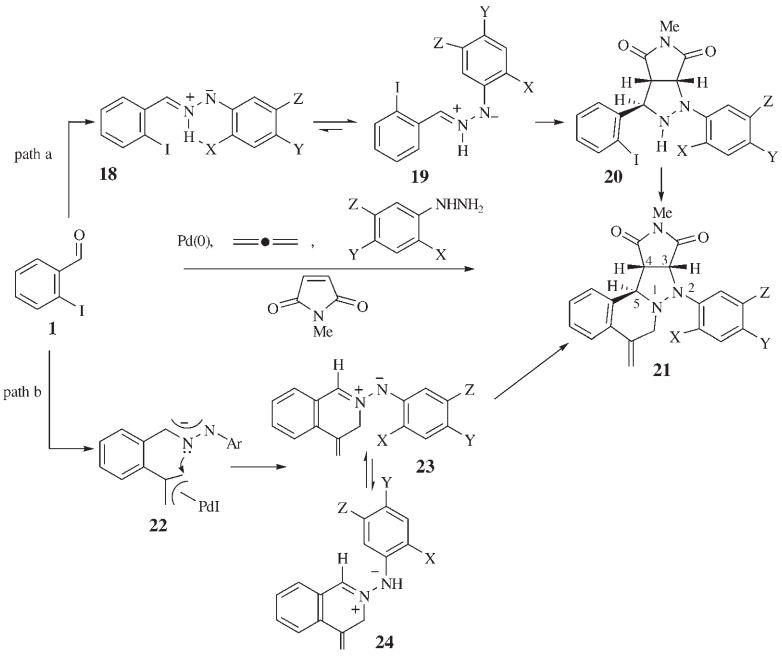

Scheme 2. The use of hydrazines in the extension of the cascade to azomethine imines.

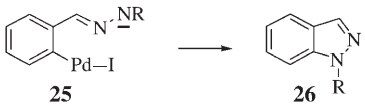

Oxime anions exhibit ambident character (O versus N) with alkylating agents,[14] which prompted a study of their use in multicomponent cascade reactions. The example shown in Scheme 3 parallels the hydrazine case and affords **27** in 62% yield.

 © 2005 Wiley-VCH Verlag GmbH & Co. KGaA, Weinheim

Table 2: Four-component azomethine imine cycloaddition/allene insertion/nucleophile incorporation cascades with hydrazines.[a]

Entry	Hydrazines	*t* [h]	Product	Yield [%]
1	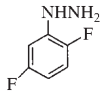	24	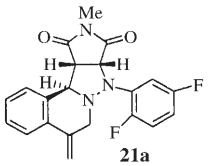 **21a**	68
2		24	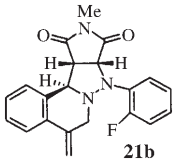 **21b**	72
3		24	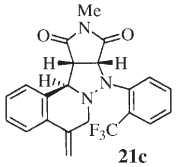 **21c**	70
4	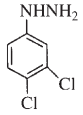	24	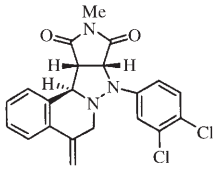 **21d**	63
5	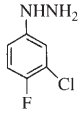	24	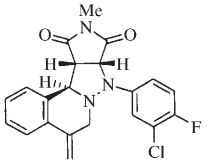 **21e**	66
6	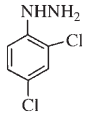	24	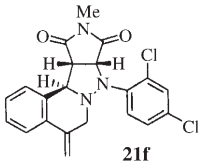 **21f**	58
7	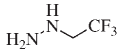	24	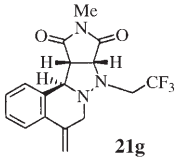 **21g**	53
8	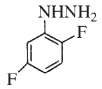	24	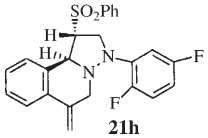 **21h**	55

[a] All reactions were carried out in toluene at 100 °C.

In conclusion, we have demonstrated novel four-component palladium catalyzed 1,3-dipolar cycloaddition/allene insertion/nucleophile incorporation cascades that proceed via intermediate azomethine ylides, azomethine imines, and nitrones. Imines undergo cycloaddition through an *endo* transition state prior to incorporation of the allene. The precise order of events in the case of hydrazines and hydroxylamines is not clear but may involve an initial incorporation of the allene followed by trapping of the π-allylpalladium species by the ambident hydrazone and oxime anions and finally cycloaddition through an *exo* transition state. Such a reversal in the relative rates of allene incorporation/cycloadduct formation would be consistent with the slower cycloaddition rates of hydrazones and oximes. These four-component cascades result in a substantial increase in molecular complexity with formation of five new bonds, two rings and two–four stereocenters.[16]

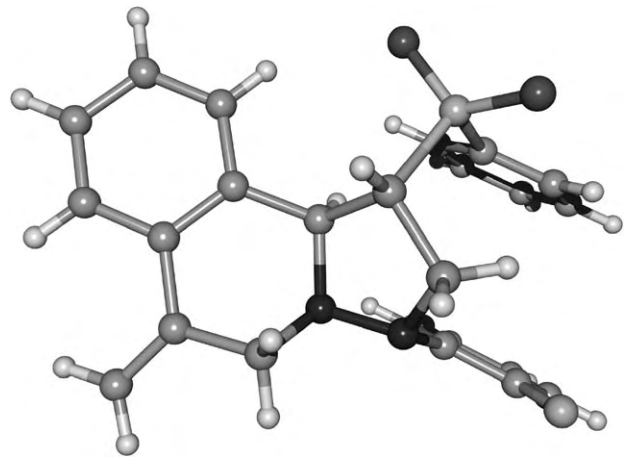

Figure 2. X-ray crystal structure of **21 h**.[15]

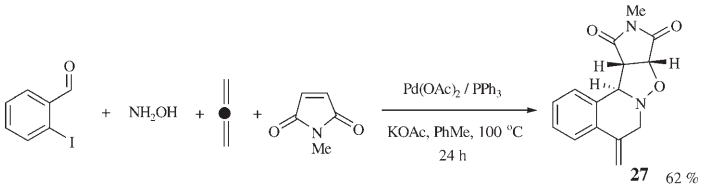

Scheme 3. Reactivity of oxime anions with alkylating agents in the multicomponent reaction.

Received: June 15, 2005
Revised: August 16, 2005
Published online: October 25, 2005

Keywords: allenes · cascade process · cycloaddition · homogeneous catalysis · multicomponent reactions

[1] a) R. Grigg, V. Sridharan, *J. Organomet. Chem.* **1999**, *576*, 65–87; b) J. Montgomery, *Angew. Chem.* **2004**, *116*, 3980–3998; *Angew. Chem. Int. Ed.* **2004**, *43*, 3890–3908
[2] J. Montgomery, *Acc. Chem. Res.* **2000**, *33*, 467–470.
[3] S. Pache, M. Lautens, *Org. Lett.* **2003**, *5*, 4827–4830.
[4] L. F. Tietze, *Chem. Rev.* **1996**, *96*, 115–136.
[5] a) A. Dömling, A. Ugi, *Angew. Chem.* **2000**, *112*, 3300–3344; *Angew. Chem. Int. Ed.* **2000**, *39*, 3168–3210; b) D. J. Ramón, M. Yus, *Angew. Chem.* **2005**, *117*, 1602–1634; *Angew. Chem. Int. Ed.* **2005**, *44*, 1602–1634.
[6] R. Zimmer, C. U. Dinesh, E. Nandanan, F. A. Kahn, *Chem. Rev.* **2000**, *100*, 3067–3126.
[7] a) X. Gai, R. Grigg, I. Koppen, J. Marchbank, V. Sridharan, *Tetrahedron Lett.* **2003**, *44*, 7445–7448; b) R. Grigg, V. Savic, C.

 © 2005 Wiley-VCH Verlag GmbH & Co. KGaA, Weinheim

Terrier, *Tetrahedron* **2002**, *58*, 8613 – 8620; c) R. Grigg, N. Kongkathip, B. Kongkathip, S. Luangkamin, A. H. Dondas, *Tetrahedron* **2001**, *57*, 7965 – 7978; d) X. Gai, R. Grigg, S. Collard, J. E. Muir, *Chem. Commun.* **2001**, 1712 – 1713; e) R. Grigg, N. Kongkathip, B. Kongkathip, S. Luangkamin, H. A. Dondas, *Tetrahedron* **2001**, *57*, 9187 – 9197.

[8] a) C. W. G. Fishwick, R. Grigg, V. Sridharan, J. Virica, *Tetrahedron* **2003**, *59*, 4451 – 4468; b) R. Grigg, M. F. Jones, M. McTiernan, V. Sridharan, *Tetrahedron* **2001**, *57*, 7979 – 7989; c) M. R. Fielding, R. Grigg, V. Sridharan, M. Thornton-Pett, C. J. Urch, *Tetrahedron* **2001**, *57*, 7737 – 7748; d) M. Gardiner, R. Grigg, M. Kordes, V. Sridharan, N. Vicker, *Tetrahedron* **2001**, *57*, 7729 – 7735.

[9] R. Grigg, V. Sridharan, *Advances in Cycloaddition*, Vol. *3* (Ed.: D. P. Curran), JAI, London, **1993**, p. 161.

[10] a) R. Grigg, J. Kemp, N. Thompson, *Tetrahedron Lett.* **1978**, *19*, 2827 – 2830; b) R. Grigg, M. Dowling, M. W. Jordan, V. Sridharan, *Tetrahedron* **1987**, *43*, 5873 – 5886; c) R. Grigg, V. Sridharan, S. Suganthan, A. W. Bridge, *Tetrahedron* **1995**, *51*, 295 – 306; d) C. W. G. Fishwick, R. Grigg, V. Sridharan, J. Virica, *Tetrahedron* **2003**, *59*, 4451 – 4468; e) M. Noguchi, S. Matsumoto, M. Shirai, H. Yamamoto, *Tetrahedron* **2003**, *59*, 4123 – 4133.

[11] a) R. J. Abraham, T. A. D. Smith, W. A. J. Thomas, *J. Chem. Soc. Perkin Trans. 2* **1996**, 1949 – 1955; b) M. H. Abraham, P. L. Grellier, D. V. Prior, J. Morris, P. J. Taylor, *J. Chem. Soc. Perkin Trans. 2* **1990**, *521*–529; c) M. H. Abraham, *Chem. Soc. Rev.* **1993**, *22*, 73 – 83; d) C. Ouvard, M. Bertlelot, C. Laurence, *J. Phys. Org. Chem.* **2001**, *14*, 804 – 810; G. Williams, personal communication.

[12] See Supporting Information.

[13] a) J. J. Song, N. K. Yee, *Org. Lett.* **2000**, *2*, 519 – 521; b) Y. M. Zhu, Y. Kiryu, H. Katayama, *Tetrahedron Lett.* **2002**, *43*, 3577 – 3580; c) K. Inamoto, M. Katsuno, T. Yoshino, I. Suzuki, K. Hiroya, T. Sakamoto, *Chem. Lett.* **2004**, *33*, 1026 – 1027; d) C. S. Cho, D. K. Lim, N. H. Heo, T. J. Kim, S. C. Shim, *Chem. Commun.* **2004**, 104 – 105; e) A. Y. Lebedev, A. S. Khartulyari, A. Z. Voskoboynikov, *J. Org. Chem.* **2005**, *70*, 596 – 602.

[14] a) J. Hamer, A. Macaluso, *Chem. Rev.* **1964**, *64*, 474 – 495; b) G. R. Delpierre, M. Lamchen, *Q. Rev. Chem. Soc.* **1965**, *19*, 329 – 348; c) H. A. Brandman, R. T. Conley, *J. Org. Chem.* **1973**, *38*, 2236 – 2238; d) T. Polonski, A. Chimiak, *Tetrahedron Lett.* **1976**, 2092 – 2095; e) G. J. Elames, C. T. Hawkins, F. W. Jackson, D. I. Smith, S. P. Standem, *Tetrahedron Lett.* **1989**, *30*, 3471 – 3472; f) R. Grigg, J. Markandu, S. Surendrakumar, *Tetrahedron Lett.* **1990**, *31*, 1191 – 1194; g) R. Grigg, J. Markandu, *Tetrahedron Lett.* **1991**, *32*, 279 – 282; h) H. Miyabe, K. Yoshida, V. K. Reddy, A. Matsumura, Y. Takemoto, *J. Org. Chem.* **2005**, *70*, 5630 – 5635.

[15] Crystal data for $C_{24}H_{22}N_2O_4$ (**15**): $0.26 \times 0.15 \times 0.14\ mm^3$, $M = 402.44$, monoclinic, space group $P2_1/n$, $a = 10.6722(2)$, $b = 14.8397(3)$, $c = 13.0511(2)$ Å, $\beta = 109.1850(9)°$, $V = 1952.14(6)$ Å^3, $Z = 4$, $\rho_{calcd} = 1.369\ mg\,m^{-3}$, $\mu = 0.094\ mm^{-1}$, $F(000) = 848$, $T = 150(2)$ K; data collection: $2.15 \le \theta \le 26°$; 3820 independent reflections were collected ($R_{int} = 0.0637$), 3322 reflections with $I > 2\sigma(I)$; structure refinement: number of parameters = 360; goodness of fit, $s = 1.017$, $wR_2 = 0.0979$, $R_1 = 0.0361$. Crystal data for $C_{24}H_{20}F_2N_2O_2S$ (**21h**): $0.30 \times 0.03 \times 0.03\ mm^3$, $M = 438.48$, orthorhombic, space group $Pna2_1$, $a = 31.7330(9)$, $b = 10.3570(2)$, $c = 6.16900(10)$ Å, $V = 2027.50(8)$ Å^3, $Z = 4$, $\rho_{calcd} = 1.436\ mg\,m^{-3}$, $\mu = 0.203\ mm^{-1}$, $F(000) = 912$, $T = 150(2)$ K; data collection: $2.75 \le \theta \le 26°$; 3345 independent reflections were collected ($R_{int} = 0.119$); 2717 reflections with $I > 2\sigma(I)$; structure refinement: number of parameters = 280; goodness of fit, $s = 1.026$; $wR_2 = 0.1078$, $R_1 = 0.0457$. CCDC 273019 (**15**) and -273011 (**21h**) contain the supplementary crystallographic data for this paper. These data can be obtained free of charge from the Cambridge Crystallographic Data Centre via www.ccdc.cam.ac.uk/data_request/cif.

[16] For general experimental procedures (Table 1, Table 2, and Scheme 3) and characterization data for selected compounds, see Supporting Information.

 © 2005 Wiley-VCH Verlag GmbH & Co. KGaA, Weinheim

Template Synthesis

DOI: 10.1002/anie.200501577

Oriented Nanoporous Lamellar Organosilicates Templated from Topologically Unsymmetrical Dendritic-Linear Block Copolymers**

Teddie Magbitang, Victor Y. Lee, Jennifer N. Cha, Hsiao-Lin Wang, W. Richard Chung, Robert D. Miller, Geraud Dubois, Willi Volksen, Ho-Cheol Kim, and James L. Hedrick**

Microstructured porous materials have potential application in a variety of areas, including separation techniques, catalysis, sensing, coatings, microelectronics, and electroop-

[*] T. Magbitang, V. Y. Lee, Dr. J. N. Cha, Dr. R. D. Miller, Dr. G. Dubois, Dr. W. Volksen, Dr. H.-C. Kim, Dr. J. L. Hedrick
IBM Almaden Research Center
650 Harry Road, San Jose, CA 95120 (USA)
Fax: (+1) 408-927-3310
E-mail: hedrick@almaden.ibm.com

H.-L. Wang, Prof. W. R. Chung
Department of Chemical and Materials Engineering
San Jose State University
San Jose, CA (USA)

[**] The authors acknowledge support from the NSF Center for Polymer Interfaces and Macromolecular Assemblies (CPIMA: NSF-DMR-0213618) and the National Institute of Standards and Technology, US Department of Commerce, for the use of the neutron research facilities. This investigation also utilized facilities supported in part by the National Science Foundation under Agreement No. DMR-9986442. We thank Robert M. Briber, Hongxia Feng, and Zhaoliang Lin for their assistance with the small-angle neutron scattering (SANS) experiments. Portions of this research were carried out at the Stanford Synchrotron Radiation Laboratory, a national user facility operated by Stanford University on behalf of the US Department of Energy, Office of Basic Energy Sciences. The SSRL Structural Molecular Biology Program is supported by the Department of Energy, Office of Biological and Environmental Research, and by the National Institutes of Health, National Center for Research Resources, Biomedical Technology Program. We thank Mike F. Toney, Hiro Tsuruta, and Igor Smolsky for their assistance with the small-angle X-ray scattering (SAXS) experiments and Philip M. Rice, Leslie E. Thompson, and Eugene A. Delenia for the transmission electron microscopy (TEM) studies.

Supporting information for this article is available on the WWW under http://www.angewandte.org or from the author.

WILEY InterScience DISCOVER SOMETHING GREAT
© 2005 Wiley-VCH Verlag GmbH & Co. KGaA, Weinheim

tics.[1] Silica-based mesoporous materials, prepared by the assembly of periodic inorganic and surfactant-based structures, have received considerable attention because of the diverse collection of possible pore sizes and shapes.[2] More recently, this concept has been extended to include lyotropic liquid crystalline assemblies,[3] ionic liquids,[4] cyclodextrin-based materials,[5] triphenylene as an electron donor (charge-transfer agents),[6] phthalocyanine-based amphiphiles,[7] and block copolymers[8] as structure-directing agents. Block copolymers have the advantage of fine-tuning the polymer/solvent/silica phase behavior through variation of the monomer type, volume composition, or macromolecular architecture.[9]

We have recently described the generation of nanoporous organosilicates by using block copolymers that exhibit unimolecular self-organization within a vitrifying organosilicate matrix. This process requires an environmentally responsive, star-shaped macromolecule that organizes the organosilicate vitrificate into nanostructures through a matrix-mediated collapse of the interior core of the core–corona polymeric structure. The insoluble core is rendered compatible in the thermosetting matrix and dispersed through the outer corona designed to be miscible with the matrix.[8c,g] The unimolecular nature of the amphiphile eliminates the complex dynamic assembly that characterizes most amphiphiles, and the curvature constraints of this architecture generate non-interconnected spherical pores up to high volume fractions (approximately 50%) upon porogen burn out. Herein, the synthesis of amphiphiles that are between conventional surfactants and block copolymers, with the shape of the former and the size of the latter, is described with the objective of templating a wide variety of porous morphologies through an amphiphile, organosilicate self-assembly process. Amphiphilic dendrons as described by Percec et al.[10] are an example of a system that self-assembles into a variety of nanostructures. Alternatively, dendritic linear hybrid AB amphiphilic block copolymers are also likely candidates, as Frechet, Meijer, Stupp, Hawker, and others[11] have shown that such architectures respond to changes in their environment through changes in the type and shape of micelles formed. In addition, these copolymers assemble into well-defined Langmuir–Blodgett monolayers that are capable of the formation of nanostructured materials with unusual properties and morphologies.[12] Wiesner and co-workers used such amphiphilic dendrimers as structure-directing agents for aluminosilicate-based materials and generated hybrids with a wide variety of nanostructured morphologies.[13] As the shape of low-molecular-weight surfactants has a pronounced effect on the type of aggregate structure formed in silica-surfactant self-assembly, we felt that a dendritic linear amphiphilic copolymer provides an excellent platform from which to tailor the size and shape of the copolymer. Herein, the responsiveness to change in the environment of the copolymer can be tuned by the type, surface functionality, and dendrimer generation together with the structure and molecular weight of the linear component.[14] Herein, we describe the use of amphiphilic dendritic linear copolymers, based on poly(ethylene oxide) (PEO) and a dendron derived from 2,2′-bis(hydroxymethyl)propionic acid (bis(MPA)),[15] as structure-directing agents for organosilicates to generate a unique, oriented perforated porous lamellar morphology.

PEO hydroxy-functionalized oligomers ($M_w = 4800$ and 9800 g mol^{-1}; polydispersity indices (PDI) = 1.03 and 1.05, respectively) were chosen as the linear component of the copolymer, as PEO has been shown to be miscible with the methyl silsequioxane (MSSQ) prepolymer over wide compositional and molecular-weight ranges.[8c,g] Dendrons derived from bis(MPA) were chosen as they decomposed cleanly and quantitatively upon thermolysis;[16] furthermore, they can be prepared by both divergent and convergent methods and provide exquisite NMR spectroscopic handles to follow the various chemical transformations.[17] Frechet and co-workers showed that hydroxy-terminated PEO is an excellent scaffold for the divergent growth of dendrons using acetal-protected anhydride derivatives of bis(MPA) and also importantly demonstrated that the PEO facilitates product purification through precipitation.[18] This divergent-growth approach was employed using acetonide-protected bis(MPA) anhydride, prepared from the self-condensation of the acetonide-protected bis(MPA) using *N*,*N*′-dicyclohexylcarbodiimide (DCC), in the presence of dimethylaminopyridine (DMAP; 0.25 mol% with respect to the anhydride) in a solvent mixture of CH_2Cl_2/pyridine (90:10). An approximate 2–4-fold excess of anhydride was used to insure quantitative conversion of the terminal hydroxy groups, and the reaction was performed at room temperature (approximately 15–18 h) under nitrogen (Scheme 1). Upon completion, the excess anhydride was treated with methanol to facilitate purification as the by-products generated are soluble in diethyl ether and the PEO copolymers do not allow polymer precipitation. Deprotection of the acetonide groups was accomplished by using Dowex 50W-X2 acidic ion-exchange resin in methanol at 54 °C for 5 h. This general procedure was repeated for each generation and for both poly(ethylene) glycol (PEG) molecular weights surveyed, thus ultimately producing up to six generations of bis(MPA) dendron "block length" in the copolymers. These transformations were followed using ^{13}C NMR spectroscopy, as the quaternary carbon atom of bis(MPA) is sensitive to the substitution of the neighboring hydroxy groups, and the spectra associated with dendritic, linear, and terminal substitution have been identified by model-compound studies. The functionalization and deprotection steps are quantitative irrespective of the generation (Figure 1). The quaternary carbon atom of the acetonide-protected first generation occurs at $\delta \approx 42$ ppm, which on deprotection shifts to $\delta \approx 50.5$ ppm. Subsequent functionalization of the first generation produces the acetonide-protected second generation ($\delta \approx 42$ ppm) and the inner first generation ($\delta \approx 46$ ppm); incomplete transformations are readily detected. The surface hydroxy groups of the dendrons for the fourth to sixth generations were subsequently functionalized by esterification with either protiated or deuterated heptanoic acid in CH_2Cl_2 using DCC/pyridinium 4-toluenesulfonate (DPTS)/DMAP.[19,20] ^{13}C NMR spectroscopy of the terminal quaternary carbon atoms of bis(MPA) clearly showed quantitative conversion into the esterification product (Figure 1). Functionalization of the polymer chain with acetonide–bis(MPA) ($\delta \approx 42$ ppm), followed by its deprotection ($\delta \approx 50.5$ ppm), is

 © 2005 Wiley-VCH Verlag GmbH & Co. KGaA, Weinheim

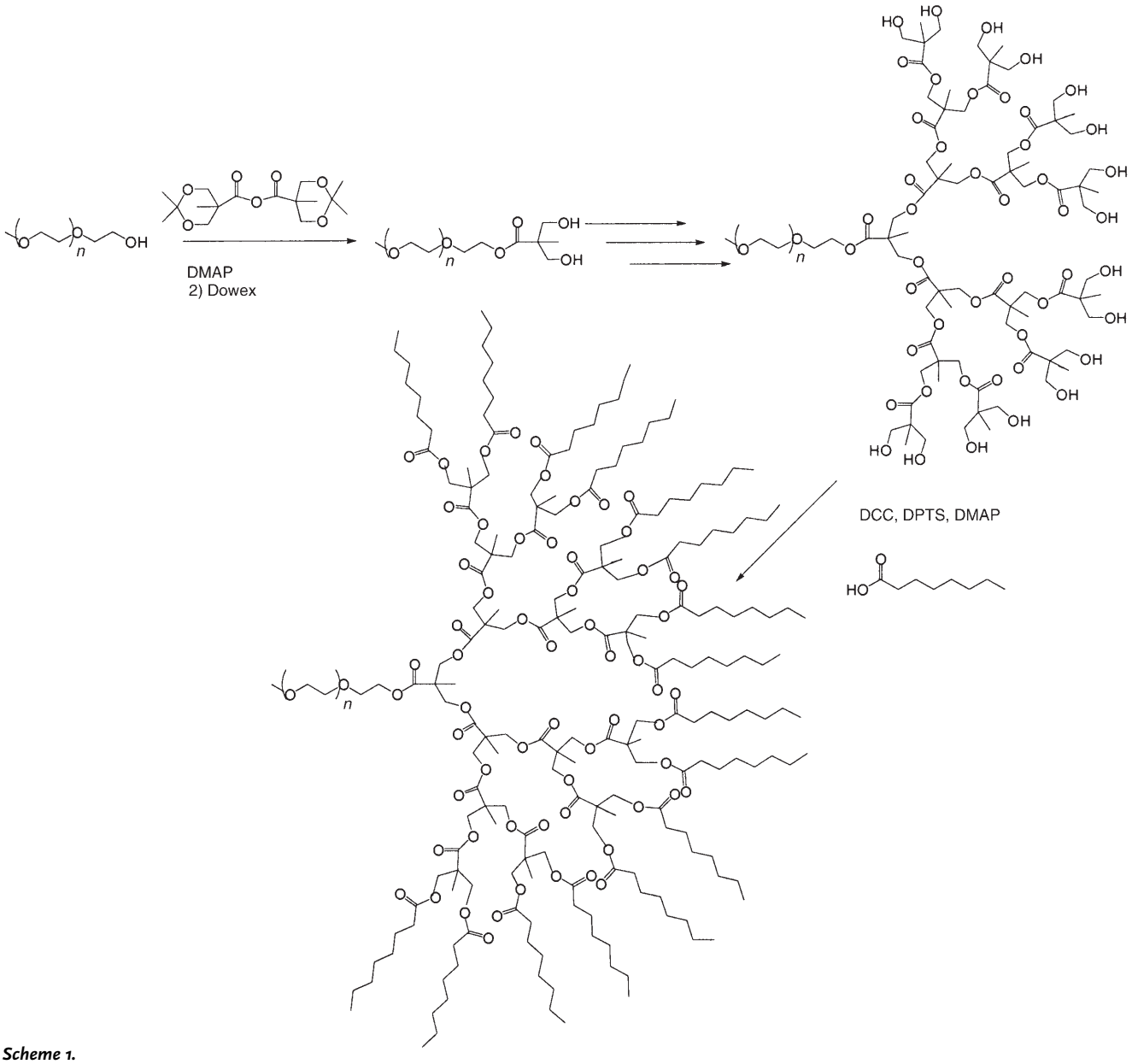

Scheme 1.

clearly seen for each generation (up to generation 5). The fifth generation is then deprotected and functionalized with heptanoic acid ($\delta \approx 46$ ppm). The general characteristics of the fourth–sixth generation copolymers prepared from each of the PEG oligomers, including the molecular weight and weight fraction of the dendron and the molecular weight and polydispersity of the entire copolymer, are given in Table 1. The size-exclusion chromatograms of the fourth–sixth generation copolymers **1a–c** (see Figure 1 and the Supporting Information) and (**2a–c**) clearly demonstrate monomodal, narrowly dispersed products (Figure 2). Thin films of these block copolymers show microphase-separated morphologies, as evidenced by the presence of two T_g values in the dynamic mechanical analysis (DMA) spectra for the third–sixth generation copolymers (Figure 3). Wiesner and co-workers studied the morphologies of similar macromolecular architectures in detail.[21]

The amphiphilic polymers were dissolved in a solution containing the MSSQ prepolymer in 1-methoxy-2-propanol, and the resulting solution was spun on a silicon wafer to produce thin films that were cured to 430 °C to effect the first network formation of the MSSQ and decomposition of the sacrificial copolymer template. Representative tan δ curves obtained from DMA for the **1a**/MSSQ hybrid (40 wt. % copolymer loading) after curing to 80 °C (minimal advancement in MSSQ molecular weight) and 150 °C (significant advancement in molecular weight of MSSQ, that is, network formation) are presented in Figure 3 (also see the Supporting Information) together with the copolymer for comparison. Irrespective of the cure temperature, a two-phase structure is clearly evident in the hybrid. The retention of the T_g value at −25 °C associated with the bis(MPA) dendron phase and the disappearance of the PEO transition (approximately −55 °C) supports the hypothesis that a two-phase structure is present

 © 2005 Wiley-VCH Verlag GmbH & Co. KGaA, Weinheim

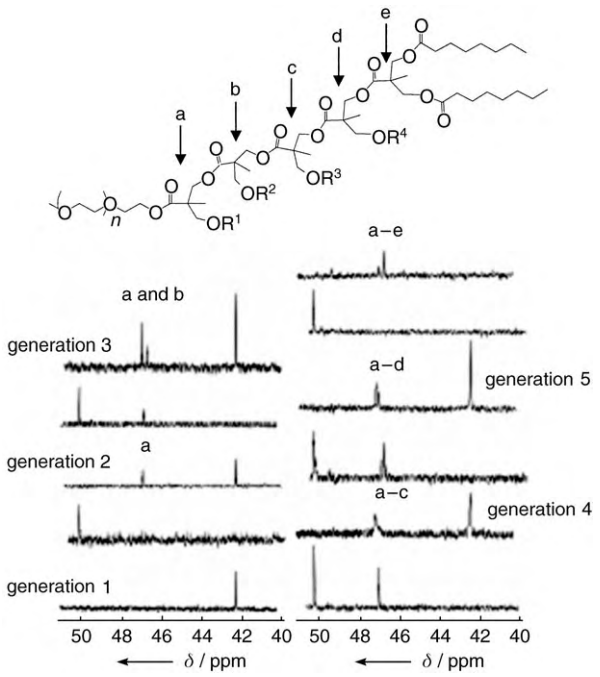

Figure 1. ^{13}C NMR spectra of copolymers **1a–c**.

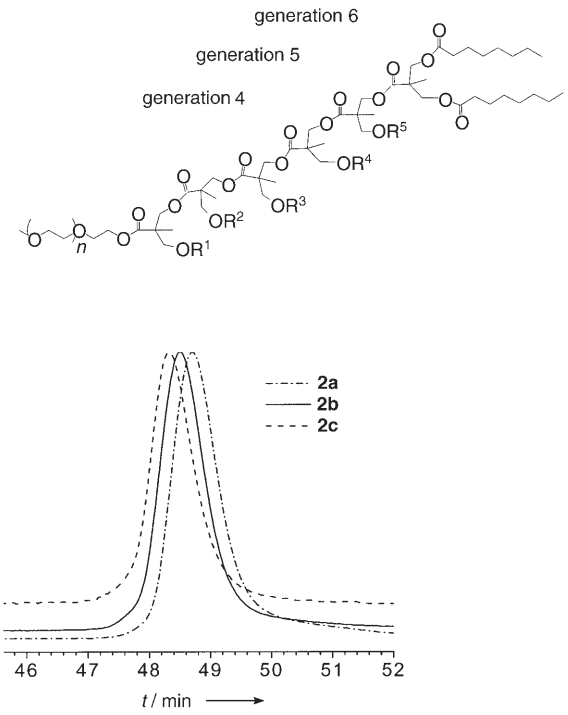

Figure 2. Size-exclusive chromatograms of copolymers **2a–c**.

Table 1: Characteristics of dendritic-linear amphiphilic copolymers.

Sample	PEO segment M_n [g mol^{-1}]	Dendron generation (M_n [g mol^{-1}])		Dendron fraction	M_n[a] [g mol^{-1}]	M_n[b] [g mol^{-1}]	PDI
1a	4800	4	(4030)	45	9000	9700	1.08
1b	4800	5	(8200)	63	13000	11300	1.03
1c	4800	6	(12000)	71	16800	14000	1.04
2a	9800	4	(4030)	29	14000	16500	1.05
2b	9800	5	(8200)	45	18000	18200	1.05
2c	9800	6	(12000)	55	21500	20000	1.04

[a] Detected by ^1H NMR spectroscopy. [b] Detected by gel-permeation chromatography.

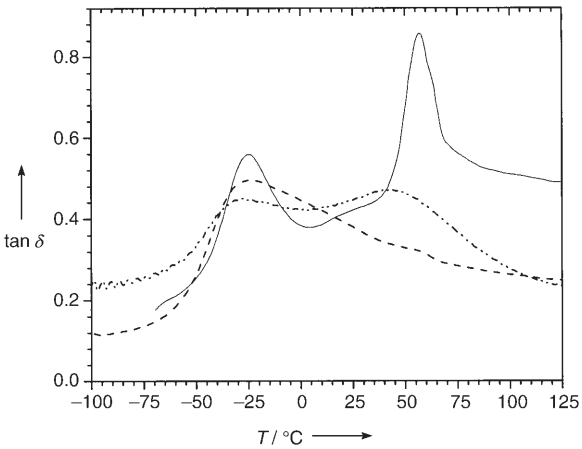

Figure 3. DMA of copolymer **1a** (——), **1a**/MSSQ mixture cured to 80 °C (–•–•) and 250 °C (----).

even prior to cure. Although it is difficult to assign with certainty, we believe it is likely that the T_g value at 50 °C is the mixed T_g values of the PEG and MSSQ phase as they are miscible. Small-angle neutron scattering (SANS) measurements of **1a** (in which the chain ends are selectively decorated with deuterated heptanoic acid) confirm the two-phase structure of the hybrid containing 40 wt.% copolymer (see the Supporting Information). This structure, generated upon spin coating, is thought to occur through a self-assembly process facilitated by the selective solubilization of the PEO by MSSQ and subsequent collapse of the dendron (namely, the structure-directing agent). Further heating of hybrid samples to 430 °C removes the block-copolymer template to create a porous thin film. For example, a porous film derived from a hybrid containing 40 wt.% **1a** has a refractive index of 1.24 and a dielectric constant of 2.00, in comparison to the dense MSSQ matrix with values of 1.37 and 2.85, respectively. Irrespective of the PEG block length or dendron generation surveyed, all refractive indices and dielectric constants were comparable for similar loading levels.

Cross-sectional transmission electron micrography (TEM) images of MSSQ mixtures containing 20, 40, and 60 wt.% of **1b** are shown in Figure 4. The sample of 20 wt.% shows a porous structure (pore sizes: 4–5 nm) with a shape that resides at the interface between the spherical and cylindrical morphologies. Conversely, mixtures that contain the higher volume fractions of copolymer manifest a nanoporous lamellar structure that is oriented parallel to the surface, and this morphology is maintained over a wide compositional range (approximately 35–70%). Small-angle X-ray scattering (SAXS) measurements on the porous films show an increasing scattering intensity with porogen volume

 © 2005 Wiley-VCH Verlag GmbH & Co. KGaA, Weinheim

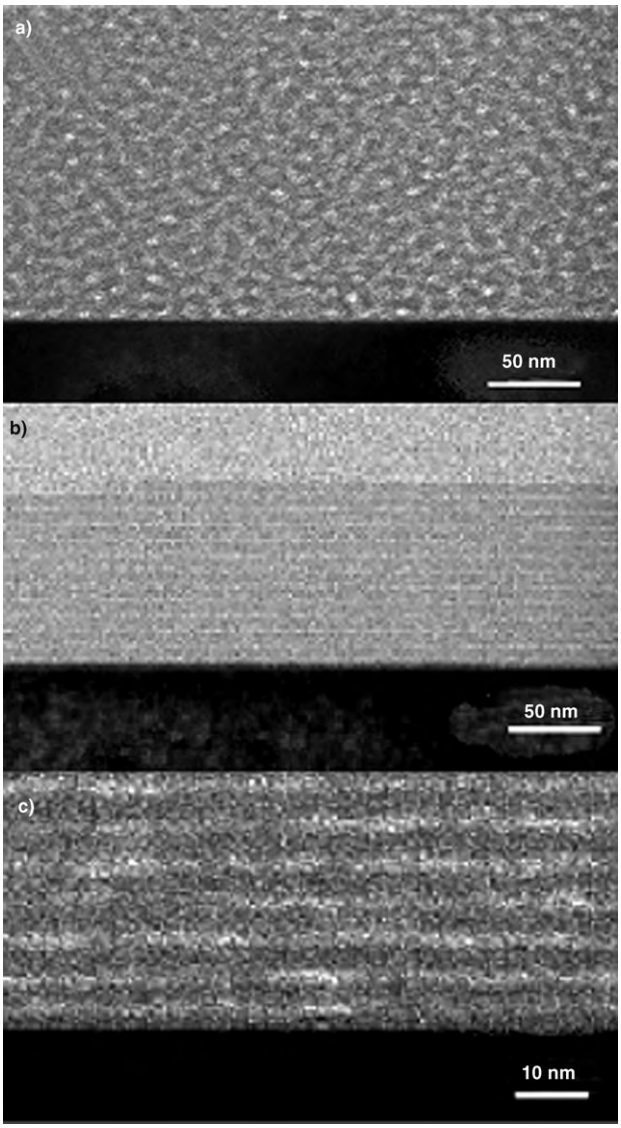

Figure 4. TEM images of copolymer **1b** with mixtures of MSSQ containing a) 20, b) 40, and c) 60 wt.% copolymer.

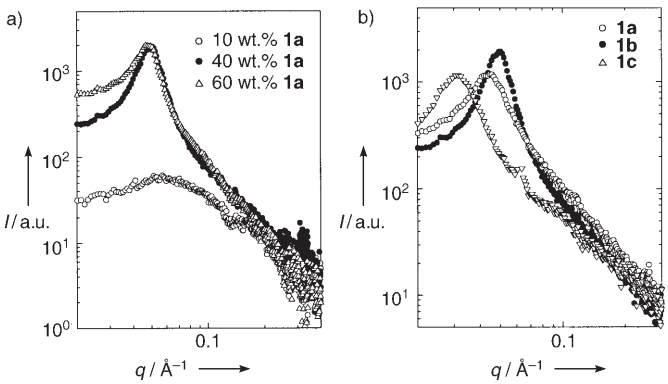

Figure 5. SAXS profiles of porous organosilicates: a) SAXS profiles as a function of weight fraction of G4-PEO5K; b) SAXS profiles of porous films generated with 40 wt.% of copolymer. The samples were prepared by thermal heating to 450 °C after spin-casting.

fraction of **1a** (Figure 5). At a loading of 40 wt.% and above, a strong interpore correlation is observed with peaks that correspond to approximately 129 Å ($2\pi/q$), and no significant change was observed by increasing the copolymer loading to 60 wt.%. Figure 5b shows the effect of PEO molecular weight and dendron generation on the pore structure. An increase in interpore distance from 129 to 137 Å was observed for a loading of 40 wt.% with increasing PEO molecular weight from 5000 to 10000. The SAXS profiles for **2a** and **2b** show the interpore distance increases from 137 to 197 Å as the dendron generation is varied from the fourth to the fifth. Although a porous morphology was observed for all calcined samples, the well-defined lamellar structure oriented parallel to the surface was observed only for the copolymer that contained the fifth generation dendron, irrespective of the PEO block length. The lamellar morphology oriented parallel to the surface was further confirmed by X-ray reflectivity (XR) by the strong scattering that satisfies the Bragg condition (40 wt.% loading of **1b**), thus indicating a layered structure with porosity oriented parallel to the substrate (Figure 6). The first-order Bragg peak corresponds to a period of approximately 107 Å ($2\pi/q$). The higher-order peaks correspond to periods of approximately 56 and 38 Å, respectively.

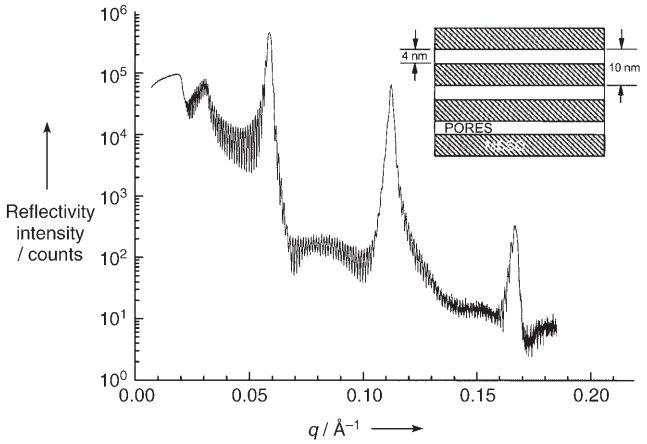

Figure 6. XR profile of porous organosilicate thin films generated with 40 wt.% **1b**. The samples were prepared by thermal heating to 450 °C after spin-casting.

In summary, environmentally responsive, topologically unsymmetrical dendritic linear diblock copolymers with a compatiblilizing linear component were used to organize a MSSQ vitrificate into nanostructures through a matrix-mediated collapse of the interior core. DMA and SANS measurements strongly suggest that the dendron is phase separated in the as-cast film, and serves as the macromolecular template for a porous lamellar morphology (XR and SAXS) at copolymer compositions above 35% volume fraction. The bulky nature of the dendron may also affect their ability to pack efficiently into the traditional spherical micelles that can form from diblock copolymers in selective solvents. The formation of elongated micellar structures, or

 © 2005 Wiley-VCH Verlag GmbH & Co. KGaA, Weinheim

"worm-like micelles", would help relieve some of the packing constraints of the dendrons and may require less distortion of the molecules from their single-molecule conformation.[11b,12c] This outcome, in turn, may explain the porous lamellar structure (4 nm) obtained between organosilicate sheets (6–9 nm) that persist over a wide temperature range. Moreover, the substrate surface SiO_2 causes the lamellar structure to orient in a parallel fashion over the entire substrate. Although inorganic hybrids with well-defined lamellar morphologies have been reported and are well characterized, this structure, although observed before,[22] is largely unstable at calcination temperatures.[8h,j,22,23]

Received: May 9, 2005
Published online: October 25, 2005

Keywords: dendrimers · hybrids · lamellar morphology · organosilicates · template synthesis

[1] For example: a) R. H. Baney, M. Itoh, A. Sakakibrar, T. Suzuki, *Chem. Rev.* **1995**, *95*, 1409; b) D. Loy, K. J. Shea, *Chem. Rev.* **1995**, *95*, 1431; c) D. Radu, C. Lai, J. Wiench, M. Pruski, V. S.-Y. Lin, *J. Am. Chem. Soc.* **2004**, *126*, 1640; d) J. L. Hedrick, T. Magbitang, E. F. Connor, T. Glauser, W. Volksen, C. J. Hawker, V. Y. Lee, R. D. Miller, *Chem. Eur. J.* **2002**, *8*, 3308; e) R. Hernandez, A. Tranvill, P. Minoofar, B. Dunn, J. I. Zink, *J. Am. Chem. Soc.* **2001**, *123*, 1248; f) R. Hernandez, H. Tseng, J. W. Wong, J. F. Stoddart, J. I. Zink, *J. Am. Chem. Soc.* **2004**, *126*, 3370; g) V. S.-Y. Lin, D. R. Radu, M.-K. Han, W. Deng, S. Kuroki, B. H. Shanks, M. Pruski, *J. Am. Chem. Soc.* **2002**, *124*, 9040; h) V. S.-Y. Lin, C.-Y. Lai, J. Huang, S.-A. Song, S. Xu, *J. Am. Chem. Soc.* **2001**, *123*, 11510; i) D. R. Radu, C.-Y. Lai, J. W. Wiench, M. Pruski, V. S.-Y. Lin, *J. Am. Chem. Soc.* **2004**, *126*, 1640; j) S. H. Tolbert, A. Firouzi, G. D. Stucky, B. F. Chmelka, *Science* **1997**, *278*, 264; k) M. Antonietti, B. Berton, C. Göltner, H.-P. Hentze, *Adv. Mater.* **1998**, *10*, 154; l) E. Krämer, S. C. Förster, Göltner, M. Antonietti, *Langmuir* **1998**, *14*, 2027; m) Q. R. Huang, H.-C. Kim, E. Huang, D. Mecerreyes, J. L. Hedrick, W. Volksen, C. W. Frank, R. D. Miller, *Macromolecules* **2003**, *36*, 7661.

[2] For example: a) C. T. Kresge, M. E. Leonowicz, W. J. Roth, J. C. Vatuli, J. S. Beck, *Nature* **1992**, *359*, 710; b) J. S. Beck, J. C. Vartuli, W. J. Roth, M. E. Leonowicz, C. T. Kresge, K. D. Schmitt, C. T. W. Chu, D. H. Olson, E. W. Sheppard, et al., *J. Am. Chem. Soc.* **1992**, *114*, 10834; c) Q. Huo, D. I. Margolese, P. Feng, T. E. Gier, G. D. Stucky, R. Leon, P. M. Petroff, U. Ciesla, F. Schüth, *Nature* **1994**, *368*, 317; d) M. E. Davies, C. Saldarriaga, C. Montes, J. Garces, C. Crowdert, *Nature* **1988**, *331*, 698; e) Q. Huo, D. I. Margolese, U. Ciesla, D. P. Feng, T. E. Gier, P. Sieger, A. Firouzi, B. F. Chmelka, F. Schüth, G. D. Stucky, *Chem. Mater.* **1994**, *6*, 1176; f) P. Yang, T. Deng, D. Zhao, P. Feng, D. Pine, B. F. Chmelka, G. M. Whitesides, G. D. Stucky, *Science* **1998**, *282*, 2244–2246; g) Y. Chujo, H. Matsuk, S. Kure, T. Saegusa, T. Yazawa, *J. Chem. Soc. Chem. Commun.* **1994**, 635.

[3] D. L. Gin, W. Gu, B. A. Pindzola, W.-W. Zhou, *Acc. Chem. Res.* **2001**, *34*, 973.

[4] Y. Zhou, J. H. Schattka, M. Antonietti, *Nano Lett.* **2004**, *4*, 477.

[5] B.-H. Han, S. Poarz, M. Antonietti, *Chem. Mater.* **2001**, *13*, 3915.

[6] A. Okabe, T. Fukushima, K. Ariga, T. Aida, *Angew. Chem.* **2002**, *114*, 3564; *Angew. Chem. Int. Ed.* **2002**, *41*, 3414.

[7] M. Kimura, K. Wada, K. Ohta, K. Hanabusa, H. Shirai, N. Kobayashi, *J. Am. Chem. Soc.* **2001**, *123*, 2438.

[8] For example: a) M. Templin, A. Franck, A. Du Chesne, H. Leist, T. Ahang, R. Ulrich, V. Schadler, U. Wiesner, *Science* **1997**, *278*, 1795; b) D. Zhao, J. Feng, Q. Huo, N. Melosh, G. H. Frederickson, B. F. Chmelka, G. D. Stucky, *Science* **1998**, *279*, 548; c) E. F. Connor, L. K. Sundberg, H.-C. Kim, J. J. Cornelissen, T. Magbitang, P. M. Rice, V. Y. Lee, C. J. Hawker, W. Volksen, J. L. Hedrick, R. D. Miller, *Angew. Chem.* **2003**, *115*, 3915; *Angew. Chem. Int. Ed.* **2003**, *42*, 3785; d) Y. Y. Yuan, P. Hentze, W. M. Arnold, B. K. Marlow, M. Antonietti, *Nano Lett.* **2002**, *2*, 1359; e) A. Jain, U. Wiesner, *Macromolecules* **2004**, *37*, 5665; f) P. Simon, R. Ulrich, H. W. Spiess, U. Wiesner, *Chem. Mater.* **2001**, *13*, 3464; g) T. Magbitang, V. Y. Lee, R. D. Miller, M. F. Toney, Z. Lin, R. M. Briber, H.-C. Kim, J. L. Hedrick, *Adv. Mater.* **2005**, *17*, 1031; h) B. Smarsly, G. Xomeritakis, K. Yu, N. Liu, H. Fan, R. A. Assink, C. A. Drewien, W. Ruland, C. J. Brinker, *Langmuir* **2003**, *19*, 7295; i) K. Yu, A. Hurd, A. Eisenburg, C. J. Brinker, *Langmuir* **2001**, *17*, 796; j) J. M. Kim, Y. Sakamoto, Y. K. Hwang, Y. U. Kwon, O. Terasaki, S. E. Park, G. D. Stucky, *J. Phys. Chem. B* **2002**, *106*, 2552; k) J. N. Cha, G. D. Stucky, D. E. Morse, T. J. Deming, *Nature* **2000**, *403*, 289; l) P. Yang, T. Deng, D. Zhao, P. Feng, D. Pine, B. F. Chmelka, G. M. Whitesides, G. D. Stucky, *Science* **1998**, *282*, 2244; m) A. Sellinger, P. M. Weiss, A. Nguyen, Y. Lu, R. A. Assink, C. J. Brinker, *Nature* **1998**, *394*, 256; n) Y. Lu, H. Fan, T. Ward, T. Reiker, C. J. Brinker, *Nature* **1999**, *398*, 223.

[9] For example: a) E. L. Thomas, *Polymer* **2003**, *44*, 6725; b) E. W. Cochran, D. C. Morse, F. S. Bates, *Macromolecules* **2003**, 36, 782; c) Z. Q. Lin, D. H. Kim, X. D. Wu, L. Boosahda, D. Stone, L. LaRose, T. P. Russell, *Adv. Mater.* **2002**, *14*, 1373.

[10] For example: a) V. Percec, C. Ahn, G. Ungar, D. Yeardley, M. Moller, S. Sheiko, *Nature* **1998**, *391*, 161; b) S. A. Prokhorova, S. S. Sheiko, C. A. Ahn, V. Percec, V. Moller, *Macromolecules* **1999**, *32*, 2653; c) Z. Liu, W. S. Zhou, S. Z. D. Cheng, V. Percec, G. Ungar, *Chem. Mater.* **2002**, *14*, 2384.

[11] For example: a) I. Gitsov, J. M. J. Frechet, *J. Am. Chem. Soc.* **1996**, *118*, 3785; b) J. C. M. Van Hest, W. M. P. L. Bars, M. H. P. van Genderen, W. W. Meijer, *Science* **1995**, *268*, 1592; c) A. Heise, J. L. Hedrick, C. W. Frank, R. D. Miller, *J. Am. Chem. Soc.* **1999**, *121*, 8647; d) Q. Ma, E. E. Remsen, T. Kowalewski, K. L. Wooley, *J. Am. Chem. Soc.* **2001**, *123*, 4627; e) Q. Zhang, E. E. Remsen, K. L. Wooley, *J. Am. Chem. Soc.* **2000**, *122*, 3642; f) J. Pyun, X. Zhou, E. Drockenmuller, C. J. Hawker, *J. Mater. Chem.* **2003**, *13*, 2653; g) L.-S. Li, S. I. Stupp, *Angew. Chem.* **2005**, *117*, 1867; *Angew. Chem. Int. Ed.* **2005**, *44*, 1833; h) F. J. Solis, S. I. Stupp, M. O. de la Cruz, *J. Chem. Phys.* **2005**, *122*, 054905; i) H. T. Jung, S. O. Kim, S. D. Hudson, V. Percec, *Appl. Phys. Lett.* **2002**, *80*, 395; j) V. Percec, A. E. Dulcey, V. S. K. Balagurusamy, Y. Miura, J. Smidrkal, M. Peterca, S. Nummelin, U. Edlund, S. D. Hudson, P. A. Heiney, H. Duan, S. N. Magonov, S. A. Vinogradov, *Nature* **2004**, *430*, 764; k) S. Liu, S. P. Armes, *J. Am. Chem. Soc.* **2001**, *123*, 9910; l) I. Gitsov, J. M. J. Frechet, *J. Am. Chem. Soc.* **1996**, *118*, 3785; m) M. A. Johnson, C. M. B. Santini, J. Iyer, S. Satija, R. Ivkov, P. T. Hammond, *Macromolecules* **2002**, *35*, 231; n) M. E. Mackay, Y. Hong, M. Jeong, B. M. Tande, N. J. Wagner, S. Hong, S. P. Gido, R. Vestberg, C. J. Hawker, *Macromolecules* **2002**, *35*, 8391.

[12] a) J. P. Kampf, C. W. Frank, E. E. Malmstrom, C. J. Hawker, *Science* **1999**, *283*, 1730; b) J. P. Kampf, C. W. Frank, E. E. Malmstrom, C. J. Hawke, *Lammuir* **1999**, *15*, 227; c) A. Wursch, M. Moller, T. Gluser, L. S. Lim, S. B. Voytek, J. L. Hedrick, C. Frank, J. G. Hilborn, *Macromolecules* **2001**, *34*, 6601; d) V. Percec, B. Barboiu, C. Grigoras, T. K. Bera, *J. Am. Chem. Soc.* **2003**, *125*, 6503; e) T. Glauser, C. M. Stancik, M. Moller, S. Voytek, A. P. Gast, J. L. Hedrick, *Macromolecules* **2002**, *35*, 5774.

[13] B. K. Cho, A. Jain, S. M. Mahajan, H. Ow, S. M. Gruner, U. Wiesner, *J. Am. Chem. Soc.* **2004**, *126*, 4070.

[14] For example: a) A. W. Bosman, H. M. Jansen, E. W. Meijer, *Chem. Rev.* **1999**, *99*, 1665; b) S. Hecht, J. M. J. Fréchet, *Angew.*

 © 2005 Wiley-VCH Verlag GmbH & Co. KGaA, Weinheim

Chem. **2001**, *113*, 76; *Angew. Chem. Int. Ed.* **2001**, *40*, 74; c) D. A. Tomalia, D. H. Dupont, *Top. Curr. Chem.* **1993**, *165*, 193; d) C. Gorman, *Adv. Mater.* **1998**, *10*, 295; e) M. Fischer, F. Vögtle, *Angew. Chem.* **1999**, *111*, 934; *Angew. Chem. Int. Ed.* **1999**, *38*, 885; f) H. Frey, *Angew. Chem.* **1998**, *110*, 2313; *Angew. Chem. Int. Ed.* **1998**, *37*, 2193; g) S. G. Grayson, J. M. J. Fréchet, *Chem. Rev.* **2001**, *101*, 3819; h) C. J. Hawker, J. M. J. Fréchet, *J. Am. Chem. Soc.* **1990**, *112*, 7368; i) E. M. Meijer, E. M. M. de Brabender-van den Berg, *Angew. Chem.* **1993**, *105*, 1370; *Angew. Chem. Int. Ed. Engl.* **1993**, *32*, 1308; j) S. Vetter, S. Koch, A. D. Schluter, *J. Polym. Sci. Part A* **2001**, *39*, 1940; k) R. Gronheid, J. Hofkens, F. Köhn, T. Weil, E. Reuther, K. Müllen, F. C. De Schryver, *J. Am. Chem. Soc.* **2002**, *124*, 2418.

[15] a) H. Ihre, O. L. Padilla De Jesu, J. M. J. Frechet, *J. Am. Chem. Soc.* **2001**, *123*, 5908; b) H. Ihre, A. Hult, E. Soderlind, *J. Am. Chem. Soc.* **1996**, *118*, 6388; c) E. Malmstrom, M. Johansson, A. Hult, *Macromolecules* **1995**, *28*, 1698; d) M. Malkoch, E. Malmstrom, A. Hult, *Macromolecules* **2002**, *35*, 8307.

[16] a) J. L. Hedrick, R. D. Miller, C. J. Hawker, K. R. Carter, W. Volksen, D. Yoon, M. Trollsås, *Adv. Mater.* **1998**, *10*, 1049; b) C. Nguyen, K. R. Carter, C. J. Hawker, J. L. Hedrick, R. Jaffy, R. D. Miller, J. Remenar, H. Rhee, P. Rice, M. Toney, D. Yoon, *Chem. Mater.* **1999**, *11*, 3080; c) C. Nguyen, C. J. Hawker, R. Miller, J. L. Hedrick, J. G. Hilborn, *Macromolecules* **2000**, *33*, 4281.

[17] a) E. Malmstrom, M. Johansson, A. Hult, *Macromolecules* **1995**, *28*, 137; b) E. Malmstrom, M. Johansson, A. Hult Macromol, *Chem. Phys.* **1996**, 197, 3199; c) M. Trollsas, J. L. Hedrick, *J. Am. Chem. Soc.* **1998**, *120*, 4644; d) M. Trollsas, B. Atthoff, H. Claesson, J. L. Hedrick, *Macromolecules* **1998**, *31*, 3439.

[18] H. Ihre, O. L. Padilla De Jesus, J. M. J. Frechet, *J. Am. Chem. Soc.* **2001**, *123*, 5908.

[19] a) J. S. Moore, S. I. Stupp, *Macromolecules* **1990**, *23*, 65; b) H. Ihre, A. Hult, E. Soderlind, *J. Am. Chem. Soc.* **1996**, *118*, 6388; c) E. Malmstrom, M. Johansson, A. Hult, *Macromolecules* **1995**, *28*, 1698.

[20] H. R. Ihre, O. L. P. De Jesus, F. C. Szoka, J. M. J. Frechet, *Bioconjugate Chem.* **2002**, *13*, 443.

[21] B.-K. Cho, A. Jain, S. M. Gruner, U. Wiesner, *Science* **2004**, *305*, 1598.

[22] For example: a) J. M. Kim, Y. Sakamoto, Y. K. Hwang, Y. Kwon, O. Terasaki, S.-E. Park, G. D. Stucky, *J. Phys. Chem. B* **2002**, *106*, 2552; b) S. H. Tolbert, C. C. Landry, G. D. Stucky, B. F. Chemlka, P. Norby, J. Hanson, A. Monnier, *Chem. Mater.* **2001**, *13*, 2247; c) K. Yu, A. J. Hurd, A. Eisenberg, C. J. Brinker, *Langmuir* **2001**, *17*, 7961.

[23] The experimental procedures used and the SEC, DMA, and SANS characterization of the copolymers are given in the Supporting Information.

 © 2005 Wiley-VCH Verlag GmbH & Co. KGaA, Weinheim

Origin of Life

DOI: 10.1002/anie.200503387

A DNA-Templated Aldol Reaction as a Model for the Formation of Pentose Sugars in the RNA World**

*Michael Oberhuber and Gerald F. Joyce**

An early stage in the history of life on Earth is thought to have involved RNA genomes and RNA catalysts, an era commonly referred to as the "RNA world".[1,2] RNA-based life would have required substantial amounts of the building blocks of RNA, such as the sugar ribose. The formation of ribose and other pentoses from simple precursors involves a substrate-specific cross-aldol reaction of glyceraldehyde and glycolaldehyde.[3] Without enzymatic control, however, a network of competing pathways, including self-aldol, isomerization, and retro-aldol reactions, gives rise to a complex mixture of compounds that includes only a small amount of pentoses and challenges even the most advanced analytical techniques.[4] While several laboratories have reported conditions that can lead to an increased yield of ribose and other pentoses from simple aldehydes,[5–9] a chemical system that allows direct and systematic investigation of the reaction of glyceraldehyde and glycolaldehyde has remained elusive. Such a system would enable examination of the kinetic and mechanistic features of this reaction, setting the stage for the development of RNA catalysts that can be used to synthesize ribose, analogous to those that may have existed in an RNA world.

The present study demonstrates a DNA-templated model system that allows the selective formation of pentoses by a cross-aldol reaction of glyceraldehyde and glycolaldehyde. DNA-templated chemistry parallels nature's approach to selectivity by exploiting the molecular recognition properties of biological macromolecules to direct the reactivity of small molecules.[10] The reactivity of the aldehydes was controlled by linking them to oligonucleotide "handles", which were recognized by Watson–Crick pairing to a complementary

[*] Dr. M. Oberhuber,[+] Prof. Dr. G. F. Joyce
Departments of Chemistry and Molecular Biology and
The Skaggs Institute for Chemical Biology
The Scripps Research Institute
La Jolla, CA 92037 (USA)
Fax: (+1) 858-784-2943
E-mail: gjoyce@scripps.edu

[+] Current address:
Institute of Organic Chemistry and
Center for Molecular Biosciences
Leopold-Franzens University of Innsbruck
6020 Innsbruck (Austria)

[**] This work was supported by NASA and The Skaggs Institute for Chemical Biology at The Scripps Research Institute. M.O. was supported by postdoctoral fellowship J2296 from the Austrian National Science Fund (FWF) and the Max Kade Foundation.

Supporting information for this article is available on the WWW under http://www.angewandte.org or from the author.

WILEY InterScience DISCOVER SOMETHING GREAT
© 2005 Wiley-VCH Verlag GmbH & Co. KGaA, Weinheim

DNA template. These handles also made it possible to use sensitive detection methods available for nucleic acids to overcome the analytical challenges. Each aldehyde was linked to a different synthetic oligonucleotide (Scheme 1), allowing

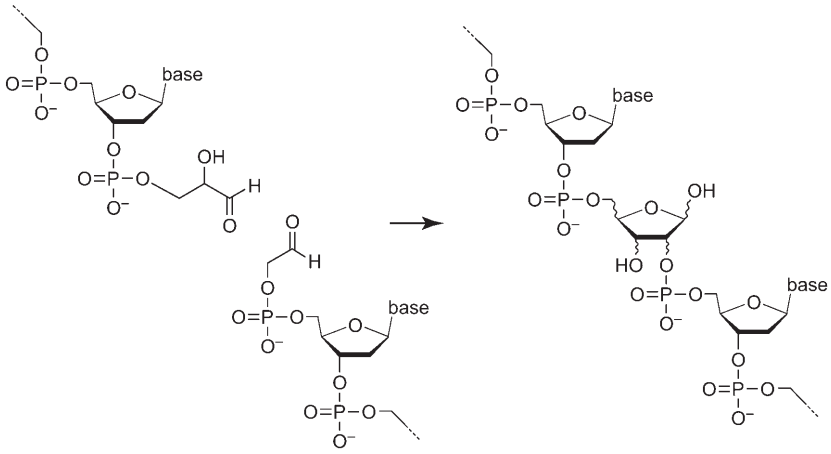

Scheme 1.

the two to be co-aligned in the desired orientation through binding to a common template. The template was designed to promote the cross-aldol reaction by increasing the effective concentration of the two juxtaposed aldehydes, at the same time suppressing undesired reactions. Over the past few years DNA templates have been shown to promote a remarkably diverse set of organic reactions.[10,11] A DNA-directed aldol reaction, however, has not yet been described.

A new class of oligonucleotide–aldehyde conjugates was synthesized by using a phosphoramidite-based approach. The synthetic strategy involved vicinal diols as aldehyde synthons, which were incorporated during solid-phase DNA synthesis and converted to the corresponding aldehyde through periodate oxidation.[12] The 5′-glyceryl-DNA conjugate was synthesized in the 5′-to-3′ direction, purified by denaturing polyacrylamide gel electrophoresis (PAGE), and oxidized to the glycolaldehyde-bearing DNA (**2-DNA$_{12}$**; Scheme 2, top).

The design of the diol precursor for the glyceraldehyde-DNA conjugate (**DNA$_9$-3**) involved a photolabile protection scheme to prevent formation of glycolaldehyde. The hydroxy group vicinal to the phosphate was protected with an *o*-NO_2-benzyl moiety, which is stable under the conditions of DNA synthesis and deprotection, and can be cleaved by irradiation with UV light following periodate oxidation.[13] The diol precursor for **DNA$_9$-3** was prepared by standard DNA synthesis using a glyceraldehyde synthon as the 3′-terminal residue. The precursor was purified by PAGE and converted to the corresponding aldehyde by oxidation and photolysis (Scheme 2, bottom). The identities of **DNA$_9$-3** and **2-DNA$_{12}$** were verified by matrix-assisted laser desorption time-of-flight (MALDI-TOF) mass spectrometry (see Supporting Information) and by DNA-templated reductive amination[11] (data not shown).

By employing the same approach, longer versions of the two DNA–aldehyde conjugates were synthesized and used to explore different formats for the template-directed reaction. The compound 5′-T_{15}GTGAAATGC-3′-glyceraldehyde (**DNA$_{24}$-3**) was efficiently [5′-^{32}P]-labeled by using [γ-^{32}P]-ATP and T4 polynucleotide kinase. It was mixed with an excess of glycolaldehyde-5′-CGATACTGATAGGACGAAGAGAT-GGCACC-3′ (**2-DNA$_{29}$**) and a complementary template that contained an unpaired thymidylate opposite the site of the juxtaposed aldehydes. Following incubation at pH 8.5 and 23 °C, the reaction mixture was analyzed by PAGE, which demonstrated formation of products with the electrophoretic mobility expected for the pentose-linked DNA (**DNA$_{24}$-5-DNA$_{29}$**) (Figure 1; lanes 2, 3, and M). There was no detectable reaction in the absence of the template or in the presence of a mismatched template (Figure 1; lanes 6 and 7, respectively). If an analogue of **DNA$_{24}$-3** was used that contained glycerol instead of glyceraldehyde, no product formation was observed (Figure 1; lane 8). Similarly, replacing **2-DNA$_{29}$** by

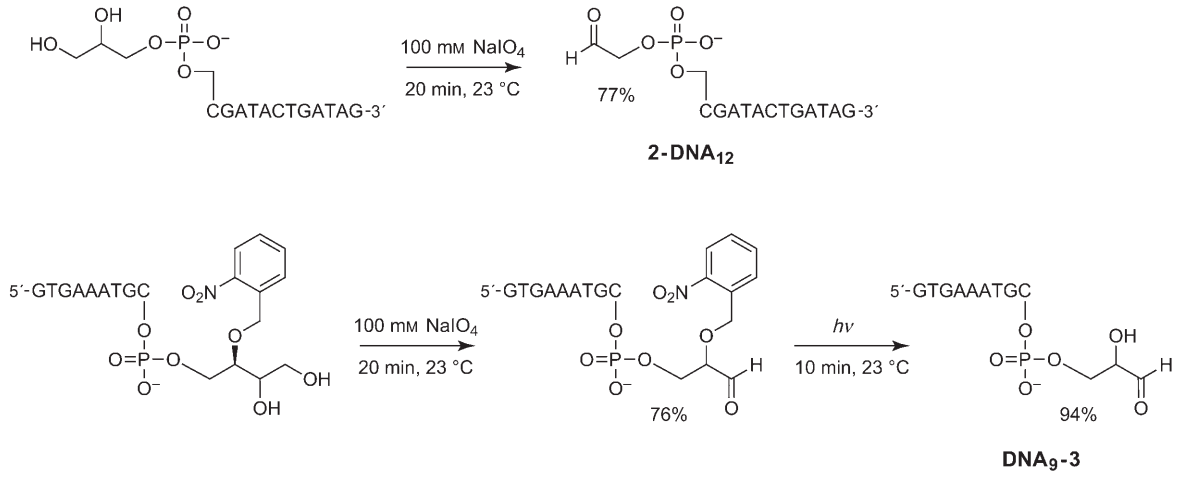

Scheme 2.

 © 2005 Wiley-VCH Verlag GmbH & Co. KGaA, Weinheim

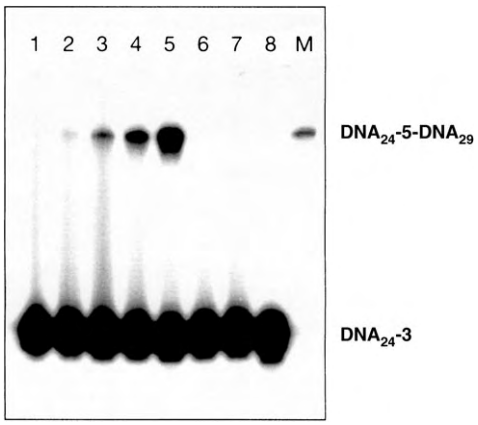

Figure 1. DNA-templated cross-aldol reaction. Reaction of 5 nM labeled **DNA_{24}-3** and 2 μM unlabeled **2-DNA_{29}** in the presence of 1 μM complementary template (lanes 2–5), no template (lane 6), or 1 μM mismatched template (lane 7). Lanes 2 and 3 correspond to reaction in the absence of L-Lys for 6 and 48 h, respectively; lanes 4 and 5 correspond to reaction in the presence of 50 mM L-Lys for 6 and 48 h, respectively; lanes 6 and 7 correspond to reaction in the absence of L-Lys for 48 h. Lane 1 contains unreacted labeled **DNA_{24}-3**; lane 8 corresponds to a control reaction (48 h) employing a labeled DNA-glycerol conjugate instead of **DNA_{24}-3**, and lane M contains a marker of the same composition as **DNA_{24}-5-DNA_{29}** but with thymidine in place of the newly-formed pentose. All reaction mixtures contained 10 mM $MgCl_2$, 100 mM NaCl, and 50 mM TAPS (pH 8.5). Reaction products were separated by denaturing 20% PAGE, an autoradiogram of which is shown.

the corresponding glycerol-containing DNA eliminated the observed reaction (data not shown).

In order to carry out mass-spectrometric analysis of the products, unlabeled **DNA_9-3** was incubated with a slight excess of **2-DNA_{12}** in the presence of a complementary template. MALDI-TOF mass spectrometry of the PAGE-purified products gave a mass consistent with the formation of a pentose linking the two substrate oligonucleotides (see Supporting Information). The **DNA_{24}-5-DNA_{29}** products were prepared similarly and analyzed by a primer extension reaction, which employed a 17 mer oligonucleotide that hybridized to the 3′ end of the product molecules and was extended by reverse transcriptase. A minor pause with substantial read-through was seen at the aldol junction (see Supporting Information), similar to the behavior of an abasic site,[14] and excluding the possibility of an unusual connectivity such as would result from the reaction of an aldehyde with a nucleobase. It was not possible to obtain sufficient material to determine the relative amounts of the four pentose sugars and their respective enantiomers. The 2′,5′-phosphodiester linkage that is formed at the aldol junction (Scheme 1) allows read-through by reverse transcriptase,[15] but the minor pause that occurs at the junction cannot be taken to indicate the presence of any particular sugar.

The rate of the DNA-templated aldol reaction was measured as a function of pH (Figure 2). Consistent with a base-catalyzed reaction, the observed pseudo-first-order rate constant increased at alkaline pH, but was nearly unchanged at neutral to acidic pH. At elevated pH and temperatures a degradation product of **DNA_{24}-3** also was detected, presumably arising from elimination of glyceraldehyde-2,3-cyclic-phosphate (data not shown). Mildly alkaline pH (8.5) and ambient temperature (23 °C) were chosen as the standard reaction conditions, for which the observed rate of reaction was about 4×10^{-6} min^{-1}.

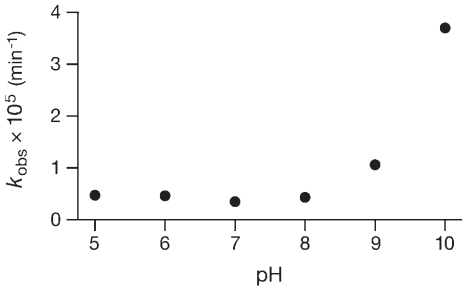

Figure 2. pH dependence of the DNA-templated aldol reaction. Reaction conditions were as described in the legend to Figure 1, except for differences in pH.

In view of the well-established role of amines as organocatalysts,[16] and with regard to their potential role as cofactors in RNA catalysis, the DNA-templated aldol reaction was studied in the presence of various amines and amino acids. A family of biological aldolases, as well as catalytic antibody aldolases that have been reported, utilize a lysine residue to catalyze aldol reactions via a Schiff-base intermediate.[17,18] This provided the impetus for experiments identifying L-Lys as a potential catalyst for the DNA-templated aldol reaction (Figure 1; lanes 4 and 5). Elevated concentrations of L-Lys accelerated the reaction up to 20-fold, but concentrations below 10 mM had no significant effect (Figure 3), suggesting a slow second-order rate of formation of the Schiff base.

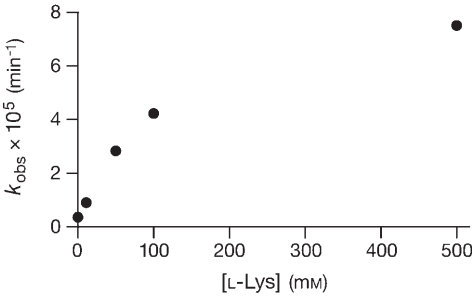

Figure 3. DNA-templated aldol reaction in the presence of varying concentrations of L-Lys. Reaction conditions were as described in the legend to Figure 1, except for the addition of 0–500 mM L-Lys.

The dipeptide Lys–Lys was similarly effective as L-Lys, but L-Pro, a well-known catalyst of aldol reactions in organic solvents,[16] was ineffective in the DNA-templated format, even at high concentrations (Figure 4). The aldol reaction also was accelerated by small aliphatic diamines, especially putrescine (Figure 4), suggesting the need for an extended aliphatic primary amine. As a negative control, the reaction was analyzed in the presence of 1M NaCl, excluding the possibility that the enhanced rate with certain amines was due to the high ionic strength of these solutions.

 © 2005 Wiley-VCH Verlag GmbH & Co. KGaA, Weinheim

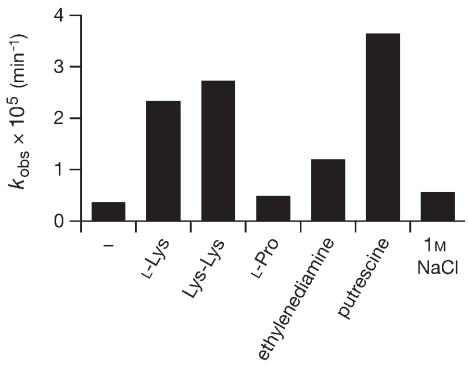

Figure 4. DNA-templated aldol reaction in the presence of various amine-containing cofactors. Reaction conditions were as described in the legend to Figure 1, except for the addition of no cofactor (lane –), 50 mM cofactor (indicated), or 1 M NaCl.

The influence of the template architecture on the aldol reaction was examined by replacing the unpaired thymidylate opposite the aldol junction with a hexaethylene glycol linker, or by placing the two aldehydes at the same end of hybridized DNA strands. Consistent with the reduced frequency of substrate encounter in these formats, the reaction rate decreased by about threefold compared to the standard format, but was similarly accelerated by the addition of 50 mM L-Lys. A variety of other template architectures were tested, but none resulted in an increased rate of reaction compared to the standard format.

In summary, this first reported example of a DNA-templated aldol reaction demonstrates how nucleic acids can selectively promote the cross-aldol reaction of glyceraldehyde and glycolaldehyde. This model system allows kinetic and mechanistic investigation of the template-directed formation of pentoses, relevant to the corresponding biosynthetic reaction in an RNA world. Aliphatic amines, such as L-Lys, were found to accelerate the reaction, emphasizing their role as potential cofactors in the RNA-catalyzed synthesis of ribose. The observed requirement for high amine concentrations may reflect the slow formation of a Schiff-base intermediate, indicating that precise positioning of the cofactor in the active site will be a crucial feature of enzymatic catalysis. A recent report by Famulok and colleagues[19] described the first example of an aldolase ribozyme, obtained by in vitro evolution, which catalyzes the reaction of a levulinic acid modified RNA and benzaldehyde-4-carboxamide. The ribozyme employs a Zn^{2+} cofactor, analogous to biological class II aldolases.[20] That work, together with the present study, suggest the plausibility of evolving aldolase ribozymes that catalyze the biosynthesis of ribose.

Experimental Section

Oligonucleotides were prepared by using a PerSeptive Biosystems Expedite 8909 Nucleic Acid Synthesis System, employing standard methods. Diol-containing oligonucleotides were synthesized by using either 3′-glyceryl CPG (Glen Research) or a solid-supported glyceraldehyde synthon (see Supporting Information). Oligonucleotides were cleaved from the solid support and deprotected by using either concentrated aqueous NH_3 at 55 °C for 2–20 h for standard DNA or 10 M $MeNH_2$ in H_2O:EtOH (1:1 v/v) at 23 °C for 14–20 h for diol-bearing DNA. All oligonucleotides were purified by PAGE. Diol precursor oligonucleotides were adsorbed on a Sep-Pak C18 resin (Waters) and oxidized with 100 mM $NaIO_4$ (ca. 3 mL), which was allowed to drip slowly through the cartridge at 23 °C over 15–20 min. After washing with H_2O (5 mL), then 10 % (v/v) MeOH (1.5 mL), the aldehyde-bearing DNA was eluted with 50 % (v/v) acetonitrile (5 mL). Photolysis was carried out at 23 °C for 10–15 min using a 100-W long-wavelength UV lamp.

DNA-templated reactions were carried out in the presence of 10 mM $MgCl_2$, 100 mM NaCl, and 50 mM 3-[(2-hydroxy-1,1-bis(hydroxymethyl)ethyl)amino]propanesulfonic acid (TAPS, pH 8.5) at 23 °C, unless otherwise stated. Aliquots were taken at 4–10 different time points and stored at −80 °C in the presence of 90 mM Tris-borate (pH 8.0), 20 mM Na_2EDTA, 10 % (w/v) sucrose, and 8 M urea. The samples were analyzed by denaturing PAGE, using a Molecular Dynamics PhosphorImager to quantify the radiolabeled material.

Supporting Information describes additional experimental procedures, including synthesis of the solid-supported glyceraldehyde synthon (Scheme S1), radiolabeling of oligonucleotides, mass-spectrometric analysis of the substrates and products of the DNA-templated aldol reaction (Figure S1), and primer extension analysis of the pentose-linked DNA (Figure S2).

Received: September 23, 2005
Published online: October 20, 2005

Keywords: enzyme models · nucleic acids · ribose · ribozymes · template synthesis

[1] W. Gilbert, *Nature* **1986**, *319*, 618.
[2] G. F. Joyce, *Nature* **2002**, *418*, 214.
[3] R. Breslow, *Tetrahedron Lett.* **1959**, 22.
[4] P. Decker, H. Schweer, R. Pohlman, *J. Chromatogr.* **1982**, *244*, 281.
[5] D. Müller, S. Pitsch, A. Kittaka, E. Wagner, C. E. Wintner, A. Eschenmoser, *Helv. Chim. Acta* **1990**, *73*, 1410.
[6] S. Pitsch, A. Eschenmoser, B. Gedulin, S. Hui, G. Arrhenius, *Origins Life Evol. Biosphere* **1995**, *24*, 297.
[7] A. Ricardo, M. A. Carrigan, A. N. Olcott, S. A. Benner, *Science* **2004**, *303*, 196.
[8] G. Springsteen, G. F. Joyce, *J. Am. Chem. Soc.* **2004**, *126*, 9578.
[9] J. Kofoed, J.-L. Reymond, T. Darbre, *Org. Biomol. Chem.* **2005**, *3*, 1850.
[10] X. Li, D. R. Liu, *Angew. Chem.* **2004**, *116*, 4956; *Angew. Chem. Int. Ed.* **2004**, *43*, 4848.
[11] Z. J. Gartner, M. W. Kanan, D. R. Liu, *Angew. Chem.* **2002**, *114*, 1874; *Angew. Chem. Int. Ed.* **2002**, *41*, 1796.
[12] H. Urata, M. Akagi, *Tetrahedron Lett.* **1993**, *34*, 4015.
[13] T. Tanaka, M. Orita, S. Uesugi, M. Ikehara, *Tetrahedron* **1988**, *44*, 4331.
[14] M. Takeshita, C.-N. Chang, F. Johnson, S. Will, A. P. Grollman, *J. Biol. Chem.* **1987**, *262*, 10171.
[15] J. R. Lorsch, D. P. Bartel, J. W. Szostak, *Nucleic Acids Res.* **1995**, *23*, 2811.
[16] J. Seayad, B. List, *Org. Biomol. Chem.* **2005**, *3*, 719.
[17] B. L. Horecker, O. Tsolas, C. Y. Lai, *Enzymes 3rd ed.* **1972**, *7*, 213.
[18] J. Wagner, R. A. Lerner, C. F. Barbas, *Science* **1995**, *270*, 1797.
[19] S. Fusz, A. Eisenführ, S. G. Srivatsan, A. Heckel, M. Famulok, *Chem. Biol.* **2005**, *12*, 941.
[20] W.-D. Fessner, A. Schneider, H. Held, G. Sinerius, C. Walter, M. Hixon, J. V. Schloss, *Angew. Chem.* **1996**, *108*, 2366; *Angew. Chem. Int. Ed. Engl.* **1996**, *35*, 2219.

 © 2005 Wiley-VCH Verlag GmbH & Co. KGaA, Weinheim

Ion Selectivity

DOI: 10.1002/anie.200501625

A Highly Active Anion-Selective Aminocyclodextrin Ion Channel**

*Nandita Madhavan, Erin C. Robert, and Mary S. Gin**

Ion-channel proteins are molecular devices found in nature that mediate the transport of charged species across cell membranes. Various functions in the human body, such as nerve and muscle excitation, hormonal secretion, cell proliferation, and homeostasis, are regulated by ion channels.[1] The efficient functioning of ion-transport machinery in nature has led to considerable interest in understanding the mechanisms by which these proteins mediate selective, regulated transmembrane ion transport.[2] Furthermore, the ability of ion channels to effect electrical signaling under aqueous saline conditions has inspired their use as biosensors,[3] therapeutic agents,[4] and other useful materials.[5] Despite the potential utility of controlled ion transport, the relative instability of proteins in vitro will likely prohibit their use in commercial applications. Advances in the synthesis of more robust artificial channels provide a viable solution to the problem of ion-channel stability, thus enabling the construction of biomimetic signaling components.

An important feature that dictates the physiological function of ion channels is ion selectivity. Ion channels can be classified as cation or anion selective on the basis of the differential permeability of ions through the channel pore. Ion channels selective for cations over anions have been widely studied, and several synthetic analogues that use β-cyclodextrin,[6] crown ethers,[7] peptides,[8] and calixarenes[9] are among the molecular scaffolds that have been developed to date. In contrast, there have been far fewer examples of synthetic channels that are selective for anions over cations. Peptidic synthetic channels developed by Gokel[10] and Matile[11] and sterol mimics developed by Regen[12] have been shown to preferentially transport anions over cations upon self-assembly within phospholipid membranes. Reported herein is a highly active, monomeric cyclodextrin-based ion channel (**1**, Figure 1) that displays not only selectivity for anions over cations but also discriminates among halide anions ($I^- > Br^- > Cl^-$).

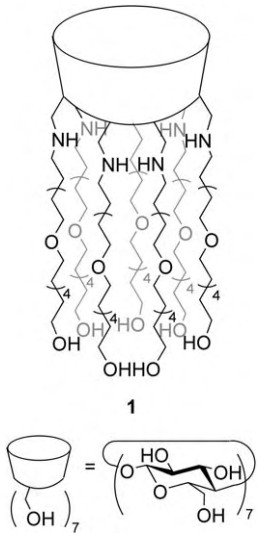

Figure 1. Structure of aminocyclodextrin channel **1**.

Channel **1** comprises a β-cyclodextrin head group with oligoether chains attached to the primary face of the cyclodextrin through amine linkages. The chains are sufficiently hydrophobic to promote insertion into a phospholipid bilayer membrane[13] and possess a length that should allow the channel to span the entire membrane.[14] Channel **1** was synthesized (Scheme 1) from pentabutylene glycol (**2**), which is readily accessible in five steps from commercially available 2,5-dimethoxytetrahydrofuran.[15,16] Conversion of **2** into the monotosylate **3** was achieved using *p*-toluenesulfonyl chloride (TsCl) and pyridine (pyr). Monotosylate **3** was heated with sodium azide at 80 °C to give the oligoether azide, which was reduced to the corresponding amine **4** using triphenylphosphine and water. N-Alkylation of neat amine **4** with the activated heptaiodocyclodextrin **5**[17] afforded channel **1**.

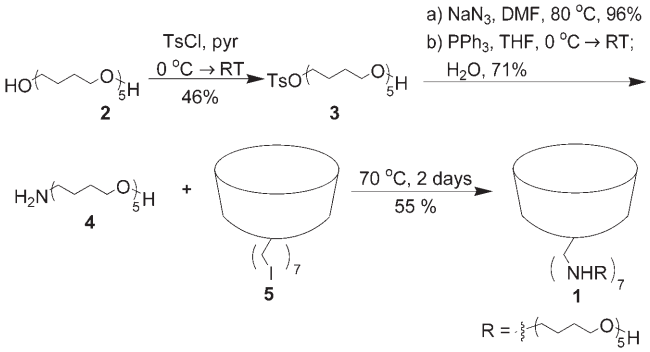

Scheme 1. Synthesis of channel **1**. DMF = dimethylformamide.

[*] N. Madhavan, E. C. Robert, Prof. M. S. Gin
Department of Chemistry
University of Illinois
Urbana, IL 61801 (USA)
Fax: (+1) 217-244-8024
E-mail: mgin@scs.uiuc.edu

[**] This research was supported by the National Science Foundation (CAREER CHE 01-34792). We thank Lisa E. Choi for early efforts toward the synthesis of channel **1**, Professor Thomas M. Fyles for helpful comments, and Professor Steven C. Zimmerman for the use of his dynamic light scattering instrument. Some of the experiments reported herein were performed at the Laboratory for Fluorescence Dynamics (LFD) at the University of Illinois at Urbana-Champaign (UIUC). The LFD is supported jointly by the National Center for Research Resources of the National Institutes of Health (PHS 5 P41-RR003155) and UIUC. Transmission electron microscopy (TEM) images were obtained at the Center for Microanalysis of Materials, University of Illinois, which is partially supported by the US Department of Energy under grant DEFG02-91-ER45439.

Supporting information for this article is available on the WWW under http://www.angewandte.org or from the author.

© 2005 Wiley-VCH Verlag GmbH & Co. KGaA, Weinheim

Initial ion-channel activity was assessed by using ^{23}Na NMR spectroscopy to study Na^+ transport across vesicle membranes (Figure 2a),[18] on the basis that other cyclodextrin-based ion channels were cation selective.[6] In the NMR experiment, a Dy^{3+} complex was used as a shift reagent to differentiate the extravesicular Na^+ ions from the internal Na^+ ions.[19] Ion transport can be visualized and quantified by the line broadening observed for the Na^+ resonances because of the exchange of the internal and external Na^+ ions. The rate of exchange is directly proportional to the line broadening observed for the internal Na^+ signal [Eq. (1)], in which ν and

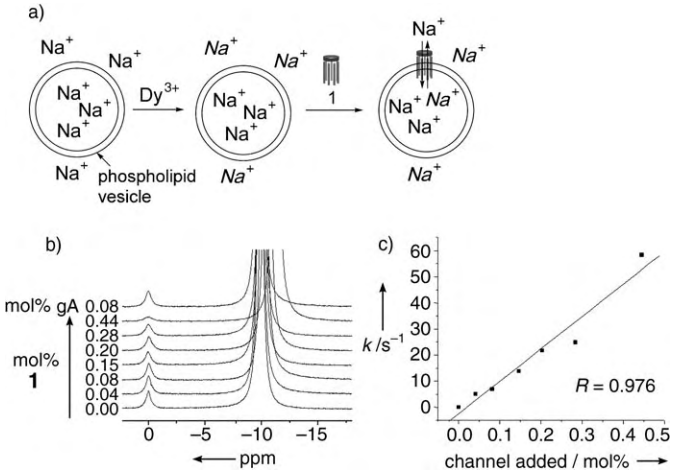

Figure 2. a) Schematic representation of the ^{23}Na NMR spectroscopic experiment (the italicized Na^+ ions represent external ions with shifted NMR peaks owing to the presence of the Dy^{3+} shift reagent). b) Stacked NMR plots that indicate line broadening observed with an increase in the channel concentration (mol% relative to phospholipid); as a comparison gramicidin A (gA) was also added. c) Linear correlation between the Na^+ exchange rates and the concentration of channel added, thus indicating that channel **1** is monomolecular.

$$k = 1/\tau = \pi(\nu - \nu_0) \quad (1)$$

ν_0 are the line widths in the presence and absence of the exchange, respectively. For the ^{23}Na NMR experiment, large unilamellar vesicles of egg-yolk phosphatidylcholine (EYPC) lipids were prepared by multiple extrusions through 0.4-μm polycarbonate membranes.[16] The vesicles were determined to be approximately 200 nm in diameter using dynamic light scattering. Addition of the $DyPPi_3$ shift reagent to the vesicle suspension followed by a solution of **1** led to significant line broadening of the internal Na^+ peak (Figure 2b), thus indicating the channel-mediated exchange of Na^+ ions across the vesicle membrane.[20] The dependence of the observed rate of Na^+ exchange (k_{obs}) on the concentration of **1** can be used to determine the aggregation state of the channel, or the number of **1** monomers that form the active structure [Eq. (2)].[21] A linear correlation ($n = 1$) between the

$$k_{obs} \propto [\text{channel}]^n \quad (2)$$

Na^+ exchange rate and the concentration of the channel indicated that the active structure formed from **1** was monomolecular (Figure 2c). Also, a comparison of the Na^+ transport rate through **1** with that for the natural ion-channel gramicidin A revealed that **1** was 36% as active as gramicidin A, thus indicating that **1** formed a highly active monomolecular ion channel.[22] This result is particularly noteworthy in light of the net charge of **1**. The multiple positive charges associated with previously studied hepta-amino, -hydroxyethylamino, and -alkylamino cyclodextrin derivatives at physiological pH values have been widely exploited for binding negatively charged phosphates to the cyclodextrin cavity.[23] In view of the similar charge densities imparted by the ammonium groups of **1** to the channel pore, it is remarkable that sodium transport is observed through the channel.

To expand the range of ions that could be assessed for transport activity, transmembrane ion-transport properties of **1** were also studied with fluorescence spectroscopy, in which the fluorescence of the pH-sensitive dye 8-hydroxypyrene-1,3,6-trisulfonic acid trisodium salt (HPTS) was used as the probe.[24] In the fluorescence assay, the HPTS dye was encapsulated inside small unilamellar vesicles (Figure 3a) approximately 50–80 nm in diameter, which were prepared by using the detergent dialysis method.[16] A pH gradient of 0.6 units was introduced by addition of a solution of NaOH (2N) to the vesicle solution, which also introduced a Na^+ concentration gradient. A solution of **1** was added to the vesicles and the activity of the channel was gauged by monitoring the change in the fluorescence intensity of the deprotonated dye. Finally, gramicidin A was added to the

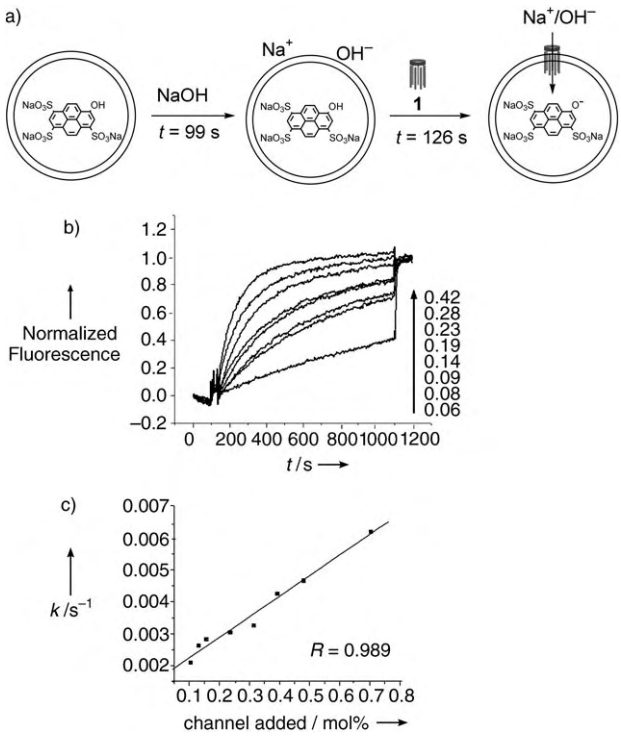

Figure 3. a) Schematic representation of the fluorescence experiment. b) Change in the fluorescence intensity of the deprotonated dye with a change in the concentration of the channel (mol%). c) Linear correlation between the rate of transport and the concentration of the channel.

 © 2005 Wiley-VCH Verlag GmbH & Co. KGaA, Weinheim

vesicles to ensure complete equilibration of the HPTS dye between the protonated and deprotonated states. Upon addition of a solution of **1** to the vesicles, an increase in the concentration of the deprotonated dye was observed, thus indicating a Na^+/H^+ antiport or Na^+/OH^- symport through **1**. Moreover, variation in the concentration of **1** induced a corresponding change in the ion-transport rate (Figure 3b). A linear correlation was observed upon plotting the rates for ion transport against the amount of **1** added, thereby confirming that **1** indeed formed a monomolecular ion channel (Figure 3c).[25]

Having established that channel **1** mediates the rapid transport of Na^+ ions through a monomolecular pore, the fluorescence assay was used to probe its ion selectivity.[26] Cation selectivity was tested by repetition of the fluorescence experiment with different alkali hydroxides (Figure 4a). The differences in rate observed for the different cations (Li^+, Na^+, and K^+) were relatively small, which is characteristic of channels with little or no selectivity among cations. Anion selectivity was investigated by variation of the counteranion (Cl^-, Br^-, and I^-) for the Na^+ ion. In this case, a consistent difference in the fluorescence profile was observed that was dependant on the nature of the anion added (Figure 4b). In all cases, the fluorescence of the deprotonated dye decreased, which indicated either an X^-/H^+ symport or X^-/OH^- antiport through the channel. For NaBr and NaI, a rapid decrease in the fluorescence intensity indicative of X^- transport was followed by a steady increase to the fully equilibrated state, thus suggesting a slower rate of Na^+ influx. A gradual decrease in fluorescence intensity was observed for NaCl, thereby indicating comparable rates for Na^+ and Cl^- transport. The curves obtained for the NaX salts were fit to exponential equations to corroborate this hypothesis. The curves obtained with NaBr and NaCl were fit to Equation (3),

$$\text{Rate} = A + Be^{-k_1 t} - Ce^{-k_2 t} \quad (3)$$

in which k_1 and k_2 represent the competing rates for ion transport.[16] However, the curve for NaI was fit to Equation (4), in which an extra term was required because of the

$$\text{Rate} = A + Be^{-k_1 t} - Ce^{-k_2 t} + De^{-k_3 t} \quad (4)$$

significant rate of I^- transport through the lipid membrane (k_3).[27] In all cases, the second exponential terms bore negative coefficients consistent with an increase in fluorescence intensity, and the k_2 values were within the same range as the rates determined for the addition of NaOH. These data are indicative of a slower increase in fluorescence intensity because of Na^+ transport. The rates (k_1) that correspond to the rapid decrease in fluorescence intensity because of X^- transport were found to vary considerably depending on the nature of the anion. The k_1 value obtained for NaCl ($0.0097\ s^{-1}$) was comparable with the rate of Na^+ transport ($k_2 = 0.0097\ s^{-1}$), the k_1 value obtained for NaBr ($0.018\ s^{-1}$) was approximately 2.7 times faster than the rate of Na^+ transport ($k_2 = 0.0066\ s^{-1}$), and the k_1 value obtained for NaI ($0.071\ s^{-1}$) was found to be significantly higher than that obtained for Br^- transport (ca. 9.5 times faster than k_2 ($0.0075\ s^{-1}$)). In addition, the k_3 value obtained for NaI ($0.002\ s^{-1}$) matched well with the rate observed for the influx of I^- ions into vesicles without channels.[28] The necessity of including a third term for membrane-permeable I^- ions corroborates the assertion that anions do indeed travel through the pore formed by **1**. Only two terms would be necessary to fit the data if anion transport only occurred through the membrane in response to Na^+ transport through the channel.

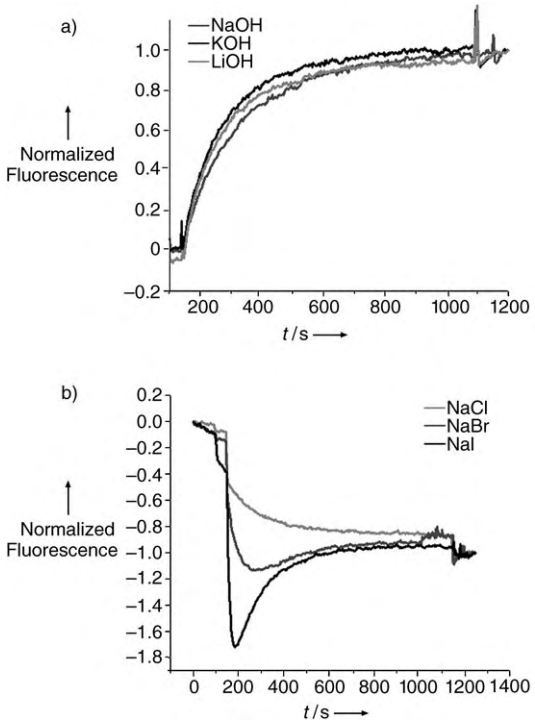

Figure 4. a) Fluorescence change of deprotonated HPTS for different cations (Li^+, Na^+, and K^+) upon addition of 1.1 mol% channel **1**. b) Fluorescence change of deprotonated HPTS for different anions (Cl^-, Br^-, and I^-) upon addition of 0.4 mol% channel **1**.

The role of electrostatics in ion selectivity has been observed with natural ion channels, wherein the charges of the amino acid residues at the pore dictate the preference of the channel for different ions.[29] Anion selective channels have a net positive charge owing to the presence of positively charged amino acids that line the pore of the channel. Channel **1** possesses a positive charge at the pore opening because of the basic amine groups at the chain-functionalized rim of the cyclodextrin. This positive charge likely leads to electrostatic interactions that favor the transport of anions over cations. The selectivity among the anions ($I^- > Br^- > Cl^-$) follows the Hofmeister series, in which various phenomena, such as protein precipitation, enzymatic activity, and polymer conformation, are influenced by the polarizability of the environmental anions.[30] The more polarizable I^- ion should face a lower activation barrier to entry into the hydrophobic interior of **1**, thus resulting in a faster rate of transport.[31]

In conclusion, the ability of aminocyclodextrin ion channel **1** to mediate transport of anions in preference to

 © 2005 Wiley-VCH Verlag GmbH & Co. KGaA, Weinheim

cations at rates that compare with, or even exceed, those of natural channel proteins is reported. The ability of this robust synthetic channel to effect conductance across a hydrophobic barrier is an important first step toward devices that take advantage of biomimetic electrical signaling under aqueous saline conditions. Investigations into the basis of anion selectivity, the range of ions that are permeable, and pH effects on ion-channel activity are currently underway.

Received: May 11, 2005
Revised: September 6, 2005
Published online: October 25, 2005

Keywords: anions · cyclodextrins · ion channels · nanostructures · sodium transport

[1] a) F. M. Ashcroft, *Ion Channels and Disease*, Academic Press, California, **2000**, pp. 1–2; b) B. Hille, *Ion Channels of Excitable Membranes*, 3rd ed., Sinauer, Sunderland, MA, **2001**, pp. 1–5.
[2] a) R. Dutzler, E. B. Campbell, R. MacKinnon, *Science* **2003**, *300*, 108–112; b) R. B. Bass, P. Strop, M. Barclay, D. C. Rees, *Science* **2002**, *298*, 1582–1587; c) D. A. Doyle, *Trends Neurosci.* **2004**, *27*, 298–302.
[3] a) S. Futaki, Y. Zhang, T. Kiwada, I. Nakase, T. Yagami, S. Oiki, Y. Sugiura, *Bioorg. Med. Chem.* **2004**, *12*, 1343–1350; b) M. Sugawara, A. Hirano, P. Bühlmann, Y. Umezawa, *Bull. Chem. Soc. Jpn.* **2002**, *75*, 187–201; c) H. Bayley, P. S. Cremer, *Nature* **2001**, *413*, 226–230; d) B. A. Cornell, V. L. B. Braach-Maksvytis, L. G. King, P. D. J. Osman, B. Raguse, L. Wieczorek, R. J. Pace, *Nature* **1997**, *387*, 580–583.
[4] a) S. Fernandez-Lopez, H.-S. Kim, E. C. Choi, M. Delgado, J. R. Granja, A. Khasanov, K. Kraehenbuehl, G. Long, D. A. Weinberger, K. M. Wilcoxen, M. R. Ghadiri, *Nature* **2001**, *412*, 452–455; b) E. A. Porter, X. Wang, H.-S. Lee, B. Weisblum, S. H. Gellman, *Nature* **2000**, *404*, 565.
[5] P. Kohli, M. Wirtz, C. R. Martin, *Electroanalysis* **2004**, *16*, 9–18.
[6] a) I. Tabushi, Y. Kuroda, K. Yokota, *Tetrahedron Lett.* **1982**, *23*, 4601–4604; b) M. J. Pregel, L. Jullien, J. Canceill, L. Lacombe, J.-M. Lehn, *J. Chem. Soc. Perkin Trans. 2* **1995**, 417–426.
[7] a) O. Murillo, I. Suzuki, E. Abel, C. L. Murray, E. S. Meadows, T. Jin, G. W. Gokel, *J. Am. Chem. Soc.* **1997**, *119*, 5540–5549; b) W. M. Leevy, M. E. Weber, P. H. Schlesinger, G. W. Gokel, *Chem. Commun.* **2005**, 89–91; c) T. M. Fyles, T. D. James, K. C. Kaye, *J. Am. Chem. Soc.* **1993**, *115*, 12315–12321.
[8] a) H. Ishida, Z. Qi, M. Sokabe, K. Donowaki, Y. Inoue, *J. Org. Chem.* **2001**, *66*, 2978–2989; b) T. D. Clark, L. K. Buehler, M. R. Ghadiri, *J. Am. Chem. Soc.* **1998**, *120*, 651–656.
[9] a) N. Yoshino, A. Satake, Y. Kobuke, *Angew. Chem.* **2001**, *113*, 471–473; *Angew. Chem. Int. Ed.* **2001**, *40*, 457–459; b) S. E. Matthews, P. Schmitt, V. Felix, M. G. B. Drew, P. D. Beer, *J. Am. Chem. Soc.* **2002**, *124*, 1341–1353.
[10] N. Djedovic, R. Ferdani, E. Harder, J. Pajewska, R. Pajewski, P. H. Schlesinger, G. W. Gokel, *Chem. Commun.* **2003**, 2862–2863.
[11] N. Sakai, D. Houdebert, S. Matile, *Chem. Eur. J.* **2003**, *9*, 223–232.
[12] G. Deng, T. Dewa, S. L. Regen, *J. Am. Chem. Soc.* **1996**, *118*, 8975–8976.
[13] Y. Kobuke, K. Ueda, M. Sokabe, *J. Am. Chem. Soc.* **1992**, *114*, 7618–7622.
[14] Pentabutylene glycol (**2**) should be approximately 33 Å based on X-ray diffraction data obtained for the analogous tributylene glycol, see: A. D. Bedells, C. Booth, *Makromol. Chem.* **1991**, *192*, 2099–2110; in combination with the aminocyclodextrin, the channel should be long enough to span a typical 35–40-Å phospholipid membrane.
[15] E. C. Knuf, J.-K. Jiang, M. S. Gin, *J. Org. Chem.* **2003**, *68*, 9166–9169.
[16] For complete experimental details, see the Supporting Information.
[17] P. R. Ashton, R. Königer, J. F. Stoddart, D. Alker, V. D. Harding, *J. Org. Chem.* **1996**, *61*, 903–908.
[18] a) F. G. Riddell, M. K. Hayer, *Biochim. Biophys. Acta* **1985**, *817*, 313–317; b) C. G. Espínola, M. Delgado, J. D. Martín, *Isr. J. Chem.* **2000**, *40*, 279–288; c) O. Murillo, S. Watanabe, A. Nakano, G. W. Gokel, *J. Am. Chem. Soc.* **1995**, *117*, 7665–7679.
[19] R. K. Gupta, P. Gupta, *J. Magn. Reson.* **1982**, *47*, 344–350.
[20] The concentration of the channel in the vesicles is reported as mol % (with respect to the lipid); the lipid content was estimated by using a modification of the Bartlett assay (details in the Supporting Information).
[21] M. Merritt, M. Lanier, G. Deng, S. L. Regen, *J. Am. Chem. Soc.* **1998**, *120*, 8494–8501.
[22] The activity relative to gramicidin A was gauged using *k* values obtained for 0.078 mol % of gramicidin A and 0.04 mol % of **1** as gramicidin A forms bimolecular ion channels.
[23] a) F. Hacket, S. Simova, H.-J. Schneider, *J. Phys. Org. Chem.* **2001**, *14*, 159–170; b) M. Ghosh, R. Zhang, R. G. Lawler, C. T. Seto, *J. Org. Chem.* **2000**, *65*, 735–741; c) D. Vizitiu, G. R. J. Thatcher, *J. Org. Chem.* **1999**, *64*, 6235–6238; d) A. V. Eliseev, H.-J. Schneider, *J. Am. Chem. Soc.* **1994**, *116*, 6081–6088.
[24] a) K. Kano, J. H. Fendler, *Biochim. Biophys. Acta* **1978**, *509*, 289–299; b) N. R. Clement, J. M. Gould, *Biochemistry* **1981**, *20*, 1534–1538.
[25] Rates were obtained by fitting the curves to a first-order exponential decay equation with the Origin 6.1 software.
[26] S. C. Hartsel, S. K. Benz, R. P. Peterson, B. S. Whyte, *Biochemistry* **1991**, *30*, 77–82.
[27] A lower channel concentration (0.3 mol %) was used in this case to obtain a curve amenable to fitting.
[28] A similar trend was observed with melittin, strongly supporting the conclusion that ion channel **1** is anion selective.[16]
[29] A. Keramidas, A. J. Moorhouse, P. R. Schofield, P. H. Barry, *Prog. Biophys. Mol. Biol.* **2004**, *86*, 161–204.
[30] a) M. C. Gurau, S.-M. Lim, E. T. Castellana, F. Albertorio, S. Kataoka, P. S. Cremer, *J. Am. Chem. Soc.* **2004**, *126*, 10522–10523; b) J. N. Sachs, T. B. Woolf, *J. Am. Chem. Soc.* **2003**, *125*, 8742–8743.
[31] Z. Qi, M. Sokabe, K. Donowaki, H. Ishida, *Biophys. J.* **1999**, *76*, 631–641.

 © 2005 Wiley-VCH Verlag GmbH & Co. KGaA, Weinheim

Heterogeneous Catalysis

DOI: 10.1002/anie.200502049

"Hydrogen-Catalyzed" Dehydrogenation: A Supercritical Conundrum**

Jason R. Hyde, Ben Walsh, and Martyn Poliakoff**

In recent years there has been increasing interest in organic reactions in supercritical carbon dioxide ($scCO_2$). These reactions have included Friedel–Crafts alkylations,[1–4] hydroformylation,[5–9] oxidation,[10–15] etherification,[16–18] and especially hydrogenation.[19–24] Apart from the environmental acceptability, the attractions of $scCO_2$ for hydrogenation are improved mass transport, ease of continuous operation, and potentially improved selectivity.[25] Much of this work has involved continuous reactors, which simplify scale-up. However, we show herein, that these reactors can produce apparently misleading results which, when correctly interpreted, can open up new routes to compounds which are difficult to synthesize otherwise.

The starting point for this paper was a report[26] of the attempted selective hydrogenation of 4-vinylcyclohex-1-ene (**V**; Scheme 1), in a small-scale (5 mL) continuous reactor. Unexpectedly, this approach resulted in the formation of ethyl benzene (**B**; which is a dehydrogenation product) even in the presence of a large excess of H_2 and at temperatures apparently as low as 40 °C. This report was significant firstly because the dehydrogenation of **V** is industrially important[27–31] and secondly because the reactor design is one which is very widely used for supercritical chemistry.

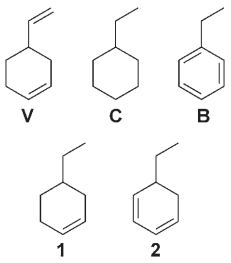

Scheme 1. Structures of ethyl cyclohexane (**C**) and ethyl benzene (**B**) formed during the dehydrogenation of 1-vinyl cyclohex-4-ene (**V**); **1** and **2** are the intermediates detected in the course of this reaction and were identified by NMR spectroscopy (see Supporting Information).

The dehydrogenation of cyclohexyl compounds to the corresponding benzene derivatives is an attractive route to aromatic compounds from cheap, plentiful biologically derived feedstocks. In batch reactors, this appears to be an overall disproportionation reaction, producing two mole of **B** for each mole of **C**. So, a surprising aspect of the reported dehydrogenation of **V** in $scCO_2$ was that **C** was not observed, making a simple disproportionation unlikely. The results presented herein provide an explanation of this conundrum and include the identification of two previously unsuspected intermediates, **1** and **2** in Scheme 1.

Initially, we investigated the effect of passing **V** + $scCO_2$ through the reactor in the absence of H_2. Our automated reactor (Figure 1)[16] was therefore programmed to ramp the temperature of the catalyst bed (Pd 2 %) from 80 °C to 200 °C over a period of 8 h at a constant pressure of 150 bar, analyzing the products by GLC every 5 minutes. Figure 2, shows that 1) in the absence of H_2, a reaction does occur; 2) this reaction yields both **B** and **C**, unlike the reaction in the presence of H_2 where **C** is not observed; 3) the ratio of **B** to **C** was found to be 2:1 close to the ratio expected for disproportionation;[27–31] 4) there are two additional products, **1** and **2**; 5) the reaction displays "light-off"[32] (i.e. there is an ignition over a small temperature interval of only 2–3 °C; similar behavior was also observed at 100, 200, and 250 bar) and 6) the reaction switches-off equally suddenly.

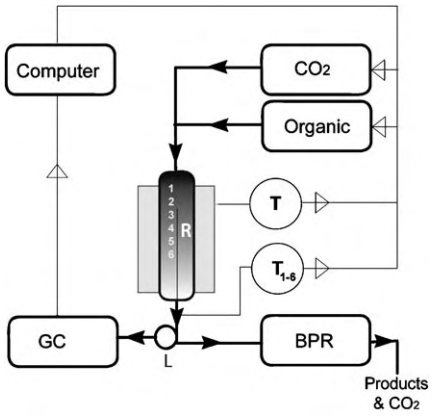

Figure 1. Schematic diagram of the automated apparatus. The organic substrates and CO_2 are delivered by HPLC pumps (Jasco PU–980 and CO_2–1580, respectively); system pressure in the reactor (R) is maintained by a Jasco Back Pressure Regulator (BPR) which also facilitates product separation. Samples of product are collected in-line by a sample loop (L; Valco/Vici) and injected into a gas chromatograph (GC) and the results are downloaded automatically to the computer. The high-pressure lines are designated by heavy filled arrowed lines, whilst data lines and the direction of data are depicted by light unfilled arrowed lines. T_{1-6} are optional thermocouples placed within the reactor.

Analysis of the product stream by off-line GC/MS showed that **2** had a parent ion with m/z 108, identical to that of **V**. By contrast **1**, had m/z 110, consistent with a partially hydrogenated product. Further experiments, detailed in the ESI, provided sufficient NMR spectroscopic data to identify the structures of **1** and **2** (see Scheme 1).

Estimating the residence times in these reactors is straightforward but slightly convoluted.[33] However, once the relationship between flow rate and residence time has

[*] Dr. J. R. Hyde, Dr. B. Walsh, Prof. M. Poliakoff
School of Chemistry
University of Nottingham
University Park, NG72RD (UK)
Fax: (+44) 115-913-058
E-mail: jason.hyde@nottingham.ac.uk
martyn.poliakoff@nottingham.ac.uk

[**] We thank the EPSRC for Grant GR/S87409 and for a CASE studentship to B.W. and Thomas Swan & Co. Ltd for support. We thank Dr. Pete Licence, Dr. Stephen Ross, and Messrs Mark Guyler, Peter Fields, Rich Wilson, David Litchfield, and James Warren for their help and support.

Supporting information for this article is available on the WWW under http://www.angewandte.org or from the author.

WILEY InterScience DISCOVER SOMETHING GREAT
© 2005 Wiley-VCH Verlag GmbH & Co. KGaA, Weinheim

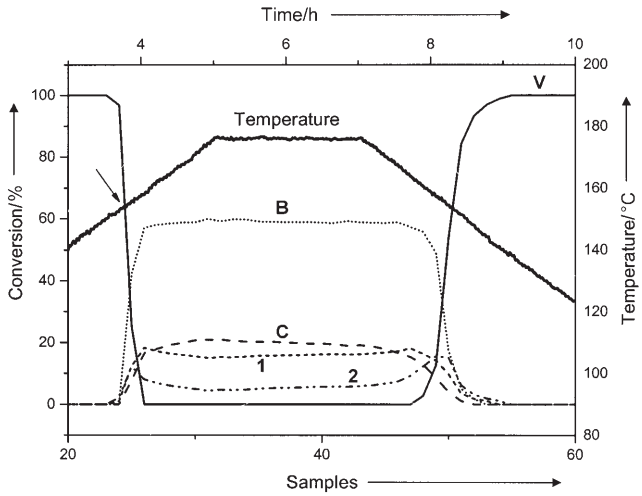

Figure 2. Plot of the product distribution observed whilst the catalyst bed is heated (bold line) between 140 and 180 °C. Note the arrowed auto-thermal ignition point at around 150 °C, and the presence of intermediates **1** and **2**. Flow rates: CO_2 1 mL min^{-1}, **V** 0.2 mL min^{-1}. The product composition was sampled every 15 minutes over the 10-hour period.

been established, it is relatively simple to investigate the variation of reaction products with residence time. Figure 3 shows that 1) reaction products are detected at residence times longer than 2 s; 2) the yields of **B** and **C** grow steadily with increasing residence time, confirming that **B** and **C** are final products; 3) the yields of **1** and **2** reach maxima and then decrease, suggesting that **1** and **2** are intermediates, and 4) the initial rates of formation of **2** and **B** are similar, suggesting that **2** is not an intermediate in the formation of **B**.

However, additional evidence for the relative positions of the different species in the reaction scheme can be obtained

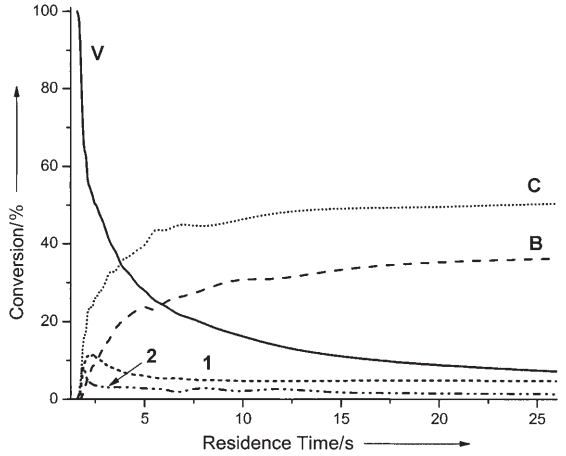

Figure 3. Plot of the product distribution for the dehydrogenation of **V** in the absence of H_2 as the residence time is varied. The traces are labeled **1**, **2**, **V**, **C**, **B** as in Scheme 1. In principle, such data can be used to model the kinetics of the reaction and hence to extract rate constants for the different stages. However, we are limited in this case by the fact that H_2 is a key component in the reaction but its concentration is unknown and indeed, will vary at different points in the reactor.

by analyzing the GC data with the new analytical technique, 2DCOR-GC,[1,34] which is an extension of the generalized correlation function to chromatographic data.[34] The 2DCOR-GC maps shown in Figure 4, are calculated from

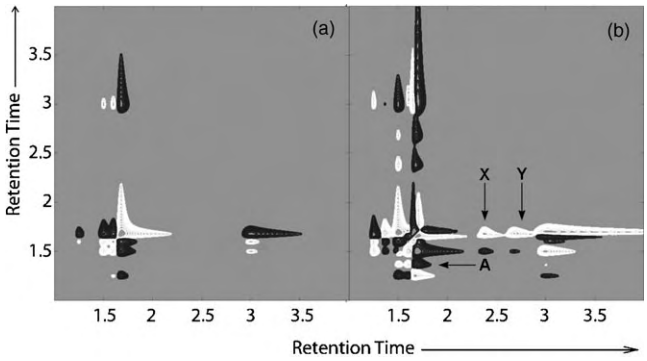

Figure 4. 2D-correlation analysis of the complete GC data from the experiment illustrated in Figure 3. This analysis is mathematically similar to the 2DCOS methodology for FTIR.[38] The principle of analysis for GC and FTIR are the same. The sequence in which the various compounds occur in response to a perturbation (in this case residence time) is obtained by comparing the signs (white positive, black negative) of the off-diagonal peaks in the synchronous and asynchronous plots and applying Noda's Rules.[38] a) Synchronous map showing the simultaneous relationships between products; b) asynchronous map showing the "out-of-phase" relationships. In this plot, further products, **A**, **X**, and **Y**, have been highlighted. High-resolution color copies are available in the Supporting Information.

the same experiment that gave the data in Figure 3. The off-diagonal peaks in Figure 4 a show that the formations of all of the products are correlated to **V** but not necessarily to each other, reflecting the existence of two parallel reaction pathways, namely hydrogenation and dehydrogenation. Together, the two maps can be used to deduce the sequence of formation of **B**, **C**, **1**, and **2**, see Scheme 2. The 2DCOR-GC maps provide evidence for two additional intermediates, **X** and **Y**, which are difficult to discern in the 1D chromatograms but are easily seen in the maps. **X** and **Y**, correlate with **2** but are formed before it. Although **X** and **Y** were not identified spectroscopically, a simple GC structural–elution simulation[35] suggests that they may have the structures shown in Scheme 2. An additional weak peak, **A** in Figure 4, was

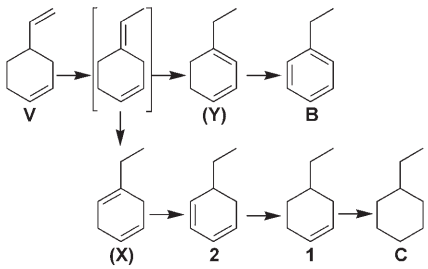

Scheme 2. Postulated mechanism for the dehydrogenation/hydrogenation of **V** to form **B** and **C**. Compounds **1** and **2**, have been identified by NMR spectroscopy, and **X** and **Y** have been tentatively identified by elution–structure relationships.

 © 2005 Wiley-VCH Verlag GmbH & Co. KGaA, Weinheim

identified as vinyl cyclohexane, by comparison with an authentic sample. Compound **A** does not correlate synchronously with any other species and is probably the product of a side reaction.

We now return to the original conundrum, namely why H_2 apparently catalyzes the dehydrogenation of **V** at temperatures close to ambient.[26] Figure 5 shows thermal images of the reactor, which reveal that H_2 causes a highly exothermic reaction and the generation of a distinct hot spot. A separate experiment with an internal thermocouple, deliberately located in the region of the hot spot, indicated that the temperature of the catalyst bed rose to approximately 200 °C. A further experiment with a series of six thermocouples positioned at regular intervals down the length of an 8 cm reactor showed that over 24 h the hot spot gradually moves down the catalyst bed; presumably the catalyst gradually becomes deactivated through charring or coking.[36] Thus, the explanation of the "catalysis" by H_2 is that hydrogenation of **V** rapidly heats a thin layer at the top of the catalyst bed to a temperature well above the light-off temperature for dehydrogenation of **V**. Since the dehydrogenation is itself exothermic, the reaction becomes almost self-sustaining and therefore can continue with almost 100% yield of **B** without the formation of **C**.

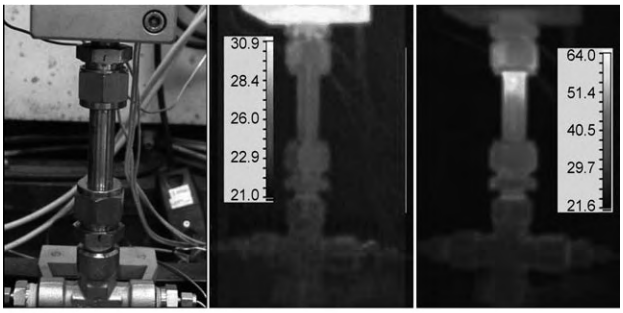

Figure 5. Evidence for hot spots during the dehydrogenation of **V** in the presence of H_2. a) photograph of the reactor; b) and c) thermal images of the same reactor with b) the pre-heater set to 40 °C, and CO_2 and **V** both flowing through it. Note the maximum temperature is 31 °C and c) with H_2 flowing and all other conditions unchanged. Note that the reactor skin has now reached nearly 65 °C. A thermocouple place at the center of the reactor reads over 200 °C. The exit temperature remained close to ambient. High-resolution color copies are available in the Supporting Information.

It is possible to suppress the dehydrogenation completely by deliberately cooling the reactor to 10 °C, although the catalyst bed itself is presumably at a higher temperature. This approach was used to generate sufficient quantities of **1** and **2** for their identification by NMR spectroscopy (see Supporting Information). Note that this low-temperature hydrogenation of **V** is a much simpler route to **2** than the original synthesis by Trost and co-workers,[37] which involved a Diels–Alder or cycloaddition reaction, and thus opens up the possibility of manufacturing this compound on a larger-scale if required.

The apparent catalytic effect of H_2 in the dehydrogenation **V** is the result of thermal hot spots generated in the catalyst bed by an initial exothermic hydrogenation "light-off" forcing the dehydrogenation reaction. The important point is that the possible presence of such hot spots in small-scale reactors should not be overlooked in other exothermic reactions in fixed bed reactors. Clearly it will be worth investigating the effects of different supercritical solvents on hot spots since different fluids can have significantly different thermal properties. In addition our study has resulted in the isolation of the diene, **2** by a potentially much simpler route than that previously reported.[37]

Many of our experiments would not have been possible on manually operated equipment because it was necessary to collect large amounts of data over a whole series of different reaction conditions, a process which would be impractically long without automation. However, handling such large volumes of data in itself presents problems and herein we have demonstrated again the value of 2DCOR-GC for presenting these data in a more easily interpretable form. Overall, one of the more important lessons from this work is that even apparently simple catalytic reactions are in reality quite complex, but that current techniques for supercritical chemistry are now capable of unraveling these complexities.

Experimental Section

Our automated continuous supercritical apparatus has recently been described in detail elsewhere.[16] Figure 1 shows a schematic of the design. Computer controlled HPLC pumps (Jasco CO_2–1580 and Jasco PU–980) deliver the CO_2 and organic substrate. The preheated CO_2/organic mixture is passed over the catalyst bed (2% $Pd/SiO_2/Al_2O_3$ supported: Johnson Matthey), which is heated by cartridge heaters and aluminum blocks. The temperature of the catalyst bed is controlled by a programmable Eurotherm. After the reaction has occurred and left the catalyst bed, the mixture of products and gases are passed through a HPLC 4-port sample loop (Valco/Vici), which samples 0.06 μL periodically into a GLC (Shimadzu GC17–A v.4), whereupon product separation and analysis is carried out. The system pressure and product separation is facilitated by a programmable Back Pressure Regulator (Jasco BPR BP-1580-81). Data analysis is performed off-line after the experimental is completed.

Received: June 14, 2005
Revised: August 23, 2005
Published online: October 31, 2005

Keywords: carbon dioxide · dehydrogenation · heterogeneous catalysis · reaction mechanisms · supercritical fluids

[1] J. R. Hyde, M. Poliakoff, R. Amandi, S. K. Ross, T. J. Lotz, *Green Chem.* **2005**, *7*, 288.
[2] J. M. Simard, M. S. Erickson, *Abstr. Pap. Am. Chem. Soc.* **1999**, *217*, 271.
[3] M. G. Hitzler, F. R. Smail, S. K. Ross, M. Poliakoff, *Chem. Commun.* **1998**, 359.
[4] J. E. Chateauneuf, K. Nie, *Abstr. Pap. Am. Chem. Soc.* **2000**, *219*, 446.
[5] W. Leitner, *Pure Appl. Chem.* **2004**, *76*, 635.
[6] A. R. Tadd, A. Marteel, M. R. Mason, J. A. Davies, M. A. Abraham, *J. Supercrit. Fluids* **2003**, *25*, 183.

 © 2005 Wiley-VCH Verlag GmbH & Co. KGaA, Weinheim

[7] A. Marteel, J. A. Davies, M. R. Mason, T. Tack, S. Bektesevic, M. A. Abraham, *Catal. Commun.* **2003**, *4*, 309.
[8] A. E. Marteel, T. T. Tack, S. Bektesevic, J. A. Davies, M. R. Mason, M. A. Abraham, *Environ. Sci. Technol.* **2003**, *37*, 5424.
[9] N. J. Meehan, A. J. Sandee, J. N. H. Reek, P. C. J. Kamer, P. van Leeuwen, M. Poliakoff, *Chem. Commun.* **2000**, 1497.
[10] M. Caravati, J. D. Grunwaldt, A. Baiker, *Catal. Today*, **2004**, *91–92*, 1.
[11] T. D. Crowe, P. J. White, *J. Am. Oil Chem. Soc.* **2003**, *80*, 569.
[12] M. L. Corazza, L. Cardozo, O. A. C. Antunes, C. Dariva, *Ind. Eng. Chem. Res.* **2003**, *42*, 3150.
[13] J. Liu, R. Zhang, L. Gao, T. Jiang, Z. M. Liu, J. He, B. X. Han, G. Y. Yang, *Chin. Chem. Lett.* **2002**, *13*, 1162.
[14] G. T. Musie, M. Wei, B. Subramaniam, D. H. Busch, *Inorg. Chem.* **2001**, *40*, 3336.
[15] G. Jenzer, M. S. Schneider, R. Wandeler, T. Mallat, A. Baiker, *J. Catal.* **2001**, *199*, 141.
[16] J. R. Hyde, M. Poliakoff, B. Walsh, *Green Chem.* **2005**, *7*, 357.
[17] W. K. Gray, F. R. Smail, M. G. Hitzler, S. K. Ross, M. Poliakoff, *J. Am. Chem. Soc.* **1999**, *121*, 10711.
[18] P. Licence, W. K. Gray, M. Sokolova, *J. Am. Chem. Soc.* **2005**, *127*, 293.
[19] S. Ichikawa, M. Tada, Y. Iwasawea, T. Ikariya, *Chem. Commun.* **2005**, 924.
[20] P. Stephenson, P. Licence, S. K. Ross, M. Poliakoff, *Green Chem.* **2004**, *6*, 521.
[21] F. Zhao, Y. Ikushima, M. Arai, *J. Catal.* **2004**, *224*, 479.
[22] F. Y. Zhao, S. Fujita, J. M. Sun, Y. Ikushima, M. Arai, *Catal. Today* **2004**, *98*, 523.
[23] T. Sato, C. V. Rode, O. Sato, M. Shirai, *Appl. Catal. B* **2004**, *49*, 181.
[24] N. Hiyoshi, C. V. Rode, O. Sato, M. Shirai, *J. Jpn. Pet. Inst.* **2004**, *47*, 410.
[25] J. R. Hyde, P. Licence, D. Carter, M. Poliakoff, *Appl. Catal. A* **2001**, *222*, 119.
[26] S. K. Ross, F. R. Smail, M. Sellin, R. Amandi, M. Poliakoff, *Chem. Eng. Trans.* **2002**, *2*, 561.
[27] S. Clark, US Patent 5321180, **1994**.
[28] R. W. Rieve, H. Shalit, US Patent 4029715, **1977**.
[29] G. Ruckelshauss, US Patent 4048243, **1997**.
[30] H. H. Vogel, H. M. Weitz, E. Lorez, R. Platz, US Patent 3903185, **1975**.
[31] D. W. Hart, L. H. Slaugh, US Patent 4375571, **1983**.
[32] O. Levenspiel, 1st ed. , *Chemical Reaction Engineering, 2nd Ed.*, Wiley, New York, **1962**, 230.
[33] The residence time was estimated by calculating the velocity of the fluid passing through the reactor per unit volume. Fluid velocity ($m s^{-1}$) was calculated at experimental temperature and pressure, and therefore requires specific data, which was obtained from appropriate equations of state, in this case from the NIST database (http://www.nist.gov).
[34] J. R. Hyde, R. A. Bourne, I. Noda, P. Stephenson, M. Poliakoff, *Anal. Chem.* **2004**, *76*, 6197.
[35] Advanced Chemistry Development, Inc., 6.08, Toronto ON, Canada, http://www.acdlabs.com, **2002**.
[36] J. H. Kim, D. J. Suh, T. J. Park, K. L. Kim, *Appl. Catal. A* **2000**, *197*, 191.
[37] B. Trost, T. Runge, L. Jungheim, *J. Am. Chem. Soc.* **1980**, *102*, 2841.
[38] I. Noda, *Appl. Spectrosc.* **1993**, *47*, 1329.

 © 2005 Wiley-VCH Verlag GmbH & Co. KGaA, Weinheim

Molecular Electronics

DOI: 10.1002/anie.200502420

Molecular AND Logic Gate Based on Electric Dichroism of a Photochromic Dihydroindolizine**

Joakim Andréasson, Yuichi Terazono, Bo Albinsson, Thomas A. Moore,* Ana L. Moore,* and Devens Gust**

Molecular switches that perform Boolean logic operations are scientifically interesting and may have technological potential.[1–4] A variety of molecule-based logic switches (AND gates, OR gates, etc.) have been reported.[5–9] In the vast majority of cases, at least one of the gate inputs requires physical addition of a chemical species. We have reported several molecular switches that employ photochromes, and function with only optical or thermal inputs.[9–12] Orientation of molecules by electric fields can lead to optically detectable electric linear dichroic phenomena.[13] The ability to control solution absorbance by using either photochromism or electric fields suggests that molecular logic gates switched by these two inputs might be realizable. Here, we report a molecular AND gate based on photochromic dihydroindolizine **1** (Scheme 1) whose two inputs are light at 366 nm and an electric field, and whose output is the electric linear dichroism (ELD) of **1**.

The dihydroindolizine[14] photochrome **1** exists in two isomeric forms. The closed, thermally stable spiro form **1c** does not absorb light significantly in the visible region (Figure 1); its longest-wavelength absorption band is at 415 nm. Irradiation of **1c** with ultraviolet light causes isomerization to the open, zwitterionic form **1o**, which absorbs in the visible region ($\lambda_{max} = 585$ nm). Compound **1o** is isomerized back to **1c** by heat or visible light. Irradiation ($\approx 1.5\ mW\,cm^{-2}$) of a solution of **1c** in 2-methyltetrahydrofuran at 366 nm at 20.5 °C, produces a photostationary state greatly enriched in **1o** with a time constant of 10.6 s. This

[*] Dr. J. Andréasson, Prof. Dr. B. Albinsson
Department of Chemistry and Bioscience
Chalmers University of Technology
41296 Göteborg (Sweden)
Fax: (+46) 31-772-3858
E-mail: a-son@chalmers.se
Dr. Y. Terazono, Prof. Dr. T. A. Moore, Prof. Dr. A. L. Moore, Prof. Dr. D. Gust
Center for the Study of Early Events in Photosynthesis
Department of Chemistry and Biochemistry
Arizona State University
Tempe, AZ 85287 (USA)
Fax: (+1) 480-965-2747
E-mail: tom.moore@asu.edu
amoore@asu.edu
gust@asu.edu

[**] We thank Prof. Bengt Nordén, Tore Eriksson, and Mattias Eng for helpful discussions and technical assistance. This work was supported by the Swedish Research Council (VR) and the U.S. National Science Foundation (CHE-0352599).

© 2005 Wiley-VCH Verlag GmbH & Co. KGaA, Weinheim

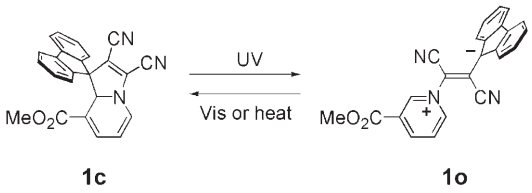

Scheme 1. Structures of the closed (**1c**) and open (**1o**) isomers of the dihydroindolizine. The thermally stable **1c** may be photoisomerized to **1o** with UV light of wavelength 366 nm and **1o** may be isomerized to **1c** with visible light or heat.

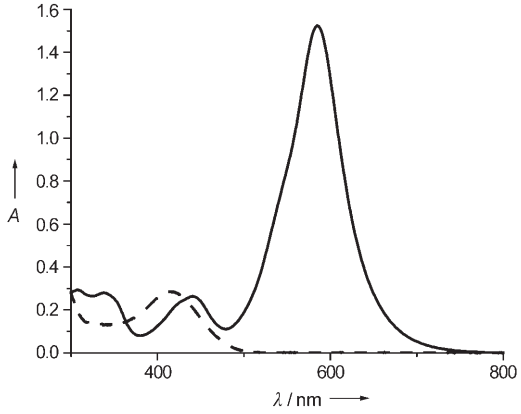

Figure 1. Absorption spectra of solutions in 2-methyltetrahydrofuran of the open (**1o** ——) and closed (**1c** -----) forms of the photochrome.

sample thermally isomerizes slowly back to **1c** ($\tau = 580$ min) in the dark. Irradiation of a sample in the **1o** state with visible light ($580\text{ nm} < \lambda < 900\text{ nm}$, $\approx 50\text{ mW cm}^{-2}$) leads to photoisomerization back to **1c** ($\tau = 9.8$ min).

ELD is the change in absorbance of plane-polarized light by a substance caused by an applied electric field. Isotropically oriented achiral molecules in an isotropic solvent have the same absorbance of plane-polarized light, regardless of the polarization. In the presence of an electric field, a molecule with a permanent dipole moment, such as **1o**, will partially align with the field. This causes orientation of the transition moment for absorption, and anisotropic behavior results. The magnitude of the absorbance change observed upon application of a field depends upon, among other things, the dipole moment and the isotropic extinction coefficient. Molecule **1o** is relatively polar, which favors alignment with an external field. It has an absorption maximum at 585 nm and could exhibit a significant ELD effect. Isomer **1c** does not absorb in the visible spectral region and is not expected to have a significant ELD response.

The ELD response for **1** was observed by using the apparatus detailed in the Experimental Section. The sample of **1** was placed in a cuvette containing two parallel, flat-plate metal electrodes separated by 1.6 mm. A beam of monochromatic plane-polarized light was passed through the sample between the electrodes, such that its plane of polarization was parallel to the electric field generated by application of a voltage across the electrodes. The intensity of the transmitted light was monitored with a photomultiplier tube. A voltage was applied across the electrodes to observe the ELD response. A 1.5 kV ac electric field (50 Hz, 940 kV m^{-1}) was used, and the change in light intensity induced by the field was measured by using lock-in detection. An ac signal from the lock-in amplifier reflects the change in absorption of the sample caused by the field (ELD response).

Figure 2 shows the ELD response (decrease in the intensity of transmitted light) for a sample of **1** that has been irradiated at 366 nm, and thereby converted into a

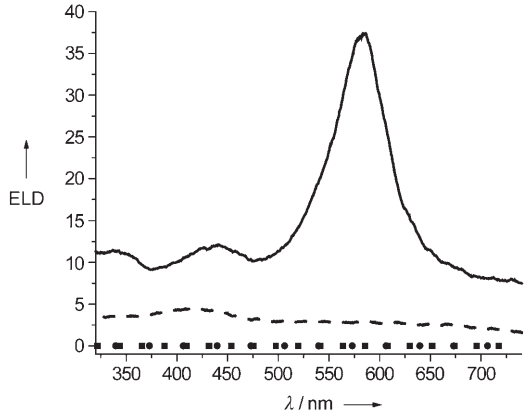

Figure 2. ELD response (arbitrary units) of a solution of **1** in 2-methyltetrahydrofuran: ——: following irradiation at 366 nm and with the application of the electric field; -----: following red light irradiation and with the application of the electric field; ●: following irradiation at 366 nm and in the absence of the electric field; and ■: following irradiation with red light and in the absence of the electric field. Note that the two data sets in the absence of the electric field overlap.

photostationary state consisting mainly of **1o**. The large band at approximately 583 nm is associated with the absorption of **1o** (Figure 1). The signal-to-noise ratio at 583 nm is very high, and the ELD response is easily observable. The ELD response and the absorption spectra are not expected to match exactly, as the ELD signal has not been corrected for the (wavelength-dependent) incident intensity nor converted into a logarithmic form. However, the lamp output as a function of wavelength is reasonably constant in this spectral region.

A similar experiment carried out with the closed form **1c** (obtained by irradiation with red light) yields a small electric-field response at the absorption maximum of approximately 416 nm (Figure 2). The response of **1c** is much smaller than that of **1o** because of differences in the dipole moment, extinction coefficient and orientation of the transition dipole. The small response in regions where **1** does not absorb is ascribed to the solvent, and it was observed even in the absence of molecule **1**. Figure 2 also shows the ELD response for **1o** and **1c** in the absence of the electric field. The response is essentially zero in both cases.

A Boolean AND logic gate requires two inputs, A and B, and an output. In the initial state with no inputs, the gate does

 © 2005 Wiley-VCH Verlag GmbH & Co. KGaA, Weinheim

not generate an output. No output is produced when either input A or input B is switched on. However, if both inputs are on, then the gate produces an output. On the basis of the ELD effects noted above, a solution of **1** can function as a molecule-based AND gate. Inputs A and B are UV irradiation at 366 nm and the application of an electric field, as discussed above. The output of the gate is the ELD signal, monitored at 583 nm.

In the initial state of the AND gate, the molecule is set in the thermally stable **1c** form. This solution does not generate an ELD response in the absence of an electric field, and the output of the gate is off (Figure 3a). Irradiation of this solution at 366 nm (input A on) generates a photostationary state containing mainly **1o**. However, in the absence of an electric field (input B off), no ELD response is observed, and the gate remains off. If, on the other hand, the original solution of **1c** is subjected to the 50 Hz electric field (input B on), only a small ELD response caused by the solvent is obtained. If a suitable threshold level is chosen, the gate in this case remains off. Alternatively, when the solution of **1c** is subjected to both irradiation at 366 nm and the electric field, photoisomerization to **1o** occurs, and **1o** gives a strong ELD response at 583 nm. The gate is switched on. Thus, the conditions for the AND function are met. After applying any combination of inputs, the gate may be reset to **1c** by irradiation with red light.

Although the purpose of this research has been to investigate a new approach to molecular gates rather than to make practical devices, the stability of **1** is important for any future applications. Figure 4a shows the ELD response of

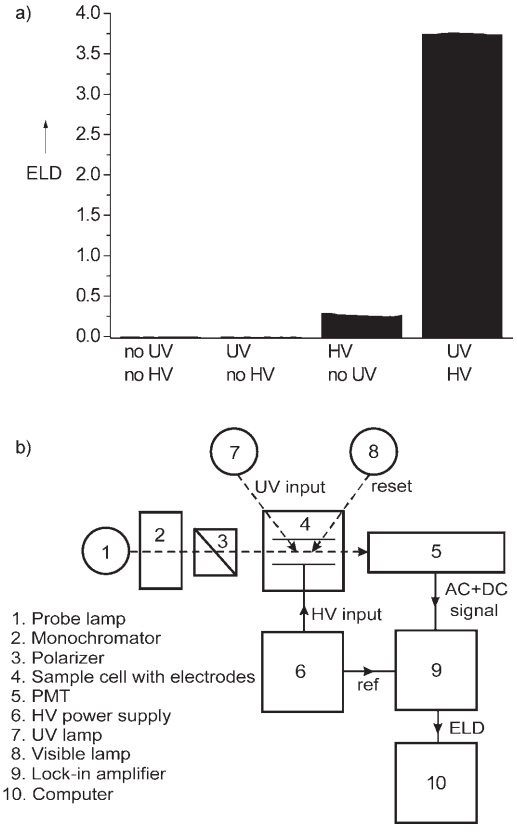

Figure 3. a) ELD response (arbitrary units) at 583 nm of **1** in 2-methyltetrahydrofuran following combinations of light (UV) and electric field (HV) inputs for the AND logic gate. Prior to the indicated inputs, the sample was in the **1c** state. The signal-to-noise ratio (variation of the ELD signal with time during a 4 s collection period, 20 data points) is shown by the small height variations within each bar. b) Schematic diagram of the experimental apparatus.

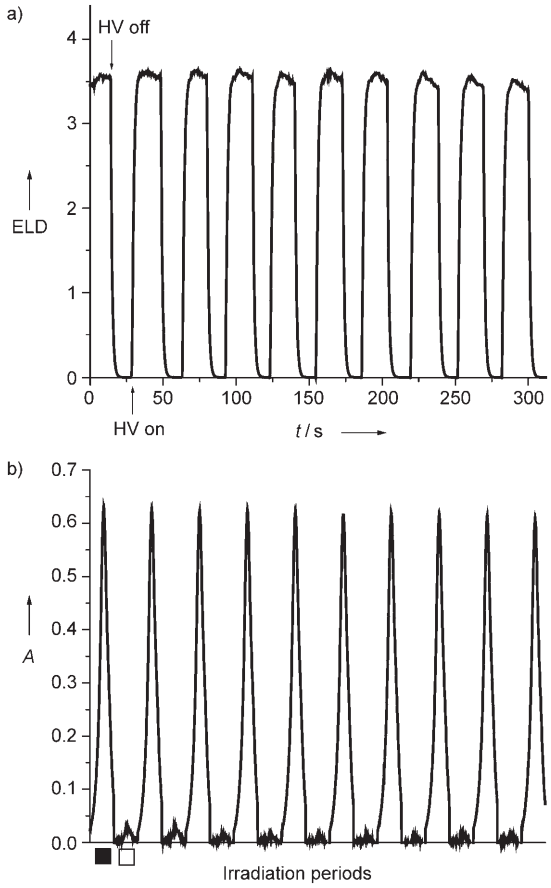

Figure 4. Cycling of the AND gate switching operations. a) The ELD signal at 583 nm from **1** in 2-methyltetrahydrofuran, measured for ca. 15 s after each switching operation, as a function of cycling of the applied voltage (HV) between 1.5 kV (HV on) and 0 V (HV off). b) Variation of the absorbance of **1**, recorded between 500 and 700 nm (where the zwitterionic isomer **1o** absorbs): after UV irradiation (■), and after red-light irradiation (□), as described in the text.

1o during application of 10 on–off cycles of the electric field. There is no degradation of the signal. Figure 4b reports the absorption between 500 and 700 nm (absorption from **1o**) after each of ten 40-s exposures to light at 366 nm alternated with nine 40-min exposures to red light. Only a small amount of photodegradation occurred after these cycles. The sample was degassed prior to the experiment with six freeze–pump–thaw cycles to a final pressure of approximately 1×10^{-4} Torr to reduce photodegradation.[15]

 © 2005 Wiley-VCH Verlag GmbH & Co. KGaA, Weinheim

This molecular AND gate does not require the addition of chemicals or translational diffusion of molecules. The times required for the photoisomerizations involved in one input and in the resetting operation are determined by the light-flux applied. The light intensities used here were chosen for convenience, rather than switching speed. The photoisomerization reactions themselves occur in ns or less. The time required for readout is ultimately limited by the time required to align the molecular dipoles sufficiently, and will be on the order of rotational diffusion times. If ac detection is employed, the frequency of the applied ac field and time constant of the cell circuit will determine the time required for detection.

The UV photonic input to the AND gate may be applied at any time prior to readout and the system will "remember" that this input was turned on because of the photoisomerization. The gate will persist in the **1o** state until thermal reversion eventually occurs. However, the second input, the ac high voltage, must be on during readout or no ELD will be detected. This behavior differs from that of photonic gates in which both inputs are photoisomerization reactions and the final state of the gate may be read out at any convenient time after the inputs have been applied and turned off.[9,12]

In summary, a solution of photochrome **1** functions as a molecule-based AND Boolean logic gate with inputs of light of 366 nm and an ac electric field. The output is the electric linear dichroism response. Resetting the gate to the initial state is accomplished by irradiation with red light. The signal-to-noise ratio is more than ample for observation of gate switching, and the sample can be cycled many times before photodegradation interferes. The apparatus is relatively simple, requiring only UV, visible, and plane-polarized light, a light-sensitive detector, an ac voltage source, and, for high sensitivity, lock-in detection.

Experimental Section

Dihydroindolizine **1** was synthesized as reported.[14] The solvent for all measurements was freshly distilled 2-methyltetrahydrofuran. Photoisomerizations of **1** were achieved by using a UVP UV lamp UVGL-25 (366 nm, ca. 1.5 $mW\,cm^{-2}$) or a 1000 W Xe/Hg-lamp at 450 W. The light from the Xe/Hg-lamp was filtered with two hot mirrors (each having $A = 1.8$ at 900 nm) to reduce the IR intensity and a long pass filter (> 580) nm. The power density at the sample was approximately 50 $mW\,cm^{-2}$.

The electric linear dichroism (ELD) measurements (Figure 3b) were performed on a JASCO J-500 A CD spectropolarimeter with the photoelastic modulator disconnected, so that the incident light was linearly polarized parallel to the applied electric field. The silica cuvette (10×10 mm) was equipped with two planar stainless-steel electrodes (9.5 mm×22 mm) connected to a 50-Hz ac high-voltage power supply. The gap between the electrodes was 1.6 mm, and the voltage was 1.5 kV, which gave a maximal field strength of 940 $kV\,m^{-1}$. The light passing between the electrodes was detected with a photomultiplier tube (PMT) connected to a lock-in amplifier (LIA; EG&G Model 124A) equipped with a differential preamplifier (EG&G Princeton Applied Research Model 116). The LIA received a 50 Hz reference signal from the high voltage power supply. The LIA detects only the ac component of the PMT response in phase with the high voltage. The output of the LIA, which represents the raw ELD response, is shown in the Figures.

Received: July 12, 2005
Published online: October 27, 2005

Keywords: electric field · linear dichroism · molecular devices · photochromism · polarized spectroscopy

[1] A. Aviram, *J. Am. Chem. Soc.* **1988**, *110*, 5687–5692.
[2] V. Balzani, A. Credi, M. Venturi, *ChemPhysChem* **2003**, *3*, 49–59.
[3] A. P. de Silva, D. B. Fox, T. S. Moody, S. M. Weir, *Pure Appl. Chem.* **2001**, *73*, 503–511.
[4] P. Ball, *Nature* **2000**, *406*, 118–120.
[5] D. Kuciauskas, P. A. Liddell, A. L. Moore, T. A. Moore, D. Gust, *J. Am. Chem. Soc.* **1998**, *120*, 10880–10886.
[6] F. M. Raymo, S. Giordani, *J. Am. Chem. Soc.* **2002**, *124*, 2004–2007.
[7] M. N. Stojanovic, T. E. Mitchell, D. Stefanovic, *J. Am. Chem. Soc.* **2002**, *124*, 3555–3561.
[8] X. Guo, D. Zhang, G. Zhang, D. Zhu, *J. Phys. Chem. B* **2004**, *108*, 11942–11945.
[9] J. Andréasson, G. Kodis, Y. Terazono, P. A. Liddell, S. Bandyopadhyay, R. H. Mitchell, T. A. Moore, A. L. Moore, D. Gust, *J. Am. Chem. Soc.* **2004**, *126*, 15926–15927.
[10] P. A. Liddell, G. Kodis, J. Andréasson, L. de la Garza, S. Bandyopadhyay, R. H. Mitchell, T. A. Moore, A. L. Moore, D. Gust, *J. Am. Chem. Soc.* **2004**, *126*, 4803–4811.
[11] S. D. Straight, J. Andréasson, G. Kodis, A. L. Moore, T. A. Moore, D. Gust, *J. Am. Chem. Soc.* **2005**, *127*, 2717–2724.
[12] S. D. Straight, J. Andréasson, G. Kodis, S. Bandyopadhyay, R. H. Mitchell, T. A. Moore, A. L. Moore, D. Gust, *J. Am. Chem. Soc.* **2005**, *127*, 9403–9409.
[13] N. Keitaro, Y. Atassi, J. A. Delaire, *Mol. Cryst. Liq. Cryst. Sci. Technol. Sect. B* **1996**, *15*, 351–358.
[14] H. Dürr in *Organic Photochromic and Thermochromic Compounds, Vol. 1* (Eds.: J. C. Crano, R. J. Guglielmetti), Plenum, New York **1999**, pp. 223–266.
[15] H. Dürr, H. Gross, *Agfa-Gevaert N. V. Neth. Research Disclosure* **1981**, *205*, 188–190.

 © 2005 Wiley-VCH Verlag GmbH & Co. KGaA, Weinheim

Coordination Chemistry

DOI: 10.1002/anie.200502231

An Efficient Design for the Rigid Assembly of Four Bidentate Chromophores in Water-Stable Highly Luminescent Lanthanide Complexes**

*Nicholas Chatterton, Yann Bretonnière, Jacques Pécaut, and Marinella Mazzanti**

The unique electronic properties of lanthanide ions (long-lived luminescence and sharp emission spectra) make them particularly suitable for the development of diagnostic tools in medical analysis.[1,2] Lanthanide complexes are increasingly used for sensor development[3] and as luminescent probes in time-resolved high-throughput assays and fluorescence imaging because of their ability to discriminate between background fluorescence and the target signal.[4–8] Numerous studies have been directed to design efficient luminescence probes containing the long-lived visible emitters Eu^{III} and Tb^{III}[9–14] and more recently near-infrared (NIR) emitters (Pr^{III}, Er^{III}, Yb^{III}, Nd^{III}).[15–18]

As the Laporte-forbidden 4f–4f transition prevents direct excitation of lanthanide luminescence, lanthanide ions require sensitization by suitable organic chromophores. Furthermore, for practical applications under physiological conditions, the lanthanide ion should be incorporated into highly stable complexes. The efficiency of ligand-to-lanthanide energy transfer, which requires compatibility between the energy levels of the ligand excited states and the accepting levels of lanthanide ions, is crucial in the design of high-performance probes.[19] Moreover, high quantum yield cannot be obtained without the prevention of nonradiative deactivation of the lanthanide excited states by O–H oscillators of coordinated or closely diffusing water molecules. The incorporation of suitable chromophores in carefully designed polydentate ligands leads to increased stability of the lanthanide chelate in solution and allows for the metal center to be well protected from water molecules. However, the tendency of lanthanide ions to adopt high coordination numbers and their lack of stereochemical preferences make the design of such ligands very challenging.[20] A successful strategy adopted by several investigators relies on tripodal architectures for the organization of three tridentate binding units in nine-coordinate Ln^{III} complexes.[21–25] The design of polydentate ligands that allow the arrangement of four bidentate moieties around a lanthanide ion has received less attention in spite of the excellent luminescent properties observed for tetrakis complexes of bidentate chomophores, such as quinolinates[26] or tropolonates.[27] Recently, octadentate ligands incorporating four bidentate chromophores have been shown to yield lanthanide complexes with very efficient emissions in the visible or NIR regions.[15,28] The structures of these complexes have not been elucidated, but the highly flexible structure of the backbone that connects the bidentate units suggests nonoptimal protection of the metal center in such systems.

Herein, we describe a new and particularly efficient way of assembling four picolinate chromophores around a lanthanide center with a multidentate ligand that yields highly luminescent and water-stable lanthanide complexes. The decadentate ligand *N*,*N*,*N*′*N*′-tetrakis[(6-carboxypyridin-2-yl)methyl]ethylenediamine (H_4tpaen) is readily obtained in five steps from commercially available pyridine-2,6-dicarboxylic acid and ethylenediamine in a yield of 26% (Scheme 1).

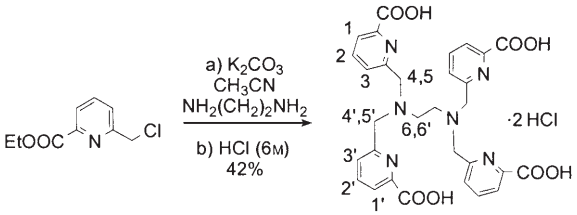

Scheme 1. Synthesis of the ligand $[H_6tpaen]^{2+}$, and its numbering scheme for NMR spectral assignment.

The water-soluble complexes of tpaen were isolated in 50–60% yield by treating the ligand with $LnCl_3{\cdot}6H_2O$ (Ln = Ce, Eu) and adjusting the pH value to approximately 6. Five deprotonation constants ($pK_{a,1} = 2.8(1)$, $pK_{a,2} = 3.2(1)$, $pK_{a,3} = 3.9(2)$, $pK_{a,4} = 5.1(1)$, and $pK_{a,5} = 7.8(1)$) were determined for the $[H_6tpaen]^{2+}$ ions by potentiometric titration as well as the stability constants of the resulting Eu^{III} and Ca^{II} complexes ($\log\beta_{EuL} = 15.3(3)$) and Ca^{II} ($\log\beta_{CaL} = 8.5$ (5); see the Supporting Information). The values of pEu = 15.7, pGd = 15.0, and pCa = 8.5 ($-\log[M]_{free}$ at pH 7.4, $[M]_{total} = 1\,\mu M$, and $[tpaa]_{total} = 10\,\mu M$) relative to the value of pEu = 14.0 for ethylenediaminetetraacetate (edta) indicate that the tpaen ligand forms lanthanide complexes of sufficient stability for potential biomedical applications and shows a good selectivity for europium with respect to calcium.

The crystal structure of the complexes [{Eu(tpaen)}K$(H_2O)_3$]·$4H_2O$ (**1**; Figure 1) and [{Ce(tpaen)}K-

[*] Dr. N. Chatterton, Dr. Y. Bretonnière, Dr. M. Mazzanti
Laboratoire de Reconnaissance Ionique
Laboratoire de Chimie Inorganique et Biologique (UMR-E 3 CEA-UJF)
Département de Recherche Fondamentale sur la Matière Condensée
CEA-Grenoble
17 rue des Martyrs, 38054 Grenoble, Cedex 09 (France)
Fax: (+33) 4-3878-5090
E-mail: mazzanti@drfmc.ceng.cea.fr
Dr. J. Pécaut
Laboratoire de Coordination et Nanochimie (UMR-E 3 CEA-UJF)
Département de Recherche Fondamentale sur la Matière Condensée
CEA-Grenoble (France)

[**] We thank Pierre Alain Bayle for help with NMR spectroscopic measurements and Emilie Robert for her contribution to the ligand synthesis. We are grateful to Daniel Imbert and Jean-Claude Bünzli for their suggestions and help with the photophysical measurements.

Supporting information for this article is available on the WWW under http://www.angewandte.org or from the author.

 © 2005 Wiley-VCH Verlag GmbH & Co. KGaA, Weinheim

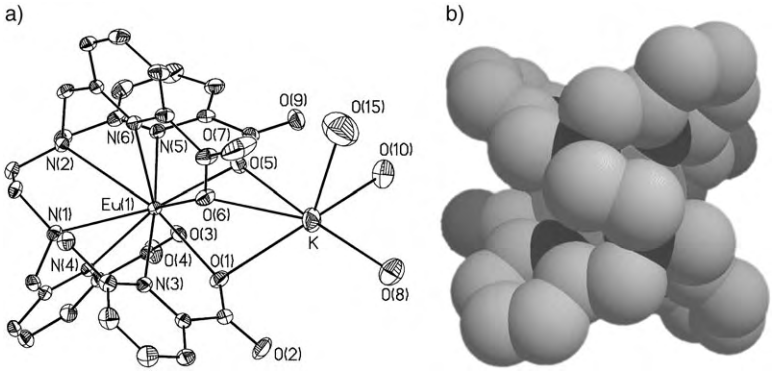

Figure 1. a) Molecular structure of $[\{Eu(tpaen)\}K(H_2O)_3]\cdot 4H_2O$ (**1**) (30% probability level). b) CPK (or space-filling) model of $[Eu(tpaen)]^+$ in **1**.

$(H_2O)_3]_2\cdot 16H_2O$ (**2**; see the Supporting Information) were analyzed by X-ray diffraction. In both complexes, the Ln^{III} ion is ten-coordinate with the four oxygen atoms (mean values of the M–O distances: 2.42(1) Å for Eu and 2.50(4) Å for Ce) and the six nitrogen atoms (mean values of the $M–N_{pyridine}$ distances: 2.65(4) Å for Eu and 2.72(1) Å for Ce, and mean values of the $M–N_{amine}$ distances: 2.91(1) Å for Eu and 2.91(4) Å for Ce) of the ligand. The bridging mode of the six-coordinate K^+ counterion differs in the two structures, thus leading to a monomeric structure for the Eu complex and to a dimeric structure for the Ce complex. The picolinate arms of the tpaen ligand wrap around the metal ion in a pseudo-C_2-symmetric helical arrangement that results in a chiral complex. Both complexes crystallize as a racemic mixture of Λ and Δ enantiomers in a centrosymmetric space group.

The ^{1}H NMR spectra of the Eu (Figure 2) and Ce complexes of tpaen in a solution of D_2O at room temperature and at pH 7 is consistent with the presence of rigid C_2-

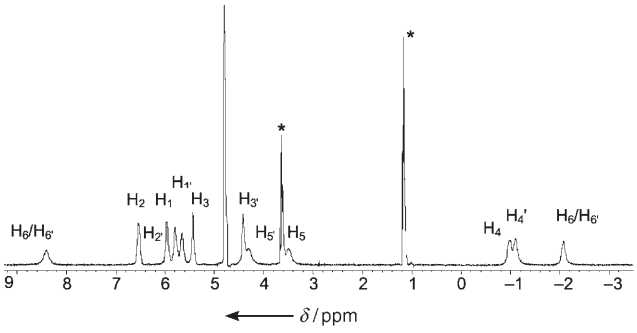

Figure 2. ^{1}H NMR spectrum at 298 K of [Eu(tpaen)]K in D_2O at pD = 6.9 (* denotes EtOH).

symmetric species in solution, in which the four chelating arms remain coordinated to the metal center on the NMR timescale. The observed symmetry is in agreement with a chiral helical solution structure, as found in the solid state. The complexes maintain their rigid structure in the temperature range 298–363 K. The presence of similar rigid C_2-symmetric species was also observed in the range 298–363 K for solutions of the tpaen complexes of La and Tb in D_2O prepared in situ. The high rigidity of these complexes in solution, rarely observed for lanthanide complexes with high denticity,[29] indicated that the arrangement of the ten donor atoms provided by the simple ethylenediamine backbone is very well adapted to lanthanide complexation, thus providing highly effective protection of the metal center from interaction with solvent molecules.

As a result, the Eu^{III} and Tb^{III} complexes of tpaen showed a bright and long-lived luminescence in solutions of both H_2O and D_2O. The observed lifetimes of the $Eu(^5D_0)$ and $Tb(^5D_4)$ levels for the $[Tb(tpaen)]^-$ and $[Eu(tpaen)]^-$ ions are in agreement with the presence of 0.04 ± 0.2 and 0.03 ± 0.2 coordinated water molecules in the Eu and Tb complexes, respectively. The luminescent properties of the visible-light emitting lanthanide ions Eu and Tb are efficiently sensitized by the ligand tpaen (Figure 3). An efficient ligand-to-metal energy transfer is

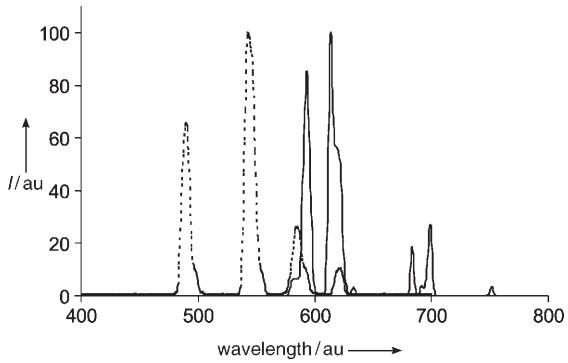

Figure 3. Normalized emission spectrum of $[Tb(tpaen)]^-$ (-----) and $[Eu(tpaen)]^-$ (——) upon ligand excitation at 274 nm.

suggested by close matching of the excitation and absorption spectra of the Eu and Tb chelates (Figure 4). The value of the quantum yield of the $[Tb(tpaen)]^-$ complex ($\Phi = 45\%$) measured relative to $[Tb(dpa)_3]^{3-}$ in aerated 0.1M tris buffer with an experimental error of 15% is one the highest reported to date.[28,30–32] The tpaen chromophore also efficiently sensitize the Eu ion to lead to a quantum yield value $\Phi =$ 7%, which is lower than that of the Tb^{III} complex but still

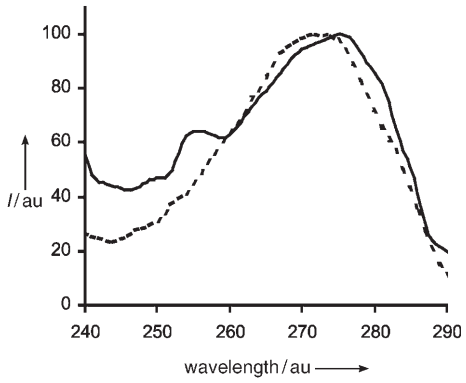

Figure 4. Absorption (•••••) and excitation spectrum (——) of [Tb-(tpaen)]$^-$ in tris Buffer.

 © 2005 Wiley-VCH Verlag GmbH & Co. KGaA, Weinheim

significantly larger than the quantum yield of lanthanide-based commercial luminescent probes.[33,34] The very intense luminescence of these ions is a result of efficient (Table 1)

Table 1: Lifetime and absolute quantum yields in tris buffer (pH 7.4; 298 K) relative to $[Eu(dpa)_3]^{3-}$ and $[Tb(dpa)_3]^{3-}$ ions.

Compound	λ_{exc} [nm]	ε [$M^{-1}cm^{-1}$]	τ_{H_2O} [ms]	τ_{D_2O} [ms]	Φ_{H_2O}
tpaen	270	15800			
[Eu(tpaen)]	274	21600	1.70(2)	3.30(1)	0.07
[Tb(tpaen)]	274	21600	3.0(1)	3.75(1)	0.45

ligand-to-metal energy transfer and effective shielding of the metal ion from radiationless deactivation. The long luminescence lifetime observed for the terbium complex in H_2O rules out the presence of a de-excitation pathway that involves back transfer from the excited state of the metal center to the ligand. This leads to a high luminescence quantum yield. The synthesis of the ligand tpaen is simple, can be performed on large scales, and can be readily modified to anchor the complex with functions capable of binding biomolecules so that highly luminescent labels for time-resolved luminescence imaging can be developed.[32]

The straightforward approach used to organize four bidentate chromophores in the decadentate ligand tpaen has yielded lanthanide chelates that are highly soluble and stable at physiological pH values. Moreover, the ligand architecture leads to a rigid structure in solution, in which the metal center is effectively protected from interaction with the solvent molecules. This approach opens a wide variety of perspectives on the development of stable visible-light or NIR emitting luminescent probes for biomedical applications from suitable chromophores; investigations towards extending this approach to other chromophores are currently in progress.

Experimental Section

A detailed description of the synthesis of the ligand *N*,*N*,*N*′*N*′-tetrakis[(6-carboxypyridin-2-yl)methyl]ethylenediamine (H_4tpaen) and of the cerium and europium complexes is given in the Supporting Information. The complexes were prepared as follows: A solution of $CeCl_3{\cdot}7H_2O$ or $EuCl_3{\cdot}6H_2O$ (0.138 mmol) in water (0.5 mL) was added to a solution of H_4tpaen (0.138 mmol) in water (6 mL) at pH 5, adjusted by the addition of KOH (0.2 M). The resulting solution was then stirred at room temperature for 2 h and its pH value was readjusted to 6 by the addition of further KOH (0.2 M). The water was then evaporated and the resulting solid was suspended in EtOH (5 mL). The insoluble salts were removed by filtration and the filtrate was evaporated. Slow evaporation of a solution of the resulting solid in water (1 mL) yielded the tpaen complexes as yellow ([Ce(tpaen)]K) or white ([Eu(tpaen)]K) crystals after 5 days in 50–60% yield. Elemental analysis (%) calcd for $[Ce(tpaen)]K{\cdot}4.5H_2O$ ($C_{30}H_{33}N_6O_{12.5}CeK$): C 42.05, H 3.88, N 9.81; found: C 41.85, H 3.67, N 9.77; elemental analysis (%) calcd for$[Eu(tpaen)]K{\cdot}6H_2O$ ($C_{30}H_{34}N_6O_{13}CeK$): C 40.22, H 4.05, N 9.38; found: C 40.03, H 4.03, N 9.19.

[Ce(tpaen)]: ^{1}H NMR (D_2O, 400 MHz, 298 K, pD = 5.4): δ = −2.03 (sbr, 2H, H6/H6′), 0.09 (sbr, 2H, H5′), 1.18 (sbr, 2H, H6/H6′), 3.25 (d, 2H, H4′), 3.51 (d, 2H, H4), 5.44 (sbr, 2H, H5), 7.97 (d, 2H, H3), 8.10 (d, 2H, H3′), 8.45 (d, 2H, H1), 8.91 (t, 2H, H2), 8.94 (d, 2H, H1′), 9.04 ppm (t, 2H, H2′).

[Eu(tpaen)]: ^{1}H NMR (D_2O, 400 MHz, 298 K, pD = 6.9): δ = −2.07 (sbr, 2H, H6/H6′), −1.11 (sbr, 2H, H4′), −0.99 (sbr, 2H, H4), 3.48 (sbr, 2H, H5), 4.28 (sbr, 2H, H5′), 4.41 (dbr, 2H, H3′), 5.43 (dbr, 2H, H3), 5.65 (sbr, 2H, H1′), 5.79 (sbr, 2H, H1), 5.96 (br, 2H, H2′), 6.53 (br, 2H, H2), 8.40 ppm (br, 2H, H6/H6′).

Crystal data for $[\{Eu(tpaen)\}K(H_2O)_3]{\cdot}4H_2O$ (**1**): $C_{30}H_{38}EuKN_6O_{15}$, M_r = 913.7, monoclinic, space group $P2(1)/n$, a = 11.995(2), b = 14.539(3), c = 21.407(5) Å, β = 106.186(3), V = 3585.2(12) Å^3, Z = 4, ρ_{calcd} = 1.693 g cm^{-3}, μ = 1.944 mm^{-1}, T = 298 K. Of the 12504 reflections collected, 5133 were unique (R_{int} = 0.0192). Refinement on all data converged at R_1 = 0.0296, wR_2 = 0.0667. Max/min residual density 0.693 and −0.528 e Å^{-3}.

Crystal data for $[\{Ce(tpaen)\}K(H_2O)_3\}_2]{\cdot}16H_2O$ (**2**): $C_{30}H_{46}CeKN_6O_{19}$, M_r = 973.95, monoclinic, space group $P2(1)/c$, a = 11.7615(10), b = 14.5931(12), c = 22.965(2) Å, β = 101.640(1), V = 3860.7(6) Å^3, Z = 4, ρ_{calcd} = 1.676 g cm^{-3}, μ = 1.374 mm^{-1}, T = 193 K. Of the 12929 reflections collected, 7459 were unique (R_{int} = 0.0310). Refinement on all data converged at R_1 = 0.0430, wR_2 = 0.1340. Max/min residual density 1.055 and −2.462 e Å^{-3}.

Data were collected using a Bruker SMART CCD area detector three-circle diffractometer $2\theta_{max}$ = 59.38° (ω scans, $Mo_{K\alpha}$ radiation, λ = 0.71073 Å, graphite monochromator). CCDC-275838 (**1**) and -275839 (**2**) contain the supplementary crystallographic data for this paper. These data can be obtained free of charge from The Cambridge Crystallographic Data Centre via www.ccdc.cam.ac.uk/data_request/cif.

The number of coordinated water molecules present in solution q were determined from lifetime measurements by using the equation of Parker and co-workers ($q = A_{Ln}(1/\tau H_2O - 1/\tau D_2O - \alpha_{Ln})$ with A_{Tb} = 5 ms, A_{Eu} = 1.2 ms, α_{Tb} = 0.06 ms^{-1}, and α_{Eu} = 0.25 ms^{-1}).[35] Quantum yields Q have been calculated by using the equation $Q_x/Q_r = A_r(\bar{\nu})n_x^2D_x/A_x(\bar{\nu})n_r^2D_r$, in which x refers to the sample, r to the reference, A to the absorbance, $\bar{\nu}$ to the excitation wavenumber used, n to the refractive index, and D to the integrated emitted intensity. The tris(dipicolinate) complexes $[Eu(dpa)_3]^{3-}$ (dpa = pyridine-2,6-dicarboxylate; Φ = 13.5%, 7.5×10^{-5} M in tris buffer 0.1 M) and $[Tb(dpa)_3]^{3-}$ (Φ = 26.5%, 6.5×10^{-5} M in tris buffer 0.1 M) were used as references for the determination of the quantum yields of Eu- and Tb-containing samples, respectively.[36] The consistency of data was checked by measuring the quantum yield of the tris(dipicolinate) complexes against rhodamine 101 (Q_{abs} = 100% in ethanol) and cresyl violet (Q_{abs} = 54% in methanol).[37]

Received: June 24, 2005

Keywords: carboxylate ligands · lanthanides · luminescence · N ligands · sensitizers

[1] J. Chen, P. R. Selvin, *J. Am. Chem. Soc.* **2000**, *122*, 657–660.
[2] S. Faulkner, J. L. Matthews, *Comprehensive Coordination Chemistry II, Vol. 9*, Elsevier, Oxford, UK, **2004**, 913–944.
[3] D. Parker, *Coord. Chem. Rev.* **2000**, *205*, 109–130.
[4] K. Matsumoto, J. Yuan in *Metal Ions in Biological Systems*: *The Lanthanides and Their Interrelations with Biosystems, Vol. 40* (Eds.: H. Sigel, A. Sigel), Marcel Dekker, New York, **2003**, pp. 191–232.
[5] D. Parker, J. A. G. Williams in *Metal Ions in Biological Systems*: *The Lanthanides and Their Interrelations with Biosystems, Vol. 40* (Eds.: H. Sigel, A. Sigel), Marcel Dekker, New York, **2003**, pp. 233–280.
[6] A. Beeby, S. W. Botchway, I. M. Clarkson, S. Faulkner, A. Parker, W. , D. Parker, J. A. G. Williams, *J. Photochem. Photobiol. B* **2000**, *57*, 83–89.
[7] M. H. V. Werts, R. H. Woundenberg, P. G. Emmerink, R. van Gassel, J. W. Hofstraat, J. W. Verhoeven, *Angew. Chem.*

 © 2005 Wiley-VCH Verlag GmbH & Co. KGaA, Weinheim

2000, *112*, 4716 – 4718; *Angew. Chem. Int. Ed.* **2000**, *39*, 4542 – 4544.
[8] L. J. Charbonnière, R. Ziessel, M. Montalti, L. Prodi, N. Zaccheroni, C. Boehme, G. Wipff, *J. Am. Chem. Soc.* **2002**, *124*, 7779 – 7788.
[9] N. Sabbatini, M. Guardigli, J.-M. Lehn, *Coord. Chem. Rev.* **1993**, *123*, 201 – 228.
[10] D. Parker, J. A. G. Williams, *J. Chem. Soc. Dalton Trans.* **1996**, 3613 – 3628.
[11] M. Latva, H. Takalo, V.-M. Mukkala, C. Matachescu, J.-C. Rodriguez-Ubis, J. Kankare, *J. Lumin.* **1997**, *75*, 149 – 169.
[12] S. Quici, M. Cavazzini, G. Marzanni, G. Accorsi, N. Armaroli, B. Ventura, F. Barigelletti, *Inorg. Chem.* **2005**, *44*, 529 – 537.
[13] G. Zucchi, A.-C. Ferrand, R. Scopelliti, J.-C. Bünzli, *Inorg. Chem.* **2002**, *41*, 2459 – 2465.
[14] F. J. Steemers, W. Verboom, D. N. Reinhoudt, E. B. van der Tol, J. W. Verhoeven, *J. Am. Chem. Soc.* **1995**, *117*, 9408 – 9414.
[15] D. Imbert, S. Comby, A.-S. Chauvin, J.-C. Bünzli, *Chem. Commun.* **2005**, 1432 – 1434.
[16] N. M. Shavaleev, L. P. Moorcraft, S. J. A. Pope, Z. R. Bell, S. Faulkner, M. D. Ward, *Chem. Eur. J.* **2003**, *9*, 5283 – 5291.
[17] D. Imbert, M. Cantuel, J.-C. Bünzli, G. Bernardinelli, C. Piguet, *J. Am. Chem. Soc.* **2003**, *125*, 15698 – 15699.
[18] S. Faulkner, S. J. A. Pope, *J. Am. Chem. Soc.* **2003**, *125*, 10526 – 10527.
[19] A. Beeby, L. M. Bushby, D. Maffeo, J. A. G. Williams, *J. Chem. Soc. Perkin Trans. 2* **2000**, 1281 – 1283.
[20] C. Piguet, J.-C. G. Bünzli, *Chem. Soc. Rev.* **1999**, *28*, 347 – 358.
[21] S. J. Archibald, A. J. Blake, S. Parsons, M. Schröder, R. E. P. Winpenny, *J. Chem. Soc. Dalton Trans.* **1997**, 173 – 179.
[22] F. Renaud, C. Piguet, G. Bernardinelli, J.-C. G. Bünzli, G. Hopfgartner, *J. Am. Chem. Soc.* **1999**, *121*, 9326 – 9342.
[23] Y. Bretonnière, R. Wietzke, M. Mazzanti, C. Lebrun, J. Pécaut, *Inorg. Chem.* **2000**, *39*, 3499 – 3505.
[24] C. Gateau, M. Mazzanti, J. Pécaut, F. Dunand, A, L. Helm, *Dalton Trans.* **2003**, 2428 – 2433.
[25] L. Charbonnière, R. Ziessel, M. Guardigli, A. Roda, N. Sabbatini, M. Cesario, *J. Am. Chem. Soc.* **2001**, *123*, 2436 – 2437.
[26] R. Van Deun, P. Fias, P. Nockemann, A. Schepers, T. N. Parac-Vogt, K. Van Hecke, L. Van Meervelt, K. Binnemans, *Inorg. Chem.* **2004**, *43*, 8461 – 8469.
[27] J. Zhang, P. D. Badger, S. J. Geib, S. Pétoud, *Angew. Chem.* **2005**, *117*, 2564 – 2568; *Angew. Chem. Int. Ed.* **2005**, *44*, 2508 – 2512.
[28] S. Petoud, S. M. Cohen, J.-C. Bünzli, K. N. Raymond, *J. Am. Chem. Soc.* **2003**, *125*, 13324 – 13325.
[29] B. G. Jenkins, R. B. Lauffer, *Inorg. Chem.* **1988**, *27*, 4730 – 4738.
[30] E. Brunet, O. Juanes, R. Sedano, J.-C. Rodriguez-Ubis, *Photochem. Photobiol. Sci.* **2002**, *1*, 613 – 618.
[31] R. S. Dickins, J. A. K. Howard, C. Maupin, J. Moloney, D. Parker, J. P. Riehl, G. Siligardi, J. A. G. Williams, *Chem. Eur. J.* **1999**, *5*, 1095 – 1104.
[32] N. Weibel, L. J. Charbonnière, M. Guardigli, A. Roda, R. Ziessel, *J. Am. Chem. Soc.* **2004**, *126*, 4888 – 4896.
[33] B. Alpha, V. Balzani, J.-M. Lehn, S. Perathoner, N. Sabbatini, *Angew. Chem.* **1987**, *99*, 1310; *Angew. Chem. Int. Ed. Engl.* **1987**, *26*, 1266 – 1267.
[34] G. Mathis, *Clin. Chem.* **1993**, *39*, 1953 – 1959.
[35] A. Beeby, I. M. Clarkson, R. S. Dickins, S. Faulkner, D. Parker, L. Royle, A. S. de Sousa, G. J. A. Williams, M. Woods, *J. Chem. Soc. Perkin Trans. 2* **1999**, 493 – 503.
[36] A.-S. Chauvin, F. Gumy, D. Imbert, J.-C. Bünzli, *Spectrosc. Lett.* **2004**, *37*, 517 – 532.
[37] D. F. Eaton, *Pure Appl. Chem.* **1988**, *60*, 1107.

 © 2005 Wiley-VCH Verlag GmbH & Co. KGaA, Weinheim

Ring Expansion

DOI: 10.1002/anie.200502650

Acyl 1,3-Migration in Rhodium-Catalyzed Reactions of Acetylenic β-Ketoesters with Aryl Boronic Acids: Application to Two-Carbon-Atom Ring Expansions**

*Tomoya Miura, Masahiko Shimada, and Masahiro Murakami**

Rhodium(I)-catalyzed carbon–carbon bond-forming reactions with organometallic reagents have recently attracted significant attention in organic chemistry.[1] We report herein a new acyl 1,3-migration catalyzed by rhodium(I) and its extension to a two-carbon-atom ring-expansion reaction [Eq. (1)].

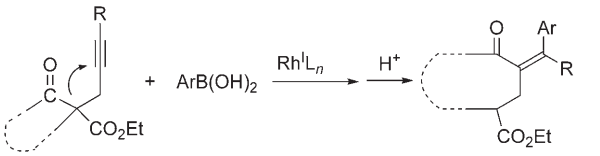

(1)

We recently reported that a cyclopentanol derivative can be synthesized from a 5-alkyn-1-one by intramolecular nucleophilic addition of an intermediate organorhodium(I) species to the ketone carbonyl group in a 5-*exo*-trig cyclization.[2] We next examined the possibility of an equivalent 4-*exo*-trig cyclization, although such a four-membered-ring formation would suffer from developing ring strain.[3] The desired 4-alkyn-1-one substructure was incorporated into the model substrate **1a**, which was readily synthesized by the alkylation reaction of a β-ketoester with 1-bromo-2-butyne. The 4-alkyn-1-one **1a** was treated with phenylboronic acid (**2a**, 2.0 equiv) in the presence of [{Rh(OH)(cod)}$_2$] (0.05 equiv of Rh) in dioxane/H_2O (100:1) at room temperature under a nitrogen atmosphere. The substrate **1a** was consumed in 16 h, and subsequent chromatographic isolation on silica gel afforded not the expected cyclobutanol derivative **3**, but rather the α,β-unsaturated ketone **4aa** in 69% yield (Scheme 1).

The following mechanism explains the production of **4aa**: A phenylrhodium(I) species is initially generated by trans-

[*] Dr. T. Miura, M. Shimada, Prof. Dr. M. Murakami
Department of Synthetic Chemistry and Biological Chemistry
Kyoto University
Katsura, Kyoto 615-8510 (Japan)
Fax: (+81) 75-383-2748
E-mail: murakami@sbchem.kyoto-u.ac.jp

[**] This work was supported by a Grant-in-Aid for Scientific Research on Priority Areas 17035044 from The Ministry of Education, Culture, Sports, Science, and Technology (MEXT).

Supporting information for this article is available on the WWW under http://www.angewandte.org or from the author.

© 2005 Wiley-VCH Verlag GmbH & Co. KGaA, Weinheim

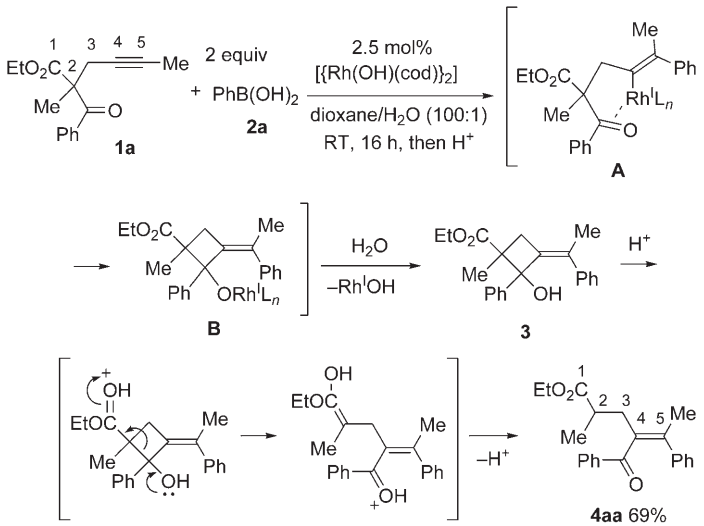

Scheme 1. Rhodium(I)-catalyzed reaction of acetylenic β-ketoester **1a** with phenylboronic acid (**2a**).

metalation of hydroxorhodium(I) with phenylboronic acid (**2a**), which then undergoes *cis*-1,2-addition to the carbon–carbon triple bond[4] in a regioselective manner directed by the ketone carbonyl group.[5] We propose that the resulting alkenyl rhodium(I) intermediate **A** undergoes intramolecular nucleophilic addition to the benzoyl group[6] in a 4-*exo* mode despite the development of ring strain. As a result, the four-membered ring carbocycle **B** is furnished as a rhodium(I) alkoxide. Hydrolysis produces the cyclobutanol **3** with regeneration of the catalytically active hydroxorhodium(I). Cleavage of the cyclobutane ring through a retro-aldol reaction is promoted by the acidic nature of silica gel during purification[7,8] to afford acyl 1,3-migration product **4aa**.

During the transformation of **1a** into **4aa**, a phenyl group was introduced at C5 of **1a**, and the resulting alkenyl rhodium intermediate facilitated migration of the benzoyl group from C2 to C4.[9] This 1,3-migration reaction was generally applicable to a variety of combinations of acetylenic β-ketoesters **1** and aryl boronic acids **2** (Table 1). Both electron-rich and -deficient aryl boronic acids were suitably reactive (Table 1, entries 1–4). *o*-Tolylboronic acid, however, failed in the acyl 1,3-migration reaction probably owing to steric reasons.[10] A better yield was obtained with 1b having an ethyl-substituted alkyne than with 1a (Table 1, entry 5).[5,6c] Methyl ketone **1c** also underwent acetyl 1,3-migration (Table 1, entry 6). The reaction of trimethylsilyl-substituted alkyne **1d** suffered from lower regioselectivity of the initial 1,2-addition and gave the product **4da** in only 25% yield (Table 1, entry 7).[11] Acetylenic β-ketoester **1e** without an α-substituent failed to undergo the cyclization reaction, probably because of the presence of a stable enol tautomer.

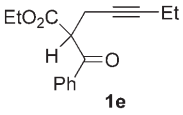

We next envisioned that if a β-ketoester moiety was installed in a cyclic skeleton, an analogous acyl 1,3-migration process would expand the ring by two carbon atoms to serve as a synthetic method for the preparation of medium-sized-ring carbocyclic skeletons.[12,13] Thus, we prepared the cyclopentanone substrate **5a** by the reaction of 2-(ethoxycarbonyl)cyclopentanone with 1-bromo-2-butyne. The cyclic substrate **5a** was treated with phenylboronic acid (**2a**) in the presence of [{Rh(OH)(cod)}$_2$] (0.05 equiv of Rh) in dioxane/H$_2$O (100:1) at room temperature for 6 h under a nitrogen atmosphere, and the resulting reaction mixture was then treated with aqueous NH$_4$Cl for 24 h to promote the retro-aldol process. As expected, the cycloheptanone **6a** was produced in 63% yield through phenyl addition and ring expansion [Eq. (2)].

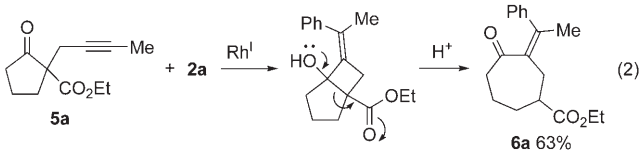

(2)

Table 1: Rhodium(I)-catalyzed acyl 1,3-migration in the reaction of **1** with **2**.[a]

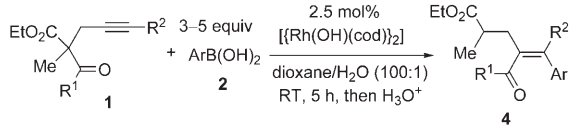

Entry	**1**	R^1	R^2	**2**	Ar	**4**	Yield [%][b]
1	**1a**	Ph	Me	**2b**	4-FC_6H_4	**4ab**	63
2	**1a**	Ph	Me	**2c**	4-MeC_6H_4	**4ac**	75
3	**1a**	Ph	Me	**2d**	3-ClC_6H_4	**4ad**	66
4	**1a**	Ph	Me	**2e**	3-$MeOC_6H_4$	**4ae**	77
5	**1b**	Ph	Et	**2a**	Ph	**4ba**	92
6	**1c**	Me	Et	**2a**	Ph	**4ca**	67
7	**1d**	Ph	TMS	**2a**	Ph	**4da**	25

[a] Reaction conditions: **1** (0.2 mmol), **2** (0.6–1.0 mmol), [{Rh(OH)(cod)}$_2$] (0.05 equiv of Rh) in dioxane/H$_2$O (2.0 mL/20 μL); then treatment with aqueous NH$_4$Cl. [b] Yields of isolated products. cod = cyclooctadiene.

As listed in Table 2, the catalytic ring-expansion process worked well with substrates of five-, six-, and eight-membered-ring structures to give the seven-, eight-, and ten-membered-ring products, respectively, in yields ranging from 49% to 66%.[14] Cyclic 1,3-diketones **5f** and **5g** also underwent the analogous ring-expansion reaction. The ring opening of intermediate cyclobutanols formed from substrates **5c**, **5d**, and **5f** under the weakly acidic conditions proceeded more slowly than that of **5a** and thus required longer times for completion (see Supporting Information).

In summary, a new rhodium(I)-catalyzed acyl 1,3-migration reaction of acetylenic β-ketoesters was developed in which an intermediate organorhodium(I) species undergoes intramolecular nucleophilic addition to a ketone carbonyl group in a 4-*exo* process, which is followed by cyclobutane cleavage through a retro-aldol reaction. On the basis of this new 1,3-migration reaction, medium-sized carbocyclic rings

 © 2005 Wiley-VCH Verlag GmbH & Co. KGaA, Weinheim

Table 2: Rhodium(I)-catalyzed two-carbon-atom ring expansion of **5** with **2a**.[a]

Entry	Substrate **5**	Product **6**	Yield [%][b]
1	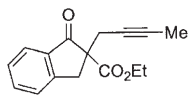 **5b**	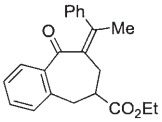 **6b**	51
2	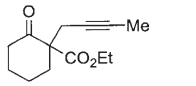 **5c**	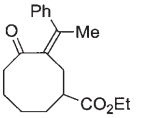 **6c**	49
3	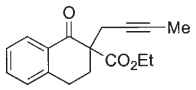 **5d**	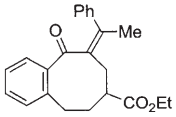 **6d**	58
4	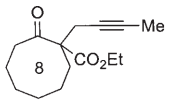 **5e**	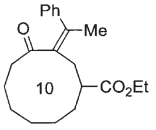 **6e**	54[c]
5	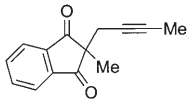 **5f**	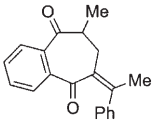 **6f**	57
6	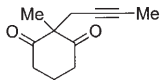 **5g**	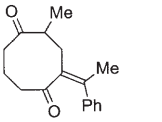 **6g**	66

[a] Reaction conditions: **5** (0.2 mmol), **2** (1.0 mmol), [{Rh(OH)(cod)}$_2$] (0.05 equiv of Rh), room temperature, dioxane/H_2O (2.0 mL/20 μL); then treatment with aqueous NH_4Cl. [b] Yields of isolated products. [c] 100 °C

that are otherwise difficult to form were constructed in a simple operation from readily available substrates.

Received: July 28, 2005
Published online: October 31, 2005

Keywords: acyl migration · boron · cyclizations · rhodium · ring expansion

[1] For reviews, see: a) K. Fagnou, M. Lautens, *Chem. Rev.* **2003**, *103*, 169–196; b) T. Hayashi, K. Yamasaki, *Chem. Rev.* **2003**, *103*, 2829–2844.
[2] T. Miura, M. Shimada, M. Murakami, *Synlett* **2005**, 667–669.
[3] a) J. E. Baldwin in *Comprehensive Organic Synthesis, Vol. 5* (Eds.: B. M. Trost, I. Fleming), Pergamon, Oxford, **1991**, pp. 63–84; b) M. T. Crimmins in *Comprehensive Organic Synthesis, Vol. 5* (Eds.: B. M. Trost, I. Fleming), Pergamon, Oxford, **1991**, pp. 123–150.
[4] For 1,2-addition of aryl rhodium(I) to an internal alkyne, see: a) T. Hayashi, K. Inoue, N. Taniguchi, M. Ogasawara, *J. Am. Chem. Soc.* **2001**, *123*, 9918–9919; b) M. Lautens, M. Yoshida, *Org. Lett.* **2002**, *4*, 123–125.
[5] An analogous 1,2-addition to dimethyl 2-(but-2-ynyl)-2-methylmalonate, which bears a methoxycarbonyl group instead of the benzoyl group in **1a**, proceeded much more slowly: T. Miura, M. Shimada, M. Murakami, *J. Am. Chem. Soc.* **2005**, *127*, 1094–1095.
[6] For intramolecular addition of an organorhodium(I) species to a ketone carbonyl group, see: a) A. Takezawa, K. Yamaguchi, T. Ohmura, Y. Yamamoto, N. Miyaura, *Synlett* **2002**, 1733–1735; b) D. F. Cauble, J. D. Gipson, M. J. Krische, *J. Am. Chem. Soc.* **2003**, *125*, 1110–1111; c) R. Shintani, K. Okamoto, Y. Otomaru, K. Ueyama, T. Hayashi, *J. Am. Chem. Soc.* **2005**, *127*, 54–55; d) T. Matsuda, M. Makino, M. Murakami, *Angew. Chem.* **2005**, *117*, 4684–4687; *Angew. Chem. Int. Ed.* **2005**, *44*, 4608–4611.
[7] When the ^{1}H NMR spectrum of the crude reaction mixture was measured prior to chromatographic purification, we observed about 50% of **3** and approximately 20% of **4aa**.
[8] Ring opening of a cyclobutanol skeleton by a retro-aldol reaction occurred much more readily than β-carbon elimination of rhodium(I) cyclobutanolates: a) T. Matsuda, M. Makino, M. Murakami, *Bull. Chem. Soc. Jpn.* **2005**, *78*, 1528–1533; see also reference [6d]; for a review on β-carbon elimination from palladium(II) cyclobutanolate, see: b) T. Nishimura, S. Uemura, *Synlett* **2004**, 201–216.
[9] For examples of photochemical acyl 1,3-migration of β,γ-unsaturated cyclic ketones, see: a) H. Suginome, M. Takemura, N. Shimoyama, K. Orito, *J. Chem. Soc. Perkin Trans. 1* **1991**, 2721–2723; b) J. Shin, W. Fenical, *J. Org. Chem.* **1991**, *56*, 1227–1233.
[10] Although *o*-tolylboronic acid underwent 1,2-addition to the carbon–carbon triple bond, the resultant alkenyl rhodium(I) intermediate was not reactive enough for the addition to the benzoyl group.
[11] A 1,2-adduct formed by addition of a phenylrhodium species with the opposite regiochemistry was obtained in 47%.
[12] For examples of ring expansion through intramolecular carbonyl addition/ring opening, see: a) C.-J. Li, D.-L. Chen, Y.-Q. Lu, J. X. Haberman, J. T. Mague, *J. Am. Chem. Soc.* **1996**, *118*, 4216–4217; b) A. E. Imai, Y. Sato, M. Nishida, M. Mori, *J. Am. Chem. Soc.* **1999**, *121*, 1217–1225; c) U. K. Tambar, B. M. Stoltz, *J. Am. Chem. Soc.* **2005**, *127*, 5340–5341; for a review, see: d) P. M. Wovkulich in *Comprehensive Organic Synthesis, Vol. 1* (Eds.: B. M. Trost, I. Fleming), Pergamon, Oxford, **1991**, pp. 892–897.
[13] For ring expansion through photochemical [2+2] cycloaddition/ring opening, see: J. D. Winkler, C. M. Bowen, F. Liotta, *Chem. Rev.* **1995**, *95*, 2003–2020, and references therein.
[14] The major by-products were the simple 1,2-adducts formed by addition to the carbon–carbon triple bond.

 © 2005 Wiley-VCH Verlag GmbH & Co. KGaA, Weinheim

Surface Chemistry

DOI: 10.1002/anie.200502160

Oxygen Storage at the Metal/Oxide Interface of Catalyst Nanoparticles**

Tobias Schalow, Mathias Laurin, Björn Brandt, Swetlana Schauermann, Sebastien Guimond, Helmut Kuhlenbeck, David E. Starr, Shamil K. Shaikhutdinov, Jörg Libuda, and Hans-Joachim Freund*

Numerous processes in chemical industry, in emission control, and in energy technology involve the application of heterogeneous catalysts consisting of nanometer-sized metal particles on high-surface-area oxides.[1,2] Often, it is found that the activity of these so-called supported catalysts critically depends not only on the size and morphology of the metal particles, but also on the support itself. At the microscopic level, the origins of such effects are poorly understood in most cases. The situation turns out to be particularly intricate for the case of oxidation reactions on supported transition-metal particles. Here, many different oxygen species may be present under reaction conditions, for example, different types of chemisorbed oxygen, subsurface oxygen, surface oxides, and bulk oxides (see e.g. Refs. [3–16] and references therein). On some transition metals such as Ru, it has indeed been shown that not the metal surface itself but surface oxides formed under reaction conditions may represent the active phase of the catalyst.[17] Also for Pd surfaces strong changes in activity have recently been observed at higher partial pressures and have been related to surface oxidation processes (Ref. [18], see also Refs. [19,20]). In most cases, however, it is unclear what the role of the different oxygen species may be during oxidation reactions.

In this contribution, we suggest a new mechanism for oxygen storage and oxidation on oxide-supported metal catalysts: For a Pd/Fe_3O_4 model catalyst it is shown that large amounts of oxygen can be reversibly accumulated in form of a thin Pd oxide layer at the metal/oxide interface. From this interface oxide layer, which is stabilized by the support, oxygen is released and migrates back onto the metallic Pd surface, where it then is available for oxidation reactions. This storage mechanism may play an important role for the kinetics of oxidation reactions, in particular under non-steady-state conditions.

The experimental approach leading to these insights is summarized in Figure 1: Briefly, we employ well-defined supported model catalysts, which are characterized in detail by surface-science methods. These systems are then probed with respect to their reactivity using molecular beam techniques. The use of model systems is motivated by the high degree of complexity of real catalysts and by experimental restrictions concerning the application of surface-science methods to these systems. Both points often preclude detailed insights into the surface chemistry and structure of real catalysts. Supported model catalysts, on the other hand, provide clean and well-defined surfaces with strongly reduced complexity and are easily accessible for most experimental techniques available in surface science.[21–23]

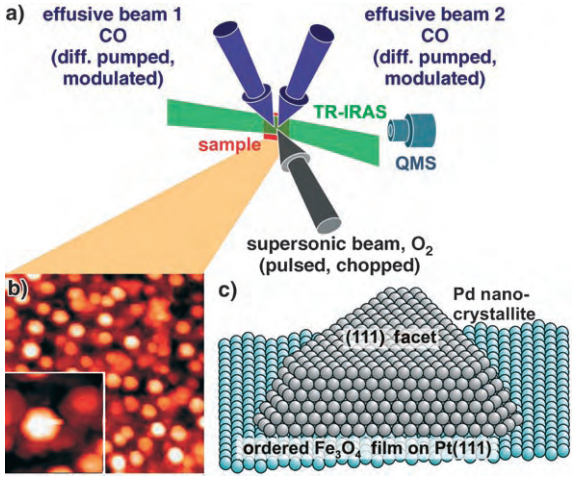

Figure 1. a) Representation of the molecular beam setup; b) STM image (100 nm × 100 nm, inset: 20 nm × 20 nm) of the Pd nanoparticles on Fe_3O_4/Pt(111) (after annealing at 600 K and oxidation and reduction at 500 K); c) model of the Pd nanoparticles.

In this study, we used Pd nanoparticles grown by metal-vapor deposition on a thin, well-ordered Fe_3O_4 film on Pt(111). The model catalyst was prepared in situ under ultrahigh-vacuum (UHV) conditions. Structure, morphology, and adsorption properties of both the Fe_3O_4 support[24,25] and the Pd particles were previously investigated in detail.[26] In Figure 1b a scanning tunnelling microscopy (STM) image of the Pd particles is shown as well as a model schematically illustrating their morphology. The three-dimensional particles have an average diameter of approximately 7 nm and contain around 3000 Pd atoms per particle. They are characterized by a well-defined crystalline shape, grow in (111) orientation with respect to the substrate, and expose a majority of (111) as well as a smaller fraction of (100) sites.

In order to study the interaction of the supported model catalyst with oxygen, we employed molecular beam (MB) methods. Molecular beams are well-established among the major experimental tools to study surface kinetics and dynamics[27–29] (for some recent examples in model catalysis see Refs. [30–32]). In this work, the technique is utilized to

[*] Dipl.-Ing. T. Schalow, Dipl.-Chem. M. Laurin, Dipl.-Chem. B. Brandt, Dipl.-Chem. S. Schauermann, Dipl.-Chem. S. Guimond, Dr. H. Kuhlenbeck, Dr. D. E. Starr, Dr. S. K. Shaikhutdinov, Priv.-Doz. Dr. J. Libuda, Prof. Dr. H.-J. Freund
Fritz-Haber-Institut der Max-Planck-Gesellschaft
Faradayweg 4–6, 14195 Berlin (Germany)
Fax: (+49) 30-8413-4309
E-mail: libuda@fhi-berlin.mpg.de

[**] This work has been funded by the Deutsche Forschungsgemeinschaft (SPP 1091) and the Fonds der Chemischen Industrie. The authors are particularly grateful to the BESSY staff for technical support.

© 2005 Wiley-VCH Verlag GmbH & Co. KGaA, Weinheim

quantitatively determine the oxygen uptake and release under exactly controlled and isothermal conditions. The MB apparatus used allows us to superimpose up to three independent reactant beams on the sample surface and facilitates simultaneous gas-phase detection (quadrupole mass spectrometry, QMS) and surface spectroscopy (time-resolved IR reflection absorption spectroscopy, TR-IRAS, see Figure 1 a).[33]

To quantitatively probe the oxygen uptake and release we performed pulsed CO titration experiments as shown in Figure 2: First, the model surface was exposed to a pulse of oxygen. After a defined delay time, short pulses of CO were applied in order to probe oxygen release by means of oxidation of CO to CO_2. The latter desorbs immediately and can be detected in the gas phase. In all experiments a supersonic beam of $^{18}O_2$ was employed in order to minimize the background signal. Experimentally, this type of pulsed titration technique allows an exact quantification of the CO_2 yield, even at very low reaction rates.

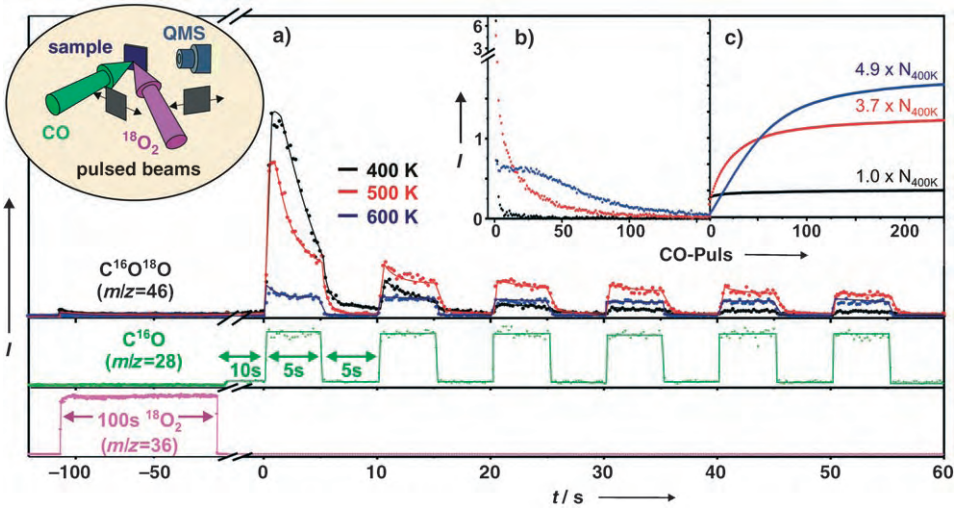

Figure 2. Pulsed CO titration experiment on the Pd/Fe_3O_4 model catalyst after oxygen exposure at different sample temperatures. Initially the model surface is exposed to a pulse of $^{18}O_2$ (100 s). After a delay time (10 s), pulses of CO (on-time 5 s, off-time 5 s) are applied to remove oxygen stored on the catalyst surface in form of CO_2: a) CO_2 formation rate; b) CO_2 yield per CO pulse; c) total CO_2 yield.

Pulsed titration experiments were performed as a function of surface temperature. At 400 K we find very high initial reaction rates, which drop to the background level within few CO pulses. The observations indicate high initial reaction probabilities and low oxygen uptake. This type of behavior is consistent with the presence of solely chemisorbed oxygen on the Pd particles and agrees well with what is expected on the basis of previous studies.[34–36] (The expected coverages of atomic oxygen would be around 0.25 monolayers (ML) on Pd(111) and around 0.5 ML on Pd(100), see Refs. [9,12] and references therein).

With increasing oxidation temperature (500–600 K) a surprising behavior is observed: The CO_2 formation rate in the first CO pulse decreases, but subsequently the rate remains finite for a long time, that is, up to 50 to 100 CO pulses. Simultaneously, the total CO_2 yield, obtained by integrating over all pulses (see Figure 2 b, c), increases drastically, indicating a nearly fivefold increase in the total oxygen release between 400 K and 600 K. Two conclusions can be drawn from these observations:

a) Partial surface oxidation of metal particles: The large oxygen release cannot be explained by surface chemisorption only. Alternatively, oxygen uptake and release by means of oxidation and reduction of the Fe_3O_4 support could be invoked. However, titration experiments on isotopically labeled supports show that oxygen exchange with the support is very slow under the experimental conditions applied in this work.[37] Therefore, we attribute the storage effect to the formation of a thin oxide layer on the Pd particles. It is well established that on Pd single crystals surface oxides can be formed under similar conditions.[10–16] Recently detailed structure models for surface oxides on both Pd(111)[13] and Pd(100)[14] were suggested on the basis of combined theoretical and experimental work. The oxygen densities in surface oxides drastically exceeds those in chemisorbed layers, allowing oxygen storage and subsequent release.[38] It is expected, however, that the oxidation behavior of small supported particles may differ from the behavior observed on single-crystal surfaces. Differences may arise, for example, from the simultaneous presence of different types of facets and low coordinated sites, from lattice distortions, and from the particle support interface. As will be discussed in a forthcoming publication,[37] the process of surface oxidation can be monitored and analyzed in detail by means of IRAS using CO as a probe molecule. For the work discussed here, the most important point to note is that metallic and oxidized surface areas coexist on the Pd particles over a large temperature region, ranging from approximately 450 K to 600 K. Within this temperature region the fraction of the metallic part decreases with increasing oxidation temperature.

b) Reactivity of partially oxidized metal particles: The low initial reaction rate after oxidation at 600 K shows that the CO reaction probability on the surface oxide is drastically lower than on the metallic surface. Consequently, for a partially oxidized surface the CO_2 yield of the first CO pulse can be interpreted as the amount of chemisorbed oxygen adsorbed on the metallic part of the Pd particles. With increasing oxidation temperatures, the amount of chemisorbed oxygen decreases as a result of the increasing fraction of the surface covered by the oxide. This result fits well with IRAS work mentioned above, showing that after oxidation at 600 K a major fraction of the particle surface is covered by surface oxides, whereas after oxidation at

 © 2005 Wiley-VCH Verlag GmbH & Co. KGaA, Weinheim

500 K only a minor part is oxidized. Accordingly, the CO_2 yield of the following CO pulses can be assigned to CO oxidation involving oxygen originating from the oxide layer. Two points are noteworthy here: Firstly, the amount of oxygen stored at 500 K is large in spite of the small degree of surface oxidation (see Figure 2c)). As shown below, this effect can be attributed to a preferential oxidation of the particle/support interface. Secondly, the CO_2 yield per pulse is initially higher at lower surface oxide coverage (500 K oxidation) than at higher coverage (600 K oxidation). This finding indicates that CO does not react directly with surface oxide. Instead, we suggest that the reduction mechanism proceeds predominantly by slow decomposition of the oxide, releasing oxygen onto the metallic Pd parts, where it readily reacts with coadsorbed CO. This model is in agreement with a detailed analysis of the transient behavior of pulsed CO titration experiments.[37] We conclude that the surface oxide layer, covering part of the particle surface, acts as an oxygen reservoir allowing storage and release of oxygen in a reversible fashion.

In view of the above results showing partial oxidation of the Pd surface, the question arises which parts of the nanoparticle are initially oxidized and, therefore, are primarily responsible for the oxygen-storage mechanism. To address these questions we have performed high-resolution photoelectron spectroscopy (PES) using synchrotron radiation (see Figure 3). For the clean Pd particles before exposure to oxygen, the Pd $3d_{5/2}$ region contains two features: a Pd bulk signal (binding energy, BE = 335.0–335.1 eV) and a surface- and interface-derived component (BE = 335.3–335.6 eV) (compare e.g. Refs. [13,14]). The surface sensitivity of the experiment can be varied by changing the photon energy. With increasing photon energy ($h\nu$) the kinetic energy of the photoelectrons increases and so does the electron escape length λ ($h\nu = 465$ eV, $\lambda \approx 4$ Å; $h\nu = 840$ eV, $\lambda \approx 9$ Å[39]). As a result, the bulk feature becomes more prominent at higher photon energy, that is, at a lower degree of surface sensitivity.

After oxidation at 600 K (at similar oxygen doses as those in MB experiments), components at higher BE are observed, which are characteristic for oxygen chemisorption and surface oxidation. Based on high-resolution PES work on single-crystal surfaces,[13,14] the Pd $3d_{5/2}$ region can be qualitatively decomposed into three regions: 1) a low BE component (335.0–335.1 eV) related to bulk Pd metal, 2) an intermediate BE region (around 335.7 eV) containing contributions from metallic Pd coordinated to chemisorbed oxygen and from specific Pd atoms in thin oxide layers, and 3) a high BE region (around 336.6–336.7 eV) due to Pd atoms in thin oxide layers only. A more detailed assignment is precluded by the large number of nonequivalent Pd atoms, exposed by the supported particle system.

Two main conclusions can be drawn from the spectra. First, the constant BE of the Pd bulk feature upon oxidation indicates that the metallic nature of the particle core is preserved and rules out significant dissolution of oxygen in the Pd lattice, the latter result being in agreement with recent theoretical studies.[16] The most surprising observation, however, is the decreasing intensity of the metallic bulk signal with increasing photon energy (similar effects also observed at other photon energies and oxidation temperatures). This finding indicates that the Pd oxide layer is not preferentially formed on the outer particle surface, that is, at the Pd/vacuum interface, but rather below the particles, that is, at the metal/support interface. As a driving force for preferential formation of a Pd interface oxide we suggest that the oxide film is stabilized by interaction with the iron oxide support. Further evidence for this hypothesis is derived from transient MB experiments showing that there is a dynamic equilibrium between chemisorbed oxygen on the metallic Pd and the interface oxide, strongly favoring formation of the latter.[37] This observation is in contrast to the oxidation behavior of Pd single crystals, on which surface-oxide formation occurs at high oxygen coverage only.[16] Finally, it should be noted that the formation of a Pd interface oxide is in agreement with the MB and IRAS experiments discussed above, showing that at 500 K substantial oxygen storage occurs without a pronounced loss of the metallic Pd surface.

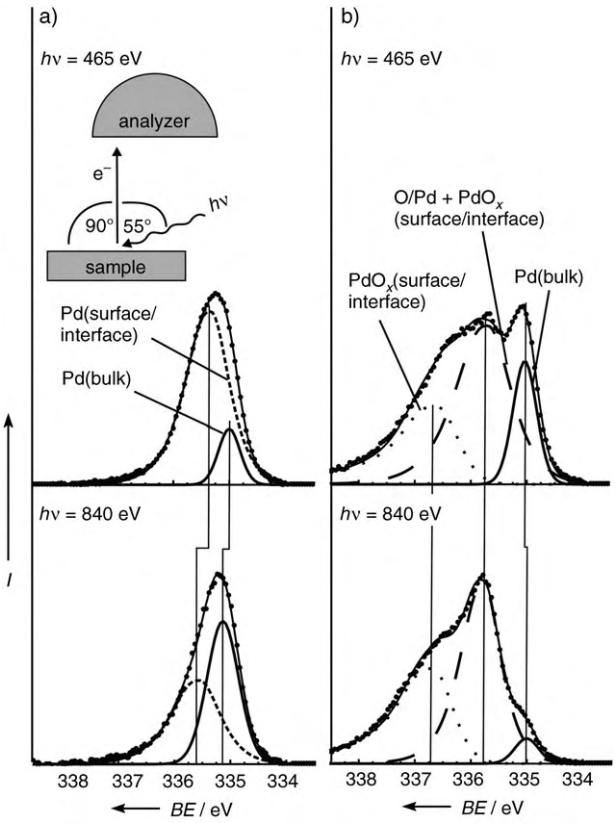

Figure 3. High-resolution core-level spectra of Pd $3d_{5/2}$ region after preparation of the model catalyst at different photon energies: a) immediately after Pd deposition and annealing in UHV to 600 K; b) after oxygen exposure at 600 K (oxygen dose: 3×10^{17} molecules cm^{-2}).

A schematic summary of our proposed oxygen-storage and CO-oxidation mechanism is depicted in Figure 4: We have shown that for a Pd/Fe_3O_4 model catalyst reversible oxygen storage and release occurs at 500 K and above through formation of thin Pd oxide layers. Preferentially the

 © 2005 Wiley-VCH Verlag GmbH & Co. KGaA, Weinheim

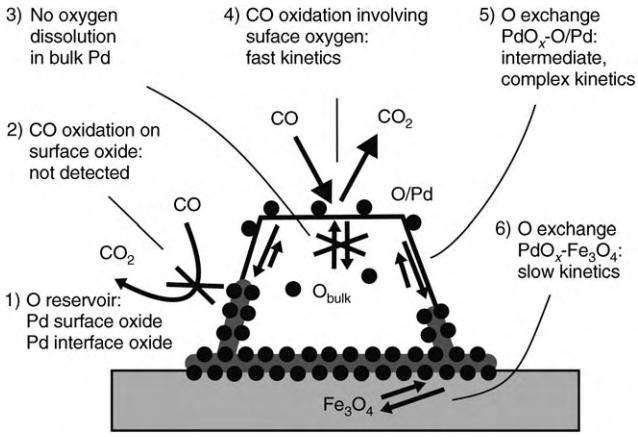

Figure 4. Illustration of the oxygen storage and CO oxidation mechanism on the Pd/Fe_3O_4-supported model catalyst.

oxide layer forms at the particle/support interface due to stabilization by the Fe_3O_4 support, before—under more drastic conditions—oxidation of the complete particle surface occurs. A dynamic equilibrium is established between oxygen chemisorbed on the metal and oxygen incorporated into the interface or surface oxides. As a result, the oxide layers can act as an oxygen reservoir for oxidation reactions. For the specific case of CO oxidation, the reaction with chemisorbed oxygen on metallic Pd is fast, whereas the reaction probability on the surface oxide is low. Thus CO oxidation occurs by release of oxygen from the interface oxide onto the metal surface, where it subsequently reacts with coadsorbed CO. Large amounts of oxygen can be stored and released by this mechanism, without substantial changes of the metal surface available. It may be anticipated that similar storage mechanisms might be active for other dispersed metal catalysts on reducible or irreducible oxide supports as well.

Experimental Section

MB and IRAS experiments were performed in a UHV apparatus at the Fritz-Haber-Institut (Berlin) which allows up to three beams to be crossed on the sample surface.[33] The CO beam (Linde, 99.997%, further purified by a gas filter (Mykrolis)) was generated by a doubly differentially pumped effusive multichannel array source and modulated by a motorized shutter. The $^{18}O_2$ beam (Campro Scientific, 95% ^{18}O, 99.7% purity) was generated from a triply differentially pumped supersonic expansion and modulated using a solenoid valve. Typical intensities of the beams were 2.1×10^{14} molecules $cm^{-2}s^{-1}$ for CO and 4.6×10^{14} molecules $cm^{-2}s^{-1}$ for O_2. For measuring the reaction rate, an automated QMS system (ABB Extrel) was employed. PES was performed at BESSY II, Beamline UE52-PGM1 with a 200-mm hemispherical energy analyzer (Scienta SES200). The energy resolution was approximately 100 meV at $h\nu = 465$ eV and 160 meV at $h\nu = 840$ eV.

The thin ($\approx$100 Å) Fe_3O_4 film was grown on Pt(111) by repeated cycles of Fe (>99.99%, Goodfellow) deposition and subsequent oxidation (see Refs. [24–26] for details). Cleanliness and quality of the oxide film was checked by IRAS of adsorbed CO (for MB experiments) and low-energy electron diffraction. Pd particles (>99.9%, Goodfellow) were grown by physical vapor deposition (Pd coverage: 2.7×10^{15} atoms cm^{-2}, sample temperature: 100 K) using a commercial evaporator (Focus, EFM 3, flux calibrated by a quartz microbalance). The particles were stabilized by annealing to 600 K in UHV and subsequent oxidation/reduction cycles at 500 K.

Received: June 21, 2005
Published online: October 25, 2005

Keywords: heterogeneous catalysis · model catalysis · nanoparticles · reaction kinetics · surface chemistry

[1] G. Ertl, H. Knoezinger, J. Weitkamp in *Handbook of Heterogeneous Catalysis* (Eds.: G. Ertl, H. Knoezinger, J. Weitkamp), VCH, Weinheim, **1997**.
[2] J. M. Thomas, W. J. Thomas, *Principle and Practice of Heterogeneous Catalysis*, VCH, Weinheim, **1997**.
[3] H. Conrad, G. Ertl, J. Küppers, E. E. Latta, *Surf. Sci.* **1977**, *65*, 235.
[4] R. Imbihl, J. E. Demuth, *Surf. Sci.* **1986**, *173*, 395.
[5] S.-L. Chang, P. A. Thiel, *J. Chem. Phys.* **1988**, *88*, 2071.
[6] X. Guo, A. Hoffman, J. T. Yates, Jr., *J. Chem. Phys.* **1989**, *90*, 5787.
[7] V. A. Bondzie, P. Kleban, D. J. Dwyer, *Surf. Sci.* **1996**, *347*, 319.
[8] E. H. Voogt, A. J. M. Mens, J. W. G. O. L. J. Gijzeman, *Surf. Sci.* **1997**, *373*, 210.
[9] F. P. Leisenberger, G. Koller, M. Sock, S. Surnev, M. G. Ramsey, F. P. Netzer, B. Klötzer, K. Hayek, *Surf. Sci.* **2000**, *445*, 380.
[10] V. A. Bondzie, P. H. Kleban, D. J. Dwyer, *Surf. Sci.* **2000**, *465*, 266.
[11] G. Zheng, E. I. Altman, *Surf. Sci.* **2000**, *462*, 151.
[12] G. Zheng, E. I. Altman, *Surf. Sci.* **2002**, *504*, 253.
[13] E. Lundgren, G. Kresse, C. Klein, M. Borg, J. N. Andersen, M. De Santis, Y. Gauthier, C. Konvicka, M. Schmid, P. Varga, *Phys. Rev. Lett.* **2002**, *88*, 246103.
[14] M. Todorova, E. Lundgren, V. Blum, A. Mikkelsen, S. Gray, J. Gustafson, M. Borg, J. Rogal, K. Reuter, J. N. Andersen, M. Scheffler, *Surf. Sci.* **2003**, *541*, 101.
[15] E. Lundgren, J. Gustafson, A. Mikkelsen, J. N. Andersen, A. Stierle, H. Dosch, M. Todorova, J. Rogal, K. Reuter, M. Scheffler, *Phys. Rev. Lett.* **2004**, *92*, 046101.
[16] M. Todorova, K. Reuter, M. Scheffler, *Phys. Rev. B* **2005**, *71*, 195403.
[17] H. Over, Y. D. Kim, A. P. Seitsonen, S. Wendt, E. Lundgren, M. Schmid, P. Varga, A. Morgante, G. Ertl, *Science* **2000**, *287*, 1474.
[18] B. L. M. Hendriksen, S. C. Bobaru, J. W. M. Frenken, *Surf. Sci.* **2004**, *552*, 229.
[19] M. R. Basset, R. Imbihl, *J. Chem. Phys.* **1990**, *93*, 811.
[20] J. Hartmann, R. Imbihl, W. Vogel, *Catal. Lett.* **1994**, *28*, 373.
[21] C. R. Henry, *Surf. Sci. Rep.* **1998**, *31*, 231.
[22] H.-J. Freund, M. Bäumer, J. Libuda, T. Risse, G. Rupprechter, S. Shaikhutdinov, *J. Catal.* **2003**, *216*, 223.
[23] D. W. Goodman, *J. Catal.* **2003**, *216*, 213.
[24] W. Weiss, W. Ranke, *Prog. Surf. Sci.* **2002**, *70*, 1.
[25] C. Lemire, R. Meyer, V. Henrich, S. K. Shaikhutdinov, H.-J. Freund, *Surf. Sci.* **2004**, *572*, 103.
[26] R. Meyer, S. K. Shaikhutdinov, H.-J. Freund, *Z. Phys. Chem.* **2004**, *218*, 2004.
[27] M. P. D'Evelyn, R. J. Madix, *Surf. Sci. Rep.* **1984**, *3*, 413.
[28] C. T. Rettner, D. J. Auerbach, *J. Chem. Phys.* **1996**, *105*, 8842.
[29] A. W. Kleyn, *Chem. Soc. Rev.* **2003**, *32*, 87.
[30] S. Schauermann, J. Hoffmann, V. Johánek, J. Hartmann, J. Libuda, H.-J. Freund, *Angew. Chem.* **2002**, *114*, 2643; *Angew. Chem. Int. Ed.* **2002**, *41*, 2532.
[31] V. Johanek, S. Schauermann, M. Laurin, J. Libuda, H.-J. Freund, *Angew. Chem.* **2003**, *115*, 3143; *Angew. Chem. Int. Ed.* **2003**, *42*, 3035.
[32] J. Libuda, H.-J. Freund, *Surf. Sci. Rep.*, in press.

 © 2005 Wiley-VCH Verlag GmbH & Co. KGaA, Weinheim

[33] J. Libuda, I. Meusel, J. Hartmann, H.-J. Freund, *Rev. Sci. Instrum.* **2000**, *71*, 4395.
[34] T. Engel, G. Ertl, *J. Chem. Phys.* **1978**, *69*, 1267.
[35] L. Piccolo, C. Becker, C. R. Henry, *Appl. Surf. Sci.* **2000**, *164*, 156.
[36] J. Libuda, I. Meusel, J. Hoffmann, J. Hartmann, L. Piccolo, C. R. Henry, H.-J. Freund, *J. Chem. Phys.* **2001**, *114*, 4669.
[37] T. Schalow, B. Brandt, M. Laurin, J. Libuda, H.-J. Freund, in preparation.
[38] G. Zheng, E. I. Altmann, *J. Phys. Chem. B* **2002**, *106*, 1048.
[39] S. Tanuma, C. J. Powell, D. R. Penn, *Surf. Interface Anal.* **1991**, *17*, 927.

 © 2005 Wiley-VCH Verlag GmbH & Co. KGaA, Weinheim

Carbohydrate Synthesis

DOI: 10.1002/anie.200502742

Short De Novo Synthesis of Fully Functionalized Uronic Acid Monosaccharides**

*Mattie S. M. Timmer, Alexander Adibekian, and Peter H. Seeberger**

Dedicated to Professor Albert Eschenmoser on the occasion of his 80th birthday

The biological importance of carbohydrates in a host of fundamental cellular processes has dramatically increased the demand for pure, synthetically derived oligosaccharides.[1] Over the past 100 years, chemical methods for the assembly of all classes of carbohydrates have been developed. This has resulted in sophisticated glycosylation reactions that allow the formation of even the most difficult glycosidic linkages with a high degree of selectivity.[2] More recently, automated methods for the rapid combination of monosaccharide building blocks on a solid phase were reported.[3] The time required to assemble an oligosaccharide has been reduced more than 100-fold, and as a result, the need for substantial quantities of and rapid access to fully functionalized building blocks has increased.

[*] Dr. M. S. M. Timmer, A. Adibekian, Prof. Dr. P. H. Seeberger
Laboratory for Organic Chemistry
Swiss Federal Institute of Technology (ETH) Zürich
ETH Hönggerberg HCI F315
Wolfgang-Pauli-Strasse 10, 8093 Zürich (Switzerland)
Fax: (+41) 44-633-1235
E-mail: seeberger@org.chem.ethz.ch

[**] This research was supported by the ETH Zürich, a Niels–Stensen Postdoctoral Fellowship (to M.T.) and a Kekulé Fellowship from the Fonds dre Chemischen Industrie (to A.A.). We thank Professor D. Seebach for helpful discussions.

Supporting information for this article is available on the WWW under http://www.angewandte.org or from the author.

A typical monosaccharide building block used in oligosaccharide assembly is equipped with different protecting groups that mask the hydroxy and amine functions and an anomeric leaving group that can be activated to induce the formation of a glycosidic linkage. These differentially protected and functionalized monosaccharides have traditionally been accessed from naturally occurring sugar starting materials through a series of protection-deprotection maneuvers. Such a process establishes the desired protecting group pattern and typically requires 6–20 steps depending on the sugar, the protecting group pattern, and the anomeric leaving group.[4]

To avoid these lengthy procedures for producing building blocks for the assembly of larger structures, efforts have been directed at the synthesis of orthogonally protected hexose monosaccharides from noncarbohydrate precursors.[5] The landmark syntheses of hexoses by Masamune, Sharpless, and co-workers[6] were enabled by the ability of new synthetic methods to introduce specific stereogenic centers selectively. The aldol reaction has also proved to be a particularly useful tool in the creation of hexoses from simple precursors. Mukaiyama and co-workers[7] reported a stereoselective synthesis of pentoses and hexoses through the use of silyl enol ethers in aldol condensations to furnish partially protected pentoses and hexoses. Unfortunately, these fundamental explorations were not investigated further than the initial proof of concept. Recently, proline-catalyzed aldol reactions were used to fashion aldo- and ketohexose precursors for Mukaiyama-type aldol reactions, which were then used to synthesize partially protected glucose, mannose, and allose monosaccharides.[8] The yields and selectivities reported for these transformations, although excellent, were highly dependent on the specific protecting groups that were chosen.

Oligosaccharide assembly requires monosaccharide building blocks that contain orthogonal protecting-group patterns and a readily activated anomeric leaving group. Herein we report a convergent route to orthogonally protected D-glucuronic and L-iduronic acid thioglycoside building blocks, which are commonly used in the assembly of heparin oligosaccharides.[9] This approach relies on the selective Mukaiyama-type aldol reaction[10] that unifies a silyl enol ether and a thioacetal-containing aldehyde (derived from the chiral pool).

Retrosynthetic analysis of the uronic acids **A** (Scheme 1) revealed that the fully protected uronic acid thioglycosides could be obtained through cyclization of the linear hexoses **B**. The open-chain hexoses can be formed, in turn, through a Mukaiyama-type aldol reaction of an appropriately protected ketene acetal **C** with a thioacetal-containing aldehyde **D**.

Synthesis of the key thioacetal aldehydes **8** and **9** commenced with readily available L-arabinose (**1**; Scheme 2). The aldehyde was converted into the corresponding thioacetal by reaction with ethanethiol in the presence of hydrochloric acid.[11] Subsequent protection of the 4,5-diol with 2,2-dimethoxypropane furnished the crystalline acetonide **2**.[12] At this stage, the protecting-group patterns for the C2 and C3 hydroxy groups were selected. The reaction of **2** with NaH, in the presence of excess benzyl bromide, afforded

 © 2005 Wiley-VCH Verlag GmbH & Co. KGaA, Weinheim

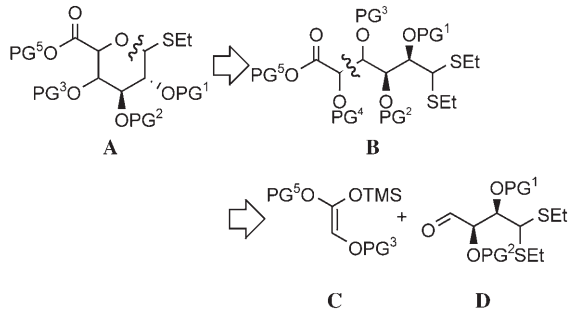

Scheme 1. Retrosynthetic analysis of uronic acid thioglycosides. PG = protecting group, TMS = trimethylsilyl.

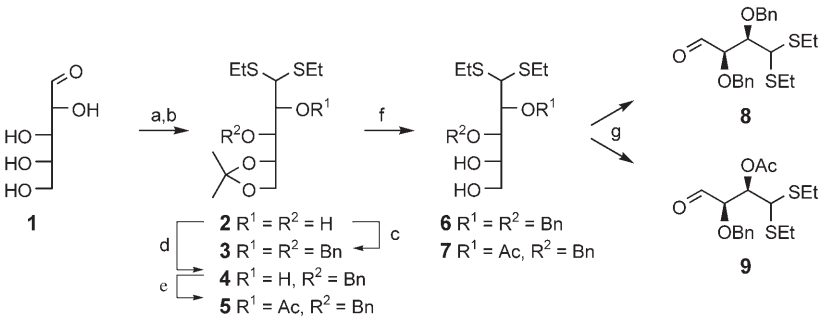

Scheme 2. Synthesis of differentially protected thioacetal aldehydes from L-arabinose: a) EtSH, conc. aq. HCl, 10 min, 77%; b) 2,2-dimethoxypropane, pyridinium *p*-toluenesulfonate (cat.), acetone, 1.5 h, 81%; c) BnBr, TBAI (cat.), NaH, DMF, 0°C, 4 h; d) nBu_2SnO, toluene, Dean–Stark trap; then BnBr, CsF, TBAI (cat.), DMF; e) Ac_2O, pyridine, 46% (two steps); f) $AcOH/H_2O$ (1:1, v/v), 50°C, 1 h, **6**: 62% (two steps: c and f), **7**: 92%; g) $NaIO_4$, H_2O/THF, 0°C, 15 min, **8**: 82%, **9**: 80%. Bn = benzyl, DMF = *N*,*N*-dimethylformamide, TBAI = tetrabutylammonium iodide.

dibenzylarabinoside **3**, whereas formation of a tin ketal of the diol **2** and subsequent monobenzylation gave **4**. After acetylation of the remaining hydroxy group in **4**, selectively protected **5** was isolated in 46% overall yield together with 45% of the 2-*O*-benzyl-3-*O*-acetyl regioisomer. Deprotection of the acetal groups in **3** and **5** was followed by sodium periodate mediated cleavage of the resulting vicinal diols to form the desired aldehydes **8** and **9** in very good overall yields. Notably, these two key intermediates are derived from cheap, commercially available starting materials (L-arabinose) through straightforward and high-yielding transformations that are readily scalable.

After this efficient route for the synthesis of thioacetal aldehydes was established, the aldol reaction/cyclization sequence was explored (Scheme 3). The $BF_3{\cdot}Et_2O$ mediated aldol reaction[13] of aldehyde **8** with silyl enol ether **10**[14] gave a 1:1:1 mixture of three products as was determined by analysis of the ^1H NMR spectrum of the crude product mixture. The three individual aldol products were isolated by column chromatography and identified after conversion into the corresponding thiopyranosides. The free hydroxy groups of **11**, **14**, and **17** were first transformed into 9-fluorenylmethyl carbonates followed by cleavage of the silyl ether in the presence of pyridine·HF to obtain the alcohols **12**, **15**, and **18**, respectively, in good overall yields. Although initial attempts to effect cyclization under various acidic conditions proved to be challenging, NIS-promoted activation of the thioacetal led to the formation of pyranose carbohydrates **13**, **16**, and **19**, respectively, in quantitative yields.

At this stage, the absolute configurations of the pyranoses were established by the ^1H NMR coupling patterns of the carbohydrate ring protons. For compound **13**, the large coupling constants ($J = 8$–10 Hz) between 2-H, 3-H, 4-H, and 5-H provided the evidence to assign the *gluco* configuration. The *ido* configuration of **16** was assigned based on the characteristically small coupling constants ($J = 1$–3 Hz) for protons 2-H to 5-H. This configuration was further corroborated by the W coupling, $^4J_{2,4} = 1.0$ Hz, which is typical of a 2,4-diaxial-substituted pyranose. The coupling pattern for the less common altruronic acid **19** was in full accordance with the reported coupling constants for altroses.[15] Notably, no trace of the *galacto* uronic acid, the fourth possible isomer, was found. This absence can be rationalized through the assumption of a nonchelating, open-chain transition state that allows only the three C–C bond formations observed and not the sterically demanding *Si*, *Si* attack that would lead to the *galacto* isomer.

Once the absolute configurations of the aldol products had been determined, the selectivity of the aldol reaction was

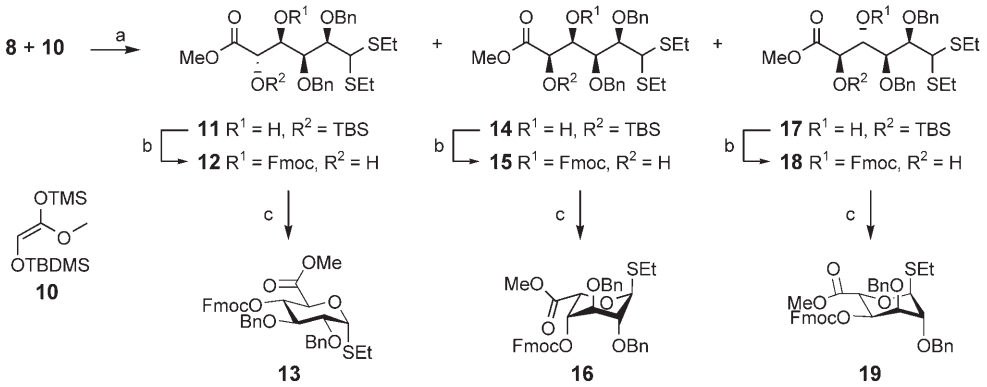

Scheme 3. Synthesis of L-glucuronic acid, L-iduronic acid, and L-altruronic acid building blocks: a) Method A: $BF_3{\cdot}Et_2O$, CH_2Cl_2, 0°C, 15 min, 93% (**11**/**14**/**17** = 1:1:1); Method B: $MgBr_2{\cdot}Et_2O$, toluene, −78→−30°C, 1 h, quant. (only **11**); b) 1. FmocCl, pyridine, 2 h; 2. HF·pyridine, THF, 16 h, **12**: 83%, **15**: 89%, **18**: 84% (two steps); c) NIS, CH_2Cl_2, 15 min, quant. (**13**, **16**, and **19**). Fmoc = 9-fluorenylmethoxycarbonyl, NIS = *N*-iodosuccinimide.

© 2005 Wiley-VCH Verlag GmbH & Co. KGaA, Weinheim

explored further. It has been shown previously that stereoselectivities can be significantly improved by the use of metal Lewis acids in a chelation-controlled Mukaiyama-type aldol reaction.[13] We envisaged that Felkin–Anh addition of a silyl enol ether to a aldehyde, in an open transition state, should preferentially furnish a glucuronic acid. Indeed, the $MgBr_2{\cdot}Et_2O$-promoted aldol reaction of the aldehyde **8** and the silyl enol ether **10** (Method B, Scheme 3) afforded glucuronic acid **11** in quantitative yield as a single diastereomer.

The $BF_3{\cdot}Et_2O$-mediated aldol reaction between the selectively protected aldehyde **9** and ketene acetal **10** was also examined (Scheme 4). Surprisingly, analysis of the crude

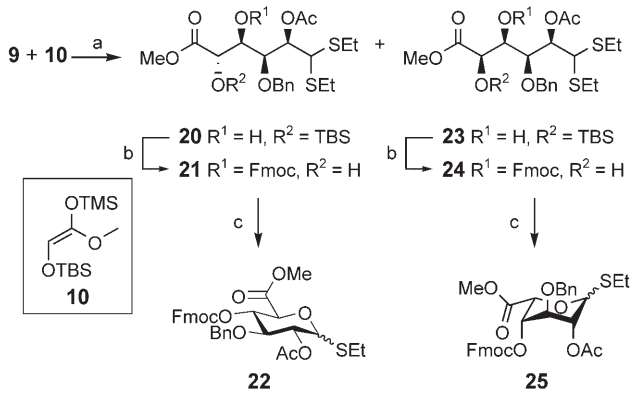

Scheme 4. Synthesis of selectively protected D-glucuronic and L-iduronic acid building blocks. a) Method A: $BF_3{\cdot}Et_2O$, CH_2Cl_2, 0 °C, 15 min, 95% (**20**/**23** = 3:2); Method B: $MgBr_2{\cdot}Et_2O$, toluene, −78 → −30 °C, 1 h, 98% (only **20**); b) 1. FmocCl, pyridine, 2 h; 2. HF·pyridine, THF, 16 h, **21**: 79%, **24**: 76% (two steps); c) NIS, CH_2Cl_2, 15 min, quant. (**22** and **25**), (α/β = 1:1).

reaction mixture by ^1H NMR spectroscopy showed a 3:2 ratio of two diastereomers, and only traces of a third. Separation of the individual isomers followed by protecting-group manipulations and NIS-mediated cyclization led to the isolation of the pyranoses **22** and **25**. Through comparison of the ^1H NMR coupling constants with those of the pyranosides **13** and **16**, thioglycoside **22** was identified as D-glucuronic acid and **25** as L-iduronic acid. Finally, the $BF_3{\cdot}Et_2O$-mediated aldol reaction between **9** and **10** (analogous to the reaction of **8** and **10**) led to the formation of the *gluco*-configured product as the only detectable diastereomer (Method B, Scheme 4).

In conclusion, a highly convergent route to orthogonally protected D-glucuronic and L-iduronic acid thioglycoside building blocks has been developed. Rapid access to substantial quantities of monosaccharides that contain practical protecting group patterns and a readily activatable anomeric leaving group will greatly facilitate oligosaccharide assembly by using automated methods. The construction of heparin analogues and the development of efficient routes to further carbohydrate building blocks are currently under investigation.

Received: August 4, 2005
Published online: November 3, 2005

Keywords: aldol reaction · carbohydrates · thioglycosides · uronic acids

[1] a) A. Varki, *Glycobiology* **1993**, *3*, 97–130; b) R. A. Dwek, *Chem. Rev.* **1996**, *96*, 683–720; c) R. Roy, *Drug Discovery Today* **2004**, *1*, 327–336; D. M. Ratner, E. W. Adams, B. R. Su, J. O'Keefe, M. Mrksich, P. H. Seeberger, *ChemBioChem* **2004**, *5*, 379–382; d) D. H. Dube, C. R. Bertozzi, *Nat. Rev. Drug Discovery* **2005**, *4*, 477–488; e) D. B. Werz, P. H. Seeberger, *Chem. Eur. J.* **2005**, *11*, 3194–3206.

[2] For recent reviews on oligosaccharide synthesis, see: a) S. Hanessian, *Preparative Carbohydrate Chemistry*, Marcel Dekker, New York, **1997**; b) *Carbohydrates in Chemistry and Biology, Vol. 1* (Eds.: B. Ernst, G. W. Hart, P. Sinaÿ), Wiley-VCH, Weinheim, **2000**; c) B. Davies, *J. Chem. Soc. Perkin Trans. 1* **2000**, 2137–2160; d) P. J. Garegg, *Adv. Carbohydr. Chem. Biochem.* **2004**, *59*, 69–113.

[3] a) T. Kanemitsu, O. Kanie, *Trends Glycosci. Glycotechnol.* **1999**, *11*, 267–276; b) P. H. Seeberger, W. C. Haase, *Chem. Rev.* **2000**, *100*, 4349–4394; c) O. J. Plante, E. R. Palmacci, P. H. Seeberger, *Science* **2001**, *291*, 1523–1527; d) P. Sears, C.-H. Wong, *Science* **2001**, *291*, 2344–2350; e) O. J. Plante, E. R. Palmacci, R. B. Andrade, P. H. Seeberger, *J. Am. Chem. Soc.* **2001**, *123*, 9545–9554; f) P. H. Seeberger, *Solid Support Oligosaccharide Synthesis and Combinatorial Carbohydrate Libraries*, Wiley, New York, **2001**; g) T. Kanemitsu, O. Kanie, *Comb. Chem. High Throughput Screening* **2002**, *5*, 339–360; h) O. J. Plante, P. H. Seeberger, *Curr. Opin. Drug Discovery Dev.* **2003**, *6*, 521–525.

[4] a) T. Ogawa, *Chem. Soc. Rev.* **1994**, *23*, 397–407; b) S. J. Danishefsky, M. T. Bilodeau, *Angew. Chem.* **1996**, *108*, 1380–1419; *Angew. Chem. Int. Ed. Engl.* **1996**, *35*, 1482–1522; c) T. Hudlicky, D. A. Entwistle, K. K. Pitzer, A. J. Thorpe, *Chem. Rev.* **1996**, *96*, 1195–1220.

[5] For recent reviews on de novo synthesis of carbohydrates, see: a) R. R. Schmidt, *Pure Appl. Chem.* **1987**, *59*, 415–424; b) A. Kirschning, M. Jesberger, K.-U. Schoning, *Synthesis* **2001**, 507–540.

[6] S. Y. Ko, A. W. M. Lee, S. Masamune, L. A. Reed, K. B. Sharpless, F. J. Walker, *Science* **1983**, *220*, 949.

[7] a) T. Mukaiyama, I. Shiina, S. Kobayashi, *Chem. Lett.* **1990**, *12*, 2201–2204; b) T. Mukaiyama, H. Anan, I. Shiina, S. Kobayashi, *Bull. Soc. Chim. Fr.* **1993**, *130*, 388–394.

[8] a) A. B. Northrup, D. W. C. MacMillan, *Science* **2004**, *305*, 1752–1755; b) D. Enders, C. Grondal, *Angew. Chem.* **2005**, *117*, 1235–1238; *Angew. Chem. Int. Ed.* **2005**, *44*, 1210–1212.

[9] For a recent review, see: C. Noti, P. H. Seeberger, *Chem. Biol.* **2005**, *12*, 731–756.

[10] a) T. Mukaiyama, K. Banno, K. Narasaka, *J. Am. Chem. Soc.* **1974**, *96*, 7503–7509; b) T. Mukaiyama, *Org. React.* **1982**, *28*, 203–331.

[11] E. Fischer, *Ber. Dtsch. Chem. Ges.* **1894**, *27*, 677.

[12] F. L. van Delft, A. R. P. M. Valentijn, G. A. van der Marel, J. H. van Boom, *J. Carbohydr. Chem.* **1999**, *18*, 165–190.

[13] D. A. Evans, M. J. Dart, J. L. Duffy, M. G. Yang, *J. Am. Chem. Soc.* **1996**, *118*, 4322–4343.

[14] K. Hattori, H. Yamamoto, *J. Org. Chem.* **1993**, *58*, 5301–5303.

[15] C. Altona, C. A. G. Haasnoot, *Org. Magn. Reson.* **1980**, *13*, 417–429.

 © 2005 Wiley-VCH Verlag GmbH & Co. KGaA, Weinheim

High-Throughput Methods

DOI: 10.1002/anie.200501766

A High-Throughput Investigation of the Role of pH, Temperature, Concentration, and Time on the Synthesis of Hybrid Inorganic–Organic Materials**

Paul M. Forster, Norbert Stock, and Anthony K. Cheetham**

Since their discovery in the 1940s, synthetic aluminosilicate zeolites have become a major research focus owing to their commercially important catalytic, ion-exchange, and sorption properties.[1] Because many of the commercially important zeolites may be synthesized without organic templates by altering simple variables such as temperature, reaction time, Si/Al ratio, and pH,[2] a detailed understanding of the role that these variables play in zeolite synthesis[3] remains one of the most important advancements in the field. Similar studies, to date, are rare for hybrid inorganic–organic systems. Instead, as a result of the remarkable success of reticular chemistry,[4] the field has focused on understanding the role of the organic molecules in determining the overall structures that hybrid materials adopt.[5] Consequently, while more than 13000 metal–organic frameworks (MOFs) have been described,[6] there are very few combinations of metal centers and ligands[+] for which more than two or three structures have been identified.[7]

The existence of five well-characterized phases of cobalt succinates containing water and/or hydroxide ions[8] offers a rare opportunity to examine the role of various reaction variables in determining which structure forms. Moreover, this family includes one-, two-, and three-dimensional systems, several of which contain infinite Co-O-Co networks,-which may display interesting magnetic[9] or catalytic[10] properties in addition to relatively high thermal stability.[11] However, since these cobalt succinate phases have been prepared by different research groups and by different procedures, a retrospective examination of the effect of the reaction conditions on the product formation is difficult.

Previously, we discovered that a very simple reaction of stoichiometric amounts of cobalt hydroxide and succinic acid in water could be used to produce the five known phases when we varied only the reaction temperature. We found that that less hydrated and increasingly dense phases form at higher temperatures.[8b] While our previous investigation was very successful in studying the role of temperature as an isolated variable, simultaneous study of additional reaction variables should provide additional insights into the chemistry of the system. Unfortunately, each increase in the number of variables raises the number of necessary reactions exponentially. The serial investigation of a large parameter spaces is impractical and most often infeasible. Recent progress in high-throughput materials science has led to the incorporation of parallel reactor systems that allow the investigation of hydrothermal syntheses. The methodology is characterized by low reagent consumption, and a complete set of parallel reactors can be set to work under identical reaction conditions. Thus, synthesis regions for various phases can be efficiently established. The application of the methodology has recently lead to a number of systematic investigations in the field of phosphonate-based inorganic–organic hybrid compounds with a focus on the role of the pH on the reaction product.[12–15] Here, we use high-throughput hydrothermal synthesis to elucidate the role of four variables in the cobalt succinate system: temperature, pH, concentration, and reaction time.

In analogy to our previous studies on the cobalt succinate system,[8b] we examined reactions of the $Co(OH)_2/C_4H_6O_4/H_2O$ system. One significant advantage is that the number of reactants is held to a minimum since the cobalt source contains the hydroxide ions necessary to deprotonate the dicarboxylic acid. Inclusion of the base in the cobalt source is also advantageous for reactions in dilute solution since weighing errors inherent to the small scale could translate into very large pH changes with other bases, such as alkali hydroxides. A second advantage is that this method does not generate salt by-products, preventing the complications from having to consider the role of different bases, additional phases that may incorporate cations from these bases,[8c] and the salt concentrations' influence on the reaction.[16] One disadvantage of this approach is that the pH cannot be determined quantitatively due to the insolubility of cobalt hydroxide, although reaction mixtures with excess metal hydroxide and succinic acid are clearly basic and acidic, respectively.

The reactions were carried out in a teflon-lined 48-reactor block with a sample volume of approximately 400 μL per reactor. We initially selected eight $Co(OH)_2/C_4H_6O_4$ ratios, six concentrations, and six temperatures, for a total of 288 reactions. The quantity of water was fixed at 200 μL, such that the vessels were filled to the same extent for most reactions. Except for reactions at very high concentrations and acidity, the amount of reactants added did not change the total volume appreciably. The reaction temperatures ranged from 75–200 °C at intervals of 25 °C. To keep the total number of

[*] N. Stock
Institut für Anorganische Chemie
Christian-Albrechts-Universität zu Kiel
Otto-Hahn-Platz 6/7, 24118 Kiel (Germany)
Fax: (+49) 431-880-1775
E-mail: stock@ac.uni-kiel.de
P. M. Forster, A. K. Cheetham
Materials Research Laboratory
University of California
Santa Barbara, CA 93106-5121 (USA)
Fax: (+1) 805-893-8797
E-mail: cheetham@mrl.ucsb.edu

[**] We thank A. Burbank for useful discussions and T. Hartmann and B. Baumgartner, STOE & CIE GmbH, Darmstadt (Germany), for collecting the X-ray powder diffraction patterns. N.S. thanks Prof. Bein for his continuous support. This work was supported by the MRL Program of the National Science Foundation under Award No. DMR00-80034.

[+] We include solvent molecules coordinated to metal centers (charged or otherwise) in the term "ligand."

 InterScience © 2005 Wiley-VCH Verlag GmbH & Co. KGaA, Weinheim

reactions reasonable, the role of time was tested by setting up identical sets of 48 reactions for 5, 25, and 75 h at 150 °C, which added a further 96 reactions. The reaction parameters investigated are summarized in Table 1.

Table 1: Summary of the temperatures, concentrations, and acid/base ratios simultaneously explored in this work.

T [°C]	75	100	125	150	175	200		
$H_2O/Co(OH)_2$	200	150	110	75	50	25		
succinic acid/$Co(OH)_2$	0.2	0.4	0.6	0.8	1	1.2	1.5	2

Of the reaction parameters investigated, the $C_4H_6O_4$/$Co(OH)_2$ ratio and temperature proved to be the most important. For concentrations and reaction times similar to those used in our previous study ($H_2O/Co^{2+} = 110$, 75 h), variation of temperature the $C_4H_6O_4/Co(OH)_2$ ratio allowed us to synthesize four of the five phases reported in the previous paper on temperature[*] as well as two new phases, summarized in Table 2. The new phases F and G both occur

Table 2: Summary of phases of cobalt succinate. For dimensionality, the overall dimensionality is given followed by the metal–oxygen–metal dimensionality in parenthesis.

Code	Phase	Dimensionality	Ref.
A	$[Co(H_2O)_4(C_4H_4O_4)]$	1 (0)	[8a]
B	$[Co(H_2O)_2(C_4H_4O_4)]$	1 (0)	[8b]
C	$[Co_4(H_2O)_2(OH)_2(C_4H_4O_4)_3]\cdot 2H_2O$	2 (2)	[8c]
D	$[Co_6(OH)_2(C_4H_4O_4)_5]\cdot 2H_2O$	3 (2)	[8d]
E	$[Co_5(OH)_2(C_4H_4O_4)_4]$	3 (2)	[8e]
F	$[Co_7(H_2O)_3(OH)_6(C_4H_4O_4)_4]\cdot 7H_2O$	2 (1)	[18]
G	"$[Co_7(H_2O)_2(OH)_{12}(C_4H_4O_4)]$"	2 (2)	[19]

under considerably more basic conditions than those in the original investigation, and they contain much more hydroxide. The powder diffraction diagram of the first of these new cobalt succinates, F, matched the simulated powder diffraction pattern for a nickel succinate material previously described by Guillou et al. using ab initio structure solution from synchrotron powder diffraction.[17] We have subsequently obtained single crystals of the cobalt analogue and will publish a complete description of the structure elsewhere.[18] The second new phase, G is easily recognized by its bright blue color, whereas the rest of the known cobalt succinates vary between pink and dark purple. Despite a significant amount of additional work using conventional autoclaves, we were unable to obtain single crystals or phase-pure powder samples of this material. However, given its color (which is indicative of the presence of tetrahedral Co^{2+} ions), the conditions under which it forms, and the position and high intensity of its first powder diffraction peak, this material is likely to be a layered hydroxide material with cationic brucite-like sheets and succinate anions between the layers. We believe that this phase is related to $[Co_7(H_2O)_2(OH)_{12}$ (ethanedisulfonate)], which forms from a similar reaction and contains both tetrahedral and octahedral Co^{2+} ions.[19]

We have constructed a crystallization diagram for temperature and $C_4H_6O_4/Co(OH)_2$ ratio (Figure 1) by choosing a fixed concentration (molar ratio $Co(OH)_2/H_2O = 1{:}110$, as used in the original study). The results are very similar for other concentrations, but deviations will be discussed shortly. Co_3O_4 and unreacted $Co(OH)_2$ have been omitted for simplicity.

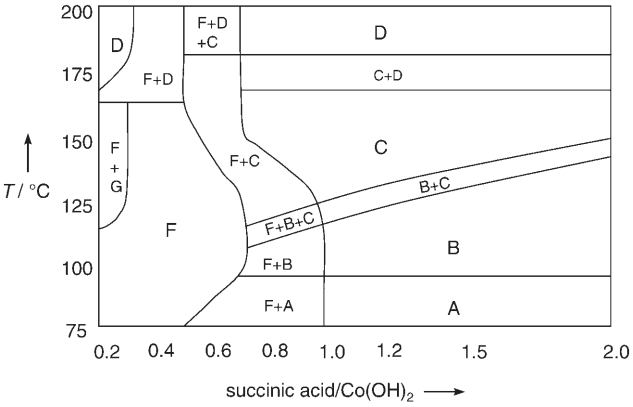

Figure 1. Crystallization diagram for the parameters reactant ratio (succinic acid/$Co(OH)_2$))and temperature at the fixed molar ratio $Co(OH)_2/H_2O = 1{:}110$. The phases are indicated by their letter code as assigned in Table 2. Unreacted $Co(OH)_2$ as well as Co_3O_4 have been omitted for clarity.

It is evident from Figure 1 that once sufficient succinic acid has been added to neutralize the hydroxide ions of $Co(OH)_2$, additional acid plays a very limited role in determining the phase. The only clear exception occurs at the boundary between the B ($[Co(H_2O)_2(C_4H_4O_4)]$) and C ($[Co_4(H_2O)_2(OH)_2(C_4H_4O_4)_3\cdot 2H_2O]$) regions, where higher concentrations of succinate were observed to favor B, while lower concentrations favored C. Since C contains hydroxide and B does not, it is reasonable that the additional amounts of acid would hinder the formation of C.

The two new phases, F ($[Co_7(H_2O)_3(OH)_6(C_4H_4O_4)_4\cdot 7H_2O]$) and G ("$[Co_7(H_2O)_2(OH)_{12}(C_4H_4O_4)]$"), encountered in this survey both occur on the basic (left) side of the phase diagram. It is surprising, given the number of groups that have studied cobalt succinates and the wide range of conditions for which F forms, that this phase has not been identified previously. More surprisingly, while the highly condensed Co–O ribbons and moderately high number of Co^{II} atoms per carboxylate group in the structure of F are more typical of hydrothermal phases, it is evident from Figure 1 that the structure forms most readily at lower temperatures. This suggests that more basic conditions may also be used to favor more condensed structures in the same

[*] Since the high-throughput autoclaves can be operated at temperatures only up 200 °C , we could not reach sufficiently high temperatures to prepare $[Co_5(OH)_2(C_4H_4O_4)_4]$ (phase E, Table 2). However, since all the other phases were obtained at the corresponding reaction conditions, we are confident that this phase would have formed at higher temperatures in this study as well.

 © 2005 Wiley-VCH Verlag GmbH & Co. KGaA, Weinheim

way that temperature does. The blue phase G described above occurs only under the most basic conditions studied at temperatures between 100 and 150 °C.

We have summarized the seven cobalt succinate phases in a ternary plot based on composition (Figure 2). It is interesting to note that the five original phases (A–E) occur along an approximate line on the left-hand side of the triangle while the two new phases (F and G) lie closer to the more basic corner of the diagram. We have added arrows indicating the effect of temperature and more basic conditions on the formation of cobalt succinate phases.

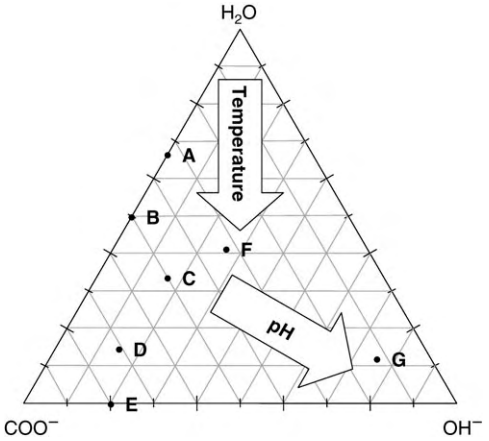

Figure 2. Ternary composition map for the seven known forms of cobalt succinate. The direction that temperature and reactant composition (indicated pH) tend to shift a reaction are indicated with arrows.

The role of reaction time, which was investigated for 150 °C only, indicated that reactions are more or less complete after one day. Corresponding crystallization diagrams for different molar ratios $H_2O/Co(OH)_2$ and $C_4H_6O_4/Co(OH)_2$ are presented in Figure 3 for the products obtained after 5, 25, and 75 h. Under strongly acidic conditions, the shortest reaction time produced phase B, which is normally found at lower temperatures, while longer reactions led almost exclusively to phase C. It is likely that some crystallites of B would form while the reactor block is heating, and that this phase may persist for some time before C, the more thermodynamically favorable phase for these conditions, forms. It is also possible that much smaller crystallites of C formed during the short reaction time, but dissolved and recrystallized as phase B while the autoclave cooled (ca. 1 h).

For intermediate acid/base ratios between 0.6 and 1.2, mixtures of phases F and C form over a wide range for the 5-h reaction, while mixtures of the two phases were observed only for the molar ratio $C_4H_6O_4/Co(OH)_2 = 0.6$ for the longer two reaction times. The most likely explanation is that F forms initially by reaction between the cobalt hydroxide and succinic acid, and that excess succinic acid then reacts with F to produce C.

Finally, under the most basic conditions (acid/base ratios of 0.6 and less), there were no differences in the phases that formed, although it was qualitatively evident that, for longer reaction times, the X-ray peaks corresponding to products

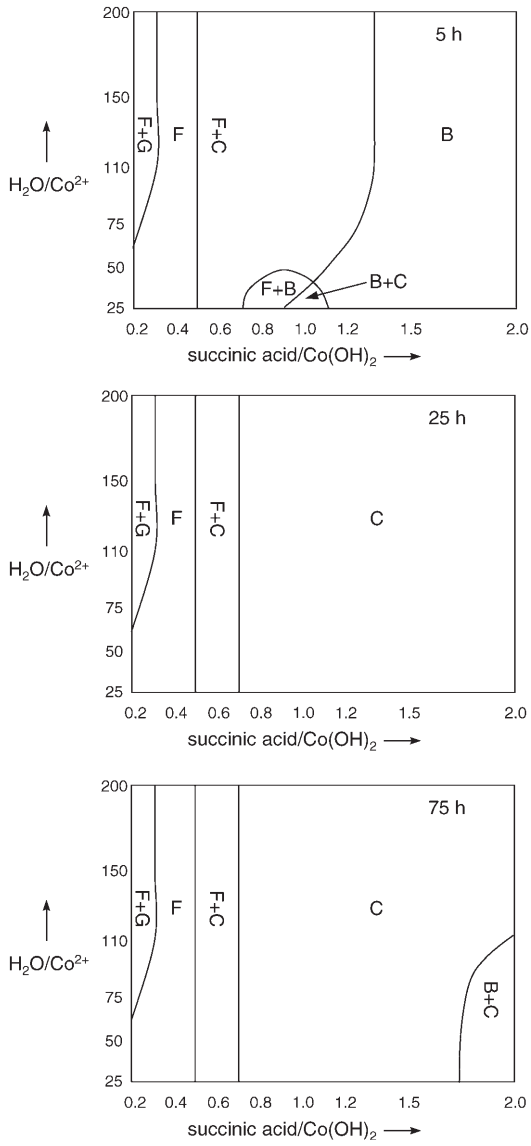

Figure 3. Crystallization diagrams for three sets of reactions carried out for 5, 25, and 75 h. These figures plot the phases observed by varying reactant composition and concentration at a fixed temperature of 150 °C.

increased in intensity relative to $Co(OH)_2$ peaks between the three time intervals. Further experiments, particularly in situ studies, will undoubtedly help to further clarify these observations.

Finally, concentration proved to be relatively unimportant. The most prominent instance where it influenced a reaction involved the formation of G. At high concentrations, G did not form at all. At lower concentrations, an increase of the relative peak height for G relative to F was noticeable as concentration dropped. Qualitatively, concentration appeared to influence crystal size. Although the effect varied considerably from reaction to reaction, the most concentrated reaction mixtures often led to the smallest crystallites for a given set of reaction conditions.

Several different groups have studied cobalt succinates during the seven years since the first example, $[Co_5(OH)_2$-

 © 2005 Wiley-VCH Verlag GmbH & Co. KGaA, Weinheim

$(C_4H_4O_4)_4]$ (phase E), was described by Livage et al. Here, we show that a simple, systematic, examination of parameter space resulted in the discovery of two additional phases in this already diverse family of materials. Furthermore, our approach shows the roles that temperature, acid/base ratio, time, and concentration play in determining which structure forms. Thanks to the rapid development of high-throughput hydrothermal methods, systematic studies such as this may be carried out in a matter of weeks, opening the door to the discovery of fascinating new compounds and an improved picture of the role that synthesis parameters play in their formation.

Experimental Section

Newly machined teflon liners for the autoclaves were used for these experiments. The machined liners were washed five times with deionized water, heated for 1 h in freshly prepared aqua regia, rinsed five times with water, heated in water to boiling for 90 min, rinsed five times with acetone, and dried at 60 °C. A similar procedure (without the acetone rinse and with an overnight soak in aqua regia) was used to clean liners for subsequent uses to insure that no nucleation centers were present.

Cobalt hydroxide (Alfa Aesar, 99.9 %) was weighed directly into the teflon liner inside an enclosed balance. The liners were handled with plastic tweezers in order to minimize weighting errors and contamination. Succinic acid (Aldrich, 99 + %) was then weighed on a piece of wax paper and added to the liner. Doubly deionized water was added as a final step using an Eppendorf pipette. The pipette was calibrated beforehand to deliver 200 μg (as verified by balance) with a consistency of better than ±1 μg. The reaction mixtures were not stirred, but sealing and moving the reaction vessel obviously resulted in some agitation.

Reactions were carried out immediately after the addition of water. Reactions were run for 75 h with two exceptions, those at 100 °C and 200 °C, which were run for 25 h. Based on our study of the kinetics, it is unlikely that this deviation affected the results. The reaction vessels were then cooled in air on a metal surface, and the mixtures were filtered as soon as possible in order to prevent dissolution of any phases stable at higher temperatures but not favored at lower temperatures. The reaction products were removed by pipette, rinsed with water followed by acetone, and dried in air at room temperature.

X-ray powder diffraction patterns were collected on a high-throughput X-ray powder diffractometer STADI P from STOE (monochromated $Mo_{K\alpha}$ radiation) equipped with a PSD detector and a horizontal *xy* stage for automated analysis without individual sample manipulation. Each sample was measured in 8 min in the range between 2 and 22° (2θ). X-ray powder diffraction patterns were compared to calculated patterns of known reaction products using Powdercell.[20] Comparisons were made for $Co(OH)_2$[21] as well as other known cobalt succinate structures.

Received: May 22, 2005
Published online: October 24, 2005

Keywords: cobalt · high-throughput methods · hydrothermal synthesis · inorganic–organic hybrid materials · succinic acid

[1] *Introduction to Zeolite Science and Practice* (Eds.: H. van Bekkum, E. M. Flanigen, P. A. Jacobs, J. C. Jansen), Elsevier, Amsterdam, **2001**.
[2] D. W. Breck, *Zeolite Molecular Sieves*, Wiley, New York, **1974**.
[3] R. Szostak, *Molecular Sieves: Principles of Synthesis and Identification*, Van Nostrand Reinhold Catalysis Series, New York, **1989**, chap. 2.
[4] O. M. Yaghi, M. O'Keeffe, N. W. Ockwig, H. K. Chae, M. Eddaoudi, J. Kim, *Nature* **2003**, *423*, 705.
[5] D. J. Chesnut, D. Hagrman, P. J. Zapf, R. P. Hammond, R. LaDuca, Jr., R. C. Haushalter, J. Zubieta, *Coord. Chem. Rev.* **1999**, *190*, 737.
[6] J. L. C. Rowsell, O. M. Yaghi, *Microporous Mesoporous Mater.* **2004**, *73*, 3.
[7] C. N. R. Rao, S. Natarajan, R. Vaidhyanathan, *Angew. Chem.* **2004**, *116*, 1490; *Angew. Chem. Int. Ed.* **2004**, *43*, 1466; .
[8] a) C. Livage, C. Egger, G. Férey, *Chem. Mater.* **2001**, *13*, 410; b) P. M. Forster, A. R. Burbank, C. Livage, G. Férey, A. K. Cheetham, *Chem. Commun.* **2004**, 368; c) C. Livage, C. Egger, G. Férey, *Chem. Mater.* **2000**, *12*, 1546; d) L.-S. Long, X.-M. Chen, M.-L. Tong, Z.-G. Sun, Y.-P. Ren, R.-B. Huang, L.-S. Zheng, *J. Chem. Soc. Dalton Trans.* **2001**, 2888; e) C. Livage, C. Egger, M. Nogues, G. Férey, *J. Mater. Chem.* **1998**, *8*, 2743.
[9] K. Barthelet, J. Marrot, D. Riou, G. Férey, *Angew. Chem.* **2002**, *114*, 291; *Angew. Chem. Int. Ed.* **2002**, *41*, 281.
[10] P. M. Forster, A. K. Cheetham, *Top. Catal.* **2003**, *24*, 79.
[11] P. M. Forster, A. K. Cheetham, *Angew. Chem.* **2002**, *114*, 475; *Angew. Chem. Int. Ed.* **2002**, *41*, 457; L. M. Zheng, T. Whitfield, X. Wang, A. J. Jacobson, *Angew. Chem.* **2000**, *112*, 4702; *Angew. Chem. Int. Ed.* **2000**, *39*, 4528.
[12] N. Stock, T. Bein, *Solid State Sci.* **2003**, *5*, 1207.
[13] N. Stock, K. Karaghiosoff, T. Bein, *Z. Anorg. Allg. Chem.* **2004**, *630*, 2535.
[14] N. Stock, T. Bein, *Angew. Chem.* **2004**, *116*, 767; *Angew. Chem. Int. Ed.* **2004**, *43*, 749.
[15] N. Stock, T. Bein, *J. Mater. Chem.* **2005**, *15*, 1384.
[16] We have noticed that the presence of salts such as KCl may have a profound effect on the product produced by a reaction in this system.
[17] N. Guillou, C. Livage, W. van Beek, M. Nogues, G. Férey, *Angew. Chem.* **2003**, *115*, 668; *Angew. Chem. Int. Ed.* **2003**, *42*, 644.
[18] P. M. Forster, A. R. Burbank, M. C. O'Sullivan, N. Guillou, C. Livage, G. Férey, N. Stock, A. K. Cheetham, *Solid State Sci.*, doi: 10.1016/j.solidstatesciences.2005.04.005.
[19] P. M. Forster, M. M. Tafoya, A. K. Cheetham, *J. Phys. Chem. Solids* **2004**, *65*, 11.
[20] W. Kraus, G. Nolze, *J. Appl. Crystallogr.* **1996**, *29*, 301.
[21] C. Mockenhaupt, T. Zeiske, H. D. Lutz, *J. Mol. Struct.* **1998**, *443*, 191.

 © 2005 Wiley-VCH Verlag GmbH & Co. KGaA, Weinheim

Bioanalysis

DOI: 10.1002/anie.200501552

Quantum Dots as Efficient Energy Acceptors in a Time-Resolved Fluoroimmunoassay**

Niko Hildebrandt, Loïc J. Charbonnière,* Michael Beck, Raymond F. Ziessel, and Hans-Gerd Löhmannsröben*

Dedicated to Professor Herbert Dreeskamp on the occasion of his 76th birthday

The last decade has witnessed the emergence of semiconductor nanoparticles as very attractive building blocks for nanotechnology. Spherically or ellipsoidally shaped nanoparticles, also called quantum dots (qdots), display size-dependent optical properties with extremely large absorption cross sections.[1] When appropriately protected from the surrounding media by a covering shell, they display narrow and symmetric emission bands with quantum yields approaching unity in some cases.[2] The inorganic cores of qdots are also more robust than organic dyes or luminescent proteins toward photobleaching.[3,4] Recent accounts have reported on the possibility of derivatizing qdot surfaces,[5] thereby offering a broad scope of opportunities for chemical and biological interactions.[6] These combined features make qdots excellent tools in analytical techniques associated with fluorescence spectroscopy, reaching sensitivity limits going down to the single particle.[4] Qdots display extremely high extinction coefficients over a wide range of wavelengths as a result of the absorption of photons with energies higher than the band gap of the semiconductor material. The resulting excitons (electron–hole pairs) recombine to generate photons with narrow emission bands. These properties make qdots excellent energy donors in fluorescence (or Förster) resonance energy transfer (FRET) experiments,[7] a technique that is ideally suited for events occurring at the nanometer scale, such as numerous biological processes. For instance, a homogeneous maltose sensor has been described in which the maltose concentration can be monitored by the recovery of qdot luminescence concomitant to the displacement of a quencher dye.[8]

Importantly, if qdots are to be used as energy acceptors, significant direct excitation may be undesirable as it limits the extent of resonance transfer and results in spurious fluorescence emission. The use of qdots as energy acceptors has proven possible in a few solid-state devices based on semiconductor quantum wells,[9] with smaller-sized qdots,[10] and with a blue-emitting polymer[11] as the energy donor, but very rarely in discrete molecular systems in solution.[12,13] Mattoussi and co-workers explained low energy-transfer efficiency from organic or inorganic donors to the qdot acceptors by the fact that the rate of FRET is much slower than the fast radiative decay rates of the donors.[12]

In the present work, we report that CdSe/ZnS core shell qdots are excellent energy acceptors in a time-resolved fluoroimmunoassay system in which a terbium chelate with long-lived luminescence lifetime is the energy donor and the strong biotin–streptavidin interaction is used for the recognition process.

The TbL chelate consisted of a terbium cation embedded in a ligand made of two 6-carboxybipyridyl arms organized on a glutamate framework (Figure 1). The terminal carboxylate function of the glutamic residue was activated with the sodium salt of *N*-hydroxysulfosuccinimide in the presence of EDC·HCl (EDC = *N*-ethyl-*N*′-(3-dimethylaminopropyl)carbodiimide hydrochloride) according to an existing procedure.[14] The activated ester, TbL*, was incubated with streptavidin in PBS buffer (pH 7.4) overnight at room temperature, and the unreacted complex was removed by extensive dialysis of the protein. The absorption spectrum of TbL-Strep is a quasi-perfect linear combination of the spectra of streptavidin and 3.5 TbL complexes (Figure 2). Material with this labeling ratio was used in all further experiments (schematically simplified by four TbL labels on streptavidin in Figure 1).

The MALDI-TOF mass spectra of the labeled tetrameric streptavidin protein show that the labeling is not simply localized on one site of each monomeric unit (see Supporting Information). While a single marker per monomer is the major species observed, monomers containing zero, two, and three labels (trace amount) are also evident in the spectrum, pointing to at least two different environments for the Tb complexes. Upon excitation in the $\pi \rightarrow \pi^*$ transitions centered on the bipyridine moities at 308 nm, the emission spectrum of TbL-Strep displays the typical emission lines of the Tb^{3+} $^5D_4 \rightarrow {}^7F_J$ ($J = 0$–6) electronic transitions (Figure 3). Excitation of the ligand resulted in an efficient energy transfer to the lanthanide cation. The labeling process did not greatly perturb the Tb environment and, in pure water, the luminescence lifetime of TbL-Strep shows a bi-exponential behavior with a major long-lived component of 1500 ± 10 μs (97 %) and

[*] Dipl.-Ing. (FH) N. Hildebrandt, Dr. M. Beck, Prof. Dr. H.-G. Löhmannsröben
Physikalische Chemie
Institut für Chemie und Interdisziplinäres Zentrum für Photonik
Universität Potsdam
Karl-Liebknecht-Strasse 24–25, 14476 Potsdam–Golm (Germany)
Fax: (+49) 331-977-5058
E-mail: hildebr@uni-potsdam.de
Dr. L. J. Charbonnière, Prof. Dr. R. F. Ziessel
Laboratoire de Chimie Moléculaire
UMR 7509-ECPM-ULP
25, rue Becquerel, 67087 Strasbourg Cedex (France)
Fax: (+33) 3-9024-2689
E-mail: charbonn@chimie.u-strasbg.fr

[**] This work was supported by the German Bundesministerium für Wirschaft und Arbeit (InnoNet program 16N0225) and the French Centre National de la Recherche Scientifique. The authors thank Frank Sellrie, Universität Potsdam, for purification of labeled streptavidin, Dr. Sophie Haebel, Universität Potsdam, for MALDI-TOF experiments, and Dr. Jennifer Weiss-Wytko and Prof. Jack Harrowfield, Université Louis Pasteur de Strasbourg, for fruitful discussions.

Supporting information for this article is available on the WWW under http://www.angewandte.org or from the author.

InterScience
© 2005 Wiley-VCH Verlag GmbH & Co. KGaA, Weinheim

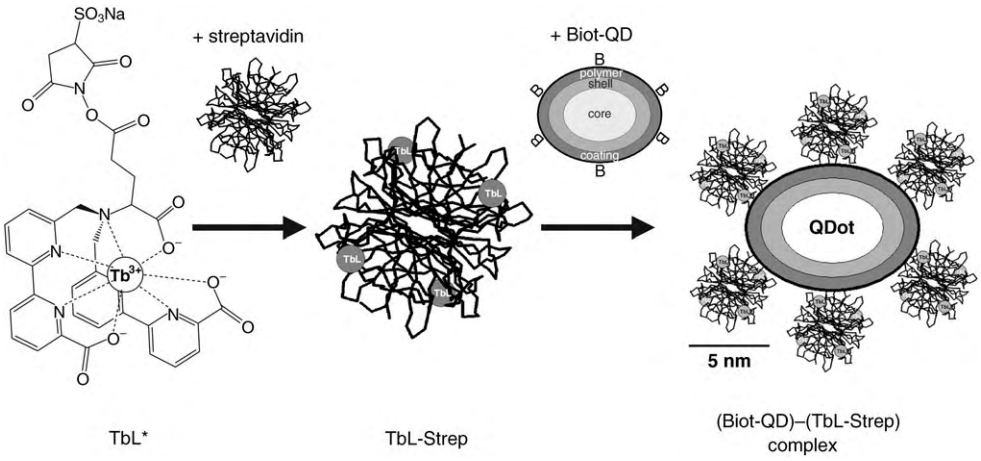

Figure 1. Schematic representation of the assembly of the Biot-QD/TbL-Strep complex. TbL-labeled streptavidin binds to biotin on the polymer surface of the qdot.

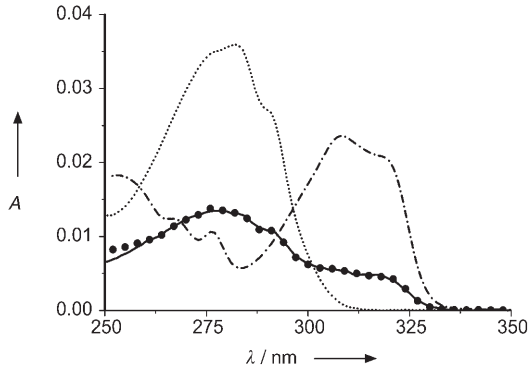

Figure 2. UV/Vis absorption spectra of streptavidin (••••, $c = 4.25 \times 10^{-7}$ M), TbL* (–•–•, $c = 2.27 \times 10^{-6}$ M), and TbL-Strep (——, $c = 1.55 \times 10^{-7}$ M) and a linear combination of streptavidin and TbL* (●).

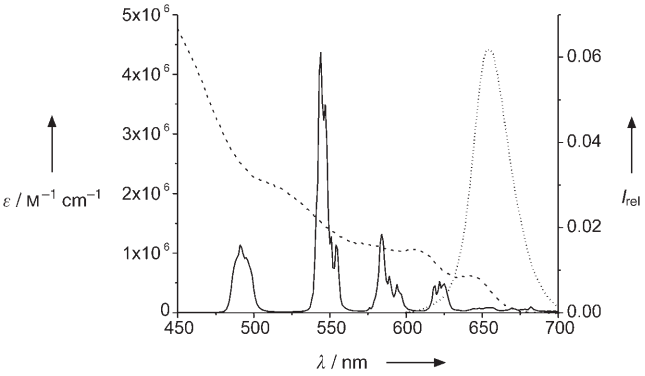

Figure 3. Normalized emission spectrum (intensity *I*) of TbL-Strep (——) and emission (·····) and absorption (-----) spectra of Biot-QD.

a minor, shorter one of 200 ± 30 μs (3%) (see Supporting Information). The longer lifetime is comparable to the value of pure TbL in water (1.48 ms).[14] In a 50 mM borate buffer containing 2% bovine serum albumin (BSA) at pH 8.3,[15] the luminescence intensity decay profile of TbL-Strep shows two exponential components. The main component remains the long-lived TbL decay with 1500 ± 50 μs (60%), and the second, with a decay time of 450 ± 30 μs (40%), results from TbL species quenched by nonspecific interactions with BSA. In this buffer, also used in the experiments, two distinct donor species are then present. The overall quantum efficiency of the system in this buffer is 14.5% (31% for pure TbL in water[14]).

As the energy-acceptor component of our fluoroimmunoassay system, an ellipsoidally shaped multilayer CdSe semiconductor core coated with a ZnS protective shell was used. The complete qdot was coated in a polymer–biotin complex, providing five to seven biotin molecules per qdot (Figure 1), with an average long axis of 10–12 nm for the biotinylated qdots (Biot-QD).[16] These nanoparticles display characteristic absorption and emission spectra with an emission maximum at 655 nm (Figure 3). Their luminescence decay profile in the borate buffer is deconvoluted with nanosecond-order multiexponential components (see Supporting Information), associated to the dispersion of the qdot in shape and size.[17]

Following Förster's theory for resonance energy transfer[18] with a refractive index of $n = 1.4$ for biomolecules in aqueous solution,[19] and assuming that the long-lived excited state lifetime of the Tb donor allows for a statistical distribution of the donor–acceptor dipoles (orientation factor $\kappa^2 = 2/3$), we calculated the Förster radius to be $R_0 = 81$ Å. This value represents the mean donor–acceptor distance at which half of the energy of the donor is transferred to the acceptor. As a result of the particularly high $\varepsilon(\lambda)$ parameters of qdots, this R_0 value is large compared to those of conventional donor–acceptor pairs (with distances ranging from 21–61 Å)[20] or pairs containing qdots as donors (47–65 Å).[7a,c]

To induce the recognition process and to probe the energy transfer, increasing amounts of Biot-QD were added to a solution of TbL-Strep ($c = 1 \times 10^{-9}$ M). Each sample was excited with a Xe-Cl excimer laser at 308 nm, and the emission was measured at 545 and 665 nm, which are the optimum spectral regions for emission from TbL-Strep and Biot-QD, respectively. Biot-QD emission was measured at 665 nm instead of 655 nm (maximum) in order to minimize the weak TbL-Strep background luminescence present at the latter wavelength (Figure 3). Emission was measured in time-resolved mode, using gated acquisition with a time window ranging from 250 to 1000 μs after the excitation pulse, which resulted in two long-lived intensities I_{665} and I_{545}. In this way

 © 2005 Wiley-VCH Verlag GmbH & Co. KGaA, Weinheim

the autofluorescence of the sample and buffer and interference associated with light scattering in the apparatus are drastically reduced.[21] Figure 4 shows the dependence of the intensity ratio R collected at two channels ($R = I_{665}/I_{545}$) as a function of Biot-QD added at varying incubation times.

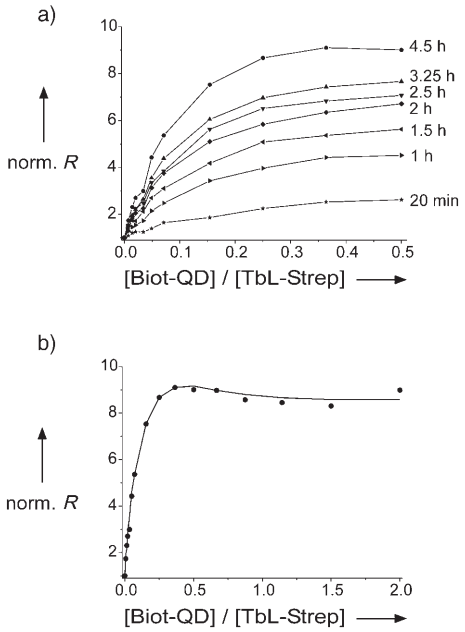

Figure 4. a) Intensity ratio R as a function of [Biot-QD]/[TbL-Strep] between values of 0 and 0.5 at varying incubation times (20 min to 4.5 h). b) R after 4.5 h (equilibrium) for [Biot-QD]/[TbL-Strep] = 0–2. Initial concentration: [TbL-Strep] = 1×10^{-9} M. In both graphs R was normalized to unity for [Biot-QD]/[TbL-Strep] = 0.

Addition of Biot-QD to TbL-Strep led to a strongly increased R for low qdot concentrations ([Biot-QD]/[TbL-Strep] < 0.2) which leveled off at higher qdot concentrations. The phenomenon evolved slowly with time (Figure 4a), reaching equilibrium after 4.5 h (Figure 4b).[22] Then, the first part of the curve, corresponding to low qdot concentrations ([Biot-QD]/[TbL-Strep] < 0.1), displayed a marked rise, mainly originating from a large long-lived qdot emission increase. At [Biot-QD]/[TbL-Strep] > 0.4, the emission ratio became almost constant. Extrapolation of the linear rising part at low concentrations led to an intersection with the plateau region at [Biot-QD]/[TbL-Strep] ≈ 0.13–0.16. This value is in excellent agreement with the number of biotin fragments per qdots mentioned by the supplier (5–7), suggesting that all biotin molecules remain accessible at the surface of the nanoparticle.

In a control experiment, dynamic energy transfer between TbL and qdots could be ruled out, as the weak linear increase of R with [Biot-QD]/[pure TbL] resulted from a stronger decrease of I_{545} compared to I_{665} (see Supporting Information). We thus take the strong increase of R with [Biot-QD]/[TbL-Strep] (Figure 4b) as clear evidence for FRET from TbL to qdots in the streptavidin-biotin complex.

Further evidence of a sensitization of qdot emission by energy transfer from terbium was obtained by measuring the decay profiles at 665 nm for various [Biot-QD]/[TbL-Strep] ratios (Figure 5). In the presence of TbL-Strep, the qdot

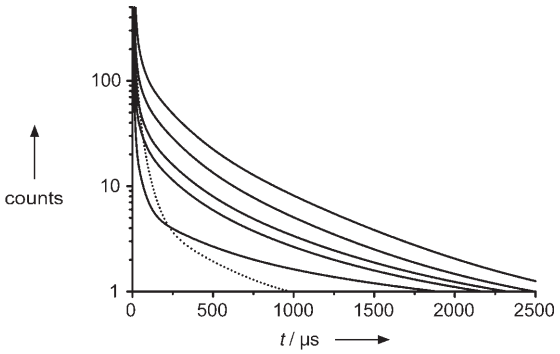

Figure 5. Intensity decay profiles at 665 nm ($\lambda_{exc} = 308$ nm) for various values of [Biot-QD]/[TbL-Strep] (0, 0.014, 0.034, 0.071 and 0.25, full lines from bottom to top, [Biot-QD] = 0–2.0×10^{-10} M) and pure Biot-QD (dotted line, [Biot-QD] = 1.0×10^{-10} M).

emission profile displays two new long-lived components of 560 ± 40 µs and 170 ± 20 µs, originating from energy transfer from the two Tb donor components. Given that the intrinsic Biot-QD decay is very prompt,[17] the long-lived components observed for Biot-QD in the presence of TbL-Strep can safely be attributed to the luminescence decays of the donors in the presence of acceptor, τ_{DAi}.[20] Calculation of the energy transfer rate and the average distance r between donor and acceptor pairs with multiexponential-decay donors gave a mean distance of $r = 72$–76 Å depending on the amount of added Biot-QD (see figure and theoretical treatment in the Supporting Information).[19] These distances reflect the assumed system configuration depicted in Figure 1 and resulted in energy-transfer rates of $k_{ET1} = (1.1 \pm 0.3) \times 10^3\ s^{-1}$ and $k_{ET2} = (3.9 \pm 0.6) \times 10^3\ s^{-1}$ as well as an efficiency of $E = 63 \pm 4\%$. It is worth pointing out that this treatment is valid for a spherically symmetric system consisting of point dipoles and does not take into account the geometric anisotropy of the ellipsoidal qdot particles and the nonrandom distribution of Tb acceptors around the nanocrystals.[24]

In short, these results show that the TbL-qdot pair is a very promising couple for FRET experiments. The use of long-lived excited state donors provides two advantages. First, efficient energy transfer to qdots becomes feasible, and the competition between radiative deactivation of the donor and energy transfer[12] swings the balance in favor of the latter. Second, the increased decay time of the qdot acceptor (up to some hundred µs) permits the use of a time-resolved acquisition mode that greatly enhances the sensitivity of the detection procedure. Under our experimental conditions, a detection limit of 3.3×10^{-12} M was estimated. The large R_0 value, which results from the very high qdot absorption,

 © 2005 Wiley-VCH Verlag GmbH & Co. KGaA, Weinheim

expands the scope of applications of energy-transfer experiments to very big proteins without the need to use large fluorescent proteins as energy donors or acceptors. Further work along these lines is currently in progress.

Experimental Section

TbL was prepared according to the literature procedure.[14] Synthesis and characterization of TbL*: [TbL]Na·4 H_2O (45 mg, 55 μmol) was suspended in 10 mL of dimethyl sulfoxide (DMSO). *N*-hydroxysulfosuccinimide sodium salt hydrate (14 mg, 60 μmol) and EDC·HCl (12 mg, 63 μmol) were added, and the solution was stirred at room temperature for 92 h, resulting in the complete dissolution of the starting complex. THF was added to precipitate the product. Upon centrifugation and drying under vacuum, [TbL*]·5 H_2O (45 mg, 81 %) was isolated as a yellow powder. Elemental analysis: calcd for $C_{33}H_{24}N_6NaO_{13}STb\cdot 5H_2O$ (%): C 38.99, H 3.37, N 8.27; found: C 39.20, H 3.56, N, 8.39; FAB$^+$-MS: m/z: 682.2 ([TbL*−$C_5H_3NNaO_7S$]$^+$, 95 %), 727.2 ([TbL*−$C_4H_3NNaO_5S$+H]$^+$, 55 %); IR (KBr): $\tilde{\nu}$ = 3447 (s), 1735 (w), 1624 (m), 1388 (w), 1231 (w), 1043 (w) cm^{-1}.

TbL-Strep labeling was performed by mixing 0.5 mg of TbL* (dissolved in 2 μL DMSO) with 1 mg of streptavidin in 200 μL PBS buffer (pH 7.4). After 1 day of incubation on a shaker at room temperature the solution was diluted in purified water (Millipore) and dialyzed.

Biotinylated qdots (Qdot 655 biotin conjugate-trial size lot no. 0603-0050) were supplied by Quantum Dot Corp. (Hayward, CA, USA). FRET measurements were performed on a modified Kryptor system (Cezanne, Nîmes, France) for time-resolved integrated single-photon counting at two channels (545 nm and 665 nm; filter-based wavelength separation) with 2-μs integration steps over 8 ms, with an OPTex XeCl excimer laser (Lambda Physik AG, Göttingen, Germany) excitation source at 20 Hz repetition rate. Qdot lifetime measurements were performed on an Andor iStar ICCD setup with monochromator and spectrograph wavelength separation (LOT-Oriel, Darmstadt, Germany) with XeCl excimer laser excitation.

Received: May 6, 2005
Revised: August 8, 2005
Published online: October 25, 2005

Keywords: FRET (fluorescence resonance energy transfer) · immunoassays · luminescence · quantum dots · terbium

[1] a) A. P. Alivisatos, *Science* **1996**, *271*, 933 – 937; b) C. B. Murray, D. J. Norris, M. G. Bawendi, *J. Am. Chem. Soc.* **1993**, *115*, 8706 – 8715.
[2] a) X. Peng, M. C. Schlamp, A. V. Kadavanich, A. P. Alivisatos, *J. Am. Chem. Soc.* **1997**, *119*, 7019; b) P. Reiss, J. Bleuse, A. Pron, *Nano Lett.* **2002**, *2*, 781 – 784.
[3] B. Dubertret, P. Skourides, D. J. Norris, V. Noireaux, A. H. Brivanlou, A. Libchaber, *Science* **2002**, *298*, 1759 – 1762.
[4] W. C. W. Chan, S. Nie, *Science* **1998**, *281*, 2016 – 2018.
[5] X. Michalet, F. F. Pinaud, L. A. Bentlila, J. M. Tsay, S. Doose, J. J. Li, G. Sundaresan, A. M. Wu, S. S. Gambhir, S. Weiss, *Science* **2005**, *307*, 538 – 544.
[6] M. Green, *Angew. Chem.* **2004**, *116*, 4221 – 4223; *Angew. Chem. Int. Ed.* **2004**, *43*, 4129 – 4131.
[7] a) E. Katz, I. Willner, *Angew. Chem.* **2004**, *116*, 6166 – 6235; *Angew. Chem. Int. Ed.* **2004**, *43*, 6042 – 6108; b) A. R. Clapp, I. L. Medintz, J. M. Mauro, B. R. Fisher, M. G. Bawendi, H. Mattoussi, *J. Am. Chem. Soc.* **2004**, *126*, 301 – 310; c) I. Geissbuehler, R. Hovius, K. L. Martinez, M. Adrian, K. Ravindranathan Thampi, H. Vogel, *Angew. Chem.* **2005**, *117*, 1412 – 1416; *Angew. Chem. Int. Ed.* **2005**, *44*, 1388 – 1392.
[8] I. L. Medintz, A. R. Clapp, H. Mattoussi, E. R. Goldman, B. M. Fisher, J. M. Mauro, *Nat. Mater.* **2003**, *2*, 630 – 638.
[9] M. Achermann, M. A. Petruska, S. Kos, D. L. Smith, D. D. Koleske, V. I. Kimov, *Nature* **2004**, *429*, 642 – 646.
[10] C. R. Kagan, C. B. Murray, M. Nirmal, M. G. Bawendi, *Phys. Rev. Lett.* **1996**, *76*, 1517 – 1520.
[11] M. Anni, L. Manna, R. Cingolani, D. Valerini, A. Creti, M. Lomascolo, *Appl. Phys. Lett.* **2004**, *85*, 4169 – 4171.
[12] A. R. Clapp, I. L. Medintz, B. R. Fisher, G. P. Anderson, H. Mattoussi, *J. Am. Chem. Soc.* **2005**, *127*, 1242 – 1250.
[13] N. N. Mamedova, A. K. Nicholas, A. L. Rogach, J. Studer, *Nano Lett.* **2001**, *1*, 281 – 286.
[14] N. Weibel, L. J. Charbonnière, M. Guardigli, A. Roda, R. Ziessel, *J. Am. Chem. Soc.* **2004**, *126*, 4888 – 4896.
[15] The choice of the buffering medium was guided by the use of this buffer for optimal photo-physical properties of qdots. Changing to PBS buffer resulted in significant losses in energy-transfer efficiency.
[16] Qdot Biotin Conjugates User Manual (Cat. # 1030-1, Cat. # 1032-1), http://www.qdots.com.
[17] a) B. R. Fisher, H. J. Eisler, N. E. Stott, M. G. Bawendi, *J. Phys. Chem. B* **2004**, *108*, 143 – 148; b) G. Schlegel, J. Bohnenberger, I. Potatova, A. Mews, *Phys. Rev. Lett.* **2002**, *88*, 137401.
[18] T. Förster, *Ann. Phys.* **1948**, *2*, 55 – 75.
[19] J. R. Lakowicz, *Principles of Fluorescence Spectroscopy*, Kluwer Academic/Plenum, New York, **1999**.
[20] B. Valeur, *Molecular Fluorescence, Principles and Applications*, Wiley-VCH, Weinheim, **2002**.
[21] L. J. Charbonnière, R. Ziessel, M. Guardigli, A. Roda, N. Sabbatini, M. Cesario, *J. Am. Chem. Soc.* **2001**, *123*, 2436 – 2437.
[22] Preliminary studies on Tb excited-state lifetimes have shown that introduction of BSA in the buffer plays a significant role. Nonspecific binding interactions of BSA and streptavidin that are able to compete with biotin-streptavidin recognition have previously been reported.[23] In our case, this nonspecific binding results in slow equilibration of the system. The interaction of BSA with streptavidin must first be disrupted before the thermodynamically favorable TbL-Strep/Biot-QD interaction can take place. Peeling off the BSA from the Tb emitting species eliminates the associated quenching processes and is probably the origin of the rising Tb emission for [Biot-QD]/[TbL-Strep] < 0.25 (see Supporting Information).
[23] J. H. F. Erkens, S. J. Dieleman, R. A. Dressendörfer, C. J. Strasburger, *J. Steroid Biochem. Mol. Biol.* **1998**, *67*, 153 – 161.
[24] H. E. Grecco, K. A. Lidke, R. Heintzmann, D. S. Lidke, C. Spagnuolo, O. E. Martinez, E. A. Jares-Erijman, T. M. Jovin, *Microsc. Res. Tech.* **2004**, *65*, 169 – 179.

 © 2005 Wiley-VCH Verlag GmbH & Co. KGaA, Weinheim

Solid-State Structures

DOI: 10.1002/anie.200503017

Fibrous Red Phosphorus**

Michael Ruck, Diana Hoppe, Bernhard Wahl, Paul Simon, Yuekui Wang, and Gotthard Seifert*

According to general chemistry textbooks, three basic allotropic modifications of elemental phosphorus exist, namely, white, red, and black phosphorus, which differ considerably in their chemical and physical properties. When white phosphorus is heated or exposed to radiation, it is transformed to amorphous red phosphorus. The structure of red phosphorus is considered to be a polymeric network of different building units, which are well-known from various compounds containing polymeric phosphorus structures.[1,2] While this network features only short or intermediate range order, further heating or irradiation leads to crystallization. Different crystalline allotropes were reported to form in this way, for example, red phosphorus IV and red phosphorus V, which were characterized by X-ray powder diffraction.[3]

Already in 1865 Hittorf found that phosphorus can also be crystallized from a melt of lead, giving red-to-violet colored platelets.[4] In 1969 Thurn and Krebs determined the structure of this crystalline type of phosphorus, called violet or Hittorf's phosphorus.[5] Up to now, it is the only structurally characterized crystalline form of red phosphorus. This modification consists of pentagonal tubes formed by covalently bonded phosphorus atoms. By comparison of the powder diffraction patterns it can be equated with red phosphorus V described earlier.

Furthermore, Thurn and Krebs reported in their work on the structure of Hittorf's phosphorus: "When white phosphorus is annealed at temperatures between 545 and 580 °C for several months, in addition to platelike crystals of Hittorf's phosphorus bunches of capillary parallel lying fibers form. […]".[5] From X-ray rotation photographs of the fibers, they proposed an arrangement of tubes of the same kind as in Hittorf's phosphorus but linked to parallel double tubes. Furthermore, they considered the constitution to be energetically stable but estimated the density to be lower than the density of Hittorf's phosphorus. Later Böcker and Häser showed in their theoretical investigations on phosphorus structures that Hittorf's phosphorus and the proposed structure of the fibrous type are energetically equivalent and the most favored of all the possible phosphorus chains.[6]

We have now confirmed the assumed structure of the fibrous type of red phosphorus using single-crystal X-ray diffraction as well as transmission electron microscopy methods. The iodine-catalyzed recrystallization of red phosphorus in a small temperature gradient yields dark red needles. In most cases the crystal quality of the fibrous phosphorus is very poor due to agglomeration and stacking faults. Frequently radial growth of fiber bunches upon the ampule wall was observed. Furthermore, needles and platelets often share edges, indicating an intergrowth of crystals of Hittorf's phosphorus and of the fibrous type. The two types can hardly be distinguished visibly; both show a bright red to deep red color and a more or less platelike shape. However, under mechanical stress crystals of the fibrous type split into thin filaments, whereas the crystal platelets of the Hittorf phosphorus type just break up into smaller platelets. In addition, the crystallization of red phosphorus from a lead melt[4,5] was carried out in order to examine whether crystals of the fibrous type can be obtained. But exclusively crystals of the Hittorf type formed by this means.

Powder diffraction patterns of sublimation products show reflections that can be assigned to Hittorf's phosphorus and numerous additional reflections. These can be assigned entirely to the fibrous type after comparison to the theoretical pattern calculated based on structural data. On comparison of the powder diffraction pattern of fibrous phosphorus with powder diffraction patterns given in ref. [3], it becomes clear that the so-called form IV of red phosphorus corresponds to the fibrous type presented here.

Under the transmission electron microscope the two crystalline forms can be differentiated easily: In Figure 1 a the high-resolution micrograph of perpendicular strands is indicative of Hittorf's phosphorus; Figure 1 b in contrast shows exclusively strands lying parallel to each other, which

[*] Prof. Dr. M. Ruck, D. Hoppe, B. Wahl
Institut für Anorganische Chemie
Technische Universität Dresden
01062 Dresden (Germany)
Fax: (+49) 351-463-37287
E-mail: michael.ruck@chemie.tu-dresden.de
Dr. P. Simon
Max-Planck-Institut für Chemische Physik fester Stoffe
Nöthnitzer Strasse 40, 01187 Dresden (Germany)
Dr. Y. Wang, Prof. Dr. G. Seifert
Institut für Physikalische Chemie und Elektrochemie
Technische Universität Dresden
01062 Dresden (Germany)

[**] We thank Dr. D. Geiger, Dr. M. Lehmann, and Prof. Dr. H. Lichte for the support of HREM.

Supporting information for this article is available on the WWW under http://www.angewandte.org or from the author.

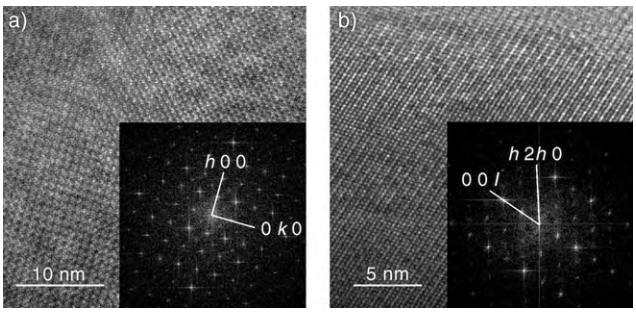

Figure 1. a) High-resolution electron micrograph showing the pseudo-tetragonal symmetry of the [001] zone of Hittorf's phosphorus at the Scherzer focus (Philips CM200 microscope), plane (*hk*0); the corresponding FFT is shown in the inset. b) High-resolution electron micrograph of fibrous phosphorus (Philips CM30 microscope), plane (*h*,2*h*,*l*); the corresponding FFT is shown in the inset.

InterScience
© 2005 Wiley-VCH Verlag GmbH & Co. KGaA, Weinheim

corresponds to fibrous phosphorus. Fast Fourier transform (FFT) of the micrographs of Hittorf's phosphorus gives images with orthogonal rows of pseudo-Bragg reflections (plane $hk0$) and reciprocal lattice parameters of $a^* \approx b^* \approx (920\,\text{pm})^{-1}$. The FFT images of fibrous phosphorus (plane $(h,2h,l)$) give lattice parameters of $|\boldsymbol{a}^* + 2\boldsymbol{b}^*| \approx (440\,\text{pm})^{-1}$ and $c^* \approx (580\,\text{pm})^{-1}$; the included angle amounts to 55.5°. The c^* axis is perpendicular to the visible fiber direction.

The crystal structure of the fibrous type of crystalline red phosphorus is closely related to the structure of Hittorf's phosphorus. Both consist of tubes with pentagonal cross section, which in turn are a regular sequence of three different building units (Figure 2). The subunits are cages of eight or nine phosphorus atoms, which we denote as *[P8]* and *[P9]* in keeping with ref. [6], and dumbbells of two phosphorus atoms, *P2*.

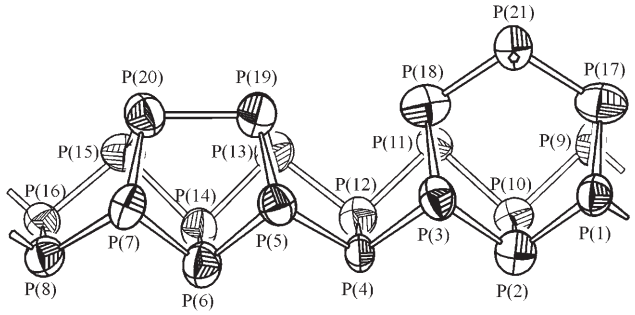

Figure 2. Repeating unit of the tubes in fibrous and in Hittorf's phosphorus (numbering of atoms in analogy to ref. [5]). Thermal ellipsoids enclose 90% probability for atomic displacement. Bond lengths are between 219(1) and 231(1) pm; the mean bond length is 221.9 pm.

The tubes can be interpreted alternatively as zigzag-shaped double chains, which form a corrugated ladder. Free valences are saturated by "roofs" of two or three phosphorus atoms. These single tubes feature the symmetry of the rod group $p2mm$ (no. 18).[7] At the medial roof atoms of the *[P9]* cages, denoted as P(21) and P(21^{i}) (Figure 3), two tubes are each connected to form double tubes with $p112/m$ symmetry (no. 11).[7] Covalent bonds of the atoms P(21) and P(21^{i}) are arranged in staggered conformation, and the corresponding lone pairs are aligned antiparallel. The arrangement resembles the energetically most favored conformation of methyl groups in 2,3-dimethylbutane.

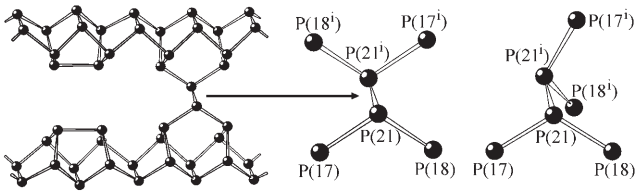

Figure 3. Linkage of the tubes in fibrous phosphorus (left; i: $-x$, $1-y$, $-z$) vs. Hittorf's phosphorus (right; i: $-x$, y, $0.5-z$). Bonding lengths and angles in the structures of fibrous and Hittorf's phosphorus[8] that differ by more than 3 SD: P(21)–P(21^{i}) 222.4(8)/217.3(1) pm; P(17)-P(21)-P(18) 111.9(3)/115.98(3)°, P(17)-P(21)-P(21^{i}) 94.7(3)/96.71(4)°, P(18)-P(21)-P(21^{i}) 93.6(3)/108.23(2)°.

In contrast, the connected tubes of Hittorf's phosphorus run perpendicularly, forming double layers of two interpenetrating but independent tube systems. These double layers are stacked in the c direction and held together by van der Waals forces. As a result of the perpendicular arrangement of two linked tubes, the described staggered conformation of the atom groups P(17)-P(21)-P(18) and P(17^{i})-P(21^{i})-P(18^{i}) cannot be attained (Figure 3, right). The consequence is a higher tension, expressed in expanded bonding angles at the atom P(21) in Hittorf's phosphorus.

The double tubes of the fibrous-type structure are stacked in the a direction with a displacement of $^{1}/_{8}\,b$ and in the c direction with a displacement $^{1}/_{4}\,b$. A distorted hexagonal pattern for the single tubes results (Figure 4). As a consequence of the packing, the $p112/m$ symmetry of the double tubes is not transferred to the crystal lattice, and the space group symmetry is $P\bar{1}$. The packing density of the tubes in Hittorf's and in fibrous phosphorus is very similar, although the arrangements of the tubes differs considerably. In contrast to the assumption in ref. [5], the calculated X-ray densities of fibrous phosphorus and Hittorf's phosphorus both amount to 2.37 g cm^{-3}. The shortest van der Waals distance in Hittorf's phosphorus is 306 pm, between atoms P(14) and P(14^{ii}) [ii: $-1-x$, $-1-y$, $-z$];[8] in fibrous phosphorus the shortest van der Waals distance is 315 pm, also between atoms P(14) and P(14^{ii}) [ii: $1-x$, $-y$, $-z$]. The observation of diffuse X-ray scattering in the diffraction pattern of many phosphorus fibers indicates alternative stacking sequences.

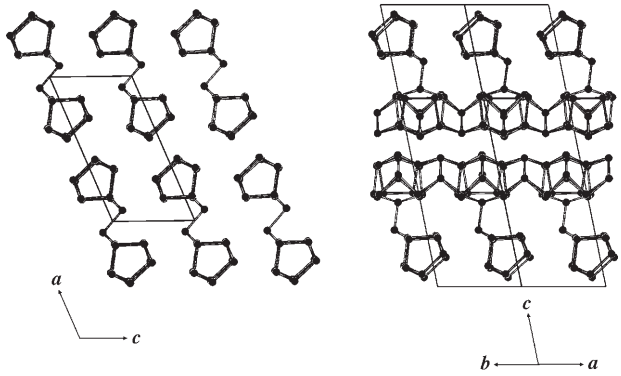

Figure 4. Left: Arrangement of the double tubes along the fiber axis in fibrous phosphorus. Right: Stacking of the layers in Hittorf's phosphorus.

Since the calculations of Böcker and Häser had focused on phosphorus clusters,[6] we have performed density functional based calculations for the bulk phases at the DFTB level[9] to investigate the relative stability of Hittorf's and fibrous phosphorus. The energy contributions of the van der Waals interactions were considered in a semiempirical a posteriori treatment.[10] Periodic boundary conditions were imposed on the systems in all calculations. Comparisons between the DFTB-optimized bond parameters and the experimental values can be found in the Supporting Informa-

 © 2005 Wiley-VCH Verlag GmbH & Co. KGaA, Weinheim

tion. Clearly, for both allotropes the calculated bond parameters are in quite good agreement with the experimental findings. For bond lengths, the standard deviations (SD) are about 1%, and the maximum deviations (MD) are less than 2%. The deviations in bond angles are SD = 0.8° and MD = 1.4° for Hittorf's phosphorus, and SD = 1.8° and MD = 3.6° for the fibrous structure. The results show that the energy differences for the two structures are all less than 0.003 eV per atom, regardless of which bond lengths (experimental or optimized) are used and whether the van der Waals interactions are included. Therefore no preferred structure could be figured out. The conclusion that neither structure is energetically preferred is in agreement with the findings of Böcker and Häser.[6]

For a better understanding of the bonding characteristics of fibrous and Hittorf's phosphorus, especially the short bridging bond P(21)–P(21^{i}) in the latter structure, we performed further calculations, using cluster models (Figure 5) at

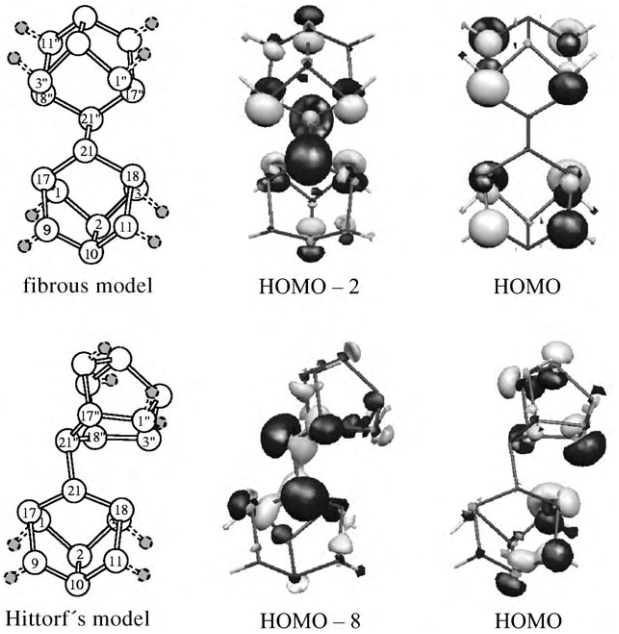

Figure 5. The cluster models ($P_{18}H_8$) used to simulate the bridge between the *[P9]* units in fibrous and in Hittorf's phosphorus (left). The highest occupied molecular orbitals (HOMO) and the orbitals close to the HOMO with dominant "lone-pair" character on the bridge atoms are shown on the right side. Note that in the configuration corresponding to Hittorf's phosphorus the orbital HOMO−8 exhibits some π-bonding characteristics between the bridge atoms, while in the fibrous structure no such contribution can be traced (see orbital HOMO−2).

the DFT/LSD/DZVP level. The fixed (X-ray) geometries of fibrous and Hittorf's phosphorus were used in these calculations. The free valences in these clusters were saturated with hydrogen (P−H = 142 pm). The results indicate that the orbitals around the HOMO show significant lone-pair character. In the fibrous structure one of these orbitals (HOMO−2), dominated by the lone-pair electrons located on the bridge atoms P(21), is only about 0.1 eV below the HOMO. In Hittorf's phosphorus the corresponding orbitals are at lower energy (1 eV below the HOMO). It seems that the twist structure in Hittorf's model is favorable to lower the energy of "lone-pair" electrons on the bridge atoms due to some π-bonding contribution, while in the fibrous structure the inversion symmetry prohibits such an effect. This accounts for the unusually short bridging bond in Hittorf's phosphorus and corresponds to the expanded bonding angles. In addition, a DFT geometry optimization of the Hittorf cluster model was also performed at the LSD/DZVP level, which confirmed that the bridging bond P(21)−P(21^{i}) is the shortest one (experimental 217.8 pm, calcd 219.5 pm).

As a general conclusion it can be stated that the fibrous type of crystalline red phosphorus bears strong structural resemblance to Hittorf's phosphorus. It represents a new crystalline modification of phosphorus. Both types of red phosphorus can be obtained in the same way. The growth mechanism is still unknown, yet experimental results indicate that homogeneous nucleation, for instance in a lead melt, leads only to Hittorf's phosphorus, whereas the growth of phosphorus fibers is preferred in case of heterogeneous nucleation. The structure model given by Thurn and Krebs as well as the theoretical predictions for the existence and stability of a fibrous type of phosphorus by Böcker and Häser thus could be confirmed.

Phosphorus tubes of similar architecture were identified in numerous compounds, such as polyphosphides (e.g. MP_{15}, M = Li–Cs;[11] M′M″P_{14}, M′ = Zn, Cd, Hg, M″ = Sn, Pb[12]); they represent quite stable possibilities of connecting phosphorus atoms.[6,11,13] Other compounds that contain exclusively polymeric tubular structures of phosphorus atoms embedded in copper halide matrices were scrutinized over the past decades.[14] Moreover, two of these phosphorus structures were extracted from their matrices.[15] The phosphorus architectures found in copper halide matrices differ from those obtained from pure amorphous red phosphorus, in all probability because the pentagonal tubes in Hittorf's and fibrous phosphorus are energetically more stable and can be arranged more densely in a crystal than the corrugated or helical phosphorus rods forming in the matrices.

Experimental Section

Synthesis: Amorphous red phosphorus (Fluka 99%; purified according to ref. [16]) was sublimed in evacuated fused-silica ampules using iodine (Merck; sublimed twice on barium oxide) as a catalyst.[17] Best results were achieved with approximately 1.0 g of phosphorus and 40 mg of iodine in an ampule of 17 cm^3. Hittorf's phosphorus and a fibrous solid were obtained. The latter showed increasing crystallinity when the temperature was increased and the temperature gradient decreased within the ampule. Sufficiently large crystals could be grown in a temperature gradient of about 10 K in the temperature range between 590 and 570 °C over several days (see also ref. [18]). At higher temperatures the phosphorus vapor pressure increases rapidly due to the increasing formation of white phosphorus in the gas phase. Therefore the samples were not heated above the given temperatures. Sublimation of red phosphorus also succeeds without catalysts. However, the generation of a gas phase is kinetically hindered, and autosublimation requires much more time.

Transmission electron microscopy: Crystallites of fibrous red phosphorus and of Hittorf's phosphorus were examined by high-resolution transmission electron microscopy (HRTEM). The inves-

 © 2005 Wiley-VCH Verlag GmbH & Co. KGaA, Weinheim

tigations were performed at the Speziallabor für Elektronenmikroskopie Triebenberg with a Philips CM200 FEG\ST Lorentz electron microscope, equipped with a field emission gun and at an acceleration voltage of 200 kV. Point resolution amounts to 2.4 Å and information limit to about 1.2 Å. A TEM Philips CM30 FEG UT/Special Tübingen at an acceleration voltage of 300 kV also equipped with a field emission gun was also used. In this case, point resolution amounts to 1.7 Å and information limit to about 0.9 Å. TEM images were processed by Digital Micrograph (Gatan, USA).

X-ray crystal structure determination: systematic name: phosphorus (*aP*42); triclinic, space group $P\bar{1}$ (no. 2), $a = 1219.8(8)$, $b = 1298.6(8)$, $c = 707.5(7)$ pm; $\alpha = 116.99(7)$, $\beta = 106.31(7)$, $\gamma = 97.91(7)°$, $V = 911(2) \times 10^6$ pm^3, $\rho_{calcd} = 2.37$ g cm^{-3}, absorption coefficient $\mu = 1.89$ mm^{-1}, $2\theta_{max} = 42.5°$, $Mo_{K\alpha}$ radiation, $\lambda = 71.073$ pm, $T = 293(2)$ K. The diffraction data were collected on an imaging plate diffraction system IPDS-I (Stoe). Numerical absorption corrections were applied. The structure was solved with SHELXS97 and refined against F_o^2 using SHELXL97.[19] All atoms were refined using anisotropic displacement parameters. Final R values: $R_1(F_o > 4\sigma(F_o)) = 0.028$, wR_2(all F_o^2) $= 0.042$; $GooF = 0.934$ for 4048 (1932 unique) reflections and 190 parameters; min./max. residual electron density ± 1.38. Atom parameters are listed in Table 1. Further details

Table 1: Atomic coordinates and equivalent displacement parameters U_{eq} of fibrous phosphorus.[a]

Atom	x	y	z	U_{eq} [pm^2]
P(1)	0.1515(5)	0.3308(4)	−0.253(1)	260(10)
P(2)	0.2754(5)	0.4729(5)	−0.2516(9)	260(20)
P(3)	0.1510(5)	0.5801(4)	−0.258(1)	270(10)
P(4)	0.2796(5)	0.7243(4)	−0.240(1)	230(10)
P(5)	0.1603(5)	−0.1640(4)	−0.2606(9)	260(10)
P(6)	0.2876(6)	−0.0284(5)	−0.263(1)	300(20)
P(7)	0.1578(5)	0.0728(4)	−0.2662(9)	270(10)
P(8)	0.2777(6)	0.2260(5)	−0.241(1)	270(20)
P(9)	0.3550(6)	0.4924(4)	0.292(1)	280(20)
P(10)	0.4123(6)	0.5813(5)	0.119(1)	280(20)
P(11)	0.3533(5)	0.7410(4)	0.2912(9)	230(10)
P(12)	0.4152(5)	0.8318(4)	0.1267(9)	240(10)
P(13)	0.3636(5)	−0.0037(4)	0.284(1)	260(10)
P(14)	0.4255(6)	0.0825(4)	0.109(1)	270(10)
P(15)	0.3598(5)	0.2365(5)	0.2835(9)	260(10)
P(16)	0.4144(5)	0.3352(4)	0.1270(9)	220(10)
P(17)	0.1587(6)	0.4055(5)	0.101(1)	340(20)
P(18)	0.1572(5)	0.6844(4)	0.097(1)	310(10)
P(19)	0.1695(5)	−0.0460(4)	0.0915(8)	320(10)
P(20)	0.1655(5)	0.1310(4)	0.0890(8)	310(10)
P(21)	0.0765(3)	0.5517(3)	0.1705(6)	310(10)

[a] Standard deviations for the last significant digit are given in parentheses. U_{eq} (in pm^2) is defined as one-third of the trace of the orthogonalized U_{ij} tensor.

of the crystal structure investigation may be obtained from the Fachinformationszentrum Karlsruhe, D-76344 Eggenstein-Leopoldshafen, Germany (e-mail: crysdata@fiz-karlsruhe.de; fax: (+49) 7247-808-666) on quoting the depository number CSD-391323.

Computational methods: The initial geometries were taken from the X-ray crystal data of Hittorf's[5] and fibrous phosphorus. To investigate the relative stability of these allotropes in the bulk phase, the initial structures were optimized using the density functional based tight-binding method (DFTB)[9] and the Γ-point approximation, as implemented in the program package *deMon*.[20] The experimental lattice constants were kept fixed during the geometry optimizations, and the convergence criterion 10^{-6} atomic units for the energy gradient was used. The validity of the gamma approximation was checked with different *k*-point sets and different sized supercells. The energy contribution of van der Waals interactions for the allotropes was calculated for fixed (X-ray) and optimized geometries. The optimized bond lengths, bond angles, and dihedral angles are given together with the corresponding experimental values in Tables 2–5 of the Supporting Information. The calculations of the clusters as models for the *[P9]* units were also performed with the program package *deMon*[20] within density functional theory (DFT) method and the local density approximation (LDA) for the exchange-correlation (XC) energy, using a DZVP basis set.

Received: August 24, 2005
Published online: October 24, 2005

Keywords: allotropy · density functional calculations · phosphorus · solid-state structures · X-ray diffraction

[1] a) G. Fasol, M. Cardona, W. Hönle, H. G. von Schnering, *Solid State Commun.* **1984**, *52*, 307; b) D. W. Bullett, *Solid State Commun.* **1985**, *55*, 257.
[2] S. R. Elliott, J. C. Dore, E. Marseglia, *J. Phys. Colloq.* **1985**, *46*, 349.
[3] a) W. L. Roth, T. W. DeWitt, A. J. Smith, *J. Am. Chem. Soc.* **1947**, *69*, 2881; b) M. Rubenstein, F. M. Ryan, *J. Electrochem. Soc.* **1966**, *113*, 1063; c) V. V. Nechaeva, N. D. Talanov, A. I. Soklakov, *Russ. J. Inorg. Chem.* **1979**, *24*, 1097.
[4] W. Hittorf, *Ann. Phys. Chem.* **1865**, *126*, 193.
[5] H. Thurn, H. Krebs, *Acta Crystallogr. Sect. B* **1969**, *25*, 125.
[6] S. Böcker, M. Häser, *Z. Anorg. Allg. Chem.* **1995**, *621*, 258.
[7] *International Tables Vol. E: Subperiodic Groups* (Eds.: V. Kopský, D. B. Litvin), Kluwer, Dordrecht, **2002**.
[8] H. G. von Schnering, X-ray single-crystal redetermination of the structure of Hittorf's phosphorus, **1993**, private communication.
[9] a) D. Porezag, T. Frauenheim, T. Köhler, G. Seifert, R. Kaschner, *Phys. Rev. B* **1995**, *51*, 12947; b) G. Seifert, D. Porezag, T. Frauenheim, *Int. J. Quantum Chem.* **1996**, *58*, 185.
[10] L. Zhechkov, T. Heine, S. Patchkovskii, G. Seifert, H. A. Duarte, *J. Chem. Theory Comp.* **2005**, *1*, 841..
[11] W. Hönle, H. G. von Schnering, *Chem. Rev.* **1988**, *88*, 243.
[12] U. D. Scholz, W. Jeitschko, *J. Solid State Chem.* **1987**, *67*, 271.
[13] "Catenation of Phosphorus Atoms": H. G. von Schnering in *Homoatomic Rings, Chains and Macromolecules of Main-Group Elements* (Ed.: A. L. Rheingold), Elsevier, Amsterdam, **1977**.
[14] a) M. H. Möller, W. Jeitschko, *J. Solid State Chem.* **1986**, *65*, 178; b) A. Pfitzner, E. Freudenthaler, *Angew. Chem.* **1995**, *107*, 1784; *Angew. Chem. Int. Ed. Engl.* **1995**, *34*, 1647; c) A. Pfitzner, E. Freudenthaler, *Z. Naturforsch. B* **1997**, *52*, 199.
[15] A. Pfitzner, M. F. Bräu, J. Zweck, G. Brunklaus, H. Eckert, *Angew. Chem.* **2004**, *116*, 4324; *Angew. Chem. Int. Ed.* **2004**, *43*, 4228.
[16] G. Brauer, *Handbuch der präparativen anorganischen Chemie, Vol. 1*, Enke, Stuttgart, **1975**.
[17] H. Schäfer, M. Trenkel, *Z. Anorg. Allg. Chem.* **1972**, *391*, 11.
[18] P. Rudolf, Diploma Thesis, Fachhochschule Reutlingen, Germany, **1983**.
[19] G. M. Sheldrick, SHELX-97, Program for Crystal Structure Determination, University of Göttingen, Germany, **1997**.
[20] A. M. Köster, G. Geudtner, A. Goursot, T. Heine, A. Vela, S. Patchkovskii, D. R. Salahub, deMon, NRC: Ottawa, Canada, **2002**.

 © 2005 Wiley-VCH Verlag GmbH & Co. KGaA, Weinheim

Kinetic Resolution

DOI: 10.1002/anie.200502631

Kinetic Resolution of Chiral Secondary Alcohols by Dehydrogenative Coupling with Recyclable Silicon-Stereogenic Silanes**

*Sebastian Rendler, Gertrud Auer, and Martin Oestreich**

Non-enzymatic kinetic resolution[1] of racemic mixtures is a competitive strategy in asymmetric synthesis for the preparation of chiral building blocks.[2,3] The general approach relies on either a chiral reagent to undergo or a chiral catalyst to promote a stereoselective reaction of one enantiomer over the other. Within the theme of the former scenario, we devised a novel concept based on an unprecedented diastereoselective transition-metal-catalyzed dehydrogenative silicon–oxygen coupling of silicon-stereogenic silanes **A** and racemic alcohols *rac*-**B** (Scheme 1).[4]

We envisioned that if a preferential reaction of **A** with (*S*)-**B** to produce diastereoenriched **C** were viable, the optical antipode (*R*)-**B** would remain in enantioenriched form. Moreover, stereospecific reductive cleavage of the silicon–oxygen bond in **C** would allow complete recovery of the resolving reagent **A**. Importantly, both silicon–oxygen bond formation and cleavage would have to proceed without any erosion of stereochemical information at the silicon atom. Herein, we describe this novel concept of utilizing silicon-stereogenic silanes **A** in a kinetic resolution reaction.

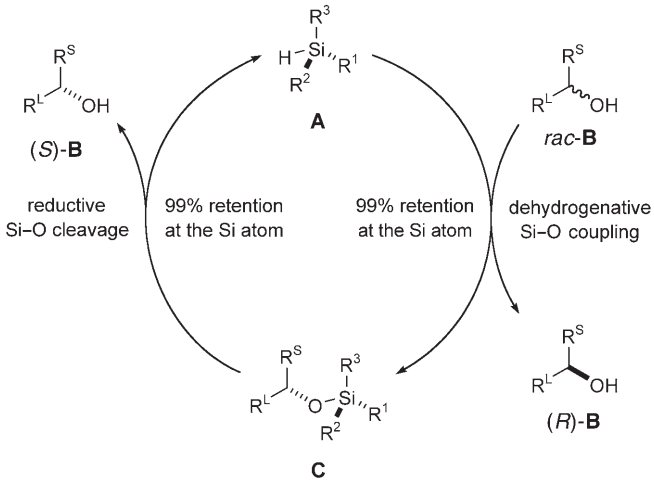

Scheme 1. Kinetic resolution with recyclable silicon-stereogenic silanes ($R^1 \neq R^2 \neq R^3$, R^L = large R, and R^S = small R groups).

We initially sought suitable reaction conditions for silane alcoholysis with a particular emphasis on the stereochemical course at the silicon atom. Several heterogeneous and homogeneous catalysts are available,[5,6] and we selected the copper(I)-catalyzed dehydrogenative coupling introduced by Lorenz and Schubert.[7] Oxygen-sensitive $[\{(Ph_3P)CuH\}_6]$[8] is effectively replaced by a robust precatalyst (CuCl, Ph_3P, NaO*t*Bu) reported by Buchwald and co-workers[9] which also enables simple variation of the phosphine ligand.

We then screened this catalyst in the methanolysis of several asymmetrically substituted silanes[10] **1**–**3** (Figure 1) followed by stereoretentive reduction with aluminum hydrides.[11] To our delight, **1**–**3** were invariably recovered with complete retention of configuration, thereby verifying the stereospecificity of the copper(I)-catalyzed dehydrogenative silicon–oxygen coupling at the asymmetrically substituted silicon atom.[12] These experiments secured the pivotal preservation of the stereochemical integrity at silicon throughout this two-step process.[13]

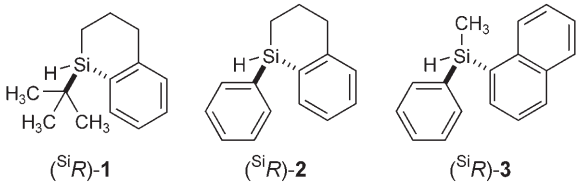

Figure 1. Silanes with silicon-centered chirality.

We then addressed the stereoselectivity of the dehydrogenative silicon–oxygen coupling of racemic alcohols with privileged silane (^{Si}R)-**1**.[14] A selected experiment (*rac*-**4**→(^{Si}S,*S*)-**5**, Scheme 2) showed that unfunctionalized secondary alcohols are essentially ineffective (d.r. ≤ 60:40). These discouraging observations led us to consider the introduction of a pendant donor (Do) in the substrate (Do = CH in **4**, Do = N in **6**), which provides a temporary residence site for the copper catalyst. We reasoned that alcohols capable of two-point binding would create more rigidity around the copper center, which in turn could be beneficial to diastereoselectivity. Consistent with our hypothesis, we were pleased to find that dehydrogenative coupling of *rac*-**6** and (^{Si}R)-**1** proceeded with substantially improved diastereoselectivity and enhanced reaction rate (*rac*-**6**→(^{Si}S,*S*)-**7**, Scheme 2).

The ideal phosphine ligand for this transformation, tri(3,5-xylyl)phosphane (**L1f**), was identified in an extensive screening of mono- and bidentate phosphine and N-heterocyclic carbene ligands (**L1**, **L2**, and **L3**, Table 1). We aimed to elucidate the influence of the ligand on the reaction rate and diastereoselectivity of the dehydrogenative coupling of *rac*-**6**

[*] Dipl.-Chem. S. Rendler, Dipl.-Chem. G. Auer, Dr. M. Oestreich
Institut für Organische Chemie und Biochemie
Albert-Ludwigs-Universität
Albertstrasse 21, 79104 Freiburg im Breisgau (Germany)
Fax: (+49) 761-203-6100
E-mail: martin.oestreich@orgmail.chemie.uni-freiburg.de

[**] Financial support was provided by the Deutsche Forschungsgemeinschaft (Emmy Noether Progamme, 2001–2006), the Fonds der Chemischen Industrie (predoctoral fellowship to S.R., 2005–2007), and the Dr. Otto Röhm Gedächtnisstiftung. The authors thank Ilona Hauser for skillful technical assistance and Gerd Fehrenbach for HPLC analyses. M.O. is indebted to Professor Reinhard Brückner for his continuous encouragement. Generous donation of Buchwald biaryl phosphine ligands by Lanxess AG (Germany) is gratefully acknowledged.

 InterScience © 2005 Wiley-VCH Verlag GmbH & Co. KGaA, Weinheim

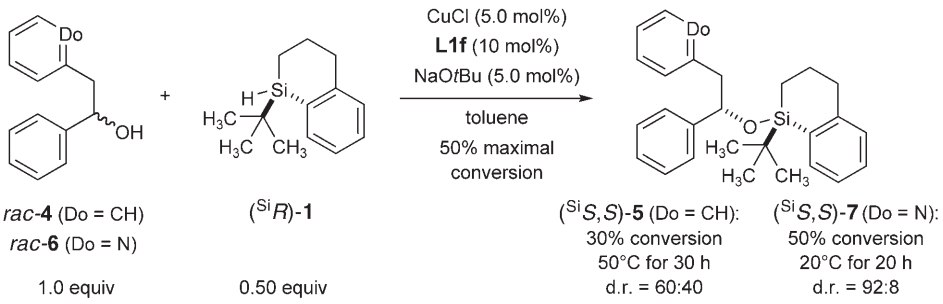

Scheme 2. Control of diastereoselectivity: Beneficial two-point binding. **L1f** = tri(3,5-xylyl)phosphane.

and (^{Si}R)-**1**.[15] A ligand/copper(I) ratio of 2:1 is usually needed to stabilize the catalyst. We began with triphenylphosphane (**L1a**), which gave ($^{Si}S,S$)-**7** under mild conditions with good diastereoselectivity (Table 1, entry 1). The reactivity decreased significantly in the presence of electron-poor phosphines **L1b–d**,[4a] yet the diastereoselectivity remained almost unaffected (Table 1, entries 2–4). Steric hindrance was not tolerated, and 2-tolyl-substituted phosphine **L1e** failed to stabilize the catalyst (Table 1, entry 5). Conversely, 3,5-xylyl-substituted phosphine **L1f** combined high reactivity with excellent diastereoselectivity at complete conversion (Table 1, entry 6). Electron-rich phosphines **L1g** and **L1h** (Table 1, entries 7 and 8), N-hetereocyclic carbene ligands[16] **L2a** and **L2b** (Table 1, entries 9 and 10), and Buchwald biaryl phosphines (not shown) were less effective. Interestingly, bidentate phospines **L3a–d** generated unreactive catalysts and led merely to moderate levels of diastereoselectivity (Table 1, entries 11–14).

These findings can be roughly rationalized by the model outlined in Scheme 3. In the rate-determining step, one of the ligands L at the copper(I) center is replaced by the weakly

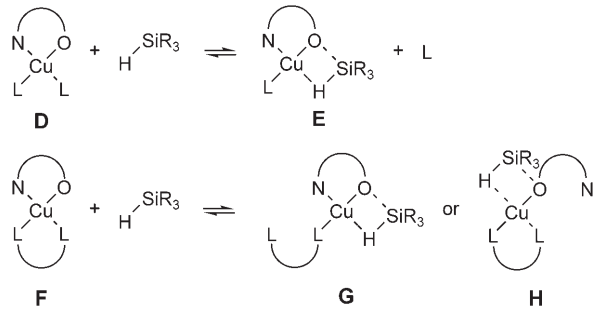

Scheme 3. Model for the postulated rate-determining step.

coordinating silane. This requires ligands with distinctly tuned σ-donor and π-acceptor strength as well as steric demand at electron-rich copper(I). In the case of monodentate ligands, a ligand must dissociate to generate a vacant coordination site (**D**→**E**). In the case of bidentate ligands, one of the chelates must open in an energetically clearly unfavorable step: 1) **F**→**G**, leaving the N,O-chelate intact, or 2) **F**→**H**, without two-point binding. The exact mechanism of the actual silicon–oxygen bond formation is still not completely understood, but is likely to involve—at least in a transition state—a pentacoordinated silicon of unknown configuration. Remarkably, a conceivable pseudorotation[17] and, hence, racemization are not observed, which indicates a concerted σ-bond metathesis.[10c]

We conducted our investigations with rationally yet empirically designed (^{Si}R)-**1**.[14] A comparison with less sterically encumbered cyclic or even acyclic silanes (^{Si}R)-**2** and (^{Si}R)-**3** impressively demonstrated once again the importance of steric demand and of three truly different substituents at the silicon atom (Scheme 4).[10c] Whereas less-hindered silanes were expectedly more reactive, diastereoselectivity collapsed in the case of cyclic (^{Si}R)-**2** (d.r. = 66:34) and was hardly observed with (^{Si}R)-**3** (d.r. = 57:43).

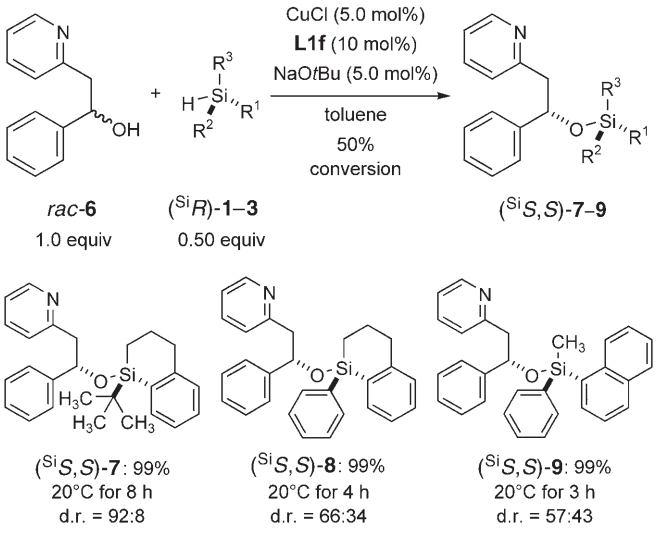

Scheme 4. Probing the steric demand and substitution pattern at the silicon atom.

This preliminary insight set the stage for an investigation of the kinetic resolution itself. As a starting point, we resolved our standard substrate *rac*-**6** by using optically enriched (^{Si}R)-**1** (96% *ee*). Both silyl ether ($^{Si}S,S$)-**7** and alcohol (*R*)-**6**[18] were isolated in quantitative yields, the latter with an encouraging 84% *ee* at 56% conversion (Table 2, entry 1). Importantly, the diastereomeric ratio of ($^{Si}S,S$)-**7** decreases with increasing conversion (d.r. = 92:8 at 50% conversion versus d.r. = 86:14 at 56% conversion). The stereoselectivity factor *s*[1] can only be estimated at larger than 10,[19] as this kinetic resolution involves an enantiomerically impure resolving reagent.[20] Indeed, we were able to verify experimentally this interesting

 © 2005 Wiley-VCH Verlag GmbH & Co. KGaA, Weinheim

Table 1: Identification of effective ligands for the conversion **6**→**7**.[a]

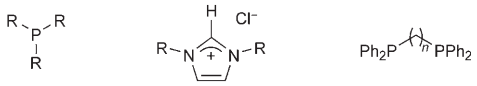

L1 **L2** **L3** (n = 1–4)

Entry	Ligand L			L/CuCl	T [°C]	t [h]	d.r.[b]	Conv. [%][c]
	L1	R						
1	**L1a**			2:1	20	48	90:10	42
2	**L1b**	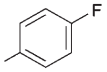		2:1	50	48	89:11	37
3	**L1c**	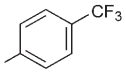		2:1	70	60	83:17	38
4	**L1d**	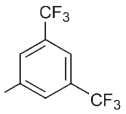		2:1	70	60	86:14	34[d]
5	**L1e**	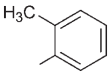		2:1	20	–	–	–[e]
6	**L1f**	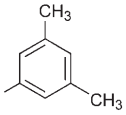		2:1	20	20	92:8	50
7	**L1g**			1:1[f]	20	24	81:19	33
8	**L1h**			2:1	50	6	75:25	21[e]
	L2	R						
9[g]	**L2a**	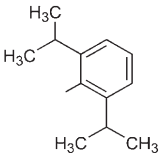 IPr·HCl		1:1	85	2	55:45	10
10[g]	**L2b**	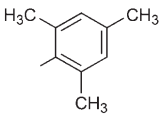 IMes·HCl		1:1	60	2	76:24	40
	L3[h]		n					
11	**L3a**	(dppm)	1	1:1	45	48	82:18	32
12	**L3b**	(dppe)	2	1:1	45	48	87:13	20
13	**L3c**	(dppp)	3	1:1	45	48	80:20	20
14	**L3d**	(dppb)	4	1:1	45	48	79:21	18

[a] Unless otherwise noted, all reactions were conducted with CuCl (5.0 mol%), **L1** (10 mol%) or **L2**/**L3** (5.0 mol%), NaO*t*Bu (5.0 mol%) with a substrate concentration of 0.1 M in toluene. [b] Determined from the ^{1}H NMR spectra of the crude reaction mixtures by integration of the baseline-separated resonance signals of diastereomeric ($^{Si}S,S$)-**7** at $\delta = 4.93$ ppm and ($^{Si}S,R$)-**7** at $\delta = 5.02$ ppm. [c] Monitored by ^{1}H NMR spectroscopic analysis and determined by integration of the baseline separated resonance signals of **6** at $\delta = 5.16$ ppm and **7** at $\delta = 4.93/5.02$ ppm. [d] Extremely slow conversion. [e] Unstable catalyst. [f] Sterically demanding **L1g** allowed an equimolar ratio of ligand and CuCl. [g] Substoichiometric amounts of NaO*t*Bu (30 mol%) were required. [h] dppm = 1,1-bis(diphenylphosphanyl)methane, dppe = 1,2-bis(diphenylphosphanyl)ethane, dppp = 1,3-bis(diphenylphosphanyl)propane, dppb = 1,4-bis(diphenylphosphanyl)butane.

example of mutual kinetic resolution.[1] For this purpose, we resolved *rac*-**6** with (^{Si}R)-**1** (32% *ee*). The optical purity of (*R*)-**6** (25% *ee*) as well as of (^{Si}R)-**1** (48% *ee*) increased as the reaction proceeded until 50% conversion was reached.[1,20]

An investigation of the substrate scope demonstrated some generality for the class of 2-pyridyl-substituted secondary alcohols (Table 2, entries 2–7). Replacement of a phenyl group (*rac*-**6**) by 1-naphthyl (*rac*-**10**) only had a marginal

 © 2005 Wiley-VCH Verlag GmbH & Co. KGaA, Weinheim

Table 2: Copper-catalyzed dehydrogenative kinetic resolution.[a]

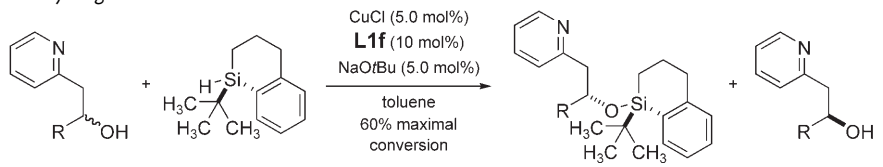

rac-**6**, *rac*-**10**–*rac*-**15** 1.0 equiv; (^{Si}R)-**1** 0.60 equiv; ($^{Si}S,S$)-**7**, ($^{Si}S,S$)-**16**–($^{Si}S,S$)-**19**, ($^{Si}S,R$)-**20**, ($^{Si}S,S$)-**21**; (*R*)-**6**, (*R*)-**10**–(*R*)-**13**, (*S*)-**14**, (*R*)-**15**

Entry	Alcohol	R	Silane (^{Si}R)-**1** *ee* [%][b]	Silyl ether Product[c]	Yield [%][d]	d.r.[e]	Conv. [%][f]	Alcohol Product[c]	Yield [%][d]	*ee* [%][g] ([α]$_D$)[h]
1	*rac*-**6**		96	($^{Si}S,S$)-**7**	99	86:14	56	(*R*)-**6**	99	84 (+)
2	*rac*-**10**	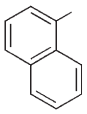	93	($^{Si}S,S$)-**16**	97	84:16	58	(*R*)-**10**	99	80 (+)
3	*rac*-**11**		95	($^{Si}S,S$)-**17**	92	88:12	50	(*R*)-**11**	99	70 (+)
4	*rac*-**12**	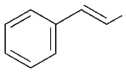	93	($^{Si}S,S$)-**18**	99	87:13	57	(*R*)-**12**	99	74 (−)
5[i]	*rac*-**13**	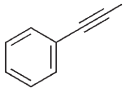	93	($^{Si}S,S$)-**19**	99[i]	74:26	64[j]	(*R*)-**13**	84[i]	89 (−)
6	*rac*-**14**		93	($^{Si}S,R$)-**20**	98	76:24	58	(*S*)-**14**	98	73 (+)
7[k]	*rac*-**15**		94	($^{Si}S,S$)-**21**	87	94:6[l]	46	(*R*)-**15**	99	68 (−)[l]

[a] Unless otherwise noted, all reactions were conducted with CuCl (5.0 mol%), **L1 f** (10 mol%), NaO*t*Bu (5.0 mol%) with a substrate concentration of 0.1 M in toluene at 25 °C. [b] HPLC analysis using a Daicel Chiralcel OJ-R column (EtOH/H_2O 80:20 at 20 °C) provided baseline separation of enantiomers. [c] Absolute configurations of (^{Si}R)-**1**[10c] and (*R*)-**6**[18] and, therefore, **7** are known. The absolute configurations of enantioenriched alcohols **10**–**15** as well as silyl ethers **16**–**21** were assigned by analogy. [d] Yield of analytically pure product isolated by flash chromatography on silica gel. [e] Determined from the ^{1}H NMR spectra of the crude reaction mixtures by integration of the baseline-separated resonance signals of the diastereomers. [f] Monitored by ^{1}H NMR analysis and determined by integration of the baseline-separated resonance signals of the alcohol and silyl ether. [g] HPLC analysis using a Daicel Chiralcel OD-H column (*n*-heptane/*i*PrOH 90:10 for **6**, **10**, **12**, and **13** and 98:2 for **11** at 20 °C) or Daicel Chiralcel AD-H column (*n*-heptane/*i*PrOH = 98:2 for **14** and **15** at 20 °C) provided baseline separation of enantiomers. [h] *c* = 0.22–0.55 in $CHCl_3$ at 20 °C. [i] Reaction accompanied by partial *Z*-selective alkyne reduction: ($^{Si}S,S$)-**19** contaminated with 7% *Z* alkene and (*R*)-**13** contaminated with 21% *Z* alkene in 57% *ee*. [j] (^{Si}R)-**1**: 0.65 equiv. [k] The reaction was performed with CuCl (10 mol%), **L1 f** (20 mol%), NaO*t*Bu (20 mol%), and (^{Si}R)-**1** (1.2 equiv) at 110 °C. [l] High diastereomeric ratio at conversion below 50% and, therefore, moderate enantiomeric excess.

effect (Table 2, entry 2), whereas the efficiency decreased with less sterically demanding vinyl (*rac*-**11**) and cinnamyl groups (*rac*-**12**) (Table 2, entries 3 and 4). For alkynyl substitution (*rac*-**13**), we probed the efficiency at higher conversion and obtained good enantiomeric purity; however, this reaction was accompanied by partial reduction of the triple bond (Table 2, entry 5). When methyl derivative *rac*-**14** was employed, the kinetic resolution was least efficient (Table 2, entry 6). Dehydrogenative coupling of branched, *t*Bu-substituted alcohol *rac*-**15** was highly diastereoselective, but conversion did not proceed beyond 50%, even at elevated temperatures (Table 2, entry 7).

Finally, our concept would only come full circle with complete recovery of the resolving reagent without racemization at the silicon atom. Reductive cleavage of the silicon–oxygen linkage in ($^{Si}S,S$)-**7** in quantitative yield liberated (^{Si}R)-**1** with an unchanged 96% *ee* (Scheme 5).

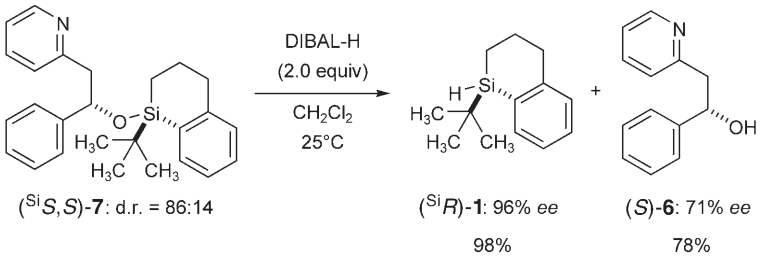

($^{Si}S,S$)-**7**: d.r. = 86:14 (^{Si}R)-**1**: 96% *ee* 98% (*S*)-**6**: 71% *ee* 78%

Scheme 5. Recycling of the resolving reagent. DIBAL-H = diisobutylaluminum hydride.

In conclusion, we have developed a novel kinetic resolution based on a diastereoselective dehydrogenative coupling of racemic alcohols and asymmetrically substituted silanes. Two-point binding of the substrates emerged as the pivotal feature for stereoselectivity. The efficiency of this strategy was exemplified by resolving a family of 2-pyridyl-substituted alcohols. Apart from the recyclability of the silicon-stereogenic silane, this two-step reaction sequence

 © 2005 Wiley-VCH Verlag GmbH & Co. KGaA, Weinheim

involves the simple separation of compounds with substantially different polarity. Further optimization and extension of substrate scope are currently underway in our laboratories.

Received: July 27, 2005
Published online: October 27, 2005

Keywords: asymmetric catalysis · copper · dehydrogenation · kinetic resolution · silicon

[1] H. B. Kagan, J. C. Fiaud in *Topics in Stereochemistry, Vol. 18* (Eds.: E. L. Eliel, S. H. Wilen), Wiley, New York, **1988**, pp. 249–330.
[2] a) E. Vedejs, M. Jure, *Angew. Chem.* **2005**, *117*, 4040–4069; *Angew. Chem. Int. Ed.* **2005**, *44*, 3974–4001; b) D. E. J. E. Robinson, S. D. Bull, *Tetrahedron: Asymmetry* **2003**, *14*, 1407–1446; c) J. M. Keith, J. F. Larrow, E. N. Jacobsen, *Adv. Synth. Catal.* **2001**, *343*, 5–26.
[3] For a brief summary of kinetic resolutions of alcohols, see: P. Somfai, *Angew. Chem.* **1997**, *109*, 2849–2851; *Angew. Chem. Int. Ed. Engl.* **1997**, *36*, 2731–2733.
[4] a) For a catalytic asymmetric alcoholysis of a prochiral dihydrosilane with chiral phosphine-modified copper(I) complexes, see: D. R. Schmidt, S. J. O'Malley, J. L. Leighton, *J. Am. Chem. Soc.* **2003**, *125*, 1190–1191; b) for the introduction of this strategy, see: R. J. P. Corriu, J. J. E. Moreau, *J. Organomet. Chem.* **1976**, *120*, 337–346.
[5] For a tabulated summary, see: J. Y. Corey in *Advances in Silicon Chemistry, Vol. 1* (Ed.: G. Larson), JAI, Greenwich, **1991**, pp. 327–387.
[6] For recent progress, see: a) Pd/C and Rh^{II}: C. N. Scott, C. S. Wilcox, *Synthesis* **2004**, 2273–2276; b) Ru^{I}: R. L. Miller, S. V. Maifeld, D. Lee, *Org. Lett.* **2004**, *6*, 2773–2776; c) Cu^{I}: H. Ito, A. Watanabe, M. Sawamura, *Org. Lett.* **2005**, *7*, 1869–1871; d) Au^{I}: H. Ito, K. Takagi, T. Miyahara, M. Sawamura, *Org. Lett.* **2005**, *7*, 3001–3004.
[7] C. Lorenz, U. Schubert, *Chem. Ber.* **1995**, *128*, 1267–1269.
[8] D. M. Brestensky, D. E. Huseland, C. McGettigan, J. M. Stryker, *Tetrahedron Lett.* **1988**, *29*, 3749–3752.
[9] D. H. Appella, Y. Moritani, R. Shintani, E. M. Ferreira, S. L. Buchwald, *J. Am. Chem. Soc.* **1999**, *121*, 9473–9474.
[10] a) L. H. Sommer, C. L. Frye, G. A. Parker, K. W. Michael, *J. Am. Chem. Soc.* **1964**, *86*, 3271–3276; b) M. Oestreich, U. K. Schmid, G. Auer, M. Keller, *Synthesis* **2003**, 2725–2739; c) M. Oestreich, S. Rendler, *Angew. Chem.* **2005**, *117*, 1688–1691; *Angew. Chem. Int. Ed.* **2005**, *44*, 1661–1664.
[11] a) L. H. Sommer, *Stereochemistry, Mechanism and Silicon*, McGraw-Hill, New York, **1965**; b) L. H. Sommer, *Intra-Sci. Chem. Rep.* **1973**, *7*, 1–44; c) R. J. P. Corriu, C. Guerin, J. J. E. Moreau in *Topics in Stereochemistry, Vol. 15* (Ed.: E. L. Eliel), Wiley, New York, **1984**, pp. 43–198.
[12] a) Inversion is favored in the presence of heterogeneous catalysts: L. H. Sommer, J. E. Lyons, *J. Am. Chem. Soc.* **1967**, *89*, 1521–1522; b) retention is favored in the presence of homogeneous catalysts: R. J. P. Corriu, J. J. E. Moreau, *J. Organomet. Chem.* **1976**, *114*, 135–144.
[13] A related strategy involving silicon–oxygen bond formation starting from chiral silyl chlorides is thwarted by their rapid chloride-induced racemization: M. Oestreich, G. Auer, M. Keller, *Eur. J. Org. Chem.* **2005**, 184–195.
[14] For a discussion of the design of silicon-stereogenic silanes, see: M. Oestreich, *Chem. Eur. J.*, DOI: 10.1002/chem.200500782.
[15] In screenings directed toward the determination of the diastereoselectivity of silane alcoholysis, we generally used racemic silane *rac*-**1**; for clarity, only one enantiomer is depicted.
[16] S. Díez-Gonzáles, H. Kaur, F. Kauer Zinn, E. D. Stevens, S. P. Nolan, *J. Org. Chem.* **2005**, *70*, 4784–4796.
[17] For pseudorotational processes at a pentavalent silicon atom incorporated into a carbocycle, see: E. P. A. Couzijn, M. Schakel, F. J. J. de Kanter, A. W. Ehlers, M. Lutz, A. L. Spek, K. Lammertsma, *Angew. Chem.* **2004**, *116*, 3522–3524; *Angew. Chem. Int. Ed.* **2004**, *43*, 3440–3442.
[18] For the absolute configuration of **6**, see: C.-Y. Yu, O. Meth-Cohn, *Tetrahedron Lett.* **1999**, *40*, 6665–6668.
[19] An *s* value was estimated based on hypothetical enantiopure (^{Si}R)-**1** (100% *ee*) by using the equation reported by Kagan:[1] $s = \ln[(100-\text{conversion})(100-ee_{(R)\text{-}6})]/\ln[(100-\text{conversion})(100+ee_{(R)\text{-}6})]$.
[20] T. O. Luukas, C. Girard, D. R. Fenwick, H. B. Kagan, *J. Am. Chem. Soc.* **1999**, *121*, 9299–9306.

 © 2005 Wiley-VCH Verlag GmbH & Co. KGaA, Weinheim

Antitumor Agents

DOI: 10.1002/anie.200501593

Synthetic Vaccines Consisting of Tumor-Associated MUC1 Glycopeptide Antigens and Bovine Serum Albumin**

*Sebastian Dziadek, Danuta Kowalczyk, and Horst Kunz**

The identification of cell-surface components that occur only on tumor but not on healthy cells is essential for a selective immunological attack on tumor tissue. About 30 years ago, Springer[1] described membrane glycoproteins containing the Thomsen–Friedenreich T antigen and the monosaccharide Tn antigen side chains as tumor-associated antigens on epithelial tumors. These T and Tn glycoproteins were described to be structurally related to the N-terminal region of asialoglycophorin. Based on this structural information, we synthesized a vaccine consisting of N-terminal glycopeptides from asialoglycophorin of M blood group specificity conjugated with bovine serum albumin (BSA)[2] and employed it in the immunization of mice. Although the monoclonal antibody (82-A6) obtained from these experiments showed affinity to epithelial tumor cells, the selectivity for tumor cells was not sufficient.[3] However, the antibody 82-A6 was capable of distinguishing clearly between asialoglycophorin of M and N

[*] Dr. S. Dziadek, D. Kowalczyk, Prof. Dr. H. Kunz
Institut für Organische Chemie
Johannes Gutenberg-Universität Mainz
Duesbergweg 10–14, 55128 Mainz (Germany)
Fax: (+49) 6131-392-4786
E-mail: hokunz@uni-mainz.de

[**] This work was supported by the Deutsche Forschungsgemeinschaft and the Stiftung Rheinland-Pfalz für Innovation. S.D. is grateful for a scholarship provided by the Fonds der Chemischen Industrie and the Bundesministerium für Bildung und Forschung.

WILEY InterScience DISCOVER SOMETHING GREAT
© 2005 Wiley-VCH Verlag GmbH & Co. KGaA, Weinheim

blood groups,[3] indicating that not only the saccharide, but also the peptide sequence, contributed to the recognized epitope. From this observation we inferred that apart from tumor-associated saccharides, tumor-selective peptide structural elements are required to render an antigen sufficiently tumor-selective.

Structural leads for the design of tumor-selective glycopeptide antigens are obtained from analyses of the tumor-associated epithelial mucin MUC1,[4] which is extensively over-expressed on tumor cells. The extracellular portion of MUC1 contains numerous repeating units of the amino acid sequence HGVTSAPDTRPAPGSTAPPA.[5] Most *O*-glycosylation sites are located within these tandem repeats. Owing to the down-regulation of a glucosaminyl transferase (C-2GnT-1) and the concomitant overexpression of sialyl transferases,[6] MUC1 on tumor cells carries short, prematurely sialylated saccharide side chains. Antibodies induced with MUC1 isolated from tumor tissues[4,5] were used to identify the peptide motif PDTRPAP as an immundominant epitope within the MUC1 tandem repeat.[7] The specificity of these anti-MUC1 antibodies was verified with synthetic Tn- and T-antigen glycopeptides.[8,9] Moreover, saturation transfer difference NMR analyses revealed the conformation of a Tn antigen pentapeptide from MUC1 bound to a monoclonal antibody.[10]

In contrast to such studies, which proved valuable for analytical purposes, immunizations with MUC1 extracted from tumor tissues as a vaccine appear not to be promising, because MUC1 from biological isolates generally displays microheterogeneity and contains structural elements that also occur on healthy cells.

For this reason we focused our attention on the development of anticancer vaccines based on defined synthetic Tn, T, and sialyl–Tn glycopeptides[11,12] from MUC1.[13] A construct, in which a glycopeptide sequence from the MUC1 tandem repeat carrying a sialyl–Tn side chain is conjugated through a polar spacer amino acid with a partial T-cell epitope from tetanus toxoid, was used to induce the proliferation of cytotoxic T cells in cell cultures of peripheral blood lymphocytes (PBLs).[14] This effect occurred exclusively in the presence of antigen-presenting cells. Apart from cytotoxic T-cell response, strong T-helper-cell-dependent antibody production is of crucial importance for the development of an efficient antitumor vaccine and requires the use of glycopeptide antigens conjugated with carrier proteins such as BSA or KLH (keyhole limpet hemocyanine).

Herein we describe the synthesis of a series of glycopeptide antigens that bear the sialyl-Tn, (2,6)-sialyl-T, (2,3)-sialyl-T, or the glycophorin (2,3-2,6-bissialyl)-T antigens and contain the partial or complete tandem repeat sequence of MUC1. We also report methods to couple these tumor-selective cell surface structures to carrier proteins or to bind them to microtiter plates. The synthetic strategy relies on the synthesis of the corresponding *O*-glycosyl amino acids, followed by sequential solid-phase glycopeptide synthesis and subsequent conjugation to proteins or immobilization.

A range *O*-glycosyl amino acids were synthesized according to a biomimetic strategy[15] starting from the same precursor. Scheme 1 illustrates the preparation of the most

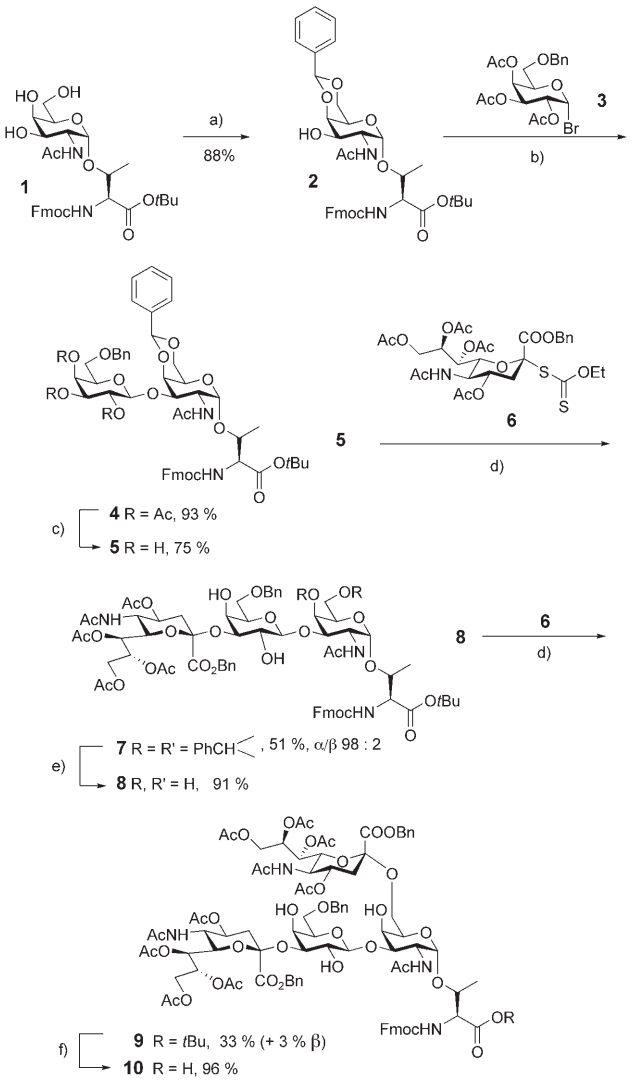

Scheme 1. a) α,α-Dimethoxytoluene, cat. *p*-TsOH, CH_3CN, 3 h; b) $Hg(CN)_2$, CH_2Cl_2/CH_3NO_2 (2:3), 4-Å molecular sieves; c) 1. NaOMe, MeOH, pH 8.5–9, 8 h; 2. Fmoc-OSu, dioxane/H_2O (1:1), NMM; d) MeSBr, AgOTf, CH_3CN/CH_2Cl_2 (2:1), −68 °C, 3-Å molecular sieves; e) 80% AcOH (aq), 80 °C; f) CF_3COOH, anisole (10:1), 2 h.

complex of the tumor-associated MUC1 saccharide antigens, the (2,3-2,6-bissialyl)-T–threonine conjugate. The *N*-Fmoc protected Tn antigen threonine *tert*-butyl ester **1**[16] deprotected at its glycan moiety served as common starting material for the synthesis of all tumor-associated mucin carbohydrate antigens. The base and acid sensitivity of the Fmoc group and the *tert*-butyl ester must be carefully taken into account in all protecting-group manipulations and glycosylation reactions. The precursor **1** was treated with α,α-dimethoxy toluene in acetonitrile in the presence of catalytic *p*-toluenesulfonic acid at pH 4 to give 4,6-benzylidene acetal **2**. Although activation of a glycosyl trichloroacetimidate[17] with trimethylsilyl trifluormethanesulfonate for 3-β-galactosylation is usually very efficient, in this case the benzylidine acetal and *tert*-butyl ester were cleaved or, after addition of sufficient amounts of molecular sieves, predominantly gave the corresponding orthoester.[18] The most successful route involved activation

 © 2005 Wiley-VCH Verlag GmbH & Co. KGaA, Weinheim

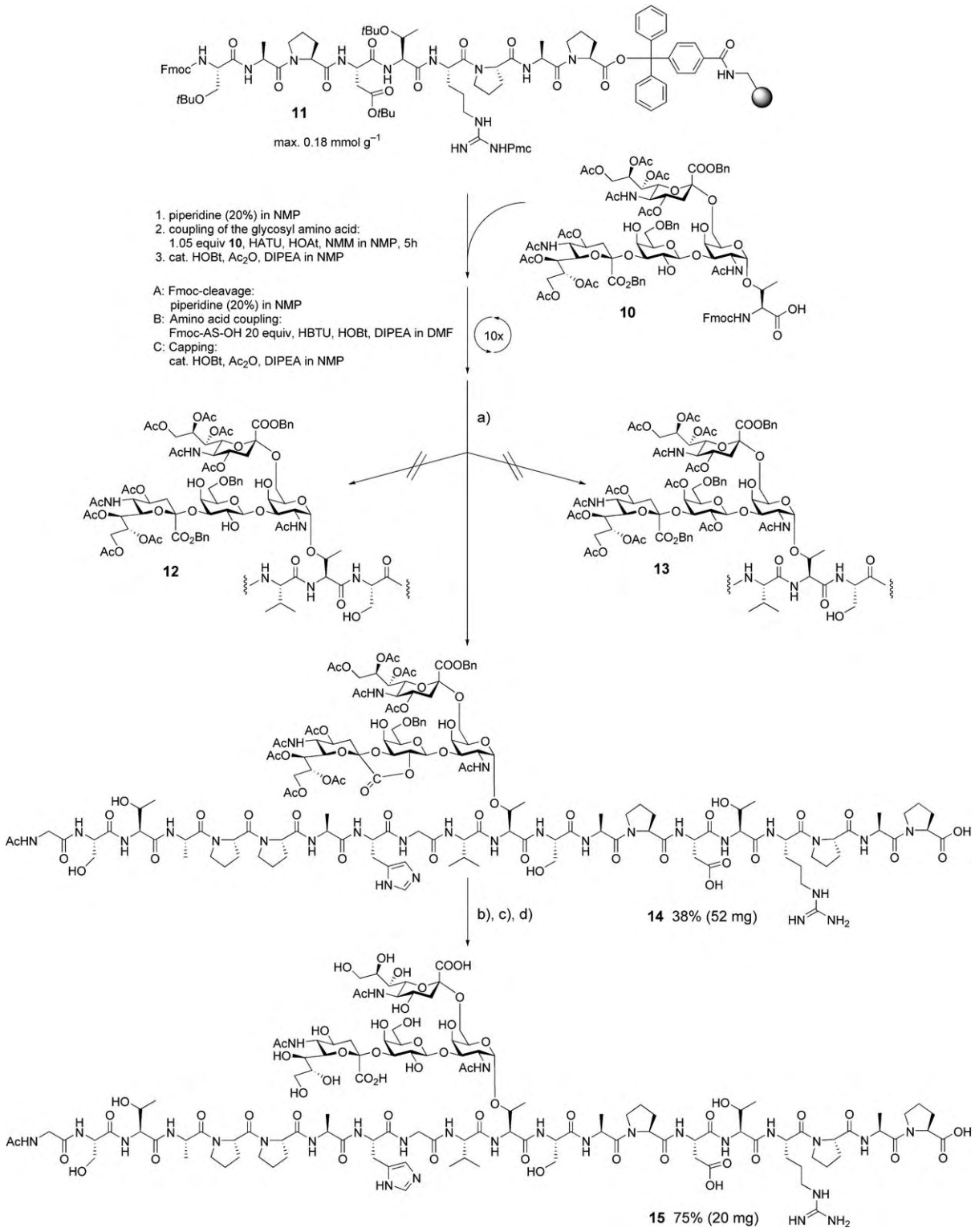

Scheme 2. a) TFA, TIS, H_2O (15:0.9:0.9); b) H_2, Pd/C (10%), MeOH; c) NaOMe/MeOH, pH 9.5; d) NaOH (aq), pH 11.5, 1 h; then AcOH. DIPEA = diisopropylethylamine.

of the 6-*O*-benzyl protected galactosyl bromide **3**[19] with mercury cyanide (according to the procedure of Helferich and Wedemeyer[20]) in nitromethane/dichloromethane which stereoselectively furnished the T-antigen–threonine conjugate **4** in high yield.

The selective *O*-deacetylation of **4** proved to be particularly challenging. On a 1-g scale, use of catalytic NaOMe in methanol under careful adjustment of the pH value to 8.5 furnished **5** in 62% yield. On a larger scale (5 g) and at pH 8.6–9, not only **5** (39%) but also the *N*-deprotected

 © 2005 Wiley-VCH Verlag GmbH & Co. KGaA, Weinheim

conjugate (46%) were formed. Subsequent *N*-acylation of the latter with 9-fluorenyl-methoxycarbonyl-*N*-hydroxy-succinimide gave more of the desired product (36%), resulting in an overall yield of 75% of **5**. Sialylation of **5** with xanthate **6** of the peracetylated sialic acid benzyl ester[14] activated with methylsulfenyl triflate[21] gave **7** with nearly complete regio- and stereoselectivity. After selective cleavage of the benzylidene acetal with aqueous acetic acid (80% *v*/*v*) at 80 °C[22] to afford **8**, a second sialylation step under identical conditions gave the bissialyl-T-antigen–threonine conjugate **9**. Although the conversion remained incomplete after 3.5 h, **9** (33%) as well as some of the corresponding β-anomer (3%) were isolated by preparative HPLC.[23] Acidolysis of the *tert*-butyl ester with trifluoroacetic acid/anisole (10:1) furnished the Fmoc-protected bissialyl-T–threonine building block **10**,[24] which was incorporated into the solid-phase synthesis without further *O*-acetylation.[25] Of the other tumor-associated glycosyl amino acid antigens, the Tn antigen **1**, T antigen **4**, and 2,3-sialyl-T antigen **7** are directly accessible by the synthetic route shown in Scheme 1, while the sialyl-Tn antigen is obtained by regioselective sialylation of **1**[14,16] and the 2,6-sialyl-T antigen through regioselective sialylation after cleavage of the benzylidene acetal in **4**.[15,26]

These building blocks were all subsequently applied in the solid-phase glycopeptide synthesis of various MUC1 tandem repeat glycopeptides, as illustrated in Scheme 2 for the bissialyl-T antigen MUC1 glycopeptide. Fmoc-proline was coupled through a trityl linker[27] to a Rapp-Tentagel polymer[28] and used to assemble the protected nonapeptide **11** from MUC1 according to the Fmoc strategy.[29] After cleavage of the Fmoc group with piperidine/*N*-methylpyrrolidone (NMP) (1:4), the *O*-glycosyl amino acid **10** (1.05 equiv) was coupled through activation with *O*-(7-azabenzotriazol-1-yl)-*N*,*N*,*N*′,*N*′-tetramethyluronium hexafluorophosphate (HATU), 1-hydroxy-7-azabenzotriazole (HOAt),[30] and *N*-methylmorpholine (NMM) in NMP. All non-glycosylated Fmoc-protected amino acids were coupled with *O*-(1H-benzotriazole-*N*,*N*,*N*′,*N*′-tetramethyluronium hexafluorophosphate (HBTU)/1-hydroxybenzotriazole (HOBt),[31] and Hünig base (*i*Pr$_2$NEt) in DMF. The remaining free amino components were capped with acetic anhydride/HOBt/*i*Pr$_2$NEt after each coupling cycle.[31c]

After completion of the peptide sequence, the trityl linker and the acid-labile side-chain protecting groups were cleaved simultaneously with trifluoroacetic acid (TFA), triisopropylsilane (TIS), and small amounts of water.[32] This cleavage procedure liberated neither the expected glycoeicosapeptide **12** with unaltered carbohydrate side chain nor the completely *O*-acetylated analogue **13** formed through the capping reactions. Instead, glycopeptide **14**,[33] which bears a lactone structure formed between the 2,3-linked sialic acid and the 2-OH group of the galactose moiety, was isolated in an overall yield of 38% after approximately 40 steps. Subsequent hydrogenolysis of the benzyl ester and benzyl ether, transesterification with NaOMe/methanol (pH 9.5), opening of the lactone with aqueous NaOH (pH 11.5), neutralization with acetic acid, lyophilization, and purification by semipreparative HPLC furnished the desired MUC1 tandem repeat glycopeptide **15**[34] in 75% yield (based on **14**).

In analogous procedures, the MUC1 eicosapeptide **16** as well as the complete tandem repeat glycopeptides from MUC1 carrying the other important tumor-associated sialyl saccharide antigens, sialyl-Tn (**17**), 2,6-sialyl-T (**18**), and 2,3-sialyl-T (**19**), were synthesized in significantly higher overall yields (Scheme 3). No formation of a lactone was observed during the acidolysis of the trityl linker in any of these syntheses.

According to the procedure illustrated in Scheme 2, the dodecapeptide **20** equipped with a triethylene glycol spacer with an amino group[14] as well as the analogous sialyl-Tn dodecapeptide **21** from MUC1 were synthesized to serve as model compounds for conjugation with bovine serum albumin (BSA) and for immobilization on microtiter plates (Scheme 4).[35] For this purpose, the N-terminal Fmoc group was removed from the resin-bound peptide and all acid-labile side-chain protecting groups were cleaved during the acidolysis of the trityl anchor. The synthesis of sialyl-Tn glycopeptide **21** required the additional removal of the carbohydrate-protecting groups by hydrogenolysis and transesterification catalyzed by NaOMe after cleavage from the resin.

To conjugate the synthetic MUC1 peptides and glycopeptides with proteins, recourse was made to the procedure described by Tietze et al.[36] for the conjugation of a lactosamine phenyl glycoside. The amino groups of the spacers of **20**

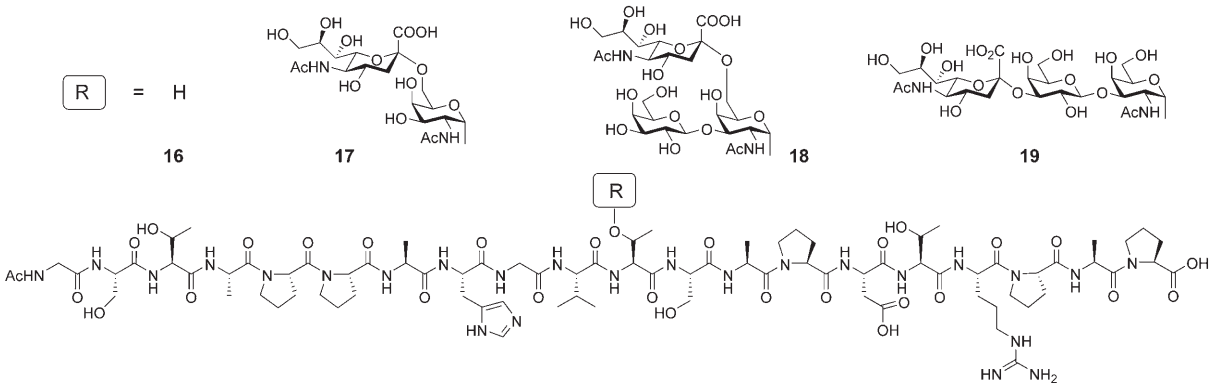

Scheme 3. Eicosapeptide **16** and the complete tandem repeat glycopeptides from MUC1 carrying sialyl-Tn (**17**), 2,6-sialyl-T (**18**), and 2,3-sialyl-T (**19**).

 © 2005 Wiley-VCH Verlag GmbH & Co. KGaA, Weinheim

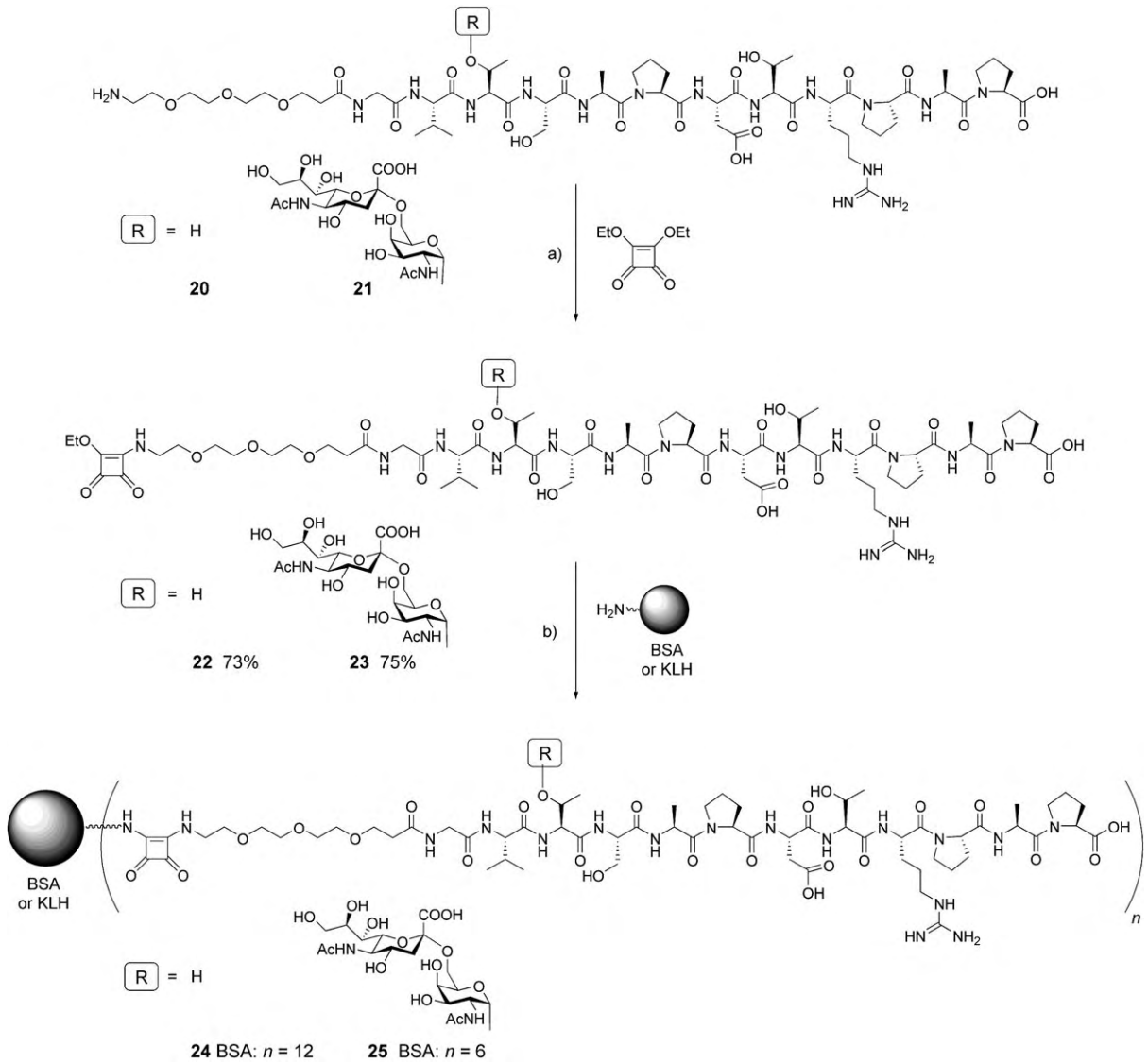

Scheme 4. a) Ethanol/water (1:1), Na_2CO_3, pH 8.0, 2 h, preparative HPLC; b) sodium borate (0.07 M), $NaHCO_3$ (0.035 M), pH 9, 24 h, gel filtration chromatography (Sephadex-G25 PD10 column), dialysis against H_2O.

and **21** were converted into the corresponding squaric monoamides **22** and **23**[37] by using diethyl squarate (3,4-diethoxy-3-cyclobutene-1,2-dione) in ethanol/water at pH 8. After purification by preparative HPLC, the activated peptide structures were coupled to BSA in a sodium borate buffer at pH 9.

Conjugation of peptide **22** resulted in a coupling yield of approximately 60% within 24 h and furnished vaccine **24** with an average degree of incorporation of 12 peptide molecules per molecule of protein as determined by MALDI-TOF MS. In the case of glycopeptide **23** the coupling to furnish **25** proceeded more slowly, and led to the incorporation of only half as many antigen molecules. Furthermore, the glycopeptide antigen equipped with the spacer was covalently immobilized on microtiter plates[38] functionalized with a secondary amine **26** (Scheme 5). The covalent linkage of the MUC1 antigen to the microtiter plates (see **27**)[39] prevents the loss of material in ELISA tests when washing with water, which had previously caused difficulties while working with glycopeptide antigens.

The immobilized and conjugated MUC1 glycopeptide antigens not only provide vaccines with a highly defined structure representing tumor-selective surface antigens but also provide tools for the verification of the structural selectivity of an immune response. The initial results are promising[40] and encourage further exploration of the entire spectrum of structures characterized by the synthetic glycopeptide antigens such as **17**, **18**, **19**, **21**, **23**, and **25** for the development of antitumor vaccines.

Received: May 10, 2005
Published online: October 25, 2005

 © 2005 Wiley-VCH Verlag GmbH & Co. KGaA, Weinheim

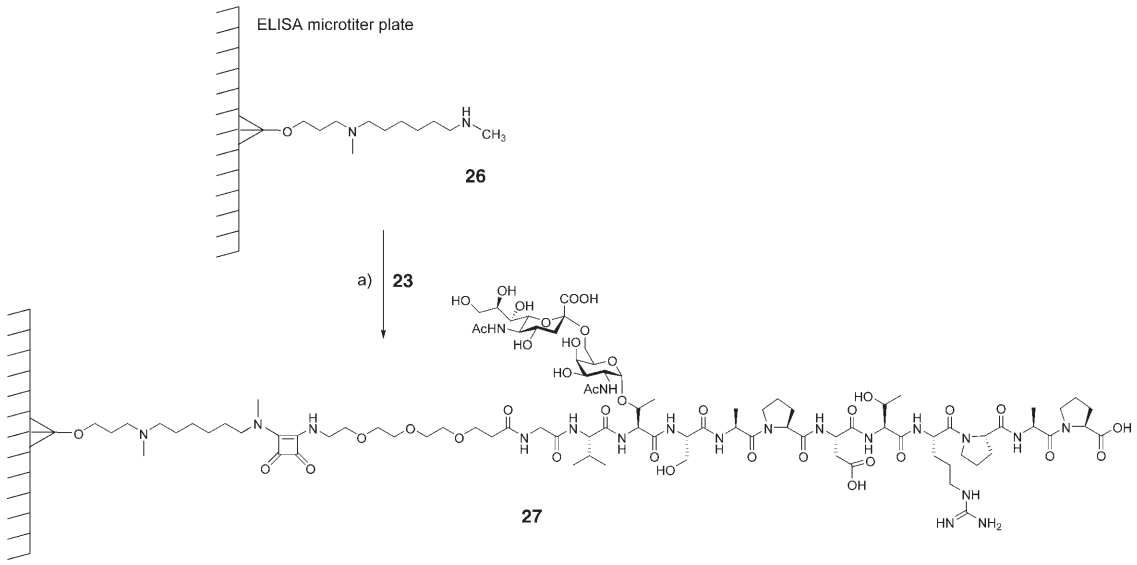

Scheme 5. a) sodium borate (0.07 M), $NaHCO_3$ (0.035 M), pH 9.

Keywords: antigens · antitumor agents · carbohydrates · glycopeptides · synthetic vaccines

[1] G. F. Springer, *Science* **1984**, *224*, 1198.

[2] H. Kunz, S. Birnbach, *Angew. Chem.* **1986**, *98*, 354; *Angew. Chem. Int. Ed. Engl.* **1986**, *25*, 360.

[3] a) W. Dippold, A. Steinborn, K.-H. Meyer zum Büschenfelde, *Environ. Health Perspect.* **1990**, *88*, 255; W. Dippold, A. Steinborn, S. Birnbach, H. Kunz, unpublished results; A. Steinborn, PhD thesis, Universität Mainz, **1990**; b) S. Dziadek, H. Kunz, *Chem. Rec.* **2004**, *4*, 308.

[4] a) S. Gendler, C. A. Lancaster, J. Taylor-Papadimitriou, T. Duhig, N. Peal, J. Burchell, L. Pemberton, E. N. Lalani, P. Wilson, *J. Biol. Chem.* **1990**, *265*, 15286; b) for a short overview, see: J. Taylor-Papadimitriou, J. M. Burchell, D. W. Miles, M. Dalziel, *Biochim. Biophys. Acta* **1999**, *1455*, 301.

[5] D. M. Swallow, S. J. Gendler, B. Griffith, G. Corney, J. Taylor-Papadimitriou, *Nature* **1987**, *328*, 82.

[6] a) I. Brockhausen, *Biochim. Biophys. Acta* **1999**, *1473*, 67; I. Brockhausen, *Biochem. Soc. Trans.* **2003**, *31*, 318; b) K. O. Lloyd, J. Burchell, V. Kundryashov, B. W. Yin, J. Taylor-Papadimitriou, *J. Biol. Chem.* **1996**, *271*, 33325; c) J. M. Burchell, A. Mungul, J. Taylor-Papadimitriou, *J. Mammary Gland. Biol. Neoplasia* **2001**, *6*, 355.

[7] a) J. Burchell, J. Taylor-Papadimitriou, M. Boshell, S. Gendler, T. Duhig, *Int. J. Cancer* **1989**, *44*, 691; b) M. R. Price, F. Hudecz, C. O'Sullivan, R. W. Baldwin, P. M. Edwards, S. B. J. Tendler, *Mol. Immunol.* **1990**, *62*, 795.

[8] a) G. F. Hanisch, S. Müller, *Glycobiology* **2000**, *10*, 439; b) S. Müller, F. G. Hanisch, *J. Biol. Chem.* **2002**, *277*, 26103; c) U. Karsten, N. Serttas, H. Paulsen, A. Danielczyk, S. Goletz, *Glycobiology* **2004**, *14*, 681.

[9] S. von Mensdorff-Pouilly, F. G. M. Snijdewint, A. A. Verstraeten, R. H. M. Verheijen, P. Kenemans, *Int. J. Biol. Markers* **2000**, *15*, 343.

[10] H. Möller, N. Serttas, H. Paulsen, J. M. Burchell, J. Taylor-Papadimitriou, B. Meyer, *Eur. J. Biochem.* **2002**, *269*, 1444.

[11] a) O. Seitz, H. Kunz, *Angew. Chem.* **1995**, *107*, 901; *Angew. Chem. Int. Ed. Engl.* **1995**, *34*, 803; b) M. Leuck, H. Kunz, *J. Prakt. Chem.* **1997**, *339*, 332; c) P. Braun, G. M. Davies, M. R. Price, P. M. Williams, S. B. J. Tendler, H. Kunz, *Bioorg. Med. Chem.* **1998**, *6*, 1531.

[12] B. Liebe, H. Kunz, *Angew. Chem.* **1997**, *109*, 629; *Angew. Chem. Int. Ed. Engl.* **1997**, *36*, 618.

[13] Other groups also synthesized mucin glycopeptides with Tn, T, and sialyl-Tn antigen saccharides: a) E. Meinjohanns, M. Meldal, A. Schleyer, H. Paulsen, K. Bock, *J. Chem. Soc. Perkin Trans.* 1 **1996**, 985; b) S. D. Kuduk, J. B. Schwarz, X.-T. Chen, P. W. Glunz, D. Sames, G. Ragapunti, P. O. Livingston, S. J. Danishefsky, *J. Am. Chem. Soc.* **1998**, *120*, 12474; c) J. B. Schwarz, S. D. Kuduk, X.-T. Chen, D. Sames, P. W. Glunz, S. J. Danishefsky, *J. Am. Chem. Soc.* **1999**, *121*, 2662; d) M. A. Reddish, L. Jackson, R. R. Koganti, D. Qui, W. Hong, B. M. Longenecker, *Glycoconjugate J.* **1997**, *14*, 549.

[14] S. Keil, C. Claus, W. Dippold, H. Kunz, *Angew. Chem.* **2001**, *113*, 379; *Angew. Chem. Int. Ed.* **2001**, *40*, 366.

[15] a) C. Brocke, H. Kunz, *Synlett* **2003**, 2052; b) S. Dziadek, H. Kunz, *Synlett* **2003**, 1623.

[16] B. Liebe, H. Kunz, *Helv. Chem. Acta.* **1997**, *80*, 1473.

[17] a) R. R. Schmidt, J. Michel, *Angew. Chem.* **1980**, *92*, 763; *Angew. Chem. Int. Ed. Engl.* **1980**, *19*, 731; b) R. R. Schmidt, *Angew. Chem.* **1986**, *98*, 213; *Angew. Chem. Int. Ed. Engl.* **1986**, *25*, 212.

[18] T. Reipen, H. Kunz, *Synthesis* **2003**, 2487.

[19] M. Lergenmüller, Y. Ito, T. Ogawa, *Tetrahedron* **1988**, *44*, 1381.

[20] B. Helferich, F. Wedemeyer, *Justus Liebigs Ann. Chem.* **1949**, *563*, 139.

[21] F. Dasgupta, P. Garegg, *Carbohydr. Res.* **1988**, *177*, C13.

[22] N. Mathieux, H. Paulsen, M. Meldal, K. Bock, *J. Chem. Soc. Perkin Trans.* 1 **1997**, 2359.

[23] **9**: $[\alpha]_D^{22} = 16.6$ ($c = 1$, $CHCl_3$); MALDI-TOF MS (dhb, positive): m/z: 1975.2 $[M+Na]^+$, 1991.2 $[M+K]^+$; HR ESI-TOF MS (positive): calcd: 1973.7271; found: 1973.7257; ^1H NMR (400 MHz, $CDCl_3$, COSY, TOSY, HMQC, HMBC): $\delta = 4.81$ ($J_{1,2} = 3.9$ Hz; 1-H), 3.32 (d, 1H, $J_{3',4'} = 2.7$ Hz; 4′-H), 2,71 (dd, 1H, $J_{3eq'',3ax''} = 12.9$ Hz, $J_{3eq'',4''} = 4.7$ Hz; 3″-H_{eq}), 2.54 ppm (dd, 1H, $J_{3eq''',3ax'''} = 12.7$ Hz, $J_{3eq''',4'''} = 4.7$ Hz; 3‴-H_{eq}).

[24] **10**: $[\alpha]_D^{22} = 20.3$ ($c = 1$, $CHCl_3$); HR ESI-TOF MS (positive): calcd: 1917.6645; found: 1917.6743 $[M+Na]^+$.

[25] The removal of *O*-acetyl groups, in particular those on the 4-OH groups of galactose moieties in sialyl-Lewis^x glycopeptides (M. Rösch, H. Herzner, W. Dippold, M. Wild, D. Vestweber, H.

 © 2005 Wiley-VCH Verlag GmbH & Co. KGaA, Weinheim

Kunz, *Angew. Chem.* **2001**, *113*, 3954; *Angew. Chem. Int. Ed.* **2001**, *40*, 3836) and in sialyl-T glycopeptides[15] can be difficult.
[26] C. Brocke, H. Kunz, *Synthesis* **2004**, 525.
[27] J. M. J. Frechét, K. E. Haque, *Tetrahedron Lett.* **1975**, *16*, 3055.
[28] E. Bayer, W. Rapp, *Chem. Pept. Proteins* **1986**, *3*, 3.
[29] L. A. Carpino, G. Y. Han, *J. Am. Chem. Soc.* **1970**, *92*, 5748.
[30] L. A. Carpino, D. Jonescu, A. El-Falham, *J. Org. Chem.* **1996**, *61*, 2460.
[31] a) R. Knorr, A. Trzeciak, W. Bannwarth, D. Gillessen, *Tetrahedron Lett.* **1989**, *30*, 1927; b) V. Dourtoglou, B. Gross, V. Lambropoulou, C. Ziondrou, *Synthesis* **1984**, 572; c) W. König, R. Geiger, *Chem. Ber.* **1970**, *103*, 788.
[32] D. A. Pearson, M. Blanchette, M. L. Baker, C. A. Guidon, *Tetrahedron Lett.* **1989**, *30*, 2739.
[33] **14**: MALDI-TOF MS (dhb, positive): *m*/*z*: 3376.0 $[M+H]^+$, 3398.0 $[M+Na]^+$, 3414.3 $[M+K]^+$; ^{1}H NMR (600 MHz, [D$_6$]DMSO, COSY, TOCSY, HMQC, HMBC): $\delta = 4.76$ (2′-H), 4.21 (4′-H), 4.01 ppm (3′-H).
[34] **15**: 19.4 mg; $[\alpha]_D^{22} = -117.4$ ($c = 1$, H$_2$O); MALDI-TOF MS (dhb, positive): *m*/*z*: 2876.6 $[M+H]^+$; ^{1}H NMR (600 MHz, [D$_6$]DMSO, COSY, HMQC, HMBC): $\delta = 4.79$ (d, 1H, $J_{1,2} = 2.1$ Hz, 1-H), 2.66 ppm (dd, 1H, $J_{3eq',3ax'} = 13.7$ Hz, $J_{3eq,4'} = 6.7$ Hz; 3″-H$_{eq}$); ^{13}C NMR (150.9 MHz, [D$_6$]DMSO, HMQC, HMBC): $\delta = 104.5$ (C1′), 98.8 (C1), 98.4 (C2″), 98.1 ppm (C2‴).
[35] According to our previous experience, the incorporation of a flexible, hydrophilic spacer is important for immunological evaluation of synthetic vaccines.[14]
[36] L. F. Tietze, C. Schröder, S. Gabius, U. Brinck, A. Goerlach-Graw, H.-J. Gabius, *Bioconjugate Chem.* **1991**, *2*, 148.
[37] **23**: $[\alpha]_D^{26} = -68.4$ ($c = 1$, H$_2$O); MALDI-TOF MS (dhb, positive): *m*/*z*: 1991.4 $[M+H]^+$; ^{1}H NMR (400 MHz, CD$_3$OD, COSY, HMQC): $\delta = 4.97$ (d, 1H, $J_{1,2} = 3.5$ Hz; 1-H), 4.76–4.64 (m, 3H; CH$_2$O-squarate, H$_\alpha$-Arg), 2.66 ppm (dd, 1H, $J_{3eq',3ax'} = 12.7$ Hz, $J_{3eq',4'} = 4.7$ Hz; 3′-H$_{eq}$).
[38] A. Bergh, B.-G. Magnusson, J. Ohlsson, U. Wellmar, U. J. Milsson, *Glycoconjugate J.* **2005**, *18*, 615.
[39] **27**: For carbohydrate detection with phenol/H$_2$SO$_4$, see reference [2].
[40] See the following Communication in this issue: S. Dziadek, A. Hobel, E. Schmitt, H. Kunz, *Angew. Chem.* **2005**, *117*, 7803; *Angew. Chem. Int. Ed.* **2005**, *44*, 7630.

 © 2005 Wiley-VCH Verlag GmbH & Co. KGaA, Weinheim

Antitumor Agents

DOI: 10.1002/anie.200501594

A Fully Synthetic Vaccine Consisting of a Tumor-Associated Glycopeptide Antigen and a T-Cell Epitope for the Induction of a Highly Specific Humoral Immune Response**

*Sebastian Dziadek, Alexandra Hobel, Edgar Schmitt, and Horst Kunz**

Tumor therapy based on nontoxic anticancer vaccines would be a valuable alternative to treatments such as chemotherapy and irradiation, which are often accompanied by significant side effects.[1] As a prerequisite for selective immunotherapy it is essential to identify antigenic target structures that distinguish a normal cell from a tumor cell as clearly as possible. In this context, glycopeptides from the tandem repeat region of the extracellular domain of the tumor-associated epithelial mucin MUC1 appear to be particularly attractive target structures.[2] MUC1 isolated from epithelial tumor cells, however, is not suitable for the induction of a tumor-selective immune response. This is due to the micro-heterogeneity of the carbohydrate moieties of these glycoproteins, which contain tumor-associated saccharide antigens but also saccharide side chains that occur in normal cells. Moreover, immunosuppressive mechanisms often prevent the organism from attacking and eliminating foreign antigens of this kind. Therefore, a further aim of antitumor vaccination is to break this tolerance by the induction of a strong immune response. With respect to tumor selectivity, apart from the initiation of a cytotoxic T cell response,[3] the induction of a selective T-helper-cell-mediated antibody production is crucial. Specific antibodies contribute decisively to the immune defense of tumors by initiating a complement-dependent lysis of both stationary as well as circulating tumor cells.

The specificity of a humoral immune response relies on the specific binding of an antigen to the membrane-bound immunoglobulin receptor of a B cell. However, in the case of the tumor-selective but only moderately immunogenic MUC1 glycopeptides, this binding itself is not sufficient to stimulate a

[*] Dr. S. Dziadek, Prof. Dr. H. Kunz
Institut für Organische Chemie
Johannes Gutenberg-Universität Mainz
Duesbergweg 10–14, 55128 Mainz (Germany)
Fax: (+49) 6131-392-4786
E-mail: hokunz@uni-mainz.de

A. Hobel, Prof. Dr. E. Schmitt
Institut für Immunologie
Johannes Gutenberg-Universität Mainz
Obere Zahlbacher Strasse 67, 55101 Mainz (Germany)

[**] This work was supported by the Deutsche Forschungsgemeinschaft and the Stiftung Rheinland-Pfalz für Innovation. S.D. is grateful for a scholarship provided by the Fonds der Chemischen Industrie and the Bundesministerium für Bildung und Forschung.

Supporting information for this article is available on the WWW under http://www.angewandte.org or from the author.

WILEY InterScience DISCOVER SOMETHING GREAT
© 2005 Wiley-VCH Verlag GmbH & Co. KGaA, Weinheim

naive B cell to proliferate and to differentiate into an antibody-secreting plasma cell. Additional stimulation by activated $CD4^+$ T helper cells is required. In turn, the T_H cells are activated when their receptor (TCR) binds to a T-cell peptide antigen presented by the major histocompatibility complex (MHC II) on the surface of a cell.[4]

We describe herein a concept for the construction of antitumor vaccines **1** in which a tumor-associated sialyl-Tn glycopeptide antigen from the tandem repeat region of MUC1 is connected to a T_H-cell peptide epitope from ovalbumin ($OVA_{323-339}$)[5] through a polar, nonimmunogenic amino acid spacer (Figure 1a). Such a synthetic vaccine should be taken up by antigen-presenting cells (APCs). After processing of construct **1**, the ovalbumin T-cell epitope[5] should be presented by MHC II complexes on APCs and recognized by the T-cell receptor (TCR). This results in the activation and differentiation of naive T cells. The activated T_H cells then stimulate those B cells that also present the corresponding T-cell epitope. It is anticipated that, according to the mechanism illustrated above (Figure 1b), recognition of the tumor-associated MUC1 glycopeptide antigen in **1** by the immunoglobulin receptor of a B cell and subsequent processing of construct **1** in the same B cell combined with additional co-stimulatory signals will initiate a strong production of specific antibodies directed against the MUC1 glycopeptide antigen.

The glycopeptide–T-cell-epitope conjugate **1** was constructed by fragment condensation on a solid phase. The MUC1 glycopeptide antigen of the sequence GVT*SAPDTRPAP chosen as the target structure contains the immunodominant motif PDTRP,[6] which is masked in MUC1 on normal cells by the large glycan side chains. The sialyl-Tn antigen, which has been identified in mammary, stomach, and colon carcinomas,[7–9] was incorporated into the peptide sequence at Thr^3 as the tumor-associated saccharide component. Examination of the aberrant glycosylation of mucines in tumor cells[10,11] reveals that the sialyl-Tn antigen may not be the most abundant, but is certainly a highly important structure in terms of tumor selectivity.

The sialyl-Tn glycopeptide from MUC1 was assembled as a protected fragment by solid-phase synthesis on the 2-phenyl-2-trimethylsilylethyl ester (PTMSEL) linker[12] (Scheme 1). For this purpose, *O*-(benzotriazol-1-yl)-*N*,*N*,*N*′,*N*′-tetramethyluronium hexafluorophosphate (HTBU)[14] and 1-hydroxybenzotriazole (HOBt) were utilized for condensing the Fmoc-protected amino acids, whereas the 7-aza analogues HATU/HOAt[16] of these reagents served for coupling the protected sialyl-Tn–threonine building block **3**.[3,12b,15] To detach side-chain-protected glycopeptide **4** from the resin, the PTMSEL anchor was cleaved with tetrabutylammonium fluoride (TBAF) trihydrate in dichloromethane.[12]

Under these almost neutral conditions, the hydrate shells of the fluoride ions remain intact, thus leaving even very sensitive protecting groups untouched. In this way, **4** could be isolated in 45% yield based on **2** after purification by preparative HPLC (Scheme 1, see Supporting Information for analytical data).

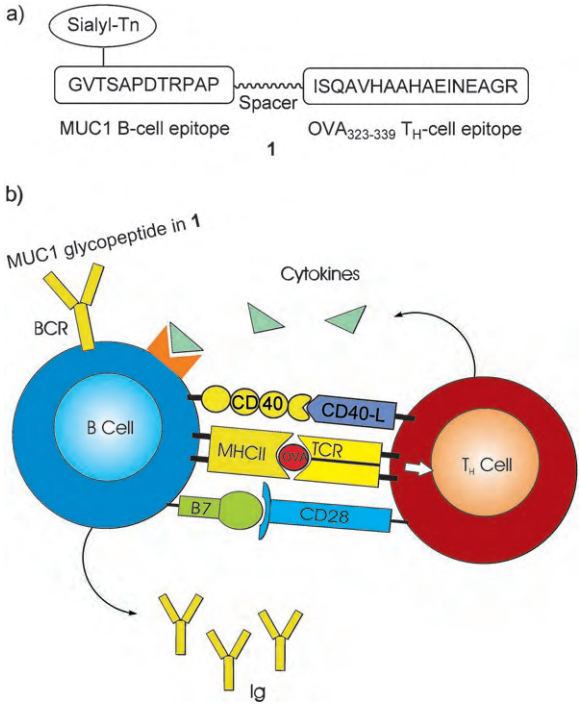

Figure 1. a) MUC1-$OVA_{323-339}$ vaccine conjugate **1**. b) T_H-cell-stimulated humoral immune response.

Parallel to this, the $OVA_{323-339}$ heptadecapeptide fragment was synthesized on a TentaGel-bound Wang linker[13,17] (**5**). After completion of the target sequence and N-terminal

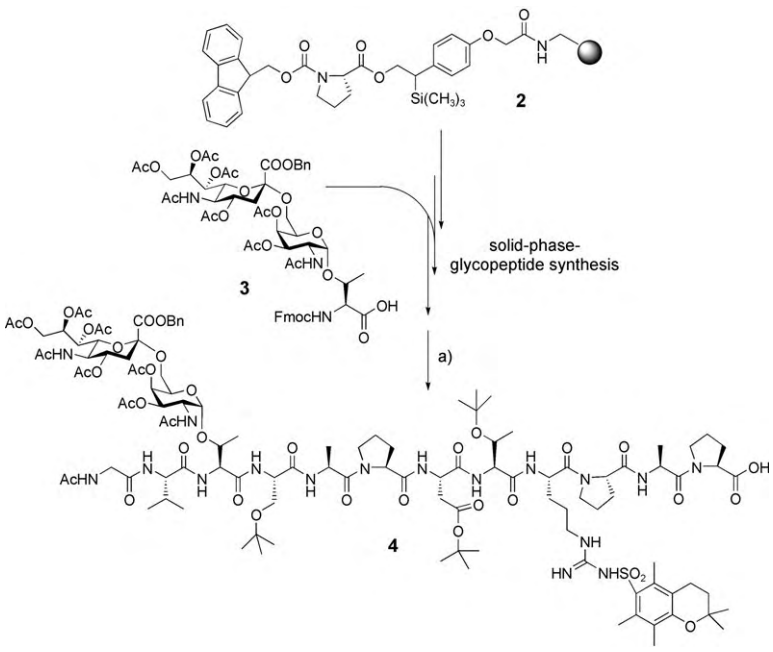

Scheme 1. Solid-phase glycopeptide synthesis: 1) cleavage of Fmoc: piperidine (20%) in NMP; 2) coupling (1.–8. Fmoc-AA-OH, HBTU, HOBt, DIPEA in DMF; 9. **3** (1.8 equiv), HATU/HOAt/NMM, DMF, 3 h; 10., 11. 2× (Fmoc-AA-OH, HBTU, HOBt, DIPEA in DMF); capping: cat. HOBt, Ac_2O, DIPEA in NMP; a) TBAF·$3H_2O$ (2×2.5 equiv), CH_2Cl_2, 2×45 min, 45% (based on **2**). NMM = *N*-methylmorpholine; Bn = benzyl; DMF = *N*,*N*-dimethylformamide.

© 2005 Wiley-VCH Verlag GmbH & Co. KGaA, Weinheim

deprotection, the Fmoc-protected triethylene glycol spacer–amino acid **6**[3] was coupled and deprotected at the N terminus to give **7** (Scheme 2).

Subsequently, the sialyl-Tn–MUC1 glycopeptide **4** activated with HATU/HOAt was coupled to the polymer-bound conjugate **7**; the excess of the carboxy fragment component **4** used was only 5% relative to the starting material **5**. The Wang linker was cleaved with a mixture of trifluoroacetic acid, triisopropylsilane, and water, and all acid-sensitive protecting groups were simultaneously removed. The construct **8** still protected in its carbohydrate moiety was isolated after purification by preparative HPLC in a yield of 42% based on **5**. Hydrogenolysis of the NeuNAc benzyl ester and removal of the *O*-acetyl groups by transesterification in methanol with catalytic NaOMe at pH 9 furnished the fully synthetic vaccine **1**, which was isolated after purification by preparative HPLC in 43% yield. Purity was confirmed by analytical HPLC and NMR spectroscopy (see Supporting Information). In the 500-MHz ^{1}H NMR spectrum of **1**, only three signals that correspond to the α-H atoms of proline were detected, thus ruling out any considerable epimerization of the *C*-terminal proline during the fragment condensation.

For the induction of a strong humoral immune response against the tumor-associated MUC1 glycopeptide antigen

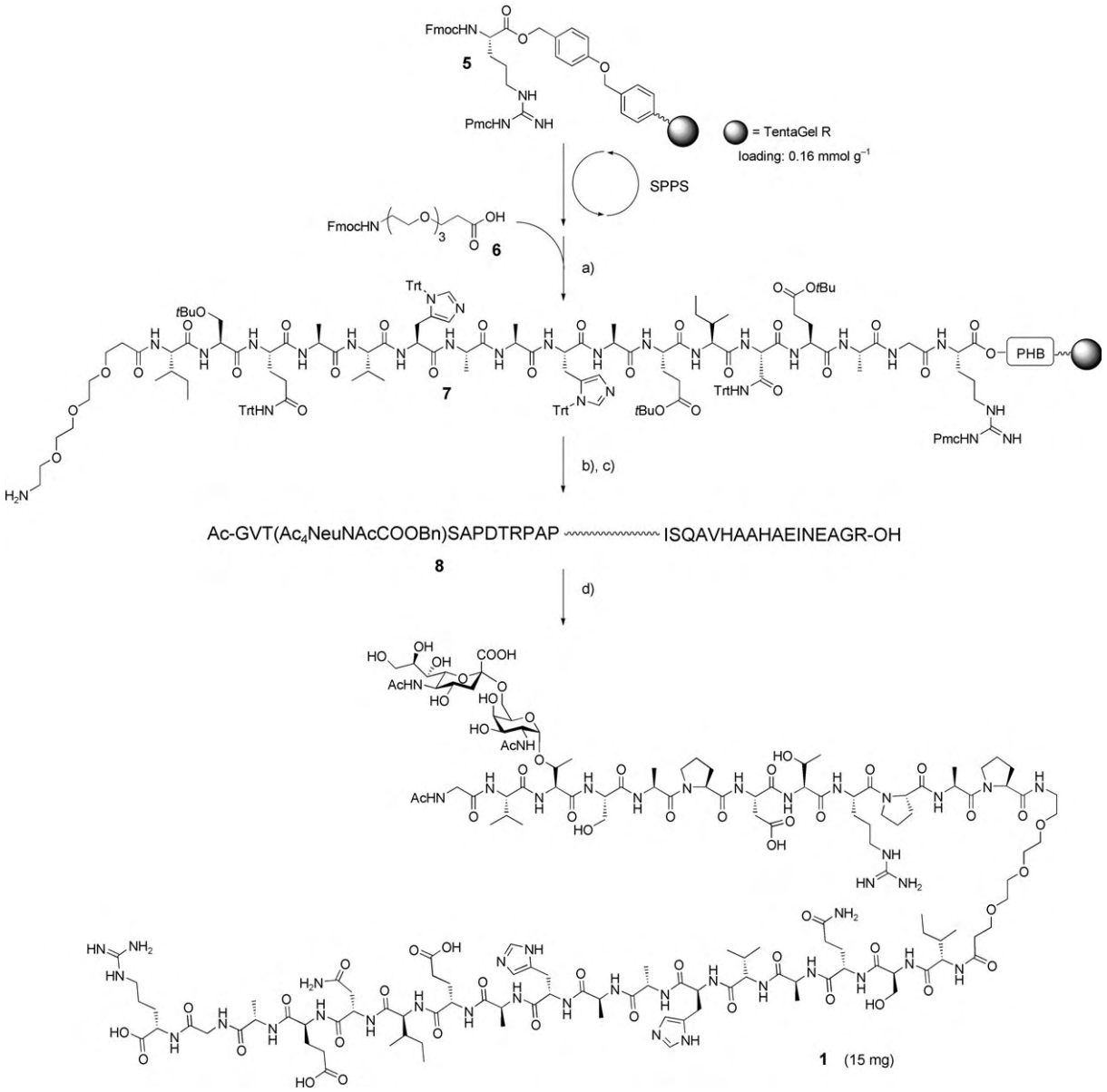

Scheme 2. SPPS: 1) cleavage of Fmoc: piperidine (20%) in NMP; 2) coupling of amino acids: Fmoc-AA-OH, HBTU, HOBt, DIPEA in DMF; 3) capping: cat. HOBt, Ac_2O, DIPEA in NMP; a) 1) piperidine in NMP; 2) coupling of the spacer molecule: **6** (10 equiv), HBTU, HOBt, DIPEA in NMP; 3) capping; 4) piperidine in NMP; b) solid-phase fragment condensation: 1) **4** (1.05 equiv), HATU, HOAt, NMM in DMF, 16 h; 2) capping; c) TFA, triisopropylsilane, water (15:0.9:0.9), 2 h, 42% after preparative HPLC; d) 1) H_2, Pd/C (10%), 21 h; 2) NaOMe, MeOH, 16 h, 43% over two steps after preparative HPLC. Trt = triphenylmethyl; Pmc = pentamethylchroman-6-ylsulfonyl.

 © 2005 Wiley-VCH Verlag GmbH & Co. KGaA, Weinheim

incorporated in vaccine **1**, transgenic mice (DO11.10), whose T cells express a receptor specific for the ovalbumin T-cell epitope ($OVA_{323-339}$) presented by MHC-II molecules ($I\text{-}A^d$),[5] were immunized with **1**. For this purpose, the synthetic vaccine **1** (10 μg) in combination with complete Freund's adjuvant (CFA) were initially injected into the footpads of three transgenic mice (mouse 4–6). Booster immunizations were performed after 21 days: vaccine **1** (10 μg) was administered intraperitoneally together with incomplete Freund's adjuvant (IFA). As a control, three DO11.10 mice received identical vaccine formulations that contained a phosphate buffer instead of the synthetic vaccine (mouse 1–3, PBS group). Five days after each immunization, blood was drawn from the tail vein of each mouse, and serum was isolated for antibody analysis. Detection of MUC1-specific antibodies in the sera of the mice was conducted by ELISA.[18] For this purpose, the wells of an ELISA plate were coated with the MUC1–sialyl-Tn glycopeptide[19] from **1** conjugated with bovine serum albumin (BSA). This neoglycoprotein unspecifically binds to the polymer surface, thereby immobilizing the highly hydrophilic glycopeptide antigen[2a] on the microtiter plate. The sera were titrated at increasing dilutions (abscissa) in a phosphate buffer (PBS), and the antibody concentration was detected photometrically by using a secondary anti-mouse antibody conjugated to horseradish peroxidase (HPO).[18] Comparing the extinctions after the

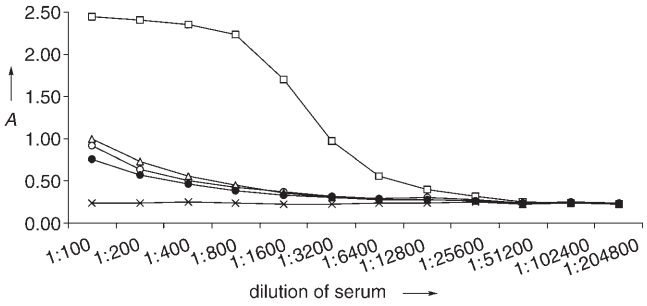

Figure 2. ELISA of sera isolated from mice immunized with **1** (after third immunization, coating of the microtiter plate with MUC1–BSA conjugate[19]): *A* at $\lambda = 414$ nm; ○: mouse 4, □: mouse 5, △: mouse 6, ●: control mouse, ×: negative control.

third immunization, a significant effect was observed (Figure 2): One of the mice (mouse 5, open squares) immunized with the synthetic MUC1-$OVA_{323-339}$ vaccine **1** exhibited a considerably elevated MUC1-specific antibody concentration, whereas the control mice (PBS mice) showed only minor unspecific reaction. Although the DO11.10 mice are genetically mostly identical, their immune responses differ individually, so it is not uncommon that only one of the three immunized mice reacted with a significantly enhanced antibody response.

When observing the development of the MUC1-specific antibody titer of mouse 5 during the immunization experiment (Figure 3), the significant increase in antibody concentration between the second and the third immunization is

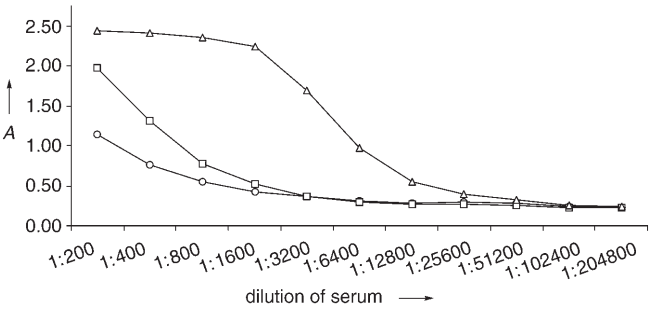

Figure 3. Development of MUC1-specific antibody titer of mouse 5. *A* at $\lambda = 414$ nm; ○: first immunization, □: second immunization, △: third immunization.

striking, clearly indicating the establishment of an immunological memory (specific IgG response).

To verify the specificity of the antibodies in the serum isolated from mouse 5, neutralization experiments with different (glyco)peptide antigens were performed at three concentration stages (1:4000, 1:8000, 1:16000) (Figure 4). In contrast to the untreated serum (open circle), incubation with the tumor-associated sialyl-Tn glycopeptide antigen **9**[2a,3,12b] contained in **1** led to nearly complete neutralization of the MUC1-specific antibodies in the isolated serum (filled squares in Figure 4a). Neither the unglycosylated dodecapeptide **10** with the same sequence from MUC1[2a,3,12b] nor the glycohexadecapeptide **11** from the tandem repeat region of MUC4[15] with identical sialyl-Tn carbohydrate component as in **9**, nor the MUC4 peptide **12**[15] were capable of neutralizing the antibody induced with vaccine **1** (Figures 4b–d).

The immunization of mice with the fully synthetic vaccine **1** consisting of a tumor-associated sialyl-Tn glycopeptide antigen from MUC1 and a T-cell epitope from ovalbumin resulted not only in the generation of a strong but also a highly specific humoral immune response directed against the tumor-associated structure. The antibody induced in this way exclusively recognizes structure **9**, consisting of peptide as well as carbohydrate components, which is contained in vaccine **1**, but not the corresponding peptide sequence **10** alone or the sialyl-Tn carbohydrate structure in combination with a different peptide sequence (**11**). This high specificity of the antibody induced with the synthetic vaccine **1** is an encouraging result for the development of efficient antitumor vaccines. Such a selective activation of the immune system directed against glycoprotein structures that only occur on tumor but not on normal cells can only be achieved with pure, preferably fully synthetic antigens that become accessible through modern chemical methodologies available today.[2a,20]

Received: May 10, 2005
Published online: October 25, 2005

Keywords: antigens · antitumor agents · glycopeptides · synthetic vaccines · T-cell epitope

 © 2005 Wiley-VCH Verlag GmbH & Co. KGaA, Weinheim

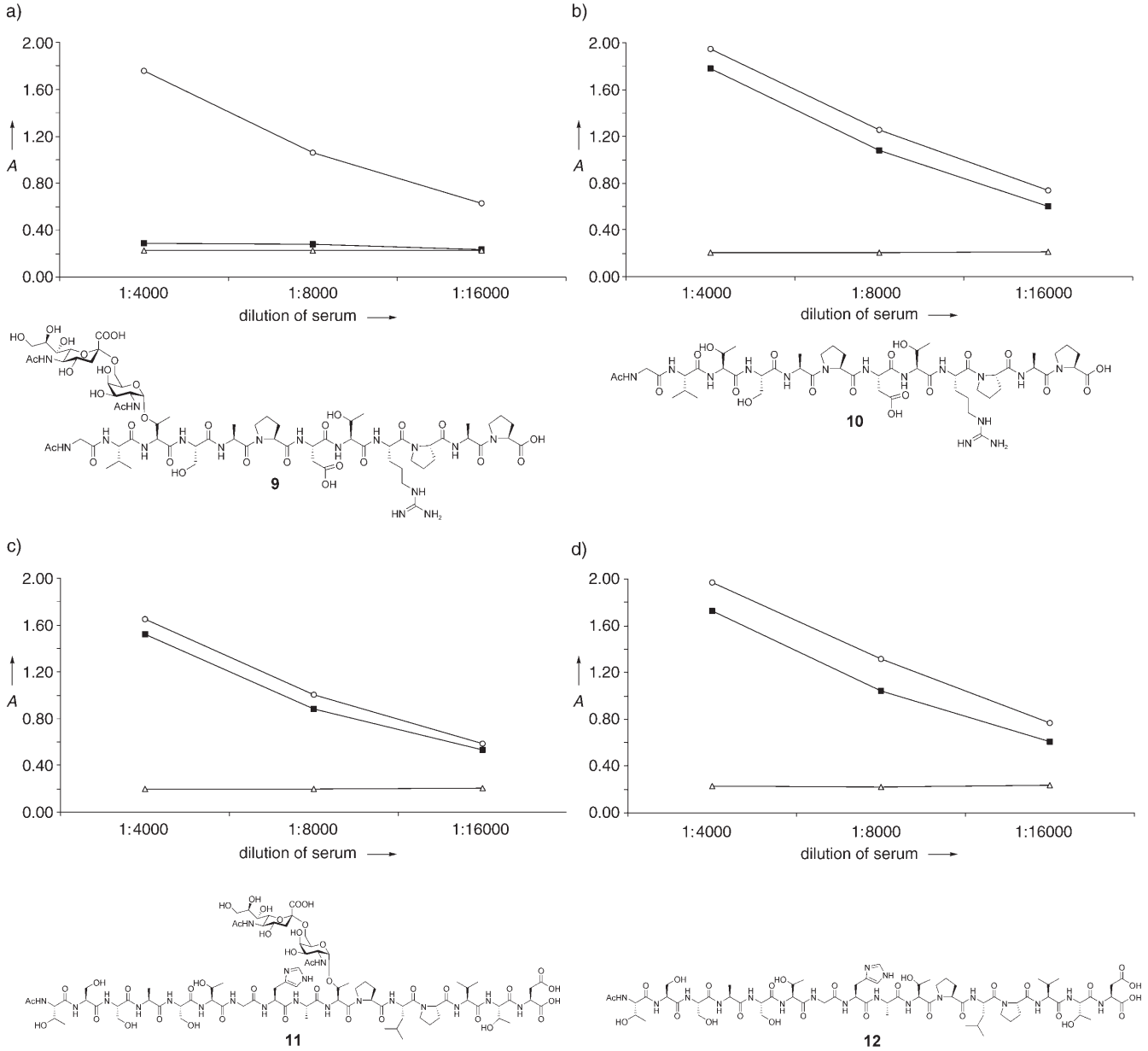

Figure 4. Neutralization of serum obtained from vaccination with **1** through (glyco)peptide antigens. *A* at $\lambda = 414$ nm; ○: serum of mouse 5 without preincubation, △: negative control, ■: serum of mouse 5 incubated with a) **9**, b) **10**, c) **11**, d) **12**.

[1] a) J. N. Blattmann, P. D. Greenberg, *Science* **2004**, *305*, 200; b) Z. Yu, N. P. Restifo, *J. Clin. Invest.* **2002**, *110*, 289; c) P. Moingeon, *Vaccine* **2001**, *19*, 1305; d) S. J. Danishefsky, J. A. Allen, *Angew. Chem.* **2000**, *112*, 883; *Angew. Chem. Int. Ed.* **2000**, *39*, 836; e) R. R. Koganty, M. A. Reddish, B. M. Longenecker, *Drug Discovery Today* **1996**, *1*, 190.

[2] For a biological background, see the previous Communication in this issue: a) S. Dziadek, D. Kowalczyk, H. Kunz, *Angew. Chem.* **2005**, *117*, 7798; *Angew. Chem. Int. Ed.* **2005**, *44*, 7624. b) for a short overview, see: S. Dziadek, C. G. Espinola, H. Kunz, *Aust. J. Chem.* **2003**, *50*, 519.

[3] S. Keil, C. Claus, W. Dippold, H. Kunz, *Angew. Chem.* **2001**, *113*, 379; *Angew. Chem. Int. Ed.* **2001**, *40*, 366.

[4] a) R. N. Germain, *Cell* **1994**, *76*, 287; b) J. A. Villadaugos, *Mol. Immunol.* **2001**, *38*, 329.

[5] K. M. Murphy, A. B. Heimberger, D. Y. Loh, *Science* **1990**, *250*, 1720.

[6] a) J. Burchell, J. Taylor-Papadimitriou, M. Boshell, S. Gendler, T. Dulig, *Int. J. Cancer* **1989**, *44*, 691; b) M. R. Price, F. Hudecz, C. O'Sullivan, R. W. Baldwin, P. M. Edwards, S. B. J. Tendler, *Mol. Immunol.* **1990**, *27*, 795; c) D. I. R. Spencer, M. R. Price, S. B. J. Tendler, C. DeMatties, T. R. E. Stadie, F.-G. Hanisch, *Cancer Lett.* **1996**, *100*, 11–15.

[7] S. H. Itzkowitz, M. Yuan, C. K. Montgomery, T. Kjeldsen, H. K. Takahashi, W. L. Bigbee, Y. S. Kim, *Cancer Res.* **1989**, *49*, 197.

[8] H. Inoue, *Obstet. Gynecol.* **1990**, *75*, 1031.

[9] a) I. Takahashi, I. Maehara, T. Kusumoto, M. Yoshida, Y. Kakej, H. Kusumoto, M. Furusawa, K. Suglimacti, *Cancer* **1993**, *72*, 18836; b) R. Soares, A. Marinho, F. Schmitt, *Pathol. Res. Pract.* **1996**, *192*, 1182.

[10] a) I. Brockhausen, *Biochim. Biophys. Acta* **1999**, *1473*, 67; I. Brockhausen, *Biochem. Soc. Trans.* **2003**, *31*, 318; b) K. O. Lloyd,

 © 2005 Wiley-VCH Verlag GmbH & Co. KGaA, Weinheim

J. Burchell, V. Kundryashov, B. W. Yin, J. Taylor-Papadimitriou, *J. Biol. Chem.* **1996**, *271*, 33325.
[11] a) T. F. Orntoft, N. Harvig, N. C. Langklide, *Int. J. Cancer* **1990**, *45*, 666; b) J. Taylor-Papadimitriou, J. M. Burchell, T. Plunkett, R. Graham, I. Correa, D. Miles, M. Smith, *J. Mammary Gland Biol.* **2002**, *7*, 209; c) F.-G. Hanisch, S. Müller, *Glycobiology* **2000**, *10*, 439.
[12] a) M. Wagner, H. Kunz, *Angew. Chem.* **2002**, *114*, 315; *Angew. Chem. Int. Ed.* **2002**, *41*, 317; b) M. Wagner, S. Dziadek, H. Kunz, *Chem. Eur. J.* **2003**, *9*, 6018.
[13] E. Bayer, W. Rapp, *Chem. Pept. Proteins* **1986**, *3*, 3.
[14] a) R. Knorr, A. Trzeciak, W. Baumwarth, D. Gillessen, *Tetrahedron Lett.* **1989**, *30*, 1927; b) V. Dourtoglou, B. Gross, V. Lambropoulou, C. Ziondrou, *Synthesis* **1984**, 572; c) W. König, R. Geiger, *Chem. Ber.* **1970**, *103*, 788.
[15] a) C. Brocke, H. Kunz, *Synlett* **2003**, 2052; b) C. Brocke, H. Kunz, *Synthesis* **2004**, 525.
[16] L. A. Carpino, D. Ionescu, A. El-Falham, *J. Org. Chem.* **1996**, *61*, 2460.
[17] S. S. Wang, *J. Am. Chem. Soc.* **1973**, *95*, 1328.
[18] The antibodies bound to the immobilized antigen were detected with a biotinylated secondary anti-mouse antibody. For the photometric analysis, horseradish peroxidase (HPO) coupled to streptavidin was utilized which catalyzes the oxidation of the colorless substrate ABTS (2,2′-azino-bis-[3-ethylbenzthiazoline-6-sulfonic acid]) by H_2O_2 to furnish a metastable green radical cation with a maximum absorbance at $\lambda = 414$ nm.
[19] The conjugate between the sialyl-Tn glycopeptide and BSA is described as compound **25** in the preceding Communication.[2a]
[20] For overviews, see, for example: a) C. Brocke, H. Kunz, *Bioorg. Med. Chem.* **2002**, *10*, 3085; b) O. Seitz, *ChemBioChem* **2000**, *1*, 214; c) H. Herzner, T. Reipen, M. Schultz, H. Kunz, *Chem. Rev.* **2000**, *100*, 4495; d) G. Arsequell, G. Valencia, *Tetrahedron Asymmetry* **1999**, *10*, 3045.

 © 2005 Wiley-VCH Verlag GmbH & Co. KGaA, Weinheim

Bioanalysis

DOI: 10.1002/anie.200502908

Direct Readout of Protein–Protein Interactions by Mass Spectrometry from Protein–DNA Microarrays**

Christian F. W. Becker, Ron Wacker, Werner Bouschen, Ralf Seidel, Branko Kolaric, Pascal Lang, Hendrick Schroeder, Oliver Müller, Christof M. Niemeyer, Bernhard Spengler, Roger S. Goody, and Martin Engelhard**

Microarray technology allows the analysis of a large number of different parameters simultaneously by using a variety of readout systems based on fluorescence, chemiluminescence, electrochemistry, radioactivity, or mass spectrometry (MS).[1] Of these readout systems mass spectrometry is unique, since it provides information on an intrinsic physical parameter of the analyte, its molecular weight. Such a readout system is especially useful to determine protein expression levels by using surface enhanced laser desorption ionization (SELDI), to determine enzyme activity through peptide-based approaches such as SAMDI (self-assembled monolayers for MALDI), and for the direct detection of cross-hybridization on DNA chips.[2–7] Particularly important is the capability of mass spectrometry to unequivocally identify specific protein–protein interactions by providing the exact molecular weight of the binding partner.[7]

To develop a microarray-based assay that combines the reversible immobilization of proteins with readout by MALDI mass spectrometry, we have utilized protein–DNA conjugates (DNA-directed immobilization, DDI). This method achieves highly specific but noncovalent and therefore reversible binding of protein–DNA conjugates to com-

[*] Dr. C. F. W. Becker, Dr. R. Seidel, B. Kolaric, P. Lang, Priv.-Doz. Dr. O. Müller, Prof. Dr. R. S. Goody, Prof. Dr. M. Engelhard
Max-Planck-Institut für molekulare Physiologie
Otto-Hahn-Strasse 11, 44227 Dortmund (Germany)
Fax: (+49) 231-1332-399
E-mail: christian.becker@mpi-dortmund.mpg.de
martin.engelhard@mpi-dortmund.mpg.de

Dr. R. Wacker, Dr. H. Schroeder
Chimera Biotec GmbH
Emil-Figge-Strasse 76A, 44227 Dortmund (Germany)

Dr. W. Bouschen, Prof. Dr. B. Spengler
Justus-Liebig Universität Giessen
Anorganische und Analytische Chemie
Schubertstrasse 60, 35392 Giessen (Germany)

Dr. H. Schroeder, Prof. Dr. C. M. Niemeyer
Universität Dortmund
Otto-Hahn-strasse 6, 44227 Dortmund (Germany)

[**] The authors thank W. Hecker for help with oligonucleotide synthesis. We are grateful for financial support from the MPG, DFG, BMBF, and VCI.

Supporting information for this article is available on the WWW under http://www.angewandte.org or from the author.

© 2005 Wiley-VCH Verlag GmbH & Co. KGaA, Weinheim

plementary, surface-attached oligonucleotides. DDI combines efficient in-solution binding of protein–DNA conjugates with spatially encoded detection in microarray format.[8–10] This approach is an addition to the widely used antibody-based immobilization of capture proteins on microarrays.[11,12]

As a model system for detecting specific protein–protein interactions by DDI and mass spectrometry, the protein pair Ras and the Ras-binding domain (RBD) of its effector molecule cRaf-1 was selected because of its medicinal relevance.[13] In addition a second protein pair, Ras and a Ras-specific antibody, was chosen. The Ras protein plays a vital role in signal transduction by cycling between its activated, GTP-bound state and its inactive, GDP-bound state.[14] The affinity of Ras:GTP for the RBD is approximately 160 nM, whereas the affinity of Ras:GDP for the RBD is around 200-fold weaker.[15] Mutations in Ras can lead to constitutive activation of the signaling cascade and occur in 30% of all solid human cancers.[16] An important reason for selecting this system was the observation that no antibody exists that can distinguish between Ras:GTP and Ras:GDP.

Functional immobilization of proteins in a controlled manner was achieved by synthesizing protein–DNA fusion proteins based on the expressed-protein ligation technique.[17,18] Similar approaches have been described for peptide–DNA and protein–PNA conjugates.[9,19,20]

The DNA-directed immobilization of protein–DNA fusion constructs through hybridization on oligonucleotide-modified microarrays is a mild procedure that combines high efficiency of adsorption and reversibility with high specificity. The immobilization strategy was initially tested with Ras–DNA and RBD–DNA conjugates on glass microarrays. The glass surface was modified with a dendritic intermediate layer and 5′-amino-modified oligonucleotides were covalently attached.[21] Three different DNA sequences were used for capturing the Ras–DNA and RBD–DNA conjugates. Two of these were fully complementary to the DNA attached to the proteins but differed in the number of nucleobases (**1**, **2**). In addition, a non-complementary capture DNA (**3**) served as a control for the specificity of DNA hybridization.

Synthesis of protein–DNA conjugates was achieved by expression of Ras and RBD in *E. coli* fused to an Mxe intein and a chitin-binding domain (CBD), which was used for affinity purification.[22] Treatment of the purified fusion proteins with mercaptoethanesulfonic acid (MESNA) liberated the corresponding C-terminal thioesters of Ras (**4**) and RBD (**5**) (see Supporting Information). These were ligated with an oligonucleotide carrying a cysteine residue at its 5′ end. The 5′-modification of the oligonucleotide was accomplished by two different routes. In the first approach a modified thymidine phosphoramidite (**6**) was introduced into the oligonucleotide (**7**) during solid-phase synthesis. Compound **6** carried a 5′-cysteine residue and was synthesized from 5′-amino thymidine (Figure 1). The second method utilized a 5′-amino oligonucleotide, covalently linked to the solid phase (**8**). The oligonucleotide was treated with an (9H-fluoren-9-ylmethoxy)carbonyl (Fmoc) protected cysteine residue (Fmoc-Cys(SBu)-OH) to produce the 5′-cysteine modified oligonucleotide **9** (see Supporting Information).[23] The oligonucleotides **7** and **9** were treated with Ras (**4**) and RBD (**5**) thioesters and produced the protein–DNA conjugates **10** and **11** (Figure 1 a–c).[19,24,25]

In initial tests conventional fluorescence readout was used to detect Ras:GppNHp–DNA (GppNHp is a nonhydrolyzable GTP analogue) on glass microarrays after incubation with a Cy5-labeled Ras-specific antibody. Specific interaction between a fully complementary surface-attached oligonucleotide **1** and the Ras–DNA conjugate **10** was clearly demon-

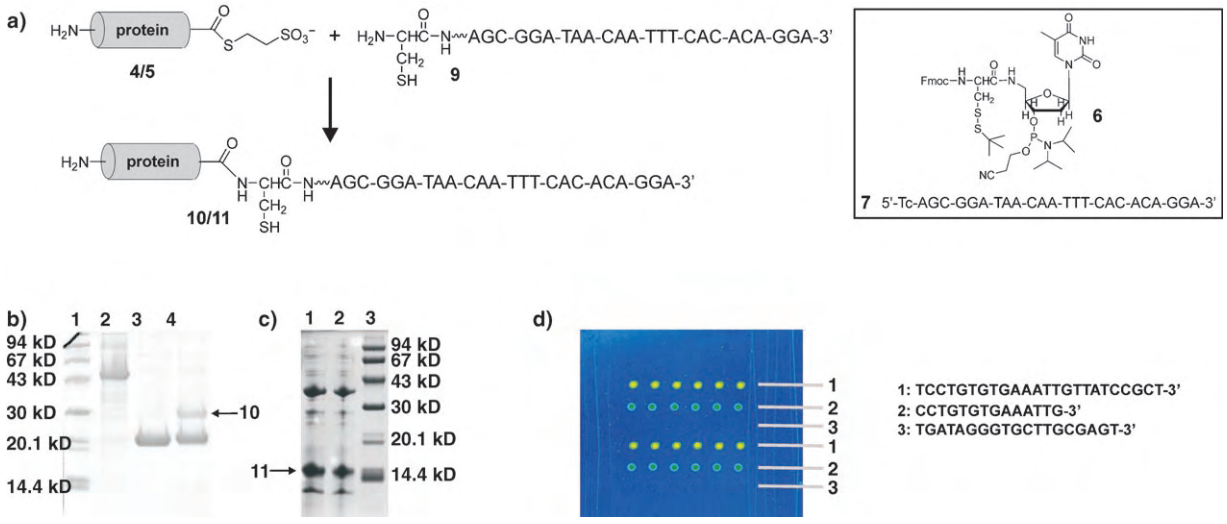

Figure 1. a) Schematic representation of the ligation reaction of protein thioesters (**4** or **5**) with 5′-Cys-modified oligonucleotide to produce the capture proteins RBD–DNA (**10**) and Ras:GppNHp–DNA (**11**). b) 12% SDS-PAGE gel of Ras-ligation reaction; 1: molecular-weight marker, 2: purified Ras–Mxe fusion protein (**2**); 3: Ras thioester (**4**); 4: Ras thioester **4**+**9** after 12 h of ligation. c) 12% SDS-PAGE gel of RBD-ligation reaction; 1: RBD thioester **5**+**9** (10 μL) after ligation; 2: RBD thioester **5**+**9** (5 μL) after ligation; 3: molecular-weight marker. d) Fluorescence image of microarray on glass slide; DNA-directed immobilization of Ras-DNA **10** on a subarray with three rows of oligonucleotides: fully complementary **1**, truncated complementary **2** and non-complementary **3**.

 © 2005 Wiley-VCH Verlag GmbH & Co. KGaA, Weinheim

strated by the strong fluorescence signal (Figure 1d). A complementary but truncated oligonucleotide **2** produced a much weaker signal (Figure 1d). The non-complementary oligonucleotide **3** did not produce a signal (Figure 1d) and was used as a negative control in all experiments to exclude any influence of the surface-attached oligonucleotide on the readout.

For the detection of analyte proteins by MALDI-MS, a different solid support had to be chosen because glass slides, owing to their poor electrical conductance properties, are inappropriate as a support. Silica wafers are easily available, have an adequate electric conductance and offer similar surface chemistry to that of glass slides. Arrays were produced in object-holder format, and contained five subarrays (18 × 9 mm) per wafer. Each subarray contained 18 to 36 spots with a diameter of approximately 200 μm (Figure 2b). In initial experiments, three different capture oligonucleotides (**1**–**3**) were spotted in rows of six spots each and the silica chips were washed and blocked with an albumin containing buffer (see Supporting Information). Subsequently the capture molecules RBD–DNA or Ras–DNA were immobilized on the surface, there then followed several washing steps and incubation with the analyte proteins (Ras:GppNHp/Ras antibody). Finally a layer of organic matrix (sinapinic acid) was deposited on the microarrays and dried (Figure 2a).

MALDI measurements were performed with a home-built post source decay (PSD) MALDI mass spectrometer (Aladim II) that allowed adjustment of the microarray plate in x, y, and z directions.[26,27] Multiple controls were performed by including a row of non-complementary oligonucleotide **3** in every subarray, as well as by measuring subarrays not treated with capture or analyte molecules and a subarray treated only with the capture molecule RBD–DNA. In the case of surface-attached, non-complementary oligonucleotide no signal, for either capture or analyte molecules, was detected. Measurement of subarrays with immobilized RBD–DNA or Ras–DNA did not produce a signal, thus demonstrating that either the conjugates were not detached from the surface or, more probably, that they were not ionized efficiently under these conditions (Figure 2c). Measurements in negative-ion mode also did not give a signal for the capture molecules.

Incubation of an RBD–DNA-loaded subarray with a 3-μM solution of C-terminally truncated Ras:GppNHp, however, produced a MALDI signal at 18862 Da for the Ras protein after only 2–20 laser pulses (calculated M_W: 18853 Da, Figure 2d). Incubating the arrays with Ras:GDP did not produce a signal, thus demonstrating that the immobilized RBD–DNA selectively binds activated Ras:GppNHp and not its inactive form (Ras:GDP). Positive results were only obtained from spots on the array that carried the oligonucleotides **1** and **2** but never for the non-complementary oligonucleotide **3**, emphasizing the specificity of the method for immobilization of both capture and analyte proteins.

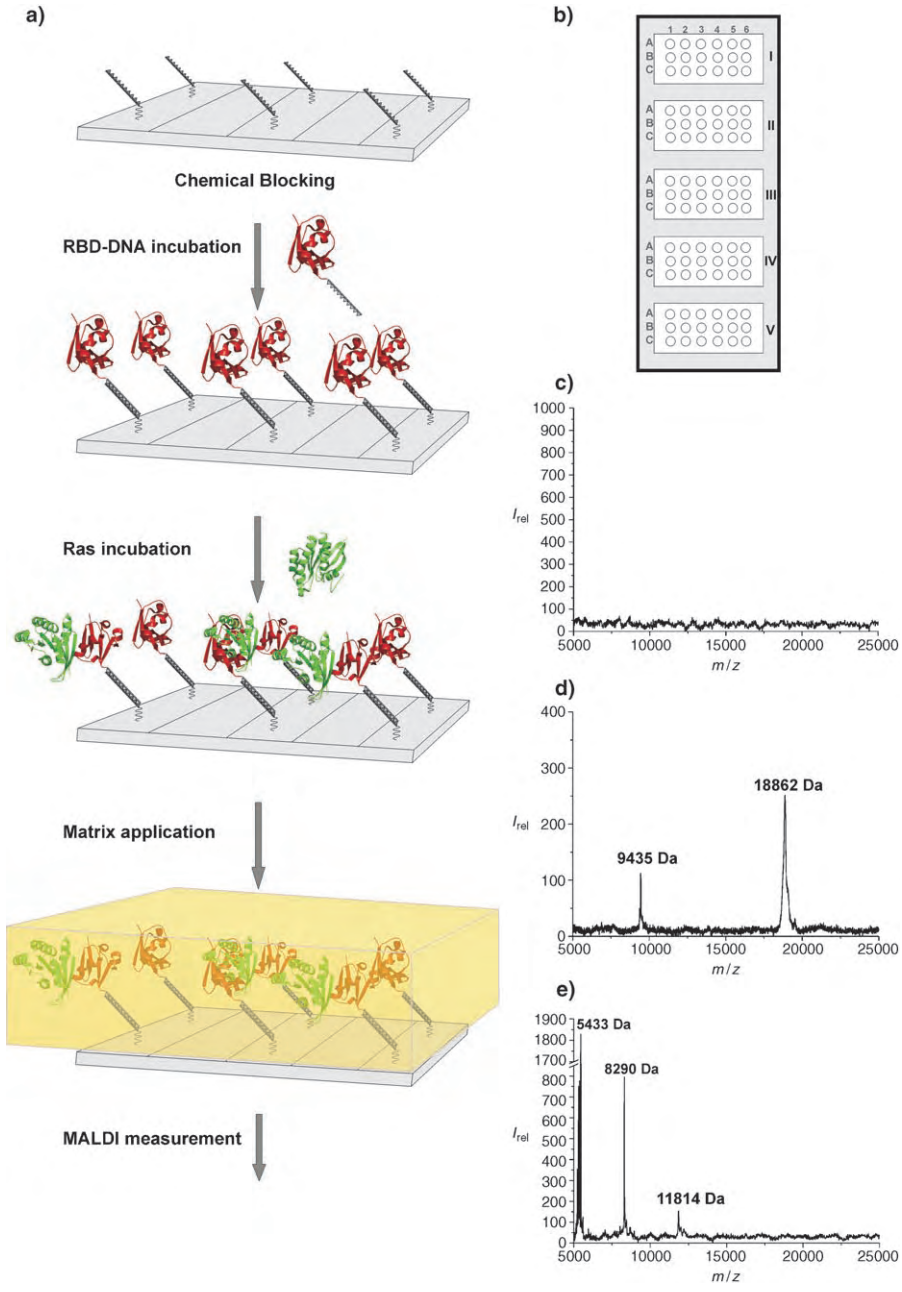

Figure 2. a) Microarray preparation. Chemical blocking of the surface after covalent attachment of oligonucleotides; DNA-directed immobilization of the capture molecule (RBD–DNA conjugate); incubation with analyte (Ras:GppNHp); matrix application; typical MALDI spectra of captured Ras:GppNHp. b) Microarray in object holder format; c) Typical MALDI spectrum of background signal (only capture molecule on the surface); d) MALDI spectrum of microarray incubated with 3-μM solution of Ras:GppNHp; e) MALDI spectrum of microarray spots with Ras–DNA as capture molecule and Ras-specific antibody as analyte.

© 2005 Wiley-VCH Verlag GmbH & Co. KGaA, Weinheim

An important advantage of this approach is its spatial resolution. Peaks in the mass spectrum were only observed for equidistant areas on the subarray that correlated very well with the spots of immobilized oligonucleotide which were brought onto the surface by an automated spotter. Based on this observation we conclude that the applied matrix solution did not fully dissolve and dislocate the analyte molecules.

To determine the scope of the method, a second protein pair was used. Ras–DNA was immobilized on one subarray and incubated with a solution of Cy5-labeled Ras-specific antibody. The corresponding mass spectrum (Figure 2e) showed a signal at 11814 Da, which can be attributed to one of the light chains of the Fab antibody. Other signals observed in this spectrum did not interfere with the identification of the analyte. Negative controls similar to those described above gave no signal.

An important aspect of analyzing protein–protein interactions is the affinity, which can be the limiting factor for measurements in physiological contexts. For the Ras–RBD interaction, which can be regarded as of intermediate affinity, the detection limit was determined by incubation of the five subarrays on one silica wafer with solutions containing 3 μM, 300 nM, 30 nM, 3 nM, and 0.3 nM Ras:GppNHp. In all cases, 80 single-laser-pulse spectra were averaged (see Supporting Information). Ras:GppNHp was detected down to an incubation concentration of 3 nM, which is 50-times below the K_D value determined for the Ras:GppNHp–RBD interaction (160 nM) in solution-phase experiments.[15] This result suggests that measurements at sample concentrations considerably below the K_D value for the interaction are possible and thus that the identification of weakly binding molecules is also possible. In addition, quantification of the analyte protein by MALDI-MS could provide information on affinities between capture and analyte protein as well as the concentration of the analyte.[28]

The successful measurement of low concentrations of activated Ras enabled the detection of activated Ras in complex mixtures originating from cell lysates. A mammalian cell line, Madine Darby canine kidney (MDCK) cells and a closely related MDCK-f3 cell line (virally transformed with the *H-Ras* gene[29–31]) were chosen to obtain fractionated cell lysates. MDCK-f3 cells express elevated levels of Ras and therefore activated Ras should be present at concentrations in amounts typical for cancer cells. After cell lysis the cytoplasmic and membrane fractions were separated. Cytoplasmic fractions were used as obtained, whereas the membrane fractions were extracted with TritonX100-containing buffer and only the soluble fraction was used.

Four subarrays were individually incubated for 30 min with the cytoplasmic fraction and the membrane extract of MDCK and MDCK-f3, then came the washing steps and application of matrix. For both membrane extracts, only a series of equidistant signals between 500 and 2000 Da was observed that arose from detergent molecules left on the surface during sample preparation, possibly impairing the detection of activated Ras. However, the cytoplasmic fraction of MDCK-f3 cells produced a broad signal, ranging from 21050 to 21700 Da, with a maximum at 21329 Da, which is in good agreement with unmodified full-length Ras (M_W 21298 Da;[32] Figure 3). This result demonstrates that activated Ras can be detected in cell lysates at concentrations well below the K_D of the Ras–RBD interaction. An increase in spectral resolution will allow the distinction of post-translationally modified isoforms of Ras in different cellular environments.

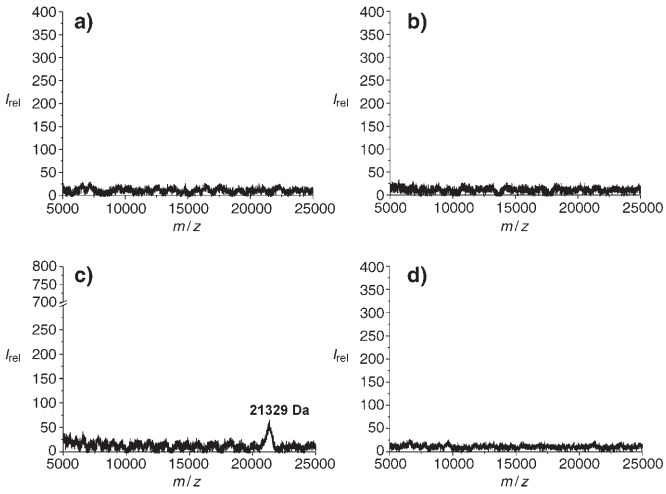

Figure 3. Microarray with RBD–DNA as capture molecule incubated with cytosolic fractions and membrane-extracts of MDCK and MDCK-f3 cells. MALDI spectrum of subarray incubated with a) cytosolic fraction of MDCK cells; b) membrane extract of MDCK cells; c) cytosolic fraction of MDCK-f3 cells showing a signal around 21329 Da; d) membrane extract of MDCK-f3 cells.

Herein we have shown that the modification of proteins by easily accessible cysteine-modified oligonucleotides using an expressed-protein ligation approach is straightforward and allows direct functional as well as highly selective immobilization of protein–DNA conjugates. A combination of the resulting DDI-based protein microarrays and MALDI mass spectrometry leads to the identification of protein–protein interactions at concentrations far below the K_D value of the chosen interaction. The selectivity and sensitivity is sufficient to identify Ras proteins in complex mixtures such as cell lysates, without interfering signals.

An additional benefit of the reversible immobilization strategy is the reusability of these microarrays with different capture molecules (e.g. protein–DNA conjugates). The advantage of MALDI detection over conventional systems such as fluorescence is the molecular-weight information obtained. In combination with proteolytic cleavage and advanced MALDI techniques, such as post source decay or composition-based sequencing FT-ICR-MS, it should be possible to identified analyte molecules directly with this approach.[33] Finally, the method described herein will permit analysis of protein–protein interactions, screening for new or unknown binding partners, or monitoring the influence of third components (drugs) on the binding event.

Received: August 16, 2005
Published online: October 24, 2005

 © 2005 Wiley-VCH Verlag GmbH & Co. KGaA, Weinheim

Keywords: mass spectrometry · microarrays · oligonucleotides · protein–DNA conjugates · proteins

[1] M. F. Templin, D. Stoll, M. Schrenk, P. C. Traub, C. F. Vohringer, T. O. Joos, *Trends Biotechnol.* **2002**, *20*, 160 – 166.
[2] J. Su, M. Mrksich, *Angew. Chem.* **2002**, *114*, 4909 – 4912; *Angew. Chem. Int. Ed.* **2002**, *41*, 4715 – 4718.
[3] V. Seibert, A. Wiesner, T. Buschmann, J. Meuer, *Pathol. Res. Pract.* **2004**, *200*, 83 – 94.
[4] D. H. Min, J. Su, M. Mrksich, *Angew. Chem.* **2004**, *116*, 6099 – 6103; *Angew. Chem. Int. Ed.* **2004**, *43*, 5973 – 5977.
[5] D. H. Min, M. Mrksich, *Curr. Opin. Chem. Biol.* **2004**, *8*, 554 – 558.
[6] U. Plutowski, C. Richert, *Angew. Chem.* **2005**, *117*, 627 – 631; *Angew. Chem. Int. Ed.* **2005**, *44*, 621 – 625.
[7] W. S. Yeo, D. H. Min, R. W. Hsieh, G. L. Greene, M. Mrksich, *Angew. Chem.* **2005**, *117*, 5616 – 5619; *Angew. Chem. Int. Ed.* **2005**, *44*, 5480 – 5483.
[8] C. M. Niemeyer, *Biochem. Soc. Trans.* **2004**, *32*, 51 – 53.
[9] M. Lovrinovic, R. Seidel, R. Wacker, H. Schroeder, O. Seitz, M. Engelhard, R. S. Goody, C. M. Niemeyer, *Chem. Commun.* **2003**, 822 – 823.
[10] R. Wacker, H. Schroeder, C. M. Niemeyer, *Anal. Biochem.* **2004**, *330*, 281 – 287.
[11] T. Kodadek, *Chem. Biol.* **2001**, *8*, 105 – 115.
[12] R. Barry, M. Soloviev, *Proteomics* **2004**, *4*, 3717 – 3726.
[13] A. Wittinghofer, H. Waldmann, *Angew. Chem.* **2000**, *112*, 4360 – 4383; *Angew. Chem. Int. Ed.* **2000**, *39*, 4193 – 4214.
[14] M. S. Boguski, F. McCormick, *Nature* **1993**, *366*, 643 – 654.
[15] J. R. Sydor, M. Engelhard, A. Wittinghofer, R. S. Goody, C. Herrmann, *Biochemistry* **1998**, *37*, 14292 – 14299.
[16] M. Barbacid, *Annu. Rev. Biochem.* **1987**, *56*, 779 – 827.
[17] T. W. Muir, *Annu. Rev. Biochem.* **2003**, *72*, 249 – 289.
[18] S. Takeda, S. Tsukiji, T. Nagamune, *Bioorg. Med. Chem. Lett.* **2004**, *14*, 2407 – 2410.
[19] D. A. Stetsenko, M. J. Gait, *J. Org. Chem.* **2000**, *65*, 4900 – 4908.
[20] Y. Singh, E. Defrancq, P. Dumy, *J. Org. Chem.* **2004**, *69*, 8544 – 8546.
[21] R. Benters, C. M. Niemeyer, D. Wöhrle, *ChemBioChem* **2001**, *2*, 686 – 694.
[22] T. C. Evans, J. Benner, M. Q. Xu, *Protein Sci.* **1998**, *7*, 2256 – 2264.
[23] R. Vinayak, *Tetrahedron Lett.* **1999**, *40*, 7611 – 7613.
[24] M. Lovrinovic, M. Spengler, C. Deutsch, C. M. Niemeyer, *Mol. Biosys.* **2005**, *1*, 64.
[25] I. Burbulis, K. Yamaguchi, A. Gordon, R. Carlson, R. Brent, *Nat. Methods* **2005**, *2*, 31 – 37.
[26] B. Spengler, *J. Mass Spectrom.* **1997**, *32*, 1019 – 1036.
[27] P. Chaurand, F. Luetzenkirchen, B. Spengler, *J. Am. Soc. Mass Spectrom.* **1999**, *10*, 91 – 103.
[28] J. Reinders, U. Lewandrowski, J. Moebius, Y. Wagner, A. Sickmann, *Proteomics* **2004**, *4*, 3686 – 3703.
[29] J. Behrens, M. M. Mareel, F. M. Vanroy, W. Birchmeier, *J. Cell Biol.* **1989**, *108*, 2435 – 2447.
[30] P. L. Hordijk, J. P. ten Klooster, R. A. van der Kammen, F. Michiels, L. C. Oomen, J. G. Collard, *Science* **1997**, *278*, 1464 – 1466.
[31] K. Vleminckx, L. Vakaet, Jr., M. Mareel, W. Fiers, F. Van Roy, *Cell* **1991**, *66*, 107 – 119.
[32] J. P. McGrath, D. J. Capon, D. H. Smith, E. Y. Chen, P. H. Seeburg, D. V. Goeddel, A. D. Levinson, *Nature* **1983**, *304*, 501 – 506.
[33] B. Spengler, *J. Am. Soc. Mass Spectrom.* **2004**, *15*, 703 – 714.

 © 2005 Wiley-VCH Verlag GmbH & Co. KGaA, Weinheim

Cluster Compounds

DOI: 10.1002/anie.200502283

$[Tl_8]^{6-}$ in Cs_8Tl_8O: A Naked Eight-Vertex *closo*-Deltaeder as a Cluster Anion**

*Andrey Karpov and Martin Jansen**

Dedicated to Professor Herbert W. Roesky on the occasion of his 70th birthday

Using NaTl as an example, Zintl developed the concept[1] that was later named after him, and which was subsequently generalized by Klemm.[2] The Zintl–Klemm approach allows a reliable and qualitative analysis of the chemical bonding in intermetallics near the ionic–metallic border-line to be performed. The classical formulation assumes that the electropositive component, for example, of a binary intermetallic phase, transfers all valence electrons to the electronegative component. The resulting anions interconnect by two-electron-two-center (2e2c) bonds to form oligomeric or polymeric substructures. Thus the anions achieve closed-shell electron configurations, which show similar structural motives to the elements with the same valence electron concentration (8-*N* rule or concept of the effective atomic number (EAN)).[3] Since then, a huge number of oligomeric and polymeric thallium anions has been discovered.[4] It may be perceived as a curiosity that among them virtually none fulfills the Zintl rules. This fact reflects some peculiarities of thallium. In accordance with its position in the periodic table, the thallium 6s orbital is contracted and energetically stabilized. In addition, the oxidation state −I is somewhat favored, because the corresponding ground state $(p_{1/2})^2$ can be considered closed-shell as a result of lifting the degeneracy of the 6p orbital through spin-orbit splitting.[5] As a consequence of the larger radial extension of the orbitals contributing to the Tl–Tl bonds, delocalized bonds play an important role in these clusters. Because of this complex interplay, completely different bonding descriptions have been considered for the thallium polyanions reported. $(Tl^-)_n$[1] and $[Tl_4]^{8-}$[6] can be classified as Zintl ions, $[Tl_5]^{7-}$[7] and $[Tl_6]^{8-}$[8] obey Wade's rules,[9] whereas $[Tl_6]^{6-}$,[10] $[Tl_7]^{7-}$,[11] $[Tl_9]^{9-}$,[7] $[Tl_{11}]^{7-}$[12] cannot be explained using any known system, and are denoted as hypoelectronic.[4] Beside these closed-shell (diamagnetic) clusters, open-shell (paramagnetic) species are also known,

[*] Dipl.-Chem. A. Karpov, Prof. Dr. M. Jansen
Max-Planck-Institut für Festkörperforschung
Heisenbergstrasse 1, 70569 Stuttgart (Germany)
Fax: (+49) 711-689-1502
E-mail: m.jansen@fkf.mpg.de

[**] We thank Dr. Ulrich Wedig for the help with the extended Hückel calculations and the Fonds der Chemischen Industrie for the continuous financial support.

Supporting information for this article is available on the WWW under http://www.angewandte.org or from the author.

© 2005 Wiley-VCH Verlag GmbH & Co. KGaA, Weinheim

for example, $[Tl_{13}]^{10-}$ (with the shape of a centered icosahedron).[13]

In the context of our investigations on aurides[14] and platinides,[15] the Tl^- ion is of particular interest to us. As part of our synthesis attempts we have also added oxygen as a third component to the binary system Cs/Tl. In this way, a further degree of freedom is introduced, thus opening additional options for the formation of appropriate compositions and packings. In the course of these studies, we discovered Cs_8Tl_8O, which contains previously unknown $[Tl_8]^{6-}$ oligoanions.

Cs_8Tl_8O was prepared from Cs, Tl, and Cs_2O, by reaction at 773 K and subsequent slow cooling to room temperature. The educts contained the required stoichiometric Tl/O ratio, however with an excess of Cs. In a second procedure the mixture was rapidly quenched from 773 K to room temperature and then heated at 473 K for 1000 h. The excess of cesium was subsequently removed by evaporation. Cs_8Tl_8O is a dark-gray brittle crystalline powder, and can be isolated as a single phase (shown by powder X-ray diffraction) in this manner. However, the products often contain an admixture of Cs_8Tl_{11},[12] as detected by powder X-ray diffraction (ca. 1–5 wt.%). The compound is extremely air- and moisture-sensitive, and thermally stable up to approximately 498 K. At this temperature, it decomposes, leaving a solid residue of Cs_8Tl_{11}. The compound Cs_8Tl_8O is formed in a wide concentration range of the constituent components (the surplus reactants do not react) and shows practically no homogeneity range. The magnetic susceptibility is temperature independent in the region 50–300 K (-72.3×10^{-10} m^3 mol$^{-1}\pm2.5\%$) and agrees fairly well with the sum of the diamagnetic core corrections $(8\chi(Tl^+)+8\chi(Cs^+)+\chi(O^{2-})=-67.1\times10^{-10}$ m^3 mol^{-1})[16] and the Larmor susceptibility of the cluster orbital electrons (-18.8×10^{-10} m^3 mol^{-1}).[17] The temperature dependence of the electrical conductivity has a gradient $(1/\rho)\,\partial\rho/\partial T=-0.36\%$ K^{-1} in the region 50→300 K (ρ(50 K) = 0.085, ρ(273 K) = 0.023 Ohm cm), which is characteristic for a semiconductor.[18] The measurement of the diffuse reflectance shows a clear absorption edge at $\lambda=465$ nm which corresponds to an optical band gap E_g of 2.7 eV, thus confirming the semiconducting nature of the sample (Figure 1).

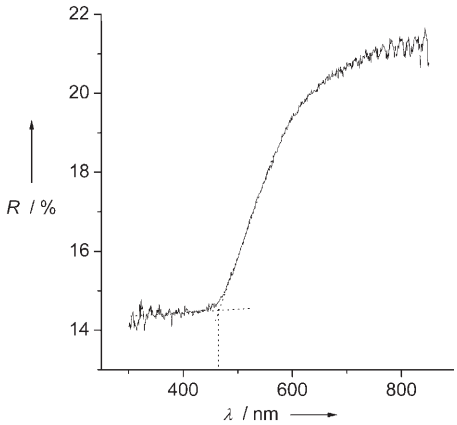

Figure 1. Diffuse reflectance spectrum of Cs_8Tl_8O. The optical band gap is defined by the intersection of the extrapolated steep rise with the base line.

According to the results of X-ray single-crystal structure analysis[19] Cs_8Tl_8O crystallizes in a novel structure type (Figure 2). The oxygen atoms are surrounded by an octahedral arrangement of six cesium atoms at a distance of 290.0(1) pm (Cs–O in Cs_2O: 287 pm).[20] Two further Cs atoms are located at a distance of 533.1(1) pm above and below each oxygen atom on the $\bar{3}$ axis of space group $R\bar{3}$. The resemblance of the Cs–O separations in Cs_8Tl_8O to those in Cs_2O is indicative for a full ionization of the Cs atoms with a charge transfer to oxygen atoms and formation of cationic $[OCs_{6+2}]^{6+}$ groups. The electrons released are accommodated by isolated ("naked") $\{Tl_8\}$ groups (point group D_{3d}, Figure 3). The Tl–Tl separations within the $[Tl_8]^{6-}$ cluster range from 311 to 326 pm, and thus are comparable to the corresponding values in other known thallium clusters. The intercluster Tl–Tl separations are clearly larger ($\geq$ 577 pm).

Topologically, the $\{Tl_8\}$ units can be regarded as being generated by condensation of an octahedron with two

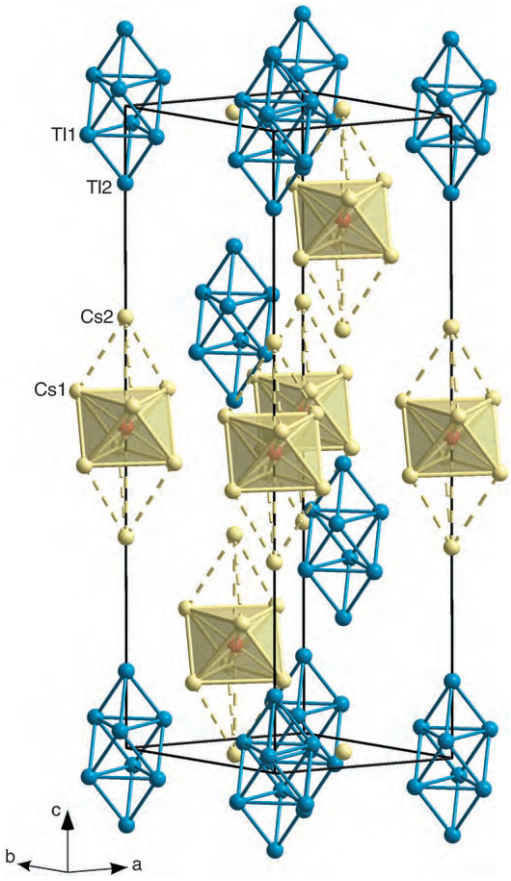

Figure 2. Crystal structure of Cs_8Tl_8O. Black lines mark the unit cell edges; $\{Tl_8\}$ clusters are blue, $\{O(Cs1)_6(Cs2)_2\}$ polyhedra are yellow.

tetrahedra (bicapped octahedron). The somewhat larger Tl–Tl distances are found in the common faces. The $\{Tl_8\}$ and $\{OCs_{6+2}\}$ groups belong to the same point group (D_{3d}), which favors the formation of a simple and highly symmetric packing. The $\{Tl_8\}$ clusters are arranged analogous to a cubic-closed packing, with the octahedral holes completely occupied by $\{OCs_{6+2}\}$ groups. The structure can therefore be

 © 2005 Wiley-VCH Verlag GmbH & Co. KGaA, Weinheim

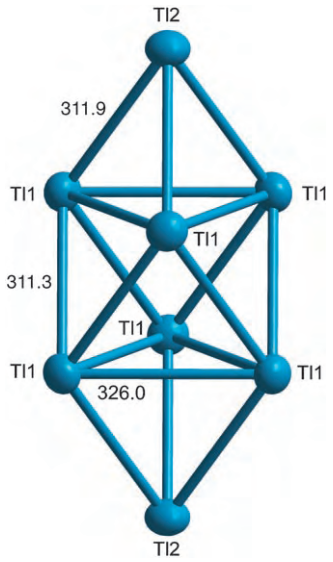

Figure 3. The $\{Tl_8\}$ cluster (thermal ellipsoids set at 50%). Interatomic distances [pm] and angles [°]: Tl1–Tl1 311.3(1) ×2, Tl1–Tl2 311.9(1), Tl1–Tl1 326.1(1) ×2, Tl2–Tl1 311.9(1) ×3; Tl1-Tl1-Tl1 63.16(3), Tl1-Tl1-Tl2 116.90(2) ×2, Tl1-Tl1-Tl1 58.42(1) ×2, Tl1-Tl1-Tl1 90 ×2, Tl1-Tl1-Tl2 58.48(1) ×2, Tl1-Tl1-Tl1 60.00, Tl1-Tl2-Tl1 63.03(3) ×3.

understood as an NaCl derivative, with one of the threefold axes of the originally cubic crystal system elongated.

Cs_8Tl_8O is the first example of a compound with an eight-vertex anionic framework in the shape of a bicapped octahedron. The earlier examples of bicapped octahedra were limited to transition metals.[21] The lack of such clusters within the boron or carbon chemistry was ascribed to the high strain of only four orbitals (per atom) contributing to the bonding.[22] When moving to the higher homologues, d orbitals are available which might reduce the angular strain. Accordingly, the first ligand-stabilized, eight-vertex, main-group-element cluster with the shape of a distorted bicapped octahedron (C_i) has recently been isolated for indium ($[In_8(2,6\text{-}Mes_2C_6H_3)_4]$, Mes = 2,4,6-$Me_3C_6H_2$).[23] Other topologies for eight-vertex cages are a distorted dodecahedron (ca. D_{2d}; $[B_8H_8]^{2-}$),[24] a distorted cube (ca. D_{2d}; $[In_8]$),[25] a rhombic prism (ca. D_{2d}; $[Sn_8]$),[26] and a square antiprism (D_{4d}; $[Sn_8]^{6-}$).[27] The latter example ($[Sn_8]^{6-}$) was the only representative of an eight-vertex, "isolated" anionic cluster known, until now.

Thirty valence electrons are available in the $[Tl_8]^{6-}$ cluster. This value is much less than the number of electrons required for 2e2c bonds within the Zintl–Klemm concept (18 edges × 2e + 8 inert pairs = 52e). The classical Wade's rules also fail at the description of this cage: in this case, for a *closo*-$[Tl_8]^{6-}$ cluster, 34 electrons would be necessary (2 × 8 + 2 skeletal electrons + 8 inert pairs = 34e). Only when employing the extended Wade–Mingos concept,[28] does the number of the electrons available correspond to the number of electrons required (electrons of the octahedron + 2 × {electrons of the tetrahedron − electrons of the common triangular face} = (4 × 6 + 2) + 2 × {(2 × 6 + 8) − (2×3+3×4)} = 30e). In this view, the two capping thallium atoms serve as electron donors for the stabilization of the electron-deficient octahedron framework ($2n \rightarrow 2n + 2$) [Eq. (1)]. As an alternative possibility of stabilizing the $[Tl_6]^{6-}$ octahedron by a strong axial compression has also been observed and discussed.[10]

$$2\,Tl^0 + [Tl_6]^{6-} = (Tl^+)_2[Tl_6]^{8-} \quad (1)$$

The closed-shell character of the $[Tl_8]^{6-}$ cluster is also qualitatively confirmed by extended Hückel calculations.[29] The bonding skeletal orbitals and the LUMO are shown in Figure 4. The LUMO (e_u) is separated from the HOMO (a_{1g}) by a remarkable band gap (0.6 eV). The band gap value is clearly underestimated, because the stabilization influence of the relativistic effects[5] is not considered.

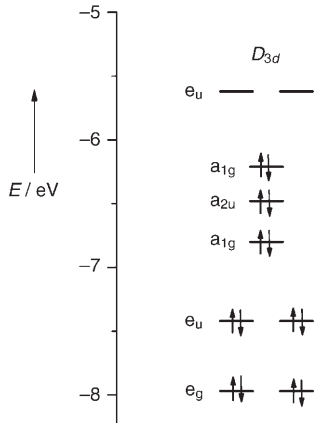

Figure 4. The MO diagram of the $\{Tl_8\}$ cluster calculated using the extended Hückel approximation.

The cluster compound reported herein provides a well defined setting for the discussion of the bonding relations. In the past, when analyzing complex compounds of oligomeric homoatomic thallium anions, incomplete charge transfer was often taken into account, as a possible correction parameter. In contrast, the details of the Cs/O substructure in Cs_8Tl_8O allows an assignment following the ionic bonding model, and therefore reasonable conclusions about the total charge of the $\{Tl_8\}$ cluster can be drawn. Although in this case neither the Zintl–Klemm concept nor Wade's rules (in their strict interpretation) apply, achieving a closed-shell electron structure appears to be the driving force for the formation of this specific structure. It is clear that for strongly delocalized bonding systems the otherwise so useful heuristic interpretation patterns are not adequate. Even only a qualitative understanding, would require an analysis of the MO term scheme of the cluster.

Experimental Section

All operations were performed under dried argon (Schlenk technique or glove-box: M.Braun, H_2O, $O_2 < 0.1$ ppm). Cs_8Tl_8O was prepared by reaction of cesium (synthesized from CsCl by a reduction with Ca and distilled twice in vacuum)[30] with thallium (Sigma-Aldrich, 99.9+ %, dried before use at 423 K in vacuum at 10^{-6} bar) and Cs_2O (synthesized from Cs by oxidation with a slight deficiency of oxygen

 © 2005 Wiley-VCH Verlag GmbH & Co. KGaA, Weinheim

followed by distillation of the excess Cs)[31] in the ratio Cs:Tl:Cs_2O 6:8:2. The mixture (1–2 g) was sealed under Ar in a tantalum ampoule, heated for 1 day at 773 K and subsequently cooled to room temperature with a rate of 1.5 K h^{-1}. In an alternative procedure, the mixture of Cs:Tl:Cs_2O in the ratio 7.5:8:1.25 was homogenized at 773 K for 1 day, quenched to room temperature and annealed at 473 K for 1000 h. The cesium excess was distilled at 363 K in both cases. Besides pure Cs_8Tl_8O, the samples often contained the thermal decomposition product Cs_8Tl_{11}. Cs_8Tl_8O is extremely sensitive to air and moisture. The atom ratio of heavy elements was additionally confirmed by energy dispersive X-ray spectroscopy (EDX) analysis (XL30TMP, Philips). The thermal stability was studied using high temperature X-ray powder diffraction (Stoe & Cie GmbH, $Mo_{K\alpha1}$, $\lambda =$ 70.93 pm, $4° < 2\theta < 40°$, T from room temperature to 623 K at 25 K intervals). The magnetization was measured using a SQUID Magnetometer (MPMS5.5, Quantum Design) in the temperature range 5–300 K at a field of 5 T. The specimen (0.1434 g) was sealed in a quartz tube under helium. The raw data were corrected for the holder contribution. The electrical conductivity measurement was performed using the four points technique (cylindrical sample, 6 mm diameter × 1 mm thickness, van der Pauw[32]) in the temperature region 5–300 K. Diffuse reflectance was recorded on a spectrophotometer (Perkin-Elmer Lambda 9) in the wavelength region 250 nm < λ < 850 nm. The sample as a finely ground powder was filled under argon into a flat quartz cuvette.

The Supporting Information contains an X-ray powder diffraction pattern of Cs_8Tl_8O and its comparison with a pattern as calculated from single-crystal data as well as the temperature dependences of the magnetization and of the electrical resistivity.

Received: June 30, 2005
Published online: October 25, 2005

Keywords: cesium · cluster compounds · relativistic effects · structure elucidation · thallium

[1] E. Zintl, W. Dullenkopf, *Z. Phys. Chem. Abt. B* **1932**, *16*, 195–205; E. Zintl, *Angew. Chem.* **1939**, *52*, 1–6.
[2] W. Klemm, *Proc. Chem. Soc. London* **1958**, 329–341; W. Klemm in *Festkörperchemie, Vol. 3* (Ed.: F. Sauter), Vieweg, Braunschweig, **1963**, pp. 233–251.
[3] E. Mooser, W. B. Pearson, *Phys. Rev.* **1956**, *101*, 1608–1609; H. Schäfer, B. Eisenmann, W. Müller, *Angew. Chem.* **1973**, *85*, 742–760; *Angew. Chem. Int. Ed. Engl.* **1973**, *12*, 694–712; H. G. von Schnering, *Angew. Chem.* **1981**, *93*, 44–63; *Angew. Chem. Int. Ed. Engl.* **1981**, *20*, 33–51; J. D. Corbett, *Chem. Rev.* **1985**, *85*, 383–397; R. Nesper, *Angew. Chem.* **1991**, *103*, 805–834; *Angew. Chem. Int. Ed. Engl.* **1991**, *30*, 789–817.
[4] J. D. Corbett, *Struct. Bonding (Berlin)* **1997**, *87*, 157–193; J. D. Corbett, *Angew. Chem.* **2000**, *112*, 682–704; *Angew. Chem. Int. Ed.* **2000**, *39*, 670–690.
[5] I. P. Grant, *Adv. Phys.* **1970**, *19*, 747–811; P. Pyykkö, *Chem. Rev.* **1988**, *88*, 563–594.
[6] D. A. Hansen, J. F. Smith, *Acta Crystallogr.* **1967**, *22*, 836–845.
[7] Z.-C. Dong, J. D. Corbett, *J. Am. Chem. Soc.* **1994**, *116*, 3429–3435.
[8] Z.-C. Dong, J. D. Corbett, *Angew. Chem.* **1996**, *108*, 1073–1076; *Angew. Chem. Int. Ed. Engl.* **1996**, *35*, 1006–1009.
[9] K. Wade, *Adv. Inorg. Chem. Radiochem.* **1976**, *18*, 1–66.
[10] Z.-C. Dong, J. D. Corbett, *J. Am. Chem. Soc.* **1993**, *115*, 11299–11303; Z.-C. Dong, J. D. Corbett, *Inorg. Chem.* **1996**, *35*, 2301–2306.
[11] D.-P. Huang, Z.-C. Dong, J. D. Corbett, *Inorg. Chem.* **1998**, *37*, 5881–5886.
[12] Z.-C. Dong, J. D. Corbett, *J. Cluster Sci.* **1995**, *6*, 187–201.
[13] Z.-C. Dong, J. D. Corbett, *J. Am. Chem. Soc.* **1995**, *117*, 6447–6455.
[14] C. Feldmann, M. Jansen, *Angew. Chem.* **1993**, *105*, 1107–1108; *Angew. Chem. Int. Ed. Engl.* **1993**, *32*, 1049–1050; C. Feldmann, M. Jansen, *J. Chem. Soc. Chem. Commun.* **1994**, 1045–1046; A. Pantelouris, G. Küper, J. Hormes, C. Feldmann, M. Jansen, *J. Am. Chem. Soc.* **1995**, *117*, 11749–11753; A.-V. Mudring, M. Jansen, *Angew. Chem.* **2000**, *112*, 3194–3196; *Angew. Chem. Int. Ed.* **2000**, *39*, 3066–3067; P. D. C. Dietzel, M. Jansen, *Chem. Commun.* **2001**, 2208–2209; A.-V. Mudring, M. Jansen, J. Daniels, S. Krämer, M. Mehring, J. P. P. Ramalho, A. H. Romero, M. Parrinello, *Angew. Chem.* **2002**, *114*, 128–132; *Angew. Chem. Int. Ed.* **2002**, *41*, 120–124.
[15] A. Karpov, J. Nuss, U. Wedig, M. Jansen, *Angew. Chem.* **2003**, *115*, 4966–4969; *Angew. Chem. Int. Ed.* **2003**, *42*, 4818–4821; A. Karpov, J. Nuss, U. Wedig, M. Jansen, *J. Am. Chem. Soc.* **2004**, *126*, 14123–14128; A. Karpov, U. Wedig, M. Jansen, *Z. Naturforsch. B* **2004**, *59*, 1387–1394; A. Karpov, U. Wedig, R. E. Dinnebier, M. Jansen, *Angew. Chem.* **2005**, *117*, 780–783; *Angew. Chem. Int. Ed.* **2005**, *44*, 770–773.
[16] H. Lueken, *Magnetochemie*, B. G. Teubner, Stuttgart, Leipzig, **1999**, p. 426.
[17] W. N. Ashcroft, D. N. Mermin, *Solid State Physics*, Holt, Rinehart and Winston, Philadelphia, **1976**, p. 649; S. C. Sevov, J. D. Corbett, *Inorg. Chem.* **1992**, *31*, 1895–1901.
[18] In the temperature region 50→5 K the resistivity decreases slightly, whereas the magnetization increases. The behavior can be ascribed to a minor contamination of the sample with paramagnetic, metallic $Cs_8Tl_{11}{\cdot}e$[12] (see Supporting Information).
[19] Crystal structure data of Cs_8Tl_8O: rhombohedral, space group $R\bar{3}$ (No. 148), $a = 898.01(6)$, $c = 3113.2(3)$ pm (powder data, $Cu_{K\alpha1}$, $\lambda = 154.06$ pm), $V = 2174.2(3) \times 10^6$ pm^3, $\rho_{calcd} =$ 6.22 g cm^{-3}, $Z = 3$, $\mu(Mo_{K\alpha}) = 54.2$ mm^{-1}, $F(000) = 3288$, $\lambda =$ 71.073 pm, Bruker AXS Smart-APEX-diffractometer, graphite monochromator, $T = 293$ K, ω-Scan, 8441 measured reflections, 1316 symmetry independent reflections ($2\theta_{max} = 58.27°$), 27 refined parameters. Atom coordinates: Tl1 (18*f*) 0.20880(7),0.99829(8),0.03983(2); Tl2 (6*c*) 0,0,0.11971(4); Cs1 (18*f*) 0.0259(1),0.5783(1),0.11748(4); Cs2 (6*c*) 2/3,1/3,0.00457(7); O1 (3*b*) 1/3,2/3,1/6. Semiempirical absorption correction (SADABS[33]). The structure solution and refinement have been performed using SHELXTL:[34] $R_1 = 0.0434$, $wR_2 = 0.1109$ (962 $F_0 > 4\sigma(F_0)$), $R_1 = 0.0627$, $wR_2 = 0.1179$ (all). Residual electron density $1.76/-1.20 \times 10^{-6}$ e pm^{-3}. Further details on the crystal structure investigations may be obtained from the Fachinformationszentrum Karlsruhe, 76344 Eggenstein-Leopoldshafen, Germany (fax: (+49) 7247-808-666; e-mail: crysdata@fiz-karlsruhe.de), on quoting the depository number CSD-415545.
[20] K. R. Tsai, P. M. Harris, E. N. Lassettre, *J. Phys. Chem.* **1956**, *60*, 338–344.
[21] P. F. Jackson, B. F. G. Johnson, J. Lewis, P. R. Raithby, *J. Chem. Soc. Chem. Commun.* **1980**, 60–61; G. Ciani, G. D'Alfonso, M. Freni, P. Romitti, A. Sironi, *J. Chem. Soc. Chem. Commun.* **1982**, 705–706.
[22] R. B. King, D. H. Rouvray, *J. Am. Chem. Soc.* **1977**, *99*, 7834–7840.
[23] N. Wiberg, T. Blank, A. Purath, G. Stößer, H. Schnöckel, *Angew. Chem.* **1999**, *111*, 2745–2748; *Angew. Chem. Int. Ed.* **1999**, *38*, 2563–2565.
[24] L. J. Guggenberger, *Inorg. Chem.* **1969**, *8*, 2771–2774.
[25] B. E. Eichler, N. J. Hardman, P. P. Power, *Angew. Chem.* **2000**, *112*, 391–393; *Angew. Chem. Int. Ed.* **2000**, *39*, 383–385.
[26] B. E. Eichler, P. P. Power, *Angew. Chem.* **2001**, *113*, 818–819; *Angew. Chem. Int. Ed.* **2001**, *40*, 796–797.

 © 2005 Wiley-VCH Verlag GmbH & Co. KGaA, Weinheim

[27] S. Bobev, S. C. Sevov, *Angew. Chem.* **2000**, *112*, 4109 – 4110; *Angew. Chem. Int. Ed.* **2000**, *39*, 4108 – 4110.
[28] D. M. P. Mingos, *Acc. Chem. Res.* **1984**, *17*, 311 – 319.
[29] Program for extended Hückel molecular orbitals and oscillator strength calculations: G. Calzaferri, R. Rytz, M. Brändle, D. Brühwiler, S. Glaus, *ICON-EDiT*, Bern, Switzerland, **1998**; Tl basis set: $H_{ss} = -11.60$ eV, $H_{pp} = -5.80$ eV with the respective orbitals exponents $\xi = 2.14$, 2.04.[35] Relativistic effects[5] are not considered.
[30] G. Brauer, *Handbuch der Präparativen Anorganischen Chemie, Vol. 2*, Ferdinand Enke, Stuttgart, **1978**, pp. 938 – 942.
[31] G. Brauer, *Handbuch der Präparativen Anorganischen Chemie, Vol. 2*, Ferdinand Enke, Stuttgart, **1978**, pp. 953 – 954.
[32] L. J. van der Pauw, *Philips Res. Rep.* **1958**, *13*, 1 – 9; "Electrical Conduction in Solid Materials" J. P. Suchet, in *International Series of Monographs in the Science of the Solid State* (Ed.: B. R. Pamplin), Pergamon, Oxford, **1975**.
[33] G. M. Sheldrick, Bruker AXS, Inc. Madison, USA, SADABS version 2.0, program for absorption correction, **2001**.
[34] G. M. Sheldrick, Bruker AXS, Inc. Madison, USA, SHELXTL version 6.12, program package for crystal structure solution and refinement, **2000**.
[35] E. Clementi, C. L. Raimondi, W. P. Reinhardt, *J. Chem. Phys.* **1967**, *47*, 1300 – 1307.

 © 2005 Wiley-VCH Verlag GmbH & Co. KGaA, Weinheim

Cover Picture

Youichi Inada, Yoshiaki Nishibayashi,* and Sakae Uemura

Diruthenium complexes with optically active thiolate-bridged ligands promote the catalytic propargylic substitution of propargylic alcohols with acetone as the nucleophile. The use of novel chiral ligands bearing a phenyl ring that can engage in a π–π interaction with a phenyl ring of the ruthenium–allenylidene moiety lead to high enantioselectivities in these processes. For more details, see the Communication by Y. Nishibayashi and co-workers on page 7715 ff.

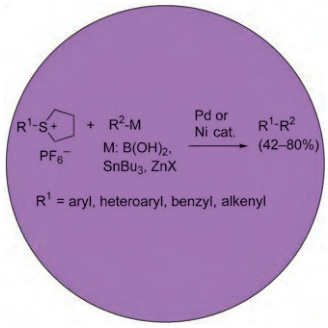

Organosulfur Reagents
In their Minireview on page 7674 ff., P. Vogel and S. R. Dubbaka describe how recent developments in the area of ligands and additives allow the cross-coupling of a large variety of reactants, including inexpensive and readily available sulfonyl chlorides.

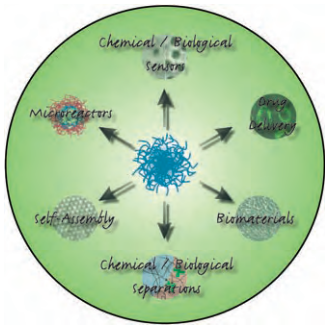

Soft Nanotechnology
Hydrogel nanoparticles are promising materials for nanotechnological and biotechnological applications. In their Review on page 7686 ff., L. A. Lyon and S. Nayak describe the advances made with these swellable materials.

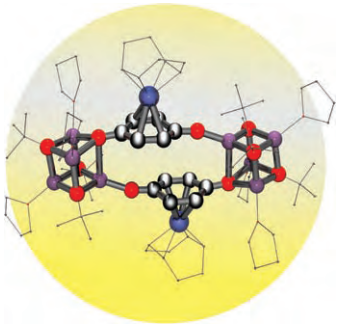

Lithium Alkoxide Cubanes
A dimeric, doubly bridged complex in which Li_4O_4 cubane units are connected by a transition-metal complex is presented by D. A. Sweigart and co-workers in their Communication on page 7710 ff.

Contents

VIP *The following Communications have been judged by at least two referees to be "very important papers" and will be published online at www.angewandte.org soon:*

*C. Drago, L. Caggiano, R. F. W. Jackson**
Vanadium-Catalyzed Sulfur Oxidation/Kinetic Resolution in the Synthesis of Enantiomerically Pure Alkyl Aryl Sulfoxides

X. Rocquefelte, S. E. Boulfelfel, M. B. Yahia, J. Bauer, J.-Y. Saillard,* J.-F. Halet**
The Structural Preferences of Boron and Carbon within MB_2C_2 (M = Mg,Sc,Ca,Y,Ln) Phases: The "Coloring Problem" Revisited by DFT Calculations

G. C. Lloyd-Jones, R. G. Margue, J. G. de Vries*
Rate Enhancement by Ethylene in the Ru-Catalyzed Ring-Closing Metathesis of Enynes: Evidence for an "Ene-then-Yne" Pathway That Diverts through a Second Catalytic Cycle

S. Klaus, H. Neumann, A. Zapf, D. Strübing, S. Hübner, J. Almena, T. Riermeier, P. Groß, M. Sarich, W.-R. Krahnert, K. Rossen, M. Beller**
A General and Efficient Method for the Formylation of Aryl and Heteroaryl Bromides

N. Martín, Á. Martín-Domenech, S. Filippone, M. Altable, L. Echegoyen,* C. M. Cardona*
Retrocycloaddition Reactions of Pyrrolidinofullerenes

Obituary

Leopold Horner (1911–2005): Nestor of Preparative Organic Chemistry — *H. Kunz* — **7664**

Meeting Reviews

All the Rave in Microwaves — *C. O. Kappe, M. Larhed* — **7666**

Highlights

Natural Product Synthesis

C. Escolano* — **7670 – 7673**

Stephacidin B, The Avrainvillamide Dimer: A Formidable Synthetic Challenge

Rising to the challenge: Stephacidin B is an antitumor antibiotic isolated from the fungi *Aspergillus ochraceus* (see picture). Recently, two elegant approaches to the enantioselective synthesis of this dimeric *N*-hydroxyindole alkaloid were reported that pave the way to a series of medicinally attractive stephacidin analogues.

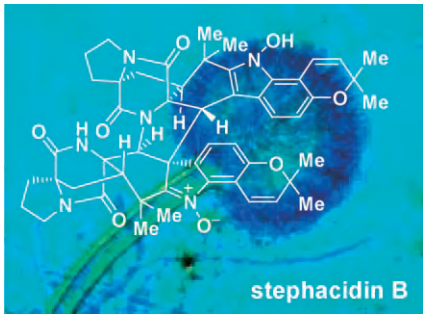

Minireviews

Organosulfur Reagents

S. R. Dubbaka, P. Vogel* — **7674 – 7684**

Organosulfur Compounds: Electrophilic Reagents in Transition-Metal-Catalyzed Carbon–Carbon Bond-Forming Reactions

Inexpensive and easily prepared organosulfur compounds, such as sulfonyl chlorides, thiol esters, thioethers, sulfonium ions, sulfoxides, sulfoximines, sulfones, sulfonates and sulfonamides, are good electrophilic partners in C–C cross-coupling reactions and arylations catalyzed by transition metals (see scheme).

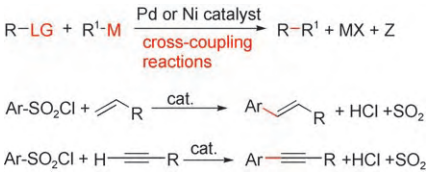

InterScience
© 2005 Wiley-VCH Verlag GmbH & Co. KGaA, Weinheim

Reviews

A swell idea: Research on hydrogel nanoparticles confirms the huge application potential of soft nanomaterials. Such nanoparticles can be made to swell and contract in response to changes in their environment. They could find uses as bioresponsive sensors, drug-delivery systems, implantable biomaterials, biotesting, and targetable chemotherapy agents. The picture shows HeLa cells containing core–shell nanoparticles as fluorescent markers.

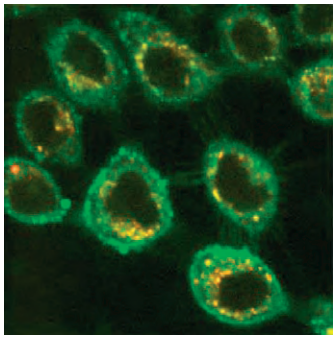

Nanotechnology

S. Nayak, L. A. Lyon* ——— **7686 – 7708**

Soft Nanotechnology with Soft Nanoparticles

Communications

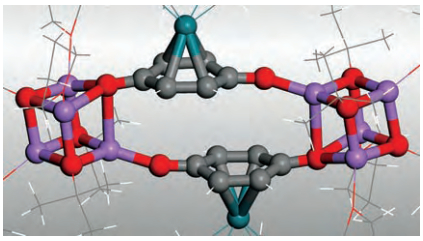

Joining the cubes: The linking of lithium $\{Li_4O_4\}$ cubanes by the bifunctional organometalloligand $[(\eta^4\text{-quinone})Rh(cod)]^-$ (cod = cyclooctadiene) results in an unprecedented doubly bridged motif. The dimeric assembly features cubane units that are connected by a transition-metal complex and that incorporate a quinone oxygen atom at one of the corners.

Cubanes

S. U. Son, J. A. Reingold, S. B. Kim, G. B. Carpenter, D. A. Sweigart* ——— **7710 – 7715**

Lithium Alkoxide $\{Li_4O_4\}$ Cubanes Bridged by Rhodium–Quinonoid Organometalloligands

Enantioselective propargylic substitution reactions of propargylic alcohols with acetone catalyzed by a diruthenium complex gives the propargylic alkylated products in good yields with up to 82% *ee*. A π–π interaction of phenyl rings between the ligand and allenylidene moieties is considered to play a crucial role in achieving such a high selectivity (see scheme; Cp*=pentamethylcyclopentadiene).

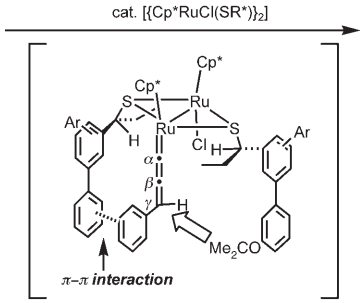

Synthetic Methods

Y. Inada, Y. Nishibayashi,* S. Uemura ——— **7715 – 7717**

Ruthenium-Catalyzed Asymmetric Propargylic Substitution Reactions of Propargylic Alcohols with Acetone

For the USA and Canada:
ANGEWANDTE CHEMIE International Edition (ISSN 1433-7851) is published weekly by Wiley-VCH PO Box 191161, D 69451 Weinheim, Germany. Air freight and mailing in the USA by Publications Expediting Inc. 200 Meacham Ave., Elmont, NY 11003. Periodicals postage paid at Jamaica NY 11431. US POSTMASTER: send address changes to *Angewandte Chemie*, Wiley-VCH, 111 River Street, Hoboken, NJ 07030. Annual subscription price for institutions: US$ 5685/5168 (valid for print and electronic / print or electronic delivery); for individuals who are personal members of a national chemical society prices are available on request. Postage and handling charges included. All prices are subject to local VAT/sales tax.

© 2005 Wiley-VCH Verlag GmbH & Co. KGaA, Weinheim

The best in chemistry –

for more than a hundred years

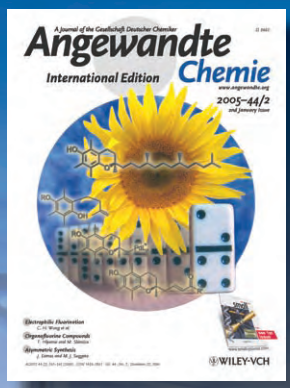

A Journal of the Gesellschaft Deutscher Chemiker

Angewandte
International Edition **Chemie**

www.angewandte.org

1888: ***The beginning of a success story***

Constant Innovations

1962: *First issue of the International Edition*
1976: *Graphical abstracts*
1979: *Cover pictures*
1988: *Centenary of Angewandte*
1989: *Routine use of color*
1991: *New section: Highlights*
1992: *Computerized editorial tracking system*
1995: *Internet service for readers*
1998: *Regular press service; full-text online*
2000: *New section: Essays; EarlyView: Communications available online ahead of the printed version*
2001: *New section: Minireviews*
2002: *Online submission of manuscripts*
2003: *Weekly publication; new section: News; new layout*
2004: *Backfiles (1962-1997); ManuscriptXpress: Online system for authors and referees*

Angewandte's advisors...

Martin Jansen
Max-Planck-Institut für Festkörperforschung, Stuttgart

»Professional presentation of the latest research in all fields of chemistry is the distinguishing characteristic that makes ***Angewandte Chemie*** *indispensable. This journal leads students to the cutting edge of chemical knowledge.«*

Angewandte Chemie International Edition *is a journal of the German Chemical Society (GDCh)*

GDCh

WILEY InterScience® DISCOVER SOMETHING GREAT

WILEY-VCH

1894504_gu

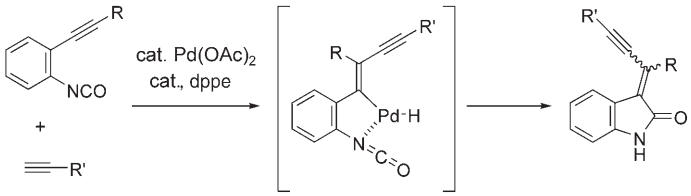

Ringing the changes for organopalladium catalysts. A new nucleophilic reactivity of organopalladium species has been revealed. The reaction between aryl isocyanates and terminal alkynes in the presence of a palladium catalyst produces oxindoles through the intramolecular vinylpalladation of isocyanates (see scheme; dppe = 1,2-bis(diphenylphosphanyl)ethane).

Palladium Catalysis

S. Kamijo,* Y. Sasaki, C. Kanazawa, T. Schüßeler, Y. Yamamoto* . **7718 – 7721**

Oxindole Synthesis through Intramolecular Nucleophilic Addition of Vinylpalladiums to Aryl Isocyanates

---

An uncommon interaction characterizes the Ni^{I}–Ni^{I} zwitterionic complex presented here. The μ-Ph moiety of the tetraphenylborate ligand coordinates synfacially to the two Ni centers (see picture) and provides two pairs of electrons through an η^2(C2,C3):η^2(C5,C6) interaction that is strengthened as a result of the electrostatic attractions between the anion and the formally cationic Ni_2 fragment.

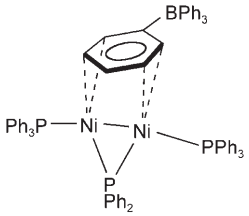

Cationic Ni_2 Fragment

Y. Chen, C. Sui-Seng, D. Zargarian* **7721 – 7725**

Tetraphenylborate as a Novel Bridging Ligand in a Zwitterionic Nickel(I) Dimer

---

When S is SO much better: Conjugate vaccines that contain S-glycosides induce carbohydrate-specific antibodies that cross react with the corresponding O-glycosides and vice versa. Four distinct systems have been examined, in each of which the antigen-specific response to S-glycosides is either comparable or superior to the response to O-glycosides.

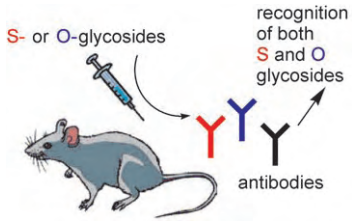

Immunochemistry

D. R. Bundle,* J. R. Rich, S. Jacques, H. N. Yu, M. Nitz, C.-C. Ling **7725 – 7729**

Thiooligosaccharide Conjugate Vaccines Evoke Antibodies Specific for Native Antigens

---

An analogue with P: Reaction of the "dithallene" $(TlAr^{Dipp_2})_2$ (**1**; $Ar^{Dipp_2} = C_6H_3$-2,6-(C_6H_2-2,6-*i*Pr_2)$_2$) with P_4 afforded $Tl_2[P_4(Ar^{Dipp_2})_2]$ (**2**), a thallium complexed diaryltetraphosphabutadienediide. The negative charge in the anion of **2** is delocalized over the P_4 array to afford an average P–P bond order of approximately 1.33.

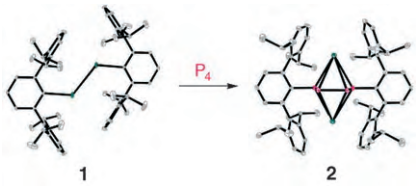

1,3-Butadiene Analogues

A. R. Fox, R. J. Wright, E. Rivard, P. P. Power* **7729 – 7733**

$Tl_2[Aryl_2P_4]$: A Thallium Complexed Diaryltetraphosphabutadienediide and its Two-Electron Oxidation to a Diaryltetraphosphabicyclobutane, $Aryl_2P_4$

© 2005 Wiley-VCH Verlag GmbH & Co. KGaA, Weinheim

Contents

Site-Ordered Solids

P. M. Mallinson, M. M. B. Allix, J. B. Claridge, R. M. Ibberson, D. M. Iddles, T. Price, M. J. Rosseinsky* _____ **7733 – 7736**

$Ba_8CoNb_6O_{24}$: A d^0 Dielectric Oxide Host Containing Ordered d^7 Cation Layers 1.88 nm Apart

Following orders: The cobalt and niobium ions in $Ba_8CoNb_6O_{24}$ are completely ordered in the seven-layer repeat of hexagonal and cubic stacking. Such site-ordered solids may find application as microwave dielectric resonators, for example, in mobile telecommunications. In the structure shown, $\{CoO_6\}$ and $\{NbO_6\}$ units are red and blue octahedra, respectively, and barium cations are black spheres.

High-Pressure Crystallography

N. Casati,* P. Macchi, A. Sironi* _____ **7736 – 7739**

Staggered to Eclipsed Conformational Rearrangement of $[Co_2(CO)_6(PPh_3)_2]$ in the Solid State: An X-ray Diffraction Study at High Pressure and Low Temperature

Under pressure: characterization of the high-pressure phase of crystalline $[Co_2(CO)_6(PPh_3)_2]$ has provided the first structural evidence for the transformation from a staggered to eclipsed arrangement of the equatorial carbonyl ligands in a dimeric transition-metal complex (see picture). A comparison with the same phenomenon observed at low temperature (though arrested in the very early stages) is presented.

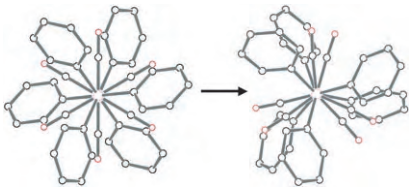

Rearrangement Reactions

D. Armesto,* M. J. Ortiz,* A. R. Agarrabeitia, N. El-Boulifi _____ **7739 – 7741**

The Effects of Triplet Sensitizers' Energies on the Photoreactivity of β,γ-Unsaturated Methyl Ketones

Triplet determines reactivity: β,γ-Unsaturated ketones **1** do not undergo the oxa-di-π-methane (ODPM) rearrangement in the presence of acetophenone or 3-methoxyacetophenone as a triplet sensitizer. However, they afford the ODPM products **2** when using triplet sensitizers with triplet energies slightly higher than those of the alkene triplets. When the triplet energies of the sensitizers are slightly lower than those of the alkene groups in **1**, ODPM rearrangement occurs along with 1,3-acyl migration to form enones **3** (see scheme).

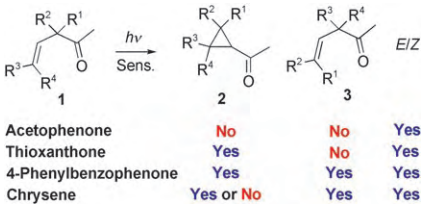

Molecular Wheels

Z.-H. Ni, H.-Z. Kou,* L.-F. Zhang, C. Ge, A.-L. Cui, R.-J. Wang, Y. Li, O. Sato* _____ **7742 – 7745**

$[Mn^{III}(salen)]_6[Fe^{III}(bpmb)(CN)_2]_6 \cdot 7H_2O$: A Cyanide-Bridged Nanosized Molecular Wheel

Heterometallic wheel: A cyanide-bridged heterometallic dodecanuclear complex featuring a nanosized molecular wheel has been synthesized based on magnetically anisotropic $[Mn(salen)]^+$ and $[Fe(bpmb)(CN)_2]^-$ building blocks. Magnetic studies reveal that the complex exhibits overall ferromagnetic intramolecular coupling (see picture) and frequency-dependent ac magnetic susceptibility. H_2bpmb = 1,2-bis(pyridine-2-carboxamido)-4-methylbenzene.

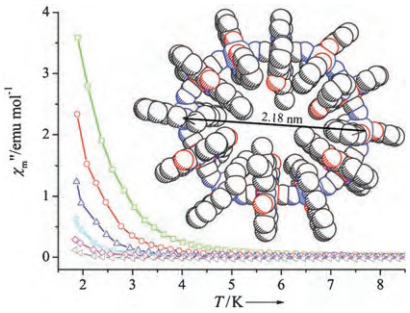

© 2005 Wiley-VCH Verlag GmbH & Co. KGaA, Weinheim

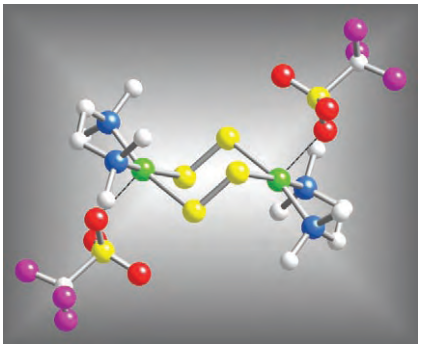

Cores for thought: Structural and spectroscopic studies show that the $\{Cu_2(S_2)_2\}^{2+}$ core of $[Cu_2(tmeda)_2(\mu\text{-}S_2)_2](OTf)_2$ (tmeda = *N*,*N*,*N*′,*N*′-tetramethylethylenediamine; OTf = trifluoromethanesulfonate) is best described as a bis(μ-disulfido(•1−))dicopper(II) complex rather than a bis(μ-disulfido(2−))-dicopper(III) complex. This complex represents a new motif in the copper–sulfur chemistry of biologically relevant, synthetic model systems.

Bioinorganic Chemistry

J. T. York, E. C. Brown, W. B. Tolman* ——— **7745 – 7748**

Characterization of a Complex Comprising a $\{Cu_2(S_2)_2\}^{2+}$ Core: Bis(μ-S_2^{2-})dicopper(III) or Bis(μ-$S_2^{\bullet-}$)dicopper(II)?

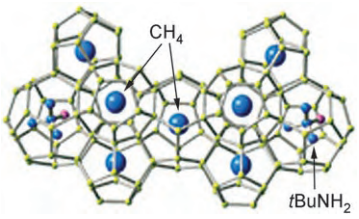

An unconventional hydrate promoter, tBuNH$_2$, forms a double hydrate upon reacting with CH_4 (see picture). This double hydrate shows different storage capacities for CH_4 depending on the concentration of tBuNH$_2$. Based on this phenomenon, a tuning concept for determining the optimum initial concentration of tBuNH$_2$ is proposed.

Gas Storage

D.-Y. Kim, J.-w. Lee, Y.-T. Seo, J. A. Ripmeester, H. Lee* — **7749 – 7752**

Structural Transition and Tuning of *tert*-Butylamine Hydrate

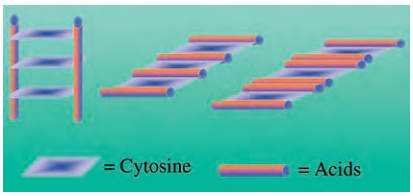

Covering the bases: Nucleobases and aromatic carboxylic acids possessing complementary functional groups have been used in the synthesis of molecular adducts with exotic architectures. The architectures obtained with cytosine as the nucleobase lead to the production of several different supramolecular structures (see picture).

Supramolecular Chemistry

S. R. Perumalla, E. Suresh, V. R. Pedireddi* ——— **7752 – 7757**

Nucleobases in Molecular Recognition: Molecular Adducts of Adenine and Cytosine with COOH Functional Groups

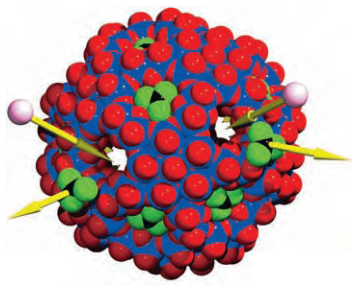

Popping corks: The protonated urea ions (C black, N/O green) that cork the pores of a polyoxomolybdate capsule (Mo blue, O red) can be reversibly removed allowing the entry of Ca^{2+} ions (pink) into the capsule. This process resembles the functioning of gated calcium channels in cell membranes.

Supramolecular Chemistry

A. Müller,* L. Toma, H. Bögge, C. Schäffer, A. Stammler ——— **7757 – 7761**

Porous Capsules Allow Pore Opening and Closing That Results in Cation Uptake

Stepping up: Density functional calculations indicate that small molecules, such as propylene oxide, chemisorb in an enantiospecific manner on intrinsically chiral, stepped Cu surfaces. As an example, the preferential adsorption configurations for the (*S*)- (right) and (*R*)-amino(fluoro)methoxy species (left) on Cu(874)^S are shown.

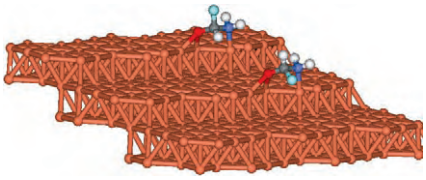

Surface Chirality

B. Bhatia, D. S. Sholl* — **7761 – 7764**

Enantiospecific Chemisorption of Small Molecules on Intrinsically Chiral Cu Surfaces

© 2005 Wiley-VCH Verlag GmbH & Co. KGaA, Weinheim

Contents

Catalyst Design

G. Klein, N. Humbert, J. Gradinaru, A. Ivanova, F. Gilardoni, U. E. Rusbandi, T. R. Ward* _____ **7764 – 7767**

Tailoring the Active Site of Chemzymes by Using a Chemogenetic-Optimization Procedure: Towards Substrate-Specific Artificial Hydrogenases Based on the Biotin–Avidin Technology

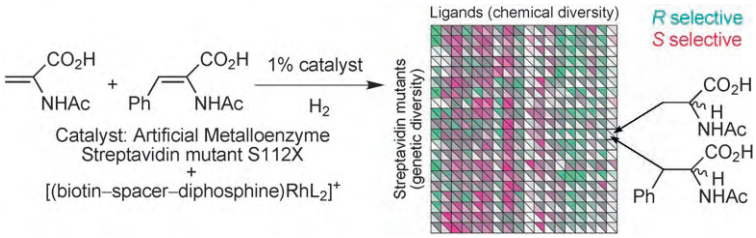

The combination of chemical- with genetic-optimization strategies (i.e. chemogenetic) allows the production of artificial hydrogenases based on the biotin–avidin technology. In the spirit of enzymes, second-coordination-sphere interactions between the host protein (streptavidin) and the substrate (an olefin) allow fine-tuning of the selectivity to produce either *R* or *S* hydrogenation products.

Directed Assembly

G. Zhang, D. Wang,* H. Möhwald _____ **7767 – 7770**

Decoration of Microspheres with Gold Nanodots—Giving Colloidal Spheres Valences

Giving directions: Microspheres are decorated with a defined number of Au nanodots by using O_2-plasma-etched colloidal crystals as masks for the deposition of Au vapor (see picture). The Au nanodots deposited on the spheres might be considered as nanoscale analogues of sp-hybridized atomic orbitals, which may be used to spatially direct the association of spheres to generate hierarchical "supraparticles".

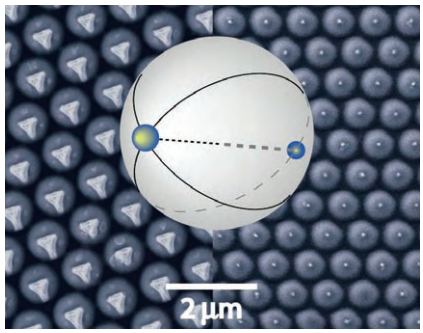

Nanotechnology

Q. Qing, F. Chen, P. Li, W. Tang, Z. Wu, Z. Liu* _____ **7771 – 7775**

Finely Tuning Metallic Nanogap Size with Electrodeposition by Utilizing High-Frequency Impedance in Feedback

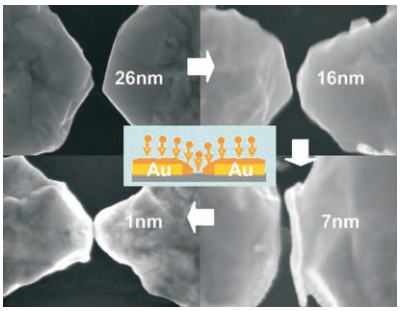

Positive feedback: Relatively large gaps can be reproducibly fabricated by utilizing the change in impedance arising from the high electric field between the electrodes in a feedback-controlled electrodeposition system. Furthermore, the gap size can be finely tuned down to around 1 nm by simply controlling subsequent deposition time (see SEM images).

Protein Structures

N. A. Lakomek, C. Farès, S. Becker, T. Carlomagno, J. Meiler,* C. Griesinger* _____ **7776 – 7778**

Side-Chain Orientation and Hydrogen-Bonding Imprint Supra-τ_c Motion on the Protein Backbone of Ubiquitin

Order parameters derived from residual dipolar couplings between NH groups reveal motion of protein backbones on a time scale slower than the correlation time τ_C. Less-mobile amides (blue and green) in ubiquitin, for example, are H-bonded and belong to residues with side chains pointing towards the hydrophobic core while more mobile ones (yellow, orange, and red) have solvent-exposed side chains and fewer H bonds.

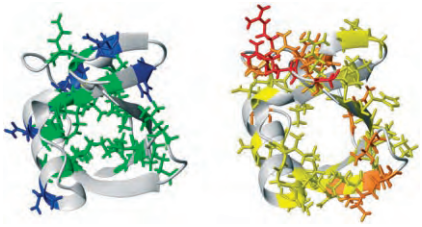

© 2005 Wiley-VCH Verlag GmbH & Co. KGaA, Weinheim

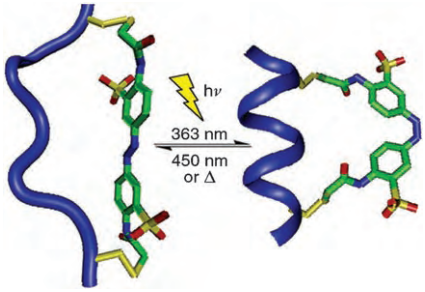

Lighting up: The conformation of the DNA-binding domain of the basic helix-loop-helix protein MyoD can be controlled through an azobenzene cross-linker in response to light flashes. The DNA binding specificity of alkylated MyoD can be modulated through the isomerization of the cross-linker to the *cis* conformer, which leads to significantly enhanced sequence selectivity.

DNA Binding

L. Guerrero, O. S. Smart, C. J. Weston, D. C. Burns, G. A. Woolley, R. K. Allemann* ——— **7778 – 7782**

Photochemical Regulation of DNA-Binding Specificity of MyoD

Close and yet fluorescent: Derivatives of Pigment Yellow 101 can exhibit small intermolecular distances in the solid-state crystal structures. Nevertheless, these compounds show strong solid-state fluorescence. X-ray structure determinations and elaborate quantum-chemical calculations indicate that the unexpected fluorescence is a property of the individual molecules which is retained in the crystal. (Excited state energies are plotted along a CNN bending mode.)

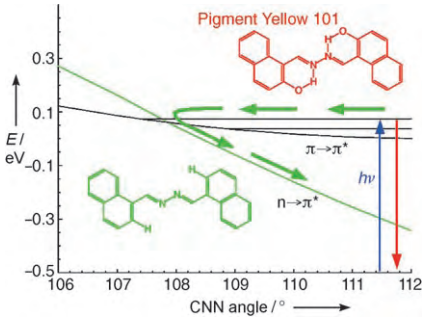

Solid-State Fluorescence

A. Dreuw,* J. Plötner, L. Lorenz, J. Wachtveitl, J. E. Djanhan, J. Brüning, T. Metz, M. Bolte, M. U. Schmidt* ——— **7783 – 7786**

Molecular Mechanism of the Solid-State Fluorescence Behavior of the Organic Pigment Yellow 101 and Its Derivatives

---

Ambidextrous ligands satisfy both Ag and Fe. The three-dimensional polymeric ions $[Ag_3Fe_2(ECN)_{12}]^{4-}$ (E = S, Se) form networks in which {Fe(1,3-μ-NCE)$_2$Ag} units are linked to form 80-membered $\{Fe_{10}Ag_{10}\}(ECNC)_{20}$ rings. The mixed-valent compound $(Pr_4N)_4[Ag_3Fe_2(SeCN)_{12}]$ is the first crystallographically characterized homoleptic selenocyanato complex of iron.

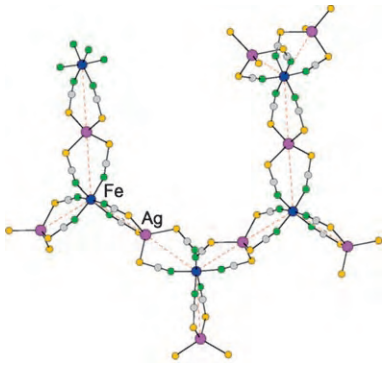

Mixed-Valent Compounds

S. Gerber, H. Gröger, J. Ensling, P. Gütlich, H. Krautscheid* ——— **7787 – 7790**

$(Pr_4N)_4[Ag_3Fe_2(ECN)_{12}]$—Anionic Network Structures with Mutual Interpenetration

---

Two $GaCl_3$ adducts of 4-bis(trimethylsilyl)amino-1,2,4,3,5-triazadiphosphole were formed in simple high-yielding reactions. The adducts were fully characterized (see structure of the monoadduct) and shown to be stable at ambient temperature. The structure, bonding, and NMR spectra of the triazadiphosphole adducts are discussed on the basis of MO, NBO, and DFT calculations.

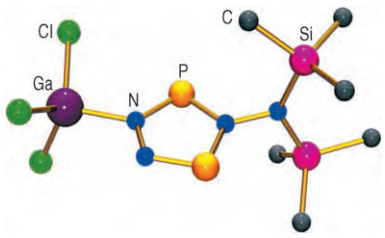

P,N Heterocycles

S. Herler, P. Mayer, J. Schmedt auf der Günne, A. Schulz,* A. Villinger, J. J. Weigand ——— **7790 – 7793**

A Triazadiphosphole

© 2005 Wiley-VCH Verlag GmbH & Co. KGaA, Weinheim

Contents

Cyclizations

A. Zulys, M. Dochnahl, D. Hollmann, K. Löhnwitz, J.-S. Herrmann, P. W. Roesky,* S. Blechert* **7794 – 7798**

Intramolecular Hydroamination of Functionalized Alkenes and Alkynes with a Homogenous Zinc Catalyst

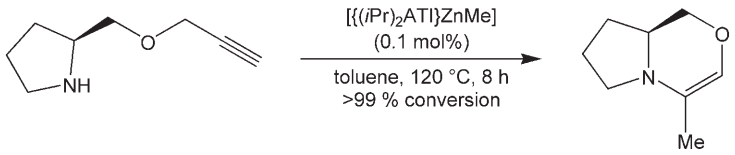

Simple and versatile: A new zinc complex catalyzes the intramolecular hydroamination of nonactivated alkynes and alkenes (see example in scheme; {(*i*Pr)$_2$ATI} = *N*-isopropyl-2-(isopropylamino)troponiminato). The catalyst is relatively robust, exhibits excellent activities, and tolerates various functional groups such as ethers, thioethers, and amides.

Coordination Modes

W. W. Seidel,* M. Schaffrath, T. Pape **7798 – 7800**

Can Acetylenedithiolate Act as a Tetradentate Bridging Ligand?

Tetradentate and ambidentate: Because the four-atom acetylenedithiolate has donor electron density on all sides of the dianion, it can link and electronically couple different metal ions. The bend-back angles of the sulfur atoms in the η^2-*C*,*C*′-acetylenedithiolate complex $[Tp'W(CO)_2(\eta^2\text{-}C_2S_2)]^-$ are sufficiently flexible to allow for a chelation of both sulfur donors to the $\{(\eta^5\text{-}C_5H_5)Ru(PPh_3)\}$ fragment (see structure).

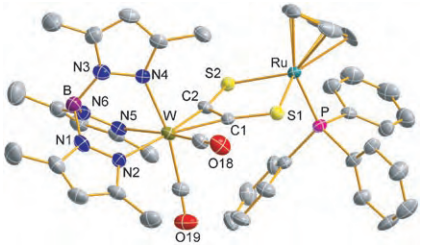

Isomerizations

M. Kreich, P. Claus* **7800 – 7804**

Direct Conversion of Linoleic Acid over Silver Catalysts in the Presence of H_2: An Unusual Way towards Conjugated Linoleic Acids

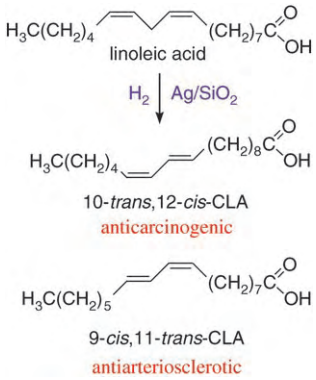

A silver lining: The isomerization of conjugated double bonds over silver catalysts in the presence of hydrogen are unusual and hitherto unknown. Silver catalysts control the selectivity of the extremely difficult isomerization of linoleic acid towards the physiologically important 9-*cis*,11-*trans*- and 10-*trans*,12-*cis*-unsaturated isomers, which are anticarcinogenic and antiarteriosclerotic agents (see scheme, CLA = conjugated linoleic acids).

WILEY InterScience® DISCOVER SOMETHING GREAT

"**Hot Papers**" are chosen by the Editors for their importance in a rapidly evolving field of high current interest. A preview with the graphical abstracts of these articles can be found on the *Angewandte Chemie* homepage in Wiley InterScience at www.angewandte.org.

All articles in *Angewandte Chemie* are published online several weeks ahead of print. They are found under the "**EarlyView**" link on the journal's homepage in Wiley InterScience.

Service

Keywords **7806**

Authors **7807**

Vacancies **A71**

Preview **7809**

© 2005 Wiley-VCH Verlag GmbH & Co. KGaA, Weinheim

Corrigendum

On page 6171 of this Communication, the sentence that begins on line 12 of the last paragraph should read "Reductive ring opening was achieved with borane–trimethylamine complex in the presence of triflic acid to give ...". On page 6172 in footnote (d) to Scheme 4, "TFA" should be changed to "triflic acid".

Highly Diastereoselective Alkylation of Aziridine-2-carboxylate Esters: Enantioselective Synthesis of LFA-1 Antagonist BIRT-377

A. P. Patwardhan, V. R. Pulgam, Y. Zhang, W. D. Wulff* _____ **6169–6172**

Angew. Chem. Int. Ed. **2005**, *44*

DOI 10.1002/anie.200500923

WILEY-VCH is an international science publisher and part of the John Wiley & Sons Publishing Group.

STM Chemistry has a position available for an

Assistant Editor (f/m)

Applicants should be self-motivated, innovative and have the desire to contribute to the development of ***Small*** – an exciting new micro- and nanoscience journal. You will be involved in all aspects of the editorial procedures, such as the reviewing process, the development of journal content, editing and proof reading manuscripts, coordination of freelance work, and contact with authors from all over the world.

Excellent organizational and communication skills, diplomacy, and flexibility are needed. A broad education in biology, medicine, chemistry, materials science or physics with an emphasis on nanoscience or technology is essential. You should be fluent in English (native speaker preferred) and be familiar with text and graphics PC programs.

The editorial office is based at WILEY-VCH in Weinheim, a pleasant small town near Heidelberg in southwest Germany.

Applicants should send their full CV with a covering letter describing their suitability for the post to:

Wiley-VCH Verlag GmbH & Co. KGaA
Human Resources
Christiane Rabe
Boschstraße 12
D-69469 Weinheim
Tel.: +49 (0) 6201-606 182
E-mail: CRabe@wiley-vch.de

WILEY-VCH

The place to be

http://www.wiley-vch.de

 © 2005 Wiley-VCH Verlag GmbH & Co. KGaA, Weinheim

Leopold Horner (1911–2005): Nestor of Preparative Organic Chemistry

Leopold Horner, Professor Emeritus at the Institute of Organic Chemistry at the Johannes Gutenberg-Universität Mainz, passed away at his home in Mainz-Bretzenheim on October 5, 2005, at the age of 94. He was fully engaged with science until his unexpected death; just a week before, he had guided Polish guests through the institute and had enquired about the seminar and lecture program for the coming winter semester.

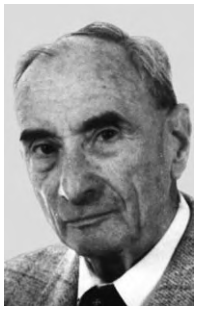

Leopold Horner was born on August 24, 1911, in Kehl am Rhein. He came into contact with chemistry at a young age as his parents ran a dyers. He endured much hardship during his childhood and adolescence: His father returned from the first world war in poor health and died in 1919. His mother, who had to raise the children and guide the company on her own through the difficult post-war years and the period of inflation, died five years later, leaving Leopold and his sister orphans. Fortunately, the children were taken in by an uncle and an aunt, who also took over the running of the dyers.

Through family solidarity and frugality, it was made possible for the young Leopold Horner, whose talent was recognized early, to attend the Oberrealschule and then to study chemistry in Heidelberg (1931). After the first Verbandsexam (known today as the Vordiplom), he moved to the Universität München where he passed the second Verbandsexam in 1935. The years of his postgraduate studies with Heinrich Wieland (Nobel Prize winner, 1927), who introduced him to the fascination of natural product chemistry, were particularly influential for Horner with regards to his research interests and his future career path as a young scientist. He obtained his doctorate in 1937 for work on vomicine—a relative of strychnine—and was appointed assistant lecturer by Heinrich Wieland. During his Habilitation, he was responsible for the preparation and execution of experiments in both organic and inorganic chemistry, which perhaps explains the remarkably wide scientific interests that were a feature of his career.

After his habilitation work on oxindoles in Munich in 1942, Horner moved to the Plastics Research Institute (Forschungsinstitut für Kunststoffe) in Frankfurt am Main. There he met his future wife, Gerda. The apartment of the young couple, and later the young family with their three children Christoph, Michael, and Irene, was frequently the venue for many friends and colleagues who were fighting for their survival during the extremely difficult time immediately before and after the end of the war. The provision of an open house and immediate aid for friends and those in need distinguished Horner and his family.

As a young assistant professor in Frankfurt, he was deeply involved in the reconstruction of the destroyed chemical institute of the university. His research concentrated on the mechanisms of polymerization induced by single-electron transfer from amines and later by two-electron transfer from phosphines. The results of this work lead to his calling to the Universität Mainz in 1953 as professor of organic chemistry. They were also the starting point of Leopold Horner's scientific work, which was characterized by a broad professional knowledge, bold interpretation, and an interdisciplinary approach.

In Mainz he carried out comprehensive studies on the chemistry of orthoquinones that included model reactions on melamine and pupurogallin formation.[1] The photochemistry of diazo compounds[2] and [2s + 2a] cycloadditions to β-lactams[3] were also investigated, as were electrochemical and catalytic hydrogen transfers of different types. Horner was also ahead of his time in the investigation of surface processes, in the process of corrosion and the reaction at silicate surfaces.[4] Organophosphorus chemistry was, however, central to his work. The principle of condensation and substitution reactions with tertiary phosphines and soft electrophiles, today known as the Appel, Mukaiyama, and Mitsunobu reactions, had already been described by Horner and his co-workers in 1959 with triphenylphosphine dihalides.[5]

The electrochemical cleavage of quaternary phosphonium salts[6] led to the unexpected discovery that tertiary phosphines with three different substituents are chiral.[7] This knowledge formed the basis of the pioneering work of Horner on enantioselective catalysis, and especially enantioselective homogeneous hydrogenation,[8] which was published independently in the same year as the work of W. S. Knowles—work that was honored by the Nobel Prize and which was also based on the chiral phosphines discovered by Horner.

Probably of even greater significance for the arsenal of preparative methods in chemistry is a previous masterly achievement of Horner: the development of PO-activated olefination.[9] In the second of his reports on this topic, Horner described the use of phosphonic acid esters as CH acidic olefination reagents as well as phosphine oxides, and was published two and three years, respectively, before Emmons et al. reported their initial experiments of this type in 1961. Without fear of contradiction, the Horner reaction can be regarded as an essential tool in the demanding field of preparative chemistry, and especially in the total synthesis of natural products and active compounds.

Horner was awarded many honors for his outstanding scientific work. He received an honorary doctorate from the Universität Karlsruhe and the Hanuš Medal of the Czech chemical society, he was also a member of the Deutsche Akademie der Naturforscher Leopoldina zu Halle and received its gold Cothenius medal. He was honored with the Liebig Commemorative Medal of the Gesellschaft Deutscher Chemiker (GDCh, German chemical society), and another particular honor for him was the conferment of Honorary Membership of the Gesellschaft Deutscher Chemiker at the 2005 Chemiedozententagung.

Horner selflessly served his university and the chemistry world in many different senior positions. He also remained especially close to his colleagues, students, and pupils and listened to their progress at congresses, seminars, and colloquia with youthful curiosity

InterScience
© 2005 Wiley-VCH Verlag GmbH & Co. KGaA, Weinheim

and alertness. His achievements remain his permanent memorial. In his courage, fighting spirit, and his warm-heartedness, Leopold Horner will always remain a model to us.

Horst Kunz
Universität Mainz
Fax: (+49) 6131-392-4786

[1] L. Horner, W. Dürckheimer, *Z. Naturforsch. B* **1959**, *14b*, 744.
[2] L. Horner, E. Spietschka, *Chem. Ber.* **1955**, *88*, 934.
[3] W. Kirmse, L. Horner, *Chem. Ber.* **1956**, *89*, 2759.
[4] L. Horner, H. Ziegler, *Liebigs Ann. Chem.* **1976**, 628.
[5] L. Horner, H. Oediger, H. Hoffmann, *Liebigs Ann. Chem.* **1959**, *626*, 26.
[6] L. Horner, A. Mentrup, *Liebigs Ann. Chem.* **1961**, *646*, 65.
[7] L. Horner, H. Winkler, A. Rapp, A. Mentrup, H. Hoffmann, P. Beck, *Tetrahedron Lett.* **1961**, *2*, 161.
[8] L. Horner, H. Siegel, H. Büthe, *Angew. Chem.* **1968**, *80*, 1034; *Angew. Chem. Int. Ed. Engl.* **1968**, *7*, 942.
[9] a) L. Horner, H. Hoffmann, H. G. Wippel, *Chem. Ber.* **1958**, *91*, 61; b) L. Horner, H. Hoffmann, H. G. Wippel, G. Klahre, **1959**, *92*, 2499.

DOI: 10.1002/anie.200503637

Novartis is pleased to announce the 2005 recipients of the

Novartis Young Investigator Award in Chemistry

Prof. Benjamin List
Max Planck Institute
Mülheim, Germany

for his outstanding contribution towards the development and application of new synthetic methodology in the area of organocatalysis

Prof. Dirk Trauner
University of California
Berkeley, USA

for his outstanding contribution towards the development of new synthetic methodology, natural product synthesis and bioorganic chemistry

The Novartis Young Investigator Award in Chemistry was created in 2002 to mark Novartis' commitment to science and innovation. The award is presented annually to outstanding scientists under the age of 40 who are active in the areas of organic or bioorganic chemistry in the broadest sense. Two winners are identified, one from Europe and one from North America, each of whom receives an unrestricted research grant.

Past winners:
Bernhard Breit, University of Freiburg (2002)
Thomas Carell, Philipps University, Marburg (2002)
Thorsten Bach, Technische Universität München (2003)
J Stephen Clark, University of Nottingham (2004)
Jonathan P Clayden, University of Manchester (2004)

NOVARTIS

© 2005 Wiley-VCH Verlag GmbH & Co. KGaA, Weinheim

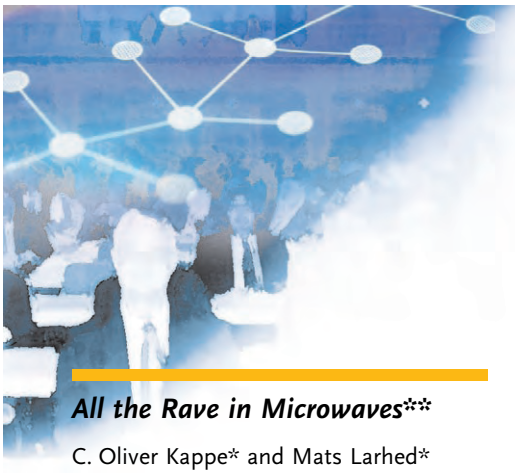

All the Rave in Microwaves**

C. Oliver Kappe* and Mats Larhed*

Over the past several years, there has been a significant growth in the area of "microwave chemistry", in particular applied to synthetic organic chemistry, drug discovery, and polymer chemistry.[1] This nonclassical heating technique has slowly moved from a laboratory curiosity to an established method that is heavily used in both academia and industry. Today, the availability of dedicated microwave reactors for chemical synthesis has removed many of the safety and reproducibility issues faced by the early pioneers in the field who employed domestic kitchen microwave ovens. Nevertheless, there is still a considerable debate on the existence of "special or nonthermal microwave effects" and a generally accepted rationalization of many of the observed effects in microwave chemistry remains elusive.

Given this background, the Gesellschaft Deutscher Chemiker (GDCh) decided to organize the first ever Symposium on Microwave-Accelerated Synthesis (M.A.S.-05) at the Heinrich-Heine University in Düsseldorf (Germany). The scientific committee, chaired by Helmut Ritter (University of Düsseldorf), put together a well-balanced interdisciplinary program that consisted of 11 invited lectures, 10 contributed oral presentations, and a poster session. During the one-and-a-half day meeting, a broad range of microwave applications in chemistry were discussed, including organic and medicinal chemistry, solid-phase peptide synthesis, oligonucleotide synthesis, polymer chemistry, microwave-assisted extractions, and the use of microwave heating in material sciences. The meeting was attended by 130 scientists, roughly two thirds of whom came from industry with the remaining one-third from academia.

The opening lecture of the symposium was given by Michael J. Collins (CEM Corporation, Matthews, USA). From the standpoint of an instrument manufacturer, Collins shared with the audience new developments and innovations in the field of microwave chemistry. The lecture focused on the controversial topic of the so-called "simultaneous cooling" technique, whereby microwave synthesis is carried out under microwave irradiation with simultaneous cooling of the reaction vessel by either compressed air or with the aid of a cooling fluid. Citing recently published work by Arvela and Leadbeater,[2] Collins presented examples of aqueous Suzuki coupling reactions of aryl chlorides using palladium-on-charcoal as the catalyst, where yields were significantly increased from 40% to 75% using the simultaneous cooling technique (Scheme 1). Another part of the lecture dealt with the important aspect of scaling up microwave chemistry. According to Collins, the preparation of kilogram quantities of products per day is technically feasible nowadays by using batch or stop-flow microwave reactors, whereas larger continuous-flow instruments for the production-scale level may be available within five years.

Following a short presentation on the use of microwave heating for the synthesis of modified oligonucleotides on controlled pore glass (cpg) surfaces by Clemens Richert (University of Karlsruhe, Germany), Hans-Georg Frank (AplaGen GmbH, Baesweiler, Germany) detailed the experiences of his laboratory in the field of microwave-assisted solid-phase peptide synthesis. While many traditional peptide chemists would be afraid of "cooking peptides" in a microwave oven through fear of side reactions, the group at AplaGen has achieved spectacular success in employing microwave heating in peptide chemistry. According to Frank, the synthesis of an otherwise problematic model peptide that mimicks the action of erythropoietin (H_2N-GGTYSCHFFGPLTWVCKPQGG-COOH) can be achieved within one day by using microwave irradiation for both the coupling and deprotection steps, as opposed to 10 days with the conventional protocol. More importantly, the peptide was obtained in significantly higher yield and purity without any racemization by using carefully controlled microwave conditions that involved intermittent cycles of short pulses of microwave irradiations and ice-bath cooling of the reaction mixture.

In the following presentation, Ulrich S. Schubert (Eindhoven University of Technology and the Dutch Polymer Institute, The Netherlands) discussed the advantages, automation issues, and scale-up possibilities of microwave irradiation for a variety of polymerization reactions, in particular for living/controlled polymerization techniques. In many instances, such polymerization reactions can be carried out much more efficiently under con-

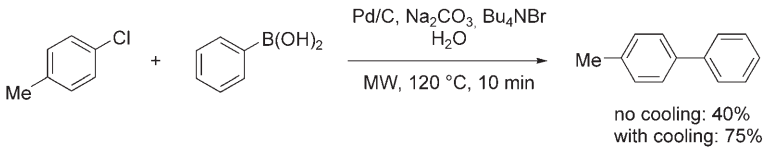

Scheme 1. The effect of the simultaneous cooling technique on a Suzuki reaction (internal temperature measurement with fiber-optic probe). MW = microwave.[2]

[*] Prof. Dr. C. O. Kappe
Institute of Chemistry, Organic and Bioorganic Chemistry
Karl-Franzens Universität Graz
Heinrichstrasse 28, 8010 Graz (Austria)
E-mail: oliver.kappe@uni-graz.at
Dr. M. Larhed
Department of Medicinal Chemistry
Organic Pharmaceutical Chemistry
BMC, Uppsala University
Box 574, SE-751 23, Uppsala (Sweden)
E-mail: mats@orgfarm.uu.se

[**] Symposium on Microwave-Accelerated Synthesis (M.A.S.-05), organized by the Gesellschaft Deutscher Chemiker (GDCh), Düsseldorf, September 14–16, 2005.

InterScience
© 2005 Wiley-VCH Verlag GmbH & Co. KGaA, Weinheim

trolled microwave heating in sealed vessels than by using conventional reflux conditions.[1b] However, the involvement of special "microwave effects" in many of these reactions is unclear. For the atom-transfer radical polymerization (ATRP) of methyl methacrylate, for example, it was demonstrated by carefully conducted kinetic studies that the obtained results were exactly the same as those obtained using oil-bath chemistry at the same reaction temperature.[3]

The contribution by Mats Larhed (Uppsala University, Sweden) described some high-speed microwave approaches for the synthesis and rapid optimization of novel hepatitis C virus NS3 and HIV-1 protease inhibitors, making extensive use of transition-metal-catalyzed carbon–carbon and carbon–heteroatom bond-forming reactions.[4]

After the lunch break, C. Oliver Kappe (University of Graz, Austria) highlighted several applications of controlled microwave heating in the area of heterocyclic chemistry. Examples included the automated synthesis and scaffold decoration of a library of dihydropyrimidones, involving multicomponent and transition-metal-catalyzed chemistries. In his lecture, Kappe emphasized the potential of high-speed microwave synthesis for the rapid testing of new ideas and for reaction optimization. In addition, he argued that microwave chemistry should not only be used as a last resort when all other options have failed (as is still the case in many laboratories) but rather as a first choice for all transformations that require heating. This is well demonstrated for the synthesis of a 4-arylquinolin-2-one derivative in which all six steps of the synthesis were successfully carried out using high-speed microwave conditions (Scheme 2).[5]

In his lecture, Joachim C. Burbiel (University of Bonn, Germany) presented several examples of microwave-assisted ring-closure and nucleophilic substitution reactions facilitating the preparation of adenosine receptor ligands of the xanthine type. In all cases, the reported ring-closure reactions were significantly faster when performed under sealed vessel microwave irradiation conditions at higher temperatures compared to the corresponding oil-bath experiments carried out at reflux temperatures. The yields, however, remained essentially unchanged.

The remainder of the afternoon session featured a series of talks on the use of microwaves in organic synthesis (Thomas J. J. Müller, University of Heidelberg, Germany; Bert U. W. Maes, University of Antwerp, Belgium), polymer chemistry (Kolio Troev, Bulgarian Academy of Sciences, Sofia, Bulgaria; Lionel L. Delaude, University of Liège, Belgium; Frank Wiesbrock, Eindhoven University of Technology and the Dutch Polymer Institute, Eindhoven, The Netherlands), as well as a presentation by Sandra Uy (University of Auckland, New Zealand) on microwave-assisted seaweed extractions.

The day ended with a poster session (32 presentations) followed by the conference dinner, which featured an Irish folk band, and allowed informal discussions among the conference participants.

Andreas Greiner (Philipps-University of Marburg, Germany) opened the Friday morning session with a short account of microwave-heated polymerization reactions.[1b] He then described systematic investigations of styrene and methyl acrylate radical (co)polymerizations under microwave irradiation and with classic heating. It was found that the choice of solvent and radical initiator is essential for microwave-assisted free radical polymerization. Despite the impressive scope of the study, no evidence for monomer selectivity or a clear correlation between microwave power and molecular weight was found.

Another highlight of the symposium was the lecture by Rainer Schobert (University of Bayreuth, Germany) with the title "Solid-Phase and Domino

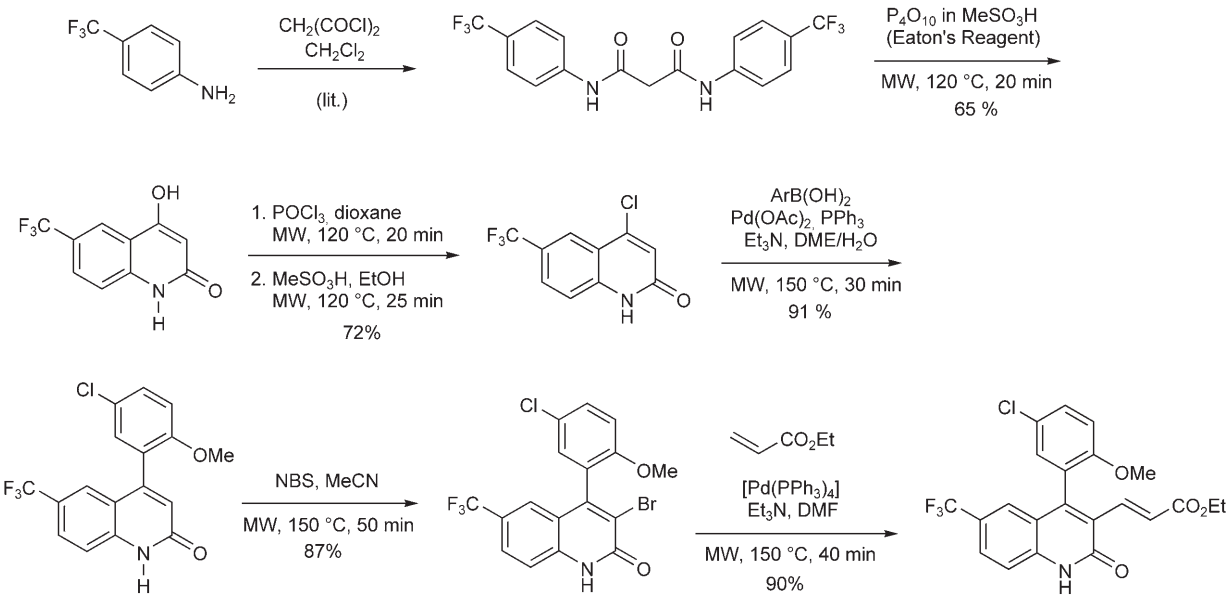

Scheme 2. Six-step "all microwave" synthesis of a 4-aryl-2-quinolinone maxi K^+ channel opener.[5] DME = 1,2-dimethoxyethane; NBS = *N*-bromosuccinimide; DMF = *N*,*N*-dimethylformamide.

 © 2005 Wiley-VCH Verlag GmbH & Co. KGaA, Weinheim

Synthesis in the Microwave—Bioactive Heterocycles in No Time". Schobert demonstrated that through careful choice of reaction parameters, a large number of 5–7 membered O and N heterocycles can be selectively prepared under controlled microwave irradiation. Among different reaction types used in his synthesis of melophlin B, both addition-Wittig cyclizations and Fries rearrangements were successfully microwave-accelerated (Scheme 3).[6]

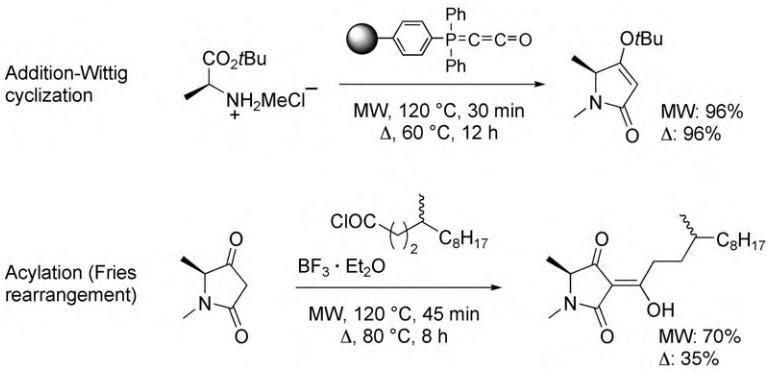

Scheme 3. Microwave-mediated improvements in the synthesis of the 3-acyltetramic acid melophlin B.[6]

Although a great variety of assembly methods and an impressive diversity of structures was established, it was also pointed out that premature linker cleavages and unwanted racemizations had been observed with high-temperature microwave heating.

Another important subject area of the symposium concerned microwave-induced inorganic materials. In a lecture by Dieter Wöhrle (University of Bremen, Germany), impressive results in microwave synthesis of structurally uniform and dye-loaded molecular sieves were presented. These novel composite materials may find use as optical switches, microlasers, and optical sensors, and in energy-transfer applications. By taking advantage of microwave heating, dye molecules were encapsulated undestroyed into molecular sieves after only 15–45 minutes of hydrothermal synthesis. Furthermore, dye-free molecular sieves were quickly and smoothly prepared using microwave conditions.

Interest in the generation of alkoxyl radicals by microwave irradiation was the topic of a lecture by Jens Hartung (Technische Universität Kaiserslautern, Germany), who showed how *N*-(alkoxy)-thiazolethiones can act as useful precursors for oxygen-centered radicals in synthetic chemistry. Hartung's work furnished two decisive results: a) regardless of the initiation source in oxyl radical chemistry (microwaves, oil-bath heating, or UV irradiation), there was no difference in the product selectivity; b) microwave heating consistently provided the shortest reaction times and highest yields.

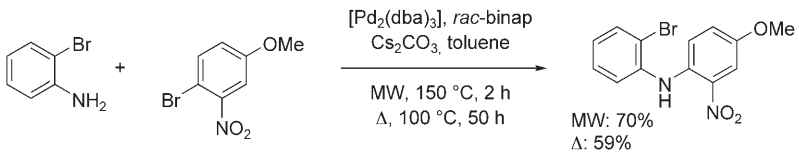

Scheme 4. Acceleration of a palladium-catalyzed intermolecular Buchwald–Hartwig *N*-arylation by single-mode microwave heating.[7] dba = dibenzylidineacetone.

In agreement with Schobert, Uwe Beifuss (University of Hohenheim, Stuttgart, Germany) stressed the beneficial use of microwave heating in heterocyclic chemistry. In the strategy employed for the synthesis of biologically active phenazines, inter- and intramolecular palladium-catalyzed *N*-arylation reactions were accelerated by microwave irradiation from days to hours (Scheme 4).[7] It was further found that a number of Brönsted and Lewis acid catalyzed cyclizations responded positively to microwave flash heating both with respect to yield and selectivity.

In addition to the invited speakers on Friday morning, Richard Hoogenboom (Eindhoven University of Technology and Dutch Polymer Institute, The Netherlands) gave an oral presentation on the scale-up of microwave-promoted polymerizations and Steven Tierney (Merck Chemical Ltd, Southampton, UK) presented novel methods for the synthesis of semiconducting polymers under high-density microwave irradiation. The final talk concerned the delicate problem of measuring reaction temperatures correctly under microwave heating. In his talk, Wilfried M. Braje (Abbott GmbH & Co. KG, Ludwigshafen, Germany) stressed that proper control experiments and measurement of reaction temperatures are of utmost importance not only for the outcome of reactions but also for the reproducibility of results.

The conference closed with the presentation of the best poster awards and the farewell comments by the chairman, Helmut Ritter. Most of the participants—if not already "riding the microwave"—will probably have gone away from this conference with a strong desire to try their next reaction under microwave conditions, although the controversial question on the existence of nonthermal microwave effects could not be resolved. As announced by the chairman, there will probably be another microwave conference organized by the GDCh in the future.[8]

[1] For recent reviews, see: a) C. O. Kappe, *Angew. Chem.* **2004**, *116*, 6408–6443; *Angew. Chem. Int. Ed.* **2004**, *43*, 6250–6285; b) F. Wiesbrock, R. Hoogenboom, U. S. Schubert, *Macromol. Rapid Commun.* **2004**, *25*, 1739–1764; for a recent book, see: C. O. Kappe, A. Stadler, *Microwaves in Organic and Medicinal Chemistry*, Wiley-VCH, Weinheim, **2005**.

 © 2005 Wiley-VCH Verlag GmbH & Co. KGaA, Weinheim

[2] R. K. Arvela, N. E. Leadbeater, *Org. Lett.* **2005**, *7*, 2101 – 2104.
[3] H. Zhang, U. S. Schubert, *Macromol. Rapid Commun.* **2004**, *25*, 1225 – 1230.
[4] a) K. Ersmark, M. Larhed, J. Wannberg, *Curr. Opin. Drug Discovery Dev.* **2004**, *7*, 417 – 427; b) X. Wu, R. Rönn, T. Gossas, M. Larhed, *J. Org. Chem.* **2005**, *70*, 3094 – 3098.
[5] T. N. Glasnov, W. Stadlbauer, C. O. Kappe, *J. Org. Chem.* **2005**, *70*, 3864 – 3870.
[6] R. Schobert, C. Jagusch, *Tetrahedron* **2005**, *61*, 2301 – 2307.
[7] M. Tietze, A. Iglesias, E. Merisor, J. Conrad, I. Klaiber, U. Beifuss, *Org. Lett.* **2005**, *7*, 1549 – 1552.
[8] For further information on microwave synthesis and upcoming conferences, see: www.maos.net

DOI: 10.1002/anie.200503543

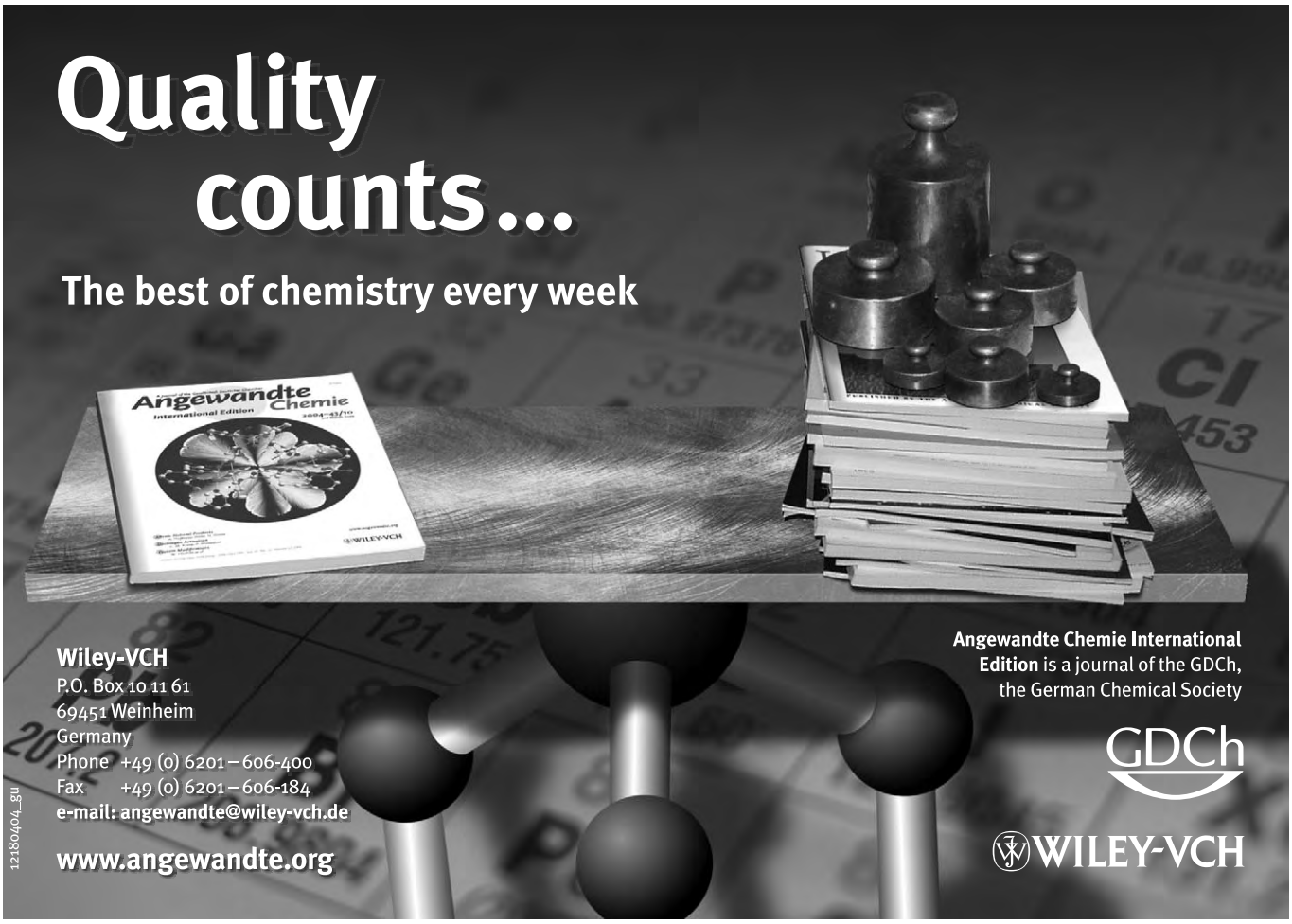

 © 2005 Wiley-VCH Verlag GmbH & Co. KGaA, Weinheim

Natural Product Synthesis

DOI: 10.1002/anie.200502383

Stephacidin B, The Avrainvillamide Dimer: A Formidable Synthetic Challenge**

*Carmen Escolano**

Keywords:
alkaloids · avrainvillamide · natural products · stephacidin · total synthesis

Nature capriciously provides us with a considerable number of alkaloids with structures that result from a combination of two identical molecules. Such a rearrangement of two molecules to create a new complex entity with different architectures, properties, and biological activity may be an intelligent energy-saving natural strategy, and thus the biosynthetic pathway to these dimeric alkaloids provides a model for a good synthetic approach.

One particularly outstanding dimeric alkaloid, in terms of its complexity, is stephacidin B. The story of stephacidin B (**1**) began a few years ago, after its isolation from the fungi *Aspergillus ochraceus* WC76466 by Qian-Cutrone et al. at Bristol-Myers Squibb (Scheme 1). Later on, the same group unambiguously elucidated the structure of this new alkaloid by a combination of NMR spectroscopy and X-ray crystallography studies.[1] The molecular architecture of **1** revealed a complex dimeric prenylated *N*-hydroxyindole alkaloid that contains 15 rings and nine stereogenic centers, but its absolute configuration remained unknown.

N-hydroxyindole and indole nitrone alkaloids, which may play important biological roles, are interesting entities rarely found in nature. In particular, the novel antitumor antibiotic stephacidin B exhibits an unusual mechanism of action. This new alkaloid has already been discussed by von Nussbaum[2] with respect to its biogenetical aspects and the mechanism of the late-stage putative biomimetic dimerization from avrainvillamide (**2**)[3] to stephacidin B (**1**). Recently, two groups of researchers led by Myers and Baran, respectively, achieved the enantioselective total synthesis of stephacidin B.[4] Furthermore, Baran et al. determined its absolute configuration as (−)-**1** and those of the biogenetically related monomeric alkaloids stephacidin A ((+)-**3**) and avrainvillamide ((+)-**2**). In this Highlight, both syntheses are compared and the most relevant aspects and the new methodology developed are discussed.

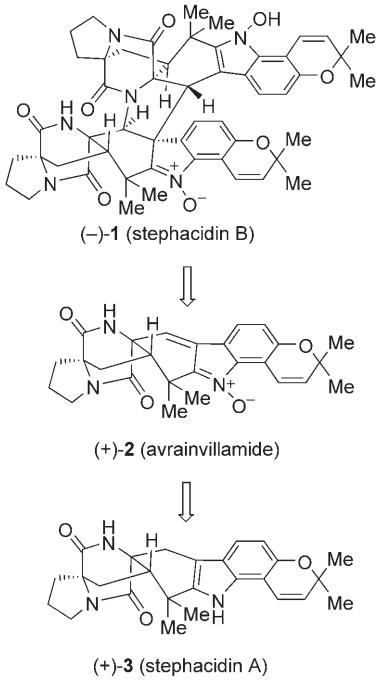

Scheme 1. Absolute chemistry of stephacidin B and related alkaloids from *Aspergillus ochraceus*.

The first synthetic concern of both groups was the total synthesis of avrainvillamide (**2**), an alkaloid with a unique oxidation pattern (3-alkylidene-3*H*-indole-1-oxide). Then, stephacidin B (**1**) was envisioned to form by dimerization of two identical units of **2**, presumably involving a Michael-like addition process. The putative dimerization was pointed out by Quian-Cutrone et al.[1] and supported by von Nussbaum[2] as well as Myers and Herzon.[4]

Myers' Approach to (−)-Avrainvillamide

In previous work, Myers and Herzon had developed a sequence to access the original 3-alkylidene-3*H*-indole-1-oxide moiety present in **2** and demonstrated the capability of this nucleus to act as a Michael acceptor.[5] Their retrosynthetic analysis is outlined in Scheme 2. The most remarkable features are 1) the simplification of avrainvillamide (**2**) by cleavage of the dihydropyrano[2,3-*g*]indole-1-oxide moiety, 2) the addition of an aminoacyl radical to a γ-phenylthiyl-substituted enamine to construct the diketopiperazine ring, 3) a Strecker-like reaction involving the addition of cyanide to an *N*-Boc-protected enamine, and 4) the use of a Corey–Bakshi–Shibata (CBS) catalyst to generate the first stereocenter and thereby set the total configuration in the final target.

The starting point of the synthesis (Scheme 3) was the enantioselective preparation of the protected allylic alcohol **8** by enantioselective reduction of the corresponding α,β-unsaturated ke-

[*] Dr. C. Escolano
Laboratorio de Química Orgánica
Facultad de Farmacia
Universidad de Barcelona
Av. Joan XXIII s/n
08028 Barcelona (Spain)
Fax: (+34) 93-402-4539
E-mail: cescolano@ub.edu

[**] I am deeply grateful to Prof. Joan Bosch and Dr. Santiago Vázquez for their invaluable advice and helpful discussions.

InterScience
© 2005 Wiley-VCH Verlag GmbH & Co. KGaA, Weinheim

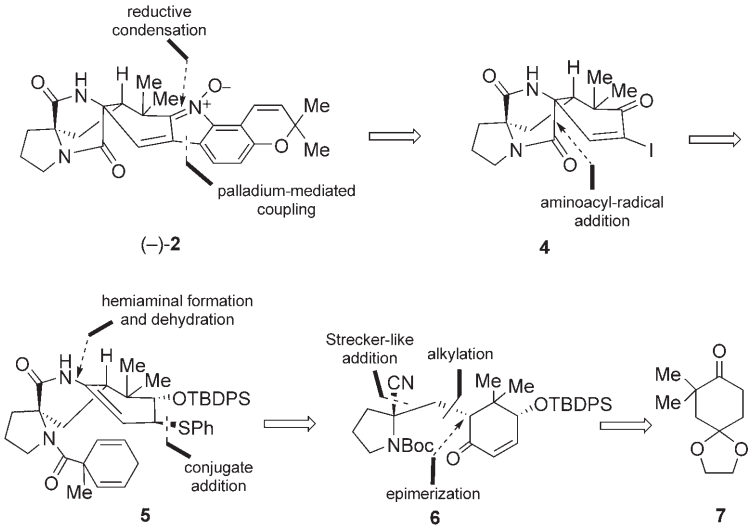

Scheme 2. Retrosynthesis of (−)-avrainvillamide by Myers and Herzon. Boc = *tert*-butyloxycarbonyl.

tone using an (*S*)-CBS catalyst. The stereochemistry of the catalyst was chosen randomly, as the absolute configuration of the final targets was still unknown. The side chain was installed by an alkylation reaction and required subsequent epimerization to give the required relative 1,3-*cis* stereochemistry. Note the unprecedented Strecker-like addition of a cyano group in the presence of hexafluoroisopropyl alcohol to an *N*-Boc enamine, and the hydrolysis under essentially neutral conditions of the resulting major *N*-Boc nitrile **6** (4:1 diastereomeric ratio) to the corresponding amide **9** using a homogeneous platinum phosphinito catalyst.[6] Conjugate addition of thiophenol with concomitant formation of a cyclic hemiaminal, followed by dehydration, cleavage of the *N*-Boc protecting group, and acylation of the pyrrolidine ring with 1-methyl-2,5-cyclohexadiene-1-carbonyl chloride furnished intermediate **5**, setting the stage for the radical-mediated elaboration of the diketopiperazine ring. This step illustrates the application of the tin-free methodology recently developed by Walton and co-workers to generate aminoacyl radicals.[7] From the advanced tetracyclic intermediate **10**, the completion of the synthesis was straightforward. After conversion of **10** into an α-iodoarene in a three-step sequence, an Ullmann-like coupling allowed the benzopyran moiety to be assembled to give *o*-nitroaryl ketone **11**, which was converted into the target heptacyclic nitrone (−)-**2** by reductive condensation with activated zinc.[8] The synthesized material was shown to be levorotatory ($[\alpha]_D = -35.1$, $CHCl_3$, 25 °C) while a dextrorotatory value ($[\alpha]_D = +10.6$, $c = 0.17$, $CHCl_3$) was described for natural **2**.[3a]

Baran's Approach to (−)-Avrainvillamide

The approach of Baran and coworkers relied on the fact that stephacidin A (**3**), a reduced monomer which is biogenetically related to stephacidin B (**1**), can be oxidized to avrainvillamide (**2**). Their retrosynthetic analysis (Scheme 4) fundamentally differs from that of Myers in that 1) the indole nucleus is already present in the starting

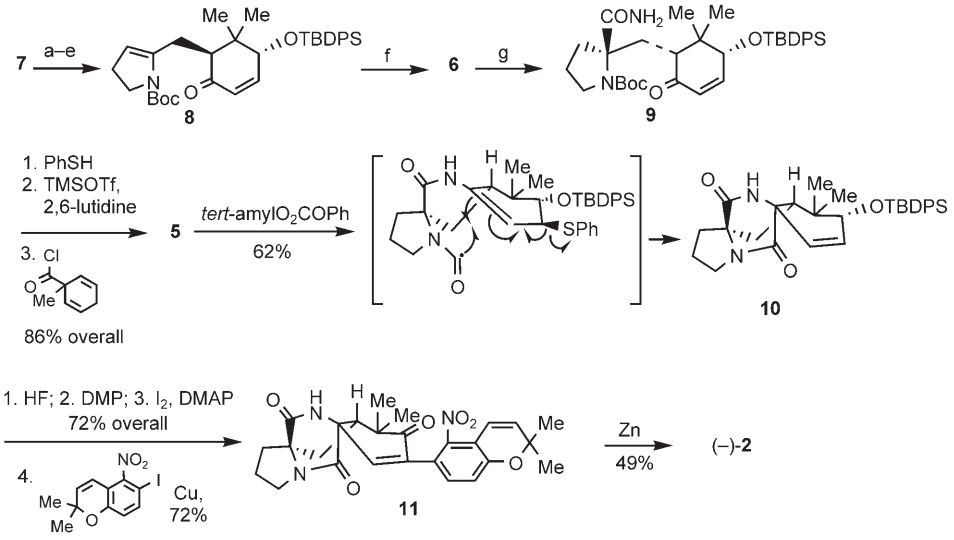

Scheme 3. a) LiHMDS, TMSCl, $Pd(OAC)_2$; b) BH_3·DMS, (*S*)-CBS catalyst; c) TBDPSOTf, 2,6-lutidine; d) 1 N H_2SO_4; e) KHMDS, *N*-(*tert*-butoxycarbonyl)-2-isopropylsulfonatemethyl-4,5-dihydropyrrole, 64% (5 steps); f) TMSCN, HFIPA, KHMDS, pivalic acid, 65%; g) [PtH(PMe_2OH)($PMe_2O)_2$H], 75% (2 steps). HMDS = hexamethyldisilazide; TMS = trimethylsilyl; DMS = dimethyl sulfide; CBS is short for Corey–Bakshi–Shibata, the catalyst is (*S*)-1-methyl-3,3-diphenylhexahydropyrrolo[1,2-*c*][1,3,2]oxazaborole; TBDPSOTf = *tert*-butyldiphenylsilyl trifluoromethylsulfonate; HFIPA = 1,1,1,3,3,3-hexafluoro-2-propanol; DMP = 1,1,1-triacetoxy-1,1-dihydro-1,2-benziodozol-3(1*H*)-one; DMAP = 4-(dimethylamino)pyridine.

 © 2005 Wiley-VCH Verlag GmbH & Co. KGaA, Weinheim

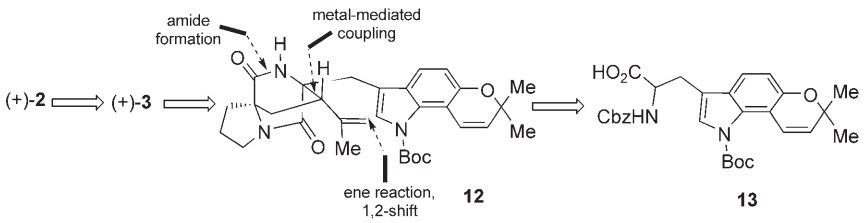

Scheme 4. Retrosynthesis of (+)-avrainvillamide by Baran et al. Cbz = carbobenzyloxy.

material, 2) one stereocenter is already fixed in one of the starting products whereas the other two stereocenters present in **2** are simultaneously installed in a rare stereocontrolled intramolecular metal-mediated oxidative coupling of enolates, and 3) the last step involves an oxidation, rather than a reduction, that leads to the unsaturated nitrone. However, a common feature of both strategies is that the configuration of the final products is determined by the absolute stereochemistry of one of the chiral reagents used in the initial steps (CBS catalyst or proline).

Guided by their previous success in the synthesis of (−)-stephacidin A[9] from an (*S*)-proline derivative, and now with a dextrorotatory natural sample of stephacidin A in hand, Baran et al. realized that their synthetic material was the unnatural enantiomer. Thus, by using (*R*)-proline they secured the preparation of the natural (+)-stephacidin A. Their synthetic pathway (Scheme 5) starts with the peptide coupling of an (*R*)-proline diester derivative **14** with the racemic tryptophan derivative **13**. The Cbz group was chemoselectively removed and the diketopiperazine ring was formed in a single step, which avoided the intramolecular cyclization to form a γ-lactam. Next, the metal-mediated oxidative coupling of enolates, a reaction that is seldom used in synthesis and never for such challenging natural targets, was envisaged to gain access to the bicyclo[2.2.2]-diazaoctane moiety in a stereocontrolled manner. Subsequent reaction with a Grignard reagent allowed the introduction of all the carbon atoms present in stephacidin A (**3**). Heating the intermediate **12** removed the Boc protecting group, and a new thermal indole annulation gave (+)-**3** ($[\alpha]_D = +68.5$, $c = 0.35$, 1:1 CH_2Cl_2/MeOH; natural (+)-**3**: $[\alpha]_D = +61.5$, $c = 0.26$, 1:1 CH_2Cl_2/MeOH). The latter transformation can be mechanistically explained by an ene reaction followed by a 1,2-shift of the spirocyclic intermediate. At that point, Somei's tungstate method which permits access to 1-hydroxyindoles from 2,3-dihydroindoles was considered.[10] In this manner, reduction of the indole ring led to indoline **18**, which surprisingly underwent chemoselective oxidation to directly give the unsaturated nitrone present in (+)-avrainvillamide (**2**) in a single step ($[\alpha]_D = +11$, $c = 0.1$, $CHCl_3$).

Biomimetic Dimerization

Preparative TLC (SiO_2, EtOAc), treatment with Et_3N/CH_3CN, or even simple evaporation of DMSO from a solution of **2** entails dimerization and furnishes the final target **1** (Scheme 6; natural sample from Bristol-Myers Squibb: $[\alpha]_D = -21.1$, $c = 0.19$, $CDCl_3$; Myers' synthetic sample: $[\alpha]_D = +91$, $c = 0.25$, CH_3CN; Baran's synthetic sample: $[\alpha]_D = -33$, $c = 0.1$, $CDCl_3$). The mechanism most probably involves a novel Michael-like 1,5-addition, which leads to the stereocontrolled formation of a new pyrrolidine connecting ring.

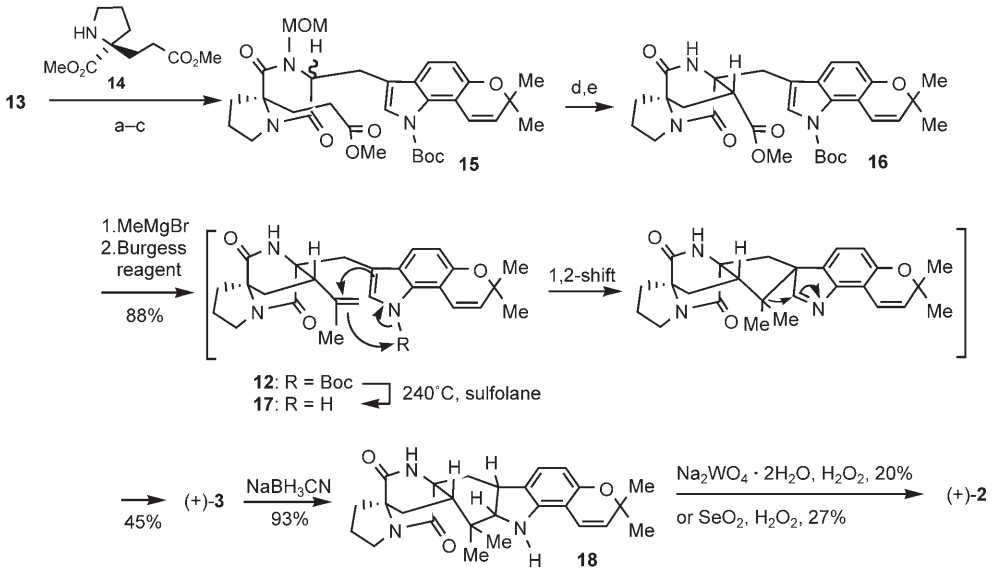

Scheme 5. a) (*R*)-methyl-2-[(2-(methoxycarbonyl)ethyl]pyrrolidine-2-carboxylate, HATU, *i*Pr_2EtN, DMF; b) $[Pd(dba)_3]\cdot CHCl_3$, Et_3SiH, Et_3N, CH_2Cl_2; then DMF/MeOH; c) NaHMDS, MOMCl, 62% (3 steps); d) LDA; $[Fe(acac)_3]$; e) *B*-bromocatecholborane, 48% (2 steps). HATU = *O*-(7-azabenzotriazol-1-yl)-*N*,*N*,*N*′,*N*′-tetramethyluronium hexafluorophosphate, DMF = *N*,*N*-dimethylformamide; dba = dibenzylideneacetone; MOM = methoxymethyl; LDA = lithium diisopropylamide; acac = acetylacetonate; Burgess reagent = $MeO_2CN^-SO_2N^+Et_3$.

 © 2005 Wiley-VCH Verlag GmbH & Co. KGaA, Weinheim

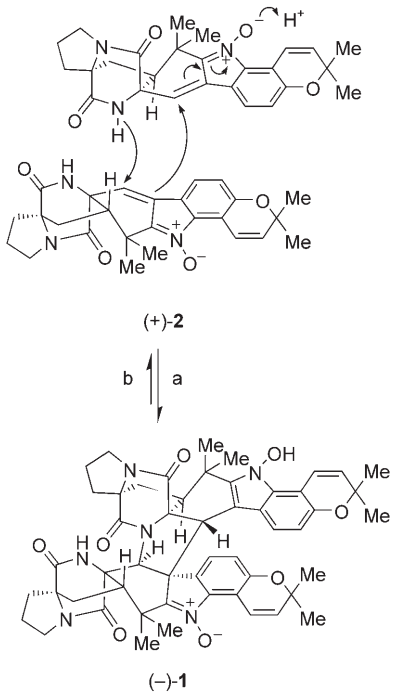

Scheme 6. Proposed dimerization mechanism from (+)-**2** to (−)-**1**: a) preparative TLC; or NEt_3 (excess), CH_3CN, 25 °C, 1 h; or DMSO/solvent removal; b) chromatography. DMSO = dimethyl sulfoxide.

Likewise, the retrodimerization to give **2** occurs spontaneously by addition of molecular sieves to a solution of **1** in $[D_6]$DMSO/CD_3CN or during chromatography of this dimeric material. In fact, reversible additions had already been observed by Myers and Herzon[5] when oxygen- and sulfur-centered nucleophiles reacted with α,β-unsaturated nitrones that are structurally related to **2**.[11]

Owing to the observed equilibration of both compounds **1** and **2** under mild conditions, Myers and Herzon[4a] cast some doubts over which compound is responsible for the biological action, suggesting that the activity observed for stephacidin B may be attributable to avrainvillamide (**2**) formed from **1** in vivo. Moreover, the possibility that stephacidin B may be an artefact in the isolation of **2** is considered. Accordingly, Baran et al. found that a solution of a natural sample of stephacidin A in DMSO contained 20% of stephacidin B, although a natural solid sample was found to be stable.[4b] The ready equilibration of avrainvillamide (**2**) and stephacidin B (**1**) illustrates the difficulty in distinguishing if the original structure of a determinate compound has been modified when extracted from its natural source or during biological testing involving chemicals and solvents.[12]

The enantioselective syntheses discussed herein have not only tackled formidable synthetic challenges but also paved the way for a series of medicinally attractive stephacidin analogues. Moreover, both sequences have expanded the arsenal of protocols for the organic chemistry community, especially in the relatively unexplored area of the chemistry of 1-hydroxyindoles.

Published online: October 27, 2005

[1] a) J. Qian-Cutrone, S. Huang, Y. Z. Shu, D. Vyas, C. Fairchild, A. Menendez, K. Krampitz, R. Dalterio, S. E. Klohr, Q. Gao, *J. Am. Chem. Soc.* **2002**, *124*, 14556–14557; b) J. Qian-Cutrone, K. D. Krampitz, Y. Z. Shu, L. P. Chang, S. E. Lowe, US Patent 6291461, **2001**.

[2] F. von Nussbaum, *Angew. Chem.* **2003**, *115*, 3176–3179; *Angew. Chem. Int. Ed.* **2003**, *42*, 3068–3071.

[3] Avrainvillamide = CJ-17,655. a) W. Fenical, P. R. Jensen, X. C. Cheng, US Patent 6066635, **2000**; b) Y. Sugie, H. Hirai, T. Inagaki, M. Ishiguro, Y.-J. Kim, Y. Kojima, T. Sakakibara, S. Sakemi, A. Sugiura, Y. Suzuki, L. Brennan, J. Duignan, L. H. Huang, J. Sutcliffe, N. Kojima, *J. Antibiot.* **2001**, *54*, 911–916.

[4] a) S. B. Herzon, A. G. Myers, *J. Am. Chem. Soc.* **2005**, *127*, 5342–5344; b) P. S. Baran, C. A. Guerrero, B. D. Hafensteiner, N. B. Ambhaikar, *Angew. Chem.* **2005**, *117*, 3960–3963; *Angew. Chem. Int. Ed.* **2005**, *44*, 3892–3895.

[5] A. G. Myers, S. B. Herzon, *J. Am. Chem. Soc.* **2003**, *125*, 12080–12081.

[6] T. Ghaffar, A. W. Parkins, *J. Mol. Catal. A* **2000**, *160*, 249–261.

[7] a) L. V. Jackson, J. C. Walton, *Chem. Commun.* **2000**, 2327–2328; b) A. F. Bella, L. V. Jackson, J. C. Walton, *Org. Biomol. Chem.* **2004**, *2*, 421–428.

[8] For a justification of the moderate yield generally observed in the reductive condensation of nitroderivatives with ketones leading to *N*-hydroxyindoles, see: K. C. Nicolaou, S. H. Lee, A. A. Estrada, M. Zak, *Angew. Chem.* **2005**, *117*, 3802–3806; *Angew. Chem. Int. Ed.* **2005**, *44*, 3736–3740.

[9] P. S. Baran, C. A. Guerrero, N. B. Ambhaikar, B. D. Hafensteiner, *Angew. Chem.* **2005**, *117*, 612–615; *Angew. Chem. Int. Ed.* **2005**, *44*, 606–609.

[10] M. Somei, *Adv. Heterocycl. Chem.* **2002**, *82*, 101–155.

[11] Nicolaou et al.[8] recently reported that 1,5-addition of alcohols, thiols, amines, and phenols to α,β-unsaturated nitrones derived from simple aromatic precursors leads to stable final products.

[12] a) F. Bracher, W. J. Eisenreich, J. Mühlbacher, M. Dreyer, G. Bringmann, *J. Org. Chem.* **2004**, *69*, 8602–8608. The authors concluded that isolated saludimerines A and B dimers are artefacts formed during the isolation process; b) For a recent example of ready monomer–dimer interconversion in panepophenanthrin, see: X. Lei, R. P. Jonson, J. A. Porco, Jr., *Angew. Chem.* **2003**, *115*, 4043–4047; *Angew. Chem. Int. Ed.* **2003**, *42*, 3913–3917; c) Somei's "1-hydroxyindole hypotheses"[10] suggest that these reactive species occur somewhat frequently in nature, but they might be transformed during extraction from natural sources to result in modified structures.

© 2005 Wiley-VCH Verlag GmbH & Co. KGaA, Weinheim

DOI: 10.1002/anie.200463007

Organosulfur Reagents

Organosulfur Compounds: Electrophilic Reagents in Transition-Metal-Catalyzed Carbon–Carbon Bond-Forming Reactions

*Srinivas Reddy Dubbaka and Pierre Vogel**

Keywords:
cross-couplings · homogeneous catalysis · sulfonamides · sulfonyl chlorides · transition metals

Transition-metal-catalyzed carbon–carbon bond-forming reactions are among the most powerful methods in organic synthesis and play a crucial role in modern materials science and medicinal chemistry. Recent developments in the area of ligands and additives permit the cross-coupling of a large variety of reactants, including inexpensive and readily available sulfonyl chlorides. Their desulfitative carbon–carbon cross-coupling reactions (Negishi, Stille, carbonylative Stille, Suzuki–Miyaura, and Sonogashira–Hagihara-type cross-couplings and Mizoroki–Heck-type arylations) are reviewed together with carbon–carbon cross-coupling reactions with other organosulfur compounds as electrophilic reagents.

1. Introduction

Transition-metal-catalyzed C–C[1] and C–heteroatom[2] bond-forming reactions are among the most powerful methods in organic synthesis.[3] They have many applications in medicinal chemistry[4] and materials science.[5–7] Their popularity stems from their tolerance of many different functional groups which allows their application in the synthesis of highly complicated molecules.[8] For C–C bond-forming reactions, one denotes two main classes: 1) reactions with a nucleophilic metallic reagent [Eq. (1)] and 2) reactions of alkene or alkyne C–H reagents with electrophilic partners RX, ArX [Eqs. (2) and (3)].

$$R\text{-}X + R^1\text{-}M \xrightarrow{\text{catalyst}} R\text{-}R^1 + MX \qquad (1)$$

M = B : Suzuki–Miyaura[1,9]
M = Sn : Stille[1,10]
M = Si : Hiyama[1,11]
M = Zn : Negishi[1,12]
M = Mg : Kumada[1,13]

$$Ar\text{-}X + \underset{R}{\diagup\!\!=} \xrightarrow{\text{cat.}} Ar\underset{R}{\diagup\!\!=} + HX \qquad (2)$$

Mizoroki–Heck[1,14]

$$Ar\text{-}X + H\text{—}\equiv\text{—}R \xrightarrow{\text{cat.}} Ar\text{—}\equiv\text{—}R + HX \qquad (3)$$

Sonogashira–Hagihara[1,15]

There have been many recent developments in the area of ligands and additives that permit the cross-coupling of a large variety of reactants[1–4,9–16] in the presence of late-transition metals (i.e. pincer complexes with Ir, Pt, Pd, and palladacycles). Other recent developments include immobilized metal catalysts that allow the easy recovery and reuse of the catalyst[17] and the use of ionic liquids.[18] The efficiency of a synthetic procedure can be improved dramatically by the use of multiple metal-catalyzed transformations, either in a domino process or in a sequential fashion.[19] There has been much progress in enantioselective palladium-catalyzed C–C bond formations.[20] It is now possible to couple inexpensive, less reactive organic chlorides by using highly active catalysts[21] or by use of microwave irradiation.[22] In the continuing search for more-economical procedures, there is more and more emphasis to avoid the formation of by-products.[23]

We have shown previously that readily available sulfonyl chlorides (RSO_2Cl, R = aryl, alkenyl, benzyl, 2-methallyl[24]) undergo desulfitative Suzuki–Miyaura,[25] Stille and carbonylative Stille,[26] Mizoroki–Heck,[27] Sonogashira–Hagihara,[28] and Negishi[29] cross-coupling reactions. We review these

[*] S. R. Dubbaka, Prof. P. Vogel
Laboratoire de glycochimie et de synthèse asymétrique
Ecole Polytechnique Fédérale de Lausanne (EPFL)
BCH, 1015 Lausanne (Switzerland)
Fax: (+41) 21-693-9375
E-mail: pierre.vogel@epfl.ch

InterScience
© 2005 Wiley-VCH Verlag GmbH & Co. KGaA, Weinheim

reactions herein together with those involving other organosulfur compounds as electrophilic reagents.

2. Reactions of Thiols, Sulfoxides, Thioethers, Aryl Sulfones, and Sulfoximines with Grignard Reagents

Wenkert and co-workers[30a–f] reported that the reactions of alkenyl sulfides, [Eq. (4)], vinyl 2-pyrimidyl sulfides,[30g] and aryl thiols and sulfides [Eq. (5)] with methyl-, phenyl-, and *p*-tolylmagnesium bromides, mediated by $[NiCl_2(PPh_3)_2]$, lead to alkenes (predominantly with retention of configuration), toluenes, and biaryl compounds, respectively.

The displacement of sulfur is faster for alkenyl sulfides than for aryl sulfides, a reactivity pattern that is similar to that

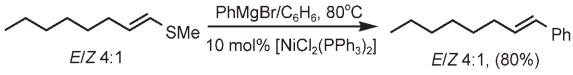

(4)

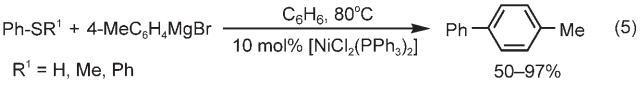

(5)

observed for enol and aryl ethers.[30e] The carbon–sulfur bond of sulfoxides[30a,f] [Eq. (6)] and sulfones[30a] [Eq. (7)] can also be replaced by a carbon–carbon linkage through nickel-catalyzed reactions with Grignard reagents. Gais and co-workers showed that alkenyl sulfoximines can also be cross-coupled either with Grignard or zinc reagents in the presence of $[NiCl_2(dppp)]$ (8 mol %) [Eq. (8)] (dppp = 1,3-bis(diphenylphosphanyl)propane).[31a–c]

Independently, Takei and co-workers showed that alkenyl and aryl sulfides can be coupled with Grignard reagents in the presence of $[NiCl_2(PPh_3)_2]$ (3 mol %) [Eq. (9)].[32] It was

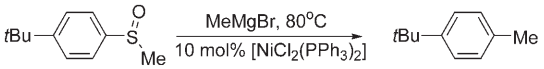

(6)

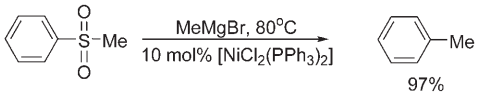

(7)

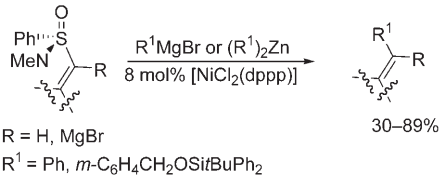

(8)

confirmed that the reactions do not occur in the absence of the Ni catalyst and that organolithium reagents are not suitable for such reactions.

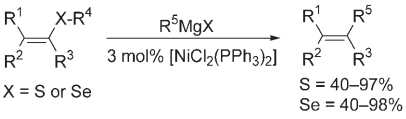

(9)

In 1980, the same group demonstrated that alkenyl, aryl, and allylic selenides also couple with Grignard reagents in the presence of catalytic amounts of $[NiCl_2(PPh_3)_2]$ or $[NiCl_2(dppp)_2]$ to give the corresponding unsaturated compounds.[33] The reactivity order of these Kumada-type cross-coupling reactions of BuMgBr, with PhSeMe, PhSMe, and PhCl catalyzed by $[NiCl_2(dppp)]$ was found to be PhSeMe $\gg$ PhCl $>$ PhSMe. The application of *ortho*-, *meta*-, and *para*-bis(alkylthio)benzenes in these reactions led to selective monoarylation and -alkylation. This allows the introduction of two different aryl or alkyl groups into the benzene ring by sequential substitution of the two substituents. Steric factors play a decisive role in the chemoselectivity of these reactions.[34]

3. Reaction of Aryl tert-Butyl Sulfones, Alkyl Arene Sulfonates, and Arene Sulfonamides with Grignard Reagents

Julia and co-workers showed that the cross-coupling reactions between vinyl *tert*-butyl sulfones[35a–c] and aryl *tert*-butyl sulfones[35d,e] with Grignard reagents take place in the presence of $[Ni(acac)_2]$ catalyst through desulfonylation [Eq. (10)] (acac = acetylacetonate). The Ni^0 species (pro-

Pierre Vogel completed his PhD at the University of Lausanne (Switzerland) in 1969 with Prof. Horst Prinzbach. After two years at Yale University with Prof. Martin Saunders, he joined the research laboratory of Syntex (Mexico City) and worked with Prof. Pierre Crabbé. He returned to the University of Lausanne and became full professor in 1977. Since 2001, he has chaired the Laboratory of Glycochemistry and Asymmetric Synthesis of the Ecole Polytechnique Fédérale de Lausanne. He obtained the Novartis lectureship (2003) and was Boehringer-Ingelheim Distinguished Lecturer for 2005.

Srinivas Reddy Dubbaka was born in MachiReddy Pally (India) in 1979. He obtained his BSc from the Kakatiya University in 1999 and MSc from the Central University of Hyderabad, India in 2001. Since 2001, he has been working towards his PhD under the supervision of Professor Pierre Vogel at the Swiss Federal Institute of Technology, Lausanne. His research focuses on the development of new organic reactions based on sulfur dioxide.

 © 2005 Wiley-VCH Verlag GmbH & Co. KGaA, Weinheim

duced from the Ni^{II} catalyst by transmetalation with two Grignard molecules and reductive elimination to form biphenyl and active Ni^0 catalyst) inserts into the vinyl or aryl $C(sp^2)$–S bond. The resulting aryl nickel(II) sulfonate complex[30b] undergoes ligand exchange with the Grignard reagent to give an unsymmetrical bisaryl complex. Finally, reductive elimination generates the C–C coupling product.[36] Notably, the $C(sp^3)$–S bond of the *tert*-butyl sulfone is never cleaved under these conditions [Eq. (10)].

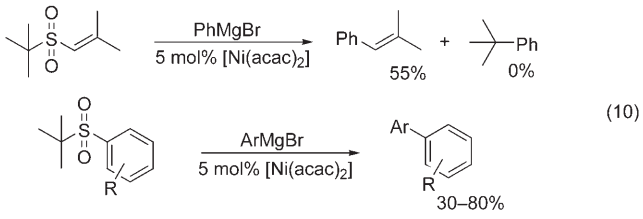

(10)

Before 2004, aryl and alkyl sulfones were not known to undergo C–C cross-coupling reactions with nonpolar nucleophiles such as boronic acids and organotin and organosilicon reagents in the presence of palladium or nickel catalysts (for polar nucleophiles, see [Eq. (10)]). However, Liu and Robins recently showed that the palladium-catalyzed Suzuki–Miyaura cross-coupling reaction of arene boronic acids and 6-[(3-methylbutyl)sulfonyl]purine nucleoside does occur with desulfonylation under suitable conditions [Eq. (11)].[37]

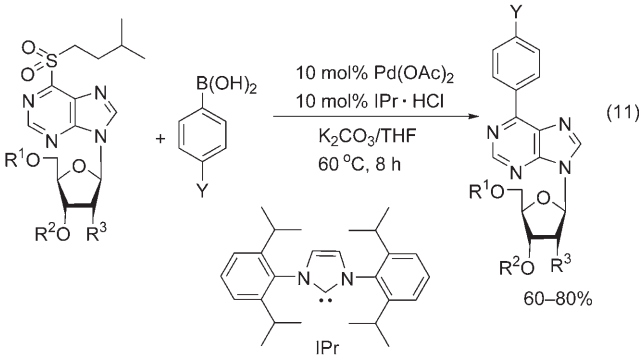

(11)

Recently, Park and co-workers found that unsymmetrical terphenyls of type **4** can be prepared in high yields by the nickel-catalyzed cross-coupling of biphenyl sulfonates **2** with aryl Grignard reagents **3** [Eq. (12)] (dppf = 1,1′-bis(diphenylphosphanyl)ferrocene).[38] Unsymmetrical biaryl compounds can also be prepared under similar conditions by reaction of alkyl arene sulfonates with aryl Grignard reagents **3**. Neopentyl arene sulfonates **1** are thus useful sources of electrophilic aryl groups. In this case, the nickel catalyst prefers to insert into the C–S rather than the C–O bond of **1** or **2**.[39] Milburn and Snieckus[40] reported the Ni^0-catalyzed C-C cross-coupling reactions between arylsulfonamides and Grignard reagents through desulfamoylation in toluene at 100 °C. As sulfonamides do not undergo Negishi coupling with aryl zinc derivatives, the method has been applied to generate unsymmetrical teraryls of type **4** [Eq. (13)].

The cross-coupling of sulfonamides and Grignard reagents represents a new variant of the Corriu–Kumada–Tamao protocol.[41] It offers the advantage of directed *ortho* metalation[42] and thus enhances its synthetic utility.[43]

4. Reaction of Sulfonium Salts, Thioethers, and Thiol Esters with Nonpolar Organometallic Compounds

Several biotransformations employ metalloenzyme-induced cleavage of carbon–sulfur bonds. The metals used by Nature are Ni, Co, Cu, and Fe.[44] Aryl and heteroaryl sulfonium salts **5** are prepared readily either by the reaction of thiolane with the corresponding halides in the presence of HPF_6, NH_4PF_6, or $NaClO_4$, or by the reaction of the corresponding thiols with 1,4-dibromobutane in the presence of NH_4PF_6.[45] Alkenyl sulfonium salts **6** can be prepared from alkenes upon reaction with Br_2/thiolane followed by the elimination of HBr and counterion exchange.[45] Liebeskind and co-workers[45] reported that electrophiles **5** and **6** undergo smooth cross-coupling reactions [Eq. (14)] with organotin reagents (Stille-type couplings), arene and heteroarene

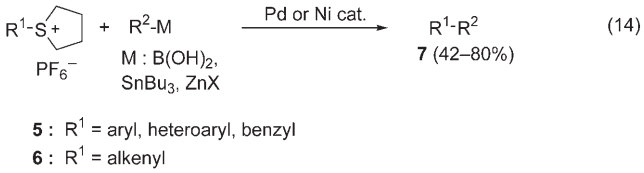

(14)

boronic acids (Suzuki–Miyaura-type couplings), and (2-thienyl)zinc chloride (Negishi-type couplings) in the presence of a Pd or Ni catalyst to give the corresponding products of C–C coupling **7**. The same group later found that triphenylphosphite, a supporting ligand for the palladium catalyst that is not readily alkylated, is uniquely effective as a ligand in hetero-

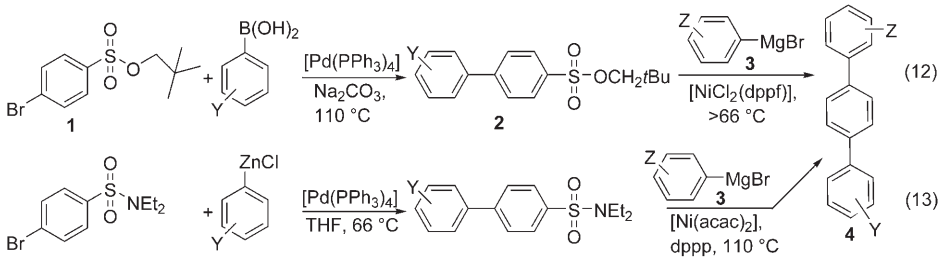

© 2005 Wiley-VCH Verlag GmbH & Co. KGaA, Weinheim

benzylic cross-coupling reactions with aryl tin, heteroaryl tin, alkenyl tin, and organozinc compounds.[46]

Inspired by the mechanism of methane production from methyl coenzyme M ($CH_3SCH_2CH_2SO_3^-$) mediated by methyl coenzyme M reductase[44c,47] (a process involving a nickel hydrocorphinoid cofactor (F_{430}) that cleaves the CH_3–S bond of $CH_3SCH_2CH_2SO_3^-$ with the generation of a CH_3–Ni intermediate, which subsequently undergoes protonation to methane), Liebeskind and co-workers developed Ni-catalyzed cross-coupling reactions of thioglycolic acids **8** with organozinc reagents [Eq. (15)].[48]

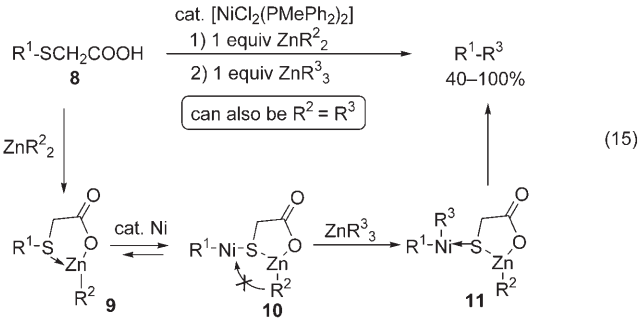

(15)

R^1 = aryl, heteroaryl, benzyl, alkenyl
R^3 = alkyl, aryl, benzyl

Experiments suggested that intermediates **9** in which the zinc center is chelated by the carboxylate moiety and the β-thioether group has a favorably activated C–S bond for nickel oxidative addition, which leads to **10**. It was also proposed that intramolecular transfer of R^2 from the zinc to the nickel center of **10** does not occur, but that an external zinc reagent interacts with the nickel center of **10** to generate the intermediate **11.**[48]

Casalnuovo and co-workers found that benzyl zinc reagents undergo Pd-catalyzed cross-coupling reactions with methylthio-substituted N-heterocycles in moderate to good yields.[49] 2-(Methylthio)pyrimidines are particularly reactive substrates for this reaction. The regioselectivity of the reactions of 2,4-bis(methylthio)pyrimidines **12** [Eq. (16)] is

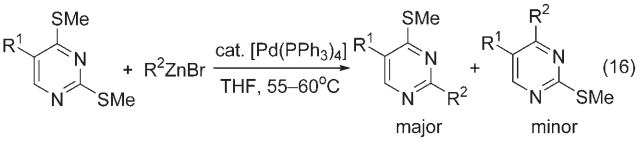

(16)

12: R^1 = H, Me
R^2 = Bn, *m*-$CF_3C_6H_4$

opposite to that of their 2,4-dichloropyrimidines analogues. This offers the possibility to prepare important heterocyclic compounds.

A new method for the preparation of substituted alkynes was reported by Liebeskind and co-workers.[50] In the presence of copper(I)–thiophene-2-carboxylate (CuTC) or copper(I)–3-methylsalicylate (CuMeSal), the Pd-catalyzed cross-coupling of thioalkyne derivatives with boronic acids affords functionalized alkynes in moderate to good yields. Thus, disubstituted alkynes can be prepared under mild, nonbasic conditions [Eq. (17)].

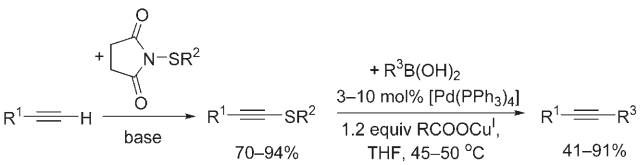

(17)

R^1 = Bu, Ph, $MeOCH_2$, *m*-$CF_3C_6H_4$, *p*-$MeOC_6H_4$, *m*-$NO_2C_6H_4$
R^2 = *p*-tolyl, Me

The same protocol was applied successfully to methylthio-substituted heterocyclic compounds and allows the synthesis of heterocyclic compounds that are important in medicinal chemistry. The proposed mechanism of this Suzuki–Miyaura-type cross-coupling reaction is shown in Scheme 1.[51] It

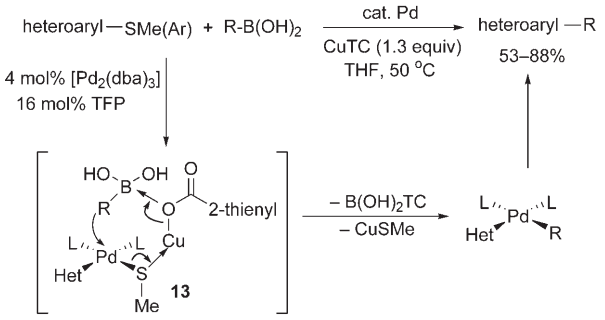

Scheme 1. Proposed mechanism by Liebeskind and Srogl for the Cu^I/Pd-catalyzed cross-coupling of heteroaromatic thioethers with boronic acids under neutral conditions.[51]

implies the formation of intermediate **13** from the oxidative addition of the C(sp^2)–S bond, rather than of the C(sp^3)–S bond, to palladium. Coordination with the copper carboxylate and the boronic acid provides the activation for the next step.

Heteroaromatic thioethers and aryl, heteroaryl, and alkenyl stannanes participate in Pd-catalyzed, Cu^I-mediated cross-coupling reactions at 50 °C in THF [Eq. (18)].[52,53] A

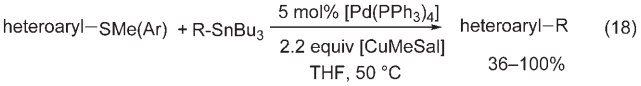

(18)

similar method was proposed for the synthesis of protected benzamidines [Eq. (19)].[54]

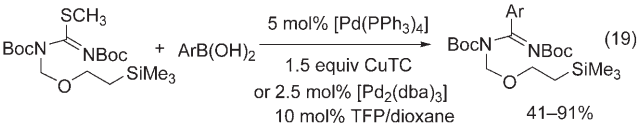

(19)

Liebeskind and Srogl designed a mild and general method for the Pd-catalyzed, Cu^I-mediated coupling of thiol esters and boronic acids under base-free conditions that produces ketones [Eq. (20)].[55] Thiol esters and *B*-alkyl-9-borabicyclo-[3.3.1]nonane derivatives also undergo smooth cross-couplings under similar conditions [Eq. (21)]. In such cases, the addition of Cs_2CO_3 facilitates the reaction.[56] A similar

© 2005 Wiley-VCH Verlag GmbH & Co. KGaA, Weinheim

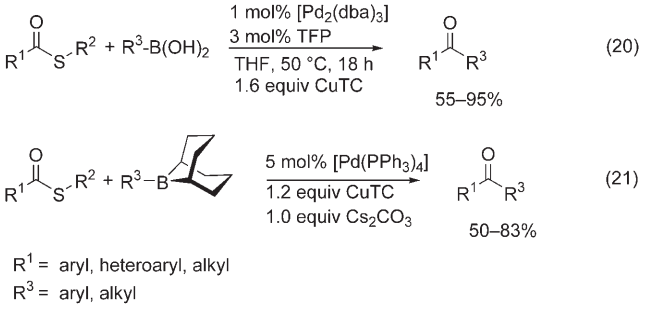

synthesis of ketones relies on the Pd-catalyzed, copper diphenylphosphinate-mediated coupling of thiol esters with organostannanes under neutral conditions.[57]

A large variety of ketones can be prepared through Fukuyama coupling. The coupling reaction between aryl esters and ethanethiol esters with organozinc derivatives and other nucleophiles (e.g. alkynes, boronic acids) takes place at ambient temperature to give the corresponding ketones [Eq. (22)].[58a–c] Ketones are also prepared by the Ni-catalyzed

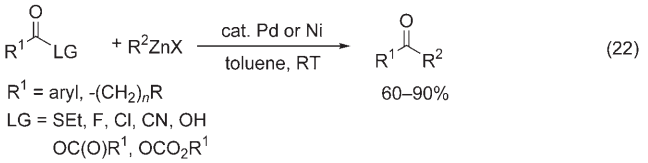

cross-coupling of organozinc and carboxylic acid fluorides, chlorides, anhydrides, and thiol esters.[58d]

5. Desulfitative C–C Cross-Coupling of Sulfonyl Chlorides

Arene and alkane sulfonyl chlorides are inexpensive and readily available compounds. They have been used for more than a century in materials science and medicinal chemistry. For instance, both α- and β-naphthalenesulfonyl chlorides obtained from naphthalene, the most abundant compound derived from coal, have been used in industry for the manufacture of drugs, pesticides, dyes, polymers, and other goods.[59] Hence it is logical to use sulfonyl chlorides as reagents in transition-metal-catalyzed C–C bond-forming reactions. However it is only recently, that this has come into practical use.

In 1966, Collman and Roper[60] reported the preparation of the iridium(III) *S*-sulfinate complex **15** by treating $[IrCl(CO)(PPh_3)_3]$ with *p*-toluenesulfonyl chloride (TsCl). They also found that upon heating to 100 °C, loss of SO_2 from **15** leads to the formation of complex **16** [Eq. (23)].

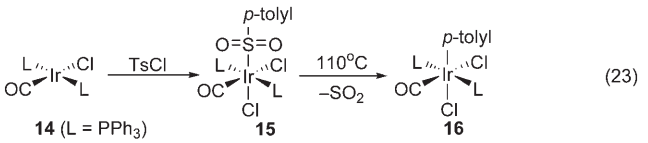

The year thereafter, Cook and Jauhal[61] reported a similar reaction sequence with $[Pt(PPh_3)_4] + TsCl \rightarrow [PtTsCl(PPh_3)_2] \rightarrow SO_2 + [Pt(C_6H_4Me)Cl(PPh_3)_2]$. In 1970, the catalytic desulfonylation of arene sulfonyl chlorides and bromides by various Rh, Ir, Ru, Pt, and Pd catalysts were investigated and proposed to proceed mainly by a metal-center-promoted mechanism and, to a smaller extent, through homolytic decomposition.[62] The first reports of transition-metal-catalyzed C–C bond-forming reactions with arene sulfonyl chlorides as reagents were those of Kasahara et al.[63] [Eq. (24)] in 1988 and of Miura and co-workers[64] [Eq. (25)]

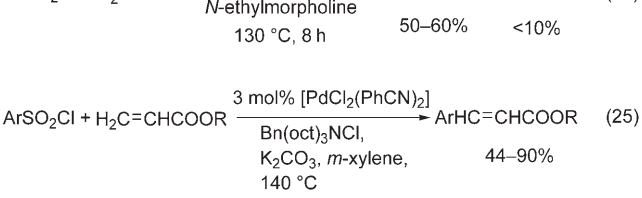

in 1989. These authors disclosed for the first time the possibility of performing desulfitative carbon vinylations (Mizoroki–Heck-type reactions) with arene sulfonyl chlorides and various alkenes in the presence of palladium catalysts.

Arene sulfonyl chlorides have also been employed in carbon carbonylation[65] and C–C homocouplings.[66] In 2003, we reported for the first time that arene and phenyl methanesulfonyl chlorides can be cross-coupled [Eq. (26)]

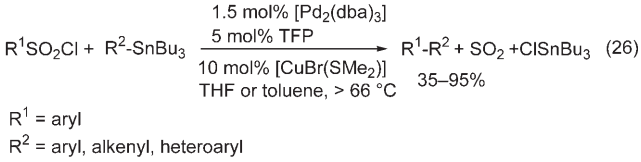

with aryl, heteroaryl, and alkenyl stannanes with concomitant loss of SO_2 in the presence of palladium and copper catalysts at temperatures above 66 °C.[26a,67] When the reaction was carried out in the presence of catalytic $[Pd(PPh_3)_4]$ in THF at 40–60 °C, the corresponding sulfones were obtained [Eq. (27)].[68]

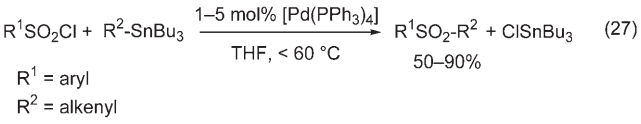

When the amount of the copper complex $[CuBr(SMe_2)]$ was increased, a rate enhancement was observed but the major product was that arising from the self-coupling of the organostannane.[69] We also examined the palladium-catalyzed carbonylative Stille cross-coupling reaction of arene

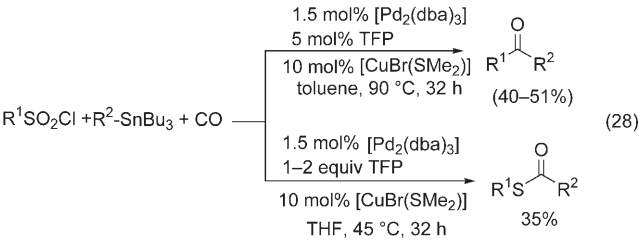

© 2005 Wiley-VCH Verlag GmbH & Co. KGaA, Weinheim

sulfonyl chlorides and organostannanes in the presence of carbon monoxide (60 bar) at 110 °C in toluene. The carbonylative cross-coupled products [Eq. (28)] were obtained in moderate yields.

When we used THF instead of toluene as solvent at 45 °C in the carbonylative Stille reaction, $R^1SC(O)R^2$ products were obtained in low yield [Eq. (28)]. The amount of thiol ester product increased with the amount of tri-2-furylphosphane (TFP) ligand, indicating that their formation resulted from the reduction of the sulfonyl chlorides to sulfenyl chlorides, which then underwent aryl carbonylation.[26a] This process is analogous to the known $[Co_2(CO)_8]$-catalyzed carbonylation of thiols[70] and to the thiocarbonylation of acetylenes with thiols and carbon monoxide catalyzed by palladium[71] or platinum complexes.[72]

When TsCl was mixed with $[PdCl_2(PhCN)_2]$ (1 equiv) and triethylamine (2 equiv) in $[D_8]$THF at 45–60 °C, a signal typical for a C–Pd bond[73a] appeared in the ^{13}C NMR spectrum after 10 min ($\delta = 145.2$ ppm). Pd^0 is generated[64,73b] in situ and undergoes oxidative addition to *p*-toluenesulfonyl chloride, thereby inserting into either the SO_2–Cl bond or the C–SO_2 bond. Subsequent rapid loss of SO_2 gives the same aryl palladium chloride in either case which in turn undergoes cross-coupling with the organostannane, in a way similar to intermediates derived from aryl halides or triflates in Stille couplings.[10] In Stille reactions, and under our conditions, the sulfonyl chloride is more reactive than the corresponding chloride or bromide. However, sulfonyl chlorides proved to be less reactive than the corresponding iodides.

Aryl and arylmethane C-glycosides have been obtained through desulfitative Stille [Eq. (29)] and carbonylative Stille [Eq. (30)] cross-coupling of tin glycals and sulfonyl chlorides.[26b]

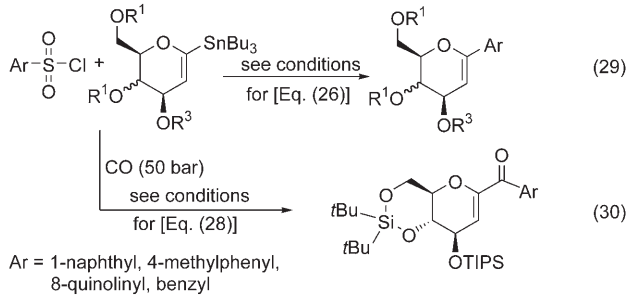

Arene, aryl methane, and alk-2-ene sulfonyl chlorides undergo Suzuki–Miyaura cross-coupling with arene, heteroarene, and alkene boronic acids in THF at reflux [Eq. (31)]. In this case too, the reactivity order is ArI > $ArSO_2Cl$ > ArBr > ArCl.[25]

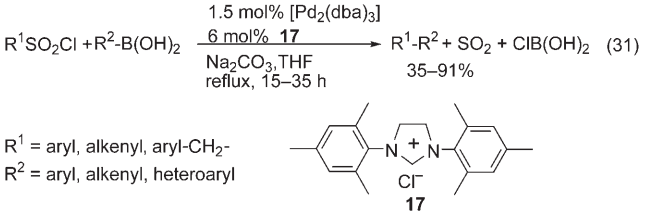

Na_2CO_3 proved to be the best activator for the boronic acids (without destroying the sulfonyl chloride) relative to other bases such as Et_3N, Cs_2CO_3, NaOAc, K_3PO_4, K_2CO_3, or Li_2CO_3. In the presence of Cs_2CO_3, we failed to observe any trace of the cross-coupling product (α-naphthalenesulfonyl chloride + 4-methylbenzeneboronic acid), even though all the starting sulfonyl chloride was consumed.

A wide range of electronically and structurally diverse sulfonyl chlorides and boronic acids were examined and proved to undergo efficient cross-coupling under our conditions. Thus, electron-rich, electron-neutral, and electron-poor arene sulfonyl chlorides reacted with boronic acids to provide the corresponding biaryl products. Self-coupling of boronic acids was observed concurrently in some cases.[74] The proportion of the latter was lower in boiling THF than in boiling dioxane, acetonitrile, 1,2-dimethoxyethane, or *p*-xylene.

The postulated mechanism of the reaction is shown in Scheme 2. Palladium(0) species arises either from $PdCl_2$ or

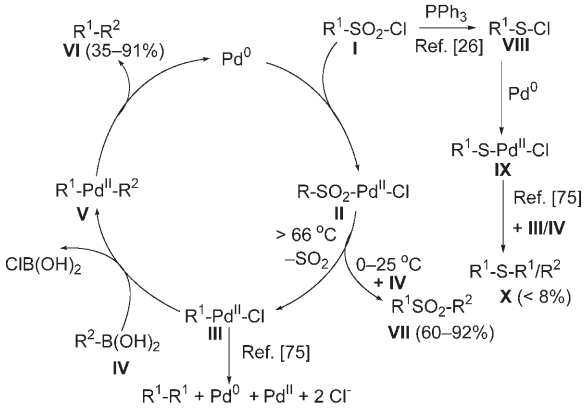

Scheme 2. Proposed catalytic cycle for Suzuki–Miyaura cross-coupling of sulfonyl chlorides and boronic acids.

from the addition of sterically hindered or electron-rich ligands to $[Pd_2(dba)_3]$. The O_2S–Cl bond of the arene sulfonyl chloride undergoes oxidative addition to the Pd^0 species to give first a chloro palladium(II) sulfinate of type **II**. At higher temperatures (> 66 °C) loss of SO_2 occurs rapidly and a Ar–Pd–Cl complex of type **III** forms which then undergoes cross-coupling with the arene boronic acids **IV**,[25] in a way similar to aryl halides or triflates in Suzuki–Miyaura condensations.[1,9]

In the presence of $[Pd(PPh_3)_4]$ catalyst, traces of diaryl sulfide were frequently observed. For instance, treatment of *p*-toluenesulfonyl chloride with 4-methoxybenzeneboronic acid in the presence of $[Pd(PPh_3)_4]$ and K_2CO_3 (3 equiv) led to Tol-S-Ar **X** (Ar = 4-methoxyphenyl), which was isolated in 8% yield. The formation of this by-product probably results from the reduction of the sulfonyl chloride to the corresponding sulfenyl chloride **VIII** by PPh_3.[26a] The Pd^0 then inserts into the S–Cl bond followed by coupling with the boronic acid **IV** (Scheme 2). In contrast, when carbenes and sterically hindered or electron-rich ligands are employed, the aryl palladium chloride intermediates **III** can give the corresponding homocoupled products[75] (Scheme 2).

© 2005 Wiley-VCH Verlag GmbH & Co. KGaA, Weinheim

At 0–25 °C, loss of SO_2 does not occur in chloro palladium(II) sulfinate **II** and, following transmetalation with arene boronic acid **IV**, yields a palladium(II) complex, which undergoes reductive elimination of the product sulfones **VII** with concomitant regeneration of the active palladium(0) catalyst.[25,76] These results show that the palladium(0) species undergoes SO_2–Cl rather than C–SO_2 oxidative addition of an arene sulfonyl chloride.

The reaction of 4-bromobenzenesulfonyl chloride (**18**) and 4-methylbenzene boronic acid (**19**) gives the corresponding bromobiaryl compound **20**, which reacts with 3-nitrobenzeneboronic acid (**21**) to generate unsymmetrical teraryl **22** in 52% yield, together with 4% of **23** (Scheme 3).

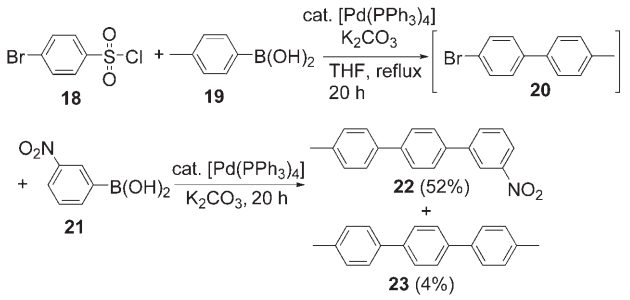

Scheme 3. Chemoselective sequential Suzuki–Miyaura cross-couplings.

When the above reactions were carried out at 0–25 °C, sulfones were formed instead of the products of Suzuki–Miyaura cross-coupling. Good yields of unsymmetrical diaryl sulfones were obtained when using $PdCl_2$ as catalyst and K_2CO_3 as base [Eq. (32)].[76]

$$\mathrm{ArSO_2Cl + Ar'\text{-}B(OH)_2} \xrightarrow[\text{acetone/H}_2\text{O (3:1)},\ \text{N}_2,\ 0\text{–}25\ ^\circ\text{C}]{2\ \text{mol\%}\ \mathrm{PdCl_2},\ \mathrm{K_2CO_3}} \mathrm{ArSO_2Ar'}\ (60\text{–}92\%) \qquad (32)$$

Ar, Ar' = aryl, heteroaryl

Preliminary results from our laboratory suggest that Negishi-type couplings can be carried out between arene sulfonyl chlorides and zinc reagents in the presence of a catalytic amount of $[Pd(PtBu_3)_2]$ in THF at reflux [Eq. (33)].[29]

$$\mathrm{R^1SO_2Cl + R^2\text{-}ZnX} \xrightarrow[\text{THF, reflux, 15 h}]{\text{cat. } [\mathrm{Pd\{P}t\mathrm{Bu_3\}_2}]} \mathrm{R^1\text{-}R^2 + SO_2 + ZnXCl} \qquad (33)$$

We reported conditions for the first palladium-catalyzed desulfitative carbon–carbon cross-coupling of arene sulfonyl chlorides with aryl and alkyl acetylenes [Eq. (34)].

$$\mathrm{ArSO_2Cl + HC{\equiv}CR} \xrightarrow[\text{15 mol\% CuI, } \mathrm{K_2CO_3}\text{, THF, 66 °C}]{\text{3 mol\% } [\mathrm{Pd_2(dba)_3}],\ \text{10 mol\% } \mathrm{P}t\mathrm{Bu_3}} \mathrm{ArC{\equiv}CR + SO_2 + HCl}\ (40\text{–}72\%) \qquad (34)$$

$[Pd_2(dba)_3]$/$PtBu_3$ and CuI proves to be the best catalyst system for the reactions in refluxing THF and in the presence of K_2CO_3.[28]

In the presence of $[PdCl_2(PhCN)_2]$ catalyst and CuI cocatalyst (5 mol% each), the reaction of TsCl with phenylacetylene leads to the desulfitative cross-coupled product in low yield ($\leq$10%). The major product was the undesired diphenylbuta-1,3-diyne (Glaser reaction).[77] However, the required cross-coupling could be seen in the presence of $[\{(\pi\text{-allyl})PdCl\}_2]$ and $PtBu_3$ (4:15 mol%). In this case, K_2CO_3 is a better base than Et_3N as it improves the competition between the desired cross-coupling and undesired homocoupling reactions. To our surprise, diaminocarbene ligands generated by α elimination of HCl from **17** (and analogous salts) led to no cross-coupling at all. Among several phosphine ligands tested, $PtBu_3$ gave the best results. It was also found that boiling THF is better than toluene or acetonitrile. A possible mechanism for these reactions is shown in Scheme 4.

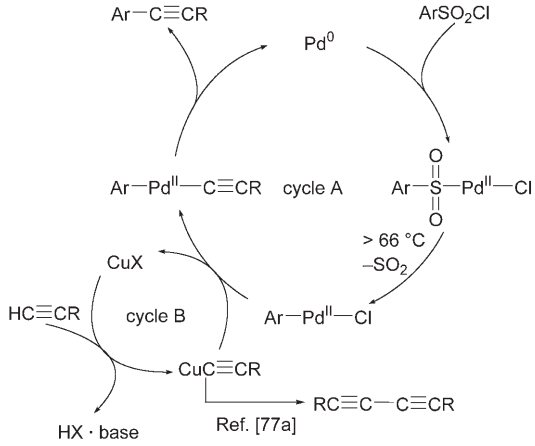

Scheme 4. Proposed catalytic cycle for the desulfitative Sonogashira–Hagihara cross-coupling of sulfonyl chlorides and terminal alkynes.

Since copper cocatalyst promotes the homocoupling of acetylenes (Glaser reaction[77]) and inhibits their cross-coupling reactions,[78] conditions have been proposed for copper-free palladium-catalyzed Sonogashira–Hagihara couplings.[79] Under the latter conditions, arene sulfonyl chlorides do not undergo desulfitative cross-couplings with acetylenes. Thus presently, CuI is still necessary as cocatalyst.

As a continuation of the work of Kasahara et al.[63] and Miura and co-workers work,[64] we explored catalysts other than $[PdCl_2(PhCN)_2]$, $Pd(OAc)_2$, $PdCl_2$, Pd black, and $[PdCl_2(PPh_3)_2]$ in the desulfitative Mizoroki–Heck type reactions

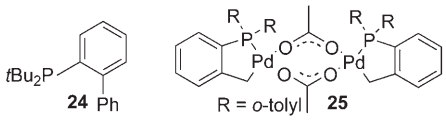

with electron-rich [Eq. (24)] and electron-poor alkenes [Eq. (25)]. We were inspired by numerous recent advances made in classic Mizoroki–Heck reactions (with aryl halide reagents in the presence of phase-transfer catalysts[80] and palladium complexes containing electron-rich ligands such as

© 2005 Wiley-VCH Verlag GmbH & Co. KGaA, Weinheim

17,[21a] P*t*Bu$_3$,[21b–c] and **24**[81] or the palladacycle **25**[82]). We found new conditions for the desulfitative Mizoroki–Heck arylation and trifluoromethylation of mono- [Eq. (35)] and

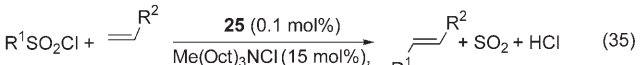

(35)

R^1 = aryl, CF_3
R^2 = COO*n*Bu, Ph, SO_2Ph

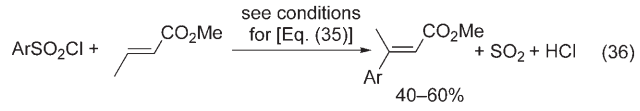

(36)

Ar = 4-F-C_6H_4, 4-NO_2-C_6H_4, 4-MeO-C_6H_4, 3-NC-C_6H_4

disubstituted olefins [Eq. (36)] with arene sulfonyl and trifluoromethanesulfonyl chlorides. *E*-1,2-Disubstituted alkenes were obtained with high stereoselectivity and 1,1,2-trisubstituted alkenes were prepared with 12:1 to 21:1 *E*/*Z* stereoselectivity. The Herrmann palladacycle **25** (0.1 mol%) is sufficient to catalyze these reactions for which electron-rich or electron-poor sulfonyl chlorides and alkenes are suitable.

Double desulfitative Mizoroki–Heck couplings have also been carried out [Eqs. (37) and (38)]. Important polymer precursors[83] have been produced in this way.

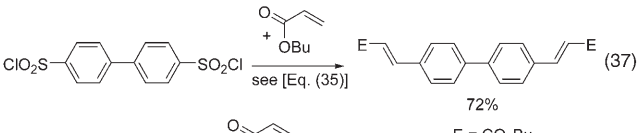

(37)

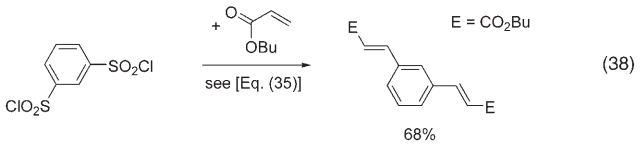

(38)

The reaction of arene sulfonyl chlorides with styrene in the presence of a catalytic amount of $PdCl_2$ or [$Pd(PPh_3)_4$] in benzene or in THF at 60 °C (instead of 140 °C) and in the presence of K_2CO_3 or NEt_3 produces the corresponding α,β-unsaturated sulfones **26**. Heating of sulfone **26** in boiling xylene in the presence of **25** (1 mol%) or [{$RhCl(C_2H_4)_2$}$_2$] (1 mol%) did not produce any traces of products of SO_2 loss after 24 h. This observation shows that sulfones **26** (Scheme 5) are not intermediates in these Heck-type reactions [see Eqs. (35)–(38)]. Kamigata and co-workers[84f] reported that [$RuCl_2(PPh_3)_2$] catalyzes the addition of sulfonyl chlorides to alkenes with the formation of the corresponding sulfones. These reactions imply $RSO_2^{\bullet}$ radical intermediates that are scavenged by the galvinoxyl free radical. This was not the case with our reactions [Eqs. (35)–(38)] catalyzed by [$Pd(PPh_3)_4$]/Et_3N because these were neither inhibited by galvinoxyl nor by 2,2,6,6-tetramethylpiperidine 1-oxyl radical (TEMPO).[27] These observations can be interpreted by the mechanism shown in Scheme 5. A palladium(0) species such as [$Pd(PPh_3)_4$] or one arising from **25**[82d] first undergoes oxidative addition into the SO_2–Cl bond of an arene sulfonyl chloride.

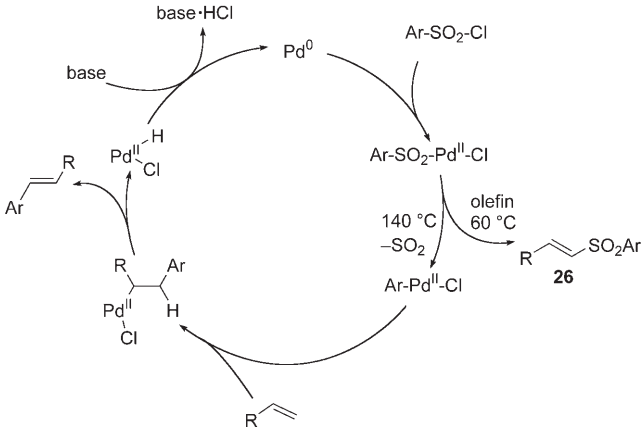

Scheme 5. Proposed catalytic cycle for sulfone synthesis and desulfitative Mizoroki–Heck type reaction between sulfonyl chlorides and olefins.

[($Pd(PPh_3)_4$] was chosen because it is known that this catalyst facilitates the reaction of arene sulfonyl chlorides with organostannanes[68] and arene boronic acids,[76]) and the alkene insertion generates the corresponding sulfone **26**. At 60 °C, loss of SO_2 does not occur, whereas at higher temperature (140 °C) SO_2 loss is rapid and forms an Ar-Pd-Cl complex, which then undergoes β addition to the olefin, followed by β elimination of chlorohydridopalladium to afford the final product of Heck coupling together with the active Pd^0 catalyst.

If phosphine- and base-free conditions are required, [{$RhCl(C_2H_4)_2$}$_2$] can be used to catalyze the desulfitative Mizoroki–Heck reactions [Eqs. (32)–(35)]. The mechanisms of these rhodium(I)-catalyzed reactions are probably similar to those for the Pd^0-catalyzed reactions (Scheme 5). We verified that the Rh-catalyzed reactions were not inhibited by radical-scavenging agents such as the galvinoxyl free radical.

Miura and co-workers reported that arene sulfonyl chlorides can be desulfitated and carbonylated with $Ti(OR)_4$ and carbon monoxide (10 atm) in the presence of palladium in acetonitrile at 150 °C to give the corresponding arene carboxylic esters [Eq. (39)].[65] They also found that, in the absence of carbon monoxide, desulfitative homocouplings

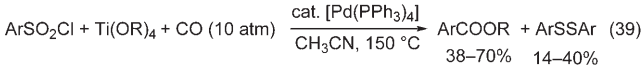

(39)

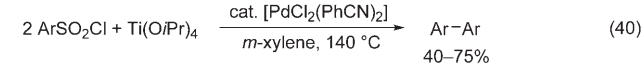

(40)

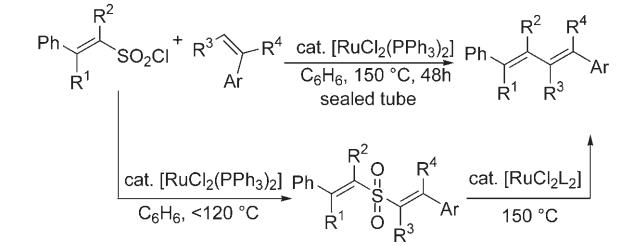

Scheme 6. Ru^{II}-catalyzed reactions of alkene sulfonyl chlorides with alkenes.

© 2005 Wiley-VCH Verlag GmbH & Co. KGaA, Weinheim

occur in *m*-xylene at reflux to give symmetrical biaryl species [Eq. (40)].[66]

Perfluoroalkene- and benzenesulfonyl chlorides add to alkenes in the presence of $[RuCl_2(PPh_3)_2]$ catalyst.[84] When the reactions are carried out at high temperature, SO_2 is eliminated and Mizoroki–Heck-type products are obtained (Scheme 6) instead of the corresponding sulfones. The process works with alkenes, arenes, and thiophene.[84c,d] The same reactions can be applied to prepare 1,3-dienes (Scheme 6).[84e,f]

6. Summary and Perspective

Organosulfur compounds are versatile electrophilic reagents for C–C cross-coupling reactions with organometallic compounds in the presence of transition-metal catalysts. Recent discoveries herald a renaissance for sulfonyl chlorides as versatile reagents for C–C coupling reactions. As arene sulfonyl chlorides are often less expensive and more reactive than corresponding aryl chlorides,[25–26] their importance in materials science and medicinal chemistry should grow in the future. Other organosulfur compounds such as sulfones, sulfoxides, sulfoximines, sulfonates, and sulfonamides can be synthesized on larger scales and engaged in Negishi- or Kumada-type cross-coupling reactions in the presence of less-expensive nickel catalysts. The reaction of substituted ketones with enantiomerically pure $LiCH_2SO(NMe)Ph$ through asymmetric elimination[31d–e] provides easy access to alkenyl sulfoximines. The latter were successfully employed in Kumada-type cross-coupling reactions, thus realizing the key step in the synthesis of important biologically active compounds.[31a–c] Based on these recent developments, organosulfur compounds should find even broader applications as coupling partners in the area of target synthesis.[85]

This work was supported by the Swiss National Science Foundation (Grant No. 2000-20100002/1). We are grateful to M. Thresen, Dr. M. Turks, Dr. Ana T. Carmona, R. Mimna, and N. Jagan Mohan Rao for their critical reading of this manuscript and suggestions.

Received: December 21, 2004
Revised: April 4, 2005
Published online: November 15, 2005

[1] a) M. Beller, A. Zapf in *Handbook of Organopalladium Chemistry for Organic Synthesis, Vol. 1* (Ed.: E.-I. Negishi), Wiley, New York, **2002**, pp. 1209–1222; b) *Metal-Catalyzed Cross-Coupling Reactions, Vol. 1&2* (Eds.: A. de Meijere, F. Diederich), 2nd ed., Wiley-VCH, Weinheim, **2004**; c) *Metal-catalyzed Cross-coupling Reactions* (Eds.: F. Diederich, P. J. Stang), Wiley-VCH, Weinheim, **1998**; d) J. Hassan, M. Sévignon, C. Gozzi, E. Schulz, M. Lemaire, *Chem. Rev.* **2002**, *102*, 1359–1470; e) for a brief historical survey of cross-coupling reactions developed during 1970s and 1980s, see: K. Tamao, T. Hiyama, E.-I. Negishi, *J. Organomet. Chem.* **2002**, *653*, 1–303; f) non-activated alkyl halides are electrophilic reagents; see: A. C. Frisch, M. Beller, *Angew. Chem.* **2005**, *117*, 680–695; *Angew. Chem. Int. Ed.* **2005**, *44*, 674–688.

[2] a) J. F. Hartwig, *Angew. Chem.* **1998**, *110*, 2154–2177; *Angew. Chem. Int. Ed.* **1998**, *37*, 2046–2067; b) J. F. Hartwig, *Acc. Chem. Res.* **1998**, *31*, 852–860; c) J. F. Hartwig, *Pure. Appl. Chem.* **1999**, *67*, 805–818; d) B. H. Yang, S. L. Buchwald, *J. Organomet. Chem.* **1999**, *576*, 125–146; e) J. P. Wolfe, S. L. Buchwald, *Angew. Chem.* **1999**, *111*, 2570–2573; *Angew. Chem. Int. Ed.* **1999**, *38*, 2413–2415; f) J. P. Wolfe, S. Wagaw, J.-F. Marcoux, S. L. Buchwald, *Acc. Chem. Res.* **1998**, *31*, 805–818; g) A. R. Muci, S. L. Buchwald, *Top. Curr. Chem.* **2002**, *219*, 131–209; h) H.-U. Blaser, A. Indolese, F. Naud, U. Nettekoven, A. Schnyder, *Adv. Synth. Catal.* **2004**, *346*, 1583–1598; i) B. Schlummer, U. Scholz, *Adv. Synth. Catal.* **2004**, *346*, 1599–1626.

[3] a) *Transition Metals for Organic Synthesis* (Eds.: M. Beller, C. Bolm), Wiley-VCH, Weinheim, **1998**; b) *Transition Metals for Organic Synthesis* (Eds.: M. Beller, C. Bolm), 2nd ed., Wiley-VCH, Weinheim, **2004**.

[4] a) A. Zapf, M. Beller, *Top. Catal.* **2002**, *19*, 101–109; b) J. G. de Vries, *Can. J. Chem.* **2001**, *79*, 1086–1092, and references therein; c) A. C. Hiller, G. A. Grassa, M. S. Viciu, H. M. Lee, C. Yang, S. P. Nolan, *J. Organomet. Chem.* **2002**, *653*, 69–82; d) U. Beutler, J. Mazacek, G. Penn, B. Schenkel, D. Wasmuth, *Chimia* **1996**, *50*, 154; e) G. A. Grassa, M. S. Viciu, J. Huang, C. Zhang, M. L. Trudell, S. P. Nolan, *Organometallics* **2002**, *21*, 2866–2873; f) G. B. Smith, G. C. Dezeny, D. L. Hughes, A. O. King, T. R. Verhoeven, *J. Org. Chem.* **1994**, *59*, 8151–8156; g) P. Moutevelis-Minakakis, M. Gianni, H. Stougiannou, P. Zoumpoulakis, A. Zoga, A. D. Vlahakos, E. Iliodromitis, T. Mavromoustakos, *Bioorg. Med. Chem. Lett.* **2003**, *13*, 1737–1740; h) K. Kawada, A. Arimura, T. Tsuri, M. Fuji, T. Komurasaki, S. Yonezawa, A. Kugimiya, N. Haga, S. Mitsumori, M. Inagaki, T. Nakatani, Y. Tamura, S. Takechi, T. Taishi, J. Kishino, M. Ohtani, *Angew. Chem.* **1998**, *110*, 1015–1017; *Angew. Chem. Int. Ed. Engl.* **1998**, *37*, 973–975.

[5] For examples of applications in optical devices, see: a) P. Bordat, R. Brown, *Chem. Phys. Lett.* **2000**, *331*, 439–445; b) W. M. F. Fabian, J. M. Kauffman, *J. Lumin.* **1999**, *85*, 137–148.

[6] For examples of applications in electrical devices, see: a) G. Schiavon, S. Zecchin, G. Zotti, S. Cattarin, *J. Electroanal. Chem.* **1986**, *213*, 53–64; b) I. B. Berlman, H. O. Wirth, O. J. Steingraber, *J. Phys. Chem.* **1971**, *75*, 318–325.

[7] For examples of applications in liquid crystals, see: a) R. S. Wright, T. K. Vinod, *Tetrahedron Lett.* **2003**, *44*, 7129–7132; b) B. S. Udaykumar, G. B. Schuster, *J. Org. Chem.* **1992**, *57*, 348–352.

[8] K. C. Nicolaou, E. J. Sorenson, *Classics in Total Synthesis*, VCH, New York, **1996**, chap. 31.

[9] a) N. Miyaura, K. Yamada, A. Suzuki, *Tetrahedron Lett.* **1979**, *20*, 3437–3440; b) A. Suzuki, *J. Organomet. Chem.* **1999**, *576*, 147–168; c) N. Miyaura, *Top. Curr. Chem.* **2002**, *219*, 11–59; d) N. Miyaura, A. Suzuki, *Chem. Rev.* **1995**, *95*, 2457–2483; e) S. P. Stanforth, *Tetrahedron* **1998**, *54*, 263–303; f) N. Miyaura in *Advances in Metal-Organic Chemistry, Vol. 6* (Ed.: L. S. Liebeskind), JAI, London, **1996**; g) T. Jeffery in *Advances in Metal-Organic Chemistry, Vol. 5* (Ed.:L. S. Liebeskind), JAI, London, **1996**.

[10] a) D. Milstein, J. K. Stille, *J. Am. Chem. Soc.* **1978**, *100*, 3636–3638; b) M. Kosugi, K. Sasazawa, Y. Shimizu, T. Migita, *Chem. Lett.* **1977**, 301–302; c) J. K. Stille, *Angew. Chem.* **1986**, *98*, 504–519; *Angew. Chem. Int. Ed. Engl.* **1986**, *25*, 508–524; d) T. N. Mitchell, *Synthesis* **1992**, 803–815; e) V. Farina, V. Krishnamurthy, W. J. Scott, *Org. React.* **1997**, *50*, 1–652; f) K. Fugami, M. Kosugi, *Top. Curr. Chem.* **2002**, *219*, 87–130; g) P. Espinet, A. M. Echavarren, *Angew. Chem.* **2004**, *116*, 4808–4839; *Angew. Chem. Int. Ed.* **2004**, *43*, 4704–4734.

[11] a) Y. Hatanaka, T. Hiyama, *J. Org. Chem.* **1988**, *53*, 918–920; b) J. Yoshida, K. Tamao, H. Yamamoto, T. Kakui, T. Uchida, M. Kumada, *Organometallics* **1982**, *1*, 542–549; c) T. Hiyama, Y.

 © 2005 Wiley-VCH Verlag GmbH & Co. KGaA, Weinheim

Hatanaka, *Pure Appl. Chem.* **1994**, *66*, 1471 – 1478; d) T. Hiyama, T. Shirakawa, *Top. Curr. Chem.* **2002**, *219*, 61 – 85.

[12] a) E.-I. Negishi, A. O. King, N. Okukado, *J. Org. Chem.* **1977**, *42*, 1821 – 1823; b) E.-I. Negishi, *Acc. Chem. Res.* **1982**, *15*, 340 – 348; c) E.-I. Negishi, L. Anastasia, *Chem. Rev.* **2003**, *103*, 1979 – 2018.

[13] a) K. Tamao, K. Sumitani, M. Kumuda, *J. Am. Chem. Soc.* **1972**, *94*, 4374 – 4376; b) R. J. P. Corriu, J. P. Masse, *J. Chem. Soc. Chem. Commun.* **1972**, 144 – 145; c) M. Yamamura, I. Moritani, S. I. Marahashi, *J. Organomet. Chem.* **1975**, *91*, C39 – C42; d) A. Minato, K. Suzuki, K. Tamao, M. Kumada, *J. Chem. Soc. Chem. Commun.* **1984**, 511 – 513; e) V. Bonnet, F. Morgin, F. Trécouret, G. Quéguiner, P. Knochel, *Tetrahedron Lett.* **2001**, *42*, 5717 – 5719; f) H. Ohmiya, T. Tsuji, H. Yorimitsu, K. Oshima, *Chem. Eur. J.* **2004**, *10*, 5640 – 5648.

[14] a) T. Mizoroki, K. Mori, A. Ozaki, *Bull. Chem. Soc. Jpn.* **1971**, *44*, 581; b) R. F. Heck, J. P. Nolley, Jr., *J. Org. Chem.* **1972**, *37*, 2320 – 2322; c) for reviews of the Heck–Mizoroki reaction, see, for example: I. P. Beletskaya, A. V. Cheprakov, *Chem. Rev.* **2000**, *100*, 3009 – 3066; d) R. F. Heck in *Comprehensive Organic Synthesis, Vol. 4* (Ed.: B. M. Trost), Pergamon, New York, **1991**, chap. 4.3; e) R. F. Heck, *Org. React.* **1982**, *27*, 345 – 390; f) G. T. Crisp, *Chem. Soc. Rev.* **1998**, *27*, 427 – 436; g) A. de Meijere, F. E. Meyer, *Angew. Chem.* **1994**, *106*, 2473 – 2506; *Angew. Chem. Int. Ed. Engl.* **1994**, *33*, 2379 – 2411; h) W. Cabri, I. Candiani, *Acc. Chem. Res.* **1995**, *28*, 2 – 7; i) for a critical overview, see: V. Farina, *Adv. Synth. Catal.* **2004**, *346*, 1553 – 1582.

[15] a) K. Sonogashira, Y. Tohda, N. Hagihara, *Tetrahedron Lett.* **1975**, *16*, 4467 – 4470; b) K. Takahashi, Y. Kuroyama, K. Sonogashira, *Synthesis* **1980**, 627 – 629; c) K. Sonogashira, *J. Organomet. Chem.* **2002**, *653*, 46 – 49; d) L. A. Agrofoglio, I. Gillaizeau, Y. Saito, *Chem. Rev.* **2003**, *103*, 1875 – 1916.

[16] a) Q. Yao, E. P. Kinney, C. Zheng, *Org. Lett.* **2004**, *6*, 2997 – 2999; b) K. H. Shaughnessy, P. Kim, J. F. Hartwig, *J. Am. Chem. Soc.* **1999**, *121*, 2123 – 2132; c) A. Ehrentraut, A. Zapf, M. Beller, *Synlett* **2000**, 1589 – 1592; d) A. S. Gruber, D. Zim, G. Ebeling, A. L. Monteiro, J. Dupont, *Org. Lett.* **2000**, *2*, 1287 – 1290; e) D. E. Bergbreiter, P. L. Osburn, Y.-S. Liu, *J. Am. Chem. Soc.* **1999**, *121*, 9531 – 9538; f) M. E. van der Bhoom, D. Milstein, *Chem. Rev.* **2003**, *103*, 1759 – 1792.

[17] a) H. Hagiwara, Y. Sugawara, K. Isobe, T. Hoshi, T. Suzuki, *Org. Lett.* **2004**, *6*, 2325 – 2328, and references therein; b) K. Okamoto, R. Akiyama, S. Kobayashi, *Org. Lett.* **2004**, *6*, 1987 – 1990; c) W. Solodenko, H. Wen, S. Leue, F. Stuhlmann, G. Sourkoni-Argirusi, G. Jas, H. Schönfeld, U. Kunz, A. Kirschning, *Eur. J. Org. Chem.* **2004**, 3601 – 3610, and references therein.

[18] For a review, see: a) T. Welton, P. J. Smith, *Adv. Organomet. Chem.* **2004**, *51*, 251 – 284; b) J. Dupont, R. F. de Souza, P. A. Z. Suarez, *Chem. Rev.* **2002**, *102*, 3667 – 3691.

[19] a) L. F. Tietze, J. M. Wiegand, C. A. Vock, *Eur. J. Org. Chem.* **2004**, 4107 – 4112, and references therein; b) C. J. Kressierer, T. J. J. Müller, *Angew. Chem.* **2004**, *116*, 6123 – 6127; *Angew. Chem. Int. Ed.* **2004**, *43*, 5997 – 6000, and references therein; c) T. Satoh, S. Ogino, M. Miura, M. Nomura, *Angew. Chem.* **2004**, *116*, 5173 – 5175; *Angew. Chem. Int. Ed.* **2004**, *43*, 5063 – 5065.

[20] For a recent review, see: a) L. F. Tietze, H. Lla, H. P. Bell, *Chem. Rev.* **2004**, *104*, 3453 – 3516; b) M. Shibasaki, E. M. Vogl, T. Ohshima, *Adv. Synth. Catal.* **2004**, *346*, 1533 – 1552.

[21] a) For a recent review on N-heterocyclic carbenes, see: W. A. Herrmann, *Angew. Chem.* **2002**, *114*, 1342 – 1363; *Angew. Chem. Int. Ed.* **2002**, *41*, 1290 – 1309; b) for a recent review on electron-rich and sterically bulky ligands, see, for example: A. F. Littke, G. C. Fu, *Angew. Chem.* **2002**, *114*, 4350 – 4386; *Angew. Chem. Int. Ed.* **2002**, *41*, 4176 – 4211; c) S. R. Dubbaka, *Synlett* **2005**, 709 – 710.

[22] For a review, see: a) C. O. Kappe, *Angew. Chem.* **2004**, *116*, 6408 – 6443; *Angew. Chem. Int. Ed.* **2004**, *43*, 6250 – 6284; b) A. K. Bose, M. S. Manhas, S. N. Subhendu, A. H. Sharma, B. K. Banik, *Synthesis* **2002**, 1578 – 1591; c) P. Lidström, J. Tierney, B. Wathey, J. Westman, *Tetrahedron* **2001**, *57*, 9225 – 9283; d) S. Caddick, *Tetrahedron* **1995**, *51*, 10403 – 10432.

[23] a) For a minireview, see: A. Zapf, *Angew. Chem.* **2003**, *115*, 5552 – 5557; *Angew. Chem. Int. Ed.* **2003**, *42*, 5394 – 5399; b) L. J. Gooßen, J. Paetzold, *Angew. Chem.* **2004**, *116*, 1115 – 1118; *Angew. Chem. Int. Ed.* **2004**, *43*, 1095 – 1098; c) T. Sugihara, T. Satoh, M. Miura, *Angew. Chem.* **2003**, *115*, 4820 – 4822; *Angew. Chem. Int. Ed.* **2003**, *42*, 4672 – 4674.

[24] For the preparation of 2-methylprop-2-enesulfonyl chloride, see: a) L. C. Bouchez, S. R. Dubbaka, M. Turks, P. Vogel, *J. Org. Chem.* **2004**, *69*, 6413 – 6418; b) S. R. Dubbaka, P. Vogel, *Tetrahedron* **2005**, *61*, 1523 – 1530, and references therein.

[25] S. R. Dubbaka, P. Vogel, *Org. Lett.* **2004**, *6*, 95 – 98.

[26] a) S. R. Dubbaka, P. Vogel, *J. Am. Chem. Soc.* **2003** *125*, 15292 – 15293; b) S. R. Dubbaka, P. Steunenberg, P. Vogel, *Synlett* **2004**, 1235 – 1238.

[27] S. R. Dubbaka, P. Vogel, *Chem. Eur. J.* **2005**, *11*, 2633 – 2641.

[28] S. R. Dubbaka, P. Vogel, *Adv. Synth. Catal.* **2004**, *346*, 1793 – 1797.

[29] S. R. Dubbaka, P. Vogel, unpublished results.

[30] a) E. Wenkert, T. W. Ferreira, E. L. Michelotti, *J. Chem. Soc. Chem. Commun.* **1979**, 637 – 638; b) E. Wenkert, M. E. Shepard, A. T. Mcphail, *J. Chem. Soc. Chem. Commun.* **1986**, 1390 – 1391; c) E. Wenkert, D. Chianelli, *J. Chem. Soc. Chem. Commun.* **1991**, 627 – 628; d) E. Wenkert, J. B. Fernandes, E. L. Michelotti, C. S. Swinndell, *Synthesis* **1983**, 701 – 703; e) E. Wenkert, E. L. Michelotti, C. S. Swinndell, *J. Am. Chem. Soc.* **1979**, *101*, 2246 – 2247; f) F. Rebière, O. Riant, L. Ricard, H. B. Kagan, *Angew. Chem.* **1993**, *105*, 644 – 648; *Angew. Chem. Int. Ed. Engl.* **1993**, *32*, 568 – 570; g) K. Itami, M. Mineno, N. Muraoka, J.-I. Yoshida, *J. Am. Chem. Soc.* **2004**, *126*, 11778 – 11779.

[31] a) I. Erdelmeier, H.-J. Gais, *J. Am. Chem. Soc.* **1989**, *111*, 1125 – 1126; b) H.-J. Gais, G. Bulow, *Tetrahedron Lett.* **1992**, *33*, 461 – 464; c) H.-J. Gais, G. Bulow, *Tetrahedron Lett.* **1992**, *33*, 465 – 468; d) H.-J. Gais, I. Erdelmeier, H. J. Linder, J. Vollhardt, *Angew. Chem.* **1986**, *98*, 914 – 915; *Angew. Chem. Int. Ed. Engl.* **1986**, *25*, 938 – 939; e) I. Erdelmeier, H. J. Linder, *Angew. Chem.* **1986**, *98*, 912 – 914; *Angew. Chem. Int. Ed. Engl.* **1986**, *25*, 935 – 937.

[32] a) H. Okamura, Y. Mitsuhira, M. Miura, H. Takei, *Chem. Lett.* **1978**, 517 – 518; b) H. Okamura, Y. Mitsuhira, M. Miura, H. Takei, *Tetrahedron Lett.* **1979**, *20*, 43 – 46, and references therein; c) for a recent example, see: K. Itami, D. Yamazaki, J.-I. Yoshida, *J. Am. Chem. Soc.* **2004**, *126*, 15396 – 15397.

[33] H. Okamura, M. Miura, K. Kosugi, H. Takei, *Tetrahedron Lett.* **1980**, *21*, 87 – 90, and references therein.

[34] M. Tiecco, L. Testaferri, M. Tingoli, E. Wenkert, *Tetrahedron* **1983**, *39*, 2289 – 2294.

[35] For vinyl *tert*-butyl sulfones, see: a) J.-L. Fabre, M. Julia, J.-N. Verpeaux, *Tetrahedron Lett.* **1982**, *23*, 2469 – 2472; b) J.-L. Fabre, M. Julia, J.-N. Verpeaux, *Bull. Soc. Chim. Fr.* **1985**, 762 – 771; c) J.-L. Fabre, M. Julia, J.-N. Verpeaux, *Bull. Soc. Chim. Fr.* **1985**, 772 – 778; for aryl *tert*-butyl sulfones, see: d) J. Clayden, M. Julia, *J. Chem. Soc. Chem. Commun.* **1993**, 1682 – 1683; e) J. Clayden, J. J. A. Cooney, M. Julia, *J. Chem. Soc. Perkin Trans. 1* **1995**, 7 – 14, and references therein.

[36] a) M. Kumuda, *Pure Appl. Chem.* **1980**, *52*, 669 – 679; b) K. Tamao, *J. Organomet. Chem.* **2002**, *653*, 23 – 26.

[37] J. Liu, M. J. Robins, *Org. Lett.* **2005**, *7*, 1149 – 1151.

[38] C.-H. Cho, I.-S. Kim, K. Park, *Tetrahedron* **2004**, *60*, 4589 – 4599.

[39] a) C.-H. Cho, H.-S. Yun, K. Park, *J. Org. Chem.* **2003**, *68*, 3017 – 3025; b) C.-H. Cho, C. B. Kim, M. Sun, K. Park, *Bull. Korean. Chem. Soc.* **2003**, *24*, 1630 – 1634.

[40] R. R. Milburn, V. Snieckus, *Angew. Chem.* **2004**, *116*, 906 – 909; *Angew. Chem. Int. Ed.* **2004**, *43*, 888 – 891.

© 2005 Wiley-VCH Verlag GmbH & Co. KGaA, Weinheim

[41] K. Tamao, K. Sumitani, Y. Kiso, M. Zembayashi, A. Fujioka, S. Kodama, I. Nakajima, A. Minato, M. Kumada, *Bull. Chem. Soc. Jpn.* **1976**, *49*, 1958 – 1969.
[42] G. Anctil, V. Snieckus, *J. Organomet. Chem.* **2002**, *653*, 150 – 160.
[43] R. R. Milburn, V. Snieckus, *Angew. Chem.* **2004**, *116*, 910 – 912; *Angew. Chem. Int. Ed.* **2004**, *43*, 892 – 894.
[44] a) J. G. Ferry, *Annu. Rev. Microbiol.* **1995**, *49*, 305 – 333; b) S. W. Ragsdale, M. Kumar, *Chem. Rev.* **1996**, *96*, 2515 – 2539; c) U. Ermler, W. Grabarse, S. Shima, M. Goubeaud, R. K. Thauer, *Science* **1997**, *278*, 1457 – 1462; d) R. G. Matthews, C. W. Goulding, *Curr. Opin. Chem. Biol.* **1997**, *1*, 332 – 339; e) C. W. Goulding, R. G. Matthews, *Biochemistry* **1997**, *36*, 15749 – 15757; f) P. E. Jablonski, W. P. Lu, S. W. Ragsdale, J. G. Ferry, *J. Biol. Chem.* **1993**, *268*, 325 – 329; g) W. Maret, B. L. Vallee, *Proc. Natl. Acad. Sci. USA* **1998**, *95*, 3478 – 3482; h) J. H. R. Kaegi, A. Schaeffer, *Biochemistry* **1988**, *27*, 8509 – 8515.
[45] J. Srogl, G. D. Allred, L. S. Liebeskind, *J. Am. Chem. Soc.* **1997**, *119*, 12376 – 12377, and references therein.
[46] a) S. Zhang, D. Marshall, L. S. Liebeskind, *J. Org. Chem.* **1999**, *64*, 2796 – 2804; b) C. Savarin, J. Srogl, L. S. Liebeskind, *Org. Lett.* **2000**, *2*, 3229 – 3231.
[47] R. P. Hausinger, *Biochemistry of Nickel*, Plenum, New York, **1993**, pp. 147 – 180.
[48] J. Srogl, W. Liu, D. Marshall, L. S. Liebeskind, *J. Am. Chem. Soc.* **1999**, *121*, 9449 – 9450.
[49] M. E. Angiolelli, A. L. Casalnuovo, T. P. Selby, *Synlett* **2000**, 905 – 907.
[50] C. Savarin, J. Srogl, L. S. Liebeskind, *Org. Lett.* **2001**, *3*, 91 – 93.
[51] L. S. Liebeskind, J. Srogl, *Org. Lett.* **2002**, *4*, 979 – 981.
[52] M. Egi, L. S. Liebeskind, *Org. Lett.* **2003**, *5*, 801 – 802.
[53] F.-A. Alphonse, F. Suzenet, A. Keromnes, B. Lebret, G. Guillaument, *Org. Lett.* **2003**, *5*, 803 – 805.
[54] C. L. Kusturin, L. S. Liebeskind, W. L. Neumann, *Org. Lett.* **2002**, *4*, 983 – 985.
[55] L. S. Liebeskind, J. Srogl, *J. Am. Chem. Soc.* **2000**, *122*, 11260 – 11261.
[56] Y. Yu, L. S. Liebeskind, *J. Org. Chem.* **2004**, *69*, 3554 – 3557.
[57] R. Wittenberg, J. Srogl, M. Egi, L. S. Liebeskind, *Org. Lett.* **2003**, *5*, 3033 – 3035.
[58] a) H. Tokuyama, S. Yokoshima, T. Yamashita, T. Fukuyama, *Tetrahedron Lett.* **1998**, *39*, 3189 – 3192; b) H. Tokuyama, S. Yokoshima, T. Yamashita, S.-C. Lin, L. Li, T. Fukuyama, *J. Braz. Chem. Soc.* **1998**, *9*, 381 – 387; c) Y. Mori, M. Seki, *Tetrahedron Lett.* **2004**, *45*, 7343 – 7345, and references therein; d) for a recent example, see: Y. Zhang, T. Rovis, *J. Am. Chem. Soc.* **2004**, *126*, 15964 – 15965.
[59] a) R. T. Morrison, R. N. Boyd, *Organic Chemistry*, 5th ed., Allyn Bacon, Boston, **1987**; b) *Kirk-Othmer Concise Encyclopedia of Chemical Technology*, Wiley-VCH, New York, **1985**.
[60] J. P. Collman, W. R. Roper, *J. Am. Chem. Soc.* **1966**, *88*, 180 – 181.
[61] C. D. Cook, G. S. Jauhal, *Can. J. Chem.* **1967**, *45*, 301 – 304.
[62] J. Blum, G. Scharf, *J. Org. Chem.* **1970**, *35*, 1895 – 1899, and references therein.
[63] a) A. Kasahara, T. Izumi, N. Kudou, H. Azami, S. Yamamato, *Chem. Ind.* **1988**, 51 – 52; b) A. Kasahara, T. Izumi, K. Miyamoto, T. Sakai, *Chem. Ind.* **1989**, 192.
[64] a) M. Miura, H. Hashimoto, K. Itoh, M. Nomura, *Tetrahedron Lett.* **1989**, *30*, 975 – 976; b) M. Miura, H. Hashimoto, K. Itoh, M. Nomura, *J. Chem. Soc. Perkin Trans. 1* **1990**, *8*, 2207 – 2211.
[65] M. Miura, K. Itoh, M. Nomura, *Chem. Lett.* **1989**, 77 – 78.
[66] M. Miura, H. Hashimoto, K. Itoh, M. Nomura, *Chem. Lett.* **1990**, 459 – 460.
[67] See also: D. F. Taber, *Org. Chem. Highlights.* **2004**, *August* 9th.
[68] S. S. Labadie, *J. Org. Chem.* **1989**, *54*, 2496 – 2498.
[69] G. H. Posner, *An Introduction to Synthesis Using Organocopper Reagents*, Wiley-Interscience, New York, **1980**.
[70] a) H. E. Holmquist, J. E. Carnahan, *J. Org. Chem.* **1960**, *25*, 2240 – 2242; b) S. C. Shim, S. Antebi, H. Alper, *J. Org. Chem.* **1985**, *50*, 147 – 149; c) S. Antebi, H. Alper, *Tetrahedron Lett.* **1985**, *26*, 2609 – 2612.
[71] H. Kunniyasu, A. Ogawa, S.-I. Miyazaki, I. Ryu, N. Kambe, N. Sonoda, *J. Am. Chem. Soc.* **1991**, *113*, 9796 – 9803.
[72] J.-I. Kawakami, M. Mihara, I. Kamiya, M. Takeda, A. Ogawa, N. Sonoda, *Tetrahedron* **2003**, *59*, 3521 – 3526.
[73] a) D. E. Berbriter, P. L. Osburn, A. Wilson, E. M. Sink, *J. Am. Chem. Soc.* **2000**, *122*, 9058 – 9064; b) For a discussion on the generation of [Pd^0L] species in situ, see: U. Christmann, R. Vilar, *Angew. Chem.* **2005**, *117*, 370 – 378; *Angew. Chem. Int. Ed.* **2005**, *44*, 366 – 374.
[74] M. M. Mañas, M. Perez, R. Pleixats, *J. Org. Chem.* **1996**, *61*, 2346 – 2351.
[75] a) F. R. S. Clark, R. O. C. Norman, C. B. Thomas, *J. Chem. Soc. Perkin Trans. 1* **1975**, 121 – 125; b) J. Hassan, L. Lavenot, C. Gozzi, M. Lemaire, *Tetrahedron Lett.* **1999**, *40*, 857 – 858; c) S. Mukhopadhyay, G. Rothenberg, D. Gitis, Y. Sasson, *J. Org. Chem.* **2000**, *65*, 3107 – 3110.
[76] B. P. Bandgar, S. V. Bettigeri, J. Phopase, *Org. Lett.* **2004**, *6*, 2105 – 2108.
[77] a) C. Glaser, *Ber. Dtsch. Chem. Ges.* **1869**, *2*, 422 – 424; b) A. S. Hay, *J. Org. Chem.* **1962**, *27*, 3320 – 3321; c) R. Rossi, A. Carpita, C. Begelli, *Tetrahedron Lett.* **1985**, *26*, 523 – 526; d) Q. Liu, D. J. Burton, *Tetrahedron Lett.* **1997**, *38*, 4371 – 4374; e) For a review of alkyne couplings, see: P. C. Siemsen, R. Livingston, F. Diederich, *Angew. Chem.* **2000**, *112*, 2740 – 2767; *Angew. Chem. Int. Ed.* **2000**, *39*, 2632 – 2657.
[78] D. Gelman, S. L. Buchwald, *Angew. Chem.* **2003**, *115*, 6175 – 6178; *Angew. Chem. Int. Ed.* **2003**, *42*, 5993 – 5996.
[79] a) V. P. W. Böhm, W. A. Herrmann, *Eur. J. Org. Chem.* **2000**, 3679 – 3681; b) A. Soheili, J. Albaneze-Walker, J. A. Murry, P. G. Dormer, D. L. Hughes, *Org. Lett.* **2003**, *5*, 4191 – 4194.
[80] a) T. Jeffery, *Tetrahedron* **1996**, *52*, 10113 – 10130; b) V. P. W. Böhm, W. A. Herrmann, *Chem. Eur. J.* **2000**, *6*, 1017 – 1025; c) C. Gürter, S. L. Buchwald, *Chem. Eur. J.* **1999**, *5*, 3107 – 3112; d) G. A. Grasa, R. Singh, E. D. Stevens, S. P. Nolan, *J. Organomet. Chem.* **2003**, *687*, 269 – 279.
[81] S. L. Buchwald, X. Huang, D. Zim, PCT Int. Appl. WO200405939, **2004**, 198 [*Chem. Abstr.* **2004**, *141*, 7178].
[82] a) W. A. Herrmann, C. Brossmer, K. Öfele, C.-P. Reisinger, T. Priermeier, M. Beller, H. Fischer, *Angew. Chem.* **1995**, *107*, 1989 – 1992; *Angew. Chem. Int. Ed. Engl.* **1995**, *34*, 1844 – 1848; b) W. A. Herrmann, C. Brossmer, C.-P. Reisinger, T. H. Reirmeier, K. Öfele, M. Beller, *Chem. Eur. J.* **1997**, *3*, 1357 – 1364; c) W. A. Herrmann, C. Brossmer, K. Öfele, M. Beller, H. Fischer, *J. Mol. Catal. A* **1995**, *103*, 133 – 146; d) V. P. W. Böhm, W. A. Herrmann, *Chem. Eur. J.* **2000**, *6*, 4191 – 4197.
[83] a) B. Wagner, D. Hueglin, PCT. Int. Appl. WO2003022790, **2003**, 42 [*Chem. Abstr.* **2003**, *138*, 254954]; b) T. Kawagushi, *Nippon Kagaku Kaishi* **1987**, *11*, 2148.
[84] For Ru^{II}-catalyzed radical additions of RSO_2Cl to alkenes and subsequent HCl eliminations, see: a) N. Kamigata, H. Sawada, M. Kobayashi, *J. Org. Chem.* **1983**, *48*, 3793 – 3796; b) N. Kamigata, T. Fukushima, Y. Terawaka, M. Yoshida, H. Sawada, *J. Chem. Soc. Perkin Trans. 1* **1991**, 627 – 633; c) N. Kamigata, T. Ohtsuka, T. Fukushima, M. Yoshida, T. Shimizu, *J. Chem. Soc. Perkin Trans. 1* **1994**, 1339 – 1346; d) N. Kamigata, M. Yoshikawa, T. Shimizu, *J. Fluorine Chem.* **1998**, *87*, 91 – 95; e) M. Kameyama, H. Shimezawa, T. Satoh, N. Kamigata, *Bull. Chem. Soc. Jpn.* **1988**, *61*, 1231 – 1235; f) N. Kamigata, J. Ozaki, M. Kobayashi, *J. Org. Chem.* **1985**, *50*, 5045 – 5050; g) For a survey of ruthenium catalyzed reactions with sulfonyl chlorides, see: N. Kamigata, T. Shimizu, *Rev. Heteroat. Chem.* **1997**, *17*, 1 – 50.
[85] T. Fukuyama, H. Tokuyama, *Aldrichimica Acta* **2004**, *37*, 87 – 95, and references therein.

 © 2005 Wiley-VCH Verlag GmbH & Co. KGaA, Weinheim

L. A. Lyon and S. Nayak

DOI: 10.1002/anie.200501321

Nanotechnology

Soft Nanotechnology with Soft Nanoparticles

*Satish Nayak and L. Andrew Lyon**

Keywords:
hydrogels · materials science · nanostructures · polymers · self-assembly

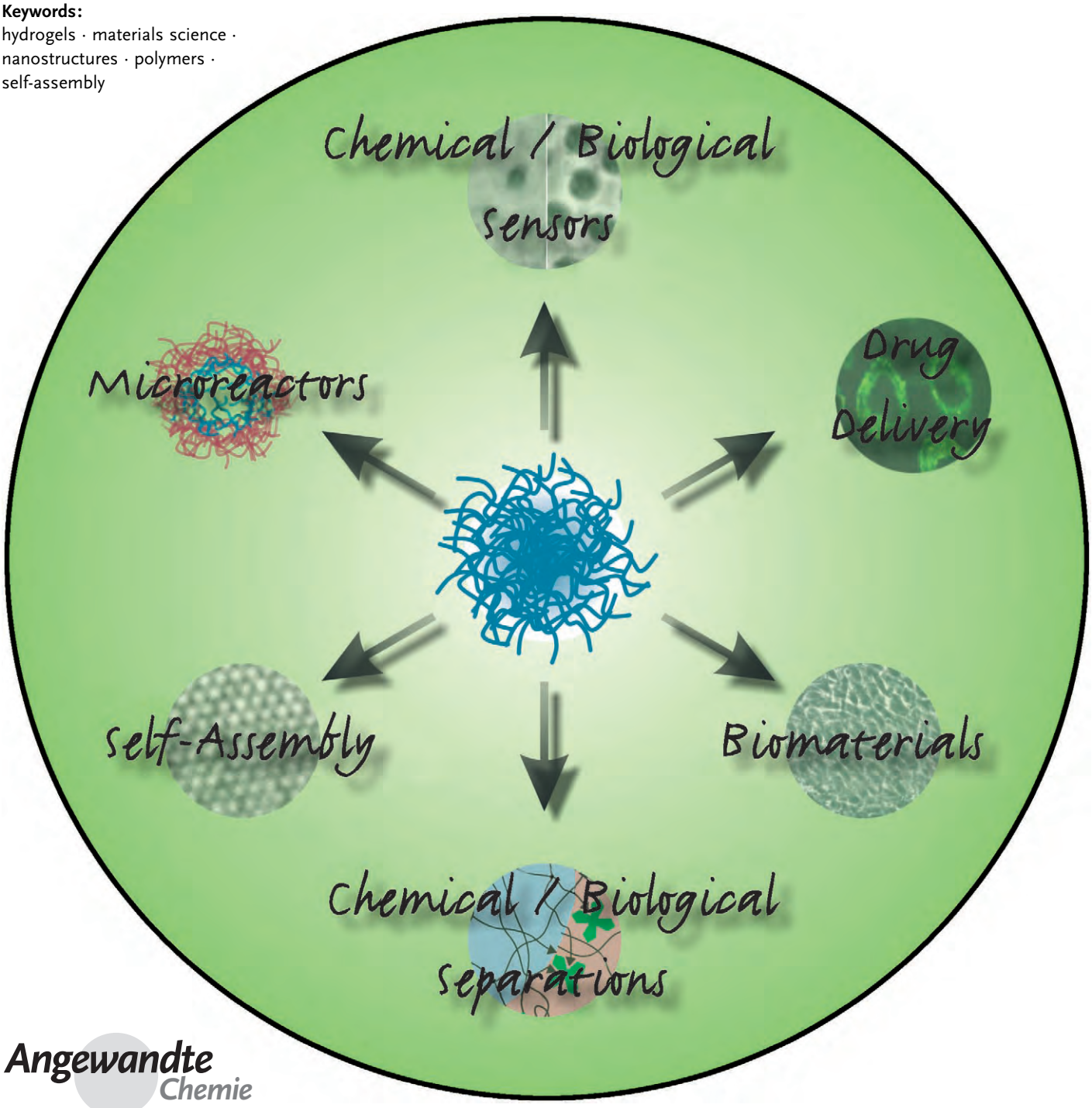

© 2005 Wiley-VCH Verlag GmbH & Co. KGaA, Weinheim

The last decade of research in the physical sciences has seen a dramatic increase in the study of nanoscale materials. Today, "nanoscience" has emerged as a multidisciplinary effort, wherein obtaining a fundamental understanding of the optical, electrical, magnetic, and mechanical properties of nanostructures promises to deliver the next generation of functional materials for a wide range of applications. While this range of efforts is extremely broad, much of the work has focused on "hard" materials, such as Buckyballs, carbon nanotubes, metals, semiconductors, and organic or inorganic dielectrics. Meanwhile, the soft materials of current interest typically include conducting or emissive polymers for "plastic electronics" applications. Despite the continued interest in these established areas of nanoscience, new classes of soft nanomaterials are being developed from more traditional polymeric constructs. Specifically, nanostructured hydrogels are emerging as a promising group of materials for multiple biotechnology applications as the need for advanced materials in the post-genomic era grows. This review will present some of the recent advances in the marriage between water-swellable networks and nanoscience.

From the Contents

1. Introduction	7687
2. Synthesis of Hydrogel Nanoparticles	7693
3. Hydrogel Particles in Nanotechnology	7697
4. Conclusions and Outlook	7705

1. Introduction

In a sense, the earliest investigators of synthetic and natural polymers were practicing nanoscience, that is, they were studying structures with spatial dimensions on the order of a few nanometers up to many microns. A similar statement could be made regarding the advent of research in molecular biology, as the dimensions of peptides, proteins, and oligonucleotides span the nanoscale. Thus, the nanometer length scale was as important in the early days of macromolecular science as it is today for nanoscientists. Many researchers in nanoscale phenomena rigidly define the nanoscale as that dimension where things become "different" (e.g. quantum confinement, dipolar plasmon oscillations, quantum conductance, etc.). Early polymer scientists may have also appreciated this philosophy, as they struggled to understand why certain arrangements of small molecules behaved in such a different fashion than their isolated molecular precursors. Indeed, polymers could be considered as the first demonstration of synthetic materials where the details of their length scale made them "different".

How then, in this modern age of nanoscience, do we define polymeric nanomaterials if most polymer chains are indeed nanometric? We could attempt to apply the above definition of differentness to some physical property of the polymer. That is, define, for a particular material, the point at which a decrease in macromolecular size leads to a discontinuity in some physical property. However, most scaling laws for polymer solution behavior begin to break down only when the polymer length approaches the persistence length of the chain, that is, the point where solutions begin to look "molecular" and not "macromolecular". While interesting physics arise from such situations, many of the desirable properties of polymers also disappear at this point. It seems then that this is a poor guideline for defining polymer nanoscience if functional materials are the overriding goals of our work. Given this conundrum, it may be the case that the redundant term "polymeric nanomaterials" cannot be rigorously defined. With this in mind, the goal of this Review is simply to explore current research in polymeric hydrogel particles, where the specific arrangement of the polymeric matter at the nanoscale imparts new properties that are not attainable from simple polymer solutions. The focus on polymer particles is important, as these discrete structures bridge the gap between more traditional areas of nanoscience and the world of soft matter. The focus on hydrogels arises from the growing need to understand how hydrophilic polymers can influence emerging areas of biotechnology.

1.1. Definition of Hydrogels

As a state of matter, gels are somewhat difficult to define, as they combine the properties of solids and fluids. They have structural integrity and do not flow appreciably when removed from their container. However, for molecules that are significantly smaller than the gel pore size, the transport of material through a gel is similar to mass transport in a fluid. Hydrogels are simply gels that swell strongly in aqueous media, and are typically composed of a hydrophilic organic polymer component that is cross-linked into a network by either covalent or noncovalent interactions.[1–3] It is the cross-linking that provides for dimensional stability, while the high solvent content gives rise to the fluid-like transport properties. The particular physical properties that result from this unusual state of matter make hydrogels ideal candidates for a number of applications. Perhaps the most widespread use

[*] Dr. S. Nayak, Prof. L. A. Lyon
Georgia Institute of Technology
School of Chemistry and Biochemistry
Atlanta, GA 30332-0400 (USA)
Fax: (+1) 404-894-7452
E-mail: lyon@chemistry.gatech.edu

 © 2005 Wiley-VCH Verlag GmbH & Co. KGaA, Weinheim

comes in the form of simple superabsorbent materials, which act to absorb and entrap water in applications where large volumes of aqueous media must be rapidly removed from a localized source. However, to have an impact in areas such as in vivo diagnostics, drug/gene delivery, chemical separations, chemical and biological sensors, and optical materials, many groups have pushed towards the synthesis of more complex polymer architectures to obtain highly functional nanomaterials. Such materials may be designed for biocompatibility, biodegradation, encapsulation, biorecognition, environmentally switchable payload release, or directed self-assembly. A number of creative synthetic methods have thus been brought to bear on this problem. In this Review, we will focus on a wide variety of approaches towards nanostructured hydrogel materials. For example, tremendous progress has been made in the assembly of amphiphilic block copolymers into dimensionally stable micellar particles. We will also address the use of stimuli-sensitive polymers in such materials, as these polymers offer new routes to hydrogels that can sense and respond to local environmental conditions. For example, it is possible to imagine the creation of a hydrogel particle that encapsulates and protects a pharmacologically active protein, only releasing it when the particle "senses" the presence of a particular disease state.

1.2. Classification of Hydrogels

Hydrogels can be classified in many ways but in this Review we will deal mostly with the classification based on type of cross-links. Cross-links are important to maintain the network structure of the hydrogels and to prevent dissolution of the hydrophilic chains. Based on the type of cross-links there are two classes of hydrogels.[4] For more detailed information on noncrystalline polymer networks, see the excellent review by Dušek and Prins.[5]

1.2.1. Physically Cross-Linked Hydrogels

The synthetic and natural hydrogels in this class have led to the concept of reversible or degradable hydrogels that undergo a transition from the three-dimensionally stable structure to a polymer solution. Most often these hydrogels have been used to encapsulate proteins,[6] cells,[7] or drugs[8] and then release them through the dissolution of the hydrogel structure. The cross-links in this class of hydrogels arise from noncovalent attractive forces between the polymer chains (Figure 1). These forces are often hydrophobic interactions, hydrogen bonding, or ionic interactions.

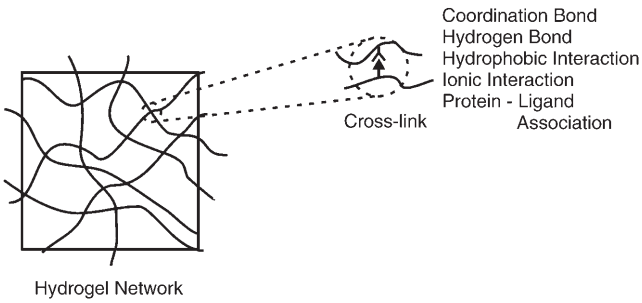

Figure 1. Physical cross-linking in hydrogels, in which the cross-links are formed by noncovalent interactions.

Alginate is a polysaccharide composed of mannuronic acid and gluconic acid, which can be cross-linked by divalent calcium ions.[4,9] The hydrogel can then be dissolved by using a chelating agent that binds to calcium ions. Alginate hydrogels have been used for encapsulating proteins and also as a matrix for the encapsulation of cells, and they often allow growth and proliferation of the cells within the encapsulating gel. Another example of cross-linking by ionic interactions is that of dextran, which lacks charged regions, but forms hydrogels in the presence of potassium ions. The reason for the cross-linking is that the ionic radius of potassium ions is such that it fits perfectly in the cage formed by six oxygen atoms of glucose units on three adjacent polymer chains.[10]

Noncovalent cross-links can also be formed in blends and interpenetrating networks of two dissimilar polymers. For example, poly(acrylic acid) and poly(methacrylic acid) form hydrogen bonds with poly(ethylene glycol), which results in formation of hydrogels. The hydrogen bond is formed between the oxygen of the poly(ethylene glycol) and carboxylic group of the poly acids. The hydrogen bonds are formed only when the acid groups are protonated, hence the hydrogel formation is pH dependent.[11,12] Oligonucleotides have also been used in the formation of hydrogels. Nagahara et al.

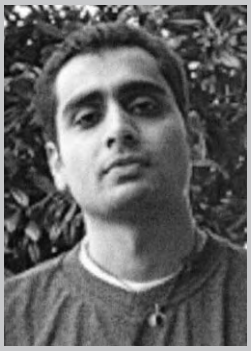

Satish Nayak received his BSc in chemistry from Ramnarain Ruia College, Mumbai and his MSc in analytical chemistry from the Institute of Science, Mumbai. He started his doctoral work on synthesizing and characterizing various types of hydrogel nanoparticles at Georgia Institute of Technology in 2000 under the supervision of Prof. L. Andrew Lyon. He successfully defended his thesis in 2004 and is currently working as a postdoctoral fellow at the University of Chicago.

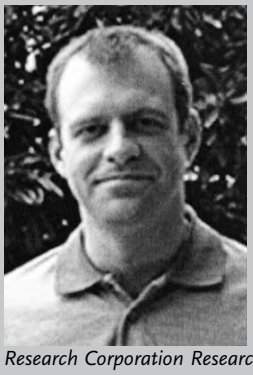

Andrew Lyon received his PhD at Northwestern University under the direction of Professor Joseph T. Hupp (1996) and was a postdoc with Professor Michael J. Natan at Penn State (1997–1998). He began his career at Georgia Tech in 1999 and was promoted to Associate Professor in 2003. His current research involves the design of stimuli-sensitive hydrogel nanoparticles, as well as the assembly of these particles into higher order structures such as photonic crystals. His awards include the NSF CAREER Award, Beckman Young Investigator Award, Research Corporation Research Innovation Award, and the Camille Dreyfus Teacher-Scholar Award.

© 2005 Wiley-VCH Verlag GmbH & Co. KGaA, Weinheim

coupled water-soluble poly(*N*,*N*-dimethylacrylamide-*co*-*N*-acryloylsuccinimide) to a single-stranded DNA.[13] At room temperature and in presence of complementary DNA, hydrogels are formed, which dissolve at temperatures above the DNA melting point.

1.2.2. Chemically Cross-Linked Hydrogels

These types of hydrogels are usually more stable than the physically cross-linked hydrogels because the cross-links are formed by covalent bonds.[4] The hydrogels formed by such cross-links have a permanent structure unless chemical labile bonds have been intentionally added to the network.

Chemically cross-linked gels are usually formed by polymerizing monomers in the presence of cross-linking agents. Poly(2-hydroxyethyl methacrylate) is a well studied hydrogel-forming polymer. It is typically synthesized by polymerizing 2-hydroxy methacrylate ($H_2C{=}C(CH_3)COOCH_2CH_2OH$) with ethylene glycol dimethacrylate ($H_2C{=}C(CH_3)COOCH_2CH_2OCO(CH_3)C{=}CH_2$) as a cross-linker. Various physical properties, such as the swelling capacity of the hydrogels are controlled by the amount of cross-linker used.[4] Hydrogels can also be formed by cross-linking of the various functional groups present on the polymer backbone. Polymers containing hydroxy, amine, or hydrazide groups can be cross-linked by using glutaraldehyde, which forms covalent bonds with each of these functionalities.[4,14,15]

Enzymes have been used in the formation of cross-linked hydrogels. In one interesting example, Sperinde et al. employed tetrahydroxy PEG (PEG = poly(ethylene glycol)) functionalized with glutaminyl groups. This polymer forms hydrogels in the presence of the enzyme transglutaminase and poly(lysine-*co*-phenylalanine), where by the enzyme catalyses the reaction between the γ-carboxyamide group of the PEG-glutaminyl polymer and ε-amine group of the lysine to form an amide bond.[16,17]

1.2.3. Other Classifications

Hydrogels can also be classified based on their size as either macrogels or microgels. Macrogels[18–20] are bulk gels where the size can be anywhere from millimeters and larger, while microgels[21,22] are colloidally stable hydrogels, and their size can vary from tens of nanometers to micrometers. Perhaps the earliest report of microgel synthesis was by Staudinger in 1935,[23] so as with most of macromolecular science, the nanoscale has been the focus for a very long time. However, given the recent interest in such materials across multiple disciplines, as well as the continued efforts in all things "nano", microgels or hydrogel nanoparticles will be the central topic of this Review.

Hydrogels can be further classified as stimuli-responsive or non-responsive gels. Non-responsive gels, as the name suggests, are merely materials that swell upon water absorption. On the other hand stimuli-responsive gels have been called "smart" materials because they respond by a change in swelling to subtle changes in the environment.[24,25] These hydrogels can be made responsive to temperature,[19] pH value,[22,26] ionic strength,[27–29] light,[30–34] electric field,[35] and biomolecules.[36–40] The responsive behavior of the hydrogels is inherited from the type of the polymer used in making the gel and/or any post-polymerization modifications that are made.

1.3. Stimuli-Sensitive Polymers

The use of stimuli-sensitive polymers in fabricating hydrogels has led to many interesting applications; in this section we illustrate a few examples. One of the most widely studied stimuli-sensitive polymers is poly(*N*-isopropylacrylamide) (pNIPAm) formed from the monomer *N*-isopropylacrylamide ($H_2C{=}CHCONHCH(CH_3)_2$). to facilitate the understanding of some of the later parts of this Review, and as most of our group's work is based on pNIPAm, it is appropriate to provide a brief background on this polymer. For an in depth understanding see the very comprehensive review by Schild.[41]

One of the earliest studies on the solution properties of PNIPAm was carried out by Heskins et al.,[42] in which they observed that the phase transition of pNIPAm is endothermic and entropy driven. Owing to this striking thermal behavior in aqueous media, pNIPAm has been widely used to make responsive hydrogels. As with most olefin-based monomers, pNIPAm has been synthesized by a variety of techniques: redox initiation, free radical initiation, ionic initiation, and also by using radiation.[41] Various functional groups have also been added to the polymer by copolymerization and post-polymerization modification, thereby giving multiresponsive and multifunctional polymers.

The behavior of any polymer in a solvent is related to the balance between solvent–solvent, solvent–polymer, and polymer–polymer interactions. For stimuli-sensitive polymers, the polymer solvation can be "switched" by strengthening one of these interactions or by weakening another. Figure 2 illustrates this concept schematically. For the case of pNIPAm in water, the polymer hydrogen bonds to water through the amide side chains. However, the isopropyl group on the side chain induces hydrophobic structuring of the water. This structured water leads to entropically driven polymer–polymer interactions by the hydrophobic effect.[41] Under the conditions where pNIPAm has a random-coil structure, the solvent–polymer interactions are stronger than the polymer–polymer interactions. At higher temperatures, the hydrogen bonds to the water molecules break and there is an entropi-

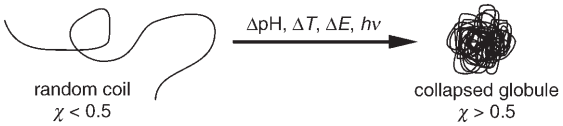

Figure 2. A stimuli-sensitive polymer undergoing phase transition as a result of a change in the solvent properties. Factors such as pH value, temperature, electric field, and light can cause these phase transitions depending on the polymer composition.

© 2005 Wiley-VCH Verlag GmbH & Co. KGaA, Weinheim

cally favored release of bound and structured water, leading to the formation of a globular polymer conformation. In this case the polymer–polymer hydrophobic interactions become stronger than the polymer–solvent interactions, and the polymer phase separates. The temperature at which this phase separation occurs is called the lower critical solution temperature (LCST). It is this behavior that makes pNIPAm a very attractive candidate for the fabrication of stimuli-responsive hydrogels. Note, however, that more than just the hydrophilic and hydrophobic side-chain contributions to polymer solvation must be considered when describing LCST behavior. For example, the polymer formed from *N*-isopropylmethacrylamide ($H_2C{=}C(CH_3)CONHCH(CH_3)_2$),[43–48] which differs from NIPAm by only a single methyl group, has a higher LCST in water, which suggests that it is more hydrophilic despite having a greater organic content. Apparently, this "increased hydrophilicity" does not arise from an increase in polymer polarity, but instead comes from a decrease in chain flexibility. This feature changes the entropic contribution to the free energy of mixing, and thus increases the LCST.

The LCST behavior of pNIPAm has been studied by a variety of techniques including UV-Vis spectroscopy, differential scanning calorimetry (DSC), light scattering, viscometry and fluorescence spectroscopy.[49–57] Wu et al. have extensively studied the phase transition of pNIPAm, where they observed that the transition is not first order, that is, the polymer does not directly go from a random coil state to a globular state, but there are other intermediate thermodynamically stable conformations (Figure 3).[52,54,58]

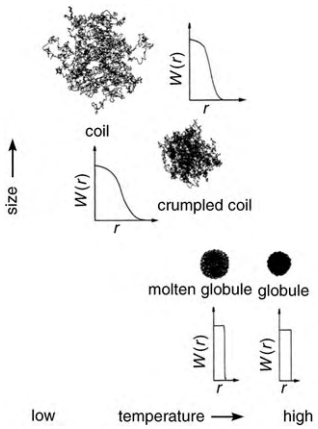

Figure 3. The thermodynamically stable states present during the phase transition of pNIPAm and the corresponding chain-density distribution along the radius for each state. Reprinted with permission from ref. [58].

There are other classes of thermoresponsive polymers that show an upper critical solution temperature (UCST). In this case the polymer is phase separated at low temperatures owing to inter- or intramolecular interactions, while at high temperatures these interactions break and the polymer dissolves or swells. Most often these interactions are hydrogen bonding or electrostatic. In one example Laschewsky and co-workers have synthesized a block copolymer of pNIPAm and 3-[*N*-(3-methacrylamidopropyl)-*N*,*N*-dimethyl]ammoniopropane sulfonate (SPP), which exhibits both LCST and UCST behavior.[59] The pNIPAm segment confers temperature sensitivity by the mechanism described above. On the other hand, SPP is a polyampholytic polymer, which at low temperatures displays strong electrostatic interactions between the oppositely charged regions of the polymers, whereas these interactions are broken at high temperatures.

Using this understanding of polymer solvation, Irie and co-workers have synthesized photoresponsive polymers by incorporating azobenzene side chains in pNIPAm.[60] Azobenzenes undergo *trans* to *cis* isomerization on UV irradiation; the transition is reversed by irradiation with visible light or by thermal relaxation. Furthermore, the dipole moment and hence the hydrophilicity of azobenzene is dependent on the isomerization state. In this fashion, the investigators were able to change the phase-transition temperature of pNIPAm by inducing isomerization of the azobenzene side chains, which in turn changed the free energy of mixing. Figure 4 shows the change in transmittance of poly-[*N*-isopropylacrylamide-*co*-*N*-(4-phenylazo-phenyl)-acrylamide] as a function of temperature before and during irradiation with UV light.

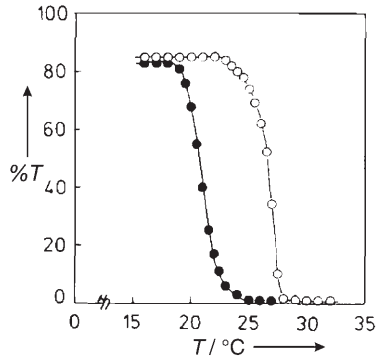

Figure 4. Temperature-dependent transmittance of the photoresponsive polymer before (●) and during (○) UV irradiation. Reprinted with permission from ref. [60]

1.4. Swelling Properties of Hydrogels

The nature of hydrogels is dependent on the type of the monomers used to synthesize them. In case of hydrogels synthesized from pNIPAm, the thermoresponsivity of the parent polymer is inherited by gels made from it. These hydrogels exhibit volume phase transition temperature (VPTT)[61] at around the LCST of pNIPAm. At temperatures higher than VPTT the hydrogel goes from a swollen (hydrophilic) state to a compact (relatively hydrophobic) state. The VPTT of the gels is dependent on several factors including cross-link density, hydrophobic-hydrophilic balance, ionic strength, and solvent composition. Correspondingly, hydrogels fabricated from titratable ionic monomers show pH-dependent swelling. The most common ionic monomers used are acrylic acid and methacrylic acid. At $pH > pK_a$ of the acid comonomer, the gel swells because of Coulombic repulsion

 © 2005 Wiley-VCH Verlag GmbH & Co. KGaA, Weinheim

between the charged monomer units and the more favorable solvation of the deprotonated monomer by the solvent. The equilibrium gel-swelling volume is a balance between the osmotic pressure of the polymer network, which is governed by polymer–solvent interactions, and the elasticity of the network.[5]

In ground-breaking work, the group of Tanaka showed that ionic thermoresponsive gels, when heated, display a discontinuous transition, while non-ionic gels undergo a continuous transition. They have also shown that the shrinking rate of the gel is inversely proportional to the square of the smallest dimension of the gel.[20,35,62–64] Taking advantage of the diffusion length scale, Yan and Hoffman have shown that polymerizing pNIPAm gels at temperatures higher than the LCST of the polymer results in gels that have large pore sizes, which in turn have faster swelling rates.[65] Reporting all the properties of hydrogels is beyond the scope of this Review; hence we have mentioned just a few important properties, and some others will be discussed in the later Sections.

The swelling behavior of hydrogels has made them useful in some interesting applications. Thermosensitive pNIPAm gels have been used in controlling the activity of enzymes. Park and Hoffman demonstrated that by immobilizing an enzyme in the gel, the diffusion of the substrate to the enzyme could be controlled by changing the pore size of the gel, which in turn depends on the temperature of the system. In this way they were able to switch the enzyme on or off by controlling the temperature.[66] Kim and Healy have synthesized pNIPAm gels with peptide cross-links. These gels can be used as an extracellular matrix mimic, where the peptide can be cleaved by a metalloproteinase, which subsequently leads to gel erosion. Figure 5 shows a schematic depiction of this process.[67]

1.5. Microgels and Nanogels

Colloidally stable particles made from hydrogels, also referred to as micro- or nanogels, have properties similar to those of their macrogel counterparts, that is, a pNIPAm microgel, just like the bulk gel, will also undergo a VPTT near the LCST of the polymer.[68,69] In addition to these properties, microgels have other characteristics of colloidal dispersions, such as zeta potentials,[69–71] and can also form ordered colloidal phases.[72–75]

Some very important studies have focused on the differences between macro- and microgels with respect to their phase behavior. For example, Wu et al. have shown that the VPTT of the microgels is slightly higher than the LCST of pNIPAm (Figure 6), and also that the transition region is less

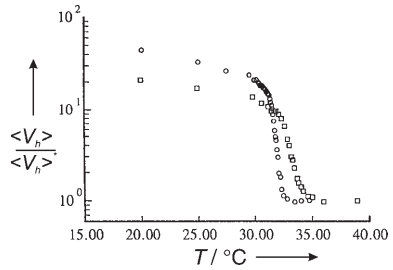

Figure 6. Deswelling ratio of linear pNIPAm chains (○) and cross-linked microgels (□) in water. Owing to the heterogeneity of the cross-links, microgels have a broader phase-transition region than the linear pNIPAm chains. Reprinted with permission ref. [76].

sharp than that of bulk gels.[76] The reason for this continuous transition is due to a greater heterogeneity in the subchain lengths of the microgels than in the traditionally prepared macrogels. When the microgels are subjected to $T >$ VPTT, the regions of the particle with longer subchain lengths collapse at a lower temperature than the regions with shorter subchains. Thus the observed phase transition for a microgel can be thought of as being the summation of the phase transitions of the different sub-networks in the particle. We have also observed this behavior in core–shell structured microgels by using fluorescent probes to interrogate cross-linker gradients.[77]

PNIPAm microgels show interesting behavior in mixed solvents owing to the cononsolvency of pNIPAm (i.e., the non-linear dependence of solvation on solvent volume fraction).[78] For example, the LCST of linear pNIPAm decreases with increasing methanol concentration until 55% methanol, beyond which the LCST increases sharply.[79] The same effect has been observed by McPhee et al. for microgels.[80] The mechanism for cononsolvency is explained by clathrate formation. Cosolvents such as water and methanol form clathrate structures, which compete with pNIPAm for the water molecules that hydrate the polymer. Hence the deswelling of the polymer is observed as the water molecules are removed from the interior of the gel by the other solvents. In related work, Daly and Saunders have studied the

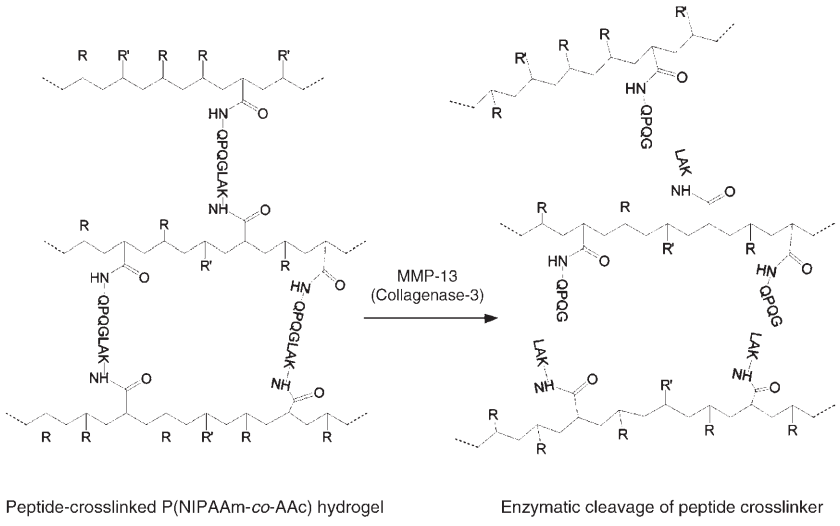

Figure 5. Peptide-cross-linked hydrogel degradation by MMP-13 (collagenase-3). The letters indicate the single-letter amino acid designations. Reprinted with permission from ref. [67].

© 2005 Wiley-VCH Verlag GmbH & Co. KGaA, Weinheim

effect of added electrolyte on the stability of the microgels. It was observed that at a particular temperature particles flocculate at higher ionic strength. The swelling ability of the particles also depends on the ionic strength of the salt and its position in the Hoffmeister series, which relates to the effect of ions on the activity of water.[70] An interesting study by Greinert and Richtering involved the modulation of polyelectrolytic pNIPAm microgels by the adsorption of oppositely charged polyelectrolytes in solution.[81] The charge compensation and bridging effect of the polyelectrolyte adsorption have a profound effect on the LCST behavior of the microgels. These studies may offer insight into the swelling phenomena observed in microgel-based polyelectrolyte multilayers,[82–85] which are discussed in Section 3.1.

Many researchers have carried out electrophoretic mobility measurements for charged particles. One of the first reports was from Pelton et al., they studied the electrokinetic behavior of pNIPAm microgels as a function of temperature and salt concentration.[86] They observed that at $T < \mathrm{VPTT}$, mobility was nearly zero owing to a low charge density on the particles, but at $T > \mathrm{VPTT}$ a sharp increase in mobility was observed. This change was attributed to the increase in charge density on the smaller deswollen particle. Since the charge per particle is constant, smaller (deswollen) particles will have a higher charge density than swollen particles. Daly and Saunders carried out a similar study and found that the onset of the increase in electrophoretic mobility was about 5–6 K higher than the VPTT of the particles. This behavior was proposed to result from a three-stage phase transition in the microgels (Figure 7).[70]

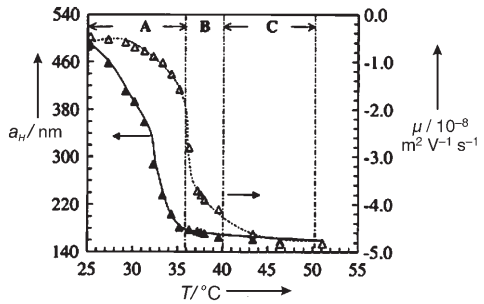

Figure 7. Electrophoretic mobility (△) and hydrodynamic radius (▲) as a function of temperature for pNIPAm microgels. The regions A, B, and C represent the three stages in the collapse of the particle. Reproduced with permission from ref. [70].

Surfactants can have a strange effect on the swelling of pNIPAm microgels. Tam et al. have observed that the microgels swell in presence of anionic surfactant.[87] They attributed this property to the interaction of the hydrophobic tail of the surfactant with the polymer network. However, in the presence of a cationic surfactant of the same chain length, no such effect was observed. Wu et al. carried out similar studies and observed by NMR spectroscopy that at concentrations less than the critical micelle concentrations (CMC), the anionic surfactants form micelles in the polymer network owing to a higher effective concentration in the network.[88] The cationic surfactants failed to form micelles in the polymer network even at very high concentration, and hence no microgel swelling was observed.

Understanding the structure of hydrogel nanoparticles is important for explaining their detailed phase-transition behavior, mass-transport through the network, and colloidal stability. Light scattering is one of the most common techniques used for structural analysis of hydrogel nanoparticles. Both dynamic and static light scattering have been used extensively and remain the standard techniques for particle characterization.[69,76,89–91] However, other techniques have allowed for even greater insight into the structure of microgels. Guillermo et al. used NMR spectroscopy to determine the cross-linker distribution in microgel particles and confirmed that these particles have a heterogeneous structure, wherein the periphery of the microgel is more loosely cross-linked than the interior.[92] Similar studies were carried out by Saunders, in which small-angle neutron scattering (SANS) was used to investigate the structural details of pNIPAm microgels synthesized by surfactant-free polymerization.[93] This study again revealed that the microgels prepared by precipitation polymerization have a heterogeneous structure, in this case it was also determined that a thin layer of loosely cross-linked chains was present at the particle periphery. Woodward et al. used DSC to determine the influence of cross-linking density on the phase transition of the particles. They observed an overall decrease in phase-transition enthalpy with increase in cross-linker density.[94] In addition to DSC they also used pulsed-gradient spin echo (PGSE) NMR spectroscopy to study the mobility of the solvent in the particle as a function of cross-linker density and observed that the diffusion of solvent is reduced with the increase in the cross-linker density, hence the particles are more rigid at high cross-linker density. Figure 8 depicts the change in relative diffusion coefficient of water in the microgels, measured by PGSE-NMR spectroscopy, for samples with different cross-linker densities.

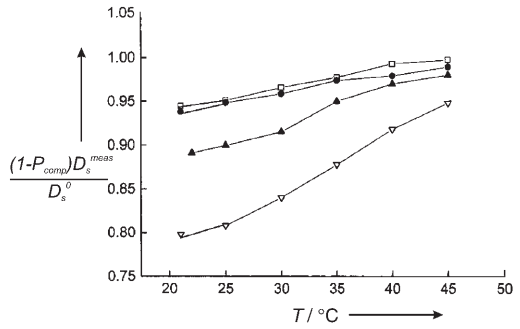

Figure 8. Relative diffusion coefficient of water inside the polymer network for 0.25% (□), 0.5% (●), 5% (▲), and 30% (△) cross-linked pNIPAm microgels as a function of temperature. The diffusion coefficient of water within the particle decreases with an increase in the cross-link density. Reprinted with permission from ref. [94].

Senff et al. have used rheometry to understand the phase behavior of microgels and to determine the effective "softness" of microgel particles.[73,95,96] This group has also carried out studies aimed at determining the internal structure of

 © 2005 Wiley-VCH Verlag GmbH & Co. KGaA, Weinheim

microgels.[97,98] Again, it was determined that the cross-link density is highest at the center of the particle and decreases gradually to the surface. They also found that the internal structure of the microgels depends on the manner in which they are synthesized. A semibatch reaction (reactants are added gradually over a certain time) gives more homogeneous morphology than a simple batch reaction (all the reactants are added at the start) This effect is attributed to the faster reactivity of the cross-linker, which gets incorporated at a faster rate during the early stages of a batch reaction. Similar behavior has also been reported by Pelton.[68,99]

2. Synthesis of Hydrogel Nanoparticles

Hydrogel Nanoparticles have been synthesized by numerous approaches. In this Section we will discuss some of the commonly used methods, where the synthetic technique being employed is typically dictated by the desired application or the type of study to be carried out.

2.1. Emulsion and Precipitation Polymerization

Surfactant-free emulsion polymerization (SFEP), or precipitation polymerization, is the most common technique to synthesize thermosensitive hydrogel particles. Although pNIPAm microgel synthesis by this method was not reported until 1986, the technique was apparently first utilized by Philip Chibante in 1978.[68,100] If carried out carefully, this method can afford particles with very narrow size distribution. In this method all the monomers, NIPAm, and the cross-linker (typically *N*,*N*′-methylenebisacrylamide (BIS)), are dissolved in water. The solution is purged with N_2 and heated to a temperature above the pNIPAm LCST (usually around 70 °C), then an initiator such as ammonium persulfate (APS) or potassium persulfate (KPS) is added.

Microgels synthesized by this method are formed by homogenous nucleation. There are good reasons for carrying out the polymerization at high temperature: the sulfate radicals, which initiate the polymerization need to be formed. After initiation the NIPAm monomer is attacked by the sulfate radical, there then follows radical propagation and chain growth. Once the chain reaches a critical length, it collapses upon itself producing precursor particles. The chain collapses because the polymerization temperature is higher than the LCST of the polymer, hence the name precipitation polymerization. The precursor particles grow by aggregation with the other precursor particles, by being captured by existing particles, by capturing growing oligoradicals, and by monomer addition. The charge imparted by the initiator stabilizes the microgels once they have reached a critical size. Figure 9 shows the proposed mechanism for precipitation polymerization. This method is extremely versatile from the standpoint of particle size control. For example, to synthesize smaller microgels, the precursor particles must be stabilized earlier in the reaction. Since there is not enough charge available from initiator fragments to stabilize small precursor particles, an ionic surfactant can be added to impart colloidal stability earlier in the reaction. Similarly, larger particles can be obtained by decreasing the surfactant concentration. Precipitation polymerization can also be used to incorporate comonomers in the microgel. We and others have copolymerized ionic monomers with pNIPAm to create pH-responsive microgels.[22,29,101–105] We have also copolymerized a hydrophobic comonomer *N*-*tert*-butylacrylamide (TBA, $H_2C{=}CHCONHC(CH_3)_3$) to give pH and temperature responsive microgels; these particles exhibit phase transitions at lower temperatures owing to the increase in hydrophobicity of the gel while retaining a pH-tunable VPTT.[105] Similarly, other functionalities can also be copolymerized into these particles by this method.

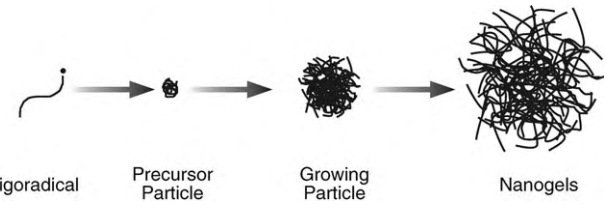

Figure 9. Precipitation polymerization of colloidal micro or nanogels from phase-separating polymers.

The presence of a cross-linker is critical in preventing the dissolution of the polymer particle as it is cooled below the LCST. However, Gao and Friskin have reported that it is possible to make pNIPAm microgels by precipitation polymerization, without using a cross-linker.[106,107] They attributed this effect to "self cross-linking" of pNIPAm chains by a chain-transfer reaction occurring at either or both of two possible sites: the hydrogen atom attached to the tertiary carbon atom on the pendant isopropyl group and the hydrogen atom on the tertiary carbon atom of the main-chain backbone. These results indicate that in precipitation polymerization the cross-link density might be higher than expected on the basis of the cross-linker concentration used in the reaction.

Precipitation polymerization has a few drawbacks. First, the method is useful only for materials that are stable at high temperatures and hence cannot be used to incorporate biological macromolecules. Also the method is best for materials which are hydrophobic so that they can attach to the collapsed precursor particle easily. Hence, if a hydrophilic comonomer is to be copolymerized, only a certain wt % can be incorporated. Beyond that wt % the growing oligomer will be too hydrophilic to undergo efficient chain collapse, thereby resulting in a very polydisperse microgel dispersion, or the complete lack of particle formation. To overcome these hurdles many researchers have used inverse microemulsion polymerization. In this method an aqueous solution of all the monomers is added to an appropriate amount of oil and surfactant and is stirred to form thermodynamically stable microemulsions. Polymerization can be initiated by having the initiator in the aqueous or in the oil phase. This method has been used to synthesize hydrogel particles with high wt % of ionic monomers; Neyret and Vincent used microemulsion polymerization to prepare zwitterionic pNIPAm microgels.[108] In this case they used a UV-activated photoinitiator

© 2005 Wiley-VCH Verlag GmbH & Co. KGaA, Weinheim

dissolved in the organic phase. McAllister et al. used the same technique to synthesize a highly cationically charged hydrogel. These particles were able to bind to DNA and can potentially be used in gene delivery.[109] One other method for preparing microgels, which is similar to microemulsion polymerization, utilizes lipids to form liposomes inside which the particle is formed. Kazakov et al. have demonstrated that liposomes can form a "nanoreactor" inside which microgels can be polymerized.[110] Figure 10 illustrates the general procedure.

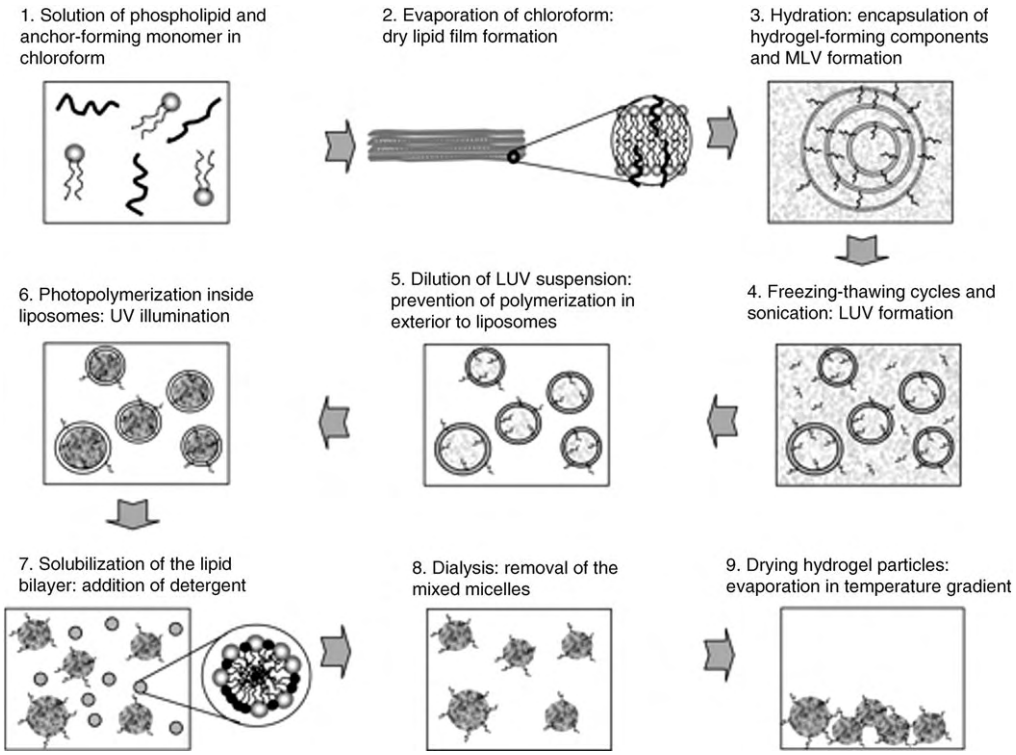

Figure 10. Hydrogel particle synthesis in liposomes. Reprinted with permission from ref. [110].

2.2. Core–Shell Structured Materials

Core–shell hydrogel particles can broadly be divided in two classes: 1) where the core is made from non-hydrogel material and the shell is made from hydrogel and 2) where both the core and the shell are made of a hydrogel-like material. In the first class of materials the core is usually made of solid material, such as polystyrene, silica or gold nanoparticles. Dingenouts et al. synthesized a polystyrene core with small amount of NIPAm as a co-monomer by SFEP.[111] The polystyrene-*co*-pNIPAm particles were stabilized by the sulfate groups from the initiator. These cores were then used as seeds for polymerizing a cross-linked shell of pNIPAm. For the shell synthesis the reaction was carried out at 80 °C, which provided a core particle with a deswollen pNIPAm-rich periphery, onto which pNIPAm polymerizing in solution aggregated by a precipitation polymerization mechanism. Xiao et al. synthesized similar particles in which pNIPAm chains were grafted onto the polystyrene core resulting in a "hairy" particle.[112]

In another example, Zha et al. have used silica particles prepared by the Stöber method[113] as a core material.[114] Vinyl groups were introduced to the surface of the particles by a silane coupling reaction. These particles were then used as seeds for precipitation polymerization of pNIPAm, which resulted in the formation of silica-core pNIPAm-shell particles. This approach allowed the synthesis of hollow pNIPAm capsules by dissolution of the silica with HF. Similarly, Kim and Lee have synthesized gold-core pNIPAm-shell particles by SFEP. The size of these citrate-stabilized gold nanoparticles was approximately 60 nm. The gold nanoparticles were then treated with oleic acid, which helps in attaching the pNIPAm hydrogel shell to the gold core during SFEP.[115]

The second type of core–shell materials is the one which has hydrogel in both the core and the shell. Our group first reported the synthesis of this type of hydrogel particles by two-stage precipitation polymerization.[22] In this method a polymer shell with the same or different structure or functionality as the core, is added onto preformed core particles thereby allowing control over the radial distribution of the functional groups in the particle. In a typical synthesis, preformed pNIPAm core particles are heated to approximately 70 °C, then the shell monomer solution is added, and polymerization is initiated. The reaction is carried out for around 4 h and then the mixture is cooled and separated by filtration. This method gives core–shell particles with no increase in polydispersity, as all the oligomers formed in solution precipitate onto the preformed core particles. To prevent heteronucleation there are several important parameters that should be controlled, including the concentration of the core, initiator, surfactant, and the shell monomer. The mechanism by which this reaction takes place is somewhat similar to that for the core microgels. Since the reaction temperature is well above the VPTT of the core particles, the particles are in a collapsed state. The collapsed particles are hydrophobic and hence they tend to capture the growing oligomers, which results in the formation of the shell.

Core–shell particles prepared in this fashion can exhibit very interesting properties.[21,43,44,77,116–119] Since the shell can be synthesized using different comonomers to the core, the particles can show multiple phase-transition behavior with

 © 2005 Wiley-VCH Verlag GmbH & Co. KGaA, Weinheim

temperature.[22,43,44] Furthermore, depending upon the cross-linker density of the shell, compression or "shrink-wrapping" of the core can be observed resulting from a cross-link gradient in the shell.[116,117,119] We have also used this synthetic method to make hollow hydrogel capsules, Figure 11.[120] To

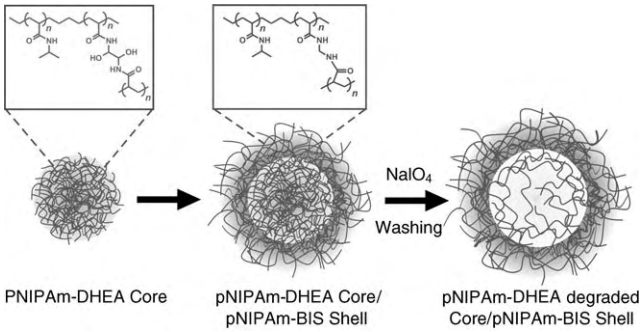

Figure 11. Preparation of thermosensitive hollow microgels by oxidation of the core cross-links. Reprinted with permission from ref. [120].

accomplish this, the core is fabricated with a degradable cross-linker and the shell with a non-degradable one. The degradable cross-linker that we have used contains a vicinal diol, which can be degraded by stoichiometric addition of periodate. After core degradation, the particles were cleaned extensively by centrifugation, after which DLS and fluorescence were used to confirm the hollow structure.

Berndt and Richtering have also synthesized core–shell particles which have two different polymers in the core and the shell.[43] In their demonstration, the core was made of pNIPAm and the shell consisted of poly(*N*-isopropylmethacrylamide) (pNIPMAm), which has a LCST of 45 °C. They studied the thermoresponsivity of these particles and found, in a similar fashion to previous work from our group, that the particles had two transitions corresponding to the LCSTs of the two polymers (Figure 12).

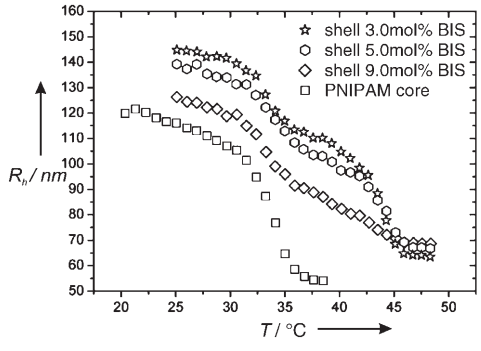

Figure 12. Hydrodynamic radius as a function of temperature for pNIPAm-core/pNIPAMAm-shell microgels with different shell cross-linker concentrations. The sample containing 3.0 mol% BIS clearly shows that the particle is undergoing two phase transitions, the first transition corresponding to the LCST of pNIPAm and the second to that of pNIPMAm. Reprinted with permission from ref. [43].

2.3. Block-Copolymer Micelles

Hydrogel nanoparticles can also be formed by using the ability of block copolymers to self-assemble into micelles.[121] Most often block copolymers are like surfactants in that they have a hydrophobic and a hydrophilic block. Depending on the polarity of the solvent and the concentration of the polymers, block copolymers can form spherical micelles. In hydrophilic solvents the hydrophobic block forms the core and the hydrophilic block is exposed to the solvent. In some cases these micelles can be cross-linked to form stable nanoparticles. For example, Zhu and Napper used pNIPAm-*b*-PEO (PEO = poly(ethylene oxide)) to form microgels.[122,123] Initially the block copolymer was synthesized using the ceric ion redox system in nitric acid at 50 °C, then addition of the cross-linker BIS formed cross-linked microgels. It was observed that the size of the microgels, as measured by DLS, was dependent on the concentration of NIPAm and PEO, and also on the rate of heating during polymerization.

The Wooley group has extensively studied cross-linked block-copolymer micelles, which they refer to as shell cross-linked knedels (SCK).[121,124–137] The size range for SCKs is around 5–200 nm. They are prepared from amphiphilic block copolymers, which self-assemble into polymeric micelles. The micelles are further stabilized by cross-linking of the side-chain functional groups in the shell of the micelles (Figure 13). The first SCK reported was fabricated from a

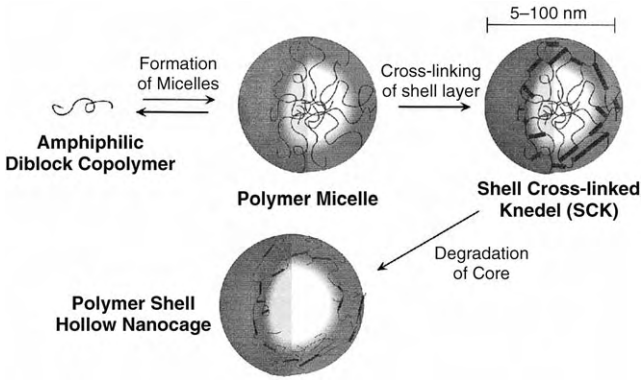

Figure 13. General synthetic approach for synthesizing SCK nanoparticles. The degradation step is used for the preparation of hollow particles. Reprinted with permission from ref. [131]

polystyrene and poly(4-vinylpyridine) block copolymer.[124] Before self-assembling the polymer into micelles, the pyridyl nitrogen was quaternized by reaction with *p*-chloromethylstyrene to impart hydrophilicity to the polymer. Once the polymer formed micelles the styrene moiety in the shell was polymerized to give the cross-linked structure. The dimensions and topologies of the particles can be controlled by varying the length of the hydrophilic and hydrophobic blocks.

The Wooley group has also prepared hydrogel-coated particles by using a polystyrene-*b*-poly(acrylic acid) copolymer.[137] The polymer self-assembled into a polystyrene core and acrylic acid shell micelle. The acrylic acid groups were

 © 2005 Wiley-VCH Verlag GmbH & Co. KGaA, Weinheim

then cross-linked by using variety of bifunctional amine cross-linkers. They have also prepared SCKs with degradable cores. In one example they used poly(ε-caprolactone)-*b*-poly(acrylic acid) copolymers. This polymer forms micelles with the caprolactone core and acrylic acid shell. The shell is cross-linked by the methods mentioned above to form SCKs, the core is then dissolved by acid or base hydrolysis.[130] In a second demonstration, they have used poly(isoprene-*b*-acrylic acid) to form hollow SCKs.[126] The micelles formed by this polymer have isoprene groups in the core and the acid groups on the periphery. The acid groups in the shell were cross-linked by amidation and the core was dissolved by isoprene oxidation, resulting in hollow capsules. The Wooley group has also synthesized an entirely hydrophilic SCK, which was pH responsive.[134] The polymer was poly(acrylic acid)-*b*-poly(methyl acrylate), which forms an acrylic acid shell and a methyl methacrylate core micelle. The shell was cross-linked, subsequent hydrolysis of the core using LiOH, which converted acrylate into acid groups, made the entire particle hydrophilic. The acid groups in the core and the shell made the SCK pH responsive.

Akiyoshi et al. have found that polysaccharides partly modified by hydrophobic groups, such as cholesterol, can form nanoparticles in water.[138] The sizes of these particles typically range from 20–30 nm with excellent monodispersity, according to size-exclusion chromatography, DLS, and TEM. These particles are not true block-copolymer micelles but are closely related to this class of particles, since the association forces are similar. These particles were first prepared in 1993 by using hydrophobized pullulan having 1.6 cholesterol groups per 100 glucose units,[138] which aggregated intermolecularly to form nanoparticles. These nanoparticles are considered to be hydrogels in which the cross-links are provided by the associated hydrophobic groups. The size of the particles can be controlled by the number of the hydrophobic groups and also by the structure of the polymers. The Akiyoshi group has also made particles in which pNIPAm was incorporated to create thermoresponsive pullulan particles. These particles can capture and entrap macromolecules, such as proteins, in the gel network.[139–142] The self-assembly of these polymers can be controlled from the molecular level (association of hydrophobic groups) to the nanoscale level (association of hydrophobized polymers) and macroscopic level (association of nanoparticles). The hierarchy of pullulan assembly is shown in Figure 14.

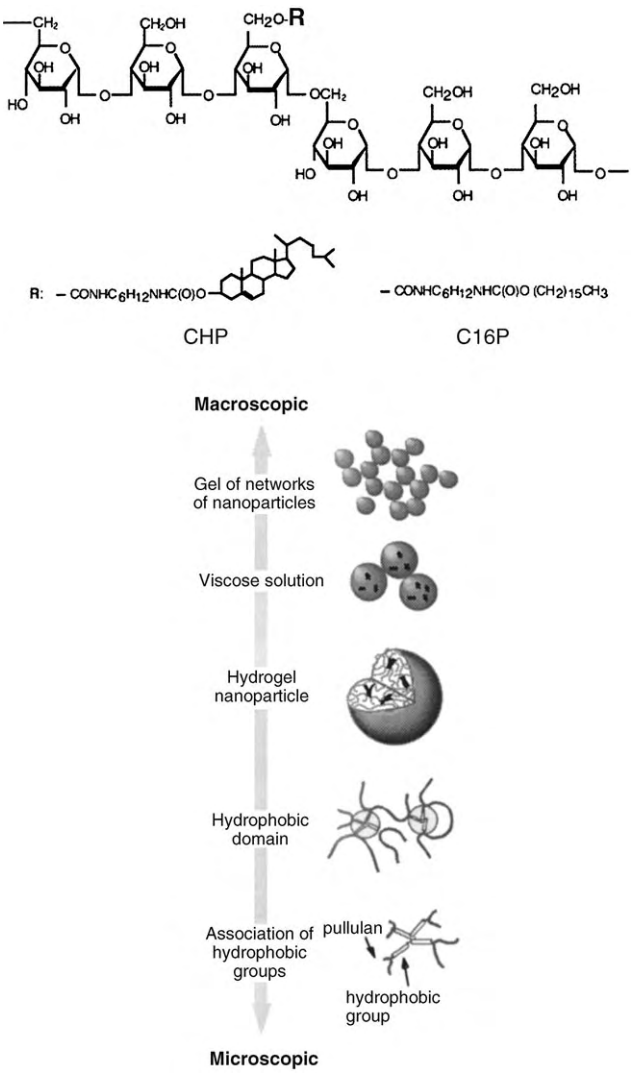

Figure 14. Chemical structure and the hierarchical self-assembly of hydrophobically modified pullulan. Reprinted with permission from ref. [142].

2.4. Post-Polymerization Modification of Hydrogels

For certain applications not all of the desired hydrogel functional groups can be added during the polymerization step. There are several reasons for this: the desired functional groups may not be stable during the polymerization step or the molecules are simply not polymerizable. This situation is true for most biomolecular structures from which hybrid gels would be prepared. To allow further functionalization of hydrogels, most often a small amount of comonomer with acidic or basic functional groups is copolymerized during the polymerization step. These functional groups are then used for the attachment of molecules that could not be directly incorporated by polymerization. This particular class of syntheses encompasses a large variety of particles, of which only a few will be mentioned in this Review.

We have created photoresponsive microgels by post-polymerization modification.[143] An amine comonomer was copolymerized in the pNIPAm microgels. This amine group was then used for attaching malachite green isothiocyanate to the microgels. Malachite green is a temperature-jump dye molecule that converts light ($\lambda_{max}^{abs} = 620$ nm) to thermal energy by nonradiative relaxation. Since the polymer is thermoresponsive, the microgels undergo deswelling when irradiated with a HeNe laser. Photoresponsive microgels exhibit dye-concentration dependent deswelling, that is, for the same laser intensity, microgels having higher concentration of malachite green deswell to a larger extent than microgels with lower concentration of the dye.

The Kawaguchi group has used post-polymerization modifications extensively for making particles with variety

 © 2005 Wiley-VCH Verlag GmbH & Co. KGaA, Weinheim

of functions.[144] For example, to synthesize a tetra-functional particle, they first synthesized standard microgels using acrylamide, BIS, methacrylic acid, and *p*-nitrophenyl acrylate as the co-monomers. The thus introduced ester side chain can be hydrolyzed to give acidic particles, or after hydrolysis can be treated with ethylene diamine to give amphoteric particles. The acid groups were also coupled with a long-chain alkyl amine to form hydrophobic particles. Finally the acid groups were coupled to an immunoglobulin G (IgG) to form bio-functionalized microgels. This particular example illustrates the tremendous versatility in microgel structure and function that is offered by post-polymerization modification.

Another interesting system involved the synthesis of pNIPAm chains bearing terminal carboxyl groups, which were then grafted to microgels. Some of the carboxy termini were then used to attach the enzyme trypsin, resulting in a particle having two different kinds of pNIPAm chains on the surface; one with trypsin and the other without it. Surprisingly, it was found that the two chains had different transition temperatures. The free chains collapsed at a lower temperature than the trypsin-conjugated chains, thereby exposing the enzyme for substrate binding. Hence by this simple construct it was possible to control the enzyme activity by controlling the temperature (Figure 15).[145]

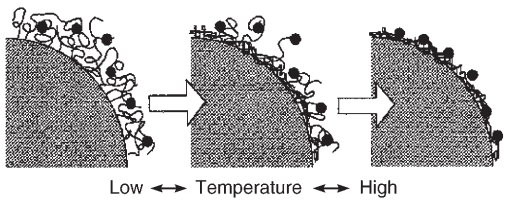

Figure 15. Changes in the surface of the particle conjugated with two different types of pNIPAm chains (filled circles depict the enzyme trypsin) with temperature. These types of phase transitions enable thermally modulated enzyme activity. Reprinted with permission from ref. [145].

Delair, et al. described the immobilization of DNA on microgels by post-polymerization modification. PNIPAm microgels with an amine comonomer were synthesized. Single-stranded DNA with an amine group at the 5′-end was treated with 1,4-phenylene diisocyanate in 1:2 ratio so that one of the isocyanates was coupled to the DNA, while the other one remained free. After purification, the DNA was coupled to the pNIPAm microgels by allowing the free isocyanate to react with the amines on the surface of the particles. The DNA particles were then used for detection of viral DNA and also for formation of two-dimensional arrays on planar substrates.[146]

Post-polymerization modification can not only be used for coupling biomolecules but also for grafting synthetic polymer chains. Hu et al. synthesized pNIPAm microgels and grafted pNIPAm chains on these particles by reversible addition fragmentation chain transfer (RAFT).[147] They then used these particles to study the thermal behavior of the grafted polymer. In another example Hu and Wu grafted PEO chains onto the microgel particles. The hydrophilic PEO chains were observed to stretch from the particle surface as the particles size decreased with increasing temperature.[148]

3. Hydrogel Particles in Nanotechnology

The synthetic methods described in the previous Sections have enabled the field to advance towards the application of hydrogel nano- and microparticles in more complex biotechnology and nanotechnology applications. In this Section, we will describe some of these applications, highlighting systems where the ability to create synthetically and topologically complex hydrogels has led to successful incorporation into advanced nanosystems.

3.1. Drug and Gene Delivery

Recently, significant efforts have been put into devising colloidal drug carriers. It has been hypothesized that an actively targeted particulate drug carrier will increase the therapeutic efficacy of a drug by delivering that drug to the diseased site, while also reducing systemic side-effects of the drug. An ideal drug carrier should be able to target and deliver only to the diseased sites, it should not induce immune response, and it should be degradable and produce nontoxic degradation products.[149]

The particulate carriers that have been most widely studied are liposomes and polymer nanoparticles. Liposomal drug carriers have been studied extensively, and a few liposomal formulations are currently available in the market, while many others are in the development "pipeline". One important drawback of liposomes is payload leakage. Since the boundary of the liposomes is a simple lipid bilayer, performance can be hampered by passive diffusion of drugs across that boundary.[150]

Among polymer particles, the most widely studied are poly(lactic acid-*co*-glycolic acid) (PLGA) particles.[151] The popularity of this material largely stems from its degradation into nontoxic by-products, which can be removed from the body by the renal system. However, this construct suffers from numerous drawbacks, as it is a very hydrophobic, immunogenic polymer with acidic degradation products. The increase in acidity associated with polymer degradation can induce nonspecific inflammatory responses, which can be very detrimental in targeted delivery applications. Non-viral gene-delivery systems have been proposed as a safer alternative to viral vectors, since they will induce host immune response to a lesser extent than viral vectors. Several cationic polymers, such as polyethyleneimine, polyamidoamine, and polylysine, have been used for non-viral gene delivery, but they all lack the biocompatibility needed for in vivo use.[152] Conversely, hydrogel nanoparticles, are a potentially useful class of materials in drug-/gene-carrier systems, but have been studied much less extensively. Herein we report a few examples of recent efforts involving nanoparticulate hydrogel delivery vehicles.

In an effort to employ naturally occurring polymers as delivery vehicles, Wang and Wu used agarose gel particles for

 © 2005 Wiley-VCH Verlag GmbH & Co. KGaA, Weinheim

protein delivery.[153] A model protein, ovalbumin was encapsulated in approximately 500-nm diameter, spherical agarose gel particles. After protein loading, it was demonstrated that the particles released ovalbumin in a temperature-dependent fashion, where the rate of protein release was higher at elevated temperatures. This effect is due to the higher swellability of agarose at higher temperature, which facilitates mass transport.

Another example of protein delivery was reported by Li et al.,[154] who demonstrated that poly(vinyl alcohol) hydrogel nanoparticles could be used for this application. These particles were prepared by an emulsion technique without incorporating any cross-linker. The model protein, bovine serum albumin (BSA) was incorporated during the particle formation. As with the previous example, the rate of release of BSA increased with temperature. The authors attribute this behavior to the decrease in the number of cross-links in the polymer network at higher temperature, thereby making the gel more "open" for the transport of BSA. Using this methodology, they were able to demonstrate release of BSA over 30 h.

Biodegradable hydrogel nanoparticles have been prepared by Kim et al. using glycidyl methacrylate dextran as the major comonomer and dimethacrylate poly(ethylene glycol) as a covalent cross-linker.[155] In this case, the particles were prepared by free-radical polymerization and a hydrophobic drug, clonazepam, was then loaded in the particles. It was found that the release rate was dependent on the pH value as well as the concentration of the enzyme dextranase, which degraded the dextran and eroded the particles.

Na and Bae have used self-assembled hydrogel particles of pullulan acetate and sulfonamide conjugates to study the release of the drug adriamycin.[156] In this case the pullulans had a pH-responsive polymer incorporated into their structure, which caused the particles to shrink and aggregate at $pH < 7$. The shrinking of the particles in turn caused the expulsion of the drug into the surrounding medium.

An interesting example of the controlled release of a drug from a microgel comes from Needham et al.[157] They used approximately 6.5-μm diameter methacrylic acid microgels as a matrix for drug encapsulation and release. While these particles are by no means in the nanoscale-range, they illustrate an interesting concept that could be extended to the nanoscale. Under conditions where the particles are deprotonated, and hence swollen (as a result of Coulombic repulsion between the negatively charged regions), the particles could be loaded with the anticancer drug doxorubicin. Upon reducing the pH value of the medium below the acid pK_a, the particles condensed. To prevent leakage of the drug from the polymer, the particles were then coated with a lipid bilayer. These lipid-coated particles were then suspended in a medium of $pH > pK_a$. Surprisingly, no gel swelling was observed and hence no drug was observed to leak from the construct. To release the drug, a series of voltage pulses was applied to electromechanically disrupt the bilayer and cause the swelling of the particle. Thus, it was illustrated that the drug could be protected and then be released on demand using a subtle stimulus. The concept is illustrated in Figure 16.

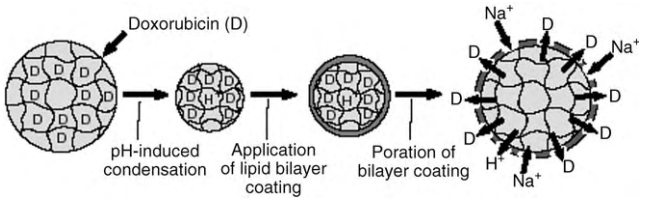

Figure 16. Loading and release of doxorubicin from lipid-coated microgels. Reprinted with permission from ref. [157], Copyright 1998 Macmillan Magazines Limited.

A similar example was published by Moore and coworkers. Again, in this example the polymer constructs are not at the nanoscale level but nonetheless provide an interesting concept.[158] A pH-sensitive gel was photopolymerized in a cylindrical shape. The gel was fabricated from 2-hydroxyethyl methacrylate, acrylic acid, and ethyleneglycol dimethacrylate. Palmitoyl chloride was then covalently bound to the surface of the gel. This modification of the gel created an ion barrier that enabled the pH-sensitive gel to remain in a condensed state even in media with a high pH value. Only when this barrier was disrupted by a surfactant did the gel swell (Figure 17). The ability of the fatty acid layer to maintain a sharp chemical gradient is analogous to the function of a cell membrane and shows the promise of creating highly non-equilibrium systems from well-designed nanomaterials.

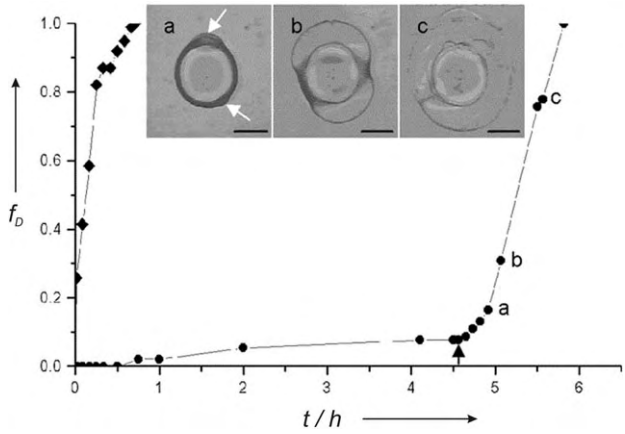

Figure 17. Lipid-modified pH-responsive gels. When the lipid-modified gel (●) is exposed to a buffer solution at pH 12, it resists swelling for a significant time, whereas the unmodified gel swells immediately (◆). The photographs show the effect of SDS on the lipid–modified gel in pH 12 buffer. The arrows indicate the points at which instabilities are first observed; swelling propagates from these points. The scale bar is 250 μm. Reprinted with permission from ref. [158].

While the previous examples were simple demonstrations of ex vivo controlled release from hydrogel particles, others have applied nanoparticulate hydrogels to in vivo delivery. For example, Hsiue et al. have used pNIPAm nanoparticles for ocular delivery.[159] Two formulations were used, one was composed of a solution of linear pNIPAm, the other was a mixture of linear pNIPAm and pNIPAm particles. The drug-

 © 2005 Wiley-VCH Verlag GmbH & Co. KGaA, Weinheim

release and cytotoxicity studies were carried out on rabbits. The drug epinephrine, which reduces intraocular pressure, was then delivered from each of the two formulations. It was observed that the intraocular pressure was decreased for around 24 h when the linear pNIPAm system was used, while the mixed system extended the therapeutic effect to about 32 h. Systems such as these are therefore potentially interesting for the clinical treatment of glaucoma.

As mentioned above, an ideal drug carrier should not induce an immune response in the host. This property is commonly achieved by making the surface of the particle hydrophilic, which can prevent opsonization (i.e. adhesion enhanced phagocytosis) by macrophages.[160] For example, Gaur et al. synthesized cross-linked poly(vinylpyrrolidine) hydrogel nanoparticles ($\approx$100 nm diameter).[161] The surface of these particles was then made hydrophilic by attaching poloxamers and poloxamines, which are PEG/poly(propylene glycol) block copolymers. In vivo studies in mice indicated that less than 1% of the dose was retained by the macrophages in the liver, and even after 8 h of injection around 5–10% of these particles were still circulating in the vasculature. This enhanced circulation time, and the lack of liver accumulation, could enable the use of such particles in drug delivery. They also reported that an increase in size and hydrophobicity of the particles increased the uptake by reticulo-endothelial system, suggesting that both factors may play a role in the ability of the body's defense mechanisms to recognize the particles as foreign invaders.

Targeting is an important property for a drug carrier, as potentially, the uptake and retention of the nano-carrier at the site of disease can be enhanced by active targeting. We have synthesized a folic acid labeled pNIPAm core–shell microgel that can target cancer cells.[162] Folic acid is a well known ligand for targeting cancer cells because most tumors overexpress folate receptors. In this demonstration, pNIPAm core–shell hydrogel particles were synthesized, in which the pNIPAm core was fluorescently labeled and the pNIPAm shell contained a small amount of a comonomer containing a primary amine. We then covalently coupled folic acid to the amine-containing hydrogel shell to localize the targeting ligand on the shell surface. When these particles were incubated with cancer cells that were overexpressing the folate receptor, the hydrogel nanoparticles were taken up by receptor-mediated endocytosis (Figure 18). It was also observed that the particles exhibited thermal cytotoxicity above the phase-transition temperature. The exact reason for this effect is not known but is suspected to be intracellular aggregation and protein adsorption onto the deswollen, hydrophobic pNIPAm particles. Since these particles apparently retain their thermoresponsivity in the cytosol, it was hypothesized that they could enable thermally triggered delivery of chemotherapeutic payloads, thereby enabling both active targeting and triggered delivery in one vehicle.

In another example of active targeting, Choi et al. used pNIPAm microgels for targeting liver cells.[163] They used pNIPAm-*co*-acrylic acid microgels that were tagged with fluorescein, while the targeting moiety in this case was galactose, which is a ligand for asialoglycoproteins. Through this ligand–receptor interaction the galactosylated microgels

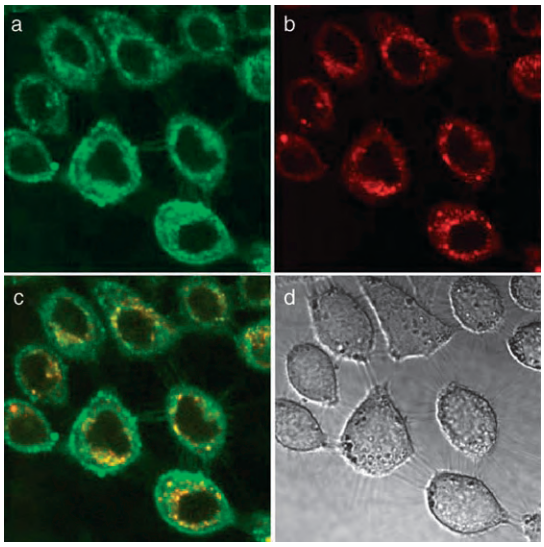

Figure 18. Confocal images of HeLa cells incubated with folate-conjugated nanoparticles. a) Green-fluorescent particle channel, b) lysotracker red-dye channel, c) overlap of both the channels and d) transmittance image of the cells. Experiments performed in collaboration with Jean Chmielewski at Purdue University.

were internalized in the cells. Furthermore, because these particles are thermoresponsive, their temperature-dependent uptake was studied. The uptake efficiency increased with the increase in temperature, which was suggested to arise from the enhanced uptake efficiency of smaller particles, although the increase in particle hydrophobicity could also enhance uptake. The Wooley group has investigated SCKs with targeting ligands such as folic acid, integrins, and peptides.[164–166] They have also demonstrated that nanoparticles coupled with a short peptide belonging to the protein transduction domain of HIV exhibited targeting ability for CHO and HeLa cell lines.

Synthetic–viral composite systems have also been explored. For example, Jana et al. prepared poly(vinylpyrrolidone) nanoparticles and encapsulated them in a reconstituted Sendai viral envelope containing only the fusion proteins.[167] These particles were incubated with human hepatoblastoma cell lines, which resulted in internalization of the polymer particles, as confirmed by fluorescence spectroscopy. Na et al. have used self-assembled polysaccharide (curdlan) particles for targeting.[168] Curdlan was hydrophobically modified with a carboxylated sulfonylurea derivative. The targeting ligand was lactobionic acid, which targets HepG2 cells. As expected, the degree of nontargeted uptake was significantly diminished relative to that for particles targeted to HepG2 cells.

Many groups have used cationic polymers, such as chitosan, for gene delivery. Chitosan is a natural cationic polysaccharide consisting of D-glucosamine and *N*-acetyl-D-glucosamine. This polymer has been shown to be biocompatible, non-immunogenic, and degradable, thereby making it potentially suitable as a delivery vehicle. In the presence of polyanions, chitosan can form hydrogel nanoparticles by complex coacervation. For example, chitosan–DNA nano-

© 2005 Wiley-VCH Verlag GmbH & Co. KGaA, Weinheim

particles have been widely studied for their application in gene delivery.[152] Targeting agents, such as transferrin, have also been conjugated to these particles to increase the internalization, while drugs such as chloroquine have been encapsulated within these particles to investigate controlled release. Mitra et al. have used chitosan to encapsulate doxorubicin, a highly toxic chemotherapeutic drug.[169] For encapsulation they first conjugated doxorubicin with dextran. This drug–dextran conjugate readily formed particles when mixed with chitosan. In vivo studies then showed that the chitosan–drug conjugate circulated in the blood longer and decreased the size of tumor to a larger extent than the free drug.

We have developed a technique to fabricate microgel thin films, which can potentially be used as drug-delivery implant devices.[85] The films are made by assembling charged microgels on a surface by a traditional layer-by-layer approach.[170] The microgels incorporated in these films retain their pH- and thermoresponsive properties.[83,85] In one example, we have loaded the microgels with insulin before assembling them into films.[82] The films then release insulin when subjected to a temperature above the microgel VPTT. The data shown in Figure 19 illustrate that this release can be thermally modu-

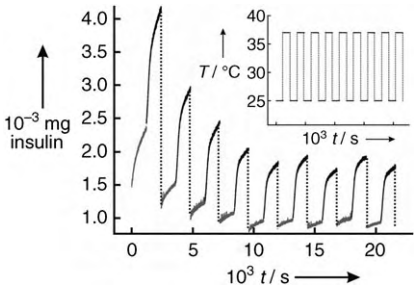

Figure 19. Insulin release during each thermal pulsing of 30-layer microgel film. Inset: the time–temperature wave form used for temperature modulation. The *x*-axis of the inset is identical to that of the main panel.

lated by alternating between heating and cooling cycles. Such films were extremely stable over extended periods of continuous thermal cycling. In addition to the release of macromolecules, these films have also been used for releasing small drug molecules such as doxorubicin.[84] Unlike in the insulin case, these films were first fabricated and then loaded with doxorubicin by thermal cycling. Similar results were obtained for the doxorubicin loaded films, where film deswelling resulted in the expulsion of the drug over many thermal cycles. These initial experiments provide a basis for creating constructs that can release therapeutic agents in a pulsed fashion when prodded by an external signal.

3.2. Encapsulation and Microreactors

The large internal free volume and hydrophilicity of hydrogels makes them useful in encapsulation of various species, such as DNA, RNA, small molecules, and proteins. When encapsulated, the hydrogel network can protect these species or release them in a controlled manner, as discussed in section 3.1. In this Section we will discuss the encapsulating property of microgels for applications other than drug delivery.

It has been observed that mass-transport rates of small molecules in hydrogels depend on the pore size, where larger pore sizes make it easier for the molecules to diffuse in the gel. In case of thermoresponsive microgels, a temperature-dependent diffusion is observed. At $T < \mathrm{VPTT}$ higher diffusion rates are observed than at $T > \mathrm{VPTT}$, owing to a decrease in the pore size of the polymer network at higher temperatures. Also, the charge on the polymer network is an important parameter, because it is easier to encapsulate molecules that are oppositely charged with respect to the polymer. In addition, a hydrophobic polymer network will enhance the encapsulation of a hydrophobic moiety.

Akiyoshi et al. have used cholesterol-bearing pullulans to encapsulate various proteins and peptides, for example, insulin, for which they observed the conformational stability of the macromolecule using circular dichroism (CD) spectroscopy.[139,140] No spontaneous release of insulin was observed from the nanoparticle, suggesting a very strong complexation in the macromolecular assembly. They observed that free insulin aggregated when subjected to heating but the encapsulated protein resisted such aggregation. They further studied the insulin stability against α-chymotrypsin activity, which degrades insulin. The pullulan-insulin complex resisted degradation to a much larger extent than the free insulin. Hence this system can potentially be used for the protection of the species of interest. Similarly, pullulans have been used as molecular chaperones for an enzyme.[141] Carbonic anhydrase B is an enzyme that denatures and aggregates at high temperature. The enzyme, in its denatured state, was complexed with the pullulans. The complex was cooled and the enzyme was released from the particles. The enzyme refolded in its native state and again became active.

SCKs have also been used for encapsulation and release of various entities. Murthy et al. have synthesized a polystyrene-*b*-poly(acrylic acid) SCK which has a thermally labile linkage at the core–shell interface.[136] After self-assembly and cross-linking of the shell, the particles were heated to 125 °C, which cleaved the bond between the polystyrene block and the poly(acrylic acid) block. The resulting release of the hydrophobic polystyrene chains occurred as a function of the cross-link density in the shell, with more heavily cross-linked shells releasing a smaller amount of hydrophobic polymer. In a further study, SCK particles were fabricated with poly(ε-caprolactone)-*b*-poly(acrylic acid).[129] Poly(ε-caprolactone) is a semicrystalline polymer with a lamellar lattice structure. In this case it was observed that at room temperature the core crystallizes and forces the particle to adopt a disc-shaped structure, which was confirmed by AFM. When the particles were heated above the melting point of the crystal, the particles adopted a spherical structure. Hence by using this novel construct it was possible to study the crystallization of poly(ε-caprolactone) in a confined system. SCKs have also been used to package DNA and thus offer protection against enzymatic degradation.[171]

 © 2005 Wiley-VCH Verlag GmbH & Co. KGaA, Weinheim

Soft nanomaterials have potential for being used as reaction vessels, which can then control the volume in which a specific reaction can take place. Liu et al. reported the use of self-assembled triblock copolymers, which they refer as shell cross-linked micelles, for preparation of gold nanoparticles.[172] The block copolymer that they used was composed of poly(ethylene oxide)-*b*-poly(glycerol monomethacrylate)-*b*-poly(diethylamino)ethyl methacrylate (PEO-GMA-DEA) as well as a second version in which the middle block was replaced by hydroxyethyl methacrylate (PEO-HEMA-DEA). These triblock copolymers form "onion like" micelles, where the core is made of DEA, the middle shell is of HEMA/GMA, and the outer shell is of PEO. After micellization, the middle shell was cross-linked with divinyl sulfone to make the structure stable. The DEA in the core was protonated by $HAuCl_4$ and subsequent in situ reduction of Au^{III} to Au^0 using $NaBH_4$. The mean size of the resultant gold nanoparticles was around 1–5 nm. The gold particles formed were not very monodisperse since each "nanoreactor" contained several gold particles and also the size was not controllable. This technique has one main advantage, that the dimensions of the nanoreactors are preserved during the reduction step as a result of the cross-linked shell. Zhang et al. have also synthesized inorganic nanoparticles in microgels.[173] They used pNIPAm-*co*-acrylic acid-*co*-2-hydroxyethyl acrylate microgels cross-linked with BIS. First the acid groups were deprotonated at high pH value and then, depending upon the type of nanoparticles desired, different precursor cations were introduced into the microgels. Three different types of nanoparticles were synthesized within the microgel matrix: CdS (a solution of Na_2S was added to a Cd^{2+}/microgel solution), Ag (an Ag^+/microgel solution was reduced by $NaBH_4$), and Fe_3O_4 (an aqueous Fe^{2+}/microgel solution was oxidized by $NaNO_2$). Most importantly, the size and polydispersity of the nanoparticles could be controlled by controlling the composition and the structure of the microgels.

3.3. Analytical Applications

Given the ability to synthesize a variety of responsive hydrogel structures, chemical and biological sensing applications remains an intriguing application. One of the earliest types of hydrogel nanoparticle employed in "sensing" was a pH-responsive particle. The simplest method of fabrication involves the use of a pH-responsive moiety, such as a weak acid, which can be copolymerized into the polymer network. At low pH value, the acid groups are protonated and the particles will be in a somewhat condensed form, while at a higher pH values at which the acid groups are deprotonated, the particles adopt a swollen structure because of Coulombic repulsion among the negatively charged regions and a change in the free energy of mixing with water. Similarly, charged microgels are responsive to ionic strength, where an oppositely charged ion neutralizes the charge and causes the gel to shrink. Similar approaches have enabled the fabrication of cross-linked block copolymer micelles that are pH-responsive. Although this approach appears to be a generalizable motif by which it is possible to imagine designing hydrogel nanoparticles that "sense" their surroundings, very little else has been done on creating hydrogel nanoparticles for real chemical-sensing applications. However, a few examples are beginning to emerge. For example, we have demonstrated that hydrogel microstructures can be rendered sensitive to protein binding, provided the interaction is multivalent and therefore results in an increase in the microgel cross-link density.[40] This approach has the potential to be extended to reversible biosensors based on antibody–antigen displacement or competitive binding. New methods for glucose sensing based on shell-restricted swelling in core–shell microgels are also currently under development.[174] It is clear that numerous opportunities exist for the design of new bioresponsive structures, and given the current focus on extending the complexity of hydrogel-nanoparticle architectures, more studies of this type can be expected in the near future.

In addition to these sensing applications, microgels have been used for the separation of proteins from complex media. Kawaguchi et al. reported that proteins could be separated using thermoresponsive microgels.[145] They used regular pNIPAm microgels and observed that at $T >$ VPTT larger amounts of protein bound to the particles than at $T <$ VPTT. The higher degree of protein adsorption at $T >$ VPTT was attributed to the hydrophobic interaction between the protein and dehydrated polymer. In an approach that utilized Coulombic interactions, Elaissari et al. used cationically charged pNIPAm microgels for the extraction of RNA. It was observed that the interaction between the cationic particles and negatively charged RNA decreased with an increase in pH value, ionic strength, or temperature, thereby indicating that adsorption was mainly governed by electrostatics.[175] In an immunoseparation study, Kondo et al. synthesized poly(styrene/NIPAm/glycidyl methacrylate) microgels. These particles were designed so that they flocculated at high temperature and at high ionic strength. Using the glycidyl methacrylate comonomer as a chemical handle for chemoligation, BSA was coupled to the particles, which were then used for the immunoseparation of anti-BSA from serum. After incubation with the serum, the particles were separated by flocculation.[176] Similarly, particles that contained magnetite were used for separation and purification, the particles could be collected by using a magnetic field.[177]

Stimuli-sensitive microgels can also be envisioned for applications in which the partition coefficient of a solute can be tuned over a wide range. For example, Kanzawa and coworkers have used the thermoresponsive properties of pNIPAm in chromatography for the separation of variety of compounds, such as steroids, peptides and proteins. Their construct uses silica particles, to which pNIPAm is grafted. These particles are an interesting stationary phase in chromatography, as the partition coefficient of a solute between the mobile and stationary phase should be strongly temperature dependent. Below the pNIPAm LCST, the particles are considered to behave as a normal, hydrophilic chromatography phase, while above the LCST, the particles should act as a hydrophobic reversed phase. The relative hydrophobicity of the polymer and the LCST can be further changed by incorporating other copolymers. Figure 20 shows chromato-

 © 2005 Wiley-VCH Verlag GmbH & Co. KGaA, Weinheim

grams for separation of steroids with respect to increasing the hydrophobic content of the stationary phase. Using these methods, it has been possible to increase the number of theoretical plates in separations of a wide range of analytes by running temperature gradients as opposed to the standard solvent-composition gradients that are the norm in most HPLC methods.[178–180] Doherty et al. have used nanogels in capillary electrophoresis (CE) based separation of DNA.[181,182] Currently CE is widely used for high-throughput DNA sequencing, in which polyacrylamide solutions are the most common sieving matrix. In the case of nanogel-based matrices, inverse emulsion polymerization was used to synthesize materials of the desired size and cross-linker concentration. These particles were synthesized from acrylamide and a small amount of BIS to obtain sparsely cross-linked networks. These nanogels were used for both conventional capillary electrophoresis and chip-based electrophoresis. In both cases they gave better selectivity and longer read lengths for single-stranded DNA than that obtained with conventional matrices.

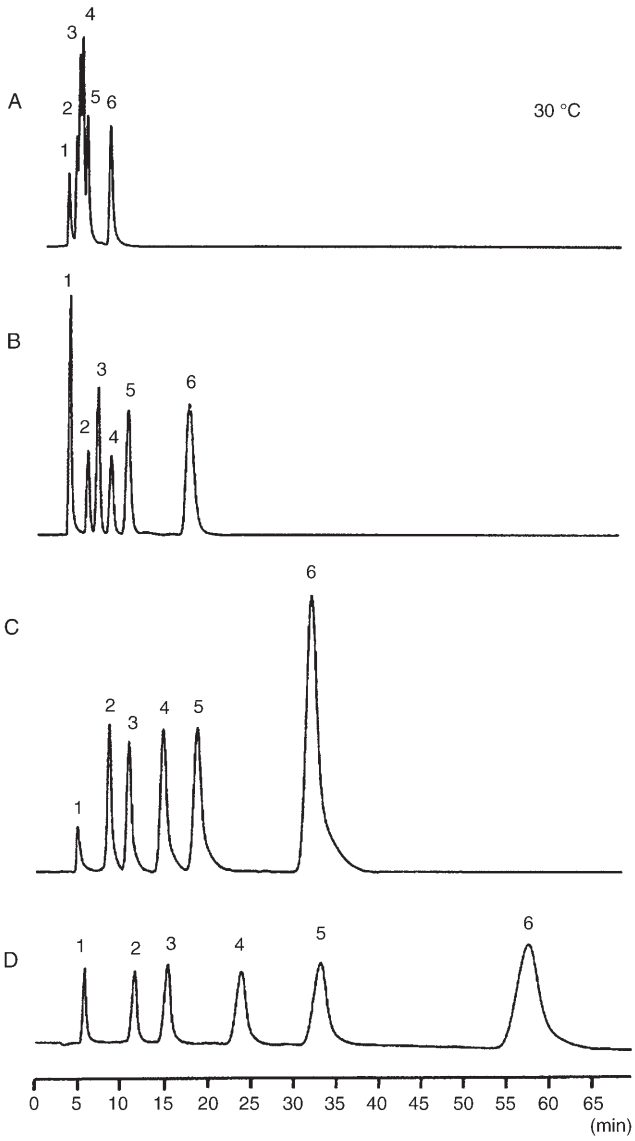

Figure 20. HPLC separations of steroid mixtures using a column packed with particles having thermally tunable hydrophobicities. The hydrogel hydrophobicity increases from A to D. The chromatograms indicate that a higher hydrophobicity results in a better separation under these mobile-phase conditions. Reprinted with permission from ref. [178].

Hydrogel nanoparticles have also been employed in a molecularly imprinted polymer (MIP) scheme. The principle behind MIP is based on both shape and molecular-recognition templating. When the polymerization is carried out in the presence of "template" molecules, it is envisioned that the polymer will rigidify around that template, forming a cavity that is optimized for binding that molecule. After the templates are removed, it is hoped that the cavity retains its shape and is able to bind and detect that particular molecule or similar molecules in a complex mixture. Ye et al. have synthesized hydrogel nanoparticles in the presence of theophylline and 17-β-estradiol. The sensing molecules were dissolved in the mixture of methacrylic acid and trimethylolpropane trimethacrylate ($[H_2C{=}C(CH_3)CO_2CH_2]_3CC_2H_5$) and then polymerized either thermally or by UV irradiation. In these studies radio ligand binding analysis was used to determine the sensitivity and selectivity of analyte binding.[183] Competition binding experiments showed high selectivity for the analyte.

In an attempt to couple simple optical interrogation of microgel behavior with responsive structures, we have developed a method to fabricate dynamically tunable microlenses that respond to light, temperature, pH value, and protein binding.[40,184–186] For this application, large (>1 micron) pNIPAm-*co*-acrylic acid particles were synthesized. These particles were then attached to a glass surface by electrostatic assembly. Since these microgels are soft, they deform upon attachment to the surface into planoconvex or hemispherical shapes. Because of the dual responsive nature of this simple polymer, the refractive index of the microgels can be controlled by temperature and pH value, where the more swollen form has a lower refractive index, with the index increasing as the gel becomes more condensed. Because of the specific shape of the microgels, the particles behave as planoconvex lenses, and the lens performance can be interrogated on a simple optical microscope (Figure 21).

In addition to these constructs we have also fabricated microlenses that respond to light.[184] In this experiment gold nanoparticles are assembled on the surface prior to attaching of the microgels. Gold nanoparticles can cause local heating when the surface plasmon modes are excited by a frequency-doubled Nd:YAG laser. We observed that only the region interrogated by the laser underwent phase transition (as a result of the local heating caused by the underlying gold-nanoparticle layer) and projected sharper images. The image quality was also controlled by the power of the laser, ambient temperature, and the pH value of the solution (Figure 22). Finally, microlenses with surface-localized ligands display dramatic changes in focal length upon protein binding, provided the protein–ligand interaction is a multivalent one.[40] This technique of fabricating microlens arrays is inexpensive, simple, and provides a method to interrogate

 © 2005 Wiley-VCH Verlag GmbH & Co. KGaA, Weinheim

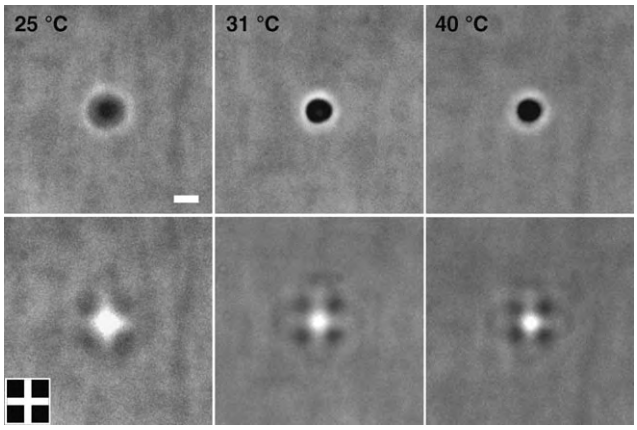

Figure 21. DIC microscopy images (top) of microgels on a glass substrate. The microgel acts as a microlens by projecting a cross pattern (bottom). The quality of the image improves with the increase in the temperature and concomitant gel deswelling. Reprinted with permission from ref. [186]

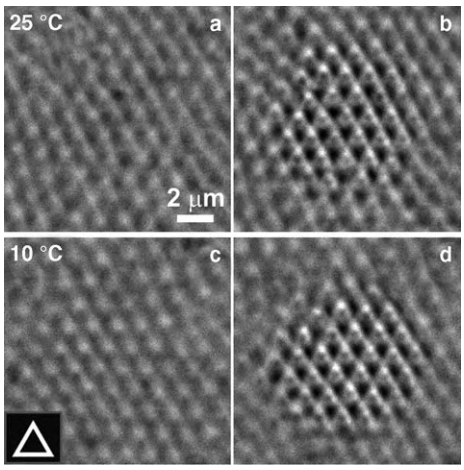

Figure 22. Photoswitching of a microlens array at 25 °C (a and b) and at 10 °C (c and d) as a function of laser power, where in the case of (b) and (d) the laser power is high enough to collapse the particles and thereby increase the microlens focusing power.[184]

single transducing elements, which makes it an attractive construct for various optical and sensing applications.

3.4. Biomaterials

Perhaps the broadest definition of biomaterials comes from the National Institutes of Health Consensus Development Conference: *"[a biomaterial is] any substance (other than a drug) or combination of substances, synthetic or natural in origin, which can be used for any period of time, as a whole or part of a system which treats, augments, or replaces any tissue, organ, or function of the body"*.[187] Research in the field of biomaterials is often linked to developing a more biocompatible system, such as making an implant or surgical device less damaging to the body. In case of hydrogels, much of the effort has been put in to coating the surface of the implants or devices with polymers or bulk gels. With the advent of responsive hydrogels, many researchers began working on making "smarter biomaterials", materials which can sense a change in the environment and respond in a programmed fashion to it. In this Section we describe a few of those examples pertaining specifically to hydrogel nanoparticles.

As mentioned previously, Kawaguchi and co-workers have studied the interaction of proteins with microgels extensively.[145,188,189] For example, the group has studied the effect of temperature on the nonspecific adsorption of proteins to thermoresponsive microgels. They have also investigated the activity of enzymes that are covalently bound to the microgels. In one example, trypsin peroxidase was attached to pNIPAm microgels and its activity was studied as a function of temperature.[190] The enzyme activity decreased with increasing temperature. This change was attributed to the decrease in the pore size which caused the decrease in the rate of diffusion of substrate to the enzyme. In a similar system with a small molecule (ubiquinone) attached to the particle, similar temperature-dependent results were obtained.

Duracher et al. have studied the adsorption of HIV-1 capsid protein p24 on polystyrene-core-pNIPAm-shell particles.[191] As predicted by numerous studies, at $T >$ VPTT of pNIPAm a higher adsorption was observed which was due to hydrophobic interactions. Similarly Urakami et al. studied the phagocytosis of polystyrene-*co*-polyacrylamide gel particles as a function of hydrophobicity. They observed that phagocytosis by granulocytes increased with the increase in polystyrene content of the particles, again presumably arising from an increase in hydrophobic association with the granulocyte.[192] In similar studies, Kimhi and Bianco-Peled used isothermal titration calorimetry (ITC) to study the adsorption of small molecules (aspartic acid and valine) to pNIPAm microgels as a function of temperature.[193] At 25 °C aspartic acid binds strongly to the polymer particles owing to the formation of hydrogen bonds, at 37 °C valine binds strongly because of the hydrophobic effect.

More advanced architectures can be prepared that take advantage of biocatalytic systems. For example, Ogawa et al. have synthesized pNIPAm microgels containing a pendant vinyl imidazole side-chain, which again allows for pH-tunable gel swelling.[38] The enzyme urease, which catalyses the hydrolysis of urea into ammonia, was then physically entrapped in the particles. As the enzyme produced ammonia, the pH value of the medium increased. Hence, in the presence of urea the particles shrank owing to the increase in pH value and subsequent deprotonation of the imidazole unit. When the substrate was removed, the particles swelled to their original size as the local pH value equilibrated with the pH value of the surrounding bath. To demonstrate the potential utility of such a biomechanical system, these particles were incorporated into a membrane. Upon introduction of urea to one of the solvent reservoirs, the permeability of the membrane increased as the particles shrank.

An important aspect of many implanted biomaterials relates to the ability of cells to adsorb and proliferate on the material surface. Even materials with low surface energies

 © 2005 Wiley-VCH Verlag GmbH & Co. KGaA, Weinheim

and hence low degrees of non-specific protein adsorption can tend to foul over time in cell culture or after implantation. Hence, it is important to evaluate fouling of biomaterials as well as to arrive at new strategies for mediating cellular recruitment at synthetic surfaces. Thus, in addition to the aforementioned protein adsorption studies, Kawaguchi and co-workers have also studied the effect of cell binding to thermoresponsive particles on a solid surface.[145] pNIPAm microspheres were deposited on a plate to produce a 2D array upon which the cell culture medium was seeded. It was observed that the cells produced more reactive oxygen species at 37 °C than at 25 °C, indicating that the cells are under more mechanical stress at the higher temperature. This stress is presumably due to stronger attachment at $T > \mathrm{VPTT}$. It was also observed that the amount of reactive oxygen species produced when the system was heated from 25 °C to 37 °C was much higher than when just incubated at 37 °C. This result was attributed to the stimulus inflicted by the dynamic deswelling process. In addition to this system a ligand–receptor system was also used a to study the mechanical stress on the cells.[145]

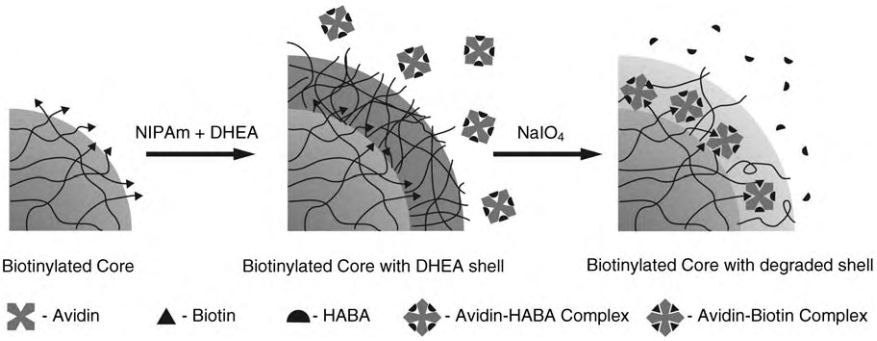

Figure 23. Permeation-selective core-shell microgels. The particles exhibit shell cross-linker-density dependent permeation of the protein.[195]

Our group has fabricated particles in which the adsorption of the proteins to the particles is reduced by using PEG grafting.[194] We used pNIPAm-core/pNIPAm-shell particles and attached PEG either to the core or to the shell by copolymerization of PEG-monomethacrylate. Reduced protein adsorption was observed for both the core- and shell-grafted PEG particles. NMR spectroscopy and protein adsorption measurements, showed that at high temperature the PEG chains phase separate to the particle surface, and because of the polymer's hydrophilicity reduce protein adsorption. For particles in which the PEG is attached to the core, the PEG chains are able to penetrate the shell and phase separate to the surface, thus reducing the surface energy of the deswollen particles.

In another example of core–shell particles that may have utility in biomaterials applications, we have prepared a system in which the shell acts a barrier between the protein in the solution and a core-localized ligand buried under the shell.[195] In this case we have synthesized a core to which biotin is attached, then added a shell containing a degradable cross-linker. Initially the cross-linker density is high enough that the pore sizes are smaller than the size of the protein avidin. As the cross-linker is degraded, the average pore size increases and allows permeation of avidin to the core, where it can bind to biotin (Figure 23). We have also observed protein-size-dependent permeation, that is, for larger proteins, more cross-links have to be degraded to allow for binding. These systems are interesting from the view of the topological complexity and also because they may be a model system for a particle that can "express" a particular functionality at the surface in response to a biological or chemical signal which disrupts shell-localized cross-links.

3.5. Colloidal Assemblies

Perhaps one of the most intriguing properties of monodispersed colloidal systems is their ability to form thermodynamically stable, ordered, periodic phases.[196] The most common of these phases is the cubic crystalline lattice observed in natural opal.[197,198] Synthetic colloidal crystals have potential applications in the field of diffractive optics, especially in the context of photonic band-gap structures.[199] Traditionally, hard sphere particles, such as silica or polystyrene beads, are used to form synthetic crystals. Recently, however a great deal of effort has been put into assembling crystals from soft colloidal precursors owing to their interesting phase behavior and the potential for creating dynamically tunable assemblies.[72–75,200–202]

Of particular interest is the potential for using microgel particles as colloidal model systems.[69,203–205] The Richtering group has extensively investigated the microgel phase diagram and has shown that deviations from hard-sphere behavior can be observed at high particle concentrations.[73,98,203,206,207] Furthermore, neutron-scattering studies have enabled the elucidation of the microgel network structure, and how that structure dictates the observed phase behavior.[207] Others have used computational methods to investigate how particle "softness" can change the effective interaction potential and the resultant phase diagram of both microgels[205,208,209] and star polymers.[210–214] Importantly, these calculations have revealed a potentially very rich phase behavior for soft colloids,[205,209,211,212] in contrast to the structures observed for hard spheres.[215]

Our group has worked intensively in the field of soft-sphere assembly, wherein we have developed methods for preparing colloidal crystals from thermoresponsive hydrogel particles. For an in-depth discussion of our work, see a recent review article on this subject.[200] One of the particular advantages of using thermoresponsive particles is that the volume phase transition allows assemblies to be annealed that have been formed by harsh methods, such as centrifugation.[72] In this fashion, it is possible to form crystals much more rapidly than those prepared by slow sedimentation of hard-sphere colloids. The thermoresponsivity of the particles has also been used to tune the Bragg peak of the crystals, both in a

 © 2005 Wiley-VCH Verlag GmbH & Co. KGaA, Weinheim

dynamic sense, and also by controlling the temperature at which the particles are centrifuged.[216]

We have also studied the phase behavior of particles that display unusual, weak attractive interactions.[217] pNIPAm-*co*-acrylic acid particles were synthesized and assembled at various volume fractions. Owing to the soft nature of the particles it was possible to overpack the system so that the effective volume fraction was greater than 100%. It was also observed that, in comparison to the hard spheres, the crystals did not melt until very low volume fraction. This property arises from multibody attractive interactions that result from dipole–dipole and ion–dipole interactions. Images corresponding to such crystals at various stages of growth are shown in Figure 24.

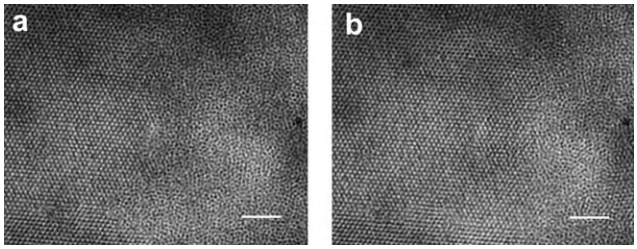

Figure 24. Growth process of weakly attractive hydrogel colloidal crystals as observed by differential interference contrast microscopy. Note that the effective particle volume fraction for this sample is approximately 40%. Panels (a) and (b) were acquired 5 minu apart; the progression of the crystal growth can be observed as the crystalline region extends further into the sample in panel (b). The scale bar is 20 μm. The unique phase behavior of these crystals is described in reference [217]. We thank Saet Byul Debord for supplying these images.

Composite colloidal crystals have also been made by incorporating gold nanoparticles, for photopatterning, into the system.[218] A frequency doubled Nd:YAG laser ($\lambda =$ 532 nm) was used to optically heat the system. In this fashion, it was possible to convert crystalline regions into glassy state (non-ordered state) and vice versa, by controlling the laser power and illumination times. Using this approach it was also possible to write patterns in the crystal assembly by a laser direct-writing approach.[219]

Asher and co-workers have fabricated polymerized colloidal crystal arrays from hydrogels for a number of applications. In one example they crystallized polystyrene beads and then polymerized the system using pNIPAm.[201] This system allows thermal tuning of Bragg diffraction, as the thermoresponsivity of the polymer chains is used to control the interparticle distance and hence the Bragg peak. These systems have also been used for detecting various analytes, where the polymer that connects the particles is responsive to the analyte and, in the presence of that analyte, causes a change in lattice spacing.[220] In one example boronic acid groups were incorporated into the crystalline array for glucose-sensing applications.[221]####Another example of polymerized colloidal crystal assembly was reported by Hu et al.[74] They synthesized two types of pNIPAm microgels, one had acrylic acid units and the other had 2-hydroxyethyl acrylate units. These nanoparticles were self-assembled to form crystals and then bonded together covalently using small linking molecules. For the acrylic acid particles epichlorohydrin was used for covalent bonding of the particles and for 2-hydroxyethyl acrylate particles divinylsulfone was used. These assemblies exhibited iridescent color patterns indicating that the particles assembled in a crystal phase. The covalent nature of the assembly provided stability to the crystal structure, which then enabled the color of the crystal to be tuned by temperature or an electric field.

4. Conclusions and Outlook

Towards the end of the last century, it was commonly thought that the term "nanotechnology" was coined exclusively for "hard materials" but this has changed as polymeric materials became more common ingredients in nanometric systems. Herein we have discussed various types of hydrogel nanoparticles and their applications in nanotechnology. As more and more research is carried out in this field, it becomes clearer that these materials hold great promise on their own, and as a bridge between more traditional nanostructures and biological systems. For example, gels that respond to a change in their environment are potentially useful in the context of truly bioresponsive structures that may enable natural systems to be manipulated in a rational fashion.

Although a great deal of research has been carried out in this field, we believe that most of the potential resources are untapped. There are opportunities for new efforts in advanced synthetic approaches to complex hydrogel nanomaterials, both in colloid synthesis (e.g. size and shape control) and in new chemoligation methods for controlled bioconjugate synthesis. The rational design of multifunctional architectures will be enabled by such efforts, thereby allowing the improvement of current applications, as well as the implementation of hydrogels in new arenas. In the case of core–shell particles reported by our group and others, the range of potential applications in which such materials can be used is just beginning to be uncovered. Early studies of the detailed structure–function relationships in hydrogel particles are now leading to the design of primitive applications-oriented nanomaterials. These proof-of-concept studies can then provide guidance for the synthesis of the second-generation of materials. In parallel, it will become increasingly important to perform detailed studies of cytotoxicity, immunogenicity, and pharamcokinetics, if these materials are to be employed in biotechnological applications. Finally, ground-level cooperation between chemists, biochemists, engineers, and clinicians is desired to enable the design, synthesis, and testing of structures that are truly applicable in clinical applications, such as drug-delivery devices, implantable biomaterials, biosensors/assays, and targeted chemotherapeutic formulations.

Received: April 15, 2005
Published online: November 11, 2005

 © 2005 Wiley-VCH Verlag GmbH & Co. KGaA, Weinheim

[1] S. H. Gehrke, *Adv. Polym. Sci.* **1993**, *110*, 82.
[2] A. S. Hoffman, *Adv. Drug Delivery Rev.* **2002**, *54*, 3.
[3] K. Yeomans, *Chem. Rev.* **2000**, *100*, 2.
[4] W. E. Hennink, C. F. van Nostrum, *Adv. Drug Delivery Rev.* **2002**, *54*, 13.
[5] K. Dusek, W. Prins, *Fortschr. Hochpolym.-Forsch.* **1969**, *6*, 1.
[6] W. R. Gombotz, S. Wee, *Adv. Drug Delivery Rev.* **1998**, *31*, 267.
[7] M. F. A. Goosen, G. M. O'Shea, H. M. Gharapetian, S. Chou, A. M. Sun, *Biotechnol. Bioeng.* **1985**, *27*, 146.
[8] M. P. Lutolf, G. P. Raeber, A. H. Zisch, N. Tirelli, J. A. Hubbell, *Adv. Mater.* **2003**, *15*, 888.
[9] P. Gacesa, *Carbohydr. Polym.* **1988**, *8*, 161.
[10] T. Watanabe, A. Ohtsuka, N. Murase, P. Barth, K. Gersonde, *Magn. Reson. Med.* **1996**, *35*, 697.
[11] D. Eagland, N. J. Crowther, C. J. Butler, *Eur. Polym. J.* **1994**, *30*, 767.
[12] A. M. Mathur, K. F. Hammonds, J. Klier, A. B. Scranton, *J. Controlled Release* **1998**, *54*, 177.
[13] S. Nagahara, T. Matsuda, *Polym. Gels Netw.* **1996**, *4*, 111.
[14] W. S. Dai, T. A. Barbari, *J. Membr. Sci.* **2000**, *171*, 79.
[15] N. A. Peppas, R. E. Benner, Jr., *Biomaterials* **1980**, *1*, 158.
[16] J. J. Sperinde, L. G. Griffith, *Macromolecules* **1997**, *30*, 5255.
[17] J. J. Sperinde, L. G. Griffith, *Macromolecules* **2000**, *33*, 5476.
[18] Y. Li, T. Tanaka, *J. Chem. Phys.* **1989**, *90*, 5161.
[19] Y. Li, T. Tanaka, *J. Chem. Phys.* **1990**, *92*, 1365.
[20] T. Tanaka, *Phys. A* **1986**, *140*, 261.
[21] D. Gan, L. A. Lyon, *J. Am. Chem. Soc.* **2001**, *123*, 7511.
[22] C. D. Jones, L. A. Lyon, *Macromolecules* **2000**, *33*, 8301.
[23] H. Staudinger, E. Husemann, *Ber. Dtsch. Chem. Ges. A* **1935**, *68*, 1618.
[24] T. Tanaka, *Phys. Rev. Lett.* **1978**, *40*, 820.
[25] K. Dusek, K. Patterson, *J. Poly. Sci. Poly. Phys. Ed.* **1968**, *6*, 1209.
[26] J. Moselhy, X. Y. Wu, R. Nicholov, K. Kodaria, *J. Biomater. Sci. Polym. Ed.* **2000**, *11*, 123.
[27] D. Duracher, F. Sauzedde, A. Elaissari, A. Perrin, C. Pichot, *Colloid Polym. Sci.* **1998**, *276*, 219.
[28] D. Duracher, F. Sauzedde, A. Elaissari, C. Pichot, L. Nabzar, *Colloid Polym. Sci.* **1998**, *276*, 920.
[29] M. J. Snowden, B. Z. Chowdhry, B. Vincent, G. E. Morris, *J. Chem. Soc. Faraday Trans.* **1996**, *92*, 5013.
[30] S. R. Sershen, S. L. Westcott, N. J. Halas, J. L. West, *J. Biomed. Mater. Res.* **2000**, *51*, 293.
[31] S. R. Sershen, S. L. Westcott, N. J. Halas, J. L. West, *Appl. Phys. Lett.* **2002**, *80*, 4609.
[32] S. R. Sershen, S. L. Westcott, J. L. West, N. J. Halas, *Appl. Phys. B* **2001**, *73*, 379.
[33] A. Suzuki, T. Ishii, Y. Maruyama, *J. Appl. Phys.* **1996**, *80*, 131.
[34] A. Suzuki, T. Tanaka, *Nature* **1990**, *346*, 345.
[35] T. Tanaka, I. Nishio, S. T. Sun, S. Ueno-Nishio, *Science* **1982**, *218*, 467.
[36] T. Miyata, N. Asami, T. Uragami, *Nature* **1999**, *399*, 766.
[37] K. Ogawa, A. Nakayama, E. Kokufuta, *Langmuir* **2003**, *19*, 3178.
[38] K. Ogawa, B. Wang, E. Kokufuta, *Langmuir* **2001**, *17*, 4704.
[39] Y. Ogawa, K. Ogawa, B. Wang, E. Kokufuta, *Langmuir* **2001**, *17*, 2670.
[40] J. Kim, S. Nayak, L. A. Lyon, *J. Am. Chem. Soc.* **2005**, *127*, 9588.
[41] H. G. Schild, *Prog. Polym. Sci.* **1992**, *17*, 163.
[42] M. Heskins, J. E. Guillet, *J. Macromol. Sci. Chem.* **1968**, *2*, 1441.
[43] I. Berndt, W. Richtering, *Macromolecules* **2003**, *36*, 8780.
[44] I. Berndt, J. S. Pedersen, W. Richtering, *J. Am. Chem. Soc.* **2005**, *127*, 9372.
[45] A. Matsumoto, S. Ikeda, A. Harada, K. Kataoka, *Biomacromolecules* **2003**, *4*, 1410.
[46] D. Duracher, A. Elaissari, F. Mallet, C. Pichot, *Macromol. Symp.* **2000**, *150*, 297.
[47] D. Duracher, A. Elaissari, C. Pichot, *Colloid Polym. Sci.* **1999**, *277*, 905.
[48] D. Duracher, A. Elaissari, C. Pichot, *J. Polym. Sci. Polym. Chem. Ed.* **1999**, *37*, 1823.
[49] F. M. Winnik, *Macromolecules* **1990**, *23*, 1647.
[50] F. M. Winnik, *Langmuir* **1990**, *6*, 522.
[51] F. M. Winnik, *Macromolecules* **1990**, *23*, 233.
[52] C. Wu, *Polymer* **1998**, *39*, 4609.
[53] C. Wu, X. Qiu, *Phys. Rev. Lett.* **1998**, *80*, 620.
[54] C. Wu, X. Wang, *Phys. Rev. Lett.* **1998**, *80*, 4092.
[55] C. Wu, S. Zhou, *Macromolecules* **1995**, *28*, 8381.
[56] C. Wu, S. Zhou, *Macromolecules* **1995**, *28*, 5388.
[57] C. Wu, S. Zhou, *Macromolecules* **1996**, *29*, 1574.
[58] X. Wang, X. Qiu, C. Wu, *Macromolecules* **1998**, *31*, 2972.
[59] M. Arotcarena, B. Heise, S. Ishaya, A. Laschewsky, *J. Am. Chem. Soc.* **2002**, *124*, 3787.
[60] D. Kungwatchakun, M. Irie, *Makromol. Chem. Rapid Commun.* **1988**, *9*, 243.
[61] M. Shibayama, T. Tanaka, *Adv. Polym. Sci.* **1993**, *109*, 1.
[62] T. Tanaka, D. J. Fillmore, *J. Chem. Phys.* **1979**, *70*, 1214.
[63] T. Tanaka, D. J. Fillmore, S.-T. Sun, I. Nishio, G. Swislow, A. Shah, *Phys. Rev. Lett.* **1980**, *45*, 1636.
[64] T. Tanaka, C. Wang, V. Pande, A. Y. Grosberg, A. English, S. Masamune, H. Gold, R. Levy, K. King, *Faraday Discuss.* **1995**, *101*, 201.
[65] Q. Yan, A. S. Hoffman, *Polymer* **1995**, *36*, 887.
[66] T. G. Park, A. S. Hoffman, *J. Biomed. Mater. Res.* **1990**, *24*, 21.
[67] S. Kim, K. E. Healy, *Biomacromolecules* **2003**, *4*, 1214.
[68] R. Pelton, *Adv. Colloid Interface Sci.* **2000**, *85*, 1.
[69] B. R. Saunders, B. Vincent, *Adv. Colloid Interface Sci.* **1999**, *80*, 1.
[70] E. Daly, B. R. Saunders, *Phys. Chem. Chem. Phys.* **2000**, *2*, 3187.
[71] H. Ohshima, K. Makino, T. Kato, K. Fujimoto, T. Kondo, H. Kawaguchi, *J. Colloid Interface Sci.* **1993**, *159*, 512.
[72] J. D. Debord, L. A. Lyon, *J. Phys. Chem. B* **2000**, *104*, 6327.
[73] H. Senff, W. Richtering, *J. Chem. Phys.* **1999**, *111*, 1705.
[74] Z. Hu, X. Lu, J. Gao, *Adv. Mater.* **2001**, *13*, 1708.
[75] T. Hellweg, C. D. Dewhurst, E. Bruckner, K. Kratz, W. Eimer, *Colloid Polym. Sci.* **2000**, *278*, 972.
[76] C. Wu, S. Zhou, *Macromolecules* **1997**, *30*, 574.
[77] D. Gan, L. A. Lyon, *J. Am. Chem. Soc.* **2001**, *123*, 8203.
[78] H. M. Crowther, B. Vincent, *Colloid Polym. Sci.* **1998**, *276*, 46.
[79] F. M. Winnik, H. Ringsdorf, J. Venzmer, *Macromolecules* **1990**, *23*, 2415.
[80] W. McPhee, K. C. Tam, R. Pelton, *J. Colloid Interface Sci.* **1993**, *156*, 24.
[81] N. Greinert, W. Richtering, *Colloid Polym. Sci.* **2004**, *282*, 1146.
[82] C. M. Nolan, M. J. Serpe, L. A. Lyon, *Biomacromolecules* **2004**, *5*, 1940.
[83] M. Serpe, L. A. Lyon, *Chem. Mater.* **2004**, *16*, 4373.
[84] M. J. Serpe, K. A. Yarmey, C. M. Nolan, L. A. Lyon, *Biomacromolecules* **2004**, *5*, 408.
[85] M. J. Serpe, C. D. Jones, L. A. Lyon, *Langmuir* **2003**, *19*, 8759.
[86] R. H. Pelton, H. M. Pelton, A. Morphesis, R. L. Rowell, *Langmuir* **1989**, *5*, 816.
[87] K. C. Tam, S. Ragaram, R. H. Pelton, *Langmuir* **1994**, *10*, 418.
[88] Y. Gao, S. C. F. Au-Yeung, S. Zhou, C. Wu, *J. Macromol. Sci. Phys.* **1997**, *36*, 417.
[89] C. Wu, S. Zhou, *J. Macromol. Sci. Phys.* **1997**, *36*, 345.
[90] Y. D. Yi, K. S. Oh, Y. C. Bae, *Polymer* **1997**, *38*, 3471.
[91] I. Varga, T. Gilanyi, R. Meszaros, G. Filipcsei, M. Zrinyi, *J. Phys. Chem. B* **2001**, *105*, 9071.
[92] A. Guillermo, J. P. C. Addad, J. P. Bazile, D. Duracher, A. Elaissari, C. Pichot, *J. Polym. Sci. Part B* **2000**, *38*, 889.
[93] B. R. Saunders, *Langmuir* **2004**, *20*, 3925.

 © 2005 Wiley-VCH Verlag GmbH & Co. KGaA, Weinheim

[94] N. C. Woodward, B. Z. Chowdhry, M. J. Snowden, S. A. Leharne, P. C. Griffiths, A. L. Winnington, *Langmuir* **2003**, *19*, 3202.
[95] H. Senff, W. Richtering, *Colloid Polym. Sci.* **2000**, *278*, 830.
[96] H. Senff, W. Richtering, C. Norhausen, A. Weiss, M. Ballauff, *Langmuir* **1999**, *15*, 102.
[97] S. Meyer, W. Richtering, *Macromolecules* **2005**, *38*, 1517.
[98] M. Stieger, W. Richtering, J. S. Pedersen, P. Lindner, *J. Chem. Phys.* **2004**, *120*, 6197.
[99] X. Wu, R. H. Pelton, A. E. Hamielec, D. R. Woods, W. McPhee, *Colloid Polym. Sci.* **1994**, *272*, 467.
[100] R. H. Pelton, P. Chibante, *Colloids Surf.* **1986**, *20*, 247.
[101] S. Zhou, B. Chu, *J. Phys. Chem. B* **1998**, *102*, 1364.
[102] K. Kratz, T. Hellweg, W. Eimer, *Ber. Bunsen-Ges.* **1998**, *102*, 1603.
[103] H. Suzuki, B. Wang, R. Yoshida, E. Kokufuta, *Langmuir* **1999**, *15*, 4283.
[104] K. Kratz, T. Hellweg, W. Eimer, *Colloids Surf. A* **2000**, *170*, 137.
[105] J. D. Debord, L. A. Lyon, *Langmuir* **2003**, *19*, 7662.
[106] J. Gao, B. J. Frisken, *Langmuir* **2003**, *19*, 5212.
[107] J. Gao, B. J. Frisken, *Langmuir* **2003**, *19*, 5217.
[108] S. Neyret, B. Vincent, *Polymer* **1997**, *38*, 6129.
[109] K. McAllister, P. Sazani, M. Adam, M. J. Cho, M. Rubinstein, R. J. Samulski, J. M. DeSimone, *J. Am. Chem. Soc.* **2002**, *124*, 15198.
[110] S. Kazakov, M. Kaholek, D. Kudasheva, I. Teraoka, M. K. Cowman, K. Levon, *Langmuir* **2003**, *19*, 8086.
[111] N. Dingenouts, S. Seelenmeyer, I. Deike, S. Rosenfeldt, M. Ballau, P. Lindner, T. Narayanan, *Phys. Chem. Chem. Phys.* **2001**, *3*, 1169.
[112] X. C. Xiao, L. Y. Chu, W. M. Chen, S. Wang, R. Xie, *Langmuir* **2004**, *20*, 5247.
[113] W. Stober, A. Fink, E. Bohn, *J. Colloid Interface Sci.* **1968**, *26*, 62.
[114] L. Zha, Y. Zhang, W. Yang, S. Fu, *Adv. Mater.* **2002**, *14*, 1090.
[115] J. H. Kim, T. R. Lee, *Chem. Mater.* **2004**, *16*, 3647.
[116] C. D. Jones, L. A. Lyon, *Langmuir* **2003**, *19*, 4544.
[117] C. D. Jones, L. A. Lyon, *Macromolecules* **2003**, *36*, 1988.
[118] D. Gan, L. A. Lyon, *Anal. Chim. Acta* **2003**, *496*, 53.
[119] C. D. Jones, J. G. McGrath, L. A. Lyon, *J. Phys. Chem. B* **2004**, *108*, 12652.
[120] S. Nayak, D. Gan, M. J. Serpe, L. A. Lyon, *Small* **2005**, *1*, 416.
[121] K. L. Wooley, *Chem. Eur. J.* **1997**, *3*, 1397.
[122] P. W. Zhu, D. H. Napper, *Macromolecules* **1999**, *32*, 2068.
[123] P. W. Zhu, D. H. Napper, *Langmuir* **2000**, *16*, 8543.
[124] K. B. Thurmond II, T. Kowalewski, K. L. Wooley, *J. Am. Chem. Soc.* **1996**, *118*, 7239.
[125] K. B. Thurmond II, T. Kowalewski, K. L. Wooley, *J. Am. Chem. Soc.* **1997**, *119*, 6656.
[126] H. Huang, E. E. Remsen, T. Kowalewski, K. L. Wooley, *J. Am. Chem. Soc.* **1999**, *121*, 3805.
[127] H. Huang, K. L. Wooley, E. E. Remsen, *Chem. Commun.* **1998**, 1415.
[128] E. E. Remsen, K. B. Thurmond II, K. L. Wooley, *Macromolecules* **1999**, *32*, 3685.
[129] Q. Zhang, C. G. Clark, Jr., M. Wang, E. E. Remsen, K. L. Wooley, *Nano Lett.* **2002**, *2*, 1051.
[130] Q. Zhang, E. E. Remsen, K. L. Wooley, *J. Am. Chem. Soc.* **2000**, *122*, 3642.
[131] K. L. Wooley, *J. Polym. Sci. Part A* **2000**, *38*, 1397.
[132] J. Liu, Q. Zhang, E. E. Remsen, K. L. Wooley, *Biomacromolecules* **2001**, *2*, 362.
[133] Q. Ma, E. E. Remsen, C. G. Clark, Jr., T. Kowalewski, K. L. Wooley, *Proc. Natl. Acad. Sci. USA* **2002**, *99*, 5058.
[134] Q. Ma, E. E. Remsen, T. Kowalewski, J. Schaefer, K. L. Wooley, *Nano Lett.* **2001**, *1*, 651.
[135] Q. Ma, E. E. Remsen, T. Kowalewski, K. L. Wooley, *J. Am. Chem. Soc.* **2001**, *123*, 4627.
[136] K. Shanmugananda Murthy, Q. Ma, C. G. Clark, Jr., E. E. Remsen, K. L. Wooley, *Chem. Commun.* **2001**, 773.
[137] H. Huang, T. Kowalewski, E. E. Remsen, R. Gertzmann, K. L. Wooley, *J. Am. Chem. Soc.* **1997**, *119*, 11653.
[138] K. Akiyoshi, S. Deguchi, N. Moriguchi, S. Yamaguchi, J. Sunamoto, *Macromolecules* **1993**, *26*, 3062.
[139] K. Akiyoshi, S. Kobayashi, S. Shichibe, D. Mix, M. Baudys, S. Wan Kim, J. Sunamoto, *J. Controlled Release* **1998**, *54*, 313.
[140] K. Akiyoshi, T. Nishikawa, S. Shichibe, J. Sunamoto, *Chem. Lett.* **1995**, 707.
[141] K. Akiyoshi, Y. Sasaki, J. Sunamoto, *Bioconjugate Chem.* **1999**, *10*, 321.
[142] K. Kuroda, K. Fujimoto, J. Sunamoto, K. Akiyoshi, *Langmuir* **2002**, *18*, 3780.
[143] S. Nayak, L. A. Lyon, *Chem. Mater.* **2004**, *16*, 2623.
[144] M. Kashiwabara, K. Fujimoto, H. Kawaguchi, *Colloid Polym. Sci.* **1995**, *273*, 339.
[145] H. Kawaguchi, K. Kisara, T. Takahashi, K. Achiha, M. Yasui, K. Fujimoto, *Macromol. Symp.* **2000**, *151*, 591.
[146] T. Delair, F. Meunier, A. Elaissari, M.-H. Charles, C. Pichot, *Colloids Surf. A* **1999**, *153*, 341.
[147] T. J. Hu, Y. Z. You, C. Y. Pan, C. Wu, *J. Phys. Chem. B* **2002**, *106*, 6659.
[148] T. Hu, C. Wu, *Macromolecules* **2001**, *34*, 6802.
[149] F. Marcucci, F. Lefoulon, *Drug Discovery Today* **2004**, *9*, 219.
[150] G. Barratt, *Cell. Mol. Life Sci.* **2003**, *60*, 21.
[151] S. Hirosue, B. G. Muller, R. C. Mulligan, R. Langer, *J. Controlled Release* **2001**, *70*, 231.
[152] H. Q. Mao, K. Roy, V. L. Troung-Le, K. A. Janes, K. Y. Lin, Y. Wang, J. T. August, K. W. Leong, *J. Controlled Release* **2001**, *70*, 399.
[153] N. Wang, X. S. Wu, *Pharm. Dev. Technol.* **1997**, *2*, 135.
[154] J. K. Li, N. Wang, X. S. Wu, *J. Controlled Release* **1998**, *56*, 117.
[155] I. S. Kim, Y. I. Jeong, S. H. Kim, *Int. J. Pharm.* **2000**, *205*, 109.
[156] K. Na, Y. H. Bae, *Pharm. Res.* **2002**, *19*, 681.
[157] P. F. Kiser, G. Wilson, D. Needham, *Nature* **1998**, *394*, 459.
[158] M. L. Kraft, J. S. Moore, *J. Am. Chem. Soc.* **2001**, *123*, 12921.
[159] G.-H. Hsiue, S.-h. Hsu, C.-C. Yang, S.-H. Lee, I. K. Yang, *Biomaterials* **2001**, *22*, 457.
[160] P. K. Ghosh, *Indian J. Biochem. Biophys.* **2000**, *37*, 273.
[161] U. Gaur, S. K. Sahoo, T. K. De, P. C. Ghosh, A. Maitra, P. K. Ghosh, *Int. J. Pharm.* **2000**, *202*, 1.
[162] S. Nayak, H. Lee, J. Chmielewski, L. A. Lyon, *J. Am. Chem. Soc.* **2004**, *126*, 10258.
[163] S. H. Choi, J. J. Yoon, T. G. Park, *J. Colloid Interface Sci.* **2002**, *251*, 57.
[164] M. L. Becker, E. E. Remsen, D. Pan, K. L. Wooley, *Bioconjugate Chem.* **2004**, *15*, 699.
[165] M. L. Becker, L. O. Bailey, K. L. Wooley, *Bioconjugate Chem.* **2004**, *15*, 710.
[166] D. Pan, J. L. Turner, K. L. Wooley, *Chem. Commun.* **2003**, 2400.
[167] S. S. Jana, D. J. Bharali, P. Mani, A. Maitra, C. M. Gupta, D. P. Sarkar, *FEBS Lett.* **2002**, *515*, 184.
[168] K. Na, K. H. Park, S. W. Kim, Y. H. Bae, *J. Controlled Release* **2000**, *69*, 225.
[169] S. Mitra, U. Gaur, P. C. Ghosh, A. N. Maitra, *J. Controlled Release* **2001**, *74*, 317.
[170] G. Decher, M. Eckle, J. Schmitt, B. Struth, *Curr. Opin. Colloid Interface Sci.* **1998**, *3*, 32.
[171] K. B. Thurmond II, E. E. Remsen, T. Kowalewski, K. L. Wooley, *Nucleic Acids Res.* **1999**, *27*, 2966.
[172] S. Liu, J. V. M. Weaver, M. Save, S. P. Armes, *Langmuir* **2002**, *18*, 8350.
[173] J. G. Zhang, S. Q. Xu, E. Kumacheva, *J. Am. Chem. Soc.* **2004**, *126*, 7908.

 © 2005 Wiley-VCH Verlag GmbH & Co. KGaA, Weinheim

[174] V. Ravaine, **2005**, personal communication.
[175] A. Elaissari, L. Holt, F. Meunier, C. Voisset, C. Pichot, B. Mandrand, C. Mabilat, *J. Biomater. Sci. Polym. Ed.* **1999**, *10*, 403.
[176] A. Kondo, T. Kaneko, K. Higashitani, *Biotechnol. Bioeng.* **1994**, *44*, 1.
[177] A. Kondo, H. Kamura, K. Higashitani, *Appl. Microbiol. Biotechnol.* **1994**, *41*, 99.
[178] H. Kanazawa, Y. Kashiwase, K. Yamamoto, Y. Matsushima, A. Kikuchi, Y. Sakurai, T. Okano, *Anal. Chem.* **1997**, *69*, 823.
[179] H. Kanazawa, T. Sunamoto, E. Ayano, Y. Matsushima, A. Kikuchi, T. Okano, *Anal. Sci.* **2002**, *18*, 45.
[180] H. Kanazawa, K. Yamamoto, Y. Kashiwase, Y. Matsushima, N. Takai, A. Kikuchi, Y. Sakurai, T. Okano, *J. Pharm. Biomed. Anal.* **1997**, *15*, 1545.
[181] E. A. S. Doherty, C. W. Kan, B. M. Paegel, S. H. I. Yeung, S. T. Cao, R. A. Mathies, A. E. Barron, *Anal. Chem.* **2004**, *76*, 5249.
[182] E. A. S. Doherty, C. W. Kan, A. E. Barron, *Electrophoresis* **2003**, *24*, 4170.
[183] L. Ye, P. A. G. Cormack, K. Mosbach, *Anal. Commun.* **1999**, *36*, 35.
[184] J. Kim, M. J. Serpe, L. A. Lyon, *Angew. Chem.* **2005**, *117*, 1357; *Angew. Chem. Int. Ed.* **2005**, *44*, 1333.
[185] M. J. Serpe, J. Kim, L. A. Lyon, *Adv. Mater.* **2004**, *16*, 184.
[186] J. Kim, M. J. Serpe, L. A. Lyon, *J. Am. Chem. Soc.* **2004**, *126*, 9512.
[187] *Contemporary Biomaterials: Material and Host Response, Clinical Applications, New Technology and Legal Aspects* (Eds.: J. W. Boretos, M. Eden), Noyes, Park Ridge, **1984**, p. 232.
[188] H. Kawaguchi, *Prog. Polym. Sci.* **2000**, *25*, 1171.
[189] H. Kawaguchi, K. Fujimoto, Y. Mizuhara, *Colloid Polym. Sci.* **1992**, *270*, 53.
[190] T. Shiroya, N. Tamura, M. Yasui, K. Fujimoto, H. Kawaguchi, *Colloids Surf. B* **1995**, *4*, 267.
[191] D. Duracher, A. Elaissari, F. Mallet, C. Pichot, *Langmuir* **2000**, *16*, 9002.
[192] Y. Urakami, Y. Kasuya, K. Fujimoto, M. Miyamoto, H. Kawaguchi, *Colloids Surf. B* **1994**, *3*, 183.
[193] O. Kimhi, H. Bianco-Peled, *Langmuir* **2002**, *18*, 8587.
[194] D. Gan, L. A. Lyon, *Macromolecules* **2002**, *35*, 9634.
[195] S. Nayak, L. A. Lyon, *Angew. Chem.* **2004**, *116*, 6874; *Angew. Chem. Int. Ed.* **2004**, *43*, 6706.
[196] A. D. Dinsmore, J. C. Crocker, A. G. Yodh, *Curr. Opin. Colloid Interface Sci.* **1998**, *3*, 5.
[197] M. J. Murray, J. V. Sanders, *Philos. Mag. A* **1980**, *42*, 721.
[198] J. V. Sanders, *Philos. Mag. A* **1980**, *42*, 705.
[199] J. D. Joannopoulos, R. D. Meade, J. N. Winn, *Photonic Crystals: Molding the Flow of Light*, Princeton University Press, Princeton, **1995**.
[200] L. A. Lyon, J. D. Debord, S. B. Debord, C. D. Jones, J. G. McGrath, M. J. Serpe, *J. Phys. Chem. B* **2004**, *108*, 19099.
[201] J. M. Weissman, H. B. Sunkara, A. S. Tse, S. A. Asher, *Science* **1996**, *274*, 959.
[202] S. Xu, J. Zhang, C. Paquet, Y. Lin, E. Kumacheva, *Adv. Funct. Mater.* **2003**, *13*, 468.
[203] S. Pyett, W. Richtering, *J. Chem. Phys.* **2005**, *122*, 034709/1.
[204] E. Bartsch, M. Antonietti, W. Schupp, H. Sillescu, *J. Chem. Phys.* **1992**, *97*, 3950.
[205] D. Gottwald, C. N. Likos, G. Kahl, H. Loewen, *Phys. Rev. Lett.* **2004**, *92*, 068301.
[206] H. Senff, W. Richtering, *Colloid Polym. Sci.* **2000**, *278*, 830.
[207] M. Stieger, J. S. Pedersen, P. Lindner, W. Richtering, *Langmuir* **2004**, *20*, 7283.
[208] C. N. Likos, N. Hoffmann, H. Lowen, A. A. Louis, *J. Phys. Condens. Matter* **2002**, *14*, 7681.
[209] D. Gottwald, C. N. Likos, G. Kahl, H. Lowen, *J. Chem. Phys.* **2005**, *122*, 074903.
[210] C. N. Likos, H. Lowen, M. Watzlawek, B. Abbas, O. Jucknischke, J. Allgaier, D. Richter, *Phys. Rev. Lett.* **1998**, *80*, 4450.
[211] M. Watzlawek, H. Lowen, C. N. Likos, *J. Phys. Condens. Matter* **1998**, *10*, 8189.
[212] M. Watzlawek, C. N. Likos, H. Lowen, *Phys. Rev. Lett.* **1999**, *82*, 5289.
[213] J. Stellbrink, J. Allgaier, M. Monkenbusch, D. Richter, A. Lang, C. N. Likos, M. Watzlawek, H. Lowen, G. Ehlers, P. Schleger, *Prog. Colloid Polym. Sci.* **2000**, *115*, 88.
[214] N. Hoffmann, C. N. Likos, H. Lowen, *J. Chem. Phys.* **2004**, *121*, 7009.
[215] P. N. Pusey, W. van Megan, *Nature* **1986**, *320*, 340.
[216] J. D. Debord, S. Eustis, S. B. Debord, M. T. Lofye, L. A. Lyon, *Adv. Mater.* **2002**, *14*, 658.
[217] S. B. Debord, L. A. Lyon, *J. Phys. Chem. B* **2003**, *107*, 2927.
[218] C. D. Jones, L. A. Lyon, *J. Am. Chem. Soc.* **2003**, *125*, 460.
[219] C. D. Jones, M. J. Serpe, L. Schroeder, L. A. Lyon, *J. Am. Chem. Soc.* **2003**, *125*, 5292.
[220] S. A. Asher, A. C. Sharma, A. V. Goponenko, M. M. Ward, *Anal. Chem.* **2003**, *75*, 1676.
[221] S. A. Asher, V. L. Alexeev, A. V. Goponenko, A. C. Sharma, I. K. Lednev, C. S. Wilcox, D. N. Finegold, *J. Am. Chem. Soc.* **2003**, *125*, 3322.

 © 2005 Wiley-VCH Verlag GmbH & Co. KGaA, Weinheim

Communications

DOI: 10.1002/anie.200503050

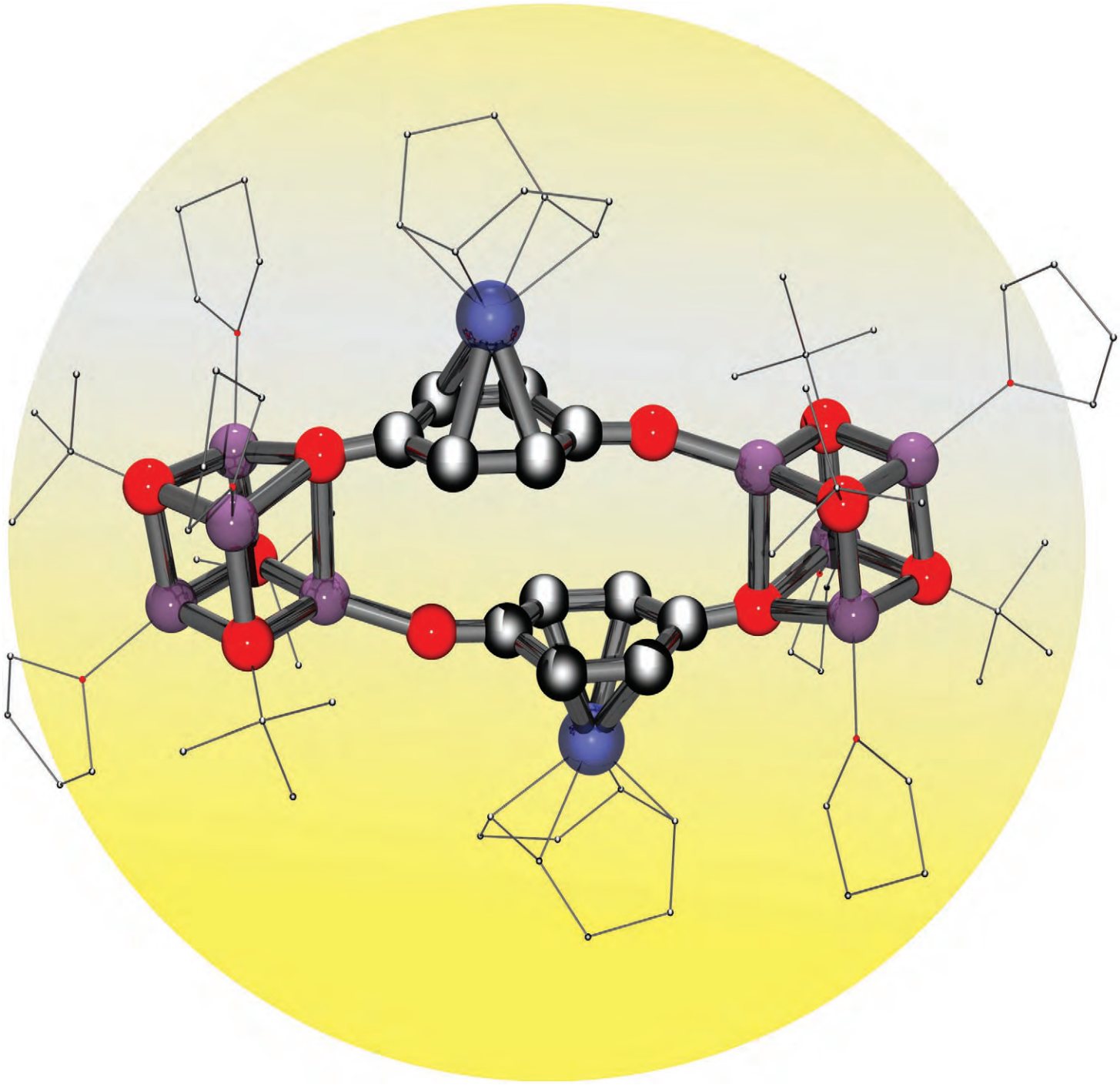

Transition-metal complexes are shown to act as ligands in the linking of Li_4O_4 cubane units. The organometallic complex $[(\eta^4\text{-quinone})Rh(cod)]^-$ is used to form a unique doubly bridged assembly, which incorporates a quinone oxygen atom at one corner of each cubane unit. For more information, see the Communication by D. A. Sweigart and co-workers on the following pages.

WILEY InterScience DISCOVER SOMETHING GREAT
© 2005 Wiley-VCH Verlag GmbH & Co. KGaA, Weinheim

Cubanes

DOI: 10.1002/anie.200503050

Lithium Alkoxide $\{Li_4O_4\}$ Cubanes Bridged by Rhodium–Quinonoid Organometalloligands**

*Seung Uk Son, Jeffrey A. Reingold, Sang Bok Kim, Gene B. Carpenter, and Dwight A. Sweigart**

Organolithium reagents with alkoxide and similar oxygen-donor ligands frequently aggregate in aprotic solvents into rectangular $\{Li_2O_2\}$ and cubic $\{Li_4O_4\}$ fragments.[1–3] Lithium $\{Li_4O_4\}$ cubane species are especially prevalent and have been extensively investigated because of the great importance of organolithium reagents in organic synthesis.[1–2] Herein, we report the synthesis and characterization of the novel lithium cubane aggregate **1**, which possesses two unprecedented features: 1) $\{Li_4O_4\}$ units that incorporate a quinone oxygen-donor atom at one of the corners and 2) $\{Li_4O_4\}$ units bridged by two rhodium $[(\eta^4\text{-benzoquinone})Rh(cod)]^-$ (cod = cyclooctadiene) organometalloligands.

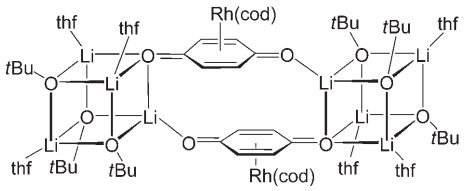

$[Li_4(OtBu)_3(thf)_3(\eta^4\text{-benzoquinone})Rh(cod)]_2$

1

It is known that Li_4O_4 cubanes can be linked or bridged by sharing a corner oxygen-donor atom. Bridged structures are also known in which the organic moiety attached to a cubane corner oxygen atom either covalently links to an oxygen atom in a second cubane or provides a donor atom that coordinates to a lithium corner in a second cubane. Examples of bridging units in these categories include carbonate and benzamide aza enolates.[4] Cubane fragments can also be linked together by "external" multifunctional donors that coordinate to two or more lithium corners.[4c,5] In these cases, the cubanes function as so-called secondary building units (SBUs) that self-assemble in the presence of multifunctional ligands or spacers to generate main-group metal-coordination networks. Spacers utilized in this manner include chloride, tetramethylethylenediamine (TMEDA), and *p*-dioxane.

Compound **1** reported herein is unique in that the bifunctional ligand that connects the cubane units is a transition-metal complex. As discussed below, it is likely that supramolecular structures analogous to **1** are accessible with a variety of transition-metal fragments.

The starting materials for the synthesis of **1** consisted of LiO*t*Bu in THF and the recently reported quinonoid complex $[(\eta^6\text{-hydroquinone})Rh(cod)]^+$ (**2**).[6] π-Coordination of a metal center to hydroquinone is known to greatly facilitate deprotonation, which is accompanied by electron transfer to the metal center and changes in the hapticity of the quinonoid ring.[6,7] In the case of **2**, neutral η^5-semiquinone and anionic η^4-quinone complexes **3** and **4**, respectively, are formed as shown in Scheme 1. π-Bonded quinone complexes analogous

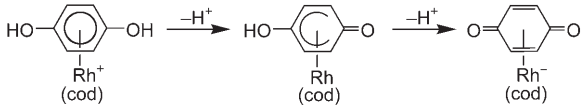

Scheme 1. Deprotonation of a π-bonded rhodium–hydroquinone complex.

to **4** have already found significant applications in the catalysis of aldehyde arylation (rhodium as the metal) and in the formation of metal–organometallic coordination networks (manganese as the metal).[6,8] Herein, it is shown that the rhodium–quinone complex **4** reacts with LiO*t*Bu in THF to afford a novel structural motif in which a quinone oxygen atom functions as a pseudo butoxide ligand in a $\{Li_4O_4\}$ cubane unit, while the other quinone oxygen atom links to a lithium atom in a second companion cubane unit.

Deprotonation of **2** in THF at room temperature with a fivefold excess of LiO*t*Bu led to a homogeneous yellow solution that slowly deposited crystals of **1** when stored at −15 °C for a period of weeks. The X-ray structure of **1** is shown in Figure 1. Each of the two $\{Li_4O_4\}$ cubanes contains three butoxide oxygen atoms and one quinone oxygen atom. Three thf ligands and an "external" quinone oxygen atom complete the pseudo tetrahedral coordination at each cubane lithium center. The quinonoid ring in **1** adopts a boat conformation with the phenolic carbon atoms C1 and C4 bent out of the C2-C3-C5-C6 diene plane away from the rhodium center by 10 and 13°, respectively. As a consequence, the {Rh(cod)} fragment is only weakly bonded to C1 and C4, and the overall structure is perhaps best described as an η^4-quinone. The relatively short C1–O1 and C4–O2 bond lengths of 1.29 and 1.26 Å support this interpretation.

The Li–O bond lengths in **1** are all in the typical 1.8–2.0 Å range, except for Li1–O1 which is much larger at 2.36(2) Å.

[*] J. A. Reingold, S. B. Kim, Prof. G. B. Carpenter, Prof. D. A. Sweigart
Department of Chemistry
Brown University
Providence, RI 02912 (USA)
Fax: (+1) 401-863-9046
E-mail: dwight_sweigart@brown.edu
Prof. S. U. Son
Department of Chemistry
Sungkyunkwan University
Suwon 440-746 (Korea)

[**] We are grateful to the donors to the Petroleum Research Fund (administered by the American Chemical Society) and to the National Science Foundation (CHE-0308640) for support of this research. We are also most grateful to Professor Ronald Lawler for insightful discussions and assistance with the NMR simulations.

Supporting information for this article is available on the WWW under http://www.angewandte.org or from the author.

© 2005 Wiley-VCH Verlag GmbH & Co. KGaA, Weinheim

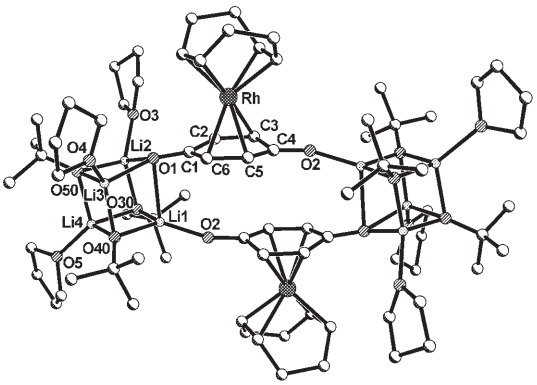

Figure 1. Crystal structure of **1** (hydrogen atoms are omitted for clarity). Selected bond lengths [Å] and angles [°]: Rh-C1 2.44(1), Rh-C2 2.30(1), Rh-C3 1.22(1), Rh-C4 2.41(1), Rh-C5 2.27(1), Rh-C6 2.28(1), C1-O1 1.29(1), C4-O2 1.26(1), Li1-O1 2.36(2), Li1-O2 1.84(2), Li1-O30 1.86(2), Li1-O40 1.95(2), Li2-O1 1.97(2), Li2-O3 1.98(2), Li2-O30 1.92(2), Li2-O50 1.88(2), Li3-O1 2.03(2), Li3-O4 1.99(2), Li3-O40 1.92(2), Li3-O50 1.93(2), Li4-O5 1.99(2), Li4-O30 1.95, Li4-O40 1.95(2), Li4-O50 1.99(2); Li2-O1-Li3 83(1), Li2-O50-Li3 88(1), O1-Li2-O50 95(1), O1-Li3-O50 92(1), Li1-O30-Li4 83(1), Li1-O40-Li4 81(1), O30-Li1-O40 99(1), O30-Li4-O40 96(1), C1-O1-Li1 97(1), O1-Li1-O2 107(1).

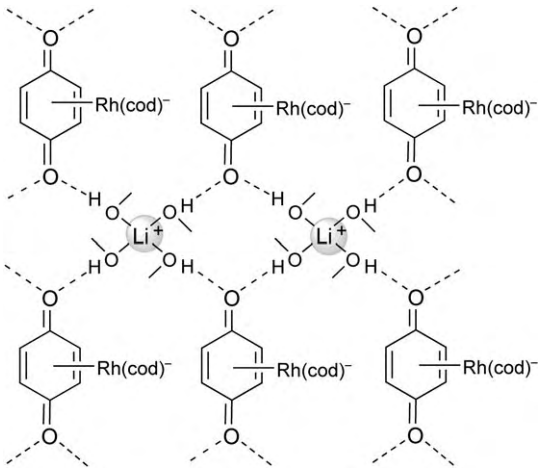

Figure 2. Hydrogen-bonding network in **5**.

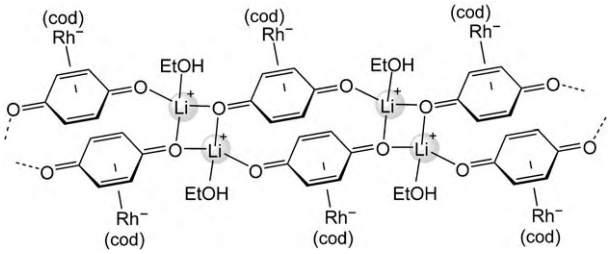

Figure 3. One-dimensional metal–organometallic coordination network **6**.

The consequence of the long Li1–O1 bond is that the O1 corner of the cubanes bends out of the O1-Li2-O50-Li3 face with a dihedral angle of 13°. The opposite face of the cubane, Li1-O30-Li4-O40, is planar to within 1°. The 13° bending of the cubane O1 corners effectively increases the separation of the two bridges from each other, which is probably the reason for the approximate 0.4-Å elongation of the Li1–O1 bond beyond that typically found in $\{Li_4O_4\}$ structures. The C1–O2 separation in **1** is just 3.1 Å, and the quinone rings partially eclipse, with a 3.2-Å ring-to-ring separation which indicates fairly strong π–π stacking interactions.[8,9] If the Li1–O1 bond length was similar to the others (ca. an average of 1.95 Å), the bridge-to-bridge separation would be greatly decreased, thus necessitating significantly different angles from those observed to avoid repulsive interactions between the bridges. In terms of the thermodynamic driving force, it is apparent that having a long Li1–O1 bond is the preferred compromise in the generation of the observed doubly bridged assembly.

To explore possible chemical processes relevant to the formation of **1**, a solution of complex **2** in THF with a fivefold excess of LiO*t*Bu was evaporated before any cubane dimer **1** had formed (one hour after mixing). The residue was washed with diethyl ether and THF. A portion of the residue dissolved in methanol afforded the salt $[Li(MeOH)_4][(\eta^4\text{-quinone})Rh(cod)]$ (**5**). The X-ray structure of **5** shows that it consists of the two-dimensional hydrogen-bonded network illustrated in Figure 2. The hydrogen bonds between the quinone oxygen atoms and the methanol ligands have average O···O distances of 2.63 Å.

The fundamentally different product **6** (Figure 3) was afforded by dissolution of the residue in ethanol instead of methanol. Complex **6** is a one-dimensional metal–organometallic coordination network (MOMN) containing rectangular $\{Li_2O_2\}$ units linked by anionic $[(\eta^4\text{-quinone})Rh(cod)]^-$ organometalloligand. Each lithium ion is bonded to three quinone oxygen atoms and one ethanol molecule. One quinone oxygen atom from each spacer molecule is bidentate and forms part of the $\{Li_2O_2\}$ ring, whereas the other oxygen atom is unidentate and propagates the network by coordinating "externally" to a lithium ion.

The X-ray structure of **6** shows that the $\{Li_2O_2\}$ rings are nearly square (internal angles: 84 and 96°) and the Li–O bond lengths average 1.94 Å, which is in the range found for most of the Li–O bonds in the cubane units in **1** (other than Li1–O1). The coordinated ethanol ligand in **6** is not hydrogen bonded. The addition of one equivalent of 1,1-bis(4-hydroxyphenyl)-methane to **6** in ethanol resulted in displacement of the quinone monodentate oxygen atom from the lithium ion and afforded the new two-dimensional network **7**, in which polymeric one-dimensional $\{Li_2O_2\}$ chains are linked through hydrogen-bonding interactions (Figure 4). The X-ray structures of **6** and **7** are given in the Supporting Information.

Having established the viability of $\{Li_4O_4\}$ and $\{Li_2O_2\}$ aggregates that incorporate a rhodium–η^4-quinone organometalloligand at a vertex, we next used NMR spectroscopy to probe any dynamic behavior that may occur. A solution of the slightly soluble cubane **1** in $[D_8]$THF gave no evidence for dynamic processes on the NMR timescale at room temperature. However, a solution of hydroquinone complex **2** in THF with ten equivalents of LiO*t*Bu, from which the **1** evolves over a period of days/weeks (see below), shows site exchange of the quinone hydrogen atoms in the deprotonated

 © 2005 Wiley-VCH Verlag GmbH & Co. KGaA, Weinheim

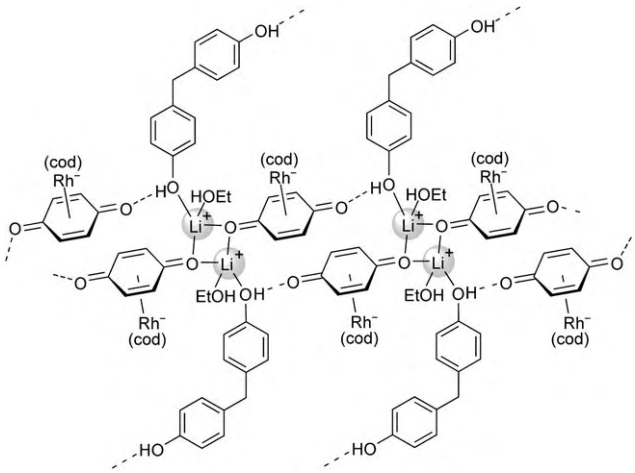

Figure 4. Two-dimensional metal–organometallic coordination network **7**.

complex $[(\eta^4\text{-benzoquinone})\text{Rh(cod)}]^-$, which is rapidly formed in situ according to Scheme 1. The NMR spectra of the quinone hydrogen atoms is illustrated in Figure 5 for the

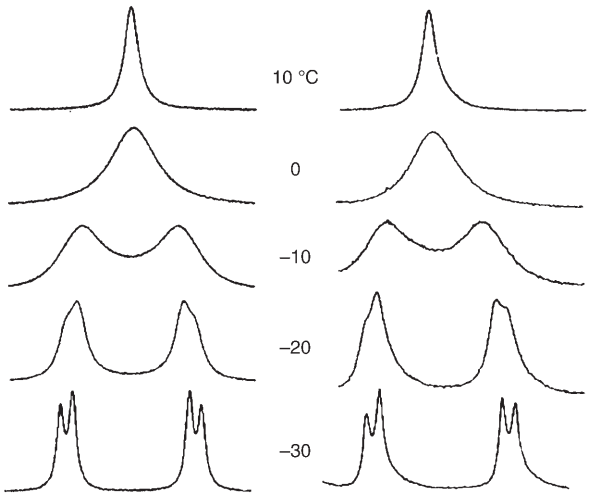

Figure 5. Simulated (left) and observed (right) ^{1}H NMR spectra of the quinone hydrogen atoms in a solution of $[(\eta^4\text{-benzoquinone})\text{Rh(cod)}]$ in $[D_8]$THF with excess LiO*t*Bu.

temperature range 10 to −30 °C. Simulations[10] of the observed two-site exchange process gave a very good fit to the Eyring equation, with the following activation parameters: $\Delta H^{\neq} = 84\ \text{kJ mol}^{-1}$ and $\Delta S^{\neq} = 110\ \text{J K}^{-1}\text{mol}^{-1}$. The process that occurs almost certainly involves differential lithium coordination to the quinone oxygen atoms, possibly as depicted in Figure 6. The ligands (L) likely include thf, although the butoxide groups may also be involved.

The actual exchange may be more complex than that illustrated, for example, species with a $\{Li_2O_2\}$ core may be present. The highly positive entropy of activation is suggestive of solvent loss in the transition state to give an activated complex such as that illustrated in Figure 6. Whatever the

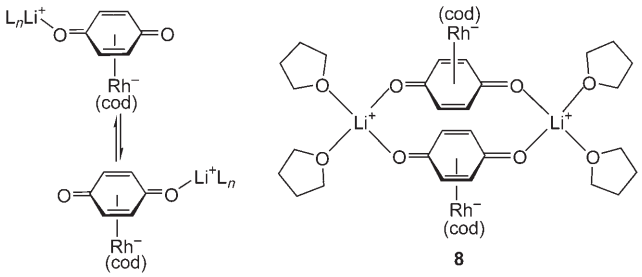

Figure 6. Dynamic coordination of the quinone oxygen atoms to lithium in a solution of THF, possibly via activated complex **8**.

specific details, the NMR behavior demonstrates that the quinone oxygen atoms can rapidly change their mode of coordination to the lithium centers in the species that exists prior to the formation of the cubane aggregate **1**.

In conclusion, it has been demonstrated that lithium alkoxide aggregates[11] can be synthesized that have two $\{Li_4O_4\}$ cubane units bridged by a quinone organometalloligand. The key to the construction of this discrete species, as well as related polymeric $\{Li_2O_2\}$ species, is the ability of the quinone oxygen atoms in $[(\eta^4\text{-quinone})\text{Rh(cod)}]^-$ to function as ligands, both as part of and external to the cubane aggregate itself. The methodology described herein should be readily extendable to anionic π-bonded quinone complexes of a variety of transition metals.

Experimental Section

All reactions were carried out under N_2 in flame-dried glassware. THF and diethyl ether solvents were HPLC grade. $[\{\text{RhCl(cod)}\}_2]$ was purchased from Strem Chemicals, Inc. The ^{1}H NMR spectra were recorded on a 300 MHz Bruker spectrometer. Elemental analyses were performed by Quantitative Technologies Inc. (New Jersey, USA).

$[\{Li_4(t\text{OBu})_3(\text{thf})_3(\eta^4\text{-benzoquinone})\text{Rh(cod)}\}_2]$ (**1**): $[(\eta^6\text{-hydroquinone})\text{Rh(cod)}]BF_4$ (**2**; 0.10 g, 0.25 mmol) in HPLC-grade THF (7 mL) was placed in a flame-dried 50-mL Schlenk flask and LiO*t*Bu (0.10 g, 1.25 mmol) was added with stirring at room temperature. A yellow precipitate of the neutral $[(\eta^5\text{-semiquinone})\text{Rh(cod)}]$ formed initially, but dissolved after addition of the base was complete. The homogeneous yellow solution was stirred for 1 h and placed in a refrigerator at −15 °C for several weeks, during which time yellow crystals of **1** formed in 68% yield of the isolated product (0.096 g, 0.085 mmol). ^{1}H NMR ($[D_8]$THF): $\delta = 5.64$ (d, $J = 7.0$ Hz, benzoquinone, 4H), 4.53 (d, $J = 6.9$ Hz, benzoquinone, 4H), 4.27 (br, cod, 8H), 2.25 (m, cod, 8H), 2.01 (m, cod, 8H), 1.15 ppm (s, *t*BuO, 54H). Washing **1** with THF and drying under vacuum produced **5**, which was characterized by NMR (see below) and elemental analysis ((%) calcd for $C_{14}O_2H_{16}Rh_1Li_1$: C 51.56, H 4.95; found: C 51.55, H 4.93).

Preliminaries for the synthesis of complexes **5**–**7**: **2** and LiO*t*Bu were combined as described above at room temperature, stirred for 1 h, and the solvent removed with a rotary evaporator. The residue was vacuum dried for 30 min, washed with diethyl ether, washed with THF, and dried again under vacuum. The residue, which contained an equivalent of $LiBF_4$, was obtained in 56% yield (0.057 g, 0.14 "mmol"). ^{1}H NMR ($[D_6]$DMSO): $\delta = 4.96$ (s, benzoquinone, 4H), 3.51 (br, cod, 4H), 2.20 (m, cod, 4H), 1.98 ppm (m, cod, 4H); elemental analysis (%) calcd for $C_{14}O_2H_{16}Rh_1Li_2B_1F_4$: C 40.05, H 3.84; found: C 40.04, H 4.17.

$[\text{Li(MeOH)}_4][\text{Rh}(\eta^4\text{-benzoquinone})(\text{cod})]$ (**5**): The residue described above (20 mg) was dissolved in methanol (1 mL), filtered

 © 2005 Wiley-VCH Verlag GmbH & Co. KGaA, Weinheim

through a celite pad, and transferred to a 5-mL vial. THF (3 mL) was carefully added to this solution as a layer, and the solution placed in a refrigerator (−15 °C) for three weeks. The yellow crystals formed in a yield of 55 % (0.011 g). ^{1}H NMR (CD_3OD): $\delta = 5.61$ (s, benzoquinone ring, 4H), 3.94 (br, cod, 4H), 2.33 (m, cod, 4H), 2.08 ppm (m, cod, 4H); elemental analysis (%) after drying under vacuum calcd for $C_{14}O_2H_{16}Rh_1Li_1$: C 51.56, H 4.95; found: C 51.50, H 4.60.

[Li(EtOH)(η^4-benzoquinone)Rh(cod)] (**6**): The residue described above (25 mg) was dissolved in ethanol (2 mL), filtered through a celite pad, and transferred to a 5-mL vial. After standing for two weeks at room temperature, yellow crystals had formed and were collected in a yield of 90 % (0.023 g). ^{1}H NMR(CD_3OD): $\delta = 5.61$ (s, benzoquinone, 4H), 3.94 (br, cod, 4H), 3.59 (q, $J = 5.2$ Hz, EtOH, 2H), 2.33 (m, cod, 4H), 2.08 (m, cod, 4H), 1.16 ppm (t, $J = 5.2$ Hz, EtOH, 3H); elemental analysis (%) after drying under vacuum calcd for $C_{14}O_2H_{16}Rh_1Li_1$: C 51.56, H 4.95; found: C 51.45, H 5.15.

[Li(EtOH)(1,1-bis(4-hydroxyphenyl)methane)(η^4-benzoquinone)Rh(cod)] (**7**): The residue described above (25 mg) and 1,1-bis(4-hydroxyphenyl)methane (18 mg) were dissolved in ethanol (2 mL), filtered through a celite pad, and transferred to a 5-mL vial. After standing for two weeks at room temperature, yellow crystals had formed and were collected in a yield of 64 % of the isolated product (0.026 g). After drying under vacuum (loss of EtOH): ^{1}H NMR ([D_6]DMSO): $\delta = 9.10$ (s, 2H, phenolic OH, 2H), 6.95 (d, J = 8.1 Hz, aryl ring, 4H), 6.64 (d, J = 8.3 Hz, aryl ring, 4H), 4.95 (s, benzoquinone, 4H), 3.68 (s, CH_2, 2H), 3.50 (br, cod, 4H), 2.20 (m, cod, 4H), 1.99 ppm (m, cod, 4H); elemental analysis (%) calcd for $C_{27}O_4H_{28}Rh_1Li_1$: C 61.61, H 5.36; found: C 61.51, H 5.91.

Dynamic NMR study: **2** (5.0 mg, 0.012 mmol) was dissolved in [D_8]THF (1.5 mL) under N_2 in an NMR tube, and Li*O*t*Bu* (9.8 mg, 0.12 mmol) was added at room temperature. The NMR tube was shaken to generate a homogeneous yellow solution, which was then used to record NMR spectra over the temperature range −78–25 °C.

Crystallography: X-ray data collection was carried out using a Bruker single-crystal diffractometer equipped with an APEX CCD area detector and controlled by SMART version 5.0. Collection was done either at 100 K. Data reduction was performed by SAINT version 6.0 and absorption corrections were applied by SADABS version 2.0. The structures were typically determined by direct methods and refined on *F* squared by use of programs in SHELXTL version 5.0. Most hydrogen atoms appeared in a difference map, or they were generally inserted in ideal positions, riding on the atoms to which they are attached. CCDC-281279 (**1**), -281276 (**5**), -281277 (**6**), and -281278 (**7**) contain the supplementary crystallographic data for this paper. These data can be obtained free of charge from The Cambridge Crystallographic Data Centre via www.ccdc.cam.ac.uk/data_request/cif.

Crystal data for **1**: $C_{38}H_{67}Li_4O_8Rh$, $M_r = 782.59$, triclinic, $P\bar{1}$, $a = 10.116(3)$, $b = 14.625(4)$, $c = 16.304(4)$ Å, $\alpha = 101.790(5)$, $\beta = 105.855(5)$, $\gamma = 107.430(4)°$, $V = 2103.3(9)$ Å^3, $Z = 2$, $\rho_{calcd} = 1.236$ g cm^{-3}, $F_{000} = 832$, $\mu = 0.451$ mm^{-1}, $\theta = 1.54$–$21.04°$, reflections collected 13816, independent reflections 4499 ($R_{int} = 0.1682$), GOF = 1.008, $R_1 = 0.0752$, $wR_2 = 0.1633$, largest diffraction peak/hole 0.826/−0.879 Å^{-3}.

Crystal data for **5**: $C_{18}H_{32}LiO_6Rh$, $M_r = 454.29$, monoclinic, $P2/c$, $a = 11.5682(12)$, $b = 8.0923(8)$, $c = 12.2963(13)$ Å, $\beta = 105.855(5)°$, $V = 1032.97(18)$ Å^3, $Z = 2$, $\rho_{calcd} = 1.461$ g cm^{-3}, $F_{000} = 472$, $\mu = 0.855$ mm^{-1}, $\theta = 1.96$–$26.42°$, reflections collected 9033, independent reflections 1956 ($R_{int} = 0.0876$), GOF = 0.961, $R_1 = 0.0420$, $wR_2 = 0.0889$, largest diffraction peak/hole 1.640/−0.726 Å^{-3}.

Crystal data for **6**: $C_{16}H_{22}LiO_3Rh$, $M_r = 372.19$, triclinic, $P\bar{1}$, $a = 6.962(2)$, $b = 7.876(3)$, $c = 14.236(5)$ Å, $\alpha = 75.933(7)$, $\beta = 85.810(8)$, $\gamma = 85.434(8)°$, $V = 753.5(4)$ Å^3, $Z = 2$, $\rho_{calcd} = 1.640$ g cm^{-3}, $F_{000} = 380$, $\mu = 1.138$ mm^{-1}, $\theta = 2.67$–$23.23°$, reflections collected 2619, independent reflections 2619 ($R_{int} = 0.0000$), GOF = 0.950, $R_1 = 0.0932$, $wR_2 = 0.2161$, largest diffraction peak/hole 1.365/−1.148 Å^{-3}.

Crystal data for **7**: $C_{29}H_{34}LiO_5Rh$, $M_r = 572.41$, triclinic, $P\bar{1}$, $a = 9.6279(7)$, $b = 10.4545(7)$, $c = 14.0917(10)$ Å, $\alpha = 79.5920(10)$, $\beta = 85.1340(10)$, $\gamma = 65.3330(10)°$, $V = 1267.69(15)$ Å^3, $Z = 2$, $\rho_{calcd} = 1.500$ g cm^{-3}, $F_{000} = 592$, $\mu = 0.711$ mm^{-1}, $\theta = 1.47$–$26.42°$, reflections collected 13673, independent reflections 10106 ($R_{int} = 0.0336$), GOF = 1.027, $R_1 = 0.0506$, $wR_2 = 0.1028$, largest diffraction peak/hole 1.005/−0.565 Å^{-3}.

Received: August 26, 2005
Published online: November 8, 2005

Keywords: cubanes · lithium · organometalloligands · quinones · rhodium

[1] a) E. Weiss, *Angew. Chem.* **1993**, *105*, 1565; *Angew. Chem. Int. Ed. Engl.* **1993**, *32*, 1501; b) M. A. Beswick, D. S. Wright in *Comprehensive Organometallic Chemistry, Vol. 1*, (Eds.: E. W. Abel, F. G. A. Stone, G. Wilkinson), Pergamon, Oxford, **1995**, p. 1.

[2] a) P. G. Williard, J. M. Salvino, *Tetrahedron Lett.* **1985**, *26*, 3931; b) H.-J. Gais, U. Dingerdissen, C. Krüger, K. Angermund, *J. Am. Chem. Soc.* **1987**, *109*, 3775; c) M. A. Nichols, A. T. McPhail, E. M. Arnett, *J. Am. Chem. Soc.* **1991**, *113*, 6222; d) P. J. Pospisil, S. R. Wilson, E. N. Jacobsen, *J. Am. Chem. Soc.* **1992**, *114*, 7585; e) S. Schütte, U. Pieper, U. Klingebiel, D. Stalke, *J. Organomet. Chem.* **1993**, *446*, 45; f) U. Piarulli, D. N. Williams, C. Floriani, G. Gervasio, D. Viterbo, *J. Chem. Soc. Chem. Commun.* **1994**, 1409; g) Y. Apeloig, I. Zharov, D. Bravo-Zhivotovskii, Y. Ovchinnikov, Y. Struchkov, *J. Organomet. Chem.* **1995**, *499*, 73; h) W. Clegg, S. T. Liddle, R. Snaith, A. E. H. Wheatley, *New J. Chem.* **1998**, *22*, 1323; i) D. R. Armstrong, J. E. Davies, R. P. Davies, P. R. Raithby, R. Snaith, A. E. H. Wheatley, *New J. Chem.* **1999**, *23*, 35; j) A. J. Hoskin, D. W. Stephan, *Organometallics* **1999**, *18*, 2479; k) C. Jones, P. C. Junk, S. G. Leary, N. A. Smithies, *J. Chem. Soc. Dalton Trans.* **2000**, 3186; l) J. Strauch, T. H. Warren, G. Erker, R. Fröhlich, P. Saarenketo, *Inorg. Chim. Acta* **2000**, *300–302*, 810; m) V. Lorenz, A. Fischer, K. Jacob, W. Bruser, F. T. Edelmann, *Chem. Eur. J.* **2001**, *7*, 848; n) T. J. Boyle, T. M. Alam, K. P. Peters, M. A. Rodriguez, *Inorg. Chem.* **2001**, *40*, 6281.

[3] a) D. Seebach, R. Amstutz, T. Laube, W. B. Schweizer, J. D. Dunitz, *J. Am. Chem. Soc.* **1985**, *107*, 5403; b) L. M. Jackman, B. D. Smith, *J. Am. Chem. Soc.* **1988**, *110*, 3829; c) M. Brehon, E. K. Cope, F. S. Mair, P. Nolan, J. E. O'Brien, R. G. Pritchard, D. J. Wilcock, *J. Chem. Soc. Dalton Trans.* **1997**, 3421; d) W. Clegg, R. P. Davies, L. Dunbar, N. Feeder, S. T. Liddle, R. E. Mulvey, R. Snaith, A. E. W. Wheatley, *Chem. Commun.* **1999**, 1401; e) T. J. Boyle, D. M. Pedrotty, T. M. Alam, S. C. Vick, M. A. Rodriguez, *Inorg. Chem.* **2000**, *39*, 5133.

[4] a) T. Maetzke, D. Seebach, *Organometallics* **1990**, *9*, 3032; b) S. C. Ball, I. Cragg-Hine, M. G. Davidson, R. P. Davies, M. I. Lopez-Solera, P. R. Raithby, D. Reed, R. Snaith, E. M. Vogl, *J. Chem. Soc. Chem. Commun.* **1995**, 2147; c) K. Hyvärinen, M. Klinga, M. Leskelä, *Polyhedron* **1996**, *15*, 2171.

[5] a) N. D. R. Barnett, R. E. Mulvey, W. Clegg, P. A. O'Neil, *J. Am. Chem. Soc.* **1993**, *115*, 1573; b) K. W. Henderson, A. R. Kennedy, L. Macdonald, D. J. MacDougall, *Inorg. Chem.* **2003**, *42*, 2839; c) D. J. MacDougall, J. J. Morris, B. C. Noll, K. W. Henderson, *Chem. Commun.* **2005**, 456.

[6] S. U. Son, S. B. Kim, J. A. Reingold, G. B. Carpenter, D. A. Sweigart, *J. Am. Chem. Soc.* **2005**, *127*, 12238.

[7] a) Y.-S. Huang, S. Sabo-Etienne, X.-D. He, B. Chaudret, *Organometallics* **1992**, *11*, 303; b) S. Sun, G. B. Carpenter, D. A. Sweigart, *J. Organomet. Chem.* **1996**, *512*, 257; c) J. Le Bras, H. Amouri, J. Vaissermann, *Organometallics* **1998**, *17*, 1116; d) M. Oh, G. B. Carpenter, D. A. Sweigart, *Organometallics* **2002**, *21*, 1290; e) J. Moussa, C. Guyard-Duhayon, P. Herson,

 © 2005 Wiley-VCH Verlag GmbH & Co. KGaA, Weinheim

H. Amouri, M. N. Rager, A. Jutand, *Organometallics* **2004**, *23*, 6231.
[8] M. Oh, G. B. Carpenter, D. A. Sweigart, *Acc. Chem. Res.* **2004**, *37*, 1.
[9] a) M. Oh, G. B. Carpenter, D. A. Sweigart, *Angew. Chem.* **2001**, *113*, 3291; *Angew. Chem. Int. Ed.* **2001**, *40*, 3191; b) M. Oh, G. B. Carpenter, D. A. Sweigart, *Organometallics* **2003**, *22*, 1437.
[10] Spectra were simulated using the program WINDNMR, which is freeware downloadable from the website of Professor Hans Reich: www.chem.wisc.edu/areas/reich/plt/windnmr.htm.
[11] a) H. Nekola, F. Olbrich, U. Behrens, *Z. Anorg. Allg. Chem.* **2002**, *628*, 2067; b) J. F. Allan, R. Nassar, E. Specht, A. Beatty, N. Calin, K. W. Henderson, *J. Am. Chem. Soc.* **2004**, *126*, 484.

 © 2005 Wiley-VCH Verlag GmbH & Co. KGaA, Weinheim

Synthetic Methods

DOI: 10.1002/anie.200502981

Ruthenium-Catalyzed Asymmetric Propargylic Substitution Reactions of Propargylic Alcohols with Acetone**

Youichi Inada, Yoshiaki Nishibayashi, and Sakae Uemura*

In sharp contrast to enantioselective allylic substitution reactions of allylic alcohol derivatives with nucleophiles catalyzed by transition metal complexes,[1] its propargylic version has not yet been developed. We recently disclosed that ruthenium-catalyzed propargylic substitution reactions of propargylic alcohols with a variety of heteroatom- and carbon-centered nucleophiles affords the corresponding functionalized propargylic compounds in high yields with complete regioselectivity.[2] The reactions were catalyzed only by thiolate-bridged diruthenium complexes[3] such as $[\{Cp^*RuCl(\mu_2\text{-}SR)\}_2]$ ($Cp^* = \eta^5\text{-}C_5Me_5$; R = Me, *n*Pr, *i*Pr) and $[Cp^*RuCl(\mu_2\text{-}SMe)_2RuCp^*(OH_2)]OTf$ (OTf = OSO_2CF_3), but not by various monoruthenium complexes,[2] and they proceeded via allenylidene complexes[4] as key intermediates under the synergistic effect of the two ruthenium atoms in the diruthenium complexes.[2]

More recently, we have prepared several diruthenium complexes bearing chiral thiolate bridging ligands and applied them as catalysts in the catalytic enantioselective propargylic alkylation of propargylic alcohols with acetone, which resulted in the formation of the propargylic alkylated compounds in good yields, but only with moderate enantioselectivity (up to 35% *ee*).[5] To achieve higher enantioselectivity, a different concept than steric repulsion between substrates and chiral ligands, which was considered in our previous system,[5] would be needed. Therefore, we envisaged a new type of chiral ligands with a phenyl ring that might interact with a phenyl ring of ruthenium–allenylidene complexes by π–π interaction.[6] In this system, nucleophilic attack of nucleophiles at the C_γ atom of the allenylidene ligand should occur from the side that is not blocked by the chiral ligand (Scheme 1). Indeed, high enantioselectivity was observed in catalytic propargylic alkylation with the second-generation catalyst (up to 82% *ee*). Preliminary results are described here.

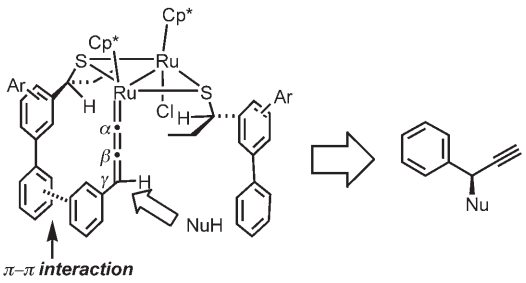

Scheme 1. Nucleophilic attack of acetone on the C_γ atom of the allenylidene complex.

A new class of chiral disulfides was prepared from the corresponding aldehydes (Scheme 2).[7] Treatment of 1-phenyl-2-propyn-1-ol (**2a**) with acetone in the presence of a catalytic amount of chiral thiolate-bridged diruthenium com-

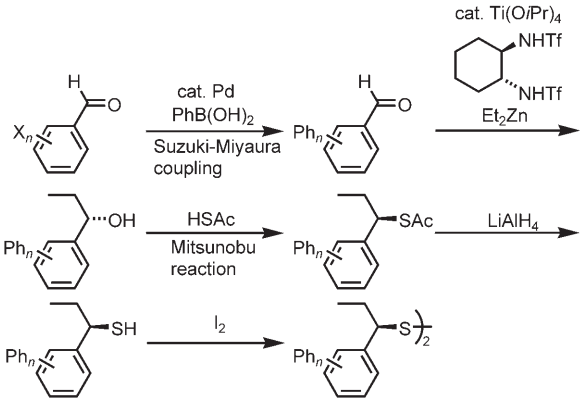

Scheme 2. Preparation of chiral disulfides.

[*] Prof. Dr. Y. Nishibayashi
Institute of Engineering Innovation
The University of Tokyo
Bunkyo-ku, Tokyo, 113-8656 (Japan)
Fax: (+81) 3-5841-1175
E-mail: ynishiba@sogo.t.u-tokyo.ac.jp
Y. Inada, Prof. Dr. S. Uemura
Department of Energy and Hydrocarbon Chemistry
Graduate School of Engineering
Kyoto University
Nishikyo-ku, Kyoto, 615-8510 (Japan)

[**] This work was supported by a Grant-in-Aid for Scientific Research for Young Scientists (A) (No.15685006) to Y.N. from the Ministry of Education, Culture, Sports, Science, and Technology, Japan. Y.I. is a recipient of the JSPS Predoctoral Fellowships for Young Scientists.

Supporting information for this article is available on the WWW under http://www.angewandte.org or from the author.

© 2005 Wiley-VCH Verlag GmbH & Co. KGaA, Weinheim

plexes, which were prepared in situ from the tetranuclear ruthenium(II) complex and the corresponding chiral disulfides in THF at room temperature for 12 h,[3,5] and NH_4BF_4 at reflux temperature for 6 h afforded the propargylic alkylated product 4-phenyl-5-hexyn-2-one (**3a**) in moderate yields with complete regioselectivity (Scheme 3). The enantiomeric excess of the product was determined by GLC on a chiral capillary column. Compared with our previous result,[5] the introduction of a phenyl group in the *meta* position of the phenyl ring of a chiral disulfide (**1a**) increased the enantioselectivity from 11 to 37% *ee*. Interestingly, introduction of a further phenyl group into the phenyl ring (**1f** and **1g**) greatly increased the enantioselectivity to 43 and 64% *ee*, respectively, but the enantioselectivity decreased when the positions of the phenyl rings were not appropriate (**1b**–**1e**). Finally, the use of a chiral disulfide (**1h**) bearing three phenyl groups on a phenyl ring achieved the highest enantioselectivity (74% *ee*).[7] Unfortunately, the introduction of a *p*-methylphenyl or *p*-*tert*-butylphenyl group on the phenyl ring of a chiral disulfide (**1i** and **1j**) did not improve the enantioselectivity. The use of **1h** as chiral ligand at lower reaction temperature did not influence the enantioselectivity. Other additives such as NH_4PF_6 did not affect the enantioselectivity. In the absence of additives such as NH_4BF_4 and NH_4PF_6, no reaction occurred. When other simple ketones such as 2-butanone and 3-methyl-2-butanone were used in place of acetone, the catalytic reactions did not proceed smoothly.

Next, the catalytic alkylation of propargylic alcohols **2** was investigated using **1h** as chiral ligand. Typical results for various alcohols **2** are shown in Table 1. The presence of substituents such as methyl, methoxy, and chloro in the benzene ring of the propargylic alcohols did not greatly affect the enantioselectivity for the products (Table 1, entries 2–4). Enantioselectivity at the same level was observed in the reactions of 1-naphthyl-2-propyn-1-ols (**2e** and **2f**) with acetone under the same reaction conditions (Table 1, entries 5 and 6). Although the reaction of propargylic alcohol bearing a phenyl group in the benzene ring (**2g**) with acetone gave the same enantioselectivity (Table 1, entry 7), the introduction of two phenyl groups at the *meta* positions of the benzene ring of the propargylic alcohols further increased the enantioselectivity to 82% *ee* (Table 1, entry 8).

Table 1: Ruthenium-catalyzed asymmetric propargylic alkylation of propargylic alcohols (**2**) with acetone.[a]

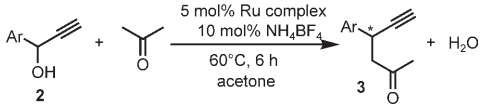

Entry	**2**, Ar	**3**, yield [%][b]	*ee* of **3** [%][c]
1	**2a**, Ph	**3a**, 56	74
2	**2b**, *o*-MeC_6H_4	**3b**, 61	72
3	**2c**, *p*-$MeOC_6H_4$	**3c**, 14	68[d]
4	**2d**, *p*-ClC_6H_4	**3d**, 57	68[d]
5	**2e**, 1-naphthyl	**3e**, 42	70
6	**2f**, 2-napthyl	**3f**, 50	70
7	**2g**, *p*-PhC_6H_4	**3g**, 50	70
8	**2h**, 3,5-$Ph_2C_6H_3$	**3h**, 58	82

[a] All reactions of **2** (0.300 mmol) with acetone were carried out in the presence of ruthenium complex (0.015 mmol, generated in situ from $[\{Cp^*RuCl\}_4]$ and **1h**) and NH_4BF_4 (0.030 mmol) in acetone (4.5 mL) at 60°C for 6 h. [b] Yield of isolated product. [c] Determined by HPLC. [d] Determined by GLC.

To obtain more information on the propargylic alkylation, the stereochemistry of the alkylated product **3a** in the reaction with **1h** as a chiral ligand was determined. Hydrogenation of the alkylated product in the presence of a catalytic amount of Pd/C under 1 atm of H_2 at room temperature for 20 h gave (*S*)-4-phenyl-2-hexanone (**4a**)[7,8] quantitatively (Scheme 4), that is, the original alkylated product **3a** has an *R* absolute configuration. This result is consistent with our proposed reaction pathway (Scheme 1), and the π–π interaction[6] of phenyl rings between the ligand and allenylidene moieties might be considered to be one of the reasons for achievement of high enantioselectivity.

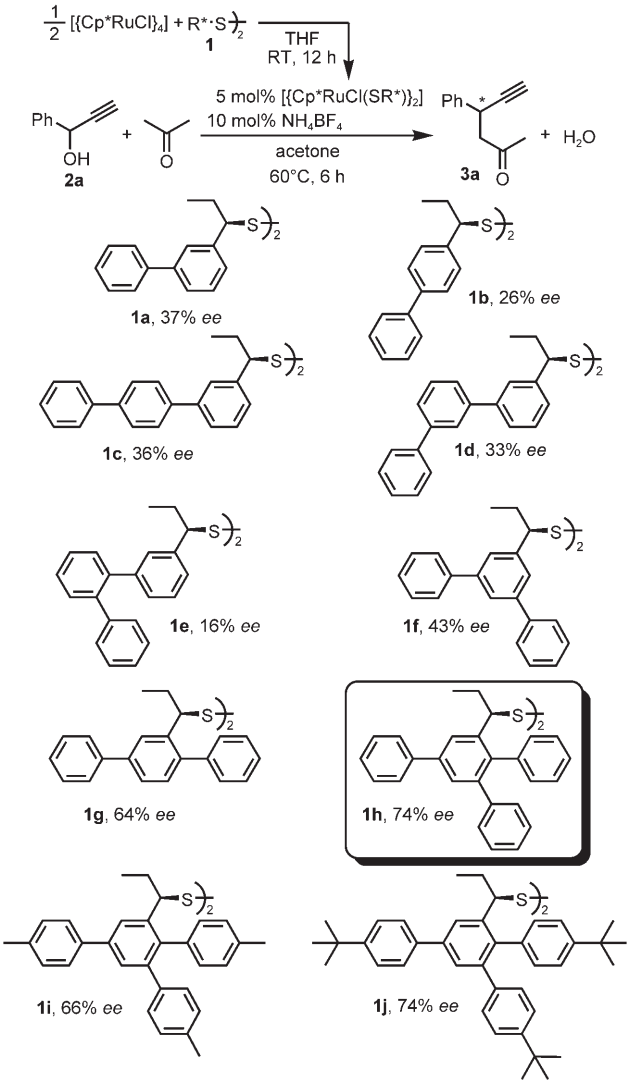

Scheme 3. Reactions of 1-phenyl-2-propyn-1-ol (**2a**) with acetone in the presence of chiral thiolate-bridged diruthenium complexes generated in situ from $[\{Cp^*RuCl\}_4]$ and chiral disulfides.

 © 2005 Wiley-VCH Verlag GmbH & Co. KGaA, Weinheim

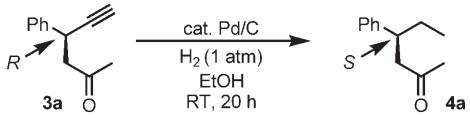

Scheme 4. Palladium-catalyzed hydrogenation of **3a**.

In summary, we have developed a diruthenium complex-catalyzed, highly enantioselective propargylic substitution reaction of propargylic alcohols with acetone to give the propargylic alkylated products with up to 82% *ee*. Here, π–π interaction of phenyl rings between the ligand and allenylidene moieties is considered to play a crucial role in achieving such a high selectivity. The method presented is in sharp contrast to the so-far-known highly diastereoselective and enantioselective propargylic substitution reactions, which use a stoichiometric amount of transition metal complexes.[9] Further work is currently in progress to improve the enantioselectivity and to broaden the scope of this enantioselective propargylic substitution reaction by using other nucleophiles.[10]

Experimental Section

Typical experimental procedure for the reaction of **2a** with acetone: $[\{Cp^*RuCl\}_4]$ (8.2 mg, 0.0075 mmol) and **1h** (11.4 mg, 0.015 mmol) were placed in a 20 mL round-bottomed flask under N_2. Anhydrous THF (1.0 mL) was added, and then the mixture was magnetically stirred for 12 h at room temperature. The solvent was evaporated in vacuo. NH_4BF_4 (3.1 mg, 0.030 mmol) and anhydrous acetone (4.5 mL) were added under N_2, and then the mixture was magnetically stirred at room temperature. After the addition of **2a** (39.7 mg, 0.30 mmol), the reaction flask was kept at 60°C for 6 h. The solvent was concentrated under reduced pressure by an aspirator, and then the residue was purified by column chromatography (SiO_2) with hexane and AcOEt to give **3a** as a pale yellow oil (30.3 mg, 0.18 mmol, 56% yield, 74% *ee*); ^{1}H NMR (270 MHz, $CDCl_3$): $\delta =$ 2.13 (s, 3H), 2.26 (s, 1H), 2.80 (dd, 1H, $J = 16$, 5.2 Hz), 3.00 (dd, 1H, $J = 16$, 8.4 Hz), 4.20 (br, 1H), 7.22–7.39 ppm (m, 5H); ^{13}C NMR (67.5 MHz, $CDCl_3$): $\delta = 30.4$, 32.4, 51.5, 71.0, 84.8, 127.1, 127.2, 128.6, 140.1, 205.4 ppm. The optical purity of **3a** was determined by HPLC analysis (column: Daicel, OD; eluent: hexane/2-propanol 97:3).

Received: August 22, 2005
Published online: October 27, 2005

Keywords: asymmetric catalysis · nucleophilic substitution · ruthenium · S ligands · synthetic methods

[1] For recent reviews, see a) J. Tsuji, *Palladium and Catalysts*, Wiley, New York, **1995**, p. 290; b) B. M. Trost, D. L. VanVranken, *Chem. Rev.* **1996**, *96*, 395; c) B. M. Trost, C. Lee in *Catalytic Asymmetric Synthesis* (Ed.: I. Ojima), Wiley-VCH, New York, **2000**, chap. 8E.

[2] a) Y. Nishibayashi, I. Wakiji, M. Hidai, *J. Am. Chem. Soc.* **2000**, *122*, 11019; b) Y. Nishibayashi, I. Wakiji, Y. Ishii, S. Uemura, M. Hidai, *J. Am. Chem. Soc.* **2001**, *123*, 3393; c) Y. Nishibayashi, M. Yoshikawa, Y. Inada, M. Hidai, S. Uemura, *J. Am. Chem. Soc.* **2002**, *124*, 11846; d) Y. Nishibayashi, M. D. Milton, Y. Inada, M. Yoshikawa, I. Wakiji, M. Hidai, S. Uemura, *Chem. Eur. J.* **2005**, *11*, 1433; e) S. C. Ammal, N. Yoshikai, Y. Inada, Y. Nishibayashi, E. Nakamura, *J. Am. Chem. Soc.* **2005**, *127*, 9428.

[3] The thiolate-bridged diruthenium complexes have been found to provide unique bimetallic reaction sites for activation and transformation of various terminal alkynes: a) Y. Nishibayashi, M. Yamanashi, I. Wakiji, M. Hidai, *Angew. Chem.* **2000**, *112*, 3031; *Angew. Chem. Int. Ed.* **2000**, *39*, 2909, and references therein; b) Y. Nishibayashi, H. Imajima, G. Onodera, M. Hidai, S. Uemura, *Organometallics* **2004**, *23*, 26; c) Y. Nishibayashi, H. Imajima, G. Onodera, Y. Inada, M. Hidai, S. Uemura, *Organometallics* **2004**, *23*, 5100.

[4] For recent examples of catalytic reactions via allenylidene complexes, see a) B. M. Trost, J. A. Flygare, *J. Am. Chem. Soc.* **1992**, *114*, 5476; b) S. M. Maddock, M. G. Finn, *Angew. Chem.* **2001**, *113*, 2196; *Angew. Chem. Int. Ed.* **2001**, *40*, 2138; c) K.-L. Yeh, B. Liu, C.-Y. Lo, H.-L. Huang, R.-S. Liu, *J. Am. Chem. Soc.* **2002**, *124*, 6510; d) S. Datta, C.-L. Chang, K.-L. Yeh, R.-S. Liu, *J. Am. Chem. Soc.* **2003**, *125*, 9294.

[5] Y. Nishibayashi, G. Onodera, Y. Inada, M. Hidai, S. Uemura, *Organometallics* **2003**, *22*, 873.

[6] For a review, see E. A. Meyer, R. K. Castellano, F. Diederich, *Angew. Chem.* **2003**, *115*, 1244; *Angew. Chem. Int. Ed.* **2003**, *42*, 1210.

[7] See Supporting Information for experimental details.

[8] M.-J. Brienne, C. Ouannes, J. Jacques, *Bull. Soc. Chim. Fr.* **1967**, 613.

[9] a) A. J. M. Caffyn, K. M. Nicholas, *J. Am. Chem. Soc.* **1993**, *115*, 6438; b) V. Cadierno, S. Conejero, M. P. Gamasa, J. Gimeno, *Dalton Trans.* **2003**, 3060; c) Y. Nishibayashi, H. Imajima, G. Onodera, S. Uemura, *Organometallics* **2005**, *24*, 4106.

[10] We have already investigated the reaction of **2a** with *p*-chloroaniline in the presence of our second generation catalyst, but good enantioselectivity was not observed.

 © 2005 Wiley-VCH Verlag GmbH & Co. KGaA, Weinheim

Palladium Catalysis

DOI: 10.1002/anie.200502252

Oxindole Synthesis through Intramolecular Nucleophilic Addition of Vinylpalladiums to Aryl Isocyanates**

Shin Kamijo, Yuya Sasaki, Chikashi Kanazawa, Thomas Schüßeler, and Yoshinori Yamamoto**

One of the main targets in the field of synthetic organic chemistry these days is the development of reactions promoted by a catalyst. Not only metal catalysts but also organo-derived catalysts have been studied and applied in various kinds of transformation.[1] Among the transition metals applied in catalytic reactions so far, palladium complexes have found wide utility in various types of transfomation.[2] In most cases, organopalladium species containing a Pd–C bond generated during the course of the reaction act either as electrophiles or as neutral species, and it is rare for these species to behave as nucleophiles.[3] Several methods have been reported to transform the electrophilic reactivity to a nucleophilic one, although these methods are generally based on the transmetalation of a C–Pd bond to a nucleophilic C–M bond in situ.[4] Recently, direct nucleophilic reactions of organopalladiums to carbon–heteroatom unsaturated bonds were discovered by us and by other groups in the allylpalladation of imines and aldehydes,[5] vinylpalladation of ketones, aldehydes, imines, and cyanides,[6] and the arylpalladation of ketones and cyanides.[7] We report herein the first example of intramolecular nucleophilic vinylpalladation of isocyanates to produce oxindoles **3**[8] from 2-(alkynyl)phenylisocyanates **1** and terminal alkynes **2** [Eq. (1)].

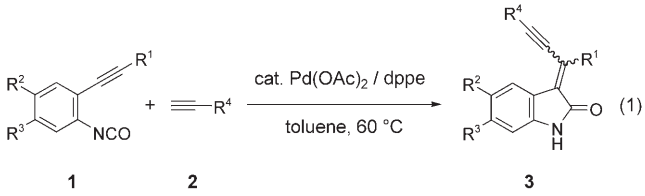

1 2 3

During the course of our investigation into the dual-role catalysis of palladium and platinum in the reaction between 2-(alkynyl)phenylisocyanates and alcohols that leads to the formation of indoles,[9] we found that a coupling reaction between 2-(alkynyl)phenylisocyanates **1** and terminal alkynes **2** took place to afford oxindoles **3**. We chose 2-(1-pentynyl)-phenylisocyanate **1a** and 1-pentyne **2a** as a standard set of starting materials for the optimization of the reaction conditions to yield the corresponding oxindole **3a** (Table 1).

Table 1: Optimization of reaction conditions for the formation of the oxindole **3a** from **1a** and **2a** [cf. Eq. (1)].[a]

Entry	Pd catalyst (mol%)	Phosphine (mol%)	*t* [h]	Yield of **3a** [%][b]
1	$Pd(OAc)_2$ (5)	tdmpp (10)	2	45[c]
2	$Pd(OCOCF_3)_2$ (5)	tdmpp (10)	>20	23[c]
3	$[(\eta^3\text{-}C_3H_5)PdCl]_2$ (2.5)	tdmpp (10)	>20	0[d]
4	$Pd_2(dba)_3\cdot CHCl_3$ (2.5)	tdmpp (10)	>20	7[c,d]
5	$Pd(OAc)_2$ (5)	ttmpp (10)	2	51[c]
6	$Pd(OAc)_2$ (5)	PPh_3 (10)	2	17[c]
7	$Pd(OAc)_2$ (5)	dppe (5)	2	62[c]
8	$Pd(OAc)_2$ (5)	dppp (5)	2	50[c,e]
9	$Pd(OAc)_2$ (5)	dppb (5)	2	26[c,e]
10	$Pd(OAc)_2$ (3)	dppe (3)	2	80[c]
11	$Pd(OAc)_2$ (3)	dppe (3)	1	80[f]
12[g]	$Pd(OAc)_2$ (3)	dppe (3)	1.5	76[e,h]

[a] dba = *trans*,*trans*-dibenzylideneacetone, tdmpp = tris(2,6-dimethoxyphenyl)phosphine, ttmpp = tris(2,4,6-trimethoxyphenyl)phosphine, dppe = 1,2-bis(diphenylphosphanyl)ethane, dppp = 1,3-bis(diphenylphosphanyl)-propane, dppb = 1,4-bis(diphenylphosphanyl)butane. [b] Yield of isolated product unless otherwise noted. [c] *E* isomer, (*E*)-**3a**, was obtained almost exclusively. [d] Substrate **1a** was recovered. [e] Yield measured by NMR spectroscopy with CH_2Br_2 as an internal standard. [f] Combined yield of the *E* and *Z* isomers (*E*)-**3a** and (*Z*)-**3a**. *E*/*Z* = 85:15. [g] The reaction was conducted at 40 °C. [h] (*E*)-**3a**/(*Z*)-**3a** = 33:67.

The reaction under a catalytic amount of $Pd(OAc)_2$ and TDMPP produced **3a** in 45% yield in 2 h (entry 1). The *E* isomer of the oxindole, (*E*)-**3a**, was obtained almost exclusively (cf. Eq. (2) for structures of (*E*)- and (*Z*)-**3a**). The combination of $Pd(OCOCF_3)$ and TDMPP catalyzed the formation of **3a** in 23% yield, but the $[(\eta^3\text{-}C_3H_5)PdCl]_2$/TDMPP catalyst did not give the corresponding oxindole **3a** at all (entries 2 and 3). The desired oxindole **3a** was also obtained from the reaction with $[Pd_2(dba)_3\cdot CHCl_3]$ and TDMPP, although the yield was rather low (entry 4). We then investigated the effects of phosphine ligands combined with $Pd(OAc)_2$. The reactivity of ttmpp was comparable to

[*] Y. Sasaki, C. Kanazawa, Prof. Dr. Y. Yamamoto
Department of Chemistry
Graduate School of Science
Tohoku University
Sendai 980-8578 (Japan)
Fax: (+81) 22-795-6784
E-mail: yoshi@mail.tains.tohoku.ac.jp
Dr. S. Kamijo
Department of Chemistry and Biochemistry
Florida State University
Tallahassee, FL 32306 (USA)
E-mail: skamijo@chem.fsu.edu
Dr. T. Schüßeler
Visiting Researcher in the summer of 2002 from:
Institut für Organische Chemie
Rheinisch-Westfälische Technische Hochschule
Professor-Pirlet-Strasse 1, 52074 Aachen (Germany)

[**] We thank members of the Research and Analytical Center for Giant Molecules at the Graduate School of Science, Tohoku University, for measurement of mass spectra, elemental analyses, and X-ray crystallographic analyses. This work was supported in part by a Grant-in-Aid for Encouragement of Young Scientists (B) from JSPS. T.S. also acknowledges JSPS for a fellowship in the Summer Program (2002).

InterScience
© 2005 Wiley-VCH Verlag GmbH & Co. KGaA, Weinheim

that of TDMPP, whereas the reactivity of PPh_3 was inferior (entries 5 and 6). The bidentate phosphine ligands in dppe, dppp, and dppb also produced the corresponding oxindole **3a** (entries 7–9). Among these catalysts, the combination of $Pd(OAc)_2$ and dppe showed the highest catalytic activity: **3a** was formed in 62% yield. When the amounts of the catalysts were reduced to 3 mol% each for $Pd(OAc)_2$ and dppe, the yield of the oxindole **3a** was increased to 80% yield with almost exclusive formation of the *E* isomer, (*E*)-**3a** (entry 10). When the reaction was quenched right after the consumption of the starting isocyanate **1a** (1 h), a mixture of the *E* and *Z* isomers of the oxindole, (*E*)-**3a** and (*Z*)-**3a**, was obtained in 80% combined yield with a ratio of 85:15 (entry 11). The reaction could proceed even at 40°C to give the oxindole in 76% combined yield with a 33:67 ratio of the *E* and *Z* isomers (entry 12).

With the optimized reaction conditions in hand, we examined the scope and limitations of the present palladium-catalyzed oxindole-forming reaction (Table 2). As mentioned above, treatment of **1a** with **2a** in the presence of a catalytic amount of $Pd(OAc)_2$ (3 mol%) and dppe (3 mol%) in toluene (0.5 M) at 60°C for 2 h afforded the *E* isomer of **3a** almost exclusively in 80% yield after isolation (entry 1). The isocyanate **1b** bearing a cyclohexyl group at the end of the acetylenic group gave the corresponding oxindole **3b** in 58% yield as the *E* isomer (entry 2). In the case of the isocyanate **1c** with a bulky *tert*-butyl substituent, the reaction did not reach completion even after 24 h, and the desired product **3c** was obtained in only 26% yield (entry 3). The phenyl-substituted isocyanate **1d** gave a complex mixture of unidentified products (entry 4). The substrates **1e** and **1f**, having electron-donating methoxy and methylthio groups, respectively, *para* to the isocyanato group, produced the corresponding oxindoles **3e** and **3f** in moderate to good yields (entries 5 and 6). The isocyanate **1g** with an electron-withdrawing chloride substituent on the benzene ring gave the desired product **3g** in 44% yield (entry 7). The reactions of isocyanates **1h** and **1i**, each bearing a substituent *para* to the alkynyl group, furnished the corresponding oxindoles **3h** and **3i**, respectively, in moderate yields (entries 8 and 9). A mixture of *E* and *Z* isomers of the corresponding oxindole, (*E*)-**3h** and (*Z*)-**3h**, was obtained in the case of **1h**, which bears an electron-donating group *para* to the alkynyl group.

Table 2: Reaction between various isocyanates **1** and **2a**.[a]

Entry	R^1	R^2	R^3	**1**	*t* [h]	**3**	Yield [%][b] (*E*/*Z*)
1	Pr	H	H	**1a**	2	**3a**	80 (>99:1)
2	cyclohexyl	H	H	**1b**	4	**3b**	58 (>99:1)
3	*t*Bu	H	H	**1c**	24	**3c**	26 (>99:1)[c]
4	Ph	H	H	**1d**	24	**3d**	–[d]
5	Pr	OMe	H	**1e**	1	**3e**	73 (>99:1)
6	Pr	SMe	H	**1f**	1	**3f**	52 (>99:1)
7	Pr	Cl	H	**1g**	1.5	**3g**	44 (>99:1)
8	Pr	H	OMe	**1h**	2	**3h**	48 (33:67)
9	Pr	H	CF_3	**1i**	24	**3i**	33 (>99:1)[e]

[a] The reaction of **1** and **2a** (2 equiv) was conducted in the presence of $Pd(OAc)_2$ (3 mol%) and dppe (3 mol%) in toluene (0.5 M) at 60°C for the time shown in the table. [b] Yield of isolated product unless otherwise noted. [c] Substrate **1c** was recovered. [d] Complex mixture. [e] Substrate **1i** was recovered.

We next investigated the reactions between the isocyanate **1a** and a variety of terminal alkynes **2** (Table 3). With increases in the bulkiness of the terminal alkynes **2a–c**, the yields of the desired products **3a**, **3j**, and **3k** decreased (entries 1–3). It is worth mentioning that the *Z* isomer of **3k** was obtained almost exclusively when bulky *tert*-butylacetylene **2c** was used as the starting material. Phenylacetylene **2d** and (trimethylsilyl)acetylene **2e** reacted to produce the corresponding oxindoles **3l** and **3m**, respectively, in moderate yields as a mixture of the *E* and *Z* isomers (entries 4 and 5). The structures of oxindoles were determined by detailed analyses of the spectroscopic data. Furthermore, the structure of the oxindoles (*E*)-**3l** and (*Z*)-**3l** were unambiguously confirmed by X-ray crystallographic analyses (Figure 1).

Table 3: Reaction between **1a** and various terminal alkynes **2**.[a]

Entry	R^4	**2**	*t* [h]	**3**	Yield [%][b] (*E*/*Z*)
1	Pr	**2a**	2	**3a**	80 (>99:1)
2	cyclohexyl	**2b**	2	**3j**	53 (>99:1)
3	*t*Bu	**2c**	20	**3k**	16 (1:>99)
4	Ph	**2d**	0.5	**3l**	67 (22:78)
5	TMS[c]	**2e**	2.5	**3m**	61 (35:65)

[a] The reaction of **1a** and **2** (2 equiv) was conducted in the presence of $Pd(OAc)_2$ (3 mol%) and dppe (3 mol%) in toluene (0.5 M) at 60°C for the time shown in the table. [b] Yield of isolated product. [c] TMS = trimethylsilyl.

The following mechanism is proposed for the unprecedented intramolecular vinylpalladation of isocyanates to form

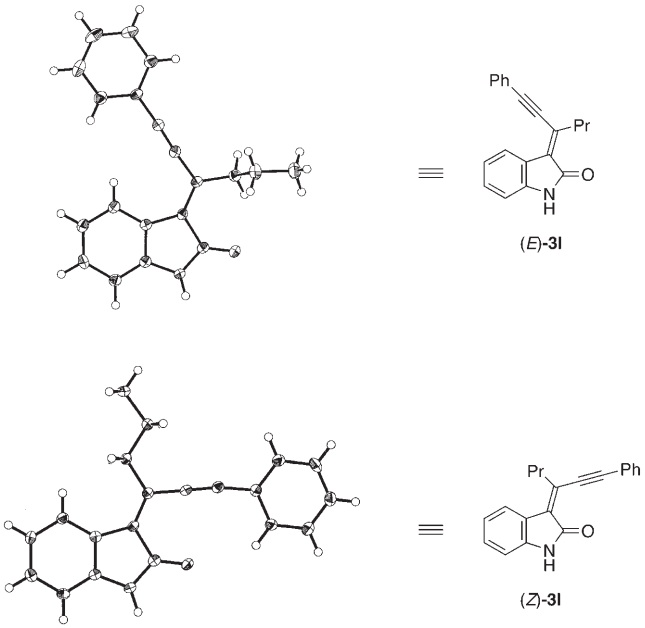

Figure 1. X-ray crystal structures of (*E*)-**3l** and (*Z*)-**3l**.

 © 2005 Wiley-VCH Verlag GmbH & Co. KGaA, Weinheim

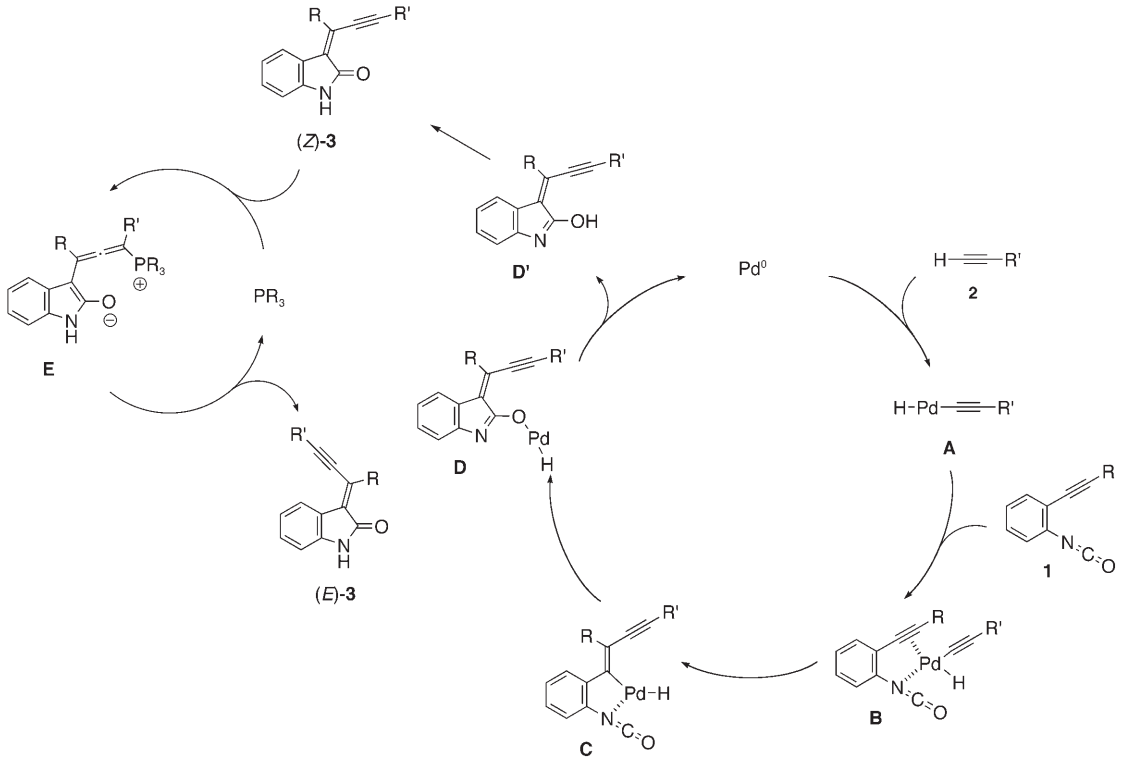

Scheme 1. Proposed mechanism for the formation of oxindoles through intramolecular vinylpalladation of isocyanates.

oxindoles (Scheme 1). A Pd^0 species is generated in situ[10] and oxidatively adds to the C–H bond of terminal alkyne **2** to give intermediate **A**. The derived species **A** would coordinate to both the alkynyl and the isocyanato moieties in **1** to form intermediate **B**, in which the palladium metal behaves as a dual-role catalyst.[9,11] Carbopalladation of the C–C triple bond in **1** yields the vinylpalladium intermediate **C**.[12] Intramolecular nucleophilic attack of the vinylpalladium species on the isocyanato group would produce the cyclized oxypalladium intermediate **D**, which would be transformed into **D′** after reductive elimination of the Pd^0. The intermediate **D′** would isomerize to the corresponding oxindole (*Z*)-**3**.

Conversion of the *Z* isomer of oxindole **3** into its *E* isomer, (*E*)-**3**, is catalyzed by the phosphine, dppe, existing in the reaction mixture. Nucleophilic addition of the phosphine to the electrophilic carbon center in the alkynyl moiety of (*Z*)-**3** would produce the zwitterionic intermediate **E**.[13] Rotation of the newly formed σ bond between the indole core and the allenyl moiety and subsequent elimination of the phosphine furnishes the corresponding *E* oxindole (*E*)-**3**. This explains well that the exclusive or predominant formations of *Z* oxindoles were observed when the reaction was conducted with the methoxy-substituted isocyanate **1h** and the bulky terminal alkynes **2c–e** as substrates. The electron flow from the properly substituted methoxy group to the enyne moiety in (*Z*)-**3i** or the steric congestion around the enyne moiety in (*Z*)-**3k–m** would hinder the nucleophilic approach of the phosphine toward the electrophilic carbon center in the alkynyl moiety in the corresponding *Z* oxindoles (entry 8 in Table 2 and entries 3–5 in Table 3). Indeed, the reaction of (*Z*)-**3a** in the presence of a catalytic amount of dppe resulted in a clean formation of (*E*)-**3a** in 2 h [Eq. (2)].

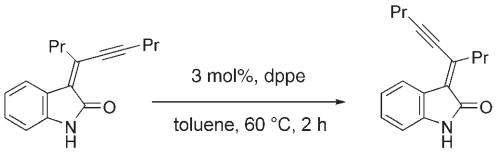

94% NMR yield (2)

We have achieved the synthesis of oxindoles **3** from aryl isocyanates **1** and terminal alkynes **2** in the presence of a catalytic amount of $Pd(OAc)_2$ and dppe. This oxindole-forming reaction most probably proceeds through the intramolecular nucleophilic attack of a vinylpalladium species on the isocyanato group. Further studies on synthetic applications and a mechanistic investigation are in progress in our laboratory.

Experimental Section

1-Pentyne (60 μL, 0.6 mmol) was added to a toluene solution (0.6 mL) of **1a** (55.6 mg, 0.3 mmol), $Pd(OAc)_2$ (2.0 mg, 0.009 mmol), and dppe (3.6 mg, 0.009 mmol) under an argon atmosphere. The solution was stirred at 60 °C for 2 h. The reaction mixture was cooled to RT, filtered through a short Florisil pad with AcOEt as

 © 2005 Wiley-VCH Verlag GmbH & Co. KGaA, Weinheim

the eluent, and concentrated. The residue was purified by silica gel column chromatography to afford (*E*)-**3a** in 68% yield (51.7 mg).

Received: June 27, 2005
Published online: November 8, 2005

Keywords: alkynes · isocyanates · nucleophilic addition · oxindoles · palladium

[1] a) B. M. Trost, *Science* **1991**, *254*, 1471 – 1477; b) P. I. Dalko, L. Moisan, *Angew. Chem.* **2004**, *116*, 5248 – 5286; *Angew. Chem. Int. Ed.* **2004**, *43*, 5138 – 5175.

[2] For reviews on palladium chemistry, see: a) J. Tsuji, *Transition Metal Reagents and Catalysts*, Wiley, Chichester, **2004**; b) *Handbook of Organopalladium Chemistry for Organic Synthesis* (Ed.: E.-i. Negishi), Wiley, New York, **2002**; c) *Metal-Catalyzed Cross-Coupling Reactions* (Eds.: F. Diederich, P. J. Stang), Wiley-VCH, Weinheim, **1998**.

[3] The Heck reaction and CO-insertion reaction are representative exceptions. In the Heck reaction, organopalladium species act as weak nucleophiles toward electron-deficient olefins to give 1,4 adducts. In the case of the CO-insertion reaction, acylpalladium species are formed by insertion of CO into the C–Pd bond of organopalladium species. See: a) R. F. Heck, *Org. React.* **1982**, *27*, 345 – 390, and references therein; b) T. Mizoroki, K. Mori, A. Ozaki, *Bull. Chem. Soc. Jpn.* **1971**, *44*, 581; c) ref. [2].

[4] Y. Tamaru in *Handbook of Organopalladium Chemistry for Organic Synthesis, Vol. 2* (Ed.: E.-i. Negishi), Wiley, New York, **2002**, pp. 1917 – 1943, and references therein.

[5] a) H. Nakamura, H. Iwama, Y. Yamamoto, *J. Am. Chem. Soc.* **1996**, *118*, 6641 – 6647; b) H. Nakamura, K. Nakamura, Y. Yamamoto, *J. Am. Chem. Soc.* **1998**, *120*, 4242 – 4243; c) K. Nakamura, H. Nakamura, Y. Yamamoto, *J. Org. Chem.* **1999**, *64*, 2614 – 2615; d) H. Nakamura, M. Bao, Y. Yamamoto, *Angew. Chem.* **2001**, *113*, 3308 – 3310; *Angew. Chem. Int. Ed.* **2001**, *40*, 3208 – 3210; e) R. A. Fernandes, A. Stimac, Y. Yamamoto, *J. Am. Chem. Soc.* **2003**, *125*, 14133 – 14139; f) O. A. Wallner, K. J. Szabó, *J. Org. Chem.* **2003**, *68*, 2934 – 2943; g) N. Solin, J Kjellgren, K. J. Szabó, *J. Am. Chem. Soc.* **2004**, *126*, 7026 – 7033.

[6] a) L. G. Quan, V. Gevorgyan, Y. Yamamoto, *J. Am. Chem. Soc.* **1999**, *121*, 3545 – 3546; b) V. Gevorgyan, L. G. Quan, Y. Yamamoto, *Tetrahedron Lett.* **1999**, *40*, 4089 – 4092; c) A. Takeda, S. Kamijo, Y. Yamamoto, *J. Am. Chem. Soc.* **2000**, *122*, 5662 – 5663; d) R. C. Larock, Q. Tian, A. A. Pletnev, *J. Am. Chem. Soc.* **1999**, *121*, 3238 – 3239; e) A. A. Pletnev, Q. Tian, R. C. Larock, *J. Org. Chem.* **2002**, *67*, 9276 – 9287; f) Q. Tian, A. A. Pletnev, R. C. Larock, *J. Org. Chem.* **2003**, *68*, 339 – 347; g) R. C. Larock, M. J. Doty, S. Cacchi, *J. Org. Chem.* **1993**, *58*, 4579 – 4583.

[7] a) L. G. Quan, M. Lamrani, Y. Yamamoto, *J. Am. Chem. Soc.* **2000**, *122*, 4827 – 4828; b) A. A. Pletnev, R. C. Larock, *Tetrahedron Lett.* **2002**, *43*, 2133 – 2136; c) A. A. Pletnev, R. C. Larock, *J. Org. Chem.* **2002**, *67*, 9428 – 9438.

[8] For recent total syntheses of oxindole alkaloids, see: a) C. Marti, E. Carreira, *Eur. J. Org. Chem.* **2003**, 2209 – 2219; b) A. Lerchner, E. Carreira, *J. Am. Chem. Soc.* **2002**, *124*, 14826 – 14827; c) H. Lin, S. J. Danishefsky, *Angew. Chem.* **2003**, *115*, 38 – 53; *Angew. Chem. Int. Ed.* **2003**, *42*, 36 – 51; d) J. M. Ready, S. E. Reisman, M. Hirata, M. W. Weiss, K. Tamaki, T. V. Ovaska, J. L. Wood, *Angew. Chem.* **2004**, *116*, 1290 – 1292; Angew. *Chem. Int. Ed.* **2004**, *43*, 1270 – 1272; e) R. M. Williams, J. Cao, H. Tsujishima, *Angew. Chem.* **2000**, *112*, 2640 – 2644; *Angew. Chem. Int. Ed.* **2000**, *39*, 2540 – 2544; f) M. Inoue, H. Sakazaki, H. Furuyama, M. Hirama, *Angew. Chem.* **2003**, *115*, 2758 – 2761; *Angew. Chem. Int. Ed.* **2003**, *42*, 2654 – 2657.

[9] S. Kamijo, Y. Yamamoto, *J. Org. Chem.* **2003**, *68*, 4764 – 4771.

[10] a) C. Amatore, E. Carré, A. Jutand, M. A. M'Barki, *Organometallics* **1995**, *14*, 1818 – 1826; b) C. Amatore, A. Jutand, A. Thuilliez, *Organometallics* **2001**, *20*, 3241 – 3249.

[11] a) N. Asao, T. Nogami, K. Takahashi, Y. Yamamoto, *J. Am. Chem. Soc.* **2002**, *124*, 764 – 765; b) I. Nakamura, G. B. Bajracharya, H. Wu, K. Oishi, Y. Mizushima, I. D. Gridnev, Y. Yamamoto, *J. Am. Chem. Soc.* **2004**, *126*, 15423 – 15430; c) G. B. Bajiracharya, I. Nakamura, Y. Yamamoto, *J. Org. Chem.* **2005**, *70*, 892 – 896.

[12] a) B. M. Trost, C. Chan, G. Ruhter, *J. Am. Chem. Soc.* **1987**, *109*, 3486 – 3487; b) B. M. Trost, M. T. Sorum, C. Chan, A. E. Harms, G. Ruhter, *J. Am. Chem. Soc.* **1997**, *119*, 698 – 708; c) M. Rubina, V. Gevorgyan, *J. Am. Chem. Soc.* **2001**, *123*, 11107 – 11108; d) C. Yang, S. P. Nolan, *J. Org. Chem.* **2002**, *67*, 591 – 593.

[13] For reviews on phosphine-mediated and -catalyzed reactions, see: a) X. Lu, C. Zhang, Z. Xu, *Acc. Chem. Res.* **2001**, *34*, 535 – 544, and references therein; b) D. H. Valentine, Jr., J. H. Hillhouse, *Synthesis* **2003**, 317 – 334, and references therein.

 © 2005 Wiley-VCH Verlag GmbH & Co. KGaA, Weinheim

Cationic Ni_2 Fragment

DOI: 10.1002/anie.200502905

Tetraphenylborate as a Novel Bridging Ligand in a Zwitterionic Nickel(I) Dimer**

*Yaofeng Chen, Christine Sui-Seng, and Davit Zargarian**

Heterolytic abstraction of anionic ligands such as halides or alkyl substituents can convert coordinatively saturated organometallic complexes into highly electrophilic, usually transient, cationic species that can serve as efficient initiators in various catalytic reactions. This strategy has been used in the development of many catalytic processes based on (quasi) square-planar d^8 metal precursors, including the recently reported systems for olefin polymerization reactions.[1]

In this context, we have shown that abstraction of Cl^- from the complexes [(R-ind)Ni(PPh_3)Cl] (R-ind = indenyl and its substituted derivatives)[2] leads to the generation of a transient species (presumed to be $[(R\text{-ind})Ni(PPh_3)]^+$) that reacts with excess substrate to promote the oligomerization or polymerization of various olefins,[3] PhC≡CH,[4] and $PhSiH_3$,[5] or catalyzes the hydrosilylation of olefins and ketones[6]

[*] Dr. Y. Chen, C. Sui-Seng, Prof. D. Zargarian
Département de Chimie
Université de Montréal
Montréal, PQ H3C3J7 (Canada)
Fax: (+1) 514-343-2468
E-mail: zargarian.davit@umontreal.ca

[**] The authors gratefully acknowledge NSERC of Canada for financial support of this study and Profs. F. Schaper and D. Gusev for many useful discussions.

Supporting information for this article is available on the WWW under http://www.angewandte.org or from the author.

© 2005 Wiley-VCH Verlag GmbH & Co. KGaA, Weinheim

(Scheme 1). We have also shown that abstraction of Cl^- in the presence of suitable ligands L gives $[(R\text{-ind})Ni(PPh_3)L]^+$ (L = PR'_3; R″CN, *t*BuNC).[3a,4c,5d] If, on the other hand, Cl^- is

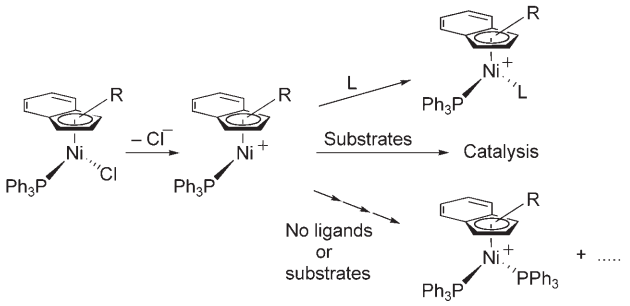

Scheme 1. Reaction pathways following abstraction of Cl^- from the complexes $[(R\text{-ind})Ni(PPh_3)Cl]$.

abstracted in the absence of sufficiently strong coordinating ligands or substrates, we obtain $[(R\text{-ind})Ni(PPh_3)_2]^+$ in low yields.[3a] Varying amounts of the latter species also form during the above-noted catalytic reactions, thus resulting in lower catalytic activities.

In the search for a strategy to circumvent this built-in deactivation pathway, we set out to determine whether placing sterically bulky substituents on the ind ligands might prevent the formation of $[(R\text{-ind})Ni(PPh_3)_2]^+$ during catalysis. An initial study showed that the catalytic activities of $[(R\text{-ind})Ni(PPh_3)Cl]$ for the hydrosilylation of styrene do increase with more bulky ind ligands (1-Me-ind < 1-$SiMe_3$-ind < 1,3-$(SiMe_3)_2$-ind).[7] To answer this question more directly, we have studied the abstraction of Cl^- from $[(1\text{-}SiMe_3\text{-}3\text{-}R\text{-ind})Ni(PPh_3)Cl]$ (R = H, **1**; $SiMe_3$, **2**) and report our findings herein.

Treatment of **1** with $NaBPh_4$ gave an initial product whose NMR spectra are consistent with the formation of $[(1\text{-}SiMe_3\text{-ind})Ni(PPh_3)_2][BPh_4]$,[8] although the ready decomposition of this new species prevented its isolation and full characterization. It appears, therefore, that the presence of one $SiMe_3$ substituent on ind destabilizes the bis(phosphane) complex but does not block its formation. In contrast, treatment of **2** with $NaBPh_4$ gave a product that was stable and isolable, but whose spectral features were not those of a bis(phosphane) cation. For instance, the $^{31}P\{^1H\}$ NMR spectrum of this product displays an A_2X system with a doublet at around $\delta = 22$ ppm and a triplet at around $\delta = 126$ ppm ($J_{P,P} = 35$ Hz), while the ^1H and ^{13}C NMR spectra contain many signals in regions typical of phenyl groups (^1H: $\delta = 6.5$–7.3 ppm; ^{13}C: $\delta = 122$–138 ppm) in addition to a few peaks farther upfield (^1H: $\delta = 5.5$–5.9 ppm; ^{13}C: $\delta = 86$–102 ppm). Significantly, the signals expected for the $(SiMe_3)_2$-ind moiety were absent from the latter spectra. In a search for clues regarding the fate of this moiety, we analyzed the reaction mixture by GC-MS and ^1H NMR spectroscopy, which enabled the detection of 3-phenyl-1,1-bis(trimethylsilyl)indene.

These spectral analyses did not, however, allow an unambiguous characterization of the main product, but X-ray diffraction analysis of single crystals obtained from repeated recrystallizations allowed us to identify it as **3**, which is a dinuclear zwitterion composed of two $(PPh_3)Ni^I$ cations bridged by the anions μ-$[PPh_2]^-$ and *syn*,μ-$[(\eta^2{:}\eta^2\text{-Ph})BPh_3]^-$ (Figure 1). The main features of this crystal structure are consistent with the solution spectra: the A_2X signals observed in the ^{31}P NMR spectrum of **3** can be assigned to a μ-PPh_2 and two PPh_3 moieties,[9] while the upfield signals in the ^1H and ^{13}C NMR spectra can be assigned to the $(\eta^2{:}\eta^2\text{-Ph})BPh_3$ moiety.

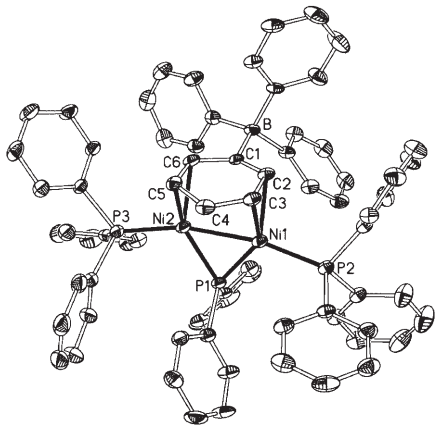

Figure 1. ORTEP view of **3**. Thermal ellipsoids are shown at the 30% probability level. Selected distances [Å] and angles [°]: Ni1-Ni2 2.4471(11), Ni1-P1 2.1397(16), Ni2-P1 2.1395(13), Ni1-P2 2.2055(15), Ni2-P3 2.1841(16), Ni1-C1 2.670(4), Ni1-C2 2.120(4), Ni1-C3 2.094(4), Ni1-C4 2.617(4), Ni2-C1 2.666(5), Ni2-C4 2.522(5), Ni2-C5 2.075(5), Ni2-C6 2.125(5), C1-C2 1.421(6), C2-C3 1.415(6), C3-C4 1.396(6), C4-C5 1.392(6), C5-C6 1.415(6), C6-C1 1.414(6); P1-Ni1-P2 116.27(6), P1-Ni2-P3 110.98(6), P2-Ni1-Ni2 168.82(5), P3-Ni2-Ni1 165.66(5), Ni2-P1-Ni1 69.76(5), P1-Ni1-Ni2 55.12(4), P1-Ni2-Ni1 55.12(4).

The most notable structural feature of **3** is the novel bonding mode of the borate moiety: although there are many precedents for complexes featuring $[(\eta^{2-6}\text{-Ph})_nBPh_{4-n}]^-$,[10,11] the formation of a complex in which one of the Ph groups bridges two metals is without precedent.[12] Interestingly, the synfacially coordinated μ-$PhBPh_3$ moiety interacts with the two NiL_2 moieties through two nonadjacent double bonds from opposite edges of the μ-arene ring, i.e., C2–C3 and C5–C6. We propose that this unusual bonding mode[13] minimizes the steric interactions between the Ph groups on the PPh_3 ligands and the borate moiety in **3**.[14]

A more complete picture of the bonding in the Ni_2-$[\mu,\eta^2,\eta^2\text{-PhBPh}_3]$ moiety emerges from a careful inspection of the individual Ni–C distances, which show that the μ-Ph ring straddles the Ni–Ni axis and is somewhat tilted, giving the following unsymmetrical Ni–C interactions: Ni1–C2 > Ni1–C3; Ni2–C6 > Ni2–C5; Ni(1/2)–C1 > Ni(1/2)–C4. Interestingly, these interactions result in only minor and more or less uniform lengthening of the C–C bond lengths within the μ-Ph ring (1.39–1.42 Å), although the dihedral angle of about 15° between the planes (C1,C2,C3,C4) and (C1,C6,C5,C4) signals a relatively significant butterfly distortion of the ring.[15,16]

It is instructive to compare the unusual Ni–arene interactions found in **3** to those in complex **4**[17], which is a rare

 © 2005 Wiley-VCH Verlag GmbH & Co. KGaA, Weinheim

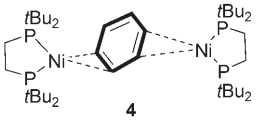

4

$Ni_2(\mu$-arene) species.[18] In contrast to **3**, the $Ni_2(\mu\text{-}C_6H_6)$ interactions in **4** are antifacial and involve two adjacent double bonds, i.e., a 1,3-diene moiety. Furthermore, the Ni–C distances are significantly shorter in **4** (ca. 2.00–2.02 vs. 2.10 Å in **3**), which is presumably due to greater backbonding possible in the Ni^0 complex. It should be noted, however, that the interactions of the Ni centers in **3** with (μ-$PhBPh_3$) are reinforced by the electrostatic attractions within this zwitterionic compound. Accordingly, the arene moiety in **3** cannot be displaced by aromatic solvents, even when heated for extended periods.

The structural parameters discussed above are consistent with a simple bonding picture involving the contribution of two pairs of electrons from $[(\mu,\eta^2,\eta^2\text{-Ph})BPh_3]^-$; when the Ni–Ni bond is taken into consideration,[19] each Ni center ends up with a total of 16 valence electrons. This is in agreement with the conclusions of a theoretical analysis[20] showing that the analogous fragment $[\{(PH_3)Pd\}_2(\mu\text{-Br})]^+$ has only two low-lying vacant orbitals of appropriate symmetry to interact with the two HOMO orbitals of a (μ-C_6H_6) ligand.

The unexpected formation of **3** from **2** raises the question of how this transformation might take place. Although definitive conclusions regarding the reaction mechanism must await further experimental evidence, the sequence of steps shown in Scheme 2 serves to rationalize the conversion

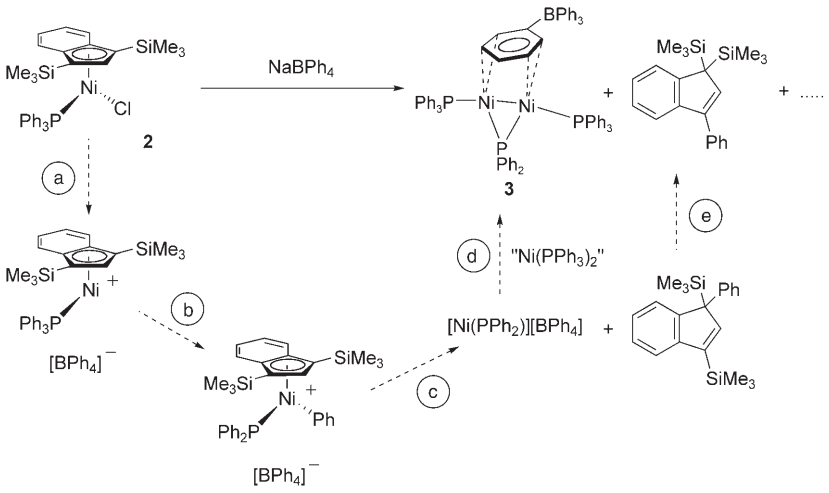

Scheme 2. Suggested pathway for the conversion of **2** into **3**.

of **2** into **3**. The proposed addition of a P–Ph bond (step b) is well known;[21] indeed, a particularly relevant example of such P–C bond activation has been observed during the formation of $[Pd_2(t\text{Bu}_2\text{PH})_2(\mu\text{-}t\text{Bu}_2\text{P})(\mu\text{-}C_6H_5O)]$, which is a closely related, isoelectronic analogue of **3**.[22] The reductive elimination from a Ni^{IV} intermediate (step c) is also quite reasonable, as is the rearrangement of the initially formed 1-phenyl-1,3-bis(trimethysilyl)indene to the observed 3-phenyl-1,3-bis(trimethysilyl)indene isomer by a silyl migration (step e).[23] Finally, comproportionation of Ni^{II} and Ni^0 species to give Ni^I dimers (step d) has been reported,[24] although the origin of the putative "$Ni^0(PPh_3)_2$" fragment is not known at this point.

We conclude that the greater steric bulk in [{($SiMe_3$)$_n$-ind}Ni(PPh_3)Cl] indeed hinders the generation of the cationic bis(phosphane) side-products that form with less bulky analogues, and this might contribute to the observed increase in the catalytic reactivity of these complexes.[7] On the other hand, the presence of $SiMe_3$ substituents on ind also opens a new decomposition pathway that, in the case of the 1,3-($SiMe_3$)$_2$-ind derivative **2**, results in the formation of the Ni^I dimer **3**. The observation of a $[(\mu,\eta^2,\eta^2\text{-Ph})BPh_3]^-$ ligand in **3** expands the range of coordination modes that should be taken into account when contemplating the use of BPh_4^- and its various analogues as weakly coordinating counterions. Preliminary experiments have shown that **3** does not react with $PhSiH_3$ or styrene, thus implying that this compound is not involved in the hydrosilylation catalysis promoted by its precursor. In view of the interesting catalytic reactivities exhibited by some Pd^I–Pd^I dimers,[25] however, future studies are planned to probe the reactivities of **3** towards other substrates.

Experimental Section

A slurry of [{1,3-($SiMe_3$)$_2$-ind}Ni(PPh_3)Cl] (191 mg, 310 μmol) and Na[BPh_4] (113 mg, 330 μmol) was stirred in Et_2O (20 mL) at room temperature for two days. The reaction mixture was then filtered and the solid residues extracted with CH_2Cl_2 (total volume ca. 15 mL). (Analysis of the filtrate is described below.) Concentration of the extracts to about 2 mL and layering with hexane (ca. 5 mL) resulted in the formation of dark-brown crystals overnight, which were isolated, washed quickly with acetone, and dried under vacuum to give **3** (30 mg, 25% yield). ^{1}H NMR (400 MHz, $CDCl_3$, 25 °C): $\delta = 7.33$–6.50 (m, 55H; Ph-H), 5.92 (brs, 2H; benzene-$H^{2,6/3,5}$), 5,79 (brs, 1H; benzene-H^4), 5.52 ppm (brs, 2H; benzene-$H^{2,6/3,5}$); ^{13}C{^{1}H} NMR (100.56 MHz, $CDCl_3$, 25 °C): $\delta = 138.5$, 136.1, 135.6, 134.8, 133.3, 132.1, 129.5, 127.1, 125.8, 122.3, 102.6, 97.1, 86.2 ppm; ^{31}P{^{1}H} NMR (161.92 MHz, $CDCl_3$, 25 °C): $\delta = 126.5$ (t, $^2J_{PP} = 35$ Hz), 22.3 ppm (d, $^2J_{PP} = 35$ Hz); elemental analysis calcd (%) for $C_{72}H_{60}BP_3Ni_2$: C 75.44, H 5.28; found: C 74.70, H 5.25.

Crystal data for **3**: monoclinic ($P2_1/n$); $a = 18.6631(6)$, $b = 13.5095(5)$, $c = 25.0944(9)$ Å; $\beta = 110.350(2)°$; $V = 5932.1(4)$ Å^3; $Z = 4$; $\rho_{calcd} = 1.283$ g cm^{-1}; Bruker AXS diffractometer; $\mu = 1.869$ mm^{-1}, $\lambda = 1.54178$ Å ($Cu_{K\alpha}$); ω scan, $\theta_{max} = 60.13°$; temperature: 223(2) K; h,k,l range: $-20 \le h \le 20$; $-14 \le k \le 15$; $-28 \le l \le 27$; 5072 reflections used ($I > 2\sigma(I)$); absorption correction multiscan SADABS; $R(F^2 > (2\sigma F^2))$, $wR(F^2)$: 0.0591, 0.1336; GOF: 0.929. CCDC-279748 contains the supplementary crystallographic data for this paper. These data can be obtained free of charge from the Cambridge Crystallographic Data Centre via www.ccdc.cam.ac.uk/data_request/cif.

 © 2005 Wiley-VCH Verlag GmbH & Co. KGaA, Weinheim

Analytical data for the filtrate from the reaction mixture: MS: *m*/*z*: 336 $[M]^+$, 321 $[M-CH_3]^+$, 263 $[M-SiMe_3]^+$, 248 $[M-SiMe_3-CH_3]^+$, 233 $[M-SiMe_3-2CH_3]^+$, 218 $[M-SiMe_3-3CH_3]^+$, 73 $[SiMe_3]^+$; ^{1}H NMR (400 MHz, $CDCl_3$, 25 °C): $\delta = 7.5$–6.9 (aromatic protons), 6.74 (s, H2 of the indenyl ring), −0.03 ppm (s, $SiMe_3$).

Received: August 16, 2005
Published online: November 8, 2005

Keywords: bridging ligands · chloride abstraction · nickel · P ligands · zwitterions

[1] a) S. D. Ittel, L. K. Johnson, M. Brookhart, *Chem. Rev.* **2000**, *100*, 1169; b) V. C. Gibson, S. K. Spitzmesser, *Chem. Rev.* **2003**, *103*, 283.

[2] D. Zargarian, *Coord. Chem. Rev.* **2002**, *233–234*, 157.

[3] a) R. Vollmerhaus, F. B. Gariépy, D. Zargarian, *Organometallics* **1997**, *16*, 4762; b) M.-A. Dubois, R. Wang, D. Zargarian, J. Tian, R. Vollmerhaus, Z. Li, S. Collins, *Organometallics* **2001**, *20*, 663; c) M.-A. Dubois, *MSc Dissertation*, Université de Montréal, **2000**.

[4] a) R. Wang, F. B. Gariépy, D. Zargarian, *Organometallics* **1999**, *18*, 5548; b) R. Wang, L. F. Groux, D. Zargarian, *J. Organomet. Chem.* **2002**, *660*, 98; c) R. Wang, L. F. Groux, D. Zargarian, *Organometallics* **2002**, *21*, 5531; d) E. Rivera, R. Wang, X. X. Zhu, D. Zargarian, R. Giasson, *J. Mol. Catal. A* **2003**, *204–205*, 325.

[5] a) F.-G. Fontaine, T. Kadkhodazadeh, D. Zargarian, *Chem. Commun.* **1998**, 1253–1254; b) F.-G. Fontaine, D. Zargarian, *Organometallics* **2002**, *21*, 401; c) F.-G. Fontaine, D. Zargarian, *J. Am. Chem. Soc.* **2004**, *126*, 8786; d) F.-G. Fontaine, *PhD Dissertation*, Université de Montréal, **2002**.

[6] F.-G. Fontaine, R.-V. Nguyen, D. Zargarian, *Can. J. Chem.* **2003**, *81*, 1299.

[7] Y. Chen, C. Sui-Seng, S. Boucher, D. Zargarian, *Organometallics* **2005**, *24*, 149.

[8] For example, the $^{31}P\{^1H\}$ NMR spectrum shows two very broad peaks at around $\delta = 30$ and 33 ppm (width at half-height approximately 400 Hz), which are assigned to the two inequivalent PPh_3 groups that are in a dissociation/re-association equilibrium. The observation in the ^{1}H NMR spectrum of a significantly downfield-shifted signal for H3 (from $\delta = 3.5$ ppm in **1** to about $\delta = 5$ ppm in the product) is also consistent with the greater ind→Ni donation in such cationic species (ref. [2]). This spectrum also shows the anticipated signals for H2 and the aromatic protons at about $\delta = 6.5$–7.5 ppm, as well as an upfield singlet for the Si-CH_3 protons at around $\delta = -0.12$ ppm.

[9] For comparison, the ^{31}P NMR signals of the μ-PPh_2 moieties in $[(CNR)_2Ni_2(\mu\text{-}PPh_2)_2(\mu\text{-}Ph_2PNHPPh_2)_2]$ (E. Simón-Manso, C. P. Kubiak, *Inorg. Chem. Commun.* **2003**, *6*, 1096) and $[Fe_2(CO)_6(\mu\text{-}PPh_2)_2]$ (E. P. Kyba, R. E. Davis, C. N. Clubb, S.-T. Liu, H. O. A. Palacios, J. S. McKennis, *Organometallics* **1986**, *5*, 869) are found at around $\delta = 190$ and 143 ppm, respectively. On the other hand, the general range for the ^{31}P NMR signal of a PPh_3 coordinated to Ni is $\delta = 25$–50 ppm.

[10] The main coordination modes of BPh_4^- and its derivatives have been reviewed: a) S. H. Strauss, *Chem. Rev.* **1993**, *93*, 927; b) M. Bochmann, *Angew. Chem.* **1992**, *104*, 1206; *Angew. Chem. Int. Ed. Engl.* **1992**, *31*, 1181.

[11] For examples of the various coordination modes encountered in complexes bearing BPh_4^- fragments, see: η^6-coordination: a) D. C. Ware, M. M. Olmstead, R. Wang, T. Henry, *Inorg. Chem.* **1996**, *35*, 2576; b) R. F. Winter, F. M. Hornung, *Inorg. Chem.* **1997**, *36*, 6197; c) M. Manger, J. Wolf, M. Laubender, M. Teichert, D. Stalke, H. Werner, *Chem. Eur. J.* **1997**, *3*, 1442; d) H. Werner, M. Manger, U. Schmidt, M. Laubender, B. Webern-doerfer, *Organometallics* **1998**, *17*, 2619; e) F. Torres, E. Sola, M. Martin, C. Ochs, G. Picazo, J. A. Lopez, F. J. Lahoz, L. A. Oro, *Organometallics* **2001**, *20*, 2716; η^2-coordination: f) M. Pasquali, C. Floriani, A. Gaetani-Manfredotti, *Inorg. Chem.* **1980**, *19*, 1191; g) A. D. Horton, J. H. G. Frijns, *Angew. Chem.* **1991**, *103*, 1181; *Angew. Chem. Int. Ed. Engl.* **1991**, *30*, 1152; h) W. J. Evans, C. A. Seibel, J. W. Ziller, *J. Am. Chem. Soc.* **1998**, *120*, 6745; η^1-, η^2-, and η^4-coordination: i) G. B. Deacon, C. M. Forsyth, *Chem. Commun.* **2002**, 2522.

[12] Multiple searches of the CCSD (up to August 6, 2005) did not lead to any complex in which one of the Ph rings of BPh_4^- is coordinated to two or more metal centers. These searches also indicated that complex **3** is the first instance of a Ni complex bearing a coordinated $[PhBPh_3]^-$.

[13] The following complexes featuring $\mu(\eta^2{:}\eta^2)$-arene ligands coordinated through nonadjacent C=C bonds have been reported: a) $[\{(t\text{Bu}_3\text{SiO})_3\text{Ta}\}_2(\mu,\eta^2{:}\eta^2\text{-}C_6H_6)]$ (D. R. Neithamer, L. Párkányi, J. F. Mitchell, P. T. Wolczanski, *J. Am. Chem. Soc.* **1988**, *110*, 4421); b) $\{AgN(SO_2F)_2(C_6H_6)\}_n$ (M. J. Begley, D. B. Sowerby, R. D. Verma, A. Vig, *J. Organomet. Chem.* **1994**, *481*, 243); c) $[\{Fe(CO)_3\}_2\{\mu,\eta^2{:}\eta^2\text{-}1,4\text{-}(CH_2NPh)_2\text{-}3,6\text{-}\eta^1,\eta^1\text{-}\{Fe(CO)_3\}_2\text{-}C_6H_2\}]$ (W. Imhof, A. Göbel, *J. Organomet. Chem.* **2000**, *610*, 102); d) $[Pd_2(GaBr_4)_2\{\mu(\eta^2{:}\eta^2\text{-arene})\}_2]$ (M. Gorlov, A. Fischer, L. Kloo, *J. Organomet. Chem.* **2004**, *689*, 489).

[14] Structural simulations have shown that rotating the borate anion in such a way as to orient a 1,3-diene moiety of the μ-$PhBPh_3$ ligand towards the Ni atoms results in significant steric interactions between the Ph groups of the PPh_3 ligand and the borate anion. The authors are grateful to Prof. F. Schaper for carrying out these simulations.

[15] For comparison, values of about 20° and 43° have been reported for the corresponding fold angles in the complexes $[Cp_2V_2(\mu\text{-}H)_2(\mu\text{-}Ph)]$ (K. Jonas, V. Wiskamp, Y.-H. Tsay, C. Krüger, *J. Am. Chem. Soc.* **1983**, *105*, 5480) and $[Cp_2Fe_2(\mu\text{-}C_6R_6)]$ (K. Jonas, G. Koepe, L. Schieferstein, R. Mynott, C. Krüger, Y.-H. Tsay, *Angew. Chem.* **1983**, *95*, 637; *Angew. Chem. Int. Ed. Engl.* **1983**, *22*, 620).

[16] For a comprehensive review on the various bonding modes observed in μ-arene complexes, see: H. Wadepohl, *Angew. Chem.* **1992**, *104*, 253; *Angew. Chem. Int. Ed. Engl.* **1992**, *31*, 247.

[17] I. Bach, K.-R. Pörschke, R. Goddard, C. Kopiske, C. Krüger, A. Rufinska, K. Seevogel, *Organometallics* **1996**, *15*, 4959.

[18] To our knowledge, the only other μ-arene complexes of Ni for which structural data are available are triple-decker complexes that involve, respectively, η^6- and $\eta^3{:}\eta^3$-arene ligands: a) J. L. Priego, L. H. Doerrer, L. H. Rees, M. L. H. Green, *Chem. Commun.* **2000**, 779; b) J. J. Schneider, D. Spickermann, D. Bläser, R. Boese, P. Rademacher, T. Labahn, J. Magull, C. Janiak, N. Seidel, K. Jacob, *Eur. J. Inorg. Chem.* **2001**, 1371; for the structure of a Ni dimer bridged by a novel benzdiyne ligand, $(\mu\text{-}C_6H_2)$, see: M. A. Bennett, J. S. Drage, K. D. Griffiths, N. K. Roberts, G. B. Robertson, W. A. Wickramasinghe, *Angew. Chem.* **1988**, *100*, 1002; *Angew. Chem. Int. Ed. Engl.* **1988**, *27*, 941.

[19] The Ni–Ni bond length of 2.4471(11) Å in **3** is within the expected range of 2.30–2.50 Å found in related Ni^I–Ni^I dimers: a) B. L. Barnett, C. Krüger, Y. H. Tsay, *Chem. Ber.* **1977**, *110*, 3900; b) R. A. Jones, A. L. Stuart, J. L. Atwood, W. E. Hunter, R. D. Rogers, *Organometallics* **1982**, *1*, 1721; c) R. Hanko, *Angew. Chem.* **1985**, *97*, 707; *Angew. Chem. Int. Ed. Engl.* **1985**, *24*, 704; d) M. J. Tenorio, M. C. Puerta, P. Valerga, *J. Chem. Soc. Dalton Trans.* **1996**, 1305; e) M. D. Fryzuk, G. K. B. Clentsmith, D. B. Leznoff, S. J. Rettig, S. J. Geiib, *Inorg. Chim. Acta* **1997**, *265*, 169–177; f) C. E. Kriley, C. J. Woolley, M. K. Krepps, E. M. Popa, P. E. Fanwick, I. P. Rothwell, *Inorg. Chim. Acta* **2000**, *300–302*, 200.

[20] L. Zhu, N. M. Kostic, *Organometallics* **1988**, *7*, 665.

 © 2005 Wiley-VCH Verlag GmbH & Co. KGaA, Weinheim

[21] a) D. R. Fahey, J. E. Mahan, *J. Am. Chem. Soc.* **1976**, *98*, 4499; b) P. E. Garrou, *Chem. Rev.* **1985**, *85*, 171; c) R. A. Dubois, P. E. Garrou, *Organometallics* **1989**, *8*, 466; d) H. Omori, H. Suzuki, Y. Take, Y. Moro-oka, *Organometallics* **1989**, *8*, 2270.
[22] M. Sommovigo, M. Pasquali, P. Leoni, D. Braga, P. Sabatino, *Chem. Ber.* **1991**, *124*, 97.
[23] For a discussion of this type of rearrangements in indenes, see: a) M. Stradiotto, P. Hazendonk, A. D. Bain, M. A. Brook, M. J. McGlinchey, *Organometallics* **2000**, *19*, 590; b) M. Stradiotto, M. J. McGlinchey, *Coord. Chem. Rev.* **2001**, *219–221*, 311.
[24] For an example of a Ni^{I}–Ni^{I} dimer formed from the reaction of Ni^{0} and Ni^{II} precursors, see ref. [19c]. For the analogous formation of Pd^{I}–Pd^{I} dimers, see: T. Murahashi, H. Kurosawa, *Coord. Chem. Rev.* **2002**, *231*, 207.
[25] a) J. P. Stambouli, R. Kuwano, J. F. Hartwig, *Angew. Chem.* **2002**, *114*, 4940; *Angew. Chem. Int. Ed.* **2002**, *41*, 4746; b) M. Prashad, X. Y. Mak, Y. Liu, O. Repic, *J. Org. Chem.* **2003**, *68*, 1163; c) U. Christmann, R. Vilar, A. J. P. White, D. J. Williams, *Chem. Commun.* **2004**, 1294.

 © 2005 Wiley-VCH Verlag GmbH & Co. KGaA, Weinheim

Immunochemistry

DOI: 10.1002/anie.200502179

Thiooligosaccharide Conjugate Vaccines Evoke Antibodies Specific for Native Antigens**

David R. Bundle, Jamie R. Rich, Sandra Jacques, Henry N. Yu, Mark Nitz, and Chang-Chun Ling*

Conjugate vaccines composed of polysaccharides or oligosaccharides covalently linked to immunogenic proteins successfully overcome the limitations of pure polysaccharide antigens, which are classical T-cell-independent antigens.[1] To date, the use of oligosaccharides to provide the recognition element of such conjugate vaccines has largely been limited to experimental, proof of concept investigations, whereas polysaccharide conjugates are successfully employed in efficacious vaccination strategies against life-threatening bacterial infections.[1–3] Intensive efforts are directed toward the synthesis and evaluation of glycopeptide and glycolipid vaccines that present tumour-associated carbohydrate antigens,[4–6] the epitopes of which may contain glycosidic linkages that are potentially susceptible to endogenous glycosyl hydrolases, for example, ganglioside-specific plasma-membrane sialidase.[7–9] Such structural features include, but are not limited to, terminal sialyl residues, the loss of which would destroy crucial recognition elements. A method for the formation of glycosidic linkages that are resistant to enzymatic or acid hydrolysis in vivo has been proposed; C-glycosides are one class of compound that has received attention.[10–12] Herein we present data for four distinct antigen systems that show, for the first time, conjugate vaccines constructed from oligosaccharides that contain a thioglycosidic linkage function as well as antigens that induce antibodies specific for O-linked oligosaccharides.

The choice of sulfur (over atoms such as carbon) to replace oxygen at the glycosidic center was based on three considerations: the ease of synthesis,[13] the existence of well-documented examples with a similar conformational preference about the thioglycosidic and aglyconic bonds both when in solution and when complexed with a protein,[14–17] and significantly lower susceptibility to enzymatic and acid hydrolysis.[18,19] Although the sulfur–carbon bond is longer than the carbon–oxygen single bond, the C–S–C bond angle is significantly smaller than the C–O–C angle, which often results in relatively small differences between the position of the carbon atoms of the glycosidic linkage.[20] However, the longer bonds and weaker stereoelectronic effect that result when oxygen is replaced with sulfur allow substantially greater flexibility.

This flexibility creates a potential obstacle to the use of thioglycoside immunogens. S-Glycosidic bonds are less constrained than the corresponding O-glycosides and can access the higher energy anti conformation in the unbound and bound state more readily. In the search for effective protective carbohydrate epitopes, it remains an open question as to whether such conformational flexibility would preclude the effective use of antigenic determinants that contain metabolically stable S-linkages. Although the structural similarity of O- and S-linked oligosaccharides is critical to this concept, their differences may also identify S-glycosides as non-self antigens and thus further enhance their immunogenicity.

To investigate the immunochemistry of S-linked oligosaccharides, we initially considered two microbial antigens and subsequently two tumour-associated ganglioside antigens (Scheme 1), in which the existence of a potentially labile sialoside linkage might account for the poor immune response toward synthetic conjugate vaccines. Amine-terminated saccharides were coupled to bovine serum albumin (BSA) or tetanus toxoid (TT) by using either of the squarate or adipate homobifunctional linkers shown in Scheme 2.[21,22] Protein

[*] Prof. Dr. D. R. Bundle, J. R. Rich, S. Jacques, Dr. H. N. Yu,[+] Dr. M. Nitz,[++] Dr. C.-C. Ling
Alberta Ingenuity Centre for Carbohydrate Science
Department of Chemistry, University of Alberta
Edmonton, AB, T6G 2G2 (Canada)
Fax: (+1) 780-492-7705
E-mail: dave.bundle@ualberta.ca

[+] Current address:
Serono Research Institute
One Technology Place, Rockland, MA 02370 (USA)

[++] Current address:
Department of Chemistry, University of Toronto
80 George Street, Toronto, ON, M5S 3H6 (Canada)

[**] We thank Mrs. Joanna Sadowska for performing ELISA experiments. S.J. was supported by a graduate scholarship from the Fond de la recherche en santé du Québec, and J.R. thanks the Natural Sciences and Engineering Research Council and Alberta Heritage Foundation for Medical Research graduate studentships. This work was supported by funds from the NSERC and the Alberta Ingenuity Centre for Carbohydrate Science.

Supporting information for this article is available on the WWW under http://www.angewandte.org or from the author.

 © 2005 Wiley-VCH Verlag GmbH & Co. KGaA, Weinheim

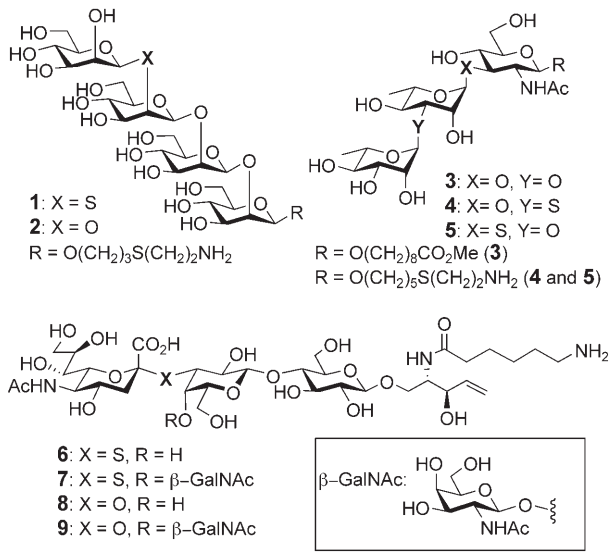

Scheme 1. S- and O-linked synthetic carbohydrate antigens described herein.

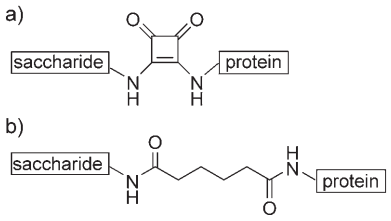

Scheme 2. Linkers used in the preparation of glycoconjugates: a) squarate linker and b) adipate homobifunctional linker.

conjugates of the O-glycosides, and for the first time S-glycosides, were evaluated for their ability to induce an antibody response. The antisera from each immunogen was then screened for binding to the immunizing and heteroatom-substituted oligosaccharides that were coupled to a heterologous protein carrier. In general, the S-glycosides induced high titer sera containing carbohydrate-specific immunoglobulin (Ig) and produced a class switch to the IgG isotype, which is associated with the development of immunological memory. Typically, the sera derived from either class of oligosaccharide displayed a similar affinity for the heterologous and homologous oligosaccharides.

Monoclonal antibodies specific for the β-1,2-mannan component of phospomannan and phospholipomannan homopolymers present in the cell wall of *Candida albicans*, protect mice against disseminated and vaginal candidiasis.[23–25] The minimal protective epitope appears to be a β-1,2-linked mannose trisaccharide.[26] Trisaccharide–TT conjugates are highly immunogenic in rabbits and bind to phospomannan when it is part of the cell wall.

Conjugation of oligosaccharides **1** and **2** to TT and BSA provided glycoconjugates for use as immunogens and ligands for ELISA screening (Table 1).[27] The results for the titrations of sera from rabbits, immunized with **10** or **12**, against a crude *C. albicans* cell-wall extract were comparable. The sera of

Table 1: Glycoconjugates for immunization and screening.

Conjugate	Oligosaccharide	Protein	Linker	n[a]
10	**1**(*S*)	TT	squarate	33
11	**1**(S)	BSA	squarate	15
12	**2**(O)	TT	squarate	28
13	**2**(O)	BSA	squarate	13
14	**3**(O)	BSA	see [29]	42
15	**4**(S)	BSA	squarate	6
16	**5**(S)	BSA	squarate	7
17	**6**(S)	TT	adipate	8
18	**6**(S)	BSA	squarate	5
19	**7**(S)	TT	adipate	8
20	**7**(S)	BSA	squarate	3
21	**8**(O)	TT	adipate	6
22	**8**(O)	BSA	squarate	10
23	**9**(O)	TT	adipate	7
24	**9**(O)	BSA	squarate	6

[a] n = incorporation.

rabbits immunized with **12** had a titre that was approximately tenfold higher than the sera from rabbits immunized with the corresponding S-linked antigen **10**, when screened against the *C. albicans* cell wall extract. Sera raised against **10** exhibited titer volumes that exceeded 1:100 000 demonstrating clearly that carbohydrate-specific antibodies to the thioglycoside cross-react with O-glycosides (Figure 1). Polyclonal sera

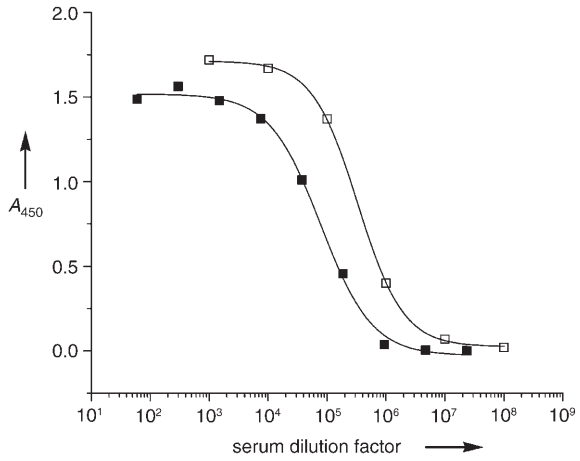

Figure 1. Titration of rabbit sera against *C. albicans* cell-wall extracts. Sera are derived from S tetrasaccharide conjugate **10** (■) and O trisaccharide conjugate **12** (□). Data are averaged for two rabbits.

raised against the thiotetrasaccharide–TT conjugate **10** and the O-linked congener **12** were titrated against the corresponding BSA conjugates **11** and **13**. These data obtained with chemically defined antigens not only show production of high titer sera, but also confirm that the S-linked antigen **11** is recognized by antibodies that are produced in response to the corresponding O-linked immunogen **12**. Furthermore, the O-linked antigen **13** is bound tightly by antibodies induced by the S-linked immunogen **10** (Figure 2).

A lipopolysaccharide (LPS) O antigen provides the second proof of concept. Variant Y *Shigella flexneri* O poly-

 © 2005 Wiley-VCH Verlag GmbH & Co. KGaA, Weinheim

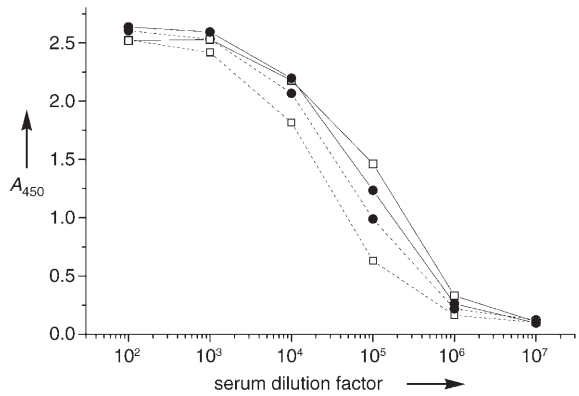

Figure 2. Titration of rabbit sera, obtained after immunization with either **10** (-----) or **12** (——), against immobilized BSA conjugates **11** (□) and **13** (●). Data are averaged for two rabbits.

saccharide has a linear tetrasaccharide repeat [→2)α-L-Rha*p*(1→2)-α-L-Rha*p*(1→3)-α-L-Rha*p*(1→3)-β-D-GlcNAc*p*(1→]. Binding studies with a monoclonal antibody SYA/J6 has identified the trisaccharide α-L-Rha*p*(1→3)-α-L-Rha*p*(1→3)-β-D-GlcNAc*p* as the minimal recognition epitope. This trisaccharide was synthesized as the O-linked structure **3** and as two monothiooligosaccharide analogues, **4** and **5**.[28–30] BSA conjugates of the three trisaccharides were prepared, and murine sera derived from immunization with each trisaccharide–BSA conjugate **14**–**16** (Table 1) were titrated against purified LPS that had been extracted from the parent *S. flexneri* bacteria (Figure 3). Recognition of LPS

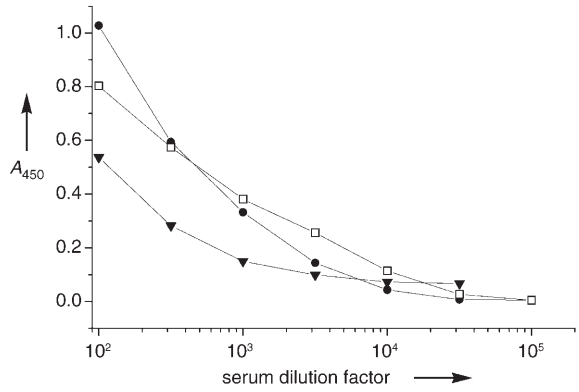

Figure 3. Binding of antibodies from polyclonal sera, derived by immunization with conjugates **14** (▼), **15** (□), and **16** (●), to immobilized *S. flexneri* LPS. Data are averaged for groups of five mice.

by immune sera derived from S-linked oligosaccharides is (represented by specific IgG) to S-glycosides appears equivalent, if not superior, to the response to O-glycosides as judged by the antibody recognition of native LPS. Consistent with these observations, antibodies to the conjugates **15** and **16** were also shown to bind the trisaccharides **4** and **5** and the tetrasaccharide α-L-Rha*p*(1→3)-α-L-Rha*p*(1→3)-β-D-GlcNAc*p*(1→2)-α-L-Rha*p* when they were immobilized on microtiter plates by noncovalent adsorption (data not shown).

Aberrant expression of gangliosides on malignant cells has highlighted the potential of these glycolipids to serve as antigens in cancer immunotherapy.[4,6] Both the trisaccharide GM_3 (α-Neu5Ac-(2→3)-β-Gal-(1→4)-β-Glc-(1→1)-ceramide) and the tetrasaccharide GM_2 (α-Neu5Ac-(2→3)-[β-GalNAc-(1→4)]-β-Gal-(1→4)-β-Glc-(1→1)-ceramide) are considered promising vaccine targets, yet their status as self-molecules and their correspondingly poor immunogenicity have hampered progress toward the development of a successful conjugate vaccine. Although endogenous enzyme hydrolysis of GM_2 is not a concern, at least in serum, extracellular enzymatic degradation of GM_3 is known.[7] We have modified the common terminal glycosidic linkage of GM_3 and GM_2 by replacement of the interresidue oxygen atom with sulfur to give the ganglioside analogues for use as antigens with potentially enhanced immunogenicity. The thiogangliosides **6** and **7**[31] and their O-linked counterparts **8** and **9**[32] bear a truncated ceramide aglycon for coupling to proteins.

The in vivo immunogenicity of ganglioside glycoconjugates (Table 1) was evaluated by ELISA. Immunization of BALB/C mice with TT conjugates (**17** and **21**) of the S- and O-linked GM_3 analogues **6** and **8** yielded a carbohydrate-specific IgG response in three out of five mice. Sera derived from either immunogen were found to cross-react with the homo- and heterosubstituted counterparts **18** and **22** (Figure 4). The

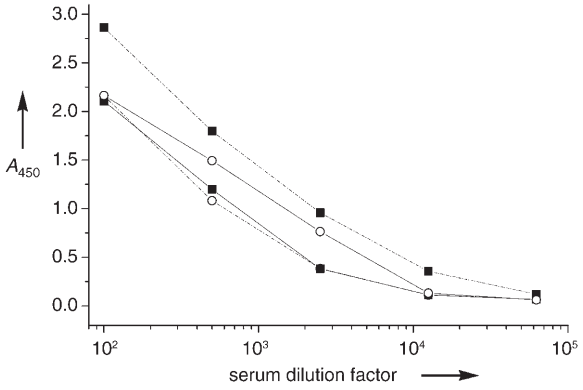

Figure 4. Binding to immobilized **22** (○) and **18** (■) by murine IgG generated from immunization of mice with **21** (——) or **17** (-----). Data are averaged for three mice from each group.

S-linked conjugate **17** was the more immunogenic of the two GM_3 analogues when screened against the immunizing carbohydrate. Cross-reactivity of these antisera with the O-glycoside was further supported by its unambiguous recognition of a α-Neu5Ac-(2→3)-β-Gal-BSA–disaccharide conjugate (see Supporting Information). Furthermore, binding of the same sera to glycoconjugate **22** could be inhibited by the addition of synthetic O-linked oligosaccharides **25** and **26** (Figure 5).[31]

Immunization with the S-GM_2–TT conjugate **19** also generated a strong carbohydrate-specific IgG response, although recognition of the immobilized glycoconjugates was restricted to the S-linked GM_2 analogue **20**. In contrast, sera to the related O-GM_2–TT conjugate **23** bound both O-

 © 2005 Wiley-VCH Verlag GmbH & Co. KGaA, Weinheim

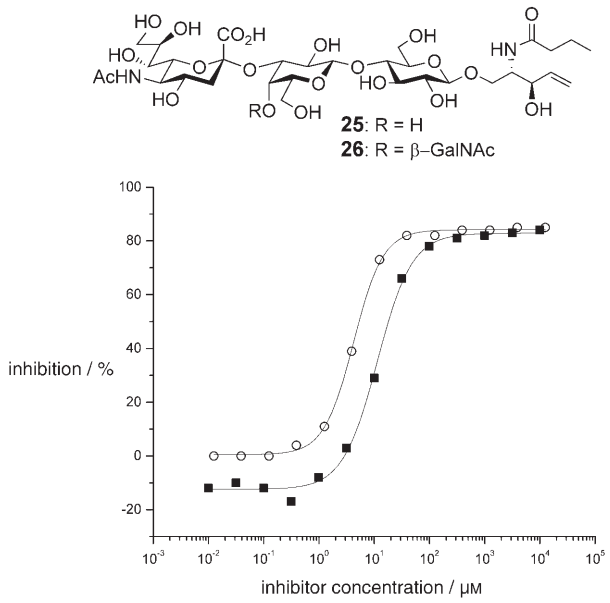

Figure 5. Synthetic oligosaccharides **25** (○) and **26** (■) inhibit the binding of polyclonal sera (IgG) against conjugate **17** to immobilized **22**. IC_{50} values were determined to be 4.2 μM (**25**) and 11.3 μM (**26**).

and S-glycosides and demonstrated equivalent or superior binding of the heterologous oligosaccharide (see Supporting Information). The apparent incongruity in the response to thioimmunogens **17** and **21**, evident in the inability of antibodies to S-GM_2 to recognize the O-glycoside, can be rationalized in terms of the flexibility of the thioglycosidic linkage in **7**. Although the *exo* anomeric effect would be expected to hold the O-linked GalNAc residue in its preferred family of low-energy conformations, the S-linked Neu5Ac should be less constrained and any steric demands imposed by vicinal substitution could be relieved by adoption of conformations that might not be populated as readily by O-linked GM_2.

S-linked immunogens, as components of conjugate vaccines, clearly generate an antigen-specific immune response that approaches (**10** and **19**) or exceeds (**15**, **16**, and **17**) the response to the native oligosaccharide. With the exception of antigens that have terminal, vicinal-branching residues (**19**), antibodies against S-glycosides demonstrate a clear cross-reactivity with the O-glycosides, which suggests a certain degree of conformational similarity. In the systems studied, superior or equivalent recognition of a heterologous oligosaccharide was demonstrated for either the O- or S-linked immunogens or both. The recognition of S-glycosides by sera derived from the native antigens may be explained by the flexibility of the thioglycosidic linkage, which may allow for an induced fit.

We have shown for the first time that carbohydrate epitopes of conjugate vaccines may be modified to contain S-linked residues and that immune responses to such vaccines are of comparable magnitude in terms of antibody titer. Furthermore, the specificity of these antibodies exhibits only a modest loss of fidelity with respect to recognition of the native O-linked epitope. We anticipate that antigens bearing critical residues attached through hydrolysis-resistant linkages will find application either in active immunotherapy or as ligands for immunoabsorption of pathological antiganglioside antibodies present in the sera of patients with certain autoimmune neuropathies.[33]

Received: June 22, 2005
Published online: November 8, 2005

Keywords: antibodies · carbohydrates · conjugate vaccines · glycoconjugates · glycosides

[1] G. Ada, D. Isaacs, *Clin. Microbiol. Infect.* **2003**, *9*, 79.
[2] V. Fernandez-Santana, F. Cardoso, A. Rodriguez, T. Carmenate, L. Pena, Y. Valdes, E. Hardy, F. Mawas, L. Heynngnezz, M. C. Rodriguez, I. Figueroa, J. N. Chang, M. E. Toledo, A. Musacchio, I. Hernandez, M. Izquierdo, K. Cosme, R. Roy, V. Verez-Bencomo, *Infect. Immun.* **2004**, *72*, 7115.
[3] D. H. Dube, C. R. Bertozzi, *Nat. Rev. Drug Discovery* **2005**, *4*, 477.
[4] C. Musselli, P. O. Livingston, G. Ragupathi, *J. Cancer Res. Clin. Oncol.* **2001**, *127 Suppl 2*, R20.
[5] S. Dziadek, C. G. Espinola, H. Kunz, *Aust. J. Chem.* **2003**, *56*, 519.
[6] P. Fredman, K. Hedberg, T. Brezicka, *BioDrugs* **2003**, *17*, 155.
[7] N. Papini, L. Anastasia, C. Tringali, G. Croci, R. Bresciani, K. Yamaguchi, T. Miyagi, A. Preti, A. Prinetti, S. Prioni, S. Sonnino, G. Tettamanti, B. Venerando, E. Monti, *J. Biol. Chem.* **2004**, *279*, 16989.
[8] J. Kopitz, C. Oehler, M. Cantz, *FEBS Lett.* **2001**, *491*, 233.
[9] T. Miyagi, T. Wada, K. Yamaguchi, K. Hata, *Glycoconjugate J.* **2004**, *20*, 189.
[10] D. Urban, T. Skrydstrup, J.-M. Beau, *Chem. Commun.* **1998**, 955.
[11] B. Kuberan, S. A. Sikkander, H. Tomiyama, R. J. Linhardt, *Angew. Chem.* **2003**, *115*, 2119; *Angew. Chem. Int. Ed.* **2003**, *42*, 2073.
[12] L. Loay, J. Riedner, P. Vogel, *Chem. Eur. J.* **2005**, *11*, 3565.
[13] J. K. Fairweather, H. Driguez, in *Carbohydrates in Chemistry and Biology, Vol. 1* (Eds.: B. Ernst, G. W. Hart, P. Sinay), Wiley-VCH, Weinheim, **2000**, pp. 531.
[14] E. Montero, M. Vallmitjana, J. A. Perez-Pons, E. Querol, J. Jimenez-Barbero, F. J. Canada, *FEBS Lett.* **1998**, *421*, 243.
[15] E. Montero, A. Garcia-Herrero, J. L. Asensio, K. Hirai, S. Ogawa, F. Santoyo-Gonzalez, F. J. Canada, J. Jimenez-Barbero, *Eur. J. Org. Chem.* **2000**, 1945.
[16] B. Aguilera, J. Jimenez-Barbero, A. Fernandez-Mayoralas, *Carbohydr. Res.* **1998**, *308*, 19.
[17] T. Weimar, U. C. Kreis, J. S. Andrews, B. M. Pinto, *Carbohydr. Res.* **1999**, *315*, 222.
[18] J. Defaye, J. Gelas, in *Studies in Natural Products Chemistry, Vol. 8* (Ed.: Atta-ur-Rahman), Elsevier, Oxford, **1991**, p. 315.
[19] J. C. Wilson, M. J. Kiefel, D. I. Angus, M. von Itzstein, *Org. Lett.* **1999**, *1*, 443.
[20] H. Yuasa, H. Hashimoto, *Trends Glycosci. Glycotechnol.* **2001**, *13*, 31.
[21] L. F. Tietze, C. Schroter, S. Gabius, U. Brinck, A. Goerlachgraw, H. J. Gabius, *Bioconjugate Chem.* **1991**, *2*, 148.
[22] X. Y. Wu, C. C. Ling, D. R. Bundle, *Org. Lett.* **2004**, *6*, 4407.
[23] Y. Han, M. H. Riesselman, J. E. Cutler, *Infect. Immun.* **2000**, *68*, 1649.
[24] Y. Han, J. E. Cutler, *J. Infect. Dis.* **1997**, *175*, 1169.
[25] Y. Han, J. E. Cutler, *Infect. Immun.* **1995**, *63*, 2714.
[26] M. Nitz, C. C. Ling, A. Otter, J. E. Cutler, D. R. Bundle, *J. Biol. Chem.* **2002**, *277*, 3440.
[27] M. Nitz, D. R. Bundle, *J. Org. Chem.* **2001**, *66*, 8411.

 © 2005 Wiley-VCH Verlag GmbH & Co. KGaA, Weinheim

[28] D. R. Bundle, S. Josephson, *Carbohydr. Res.* **1980**, *80*, 75.
[29] B. M. Pinto, D. R. Bundle, *Carbohydr. Res.* **1983**, *124*, 313.
[30] H. N. Yu, PhD thesis, University of Alberta, **2002**.
[31] J. R. Rich, W. W. Wakarchuk, D. R. Bundle, *Chem. Eur. J.* 2006, in press, DOI: 10.1002/chem.200500518.
[32] S. Jacques, J. R. Rich, C. -C. Ling, D. R. Bundle, *Org. Biomol. Chem.* **2005**, in press.
[33] S. M. Andersen, C. C. Ling, P. Zhang, K. Townson, H. J. Willison, D. R. Bundle, *Org. Biomol. Chem.* **2004**, *2*, 1199.

 © 2005 Wiley-VCH Verlag GmbH & Co. KGaA, Weinheim

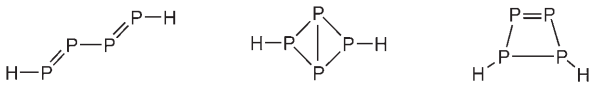

A B C

Scheme 1.

1,3-Butadiene Analogues

DOI: 10.1002/anie.200502865

$Tl_2[Aryl_2P_4]$: A Thallium Complexed Diaryltetraphosphabutadienediide and its Two-Electron Oxidation to a Diaryltetraphosphabicyclobutane, $Aryl_2P_4$**

*Alexander R. Fox, Robert J. Wright, Eric Rivard, and Philip P. Power**

The synthesis and characterization of multiply bonded heavier main group element compounds is a major area of interest in organometallic chemistry.[1] A primary focus of this work has been the stabilization of homonuclear multiply bonded dimeric species of the heavier group 13, 14, and 15 elements and the study of their reactivity.[2] More recently this has led to the stabilization of multinuclear conjugated heavier element arrays containing more than two multiply bonded heavier elements.[3] For example, Weidenbruch and co-workers have prepared silicon[3a] and germanium[3b] analogues of 1,3-butadiene with the use of bulky triisopropylphenyl substituents and have been shown by spectroscopy that they display conjugation. However, the corresponding tetraphosphabutadienes (P_4R_2) and heavier group 15 congeners have not been isolated.[4] Calculations on three parent P_4H_2 isomers (**A**–**C**, Scheme 1) revealed that the tetraphosphabutadiene (**A**) is ca. 20 kcal mol^{-1} less stable than the tetraphosphacyclobutane isomer **B**, while the tetraphosphacyclobutene isomer **C** is 10.7 kcal mol^{-1} less stable than **B**.[5]

The prediction that **A** is the least stable isomer suggests that the preparation of substituted analogues of **A** is a formidable challenge. We were led to consider the existence of stable species with structural frameworks related to **A** during the investigations of reactions of the recently reported "dithallene"[2a] $(TlAr^{Dipp_2})_2$ ($Ar^{Dipp_2} = C_6H_3$-2,6-(C_6H_2-2,6-iPr$_2$)$_2$) with white phosphorus.[6] We now report that the reaction of the weakly dimerized "dithallene" $(TlAr^{Dipp_2})_2$ with P_4 results in aryl group transfer to phosphorus to afford $Tl_2[P_4(Ar^{Dipp_2})_2]$ (**1**), a thallium salt of the diaryltetraphosphabutadienediide, which is a doubly reduced analogue of **A** [Eq. (1)]. Furthermore, we describe the facile two-electron oxidation of **1** by I_2 to yield the neutral diaryltetraphosphabicyclobutane, $P_4(Ar^{Dipp_2})_2$ (**2**), a substituted analogue of **B** [Eq. (2)].

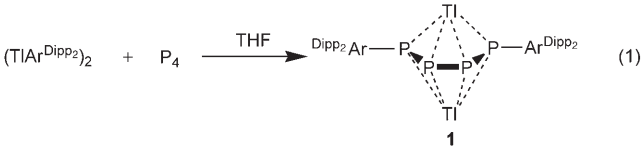

(1)

1

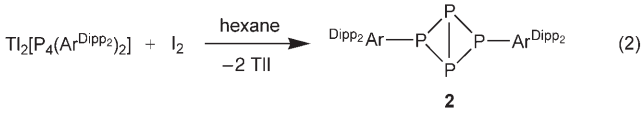

(2)

2

Reaction of $(TlAr^{Dipp_2})_2$ with P_4 in THF and subsequent recrystallization from hexane yielded **1** as burgundy crystals in 40 % yield. Complex **1** was characterized by ^{1}H, ^{13}C, ^{31}P, and $^{203/205}$Tl NMR spectroscopy, UV/Vis spectroscopy, and single-crystal X-ray crystallography. The structure[7a] of **1** (Figure 1) revealed a planar C(1)-P(1)-P(2)-P(2A)-P(1A)-C(1A) dianionic core with a *cis* conformation which is complexed to Tl(1) and Tl(1A) ions disposed equidistant above and below the P_4C_2 array (Tl–P distances 3.032(3)–3.168(3) Å). The Tl^I centers also interact with the flanking Dipp substituents of Ar^{Dipp_2} (Tl–centroid distances are 3.290(3) and 3.204(3) Å).

The Tl–centroid distances in **1** are greater than those in $[(Mes)_6Tl_4(GaBr_4)_4]$[8a] (2.94–3.03 Å), $TlN(Me)Ar^{Mes_2}$[8b] (3.03 Å), and $[Tl\{N[C(C_3F_7)N(Ar)]_2\}]$[8c] (ca. 3.0 Å; Ar = Mes or Dipp) and are substantially greater than the Tl–centroid distances (2.49 Å) observed in the dimer $[C_5(CH_2Ph)_5Tl]_2$.[2b] Calculated Tl–arene interaction energies vary from very weak (ca. 3 kcal mol^{-1})[8b] to relatively strong (ca. 20 kcal mol^{-1})[8c] depending on the model.[9] The Tl–arene interaction energies in **1** are probably weak, however, they may be responsible for the *cis* conformation. The P–P distances in **1** are almost identical (P(1)–P(2) 2.136(4); P(2)–P(2A) 2.143(6) Å) and lie between those observed in doubly-bonded diphosphenes[10] (1.98–2.05 Å) and typical P–P single bonds[11] (ca. 2.21 Å).

[*] A. R. Fox, R. J. Wright, Dr. E. Rivard, Prof. P. P. Power
Department of Chemistry
University of California
One Shields Avenue, Davis, CA 95616 (USA)
Fax: (+1) 530-752-8995
E-mail: pppower@ucdavis.edu

[**] The authors thank the National Science Foundation for financial support. E.R. thanks NSERC of Canada for a Postdoctoral Fellowship. We also thank Professor M. M. Olmstead and Dr. J. de Ropp for assistance with crystallographic and NMR spectroscopic studies.

 © 2005 Wiley-VCH Verlag GmbH & Co. KGaA, Weinheim

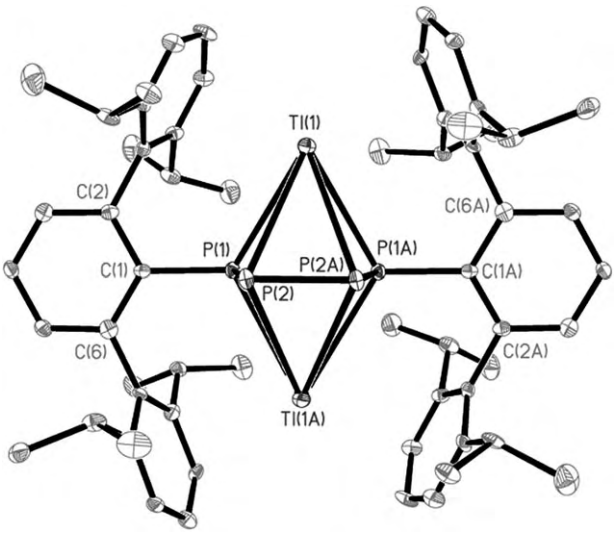

Figure 1. Thermal ellipsoid (30%) plot of **1**. H atoms are not shown for clarity. Selected bond lengths [Å] and angles [deg]: P(1)–C(1) 1.868(11), P(1)–P(2) 2.136(4), P(2)–P(2A) 2.143(6), Tl(1)–P(1) 3.066(3), Tl(1)–P(1A) 3.032(3), Tl(1)–P(2) 3.168(3), Tl(1)–P(2A) 3.144(3); C(1)-P(1)-P(2) 100.7(3), P(1)-P(2)-P(2A) 101.75(10), C(1)-P(1)-Tl(1) 120.9(3), C(1)-P(1)-Tl(1A) 117.8(3).

The ^{205}Tl NMR spectrum of **1** consisted of a broad signal (1750 Hz at half height) at ca. 2730 ppm, which is within the range observed for Tl^{I} compounds.[12] There is a pair of satellite signals ($^{2}J_{^{205}Tl,^{203}Tl} \approx 12000$ Hz) arising from coupling to the ^{203}Tl isotope (Figure 2). A pseudo-quintet pattern is superimposed on the three broad signals, which presumably results from the similar $^{1}J_{^{205}Tl,P(1)}$ and $^{1}J_{^{205}Tl,P(2)}$ coupling constants of ca. 500 Hz. The ^{203}Tl NMR spectrum consists of the same pseudo-quintet pattern, with a pair of ^{205}Tl satellite signals ($^{2}J_{^{203}Tl,^{205}Tl} \approx 12000$ Hz). However, because of the greater abundance of the ^{205}Tl isotope (^{203}Tl 29.5%, ^{205}Tl 70.5%), the ^{205}Tl satellite signals are larger. The large size of the $^{2}J_{^{205}Tl,^{203}Tl}$ coupling constant (ca. 12000 Hz) in both spectra is noteworthy.[13] The pseudo quintet displayed in the Tl NMR spectra indicates that the association of the thallium ions and the P_4 array is preserved in solution.

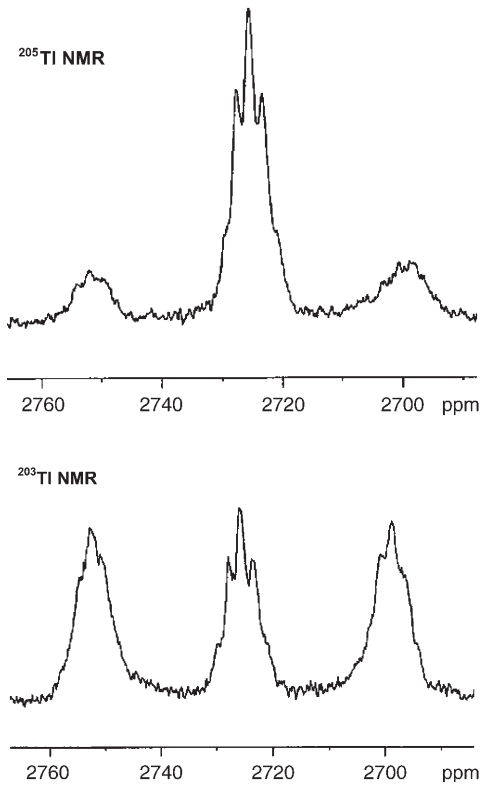

Figure 2. ^{205}Tl and ^{203}Tl NMR spectra of **1**.

The ^{31}P NMR spectrum revealed two broad multiplets (width at half height ca. 850 Hz) at 280 and 185 ppm, likely due to $^{1}J_{P,P}$, $^{1}J_{^{205}Tl,P}$, and $^{1}J_{^{203}Tl,P}$ coupling. Variable-temperature spectroscopy in the range −90 to 60 °C did not allow for extraction of specific coupling constants. The UV/Vis spectrum displayed three intense absorptions at 322, 432, and 546 nm ($\varepsilon = 1000$–$13000\ mol^{-1}\,L\,cm^{-1}$), where the longer-wavelength absorptions are probably due to the orbitally allowed $\pi \rightarrow \pi^*$ and $n \rightarrow \pi^*$ transitions.

Compound **1** is a thallium complexed diaryltetraphosphabutadienediide and can formally be derived from the two-electron reduction of the neutral diaryltetraphosphabutadiene. This affords a 6π system where two bonding forms are possible: the negative charge can be localized on the terminal phosphorus atoms (**I**) or the negative charge can be delocalized over the entire P_4 unit (**II**) (Scheme 2).

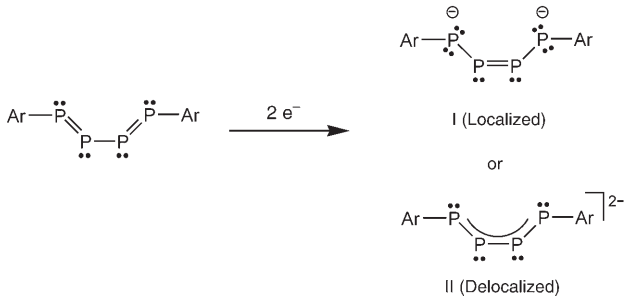

Scheme 2.

The isolated dianions of substituted 1,3-butadiene[14] and 1,2-bis(diphosphinyl)ethenes,[15] which are isoelectronic to **1**, display a localized bonding pattern analogous to structure **I**, where minimization of the Coulombic repulsion between the two negative charges is achieved. However, the P–P distances in **1** are nearly identical suggesting that a more delocalized bonding scheme (structure **II**) is present, which gives a formal P–P bond order of 1.33.[16] The Tl–P interactions may be responsible for decreasing intrachain electronic repulsion in **1**.

The synthesis of a neutral diaryltetraphosphabutadiene derivative analogous to **A** was attempted by oxidation of **1**. However, reaction of **1** with I_2 gave $P_4(Ar^{Dipp_2})_2$ as the diaryltetraphosphabicyclobutane isomer.[7c,17] It seems likely that a species with a structure analogous to **A** is generated initially but that this isomerizes to **2**.[18] The isomerization is reminiscent to that of 1,3-butadiene to bicyclobutane which

 © 2005 Wiley-VCH Verlag GmbH & Co. KGaA, Weinheim

has been well explored in the classic work of Woodward and Hoffmann.[19]

The ^{31}P NMR spectrum of **2** gave two triplet resonances centered at $\delta = -331.8$ (bridgehead P atoms) and $\delta = -163.0$ ppm ($^{1}J_{P,P} = 189$ Hz), consistent with either a rigid *trans*,*trans*-diaryltetraphosphabicyclobutane, or a fluxional structure with C_{2v} symmetry. Previously reported disubstituted tetraphosphabicyclobutanes, R_2P_4 (R = 2,4,6-*t*Bu$_3$C$_6$H$_2$ (**3**),[17a] (Me$_3$Si)$_2$N (**4**),[17b] [(Me$_3$Si)$_2$N]$_2$P (**5**),[17c]) crystallized in the *trans*,*trans* configuration. However, unlike **2**, the ^{31}P NMR spectra of **4** and **5** showed evidence for both the C_s-symmetric *cis*,*trans* conformer and *trans*,*trans* conformer in solution. In contrast, the ^{31}P NMR spectrum of the Mes* substituted **3** afforded only two resonances ($\delta = -272$ and -130 ppm) with chemical shift values similar to **2**.

The crystal structure (**2a**; from benzene)[7b] revealed a *trans*,*trans* structure (Figure 3), which is similar to a range of previously structurally characterized tetraphosphabicyclobutanes and is consistent with the ^{31}P NMR spectrum of **2** in solution ([D$_8$]THF, −90 to 60 °C). However, crystals of **2** grown from hexane[7c] displayed a *cis*,*trans* structure (**2b**), an isomeric form that has not been observed in the solid state. The P–P distances, including the bridgehead P–P bonds, of **2a** (2.203(1)–2.207(2) Å) and **2b** (2.205(2)–2.243(2) Å) are similar and consistent with P–P single bonding. The bridgehead P–P bonds (**2a**, 2.203(2); **2b**, 2.219(2) Å) are ca. 0.10 Å longer than in **4** and ca. 0.05 Å longer than in **3** and **5**. The P_4 fold angle of **2a** is 92.9° and falls only slightly outside of the known range (95.2–95.6°) for **3**–**5**. However, the P_4 fold angle of 71.9° in **2b** is accompanied by a widening of the P(1)-P(2)-P(4) (89.33(7)°) and P(1)-P(3)-P(4) (88.66(7)°) angles resulting from alleviation of the steric interactions between the two Ar^{Dipp_2} substituents. Calculations regarding the relative stability of the *trans*,*trans* and *cis*,*trans* conformations of P_4H_2 indicate that the *trans*,*trans* isomer is more stable, but only by 1.2 kcal mol^{-1}.[20] Since both isomers are obtainable in the solid state, crystal packing effects probably dictate the solid state conformation.

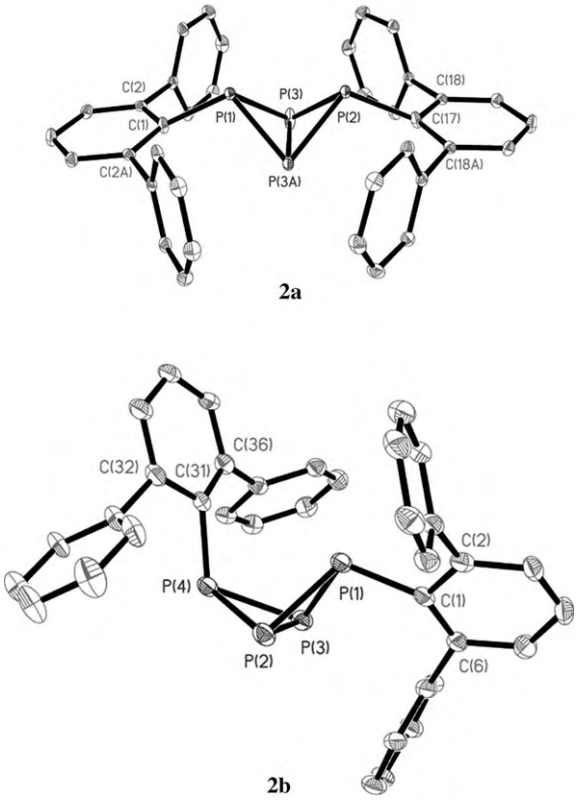

Figure 3. Thermal ellipsoid (30%) plots of **2a** and **2b**. H atoms and isopropyl groups on Ar^{Dipp_2} are not shown for clarity. Selected bond lengths [Å] and angles [deg]: **2a**: P(1)–C(1) 1.866(3), P(2)–C(17) 1.887(3), P(1)–P(3) 2.207(1), P(2)–P(3) 2.201(1), P(3)–P(3A) 2.203(2); P(1)-P(3)-P(2) 77.81(4); the P_4 fold angle, defined as the dihedral angle between the P(1)-P(3)-P(3A) and P(2)-P(3)-P(3A) planes, is 92.9. **2b**: P(1)–C(1) 1.874(6), P(1)–P(2) 2.205(2), P(1)–P(3) 2.243(2), P(2)–P(4) 2.216(2), P(2)–P(3) 2.219(2), P(3)–P(4) 2.205(2), P(4)–C(31) 1.821(6); P(1)-P(2)-P(4) 89.33(7), P(1)-P(3)-P(4) 88.66(7); the P_4 fold angle, defined as the dihedral angle between the P(1)-P(2)-P(4) and P(4)-P(3)-P(2) planes, is 71.9°.

In conclusion, the thallium complexed diaryltetraphosphabutadienediide (**1**) has been synthesized from the reaction of (Ar^{Dipp_2}Tl)$_2$ and white phosphorus. The negative charge is delocalized over the P_4 array, as suggested by the essentially equal P–P distances and planar P_4C_2 core, to afford an average P–P bond order of approximately 1.33. Reaction of **1** with I_2 afforded the diaryltetraphosphabicyclobutane **2** which depending on the solvent of crystallization can be obtained as either the *trans*,*trans* (**2a**) or the *cis*,*trans* isomer (**2b**). Future work will focus on evaluating the ability of **1** as a $[P_4Aryl_2]^{2-}$ transfer agent, and exploring the reduction chemistry of **2**.

Experimental Section

All manipulations were carried out under anhydrous and anaerobic conditions.

1: An aluminum foil-wrapped 100-mL Schlenk flask was charged with equimolar portions of (Ar^{Dipp_2}Tl)$_2$ (0.916 g, 0.761 mmol) and freshly distilled white P_4 (0.094 g, 0.76 mmol). This mixture was placed in a water–ice bath and, with vigorous magnetic stirring, THF (ca. 60 mL) that had been pre-cooled to 0 °C was added. The resulting deep red solution was stirred for 12 h, whereupon it was filtered from some precipitate (presumably Tl metal) using a glass-fiber tipped cannula. The solvent was removed under a dynamic vacuum and the residue was washed with ca. 15 mL of cold hexane. The product was obtained as a burgundy microcrystalline solid that is sparingly soluble in hydrocarbon solvents and does not display any detectable light sensitivity. Redissolving with warm hexane (ca. 35 mL) followed by overnight cooling to ca. −15 °C afforded X-ray quality crystals of **1**. Yield: 0.205 g, 40%; Mp: darkens at 130 °C, 226 °C (dec.) ^{1}H NMR (300.1 MHz, [D$_8$]THF, 25 °C): $\delta = 0.96$ (d, 24 H, CH(C*H*$_3$)$_2$, $^{3}J_{H,H} = 6.9$ Hz), 1.33 (d, 24 H, CH(C*H*$_3$)$_2$, $^{3}J_{H,H} = 6.9$ Hz), 2.70 (sept, 8 H, C*H*(CH$_3$)$_2$, $^{3}J_{H,H} = 6.9$ Hz), 6.88 (d, 4 H, *m*-C$_6$H$_3$, $^{3}J_{H,H} = 7.5$ Hz), 6.99 (t, 4 H, *p*-dipp, $^{3}J_{H,H} = 7.7$ Hz), 7.11–7.16 (t, partially buried, *p*-C$_6$H$_3$), 7.11 ppm (d, 8 H, *m*-dipp, $^{3}J_{H,H} = 8.1$ Hz); ^{13}C{^{1}H} NMR: (75.5 MHz, [D$_8$]THF, 25 °C): $\delta = 24.1$ (*o*-CH(*C*H$_3$)$_2$), 26.0 (*o*-CH(*C*H$_3$)$_2$), 31.8 (*o*-CH(*C*H$_3$)$_2$), 124.4 (*p*-C$_6$H$_3$), 126.5 (*p*-dipp), 129.4 (*i*-C$_6$H$_3$), 130.8 (*m*-C$_6$H$_3$), 142.6 (*o*-C$_6$H$_3$), 144.5 (*i*-dipp), 147.5 (*o*-dipp), 148.1 ppm (*m*-dipp); ^{31}P{^{1}H} NMR (121.5 MHz, [D$_8$]THF, 50 °C, referenced externally to 85% H$_3$PO$_4$): $\delta = 185$ (m), 280 ppm (m); ^{205}Tl NMR (230.71 MHz, [D$_8$]THF, 25 °C, referenced externally to TlNO$_3$(aq)): $\delta = 2730$ ppm (m, $^{2}J_{^{205}Tl,^{203}Tl} \approx 12000$ Hz); ^{203}Tl NMR (228.47 MHz, [D$_8$]THF, 25 °C, referenced externally to TlNO$_3$(aq)): $\delta = 2730$ ppm (m, $^{2}J_{^{205}Tl,^{203}Tl} = 12000$ Hz); UV/Vis (hexanes) λ_{max} [nm] (ε in mol^{-1} L cm^{-1}): 222 (45000), 322 (13000), 432 (990), 546 (2400).

 © 2005 Wiley-VCH Verlag GmbH & Co. KGaA, Weinheim

2: I_2 (0.068 g, 0.270 mmol) was dissolved in hexane (80 mL). This solution was added dropwise to **1** (0.355 g, 0.267 mmol) dissolved in hexane (20 mL). Upon complete addition the color of the solution had changed from deep red to colorless. The slurry was stirred for 2 h and the precipitate (TlI) was removed by filtration through a Celite-padded frit. The solution was concentrated to ca. 10 mL and storage at ca. −20 °C overnight afforded colorless X-ray quality crystals of **2b**. Yield: 0.130 g, 53 %; Mp > 320 °C. ^{1}H NMR (300.1 MHz, [D$_8$]THF, 25 °C): $\delta = 0.93$ (d, 24 H, CH(CH_3)$_2$, $^3J_{H,H} = 6.6$ Hz), 1.13 (d, 24 H, CH(CH_3)$_2$, $^3J_{H,H} = 6.9$ Hz), 2.31 (sept, 8 H, CH(CH$_3$)$_2$, $^3J_{H,H} = 6.6$ Hz), 6.94 (d, 4 H, *m*-C$_6$H$_3$, $J_{HH} = 7.5$ Hz), 7.14 (d, 8 H, *m*-dipp, $J_{H,H} = 7.8$ Hz), 7.20 (t, 4 H, *p*-C$_6$H$_3$, $J_{H,H} = 7.8$ Hz), 7.37 ppm (t, 4 H, *p*-dipp, $J_{H,H} = 7.8$ Hz); ^{13}C{^{1}H} NMR (75.5 MHz, [D$_8$]THF, 25 °C): $\delta = 22.9$ (CH(*C*H$_3$)$_2$), 25.2 (CH(*C*H$_3$)$_2$), 30.8 (CH(CH$_3$)$_2$), 123.1 (*m*-dipp), 127.0 (*p*-C$_6$H$_3$), 129.0 (*m*-C$_6$H$_3$), 129.3 (*p*-dipp), 135.5 (m, *i*-C$_6$H$_3$), 138.7 (*o*-C$_6$H$_3$), 145.4 (m, *i*-dipp), 146.5 ppm (*o*-dipp); ^{31}P NMR (121.5 MHz, [D$_8$]THF, 25 °C): $\delta = -331.8$ (t, 2 P, bridgehead, $^1J_{P,P} = 189.2$ Hz), −163.0 ppm (t, 2 P, terminal, $^1J_{P,P} = 189.2$ Hz). X-ray quality crystals of **2a** were obtained by dissolving **2b** in C$_6$D$_6$ followed by slow cooling to 7 °C. The spectroscopic properties of **2a** (in [D$_8$]THF) were identical to those of **2b** (in [D$_8$]THF).

Received: August 11, 2005

Keywords: bond order · multiple bonds · phosphabutadiene · phosphorus · thallium

[1] a) P. P. Power, *Chem. Rev.* **1999**, *99*, 3463; b) M. Weidenbruch, *J. Organomet. Chem.* **2002**, *646*, 39; c) M. Weidenbruch, *Organometallics* **2003**, *22*, 4348.

[2] For neutral homonuclear Group 13 formally double bonded analogues see: a) R. J. Wright, A. D. Phillips, S. Hino, P. P. Power, *J. Am. Chem. Soc.* **2005**, *127*, 4794; b) H. Schumann, C. Janiak, J. Pickhardt, U. Börner, *Angew. Chem.* **1987**, *99*, 788; *Angew. Chem. Int. Ed. Engl.* **1987**, *26*, 789; ; c) M. S. Hill, P. B. Hitchcock, R. Pongtavornpinyo, *Angew. Chem.* **2005**, *117*, 4303; *Angew. Chem. Int. Ed.* **2005**, *44*, 4231; d) R. J. Wright, A. D. Phillips, N. J. Hardman, P. P. Power, *J. Am. Chem. Soc.* **2002**, *124*, 8538; e) N. J. Hardman, R. J. Wright, A. D. Phillips, P. P. Power, *J. Am. Chem. Soc.* **2003**, *125*, 2667; f) R. J. Wright, A. D. Phillips, P. P. Power, *J. Am. Chem. Soc.* **2003**, *125*, 10784; for neutral homonuclear Group 14 alkyne analogues see: g) A. Sekiguchi, R. Kinjo, M. Ichinohe, *Science* **2004**, *305*, 1755; h) N. Wiberg, W. Niedermayer, G. Fischer, H. Nöth, M. Suter, *Eur. J. Inorg. Chem.* **2002**, 1066; i) L. Pu, A. D. Phillips, A. F. Richards, M. Stender, R. S. Simons, M. M. Olmstead, P. P. Power, *J. Am. Chem. Soc.* **2003**, *125*, 11626; j) L. Pu, B. Twamley, P. P. Power, *J. Am. Chem. Soc.* **2000**, *122*, 3524; for neutral homonuclear Group 14 alkene analogues see ref. [1] and k) R. West, M. Fink, J. Michl, *Science* **1981**, *214*, 1343; for homonuclear Group 15 alkene analogues see ref. [1a] and l) M. Yoshifuji, I. Shima, N. Inamoto, K. Hirotsu, T. Higuchi, *J. Am. Chem. Soc.* **1981**, *103*, 4587; m) N. Tokitoh. Y. Arai, R. Okazaki, S. Nagase, *Science* **1997**, *277*, 78.

[3] a) M. Weidenbruch, S. Willms, W. Saak, G. Henkel, *Angew. Chem.* **1997**, *109*, 2612; *Angew. Chem. Int. Ed. Engl.* **1997**, *36*, 2503; b) H. Schäfer, W. Saak, M. Weidenbruch, *Angew. Chem.* **2000**, *112*, 3847; *Angew. Chem. Int. Ed.* **2000**, *39*, 3703.

[4] For a review on carbon substituted tetraphosphabutadienes such as 1,3-diphosphabutadienes and 2,3-diphosphabutadienes see: a) K. B. Dillon, F. Mathey, J. F. Nixon, *Phosphorus: The Carbon Copy*, Wiley, Chichester, **1998**; for P=C polymers see: b) V. A. Wright, D. P. Gates, *Angew. Chem.* **2002**, *114*, 2495; *Angew. Chem. Int. Ed.* **2002**, *41*, 2389; c) D. P. Gates, *Top. Curr. Chem.* **2005**, *250*, 107; for cobalt complexed tetraphosphabutadienes see: d) F. Cecconi, C. A. Ghilardi, S. Midollini, A. Orlandini, *J. Am. Chem. Soc.* **1984**, *106*, 3667; e) F. Cecconi, C. A. Ghilardi, S. Midollini, A. Orlandini, *Inorg. Chem.* **1986**, *25*, 1766; for related transition metal complexes: f) O. J. Scherer, M. Swarowsky, H. Swarowsky, G. Wolmershäuser, *Angew. Chem.* **1988**, *100*, 738; *Angew. Chem. Int. Ed. Engl.* **1988**, *27*, 694; g) V. A. Miluykov, O. G. Sinyashin, P. Lönnecke, E. Hey-Hawkins, *Mendeleev Commun.* **2003**, 212; h) O. J. Scherer, T. Hilt, G. Wolmershäuser, *Organometallics* **1998**, *17*, 4110; i) O. J. Scherer, R. Winter, G. Wolmershäuser, *Z. Anorg. Allg. Chem.* **1993**, *619*, 827; for an arsenic compound see for example: j) O. J. Scherer, J. Vondung, G. Wolmershäuser, *J. Organomet. Chem.* **1989**, *376*, C35.

[5] W. W. Schoeller, U. Tubbesing, *Chem. Ber.* **1996**, *129*, 419.

[6] The reaction of K(Si*t*Bu$_3$) with P$_4$ afforded several products, one of which, K$_2$P$_4$(Si*t*Bu$_3$)$_2$, was assigned the tetraphosphabutadienediide structure analogous to **1** on the basis of ^{31}P NMR spectroscopy. See: H.-W. Lerner, M. Bolte, K. Karaghiosoff, M. Wagner, *Organometallics* **2004**, *23*, 6073.

[7] Crystallographic data for **1**, **2a**, **2b**: Recorded at 90 K with Mo$_{K\alpha}$ radiation ($\lambda = 0.71073$ Å): **1** $a = 18.690(4)$, $b = 18.690(4)$, $c = 16.783(9)$ Å, $\alpha = \beta = 90°$, $\gamma = 120°$, trigonal, space group $P3_221$, $Z = 3$, $R1 = 0.0418$ for 5243 ($I > 2\sigma(I)$) data, w$R2$ (all data) = 0.1418; **2a** $a = 15.990(3)$, $b = 26.291(5)$, $c = 16.876(3)$ Å, $\alpha = \beta = \gamma = 90°$, orthorhombic, space group *Pnma*, $Z = 4$, $R1 = 0.0402$ for 4674 ($I > 2\sigma(I)$) data, w$R2$ (all data) = 0.1018; **2b** $a = 13.600(3)$, $b = 22.500(4)$, $c = 19.418(7)$ Å, $\alpha = 90°$, $\beta = 117.57(2)°$, $\gamma = 90°$, monoclinic, $P2_1/c$, $Z = 4$, $R1 = 0.0882$ for 4381 ($I > 2\sigma(I)$) data, w$R2$ (all data) = 0.2275. CCDC-279795 (**1**), CCDC-279797 (**2a**), CCDC-279796 (**2b**) contain the supplementary crystallographic data for this paper. These data can be obtained free of charge from the Cambridge Crystallographic Data Centre via www.ccdc.cam.ac.uk/data_request/cif.

[8] a) H. Schmidbaur, W. Bublak, J. Riede, G. Müller, *Angew. Chem.* **1985**, *97*, 402; *Angew. Chem. Int. Ed. Engl.* **1985**, *24*, 414; b) R. J. Wright, M. Brynda, P. P. Power, *Inorg. Chem.* **2005**, *44*, 3368; c) H. V. R. Dias, S. Singh, T. R. Cundari, *Angew. Chem.* **2005**, *117*, 4985; *Angew. Chem. Int. Ed.* **2005**, *44*, 4907.

[9] An interaction energy of 42 kcal mol^{-1} [8c] has been recently calculated for the bis-benzene complex [Tl(η^6-benzene)$_2$]$^+$, that is 21 kcal mol^{-1} for each Tl–arene interaction, while an interaction energy of 3 kcal mol^{-1} was calculated for the model complex TlN(Me)Ph–benzene.[8b]

[10] Structural data for over 20 organo-diphosphenes have been published; see ref. [1a].

[11] J. Emsley, *The Elements*, Clarendon, Oxford, **1995**, pp. 140–141.

[12] a) J. Mason, *Multinuclear NMR*, Plenum, New York, **1987**, p. 285; b) I. R. Shapiro, D. M. Jenkins, J. C. Thomas, M. W. Day, J. C. Peters, *Chem. Commun.* **2001**, 2152.

[13] The $^2J_{^{205}Tl,^{203}Tl}$ coupling constants in a variety of Tl^I alkoxides vary from 2200 to 2800 Hz, see: P. J. Burke, R. W. Matthews, D. G. Gillies, *J. Chem. Soc. Dalton.* **1980**, 1439.

[14] a) H. Bock, C. Näther, K. Ruppert, *J. Chem. Soc. Chem. Commun.* **1992**, 765; b) H. Bock, C. Näther, K. Ruppert, Z. Havlas, *J. Am. Chem. Soc.* **1992**, *114*, 6907.

[15] C. Tirla, N. Mézailles, L. Ricard, F. Mathey, P. Le Floch, *Inorg. Chem.* **2002**, *41*, 6032.

[16] Assuming that disubstituted tetraphosphabutadienes possess frontier orbitals qualitatively similar to 1,3-butadiene, addition of two electrons to the partially antibonding LUMO lowers the overall P–P bond order to 1.33.

[17] a) R. Riedel, H.-D. Hausen, E. Fluck, *Angew. Chem.* **1985**, *97*, 1050; *Angew. Chem. Int. Ed. Engl.* **1985**, *24*, 1056; for other disubstituted tetraphosphabicyclobutanes see: b) E. Niecke, R. Ruger, B. Krebs, *Angew. Chem.* **1982**, *94*, 553; *Angew. Chem. Int. Ed. Engl.* **1982**, *21*, 544; c) J.-P. Bezombes, P. B. Hitchcock, M. F. Lappert, J. E. Nycz, *Dalton Trans.* **2004**, 499; d) H.-P. Schrodel, H. Nöth, M. Schmidt-Amelunxen, W. W. Schoeller, A Schmidpeter, *Chem. Ber.* **1997**, *130*, 1801; e) A. H. Cowley, P. C. Knüppel, C. M. Nunn, *Organometallics* **1989**, *8*, 2490; f) P.

 © 2005 Wiley-VCH Verlag GmbH & Co. KGaA, Weinheim

Jutzi, R. Kroos, A. Müller, M. Penk, *Angew. Chem.* **1989**, *101*, 628; *Angew. Chem. Int. Ed. Engl.* **1989**, *28*, 600.
[18] E. Niecke, O. Altmeyer, M. Nieger, F. Knoll, *Angew. Chem.* **1987**, *99*, 1299; *Angew. Chem. Int. Ed. Engl.* **1987**, *26*, 1256.
[19] R. B. Woodward, R. Hoffmann, *The Conservation of Orbital Symmetry*, VCH, New York, **1985**, p. 75.
[20] W. W. Schoeller, C. Lerch, *Inorg. Chem.* **1983**, *22*, 2992.

 © 2005 Wiley-VCH Verlag GmbH & Co. KGaA, Weinheim

Site-Ordered Solids

DOI: 10.1002/anie.200500135

$Ba_8CoNb_6O_{24}$: A d^0 Dielectric Oxide Host Containing Ordered d^7 Cation Layers 1.88 nm Apart**

*Phillip M. Mallinson, Mathieu M. B. Allix, John B. Claridge, Richard M. Ibberson, David M. Iddles, Tim Price, and Matthew J. Rosseinsky**

The search for multiproperty materials,[1] in which one cooperative phenomenon can control another through modulation of the local structure and bonding, is complicated by the need to separate the chemical units responsible for these different properties. Thus, rules are required for the synthesis of materials that assemble with spatial segregation of the elements conferring distinct properties. These rules should be sufficiently strict to operate at the high synthesis temperatures required for processing many inorganic materials.

This challenging synthetic task can be addressed by exploiting the diversity of site chemistries[2] available in a complex perovskite structure and harnessing the combination of the specific bonding requirements of the d^0 cations and the site symmetries in the structure to drive the cation ordering. Here we present the functional material $Ba_8CoNb_6O_{24}$ comprising isolated single layers of Co^{2+} d^7 cations separated by intervening d^0 cation layers and 1.88 nm away from the next Co^{2+} layer. Most remarkable is that this long-range ordering is driven despite the low concentration of Co^{2+} cations in the structure. These site-ordered solids are then processed to permit their evaluation as microwave dielectric resonators.

In the chemistry of transition-metal oxides, elements in the d^0 oxidation state (particularly Ta^V, Ti^{IV}, and Nb^V), with their characteristic directional M–O multiple bonding, are the basic components of ferroelectric, relaxor, and high-permittivity materials.[3] Transition-metal centers that bear d electrons (d^n centers) confer magnetic, optical, and electronic properties on materials. The development of extended metal oxide networks in which d^n centers can be separated by long distances with precise site order within a d^0 matrix offers great potential in materials design. The ordering of cations of different sizes and charges is possible on the octahedral B site of the ABO_3 perovskite structure[4]—hexagonal stacking of the AO_3 close-packed layers produces face-sharing octahedral sites in addition to the corner-sharing sites characteristic of a cubic stacking sequence. The face-sharing sites thus introduced are favorable locations for cation vacancies, with mixed hexagonal and cubic stacking sequences resulting in the family of "hexagonal perovskites".[5]

Complex tantalum oxides are widely employed as microwave resonators in mobile telecommunications, but the cost of raw materials makes niobium-based alternatives desirable. The eight-layer hexagonal perovskite $Ba_8ZnTa_6O_{24}$ adopts a $(chcc)_2$ sequence (an AO_3 layer (B) is described as h if its two neighboring layers are the same (ABA) or c if they are different (ABC)) and has interesting dielectric properties with a moderately high Q of 20800 at 3.28 GHz ($Q = (\tan\delta)^{-1}$).[6] Our initial investigations on the Nb analogue $Ba_8ZnNb_6O_{24}$ consistently lead to the synthesis of polyphasic material with several competing stacking sequences of hexagonal and cubic layers.

Investigation of the cobalt-substituted niobate $Ba_8CoNb_6O_{24}$ revealed that this composition afforded single-phase material with an eight-layer ($c \approx 18$ Å , BaO_3 layer thickness ≈ 2.3 Å) repeat in contrast to the mixed phases in the Ba-Zn-Nb-O field at this composition. Surprisingly, although $Ba_8CoTa_6O_{24}$ is isostructural with $Ba_8ZnTa_6O_{24}$ and tolerance factor effects associated with stacking sequence changes[5] are absent, the new Nb phase adopts a different eight-layer stacking sequence in which two hexagonal ABA AO_3 layer units are adjacent to each other in an ccchhccc motif (Figure 1).[7] High-resolution electron microscopy images directly demonstrate that this sequence is adopted without stacking faults (Figure 2a). The $P\bar{3}m1$ space-group symmetry is confirmed by electron diffraction (Figure 2b,c) and the cation composition and homogeneity by energy dispersive spectroscopy (EDS) in the electron microscope. Although all the occupied octahedra in such a sequence are corner sharing, and the triple layer of face-sharing octahedral sites in the hh region of the structure

[*] P. M. Mallinson, Dr. M. M. B. Allix, Dr. J. B. Claridge, Prof. M. J. Rosseinsky
Department of Chemistry
The University of Liverpool
Liverpool L69 7ZD (UK)
Fax: (+44) 151-794-3587
E-mail: m.j.rosseinsky@liverpool.ac.uk
Dr. R. M. Ibberson
ISIS Facility
CCLRC – Rutherford Appleton Laboratory
Chilton, Didcot
Oxon OX11 0QX (UK)
Dr. D. M. Iddles, T. Price
Filtronic Comtek, Ceramics Division
Enterprise Drive, Station Road, Four Ashes
Wolverhampton WV10 7DB (UK)

[**] We thank EPSRC for Portfolio Partnership funding and CCLRC and the CCLRC Centre for Materials Physics and Chemistry for partial support of P.M. (grant ref. CMPC03106).

Supporting information for this article is available on the WWW under http://www.angewandte.org or from the author.

 © 2005 Wiley-VCH Verlag GmbH & Co. KGaA, Weinheim

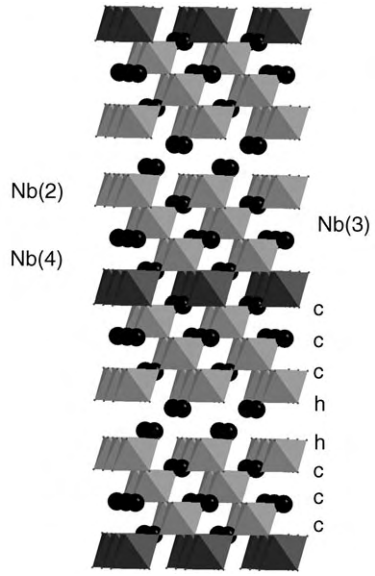

Figure 1. The cchhccc stacking sequence of $Ba_8CoNb_6O_{24}$ shows strict ordering of the Co^{2+} cations (comprising only 12.5% of the total octahedral-site cations) on the central layer of octahedral sites within the seven-block unit of corner-sharing octahedra. Cobalt- and niobium-centered octahedra are shown in dark gray and light gray, respectively, and barium cations are represented as black spheres. The layer of vacant octahedral sites in the hh region of the stacking sequence produces a structure consisting solely of corner-sharing octahedra.

results in a central layer of vacant sites (Figure 1), $Ba_8CoNb_6O_{24}$ displays essentially complete ordering of the Co^{2+} and Nb^{5+} cations. Refinement of high-resolution time-of-flight neutron powder diffraction data reveal the superiority of fully ordered ($\chi^2 = 2.92$) over fully disordered ($\chi^2 = 3.15$) models; permitting antisite disorder between the single Co (*1a*) and three crystallographically distinct Nb sites results in 95(3)% Co occupancy of the *1a* site and pure Nb(2) and Nb(3) sites within 1σ; improvements in agreement indices when site disorder was permitted were insignificant. (The atomic displacement parameters in the partially ordered model are unphysical, with several atoms refining to negative values, and the convergence was not robust). The fully site-ordered model was thus adopted (Table 1 and Table 2) The bond valence sums for Co^{2+} and Nb^{5+} on the *1a* site are 1.95 (3% deviation from expected) and 3.51 (30% deviation), respectively, while the maximum deviation from the ideal bond valence of 5 for Nb^{5+} cations on the other three sites in the structure is 8%. As the Nb^{5+} bond valence in fully site-ordered $Ba_3MgNb_2O_9$ is 4.66,[8] both the site occupancies and bond-valence considerations indicate that the cation site order is complete in $Ba_8CoNb_6O_{24}$.

The *1a* sites solely occupied by Co^{2+} are at the centers of the seven-layer blocks of corner-sharing octahedra. This is surprising as a statistical distribution of cobalt cations over the four available sites might have been expected given their low concentration (only 12.5% of the octahedral sites are occupied by Co^{2+}) and the existence of only corner-sharing sites in the structure. The *1a* site is the most regular environment amongst the four symmetry-inequivalent octahedral sites, as it is located necessarily at a center of symmetry

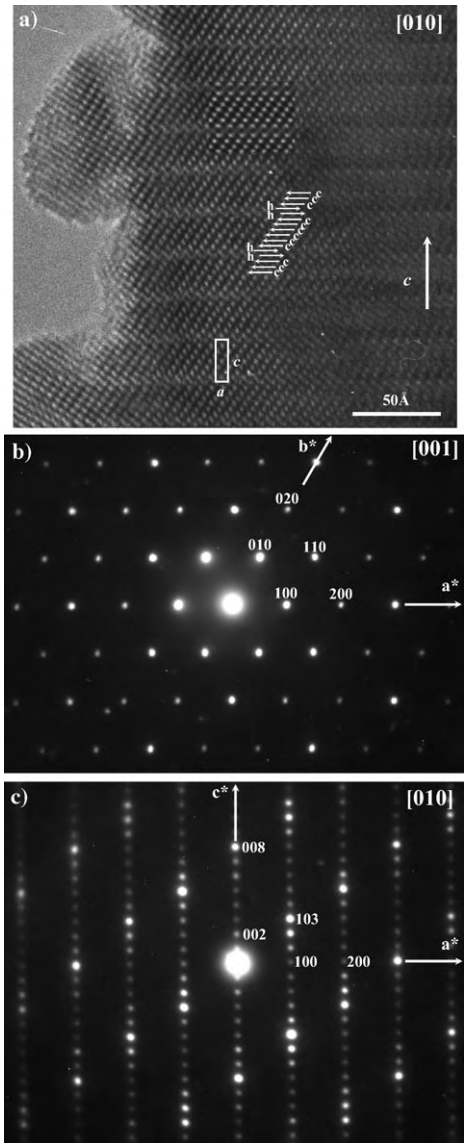

Figure 2. a) HREM image of $Ba_8CoNb_6O_{24}$ recorded along the [010] direction. The simulated image is embedded. Experimental [001] (b) and [010] (c) electron diffraction patterns.

as a result of the odd number of occupied layers in the stacking sequence. The symmetry-imposed requirement that all the bond lengths between oxygen and the central atom on this site are equal is inconsistent with the multiple-bonding preference of Nb^{5+}, which is often displaced from the center of an octahedral environment to form multiple bonds to oxygen (Figure 3a). This in turn favors all the Co^{2+} cations, which are more commonly found in centrosymmetric oxide octahedra (Figure 3b), occupying the site to avoid forcing Nb^{5+} into an unfavorable environment. The availability of the distinctly bonded *1a* site together with the cation charge difference (which is more pronounced here than between the cations with charges of +3, +4, and +5 of site-disordered $Ba_8In_{0.5}Ti_2Nb_{4.5}O_{24}$)[7] drives the strict site ordering and resulting extreme long-range separation of the cobalt cation layers. This strict site ordering results in the separation of Co^{2+} layers by 1.88 nm along *c*. Ordering over this distance

 © 2005 Wiley-VCH Verlag GmbH & Co. KGaA, Weinheim

Table 1: Refined coordinates of $Ba_8CoNb_6O_{24}$. Space group $P\bar{3}m1$; $a = 5.789813(10)$, $c = 18.89355(6)$ Å; $\chi^2 = 2.9$ $R(F^2) = 5.88\,\%$ $R(F) = 4.34\,\%$. The global instability index,[14] which measures the mean deviation of the bond valence sum of all ions in the structure from their formal valence, is 0.21, which is consistent with that observed in high-permittivity niobates based on site-ordered cubic perovskites.[8] The weighted average deviation from the ideal bond valence sums is 0.058, which is consistent with those observed in cubic perovskite niobates. The valence sums at Ba of over 2 indicate compression around these sites, as is commonly observed in perovskite niobates.[8]

	x	*y*	*z*	100 U [Å^{-2}]	Symm.	Site	BVS[a]
Ba1	0	0	0.1862(2)	0.9(1)	3*m*	2c	2.45
Ba2	1/3	2/3	0.0609(3)	0.77(9)	3*m*	2d	2.32
Ba3	1/3	2/3	0.4564(2)	0.70(9)	3*m*	2d	2.08
Ba4	1/3	2/3	0.6826(2)	0.12(8)	3*m*	2d	2.51
Co1	0	0	0	0.1(2)	$\bar{3}m$	1a	1.95
Nb2	0	0	0.3849(1)	0.44(6)	3*m*	2c	4.93
Nb3	1/3	2/3	0.2549(2)	0.52(8)	3*m*	2d	4.64
Nb4	1/3	2/3	0.8789(1)	0.61(9)	3*m*	2d	4.58
O1	0.1679(2)	0.8321(2)	0.3074(1)	0.82(6)	*m*	6i	2.03
O2	0.1630(2)	0.8369(2)	0.5706(1)	1.05(6)	*m*	6i	2.15
O3	0.1710(3)	0.8289(3)	0.9351(1)	0.72(4)	*m*	6i	2.03
O4	0.4985(2)	0.5014(2)	0.1868(1)	0.92(6)	*m*	6i	1.94

[a] BVS is the bond valence sum for the atom.

Table 2: Bond lengths [Å] and angles [°] in $Ba_8CoNb_6O_{24}$. The magnitude of the off-center distortion at the Nb sites, computed as $1/6 \sum_{n=1,6} ((d_n - \bar{d})/\bar{d})^2$, where $\bar{d}$ is the mean bond length at the site, is 0.0094 (Nb2), 0.0017 (Nb3), and 0.0014 (Nb4) compared with 0.0016 in fully site-ordered $Ba_3MgNb_2O_9$.[8]

Co1–O3	×6	2.108(3)	Nb3–O1	×3	1.933(4)
O3-Co1-O3	×6	89.6(1)	Nb3–O4	×3	2.097(3)
O3-Co1-O3	×6	90.4(1)	O1-Nb3-O1	×3	96.0(2)
O3-Co1-O3	×3	180.0(1)	O1-Nb3-O4	×3	173.1(2)
			O1-Nb3-O4	×6	88.60(7)
Nb2–O1	×3	2.231(3)	O4-Nb3-O4	×3	86.3(2)
Nb2–O2	×3	1.837(3)			
O1-Nb2-O1	×3	81.6(1)	Nb4–O3	×3	1.942(4)
O1-Nb2-O2	×3	166.2(2)	Nb4–O4	×3	2.095(3)
O1-Nb2-O2	×6	87.9(1)	O3-Nb4-O3	×3	93.0(2)
O2-Nb2-O2	×3	100.8(2)	O3-Nb4-O4	×3	176.7(2)
			O3-Nb4-O4	×6	89.2(1)
			O4-Nb4-O4	×3	88.4(1)

over purely six coordinate sites is unusual (Mn^{2+} and W^{6+} are ordered within a three-layer block in $Ba_2La_2MnW_2O_{10}$, where the concentration of the centrosymmetric cation is considerably higher than the present case[9]), although discrete Fe^{3+} tetrahedral layers are observed separated by mixed iron/titanium octahedral layers in complex barium iron titanium oxides.[10]

The Nb(2) site adjacent to the layer of vacant octahedral sites has the most pronounced off-center displacement of Nb^{5+} towards a triangular face of the octahedral oxide environment along the threefold axis due to the absence of other cations competing for bonding with the O2 oxide anions. The other two Nb sites, which share all their coordinating oxide anions with neighboring B site cations, have off-center displacements similar to those observed in fully site-ordered $Ba_3MgNb_2O_9$,[8] in accord with the proposed structural model for $Ba_8CoNb_6O_{24}$. It is interesting to note that the separation of the BaO_3 layers neighboring the vacant site is at 1.65 Å consistent with that of $Ba_5Nb_4O_{15}$ but distinctly shorter than found in the Q blocks of ferrites,[11] where the corresponding distance is 2.15 Å.

Magnetization data for $Ba_8CoNb_6O_{24}$ obeyed the Curie–Weiss law between 2 and 300 K with an effective moment of 4.06 μ_B per Co (the spin-only value is 3.87 μ_B) and −4.26(6) K antiferromagnetic Weiss constant) and no irreversibility between field and zero-field cooled runs (Figure 4). This is consistent with the structural model of Co^{2+} cations with near-neighbor Co–Co distances within the layer of 5.786 Å without direct Co-O-Co superexchange pathways. Deviations from the spin-only prediction are commonly observed for

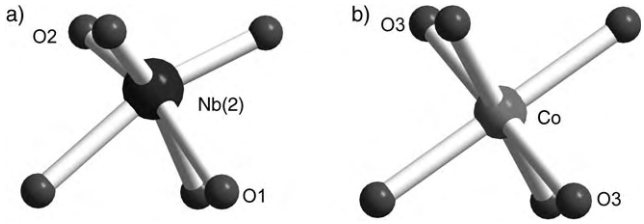

Figure 3. a) The asymmetric multiple bonding to oxide by Nb^{5+} produces displacement of Nb(2) from the center of the octahedron towards the face of three O2 oxide anions bordering the layer of vacant face-sharing octahedral sites, whereas in b) the Co^{2+} cation is located in a centrosymmetric environment that does not permit ordered displacements of the type required to optimize the bonding at Nb. The *c* axis (layer stacking direction) is vertical in both structures.

octahedral Co^{2+}—the slight enhancement of the magnetic moment over the spin-only value results from incomplete quenching of the orbital contribution from the $^4T_{1g}$ state of high-spin Co^{2+} by the trigonal ligand field, and agrees with the value of 4.1 μ_B observed for Co^{2+} in anatase.[12]

For oxides containing metals with variable oxidation states, hopping conduction offers a mechanism for dielectric loss. However, the Co^{2+} oxidation state seems robust in $Ba_8CoNb_6O_{24}$, as indicated both by the magnetic data and the invariance of the cell parameters to processing conditions. The phase can be processed into resonators with a density of 89.6 % of the crystallographic density with a relative permittivity of 31: Q values are sensitive to processing, but resonators with the most dense microstructure (scanning electron micrographic images of sectioned high-Q material shown in Figure S2 and S3 reveal lath- and platelike grains $\geqq 10$ μm thick and of similar aspect to but with larger dimensions than those for $Ba_8ZnTa_6O_{24}$[13]) have Q of 16700 at 3.2 GHz ($Qf = 53200$ GHz). The temperature coefficient of the resonant frequency, τ_f, is 16 ppm K^{-1}. EDS analysis of the grains (Figure S2) at both interior and exterior surfaces of the

 © 2005 Wiley-VCH Verlag GmbH & Co. KGaA, Weinheim

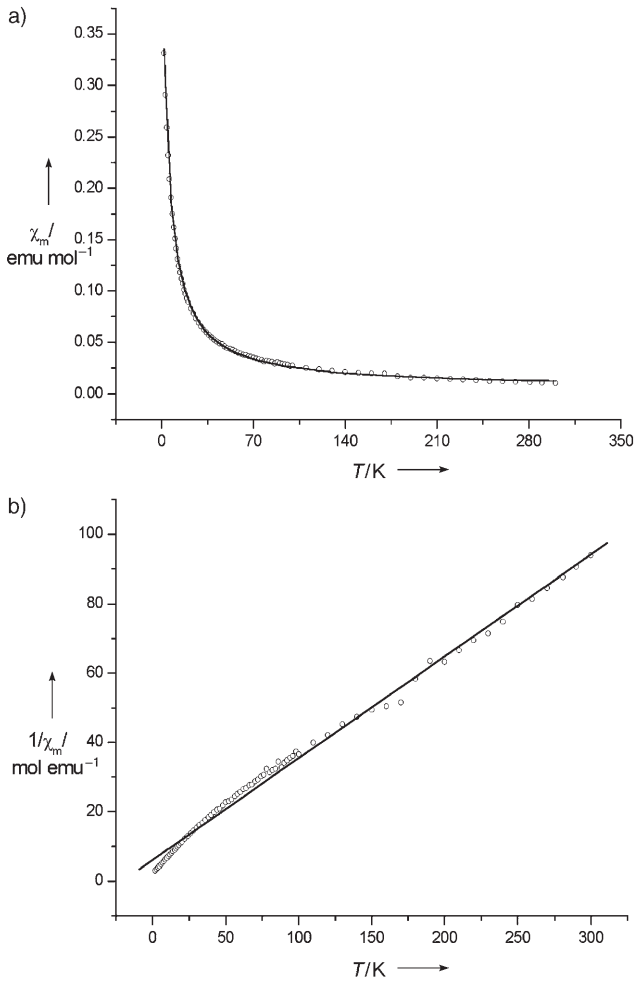

Figure 4. a) Fit of the magnetic susceptibility of $Ba_8CoNb_6O_{24}$ to the Curie–Weiss law. A single-ion Kotani fit gives an unphysical value for the spin-orbit coupling constant and thus the assignment of the observed value of θ to exchange coupling between the cobalt cations is preferred. b) Plot of the inverse susceptibility versus temperature.

resonator ceramics confirms the homogeneity of the Co distribution and the absence of $Ba_3CoNb_2O_9$ perovskite.

The structure of $Ba_8CoNb_6O_{24}$ shows that subtle differences in bonding are sufficient to produce long-range order over nanometer-distance scales even in high-temperature reactions producing complex structures containing solely six coordinate corner-sharing sites. The extension of this motif to compositionally more complex arrays in which three or more metal centers can be manipulated spatially in this manner is now a significant challenge.

Received: January 13, 2005
Revised: August 22, 2005
Published online: November 7, 2005

Keywords: cations · dielectric materials · perovskite phases · transition-metal oxides · X-ray diffraction

[1] B. B. Van Aken, T. T. M. Palstra, A. Filippetti, N. A. Spaldin, *Nat. Mater.* **2004**, *3*, 164.
[2] N. Floros, C. Michel, M. Hervieu, B. Raveau, *J. Solid State Chem.* **2002**, *168*, 11.
[3] T. A. Vanderah, *Science* **2002**, *298*, 1182.
[4] M. T. Anderson, K. B. Greenwood, G. A. Taylor, K. R. Poeppelmeier, *Prog. Solid State Chem.* **1993**, *22*, 197.
[5] G. Trolliard, N. Teneze, P. Boullay, D. Mercurio, *J. Solid State Chem.* **2004**, *177*, 1188.
[6] S. M. Moussa, J. B. Claridge, R. M. Ibberson, M. J. Rosseinsky, S. Clarke, D. Iddles, T. Price, D. C. Sinclair, *Appl. Phys. Lett.* **2003**, *82*, 4537.
[7] B. Mossner, S. Kemmler-Sack, *J. Less-Common Met.* **1986**, *120*, 203.
[8] M. W. Lufaso, *Chem. Mater.* **2004**, *16*, 2148.
[9] Z. Li, J. Sun, L. You, Y. Wang, J. Lin, *J. Alloys Compd.* **2004**, *379*, 117.
[10] T. Siegrist, T. A. Vanderah, *Eur. J. Inorg. Chem.* **2003**, 1483.
[11] M. C. Cadee, D. J. W. Ijdo, *J. Solid State Chem.* **1981**, *40*, 314.
[12] A. Manivannan, G. Glaspell, M. S. Seehra, *J. Appl. Phys.* **2003**, 6994.
[13] P. K. Davies, A. Borisevich, M. Thirumal, *J. Eur. Ceram. Soc.* **2003**, *23*, 2461.
[14] A. Salinas-Sanchez, J. L. Garcia-Munoz, J. Rodriguez-Carvajal, R. Saez-Puche, J. L. Martinez, *J. Solid State Chem.* **1992**, *100*, 201.

 © 2005 Wiley-VCH Verlag GmbH & Co. KGaA, Weinheim

High-Pressure Crystallography

DOI: 10.1002/anie.200502241

Staggered to Eclipsed Conformational Rearrangement of $[Co_2(CO)_6(PPh_3)_2]$ in the Solid State: An X-ray Diffraction Study at High Pressure and Low Temperature**

Nicola Casati, Piero Macchi, and Angelo Sironi**

Single-crystal high-pressure (HP) crystallography is a growing field, but studies on organometallics are relatively rare despite the many interesting behaviors inferred from HP spectroscopy.[1] Molecular solids, being held together by

[*] N. Casati, Dr. P. Macchi, Prof. A. Sironi
Dipartimento di Chimica Strutturale e Stereochimica Inorganica
Università degli Studi di Milano and Istituto di Scienze e Tecnologie Molecolari del CNR (ISTM-CNR)
Via Venezian 21, 20133 Milan (Italy)
Fax: (+39) 025-031-4454
E-mail: angelo.sironi@istm.cnr.it

[**] We thank Prof. Bruni for the use of the spectrometer to perform the high-pressure measurements.

Supporting information for this article is available on the WWW under http://www.angewandte.org or from the author.

WILEY InterScience DISCOVER SOMETHING GREAT
© 2005 Wiley-VCH Verlag GmbH & Co. KGaA, Weinheim

relatively weak forces, have high compressibilities; organometallics, in addition, have soft metal-centered bonds. Thus, at HP it should be possible to observe significant changes in both inter- and intramolecular distances.

We have recently discussed the nature of M–M bonds of metal carbonyl clusters using experimental and theoretical charge densities;[2] here we report the first attempt to "directly" observe the behavior of a M–M bonded system under pressure. As suggested by HP spectroscopy, $[Mn_2(CO)_{10}]$, $[Re_2(CO)_{10}]$, and $[MnRe(CO)_{10}]$ undergo a staggered to eclipsed conformational rearrangement of the equatorial carbonyl ligands,[3] which seems to be associated with a reconstructive phase transition (PT) and extensive crystal fragmentation.

To obtain "indirect" proof of this process we considered a related species, $[Co_2(CO)_6(PPh_3)_2]$ (**1**), which at room temperature and pressure (RT and RP) has an unsupported M–M bond and a staggered arrangement of equatorial CO ligands. In the solid state, **1** is isomorphous to $[Co_2(CO)_6(AsPh_3)_2]$ (**2**), which is known to undergo a reversible "crystal to crystal" PT (at $T \approx 200$ K) characterized by an incipient staggered to eclipsed rearrangement.[4] Thus, according to the well-known relationship between low-temperature (LT) and HP changes, **1** (as well as **2**) should be the ideal candidate for a single-crystal HP diffraction study of this process. Here we report the detailed crystallographic analysis of the structural behavior of **1** on lowering T (down to 28 K) and on raising P (up to 46 kbar).[5]

At RT and RP, **1** crystallizes in the trigonal space group $R\bar{3}$ and lies about a $\bar{3}$ symmetry element (*b* in Wickoff notation). The molecule (Figure 1) consists of two trigonal-bipyramidal cobalt atoms linked by an unsupported Co–Co bond along the axial direction. The remaining axial site of each metal center is occupied by a PPh_3 group and three CO ligands are bound in the equatorial positions. Given the observed crystallographic symmetry the CO ligands are constrained to be exactly staggered, and the same occurs for the phenyl groups of the triphenylphosphane ligands. In the crystal, molecules of **1** stack on top of each other in columns (parallel to *c*, Figure 2a), the projections of which define a hexagonal motif in the *ab* plane (Figure 2b). The packing along the columns is dominated by the presence of "sextuple embraces" between opposite PPh_3 groups.[6] The six neighboring columns are shifted along the *c* axis by $\pm 1/3$ (three upwards, three downwards) to allow the optimization of "lateral" interactions (π stacking of phenyl groups and CH···O contacts).

On lowering the temperature below 120 K or on increasing the pressure above 13 kbar, we observed a reversible solid–solid PT,[7] in which doubling of the *c* axis reduces the molecular symmetry from $\bar{3}$ to 3 without losing the crystal symmetry class ($\bar{3}$). After the PT, the perfect staggering of the ligands no longer holds and different structural changes are observed, the most striking of which is the rapid progress toward eclipsing of the two sets of CO ligands.

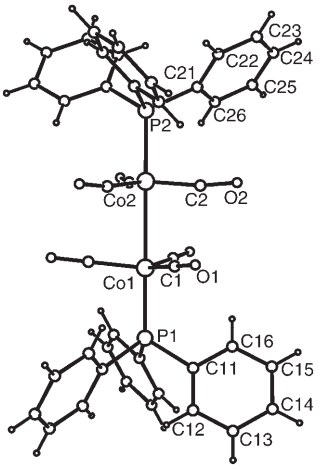

Figure 1. $[Co_2(CO)_6(PPh_3)_2]$ (**1**); independent atoms of the HP/LT phases are labeled. Before the transition the presence of an intramolecular inversion center halves the asymmetric unit and limits the significant degrees of freedom to a few angles (C11-P1-Co1-O1, C16-C11-P1-Co1, and Co2-Co1-C1) and bond lengths (Co1-Co2 and Co1-P1). After the transition the inversion center is lost, the CO-Co-Co-CO and Ph-P-P-Ph torsions are freed, and the above-mentioned parameters doubled.

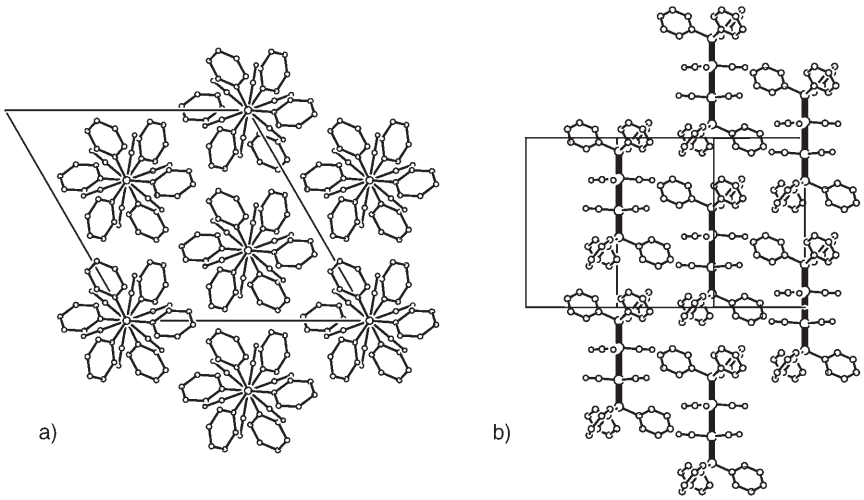

Figure 2. Crystal packing of **1** under ambient conditions. a) View normal to (001). b) View normal to (100).

Temperature-induced structural modifications are mainly due to reduced atomic motion and span a limited region of the molecular potential energy surface (at 28 K the OC-Co-Co-CO angle is ca. 56°), but larger effects are expected and found on increasing the pressure (at 46 kbar the OC-Co-Co-CO angle is as small as ca. 20°).

To estimate the energies associated with the observed molecular deformations, we performed a series of constrained DFT gas-phase optimizations of $[Co_2(CO)_6(PH_3)_2]$ (mimicking **1**, see Table 1), which showed a correlation between CO eclipsing and Co–Co elongation (the eclipsed conformer is ca. 0.2 Å longer and 10 kcal mol^{-1} less stable than the staggered one).[8] Further insight is offered by normal-mode analysis of the staggered conformer: H-P-P-H (33 cm^{-1}), OC-Co-Co-CO

 © 2005 Wiley-VCH Verlag GmbH & Co. KGaA, Weinheim

Table 1: The main molecular and intermolecular distances [Å] and angles and torsion angles [°] of **1** as measured at different values of the independent variables *P* and *T* (experimentally) and of the carbonyl torsion (DFT calculations).

	OC-Co-Co-CO	Co-P-C-C		Co-Co-CO		Co-Co	Co-P		P···P	
P [kbar]										
0.001	60	43.9(5)		86.6(5)		2.67(1)	2.21(1)		6.80(3)	
8	60	43.2(11)		87.4(10)		2.61(3)	2.17(3)		6.76(6)	
13	46.1(5)	33.6(7)	49.1(9)	82.5(10)	89.6(11)	2.69(2)	2.18	2.16	7.00(4)	6.31(4)
26	24.5(3)	32.9(5)	48.8(6)	82.4(7)	95.3(7)	2.76(1)	2.22(2)	2.15(2)	6.99(4)	6.55(4)
34	22.5(3)	32.8(4)	50.2(5)	82.1(6)	96.6(5)	2.72(1)	2.20(1)	2.14(1)	6.96(3)	6.55(3)
46	21.6(3)	32.4(5)	50.4(6)	81.2(7)	96.2(6)	2.72(1)	2.20(2)	2.16(2)	6.91(3)	6.44(3)
T [K]										
298(2)[a]	60	43.8(1)		86.6(1)		2.6610(5)	2.1914(6)		6.853(1)	
120(2)	59.66(7)	42.86(8)	43.46(8)	86.2(1)	86.1(1)	2.6492(2)	2.1860(9)	2.1880(9)	6.839(1)	6.793(1)
90(2)	5750(2)	40.45(4)	45.43(4)	85.7(1)	86.6(1)	2.6494(4)	2.1886(5)	2.1868(5)	6.9454(9)	6.677(1)
60(2)	56.05(4)	39.17(6)	46.50(6)	85.5(1)	86.8(1)	2.6510(6)	2.1872(9)	2.1852(9)	7.007(1)	6.608(1)
28(2)	55.57(4)	38.56(6)	46.93(6)	85.3(1)	86.8(1)	2.6528(6)	2.1888(8)	2.1865(9)	7.034(1)	6.584(1)
E [kcal mol^{-1}][b]										
0.0	60.0	–	–	86.6		2.652	2.205		–	–
0.7	50.0	–	–	87.2	87.2	2.670	2.208	2.208	–	–
2.8	40.0	–	–	88.5	88.4	2.700	2.208	2.208	–	–
5.3	30.0	–	–	89.9	89.9	2.749	2.207	2.207	–	–
7.6	20.0	–	–	91.1	91.1	2.790	2.207	2.207	–	–
9.1	10.0	–	–	91.8	91.8	2.820	2.206	2.206	–	–
9.7	0.0	–	–	92.1		2.831	2.206		–	–

[a] Room temperature. [b] Relative energies for $[Co_2(CO)_6(PH_3)_2]$.

(47 cm^{-1}); Co-Co-CO (96 cm^{-1}); and Co–Co (156 cm^{-1}), Co–P (320 cm^{-1}) are the softer torsional, bending, and stretching modes, respectively.

These computations, although neglecting effects of crystal packing, clearly highlight the most accessible deformation modes of the molecule. However, before the PT, Ph-P-P-Ph and OC-Co-Co-CO torsions are locked in by the crystal symmetry; thus, other deformation modes must occur, even if associated with higher energies. Indeed, at 8 kbar we observed significant compression of the Co–Co and Co–P bonds.

After the PT, other intramolecular degrees of freedom become available (see legend to Figure 1) and the response of the molecule to the "external field" can be different. For example, the Co–Co bond elongates, that is, its stretching energy is released and redistributed over the softer deformation modes now available. However, using as reference the values calculated for the isolated molecule (at different OC-Co-Co-CO torsion angles) we were able to identify, above the PT, a continuous (relative) compression of the Co–Co bond, in spite of its actual (absolute) elongation (see Table 1 and Supporting Information).

As the pressure increases, the *ab* plane shrinks (see Supporting Information) and a series of concatenated deformations occurs. We suggest the following order of (major) events (see Figure 3): P2-bound phenyl groups come into contact with the neighboring Co1-bound CO ligands, which rotate about the threefold axis and bend toward the Co2-bound ones, which in turn are pushed away. At the same time, a translation along the *c* axis of the whole molecule generates an alternation of closely (P2···P2) and loosely (P1···P1) packed sextuple embraces (like a Peierls distortion), and thus the P2-bound phenyl groups are forced to become less parallel to the molecular axis, and the opposite behavior is exhibited by their P1-bound counterparts).

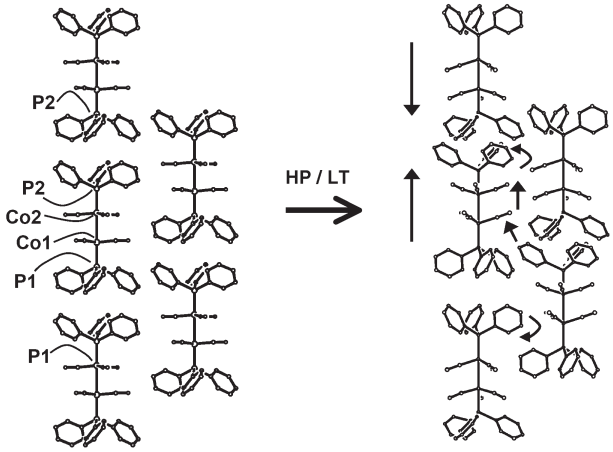

Figure 3. Schematic representation of the pressure-induced concatenated effects: bending of Co ligands, shifting of molecules, torsion of phenyl groups, and shortening of Co–P bonds.

Noteworthily, the shortening of the P2···P2 distance within the sextuple embrace is paralleled by shrinking of the related Co2–P2 bond. This is quite extraordinary as this deformation is associated with a rather deep energy well.

The interesting outcome of our experiments is that *T* and *P* induce not only modifications in the intermolecular packing but also a continuous variation of the molecular stereochemistry.

High-pressure (more than LT) crystallography is a very powerful tool for exploring the molecular potential energy surface quite far from the stationary points. Here, for

 © 2005 Wiley-VCH Verlag GmbH & Co. KGaA, Weinheim

example, we could observe the previously undetected eclipsing of a staggered carbonyl metal dimer and the consequent "molecular response" (mainly Co–Co elongation), together with crystal effects leading to the compression of the more energetic Co–P bond.

As **2** undergoes the same transition as **1**, but at higher *T*, very likely it will also undergo a lower pressure PT. Presently we are performing HP experiments on **2**, to possibly take a wider picture of the molecular rearrangements.

Experimental Section

HP experiments were conducted on one side of a Merrill Basset diamond anvil cell equipped with 600 μm culet diamonds. The sample, a hexagonal single crystal of dimensions $0.18 \times 0.18 \times 0.1$ mm was loaded in a W gasket with a 300 μm hole pre-indented to 200 μm. Diffraction data at HP were collected on a Smart-APEX CCD Bruker diffractometer following literature methods.[9] Pressure was measured by the ruby fluorescence method, using a JASCO TRS-300 spectrometer equipped with a Kr laser source.

Details of the DFT calculations and crystallography can be found in the Supporting Information.

Received: June 25, 2005
Revised: September 1, 2005

Keywords: carbonyl ligands · high-pressure chemistry · phase transitions · X-ray diffraction

[1] For example, see C. M. Edwards, I. S. Butler, *Coord. Chem. Rev.* **2000**, *199*, 1 – 53.
[2] P. Macchi, A. Sironi, *Coord. Chem. Rev.* **2003**, *238*/239, 383 – 412.
[3] D. M. Adams, P. D. Hatton, A. C. Shaw, *J. Phys. Condens. Matter* **1991**, *3*, 6145.
[4] P. Macchi, L. Garlaschelli, S. Martinengo, A. Sironi, *Inorg. Chem.* **1998**, *37*, 6263.
[5] Details for all structures are available as Supporting Information. CCDC 276054–276064 contain the supplementary crystallographic data for this paper. These data can be obtained free of charge from the Cambridge Crystallographic Data Centre via www.ccdc.cam.ac.uk/data_request/cif.
[6] I. Dance in *The Crystal as Supramolecular Entity* (Ed.: G. R. Desiraju), Wiley, Chichester, **1995**.
[7] The reversibility was confirmed by probing the crystal after the pressure was completely released.
[8] An elongation of 0.014 Å has been observed for the $[Cr_2(CO)_{10}]^{2-}$ anion on going from the staggered (Cr–Cr 2.976 Å, [2,2,2-Crypt-Na]$^+$ salt, H. Borrmann, A. M. Pirani, G. J. Schrobilgen, *Acta Crystallogr. Sect. C* **1997**, *53*, 19) to the eclipsed conformation (Cr–Cr 3.090 Å, [2,2,2-Crypt-K]$^+$ salt, H. Borrmann, A. M. Pirani, G. J. Schrobilgen, *Acta Crystallogr. Sect. C* **1997**, *53*, 1007). A detailed explanation for this behavior can be found in A. Sironi, *Metal Clusters in Chemistry, Vol. 2* (Eds.: P. Braunstein, L. A. Oro, P. R. Raithby), Wiley-VCH, Weinheim, **1999**, pp. 937 – 959.
[9] A. Dawson, D. R. Allan, S. Parsons, M. Ruf, *J. Appl. Crystallogr.* **2004**, *37*, 410.

 © 2005 Wiley-VCH Verlag GmbH & Co. KGaA, Weinheim

Rearrangement Reactions

DOI: 10.1002/anie.200502619

The Effects of Triplet Sensitizers' Energies on the Photoreactivity of β,γ-Unsaturated Methyl Ketones**

Diego Armesto, Maria J. Ortiz,**
Antonia R. Agarrabeitia, and Noureddin El-Boulifi

The photochemistry of β,γ-unsaturated ketones has been a topic of great interest to organic photochemists for many years.[1] The results of studies in this area show that these substances undergo a 1,3-acyl migration on direct irradiation and an oxa-di-π-methane (ODPM) rearrangement in the presence of triplet sensitizers. Both processes usually occur with high chemical and quantum efficiencies and high degrees of stereoselectivity.[1] As a result, the photochemical 1,3-acyl migration and ODPM rearrangement reactions have found important synthetic applications.[1] Despite the fact that a large majority of β,γ-unsaturated ketones undergo triplet-state ODPM reactions, some acyclic compounds in this series, even those having substitution patterns that are known to favor this reaction, are unreactive.[1a] For example, it has been reported that the β,γ-unsaturated ketones **1a**,[2] **1b**[3] **1c**,[4] and **1d**[2] do not undergo the ODPM rearrangement in the presence of acetophenone or 3-methoxyacetophenone. Instead, under these conditions **1a** and **1b** undergo alkene *E*/*Z* isomerization.

To gain a better understanding of this unusual behavior, we have carried out a more detailed study in which we have probed the photochemistry of enones **1a–e** by using a variety of other triplet sensitizers. The results arising from this effort reveal that these acyclic β,γ-unsaturated ketones do indeed undergo the ODPM process when the triplet energies of the sensitizers used to promote the reaction are close to those of the triplet states of the alkene moieties, and that the ODPM reactivity of these substrates is intimately related to the features of the triplet formed in the energy-transfer processes.

In this study, solutions of β,γ-unsaturated ketones **1a–e** containing sensitizers of varying triplet energies[5] (acetophenone: $E_T = 74$ kcal mol^{-1}; 3-methoxyacetophenone: $E_T = 71$ kcal mol^{-1}, depending on the absorption properties of the enone; thioxanthone: $E_T = 63$ kcal mol^{-1}; 4-phenylbenzophe-

[*] Prof. Dr. D. Armesto, Prof. Dr. M. J. Ortiz, Prof. Dr. A. R. Agarrabeitia, N. El-Boulifi
Departamento de Quimica Organica I
Facultad de Ciencias Quimicas
Universidad Complutense
28040 Madrid (Spain)
Fax: (+34) 913-944-103
E-mail: darmesto@quim.ucm.es
mjortiz@quim.ucm.es

[**] The authors thank the Universidad Complutense (PR1/05-13271) for financial support.

Supporting information for this article is available on the WWW under http://www.angewandte.org or from the author.

© 2005 Wiley-VCH Verlag GmbH & Co. KGaA, Weinheim

none: $E_T = 61$ kcal mol^{-1}; chrysene: $E_T = 57$ kcal mol^{-1}) were irradiated in an immersion apparatus through Pyrex using a 400-W medium-pressure mercury arc lamp. The results of an earlier study showed that irradiation of the β,γ-unsaturated ketone **1a**[2] (the E_T of the styrene chromophore is about 62 kcal mol^{-1})[5] with acetophenone triplet sensitization (E_T = 74 kcal mol^{-1}) for 5 h led to 91% recovery of the enone as a 1:1 mixture of *E* and *Z* isomers. In contrast, irradiation of **1a** (1:2 mixture of *E* and *Z* isomers) in CH_2Cl_2 with thioxanthone ($E_T = 63$ kcal mol^{-1}) as the sensitizer for 8.5 h resulted in formation of the ODPM product (*E*)-**2a** (50%) and recovered starting material **1a** (20%), as a 2:3 mixture of *E*- and *Z*-isomers (Scheme 1). Likewise, irradiation of **1a** (1:2, *E*/*Z*)

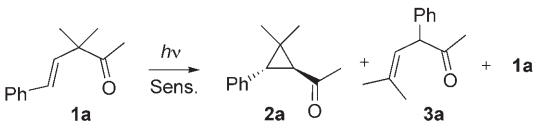

	2a	3a	1a
Acetophenone	—	—	91%
Thioxanthone	50%	—	20%
4-Phenylbenzophenone	10%	28%	35%
Chrysene	—	6%	56%

Scheme 1. Photoreactivity of enone **1a** using different triplet sensitizers. Sens.=sensitizer.

with 4-phenylbenzophenone ($E_T = 61$ kcal mol^{-1}) as sensitizer for 8.5 h promoted formation of the ODPM product (*E*)-**2a** (10%), the 1,3-acyl migration product **3a** (28%), and recovered starting material **1a** (35%), as a 2:5 mixture of *E* and *Z* isomers (Scheme 1). In this case, three different types of photochemical reactions, namely *E*/*Z* isomerization, ODPM rearrangement, and 1,3-acyl migration, take place from the triplet excited state of **1a**, a phenomenon rarely observed in photochemistry.[6] Finally, when the photoreaction of **1a** was carried out with chrysene ($E_T = 57$ kcal mol^{-1}) as the triplet sensitizer, **3a** (6%) and recovered starting material **1a** (56%, 1:6 mixture of *E* and *Z* isomers) were isolated (Scheme 1).

To the best of our knowledge, these unusual observations, which suggest that the excited-state reaction pathways followed by enone **1a** depends on the triplet energy of the sensitizer, are unprecedented. In order to determine if this behavior is observed with other β,γ-unsaturated ketones, the photochemistry of ketones **1b–e** was also explored. We found that (*E*)-**1b** behaves in a similar manner to **1a** in photoreactions promoted by the triplet sensitizers listed above. The only difference observed in this case is that the ODPM photoproduct **2b** is also formed in low yield, along with **3b** as the major product, when chrysene is used as triplet sensitizer (Scheme 2 and Table 1). The diphenylvinyl chromophore in **1c** has a triplet energy of about 53–62 kcal mol^{-1},[7] and irradiation of **1c** with 3-methoxyacetophenone ($E_T = 71$ kcal mol^{-1}) as the sensitizer leads to recovered starting material

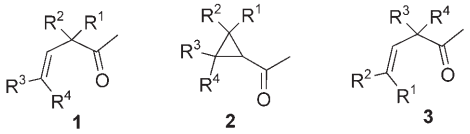

1a, **2a**, **3a**: $R^1 = R^2$ = Me, R^3 = Ph, R^4 = H
1b, **2b**, **3b**: $R^1 = R^2 = (CH_2)_4$, R^3 = Ph, R^4 = H
1c, **2c**, **3c**: $R^1 = R^2$ = Me, $R^3 = R^4$ = Ph
1d, **2d**, **3d**: $R^1 = R^2$ = Me, $R^3 = R^4$ = CN
1e, **2e**, **3e**: $R^1 = R^2$ = Me, $R^3 = (Me)_2C{=}CH$, R^4 = H

Scheme 2. Starting enones and photoproducts.

Table 1: Reaction conditions and yields of isolated products in the irradiation of β,γ-unsaturated ketones **1** in the presence of triplet sensitizers.

Substrate	Irrad. time [h]	Triplet sensitizer	Estimated ΔE_{D-A} [kcal mol^{-1}]	ODPM (yield [%])	1,3-Acyl migration (yield, [%])	Starting material (yield [%])
1a	5	acetophenone	12	–	–	91[2]
1a	8.5	thioxanthone	1	**2a** (50)	–	20
1a	8.5	4-phenylbenzophenone	−1	**2a** (10)	**3a** (28)	35
1a	8.5	chrysene	−5	–	**3a** (6)	56
1b	11	acetophenone	12	–	–	83[a]
1b	11	thioxanthone	1.7	**2b** (68)	–	30
1b	11	4-phenylbenzophenone	−1	**2b** (51)	**3b** (15)	15
1b	11	chrysene	−5	**2b** (8)	**3b** (22)	65
1c	11	3-methoxyacetophenone	13[b]	–	–	80[4]
1c	10	thioxanthone	5[b]	**2c** (39)	–	45
1c	10	4-phenylbenzophenone	3[b]	**2c** (20)	**3c** (10)	56
1c	10	chrysene	−1[b]	–	**3c** (23)	40
1d	14	acetophenone	14	–	–	60[2]
1d	25	thioxanthone	3	**2d** (39)	–	50
1d	25	4-phenylbenzophenone	1	**2d** (16)	**3d** (6)	63
1d	25	chrysene	−3	**2d** (10)	**3d** (8)	40
1e	5.5	3-methoxyacetophenone	12	–	–	72
1e	5.5	thioxanthone	4	**2e** (20)	–	32
1e	5.5	4-phenylbenzophenone	2	**2e** (53)	**3e** (7)	20
1e	5.5	chrysene	−2	**2e** (23)	**3e** (30)	27

[a] Reinvestigated by us. Compound **1b**[3] was previously reported without experimental details. [b] An average energy value of 58 kcal mol^{-1} [7] was used for the triplet energy of the diphenylvinyl unit present in **1c**.

 © 2005 Wiley-VCH Verlag GmbH & Co. KGaA, Weinheim

(80%) exclusively.[4] When thioxanthone is used as sensitizer, **1c** reacts to form the ODPM photoproduct **2c** (39%) exclusively, and both **2c** (20%) and **3c** (10%) are obtained when the process is sensitized by 4-phenylbenzophenone. Finally, the chrysene-sensitized photoreaction of **1c** gives only **3c** (23%) (Scheme 2 and Table 1).

The photochemical behavior of dicyano-substituted enone **1d**, which has a triplet energy of about 60 kcal mol^{-1},[7] also follows the general pattern described above. Thus, the acetophenone-sensitized reaction of this substrate leads to recovered starting material (60%) only.[2] With thioxanthone, the photoreaction of **1d** gives the ODPM product **2d** (39%) exclusively, and with 4-phenylbenzophenone **2d** (16%) and **3d** (6%) are obtained. Finally, chrysene sensitization also transforms **1d** into **2d** (10%) and **3d** (8%) (Scheme 2 and Table 1).

The photochemistry of β,γ-unsaturated ketone **1e**, which contains a piperylene group ($E_T = 59$ kcal mol^{-1}),[5] was studied to test the generality of this novel reactivity profile. Irradiation of **1e** (1:6 mixture of *E* and *Z* isomers) with 3-methoxyacetophenone as the sensitizer gives rise to *E*/*Z* isomerization (3:2, *E*/*Z*) only. However, with thioxanthone the ODPM product **2e** (20%) is formed in addition to recovered starting material **1e** (3:2 mixture of *E*- and *Z*-isomers). With 4-phenylbenzophenone as the triplet sensitizer, **2e** (53%) and **3e** (7%) are generated along with recovered **1e** (1:1, *E*/*Z*). Chrysene sensitization ($\Delta E_{D-A} \approx -2$ kcal mol^{-1}) also affords **2e** (23%), **3e** (30%), and **1e** (3:1, *E*/*Z*) (Scheme 2 and Table 1).

In summary, we have explored triplet-sensitized reactions of the acyclic β,γ-unsaturated methyl ketones **1a–e** by using sensitizers with different triplet energies. It has been reported that **1a–d**[2–4] do not undergo an ODPM rearrangement when acetophenone and 3-methoxyacetophenone are used as triplet sensitizers: under these conditions, **1a** and **1b** instead undergo alkene *E*/*Z* isomerization. Enone **1e** behaves similarly in that it undergoes *E*/*Z* isomerization exclusively when irradiated in the presence of 3-methoxyacetophenone as triplet sensitizer. Both of the sensitizers used in these processes have triplet energies that are about 12 kcal mol^{-1} higher than those of the alkene moieties present in the β,γ-unsaturated enones. In contrast, photoreactions of enones **1a–e** with triplet sensitizers having triplet energies that are about 5 and 1 kcal mol^{-1} higher than those of the alkene triplets follow ODPM rearrangement pathways to afford cyclopropyl ketones **2a–e** (Scheme 2). An ODPM rearrangement still takes place (albeit inefficiently) even when the triplet energies of the sensitizer are slightly lower (ca. −1 to −5 kcal mol^{-1}) than those of the alkene groups in **1a–e**, and a new process involving 1,3-acyl migration to form enones **3a–e** (Scheme 2) becomes competitive.

These results clearly show that the energy of the triplet sensitizer plays an important role in determining the outcome of triplet-sensitized reactions of β,γ-unsaturated ketones **1a–e**. The reactivity patterns suggest that, regardless of their triplet energies, all sensitizers promote photo-*E*/*Z* isomerization of the alkene moiety. However, the "hot" triplet excited states, with a large excess of vibrational energy, that are formed when sensitizers with a high triplet energy are used deactivate by *E*/*Z* isomerization exclusively. "Warm" triplet excited states of the alkene chromophores in the β,γ-unsaturated ketones are formed upon lowering the triplet energy of the sensitizer, and these undergo ODPM rearrangements in addition to the *E*/*Z* isomerization, and sensitizers that have a triplet energy close to that of the alkene groups give "cold" triplet excited states that undergo *E*/*Z* isomerization, 1,3-acyl migration, and ODPM rearrangement. Finally, when the energy of the sensitizer is slightly lower than that of the alkene, the efficiency of the ODPM rearrangement reaction path falls or is totally suppressed and *E*/*Z* isomerization and 1,3-acyl migration become the main routes followed.

It is interesting to view the conclusions presented above in the context of basic photochemical principles. Triplet sensitization is a standard method to promote triplet reactivity in molecules that do not undergo spontaneous intersystem crossing from their singlet excited states. This topic is discussed in great detail in all standard photochemical textbooks and monographs.[8] However, no reports exist, to the best of our knowledge, in the massive amount of literature on this topic that show that triplet excited states generated by intermolecular energy transfer can undergo different reactions depending on the energy of the triplet sensitizer used. Consequently, the generality of these novel findings and the accuracy of our mechanistic postulates will be tested in further studies we plan to carry out in this area.

Received: July 26, 2005
Revised: September 13, 2005
Published online: November 3, 2005

Keywords: isomerization · ketones · photochemistry · rearrangement · sensitizers

[1] For recent reviews, see: a) H. E. Zimmerman, D. Armesto, *Chem. Rev.* **1996**, *96*, 3065–3112; b) S. Vishwakarma, *CRC Handbook of Organic Photochemistry and Photobiolology, 2nd ed.* (Eds.: W. Horspool, F. Lenci), CRC, New York, **2004**, chap. 78 and 79; c) V. J. Rao, A. G. Griesbeck, *Molecular and Supramolecular Photochemistry, Vol. 12*, *Synthetic Organic Photochemistry* (Eds.: A. G. Griesbeck, J. Mattay), Marcel Dekker, New York, **2005**, pp. 189–210.

[2] D. Armesto, M. J. Ortiz, A. R. Agarrabeitia, M. Martin-Fontecha, *Org. Lett.* **2005**, *7*, 2687–2690.

[3] A. J. A. van der Weerdt, H. Cerfontain, *Recl. Trav. Chim. Pays-Bas* **1977**, *96*, 247–248.

[4] D. Armesto, M. J. Ortiz, S. Romano, A. R. Agarrabeitia, M. G. Gallego, A. Ramos, *J. Org. Chem.* **1996**, *61*, 1459–1466.

[5] S. L. Murov, I. Carmichael, G. L. Hug, *Handbook of Photochemistry, 2nd ed.*, Marcel Dekker, New York, **1993**.

[6] D. Armesto, M. J. Ortiz, A. R. Agarrabeitia, S. Aparicio-Lara, *Synthesis* **2001**, 1149–1158.

[7] H. E. Zimmerman, D. Armesto, M. G. Amezua, T. P. Gannett, R. P. Johnson, *J. Am. Chem. Soc.* **1979**, *101*, 6367–6383.

[8] See, for example: a) G. J. Calvert, J. N. Pitts, *Photochemistry*, Wiley, New York, **1966**; b) N. J. Turro, *Modern Molecular Photochemistry*, Benjamin Cummings, Menlo Park, **1978**; c) A. Gilbert, J. Baggott, *Essentials of Molecular Photochemistry*, Blackwell, Oxford, **1991**.

 © 2005 Wiley-VCH Verlag GmbH & Co. KGaA, Weinheim

Molecular Wheels

DOI: 10.1002/anie.200502699

$[Mn^{III}(salen)]_6[Fe^{III}(bpmb)(CN)_2]_6 \cdot 7H_2O$: A Cyanide-Bridged Nanosized Molecular Wheel**

Zhong-Hai Ni, Hui-Zhong Kou, Li-Fang Zhang, Chunhua Ge, Ai-Li Cui, Ru-Ji Wang, Yadong Li, and Osamu Sato**

In the past decade, the design and synthesis of metallamacrocycles has attracted extensive interest in several research fields, including materials chemistry,[1] magnetochemistry,[2] supramolecular chemistry,[3] and molecular nanotechnology.[4] Many structurally appealing metallamacrocycles[1–8] have been synthesized and some unique physical properties have been observed to date. However, most of them are homometallic $[M–O]_n$,[2,3,5] $[M–N–O]_n$,[1,6] or $[M–N–N]_n$[7] cyclic clusters, which are easier to construct than heterometallic cycles. More significantly, as far as magnetic properties are concerned, homometallic compounds are usually antiferromagnetic and therefore in a low-spin ground state, which is unfavorable for single-molecule magnets (SMMs) because the observation of such phenomena requires a high-spin ground state and significant uniaxial magnetic anisotropy.[2,5,7]

As one of the more well-known linkers, the CN^- group has been used extensively to assemble heterometallic compounds because the topological structures and the nature of the magnetic interactions between different metal ions can be readily controlled and anticipated. Therefore, we have endeavored to synthesize large, cyanide-bridged, heterometallic cycles that might exhibit high-spin ground states and even single-molecule magnet behavior. Cyanide-bridged metallamacrocycles are still scarce, and only a few tetranuclear cyclic squares[9] have been synthesized by rational design.

Recently, we have shown that the use of the rigid building block *trans*-$[Fe^{III}(bpb)(CN)_2]^-$ (H_2bpb = 1,2-bis(pyridine-2-carboxamido)benzene) is a suitable strategy for the construction of low-dimensional heterometallic species.[10] In this study, we prepared a new cyanide-containing analog $[Fe^{III}(bpmb)(CN)_2]^-$ (H_2bpmb = 1,2-bis(pyridine-2-carboxamido)-4-methylbenzene).[11] We inferred that the reaction of $[Fe(bpb)(CN)_2]^-$ or $[Fe(bpmb)(CN)_2]^-$ with $[Mn(salen)]^+$ ($salen^{2-}$ = *N*,*N*′-ethylenebis(salicylideneaminato) dianion) might lead to a one-dimensional, polynuclear or metallacyclic compound. Indeed, we have successfully obtained a unique cyanide-bridged, dodecanuclear, nanosized molecular wheel $[\{Mn(salen)\}_6\{Fe(bpmb)(CN)_2\}_6]\cdot 7H_2O$ (**1**) with a repeating [-Fe-CN-Mn-NC-]$_6$ unit. Herein we report the synthesis of this novel metallamacrocycle together with the new one-dimensional chain complex $[\{Mn^{III}(salen)\}\{Fe^{III}(bpb)(CN)_2\}]_\infty$ (**2**). To the best of our knowledge, complex **1** is the largest cyanide-bridged heterometallic metallamacrocycle to date.

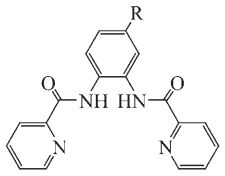

R = CH_3, H_2bpmb
R = H, H_2bpb

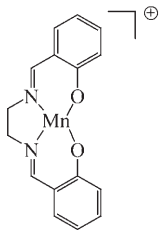

$[Mn(salen)]^+$

Compounds **1** and **2** were synthesized by the slow evaporation of a solution of equimolar amounts of $[Mn(salen)]ClO_4$ and $K[Fe(bpmb)(CN)_2]$ or $K[Fe(bpb)(CN)_2]$ in MeOH/MeCN/H_2O (6:3:1) at room temperature. An X-ray single-crystal structural analysis[12] showed that complex **1** is comprised of six Mn^{III} and six Fe^{III} ions alternately bridged by cyanide ligands to give a centrosymmetrical, elliptical, dodecanuclear molecular wheel (Figure 1), while complex **2** has a neutral infinite chain structure in which alternating $[Fe(bpb)(CN)_2]^-$ and $[Mn(salen)]^+$ fragments are linked by the cyanide ligands in $[Fe(bpb)(CN)_2]^-$ (Figure 2).

All bond distances and bond angles in complexes **1** and **2** are in the normal range. The Fe–C bond lengths (1.941(6)–1.984(6) Å for **1** and 1.956(4)–1.990(4) Å for **2**) are in good agreement with those observed previously in related compounds.[10,11] The Mn–$N_{cyanide}$ bonds range from 2.258(5) to 2.354(4) Å for **1** and from 2.301(3) to 2.439(3) Å for **2**. The Fe–C≡N bond angles in the two complexes are approximately linear (173.5(4)–178.2(5)°), except for N2≡C2–Fe1 in complex **1** (168.5(5)°). However, the Mn–N≡C bond angles (140.8(4)–163.3(5)° for **1** and 151.8(3)–158.6(3)° for **2**) deviate significantly from strict linearity. The shortest intermolecular metal–metal separations are 6.808 and 5.387 Å for **1** and **2**, respectively. In addition, the cell packing diagram (Figure 3) of complex **1** along the *a* axis shows a highly ordered pattern.

[*] Z.-H. Ni, Dr. H.-Z. Kou, L.-F. Zhang, Dr. C. Ge, Dr. A.-L. Cui, Prof. R.-J. Wang, Prof. Dr. Y. Li
Department of Chemistry
Tsinghua University
Beijing 100084 (P. R. China)
Fax: (+86) 10-6279-5477
E-mail: kouhz@mail.tsinghua.edu.cn
Prof. Dr. O. Sato
Institute for Materials Chemistry and Engineering
Kyushu University
6-1 Kasuga-koen, Kasuga, Fukuoka 816-8580 (Japan)
Fax: (+81) 92-583-7787
E-mail: sato@chem.kyushu.ac.jp

[**] This work was supported by the National Natural Science Foundation of China (project nos. 20201008 and 50272034) and the Fok Ying Tong Education Foundation. H_2bpmb = 1,2-bis(pyridine-2-carboxamido)-4-methylbenzene; $salen^{2-}$ = *N*,*N*′-ethylenebis(salicylideneaminato) dianion.

Supporting information for this article is available on the WWW under http://www.angewandte.org or from the author.

InterScience
© 2005 Wiley-VCH Verlag GmbH & Co. KGaA, Weinheim

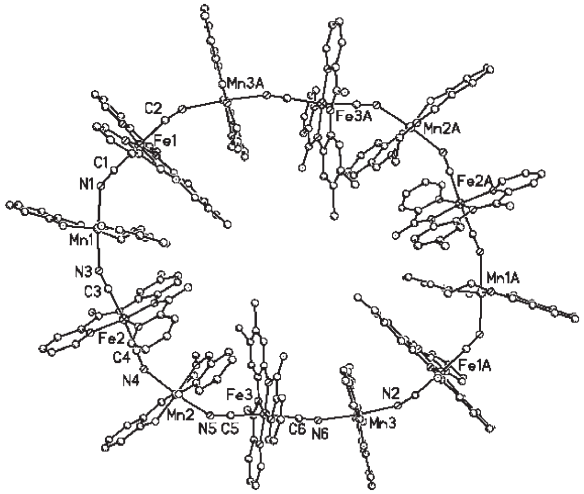

Figure 1. Structure of $[\{Mn(salen)\}_6\{Fe(bpmb)(CN)_2\}_6]\cdot 7H_2O$ (**1**). All solvent molecules and hydrogen atoms have been omitted for clarity. Selected bond lengths [Å] and angles [°]: Mn1–N1 2.354(4), Mn1–N3 2.322(4), Mn2–N4 2.290(5), Mn2–N5 2.258(5), Mn3–N2 2.327(5), Mn3–N6 2.309(5); Mn1–N1–C1 140.8(4), Mn1–N3–C3 151.7(4), Mn2–N4–C4 147.6(4), Mn2–N5–C5 147.8(4), Mn3–N6–C6 163.3(5), Mn3–N2–C2 158.0(4). Separations between opposite metal atoms [Å]: Fe1···Fe1a 21.152, Fe2···Fe2a 19.804, Fe3···Fe3a 17.728, Mn1···Mn1a 21.778, Mn2···Mn2a 19.776, Mn3···Mn3a 19.349.

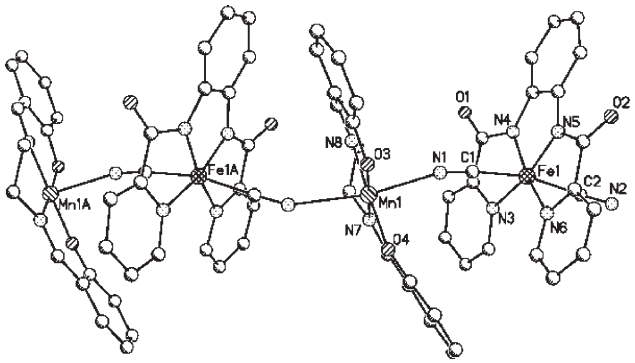

Figure 2. Structural unit of $[\{Mn(salen)\}\{Fe(bpb)(CN)_2\}]_\infty$ (**2**). Hydrogen atoms have been omitted for clarity. Selected bond lengths [Å] and angles [°]: Mn1–N1 2.301(3), Mn1–N2 2.439(3); Mn1–N1–C1 158.6(3), Mn1–N2–C2 151.8(3). The neighboring Fe···Mn distance is 5.280 Å.

It is worth noting that the largest intramolecular metal–metal distance is 2.178 nm, which corresponds to the major axis of the ellipse; the minor axis of the ellipse corresponds to a metal–metal separation of 1.773 nm, which indicates that complex **1** is a nanosized molecular wheel.

Similar to the wheel compounds previously reported,[1–8] the mechanism for the formation of wheel or chain structures is very subtle, and we have not yet been able to isolate the wheel compound containing $[Fe(bpb)(CN)_2]^-$ or the 1D compound with $[Fe(bpmb)(CN)_2]^-$. This indicates that only these two compounds are formed under the present synthetic conditions, as further proven by the powder XRD patterns (see Supporting Information). Steric effects are likely to be responsible for formation of the molecular wheel structure,

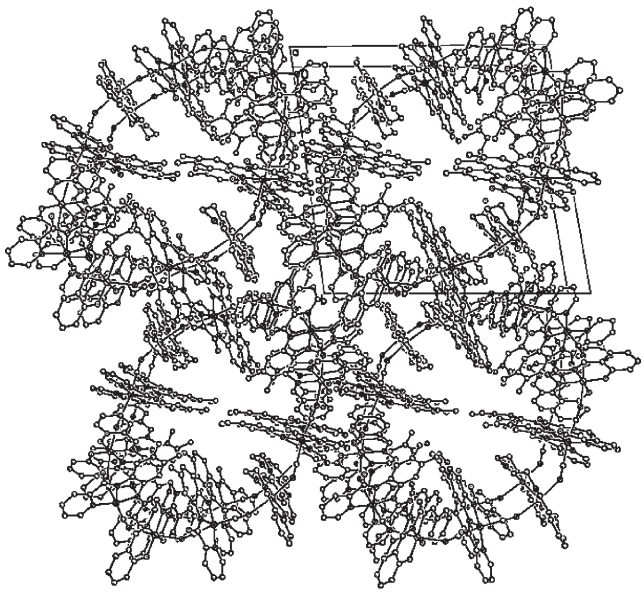

Figure 3. Cell packing diagram of complex **1** along the *a* axis showing the ordered architectural pattern.

although other factors (e.g. solvents) probably contribute. In this context, the study of the wheel-formation process and mechanism is worthwhile.

The magnetic susceptibilities of complexes **1** and **2** were measured in the range 5–300 K in an external magnetic field of 1000 Oe. As shown in Figure 4, the room temperature $\chi_m T$

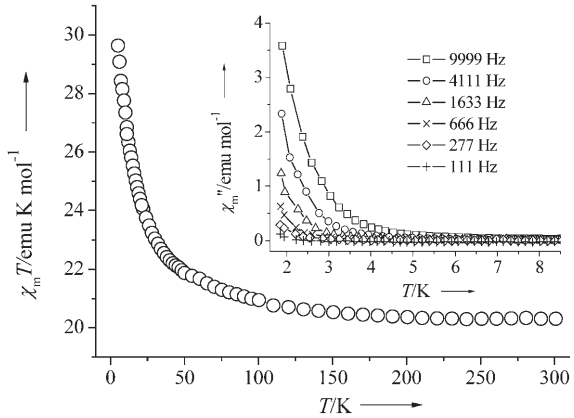

Figure 4. Temperature dependence of $\chi_m T$ for **1** at a field of 1000 Oe. Inset: the out-of-phase (χ_m'') signals in the ac susceptibility for **1**.

value for **1** is 20.3 emu K mol^{-1}, which is close to the spin-only value of 20.25 emu K mol^{-1} for six high-spin Mn^{III} ($S = 2$) and six low-spin Fe^{III} ($S = 1/2$) ions assuming that $g = 2.00$. When the temperature is decreased, the $\chi_m T$ value of complex **1** gradually increases and reaches 29.64 emu K mol^{-1} at 5 K. The reciprocal magnetic susceptibilities in the 5–300 K range obey the Curie–Weiss law, with a Curie constant, C, of 20.06 emu K mol^{-1} and a Weiss constant, θ, of $+3.5$ K. The behavior of $\chi_m T$ and the positive Weiss constant confirm the presence of overall ferromagnetic interactions in complex **1**.

 © 2005 Wiley-VCH Verlag GmbH & Co. KGaA, Weinheim

The field dependence of the magnetization for **1** at 2 K shows that the experimental values below 8 kOe are higher than the Brillouin curve corresponding to six noninteracting S_{Mn} and six S_{Fe} spins, thus confirming the overall ferromagnetic Mn^{III}–Fe^{III} coupling (see Supporting Information). The high-field magnetization values are lower than calculated, which may be due to the zero-field splitting effect of Mn^{III}.

For complex **2**, the room temperature $\chi_m T$ value is 3.45 emu K mol^{-1}, which is close to the spin-only value of 3.375 emu K mol^{-1} for one Mn^{III} ($S=2$) and one Fe^{III} ($S=1/2$) ion. As the temperature decreases, $\chi_m T$ remains nearly constant until about 50 K, and then decreases rapidly to 1.50 emu K mol^{-1} at 5 K (Figure 5). The Curie–Weiss law gives

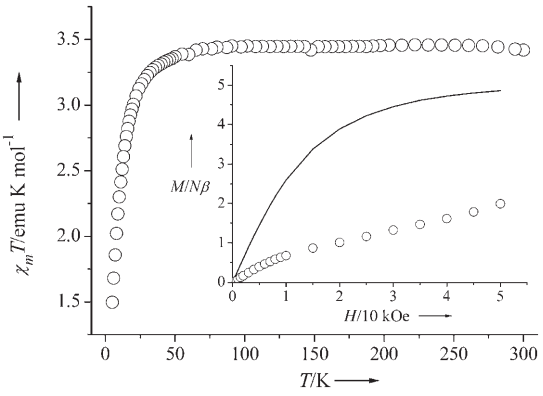

Figure 5. Temperature dependence of $\chi_m T$ for **2** at a field of 1000 Oe. Inset is the field dependence of the magnetization at 2.0 K. The line represents the Brillouin function that corresponds to noninteracting $S = S_{Mn} + S_{Fe}$ with $g = 2.0$.

a Curie constant of 3.52 emu K mol^{-1} and a Weiss constant of −3.2 K. The field dependence of the magnetization for **2** shows that the experimental values are significantly lower than the Brillouin curve corresponding to one noninteracting S_{Mn} and one S_{Fe} spin, as displayed in the inset of Figure 5. This suggests an overall antiferromagnetic Mn^{III}–Fe^{III} interaction in **2**. Similar to other cyanide-bridged high-spin Mn^{III} (d^4, $(t_{2g})^3(e_g)^1$) and low-spin Fe^{III} (d^5, $(t_{2g})^5$) systems, both ferromagnetic and antiferromagnetic contributions coexist. The overall magnetic interaction is determined by the coordination environment and configurations of the Mn^{III} and Fe^{III} ions to some extent. Therefore, the inversion of the magnetic coupling for **1** and **2** may be attributed to the different average Mn−N≡C angles of 151.4(5)° for **1** and 155.2(3)° for **2**, and the different linking of the $[Mn(salen)]^+$ unit to the $[Fe(bpmb)(CN)_2]^-$ or $[Fe(bpb)(CN)_2]^-$ building blocks, which can alter the overlap between the magnetic orbitals.[13]

As the largest cyanide-bridged, heterometallic, macrocyclic complex with ferromagnetic exchange between anisotropic Mn^{III} ions and low-spin Fe^{III} ions, **1** might represent a new type of SMM. One of the most important characteristics of an SMM is the observation of a frequency-dependent, out-of-phase (χ_m'') ac susceptibility signal. Thus, ac magnetic susceptibility measurements were performed in a 3 Oe ac field oscillating at 111–9999 Hz with a zero dc field (inset of Figure 4). Indeed, there is an obvious frequency-dependent χ_m'' signal below 4 K, along with a clear frequency-dependent decrease in the $\chi_m' T$ signals (see Supporting Information). These results are very similar to those observed for the recently published complexes $[\{Mn^{II}(tmphen)\}_3\{Mn^{III}(CN)_6\}_2]$[14a] (tmphen = 3,4,7,8-tetramethyl-1,10-phenanthroline), $[(Tp)_8(H_2O)_6Cu^{II}_6Fe^{III}_8(CN)_{24}]^{4+}$ (Tp^- = hydrotris(pyrazolyl)borate),[14b] $[Mn^{II}_4Mn^{III}_{22}(pdol)_{12}(\mu_3\text{-}CH_3O)_{12}(\mu_3\text{-}O)_{10}(\mu_4\text{-}O)_6(N_3)_6]$ ($pdol^{2-}$ = dipridylketonediolate ion),[14c] and $[Dy_6Mn_6(H_2shi)_4(Hshi)_2(shi)_{10}(CH_3OH)_{10}(H_2O)_2]\cdot 9CH_3OH\cdot 8H_2O$[14d] ($H_3shi$ = salicylhydroxamic acid), all of which have been considered as SMMs. Unfortunately, there is no maximum for the χ_m'' signals down to 2 K, and the observation of hysteretic behavior at 2 K was not possible. Thus, measurements are underway at lower temperatures to check hysteresis and to confirm whether the frequency dependence is in accord with Arrhenius-type behavior.

In summary, we have successfully synthesized a unique nanosized, dodecanuclear, molecular wheel that is the largest cyanide-bridged, heterometallic, supramolecular macrocycle known to date. Magnetic measurements indicate that **1** exhibits an interesting frequency-dependent ac magnetic susceptibility. The present study demonstrates that this synthetic route may be a promising approach to cyanide-bridged heterometallic macrocycles that may potentially exhibit SMM behavior. We are currently investigating other Mn^{III}–Schiff base building blocks and various pyridine carboxamine ligands similar to H_2bpb and H_2bpmb. Moreover, we will try to introduce other metal ions such as anistropic Ru^{III} and Mn^{III} into the system in place of the low-spin Fe^{III} ion, which may improve the magnetic properties.

Experimental Section

Complexes **1** and **2** were synthesized by the reaction of $[Mn(salen)]ClO_4$ (42.0 mg, 0.1 mmol) and $K[Fe(bpmb)(CN)_2]$[11] (48.0 mg, 0.1 mmol) or $K[Fe(bpb)(CN)_2]$[11] (46.5 mg, 0.1 mmol) in MeOH/MeCN/H_2O (10 mL, volume ratio 6:3:1) at room temperature. Uniform, well-shaped, red-brown single crystals were collected after about three days. Both **1** and **2** were isolated in high yield (ca. 60%). $C_{220}H_{176}Fe_6Mn_6N_{48}O_{31}$ (**1**) calcd: C 56.79, H 3.81, N 14.45; found: C 56.38, H 3.60, N 14.25. IR: $\tilde{\nu}$ = 2122 (m, C≡N), 1622 cm^{-1} (vs, C=O). $C_{36}H_{26}FeMnN_8O_4$ (**2**) calcd: C 58.01, H 3.52, N 15.03; found: C 57.65, H 3.57, N 15.07. IR: $\tilde{\nu}$ = 2134(m, C≡N), 2109 (m, C≡N), 1619 cm^{-1} (vs, C=O).

Received: August 1, 2005
Revised: September 15, 2005
Published online: November 3, 2005

Keywords: cyanides · iron · magnetic properties · manganese · metallacycles

[1] a) J. J. Bodwin, A. D. Cutland, R. G. Malkani, V. L. Pecoraro, *Coord. Chem. Rev.* **2001**, *216–217*, 489–512; b) V. L. Pecoraro, J. J. Bodwin, A. D. Cutland, *J. Solid State Chem.* **2000**, *152*, 68–77.

[2] a) A. J. Tasiopoulos, A. Vinslava, W. Wernsdorfer, K. A. Abboud, G. Christou, *Angew. Chem.* **2004**, *116*, 2169–2173; *Angew. Chem. Int. Ed.* **2004**, *43*, 2117–2121; b) C. Cadiou, M. Murrie, C. Paulsen, V. Villar, W. Wernsdorfer, R. E. P. Winpenny, *Chem. Commun.* **2001**, 2666–2667.

 © 2005 Wiley-VCH Verlag GmbH & Co. KGaA, Weinheim

[3] a) A. Müller, C. Serain, *Acc. Chem. Res.* **2000**, *33*, 2 – 10; b) T. B. Liu, E. Diemann, H. L. Li, A. W. M. Dress, A. Müller, *Nature* **2003**, *426*, 59 – 62.

[4] S. Leininger, B. Olenyuk, P. J. Stang, *Chem. Rev.* **2000**, *100*, 853 – 908.

[5] a) K. L. Taft, C. D. Delfs, G. C. Papaefthymiou, S. Foner, D. Gatteschi, S. J. Lippard, *J. Am. Chem. Soc.* **1994**, *116*, 823 – 832; b) A. Caneschi, A. Cornia, A. C. Fabretti, D. Gatteschi, *Angew. Chem.* **1999**, *111*, 1372 – 1374; *Angew. Chem. Int. Ed.* **1999**, *38*, 1295 – 1297; c) O. Cador, D. Gatteschi, R. Sessoli, F. K. Larsen, J. Overgaard, A.-L. Barra, S. J. Teat, G. A. Timco, R. E. P. Winpenny, *Angew. Chem.* **2004**, *116*, 5308 – 5312; *Angew. Chem. Int. Ed.* **2004**, *43*, 5196 – 5200; d) S. S. Mal, U. Kortz, *Angew. Chem.* **2005**, *117*, 3843 – 3846; *Angew. Chem. Int. Ed.* **2005**, *44*, 3777 – 3780; e) E. J. L. McInnes, C. Anson, A. K. Powell, A. J. Thomson, S. Poussereau, R. Sessoli, *Chem. Commun.* **2001**, 89 – 90; f) R. W. Saalfrank, I. Bernt, M. M. Chowdhry, F. Hampel, G. B. M. Vaughan, *Chem. Eur. J.* **2001**, *7*, 2765 – 2769.

[6] a) A. D. Cutland, J. A. Halfen, J. W. Kampf, V. L. Pecoraro, *J. Am. Chem. Soc.* **2001**, *123*, 6211 – 6212; b) C. Dendrinou-Samara, G. Psomas, L. Iordanidis, V. Tangoulis, D. P. Kessissoglou, *Chem. Eur. J.* **2001**, *7*, 5041 – 5051; c) T. C. Stamatatos, S. Dionyssopoulou, G. Efthymiou, P. Kyritsis, C. P. Raptopoulou, A. Terzis, R. Vicente, A. Escuer, S. P. Perlepes, *Inorg. Chem.* **2005**, *44*, 3374 – 3376.

[7] a) B. Kwak, H. Rhee, S. Park, M. S. Lah, *Inorg. Chem.* **1998**, *37*, 3599 – 3602; b) S.-X. Liu, S. Lin, B.-Z. Lin, C.-C. Lin, J.-Q. Huang, *Angew. Chem.* **2001**, *113*, 1118 – 1121; *Angew. Chem. Int. Ed.* **2001**, *40*, 1084 – 1087; c) R. P. John, K. Lee, M. S. Lah, *Chem. Commun.* **2004**, 2660 – 2661; d) S. Lin, S.-X. Liu, Z. Chen, B.-Z. Lin, S. Gao, *Inorg. Chem.* **2004**, *43*, 2222 – 2224.

[8] a) M. Fujita, Y. J. Kwon, S. Washizu, K. Ogura, *J. Am. Chem. Soc.* **1994**, *116*, 1151 – 1152; b) B. Grossmann, J. Heinze, E. Herdtweck, F. H. Köhler, H. Nöth, H. Schwenk, M. Spiegler, W. Wachter, B. Weber, *Angew. Chem.* **1997**, *109*, 384 – 386; *Angew. Chem. Int. Ed. Engl.* **1997**, *36*, 387 – 389; c) X.-C. Huang, J.-P. Zhang, X.-M. Chen, *J. Am. Chem. Soc.* **2004**, *126*, 13218 – 13219; d) H. Piotrowski, G. Hilt, A. Schulz, P. Mayer, K. Polborn, K. Severin, *Chem. Eur. J.* **2001**, *7*, 3196 – 3208; e) X. Wang, J. J. Vittal, *Inorg. Chem.* **2003**, *42*, 5135 – 5142; f) C.-H. Chang, K. C. Hwang, C.-S. Liu, Y. Chi, A. J. Carty, L. Scoles, S.-M. Peng, G.-H. Lee, J. Reedijk, *Angew. Chem.* **2001**, *113*, 4787 – 4789; *Angew. Chem. Int. Ed.* **2001**, *40*, 4651 – 4653.

[9] a) D. Li, S. Parkin, G. Wang, G. T. Yee, A. V. Provirin, S. M. Holmes, *Inorg. Chem.* **2005**, *44*, 4903 – 4905; b) H. Oshio, H. Onodera, T. Ito, *Chem. Eur. J.* **2003**, *9*, 3946 – 3950; c) H. Oshio, O. Tamada, H. Onodera, T. Ito, T. Ikoma, S. Tero-Kubota, *Inorg. Chem.* **1999**, *38*, 5686 – 5689; d) J. Kim, S. Han, I.-K. Cho, K. Y. Choi, M. Heu, S. Y. B. J. Suh, *Polyhedron* **2001**, *20*, 1333 – 1339; e) F. Karada, E. J. Schelter, A. V. Prosvirin, J. Bacsa, K. R. Dunbar, *Chem. Commun.* **2005**, 1414 – 1416; f) H.-Z. Kou, S. Gao, C.-H. Li, D.-Z. Liao, B.-C. Zhou, R.-J. Wang, Y. Li, *Inorg. Chem.* **2002**, *41*, 4756 – 4762.

[10] a) Z.-H. Ni, H.-Z. Kou, L. Zheng, R.-J. Wang, A.-L. Cui, O. Sato, *Inorg. Chem.* **2005**, *44*, 2050 – 2059; b) Z.-H. Ni, H.-Z. Kou, L. Zheng, Y.-H. Zhao, L.-F. Zhang, R.-J. Wang, A.-L. Cui, O. Sato, *Inorg. Chem.* **2005**, *44*, 4728 – 4736.

[11] K[Fe(bpmb)$(CN)_2$] was prepared in a similar way to K-[Fe(bpb)$(CN)_2$]: M. Ray, R. Mukherjee, J. F. Richardson, R. M. Buchanan, *J. Chem. Soc. Dalton Trans.* **1993**, 2451 – 2457; S. K. Dutta, U. Beckmann, E. Bill, T. Weyhermüller, K. Wieghardt, *Inorg. Chem.* **2000**, *39*, 3355 – 3364.

[12] Crystal data for **1**: $C_{220}H_{176}Fe_6Mn_6N_{48}O_{31}$, $M_w = 4652.83$, $T = 293$ K, triclinic, space group $P\bar{1}$, $a = 13.678(4)$, $b = 20.845(8)$, $c = 20.892(9)$ Å, $\alpha = 81.38(2)$, $\beta = 86.10(2)$, $\gamma = 76.84(2)°$, $U = 5731(4)$ Å^3, $Z = 1$, $\rho_{calcd} = 1.348$ g cm^{-3}, $\mu = 0.762$ mm^{-1}, λ(Mo K_α) = 0.71073 Å, 19761 unique reflections, 9621 observed reflections ($I > 2\sigma(I)$). $R1 = 0.0601$, $wR2 = 0.1571$ (all data), GOF = 0.998 based on 1403 parameters. **2**: $C_{36}H_{26}FeMnN_8O_4$, $M_w = 745.44$, $T = 293$ K, monoclinic, space group $P2_1/c$, $a = 9.2153(15)$, $b = 16.654(2)$, $c = 20.342(3)$ Å, $\beta = 93.664(15)°$, $U = 3115.5(8)$ Å^3, $Z = 4$, $\rho_{calcd} = 1.589$ g cm^{-3}, $\mu = 0.928$ mm^{-1}, λ(Mo K_α) = 0.71073 Å, 5473 unique reflections, 4125 observed reflections ($I > 2\sigma(I)$). $R1 = 0.0476$, $wR2 = 0.1604$ (all data), GOF = 1.067 based on 451 parameters. CCDC-279245 and -279246 contain the supplementary crystallographic data for this paper. These data can be obtained free of charge from the Cambridge Crystallographic Data Centre via www.ccdc.cam.ac.uk/data_request/cif.

[13] H. Miyasaka, N. Matsumoto, H. Okawa, N. Re, E. Gallo, C. Folriani, *J. Am. Chem. Soc.* **1996**, *118*, 981 – 994.

[14] a) C. P. Berlinguette, D. Vaughn, C. Cañada-Vilalta, J. R. Galán-Mascarós, K. R. Dunbar, *Angew. Chem.* **2003**, *115*, 1561 – 1564; *Angew. Chem. Int. Ed.* **2003**, *42*, 1523 – 1526; b) S. Wang, J.-L. Zuo, H.-C. Zhou, H. J. Choi, Y. Ke, J. R. Long, X.-Z. You, *Angew. Chem.* **2004**, *116*, 6066 – 6069; *Angew. Chem. Int. Ed.* **2004**, *43*, 5940 – 5943; c) C. Dendrinou-Samara, M. Alexiou, C. M. Zaleski, J. W. Kampf, M. L. Kirk, D. P. Kessissoglou, V. L. Pecoraro, *Angew. Chem.* **2003**, *115*, 3893 – 3896; *Angew. Chem. Int. Ed.* **2003**, *42*, 3763 – 3766; d) C. M. Zaleski, E. C. Depperman, J. W. Kampf, M. L. Kirk, V. L. Pecoraro, *Angew. Chem.* **2004**, *116*, 4002 – 4004; *Angew. Chem. Int. Ed.* **2004**, *43*, 3912 – 3914.

 © 2005 Wiley-VCH Verlag GmbH & Co. KGaA, Weinheim

Bioinorganic Chemistry

DOI: 10.1002/anie.200503134

Characterization of a Complex Comprising a $\{Cu_2(S_2)_2\}^{2+}$ Core: Bis(μ-S_2^{2-})dicopper(III) or Bis(μ-$S_2^{\cdot-}$)dicopper(II)?**

*John T. York, Eric C. Brown, and William B. Tolman**

Copper–sulfur interactions play a critical role in the function of several classes of biological molecules, with the soft, polarizable nature of sulfur being uniquely suited for modulating the electronic structure and reactivity of copper-protein active sites. For example, copper–thiolate bonds with significant covalent character in type 1 monocopper and

[*] J. T. York, Dr. E. C. Brown, Prof. W. B. Tolman
Department of Chemistry and
Center for Metals in Biocatalysis
University of Minnesota
207 Pleasant Street SE, Minneapolis, MN 55455 (USA)
Fax: (+1) 612-624-7029
E-mail: tolman@chem.umn.edu

[**] This work was supported by grants from the National Institutes of Health (GM-47365 to W.B.T. and GM-68307 to E.C.B.).

Supporting information for this article is available on the WWW under http://www.angewandte.org or from the author.

© 2005 Wiley-VCH Verlag GmbH & Co. KGaA, Weinheim
InterScience

mixed-valent dicopper "Cu_A" centers mediate electronic delocalization, which facilitates electron-transfer reactions.[1] The inorganic sulfur recently identified in the "Cu_Z" site of nitrous oxide reductase, which features four copper ions linked by a μ_4-sulfido ligand and attached to the protein through multiple histidine imidazolyl ligands, has also been postulated to play a role in electronic delocalization.[2,3] To gain insight into the properties of the unique "Cu_Z" catalytic cluster through the study of synthetic model complexes, the chemistry of copper–sulfur complexes containing N-donor ligands needs to be developed. In efforts towards this aim, complexes with (μ-η^2:η^2-disulfido(2-))dicopper(II)[4a,b] or (*trans*-μ-1,2-disulfido(2-))dicopper(II)[4c,d] cores have been isolated by using sterically bulky multidentate N-donor coligands. We recently discovered that reactions of the copper(I) complexes [Cu(tmeda)(MeCN)]SbF_6 (**1a**) and [Cu(tmchd)(MeCN)]PF_6 with S_8 yield clusters with fully delocalized mixed-valent $\{Cu_3(\mu\text{-}S)_2\}^{3+}$ cores (Scheme 1).[5,6] Herein, we report that the reaction of [Cu(tmeda)(MeCN)]OTf (**1b**)[5] with S_8 instead yields a complex with a heterocyclic $\{Cu_2(\mu\text{-}1,2\text{-}S_2)_2\}^{2+}$ core,[7] for which an unexpected electronic structure is proposed on the basis of structural and spectroscopic data.

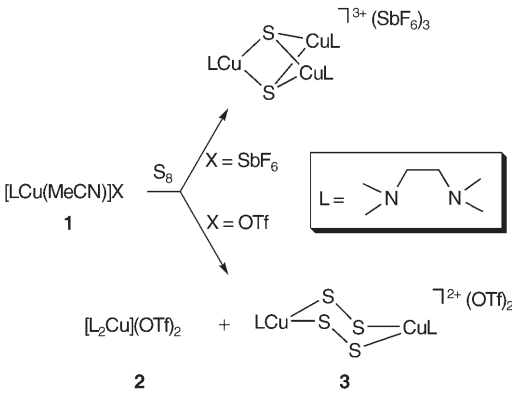

Scheme 1.

The addition of excess elemental sulfur (4 equiv) to a colorless solution of **1b** in THF or CH_2Cl_2 at room temperature resulted in the gradual development of a deep-blue color. Two products were isolated from the reaction mixture by removal of solvent, filtration, and fractional crystallization/precipitation, and were structurally characterized by X-ray diffraction (Scheme 1).[8] The blue–green complex [Cu(tmeda)$_2$](OTf)$_2$ (**2**, see Supporting Information) is a minor product (13% yield) that apparently derives from partial disproportionation of **1b**, as small amounts of metallic copper were also observed. The dark-blue complex $[Cu_2(tmeda)_2(\mu\text{-}1,2\text{-}S_2)_2](OTf)_2$ (**3**, Figure 1) was isolated in 63% yield, and features two square-pyramidal copper centers, each with two S and two N donors occupying equatorial positions and a weakly coordinated axial triflate anion.

In assessing the structural parameters for **3**, two extreme resonance formulations may be considered for its $\{Cu_2(\mu\text{-}1,2\text{-}S_2)_2\}^{2+}$ core: two Cu^{III} ions bridged by disulfide(2-) ions (S_2^{2-}), or two Cu^{II} ions bridged by disulfide($\cdot$1−) ions ($S_2^{\cdot-}$).[9] Similar resonance forms have been invoked in ruthenium and iron complexes.[7d,10] The Cu–N bond lengths in **3** of 2.032(3) and 2.058(3) Å are significantly longer than those in Cu^{III} complexes with similar diamine ligands (Cu–N $\approx$1.93 Å),[11] and are more consistent with those in Cu^{II}–N(amine) complexes (Cu–N 2.06–2.17 Å in **2**). The S–S bond length in **3** is 1.950(1) Å, which falls between that of free S_2 (S=S 1.892 Å) and H_2S_2 (S–S 2.055 Å).[12] As a comparison, the S–S bonds in transition-metal μ-1,2-disulfido(2-) complexes typically range from 2.01 to 2.06 Å;[7,10a,b,d,13,14] the only structurally characterized (*trans*-μ-1,2 disulfido(2-))dicopper(II) complex has a S–S bond length of 2.044 Å.[4c] In summary, the X-ray structural data are most consistent with a bis(μ-disulfido($\cdot$1−))dicopper(II) formulation for **3**.

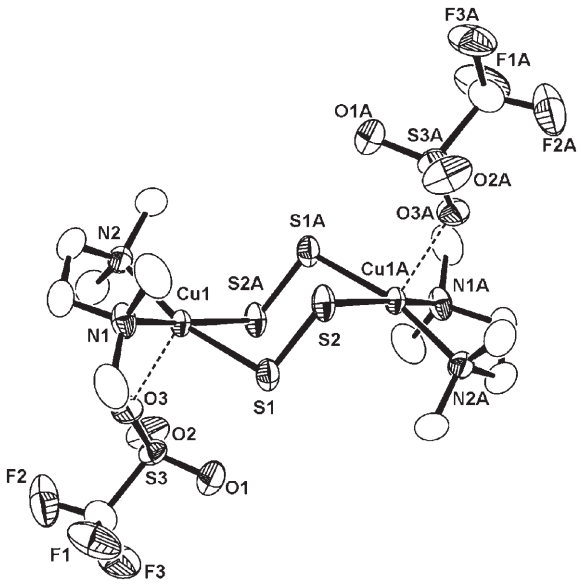

Figure 1. Molecular structure of **3** (50% ellipsoids, H atoms excluded, only heteroatoms labeled). Selected interatomic distances [Å]: S1-S2, 1.9500(13); Cu1-S1, 2.2696(11); Cu1-S, 2.2729(12); Cu1-N1, 2.032(3); Cu1-N2, 2.058(3); Cu1-O3, 2.304(2).

Further insight is provided by spectroscopic data. Complex **3** is EPR silent (X-band, 20 K) and exhibits a sharp, well-resolved ^{1}H NMR spectrum, indicative of a diamagnetic ground state; this is consistent with either resonance formulation if one invokes strong antiferromagnetic coupling in the case of the bis(μ-disulfido($\cdot$1−))dicopper(II) species. The UV/Vis spectrum of **3** in THF at 25 °C has intense absorption features at 251 ($\varepsilon = 11\,000\,M^{-1}cm^{-1}$), 394 ($\varepsilon = 9000\,M^{-1}cm^{-1}$), and 575 nm ($\varepsilon = 6400\,M^{-1}cm^{-1}$), which bleach upon exposure to air (Figure 2a). Unlike many *trans*-disulfido(2-)-bridged complexes,[4c,9c,13e,13f,15] **3** exhibits no absorption features generally attributable to the 4-center–6-electron $\{M_2S_2\}$ chromophore in the near-IR region of the spectrum. Resonance Raman spectra (Figure 2b) of a frozen solution of **3** in THF obtained by using 514.5-nm laser excitation wavelength reveal strong S-isotope sensitive bands at 613 and 336 cm^{-1} that are consistent with ν(S–S) and ν(Cu–S) vibrations, respectively ($\Delta^{34}S_{exptl} = 19$ and $9\,cm^{-1}$; $\Delta^{34}S_{calcd} = 18$ and $7\,cm^{-1}$). The ν(S–S) vibration at 613 cm^{-1} is at a much higher wavenumber

 © 2005 Wiley-VCH Verlag GmbH & Co. KGaA, Weinheim

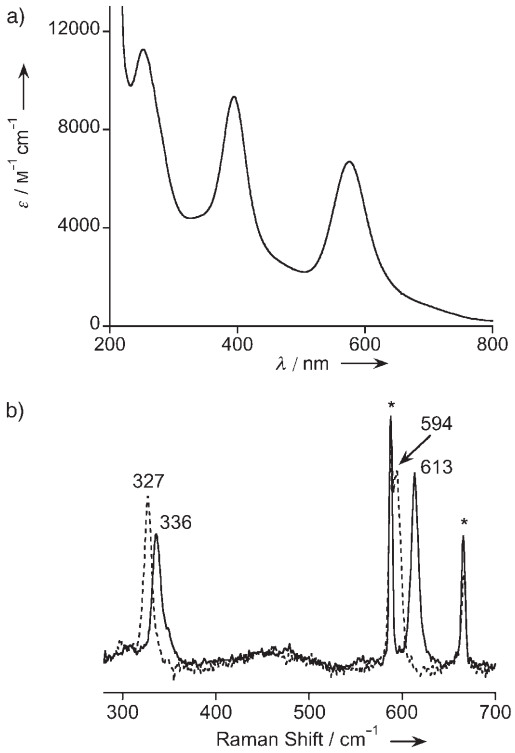

Figure 2. a) UV/Vis spectrum of **3** in THF at 25 °C. b) Resonance Raman spectrum of **3** in THF at −196 °C, $\lambda_{ex} = 514.5$ nm (^{32}S, solid line; ^{34}S, dashed line; asterisks indicate peaks arising from the solvent).

than that normally observed in μ-disulfido(2-) complexes,[9b,g,14c,16] including dicopper examples, which have ν(S–S) vibrations in the range from around 450 to 500 cm^{-1}.[4] Indeed, comparison with published ν(S–S) values for Na_2S_2 (446 cm^{-1}),[17] $S_2^{\bullet-}$ (601 cm^{-1}),[18] and doubly bonded S_2 (718 cm^{-1})[19] clearly supports a $S_2^{\bullet-}$ formulation for the bridging ligands in **3**.

In summary, the combined structural and spectroscopic data indicate that **3** is best described as a bis(μ-disulfido-(·1−))dicopper(II) complex,[9] which represents a new motif in copper–sulfur chemistry. The lack of further reduction of the sulfur ligands to yield a bis(μ-disulfido(2-))dicopper(III) species can be rationalized on the basis of the relatively low electronegativity of sulfur (relative to that of oxygen). A further intriguing aspect is the fact that **3** is the major product of the reaction of S_8 with **1b**, but under identical conditions, the reaction with **1a** yields the mixed-valent cluster $[Cu_3S_2(tmeda)_3](SbF_6)_3$.[5] The better coordinating ability of OTf^- relative to that of SbF_6^- may be in part responsible for the divergent reactivity, but the nature of the N-donor ligand also is important, as both the PF_6^- and OTf^- salts of [Cu(tmchd)(MeCN)]$^+$ yield the bis(μ-sulfido)tricopper cluster.[20] Future studies will address this effect of counterion, as well as aspects of the reactivity of **3**.

Experimental Section

All solvents and reagents were obtained from commercial sources and used as received unless noted otherwise. The solvents tetrahydrofuran (THF), pentane, diethyl ether, and dichloromethane were passed through solvent purification columns (Glass Contour, Laguna, CA) prior to use. All metal complexes were prepared and stored in a Vacuum Atmospheres inert-atmosphere glove box under a dry nitrogen atmosphere or were manipulated by using standard Schlenk line techniques. Labeled elemental sulfur (^{34}S, 99 % enrichment) was purchased from Cambridge Isotope Laboratories, Inc. NMR spectra were recorded on a Varian VI-300 or VXR-300 spectrometer. Chemical shifts (δ) for ^1H or ^{13}C NMR spectra were referenced to residual protons in the deuterated solvent. UV/Vis spectra were recorded on a HP8453 (190–1100 nm) diode-array spectrophotometer. X-band EPR spectra were recorded on a Bruker E-500 spectrometer with an Oxford Instruments EPR-10 liquid-helium cryostat. Resonance Raman spectra were recorded on an Acton 506 spectrometer by using a Princeton Instruments LN/CCD-11100-PB/UVAR detector and ST-1385 controller interfaced with Winspec software. The spectra were obtained at −196 °C by using a backscattering geometry. Samples were frozen in an NMR tube by submersion in a dewar flask containing liquid nitrogen. Raman shifts were externally referenced to liquid indene. ESI mass spectra were obtained on a Bruker BioTOF II spectrometer. The ligand tmeda was purchased from Aldrich Chemical Co. and used as received. The complex [Cu(MeCN)$_4$]OTf was prepared according to a published procedure.[21] Crystallographic information on **2** are listed in the Supporting Information.

[Cu(tmeda)(MeCN)]OTf (**1b**): A solution of tmeda (0.055 g, 0.47 mmol) in CH_2Cl_2 (2 mL) was added to a solution of [Cu(MeCN)$_4$]OTf (0.160 g, 0.43 mmol) in CH_2Cl_2 (4 mL). The reaction was stirred for 30 minutes, filtered through celite, and the filtrate concentrated under reduced pressure to approximately 2 mL. Addition of pentane (10 mL) resulted in the precipitation of a white solid, which was collected, washed with diethyl ether (3 × 5 mL), and dried under vacuum. Yield: 148 mg (93 %); ^1H NMR (CD_2Cl_2, 300 MHz): $\delta = 2.56$ (s, 4H), 2.52 (s, 12H), 2.23 ppm (s, 3H); ^{13}C NMR (CD_2Cl_2, 75 MHz): $\delta = 120.7$ ($J_{C,F} = 320$ Hz), 115.9, 57.9, 48.1, 2.1 ppm; ESIMS: calcd for [Cu(tmeda)(MeCN)]$^+$: m/z 220.0870; found: 220.0853.

$[Cu_2(S_2)_2(tmeda)_2](OTf)_2$ (**3**): Elemental sulfur (0.117 g, 0.46 mmol) was added to a solution of **1b** (0.170 g, 0.46 mmol) in THF (15 mL). The solution was stirred for 18 h at room temperature, during which time it turned deep blue. The solvent was removed by vacuum and the resulting residue was extracted with THF (10 mL) and filtered through celite. The filtrate was placed in a freezer at −20 °C overnight. Two different forms of crystals of **2** were formed, along with excess sulfur, which were collected by filtration and separated mechanically (0.035 g, 13 % yield). Elemental analysis (%) calcd for $C_{14}H_{32}N_4CuS_2O_6F_6$ (**2**): C 28.30, H 5.43, N 9.43; found: C 27.70, H 5.14, N 9.13. The solvent was removed from the filtrate in vacuo to give **3** as a dark blue powder. The solid was washed with diethyl ether (2 × 5 mL) and dried under vacuum. Purple crystals of **3** were grown from a solution in THF by slow diffusion of pentane at −20 °C. Yield: 115 mg (63 %); ^1H NMR (CD_2Cl_2, 300 MHz): $\delta = 2.49$ (s, 8H), 2.37 ppm (s, 24H); UV/Vis (THF): λ_{max} (ε, $M^{-1}cm^{-1}$) = 251 (11 000), 394 (9000), 575 nm (6400); elemental analysis (%) calcd for $C_{14}H_{32}N_4Cu_2S_6O_6F_6$ (**3**): C 21.40, H 4.10, N 7.13; found: C 21.84, H 4.05, N 6.94.

Received: September 2, 2005
Published online: November 3, 2005

Keywords: bioinorganic chemistry · bridging ligands · copper · N ligands · sulfur

 © 2005 Wiley-VCH Verlag GmbH & Co. KGaA, Weinheim

[1] D. W. Randall, D. R. Gamelin, L. B. LaCroix, E. I. Solomon, *J. Biol. Inorg. Chem.* **2000**, *5*, 16.

[2] a) K. Brown, K. Djinovic-Carugo, T. Haltia, I. Cabrito, M. Saraste, J. J. G. Moura, I. Moura, M. Tegoni, C. Cambillau, *J. Biol. Chem.* **2000**, *275*, 41133; b) T. Haltia, K. Brown, M. Tegoni, C. Cambillau, M. Saraste, K. Mattila, K. Djinovic-Carugo, *Biochem. J.* **2003**, *369*, 77.

[3] a) T. Rasmussen, B. C. Berks, J. Sanders-Loehr, D. M. Dooley, W. G. Zumft, A. J. Thomson, *Biochemistry* **2000**, *39*, 12753; b) M. L. Alvarez, J. Ai, W. Zumft, J. Sanders-Loehr, D. M. Dooley, *J. Am. Chem. Soc.* **2001**, *123*, 576; c) P. Chen, S. DeBeer George, I. Cabrito, W. E. Antholine, J. J. G. Moura, I. Moura, B. Hedman, K. O. Hodgson, E. I. Solomon, *J. Am. Chem. Soc.* **2002**, *124*, 744; d) P. Chen, I. Cabrito, J. J. G. Moura, I. Moura, E. I. Solomon, *J. Am. Chem. Soc.* **2002**, *124*, 10497; e) S. Ghosh, S. I. Gorelsky, P. Chen, I. Cabrito, J. J. G. Moura, I. Moura, E. I. Solomon, *J. Am. Chem. Soc.* **2003**, *125*, 15708.

[4] a) E. C. Brown, N. W. Aboelella, A. M. Reynolds, G. Aullón, S. Alvarez, W. B. Tolman, *Inorg. Chem.* **2004**, *43*, 3335; b) K. Fujisawa, Y. Moro-oka, N. Kitajima, *J. Chem. Soc. Chem. Commun.* **1994**, 623; c) M. E. Helton, P. Chen, P. P. Paul, Z. Tyeklar, R. D. Sommer, L. N. Zakharov, A. L. Rheingold, E. I. Solomon, K. D. Karlin, *J. Am. Chem. Soc.* **2003**, *125*, 1160; d) P. Chen, K. Fujisawa, M. E. Helton, K. D. Karlin, E. I. Solomon, *J. Am. Chem. Soc.* **2003**, *125*, 6394.

[5] Abbreviations used: tmeda = *N*,*N*,*N*′,*N*′-tetramethylethylenediamine; tmchd = *N*,*N*,*N*′,*N*′-tetramethylcyclohexane-1,2-diamine; OTf = trifluoromethanesulfonate.

[6] E. C. Brown, J. T. York, W. E. Antholine, E. Ruiz, S. Alvarez, W. B. Tolman, *J. Am. Chem. Soc.* **2005**, *127*, 13752.

[7] Similar core geometries have been reported with other transition metals: a) J. Amarasekera, T. B. Rauchfuss, A. L. Rheingold, *Inorg. Chem.* **1987**, *26*, 2017; b) D. M. Giolando, T. B. Rauchfuss, A. L. Rheingold, S. R. Wilson, *Organometallics* **1987**, *6*, 667; c) R. J. Pleus, W. Saak, S. Pohl, *Z. Anorg. Allg. Chem.* **2001**, *627*, 250; d) P. M. Treichel, R. A. Crane, K. J. Haller, *Polyhedron* **1990**, *9*, 1893.

[8] X-ray structural analysis of **3**: An X-ray quality crystal was mounted on a Siemens SMART Platform CCD diffractometer for data collection. A randomly oriented region of reciprocal space was surveyed to the extent of one sphere and to a resolution of 0.84 Å. The intensity data were corrected for absorption and decay by using SADABS (R. Blessing, *Acta Crystallogr. Sect. A* **1995**, *51*, 33). Final cell constants were calculated from the *xyz* centroids of strong reflections from the actual data collection after integration with SAINT (SAINT version 6.2, Bruker Analytical X-ray Systems, Madison, WI, **2001**). The structure was solved by direct methods with SHELXL97 software (SHELXTL version 6.10, Bruker Analytical X-Ray Systems, Madison, WI, **2000**). Full-matrix least-squares/difference Fourier cycles were performed by using SHELXL97 software, which located the remaining non-hydrogen atoms. All non-hydrogen atoms were refined with anisotropic displacement parameters. All hydrogen atoms were placed in ideal positions and refined as riding atoms with relative isotropic displacement parameters. $C_{14}H_{32}N_4F_6O_6S_6Cu_2$, $M_r = 785.88$, monoclinic, space group $P2(1)/n$, $a = 8.697(5)$, $b = 13.269(5)$, $c = 13.029(5)$ Å, $\beta = 92.481(5)°$, $V = 1502.1(12)$ Å^3, $Z = 2$, $\rho_{calcd} = 1.737$ g cm^{-3}, $\lambda(Mo_{K\alpha}) = 0.71069$ Å, $T = 173(2)$ K, crystal dimensions $0.25 \times 0.25 \times 0.20$ mm^3, $\mu(Mo_{K\alpha}) = 1.906$ mm^{-1}, θ range from 2.19 to 25.06°, 7497 measured reflections, 2651 independent reflections ($R_{int} = 0.0243$), R_1 ($I > 2\sigma(I) = 0.0314$), wR_2 ($I > 2\sigma(I)) = 0.0710$, GOF = 1.027, 172 parameters, final difference map within 0.569 and −0.230 e Å^{-3}. The crystallographic data for the two forms of **2** are given in the Supporting Information. CCDC-282801–282803 contain the supplementary crystallographic data for this paper. These data can be obtained free of charge from The Cambridge Crystallographic Data Centre via www.ccdc.cam.ac.uk/data_request/cif.

[9] The $S_2^{\bullet-}$ ion is often referred to as "supersulfide" in the literature, but, according to the IUPAC recommendations, it should be denoted as "disulfide(1−)"; see: W. H. Koppenol, *Pure Appl. Chem.* **2000**, *72*, 437.

[10] a) A. Terzis, R. Rivest, *Inorg. Chem.* **1973**, *12*, 2132; b) R. C. Elder, M. Trkula, *Inorg. Chem.* **1977**, *16*, 1048; c) R. Schneider, K. Weighardt, B. Nuber, *Inorg. Chem.* **1993**, *32*, 4935; d) P. J. Vergamini, R. R. Ryan, G. J. Kubas, *J. Am. Chem. Soc.* **1976**, *98*, 1980; e) H. Sugiyama, Y. Lin, K. Matsumoto, *Angew. Chem.* **2000**, *112*, 4224; *Angew. Chem. Int. Ed.* **2000**, *39*, 4058; f) K. Matsumoto, H. Sugiyama, *Acc. Chem. Res.* **2002**, *35*, 915; g) S. Kim, E. S. Otterbein, R. P. Rava, S. S. Isied, J. S. Filippo, J. V. Waszcyak, *J. Am. Chem. Soc.* **1983**, *105*, 336.

[11] a) A. P. Cole, D. E. Root, P. Mukherjee, E. I. Solomon, T. D. P. Stack, *Science* **1996**, *273*, 1848; b) V. Mahadevan, Z. Hou, A. P. Cole, D. E. Root, T. K. Lal, E. I. Solomon, T. D. P. Stack, *J. Am. Chem. Soc.* **1997**, *119*, 11996.

[12] a) R. Steudel, *Angew. Chem.* **1975**, *87*, 683; *Angew. Chem. Int. Ed. Engl.* **1975**, *14*, 655; b) B. Meyer, *Chem. Rev.* **1976**, *76*, 370.

[13] A. Müller, W. Jaegermann, J. H. Enemark, *Coord. Chem. Rev.* **1982**, *46*, 245.

[14] a) A. V. Firth, D. W. Stephan, *Inorg. Chem.* **1998**, *37*, 4726; b) K. B. Capps, G. D. Whitener, A. Bauer, K. A. Abboud, I. M. Wasser, K. P. C. Vollhardt, C. D. Hoff, *Inorg. Chem.* **2002**, *41*, 3212; c) P. B. Glaser, P. W. Wanandi, T. D. Tilly, *Organometallics* **2004**, *23*, 693; d) M. W. Droege, H. Taube, *Inorg. Chem.* **1987**, *26*, 3316; e) J. D. Franolic, M. Millar, S. A. Koch, *Inorg. Chem.* **1995**, *34*, 1981; f) D. Sellmann, G. Mahr, F. Knoch, *Angew. Chem.* **1991**, *103*, 1493; *Angew. Chem. Int. Ed. Engl.* **1991**, *30*, 1477; g) C. M. Bollinger, T. B. Rauchfuss, A. L. Rheingold, *Organometallics* **1982**, *1*, 1551; h) T. B. Rauschfuss, D. P. S. Rogers, S. R. Wilson, *J. Am. Chem. Soc.* **1986**, *108*, 3114.

[15] a) D. Sellmann, F. W. Heinemann, T. Gottschalk-Gaudig, *Z. Naturforsch. B* **1999**, *54*, 1122; b) D. Sellmann, P. Lechner, F. Knoch, M. Moll, *J. Am. Chem. Soc.* **1992**, *114*, 922; c) J. A. Amarasekera, T. B. Rauchfuss, S. R. Wilson, *Inorg. Chem.* **1987**, *26*, 3328.

[16] a) C. R. Brulet, S. S. Isied, H. Taube, *J. Am. Chem. Soc.* **1973**, *95*, 4758; b) W. M. Scovell, T. G. Spiro, *Inorg. Chem.* **1974**, *13*, 304; c) M. M. T. Khan, M. R. H. Siddiqui, *Inorg. Chem.* **1991**, *30*, 1157; d) K. Matsumoto, T. Matsumoto, M. Kawano, H. Ohnuki, Y. Shichi, T. Nishide, T. Sato, *J. Am. Chem. Soc.* **1996**, *118*, 3597.

[17] A. Müller, W. Jaegermann, *Inorg. Chem.* **1979**, *18*, 2631.

[18] Measured in crystalline KI: J. Rolfe, *J. Chem. Phys.* **1968**, *49*, 4193.

[19] K. K. Yee, R. F. Barrow, A. Rogstad, *J. Chem. Soc. Faraday Trans. 2* **1972**, *68*, 1808.

[20] J. T. York, E. C. Brown, W. B. Tolman, unpublished results.

[21] G. J. Kubas, *Inorg. Synth.* **1979**, *19*, 90.

 © 2005 Wiley-VCH Verlag GmbH & Co. KGaA, Weinheim

Gas Storage

DOI: 10.1002/anie.200502376

Structural Transition and Tuning of *tert*-Butylamine Hydrate**

*Do-Youn Kim, Jong-won Lee, Yu-Taek Seo, John A. Ripmeester, and Huen Lee**

Gas hydrates, or more generally clathrate hydrates, are a type of inclusion compound and take the form of nonstoichiometic solid crystalline materials formed from water and small guest molecules.[1] Under sufficient pressure of the guest material and at specific temperatures, 3D hydrate structures are formed by the stacking of polyhedral cages of hydrogen-bonded water molecules. Suitably sized guest molecules are enclathrated in cages and their presence stabilizes the compounds formed. Although the guest molecules are physically enclosed within the cages, there are no direct chemical bonds between host water molecules and guest molecules.

In general gas hydrates form three distinct structural families known as structure I (sI), structure II (sII), and structure H (sH), which differ in the combination of cage types required to build a 3D structure.[2] In addition, there are a variety of more complex clathrate hydrate structures, labeled as types III–VII[2] and structure T (sT).[3] It is clear that many of the physical attributes of gas hydrates remain unknown and thus need to be examined in more detail. The gas hydrates are of particular interest in the fields of energy research and environmental science because of the possible applications for the storage of natural gas,[4] sequestration of CO_2 in the deep ocean,[5] and separation of greenhouse gases from flue gas.[6] It is noteworthy that for lowering the pressure of hydrate formation without significant reduction of the capacity to store CH_4, the use of sH hydrate was suggested.[7] Many experimental and theoretical works to understand macroscopic phase behavior and microscopic structural characteristics of the pure and mixed hydrates have been reported.[8–12] Most recently, we proposed a tuning mechanism to increase the storage capacity of hydrogen in double hydrogen hydrate.[13]

Herein, we report a structural transition of the simple amine hydrate to produce a novel double (CH_4 + tBuNH$_2$) hydrate as confirmed by using microscopic analytical methods. Powder X-ray diffraction (PXRD) was adopted as the primary method to identify the structure of the gas hydrates and to provide lattice parameters. More importantly, the distribution of guest molecules over the hydrate cages was investigated by NMR spectroscopy, as it is imperative to establish a mutual consistency between the structures from PXRD and the structure-specific chemical-shift signatures from NMR spectroscopy to obtain a more complete description of the hydrates. In addition, the corresponding hydrate compositions were determined from a quantitative analysis of the NMR spectroscopic results. We note that during sample preparation in a high-pressure vessel, the composition of the aqueous phase continuously changes. However, for this work we have focused only on the final equilibrium compositions that are spontaneously determined by the pressure of CH_4 gas, system temperature, and initial concentration of tBuNH$_2$.

The tBuNH$_2$ clathrate hydrate, $16\,(CH_3)_3CNH_2{\cdot}156\,H_2O$, which Jeffrey designated as a type VI structure,[2] is a true clathrate as there is no evidence of hydrogen bonding between host water and guest amine molecules. tBuNH$_2$ molecules occupy large complex cages with 17 sides ($4^3 5^9 6^2 7^3$) while the small cages ($4^4 5^4$) remain empty.[14] Figure 1 represents the PXRD patterns of both pure tBuNH$_2$ and double (CH_4 + tBuNH$_2$) hydrate at 113.15 K. According to a previous report,[14] the structure of pure tBuNH$_2$ hydrate is cubic (space group $I\bar{4}3d$) with a unit cell dimension of 18.81 ± 0.02 Å. The PXRD patterns of pure tBuNH$_2$ hydrate samples are consistent with the reported single-crystal structure;[14] the slightly smaller unit cell dimension of 18.7117 ± 0.0019 Å arises from the different temperatures at which the parameter was measured. In Figure 1a, all of the observed reflections for pure tBuNH$_2$ hydrate were attributed to type VI structure,[2] as indexed by the Checkcell program.[15] However, it should be noted that there are clear structural differences when we compare the PXRD patterns for pure tBuNH$_2$ hydrate with those of the double (CH_4 + tBuNH$_2$) hydrate. The introduction of CH_4 molecules as guests changes the structure of the pure tBuNH$_2$ hydrate. Preliminary X-ray results suggested that the transformed structure is a cubic sII hydrate, $16S{\cdot}8L{\cdot}136\,H_2O$, with space group $Fd3m$. Because the ideal mole ratio of liquid guest (tBuNH$_2$) is 5.6 when it completely fills the large cages of the host (water), we chose to prepare a double (CH_4 + 5.6 mol % tBuNH$_2$) hydrate to verify the structural transition. The collected PXRD patterns were indexed by using the Checkcell program,[15] and the unit cell dimension was determined to be 17.3060 ± 0.0033 Å (see Supporting Information). The resulting refined pattern (Figure 1b) agrees with the reported value for a face-centered-cubic sII hydrate with $a = 17.31 \pm 0.01$ Å.[16]

[*] D.-Y. Kim, Prof. H. Lee
Department of Chemical & Biomolecular Engineering
Korea Advanced Institute of Science and Technology (KAIST)
373–1, Guseong-dong, Yuseong-gu, Daejeon, 305-701 (Korea)
Fax: (+82) 42-869-3910
E-mail: h_lee@kaist.ac.kr
Dr. Y.-T. Seo
Hydrogen System Research Center
Hydrogen & Fuel Cell Research Department
Korea Institute of Energy Research (KIER)
P.O. Box 103, Jang-dong, Yuseong-gu, Daejeon 305-701 (Korea)
Dr. J.-w. Lee, Dr. J. A. Ripmeester
The Steacie Institute for Molecular Sciences
National Research Council of Canada
100 Sussex Drive, Ottawa, Ontario, K1A OR6 (Canada)

[**] This research was performed by the National Research Laboratory (NRL) Program of KOSEF funded by the Ministry of Science and Technology of Korea, and also partially supported by the Brain Korea 21 Project.

Supporting information for this article is available on the WWW under http://www.angewandte.org or from the author.

 © 2005 Wiley-VCH Verlag GmbH & Co. KGaA, Weinheim

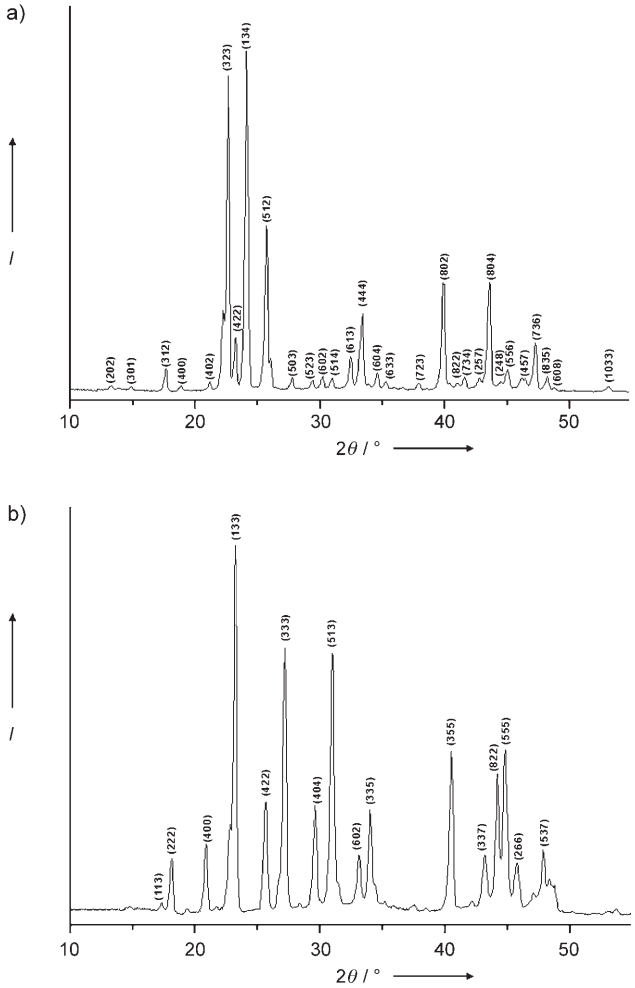

Figure 1. Powder X-ray diffraction patterns: a) pure tBuNH$_2$ hydrate, $a = 18.7117 \pm 0.0019$ Å; b) double (CH_4 + tBuNH$_2$) hydrate, $a = 17.3060 \pm 0.0033$ Å.

One of the objectives of this work was to determine the guest distribution of the two types of guest molecules and to use this information to find the equilibrium composition of the double hydrate. Although the 5^{12} cages are common to many hydrate structures, the symmetry and size of these small cages in the structures are somewhat different and their interactions with guest molecules are also different.[17] Accordingly, encaged guest molecules show different chemical shifts in the NMR spectrum which were used for structural assignments and the identification of guest distribution in cages of pure tBuNH$_2$ hydrate and double (CH_4 + tBuNH$_2$) hydrate that range from a concentration of tBuNH$_2$ from 9.3 to 1.0 mol%. Figure 2 shows ^{13}C magic-angle spinning (MAS) NMR spectra of pure tBuNH$_2$ hydrate and double (CH_4 + tBuNH$_2$) hydrate, which were used to assign the chemical shifts of tBuNH$_2$ molecules as well as those of CH_4 molecules in the hydrate cages. The spectrum of pure tBuNH$_2$ hydrate (Figure 2a) is consistent with the tBuNH$_2$ molecules occupying the large cages of this hydrate, as attested by signals at $\delta = 47.3$ (-C(CH$_3$)$_3$) and 31.6 ppm (-C(CH$_3$)$_3$); the signal intensities reflect the molecular formula. Figures 2b and c show the ^{13}C NMR spectra of double (CH_4 + tBuNH$_2$) hydrate (tBuNH$_2$ concentrations of 9.3 and 7.0 mol%, respectively), which both have CH_4 and tBuNH$_2$ as guest molecules. The CH_4 molecules occupy only the small cages of the double hydrate, as indicated by a single signal at about $\delta = -4.7$ ppm. At the same time, tBuNH$_2$ molecules are present in the large cages, which can be identified by two resonances ($\delta = 46.5$ and 33.1 ppm). However, at these concentrations of tBuNH$_2$, the pure tBuNH$_2$ hydrate and the double (CH_4 + tBuNH$_2$) hydrate are found to coexist as the NMR signals characteristic of both hydrates appear downfield of the NMR spectrum. As the concentration of tBuNH$_2$ decreases further, the relative amount of double hydrate increases so that the number of encaged CH_4 molecules in the small cages also increases. When the concentrations of tBuNH$_2$ were 5.6 or 4.5 mol% (Figures 2d and e), only the double hydrate was found, as just three peaks were obtained for the double (CH_4 + tBuNH$_2$) hydrate. In contrast, pure sI CH_4 hydrate also formed in addition to the double hydrate (sII) when the concentration of tBuNH$_2$ was lowered to 3.0 mol% and 1.0 mol% (Figures 2f and g).

The distribution of CH_4 molecules throughout the cages in the pure CH_4 hydrate and in the double hydrate was investigated for concentrations of tBuNH$_2$ from 3.0 to 1.0 mol%; expanded NMR spectra are presented in Figure 3. In the ^{13}C NMR spectra of the sII double hydrate, two CH_4 resonances at $\delta = -4.7$ (small cage) and -8.3 ppm (large cage) are present, and the resonance of CH_4 molecules in a large cage is clearly seen below 3.0 mol% of tBuNH$_2$. Moreover, the number of encaged CH_4 molecules in the large cages of the double hydrate continues to increase as the concentration of tBuNH$_2$ decreases down to 1.0 mol%. In this region, when the aqueous tBuNH$_2$ solution was cooled below the phase boundary of pure CH_4 hydrate, it was found that pure CH_4 hydrate also formed as indicated by two resonances at $\delta = -4.3$ and -6.7 ppm, which are characteristic of CH_4 molecules trapped in small and large cages of sI hydrate, respectively. As the concentration of tBuNH$_2$ decreases, the amount of pure CH_4 hydrate formed becomes larger because the amount of water participating in the formation of the double hydrate decreases. In the case of 1.0 mol% of tBuNH$_2$, four NMR signals indicate the presence of CH_4 molecules enclathrated in each of the four hydrate cages of pure (sI) and double hydrate (sII). Therefore, Figure 3e precisely indicates the coexistence and guest distribution of CH_4 molecules in pure sI CH_4 hydrate and the sII double hydrate. In our experiments, the relative amount of sI and sII hydrate observed at low concentrations of tBuNH$_2$ is a variable that depends on the amount of excess water present and the reaction time. For practical purposes, it is desirable to work at a pressure that is just below the point at which sI hydrate appears. Therefore, the appearance of the spectra is not necessarily characteristic of the equilibrium distribution of the various hydrates. Note that the signal intensity in Figure 2 and Figure 3 does not directly represent the absolute amount of formed hydrates.

For several concentrations of tBuNH$_2$, the ratio of signal areas for CH_4 molecules in large cages to that of small cages of the double hydrates is plotted in Figure 4. As described above, the CH_4 molecules can occupy only the small cages of

 © 2005 Wiley-VCH Verlag GmbH & Co. KGaA, Weinheim

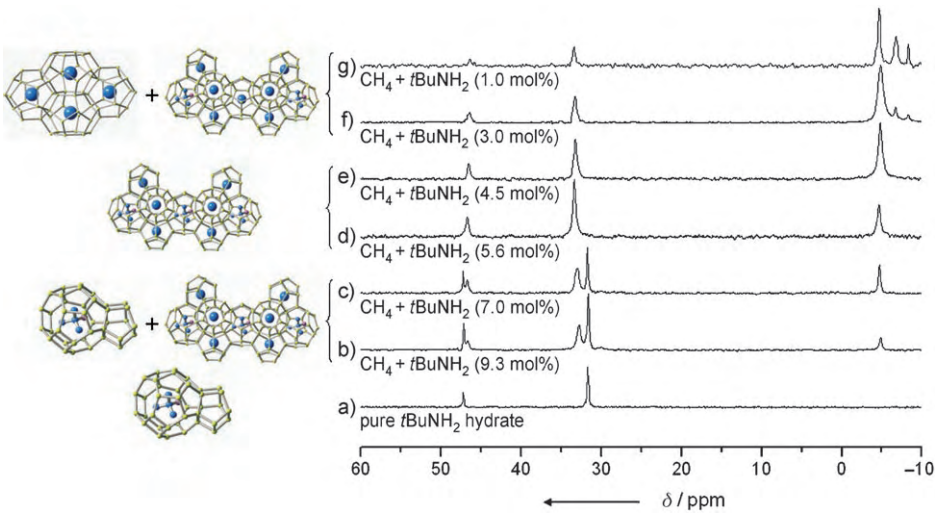

Figure 2. ^{13}C MAS NMR spectra and structural diagrams of the pure and double hydrates: a) pure tBuNH$_2$ hydrate; b) and c) both pure tBuNH$_2$ hydrate and sII double hydrate coexisted (9.3 and 7.0 mol% tBuNH$_2$, respectively); d) and e) only the sII double hydrate formed (5.6 and 4.5 mol% tBuNH$_2$, respectively); f) and g) both pure sI CH_4 hydrate and sII double hydrate coexisted (3.0 and 1.0 mol% tBuNH$_2$, respectively). All samples, except for the pure tBuNH$_2$ hydrate, were prepared for NMR analysis by using the same experimental procedure (see text, Experimental Section, and Supporting Information for details). Hydrogen atoms were omitted in the structural diagrams.

resulting values are shown in Figure 4. A value of 1.46, the lowest mole ratio of CH_4 to tBuNH$_2$ found, indicates that about 75% of the small cages are occupied by CH_4 molecules in the double hydrate; if all small and large cages encapsulate the CH_4 and tBuNH$_2$ molecules in the double hydrate, respectively, the mole ratio of CH_4 to tBuNH$_2$ becomes 2.0. As the concentration of tBuNH$_2$ decreases, the number of CH_4 molecules captured in cages increases. Based on the assumption that the occupancy of the small cage by CH_4 molecules is 0.75 (according to the result obtained for 5.6 mol% of tBuNH$_2$), the remaining CH_4 molecules should be confined in large cages of the double hydrate, which is about 31% of the large cages at 1.0 mol% of tBuNH$_2$.[18]

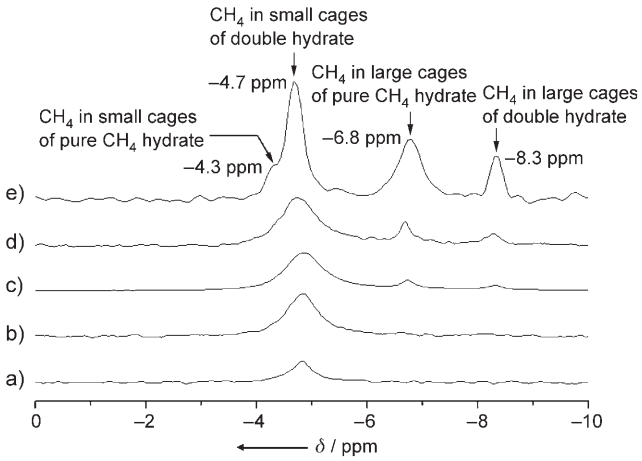

Figure 3. Expanded ^{13}C MAS NMR spectra of double (CH_4 + tBuNH$_2$) hydrates. Concentrations of tBuNH$_2$: a) 5.6; b) 4.0; c) 3.0; d) 2.0; e) 1.0 mol%.

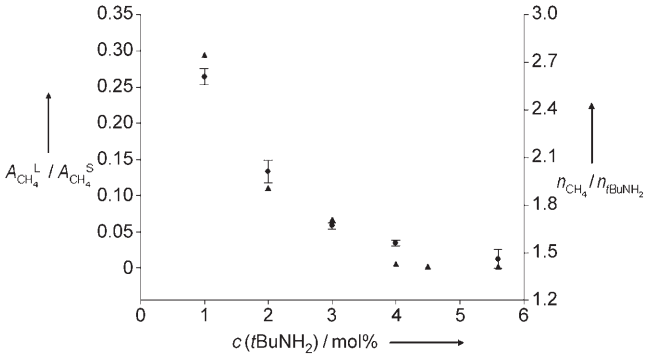

Figure 4. The area ratio (▲) of ^{13}C MAS NMR signals for CH_4 molecules occluded in large and small cages and the CH_4/tBuNH$_2$ mole ratio (●) in the double hydrate.

the double hydrate up to 4.5 mol% but occupy both small and large cages of the double hydrate below concentrations of 4.0 mol% of tBuNH$_2$. The ratio of the integrated intensities for the two signals was 0.04 at 4.0 mol% but jumped to 0.294 at 1.0 mol% of tBuNH$_2$. To check the actual amount of CH_4 molecules stored in the hydrate phase, we measured the volume of CH_4 gas released from the double hydrate samples. The samples were prepared at 70 bar and 283.65 K to eliminate the possible formation of pure CH_4 hydrates that may result from a reaction between residual water and CH_4 gas in the low concentration region of tBuNH$_2$. The measured volume of CH_4 gas was converted into moles by considering the compressibility factor of the CH_4 molecule, and the Thus, the amount of CH_4 in the sII double hydrate can be tuned by decreasing the concentration of tBuNH$_2$.

The results reported in this study show for the first time that a structural transition occurs in tBuNH$_2$ hydrate according to the initial concentration of tBuNH$_2$ when small molecules such as CH_4 are introduced. The structural transition was confirmed by PXRD and analysis of the solid-state NMR spectrum. At sufficiently low concentrations of tBuNH$_2$, pure CH_4 hydrate (sI) and double (CH_4 + tBuNH$_2$) hydrate (sII) coexist when crossing the corresponding phase boundary so that there is a complex mixture of solid phases. Moreover, it is shown that the storage capacity of CH_4 gas in the hydrate phase increases drastically as the initial concentration of tBuNH$_2$ decreases. These results confirm that the gaseous distribution of guest molecules and the hydrate composition can be altered by adjusting the concen-

 © 2005 Wiley-VCH Verlag GmbH & Co. KGaA, Weinheim

tration of the liquid guest. This "tuning mechanism" plays an important role in understanding the dynamics of hydrate cages and should be one of the strategies used to enhance the gas-storage capacity of double-hydrate systems, including a water-soluble liquid hydrate promoter for application to gas storage and transportation areas.

Experimental Section

The PXRD patterns were recorded at 113.15 K on a Rigaku Geigerflex diffractometer (D/Max-RB) by using graphite-monochromatized $Cu_{K\alpha 1}$ radiation ($\lambda = 1.5406$ Å) in the $\theta/2\theta$ scan mode. The XRD experiments were carried out in step mode with a fixed time of 10 s and a step size of 0.05° for $2\theta = 10$–60°, thus rendering a total acquisition time of approximately 2 h for each hydrate sample.

To identify hydrate structure and guest distribution, a Bruker DSX 400 MHz solid-state NMR spectrometer was used. The powdered samples were placed in a zirconia rotor with an outer diameter of 4 mm, which was loaded into a variable temperature probe. The initial temperature (T) and pressure (P) were 293.15 K and 70 bar, respectively, and then T was gradually reduced to 270.15 K. The pure tBuNH$_2$ hydrate was made by freezing an aqueous solution of tBuNH$_2$ (9.3 mol%, the ideal stoichiometric concentration of tBuNH$_2$ hydrate) at 243.15 K. All ^{13}C NMR spectra were recorded at a Larmor frequency of 100.6 MHz with MAS at about 3 kHz. A pulse length of 2 μs and pulse repetition delay of 40 s under proton decoupling were employed with a radio frequency field strength of 50 kHz, which corresponded to 5-μs 90° pulses. The downfield carbon resonance signal of adamantane, which was assigned a chemical shift of $\delta = 38.3$ ppm at 300 K, was used as an external chemical shift reference. For the mixed hydrate samples, $^{13}CH_4$ gas was used to obtain higher-intensity CH_4 signals.

Received: July 8, 2005

Keywords: clathrates · host–guest systems · inclusion compounds · NMR spectroscopy · water chemistry

[1] E. D. Sloan, *Clathrate Hydrates of Natural Gas*, 2nd ed., Dekker, New York, **1998**.
[2] G. A. Jeffrey in *Inclusion Compounds, Vol. 1* (Eds.: J. L. Atwood, J. E. D. Davies, D. D. MacNicol), Academic Press, London, **1984**, pp. 135–190.
[3] K. A. Udachin, C. I. Ratcliffe, J. A. Ripmeester, *Angew. Chem.* **2001**, *113*, 1343–1345; *Angew. Chem. Int. Ed.* **2001**, *40*, 1303–1305.
[4] J. S. Gudmundsson, M. Mork, O. F. Graff, *Proceedings of the 4th International Conference on Gas Hydrates*, Yokohama, **2002**, pp. 997–1002.
[5] H. Teng, A. Yamasaki, M. K. Chun, H. Lee, *Energy* **1997**, *22*, 1111–1117.
[6] S.-P. Kang, H. Lee, *Environ. Sci. Technol.* **2000**, *34*, 4397–4400.
[7] A. A. Khokhar, J. S. Gudmundsson, E. D. Sloan, *Fluid Phase Equilib.* **1998**, *105–151*, 383–392.
[8] S. Takeya, A. Hori, T. Hondoh, T. Uchida, *J. Phys. Chem. B* **2000**, *104*, 4164–4168.
[9] Y.-T. Seo, H. Lee, *J. Phys. Chem. B* **2001**, *105*, 10084–10090.
[10] S. Subramanian, E. D. Sloan, *J. Phys. Chem. B* **2002**, *106*, 4348–4355.
[11] Y.-T. Seo, H. Lee, I. Moudrakovski, J. A. Ripmeester, *ChemPhysChem* **2003**, *4*, 379–382.
[12] Y.-T. Seo, H. Lee, *J. Phys. Chem. B* **2004**, *108*, 530–534.
[13] H. Lee, J.-W. Lee, D.-Y. Kim, J.-S. Park, Y.-T. Seo, H. Zeng, I. L. Moudrakovski, C. I. Ratcliffe, J. A. Ripmeester, *Nature* **2005**, *434*, 743–746.
[14] R. K. McMullan, G. A. Jeffrey, T. H. Jordan, *J. Chem. Phys.* **1967**, *47*, 1229–1234.
[15] J. Laugier, B. Bochu, Laboratoire des Materiaux et du Génie Physique, Ecole Supérieure de Physique de Grenoble. Available at http://www.ccp14.ac.uk.
[16] T. C. W. Mak, R. K. McMullan, *J. Chem. Phys.* **1965**, *42*, 2732–2737.
[17] J. A. Ripmeester, C. I. Ratcliffe, *J. Phys. Chem.* **1988**, *92*, 337–339.
[18] In this case, by assuming that $\theta^{S}_{CH_4} = 0.75$ and $\theta^{L} = \theta^{L}_{CH_4} + \theta^{L}_{t\mathrm{BuNH_2}} = 1$ due to stability of sII hydrate, we could determine the number of moles of guest molecules, CH_4 and tBuNH$_2$, in small and large cages of double hydrate, which was in agreement with $n_{CH_4}/n_{t\mathrm{BuNH_2}} = 2.61$. From the resulting values, it appears that the final composition of double hydrate is $(12\,CH_4)_S\left(\frac{2.46\,CH_4}{5.54\,t\mathrm{BuNH_2}}\right)_L \cdot 136\,H_2O$.

 © 2005 Wiley-VCH Verlag GmbH & Co. KGaA, Weinheim

Supramolecular Chemistry

DOI: 10.1002/anie.200502434

Nucleobases in Molecular Recognition: Molecular Adducts of Adenine and Cytosine with COOH Functional Groups**

*Sathyanarayana Reddy Perumalla, E. Suresh, and Venkateswara Rao Pedireddi**

The current advancements in the areas of solid-state chemistry, supramolecular chemistry, and crystal engineering of molecular complexes, including metal–organic hybrids, illustrate the ability of a variety of organic compounds possessing specific functional groups to create exotic supramolecular assemblies with tailor-made properties after either self-

[*] S. R. Perumalla, Dr. V. R. Pedireddi
Solid State & Supramolecular Structural Chemistry Lab
Division of Organic Chemistry
National Chemical Laboratory
Dr. Homi Bhabha Road, Pune 411 008 (India)
Fax: (+91) 202-589-3153
E-mail: vr.pedireddi@ncl.res.in

Dr. E. Suresh
Central Salt and Marine Chemicals Research Institute
Bhavnagar 364 002 (India)

[**] We thank Dr. S. Sivaram (Director, NCL) and Dr. K. N. Ganesh (Head, Division of Organic Chemistry, NCL) for their constant support and encouragement. We also thank DST and BRNS for funding ongoing research projects and the University Grants Commission (UGC) for the award of a Junior Research Fellowship (JRF) to S.R.P.

Supporting information for this article is available on the WWW under http://www.angewandte.org or from the author.

WILEY InterScience DISCOVER SOMETHING GREAT
© 2005 Wiley-VCH Verlag GmbH & Co. KGaA, Weinheim

assembly processes or molecular recognition of complimentary functional moieties.[1–5] For example, numerous assemblies of trimesic acid,[6] 1,2,4,5-benzenetetracarboxylic acid,[7] cyanuric acid,[8] trithiocyanuric acid,[9] and related compounds demonstrate the spectrum of versatile assemblies available in the literature.

In fact, the molecular recognition of complimentary nucleobases (adenine (A) and thymine (T); guanine (G), and cytosine (C)) through the formation of A-T and G-C base pairs leads to the complex structure of DNA.[10] However, it is rather surprising that utilization of the native nucleobases in molecular recognition studies for the creation of adducts or assemblies is rare, except for a few studies reported by Sasada and co-workers conducted as part of a study on the interactions of nucleic acids and amino acids.[11] An analysis of the Cambridge Structural Database (CSD),[12] with conquest version 1.7, reveals that only a handful of structures of molecular adducts of nucleobases are known.

Considering the present developments in the areas of nucleic acid/protein interactions, and in particular, the interaction of nucleobases with bioactive molecules, we believe that evaluation of a large cluster of molecular adducts of nucleobases is essential as it would enable the formulation of ideal basis sets for accurate predictions in biomolecular modeling experiments.

In this context, the potential ability of the nucleobases having both acceptor and donor functionalities (Scheme 1) led us to initiate the synthesis of numerous molecular adducts of nucleobases with the complimentary carboxylic acid derivatives shown in Scheme 1. However, we noted that only A and C formed complexes readily while G, T, and uracil (U) did not yield any complexes: XRD analysis of the resulting precipitates revealed a mixture of reactants.[13] Thus, herein we report the molecular adducts of A with benzoic acid (BA); C with BA, phthalic acid (PA) and isophthalic acid (IA) as single crystals; we also report the adducts of A with the dicarboxylic acids in the crystalline powder form. These adducts can serve as representative examples in future studies of supramolecular assemblies involving nucleobases as well as for better evaluation of biological studies.

Cocrystallization of A and BA from a CH_3OH solution gave good quality single crystals and structure determination by XRD methods revealed that the adduct of A and BA formed in a 1:2 ratio.[14] In the crystal lattice, molecules of A and BA interact with each other through the formation of a cyclic arrangement of hydrogen bonds involving COOH, NH_2, and hetero N atoms (N^1 and N^7)[15] similar to Watson–Crick and Hoogsteen base pairs. The 2D recognition pattern and molecular arrangement is shown in Figure 1. Thus, BA interacts with A through both the pyrimidine and imidazole rings with the formation of O–H···N (H···N, 1.83 and 1.86 Å)

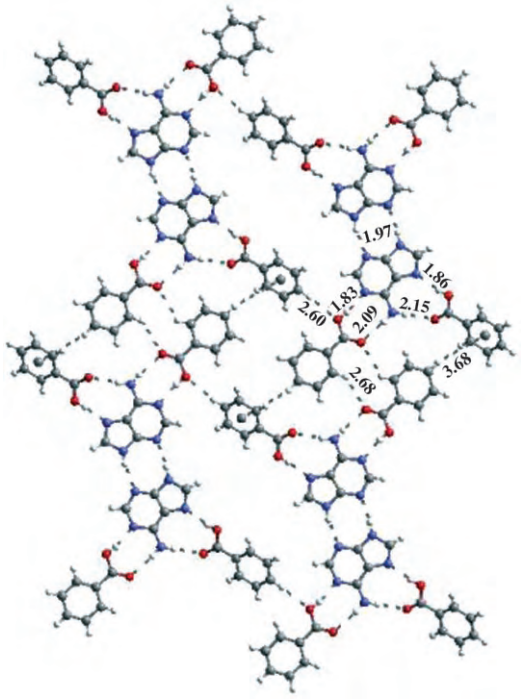

Figure 1. Arrangement of adenine (A) and benzoic acid (BA) in the molecular adduct. Hydrogen bonds are shown as dashed lines. Lines between hydrogen atoms and the center of the phenyl moiety of BA molecules represent C–H···π interactions.

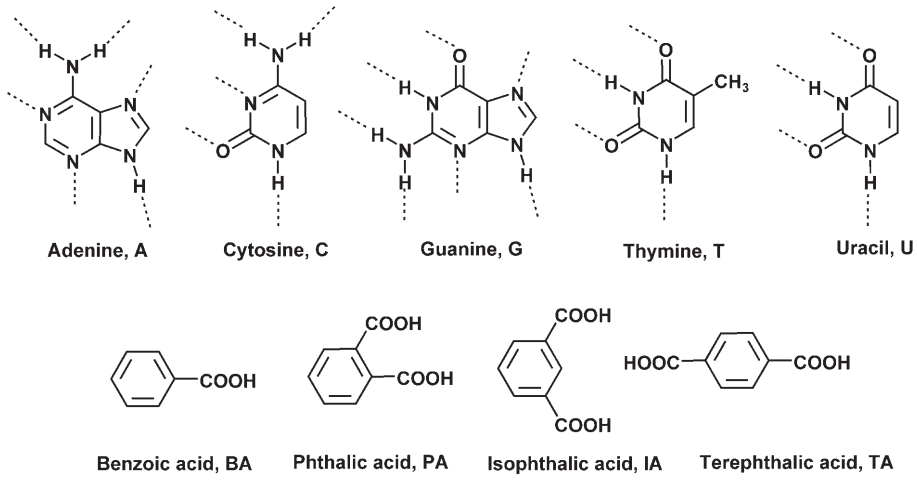

Scheme 1.

and N–H···O (H···O, 2.09 and 2.15 Å) hydrogen bonds. Furthermore, the 1:2 units are held together by centrosymmetric N–H···N hydrogen bonds between the pyrimidine N^3 atom and imidazole NH at the 9-position. The H···N distance is 1.97 Å. Such aggregates form 1D networks through a cyclic arrangement of C–H···O hydrogen bonds (H···O, 2.68 Å) formed between BA molecules to yield infinite molecular tapes. The adjacent tapes are held together by further single C–H···O hydrogen bonds (H···O, 2.60 Å) as well as C–H···π interactions (3.68 Å; Figure 1).

 © 2005 Wiley-VCH Verlag GmbH & Co. KGaA, Weinheim

We also anticipated similar interactions with dicarboxylic acids but unfortunately, to date, we have not been successful in obtaining single crystals for the evaluation of intermolecular interactions.[16] However, evidence for the formation of adducts has been obtained by XRD analysis of the residues isolated from cocrystallization experiments.[13] Nevertheless, we were able to isolate single crystals for the adducts of cytosine, except with terephthalic acid, and the analyses disclose intriguing features.

In the 1:1 molecular adduct of C and BA, however, two molecules of each C and BA, are present in the asymmetric unit.[14] While one pair of C and BA exists in a neutral form, in the other pair proton transfer from the COOH group to the pyrimidine N^3 atom occurs. Furthermore, the interaction between C and BA is established through N^1, such that each deprotonated acid interact with both the symmetry-independent molecules of C, while the adjacent molecules of C exist as dimers connected together by a triple hydrogen bond involving N^3H, carbonyl, and the NH_2 groups, thus resembling a pseudo Watson–Crick pattern. A pictorial representation of the interactions between the cytosine and BA molecules is shown in Figure 2. The hydrogen bond lengths (H···O and H···N) in the cytosine duplex are 1.65, 1.84, and 1.94 Å (Figure 2a). Furthermore, the adjacent cytosine dimers are held together by two N–H···O hydrogen bonds with H···O distances of 2.13 and 2.15 Å, formed by NH_2 and carbonyl groups (Figure 2b). An intriguing ladderlike structure is formed in the 3D arrangement of these species (Figure 2c).

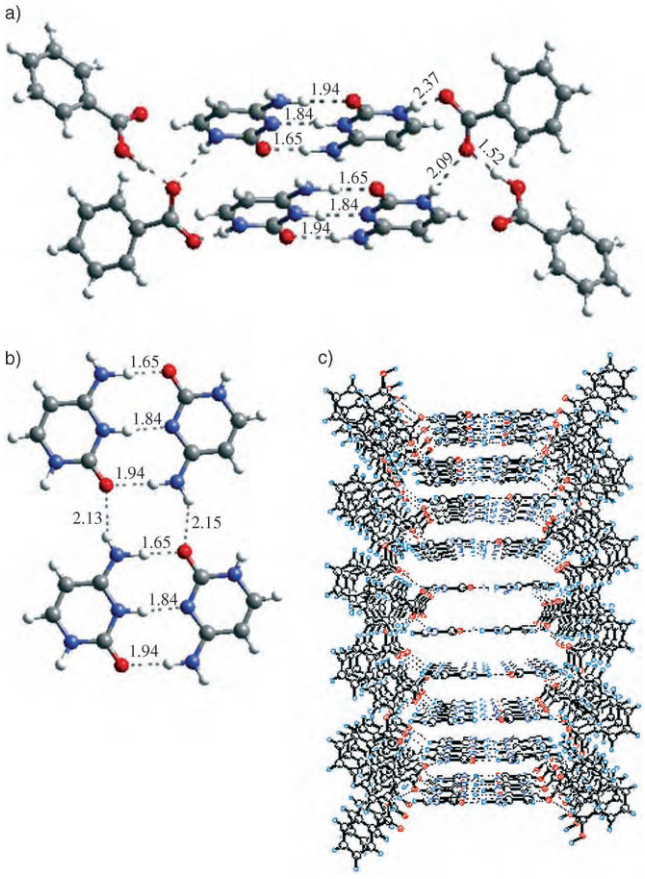

Figure 2. a) Recognition pattern between cytosine (C) and benzoic acid (BA) in the molecular adduct. b) Duplexes of cytosine residues connected together by N–H···O hydrogen bonds. c) 3D packing of C and BA in the molecular adduct forming a supramolecular ladder.

The interaction of C with PA and IA is much more interesting, with the formation of novel supramolecular structures. In both the adducts the cytosine dimers were observed as found in the complex with BA. The molecular packing in a typical 2D arrangement of the adduct between C and PA is shown in Figure 3. The adduct of C with PA is a 2:1

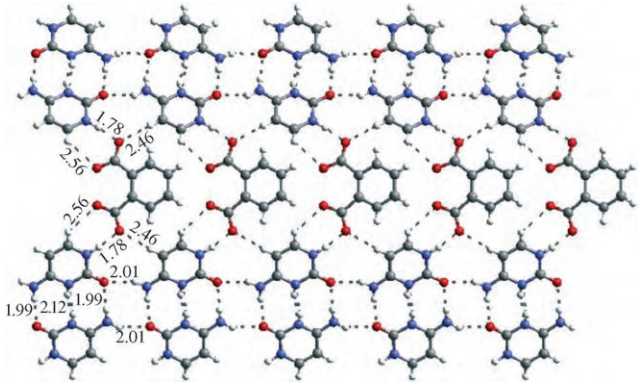

Figure 3. Arrangement of molecules of cytosine (C) and phthalic acid (PA) in the adduct forming a pillarlike structure.

complex,[14] with C and PA interacting through the deprotonated carboxyl groups of PA and C to form cyclic hydrogen-bonding patterns consisting of N–H···O (H···O, 1.78 Å) and C–H···O (H···O, 2.56 Å). Such adjacent units further interact with each other through molecules of C to yield dimers of C connected by triple hydrogen bonds, as observed in the complex of C and BA, but with different hydrogen bond lengths (H···O, 1.99 and H···N, 2.12 Å). As a result, crinkled chains are formed in the 2D arrangement (Figure 3) which are further held together by N–H···O hydrogen bonds (H···O, 2.01 Å) between molecules of C, and by C–H···O hydrogen bonds (H···O, 2.46 Å) between C and PA molecules. Thus, in each sheet the PA molecules appear as though they are inserted between tapes of C molecules.

Although 3D packing into a stacked sheets arrangement prevails in the adduct of C with IA,[14] as observed in the adduct with PA, the molecular packing is quite different within the 2D arrangement (Figure 4). Molecules of IA and C appear to exist as homomeric chains formed by strong hydrogen bonds such that while the adjacent IA molecules are held together by catemeric type O–H···O hydrogen bonds (H···O, 1.80 Å) through COOH and COO^-, molecules of C are held together by two different hydrogen bonding networks. Further, the adjacent chains are held together by a centrosymmetric cyclic arrangement of C–H···O hydrogen bonds (H···O, 2.69 Å) as shown in Figure 4b, which leads to the formation of a quartet of IA molecules (Figure 4c). In the two patterns of C, one of them is identical to that observed in

 © 2005 Wiley-VCH Verlag GmbH & Co. KGaA, Weinheim

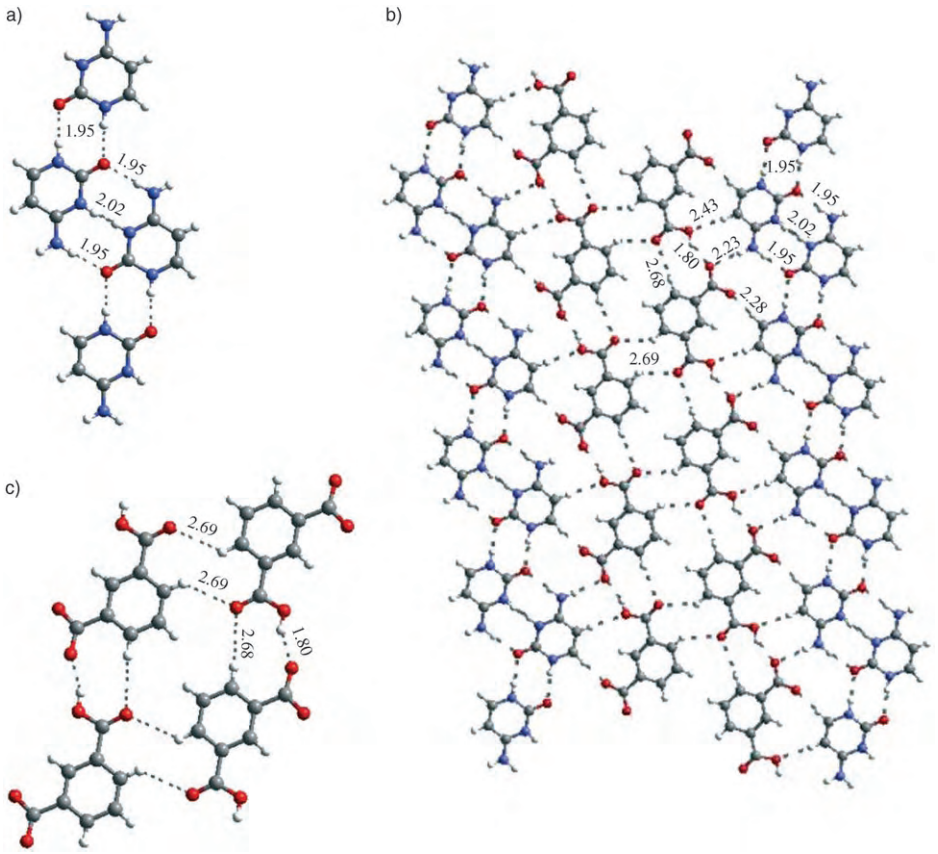

Figure 4. a) Interaction of the adjacent triple hydrogen-bonded duplexes of cytosine (C) through a dimeric hydrogen-bonding pattern. b) 2D arrangement of C and isophthalic acid (IA) in the crystal lattices of their adduct. c) Quartet arrangement of IA molecules.

the complex formed between C and PA with a triple hydrogen-bonding pattern. In contrast to the patterns observed in the complexes with BA and PA, the triplet dimers are further held together by dimeric hydrogen-bonding patterns in the adduct with **IA** through N–H···O hydrogen bonds (H···O, 1.95 Å) formed between pyridyl NH rather than NH_2 groups (Figure 4a).

Comparisons of the three adducts of C discussed above show that in all cases C exists as dimers connected together by triple hydrogen bonds and yields molecular tapes. These molecular tapes are arranged in the crystal lattice as rungs in a ladderlike structure with BA, but are sandwiched in the 2D arrangement in the adducts of PA and IA. A schematic representation of systematic variations in the arrangement of molecules in the different adducts is shown in Figure 5.

In conclusion, we have reported the formation of 3D assemblies of molecular adducts of cytosine with benzoic, phthalic, and isopthalic acids, as well as the adduct of adenine with benzoic acid. It was noted that cytosine and adenine both show the tendency to form duplexes, irrespective of the nature of the other species involved in the recognition process. Furthermore, by correlating the patterns obtained in this study with the patterns observed in other structures available in the literature, it appears that cytosine duplexes with triple hydrogen-bonding patterns are predominant in the vicinity of COOH functional groups. The cocrystallization studies with molecules containing COOH functional groups also shows that adenine binds with the other molecules through the N^1 and N^7 sites, in a similar manner to binding generally observed with thymine in the DNA structure. However, cytosine participated in molecular recognition preferentially through the N^1-position, which is generally connected to the sugar moiety in DNA, but mimics the hydrogen-bonding pattern that it forms with guanine in a G-C base pair by a homomeric process. Although these results are quite intriguing, a large number of synthetic studies of molecular adducts of nucleobases and their systematic analysis need to be made to address several problems in biological studies. We are engaged in the synthesis of cocrystals of nucleobases with different functional moieties, aimed in particular to identify groups that could interact with guanine and thymine.

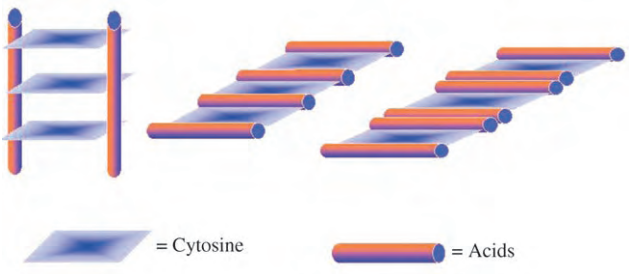

Figure 5. Schematic representation of the packing of molecules in the adducts of cytosine (C) with (left) benzoic acid (BA), (middle) phthalic acid (PA), and (right) isophthalic acid (IA).

Received: July 12, 2005
Published online: November 7, 2005

Keywords: carboxylic acids · hydrogen bonds · molecular recognition · nucleobases · supramolecular chemistry

[1] a) M. Lahav, G. M. J. Schmidt, *J. Chem. Soc. B* **1967**, 239–243; b) J. Hulliger, *Angew. Chem.* **1994**, *106*, 151–171; *Angew. Chem. Int. Ed. Engl.* **1994**, *33*, 143–162; c) L. R. MacGillivray, J. L.

 © 2005 Wiley-VCH Verlag GmbH & Co. KGaA, Weinheim

Reid, J. A. Ripmeester, *J. Am. Chem. Soc.* **2000**, *122*, 7817 – 7818; d) M. Jansen, *Angew. Chem.* **2002**, *114*, 3896 – 3917; *Angew. Chem. Int. Ed.* **2002**, *41*, 3746 – 3766; e) L. R. MacGillivray, J. L. Reid, J. A. Ripmeester, G. S. Papaefstathiou, *Ind. Eng. Chem. Res.* **2002**, *41*, 4494 – 4497; f) O. Saied, T. Maris, J. D. Wuest, *J. Am. Chem. Soc.* **2003**, *125*, 14956 – 14957; g) F. Guo, K. D. M. Harris, *J. Am. Chem. Soc.* **2005**, *127*, 7314 – 7315; h) F. Remenar, S. L. Morissette, M. L. Peterson, B. Moulton, J. M. MacPhee, H. R. Guzman, O. Almarsson, *J. Am. Chem. Soc.* **2003**, *125*, 8456 – 8457.

[2] a) J.-M. Lehn, *Supramolecular Chemistry: Concepts and Perspectives*, VCH, Weinheim, **1995**; b) J. L. Atwood, J. E. D. Davies, D. D. MacNicol, F. Vögtle, *Comprehensive Supramolecular Chemistry*, Pergamon, Oxford, **1996**; c) G. A. Jeffrey, W. Saenger, *Hydrogen Bonding in Biological Structures*, Springer, Berlin, **1991**; d) G. A. Jeffrey, *An Introduction to Hydrogen Bonding*, Oxford University Press, New York, **1997**; e) G. R. Desiraju, *Crystal Engineering: The Design of Organic Solids*, Elsevier, Amsterdam **1989**.

[3] a) J.-M. Lehn, *Angew. Chem.* **1990**, *102*, 1347 – 1362; *Angew. Chem. Int. Ed. Engl.* **1990**, *29*, 1304 – 1319; b) L. J. Prins, D. N. Reinhoudt, P. Timmerman, *Angew. Chem.* **2001**, *113*, 2446 – 2492; *Angew. Chem. Int. Ed.* **2001**, *40*, 2382 – 2426; c) G. R. Desiraju, *Angew. Chem.* **1995**, *107*, 2541 – 2558; *Angew. Chem. Int. Ed. Engl.* **1995**, *34*, 2311 – 2327; d) M. C. T. Fyfe, J. F. Stoddart, *Acc. Chem. Res.* **1997**, *30*, 393 – 401; e) G. M. Whitesides, E. E. Simanek, J. P. Mathias, C. T. Seto, D. N. Chin, M. Mammen, D. M. Gordon, *Acc. Chem. Res.* **1995**, *28*, 37 – 44; f) K. Biradha, *CrystEngComm* **2003**, *5*, 374 – 384; g) S. Sivakova, S. J. Rowan, *Chem. Soc. Rev.* **2005**, 9 – 21; h) R. P. Sijbesma, E. W. Meijer, *Chem. Commun.* **2003**, 5 – 16.

[4] a) G. R. Desiraju, *Nature* **2001**, *412*, 397 – 400; b) B. Kahr, *Cryst. Growth Des.* **2004**, *4*, 3 – 9; c) M. D. Hollingsworth, *Science* **2002**, *295*, 2410 – 2413; d) D. Braga, *Chem. Commun.* **2003**, *9*, 2751 – 2754; e) C. V. K. Sharma, *Cryst. Growth Des.* **2002**, *2*, 465 – 474; f) S. A. Bourne, K. C. Corin, L. R. Nassimbeni, F. Toda, *Cryst. Growth Des.* **2005**, *5*, 379 – 382; g) J. A. Bis, M. J. Zaworotko, *Cryst. Growth Des.* **2005**, *5*, 1169 – 1179; h) M. Lee, B.-K. Cho, K. J. Ihn, W.-K. Lee, N.-K. Oh, W.-C. Zin, *J. Am. Chem. Soc.* **2001**, *123*, 4647 – 4648; i) C. B. Aakeröy, J. Desper, J. F. Urbina, *Chem. Commun.* **2005**, 2820 – 2822; j) L. E. Cheruzel, M. S. Mashuta, R. M. Buchanan, *Chem. Commun.* **2005**, 2223 – 2225; k) N. Malek, T. Maris, M.-È. Perron, J. D. Wuest, *Angew. Chem.* **2005**, *117*, 4089 – 4093; *Angew. Chem. Int. Ed.* **2005**, *44*, 4021 – 4025.

[5] a) N. W. Ockwig, O. Delgado-Friedrichs, M. O'Keeffe, O. M. Yaghi, *Acc. Chem. Res.* **2005**, *38*, 176 – 182; b) S. Kitagawa, R. Kitaura, S. I. Noro, *Angew. Chem.* **2004**, *116*, 2388 – 2430; *Angew. Chem. Int. Ed.* **2004**, *43*, 2334 – 2375; c) J. Y. Lu, *Coord. Chem. Rev.* **2003**, *246*, 327 – 347; d) G. S. Papaefstathiou, L. R. MacGillivray, *Coord. Chem. Rev.* **2003**, *246*, 169 – 184; e) X. Shi, G. Zhu, G. Li, Q. Fang, G. Wu, G. Tian, M. Xue, X. Zhao, R. Wang, S. Qiu, X. Wang, *Cryst. Growth Des.* **2005**, *5*, 207 – 213; f) M. W. Hosseini, *Acc. Chem. Res.* **2005**, *38*, 313 – 323; g) B. Kesanli, Y. Cui, W. Lin, M. R. Smith, E. W. Bittner, B. C. Bockrath, *Angew. Chem.* **2005**, *117*, 74 – 77; *Angew. Chem. Int. Ed.* **2005**, *44*, 72 – 75.

[6] a) K. Biradha, D. Dennis, V. A. Mackinnon, C. V. K. Sharma, M. J. Zaworotko, *J. Am. Chem. Soc.* **1998**, *120*, 11894; b) P. Holy, J. Zavada, I. Cisarova, J. Podlaha, *Angew. Chem.* **1999**, *111*, 393 – 395; *Angew. Chem. Int. Ed.* **1999**, *38*, 381 – 383; c) S. V. Kolotuchin, E. E. Fenlon, S. R. Wilson, C. J. Loweth, S. C. Zimmerman, *Angew. Chem.* **1995**, *107*, 2873 – 2876; *Angew. Chem. Int. Ed. Engl.* **1995**, *34*, 2654 – 2657; d) S. V. Kolotuchin, P. A. Thiessen, E. E. Fenlon, S. R. Wilson, C. J. Loweth, S. C. Zimmerman, *Chem. Eur. J.* **1999**, *5*, 2537 – 2547; e) R. E. Melendez, C. V. K. Sharma, M. J. Zaworotko, C. Bauer, R. D. Rogers, *Angew. Chem.* **1996**, *108*, 2355 – 2357; *Angew. Chem. Int. Ed. Engl.* **1996**, *35*, 2213 – 2215; f) F. A. A. Paz, J. Klinowski, *CrystEngComm* **2003**, *5*, 238 – 244; g) C. V. K. Sharma, M. J. Zaworotko, *Chem. Commun.* **1996**, 2655 – 2656; h) O. Ermer, J. Neudörfl, *Chem. Eur. J.* **2001**, *7*, 4961 – 4980; i) O. Ermer, J. Neudörfl, *Helv. Chim. Acta*, **2001**, *84*, 1268 – 1313; j) B.-Q. Ma, P. Coppens, *Chem. Commun.* **2003**, 2290 – 2291; k) R. Liu, K.-F. Mok, S. Valiyaveettil, *New J. Chem.* **2001**, 890 – 892; l) O. Ermer, J. Neudörfl, *Chem. Eur. J.* **2001**, *7*, 4961 – 4980.

[7] a) K. K. Arora, V. R. Pedireddi, *J. Org. Chem.* **2003**, *68*, 9177 – 9185; b) N. Shan, W. Jones, *Tetrahedron Lett.* **2003**, *44*, 3687 – 3689; c) O. Fabelo, L. Caòadillas-Delgado, F. S. Delgado, P. Lorenzo-Luis, M. M. Laz, M. Julve, C. Ruiz-Pérez, *Cryst. Growth Des.* **2005**, *5*, 1163 – 1167; d) M. Du, Z.-H. Zhang, X.-J. Zhao, *Cryst. Growth Des.* **2005**, *5*, 1247 – 1254.

[8] a) A. Ranganathan, V. R. Pedireddi, C. N. R. Rao, *J. Am. Chem. Soc.* **1999**, *121*, 1752 – 1753; b) V. R. Pedireddi, D. Belhekar, *Tetrahedron* **2002**, *58*, 2937 – 2941; c) J. A. Zerkowski, C. T. Seto, G. M. Whitesides, *J. Am. Chem. Soc.* **1992**, *114*, 5473 – 5475; d) G. J. Sanjayan, V. R. Pedireddi, K. N. Ganesh, *Org. Lett.* **2000**, *2*, 2825 – 2828; e) C. T. Seto, G. M. Whitesides, *J. Am. Chem. Soc.* **1990**, *112*, 6409 – 6411.

[9] a) S. Ahn, B. M. Kariuki, J. PrakashaReddy, V. R. Pedireddi, S. Chatterjee, A. Ranganathan, C. N. R. Rao, K. D. M. Harris, *Chem. Eur. J.* **2005**, *11*, 2433 – 2439; b) S. Aoki, M. Shiro, E. Kimura, *Chem. Eur. J.* **2002**, *8*, 929 – 939; c) S. V. Kolotuchin, S. C. Zimmerman, *J. Am. Chem. Soc.* **1998**, *120*, 9092 – 9093; d) A. Ranganathan, V. R. Pedireddi, S. Chatterjee, C. N. R. Rao, *J. Mater. Chem.* **1999**, *9*, 2407 – 2411; e) P. A. W. Dean, M. Jennings, T. M. Houle, D. C. Craig, I. G. Dance, J. M. Hook, M. L. Scudder, *CrystEngComm* **2004**, 543 – 548; f) X. Li, D. N. Chin, G. M. Whitesides, *J. Org. Chem.* **1996**, *61*, 1779 – 1786.

[10] J. D. Watson, F. H. C. Crick, *Nature* **1953**, *171*, 964 – 967.

[11] a) M. Ohki, A. Takenaka, H. Shimanouchi, Y. Sasada, *Bull. Chem. Soc. Jpn.* **1975**, *48*, 848 – 852; b) A. Takenaka, Y. Sasada, *Bull. Chem. Soc. Jpn.* **1982**, *55*, 680 – 686; c) S. Fujitha, A. Takenaka, Y. Sasada, *Bull. Chem. Soc. Jpn.* **1983**, *56*, 2234 – 2237.

[12] F. H. Allen, O. Kennard, *Chem. Des. Automat. News.* **1993**, *8*, 31 – 37.

[13] Powder patterns are given in the Supporting Information.

[14] Crystal data for adenine and benzoic acid adduct: $C_5H_5N_5{\cdot}2\,C_7H_6O_2$, $M_r = 379.38$, colorless blocks, $0.32 \times 0.21 \times 0.13$ mm, space group $P\bar{1}$, $a = 6.949(2)$, $b = 10.324(3)$, $c = 14.286(5)$ Å, $\alpha = 80.46(1)$, $\beta = 76.40(1)$, $\gamma = 71.21(1)^\circ$, $V = 938.6(5)$ Å^3, $Z = 2$, $\rho_{calcd} = 1.342$ g cm^3, $\mu = 0.097$ mm^{-1}, $2\theta = 56.66$, $(Mo_{K\alpha}) = 0.71073$ Å, $T = 298(2)$ K, 8200 total reflections, $R_1 = 0.070$ and $wR_2 = 0.148$ for 4268 reflections. Crystal data for cytosine and benzoic acid adduct: $C_7H_6O_2{\cdot}C_4H_6N_3O{\cdot}C_7H_5O_2{\cdot}C_4H_5N_3O$, $M_r = 466.46$, colorless needles, $0.35 \times 0.24 \times 0.14$ mm, space group $P2_1/c$, $a = 22.410(1)$, $b = 7.450(1)$, $c = 13.060(1)$ Å, $\beta = 91.918(1)^\circ$, $V = 2179.2(4)$ Å^3, $Z = 4$, $\rho_{calcd} = 1.422$ g cm^3, $\mu = 0.106$ mm^{-1}, $2\theta = 56.58$, $(Mo_{K\alpha}) = 0.71073$ Å, $T = 298(2)$ K, 12642 total reflections, $R_1 = 0.079$ and $wR_2 = 0.160$ for 5066 reflections. Crystal data for cytosine and phthalic acid adduct: $2\,C_4H_6N_3O{\cdot}C_8H_4O_4$, $M_r = 388.35$, colorless needles, $0.35 \times 0.22 \times 0.13$ mm, space group $P2_1/m$, $a = 3.684(1)$, $b = 29.770(4)$, $c = 7.338(1)$ Å, $\beta = 92.76(1)^\circ$, $V = 803.8(3)$ Å^3, $Z = 2$, $\rho_{calcd} = 1.604$ g cm^3 $\mu = 0.126$ mm^{-1}, $2\theta = 56.44$, $(Mo_{K\alpha}) = 0.71073$ Å, $T = 298(2)$ K, 4517 total reflections, $R_1 = 0.057$ and $wR_2 = 0.169$ for 1847 reflections. Crystal data for cytosine and isophthalic acid adduct: $C_4H_5N_3O{\cdot}C_8H_6O_4$, $M_r = 277.24$, colorless needles, $0.32 \times 0.25 \times 0.13$ mm, space group $P\bar{1}$, $a = 8.588(1)$, $b = 8.963(2)$, $c = 9.061(2)$ Å, $\alpha = 100.81(1)$, $\beta = 105.20(1)$, $\gamma = 113.08(1)^\circ$, $V = 585.1(2)$ Å^3, $Z = 2$, $\rho_{calcd} = 1.574$ g cm^3 $\mu = 0.125$ mm, $2\theta = 56.56$, $(Mo_{K\alpha}) = 0.71073$ Å, $T = 298(2)$ K, 5071 total reflections, $R_1 = 0.040$ and $wR_2 = 0.111$ for 2651 reflections. CCDC-281299–281302 contain the supplementary crystallographic data for this paper. These data can be obtained free of

 © 2005 Wiley-VCH Verlag GmbH & Co. KGaA, Weinheim

charge from the Cambridge Crystallographic Data Centre via www.ccdc.cam.ac.uk/data_request/cif.
[15] Labeling of N atoms have been adopted from IUPAC labeling of atoms in the nucleobases.
[16] In the literature, a 3:1 adduct of phthalic acid and adenine is known as an hexahydrate,[11b] in which the phthalic acid was produced in situ as an hydrolyzed product of *N*,*N*-phthaloyl-DL-glutamic acid. A comparison of the simulated powder patterns of it with the one we obtained show drastic differences,[13] thus suggesting the possibility of a new solid-state structure of phthalic acid and adenine in our adduct.

 © 2005 Wiley-VCH Verlag GmbH & Co. KGaA, Weinheim

Supramolecular Chemistry

DOI: 10.1002/anie.200502202

Porous Capsules Allow Pore Opening and Closing That Results in Cation Uptake**

Achim Müller, Liviu Toma, Hartmut Bögge, Christian Schäffer, and Anja Stammler*

Dedicated to Prof. Herbert W. Roesky on the occasion of his 70th birthday

Structurally well-defined spherical porous molybdenum oxide based nanocapsules of the type $\{Pentagon\}_{12}\{Linker\}_{30}$[1,2] can be described as artificial cells as they allow the modeling—in solution studies—of passive biological ion transport[3a,b] as well as cell response to stimuli[3c] (see also ref. [4]); for biochemically related literature, see ref. [5a]. Specifically we refer herein to spherical, nanoscale, porous capsules/artificial cells of the type $[\{(Mo)Mo_5O_{21}(H_2O)_6\}_{12}\{Mo_2O_4(ligand)\}_{30}]^{n-}$,[1,2] the overall charges and internal surfaces of which can be fine-tuned by changing the ligands, thus allowing the type and structure of encapsulates to be influenced.[4] Most important, the 20 $\{Mo_9O_9\}$-type pores have crown-ether-like function and can be opened and closed with noncovalently bonded guests in a supramolecular fashion.[6a] Herein we will refer to the special situation of (protonated) urea molecules as guest species,[6b] which are found in all 20 of the capsule pores. Interestingly, after exposition of a solution of this type of capsule to Ca^{2+} ions the Ca^{2+} ions are incorporated, however, in the final precipitated product all 20 pores are again closed with the urea-type guests. This situation is not only of some interest regarding modeling of cell environment interactions but fundamentally shows in an example that supramolecular chemistry is, according to J.-M. Lehn,[5b] a "dynamic chemistry/science": the interaction between the parts, that is, the capsule pores and the "corks"/guests, is based on lability, which allows an easy exchange corresponding to the reversibility of noncovalent interactions. Furthermore, we should note that "*calcium probably fulfills a greater variety of biological functions than any other cation*";[6c] this includes for instance the special role of Ca^{2+} ions in information mediation in connection with the ubiquitous presence of Ca^{2+} channels in excitable cells.[5a] In the present case, the up-taken Ca^{2+} ions influence/direct the structure of the capsule encapsulates, that is, of the water-molecule-based assembly.

Exposition of an aqueous solution of **1**[6d]—where the 20 pores are closed with protonated urea molecules—to Ca^{2+} ions leads finally to the precipitation of **2** which was characterized by elemental analysis, thermogravimetry (to determine the number of crystal water molecules), redox titration (to determine the number of Mo^V centers), bond valence sum (BVS) calculations,[7] spectroscopic methods (IR, Raman), and single-crystal X-ray structure analysis.[8,9]

$$(H^+ \cdot OC(NH_2)_2)_{23}(NH_4)_{29-n}[\{(H^+ \cdot OC(NH_2)_2)_{20} + (H_2O)_{81-n} + (NH_4)_n\} \subset \{(Mo^{VI})Mo^{VI}{}_5O_{21}(H_2O)_6\}_{12}\{Mo^V{}_2O_4(SO_4)\}_{30}] \cdot \approx 100\,H_2O \equiv (H^+ \cdot OC(NH_2)_2)_{23}(NH_4)_{29-n}\mathbf{1a} \cdot \approx 100\,H_2O \quad \mathbf{1}^{[10]}$$

$$(H^+ \cdot OC(NH_2)_2)_{15}(NH_4)_{21-n}[\{(H^+ \cdot OC(NH_2)_2)_{20} + Ca_8 + (H_2O)_{60} + (NH_4)_n\} \subset \{(Mo^{VI})\,Mo^{VI}{}_5O_{21}(H_2O)_6\}_{12}\{Mo^V{}_2O_4(SO_4)\}_{30}] \cdot \approx 150\,H_2O \equiv (H^+ \cdot OC(NH_2)_2)_{15}(NH_4)_{21-n}\mathbf{2a} \cdot \approx 150\,H_2O \quad \mathbf{2}$$

According to the X-ray crystallographic results, the capsule **2a** (Figure 1) shows the characteristic basic polyoxomolybdate skeleton[1,2]—the artificial cell's "inorganic membrane"[4b]—that is present in **1a**,[10] and which also occurs in other spherical capsules.[1,2,4] However, in **2a** there are additionally 20 protonated urea guests closing the 20 $\{Mo_9O_9\}$ pores/rings through noncovalent (that is, hydrogen-bond) interactions[6ab], and, encapsulated Ca^{2+} ions; furthermore, the structure of the encapsulated water-molecule assembly is different in **2a** from that of **1a**. (The presence of Ca^{2+} can also be demonstrated by IR spectroscopy by the shift of a specific sulfate band from 1036 in **1** to 1057 cm^{-1} in **2**; see ref. [3a].) The eight calcium cations found in **2a** are disordered over 20 equivalent positions below the $\{Mo_9O_9\}$ pore openings at the end of the channels (Figure 1), that is, on the C_3 axes, and exhibit the expected octahedral coordination environment which is formed by three oxygen atoms of three sulfate ligands and three oxygen atoms belonging to the encapsulated water shell/assembly (see below and ref. [4]). Whereas **1a** shows the known structure of the NH_4^+/H_2O assembly within a capsule containing SO_4^{2-} ligands,[4a] in **2a** a

[*] Prof. Dr. A. Müller, L. Toma, Dr. H. Bögge, C. Schäffer, A. Stammler
Lehrstuhl für Anorganische Chemie I
Fakultät für Chemie der Universität
Postfach 100131, 33501 Bielefeld (Germany)
Fax: (+49) 521-106-6003
E-mail: a.mueller@uni-bielefeld.de

[**] Financial support from the Deutsche Forschungsgemeinschaft, the Fonds der Chemischen Industrie, the Volkswagenstiftung, the German–Israeli Foundation for Scientific Research and Development (GIF), and the European Union is gratefully acknowledged. L.T. thanks the Graduiertenkolleg "Strukturbildungsprozesse" of the University of Bielefeld for a fellowship. Furthermore, the contributions from Dr. Alice Merca and Dr. Soumyajit Roy (preparation of the educt) as well as Dr. Andreas Mix (NMR spectra) are acknowledged.

 © 2005 Wiley-VCH Verlag GmbH & Co. KGaA, Weinheim

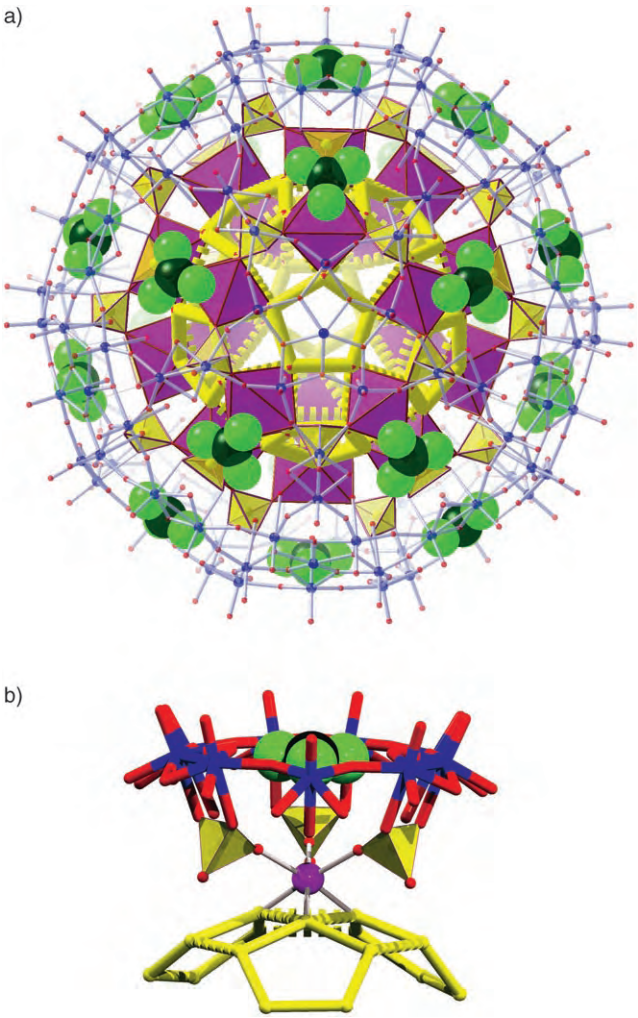

Figure 1. a) Structure of the capsule **2a** with the skeleton in ball-and-stick representation (Mo blue, O red), sulfate ligands (yellow tetrahedra), Ca^{2+} ions in the octahedral coordination of oxygen atoms (pink octahedra), the rhombicosidodecahedral $(H_2O)_{60}$ water assembly inside the capsule (yellow wire-frame representation, solid and dotted lines), and the protonated urea corks (space-filling representation, C dark green, N/O (urea) green). b) For clarity one segment of **2a** is shown separately (same color code as in (a)).

pure, well-defined water assembly/shell $\{H_2O\}_{60} \approx 12\{H_2O\}_5$ (radius 6.81–7.12 Å; occupation factor 1 for the O atoms) acting as ligand to the Ca^{2+} ions is observed,[11a] the formation and positioning of which is directed by the abundance of the fixed Ca^{2+} ions. (Though the exact NH_4^+ and H_2O positions in **1a** cannot be distinguished by X-ray crystallography because of a related disorder, there is clear evidence that NH_4^+ ions are involved in the formation of the central $\{X_{20}\}$ dodecahedron.[11a]) The $(H_2O)_{60}$ shell of **2a** corresponds to a distorted rhombicosidodecahedron which might be regarded as an unprecedented polydentate/macrocyclic ligand for the calcium ions or other cations.

Recall that we start with a capsule **1a** closed by the protonated urea "corks" and detect Ca^{2+} ions afterwards in the capsule **2a**, the pores of which are again closed by the same corks. The inorganic membrane pores are definitely not permanently closed, and in solution only a fraction of the pores is always (statistically) open (Figure 2). This problem related to the "behavior" of the corks in solution cannot of course be solved by an X-ray crystallography study. On the other hand, preliminary ^1H NMR spectra of solutions of **2** in DMF at room temperature clearly indicate the abundance of oxygen-protonated urea species in the pores.[11b] (Oxygen protonation would agree with earlier results for the protonation sites of urea determined by IR and ^{17}O NMR spectroscopy.[6b]) In this case, the peak-intensity analysis reveals that approximately a third of the capsule pores are occupied.[11c] Interesting, in this context, is the possibility of stabilizing the OH-type protonated urea species by integration into the pores. Furthermore, a well-defined temperature-dependent equilibrium can—in the case of guest cations exhibiting a much higher affinity[6a] for the pores than protonated urea—be easily studied by NMR spectroscopy in different solvents.[11d] With such guests the remarkable situation arises in which all the 20 pores are completely closed at lower temperatures and can be (reversibly) opened on heating with the consequence that uptake of different types of cations only occurs at higher temperatures (temperature gating). This process can be demonstrated nicely by ^1H- and metal-NMR spectroscopy studies including EXSY data.[11d]

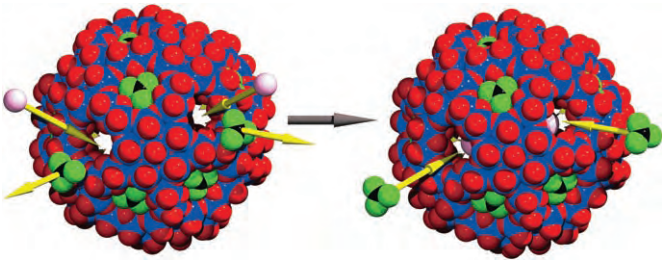

Figure 2. Space-filling representation demonstrating a simplified view of the Ca^{2+} ion uptake based on the capsule **1a**. In the anions of **1** the pores are closed. Treating a solution of **1** with Ca^{2+} ions leads to cation uptake (left) while in the final product **2** the pores again are closed (right; Mo blue, O red, C black, N/O(urea) green, Ca^{2+} pink, yellow arrows indicate direction of motion).

Under the conditions employed the Ca^{2+} ions cannot pass through the pores with their hydrate coat: for an effective trafficking the comparably large Ca^{2+} complexes must release their water ligands and some of these ligands are "taken up" again inside the artificial cell. (Note: the inorganic membrane pores are semipermeable allowing uptake and release of water but not of organic solvents such as DMF or DMSO.[3b,11d]) A condition for the uptake is therefore that the affinity of Ca^{2+} ions for the H_2O ligands is not too strong. This condition is met in this case as the water ligand "mean residence time" is of the order around 10^{-8} s at room temperature,[12] which is comparable to the published water exchange rate constant of $6–9 \cdot 10^8\ s^{-1}$.[13ab,14] As $[Ca(H_2O)_6]^{2+}$ shows a much greater lability compared to the related Be^{2+} and Mg^{2+} hydrate complexes, Be^{2+} and Mg^{2+} should therefore both show a different behavior with respect to their inter-

 © 2005 Wiley-VCH Verlag GmbH & Co. KGaA, Weinheim

actions with the capsule(s).[14] In this context there is another attractive aspect which is related to the possibility of trapping complete hydrate complexes above the capsules' pores based on hydrogen-bond interactions between the O atoms of the $\{Mo_9O_9\}$ pores/rings and the H_2O ligands. But this type of trapping only occurs for the present type of hydrate complex, which has a low stability-constant value, with less negatively charged capsules, for example, those with linkers containing less negatively charged ligands, such as acetates (instead of sulfates), where the capsule–cation interaction is weaker.[15] Interesting in this context is that the coordination environment of calcium ions in water is not very well defined, and correspondingly different coordination numbers for Ca^{2+} ions are reported in the literature.[13a] This gives, in principle, the option to trap different hydrate complexes in this or in related metal complexes at the capsule surface sites under different conditions,[13c] including different capsule charges (so called "Sphere Surface Chemistry").

An aspect of more general interest in this context is the chance to carry out systematic studies on the interaction between the capsules/artificial cells—the pores of which are partially or temporarily closed with different kinds of complementary guests—and a series of different hydrated cations present in solution; this would allow information to be obtained on the properties and behavior of hydrate complexes. The entrance of appropriate cations can nicely be studied in solution with NMR spectroscopy.[3a,b] Importantly, most of the biological ion pores/channels are not continuously open (note: the K^+ ion leak channels are) they are gated, that is, they can open and then close again.[5a] The opening is due to a response to specific stimuli, for example, corresponding to a change in the voltage across the membrane (leading to the channel protein conformational changes), a mechanical stress, or binding of a ligand.[5a] Referring to the present situation, the abundance of a large number of added cations, such as Ca^{2+}, in the vicinity or at the surface of the highly charged capsule decreases the capsule's charge, that is, diminishes the formal electrochemical gradient.[5a] This can 1) facilitate the release of guests such as protonated (even comparably strongly bonded) organic bases complementary to the $\{Mo_9O_9\}$ pores, and 2) allow subsequent entering of the cations (voltage gating of channels[5a]). In the case of more strongly bonded guests (see above and ref. [6]), this leads to complete pore closing at lower temperatures and cation uptake is observed only at higher temperatures (temperature gating (see above)). Once the cations are encapsulated the charge distribution changes, which might again influence the gating of the pores.

In the present system cation entrance is interesting because of the following facts: Voltage-gated calcium channels—ubiquitous in excitable cells in which Ca^{2+} functions as the ubiquitous intracellular messenger—play a key role in various physiological processes, such as muscle contraction, hormone and neurotransmitter secretion, and neuronal excitability. Several extracellular signals can induce an increase in the cytosolic Ca^{2+} ion concentration by 10–20-fold, which triggers the response.[5a,16,17] An interesting result of the present study is also that the uptake of Ca^{2+} ions leads to a "response in the cavity" in the form of a change in the structure of the encapsulates, that is, of the water/electrolyte based assembly.

Experimental Section

Synthesis of **1** (see also ref. [10]): A mixture of $(NH_4)_{42}[\{(Mo)Mo_5O_{21}(H_2O)_6\}_{12}\{Mo_2O_4(CH_3COO)\}_{30}]\cdot\approx[10\,CH_3COONH_4+300\,H_2O]$ (1.0 g, 0.04 mmol),[2d] ammonium sulfate (4.0 g, 30 mmol), urea (3.0 g, 50 mmol), and water (100 mL) was acidified with 16% HCl (8 mL) in a 250-mL conical flask (covered with a watch-glass) and stirred for 45 min at room temperature. The solution was kept in an open 250-mL beaker at around 23 °C for 10 days. Then the precipitated brown rhombohedral crystals of **1** were collected by filtration and dried in air. Yield: 0.35 g (35% based on Mo); elemental analyses (%) calcd N 5.69, H 2.62, C 1.82; found: N 5.6, H 2.7, C 1.8.

Characteristic IR bands: (KBr pellet, some characteristic bands for the range 1700–500 cm^{-1}): $\tilde{\nu}=1703$ [w, $\delta(ureaH^+)$], 1622 [s, $\delta(H_2O)$], 1555 [w, $\delta(ureaH^+)$], 1402 [m, $\delta(NH_4)$], 1196 (w), 1140 (m), 1036 (w) [all $\nu_{as}(SO_4)$], 972 [s, ν(Mo=O)], 852 (m), 795 (s), 723 (s), 630 (w), 569 cm^{-1} (s). (The $ureaH^+$ bands are influenced by the hydrogen bonds in the pores and are rather different from those of urea itself.)

Characteristic Raman bands: (solid state, KBr dilution, $\lambda_e\approx1064$ nm): $\tilde{\nu}=950$ [m, ν(Mo=O)], 880 [ν_s ($O_{bridging}$ breathing/A_{1g})], 372 (m), 303 cm^{-1} (w).

2: A mixture of **1** (2.0 g, 0.07 mmol), $CaCl_2\cdot2H_2O$ (0.5 g, 3.40 mmol), and water (50 mL; pH < 2) was stirred for 2 h at room temperature. The solution was then kept in an open 250-mL beaker at about 23 °C and after one week the precipitated brown rhombohedral crystals were collected by filtration through a glass frit (D2) and dried in air. Yield: 0.6 g (30% based on Mo); elemental analyses (%) calcd N 4.47, C 1.47, H 2.55, Ca 1.12; found: N 4.5, C 1.5, H 2.4, Ca 1.1.

Characteristic IR bands: (KBr pellet, some characteristic bands for the range 1700–500 cm^{-1}): $\tilde{\nu}=1703$ [w, $\delta(ureaH^+)$], 1624 [s, $\delta(H_2O)$], 1555 [w, $\delta(ureaH^+)$], 1402 [s, $\delta(NH_4)$], ≈1200 (sh), 1143 (m-s), 1057 (w) [all $\nu_{as}(SO_4)$], 976 (s), 947 (w) [both ν(Mo=O)], 854 (m), 796 (s), 725 (s), 632 (w), 573 cm^{-1} (s).

Characteristic Raman bands: (solid state, KBr dilution, $\lambda_e\approx1064$ nm): $\tilde{\nu}=950$ [m, ν(Mo=O)], 879 [ν_s ($O_{bridging}$ breathing/A_{1g})], 372 (m), 302 cm^{-1} (w).

The chemical formulae of **1** and **2** refer to the maximum possible number of crystal water molecules which correspond to the related volume calculated from the cell volume and the sum of volumes of all cell ingredients excluding those of the crystal water molecules. The given calculated values for C, N, Ca are related to a formula with 50 crystal water molecules less than given (note: **1** and **2** as all similar compounds show slow weathering, that is, loss of crystal water).

Received: June 23, 2005
Published online: November 8, 2005

Keywords: calcium · ion transport · molybdenum · polyoxometalates · porous capsules

[1] L. Cronin in *Comprehensive Coordination Chemistry II, Vol. 7* (Eds.: J. A. McCleverty, T. J. Meyer), Elsevier, Amsterdam, **2004**, pp. 1–56.

[2] a) A. Müller, P. Kögerler, C. Kuhlmann, *Chem. Commun.* **1999**, 1347–1358; b) A. Müller, S. Roy, *Coord. Chem. Rev.* **2003**, *245*, 153–166; c) L. Cronin, E. Diemann, A. Müller in *Inorganic Experiments*, 2nd ed. (Ed.: J. D. Woollins), Wiley-VCH, Weinheim, **2003**, pp. 340–346; d) A. Müller, S. K. Das, E. Krickemeyer, C. Kuhlmann, *Inorg. Synth.* (Ed.: J. R. Shapley) **2004**, *34*, pp. 191–200; e) A. Müller, S. Roy in *The Chemistry of Nanomaterials: Synthesis, Properties and Applications* (Eds.: C. N. R. Rao, A. Müller, A. K. Cheetham), Wiley-VCH, Wein-

 © 2005 Wiley-VCH Verlag GmbH & Co. KGaA, Weinheim

heim, **2004**, pp. 452 – 475; f) N. Hall, *Chem. Commun.* **2003**, 803 – 806.

[3] This finding is based on ^{7}Li NMR solution studies: a) A. Müller, D. Rehder, E. T. K. Haupt, A. Merca, H. Bögge, M. Schmidtmann, G. Heinze-Brückner, *Angew. Chem.* **2004**, *116*, 4566 – 4570; *Angew. Chem. Int. Ed.* **2004**, *43*, 4466 – 4470; corrigendum: A. Müller, D. Rehder, E. T. K. Haupt, A. Merca, H. Bögge, M. Schmidtmann, G. Heinze-Brückner, *Angew. Chem.* **2004**, *116*, 5225; *Angew. Chem. Int. Ed.* **2004**, *43*, 43, 5115 (see also: M. Gross, *Chem. World* **2004**, *1*, 18) and; b) E. T. K. Haupt, C. Wontorra, D. Rehder, A. Müller, *Chem. Commun.* **2005**, 3912 – 3914; c) A. Müller, E. Krickemeyer, H. Bögge, M. Schmidtmann, S. Roy, A. Berkle, *Angew. Chem.* **2002**, *114*, 3756 – 3761; *Angew. Chem. Int. Ed.* **2002**, *41*, 3604 – 3609.

[4] a) A. Müller, E. Krickemeyer, H. Bögge, M. Schmidtmann, B. Botar, M. O. Talismanova, *Angew. Chem.* **2003**, *115*, 2131 – 2136; *Angew. Chem. Int. Ed.* **2003**, *42*, 2085 – 2090; b) A. Müller, H. Bögge, M. Henry, *C. R. Chim.* **2005**, *8*, 47 – 56; c) M. Henry, H. Bögge, E. Diemann, A. Müller, *J. Mol. Liq.* **2005**, *118*, 155 – 162; d) A. Müller, S. K. Das, S. Talismanov, S. Roy, E. Beckmann, H. Bögge, M. Schmidtmann, A. Merca, A. Berkle, L. Allouche, Y. Zhou, L. Zhang, *Angew. Chem.* **2003**, *115*, 5139 – 5198; *Angew. Chem. Int. Ed.* **2003**, *42*, 5039 – 5044.

[5] a) B. Alberts, A. Johnson, J. Lewis, M. Raff, K. Roberts, P. Walter, *Molecular Biology of the Cell*, 4th ed., Garland Science, New York, **2002**; b) J.-M. Lehn, *Proc. Natl. Acad. Sci. USA* **2002**, *99*, 4763 – 4768, and references therein.

[6] a) The first published example referred to the integration of $20[C(NH_2)_3]^+$ ions into the $20\{Mo_9O_9\}$ pores/rings in the same way as into a crown ether host, that is, the O···H–N bonding is comparable to that in crown ether hosts; for details see ref. [3c]. The pore(host)–guest interactions with other protonated bases such as $H^+{\cdot}OC(NH_2)_2$ (see below) and $HC(NH_2)_2^+$ (unpublished results; see also comments in the text) are as expected weaker, while with the increasing basicity of the corresponding unprotonated base—which is lowest in case of urea—the stability of the protonated species increases (H. R. Christen, F. Vögtle, *Organische Chemie, Vol. 1*, Salle and Sauerländer, Frankfurt am Main, **1992**, p. 452); b) Urea is, apart from its biological (e.g., protein denaturation) and industrial importance (see, for example, J. W. Steed, J. L. Atwood, *Supramolecular Chemistry*, Wiley, New York, **2000**, p. 273), especially interesting structurally and chemically: firstly because of the abundance of the (complementary) hydrogen-bonding sites giving rise to the remarkable cage/inclusion structures (see, for example, G. A. Jeffrey, *An Introduction to Hydrogen Bonding*, Oxford University Press, New York, **1997**, p. 175), and secondly to the (in principle) different sites for protonation, that is, at the N and O atoms. The OH type species is stabilized by the contribution of the mesomeric border structure exhibiting the $C{=}NH_2^+$ fragment (K. P. C. Vollhardt, N. E. Schore, *Organische Chemie*, Wiley-VCH, 3. Aufl, Weinheim, **2000**, p. 956; see also: H. Beyer, W. Walter, *Lehrbuch der Organischen Chemie*, Hirzel, Stuttgart, 21. Aufl., **1988**, p. 356). Important in this case is that O protonation allows hydrogen-bond interactions in the pores in three directions. The problem of protonated sites was controversial for a long time starting from Alfred Werner's opinion: From vibrational spectra of normal urea salts, for example, with the $PtCl_6^{2-}$ ion, it was concluded for the first time that the preferable site of protonation is the O atom (W. Kutzelnigg, R. Mecke, *Chem. Ber.* **1961**, *94*, 1706 – 1716). Also from ^{17}O NMR spectroscopy studies over a wide pH range, from aqueous solution to fluoro sulfonic acid, it was concluded that (the first) protonation takes place at the O atom; in a magic acid even double protonation was observed (B. Valentine, T. E. St. Amour, D. Fiat, *Org. Magn. Reson.* **1984**, *22*, 697–700); c) W. Kaim, B. Schwederski, *Bioinorganic Chemistry: Inorganic Elements in the Chemistry of Life*, Wiley, Chichester, **1994**, p. 293; d) Note: this type of capsules is stable in solution at pH values between 1.5 and 4 and under exclusion of oxygen.

[7] I. D. Brown in *Structure and Bonding in Crystals, Vol. II* (Eds.: M. O'Keeffe, A. Navrotsky), Academic Press, New York, **1981**, pp. 1 – 30.

[8] Crystal data for **2**: $C_{35}H_{823}Ca_8Mo_{132}N_{91}O_{809}S_{30}$, $M_r = 29415.4\ g\,mol^{-1}$, rhombohedral, space group $R\bar{3}$, $a = 32.8169(7)$, $c = 73.921(2)$ Å, $V = 68944(3)$ Å^3, $Z = 3$, $\rho = 2.125\ g\,cm^{-3}$, $\mu = 1.96\ mm^{-1}$, $F(000) = 42978$, crystal size $= 0.40 \times 0.30 \times 0.30\ mm^3$. Crystals of **2** were removed from the mother liquor and immediately cooled to 183(2) K on a Bruker AXS SMART diffractometer (three circle goniometer with 1 K CCD detector, $Mo_{K\alpha}$ radiation, graphite monochromator; hemisphere data collection in ω at 0.3° scan width in three runs with 606, 435, and 230 frames ($\varphi = 0$, 88 and 180°) at a detector distance of 5.00 cm). A total of 115162 reflections ($1.55 < \Theta < 27.01°$) were collected of which 32366 reflections were unique ($R(\mathrm{int}) = 0.0290$). An empirical absorption correction using equivalent reflections was performed with the program SADABS 2.10. The structure was solved with the program SHELXS-97 and refined using SHELXL-97 to $R = 0.0389$ for 27502 reflections with $I > 2\sigma(I)$, $R = 0.0487$ for all reflections; max./min. residual electron density 1.87 and $-1.85\ e\,Å^{-3}$ (SHELXS/L, SADABS from G. M. Sheldrick, University of Göttingen, **1997/2003**; structure graphics with DIAMOND 3.0, http://www.crystalimpact.com/ and with POV-Ray 3.6, http://www.povray.org/).

[9] The basic structure of the educt **1**[10], for which the synthesis is also given (see Experimental Section), corresponds to that of **2**.

[10] a) S. Roy, Thesis, Faculty of Chemistry, University of Bielefeld, **2005**; b) A. Müller, A. Merca, S. Roy, H. Bögge, M. Schmidtmann, unpublished results.

[11] a) The shell system in the cavity of **1a** spanned by $n\,NH_4^+/m\,H_2O = X$ centers with $m \gg n$ is X_{60} (distorted rhombicosidodecahedron) + X_{20} (dodecahedron) + X (in the center) and is also found, for example, in an ammonium/sulfate-based capsule with open pores;[4a] the X_{60} shell is geometrically similar to the known pure water assembly $\{H_2O\}_{60}$ shell such as that in **2a** (see also ref. [4b,c]). There is clear evidence that the NH_4^+ ions in **1a** are rather strongly fixed in the cavity, as shown by combined thermogravimetry, mass spectroscopy, and temperature-dependent elemental analyses studies up to 450 °C; remarkably, the release of the "last" NH_3 molecules out of the capsules upon heating occurs at rather high temperatures (A. Malecki, A. Bielanski, E. Diemann, A. Müller, unpublished results). On the other hand it is evident that a change of the positions of the NH_4^+ ions during the conversion of **1a** into **2a** occurs while a Ca^{2+}–NH_4^+ counter transport takes place which leads to very small values of n in **2** and is currently being investigated in detail by ^{15}N HSQC NMR spectroscopy (E. T. K. Haupt, A. Müller, unpublished results); b) A. Mix, H. Bögge, T. Mitra, D. Rehder, A. Müller, unpublished results; c) In an aqueous solution of **1** the ratio of open to closed pores is unknown. The complete pore closing observed in solid **2** is to some extent influenced by the fact that it lowers the capsule charge and leads to a lower solubility of **2**; d) A. Mix, H. Bögge, D. Rehder, T. Mitra, M. Schmidtmann, A. Müller, unpublished results.

[12] F. A. Cotton, G. Wilkinson, C. A. Murillo, M. Bochmann, *Advanced Inorganic Chemistry*, 6th ed., Wiley, New York, **1999**, page 59.

[13] a) D. T. Richens, *The Chemistry of Aqua Ions: Synthesis, Structure and Reactivity: A Tour Through the Periodic Table of the Elements*, Wiley, Chichester, **1997**; b) See also: H. Krüger, *Chem. Soc. Rev.* **1982**, *11*, 227 – 256; c) Regarding unprecedented coordination numbers it should be mentioned in this context that recently for the first time evidence for a fivefold coordination of a trivalent metal aqua ion, that is, of Al^{III} could be obtained

 © 2005 Wiley-VCH Verlag GmbH & Co. KGaA, Weinheim

(T. W. Swaddle, J. Rosenqvist, P. Yu, E. Bylaska, B. L. Phillips, W. H. Casey, *Science* **2005**, *308*, 1450 – 1453).

[14] The exchange rate for water ligands in the Ca^{2+} complex is, for instance, too fast to be measured by dynamic NMR spectroscopy.[13]

[15] A. Müller, L. Toma, H. Bögge, M. Schmidtmann unpublished results; see also Ref. [4b].

[16] a) B. Hille, *Ion Channels of Excitable Membranes*, 3rd ed., Sinauer, Massachusetts, **2001**; b) D. E. Clapham, *Nature* **2003**, *426*, 517 – 524.

[17] The surface of the excitable cell type mentioned holds thousands of related channels that precisely control the timing and entry of Ca^{2+} ions. Furthermore, the inhibition of the Ca^{2+} ion entry through channels by antagonists/entry blockers is of tremendous importance for the treatment of hypertony and coronary heart diseases because an excess of Ca^{2+} ions in the cells has to be avoided, a situation which nature can normally remedy through an effective control by Ca^{2+} ion pumps (T. A. Scott, E. I. Mercer, *Concise Encyclopedia Biochemistry and Molecular Biology*, 3rd ed., de Gruyter, New York, **1997**; E. Mutschler, *Arzneimittelwirkungen*, Wissenschaftliche Verlagsgesellschaft, Stuttgart, **1986**, p. 447).

 © 2005 Wiley-VCH Verlag GmbH & Co. KGaA, Weinheim

Surface Chirality

DOI: 10.1002/anie.200501655

Enantiospecific Chemisorption of Small Molecules on Intrinsically Chiral Cu Surfaces**

*Bhawna Bhatia and David S. Sholl**

Solid surfaces that define chiral interfaces are of great interest for potential applications in chiral processing.[1–4] The observation that highly stepped metal surfaces are intrinsically chiral has created interest in the use of these surfaces for enantiospecific separations and catalysis.[5–9] An enantiospecific separation based on the reversible adsorption of molecules on a chiral Cu surface has recently been demonstrated.[10] Chemisorption of enantiopure amino acids on low-index Cu surfaces has been shown to lead to the spontaneous formation of homochiral surface facets.[11] A number of common mineral surfaces are also intrinsically chiral.[12] Enantiospecific adsorption on chiral surfaces is controlled by the preferred locations and orientations of adsorbed molecules, but assessment of these properties experimentally is extremely challenging. Below, we present predictions of the preferred binding configurations of two small species on a chiral Cu surface, Cu(874), made by using density functional theory (DFT) calculations.

Previous theoretical studies of molecular adsorption on chiral metal surfaces have focused on physisorbed molecules, which can be described using empirical potentials.[6,8,9,13] DFT has been used to study the chemisorption of $HSCH_2CHNH_2CH_2P(CH_3)_2$ on a chiral Au surface,[14] thus predicting a binding-energy difference between the two molecular enantiomers of 0.09 eV. Unfortunately, neither this molecule nor the Au surface used in these calculations have been characterized experimentally. Herein, we consider a chiral Cu surface of the type that has been used in a number of experiments[15–18] and examine two molecular adsorbates, one of which, propylene oxide, has been used in several experimental studies of surface chirality.[1,16,19] We recently used DFT methods very similar to those used below to determine the structure of chiral adlayers of amino acids on low-index Cu surfaces and found very good agreement between the calculated structures and those observed experimentally.[20,21]

Our calculations examined the adsorption of the amino(fluoro)methoxy (FAM) species and propylene oxide on a Cu(874) surface. A schematic view of these moieties as they bind on Cu surfaces is shown in Figure 1. Cu(874) is intrinsically chiral because of the kinked steps that separate its (111)-oriented terraces (Figure 2).[5–9] Using the standard notation for defining the chirality of these surfaces,[5–9] the surface shown in Figure 2 and used in our calculations is denoted Cu(874)^S. Real chiral Cu surfaces exhibit a distribution of step and kink lengths because of the thermal motion of step-edge atoms.[22,23] Detailed models of these step distributions suggest that the structures that define Cu(874) are representative of a large number of surface orientations with (111)-oriented terraces.[13,24] Cu(643), which has been used in most experiments of intrinsically chiral metal surfaces, also has (111)-oriented terraces.[10] The unit cell of Cu(874) is somewhat larger than Cu(643), thus making it more suitable for calculations in which the effect of adsorbate–adsorbate interactions is minimal.

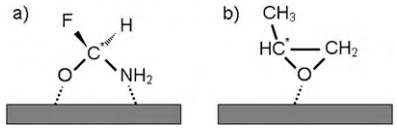

Figure 1. Schematic representations of a) FAM and b) PO binding on a metal surface. In each species, the chiral center is denoted by an asterisk and bonds with the surface are shown with dashed lines.

A challenging aspect of examining molecular adsorption on stepped metal surfaces computationally is that large numbers of adsorption configurations must be examined.[14,18] This task can be simplified if some information is available on

[*] B. Bhatia, Prof. D. S. Sholl
Department of Chemical Engineering
Carnegie Mellon University
Pittsburgh, PA 15213 (USA)
Fax: (+1) 412-268-7319
E-mail: sholl@andrew.cmu.edu

[**] Financial support from the National Science Foundation (CTS-0216170), the US Department of Energy (DE-FG02-03ER15473), and the Alfred P. Sloan Foundation (DSS) is gratefully acknowledged.

Supporting information for this article is available on the WWW under http://www.angewandte.org or from the author.

 © 2005 Wiley-VCH Verlag GmbH & Co. KGaA, Weinheim

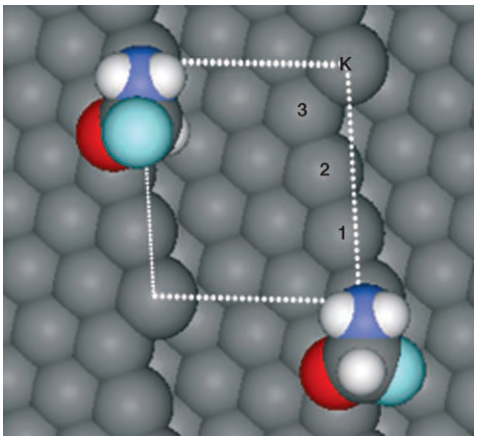

Figure 2. The most favorable binding geometries of *R*-FAM (top left) and *S*-FAM (bottom right) on Cu(874)^S as computed by using DFT. Dashed lines indicate a single surface unit cell. The surface-kink atom (K) and step-edge atoms (1–3) are labeled.

the types of binding sites preferred by the moieties of interest. We first examined the adsorption of methoxy (OCH_3), chlorofluoromethoxy (OCHClF), methylamine (H_3CNH_2), and chlorofluoromethylamine ($HClFCNH_2$) species on Cu(111) (see the Supporting Information). We previously used DFT to examine the adsorption of fluoroethoxy species on Cu(111) and found excellent agreement between the calculated and experimental adsorption geometries and energies.[25] Both methoxy (amine) species were found to favor threefold fcc (top) sites, with each forming a single bond with the surface. We then examined the adsorption of chlorofluoromethoxy and chlorofluoromethylamine species on Cu(874) for multiple positions of these species near the step edge; both favor adsorption on the upper edge of the surface step. Binding energies on the stepped surface were 0.33–0.40 eV more stable than on Cu(111). Based on this observation, we only consider configurations with molecules bound to step edges in the calculations described below. The difference between the binding energy of terrace and step sites is larger for the amine than the methoxy species. The preferred binding site for the amine is on top of the kink atom shown in Figure 2.

Based on our preliminary calculations, we investigated the adsorption of *R*- and *S*-FAM on Cu(874)^S in detail. For *S*-FAM, we considered configurations with the amino group on top of atoms K, 1, 2, and 3 in Figure 2. For each configuration, six distinct rotations of the N–O direction about the surface normal were considered. For each of these configurations, two distinct orientations that differ in the angle formed by C–H and C–F with respect to the surface normal were examined. This procedure yields 48 distinct configurations for *S*-FAM/Cu(874)^S. An equivalent set of 48 configurations for *R*-FAM was also examined. From these 96 configurations, we excluded 64 states in which the O atom was located in what could be considered a pure terrace site. The remaining 32 states were geometrically optimized by using $3\times3\times1$ *k* points. The 21 states with the most favored energies from these calculations were further optimized with $7\times7\times1$ *k* points and dipole corrections.

Two views of the most favored adsorption configurations for *S*- and *R*-FAM on Cu(874)^S are shown in Figures 2 and 3. There is a significant energy difference between the two

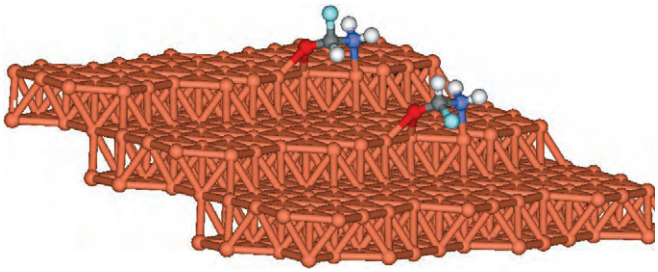

Figure 3. Side view of *R*- (left) and *S*-FAM (right) on Cu(874)^S.

enantiomers, as the *R*-FAM binding to the surface is 0.13 eV stronger than the *S*-FAM binding. This difference is the largest enantiospecific adsorption-energy difference that has been predicted or observed to date for molecular adsorption on a chiral metal surface. The origin of this enantiospecific binding can be understood as follows: Both enantiomers bind to the same surface atoms (see Figure 3). These bonds, as characterized by the Cu–O and Cu–N distances (see the Supporting Information), are essentially the same for the two adsorbed enantiomers. These surface bonds constrain the C–F bond to point towards (away from) the surface for *S*-FAM (*R*-FAM) and vice versa for the C–H bond. The energy difference between the adsorbed enantiomers arises from the different local environments of the F atom; the more stable *R* enantiomer has the F atom far from the surface. The energetic preference for F atoms to not lie close to a Cu surface has been observed before with DFT calculations and experiments for 2-fluoroethoxy/Cu(111).[25] Interactions between the F atom and step edge in *S*-FAM induce slight distortions in the molecule; the O-C-F bond angle is 114° for adsorbed *S*-FAM but 109° for *R*-FAM.

Many local minima exist for *R*- and *S*-FAM on Cu(874)^S. For *R*-FAM, the next four most favorable states had energies of 0.12, 0.18, 0.20, and 0.22 eV relative to the most stable state. For *S*-FAM, the next four locally stable states had energies of 0.16, 0.19, 0.21, and 0.23 eV relative to the favored configuration of *R*-FAM. The distribution of energy minima accessible to each adsorbed enantiomer is shown in Figure 4.

The species treated above exhibits strongly enantiospecific binding on Cu(874)^S but suffers from the serious drawback that it is not readily available for experiments. To address this point, we performed similar calculations for propylene oxide (PO) on Cu(874)^S. PO has previously been used experimentally as a probe for enantiospecific binding on both intrinsically chiral metal surfaces[16] and chirally templated surfaces.[1,19] We first examined the adsorption of PO on Cu(111) and found that the molecule favors a configuration in which the terminal methyl group is oriented away from the surface. Test calculations with PO on Cu(874)^S showed that PO binds much more strongly to step-edge sites than to terrace sites, so only adsorption configurations with the molecule above the step edge were considered

 © 2005 Wiley-VCH Verlag GmbH & Co. KGaA, Weinheim

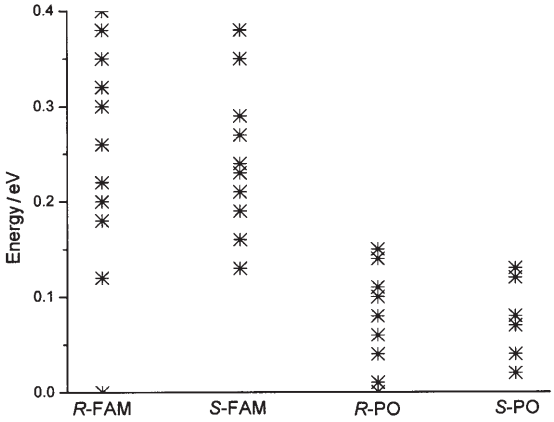

Figure 4. Energies of the distinct local minima observed for FAM and PO adsorbed on Cu(874)^S measured relative to the energy of the most favorably bound configuration of either enantiomer of the species of interest. These results are from calculations using $3\times3\times1$ *k* points. Calculations using $7\times7\times1$ *k* points were performed for 21 states of FAM and 15 states of PO; the figure does not change appreciably if these energies are plotted.

further. A set of configurations sampling the placement and orientation of *S*- and *R*-PO were examined by using methods analogous to our calculations for FAM. In all, 23 configurations were examined. The most stable orientations for each enantiomer on the surface are shown in Figures 5 and 6. Both

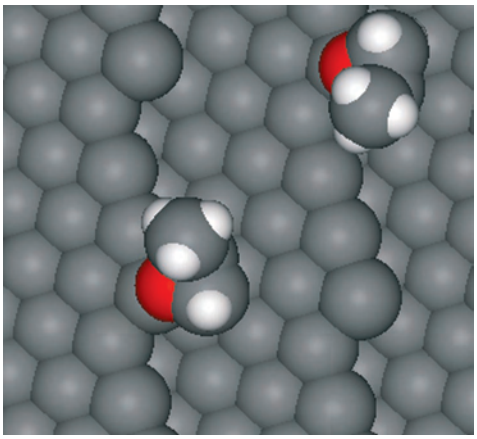

Figure 5. The most favorable binding geometries of *R*- (bottom left) and *S*-PO (top right) on Cu(874)^S, as computed by using DFT.

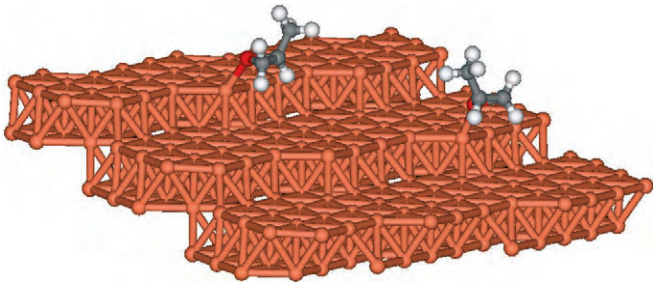

Figure 6. Side view of *R*- (left) and *S*-PO (right) on Cu(874)^S.

enantiomers favor geometries with the O atom above the surface-kink atom and the terminal methyl group oriented away from the surface. The calculated energy difference between the two adsorbed enantiomers is much smaller than the energy difference for FAM; for PO, the energy difference is 0.02 eV with the *R* enantiomer being favored. Energy differences of this magnitude lie close to the limit of those that can be reliably distinguished with DFT, but the distinct orientations of the adsorbed molecules in Figure 5 and the other less favored adsorption configurations described below make it clear that the adsorption of PO on Cu(874)^S is enantiospecific. The energy differences between adsorbed enantiomers of PO are considerably smaller than those described above for FAM. This difference can be understood by noting that the enantiomers differ by which atom, F or H, interacts with the step edge for FAM in its favored configurations. For PO, the same atoms, both H, interact with the step edge for both adsorbed enantiomers, which strongly limits the size of the energy difference between the adsorbed enantiomers.

Similar to FAM, multiple local minima exist for PO on Cu(874)^S, as shown in Figure 4. Because of the relatively small energy differences between these minima, a distribution of states would be observed in any experiment that probes these species. This observation is consistent with the experimental observation that thermal desorption spectra from the most strongly bound surface states of *R*- and *S*-PO on Cu(643) yield broad features that cannot be readily analyzed in terms of adsorption enantiospecificity.[16] Desorption from other surface sites associated with higher surface coverages of PO has been seen experimentally to be enantiospecific.[16] We have not attempted to characterize these states computationally, as it would require the examination of large numbers of coadsorption configurations.

Our DFT calculations have provided two examples of the enantiospecific adsorption of small molecules on a chiral Cu surface, Cu(874)^S. Calculations of this type will be a great assistance to complement experimental studies of molecular adsorption on chiral surfaces.[10–12] By examining the adsorption of a variety of functional groups on stepped metal surfaces, DFT calculations can be used to understand what aspects of molecular architecture can lead to highly enantiospecific interactions with chiral metal surfaces. Similarly, performing analogous calculations on a range of chiral surfaces will provide insight into the role of surface structure on enantiospecific adsorption.[10]

Experimental Section

Our plane-wave DFT calculations were performed with the Vienna ab initio Simulation Package with the ultrasoft pseudopotentials available in this package.[26,27] The results reported above used the generalized gradient approximation (GGA) with the PW91 functional. A small number of configurations were also examined with the rPBE functional within the PAW formalism. The energy differences between configurations with the rPBE-PAW calculations were found to coincide with those of the GGA-PW91 calculations. All GGA calculations used a plane-wave expansion with a cutoff of 425 eV and Fermi-level smearing with a width of 0.2 eV. Geometries were relaxed until the forces on all unconstrained atoms were less than 0.03 eV Å^{-1}.

 © 2005 Wiley-VCH Verlag GmbH & Co. KGaA, Weinheim

Final results were computed using a $7 \times 7 \times 1$ *k*-point mesh and dipole corrections. Prior to these calculations, the most favorable configurations were determined using $3 \times 3 \times 1$ *k* points as described above.

In our calculations, the DFT-optimized lattice parameter for Cu was used to define the periodicity of the material in the plane of the surface. The computational supercell contained a single surface unit cell of $Cu(874)^S$ with a vacuum spacing greater than 10 Å in the direction of the surface normal. The surface unit cell is shown in Figure 2. This computational supercell contains 32 metal atoms. Our calculations were performed using slabs equivalent in thickness to three (111)-oriented layers. Molecules were adsorbed on only one side of the slab, and all degrees of freedom of all the metal atoms and the molecule were allowed to relax in all energy minimization calculations. A limited number of calculations, in which all the metal atoms were constrained in their bulk positions, indicated that surface relaxation is not a dominant effect in the relative adsorption energies of the most stable molecular configurations we examined.

Received: May 13, 2005
Revised: July 28, 2005

Keywords: chemisorption · density functional calculations · enantioselectivity · surface chemistry

[1] D. Stacchiola, L. Burkholder, W. T. Tysoe, *J. Am. Chem. Soc.* **2002**, *124*, 8984.
[2] A. M. Berg, D. L. Patrick, *Angew. Chem.* **2005**, *117*, 1855; *Angew. Chem. Int. Ed.* **2005**, *44*, 1821.
[3] J. A. Switzer, H. M. Kothari, P. Poizot, S. Nakanishi, E. W. Bohannan, *Nature* **2003**, *425*, 490.
[4] S. M. Barlow, R. Raval, *Surf. Sci. Rep.* **2003**, *50*, 201.
[5] C. F. McFadden, P. S. Cremer, A. J. Gellman, *Langmuir* **1996**, *12*, 2483.
[6] D. S. Sholl, *Langmuir* **1998**, *14*, 862.
[7] A. Ahmadi, G. Attard, J. Feliu, A. Rodes, *Langmuir* **1999**, *15*, 2420.
[8] D. S. Sholl, A. Asthagiri, T. D. Power, *J. Phys. Chem. B* **2001**, *105*, 4771.
[9] R. M. Hazen, D. S. Sholl, *Nat. Mater.* **2003**, *2*, 367.
[10] J. D. Horvath, A. Koritnik, P. Kamakoti, D. S. Sholl, A. J. Gellman, *J. Am. Chem. Soc.* **2004**, *126*, 14988.
[11] X. Y. Zhao, R. G. Zhao, W. S. Yang, *Langmuir* **2000**, *16*, 9812.
[12] R. M. Hazen, T. R. Filley, G. A. Goodfriend, *Proc. Natl. Acad. Sci. USA* **2001**, *98*, 5487.
[13] T. D. Power, A. Asthagiri, D. S. Sholl, *Langmuir* **2002**, *18*, 3737.
[14] Z. Sljivancanin, K. V. Gothelf, B. Hammer, *J. Am. Chem. Soc.* **2002**, *124*, 14789.
[15] A. J. Gellman, J. D. Horvath, M. T. Buelow, *J. Mol. Catal. A* **2001**, *167*, 3.
[16] J. D. Horvath, A. J. Gellman, *J. Am. Chem. Soc.* **2001**, *123*, 7953.
[17] J. D. Horvath, A. J. Gellman, *J. Am. Chem. Soc.* **2002**, *124*, 2384.
[18] P. Kamakoti, J. Horvath, A. J. Gellman, D. S. Sholl, *Surf. Sci.* **2004**, *563*, 206.
[19] D. Stacchiola, L. Burkholder, T. Zheng, M. Weinert, W. T. Tysoe, *J. Phys. Chem. B* **2005**, *109*, 851.
[20] R. B. Rankin, D. S. Sholl, *Surf. Sci.* **2004**, *548*, 301.
[21] R. B. Rankin, D. S. Sholl, *Surf. Sci.* **2005**, *574*, L1.
[22] X. Y. Zhao, S. S. Perry, *J. Mol. Catal. A* **2004**, *216*, 257.
[23] M. Giesen, S. Dieluweit, *J. Mol. Catal. A* **2004**, *216*, 263.
[24] A. Asthagiri, P. J. Feibelman, D. S. Sholl, *Top. Catal.* **2002**, *18*, 193.
[25] X. Li, A. J. Gellman, D. S. Sholl, *J. Mol. Catal. A* **2005**, *228*, 77.
[26] G. Kresse, J. Hafner, *Phys. Rev. B* **1993**, *48*, 13115.
[27] G. Kresse, J. Furthmuller, *Comput. Mater. Sci.* **1996**, *6*, 15.

 © 2005 Wiley-VCH Verlag GmbH & Co. KGaA, Weinheim

Catalyst Design

DOI: 10.1002/anie.200502000

Tailoring the Active Site of Chemzymes by Using a Chemogenetic-Optimization Procedure: Towards Substrate-Specific Artificial Hydrogenases Based on the Biotin–Avidin Technology**

*Gérard Klein, Nicolas Humbert, Julieta Gradinaru, Anita Ivanova, François Gilardoni, Untung E Rusbandi, and Thomas R. Ward**

Dedicated to Professor George M. Whitesides

Catalysis offers efficient means to produce enantiopure products. Traditionally, enzymatic and homogeneous catalysis have evolved independently to afford mild, robust, active, and highly selective catalysts.[1,2] Both systems are often considered complementary in terms of substrate and reaction scope, operating conditions, enantioselectivity mechanism, reaction medium, etc. For the optimization of activity and selectivity, directed-evolution methodologies (combined with an efficient selection or screening tool) outperform combinatorial ligand libraries.[3–13] With the hope of alleviating some of the inherent limitations of both enzymatic and organometallic catalysis, two approaches have recently witnessed a revival: 1) organocatalysis[14–19] and 2) artificial metalloenzymes based on either covalent[20,21] or supramolecular anchoring[22] of a catalytic moiety in a macromolecular host.[23–30]

Inspired by the early works of Whitesides and Wilson,[22] we recently reported artificial metalloenzymes based on the biotin–avidin technology.[31–35] Herein, we report our efforts to produce substrate-specific and *S*-selective artificial metalloenzymes based on the biotin–avidin technology for the hydrogenation of α-acetamidodehydroamino acids.

The starting point for the chemogenetic-optimization procedure presented herein is the identification of [Rh(cod)-(biot–**1**)]$^+$⊂S112G Sav (cod = 1,5-cyclooctadiene, biot =

[*] Dr. G. Klein,[+] N. Humbert,[+] Dr. J. Gradinaru, A. Ivanova, Dr. F. Gilardoni, U. E Rusbandi, Prof. T. R. Ward
Institute of Chemistry, University of Neuchâtel
Av. Bellevaux 51, CP 2, 2007 Neuchâtel (Switzerland)
Fax: (+41) 327-182-511
E-mail: thomas.ward@unine.ch

[+] Both authors contributed equally to the work.

[**] We thank Professor C. R. Cantor for the streptavidin gene and Professors P. Schürmann and J.-M. Neuhaus for their help in setting up the protein production. This work was funded by the Swiss National Science Foundation (Grants FN 620-57866.99 and FN 200021-105192/1 as well as NRP 47 "Supramolecular Functional Materials"), CERC3 (Grant FN20C321-101071), the Roche Foundation, the Canton of Neuchâtel, as well as the FP6 Marie Curie Research Training Network (MRTN-CT-2003-505020). Umicore Precious Metals Chemistry is acknowledged for a loan of rhodium.

Supporting information for this article is available on the WWW under http://www.angewandte.org or from the author.

InterScience
© 2005 Wiley-VCH Verlag GmbH & Co. KGaA, Weinheim

biotin, Sav = streptavidin, Scheme 1) as the best ligand–protein combination for the enantioselective reduction of α-acetamidoacrylic acid (up to 96 % *ee* in favor of (*R*)-acetamidoalanine (*N*-AcAla)).[32,33] These observations prompted us to perform saturation mutagenesis at position 112 of WT-Sav. The resultant 20 proteins were combined with the biotinylated catalyst precursors [Rh(biot-spacer-P_2)cod]BF_4 (P = diphenylphosphine donor; Scheme 1) to afford 360 artificial metalloenzymes. To gain broader insight into the substrate specificity, the catalytic runs were performed on both α-acetamidoacrylic acid and α-acetamidocinnamic acid simultaneously (both 50 equiv, Scheme 1). Control experiments established that the selectivity and conversion are identical to those obtained with a single substrate (i.e. no autoinduction).[6,36] The detailed experimental procedure is provided in the Supporting Information.

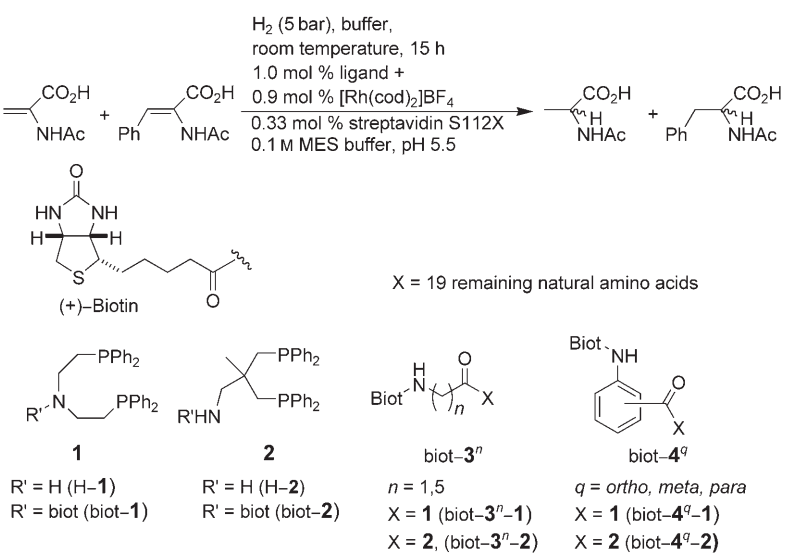

Scheme 1. Operating conditions used for the chemogenetic optimization of artificial hydrogenases in the reduction of α-acetamidoacrylic acid and α-acetamidocinnamic acid (50 equiv of each with respect to the ligand). MES buffer solution is composed of 4-morpholineethanesulfonic acid that is pH adjusted with sodium hydroxide.

The results of the chemogenetic-screening experiments with both substrates are summarized in Figure 1 by using a fingerprint display for each substrate–protein–ligand combination.[37] The selectivity is color coded: pink for *S*-selective and green for *R*-selective ligand–protein combinations. The intensity of the color reflects the percentage of conversion.[38] Both substrates are displayed as two hypotenuse-sharing triangles (HyShaTri) for each ligand–protein matrix element. This convenient display allows rapid identification of interesting ligand–protein combinations. Selected results are collated in Table 1 and a summary, including all catalytic runs (as well as multiple reproduction of selected experiments), is provided in the Supporting Information.

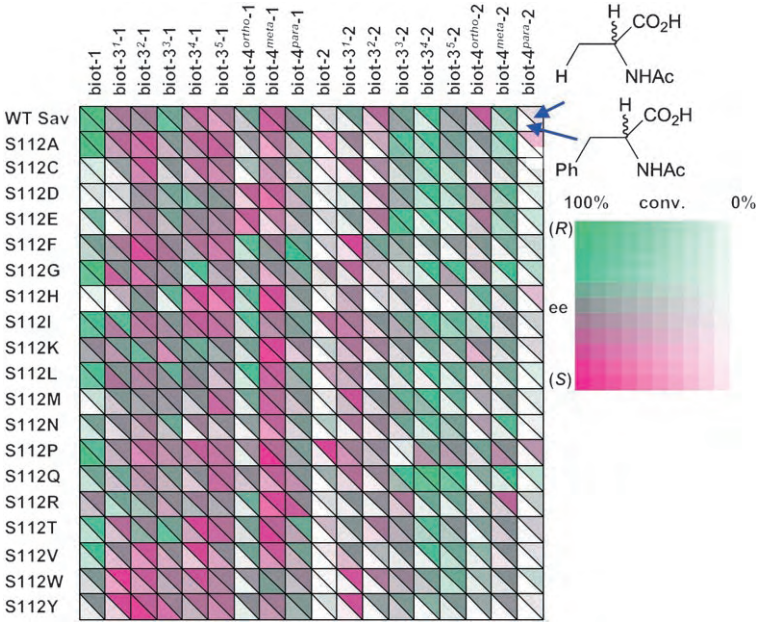

Figure 1. Fingerprint display of the results for the chemogenetic optimization for the reduction of α-acetamidoacrylic acid (top triangle) and α-acetamidocinnamic acid (bottom triangle) in the presence of 18 biotinylated ligands and 20 streptavidin isoforms obtained by saturation mutagenesis at position 112.

Analysis of the results that are displayed graphically in Figure 1 reveals several noteworthy general features:

1) Most ligand–protein combinations yield distinctively different results for both substrates. This trend is reflected by the differences in color (selectivity) and/or intensity (activity) for two HyShaTri (Figure 1). In general, enantioselectivity for *N*-AcPhe was higher than for *N*-AcAla; however, the reverse trend was observed for conversion as the smaller substrates systematically display higher yields.
2) The chemical optimization brings more diversity than the genetic counterpart. This is best illustrated through the comparison of line vectors (i.e. chemical optimization) with column vectors (i.e. genetic optimization). The line vector S112P yields reduction products with both *R* and *S* configurations in respectable *ee* values for *N*-AcPhe (Table 1, entries 5 and 8).
3) Overall, the ligand scaffold **1** outperformed the ligand scaffold **2** both in terms of enantioselectivity and conversion. The best spacer–ligand combinations are biot–**1** (which yields *R* products, Table 1, entries 1–5) and biot–**4**^{meta}–**1**, in combination with cationic amino acid residues in position 112 (which yields *S* products, Table 1, entries 6–9). We speculated that the cationic side chains interact through ionic hydrogen bonds with the carboxylate functionality of the substrate, thus favoring coordination of one of the prochiral faces of the substrate.
4) The most pronounced differences in substrate selectivity (in terms of conversion) are observed with biot–**3**^{1}–**2** in combination with aromatic residues in position 112 (Table 1, entries 10–12).
5) For the biot-**1** vector, the lowest conversions were obtained with mutants that had a potentially coordinating amino acid side chain in position 112 and included S112C (Table 1, entry 3), S112D, S112H, and S112M (to a lesser extent S112E and S112Y as well, Figure 1). We speculated

 © 2005 Wiley-VCH Verlag GmbH & Co. KGaA, Weinheim

Table 1: Numerical summary of selected results of the catalytic experiments.

Entry	Ligand	Protein	*ee* *N*-AcPhe[1]	*ee* *N*-AcAla[2]	Conv. *N*-AcPhe	Conv. *N*-AcAla
1	biot–**1**	WT Sav	93(*R*)	94(*R*)	84	quant.[3]
2	biot–**1**	S112A	94(*R*)	93(*R*)	94	quant.[3]
3	biot–**1**	S112C	90(*R*)	76(*R*)	10	19
4	biot–**1**	S112G	94(*R*)	93(*R*)	77	quant.[3]
5	biot–**1**	S112P	87(*R*)	31(*R*)	96	quant.[3]
6	biot–**4**^{meta}–**1**	S112H	81(*S*)	58(*S*)	88	quant.[3]
7	biot–**4**^{meta}–**1**	S112K	88(*S*)	63(*S*)	89	quant.[3]
8	biot–**4**^{meta}–**1**	S112P	78(*S*)	36(*S*)	quant.[3]	quant.[3]
9	biot–**4**^{meta}–**1**	S112R	86(*S*)	63(*S*)	71	quant.[3]
10	biot–**3**^{1}–**2**	S112F	36(*S*)	64(*S*)	20	quant.[3]
11	biot–**3**^{1}–**2**	S112W	33(*S*)	59(*S*)	8	96
12	biot–**3**^{1}–**2**	S112Y	42(*S*)	55(*S*)	10	quant.[3]
13	biot–**3**^{4}–**2**	S112Q	92(*R*)	87(*R*)	77	quant.[3]

[1] *N*-AcPhe = α-acetamidophenylalanine; [2] *N*-AcAla = α-acetamidoalanine; [3] quant. = quantitative conversion. Reproducibility: *ee* ± 1.5% (when *ee* > 60%; up to *ee* ± 5% with low *ee* values) and conversion ± 10%. All listed experiments were performed at least in duplicate.

that these Lewis basic side chains coordinate to the rhodium center, thus interfering with the catalytic cycle.

6) Introduction of a glutamine in position 112 yields *R*-selective artificial metalloenzymes when combined with biot-**3**^{4}-**2** (92% *ee* (*R*), Table 1, entry 13).

This study thus demonstrates the potential of saturation mutagenesis at position 112 coupled with chemical optimization to yield both *R* and *S* reduction products as well as substrate-specific artificial metalloenzymes. Although general trends in enantioselectivity are mostly dictated by the biot–spacer–ligand scaffold (chemical optimization), saturation mutagenesis (genetic optimization) provides the critical second-coordination-sphere interactions between the host protein and the prochiral substrate. It is precisely such crucial weak interactions between a catalyst and its substrate that distinguish enzymatic from homogeneous systems.[41]

Received: June 10, 2005
Revised: September 11, 2005
Published online: November 8, 2005

Keywords: asymmetric catalysis · combinatorial chemistry · hydrogenation · metalloenzymes · mutagenesis

[1] K. Faber, *Biotransformations in Organic Chemistry, 5th ed.*, Springer, Berlin, **2004**.
[2] *Comprehensive Asymmetric Catalysis* (Eds.: E. N. Jacobsen, A. Pfaltz, H. Yamamoto), Springer, Berlin, **1999**.
[3] M. T. Reetz, *Proc. Natl. Acad. Sci. USA* **2004**, *101*, 5716.
[4] M. T. Reetz, *Angew. Chem.* **2002**, *114*, 1391; *Angew. Chem. Int. Ed.* **2002**, *41*, 1335.
[5] S. V. Taylor, P. Kast, D. Hilvert, *Angew. Chem.* **2001**, *113*, 3408; *Angew. Chem. Int. Ed.* **2001**, *40*, 3310.
[6] C. Gennari, U. Piarulli, *Chem. Rev.* **2003**, *103*, 3071.
[7] B. Jandeleit, D. J. Schaefer, T. S. Powers, H. W. Turner, W. H. Weinberg, *Angew. Chem.* **1999**, *111*, 2648; *Angew. Chem. Int. Ed.* **1999**, *38*, 2494.
[8] M. T. Reetz, *Angew. Chem.* **2001**, *113*, 292; *Angew. Chem. Int. Ed.* **2001**, *40*, 284.
[9] D. Wahler, J.-L. Reymond, *Curr. Opin. Chem. Biol.* **2001**, *5*, 152.
[10] M. Breuer, K. Ditrich, T. Habicher, B. Hauer, M. Kesseler, R. Stürmer, T. Zelinski, *Angew. Chem.* **2004**, *116*, 806; *Angew. Chem. Int. Ed.* **2004**, *43*, 788.
[11] A. J. J. Straathof, S. Panke, A. Schmid, *Curr. Opin. Biotechnol.* **2002**, *13*, 548.
[12] H.-U. Blaser, F. Spindler, M. Studer, *Appl. Catal. A* **2001**, *221*, 119.
[13] H.-U. Blaser, *Chem. Commun.* **2003**, 293.
[14] H. Pracejus, H. Mätje, *J. Prakt. Chem.* **1964**, *24*, 195.
[15] U. Eder, G. Sauer, R. Wiechert, *Angew. Chem.* **1971**, *83*, 492; *Angew. Chem. Int. Ed. Engl.* **1971**, *10*, 496.
[16] A. Berkessel, H. Gröger, *Asymmetric Organocatalysis*, Wiley-VCH, Weinheim, **2005**.
[17] P. I. Dalko, L. Moisan, *Angew. Chem.* **2004**, *116*, 5248; *Angew. Chem. Int. Ed.* **2004**, *43*, 5138.
[18] U. Kazmaier, *Angew. Chem.* **2005**, *117*, 2224; *Angew. Chem. Int. Ed.* **2005**, *44*, 2186.
[19] Special Issue on Asymmetric Organocatalysis, *Acc. Chem. Res.* **2004**, *37*, 487.
[20] E. T. Kaiser, D. S. Lawrence, *Science* **1984**, *226*, 505.
[21] Z.-P. Wu, D. Hilvert, *J. Am. Chem. Soc.* **1989**, *111*, 4513.
[22] M. E. Wilson, G. M. Whitesides, *J. Am. Chem. Soc.* **1978**, *100*, 306.
[23] D. Qi, C.-M. Tann, D. Haring, M. D. Distefano, *Chem. Rev.* **2001**, *101*, 3081.
[24] B. G. Davis, *Curr. Opin. Biotechnol.* **2003**, *14*, 379.
[25] C. M. Thomas, T. R. Ward, *Chem. Soc. Rev.* **2005**, *34*, 337.
[26] G. Roelfes, B. L. Feringa, *Angew. Chem.* **2005**, *117*, 3294; *Angew. Chem. Int. Ed.* **2005**, *44*, 3230.
[27] M. Ohashi, T. Koshiyama, T. Ueno, M. Yanase, H. Fujii, Y. Watanabe, *Angew. Chem.* **2003**, *115*, 1035; *Angew. Chem. Int. Ed.* **2003**, *42*, 1005.
[28] J. R. Carey, S. K. Ma, T. D. Pfister, D. K. Garner, H. K. Kim, J. A. Abramite, Z. Wang, Z. Guo, Y. Lu, *J. Am. Chem. Soc.* **2004**, *126*, 10812.
[29] A. Mahammed, Z. Gross, *J. Am. Chem. Soc.* **2005**, *127*, 2883.
[30] T. Ueno, T. Koshiyama, M. Ohashi, K. Kondo, M. Kono, A. Suzuki, T. Yamane, Y. Watanabe, *J. Am. Chem. Soc.* **2005**, *127*, 6556.
[31] M. Wilchek, E. A. Bayer in *Methods in Enzymology, Vol. 184*, Academic Press, San Diego, **1990**.
[32] J. Collot, J. Gradinaru, N. Humbert, M. Skander, A. Zocchi, T. R. Ward, *J. Am. Chem. Soc.* **2003**, *125*, 9030.
[33] M. Skander, N. Humbert, J. Collot, J. Gradinaru, G. Klein, A. Loosli, J. Sauser, A. Zocchi, F. Gilardoni, T. R. Ward, *J. Am. Chem. Soc.* **2004**, *126*, 14411.
[34] T. R. Ward, *Chem. Eur. J.* **2005**, *11*, 3798.
[35] C. Letondor, N. Humbert, T. R. Ward, *Proc. Natl. Acad. Sci. USA* **2005**, *102*, 4683.
[36] T. Satyanarayana, H. B. Kagan, *Adv. Synth. Catal.* **2005**, *347*, 737.
[37] D. Wahler, F. Badalassi, P. Crotti, J.-L. Reymond, *Chem. Eur. J.* **2002**, *8*, 3211.
[38] To generate the RGB codes for a catalytic experiment yielding one of the products in *x*% yield, *y*%(*R*), and *z*%(*S*) (100% − *y*% = *z*% (*S*)), the following formulas were imple-

 © 2005 Wiley-VCH Verlag GmbH & Co. KGaA, Weinheim

mented in an Excel macro: RGB1 = [100−(*y***x*)/100]*2.55; RGB2 = [100−(*z***x*)/100]*2.55; RGB3 = 0.5*(RGB1+RGB2).

[39] To solubilize both substrates, MES buffer solution (0.1M, pH 5.5) was used. Compared with the buffer solution traditionally used for α-acetamidoacrylic acid (0.1M acetate, pH 4.0), slightly lower conversions (up to −5%) and lower enantioselectivities (up to −3%) were occasionally encountered. For the sake of coherence, all results presented herein are based on the dual substrate screening which must be performed in 0.1M MES (pH 5.5). This is because of the low solubility of α-acetamidocinnamic acid in 0.1M acetate buffer at pH 4.0. The results reported previously for *N*-AcAla (96% *ee* (R) with the biot–**1**–S112G) can be attained only with an 0.1M acetate buffer (pH 4.0).[32,33]

[40] W. S. Knowles, *Acc. Chem. Res.* **1983**, *16*, 106.

[41] For a recent example of the exploitation of second-coordination-sphere interactions in organocatalysis, see: T. P. Yoon, E. N. Jacobsen, *Angew. Chem.* **2005**, *117*, 470; *Angew. Chem. Int. Ed.* **2005**, *44*, 466.

 © 2005 Wiley-VCH Verlag GmbH & Co. KGaA, Weinheim

Directed Assembly

DOI: 10.1002/anie.200502117

Decoration of Microspheres with Gold Nanodots—Giving Colloidal Spheres Valences**

Gang Zhang, Dayang Wang, and Helmuth Möhwald*

To obtain a large variety of structures from colloids, one has to lend colloidal spheres a multiplicity of directed interactions that are analogous to those of atoms. This directionality is achieved in the work presented herein by combining the building of colloidal crystals with Au evaporation and plasma etching. The resulting colloidal spheres exhibit two, three, four, or five nanosized Au dots that are analogous to sp-hybridized atomic orbitals.

Colloidal spheres have been extensively investigated due to their broad spectrum of industrial and fundamental applications, especially their use in photonic crystals.[1–4] Various colloidal spheres, organic and inorganic, can be produced that are exceedingly monodisperse in terms of size and shape. Nevertheless, their surfaces still remain chemically homogeneous or heterogeneous in an undefined way despite there being well-established methods to modify surfaces. This surface chemistry renders the coupling of spheres spatially isotropic, so it is difficult to spatially direct the organization of the spheres. They self-assemble only into simple and energy-favorable structures such as face-centered-cubic (fcc) or hexagonal-close-packing (hcp) arrays. In this respect, colloidal spheres have changed little in at least a century.

The ability to spatially direct the integration of spheres or selectively link other nano-objects on spheres necessitates the spatially selective attachment of functional sites on colloidal spheres, thus creating analogues of valency of atoms and breaking the spatially isotropic coupling into anisotropic coupling. Up to date, however, little effort has been shown to address this challenge. Nelson theoretically testified the possibility of creating valences on microspheres by coating them with anisotropic objects such as nanorods.[5] Fitzmaurice and co-workers immobilized linear aggregates of Au nanoparticles on silica microspheres by fixing nanoporous membranes on microspheres to template the self-assembly of nanoparticles.[6] The controlled deposition of Au vapor allows capping of microspheres with half an Au shell.[7–9] Using the upper single layers of colloidal crystals as masks during Au vapor deposition, we recently demonstrated a simple and versatile way of fabricating various Au patterns on the upper halves of the lower spheres, whose dimension and feature are predominantly manipulated by the orientation of the template crystals.[10] Our methodology is demonstrably independent of the size and surface chemistry of the spheres. As the size of the Au patterns is comparable to that of the spheres, they may not be ideal as valences to direct the coupling of the spheres. Herein we have used the upper bilayers of polystyrene (PS) colloidal crystals that have been etched by O_2 plasma as masks for Au deposition on the spheres of the lower layers. This process allows decoration of microspheres with two, three, four, and five Au nanodots, whose arrangements are linear, trigonal, tetrahedral, or right-pyramidal in space, respectively. In terms of configuration, these Au nanodots might be considered as nanoscale analogues of the sp-hybridized chemical valences in, for example, carbon and silicon atoms.

Our previous study reported the formation of one Au nanodot on the upper half of a shell of microspheres by using the upper bilayers of their colloidal crystals.[10] However, the smaller interstices in the upper bilayers cause a non-uniform diffusion of Au vapor, so the dimension and features of the Au dots obtained in our previous study were not uniform or clear-cut as compared with those of patterns derived from a single-layer template.[10] To circumvent this non-uniform diffusion of Au vapor, in the present work we etched slightly PS colloidal crystals with O_2 plasma prior to Au vapor deposition. Yang and co-workers suggested that the shadow of the upper layers in the colloidal crystals renders the plasma etching anisotropic, which not only increases the interstice sizes between spheres but also allows the creation of new interstitial shapes.[11]

Figure 1 schematically represents our procedure for the fabrication of Au nanodots on microspheres by using the upper bilayers of O_2-plasma-etched colloidal crystals as masks for Au vapor deposition. In this work, we organized 270 or 920 nm PS spheres through a dip-coating process. After optimizing the withdrawing speed and the concentration of

[*] Dr. G. Zhang, Dr. D. Wang, Prof. H. Möhwald
Max Planck Institute of Colloids and Interfaces
14424 Potsdam (Germany)
Fax: (+49) 331-567-9202
E-mail: dayang.wang@mpikg-golm.mpg.de

[**] This work is supported by the Max Planck Society.

Supporting information for this article is available on the WWW under http://www.angewandte.org or from the author.

© 2005 Wiley-VCH Verlag GmbH & Co. KGaA, Weinheim

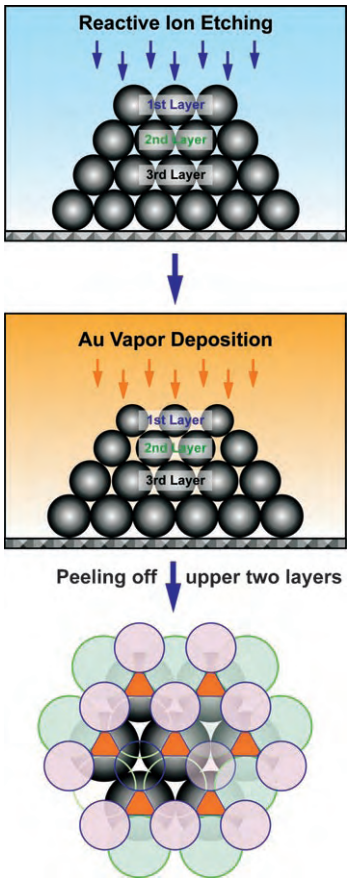

Figure 1. Construction of Au nanodots on microspheres by combining Au vapor deposition and the use of the upper bilayers of O_2-plasma-etched colloidal crystals with (111) facets parallel to the substrates as masks. The orange areas represent Au domains that remained on spheres after removal of the upper two layers.

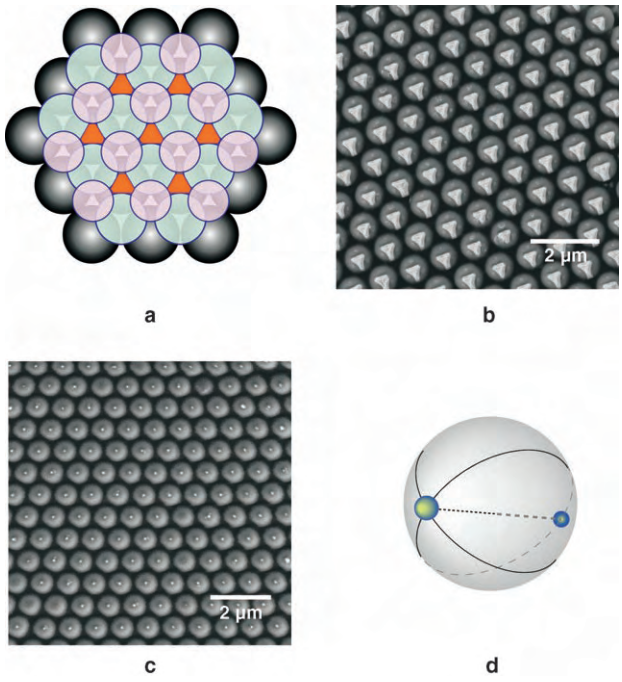

Figure 2. a) Au patterns obtained atop spheres in the third layer in O_2-plasma-etched colloidal crystals with an fcc structure by using the upper bilayers as a mask during Au vapor deposition. The stacking symmetry of the crystals is ABCABC and their (111) facets are parallel to the substrates. The spheres in the first, second, and third layers are highlighted by pink, light green, and black, respectively; the Au patterns on the third layer spheres are orange. The incidence angle between Au vapor flow and the normal direction of the crystals films is set as 0°. b) SEM image of the resulting Au patterns deposited on the upper halves of 925 nm PS spheres in the third layer obtained by templating their fcc colloidal crystals that had been etched by O_2 plasma for 10 min and coated with a 100 nm thick Au layer. The size of the resulting Au dots is in the range of 350–400 nm. c) SEM image of the Au patterns obtained on the lower halves of these spheres; the size of the resulting dots is around 80 nm. d) Schematic illustration of the spatial configuration of two Au nanodots constructed on microspheres.

PS suspensions, we constructed colloidal crystals with four or five layers of PS spheres on silicon wafers, in which single-crystal domains of a pure fcc structure extended over 50 μm and the preferential orientation parallel to the substrate was (111). In this packing structure, the spheres in the third layer are located just underneath the interstices in the upper bilayers, thus allowing Au vapor to reach them. After O_2-plasma etching, the PS spheres in the top layers are reduced in size due to direct exposure to O_2-plasma flow (see Figure 2a and Supporting Information), thus increasing the interstitial sizes between PS spheres. In this work, however, we found that prolonged plasma etching usually caused fusion of the spheres in colloidal crystals, which made it difficult to remove the upper layers. Hence the plasma-etching period was fixed at 3 min for 270 nm PS spheres and 10 min for 920 nm PS spheres. After Au vapor deposition and removal of the upper two layers with adhesive tape, a triangular Au dot was found exclusively atop the spheres. This can be seen by scanning electron microscopy (SEM, Figure 2b). The structural profiles of the resulting triangular dots were analyzed by atomic force microscopy (AFM; see Supporting Information), which indicated that the thicknesses of the triangular dots increase with an increase in the period of Au deposition.

After these third-layer PS spheres with a triangular Au nanodot on their upper halves were peeled off from the crystals, we observed a round Au nanodot on the apex of their lower halves (Figure 2c). According to the AFM analysis (see Supporting Information), the size and thickness of the resulting round Au nanodots increases with an increase in the Au vapor-deposition time. Thus, from a combination of the results shown in Figures 2b and c, we conclude that the PS spheres in the third layer are decorated with two Au nandots. These two dots are arranged opposite each other in the great circle of the sphere, as illustrated schematically in Figure 2d. In this scenario, the configuration of these two Au nanodots on a microsphere resembles that of the sp-hybridized atomic orbital of carbon atoms.

When the colloidal crystals with four layers of spheres were used, we found that round Au nanodots were visible on the lower halves not only of the third-layer spheres but also of the second-layer spheres and of the first-layer spheres, but not of the fourth-layer spheres that are attached directly to the substrate. The formation of these round Au dots is not

 © 2005 Wiley-VCH Verlag GmbH & Co. KGaA, Weinheim

entirely explained so far. We speculate that when the Au vapor diffuses from the top layers into the lower layers in colloidal crystals through the interstitial voids between the spheres, it might be scattered or reflected back by the surface of the spheres or the substrate. The scattered or reflected vapor should condense on the lower halves of the spheres, opposite to the flow of the Au vapor, which should lead to the formation of the round Au dots. An investigation into the origin of this round Au nanodot is underway.

The features of Au patterns constructed on the spheres in the third layers in colloidal crystals are expected to be strongly dependent on the stacking structure of the colloidal crystals, ABCABC (fcc) or ABAB (hcp). However, so far we have had difficulty in controlling the stacking structures of colloidal crystals due to the exceedingly narrow energy difference between these two stacking structures.[12] The crystals, constructed by the existing methods, usually are a mixture of ABCABC (fcc) or ABAB (hcp) stacking structures. In the dip-coating process, we found that the rapid withdrawing speed led to the formation of more ABAB stacking structures. In an hcp array, the spheres in the third layer are positioned just under the spheres of the first layer, thus leaving air channels behind that allow Au vapor to penetrate freely through the whole crystal with little deposition on the lower-layer spheres. After plasma etching, the spheres in the first layer were smaller than those in the third layer, which may allow Au deposition on the edges of the latter (Figure 3a). After Au vapor deposition and removal of the upper two layers, three small triangular Au nanodots were observed on the edge of the upper halves of the spheres, which were arranged in a trigonal array (Figure 3c). In the current work, we learned that the number of Au dots atop the spheres is dependent on the incidence angle of the Au evaporation, the angle between the vapor flow and the normal direction of the sample surfaces.[13,14] If the incidence angle is increased from 0° to 10° (Figure 3b), the number of Au dots is reduced from three to two. Figure 3d reveals that the edges of the upper halves of the spheres are decorated with one large and one small triangular nanodots. In this case, one round Au nanodot was also found on the lower halves of the spheres in third layer in a way similar to that shown in Figure 2c. As shown in Figures 3e and f, the arrangement of Au nanodots on spheres can be expected to be tetrahedral (four dots) and trigonal (three dots), thus resembling nanoscale analogues of sp^3- and sp^2-hybridized molecular orbitals.

Thanks to enormous efforts in the past decade, it is possible to grow colloidal crystals with defined crystal orientation parallel to substrates. By use of substrates with V-shaped grooves, one can construct fcc colloidal crystals with a preferential plane of (100) parallel to the substrates.[15,16] In this square close-packing structure (ABAB stacking), the spheres in the third layers are located exclusively underneath those of the top layers. Therefore, no Au vapor may reach the third layer.[10] After plasma etching, four air gaps were opened up in the upper bilayers to allow the penetration of Au vapor (Figure 4a and Supporting Information). After Au vapor deposition and removal of the upper two layers, we constructed four rectangular Au nanodots on the edges of the upper halves of the PS spheres on the third layer (Figure 4b).

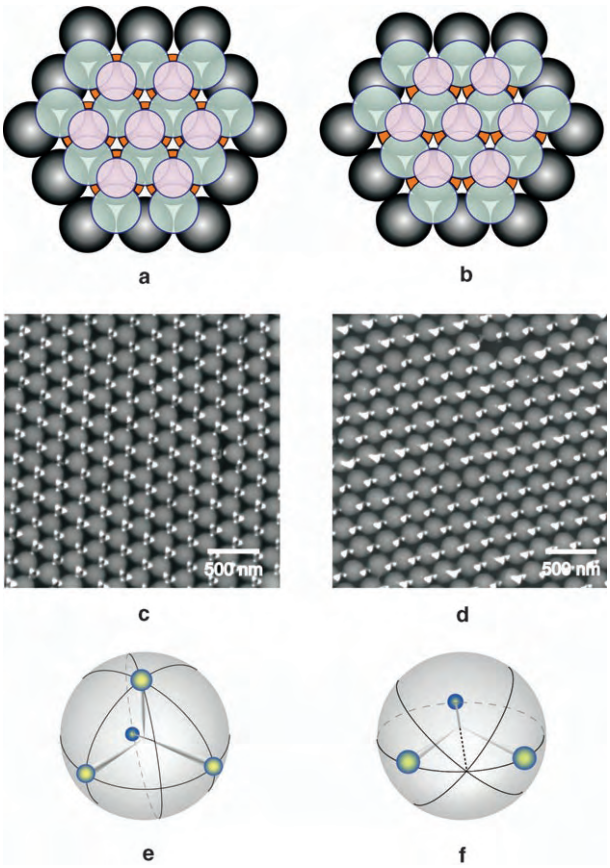

Figure 3. a, b) Au patterns atop the spheres in the third layer obtained by using the upper bilayers as a mask during Au vapor deposition in O_2-plasma-etched colloidal crystals with an ABAB stacking symmetry. The incidence angle between Au vapor flow and the normal direction of the crystal films is set as 0° (a) and 10° (b). c, d) SEM images of the Au patterns on the upper halves of 270 nm PS spheres in their hcp colloidal crystals, constructed at an incidence angle of 0° (c) and 10° (d). The crystals were etched by O_2 plasma for 3 min and coated by an Au layer 30 nm thick. c) Three Au dots of 20–45 nm in size on the edge of the PS spheres. d) One 90 nm and one 25 nm dot on the sphere edge. e, f) Spatial configurations of the resulting four (e) and three Au nanodots (f) on microspheres.

One round Au dot also formed on the center of the lower half of the spheres (see Supporting Information). As depicted in Figure 4c, five Au nanodots with a right-pyramidal configuration are therefore linked on one PS sphere. When the incidence angle of the Au vapor flow was set as 10°, only three rectangular Au nanodots—one big and two small—were obtained (Figure 4d). The spatial configuration of these three dots is expected to be similar to that shown in Figure 3e.

It is worth noting that the decoration of Au nanodots on microspheres is independent of the diameter of the spheres and is extendable to other polymer spheres. Nevertheless, the mechanical stability of the Au nanodots deposited on PS microspheres is currently poor. Redispersion of the PS spheres coated with Au dots into water resulted in the detachment of the Au dots, thus limiting their usage for directing self-assembly of spheres. To circumvent this drawback, we are currently extending our procedure to silica spheres with the aid of highly reactive ion etching. Further-

 © 2005 Wiley-VCH Verlag GmbH & Co. KGaA, Weinheim

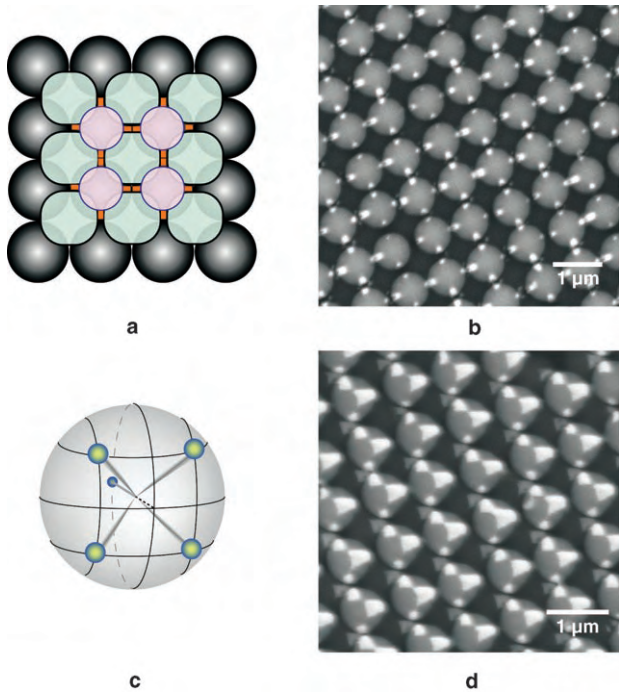

Figure 4. a) Au patterns atop the spheres in the third layers obtained by using the upper bilayers as a mask during Au vapor deposition in O_2-plasma-etched fcc colloidal crystals with (100) facets parallel to the substrates. The incidence angle is 0°. b) SEM image of the resulting Au patterns on the upper halves of 925 nm PS spheres in the third layer obtained by templating their colloidal crystals that had been etched by O_2 plasma for 10 min and coated with an Au layer 100 nm thick. The size of the resulting dots is in the range of 50–150 nm. c) Spatial configuration of the five Au nanodots constructed on the spheres. d) SEM image of the Au patterns atop the spheres in the third layer obtained at an incidence angle of 10°, which reveals a large Au dots (200 nm × 400 nm) and two small dots (about 150 nm).

more, the selective fabrication of colloidal crystals with either fcc or hcp structures is also a promising extension of this work.

In summary, we have demonstrated the feasibility of the decoration of PS microspheres with two, three, four, or five Au nanodots by using their colloidal crystals, etched by O_2 plasma, as masks for Au vapor deposition. The number of dots per sphere can be manipulated by use of different crystal structures and by altering the conditions of Au vapor deposition. The Au nanodots deposited on the spheres are arranged in a linear, trigonal, tetrahedral, or right-pyramidal fashion, which provides the nanoscale analogues of sp-hybridized atomic orbitals of carbon. The Au nanodots obtained on microspheres can be used as the bonding site to dictate the integration of the spheres, thus paving a new way to colloidal self-assembly—colloidal valent chemistry of spheres[5]—to create hierarchical and complex "supraparticles".[17]

Experimental Section

Aqueous suspensions (10 wt %) of polystyrene of 270 and 925 nm in diameter were purchased from Microparticles GmbH, Germany. The crystallization of these spheres on silicon wafers was conducted by a dip-coating process. The withdrawing speeds were optimized in the range of 0.5–5 $\mu m\,s^{-1}$ and the concentration of these spheres in the range of 1.0–2.0 wt % for 270 nm spheres and 3.0–5.0 wt % for 925 nm spheres to produce crystals with four or five layers of spheres. By using a plasma cleaner (PDC-32G, Germany), O_2-plasma etching was performed at a pressure of 0.2 mbar and a power density of 100 W. The optimal etching period was adjusted to 3 min for 270 nm PS colloidal crystals and 10 min for those of 925 nm. Au vapor deposition was conducted in a high-vacuum coater (Edwards Auto 306, UK) at a pressure of 10^{-7} mbar and a deposition speed of $0.02\,nm\,s^{-1}$. By varying the deposition time, Au layers of 30, 50, 100, and 200 nm thick were deposited within the plasma-etched colloidal crystals. Note that prior to Au deposition, the crystals were coated with chromium layers 5 nm thick. The incidence angles between the Au vapor flow and the normal direction of the samples were adjusted by tilting the samples on the sample holding blocks within the thermal deposition chamber.

After Au deposition, we placed double-sided adhesive tapes on the Au-coated surfaces of colloidal crystals and subsequently covered glass slides atop the adhesive tapes.[10] The glass slides were pressed at a pressure of $0.2\,kg\,cm^{-2}$ for 5 min, then the upper two layers were stripped off to leave an Au pattern on the spheres in the third layers. A similar process allowed the spheres in the third layers to be removed from the crystals. Both sides of the third-layer spheres were visualized by SEM. SEM images were recorded with a Gemini LEO 1550 instrument operated at 3 kV. To directly reveal the Au patterns on colloidal spheres, the samples were not sputtered by thin Au films before SEM measurements. AFM imaging was performed by using the Nanoscope Dimension 3100 system operating in tapping mode.

Received: June 17, 2005
Published online: November 8, 2005

Keywords: colloids · gold · nanostructures · self-assembly

[1] Y. Xia, B. Gates, Y. Yin, Y. Lu, *Adv. Mater.* **2000**, *12*, 693–713.
[2] D. Wang, H. Möhwald, *J. Mater. Chem.* **2004**, *14*, 459–468.
[3] A. Arsenault, S. Fournier-Bidoz, B. Hatton, H. Míguez, N. Tétreault, E. Vekris, S. Wong, S. M. Yang, V. Kitaev, G. A. Ozin, *J. Mater. Chem.* **2004**, *14*, 781–794.
[4] A. van Blaaderen, *MRS Bull.* **1998**, *23*, 39–43.
[5] D. R. Nelson, *Nano Lett.* **2002**, *2*, 1125–1129.
[6] a) L. Nagle, D. Ryan, S. Cobbe, D. Fitzmaurice, *Nano Lett.* **2003**, *3*, 51–53; b) L. Nagle, D. Fitzmaurice, *Adv. Mater.* **2003**, *15*, 933–935.
[7] J. C. Love, B. D. Gates, D. B. Wolfe, K. E. Paul, G. M. Whitesides, *Nano Lett.* **2002**, *2*, 891–894.
[8] Z. Bao, L. Chen, M. Weldon, E. Chandross, O. Cherniavskaya, Y. Dai, J. Tok, *Chem. Mater.* **2002**, *14*, 24–26.
[9] Y. Lu, H. Xiong, X. Jiang, Y. Xia, M. Prentiss, G. M. Whitesides, *J. Am. Chem. Soc.* **2003**, *125*, 12724–12725.
[10] G. Zhang, D. Wang, H. Möhwald, *Nano Lett.* **2005**, *5*, 143–146.
[11] D. Choi, H. K. Yu, S. G. Jang, S. M. Yang, *J. Am. Chem. Soc.* **2004**, *126*, 7019–7025.
[12] B. J. Alder, B. P. Carter, D. A. Young, *Phys. Rev.* **1969**, *183*, 831–833.
[13] a) C. L. Haynes, A. D. McFarland, M. T. Smith, J. C. Hulteen, R. P. van Duyne, *J. Phys. Chem. B* **2002**, *106*, 1898–1902; b) C. L. Haynes, R. P. van Duyne, *J. Phys. Chem. B* **2001**, *105*, 5599–5611.
[14] a) A. Kosiorek, W. Kandulski, P. Chudzinski, K. Kempa, M. Giersig, *Nano Lett.* **2004**, *4*, 1359–1363; b) J. Rybczynski, U. Ebels, M. Giersig, *Colloids Surf. A* **2003**, *219*, 1–6.
[15] S. Yang, G. Ozin, *Chem. Commun.* **2000**, 2507–2508.
[16] Y. Yin, Y. Xia, *Adv. Mater.* **2002**, *14*, 605–608.
[17] V. N. Manoharan, M. T. Elsesser, D. J. Pine, *Science* **2003**, *301*, 483–487.

 © 2005 Wiley-VCH Verlag GmbH & Co. KGaA, Weinheim

Nanotechnology

DOI: 10.1002/anie.200502680

Finely Tuning Metallic Nanogap Size with Electrodeposition by Utilizing High-Frequency Impedance in Feedback**

*Quan Qing, Fang Chen, Peigang Li, Weihua Tang, Zhongyun Wu, and Zhongfan Liu**

Nanomaterials and molecules have shown quite remarkable features for nanoscale devices when they are organized in fine structures either by top-down techniques or bottom-up approaches.[1–3] Making metallic pairs with gap sizes commensurate with the objects of interest so that such system can interact with the outside is one of the key issues that remains a challenge. The desired distance between electrodes ranges from less than 1 nm up to more than 100 nm for different systems involving small molecules,[4] nanoparticles,[5] nanotubes,[1a] and biomolecules such as DNA chains.[2d]

Conventional top-down techniques such as electron-beam lithography still suffers from a disadvantage in terms of yield when the feature size approaches 10 nm or below. However, recent reports have shown very promising results on the shrinkage of the gap size of a predefined pattern by electrodeposition with an active feedback loop. Compared with other techniques, such as break junction, which mechanically tears a narrow metallic wire,[6] and electromigration, which splits a very thin metallic layer by current-induced migration,[7] the electrochemical method is arguably more versatile with a controllable gap range.[8]

The feedback signal of such electrochemical systems normally utilizes a dc voltage or ac voltage of very low frequency (< 10 Hz)[9,10] to detect the occurrence of electron tunneling through the gap during metal deposition, or uses one of the electrodes as the reference to sense the sharp potential drop when the electrodes grow within the electrical double layer.[8] The electrochemical process is stopped when the feedback signal shows significant change, which results in a gap size normally around 1 nm in the tunneling region in the first case, or below 10 nm for the latter. These systems show the controllability of such a feedback design, but they also pose several problems, such as a very narrow range of available gap size or an asymmetric deposition behavior. These limitations can be mainly attributed to the low frequency of the feedback signal, electrodes playing different roles during deposition, or the features that are needed to arbitrarily separate the ac signal from the dc deposition current.

In the present study we used a very different system design, which showed very interesting frequency dependency on the final gap size in a previous study.[11] Herein we investigate this behavior in detail with improved electrode geometry[12] and demonstrate that a gap size larger than 10 nm can be obtained reproducibly by using a high-frequency feedback signal. We will discuss the mechanism of the prominent impedance change over a complete deposition process by reference to the amplitude and phase-shift data, and show that the gap size can be further tuned down to around 1 nm simply by controlling the subsequent deposition time. This method is unique in that it indicates the distinctive behavior of the high-frequency impedance in such a nanoscale electrochemical system, and it provides a very flexible and common way to fabricate nanogaps for various applications.

We first prepared an initial metallic electrode pair which was over 200 nm apart. The gap was then narrowed by controlled electrodeposition. A sharp tip-against-tip geometry of the initial electrodes was found to be more favorable than a flat-top configuration for a reproducible feedback signal and a good final shape.[10,12,13] This geometry was achieved in two steps: First, a metal bar of length 50 μm and width 5 μm was fabricated by using a conventional photolithography technique, which was followed by metal evaporation (15 nm Ti covered by 85 nm Au) and lift-off. The bar was then carved in the middle by a focused ion beam to form two sharp tips with a distance ranging from 200 to 500 nm (Figure 1a). A small amount of SiO_2 under the metal in this area was also etched away to make sure that the tips were isolated. The sample was then immersed in concentrated HNO_3 for 30 minutes and washed with sufficient Milli-Q water to remove the residue Ga^{3+} ions that became doped during the course of the ion bombardment.

A schematic diagram of the feedback system is shown in Figure 1b.[11] Briefly, both electrodes of the gap were used as cathodes to symmetrically deposit metal, Au in our experiments. The unique symmetric design ensures that the ac signal travels only in the symmetric circuit loop, while the faradic current can be recorded independently on the electrochemical workstation. The ac voltage (V_s) at one of the electrodes was analyzed by a two-phase lock-in amplifier and its amplitude (V_m) was used as the feedback signal. This ac voltage has a very simple relationship to the impedance of the gap,[11] and shows a prominent decay when the gap distance is close enough.

Figure 1c gives the typical V_m–t curves for a complete deposition process using different ac frequencies. The curves are composed of three stages: 1) the sudden decay in the first few seconds of the Au deposition, which is attributed to the charging process of the double layer; 2) a plateau before the

[*] Dr. Q. Qing, Dr. F. Chen, Dr. Z. Wu, Prof. Z. Liu
Center for Nanoscale Science and Technology
College of Chemistry and Molecular Engineering
Peking University
Beijing 100871 (P.R. China)
Fax: (+86) 10-6275-7157
E-mail: zfliu@pku.edu.cn
Dr. P. Li, Prof. W. Tang
Institute of Physics
Chinese Academy of Science (P.R. China)

[**] We are thankful for the financial support from The Ministry of Science and Technology of China (973 program, 2001CB6105) and The National Natural Science Foundation of China (NSFC Key project, 90301006).

Supporting information for this article is available on the WWW under http://www.angewandte.org or from the author.

 © 2005 Wiley-VCH Verlag GmbH & Co. KGaA, Weinheim

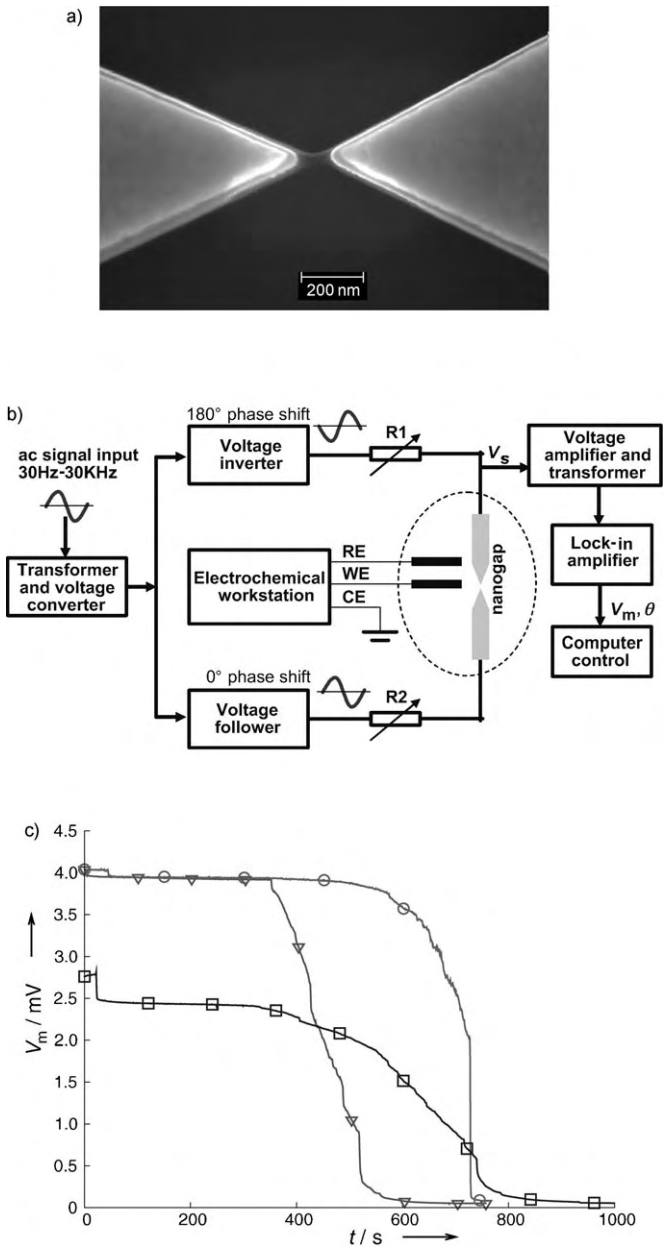

Figure 1. a) SEM image of the initial electrode pair. b) Schematic diagram of the electrodeposition system. The parts in the circle were immersed in solution. R1 and R2 were both set to 1 KΩ. c) The time evolution of V_m for different ac frequencies in a complete deposition process. ▽: 70 Hz, ○: 300 Hz, □: 3 KHz.

gap distance enters the critical region; and 3) a prominent decrease as the electrodes grow close enough and finally down to zero when a metallic contact is established.

A computer program was used to record the V_m signal and to detect the beginning of stage 3.[11] In other words, when the program detected an accelerated decrease in the value of V_m after the plateau (stage 2), it would take action—either stopping the deposition or doing so after a programmed period of time. We define the interval of time between the actual inflexion of the curve and the point at which the program reacted as Δt. The algorithm for such detection means we normally get a minimum Δt value of around seven seconds.

Three samples prepared at 3 KHz are presented in Figure 2. These samples showed consistent Δt values of around seven seconds (Figure 2a), which is a measure of the stability of the program algorithm and is consistent with a gap distance of around 30 nm (Figure 2b). It should be noted that the different initial gap distances of these samples did not show any critical effect on the final gap size. These results demonstrate persuasively the reproducibility of the system.[14]

Current mechanisms for the change in the feedback signal involve electron tunneling and the electrical double layer. The tunneling region in a vacuum is known to be only a few angstroms, while in solution it may be slightly larger because of the screening effect of ions.[15,16] Furthermore, the thickness of the electrical double layer is very sensitive to the ion strength in solution, but can be considered to be less than 1 nm in the buffer solution used in our experiments.[17] So our results here reach far beyond these regions, and imply quite a different story.

The first evidence of the mechanism lies in the different patterns of the third stages of the V_m–t curves shown in Figure 1c. At low frequencies, such as 70 and 300 Hz, the curves showed clear discrete behavior, which, when converted into conductance between the electrodes, gave steps at multiples of quantum conductance.[14] As for the 3 KHz case, the value of V_m decreased smoothly down to zero. The quantum conductance behavior clearly proved that the decrease in the feedback signal at low ac frequency reflected primarily the tunneling event and the quantum contact between the two electrodes. This is in good agreement with other reported results.[9] However, the capacitive reactance was actively involved at high ac frequency.

We can easily calculate the resistance and capacitive reactance from the amplitude and phase-shift data that were recorded simultaneously. Figure 3a and c give the raw data at a frequency of 300 Hz and 3 KHz, respectively. Similar to the amplitude signal, the phase-shift signal also showed a steady state followed by a remarkable increase.[18] Figure 3b gives the calculated resistance and capacitive reactance at 300 Hz on using an equivalent circuit of a resistor and a capacitor in parallel. Figure 3d shows the calculated resistance and capacitive reactance for 3 KHz obtained using an equivalent circuit of a resistor in series with a capacitor.

It can be seen from Figure 3b that the change of resistance and capacitive reactance was composed of two parts. In Part I only the resistance was decreasing while the capacitive reactance remained almost constant, while in Part II the capacitive reactance showed a radical increase, which is because the equivalent circuit was no longer valid in this region, since a quantum contact was formed. This effect was evidenced by the steps in the enlarged R–t curves of this region of the graph (inset of Figure 3b). The controlling program always stopped the deposition in Part I, where the change of resistance dominated. In sharp contrast, the resistance and capacitive reactance at 3 KHz decreased together to zero, as shown in Figure 3d.

The surface area of the electrodes and the frequency can be considered as constant within this region, so the media

 © 2005 Wiley-VCH Verlag GmbH & Co. KGaA, Weinheim

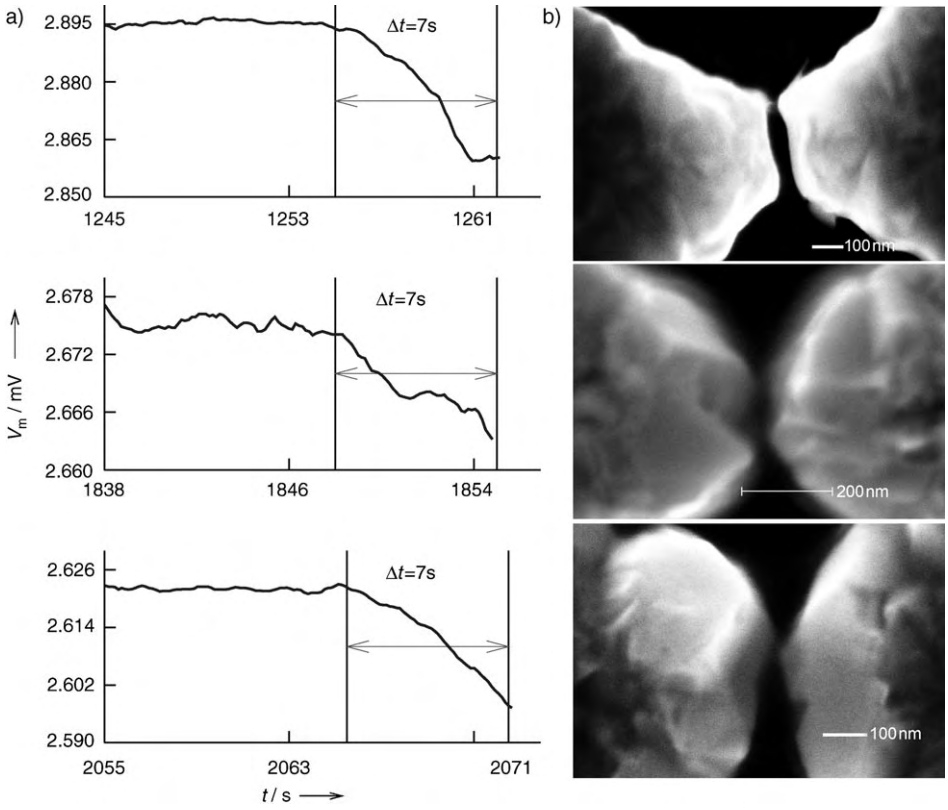

Figure 2. a) The V_m–t curves of three samples prepared at 3 KHz, only the last part is shown. The controlling program stopped the deposition at the last point. Δt is defined as the interval between the inflexion of the curve and the last point. b) The SEM images of the resulting gap in the three samples prepared as in (a), with a gap distance of 27, 35, and 25 nm, respectively.

between the electrodes could be the real cause of the behavior at 3 KHz. Considering the fact that there was an electric field of $10^5\,V\,m^{-1}$ between the electrodes (established by the feedback ac signal), the distribution of ions could be seriously perturbed, that is, the ions could be pushed and pulled according to the ac frequency between the electrodes. The solvent molecules could also be highly polarized, which will affect the dielectric constant.

In short, there will be a detectable change in the impedance for a frequency at which the capacitive reactance plays a dominant role, namely, when the nanogap shrinks to the extent that makes the electric field strong enough. This change is mainly affected by the field strength and the media between the electrodes, and thus is relatively stable. The frequency of the ac feedback signal can tune the ratio of the capacitive reactance, and the amplitude controls the strength of the electric field. The gap distance can be easily controlled by carefully tuning these two parameters.

Since the break point of the high-frequency feedback signal at which the gap distance was still relatively large can be detected very reproducibly, and the electrodeposition in the constant current mode evolved slowly and steadily, the gap size can be further developed by simply controlling the subsequent deposition time. For a frequency of 3 KHz, the deposition was stopped at $\Delta t = 9$, 25, 42, and 62 s on four samples, and the gap size was found to decrease from 26 nm to 16 nm, to 7 nm, and finally to around 1 nm, respectively (Figure 4). A simple analysis of these data showed a very good linear relationship between the final distance and the time, from which a deposition rate of $0.5\,nm\,s^{-1}$ can be calculated. In comparison, for a frequency of 300 Hz, gap sizes remained around or below 1 nm for $\Delta t = 7$ s and $\Delta t = 15$ s, which could not be measured directly by SEM (Figure 5). This result also indicated that only a very small portion of the deposited metal atoms helped to decrease the distance when the gap was less than 1 nm. This set of data is very clear proof of the important role that the high-frequency impedance plays in controlling the gap distance over a wider range.

The feedback signal at low frequencies could also establish an electric field strong enough to affect the movement of the ions between the electrodes. However, because the capacitive reactance was insignificant in the total impedance, it could not be observed. Furthermore, at a sufficiently high frequency, the electric field would change its direction before the ions could finish their movement across the short distance within a half cycle, which would cause them to oscillate between the electrodes.[19] This dynamic behavior could not be observed in our system because the surface area of the electrodes was large, and the impedance at such high frequencies was practically zero. The frequency range of the system could be expanded, and more information could be revealed by using a mask to minimize the surface area.

In summary, we have demonstrated that the high-frequency impedance of a pair of nanoscale electrodes can be greatly affected by a strong electric field between them. Utilization of this impedance change in the feedback loop enables nanogaps of 30 nm to be formed very reproducibly at a frequency of 3 KHz by an electrodeposition system. This distance is affected by the frequency and the amplitude of the ac signal, and the gap can be further finely tuned to around 1 nm by simply controlling the subsequent deposition time. This feedback system is stable and flexible, as well as providing a new strategy to prepare wide ranges of nanogaps for various applications. Furthermore, this method can also be used to study the impedance of a confined, nanoscale electrochemical system that is either in equilibrium or dynamic, for example, with a redox reaction proceeding on the surface. The dynamic behavior of molecules of special interest, such as DNA chains, proteins, or molecules with binding groups, could also be revealed with this system.

 © 2005 Wiley-VCH Verlag GmbH & Co. KGaA, Weinheim

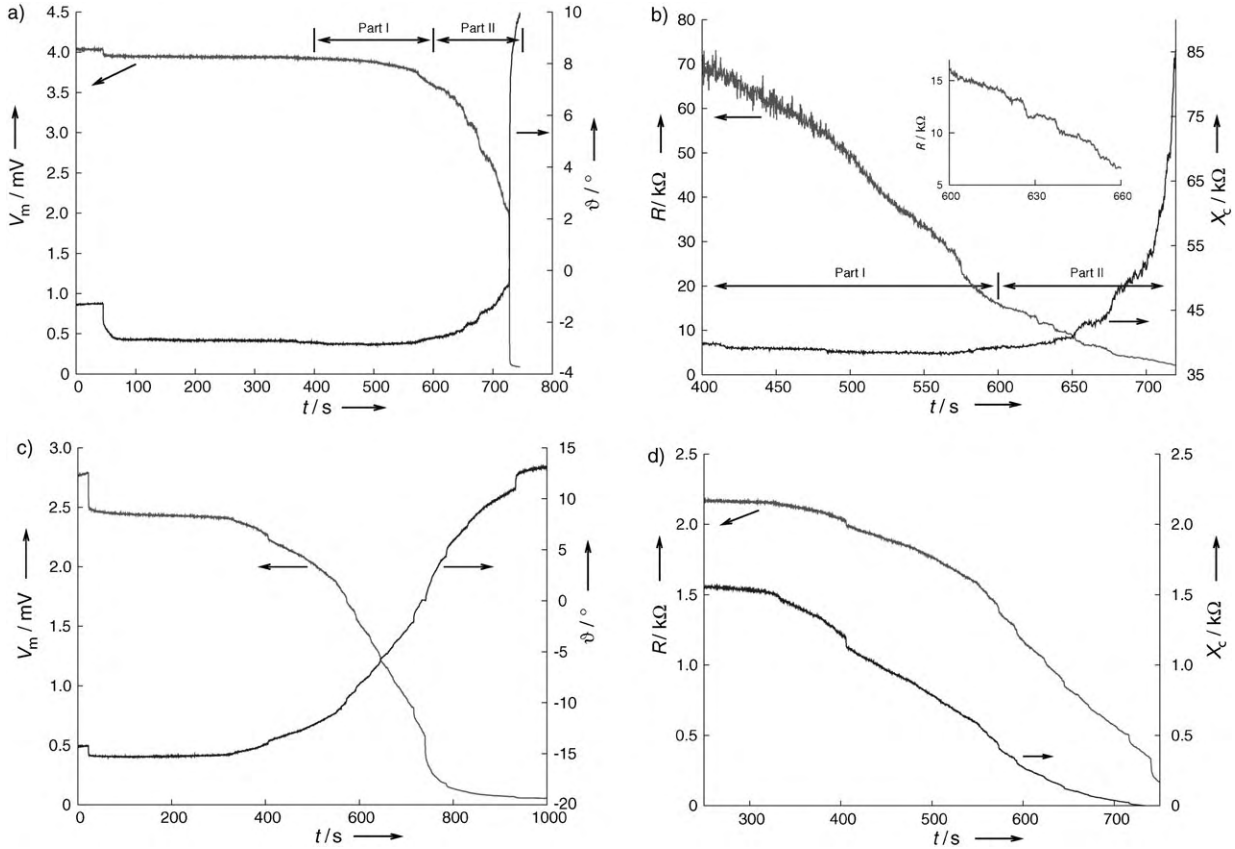

Figure 3. a) The amplitude (V_m) and phase-shift (θ) data versus time collected in a complete deposition at 300 Hz. b) Calculated resistance and capacitive reactance data according to (a) using an equivalent circuit of a resistor and a capacitor in parallel. Inset: enlarged *R*–*t* curve of Part II. c) The amplitude (V_m) and phase-shift (θ) data versus time collected in a complete deposition at 3 KHz. d) Calculated resistance and capacitive reactance data according to (c) using an equivalent circuit of a resistor and a capacitor in series.

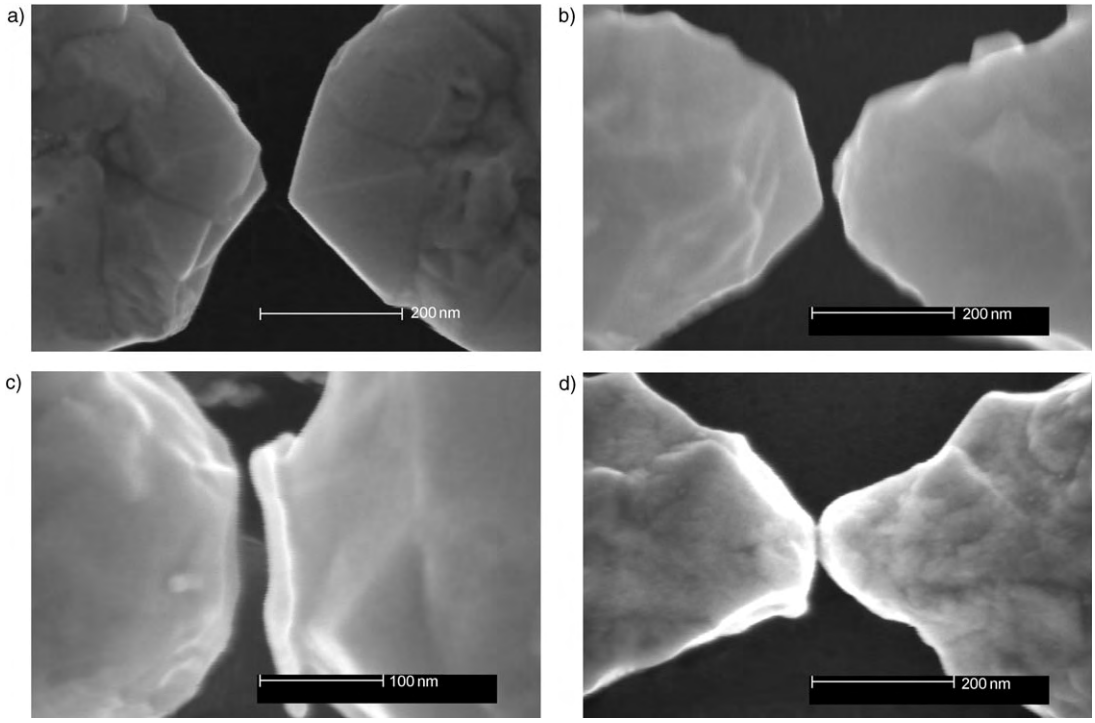

Figure 4. SEM images of the samples prepared at 3 KHz with different Δt values: a) $\Delta t = 9$ s, $d = 26$ nm; b) $\Delta t = 25$ s, $d = 16$ nm; c) $\Delta t = 42$ s, $d = 7$ nm; d) $\Delta t = 62$ s, $d = \approx 1$ nm.

 © 2005 Wiley-VCH Verlag GmbH & Co. KGaA, Weinheim

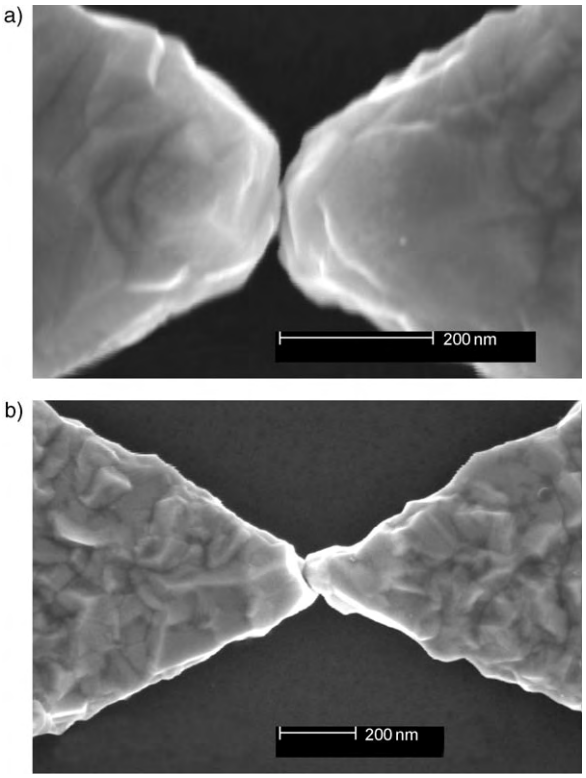

Figure 5. SEM images of the samples prepared at 300 Hz with different Δt values: a) $\Delta t = 7$ s, $d < 1$ nm; b) $\Delta t = 15$ s, $d < 1$ nm.

Experimental Section

The dc deposition was achieved with a commercial electrochemical station (CHI660B), and the current density was constant at 0.3 mA cm^{-2}. The electrolyte solution consisted of 0.1 M $KAu(CN)_2$ and 0.1 M potassium citrate buffer (pH 5.45). All solutions were prepared with analytic grade reagents and Milli-Q water (resistance: 18 MΩ). The electrochemical cell was elaborately designed to keep a constant electrode area exposed in the solution; in this study, the surface area was 0.30 ± 0.05 mm^2, as measured by an optical microscope.

Both electrodes of the gap were used as cathodes. A symmetric ac circuit composed of two 1 KΩ resistors and two ac sources with a phase difference of 180° was connected to them. The frequency could be adjusted from 30 Hz to 30 KHz, which resulted in different gap sizes ranging from less than 1 nm to 70 nm. The amplitude of the sources was normally set to 4 mV. The ac signals were monitored with a two-phase lock-in amplifier (Model 5206, EG&G Princeton Applied Research). In cases when we needed to record both amplitude and phase-shift data, a Keithley 4200 semiconductor characterization system was programmed for multichannel measurements. Otherwise a Keithley 6517a electrometer was used to collect real-time data. The electrodes with a nanogap separation after electrodeposition were imaged by scanning electron microscopy (SEM, XL30S-FEG, 15 kV).

Received: July 30, 2005
Published online: November 3, 2005

Keywords: electrochemistry · electrodeposition · electron microscopy · nanogap · nanotechnology

[1] a) S. J. Tans, A. R. M. Verschueren, C. Dekker, *Nature* **1998**, *393*, 49; b) A. Javey, J. Guo, M. Paulsson, Q. Wang, D. Mann, M. Lundstrom, H. J. Dai, *Phys. Rev. Lett.* **2004**, *92*, 106804.
[2] a) H. W. Fink, C. Schonenberger, *Nature* **1999**, *398*, 407; b) Y. Okahata, T. Kobayashi, K. Tanaka, M. Shimomura, *J. Am. Chem. Soc.* **1998**, *120*, 6165; c) A. J. Storm, J. Noort, S. Vries, C. Dekker, *Appl. Phys. Lett.* **2001**, *79*, 3881; d) D. Porath, A. Bezryadin, S. Vries, C. Dekker, *Nature* **2000**, *403*, 635.
[3] a) J. Park, A. N. Pasupathy, J. I. Goldsmith, C. Chang, Y. Yaish, J. R. Petta, M. Rinkoski, J. P. Sethna, H. D. Abruna, P. L. McEuen, D. C. Ralph, *Nature* **2002**, *417*, 722; b) W. Liang, M. P. Shores, M. Bockrath, J. R. Long, H. K. Park, *Nature* **2002**, *417*, 725; c) H. B. Yu, Y. Luo, K. Beverly, J. F. Stoddart, H. R. Tseng, J. R. Heath, *Angew. Chem.* **2003**, *115*, 5884; *Angew. Chem. Int. Ed.* **2003**, *42*, 5706.
[4] a) B. Q. Xu, N. J. Tao, *Science* **2003**, *301*, 1221; b) X. Y. Xiao, B. Q. Xu, N. J. Tao, *Nano. Lett.* **2004**, *4*, 267.
[5] D. L. Klein, P. L. McEuen, J. E. B. Katari, R. Roth, A. P. Alivisatos, *Appl. Phys. Lett.* **1996**, *68*, 2574.
[6] a) C. J. Muller, J. M. Ruitenbeek, L. J. de Jongh, *Physica C* **1992**, *191*, 485; b) C. J. Mulle, O. R. de Bruyn, *J. Appl. Phys.* **1995**, *77*, 5231.
[7] a) H. K. Park, A. K. L. Lim, A. P. Alivisatos, J. Park, P. L. McEuen, *Appl. Phys. Lett.* **1999**, *75*, 301; b) R. S. Sorbello, *Phys. Rev. B* **1989**, *39*, 4984; c) P. F. Qi, A. Javey, M. Rolandi, Q. Wang, E. Yenilmez, H. J. Dai, *J. Am. Chem. Soc.* **2004**, *126*, 11774.
[8] J. Xiang, B. Liu, S. T. Wu, B. Ren, F. Z. Yang, B. W. Mao, Y. L. Chow, Z. Q. Tian, *Angew. Chem.* **2005**, *117*, 1291; *Angew. Chem. Int. Ed.* **2005**, *44*, 1265.
[9] a) C. Z. Li, N. J. Tao, *Appl. Phys. Lett.* **1998**, *72*, 894; b) C. Z. Li, H. X. He, N. J. Tao, *Appl. Phys. Lett.* **2000**, *77*, 3995.
[10] a) A. F. Morpurgo, C. M. Marcus, D. B. Robinson, *Appl. Phys. Lett.* **1999**, *74*, 2084; b) Y. V. Kervennic, H. S. J. van der Zant, A. F. Morpurgo, L. Gurevich, L. P. Kouwenhoven, *Appl. Phys. Lett.* **2002**, *80*, 321; c) M. M. Deshmukh, A. L. Prieto, Q. Gu, H. K. Park, *Nano. Lett.* **2003**, *3*, 1383.
[11] F. Chen, Q. Qing, L. Ren, Z. Y. Wu, Z. F. Liu, *Appl. Phys. Lett.* **2005**, *86*, 123105.
[12] The large initial distance and flat geometry of the electrodes results in final electrodes which have a very high number of randomly distributed protuberances. This introduces extra diffusion limitation and shielding of electric fields, etc. The effect of frequency in this more complex system is thus less dominant and may show rather different behavior.
[13] C. S. Yang, J. Thiltges, B. Doudin, M. J. Johnson, *J. Phys. Condens. Matter* **2002**, *14*, L765.
[14] See Supporting Information.
[15] W. Schmickler, D. Henderson, *J. Electroanal. Chem. Interfacial Electrochem.* **1990**, *290*, 283.
[16] A. Vaught, T. W. Jing, S. M. Lindsay, *Chem. Phys. Lett.* **1995**, *236*, 306.
[17] A. J. Bard, L. R. Faulkner, *Electrochemical methods: fundamentals and applications, 2nd ed.*, Wiley, New York, **2001**, chap. 13.
[18] When the amplitude of the input signal becomes very small, the phase-shift output of the lock-in amplifier used stays at a relatively constant value of around 10°. Thus, when the amplitude has approached zero the last portion of the phase-shift data should be considered as inaccurate and invalid for calculation of the impedance.
[19] Consider, for example, the SO_4^{2-} ion with a mobility of 8.27×10^{-8} m^2 s^{-1} V^{-1} in a electric field of 10^5 V m^{-1}. It will take 3.6×10^{-6} s for the ion to get through a 30 nm gap, which corresponds to a frequency of 551 KHz. In real systems, this frequency could be significantly lower because of the absorption of ions as well as the changes of the solution viscosity under the high electric field.

 © 2005 Wiley-VCH Verlag GmbH & Co. KGaA, Weinheim

Protein Structures

DOI: 10.1002/anie.200502573

Side-Chain Orientation and Hydrogen-Bonding Imprint Supra-τ_c Motion on the Protein Backbone of Ubiquitin**

Nils A. Lakomek, Christophe Farès, Stefan Becker, Teresa Carlomagno, Jens Meiler, and Christian Griesinger**

Knowledge about protein dynamics is crucial for the understanding of protein function.[1] NMR spectroscopy can characterize the amplitudes and rates of motions that are either faster than the rotational correlation time τ_c (sub-τ_c motion) with heteronuclear relaxation experiments or between approximately 50 μs and 10 ms (μs/ms motion) with relaxation dispersion.[2,3] The extent of motions occurring in folded proteins on the time scale between the rotational correlation time τ_c and the μs/ms range (supra-τ_c motion) has been a matter of debate.[4] However, the functional relevance of such motions has recently been shown for the aggregation rate of natively unfolded proteins involved in neurodegenerative diseases.[5] Very recently, motions on this supra-τ_c time scale have been observed in a 0.2 μs molecular dynamics simulation of ubiquitin.[6]

Residual dipolar couplings (rdcs) were recognized early on as an ideal tool to widen the time window of dynamics that can be characterized by NMR spectroscopy, since they are sensitive to motional averaging occurring over the sub- *and* supra-τ_c time scales (ps to ms).[4] We recently analyzed NH rdcs of ubiquitin measured in 31 different alignment conditions and derived the order parameters $S^2_{rdc} = \frac{4\pi}{5} \sum_{M=-2}^{2} \langle Y_{2,M}(\theta',\phi') \rangle|^{ms}_0 \langle Y^*_{2,M}(\theta',\phi') \rangle|^{ms}_0$.[4c,7] To differentiate between the sub- and supra-τ_c time scale, these order parameters were compared to Lipari–Szabo order parameters S^2_{LS} that are derived from conventional relaxation time measurements and that are only sensitive to the sub-τ_c time scale.[8,9]

Interestingly, a periodic variation of the S^2_{rdc} value can be observed with a periodicity of two residues in the β strands of ubiquitin (amino acids 2–6, 12–16, 41–45, 66–71), while it is largely absent from the S^2_{LS} and exchange-rate data. Most prominently, the S^2_{rdc} values are larger for residues Gln 41, Leu 43, and Phe 45, and smaller for residues Arg 42 and Ile 44 in the β strand 41–45 (Figure 1). Correspondingly, the side chains of residues Gln 41, Leu 43, and Phe 45 point towards the hydrophobic core (core residues), whereas the side chains of Arg 42 and Ile 44 are exposed to solvent (exposed residues). Thus, the alternating pattern of the S^2_{rdc} values seems to correlate with the orientation of the side chains towards the solvent or away from it (Figure 2).

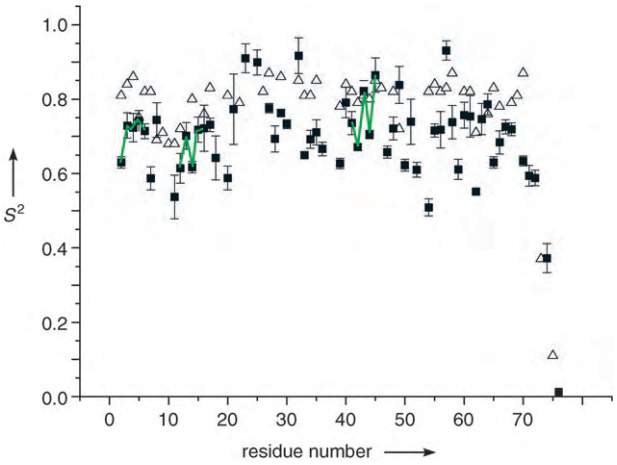

Figure 1. Comparison of the Lipari–Szabo order parameter S^2_{LS} (△) and the rdc derived order parameter S^2_{rdc} (■) as a function of residue number. The marked periodic variations of the S^2_{rdc} values are indicated by lines connecting sequential residues.

The observation that solvent-exposed residues exhibit reduced S^2_{rdc} values relative to core residues holds not only for the β strands but also for the rest of the protein. The amino acids of ubiquitin (1d3z) are color coded in Figure 3 according to the S^2_{rdc} value of the backbone amide groups. Residues with less-mobile NH vectors (blue and green) have side chains predominantly pointing towards the hydrophobic core (Figure 3a), while for those with more-mobile NH vectors (yellow, orange, and red), the side chains are solvent-exposed (Figure 3b).

To investigate this effect quantitatively, an order parameter for only the supra-τ_c time scale is derived: $S^2_{rdc}/S^2_{LS} = \frac{4\pi}{5} \sum_{M=-2}^{2} \langle Y_{2,M}(\theta',\phi') \rangle|^{ms}_{\tau_c} \langle Y^*_{2,M}(\theta',\phi') \rangle|^{ms}_{\tau_c}$. For residues with supra-τ_c motions, we expect a value for S^2_{rdc}/S^2_{LS} smaller than 1, while it should be 1 in the absence of such motions (see the Supporting Information).

[*] Prof. Dr. J. Meiler
Vanderbilt University
Department of Chemistry
Center of Structural Biology
465 21st Ave South, Nashville, TN 37232-8725 (USA)
Fax: (+1) 615-936-2211
E-mail: jens@jens-meiler.de

Dipl.-Phys. N. A. Lakomek, Dr. C. Farès, Dr. S. Becker, Dr. T. Carlomagno, Prof. Dr. C. Griesinger
Max Planck Institut für Biophysikalische Chemie
Am Fassberg 11, 37077 Göttingen (Germany)
Fax: (+49) 551-201-2202
E-mail: cigr@nmr.mpibpc.mpg.de

[**] This work was supported by the MPG, the DFG, and the Fonds der Chemischen Industrie (to C.G.). We thank Dirk Lennartz (Bayer Leverkusen), Vinesh Vijayan, and Karel Kubicek (both MPI Göttingen) for useful discussions and help with the measurement of dipolar couplings used for this analysis, and Karin Giller for expert technical help expressing ubiquitin. Nico Tjandra (NIH, Washington) kindly provided Lipari–Szabo order parameters of backbone amide groups at 35 °C. J.M. thanks the Human Frontier Science Program (HFSP) for financial support.

Supporting information for this article is available on the WWW under http://www.angewandte.org or from the author.

InterScience
© 2005 Wiley-VCH Verlag GmbH & Co. KGaA, Weinheim

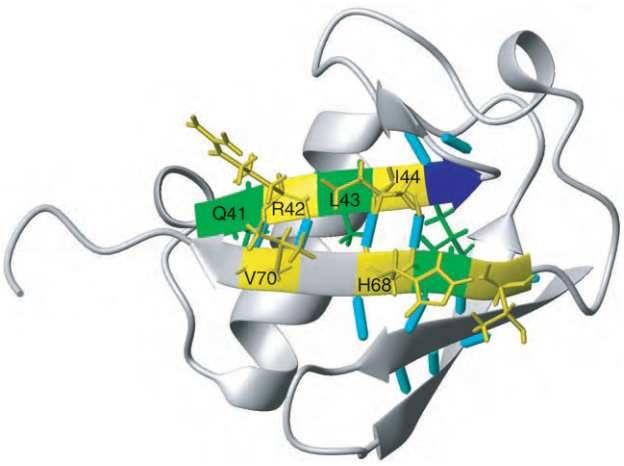

Figure 2. The residues 41–45 and 66–71 of the ubiquitin β strands (1d3z) are color-coded according to the rdc-based order parameters S^2_{rdc} (yellow $0.63 \le S^2_{rdc} < 0.73$, green $0.73 \le S^2_{rdc} < 0.83$, blue $S^2_{rdc} \ge 0.83$, gray unknown). Hydrogen bridges are displayed as cyan rods. The alternating pattern of S^2_{rdc} order parameters in residues 41–45 of the β strand is clearly correlated with the side-chain orientation.

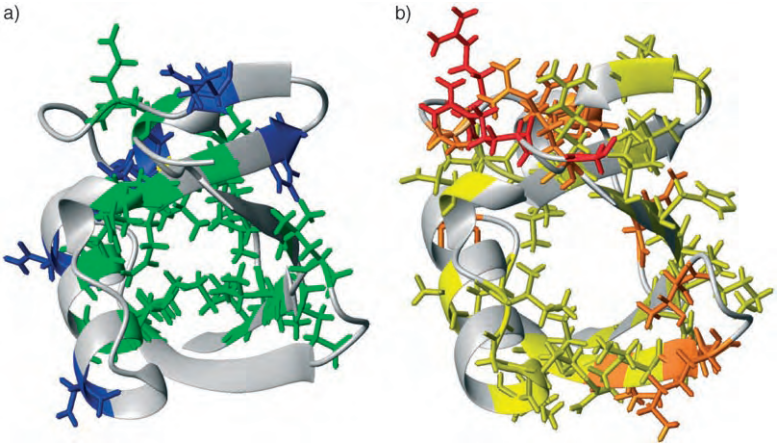

Figure 3. Residues of ubiquitin (1d3z) are color-coded with respect to the rdc-based order parameters S^2_{rdc} (red $S^2_{rdc} < 0.53$, orange $S^2_{rdc} < 0.63$, yellow $S^2_{rdc} < 0.73$, green $S^2_{rdc} < 0.83$, blue $S^2_{rdc} \ge 0.83$, gray unknown) and are distinguished between large (a) and small (b) S^2_{rdc} values. Interestingly, most of the residues with larger backbone amide S^2_{rdc} values have side chains pointing to the core (a), whereas residues with solvent-exposed side chains show smaller order parameters (b).

Core residues show an average S^2_{rdc}/S^2_{LS} value of 0.91 ± 0.02 as compared to 0.86 ± 0.02 for solvent-exposed residues (Table 1), while the exposure of the previous side chain does not have a significant influence (0.86 ± 0.02 versus 0.87 ± 0.02). Furthermore, 90% of the core residues have a S^2_{rdc}/S^2_{LS} value greater than 0.85. In contrast, this is true for only 55% of the solvent-exposed residues (Figure 4a). Thus, the supra-τ_c time order parameter of the NH vector is on average 0.05 ± 0.03 larger if the side chain is buried in the protein core.

We also investigated the influence of backbone hydrogen bonds on the supra-τ_c order parameter S^2_{rdc}/S^2_{LS}. For this, each NH group was classified according to the number of backbone hydrogen bonds on the corresponding peptide plane, including the amino acids NH_i and the preceding carbonyl group CO_{i-1} (see the Supporting Information).

The average S^2_{rdc}/S^2_{LS} values (Table 1) reveal a dependence on the number of hydrogen bonds, and increases from 0.82 ± 0.05 to 0.86 ± 0.02 to 0.90 ± 0.02 as the number of hydrogen bonds increases from zero, to one, to two. Although 83% of residues with two backbone hydrogen bonds have S^2_{rdc}/S^2_{LS} values greater than 0.85, this is true for only 61% of the residues that are involved in only one hydrogen bond (Figure 4b).

In conclusion, side-chain orientation and hydrogen bonds influence supra-τ_c motions of the backbone amide groups to the same extent. The hydrogen-bridge dependency correlates with the secondary structure of the protein whereas solvent exposure is a property of the tertiary structure. It is interesting that the side-chain mobility is apparently transmitted only along the ϕ angle and not along the ψ angle (see the Supporting Information). The investigation of this effect is beyond the scope of this paper. One possibility for this finding could be that the side-chain motion is coupled with pyramidalization of the neighboring NH group in a dissipative manner; this NH group is closer than the NH group of the following amino acid. However, the reason could also be the different rotation barriers around the ϕ and the ψ angles arising from the constitutional difference of these two moieties. The finding that the side-chain orientation influences the supra-τ_c motions of the backbone has been independently observed by Blackledge and co-workers.[10] Alignment tensor fluctuations that have been proposed[13] as an alternative to supra-tc-motion would affect parallel NH vectors identically. However, as NH vectors are parallel in β-sheets, such fluctuations do not affect our conclusions.

Table 1: Average order parameters for core and exposed residues and for residues involved in 0,1, or 2 hydrogen bonds.[a]

	Exposure				Hydrogen bridges		
	solvent(i)	core(i)	solvent($i-1$)	core($i-1$)	0	1	2
S^2_{LS}	0.80 ± 0.01	0.82 ± 0.01	0.80 ± 0.01	0.81 ± 0.01	0.74 ± 0.02	0.81 ± 0.01	0.83 ± 0.01
S^2_{rdc}	0.69 ± 0.02	0.75 ± 0.02	0.71 ± 0.01	0.70 ± 0.02	0.65 ± 0.03	0.70 ± 0.02	0.77 ± 0.02
S^2_{rdc}/S^2_{LS}	0.86 ± 0.02	0.91 ± 0.02	0.87 ± 0.02	0.86 ± 0.02	0.82 ± 0.05	0.86 ± 0.02	0.90 ± 0.02

[a] The NH_i order parameter was correlated with the side-chain orientation of the same residue (i) and the orientation of the previous residue ($i-1$). Whereas a strong dependence on the side chain orientation is obtained for the first case, no correlation is observed for the second case, thus indicating that mobility is transferred only along the φ and not the ψ angle.

Experimental Section

A model free analysis on backbone NH rdcs has been performed on ubiquitin by Lakomek et al.[7]

The analysis of order parameters has been performed with Origin 6.1 and hydrogen bonds have been reported in the literature (see Supporting Information).[11,12] Figures 2 and 3 have been

 © 2005 Wiley-VCH Verlag GmbH & Co. KGaA, Weinheim

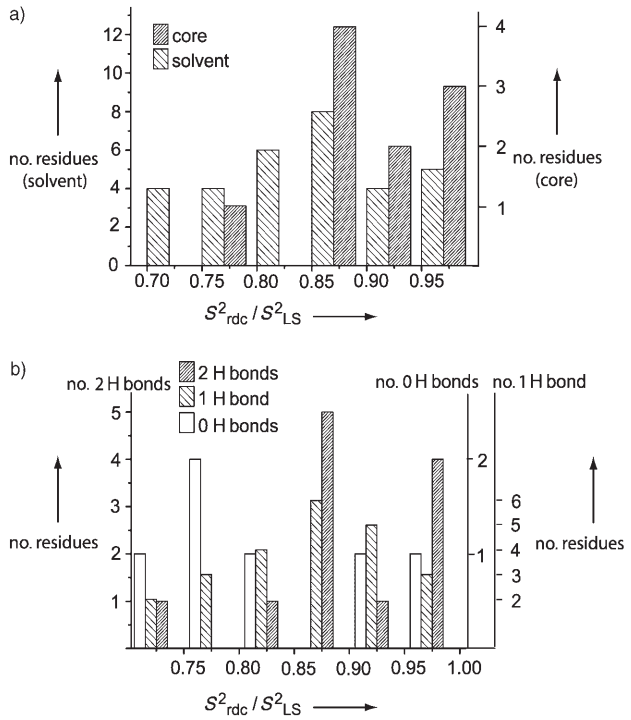

Figure 4. Histogram plot of the distribution of S^2_{rdc}/S^2_{LS} values. The residues are classified as core or solvent-exposed residues (a) or with respect to the number of backbone hydrogen bonds (b). The average S^2_{rdc}/S^2_{LS} order parameter is 0.91 ± 0.02 for core and 0.86 ± 0.02 for solvent-exposed residues. The values are 0.90 ± 0.02 for residues involved in two backbone hydrogen bonds, 0.86 ± 0.02 for one hydrogen bond, and 0.82 ± 0.05 for residues that are not involved in backbone hydrogen bonds. a) Core residues have a strong tendency for higher S^2_{rdc}/S^2_{LS} order parameters: 9 out of 10 core residues have a S^2_{rdc}/S^2_{LS} value greater than 0.85. b) Residues involved in two hydrogen bonds have higher S^2_{rdc}/S^2_{LS} values than those without any.

prepared with MOLMOL 2K.1 by using the ubiquitin structure (pdb 1d3z).

Received: July 22, 2005
Published online: November 8, 2005

Keywords: molecular dynamics · natural products · NMR spectroscopy · protein structures

[1] a) L. E. Kay, *Nat. Struct. Biol.* **1998**, *5*, 513 – 517; b) F. Massi, M. J. Grey, A. G. Palmer, *Protein Sci.* **2005**, *14*, 735 – 742.
[2] a) L. E. Kay, D. A. Torchia, A. Bax, *Biochemistry* **1989**, *28*, 8972 – 8979; b) N. Tjandra, S. E. Feller, R. W. Pastor, A. Bax, *J. Am. Chem. Soc.* **1995**, *117*, 12562 – 12566; c) A. G. Palmer, *Chem. Rev.* **2004**, *104*, 3623 – 3640.
[3] a) K. D. Kopple, K. K. Bhandary, G. Kartha, Y.-S. Wang, K. N. Parameswaran, *J. Am. Chem. Soc.* **1986**, *108*, 4637 – 4642; b) M. Akke, A. Palmer, *J. Am. Chem. Soc.* **1996**, *118*, 911 – 912; c) A. G. Palmer, C. D. Kroenke, J. P. Loria, *Methods Enzymol.* **2001**, *204*, 204 – 238.
[4] a) J. R. Tolman, J. M. Flanagan, M. A. Kennedy, J. H. Prestegard, *Nat. Struct. Biol.* **1997**, *4*, 292 – 297; b) A. Bax, N. Tjandra, *Nat. Struct. Biol.* **1997**, *4*, 254 – 256; c) J. Meiler, W. Peti, J. Prompers, C. Griesinger, R. Brueschweiler, *J. Am. Chem. Soc.* **2001**, *123*, 6098 – 6107; d) W. Peti, J. Meiler, R. Brueschweiler, C. Griesinger, *J. Am. Chem. Soc.* **2002**, *124*, 5822 – 5833; e) J. Meiler, W. Peti, C. Griesinger, *J. Am. Chem. Soc.* **2003**, *125*, 8072 – 8073; f) G. M. Clore, C. D. Schwieters, *J. Am. Chem. Soc.* **2004**, *126*, 2923 – 2938.
[5] a) C. W. Bertoncini, Y. S. Jung, C. O. Fernandez, W. Hoyer, M. Zweckstetter, E. A. Jares-Erijman, V. Subramanian, C. Griesinger, T. M. Jovin, *EMBO J.* **2004**, *23*, 2039 – 2046; b) C. W. Bertoncini, Y. S. Jung, C. O. Fernandez, W. Hoyer, C. Griesinger, T. M. Jovin, M. Zweckstetter, *Proc. Natl. Acad. Sci. USA* **2005**, *102*, 1430 – 1435.
[6] A. J. Nederveen, A. Bonvin, *J. Chem. Theory Comput.* **2005**, 1, 363 – 374.
[7] N. A. Lakomek, T. Carlomagno, S. Becker, J. Meiler, C. Griesinger, submitted to *J. Biomol. NMR*.
[8] a) G. Lipari, A. Szabo, *J. Am. Chem. Soc.* **1982**, *104*, 4546 – 4559; b) G. Lipari, A. Szabo, *J. Am. Chem. Soc.* **1982**, *104*, 4559 – 4570.
[9] S.-L. Chang, N. Tjandra, *J. Magn. Reson.* **2005**, *174*, 43 – 53.
[10] G. Bouvignies, P. Bernado, S. Meier, K. Cho, R. Brueschweiler, M. Blackledge, *Proc. Natl. Acad. Sci. USA* **2005**, in press.
[11] R. Konradi, M. Billeter, K. Wuethrich, *J. Mol. Graphics* **1996**, *14*, 51 – 55.
[12] F. Cordier, S. Grzesiek, *J. Am. Chem. Soc.* **1999**, *121*, 1601 – 1602.
[13] M. Louhivuori, R. Otten, A. Annila, *XXVII Finnish NMR symposium* (Iso-Syöte, Finland), October 8 – 10, 2005.

 © 2005 Wiley-VCH Verlag GmbH & Co. KGaA, Weinheim

DNA Binding

DOI: 10.1002/anie.200502666

Photochemical Regulation of DNA-Binding Specificity of MyoD**

*Lucia Guerrero, Oliver S. Smart, Chris J. Weston, Darcy C. Burns, G. Andrew Woolley, and Rudolf K. Allemann**

The first step in the expression of genetic information, namely the synthesis of RNA from a DNA template, is tightly regulated by DNA-binding proteins called transcription factors. The recognition of DNA by many transcription

[*] L. Guerrero, Prof. Dr. R. K. Allemann
School of Chemistry, Cardiff University
Main Building, Park Place, Cardiff, CF10 3AT (UK)
Fax: (+44) 29-2087-4030
E-mail: allemannrk@cardiff.ac.uk

O. S. Smart, Dr. C. J. Weston
School of Biosciences, University of Birmingham
Edgbaston, Birmingham, B15 2TT (UK)

Dr. D. C. Burns, Prof. Dr. G. A. Woolley
Department of Chemistry, University of Toronto
80 St George Street, Toronto, M5S 3H6 (Canada)

[**] The authors thank Dr. Elizebeth Turner for help in the early stages of this project. The BBSRC (R.K.A., O.S.S.), NSERC (G.A.W.) and the EPSRC (L.G.) supported this work financially.

Supporting information for this article is available on the WWW under http://www.angewandte.org or from the author.

WILEY InterScience DISCOVER SOMETHING GREAT
© 2005 Wiley-VCH Verlag GmbH & Co. KGaA, Weinheim

factors relies on short α helices that bind in the major groove. Isolated α-helical peptides could therefore be used to interfere selectively with protein–DNA interactions. However, isolated peptides do not normally adopt well-defined secondary structures, and the recognition helices in DNA binding proteins often rely on interactions with other proteins for stability with the potential for selectivity modulation.[1–7] For instance, the activity of the muscle-specific transcription factor MyoD is regulated through interaction with coactivators from the myocyte enhancer factor-2 (MEF-2) family.[8] MyoD belongs to a family of transcription factors that rely on a basic helix-loop-helix (bHLH) domain for DNA binding. MyoD dimerizes through the HLH domain and contacts the major groove of the DNA target sequences through its N-terminal recognition α helix. The production of MyoD in a wide variety of cell types, including fibroblasts and myoblasts, activates a cascade of genes that eventually results in cellular differentiation and the production of muscle cells.[9] The physiological activity of MyoD depends on the presence of DNA sequences that contain the symmetrical core motif CANNTG (E-box) that is found in the promoters and enhancers of many muscle specific genes, such as the creatine kinase enhancer.[10] In stark contrast to its high physiological specificity, MyoD displays only limited DNA-binding specificity in vitro.[11] The specificity of transcriptional activation that is needed to explain the physiological specificity of MyoD is therefore most likely achieved through cooperative interactions with other components of the transcriptional machinery such as MEF-2C.[8]

The identification of mechanisms to control the DNA-binding properties of transcription factors such as MyoD would permit the regulation of their activity. Previously, we have shown that stabilization of the DNA-recognition helix of MyoD, through two disulfide bonds from an N-terminally fused apamin extension, led to a tenfold increase in the DNA-binding specificity.[12] However, due to the lability of disulfide bonds in cells, the application of such apamin-stabilized recognition helices is limited. Furthermore, it would be desirable to control the properties of DNA-binding proteins in response to external signals such as light.

Previous work had shown significant stabilization of the α-helical conformation of peptides linked through cysteine residues in an i, $i+7$ spacing, to azobenzene-derived cross-linkers in their *cis* configuration (Figure 1a).[13] Met 116 and Ser 123, which are located on the water-exposed face of the recognition helix of MyoD, were therefore replaced with cysteine residues (Figure 1b). MyoD-bHLH-M116C-S123C was alkylated with 3,3′-bis(sulfo)-4,4′-bis(chloroacetamido)-azobenzene to generate photoMyoD (Figure 1c).[14] The i, $i+7$ spacing avoided unfavourable steric interactions between residues in the helix and the cross-linker. Furthermore, this spacing maximized the conformational differences in the *cis* and *trans* configurations of the cross-linker of the residues that make specific contacts to the nucleobases, namely Arg 111, Thr 115, and Glu 118.[15]

UV/Vis spectroscopy was used to follow the isomerization of photoMyoD. When the cross-linker was in its thermally stable *trans* configuration, the spectrum showed the strong maximum at 363 nm typical for amide-substituted azobenzene π–π* transitions (Figure 2).[16] However, irradiation with light at a wavelength of 360 nm led to the loss of that absorption maximum. The percentage of isomerization was determined by HPLC separation of the irradiated material and through monitoring the elution profile at the isosbestic point of 315 nm. Of the irradiated material, 61 % was found to be in the *cis* configuration, which is a value typically achieved by photoisomerization of *trans* azobenzenes.[13,17] The thermal reversion of irradiated photoMyoD to the *trans* configuration occurred with a half life of 193 min at 15 °C.

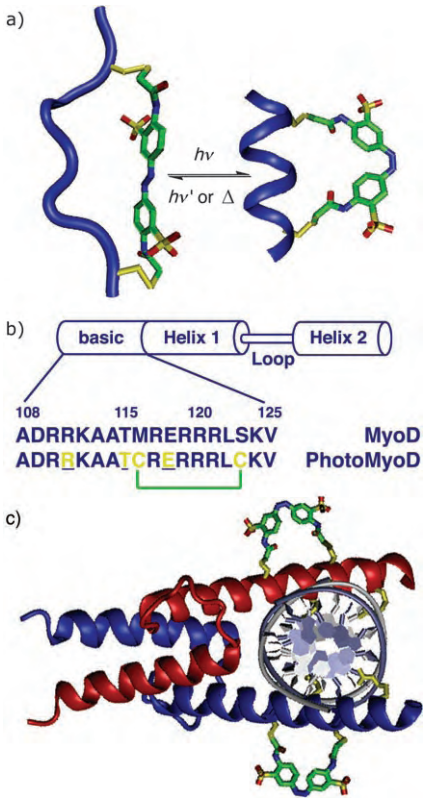

Figure 1. a) Sketch of the proposed structures of the basic regions of *trans* and *cis* photoMyoD indicating the conformational switch induced by the isomerization of the azobenzene cross-linker. b) Primary amino acid sequence of the basic region of MyoD and of photoMyoD. The residues that make specific contacts to the nucleobases in the X-ray crystal structure of the DNA complex of MyoD-bHLH[15] are underlined. c) Model of the DNA complex of photoMyoD with the cross-linker in its *cis* configuration. The DNA is complexed by the recognition helices of the two bHLH subunits of the dimeric protein. The cross-linker is located on the water-exposed face of the helices. The coordinates were from the crystal structure of MyoD-bHLH and DNA.[15]

CD spectroscopy revealed that the unalkylated MyoD-bHLH-M116C-S123C displayed only approximately 10 % helicity as judged from the mean residue ellipticity at 222 nm ($[\Theta]_{r,222} = -3658 \pm 232$ deg cm^2 dmol^{-1}) (Figure 3). The unalkylated form therefore existed predominantly in a random coil conformation like the parent MyoD-bHLH domain, which adopts an α-helical conformation only upon DNA binding.[11] The mean residue ellipticity of dark-adapted photoMyoD, in which the cross-linker is in its *trans* configuration, was similar to that of the non-cross-linked protein ($[\Theta]_{r,222} = -3328 \pm 345$ deg cm^2 dmol^{-1}). However, upon irra-

 © 2005 Wiley-VCH Verlag GmbH & Co. KGaA, Weinheim

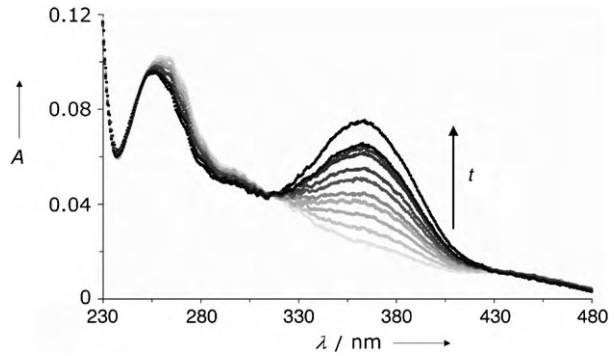

Figure 2. UV/Vis absorption spectra showing the photoisomerization of dark-adapted photoMyoD to the light-induced state. Black line (top) is the spectrum of dark-adapted photoMyoD (2 μM in 5 mM potassium phosphate buffer, pH 8.0, 15 °C). Light gray line (bottom) is the spectrum obtained immediately after exposure to 360 nm light. The intermediate curves show the spectra at varying times after photoisomerization (30, 60, 100, 135, 200, 260, 370, 430, 490 min). The sample was kept in the dark at 15 °C throughout the experiment.

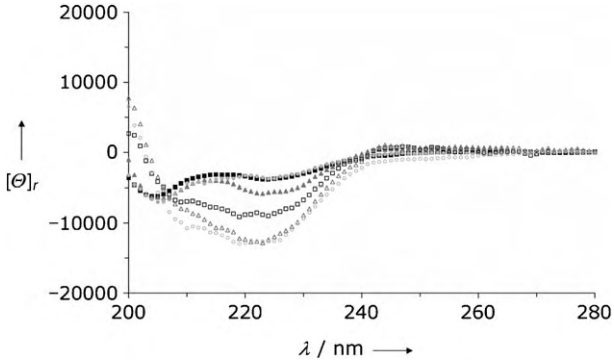

Figure 3. CD spectra showing DNA binding of MyoD-bHLH-M116C-S123C and photoMyoD. The protein concentrations were 2 μM in potassium phosphate (5 mM, pH 8.0) at 5 °C. ■ dark-adapted photoMyoD, ● non-cross-linked MyoD-bHLH-M116C-S123C, ▲ irradiated photoMyoD, ○ non-cross-linked MyoD-bHLH-M116C-S123C plus MCK-S (1 equiv, 1 μM), □ dark-adapted photoMyoD plus MCK-S (1 equiv, 1 μM); △ irradiated photoMyoD plus MCK-S (1 equiv, 1 μM). Mean residue ellipticity, [Θ]r, is in units of deg cm^2 dmol^{-1}.

diation with light of wavelength 360 nm, the mean residue ellipticity was reduced to -5597 ± 346 deg cm^2 dmol^{-1}. Given that this irradiated state of photoMyoD contained 39 % of the *trans* conformer, the mean residue ellipticity of pure *cis* photoMyoD could be calculated as -7060 ± 611 deg cm^2 dmol^{-1}. This corresponded to 19 % helicity or approximately 11 amino acids of the bHLH domain. It was not surprising that little helix induction was seen outside the eight residues spanned by the cross-linker as even at high concentrations where bHLH domains are folded dimers, the basic domain remains unstructured in the absence of DNA most likely owing to the electrostatic interactions of its many positively charged residues.[18]

The DNA-binding reactions of dark-adapted and irradiated photoMyoD, as well as that of the non-cross-linked parent protein, were studied with CD spectroscopy by using an oligonucleotide (MCK-S) comprised of 17 base pairs of the IgH enhancer-like element of the muscle-specific creatine kinase enhancer with the central E-box sequence, CAGGTG. Like MyoD-bHLH,[11] the non-cross-linked protein underwent a transition from a mostly disordered conformation to a mainly α-helical structure upon the addition of MCK-S (Figure 3). The observed value for the mean residue ellipticity at 222 nm, $[\Theta]_{r,222} = -13030 \pm 228$ deg cm^2 dmol^{-1}, indicated that the introduction of the two cysteine residues did not alter the DNA-binding properties of MyoD. The CD spectrum of the MCK-S complex of dark-adapted photoMyoD was characterized by $[\Theta]_{r,222} = -8913 \pm 182$ deg cm^2 dmol^{-1}, which indicates a significant loss of α-helical character. The CD spectrum of the DNA complex of irradiated photoMyoD was of a similar shape and intensity as that of the DNA complex of the non-alkylated protein. The value for $[\Theta]_{r,222}$ was reduced to -12130 ± 205 deg cm^2 dmol^{-1}. When the solution of the MCK-S complex of dark-adapted photoMyoD was irradiated with 360-nm light, the resultant CD spectrum was virtually identical to that of a solution of irradiated photoMyoD and DNA (Figure 3). This therefore indicated that the presence of DNA did not prevent the isomerization process.

The apparent dissociation constants of the DNA complexes of dark-adapted and irradiated photoMyoD were determined by using measurements of the fluorescence anisotropy.[12,19–22] The addition of protein to a solution of fluorescently labeled, double-stranded oligonucleotides resulted in a saturable increase in the fluorescence anisotropy, indicating that the protein had bound to the DNA in solution (Figure 4). The titration curves were fit to the Langmuir isotherm $\Phi_{Fit} = 1/(1 + K_D^n/[P]^n)$. For complexes with MCK-S, the best results were obtained for a model of cooperative two-state binding of two protein monomers to one DNA duplex as is commonly observed for bHLH proteins.[11,18,23] These fits yielded the apparent dissociation constant (K_D) from which the concentration of the protein, at which half-maximal DNA binding occurs ($[P]_{1/2}$) was calculated (see Supporting Information).

The K_D value for the MCK-S complex of dark-adapted photoMyoD ($1.5 \pm 0.38 \times 10^{-14}$ M^2) was similar to that of non-alkylated MyoD-bHLH-M116C-S123C ($8.8 \pm 2.2 \times 10^{-15}$ M^2). The stability of the MCK-S complex of irradiated photoMyoD, however, was increased significantly, and its apparent dissociation constant was reduced by more than three orders of magnitude to $4.4 \pm 0.16 \times 10^{-18}$ M^2. To the best of our knowledge, this almost 60-fold decrease in $[P]_{1/2}$ is the biggest change in DNA affinity caused by covalent helix stabilization reported to date.

The DNA-binding specificities of dark-adapted and irradiated photoMyoD were measured by comparison of the apparent dissociation constants of their complexes with MCK-S and with the oligonucleotide NoE-box (same base composition as MCK-S but with a scrambled sequence and without an E-box).[12] The bHLH proteins MASH-1 and MyoD have been shown previously not to distinguish efficiently between MCK-S and NoE-box.[11,23–25] Similarly, the K_D values for binding of non-alkylated MyoD-bHLH-M116C-S123C to MCK-S and NoE-box ($5.9 \pm 1.0 \times 10^{-15}$ M^2) were identical (Figure 4 and Supporting Information) and in

 © 2005 Wiley-VCH Verlag GmbH & Co. KGaA, Weinheim

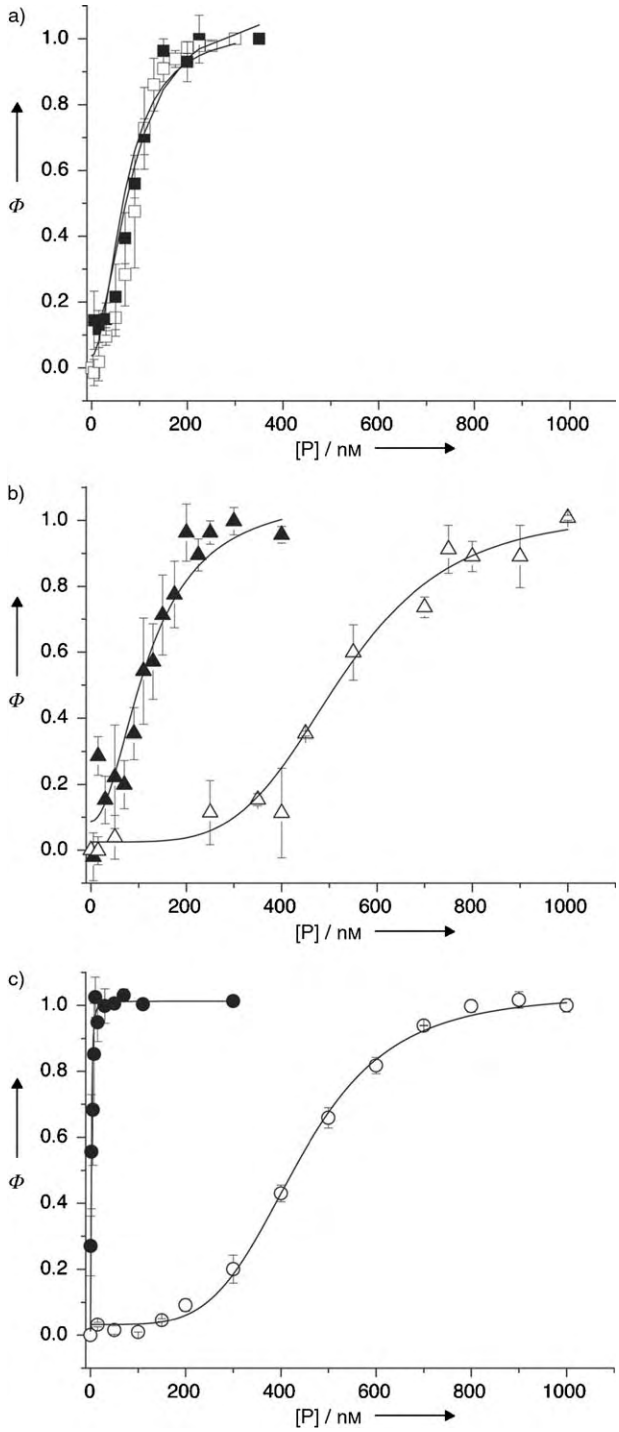

Figure 4. Characterization of DNA binding of non-cross-linked MyoD-bHLH-M116C-S123C and dark-adapted and irradiated photoMyoD measured by fluorescence anisotropy. Fraction (Φ) of bound MCK-S (solid symbols) and NoE-box (open symbols) in the complexes of a) MyoD-bHLH-M116C-S123C, b) dark-adapted and c) irradiated photoMyoD is plotted against the concentration of the free protein (P).

agreement with a previous study of MyoD-bHLH.[12] The association of MyoD-bHLH-M116C-S123C and NoE-box also displayed cooperative binding of two protein monomers per duplex DNA as had been observed for the MCK-S complex (Figure 4).

Dark-adapted photoMyoD showed only a slight increase in DNA-binding specificity. Although it bound MCK-S with comparable affinity to the non-alkylated parent protein MyoD-bHLH-M116C-S123C, the stability of its complex with NoE-box was reduced ($2.7 \pm 0.05 \times 10^{-13}$ M^2). In strong contrast, a reduction in affinity of irradiated photoMyoD for NoE-box ($1.9 \pm 0.06 \times 10^{-13}$ M^2) was accompanied by a dramatic increase in its affinity for MCK-S. The K_D value of the MCK-S complex of the irradiated protein ($4.4 \pm 0.16 \times 10^{-18}$ M^2) was reduced approximately 3400-fold relative to that of the dark-adapted state, whereas the K_D values of the NoE-box complexes of irradiated and dark-adapted photoMyoD ($2.7 \pm 0.05 \times 10^{-13}$ M^2) were similar.

At the high concentrations of irradiated and dark-adapted photoMyoD required to bind to the NoE-box duplex, the mechanism of DNA binding appeared to be altered when compared to the high-affinity binding reaction observed for binding to specific DNA. The best fit to the Langmuir isotherm for binding to noncognate DNA was obtained for binding orders of approximately 4.5 (Figure 4). This may be a consequence of interactions between the alkylated proteins at these elevated concentrations possibly through their aromatic cross-linkers.

The introduction of an azobenzene-derived photo-cross-linker into the DNA-recognition helix of the transcriptional activator MyoD produced a DNA-binding protein, the activity of which could be controlled by light pulses. In its irradiated state, in which the cross-linker was predominantly in the *cis* configuration, significant stabilization of the recognition helix and of the specific DNA complex was observed relative to the dark-adapted state. Because the affinity for heterologous DNA sequences was comparable for the dark-adapted and the irradiated proteins, photoactivation generated increases in the DNA-binding specificity of more than two orders of magnitude. Such photocontrolled DNA-binding proteins could serve as building blocks for the generation of reagents to control developmental processes and therapeutics. The activity of transcriptional activators is typically regulated through interaction with other protein domains, and these interfaces have proven difficult to target with small molecules. Reinforcing the native structure of DNA-recognition elements may be an alternative strategy to target these interactions and interfere with biological processes in a specific and controlled fashion.

Received: July 29, 2005

Keywords: azo compounds · DNA · fluorescence anisotropy · photoisomerization · transcription factors

[1] S. Wagner, M. R. Green, *Science* **1993**, *262*, 395.
[2] A. M. Baranger, C. R. Palmer, M. K. Hamm, H. A. Giebler, A. Brauweiler, J. K. Nyborg, A. Schepartz, *Nature* **1995**, *376*, 606.
[3] G. Perini, S. Wagner, M. R. Green, *Nature* **1995**, *376*, 602.
[4] C. R. Palmer, L. D. Gegnas, A. Schepartz, *Biochemistry* **1997**, *36*, 15349.
[5] G. Natoli, M. L. Avantaggiati, P. Chirillo, E. Demarzio, D. Collepardo, M. Falco, C. Balsano, M. Levrero, *J. Hepatol.* **1995**, *22*, 14.

 © 2005 Wiley-VCH Verlag GmbH & Co. KGaA, Weinheim

[6] C. Balsano, O. Billet, M. Bennoun, C. Cavard, A. Zider, G. Grimber, G. Natoli, P. Briand, M. Levrero, *J. Hepatol.* **1994**, *21*, 103.
[7] R. Grassmann, C. Dengler, I. Mullerfleckenstein, B. Fleckenstein, K. McGuire, M. C. Dokhelar, J. G. Sodroski, W. A. Haseltine, *Proc. Natl. Acad. Sci. USA* **1989**, *86*, 3351.
[8] E. N. Olson, M. Perry, R. A. Schulz, *Dev. Biol.* **1995**, *172*, 2.
[9] E. N. Olson, *Genes Dev.* **1990**, *4*, 1454.
[10] J. N. Buskin, S. D. Hauschka, *Mol. Cell. Biol.* **1989**, *9*, 2627.
[11] A. G. Künne, D. Meierhans, R. K. Allemann, *FEBS Lett.* **1996**, *391*, 79.
[12] E. C. Turner, C. H. Cureton, C. J. Weston, O. S. Smart, R. K. Allemann, *Chem. Biol.* **2004**, *11*, 69.
[13] D. G. Flint, J. R. Kumita, O. S. Smart, G. A. Woolley, *Chem. Biol.* **2002**, *9*, 391.
[14] Z. Zhang, D. C. Burns, J. R. Kumita, O. S. Smart, G. A. Woolley, *Bioconjugate Chem.* **2003**, *14*, 824.
[15] P. C. M. Ma, M. A. Rould, H. Weintraub, C. O. Pabo, *Cell* **1994**, *77*, 451.
[16] H. Rau, *Photoisomerisation of azobenzenes*, CRC, Boca Raton, **1990**.
[17] C. Renner, J. Cramer, R. Behrendt, L. Moroder, *Biopolymers* **2000**, *54*, 501.
[18] A. G. E. Künne, M. Sieber, D. Meierhans, R. K. Allemann, *Biochemistry* **1998**, *37*, 4217.
[19] J. Weiel, J. W. B. Hershey, *J. Biol. Chem.* **1982**, *257*, 1215.
[20] J. Weiel, J. W. B. Hershey, *Biochemistry* **1981**, *20*, 5859.
[21] T. Heyduk, J. C. Lee, *Proc. Natl. Acad. Sci. USA* **1990**, *87*, 1744.
[22] T. Heyduk, Y. Ma, H. Tang, R. H. Ebright, *Methods Enzymol.* **1996**, *274*, 492.
[23] D. Meierhans, C. Elariss, M. Neuenschwander, M. Sieber, J. F. Stackhouse, R. K. Allemann, *Biochemistry* **1995**, *34*, 11026.
[24] A. G. E. Künne, R. K. Allemann, *Biochemistry* **1997**, *36*, 1085.
[25] A. G. E. Künne, D. Meierhans, R. K. Allemann, *FEBS Lett.* **1996**, *391*, 79.

 © 2005 Wiley-VCH Verlag GmbH & Co. KGaA, Weinheim

Solid-State Fluorescence

DOI: 10.1002/anie.200501781

Molecular Mechanism of the Solid-State Fluorescence Behavior of the Organic Pigment Yellow 101 and Its Derivatives**

Andreas Dreuw, Jürgen Plötner, Lisa Lorenz, Josef Wachtveitl, Juste E. Djanhan, Jürgen Brüning, Thomas Metz, Michael Bolte, and Martin U. Schmidt**

Many organic colorants that fluoresce in solution (e.g. fluoresceine) lose this property when they are crystallized. Pigment Yellow 101 (P.Y.101, **2**; $R^1 = H$, $R^2 = OH$) is the only commercial organic yellow pigment[1,2] that exhibits fluorescence also in the crystalline state. P.Y.101 has been known since 1899 and has been produced industrially for decades. It is used, for example, as a pigment for viscose, for printing inks, and for artists' applications. Analysis of the fluorescence properties of the derivatives **1** ($R^1 = R^2 = H$) **3** ($R^1 = H$, $R^2 = OCH_3$), and **4** ($R^1 = CH_3$, $R^2 = OH$) reveals an unexpected behavior: Pigments **1** and **3** do not fluoresce, neither in solution nor in the solid state. However, pigment **4** does exhibit fluorescence like **2** both in solution and in the solid state (Table 1).

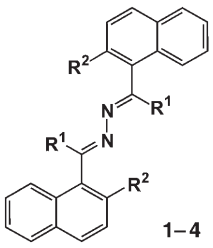

1–4

This is remarkable for two reasons: 1) Compounds **2** and **4** are fluorescent in contradiction to an empirical rule that states that pigments with OH groups usually do not fluoresce. Here, only the pigments with OH groups exhibit fluorescence. 2) The fluorescent pigments remain fluorescent upon crystallization, although compound **4** displays short intermolecular distances in the crystal, which should lead to fluorescence quenching.[3] To understand the influence of the OH groups on the fluorescence of the pigments we performed extensive quantum-chemical calculations employing methods based on time-dependent density functional theory (TDDFT). In the following presentation of our theoretical study, we focus on the pigments **1** and **2**, but analogous results have been found for **3** and **4**.

The calculated geometrical parameters of the ground states of the individual molecules **1** and **2** agree very well with the X-ray crystal structure (see the Supporting Information). For all the molecules, excitation into the lowest-lying optically allowed state leads to bond-length equilibration of the N–N, C=N, and C–C bonds of the bisazomethine substructure, in other words, to a transition of the C=N–N=C to a C=N=N=C fragment (see the Supporting Information). The absorption and fluorescence spectra of the individual molecules have been calculated and compared with experimental spectra as shown in Figure 1 for **2**. The calculated excited states are shifted about 77 nm to smaller wavelengths (higher energy) to match the 0→0 transition of the strongly allowed and thus experimentally observed absorption band. The good agreement between theory and experiment in this case is striking. The experimentally observed absorption band at 413 nm (λ_{max}) exhibits a pronounced vibrational fine structure that points to a mode with a frequency of about 1400 cm^{-1} (Figure 1), which is excited upon optical transition from the ground state. This frequency corresponds to a typical value for symmetric stretching vibrations ν_s involving the bisazomethine subunit. This is also in agreement with the change of the equilibrium geometries from the ground state to the optically allowed excited state S_1 in the case of **2** (see the Supporting Information).

To answer the question why pigments **2** and **4** fluoresce while **1** and **3** do not, their excited states were calculated (Table 2). The relevant states and the corresponding orbitals are displayed in Figure 2. In the case of **1** and **3**, the energetically lowest excited state S_1 corresponds to a for-

Table 1: Crystal structure data and fluorescence properties of the pigments **1**–**4**.

	1	**2**	**3**	**4**
R^1	H	H	H	CH_3
R^2	H	OH	OCH_3	OH
Fluorescence in solution	no	yes	no	yes
Fluorescence in crystal	no	strong	no	strong
Space group	$P2_1/n$	$P2_1/n$	$P2_1/n$	$C2/c$
Z (molecules/unit cell)	2	2	2	4
Center-to-center distance [Å]	6.085	6.114	7.007	3.863

[*] Dr. A. Dreuw, Dipl.-Chem. J. Plötner, Dipl.-Chem. L. Lorenz, Prof. Dr. J. Wachtveitl
Institut für Physikalische und Theoretische Chemie
Johann Wolfgang Goethe-Universität Frankfurt
Marie Curie-Strasse 11, 60439 Frankfurt/Main (Germany)
Fax: (+49) 69-798-29709
E-mail: andreas.dreuw@theochem.uni-frankfurt.de
Dipl.-Chem. J. E. Djanhan, J. Brüning, Dr. M. Bolte, Prof. Dr. M. U. Schmidt
Institut für Anorganische und Analytische Chemie
Johann Wolfgang Goethe-Universität Frankfurt
Marie Curie-Strasse 11, 60439 Frankfurt/Main (Germany)
Fax: (+49) 69-798-29235
E-mail: m.schmidt@chemie.uni-frankfurt.de
Dr. T. Metz
Clariant GmbH
Div. Pigments & Additives
Pigments Research, G 834
65926 Frankfurt/Main (Germany)

[**] A.D. is supported by the Deutsche Forschungsgemeinschaft as an Emmy Noether fellow. The authors thank Antje Lemanczyk and Uwe Jobstmann (Clariant GmbH) for syntheses, Dr. Jürgen Glinnemann and Dr. Chunhua Hu (Universität Frankfurt) for recrystallizations, and Edith Alig (Universität Frankfurt) for X-ray powder diffraction diagrams.

Supporting information for this article is available on the WWW under http://www.angewandte.org or from the author.

 © 2005 Wiley-VCH Verlag GmbH & Co. KGaA, Weinheim

Table 2: Excitation energies (given as wavelengths λ in [nm]) and oscillator strengths (in brackets) as well as the character of the transitions are given for the five energetically lowest-lying excited states of the pigments **1**–**4** as calculated by TDDFT/BP86/DZP.

	1		**2**		**3**		**4**	
State	λ_{ex} (osc)	Character	λ_{ex} (osc)	Character	λ_{ex} (osc)	Character	λ_{ex} (osc)	Character
S_1	532 (0.00)	n→π*	510 (0.69)	π→π*	559 (0.00)	n→π*	506 (0.41)	π→π*
S_2	479 (0.76)	π→π*	469 (0.00)	π→π*	494 (0.62)	π→π*	480 (0.00)	π→π*
S_3	452 (0.00)	π→π*	416 (0.00)	π→π*	464 (0.00)	π→π*	402 (0.00)	π→π*
S_4	399 (0.00)	π→π*	413 (0.00)	π→π*	429 (0.00)	π→π*	401 (0.00)	π→π*
S_5	371 (0.00)	π→π*	409 (0.00)	n→π*	383 (0.00)	π→π*	391 (0.00)	n→π*

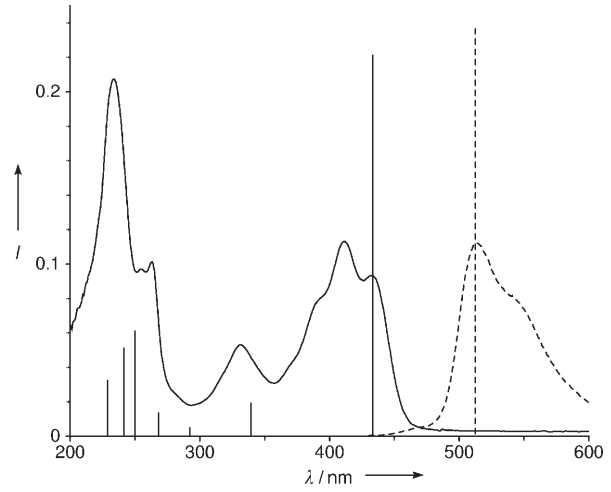

Figure 1. Comparison of the measured absorption (solid line) and fluorescence (dashed line) spectra with the corresponding calculated transitions (vertical lines) of **2**. The calculated wavelengths are all shifted by 77 nm to smaller wavelengths (see text).

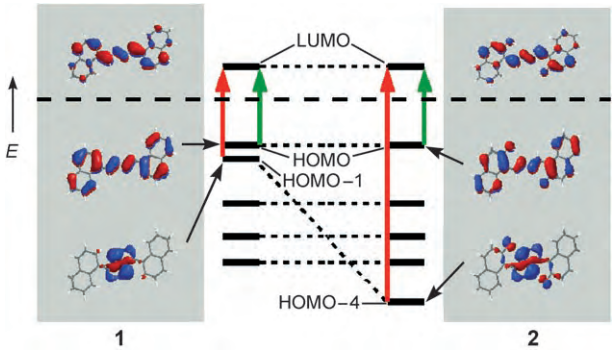

Figure 2. Energy diagrams of the molecular orbitals involved in the allowed π→π* transitions (green) and forbidden n→π* transitions (red) of pigments **1** and **2**. In **2** the n orbitals corresponding to the lone pairs are strongly stabilized by hydrogen bonds. Thus, the corresponding nπ* state becomes much higher in energy than the ππ* state. Note that the lengths of the arrows are not related to the transition energies of the corresponding states (see text).

bidden nπ* state, which is represented mostly by a HOMO-1→LUMO transition (red arrow). The second lowest state S_2 corresponds to an optically allowed ππ* state and can considered to arise almost exclusively a HOMO→LUMO transition (green arrow). Astonishingly, the HOMO−1→LUMO transition is lower in energy than the HOMO→LUMO transition, but this results from additional admixtures of other transitions into the wavefunction of the dark nπ* state which lower its energy substantially. In **2** and **4**, the allowed HOMO→LUMO transition leads to the energetically lowest-lying state S_1, and the forbidden n→π* transition leads to the fifth lowest-lying state S_5, owing to a strong stabilization of the nitrogen lone-pair orbital by the hydrogen bonds of the OH groups. The hydrogen bonds in **2** and **4** lower the energy of the n orbital, thus increasing the excitation energy for the n→π* transition. Hence the order of the excited states of the pigments **1**–**4** already explains the molecular fluorescence behavior of the pigments in solution.

To allow for fluorescence quenching in pigments **1** and **3**, a suitable reaction pathway on the potential energy surface of the excited state should exist that leads from the allowed S_2 (ππ*) state to the optically forbidden S_1 (nπ*) state. Most likely this pathway corresponds to a vibrational mode of the system. Several different modes have been considered, but only CNN bending proved to be relevant. The calculated potential energy curves of the three lowest excited states of **1** along the CNN angle are shown in Figure 3. The structure of the S_2 state has been reoptimized along this coordinate. For decreasing CNN angles, the dark S_1 state is strongly destabilized; its energy increases and crosses that of the S_2 state at a CNN angle of 108°. Even if one assumes a low vibrational frequency of only 300 cm^{-1}, already the second vibrational level of the S_2 state lies energetically above the state crossing as indicated in Figure 3. Consequently, every mode that

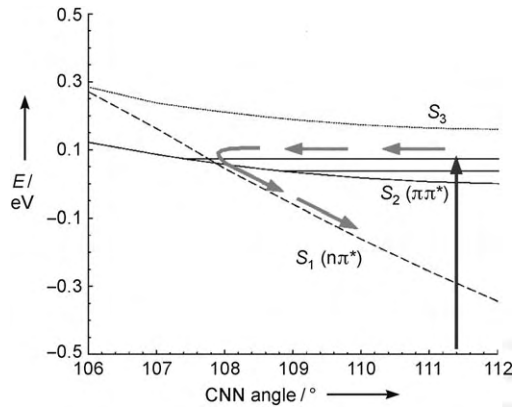

Figure 3. Calculated potential energy curves of pigment **1** along the CNN-bending vibration. Since a curve crossing between the state S_2 (optically allowed ππ* state) and the state S_1 (forbidden nπ* state) occurs, this vibrational motion is an efficient pathway for fluorescence quenching in pigment **1** (gray arrows).

 © 2005 Wiley-VCH Verlag GmbH & Co. KGaA, Weinheim

contains a CNN-bending contribution will lead to state crossings. Based on simple geometric arguments, it can be expected that CNN bending is strongly coupled to the Franck–Condon-active symmetric stretching mode, thus allowing very efficient fluorescence quenching in **1** and **3**.

To understand why the molecular fluorescence properties of **1**–**4** are retained when the compounds are crystallized, we determined the structures of all compounds by single-crystal X-ray diffraction.[4] Structural details and different conformers of the pigments are discussed in the Supporting Information. Compounds **1**–**3** form isostructural arrangements in which the distances between the centers of the molecules are 6 to 7 Å (Table 1). The crystal structure of the simplest derivative **1** is displayed in Figure 4. Lattice-energy calculations demonstrate that CNN bending is also possible in the crystals. If, in a crystal of compound **1** or **3** consisting of molecules with the ground-state geometry only, a single molecule adopts the geometry of the excited state (CNN angle 108°, near the crossing between the S_1 and S_2 states), the lattice energy drops by 0.2 kJ mol^{-1}. Consequently, the vibration responsible for fluorescence quenching is not hampered by the crystal lattice, but is on the contrary even slightly facilitated. Thus nonfluorescent pigments **1** and **3** remain nonfluorescent in the crystal.

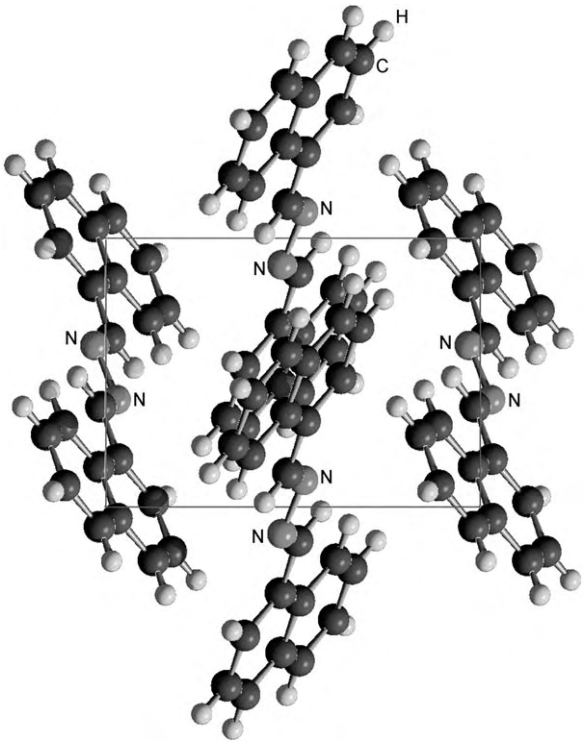

Figure 4. Crystal structure of the unsubstituted compound **1**. SCHAKAL plot,[11] view along [001], *a* axis horizontal, *b* axis vertical.

The crystal structure of **4** is different from the structures of pigments **1**–**3**. In crystals of **4** the molecules are stacked almost on top of each other, leading to short intermolecular distances of only 3.86 Å (Figure 5). According to a rule formulated by Langhals et al.,[3] solid-state fluorescence strongly depends on the intermolecular distance and is usually quenched when the distance between the chromophores is less than 5–6 Å as a result of enhanced exciton–phonon coupling. This typically results in electron-transfer (ET) quenching. Here, the observed solid-state fluorescence contradicts this rule: pigment **4** exhibits strong solid-state fluorescence, despite the short intermolecular distance of only 3.86 Å.

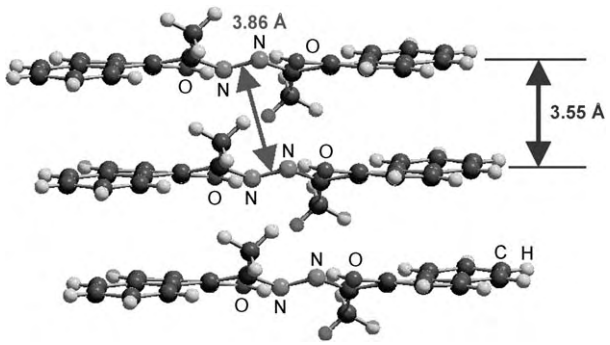

Figure 5. Molecular packing in the crystal structure of the strongly fluorescent pigment **4**. The small intermolecular distance of only 3.86 Å and the pronounced stacking of the planar pigment molecules in the crystal are apparent.

However, ET quenching can most likely be excluded. Calculations of the excited states of pigment dimers in the relative orientation taken from the crystal structures using a recently suggested hybrid approach[5] revealed that the required charge-transfer (CT) excited states are energetically not accessible. The lowest CT excited state of the dimer of **4** exhibits an excitation energy of about 3.0 eV (413 nm) and is thus higher in energy than the optically allowed state. Based on these findings, the solid-state fluorescence of Pigment Yellow 101 (**2**) and its derivative **4** can be interpreted as a molecular property retained in the crystal.

In this work we have demonstrated that the pigments **1**–**4** do not obey empirical rules for solid-state fluorescence. It has been shown that the optically allowed excited states of **2** and **4** can decay only by fluorescence, while the excited states of **1** and **3** can efficiently decay to a low-lying dark nπ* state through CNN bending of the bisazomethine substructure. This is also possible in the crystal lattice. Crystal-packing-controlled electron-transfer quenching has been ruled out as a possible quenching pathway. The fluorescence behavior of Pigment Yellow 101 and its derivatives is explained as a molecular property that is retained in the solid state. Moreover, the O–H···N bond has been proven to be essential for fluorescence. This insight may stimulate syntheses of new pigments based on substituted 2-hydroxynaphthalenes. Indeed, all compounds synthesized so far exhibit solid-state fluorescence.

Experimental Section

Syntheses and crystallization: The pigments **1**–**4** were synthesized by condensation of hydrazine with the corresponding formyl- and acetylnaphthalene derivatives.[6] Crystals of **1** were grown by slowly

 © 2005 Wiley-VCH Verlag GmbH & Co. KGaA, Weinheim

cooling a heated dilute solution of **1** in CH_3OH/C_2H_5OH (1:1); for **2**, DMF was used, for **3** and **4** xylene/mesitylene (1:1) was used.

UV/Vis spectra were recorded with a Specord S100 spectrophotometer from Analytik Jena. Concentration of **2** in dichloromethane (LiChrosolv, Merck) was 3 μM in order to obtain an optical density of 0.1 (at 411 nm). The spectrum was recorded versus pure dichloromethane with an integration time of 38 ms and 100 accumulations. Fluorescence spectra were measured with a Cary Eclipse fluorescence spectrophotometer from Varian. For **2** the excitation wavelength was 410 nm, and the spectrum was recorded at high PMT voltage (800 V) with a scan rate of 120 nm min^{-1}.

The calculations were performed using the TURBOMOLE package of programs.[7] The ground-state and excited-state properties were calculated using DFT and TDDFT,[8,9] respectively, employing the BP86 exchange-correlation (xc) functional in combination with the double-zeta polarization (DZP) basis set.[10] An extensive study of various xc-functional/basis set combinations has been performed, the details of which shall be published elsewhere. Lattice-energy minimizations: DREIDING force field, with especially developed force-field parameters for the C=N and N–N bond streching, C–C=N and C=N–N angle bending, and C–C=N–N and C=C–C=N torsions in order to exactly reproduce the crystal structure of **2** with ground-state molecules.

Received: May 23, 2005
Revised: August 2, 2005

Keywords: density functional calculations · dyes/pigments · fluorescence · solid-state structures · UV/Vis spectroscopy

[1] W. Herbst, K. Hunger, *Industrial Organic Pigments*, 3rd ed., Wiley-VCH, Weinheim, **2004**, p. 570.

[2] Some other organic and organometallic compounds also show solid-state fluorescence, for example, diketopyrrolopyrrole dyestuffs (see, for example, ref. [3]), tris(8-hydroxyquinoline)-aluminum(III) (see, for example, C. W. Tang, S. A. Van Slyke, *Appl. Phys. Lett.* **1987**, *51*, 913–915; M. Brinkmann, G. Gadret, M. Muccini, C. Taliani, N. Masciocchi, A. Sironi, *J. Am. Chem. Soc.* **2000**, *122*, 5147–5157), 3,4,6-triphenyl-α-pyrone (K. Hirano, S. Minakata, M. Komatsu, J. Mizuguchi, *J. Phys. Chem. A* **2002**, *106*, 4868–4871), and 2-(*ortho*-hydroxyaryl)-azoles (A. Graness, G. Graness, *Z. Phys. Chem.* **1986**, *267*, 173–179), but to our knowledge none of them has been used industrially as a pigment.

[3] H. Langhals, T. Potrawa, H. Nöth, G. Linti, *Angew. Chem.* **1989**, *101*, 497–499; *Angew. Chem. Int. Ed. Engl.* **1989**, *28* 478–480.

[4] Crystallographic data for **1**: $C_{22}H_{16}N_2$, $M_w = 308.37$ g mol^{-1}, monoclinic, space group $P2_1/n$ (no. 14), $a = 8.4352(14)$, $b = 6.0856(14)$, $c = 15.742(3)$ Å, $\beta = 91.977(13)°$, $V = 807.6(3)$ Å^3, $Z = 2$, $\rho_{calcd} = 1.268$ g cm^{-3}, $T = -173$ °C, 8623 measured reflections, 1577 unique reflections ($R_{int} = 0.268$), 932 with $I > 2(I)$ used in refinement, $R = 0.097$, $wR2 = 0.164$, GOF = 0.880. Crystallographic data for **2**: $C_{22}H_{16}N_2O_2$, $M_w = 340.37$ g mol^{-1}, monoclinic, space group $P2_1/n$ (no. 14), $a = 8.4400(6)$, $b = 6.1140(6)$, $c = 16.0146(11)$ Å, $\beta = 91.565(6)°$, $V = 826.08(12)$ Å^3, $Z = 2$, $\rho_{calcd} = 1.368$ g cm^{-3}, $T = -100$ °C, 12959 measured reflections, 2384 unique reflections ($R_{int} = 0.054$), 2088 with $I > 2(I)$ used in refinement, $R = 0.052$, $wR2 = 0.140$, GOF = 1.053. Crystallographic data for **3**: $C_{24}H_{20}N_2O_2$, $M_w = 368.42$ g mol^{-1}, monoclinic, space group $P2_1/n$ (no. 14), $a = 10.2314(11)$, $b = 7.0071(7)$, $c = 13.2469(15)$ Å, $\beta = 100.993(8)°$, $V = 932.28(17)$ Å^3, $Z = 2$, $\rho_{calcd} = 1.312$ g cm^{-3}, $T = -173$ °C, 8654 measured reflections, 2120 unique reflections ($R_{int} = 0.048$), 1768 with $I > 2(I)$ used in refinement, $R = 0.045$, $wR2 = 0.112$, GOF = 1.044. Crystallographic data for **4**: $C_{24}H_{20}N_2O_2$, $M_w = 368.42$ g mol^{-1}, monoclinic, space group $C2/c$ (no. 15), $a = 30.985(4)$, $b = 3.8628(3)$, $c = 14.4975(14)$ Å, $\beta = 94.831(8)°$, $V = 1729.0(3)$ Å^3, $Z = 4$, $\rho_{calcd} = 1.415$ g cm^{-3}, $T = -173$ °C, 10746 measured reflections, 1968 unique reflections ($R_{int} = 0.071$), 1558 with $I > 2(I)$ used in refinement, $R = 0.048$, $wR2 = 0.109$, GOF = 1.035. Further details on the crystal structure investigation may be obtained from the Fachinformationszentrum Karlsruhe, 76344 Eggenstein-Leopoldshafen, Germany (fax: (+49) 7247-808-666; e-mail: crysdata@fiz-karlsruhe.de), on quoting the depository numbers CSD-268945 (for **1**), CSD-268942 (for **2**), CSD-268944 (for **3**), and CSD-268943 (for **4**). For **2** see also D. Guo, J. Li, J. Xie, C. Duan, Q. Meng, *Chin. J. Inorg. Chem.* **2002**, *18*, 1215–1220.

[5] A. Dreuw, M. Head-Gordon, *J. Am. Chem. Soc.* **2004**, *126*, 4007–4016.

[6] a) N. Schapiro, *Ber. Dtsch. Chem. Ges.* **1933**, *66*, 1103–1106; b) E. R. Blout, R. M. Gofstein, *J. Am. Chem. Soc.* **1945**, *67*, 13–16; c) S. S. Mathur, H. Suschitzky, *J. Chem. Soc. Perkin Trans.* **1975**, 2479–2483; d) R. K. Sharma, J. P. Tandon, *J. Prakt. Chem.* **1980**, *322*, 161–168.

[7] TURBOMOLE Version 5.6, a) R. Ahlrichs, M. Bär, M. Häser, H. Horn, C. Kölmel, *Chem. Phys. Lett.* **1989**, *162*, 165–169; b) M. Häser, R. Ahlrichs, *J. Comput. Chem.* **1989**, *10*, 104–111; c) H. Weiss, R. Ahlrichs, M. Häser, *J. Chem. Phys.* **1993**, *99*, 1262–1270.

[8] R. G. Parr, W. Yang, *Density Functional Theory of Atoms and Molecules*, Oxford University Press, Oxford, **1989**.

[9] M. E. Casida in *Recent Advances in Density Functional Methods, Part I* (Ed.: D. P. Chon), World Scientific, Singapore, **1995**, p. 155–192.

[10] a) A. D. Becke, *Phys. Rev. A* **1988**, *38*, 3098–3100; b) J. P. Perdew, *Phys. Rev. B* **1986**, *34*, 7406; c) T. H. Dunning, Jr., *J. Chem. Phys.* **1970**, *53*, 2823–2833.

[11] E. Keller, SCHAKAL99, Universität Freiburg, Germany, **1999**.

 © 2005 Wiley-VCH Verlag GmbH & Co. KGaA, Weinheim

Mixed-Valent Compounds

DOI: 10.1002/anie.200502287

$(Pr_4N)_4[Ag_3Fe_2(ECN)_{12}]$—Anionic Network Structures with Mutual Interpenetration**

*Stefan Gerber, Henriette Gröger, Jürgen Ensling, Philipp Gütlich, and Harald Krautscheid**

Dedicated to Professor Dieter Fenske

The synthesis and characterization of compounds with extended network structures has become a fast growing field of research.[1] In some cases these compounds show porous structures with large cavities, in others the formation of the cavities is prevented by interpenetration of the networks. 1998 Batten and Robson reviewed[2] network structures with mutual interpenetration, mostly formed by self-aggregation. Following this concept, it is possible, for example, to synthesize heteronuclear polymeric complexes, if SCN^- ions are coordinating to metal ions with different Lewis acidities.[3] In keeping with Pearson's HSAB principle,[4] the SCN^- ion acts as an ambidentate ligand; it coordinates to hard Lewis acids mainly through the N atom and to soft Lewis acids through the S atom. The central Fe^{II} and Fe^{III} atoms in the homoleptic complexes $(Et_4N)_4[Fe(NCS)_6]$[5] and $(Me_4N)_3[Fe(NCS)_6]$,[6] respectively, are coordinated octahedrally by six thiocyanato-N ligands, whereas in $K[Ag(SCN)_2]$, $K_4[Ag_2(SCN)_6]$, $K_3[Ag(SCN)_4]$, and $Rb_2[Ag(SCN)_3]$[7] terminal or bridging thiocyanato ligands are bound tetrahedrally through S atoms. If SCN^- ions are offered Fe^{2+}, Fe^{3+}, and Ag^+ ions at the same time, the two coordination motives are combined in such a way that $Fe(NCS)_6$ octahedra and $Ag(SCN)_4$ tetrahedra are linked, as the structures of $(Et_4N)_2[Ag_2Fe(SCN)_6]$, $(Bu_4N)_4[Ag_2Fe_2(SCN)_{12}]$,[5] and $(Me_3NPh)_6[Ag_6Fe_3(SCN)_{18}]$[8] show.

[*] S. Gerber, Prof. Dr. H. Krautscheid
Institut für Anorganische Chemie
Universität Leipzig
Johannisallee 29, 04103 Leipzig (Germany)
Fax: (+49) 341-973-6199
E-mail: krautscheid@rz.uni-leipzig.de
H. Gröger
Institut für Anorganische Chemie
Universität Karlsruhe (TH) (Germany)
Dr. J. Ensling, Prof. Dr. P. Gütlich
Institut für Anorganische und Analytische Chemie
Universität Mainz (Germany)

[**] This work was supported by the Fonds der Chemischen Industrie. We thank Dr. M. T. Kelemen (Physikalisches Institut, Universität Karlsruhe) for measuring the magnetic susceptibility, Dr. P. Scheer (Forschungszentrum Karlsruhe) for the thermochemical measurements. H.K. thanks Prof. D. Fenske (Universität Karlsruhe) for his invaluable support. E = S, Se.

Supporting information for this article is available on the WWW under http://www.angewandte.org or from the author.

Here we report on the heteronuclear, mixed-valent coordination compounds **1** and **2**, which contain Fe^{2+}, Fe^{3+}, and Ag^+ ions and are formed according to Equation (1) in nitromethane and crystallized by addition of diethyl ether. The partial reduction of the Fe^{3+} ions is due to the reducing effect of thiocyanate, which is oxidized to $(SCN)_2$ and subsequent products.[9]

$$2\,(Pr_4N)_3[Fe(NCE)_6] + 3\,AgECN \xrightarrow{MeNO_2} (Pr_4N)_4[Ag_3Fe_2(ECN)_{12}] + 2\,(Pr_4N)SCN + {}^1/_2\,(SCN)_2 \quad (1)$$

1: E = S

2: E = Se

The X-ray structure analyses show that **1** and **2** are isostructural and crystallize in the space group $I\bar{4}2d$.[10] As expected, Ag^+ ions are coordinated tetrahedrally to SCN^- and $SeCN^-$ ions through S and Se atoms, respectively, and Fe^{2+} and Fe^{3+} ions are coordinated octahedrally through the N atoms of SCN^- and $SeCN^-$ (Figure 1a). Two 1,3-μ_2 bridging ligands link single Fe and Ag atoms in such a way that each Fe atom is surrounded by three Ag atoms in a trigonal-planar arrangement with Ag···Fe distances of 560.5 and 560.8 pm in **1** and 568.3 and 570.6 pm in **2**. Each Ag atom is connected to two Fe atoms by two ECN^- ligands each (Fe···Ag···Fe > 174°). As shown in Figure 1b (Ag···Fe drawn as dotted lines), this connectivity results in a three-dimensional Fe_2Ag_3 network, whose topology corresponds to the *(10,3)-b* network of $\alpha ThSi_2$ (Figure 1c) and shows the highest possible tetragonal symmetry for this type of network.[2,11]

In this way channels are formed with a width of 1.2 nm × 2.7 nm in direction of the crystallographic *a* and *b* axes. These cavities are partially occupied according to the interpenetration of three of these *(10,3)-b* $[Ag_3Fe_2(ECN)_{12}]^{4-}$ nets, as shown in Figure 2. The Pr_4N^+ ions are located in the remaining cavities. After crystallization **1** is hardly soluble in nitromethane. The Pr_4N^+ ions could not be exchanged for Me_4N^+ ions. Similar three-dimensional networks with mutual interpenetration are found in $[Ag(H_2NC_{12}H_{24}NH_2)_2]^+$ and $[Ag_2(pz)_3]^{2+}$ ions (pz = pyrazine).[12]

Complexometric titrations show that **1** is a mixed-valent compound, whereas all Fe atoms occupy equivalent positions according to the X-ray structure analysis. Therefore Fe^{II} and Fe^{III} centers are undistinguishable by crystallographic means. The Fe–N bond lengths (210.1–212.2(2) pm in **1** and 209.9–211.1(4) pm in **2**) are between those observed in $(Me_4N)_3[Fe^{III}(NCS)_6]$[6] (204.8 pm) and $(Et_4N)_4[Fe^{II}(NCS)_6]$[5] (217.6 pm). The thermal ellipsoids of the N atoms are almost spherical and do not indicate differing Fe–ligand distances (Figure 1a). Differential thermal analysis/thermogravimetric analysis of **1** shows a phase transition at 161 °C (endothermic) and a thermal stability up to 250 °C under N_2.[13] Single crystals of **1** show no significant electric conductivity. Numerous complexes of SCN^- are known with Fe^{II} and also with Fe^{III} central atoms. In contrast, only a few iron complexes of $SeCN^-$ have been characterized by X-ray structure analysis, in many of which, however, also other ligands are present.[14] Only one mixed-valent iron complex with SCN^- and $SeCN^-$ ligands has been reported, but its crystal structure was not described.[15]

 © 2005 Wiley-VCH Verlag GmbH & Co. KGaA, Weinheim

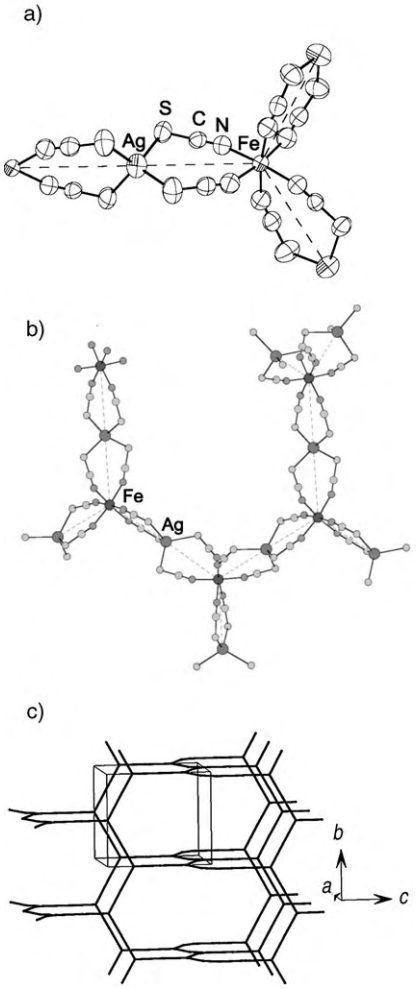

Figure 1. a), b) Fragments of the structure of the three-dimensional polymeric $[Ag_3Fe_2(SCN)_{12}]^{4-}$ ion in **1** (thermal ellipsoids with 70% probability). For clarity, Ag···Fe distances are marked with dashed lines. Distances [pm] and angles [°] in **1** [**2**]: Fe–N 210.1–212.2(2) [209.9–211.1(4)]; Ag–S 260.99–262.08(8) [Ag–Se 270.52–271.22(6)], C–N 115.5–116.3(3) [116.3–116.9(5)], C–S 163.3–163.7(3) [C–Se 178.0–178.3(4)]; N-Fe-N 83.14–93.74(8), 171.4–175.5(1) [83.3–94.3, 171.4–176.5(2)], S-Ag-S 91.18–119.39(4) [Se-Ag-Se 88.65–121.38(2)], S-C-N 177.7–178.6(3) [Se-C-N 178.1–179.5(4)]. c) *(10,3)-b* Network of α-$ThSi_2$ and of the Ag and Fe atoms in **1** and **2**, respectively; the Fe atoms occupy the positions of the Si atoms (linking position), between them are the Ag atoms. A section of the $[Ag_3Fe_2(SCN)_{12}]^{4-}$ network including the tetragonal unit cell is shown (view approximately along the *a* axis).

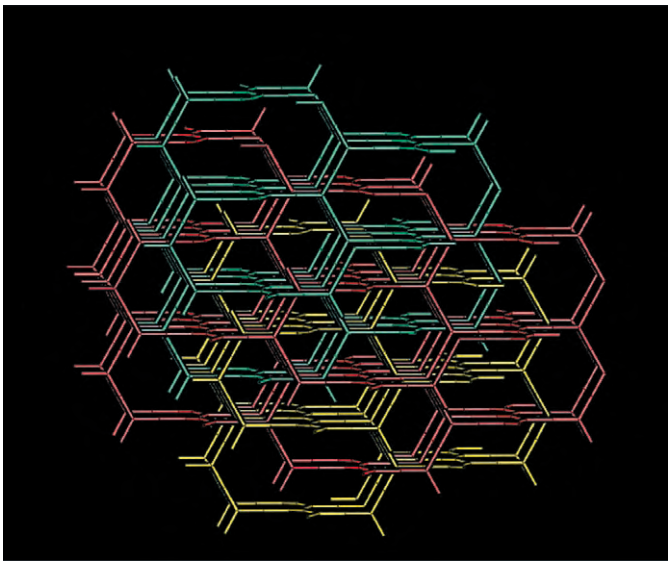

Figure 2. Interpenetration of three *(10,3)-b* nets in the structures of the anions of **1** and **2**; only the Ag···Fe lines are shown.

The IR spectrum of **1** shows intense vibrational resonances at 2112 (s) and 2069 (vs) cm^{-1}, which can be attributed to the stretching vibrations ν_{CN} of the SCN^- ligands. Because of the 1,3-μ bridging mode of the SCN^- ligands, these absorptions are slightly shifted compared to those of the mononuclear complexes with terminal N-bonded SCN^- ligands.[16] For comparison, the ν_{CN} frequencies are 2069 cm^{-1} in $(Pr_4N)_3[Fe(NCS)_6]$, 2085 cm^{-1} in $(Et_4N)_4[Fe(NCS)_6]$ and 2125, 2076, and 2042 cm^{-1} in $(Bu_4N)_4[Ag_2Fe_2(SCN)_{12}]$.[5]

The almost-black crystals of **1**, which appear red in thin layers, show a very strong absorption at 525 nm in the UV/Vis spectrum, which is interpreted as a ligand-to-metal charge-transfer (LMCT) transition.[17] The peak is broadened compared to that of the starting compound $(Pr_4N)_3[Fe(NCS)_6]$ ($\lambda_{max} = 480$ nm), and like the absorption of $(Bu_4N)_4[Ag_2Fe_3(SCN)_{12}]$ ($\lambda_{max} = 530$ nm) it is shifted to lower energy as a result of the coordination of the ligand S atoms to Ag^+.[5] The high intensity of the LMCT absorption prevents the identification of an intervalence charge-transfer (IVCT) absorption.

At room temperature the magnetic moment of **1** is $\chi = 2.88 \times 10^{-2}$ emu mol^{-1} (after subtraction of the diamagnetic increments).[18,19] Between 100 K and 300 K the magnetic susceptibility follows approximately Curie's law with a Curie constant of $C = 8.35$. If one assumes $\mu_{eff}(Fe^{3+}) = 5.92\,\mu_B$ as the spin-only value for the high-spin Fe^{3+} ions, the Fe^{2+} ions contribute $\mu_{eff}(Fe^{2+}) = 5.64\,\mu_B$. The magnetic moment for high-spin Fe^{2+} complexes in octahedral ligand fields is typically between 5.1 and $5.7\,\mu_B$.[19] Below 100 K the χT function drops off slightly. Apparently at these temperatures there are no significant exchange interactions between the Fe ions, which have separations of 1121 pm within and 1104 pm between two networks. According to the structure analysis, the Fe^{2+} and Fe^{3+} ions occupy equivalent positions, whereas the Mössbauer spectra can be interpreted as the superposition of signals of Fe^{2+} and Fe^{3+} (Figure 3). At room temperature, 130 K, and 4.2 K the spectra show quadrupole doublets with temperature-dependent splittings ranging from 0.38 mm s^{-1} at room temperature to 0.65 mm s^{-1} at 4.2 K. This signal with an isomeric shift of 1.15 to 1.27 mm s^{-1} can be assigned to high-spin Fe^{2+}. The comparatively small quadrupole splitting is a result of the almost equal contributions of the valence electrons and the lattice to the electric field gradient with opposite signs. The contribution of the valence electrons is responsible for the temperature dependence of the quadrupole splitting. The strongly broadened signal with an isomeric shift of about 0.5 mm s^{-1} indicates Fe^{3+} in a high-spin state. At room temperature both portions of the peak area are almost equal, but shift with decreasing temperature in favor of the

 © 2005 Wiley-VCH Verlag GmbH & Co. KGaA, Weinheim

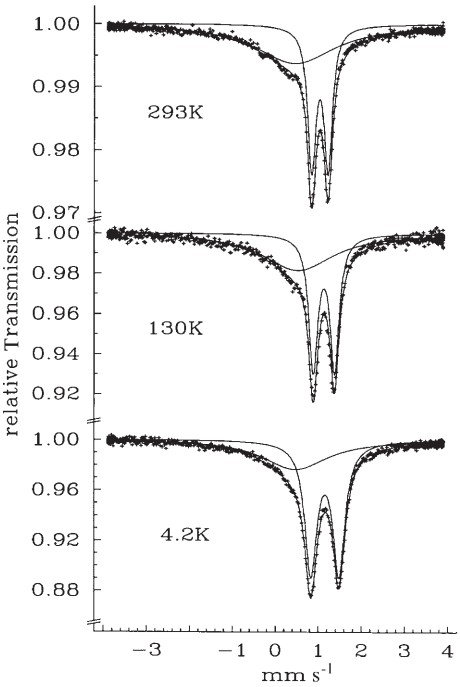

Figure 3. Mössbauer spectra of **1** at 293, 130, and 4.2 K. IS = isomeric shift, QS = quadrupole splitting, hs = high spin.

Fe^{2+} high-spin component. Probably spin relaxation leads to the strong broadening of the Fe^{3+} signal, since the relaxation times are comparable with the typical time window for the ^{57}Fe Mössbauer experiment.

The broad intervalence bands of $[(CN)_5Fe\text{-}ECN\text{-}Fe(CN)_5]^{6-}$ (E = S, Se) at $\lambda = 1300$ nm with half widths of 3550 and 3090 cm^{-1} show that exchange interactions through bridging SCN^- and $SeCN^-$ ligands, respectively, are possible.[15] These complexes can be assigned to class II in the sense of the Robin Day classification[20] with localized oxidation states, since the ν_{CN} frequencies for the $Fe^{II}(CN)_5$ and $Fe^{III}(CN)_5$ fragments are distinguishable. The Fe ions in $[(CN)_5Fe(\mu\text{-tz})Fe(CN)_5]^{5-}$ (μ-tz = 1,2,4,5-tetrazine), however, cannot be distinguished by either IR or Mössbauer spectroscopy, and can therefore be assigned to class III, which is also supported by a minor solvent dependence of the significantly sharper intervalence charge-transfer band at 2495 cm^{-1}.[21] Because in **1** the Fe^{2+} and the Fe^{3+} ions have similar chemical environments, the magnetic features correspond to those of the isolated complexes, and these ions also give rise to distinct signals in the Mössbauer spectra, **1** should be considered a Robin Day class II mixed-valent compound.

Experimental Section

1: Equimolar quantities of $(Pr_4N)_3[Fe(NCS)_6]$ (550 mg, 0.57 mmol) (prepared according to reference [22] and recrystallized from CH_2Cl_2/hexane), $AgNO_3$ (96 mg), and $(Pr_4N)SCN$ (139 mg) were stirred in nitromethane (5 mL) at room temperature. After 10 h the red–black solution was filtered and 15 mL of diethyl ether was condensed into the solution. After one week, black crystals of **1**, which in thin layers appear red, were isolated, washed with nitromethane and diethyl ether, and dried in vacuum. Yield: 50 mg (0.027 mmol, 14%); elemental analysis calcd (%) for $C_{60}H_{112}N_{16}Ag_3Fe_2S_{12}$: C 38.4, H 6.7, N 11.9, Fe 5.9; found: C 38.3, H 6.3, N 12.0, Fe 5.9.

Coordination compound **2** was obtained as dark blue crystals in small yield by reaction of AgSeCN with $Fe(ClO_4)_3$ and $(Pr_4N)SeCN$.

The amount of Fe^{2+} and Fe^{3+} in **1** was determined by complexometric titration under N_2 with 0.01M EDTA solution with 5-sulfosalicylic acid as indicator: Compound **1** (85 mg, 0.0453 mmol) was stirred with an excess of $AgNO_3$ in water acidified with HNO_3. Insoluble AgSCN was filtered off, and the resulting solution was titrated with EDTA solution to determine the Fe^{3+} content. The point of equivalence was reached after addition of EDTA solution (4.55 mL). After oxidation of the Fe^{2+} ions with added H_2O_2, the titration was continued until the second point of equivalence is reached after the addition of EDTA solution (4.40 mL).

Received: June 30, 2005
Published online: November 4, 2005

Keywords: coordination polymers · interpenetrating networks · Moessbauer spectroscopy · selenocyanates · thiocyanates

[1] S. Kaskel, *Nachr. Chem.* **2005**, *53*, 394; S. Kaskel in *Handbook of Porous Solids, Vol. 2* (Eds.: F. Schüth, K. S. W. Sing, J. Weitkamp), Wiley-VCH, Weinheim, **2002**, p. 1190; S. Kitagawa, R. Kitaura, S. Noro, *Angew. Chem.* **2004**, *116*, 2388; *Angew. Chem. Int. Ed.* **2004**, *43*, 2334.

[2] S. R. Batten, R. Robson, *Angew. Chem.* **1998**, *110*, 1559; *Angew. Chem. Int. Ed.* **1998**, *37*, 1461.

[3] J. Burmeister, *Coord. Chem. Rev.* **1966**, *1*, 205; J. Burmeister, *Coord. Chem. Rev.* **1968**, *3*, 225; J. Burmeister, *Coord. Chem. Rev.* **1990**, *105*, 77; P. P. Singh, *Coord. Chem. Rev.* **1980**, *32*, 33.

[4] R. G. Pearson, *J. Am. Chem. Soc.* **1963**, *85*, 3533; M. K. Kroeger, R. S. Drago, *J. Am. Chem. Soc.* **1981**, *103*, 3250.

[5] H. Krautscheid, S. Gerber, *Z. Anorg. Allg. Chem.* **1999**, *625*, 2041.

[6] U. Müller, *Acta Crystallogr. Sect. B* **1977**, *33*, 2197.

[7] H. Krautscheid, S. Gerber, *Acta Crystallogr. Sect. C* **2001**, *57*, 781; G. Thiele, *Z. Anorg. Allg. Chem.* **1984**, *515*, 199.

[8] S. Gerber, H. Krautscheid, T. Gelbrich, H. Vollmer, *Z. Anorg. Allg. Chem.* **2004**, *630*, 1427.

[9] E. Itabashi, *Inorg. Chem.* **1985**, *24*, 4024; D. Rehorek, E. G. Janzen, *Inorg. Chim. Acta* **1986**, *118*, L29.

[10] Crystal data: **1** ($C_{60}H_{112}N_{16}Ag_3Fe_2S_{12}$): STOE IPDS-2T diffractometer, $M_m = 1877.7$ g mol^{-1}, crystal size $0.14 \times 0.18 \times 0.22$ mm^3, tetragonal, space group $I\bar{4}2d$ (no. 122), $a = 1960.65(7)$ $c = 2218.1(1)$ pm, $V = 8526.6(6) \times 10^6$ pm^3, $Z = 4$, $T = 200$ K, $\rho_{calcd} = 1.463$ g cm^{-3}, $\mu = 1.347$ mm^{-1}, $\lambda = 71.073$ pm ($Mo_{K\alpha}$), $T_{min} = 0.775$, $T_{max} = 0.840$, 22659 measured, 4652 independent reflections, $R_{int} = 0.036$, 4285 with $I > 2\sigma(I)$, 201 parameters, propyl groups disordered, H atoms in idealized positions, R_1 (observed reflections) = 0.029, wR_2 (all data) = 0.060, Flack parameter $x = -0.04(2)$, max./min. residual electron density peaks 0.35/−0.47 e/10^6 pm^3; **2** ($C_{60}H_{112}N_{16}Ag_3Fe_2Se_{12}$): STOE IPDS diffractometer, $M_m = 2440.5$ g mol^{-1}, crystal size $0.12 \times 0.14 \times 0.35$ mm,

 © 2005 Wiley-VCH Verlag GmbH & Co. KGaA, Weinheim

tetragonal, space group $I\bar{4}2d$ (no. 122), $a = 1986.21(8)$ $c = 2262.09(10)$ pm, $V = 8924.0(6) \times 10^6$ pm^3, $Z = 4$, $T = 213$ K, $\rho_{calcd} = 1.816$ g cm^{-3}, $\mu = 3.123$ mm^{-1}, $\lambda = 56.087$ pm ($Ag_{K\alpha}$), $T_{min} = 0.5521$, $T_{max} = 0.7134$, 40179 measured, 4880 independent reflections, $R_{int} = 0.0465$, 4501 with $I > 2\sigma(I)$, 183 parameters, propyl groups disordered, H atoms in idealized positionen, R_1 (observed reflections) = 0.030, wR_2 (all data) = 0.069, Flack parameter $x = 0.01(2)$, max./min. residual electron density peaks 0.74/−0.47 e/10^6 pm^3; structure solution and refinement: SHELXS-97 (Sheldrick, 1990) and SHELXL-97 (Sheldrick, 1997). Graphical presentation: Diamond2 (Brandenburg, 1999), Schakal92 (Keller, 1992). CCDC 193054 (**1**) and CCDC-193055 (**2**) contain the supplementary crystallographic data for this paper. These data can be obtained free of charge from the Cambridge Crystallographic Data Centre via www.ccdc.cam.ac.uk/data_request/cif.

[11] A. F. Wells, *Structural Inorganic Chemistry*, 5th ed., Clarendon, Oxford, **1984**.

[12] L. Carlucci, G. Ciani, D. M. Proserpio, S. Rizzato, *Chem. Eur. J.* **2002**, *8*, 1519; L. Carlucci, G. Ciani, D. M. Proserpio, A. Sironi, *J. Am. Chem. Soc.* **1995**, *117*, 4562.

[13] Differential thermal analysis/thermogravimetry: Netzsch STA 409C, heating rate 5 K min^{-1}, N_2 atmosphere.

[14] A. Ozarowski, Yu. Shunzhong, B. R. McGarvey, A. Mislankar, J. E. Drake, *Inorg. Chem.* **1991**, *30*, 3167; T. J. Mizoguchi, S. J. Lippard, *Inorg. Chem.* **1997**, *36*, 4526; N. Moliner, M. Carmen Munoz, J. A. Real, *Inorg. Chem. Commun.* **1999**, *2*, 25; N. Moliner, M. Carmen Munoz, S. Letard, J.-F. Letard, X. Solans, R. Burriel, M. Castro, O. Kahn, J. A. Real, *Inorg. Chim. Acta* **1999**, *291*, 279.

[15] V. Palaniappan, R. M. Singru, U. C. Agarwala, *Inorg. Chem.* **1988**, *27*, 181.

[16] A. H. Norbury, *Adv. Inorg. Chem. Radiochem.* **1975**, *17*, 231.

[17] I. M. Walker, P. J. McCarthy, *Inorg. Chem.* **1984**, *23*, 1842; H. H. Schmidtke, *Ber. Bunsen-Ges.* **1967**, *71*, 1138.

[18] The magnetic susceptibility was measured in the temperature range 3–300 K at magnetic fields of 10000 and 1000 Oe using a SQUID magnetometer. The data were corrected for the contribution of ferromagnetic impurities.

[19] A. Weiss, H. Witte, *Magnetochemie*, VCH, Weinheim, **1973**.

[20] M. B. Robin, P. Day, *Adv. Inorg. Chem. Radiochem.* **1967**, *10*, 248.

[21] M. Glöckle, W. Kaim, A. Klein, E. Roduner, G. Hübner, S. Zalis, J. van Slageren, F. Renz, P. Gütlich, *Inorg. Chem.* **2001**, *40*, 2256.

[22] H. H. Schmidtke, D. Gathoff, *Fasciculus* **1967**, *6*, 1631.

 © 2005 Wiley-VCH Verlag GmbH & Co. KGaA, Weinheim

P,N Heterocycles

DOI: 10.1002/anie.200502475

A Triazadiphosphole**

Sebastian Herler, Peter Mayer,
*Jörn Schmedt auf der Günne, Axel Schulz,**
Alexander Villinger, and Jan J. Weigand

In memory of Erhard Kurras

Phosphorus–nitrogen compounds with low-coordinated phosphorus(III) atoms are a well-established group of compounds.[1–3] However, covalent azide analogues such as R-PNN and R-NNP (R = organic group) are not yet known. As part of our research directed toward the synthesis of (TMS)PNN and (TMS)NNP species, we have recently investigated the elimination of trimethylsilylchloride (TMSCl) in the thermal decomposition of *N*,*N*′,*N*′-[tris(trimethylsilyl)hydrazino]dichlorophosphane (**1**).[4] This experimental and theoretical study revealed rather large activation barriers (38–45 kcal mol^{-1}) for the successive intrinsic elimination of TMSCl in **1** and led to the conclusion that Lewis acids should be used to eliminate TMSCl at ambient temperature. In this context, we have studied the reactions of **1** with gallium trichloride as a Lewis acid.[5]

Compound **1** is stable in dichloromethane at ambient temperature for several days as shown by ^{31}P NMR studies ($\delta(^{31}P) = 166.6$ ppm).[4] However, the ^{31}P NMR spectra for reaction mixtures of **1** (2 equiv) and $GaCl_3$ (1 equiv) in CH_2Cl_2 at ambient temperature show rapid, quantitative formation of the new phosphorus species **2** within 2 h (Scheme 1).[6] Two new different phosphorus resonances belonging to only one species are observed in the range typical for dicoordinated phosphorus(III) compounds (doublets at $\delta(^{31}P) = 317.2$ (P1) and 292.1 ppm (P2),[7a] $^2J_{P,P} = 22.1$ Hz; cf. 265.1 ppm, $^2J_{P,P} = 22.7$ Hz for a 1,2,3,5-diazadiphosphole (RN_2P_2C, R = Me)[8]). Removal of the solvent resulted in a yellow polycrystalline powder. ^{31}P MAS NMR studies proved the existence of the same species in the solid state as that observed in the solvent ^{31}P NMR experiment. Because there are two independent molecules in the unit cell, four resonances at $\delta(^{31}P) = 318/312$ (P1 or P3) and 296/285 ppm (P2 or P4) were found in the ^{31}P MAS NMR spectrum (Figures 1 and 2). Interestingly, we were able to

[*] S. Herler, Dr. P. Mayer, Dr. J. Schmedt auf der Günne, Dr. A. Schulz, A. Villinger, Dr. J. J. Weigand
Department Chemie und Pharmazie
Ludwig-Maximilians-Universität München
Butenandtstrasse 5–13 (Haus D), 81377 München (Germany)
Fax: (+49) 89-2180-77492
E-mail: axel.schulz@cup.uni-muenchen.de

[**] A.S. thanks Prof. Dr. T. M. Klapötke (LMU München) for his generous support and Prof. Dr. A. Schmidpeter, Dr. K. Karaghiosoff, and Dr. B. Krumm for their interest, help, and advice.

Supporting information for this article is available on the WWW under http://www.angewandte.org or from the author.

© 2005 Wiley-VCH Verlag GmbH & Co. KGaA, Weinheim

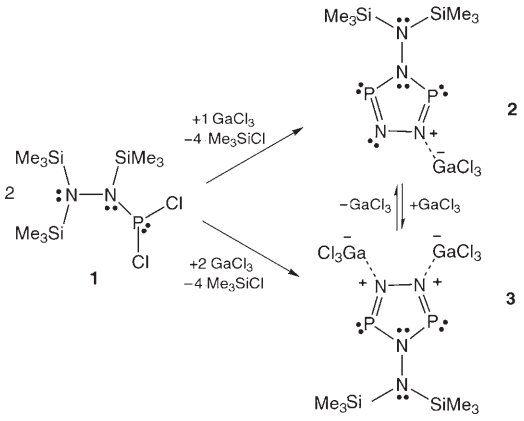

Scheme 1. Synthesis of $GaCl_3$ adducts **2** and **3** of 4-bis(trimethylsilyl)-amino-1,2,4,3,5-triazadiphosphole.

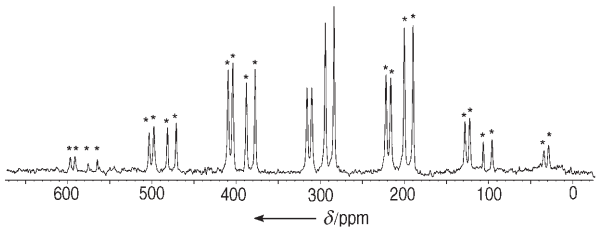

Figure 1. ^{31}P MAS spectrum of **3**. The four resonances arise from two independent molecules in the unit cell (spinning side bands are marked with asterisks).

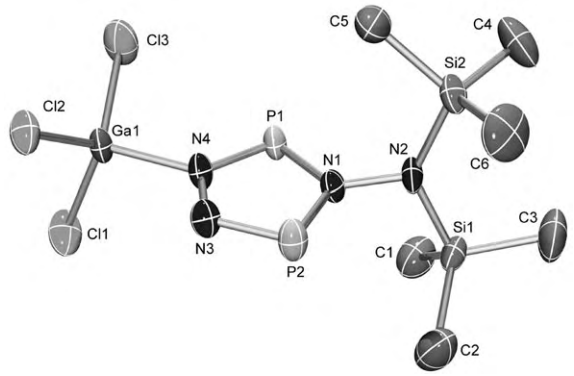

Figure 2. ORTEP drawing of the molecular structure of one independent molecule of **2** in the crystal.[9] Thermal ellipsoids with 50% probability at 200 K (hydrogen atoms omitted for clarity). Selected bond lengths [Å] and angles [°]: Ga1—N4 1.978(3), P1—N1 1.670(4), P1—N4 1.633(4), P2—N1 1.694(4), P2—N3 1.603(4), N1—N2 1.451(5), N3—N4 1.380(5); N1-P1-N4 93.2(2), N1-P2-N3 96.1(2), P1-N1-P2 116.4(2), P1-N4-N3 119.6(3), P2-N3-N4 114.8(3), P1-N1-N2 120.5(3), P2-N1-N2 122.9(3).[7b]

assign these two groups of resonances on the basis of the excellent agreement between theoretically and experimentally obtained values of the ^{31}P chemical shift tensor (δ_{iso}, δ_{aniso}, see the Supporting Information).[7a–b,9]

Crystals suitable for X-ray diffraction were obtained from a yellow hexane/CH_2Cl_2 solution of **2** after stepwise removal of solvent at −10 °C. Single-crystal X-ray studies revealed a surprising $GaCl_3$ adduct **2** of the hitherto unknown 4-bis(trimethylsilyl)amino-1,2,4,3,5-triazadiphosphole (Figure 2).[7b]

The $GaCl_3$-induced elimination of TMSCl (Scheme 1) from species **1** at ambient temperature leads to **2** quickly and in high yields (reaction time 2 h, yield > 95%). A solution of **2** in CH_2Cl_2 is stable for at least four weeks (according to ^{31}P NMR experiments). Adding yet another equivalent of $GaCl_3$ to a solution of **2** results immediately in the formation of a new species: the $GaCl_3$ diadduct **3** of 4-bis(trimethylsilyl)amino-1,2,4,3,5-triazadiphosphole (Scheme 1) as shown by ^{31}P NMR studies (CH_2Cl_2 solution: 304.6 ppm, solid (MAS): 298 ppm). The same product is formed from the reaction of **1** (1 equiv) and $GaCl_3$ (1 equiv). Removal of the solvent again results in a yellow polycrystalline powder (**3**, yield > 95%). X-ray quality crystals were obtained from a saturated solution of **3** in CH_2Cl_2 (Figure 3).[7b]

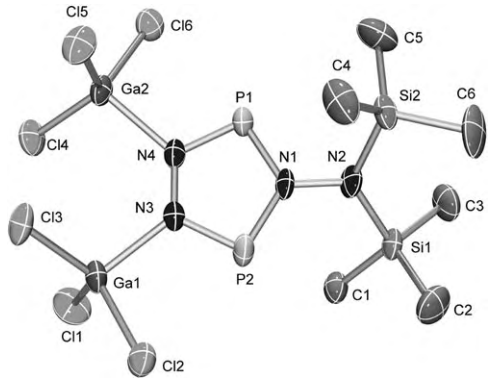

Figure 3. ORTEP drawing of the molecular structure of **3** in the crystal. Thermal ellipsoids with 50% probability at 200 K (hydrogen atoms omitted for clarity). Selected bond lengths [Å] and angles [°]: Ga1—N3 2.036(4), Ga2—N4 2.035(4), P1—N1 1.682(3), P1—N4 1.630(4), P2—N1 1.675(3), P2—N3 1.637(4), N1—N2 1.414(5), N3—N4 1.379(5); N1-P1-N4 94.4(2), N1-P2-N3 94.4(2), P1-N1-P2 117.1(2), P1-N4-N3 117.1(3), P2-N3-N4 116.9(3), P1-N1-N2 121.5(3), P2-N1-N2 121.4(3).[7b]

Both species **2** and **3** are air and moisture sensitive but stable under argon atmosphere over a long period as solids and in common organic solvents (e.g. benzene, CH_2Cl_2, ether). The yellow color of **2** and **3** vanishes rapidly when traces of H_2O are present. Compounds **2** and **3** are easily prepared in bulk and are infinitely stable when stored in a sealed tube and kept cool at 4 °C in the dark. This together with the very good solubility in almost all common organic solvents makes both compounds good precursors for further synthesis.[7a–d] Compound **2** is thermally stable up to over 130 °C, while **3** can be heated only up to 96 °C. At these temperatures decomposition starts, accompanied by a slow elimination of TMSCl (MS experiments).

Compound **2** crystallizes in the triclinic space group $P\bar{1}$ with two independent molecules in the unit cell consistent with the ^{31}P MAS NMR data (Figure 1).[7b,9] In agreement with our DFT calculations,[7c] the molecule adopts a staggered configuration with the planar five-membered P_2N_3 ring

 © 2005 Wiley-VCH Verlag GmbH & Co. KGaA, Weinheim

almost perpendicular to the Si1-N2-Si2 plane (P1-N1-N2-Si2 92.3(3), P2-N1-N2-Si1 84.7(3)°). Upon formation of the $GaCl_3$ adduct, the C_{2v} symmetry of the P_2N_3 ring is slightly distorted, with two shorter P–N bonds (P1–N4 1.633(4), P2–N3 1.603(4) Å) and two longer P–N bonds (P1–N1 1.670(4), P2–N1 1.694(4) Å). These P–N distances between 1.63 and 1.70 Å are substantially shorter than the sum of the covalent radii (d_{cov}: N–P 1.8, N=P 1.6 Å),[10,11] which indicates partial double-bond character for the P–N bonds. A similar situation is found for the N3–N4 bond (1.380(5) Å) of the P_2N_3 ring, which also lies in the range between a single and a double bond (d_{cov}: N–N 1.4, N=N 1.2 Å). The N1–N2 bond is a typical single bond, with a length of 1.451(5) Å. The Ga–N bond length of 1.978(3) Å (Ga1–N4) is slightly shorter than those found for the adducts $Cl_3Ga{\cdot}NMe_2SiMe_2NMe_2$ (2.003(5) Å),[12] $MeCl_2Ga{\cdot}H_2N{-}NHtBu$ (2.023(7) Å),[13] and the dimeric gallium amide $[\{Me_2Ga{-}N(Ph)SiMe_3\}_2]$ (2.071(2) Å).[14] The P-N-N angles (114–123°) are rather large compared to the N-P-N angles (93–96°), and the Cl-Ga-Cl angles decrease upon adduct formation (110–115°).

The structural features of **3** are very similar to those of **2** (Figure 3).[7b] The P–N, N–N, and Si–N bond lengths and all angles within the $\{P_2N_3\text{-}N(TMS)_2\}$ fragment do not change much upon addition of a second $GaCl_3$ molecule. However, as expected, the two Ga–N distances in **3** (Ga1–N3 2.036(3) and Ga2–N4 2.034(4) Å) are slightly longer than those in **2** (cf. Ga1–N4 1.978(3), Ga2–N8 1.968(3) Å)[7b,9] due to steric repulsion and a weaker donor–acceptor bond (smaller charge transfer, see below). It is interesting to note that for both adducts **2** and **3** noticeable $H_{TMS}\cdots Cl_{GaCl_3}$ contacts are found (**2**: 2.855(1); **3**: 2.840(1) Å), which are shorter than the sum of the van der Waals radii (d_{vdW}: H···Cl 2.95 Å).[7b,15] This intermolecular interaction links the molecules as a chainlike structure in the solid.

Adducts such as **2** and **3** are typical charge-transfer complexes, and the bond between the $GaCl_3$ and the RP_2N_3 fragments can be considered a donor–acceptor bond.[16] The calculated gas-phase Gibbs energy[7c] for the formation of the monoadduct, $P_2N_3\text{-}N(TMS)_2 + GaCl_3 \rightarrow$ **2** ($\Delta G_{298} = -7.8$ kcal mol^{-1}), is in agreement with the experiment since no equilibrium between **2** and the dissociated fragments could be observed in ^{31}P NMR studies. The diadduct formation, **2** + $GaCl_3 \rightarrow$ **3**, is a true equilibrium reaction at the B3LYP level of theory[7c] ($\Delta G_{298} = 0.6$ kcal mol^{-1}, Scheme 1). However, this was not evident in the ^{31}P NMR experiments since only species **3** was detected.[16] According to NBO analysis (NBO = natural bond orbital),[17] the charge transfer is about 0.16 *e* in **2** and 0.11 *e* per $GaCl_3$ fragment in **3**.[7e] The P–N σ and π bonds are highly polarized, while the adjacent N1–N2 and N3–N4 in **2** and **3** are almost ideally covalent (Figure 2 and Figure 3).[7e] The nitrogen atoms N1 and N2 have almost planar surroundings (e.g. **2**: Si2-N2-N1-Si3 174.9, Si1-N1-P1-N2 174.7°; all N-N-X (X = P, Si) angles are between 113 and 123°). Hence, as indicated by NBO analysis, the lone pair (LP) on each nitrogen atom in **2** and **3** is localized in a pure p-type atomic orbital (p-AO). The two lone pairs are also perpendicular to each other. As a consequence the p-AO lone pair of N2 atom lies in the ring plane and does not contribute to the π-electron system of the P_2N_3 ring whereas, the p-AO lone pair of N1 is part of the 6π-electron system of the P_2N_3 ring, as indicated by an investigation of the noncovalent effects.[17] There are no significant intramolecular interactions (noncovalent effects) between the bis(trimethylsilyl)amino group and the ring. Hence, neither the lone pair of the amino group nor the TMS groups stabilize the P_2N_3 ring significantly.

Over the past 50 years only a very small number of planar five-membered-ring molecules and ions containing only the elements phosphorus(III) and/or nitrogen have been isolated and fully characterized (Scheme 2). Only three are known:

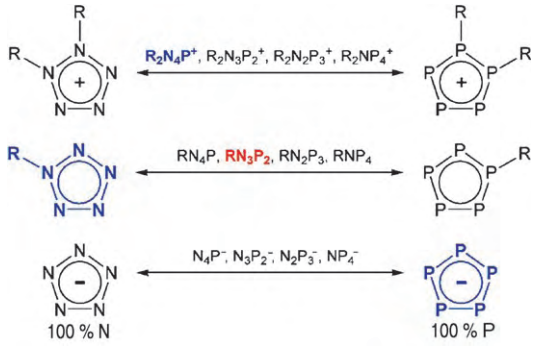

Scheme 2. Binary P-N five-membered rings with P^{III} atoms. Species in blue are known and fully characterized, the triazadiphosphole is in red. (R = organic or inorganic group).

The neutral pentazole derivatives, RN_5,[18] the pentaphosphacyclopentadienide anion, P_5^-,[19] and the 1-alkyl-4-aryltetraazaphospholium cations, $R_2N_4P^+$ (as tetrachloroaluminate).[20] Additionally, the pentazolate anion, *cyclo*-N_5^-, has been detected recently.[21] Since the electronic structures of these three classes of planar ring systems and the novel triazadiphosphole all have $(4n+2)$ π electrons and therefore formally obey the Hückel rule, these compounds are related to aromatic hydrocarbons.[22]

Formally, the formation of the P_2N_3 ring in **2** and **3** might be regarded as a [3+2] cycloaddition of NNP^- and $(TMS)_2NNP^+$ ions or as a dimerization of an azide analogue of (TMS)NNP, which has been stabilized by cycloaddition followed by a 1,4-shift of one TMS group. We assume that in the first step a 1,2-elimination of TMSCl in **1** occurs assisted by $GaCl_3$. All together two TMSCl molecules are eliminated from **1**, and two condensation steps followed by adduct formation are needed. The exclusive formation of **2** and **3** demonstrates the thermodynamic preference for the five-membered framework over the six-membered alternatives and is consistent with the prominence of the known binary five-membered-ring PN cations, and polyphosphorus anions.[19,20]

In conclusion, we present here an easy, high-yielding (> 95 %) synthetic procedure and full characterization (see the Supporting Information) of the first triazadiphosphole stabilized as a $GaCl_3$ mono- and diadduct.[7a–d] Moreover, **2** and **3** are rare examples of structurally characterized Lewis acid–base adducts involving a ring atom within a PN ring.[23] Because of the astonishing stability of **2** and **3** in solution as

 © 2005 Wiley-VCH Verlag GmbH & Co. KGaA, Weinheim

well as in solid, both compounds may have great synthetic potential, for example, as sources for binary PN or ternary PNGa species.

Received: July 15, 2005
Revised: August 17, 2005
Published online: October 31, 2005

Keywords: bonding analysis · Lewis acid–base adducts · P,N heterocycles · structure determination · triazadiphospholes

[1] a) E. Niecke, W. Flick, *Angew. Chem.* **1973**, *85*, 586 – 587; *Angew. Chem. Int. Ed. Engl.* **1973**, *12*, 585 – 586; b) E. Niecke, W. Flick, *Angew. Chem.* **1974**, *86*, 128 – 129; *Angew. Chem. Int. Ed. Engl.* **1974**, *13*, 134 – 135; c) O. J. Scherer, N. Kuhn, *Chem. Ber.* **1974**, *107*, 2123 – 2125; d) O. J. Scherer, N. Kuhn, *J. Organomet. Chem.* **1974**, *82*, C3 – C6; e) O. J. Scherer, N. Kuhn, *Angew. Chem.* **1974**, *86*, 899 – 900; *Angew. Chem. Int. Ed. Engl.* **1974**, *13*, 811 – 812; f) E. Niecke, W. Flick, *Angew. Chem.* **1975**, *87*, 355 – 356; *Angew. Chem. Int. Ed. Engl.* **1975**, *14*, 363 – 364; g) R. Appel, M. Halstenberg, *Angew. Chem.* **1975**, *87*, 810; *Angew. Chem. Int. Ed. Engl.* **1975**, *14*, 768; h) E. Niecke, R. Kröher, *Angew. Chem.* **1976**, *88*, 758 – 759; *Angew. Chem. Int. Ed. Engl.* **1976**, *15*, 692 – 693; i) S. Pohl, *Angew. Chem.* **1976**, *88*, 723 – 724; *Angew. Chem. Int. Ed. Engl.* **1976**, *15*, 687 – 688; j) A. Schmidpeter, J. Luber, H. Tautz, *Angew. Chem.* **1977**, *89*, 554 – 555; *Angew. Chem. Int. Ed. Engl.* **1977**, *16*, 546 – 547; k) R. O. Day, A. Schmidpeter, R. R. Holmes, *Inorg. Chem.* **1983**, *22*, 3696 – 3699; l) N. Burford, J. A. C. Clyburne, P. K. Bakshi, T. S. Cameron, *J. Am. Chem. Soc.* **1993**, *115*, 8829 – 8830; m) N. Burford, T. S. Cameron, J. A. C. Clyburne, K. Eichele, K. N. Robertson, S. Sereda, R. E. Wasylishen, W. A. Whitla, *Inorg. Chem.* **1996**, *35*, 5460 – 5467; n) A. Schmidpeter, *Heteroat. Chem.* **1999**, *10*, 529 – 537; o) N. Burford, A. D. Phillips, H. A. Spinney, M. Lumsden, U. Werner-Zwanziger, M. J. Ferguson, R. McDonald, *J. Am. Chem. Soc.* **2005**, *127*, 3921 – 3927.

[2] a) E. Niecke, D. Gudat, *Angew. Chem.* **1991**, *103*, 251 – 270; *Angew. Chem. Int. Ed. Engl.* **1991**, *30*, 217 – 237; b) A. Schmidpeter, *Phosphorus Sulfur* **1986**, *28*, 71 – 89, and references therein.

[3] *Multiple Bonds and Low Coordination in Phosphorus Chemistry* (Ed.: M. Regitz, O. J. Scherer), Thieme, Stuttgart, **1990**, and references therein.

[4] G. Fischer, S. Herler, P. Mayer, A. Schulz, A. Villinger, J. J. Weigand, *Inorg. Chem.* **2005**, *44*, 1740 – 1751.

[5] N. Burford, K. D. Conroy, J. C. Landry, P. J. Ragogna, M. J. Ferguson, R. McDonald, *Inorg. Chem.* **2004**, *43*, 8245 – 8251.

[6] If less than 1 equiv of $GaCl_3$ is used, the reaction is not complete, i.e. both compounds **2** and **1** are observed.

[7] See the Supporting Information: a) Chemical shifts (^{1}H, ^{13}C, ^{29}Si{^{1}H}, ^{31}P, ^{31}P-MAS NMR), assignment was based the excellent agreement between theoretically and experimentally obtained shifts ($\delta(^{31}P)$) and coupling constants; b) crystal data; c) computational details, calculated structural and vibrational data of all described species (B3LYP), approximate assignment and trends; d) full description of the experimental data, technique and details; e) summary of the NBO analysis for **2** and **3**: 1) partial charges, 2) hybridization effects, 3) polarization, and 4) Wiberg bond indices.

[8] a) A. Schmidpeter, C. Leyh, K. Karaghiosoff, *Angew. Chem.* **1985**, *97*, 127 – 128; *Angew. Chem. Int. Ed. Engl.* **1985**, *24*, 124 – 125; b) J. C. Tebby, *Handbook of Phosphorus-31 Nuclear Magnetic Resonance Data*, CRC, Boston, **1991**.

[9] The structural parameters of second independent molecule are almost identical to those of the first; hence, we have only discussed the data of the first molecule.

[10] A. F. Holleman, E. Wiberg, N. Wiberg, *Lehrbuch der Anorganischen Chemie*, 101. Aufl., de Gruyter, Berlin, **1995**, Anhang V.

[11] E. Niecke, O. Altmeyer, M. Nieger, *J. Chem. Soc. Chem. Commun.* **1988**, 945 – 946.

[12] W. R. Nutt, J. S. Blanton, A. M. Boccanfusco, L. A. Silks III, A. R. Garber, J. D. Odom, *Inorg. Chem.* **1991**, *30*, 4136 – 4140.

[13] H. Nöth, T. Seifert, *Eur. J. Inorg. Chem.* **2002**, 602 – 612.

[14] S. D. Waezsada, C. Rennekamp, H. W. Roesky, C. Röpken, E. Parisini, *Z. Anorg. Allg. Chem.* **1998**, *624*, 987 – 990.

[15] a) A. Bondi, *J. Phys. Chem.* **1964**, *68*, 441 – 451; b) see Figure S3 and S4 in the Supporting Information.

[16] It is known that for adducts in the solid state and gas phase, structural data and donor–acceptor energies can be quite different. Leopold et al. have indicated that the donor–acceptor bond is much shorter in the solid state than in the gas phase, and this change has been associated with the substantial dipole moment of the adduct. D. L. Fiacco, Y. Mo, S. W. Hunt, M. E. Ott, A. Roberts, K. R. Leopold, *J. Phys. Chem. A* **2001**, *105*, 484 – 493, and references therein.

[17] a) E. D. Glendening, A. E. Reed, J. E. Carpenter, F. Weinhold, *NBO Version 3.1*; b) A. E. Reed, L. A. Curtiss, F. Weinhold, *Chem. Rev.* **1988**, *88*, 899 – 926.

[18] a) R. Huisgen, I. Ugi, *Chem. Ber.* **1957**, *90*, 2914 – 2927; b) I. Ugi, H. Perlinger, L. Behringer, *Chem. Ber.* **1958**, *91*, 2324 – 2330; c) I. Ugi, R. Huisgen, *Chem. Ber.* **1958**, *91*, 531 – 537; J. D. Wallis, J. D. Dunitz, *J. Chem. Soc. Chem. Commun.* **1983**, 910.

[19] a) M. Baudler, D. Düster, D. Z. Ouzounis, *Z. Anorg. Allg. Chem.* **1987**, *544*, 87 – 94; b) O. J. Scherer, T. Brück, *Angew. Chem.* **1987**, *99*, 59; *Angew. Chem. Int. Ed. Engl.* **1987**, *26*, 59; c) M. Baudler, D. Z. Ouzounis, *Naturforsch. B* **1989**, *44*, 381 – 382; d) M. Baudler, *Angew. Chem.* **1987**, *99*, 429 – 451; *Angew. Chem. Int. Ed. Engl.* **1987**, *26*, 419 – 441.

[20] G. David, E. Niecke, M. Nieger, V. van der Goenna, W. W. Schöller, *Chem. Ber.* **1993**, *126*, 1513 – 1517.

[21] a) A. Hahma, E. Holmberg, N. Hore, R. Tryman, S. Wallin, H. Östmark, *33rd International Annual Conference of ICT*, Karlsruhe, Germany, **2002**, 62/1; b) A. Vij, J. G. Pavlovich, W. W. Wilson, V. Vij, K. O. Christe, *Angew. Chem.* **2002**, *114*, 3177 – 3180; *Angew. Chem. Int. Ed.* **2002**, *41*, 3051 – 3054; c) H. Östmark, S. Wallin, T. Brinck, P. Carlqvist, R. Claidge, E. Hedlun, L. Yudina, *Chem. Phys. Lett.* **2003**, *379*, 539 – 546; d) C. John, L. A. Burke, *Chem. Commun.* **2003**, *8*, 1016 – 1017; e) L. Belau, Y. Haas, S. Zilberg, *J. Phys. Chem. A* **2004**, *108*, 11715 – 11720; f) P. Carlqvist, H. Östmark, T. Brinck, *J. Org. Chem.* **2004**, *69*, 3222 – 3225.

[22] a) A. Schmidpeter, K. Karaghiosoff, *Heterophospholes in Multiple Bonding and Low Corrdination in Phosphorus Chemistry* (Eds.: M. Regitz, O. J. Scherer), Thieme, Stuttgart, **1990**, pp. 258 – 286; b) J. D. Woolins, *Non-Metal Rings, Cages, and Clusters*, Wiley, Chichester, **1988**.

[23] E. Rivard, A. Lough, T. Chivers, I. Manners, *Inorg. Chem.* **2004**, *43*, 802 – 811.

 © 2005 Wiley-VCH Verlag GmbH & Co. KGaA, Weinheim

Cyclizations

DOI: 10.1002/anie.200502006

Intramolecular Hydroamination of Functionalized Alkenes and Alkynes with a Homogenous Zinc Catalyst**

Agustino Zulys, Maximilian Dochnahl, Dirk Hollmann, Karolin Löhnwitz, Jost-Steffen Herrmann, Peter W. Roesky, and Siegfried Blechert**

Dedicated to Professor Dr. Herbert W. Roesky on the occasion of his 70th birthday

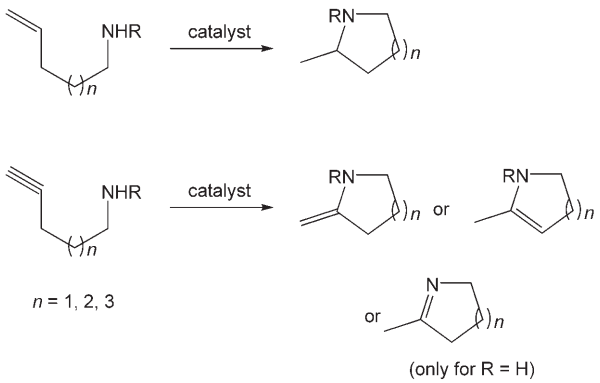

Scheme 1. Intramolecular hydroamination of alkenes and alkynes.

The catalytic addition of an organic amine N–H bond to alkenes or alkynes (hydroamination) to give nitrogen-containing molecules is of great interest to both academic and industrial researchers.[1] At present, most amines are made in multistep syntheses, and as such hydroamination offers an attractive alternative to give nitrogen-containing molecules that are important for fine chemicals, pharmaceuticals, and as useful chiral building blocks. Hydroamination can be catalyzed by d- and f-block transition metals, alkali metals,[2] as well as by calcium compounds, as shown very recently.[3] Early transition metals (Group 4[1d] and especially the lanthanides[1b]) are highly efficient catalysts for the hydroamination reaction of various C–C multiple bonds (Scheme 1), but the high sensitivity of these catalysts towards moisture and air limits their application. Furthermore, they show a very limited tolerance to polar functional groups. On the other hand, late-transition-metal catalysts offer the advantage of greater polar-functional-group compatibility; however, most of these catalysts are based on relatively expensive platinum[4] or on nickel,[5] which has only limited use in the synthesis of pharmaceuticals. Moreover, most of the late-transition-metal catalysts show limited scope, modest selectivity, and sluggish rates in their reactions with non-activated substrates. The scope of catalytic hydroamination was reviewed recently.[1]

Herein we report a new zinc-based catalyst, [*N*-isopropyl-2-(isopropylamino)troponiminato]methylzinc [{(iPr)$_2$ATI}-ZnMe] (**I**), for the hydroamination of non-activated double and triple bonds. Catalyst **I** is compatible with various polar functional groups such as ethers, amides and hydroxylamines. Furthermore, the complex is relatively robust in air and shows excellent catalytic activity. To the best of our knowledge, the only previously investigated molecular zinc compound used in catalytic hydroamination is zinc triflate, which in the presence of amines is only sparingly soluble in toluene.[6,7] Moreover, the intermolecular hydroamination of activated acetylenes by zinc-exchanged montmorillonite clay was reported recently.[8] Compared to other late-transition-metal catalysts, zinc compounds are relatively cheap and nontoxic. Furthermore Zn^{II} is stable against deactivation as it cannot be reduced to the metal under the reaction conditions.[6b]

Compound **I**, which is easily available from {(iPr)$_2$ATI}H and $ZnMe_2$ (Scheme 2), was reported previously by us as an intermediate in the synthesis of aminotroponiminate zinc

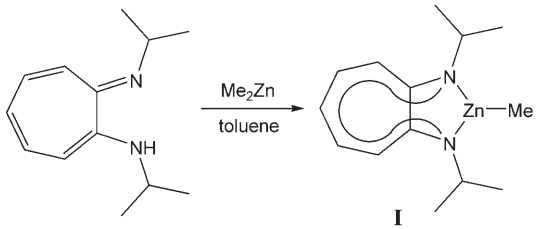

Scheme 2. Synthesis of [{(iPr)$_2$ATI}ZnMe] (**I**).

alkoxides.[9] Besides the catalytic properties, we now report the solid-state structure of **I**, which was established by single-crystal X-ray diffraction.[10] Compound **I** is a monomer in the solid state, and therefore the zinc atom has a trigonal-planar coordination sphere (Figure 1). The bond lengths and angles around the zinc center are in the expected range. In contrast to early-transition-metal–alkyl complexes, compound **I** is relatively robust towards moisture and air and thus no special experimental techniques are required for its use. This

[*] M.Sc. A. Zulys, Dipl.-Chem. K. Löhnwitz, Dipl.-Chem. J.-S. Herrmann, Prof. Dr. P. W. Roesky
Institut für Chemie und Biochemie
Freie Universität Berlin
Fabeckstrasse 34–36, 14195 Berlin (Germany)
Fax: (+49) 30-8385-2440
E-mail: roesky@chemie.fu-berlin.de
Dipl.-Chem. M. Dochnahl, Dipl.-Chem. D. Hollmann, Prof. Dr. S. Blechert
Institut für Chemie
Technische Universität Berlin
Strasse des 17. Juni 135, 10623 Berlin (Germany)
Fax: (+49) 30-3142-3619
E-mail: blechert@chem.tu-berlin.de

[**] This work was supported by the Deutsche Forschungsgemeinschaft (Graduiertenkolleg: "Synthetische, mechanistische und reaktionstechnische Aspekte von Metallkatalysatoren"). M.D. thanks the Fonds der Chemischen Industrie for a fellowship (K174/11).

Supporting information for this article is available on the WWW under http://www.angewandte.org or from the author.

InterScience
© 2005 Wiley-VCH Verlag GmbH & Co. KGaA, Weinheim

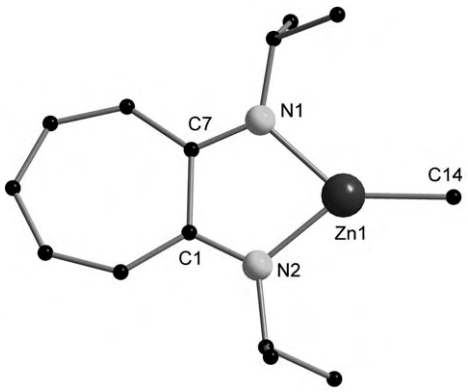

Figure 1. Solid-state structure of **I**. Hydrogen atoms have been omitted. Selected distances [pm] and angles [°]: Zn1–C14 194.1(5), Zn1–N1 198.0(4), Zn1–N2 195.5(4); C14-Zn1-N1 138.5(2), C14-Zn1-N2 139.6(2), N1-Zn1-N2 81.94(14).

behavior is very different to that of the starting material $ZnMe_2$, which is pyrophoric (see Supporting Information). The stability of compounds of the general formula [LZnMe] (L = ligand) has been described before.[11]

The goal of the current study was to explore the scope, selectivity, and functional-group tolerance of the intramolecular hydroamination reaction catalyzed by **I**. For this reason, several substrates bearing different functional groups and leading to different ring sizes were synthesized. The results are given in Table 1 and demonstrate that **I** exhibited good activity in this reaction. The best conditions were found to be when the reaction was carried out in benzene as the solvent at a temperature of 120 °C; under these conditions, total conversion occurred within reasonable reaction times in most cases. In the majority of cases it was possible to lower the catalyst loading from 10 to 1 mol %, and it was also found that the reaction rate could be accelerated by the addition of an equimolar amount (based on **I**) of $[PhNMe_2H][B(C_6F_5)_4]$ as a cocatalyst.

Interestingly, cyclization of propargyl ethers that bear a secondary amine moiety opened a new route to the corresponding 1,4-oxazines, as the double bond migrates to give the thermodynamically more stable vinyl ether. [12] A comparison of the reaction times of the α-branched amino ether **2a** and the corresponding primary amine **3a** demonstrates the greater propensity of secondary amines to react: even though the catalyst loading for substrate **3a** was 20 times higher, the reaction time was nearly double that for substrate **2a**. On the other hand, bulkier substituents, such as an isopropyl group α to the amine moiety, caused a significant decrease in the reaction rate. Nevertheless, valine derivative **4a** could be completely converted into the oxazine **4b** by the addition of 10 mol % of the catalyst/activator system.

To our surprise, the incorporation of large substituents in the β position had no beneficial effect on the cyclization. Therefore, amino benzyl ether **5a** was cyclized within the same time as substrate **3a**. Cyclic secondary amines, such as proline derivative **6a**, exhibited very high reactivity under these reaction conditions (Table 1, entry 6). Substituted amides underwent cyclization to the corresponding lactams (Table 1, entries 7 and 8). Depending on the reaction conditions, two different products were observed. When the reaction was performed in the absence of the cocatalyst, the cyclized product **7b** with an exocyclic double bond was detected. On the other hand, a 6:1 mixture of the isomerized dihydropyridone **8b** and δ-valerolactam **7b** was observed when an equal amount of the cocatalyst was added.

We were also able to cyclize methionine derivative **9a** to the dihydropyrazinone **9b**. This substrate is of particular interest as it contains both an amide functionality and a thioether group. To the best of our knowledge, this constitutes the first hydroamination of a compound bearing a thioether moiety, which is most likely incompatible with most well-known catalysts for hydroamination. The cyclization of phenylalanine propargylamide (**10a**) revealed an influence of the catalyst concentration on the structure of the product (Table 1, entries 10 and 11): When 10 mol % of the catalyst was used complete conversion into the resulting dihydropyrazinone **11b** was observed. In contrast, when only 5 mol % of the catalyst was added, only the methylene piperazinone **10b** was formed. Moreover we were able to apply our catalytic system to alkynes that bear an hydroxylamine functionality to afford cyclic nitrones (Entry 12).[13] Carbonic acid hydrazide **13a** was also cyclized to the resulting *N*-aminopiperidinone **13b**. Interestingly, the more-electron-poor nitrogen atom added preferentially to the triple bond, thus indicating that ring size has a larger influence than electronic effects on the outcome of the reaction. We were pleased to find that our system catalyzes the formation of seven-membered rings (Table 1, entry 14). It can be concluded that the rate of cyclization for aminoalkynes follows the order five-membered > six-membered ≫ seven-membered ring, consistent with classical, stereoelectronically controlled, cyclization processes.[1b]

With these results in hands, we also investigated the intramolecular hydroamination of non-activated alkenes (Table 2). However, it is well known that the hydroamination of alkenes is significantly slower than that of alkynes.[1g,3,4] Substrates that bear bulky geminal substituents β to the amino group (Thorpe–Ingold effect)[14] could be cyclized with reasonable catalyst/activator loadings of 5 mol % with moderate reaction times (Table 2, entries 1–3). Substrate **16a** was the most reactive and gave the corresponding pyrrolidine within 5 h. Compound **18a**, which is known to be a difficult substrate for this reaction, was converted into 2,5-dimethylpyrrolidine (**18b**) in modest yield.

In conclusion, compound **I** has proved to be an efficient catalyst for homogenous intramolecular hydroamination reactions and has a number of practical advantages, such as particularly high functional-group tolerance, good activity in the catalytic conversion of non-activated C–C multiple bonds, and a relatively high stability towards moisture and air. The reaction conditions allowed the manipulation of a multitude of polar functional groups, including ethers, thioethers, and amides. It is also notable that seven-membered heterocycles can be accessed. These advantages lead us to hope that **I**, which is an easily accessible reagent, will find further application as a hydroamination catalyst.

 © 2005 Wiley-VCH Verlag GmbH & Co. KGaA, Weinheim

Table 1: Intramolecular hydroamination of functionalized alkynes.[a]

Entry	Substrate		Product		cat. **I** [mol%]	Activ.[b] [mol%]	*t* [h]	Conv. [%][c]
1	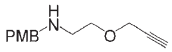	**1a**		**1b**	1 1	– 1	144 39	>99[d] >99[d]
2	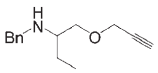	**2a**	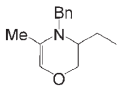	**2b**	1 0.1 1	– 0.1 1	72 8 45	>99 >99, (91)[e] >99[d]
3	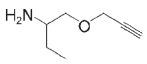	**3a**	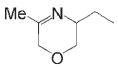	**3b**	10 2	– 2	144 14	>99 >99, (70)[e]
4	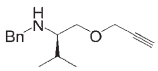	**4a**	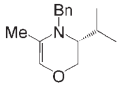	**4b**	1 10 1	– 10 1	96 1.5 144	19 >99 94
5	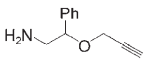	**5a**	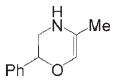	**5b**	10 2	– 2	6 14	>99 >99
6	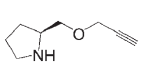	**6a**		**6b**	1 0.1	– 0.1	4 8	95 >99
7	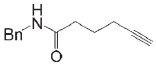	**7a**		**7b**	10	–	60	25
8	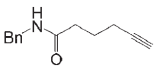	**7a**	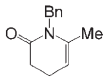	**8b**	10	10	60	>99[f]
9	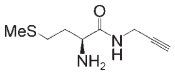	**9a**	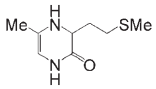	**9b**	10	–	15	92
10	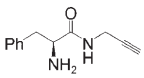	**10a**	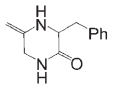	**10b**	5	–	72	51
11	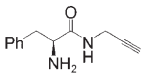	**10a**	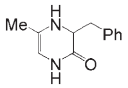	**11b**	10	–	15	>99
12	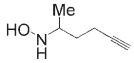	**12a**	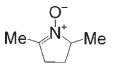	**12b**	1 0.5	– 0.5	5 4	98[d] >99[d]
13	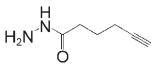	**13a**		**13b**	10	–	14	>99
14	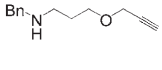	**14a**		**14b**	5	–	312	>99

[a] Reaction conditions: amine (430 μmol), catalyst **I**, benzene (0.5 mL), 120°C. [b] Activator: $[PhNMe_2H][B(C_6F_5)_4]$. [c] Determined by ^1H NMR spectroscopy. [d] The reaction was carried out at 60°C. [e] Yield of isolated product; the reaction was performed on a 2-mmol scale. [f] **8b**/**7b** = 6:1.

© 2005 Wiley-VCH Verlag GmbH & Co. KGaA, Weinheim

Table 2: Intramolecular hydroamination of alkenes.[a]

Entry	Substrate		Product		cat. **I** [mol%]	Activ.[b] [mol%]	*t* [h]	Conv. [%][c]
1	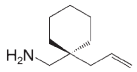	**15a**	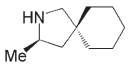	**15b**	10	–	30	87[d]
					5	–	28	>99
					5	5	8	80
2	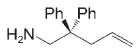	**16a**	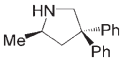	**16b**	10	–	12	>99
					10	–	24	69[d]
					5	5	5	>99
3	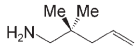	**17a**	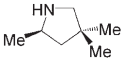	**17b**	13.3	–	72	>99
					5	5	52	46
4	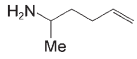	**18a**	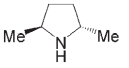	**18b**	10	10	36	19

[a] Reaction conditions: amine (430 μmol), catalyst **I**, benzene (0.5 mL), 120°C. [b] Activator: $[PhNMe_2H][B(C_6F_5)_4]$. [c] Determined by ^1H NMR spectroscopy. [d] Yield of isolated product; the reaction was carried out at 100°C in toluene.

Experimental Section

I: A solution of $ZnMe_2$ (2.0 M in toluene; 0.64 mL, 1.28 mmol, 1.05 equiv) was diluted in toluene (25 mL) and cooled to −78°C. A solution of {(*i*Pr)$_2$ATI}H (250 mg, 1.22 mmol) in toluene (25 mL) was added. The reaction mixture was slowly warmed up to room temperature, and gas was evolved for about 3 h. The solution was then filtered off, the solvent was evaporated under reduced pressure. The resulting yellow solid was washed with *n*-pentane (3 × 10 mL) and dried under vacuum. Yield: 287 mg (83%). ^1H NMR (C_6D_6, 400 MHz, 25°C): $\delta = 0.00$ (s, 3H; $ZnCH_3$), 1.14 (d, $J = 6.1$ Hz, 12H; $NCH(CH_3)_2$), 3.76 (sept, $J = 6.2$ Hz, 2H; $NCH(CH_3)_2$), 6.35 (d, $J =$ 9.4 Hz, 1H; H_{Ar}), 6.57 (d, $J = 10.2$ Hz, 2H; H_{Ar}), 6.95 ppm (dd, $J =$ 9.4 Hz, 10.2 Hz, 2H; H_{Ar}); $^{13}C\{^1H\}$ NMR (C_6D_6, 100.4 MHz, 25°C): $\delta = -9.9$ ($ZnCH_3$), 24.5 ($NCH(CH_3)_2$), 48.3 ($NCH(CH_3)_2$), 111.6 (C_{Ar}), 117.7 (C_{Ar}), 134.5 (C_{Ar}), 160.2 ppm (C_{Ar}); MS (EI): *m*/*z* (%): 282 (33) $[M]^+$, 267 (51) $[M-CH_3]^+$, 204 (24) $[M-ZnCH_3]^+$.

NMR-tube-scale intramolecular hydroamination: All NMR-tube-scale reactions were prepared in an N_2-filled glovebox. The aminoalkynes (430 μmol) were dissolved in [D_6]benzene (0.5 mL) and then added to the catalyst (e.g. 4.30 μmol for 1 mol%). The mixture was injected into an NMR tube, which was removed from the glovebox and flame-sealed under vacuum. The reaction mixture was then heated to the appropriate temperature for the stated duration of time. All products were analyzed by ^1H, ^{13}C, ^{13}C DEPT, COSY, and HMQC NMR spectroscopy and by IR, MS, and HRMS when possible. The ratio between the reactant and the product was calculated by comparison of the integrations of the corresponding signals in the ^1H NMR spectra. The concentration of the catalyst was controlled by comparing the integration of a well-resolved signal for the heterocyclic product with that for a signal for a catalyst ligand.

Received: June 10, 2005
Revised: August 17, 2005
Published online: November 4, 2005

Keywords: cyclization · heterocycles · homogenous catalysis · hydroamination · zinc

[1] For leading reviews, see: a) K. C. Hultzsch, *Adv. Synth. Catal.* **2005**, *347*, 367–391; b) S. Hong, T. J. Marks, *Acc. Chem. Res.* **2004**, *37*, 673–686; c) I. Bytschkov, S. Doye, *Eur. J. Org. Chem.* **2003**, 935–946; d) F. Pohlki, S. Doye, *Chem. Soc. Rev.* **2003**, *32*, 104–114; e) T. E. Müller in J. T. Horváth, *Encyclopedia of Catalysis*, Wiley, New York, **2002**; f) J. Seayad, A. Tillack, C. G. Hartung, M. Beller, *Adv. Synth. Catal.* **2002**, *344*, 795–813; g) J.-J. Brunet, D. Neibecker in *Catalytic Heterofunctionalization* (Eds.: A. Togni, H. Grützmacher), VCH, Weinheim, **2001**, pp. 91–141; h) M. Nobis, B. Drießen-Hölscher, *Angew. Chem.* **2001**, *113*, 4105–4108; *Angew. Chem. Int. Ed.* **2001**, *40*, 3983–3985; i) M. Johannsen, K. A. Jørgensen, *Chem. Rev.* **1998**, *98*, 1689–1708; j) T. E. Müller, M. Beller, *Chem. Rev.* **1998**, *98*, 675–704; k) D. M. Roundhill, *Chem. Rev.* **1992**, *92*, 1–27.

[2] A. Ates, C. Quinet, *Eur. J. Org. Chem.* **2003**, *9*, 1623–1626.

[3] M. R. Crimmin, I. J. Casely, M. S. Hill, *J. Am. Chem. Soc.* **2005**, *127*, 2042–2043.

[4] Rh: a) M. Utsunomiya, R. Kuwano, M. Kawatsura, J. F. Hartwig, *J. Am. Chem. Soc.* **2003**, *125*, 5608–5609; Ir: b) R. Dorta, P. Egli, F. Zürcher, A. Togni, *J. Am. Chem. Soc.* **1997**, *119*, 10857–10858; Pd: c) M. Utsunomiya, J. F. Hartwig, *J. Am. Chem. Soc.* **2003**, *125*, 14286–14287; K. Li, K. K. Hii, *Chem. Commun.* **2003**, *10*, 1132–1133; Pt: d) J.-J. Brunet, N. C. Chu, O. Diallo, *Organometallics* **2005**, *24*, 3104–3110; e) C. F. Bender, R. A. Widenhoefer, *J. Am. Chem. Soc.* **2005**, *127*, 1070–1071.

[5] L. Fadini, A. Togni, *Chem. Commun.* **2003**, *1*, 30–31.

[6] a) J. Bodis, T. E. Müller, J. A. Lercher, *Green Chem.* **2003**, *5*, 227–231; b) V. Neff, T. E. Müller, J. A. Lercher, *Chem. Commun.* **2002**, *8*, 906–907; c) T. E. Müller, A.-K. Pleier, *J. Chem. Soc. Dalton Trans.* **1999**, *4*, 583–588.

[7] T. E. Müller, M. Grosche, E. Herdtweck, A.-K. Pleier, E. Walter, Y.-K. Yan, *Organometallics* **2000**, *19*, 170–183.

[8] G. V. Shanbang, S. B. Halligudi, *J. Mol. Catal. A* **2004**, *222*, 223–228.

[9] J.-S. Herrmann, G. A. Luinstra, P. W. Roesky, *J. Organomet. Chem.* **2004**, *689*, 2720–2725.

[10] Single-crystal X-ray diffraction data for **1**: $C_{14}H_{22}N_2Zn$ ($M_r =$ 283.71): Bruker Smart 1000 CCD, space group $P2_1/c$ (No. 14); $a = 1579(3)$, $b = 906(2)$, $c = 2176(4)$ pm, $\beta = 109.40(4)°$; $T =$ 173 K, $Z = 8$, $V = 2935(10) \times 10^6$ pm^3, $\rho = 1.284$ g cm^{-3}, $2\theta_{max} =$ 55°, 16208 reflections collected, 6333 unique reflections ($R_{int} =$ 0.0593). The structure was solved by Patterson methods (SHELXS-97 and SHELXL-97)[15] and refined by full-matrix least-square techniques with $I > 2\sigma(I)$ to $R1 = 0.0412$ and w$R2 =$ 0.1097. CCDC-274802 contains the supplementary crystallographic data for this paper. These data can be obtained free of charge from The Cambridge Crystallographic Data Centre via www.ccdc.cam.ac.uk/data_request/cif.

[11] M. P. Coles, P. B. Hitchcock, *Eur. J. Inorg. Chem.* **2004**, *13*, 2662–2672.

[12] Recently a copper mediated approach to 3,4-dihydro-2*H*-benzoxazines was published. However the products were obtained in moderate yields only: Y.-G. Zhou, P.-Y. Yang, X.-W. Han, *J. Org. Chem.* **2005**, *70*, 1679–1683.

[13] Activated olefins: A. Padwa, G. S. K. Wong, *J. Org. Chem.* **1986**, *51*, 3125–3133; non-activated olefins: E. C. Davison, I. T. Forbes, A. B. Holmes, J. A. Warner, *Tetrahedron* **1996**, *52*, 11601–11624.

[14] a) R. M. Beesley, C. K. Ingold, J. F. Thorpe, *J. Chem. Soc.* **1915**, *107*, 1080–1106; b) C. K. Ingold, *J. Chem. Soc.* **1921**, *119*, 305–

 © 2005 Wiley-VCH Verlag GmbH & Co. KGaA, Weinheim

329; c) A. J. Kirby, *Adv. Phys. Org. Chem.* **1980**, *17*, 183–278; d) M. E. Jung, J. Gervay, *J. Am. Chem. Soc.* **1991**, *113*, 224–232.
[15] a) G. M. Sheldrick, SHELXS-97, Program for Crystal Structure Solution, University of Göttingen, Germany, **1997**; b) G. M. Sheldrick, SHELXL-97, Program for Crystal Structure Refinement, University of Göttingen, Germany, **1997**.

 © 2005 Wiley-VCH Verlag GmbH & Co. KGaA, Weinheim

Coordination Modes

DOI: 10.1002/anie.200502489

Can Acetylenedithiolate Act as a Tetradentate Bridging Ligand?**

Wolfram W. Seidel, Markus Schaffrath, and Tania Pape*

Acetylenedithiolate is a small, intriguing bridging ligand. The four-atom dianion is potentially tetradentate and ambidentate at the same time, but its coordination chemistry has yet not been investigated. This gap is astonishing since η^2 binding at the triple bond and coordination of metal ions at the sulfur donors would allow the straightforward linkage of Werner-type complex ions with organometallic moieties. Separately, both binding options have already been demonstrated with alkynethiolates[1] and acetylenedisulfides.[2] However, the combination of the two binding modes in a bimetallic complex with acetylenedithiolate raises the question of whether the bend-back of the sulfur substituents upon coordination of the triple bond would be flexible enough to allow for chelate coordination of both thiolate donors at a second metal ion. Herein we report μ-η^2-*C*,*C*′-η^2-*S*,*S*′-binding of acetylenedithiolate.

Our approach to the controlled introduction of acetylenedithiolate in metal complexes comprises the synthesis of stable alkyne complexes with bis(benzylthio)acetylene and subsequent reductive removal of the benzyl groups in the complex. Recently we reported on the cleavage of one benzyl group from the cationic complex $[Tp'W(CO)_2\{\eta^2\text{-}(BnS)CC(SBn)\}]^+$ (Tp′ = hydrotris(3,5-dimethylpyrazolyl)borate, Bn = benzyl) leading to the neutral thioalkyne complex $[Tp'W(CO)_2\{\eta^2\text{-}(BnS)CC(S)\}]$ (**1**).[3] We found now that the second benzyl group can be cleaved similarly by the one-electron reduction of **1** with retention of the complex topology (Scheme 1). Reaction of **1** with one equivalent of C_8K in THF at −78 °C resulted in an intensively purple solution. Upon warming to ambient temperature the solution turned brown, and $K[Tp'W(CO)_2\{\eta^2\text{-}(S)CC(S)]$ (K-**2**) was isolated by precipitation.

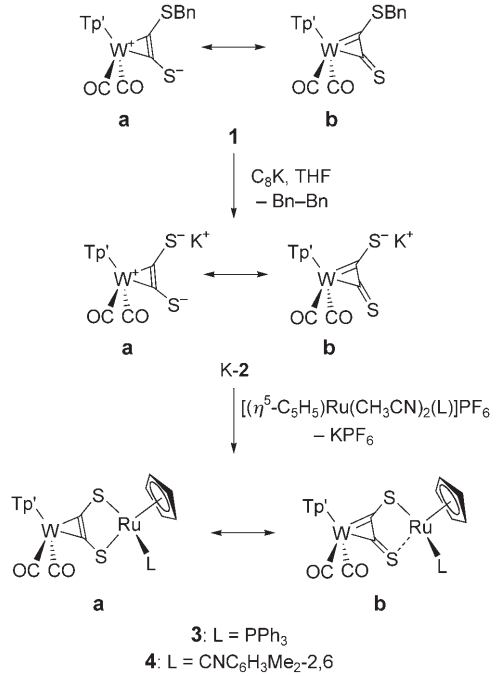

Scheme 1. Synthesis of K-**2**, **3**, and **4**.

The identity of K-**2** was proven by IR, ESI-MS, and particularly ^{13}C NMR spectroscopy. The CO valence frequencies of K-**2** are shifted to lower energy with respect to **1** by 34 and 25 cm^{-1}, respectively. The C_s symmetry of K-**2** is reflected in the ^{13}C NMR spectrum, in which two alkyne resonances are observed only at −60 °C because of rotation of the alkyne ligand at the metal center.[4] However, the large shift difference (291 vs. 252 ppm) and the very low-field shift of one of the alkyne resonances with respect to reference values of tungsten(II) four-electron-donor alkyne complexes (cf. 180–240 ppm[4]) point to the contribution of resonance structure K-**2b** displaying a thioketo function.

To address the essential question whether $\mathbf{2}^-$ acts primarily as a mono- or a bidentate sulfur ligand, we reacted K-**2** with both $[(\eta^5\text{-}C_5H_5)RuCl(PPh_3)_2]$ and $[(\eta^5\text{-}C_5H_5)Ru(PPh_3)(CH_3CN)_2]PF_6$. Surprisingly both reactions yielded the same blue, neutral product **3**, which is characterized by a singlet at 55 ppm in the ^{31}P NMR spectrum and by slightly increased CO stretching frequencies compared to those of K-**2**. The structure determination of **3** disclosed that both sulfur donors of an individual acetylenedithiolate in $[\{Tp'W(CO)_2\}(C_2S_2)\{(\eta^5\text{-}C_5H_5)Ru(PPh_3)\}]$ (**3**) are coordinated to ruthenium in a chelate-like fashion, while the alkyne unit is stabilized by η^2 coordination with the tungsten center (Figure 1).[5]

[*] Dr. W. W. Seidel, Dipl.-Chem. M. Schaffrath, T. Pape
Institut für Anorganische und Analytische Chemie
Westfälische Wilhelms-Universität Münster
Corrensstrasse 36, 48149 Münster (Germany)
Fax: (+49) 251-833-3108
E-mail: seidelww@uni-muenster.de

[**] This research was supported by the Deutsche Forschungsgemeinschaft. W.W.S. thanks Prof. F. E. Hahn for generous support, Dr. K. Bergander for the variable-temperature NMR measurements, and Dr. E. Bill (MPI Mülheim) for the EPR measurement.

Supporting information for this article is available on the WWW under http://www.angewandte.org or from the author.

InterScience
© 2005 Wiley-VCH Verlag GmbH & Co. KGaA, Weinheim

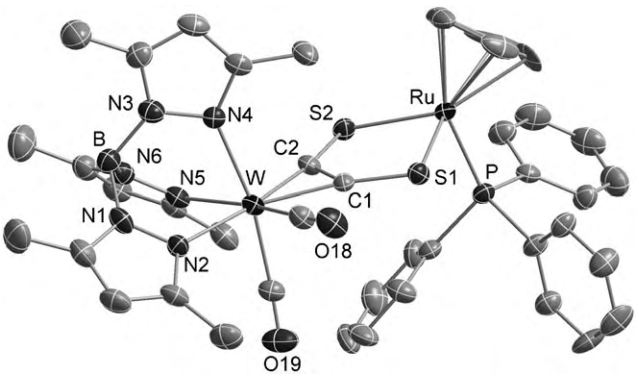

Figure 1. Solid-state structure of **3**. Selected bond lengths [Å] and angles [°]: W–C1 2.066(7), W–C2 2.049(6), C1–C2 1.391(9), C1–S1 1.665(7), C2–S2 1.677(7), Ru–S1 2.396(2), Ru–S2 2.369(2); C1-C2-S2 119.5(5), C2-C1-S1 127.5(5), S1-Ru-S2 85.5(1), Ru-S1-C1 101.3(2), Ru-S2-C2 105.2(2).

The C1–C2 alkyne bond determined to 1.391(9) Å is markedly elongated. The bond angles C1-C2-S2 and C2-C1-S1 amount to 119.5° and 127.5°, respectively, and hence they are close to the ideal value of 120° for sp^2 carbon atoms. This remarkable bend of the sulfur substituents on the coordinated alkyne is a consequence of a strong chelate effect, because the bond angles found in complexes of alkynes with free substituents are distinctively larger. Thus the corresponding C-C-S angles in **1** amount to 144.9° and 132.5°, respectively.[3] The planarity of the five-membered chelate ring is reflected in the angle sum of 539° with an acute S1-Ru-S2 angle (85.5°). The strong tendency to form the Ru-S-C-C-S chelate ring is supported by the fact that even the phosphine is substituted in $[(\eta^5\text{-}C_5H_5)Ru(PPh_3)_2Cl]$. The W–C1/W–C2 and the C1–S1/C2–S2 distances are equal within the margin of error, which is reflected in resonance structure **3a**. However, the strikingly larger C2-C1-S1 angle (compared with C1-C2-S2), which is in accordance with the longer Ru–S1 bond (2.396(2) Å) (compared to Ru–S2, 2.369(2) Å), indicates the contribution of resonance structure **3b**.

The observation of two ^{13}C NMR resonances for the CO ligands and for the alkyne carbon atoms in solution at −60 °C can be explained by the alignment of one CO ligand with the C1–C2 vector as found in the solid state. However, variable-temperature ^1H and ^{13}C NMR investigations revealed a roughly 90° oscillation process of the $\{Tp'W(CO)_2\}$ unit at the alkyne, rendering the CO ligands and the alkyne carbon atoms indistinguishable. The activation barrier was determined to be $\Delta G^*_{298} = 48.8\ kJ\,mol^{-1}$ by line-shape analysis. The similarity of the spectroscopic data of K-**2** and **3** provide evidence that the chelation of both sulfur donors to ruthenium and the resulting angle distortion at the alkyne does little to interfere with the η^2-*C*,*C*′ binding of the alkyne at the tungsten center.

The structure of the five-membered chelate ring in **3** is reminiscent of dithiolene complexes, where the backbone is stabilized by carbon-based substituents instead of a π-bound metal complex moiety. Stability in more than one oxidation state is a typical feature of dithiolene complexes.[6] Indeed, voltammetric studies with **3** show a reversible redox process at −250 mV versus Fc/Fc^+. The stoichiometric oxidation of **3** with $[(\eta^5\text{-}C_5H_5)_2Fe]PF_6$ yielding the corresponding complex **3**-PF_6 causes a distinct increase of the stretching frequencies of the tungsten-bound CO ligands ($\Delta\tilde{\nu} = 55$ and $59\ cm^{-1}$). However, the EPR spectrum of **3**-PF_6 in a frozen CH_2Cl_2/THF solution (Figure 2) displays a strong hyperfine coupling to phosphorus (43 to 70 G). This observation points to a SOMO, which is predominantly localized at ruthenium.[7]

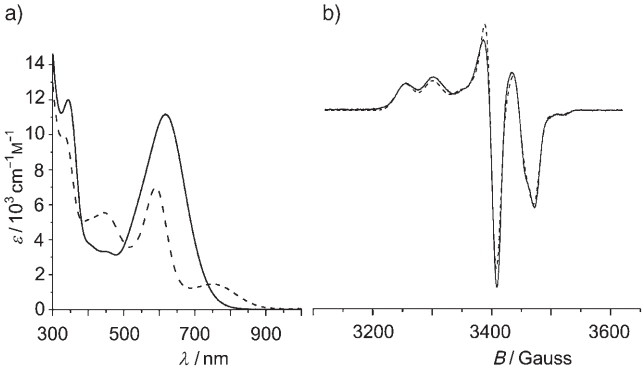

Figure 2. a) UV/Vis spectra of **3** (——) and **3**-PF_6 (-----) in CH_2Cl_2; b) X-band EPR spectrum of **3**-PF_6 in a frozen CH_2Cl_2/THF solution (experimental ——, calculated -----).

In order to compare the effect of the oxidation on both metal atoms the ruthenium center was furnished with an IR probe. For this purpose complex **4** was synthesized, in which the phosphine in **3** is replaced by 2,6-dimethylphenylisocyanide. Remarkably, the oxidation of **4** to $\mathbf{4}^+$ not only leads to a frequency increase for the tungsten-bound CO ligands, but also for the ruthenium-coordinated isocyanide ($\Delta\tilde{\nu} = 88\ cm^{-1}$). Accordingly, one-electron oxidation affects both metal centers to a comparable extent, which indicates a highly delocalized HOMO for **3** and **4**. The comparison of the electronic spectra of **3** and $\mathbf{3}^+$ (Figure 2) confirms the expected hypsochromic shift of the individual charge-transfer bands owing to the oxidation. The alteration of the ratio of the extinction coefficients points to changes in the electronic structure. The additional low-energy absorption at 758 nm in the UV/Vis spectrum of $\mathbf{3}^+$ can be interpreated as an intervalence transfer into the SOMO at ruthenium.[8]

The affirmative answer to the question in the title raises another challenging problem. Can acetylenedithiolate also act as a dithiolate chelate ligand without coordination at the triple bond? Alkyne complexes of acetylenedithiolate are related to complexes of ethenedithione according to **E** (Scheme 2) by a two-electron transfer. The smooth transition between the formulation of thiolates and thiones is obvious in

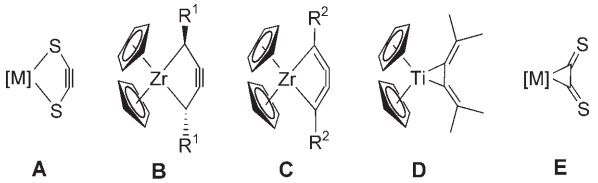

Scheme 2. Coordination modes of C_2X_2 ligands (X = S, CR_nH_{2-n}, CR).

 © 2005 Wiley-VCH Verlag GmbH & Co. KGaA, Weinheim

the complexes described herein. The rather paradoxical idea of having an acetylenedithiolate chelate ligand without coordination at the triple bond is realized in structure **A**. This type of linkage isomerism **A**/**E** has actually been established in corresponding carbon-based ligand systems by isolation of unusual zirconacyclopent-3-ynes **B**,[9] zirconacyclocumulenes **C**,[10] and the titana[3]radialene **D**.[11]

In conclusion, we present here a facile access to η^2-*C*,*C*′-acetylenedithiolate complexes and a full characterization of the first heterobimetallic complex containing acetylenedithiolate as an η^2-*C*,*C*′-η^2-*S*,*S*′-bridging ligand. Further investigations are necessary to verify the general applicability of alkyne complexes with acetylenedithiolate as dithiolate chelate ligands.

Experimental Section

K-**2**: At −78 °C C_8K (68 mg, 0.5 mmol) was added to a solution of **1** (300 mg, 0.42 mmol) in THF (10 mL) leading to an intensively purple solution. After 12 h of stirring at room temperature the now-brown solution was filtered through a pad of celite and layered with 60 mL of *n*-hexane. The brown precipitate K-**2** (42 %) formed overnight was sufficiently pure for further experiments.

3: $[(\eta^5\text{-}C_5H_5)RuCl(PPh_3)_2]$ (218 mg, 0.3 mmol) was added to a solution of K-**2** (200 mg, 0.3 mmol) in THF (30 mL). The solution turned green at ambient temperature and finally blue in the course of 12 h at reflux. Complex **3** (80 mg, 25 %) was isolated by chromatographic purification at SiO_2 using toluene as eluent. Crystallization was achieved by gas-phase diffusion of *n*-hexane into a THF solution of **3**. C,H,N analysis (%) calcd for $C_{42}H_{42}BN_6O_2PRuS_2W$: C 47.88, H 4.02, N 7.98; found: C 47.85, H 4.19, N 7.85. Complex **3** was also obtained after 12 h at room temperature using $[(\eta^5\text{-}C_5H_5)Ru(PPh_3)(CH_3CN)_2]PF_6$.

Complex **4** was obtained analogously from $[(\eta^5\text{-}C_5H_5)Ru(CNC_6H_3Me_2\text{-}2,6)(CH_3CN)_2]PF_6$ after reaction for 12 h at room temperature. C,H,N analysis (%) calcd for $C_{33}H_{36}BN_7O_2RuS_2W$ **4**: C 42.96, H 3.93, N 10.63; found: C 43.07, H 4.05, N 10.53.

3-PF_6: A solution of **3** (42 mg, 0.04 mmol) in CH_2Cl_2 (10 mL) was treated with $[(\eta^5\text{-}C_5H_5)_2Fe]PF_6$ (13 mg, 0.04 mmol). After 30 min the solvent was evaporated in vacuo, and the product was washed with Et_2O in order to remove ferrocene. Complex **3**-PF_6 was obtained as purple needles by gas-phase diffusion of Et_2O into a CH_2Cl_2 solution. Complex **4**-PF_6 was obtained analogously from **4** (37 mg, 0.04 mmol).

Spectroscopic data of K-**2**, **3**, **4**, **3**-PF_6, and **4**-PF_6 are included in the Supporting Information.

Received: July 17, 2005
Published online: November 4, 2005

Keywords: alkyne ligands · bridging ligands · coordination modes · S ligands · structure determination

[1] a) T.-Y. Lee, A. Mayr, *J. Am. Chem. Soc.* **1994**, *116*, 10300; b) A. F. Hill, J. M. Malget, A. J. P. White, D. J. Williams, *Chem. Commun.* **1996**, 721; c) W. Weigand, *Z. Naturforsch. B* **1991**, *46*, 1333; d) H. Sugiyama, Y. Hayashi, H. Kawaguchi, K. Tatsumi, *Inorg. Chem.* **1998**, *37*, 6773; e) I. Ara, E. Delgado, J. Fornies, E. Hernandes, E. Lalinde, N. Mansilla, M. T. Moreno, *J. Chem. Soc. Dalton Trans.* **1998**, 3199; f) Y. Sunada, Y. Hayashi, H. Kawaguchi, K. Tatsumi, *Inorg. Chem.* **2001**, *40*, 7072.

[2] a) J. A. Connor, G. A. Hudson, *J. Organomet. Chem.* **1978**, *160*, 159; b) D. C. Miller, R. J. Angelici, *J. Organomet. Chem.* **1990**, *394*, 235; c) D. C. Miller, R. J. Angelici, *Organometallics* **1990**, *9*, 79; d) C. Benisch, R. Gleiter, T. H. Staeb, B. Nuber, T. Oeser, H. Pritzkow, F. Rominger, *J. Organomet. Chem.* **2002**, *641*, 102.

[3] W. W. Seidel, M. D. Ibarra Arias, M. Schaffrath, K. Bergander, *Dalton Trans.* **2004**, 2053.

[4] J. L. Templeton, *Adv. Organomet. Chem.* **1989**, *29*, 1.

[5] Crystal data of **3**·2 THF: $C_{50}H_{58}BN_6O_4PRuS_2W$, $M_r = 1197.84$, monoclinic, $P2(1)/c$, $a = 10.1737(12)$, $b = 19.978(2)$, $c = 24.820(3)$ Å, $\beta = 99.557(3)°$, $V = 4974.6(10)$ Å^3, $Z = 4$, $\rho_{calcd} = 1.599$ g cm^{-3}, $T = 173(2)$ K, $2\Theta_{max} = 50°$, $\mu(Mo_{K\alpha}) = 2.78$ mm^{-1}; 39691 reflections measured, of which 8738 were unique, 7329 reflection observed ($R_{int} = 0.0622$), final *R* indices: $R1 = 0.0506$ ($I > 2\sigma(I)$), w$R2 = 0.1004$ (obsd data). CCDC-278210 contains the supplementary crystallographic data for this paper. These data can be obtained free of charge from the Cambridge Crystallographic Data Centre via www.ccdc.cam.ac.uk/data_request/cif.

[6] K. Wang, *Prog. Inorg. Chem.* **2004**, *52*, 267.

[7] M. P. Castellani, N. G. Connelly, R. D. Pike, A. L. Rieger, P. H. Rieger, *Organometallics* **1997**, *16*, 4369; see also the Supporting Information.

[8] C. Creutz, *Prog. Inorg. Chem.* **1983**, *30*, 1.

[9] a) N. Suzuki, M. Nishiura, Y. Wakatsuki, *Science* **2002**, *295*, 660; b) N. Suzuki, N. Aihara, H. Takahara, T. Watanabe, M. Iwasaki, M. Saburi, D. Hashizume, T. Chihara, *J. Am. Chem. Soc.* **2004**, *126*, 60.

[10] a) P.-M. Pellny, F. G. Kirchbauer, V. V. Burlakov, W. Baumann, A. Spannenberg, U. Rosenthal, *J. Am. Chem. Soc.* **1999**, *121*, 8313; b) U. Rosenthal, *Angew. Chem.* **2004**, *116*, 3972; *Angew. Chem. Int. Ed.* **2004**, *43*, 3882.

[11] A. Maercker, A. Groos, *Angew. Chem.* **1996**, *108*, 216; *Angew. Chem. Int. Ed. Engl.* **1996**, *35*, 210.

 © 2005 Wiley-VCH Verlag GmbH & Co. KGaA, Weinheim

Isomerizations

DOI: 10.1002/anie.200501852

Direct Conversion of Linoleic Acid over Silver Catalysts in the Presence of H_2: An Unusual Way towards Conjugated Linoleic Acids

*Markus Kreich and Peter Claus**

Dedicated to Professor Gerhard Zimmermann on the occasion of his 75th birthday

In the search for anticarcinogenic substances towards the end of the 1980s, isomers of linoleic acid were discovered in beef and dairy products and proved to be potential mutagen

[*] Dipl.-Ing. M. Kreich, Prof. Dr. P. Claus
Ernst-Berl-Institut/Technical Chemistry II
Technical University of Darmstadt
64287 Darmstadt (Germany)
Fax: (+49) 6151-16-4788
E-mail: claus@ct.chemie.tu-darmstadt.de

Supporting information for this article is available on the WWW under http://www.angewandte.org or from the author.

WILEY InterScience DISCOVER SOMETHING GREAT
© 2005 Wiley-VCH Verlag GmbH & Co. KGaA, Weinheim

inhibitors.[1,2] Owing to the conjugated double bonds present in these isomers, they were called CLAs (conjugated linoleic acids). Food that is modified by the addition of CLAs (so-called functional foods) offers specific benefits and advantages for human health.[3] Although functional food has been at the center of traditional Chinese medicine for over 2000 years, the amount of research has only increased since the physiological benefits CLAs were proved. Most of this research has been in the field of food chemistry and is particularly anchored in a framework program of the European Union.[4,5] These studies have shown that CLAs exhibit a variety of positive qualities. Besides their anticarcinogenic and antioxidative qualities, they also influence the fat and muscle content in the body and display antiarteriosclerotic qualities. The latest theories attribute these qualities to the 9-*cis*,11-*trans* and the 10-*trans*,12-*cis* isomer.[6–10] The influence of the other CLA isomers on these qualities are largely unknown.

The established and industrial approach to the production of CLA is isomerization under alkaline conditions, which converts linoleic acids and their alkyl esters with alkali bases or potassium alkoxides into CLAs.[11] Subsequent neutralization with acid—typically phosphoric acid—is necessary. The alkali bases, solvents (e.g. DMSO and propylene glycol), and phosphoric acid are disadvantageous from an ecological and economic point of view. The enzyme-catalyzed production of CLA is known from biochemistry;[12] in nature, this process occurs in the rumen of cattle by means of *Butyrivibrio fibrisolvens*.[13,14] Homogeneous catalysts such as [{RhCl-$(C_8H_{14})_2$}$_2$] and [RhCl$(PPh_3)_3$] have also been applied in the isomerization of soybean oil.[15]

Very little work has been carried out on the production of CLA under heterogeneous catalysis, in which the problem of catalyst separation is avoided. This is due to the fact that the CLA have only received attention in the last few years as a result of investigations in the pharmaceutical field. On the other hand, direct CLA production is a very complex and difficult process. It is easy to find a catalyst that hydrogenates linoleic acid directly to stearic acid. In contrast, the search for a heterogeneous catalyst that favors selective isomerization to the physiologically important 9-*cis*,11-*trans* and 10-*trans*,12-*cis*-CLAs has proved to be much more challenging (Scheme 1).

In experiments described in the literature with heterogeneous ruthenium catalysts supported on Al_2O_3 and carbon, the catalyst was first covered with hydrogen, and linoleic acid was subsequently converted into CLA under nitrogen.[16] In order to produce CLA at all, this two-step reaction is necessary owing to the catalyst properties and the subsequent reactions competing with the desired isomerization. On the one hand, the excellent hydrogenation qualities of ruthenium catalysts results in the complete and rapid conversion of linoleic acid under hydrogen to give to stearic acid via oleic acid. On the other hand, it is clear that only a small quantity of hydrogen is required for the isomerization of linoleic acid into CLAs. It is therefore a fine line between the high activity of the catalyst, but under formation of unwanted hydrogenation products (oleic acid, stearic acid), and an increased selectivity towards CLAs controlled by the surface concentration of hydrogen over the catalyst.

Although we first achieved good results with ruthenium catalysts (Ru/C, Ru/Al_2O_3) in agreement with literature reports,[16] the two-step reaction (chemisorptive preadsorption of hydrogen onto the Ru catalyst followed by deactivation and chemical reaction in the semi-batch-mode under N_2) was a constant point of criticism in our considerations. The use of typical hydrogenation metal catalysts (e.g. Ni) promised no improvement, as was already discussed amply in the literature.[16c]

We describe herein a completely new and highly selective method for the synthesis of CLAs over heterogeneous silver catalysts and in the constant presence of hydrogen. According

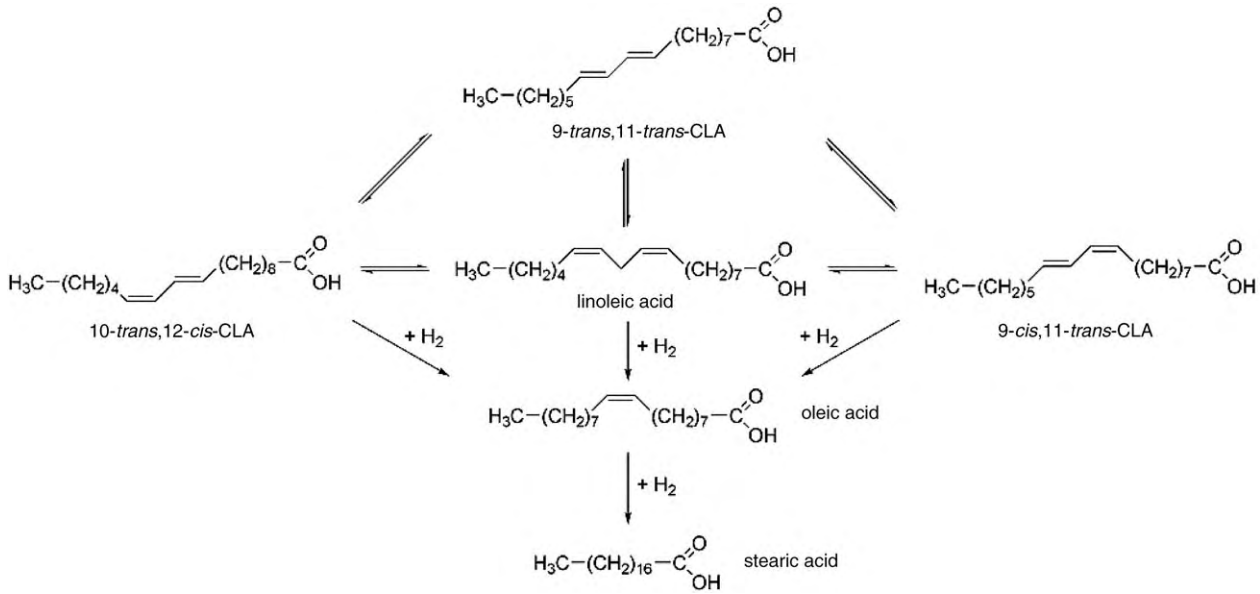

Scheme 1. Reaction network for the hydrogenation/isomerization of linoleic acid.

 © 2005 Wiley-VCH Verlag GmbH & Co. KGaA, Weinheim

to the literature, silver is the metal with the lowest hydrogen-binding energy; experimental results and DFT calculations, although for Ag single crystals, showed weakly bound hydrogen on Ag.[17,18] Moreover, our work in the field of selective hydrogenation of polyunsaturated organic substances shows a much lower C=C hydrogenation activity over silver.[19] This reactivity is the exact prerequisite of the reaction network, which calls for a suppression of the parallel and/or consecutive hydrogenations to oleic acid and stearic acid. During isomerization experiments with silver catalysts carried out in the same way as those with ruthenium catalysts (i.e. under nitrogen after preactivation of the catalyst with hydrogen), we did not observe any conversions, as expected. As the success of the reaction depends on the surface coverage by hydrogen, as mentioned above, it seemed reasonable in the case of a metal such as silver to change the reaction procedure and to convert linoleic acid in the semi-batch-mode under hydrogen. At first, the catalyst was preactivated with hydrogen as in the case of the Ru catalysts.

We achieved surprisingly good results with respect to the direct synthesis of CLA (Table 1). Despite the simple reaction procedure under hydrogen, linoleic acid underwent 90% conversion on average after 90 min over Ag/SiO_2 using different grain fractions. The selectivity towards CLAs reached values between 60 and 67%. This shows at the same time that the particle size does not exhibit a noticeable influence on the catalytic properties. Therefore, there is no evidence of mass transport limitation in the examined area of ≤ 500 μm. The formation of the 9-*trans*,11-*trans* isomer was preferred at high conversions. The linoleic acid conversion increased with the reaction temperature, thus the physiologically important 9-*cis*,11-*trans*- and 10-*trans*,12-*cis* isomers were always the main components of the products. Furthermore, it was observed that the selectivity towards the hydrogenation products oleic acid and stearic acid decreased with decreasing substrate/catalyst mass ratio. Consequently, a desirable practical result is the increase in isomerization/hydrogenation ratio. From the selectivity–conversion data, CLA yields of up to 60% can be calculated, depending on the reaction conditions applied. Furthermore, the conversion of linoleic acid was carried out without previous contact of the Ag catalyst with hydrogen; this occurred primarily at the beginning of the reaction by switching from nitrogen to H_2. These experiments delivered the same degrees of conversion and selectivity as those with preactivation.

To understand the different effects of hydrogen on the Ru catalyst (hydrogenation to stearic and oleic acid) and the Ag catalyst (isomerization to 9-*cis*,11-*trans*- and 10-*trans*,12-*cis*-CLA), calorimetric experiments of H_2 adsorption were carried out with these catalysts. As seen in Figure 1a, at first an irreversible hydrogen adsorption occurs at the ruthenium catalyst. A reversible adsorption can be recognized only beyond the appearance of a saturation point (after the sixth pulse). The adsorption heat of the hydrogen determined from the calorimetric experiments has been estimated to about 90 kJ mol^{-1} from which a Ru–H bond strength of approximately 260 kJ mol^{-1} can be calculated.[20] On the silver catalyst (Figure 1B) only reversible hydrogen adsorption appears; an irreversible chemisorption could not be verified.[21] Therefore, we can distinguish between strongly adsorbed hydrogen on ruthenium and weakly adsorbed hydrogen in the case of the silver catalyst.[22] These findings suggest that the differences in the reactivity/selectivity patterns (hydrogenation activity on Ru versus isomerization activity on Ag) are based on differences in the hydrogen adsorption behavior of the active metal catalyst. It is clear that the weakly bound hydrogen plays a key role in the selective isomerization of conjugated double bonds (to CLA). A very similar situation is present in the case of the control of the intramolecular selectivity with respect to the hydrogenation of conjugated C=C–C=O double bonds.[19] With weakly chemisorbed hydrogen, a discrimination of the hydrogenation of the C=O- in contrast to the C=C-bond is possible; the latter is hardly hydrogenated by the weakly bonded hydrogen.[19,23] For the conversion of linoleic acid in the presence of H_2, an addition–elimination mechanism according to Horiuti–Polanyi[16g,20] is assumed, which is typical for the isomerization of C=C-double bonds in alkenes and alkadienes (Scheme 2). According to this mechanism, the selectivity of the reaction is decided by the type of reaction of the half-hydrogenated

Table 1: Catalytic properties of Ag/SiO_2 in the conversion of linoleic acid.[a]

Conditions	X_{LS} [%]	$S_{9\text{-}cis,11\text{-}trans}$ [%]	$S_{10\text{-}trans,12\text{-}cis}$ [%]	$S_{9\text{-}trans,11\text{-}trans}$ [%]	$S_{hydr.}$[e] [%]	S_{NP}[f] [%]	Σ_{CLA}[g] [%]	CLA/Hydr.
Variation of catalyst particle size:[b]								
< 63 μm	90	15	13	32	19	21	60	3.2
63–200 μm	91	20	14	33	17	16	67	3.9
200–500 μm	86	20	14	33	20	13	67	3.4
Variation of the temperature:[c]								
383 K	35	25	19	15	31	10	59	1.9
398 K	44	29	19	13	33	6	61	1.8
438 K	69	35	26	20	12	7	81	6.8
Variation of the substrate/catalyst mass ratio:[d]								
2	16	7	7	14	61	11	28	0.5
0.5	38	29	20	24	27	–	73	2.7
0.24	86	20	13	32	19	16	65	3.4

[a] $t = 90$ min; X_{LS}=conversion; S_i=selectivity. [b] $T = 438$ K, $m_{cat} = 0.8$ g. [c] $m_{cat} = 0.8$ g, $d_{cat} = 200$–500 μm. [d] $T = 438$ K, $d_{cat} = 200$–500 μm. [e] Selectivity towards hydrogenation products (oleic acid + stearic acid). [f] Unidentified products. [g] Sum of CLAs. Hydr.=hydrogenation.

 © 2005 Wiley-VCH Verlag GmbH & Co. KGaA, Weinheim

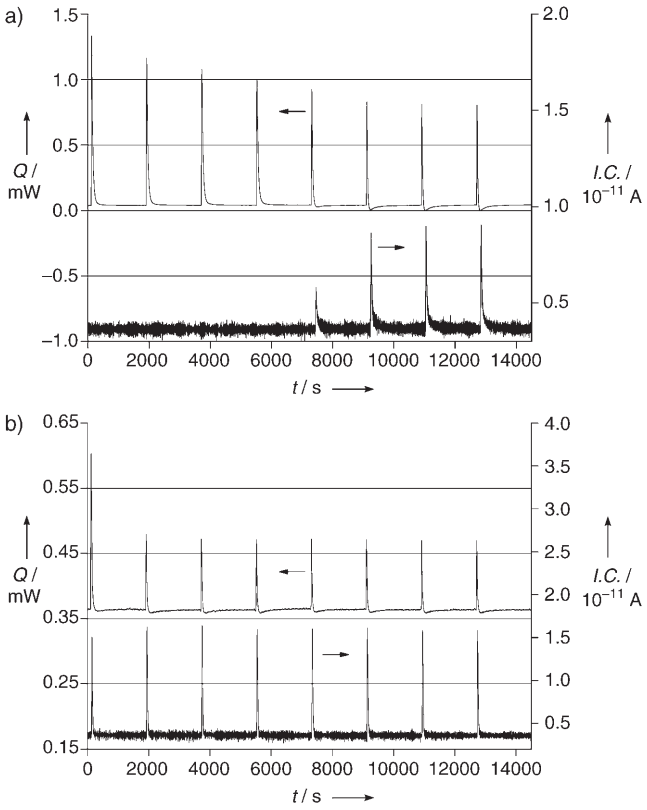

Figure 1. Results of calorimetric measurements of H_2 adsorption over Ru/C (a) and Ag/SiO_2 (b) catalysts in the presence of H_2 ($T_{ads} = 293$ K (a), 423 K (b)). The heat flow of the DSC (left ordinate) and the H_2 signal of the mass spectrometer (right ordinate) are shown. DSC = differential scanning calorimeter.

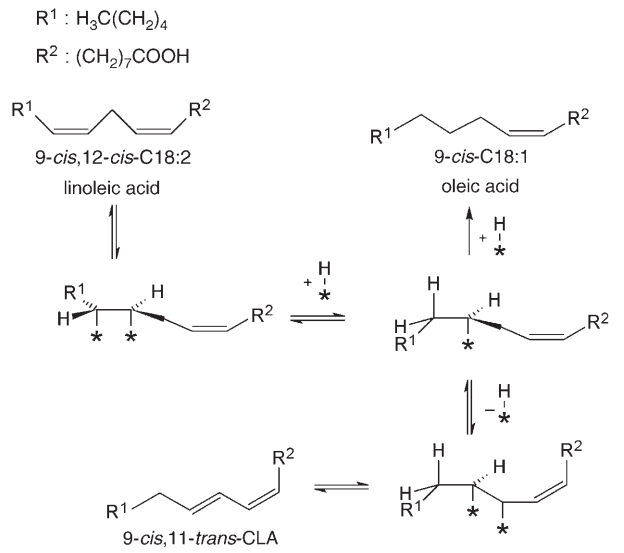

Scheme 2. Horiuti–Polanyi mechanism for the hydrogenation/isomerization of linoleic acid: weakly bonded hydrogen (on Ag) causes the desired CLA formation through an addition/elimination mechanism, whereas strongly bonded hydrogen (on Ru) causes the formation of oleic acid through consecutive H addition.

intermediate: addition of a further chemisorbed hydrogen atom under hydrogenation to give undesired oleic acid in the case of catalysts with high affinity to hydrogen chemisorption (Ru) versus elimination of a hydrogen atom with desired CLA formation in the case of weakly bonded hydrogen (Ag). Investigations are currently underway to examine the activation/adsorption of hydrogen on silver catalysts, which is rather unusual and is in contrast to the oxygen chemisorption known from oxidation catalysis, but comparable with gold catalysts.[24] Transient experiments with a Ag/SiO_2 catalyst preconditioned with H_2 in a TAP (temporal analysis of products) reactor and subsequent D_2 pulses revealed the formation of H–D and, thus, that H_2 dissociation must occur. This is not noticed over pure silver or SiO_2.[25]

The results presented herein show not only a direct route to CLAs but also a completely new method for the isomerization of (conjugated) double bonds. The prospects for the isomerization of linoleic acid to CLA in the presence of hydrogen and silver catalysts are obvious. After optimization of important catalyst properties (e.g. support material, silver particle size, and metal loading) the high CLA selectivity and yield as well as the simple reaction procedure in the presence of hydrogen permit the assignment to a continuous operation coupled with simple catalyst separation. Despite the high CLA selectivity, the product spectrum has to be further improved with respect to potential use in functional food. In particular, the fraction of 9-*trans*,11-*trans*-CLA must be decreased. Fundamentally, nothing should stand in the way of applying the presented principle of direct conversion of linoleic acid into CLAs over silver catalysts in the presence of H_2 as an alternative for the alkaline isomerization.

Experimental Section

General: The experiments were carried out in a 250-mL four-necked quartz-glass reactor, which was equipped with a reflux condenser, a drip funnel, a thermometer, a stirrer bar, and a gas-inlet tube. A magnetic stirrer with an oil bath was used as for heating and stirring. The Ag/SiO_2 catalyst was synthesized by incipient wetness impregnation from silver lactate (Fluka 85210) and SiO_2 (Alfa Aesar, "large pore") (Ag-content via ICP-OES: 7.7 wt %). The catalyst was dried at 353 K and reduced at 598 K under H_2 flow. A TEM examination (Philips CM 200 UT) resulted in an average Ag particle size of 14 nm. The Ru/C catalyst was a commercial product of Fluka (Ru content: 5 wt %). The calorimetric measurements of H_2 adsorption were carried out with a DSC 111 (Setaram) with mass spectrometer (Pfeiffer Vakuum) coupled to a pulse apparatus.

Example of an isomerization experiment: The catalyst ($m_{cat} = 800$ mg, grain fraction $d_{cat} = 200$–500 μm) was introduced into the reactor, and the mixture of linoleic acid (Aldrich, purity > 99 %) and *n*-decane was placed in the dropping funnel ($V = 70$ mL, $c_{LA} = 0.01$ mol L^{-1}). Nitrogen (100 mL min^{-1}) was flushed through the apparatus for 15 min to create an inert atmosphere and for degassing the linoleic acid/*n*-decane mixture. The catalyst was then activated under hydrogen flow (100 mL min^{-1}) for 1.5 h (including heating time) at 438 K. The linoleic acid/*n*-decane mixture was then added to the catalyst; this represents the starting time of the reaction ($t = 0$). The reaction mixture was kept at a reaction temperature of 438 K under permanent stirring (1100 rpm). Hydrogen (100 mL min^{-1}) was flushed through the mixture as reaction gas. Subsequent analysis was performed by means of temperature-programmed capillary gas chromatography (with FID) through an Agilent HP-5 column ($l = 25$ m, $d_i = 0.20$ mm, $t_f = 0.11$ mm), carried out according to the literature.[16b] Heptadecanoic acid was used as an internal GC standard. The samples were concentrated in a heating block and

 © 2005 Wiley-VCH Verlag GmbH & Co. KGaA, Weinheim

silylated with bis(trimethylsilyl)trifluoroacetamide (BSTFA) (80 μL) and trimethylchlorosilane (TMCS) (40 μL). Details of the analysis as well as a chromatogram example can be found in the Supporting Information.

Received: May 27, 2005
Revised: August 3, 2005

Keywords: conjugated linoleic acids · functional foods · heterogeneous catalysis · hydrogen · isomerization · silver

[1] Y. L. Ha, N. K. Grimm, M. W. Pariza, *Carcinogenesis* **1987**, *8*, 1881 – 1887.
[2] Y. L. Ha, N. K. Grimm, M. W. Pariza, *J. Agric. Food Chem.* **1989**, *37*, 75 – 81.
[3] *Ernährungsumschau* **1995**, *42*, 452.
[4] "Lebensmittelchemie 2000": J. Fritsche, *Nachr. Chem.* **2001**, *49*, 374 – 381.
[5] European Commission, Fifth Framework Program, KA1–FOOD, NUTRITION & HEALTH EUR 19422: FUNCLA: Conjugated linoleic acid (CLA) in functional food: A potential benefit for overweight middle-aged Europeans, http://europa.eu.int/comm/research/quality-of-life/ka1/volume2/qlk1-1999-00076.htm
[6] P. R. O'Quinn, J. L. Nelssen, R. D. Goodband, M. D. Tokach, *Anim. Health Res. Rev.* **2000**, *1*, 35 – 46.
[7] L. D. Whigham, M. E. Cook, R. L. Atkinson, *Pharmacol. Res.* **2000**, *42*, 503 – 510.
[8] S. F. Chin, W. Liu, M. Storkson, Y. L. Ha, M. W. Pariza, *J. Food Compos. Anal.* **1992**, *5*, 185 – 197.
[9] V. Mougios, A. Matsakas, A. Petridou, S. Ring, A. Sagredos, A. Melissopoulou, N. Tsigilis, M. Nikolaidis, *J. Nutr. Biochem.* **2001**, *12*, 585 – 594.
[10] J. D. Palombo, A. Ganguly, B. R. Bistrian, M. P. Menard, *Cancer Lett.* **2002**, *177*, 163 – 172.
[11] a) S. Busch, L. Zander, W. Albiez, P. Horlacher, A. Westfechtel (Cognis), DE 102 36 086A1, **2002** [*Chem. Abstr.* **2004**, *140*, 183582]; b) P. Horlacher, K.-H. Ruf, F. Timmermann, W. Adams, R. von Kries, (Cognis), DE 102 59 157A1, **2002** [*Chem. Abstr.* **2004**, *141*, 73307].
[12] M. W. Pariza, X.-Y. Yang, US 5 856 149, **1999** [*Chem. Abstr.* **1999**, *130*, 94531].
[13] J. R. Kepler, K. P. Hirons, J. J. McNeill, S. B. Tove, *J. Biol. Chem.* **1966**, *241*, 1350 – 1354.
[14] T. Y. Lin, C.-W. Lin, Y.-J. Wang, *Food Chem.* **2003**, *83*, 27 – 31.
[15] X. Dong, S. Chung, Ch. K. Reddy, L. E. Ehlers, *J. Am. Oil Chem. Soc.* **2001**, *78*, 447 – 453.
[16] a) A. Bernas, N. Kumar, P. Mäki-Arvela, E. Laine, B. Holmbom, T. Salmi, D. Murzin, *Chem. Commun.* **2002**, *10*, 1142 – 1143; b) A. Bernas, P. Laukkanen, N. Kumar, P. Mäki-Arvela, J. Väyrynen, E. Laine, B. Holmbom, T. Salmi, D. Murzin, *J. Catal.* **2002**, *210*, 354 – 366; c) A. Bernas, N. Kumar, P. Mäki-Arvela, N. V. Kul'kova, B. Holmbom, T. Salmi, D. Murzin, *Appl. Catal. A* **2003**, 245, 257 – 275; d) A. Bernas, P. Mäki-Arvela, N. Kumar, B. Holmbom, T. Salmi, D. Murzin, *Ind. Eng. Chem. Res.* **2003**, *42*, 718 – 727; e) A. Bernas, D. Murzin, *React. Kinet. Catal. Lett.* **2003**, *78*, 3 – 10; f) A. Bernas, N. Kumar, P. Laukkanen, J. Väyrynen, T. Salmi, D. Murzin, *Appl. Catal. A* **2004**, *267*, 121 – 133; g) A. Bernas, N. Kumar, P. Mäki-Arvela, B. Holmbom, T. Salmi, D. Murzin, *Org. Process Res. Dev.* **2004**, *8*, 341 – 352.
[17] J. Greeley, M. Mavrikakis, *J. Phys. Chem. B* **2005**, *109*, 3460 – 3471.
[18] "Hydrogen Sorption on Pure Metal Surfaces": C. Christmann in *Hydrogen Effects in Catalysis, Fundamentals and Practical Applications* (Eds.: Z. Paál, P. G. Menon), Marcel Dekker, New York, **1988**, p. 12.
[19] P. Claus, *Top. Catal.* **1998**, *5*, 51 – 62.
[20] The Microkinetics of Heterogeneous Catalysis (Eds.: J. A. Dumesic, D. F. Rudd, L. M. Aparicio, J. E. Rekoske, A. A. Trevino), ACS Professional Reference Book, Washington, DC, **1993**.
[21] The detailed quantitative evaluation shows that the areas under the peaks for adsorption (exothermic signal) and desorption (endothermic signal) are identical.
[22] This is also confirmed by TPD experiments: Whereas a hydrogen desorption peak appears at the ruthenium catalyst at 125 °C, the silver catalyst does not show any corresponding signal.
[23] T. Takeuchi, T. Asano, *Z. Phys. Chem.* **1963**, *36*, 118 – 125.
[24] Special Issue "Catalysis by Gold" (Eds.: G. Hutchings, M. Haruta), P. Claus, *Appl. Catal. A* **2005**, *251*, 222 – 229.
[25] M. Bron, E. Kondratenko, A. Trunschke, P. Claus, *Z. Phys. Chem.* **2004**, *218*, 405 – 423.

 © 2005 Wiley-VCH Verlag GmbH & Co. KGaA, Weinheim

Cover Picture

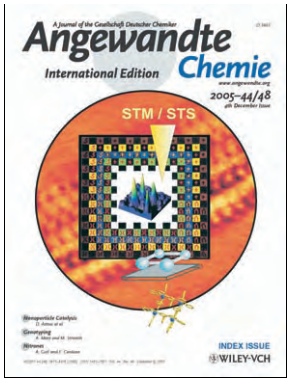

Mohammad Sahabul Alam, Stefan Strömsdörfer, Viacheslav Dremov, Paul Müller,* Jens Kortus, Mario Ruben,* and Jean-Marie Lehn*

***"I find in the square** specific settings, divisible areas, number structures, possibilities of time, measure and rhythm as well as the essential form of color which can be placed in the square to interplay with number forms.*" This statement by Alfred Jensen (his painting "The River Diagram" is shown in the cover picture) might also hold for research on molecular squares. In their Communication on page 7896 ff., M. Ruben, J.-M. Lehn, and P. Müller et al. describe the spectroscopic dissecting of a single molecular square into regions of different electronic properties by STM/STS techniques.

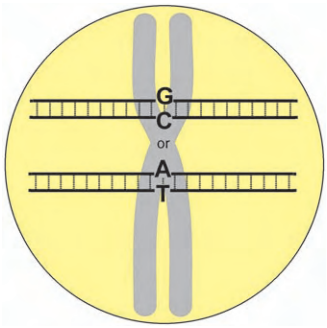

Genotyping
Modern techniques for the detection of single-nucleotide polymorphisms combine the amplification step with the actual analysis in a closed vessel. This one-pot operation is discussed by A. Marx and M. Strerath in their Minireview on page 7842 ff.

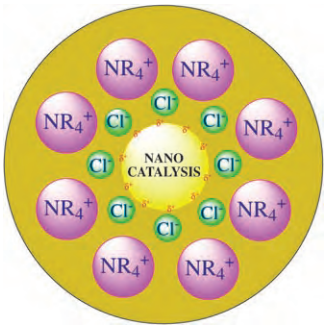

Nanoparticle Catalysts
The use of catalytic metal nanoparticles has developed into a multidisciplinary theme linking materials science and organic synthesis. The recent advances are presented by D. Astruc et al. in their Review on page 7852 ff.

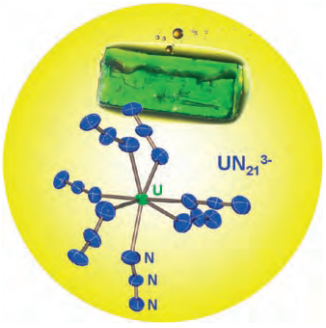

Binary Actinide Azides
In their Communication on pp. 7874 ff, M.-J. Crawford and co-workers describe the synthesis and structure of the first homoleptic azide of an actinide. The $[U(N_3)_7]^{3-}$ ion, which was characterized as the $(Bu_4N)_3[U(N_3)_7]$ salt, is the first structurally characterized heptaazide.

Contents

VIP *The following Communications have been judged by at least two referees to be "very important papers" and will be published online at www.angewandte.org soon:*

*C. Drago, L. Caggiano, R. F. W. Jackson**
Vanadium-Catalyzed Sulfur Oxidation/Kinetic Resolution in the Synthesis of Enantiomerically Pure Alkyl Aryl Sulfoxides

X. Rocquefelte, S. E. Boulfelfel, M. B. Yahia, J. Bauer, J.-Y. Saillard,* J.-F. Halet**
The Structural Preferences of Boron and Carbon within MB_2C_2 (M = Mg,Sc,Ca,Y,Ln) Phases: The "Coloring Problem" Revisited by DFT Calculations

G. C. Lloyd-Jones, R. G. Margue, J. G. de Vries*
Rate Enhancement by Ethylene in the Ru-Catalyzed Ring-Closing Metathesis of Enynes: Evidence for an "Ene-then-Yne" Pathway That Diverts through a Second Catalytic Cycle

S. Klaus, H. Neumann, A. Zapf, D. Strübing, S. Hübner, J. Almena, T. Riermeier, P. Groß, M. Sarich, W.-R. Krahnert, K. Rossen, M. Beller**
A General and Efficient Method for the Formylation of Aryl and Heteroaryl Bromides

N. Martín, Á. Martín-Domenech, S. Filippone, M. Altable, L. Echegoyen,* C. M. Cardona*
Retrocycloaddition Reactions of Pyrrolidinofullerenes

Meeting Reviews

Boron—A Meeting Point — *H. Braunschweig, D. Rais* ____ **7826**

Books

Artificial Enzymes — Ronald Breslow — *reviewed by M. Meldal* ____ **7829**

Highlights

Organic Synthesis

F. Cardona, A. Goti* ____ **7832 – 7835**

The Discovery of Novel Metal-Induced Reactions of Nitrones: Not Only Electrophiles and Reagents for [3+2] Cycloadditions

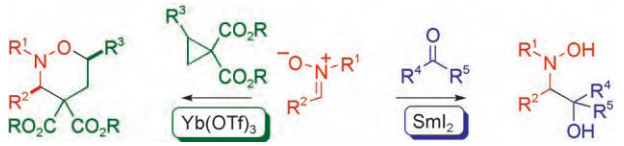

Tales of the unexpected: A multitude of new reactions have been discovered for nitrones, the chemistry of which was considered well established. Two of them, a formal [3+3] cycloaddition and a pinacol-type coupling (see scheme) are induced by lanthanide derivatives and appear particularly promising and attractive for the synthesis of natural products and complex molecules.

Essays

History of Chemistry

A. de Meijere* ____ **7836 – 7840**

Adolf von Baeyer: Winner of the Nobel Prize for Chemistry 1905

The 100th anniversary of the awarding of the Nobel Prize for Chemistry to Adolf von Baeyer (1835–1912) is drawing to a close. Nevertheless, his scientific work, especially that on organic dyes, *C*-nitroso compounds, and on hydroaromatic compounds have had and continue to have a profound effect on chemistry and on the chemical industry.

© 2005 Wiley-VCH Verlag GmbH & Co. KGaA, Weinheim

Minireviews

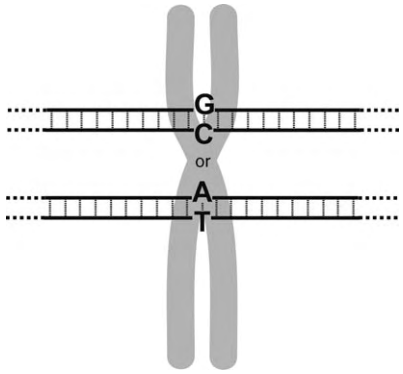

G/C or A/T: that is the question! Nucleotide variations in the human genome, such as single-nucleotide polymorphisms (see picture), can be linked directly to diseases and also to side effects of drugs. Efficient, cost-effective processes that can be conducted in a closed reaction tube allow directly analysis of genomic DNA without preamplification.

Genomics

M. Strerath, A. Marx* ____ **7842 – 7849**

Genotyping—From Genomic DNA to Genotype in a Single Tube

Reviews

The smaller, the better: Metal nanoparticle catalysis is an expanding area at the interface between homogeneous and heterogeneous catalysis. Moreover, its applications in the synthesis of fine organic chemicals, fuel-cell technology, and environmental issues are of growing importance. This Review shows the interdisciplinary character of this catalysis and presents the main recent advances. The picture shows the morphology of an electrosteric stabilized nanoparticle.

Nanoparticle Catalysts

D. Astruc,* F. Lu, J. R. Aranzaes ____ **7852 – 7872**

Nanoparticles as Recyclable Catalysts: The Frontier between Homogeneous and Heterogeneous Catalysis

Communications

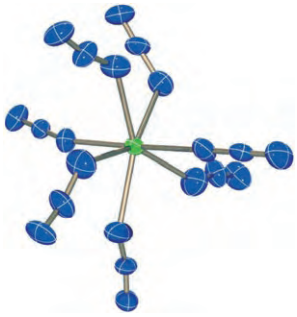

More stable than it seems: The binary uranium–nitrogen anion $U(N_3)_7^{3-}$ was synthesized and characterized as the $(Bu_4N)_3[U(N_3)_7]$ salt. The $U(N_3)_7^{3-}$ ion is the first structurally characterized heptaazide and is the first homoleptic azide of an actinide. The crystal structure shows a pentagonal-bipyramidal arrangement of the azide ligands around the central uranium(IV) atom (see structure; N: blue; U: green).

Azide Complexes

M.-J. Crawford,* A. Ellern, P. Mayer ____ **7874 – 7878**

UN_{21}^{3-}: A Structurally Characterized Binary Actinide Heptaazide Anion

For the USA and Canada:
ANGEWANDTE CHEMIE International Edition (ISSN 1433-7851) is published weekly by Wiley-VCH PO Box 191161, D 69451 Weinheim, Germany. Air freight and mailing in the USA by Publications Expediting Inc. 200 Meacham Ave., Elmont, NY 11003. Periodicals postage paid at Jamaica NY 11431. US POSTMASTER: send address changes to *Angewandte Chemie*, Wiley-VCH, 111 River Street, Hoboken, NJ 07030. Annual subscription price for institutions: US$ 5685/5168 (valid for print and electronic / print or electronic delivery); for individuals who are personal members of a national chemical society prices are available on request. Postage and handling charges included. All prices are subject to local VAT/sales tax.

© 2005 Wiley-VCH Verlag GmbH & Co. KGaA, Weinheim

The best in chemistry –

for more than a hundred years

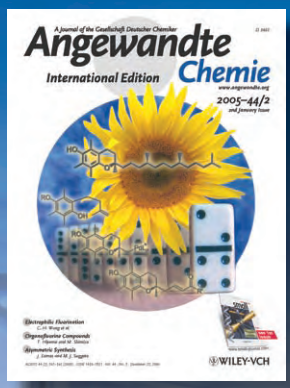

A Journal of the Gesellschaft Deutscher Chemiker

Angewandte
International Edition **Chemie**

www.angewandte.org

Angewandte's advisors...

Wolfgang A. Herrmann
Technische Universität München

»**Angewandte Chemie** is at home in Germany and successful in the world. This journal has developed as the international community of chemists has grown together. Today, **Angewandte** is of central importance for modern chemists. It is the only journal I afford not to hurry through in the office – it's my "home is my castle journal"!«

1888: **The beginning of a success story**

Constant Innovations

1962: First issue of the International Edition
1976: Graphical abstracts
1979: Cover pictures
1988: Centenary of Angewandte
1989: Routine use of color
1991: New section: Highlights
1992: Computerized editorial tracking system
1995: Internet service for readers
1998: Regular press service; full-text online
2000: New section: Essays; EarlyView: Communications available online ahead of the printed version
2001: New section: Minireviews
2002: Online submission of manuscripts
2003: Weekly publication; new section: News; new layout
2004: Backfiles (1962-1997); ManuscriptXpress: Online system for authors and referees

Angewandte Chemie International Edition is a journal of the German Chemical Society (GDCh)

GDCh

WILEY InterScience® DISCOVER SOMETHING GREAT

WILEY-VCH

1908/1506_gu

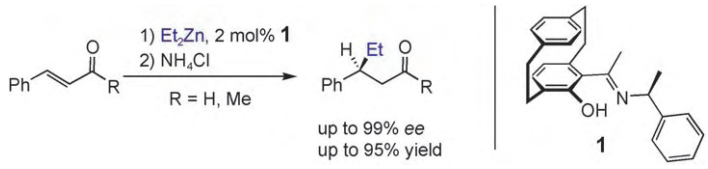

The ligand makes it possible: The asymmetric conjugate addition of diethylzinc to α,β-unsaturated aldehydes and ketones occurs with catalytic amounts of the paracyclophaneketimine ligand **1** without further additives.

Synthetic Methods

S. Bräse,* S. Höfener ——— **7879 – 7881**

Asymmetric Conjugate Addition of Organozinc Compounds to α,β-Unsaturated Aldehydes and Ketones with [2.2]Paracyclophaneketimine Ligands without Added Copper Salts

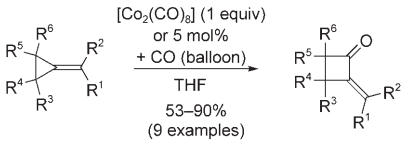

Activation of C–C bonds in cyclopropanes with a cobalt complex: Methylenecyclopropanes react with one equivalent of $[Co_2(CO)_8]$ under mild conditions to give 2-methylenecyclobutanones in moderate to good yields (up to 85%). The reaction also proceeds with a catalytic amount of the cobalt complex under an atmosphere of CO (balloon) to give products in good yields (up to 90%; see scheme).

C–C Activation

T. Kurahashi, A. de Meijere* **7881 – 7884**

C–C Bond Activation by Octacarbonyldicobalt: [3+1] Cocyclizations of Methylenecyclopropanes with Carbon Monoxide

Inside out: Deiodination of $R^*_3Si_4I_5$ ($R^* = SitBu_3$) with NaR* affords the silicon compound $Si_8R^*_6$. A Si_2 dumbbell-(Si1–Si2) is present in this novel cluster framework, embedded as in a sandwich compound between two $Si_3R^*_3$ rings (see structure; the *t*Bu methyl groups are not shown). The Si atoms of the dumbbell are "inverse-tetrahedrally" coordinated by four Si atoms.

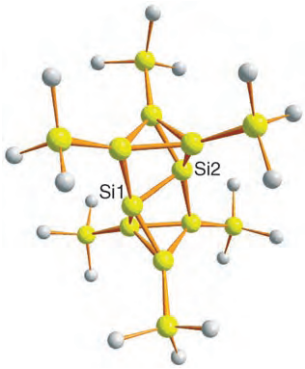

Silicon Clusters

G. Fischer, V. Huch, P. Mayer, S. K. Vasisht, M. Veith, N. Wiberg* ——— **7884 – 7887**

$Si_8(SitBu_3)_6$: A Hitherto Unknown Cluster Structure in Silicon Chemistry

Shedding light: Efficient activation of cyclic nucleoside monophosphates (cNMPs) can be achieved upon one- and two-photon flash photolysis of novel photolabile coumarinylmethyl esters of cAMP and cGMP (A = adenosine, G = guanosine) as well as their 8-bromo-substituted derivatives. The phototriggers show high solubility in water and permit space- and time-resolved investigations of the molecular mechanisms of cyclic nucleotide dependent processes.

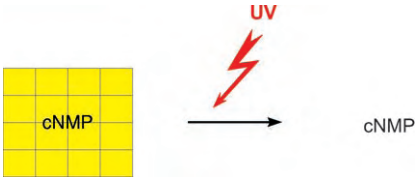

Photoactivatable Compounds

V. Hagen,* B. Dekowski, V. Nache, R. Schmidt, D. Geißler, D. Lorenz, J. Eichhorst, S. Keller, H. Kaneko, K. Benndorf, B. Wiesner ——— **7887 – 7891**

Coumarinylmethyl Esters for Ultrafast Release of High Concentrations of Cyclic Nucleotides upon One- and Two-Photon Photolysis

© 2005 Wiley-VCH Verlag GmbH & Co. KGaA, Weinheim

Contents

Nanoparticle Synthesis

S. Polarz,* A. V. Orlov, M. W. E. van den Berg, M. Driess _____ **7892 – 7896**

Molecular Encoding at the Nanoscale: From Complex Cubes to Bimetallic Oxides

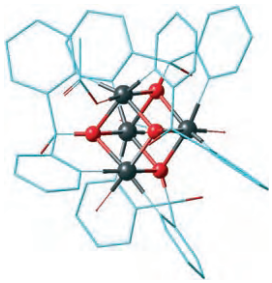

Simple metal acetates react to give bimetallic heterocubanes of the type $[M^1_{4-y}M^2_yO_4]$ (see structure, $M^{1,2}$ = Mn, Co, Ni, Zn), which in turn are precursors for the selective formation of bimetallic oxide nanoparticles with a controlled composition. The size of the particles can be controlled by adjusting the thermolysis temperature.

Surface Chemistry

M. S. Alam, S. Strömsdörfer, V. Dremov, P. Müller,* J. Kortus, M. Ruben,* J.-M. Lehn* _____ **7896 – 7900**

Addressing the Metal Centers of [2 × 2] Co^{II}_4 Grid-Type Complexes by STM/STS

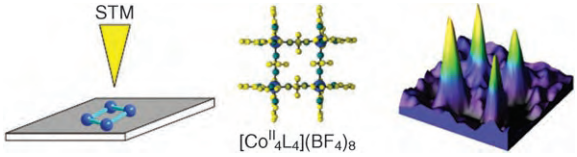

The controlled deposition of grid-type [2 × 2] Co^{II}_4 complexes onto graphite rendered free-standing 0D, 1D, and 2D molecular arrangements, which were examined by STM techniques. Scanning tunneling spectroscopy (STS) investigations enabled the direct addressing of the metal centers at the single-molecule level (see image). The experimentally determined intramolecular positions of the Co^{II} centers are in agreement with DFT calculations of the molecule.

Reaction Mechanisms

S. Laimgruber, W. J. Schreier, T. Schrader, F. Koller, W. Zinth, P. Gilch* **7901 – 7904**

The Photochemistry of *o*-Nitrobenzaldehyde as Seen by Femtosecond Vibrational Spectroscopy

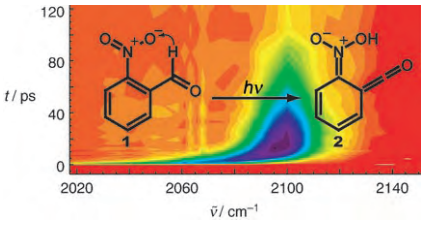

A ketene comes and goes: The first intermediate in the photoredox reaction of *o*-nitrobenzaldehyde (**1**) is identified as ketene **2**. In a femtosecond IR experiment a resonance at 2100 cm^{-1} corresponding to the ketene stretching vibration appears less than one picosecond after photoexcitation. The 90-ps decay of this band is a manifestation of a nucleophilic addition to the C=C double bond, which is supported by other spectroscopic experiments (IR and Raman).

Glasses

M. Eichelbaum, K. Rademann,* R. Müller, M. Radtke, H. Riesemeier, W. Görner _____ **7905 – 7909**

On the Chemistry of Gold in Silicate Glasses: Studies on a Nonthermally Activated Growth of Gold Nanoparticles

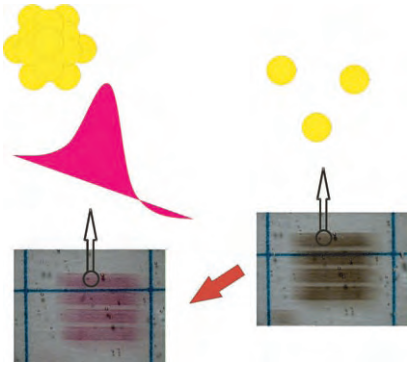

Gold in glass: Activating gold silicate glasses with synchrotron X-rays results in the spatial reduction of cationic gold to gold atoms. Subsequent annealing allows the growth of nanoparticles with defined sizes and tailored optical properties (see picture). This opens up new vistas in functionalizing chemically and mechanically stable glasses for integrated nanophotonic applications.

© 2005 Wiley-VCH Verlag GmbH & Co. KGaA, Weinheim

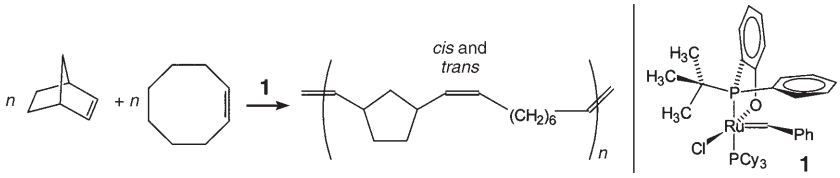

Back and forth like a metronome is how the carbene moiety swings in a dual-site catalyst which produces a predominantly alternating copolymer of norbornene and cyclooctene from a one-pot reaction of appropriate mixtures of the two monomers (see scheme). The alternating sequence of the polymer was confirmed by NMR spectroscopy and gel-permeation gravimetric analysis.

Copolymerization

M. Bornand, P. Chen* ____ **7909 – 7911**

Mechanism-Based Design of a ROMP Catalyst for Sequence-Selective Copolymerization

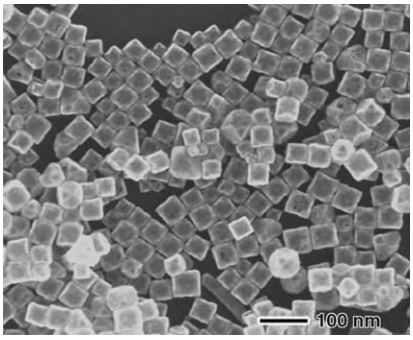

Inside out: Corrosive pitting and etching can be combined in a simple, elegant, and powerful method to transform single-crystal Pd nanocubes into nanoboxes (see SEM image) and nanocages in a one-pot synthesis without the involvement of exotic templates. Emptying the interiors enables the surface plasmon resonance peaks of the Pd nanostructures to be tuned from 410 to 520 nm.

Nanostructures

Y. Xiong, B. Wiley, J. Chen, Z.-Y. Li, Y. Yin, Y. Xia* ____ **7913 – 7917**

Corrosion-Based Synthesis of Single-Crystal Pd Nanoboxes and Nanocages and Their Surface Plasmon Properties

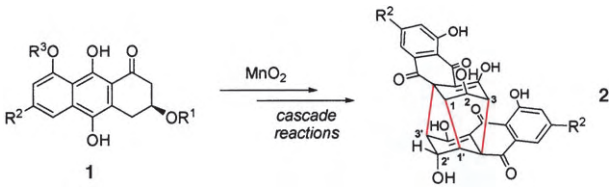

The cytoskyrin cascade: The total syntheses of the bisanthraquinones **2** (+)-2,2′-*epi*-cytoskyrin A (R^2 = OMe) and (+)-rugulosin (R^2 = Me) has been achieved through a cascade sequence from anthradihydroquinone monomeric units **1**.

Natural Product Synthesis

K. C. Nicolaou,* Y. H. Lim, C. D. Papageorgiou, J. L. Piper ____ **7917 – 7921**

Total Synthesis of (+)-Rugulosin and (+)-2,2′-*epi*-Cytoskyrin A through Cascade Reactions

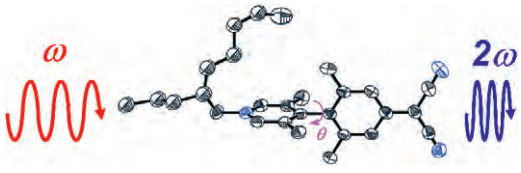

Nonlinear optics: Twisted π-electron system electrooptic (EO) chromophores with exceptional molecular hyperpolarizabilities ($-488\,000 \times 10^{-48}$ esu at 1907 nm) were designed and synthesized. Crystallographic analysis reveals large twist angles and a highly charge-separated zwitterionic ground state. Experiments on poled host–guest polymers containing these chromophores show them to be promising candidates for EO applications.

Electrooptic Systems

H. Kang, A. Facchetti, P. Zhu, H. Jiang, Y. Yang, E. Cariati, S. Righetto, R. Ugo, C. Zuccaccia, A. Macchioni, C. L. Stern, Z. Liu, S.-T. Ho, T. J. Marks* **7922 – 7925**

Exceptional Molecular Hyperpolarizabilities in Twisted π-Electron System Chromophores

© 2005 Wiley-VCH Verlag GmbH & Co. KGaA, Weinheim

Contents

Sensors

K.-J. Chang, D. Moon, M. S. Lah, K.-S. Jeong* ——— **7926 – 7929**

Indole-Based Macrocycles as a Class of Receptors for Anions

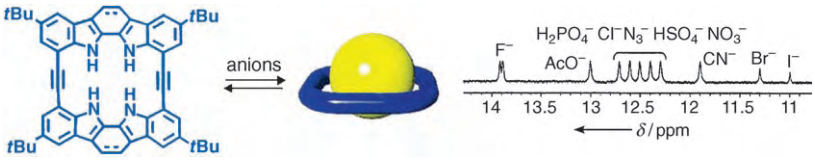

Shift work: The identity of an anion complexed to indole-based macrocycles can be determined by the NMR chemical shift of the NH protons (see picture). The difference in the chemical shifts arises from a difference in the strength of the hydrogen-bonding interactions between the macrocycles and the anions.

Nanotubes

C. Zhi,* Y. Bando, C. Tang, S. Honda, K. Sato, H. Kuwahara, D. Golberg ——— **7929 – 7932**

Characteristics of Boron Nitride Nanotube–Polyaniline Composites

A self-organized film of boron nitride nanotube–polyaniline (BNNT–PANI) composite is fabricated by using a simple solution method. The BNNTs are fully coated with PANI as a result of strong interactions between these components (see picture). Mechanically tough, BNNTs may have potential as stabilizing additives to PANI or other polymers.

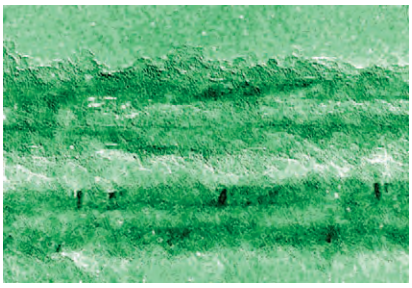

Nanotubes

C. Zhi,* Y. Bando, C. Tang, S. Honda, K. Sato, H. Kuwahara, D. Golberg ——— **7932 – 7935**

Covalent Functionalization: Towards Soluble Multiwalled Boron Nitride Nanotubes

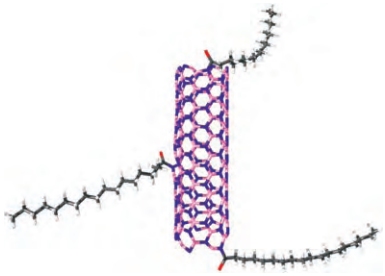

Playing with the band: Long alkyl chains are bound to boron nitride nanotubes (BNNTs) from the reaction of stearoyl chloride with amino groups on the BNNTs; the resulting functionalized BNNTs (see picture) are soluble in many organic solvents. Cathodoluminescence and UV/Vis absorption experiments indicate that the long alkyl chains may induce drastic changes in the band structure of BNNTs.

VIP **Sensors**

A. Buryak, K. Severin* ——— **7935 – 7938**

Dynamic Combinatorial Libraries of Dye Complexes as Sensors

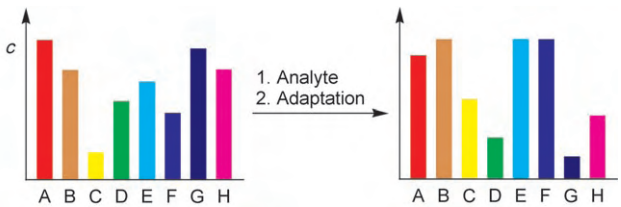

A simple solution: Simply dissolving three commercially available dyes and two metal salts in a buffer is sufficient to create a sensor which allows the identification of dipeptides with high selectivity by using UV/Vis spectroscopy (see picture for the adaptive behaviour of a dynamic mixture of colored compounds A–H).

© 2005 Wiley-VCH Verlag GmbH & Co. KGaA, Weinheim

Metallomacrocyclic arrays containing eight copper(II) centers (see picture; green Cu, blue N, red O, yellow S) were obtained by using a heptadentate thiocarbohydrazone ligand with a particular conformational and configurational flexibility, as well as an appropriate arrangement of metal-binding sites, coordination ability, and acid–base properties.

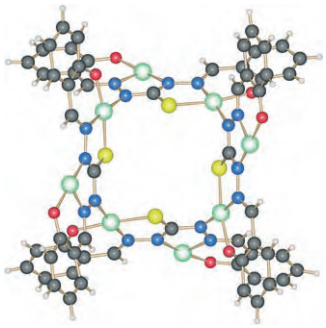

Cluster Compounds

D. Dragancea, V. B. Arion,* S. Shova, E. Rentschler, N. V. Gerbeleu* ——— **7938 – 7942**

Azine-Bridged Octanuclear Copper(II) Complexes Assembled with a One-Stranded Ditopic Thiocarbohydrazone Ligand

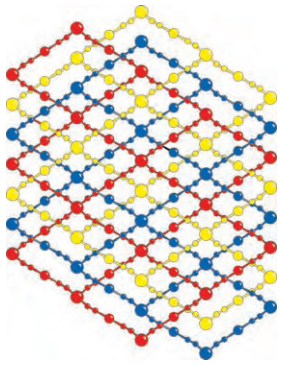

Caught in the net: A series of mixed copper(I)–silver(I) cyanide complexes of the form $A[Ag_2Cu(CN)_4]$ (A = K, Rb, Cs) have been found to form interpenetrating layer structures and three-dimensional networks (see picture). Two different forms of the Rb and Cs compounds are observed, which are both topological isomers and polymorphs.

Network Structures

A. M. Chippindale,* S. M. Cheyne, S. J. Hibble* ——— **7942 – 7946**

Interpenetrating Copper–Silver Cyanometallate Networks: Polymorphs and Topological Isomers

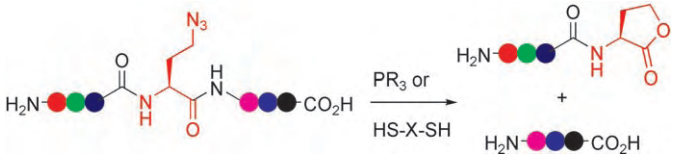

A gentle break: Cleavage of peptides containing the non-natural but proteogenic amino acid azido homoalanine can be accomplished by phosphine- or dithiol-mediated reductive activation of the azide functionality in aqueous buffers (see scheme). The resulting C-terminal lactone of one peptide fragment allows facile further derivatization.

Protein Chemistry

J. W. Back,* O. David, G. Kramer, G. Masson, P. T. Kasper, L. J. de Koning, L. de Jong, J. H. van Maarseveen, C. G. de Koster ——— **7946 – 7950**

Mild and Chemoselective Peptide-Bond Cleavage of Peptides and Proteins at Azido Homoalanine

Quality control: UDP-glucose:glycoprotein glucosyltransferase (UGGT) works as the folding sensor in glycoprotein quality control. It glucosylates the Man9GlcNAc2 of misfolded glycoproteins to produce Glc1Man9GlcNAc2, which is a ligand of calnexin and calreticulin. The synthetic substrate Man9GlcNAc2-MTX can be used for the quantitative analysis of UGGT. UDP = uridine 5′-diphosphate, Glc = D-glucose, Man = D-mannose, GlcNAc = *N*-acetyl-D-glucosamine, MTX = methotrexate.

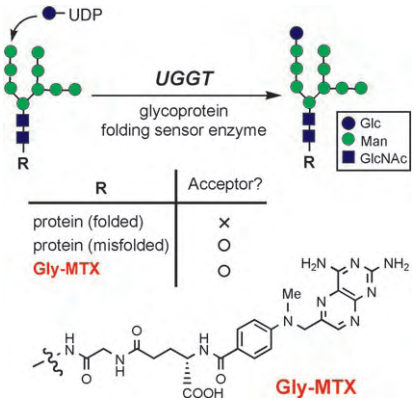

Protein Folding

K. Totani, Y. Ihara, I. Matsuo, H. Koshino, Y. Ito* ——— **7950 – 7954**

Synthetic Substrates for an Endoplasmic Reticulum Protein-Folding Sensor, UDP-Glucose: Glycoprotein Glucosyltransferase

© 2005 Wiley-VCH Verlag GmbH & Co. KGaA, Weinheim

Contents

Self-Assembly

K. Zeckert, J. Hamacek, J.-M. Senegas, N. Dalla-Favera, S. Floquet, G. Bernardinelli,* C. Piguet* ——— **7954 – 7958**

Predictions, Synthetic Strategy, and Isolation of a Linear Tetrametallic Triple-Stranded Lanthanide Helicate

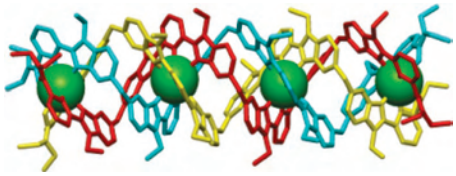

Complex twists: Following theoretical thermodynamic predictions, it is seen that the tetrametallic triple-stranded lanthanide helicate $[Ln_4L_3]^{12+}$ (see structure) dominates the speciation in solution at millimolar concentrations, despite its high positive charge. Isolation of the europium complex in the solid state unambiguously establishes its nanometric triple-helical structure.

Crown Compounds

A. Decken, H. D. B. Jenkins,* C. Knapp, G. B. Nikiforov, J. Passmore,* J. M. Rautiainen ——— **7958 – 7961**

The Autoionization of $[TiF_4]$ by Cation Complexation with [15]Crown-5 To Give $[TiF_2([15]crown\text{-}5)][Ti_4F_{18}]$ Containing the Tetrahedral $[Ti_4F_{18}]^{2-}$ Ion

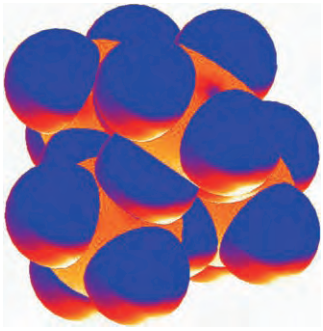

It's the crown that does it: The autoionization of $[TiF_4]$ has been promoted by complexation with [15]crown-5 to produce $[TiF_2([15]crown\text{-}5)][Ti_4F_{18}]$, which contains the new tetrahedral ion $[Ti_4F_{18}]^{2-}$ (see picture). The thermodynamics of the $[Ti_4F_{18}]^{2-}$ ion relative to the $[Ti_2F_9]^-$ ion in the gas, solution, and solid states were calculated by density functional methods.

Multicomponent Arylation

L. El Kaïm,* L. Grimaud,* J. Oble ——— **7961 – 7964**

Phenol Ugi–Smiles Systems: Strategies for the Multicomponent N-Arylation of Primary Amines with Isocyanides, Aldehydes, and Phenols

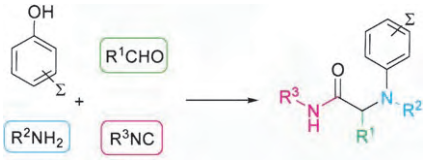

A Smiles rearrangement is the key step in the efficient coupling of primary amines with isocyanides, carbonyl compounds, and electron-deficient substituted phenols to form *N*-aryl amines (see picture). The presence of a nitro or ester group on the resulting adduct allows applications in heterocyclic synthesis.

Organogels

K. T. Kim, C. Park, G. W. M. Vandermeulen, D. A. Rider, C. Kim, M. A. Winnik,* I. Manners* ——— **7964 – 7968**

Gelation of Helical Polypeptide–Random Coil Diblock Copolymers by a Nanoribbon Mechanism

Thermoreversible gelation of diblock copolymers of a helical polypeptide, poly(γ-benzyl-L-glutamate) and random-coil polymers such as polyferrocenylsilanes in dilute solution has been discovered (see picture). A new mechanism for self-assembly of block copolymers of helical polypeptides is proposed.

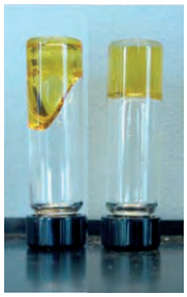

© 2005 Wiley-VCH Verlag GmbH & Co. KGaA, Weinheim

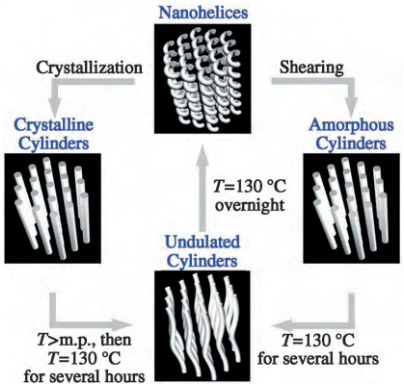

Spring-loaded polymers: The nanohelical structure of poly(L-lactide) (PLLA) in the polystyrene (PS) matrix of chiral PS-PLLA block copolymers displays springlike behavior in response to an applied stimulus. The self-assembled nanohelices are transformed into cylinders by crystallization or shearing (see picture). This thermally reversible phase behavior may be used for manipulating switchable nanohelical structures.

Switchable Nanostructures

Y.-W. Chiang, R.-M. Ho,* B.-T. Ko, C.-C. Lin ——— **7969 – 7972**

Springlike Nanohelical Structures in Chiral Block Copolymers

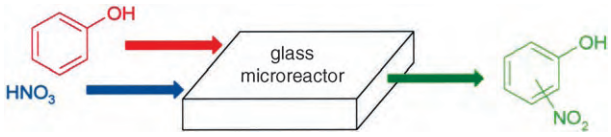

Scaled-down approach: The nitration of phenol is an autocatalytic, strongly exothermic reaction and is thus difficult to handle on an industrial scale. Continuous nitration in a microreactor (see picture) affords higher yields and enhanced process safety, thanks to good heat exchange and mixing properties, as well as rapid radical propagation under sufficiently harsh conditions.

Synthetic Methods

L. Ducry,* D. M. Roberge* **7972 – 7975**

Controlled Autocatalytic Nitration of Phenol in a Microreactor

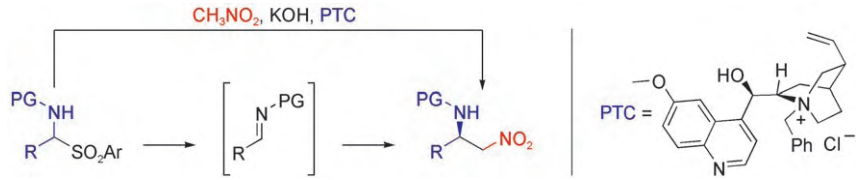

A general approach to the catalytic asymmetric aza-Henry reaction has been developed. The combination of a commercially available phase-transfer catalyst (PTC) with a base is able to promote the in situ formation of *N*-carbamoyl imines from α-amido sulfones and activate nitromethane towards the asymmetric addition reaction, thus furnishing *N*-carbamoyl-protected β-nitroamines in good yields and with up to 98% *ee* (see scheme; PG = protecting group).

Asymmetric Synthesis

F. Fini, V. Sgarzani, D. Pettersen, R. P. Herrera,* L. Bernardi,* A. Ricci ——— **7975 – 7978**

Phase-Transfer-Catalyzed Asymmetric Aza-Henry Reaction Using *N*-Carbamoyl Imines Generated In Situ from α-Amido Sulfones

Aluminum-stabilized copper colloids with a size of about 5 nm (see picture) are the key to a quasi-homogeneous version of the heterogeneously catalyzed synthesis of methanol from synthesis gas over $Cu/ZnO/Al_2O_3$. The catalyst productivity is very high in spite of the absence of ZnO.

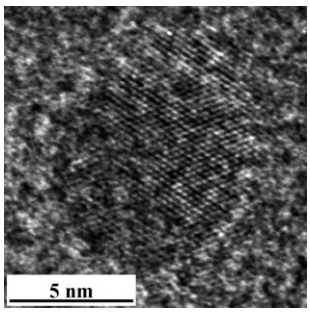

Catalyst Research

S. Vukojević, O. Trapp, J.-D. Grunwaldt, C. Kiener, F. Schüth* ——— **7978 – 7981**

Quasi-Homogeneous Methanol Synthesis Over Highly Active Copper Nanoparticles

© 2005 Wiley-VCH Verlag GmbH & Co. KGaA, Weinheim

Contents

Natural Product Synthesis

T. K. M. Shing,* Y. Y. Yeung **7981 – 7984**

Total Synthesis of (−)-Samaderine Y from (*S*)-(+)-Carvone

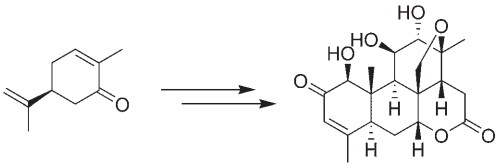

(*S*)-(+)-carvone (−)-samaderine Y

Elegant, efficient, and enantiospecific describe the first total synthesis of the quassinoid (−)-samaderine Y (see scheme), which has been shown to display in vitro cytotoxicity and is of interest as a potential antitumor agent. Its synthesis has been accomplished from (*S*)-(+)-carvone in 21 steps.

Substituted Fullerenes

I. E. Kareev, I. V. Kuvychko, A. A. Popov, S. F. Lebedkin, S. M. Miller, O. P. Anderson, S. H. Strauss,* O. V. Boltalina* **7984 – 7987**

High-Temperature Synthesis of the Surprisingly Stable C_1-$C_{70}(CF_3)_{10}$ Isomer with a *para*^{7}–*meta*–*para* Ribbon of Nine $C_6(CF_3)_2$ Edge-Sharing Hexagons

From the equator to the pole: The high-temperature, high-yield C_1 isomer of $C_{70}(CF_3)_{10}$ has an unprecedented structure. The CF_3 groups belong to a *para*^{7}–*meta*–*para* ribbon of edge-sharing $C_6(CF_3)_2$ hexagons, which wraps around the equator of the C_{70} cage and then climbs up to one of the poles. Calculations demonstrate that this isomer is more stable than the structures observed for $C_{70}Br_{10}$ and $C_{70}(t\text{BuOO})_{10}$.

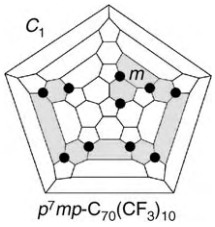

p^7mp-$C_{70}(CF_3)_{10}$

Photofunctional Materials

Y. Du, M. Yang, J. Yu,* Q. Pan, R. Xu* **7988 – 7990**

An Unexpected Photoelectronic Effect from $[Co(en)_3]_2(Zr_2F_{12})(SiF_6)\cdot 4H_2O$, a Compound Containing an H-Bonded Assembly of Discrete $[Co(en)_3]^{3+}$, $(Zr_2F_{12})^{4-}$, and $(SiF_6)^{2-}$ Ions

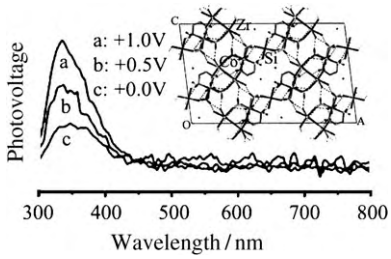

Hydrogen-bonded network: A hydrothermal synthesis delivers the titled compound, which consists of an H-bonded network of discrete $[Co(en)_3]^{3+}$, $(Zr_2F_{12})^{4-}$, and $(SiF_6)^{2-}$ ions. It exhibits an unexpected photoelectronic effect in the near-UV region (see figure).

WILEY InterScience® DISCOVER SOMETHING GREAT

"**Hot Papers**" are chosen by the Editors for their importance in a rapidly evolving field of high current interest. A preview with the graphical abstracts of these articles can be found on the *Angewandte Chemie* homepage in Wiley InterScience at www.angewandte.org.

All articles in *Angewandte Chemie* are published online several weeks ahead of print. They are found under the "**EarlyView**" link on the journal's homepage in Wiley InterScience.

Service

Keywords **7992**

Authors **7993**

Vacancies **7831**

Index **7997**

Preview **8077**

© 2005 Wiley-VCH Verlag GmbH & Co. KGaA, Weinheim

The editorial staff and the publishers thank all readers, authors, referees, and advertisers for their interest and support over the past year and wish them all a happy new year.

Unique series on Optical Design

- gives a unique overview for both newcomers and professionals in academia and industry
- balances comprehensive introduction with latest research results in a uniform style
- features over 3,000 color illustrations that facilitate access to complex problems
- written by experts at the world's leading manufacturer of optical systems

6 Volume Set

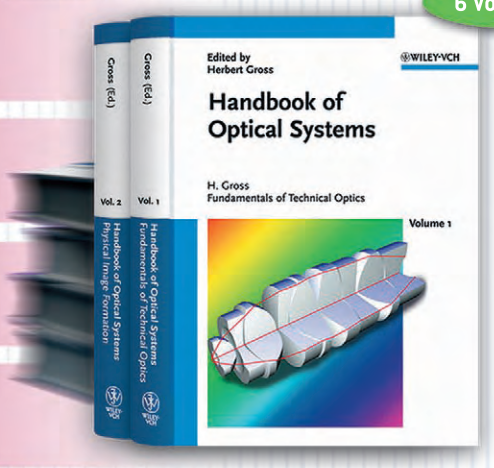

Price of each volume if purchased as part of the set:
€ 248.00 / £ 175.00 / US$ 335.00
Each volume will be invoiced and despatched upon publicaton.

Single volume price:
Approx € 298.00 / £ 210.00 / US$ 400.00

Set price:
€ 1488.00 / £ 1050.00 / US$ 1905.00

Publication dates:
Volumes 1 and 2: 2005
Volumes 3 and 4: Spring 2006
Volumes 5 and 6: Fall 2007

ISBN 3-527-40382-5

15033409_bu

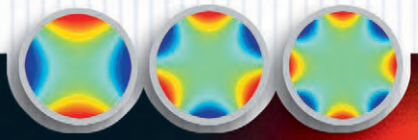

Wiley-VCH • Tel.: +49 (0) 6201 - 606 400
Fax: +49 (0) 6201 - 606 184
e-Mail: service@wiley-vch.de • www.wiley-vch.de

WILEY-VCH

© 2005 Wiley-VCH Verlag GmbH & Co. KGaA, Weinheim

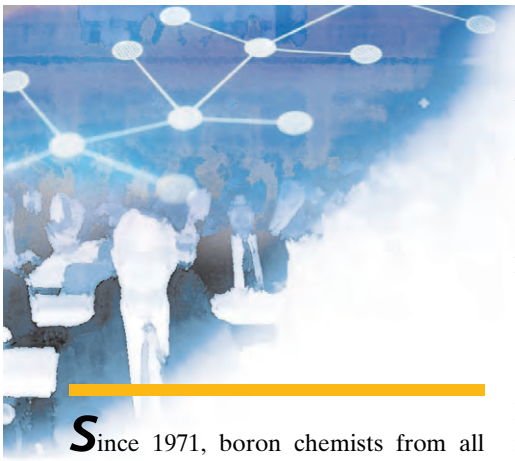

Boron—A Meeting Point**

Holger Braunschweig and Daniela Rais*

Since 1971, boron chemists from all over the world meet every three years at the IMEBORON conference. The 12th meeting in this series was hosted by Y. Yamamoto in Sendai, Japan, during September 11–15, 2005. A scientific program comprising 22 invited lectures and 75 keynote lectures and short presentations was delivered to an audience of 300 participants from more than 20 countries, emphasizing the importance of the IMEBORON conferences in fostering international collaboration within the boron chemistry community. This year's meeting, which was overshadowed by the loss of Nobel laureate H. C. Brown, who died last year at the age of 92, offered contributions on all modern research areas of boron chemistry, focusing on applications of boron-containing compounds in catalysis, organic synthesis, and pharmaceutical chemistry, materials chemistry, and the evergreen area of cluster chemistry.

Highlights of the contributions on catalysis were the three invited lectures given by N. Miyaura (Hokkaido University), T. B. Marder (University of Durham), and M. R. Smith III (Michigan State University). After a brief historical overview on the evolution of transition-metal-catalyzed hydrocarbon borylation, culminating in the identification of $[(cod)Ir(OMe)]_2$ (cod = 1,5-cyclooctadiene) as the optimal catalyst precursor for aromatic borylation (Scheme 1), Miyaura described highly selective syntheses of aryl-, heteroaryl-, and alkenylboronate esters through iridium-catalyzed functionalization of C–Hbonds with pinacolborane and bis(pinacolato)diborane(4) .

The preferential borylation of sites that are distant from any substituent or ring junction was exploited by Marder and co-workers to achieve selective functionalization of polycyclic hydrocarbons, such as perylenes, in positions that are otherwise difficult to access through alternative electrophilic substitutions. Very recent developments on the borylation of pyridines and 2,2′-bipyridines were also presented, including rare examples of functionalization at the position *ortho* to the pyridinyl nitrogen atom or to a substituent on the pyridinyl ring.

The remarkable chemoselectivity of the iridium-catalyzed borylation process for aromatic C–H bonds, in the presence of other potentially reactive C–X sites (X = Cl, Br, I, etc.), was highlighted in the lecture by Smith.[1] This important feature allowed for further elaboration of the borylated products in one-pot catalytic cascade reactions, in which borylation was coupled with, most notably, Suzuki–Miyaura cross-coupling reactions to produce variously substituted biaryls.

Reports on the utilization of boron-containing compounds as reagents or intermediates in organic syntheses represented a prominent part of the conference program. The application of enantiomerically enriched B-allyl- or B-alkynyl-10-trimethylsilyl-9-bora[3.3.2]-bicyclodecanes to allylboration reactions of *N*-trimethylsilyl-substituted aromatic aldimines or 1,4-additions to their *N*-acyl-substituted analogues, leading to the asymmetric synthesis of secondary alkyl homoallylic amines or propargyl amides, respectively, was discussed by J. A. Soderquist (University of Puerto Rico).

The asymmetric synthesis of homoallylic amines through allylboration of *N*-metalloimines with α-pinene-based organoboron reagents was addressed in the contribution offered by P. V. Ramachandran (Purdue University), while allylic organoboranes and their application to the synthesis of a variety of

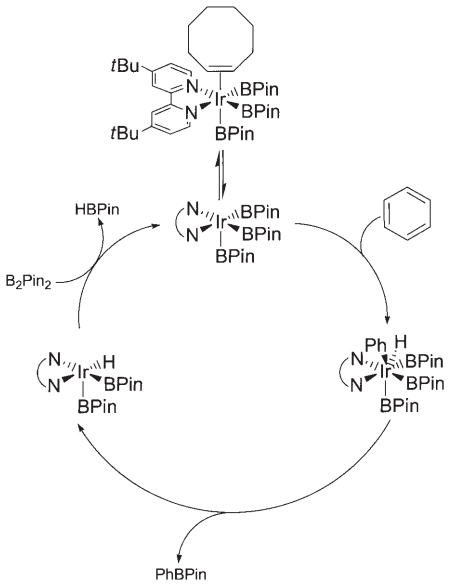

Scheme 1. Catalytic cycle for the iridium-catalyzed aromatic borylation reaction. Pin = pinacolate.

[*] Prof. Dr. H. Braunschweig, Dr. D. Rais
Bayerische Julius-Maximilians-Universität Würzburg
Institut für Anorganische Chemie
Am Hubland
97074 Würzburg (Germany)
Fax: (+49) 931-888-4623
Tel.: (+49) 931-888-5260
E-mail: h.braunschweig@mail.uni-wuerzburg.de

[**] 12th International Conference on Boron Chemistry in Sendai, Japan, September 11–15, 2005.

InterScience
© 2005 Wiley-VCH Verlag GmbH & Co. KGaA, Weinheim

nitrogen-containing bicyclic and cage-type compounds were described by Y. N. Bubnov (Russian Academy of Sciences, Moscow). The synthesis of nitrogen-containing heterocycles and a variety of amine derivatives through one-step, three-component reactions between organoboron compounds, amines, and carbonyl substrates was described by N. A. Petasis (University of Southern California).

M. Suginome (Kyoto University) delineated the successful efforts of his research group towards the utilization of aminoboranes as "iminium ion generators" in amination reactions. Diaminoboranes that incorporate nucleophilic groups, such as a cyano substituent, and the aminoborane-based "universal iminium ion generator" *N*,*N*-diisopropyl-4*H*-benzo[d][1,3,2]-dioxaboririn-2-amine, which is designed to aid reactions in the presence of external nucleophiles and free amines as the amino source, were employed in Mannich-type transformations.

P_π–π^* conjugation between a π-conjugated system and the vacant p orbital of an sp^2-hybridized boron atom confers intriguing electronic and photophysical properties to boron-containing materials. Y. Chujo (Kyoto University) detailed the optical properties associated with conjugated polymers featuring pyrazabole units and triply bridged poly(pyrazabole)s in the main chain, while the stereoselective hydroboration of di- and triethynyl-substituted aromatic systems and the subsequent application of the resulting vinylboronate esters to Suzuki–Miyaura cross-coupling reactions with chromophore-containing coupling partners were employed by S. O. Kang (Korea University) in the synthesis of fluorescent dyes and light-emitting polymers. Further efforts towards the synthesis of fully conjugated electron-rich borole-containing systems, as well as the development of green/blue-luminescent materials based on phenoxyoxazolylboron compounds were also sketched.

A number of fascinating systems were highlighted by S. Yamaguchi (Nagoya University) in his lecture. Highly conjugated materials comprising the dibenzoborole unit and their photophysical properties were presented. The concept of π-conjugated molecular bundles that stem from a sixfold functionalization of the hexagonal borazine core with π-conjugated substituents was also introduced, and the great potential of this molecular motif for the generation of new π-electron materials was highlighted (Figure 1).[2] Interestingly, the propensity of the boron center to interact reversibly with Lewis bases, modifying its hybridization and interrupting the π conjugation with the organic framework, was utilized, for instance, in designing boron-based colorimetric sensors for fluoride anion. The design of similar chemosensors for the quantitative detection of glucose and other saccharides was illustrated by S. Shinkai (Kyushu University).

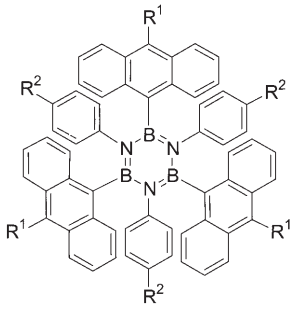

Figure 1. Borazine-based π-conjugated molecular bundle.

Fluorescent conjugated materials with a boron–nitrogen core were also presented by W. E. Piers (University of Calgary). Cyclization reactions of 2,6-dialkynylpyridine adducts of borabenzenes yield luminescent B–N analogues of pyrene. The photophysical properties of various pyridazine-2,2′-diborabiphenyl adducts and their reduction products were also reported.

Numerous contributions focused on fundamental aspects as well as novel and applicative developments of carborane chemistry, a multifaceted topic of long-standing interest for the boron chemistry community. Particularly impressive for their quality of results and future applications were the lectures held by M. F. Hawthorne (University of California, Los Angeles) and L. G. Sneddon (University of Pennsylvania). On the basis of the known chemistry of Ni^{III} and Ni^{IV} *commo*-bis-7,8-dicarbollyl metallacarboranes, Hawthorne described his group's efforts towards the design and synthesis of rotary molecular motors powered by a redox process.[3] Oxidation of Ni^{III} to Ni^{IV} determines a change from a transoid, that is, a disposition where the two carbon atoms on the cages are related through an inversion center, to a cisoid disposition of the two carborane cages. Such redox-driven interconversion of the two geometries constitutes the basis for the rotational motion, which can be induced chemically, electrochemically, or photochemically (Figure 2).

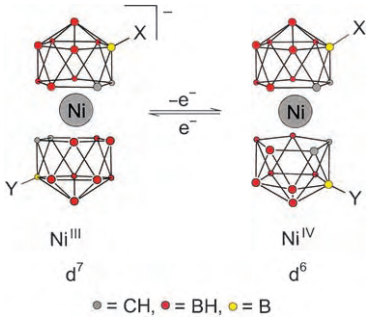

Figure 2. Nickelacarborane-based rotary molecular motors.

The lecture by Sneddon related to recent developments concerning the reactions of polyborane with unsaturated organic substrates in ionic liquids. Functionalized decaboranes are obtained in high yields upon metal-free hydroboration of polyborane olefins, while insertion rather than hydroboration occurs with a variety of alkynes, providing a new, versatile one-step route to functionalized *ortho*-carborane clusters. A survey of the reactivity of Group VI to IX metallaboranes with alkynes was provided by T. P. Fehlner (University of Notre Dame), while details on the chemistry of bis- and tris-mercaptoborates and lanthanacarboranes were provided by S. Shore (Ohio State University) and N. S. Hosmane (Northern Illinois University), respectively.

Reports on pharmacologically active boron-containing compounds were also presented. After an interesting overview on the mechanisms and consequences of biofilm formation, M. Srebnik (Hebrew University) presented his results on the synthesis and antimicrobial activity evaluation of differently substituted oxaborolidines. The quest for engineering porous supramolecular networks

© 2005 Wiley-VCH Verlag GmbH & Co. KGaA, Weinheim

based on hydrogen-bonding interactions between boronic acids was detailed in the lecture given by J. D. Wuest (Université de Montréal), while N. C. Norman (University of Bristol) commented on the first structural determination of diboronic acid, $B_2(OH)_4$, and provided details on a synthetic route to pure boron(II) oxide, together with spectroscopic and analytical data on this elusive compound.

In conclusion, a comprehensive overview of all modern aspects of boron chemistry was presented, demonstrating the importance of boron-containing compounds in topical areas of research, such as the functionalization of hydrocarbons and materials science. The boron community looks forward to IMEBORON XIII, the next event in the series, which will be hosted by F. Teixidor in Barcelona-Girona in 2008.

[1] J.-Y. Cho, M. K. Tse, D. Holmes, R. E. Maleczka, Jr, M. R. Smith III, *Science* **2002**, *295*, 305.
[2] A. Wakamiya, T. Ide, S. Yamaguchi, *J. Am. Chem. Soc.* **2005**, *127*, 14859.
[3] M. F. Hawthorne, J. I. Zink, J. M. Skelton, M. J. Bayer, C. Liu, E. Livshits, R. Baer, D. Neuhauser, *Science* **2004**, *303*, 1849.

DOI: 10.1002/anie.200503703

Concise Insight of 20 Years of Research

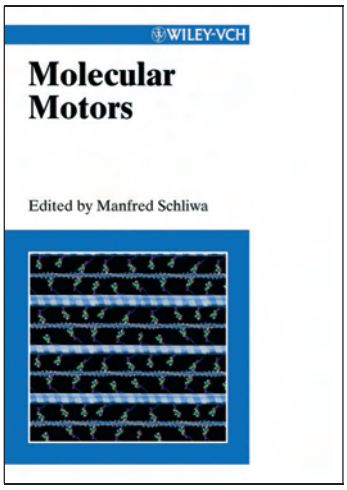

2002. XXII, 582 pages, 129 figures 48 in color, 20 tables. Hardcover. ISBN 3-527-30594-7 € 179.- /£ 125.- /US$ 245.-

MANFRED SCHLIWA, University of Munich, Germany (Ed.)

Molecular Motors

Cell motility, virus transport and developmental asymmetry are examples of biological processes related to the function or malfunction of the minute machinery of molecular motors. This handbook brings together current knowledge on the functionality, regulation, and interactions of cytoskeletal, DNA, and rotary motors. Leading experts present principles and applications ranging from atomic structure, biochemistry, and biophysics to cell biology, developmental biology and pathology - all set to become a "classic" in the years to come.

"...essential reading for graduate students in the field of cell motility and molecular motors... recommend it enthusiastically..."
- Nature Cell Biology

22540509_kn

Register now for the free
WILEY-VCH Newsletter!
www.wiley-vch.de/home/pas

WILEY-VCH • P.O. Box 10 11 61 • D-69451 Weinheim, Germany
Fax: +49 (0) 62 01 - 60 61 84
e-mail: service@wiley-vch.de • http://www.wiley-vch.de

WILEY-VCH

 © 2005 Wiley-VCH Verlag GmbH & Co. KGaA, Weinheim

Organic Synthesis

DOI: 10.1002/anie.200502640

The Discovery of Novel Metal-Induced Reactions of Nitrones: Not Only Electrophiles and Reagents for [3+2] Cycloadditions

*Francesca Cardona and Andrea Goti**

Keywords:
cycloaddition · nitrones · organic synthesis · samarium · ytterbium

Dedicated to Professor Dr. Rolf Huisgen on the occasion of his 85th birthday

Nitrones **1** have been known for more than a century, and their main reactivities as electrophiles towards organometallic reagents (Scheme 1, reaction A)

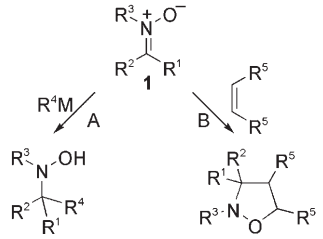

Scheme 1. Reactions of nitrones as electrophiles and 1,3-dipoles.

and as 1,3-dipolar reagents in cycloadditions (Scheme 1, reaction B) have long been recognized.[1] Nowadays, these reactions are employed profusely and nitrones have assumed a prominent role as extremely useful and reliable intermediates in synthetic applications, most notably through the exploitation of diastereo- and enantioselective procedures.[2]

In the last few years a multitude of novel reactions involving nitrones have been discovered which yield structurally diverse and highly functionalized useful products. Most of the new C–C bond-forming reactions have been effected by the use of metal derivatives, which alter the usual nitrone reactivity. The reactions which showed broader scope and potential, and have already witnessed useful synthetic application, are two metal-mediated cycloadditions, namely a formal [2+2] (the Kinugasa reaction, which affords β-lactam derivatives and has recently been reviewed)[3] and a formal [3+3] cycloaddition, as well as a coupling reaction based on umpolung reactivity of a nitrone as a nucleophile.[4] The two latter reactions are illustrated herein.

Young and Kerr discovered a completely new [3+3] cycloaddition of nitrones **2**, which reacted with 1,1-cyclopropane diesters **3** under $Yb(OTf)_3$ catalysis to give the quite uncommon tetrahydro-1,2-oxazine ring (Scheme 2).[5,6] This structural unit occurs in a few natural products, such as FR900482 and related compounds.[7]

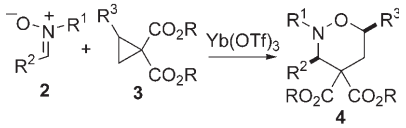

Scheme 2. [3+3] Cycloaddition of nitrones **2**. Tf = trifluoromethanesulfonyl.

This unique reaction, which has been described as a homo [3+2] dipolar cycloaddition, was completely regioselective and stereoselective, and afforded the *cis* adducts **4** exclusively. The same authors developed a three-component version of this reaction, in which the nitrones were formed in situ by reaction of hydroxylamines with aldehydes.[8] Screening of a number of other Lewis acids showed that anhydrous MgI_2 is also an effective promoter of the reaction, and acts in a complementary manner to $Yb(OTf)_3$.[9] In some cases the reaction with MgI_2 was not completely *cis*-diasteroselective, and some of the *trans* isomer were formed.

Very recently, Sibi et al. accomplished the first enantioselective version of this reaction. Asymmetric induction was achieved by addition of nitrones **5** to activated cyclopropanes **6** under catalysis by Lewis acids in the presence of chiral bis(oxazoline) ligands (Scheme 3).[10] The best results were achieved with $Ni(ClO_4)_2$ and ligand **7** (up to 99% yields and 89–99% *ee*). In contrast to $Yb(OTf)_3$, this chiral catalyst gave almost no *cis*/*trans* diastereoselectivity, but gave excellent enantioselectivity for both diastereoisomers of **8**.

Several different pathways have been proposed by the authors to explain

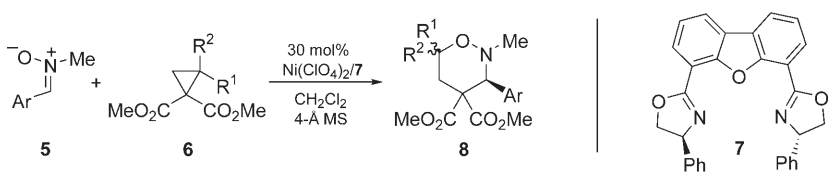

Scheme 3. Enantioselective [3+3] cycloaddition of nitrones. MS = molecular sieves.

[*] Dr. F. Cardona, Prof. A. Goti
Dipartimento di Chimica Organica
"Ugo Schiff" and ICCOM-CNR
Università di Firenze
via della Lastruccia 13
50019 Sesto Fiorentino (FI), Italy
Fax: (+39) 055-457-3531
E-mail: andrea.goti@unifi.it

InterScience
© 2005 Wiley-VCH Verlag GmbH & Co. KGaA, Weinheim

the findings of this interesting addition of nitrones to activated cyclopropanes,[9,10] which depends on the metal catalyst employed. The mechanism proposed by Ganton and Kerr[9] is outlined in Scheme 4, and accounts for the formation of the *cis* isomer through ring closure of the initially formed chairlike intermediate **A**. The *trans* isomer would be generated by a chair-flip or conformational change of the iminium ion in intermediate **A**. However, more detailed studies are needed to clarify the intimate mechanistic aspects of the reaction.

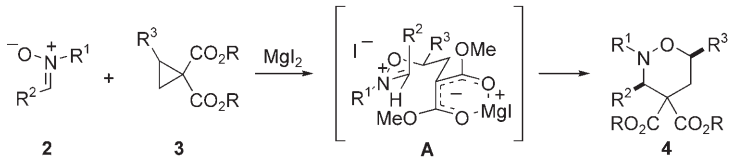

Scheme 4. Proposed mechanism for the addition of nitrones to activated cyclopropanes.

Although the scope of this novel [3+3] cycloaddition is clearly limited by the need for cyclopropanes substituted with two strongly electron-withdrawing groups in the geminal positions, its synthetic utility has already been demonstrated by an elegant approach to the tetracyclic core of nakadomarin A (Scheme 5). Nakadomarin A is an uncommon alkaloid related to manzamines recently isolated from a sea sponge[11] which possesses a range of useful bioactivities (anticancer, antifungal, antibacterial). The 3,2′-linked oxazine–furan motif in **12** was assembled by a key three-component cycloaddition catalyzed by $Yb(OTf)_3$.[12] A selective reduction of the ester group *cis* to the furyl substituent followed by Horner–Emmons olefination then furnished compound **13**, which underwent a Heck reaction to **14**. Hydrogenolysis of the N–O bond and subsequent mesylation gave the fused 5,5,5 tricyclic moiety **15** of the alkaloid, on which the fused six-membered ring was assembled by straightforward synthetic transformations to give compound **16** (Scheme 5).

Another lanthanide compound was the key for the recently discovered umpolung reactivity of nitrones, which react with electrophiles at the carbon atom in the presence of SmI_2. These coupling reactions also appear to be of broad scope and several applications have already been reported. The method was first described by Py and coworkers for aldehydes or ketones **17** as the acceptors and afforded β-hydroxyamino alcohol derivatives **18** (Scheme 6, reaction A).[13]

An initial chemoselective single-electron transfer (SET) from SmI_2 to the nitrone was ascertained, and a subsequent radical coupling was proposed to occur.[14] However, no conclusive proof of the mechanism of this and the related subsequent reactions has been obtained, and a process involving further reduction of the initially formed radical by a second equivalent of SmI_2 followed by nucleophilic attack of the generated carbanionic species cannot be ruled out. Irrespective of the mechanism, the method turned out to be of considerable scope, and several examples of acyclic and exocyclic nitrones reacting with a large series of aldehydes, ketones, and oxoaldehydes, either in an inter- or intramolecular fashion, were reported. Nitrones proved to be far superior to imines, oximes, and hydra-

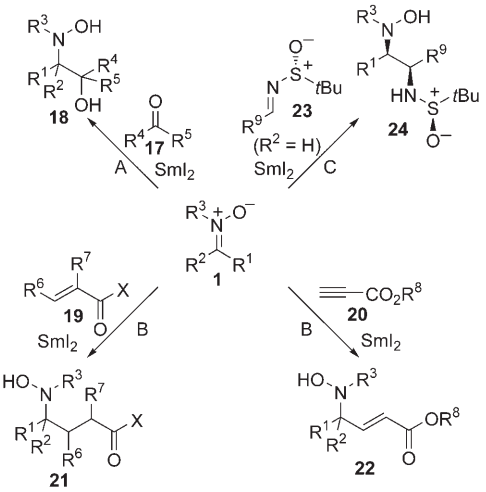

Scheme 6. Examples of the umpolung reactivity of nitrones.

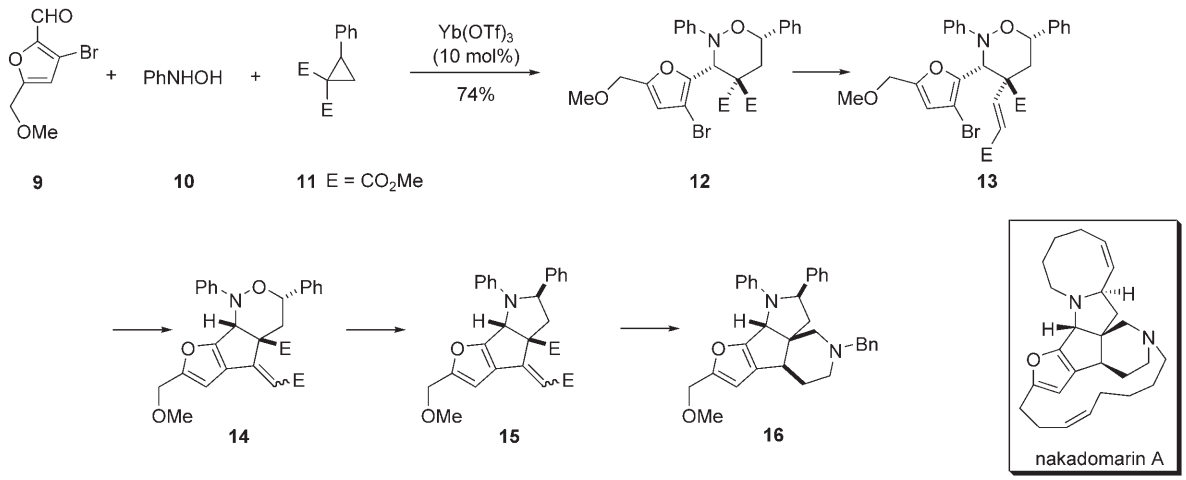

Scheme 5. Use of the [3+3] cycloaddition for the synthesis of the tetracyclic core of nakadomarin A.

 © 2005 Wiley-VCH Verlag GmbH & Co. KGaA, Weinheim

zones for this intermolecular coupling reaction.

Interestingly, reduction of the hydroxyamino functionality to the corresponding amino group was also accomplished when an excess of SmI_2 (6 equiv) was used, and afforded β-amino alcohols directly. This reaction is exemplified by the domino intramolecular coupling/deoxygenation of **25** to the amino alcohol **27** (Scheme 7).[13]

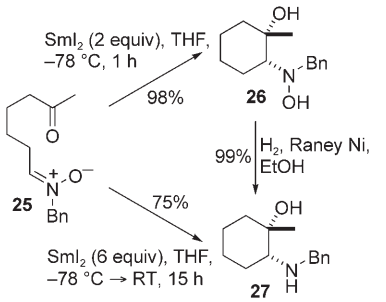

Scheme 7. Domino intramolecular coupling/deoxygenation of **25**. Bn = benzyl.

A highly stereoselective version employing planar chiral tricarbonylchromium complex **28** of *C*-arylnitrones has been developed, which afforded β-hydroxyamino and β-amino alcohols **29** and **30** (Scheme 8), respectively, in excellent yield. The reaction also often gave one diastereoisomer exclusively as a result of a highly preferred approach of the ketone or aldehyde to the face of the nitrone opposite to the bulky (tricarbonyl)chromium moiety.[15] Enantiomerically pure starting nitrones resulted in an enantioselective synthesis of benzylamines after decomplexation.

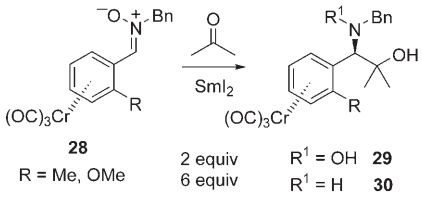

Scheme 8. Stereoselective version of the intramolecular SmI_2-mediated coupling reaction.

A variation of this reaction which employed conjugated unsaturated esters or amides as the acceptors (Scheme 6, reactions B) was reported independently soon afterwards by Py and co-workers as well as by Riber and Skrydstrup.[16] Again, a large number of acyclic as well as exo- and endocyclic nitrones, including chiral ones, has been shown to take part in the reaction. Not only are acrylates and acrylamides **19** suitable partners as acceptors, but even propiolates **20**, for which intermolecular SmI_2-induced additions had not been recorded previously, can be used. These acceptors afford γ-hydroxyamino esters and amides **21**, and γ-hydroxyamino-α,β-*E*-unsaturated esters **22**, respectively, through conjugate addition reactions. The adducts of acrylic derivatives have been transformed into γ-amino acids or into small peptides containing γ-amino acids.[16b] The reactions must be performed at low temperature (−78 °C) to achieve a fine balance of chemoselectivity when using reagents possessing similar reactivity: reduction and homocoupling of the acceptor compete at higher temperature. The effect of added water is very important, and results generally in rate acceleration and improvement in the reaction yield. Methacrylates and (*E*)-crotonates can also be used in this reaction to furnish products with high diastereoselectivity (up to > 90:10 d.r.) in favor of the *syn* and *anti* isomers, respectively.

Chiral auxiliaries have been used, either as substituents at the nitrone nitrogen atom or at the unsaturated ester or amide, to achieve enantioselectivity (Scheme 9).[16,17] The latter approach afforded up to 90:10 d.r. (for example, in the synthesis of γ-hydroxyaminoester **33**),[16b] while the former one gave moderate to very good enantioselectivity for *N*-benzyl-type substituents[16a] and excellent enantioselectivity for *N*-glycosylnitrones, such as **34**.[17] In this case, opposite absolute configuration at the new stereogenic center was achieved by changing the carbohydrate auxiliary from a D-mannose to a D-ribose derivative.

More recently, a very interesting variant of these reactions has been discovered, which employs enantiopure *N*-*tert*-butylsulfinylimines **23** as acceptors (Scheme 6, reaction C), and affords vicinal *N*-hydroxy-*N*′-sulfinyldiamines **24** which could be transformed into 1,2-diamines by reductive procedures and treatment with acid.[18] This reaction was the first example of an enantioselective cross-coupling between two different imine species. The addition reaction was highly stereoselective (> 7:1 d.r., but in many cases only one diastereoisomer was detected), and ultimately gave enantiomerically pure diamines that are relevant for use in natural products synthesis and as chiral ligands in asymmetric catalysis. The high level of stereoselectivity in the addition was rationalized on the basis of a preferred chelated transition state with the *Si* face of the nitrone approaching the less hindered *Si* face of the sulfinylimine to accommodate the two substituents R^1 and R^8 at the reacting carbon atoms in an antiperiplanar conformation (Figure 1).

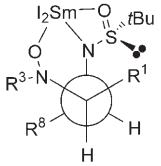

Figure 1. Transition-state model proposed for the SmI_2-mediated addition of nitrones to sulfinylimines.

Full exploitation of these versatile and

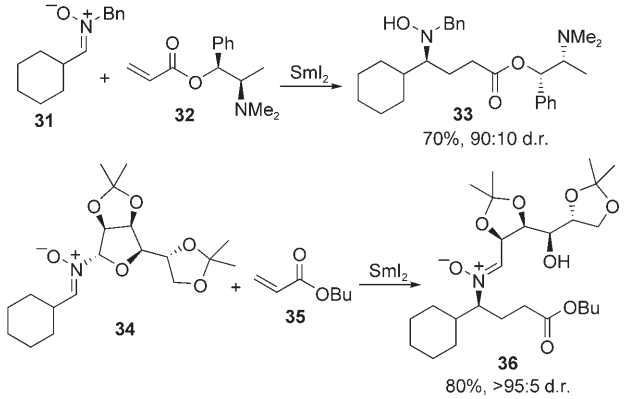

Scheme 9. Use of chiral auxiliaries to achieve enantioselectivity.

 © 2005 Wiley-VCH Verlag GmbH & Co. KGaA, Weinheim

flexible new procedures involving nitrones is likely to warrant access to many structurally diverse nitrogen compounds in the near future. This proposal is corroborated by the elegant applications already reported. An intramolecular nitrone–ketone coupling was the key step for the synthesis of the aminocyclopentitol 1-epitrehazolamine (Scheme 10).[19] The coupling of acrylates with chiral nitrones were strategic in the synthesis of (*S*)-vigabatrin,[20] an irreversible inhibitor of GABA amino transferase, and of the pyrrolizidine alkaloid hyacinthacine A_2 (Scheme 10).[21,22]

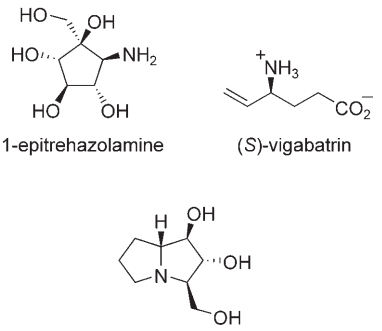

Scheme 10. Natural products synthesized by the SmI_2-induced coupling of nitrones with electrophiles.

These novel reactions serve to exemplify the extent to which unexpected and undisclosed new reactivities may come to light when metals come into play, even when "old" compounds, whose chemistry is considered completely known, are concerned.

[1] For a review on the pioneering contributions from Huisgen's research group to the field of 1,3-dipolar cycloadditions, see: a) R. Huisgen, *Angew. Chem.* **1963**, *75*, 604–637; *Angew. Chem. Int. Ed. Engl.* **1963**, *2*, 565–598; for early reviews on nitrones, see: b) L. I. Smith, *Chem. Rev.* **1938**, *38*, 193–285; c) J. Hamer, A. Macaluso, *Chem. Rev.* **1964**, *64*, 473–495.

[2] Reviews: a) P. Merino in *Science of Synthesis, Vol. 27* (Ed.: A. Padwa), Thieme, Stuttgart, **2004**, pp. 511–580; b) J. J. Tufariello in *1,3-Dipolar Cycloaddition Chemistry, Vol. 2* (Ed.: A. Padwa), Wiley, New York, **1984**, pp. 83–168; c) M. Frederickson, *Tetrahedron* **1997**, *53*, 403–425; d) K. V. Gothelf, K. A. Jørgensen, *Chem. Rev.* **1998**, *98*, 863–909; e) R. C. F. Jones, J. N. Martin in *Synthetic Applications of 1,3-Dipolar Cycloaddition Chemistry Toward Heterocycles and Natural Products*, *The Chemistry of Heterocyclic Compounds, Vol. 59* (Eds.: A. Padwa, W. H. Pearson), Wiley, New York, **2002**, pp. 1–81.

[3] J. Marco-Contelles, *Angew. Chem.* **2004**, *116*, 2248–2250; *Angew. Chem. Int. Ed.* **2004**, *43*, 2198–2200.

[4] For other recently discovered unusual reactions of nitrones, see: a) S. Hanessian, M. Bayrakdarian, *Tetrahedron Lett.* **2002**, *43*, 967–971; b) A. Bøgevig, K. V. Gothelf, K. A. Jørgensen, *Chem. Eur. J.* **2002**, *8*, 5652–5661; c) M. A. Voinov, I. A. Grigor'ev, L. B. Volodarsky, *Tetrahedron* **2000**, *56*, 4071–4077.

[5] I. S. Young, M. A. Kerr, *Angew. Chem.* **2003**, *115*, 3131–3134; *Angew. Chem. Int. Ed.* **2003**, *42*, 3023–3026.

[6] Closely related synthetically valuable dihydro-1,2-oxazines have recently been accessed by Reissig and co-workers through a two-step [3+3] cyclization process from lithiated alkoxyallenes and nitrones: M. Helms, W. Schade, R. Pulz, T. Watanabe, A. Al-Harrasi, L. Fišera, I. Hlobilová, G. Zahn, H.-U. Reissig, *Eur. J. Org. Chem.* **2005**, 1003–1019, and references therein.

[7] I. Uchida, T. Shigehiro, K. Hiroshi, K. Sumio, M. Hashimoto, T. Tada, K. Shigetaka, Y. Morimoto, *J. Am. Chem. Soc.* **1987**, *109*, 4108–4109.

[8] I. S. Young, M. A. Kerr, *Org. Lett.* **2004**, *6*, 139–141.

[9] M. D. Ganton, M. A. Kerr, *J. Org. Chem.* **2004**, *69*, 8554–8557.

[10] M. K. Sibi, Z. Ma, C. P. Jasperse, *J. Am. Chem. Soc.* **2005**, *127*, 5764–5765.

[11] J. Kobayashi, D. Watanabe, N. Kawasaki, M. Tsuda, *J. Org. Chem.* **1997**, *62*, 9236–9239.

[12] I. S. Young, J. L. Williams, M. A. Kerr, *Org. Lett.* **2005**, *7*, 953–955.

[13] G. Masson, S. Py, Y. Vallée, *Angew. Chem.* **2002**, *114*, 1850–1853; *Angew. Chem. Int. Ed.* **2002**, *41*, 1772–1775.

[14] Although nitrones have been largely used as spin traps for short-lived reactive free radicals, only a few reports document their use in synthetically useful radical additions; for a recent example of a chiral nitrone employed in radical additions for the enantioselective synthesis of α-amino acids, see: M. Ueda, H. Miyabe, M. Teramachi, O. Miyata, T. Naito, *Chem. Commun.* **2003**, 426–427.

[15] M. Chavarot, M. Rivard, F. Rose-Munch, E. Rose, S. Py, *Chem. Commun.* **2004**, 2330–2331.

[16] a) G. Masson, P. Cividino, S. Py, Y. Vallée, *Angew. Chem.* **2003**, *115*, 2367–2370; *Angew. Chem. Int. Ed.* **2003**, *42*, 2265–2268; b) D. Riber, T. Skrydstrup, *Org. Lett.* **2003**, *5*, 229–231.

[17] S. A. Johannesen, S. Albu, R. G. Hazell, T. Skrydstrup, *Chem. Commun.* **2004**, 1962–1963.

[18] Y.-W. Zhong, M.-H. Xu, G.-Q. Lin, *Org. Lett.* **2004**, *6*, 3953–3956.

[19] G. Masson, C. Philouze, S. Py, *Org. Biomol. Chem.* **2005**, *3*, 2067–2069.

[20] G. Masson, W. Zeghida, P. Cividino, S. Py, Y. Vallée, *Synlett* **2003**, 1527–1529.

[21] S. Desvergnes, S. Py, Y. Vallée, *J. Org. Chem.* **2005**, *70*, 1459–1462.

[22] For a different synthesis of hyacinthacine A_2 based on cycloaddition to the same nitrone, see: F. Cardona, E. Faggi, F. Liguori, M. Cacciarini, A. Goti, *Tetrahedron Lett.* **2003**, *44*, 2315–2318.

 © 2005 Wiley-VCH Verlag GmbH & Co. KGaA, Weinheim

History of Chemistry

DOI: 10.1002/anie.200503351

Adolf von Baeyer: Winner of the Nobel Prize for Chemistry 1905

*Armin de Meijere**

Keywords:
benzene · history of chemistry · indigo · nitroso compounds · von Baeyer, Adolf

On December 10, 1905, Johann Friedrich Wilhelm Adolf Ritter von Baeyer (*October 31, 1835 in Berlin, † August 20, 1917 in Starnberg) received the Nobel Prize for Chemistry of the Royal Swedish Academy of Sciences in Stockholm. It was the fifth Nobel Prize for chemistry at all, and it was awarded to von Baeyer "in recognition of his services in the advancement of organic chemistry and the chemical industry, through his work on organic dyes and hydroaromatic compounds". Adolf von Baeyer was a doctoral student in the group of Kekulé in Heidelberg until 1858. He succeeded Justus von Liebig as director of the Chemical Laboratory of the Bavarian Academy of Sciences in Munich in 1875. This latter period was preceded by 12 fruitful years as Professor at the "Gewerbeinstitut" (forerunner to the Technical University) in Berlin and 3 years at the University of Strasbourg, after his Habilitation in 1860 in Berlin. Even before his time in Munich he described the first synthesis of barbituric acid (1864), the polycondensation of phenol with formaldehyde (1872), the structural elucidation of compounds within the uric acid group (from 1860) and other *N*-heteroarenes (from 1868), the preparation of phthaleins (from 1869), nitroso compounds (from 1869), as well as hydroaromatic compounds (from 1866) and their transformations into benzene derivatives. An excellent review of Adolf von Baeyer's scientific achievements has been provided in an article by Rolf Huisgen that appeared in this journal twenty years ago.[1] On the occasion of the 100th anniversary of the Nobel Prize being awarded to Adolf von Baeyer, some thoughts on the current relevance of his research are mentioned here.[#]

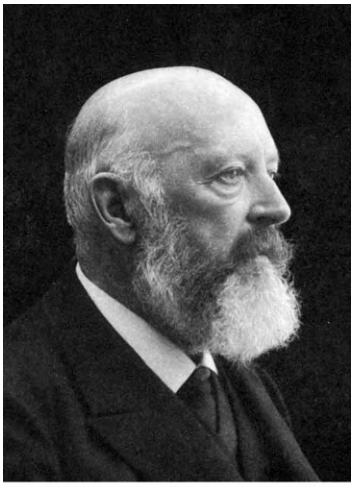

Adolf von Baeyer
(1835–1917)

Quite personally, I became interested in the scientific work of von Baeyer at the very beginning of my work towards my first thesis (Master's degree). At that time I was engaged in the synthesis and conformational analysis of cyclopropane derivatives, especially of bicyclopropyl, by spectroscopic methods. Naturally, I had become acquainted with von Baeyer's theory of ring strain during my undergraduate education, but it was not until I prepared my sample lecture for my Habilitation 10 years later that I read the original paper concerning this often quoted theory.[2] I was surprised to find that this publication entitled "On Polyacetylene Compounds" in reality described the synthesis of a series of oligoacetylene derivatives such as diacetylene dicarboxylic acid, tetraacetylene dicarboxylic acid, diiodoacetylene, and diiododiacetylene. In the context of his conjectures concerning the observed explosive properties of the new acetylenes, von Baeyer expressed some thoughts about the "*Theory of Ring Closure and the Double Bond*" in an appendix ("Theoretical considerations") and he summarized these in one core sentence after six generally accepted sentences about the bonding ability of the carbon atom (Figure 1): "*The four valences of the carbon atom act in the directions that connect the center of a sphere with the corners of a tetrahedron and that form an angle of 109° 28′ with each other. The direction of the attraction can experience a deviation that will, however, cause an increase in strain correlating with the degree of this deviation.*"

These considerations of von Baeyer were initiated by the fact that his young English doctoral associate, William Henry Perkin, had just prepared the first cyclopropane derivatives in his laboratory in Munich,[3] even though

[*] Prof. Dr. A. de Meijere
Institut für Organische und Biomolekulare Chemie
Georg-August-Universität Göttingen
Tammannstrasse 2
37077 Göttingen (Germany)
Fax: (+49) 551-399-475
E-mail: armin.demeijere@chemie.uni-goettingen.de

[#] To commemorate the 50th anniversary of his appointment as lecturer and the 75th birthday of his teacher Adolf von Baeyer, one of the most outstanding industrial chemists of the 20th century, Carl Duisberg, established the "Adolf von Baeyer Medal" on May 19, 1910. Since then, the German Chemical Society has awarded this prize in irregular intervals to a total of 47 chemists, predominantly Germans.

InterScience
© 2005 Wiley-VCH Verlag GmbH & Co. KGaA, Weinheim

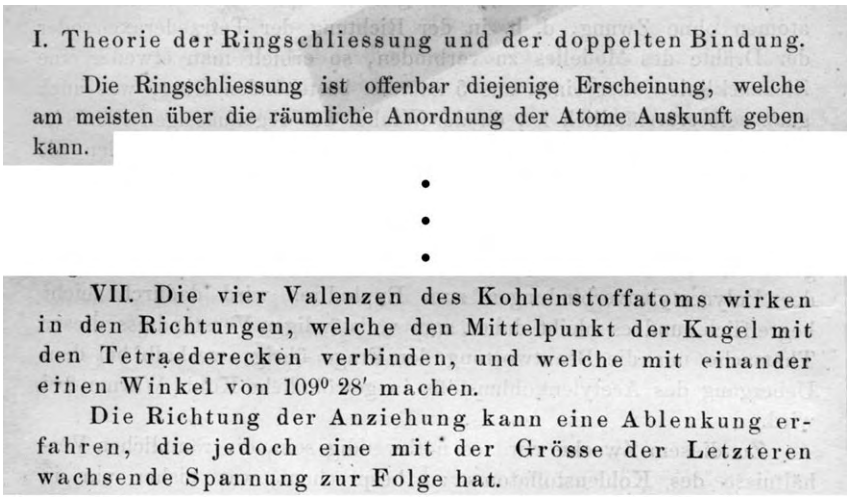

I. Theorie der Ringschliessung und der doppelten Bindung.

Die Ringschliessung ist offenbar diejenige Erscheinung, welche am meisten über die räumliche Anordnung der Atome Auskunft geben kann.

•
•
•

VII. Die vier Valenzen des Kohlenstoffatoms wirken in den Richtungen, welche den Mittelpunkt der Kugel mit den Tetraederecken verbinden, und welche mit einander einen Winkel von 109° 28′ machen.

Die Richtung der Anziehung kann eine Ablenkung erfahren, die jedoch eine mit der Grösse der Letzteren wachsende Spannung zur Folge hat.

Figure 1. Reproduction of the passage from reference [2], in which von Baeyer expresses his thoughts on the origin of ring strain. (*I. Theory of Ring Closure and of the Double Bond. The ring closure is apparently the phenomenon that can provide the most detailed information about the arrangement of atoms. ... VII. " The four valences of the carbon atom act in the directions that connect the center of a sphere with the corners of a tetrahedron and that form an angle of 109° 28′ with each other. The direction of the attraction can experience a deviation that will, however, cause an increase in strain correlating with the degree of this deviation."*

Adolf von Baeyer himself and especially his meanwhile famous former student Viktor Meyer only a few years earlier had doubted whether three-membered carbon rings could exist at all.[4] During his studies, Perkin observed that cyclopropane derivatives undergo ring-opening reactions upon treatment with strong acids such as hydrogen bromide, and Adolf von Baeyer explained this behavior with an inherent ring strain that leads to an enhanced reactivity. It is also remarkable that Perkin published the first syntheses of small-ring molecules with his own name only, without that of his thesis mentor Adolf von Baeyer.

Subsequently, von Baeyer was criticized for his theory of ring strain, because he also conceived six- and higher-membered rings as being planar with bonding angles that deviated from the tetrahedral arrangement. The concept of ring strain, however, is as valid today just as it was 120 years ago for three- and four-membered rings, but in the meantime it is known that the total strain of a ring consists of three increments: one for angle strain (Baeyer strain), one for conformational strain (Pitzer strain) and a third for transannular strain (van der Waals strain).[5] The latter two concepts, however, became common knowledge only some 40 years later, and thus it is now well understood why seven-membered and larger rings—only the cyclohexane ring is unstrained—experience a certain degree of strain in spite of their not being planar. Incidentally, Adolf von Baeyer included ethylene in his concept of ring strain, and was thereby the first to consider ethylene as a two-membered ring. Through the work of Pauling (1931, 1958) it has become well known that ethylene, like the cyclopropane ring, can be described in terms of bent bonds, and that this theoretical description is an equivalent alternative to the more popular description with σ and π bonds first formulated by Erich Hückel in 1930.

Thus, Adolf von Baeyer became famous with an initially peripheral remark in one of his 305 publications,[1,6] and his concept of strain in small rings is mentioned in every first-year organic chemistry lecture as well as in every decent organic textbook. Baeyer's contributions to the chemistry of acetylenes and diacetylenes (a total of five publications), like the cited reference [2], continue to have an impact in modern times. Because of their manifold reactivities, acetylenes have always been popular and frequently applied building blocks for organic syntheses. Indeed, a whole branch of the chemical industry that existed into the 1960s was based on the chemistry of acetylenes and thus on the original contributions of Baeyer and later Reppe.[7] Acetylene chemistry has recently gained popularity once again, as acetylene derivatives are being used increasingly to construct some of the most unusual molecular architectures, most of them with several triple bonds. Such compounds may eventually achieve economic importance as so-called nanomaterials.[8]

Early on in my career, I also became acquainted with another two of the 14 major research areas of von Baeyer:[1,9] The chemistry of nitroso compounds and that of indigo. Both were research topics of my thesis mentor Wolfgang Lüttke in Göttingen. Lüttke et al. elucidated the basic chromophore of indigo by quantum-chemical calculations[10] and proved the theoretical predictions by experimental studies.[11,12] Naturally, the formation of indigo from *o*-nitrobenzaldehyde and acetone upon addition of dilute sodium hydroxide, barium hydroxide, or ammonia[13] discovered by von Baeyer, was adopted towards the synthesis of new, variously substituted indigo derivatives. Baeyer at his time had not innocently accepted this observation, but started "*a deeper investigation of the events that took place during this remarkable reaction*" (Figure 2).

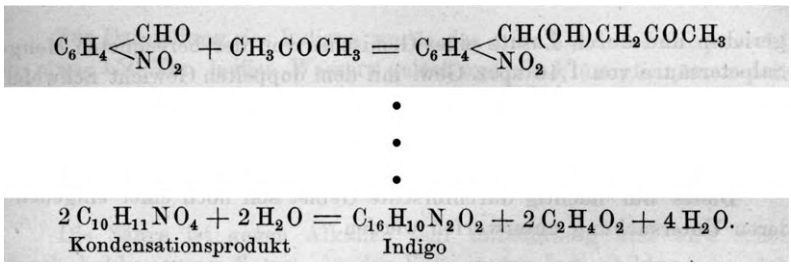

$$C_6H_4\!<\!\begin{matrix}CHO\\NO_2\end{matrix} + CH_3COCH_3 = C_6H_4\!<\!\begin{matrix}CH(OH)CH_2COCH_3\\NO_2\end{matrix}$$

•
•
•

$$2\,C_{10}H_{11}NO_4 + 2\,H_2O = C_{16}H_{10}N_2O_2 + 2\,C_2H_4O_2 + 4\,H_2O.$$

Kondensationsprodukt — Indigo

Figure 2. Equations for the formation of indigo from *o*-nitrobenzaldehyde and acetone, as presented in the original publication.[13] Kondensationsprodukt = condensation product.

© 2005 Wiley-VCH Verlag GmbH & Co. KGaA, Weinheim

He observed that indigo is only formed upon treatment of the aldol product (in the original publication this is called "condensation product") with dilute aqueous sodium hydroxide (or aqueous barium hydroxide or ammonia)—and not from the condensation product of *o*-nitrobenzaldehyde and acetone, *o*-nitrocinnamyl methyl ketone—and that the yield of indigo is even considerably better, when the aldol is first isolated and then treated with sodium hydroxide. Water plays an important role in this cyclizing condensation, and acetic acid is cleaved off. The mechanism of this multistep transformation was only fully elucidated in 1932 by Tanasescu and Georgescu.[14]

Even though this synthesis of indigo was not applied in its industrial production (just like the very first sequence from phenylacetic acid via isatin[15] and two additional syntheses, which were also developed by von Baeyer), it has substantially contributed to the final elucidation of the structure, which von-Baeyer disclosed in 1883 with a certain degree of pride (Figure 3).[16] The structural elucidation and the first syntheses by von Baeyer soon thereafter also formed the basis of the industrial production of indigo from anthranilic acid, which was developed at the Badische Anilin- und Sodafabrik (BASF) by Heumann.[17] The economic importance of this synthetic access to the "king of natural dyestuffs" was immense, and the fame of von Baeyer grew accordingly. Because of the timeless popularity of denim clothing, BASF still produces indigo, in spite of the fact that much better nonfading and hard-wearing synthetic dyes have long been available. But jeans, even when brand new, are preferred by their owners to look worn.

For von Baeyer, the intense occupation with indigo had developed from his previous studies of compounds within the uric acid group (13 publications between 1860 and 1866) as well as nitrogen-containing heteroaromatic compounds (21 publications between 1868 and 1883). He was not the first to conduct research in these areas, as he later stated in a lecture "On the History of the Indigo Synthesis," which he gave at a ceremonial meeting of the German Chemical Society on October 20, 1900: "*My studies on isatin originated from those on uric acid. They were initiated by Adolf Schlieper, who in 1860 asked me to continue his research, which he had carried out 15 years earlier in the laboratory of Liebig.*"[16] But the *N*-nitrosoamines as well as the aromatic and aliphatic *C*-nitroso compounds and their chemistry were developed by von Baeyer himself, in part together with Heinrich Caro (Figure 4) from the very beginning.[19,20]

Whereas he published only two papers on *N*-nitroso compounds, he occupied himself with *C*-nitroso compounds (at that time called "real nitroso structures") more intensively (12 publications) and for a longer period of time (1869–1902). It was once again Viktor Meyer [21] who questioned this work, believing that "*there is an unsurmountable natural aversion to the formation of real nitroso compounds, in which the nitroso group is bound to carbon through its nitrogen*" and who also doubted that the "*nitrosobenzene*" discovered by von Baeyer "*was a real nitroso structure.*" Of course, one has to take into account that all this happened long before modern spectroscopic methods,[22] and that proof for the constitution of novel compounds could only be obtained by elemental analysis, molecular-mass determination, melting and boiling points, as well as chemical transformations of known compounds into the new ones or of the new ones into known compounds. Baeyer succeeded in proving his structural assignment in the case of *C*-nitroso compounds, among others, with the observation that the blue products formed by the addition of nitrosyl chloride to tetramethylethylene, to $\Delta^{4(8)}$-terpenol acetate, and to other unsaturated terpenes, re-formed the olefins by cleaving off nitrosyl chloride upon heating.

Although the *N*-nitroso compounds, especially *N*-nitrosodimethylamine, enjoyed a short period of preparative applications,[23] they rapidly became infamous after the discovery of their carcinogenicity and after traces were even detected in beer. This has long been circumvented by modification of

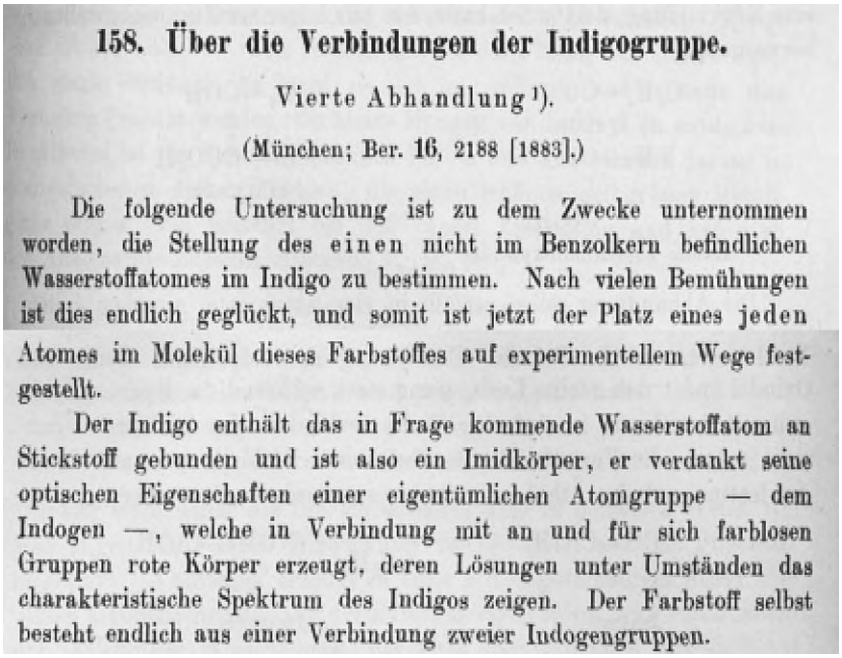

158. Über die Verbindungen der Indigogruppe.

Vierte Abhandlung [1]).

(München; Ber. 16, 2188 [1883].)

Die folgende Untersuchung ist zu dem Zwecke unternommen worden, die Stellung des einen nicht im Benzolkern befindlichen Wasserstoffatomes im Indigo zu bestimmen. Nach vielen Bemühungen ist dies endlich geglückt, und somit ist jetzt der Platz eines jeden Atomes im Molekül dieses Farbstoffes auf experimentellem Wege festgestellt.

Der Indigo enthält das in Frage kommende Wasserstoffatom an Stickstoff gebunden und ist also ein Imidkörper, er verdankt seine optischen Eigenschaften einer eigentümlichen Atomgruppe — dem Indogen —, welche in Verbindung mit an und für sich farblosen Gruppen rote Körper erzeugt, deren Lösungen unter Umständen das charakteristische Spektrum des Indigos zeigen. Der Farbstoff selbst besteht endlich aus einer Verbindung zweier Indogengruppen.

Figure 3. Introduction in the paper by von Baeyer on the final elucidation of the indigo structure. ***158. On the Compounds of the Indigo Group.*** **Fourth treatise**[1]. *(Munich; Ber.* ***16****, 2188 [1883].) The following investigation has been carried out in order to determine the position of the pne hydrogen atom in indigo which is not attached to the benzene nucleus. After many efforts, this has been successful, and thus the position of each atom in the molecule of this dye has now been determined experimentally. Indigo contains the hydrogen in question bound to nitrogen and thereby is an imide structure; it owes its optical properties to a peculiar atom grouping—the indogen—which, in connection with groups that are themselves colorless, generates red bodies, solutions of which possibly show the characteristic spectrum of indigo. The dyestuff itself consists of a composition of two indogen groups.*

 © 2005 Wiley-VCH Verlag GmbH & Co. KGaA, Weinheim

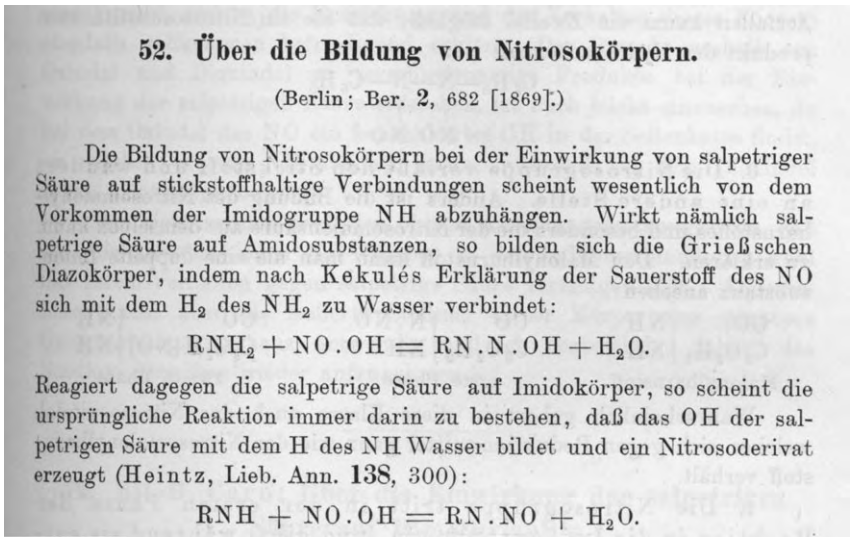

52. Über die Bildung von Nitrosokörpern.

(Berlin; Ber. 2, 682 [1869].)

Die Bildung von Nitrosokörpern bei der Einwirkung von salpetriger Säure auf stickstoffhaltige Verbindungen scheint wesentlich von dem Vorkommen der Imidogruppe NH abzuhängen. Wirkt nämlich salpetrige Säure auf Amidosubstanzen, so bilden sich die Grießschen Diazokörper, indem nach Kekulés Erklärung der Sauerstoff des NO sich mit dem H_2 des NH_2 zu Wasser verbindet:

$$RNH_2 + NO.OH = RN.N.OH + H_2O.$$

Reagiert dagegen die salpetrige Säure auf Imidokörper, so scheint die ursprüngliche Reaktion immer darin zu bestehen, daß das OH der salpetrigen Säure mit dem H des NH Wasser bildet und ein Nitrosoderivat erzeugt (Heintz, Lieb. Ann. 138, 300):

$$RNH + NO.OH = RN.NO + H_2O.$$

Figure 4. Excerpt from the paper "On the Formation of Nitroso Bodies".[20] *The formation of nitroso bodies upon the action of nitrous acid on nitrogen-containing compounds appears essentially to depend on the occurrence of the imido group NH. Upon the action of nitrous acid on amido compounds, Griess's diazo structures are formed, in which according to Kekulé's explanation, the oxygen of the NO has combined itself with the H_2 of the NH_2 to yield water:* (see equation)- *However, when nitrous acid acts upon imido structures, the initial reaction appears to be that in which the OH of the nitrous acid forms water with the H of the NH, and thus generates a nitroso derivative (Heinz, Lieb. Ann.* ***138****, 300):* (See equation)

the malting process. *N*-nitroso compounds have since also been virtually banned as synthetic building blocks from the chemical laboratory. The *C*-nitroso compounds,[24] on the other hand, are experiencing a renaissance as versatile reagents for the preparation of nitrogen-containing open-chain and cyclic compounds.[25]

One might call it a typical research topic of time past, and to a certain degree it certainly was: The constitution of benzene and of hydroaromatic compounds. Adolf von Baeyer himself chose the area of organoarsenic compounds for his doctoral thesis, and he carried it out in association with Kekulé, when the latter still was a lecturer in Heidelberg. After he obtained his doctoral degree in Berlin in 1858, Baeyer followed Kekulé as an assistant to the University of Gent and returned to Berlin in 1860 for his habilitation. Occasionally, he called himself an autodidact, yet he was provably one of the most passionate disciples of Kekulé, as he himself stated in a letter to Kekulé in 1864: "*Your outline on aromatic compounds caught my attention only recently. It reminded me vividly how much I am your follower, since a few months ago I presented the theory of the aromatic group in the same form, with almost the same words.*" Kekulé had presented his structural theory[26] in 1858, and had published his thoughts about the constitution of benzene[27] in 1865. Subsequently, von Baeyer occupied himself intensively with these ideas, which were significantly ahead of the times.

The papers of Baeyer on this topic represent the largest block of his publications (40 out of 305). Initially, his questions were born out of skepticism with regard to the constitutional formula of Kekulé, but according to the results of his own investigations concerning the reduction of phthalic acid and terephthalic acid with sodium amalgam—a predecessor of the Birch reduction discovered much later—upon the addition of bromine to the dihydro derivatives and upon further transformation of the bromine adducts, he concluded with incredible logic that other structural proposals, such as that of Ladenburg and of Dewar, did not really represent the properties of benzene. At most, he flirted for a while with a modified version of the structural proposal of Adolf Claus (1867) with one valence each from the six carbon atoms connected with each other in a cycle, pointing into the center of the ring. As the main speaker at the famous Benzene Festival of the German Chemical Society in honor of August von Kekulé 25 years after his publication of the cyclic benzene formula, Baeyer made the point:[28] "*In your theory of benzene, you have for the first time expressed the thought that the atoms of carbon cannot only form simple and branched chains, but also rings.*"

Building on this basic idea of Kekulé, Baeyer made significant early contributions to the understanding of the chemistry of aromatic compounds, and thereby provided the foundations for this blooming field in chemical industry—the exact thoughts expressed on the certificate of his Nobel Prize. Thus, it is no wonder that Adolf von Baeyer is recognized for his extremely important contribution to organic chemistry which extends even into modern times. And above all, it must be stressed that he performed most of his experiments with his own hands.

[1] "Adolf von Baeyer's Scientific Achievements—A Legacy": R. Huisgen, *Angew. Chem.* **1986**, *98*, 297–311; *Angew. Chem. Int. Ed. Engl.* **1986**, *25*, 297–311.

[2] A. von Baeyer, *Ber. Dtsch. Chem. Ges.* **1885**, *18*, 2269–2281.

[3] For a descriptive summary of the earlier papers, see: W. H. Perkin, *J. Chem. Soc.* **1929**, 1347–1363.

[4] V. Meyer, *Justus Liebigs Ann. Chem.* **1876**, *180*, 192–206.

[5] a) A. de Meijere, *Angew. Chem.* **1979**, *91*, 867–884; *Angew. Chem. Int. Ed. Engl.* **1979**, *18*, 809–826; b) K. B. Wiberg, *Angew. Chem.* **1986**, *98*, 312–322; *Angew. Chem. Int. Ed. Engl.* **1986**, *25*, 312–322.

[6] *Adolf von Baeyer's Collected Works* (*edited by his students and friends on the occasion of his 70th birthday*), Vieweg, Braunschweig, **1905**.

[7] a) W. Reppe, *Neue Entwicklungen auf dem Gebiete der Chemie des Acetylens und Kohlenoxyds*, Springer, Berlin, **1949**; b) W. Reppe, *Chemie und Technik der Acetylen-Druck-Reaktionen*, Verlag Chemie, Weinheim, **1951** (2nd ed. 1952).

[8] a) *Modern Acetylene Chemistry* (Eds.: F. Diederich, P. J. Stang, R. Tykwinski), Wiley-VCH, Weinheim, **1995** (1st ed.), **2004** (2nd ed.); see also the Nobel lecture: b) H. Shirakawa, *Angew. Chem.* **2001**, *113*, 2642–2648; *Angew. Chem. Int. Ed.* **2001**, *40*, 2574–2580.

[9] R. Willstätter et al., *Die Naturwissenschaften* **1915**, *3*, 559–599.

 © 2005 Wiley-VCH Verlag GmbH & Co. KGaA, Weinheim

[10] "The Chromophoric System of the Indigo Dyestuffs": M. Klessinger, W. Lüttke, *Tetrahedron* **1963**, *19* (Suppl. 2), 315 – 335.
[11] "Theoretically and Experimentally Determined Properties of the Basic Chromophore of Indigo": W. Lüttke, H. Hermann, M. Klessinger, *Angew. Chem.* **1966**, *78*, 638 – 639; *Angew. Chem. Int. Ed. Engl.* **1966**, *5*, 598 – 599.
[12] "4,4,4′,4′-Tetramethyl-$\Delta^{2,2}$-bipyrrolidine-3,3′-dione, a Compound with the Basic Chromophore of Indigo": E. Wille, W. Lüttke, *Angew. Chem.* **1971**, *83*, 853 – 854; *Angew. Chem. Int. Ed. Engl.* **1971**, *10*, 803 – 804.
[13] A. von Baeyer, V. Drewsen, *Ber. Dtsch. Chem. Ges.* **1882**, *15*, 2856 – 2864.
[14] I. Tanasescu, A. Georgescu, *Bull. Soc. Chim. Fr.* **1932**, *51*, 234 – 240.
[15] A. von Baeyer, *Ber. Dtsch. Chem. Ges.* **1878**, *11*, 1228 – 1229.
[16] A. von Baeyer, *Ber. Dtsch. Chem. Ges.* **1883**, *16*, 2188 – 2204.
[17] Deutsche Patentschrift No. 54626, Badische Anilin- und Sodafabrik, Ludwigshafen, May 6, 1890.
[18] A. Baeyer, *Ber. Dtsch. Chem. Ges.* **1900**, *33*, LI (special issue).
[19] A. Baeyer, H. Caro, *Ber. Dtsch. Chem. Ges.* **1874**, *7*, 809 – 811.
[20] A. Baeyer, *Ber. Dtsch. Chem. Ges.* **1869**, *2*, 682 – 684.
[21] V. Meyer, *Ber. Dtsch. Chem. Ges.* **1888**, *21*, 1291 – 1295.
[22] The first IR spectroscopic characterizations of nitroso compounds were reported from 1954 onward: W. Lüttke, *Angew. Chem.* **1954**, *66*, 159; W. Lüttke, *Z. Elektrochem.* **1957**, *61*, 302 – 313; W. Lüttke, *Z. Elektrochem.* **1957**, *61*, 976 – 986.
[23] For a Review, see: D. Seebach, D. Enders, *Angew. Chem.* **1975**, *87*, 1 – 18; *Angew. Chem. Int. Ed. Engl.* **1975**, *14*, 15 – 32.
[24] For an overview, see: B. G. Gowenlock, G. B. Richter-Addo, *Chem. Rev.* **2004**, *104*, 3315 – 3340.
[25] For a recent review, see: H. Yamamoto, N. Momiyama, *Chem. Commun.* **2005**, 3514 – 3525.
[26] A. Kekulé, *Ann. Chem. Pharm.* **1858**, *106*, 129 – 159.
[27] A. Kekulé, *Bull. Soc. Chim. Fr. [2]* **1865**, *3*, 98 – 111.
[28] A. von Baeyer, *Ber. Dtsch. Chem. Ges.* **1890**, *23*, 1272 – 1287.

 © 2005 Wiley-VCH Verlag GmbH & Co. KGaA, Weinheim

Genomics

DOI: 10.1002/anie.200501444

Genotyping—From Genomic DNA to Genotype in a Single Tube

*Michael Strerath and Andreas Marx**

Keywords:
DNA recognition · DNA · genomics · polymerase chain reaction · single-nucleotide polymorphisms

Nucleotide variations in the human genome, such as single-nucleotide polymorphisms, have been researched more intensively since it became apparent that these deviations are linked to various diseases and also several side effects of drugs. The investigation of genomic DNA in the laboratory requires routine methods that are time-, labour-, and cost-effective. These criteria are fulfilled by so-called closed-tube methods, which are applied directly to isolated genomic DNA without any preamplification.

1. Introduction

Within the entire human genome, which comprises approximately three billion base pairs, individuals differ in approximately 0.1 % of their nucleotide sequence.[1,2] The most common of these three million sequence variations are single-nucleotide polymorphisms (SNPs).[3–5] SNPs are defined as sites in the genome at which the less-common variant has a frequency of at least 1 % in the population. There is a direct link between some of these dissimilarities and certain diseases, a topic dealt with in pharmacogenomics. Additionally, different effects of drugs on different patients can also be linked to SNPs.[3,5,6] Thus, considerable efforts are focused on finding new SNPs and elucidating their connection to certain phenotypes. To date, nearly 1.8 million SNPs have been discovered and characterized through a variety of methods. First, methods are needed to identify unknown nucleotide variations so that their medicinal relevance can be investigated. Once the exact sequence is known, other methods are required for high-throughput screening of populations in the search for known SNPs or to analyze individuals for SNP patterns. Thus, time-, labor-, and cost-effective analytical methods are clearly essential to allow routine studies of such nucleotide variations in the laboratory.[7–15] The efficacy of these methods is decisive for further advances in pharmacogenetics, which may, in the future, allow a therapy that is tailored to the genetic constitution of the individual. Treatments with drugs that are ineffective or cause severe side effects due to the genetic basis of the individual may be avoided.

Many methods are known for SNP diagnosis, but none has prevailed so far.[8–15] An important criterion for progress in this field is that the number of working steps must be kept to a minimum. However, most known methods require preamplification of the genomic target sequence through the polymerase chain reaction (PCR) prior to the actual analytical detection step. Hence, these methods usually involve at least two steps.[7–14] Methods that allow genotyping in one step directly from genomic DNA without preamplification would be ideal. In this Minireview, we focus on procedures of the latter type and discuss methods that link the amplification step with analysis in a closed-tube reaction. Furthermore, we focus on applications that exploit the properties of many enzymes to preferentially process canonically paired (according to the Watson–Crick rule) DNA constructs. For a general overview of methods applied in DNA diagnostics, we refer to several excellent reviews published recently.[7–15]

2. Sequence-Specific Invasive Cleavage of Oligonucleotide Probes: The Invader Assay

The invader assay can be divided into two reactions.[16,17] First, two oligonucleotides termed "signal probe" and "invasive probe" simultaneously anneal to a genomic DNA target sequence. The sequences of both probes are designed to form a characteristic structure when they bind to the target sequence (see Scheme 1 a).

The signal probe consists of two regions: one is complementary to the target and the other consists of a 5′-arm (Flap) and is not complementary to the target and invasive probes. The formed structure is recognized by certain 5′-3′-nucleases,

[*] Dipl.-Chem. M. Strerath, Prof. Dr. A. Marx
Fachbereich Chemie
Universität Konstanz
Universitätsstrasse 10, M 726, 78457 Konstanz (Germany)
Fax: (+49) 7531-885-140
E-mail: Andreas.Marx@uni-konstanz.de

InterScience
© 2005 Wiley-VCH Verlag GmbH & Co. KGaA, Weinheim

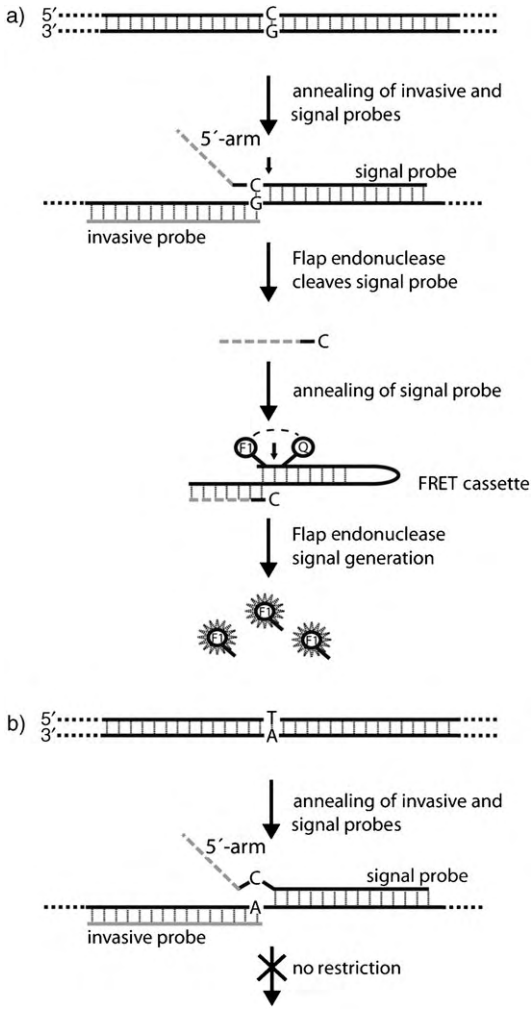

Scheme 1. Genotyping by means of the invader assay. Through annealing of two oligonucleotide probes (signal and invasive probe) a triplex structure is formed at the position of interest. a) In the case of a perfectly matched triplex, the Flap endonuclease is able to cleave the signal probe at the indicated position and the 5′-arm of the signal probe is released. The released 5′-arm anneals sequence specifically to a FRET cassette and catalyzes its restriction by the Flap endonuclease. This restriction cause a spatial separation between the fluorophore (F1) and the quencher molecule (Q), and a fluorescent signal is generated. b) If a noncanonical triplex is formed owing to the presence of a single-nucleotide variation, efficient restriction of the formed triplex structure is prevented, and the FRET cassette remains intact, thus causing quenching of fluorescence.

for example, Flap endonuclease I of *Archaeoglobus fulgidus* or DNA polymerase of *Thermus aquaticus* (which exhibits 5′-3′-exonuclease activity). The signal probe is cleaved at the indicated position to release an oligonucleotide,[18] which is composed of the 5′-arm and one nucleotide derived from its target-specific region. Remarkably, the cleavage rate is significantly enhanced by the presence of the invasive probe.[18,19] Furthermore, it is crucial to the cleavage process that the signal probe and target sequence are fully complementary at the SNP site. The discrimination between single-nucleotide variations in the invader assay derives from the ability of the enzyme to cleave canonical target–signal-probe complexes selectively. Single-nucleotide variations within the target site (e.g. because of a single-nucleotide polymorphism) result in a mismatched complex that is cleaved significantly less efficiently (Scheme 1b). If reactions are performed at elevated temperatures with an excess of the signal probe, the generated fluorescence signal will be amplified owing to the dissociation of the cleaved signal probe from the target and repeated annealing of a new and uncleaved signal probe.[19]

The signal can be amplified further by using a subsequent reaction step. In this second reaction, the cleaved strand anneals to a fluorescence resonance energy transfer (FRET) cassette and invades a short hairpin, which has a fluorophore and quencher pair at its 5′-end. Cleavage of the hairpin construct at the indicated position is again executed by the 5′-3′-exonuclease function of the enzymes mentioned above. The cleavage liberates the dye and generates a fluorescence signal owing to the separation of the fluorophore and the quencher. Therefore, the cleaved signal probe catalyzes the cleavage of a FRET cassette and releases a fluorophore in the second step of the invader assay.[20] In practice, both reactions are carried out in the same reaction tube, and an overall signal amplification of up to 10^7-fold within 4 h has been reported.[20] Direct SNP analysis can be performed from samples containing 10–100 ng of human genomic DNA.[17]

Michael Strerath studied chemistry at the University of Düsseldorf (Germany) where he completed his thesis work for his undergraduate degree under the guidance of Stefan Kubik in 2001. In the same year he moved to the University of Bonn, where he started his PhD with Andreas Marx. In 2004 he followed Andreas Marx to Konstanz University, where he completed his PhD studies on chemical und genetic approaches for genome analysis. Since August 2005 he has been working with Direvo Biotech AG in Cologne.

Andreas Marx studied Chemistry in Freiburg, Sussex, and Bochum, where he completed his Diplom with Peter Welzel in 1994. He obtained his PhD in 1997 with Bernd Giese at Basel University. After postdoctoral studies with Hisashi Yamamoto at Nagoya University as a EU/JSPS fellow, he started his independent research on the chemical biology of nucleic acids associated with Michael Famulok at Bonn University and obtained his habilitation in organic chemistry and biochemistry in 2003. Since January 2004 he has held the Chair of Organic Chemistry–Cellular Chemistry at Konstanz University.

© 2005 Wiley-VCH Verlag GmbH & Co. KGaA, Weinheim

3. Genotyping through the 5′-3′-Exonuclease Activity of DNA Polymerases: The TaqMan Assay

The 5′-3′-nuclease proficiency of DNA polymerase of *Thermus aquaticus* is exploited in the TaqMan assay.[21] The characteristic steps of this approach are the DNA synthesis by DNA polymerase, partial strand displacement, and cleavage of a FRET DNA probe by the enzyme to generate a fluorescence signal through separation of the fluorophore and quencher (Scheme 2).[21–24]

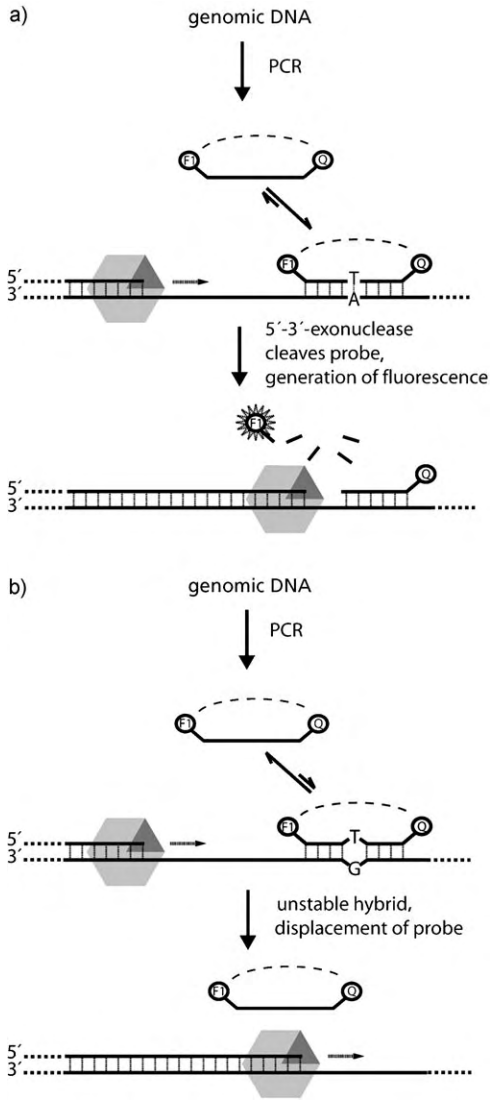

Scheme 2. The TaqMan assay. a) The target sequence is amplified through a PCR by using *Taq* DNA-polymerase that exhibits 5′-3′-nuclease activity. The probe sequence is complementary to one allelic variant. b) In the case of the other allele, a mispaired complex is formed. The perfectly matched hybrid (a) is thermodynamically stable, whereas the mispaired hybrid (b) is thermodynamically unstable at the applied temperature. As strand extension proceeds, the 5′-3′-nuclease activity of *Taq* DNA-polymerase cleaves canonically bound probes and releases the fluorophore, thus resulting in the generation of a signal. In the case of noncanonical probe–target sequences, the displacement of a portion of the probe by the DNA polymerase lowers the thermodynamic stability even further, and the probe is released. Thus, cleavage of the probe is prevented and hence no signal is generated.

Several factors contribute to the capability of this approach to discriminate between single-nucleotide variations. First, probes with complementary sequences form duplexes with the target site that are inherently more stable than those that contain mismatches.[22] Accordingly, judicious tuning of the annealing and extension temperatures in the PCR favors formation of a perfectly matched duplex over a mismatched duplex. Duplex formation is mandatory for the 5′-3′-nuclease action of the DNA polymerase. Recognition and cleavage by an enzyme occur at the bifurcated end of a duplex. Therefore one to three nucleotides at the 5′-end of the probe must be displaced prior to cleavage of the probe. This further destabilizes a mismatched probe and promotes its dissociation, thereby preventing cleavage and signal formation. A crucial parameter for the success of this approach is the design of the probe. The probe must be long enough to build stable duplexes at the extension temperature ($\approx 70\,^{\circ}C$), but must be short enough to discriminate sufficiently between single-nucleotide variations within the target site. It has been shown that probes that are conjugated with a minor-groove binder have higher binding affinity to a complementary sequence and can still be processed by enzymes (Figure 1).[22,25,26] This allows application of shortened fluorogenic probes, which have better sequence selectivity.

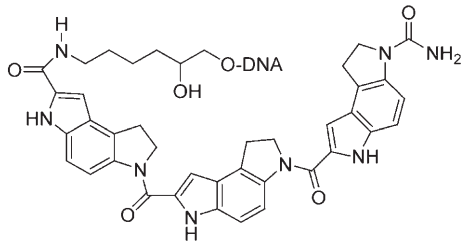

Figure 1. Structure of the DNA minor groove binder conjugated to DNA.

The entire process is carried out in a closed tube and does not require further post-PCR handling and processing steps. Additionally, the analysis can be conducted and monitored in real-time. The assay is sensitive and only minute amounts of genomic DNA (2–20 ng) are required.[22]

4. Genotyping through DNA Polymerase Selectivity: Allele-Specific Amplification

A conceptually simple approach to detect allele variations is realized in allele-specific amplification (ASA). ASA is used to determine nucleotide variations through either the presence or absence of a DNA product obtained by PCR amplification. The principle of ASA is based on the formation of matched or mismatched primer-template complexes through allele-specific primer probes. PCR amplification by a DNA polymerase proceeds from matched 3′-primer termini, whereas a mismatched primer terminus inhibits amplification (Scheme 3).[27–34]

© 2005 Wiley-VCH Verlag GmbH & Co. KGaA, Weinheim

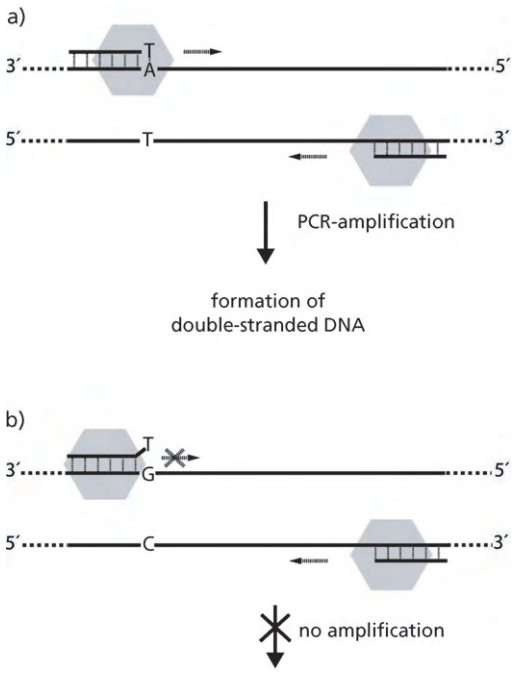

Scheme 3. Allele-specific amplification. The PCR primer pair is designed to amplify a part of the genomic DNA of interest. A 3′-end of a primer strand is positioned opposite to the SNP position, resulting in a matched (a) or a mismatched (b) complex, depending on the nature of the target nucleotide. In the case of the matched hybrid, the DNA polymerase elongates the primer which results in the exponential amplification of the PCR product. The elongation of the mismatched primer is hampered, and thus the formation of the PCR product is prevented.

Ideally, the extension of a mismatched primer end by the DNA polymerase should be discriminated. In the case of a mismatch, exponential product formation by PCR is prevented, in contrast to the situation when both primers are complementary to the target site. Product formation can be detected by gel chromatography or monitored in real-time by using a double-stranded-DNA-specific dye (e.g. SybrGreen I), which shows fluorescence after binding to the PCR product in a sequence-independent manner.[35] The main advantage of this approach is that no relatively expensive fluorescence probes are required. However, only the formation of double-stranded DNA is detected without any sequence specificity and therefore false signals are generated from unspecific amplification, for example, the formation of primer dimers. To prevent the detection of false amplificates, sequence-specific FRET probes (e.g. molecular beacons) can be employed.[36] Such probes bind sequence specifically to the amplificate and thus link signal generation to amplification of the desired sequence. In many cases, however, the method still requires tedious costly and time-consuming optimization. Accordingly, any factors that increase the selectivity and reliability of the allele-specific PCR approach should have a significant impact on the reliability and robustness of direct SNP analysis by ASA.

Recently, it was reported that the selectivity of allele-specific PCR can be significantly increased through the employment of chemically modified primer probes.[37–41] Significantly higher amplification selectivity is observed by application of primer probes that bear small 4′-C-modifications such as vinyl (**1**) or methoxymethylene (**2**) groups at the 3′-end. A commercially available 3′-5′-exonuclease-deficient variant of a DNA polymerase from *Thermococcus litoralis* (Vent(exo−) DNA polymerase) was used for amplification (Scheme 4).[37–39]

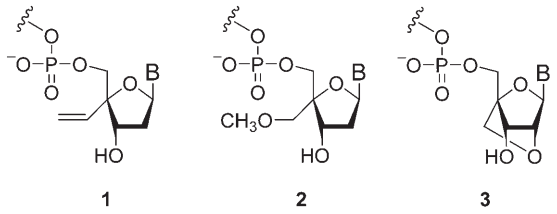

Scheme 4. Structures of modified primer strands employed in allele-specific PCR. B = nucleobase.

As already mentioned, the identification of single-nucleotide variations within genes is feasible in real time. This makes real-time PCR a rapid and convenient tool for the identification and analysis of allele variations. Interestingly,

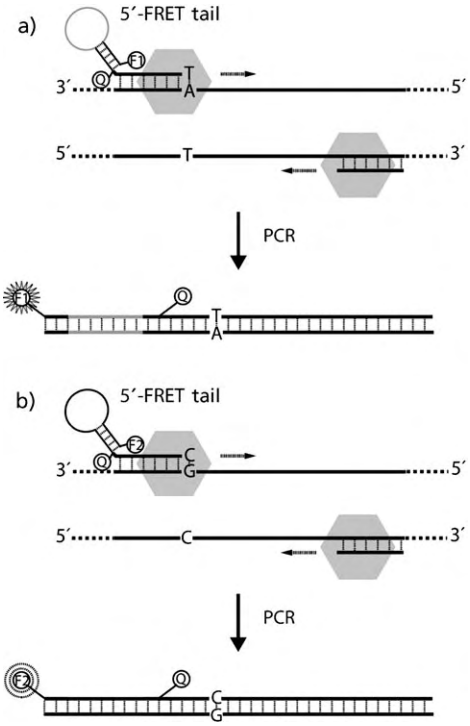

Scheme 5. Multiplex allele-specific amplification. Each allele-specific primer is coupled to a specific oligonucleotide that is not complementary to the target tail sequence and forms a hairpin structure. Each stemloop bears a fluorophore–quencher FRET pair. During PCR the primer strands are elongated in an allele-specific manner, and the loop sequence is linearized. This leads to a separation of the fluorophore and quencher, and a fluorescent signal is generated. The wavelength of the construct is therefore coupled to the allelic variant, as shown for genotype A (signal F1 in (a)) and genotype G (signal F2 in (b)) as examples.

 © 2005 Wiley-VCH Verlag GmbH & Co. KGaA, Weinheim

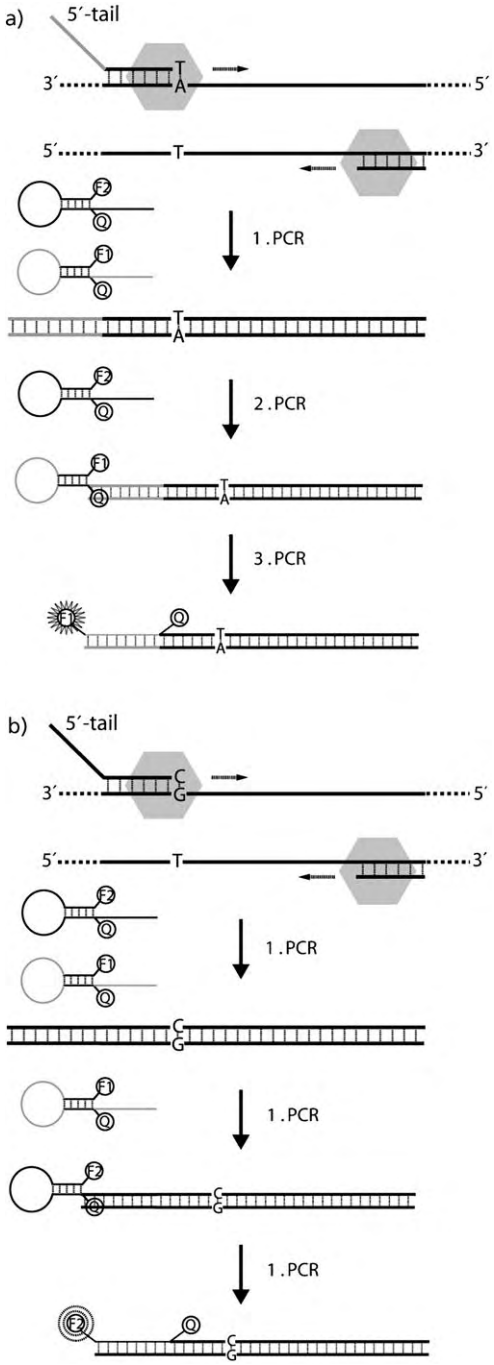

Scheme 6. Multiplex allele-specific amplification. Each allele-specific primer bears a specific tail sequence that is not complementary to the target sequence. During PCR, the allele-specific primer is elongated, and the tail complementary sequence is added to the PCR product. An allele-specific primer bearing a priming and a stem loop structure hybridizes to this sequence and is therefore coupled to the PCR product. During the proceeding PCR, the stem loop is linearized and results in a fluorescence signal. The wavelength of the construct is therefore coupled to the allelic variant as shown for genotype A (signal F1 in (a)) and genotype G (signal F2 in (b)).

modified building blocks that are bridged with a 2′-*O*-4′-*C*-methylene bridge (**3**) at the 3′-end of primer probes exhibit similar features (Scheme 4).[42]

So-called multiplex reactions in which two allele variants are differentiated in a single reaction tube are realized by adding a specific 5′-tail sequences to each allele-specific primer. The signal generation is thereby directly linked to the allele-specific primer in the PCR amplification. Two hairpin FRET structures bearing different fluorophores (which emit at different wavelengths) are added as an overhang sequence to the discriminating primer (Scheme 5).[36] During PCR, the overhang becomes double stranded and the hairpin is opened, thus resulting in an allele-specific fluorescence signal.

In another approach, a specific tail-complementary sequence is added which can be detected by the use of overhang primers as described above.[43] This method has the advantage that the primers that bear the overhang FRET cassette are independent of the target sequence and can therefore be used in a universal manner (Scheme 6). The same pair of FRET primers can be used for each sequence, and only the simple, allele-specific primers are varied. Allele discrimination was achieved with 40 ng of genomic DNA.

The ability of the enzyme to discriminate between mismatched primer ends was increased by mutating the DNA polymerase. A *Taq* DNA polymerase variant was identified that exhibits significantly higher single-nucleotide discrimination than the wild-type enzyme in allele-specific PCR.[44] This goal was accomplished through a combinatorial approach by randomization of a gene cassette of a DNA polymerase and subsequent screening for variants with higher mismatch-discriminating properties.

DNA diagnostic methods that do not employ labeled probes are highly promising candidates for further developments in terms of selectivity and robustness, as costly fluorescent probes could be replaced by standard primer strands that are required for PCR amplification anyway.

5. Isothermal Genotyping by Circularized Oligonucleotide Probes: Padlock Probes and Rolling Circle Amplification (RCA)

Padlock probes are circularized single-stranded oligonucleotides made up of 70–110 nucleobases. They are designed in an open circle form with two target-complementary regions at each end (see Scheme 7).[45]

In the presence of a complementary target sequence, the two ends of the open-circle oligonucleotides are covalently connected by a DNA ligase to form circularized padlock probes. It is possible to degrade open probes that are not ligated as a result of a noncanonical target sequence by treatment with exonucleases, whereas closed circles are resistant and remain intact. In many applications, the formation of circularized probes is followed by isothermal amplification by using a primer derived from a central region of the padlock probe. This results in hundreds of tandemly linked copies of the padlock probe. For this copy process, termed rolling circle amplification (RCA),[46] a DNA polymerase with strand-displacing properties is required. Typically, DNA polymerase Φ29 is used, but there are also applications in which thermostable DNA polymerases are employed.[47,48]

© 2005 Wiley-VCH Verlag GmbH & Co. KGaA, Weinheim

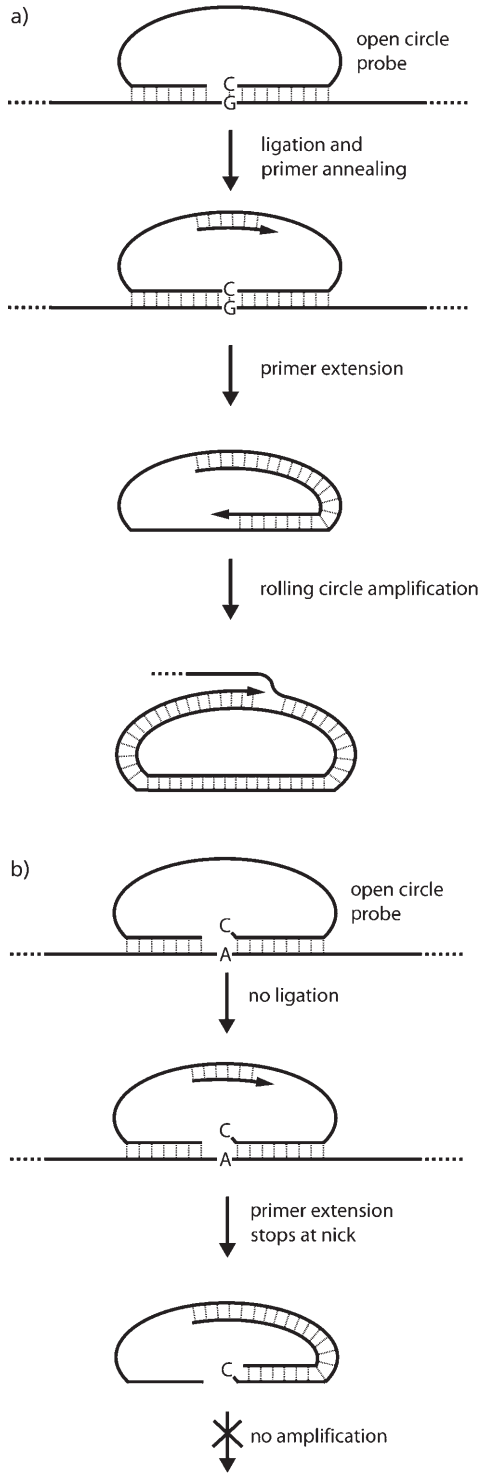

Scheme 7. Rolling circle amplification (RCA). a) In the first step, the open-circle probe (OCP) anneals to the target sequence with both of its target-complementary regions. Both ends lie adjacent to each other and form a nick. In the case of one allelic variant the 3′-end forms a perfectly matched hybrid (a). In the other case, a mismatch is formed (b). The perfectly matched ends are ligated by a DNA ligase and a circular molecule is generated. In the case of the mismatched complex, ligation cannot take place. The reaction mixture also contains an oligonucleotide that is complementary to a part of the OCP and that can serve as a primer. A DNA polymerase elongates this primer and stops at the nick site of the OCP in the case of a nonligated molecule (b). In contrast, if the probe is circularized by the DNA ligase, the elongation can proceed (a). After one round of amplification, the already hybridized oligonucleotide sequence is removed by the DNA polymerase strand. This results in thousands of tandem repeats of the complementary sequence of the closed circle.

The most common applications of padlock probes in allele diagnostics make use of the mismatch-discriminating properties of various enzymes, often in combination with hybridization assays. In the DNA-ligase-dependent method, the open-circle probe is designed to form either a perfectly matched or a single-mismatched 3′-complementary region according to the target sequence.[46] The mismatch-discriminating properties of the DNA ligase applied allow circularization of the probe in the former case. In contrast, no ligation occurs in the second case owing to the mismatched primer–target complex.[49] Additionally, the 5′-complementary part of the open-circle probes (OCP) is designed to hybridize tightly with the target sequence. On the other hand, the 3′-region is in an association–dissociation equilibrium with the target because of a calculated dissociation temperature that is 10 °C lower than the reaction temperature of 60 °C.[50] Accordingly the specificity of the ligation reaction is enhanced owing to the favorable hybridization of the perfectly matched OCP. After ligation, linear isothermal RCA can be used to determine whether the probe was circularized or not.

An additional application of padlock probe ligation followed by RCA makes use of the mismatch-discriminating properties of DNA polymerases.[47] The OCP is designed to form a gap of typically seven nucleotides between the target complementary parts (Scheme 8). This gap includes the sequence context surrounding the SNP site to be studied. In a first step, a DNA polymerase is used to fill the gap by copying the sequence context into the padlock probe. After the gap-filling reaction, a DNA ligase is used to circularize the probe. Subsequently, the circular padlock is amplified by RCA. The linear single-stranded product bears hundreds of tandemly linked repeated copies of the padlock probe, including the incorporated sequence context. These sequences are hybridized to an allele-specific primer (P2) and form either a perfectly matched (Scheme 8a) or mismatched (Scheme 8b) 3′-end.

Afterwards, the mismatch-discriminating properties of a DNA polymerase such as Vent(exo−) are used in an allele-specific amplification to distinguish the allelic variants. The products of this second amplification represent tandem repeats of the original padlock probe. These sequences bear multiple binding sites for the first RCA primer (P1). The extension of primers bound to these sites generates a continuous pattern of double-stranded DNA with branches and is therefore called hyperbranching RCA (HRCA). In contrast to allele-specific PCR, mispriming events will only incorporate the incorrect base in the primer itself so that nonspecific priming is a nonpropagating event in HRCA. By this method up to 10^9 copies of each circle can be generated in 90 min.[47]

 © 2005 Wiley-VCH Verlag GmbH & Co. KGaA, Weinheim

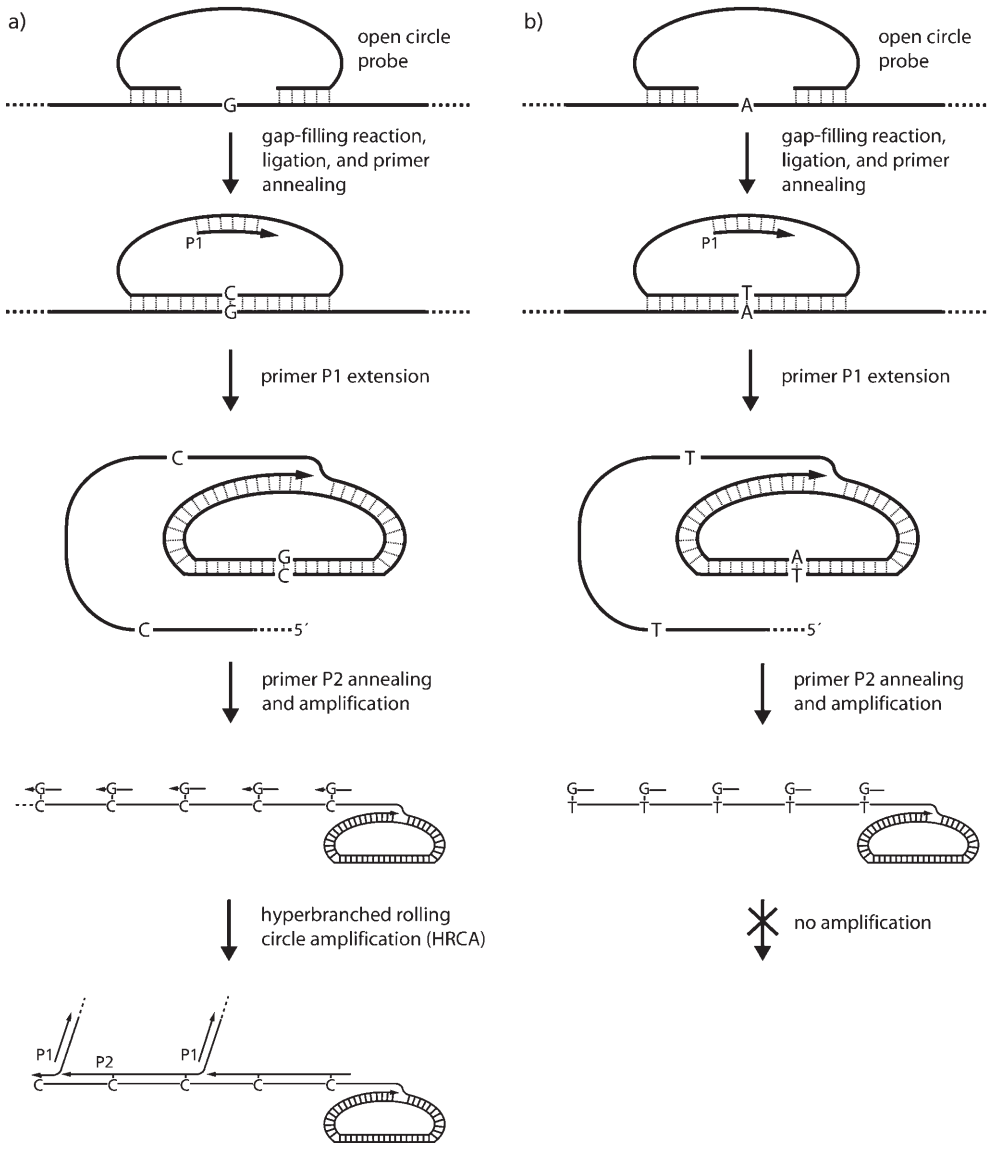

Scheme 8. Hyperbranching rolling circle amplification (HRCA). The two ends of the open-circle probe hybridize to the target strand in such a way that a short gap is formed. In a first gap-filling reaction, a DNA polymerase closes the gap by copying a part of the target sequence into the probe. Subsequently, a ligase circularizes the probe and RCA can proceed, starting from the primer P1. The single-stranded product includes repetitions of the short incorporated sequence containing the SNP site. A second oligonucleotide with a 3′-end is complementary to one allelic variant at the SNP site and serves as a primer (P2) in a second reaction. It can only be elongated when it is perfectly matched (a), whereas no extension proceeds in the mismatched case (b). The product of this extension consists of the original circle probe sequence. Thus the first primer P1 can bind to these new synthesized products, and the target sequence is amplified. The result is the amplification of a highly branched DNA product.

In 2001, Qi et al. introduced a procedure to perform DNA probe ligation and RCA under identical buffer conditions which enabled closed-tube or closed microplate formats.[48]

6. Outlook

Currently, all known methods exhibit advantages and disadvantages, and none of the described procedures has prevailed so far. Thus, improvements are needed to facilitate general application in daily practice.

To ensure allelic discrimination in a more robust and selective manner, methods that use enzymes in the discriminating step might be further optimized by mutagenic engineering the respective enzymes. The high costs associated with the assays are still a matter of concern and prevent general application. These costs could be reduced by the development of methods that do not make use of probes with covalently linked dyes, as their synthesis is time- and cost-intensive.

The development of cheaper and faster closed-tube detection methods should put the aim of adopting SNP detection for general use in clinical practice within reach.

Received: April 27, 2005
Published online: October 10, 2005

 © 2005 Wiley-VCH Verlag GmbH & Co. KGaA, Weinheim

[1] J. C. Venter et al. , *Science* **2001**, *291*, 1304.
[2] R. Sachidanandam et al. , *Nature* **2001**, *409*, 928.
[3] W. E. Evans, M. V. Relling, *Science* **1999**, *286*, 487.
[4] L. Licinio, M. Wong, *Pharmacogenomics*, Wiley-VCH, Weinheim, **2002**.
[5] J. J. McCarthy, R. Hilfiker, *Nat. Biotechnol.* **2000**, *18*, 505.
[6] M. V. Relling, T. Dervieux, *Nat. Rev. Cancer* **2001**, *1*, 99.
[7] B. W. Kirk, M. Feinsod, R. Favis, R. M. Kliman, F. Barany, *Nucleic Acids Res.* **2002**, *30*, 3295.
[8] A. C. Syvanen, *Nat. Rev. Genet.* **2001**, *2*, 930.
[9] M. M. Shi, *Am. J. Pharmacogenomics* **2002**, *2*, 197.
[10] I. G. Gut, *Hum. Mutat.* **2001**, *17*, 475.
[11] R. M. Twyman, S. B. Primrose, *Pharmacogenomics* **2003**, *4*, 67.
[12] R. M. Twyman, *Curr. Top. Med. Chem.* **2004**, *4*, 1423.
[13] P. Y. Kwok, *Annu. Rev. Genomics Hum. Genet.* **2001**, *2*, 235.
[14] P. Y. Kwok, X. Chen, *Curr. Issues Mol. Biol.* **2003**, *5*, 43.
[15] K. Nakatani, *ChemBioChem* **2004**, *5*, 1623.
[16] L. Fors, K. W. Lieder, S. H. Vavra, R. W. Kwiatkowski, *Pharmacogenomics* **2000**, *1*, 219.
[17] "Single Nucleotide Polymorphisms": V. Lyamichev, B. Neri in *Methods in Molecular Biology, Vol. 212* (Ed.: P.-Y. Kwok), Humana, Totowa, NY, **2003**, p. 229.
[18] V. Lyamichev, M. A. Brow, J. E. Dahlberg, *Science* **1993**, *260*, 778.
[19] V. Lyamichev, A. L. Mast, J. G. Hall, J. R. Prudent, M. W. Kaiser, T. Takova, R. W. Kwiatkowski, T. J. Sander, M. de Arruda, D. A. Arco, B. P. Neri, M. A. Brow, *Nat. Biotechnol.* **1999**, *17*, 292.
[20] J. G. Hall, P. S. Eis, S. M. Law, L. P. Reynaldo, J. R. Prudent, D. J. Marshall, H. T. Allawi, A. L. Mast, J. E. Dahlberg, R. W. Kwiatkowski, M. de Arruda, B. P. Neri, V. I. Lyamichev, *Proc. Natl. Acad. Sci. USA* **2000**, *97*, 8272.
[21] P. M. Holland, R. D. Abramson, R. Watson, D. H. Gelfand, *Proc. Natl. Acad. Sci. USA* **1991**, *88*, 7276.
[22] "Single Nucleotide Polymorphisms": K. J. Livak in *Methods in Molecular Biology, Vol. 212* (Ed.: P.-Y. Kwok), Humana, Totowa, NY, **2003**, pp. 129 – 147.
[23] L. G. Lee, C. R. Connell, W. Bloch, *Nucleic Acids Res.* **1993**, *21*, 3761.
[24] P. M. Holland, R. D. Abramson, R. Watson, D. H. Gelfand, *Clin. Chem.* **1992**, *38*, 462.
[25] a) I. Afonina, M. Zivarts, I. Kutyavin, E. Lukhtanov, H. Gamper, R. B. Meyer, *Nucleic Acids Res.* **1997**, *25*, 2657; b) I. V. Kutyavin, E. A. Lukhtanov, H. B. Gamper, R. B. Meyer, *Nucleic Acids Res.* **1997**, *25*, 3718.
[26] I. V. Kutyavin et al., *Nucleic Acids Res.* **2000**, *28*, 655.
[27] S. Germer, R. Higuchi, *Genome Res.* **1999**, *9*, 72.
[28] R. A. Gibbs, P. N. Nguyen, C. T. Caskey, *Nucleic Acids Res.* **1989**, *17*, 2437.
[29] S. Germer, M. J. Holland, R. Higuchi, *Genome Res.* **2000**, *10*, 258.
[30] D. Y. Wu, L. Ugozzoli, B. K. Pal, R. B. Wallace, *Proc. Natl. Acad. Sci. USA* **1989**, *86*, 2757.
[31] L. Shively, L. Chang, J. M. LeBon, Q. Liu, A. D. Riggs, J. Singer-Sam, *Biotechniques* **2003**, *34*, 498.
[32] Z. Guo, Q. Liu, L. M. Smith, *Nat. Biotechnol.* **1997**, *15*, 331.
[33] Y. Ishikawa, K. Tokunaga, K. Kashiwase, T. Akaza, K. Tadokoro, T. Juji, *Hum. Immunol.* **1995**, *42*, 315.
[34] J. Wilhelm, H. Reuter, B. Tews, A. Pingoud, M. Hahn, *Biol. Chem.* **2002**, *383*, 1423.
[35] J. Wilhelm, A. Pingoud, *ChemBioChem* **2003**, *4*, 1120.
[36] I. A. Nazarenko, S. K. Bhatnagar, R. J. Hohman, *Nucleic Acids Res.* **1997**, *25*, 2516.
[37] M. Strerath, A. Marx, *Angew. Chem.* **2002**, *41*, 4961; *Angew. Chem. Int. Ed.* **2002**, *41*, 4766.
[38] M. Strerath, J. Gaster, D. Summerer, A. Marx, *ChemBioChem* **2004**, *5*, 333.
[39] M. Strerath, J. Gaster, A. Marx, *ChemBioChem* **2004**, *5*, 1585.
[40] J. Gaster, A. Marx, *Chem. Eur. J.* **2005**, *11*, 1861.
[41] B. Tews, J. Wilhelm, D. Summerer, M. Strerath, A. Marx, P. Friedhoff, A. Pingoud, M. Hahn, *Biol. Chem.* **2003**, *384*, 1533.
[42] D. Latorra, K. Campbell, A. Wolter, J. M. Hurley, *Hum. Mutat.* **2003**, *22*, 79.
[43] M. V. Myakishev, Y. Khripin, S. Hu, D. H. Hamer, *Genome Res.* **2001**, *11*, 163.
[44] D. Summerer, N. Z. Rudinger, I. Detmer, A. Marx, *Angew. Chem.* **2005**, *117*, 4791 – 4794; *Angew. Chem. Int. Ed.* **2005**, *44*, 4712 – 4715.
[45] M. Nilsson, H. Malmgren, M. Samiotaki, M. Kwiatkowski, B. P. Chowdhary, U. Landegren, *Science* **1994**, *265*, 2085.
[46] J. Baner, M. Nilsson, M. Mendel-Hartvig, U. Landegren, *Nucleic Acids Res.* **1998**, *26*, 5073.
[47] P. M. Lizardi, X. Huang, Z. Zhu, P. Bray-Ward, D. C. Thomas, D. C. Ward, *Nat. Genet.* **1998**, *19*, 225.
[48] X. Qi, S. Bakht, K. M. Devos, M. D. Gale, A. Osbourn, *Nucleic Acids Res.* **2001**, *29*, E116.
[49] U. Landegren, R. Kaiser, J. Sanders, L. Hood, *Science* **1988**, *241*, 1077.
[50] A. F. Faruqi, S. Hosono, M. D. Driscoll, F. B. Dean, O. Alsmadi, R. Bandaru, G. Kumar, B. Grimwade, Q. Zong, Z. Sun, Y. Du, S. Kingsmore, T. Knott, R. S. Lasken, *BMC Genomics* **2001**, *2*, 4.

© 2005 Wiley-VCH Verlag GmbH & Co. KGaA, Weinheim

Nanoparticle Catalysts

DOI: 10.1002/anie.200500766

Nanoparticles as Recyclable Catalysts: The Frontier between Homogeneous and Heterogeneous Catalysis

Didier Astruc, Feng Lu, and Jaime Ruiz Aranzaes*

Keywords:
C–C coupling · dendrimers · gold · nanoparticles · palladium · supported catalysts

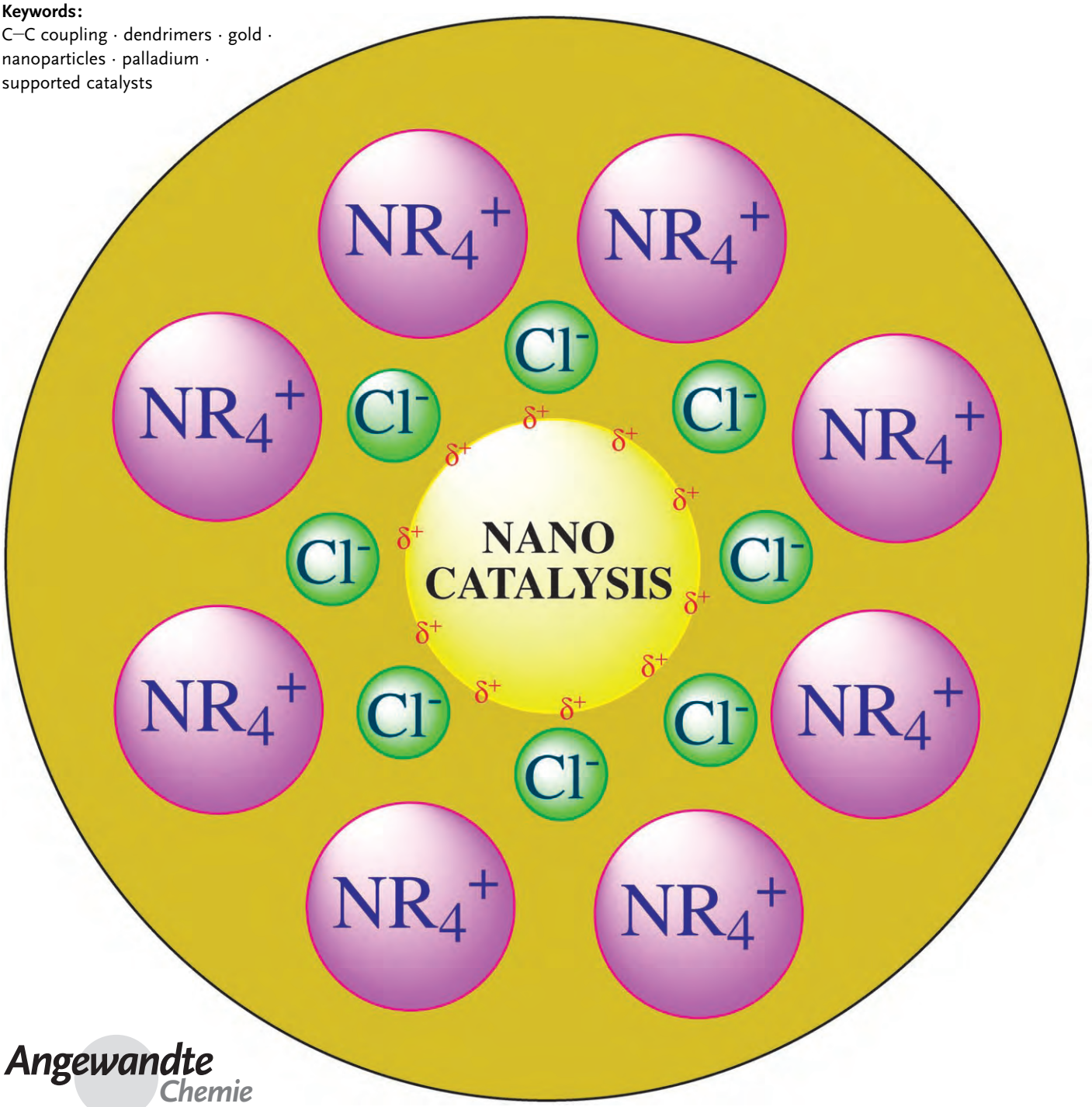

© 2005 Wiley-VCH Verlag GmbH & Co. KGaA, Weinheim

Interest in catalysis by metal nanoparticles (NPs) is increasing dramatically, as reflected by the large number of publications in the last five years. This field, "semi-heterogeneous catalysis", is at the frontier between homogeneous and heterogeneous catalysis, and progress has been made in the efficiency and selectivity of reactions and recovery and recyclability of the catalytic materials. Usually NP catalysts are prepared from a metal salt, a reducing agent, and a stabilizer and are supported on an oxide, charcoal, or a zeolite. Besides the polymers and oxides that used to be employed as standard, innovative stabilizers, media, and supports have appeared, such as dendrimers, specific ligands, ionic liquids, surfactants, membranes, carbon nanotubes, and a variety of oxides. Ligand-free procedures have provided remarkable results with extremely low metal loading. The Review presents the recent developments and the use of NP catalysis in organic synthesis, for example, in hydrogenation and C–C coupling reactions, and the heterogeneous oxidation of CO on gold NPs.

From the Contents

1. Introduction	7853
2. Pioneering Studies	7854
3. Stabilizors for Metal Nanoparticles	7854
4. Ionic liquids as Media for Metal-Nanoparticle Catalysis	7860
5. Solid Supports for Metal Nanoparticles	7861
6. The New Gold Rush	7864
7. Summary of Mechanistic Information	7865
8. Prospects for Organic Synthesis	7866
9. Conclusion	7867

1. Introduction

In a recent "Focus" Article in *Chemical Communications*, Somorjai emphasized that catalysis is the central field of nanoscience and nanotechnology,[1a] and finds parallels between enzyme catalysis and heterogeneous catalysis, even though this idea in reality remains a dream. As admitted by Somorjai, selectivity is still a major problem in heterogeneous catalysis that involves the top-down approach, even though up-to-date techniques, such as size-reduction lithography, permit access to nanocatalysts.[1] On the other side of the catalysis world, mononuclear transition-metal complexes have recently achieved an amazing level of performance in terms of selectivity;[2] just think of the amazing progress in C–C coupling[2a–c] and metathesis[2d] reactions. The ultimate goals of recoverable catalysts, their criteria of evaluation, and their role in "Green Chemistry" have been emphasized in recent articles.[3]

Many important homogeneous catalysts are used in industry in biphasic systems or by fixation on supports, the bridge between these two approaches is now being built through the use of nanoparticles (NPs; sometimes called giant clusters, nanoclusters, or colloids) whose activity is very high under mild conditions because of their very large surface area.[4–11] This frontier domain is sometimes called "semi-heterogeneous". Contrary to classic heterogeneous catalysts,[1] these NPs are synthesized by the bottom-up approach from molecular precursors including a metal salt, a molecular stabilizer, and a reducing agent (a typical preparation is given in Equation (1); M = Metal from Group 8–10, X = Cl or Br, R = C_{4-12} alkyl, Red = M′H with M′ = H, Li, $LiBEt_3$, $NaBEt_3$, $KBEt_3$).[4–7,11] Physical means of preparation,[6–8,10,11] such as the electrochemical route developed by Reetz,[7] are also numerous.[4,5,7,11]

$$MX_n(NR_4)_m + (n-m)\,Red \xrightarrow{THF} M_{NP} + (n-m)(Red^+X^-) + m\,(NR_4{}^+X^-) \quad (1)$$

Another modern synthesis, inspired by the 150-year old method of Faraday[8a,b] and popularized by Schiffrin's group in 1993,[8a,c] involves reduction by $NaBH_4$ of a metal precursor such as $HAuCl_4$[8a,c] or Na_2PdCl_4[8d] in a biphasic organic-solvent–water system in the presence of the phase-transfer reagent $[N(C_8H_{17})_4]Br$ and subsequent addition of a stabilizer such as a thiol for AuNPs and (4-dimethylamino)pyridine in the case of PdNPs. NPs can be soluble and thus act homogeneously (soluble AuNPs were discovered over 2500 years ago and were used for aesthetic and curative purposes).[8a] The stabilization of NPs during their synthesis can be by electrostatic, steric, electrosteric (a combination of steric and electrostatic, see Figure 1) means or through the use of ligands.[4,5,8,11] M^0NP synthesis can also be carried out by the vaporization of the atomic metal or of M^0 complexes.[11] In view of the catalyst recycling, NP catalysts often are immobilized or grafted on inorganic or organic polymer supports.[4,5,8,11] There are many reviews on the numerous synthetic routes for NPs,[4–11] and herein in we will not cover

[*] Prof. D. Astruc, Dr. F. Lu, Dr. J. R. Aranzaes
Molecular Nanosciences and Catalysis Group, LCOO
UMR CNRS N°5802, Université Bordeaux I
33405 Talence Cedex (France)
Fax: (+33) 556-84-69-94
E-mail: d.astruc@lcoo.u-bordeaux1.fr

 © 2005 Wiley-VCH Verlag GmbH & Co. KGaA, Weinheim

this aspect in detail. We will rather focus on catalysis with emphasis on the most recent work, after a brief survey of the background. For this Review, we will classify and discuss the categories of NP catalysts by the type of support.

2. Pioneering Studies

The use of NPs in catalysis appeared in the 19th century with photography (AgNPs) and the decomposition of hydrogen peroxide (PtNPs).[5d] Pioneering catalytic applications of NPs were reported in 1940 by Nord on nitrobenzene reduction,[9a] in 1970 by Parravano on hydrogen-atom transfer between benzene and cyclohexane and oxygen-atom transfer between CO and CO_2 using AuNPs.[9b] The real breakthrough came with Haruta's seminal studies on oxide-supported AuNP-catalyzed CO oxidation by O_2 at low temperatures.[9c–e] In the 1970s, Bond and Sermon[9f] and Hirai et al.[9g] disclosed AuNP-catalyzed olefin hydrogenation. In 1986 Lewis demonstrated the colloidal mechanism for the catalysis of olefin hydrosilylation by silanes using organometallic complexes of Co, Ni, Pd, or Pt including the Speier catalyst (alcoholic H_2PtCl_6).[9h] These catalysts were formerly believed to follow the classic monometallic organometallic mechanism (oxidative addition of the Si–H bond of the silane onto the transition-metal center and subsequent alkene insertion and reductive elimination). That decade saw the beginning of extended NP catalytic studies especially in the fields of redox catalysis, photocatalysis (photocatalytic water splitting and photo-hydrogenation of alkenes, alkynes, and CO_2),[10a–g] hydrogenation of unsaturated substrates, and oxidation.[10h,i] In the mid-1990s, pioneering studies of PdNP catalysis were reported by Reetz for Heck C–C coupling, such as the reaction between butyl acrylate and iodobenzene or aryl bromides and styrene.[7]

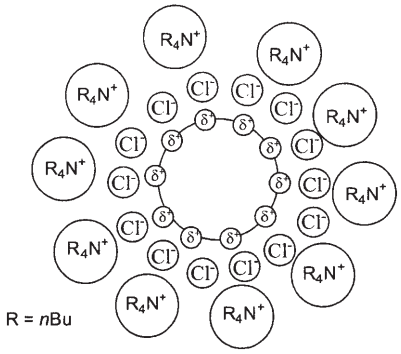

Figure 1. "Electrosteric" (that is electrostatic and steric) stabilization of metal nanoparticles obtained by reduction of a metal chloride salt in the presence of a tetra-*N*-alkylammonium cations. The halide anions provide electrostatic stabilization, and the tetrabutylammonium cations steric stabilization) (Bönnemann-type synthesis based on Equation (1)). The presence of chloride or other anions (and not the ammonium cations) at the nanoparticle surface was demonstrated. Anions stabilized IrNPs in the following order: polyoxometallate > citrate > polyacrylate ≈ chloride. Thus, the stabilization of metal NPs by anions can also have an important steric component.[25f,g]

Didier Astruc, born in Versailles, 1946, obtained his PhD in Rennes with Prof. R. Dabard (ferrocenes-cages) and was a NATO post-doctoral fellow at MIT with Prof. R. R. Schrock. He has been a Senior Member of l'Institut Universitaire de France since 1995, a Member of the French CNRS committee since 2000, and the President of the Coordination Chemistry Division of Société Chimique de France since January 2002. He was awarded numerous prizes including the 1989 Humboldt Prize and the 2000 Le Bel Prize. His research interests are now mainly focused on metallodendrimers and nanoparticles.

Feng Lu obtained his PhD under the supervision of Prof. C. Elschenbroich in Marburg in 2002, then joined Professor Didier Astruc at University BordeauxI with where he worked for a year on nanoparticle catalysis. He is presently a post-doc with Professor Chistopher B. Gorman in North Carolina State University at Raleigh working on metallodendrimers. His research interests cover biocatalysts, biosynthesis, dendrimers, electron transfer, molecular electronics, organometallic chemistry, and solar energy conversion.

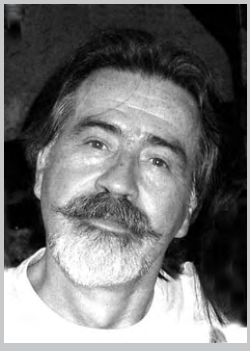

Jaime Ruiz Aranzaes studied at the Catholic University Santiago (Chile) where he passed his Master degree in chemistry with Professor E. Roman, then moved to Bordeaux to prepare a PhD on the kinetics of substitution reactions of 19-electron complexes with Professor Didier Astruc and then his Habilitation on polyaromatic-iron chemistry. He is presently guiding a research group in the same laboratory, his interests being in the area of the synthesis, chemistry, electrochemistry, and physical properties of redox-active nano-organometallics.

The first years of the 21st century have seen an exponential growth in the number of publications in the NP field. The main goals are 1) improving catalyst activities and selectivities and 2) understanding the catalytic mechanisms.[11] The modes of preparation of catalytically active NPs have been diversified and currently include impregnation,[12a] co-precipitation,[12a,b] deposition/precipitation,[12c] sol–gel,[12a,d] gas-phase organometallic deposition,[12f] sonochemical,[12g] micro-emulsion,[12h] laser ablation,[12i] electrochemical,[12j] and cross-linking.[12k]

3. Stabilizors for Metal Nanoparticles

3.1. Polymers

Polymers provide stabilization for metal NPs through the steric bulk of their framework, but also by binding weakly to the NP surface through heteroatom that play the role of ligands. Poly(*N*-vinyl-2-pyrrolidone) (PVP) is the most used polymer for NP stabilization and catalysis, because it fulfill both steric and ligand requirements (Scheme 1).[5f] PVP-

 © 2005 Wiley-VCH Verlag GmbH & Co. KGaA, Weinheim

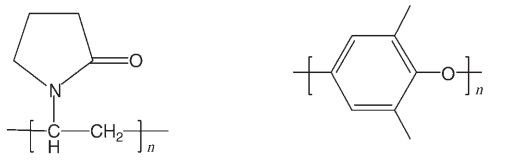

Scheme 1. Two major polymer families used as metal NP supports for catalysis.

stabilized Pt-, Pd-, and RhNPs, that are synthesized by the reduction of the corresponding metal halide in refluxing ethanol and immobilized in an ionic liquid, 1-*n*-butyl-3-methylimidazolium hexafluorophosphate ([BMI][PF_6]), are very efficient olefin and benzene hydrogenation catalysts at 40 °C that can be recycled without loss of activity.[12k]

Using standard PVP-stabilized NP catalysts, parameters such as size and stability during the catalytic process have been examined. For instance, decreasing the PdNP size down to 3 nm in the Suzuki reaction improved the catalytic activity, suggesting that the low-coordination-number vertex and edge atoms on the particle surface are the active catalytic sites.[13] Many other polymers have recently been used as efficient supports for NP catalysis: polyurea (Scheme 2),[14a] polyac-

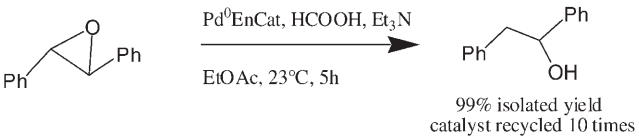

Scheme 2. Ring-opening hydrogenolysis of epoxides catalyzed by PdNPs (2 nm) microencapsulated in polyurea. The system can be recycled at least ten times with 97–99% yield.[14a]

rylonitrile and/or polyacrylic acid (Figure 2),[14b] multilayer polyelectrolyte films (Figure 3),[14c] polysilane micelles with cross-linked shells (Scheme 3),[14d] polysiloxanes (Scheme 4),[14e] oligosaccharides,[14f] copolymers synthesized by aqueous reversible addition–fragmentation chain-transfer polymerization,[14g] π-conjugated conducting polypyrroles,[14h] poly(4-vinylpyridine),[14h] poly(*N*,*N*-dialkylcarbodiimide,[14i] polyethylene glycol,[14j] chitosan[14k] and hyperbranched aromatic polyamides (aramids).[14l] Classic surfactants such as sodium dodecylsulfate (SDS) are also used as NP stabilizers for catalysis.[14m] Water-soluble polymers have been used with success for selective hydrogenation of cyclic versus noncyclic olefins.[5d]

A very important concept pioneered in the 1970s is that of catalysis using two different metals such as Au and Pd in the same NP.[15] This idea has been beautifully developed by Toshima's group who used PVP to stabilize core–shell bimetallic Au–PdNPs, that is, NPs in which the core is Au and the shell is Pd (Figure 4).[16] After co-reduction, the structure is controlled by the order of reduction potentials of both ions and coordination abilities of both atoms to PVP. The location of Au in the core and Pd on the shell was

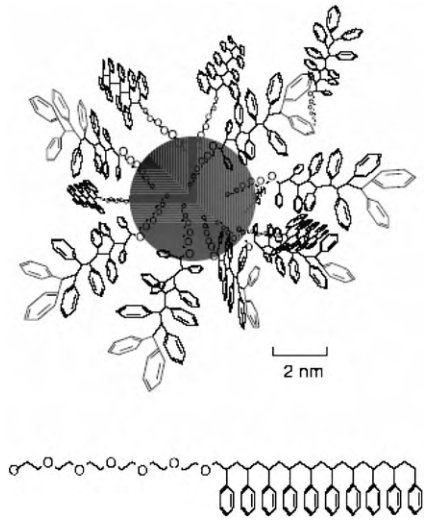

Figure 2. PdNP adsorbed on polyacrylic acid block copolymer as hydrogenation catalyst: the PdNP is stabilized through the block copolymer. Reprinted with permission from ref. [14c].

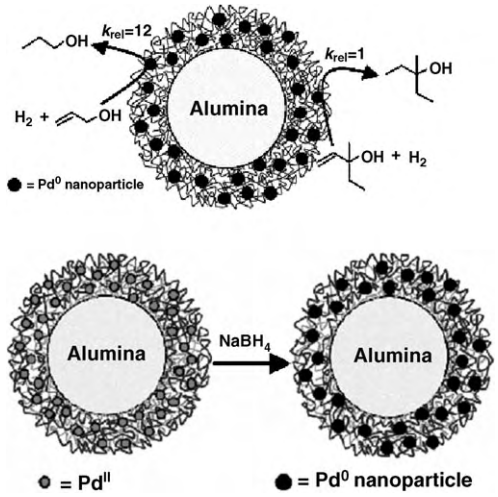

Figure 3. Principle of the formation of PdNPs in multilayer polyelectrolyte films for selective hydrogenation (the layer-by-layer deposition is both convenient and versatile). Reprinted with permission from ref. [14d].

demonstrated by extended X-ray absorption fine structure spectroscopy (EXAFS), and it was shown that such heterobimetallic Au-cored PdNPs are more active in catalysis than simple PVP-stabilized PdNPs. Thus, the Au core enhances the catalytic properties of PdNPs at the PdNP surface.[5f,g] Conversely, design strategies can lead to the opposite core–shell structure (Pd core, Au shell), and specific catalytic properties were obtained for methylacrylate hydrogenation.[16]

Cyclohexene hydrogenation was catalyzed with PdNPs stabilized by highly branched amphiphilic polyglycerol (75% esterified with palmitoyl chloride) and this system was used in a continuously operating membrane reactor to enable recovery and recycling of the PdNP catalyst.[16c]

 © 2005 Wiley-VCH Verlag GmbH & Co. KGaA, Weinheim

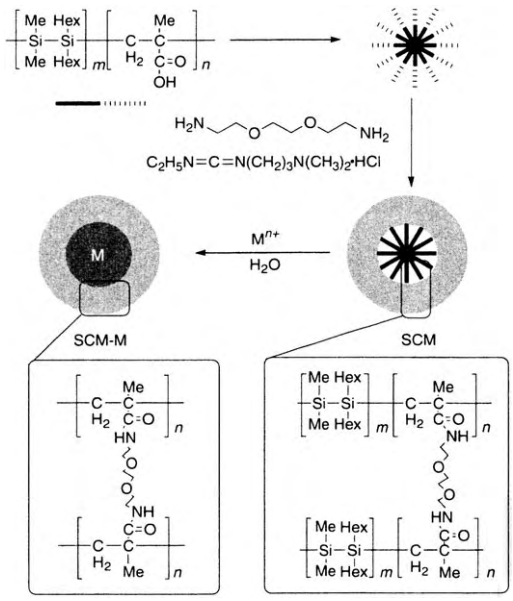

Scheme 3. Schematic illustration of the synthesis of metal NPs derived from polysilane-shell cross-linked micelle templates (Reprinted with permission from ref. [14f]).

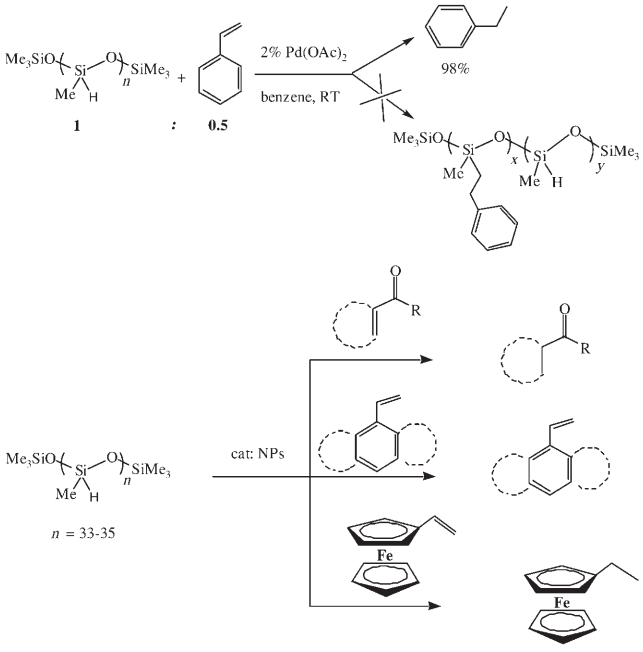

Scheme 4. Polysiloxane-supported PdNPs, generated by reduction of $Pd(OAc)_2$ with polymethylhydrosiloxane, as recyclable chemoselective hydrogenation catalysts. Top: selective reduction of styrene, bottom: reduction of alkenes.[14e].

3.2. Dendrimers

Dendrimers, like polymers, are macromolecules; but unlike polymers, there are perfectly defined on the molecular level with a polydispersity of 1.0.[17] Having shapes that resemble molecular trees or cauliflowers, they become globular after a few generations, and thus behave as molecular boxes[17c] that can entrap and stabilize metal NPs especially if there are heteroatoms in the dendrimer's interiors.[17d,18] The dendritic branches and termini can serve as gates to control the access of small substrates into the dendrimer and thus to the encapsulated NP. Finally, the dendrimer terminal groups can be chosen to provide the desired solubility in organic, aqueous, or fluorous medium. The formation of NPs stabilized by dendrimers for catalysis has been proposed in 1998 by the three research groups of Crooks,[18] Tomalia[19a,b] and Esumi.[19c–e] Metal NPs were introduced inside the dendrimers,[18,19a,b] or at the dendrimer periphery.[19c–e] The former strategy has proved very successful because of the molecular definition of dendrimers and their ability to serve as a box and generation-dependent filter of substrates.

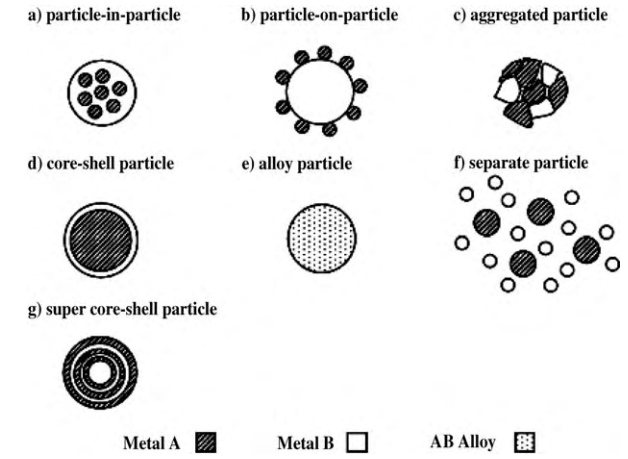

Figure 4. Representative morphologies of bimetallic nanoparticles. Reprinted with permission from ref. [16a].

Crooks and co-workers complexed metal ions (Cu^{2+}, Au^{3+}, Pt^{2+}, Pd^{2+}, Fe^{3+}, Ru^{3+}) to the inner nitrogen atoms of the tertiary amines of poly(amidoamine) (PAMAM) dendrimers. The reduction of the metal ions to M^0 by $NaBH_4$ provoked the agglomeration of the metal atoms to NPs inside the dendrimer.[18] When the terminal amino groups were protonated at pH 2 prior to complexation by metal ions, the metal ions proceeded selectively onto the inner nitrogen atoms resulting in water solubility of the dendrimer and subsequent catalytic activity in water. For example, the selective hydrogenation of allylic alcohol and *N*-isopropyl acrylamide was catalyzed in water by such PAMAM dendrimer–PdNPs (Figure 5 and Scheme 5). Terminal amino groups can be converted into amide groups by the addition of decanoic acid so that the dendrimer–NP catalyst becomes soluble in toluene. In this solvent the catalyst hydrogenates the substrates more rapidly than in water. Alternatively, a perfluorinated polyether "ponytail" can be covalently grafted to the PAMAM dendrimer PdNP catalyst making it soluble in supercritical CO_2. This catalyst was shown to perform classic palladium-catalyzed Heck coupling between aryl halides and methacrylate yielding predominantly (97%) *trans*-cinnamaldehyde. Oxidation[18] and reduction[20] catalysis could also be performed using such dendrimer-encapsulated NPs.

 © 2005 Wiley-VCH Verlag GmbH & Co. KGaA, Weinheim

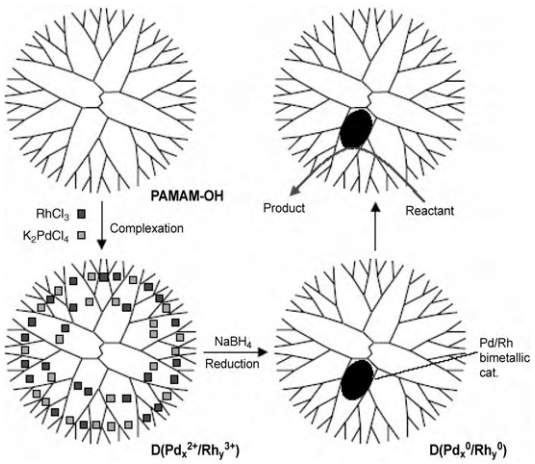

Figure 5. Strategy pioneered by Crooks for the catalysis by nanoparticles encapsulated in PAMAM or PPI dendrimers: complexation of a metal cation to the inner nitrogen atoms of tertiary amines, then reduction to metal(0) by $NaBH_4$, and aggregation giving the NPs inside the dendrimer. The use of PPI dendrimers requires control of the pH value before metal ion complexation to ensure protonation of the terminal amino groups ($pK_a = 9.5$), not the inner ones ($pK_a = 5.5$). In the PAMAM series, OH-terminated dendrimers are used.[18f] Specifically, the preparation of dendrimer-encapsulated bimetallic NPs is shown. Reprinted with permission from ref. [23].

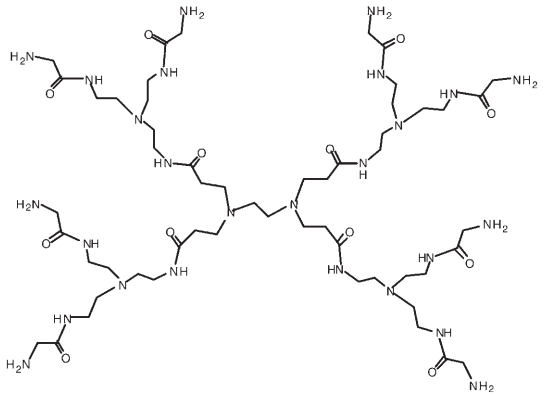

G1 PAMAM Dendrimer

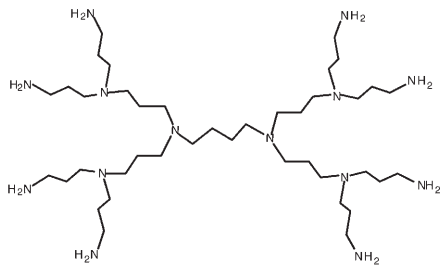

G1 PPI Dendrimer

Scheme 5. The two families of commercial dendrimers considered as metal nanoparticle supports for catalysis (only the first generation (G1) is represented). PPI dendrimers are smaller then PAMAM (2.8 nm versus 4.5 nm for G4, respectively), but more stable (470 °C versus 100 °C respectively).[11b]

El Sayed and co-workers investigated the effect of the generation of the PAMAM dendrimer on the catalytic activity in the Suzuki C–C coupling reaction between phenyl iodide and phenylboronic acid at 80 °C.[21] Generations 3 and 4 were found to be good stabilizers (in contrast to generation 2). These dendrimers stabilize the metal NPs by preventing their agglomeration, but they do not fully passivate the metal surface. The PAMAM-dendrimer-stabilized PdNPs (1.3 ± 0.1 nm) were compared to PVP-stabilized PdNPs (2.1 ± 0.1 nm) for this Suzuki reaction carried out in MeCN:H_2O 3:1 at 100 °C. The mechanism was found to be similar in both cases with phenylboronic acid adsorption onto the NPs, but the turnover ratio for the 2nd cycle:1st cycle was higher for the dendrimer-PdNP catalyst.

Using a different mode of synthesis, 4th-generation (G4) PAMAM-dendrimer-stabilized PdNPs (3.2 ± 1 nm) where prepared by Christensen and co-workers.[22a] With this catalytic system Suzuki coupling occurs with iodobenzene in EtOH at 78 °C, whereas bromobenzene requires a temperature of 153 °C in DMF.[22a] The amount of catalyst was only 0.055 %, which is significantly smaller than traditional catalysts. It was suggested that, since the G4-dendrimer diameter is only 4.5 nm, the PdNPs are stabilized, rather than encapsulated, by the dendrimer.

In studies with 3rd to 5th-generation poly(propylene imine) (PPI) dendrimers that were functionalized by reaction with triethoxybenzoic acid chloride, the dendrimer-stabilized PdNP catalyst led to substrate specificity for the hydrogenation of polar olefins, owing to the strong interaction between polar substrates and the inner tertiary amino groups.[22b,c] For example, in competitive hydrogenation reactions of 3-cyclohexene-1-methanol and cyclohexene, G5-PdNPs gave only reduction of the 3-cyclohexene-1-methanol whereas the traditional Pd/C catalyst gave incomplete hydrogenation of both compounds under the same conditions (Figure 6). For third-generation PdNP-cored dendrimers catalytic activity has been found for the Heck reaction of iodobenzene with ethylacrylate in refluxing toluene (75 % yield) and Suzuki reactions of iodo- and bromobenzene with $PhB(OH)_2$ in refluxing ethanol (42–47 % yield) have been observed. No activity was obtained for hydrogenation reactions, however.[22d]

The encapsulation strategy has recently been extended to bimetallic NP catalysts,[23] evidence that these NPs are bimetallic being provided by single-particle X-ray dispersive spectroscopy (EDS).[17a,b] It was shown that the G4-PAMAM Pd–MNPs (M = Pt or Au) more efficiently catalyze allylic alcohol hydrogenation than the analogous monometallic Pt or Pd catalyst or a mixture of both (Scheme 6).[18i,k]

When a PdNP was located at the dendritic core of G3-TEBA dendrimer, Heck and Suzuki coupling could be obtained in 38 % to 90 % yield in refluxing toluene or ethanol for a day. The form of NPs within the dendrimer is not clear despite TEM studies. Are the NPs really completely inside the dendrimer? Is the dendritic core encapsulated in the NP? Are there several close NPs in the dendrimer cavities or are they connected? Likewise, more work is called for in order to understand the very nature of the catalytically active Pd species.

 © 2005 Wiley-VCH Verlag GmbH & Co. KGaA, Weinheim

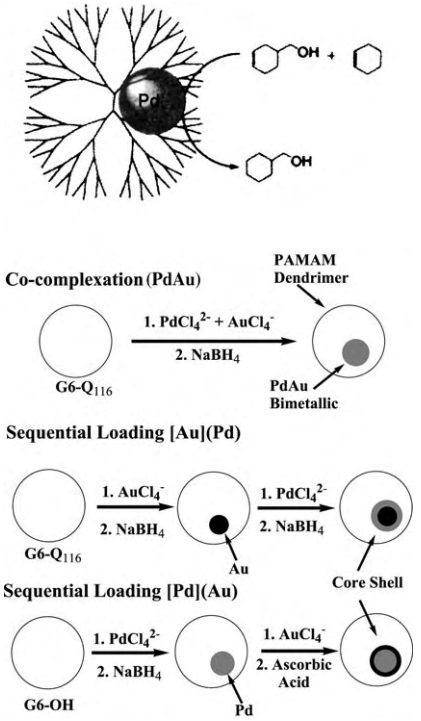

Figure 6. Modes of synthesis of PAMAM-dendrimer-encapsulated heterobimetallic Pd–AuNPs. Reprinted with permission from ref. [18k].

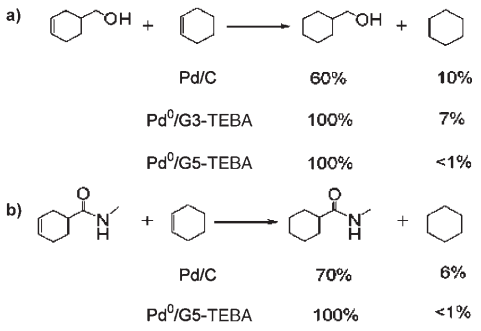

Scheme 6. Competitive hydrogenation of a) 3-cyclohexene-1-methanol and cyclohexene b) *N*-methyl-3-cyclohexene-1-carboxamide and cyclohexene using various palladium catalysts. TEBA = triethoxybenzamide-terminated poly(propylene imine) dendrimer. Reprinted with permission from ref. [22b].

A different dendrimer-stabilizing strategy involves coordination of the NPs by the surface amino groups of PAMAM and PPI dendrimers,[19c–e] and these catalysts were used for various catalytic reactions including the reduction of 4-nitrophenol. In this case, the PdNPs may be surrounded by a number of dendrimers that can also bridge the nanoparticles.

In both situations, the dendrimers clearly stabilize small nanoparticles by a combination of polyligand and steric effects. Whether these dendrimer-stabilized PdNPs are the active species in palladium-catalysis or reservoirs of much smaller, very active palladium fragments, is unclear.

3.3. Ligands

The introduction of ligands as NP stabilizers is of special interest, because it focuses on the precise molecular definition of the catalytic materials. This strategy potentially allows optimization of the parameters that govern the efficiency in catalytic reactions, including enantioselective ones.

Gladysz showed that thermomorphic fluorous palladacycles act as PdNP catalyst precursors for the Heck reaction at 80–140 °C in DMF and gave very high turnover numbers.[24a] Molecular palladium complexes, such as palladacycles and other palladium salts, were also used as PdNP precursors. Treatment with CO in DMF or toluene at room temperature gave PdNPs that catalyzed nucleophilic substitution/carbonylation/amination affording *iso*-indolinones at room temperature.[24b] PdNPs capped with special ligands such as polyoxometallates[25] and cyclodextrins[26] were shown to be active for the catalysis of the hydrogenation of unsaturated substrates and for the Suzuki, Heck, and Stille reactions. For example, perthiolated β-cyclodextrin-PdNPs (1%), in the presence of K_2CO_3 or $Ba(OH)_2$, catalyze the coupling of iodo- and bromoarenes and iodoferrocene to phenyl boronic acid in refluxing in MeCN:H_2O, 1:1 (v/v).[26a] These 3 nm PdNPs are also active for the hydrogenation of water-soluble alkenes.[26b,c] The simplest dodecathiolate-PdNPs catalyze the Suzuki reaction of haloarenes including chloroarenes with phenylboronic acid even at ambient temperature, and the catalyst can be recycled several times.[27]

Another very simple mode of stabilization involves addition of silanes R_3SiH, such as *tert*-butyldimethylsilane, to PdX_2 ($X = Cl^-$, OAc^-) in *N*,*N*-dimethylacetamide. The black NP solution formed in this way catalyzes silane alcolysis of sugars[28a] and selective cross-coupling of the silane with phenyl and vinyl thioethers giving the corresponding thiosilanes and silthianes [Eq. (2); R and R′ = alkyl, aryl; DMA = *N*,*N*′-dimethylacetamide; $T = 25\,^{\circ}C$]:[28b]

$$RSR' + HSi(t\mathrm{Bu})Me_2 \xrightarrow[DMA]{PdNPs} HSi(t\mathrm{Bu})Me_2 + R'H \qquad (2)$$

The synthesis of core–shell NPs that have a cheap-metal core, such as nickel, and a noble metal shell, such as palladium, has been achieved by the thermal decomposition (235 °C) of the Pd and Ni precursors ([$Ni(acac)_2$] + [$Pd(acac)_2$] + trioctylphosphine; acac = 2,4-pentanedione), the nickel complex decomposes before the palladium one. The nickel-cored PdNPs show a much better activity than PdNPs without nickel, but with the same amount of Pd atoms, for the Sonogashira coupling of *p*-bromoacetophenone with phenylacetylene in toluene at 80 °C, although *p*-chloroacetophenone was unreactive.[28c]

Enantioselective reactions have been carried out with metal NPs.[29–30] The first example of an asymmetric reaction catalyzed by metal NPs was reported by the group of Lemaire, Besson, and Galez in 1994 for the RhNP-catalyzed hydrogenation of 2-methylanisole *o*-cresol trimethylsilyl ether induced by a RhNP with a chiral amine, R-dioctylcyclohexyl-1-ethylamine, as ligand.[29] The hydrogenation of ethyl pyruvate was found by Bönnemann and co-workers[30a] to be efficiently catalyzed by Pt- or PdNPs with cinchonidine

 © 2005 Wiley-VCH Verlag GmbH & Co. KGaA, Weinheim

ligands (75–80% *ee*, Scheme 7). The *ee* value was later improved (up to 95–98%).[30b–d] Fujihara and co-workers reported 2,2′-bis(diphenylphosphino)-1,1′-binaphtyl (binap)—stabilized PdNPs with a diameter of 2.0 ± 0.5 nm

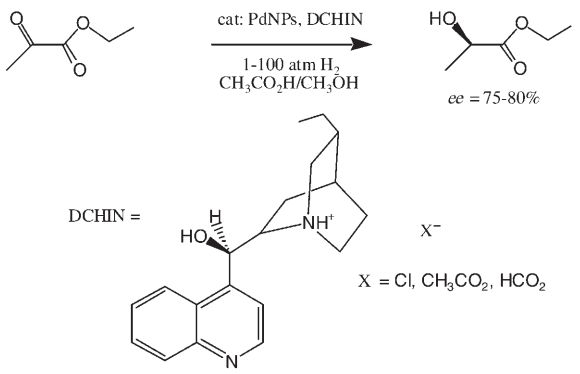

Scheme 7. Enantioselective hydrogenation of ethyl pyruvate catalyzed by cinchonidine-PtNP or cinchonidine-PdNPs.[30a]

and narrow size distribution. It was found that these binap–PdNPs catalyze the asymmetric hydrosilylation of styrene under mild conditions (*ee* 95% at 0°C), whereas mononuclear binap–Pd complexes are inactive.[30e] Recently, the Gomez and Chaudret groups reported enantioselective allylic alkylation reactions with 97% *ee* that were catalyzed by PdNPs stabilized by a chiral xylofuranide diphosphite.[30f] In the above mentioned reports it is suggested that the nanoparticles themselves are catalytically active. However, the nature of the catalytically active species (and even whether catalysis actually occurs on the NP surface) remains unclear. The catalytically active species could also be much smaller Pd fragments, that are leached from the NP, and to which the asymmetric ligand is bound. In any case, regardless of the mechanism, the selectivity obtained is remarkable.

3.4. "Ligand-free" Heck Reactions Using Low Palladium Loading and the Resulting Mechanistic Implications

The original work by Mizoroki et al.,[31a] then by Heck et al.[31b] on the palladium-catalyzed coupling reaction of aryl iodides with olefin used a palladium salt ($PdCl_2$ and $Pd(OAc)_2$, respectively), a base (NaOAc and NBu_3, respectively) and a solvent (methanol and *N*-methylpyrolidone, respectively), but no phosphine or other ligand. Beletskaya and co-workers reported a similar phosphine-free reaction of iodo- and bromoarenes in water, and the palladium loading was as low as 0.0005 mol% (for which the term "homeopathic dose" was used) in the case of 3-iodobenzoic acid.[31c] Likewise, the Reetz[31d,n] and de Vries[31e,n] groups reported extremely efficient Heck catalysis with similarly low palladium-loadings for the coupling between aryl bromides and styrene in organic solvents. Reetz also found that PdNPs are formed when $PdCl_2$, $Pd(OAc)_2$, or $Pd(NO_3)_2$ is warmed in THF in the presence of a tetrabutyl ammonium carboxylate that functions as a reducing and stabilizing agent.[31f] Heating $Pd(OAc)_2$ in polar solvents such as propylene carbonate also generated PdNPs. PdNPs generated in this way from $Pd(OAc)_2$[31d–f] or palladacycles[31g–i] are active catalysts in the Heck reaction, this was demonstrated by monitoring the reactions using TEM.[31j]

Very interestingly, it was found that the palladium catalyst "improves" upon lowering the palladium loading. The proposal to account for this observation was an equilibrium between small (monomeric or dimeric) catalytically active palladium species and the PdNPs which serve as a catalyst reservoir.[31d,h,k] When the catalyst concentration is too high, inactive palladium black forms (Scheme 8). This result

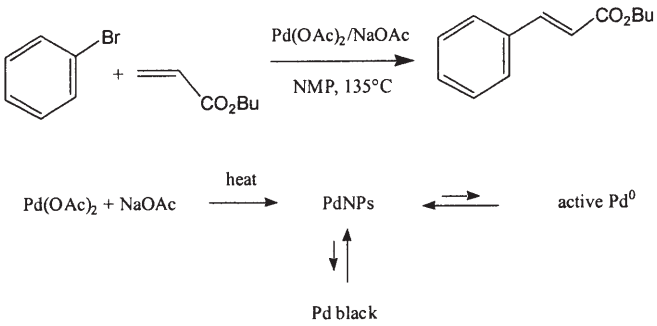

Scheme 8. Heck-type reactions catalyzed by extremely low loadings of palladium salts.[31d,f,j,n]

indicates that the rate of the catalytic reaction must be extremely high, since most of the palladium is in the form of PdNPs. This type of Heck reaction seems quite general for aryl bromides and has been scaled up by the firm DSM to kilogram scale to prepare a drug intermediate.[31e] Likewise, a range of enantiopure substituted *N*-acetylphenylalanines were obtained from methyl *N*-acetamido acrylate and various bromoarenes at very low palladium loading in the absence of other ligands, followed by rhodium-catalyzed hydrogenation.[31l] De Vries reported a similar behavior for the Suzuki reaction of aryl bromides with a turnover frequency (TOF) of up to 30000 mole of product per mole of catalyst per hour.[31m] The precise nature of the active species in these palladium-catalyzed C–C coupling reactions is not known, and it may well be an monomeric- or dimeric Pd^0 species to which an anionic ligand (Cl^- or OAc^-) is bound. This type of reaction is very important in terms of "Green Chemistry" as in it waste is minimized through the absence of added ligand and by such low palladium loadings.[31n] This concept could be extended to other types of catalysis, and indeed other examples of NP catalysts are known for platinum-catalyzed hydrosilylation[5c] and ruthenium-catalyzed hydrogenation.[31o–q] RuNPs have also been shown to catalyze the Heck reaction.[31r]

3.5. Micelles, Microemulsions and Surfactants

"Fluorous" strategies[32] have been used on various occasions for NP catalysis for instance by the Crooks[17] and Gladysz[3,24a] groups. Fluoro surfactants can also serve as micellar stabilizers for PdNPs in water-in-supercritical CO_2

© 2005 Wiley-VCH Verlag GmbH & Co. KGaA, Weinheim

($scCO_2$) microemulsions. Such systems were used as hydrogenation catalysts for simple olefins[32b–d] and citral.[32e] In these systems, hydrogen can work both as a reducing agent for palladium salts and for the unsaturated substrate. Ultrafine PdNPs in reverse micelles (KBH_4 used to reduce the Pd^{II} precursors) enabled the catalytic hydrogenation of allylic alcohol and styrene in the solvent isooctane, although the bis(2-ethylhexyl) sulfosuccinate surfactant inhibited the hydrogenation activity (Scheme 9).[32f] The oxidation of

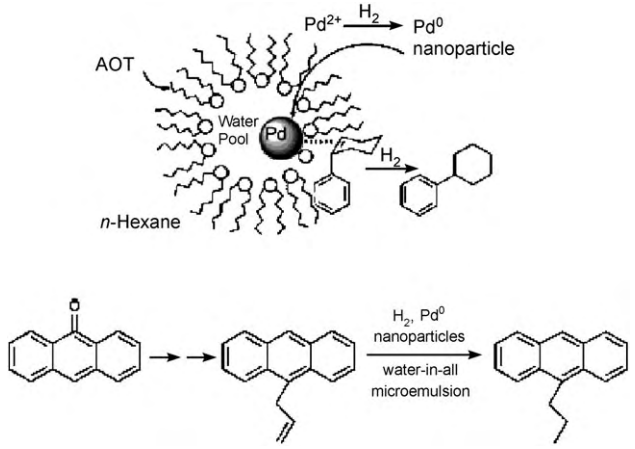

Scheme 9. Hydrogenation of 10-(3-propenyl) anthracene catalyzed by PdNPs in water-in-oil microemulsion (the reaction is much faster than with Pd/C catalysts). AOT = sodium-5-14-diethyl-8,11-dioxo-7,12-dioxaoctadecane-2-sulfonate. Reprinted with permission from ref. [32f].

N,*N*,*N*′,*N*′-tetramethyl-*p*-phenylenediamine by $[Co(NH_3)_5Cl]^{2+}$ was catalyzed by PdNPs in an aqueous/AOT/*n*-heptane microemulsion.[32g] Functional olefins such as 4-methoxycinnamic acid were selectively hydrogenated in $scCO_2$ using PdNPs in a water-in-$scCO_2$ microemulsion, as was nitrobenzene (to aniline).[32h] Oxidation of cyclooctane by *tert*-butylhydroperoxide (*t*BHP) was catalyzed by FeNPs in reverse microemulsion or with RuNPs in biphasic water/cyclooctane solvent. The catalyst could be recycled without loss of activity (Scheme 10).

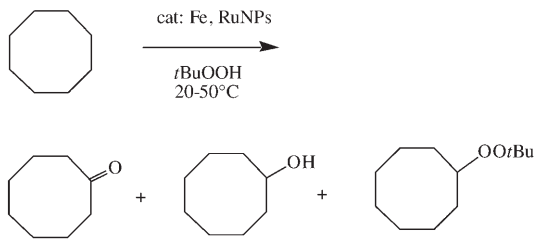

Scheme 10. Cyclooctane oxidation catalyzed by FeNPs in reverse microemulsions or by RuNPs in biphasic water–organic media.[49]

4. Ionic liquids as Media for Metal-Nanoparticle Catalysis

Ionic liquids (ILs) are valuable media for catalysis with PdNPs. The substituted imidazolium cation is bulky, favoring the electrosteric stabilization of NPs (as do tBu_4N^+ ions in Figure 1). The size of the imidazolium cation (that can eventually be tuned by the choice of the *N*-alkyl substituents) also has an important influence on the stabilization, size, and solubility of the NPs, factors which play a role in catalysis. However, ILs are non-innocent, at high temperatures they readily produce palladium-*N*-heterocyclic carbene complexes from PdNPs upon deprotonation of the imidazolium salt. Thus, these carbene ligands can be bound to the NP surface or form mononuclear mono- or biscarbene complexes with palladium atoms that have been leached from the PdNP surface.[33]

IrNPs in 1-*n*-butyl-3-methylimidazolium hexafluorophosphate ([BMIM][PF_6]) were used directly for the hydrogenation of olefins, and good results were obtained.[33b] Phenanthroline (phen) stabilized PdNPs prepared in [BMIM][PF_6] according to the method reported by Schmid and co-workers[33c] (but without using acetic acid as the solvent: $Pd(OAc)_2 + Phen{\cdot}H_2O + 1$ atm H_2 in the IL at room temperature), efficiently catalyzed the hydrogenation of olefins and the selective hydrogenation of cyclohexadiene to cyclohexene under mild conditions (1 atm H_2, 40 °C). Under these conditions, formation of palladium carbene complexes from the BMIM ions does not occur, thus the IL simply plays the role of a PdNP-stabilizing solvent. This catalyst could be reused several times,[33d] and it was much more active than phenanthroline-protected PdNPs supported on TiO_2 for the hydrogenation of 1-hexene.[6b] It was found that PdNPs, formed by reaction of $Pd(OAc)_2$ with tetrabutylammonium acetate dissolved in tetrabutylammonium bromide, efficiently catalyzed the stereospecific reaction of cinnamates with aryl halides to give β-aryl-substituted cinnamic esters.

As indicating in the beginning of this section, the role of the IL is crucial in both the PdNP formation and for the stereospecifity of C–C coupling that could not be obtained in previous studies of PdNP-catalyzed Heck reactions.[33e–g] Salts of *N*-butyronitrile pyridinium cation react with $PdCl_2$ to give dinitrile complexes that turn black upon addition of phenyltributylstannane, and the PdNPs formed catalyze Stille and Suzuki C–C coupling reactions. It is believed that the nitrile groups coordinate to the PdNP surface, which results in PdNP stabilization.[33h]

PdNPs are formed from palladium acetate in the presence of 1,3-dibutylimidazolium salts. It was suggested that N-heterocyclic palladium carbene complexes are generated which form the PdNPs that catalyze Suzuki coupling.[33i] Such carbene complexes were shown to form and catalyze the Heck reaction, and it is strongly suspected that the catalytically active species are in fact PdNPs which form under these conditions.[33e,j] Indeed, heating these N-heterocyclic palladium carbene complexes lead to PdNP formation after ligand loss (Scheme 11). The selectivity of the reactions in such IL media also depends on the solubility, and the solubility difference can be used for the extraction of the product.[33k–m]

Ionic liquids are favorable media for the electrostatic stabilization of preformed NPs at room temperature and subsequent catalysis. At high temperature they give palladium-carbene complexes upon deprotonation of the imida-

 © 2005 Wiley-VCH Verlag GmbH & Co. KGaA, Weinheim

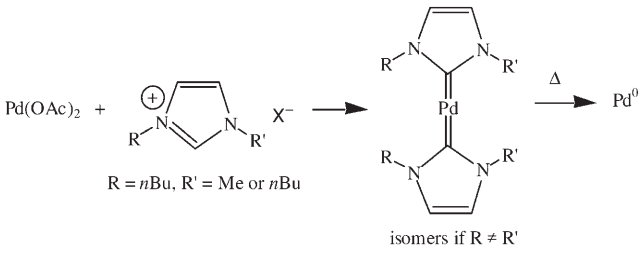

Scheme 11. Formation of palladium carbene complexes by the reaction between palladium acetate and imidazolium salts. Subsequent decomplexation at high temperature gives catalytically active PdNPs for Heck-type reactions.[33e,i,j]

zolium cation, these carbene complexes in turn generate, PdNP catalysts.

5. Solid Supports for Metal Nanoparticles

5.1. Oxide supports

A large number of recent reports (for earlier reports, see refs [6] and [11]) focus on the catalytic properties of NPs supported on metal oxides, including oxides of Si,[34,35] Al,[36] Ti,[37] Zr,[43] Ca,[38] Mg,[39,43] and Zn.[39g] These oxides take various forms, such as SiO_2 aerogels or sol–gels such as Gomasil G-200, high-surface silica (for example, see Scheme 12), M41S silicates and alumimosilicates, MCM-41

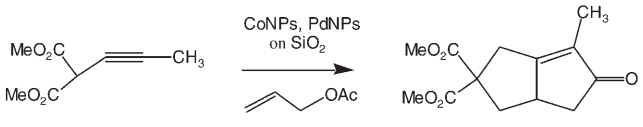

Scheme 12. Sequential allylic alkylation and Pauson–Khand reactions for the one-pot syntheses of bicyclic enones. Both are catalyzed by CoNPs and PdNPs supported on silica.[35c]

mesoporous silicates such as HMS and SBA-15 silica, silica spheres,[35b] microemulsions (SiO_2), hydroxyapatite (Ca^{2+}),[38] hydrotalcite (Mg^{2+}, Al^{3+}),[39] zeolites (SiO_2, Al_2O_3),[40] molecular sieves (Figure 7)[41] and alumina membranes (Figure 8).[36a] Thus, despite the large variety of supports, the majority of them deal with a form of silica. The catalytic reactions examined with these supported NPs are hydrogenation reactions, including selective ones, of unsaturated substrates, Heck and other C–C coupling reactions, and oxidation of CO and alcohols using molecular oxygen. The heterogenization of polymer- or dendrimer-stabilized NPs on a solid supports such as silica brings the classic advantages of heterogeneous catalysis, that is, stability to high temperatures, easy removal from the reaction medium, and the bottom-up approach of NP synthesis. A few outstanding recent examples are discussed below, and Table 1 gathers references for each NP-catalyzed reaction.

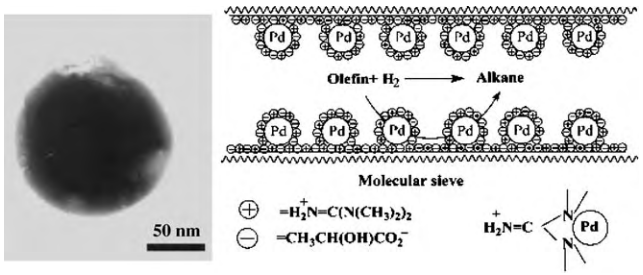

Figure 7. Transmission electron micrograph (left) of a molecular sieve with supported PdNPs (right). The catalyst, active in hydrogenation of olefins, contains 20 wt% ionic liquid as the stabilizer whose average layer thickness is 0.4 nm.[41b]

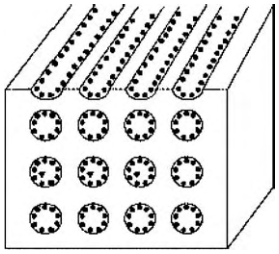

Figure 8. Schematic representation of a section of alumina membrane loaded with metal nanoparticles as would be used for the gas-phase catalysis of 1,3-butadiene hydrogenation (PdNPs) and CO oxidation (RuNPs).[36a]

PtNPs and bimetallic dendrimer-stabilized Pd–AuNPs were adsorbed onto a high-surface silica support and thermally activated to remove the dendrimers (Figure 9). The Chandler group showed that these NPs were smaller than 3 nm and highly active for CO oxidation catalysis near room temperature. The hydrogenation of toluene was also efficiently carried out.[34] The fabrication of uniform hollow spheres with nanometer to micrometer dimensions having tailored properties has recently been intensively studied using various procedures.[42] Monodisperse palladium nanospheres of 300 nm catalyzed Suzuki coupling of iodothiophene with phenylboronic acid using 3 mol% Pd catalyst in ethanol under reflux. Under the same conditions 15 mol% Pd catalyst was used to couple bromobenzene (Figure 9).[35b] Treating hydroxyapatite, $[Ca_{10}(PO_4)_6(OH)_2]$, with $[PdCl_2(CH_3CN)_2]$ gives a monomeric $PdCl_2$ species chemisorbed on the hydroxyapatite surface that, in the presence of alcohol, is readily transformed into supported PdNPs with narrow size distribution. These PdNPs catalyze the oxidation of 1-phenylethanol under atmospheric O_2 pressure in solvent-free conditions with very high turnover numbers of up to 236000 and a remarkable turnover frequency of 9800 h^{-1}. The work up is easy and the catalyst is recyclable without requiring additives to complete the catalytic cycles.[38]

Hydrotalcite anionic clays are layered double hydroxides of formula $M^{2+}_{1-x}M^{3+}_{x}(OH)_2(A^{n-})_{x/n}\cdot y\,H_2O$ (where A^{n-} is CO_3^{3-}, Cl^-, or NO_3^-) in which the anion can easily be exchanged. These materials, after calcination at temperatures over 723 K, serve as supports for noble-metal catalysts, for example, C–C coupling[39d] and selective semi-hydrogenation

 © 2005 Wiley-VCH Verlag GmbH & Co. KGaA, Weinheim

Table 1: Overview of metal-nanoparticle-catalyzed reactions.

Reaction	Ref.	Reaction	Ref.
Hydrogenations			
Simple olefins and dienes	[2, 6b, 10d–i, 12, 14d,f,j,k,l, 16, 17a,b, 22b–d, 23, 26, 31l,o–q, 32, 33, 35a,i, 36a, 40a, 41, 43d, 44b,h, 46a–d, 58, 61]	Amination of aryl halides and sulfonates (ArX + RNHR' → Ar-N(R)R')	[44k–o, 74b, 77]
Alkynes	[14c, 37b, 39, 40b, 62, 63]	Hydrosilylation	[9h, 48]
CO_2	[10, 82]	Coupling of silanes	[28a,b]
Arene rings	[12a, 29, 33k,m, 34, 37b, 65–70]	Hydroxycarbonylation of olefins	[75]
Arene rings of bibenzo-[18]crown-6	[64]	[3+2] Cycloaddition	[55]
Acrolein	[12b, 78]	McMurry coupling	[56, 57]
Methylacrylate	[16]		
		Oxidation reactions	
Allylic alcohols	[14d, 17b]	CO	[8a, 9d,e, 11j, 17, 34, 36a,b,e, 37c,d, 45, 50b, 80]
N-isopropylacrylamide	[17b]	Dihydrogen	[46f]
Ethylpyruvate	[30a, 63]	Aromatic amines	[33g, 46g]
Citral	[32c,d,e]	Alkyl amines	[9d]
Styrene	[18i]	1-Phenylethanol	[38]
trans-Stilbene	[32h,f]	CH_3OH elektrooxidation	[47]
Opening of epoxides	[14a]	Cyclooctane	[49]
Dehydrolinalole	[14b]	Cyclohexane	[46n]
Citronellal	[59b]	Ethene und propene epoxidation	[50]
9-Decen-1-ol	[35n]	Glucose	[51, 46m]
Functionalized olefins	[9f,g, 14e, 22b,d, 32h, 33k,m]	Diol, glycerol, ethylene glycole	[46c,e, 81]
Polar olefins	[22b]	Oxalate	[46m]
Nitroaromatics	[9a, 59c, 61]	*Aminations*	[24b, 43j]
Ketones, benzonitrile	[14h, 33l, 35d,i]		
		Carbonylations	
Cinnamaldehyd	[47, 59a]	Aryl halides	[24b]
Asymmetric hydrogenation	[29]	Methanol	[52]
Coupling reactions		*Miscellaneous reactions*	
Heck coupling (ArX + olefin → arylolefin)	[7, 8b, 14f, 17f, 18i, 22, 24a, 31a–n, 32n, 33e–g,i,j, 35g,n, 40b, 43a–f, 44a–k, 53, 71–73]	Allylic alkylation	[30f, 31, 35c, 57]
Suzuki coupling (ArX + Ar'B(OH)$_2$ → Ar-Ar')	[13a,b, 14i, 17i–k, 21–23, 24a, 25–27, 31m,n, 33e,h,i, 34b, 35b,o, 43c, 44c–e,l, 54, 72f, 74a, 76]	Mannich reaction	[57]
Sonogashira coupling (ArX + alkyne → arylalkyne)	[28c, 43g,h,i]	Pauson–Khand reaction	[11h, 35c]
Stille coupling (ArX + Bu_3SnR → Ar-R)	[33h]	Hydroconversion of hydrocarbon	[40a]
Negishi coupling (ArCl + RZnX → Ar-R)	[44m]	Combustion: alkanes, arenes, alcohols	[32e, 35j, 79]
Kumada coupling (ArCl + RMgX → Ar-R)	[44j,k]	Methanol reforming	[36c, 39g]
Dehydrohalogenation of arylhalides	[44i,n]		

of alkynes[39e] have been obtained. Immobilization of a PdNP catalyst on a solid surface such as molecular sieves was achieved by using the ionic liquid 1,1,3,3-tetramethylguanidinium lactate. This system was used for solvent-free hydrogenation of alkenes and gave high activity and stability (for instance with a cyclohexene/palladium mol ratio of 12000:1, 100% conversion was obtained in 10 h at 20°C with a TOF of 20 min^{-1}).[41b] The PdNPs whose size remains unchanged (1–2 nm) during the catalysis, are stabilized by guanidinium ions.[33d] Ag–PdNPs prepared directly in ultrathin TiO_2 gel films by a stepwise ion-exchange/reduction method showed an activity in methyl acrylate hydrogenation 267-times higher than commercial palladium black and 1.6-times higher than PdNPs that did not contain Ag. This outstanding activity was explained by the large fraction of the surface-exposed palladium atoms.[37c] Polyelectrolyte multilayers serve as supports the PdNP catalysts for the selective hydrogenation of allylic alcohols, a reaction in which the isomerization is suppressed. To prepare this catalyst, polyacrylic acid and a polyethyleneimine palladium(II) complex were alternatively

 © 2005 Wiley-VCH Verlag GmbH & Co. KGaA, Weinheim

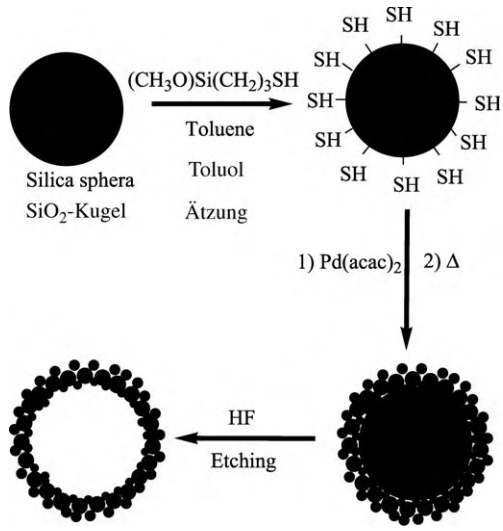

Figure 9. Principle of the formation of hollow PdNP spheres used for the catalysis of Suzuki reactions in refluxing ethanol with K_3PO_4 as a base. With 2-iodothiophene and phenylboronic acid (cat: 3% Pd spheres), at least seven cycles could be achieved with 95–97% yields, ref. [35b].

adsorbed on 150-mm diameter alumina particles, and subsequent reduction of Pd^{II} to PdNPs was carried out using $NaBH_4$.[14d]

The mechanisms of oxide-supported PdNP catalysis are a long way from being understood. The oxide support however has a strong influence on the activity. For instance, in the Heck reaction, the activity is dominated by the support in the order: C (84%) ~ H-Mordenite (83%) > ZrO_2 (49%) ~ TiO_2 (45%) > MgO (37%) = ZnO (37%) > SiO_2 (7%). The good activity of zeolites in this reaction is seemingly due to a better stabilization of the active species in the cavities and to a better dispersion of PdNPs on the oxide support. There are many heterogeneous-catalysis studies that discuss the influence of parameters (solvent, catalyst, base, temperature, recycling activity, NP size). Indeed, Djakovitch and Köhler have proposed that, since the results are often similar for homogeneous and heterogeneous systems in terms of selectivity, the "heterogeneous mechanism" proceeds by leaching of molecular palladium species into the solution (a phenomenon favored in DMF). On the other hand, dehalogenation is more favored on a heterogeneous support than with a homogeneous catalyst. Thus, it has been proposed that supported PdNPs are responsible for dehalogenation.[43]

The heterogeneous palladium-catalyzed Heck reaction has been extended to important α-arylated carbonyl derivatives, and the model arylation of diethylmalonate has been examined. The NaY-supported PdNP catalyst showed a limited activity, giving yields comparable to those obtained with the homogeneous ($Pd(OAc)_2$/4 PPh_3) system, but the palladium concentration used is only 2% and the recyclability is good. The amination of halogenoarenes has also been investigated with MgO-supported PdNPs and ZrO_2-supported PdNPs, the amphoteric supports give the best yields, which would indicate that they favor the rate-limiting C–N coupling in the reductive-elimination step. For this reaction, the zeolite supports give a better *para* selectivity presumably because of the "shape selectivity" properties of this material.[43]

The Heck and Suzuki reactions have also been catalyzed by alumina-supported RuNPs.[43c] Hydroxyapatite-supported RuNPs were recently found to be efficient and recyclable catalysts for *cis*-dihydroxlation and oxidative cleavage of alkenes.[43d] Supported RuNPs in the pores of mesoporous Al-MCM-41 materials were prepared by H_2 reduction of adsorbed $[Ru(NH_3)_6]^{2+}$. Their activity in benzene hydrogenation reactions was studied and found to be more efficient when 330 ppm H_2S was added to the H_2 than when H_2S was not present.[43d]

Little is known concerning the catalytically active species of oxide-supported NPs, and it is possible that the supported NPs are only reservoirs of much smaller catalytically active palladium fragments.

5.2. Carbon Supports

Charcoal is a classic commercial support for catalysts, (for example Pd/C). Using the general synthetic method developed by Bönnemann (the reduction of quaternary ammonium salts of metal cations in THF) the charcoal is impregnated simply by stirring in the NP suspension. These charcoal-supported metal NPs have been used for a variety of catalyzed reactions.[7,29a,35a,41a,c] This procedure was also used by Reetz et al. to support their electrochemically prepared metal NPs including catalytically active bimetallic NPs.[8,35a] Activated carbons that are suitable as support materials in catalytic processes need to be prepared and modified so that adequate surface area, porosity, and pore size distribution are obtained. Purification by acid treatment and elution processes are required to remove ash, extractable sp^3 material, and contaminants. Treating and conditioning supports leads to optimal interactions between the precious metal and the support during impregnation and ensures dispersibility in the reaction media.

The detailed identification of the specific properties of the surface atomic layers of carboneous supports used for the preparation of Pd/C catalysts has been studied recently by means of inelastic incoherent neutron scattering. This technique allows the behavior of activated carbons and carbon blacks in the presence of adsorbed hydrogen to be studied and the vibrational states of protons on and inside carbon-supported PdNPs and PtNPs to be identified.[44a] Well-known and typical applications of such materials are the hydrogenation reactions that are important for the synthesis of fine-chemicals intermediates, vitamins, and pharmaceuticals.[2,44b] Such Pd/C catalysts were also reported for the Suzuki and other C–C forming reactions.[44c–e]

It was shown that the catalysis proceeds with palladium dissolution/reprecipitation, the palladium concentration in solution being highest at the beginning of the reaction and minimal (< 1 ppm) at the end of the reaction. The mechanism is quasi-homogeneous, and small palladium species in solution act as the catalytically active species.[44f,g] The palladium

 © 2005 Wiley-VCH Verlag GmbH & Co. KGaA, Weinheim

is leached and, at the end of the reaction redeposited, which provides an excellent recovery of the precious metal from the reaction mixture.[44f,g] The precipitation of the catalyst at the end of the reaction significantly changes its state and decreases its activity, however, making its reuse unattractive.[44f]

Köhler et al. also showed that optimization of the Pd/C catalyst (temperature, solvent, base, and palladium loading) for the Heck reaction of unactivited bromobenzene at 140 °C, allows turnover frequencies (TOFs) of up to 9000 mole of product per mole of catalyst per hour (the highest ever reported) to be reached and palladium concentration down to 0.005 mol % to be developed. The efficiency of this catalyst is far higher than, for instance, palladium on mesoporous silica and palladium on zeolites, and TOFs are higher than homogeneous palladium catalysts. The turnover numbers (TONs), however, are surpassed by those of the best homogeneous catalysts.[44f] As indicated above, the efficiency of the Pd/C catalyst strongly depends on the palladium dispersion, oxidation state in the fresh catalyst (in situ reduction of Pd^{II} to active Pd^0 under the Heck reaction conditions leads to the best dispersion and activity), impregnation method, and pre-treatment. Interestingly, exclusion of air and moisture is not necessary, however. The fact that no dehalogenation of bromobenzene to benzene is found confirms the homogeneous mechanism, whereas surface heterogeneous catalysis might be responsible for dehalogenation under different conditions.

Heterogeneous Ni/C catalysis[44h–o] is also mainly known for the hydrogenation of unsaturated compounds.[44h] Recent reports, however, concern hydrodehalogenation of aryl halides (including aryl chlorides),[44i,n] Kumada,[44j,k] Suzuki,[44l] and Negishi-type C–C coupling[44m] and aromatic amination.[44k–o] Whereas the mechanism for heterogeneous hydrogenation follows true surface chemistry with dihydrogen chemisorption onto the metal surface,[44p] C–C and C–N coupling reactions involve nickel bleed from the carbon support, a one-time event at the very beginning of the reactions. There is an equilibrium for between homogeneous nickel species located inside and outside the carbon pores which strongly favors the former. Thus, unlike in the Pd/C case, only traces of metal are detectable in solution. The nickel is completely recovered on charcoal, making this heterogeneous catalyst interesting for applications. These reactions appear to be due to a combination of heterogeneous and homogeneous catalysis.[44k,n]

Recently, new supports such as high-area carbon have been used to prepare bimetallic Pt–RuNPs that catalyze methanol electrooxidation with enhanced activities compared to commercial catalysts.[46i–l] Pd-, Rh-, and RuNPs, deposited onto functionalized carbon nanotubes by hydrogen reduction of metal-β-diketone precursors are effective catalysts for hydrogenation of olefins, such as *trans*-stilbene in $scCO_2$[32g]. Comparison of the properties of carbon nanotube and activated carbon supports were carried out for Heck and Suzuki reactions, aerobic alcohol oxidation, and selective hydrogenation.[44q]

6. The New Gold Rush

In the AuNP-catalyzed CO oxidation to CO_2 by O_2 that can occur down to 200 K, the oxide support (Fe_2O_3, TiO_2 or Co_3O_4) is indispensable.[9c,d] The mechanism is not clear, however.[45a] A new "gold rush"[9d,e,45] is now following Haruta's crucial work on catalysis with AuNPs.[9c,d] This finding of low-temperature catalysis of CO oxidation is of great interest, because the Pt/Pd catalysts that are currently used in cars for CO oxidation work only at temperatures above 200 °C. Thus, CO pollution essentially occurs during the first five minutes after starting the engine. The low-temperature, supported-AuNP-catalyzed CO oxidation clearly could solve this problem.

CO can be selectively oxidized by O_2 in the presence of H_2 which allows H_2 to be purified from residual CO. There are many other challenges in catalytic oxidation chemistry that can be addressed using this type of catalyst (see below). Of the various ways to prepare supported AuNP catalysts, it is considered that Haruta's deposition–precipitation procedure is the most suitable [Eq. (3)]:[9d]

$$\begin{aligned} &HAuCl_{4(aq)} + NaOH \rightarrow [Au(OH)_4]^- \; Na^+_{(aq)} \; (pH\,6-10) \rightarrow \\ &Au(OH)_3/Support \rightarrow wash,\ dry\ then \\ &calcinate\ at\ 563-673\ K \rightarrow AuNP/Support \end{aligned} \quad (3)$$

The optimum size of the AuNPs is 3 nm, stable hemispherical NPs, are formed, their size being controlled by the calcination temperature (optimum 570 K). The best support is TiO_2, for a good dispersion of the AuNPs the addition of Mg citrate is necessary during or after coprecipitation).

It has been shown that oxidation of CO by O_2 to CO_2 can also be catalyzed in the gas phase by the cluster Au_6^- (Figure 10),[45c] and calculations with Au_{10} predict CO oxidation by O_2 below room temperature.[45d] Although the mechanism was thus depicted with AuNPs alone[45c,d] (Figure 10), the activation by the oxide support is also

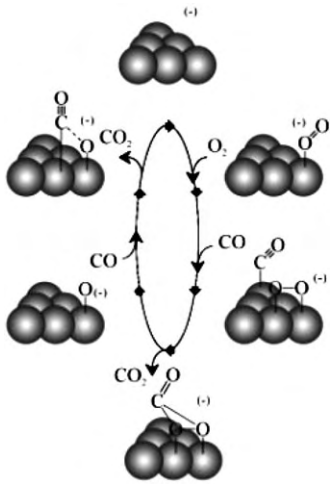

Figure 10. Proposed schematic mechanism of the Au_6^- catalyzed formation of CO_2 from CO and O_2 in the gas phase (Reprinted with permission from ref. [44c].

 © 2005 Wiley-VCH Verlag GmbH & Co. KGaA, Weinheim

needed and must be involved in the mechanism. It is probable that the oxide favors the polarization of the adsorbed CO molecule to provoke electrophilic attack on the CO carbon atom by AuNP-support-activated O_2 (in the form of superoxide or a related nucleophilic oxygen species).[9d,e,45b] It is also suggested that CO adsorbs on the edge and step sites of AuNP surfaces and O_2 adsorbs on support surfaces.[50b]

Applications of supported AuNPs are expected both in the catalytic removal of CO produced at ambient temperature by engines and in the removal of CO traces from dihydrogen streams feeding the fuel cells. There has been a tremendous increase recently in the number of reports focusing on this area of supported AuNP-catalyzed CO oxidation, TiO_2 becoming the dominant support.[45] Besides CO oxidation, other supported-AuNP-catalyzed reactions have been disclosed, confirming that supported AuNPs are now a very popular means to catalytically activate dihydrogen and dioxygen. The following applications have been reported:

- Hydrogenation of 1,4-butadiene to butenes,[46a] acrylaldehyde to allylic alcohol,[46b] citral to geraniol and nerol,[46c] and benzalacetone to phenyl-3-butene-2-ol.[46d]
- Oxidation (using O_2 or air) of alcohols to aldehydes,[46c] *o*-hydroxybenzyl alcohol to salicylic aldehyde,[46d] ethane-1,2-diol to glycolate,[46c] other diols to hydroxymonocarboxylates,[46e] β-amino alcohols to β-amino-acids,[46e] aliphatic aldehydes to carboxylic acids,[46e] D-glucose to gluconic acid[46e] or oxalate,[46m] dihydrogen to hydrogen peroxide,[45f] aromatic amines (with CO) to carbamate,[46g] propene to propene oxide,[45h] and cyclohexane to cyclohenol and cyclohexanone.[46n–o] Alcohols, in particular methanol, are also oxidized electrochemically, with supported AuNPs being more active electrocatalysts than AuNPs alone.[47]

Other applications of supported AuNP-catalyzed reactions are numerous. They include:

- Oxidative decomposition by Fe_2O_3-supported AuNPs of bad-smelling alkylamines responsible for unpleasant atmosphere in toilets.[9d]
- Oxidative decomposition of dioxin coming from incinerator outlet gases by La_2O_3-supported AuNPs integrated with Pd/SnO_2 and Ir/La_2O_3.[9d]
- Direct epoxidation of propylene to propylene oxide by TiO_2(MCM48)-supported AuNPs.[9d]
- Sensors using Co_2O_3-supported AuNPs that are able to simultaneously detect H_2 and CO at low concentration levels.[9e]
- CO safety masks for efficient removal of CO from contaminated atmospheres.[9e,45f]
- Various liquid-phase synthetic processes.

7. Summary of Mechanistic Information

Hydrogenation of unsaturated substrates under ambient conditions can be catalyzed by a large variety of unsupported or supported metal NPs of 1 to 5 nm size and, in the mechanistically studied cases, proceeds by the classic heterogeneous surface mechanism involving dihydrogen chemisorption. The use of core–shell bimetallic NPs, where by the metal core activates the metal surface of the NP, improves the catalytic efficiency compared to the monometallic NPs. For soluble metal NPs active at room temperature, hydrogenation presumably proceeds on the edge of polyhedral NPs without leaching.

The finding that dehalogenation of halogenoarenes occurs in the course of heterogeneously catalyzed C–C bond-formation reactions is explained by a heterogeneous mechanism.[43] It has been proposed that defects on the PdNP surface are involved in the mechanism of C–C bond formation in the Heck reaction, that is, the activity should be related to the number of low-coordinate surface atoms.[83] It has also been suggested that flat π-adsorption of the aromatic ring of the aryl halide over a "large" PdNP is responsible of activation of the C–X bond prior to formation of a σ-aryl-palladium complex at the PdNP surface.[84] However, the homogeneous mechanism according which the catalytic activity is due to palladium species leaching from the heterogeneous catalyst (Pd/C or Pd/MO_x) into the solution is presently preferred. This "leaching mechanism",[43,85,86] first proposed by Julia et al. in 1973,[85] is now firmly established especially by the recent work by Djakovitch and Köhler using astute experiments in which the selectivities obtained in homogeneous and heterogeneous catalysis are compared.[43e] Charcoal-supported catalysts are superior to oxide-supported catalyst in terms of efficiency and selectivity. PdNPs on NaY zeolites are also very efficient catalysts, and the catalytically active Pd^0 species could be retained in the zeolite pores or re-adsorbed at the surface by dissolution–readsorption.[43e,f] The thermal treatment has an important influence on the mechanism, as Pd^{II} species surrounded by oxygen atoms in the zeolite pores could give leaching whereas Pd^0NP entrapped the zeolite pores would still react by a heterogeneous mechanism.[87a] The exact nature of these exceedingly reactive species involved in the homogeneous mechanism is not known: they could be mono- or bimetallic metal species[87b] or very small metal clusters containing only a few atoms. They could be neutral or be coordinated to an anionic ligand (for example, halide, acetate) making them anionic which could facilitate the oxidative addition of the aryl–halogen bond.[88]

The finding that unsupported palladium salts are active even under "homeopathic" (extremely low) concentration in the "absence" of ligand (except halide or acetate) was taken together with the facts that PdNPs were confirmed and that dilution improved the catalysis led Reetz to propose an equilibrium between PdNPs and catalytically active palladium fragments.[31j,n] Thus, in the Heck reaction, there is a good parallel between homogeneous catalysis and catalysis by supported PdNPs. In the homogeneous case, the PdNPs are the reservoir of active palladium species, and in the supported Pd/C catalysis, the charcoal or zeolite is the reservoir of palladium species that are also catalytically active in solution. These active species could be of similar nature in both supported and unsupported cases.

© 2005 Wiley-VCH Verlag GmbH & Co. KGaA, Weinheim

Such a mixture homogeneous and heterogeneous catalysis was also found or Ni/C catalysis of a variety of C–C and C–N coupling reactions (Kumada, Suzuki, Negishi, Heck, amination of bromoarenes). The leaching of nickel species was demonstrated in all these cases. However, the amount of leached metal is much less important than in the palladium case; with nickel the amount of leaching remained essentially constant and extremely low throughout the reactions. Besides supported NP metal catalysts, some unsupported, but ligand-coordinated PdNPs are active and recyclable catalysts for the Suzuki C–C coupling reaction at room temperature.[27] It is possible that, under such mild conditions, the PdNPs do not loose palladium atoms or clusters of atoms in the solution, and that catalysis occurs at the edge of the polyhedral PdNP itself, but this remains to be ascertained.

It is clear that care should be exercised in classifying the NP-catalyzed reactions as homogeneous or heterogeneous as the frontier is fuzzy, as exemplified by the above homogeneous mechanism of reactions on heterogeneous supports.

Techniques that allow investigation of the leaching of metal species from the supported metal to the solution are crucial to mechanistic investigations and include transmission electron microscopy (TEM), energy dispersion X-ray analysis (EDX), and X-ray diffraction. Data are recorded from samples before and after catalytic runs for comparison. Sometimes, experiments carried out with and without PPh_3 or a polymer phosphine are compared to investigate the importance of such ligands on the activity of the leached metal species in solution. The metal content in solution can also be determined by inductively coupled plasma atomic emission spectroscopy (ICP-AES) after filtration of the hot or cooled reaction mixture. Comparison of the selectivities obtained with homogeneous and heterogeneous catalysts is also a powerful means to investigate whether heterogeneous catalysis proceeds by an active leached species.[43e]

Concerning the important AuNP catalysis of CO oxidation by O_2, recent studies by Haruta's group indicate that the TOF increases with decreasing AuNP diameter. The enhancing effect of moisture on the metal oxide support was demonstrated. Kinetic studies showed that the rate of CO oxidation is independent of the CO concentration and only slightly dependent on the O_2 concentration in the low concentration range down to 0.1 vol%. This result suggests that both CO and O_2 are adsorbed on the catalyst surface to near saturation and that the rate-determining step is the reaction between the two adsorbed species. Isotope effects also are a useful technique contributing to mechanistic investigations. Some logical mechanistic trends are apparent and have been proposed, in particular by Haruta, although the precise mechanism is unknown and still the subject of scrutiny. Adsorption of CO and O_2 must occur at the NP periphery on edges and corners. The Au-coordinated CO must be polarized ($C^{\delta+}$–$O^{\delta-}$) upon coordination, and the dioxygen molecule must also be polarized or reduced to the superoxide anion by AuNPs. Then $O_2^{\bullet-}$ could attack the positively polarized CO carbon atom. The role of the oxide support might be to facilitate the polarization of either molecule or both, this role however is more difficult to evaluate. The support may also have a crucial role in the cleavage of the superoxide species or negatively polarized oxygen atom of the O_2 molecule before, during, or after CO binding.[45] Haruta recently depicted his mechanistic proposal as follows [Eq (4)–Eq (6)]:[11j]

$$O_2 + Au_{NP}/TiO_2 \rightarrow Au_{NP}/TiO_2 \cdots O_2 \quad (4)$$

$$Au/TiO_2 \cdots O_2 + 2\,Au_{NP}CO \rightarrow OCAu_{NP}{=}O + CO_2 + TiO_2 \quad (5)$$

$$OCAu_{NP}{=}O \rightarrow Au_{NP} + CO_2 \quad (6)$$

Clarification should be provided by theoretical work involving not only AuNPs but all the four components of the reaction including the TiO_2 support. Intriguingly, the Corma group reported that Au^{3+} on CeO_2 catalyzed the homocoupling of phenylboronic acid, and the catalytic cycle was proposed to involve the interconversion of Au^{3+} and Au^{+}.[87c] Spectroscopic studies, by the same research group, of Au supported on nanocrystalline CeO_2 showed that CO was bonded to Au^{3+}, Au^{+}, and Au^{0} species, whereas the active form of O_2 was bonded to CeO_2 as superoxide η^1-O_2^-, confirming the nucleophilic attack on the electron-deficient carbon atom of CO by superoxide on the way to CO_2.[87d]

8. Prospects for Organic Synthesis

The discovery of the catalytic formation of C–C and C–N bonds by palladium catalysts has been a considerable advance for organic chemistry. It became possible to easily functionalize olefins, alkynes, and aromatics. Yet, the problems of catalyst recovery and pollution by phosphines were unsolved. These aspects are crucial for the pharmaceutical industry, because the presence of metal and phosphine contaminants in drugs is unacceptable. These problems are largely solved by the use of Supported NP catalysts which allows catalyst removal from the reaction mixture by simple filtration. The carbon and NaY zeolite supports (the best ones) are reservoirs of metal species that retain these metal species subsequent to reaction in solution. The amount of metal left in solution is in the ppm range. Moreover, such types of catalyst are phosphine free. The firm DSM employ this method for the synthesis on the kg-scale of pharmaceutical intermediates, and it is likely that this type of procedure will find use throughout the pharmaceutical and other industries.

The Heck reaction is a key reaction in the production of fine chemicals on multiton scale per year[89] for which the use of NP catalysts could be possible. It is used for the production of the herbicide prosulfuron,[90] the anti-inflamatory naproxen,[91] or the anti-asthma singulair.[92] On the other hand, in terms of "Green Chemistry", it is likely that procedures involving chemicals such as ionic liquids, micelles, surfactants, and other additives in homogeneous solution will be of interest.

Given the extraordinary recent advances in AuNP-catalyzed reactions, it is clear that many applications in oxidation catalysis will very soon penetrate the every-day world of organic chemists. In addition there is considerable interest from materials scientists for the reduction of car

 © 2005 Wiley-VCH Verlag GmbH & Co. KGaA, Weinheim

pollution and in H_2 purification through the removal of residual CO.

9. Conclusion

The design and use of metal NP catalysis is now well advanced thanks to the efforts of pioneers and advent of modern characterization techniques. A large variety of NP preparation modes, a variety of materials that can serve as supports or grafting cores, and several media are available. Monodisperse, small (1–10 nm) supported metal NPs are available for many important reactions. Bi- and trimetallic NP catalysts are often more efficient than those containing only one type of metal. Compared surface studies on palladium single crystals and PdNP have even shown that alkene hydrogenation is only catalyzed by PdNPs.[32i] These advances have considerably improved the selectivity of NP-catalyzed reactions, especially the heterogeneously catalyzed hydrogenation of unsaturated substrates. High enantioselectivity has been obtained, although it has not yet been demonstrated that asymmetric induction occurs at the metal NP surface and not on more reactive leached monometallic complex fragments. For example, in the Pd/C and Ni/C catalyzed C–C and C–N bond forming reactions, the mechanism involves such a leaching pathway with recovery of the metal on the support at the end of the reaction. More mechanistic studies are called for to understand the nature of the very active metal species in solution. The activation of aryl chlorides for C–C coupling reactions still remains a key challenge because organometallic catalysts are presently more efficient than metal NP catalysts. A major recent finding was the removal of these NP catalysts by filtration, although recycling and efficient re-use many times of supported NP catalysts remains a challenge.

Altogether, the field of metal NP catalysis is a fascinating one, as exemplified by the new gold rush and its very attractive perspectives in oxidation chemistry and by the ligand-free palladium and nickel catalysts that are employed in "homeopathic" amounts. The metal NP field is presently expanding dramatically, and it is anticipated that these key challenges will be met in the near future, and that this area will find many more applications in tomorrow's laboratory and industry.

Received: March 1, 2005
Revised: June 14, 2005
Published online: November 22, 2005

[1] a) J. Grunes, J. Zhu, G. A. Somorjai, *Chem. Commun.* **2003**, 2257 (Focus Article); b) G. A. Somorjai, *Introduction to Surface Chemistry and Catalysis*, Wiley, New York, **1994**; J. M. Thomas, W. J. Thomas, *Principles and Practice of Heterogeneous Catalysis*, VCH, Weinheim, **1997**; A. Eppler, G. Rupprechter, L. Guczi, G. A. Somorjai, *J. Phys. Chem. B* **1997**, *101*, 9973; G. A. Somorjai, R. M. Rioux, *Catal. Today* **2005**, *100*, 201; E. J. Puddephat, *Met. Clusters Chem.* **1999**, *22*, 1179; C. R. Henry, *Appl. Surf. Sci.* **2000**, *164*, 252; T. P. St. Clair, D. W. Goodman, *Top. Catal.* **2000**, *13*, 5; M. Bowker, R. A. Bennet, A. Dickinson, D. James, R. Smith, P. Stone, *Stud. Surf. Sci. Catal.* **2001**, *133*, 3; M. Kralik, A. Biffis, *J. Mol. Catal. A* **2001**, *177*, 113; J. M. Thomas, R. Raja, *Chem. Rec.* **2001**, *1*, 448; C. Mohr, P. Claus, *Sci. Prog.* **2001**, *84*, 311; J. M. Thomas, B. F. G. Johnson, R. Raja, G. Sankar, P. A. Midgley, *Acc. Chem. Res.* **2003**, *36*, 20.

[2] a) *Applied Homogeneous Catalysis with Organometallic Compounds, Vols. 1 and 2* (Eds.: B. Cornils, W. A. Herrmann), Wiley-VCH, Weinheim, **1996**; b) W. A. Herrmann, B. Cornils, *Angew. Chem.* **1997**, *109*, 1074; *Angew. Chem. Int. Ed. Engl.* **1997**, *36*, 1048; c) *Metal-Catalyzed Cross-Coupling Reactions* (Eds.: F. Diederich, P. J. Stang), Wiley-VCH, Weinheim, **1998**; *Metal-Catalyzed Cross-Coupling Reactions, Vols. 1 and 2* (Eds.: A. de Mejere, F. Diederich), Wiley-VCH, Weinheim, **2004**; d) *Handbook of Metathesis, Vols. 1–3* (Ed.: R. H. Grubbs), Wiley-VCH, Weinheim, **2003**.

[3] J. A. Gladysz, *Pure Appl. Chem.* **2001**, *73*, 1319; J. Gladysz, *Chem. Rev.* **2002**, *102*, 3215 (introduction to a special issue on recoverable catalysts).

[4] a) *Nanoparticles* (Ed.: G. Schmid), Wiley-VCH, Weinheim, **2004**; b) R. G. Finke in *Metal Nanoparticles. Synthesis, Characterization and Applications* (Eds.: D. L. Feldheim, C. A. Foss, Jr.), Marcel Dekker, New York, **2002**, chap. 2, p. 17; c) *Nanoparticles and Nanostructured Films. Preparation, Characterization and Applications* (Ed.: J. H. Fendler), Wiley-VCH, Weinheim, **1998**; G. Schmid in *Nanoscale Materials in Chemistry* (Ed.: K. J. Klabunde), Wiley-Interscience, New York, **2001**, p. 15.

[5] Early reviews on NP catalysis: a) J. B. Michel, J. T. Scharz in *Catalyst Preparation Science, Vol. IV* (Eds.: B. Delmon, P. Grange, P. A. Jacobs, G. Poncelet), Elsevier, Amsterdam, **1987**, p. 669; b) G. Schmid, *Chem. Rev.* **1992**, *92*, 1709; c) L. N. Lewis, *Chem. Rev.* **1993**, *93*, 2693; d) J. S. Bradley in *Clusters and Colloids* (Ed.: G. Schmid), VCH, Weinheim, **1994**, chap. 6, p. 459; e) *Catalysis by Di- and Polynuclear Metal-Cluster Complexes* (Eds.: L. N. Lewis, R. D. Adams, F. A. Cotton), Wiley-VCH, New York, **1998**, p. 373; f) N. Toshima in *Fine Particles Sciences and Technology. From Micro- to New Particles* (Ed.: E. Pellizzetti), Kluwer, Dordrecht, **1996**, p. 371; g) N. Toshima, T. Yonezawa, *New J. Chem.* **1998**, *22*, 1179.

[6] a) H. Bönnemann, W. Brijoux, T. Joussen, *Angew. Chem.* **1990**, *102*, 324; *Angew. Chem. Int. Ed. Engl.* **1990**, *29*, 273; b) H. Bönnemann, W. Brijoux, R. Brinkmann, E. Dinjus, , T. Joussen, B. Korall, *Angew. Chem.* **1991**, *103*, 1344; *Angew. Chem. Int. Ed. Engl.* **1991**, *30*, 1312; H. Bönnemann, W. Brijoux in *Active Metals: Preparation, Characterization, Applications* (Ed.: A. Fürstner), VCH, Weinheim, **1996**, p. 339.

[7] a) M. T. Reetz, W. Helbig, *J. Am. Chem. Soc.* **1994**, *116*, 7401; b) M. T. Reetz, S. A. Quaiser, *Angew. Chem.* **1995**, *107*, 2461; *Angew. Chem. Int. Ed. Engl.* **1995**, *34*, 2240; c) M. T. Reetz, W. Helbig, S. A. Quaiser in *Active Metals: Preparation, Characterization, Applications* (Ed.: A. Fürstner), VCH, Weinheim, **1996**, p. 279; d) M. T. Reetz, R. Breinbauer, K. Wanninger, *Tetrahedron Lett.* **1996**, *37*, 4499; e) M. T. Reetz, G. Lohmer, *Chem. Commun.* **1996**, 1921; for recent reports on PdNP catalysis, see refs. [31d,f,j,n] and [41c].

[8] a) M.-C. Daniel, D. Astruc, *Chem. Rev.* **2004**, *104*, 293; b) M. Faraday, *Philos. Trans. R. Soc. London* **1857**, *151*, 183; c) M. Brust, M. Walker, D. Bethell, D. J. Schiffrin, R. J. Whyman, *J. Chem. Soc. Chem. Commun.* **1994**, 801; d) D. I. Gittins, F. Caruso, *Angew. Chem.* **2001**, *113*, 3089; *Angew. Chem. Int. Ed.* **2001**, *40*, 3001.

[9] a) L. D. Rapino, F. F. Nord, *J. Am. Chem. Soc.* **1941**, *63*, 2745; L. D. Rapino, F. F. Nord, *J. Am. Chem. Soc.* **1941**, *63*, 3268; K. E. Kavanagh, F. F. Nord, *J. Am. Chem. Soc.* **1943**, *65*, 2121; b) D. Y. Cha, G. Parravano, *J. Catal.* **1970**, *18*, 320; G. Parravano, *J. Catal.* **1970**, *18*, 320; c) M. Haruta, T. Kobayashi, H. Sano, N. Yamada, *Chem. Lett.* **1987**, 405; M. Haruta, N. Yamada, T. Kobayashi, S. Lijima, *J. Catal.* **1989**, *115*, 301; CO-Oxidation bei 200 K: M. Haruta, S. Tsuboda, T. Kobayashi, H. Kagehiama, M. J. Genet,

 © 2005 Wiley-VCH Verlag GmbH & Co. KGaA, Weinheim

B. Demon, *J. Catal.* **1993**, *144*, 175; d) M. Haruta, CATTECH **2002**, *6*, 102; e) for other recent reviews on AuNP-catalyzed CO oxidation by O_2, see ref. [11j], [50b] and: T. V. Choudary, D. W. Goodman, *Top. Catal.* **2002**, *21*, 25; G. Schmid, B. Corain, *Eur. J. Inorg. Chem.* **2003**, 3081; see also ref. [8a]; f) G. C. Bond, P. A. Sermon, *Gold Bull.* **1973**, *6*, 102; g) H. Hirai, Y. Nakao, N. J. Toshima, *Macromol. Sci. Chem. A* **1978**, *12*, 1117; H. Hirai, Y. Nakao, N. J. Toshima, *Macromol. Sci. Chem. A* **1979**, *13*, 727; h) L. N. Lewis, N. Lewis, *J. Am. Chem. Soc.* **1986**, *108*, 7228 (for further discussions, see also references [5c] and [5e]).

[10] For examples, see: a) A. Moradpour, E. Amouyal, P. Keller, H. Kagan, *Nouv. J. Chim.* **1978**, *2*, 547; b) A. Henglein, *J. Phys. Chem.* **1979**, *83*, 2858; c) A. Henglein, J. Lillie, *J. Am. Chem. Soc.* **1981**, *103*, 1059; d) K. Kurihara, J. H. Fendler, I. J. Ravet, *J. Mol. Catal.* **1986**, *34*, 325; e) M. Boutonnet, J. Kizling, R. Touroude, G. Maire, P. Stenius, *Appl. Catal.* **1986**, *20*, 163; f) Y. Degani, I. J. Willner, *J. Chem. Soc. Perkin Trans. 2* **1986**, 37; g) I. Willner, R. Maidan, D. Mandler, H. Dürr, G. Dörr, K. Zengerle, *J. Am. Chem. Soc.* **1987**, *109*, 6080; h) J. S. Bradley, E. W. Hill, M. E. Leonowitz, H. Witzke, *J. Mol. Catal.* **1987**, *41*, 59; i) C. Larpent, H. Patin, *J. Mol. Catal.* **1988**, *44*, 191.

[11] Recent reviews on NP catalysis: a) M. A. El-Sayed, *Acc. Chem. Res.* **2001**, *34*, 257; b) R. M. Crooks, M. Zhao, L. Sun, V. Chechik, L. K. Yeung, *Acc. Chem. Res.* **2001**, *34*, 181; c) "Polymer-Stabilized Metal Nanoparticles: Preparation, Characterization and Applications": T. Yonezawa, N. Toshima in *Advanced Functional Molecules and Polymers, Vol. 2* (Ed.: H. S. Nalwa), Accelerated Development, **2001**, chap. 3, p. 65; A. B. R. Mayer, *Polym. Adv. Technol.* **2001**, *12*, 96; d) H. Bönnemann, R. Richards, *Synth. Methods Organomet. Inorg. Chem.* **2002**, *10*, 209; e) A. Roucoux, J. Schulz, H. Patin, *Chem. Rev.* **2002**, *102*, 27; f) I. I. Moiseev, M. N. Vargaftik, *Russ. J. Gen. Chem.* **2002**, *72*, 512; g) A. T. Bell, *Science* **2003**, *299*, 1688; h) M. Moreno-Manas, R. Pleixats, *Acc. Chem. Res.* **2003**, *36*, 638; i) B. F. G. Johnson, *Top. Catal.* **2003**, *24*, 147; j) AuNP-catalyzed CO oxidation: M. Haruta, *J. New Mater. Electrochem. Syst.* **2004**, *7*, 163.

[12] a) X.-D. Mu, D. G. Evans, Y. Kou, *Catal. Lett.* **2004**, *97*, 151; b) P. Claus, A. Brückner, C. Möhr, H. Hofmeister, *J. Am. Chem. Soc.* **2000**, *122*, 11430; c) A.-I. Kozlov, A. P. Kozlova, K. Asakura, Y. Matsui, T. Kogure, T. Shido, Y. Iwazawa, *J. Catal.* **2000**, *196*, 56; d) A. Martino, S. A. Yamanaka, J. S. Kawola, D. A. Ly, *Chem. Mater.* **1997**, *9*, 423; e) T. Li, J. Moon, A. A. Morrone, J. J. Mecholsky, D. R. Talham, J.-H. Adair, *Langmuir* **1999**, *15*, 4328; f) U.-A. Paulus, U. Endruschat, G.-J. Feldmeyer, T.-J. Schmidt, H. Bönnemann, J.-J. Behm, *J. Catal.* **2000**, *195*, 383; g) Y. Mizukoshi, R. Oshima, Y. Mizukoshi, Y. Nagata, *Langmuir* **1999**, *15*, 2733; h) S. Papp, I. Dekany, *Colloid Polym. Sci.* **2001**, *279*, 449; i) C. B. Hwang, Y.-S. Fu, Y.-L. Lu, S.-W. Jang, P.-T. Chou, C.-R. Wang, S.-J. Yu, *J. Catal.* **2000**, *195*, 336; j) K.-T. Wu, Y.-D. Yao, C.-R. C. Wang, P. F. Chen, E.-T. Yeh, *J. Appl. Phys.* **1999**, *85*, 5959; k) R. P. Andres, J.-D. Bielefeld, J.-I. Henderson, D.-B. Janes, V.-R. Kolagunta, C.-P. Kubink, W. Mahoney, R.-G. Osifchin, R. Reifenberger, *Science* **1996**, *273*, 1690.

[13] a) R. Narayanan, M. A. El-Sayed, *J. Am. Chem. Soc.* **2003**, *125*, 8340; b) Y. Li, E. Boone, M. A. El-Sayed, *Langmuir* **2002**, *18*, 4921.

[14] a) S. V. Ley, C. Mitchell, D. Pears, C. Ramarao, J.-Q. Yu, W.-Z. Zhou, *Org. Lett.* **2003**, *5*, 4665; b) M. M. Demir, M. A. Gulgun, Y. Z. Menceloglu, B. Erman, S. S. Abramchuk, E. E. Makhaeva, A. R. Khokhlov, V. G. Matveeva, M. G. Sullman, *Macromolecules* **2004**, *37*, 1787; c) L. R. Gröschel, A. Haidar, K.-H. Beyer, R. Reichert, R. Schomäcker, *Catal. Lett.* **2004**, 95, 67; d) S. Kidambi, J.-H. Dai, J. Lin, M. L. Bruening, *J. Am. Chem. Soc.* **2004**, *126*, 2658; e) B. P. S. Chauhan, J. S. Rathore, T. Bandoo, *J. Am. Chem. Soc.* **2004**, *126*, 8493; f) T. Sanji, Y. Ogawa, Y. Nakatsuka, M. Tanaka, H. Sakurai, *Chem. Lett.* **2003**, *32*, 980; g) A. B. Lowe, B. S. Sumerlin, M. S. Donovan, C. L. McCormick, *J. Am. Chem. Soc.* **2002**, *124*, 11562; h) A. Drelinkiewicza, A. Waksmundzka, W. Makowski, J. W. Sobczak, A. Krol, A. Zieba, *Catal. Lett.* **2004**, *94*, 143; i) Y.-B. Liu, C. Khemtong, J. Hu, *Chem. Commun.* **2004**, 398; j) U. R. Pillai, E. Sahle-Demessie, *J. Mol. Catal. A* **2004**, *222*, 153; k) M. Adlim, M. Abu Bakar, K. Y. Liew, J. Ismail, *J. Mol. Catal. A* **2004**, *212*, 141; l) D. Tabuani, O. Monticelli, A. Chincarini, C. Bianchini, F. Vizza, S. Moneti, S. Russo, *Macromolecules* **2003**, *36*, 4294; m) C. C. Yang, C. C. Wan, Y. Y. Wang, *J. Colloid Interface Sci.* **2004**, *279*, 433.

[15] J. H. Sinfelt, *Acc. Chem. Res.* **1977**, *10*, 15; J. H. Sinfelt, *Bimetallic Catalyst: Discoveries, Concepts and Applications*, Wiley, New York, **1983**; J. H. Sinfelt, *Int. Rev. Phys. Chem.* **1988**, *7*, 281.

[16] a) J.-H. He, I. Ichinose, T. Kunitake, A. Nakao, Y. Shiraishi, N. Toshima, *J. Am. Chem. Soc.* **2003**, *125*, 11034; b) Y. Shiraishi, D. Ikenaga, N. Toshima, *Aust. J. Chem.* **2003**, *56*, 1025; c) R. Sablong, U. Schlotterbeck, D. Vogt, S. Mecking, *Adv. Synth. Catal.* **2003**, *345*, 333.

[17] a) *Dendrimers and Nanosciences* (Ed.: D. Astruc), Elsevier, Paris, **2003**, *6* (special issue *C. R. Chim.*, vol. 8–10); b) G. R. Newkome, C. N. Moorefield, F. Vögtle, *Dendrimers and Dendrons: Concepts, Synthesis, Applications*, Wiley-VCH, Weinheim, **2001**; c) J. F. G. A. Jansen E. M. M. de Brabander-van den Berg, E. W. Meijer, *Science* **1994**, *266*, 1226; d) D. A. Tomalia, A. M. Naylor, W. A. Goddard III, *Angew. Chem.* **1990**, *102*, 119; *Angew. Chem. Int. Ed. Engl.* **1990**, *29*, 138.

[18] a) M. Zhao, L. Sun, R. M. Crooks, *J. Am. Chem. Soc.* **1998**, *120*, 4877; b) M. Zhao, R. M. Crooks, *Angew. Chem.* **1999**, *111*, 375; *Angew. Chem. Int. Ed.* **1999**, *38*, 364; c) V. Chechik, M. Zhao, R. M. Crooks, *J. Am. Chem. Soc.* **1999**, *121*, 4910; d) M. Zhao, R. M. Crooks, *Adv. Mater.* **1999**, *11*, 217; e) V. Chechik, M. Zhao, R. M. Crooks, *J. Am. Chem. Soc.* **2000**, *122*, 1243; f) For reviews of the dendrimer-encapsulated-NP approach see refs. [11b] and [17g]; g) R. M. Crooks, M. Zhao, L. Sun, V. Chechik, L. K. Yeung, *Acc. Chem. Res.* **2001**, *34*, 181; h) L. K. Yeung, R. M. Crooks, *Nano Lett.* **2001**, *1*, 14; i) L. K. Yeung, C. T. Lee, K. P. Jonston, R. M. Crooks, *Chem. Commun.* **2001**, 2290; j) R. W. Scott, A. F. Datye, R. M. Crooks, *J. Am. Chem. Soc.* **2003**, *125*, 3708; k) Y. Niu, R. M. Crooks in *Dendrimers and Nanosciences* (Ed.: D. Astruc), Elsevier, Paris (*C. R. Chim.* **2003**, *6*, 1049); l) R. W. Scott, O. M. Wilson, S.-K. Oh, E. A. Kenik, R. M. Crooks, *J. Am. Chem. Soc.* **2004**, *126*, 15583; m) Y.-G. Kim, S.-K. Ho, R. M. Crooks, *Chem. Mater.* **2004**, *16*, 167; R. W. J. Scott, C. Sivadinarayana, O. M. Wilson, Z. Yan, D. W. Goodman, R. M. Crooks, *J. Am. Chem. Soc.* **2005**, *127*, 1380; J.-H. Liu, A.-Q. Wang, Y.-S. Shi, H.-P. Lin, C.-Y. Mou, *J. Phys. Chem. B* **2005**, *109*, 40.

[19] a) L. Balogh, D. A. Tomalia, *J. Am. Chem. Soc.* **1998**, *120*, 7355; b) L. Balogh, D. R. Swanson, D. A. Tomalia, G. L. Hagnauer, A. T. McManus, *Nano Lett.* **2001**, *1*, 18; c) K. Esumi, A. Susuki, N. Aihara, K. Usui, K. Torigoe, *Langmuir* **1998**, *14*, 3157; d) K. Esumi, K. Satoh, A. Suzuki, K. Torigoe, *Shikizai Kyokaishi* **2000**, *73*, 434; e) K. Esumi, R. Isono, T. Yoshimura, *Langmuir* **2004**, *20*, 237.

[20] E. Kunio, M. Keiko, Y. Tomokazu, *J. Colloid Interface Sci.* **2002**, *254*, 402.

[21] a) Y. Li, M. A. El Sayed, *J. Phys. Chem. B* **2001**, *105*, 8938; b) R. Narayanan, M. A. El-Sayed, *J. Phys. Chem. B* **2004**, *108*, 8572.

[22] a) M. Pittelkow, K. Moth-Poulsen, U. Boas, J. B. Christensen, *Langmuir* **2003**, *19*, 7682; b) M. Ooe, M. Murata, T. Mizugaki, K. Ebitani, K. Kaneda, *Nano Lett.* **2002**, *2*, 999; c) K. Mori, T. Hara, T. Mizugaki, K. Ebitani, K. Kaneda, *J. Am. Chem. Soc.* **2004**, *126*, 10657; d) K. R. Gopidas, J. K. Whitesell, M.-A. Fox, *Nano Lett.* **2003**, *3*, 1757.

[23] Y.-M. Chung, H.-K. Rhee, *J. Mol. Catal. A* **2003**, *206*, 291.

 © 2005 Wiley-VCH Verlag GmbH & Co. KGaA, Weinheim

[24] a) C. Rocaboy, J. A. Gladysz, *Org. Lett.* **2002**, *4*, 1993; b) R. Grigg, L.-X. Zhang, S. Collard, A. Keep, *Tetrahedron Lett.* **2003**, *44*, 6979.

[25] Polyoxometallate-stabilized metal NPs and their catalytic function: a) J. D. Aiken III, R. G. Finke, *J. Am. Chem. Soc.* **1999**, *121*, 8803; b) S. Ozkar, R. G. Finke, *J. Am. Chem. Soc.* **2002**, *124*, 5796; c) A. M. Fargo, J. F. Odzak, F. S. Lai, B. C. Gates, *Nature* **2002**, *415*, 623; d) V. Kogan, Z. Aizenshtat, R. Popovitz-Biro, R. Neumann, *Org. Lett.* **2002**, *4*, 3529; e) M. Ohde, H. Yukiohde, C. M. Wai, *Chem. Commun.* **2002**, 2388; f) anion-mediated adsorption of the tetra-*n*-butyl ammonium cation on surfaces and metal NPs: Z. Deng, D. E. Irish, *J. Phys. Chem.* **1994**, *98*, 11169; S. Özkar, R. G. Finke, *J. Am. Chem. Soc.* **2002**, *124*, 5796; g) ealiest report of ammonium-stabilized metal NPs: J. Kiwi, M. Grätzel, *J. Am. Chem. Soc.* **1979**, *101*, 7214.

[26] a) L. Strimbu, J. Liu, A. E. Kaifer, *Langmuir* **2003**, *19*, 483; b) J. Alvarez, J. Liu, E. Roman, A. E. Kaifer, *Chem. Commun.* **2000**, 1151; c) J. Liu, J. Alvarez, W. Ong, E. Roman, A. E. Kaifer, *Langmuir* **2001**, *17*, 6762.

[27] F. Lu, J. Ruiz, D. Astruc, *Tetrahedron Lett.* **2004**, *45*, 9443.

[28] a) M.-K. Chung, G. Orlova, J. D. Goddart, M. Schlaf, R. Harris, T. J. Beveridge, G. White, F. R. Hallett, *J. Am. Chem. Soc.* **2002**, *124*, 10508; b) M.-K. Chung, M. Schlaf, *J. Am. Chem. Soc.* **2004**, *126*, 7386; c) S. U. Son, Y. Jang, J. Park, H. B. Na, H. M. Park, H. J. Yun, J. Lee, T. Hyeon, *J. Am. Chem. Soc.* **2004**, *126*, 5026, and references therein.

[29] K. Nasar, F. Fache, M. Lemaire, M. Draye, J. C. Béziat, M. Besson, P. Galez, *J. Mol. Catal.* **1994**, *87*, 107.

[30] a) H. Bönnemann, G. A. Braun, *Chem. Eur. J.* **1997**, *3*, 1200; b) J. U. Köhler, J. S. Bradley, **1998**, *14*, 2730; c) X. Zuo, H. Liu, D. Guo, X. Yang, *Tetrahedron* **1999**, *55*, 203; d) M. Studer, H.-U. Blaser, C. Exner, *Adv. Synth. Catal.* **2003**, *345*, 45; e) M. Tamura, H. Fujihara, *J. Am. Chem. Soc.* **2003**, *125*, 15742; f) S. Jansat, M. Gomez, K. Philippot, G. Muller, E. Guiu, C. Claver, S. Castillon, B. Chaudret, *J. Am. Chem. Soc.* **2004**, *126*, 1592.

[31] a) T. Mizoroki, K. Mori, A. Ozaki, *Bull. Soc. Chem. Jpn.* **1971**, *44*, 581; b) R. F. Heck, J. P. Nolley, Jr., *J. Org. Chem.* **1972**, *37*, 2320; c) I. P. Beletskaya, A. V. Cheprakov, *Chem. Rev.* **2000**, *100*, 3009; d) M. T. Reetz, E. Westermann, R. Lomer, G. Lohmer, *Tetrahedron Lett.* **1998**, *39*, 8449; e) A. H. M. de Vries, J. M. C. A. Mulders, J. H. M. Mommers, H. J. W. Henderckx, J. G. de Vries, *Org. Lett.* **2003**, *5*, 3285; f) M. T. Reetz, M. Maase, *Adv. Mater.* **1999**, *11*, 773; g) C. Rocaboy, J. A. Gladysz, *New J. Chem.* **2003**, *27*, 39; h) M. Nowotny, U. Hanefeld, H. van Koningsveld, T. Maschmeyer, *Chem. Commun.* **2000**, 1877; i) I. P. Beletskaya, A. N. Kashin, N. B. Karlstedt, A. V. Mitin, A. V. Chepakov, G. M. Kazankov, *J. Organomet. Chem.* **2001**, *622*, 89; j) M. T. Reetz, E. Westermann, *Angew. Chem.* **2000**, *112*, 170; *Angew. Chem. Int. Ed.* **2000**, *39*, 165 (see also E. Westermann, Dissertation, Ruhr-Universität Bochum, **1999**); k) T. Rosner, J. Le Bars, A. Pfaltz, D. G. Blackmond, *J. Am. Chem. Soc.* **2001**, *123*, 1848; l) C. E. Williams, J. M. C. A. Mulders, J. G. de Vries, A. H. M. de Vries, *J. Organomet. Chem.* **2003**, *687*, 494; m) J. G. de Vries, A. H. M. de Vries, *Eur. J. Org. Chem.* **2003**, 799; n) focus article on ligand-free Heck reactions using extremely low Pd loading: M. T. Reetz, J. G. de Vries, *Chem. Commun.* **2004**, 1559; o) K. Pelzer, O. Vidoni, K. Philippot, B. Chaudret, V. Colliere, *Adv. Funct. Mater.* **2003**, *13*, 118; p) P. J. Dyson, D. J. Ellis, G. Laurenczy, *Adv. Synth. Catal.* **2003**, *345*, 211; q) J. A. Widegren, R. G. Finke, *J. Mol. Catal. A* **2003**, *198*, 317; r) Y. Na, S. Park, S. B. Han, H. Han, S. Ko, S. Chang, *J. Am. Chem. Soc.* **2004**, *126*, 250.

[32] a) I. T. Horvath, J. Rabai, *Science* **1994**, *266*, 72; I. T. Horvath, *Acc. Chem. Res.* **1998**, *31*, 641; L. P. Barthel-Rosa, J. A. Gladysz, *Coord. Chem. Rev.* **1999**, *578*, 190; b) H. Ohde, C. M. Wai, H. Kim, M. Ohde, *J. Am. Chem. Soc.* **2002**, *124*, 4540; c) P. Meric, K. M. K. Yu, S. C. Tsang, *Catal. Lett.* **2004**, *95*, 39; d) P. Meric, K. M. K. Yu, S. C. Tsang, *Langmuir* **2004**, *20*, 8537; e) K. M. K. Yu, C. M. Y. Yeung, D. Thompsett, S. C. Tsang, *J. Phys. Chem. B* **2003**, *107*, 4515; f) B.-H. Yoon, H. Kim, C. M. Wai, *Chem. Commun.* **2003**, 1040; g) H. Ohde, C. M. Wai, H. Kim, J. Kim, M. Ohde, *J. Am. Chem. Soc.* **2002**, *124*, 4540; h) X. R. Ye, Y.-H. Lin, C. M. Wai, *Chem. Commun.* **2003**, 642; i) A. M. Doyle, S. K. Shaikhutdinov, S. D. Jackson, H.-J. Freund, *Angew. Chem.* **2003**, *115*, 5398; *Angew. Chem. Int. Ed.* **2003**, *42*, 5240.

[33] a) J. Dupont, R. F. de Souza, P. A. Z. Suarez, *Chem. Rev.* **2002**, *102*, 3667; b) J. Dupont, G. S. Fonseca, A. P. Umpierre, P. F. P. Fichtner, S. R. Teixiera, *J. Am. Chem. Soc.* **2002**, *124*, 4228; c) G. Schmid, M. Harms, J. O. Malm, J. O. Bovin, J. van Ruitenbeck, H. W. Zandbergen, W. T. Fu, *J. Am. Chem. Soc.* **1993**, *115*, 2047; d) J. Huang, T. Jiang, H. Gao, Y. Chang, G. Zhao, W. Wu, *Chem. Commun.* **2003**, 1654; e) V. Calo, A. Nacci, A. Monopoli, S. Laera, N. Cioffi, *J. Org. Chem.* **2003**, *68*, 2929; f) V. Calo, A. Nacci, A. Monopoli, A. Detomaso, P. Illiade, *Organometallics* **2003**, *22*, 4193; g) M. Spiro, D. M. De Jesus, *Langmuir* **2000**, *16*, 2664; M. Spiro, D. M. De Jesus, *Langmuir* **2000**, *16*, 4896; G. Battistuzzi, S. Cacchi, G. Fabrizi, *Synlett* **2002**, 439; h) D. Zhao, Z. Fei, T. Geldbach, R. Scopelliti, P. J. Dyson, *J. Am. Chem. Soc.* **2004**, *126*, 15876; i) R. R. Deshmukh, R. Rajagopal, K. V. Srinivasan, *Chem. Commun.* **2001**, 1544; j) L. Xu, W. Chen, J. Xiao, *Organometallics* **2000**, *19*, 1123; k) C. W. Scheeren, G. Machado, J. Dupont, P. F. P. Fichtner, S. R. Texeira, *Inorg. Chem.* **2003**, *42*, 4738; l) E. T. Silveira, A. P. Umpierre, L. M. Rossi, G. Machado, J. Morais, G. V. Soares, I. J. R. Baumvol, S. R. Teixeira, P. F. P. Fichtner, J. Dupont, *Chem. Eur. J.* **2004**, *10*, 3734; m) G. S. Fonseca, J. D. Scholten, J. Dupont, *Synlett* **2004**, *9*, 1525.

[34] a) H.-F. Lang, R. A. May, B. L. Iversen, B. D. Chandler, *J. Am. Chem. Soc.* **2003**, *125*, 14832; b) H.-F. Lang, S. Maldonado, K. J. Stevenson, B. D. Chandler, *J. Am. Chem. Soc.* **2004**, *126*, 12949.

[35] a) J. P. M. Niederer, A. B. J. Arnold, W. F. Hölderich, B. Tesche, M. Reetz, H. Bönnemann, *Top. Catal.* **2002**, *18*, 265; b) S.-W. Kim, M. Kim, W. Y. Lee, T. Hyeon, *J. Am. Chem. Soc.* **2002**, *124*, 7642; c) K. H. Park, S. U. Son, Y. K. Chung, *Org. Lett.* **2002**, *4*, 4361; d) R. Abu-Reziq, D. Avnir, J. Blum, *J. Mol. Catal. A* **2002**, *187*, 277; e) A. Horvath, A. Beck, Z. Koppany, A. Sarkany, L. Guczi, *J. Mol. Catal. A* **2002**, *182*, 295; f) A.-M. Huang, Z.-F. Liu, C. Lai, J.-D. Hua, *J. Appl. Polym. Sci.* **2002**, *85*, 989; g) A. Molnar, A. Papp, K. Miklos, P. Forgo, *Chem. Commun.* **2003**, 2626; h) T. Sanji, Y. Ogawa, Y. Nakatsuka, M. Tanaka, H. Sakurai, *Chem. Lett.* **2003**, *32*, 980; i) O. Dominguez-Quintero, S. Martinez, Y. Henriquez, L. D'Ornelas, H. Krentzien, J. Osuna, *J. Mol. Catal. A* **2003**, *197*, 185; j) I. Yuranov, P. Moeckli, E. Suvorova, P. Buffat, L. Kiwi-Minsker, A. Renken, *J. Mol. Catal. A* **2003**, *192*, 239; k) B. Corain, P. Guerriero, G. Schiavon, M. Zapparoli, M. Kralik, *J. Mol. Catal. A* **2004**, *211*, 237; M. Kralik, V. Ktratky, P. Centomo, P. Guerriero, S. Lora, B. Corain, *J. Mol. Catal. A* **2003**, *195*, 219; l) P. Canton, *Catal. Lett.* **2003**, *88*, 14; m) V. Johanek, *Surf. Sci.* **2004**, *561*, L218; n) T. G. Galow, U. Dreshler, J. A. Hanson, V. M. Rotello, *Chem. Commun.* **2002**, 1076; o) R. B. Bedford, U. G. Singh, R. I. Walton, R. T. Williams, S. A. Davis, *Chem. Mater.* **2005**, *17*, 701.

[36] a) H.-P. Kormann, G. Schmid, K. Pelzer, K. Philippot, B. Chaudret, *Z. Anorg. Allg. Chem.* **2004**, *630*, 1913; b) M. Yashima, L. K. L. Falk, A. E. C. Palmqvist, K. Holmberg, *J. Colloid Interface Sci.* **2003**, *268*, 348; c) S. Schauermann, J. Hoffmann, V. Johanek, J. Hartmann, J. Libuda, H.-J. Freund, *Angew. Chem.* **2002**, *114*, 2643; *Angew. Chem. Int. Ed.* **2002**, *41*, 2532; d) M. Heemeier, A. F. Carlsson, M. Naschitzki, M. Schmal, M. Bäumer, H.-J. Freund, *Angew. Chem.* **2002**, *114*, 4242; *Angew. Chem. Int. Ed.* **2002**, *41*, 4073; e) V. Johanek, M. Laurin, J. Hoffmann, S. Schauermann, A. W. Grant, B. Kasemo, J. Libuda, H.-J. Freund, *Surf. Sci.* **2004**, *561*, L218.

 © 2005 Wiley-VCH Verlag GmbH & Co. KGaA, Weinheim

[37] a) K. Ebitani, Y. Fujie, K. Kaneda, *Langmuir* **1999**, *15*, 190; b) K.-M. Choi, T. Akita, T. Mizugaki, K. Ebitani, K. Kaneda, *New J. Chem.* **2003**, *27*, 324; c) L. Guczi, A. Beck, A. Horvath, Zs. Koppany, G. Stefler, K. Frey, I. Sajo, O. Geszti, D. Bazin, J. Lynch, *J. Mol. Catal. A* **2004**, *204*, 545.

[38] K. Mori, T. Hara, T. Mizugaki, K. Ebitani, K. Kaneda, *J. Am. Chem. Soc.* **2004**, *126*, 10657.

[39] a) T. Nishimura, N. Kakiuchi, M. Inoue, S. Uemura, *Chem. Commun.* **2000**, 124; b) N. Kakiuchi, Y. Maeda, T. Nishimura, S. Uemura, *J. Org. Chem.* **2001**, *66*, 6220; c) Lit. [36c]; d) Lit. [36d]; e) B. M. Choudary, S. Mahdi, N. S. Chowdari, M. L Kantam, B. Streedhar, *J. Am. Chem. Soc.* **2002**, *124*, 14127; f) A. Mastalir, Z. Kiraly, *J. Catal.* **2003**, *220*, 372; g) S. Bertarione, D. Scarano, A. Zecchina, V. Johanek, J. Hoffmann, S. Schauermann, J. Libuda, G. Rupprechter, H.-J. Freund, *J. Catal.* **2004**, *123*, 64; h) P. Pfeifer, K. Schubert, M. A. Liauw, G. Emig, *Appl. Catal. A* **2004**, *270*, 165.

[40] G. Riahi, D. Guillemot, M. Polisset-Tfoin, A. A. Khodadadi, J. Fraissard, *Catal. Today* **2002**, *72*, 115; M. Mtelkar, C. V. Rode, R. V. Chaudhari, S. S. Joshi, A. M. Nalawade, *Appl. Catal. A* **2004**, *273*, 11.

[41] a) N. Toshima, Y. Shiiraishi, T. Teranishi, M. Mitake, T. Tominaga, H. Watanabe, W. Brijoux, H. Bönnemann, G. Schmid, *Appl. Organomet. Chem.* **2001**, *15*, 178; b) J. Huang, T. Jiang, H.-X. Gao, B.-X. Han, Z.-M. Liu, W.-Z. Wu, Y.-H. Chang, G.-Y. Zhao, *Angew. Chem.* **2004**, *116*, 1421; *Angew. Chem. Int. Ed.* **2004**, *43*, 1397; c) M. T. Reetz, H. Schulenburg, M. Lopez, B. Spliethoff, B. Tesche, *Chimia* **2004**, *58*, 896.

[42] F. Caruso, *Adv. Mater.* **2001**, *13*, 11; F. Caruso, R. A. Caruso, H. Möhwald, *Science* **1998**, *282*, 1111; Y. Lin, Y. Lu, B. Gates, Y. Xia, *Chem. Mater.* **2001**, *13*, 1146.

[43] a) M. Wagner, K. Köhler, L. Djakovitch, M. Muhler, *Top. Catal.* **1999**, 13, 319; b) K. Köhler, L. Djakovitch, M. Wagner, *Catal. Today* **2001**, *66*, 105; c) L. Djakovitch, K. Köhler, *J. Am. Chem. Soc.* **2001**, *123*, 5990; d) A. Nejjar, C. Pinel, L. Djakovitch, *Adv. Synth. Catal.* **2003**, *345*, 612; e) L. Djakovitch, M. Wagner, C. G. Hartung, M. Beller, K. Köhler, *J. Mol. Catal. A* **2004**, *219*, 121; f) S. Pröckl, W. Kleist, M. A. Gruber, K. Köhler, *Angew. Chem.* **2004**, *116*, 1917; *Angew. Chem. Int. Ed.* **2004**, *43*, 1881; g) L. Djakovitch, P. Rollet, *Adv. Synth. Catal.* **2004**, *346*, 1782; h) L. Djakovitch, P. Rollet, *Tetrahedron Lett.* **2004**, *45*, 1367; i) S. Chouzier, M. Gruber, L. Djakovitch, *J. Mol. Catal. A* **2004**, *212*, 43; j) J. Penzien, C. Haessner, A. Jentys, K. Köhler, T. E. Müller, J. A. Lercher, *J. Catal.* **2004**, *121*, 302.

[44] a) P. W. Albers, J. G. E. Krauter, D. K. Ross, R. G. Heidenreich, K. Köhler, S. F. Parker, *Langmuir* **2004**, *20*, 8254; b) P. Rylander, *Catalytic Hydrogenation in Organic Synthesis*, Academic Press, New York, **1979**; c) M. L. Toebes, J. A. van Dillen, K. P. de Jong, *J. Mol. Catal. A* **2001**, *173*, 75; d) C. R. Le Blond, A. T. Andrews, Y. Sun, J. R. Sowa, Jr., *Org. Lett.* **2001**, *3*, 1555; e) E. B. Mobufu, J. H. Clark, D. J. Macquarrie, *Green Chem.* **2001**, *3*, 23; f) R. G. Heidenreich, J. G. E. Krauter, J. Pietsch, K. Köhler, *J. Mol. Catal. A* **2002**, *182–183*, 499; K. Köhler, R. G. Heidenreich, J. G. E. Krauter, J. Pietsch, *Chem. Eur. J.* **2002**, *8*, 622; g) F. Zhao, K. Kurakami, M. Shirai, M. Arai, *J. Catal.* **2000**, *194*, 479; h) see, for example: B. Coq, F. Figueras, P. Geneste, C. Moreau, P. Moreau, M. Warawdekar, *J. Mol. Catal.* **1993**, *78*, 211; i) V. A. Yakovlev, V. V. Terskikh, V. I. Simagina, V. A. Likholobov, *J. Mol. Catal. A* **2000**, *153*, 231; j) P. Styring, C. Grindon, C. M. Fisher, *Catal. Lett.* **2001**, *77*, 219; k) B. H. Lipshutz, S. Tasler, W. Chrisman, B. Spliethoff, B. Tesche, *J. Org. Chem.* **2003**, *68*, 1177; l) B. H. Lipshutz, J. A. Sclafani, P. A. Blomgren, *Tetrahedron* **2000**, *56*, 2139; m) B. H. Lipshutz, P. A. Blomgren, *J. Am. Chem. Soc.* **1999**, *121*, 5819; n) B. H. Lipshutz, *Adv. Synth. Catal.* **2001**, *343*, 313; o) B. H. Lipshutz, H. Ueda, *Angew. Chem.* **2000**, *112*, 4666; *Angew. Chem. Int. Ed.* **2000**, *39*, 4492; p) F. Zaera, *Acc. Chem. Res.* **2002**, *35*, 129; K. Anderson, S. C. Fernandez, C. Hardacre, P. C. Marr, *Inorg. Chem. Commun.* **2004**, *7*, 73; q) A. Corma, H. Garcia, A. Leyva, *J. Mol. Catal. A* **2005**, *230*, 97.

[45] a) For recent reports on the oxide-support-AuNP-catalyzed CO oxidation by O_2 and its mechanism, see refs. [9e, 11j, 50b] and: G. C. Bond, D. T. Thompson, *Catal. Rev. Sci. Eng.* **1999**, *41*, 319; G. C. Bond, D. T. Thompson, *Gold Bull.* **2000**, *33*, 41; b) A. Wolf, F. Schüth, *Appl. Catal. A* **2002**, *226*, 1; c) W. T. Wallace, R. L. Whetten, *J. Am. Chem. Soc.* **2003**, *125*, 7499; d) N. Lopez, J. K. Norskov, *J. Am. Chem. Soc.* **2002**, *124*, 11262; e) S. Schimpf, M. Lucas, C. Mohr, U. Rodemerk, A. Brückner, J. Radnik, H. Hofmeister, P. Claus, *Catal. Today* **2002**, *72*, 63; A. Zwijnenburg, M. Saleh, M. Makkee, J. A. Moulijn, *Catal. Today* **2002**, *72*, 59; M. Daté, Y. Ichihashi, T. Yamashita, A. Chiorini, F. Boccuzzi, M. Haruta, *Catal. Today* **2002**, *72*, 89; T. Akita, P. Lu, S. Ichikawa, K. Tanaka, M. Haruta, *Surf. Interface Anal.* **2001**, *31*, 73; C.-M. Yang, M. Kalwei, F. Schüth, K.-J. Chao, *Appl. Catal. A* **2003**, *254*, 289; K. Mallick, M. S. Scurrell, S. Mike, *Appl. Catal. A* **2003**, *253*, 527; R. B. Cuenya, S.-H. Baeck, T. F. Jaramillo, E. W. McFarland, *J. Am. Chem. Soc.* **2003**, *125*, 12928; L. Guczi, A. Beck, A. Horvath, Zs. Koppany, G. Stefler, K. Frey, I. Sajo, O. Geszti, D. Bazin, J. Lynch, *J. Mol. Catal. A* **2003**, *204*, 545; L. Fan, N. Ichikuni, S. Shimazu, T. Uemarsu, *Appl. Catal. A* **2003**, *246*, 87; T. F. Jaramillo, S.-H. Baeck, B. R. Cuenya, E. W. McFarland, *J. Am. Chem. Soc.* **2003**, *125*, 7148; H. Araki, A. Fukuoka, Y. Sakamoto, S. Inagaki, N. Sugimoto, Y. Fukushima, M. Ichikawa, *J. Mol. Catal. A* **2003**, *199*, 95; M. Okumura, S. Tsubota, M. Haruta, *J. Mol. Catal. A* **2003**, *199*, 73; H. Hakkinen, S. Abbet, A. Sanchez, U. Heiz, U. Landman, *Angew. Chem.* **2003**, *115*, 1335; *Angew. Chem. Int. Ed.* **2003**, *42*, 1297; L. Guczi, G. Petoe, A. Beck, K. Frey, O. Geszti, G. Molnar, C. Daroczi, *J. Am. Chem. Soc.* **2003**, *125*, 4332; L. Guczi, P. Gabor, A. Beck, K. Frey, O. Geszti, G. Molnar, C. Daroczi, *J. Am. Chem. Soc.* **2003**, *125*, 4332; S. Carretin, P. Conception, A. Corma, J. M. Lopez Nieto, V. F. Puntes, *Angew. Chem.* **2004**, *116*, 2592; *Angew. Chem. Int. Ed.* **2004**, *43*, 2538; J.-H. Liu, Y.-S. Chi, H.-P. Lin, C.-Y. Mou, B.-Z. Wan, *Catal. Today* **2004**, *93*, 141; S.-H. Wu, X.-C. Zheng, S.-R. Wang, D.-Z. Han, W.-P. Huang, S.-M. Zhang, *Catal. Lett.* **2004**, *97*, 17; J. Chou, N. R. Franklin, S.-H. Baeck, T. F. Jaramillo, E. W. McFarland, *Catal. Lett.* **2004**, *95*, 107; S. H. Overbury, L. Ortiz-Soto, H. Zhu, B. Lee, M. D. Amiridis, S. Dai, *Catal. Lett.* **2004**, *95*, 99; L. Guczi, G. Petoe, A. Beck, Z. Paszti, *Top. Catal.* **2004**, *29*, 129; S.-H. Wu, X.-C. Zheng, S.-R. Wang, D.-Z. Han, W.-P. Huang, S.-M. Zhang, *Catal. Lett.* **2004**, *96*, 49; L. M. Molina, B. Hammer, *Phys. Rev. B* **2004**, *69*, 155424; B. Schumacher, Y. Denkwitz, V. Plzak, M. Kinne, R. J. Behm, *J. Catal.* **2004**, *124*, 449; M. Daté, M. Okumura, S. Tsubota, M. Haruta, *Angew. Chem.* **2004**, *116*, 2181; *Angew. Chem. Int. Ed.* **2004**, *116*, 2129; D. A. Bulushev, I. Yuranov, E. I. Suvurova, P. A. Buffat, L. Kiwi-Minsker, *J. Catal.* **2004**, *124*, 8; P. Konova, A. Naydenov, Cv. Venkov, D. Mehandjiev, D. Andreeva, T. Tabakova, *J. Mol. Catal. A* **2004**, *213*, 235; R. Zanella, S. Giorgio, C.-H. Shin, C. R. Henry, C. Louis, *J. Catal.* **2004**, *122*, 357; K. Mallick, M. J. Witcomb, M. S. Scurrell, *Appl. Catal. A* **2004**, *259*, 163; S. Y. Lai, H. Zhang, C. F. Ng, *Catal. Lett.* **2004**, *92*, 107; S. Arrii, F. Morfin, A. Renouprez, J. L. Rousset, *J. Am. Chem. Soc.* **2004**, *126*, 1199; Y. Gong, Z. Hou, H. Xin, *J. Phys. Chem. B* **2004**, *108*, 17796; L. Fu, N. Q. Wu, J. H. Yang, F. Qu, D. L. Johnson, M. C. Kung, H. H. Kung, V. P. Dravid, *J. Phys. Chem. B* **2005**, *109*, 3704; M. Date, M. Haruta, *Shokubai* **2005**, *47*, 8; M. Lomello-Tafin, A. A. Chaou, F. Morfin, V. Caps, J.-L. Rousset, *Chem. Commun.* **2005**, 388; G. J. Hutchings, *Catal. Today* **2005**, *100*, 55.

[46] a) M. Okumura, S. Nakamara, S. Tsubota, T. Nakamura, M. Azuma, *Catal. Lett.* **1998**, *51*, 53; M. Okumura, T. Akita, M. Haruta, *Catal. Today* **2002**, *74*, 265; b) C. Mohr, H. Hofmeister, P. Claus, *J. Catal.* **2003**, *213*, 86; c) S. Biella, M. Rossi, *Chem. Commun.* **2003**, 378; S. Biela, G. L. Castiglioni, C. Fumagalli, L. Prati, M. Rossi, *Catal. Today* **2002**, *72*, 43; d) C. Milone, R.

 © 2005 Wiley-VCH Verlag GmbH & Co. KGaA, Weinheim

Ingoglia, G. Neri, A. Pistone, S. Galvagno, *Appl. Catal. A* **2001**, *211*, 251; C. Milone, M. L. Tropeano, G. Gulino, G. Neri, R. Ingoglia, S. Galvano, *Chem. Commun.* **2002**, 868; e) F. Porta, L. Prati, M. Rossi, S. Collucia, G. Martra, *Catal. Today* **2000**, *61*, 165; f) P. Landon, P. J. Collier, A. J. Papworth, C. J. Kiely, G. J. Hutchings, *Chem. Commun.* **2002**, 2058; g) F. Shi, Y. Deng, *J. Catal.* **2002**, *211*, 548; S.-W. Kim, S. U. Son, S. S. Lee, T. Hyeon, Y. K. Chung, *Chem. Commun.* **2001**, 2212; h) C. W. Corti, R. J. Holliday, D. T. Thompson, *Gold Bull.* **2002**, *35*, 11; i) C. Mohr, T. Akita, M. Aruta, *Catal. Today* **2003**, *213*, 86; j) S. U. Son, S. I. Lee, Y. K. Chung, S.-W. Kim, T. Hyeon, *Org. Lett.* **2002**, *4*, 277; k) S. U. Son, K. H. Park, Y. K. Chung, *Org. Lett.* **2002**, *4*, 3983; l) S. U. Son, K. H. Park, Y. K. Chung, *J. Am. Chem. Soc.* **2002**, *124*, 6838; m) M. Tominaga, T. Shimazoe, N. Toshihiro, M. Nagashima, I. Tanigushi, *Chem. Lett.* **2005**, *34*, 202; n) G. Lue, D. Ji, G. Qian, Y. Qi, X. Wang, J. Suo, *Appl. Catal. A* **2005**, *280*, 175; o) K. Zhu, J. Hu, R. Richards, *Catal. Lett.* **2005**, *100*, 195; p) G. Lü, D. Ji, G. Qian, Y. Qi, X. Wang, J. Suo, *Appl. Catal. A* **2005**, *280*, 175.

[47] M. M. Maye, J. Luo, Y. Lin, M. H. Engelhard, H. Mark, M. Hepel, C.-J. Zhong, *Langmuir* **2003**, *19*, 125, and references therein; C. Roth, I. Hussain, M. Bayati, R. J. Nichols, D. J. Schiffrin, *Chem. Commun.* **2004**, 1532; H. Tang, J. H. Chen, M. Y. Wang, L. H. Nie, Y. F. Kuang, S. Z. Yao, *Appl. Catal. A* **2004**, *275*, 43; for a recent review, see ref. [8a]. With supported PtNPs and Pt–RuNPs: Z. Liu, X. Y. Ling, X. Su, J. Y. Lee, *J. Phys. Chem. B* **2004**, *108*, 8234; J. Solla-Gullon, F. J. Vidal-Iglesias, V. Montiel, A. Aldaz, *Electrochim. Acta* **2004**, *49*, 5079; X. Zhang, F. Zhang, K.-Y. Chan, *J. Mater. Sci.* **2004**, *39*, 5845; Z. He, J. Chen, D. Liu, H. Zhou, Y. Kuang, *Diamond Relat. Mater.* **2004**, *13*, 1764; E. V. Spinace, A. O. Neto, M. Linardi, *J. Power Sources* **2004**, *129*, 121; K. Zhu, J. Hu, R. Richards, *Catal. Lett.* **2005**, *100*, 195; G. M. Veith, A. R. Lupini, S. J. Pennycook, G. W. Ownby, N. J. Dudney, *J. Catal.* **2005**, *231*, 151; S.-H. Baeck, T. F. Jaramillo, A. Kleiman, E. W. McFarland, *Measur. Sci. Technol.* **2005**, *16*, 54; C. Bock, C. Paquet, M. Couillard, G. A. Botton, B. R. MacDougall, *J. Am. Chem. Soc.* **2004**, *126*, 8028.

[48] a) G. Schmid, H. West, H. Mehles, A. Lehnert, *Inorg. Chem.* **1997**, *36*, 891; b) A. M. Caporusso, L. A. Aronica, E. Schiavi, G. Martra, G. Vitulli, P. Salvadori, *J. Organomet. Chem.* **2005**, *690*, 1063.

[49] C. Larpent, F. Brisse-Le Menn, H. Patin, *New J. Chem.* **1991**, *15*, 361; C. Larpent, F. Brisse-Le Menn, H. Patin, *J. Mol. Catal.* **1991**, *65*, L35; C. Larpent, E. Bernard, F. Brisse-Le Menn, H. Patin, *J. Mol. Catal. A* **1997**, *116*, 277; F. Launay, H. Patin, *New J. Chem.* **1997**, *21*, 247; F. Launay, A. Roucoux, H. Patin, *Tetrahedron Lett.* **1998**, *39*, 1353; see also ref. [10].

[50] a) Y. Shiraishi, N. Toshima, *J. Mol. Catal. A* **1999**, *141*, 187; Y. Shiraishi, N. Toshima, *Colloids Surf. A* **2000**, *169*, 59; b) M. Haruta, *Stud. Surf. Sci. Catal.* **2003**, 14; M. Haruta, *Sci. Technol. Catal.* **2002**, 31; c) H. Tang, J. H. Chen, M. Y. Wang, L. H. Nie, Y. F. Kuang, S. Z. Yao, *Appl. Catal. A* **2004**, *275*, 43; A. K. Sinha, S. Seelan, M. Okumura, T. Akita, S. Tsubota, M. Haruta, *J. Phys. Chem. B* **2005**, *109*, 3956.

[51] H. Bönnemann, W. Brijoux, A. Schulze Tilling, K. Siepen, *Top. Catal.* **1997**, *4*, 217; H. Bönnemann, W. Brijoux, A. Schulze Tilling, T. Shilling, B. Tesche, K. Seevogel, R. Franke, J. Hormes, G. Köhl, J. Pollmann, J. Rothe, W. Vogel, *Inorg. Chim. Acta* **1998**, *270*, 95.

[52] Q. Wang, H. Liu, M. Han, X. Li, D. Jiang, *J. Mol. Catal. A* **1997**, *118*, 145.

[53] M. Beller, H. Fischer, K. Köhlein, C.-P. Reisinger, W. A. Herrmann, *J. Organomet. Chem.* **1996**, *520*, 257.

[54] M. T. Reetz, R. Breinbauer, K. Wanninger, *Tetrahedron Lett.* **1996**, *37*, 4499.

[55] M. T. Reetz, R. Breinbauer, P. Wedemann, P. Binger, *Tetrahedron* **1998**, *54*, 1233.

[56] M. T. Reetz, S. A. Quaiser, C. Merk, *Chem. Ber.* **1996**, *129*, 741.

[57] K. Manabe, Y. Mori, T. Wakabayashi, S. Nagayama, S. Kobayashi, *J. Am. Chem. Soc.* **2000**, *122*, 7202.

[58] A. B. R. Mayer, J. E. Mark, R. E. Morris, *Polym. J.* **1997**, *275*, 333; A. Borsla, A. M. Wilhelm, H. Delmas, *Catal. Today* **2001**, *66*, 389.

[59] a) W. Liu, H. Liu, X. An, X. Ma, Z. Liu, L. Quiang, *J. Mol. Catal. A* **1999**, *147*, 73, and references therein; b) W. Yu, H. Liu, M. Liu, Z. Liu, *React. Funct. Polym.* **2000**, *44*, 21; c) X. Yang, Z. Deng, H. Liu, *J. Mol. Catal. A* **1999**, *144*, 123.

[60] N. Pradhan, A. Pal, T. Pal, *Langmuir* **2001**, *17*, 1800.

[61] H. Hirai, N. Yakura, Y. Seta, S. Hodoshima, *React. Funct. Polym.* **1998**, *37*, 121.

[62] G. Schmid, V. Maihack, F. Lantermann, S. Peschel, *J. Chem. Soc. Dalton Trans.* **1996**, 589.

[63] H. Bönnemann, G. A. Braun, *Angew. Chem.* **1996**, *108*, 2120; *Angew. Chem. Int. Ed. Engl.* **1996**, *35*, 1992.

[64] P. Drogna-Landré, M. Lemaire, D. Richard, P. Gallezot, *J. Mol. Catal.* **1993**, *78*, 257; P. Drogna-Landré, D. Richard, M. Draye, P. Gallezot, M. Lemaire, *J. Catal.* **1994**, *147*, 214.

[65] W. D. Harman, *Chem. Rev.* **1997**, *97*, 1953.

[66] Y. Lin, R. G. Finke, *Inorg. Chem.* **1994**, *33*, 4891; J. A. Widegren, R. G. Finke, *J. Mol. Catal. A* **2003**, *198*, 317; J. A. Widegren, R. G. Finke, *Inorg. Chem.* **2002**, *41*, 1558.

[67] a) H. Yang, H. Gao, R. Angelici, *Organometallics* **2000**, *19*, 622; b) J.-L. Pellegatta, C. Blancy, V. Collière, R. Choukroun, B. Chaudret, P. Cheng, K. Philippot, *J. Mol. Catal. A* **2002**, *178*, 55.

[68] J. Blum, I. Amer, A. Zoran, Y. Sasson, *Tetrahedron Lett.* **1983**, *24*, 4139; J. Foise, R. Kershaw, K. Dwight, A. Wold, *Mater. Res. Bull.* **1985**, *20*, 147.

[69] "Two-Phase Hydrogenation Method and Colloidal Catalysts for the Preparation of Cyclohexanes from Benzenes": R. W. Albach, M. Jautelat (A.G. Bayer), Ger. Offen. DE 19807995 A1, **1999**, Germany.

[70] J. Schulz, A. Roucoux, H. Patin, *Chem. Commun.* **1999**, 535; J. Schulz, A. Roucoux, H. Patin, *Chem. Eur. J.* **2000**, *6*, 618; J. Schulz, S. Levigne, A. Roucoux, H. Patin, *Adv. Synth. Catal.* **2002**, *344*, 266; A. Roucoux, J. Schulz, H. Patin, *Adv. Synth. Catal.* **2003**, *345*, 222; V. Mévellec, A. Roucoux, E. Ramirez, K. Philippot, B. Chaudret, *Adv. Synth. Catal.* **2004**, *346*, 72.

[71] T. Jeffery, *Tetrahedron* **1996**, *52*, 10113.

[72] S. Klingelhöfer, W. Heitz, A. Greiner, S. Oestreich, S. Förster, M. Antonietti, *J. Am. Chem. Soc.* **1997**, *119*, 10116; J. Walter, J. Heiermann, G. Dyker, S. Hara, H. Shioyama, *J. Catal.* **2000**, *189*, 449; F. Zhao, B. M. Bhanage, M. Shirai, M. Arai, *Chem. Eur. J.* **2000**, *6*, 843; B. M. Choudary, N. S. Chowdari, K. Jyoti, N. S. Kumar, M. L. Kantam, *Chem. Commun.* **2002**, 586; J. Le Bars, U. Sprecht, J. S. Bradley, D. G. Blackmond, *Langmuir* **1999**, *15*, 7621; M. Moreno-Manas, R. Pleixats, S. Villaroya, *Organometallics* **2001**, *20*, 4524.

[73] For recent reviews on Heck reaction, see ref. [31c,n] and: a) S. Bräse, A. de Meijere in *Metal-Catalyzed Cross-Coupling Reactions* (Eds.: F. Diederich, P. J. Stang), Wiley-VCH, Weinheim, **1998**, p. 99; b) N. J. Whitcombe, K. K. Hii, S. E. Gibson, *Tetrahedron* **2001**, *57*, 7449; c) B. M. Bhanage, M. Arai, *Catal. Rev.* **2001**, *43*, 315; d) A. F. Little, G. C. Fu, *Angew. Chem.* **2002**, *114*, 4350; *Angew. Chem. Int. Ed.* **2002**, *41*, 4176; e) M. Larhed, A. Hallberg in *Handbook of Organopalladium Chemistry for Organic Synthesis, Vol. 1* (Ed.: E.-i. Negishi), Wiley, Hoboken, **2002**, p. 1133; f) W. Hieringer in *Applied Homogeneous Catalysis with Organometallic Compounds, Vol. 2*, 2nd ed. (Eds.: B. Cornils, W. A. Herrmann), Wiley-VCH, Weinheim, **2002**, p. 721; g) B. M. Bhanage, S.-i. Fujita, M. Arai, *J. Organomet. Chem.* **2003**, *687*, 211; h) M. Shibasaki, E. M. Vogl, T. Oshima in *Comprehensive Asymmetric Catalysis, Vol. Suppl. 2004* (Eds.: E. N. Jacobsen, A. Pfaltz, H. Yamamoto), Springer, Heidelberg, **2004**, p. 73.

 © 2005 Wiley-VCH Verlag GmbH & Co. KGaA, Weinheim

[74] a) For a recent review on the Suzuki reaction, see: A. Suzuki in *Modern Arene Chemistry* (Ed.: D. Astruc), Wiley-VCH, Weinheim, **2003**, p. 53; b) for a recent review on amination of aryl halides and sulfonates, see: J. F. Hartwig in *Modern Arene Chemistry* (Ed.: D. Astruc), Wiley-VCH, Weinheim, **2003**, p. 107.
[75] F. Bertoux, E. Monflier, Y. Castanet, A. Mortreux, *J. Mol. Catal. A* **1999**, *143*, 23.
[76] M. T. Thathagar, J. Beckers, G. Rothenberg, *J. Am. Chem. Soc.* **2002**, *124*, 11858.
[77] L. Djakovitch, M. Wagner, K. Köhler, *J. Organomet. Chem.* **1999**, *592*, 225; B. H. Lipshutz, H. Ueda, *Angew. Chem.* **2000**, *112*, 4666; *Angew. Chem. Int. Ed.* **2000**, *39*, 4492.
[78] C. Mohr, H. Hofmeister, J. Radnik, P. Claus, *J. Am. Chem. Soc.* **2003**, *125*, 1905; K. Chen, Z. Zhang, Z. Cui, D. Yang, *Gaofenzi Xuebao* **2000**, 180 [*Chem. Abstr.* **2000**, *133*, 159490].
[79] S. Scire, S. Minico, C. Crisafulli, C. Satriano, A. Pistone, *Appl. Catal. B* **2003**, *40*, 43.
[80] C. T. Campbell, *Science* **2004**, *306*, 234.
[81] a) H. Berndt, A. Martin, I. Pitsch, U. Prusse, K.-D. Vorlop, *Catal. Today* **2004**, *91*, 191; S. Carrettin, P. McMorn, P. Johnston, K. Griffin, C. J. Kiely, G. A. Attard, G. J. Hutchings, *Top. Catal.* **2004**, *27*, 131; b) S. Biella, F. Porta, L. Prati, M. Rossi, *Catal. Lett.* **2003**, *90*, 23.
[82] A. Venugopal, M. S. Scurrel, *Appl. Catal. A* **2004**, 258, 241.
[83] a) R. L. Augustine, S. T. O'Leary, *J. Mol. Catal. A* **1995**, *277*, 95; b) J. Le Bars, U. Specht, J. S. Bradley, D. G. Blackmond, *Langmuir* **1999**, *15*, 7621; c) B. M. Choudary, S. Madhi, N. S. Chowdari, M. L. Kantam, B. Sreedhar, *J. Am. Chem. Soc.* **2002**, *124*, 14127.
[84] K. Kaneda, M. Higushi, T. Himanaka, *J. Mol. Catal. A* **2001**, *63*, L33.
[85] M. Julia, M. Duteil, C. Grard, E. Kunz, *Bull. Soc. Chim. Fr.* **1993**, 2791; M. Julia, M. Duteil, *Bull. Soc. Chim. Fr.* **1993**, 2791.
[86] a) F. Zhao, B. M. Bhanage, M. Shirai, M. Arai, *Chem. Eur. J.* **2001**, *7*, 843; b) F. Zhao, M. Shirai, Y. Ikushima, M. Arai, *J. Mol. Catal. A* **2002**, *180*, 211; c) F. Zhao, M. Arai, *React. Kinet. Catal. Lett.* **2004**, *81*, 281; d) A. Eisenstadt in *Catalysis of Organic Reactions, Vol. 1* (Ed.: F. E. Herkes), Marcel Dekker, Basel, **1998**, p. 415.
[87] a) M. Dams, L. Drijkoningen, B. Pauwels, G. Van Tendeloo, D. E. De Vos, P. A. Jacobs, *J. Catal.* **2002**, *209*, 225; b) J. Evans, L. O'Neill, V. L. Kambhampati, G. Rayner, S. Turin, A. Genge, A. J. Dent, T. Neisius, *J. Chem. Soc. Dalton Trans.* **2002**, 2207; c) S. Carrettin, J. Guzman, A. Corma, *Angew. Chem.* **2005**, *117*, 2282; *Angew. Chem. Int. Ed.* **2005**, *44*, 2242; d) J. Gurman, S. Carretin, A. Corma, *J. Am. Chem. Soc.* **2005**, *127*, 3286.
[88] For homogeneous palladium catalysis, Amatore and Jutand have proposed the intermediacy of anionic catalytically active Pd^0 species when anionic ligands are present: see C. Amatore, A. Jutand, *Acc. Chem. Res.* **2000**, *33*, 314, and references therein.
[89] a) C. E. Tucker, J. G. de Vries, *Top. Catal.* **2002**, *19*, 111; b) M. Beller, A. Zapf in *Handbook of Organopalladium Chemistry for Organic Synthesis, Vol. 1* (Ed.: E.-i. Negishi), Wiley, Hoboken, **2002**, p. 1209.
[90] P. Baumeister, W. Meyer, K. Oertle, G. Seifert, H. Seifert, H. Steiner, *Chimia* **1997**, *51*, 144.
[91] J. McChesney, *Spec. Chem.* **1999**, *6*, 98.
[92] I. Shinkai, A. O. King, R. D. Larsen, *Pure Appl. Chem.* **1994**, *66*, 1551.

 © 2005 Wiley-VCH Verlag GmbH & Co. KGaA, Weinheim

Communications

DOI: 10.1002/anie.200502484

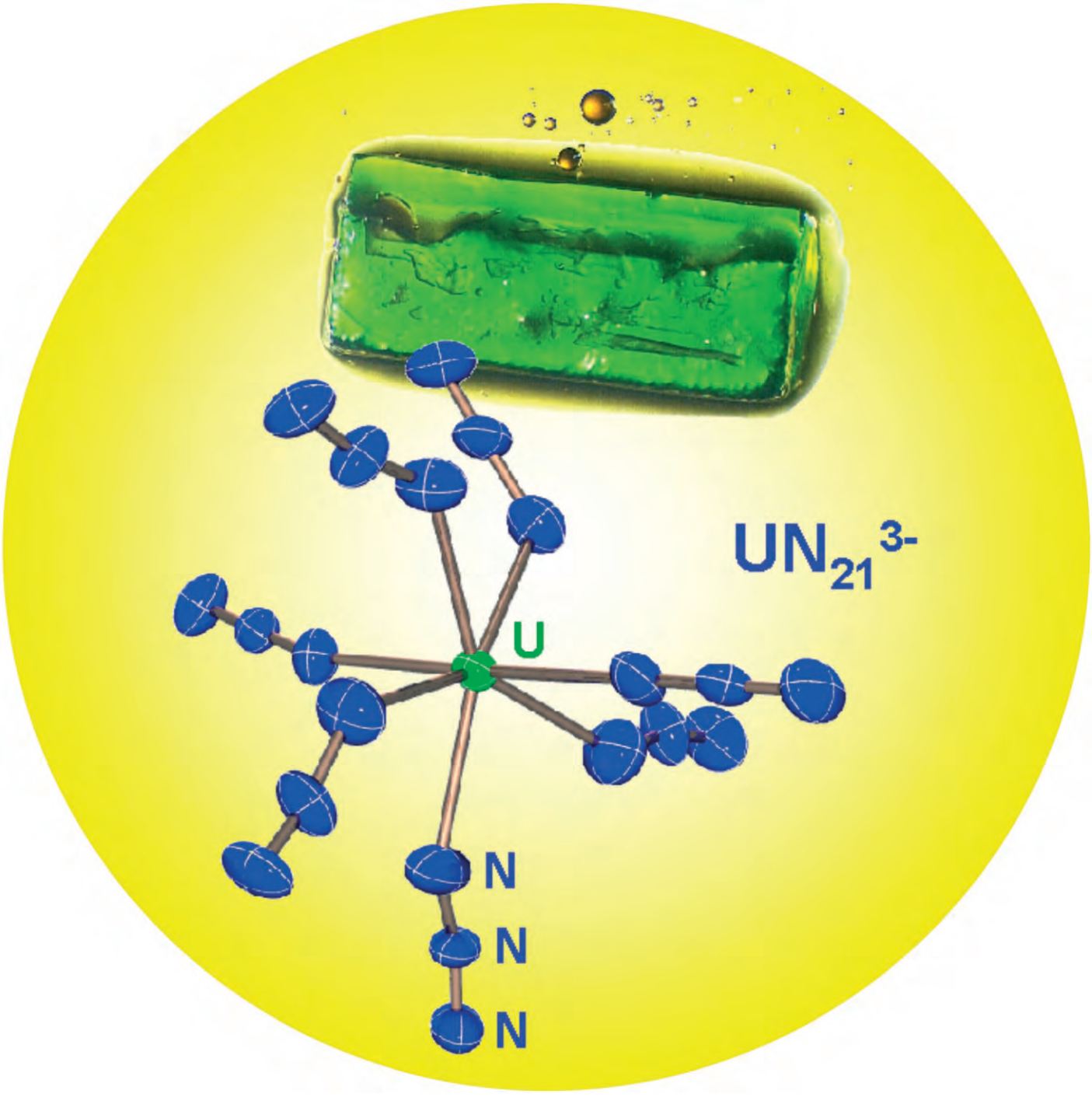

The UN_{21}^{3-} ion, which was characterized as the $(Bu_4N)_3[U(N_3)_7]$ salt, is not only the first homoleptic azide of an actinide but also the first structurally characterized heptaazide. For more information on this fascinating structure, see the Communication by M.-J. Crawford and co-workers on the following pages.

WILEY InterScience DISCOVER SOMETHING GREAT
© 2005 Wiley-VCH Verlag GmbH & Co. KGaA, Weinheim

Azide Complexes

DOI: 10.1002/anie.200502484

UN_{21}^{3-}: A Structurally Characterized Binary Actinide Heptaazide Anion**

Margaret-Jane Crawford, Arkady Ellern, and Peter Mayer*

Although the chemistry of uranium has been extensively investigated, many small, conceptually simple uranium compounds have not been unambiguously characterized, or are missing from the literature completely. The synthesis and characterization of such uranium compounds is particularly interesting, because uranium is the heaviest element that can be handled in the laboratory in small quantities without special techniques. Recent advances in computational chemistry have made the study of small uranium systems possible, thereby opening up a large and interesting aspect of actinide chemistry.[1] We recently reported the first structurally characterized actinide isocyanate,[2] which alerted us to the absence in the literature of any report describing the synthesis of a homoleptic uranium or actinide azide. Pyykkö et al. have recently reported computational investigations into the binary $Th(N_3)_4$ molecule,[3] which they predicted should possess linear azide units. However, despite this exciting prediction, to the best of our knowledge, no synthetic report describing a homoleptic thorium azide exists in the literature.

A few structurally characterized uranium azides have previously been reported, namely polymeric uranyl(VI) azide anions[4] and the $[UO_2\{(CF_3CO)_2CH\}_2N_3]^-$ ion,[5] as well as the uranium(IV) compound $[\{(ArO)_3tacn\}U(N_3)]$ ($(ArOH)_3tacn$ = 1,4,7-tris(3,5-di-*tert*-butyl-2-hydroxybenzyl)-1,4,7-triazacyclononane).[6] The $[UO_2(N_3)_4]^{2-}$ ion has been extensively investigated and unambiguously characterized by Beck and co-workers,[7] and we have recently reported the crystal structures of salts containing $[UO_2(N_3)_4]^{2-}$ and related anions.[8] However, in all of the above-mentioned compounds no binary U–N system was isolated. This is surprising because the synthetic chemistry of binary azides has undergone a renaissance.[9] In addition to the synthesis and structural characterization of IN_3 in the solid state,[10] many new main group and transition-metal anionic azide species have been synthesized.[11] The strategy of synthesizing salts containing binary azide anions in combination with large bulky cations has been used to prepare a wide range of binary azide anions, many salts of which could be structurally characterized in the solid state, and were usually found to be less explosive than neutral binary azides. Some examples include the $As(N_3)_6^-$,[11a,b] $Sn(N_3)_6^{2-}$,[11c,d] $Au(N_3)_4^{2-}$,[11e,f] $Si(N_3)_6^{2-}$,[11g] $Pd(N_3)_4^{2-}$,[11h] $Pt(N_3)_4^{2-}$,[11i] $B(N_3)_4^-$,[11j,k] $Ge(N_3)_6^{2-}$,[11l] $Pt(N_3)_6^{2-}$,[11i,m,n] $Te(N_3)_6^{2-}$,[11o] $Te(N_3)_5^-$,[11p] $I(N_3)_2^-$,[11q,r] $Sb(N_3)_6^-$,[11s] and $Ti(N_3)_6^{2-}$[11t] ions. Detailed discussions of the chemistry of covalent azides are available in excellent review articles by Dehnicke[12] and Klapötke et al.[9]

Since salts containing the binary azide anions are generally more thermally stable and less explosive, particularly when large bulky cations are employed, we set out to investigate the synthesis of a binary uranium azide anion. The convenient synthesis of the $(R_4N)_2[UX_6]$ (R = alkyl; X = Cl, Br) salts,[13] as well as the previous reports on the synthesis and structural characterization of salts of the octaisothiocyanatouranate anion $U(NCS)_8^{4-}$,[14] made the synthesis of a uranium(IV) azide a particularly interesting and promising target. Herein, we report on the synthesis and characterization including the single-crystal structure determination of the binary uranium(IV) heptaazide anion in the $(Bu_4N)_3[U(N_3)_7]$ salt.

The reaction of the uranium(IV) compound $(Bu_4N)_2[UCl_6]$ with two equivalents of Bu_4NBr and eight equivalents of silver azide at room temperature resulted in an immediate color change of the solution from pale green to emerald green. On leaving the reaction mixture to stir overnight (ca. 12 h), an extremely air-sensitive, clear emerald green solution was obtained which could be separated from the insoluble side products.

Large dark green crystals were obtained on cooling a solution of the crude product in $CH_3CN/CFCl_3$. X-ray diffraction revealed that these crystals were not the salt containing the octaazidouranate anion, $(Bu_4N)_4[U(N_3)_8]$, which was expected based on the stoichiometry used, but the heptaazide $(Bu_4N)_3[U(N_3)_7]$ (**1a**) [Eq. (1)]. It is worth mentioning, that to the best of our knowledge no structurally characterized octaazide of any element has been reported. Nevertheless, the isolation of the heptaazide was initially surprising, because preliminary results from our laboratory indicate that from a related reaction, the octaisoselenocyanatouranate anion can be prepared in the form of the $(Pr_4N)_4[U(NCSe)_8]\cdot 2\,CFCl_3$ salt,[8b] in analogy to the previously reported salts of the $U(NCS)_8^{4-}$ ion.[14]

$$(Bu_4N)_2[UCl_6] + Bu_4NBr + 7\,AgN_3 \xrightarrow{CH_3CN} (Bu_4N)_3[U(N_3)_7] + 6\,AgCl + AgBr \quad (1)$$

According to the X-ray structure determination **1a** crystallizes in the cubic space group $Pa\bar{3}$, with one uranium

[*] Dr. M.-J. Crawford, Dr. P. Mayer
Department of Chemistry and Biochemistry
Ludwig-Maximilians University
Butenandtstrasse 5–13 (Haus D), 81377 Munich (Germany)
Fax: (+49) 89-2180-77492
E-mail: mjc@cup.uni-muenchen.de
Dr. A. Ellern
Department of Chemistry
Iowa State University
1711 Gilman Hall, Ames, IA 50011 (USA)

[**] This work was funded by the Deutsche Forschungsgemeinschaft (CR 138/1-1, CR 138/1-2) and Ludwig-Maximilians University. In addition, the Ludwig-Maximilians University Munich is thanked for the award of a Habilitation scholarship through the "Hochschul- und Wissenschaftsprogram (HWP)" within the program "Programm zur Förderung der Chancengleichheit für Frauen in Forschung und Lehre". Prof. Dr. T. M. Klapötke is thanked for his generous support of this work and stimulating discussions. Prof. Dr. A. Türler and Dr. R. Henkelmann (TU Munich) are thanked for their advice throughout this study. Prof. Dr. P. Klüfers is thanked for a generous allocation of X-ray diffractometer time.

 © 2005 Wiley-VCH Verlag GmbH & Co. KGaA, Weinheim

atom and one of three crystallographically independent azide groups located on a C_3 symmetry axis. This results in a monocapped octahedron (1:3:3) arrangement of the azide ligands around the central uranium atom. The N_α atoms of six of the azide ligands are positioned at the corners of a trigonal antiprism, whereas the seventh azide group is located along the C_3 axis. The U–N bond lengths in **1a** range from 2.32(2) to 2.40(2) Å, and it is worth noting that the shortest anion–anion contact, between N6 and N3^i (with $i = y, {}^1/_2-z, -{}^1/_2+x$), is very long (6.72(3) Å; Figure 1) Despite several recrystallization attempts using this method, we did not obtain a better quality structure, therefore we decided to use CH_3CH_2CN as the solvent instead of CH_3CN, because the $(Bu_4N)_3(N_3)_7$ salt is less soluble in CH_3CH_2CN. The reaction using $(Bu_4N)_2[UBr_6]$ and CH_3CH_2CN as the solvent, proceeded analogously to that observed when $(Bu_4N)_2[UCl_6]$ and CH_3CN were used. Although eight equivalents of AgN_3 were used, again only the heptaazide was isolated [Eq. (2)].

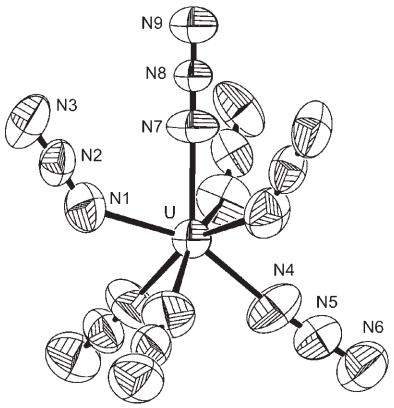

Figure 1. Molecular structure of the $U(N_3)_7^{3-}$ ion in **1a** as determined by single-crystal X-ray diffraction on crystals obtained from CH_3CN/$CFCl_3$ solution (thermal ellipsoids at the 25% probability level).

$$(Bu_4N)_2[UBr_6] + Bu_4NBr + 7\,AgN_3 \rightarrow (Bu_4N)_3[U(N_3)_7] + 7\,AgBr \quad (2)$$

After separation of the green solution from the insoluble solid, the solvent was removed under vacuum at room temperature to yield a sticky green solid **1b**, which was characterized by using IR spectroscopy and after recrystallization from CH_3CH_2CN, by using single-crystal X-ray diffraction (Figure 2). The single-crystal structure of the $U(N_3)_7^{3-}$ ion in **1b**, which was recrystallized from a saturated CH_3CH_2CN solution as the $(Bu_4N)_3[U(N_3)_7]$ salt, clearly shows a distorted pentagonal-bipyramid 1:5:1 arrangement of seven azide ligands around the central uranium(IV) atom. The U–N_α bond lengths of 2.323(6)–2.431(7) Å are significantly shorter than the U–N bond lengths observed in the related $U(NCS)_8^{4-}$ ion in $Cs_4[U(NCS)_8]$ (d(U–N) = 2.441(7)–2.446(5) Å),[14b] and are in reasonable agreement with those observed in $(Et_4N)_4[U(NCS)_8]$ (d(U–N) = 2.379 Å).[14a] Interestingly, the U–N bond lengths in the $U(N_3)_7^{3-}$ ion vary considerably (as was also observed for the Te–N bond lengths in the $Te(N_3)_6^{2-}$ ion),[11o] and can be separated into the five longer equatorial U–N distances (d(U–N) = 2.374(8)–2.431(7) Å) and two shorter axial U–N bond lengths (d(U–N) = 2.329(6) and 2.323(6) Å). The shorter axial U–N bond lengths are in good agreement with the VSEPR model, according to which the axial positions in a pentagonal bipyramid are sterically less crowded than the equatorial positions. The N_α–N_β bond lengths in the $U(N_3)_7^{3-}$ ion ($d(N_\alpha$–$N_\beta)$ = 1.162(8)–1.246(9) Å) are all longer than the corresponding N_β–N_γ bond lengths, as is to be expected ($d(N_\beta$–$N_\gamma)$ = 1.055(8)–1.150(7) Å), in nice agreement with the structures of various binary azide anions, such as $Ti(N_3)_6^{2-}$.[11t] The N_α-N_β-N_γ angles of the five equatorial azide groups (164(1)–168.1(8)°) deviate from linearity considerably more than the two axial N_α-N_β-N_γ angles, which are essentially linear (179.5(7) and 178.9(9)°).

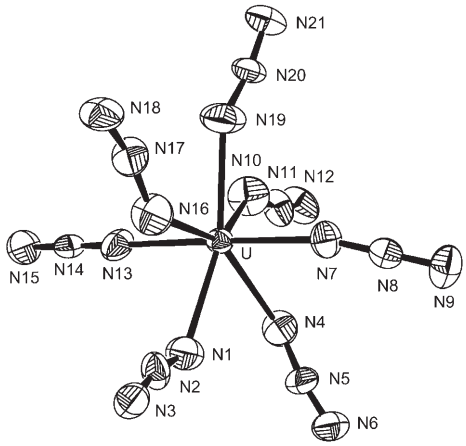

Figure 2. Molecular structure of the $U(N_3)_7^{3-}$ ion in **1b** as determined by single-crystal X-ray diffraction on crystals obtained from CH_3CH_2CN (thermal ellipsoids at the 25% probability level). Selected bond lengths [Å] and angles [°]: U–N1 2.431(7), U–N4 2.429(7), U–N7 2.329(6), U–N10 2.391(8), U–N13 2.323(6), U–N16 2.385(7), U–N19 2.374(8), N1–N2 1.223(8), N2–N3 1.081(7), N4–N5 1.239(9), N5–N6 1.085(8), N7–N8 1.172(7), N8–N9 1.150(7), N10–N11 1.174(9), N11–N12 1.055(8), N13–N14 1.162(8), N14–N15 1.133(8), N16–N17 1.246(9), N17–N18 1.093(8), N19–N20 1.20(1), N20–N21 1.093(7); U-N1-N2 130.5(5), N1-N2-N3 166.2(8), U-N4-N5 121.5(5), N4-N5-N6 168.1(8), U-N7-N8 162.0(5), N7-N8-N9 179.5(7), U-N10-N11 141.9(7), N10-N11-N12 164(1), U-N13-N14 178.6(7), N13-N14-N15 178.9(9) U-N16-N17 135.8(6), N16-N17-N18 165.0(9), U-N19-N20 140.2(8), N19-N20-N21 165.4(9), N4-U-N19 139.1(3), N7-U-N10 104.2(3), N7-U-N13 176.5(2), N7-U-N16 90.6(2), N4-U-N10 74.1(3), N10-U-N19 73.1(3), N16-U-N19 74.0(3), N1-U-N16 72.5(3), N1-U-N4 72.4(2).

The N_α-U-N_α angles between the N_α atoms of neighboring azide groups all lie between 72.4(2) and 74.1(3)°. Whereas the U-N_α-N_β angles are distinctly bent for six out of the seven ligands ($\sphericalangle$(U-N_α-N_β) = 121.5(5)–162.0(5)°), one of the axial azide ligands is bound to the uranium atom in an essentially linear array with a U-N_α-N_β angle of 178.6(7)°. The nitrogen atom N10 deviates the most (−0.457(9) Å) from the equatorial plane, which is defined by the atoms N1, N4, N10, N16, and N19. In addition, the axial U–N7 and U–N13 bonds are oriented 86.8(2)° and 88.4(3)°, respectively, to the equatorial plane. Interestingly, the packing diagram of **1b** indicates that the $U(N_3)_7^{3-}$ ions are surrounded on all sides by tetrabutyl-

 © 2005 Wiley-VCH Verlag GmbH & Co. KGaA, Weinheim

ammonium cations. In addition, the shortest anion–anion contact, between N6 and N15^{i} (with $i = x, \frac{1}{2}-y, \frac{1}{2}+z$), was found to be very long (5.34(1) Å; Figure 3).

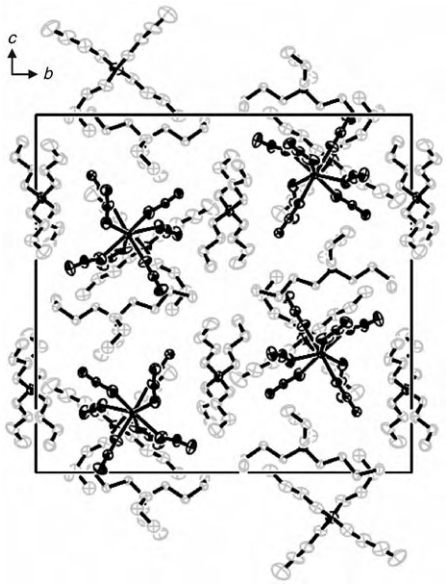

Figure 3. A view of the unit cell of **1b** along the *a* axis (crystals grown from CH_3CH_2CN solution). Thermal ellipsoids are drawn at the 25% probability level; hydrogen atoms are omitted for clarity.

We have not established the friction or impact sensitivity of solid $(Bu_4N)_3[U(N_3)_7]$, because of its extreme air sensitivity. Exposing the reaction mixture to air for a few minutes resulted in a rapid color change of the clear solution from green to yellow (which is indicative for the formation of a uranyl (uranium(VI)) species), and finally brown. Interestingly, for uranium(VI), the $[UO_2(NCS)_5]^{3-}$ ion possesses five SCN^- ligands in the equatorial plane,[15] whereas salts of the related uranium(VI) azide anions, $[UO_2(N_3)_4]^{2-}$ show only four azide ligands in the plane perpendicular to the uranyl axis.[7,8] For the homoleptic uranium(IV) anions, the eight-coordinate $U(NCS)_8^{4-}$ anion is formed,[14] whereas with azide ligands, the seven-coordinate $U(N_3)_7^{3-}$ ion was formed. Interestingly, the synthesis and characterization by IR spectroscopy of the uranium(VI) azide $[UCl_4(N_3)_2]$ has been reported,[16] however, the reaction of UF_6 with CsN_3 led to $CsUF_6$ and N_2.[17] However, the uranium(VI) hexakisamido complex $[U(dbabh)_6]$ (Hdbabh = 2,3:5,6-dibenzo-7-azabicyclo-[2.2.1]hepta-2,5-diene) has recently been described, in which the central uranium(VI) atom is coordinated by six amide nitrogen atoms.[18]

Although the $U(N_3)_7^{3-}$ ion is the first structurally characterized covalent heptaazide, the first covalent heptaazides to be synthesized and isolated were salts containing the highly shock-sensitive $Mo(N_3)_7^-$ and $W(N_3)_7^-$ anions reported by Christe et al., in which the central metal atom is in the +VI oxidation state.[19] In contrast to $Ph_4P[Mo(N_3)_7]$ and Ph_4P-$[W(N_3)_7]$, which were characterized by using low-temperature Raman spectroscopy and exploded violently when being warmed to room temperature, the $(Bu_4N)_3[U(N_3)_7]$ compound was found to be stable both in CH_3CH_2CN solution and in the solid state at room temperature for some time. In the previous report of the $Mo(N_3)_7^-$ and $W(N_3)_7^-$ ions, computational investigations on the $W(N_3)_7^-$ ion located two stable minima, namely the 1:5:1 and 1:4:2 structures, the former of which was calculated to be more favorable in energy by 3.3 kcal mol^{-1}.[19] This is in very good agreement with our experimental observations for the $U(N_3)_7^{3-}$ ion in compound **1b**, for which the 1:5:1 structure was observed. It should be noted however, that the calculated energy difference between the pentagonal bipyramid and monocapped trigonal prism for $W(N_3)_7^-$ was found to be very small.[19]

The synthesis and structural characterization of the homoleptic $U(N_3)_7^{3-}$ ion now raises the question whether further uranium azides can be synthesized, isolated, and structurally characterized, in which the central uranium atom is in an oxidation state other than +IV. In addition, an interesting investigation would be the synthesis and characterization of the neutral homoleptic azides $U(N_3)_4$ and $U(N_3)_6$, or related species such as $[U(N_3)_4L_x]$ (L = neutral coordinating ligand).

Experimental Section

$(Bu_4N)_2[UBr_6]$, $(Bu_4N)_2[UCl_6]$, and AgN_3 were prepared according to literature procedures.[13,20] Bu_4NBr (Fluka) was used as received. CH_3CN and CH_3CH_2CN were dried over P_4O_{10} and distilled twice immediately prior to use. The IR spectrum of the reaction product was recorded between KBr plates. The samples for IR spectroscopy were prepared in a glove-box under a nitrogen atmosphere and were recorded by using a Perkin Elmer FT-IR Spectrum One spectrometer. Standard procedures for working under inert gas atmospheres were used.

Caution! All covalent azides should be handled with extreme caution, because they can detonate unexpectedly due to friction or shock. Under no circumstances should AgN_3 or $(Bu_4N)_3[U(N_3)_7]$ be handled on larger scales, and the work should only be undertaken by experienced experimental chemists with the appropriate safety precautions (Kevlar gloves, leather jacket, face shield, earthing stripes, ear protectors, Teflon spatulas). Even using the above-mentioned precautions, violent explosions may occur, and disregarding the necessary stringent safety precautions can result in serious injury, even if reactions are carried out on a small scale.

1b: $(Bu_4N)_2[UBr_6]$ (0.601 g, 0.5 mmol), Bu_4NBr (0.322 g, 1.0 mmol), and AgN_3 (0.60 g, 4.0 mmol) were added to a 25-mL Schlenk flask under a nitrogen purge. On addition of rigorously dried CH_3CH_2CN (10 mL), a clear emerald green solution formed. The reaction vessel was covered in aluminum foil and the mixture was left to stir at room temperature for 5 h, after which time the insoluble side products were allowed to settle and separated from the green solution. The volume of the filtrate was reduced under vacuum and the vessel was then cooled, whereby emerald green crystals formed in moderate yield. The crystals were found to be stable for several hours when the vessel was maintained under an argon atmosphere in the dark at 4°C, but were extremely air-sensitive. IR (KBr plates, resolution 4 cm^{-1}): $\tilde{\nu}$ 3378 (w), 2961 (m), 2934 (m), 2874 (m), 2112 (m), 2055 (s), 2013 (m), 1983 (w), 1555 (w, br), 1471 (m. br), 1344 (m), 1333 (w), 1281 (w), 1262 (w), 1155 (m), 1066 (w), 1026 (w), 898 (w), 880 (w), 795 (w), 732 (w), 611 cm^{-1} (w).

Crystal data for $(Bu_4N)_3[U(N_3)_7]$ recrystallized from CH_3CH_2CN (**1b**): $C_{48}H_{108}N_{24}U$, $M_r = 1259.56$, yellow-green block, $0.20 \times 0.31 \times 0.42$ mm^3, monoclinic, space group $P2_1/c$, $a = 11.9064(1)$, $b = 24.1556(2)$, $c = 23.5762(2)$ Å, $\beta = 101.7397(6)°$, $V = 6638.8(1)$ Å^3, $Z = 4$, $\rho_{calcd} = 1.260$ g cm^{-3}, $\mu = 2.494$ mm^{-1}, $F(000) = 2624$, Nonius Kappa

 © 2005 Wiley-VCH Verlag GmbH & Co. KGaA, Weinheim

CCD diffractometer, $Mo_{K\alpha}$ radiation, $\lambda = 0.71073$ Å, $T = 200$ K, $\theta = 4.0$–$27.5°$, $-15 \le h \le 15$, $-30 \le k \le 31$, $-30 \le l \le 28$, reflections collected: 75322, independent reflections: 15150 ($R_{int} = 0.058$), observed reflections: 10479, structure solution: Sir 97,[21] direct methods, $R1[I > 2\sigma(I)] = 0.0535$, Final w$R2$ (all data) = 0.1342, Goof = 1.048.

1a: An alternative procedure using $(Bu_4N)_2[UCl_6]$ instead of $(Bu_4N)_2[UBr_6]$ and acetonitrile instead of CH_3CH_2CN was also employed. After the volume of CH_3CN had been reduced in the reaction vessel under vacuum to form a saturated solution, $CFCl_3$ (20 mL) was added under an argon purge, and the vessel was then cooled to −28 °C, whereby emerald green crystals formed in low yield. The crystals were found to be stable for several weeks when the vessel was maintained under an argon atmosphere in the dark at 4 °C, but were extremely air-sensitive.

Crystal data for $(Bu_4N)_3[U(N_3)_7]$ recrystallized from $CH_3CN/CFCl_3$ (**1a**): $C_{48}H_{108}N_{24}U_1$, $M_r = 1259.56$, green block, $0.22 \times 0.24 \times 0.26$ mm^3, cubic, space group $Pa\bar{3}$, $a = 23.8368(3)$ Å, $V = 13543.9(3)$ Å^3, $Z = 8$, $T = 200$ K, $\rho_{calcd} = 1.235$ g cm^{-3}, $\mu = 2.445$ mm^{-1}, $F(000) = 5248$, Nonius Kappa CCD, $Mo_{K\alpha}$ radiation, $\lambda = 0.71073$ Å, $T = 200$ K, $\theta = 3.2$–$21.0°$, $-23 \le h \le 24$, $-24 \le k \le 24$, $-23 \le l \le 22$, reflections collected: 61063, independent reflections: 2409 ($R_{int} = 0.079$), observed reflections: 1599 [$I > 2\sigma(I)$], structure solution: Sir 97,[21] direct methods, final R indices: $R1[I > 2\sigma(I)]$: = 0.0718, final w$R2$ (all data) = 0.2142, Goof = 1.054.

CCDC-278412 and CCDC-278413 contain the supplementary crystallographic data for this paper. These data can be obtained free of charge from The Cambridge Crystallographic Data Centre via www.ccdc.cam.ac.uk/data_request/cif.

Received: July 16, 2005
Revised: October 19, 2005
Published online: November 25, 2005

Keywords: azides · pseudohalides · structure elucidation · uranium

[1] a) N. Kaltsoyannis, *Chem. Soc. Rev.* **2003**, *32*, 9; b) G. Schreckenbach, P. J. Hay, R. L. Martin, *J. Comput. Chem.* **1999**, *20*, 70; c) M. Straka, M. Patzschke, P. Pyykkö, *Theor. Chem. Acc.* **2003**, *109*, 332.

[2] M.-J. Crawford, P. Mayer, H. Nöth, M. Suter, *Inorg. Chem.* **2004**, *43*, 6860.

[3] L. Gagliardi, P. Pyykkö, *Inorg. Chem.* **2003**, *42*, 3074.

[4] P. Charpin, M. Lance, M. Nierlich, D. Vigner, *Acta Crystallogr. Sect. C* **1986**, *42*, 1691.

[5] L. Prasad, E. J. Gabe, B. Glavincevski, S. Brownstein, *Acta Crystallogr. Sect. C* **1983**, *39*, 181.

[6] I. Castro-Rodrigues, K. Olsen, P. Gantzel, K. Meyer, *J. Am. Chem. Soc.* **2003**, *125*, 4565.

[7] a) C. Oetker, W. Beck, *Spectrochim. Acta Part A* **1973**, *29*, 1975; b) W. Beck, W. P. Fehlhammer, P. Poellmann, E. Schuierer, K. Feldl, *Chem. Ber.* **1967**, *100*, 2335; c) W. Beck, E. Schuierer, P. Poellmann, W. P. Fehlhammer, *Z. Naturforsch. B* **1966**, *21*, 811.

[8] a) M.-J. Crawford, Oral presentation, Finnish Winter School, Helsinki University (Finland), 13–17 December, **2004**; b) M.-J. Crawford, Habilitation thesis, Ludwig-Maximilians University, Munich, **2005**.

[9] a) I. C. Tornieporth-Oetting, T. M. Klapötke, *Angew. Chem.* **1995**, *107*, 559; *Angew. Chem. Int. Ed. Engl.* **1995**, *34*, 511; b) T. M. Klapötke, *Chem. Ber.* **1997**, *130*, 443.

[10] P. Buzek, T. M. Klapötke, P. von R. Schleyer, I. C. Tornieporth-Oetting, P. S. White, *Angew. Chem.* **1993**, *105*, 285; *Angew. Chem. Int. Ed. Engl.* **1993**, *32*, 275.

[11] a) T. M. Klapötke, H. Nöth, T. Schütt, M. Warchhold, *Angew. Chem.* **2000**, *112*, 2197; *Angew. Chem. Int. Ed.* **2000**, *39*, 2108; b) K. Karaghiosoff, T. M. Klapötke, B. Krumm, H. Nöth, T. Schutt, M. Suter, *Inorg. Chem.* **2002**, *41*, 170; c) D. Fenske, H.-D. Domer, K. Dehnicke, *Z. Naturforsch.* **1983**, *38*, 1301; d) F. Petillon, M.-T. Vouinou, J.-E. Guerchais, *Bull. Soc. Chim. Fr.* **1969**, 4293; e) W. Beck, H. Nöth, *Chem. Ber.* **1984**, *117*, 419; f) W. Beck, T. M. Klapötke, P. Klüfers, G. Kramer, C. M. Rienäcker, *Z. Anorg. Allg. Chem.* **2001**, *627*, 1669; g) A. C. Fillipou, P. Portius, G. Schnakenburg, *J. Am. Chem. Soc.* **2002**, *124*, 12396; h) W. Beck, T. M. Klapötke, J. Knizek, H. Nöth, T. Schütt, *Eur. J. Inorg. Chem.* **1999**, 523; i) B. Neumüller, F. Schmock, S. Schlecht, K. Dehnicke, *Z. Anorg. Allg. Chem.* **2000**, *626*, 1792; j) W. Fraenk, T. Habereder, A. Hammerl, T. M. Klapötke, B. Krumm, P. Mayer, H. Nöth, M. Warchhold, *Inorg. Chem.* **2001**, *40*, 1334; k) W. Fraenk, H. Nöth, T. M. Klapötke, M. Suter, *Z. Naturforsch. B* **2002**, *57*, 621; l) A. C. Fillipou, P Portius, D. U. Neumann, K.-D. Wehrstedt, *Angew. Chem.* **2000**, *112*, 4524; *Angew. Chem. Int. Ed.* **2000**, *39*, 4333; m) W. Beck, W. P. Fehlhammer, K. Feldl, T. M. Klapötke, G. Kramer, P. Mayer, H. Piotrowski, P. Pöllmann, W. Ponikwar, T. Schütt, E. Schuierer, M. Vogt, *Z. Anorg. Allg. Chem.* **2001**, *627*, 1751; n) see also: S. Schröder, W. Preetz, *Z. Anorg. Allg. Chem.* **2001**, *627*, 390; o) R. Haiges, J. A. Boatz, A. Vij, M. Gerken, S. Schneider, T. Schroer, K. O. Christe, *Angew. Chem.* **2003**, *115*, 6027; *Angew. Chem. Int. Ed.* **2003**, *42*, 5847; p) T. M. Klapötke, B. Krumm, P. Mayer, I. Schwab, *Angew. Chem.* **2003**, *115*, 6024; *Angew. Chem. Int. Ed.* **2003**, *42*, 5843; q) R. Dübgen, K. Dehnicke, *Naturwissenschaften* **1978**, *65*, 535; r) U. Müller, R. Dübgen, K. Dehnicke, *Z. Anorg. Allg. Chem.* **1980**, *463*, 7; s) R. Haiges, J. A. Boatz, A. Vij, V. Vij, M. Gerken, S. Schneider, T. Schroer, M. Yousufuddin, K. O. Christe, *Angew. Chem.* **2004**, *116*, 6844; *Angew. Chem. Int. Ed.* **2004**, *43*, 6676; t) R. Haiges, J. A. Boatz, S. Schneider, T. Schroer, M. Yousufuddin, K. O. Christe, *Angew. Chem.* **2004**, *116*, 3210; *Angew. Chem. Int. Ed.* **2004**, *43*, 3148.

[12] a) K. Dehnicke, *Angew. Chem.* **1979**, *91*, 527; *Angew. Chem. Int. Ed. Engl.* **1979**, *18*, 507; b) K. Dehnicke, *Angew. Chem.* **1967**, *79*, 253; *Angew. Chem. Int. Ed. Engl.* **1967**, *6*, 240; c) K. Dehnicke, *Adv. Inorg. Chem. Radiochem.* **1983**, *26*, 169.

[13] a) J. L. Ryan, *J. Inorg. Nucl. Chem.* **1971**, *33*, 153; b) E. Saritzky, J. Singer, *Acta Crystallogr.* **1956**, *5*, 536.

[14] a) R. Countryman, W. S. McDonald, *J. Inorg. Nucl. Chem.* **1971**, *33*, 2213; b) G. Bombieri, P. T. Moseley, D. Brown, *J. Chem. Soc. Dalton Trans.* **1975**, 1520.

[15] a) K. W. Bagnall, *MTP International Review of Science*, Butterworths University Park Press, London, **1972**, *7*, 139; b) G. Bombieri, E. Forsellini, R. Graziani, G. C. Pappalardo, *Transition Met. Chem.* **1979**, *4*, 70; c) N. W. Alcock, M. M. Roberts, D. Brown, *Acta Crystallogr. Sect. B* **1982**, *38*, 2870.

[16] W. Kolitsch, U. Müller, *Z. Anorg. Allg. Chem.* **1974**, *410*, 21.

[17] B. Glavincevski, S. Brownstein, *Inorg. Chem.* **1981**, *20*, 3580.

[18] K. Mayer, D. J. Mindola, T. A. Baker, W. M. Davis, C. C. Cummins, *Angew. Chem.* **2000**, *112*, 3191; *Angew. Chem. Int. Ed.* **2000**, *39*, 3063.

[19] R. Haiges, J. A. Boatz, R. Bau, S. Schneider, T. Schroer, M. Yousufuddin, K. O. Christe, *Angew. Chem.* **2005**, *117*, 1894; *Angew. Chem. Int. Ed.* **2005**, *44*, 1860.

[20] G. Brauer, *Handbuch der Präparativen Anorganischen Chemie*, 3rd ed., Enke, Stuttgart, **1975**/**1981**.

[21] A. Altomare, M. C. Burla, M. Camalli, G. L. Cascarano, C. Giacovazzo, A. Guagliardi, A. G. G. Moliterni, G. Polidori, R. Spagna, *J. Appl. Crystallogr.* **1999**, *32*, 115.

 © 2005 Wiley-VCH Verlag GmbH & Co. KGaA, Weinheim

Synthetic Methods

DOI: 10.1002/anie.200501732

Asymmetric Conjugate Addition of Organozinc Compounds to α,β-Unsaturated Aldehydes and Ketones with [2.2]Paracyclophaneketimine Ligands without Added Copper Salts**

Stefan Bräse and Sebastian Höfener*

Dedicated to Professor Henri B. Kagan on the occasion of his 75th birthday

Asymmetric catalysis has established itself as a versatile method in modern synthetic chemistry. In particular, many transformations with almost complete enantioselectivity are possible today through the use of chiral ligands. One example is the conjugate addition of organometallic reagents to α,β-unsaturated carbonyl compounds, especially to ketones.[1] In the presence of copper additives different ligand systems give almost complete stereocontrol. The copper ions influence the electronic properties of the carbonyl group, they determine which alkyl or aryl residues are transferred, and they act as bridging units in the transition state.[2,3] As an extension of the non-enantioselective copper-free 1,4-addition to α,β-unsaturated aldehydes described previously by Knochel et al.,[4] we present here for the first time a highly enantioselective copper-free variant.

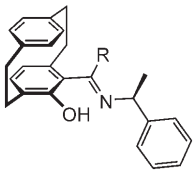

(R_p,*S*)-**1a**: R = Me
(R_p,*S*)-**1b**: R = Ph

Over the last few years we have been able to demonstrate that readily accessible, configurationally stable, planar and centrochiral ketimines **1** with a [2.2]paracyclophane framework[5] are highly suitable for the asymmetric addition of alkyl[6] and alkenyl residues[7] to aliphatic aldehydes. In addition, these ligands have proved to be useful in the addition of alkyl[8] and aryl residues[9] to *N*-acylimines.

Since the addition to *N*-acylimines is comparable to a conjugate addition, we postulated that α,β-unsaturated aldehydes and ketones could also be suitable as substrates. Therefore different α,β-unsaturated aldehydes were tested under standard reaction conditions (2 mol% ligand **1**, 4 equiv $ZnEt_2$ or 2 equiv diisopropylzinc, −20 °C) (Table 1, entries 1–7). Unlike all previously described ligands,[10] the ketimines **1** also transformed α,β-unsaturated aldehydes **2** into the respective 1,4-addition products **3** in a highly enantioselective manner. This even takes place with a relatively small amount of catalyst, 2 mol%, without the addition[11] of compounds having a soft metal center (copper, nickel, or indium[12]). The 1,2-addition products **4** were also formed in most cases, but with only moderate enantioselectivity. The reason is that with α,β-unsaturated aldehydes, unlike, for example, benzaldehyde,[13] the uncatalyzed reaction also takes place. Other ligands (dimethylaminoethanol, 3-*exo*-(dimethylamino)isoborneol (DAIB)) gave, as described in the literature,[10] only 1,2-addition products **4**.

The ratio between 1,2- and 1,4-addition was temperature dependent: low temperatures increased the proportion of the more thermodynamically favorable 1,4 products. However, the reaction rate dropped to such an extent that a compromise between acceptable reaction rate and selectivity had to be found.

In the addition of diethylzinc to cinnamaldehyde (**2a**, entries 1–3 in Table 1) or its derivatives *o*-methoxycinnamaldehyde (**2b**, entry 5) and *p*-chlorocinnamaldehyde (**2c**, entry 6) and also 3-thiophen-3-yl-propenal (**2d**, entry 7) the yield of the 1,4 product was as high as 52% with enantiomeric excesses of between 96 and 98% *ee*. Better regioselectivity was obtained with 6-methoxy-2,2-dimethyl-2*H*-chromene-3-carbaldehyde (**2e**) after 62 h at 0 °C. Here both (S_p,*S*)-**1a** (Table 1, entry 9) and (R_p,*S*)-**1a** (entry 8) gave the 1,4 product in 78–80% yield and 97 and 96% *ee*, respectively. In both cases the *syn* diastereomers were formed preferentially (74% *de* with (S_p,*S*)-**1a**, 77% *de* with (R_p,*S*)-**1a**), which was confirmed by NOE experiments. The addition of diisopropylzinc to cinnamaldehyde (**2a**) was also successful; the 1,4 product was formed with a yield of 39% at 91% *ee* (entry 4).

Whereas in the 1,4-addition to aldehydes temperatures of −20 °C (or 0 °C) are of advantage for selectivity reasons, 1,4-additions to ketones such as benzylideneacetone (**2f**) and 3-octen-2-one (**2g**) can be carried out at room temperature (Table 1, entries 10–12). The 1,2-addition products were never formed as by-products, only the corresponding aldol addition products. However, in the case of benzylideneacetone their fraction could be reduced from 15 to 5% by increasing the amount of ligand from 2 to 4 mol% (Table 1, entries 10 and 11). The enantioselectivities varied between 73 and 90% *ee* for the ketones. Ketones were also successfully reacted with diisopropylzinc (see the Supporting Information).

The diastereomeric ketimine ligands (S_p,*S*)-**1a** and (R_p,*S*)-**1a** led in each case to the complementary main enantiomers of the 1,4- and 1,2-addition products. This pivotal influence of the planar chirality on product configuration confirms previous investigations on 1,2-additions to saturated aldehydes, which also indicated the strongly dominating effect of the planar chirality as opposed to the centrochirality of the ligands.[14]

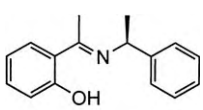

(*S*)-**5**

The nonplanar analogue **5** of the paracyclophaneketimine ligand **1** also catalyzed conjugate addition, albeit

[*] Prof. Dr. S. Bräse, Dr. S. Höfener
Institut für Organische Chemie
Universität Karlsruhe (TH)
Fritz-Haber-Weg 6, 76131 Karlsruhe (Germany)
Fax: (+49) 721-608-8581
E-mail: braese@ioc.uka.de

[**] This research was supported by the Fonds der Chemischen Industrie. We thank Alexander Tung-Qiang Wong and Jens Adler for their contributions to the experimental work.

Supporting information for this article is available on the web under http://www.angewandte.com or from the author.

 © 2005 Wiley-VCH Verlag GmbH & Co. KGaA, Weinheim

Table 1: Asymmetric conjugate addition of diethylzinc and diisopropylzinc to aldehydes and ketones.

2a–e → **3a–e** (1,4-Addition) + **4a–e** (1,2-Addition)

a: R^1 = Ph; R^2 = H
b: R^1 = *o*-$MeOC_6H_4$; R^2 = H
c: R^1 = *p*-ClC_6H_4; R^2 = H
d: R^1 = 3-C_4H_3S; R^2 = H

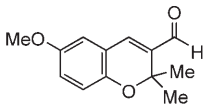

2e

Entry	Substr.	Variant[a]	R	*T* [°C]	Ligand	1,4 Product		1,2 Product	
						Yield [%][b]	*ee* [%][c]	Yield [%][b]	*ee* [%][c]
1	**2a**	B[f]	Et	−20	(R_p,*S*)-**1a**	43	98(*S*)	23	69
2	**2a**	B[f]	Et	−20	(S_p,*S*)-**1a**	36	99(*R*)	37	58
3	**2a**	B[f]	Et	−20	(S_p,*S*)-**1b**	46	97(*R*)	38	53
4	**2a**	D[f]	*i*Pr	−20	(S_p,*S*)-**1a**	39	91	22	n.d.[d]
5	**2b**	B[f]	Et	−20	(S_p,*S*)-**1a**	52	97	13	n.s.[e]
6	**2c**	A[f]	Et	−20	(S_p,*S*)-**1a**	42	96	34	57
7	**2d**	A[f]	Et	−20	(R_p,*S*)-**1a**	45	99	31	50
8	**2e**	C	Et	0	(R_p,*S*)-**1a**	80	96	4	n.d.[d]
9	**2e**	C	Et	0	(S_p,*S*)-**1a**	78	97	12	n.d.[d]
10	**2f**	E[g]	Et	RT	(S_p,*S*)-**1a**	85	87(*R*)	–	–
11	**2f**	E[g,h]	Et	RT	(S_p,*S*)-**1a**	95	90(*R*)	–	–
12	**2g**	E[g]	Et	RT	(S_p,*S*)-**1a**	88	73	–	–

[a] See Experimental Section for details. [b] Determination by GC on an achiral stationary phase (HP1). [c] Determination by GC on a chiral stationary phase (CP-Chirasil-Dex for entries 1–8 and 11; Lipodex E for entries 9 and 10). [d] n.d. = not determined. [e] n.s. = no separation of enantiomers on chiral stationary phase. [f] The condensation product of the 1,2 product was also identified by GC-MS. [g] The aldol products were formed as by-products. [h] Amount of catalyst used: 4 mol%.

with a poorer ratio of 1,2- to 1,4-addition products and lower enantioselectivities. The reaction of cinnamaldehyde (**2a**) at −20 °C gave the 1,2 and 1,4 products in a ratio 2.3:1 (with 17% *ee* for the 1,4 product and 4% *ee* for the 1,2 product).

Here the first copper-free[11] asymmetric 1,4-addition of diethylzinc or diisopropylzinc to α,β-unsaturated aldehydes and ketones has been described. This methodology supplements the spectrum of synthetic methods for β-chiral aldehydes and ketones.[15] The application to the synthesis of biologically active compounds and the extension of the substrate spectrum represents further objectives of our investigations.

Experimental section

Variant A: The ligand (0.01 mmol) and the aldehyde (0.5 mmol) were placed in a 10-mL flask. The reaction vessel was purged with argon and cooled to −20 °C before a solution of diethylzinc (1M in toluene or hexane; 1 mL, 1 mmol) was added. The reaction mixture was stirred for 24 h at this temperature before more diethylzinc solution (1 mL) was added. The reaction mixture was then stirred at −20 °C for 38 h, warmed to room temperature, and stirred for a further 24 h. The reaction was quenched by the addition of semisaturated ammonium chloride solution (3 mL). The reaction mixture was treated with diethyl ether, filtered, and separated in a separating funnel. The organic phase was washed three times with deionized water and dried over magnesium sulfate. GC chromatograms were recorded for these solutions. The solution was then concentrated under reduced pressure, and the regioisomers were separated by column chromatography on silica 60 (eluent: cyclohexane/ethyl acetate).

Variant B: The same as variant A but the twice the quantities were used.

Variant C: The same as variant A, but the reaction was carried out at 0 °C (62 h) and not warmed to room temperature.

Variant D: The ligand (S_p,*S*)-**1a** (0.01 mmol) and cinnamaldehyde (0.5 mmol) were mixed. The reaction vessel was purged with argon and cooled to −20 °C before a solution of diisopropylzinc (1M in toluene; 1 mL, 1 mmol) was added. The reaction mixture was then stirred for 62 h at −20 °C before the reaction was quenched by the addition of semisaturated ammonium chloride solution (3 mL) and worked up as in variant A.

Variant E: (S_p,*S*)-**1a** (0.01 mmol) and the ketone (0.5 mmol) were placed in a 10-mL flask. The reaction vessel was purged with argon before diethylzinc or diisopropylzinc solution was added (1M in hexane or toluene; 1 mL, 1 mmol). After 62 h stirring at room temperature the reaction was quenched by the addition of semisaturated ammonium chloride solution (3 mL) and worked up as in variant A.

Received: May 19, 2005
Revised: August 17, 2005
Published online: November 17, 2005

Keywords: aldehydes · asymmetric catalysis · conjugate additions · cyclophanes · zinc

[1] N. Krause, A. Hoffmann-Röder, *Synthesis* **2001**, 171–196.
[2] Selected examples of conjugate addition of cuprates to α,β-unsaturated ketones: a) R. R. Cesati, J. De Armas, A. H. Hoveyda, *J. Am. Chem. Soc.* **2004**, *126*, 96–101; b) S. Jeon, P. J. Walsh, *J. Am. Chem. Soc.* **2003**, *125*, 9544–9545; c) B. Breit, A. C. Laungani, C. Andy, *Tetrahedron: Asymmetry* **2003**, *14*, 3823–3826; d) I. J. Krauss, J. L. Leighton, *Org. Lett.* **2003**, *5*, 3201–3203; e) B. L. Feringa, R. Badorrey, D. Peña, S. R. Harutyunyan, A. J. Minnaard, *Proc. Natl. Acad. Sci. USA* **2004**, *101*, 5834–5838; f) Y. Ma, C. Song, C. Ma, Z. Sun, Q. Chai, M. B. Andrus, *Angew. Chem.* **2003**, *115*, 6051–6054; *Angew. Chem. Int. Ed.* **2003**, *42*, 5871–5874; g) B. E. Rossiter, N. M. Swingle, *Chem. Rev.* **1992**, *92*, 771; h) A. Alexakis, S. Mutti, J. F. Normant, *J. Am. Chem. Soc.* **1991**, *113*, 6332–6334; i) Nickel catalyzed: K. Soai, S. Yokoyama, T. Hayasaka, K. Ebihara, *J. Org. Chem.* **1988**, *53*, 4148–4149; j) B. L. Feringa, R. Naasz, R. Imbos, L. A. Arnold in *Modern Organocopper Chemistry* (Ed.: N. Krause), Wiley-VCH, Weinheim, **2002**, pp. 224–258.
[3] Conjugate addition of cuprates to α,β-unsaturated aldehydes: G. H. Posner, *Org. React.* **1972**, *19*, 1–113.
[4] a) P. Knochel, *Sci. Synth.* **2004**, *3*, 5–90; b) P. Jones, C. K. Reddy, P. Knochel, *Tetrahedron* **1998**, *54*, 1471–1490.
[5] V. Rozenberg, T. Danilova, E. Sergeeva, E. Vorontsov, Z. Starikova, K. Lysenko, Y. Belokon, *Eur. J. Org. Chem.* **2000**, 3295–3303.

 © 2005 Wiley-VCH Verlag GmbH & Co. KGaA, Weinheim

[6] S. Dahmen, S. Bräse, *Chem. Commun.* **2002**, 26 – 27.
[7] S. Dahmen, S. Bräse, *Org. Lett.* **2001**, *3*, 4119 – 4122.
[8] S. Dahmen, S. Bräse, *J. Am. Chem. Soc.* **2002**, *124*, 5941 – 5942.
[9] N. Hermanns, S. Dahmen, C. Bolm, S. Bräse, *Angew. Chem.* **2002**, *114*, 3844 – 3846; *Angew. Chem. Int. Ed.* **2002**, *41*, 3692 – 3694.
[10] Selected examples: a) W. A. Nugent, *Org. Lett.* **2002**, *4*, 2133 – 2136; b) C. M. Sprout, C. T. Seto, *J. Org. Chem.* **2003**, *68*, 7788 – 7794; c) D. H. Park, H. J. Choi, S. Lee, *Bull. Korean Chem. Soc.* **2003**, *24*, 1559 – 1560; d) J. Long, K. Ding, *Angew. Chem.* **2001**, *113*, 562 – 565; *Angew. Chem. Int. Ed.* **2001**, *40*, 544 – 547; e) X. Yang, J. Sheng, C. Da, H. Wang, W. Su, R. Wang, A. S. C. Chan, *J. Org. Chem.* **2000**, *65*, 295 – 296.
[11] According to ICPMS measurements the copper content of the commercial diethylzinc solutions used is (50 ± 5) μM or less. This gives a ligand/copper ratio of at least 100:1 and a zinc/copper ratio of at least 20000:1. We assume that these copper ions do not play any role in the catalyst cycle since other catalysts show no cuprate-like behavior. We thank Dr. Zsolt Berner, Institut für Mineralogie und Geochemie der Universität Karlsruhe (TH), for carrying out these measurements.
[12] B. G. Kelly, D. G. Gilheany, *Tetrahedron Lett.* **2002**, *43*, 887 – 890.
[13] M. Yamakawa, R. Noyori, *J. Am. Chem. Soc.* **1995**, *117*, 6327 – 6335.
[14] S. Höfener, F. Lauterwasser, S. Bräse, *Adv. Synth. Catal.* **2004**, *346*, 755 – 759.
[15] a) Diastereoselective addition: P. Mangeney, A. Alexakis, J. F. Normant, *Tetrahedron Lett.* **1986**, *27*, 3143 – 3146; asymmetric hydroformylation: G. Consiglio, F. Morandini, M. Scalone, P. Pino, *J. Organomet. Chem.* **1985**, *279*, 193 – 202; diastereoselective alkylation: T. Mukaiyama, H. Teruaki, T. Miwa, K. Narasaka, *Chem. Lett.* **1982**, 1637 – 1640; H. Ahlbrecht, D. Enders, L. Santowski, G. Zimmerman, *Tetrahedron Lett.* **1980**, *21*, 3175 – 3178; b) W. Langer, D. Seebach, *Helv. Chim. Acta* **1979**, *62*, 1710 – 1722; enantioselective isomerization: K. Tanaka, S. Qiao, M. Tobisu, M. M.-C. Lo, G. Fu, *J. Am. Chem. Soc.* **2000**, *122*, 9870 – 9871.

 © 2005 Wiley-VCH Verlag GmbH & Co. KGaA, Weinheim

C–C Activation

DOI: 10.1002/anie.200502596

C–C Bond Activation by Octacarbonyldicobalt: [3+1] Cocyclizations of Methylenecyclopropanes with Carbon Monoxide**

*Takuya Kurahashi and Armin de Meijere**

The activation of carbon–carbon σ bonds under the influence of transition metals remains a fundamental challenge in organometallic chemistry.[1] Methylenecyclopropane and its derivatives were among the first substrates for which involvement of C–C single bonds in transition-metal-catalyzed cycloaddition reactions was observed.[2] In particular, the cycloadditions of methylenecyclopropanes as a C_3 component across C–C multiple bonds have been thoroughly investigated.[3] Surprisingly, only a limited number of transition metals such as Ni, Pd, and Pt have been explored. In recent years, cobalt complexes have been demonstrated to facilitate new types of C–H and C–C bond activation.[4,5] Alper et al. as well as other groups have shown that cobalt-catalyzed carbonylative ring expansions of epoxides and aziridines are useful and efficient procedures for the synthesis of β-lactones and β-lactams, respectively.[6]

In connection with our recently reported cobalt-catalyzed [5+1] cocyclization of vinylcyclopropanes with carbon monoxide leading to cyclohexenones, we found carbonylcobalt complexes to show the highest activity among the transition-metal complexes examined.[7] In view of the observed unique reactivity of the octacarbonyldicobalt complex, we have set out to further explore carbonylative ring-expansion reactions, and here we report a novel [3+1] cocyclization of methylenecyclopropanes with carbon monoxide under cobalt catalysis.

Initially, heptylidenecyclopropane (**1a**) was treated with one equivalent of octacarbonyldicobalt in THF at 50 °C for 12 h, and this led to a mixture of (2*E*)- and (2*Z*)-2-heptylidenecyclobutanone (**2a**) in 85 % yield (Table 1).[8] In other solvents such as toluene, dichloroethane, hexane, and acetonitrile the yields were lower. Among the carbonylmetal complexes examined, octacarbonyldicobalt gave the best

[*] Dr. T. Kurahashi, Prof. Dr. A. de Meijere
Institut für Organische und Biomolekulare Chemie
Georg-August-Universität Göttingen
Tammannstrasse 2, 37077 Göttingen (Germany)
Fax: (+49) 551-399-475
E-mail: armin.demeijere@chemie.uni-goettingen.de

[**] Cyclopropyl Building Blocks for Organic Synthesis, Part 121. This work was supported by the State of Lower Saxony and the Fonds der Chemischen Industrie. T.K. is indebted to the Alexander von Humboldt Foundation for a research fellowship. The authors are grateful to Dr. Burkhard Knieriem, Göttingen, for his careful proofreading of the final manuscript. For Part 120 see: T. Kurahashi, A. de Meijere, *Synlett* **2005**, 2619–2622. Part 119: S. Dalai, M. Limbach, L. Zhao, M. Tamm, M. Sevvana, A. de Meijere, *Synthesis* **2005**, in press.

© 2005 Wiley-VCH Verlag GmbH & Co. KGaA, Weinheim

Table 1: $[Co_2(CO)_8]$-mediated and -catalyzed [3+1] cocyclization of 1′-substituted methylenecyclopropanes with carbon monoxide.[8]

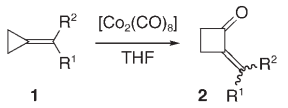

1 2

Substrate	R^1	R^2	T [°C]	t [h]	Prod.	Yield [%]	E/Z[a]
1a	*n*-C_6H_{13}	H	50	12	**2a**	85	73:27
1a	*n*-C_6H_{13}	H	60	12	**2a**	88[b]	71:29
1b	Ph	H	100	12	**2b**	80	98:2
1b	Ph	H	60	12	**2b**	< 1[b]	
1c	-$(CH_2)_5$-		50	24	**2c**	5	
1d	Me	Me	50	24	**2d**	27	
1d	Me	Me	60	48	**2d**	15[b]	
1e		H	50	24	**2e**	53	98:2

[a] The diastereomer ratio was determined by integration of corresponding ^{1}H NMR signals for the crude product. [b] Reaction carried out with a catalytic amount (5 mol%) of $[Co_2(CO)_8]$ under an atmosphere of CO (balloon).

yield of this product. With $[Cr(CO)_6]$, $[Mo(CO)_6]$, $[W(CO)_6]$, and $[Fe(CO)_5]$ the yields were very low (5, 8, < 1, and < 1%, respectively). The reactivity of methylenecyclopropanes with an electron-withdrawing group in the 1′ position was lower, and the reaction of $[Co_2(CO)_8]$ with (phenylmethylene)cyclopropane (**1b**) at 50°C gave only a trace amount of the corresponding benzylidenecyclobutanone **2b**. However, at elevated temperature (100°C) **1b** furnished the product **2b** in 80% yield with a diastereomeric excess of 96%. More electron-deficient methylenecyclopropanes such as (bromomethylene)cyclopropane and *tert*-butyl methylenecyclopropane-1′-carboxylate did not react with $[Co_2(CO)_8]$ even at 100°C. Sterically encumbered 1′,1′-disubstituted methylenecyclopropanes such as **1c** and **1d** reacted sluggishly to give **2c** and **2d** in 5 and 27% yield, respectively. With the alkenyl-substituted methylenecyclopropane **1e**, $[Co_2(CO)_8]$ reacted at the methylenecyclopropane moiety selectively to give the corresponding cyclobutanone **2e** in moderate yield. Unsubstituted methylenecyclopropane and bicyclopropylidene also reacted with $[Co_2(CO)_8]$ even at 25°C, yet no low-molecular-weight products could be isolated.

Methylenecyclopropanes **3** with substituents at the 2- and 3-positions were also tested (Table 2). Indeed, 2-hexyl- (**3f**) and 2-phenylmethylenecyclopropane (**3g**) reacted with $[Co_2(CO)_8]$ to give the corresponding 3- and 4-substituted 2-methylenecyclobutanones **4f/5f** and **4g/5g** in 84 and 71% yield, respectively. In both cases, the regioisomer of type **4** predominated by a factor of about four. 2-Methyl-2-phenyl- (**3h**) and (2,2,3,3-tetramethyl)methylenecyclopropane (**3i**) also readily reacted to furnish the di- and tetrasubstituted 2-methylenecyclobutanones in good yields. The reaction tolerates ester functionalities and other C–C double bonds as exemplified by the successful transformations of **3j** and **3k** to **4j/5j** and **4k/5k**, respectively. Even the unprotected 4-(hydroxymethyl)methylenespiropentane (**3l**) reacted with $[Co_2(CO)_8]$ to give the regioisomeric methylenespiro[2.3]hexanones **4l** and **5l** in a ratio of 86:14 in 66% yield (Scheme 1).

These transformations of methylenecyclopropanes to 2-methylenecyclobutanones, which are essentially insertions of carbon monoxide into the proximal C–C single bonds of the methylenecyclopropanes **1** and **3**, also proceed in the presence of only 5 mol% of $[Co_2(CO)_8]$ [9] under an atmosphere of

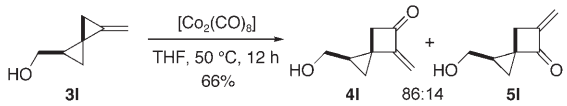

3l 4l 86:14 5l

Scheme 1. $[Co_2(CO)_8]$-mediated and -catalyzed [3+1] cocyclization of **3l** and carbon monoxide.

Table 2: $[Co_2(CO)_8]$-mediated and -catalyzed [3+1] cocyclization of 2- and 2,3-substituted methylenecyclopropanes and carbon monoxide.

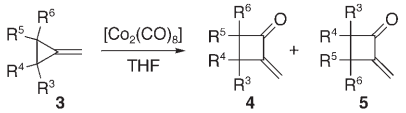

3 4 5

Substrate	R^3	R^4	R^5	R^6	T [°C]	t [h]	Prod.	Yield [%]	**4/5**[a]
3f	*n*-C_6H_{13}	H	H	H	50	12	**4f + 5f**	84	81:19
3f	*n*-C_6H_{13}	H	H	H	60	12	**4f + 5f**	90[b]	85:15
3g	Ph	H	H	H	RT	12	**4g + 5g**	71	83:17
3g	Ph	H	H	H	40	12	**4g + 5g**	62[b]	82:18
3h	Ph	Me	H	H	50	12	**4h + 5h**	67	89:11
3i	Me	Me	Me	Me	50	12	**4i**	81	
3i	Me	Me	Me	Me	60	24	**4i**	75[b]	
3j	$AcOCH_2$	H	H	H	50	12	**4j + 5j**	62	78:22
3k	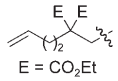 E = CO_2Et	H	H	H	50	24	**4k + 5k**	58	95:5

[a] The ratio of regioisomers **4**:**5** was determined by integration of corresponding ^{1}H NMR signals for the crude product. [b] Reaction carried out with a catalytic amount (5 mol%) of $[Co_2(CO)_8]$ under an atmosphere of CO (balloon).

 © 2005 Wiley-VCH Verlag GmbH & Co. KGaA, Weinheim

carbon monoxide (provided by a balloon). For example, **1a** thus reacted at 60 °C to furnish **2a** in 88 % yield.[8] 1′-Phenylmethylenecyclopropane (**1b**) did not yield the cyclobutanone **2b** at 60 °C under these conditions. Even at elevated temperature (100 °C in dioxane) only a trace amount of the product **2b** was identified. The 1′,1′-disubstituted methylenecyclopropane **1d** reacted sluggishly to give **2d** in 15 % yield. But 2-substituted and 2,3-oligosubstituted methylenecyclopropanes such as **3f** and **3g** did give the corresponding products **4f**/**5f** and **4g**/**5g**, respectively, in good yields. Even the tetrasubstituted methylenecyclopropane **3i** readily provided the product **4i** in 75 % yield.

Mechanistically, this formation of cyclobutanones **2** from methylenecyclopropane **1** is initiated by exchange of one or two CO ligands of the $[Co_2(CO)_8]$ complex with a methylenecyclopropane ligand. The resulting alkene complex, resembling a cobaltaspiropentane **8B**,[10] can either undergo migratory CO insertion to give the cobaltaspiro[2.3]hexanone **7** or a (cyclopropylmethyl)metal-to-homoallylmetal rearrangement[11] to yield an alkylidenecobaltacyclobutane **9**. Subsequent (cyclopropylmethyl)metal-to-homoallylmetal rearrangement[10] of **7** or migratory CO insertion in **9** leads to an alkylidenecobaltacyclopentanone **6**, which undergoes reductive elimination to give the alkylidenecyclobutanone **2** (Scheme 2).

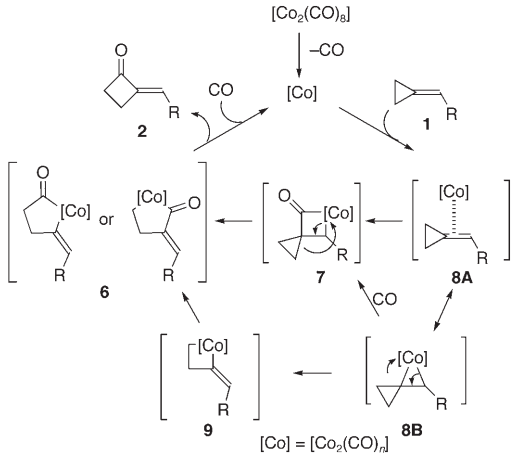

Scheme 2. Mechanistic rationalization of the cobalt-catalyzed [3+1] cocyclization of methylenecyclopropanes with carbon monoxide.

In conclusion, a new cobalt-mediated and -catalyzed [3+1] carbonylative cocyclization of methylenecyclopropanes to give 2-alkylidenecyclobutanones under mild conditions has been developed. Thus, for the first time cobalt has been demonstrated to be an efficient transition metal for the activation of strained carbon–carbon σ bonds.[12] In comparison with rhodium, ruthenium, and nickel complexes, which are usually used for the activation of carbon–carbon bonds, octacarbonyldicobalt is significantly less expensive.

Received: July 25, 2005
Published online: November 15, 2005

Keywords: C–C activation · carbon monoxide · cycloaddition · transition metals

[1] For reviews see: a) C.-H. Jun, *Chem. Soc. Rev.* **2004**, *33*, 610–618; b) M. E. van der Boom, D. Milstein, *Chem. Rev.* **2003**, *103*, 1759–1792; c) M. Murakami, Y. Ito in *Topic in Organometallic Chemistry, Vol. 3* (Ed.: S. Murai), Springer, Berlin, **1999**, pp. 97–129; d) R. H. Crabtree, *Chem. Rev.* **1985**, *85*, 245–269.

[2] a) R. Noyori, Y. Kumagai, I. Umeda, H. Takaya, *J. Am. Chem. Soc.* **1972**, *94*, 4018–4020; b) P. Binger, M. J. Doyle, R. Benn, *Chem. Ber.* **1983**, *116*, 1–10.

[3] For reviews see: a) A. Brandi, S. Cicchi, F. M. Cordero, A. Goti, *Chem. Rev.* **2003**, *103*, 1213–1270; b) I. Nakamura, Y. Yamamoto, *Adv. Synth. Catal.* **2002**, *344*, 111–129; c) M. Lautens, W. Klute, W. Tam, *Chem. Rev.* **1996**, *96*, 49–92; d) "Carbocyclic Three-Membered Ring Compounds" in *Methods of Organic Chemistry (Houben-Weyl), Vol. E17* (Ed.: A. de Meijere), Thieme, Stuttgart, **1996**; e) P. Binger, H. M. Büch in *Top. Curr. Chem., Vol. 135* (Ed.: A. de Meijere), Springer, Berlin, **1987**, pp. 77–151.

[4] For reviews concerning cobalt complexes in organic synthesis see: M. E. Welker, *Current Org. Chem.* **2001**, *5*, 785–807, and references therein.

[5] a) D. T. Shay, G. P. A. Yap, L. N. Zakharov, A. L. Rheingold, K. H. Theopold, *Angew. Chem.* **2005**, *117*, 1532–1534; *Angew. Chem. Int. Ed.* **2005**, *44*, 1508–1510; b) H.-F. Klein, S. Camadanli, R. Beck, D. Leukel, U. Flörke, *Angew. Chem.* **2005**, *117*, 997–999; *Angew. Chem. Int. Ed.* **2005**, *44*, 975–977; c) T. L. Dzwiniel, J. M. Stryker, *J. Am. Chem. Soc.* **2004**, *126*, 9184–9185; d) T. L. Dzwiniel, N. Etkin, J. M. Stryker, *J. Am. Chem. Soc.* **1999**, *121*, 10640–10641.

[6] a) V. Mahadevan, Y. D. Y. L. Getzler, G. W. Coates, *Angew. Chem.* **2002**, *114*, 2905–2908; *Angew. Chem. Int. Ed.* **2002**, *41*, 2781–2784; b) Y. D. Y. L. Getzler, V. Mahadevan, E. B. Lobkovsky, G. W. Coates, *J. Am. Chem. Soc.* **2002**, *124*, 1174–1175; c) J. T. Lee, P. J. Thomas, H. Alper, *J. Org. Chem.* **2001**, *66*, 5424–5426; d) P. Davoli, I. Moretti, F. Prati, H. Alper, *J. Org. Chem.* **1999**, *64*, 518–521; e) M. E. Piotti, H. Alper, *J. Am. Chem. Soc.* **1996**, *118*, 111–116; f) D. Robert, H. Alper, *Organometallics* **1984**, *3*, 1767–1769.

[7] T. Kurahashi, A. de Meijere, *Synlett* **2005**, 2619–2622.

[8] Representative procedure: In an oven-dried Schlenk flask (250 °C) were placed $[Co_2(CO)_8]$ (17 mg, 0.05 mmol) and freshly distilled anhydrous THF (10 mL) under an argon atmosphere. To the resulting dark red solution was added **1a** (138 mg, 1 mmol), and the mixture was stirred at 60 °C under an atmosphere of CO provided by a balloon attached to the flask. The progress of the reaction was monitored by TLC. Upon completion, the initially dark green solution turned pale brown. The cooled reaction mixture was diluted with diethyl ether (20 mL) and stirred under air for 1 h. Filtration through a pad of Celite and purification by Kugelrohr distillation gave **2a** (146 mg, 0.88 mmol, 88 %) as a pale yellow oil. $R_f = 0.29$ (hexane/diethyl ether 10:1). ^{1}H NMR ($CDCl_3$, 500 MHz): $\delta =$ 6.26 (tt, $J = 7.6$, 2.8 Hz, 1H; CH), 2.91 (t, $J = 8.2$ Hz, 2H; CH_2CO), 2.58 (m, 2H; CH_2), 2.07 (m, 2H; CH_2), 1.47–1.39 (m, 2H; CH_2), 1.35–1.25 (m, 6H; 3 CH_2), 0.88 ppm (t, $J = 6.9$ Hz, 3H; CH_3); ^{13}C NMR ($CDCl_3$, 125 MHz): $\delta = 199.4$ (CO), 147.8 (C), 131.1 (CH), 43.3 (CH_2CO), 31.6 (CH_2), 29.0 (CH_2), 28.8 (CH_2), 28.2 (CH_2), 22.5 (CH_2), 20.2 (CH_2), 14.0 ppm (CH_3). IR (neat): $\tilde{\nu} = 2929$, 2857, 1757, 1670, 1457, 1394, 1222, 1098, 1006, 893, 727, 668 cm^{-1}; MS (EI): m/z: 166 ($[M]^+$, 2), 151 ($[M-Me]^+$, 1), 109 ($[M-Bu]^+$, 48), 81 (52), 68 (58), 55 (39), 43 (76), 41 (100); elemental analysis calcd (%) for $C_{11}H_{18}O$: C 79.46, H 10.91; found: C 79.16, H 10.68. Spectroscopic data of the minor diastereomer ($R_f = 0.41$): ^{1}H NMR ($CDCl_3$, 500 MHz): $\delta = 5.58$

 © 2005 Wiley-VCH Verlag GmbH & Co. KGaA, Weinheim

(tt, $J = 7.8$, 2.2 Hz, 1H; CH), 2.85 (t, $J = 8.3$ Hz, 2H; CH_2CO), 2.56 (m, 2H; CH_2), 2.46 (m, 2H; CH_2), 1.41–1.23 (m, 8H; 4 CH_2), 0.87 ppm (t, $J = 6.6$ Hz, 3H; CH_3). ^{13}C NMR ($CDCl_3$, 125 MHz): $\delta = 200.3$ (CO), 146.2 (C), 136.2 (CH), 43.2 (CH_2CO), 31.6 (CH_2), 29.6 (CH_2), 29.1 (CH_2), 28.8 (CH_2), 22.5 (CH_2), 20.9 (CH_2), 14.0 ppm (CH_3). IR (neat): $\tilde{\nu} = 2926$, 2856, 1752, 1663, 1559, 1457, 1394, 1072, 706, 668 cm^{-1}. MS (EI): m/z: 166 ($[M]^+$, 2), 151 ($[M-Me]^+$, 1), 109 ($[M-Bu]^+$, 51), 81 (56), 68 (67), 55 (41), 43 (75), 41 (100). The diastereomer ratio was determined according to the integrals of distinguishable signals in the ^1H NMR spectrum of the crude product mixture: major isomer $\delta = 6.26$ ppm (tt, $J = 7.6$, 2.8 Hz, 1H; CH); minor isomer $\delta =$ 5.58 ppm (tt, $J = 7.8$, 2.2 Hz, 1H; CH).

[9] Among the various cobalt complexes which, according to literature reports, are active in the Pauson–Khand reaction, the best one $[Co(acac)_2]/NaBH_4$ (better than $[CpCo(CO)_2]$, $CoCl_2$, and $[CoCl(PPh_3)_3]$) did not show any catalytic activity in the current transformation. Cf. N. Y. Lee, Y. K. Chung, *Tetrahedron Lett.* **1996**, *37*, 3145–3148.

[10] a) T. Sugihara, M. Yamaguchi, M. Nishizawa, *Chem. Eur. J.* **2001**, *7*, 1589–1595; b) J. Foerstner, S. Kozhushkov, P. Binger, P. Wedemann, M. Noltemeyer, A. de Meijere, H. Butenschön, *Chem. Commun.* **1998**, 239–240.

[11] For cyclopropylmethylmetal rearrangements with transition metals see: a) R. C. Larock, S. Varaprath, *J. Org. Chem.* **1984**, *49*, 3432–3435; b) P. A. Wender, C. O. Husfeld, E. Langkopf, J. A. Love, N. Pleuss, *Tetrahedron* **1998**, *54*, 7203–7220; c) A. de Meijere, H. Nüske, M. Es-Sayed, T. Labahn, M. Schroen, S. Bräse, *Angew. Chem.* **1999**, *111*, 3881–3884; *Angew. Chem. Int. Ed.* **1999**, *38*, 3669–3672; d) B. M. Trost, F. D. Toste, H. Shen, *J. Am. Chem. Soc.* **2000**, *122*, 2379–2380; e) H. Nüske, M. Noltemeyer, A. de Meijere, *Angew. Chem.* **2001**, *113*, 3509–3511; *Angew. Chem. Int. Ed.* **2001**, *40*, 3411–3413; f) P. A. Wender, T. J. Williams, *Angew. Chem.* **2002**, *114*, 4732–4735; *Angew. Chem. Int. Ed.* **2002**, *41*, 4550–4553; g) T. Kawasaki, S. Saito, Y. Yamamoto, *J. Org. Chem.* **2002**, *67*, 4911–4915; h) S. Saito, M. Masuda, S. Kamagawa, *J. Am. Chem. Soc.* **2004**, *126*, 10540–10541.

[12] One of the referees proposed that the previously reported reaction of 1*H*-cyclopropa[*b*]arenes with tris(acetonitrile)tricarbonylchromium to afford cyclobutaarene-1-ones should be cited as a precedent: P. Müller, G. Bernadinelli, Y. Jacquier, A. Ricca, *Helv. Chim. Acta* **1989**, *72*, 1618–1626.

 © 2005 Wiley-VCH Verlag GmbH & Co. KGaA, Weinheim

Silicon Clusters

DOI: 10.1002/anie.200501289

$Si_8(SitBu_3)_6$: A Hitherto Unknown Cluster Structure in Silicon Chemistry**

*Gerd Fischer, Volker Huch, Peter Mayer, Sham Kumar Vasisht, Michael Veith, and Nils Wiberg**

Dedicted to Professor Peter Paetzold on the occasion of his 70th birthday

In a 1991 Review article on the then recent chemistry of cluster compounds of heavy elements of the fourth main group (Si, Ge, Sn, Pb) Masamune and co-workers[1] considered the synthesis of a tetrasilatetrahedrane, a disilyne, and a 1,1,1-pentasilapropellane (that is, a compound of strained anellated Si_3 rings, a compound with a Si–Si triple bond, and a compound with "inverse tetrahedral" Si atoms) as the greatest challenges of silicon chemistry.

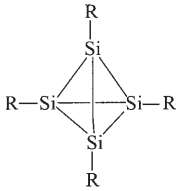

tetrasilatetrahedrane

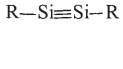

disilyne

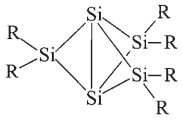

1,1,1-pentasilapropellane

In 1993 we isolated the first tetrasilatetrahedrane with the orange-colored $Si_4R^*_4$ ($R^* = SitBu_3$; "supersilyl")[2] and in 2002 the first disilyne, which is metastable at room temperature, with the yellow $R^*_2MeSi\text{-}Si{\equiv}Si\text{-}SiMeR^*_2$. The latter compound was confirmed by mass spectrometry and NMR spectroscopy as well as chemically and by ab initio studies.[3] In the meanwhile Sekiguchi and co-workers synthesized in a similar way a second tetrasilatetrahedrane (Si_4R_4; $R = [(Me_3Si)_2CH]_2MeSi$) and a second disilyne (Si_2R_2; $R = [(Me_3Si)_2CH]_2iPrSi$), whose structure was elucidated experimentally by X-ray crystallographic analysis.[4] Herein we report the synthesis of a silicon cluster $Si_8R^*_6$ with "inverse

[*] Dr. G. Fischer, Dr. P. Mayer, Prof. Dr. S. K. Vasisht, Prof. Dr. N. Wiberg
Department Chemie und Biochemie
Ludwig-Maximilians-Universität München
Butenandtstrasse 5–13 (Haus D), 81377 München (Germany)
Fax: (+49) 89-2180-77867
E-mail: niw@cup.uni-muenchen.de
Dr. V. Huch, Prof. Dr. M. Veith
Institut für Anorganische Chemie
Universität des Saarlandes
Im Stadtwald, 66123 Saarbrücken (Germany)

[**] Silicon compounds, Part 162. We gratefully acknowledge financial support from the Deutsche Forschungsgemeinschaft. Part 161: Reference [3b]

InterScience
© 2005 Wiley-VCH Verlag GmbH & Co. KGaA, Weinheim

tetrahedral" Si atoms and thereby present a member of the third compound class mentioned at the outset.[5]

The high thermal stability of tetrasupersilyl tetrahedrotetrasilane $Si_4R^*_4$ (**1**)[2] led us to postulate the existence of a ditetrahedranyl $RR^*_3Si_4{-}Si_4R^*_3$ (**5a**), which should be accessible by metathesis from $MSi_4R^*_3$ and $R^*_3Si_4X$ (M = alkali metal, X = halogen). We found that the action of sodium

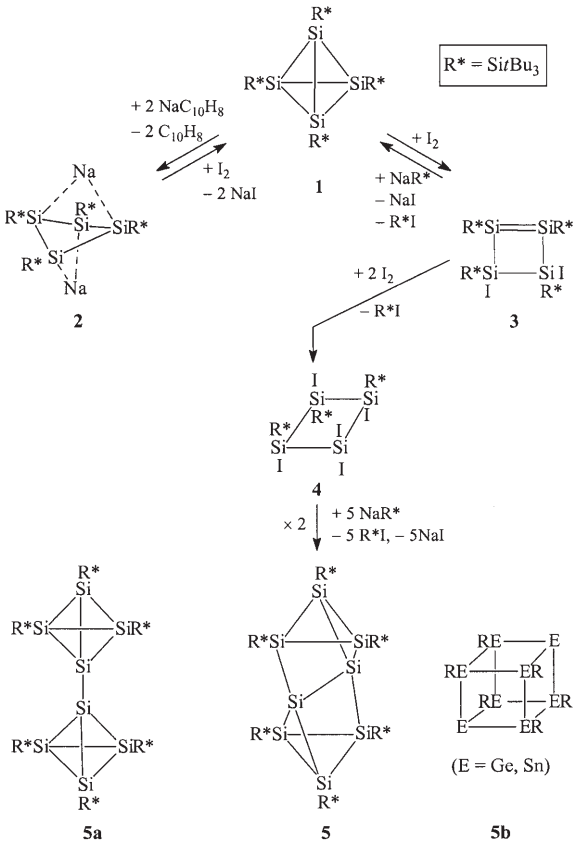

naphthalide ($NaC_{10}H_8$) on **1** in THF at −78 °C did not lead to the elimination of NaR* to the desired substitution product $NaSi_4R^*_3$. Furthermore, the reaction of **1** with iodine in benzene at 6 °C did not proceed with elimination of R*I to form $R^*_3Si_4I$. Instead, the reactions gave the addition products **2** (structure deduced from products of subsequent reactions with MeOH and Me_2SO_4) and **3**, respectively (structure elucidated by X-ray crystallographic analyis).[6] The compounds **2** and **3** readily revert back to **1** by reaction with I_2 and NaR*, respectively. Treatment of the cyclotetrasilene **3** with excess iodine in benzene at room temperature leads to the loss of R*I[7] to afford the pale yellow cyclotetrasilane *trans,trans*-$R^*_3Si_4I_5$ (**4**; Figure 1[8]), which in turn is iodinated to the cyclotetrasilane *trans*-$R^*_2Si_4I_6$ in boiling benzene.[9]

The complete deiodination of pentaiodide **4** with NaR* in THF resulted in a violet product with the sought-after composition $Si_8R^*_6$ (confirmed by mass spectrometry). However, X-ray crystal-structure analysis revealed that this cluster does not correspond to structure **5a**, but instead to **5** (Figure 2[10]). This structure exhibits the following features:

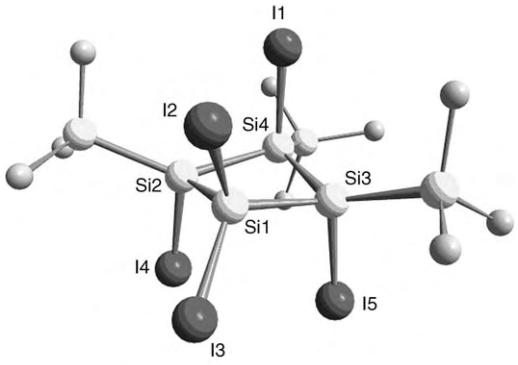

Figure 1. Molecular structure of **4** and selected bond lengths [Å] and angles [°] (methyl groups have been omitted for clarity): Si1-Si2 2.384(11), Si1-Si3 2.384(10), Si2-Si4 2.507(11), Si3-Si4 2.511(12), Si1-I2 2.466(9), Si1-I3 2.466(9), Si2-I4 2.487(9), Si3-I5 2.506(9), Si4-I1 2.485(9); Si2-Si1-Si3 97.2(4), Si1-Si2-Si4 84.2(4), Si1-Si3-Si4 84.1(3), Si2-Si4-Si3 90.9(4); Si1-Si2-Si4-Si3/Si2-Si4-Si3-Si1 14.0, Si4-Si3-Si1-Si2/Si3-Si1-Si2-Si4 14.9.

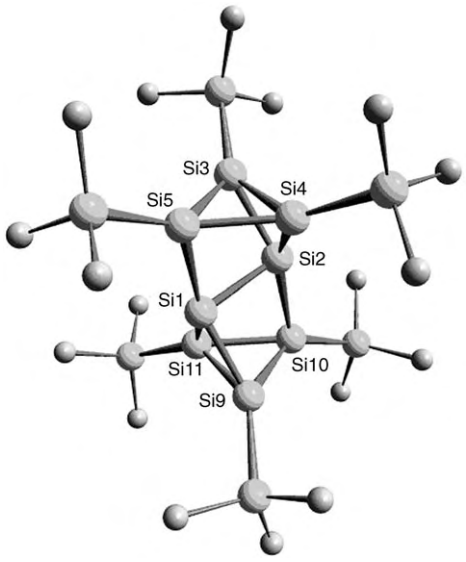

Figure 2. Ball-and-stick representation of the molecular structure of **5**. In the crystal Si1 and Si2 occupy three different positions A, B, and C, which can be approximately transformed into one another by rotation about a threefold noncrystallographic axis. The axis runs through the midpoint of the three-membered rings Si3,Si4,Si5 and Si9,Si10,Si11. Only position C is shown in the figure (methyl groups have been omitted for clarity). Selected bond lengths [Å]: Si3-Si4 2.40(1), Si4-Si5 2.40(1), Si3-Si5 2.39(1), Si9-Si10 2.39(1), Si10-Si11 2.41(1), Si9-Si11 2.40(1). Averaged bond lengths [Å] and angles [°]: Si1-Si2 2.29(1), Si1-Si(9, 11) and Si2-Si(3, 4) 2.33(2), Si1-Si5 und Si2-Si10 2.57(1); Si-Si-Si in the rings Si3,Si4,Si5 and Si9,Si10,Si11: 60.0(1), Si9-Si1-Si11 62.0(2), Si3-Si2-Si4 62.0(3), Si2-Si1-Si(9,11) 92.5(4), Si1-Si2-Si(3,4) 92.4(4), Si2-Si1-Si5 81.7(4), Si1-Si2-Si10 81.2(4), Si(9,11)-Si1-Si5 148.6(9), Si(3,4)-Si2-Si10 148.5(9).

1) **5** contains an unsubstituted Si_2 dumbbell with a short Si–Si single bond of only 2.29(1) Å (normally 2.34 Å). 2) The Si_2 dumbbell is embedded as in a sandwich compound between two almost parallel $Si_3R^*_3$ rings situated on a lattice vacancy where each Si atom of the dumbbell forms two Si–Si bonds of

 © 2005 Wiley-VCH Verlag GmbH & Co. KGaA, Weinheim

normal length (2.33 Å) to one Si_3 ring and a long Si–Si bond (2.75 Å) to the other. 3) X-ray crystal-structure analysis showed that the atoms of the Si_2 dumbbell are distributed over six sites, which can be explained by a disorder of the molecules of **5** in the crystal. 4) The atoms of the Si_2 dumbbell are "inverse tetrahedrally" coordinated by four Si atoms.

Clearly the Si_2 dumbbell is not aligned vertically to the $Si_3R^*_3$ rings as in **5a,** although the atoms of the Si_2 dumbbell in such a structure would be arranged in the usual tetrahedral geometry of tetravalent Si atoms. It is noted in this context that the Ge and Sn atoms of the clusters Ge_8R_6[11] and Sn_8R_6,[12] homologues of $Si_8R^*_6$, are localized at the corners of a cube (in terms of the formulation of **5b**); however, the substituent-free Ge and Sn atoms are not "inverse tetrahedrally" coordinated as they bond only to three atoms (not four).

Theoretical studies[13] must now explain why the cluster $Si_8R^*_6$ adopts structure **5**, and not a bis(tetrahedranyl) structure **5a** or a hexahedranyl structure **5b** (E = Si), which would arise from **5** by stretching the Si–Si bond of the dumbbell. Steric effects do not play a role in this case, but clearly the Si–Si bond in the dumbbell is strong, as chlorination of **5** with CCl_4 does not give the dichloride of **5b** but the cyclotrisilane *cis*,*cis*-$R^*_3Si_3Cl_3$, and possibly Si_2Cl_6.[14]

Experimental section

4: A solution of iodine (0.660 g, 2.60 mmol) in benzene (20 mL) was added dropwise over 1 h, with ice cooling, to a suspension of **1** (0.740 g, 0.81 mmol) in benzene (50 mL) with the exclusion of light. The reaction mixture was allowed to warm to room temperature over about 12 h before the solvent and the excess iodine were removed under vacuum (oil pump). The pale yellow solid residue was washed five to six times with a little *n*-heptane to remove iodine residues and heptane-soluble by-products (e.g. tBu_3SiH), dried under vacuum, and then extracted for 5 h with benzene (25 mL) in a Soxhlet extractor. Pure **4** (0.846 g, 0.63 mmol, 77%) was obtained from the solution. ^{29}Si NMR (C_6D_6, 400 MHz, 23 °C): $\delta = 47.1$ (2 Si*t*Bu$_3$), 41.7 (Si*t*Bu$_3$), −39.0 ppm (3 SiIR*) (A signal for the SiI_2 group was expected in the upfield region, but could not be found owing to the poor solubility of the substance and the mostly low intensity of the ^{29}Si NMR signals for SiI_2 groups. The ^{29}Si NMR signals for two of the three SiIR* groups clearly appear at the same shift.); ^{1}H NMR (C_6D_6, 400 MHz, 23 °C): $\delta = 1.53$ (s; 2 Si*t*Bu$_3$), 1.47 ppm (s; Si*t*Bu$_3$); ^{13}C NMR (C_6D_6, 400 MHz, 23 °C): $\delta = 33.9$ (6 C*Me*$_3$), 33.4 (3 C*Me*$_3$), 27.8 (6 *C*Me$_3$), 26.7 ppm (3 *C*Me$_3$); MS (70 eV, DEI): *m*/*z* (%): 1344 (0.05) [M^+], 1287 (0.05) [$M-t$Bu]$^+$, 1145 (3) [M−R*]$^+$, 1018 (11) [$R^*_2Si_4I_4$]$^+$, 946 (100) [$R^*Si_4I_5$]$^+$, 889 (6) [$R^*Si_4I_5-t$Bu]$^+$, 819 (2) [$R^*Si_4I_4$]$^+$.

5: A solution of NaR* (1.25 mmol) in THF was added dropwise over 1 h to a vigorously stirred suspension of **4** (0.675 g, 0.50 mmol) in THF (50 mL) at −78 °C. The reaction mixture was allowed to warm to room temperature over about 12 h, a third of the solvent was removed under vacuum, and the residue was filtered. The orange-red filtrate contained, among other products, tBu_3SiI and the main component NaI. The violet residue was washed with *n*-heptane and dried under vacuum. Soxhlet extraction for one week with benzene (30 mL) gave pure **5** (0.272 g, 0.19 mmol, 77%); m.p. > 300 °C (lightening in color to yellow above ≈175 °C). ^{1}H NMR (D_8[toluene], 400 MHz, 60 °C): $\delta = 1.43$ ppm (br; Si*t*Bu$_3$) (Owing to the extremely low solubility of **5** in organic media the NMR spectra were recorded at 60 °C. Only one broad signal instead of the expected two appeared in the ^{1}H NMR spectrum; no ^{29}Si NMR signals were observed, even at 60 °C. Solid-state ^{29}Si NMR studies (MAS frequency 12 KHz, single pulse measurement) have thus far produced no meaningful results (signals at $\delta = 45.7$ and 32.0 ppm may possibly be assigned to Si atoms of 2 Si*t*Bu$_3$ and 1 Si*t*Bu$_3$, respectively.); MS (FAB$^+$, Xe, NBA): *m*/*z* (%): 1420.0 (4) [M^+], 1221.8 (21) [M−R*]$^+$, 1021.7 (9) [M−R*−R*H]$^+$, 821.4 (2) [$R^*_3Si_8$]$^+$, 737.7 (8) [$R^*_3Si_5$]$^+$, 709.7 (31) [$R^*_3Si_4$]$^+$, 681.7 (100) [$R^*_3Si_3$]$^+$.

Received: April 13, 2005
Revised: August 12, 2005
Published online: November 15, 2005

Keywords: cluster compounds · silicon · structure elucidation · X-ray diffraction

[1] T. Tsumuraya, S. A. Batcheller, S. Masamune, *Angew. Chem.* **1991**, *103*, 916; *Angew. Chem. Int. Ed. Engl.* **1991**, *30*, 902.

[2] N. Wiberg, C. M. M. Finger, K. Polborn, *Angew. Chem.* **1993**, *105*, 1140; *Angew. Chem. Int. Ed. Engl.* **1993**, *32*, 1055.

[3] a) N. Wiberg, W. Niedermayer, G. Fischer, H. Nöth, M. Suter, *Eur. J. Inorg. Chem.* **2002**, 1066; b) N. Wiberg, S. K. Vasisht, G. Fischer, P. Mayer, *Z. Anorg. Allg. Chem.* **2004**, *630*, 1823, and references therein.

[4] M. Ichinohe, M. Toyoshima, R. Kinjo, A. Sekiguchi, *J. Am. Chem. Soc.* **2003**, *125*, 13328; A. Sekiguchi, R. Kinjo, M. Ichinohe, *Science* **2004**, *305*, 1755; see also: M. Tanaka, A. Sekiguchi, *Angew. Chem.* **2005**, *117*, 5971; *Angew. Chem. Int. Ed.* **2005**, *44*, 5821.

[5] In a publication that appeared after submission of this manuscript, the silicon cluster Si_5R_6 (R = 2,4,6-C_6H_2iPr$_3$) with a "naked" inverse-tetrahedral silicon framework atom was reported: D. Scheschkewitz, *Angew. Chem.* **2005**, *117*, 3014; *Angew. Chem. Int. Ed.* **2005**, *44*, 2954.

[6] N. Wiberg, H. Auer, H. Nöth, J. Knizek, K. Polborn, *Angew. Chem.* **1998**, *110*, 3030; *Angew. Chem. Int. Ed.* **1998**, *37*, 2869; N. Wiberg, H. Auer, S. Wagner, K. Polborn, G. Kramer, *J. Organomet. Chem.* **2001**, *619*, 110; N. Wiberg in *Silicon Chemistry* (Eds.: P. Jutzi, U. Schubert), Wiley-VCH, Weinheim, **2003**, p. 85.

[7] N. Wiberg, H. Auer, K. Polborn, M. Veith, V. Huch in *Organosilicon Chemistry IV* (Eds.: N. Auner, J. Weis), Wiley-VCH, Weinheim, **2000**, p. 124.

[8] X-ray crystal-structure analysis of **4**: $C_{36}H_{81}I_5Si_7 \cdot 0.5\,C_6H_6$, colorless needles, $0.4 \times 0.1 \times 0.1$ mm^3, $M_r = 1384.19$ g mol^{-1}; monoclinic, space group *C*2/*c*; $a = 42.644(9)$, $b = 9.162(2)$, $c = 30.989(6)$ Å, $\beta = 98.81(3)°$, $V = 11965(4)$ Å^3, $Z = 8$, $\mu(Mo_{K\alpha}) = 2.763$ mm^{-1}, $T = 293(2)$ K, $F(000) = 5448$. On a Stoe-IPDS diffractometer, 23102 reflections were measured with $Mo_{K\alpha}$ radiation to $2\Theta_{max.} = 41.92°$ of which 6088 were independent and used for all calculations. The structure was solved by direct methods and refined anisotropically against F^2. The refinement of the H atoms was carried out with the Reiter model. $R1 = 0.068$, $wR2(F^2) = 0.2920$, GOF(F^2) = 1.543. CCDC-159341 (**4**) contains the detailed crystallographic data for this structure analysis. The data may be obtained free of charge from the Cambridge Crystallographic Data Centre under www.ccdc.cam.ac.uk/data_request/cif.

[9] A solution of iodine (1.220 g, 4.80 mmol) in benzene (20 mL) was added dropwise over 30 min to a suspension of **1** (1.094 g, 1.20 mmol) in benzene (50 mL). The reaction mixture was heated at reflux (48 h), during which time the color of the reaction mixture lightened to pale pink. After removal of all volatile components under reduced pressure (oil pump) and washing with *n*-heptane (≥ 4 × 3 mL) the solid residue was dried under vacuum and then extracted for 3 h with hot benzene (15 mL). The extract was cooled, and pale yellow *trans*-$R^*_2Si_4I_6$ crystallized (1.070 g, 0.84 mmol, 70%). In a similar manner, the

 © 2005 Wiley-VCH Verlag GmbH & Co. KGaA, Weinheim

reaction of **3** with iodine in boiling benzene gave *trans*-$R^*_2Si_4I_6$. ^{1}H NMR (C_6D_6, 400 MHz, 23 °C): $\delta = 1.39$ ppm (54 H; 2 Si*t*Bu$_3$); ^{29}Si NMR (C_6D_6, 400 MHz, 23 °C): $\delta = 37.5$ (2 Si*t*Bu$_3$), −58.0 ppm (2 SiIR*) (No signals were observed for SiI_2 groups.); ^{13}C NMR (C_6D_6, 400 MHz, 23 °C): $\delta = 26.7$ (6 *C*Me$_3$), 33.1 ppm (6 *Me*$_3$C); MS (70 eV, DEI): *m*/*z* (%): 1272 (0.4) [M^+], 1214 (4) [$M-t$Bu]$^+$, 1145 (0.4) [$M-$I]$^+$, 1173 (0.7) [$M-$R*]$^+$, 1018 (2) [$R^*_2Si_4I_4$]$^+$, 946 (100) [$R^*Si_4I_5$]$^+$, 889 (10) [$R^*Si_4I_5-t$Bu]$^+$, 819 (3) [$R^*Si_4I_4$]$^+$. For X-ray crystal-structure analysis of *trans*-$R_2Si_4I_6$, see reference [7].

[10] X-ray crystal-structure analysis of **5**: $C_{78}H_{168}Si_{14}$, violet crystals, $0.01 \times 0.05 \times 0.1$ mm^3, $M_r = 1499.38$ g mol^{-1}; triclinic, space group $P\bar{1}$; $a = 12.948(2)$, $b = 15.651(2)$, $c = 25.251(5)$ Å, $\alpha = 78.531(10)$, $\beta = 80.246(11)$, $\gamma = 75.450(10)°$, $V = 4815.1(14)$ Å^3, $Z = 2$, $\mu(Mo_{K\alpha}) = 0.222$ mm^{-1}, $T = 103(2)$ K, $F(000) = 1664$. On a Stoe-IPDS diffractometer, 33637 reflections were measured with $Mo_{K\alpha}$ radiation to $2\Theta_{max.} = 34.84°$ of which 6354 were independent and used for all calculations. The structure was solved by direct methods and refined anisotropically against F^2. Refinement of the H atoms was carried out with the Reiter model. $R1 = 0.068$, $wR2(F^2) = 0.1198$, GOF(F^2) = 1.034. CCDC-277488 (**5**) contains the detailed crystallographic data for this structure analysis. The data may be obtained free of charge from the Cambridge Crystallographic Data Centre under www.ccdc.cam.ac.uk/data_request/cif. Comments: a) No libration correction was carried out. However, the anisotropic temperature factors at the respective atoms are very small and have no pronounced preferred orientation (they are thus almost isotropic). Naturally, in the case of disorder, greater errors in the position parameters can be assumed. However, the deflection parameters did not indicate any excessive deviation. b)If the data set of **5** is expanded to a 2Θ value of 48.0° the R value deteriorates to $R1 = 0.0682$ ($wR2 = 0.11494$). The averaged values (see legend to Figure 2 are, however, not changed by this; thus the structure solution is indirectly confirmed. c) The comparably weak coordination of the Si_2 dumbbell could explain the small Si1–Si2 distance (the higher the coordination number of an atom, the longer are the bonds; Si1 and Si2 are the only atoms in **5** not to carry a R* ligand).

[11] A. Schnepf, R. Köppe, *Angew. Chem.* **2003**, *115*, 940; *Angew. Chem. Int. Ed.* **2003**, *42*, 911.

[12] N. Wiberg, H.-W. Lerner, S. Wagner, H. Nöth, T. Seifert, *Z. Naturforsch. B* **1999**, *54*, 877.

[13] Dr. M. Karni, Dept. Chem. for Computational Quantum Chemistry, Technion-Israel Institute of Technology, Haifa 32000, Israel.

[14] N. Wiberg, unpublished results.

 © 2005 Wiley-VCH Verlag GmbH & Co. KGaA, Weinheim

Photoactivatable Compounds

DOI: 10.1002/anie.200502411

Coumarinylmethyl Esters for Ultrafast Release of High Concentrations of Cyclic Nucleotides upon One- and Two-Photon Photolysis**

Volker Hagen, Brigitte Dekowski, Vasilica Nache, Reinhard Schmidt, Daniel Geißler, Dorothea Lorenz, Jenny Eichhorst, Sandro Keller, Hiroshi Kaneko, Klaus Benndorf, and Burkhard Wiesner*

Biologically inert, photoactivatable precursors ("caged" compounds) of cyclic nucleoside monophosphates (cNMPs) are powerful tools for studying the spatiotemporal dynamics of cyclic nucleotide dependent processes. Among these compounds, (coumarin-4-yl)methyl esters of cNMPs are most useful because they show no background bioactivity, are stable to solvolysis, and can be photolyzed efficiently and extremely quickly.[1,2] Recently, we introduced [7-(diethylamino)coumarin-4-yl]methyl (DEACM) esters of cNMPs as caged compounds.[3,4] Compared with other coumarinylmethyl-caged cNMPs, the DEACM esters photorelease cNMPs with higher photosensitivity at long-wavelength irradiation (up to 436 nm), thus minimizing or even preventing damage to cellular components and chromophores by photobleaching.

Herein, we describe the development of the 7-[bis(carboxymethyl)amino]-substituted coumarinylmethyl building blocks **1** and **2** (structures in Scheme 1) for the caging of phosphates and other functionalities. With the axial and the equatorial diastereomers of the {7-[bis(carboxymethyl)amino]coumarin-4-yl}methyl (BCMACM) esters of cAMP, cGMP, 8-Br-cAMP, and 8-Br-cGMP **3**–**6** (Scheme 1), we present new variants of the DEACM-caged cNMPs, which maintain their favorable properties and additionally have much higher aqueous solubility by virtue of their anionic

[*] Dr. V. Hagen, B. Dekowski, D. Geißler, D. Lorenz, J. Eichhorst, S. Keller, Dr. B. Wiesner
Forschungsinstitut für Molekulare Pharmakologie
Robert-Rössle-Strasse 10, 13125 Berlin (Germany)
Fax: (+49) 30-94793-159
E-mail: hagen@fmp-berlin.de
V. Nache, Prof. Dr. K. Benndorf
Institut für Physiologie II
Friedrich-Schiller-Universität Jena (Germany)
Prof. Dr. R. Schmidt
Institut für Physikalische und Theoretische Chemie
Johann-Wolfgang-Goethe-Universität Frankfurt (Germany)
H. Kaneko
Institut für Zoologie
Universität Heidelberg (Germany)

[**] This work was supported by the Fonds der Chemischen Industrie. We thank Dr. E. Krause for mass-spectrometric and R. Lechler for NMR measurements.

Supporting information for this article is available on the WWW under http://www.angewandte.org or from the author.

 © 2005 Wiley-VCH Verlag GmbH & Co. KGaA, Weinheim

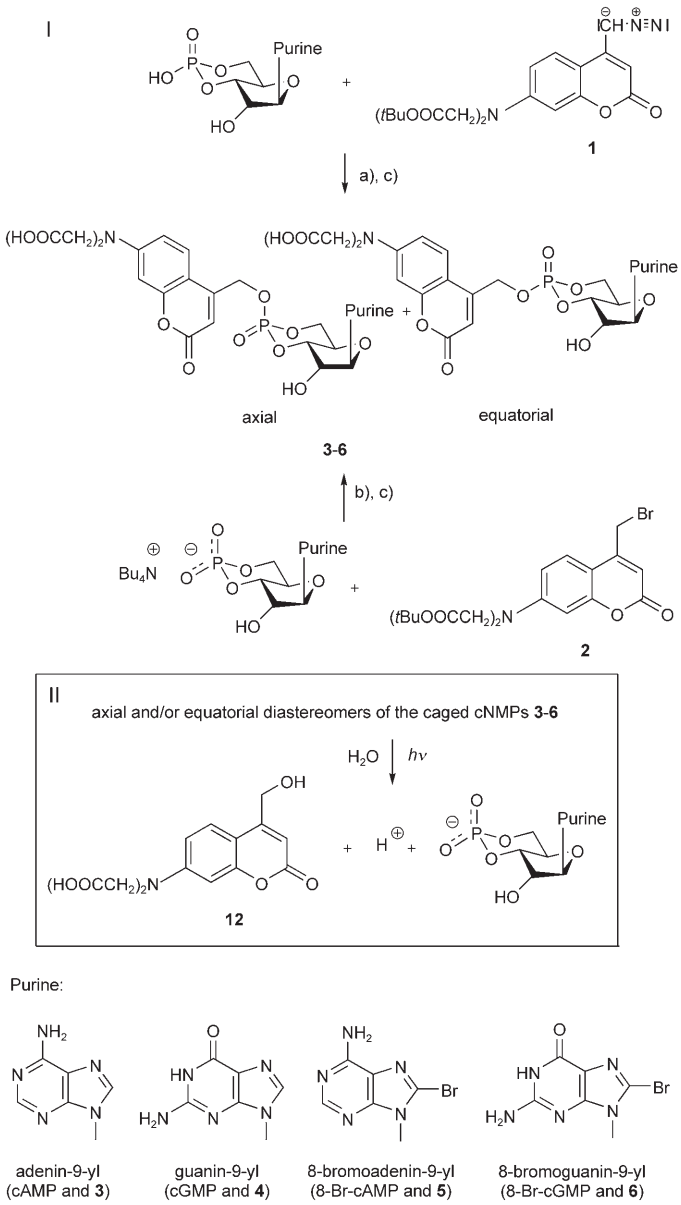

Scheme 1. Synthesis (I) and photolysis (II) of **3**–**6**: a) DMSO/CH_3CN (1:4), 60 °C, 24 h; b) CH_3CN, 85 °C, 5 h; c) TFA/CH_2Cl_2/H_2O (75:24:1), room temperature, 20 min.

centers. Furthermore, we show that the new caged compounds photorelease cNMPs upon one- as well as two-photon excitation and that it is possible to determine quantitatively the amount of cyclic nucleotide photoreleased inside a cell by fluorescence measurements.

The compounds **3**–**6** were prepared as shown in Scheme 1 I by alkylation of the free acid form of the respective cNMP with the 4-(diazomethyl)coumarin **1** (Method A) or by reaction of the tetra-*n*-butylammonium salts of the cNMPs with the 4-(bromomethyl)coumarin **2** (Method B) according to procedures described earlier for other coumarinylmethyl esters of cNMPs[5,6] and by subsequent removal of the *tert*-butoxy protecting groups with trifluoroacetic acid (TFA).

The synthesis of the key compounds **1** and **2** is outlined in Scheme 2. 7-Amino-4-methylcoumarin (**7**) was treated with an excess of bromoacetic acid *tert*-butyl ester in the presence of diisopropylethylamine to yield a mixture of **8** and **9**, which was separated by flash chromatography to provide the two products in yields of 27% and 31%, respectively. SeO_2 oxidation of **9** gave the corresponding aldehyde **10** in a yield of 80%. Condensation of **10** with tosylhydrazide furnished the corresponding hydrazone (84% yield), which was transformed into **1** by triethylamine-mediated Bamford–Stevens reaction (87% yield). Compound **2** was best prepared (81% yield) from the alcohol **11**, which was synthesized in 74% yield from **10** by reduction with $NaBH_4$, by mesylation and subsequent displacement of the mesyl group using LiBr in THF. Our attempts to convert **9** directly into **2** by utilizing *N*-bromosuccinimide were not successful as they resulted mainly in bromo substitution in position 3 of the coumarin ring.

Alkylation of the cNMPs using Method A gave relatively low product yields for the *tert*-butoxy-protected derivatives of **3** (12%) and **6** (7%) but an acceptable yield for the corresponding analogue of **4** (25%). The reaction of **1** with 8-Br-cAMP yielded only traces of **5**. However, the alternative esterification by Method B gave relatively high product yields for the *tert*-butoxy-protected derivatives of **3** (38%) and **5** (49%), an acceptable yield for the corresponding derivative of **6** (18%), and only negligible amounts of the analogue of **4**. Compared with the syntheses of other caged cNMPs,[2,3,7] **3**–**6** can be prepared with good yields by Method A for the synthesis of **4** and Method B for the preparation of **3**, **5**, and **6**, particularly because the product yields represent typical rather than optimal conditions.

Both synthetic procedures resulted in diastereomeric mixtures of the *tert*-butoxy-protected caged compounds. The ratios of the axial to the equatorial diastereomers were approximately 2:3 (Method A) and from 2:1 to 4:1 (Method B). The diastereomers were separated by reversed-phase HPLC on a preparative scale. In all cases, the axial isomers showed lower retention times than the equatorial isomers. TFA deprotection of the *tert*-butoxy-protected diastereomers of the esters resulted in the pure axial and equatorial isomers of **3**–**6** with approximately quantitative yields (see the Supporting Information for preparative details and analytical characterization). The isomers were assigned by ^{31}P NMR spectroscopy.[8,9]

Like other coumarinylmethyl-caged cNMPs, compounds **3**–**6** are highly resistant to spontaneous hydrolysis in the dark. HPLC monitoring of the pure diastereomers of the caged compounds in aqueous HEPES buffer at pH 7.2 during a 24-h period revealed no measurable formation ($<0.5\%$) of the free cNMPs at room temperature (HEPES = 2-[4-(2-hydroxyethyl)-1-piperazinyl]ethanesulfonic acid). All the compounds are readily soluble in aqueous HEPES buffer at pH 7.2 (Table 1), which is a prerequisite for the administration of large concentrations of phototriggers in cells or around membrane patches at the tip of glass pipettes when the patch–clamp technique is used. As expected, the hydrophilic caged cNMPs do not measurably partition into model lipid membranes at pH 7.2. This was demonstrated by the lack of reaction heats when compounds **3** and **5** were titrated with

 © 2005 Wiley-VCH Verlag GmbH & Co. KGaA, Weinheim

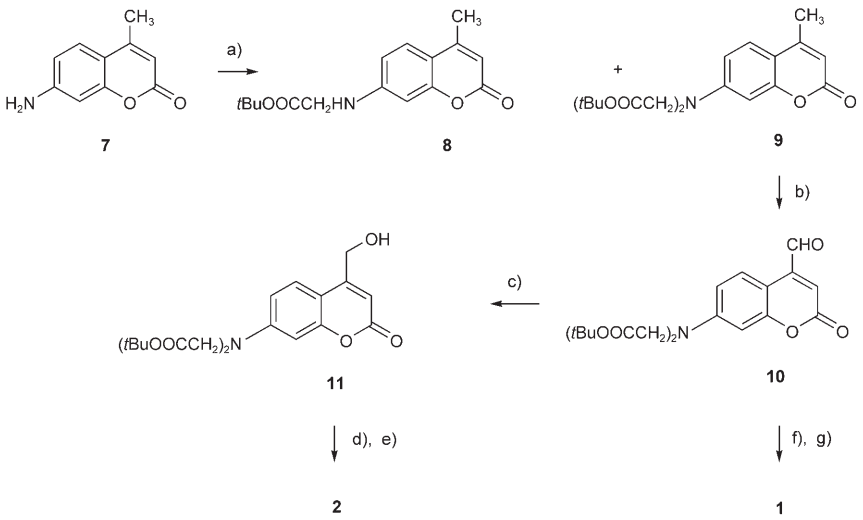

Scheme 2. Synthesis of **1** and **2**: a) $BrCH_2COOtBu$ (3 equiv), iPr_2EtN, NaI, CH_3CN, reflux, 24 h; b) SeO_2, *p*-xylene, reflux, 6 h; c) $NaBH_4$, MeOH, room temperature, 2 h; d) CH_3SO_2Cl, Et_3N, CH_2Cl_2, 5 °C, 20 min; e) LiBr, THF, room temperature, 1.5 h; f) *p*-tosylhydrazide, EtOH, room temperature, 1.5 h; g) Et_3N, MeOH, room temperature, 3 h.

Table 1: Long-wavelength absorption maxima (λ_{abs}^{max}), extinction coefficients, (ε^{max}), photochemical quantum yields (ϕ_{chem}), fluorescence maxima (λ_f^{max}), fluorescence quantum yields (ϕ_f), lifetimes of the lowest excited singlet state (τ), and solubilities (*s*) of the BCMACM esters **3**–**6** and of **12** in CH_3CN/HEPES-KCl buffer (5:95), pH 7.2.

Compound	λ_{abs}^{max} [nm]	ε^{max} [$M^{-1}cm^{-1}$]	ϕ_{chem}[a]	λ_f^{max} [nm]	ϕ_f[b]	τ [ns]	*s* [mM]
3 (axial)	384	17000	0.26	483	0.007	0.07[c]	>2
3 (equatorial)	383	17900	0.30	484	0.007	0.06[c]	>1
4 (axial)	386	18000	0.25	482	0.008	0.07[c]	>2
4 (equatorial)	383	18700	0.30	480	0.011	0.10[c]	>1
5 (axial)	384	18500	0.23	486	0.012	0.11[c]	≈1
5 (equatorial)	383	18100	0.26	483	0.025	0.23[c]	≈1
6 (axial)	387	18100	0.25	479	0.015	0.13[c]	≈1
6 (equatorial)	282	18400	0.29	487	0.023	0.21[c]	≈1
12	376	18400	–	479	0.17	1.59[d]	–

Estimated average uncertainties: [a] 15%, [b] 8%. [c] Calculated as $\tau = \tau_{12} \times \phi_f / \phi_f^{12}$,[13] τ_{12} = fluorescence lifetime of **12**, ϕ_f^{12} = fluorescence quantum yield of **12**. [d] Measured fluorescence lifetime of **12**.

lipid vesicles at different temperatures (see the Supporting Information for details). Nevertheless, the caged compounds rapidly enter live cells, probably using transport proteins or by endocytosis, and HEK293 cells could be loaded with **6** by incubation with a 50-μM buffered (pH 7.2) solution.

Photoactivation of the axial or equatorial diastereomers of the (coumarin-4-yl)methyl esters **3**–**6** by irradiation with wavelengths of 330–430 nm in aqueous buffer leads to the 7-[bis(carboxymethyl)amino]-4-(hydroxymethyl)coumarin **12**, a proton, and the respective "free" cNMP anion (Scheme 1 II). The photoreaction is efficient and clean and gives about 90–95% of the cNMP. Indications of a significant triplet-state population were not found. In fact, the lifetimes of the lowest excited singlet states S_1 are extremely short, about 0.1 ns (see Table 1). We assume that the photochemical conversion proceeds by means of a photochemical S_N1 mechanism (solvent-assisted photoheterolysis) from S_1 via a singlet ion pair. This ion pair decays mainly by recombination to the singlet ground state.[10] Competitively, separation of the ion pair by the polar solvent (formation of the cNMP anion) and subsequent hydrolysis of the coumarinylmethyl carbocation or, alternatively, direct reaction of a water molecule from the solvent cage of the ion pair with its carbocation followed by a very fast deprotonation step may take place.[10,11] Such a photolysis pathway implies that product formation is very fast. Indeed, time-resolved fluorescence measurements upon single-pulse excitation (0.5 ns half-width, 337 nm) of the axial diastereomers of **3** and **4** revealed fluorescence contributions from **12**. Because pure solutions of the caged compounds were irradiated, **12** must have been formed and excited during the photolysis pulse. Actually, deconvolution of the fluorescence signals with a biexponential decay function yielded rise times of the fluorescence of **12** of about 0.7 ns and 0.4 ns for the axial diastereomers of **3** and **4**, respectively. The rate constants of cNMP formation are the quotients of the efficiencies of product formation from the ion pairs and the fluorescence rise times of **12**.[10] Considering the corresponding efficiencies of product formation of 0.27 for **3** and 0.26 for **4**, we obtain for the rate constants values of $4 \times 10^8\ s^{-1}$ and $6 \times 10^8\ s^{-1}$, respectively. As the quantum yields, ϕ_{chem} and ϕ_f, do not vary much (Table 1), it is expected that the equatorial diastereomers of **3** and **4** as well the diastereomers of **5** and **6** photorelease the cNMPs with similar rates.

The photochemical characteristics of the BCMACM esters **3**–**6** in HEPES buffer (pH 7.2) are summarized in Table 1. The absorption and the fluorescence spectra show maxima at 382–387 nm and 479–487 nm, respectively, and correspond to those of the DEACM esters. The single-photon photochemical quantum yields, ϕ_{chem}, as well as the extinction coefficients, ε^{max}, are high for caged compounds, which results in excellent photosensitivity at long-wavelength irradiation. As a consequence, even moderate UV/Vis irradiation is sufficient to obtain large amounts of free cNMP.

The combination of the high photosensitivity and the good solubility of **3**–**6** also permits the generation of large instantaneous cNMP concentration jumps. This could be

 © 2005 Wiley-VCH Verlag GmbH & Co. KGaA, Weinheim

demonstrated by means of cyclic nucleotide gated (CNG) ion channels of the rod photoreceptor, which are activated by cGMP. The CNGA1 subunit of these channels was expressed heterologously in *Xenopus* oocytes, and the current conducted by these channels was measured in inside-out patches with the patch–clamp technique. For example, with 400 μM **4** in the bath solution, a 150-μs light flash generated concentration jumps of free cGMP from zero to 72 μM. Figure 1

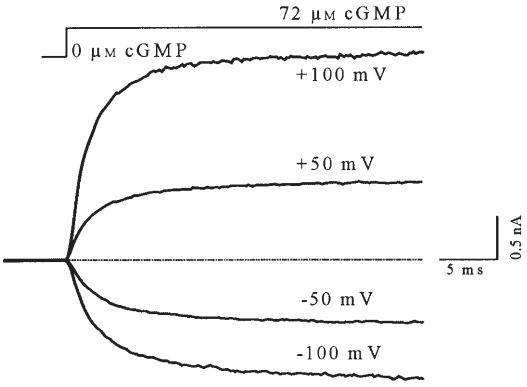

Figure 1. Activation of homotetrameric CNGA1 channels by jumps in cGMP concentration upon photolysis of **4** (axial isomer). The channels were expressed heterologously in *Xenopus* oocytes, and the recordings were performed in inside-out patches containing a high number of channels. The concentration of free cGMP was determined from the steady-state current of the traces referred to the steady-state current at saturating cGMP and the concentration–response relationship for these channels.[15] Before the flash, no current was present. The four traces at the indicated voltages were recorded from the same patch and were corrected for small leak currents by subtracting the respective traces recorded in the absence of cyclic nucleotide.

illustrates the resulting activation time courses at four transmembrane voltages. The time courses are highly resolved and are therefore most appropriate to give information on the molecular mechanisms underlying the activation gating of these channels. At maximum concentrations, **4** allowed us to elicit larger cGMP concentration jumps than the DEACM ester of cGMP.

BCMACM-caged cNMPs are highly sensitive not only to one-photon but also to two-photon excitation. Images obtained by confocal laser scanning microscopy (Figures 2 and 3) indicate that upon photolysis of **6**, 8-Br-cGMP mediates the entry of Ca^{2+} ions into HEK293 cells expressing the cGMP-gated ion channel of the cone photoreceptor (CNGA3). UV (argon laser, 364 nm) as well as IR light (Cameleon diode-pumped laser, 745 nm) evoked a saturable increase in the fluorescence intensity of the Ca^{2+} indicator FLUO-4, which indicates Ca^{2+}-ion influx through CNG channels. Addition of excess Mg^{2+} to the used Ca^{2+} buffer blocked Ca^{2+} influx, and neither UV nor IR irradiation in the absence of **6** led to changes in the fluorescence signal of the cells (not shown). High sensitivity to two-photon photolysis has been described earlier for (6-bromo-7-hydroxycoumarin-4-yl)methyl-caged compounds[2,12] and recently for (6,7-dimethoxycoumarin-4-yl)methyl diethyl phosphate as well as sodium [7-(dimethylamino)coumarin-4-yl]methyl sul-

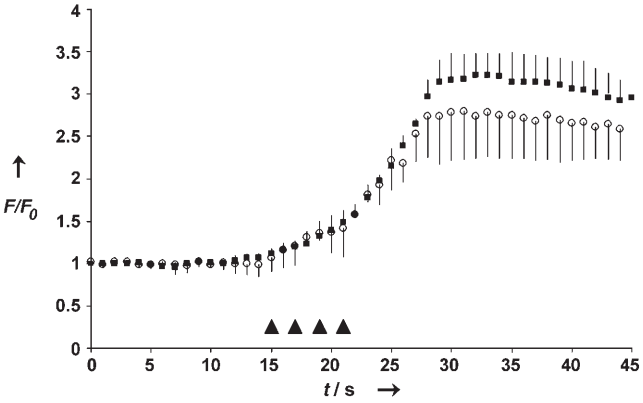

Figure 2. Time course of the Ca^{2+} influx through CNG channels into HEK293 cells expressing the CNGA3 channel after photorelease of 8-Br-cGMP from **6** (axial isomer) by exposure to UV light (364 nm, one-photon excitation, ■) and to IR light (745 nm, two-photon excitation, ○), respectively. The cells were preincubated with 4 μM FLUO-4/AM (30 min) and 50 μM **6** (20 min). The fluorescence intensity F of the Ca^{2+} indicator FLUO-4 was recorded before and after irradiation (▲). There was no significant difference between the two curves. F/F_0 = relative fluorescence intensity (mean values ± standard deviations obtained from three cells).

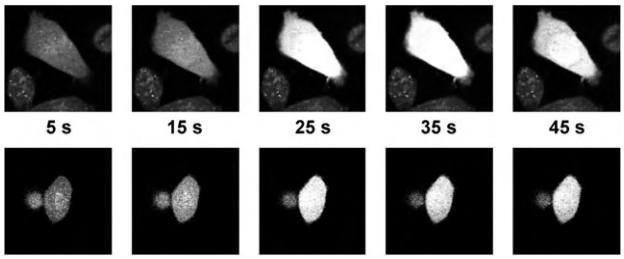

Figure 3. Fluorescence intensity of the Ca^{2+} indicator FLUO-4 in two CNGA3-transfected HEK293 cells before and after photorelease of 8-Br-cGMP from **6** (axial isomer) by exposure to UV (364 nm, upper row) or to IR light (745 nm, lower row). The cells were preincubated with 4 μM FLUO-4/AM (30 min)and 50 μM **6** (20 min). The indicated times correspond to those given in Figure 2. The fluorescence intensity is represented in an 8-bit gray scale.

fate.[13] Direct comparison of the time course for two-photon uncaging of **6** (axial isomer) with that of *N*-[(6-bromo-7-hydroxycoumarin-4-yl)methoxycarbonyl]-L-glutamic acid (Bhc-glu)[12] reveals that **6** photodecomposes initially 1.3 times faster than Bhc-glu under identical conditions (Figure 4). Because Bhc-glu displays a two-photon uncaging action cross-section, δ_u, at 740 nm of about 10^{-50} $cm^4 s\,photon^{-2}$, the two-photon action cross-section of **6** should be slightly larger than 10^{-50} $cm^4 s\,photon^{-2}$. Similar δ_u values are expected also for the equatorial isomer of **6** as well as for the diastereomers of **3**–**5**.

The fluorescence quantum yields ϕ_f of **3**–**6** are one order of magnitude smaller than that of the photoreleased alcohol **12** (Table 1). Compound **12** fluoresces also inside cells (see the Supporting Information), in contrast to 7-(diethylamino)-4-(hydroxymethyl)coumarin whose fluorescence is totally quenched inside HEK293 cells.[4] Thus, fluorescence spectro-

 © 2005 Wiley-VCH Verlag GmbH & Co. KGaA, Weinheim

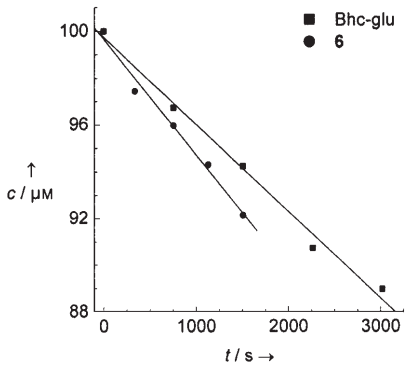

Figure 4. Initial time course of the two-photon photolysis of **6** (axial isomer) and Bhc-glu upon 740-nm irradiation in HEPES buffer, pH 7.2. The concentrations of **6** and Bhc-glu (starting concentrations 100 μM) were determined by RP-HPLC. Solid lines are linear regression lines. **6**: $c/\mu m = -0.0049t/s + 99.65$ ($R^2 = 0.987$); Bhc-glu: $c/\mu m = -0.0037t/s + 99.74$ ($R^2 = 0.991$). c = concentrations of the caged compounds.

scopic visualization of the progress of cNMP photorelease from BCMACM-caged cNMPs within cells becomes possible, as demonstrated in Figure 5. The generation of 8-Br-cGMP

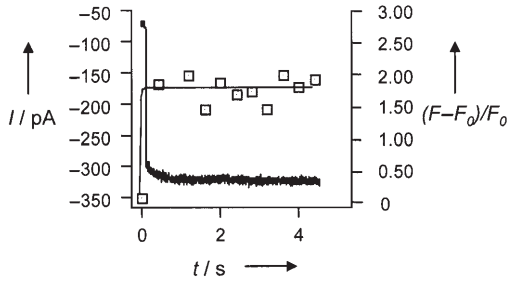

Figure 5. Monitoring the photorelease of 8-Br-cGMP from **6** within a CNGA3-transfected HEK293 cell by measuring the total whole-cell current and the fluorescence emitted from liberated **12** using excitation at 360 nm. The cell was loaded in the whole-cell configuration of the patch–clamp technique with 80 μM **6** and irradiated. The change in current amplitude and the fluorescence intensity increase (□) show photolytic liberation of 8-Br-cGMP.

from **6** in CNGA3-transfected HEK293 cells was monitored simultaneously by current recordings resulting from CNG-channel activation and by the fluorescence emitted from the liberated photoproduct **12** upon excitation at 360 nm. Since the fluorescence signal can be calibrated,[14] it is possible to quantify cNMP release from BCMACM esters of cNMPs using fluorescence spectroscopy. In addition to the high solubility of BCMACM-caged cNMPs in aqueous buffer, the possibility of visualizing and quantifying the release process within cells is a considerable advantage of BCMACM-caged cNMPs over the DEACM-caged analogues.

In conclusion, we have developed a photolabile coumarinylmethyl protecting group bearing a dianionic substituent and used this protecting group for the caging of cNMPs. The caged cNMPs exhibit high photosensitivities at long-wavelength irradiation and allow large and instantaneous cNMP concentration jumps upon one- and two-photon excitation within cells under physiological conditions. This approach can extend decisively the tools available for the study of space- and time-dependent aspects of cNMP-triggered processes. Finally, the novel protecting group should be useful in the caging and uncaging of other biomolecules with phosphate, carboxylate, and other functionalities. Exemplarily, the BCMACM ester of phenylacetic acid has already been prepared. The caged compound shows high solubility in aqueous buffer and can be photolyzed rapidly and efficiently ($\phi_{chem} = 0.02$, $\varepsilon^{max} = 20000$) in the visible-wavelength region.

Received: July 11, 2005
Revised: August 22, 2005
Published online: November 4, 2005

Keywords: ion channels · nucleotides · photoactivatable compounds · photolysis · signal transduction

[1] V. Hagen, K. Benndorf, U. B. Kaupp in *Dynamic Studies in Biology: Phototriggers, Photoswitches and Caged Biomolecules* (Eds.: M. Goeldner, R. S. Givens), Wiley-VCH, Weinheim, **2005**, pp. 155–178.
[2] T. Furuta, H. Takeuchi, M. Isozaki, Y. Takahashi, M. Kanehara, M. Sugimoto, T. Watanabe, K. Noguchi, T. M. Dore, T. Kurahashi, M. Iwamura, R. Y. Tsien, *ChemBioChem* **2004**, *5*, 1119–1128.
[3] V. Hagen, J. Bendig, S. Frings, T. Eckardt, S. Helm, D. Reuter, U. B. Kaupp, *Angew. Chem.* **2001**, *113*, 1078–1080; *Angew. Chem. Int. Ed.* **2001**, *40*, 1046–1048.
[4] V. Hagen, S. Frings, B. Wiesner, S. Helm, U. B. Kaupp, J. Bendig, *ChemBioChem* **2003**, *4*, 434–442.
[5] T. Furuta, M. Iwamura, R. Y. Tsien, *Methods Enzymol.* **1998**, *291*, 50–63.
[6] V. Hagen, J. Bendig, S. Frings, B. Wiesner, B. Schade, S. Helm, D. Lorenz, U. B. Kaupp, *J. Photochem. Photobiol. B* **1999**, *53*, 91–102.
[7] L. Wang, J. E. T. Corrie, J. F. Wootton, *J. Org. Chem.* **2002**, *67*, 3474–3478.
[8] J. Engels, E. J. Schlaeger, *J. Med. Chem.* **1977**, *20*, 907–911.
[9] J. Engels, *Bioorg. Chem.* **1979**, *8*, 9–16.
[10] R. Schmidt, D. Geißler, V. Hagen, J. Bendig, *J. Phys. Chem. A* **2005**, *109*, 5000–5004.
[11] B. Schade, V. Hagen, R. Schmidt, R. Herbrich, E. Krause, T. Eckardt, J. Bendig, *J. Org. Chem.* **1999**, *64*, 9109–9117.
[12] T. Furuta, S. S.-H. Wang, J. L. Dantzker, T. M. Dore, W. J. Bybee, E. M. Callaway, W. Denk, R. Y. Tsien, *Proc. Natl. Acad. Sci. USA* **1999**, *96*, 1193–1200.
[13] D. Geißler, Y. N. Antonenko, R. Schmidt, S. Keller, O. O. Krylova, B. Wiesner, J. Bendig, P. Pohl, V. Hagen, *Angew. Chem.* **2005**, *117*, 1219–1223; *Angew. Chem. Int. Ed.* **2005**, *44*, 1195–1198.
[14] V. Hagen, S. Frings, J. Bendig, D. Lorenz, B. Wiesner, U. B. Kaupp, *Angew. Chem.* **2002**, *114*, 3775–3777; *Angew. Chem. Int. Ed.* **2002**, *41*, 3625–3628.
[15] V. Nache, J. Kusch, V. Hagen, K. Benndorf, unpublished results.

 © 2005 Wiley-VCH Verlag GmbH & Co. KGaA, Weinheim

Nanoparticle Synthesis

DOI: 10.1002/anie.200501212

Molecular Encoding at the Nanoscale: From Complex Cubes to Bimetallic Oxides**

Sebastian Polarz, Andrey V. Orlov, Maurits W. E. van den Berg, and Matthias Driess*

Nanoparticles,[1,2] in particular those of semiconducting metal oxides like ZnO, have received increasing attention because of their high potential as components in nanotechnological devices. In general, materials containing more than one type of metal should display higher complexity and a wider range of properties.[3] So far only little attention has been paid to bi- or multimetallic oxide nanostructures, although a diverse spectrum of properties can be envisioned for such oxides.[4] Multimetallic oxides have been known in solid-state chemistry for a long time, but the high processing temperatures typically applied make them less suitable for the preparation of nanoscaled materials.[5] In addition, optimum dispersity of the two metals inside the nanostructures would play a pivotal role for the rational synthesis and adjustment of properties of those systems. Optimum dispersity is ensured when the respective elements are distributed on the molecular level.[6] In this respect, the use of molecular single-source precursors could potentially solve this problem by the creation of molecular building blocks suitable for bottom-up formation of oxides or other materials. Correlated to the molecular design of the precursor are low thermolysis temperatures resulting in reduced particle growth.[7] However, the preparation of a specific precursor resulting in a specific oxide is difficult,[8] especially if bi- or multimetallic oxide nanostructures are targeted.[4,9] Some examples for such single-source precursors exist already.[10–16] In most cases these heterometallic precursors are alkoxides and are thus very moisture sensitive.[17–19]

Our goal is to identify a new precursor system that enables access to a large variety of nanoscaled bimetallic oxides, and at the same time is readily available and stable. One particular type of bimetallic oxide of current interest is metal oxide semiconductors (for instance ZnO) doped with paramagnetic metal ions like Mn^{2+} and Ni^{2+}. Since such metal-doped oxides are expected to display considerable magnetoresistivity, they are promising materials for "spintronics".[20,21] Heterometallic precursors for this type of materials are currently unknown.

Herein, we report on the intriguing properties of molecular clusters having heterocubane architecture $[M^1_{4-y}M^2_y(LH)_4]^{4+}(OAc)_{4-x}(ClO_4)_x$ ($\cong [M^1_{4-y}M^2_yO_4]$; see Scheme 1) with a singly deprotonated dipyridyldiol (LH) as a chelating ligand, and their exploitation for the preparation of metal-doped transition-metal oxides. We show that 1) monometallic $[M_4O_4]$ clusters are single-source precursors for nanoscaled oxides; 2) any combination and permutation of bimetallic clusters $[M^1_{4-y}M^2_yO_4]$ containing the metals $M^{1,2}$ = Mn, Co, Ni, Zn are easily accessible; and 3) these bimetallic clusters can be used to prepare nanoscaled bimetallic oxides. The oxo clusters introduced here are the smallest possible molecular building blocks for the desired bimetallic oxide nanostructures (see Scheme 1).

1) Preparation of nanoscaled oxides from $[M_4O_4]$ precursors. In order to probe the capacity of the described clusters as reliable precursors, the thermolysis behavior of the different monometallic compounds $[M_4O_4]$ was studied by thermogravimetric analysis (TGA) and powder X-ray diffraction (PXRD). The data for the $[Zn_4O_4]$ cluster shown in Figure 1 are representative. Since phase-pure zinc oxide is obtained both under argon as well as under oxidative (20 vol% O_2) conditions as proven by PXRD, $[Zn_4O_4]$ is a suitable single-source precursor for ZnO. The presence of oxygen facilitates the complete removal of the organic ligands as proven by TG analysis. Apart from the fact that one can obtain nanocrystalline ZnO, it is also possible to control the size of the ZnO particles by heating the $[Zn_4O_4]$ precursor to a particular temperature T_d and maintaining this temperature for 3 h in order to oxidize off the organic shell. Under these conditions, the size of the ZnO particles (determined by the Scherrer equation) depends nearly linearly on the thermolysis temperature T_d (similar to the Ni–ZnO system shown below). Similar behavior was found for the alternative monometallic precursors with the difference that the oxidation state of the resulting materials may be sensitive to the presence of oxygen during thermolysis [Eq. (1a–d)]. Oxidizing conditions were selected for the preparation of bimetallic oxides.

$$Zn^{II}O \xleftarrow{ox.} [Zn_4O_4] \xrightarrow{inert} Zn^{II}O \quad (1a)$$

$$Co^{II}O \xleftarrow{ox.} [Co_4O_4] \xrightarrow{inert} Co^{II}O \quad (1b)$$

$$Mn^{III}_2O_3 \xleftarrow{ox.} [Mn_4O_4] \xrightarrow{inert} Mn^{II}O \quad (1c)$$

$$Ni^{II}O \xleftarrow{ox.} [Ni_4O_4] \xrightarrow{inert} Ni^0 \quad (1d)$$

2) Preparation of bimetallic heterocubanes $[M^1_{4-y}M^2_yO_4]$ as precursors. Instead of employing pure metal acetates in the synthesis of the single-metal clusters, we used mixtures of metal acetates in order to synthesize bimetallic heterocubanes, which were hitherto unknown (Scheme 1). In fact, we could prepare all possible combinations and permutations of the mixed bimetallic clusters $[M^1_{4-y}M^2_yO_4]$ ($M^{1,2}$ = Mn, Co, Ni, Zn; see Scheme 1) in single-crystalline form (see the Supporting Information). Because of the cationic character of the

[*] Dr. S. Polarz, A. V. Orlov, Prof. Dr. M. Driess
Institute of Chemistry
Technical University Berlin
Strasse des 17. Juni 135, 10623 Berlin (Germany)
Fax: (+49) 30-314-29732
E-mail: sebastian.polarz@tu-berlin.de
Dr. M. W. E. van den Berg
Department of Chemistry
Ruhr-University Bochum
Universitätsstrasse 150, 44780 Bochum (Germany)

[**] S.P. gratefully acknowledges funding from the DFG (Emmy-Noether program). We thank W. Grünert for valuable discussions.

Supporting information for this article is available on the WWW under http://www.angewandte.org or from the author.

InterScience
© 2005 Wiley-VCH Verlag GmbH & Co. KGaA, Weinheim

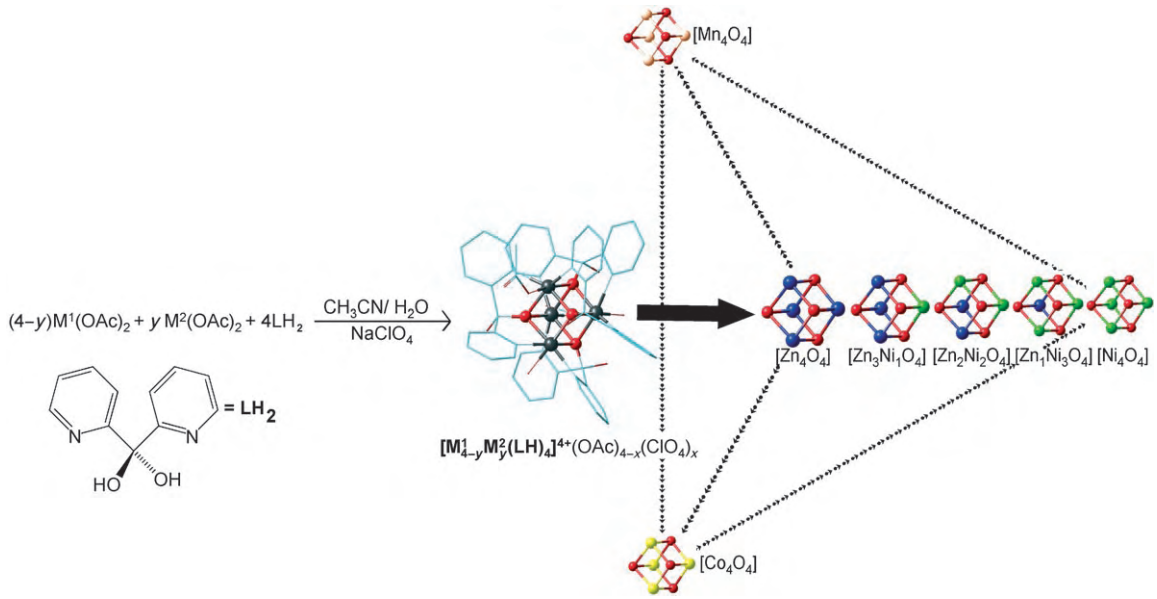

Scheme 1. Possible combinations and permutations of metals in bimetallic clusters. The chemical equation describes the general synthetic route to the heterometallic clusters. The central M_4O_4 motif is highlighted in the structural plot. (A structure determined by single-crystal X-ray analysis is shown in the Supporting Information.) The tetrahedron on the right outlines the possibilities for accessible precursor systems: monometallic clusters are located at the corners, bimetallic clusters along the edges, and trimetallic clusters (not shown) along the faces.

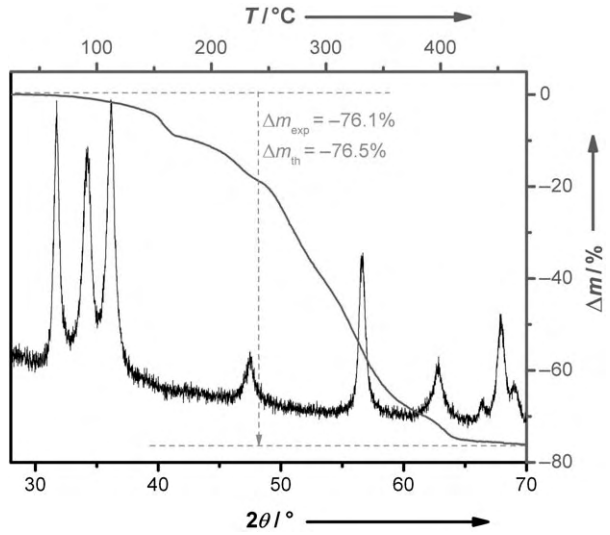

Figure 1. Powder X-ray diffraction pattern for the thermolyzed $[Zn_4O_4]$ cluster (black) and the thermogravimetric trace (gray) for its thermolysis. It is seen that the experimentally observed mass loss is very close to the theoretical mass loss for the transformation to ZnO.

oxo cluster core, the formation of the molecules can be followed by electrospray ionization mass spectrometry (ESI-MS). The spectra were recorded for acetonitrile solutions obtained from dissolving exactly one single crystal. ESI-MS gives a reliable picture of the true compositional distribution of the obtained clusters. The results are shown for the combinations Zn/Ni, Zn/Co, and Co/Ni as proof of principle (Figure 2). The most intensive signals in the spectra can be attributed to cluster ions of the type $[M^1_{4-y}M^2_y(LH)_2(L)_2]^{2+}$ (denoted as $[M^1_{4-y}M^2_yO_4]^{2+}$). Here, all counterions are solvent separated, but two dipyridyldiol functions in the cluster cations are additionally deprotonated, resulting in a net charge of +2. Signals related to singly charged species and complexes with different ratios of perchlorate to acetate were also seen in the spectra, but we focussed on the most intensive signal mentioned above. A broad signal centred around m/z 550 was observed (Figure 2a) when the synthesis mixture with the molar ratio of $Zn^{2+}/Ni^{2+} = 3:1$ was used. If one calculates the theoretical pattern expected for different cluster compositions, this signal is found to correspond to a superposition of several species. Deconvolution of the signal indicates that the solution contains roughly 73% $[Zn_3NiO_4]^{2+}$ as well as 22% $[Zn_4O_4]^{2+}$ and 5% $[Zn_2Ni_2O_4]^{2+}$. This is not surprising since the formation of clusters of different compositions is entropically favored. We also checked that there is no interchange equilibrium in solution. Pure $[Zn_4O_4]$ and pure $[Ni_4O_4]$ were dissolved together, and the ESI mass spectrum was recorded after two weeks. No formation of mixed clusters was found under these conditions. This and the fact that we used only one single crystal for each solution for ESI-MS measurement is clear proof that the bimetallic clusters are not an artifact but that they exist in solution as well as in the solid state.

Similarly, for the molar ratio $Zn^{2+}/Co^{2+} = 1:1$ (Figure 2b) not only the expected $[Zn_2Co_2]^{2+}$ but also the other permutations ($[Co_4O_4]^{2+}$, $[ZnCo_3O_4]^{2+}$, $[Zn_3CoO_4]^{2+}$) are observed in lower amounts as well. In principle all combinations of mixed-metal clusters ($M^{1,2}$ = Mn, Co, Ni, Zn) can be obtained. This is shown for the formation of mixed clusters starting from the molar ratio $Ni^{2+}/Co^{2+} = 1:1$ (Figure 2c). However, for addressing the mixed-metal clusters as precursors it would be even more desirable if one could obtain only one molecular species instead of a mixture of cluster compounds. To investigate this, the Zn/Ni system was chosen as a model

 © 2005 Wiley-VCH Verlag GmbH & Co. KGaA, Weinheim

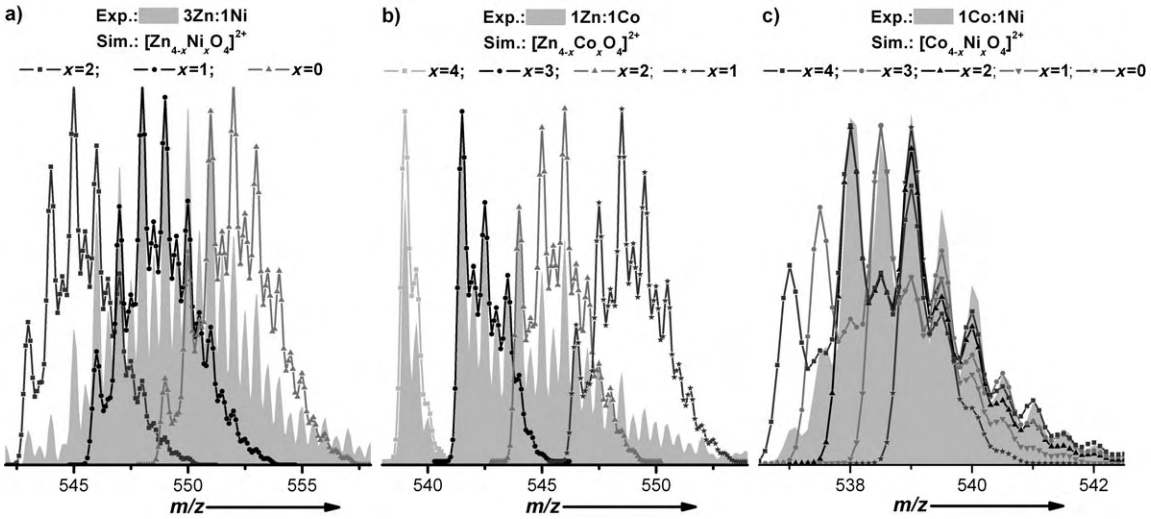

Figure 2. ESI mass spectra of mixed-metal clusters: a) Zn/Ni, b) Zn/Co, and c) Co/Ni. The light gray areas represent the measured spectra (Exp.), while the straight lines with symbols show the simulated patterns for a particular cluster composition (Sim.).

system. By changing the initial molar ratios of metal ions Zn^{2+}/Ni^{2+} from 3:1 to 1:1 (Figure 3a), the center of the cluster distribution can be moved towards clusters containing more Ni (cf. Figure 2a) but the width of the distribution is not affected.

Because the clusters are well soluble in acetonitrile as well as in water, we investigated whether the clusters of different compositions can be separated by chromatography. We performed HPLC on silica gel with a sodium acetate buffer as eluent. Indeed, fractions were collected with a narrower distribution of clusters (Figure 3b). The resulting pattern shows very good agreement with the pattern expected for a pure $[Zn_3NiO_4]^{2+}$ cluster (see Figure 2a).

3) Preparation of bimetallic oxide nanoparticles from mixed-metal clusters. The pure $[Zn_3NiO_4]$ compound obtained after chromatography was further used for the synthesis of oxidic materials. The formation of a nickel-doped zinc oxide is further complicated by the different coordination geometries (tetrahedral for Zn^{2+} in ZnO; octahedral for Ni^{2+} in NiO). Thermodynamically, this leads to a positive free mixing enthalpy. The formation of a spinell could be an alternative to the demixing, but spinells are not known for the Ni/Zn/O system. It is thus expected that for thermolysis of the $[Zn_3NiO_4]$ precursor demixing occurs resulting in a "zinc-saturated" NiO phase and a "nickel-saturated" ZnO phase. This is indeed the case as can seen from the XRD pattern of a sample where $[Zn_3NiO_4]$ had been decomposed at $T = 500\,^{\circ}C$ and tempered at this temperature for three hours (Figure 4a). The reflections can be attributed to $Ni_{0.7}Zn_{0.3}O$ (particle diameter $D_p = 44.1$ nm) and ZnO. The formation of the known $Ni_{0.7}Zn_{0.3}O$ phase is also very reasonable as Zn^{2+} can easily adopt octahedral coordination.

If, on the other hand, the precursor is thermolyzed at lower temperature, smaller particles result. It was already mentioned that under the described conditions the relationship between T_d and the particle size is practically linear (Figure 4c). Thus, particle size can be adjusted to a certain extent. Particles resulting from $T_d = 250\,^{\circ}C$ are only 10.1 nm

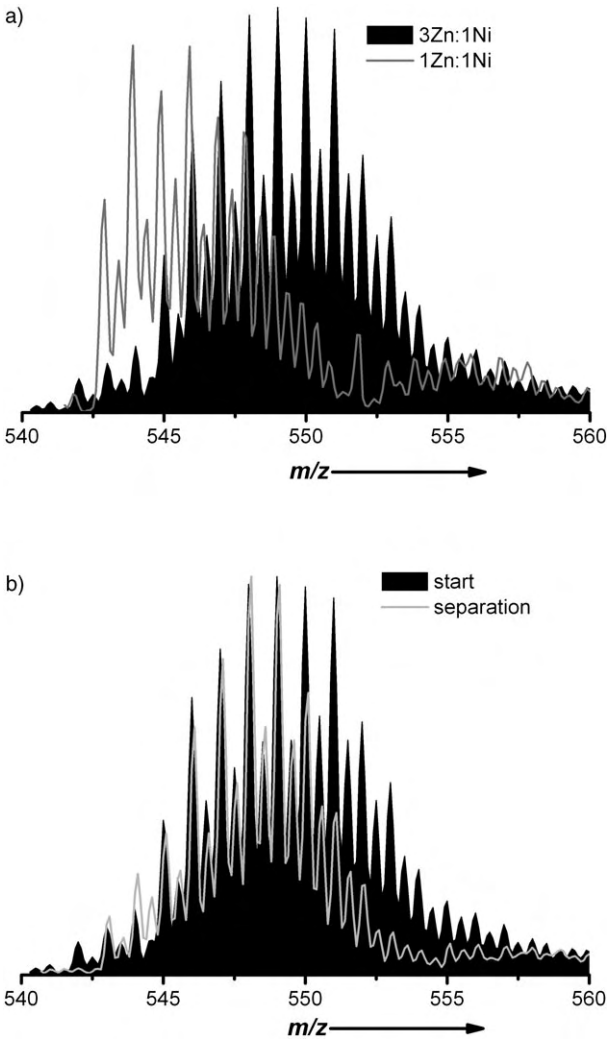

Figure 3. Change of the distribution of mixed Zn/Ni clusters from the initial distribution (black curve) a) upon adjustment of the initial ratio of metal acetates (gray line) and b) after chromatographic separation (gray line).

 © 2005 Wiley-VCH Verlag GmbH & Co. KGaA, Weinheim

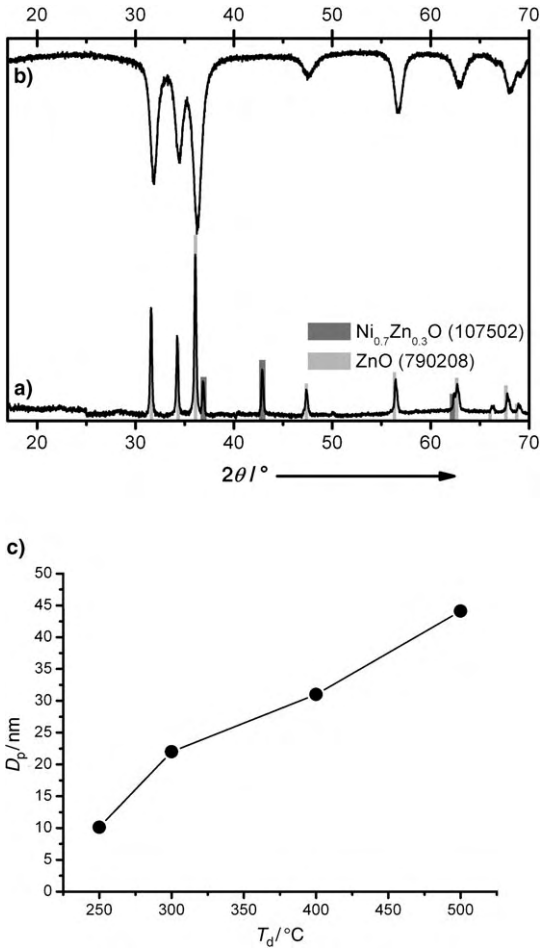

Figure 4. Powder X-ray diffraction patterns for material obtained by decomposition of $[Zn_3Ni]$ at a) $T_d = 500\,°C$ and b) $T_d = 250\,°C$. c) Dependence of particle size on decomposition temperature.

in size. Surprisingly, only the reflections of ZnO are found for the small particles, and a NiO phase is not detectable by X-ray diffraction (Figure 4b). EDX spectra (see the Supporting Information) recorded on agglomerates of such particles indicate that these particles contain $\approx 30\,\%$ nickel. However, it can not be excluded by EDX alone that the agglomerates do not contain particles of different composition. Nevertheless, TEM images indicate that these agglomerates are not amorphous and that the size of the constituent particles is very similar to that determined by means of X-ray scattering data (see SI2 in the Supporting Information). Therefore, it seems unlikely that an amorphous NiO phase, which would have been invisible in PXRD, is present in this material.

Another model which, at this point, can also not be excluded is that a thin NiO layer covers the ZnO nanoparticles. To consider this possibility in more detail, the local structures of the Zn and Ni centers were determined from K-edges (at 9659.0 and 8333.0 eV, respectively) by X-ray absorption spectroscopy (XAS) for the sample prepared at $T_d = 250\,°C$. Whereas from XRD results it is not possible to exclude small, amorphous NiO particles dispersed in ZnO, the XAS results indicate that the crystalline environment of Ni does not permit such an interpretation. The Ni–O distance fitted to the first feature in the Fourier transform of χ was found to be 2.07 Å, indicating a coordination number of Ni^{2+} of the order of 4. Furthermore, the Ni–Ni distance is clearly too small to be explained by the presence of a separate NiO phase (Figure 5). Small deviations in the Ni X-ray absorption

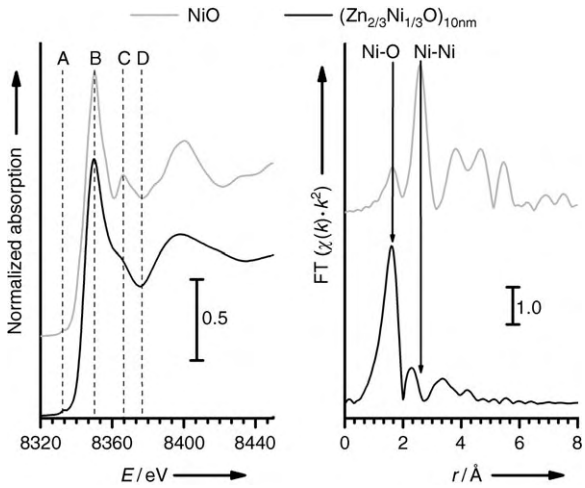

Figure 5. Ni K-edge XAS spectra of NiO and $[Zn_3NiO_4]$ ($T_d = 250\,°C$). Left: The XANES features A, B, C, and D. Right: The Fourier transform (not corrected for phase shifts).

near-edge spectrum (XANES) confirm this hypothesis. A NiO layer on top of the ZnO particles would have given a Ni–Ni distance close to the value expected for NiO. Therefore, we propose a model in which Ni^{2+} centers have replaced Zn^{2+} in the ZnO lattice. This assumption is further supported by modeling of the XAS data taking this model into account (see SI3 in the Supporting Information).

If one considers all the data together (the precursor architecture, the mild thermolysis conditions, TEM/EDX, PXRD, EXAFS), it appears that the molecular preorganization determined in $[Zn_3NiO_4]$ can lead to a Ni-doped ZnO but only for small particle sizes.

The findings reported here indicate that by forcing matter into the nanoscale, it is not only possible to manipulate the properties of ensembles of atoms (band gap) but also to alter the chemistry of individual atoms. It could be shown as soon as the particles are small enough, the chemical behavior of Ni^{2+} changes. It was possible to mix two species with each other that normally would segregate (demixing into ZnO and NiO).

The reason for this unusual behavior is presumably very simple. On the nanoscale, the total free energy of a system, ΔG_{tot}, is increasingly dependent on the free interface energy as particles become smaller, $dG \propto (\partial G/\partial A)\mathrm{d}A$, a relationship well established in colloid science. Thus, for the bulk (large particles) ΔG_{tot} is mainly determined by the free mixing energy, ΔG_{mix}, and free interface energy, ΔG_{if}, is negligible. However, the situation changes for the nanoscale: ΔG_{mix} and ΔG_{if} are antidromic in a certain sense. While a positive ΔG_{mix} results in demixing and thus the formation of two new particles, the formation of smaller particles from a larger one

 © 2005 Wiley-VCH Verlag GmbH & Co. KGaA, Weinheim

is countered by ΔG_{if}, which is always positive. Therefore, under conditions where transport of matter is restricted, as under the moderate thermolysis temperatures used here for the preparation of the small oxidic nanoparticles, free interface energy overcompensates the free demixing energy, and thus demixing does not occur. This, in turn, leads to the formation of particles with unusual fine structure, for example, the ZnO particles doped with high content of tetrahedral Ni^{2+} atoms. Because the "game" of pitting ΔG_{if} against ΔG_{mix} is so fundamental, it can certainly be applied to many other systems as well.

Received: April 6, 2005
Revised: September 5, 2005
Published online: November 21, 2005

Keywords: heterocubanes · metal acetates · nanoparticles · transition-metal oxides

[1] J. H. Fendler, F. C. Meldrum, *Adv. Mater.* **1995**, *7*, 607.
[2] C. N. R. Rao, G. U. Kulkarni, P. J. Thomas, P. P. Edwards, *Chem. Soc. Rev.* **2000**, *29*, 27.
[3] N. Toshima, T. Yonezawa, *New J. Chem.* **1998**, *22*, 1179.
[4] M. Niederberger, N. Pinna, J. Polleux, A. Antonietti, *Angew. Chem.* **2004**, *116*, 2320; *Angew. Chem. Int. Ed.* **2004**, *43*, 2270.
[5] M. Jansen, *Angew. Chem.* **2002**, *114*, 3896; *Angew. Chem. Int. Ed.* **2002**, *41*, 3746.
[6] N. Herron, D. L. Thorn, *Adv. Mater.* **1998**, *10*, 1173.
[7] V. Ischenko, S. Polarz, D. Grote, V. Stavarache, K. Fink, M. Driess, *Adv. Funct. Mater.* **2005**, DOI: 10.1002/adfm.200500087.
[8] S. L. Cumberland, K. M. Hanif, A. Javier, G. A. Khitrov, G. F. Strouse, S. M. Woessner, C. S. Yun, *Chem. Mater.* **2002**, *14*, 1576.
[9] M. Niederberger, G. Garnweitner, N. Pinna, M. Antonietti, *J. Am. Chem. Soc.* **2004**, *126*, 9120.
[10] S. Mathur, M. Veith, M. Haas, A. Shen, N. Lecerf, V. Huch, S. Hufner, R. Haberkorn, H. P. Beck, M. Jilavi, *J. Am. Ceram. Soc.* **2001**, *84*, 1921.
[11] J. F. Eichler, O. Just, W. S. Rees, *J. Mater. Chem.* **2004**, *14*, 3139.
[12] G. A. Seisenbaeva, E. V. Suslova, M. Kritikos, V. G. Kessler, L. Rapenne, M. Andrieux, F. Chassagneux, S. Parola, *J. Mater. Chem.* **2004**, *14*, 3150.
[13] S. Mathur, M. Veith, R. Rapalaviciute, H. Shen, G. F. Goya, W. L. Martins, T. S. Berquo, *Chem. Mater.* **2004**, *16*, 1906.
[14] J. H. Thurston, T. O. Ely, D. Trahan, K. H. Whitmire, *Chem. Mater.* **2003**, *15*, 4407.
[15] H. O. Davies, A. C. Jones, T. J. Leedham, P. O'Brien, A. J. P. White, D. J. Williams, *J. Mater. Chem.* **1998**, *8*, 2315.
[16] C. L. Carnes, P. N. Kapoor, K. J. Klabunde, J. Bonevich, *Chem. Mater.* **2002**, *14*, 2922.
[17] M. Veith, S. Mathur, C. Mathur, *Polyhedron* **1998**, *17*, 1005.
[18] L. G. Hubert-Pfalzgraf, *Coord. Chem. Rev.* **1998**, *180*, 967.
[19] L. G. Hubert-Pfalzgraf, *Inorg. Chem. Commun.* **2003**, *6*, 102.
[20] Y. Ohno, D. K. Young, B. Beschoten, F. Matsukura, H. Ohno, D. D. Awschalom, *Nature* **1999**, *402*, 790.
[21] P. Ball, *Nature* **2000**, *404*, 918.
[22] M.-L. Tong, S.-L. Zheng, J.-X. Tong, H. K. Lee, X.-M. Chen, *J. Chem. Soc. Dalton Trans.* **2002**, *124*, 1727.

 © 2005 Wiley-VCH Verlag GmbH & Co. KGaA, Weinheim

Surface Chemistry

DOI: 10.1002/anie.200502743

Addressing the Metal Centers of [2 × 2] Co^{II}_4 Grid-Type Complexes by STM/STS**

Mohammad Sahabul Alam, Stefan Strömsdörfer, Viacheslav Dremov, Paul Müller, Jens Kortus, Mario Ruben,* and Jean-Marie Lehn**

The adsorption of functional molecules on solid substrates is increasingly becoming an important aspect of nanoscience and sensing technology. Molecular and supramolecular electronics, understood as the integration of molecular structures to supplement specific functionalities on an integrated circuit chip, is a promising alternative approach for reducing both the feature size and the cost per functional unit. Driven by its characteristic control of the self-assembly process with nanometer accuracy, supramolecular chemistry has a deep impact on the realization of new concepts in molecular electronics. In particular, it plays a leading role in the future development of electronic devices at the solid-state/air interface; the intrinsic physical properties of supramolecular nanostructures can be screened in view of potential applications in nanotechnology.[1]

Recent progress in supramolecular coordination chemistry allows access to a broad variety of transition-metal complexes of grid-type architecture comprising two-dimensional arrays of metal ions interconnected by a set of organic

[*] MSc M. S. Alam, Dipl.-Phys. S. Strömsdörfer, Dr. V. Dremov, Prof. Dr. P. Müller
Physikalisches Institut III
Universität Erlangen-Nürnberg
Erwin-Rommel-Strasse 1, 91058 Erlangen (Germany)
Fax: (+49) 9131-15249
E-mail: phm@physik.uni-erlangen.de

Dr. M. Ruben
Institut für Nanotechnologie
Forschungszentrum Karlsruhe GmbH
76021 Karlsruhe(Germany)
Fax: (+49) 724-782-6434
E-mail: mario.ruben@int.fzk.de

Dr. J. Kortus
Institut de Physique et Chimie des Matériaux de Strasbourg
23, rue du Loess, BP 43, 67034 Strasbourg (France)
and
MPI for Solid-State Research
Heisenbergstrasse 1, 70569 Stuttgart (Germany)

Prof. Dr. J.-M. Lehn
ISIS
Université Louis Pasteur
8, Allée Gaspard Monge, BP 70028
67083 Strasbourg cedex (France)
Fax: (+33) 390-245-140
E-mail: lehn@isis.u-strasbg.fr

[**] This research was supported by the German Science Foundation through DFG-SFB 583 (P.M.) and the ESF-EUROCORES-SONS project "FunSMARTs" (M.R.). STM: scanning tunneling microscopy, STS: scanning tunneling spectroscopy

 WILEY InterScience DISCOVER SOMETHING GREAT © 2005 Wiley-VCH Verlag GmbH & Co. KGaA, Weinheim

ligands. They appear to be of particular interest as a basis for information storage functions, logic, sensing, and electrical switches.[2–5] Complexes of the $[n \times m]$ M^{II} type have been found to exhibit very interesting structural,[3] optical,[4] magnetic,[5] and, in particular the $[2 \times 2]$ Co^{II}_4 species, remarkable electronic properties.[6]

The synthesis and the structural characteristics of polypyridine-derived, multinuclear metal complexes of the $[2 \times 2]$ Co^{II} grid-type (Figure 1) have been reported earlier.[7] The

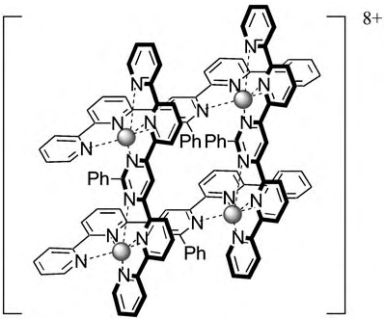

Figure 1. Representation of the $[Co^{II}_4L_4]^{8+}$ complex (L = 4,6-bis(2,2′-bipyrid-6-yl)-2-phenylpyrimidine). Each Co^{II} center is coordinated by six N donor atoms (dotted lines).[6,7]

central focus of the work presented here is to address two key challenges in the realization of composite solid-state molecule device architectures: the controlled deposition and organization of this class of molecules on solid surfaces and the addressing of individual subunits (here, metal centers) inside the $[2 \times 2]$ Co^{II} grid-type complex.

Experimentally, we applied scanning tunneling microscopy (STM) and scanning tunneling spectroscopy (STS) techniques to free-standing 1D and 2D ensembles as well as to single molecules of the $[2 \times 2]$ Co^{II}_4 type deposited onto highly oriented pyrolytic graphite (HOPG). STM studies of densely packed monolayers of $[Co^{II}_4L_4]^{8+}$ grid complexes on graphite have already been reported.[8,9] In order to study the specific features of the electronic properties at the single-molecule level, we concentrated our work on isolated, free-standing molecules. Related work on the investigation of specific functionalities of supramolecular nanostructures on surfaces was reviewed recently.[10,11]

Since the structural and electronic informations of STM measurements are strongly entwined,[12] the interpretation and analysis of the images of rather complex molecules is not straightforward. In addition, a pure topographical image of the van der Waals surface of $[2 \times 2]$ grid-like species would not be very useful as it would appear as a more or less featureless "blob" mapping the surface of a pile of more than 200 atoms. However, scanning tunneling spectroscopy (STS) measurements can provide direct information about the molecular energy levels, especially those close to the Fermi level. Functional units of atoms can be distinguished by selective mapping of certain energy regions, provided that their corresponding orbitals are well separated in energy. In general, such STS experiments are carried out under very rigorous conditions (metallic single crystals, ultrahigh-vacuum conditions with low temperatures) to minimize the coupling of the system with the environment.[13] However, it was also shown that under certain conditions room-temperature STM experiments could detect local changes in the electronic properties of molecules resulting, for example, from intramolecular acceptor–donor,[14a] intermolecular π–π,[14b] and charge-transfer interactions.[14c]

Using a homebuilt STM working under ambient conditions, we succeeded in combining high-resolution topography mapping with simultaneous measurement of current–voltage characteristics (STS) on single molecules deposited on HOPG surfaces. The electrical conductivity of molecules is not only of fundamental interest but is also of considerable significance in device applications.[15]

The investigated samples were prepared by depositing a drop of a solution of $[Co^{II}_4L_4]^{8+}$ molecules in acetonitrile (10^{-9} M). Different molecular arrangements of Co $[2 \times 2]$ grid complexes on the HOPG surface could be observed after repeated scanning under relatively mild tunneling conditions (Figure 2). At low coverage the grid complexes get trapped

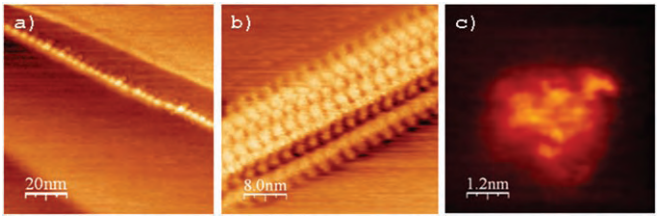

Figure 2. STM images of $[2 \times 2]$ Co^{II}_4 grid complexes deposited onto a HOPG surface. a) At low concentrations the $[Co^{II}_4L_4]^{8+}$ complexes are aligned along graphite steps into 1D chains (set point current 5 pA, set point voltage 100 mV). b) 2D crystal formed from $[Co^{II}_4L_4]^{8+}$ molecules along a graphite step (set point current 200 pA, set point voltage 100 mV). c) An isolated molecule with submolecular resolution (set point current 200 pA, set point voltage 500 mV).

along the step edges of HOPG, and it was possible to obtain continuous 1D chains several hundred nanometers in length (Figure 2a), as well as 2D arrays of densely packed grids (Figure 2b). The ordered 2D structures form spontaneously and start to grow from single nucleation points, which can be considered the 2D equivalent of a crystallization process. At very low coverage, a well-ordered distribution of isolated units is found, even at room temperature where thermal mobility becomes appreciable, which demonstrates the delicate adsorbate–substrate interactions in this system.[16]

In Figure 2c, we show a high-resolution STM image of a single $[2 \times 2]$ Co^{II}_4 complex. The image appears as a bright uniform spot with a cross-section of about 1.7 nm surrounded by a less defined halo, which can be caused by contributions from the BF_4 anions and solvent molecules, and corresponds to the molecular size extracted from single-crystal X-ray diffraction studies (1.65 nm).[7] Additionally, a quadratic set of slightly brighter spots can be observed on top of the structure anticipating the positions of the cornerstone metal ions. Besides these faint features, as expected, STM topography

 © 2005 Wiley-VCH Verlag GmbH & Co. KGaA, Weinheim

cannot provide any further information on the intramolecular structure.

In order to investigate the electronic properties of the deposited $[Co^{II}_4L_4]^{8+}$ molecules, we applied current imaging tunneling spectroscopy (CITS) techniques to the molecule–substrate system. CITS techniques have been developed for scanning tunneling spectroscopy (STS) of a sample surface and consist in the recording of current–voltage (I–V) characteristics at every pixel position of the topography map while maintaining a constant tip to surface distance.[17–19] The I–V data set can be sorted such that it provides both a height (topography) map, taken at constant current, and several tens of current (CITS) maps, taken at constant voltage. The current contrast changes significantly when at certain bias voltages new molecular energy levels come into play. Although this technique has been applied successfully to semiconductor materials, its application to organic molecules is rather difficult because of mobility or instability of the molecules, drift, etc.[20] Nevertheless, if there would be energy regions where the molecular levels result exclusively from some functional subgroups of atoms, a selective screening of parts of the molecule would be possible.

We successfully applied CITS techniques to the [2 × 2] Co^{II}_4 grid-type complex. We confined our investigations to negative sample-to-tip bias voltages, that is, to the spectroscopy of occupied levels. Figure 3a shows a constant current topography imaging. Figure 3b shows the current map taken at a bias of −0.942 V in the same scan. The tunneling resistance was set to 1 GΩ. Thereby, the topographic image presents a rather featureless structure with a diameter of approximately 1.7 nm, while the CITS current map reveals a quadratic array of four bright spots representing sharp peaks of the tunneling current. In Figure 3c the set of I–V characteristics measured at 32 equidistant positions along a line between the two arrows in Figure 3b is shown. The background current arising from the graphite surface was subtracted. Two ridges are revealed which are approximately 0.7 nm apart. This is in accord to the distance between two neighboring Co ions.[7]

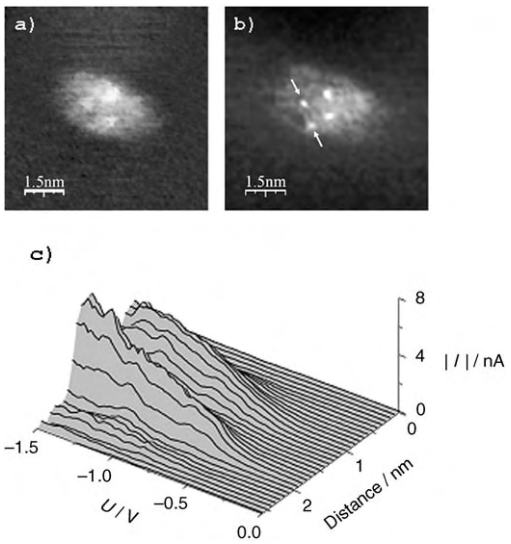

Figure 3. a) Topographic map of a [2 × 2] Co^{II}_4 grid. b) Simultaneously recorded current (CITS) image, taken at a voltage of −0.942 V. A quadratic array of bright spots can be detected with a spot-to-spot distance of approximately 0.7 nm. c) Representation of a set of I–V characteristics measured at positions between the two arrows in Figure 3b.

Since all distances between the peaks in the CITS pictures correspond to the Co–Co distances in the molecule, we conclude that we have mapped local maxima of the density of states situated at the positions of the Co ions. We note that in spite of the high resolution of the images no features arising from the bis(bipyridyl)pyrimidine ligands were observed. This can be expected because the electronic states of the ligands are located far from the Fermi level E_F.[19,21–24] As a consequence, these states do not play a significant role in the tunneling current at bias voltages down to −1.5 V. This is further confirmed by DFT calculations (vide infra).

Coming back to Figure 3c, we note that below a threshold of approximately −0.6 V the tunneling current at the positions of the bright spots increases drastically. This can be clearly seen in the set of 3D current maps presented in Figure 4.

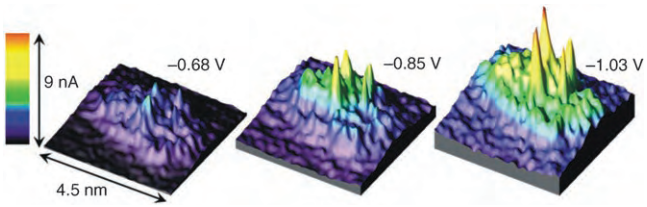

Figure 4. Set of 3D current images representing the central part of Figure 3b at different tunnel biases.

The DFT calculations show that the highest occupied molecular orbitals (HOMO) are build from Co d states. The energy gap between the highest occupied and the lowest unoccupied molecular orbital (LUMO) obtained from these calculations is 0.53 eV. The eightfold positively charged grid molecule is highly electronegative. Therefore it seems plausible that the Fermi level will be pinned at the energy position of the LUMO. This would explain the strong increase in tunneling current around −0.6 eV observed experimentally, because tunneling from the HOMO starts at this energy. In the following, all energies are given with respect to the Fermi level. The first three occupied orbitals are quasi degenerate in energy being separated in energy by only a few meV, followed by states at −0.55 and −0.60 eV and sets of states around −0.62 and −0.67 eV. Below −0.7 eV there is an energy gap of about 0.3 eV until the remaining states which exhibit d character are found around −1 eV. As evidenced by Figure 5a, all these states are localized near the position of the Co atoms. Figure 5a shows a superposition of the crystal structure, the above-mentioned orbitals in an energy window between the Fermi level and −0.7 eV (in red), and a color-coded contour plot of the electron density corresponding to these orbitals at a plane parallel to the Co atoms at a distance

 © 2005 Wiley-VCH Verlag GmbH & Co. KGaA, Weinheim

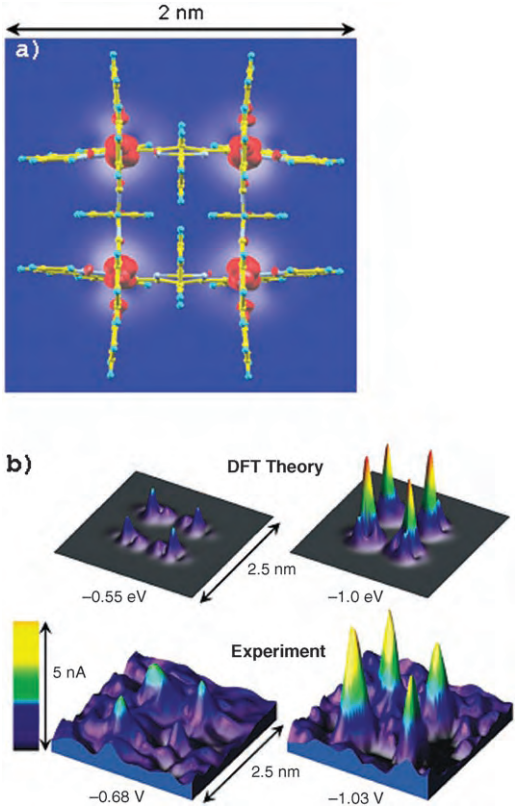

Figure 5. a) DFT calculation of occupied orbitals within an energy window between E_F and −0.7 eV and the electron density map in superposition with the crystal structure data. b) 3D representation of DFT-calculated electron density maps within an energy window between E_F and −0.55 eV and between E_F and −1 eV (upper row). Lower row: Central section of the measured CITS maps of Figure 4.

of 7 Å (white halo around the orbitals). A 3D representation of the electron density maps is repeated in Figure 5b, upper row, using the same coloring scheme as the experimental data. Two energy windows are shown: The first one covers the range between E_F and the HOMO (−0.55 eV), while the second one covers the full range between E_F and all states exhibiting 3d character (−1 eV). Considering that DFT usually underestimates band gaps, the HOMO–LUMO gap seems to be underestimated by 150 meV compared to experiment. If one assumes the validity of the Tersoff–Hamann approximation, the theoretical distribution at −0.55 eV should then conform to the map of tunneling currents at a bias of −0.7 eV, etc. The lower row of Figure 5b shows the central part of the CITS current maps of Figure 4 with subtracted background. The accordance with the electron density maps from the DFT calculation is striking. Of course, the DFT calculations do not include possible interactions between molecule and substrate. This might account for some of the discrepancies between theory and measurements.

Intuitively, one would assume that the weakest bonds, in other words, the supramolecular coordination interactions, should dominate the molecular orbitals near the Fermi level of the molecule. A comparison of our measurements with the DFT calculations confirms clearly this assumption. Thus, STS spectroscopy directly addresses the metal centers in a rather complex (supra)molecular entity. If this explanation can be applied also to other supramolecular species with metal centers, our method would allow a selective mapping of the functional units within the supramolecular architecture, even if these units are embedded into a complex set of organic ligands.

In conclusion, [2 × 2] Co^{II}_4 grid-type complexes on HOPG substrates were imaged using STM with submolecular resolution. At very low coverage, the molecules were shown to align preferably with the step edges of the HOPG surface. The size of the molecules observed is in agreement with the data determined by X-ray crystallography. STS measurements at room temperature allowed us to address directly the metal centers of the supramolecular architectures at the expected locations and in agreement with DFT calculations. It is to be expected that single-molecule spectroscopic techniques such as CITS, together with break junction techniques[25] or spin-polarized STM,[26] might constitute a significant part of the future tool kit needed for achieving the directed construction and controlled manipulation of fully electronically functional molecular designs.

Experimental Section

STM measurements: All measurements were carried out with a homebuilt low-drift STM head equipped with commercially available low-current-control electronics (RHK technology) under ambient conditions. For high-resolution STM studies a HOPG substrate was freshly cleaved. Afterwards, the substrate was imaged by STM to characterize the tip resolution. We calibrated distances in the STM images by observing atomic spacing on highly oriented pyrolytic graphite (HOPG). After imaging the graphite surface successfully, we deposited a droplet of a solution of the molecule under study and let the droplet run down the graphite surface. Concentrations were around 10^{-9} M. Typically for the STM measurements, tunneling currents between 5 and 200 pA were employed. The bias voltage was between ±50 and ±500 mV. The scan frequency was varied between 2 and 5 Hz. Resolution was 256 × 256 points for topography, and 128 × 128 in the STS measurements. In STS mode, current–voltage (*I–V*) curves were recorded simultaneously with a constant-current STM image with the interrupted-feedback loop technique. The scan range of voltages was typically from −1.5 to 0.1 V relative to the tip potential. Typically, tunneling resistances of the order of 1 GΩ were set. We used mechanically cut Pt–Ir (90:10) tips from wires with a diameter of 0.25 mm. Figures 2, 3a, b, 4, and 5 were produced using the program WSxM (Nanotec Electrónica, Madrid). The molecule $[Co^{II}_4L_4](BF_4)_8$ was synthesized as described previously.[7]

DFT calculations: The first-principles density functional theory (DFT) calculations have been carried out using the Naval Research Laboratory Molecular Orbital Library (NRLMOL) program package, which is an all-electron implementation of DFT. NRLMOL combines large Gaussian orbital basis sets, numerically precise variational integration, and an analytic solution of Poisson's equation in order to accurately determine the self-consistent potentials, secular matrix, total energies, and Hellmann–Feynman–Pulay forces.[27] Starting from the X-ray structure, we generated an isolated single Co [2 × 2] grid molecule without counterions for the calculation. This resulted in a cluster of 228 atoms used for the DFT calculation. To reduce the numerical cost we used a D_2 symmetry found in the isolated cluster. The basis set for each Co contained 11 s-like, 5 p-like, and 4 d-like contracted Gaussian orbitals with 20 exponents ranging from 0.048 to 4.2×10^6. Nitrogen and carbon had the same number of contracted orbitals (8 s, 4 p, and 3 d), with 13 bare Gaussians between 0.094 and 5.17×10^4 for N and 12 bare Gaussians between 0.077 and

 © 2005 Wiley-VCH Verlag GmbH & Co. KGaA, Weinheim

2.22×10^4 for C. Finally, hydrogen had 6 s-like, 3 p-like, and 1 d-like orbital with six exponents between 0.074 and 77.84. For all orbitals not corresponding to an atomic orbital we used the longest ranged single Gaussians. This basis set resulted in a total number of 3372 orbitals for each symmetry representation of the complete cluster. The calculations have been carried out for the charged 8+ state using the generalized gradient approximation of Perdew, Burke, and Ernzerhof[28] to the exchange and correlation functional. The self-consistent charge density was obtained from a spin-polarized calculation with antiferromagnetic order of the Co ions on a dense real-space grid. The figure corresponds to a cut plane parallel to the Co atoms at a distance of 7 Å.

Received: August 4, 2005
Published online: November 28, 2005

Keywords: density functional calculations · scanning probe microscopy · self-assembly · supramolecular chemistry · surface chemistry

[1] a) J.-M. Lehn, *Supramolecular Chemistry. Concepts and Perspectives*, VHC, Weinheim, **1995**, chap. 9 and p. 200; b) J.-M. Lehn, *Science* **2002**, *295*, 2400; J.-M. Lehn, *Proc. Natl. Acad. Sci. USA* **2002**, *99*, 4763.
[2] M. Ruben, J. Rojo, F. J. Romero-Salguero, L. H. Uppadine, J.-M. Lehn, *Angew. Chem.* **2004**, *116*, 3728; *Angew. Chem. Int. Ed.* **2004**, *43*, 3644; M. Ruben, *Angew. Chem.* **2005**, *117*, 1620; *Angew. Chem. Int. Ed.* **2005**, *44*, 1594.
[3] Structural properties: P. N. W. Baxter, J.-M. Lehn, J. Fischer, M.-T. Youinou, *Angew. Chem.* **1994**, *106*, 2432; *Angew. Chem. Int. Ed. Engl.* **1994**, *33*, 2284; P. N. W. Baxter, J.-M. Lehn, G. Baum, D. Fenske, *Angew. Chem.* **1997**, *109*, 2067; *Angew. Chem. Int. Ed. Engl.* **1997**, *36*, 1978; M. Barbiou, J.-M. Lehn, *J. Am. Chem. Soc.* **2003**, *125*, 10257.
[4] Optical properties: M. Ruben, J.-M. Lehn, G. Vaughan, *Chem. Commun.* **2003**, 1338.
[5] Magnetic properties: O. Waldmann, J. Hassmann, P. Müller, G. S. Hanan, D. Volkmer, U. S. Schubert, J.-M. Lehn, *Phys. Rev. Lett.* **1997**, *78*, 3390; E. Breuning, M. Ruben, J.-M. Lehn, F. Renz, Y. Garcia, V. Ksenofontov, P. Gütlich, E. Wegelius, K. Rissanen, *Angew. Chem.* **2000**, *112*, 2563; *Angew. Chem. Int. Ed.* **2000**, *39*, 2504; M. Ruben, E. Breuning, J.-M. Lehn, V. Ksenofontov, F. Renz, P. Gütlich, G. Vaughan, *Chem. Eur. J.* **2003**, *9*, 4422; M. Ruben, U. Ziener, J.-M. Lehn, V. Ksenofontov, P. Gütlich, G. B. M. Vaughan, *Chem. Eur. J.* **2005**, *11*, 94.
[6] Electronic properties: a) M. Ruben, E. Breuning, J.-P. Gisselbrecht, J.-M. Lehn, *Angew. Chem.* **2000**, *112*, 4312; *Angew. Chem. Int. Ed.* **2000**, *39*, 4139; b) M. Ruben, E. Breuning, M. Barboiu, J.-P. Gisselbrecht, J.-M. Lehn, *Chem. Eur. J.* **2003**, *9*, 291; D. M. Bassani, J.-M. Lehn, S. Serroni, F. Puntoriero, S. Campagna, *Chem. Eur. J.* **2003**, *9*, 5936.
[7] J. Rojo, F. J. Romero-Salguero, J.-M. Lehn, G. Baum, D. Fenske, *Eur. J. Inorg. Chem.* **1999**, 1421.
[8] A. Semenov, J. P. Spatz, J.-M. Lehn, C. H. Weidl, U. S. Schubert, M. Möller, *Appl. Surf. Sci.* **1999**, *144–145*, 456; A. Semenov, J. P. Spatz, M. Möller, J.-M. Lehn, B. Sell, D. Schubert, C. H. Weidl, U. S. Schubert, *Angew. Chem.* **1999**, *111*, 2701; *Angew. Chem. Int. Ed.* **1999**, *38*, 2547.
[9] U. Ziener, J.-M. Lehn, A. Mourran, M. Möller, *Chem. Eur. J.* **2002**, *8*, 951.
[10] S. De Feyter, F. C. De Schryver, *Chem. Soc. Rev.* **2003**, *32*,139.
[11] P. Samorí, *Chem. Soc. Rev.* **2005**, *34*, 551.
[12] Ó. Paz, I. Brihuega, J. M. Gómez-Rodríguez, J. M. Soler, *Phys. Rev. Lett.* **2005**, *94*, 056103.
[13] a) W. Ho, *J. Chem. Phys.* **2002**, *117*, 11033; b) P. Wahl, L. Diekhöner, M. A. Schneider, L. Vitali, G. Wittich, K. Kern, *Phys. Rev. Lett.* **2004**, *93*, 176603.
[14] a) A. Miura, Z. Chen, H. Uji-i, S. De Feyter, M. Sdanowska, P. Jonkhejm, A. P. H. J. Schenning, B. Mejer, F. Würthner, F. C. De Schryver, *J. Am. Chem. Soc.* **2003**, *125*, 14968; b) A. Gesquiere, S. De Feyter, F. C. De Schryver, *Nano Lett.* **2001**, *1*, 201; c) F. Jäckel, M. D. Watson, K. Müllen, J. P. Rabe, *Phys. Rev. Lett.* **2004**, *92*, 188303.
[15] S. Datta, W. Tian, S. Hong, R. Reifenberger, J. I. Henderson, C. P. Kubiak, *Phys. Rev. Lett.* **1997**, *79*, 2530; R. E. Palmer, Q. Guo, *Phys. Chem. Chem. Phys.* **2002**, *4*, 4275.
[16] J. V. Barth, J. Weckesser, C. Cai, P. Günter, L. Bürgi, O. Jeandupeux, K. Kern, *Angew. Chem.* **2000**, *112*, 1285; *Angew. Chem. Int. Ed.* **2000**, *39*, 1230.
[17] R. J. Hamers, R. M. Tromp, J. E. Demuth, *Phys. Rev. Lett.* **1986**, *56*, 1974.
[18] S. Novokmet, M. S. Alam, V. Dremov, F. W. Heinemann, P. Müller, R. Alsfasser, *Angew. Chem.* **2005**, *117*, 813; *Angew. Chem. Int. Ed.* **2005**, *44*, 803.
[19] A. M. Ako, H. Maid, S. Sperner, S. H. H. Zaidi R. W. Saalfrank, M. S. Alam, P. Müller, F. W. Heinemann, *Supramol. Chem.* **2005**, *17*, 315.
[20] M. Rivera, R. L. Williamson, M. J. Miles, *J. Vac. Sci. Technol. B* **1996**, *14*, 1472.
[21] Z. Klusek, W. Kozlowski, *J. Electr. Spect. Relt. Phenom.* **2000**, *107*, 63.
[22] D. P. E. Smith, *J. Vac. Sci. Technol. B* **1991**, *9*, 1119.
[23] H. Nejoh, *Appl. Phys. Lett.* **1990**, *57*, 2907.
[24] M. Shigeno, M. Ohmi, M. Suginoya, W. Mizutani, *Mol. Cryst. Liq. Cryst.* **1991**, *199*, 141.
[25] M. A. Reed, C. Zhou, C. J. Muller, T. P. Burgin, J. M. Tour, *Science* **1997**, *278*, 252.
[26] M. Bode, *Rep. Prog. Phys.* **2003**, *66*, 523; A. R. Smith, R. Yang, W. R. L. Lambrecht, A. Dick, J. Neugebauer, *Surf. Sci.* **2004**, *561*, 154.
[27] M. R. Pederson, K. A. Jackson, *Phys. Rev. B* **1990**, *41*, 7453; K. A. Jackson, M. R. Pederson, *Phys. Rev. B* **1990**, *42*, 3276; D. V. Porezag, M. R. Pederson, *Phys. Rev. A* **1999**, *60*, 2840; M. R. Pederson, D. V. Porezag, J. Kortus, D. C. Patton, *Phys. Status Solidi B* **2000**, *217*, 197.
[28] J. P. Perdew, K. Burke, M. Ernzerhof, *Phys. Rev. Lett.* **1996**, *77*, 3865.

 © 2005 Wiley-VCH Verlag GmbH & Co. KGaA, Weinheim

Reaction Mechanisms

DOI: 10.1002/anie.200501642

The Photochemistry of *o*-Nitrobenzaldehyde as Seen by Femtosecond Vibrational Spectroscopy**

*Stefan Laimgruber, Wolfgang J. Schreier, Tobias Schrader, Florian Koller, Wolfgang Zinth, and Peter Gilch**

Owing to their rich photochemistry, aromatic nitro compounds find applications wherever temporal and spatial control of chemical and biological activity is desired. The production of DNA chips relies on such compounds as photolabile protecting groups.[1] Composites of aromatic nitro compounds and bioactive molecules are used in experiments on photoactivatable ("caged") compounds.[2] Mechanistic studies of these reactions point to an initial hydrogen transfer from a residue situated in *ortho* position to the nitro group.[3] Secondary processes at the residue then lead to a bond fission which releases the molecule of interest. In the present study we supply firm experimental data on the mechanism of one of these reactions, the photochemical transformation of *o*-nitrobenzaldehyde (NBA) to *o*-nitrosobenzoic acid or the corresponding ester.

This intramolecular redox reaction first described by Ciamician and Silber in 1901[4] proceeds with a quantum yield of 50% nearly irrespective of the solvent properties.[5] It has been addressed twice by time-resolved techniques. In 1980 George and Scaiano[5] used laser flash photolysis with a time resolution of some nanoseconds and found transients with solvent-dependent lifetimes ranging from 50 ns to $\lesssim$ 1 ns. They associated these transients with the triplet state of NBA. A pump–probe experiment with a time resolution of 35 ps reported by Yip and Sharma[6] in 1989 revealed a transient with a lifetime of 74 ps for NBA in aqueous acetonitrile. Based on the strong solvent dependence and the observed spectroscopic signature, they argued that the transient should be assigned to a ketene intermediate and not to a triplet state. We here re-address this reaction with modern femtosecond (vibrational) spectroscopy. Thereby, we not only profit from an improved time resolution but also use the distinct features of vibrational spectroscopy to identify intermediates. Based on these results we will give clear-cut evidence for the involvement of the ketene intermediate and describe its formation dynamics and its transformation into further intermediates.

In the present experiments solutions of NBA were excited with laser pulses of 100–200 fs centered at a wavelength of approximately 260 nm, whereby the photoreaction is initiated. The spectral changes induced by this excitation were probed by three detection schemes: transient Vis absorption, transient IR, and (stimulated) Raman spectroscopy. The particulars of the IR experiment can be found in reference [7], the other techniques use well-known principles.[8–10] Details will be presented in a forthcoming publication. Since in alcoholic solution NBA is transformed into the respective hemiacetals on the timescale of a few hours,[11] sample solutions were always freshly prepared immediately before the measurements.

Transient Vis spectroscopy is best suited to study the kinetics of the process. Optical excitation of NBA results in an induced absorption centered around 500 nm which rises within the instrumental response time ($\approx$200 fs). This absorption evolves on multiple timescales (Figure 1a). A global analysis of the data affords three kinetic components with time constants of 0.4 ps (± 20%), 90 ps (± 30%), and 3 ns$^{+65\%}_{-35\%}$. Adding water reduces the second time constant, which goes down to 13 ps for ethanol/water 1:1 (v/v) (Figure 1b). The other time constants are virtually unaffected. As optical excitation results in the population of an excited singlet state, the 0.4-ps component must be associated

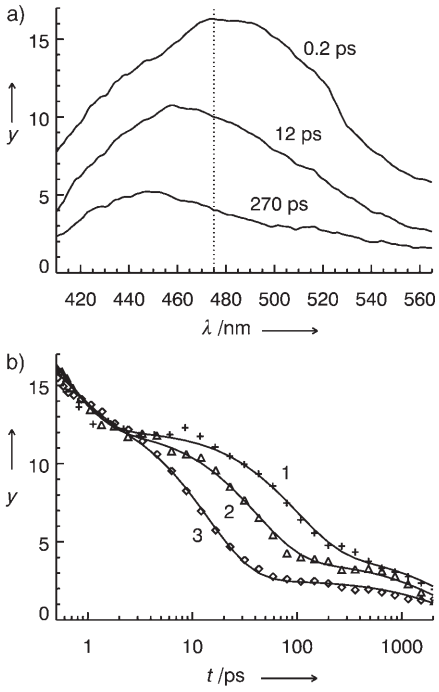

Figure 1. Femtosecond transient Vis spectroscopy of the photorearrangement of NBA following excitation at 258 nm. y: Difference absorbance ΔA in mOD (milliunits of optical density). a) Transient spectra recorded at characteristic times after photoexcitation. The dotted line marks the wavelength for the time traces in (b). b) Dependence of the absorption time trace at 475 nm on the water content of the solvent (1: 0%, 2: 10%, and 3: 50 vol.% water in ethanol). Note the logarithmic time axis.

[*] Dipl.-Phys. S. Laimgruber, Dipl.-Phys. W. J. Schreier, Dipl.-Phys. T. Schrader, Dipl.-Phys. F. Koller, Prof. Dr. W. Zinth, Priv.-Doz. Dr. P. Gilch
Department für Physik
Ludwig-Maximilians-Universität
Oettingenstrasse 67, 80538 München (Germany)
Fax: (+49) 892-180-9202
E-mail: Peter.Gilch@physik.uni-muenchen.de

[**] Financial support by the Deutsche Forschungsgemeinschaft (Project Zi277/11-1) is gratefully acknowledged. We thank Prof. Richard R. Schmidt for pointing out the possibility of an intramolecular reaction of the ketene.

 © 2005 Wiley-VCH Verlag GmbH & Co. KGaA, Weinheim

with the depletion of the excited state. The spectral signature of the 90-ps (in ethanol) component resembles that reported for a ketene intermediate (structure given in Scheme 1) obtained by matrix isolation spectroscopy.[12] This similarity and the water dependence suggest that the first intermediate is a ketene. However, as inspection of Figure 1a shows, the absorption signatures are not that discriminative, and intermediates that might respond to the water content are numerous.

Transient IR spectroscopy may deliver clear-cut evidence for the presence of a ketene intermediate. Ketenes feature a strong and very characteristic IR resonance centered around 2100 cm^{-1},[13] which is due to the stretching vibration of the ketene group. Matrix isolation spectroscopy of the ketene form of NBA delivers a resonance peaking at 2118 cm^{-1} for this vibration.[12] Upon 267-nm excitation of NBA a transient IR signal in the 2100-cm^{-1} range is observed (Figure 2). A

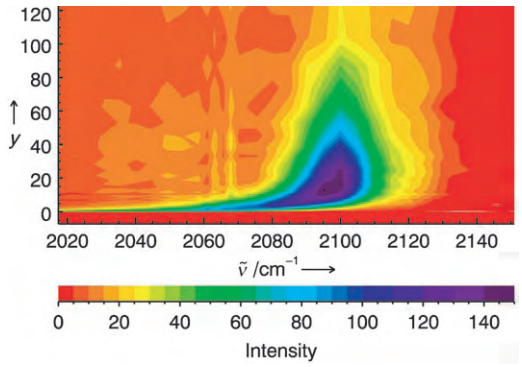

Figure 2. Contour representation of transient IR absorption of NBA in ethanol after excitation with 267-nm laser pulses. *y*: Delay time *t* in ps.

transient IR band rises rapidly within ≈400 fs. Immediately after its appearance the band peaks at 2040 cm^{-1} and then experiences a frequency up-shift to 2100 cm^{-1} proceeding with a characteristic time of ≈10 ps. Following that shift the signal decays with a time constant of 60 ps (± 20%), which is close to the time constant of 90 ps (± 30%) derived from the Vis experiment. Thus, in the course of the photorearrangement of NBA the ketene intermediate is formed within 0.4 ps. A frequency shift of an IR resonance is a marker for vibrational excitation (see, for example, reference [7]). The relaxation of this shift thus represents the vibrational cooling of the nascent ketene intermediate.

The ketene then reacts with a time constant of 60–90 ps. The presence of a further kinetic component in the Vis experiments (3 ns) indicates that the product of this reaction is *not* the final nitroso form but a second intermediate. The strong solvent dependence of the ketene lifetime (Figure 1b and reference [6]) could be interpreted as a signature for a reaction of the solvent and the ketene. The product of such a reaction could be a solvent adduct. Several tautomeric forms of this adduct are conceivable (referred to as **A**–**C** in Scheme 1). One suggested form, an enol tautomer (**A**),[5] would result from a formal addition of an ethanol to the C=O bond of the ketene. From a formal addition to the C=C bond (at least) two potential adduct forms may result (tautomers **B** and **C**). The solvent could also act catalytically promoting an intramolecular addition to the ketene function. The intramolecular reaction could also proceed by means of a C=C or a C=O addition. One potential product of a C=C addition is the lactone **D**. The IR experiments give a first indication for an addition to the C=C bond: In the spectral region of carbonyl stretching vibrations around 1700 cm^{-1} we observe the rise of an IR band (data not shown) concomitant with the decay of ketene. The second intermediate thus seems to bear a carbonyl group as contained in the ester function of the forms **B**, **C**, and **D**. A nonambiguous distinction between these forms based on the present IR data alone is not possible. Further information might be supplied by Raman spectroscopy.

Femtosecond stimulated Raman spectroscopy allows the recording of transient and stationary Raman spectra with a tremendous improvement in signal-to-noise ratio over that of conventional Raman spectroscopy.[8–10] The stationary stimulated Raman spectrum of the NBA sample is depicted in Figure 3, upper part. In these experiments the Raman pump

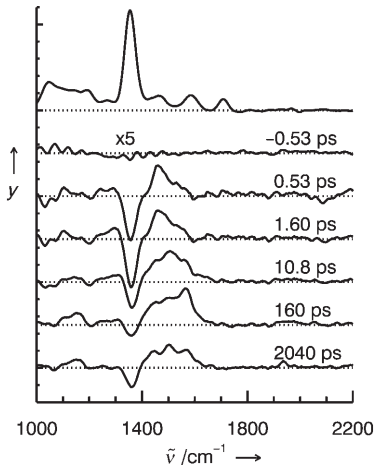

Figure 3. Steady-state and time-resolved stimulated Raman spectra of NBA in ethanol. *y*: Raman intensity *I* and change in Raman intensity Δ*I*. The uppermost trace is the spectrum of NBA (with the solvent contribution subtracted). The traces below are difference Raman spectra at the delay times given in the figure.

pulse had a wavelength of 388 nm, thereby fulfilling a (pre-) resonance condition for NBA and its products. The Raman spectrum of NBA is dominated by a strong peak at 1360 cm^{-1} due to the symmetric stretching vibration of the nitro group.[14] Upon photoexcitation at 260 nm this band experiences bleaching and adjacent to it new Raman resonances emerge (Figure 3, lower part). The bleaching is caused by the decrease of the concentration of ground-state NBA due to the photoexcitation. In the course of the reaction it partially recovers since the quantum yield of the reaction is only 50%

 © 2005 Wiley-VCH Verlag GmbH & Co. KGaA, Weinheim

(see above). The emerging new bands are Raman resonances of intermediates. Strong resonances can be found between 1400 and 1700 cm^{-1}—a range characteristic for C=C and C=N stretching vibrations.[14]

To extract structural information from these Raman resonances, we compared them with results of DFT calculations (B3LYP, 6-311G** as implemented in Gaussian 98[15]). The spectra were calculated for geometry-optimized structures. In the case of NBA the initial geometry was based on a X-ray structure.[16,17] As the calculations do not include anharmonicities, solvent effects, and resonance Raman enhancements, only a *qualitative* agreement between experimental and calculated spectra is expected. Still, considering these shortcomings, the calculated spectrum of NBA rather nicely reproduces the experimental features (Figure 4, trace 1). For instance, the symmetric NO_2 stretching mode around 1350 cm^{-1} dominates both spectra, there is a close match of resonance frequencies, and the intensities agree qualitatively. This gives some confidence that this comparison may be used to draw conclusions on structures of intermediates. The experiment yields difference spectra of intermediates, whereas the output of calculations are absolute spectra. Prior to the comparison, the experimental spectra were therefore transformed into absolute spectra by correcting for the NBA bleaching. At a delay time of 10 ps the dominant intermediate is the (vibrationally relaxed) ketene form. The experimental spectrum at that instant (Figure 4, trace 2) is indeed in qualitative agreement with the calculated spectrum of the ketene intermediate. The DFT calculation tells us that the highest peak in the Raman spectrum is due to the *cis*-butadiene motif in the ketene intermediate. This type of vibration is also present on *o*-quinones and is known to have strong Raman intensities (see, for example, reference [18]). Thus, the presence of a strong resonance in that region of the spectrum recorded at a delay time of 160 ps is very telling.

Of the proposed structures (**A**–**D** in Scheme 1) for the second intermediate, we include only **B**–**D** in our comparison since IR spectroscopy rules out structure **A**. Among structures **B**–**D** the form **B** stands out as it contains an aromatic ring and not a *cis*-butadiene motif. The spectrum of form **B** (green dotted line in Figure 4, trace 3) shows the largest deviation from the experimental spectrum. For instance, it features strong bands at 1200 and 1670 cm^{-1} which are absent in the experimental spectrum. The agreement between forms **C** and **D** and the experiment—though not quantitative—is much better. The calculated spectra of **C** and **D** are so similar that a distinction between the two is not yet possible. Clearly, the data favor *cis*-butadiene-like structures (**C** and **D**) over aromatic ones (**B**). The second intermediate then supposedly transforms to the final nitroso product within $\approx$3 ns. The adduct **C** is expected to form the nitroso ester, whereas the lactone **D** should yield the acid. Both products are compatible with our spectroscopic results (Figure 4, trace 4).

Let us now summarize our spectroscopic findings and combine them with prior results to arrive at a comprehensive picture of the photoredox reaction of NBA (see Scheme 1). The photoexcited (singlet) state of

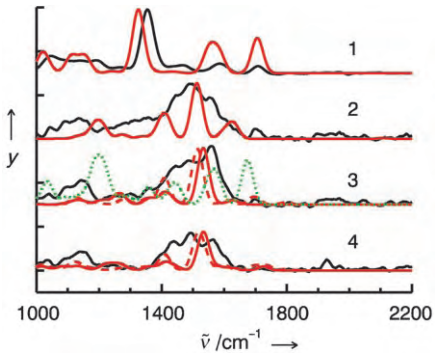

Figure 4. Experimental stimulated Raman spectra (black) in comparison with computed spectra (in color). y: Raman intensity *I*. The frequency axis for the computed spectra was scaled by 0.96,[22] the linewidths were adjusted to the experimental resolution, and the depolarization ratio was accounted for. 1: Steady-state spectra of NBA. 2–4: Experimental transient spectra (obtained by adding a properly scaled NBA spectrum to the difference spectra from Figure 3) are overlaid with computed spectra of suggested intermediates. 2: Ketene intermediate vs. 10-ps spectrum. 3: Second intermediate (structures **B** (green), **C** (red), **D** (red, dashed)) vs. 160-ps spectrum. 4: Nitroso ester product + structure **C** (red) and nitroso acid product + structure **D** (red, dashed) vs. 2-ns spectrum. Note that at 2 ns the product formation is not terminated and a mixture of the second intermediate and the final product has to be compared with the experimental spectrum.

NBA is depopulated with a time constant of 400 fs. The product formed thereby is a ketene, which results from the transfer of a hydrogen atom from the aldehyde group to the nitro group. Comparison of the visible and IR femtosecond transients with matrix isolation experiments unequivocally shows that the ketene is formed in its electronic ground state. Furthermore, a biradical form often discussed[5,19] is not involved or if so its lifetime is considerably shorter than 400 fs. The transformation of NBA to the ketene intermediate calls for a considerable reorganization of the molecular

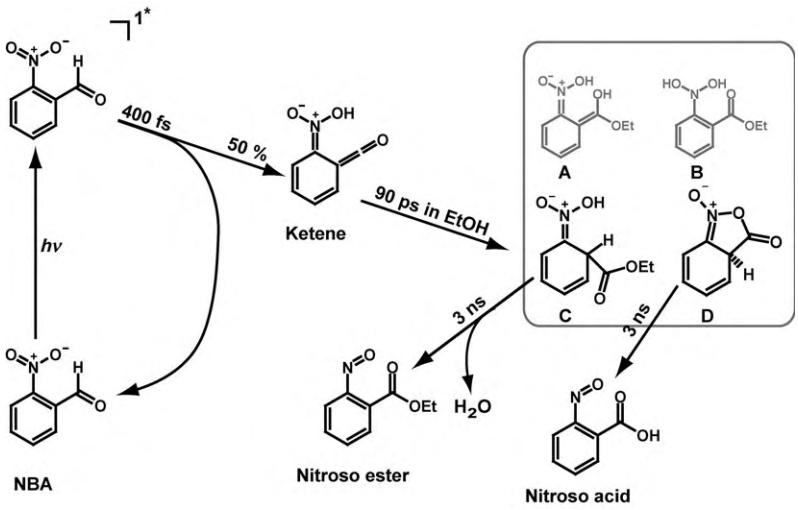

Scheme 1. Time constants and suggested intermediates of the photoredox reaction of NBA. The structures **C** and **D** and their reactions are compatible with our spectroscopic data.

© 2005 Wiley-VCH Verlag GmbH & Co. KGaA, Weinheim

structure. For instance, the C–O distance in the aldehyde is 1.208 Å, whereas it is 1.156 Å in the ketene (values from the DFT structures). This reorganization results in a high vibrational excitation of the stretching mode of the nascent ketene. That excitation is clearly seen in the IR experiment as an initial decrease of the ketene resonance frequency. As the ketene relaxes vibrationally, the resonance moves to its (higher) equilibrium value—a process which here takes about 10 ps. In the next step the ketene undergoes an addition reaction. The rate constant of this process depends on the nature of the solvent. In pure ethanol the reaction takes about 90 ps (± 30 %) and yields a second intermediate. The second intermediate results most likely from an addition to the C=C bond of the ketene. The addition of an ethanol solvent molecule as well as an intramolecular addition are in line with the present spectroscopic results. In either case, the most probable addition product bears an ester function and a *cis*-butadiene motif. During the last (3-ns) step the aromaticity of the phenyl ring is reestablished and the nitroso product formed. It has been found that NBA in ethanol photoreacts to give the nitroso ester.[4] This seems to point to the intermolecular reaction via the adduct form **C**. Yet, this product identification is based on a continuous-wave irradiation experiment. During the time it takes to phototransform the sample, NBA might also thermally react to give the hemiacetal. This is known to photoreact to give the nitroso ester.[21] Thus, a final decision cannot be based on the nature of the product.

Relying on our data, we will now address the quantum yield of the reaction. The quantum yield for the formation of the nitroso product is close to 50 % irrespective of the solvent.[5] As the lifetime of the ketene intermediate strongly depends on the solvent (13 ps in a 1:1 ethanol/water mixture and 24 ns in acetonitrile[6]), it can be excluded that the ketene intermediate is partially reconverted to the NBA starting material—otherwise the quantum yield would be strongly solvent dependent. So either the ground state is replenished during the decay of the electronically excited state or the adduct not only forms the nitroso product but also regenerates the starting material. The latter possibility can be excluded again on the grounds of the solvent independence of the overall quantum yield. Even in solvents like benzene where no addition product can be formed the quantum yield is $\approx$50 %. Thus, the branching must occur during an earlier stage—the decay of the electronically excited state. This decay is promoted by the motion of the hydrogen atom from the aldehyde moiety to the nitro group. The motion brings the ground- and excited-state surfaces in energetic vicinity and internal conversion takes place. Thereby, the ketene intermediate is formed and the ground state is partially recovered. Once formed, the ketene reacts to give the nitroso product with a high yield of $\approx$100 %.

The photoredox reaction of NBA was first described more than 100 years ago, and its study marked the beginning of modern photochemistry.[20] Previous experiments on its mechanism were limited by the time resolutions and the spectroscopic techniques used. Now with femtosecond experiments, particularly femtosecond vibrational spectroscopy, we can map out an "evidenced-based" mechanism based on a ketene intermediate for this reaction. It is foreseeable that this approach will shed light on the mechanisms of many other photoreactions.

Received: May 12, 2005
Revised: September 8, 2005
Published online: November 15, 2005

Keywords: femtochemistry · hydrogen transfer · nitroarenes · photochemistry · reaction mechanisms

[1] X. L. Gao, E. Gulari, X. C. Zhou, *Biopolymers* **2004**, *73*, 579–596.
[2] S. R. Adams, R. Y. Tsien, *Annu. Rev. Physiol.* **1993**, *55*, 755–784.
[3] J. A. Mccray, D. R. Trentham, *Annu. Rev. Biophys. Biophys. Chem.* **1989**, *18*, 239–270.
[4] G. Ciamician, P. Silber, *Ber. Dtsch. Chem. Ges.* **1901**, *35*, 2040–2046.
[5] M. George, J. Scaiano, *J. Phys. Chem.* **1980**, *84*, 492–496.
[6] R. W. Yip, D. K. Sharma, *Res. Chem. Intermed.* **1989**, *11*, 109–116.
[7] T. Schrader, A. Sieg, F. Koller, W. Schreier, Q. An, W. Zinth, P. Gilch, *Chem. Phys. Lett.* **2004**, *392*, 358–364.
[8] M. Yoshizawa, M. Kurosawa, *Physs Rev. A* **1999**, *61*, 013808.
[9] D. W. McCamant, P. Kukura, R. A. Mathies, *J. Phys. Chem. A* **2003**, *107*, 8208–8214.
[10] D. W. McCamant, P. Kukura, S. Yoon, R. A. Mathies, *Rev. Sci. Instrum.* **2004**, *75*, 4971–4980.
[11] D. Jannakoudakis, G. Stalidis, G. Kokkinidis, *Chim. Chron.* **1972**, *1*, 55–67.
[12] S. Kuberski, J. Gebicki, *J. Mol. Struct.* **1992**, *275*, 105–110.
[13] J. L. Duncan, A. M. Ferguson, J. Harper, K. H. Tonge, *J. Mol. Spectrosc.* **1987**, *125*, 196–213.
[14] *Infrared and Raman Spectroscopy* (Ed.: B. Schrader), VCH, Weinheim, **1995**.
[15] M. Frisch, et al., Gaussian 98, Revision A.7.
[16] P. Coppens, *Acta Crystallogr.* **1964**, *20*, 573–578.
[17] P. Coppens, G. M. J. Schmidt, *Acta Crystallogr.* **1964**, *20*, 222–228.
[18] R. T. Packard, R. L. McCreery, *J. Phys. Chem.* **1988**, *92*, 6345–6351.
[19] J. Choi, M. Hirota, M. Terazima, *J. Phys. Chem. A* **2001**, *105*, 12–18.
[20] H. D. Roth, *Pure Appl. Chem.* **2001**, *73*, 395–403.
[21] A. A. Pashayan, A. L. Prokhoda, S. A. Sarkisyan, *High Energy Chem.* **1977**, *11*, 41–46.
[22] W. Koch, W. M. Holthausen, *A Chemist's Guide to Density Functional Theory*, 2nd ed., Wiley-VCH, Weinheim, **2000**.

 © 2005 Wiley-VCH Verlag GmbH & Co. KGaA, Weinheim

Glasses

DOI: 10.1002/anie.200502174

On the Chemistry of Gold in Silicate Glasses: Studies on a Nonthermally Activated Growth of Gold Nanoparticles**

Maik Eichelbaum, Klaus Rademann, Ralf Müller, Martin Radtke, Heinrich Riesemeier, and Wolf Görner*

The history of gold-ruby glasses goes back to the Roman Empire. However, the first known written report about the manufacturing of these glasses was published in 1689 by the German pharmacist and alchemist Johannes Kunckel.[1] Colorless glasses containing the "magic" noble metal gold become characteristically ruby-colored after annealing because of the formation of gold colloids. The absorption of light is caused by an excitation of a collective oscillation of gold valence electrons. The quantum of this plasma oscillation is called the surface plasmon.[2] The surface plasmon resonance frequency mainly depends on the size, shape, topology, and dielectric environment of metal clusters.[3] By changing these parameters it should be possible to create materials that can be used in nanophotonic devices. A large nonlinear optical response with a fast response time is needed for applications in the field of optical computing. Plasmonic materials are exceptionally promising candidates for ultrafast optical switches and modulators because of their large third-order nonlinear susceptibility $\chi^{(3)}$. A second advantage is a response time in the range of picoseconds, which would therefore enable processors with terahertz frequencies.[4]

Another challenging problem is the chemical and mechanical stability of these materials. Gold clusters in glass matrices exhibit the extended stability required for the fabrication of nanodimensional optoelectronic circuits and optical memory with ultrahigh recording speed and storage density. With synchrotron radiation it is already possible to create very small devices, circuits, and even miniaturized lasers by UV and X-ray lithography. We have now succeeded in the spatial synthesis of gold nanoparticles of defined size and with a sharp size distribution by activation of gold silicate glasses with synchrotron radiation and subsequent heating of the samples. Understanding the chemical and physical processes of cluster formation is fundamental for the directed modification of the size, shape, and topology of gold clusters and hence for the creation of structures with a specific functionality. Therefore we have studied the activation caused by the reduction of gold ions to atoms as well as the nucleation and the growth of the gold nanoparticles in gold silicate glasses by UV/Vis spectroscopy, X-ray absorption near-edge spectroscopy (XANES), transmission electron microscopy (TEM), and high-resolution transmission electron microscopy (HRTEM).

Soda–lime–silicate glasses were doped with 0.02 mol% $AuCl_3$ by melting the component materials at 1450 °C. Selected samples were irradiated with a photon flux density of 10^{12} photons $mm^{-2}s^{-1}$ on a defined area with hard X-ray radiation (32 keV) for 300 s in the Berlin electron storage ring (BESSY II).[5] During this irradiation the activated area turned brownish (Figure 1a). Maxima at 315, 440, and 620 nm can be identified in the extinction spectrum of the activated sample (Figure 2, curve b). These peaks can be assigned to defect centers in the SiO_2 framework.

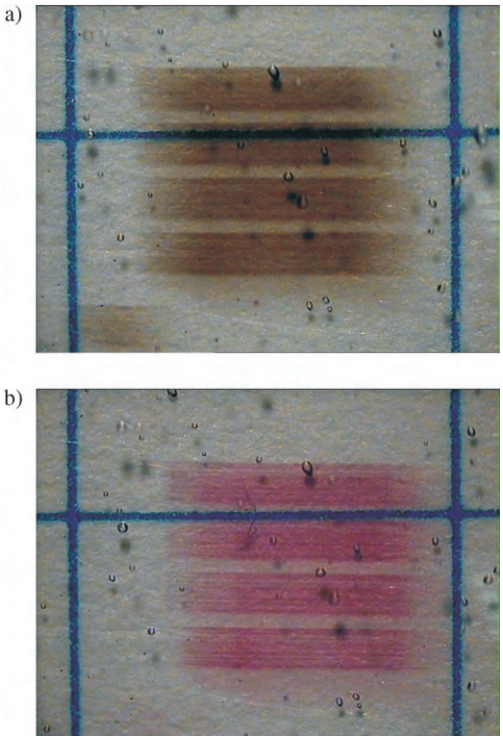

Figure 1. Light-microscopy images of a gold silicate glass after activation with 32-keV synchrotron radiation a) before thermal annealing, b) after annealing at 550 °C for 30 min. The pattern consists of spots with a size of 0.5×1.0 mm^2. The distance between the lines of the blue grid is 5 mm.

In general, the absorption at 315 nm in soda–lime–silicate glasses is caused by holes trapped in oxygen vacancies that neighbor alkali-metal ions (E′ centers).[6] This extinction is obviously much stronger in gold-doped samples than in undoped ones (Figure 2, curve a). Antonietti et al. recently reported TD-DFT (time-dependent density functional theory) cluster model calculations of optical transitions in

[*] Dipl.-Chem. M. Eichelbaum, Prof. Dr. K. Rademann
Institut für Chemie
Humboldt-Universität zu Berlin
Brook-Taylor-Strasse 2, 12489 Berlin (Germany)
Fax: (+49) 30-2093-5559
E-mail: klaus.rademann@chemie.hu-berlin.de
Dr. R. Müller, Dr. M. Radtke, Dr. H. Riesemeier, Prof. Dr. W. Görner
Bundesanstalt für Materialforschung und -prüfung (BAM)
Unter den Eichen 87, 12205 Berlin (Germany)

[**] The authors thank Mr. Schadrack and Mrs. Koslowski (BAM) for their help in preparing glass samples and Prof. Dr. Schlögl, Dr. Su, and Mr. Klein-Hoffmann (Fritz-Haber-Institut der Max-Planck-Gesellschaft) for TEM analysis. This work was supported financially by the Fonds der Chemischen Industrie.

© 2005 Wiley-VCH Verlag GmbH & Co. KGaA, Weinheim

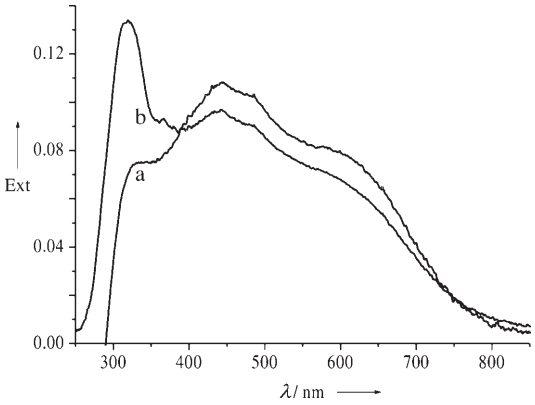

Figure 2. Extinction spectra of silicate glasses activated with 32-keV synchrotron radiation. a) Undoped glass sample; b) Au^{III}-doped (0.02 mol%) glass sample.

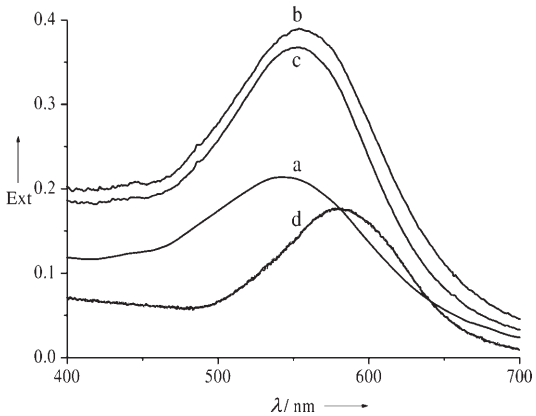

Figure 3. Extinction spectra of gold silicate glasses after activation with synchrotron radiation and subsequent annealing for a) 45 min at 550 °C, b) 45 min at 590 °C, and c) 15 min at 630 °C. d) Spectrum after only annealing for 240 min at 590 °C.

gold atoms bound to silicate defect centers.[7] The highest calculated oscillator strength of possible gold–defect bonds is predicted at 4.02 eV (308 nm) for gold atoms bound to E′ centers. Therefore the peak at 315 nm in the experimental spectrum could be assigned to gold atoms that were generated by activating the glass sample with X-rays.

Peaks at 440 and 620 nm can be attributed to the NBO (nonbridging oxygen) centers HC_1 and HC_2 (holes trapped in SiO_4 tetrahedrons with three or two nonbridging oxygen atoms, respectively).[6] These extinction maxima do not differ very much in doped and undoped samples (Figure 2). The irradiated glasses were subsequently annealed in a muffle furnace. After 10 min of thermal treatment at 450 °C the glasses became colorless again. Apparently the color centers consisting of electrons and holes recombine and their absorption vanishes. When the glass samples were annealed at a higher temperature of 550 °C, the color of the activated array changed to red within 30 min (Figure 1 b).

The red color corresponds to a peak at 540 nm in the extinction spectrum. This extinction can be attributed to the surface plasmon resonance (SPR) of gold nanoparticles.[2,8] When the activated gold silicate glass was annealed for 45 min at 550 °C instead of for 30 min, the extinction peak shifted to 549 nm (Figure 3, curve a). A remarkable red shift of the SPR with increasing duration of thermal treatment was also observed when samples were annealed at 590 °C (SPR peak after 10 min at 547 nm and after 45 min at 556 nm) and 630 °C (SPR peak after 5 min at 547 nm and after 15 min at 554 nm) (Figure 3, curves b and c, respectively).

The optical properties of spherical metal clusters can be described with the Mie theory using the complex dielectric function $\varepsilon^{\text{sphere}} = \varepsilon_1^{\text{sphere}} + i\,\varepsilon_2^{\text{sphere}}$ of the metal and the refraction index of the matrix material n_m.[2,9] For clusters with radii between 1 and 10 nm the extinction Ext can be formulated within a quasi-static approximation under the exclusive consideration of dipolaric excitations [Eq. (1)].[2] Fitting to

$$\text{Ext} = (\lg e)\, C\, d \frac{18\pi n_m^3}{\lambda} \frac{\varepsilon_2^{\text{sphere}}}{(\varepsilon_1^{\text{sphere}} + 2\,n_m^2)^2 + (\varepsilon_2^{\text{sphere}})^2} \quad (1)$$

the height of the extinction maximum in the experimental spectrum is achieved by varying the filling factor C. The refraction index of the glass matrix n_m is 1.52 and the thickness of the sample d is 1.00 mm.

The dielectric function of a metallic sphere $\varepsilon^{\text{sphere}}$ can be calculated from the dielectric function of the bulk material $\varepsilon^{\text{bulk}}$, if one considers its dependence on the sphere radius R caused by the effect of the limited mean free path of electrons ℓ_∞ as described by Equations (2) and (3).[2] Values for $\varepsilon_1^{\text{bulk}}$ and

$$\varepsilon_1^{\text{sphere}}(\omega,R) = \varepsilon_1^{\text{bulk}}(\omega) + \omega_p^2\left(\frac{1}{\omega^2+\Gamma_\infty^2} - \frac{1}{\omega^2+\Gamma(R)^2}\right) \quad (2)$$

$$\varepsilon_2^{\text{sphere}}(\omega,R) = \varepsilon_2^{\text{bulk}}(\omega) + \frac{\omega_p^2}{\omega}\left(\frac{\Gamma(R)}{\omega^2+\Gamma(R)^2} - \frac{\Gamma_\infty}{\omega^2+\Gamma_\infty^2}\right) \quad (3)$$

$\varepsilon_2^{\text{bulk}}$ were taken from ref. [10]. The Drude plasma frequency ω_p of gold is $1.37\times10^{16}\ \text{s}^{-1}$ and the halfwidth $\Gamma(R)$ is given by Equation (4) with the Fermi velocity being $\upsilon_{\text{Fermi}} = 1.40\times$

$$\Gamma(R) = \Gamma_\infty + \frac{\upsilon_{\text{Fermi}}}{R} = \frac{\upsilon_{\text{Fermi}}}{\ell_\infty} + \frac{\upsilon_{\text{Fermi}}}{R} \quad (4)$$

$10^6\ \text{m s}^{-1}$ and the mean free path of electrons being $\ell_\infty =$ 42 nm.

Transmission electron microscopy (TEM) was used to determine the mean cluster radius R of the gold nanoparticles in two samples to be 3.2 ± 0.9 nm (sample had been activated and annealed for 45 min at 550 °C) and 6.2 ± 1.5 nm (sample had been activated and annealed for 15 min at 630 °C). The shape of the curve and the halfwidth of SPR in the experimental UV/Vis spectra are very well described by calculating the extinction spectra for gold spheres with radii of 3.2 and 6.2 nm, respectively (Figure 4). The red shift of SPR with increasing cluster size cannot be explained with Mie theory for radii between 1 and 10 nm. Only for remarkably larger nanoparticles should red shifts and broadening of SPR caused by retardation effects be expected.[2,8a]

Equation (1) is valid only for spherical clusters. For the investigation of the shape of the gold particles, HRTEM images of the gold glass samples were made (Figure 5 a,b).

 © 2005 Wiley-VCH Verlag GmbH & Co. KGaA, Weinheim

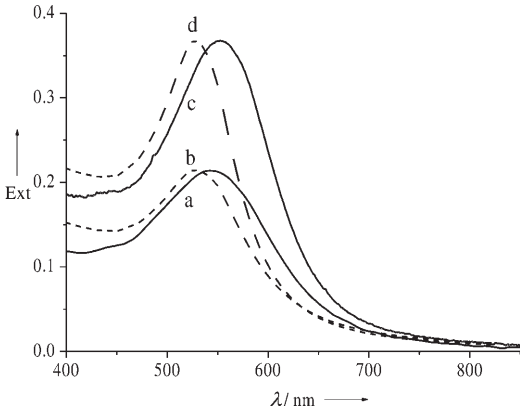

Figure 4. Experimental (solid lines) and calculated extinction spectra (dashed lines) of gold clusters in silicate glasses. a) Spectrum measured for a gold silicate glass that was activated with synchrotron radiation activated and subsequently annealed for 45 min at 550°C; b) spectrum calculated for gold spheres with $R = 3.2$ nm; c) spectrum measured for a gold silicate glass that was activated with synchrotron radiation and subsequently annealed for 15 min at 630°C; d) spectrum calculated for gold spheres with $R = 6.2$ nm.

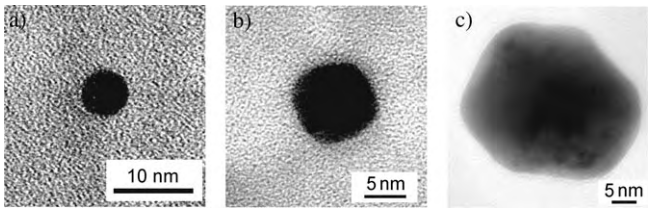

Figure 5. HRTEM images of characteristic gold clusters in gold silicate glasses. Samples were activated with synchrotron radiation and subsequently annealed for a) 45 min at 550°C and b) for 15 min at 630°. c) Sample was only annealed (240 min at 590°C).

Thus it appears that the shape of nanoparticles is approximately spherical. When the glasses were not activated by synchrotron radiation, a violet stain could be observed only after they had been annealed for 60 min at 590°C. The maximum of the observed SPR in the extinction spectrum was shifted from 574 nm (after annealing for 60 min) to 580 nm (after annealing for 240 min) (Figure 3, curve d). TEM images give a mean cluster radius of 27 ± 3 nm, and HRTEM images indicate a distinct deviation of particle shape from an ideal spherical symmetry (Figure 5c).

In 1951 Weyl tried to explain the violet stain of gold-ruby glasses after defined thermal treatment by a nonspherical shape of gold colloids. Thus the typical ruby color would be observed only for spherical particles.[1b] Experiments conducted by Doremus et al. confirm that the effect of particle size on the SPR frequency is marginal.[8c] They examined the growth of gold nanoparticles with radii between 3 and 6 nm in borosilicate glass and found a SPR wavelength of 525 nm. This value, which was independent of cluster size, is also in agreement with our calculations.

As a result of long annealing times of up to 150 h and the low diffusion constant in borosilicate glasses one can assume that the spherical nanoparticles are formed by a very slow growth process. Therefore red shifts of SPR observed in our samples could be explained by an increasing deviation of gold clusters from spherical shape. Studies on noble-metal ellipsoids in glass matrices would also confirm this thesis because of the observation of a red shift of SPR with increasing aspect ratio (and consequently an increasing deviation of spherical shape).[3] This property of our gold silicate glasses is very interesting because a shift of SPR can be achieved in unexpectedly small clusters within a very short period of time only by changing the annealing temperature and thus the optical properties can be modified very easily.

In activated glasses cluster growth occurs at a lower temperature and within a shorter period of time than in nonactivated samples. Light microscopy and TEM images show that the distribution of gold nanoparticles is more homogenous and cluster density is much higher than in exclusively annealed gold glasses. An explanation therefore could be that the activation with synchrotron radiation leads through a reductive process to a very high density of gold atoms, which can diffuse much easier through the glass matrix than bound, oxidized gold species. Thereby an effective cluster growth is facilitated when the samples are annealed at a temperature near the glass transformation temperature.

The chemistry of gold in glass is so far a mystery. The only certainty is that the glass compounds are doped with gold(III) before the melting process starts. Assumptions of the oxidation state in the resulting glass are contradictory. However, recent experiments come to the conclusion that the noble metal is mainly in cationic form before either annealing or activation.[11] Furthermore, one must assume that the gold cations undergo reduction to produce the coloring gold colloids.[2,8b–d]

We used Au L_{III}-edge XANES spectroscopy to study the effect of synchrotron radiation on the oxidation state. XANES spectroscopy is a reliable method for determining oxidation states and is also an established method for the qualitative analysis of gold nanoparticles.[12] In our studies a gold film with a thickness of 40 nm on silica glass, gold(I) cyanide, and gold(III) oxide were used as reference materials. Cationic gold standards show distinct white lines (caused by transitions of 2p electrons into vacant 5d states) at 11922 eV (Au^{III}) and 11926 eV (Au^{I}) and can be clearly distinguished from Au^0 samples, whose spectra do not show any white lines. A XANES spectrum was recorded for the activated area of a gold silicate glass. If the oxidation values $\pm$0, +I, and/or +III of gold exist in the sample, its spectrum should be composed additively of the reference spectra. Therefore the spectra of the gold film and gold(III) oxide were added in different proportions (Figure 6), and the L_{III} edges of the gold film and gold silicate glass were found to match up almost exactly. The white line at 11922 eV in the glass spectrum also indicates a minor fraction of gold(III).

XANES spectra of glass samples were furthermore compared with spectra obtained by combination of oxidation values $\pm$ 0 and +I (Figure 7). It is remarkable that the white line of AuCN at 11926 eV differs clearly from the white line of the activated glass sample. Indeed one cannot exclude a significant influence of ligands in the vicinity of Au^{I} on the XANES spectrum. This effect should be clarified by inves-

 © 2005 Wiley-VCH Verlag GmbH & Co. KGaA, Weinheim

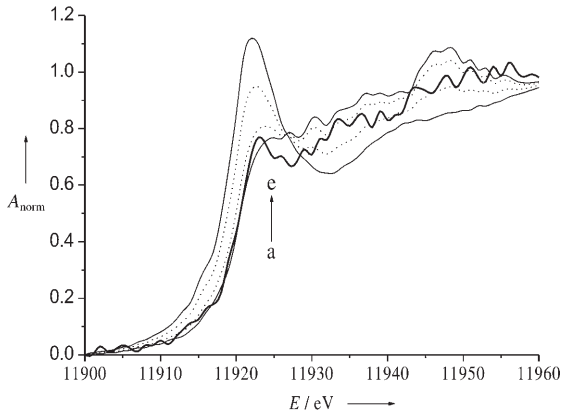

Figure 6. Normalized Au L_{III}-edge XANES spectra of different gold samples (solid lines) and spectra composed additively of reference spectra (dashed lines) obtained from a) gold silicate glass activated with synchrotron radiation; b) Au film; c) 0.2 Au_2O_3 + 0.8 Au film; d) 0.6 Au_2O_3 + 0.4 Au film; e) Au_2O_3.

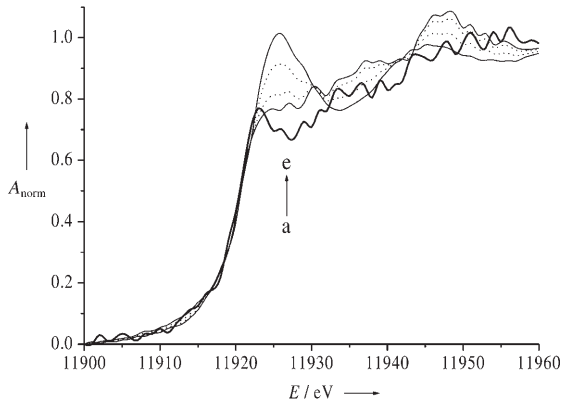

Figure 7. Normalized Au L_{III}-edge XANES spectra of different gold samples (solid lines) and spectra composed additively of reference spectra (dashed lines) obtained from a) gold silicate glass activated with synchrotron radiation; b) Au film; c) 0.2 AuCN + 0.8 Au film; d) 0.6 AuCN + 0.4 Au film; e) AuCN.

tigating further reference materials especially compounds with linearly coordinated oxygen ligands (e.g. CsAuO) as they would be expected in glass.

Although XANES measurements were conducted with photon flux densities (10^{10} photons $mm^{-2} s^{-1}$) well below activating densities (10^{12} photons $mm^{-2} s^{-1}$), occurrence of color centers could be observed in nonactivated samples, too, as a result of long measurement times. Hence it is not possible to get information about the oxidation state before synchrotron irradiation. In future work fast XANES spectroscopy must be used, because this method would provide a determination of oxidation values in a very short period.

In conclusion, activation of gold silicate glasses with synchrotron radiation allows spatial reduction of cationic gold. By subsequent annealing, gold clusters with a sharp size distribution can be synthesized within a short period of time. With increasing cluster size a red shift of surface plasmon resonance is observed in the extinction spectra. This effect can be explained by the increasing deviation from spherical symmetry with the increase in gold cluster size. Au L_{III}-edge XANES spectra of activated gold silicate glasses can be described best by a combination of the spectra of a gold film and an Au_2O_3 reference. This indicates that cationic gold species were found at least as minor compounds in the glass samples investigated. Because of the short wavelength used it should be possible to create nanostructures in glasses with X-ray lithography. This could provide an opportunity for developing nanophotonic devices in glass matrices for opto-electronic circuits, whose surface plasmon resonance could be tuned over a wide range of wavelengths by changing the size and shape of the gold nanoparticles.[13]

Experimental Section

Glasses composed of 70 SiO_2·20 Na_2O·10 CaO (values in mol %) were doped with 0.02 mol % $AuCl_3$·2 H_2O. Reagent-grade SiO_2, Na_2CO_3, $CaCO_3$, and $AuCl_3$·2 H_2O were used as starting materials. Approximately 35-g batches were mixed and melted at 1450 °C for 90 min in an electric furnace. The glass melt was then slowly cooled down to room temperature and cut, and samples were polished to sizes of 10 × 10 × 1.00 mm^3.

Selected samples were irradiated ("activated") on an area of approximately 2.0 × 1.5 mm^2 with synchrotron radiation from BESSY II with 32 keV for 300 s. In the subsequent thermal treatment the glass samples were placed into a platinum crucible and annealed in a muffle furnace. XANES spectroscopy was also recorded at BESSY II. Au L_{III}-edge XANES spectra were acquired in fluorescence mode (detection at the Au L_α line at 9707 eV) between 11 900 eV and 11 960 eV with an increment of 1 eV. Peak integration was determined with the program QXAS 3.5. The background spectra was corrected by subtracting the absorption value at 11 900 eV and normalizing the value at 11 960 eV to unity. Extinction spectra were acquired with a StellarNet EPP2000C-50 spectrometer and a Mikropack DH-2000 deuterium/halogen light source. For the activated samples a nonactivated area of the same glass was defined as the reference, and its spectrum was subtracted from the extinction spectrum of the activated area. For exclusively thermally treated samples an untreated glass with the same composition was defined as the reference, and its spectrum was subtracted from the extinction spectrum.

TEM measurements were made at Fritz-Haber-Institut der Max-Planck-Gesellschaft in Berlin with the microscope Philips CM 200 LaB_6 operating at an acceleration voltage of 200 kV.

Received: June 21, 2005
Revised: August 2, 2005
Published online: October 31, 2005

Keywords: glasses · gold · nanostructures · surface plasmon resonance · X-ray absorption spectroscopy

[1] a) J. Kunckel, *Ars Vitraria Experimentalis oder vollkommene Glasmacher-Kunst*, Frankfurt, **1689**; b) W. A. Weyl, *Coloured Glasses*, Society of Glass Technology, Sheffield, **1951**.
[2] U. Kreibig, M. Vollmer, *Optical Properties of Metal Clusters*, Springer, Berlin, **1995**.
[3] K. L. Kelly, E. Coronado, L. L. Zhao, G. C. Schatz, *J. Phys. Chem. B* **2003**, *107*, 668–677.
[4] K. Hirao, T. Mitsuyo, J. Si, J. Qiu, *Active Glass for Photonic Devices*, Springer, Berlin, **2001**; J. Sasei, K. Hirao, *J. Appl. Phys.* **2001**, *89*, 4548–4553; M. Ando, K. Kadono, M. Haruta, T.

 © 2005 Wiley-VCH Verlag GmbH & Co. KGaA, Weinheim

Sakaguchi, M. Miya, *Nature* **1995**, *374*, 625 – 627; K. Fukumi, A. Chayahara, K. Kadono, T. Sakaguchi, Y. Horino, M. Miya, K. Fujii, J. Hayakawa, M. Saton, *J. Appl. Phys.* **1994**, *75*, 3075 – 3080; Y. Menke, M. Ferraris, C. Corbari, J. Fage-Pedersen, *J. Non-Cryst. Solids* **2004**, *345&346*, 366 – 371.

[5] H. Riesemeier, K. Ecker, W. Görner, B. R. Müller, M. Radtke, M. Krumrey, *X-Ray Spectrom.* **2005**, *34*, 160 – 163.

[6] A. Bishay, *J. Non-Cryst. Solids* **1970**, *3*, 54 – 114.

[7] J.-M. Antonietti, M. Michalski, U. Heiz, H. Jones, K. H. Lim, N. Rösch, A. Del Vitto, G. Pacchioni, *Phys. Rev. Lett.* **2005**, *94*, 213 402.

[8] a) C. Sönnichsen, T. Franzl, T. Wilk, G. von Plessen, J. Feldmann, *New J. Phys.* **2002**, *5*, 93.1 – 93.8, b) J. Qiu, X. Jiang, C. Zhu, M. Shirai, J. Si, N. Jiang, K. Hirao, *Angew. Chem.* **2004**, *116*, 2280 – 2284; *Angew. Chem. Int. Ed.* **2004**, *43*, 2230 – 2234; c) P. Rao, R. Doremus, *J. Non-Cryst. Solids* **1996**, *203*, 202 – 205; d) J. Vosburgh, R. H. Doremus, *J. Non-Cryst. Solids* **2004**, *349*, 309 – 314.

[9] G. Mie, *Ann. Phys.* **1908**, *25*, 377 – 445.

[10] M. Quinten, *Z. Phys. B* **1996**, *101*, 211 – 217.

[11] F. E. Wagner, S. Haslbeck, L. Stievano, S. Calogero, Q. A. Pankhurst, K.-P. Martinek, *Nature* **2000**, *407*, 691 – 692.

[12] S. Matsuo, T. Tsukomato, A. Kamigaki, Y. Okaue, T. Yokoyama, H. Wakita, *X-Ray Spectrom.* **2003**, *32*, 158 – 160; R. E. Benfield, D. Grandjean, M. Kröll, R. Pugin, T. Sawitowski, G. Schmid, *J. Phys. Chem. B* **2001**, *105*, 1961 – 1970.

[13] W. L. Barnes, A. Dereux, T. W. Ebbesen, *Nature* **2003**, *424*, 824 – 830; J. R. Krenn, B. Lamprecht, H. Ditlbacher, G. Schider, M. Salerno, A. Leitner, F. R. Aussenegg, *Europhys. Lett.* **2002**, *60*, 663 – 669; V. A. Podolskiy, A. K. Sarychev, E. E. Narimana, V. M. Shalaev, *J. Opt. A* **2005**, *7*, S32-S37.

 © 2005 Wiley-VCH Verlag GmbH & Co. KGaA, Weinheim

Copolymerization

DOI: 10.1002/anie.200502606

Mechanism-Based Design of a ROMP Catalyst for Sequence-Selective Copolymerization

*Marc Bornand and Peter Chen**

We report here the mechanism-based design of a ring-opening metathesis polymerization (ROMP)[1] catalyst which preferentially assembles a mixture of cyclooctene and norbornene into an alternating copolymer. While there have been reports of regular copolymerizations, highly selective examples are uncommon outside of free-radical polymerization, with the 1:1 alternating copolymers of ethylene and carbon monoxide,[2] or of epoxides and carbon dioxide,[3] being perhaps the most prominent examples. Given that the exemplary functional characteristics of biopolymers, for example, structural or catalytic functions in polypeptides, information storage and transmission in polynucleotides, and molecular recognition in polysaccharides, derive ultimately from sequence-selective copolymerization of simple monomer units, one can presume that synthetic polyolefins, as high-performance materials, would be substantially enhanced if even simple sequence-selective copolymerizations could be achieved routinely. Treating regular copolymerization more generally as a problem in metal-catalyzed organic synthesis, one sees that the issue is not stereoselectivity, or even regioselectivity. We seek to introduce into polymerization catalysts the element of chemoselectivity, which is the most basic kind of selectivity in organic synthesis. We encode the sequence information in the catalyst itself, and in this present study succeed in the most primitive, two-component, alternating sequence of ring-opening metathesis copolymerization.

Phosphine ligand **1** was prepared by sequential alkylation and arylation of phenyldichlorophosphine with *t*BuMgCl and *ortho*-methoxyphenyllithium, isolation by careful distillation, cleavage of the methyl ether by BBr_3, and then deprotonation with NaH. Reaction of one equivalent of **1** and $[(Cy_3P)_2RuCl_2(=CHPh)]$ (**2**, Scheme 1) resulted in phosphine exchange,

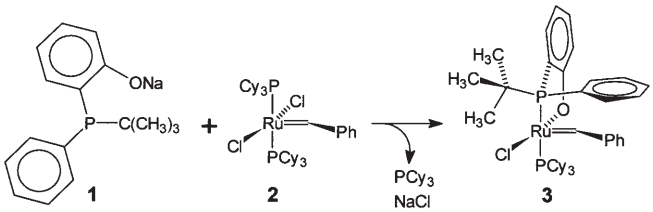

Scheme 1. Synthesis of the chemoselective ROMP catalyst **3**. Cy = cyclohexyl.

followed by elimination of NaCl. A similar approach has been reported by Hoveyda and co-workers for the preparation of a tethered, second-generation metathesis catalysts.[4] The resulting carbene complex **3** was purified by column chromatography under rigorous exclusion of oxygen, and checked by ^1H and ^{31}P NMR spectroscopy, as well as ESI-MS, to confirm that a single compound was prepared. Importantly, no other carbene species was present (analytical details and further information on the synthesis of **1** and **3** can be found in the Supporting Information). Polymerization of norbornene, cyclooctene, and mixtures thereof, together with 0.05 mol% catalyst, were conducted under dry N_2 at room temperature in either dichloromethane or cyclooctene as solvent. In experiments with cyclooctene as solvent, the norbornene is consumed quantitatively after 17 h. If a less-coordinating solvent, such as CH_2Cl_2, is used, then norbornene is consumed much more rapidly, with phenomenological rates comparable to those observed with catalyst **2** under the same conditions. The resulting polymer was isolated by removal of solvent at 0.01 mbar pressure until no further weight loss was seen. In copolymerizations with **3**, the weight of the dry polymer corresponded to the weight of norbornene, plus up to one equivalent of cyclooctene. The polymer samples were characterized by ^1H and ^{13}C NMR spectroscopy (Varian Gemini 300 MHz for ^1H, and 75.4 MHz for ^{13}C; $CDCl_3$) and gel

[*] Dr. M. Bornand, Prof. Dr. P. Chen
Laboratorium für Organische Chemie
Eidgenössische Technische Hochschule (ETH)
Zürich (Switzerland)
Fax: (+41) 44-632-1280
E-mail: chen@org.chem.ethz.ch

Supporting information for this article is available on the WWW under http://www.angewandte.org or from the author.

© 2005 Wiley-VCH Verlag GmbH & Co. KGaA, Weinheim

permeation chromatography (PL-GPC-220, 1,3,5-trichlorobenzene, 180 °C, PLgel 10 μm column) with refractive index and viscometry detection calibrated against polyethylene standards. Reference polymer samples were prepared analogously with $[(Cy_3P)_2RuCl_2(=CHPh)]$ (**2**) for comparison. The ^{13}C resonances were assigned with the help of group equivalents, which gave good predictions for the homopolymers. The relaxation time was set to $t_2 = 5$ s so that reliable integrations could be taken from the ^{13}C NMR spectra.

While the ordinary ruthenium carbene complex **2** polymerizes both norbornene and cyclooctene efficiently, complex **3** shows almost no reactivity with cyclooctene alone under the conditions of the experiment, but is nevertheless as active (qualitatively) as **2** in ROMP of norbornene. More interesting is the behavior with respect to copolymerization. Polymerization catalyzed by **3** in cyclooctene with various amounts of norbornene proceeds until the norbornene is exhausted and then stops, but the resultant polymer ($M_w \approx 10^6$, $M_w/M_n \approx 5$) contains increasingly long stretches of alternating copolymer as the ratio of norbornene to cyclooctene decreases. GPC analysis indicates that the polymer is not a physical mixture of the homopolymers of norbornene and cyclooctene. Both the viscosity and refractive index traces show a single, smooth, monomodal peak at the same retention time, which is significant because norbornene homopolymer would not appear in the latter trace, its refractive index being coincidentally the same as that of the 1,3,5-trichlorobenzene solvent. Moreover, the ^{13}C NMR spectra (Figure 1) of the homopolymers of norbornene and cyclooctene, as well as the copolymers with various ratios of the two monomers, demonstrate that alternate incorporation of cyclooctene and norbornene is preferred for complex **3** but not for ROMP catalyst **2**.

Catalyst **2** in norbornene/cyclooctene mixtures forms predominantly norbornene homopolymer until the norbornene is exhausted, and then proceeds to homopolymerize cyclooctene. As the norbornene is increasingly dilute, the ^{13}C NMR signals arising from its homopolymer disappear because of the increasing preponderance of cyclooctene polymer. Catalyst **3**, on the other hand, displays an increasing preference for the production of the alternating copolymer as the amount of norbornene, relative to cyclooctene, is decreased, with about two-thirds of the olefinic linkages in the copolymer comprising the alternating stretches in the best cases seen so far. Preliminary results for the negative control with a symmetrical analogue of **3** having two *tert*-butyl groups instead of one phenyl and one *tert*-butyl show that the symmetrical catalyst **4** (see Supporting Information for synthesis and characterization) homopolymerizes norbornene well and cyclooctene poorly. No alternating copolymer is formed in the negative control for mixtures of norbornene and cyclooctene.

The design concept for **3** derives from our earlier mechanistic work on olefin metathesis. Secondary deuterium isotope effects, measured in the gas phase, indicated that the structure of the rate-determining transition state for the metathesis reaction catalyzed by the first-generation ruthenium catalyst was a metallacyclobutane.[5] Computational work from our own research group,[6,7] as well as others,[8,9]

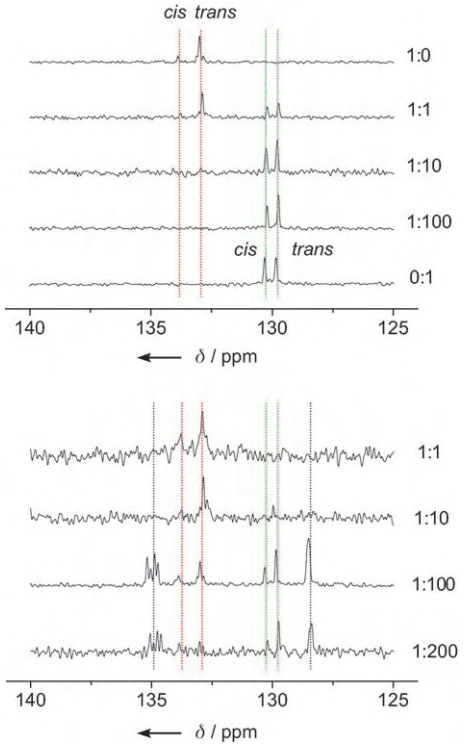

Figure 1. Olefinic regions of the ^{13}C NMR spectra of the polymer samples prepared from norbornene/cyclooctene mixtures at different mole ratios. The top spectra show results for catalyst **2**; spectra for catalyst **3** are at the bottom. The olefinic carbon resonances for the ring-opening metathesis polymer of norbornene are marked with red dotted lines, the resonances for the polymer from cyclooctene are marked in green. The black dotted lines mark the resonances for the alternating copolymer. There are at least two partially resolved signals in the high-field resonance, assigned to the end of the double bond derived from cyclooctene (*cis* and *trans*), whereas there are four signals in the low-field resonance, assigned to the end derived from norbornene. One presumes that, not only the *cis* and *trans* configuration of the double bond, but also the *cis* and *trans* configuration of the next double bond, causes the splitting.

however, found minima at the metallacyclobutane structure. Experimental observation of the olefin π complex by Snapper and co-workers[10] and a ruthenacyclobutane intermediate by Romero and Piers[11] supported the DFT calculations. In our computations, we did find, however, that the rate-determining transition step for olefin metathesis by **2** was a rotation of the tricyclohexylphosphine ligand in a metallacyclobutane structure,[6] which is in fact consistent with the isotope effect studies, the other computational work, and the solution-phase observations. For a degenerate metathesis reaction, the rotation is required by microscopic reversibility. If the rotation were, however, to be prevented, and, furthermore, the phosphine were to bear two different substituents, then the mechanism would require that the active site would swing back and forth with each productive metathesis step between two distinct states in a motion reminiscent of a windshield wiper. The two sites can be made sterically or electronically different enough so that chemoselectivity in an appropriate mixture of two substrates can be achieved. Scheme 2 depicts the catalytic cycle for ROMP of cycloalkenes by **3**. The carbene moiety in the propagating species can lie either on

 © 2005 Wiley-VCH Verlag GmbH & Co. KGaA, Weinheim

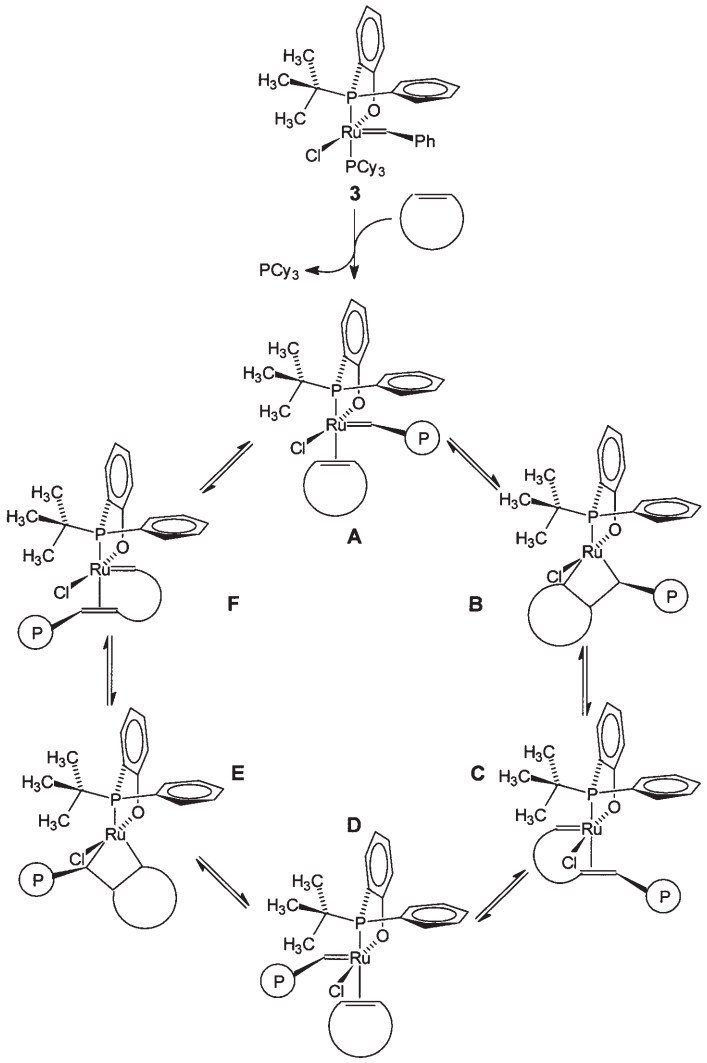

Scheme 2. Catalytic cycle for ROMP of cycloalkenes with catalyst **3**.

the right, as in species **A**, or on the left, as in species **D**. Molecular modeling studies indicate that **A** is much less sterically crowded than **D**, which breaks what would have been a degeneracy in the more usual case of a rotatable phosphine or a phosphine with at least two identical substituents.

If we consider the productive direction around the catalytic cycle for ROMP (**A**→**B**→**C**→**D**→**E**→**F**→**A**) with each step reversible, it would be expected that the forward reaction **A**→**B**→**C** would only occur if there is a large strain release in the **B**→**C** step so that the intermediate metallacyclobutane **B** would preferentially partition forward to **C** rather than return to **A**. On the other hand, the reaction **D**→**E**→**F** should proceed in the forward direction for any cycloalkene, strained or not, because the metallacyclobutane **E** should partition forward to the sterically less hindered carbene **F**. Consequently, the intermediate **A** can only incorporate norbornene into the growing chain, but intermediate **D** can take either norbornene or cyclooctene, the probability being largely determined by the relative concentrations. Accordingly, dilute concentrations of norbornene in a cyclooctene solution yields a largely 1:1 alternating copolymer.

Complex **3** is the simplest implementation of the general concept. It is a dual-site catalyst in which one site shows chemoselectivity and the other not, which, together with a concentration difference between the two monomers, constitutes the bare minimum case for an alternating copolymerization. Selectivity at both sites would eliminate the need for widely divergent concentrations of the two monomers, but even such a restriction can be easily accommodated by slow addition of one monomer into a neat solution of the other. One might expect similar behavior from an unsymmetrically substituted N-heterocyclic carbene complex reported by Mol and co-workers,[12] but the complex did not even polymerize norbornene well, presumably because of the much-too-large adamantyl substituent. One should note that a similar example of a dual-site catalyst can be found in the C_1- or C_s-symmetric metallocene catalysts for syndiotactic polypropylene.[13] In these systems, the activated catalyst alternately selects for the *re* and *si* face of the single monomer, propylene, but there is no documented case where selective copolymerization has been reported with these catalysts. The alternating selectivity has other potential uses as well. Selective oligomerization and selective ring-closing metathesis should be achievable with the new, designer catalyst architecture. Furthermore, while the designed structure demonstrates the target selectivity, no optimization of the catalyst has been attempted yet. Further work in this direction is underway.

Received: July 25, 2005

Keywords: alkenes · copolymerization · homogeneous catalysis · metathesis · ruthenium

[1] K. J. Ivin, J. C. Mol, *Olefin Metathesis and Metathesis Polymerization*, Academic Press, New York, **1997**.
[2] E. Drent, J. A. M. van Broekhoven, M. J. Doyle, *J. Organomet. Chem.* **1991**, *417*, 235.
[3] D. J. Darensbourg, M. W. Holtcamp, *Coord. Chem. Rev.* **1996**, *153*, 155.
[4] J. J. Van Veldhuizen, D. G. Gillingham, S. B. Garber, O. Kataoka, A. H. Hoveyda, *J. Am. Chem. Soc.* **2003**, *125*, 12502.
[5] C. Adlhart, C. Hinderling, H. Baumann, P. Chen, *J. Am. Chem. Soc.* **2000**, *122*, 8204.
[6] C. Adlhart, P. Chen, *Angew. Chem.* **2002**, *114*, 4668; *Angew. Chem. Int. Ed.* **2002**, *41*, 4484.
[7] C. Adlhart, P. Chen, *J. Am. Chem. Soc.* **2004**, *126*, 3496.
[8] L. Cavallo, *J. Am. Chem. Soc.* **2002**, *124*, 8965.
[9] S. F. Vyboishchikov, M. Bühl, W. Thiel, *Chem. Eur. J.* **2002**, *8*, 3962.
[10] J. A. Tallarico, P. J. Bonitatebus, M. L. Snapper, *J. Am. Chem. Soc.* **1997**, *119*, 7157.
[11] P. E. Romero, W. E. Piers, *J. Am. Chem. Soc.* **2005**, *127*, 5032.
[12] M. B. Dinger, P. Nieczypor, J. C. Mol, *Organometallics* **2003**, *22*, 5291.
[13] Y. van der Leek, K. Angermund, M. Reffke, R. Kleinschmidt, R. Goretzki, G. Fink, *Chem. Eur. J.* **1997**, *3*, 585.

 © 2005 Wiley-VCH Verlag GmbH & Co. KGaA, Weinheim

Nanostructures

DOI: 10.1002/anie.200502722

Corrosion-Based Synthesis of Single-Crystal Pd Nanoboxes and Nanocages and Their Surface Plasmon Properties**

*Yujie Xiong, Benjamin Wiley, Jingyi Chen, Zhi-Yuan Li, Yadong Yin, and Younan Xia**

Corrosion can be broadly defined as "the damage to metal caused by reactions with its environment," and may take place in many different forms such as pitting, crevice etching, intergranular exchange, galvanic replacement, and dealloying.[1] Although corrosion is generally undesirable (automobile corrosion alone costs $16 billion annually!), it can be exploited as a versatile route to porous structures such as metal membranes.[2] While many solution-phase methods have been developed for synthesizing nanoparticles with well-controlled shapes,[3] it is still a great challenge to generate hollow nanostructures without involving exotic templates. We recently found that the galvanic replacement reaction between Ag templates and $HAuCl_4$ in an aqueous medium could lead to the formation of hollow nanostructures with controllable void size, wall porosity, and shell thickness.[4] More interestingly, the surface plasmon resonance (SPR) peaks of the resultant nanostructures could be continuously shifted from the blue (400 nm) to the near infrared (1200 nm) region by controlling the molar ratio of Ag to $HAuCl_4$ and thus the extent of replacement, alloying, and dealloying. Ideally, one would prefer a one-step synthesis that is able to tune the SPR properties of metal nanostructures without the requirement of templates made of a different metal. Here we demonstrate that corrosive etching of single-crystal Pd nanocubes could be used to transform them into nanoboxes and nanocages by controlling the reaction time.

As demonstrated in previous studies, Pd nanoparticles play an important role in hydrogen storage,[5] serve as the primary catalyst for the reduction of pollutants emitted from automobiles,[6] and facilitate organic reactions such as Suzuki, Heck, and Stille couplings.[7] Their performance could be tuned or improved for most of these applications by processing Pd nanostructures into hollow ones. For example, although solid Pd nanoparticles usually lose their catalytic activity after one round of Suzuki coupling reactions,[7a] hollow Pd spheres remained highly active for at least 24 rounds of reactions.[7b] While the SPR properties of Au and Ag have enabled many applications such as colorimetric sensing, nanoscale wave-guiding, and enhancement of electromagnetic fields and light transmission,[8] the SPR properties of Pd nanoparticles remain largely unexplored since Pd particles less than 10 nm in size give no resonance peak in the visible and near infrared regions.[9] Furthermore, the specific sensitivity of Pd towards hydrogen makes it especially interesting for fabricating SPR-based sensors for hydrogen gas.[10] We found by using discrete dipole approximation (DDA) calculations[11] that the resonant peak of Pd nanoshells with outer diameters of 48 nm could be tuned from 530 to 870 nm by tailoring their wall thickness from 6 to 3 nm. To demonstrate that Pd nanostructures with hollow interiors could indeed exhibit tunable SPR extinction peaks in the visible region we have synthesized single-crystal Pd nanoboxes and nanocages by a self-templating, corrosive pitting process.

The synthesis was conducted in a solution containing ethylene glycol, water, and poly(vinyl pyrrolidone) (PVP) with the addition of Na_2PdCl_4 as a precursor to Pd. The reaction can be divided into six distinctive stages based on both microscopic and spectroscopic observations. Reduction of $[PdCl_4]^{2-}$ to Pd atoms dominated up until $t = 18$ h (Figure 1a), with the Pd atoms nucleating and growing into nanocubes (with slightly truncated corners) with edge lengths of approximately 48 nm. Oxidative etching of the Pd nanocubes by O_2 (that is, corrosion) started to surpass the reduction process at $t = 20$ h. Small pits were observed in the surfaces of individual Pd nanocubes (Figure 1b), thus implying that the corrosion was initiated locally rather than uniformly over the entire surface of each cube. Over the next hour the interior of each cube became increasingly empty while the size of the hole in the surface started to shrink to form a box with relatively thick walls (Figure 1c). After another hour the void was further increased in size and each Pd cube evolved into a completely empty box with somewhat

[*] Dr. Y. Xiong, J. Chen, Prof. Y. Xia
Department of Chemistry
University of Washington
Seattle, WA 98195 (USA)
Fax: (+1) 206-685-8665
E-mail: xia@chem.washington.edu
B. Wiley
Department of Chemical Engineering
University of Washington
Seattle, WA 98195 (USA)
Prof. Z.-Y. Li
Laboratory of Optical Physics
Institute of Physics
Chinese Academy of Sciences
Beijing 100080 (P.R. China)
Dr. Y. Yin
The Molecular Foundry
Lawrence Berkeley National Laboratory
Berkeley, CA 94720 (USA)

[**] This work was supported in part by a grant from the NSF (DMR-0451788), a DARPA-DURINT subcontract from Harvard University, and a fellowship from the David and Lucile Packard Foundation. Y.X. is a Camille Dreyfus Teacher Scholar (2002). B.W. and J.C. thank the Center for Nanotechnology at the University of Washington for an IGERT (funded by the NSF, DGE-9987620) and a Nanotech fellowship, respectively. Z.-Y.L. was supported by the National Key Basic Research Special Foundation of China (Grant no. 2004CB719804). Y.Y. was supported by the Director, Office of Science, U.S. Department of Energy, under Contract DE-AC03-76SF00098. This work used the Nanotech User Facility (NTUF), a member of the National Nanotechnology Infrastructure Network (NNIN) funded by the NSF. We thank the Molecular Foundry at the Lawrence Berkeley National Laboratory for HRTEM analysis.

Supporting information for this article is available on the WWW under http://www.angewandte.org or from the author.

 © 2005 Wiley-VCH Verlag GmbH & Co. KGaA, Weinheim

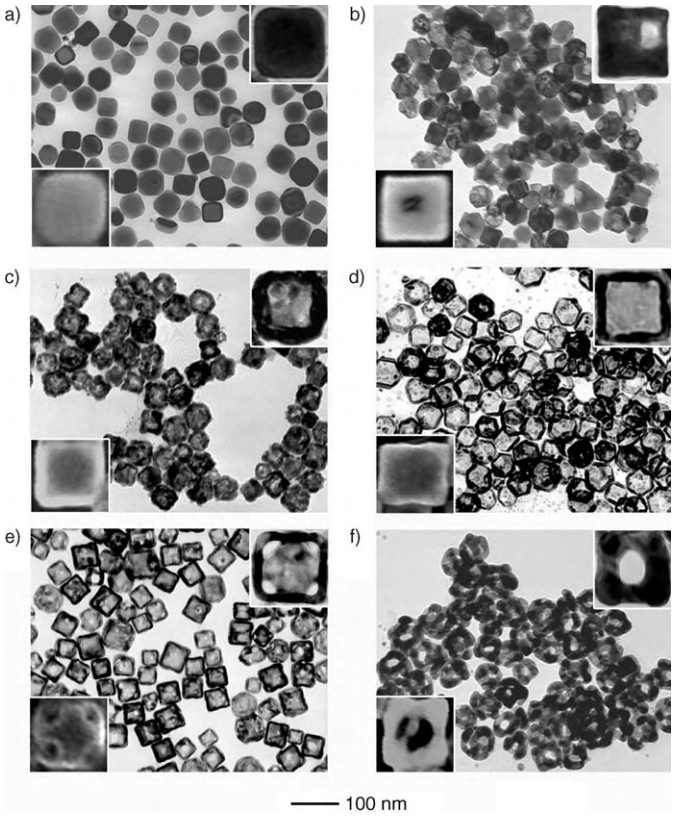

Figure 1. TEM images of the products at different reaction stages: a) $t = 18$ h; b) $t = 20$ h; c) $t = 21$ h; d) $t = 22$ h; e) $t = 24$ h; and f) $t = 28$ h. Note that the 100-nm bar applies to all images. The upper right and lower left insets show enlarged TEM and SEM images of an individual particle taken from each product, respectively.

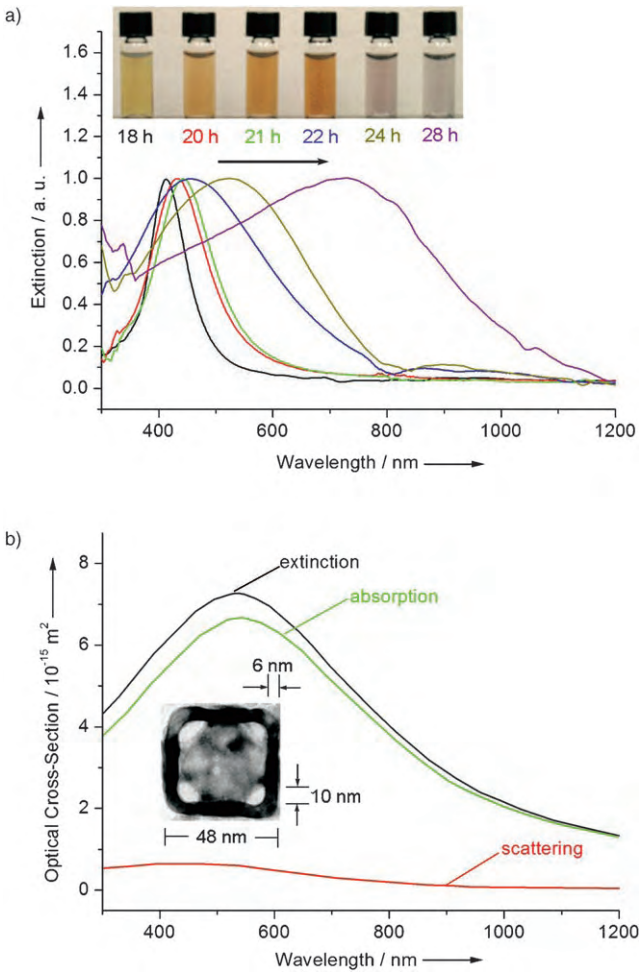

Figure 2. Surface plasmon properties of the Pd nanostructures shown in Figure 1: a) UV/Vis extinction spectra recorded from aqueous suspensions of the as-synthesized samples (see the inset, all spectra are normalized against the intensities of their strongest peaks); and b) DDA calculation of extinction, scattering, and absorption cross-sections of the Pd nanocage depicted in the inset.

truncated corners (Figure 1 d). Note that the hole in the surface had by now disappeared so that the nanobox was enclosed by a smooth, thin wall with a thickness of about 8 nm. Small holes appeared at the corners of each nanobox if the reaction was continued beyond this point. Holes of about 10 nm in diameter punctured each corner at $t = 24$ h (Figure 1 e), thus turning the nanobox into a cage. The Pd nanocage had an edge length of approximately 48 nm and was characterized by a uniform wall thickness of about 6 nm. It is worth noting that the outer diameter of the nanobox and nanocage exhibited no significant change relative to the initial Pd nanocube. The nanocage finally evolved into a ring (probably through additional etching and Ostwald ripening), thus causing the wall thickness to increase slightly from 6 to 10–20 nm (Figure 1 f).

The Pd nanostructures displayed distinctive colors since SPR is strongly dependent on wall thickness. As shown by the inset in Figure 2 a, the aqueous suspensions changed from yellow to orange to purple as the solid Pd nanocubes were transformed into hollow boxes and then porous cages. Figure 2 a shows the UV/Vis extinction spectra recorded from the six aqueous suspensions. The Pd nanocubes exhibited an SPR peak at 410 nm, which was consistent with the results of DDA calculations (see the Supporting Information).[11] The SPR peak was red-shifted to 430 nm as holes appeared in their surfaces. The formation of hollow structures with thick walls (and relatively rough inner surfaces) resulted in the sample exhibiting an SPR peak at 443 nm. The extinction peak was further shifted to 452 nm as the wall of the nanoboxes was thinned to 8 nm. Once the product had evolved into nanocages with an edge length of 48 nm and a wall thickness of 6 nm, the SPR peak was shifted to 520 nm, which matched the calculated spectra (Figure 2 b). The extinction (C_{ext}), absorption (C_{abs}), and scattering (C_{sca}) cross-sections are related by the following equation: $C_{ext} = C_{abs} + C_{sca}$.

Figure 3 a and b show typical SEM and TEM images of the Pd nanoboxes at relatively low magnifications which indicate that over 95% of the hollow structures inherited the truncated, cubic shape of the initial cubes. The fringes in the HRTEM images (Figure 3 c and d) showed a period of 2.0 Å, which was consistent with the {200} lattice spacing of face-centered-cubic Pd. These images also displayed well-resolved, continuous fringes with the same orientation, thus implying that the Pd nanobox, like the starting Pd nanocube, was a piece of single crystal. The inset of Figure 3 c shows a

 © 2005 Wiley-VCH Verlag GmbH & Co. KGaA, Weinheim

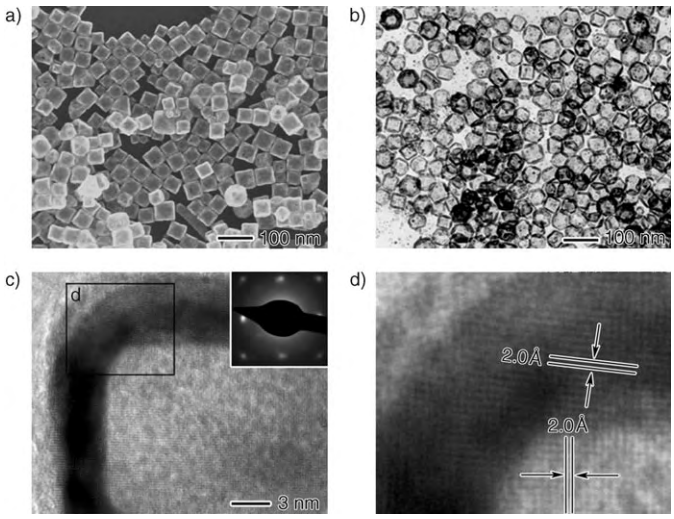

Figure 3. Electron microscopy characterization of the Pd nanoboxes obtained at $t = 22$ h: a) SEM image; b) TEM image; and c, d) high-resolution TEM images. The inset of (c) shows an electron diffraction pattern taken from the side surface of an individual Pd nanobox.

nanoprobe electron diffraction (ED) pattern obtained by aligning the beam perpendicular to one of the side faces of a cubic box. The spots could be indexed to the {200} diffraction of face-centered-cubic Pd. This diffraction pattern also suggests that the Pd nanobox was a single crystal with its symmetry similar to that of the initial Pd nanocube, which was enclosed by {100} facets. Both powder XRD and microprobe ED patterns (see the Supporting Information) further confirms the high phase purity and crystallinity of the Pd nanoboxes.

To analyze the corrosive etching process that transformed Pd nanocubes into nanocages we recorded UV/Vis spectra of the solution at different stages of the reaction (see the Supporting Information, the Pd nanoparticles were removed by centrifugation before the spectra were taken). The extinction peak at 242 nm (see the Supporting Information) corresponds to $[PdCl_4]^{2-}$ while that at 278 nm can be attributed to water-substituted $[PdCl_4]^{2-}$ ($[PdCl_{4-n}(H_2O)_n]^{(2-n)-}$) species.[12] The peak at 242 nm disappeared quickly when $[PdCl_4]^{2-}$ was reduced by ethylene glycol to generate Pd atoms and then nanocubes (see the Supporting Information). The concentration of water-substituted $[PdCl_4]^{2-}$ steadily increased as the nanocubes were etched by corrosive pitting. Similar to the corrosion of bulk metals,[13] O_2, Cl^- ions, and H_2O are all instrumental for the initiation of pitting on the surfaces of Pd nanocubes. As documented in the literature, corrosion most commonly occurs when the O_2 in air is dissolved in a thin film of water on the surface of a metal, thereby picking up electrons from the cathode to form hydroxide ions that then migrate towards the anode.[1] If the anode and cathode are located at different sites on the metal surface because of differences in the local environment (for example, surface heterogeneity and/or concentrations of ions), either pitting or crevice corrosion will take place.[1] Like the corrosion of bulk metals, adsorption of chloride ions can greatly increase the rate of surface diffusion and therefore expedite the pitting process.[13] On the other hand, the presence of a small amount of water can enhance the solubility of O_2 and profoundly increase the corrosion rate.[1] In addition to the augmentation by O_2, Cl^- ions, and H_2O, the amount of PVP was also found to be critical to the formation of hollow Pd nanostructures through a corrosion process. A large amount of PVP (with the ratio of PVP to Pd being 15:1) could ensure that the surface of each Pd nanocube was effectively covered by this polymer. In addition, the surface of each Pd nanocube is likely covered by a thin layer of palladium oxide.[13a] Both of these factors could make the surface of a Pd nanocube less reactive than the freshly exposed interior once the pitting process has started.[13b]

Figure 4 summarizes all the major steps involved in the corrosive etching process. Compared with the system without water (which produced Pd particles ca. 8 nm in size),[12b] the presence of water significantly accelerated the oxidative etching of Pd, and thus reduced the number of seeds formed in the nucleation step. As we have recently demonstrated in a case where Fe^{III} ions were added as the oxidative etchant,[14] a decrease in the number of seeds resulted in formation of Pd nanocubes with larger sizes when the concentration of the Pd precursor was maintained. As in the corrosion of bulk metals, the presence of water also facilitated the pitting process. Once a pit was formed at a specific site on the surface of a Pd cube (step a), further corrosion would occur preferentially inside

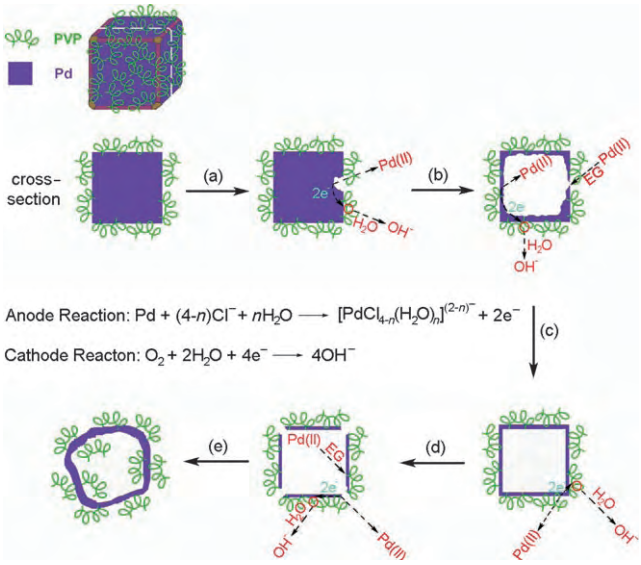

Figure 4. Schematic illustration summarizing all the major morphological changes involved in the synthesis of Pd nanoboxes and nanocages by corrosive etching: a) Pitting at a specific site on the surface of a nanocube where the O_2 dissolved in the solvent received electrons from the cathode and generated hydroxide ions that migrated towards the anode; b) formation of hollow structures after further etching of the interior of the nanocube, and the concentration of water-substituted $[PdCl_4]^{2-}$ increased; c) formation of a completely enclosed Pd nanobox by reducing the water-substituted $[PdCl_4]^{2-}$ species to form Pd atoms at the edge of each hole; d) formation of nanocages by dissolving Pd from the corners of the nanobox; and e) reconstruction of the nanocage by relocating all the holes from the corners to side faces and thickening of the wall as a result of additional reduction of the water-substituted $[PdCl_4]^{2-}$ species.

© 2005 Wiley-VCH Verlag GmbH & Co. KGaA, Weinheim

the pit, thus leading to formation of a hollow nanostructure (step b). As etching was continued, the concentration of water-substituted $[PdCl_4]^{2-}$ sufficiently increased to allow the reduction by ethylene glycol to take place at the edge of a hole, thus causing it to gradually shrink in size. Since the reduction of water-substituted $[PdCl_4]^{2-}$ by ethylene glycol was minimal, most of these ionic species were retained in the solution rather than being reduced and deposited onto the outer surface of the Pd nanoboxes. This argument is supported by the UV/Vis spectra (see the Supporting Information), and it is for this reason why the outer dimensions of the Pd nanocubes, nanoboxes, and nanocages were essentially the same. It is the combination of continuous etching of the Pd nanocube from the interior and some reduction of the Pd^{II} species at the edge of the hole that resulted in the formation of Pd nanobox by $t = 22$ h (step c). It is worth pointing out that such a self-templating and self-etching process has also been observed in the solution-phase synthesis of ZnO microtubes.[15] The Pd nanoboxes were as unstable as the nanocubes when exposed to the corrosive environment. Under the illumination of light, the electric field intensity should concentrate at the corners, thus increasing the surface charge at these sites.[16] As a result, corrosive etching of the Pd nanoboxes preferentially occurred at the corners, thus leading to the formation of Pd nanocages with all eight corners being truncated (step d). This is different from the synthesis performed in the dark (see the Supporting Information). Further corrosion caused these holes to increase in dimension until the Pd nanocages evolved into rings. At the same time, continuous reduction of the water-substituted $[PdCl_4]^{2-}$ species occurred on the exterior surface of the nanocages, which led to the formation of nanorings (step e). This course of materials transfer resembles the conventional "Ostward ripening" process. Overall, the void size, shell thickness, and wall porosity of Pd hollow nanostructures were determined by the net difference between two opposite reactions: the reduction of the Pd^{II} precursor to form Pd^0 atoms, and the oxidation of Pd (both atoms and nanostructures) into Pd^{II} species.

In summary, metal corrosion is a familiar and common natural phenomenon that, while normally viewed as a detrimental process that destroys the usefulness of tools and machines, can also serve as a simple, elegant, and powerful method for the fabrication of hollow nanostructures with controllable optical properties. More specifically, corrosive pitting and etching could be combined to transform single-crystal Pd nanocubes into nanoboxes and nanocages in a one-pot synthesis without the involvement of exotic templates. The SPR peaks of Pd nanostructures could be tuned from 410 to 520 nm by empting their interiors. Our DDA calculations indicated that the SPR peak of the Pd nanocages with edge lengths of 48 nm could be further red-shifted to 870 nm by decreasing their wall thickness to 3 nm.

Experimental Section

In a typical synthesis, ethylene glycol (5 mL, J. T. Baker) was placed in a 3-neck flask (equipped with a reflux condenser and a teflon-coated magnetic stirring bar) and heated in air at 100 °C for 1 h. Meanwhile, palladium(II) sodium chloride (0.0486 g, Na_2PdCl_4, Aldrich) and poly(vinyl pyrrolidone) (0.2747 g, PVP, M.W. = 55000, Aldrich) were dissolved at room temperature in ethylene glycol (3 mL) and water (3 mL), respectively. These two solutions (with the molar ratio between Pd and the repeating unit of PVP being 1:15) were then injected simultaneously into the flask with a syringe pump at a rate of 45 mL h^{-1}. Heating of the reaction at 100 °C was continued in air for 28 h. A set of samples were taken over the course of a synthesis with a glass pipette. To minimize temperature perturbation during sampling, the glass pipette was held just above the solution and preheated for 30 s before immersion. For the argon-protected synthesis, all other experimental parameters were kept the same except for the continuous bubbling of argon. The samples were washed with acetone and then with ethanol several times before they were centrifuged at a rate of 6000 rpm for 10 min to remove most of the ethylene glycol and excess PVP. The samples were characterized by transmission electron microscopy (TEM), high-resolution TEM, scanning electron microscopy (SEM), electron diffraction (ED), and powder X-ray diffraction (PXRD).

TEM images and microprobe ED patterns were recorded on a Phillips 420 transmission electron microscope operated at 120 kV. HRTEM images and nanoprobe ED patterns were taken on a Jeol 2010 LaB6 high-resolution transmission electron microscope operated at 200 kV. PXRD patterns were recorded on a Philips 1820 diffractometer equipped with a $Cu_{K\alpha}$ radiation source ($\lambda = 1.54180$ Å). SEM images were taken on a FEI field-emission scanning electron microscope (Sirion XL) operated at an accelerating voltage of 20 kV. UV/Vis spectra were obtained using a Hewlett–Packard 8452A diode array spectrophotometer.

The calculation used in the article is based on the DDA method.[11] DDA is a computational method developed for studying both the scattering and absorption of electromagnetic radiation by particles with sizes on the order of or smaller than the wavelength of incident light. In the calculation, the particle is divided into an array of N polarizable point dipoles, each of which is characterized by a polarizability of $\boldsymbol{\alpha}_i$. When the system is excited by a monochromatic incident plane wave $\boldsymbol{E}_{inc}$, each dipole of the system will be subjected to an electric field that can be split in two contributions: 1) the incident radiation field $\boldsymbol{E}_{i,inc}$ and 2) the field radiated by all of the other induced dipoles $\boldsymbol{E}_{i,dip}$. The sum of both fields is the so-called local field at each dipole ($\boldsymbol{E}_{i,loc} = \boldsymbol{E}_{i,inc} + \boldsymbol{E}_{i,dip}$). Each dipole can be expressed as an oscillating polarization with the dipole moment being $\boldsymbol{P}_i = \boldsymbol{\alpha}_i \boldsymbol{E}_{i,loc}$. Both absorption and scattering cross-sections (C_{abs} and C_{sca}) can be obtained directly from $\boldsymbol{P}_i$. The refractive index of bulk Pd was used in all calculations reported in this article, and the nanoparticle was assumed to be surrounded by and filled with water (when it became porous).

Received: August 3, 2005
Published online: November 22, 2005

Keywords: corrosion · nanostructures · palladium · scanning probe microscopy · surface plasmon resonance

[1] S. A. Bradford, *Corrosion Control*, 2nd ed., CASTI Publishing, Edmonton, Canada, **2001**, pp. 1–51.
[2] Y. Ding, J. Erlebacher, *J. Am. Chem. Soc.* **2003**, *125*, 7772–7773.
[3] a) F. Kim, S. Connor, H. Song, T. Kuykendall, P. Yang, *Angew. Chem.* **2004**, *116*, 3759–3763; *Angew. Chem. Int. Ed.* **2004**, *43*, 3673–3677; b) V. F. Puntes, K. M. Krishnan, A. P. Alivisatos, *Science* **2001**, *291*, 2115–2117; c) L. A. Gugliotti, D. L. Feldheim, B. E. Eaton, *Science* **2004**, *304*, 850–852; d) X. Teng, H. Yang, *Nano Lett.* **2005**, *5*, 885–891.
[4] a) Y. Sun, Y. Xia, *Science* **2002**, *298*, 2176–2179; b) Y. Sun, Y. Xia, *J. Am. Chem. Soc.* **2004**, *126*, 3892–3901; c) B. Wiley, Y.

 © 2005 Wiley-VCH Verlag GmbH & Co. KGaA, Weinheim

Sun, J. Chen, H. Cang, Z.-Y. Li, X. Li, Y. Xia, *MRS Bull.* **2005**, *30*, 356 – 361.
[5] Y. Sun, Z. Tao, J. Chen, T. Herricks, Y. Xia, *J. Am. Chem. Soc.* **2004**, *126*, 5940 – 5941.
[6] Y. Nishihata, J. Mizuki, T. Akao, H. Tanaka, M. Uenishi, M. Kimura, T. Okamoto, N. Hamada, *Nature* **2002**, *418*, 164 – 167.
[7] a) Y. Li, X. M. Hong, D. M. Collard, M. A. El-Sayed, *Org. Lett.* **2000**, *2*, 2385 – 2388; b) S.-W. Kim, M. Kim, W. Y. Lee, T. Hyeon, *J. Am. Chem. Soc.* **2002**, *124*, 7642 – 7643; c) M. T. Reetz, E. Westermann, *Angew. Chem.* **2000**, *112*, 170 – 173; *Angew. Chem. Int. Ed.* **2000**, *39*, 165 – 168; d) S. U. Son, Y. Jang, J. Park, H. B. Na, H. M. Park, H. J. Yun, J. Lee, T. Hyeon, *J. Am. Chem. Soc.* **2004**, *126*, 5026 – 5627.
[8] Y. Xia, N. J. Halas, *MRS Bull.* **2005**, *30*, 338 – 343.
[9] J. A. Creighton, D. G. Eadon, *J. Chem. Soc. Faraday Trans.* **1991**, *87*, 3881 – 3891.
[10] P. Tobiška, O. Hugon, A. Trouillet, H. Gagnaire, *Sens. Actuators B* **2001**, *74*, 168 – 172.
[11] a) W. H. Yang, G. C. Schatz, R. P. Van Duyne, *J. Chem. Phys.* **1995**, *103*, 869 – 875; b) K. L. Kelly, E. Coronado, L. L. Zhao, G. C. Schatz, *J. Phys. Chem. B* **2003**, *107*, 668 – 677; c) I. O. Sosa, C. Noguez, R. G. Barrera, *J. Phys. Chem. B* **2003**, *107*, 6269 – 6275.
[12] a) B. Veisz, Z. Király, *Langmuir* **2003**, *19*, 4817 – 4824; b) Y. Xiong, J. Chen, B. Wiley, Y. Xia, S. Aloni, Y. Yin, *J. Am. Chem. Soc.* **2005**, *127*, 7332 – 7333.
[13] a) R. C. Newman, K. Sieradzki, *Science* **1994**, *263*, 1708 – 1709; b) J. C. Scully, *The Fundamentals of Corrosion*, 3rd ed., Pergamon, Oxford, **1990**, pp. 1 – 57.
[14] Y. Xiong, J. Chen, B. Wiley, Y. Xia, Y. Yin, Z.-Y. Li, *Nano Lett.* **2005**, *5*, 1237 – 1242.
[15] L. Vayssieres, K. Keis, A. Hagfeldt, S. E. Lindquist, *Chem. Mater.* **2001**, *13*, 4395 – 4398.
[16] a) J. P. Kottmann, O. J. F. Martin, D. R. Smith, S. Schultz, *Phys. Rev. B* **2001**, *64*, 235402(1 – 10); b) A. J. Haes, C. L. Haynes, A. D. McFarland, G. C. Schatz, R. P. Van Duyne, S. Zhou, *MRS Bull.* **2005**, *30*, 368 – 375.

 © 2005 Wiley-VCH Verlag GmbH & Co. KGaA, Weinheim

Natural Product Synthesis

DOI: 10.1002/anie.200503678

Total Synthesis of (+)-Rugulosin and (+)-2,2′-*epi*-Cytoskyrin A through Cascade Reactions**

K. C. Nicolaou, Yee Hwee Lim, Charles D. Papageorgiou, and Jared L. Piper*

We have previously reported[1] the development of the "cytoskyrin cascade" as a facile and efficient entry into the growing class of modified bisanthraquinones that includes cytoskyrin A (**1a**),[2] graciliformin (**1b**),[3] and rugulosin (**2b**; Figure 1).[1c,4] Isolated from a number of fungi and lichens,[4b]

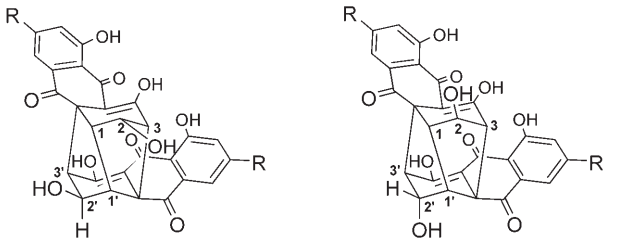

R = OMe: (+)-cytoskyrin A (**1a**)
R = Me: (+)-graciliformin (**1b**)

R = OMe: (+)-2,2'-*epi*-cytoskyrin A (**2a**)
R = Me: (+)-rugulosin (**2b**)

Figure 1. Selected naturally occurring modified bisanthraquinones.

the latter compound (**2b**) was recently found to exhibit anti-HIV properties,[5] in addition to its originally reported cytotoxic activity[4b] that it shares with cytoskyrin A (**1a**).[2] Given the occurrence of both graciliformin (**1b**) and rugulosin (**2b**) in nature, it will not be surprising if 2,2′-*epi*-cytoskyrin A (**2a**) is someday discovered as a natural product, for its structural relationship to cytoskyrin A (**1a**) is the same as that of **2b** to **1b**. The multistep "cytoskyrin cascade" was demonstrated on a model system that differed from the

[*] Prof. Dr. K. C. Nicolaou, Y. H. Lim, Dr. C. D. Papageorgiou, Dr. J. L. Piper
Department of Chemistry and
The Skaggs Institute for Chemical Biology
The Scripps Research Institute
10550 North Torrey Pines Road, La Jolla, CA 92037 (USA)
Fax: (+1) 858-784-2469
E-mail: kcn@scripps.edu
and
Department of Chemistry and Biochemistry
University of California, San Diego
9500 Gilman Drive, La Jolla, CA 92093 (USA)

[**] We thank Dr. D. H. Huang, Dr. G. Siuzdak, and Dr. R. K. Chadha for NMR spectroscopic, mass spectrometric, and X-ray crystallographic assistance, respectively. Financial support for this work was provided by grants from the National Institutes of Health (USA) and the Skaggs Institute for Chemical Biology, a predoctoral fellowship from the A*STAR NSS Overseas PhD Scholarship (to Y.H.L.), and a postdoctoral fellowship from the George E. Hewitt Foundation (to J.L.P.).

© 2005 Wiley-VCH Verlag GmbH & Co. KGaA, Weinheim

natural products by the absence of a hydroxy group at the C2 and C2′ positions (see Figure 1). The presence of these hydroxy groups was considered to be problematic for a total synthesis involving dimerization of two monomeric units, as their elimination was anticipated to be favored by aromatization, and hence facile. Although nature is probably carrying out this dimerization process with a hydroxy group in place, a recent report[1b] confirmed that attempts to synthesize the monomeric anthradihydroquinone featuring a benzyl-protected hydroxy group at the C2 and C2′ positions resulted in elimination of benzyl alcohol. Herein, we report the first biomimetic, asymmetric total synthesis of (+)-2,2′-*epi*-cytoskyrin A (**2a**) and (+)-rugulosin (**2b**) through the "cytoskyrin cascade", under conditions that successfully overcome the above-mentioned challenges.

There are four possible spatial arrangements (**A**–**D**) for the dimerization of the monomeric anthraquinones, two *endo* (**A**, **B**) and two *exo* (**C**, **D**) arrangements, which are further distinguished by the faciality of approach, the one from the top (**B**, **D**) and the one from below (**A**, **C**), as demonstrated in Figure 2. The two *endo* alignments (**A** and **B**) are equivalent and are unlikely, if not impossible, due to structural constraints. The *exo-syn* arrangement (**C**) would place the two substituted hydroxy groups (OR^1) in a *syn* arrangement resulting in the build-up of significant steric congestion and should, therefore, be disfavored. A pathway through such an arrangement would form *ent*-cytoskyrin (*ent*-**1a**) and *ent*-graciliformin (*ent*-**1b**) through the intermediacy of *O*-bridged dimers **3**. The alternative *exo-anti* arrangement (**D**), places these two interfering groups opposite to each other, hence minimizing the steric congestion and allowing the generation of 2,2′-*epi*-cytoskyrin A (**2a**) and rugulosin (**2b**). It is interesting to note that while the chirality of the monomeric anthraquinone is responsible for determining the absolute configuration of the cage, the diastereoselectivity of the dimerization step controls the relative stereochemistry of the C2 and C2′ centers relative to the rest (epimeric stereochemistry) in the final product of the cascade sequence (see also caption, Figure 2).

Reasoning that the nature of the groups (R^1) residing on the C2/C2′ hydroxy groups may make a difference in the outcome of the anticipated reactions, we proceeded to construct different monomeric units as starting materials for the cascade. Scheme 1 summarizes the synthesis of hydroquinones **11a**–**11c** featuring a Hauser annulation[6] to construct the requisite tricyclic system. Thus, protection of the known diacetate **5**[7] with MOMCl or TBSCl followed by desymmetrization using porcine liver esterase (PLE) at pH 8 afforded alcohols **6a**[8] or **6b**[7] in 95 and 90% yield, respectively, over the two steps. PCC oxidation under buffered conditions using NaOAc followed by brief (10 min) exposure to DBU at 25 °C furnished the desired enones **7a** or **7b** in 68 and 67% yield, respectively, over the two steps. The other partners for the Hauser annulation, nitriles **10a** and **10b** were synthesized as shown in Scheme 1. Thus, protection of the commercially available salicylic acids **8a** or **8b** with excess TBSCl followed by treatment with $(COCl)_2$ and a catalytic amount of DMF in CH_2Cl_2 at 0 °C afforded the corresponding acid chlorides, which were quenched with Me_2NH to furnish

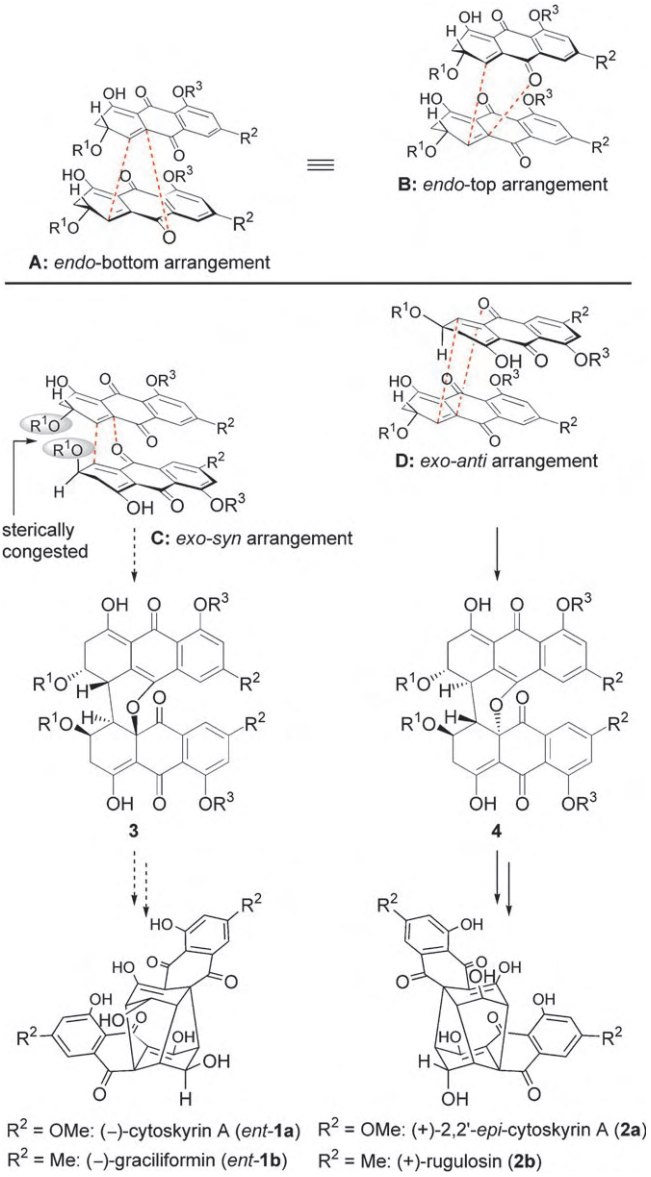

Figure 2. Stereoselectivity considerations for the dimerization step of anthradihydroquinones to modified bisanthraquinones. The shown enantiomers of the starting anthraquinones correspond to *ent*-**1a**, *ent*-**1b**, **2a**, and **2b**. Should the pathway involving arrangement **C** be possible, the opposite enantiomers would have been needed to obtain natural cytoskyrin A (**1a**) and graciliformin (**1b**).

amides **9a** or **9b** in 85 and 74% yield, respectively, over the three steps. *Ortho*-lithiation of amides **9a** or **9b** using *t*BuLi and TMEDA at −78 °C and subsequent quenching with freshly distilled DMF yielded the corresponding aldehydes. Exposure of the latter compounds to TMSCN, a catalytic amount of KCN, [18]crown-6, and AcOH afforded the deprotected nitrile compounds, which were finally treated with MOMCl and iPr_2NEt at 0 °C to furnish the required building blocks **10a** and **10b** in 64 and 50% yield, respectively, over the three steps.

With the two fragments in hand, the stage was now set for the synthesis of the requisite anthradihydroquinones **11a**–**11c**. Treatment of nitriles **10a** or **10b** with LHMDS in THF at

 © 2005 Wiley-VCH Verlag GmbH & Co. KGaA, Weinheim

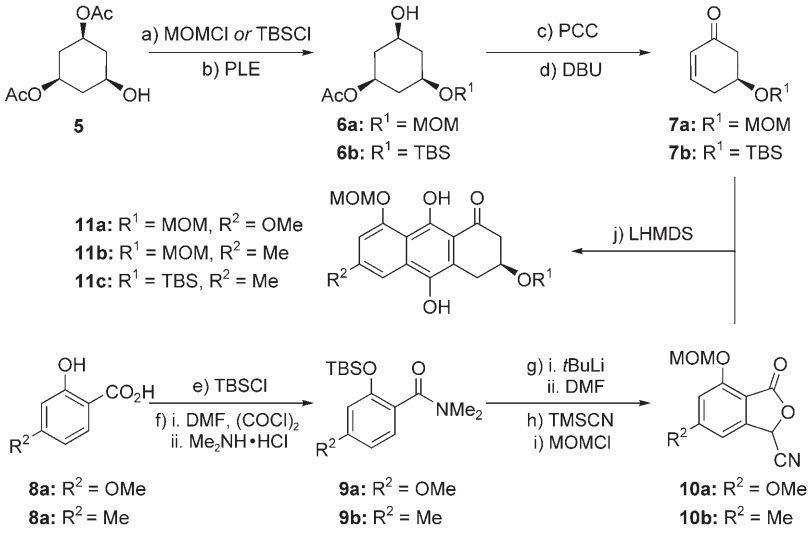

Scheme 1. Reagents and conditions: a) MOMCl (3.8 equiv), *i*Pr_2NEt (3.8 equiv), CH_2Cl_2, 25 °C, 1.5 h; TBSCl (3.8 equiv), imid (3.8 equiv), CH_2Cl_2, 25 °C, 48 h; b) PLE (1.0 equiv), buffer pH 8 (0.1 M), *t*BuOH (8% v/v), 25 °C, 4 h, 95% (**6a**), 90% (**6b**) over two steps;[8] c) PCC (3.0 equiv), NaOAc (3.0 equiv), CH_2Cl_2, 25 °C, 12 h; d) DBU (1.0 equiv), CH_2Cl_2, 25 °C, 10 min, 68% (**7a**), 67% (**7b**) over two steps; e) TBSCl (4.0 equiv), imid (6.0 equiv), DMF, 25 °C, 16 h; f) i. $(COCl)_2$ (1.25 equiv), DMF (cat.), CH_2Cl_2, 0 °C, 2 h; ii. $Me_2NH{\cdot}HCl$ (1.0 equiv), Et_3N (3.0 equiv), CH_2Cl_2, 0 °C, 30 min, 85% (**9a**), 74% (**9b**) over three steps; g) TMEDA (3.0 equiv), *t*BuLi (3.0 equiv), DMF (3.0 equiv), THF, −78→25 °C, 12 h; h) KCN (0.2 equiv), [18]crown-6 (0.2 equiv), TMSCN (1.4 equiv), CH_2Cl_2, 25 °C, 4 h; then AcOH, 12 h; i) MOMCl (1.5 equiv), *i*Pr_2NEt (1.2 equiv), CH_2Cl_2, 0 °C, 1 h, 64% (**10a**), 50% (**10b**) over three steps; j) **10** (1.1 equiv), THF, LHMDS (1.1 equiv), −78 °C; then **7** (1.0 equiv), −78→0 °C, 2 h, (submitted directly to the cascade). MOM = methoxymethyl; TBS = *tert*-butyldimethylsilyl; PLE = porcine liver esterase; PCC = pyridinium chlorochromate; DBU = 1,8-diazabicyclo[5.4.0]undec-7-ene; DMF = *N*,*N*′-dimethylformamide; TMEDA = tetramethylethylenediamine; THF = tetrahydrofuran; TMS = trimethylsilyl; LHMDS = lithium bis(trimethylsilyl)amide.

−78 °C, followed by addition of **7a** or **7b** (−78→0 °C) gave crude anthradihydroquinones **11a**–**11c**, which were directly subjected to the cytoskyrin cascade[1a] (Scheme 2). We had already established the facilitating role[1a] of MnO_2 and anticipated that the mild reaction conditions employed for the cascade coupled with the expected reluctance of the final compound to lose its alkoxy groups by virtue of Bredt's rule[9] would enable arrival at compounds **2a** and **2b**, provided that the feared elimination/aromatization pathway from the monomeric anthraquinones did not predominate. Indeed, exposure of **11a** or **11b** to MnO_2 (1.5 wt equiv) in a concentrated CH_2Cl_2 solution (0.35 M) at 25 °C for 30 min resulted in the formation of dimeric compounds **4a** or **4b** as single diastereoisomers in 64 and 32% yield, respectively, through a sequence featuring oxidation to the corresponding anthraquinone (**12a** or **12b**) and dimerization of its easily generated, under the reaction conditions, enol form. It was found that when crude **11a** or **11b** were used, the cascade was shutdown at the stage of **4a** or **4b**. This occurrence was attributed to an, as yet unknown, impurity[10] carried through from the Hauser annulation which hindered the oxidation of **4a** or **4b** to **13a** or **13b**, impeding the cascade. Prolonged exposure of the thus-obtained **4a** or **4b** to MnO_2 (12 h) resulted in quantitative formation of **16a** or **16b**, presumably through two successive retro-Michael reactions (see Scheme 3) followed by elimination and aromatization. However, treatment of purified **4a** or **4b** (flash column chromatography on silica gel) with MnO_2 (1.5 wt equiv) and Et_3N (5.0 equiv, added as soon as **14a** or **14b** were observed by thin layer chromatography (TLC), ca. 6 h) in CH_2Cl_2 at 45 °C for 12 h resulted in the formation of **15a** or **15b** in 71 and 81% yield, respectively, through the intermediacy of fleeting compounds **13a** or **13b** and **14a** or **14b**.

Use of carefully purified **11a** or **11b** (preparative TLC) enabled the realization of an impressive seven-step cascade sequence featuring the transformation of tricyclic monomers **11a** or **11b** into nonacyclic systems **15a** or **15b** in 60 and 50% yield, respectively, involving a sequence of alternating oxidations and double Michael reactions as shown in Scheme 2. The remaining mass was accounted for by the formation of aromatized monomers **16a** or **16b** in 40 and 50% yield, respectively. This cascade required treatment of **11a** or **11b** with MnO_2 (1.5 wt equiv) in CH_2Cl_2 (0.35 M) for 10 min at 25 °C, conditions that led to the formation of **4a** or **4b** as indicated by TLC, followed by tenfold dilution with CH_2Cl_2 and addition of a further 1.5 wt equiv of MnO_2 until the formation of **14a** or **14b** was complete (6 h). Finally, addition of Et_3N (5.0 equiv) and heating to 45 °C for 6 h furnished **15a** or **15b**. Exposure of the latter compounds (**15b** or **15b**) to concentrated HCl in a mixture of MeOH and THF (20:1) resulted in global deprotection, affording (+)-2,2′-*epi*-cytoskyrin A (**2a**) or (+)-rugulosin (**2b**) in 93 and 98% yield, respectively. The ^{1}H NMR spectrum of (+)-rugulosin (**2b**) in [D_6]DMSO was identical to that reported in the literature[4c] for the naturally occurring substance. Besides being anticipated on the basis of the above arguments (Figure 2), the stereochemistry of **2a** was firmly established through spectroscopic analysis. Thus, the ^{1}H NMR spectrum of synthetic (+)-2,2′-*epi*-cytoskyrin A (**2a**) exhibited doublets for H3/H3′ ($\delta = 2.85$, $J = 4.8$ Hz) and H2/H2′ ($\delta = 4.49$, $J = 4.8$ Hz), while in the spectrum reported for naturally occurring cytoskyrin A (**1a**)[2] both signals for H3/H3′ ($\delta = 2.85$) and H2/H2′ ($\delta =$ 4.00) appear as singlets. If **2a** was to have the same stereochemistry as cytoskyrin (**1a**) at C2/C2′, the dihedral angle of H1/H1′-H2/H2′ and H2/H2′-H3/H3′ would have been 78° and 85°, respectively (manual molecular models)[3] and hence the signals for H3/H3′ and H2/H2′ would have been singlets. Crystals of synthetic rugulosin (**2b**) obtained by slow crystallization from acetone containing 1% Et_3N over MeOH vapors yielded to X-ray crystallographic analysis (see ORTEP drawing,[11] Figure 3), proving unambiguously its structure and, indirectly, rendering further support for the assigned structure of (+)-2,2′-*epi*-cytoskyrin A due to the striking closeness of the ^{1}H NMR spectra of **2a** and **2b**.

Having established a viable pathway to 2,2′-*epi*-cytoskyrin A (**2a**) and rugulosin (**2b**) starting from **11a** or **11b**,

 © 2005 Wiley-VCH Verlag GmbH & Co. KGaA, Weinheim

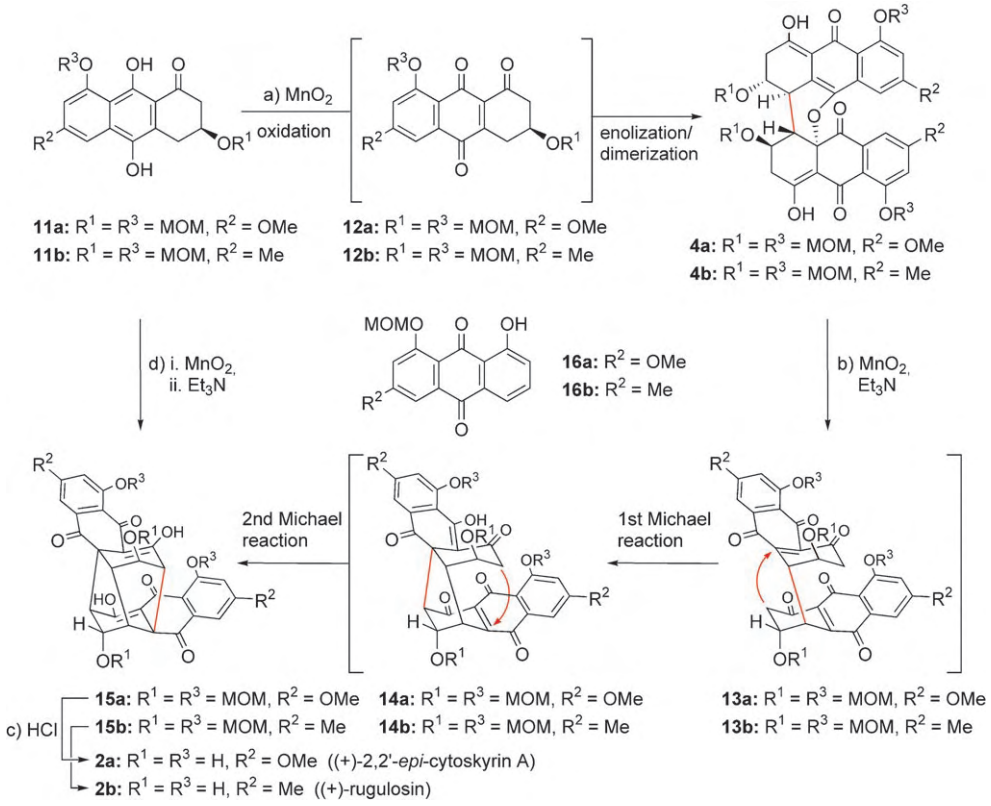

Scheme 2. The cytoskyrin cascade: synthesis of (+)-2,2′-*epi*-cytoskyrin A (**2a**) and (+)-rugulosin (**2b**) from anthradihydroquinone **11a** or **11b**, respectively. Reagents and conditions: a) MnO_2 (1.5 wt equiv), CH_2Cl_2 (0.35 M), 25 °C, 1 h, 64% (**4a**), 32% (**4b**) over five steps; b) MnO_2, (1.5 wt equiv), Et_3N (5.0 equiv), CH_2Cl_2, 25→45 °C, 12 h, 71% (**15a**), 81% (**15b**) over three steps; c) conc. HCl, MeOH, THF, 60 °C, 12 h, 93% (**2a**), 98% (**2b**); d) MnO_2 (1.5 wt equiv), CH_2Cl_2, 25 °C, 10 min; then MnO_2 (1.5 wt equiv), Et_3N (5.0 equiv), 25→45 °C, 12 h, 60% (**15a**), 40% (**16a**), 50% (**15b**), 50% (**16b**).

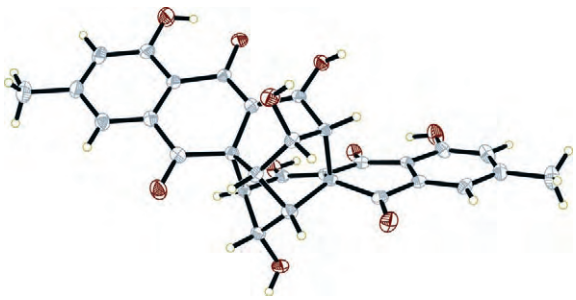

Figure 3. ORTEP drawing of rugulosin (**2b**) derived from X-ray crystallographic studies (O burgundy, C gray, H yellow). The molecule of Et_3N per molecule of **2b** is not shown. The crystallographic analysis did not reveal the absolute stereochemistry of **2b**, which was assigned as shown, on the basis of the absolute stereochemistry of the starting material and its positive optical rotation.[1c,4]

respectively, we then proceeded to investigate TBS-anthradihydroquinone **11c** as a substrate for the cytoskyrin cascade. It was reasoned that the sheer bulk of the TBS group as compared to the smaller MOM moiety was expected to retard both Michael reactions, an occurrence that could result in the isolation of some of the postulated intermediates of the cascade. Scheme 3 summarizes our findings, which indeed included the isolation of two of the reactive species involved, quinone **12c** and highly labile dimer **18**, both of which were characterized by ^{1}H NMR spectroscopy (see Table 1). Thus treatment of **11c** with MnO_2 (1.5 wt equiv) in a concentrated CH_2Cl_2 solution (0.35 M) at 25 °C for 30 min resulted in the slow formation of quinone **12c**, dimer **18**, product **4c**, and aromatized system **16b**. Moreover, compound **18**, upon standing in $CDCl_3$, slowly and quantitatively converted into **4c** and **16b** (**4c**/**16b** ≈ 1:3, as determined by ^{1}H NMR spectroscopy). This suggests that compounds **12c**, **17**, and **18** are in equilibrium with each other and that the rate of aromatization of **17** to **16b** is faster than the second Michael reaction within dimer **18** that leads to the desired compound **4c**. These observations were consistent with a stepwise mechanism for the cytoskyrin cascade involving two consecutive Michael reactions as shown in Figure 3, at least in the case of the TBS-protected derivative **11c**.

The described chemistry demonstrates the power of cascade reactions in chemical synthesis[12] and underscores the applicability of such processes in situations facing seemingly intransigent synthetic challenges. Further applications of these remarkable cascade reactions to the synthesis of other natural and designed members of the bisanthraquinone class should be forthcoming.

Received: October 17, 2005
Revised: November 2, 2005

 © 2005 Wiley-VCH Verlag GmbH & Co. KGaA, Weinheim

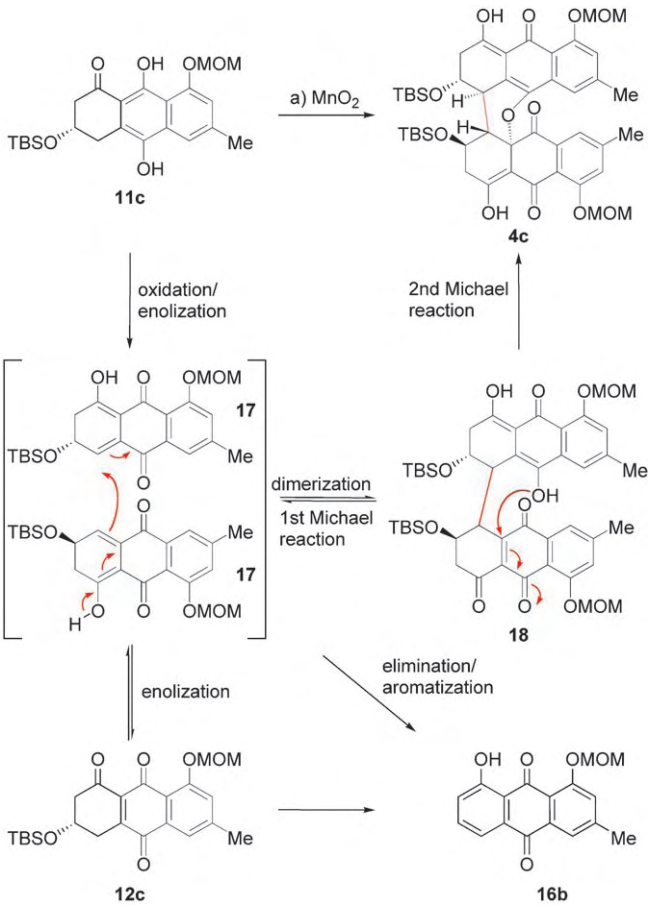

Scheme 3. Mechanistic investigation of the dimerization cascade (**11c** to **4c**). Reagents and conditions: a) MnO_2 (1.5 wt equiv), CH_2Cl_2 (0.35 M), 25 °C, 1 h, 20% **4c**; 30% **18**; 45% **16b**; 5% **12c**; ratio of products dependent on reaction time.

Keywords: anthraquinones · biomimetic synthesis · Michael reaction · natural products · total synthesis

Table 1: Selected physical properties for compounds **2a**, **2b**, **4c**, **12c**, **16b**, and **18**.

2a: $R_f = 0.53$ (benzene/acetone 2:1, oxalic acid impregnated TLC); ^{1}H NMR (500 MHz, [D$_8$]THF): $\delta = 14.60$ (2H, s), 12.10 (2H, s), 7.19 (2H, d, $J = 2.3$ Hz), 6.79 (2H, d, $J = 2.3$ Hz), 4.49 (2H, d, $J = 4.8$ Hz), 3.92 (6H, s), 3.41 (2H, br), 2.85 ppm (2H, d, $J = 4.8$ Hz); ^{13}C NMR (125 MHz, [D$_8$]THF): $\delta = 194.3$, 186.5, 182.5, 167.1, 165.5, 135.2, 111.8, 108.0, 107.4, 107.1, 69.9, 67.9, 59.0, 56.4, 49.4 ppm; HRMS (ESI-TOF): m/z calcd for $C_{30}H_{21}O_{12}^-$ $[M-H]^-$: 573.1038; found: 573.1031.

2b: $R_f = 0.50$ (benzene/acetone 4:1, oxalic acid impregnated TLC); ^{1}H NMR (500 MHz, [D$_6$]DMSO): $\delta = 14.70$ (2H, s), 11.39 (2H, s), 7.46 (2H, s), 7.20 (2H, s), 4.39 (2H, d, $J = 6.0$ Hz), 3.37 (2H, s), 2.78 (2H, d, $J = 6.0$ Hz), 2.43 ppm (6H, s); ^{13}C NMR (125 MHz, [D$_8$]THF): $\delta = 186.0$, 184.6, 162.8, 160.4, 148.7, 133.5, 124.7, 121.3, 115.7, 107.6, 70.1, 68.0, 59.3, 49.5, 22.0 ppm; HRMS (ESI-TOF): m/z calcd for $C_{30}H_{21}O_{10}^-$ $[M-H]^-$: 541.1140; found: 541.1136.

4c: $R_f = 0.43$ (MeOH/CH_2Cl_2 2:100); ^{1}H NMR (500 MHz, $CDCl_3$): $\delta = 16.28$ (1H, s), 14.79 (1H, s), 7.20 (1H, br), 6.81 (1H, br), 6.53 (1H, br), 6.30 (1H, br), 5.47–5.44 (2H, m), 5.36–5.30 (2H, m), 4.48 (1H, ddd, $J = 11.0$, 11.0, 4.8 Hz), 4.15 (1H, ddd, $J = 11.0$, 11.0, 4.8 Hz), 3.62 (3H, s), 3.57 (3H, s), 3.32 (1H, d, $J = 11.0$ Hz), 3.08 (1H, d, $J = 11.0$ Hz), 3.06 (1H, dd, $J = 17.8$, 4.8 Hz), 2.87 (1H, dd, $J = 17.8$, 4.8 Hz), 2.74 (1H, dd, $J = 17.8$, 11.0 Hz), 2.66 (1H, dd, $J = 17.8$, 11.0 Hz), 2.17 (3H, s), 1.99 (3H, s), 0.98 (9H, s), 0.94 (9H, s), 0.25 (3H, s), 0.20 (3H, s), 0.07 (3H, s), 0.00 ppm (3H, s).

12c: $R_f = 0.13$ (MeOH/CH_2Cl_2 1:100); ^{1}H NMR (500 MHz, $CDCl_3$): $\delta = 7.10$ (1H, s), 7.00 (1H, s), 5.20 (2H, s), 4.55 (1H, br), 3.63–3.53 (2H, m), 3.52 (3H, s), 2.88–2.81 (1H, m), 2.83–2.79 (1H, m), 2.23 (3H, s), 0.79 (9H, s), 0.10 (3H, s), 0.07 ppm (3H, s).

16b: $R_f = 0.85$ (MeOH/CH_2Cl_2 5:100); ^{1}H NMR (500 MHz, $CDCl_3$): $\delta = 13.03$ (1H, s), 7.85 (1H, brs, 7.78 (1H, d, $J = 7.5$ Hz), 7.62 (1H, dd, $J = 7.5$, 8.5 Hz), 7.29 (1H, d, $J = 8.5$ Hz), 7.39 (1H, brs), 5.41 (2H, s), 3.60 (3H, s), 2.51 (3H, s) ppm (3H, s); HRMS (ESI-TOF): m/z calcd for $C_{17}H_{14}O_5Na^+$ $[M+Na]^+$: 321.0733; found: 321.0731.

18: $R_f = 0.24$ (MeOH/CH_2Cl_2 2:100); ^{1}H NMR (500 MHz, $CDCl_3$): $\delta = 16.24$ (1H, s), 7.59 (1H, s), 7.49 (1H, s), 7.40 (1H, s), 7.34 (1H, s), 5.39–5.37 (2H, m), 5.33–5.31 (2H, m), 4.41–4.40 (1H, m), 4.31–4.29 (1H, m), 4.06–4.05 (1H, m), 3.90–3.89 (1H, m), 3.61 (3H, s), 3.56 (3H, s), 3.00 (1H, dd, $J = 5.3$, 1.8 Hz), 2.48 (3H, s), 2.46 (3H, s), 2.17–2.13 (2H, m), 2.00 (2H, dd, $J = 18.5$, 3.5 Hz), 0.74 (9H, s), 0.63 (9H, s), 0.13 (3H, s), 0.03 (3H, s), −0.08 (3H, s), −0.11 ppm (3H, s).

[1] a) K. C. Nicolaou, C. D. Papageorgiou, J. L. Piper, R. K. Chadha, *Angew. Chem.* **2005**, *117*, 5996–6001; *Angew. Chem. Int. Ed.* **2005**, *44*, 5846–5851; See also: b) B. B. Snider, X. Gao, *J. Org. Chem.* **2005**, *70*, 6863–6869; c) D.-M. Yang, U. Sankawa, Y. Ebizuka, S. Shibata, *Tetrahedron* **1976**, *32*, 333–335.

[2] S. F. Brady, M. P. Singh, J. E. Janso, J. Clardy, *Org. Lett.* **2000**, *2*, 4047–4049.

[3] H. Ejiri, U. Sankawa, S. Shibata, *Phytochemistry* **1975**, *14*, 277–279.

[4] a) Y. Ogihara, N. Kobayashi, S. Shibata, *Tetrahedron Lett.* **1968**, 1881–1886; b) S. Shibata, *Pure Appl. Chem.* **1973**, *33*, 109–128; c) N. Takeda, S. Seo, Y. Ogihara, U. Sankawa, I. Iitaka, I. Kitagawa, S. Shibata, *Tetrahedron* **1973**, *29*, 3703–3719; d) S. Seo, U. Sankawa, Y. Ogihara, Y. Iitaka, S. Shibata, *Tetrahedron* **1973**, *29*, 3721–3726.

[5] S. B. Singh, H. Jayasuriya, R. Dewey, J. D. Polishook, A. W. Dombrowski, D. L. Zink, Z. Guan, J. Collado, G. Platas, F. Pelaez, P. J. Felock, D. J. Hazuda, *J. Ind. Microbiol. Biotechnol.* **2003**, *30*, 721–731.

[6] F. M. Hauser, S. Chakrapani, W. P. Ellenberger, *J. Org. Chem.* **1991**, *56*, 5248–5250.

[7] U. R. Kalkote, S. R. Ghorpade, S. P. Chavan, T. Ravindranathan, *J. Org. Chem.* **2001**, *66*, 8277–8281.

[8] The enantiomeric ratio (e.r.) of compound **6a** was determined by Mosher ester analysis (^{1}H NMR and HPLC) to be 85:15. Optimization of this desymmetrization reaction is currently underway. The e.r. of **6b** was assumed to be the same (i.e. 98:2) as in reference [7].

[9] a) J. Bredt, H. Thouet, J. Schmitz, *Justus Liebigs Ann. Chem.* **1924**, *427*, 1; b) S. I. Weissman, *J. Am. Chem. Soc.* **1967**, *89*, 5966–5968; c) W. F. Maier, P. R. Schleyer, *J. Am. Chem. Soc.* **1981**, *103*, 1891–1900.

[10] The impurities that impeded the cascade were carried through from the Hauser annulation and were not batch specific.

[11] CCDC-286831 (**2b**) contains the supplementary crystallographic data for this paper. These data can be obtained free of charge from The Cambridge Crystallographic Data Centre via www.ccdc.cam.ac.uk/data_request/cif.

[12] For a review highlighting a number of cascade reactions in total synthesis, see: K. C. Nicolaou, T. Montagnon, S. N. Snyder, *Chem. Commun.* **2003**, 551–564.

 © 2005 Wiley-VCH Verlag GmbH & Co. KGaA, Weinheim

Electrooptic Systems

DOI: 10.1002/anie.200501581

Exceptional Molecular Hyperpolarizabilities in Twisted π-Electron System Chromophores**

*Hu Kang, Antonio Facchetti, Peiwang Zhu, Hua Jiang, Yu Yang, Elena Cariati, Stefania Righetto, Renato Ugo, Cristiano Zuccaccia, Alceo Macchioni, Charlotte L. Stern, Zhifu Liu, Seng-Tiong Ho, and Tobin J. Marks**

Molecule-based electrooptic (EO) materials are of intense research interest for understanding how light interacts with matter and for applications in photonic technologies such as high-speed optical communications, integrated optics, and optical data processing and storage.[1] In such materials, the second-order susceptibility tensor governing EO response (r_{33}), is governed both by the net polar microstructural order and the microscopic molecular first hyperpolarizability tensor (β). Large β values are essential for large EO response, and the quest for higher performance EO chromophores presents a daunting challenge.[1] To date, effective chromophores have been designed according to similar principles embodied in the classical "two-level" model: conjugated π systems end-capped with donor (D) and acceptor (A) moieties.[2] Elegant efforts have sought maximum β by optimizing D and A strengths and conjugation pathways,[3] directed by "bond length alternation"[4] and "auxiliary donor and acceptor" models.[5] Such strategies utilize extended *planar* π-conjugation, resulting in chromophores that are inherently elaborate structurally, complicating synthesis and introducing potential chemical, thermal, and photochemical instabilities.[6] Alternative routes to very large-β chromophores would clearly be desirable, and there is growing evidence that simple two-level systems may not provide access.[7]

Recent theoretical work suggests that unconventional chromophores with *twisted* π-electron systems bridging D and A substituents (TICTOID = twisted intramolecular charge-transfer; Scheme 1) may exhibit unprecedented hyperpolarizabilities through non-classical mechanisms.[8] These would have relatively simple biaryl structures in which β is sterically tunable through R^1, R^2 modification of the interplanar dihedral angle (θ). Large β magnitudes are predicted at $\theta \approx 70$–$85°$,[8a] with twist-induced reduction in D–π–A conjugation leading to charge-separated zwitterionic ground states. The intriguing question is whether such molecules, with small numbers of π-electrons, could thereby exhibit far larger β values than conventional planar chromophores.

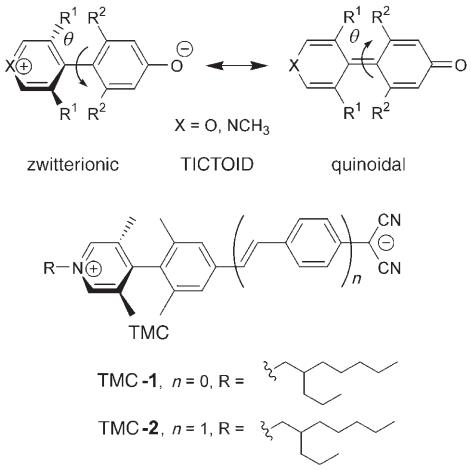

Scheme 1. Structures of TICTOID and TMC (twisted π-electron system molecular chromophore).

We report here the first realization of such TICTOID chromophores, that they have unprecedented hyperpolarizabilities on the order of 10–20× larger than previously observed,[1–5] and that these are not simple two-level systems. The new chromophores (Scheme 1) were designed according to the following criteria: 1) Synthetically challenging tetra-*ortho*-alkylbiaryl cores should enforce large interplanar angles, judging from bimesityl ($\theta \approx 90°$).[9] 2) Dicyanomethanide and pyridinium groups should be effective D and A substituents, with dicyanomethanide more stable than phenoxide.[10] 3) Pyridine alkylations should enhance solubility and processability (TMC-1 and TMC-2), with styrenic substitution further enhancing β (TMC-2).

TMC syntheses (Scheme 2) begin with precursor **1**, synthesized as reported elsewhere.[10] Pd-catalyzed $NaCH(CN)_2$ coupling affords **2**, which is then regioselectively quaternized[11] and deprotonated to afford TMC-1. Precursor **3** is synthesized by Pd-catalyzed coupling of 1-iodo-4-vinylbenzene with $NaCH(CN)_2$. Subsequent Heck-coupling of **1** and **3** affords precursor **4**, which is then alkylated and

[*] H. Kang, Dr. A. Facchetti, Dr. P. Zhu, Dr. H. Jiang, Dr. Y. Yang, C. L. Stern, Prof. T. J. Marks
Department of Chemistry and the Materials Research Center
Northwestern University
2145 Sheridan Road, Evanston, IL 60208-3113 (USA)
Fax: (+1) 847-491-2990
E-mail: t-marks@northwestern.edu
Dr. Z. Liu, Prof. S.-T. Ho
Department of Electrical and Computer Engineering
Northwestern University
2145 Sheridan Road, Evanston, IL 60208 (USA)
Prof. E. Cariati, S. Righetto, Prof. R. Ugo
Dipartimento di Chimica Inorganica Metallorganica e Analitica and Centro di Eccellenza CIMAINA
dell'Università di Milano
and Unità di Ricerca dell'INSTM di Milano
Via Venezian 21, 20133 Milano (Italy)
Dr. C. Zuccaccia, Prof. A. Macchioni
Dipartimento di Chimica
Università di Perugia
Via Elce di Sotto 8, 06123 Perugia (Italy)

[**] Supported by DARPA/ONR (SP01P7001R-A1/N00014-00-C), the NSF-Europe Program (DMR-0353831), and MIUR(PRIN 2004–2005). We thank Dr. S. Keinan and Prof. M. Ratner for computational collaboration.

Supporting information for this article is available on the WWW under http://www.angewandte.org or from the author.

InterScience DISCOVER SOMETHING GREAT
© 2005 Wiley-VCH Verlag GmbH & Co. KGaA, Weinheim

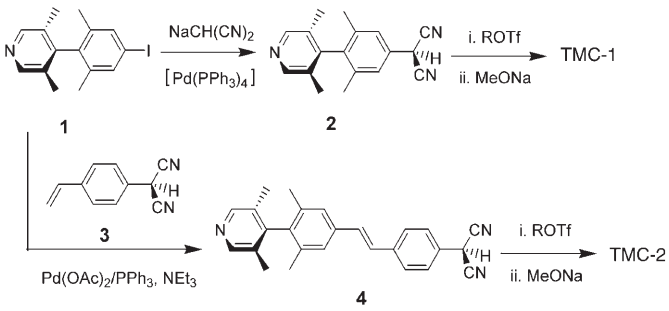

Scheme 2. Synthesis of twisted π-electron chromophores. Tf = trifluoromethanesulfonyl.

deprotonated to yield TMC-2. The new zwitterions are air- and moisture-stable, purifiable by column chromatography, and were characterized by conventional techniques.[12] Thermogravimetric analysis indicates very high chromophore thermal stability ($T_d \approx 306\,°C$ for TMC-1, $\approx 330\,°C$ for TMC-2),[12] while ^1H NMR indicates stability in [D$_6$]DMSO solution at 150 °C for periods of hours under air.

Single-crystal diffraction data for TMC-1[13] reveal a large arene–arene dihedral twist angle (89°; Figure 1). The fact that twisting is governed primarily by tetra-*ortho*-methylbiaryl

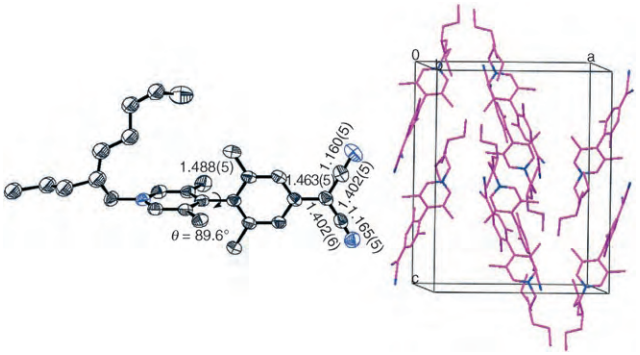

Figure 1. Left: ORTEP drawing (50% probability ellipsoids) of the TMC-1 molecule. Hydrogen atoms are omitted for clarity. Right: Packing diagram.

steric interactions and is independent of chromophore architecture is argued by nearly identical angles in several other TMC-type molecules.[10] The TMC-1 (ring)C–C(ring) distance (1.488(5) Å) is close to that in typical biphenyls ($\approx$1.487 Å),[14] indicating steric crowding, consequent reduction in inter-ring π-conjugation, and departure from quinoidal structures where (ring)C=C(ring) $\approx$ 1.349 Å.[14] The phenylenedicyanomethanide fragment displays different bond length patterns than in typical TCNQs;[14,15] the (NC)$_2$C-bound phenylene ring has less quinoidal character, and the (dicyanomethanide)C–C(aryl) distance (1.463(5) Å) lacks TCNQ C=C(CN)$_2$ exocyclic character ($\approx$1.392 Å).[14] This metrical pattern indicates negative charge localization on the C(CN)$_2$ group, also evident from C–CN bond shortening and C≡N bond elongation (TCNQ distances are 1.427 Å and 1.144 Å, respectively).[14] Finally, there is significant pyridinium aromatic character, with molecular dimensions paralleling those in *N*-methyl-*p*-phenylpyridinium salts[16] rather than in cyclopentadienylidene-1,4-dihydropyridines.[17] Together, these metrical parameters confirm a charge-separated zwitterionic TICTOID ground state. Importantly, close correspondence between solid-state ^{13}C NMR and optical spectra and those recorded in solution[12] argue that this structure persists essentially unchanged in solution.[18] As might be expected, the present zwitterion packs centrosymmetrically in pairs (Figure 1), likely a result of electrostatic dipole–dipole interactions (reasonable considering the large computed dipole moments).[19]

Optical spectra further support a zwitterionic ground state, with oscillator strengths unexceptional for two-level chromophores.[1–5] Thus, TMC-1 exhibits two fairly short wavelength maxima, assigned to pyridinium and phenyl subfragment high-energy intra-ring excitations, and one low-energy inter-subfragment charge-transfer (CT) excitation (Figure 2a).[8] The TMC-1 CT bands exhibit strong negative

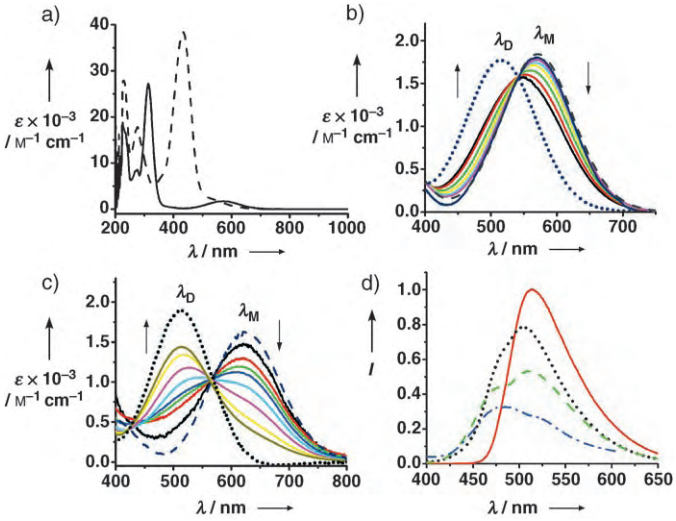

Figure 2. a) Optical absorption spectra of TMC chromophores in CH_2Cl_2 solution. Solid line: TMC-1; dashed line: TMC-2. b, c) Concentration-dependent TMC-1 spectra in CH_2Cl_2 solution (b) (3.0×10^{-3}–2.0×10^{-5} M) and in $CHCl_3$ solution (c) (5.6×10^{-4}–4.5×10^{-6} M). Arrows indicate changes in CT bands upon dilution. The monomer (dashed line) and dimer (dotted line) spectra were derived from the data at two different concentrations and $K_{dimerize}$. d) Variable-concentration fluorescence spectra (λ_{ex} = 300–350 nm) of TMC-2 in CH_2Cl_2. Intensities are normalized. I = fluorescence intensity. Solid line: 5×10^{-4} M, dotted line: 5×10^{-5} M, dashed line: 5×10^{-6} M, dash-dotted line: 2.5×10^{-6} M.

solvatochromism – large blue-shifts with increasing the solvent polarity (Table 1), indicating that the ground state dipole moment is substantially larger than in the excited state, consistent with the dominant zwitterionic ground state (and a negative β). TMC aggregation observed in the solid state is further evidenced in CH_2Cl_2 solution by concentration-dependent optical spectra (Figure 2b), exhibiting a red-shift and increase of CT band intensity upon dilution in the range of 10^{-3}–10^{-4} M (H-aggregation), with an isosbestic point supporting well-defined aggregation equilibria.[20]

To estimate binding energetics, the TMC-1 extinction coefficient was analyzed[20] as a function of concentration,

 © 2005 Wiley-VCH Verlag GmbH & Co. KGaA, Weinheim

Table 1: Solvatochromic optical spectroscopic data and estimated changes in dipole moment from ground to excited state for TMC chromophores in selected solvents.[a]

Solvent (E_T)	TMC-1			TMC-2		
	λ_{max} (ε)[b]	λ_{max} (ε)[c]	$\Delta\mu$[d]	λ_{max} (ε)[b]	λ_{max} (ε)[c]	$\Delta\mu$[d]
MeOH (0.76)	297	451		397	–	
DMF (0.40)	310	478		427	–	
			64			151
CH_2Cl_2 (0.31)	314 (27200)	569 (1840)		433 (38400)	540[e] (2090)	
THF (0.21)	320	592		451	578[e]	

[a] λ_{max} in nm, ε in $M^{-1}cm^{-1}$, $\Delta\mu$ in 10^{-30} C m. Solvent polarity given by the normalized E_T parameter. [b] Assigned to intra-subfragment excitation. Another high-energy subfragment excitation overlaps with the solvent (except CH_2Cl_2) and is not tabulated here. [c] Assigned to low-energy inter-subfragment charge-transfer (CT) excitation. [d] DFT-derived change in dipole moment from ground to excited state. [e] Deconvoluted from the subfragment excitation band and assigned to inter-subfragment CT.

assuming a simple dimerization model, and yields $K_{dimerize} = 250 \pm 30\,M^{-1}$ and $\Delta G^{o}_{dimerize} = -13.6 \pm 0.3\,kJ\,mol^{-1}$ in CH_2Cl_2. Concentration-dependent TMC-1 studies (Figure 2c) in less polar $CHCl_3$ yield larger $K_{dimerize}$ and $\Delta G^{o}_{dimerize}$ values of $13300 \pm 1420\,M^{-1}$ and $-23.5 \pm 0.3\,kJ\,mol^{-1}$, respectively, not unexpectedly indicating that the aggregation is weaker in more polar solvents and also somewhat stronger than in typical planar merocyanine zwitterions.[20]

The TMC-2 spectrum features an intense band at 433 nm in CH_2Cl_2 doubtless involving stilbenyl subfragment excitation,[8b] overlapping a weaker CT band centered at 540 nm (Figure 2a). Both subfragment and CT bands again exhibit negative solvatochromism (Table 1). Variable-concentration TMC-2 fluorescence spectra (Figure 2d) reveal a clear transition from dimer (515 nm) to monomer (485 nm) in the range of 5×10^{-4}–2.5×10^{-6} M, providing confirmation of aggregation.

Additional quantitative information on the state of TMC chromophore aggregation is provided by PGSE (pulsed field gradient spin-echo) NMR spectroscopy (Figure 3).[21] Here, experimentally determined translational self-diffusion coefficients (D_t), hydrodynamic radii (r_H), volumes (V_H), and the ratio between V_H and the van der Waals volume afford aggregation numbers (N) readily identifying the aggregation level in solution ($N = 1.0$, 1.5, or 2.0 means 100% monomer, 50% monomer + 50% dimer, or 100% of dimer, respectively).[21c] The trends in N versus $\log c$ (Figure 3) clearly show that monomer predominates in [D$_6$]DMSO (ε_r^{25} = relative permittivity at 25 °C = 46.45) for both TMC-1 and TMC-2 over the entire concentration range (see Supporting Information). In CD_2Cl_2 ($\varepsilon_r^{25} = 8.93$), TMC-1 is exclusively monomeric only at the lowest concentrations examined (4×10^{-6} M, Supporting Information) while dimers (see Supporting Information) and even larger aggregates (Figure 3, Supporting Information) are present at the highest concentrations (Figure 3). TMC-2 exhibits a greater aggregation tendency and is not exclusively monomeric even at 5×10^{-6} M (see Supporting Information). For TMC-2, aggregates larger than dimers are present at the highest concentrations (Figure 3, Supporting Information).

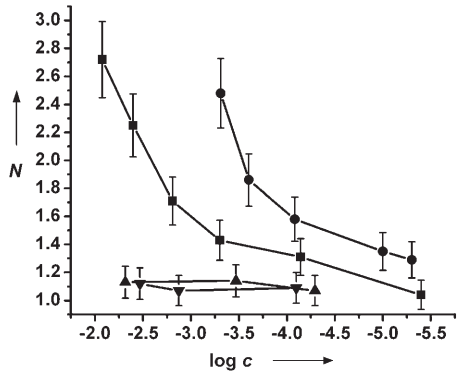

Figure 3. PGSE NMR-derived aggregation numbers (N) as a function of concentration for chromophores TMC-1 in CD_2Cl_2 (●) and [D$_6$]DMSO (▲), and TMC-2 in CD_2Cl_2 (■) and [D$_6$]DMSO (▼). Lines are drawn as guides to the eye. c = concentration [M].

Hyperpolarizabilities were measured at 1907 nm in CH_2Cl_2 by electric field-induced second harmonic generation (EFISH)[22] and track the same concentration-dependence as observed in the optical and PGSE spectra. Thus, the TCM-1 and TCM-2 $\mu\beta$ values show pronounced concentration dependence due to the aforementioned aggregation effects (Figure 4). The TCM-1 $\mu\beta$ rapidly increases as concentration falls, with $\mu\beta$ saturating at a very large[1–5] $-24000 \pm 4320 \times 10^{-48}$ esu at 5×10^{-6} M. The increase with dilution indicates dissociation of (presumably centrosymmetric) aggregates, paralleling the PGSE data, as expected. Note that $\mu\beta$ approaches a maximum at concentrations where the PGSE measurements indicate the presence of more than 80% monomer. TCM-2 deaggregation occurs at somewhat lower concentrations (10^{-5}–10^{-6} M), in good agreement with the PGSE data, with an unprecedented $\mu\beta$ value of $-488000 \pm 48800 \times 10^{-48}$ esu at 8×10^{-7} M.[23] From the reliably computed μ[19] we estimate $\beta_{0.65eV} \approx 9800 \times 10^{-30}$ esu. To our knowledge, these are the largest off-resonance $\mu\beta$ and β values ever achieved for any molecule.[1–5]

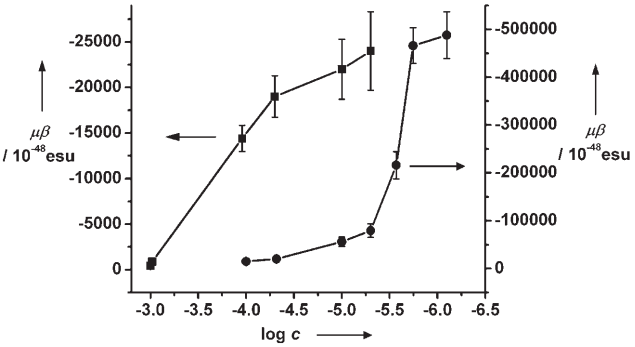

Figure 4. EFISH-derived $\mu\beta$ data for chromophores TMC-1 (■) and TMC-2 (●) versus concentration in CH_2Cl_2 at 1907 nm. Lines are drawn as guides to the eye. c = concentration [M].

 © 2005 Wiley-VCH Verlag GmbH & Co. KGaA, Weinheim

Preliminary Teng and Man[24] measurements on poled TMC-1 and TMC-2 containing guest–host polymers reveal very large EO coefficients (r_{33}) at 1310 nm. Poly(vinylphenol) films containing 10 wt % TMC-1 and 5 wt % TMC-2, poled at 100 $V\,\mu m^{-1}$, exhibit nonresonant r_{33} responses of 48 and 320 $pm\,V^{-1}$, respectively. Lower EO responses are observed in less polar matrices, presumably due to the aggregation. These results suggest obvious molecular and macromolecular modification strategies, currently under investigation, to address the aggregation issue and to further enhance r_{33}.

In summary, twisted π-electron system chromophores have been prepared and exhibit exceptional molecular hyperpolarizabilities, with nonresonant $\mu\beta$ values as high as -488000×10^{-48} esu, while preliminary poled guest–host experiments indicate promise for EO applications. An interesting observation here is that the ultralarge hyperpolarizabilities exhibited by these unconventional chromophores seem far beyond classical two-level behavior. Kuzyk argues that the β responses of all organic chromophores prepared to date fall far short of the theoretical quantum limits, for reasons that are presently not entirely clear.[25] Twisted π-electron system chromophores may provide new insight into the reasons.

Received: May 10, 2005
Revised: September 20, 2005
Published online: November 21, 2005

Keywords: chromophores · electrooptics · nonlinear optics · pi systems · zwitterions

[1] Recent reviews of EO materials: a) L. R. Dalton, *Pure Appl. Chem.* **2004**, *76*, 1421–1433; b) F. Kajzar, K.-S. Lee, A. K.-Y. Jen, *Adv. Polym. Sci.* **2003**, *161*, 1–85; c) M. G. Kuzyk, *Phys. Rev. Lett.* **2000**, *85*, 1218–1221; d) *Molecular Nonlinear Optics: Materials, Phenomena and Devices* (Ed.: J. Zyss), *Chem. Phys.* **1999**, *245* (Special issue); e) T. Verbiest, S. Houbrechts, M. Kauranen, K. Clays, A. Persoons, *J. Mater. Chem.* **1997**, *7*, 2175–2189; f) S. R. Marder, B. Kippelen, A. K.-Y. Jen, N. Peyghambarian, *Nature* **1997**, *388*, 845–851.

[2] S. R. Marder, D. N. Beratan, L.-T. Cheng, *Science* **1991**, *252*, 103–106.

[3] a) K. Staub, G. A. Levina, S. Barlow, T. C. Kowalczyk, H. S. Lackritz, M. Barzoukas, A. Fort, S. R. Marder, *J. Mater. Chem.* **2003**, *13*, 825–833; b) A. Abbotto, L. Beverina, S. Bradamante, A. Facchetti, C. Klein, G. A. Pagani, M. Redi-Abshiro, R. Wortmann, *Chem. Eur. J.* **2003**, *9*, 1991–2007; c) A. K.-Y. Jen, H. Ma, X. Wu, J. Wu, S. Liu, S. R. Marder, L. R. Dalton, C.-F. Shu, *SPIE Proc.* **1999**, *3623*, 112–119.

[4] S. R. Marder, L. T. Cheng, B. G. Tiemann, A. C. Friedli, M. Blanchard-Desce, J. W. Perry, J. Skindhoej, *Science* **1994**, *263*, 511–514.

[5] I. D. L. Albert, T. J. Marks, M. A. Ratner, *J. Am. Chem. Soc.* **1997**, *119*, 6575–6582.

[6] A. Galvan-Gonzalez, K. D. Belfield, G. I. Stegeman, M. Canva, S. R. Marder, K. Staub, G. Levina, R. J. Twieg, *J. Appl. Phys.* **2003**, *94*, 756–763, and references therein.

[7] a) S. Di Bella, *New J. Chem.* **2002**, *26*, 495–497; b) G. Meshulam, G. Berkovic, Z. Kotler, *Opt. Lett.* **2001**, *26*, 30–32; c) S. Brasselet, J. Zyss, *J. Nonlinear Opt. Phys. Mater.* **1996**, *5*, 671–693; d) I. Ledoux, J. Zyss, *Pure Appl. Opt.* **1996**, *5*, 603–612.

[8] a) S. Keinan, E. Zojer, J.-L. Bredas, M. A. Ratner, T. J. Marks, *THEOCHEM* **2003**, *633*, 227–235; b) I. D. L. Albert, T. J. Marks, M. A. Ratner, *J. Am. Chem. Soc.* **1998**, *120*, 11174–11181; c) S. Keinan, M. A. Ratner, T. J. Marks, unpublished computations.

[9] R. Fröhlich, H. Musso, *Chem. Ber.* **1985**, *118*, 4649–4651.

[10] H. Kang, A. Facchetti, C. Stern, A. L. Rheingold, W. S. Kassel, T. J. Marks, *Org. Lett.* **2005**, *7*, 3721–3724.

[11] A. Abbotto, S. Bradamante, A. Facchetti, G. A. Pagani, *J. Org. Chem.* **1997**, *62*, 5755–5765.

[12] See Supporting Information.

[13] TMC-1 crystals were grown from saturated acetonitrile solutions. All measurements were made on a Bruker SMART CCD diffractometer with graphite-monochromated $Mo_{K\alpha}$ (0.71073 Å) radiation at 153(2) K. The structure was solved by direct methods and Fourier techniques with SHELXTL. Non-hydrogen atoms were refined anisotropically. The hydrogen atoms were included in idealized positions, but not refined. $C_{28}H_{37}N_3$, $M=415.60$, orthorhombic, *Pbca*, $a=15.6106(16)$, $b=16.1279(17)$, $c=19.714(2)$ Å, $V=4963.2(9)$ Å^3, $Z=8$, $\rho_{cald}=1.110\,g\,cm^{-3}$, $2\theta_{max}=57.64°$. Of the 43353 reflections which were collected, 6031 were independent ($R_{int}=0.0654$), 269 parameters, $R_1=0.0865$ (for reflections with $I>2\sigma(I)$), $wR_2=0.3100$ (for all reflections). CCDC 282594 contains the supplementary crystallographic data for this paper. These data can be obtained free of charge from The Cambridge Crystallographic Data Centre via www.ccdc.cam.ac.uk/data_request/cif.

[14] F. H. Allen, O. Kennard, D. G. Watson, L. Brammer, A. G. Orpen, R. Taylor, *J. Chem. Soc. Perkin Trans. 2* **1987**, S1.

[15] J. C. Cole, J. M. Cole, G. H. Cross, M. Farsari, J. A. K. Howard, M. Szablewski, *Acta Crystallogr. Sect. B* **1997**, *53*, 812–821.

[16] A. Das, J. C. Jeffery, J. P. Maher, J. A. McCleverty, E. Schatz, M. D. Ward, G. Wollermann, *Inorg. Chem.* **1993**, *32*, 2145–2155.

[17] H. L. Ammon, G. L. Wheeler, *J. Am. Chem. Soc.* **1975**, *97*, 2326–2336.

[18] Variations in θ should significantly affect the relative contributions of quinoid versus zwitterion structures, hence ^{13}C NMR and optical spectra.

[19] DFT-derived ground state dipole moments are 27.0 and 50.6 D for TMC-1 and TMC-2, respectively (S. Keinan, M. A. Ratner, T. J. Marks).

[20] Merocyanine dye aggregation studies reveal CT band blue-shifts due to centrosymmetric dimers: F. Würthner, S. Yao, T. Debaerdemaeker, R. Wortmann, *J. Am. Chem. Soc.* **2002**, *124*, 9431–9447.

[21] a) C. S. Johnson, Jr., *Prog. Nucl. Magn. Reson. Spectrosc.* **1999**, *34*, 203–256; b) P. Stilbs, *Prog. Nucl. Magn. Reson. Spectrosc.* **1987**, *19*, 1–45; c) D. Zuccaccia, A. Macchioni, *Organometallics* **2005**, *24*, 3476–3486; d) C. Zuccaccia, N. G. Stahl, A. Macchioni, M.-C. Chen, J. A. Roberts, T. J. Marks, *J. Am. Chem. Soc.* **2004**, *126*, 1448–1464.

[22] a) D. Roberto, R. Ugo, S. Bruni, E. Cariati, F. Cariati, P. Fantucci, I. Invernizzi, S. Quici, I. Ledoux, J. Zyss, *Organometallics* **2000**, *19*, 1775–1788; b) I. Ledoux, J. Zyss, *Chem. Phys.* **1982**, *73*, 203–213; c) K. D. Singer, A. F. Garito, *J. Chem. Phys.* **1981**, *75*, 3572–3580.

[23] EFISH measurements in DMF confirm the very large TCM-2 response, with $\mu\beta=-84000\times10^{-48}$ esu at 1.1×10^{-6} M. That the magnitude of β is lower in more polar solvents is common for zwitterions.[3b]

[24] a) C. C. Teng, H. T. Man, *Appl. Phys. Lett.* **1990**, *56*, 1734–1736; b) J. S. Schildkraut, *Appl. Opt.* **1990**, *29*, 2839–2842.

[25] K. Tripathy, J. P. Moreno, M. G. Kuzyk, B. J. Coe, K. Clays, A. M. Kelley, *J. Chem. Phys.* **2004**, *121*, 7932–7945.

 © 2005 Wiley-VCH Verlag GmbH & Co. KGaA, Weinheim

Sensors

DOI: 10.1002/anie.200503121

Indole-Based Macrocycles as a Class of Receptors for Anions**

*Kyoung-Jin Chang, Dohyun Moon, Myoung Soo Lah, and Kyu-Sung Jeong**

The development of synthetic receptors and chemosensors for anions[1] has attracted much attention in recent years as the fundamental role of anions in biological and chemical processes has become increasingly understood. Biomacromolecules such as sulfate-binding proteins and a CIC chloride channel make use of hydrogen bonds as a major driving force to bind or transport anions through cell membranes.[2] Similarly, hydrogen-bonding interactions are widely implemented for the construction of artificial receptors, and amido and ureido groups have frequently been incorporated for this purpose.[1,3,4] Furthermore, the pyrrolic NH group has also been used as a hydrogen-bond donor to an anion, as demonstrated in calixpyrroles,[5] expanded porphyrinoids,[6] and amidopyrroles.[7]

Herein, we describe the synthesis and binding properties of indole-based macrocycles **1** and **2**, which can function as a new class of synthetic receptors for anions.[8] The macrocycles contain a well-defined internal cavity surrounded by four indole NH hydrogen atoms, thus are capable of binding anions strongly through hydrogen-bonding interactions. More interestingly, **1** and **2** showed separate sets of ^{1}H NMR signals for the free macrocycles and their complexes at room temperature in all cases and thus can serve as chemosensors for anions based on ^{1}H NMR chemical shifts.

The synthesis of **1** and **2** is outlined in Scheme 1. The key molecular building block 7,7′-diiodo-2,2′-biindole (**4**) was prepared by oxidative dimerization ($Cu(OAc)_2$, 95%)[9] followed by double indolization (CuI, 81%)[10] of 4-*tert*-butyl-2-ethynyl-6-iodoanilne (**3**).[11] In turn, **4** was converted into a diethynyl derivative **5**. After numerous unsuccessful attempts,[12] the coupling reaction of **4** and **5** under the copper-free conditions described by Soheili et al. gave **1** in a reasonable yield (64%).[13] Similarly, the ethynylene-bridged macrocycle **2** was synthesized from compound **6**,[11] and the yield for the final coupling step was 73%. The structures of **1** and **2** were elucidated by elemental analyses, ^{1}H NMR spectroscopy (including ^{1}H-^{1}H NOESY experiments), and FAB mass spectrometry.

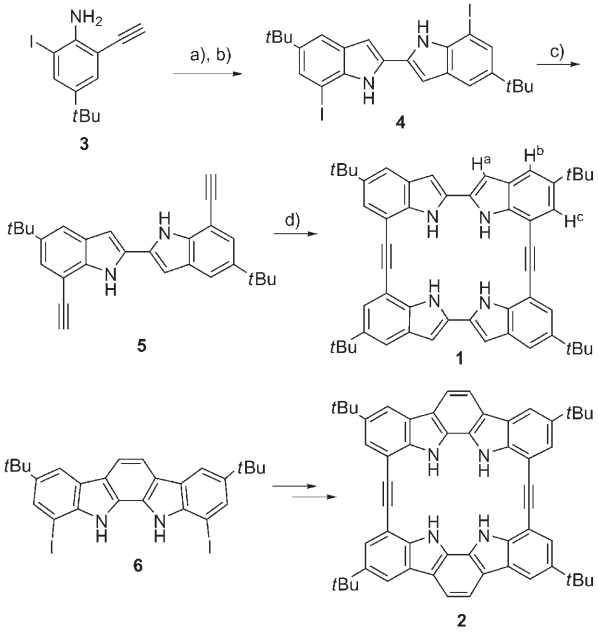

Scheme 1. Reaction conditions: a) $Cu(OAc)_2 \cdot H_2O$, pyridine, RT, 95%; b) CuI, DMF, 100–110°C, 81%; c) $[Pd(dba)_2]$, CuI, PPh_3, TMS-acetylene, Et_3N/THF, 54–55°C, 80%, then K_2CO_3, MeOH, RT, 90%; d) $[(allylPdCl)_2]$, P(*t*Bu)$_3$, DABCO, CH_3CN/toluene, RT, 64%. dba = *trans*,*trans*-dibenzylidineacetone, TMS = trimethylsilyl, DABCO = 1,4-diazabicyclo[2.2.2]octane.

Computer modeling studies show that **1** and **2** are highly rigid, flat structures[14] as a result of full conjugation of all the indole rings without any flexible bonds (see the Supporting Information). The cavity sizes of **1** and **2** are nearly identical; the diagonal distances between the NH hydrogen atoms in the internal cavities are 3.7 Å for **1** and 3.6 Å for **2**. The widths and heights of the cavities of **1** and **2** are 2.5 and 2.7 Å, and 2.8 and 2.3 Å, respectively. These structural features were confirmed by single-crystal X-ray diffraction analysis[15] of the complex formed between **2** and $Bu_4N^+Cl^-$ (Figure 1). The chloride ion is located in the middle of four indole NH groups and stabilized by four hydrogen bonds with N···Cl$^-$ distances of 3.14(±0.01) Å. The chloride ion is only partially inserted into the cavity of **2**, which implies that the internal size is slightly too small for the chloride ion. It is also worth mentioning that the tetrabutylammonium countercation sits in the plane of the aryl rings, possibly as a consequence of cation–π interactions.The binding properties of **1** and **2** in solution were studied first by ^{1}H NMR spectroscopy. The symmetrical nature of **1** and **2** results in the ^{1}H NMR spectra being very simple; for example, **1** exhibits only five singlets at $\delta = 10.9$ (NH), 7.15 (H_c), 7.01 (H_b), 6.56 (H_a), and 1.24 ppm (*t*Bu) in CD_3CN. Addition of an anion (0.5 equiv) resulted in a new set of ^{1}H NMR signals corresponding to its complex

[*] K.-J. Chang, Prof. Dr. K.-S. Jeong
Center for Bioactive Molecular Hybrids and Department of Chemistry
Yonsei University
Seoul 120-749 (Korea)
Fax: (+82) 2-364-7050
E-mail: ksjeong@yonsei.ac.kr
D. Moon, Prof. Dr. M. S. Lah
Department of Chemistry and Applied Chemistry
College of Science and Technology
Hanyang University
1271 Sa-1-dong, Ansan, Kyunggi-do 426-791 (Korea)

[**] This work was supported by a Korea Research Foundation Grant (KRF-2004-041-C00215) and the Center for Bioactive Molecular Hybrids (CBMH).

Supporting information for this article is available on the WWW under http://www.angewandte.org or from the author.

InterScience
© 2005 Wiley-VCH Verlag GmbH & Co. KGaA, Weinheim

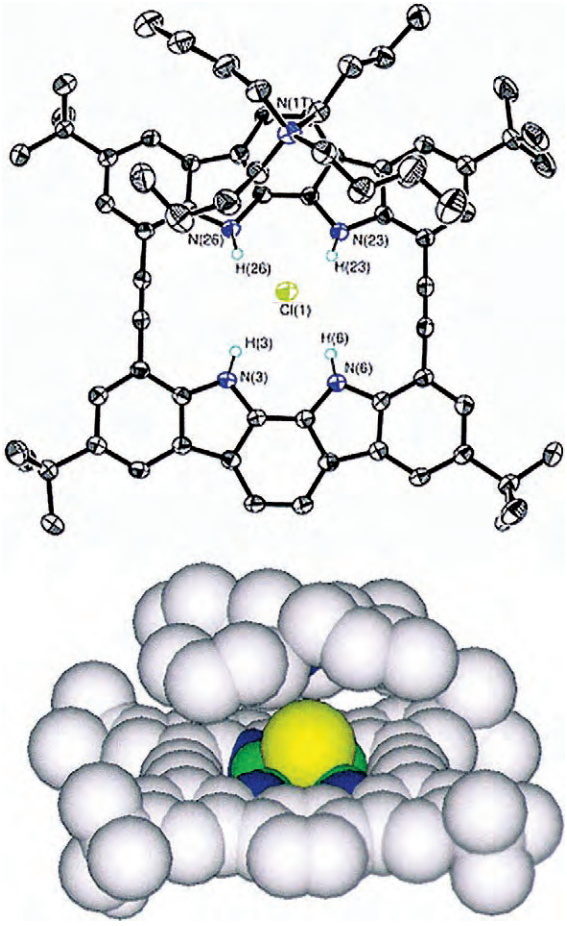

Figure 1. Crystal structures of the complex formed between **2** and $Bu_4N^+Cl^-$: Ortep plot (top) and CPK representation (bottom). Displacement ellipsoids represent 50% probability. Hydrogen-bonding distances and angles between the indole nitrogen atoms and chloride ion are 3.13–3.15 Å and 149–153°, respectively.

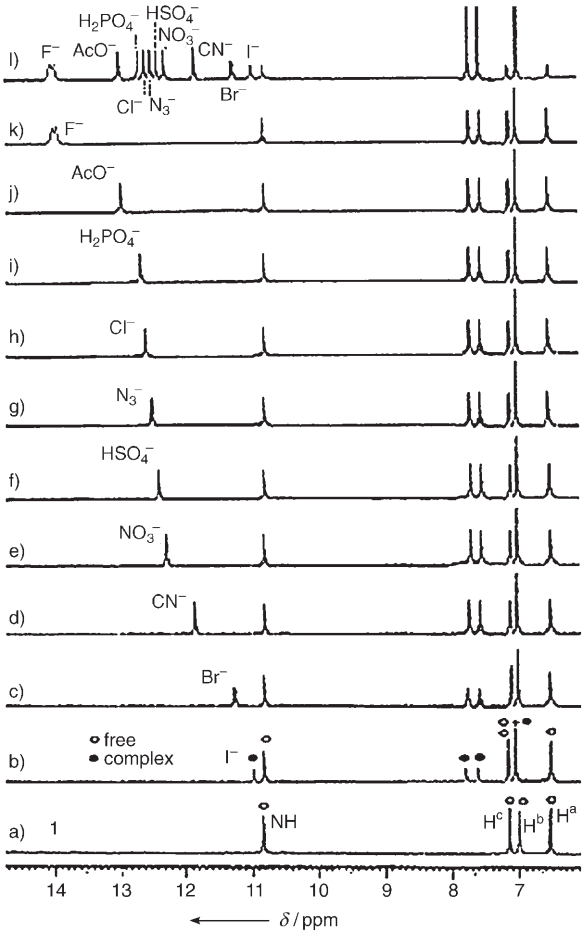

Figure 2. Partial ^{1}H NMR spectra (500 MHz, CD_3CN, 298 K) of a) **1** (1.0×10^{-4} M); b–k) **1** containing approximately 0.5 equivalents of I^-, Br^-, CN^-, NO_3^-, HSO_4^-, N_3^-, Cl^-, $H_2PO_4^-$, AcO^-, and F^-, respectively, and l) **1** (2.0×10^{-4} M) containing approximately 0.1 equivalents of each of 10 different anions. The anions were used as their tetrabutylammonium salts.

that appear at the expense of those of the free macrocycles **1** and **2**, as a consequence of slow exchange on the NMR time scale at ambient temperature (Figure 2). In particular, the NH signals of the complexes were significantly shifted downfield as a result of the formation of hydrogen bonds between the macrocycle and the anions. It should be mentioned that separate sets of ^{1}H NMR signals were observed even with the weakly binding anions Br^- and I^- at room temperature. This type of slow exchange is quite unusual for macrocycles, regardless of the binding strength.[16] All the anions studied gave different chemical shifts for the NH protons of the complexes, and ranged from $\delta = 10.7$ (I^-) to 13.9 ppm (F^-; Table 1).

The NH signals of the complexes appear as a sharp singlet in all cases except for **1**·F^-, which split into a doublet as a consequence of coupling between the NH protons and the bound fluoride nucleus. These NH signals have allowed us to identify and analyze an anion at a micromolar concentration (for example, 5.0×10^{-6} M for Cl^-) by ^{1}H NMR (500 MHz) spectroscopy. Furthermore, the NH signals of all 10 complexes were nicely resolved at room temperature when 10 different anions were added at the same time to a solution of **1** (2.0×10^{-4} M) in CD_3CN. The macrocycle **2** also showed identical spectroscopic behaviors when complexed with anions, but the NH chemical shifts of the complexes were slightly different from those derived from **1** (see the Supporting Information). As a result, the presence of an anion can be detected qualitatively and even quantitatively from the NH chemical shifts and ^{1}H NMR integrals. Therefore, **1** and **2** can be considered as chemical shift based chemosensors capable of sensing and analyzing anions in solution.

The association constants between the macrocycles and anions were determined by UV/Vis titration experiments in CH_3CN at 295 ± 1 K. Incremental addition of an anion to a solution of the macrocycle in CH_3CN (2.0×10^{-5} M) led to gradual changes in the UV absorption spectra, with isosbestic points at several different wavelengths. The association constants (K_a) were determined by nonlinear fitting analyses of the titration curves (Table 1).[17] Job's plots[17b] showed that **1** and **2** formed 1:1 complexes with all of the anions except Br^- and I^-. These larger halides form 2:1 macrocycle/anion complexes, possibly sandwich-type complexes as observed in

 © 2005 Wiley-VCH Verlag GmbH & Co. KGaA, Weinheim

Table 1: Association constants (K_a, M^{-1}) and NH chemical shifts of complexes (CD_3CN) formed between **1** and **2** and anions.

Anion	NH chemical shift[a] (δ, ppm)		Association constant (K_a, M^{-1})[b]	
	1	**2**	**1**	**2**
F^-[c]	13.9	13.9	2.0×10^8	5.6×10^8
AcO^-	13.0	12.8	5.9×10^6	6.5×10^6
$H_2PO_4^-$	12.7	12.5	2.1×10^6	3.2×10^6
Cl^-	12.6	12.3	1.5×10^6	2.1×10^6
N_3^-	12.5	12.1	8.8×10^5	9.1×10^5
HSO_4^-	12.4	12.0	6.5×10^5	6.8×10^5
NO_3^-	12.3	11.8	3.9×10^5	3.9×10^5
CN^-	11.9	11.5	6.5×10^4	7.5×10^4
Br^-	11.3	10.9	$K_1=1.9\times10^3$	$K_1=1.9\times10^3$
			$K_2=10$	$K_2=14$
I^-	11.0	10.7	$K_1=3.1\times10^2$	$K_1=3.0\times10^2$
			$K_2=6$	$K_2=5$

[a] The NH chemical shifts of the free macrocycles **1** and **2** are $\delta=10.9$ and 10.6 ppm, respectively. [b] Titrations were all duplicated in CH_3CN at 295 ± 1 K and the errors in the K_a values were within $\pm6\%$. The CH_3CN containing less than 0.05% water was used directly as purchased. [c] The association constants between macrocycles and fluoride ions were determined by competition experiments with chloride by using ^1H NMR spectroscopy.

the binding mode of alkali metals with crown ethers having small cavities.[18] As anticipated from the cavity size, macrocycles **1** and **2** generally show similar binding affinities toward anions. The association constants for a series of halides decrease dramatically in the order $F^- > Cl^- \gg Br^- > I^-$. This large difference is probably attributed to the charge density of the anion surfaces and to the size complementarities of the anions and the internal cavity. Finally, it should be noted that there is a good linear relationship between the binding affinities and the NH chemical shifts of the complexes (see the Supporting Information).

In conclusion, macrocycles **1** and **2** strongly bind various anions through hydrogen-bonding interactions and function as chemosensors capable of distinguishing between anions on the basis of the ^1H NMR chemical shifts of the complex. We are currently developing more practical and selective chemosensors for anionic species by incorporating a chromophore or a fluorophore and by tuning the cavity size.

Received: September 2, 2005
Published online: November 10, 2005

Keywords: anions · heterocycles · hydrogen bonds · macrocycles · sensors

[1] For reviews, see: a) P. D. Beer, *Acc. Chem. Res.* **1998**, *31*, 71–80; b) P. D. Beer, P. A. Gale, *Angew. Chem.* **2001**, *113*, 502–532; *Angew. Chem. Int. Ed.* **2001**, *40*, 486–516; c) C. R. Bondy, S. J. Loeb, *Coord. Chem. Rev.* **2003**, *240*, 77–99; d) K. Choi, A. D. Hamilton, *Coord. Chem. Rev.* **2003**, *240*, 101–110; e) P. A. Gale, *Coord. Chem. Rev.* **2003**, *240*, 191–221; f) C. Suksai, T. Tuntulani, *Chem. Soc. Rev.* **2003**, *32*, 192–202; g) R. Martínez-Máñez, F. Sancenón, *Chem. Rev.* **2003**, *103*, 4419–4476; h) C. Bowman-James, *Acc. Chem. Res.* **2005**, *38*, 671–678.

[2] a) J. W. Pflugrath, F. A. Quiocho, *Nature* **1985**, *314*, 257–260; b) H. Luecke, F. A. Quiocho, *Nature* **1990**, *347*, 402–406; c) R. Dutzler, E. B. Campbell, M. Cadene, B. T. Chait, R. MacKinnon, *Nature* **2002**, *415*, 287–294.

[3] For selected recent examples of (thio)ureido-based receptors, see: a) A. V. Koulov, T. N. Lambert, R. Shukla, M. Jain, J. M. Boon, B. D. Smith, H. Li, D. N. Sheppard, J.-B. Joos, J. P. Clare, A. P. Davis, *Angew. Chem.* **2003**, *115*, 5081–5083; *Angew. Chem. Int. Ed.* **2003**, *42*, 4931–4933; b) C. R. Bondy, P. Gale, S. J. Loeb, *J. Am. Chem. Soc.* **2004**, *126*, 5030–5031; c) M. Vázquez, L. Fabbrizzi, A. Taglietti, R. M. Pedrido, A. M. González-Noya, M. R. Bermejo, *Angew. Chem.* **2004**, *116*, 1996–1999; *Angew. Chem. Int. Ed.* **2004**, *43*, 1962–1965; d) J. Y. Kwon, Y. J. Jang, S. K. Kim, K.-H. Lee, J. S. Kim, J. Yoon, *J. Org. Chem.* **2004**, *69*, 5155–5157; e) S. Zhang, L. Echegoyen, *J. Am. Chem. Soc.* **2005**, *127*, 2006–2011; f) J. P. Clare, A. J. Ayling, J.-B. Joos, A. L. Sission, G. Magro, M. N. Pérez-Payán, T. N. Lambert, R. Shukla, B. D. Smith, A. P. Davis, *J. Am. Chem. Soc.* **2005**, *127*, 10739–10746; g) E. J. Cho, B. J. Ryu, Y. J. Lee, K. C. Nam, *Org. Lett.* **2005**, *7*, 2607–2609.

[4] For selected recent examples of amido-based receptors, see: a) S. O. Kang, J. M. Llinares, D. Powell, D. Van der Velde, K. Bowman-James, *J. Am. Chem. Soc.* **2003**, *125*, 10152–10153; b) K. Choi, A. D. Hamilton, *J. Am. Chem. Soc.* **2003**, *125*, 10241–10249; c) D. Curiel, P. D. Beer, *Chem. Commun.* **2005**, 1909–1911.

[5] a) P. A. Gale, J. L. Sessler, V. Král, *Chem. Commun.* **1998**, 1–8; b) P. A. Gale, P. Anzenbacher, Jr., J. L. Sessler, *Coord. Chem. Rev.* **2001**, *222*, 57–102; c) P. Piątek, V. M. Lynch, J. L. Sessler, *J. Am. Chem. Soc.* **2004**, *126*, 16073–16076; d) K. A. Nielsen, W.-S. Cho, J. O. Jeppesen, V. M. Lynch, J. Becher, J. L. Sessler, *J. Am. Chem. Soc.* **2004**, *126*, 16296–16297; e) J. L. Sessler, E. Katayev, G. D. Pantos, P. Scherbakov, M. D. Reshetova, V. N. Khrustalev, V. M. Lynch, Y. A. Ustynyuk, *J. Am. Chem. Soc.* **2005**, *127*, 11442–11446.

[6] For reviews, see: a) J. L. Sessler, J. M. Davis, *Acc. Chem. Res.* **2001**, *34*, 989–997; b) J. L. Sessler, S. Camiolo, P. A. Gale, *Coord. Chem. Rev.* **2003**, *240*, 17–55.

[7] For a review, see: P. A. Gale, *Chem. Commun.* **2005**, 3761–3772.

[8] For indolocarbazole-based anion sensors, see: D. Curiel, A. Cowley, P. D. Beer, *Chem. Commun.* **2005**, 236–238.

[9] a) T. M. Cresp, J. Ojima, F. Sondheimer, *J. Org. Chem.* **1977**, *42*, 2130–2138; b) Y. Tobe, N. Utsumi, K. Kawabata, A. Nagano, K. Adachi, S. Araki, M. Sonada, K. Hirose, K. Naemura, *J. Am. Chem. Soc.* **2002**, *124*, 5350–5364.

[10] For the preparation of an indole ring, see: J. Ezquerra, C. Pedregal, C. Lamas, *J. Org. Chem.* **1996**, *61*, 5804–5812.

[11] Compound **3** was prepared from 4-*tert*-butylanilne in two steps, and compound **6** was prepared by the reaction of **4** with (dimethylamino)acetaldehyde diethyl acetal (see the Supporting Information).

[12] The coupling reactions in the presence of copper iodide and/or at higher temperature under various conditions always resulted in complicated mixtures without any discrete, separable spots on the TLC plates and a major product in the ^1H NMR spectra.

[13] A. Soheili, J. Albaneze-Walker, J. A. Murry, P. G. Dormer, D. L. Hughes, *Org. Lett.* **2003**, *5*, 4191–4194.

[14] For the synthesis of sp^3-carbon-bridged, puckered calix[*n*]indoles, see: a) D. StC. Black, M. C. Bowyer, N. Kumar, P. S. R. Mitchell, *J. Chem. Soc. Chem. Commun.* **1993**, 819–821; b) D. StC. Black, D. C. Craig, N. Kumar, *Tetrahedron Lett.* **1995**, *36*, 8075–8078.

[15] Single crystals of $\mathbf{2}\cdot Bu_4N^+Cl^-$ were obtained by slow vapor diffusion of diethyl ether into a solution of **2** and $Bu_4N^+Cl^-$ (1:1) in CH_3CN/CH_2Cl_2. The data collection was performed at $-100\,°C$ with $Mo_{K\alpha}$ radiation ($\lambda=0.71073$ Å) on a Bruker SMART CCD equipped with a graphite crystal, incident-beam

 © 2005 Wiley-VCH Verlag GmbH & Co. KGaA, Weinheim

monochromator. Cell constants and orientation matrices for data collection were obtained from least-squares refinement with a set of 45 narrow-frame (0.3° in ω) scans. The SMART and SAINT software packages were used for data collection and integration, respectively. Collected data were corrected for absorbance by using SADABS based upon Laue symmetry using equivalent reflections. The structure was solved by direct methods and refined by full-matrix least-squares calculations with the SHELXTL-PLUS software package (version 5.1). All non-hydrogen atoms were refined anisotropically; hydrogen atoms except those on the nitrogen atoms were assigned isotropic displacement coefficients U(H) = 1.2U (C) or 1.5U (C_{methyl}), and their coordinates were allowed to ride on their respective atoms. Four hydrogen atoms on the nitrogen atoms could be found in the difference Fourier map and refined with isotropic displacement coefficients. Crystal data for **2**·Cl^- at 173 K: $C_{72}H_{88}N_5Cl$, $0.38 \times 0.33 \times 0.30$ mm^3, orange crystal, monoclinic, space group $P2_1/c$, $a = 15.664(2)$ Å, $b = 19.343(2)$ Å, $c = 20.201(2)$ Å, $\beta = 92.752(2)°$, $V = 6114(1)$ Å^3, $Z = 4$; $M_r = 1058.92$, $\rho_{calcd} = 1.150$ g cm^{-3}, $\mu(Mo_{K\alpha}) = 0.109$ mm^{-1}, final R1 = 0.0554 for 14549 reflection of $I > 2\sigma(I)$, $R1 = 0.1111$, $wR2 = 0.1633$ for all 37737 reflections. CCDC-288190 contains the supplementary crystallographic data for this paper. These data can be obtained free of charge from The Cambridge Crystallographic Data Centre via www.ccdc.cam.ac.uk/data_request/cif.

[16] For a molecular capsule which shows slow exchange of anions on the NMR time scale, see: a) O. Hayashida, A. Shivanyuk, J. Rebek, Jr., *Angew. Chem.* **2002**, *114*, 3573 – 3576; *Angew. Chem. Int. Ed.* **2002**, *41*, 3423 – 3426; b) J. Rebek, Jr., *Angew. Chem.* **2005**, *117*, 2104 – 2115; *Angew. Chem. Int. Ed.* **2005**, *44*, 2068 – 2078.

[17] a) J. R. Long, R. S. Drago, *J. Chem. Educ.* **1982**, *59*, 1037 – 1089; b) K. A. Connors, *Binding Constants*, Wiley, New York, **1987**.

[18] a) S. Shinkai, T. Nakaji, T. Ogawa, K. Shigematsu, O. Manabe, *J. Am. Chem. Soc.* **1981**, *103*, 111 – 115; b) "Crown ethers and Analogue Compounds": H. Tsukube in *Studies in Organic Chemistry 45* (Ed.: M. Hiraoka), Elsevier, Amsterdam, **1992**, chap. 3.

 © 2005 Wiley-VCH Verlag GmbH & Co. KGaA, Weinheim

Nanotubes

DOI: 10.1002/anie.200502591

Characteristics of Boron Nitride Nanotube–Polyaniline Composites**

Chunyi Zhi, Yoshio Bando, Chengchun Tang, Susumu Honda, Kazuhiko Sato, Hiroaki Kuwahara, and Dmitri Golberg*

Significant efforts have been made to design and fabricate nanotube-based composites since the pioneering report on carbon nanotube (CNT)–polymer composites by Ajayan et al.[1] These composites are expected to have useful electrical and optical properties, thermal conductivity, and superior mechanical strength compared to unprocessed polymers.[2,3] Polyaniline (PANI), a typical electroconductive polymer, is a promising candidate for the fabrication of nanotube-based composites due to its stability and redox properties. Significant progress has been achieved with respect to the processing and property improvements of PANI–CNT composites.[4] For real-device applications, the two important factors—functionality and processability—should be considered. These parameters primarily depend on the efficiency of interactions between the nanotubes and polymer chains within a composite material. To enhance these interactions, the PANI–CNT composites are typically fabricated by in situ polymerization.

Boron nitride nanotubes (BNNTs), which are structurally similar to CNTs, have been predicted to behave like wide-band-gap semiconductors independent of radius, chirality, and the number of tubular shells.[5] Interestingly, the electrical polarization induced by broken symmetry along the BNNT axis has been predicted in a theoretical study; this is quite distinct from the case of CNTs.[6] Moreover, BNNTs have superb mechanical properties, thermal conductivity, and resistance to oxidation at high temperatures.[7–11] These factors may promote effective BNNT usage in nanocomposites. However, to the best of our knowledge, no BNNT–polymer composites have been reported to date. Studies of BNNTs–polymer composites are absent because it is extremely difficult to obtain a highly pure BNNT phase with a yield high enough to fabricate and test a composite

[*] Dr. C. Zhi, Prof. Y. Bando, Dr. C. Tang, Prof. D. Golberg
Advanced Materials Laboratory
National Institute for Materials Science (NIMS)
Namiki 1-1, Tsukuba, Ibaraki 305-0044 (Japan)
Fax: (+81) 29-851-6280
E-mail: zhi.chunyi@nims.go.jp
Dr. S. Honda, Dr. K. Sato, Dr. H. Kuwahara
Innovation Research Institute, Teijin Ltd.
2-1, Hinode-cho, Iwakuni, Yamaguchi 740-8511 (Japan)

[**] We thank Drs. Y. Uemura, M. Mitome, K. Kurashima, R. Z. Ma, and T. Sasaki for their cooperation and kind help.

Supporting information for this article is available on the WWW under http://www.angewandte.org or from the author.

© 2005 Wiley-VCH Verlag GmbH & Co. KGaA, Weinheim

material, although many methods have been probed to synthesize BNNTs.[12–16]

In the study presented herein, large quantities of highly pure BNNTs were synthesized by chemical vapor deposition with boron and metal oxide as the reactants.[17,18] PANI–BNNTs composites were fabricated by simple solution mixing to give self-organized composite films. Detailed comparative characterization of the composite samples and initial materials constituting them was then carried out. The morphology of the composites was analyzed by using scanning and transmission electron microscopy (SEM, TEM), which both revealed uniform coverage of a BNNT surface with PANI. Additional characterization was performed by using Raman spectroscopy, UV/Vis absorption, and X-ray diffraction (XRD). All results indicated strong interactions between PANI and BNNTs within the composites.

BNNTs and a nonconducting soluble emeraldine-based form of PANI (EB) were mixed and sonicated in *N*,*N*-dimethylformamide to form a solution. The solution was then left at room temperature for over 12 h during which a self-organized composite film formed at the bottom of the reaction vessel. It is worth noting that when the same process was carried out with a solution of CNT and EB, no film was deposited. This result indicates that BNNTs display stronger interactions with EB than CNTs. A BNNT–EB film was removed from the reaction vessel and mounted on a silicon wafer for further characterization and testing.

Figure 1 depicts typical SEM images of a composite film. Figure 1a shows the BNNTs embedded in an EB matrix; some BNNTs are out of the matrix because the film broke during its mounting on a silicon wafer. During the long irradiation times, the film shrank and broke, thus allowing the BNNTs to become clearly visible (Figure 1b). The morphology of BNNTs within the composites is similar to that of pure BNNTs, as revealed by SEM. However, notable differences were observed by TEM. Figure 2a shows a low magnification TEM image of a composite. Although the BNNTs are covered by EB, they still retain a perfect crystalline structure, as revealed by a high-resolution TEM image (Figure 2b). Typically, BNNTs are not wetted by most materials (see Supporting Information). In contrast, in the present experiments all BNNTs were well covered by EB, although some BNNTs protruded from the matrix during SEM observations. This coverage indicates strong interactions between BNNTs and EB. The origin of these interactions may be analogous to that found in a solution of BNNT/poly(*m*-phenylenevinylene-co-2,5-dioctoxy-*p*-phenylenevinylene):[19] the PANI ring units may come sufficiently close to a hexagonal BNNT surface to lead to efficient π–π interactions.[4] The interactions between BNNT and PANI are stronger than between CNT and PANI due to electrical polarization in BNNTs induced by broken symmetry.[6]

Raman spectroscopy was used to gain insight into the origin of the strong interactions between EB and BNNTs. As shown in Figure 3, two dominant peaks at 1350 and 1579 cm^{-1} are present in the Raman spectrum of pure EB. Only one peak at 1365 cm^{-1} is visible in the spectrum of BNNTs. It is surprising that the marked peak shifts are observed in the Raman spectrum of the composite. The BNNT-related peak

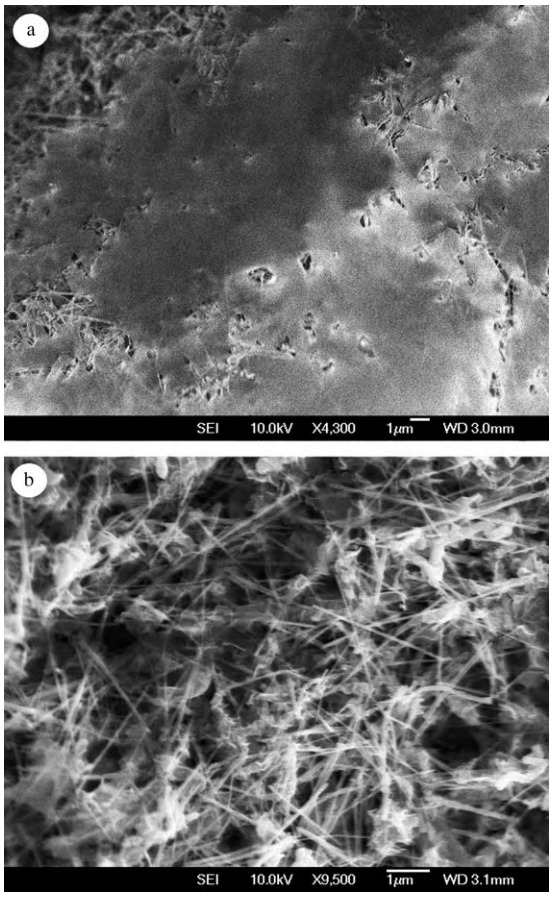

Figure 1. SEM images of an EB–BNNT composite a) before and b) after a long period (10–15 s) of electron-beam irradiation inside the scanning electron microscope.

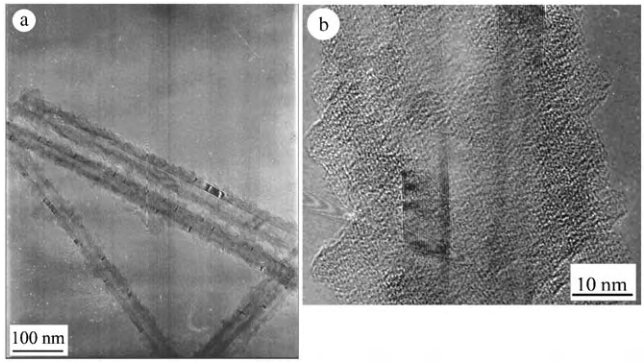

Figure 2. a) Low magnification TEM image and b) high-resolution TEM image of an EB–BNNT composite.

shifts to 1352 cm^{-1}, while the EB-related peak at 1579 cm^{-1} shifts to 1589 cm^{-1} (the peak at 1350 cm^{-1} cannot be identified in the spectrum because it is too weak and overlaps with the BNNT-related peak). Raman peak shifts have not been observed during studies of CNT–PANI composites. It is well known that the Raman spectra of CNTs consist of a G band (in-plane stretching, E_{2g} mode) and a D band induced by the disordering or an amorphous C residue. For single-walled

 © 2005 Wiley-VCH Verlag GmbH & Co. KGaA, Weinheim

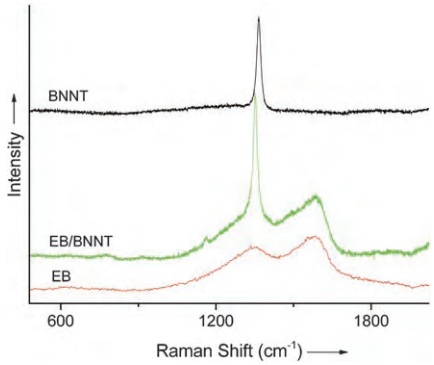

Figure 3. Raman spectra of BNNTs, EB, and an EB–BNNT composite film.

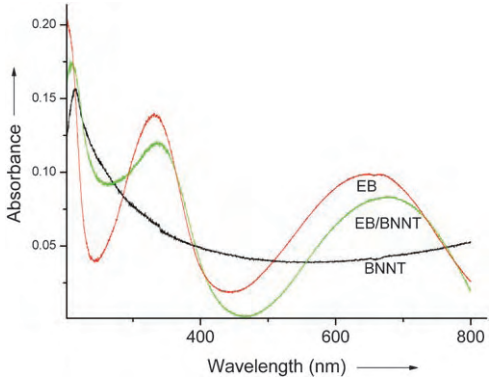

Figure 4. UV/Vis absorption spectra of BNNTs, EB, and an EB–BNNT composite film.

CNTs, evidence of a radial breathing mode (RBM) can also be observed, which is associated with a symmetric movement of all C atoms in the radial direction. The D and G bands are usually not changed in the Raman spectra of CNT–polymer composites, whereas the RBM may shift to somewhat lower frequencies. This fact is supposed to highlight that the breathing mode of single-walled CNTs is largely affected by the particular surrounding of an individual tube.[20] It is clear that a different mechanism should be assigned to explain the large Raman shifts observed in our experiments. Raman spectra are associated with the lattice vibrations. These vibrations are affected by the atomic structure, chemical bonds, and/or electronic structure through electron–phonon coupling. For BNNTs, the shifts may be caused by the prominent variations of the electronic structure rather than the atomic structure. The BNNTs are structurally stable, and it is doubtful that EB, which only covers the BNNT surface, may affect the entire atomic structure of the nanotube. For EB, the shift may be caused by conformation-induced changes in the electronic structure. Generally, given the fact that this phenomenon has not been observed for the CNT composites, we suggest that the peak shift may be related to the electrical polarization solely peculiar to BNNTs.[6] Nevertheless, strong interactions between EB and BNNTs have been demonstrated here by these Raman studies. These interactions may facilitate the charge-transfer processes between the two components. A detailed mechanism of the prominent Raman shifts for the novel composites is still not clear and is the subject of on-going research.

To reveal the influence of the interactions within the composites on the electronic structures of the constituting EB and BNNTs, we performed UV/Vis absorption measurements. Figure 4 shows the UV/Vis absorption spectra of EB, a composite film, and a BNNT film retracted from the composite film by heating the sample at 700 °C in air. For EB, two broad peaks are visible with maximums at 332 nm and 650 nm, which correspond to the π–π^* transitions centered at the benzenoid unit of EB and on the quinoid exciton band, respectively.[21] The peak at 332 nm shifts to 338 nm and that at 650 nm shifts to 673 nm for the composite. For BNNTs, the peak corresponding to a band-gap transition shifts from 214 nm (pure BNNT film) to 210 nm (composite film). This shift implies that BNNTs may have a dopant effect, which was first mentioned for CNT–PANI composites.[4b] However, it is hard to expect a drastic improvement in the conductivity of the present EB–BNNT composites as EB is a nonconducting form of PANI and BNNT is a wide-band-gap semiconductor. In CNT–PANI composites, CNTs can act as conducting bridges, which leads to an increase in conductivity, whereas the present BNNTs cannot. Further investigations on the dopant effect within the composites by using luminescence experiments are underway.

The strong interactions in the EB–BNNT composites may influence the conformation of EB.[4a] Consequently, the ordered structures of a EB–BNNT composite were investigated by XRD, as shown in Figure 5. For BNNTs, the peaks

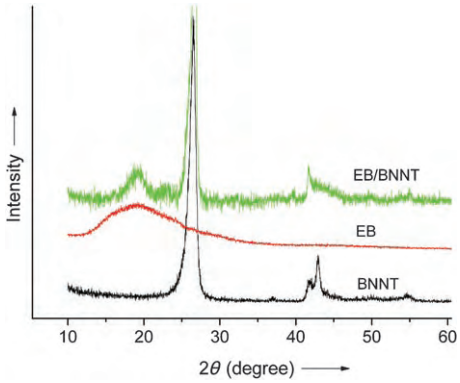

Figure 5. XRD of BNNTs, EB, and an EB–BNNT composite powder.

at $2\theta = 26°$, 41°, 43°, and 54° correspond to the (002), (100), (101), and (004) reflections, respectively. Pure EB displays only a very broad peak centered at 19°. However, for the composite, the EB-related peak becomes much sharper (the full-width half maximum decreases from 10 to 3°). This peak sharpening indicates that the structure of EB within a composite becomes more ordered. The strong nanotube–polymer interactions may lead to such ordering. The above-mentioned EB Raman shifts may be another reflection of this ordering.

© 2005 Wiley-VCH Verlag GmbH & Co. KGaA, Weinheim

In summary, BNNTs–EB composites were fabricated by using simple solution mixing. A composite film can be obtained through self-organization, which is indicative of the strong interactions between BNNT and PANI. Proof of this interaction is given by Raman, UV/Vis absorption, and XRD experiments. BNNT may exhibit a dopant effect to PANI due to charge transfer. PANI becomes more ordered in a composite with respect to its pure form. The present studies reveal that mechanically tough BNNTs may find application as an effective composite additive in EB in order to improve the polymer processing and handling due to the strong BNNT–polymer interactions. In addition, the optical properties of the newly fabricated EB–BNNT composites may be of significant interest.

Experimental Section

An induction furnace was used to synthesize BNNTs. In a typical experimental run, a mixture of MgO, FeO, and boron powder was heated in a boron nitride crucible to 1400 °C. Ammonia gas was then introduced into the system to react with gaseous Mg and Fe and gaseous B_2O_2 was produced. After two hours, a white product was collected from a BN tube attached to the reaction chamber. The BNNT–PANI composites were fabricated by simple mixing and sonication of BNNTs and EB in the *N*,*N*-dimethylformamide. A self-organized composite film was recovered from the bottom of the reaction vessel. An SEM (JEOL SM67F) was used to characterize the products. The microstructure was investigated by using a JEOL-3000F high-resolution field-emission TEM operated at 300 kV. A Reinshaw 2000 Micro-Raman system with a 30 mW Ar^+ laser of wavelength of 514 nm was used to study the lattice vibrations of the fabricated composites. The UV/Vis absorption experiments were performed by using a HITACHI U-4100 spectrometer. XRD patterns of the samples were recorded on a RINT2200 X-ray diffractometer with standard $Cu_{K\alpha}$ radiation.

Received: July 25, 2005
Published online: November 15, 2005

Keywords: boron · conducting materials · mechanical properties · nanotubes · noncovalent interactions · polymers

[1] P. M. Ajayan, O. Stephan, C. Colliex, D. Trauth, *Science* **1994**, *265*, 1212.
[2] R. Andrews, M. C. Weisenberger, *Curr. Opin. Solid State Mater. Sci.* **2004**, *9*, 31.
[3] P. J. F. Harris, *Int. Mater. Rev.* **2004**, *49*, 31.
[4] a) R. Sainz, A. M. Benito, M. T. Martinez, J. F. Galindo, J. Sotres, A. M. Baró, B. Coraze, O. Chauvet, W. K. Maser, *Adv. Mater.* **2005**, *17*, 278; b) H. Zengin, W. Zhou, J. Jin, R. Czerw, D. W. Smith, J. L. Echegoyen, D. L. Carroll, S. H. Foulger, J. Ballato, *Adv. Mater.* **2002**, *14*, 1480; c) H. J. Choi, S. J. Park, S. T. Kim, M. S. Jhon, *Diamond Relat. Mater.* **2005**, *14*, 766; d) X. Zhang, J. Zhang, Z. Liu, *Appl. Phys. A* **2005**, *80*, 1813.
[5] X. Blase, A. Rubio, S. G. Louie, M. L. Cohen, *Europhys. Lett.* **1994**, *28*, 335.
[6] E. J. Mele, P. Král, *Phys. Rev. Lett.* **2002**, *88*, 056803.
[7] E. Hernandez, C. Goze, P. Bernier, A. Rubio, *Phys. Rev. Lett.* **1998**, *80*, 4502.
[8] A. P. Suryavanshi, M. Yu, J. Wen, C. Tang, Y. Bando, *Appl. Phys. Lett.* **2004**, *84*, 2527.
[9] D. Golberg, Y. Bando, K. Kurashima, T. Sato, *Scr. Mater.* **2001**, *44*, 1561.
[10] Y. Xiao, X. H. Yan, J. X. Cao, J. W. Ding, Y. L. Mao, J. Xiang, *Phys. Rev. B* **2004**, *69*, 205415.
[11] C. W. Chang, W. Q. Han, A. Zettl, *Appl. Phys. Lett.* **2005**, *86*, 173102.
[12] N. G. Chopra, R. J. Luyken, K. Cherrey, V. H. Crespi, M. L. Cohen, S. G. Louie, A. Zettl, *Science* **1995**, *269*, 966.
[13] A. Loiseau, F. Willaime, N. Demoncy, N. Schramchenko, G. Hug, C. Colliex, H. Pascard, *Carbon* **1997**, *35*, 743.
[14] T. Laude, Y. Matsui, A. Marraud, B. Jouffrey, *Appl. Phys. Lett.* **2000**, *76*, 3239.
[15] W. Q. Han, W. Mickelson, J. Cumings, A. Zettl, *Appl. Phys. Lett.* **2002**, *81*, 1110.
[16] Y. Chen, L. T. Chadderton, J. F. Gerald, J. S. Williams, *Appl. Phys. Lett.* **1999**, *74*, 2960.
[17] C. Tang, Y. Bando, T. Sato, K. Kurashima, *Chem. Commun.* **2002**, 1290.
[18] C. Y. Zhi, Y. Bando, C. Tang, D. Golberg, *Solid State Commun.* **2005**, *135*, 67.
[19] C. Y. Zhi, Y. Bando, C. Tang, D. Golberg, R. Xie, T. Sekiguchi, *J. Am. Chem. Soc.*, accepted.
[20] Q. Zhao, H. D. Wagner, *Philos. Trans. R. Soc. London Ser. A* **2004**, *362*, 2407.
[21] S. Quillard, G. Louarn, S. Lefrant, A. G. MacDiarmid, *Phys. Rev. B* **1994**, *50*, 12496.

 © 2005 Wiley-VCH Verlag GmbH & Co. KGaA, Weinheim

Nanotubes

DOI: 10.1002/anie.200502846

Covalent Functionalization: Towards Soluble Multiwalled Boron Nitride Nanotubes**

Chunyi Zhi, Yoshio Bando, Chengchun Tang, Susumu Honda, Kazuhiko Sato, Hiroaki Kuwahara, and Dmitri Golberg*

In many respects, a boron nitride nanotube (BNNT) has advantageous properties when compared to a standard carbon nanotube (CNT). For example, BNNTs are stable wide-band-gap semiconductors, independent of diameter and chirality.[1] In contrast, the electrical performance of a CNT is a complex function of many structural parameters, which are difficult to control.[2] BNNTs exhibit excellent mechanical properties, high thermal conductivity, and superb resistance

[*] Dr. C. Zhi, Prof. Y. Bando, Dr. C. Tang, Prof. D. Golberg
Advanced Materials Laboratory
National Institute for Materials Science (NIMS)
Namiki 1–1, Tsukuba, Ibaraki 305-0044 (Japan)
Fax: (+81) 29-851-6280
E-mail: zhi.chunyi@nims.go.jp
Dr. S. Honda, Dr. K. Sato, Dr. H. Kuwahara
Innovation Research Institute, Teijin Ltd.
2–1, Hinode-cho, Iwakuni, Yamaguchi 740-8511 (Japan)

[**] We thank Drs Y. Uemura, M. Mitome, K. Kurashima, R. Z. Ma, and T. Sasaki for cooperation and kind help.

WILEY InterScience DISCOVER SOMETHING GREAT
© 2005 Wiley-VCH Verlag GmbH & Co. KGaA, Weinheim

to oxidation.[3–8] Therefore BNNTs are thought to be primarily useful in nanoscale semiconductors working in oxidative or hazardous environments at high temperatures, and as an additive in composites that leads to the improvement of mechanical properties and thermal conductivity of the matrix.

However, to date there has been a lack of notable progress in the above-mentioned fields. Many unanswered questions, such as how to adjust the electronic structure of BNNTs, how dispersible BNNTs are in a solvent, and how to produce clean BNNTs in high yield, has hampered the expected breakthroughs.

The functionalization of CNTs is a vital tool in tailoring their properties and engineering devices, and significant efforts have been undertaken with respect to this functionalization. Intense research has been carried out on soluble CNTs, CNT composites, and CNT compatibility with biological systems.[9–13] As for the BNNT system, only recently Xie et al. have obtained good BNNT dispersion through their functionalization with amine-terminated oligomeric poly(ethylene glycol).[14] The functionalized BNNTs were easily retracted, which indicates that the interactions between the amino groups and the BNNTs are noncovalent. In addition, contamination with carbon was a major concern as the BNNTs were produced by a CNT substitution reaction.[8] To date, the covalent-bond chemistry of BNNTs and related functionalization has long been awaited but not reported. The ability to functionalize BNNTs with covalently bonded groups should allow the tailoring of their properties and of the materials made out of them.

Herein, we report how pure multiwalled BNNTs are synthesized in high yield by carbon-free chemical vapor deposition (CVD).[15,16] A mixture of boron and metal oxide served as the reactant during the synthesis and an original approach was then developed to functionalize BNNTs with an organic residue through the formation of a covalent bond. This method led to highly soluble products. Cathodoluminescence (CL) and UV/Vis absorption experiments revealed variations in the electronic structure of the BNNTs after functionalization, which may pave a way to tune the band gap of the BNNTs.

The functionalization methodology is based on the chemical reaction between the COCl group of stearoyl chloride and amino groups on the BNNTs, as shown in Scheme 1. A similar reaction has been widely applied to modify CNTs.[9] In contrast to the starting material (multiwalled BNNTs), which is insoluble in organic solvents, the functionalized BNNTs (f-BNNTs) are soluble in solvents such as chloroform, *N*,*N*-dimethylacetamide, tetrahydrofuran, *N*,*N*-dimethylformamide, acetone, toluene, and ethanol. The solubility of f-BNNTs in *N*,*N*-dimethylacetamide is $>0.5\,g\,L^{-1}$. Very dilute BNNT solutions are almost totally transparent and white concentrated BNNT solutions are visually nonscattering. No precipitation was observed when the sample was kept over a long period under ambient conditions.

Transmission electron microscopy (TEM) was used to confirm the presence of BNNTs in solution and to check the morphology of the f-BNNTs. The results are shown in Figure 1. f-BNNTs in solution are well dispersed and retain

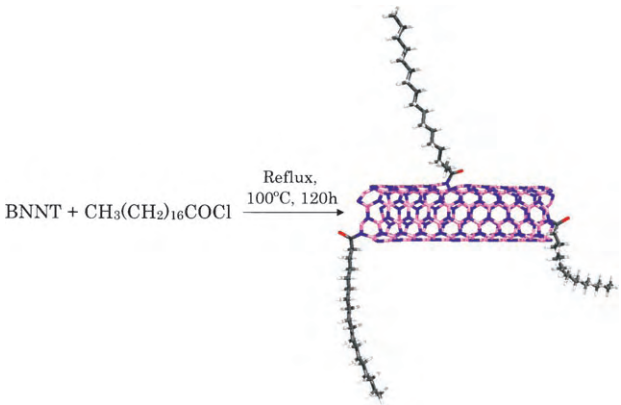

Scheme 1. Schematic representation of the designed reaction to give a functionalized nanotube.

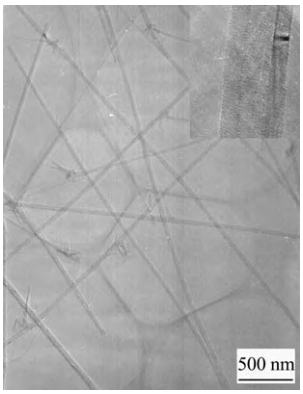

Figure 1. TEM images of f-BNNTs. Inset: a high-magnification TEM image revealing a tubular structure of the f-BNNT and an amorphous layer on its surface.

a characteristic 1D tubular morphology. An amorphous layer can be observed on their surface. On average, the f-BNNTs are slightly shorter than the original BNNTs, which is caused by stirring of the reaction mixture for a long period during functionalization.

To reveal the functionalization mechanism, Fourier-transformed infrared (FTIR) spectroscopy was used to compare the original BNNTs with f-BNNTs (Figure 2. The absorptions corresponding to C=O (1774 and 1630 cm^{-1}) and C–H bonds (bending vibrations: 1016, 1078, 1163, and 1193 cm^{-1}, stretching vibrations: 3033 2959 and 2925 cm^{-1}(weak)) can be clearly identified in the FTIR spectrum of f-BNNTs, which indicates that long alkyl chains are bonded to the BNNTs. It is worth noting that for stearoyl chloride, the peaks related to C=O appear at 1712 and 1807 cm^{-1}, while they appear at 1774 and 1630 cm^{-1} for the f-BNNTs. This shift implies that the COCl functional group participates in the chemical reaction. As a reductive NH_3 gas is used during the CVD synthesis of BNNTs from boron and metal oxide,[15,16] we assume that there are some amino groups present on the side walls of the BNNTs, as well as at their open ends. Their presence ensures that long alkyl chains can bond through the chemical reaction between COCl and the amino groups. The effect is similar to that observed in CNTs, whose defects can be oxidized to form

 © 2005 Wiley-VCH Verlag GmbH & Co. KGaA, Weinheim

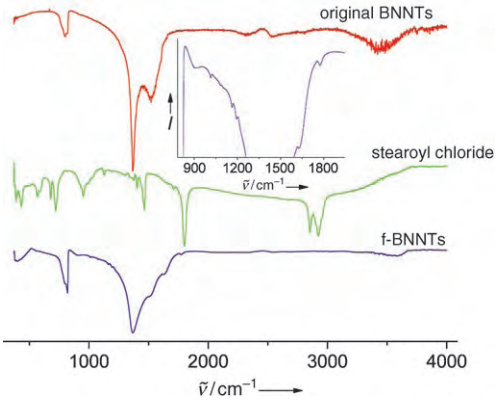

Figure 2. Comparative FTIR spectra of original BNNTs, stearoyl chloride, and f-BNNTs. Inset: an enlarged profile of additional peaks that only appear in the spectrum of f-BNNTs.

reactive groups, and subsequently long-chain alkyl amines can be coupled to carboxy groups activated with $SOCl_2$.[17] In addition, the chemical reaction also induces notable variations in BNNT-related FTIR peaks, namely, the disappearance of peaks corresponding to multiphonon processes (2313 and 2530 cm^{-1}) and abatement of splitting of the E_{1u}(TO) and E_{1u}(LO) modes (TO: transverse optic; LO: longitudinal optic).[18] An investigation into the detailed mechanism that causes these changes is underway.

Given that variations in the optical properties have also been observed for CNTs after functionalization[19,20] and that UV emission has been observed for BNNTs,[18] we performed CL measurements on the f-BNNTS. A f-BNNTs powder was chosen as the sample to be analyzed as solutions are not suitable for CL experiments. Figure 3 compares the room-

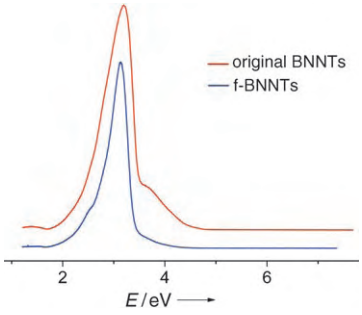

Figure 3. Comparative CL spectra of original BNNTs and f-BNNTs.

temperature CL spectrum of original BNNTs with that of f-BNNTs. As previously reported, the spectrum of original BNNTs shows a dominant peak at about 3.25 eV and a shoulder at about 4.05 eV, which is thought to originate from B or N vacancies.[18] Peaks related to the band transition should appear at about 5.5 eV, which can only be observed from low-temperature CL experiments. In the spectrum of the f-BNNTs, there is a new shoulder at about 2.50 eV. One possible explanation for this emission is that a new defect-related band is introduced into the energy gap of BNNTs. This, in turn, implies that a long alkyl chain protruding from a side wall or open end of a BNNT may lead to a dopant effect. The dopant effect may be induced by a charge transfer between the BNNT and the alkyl chain.[9] Another possibility is that the shoulder at about 2.50 eV may solely originate from the long alkyl chains, which means that we detect a kind of surface-state luminescence. If so, the intensity of the shoulder emission may provide a way to estimate the density of alkyl chains on the surface of a BNNT.

To probe the influence of long alkyl chains on the electronic structure of BNNTs, UV/Vis absorption experiments were performed. A solution sample cannot be used for these experiments as most organic solvents are totally opaque to wavelengths shorter than 250 nm (4.96 eV), and a BNNT has an even larger band gap according to a previous study.[1] Therefore, BNNT films were used as samples. Figure 4

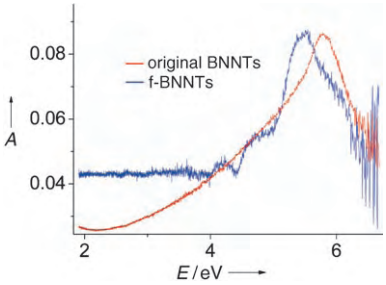

Figure 4. Comparative UV/Vis absorption spectra of original BNNTs and f-BNNTs.

compares the UV/Vis absorption spectrum of BNNTs with that of f-BNNTs. The peak at 5.80 eV dominates the BNNT spectrum; it corresponds to the band-gap transition and indicates a band gap in the range of 5.2 to 5.5 eV.

More features appear in the spectrum of the f-BNNT. First, the dominant peak shifts to about 5.45 eV and displays a shoulder at 5.8 eV. This shoulder clearly corresponds to the peak of the band-gap transition mentioned above. Second, new peaks at about 4.68 and 4.20 eV appear. The shift of the main peak indicates that some new electronic states are present in the energy-gap region of the f-BNNTs. If the long alkyl chain acts as a carbon dopant, it may be that the additional electronic states appear in the top of the valence band and the bottom of the conduction band. It was reported that in boron carbonitride (BCN) nanotubes, the carbon content may affect the band gap. Typically in BCN nanotubes, the width of the band gap decreases with an increase in carbon concentration.[21] However, it is difficult to control precisely the atomic concentration of carbon within BCN nanotubes at the stage of tube growth.

In contrast, the process of postsynthesis chemical modification of BNNTs may be easily controlled. Specifically, the density of alkyl chains on the BNNT surface can be adjusted by controlling the reaction time and temperature. Alternatively, a defunctionalization process could be developed to further adjust the alkyl-chain density as with CNTs.[22] The peaks at 4.68 and 4.20 eV imply that the dopant effect of alkyl chains on BNNTs is real. This doping is crucial for the engineering of the wide band gap. Chen et al. have used a long alkyl chain to decorate single-walled CNTs.[9] Variations in the band structure of the decorated CNTs have indeed been observed in absorption experiments. The influence of an alkyl chain on BNNTs may be even larger than that on CNTs as

 © 2005 Wiley-VCH Verlag GmbH & Co. KGaA, Weinheim

carbon atoms are already present in CNTs but are heteroatomic for BNNTs. This factor makes the modification of BNNTs with organic groups highly promising.

In summary, an original methodology has been developed to functionalize multiwalled BNNTs with long alkyl chains and the resultant functionalized BNNTs are soluble in many organic solvents. The CL and UV/Vis absorption experiments indicate that long alkyl chains may induce drastic changes in the band structure of BNNTs. These findings may be the beginning of significant progress in the chemistry of BNNTs and their functionalization paves the way to controllable tailoring of their electronic structure and to band-gap engineering.

Experimental Section

An induction furnace was used to synthesize multiwalled BNNTs. The detailed procedure is described elsewhere.[15,16] The as-prepared BNNTs were heated to about 1900 °C in nitrogen to remove impurities and metal catalysts. For functionalization, the BNNTs were immersed in stearoyl chloride, the mixture was stirred, heated to 100 °C, and annealed over 120 h. After centrifugation, the remaining solid was washed with chloroform and *N*,*N*-dimethylformamide repeatedly to afford f-BNNTs.

The microstructure was analyzed by using a JEOL-3000F high-resolution field-emission TEM operated at 300 kV. FTIR spectra were collected by using a Perkin Elmer FTIR spectrometer with a laser wavelength of 1024 nm. The CL spectra were recorded in a charge-coupled device (spectra view 2D; Jobin Yvon, France).

The UV/Vis absorption experiments were performed by using a Hitachi U-4100 spectrometer. The f-BNNTs were dissolved firstly in chloroform, a few drops of the solution were dripped onto a clean quartz wafer, then the solvent was allowed to evaporate. A uniform compact film suitable for UV/Vis absorption experiments was thus obtained. For the original BNNTs, a technique developed in our previous studies was used to make a film.[23] Briefly, a conjugated polymer, poly(*m*-phenylenevinylene-*co*-2,5-dioctoxy-*p*-phenylenevinylene), was used to wrap the BNNTs, which allows them to be dissolved. Composite films were first made by dripping a solution of the BNNTs onto a quartz wafer; the original uniform BNNT film was obtained by heating the composite film to 700 °C in air to remove the polymer.

Received: August 10, 2005
Published online: November 15, 2005

Keywords: alkylation · boron · electronic structure · nanotubes · nitrogen

[1] X. Blase, A. Rubio, S. G. Louie, M. L. Cohen, *Europhys. Lett.* **1994**, *28*, 335.
[2] E. J. Mele, P. Král, *Phys. Rev. Lett.* **2002**, *88*, 056803.
[3] E. Hernandez, C. Goze, P. Bernier, A. Rubio, *Phys. Rev. Lett.* **1998**, *80*, 4502.
[4] A. P. Suryavanshi, M. Yu, J. Wen, C. Tang, Y. Bando, *Appl. Phys. Lett.* **2004**, *84*, 2527.
[5] D. Golberg, Y. Bando, K. Kurashima, T. Sato, *Scr. Mater.* **2001**, *44*, 1561.
[6] Y. Xiao, X. H. Yan, J. X. Cao, J. W. Ding, Y. L. Mao, J. Xiang, *Phys. Rev. B* **2004**, *69*, 205415.
[7] C. W. Chang, W. Q. Han, A. Zettl, *Appl. Phys. Lett.* **2005**, *86*, 173102.
[8] W. Q. Han, Y. Bando, K. Kurashima, T. Sato, *Appl. Phys. Lett.* **1998**, *73*, 3085.
[9] J. Chen, M. A. Hamon, H. Hui, Y. Chen, A. M. Rao, P. C. Eklund, R. C. Haddon, *Science* **1998**, *282*, 95.
[10] J. Chen, H. Liu, W. A. Weimer, M. D. Halls, D. H. Waldeck, G. C. Walker, *J. Am. Chem. Soc.* **2002**, *124*, 9034.
[11] V. Georgakilas, K. Kordatos, M. Proto, D. M. Guldi, M. Holzinger, A. Hirsch, *J. Am. Chem. Soc.* **2002**, *124*, 760.
[12] A. Star, J. F. Stoddart, D. Steuerman, M. Diehl, A. Boukai, E. W. Wong, X. Yang, S. W. Chung, H. Choi, J. R. Heath, *Angew. Chem.* **2001**, *113*, 1771; *Angew. Chem. Int. Ed.* **2001**, *40*, 1721.
[13] A. Bianco, M. Prato, *Adv. Mater.* **2003**, *15*, 1765.
[14] S. Xie, W. Wang, K. A. S. Fernando, X. Wang, Y. Lin, Y. Sun, *Chem. Commun.* **2005**, 3670.
[15] C. Tang, Y. Bando, T. Sato, K. Kurashima, *Chem. Commun.* **2002**, 1290.
[16] C. Y. Zhi, Y. Bando, C. Tang, D. Golberg, *Solid State Commun.* **2005**, *135*, 67.
[17] A. Hirsch, *Angew. Chem.* **2002**, *114*, 1993; *Angew. Chem. Int. Ed.* **2002**, *41*, 1853; .
[18] C. Y. Zhi, Y. Bando, C. Tang, D. Golberg, R. Xie, T. Sekigushi, *Appl. Phys. Lett.* **2005**, *86*, 213110.
[19] Y. Sun, S. R. Wilson, D. I. Schuster, *J. Am. Chem. Soc.* **2001**, *123*, 5348.
[20] M. A. Hamon, M. E. Itkis, S. Niyogi, T. Alvaraez, C. Kuper, M. Menon, R. C. Haddon, *J. Am. Chem. Soc.* **2001**, *123*, 11292.
[21] C. Y. Zhi, J. D. Guo, X. D. Bai, E. G. Wang, *Appl. Phys. Lett.* **2002**, *91*, 5325.
[22] K. Fu, W. Huang, Y. Lin, L. A. Riddle, D. L. Carroll, Y. Sun, *Nano Lett.* **2001**, *1*, 439.
[23] C. Y. Zhi, Y. Bando, C. Tang, D. Golberg, R. Xie, T. Sekiguchi, *J. Am. Chem. Soc.*, accepted.

 © 2005 Wiley-VCH Verlag GmbH & Co. KGaA, Weinheim

Sensors

DOI: 10.1002/anie.200502827

Dynamic Combinatorial Libraries of Dye Complexes as Sensors**

*Andrey Buryak and Kay Severin**

Mixtures of compounds which are formed by the combinatorial assembly of molecular building blocks under thermodynamic control are generally referred to as "dynamic

[*] A. Buryak, Prof. K. Severin
Institut des Sciences et Ingénierie Chimiques
École Polytechnique Fédérale de Lausanne (EPFL)
1015 Lausanne (Switzerland)
Fax: (+41) 21-693-9305
E-mail: kay.severin@epfl.ch

[**] This work was supported by the COST action D31, by the Swiss National Science Foundation, and by the EPFL. We thank Dr. Jean-Marie Helbling, Institute of Mathematics, EPFL, for helpful discussions.

Supporting information for this article is available on the WWW under http://www.angewandte.org or from the author.

© 2005 Wiley-VCH Verlag GmbH & Co. KGaA, Weinheim

combinatorial libraries" (DCLs).[1,2] DCLs are adaptive chemical networks. The addition of a target molecule that selectively interacts with some members of the library may result in a re-equilibration, and this adaptation can be used to identify library members with a high affinity for the respective target molecule. So far, DCLs have mainly been used to study receptors, catalysts, enzyme inhibitors, and new materials.[1,2] Herein, we describe a different application: the utilization of DCLs as sensors.[3]

The relative concentrations of the members of a DCL depend on the environment (solvent, pH, absence or presence of target molecules etc.). A certain library composition is thus a characteristic feature of the environment. It is possible to use the DCL as a sensor if the DCL composition can be transduced into a specific signal output. Up to now DCLs have mainly been analyzed by HPLC, mass spectrometry, and NMR spectroscopy.[1,2] For sensing purposes, however, a fast and cheap analysis method such as fluorescence or UV/Vis spectroscopy would be advantageous. To use the latter technique, we have constructed a DCL of metal–dye complexes in which the library members have a different color. Any re-equilibration will, therefore, result in a variation in the UV/Vis spectrum of the mixture (Figure 1). We show herein that such a library can be used to identify dipeptides in aqueous solution with high selectivity.

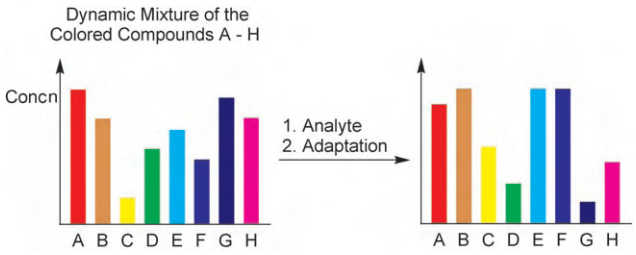

Figure 1. The adaptive behavior of a DCL upon addition of an analyte can be used to identify this analyte by UV/Vis spectroscopy given that the library members possess a characteristic color.

We have used the commercially available dyes arsenazo I (**1**), methylcalcein blue (**2**), and glycine cresol red (**3**) in combination with the metal salts $CuCl_2$ and $NiCl_2$ to generate a DCL in which the library members have a characteristic color (Scheme 1). The dyes form stable complexes with Cu^{2+} and Ni^{2+} ions in buffered aqueous solution (2-(*N*-cyclohexylamino)ethanesulfonic acid (CHES) buffer, pH 8.4), as evidenced by UV/Vis titration experiments. This result is in agreement with reports on the high affinity of these dyes for metal ions.[4–6] Job plot analyses[7] revealed that complexes with more than one ligand per metal ion were formed for several combinations in addition to 1:1 complexes (see the Supporting Information).

The individual metal–dye complexes are able to undergo ligand-exchange reactions. This was evidenced by the fact that the UV/Vis spectra of solutions containing a mixture of two dyes and one metal were different from the sum of the spectra of the individual metal–dye mixtures. The same was true for

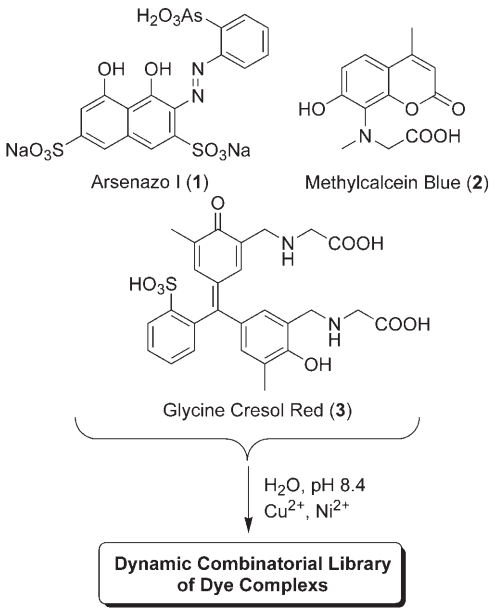

Scheme 1. Generation of a DCL of metal–dye complexes by mixing arsenazo I, methylcalcein blue, and glycine cresol red with $CuCl_2$ and $NiCl_2$ in buffered aqueous solution.

the experiments with two metal ions and one dye molecule (see the Supporting Information).

This data confirmed that solutions of the dyes **1**–**3** and the two metal salts contain a complex mixture of metal–dye complexes and that these complexes are in a dynamic equilibrium with small amounts of free metal ions and dye molecules. Any disturbance of this equilibrium by addition of an analyte was expected to result in a characteristic change of color.

We decided to use dipeptides as analytes to demonstrate this proposal.[8] Dipeptides are known to form stable complexes with Cu^{2+} and Ni^{2+} ions[9] and may therefore displace some of the dyes from the metal ions.[10] This process should lead to an increase in the free dye concentration as well as to a re-equilibration of the remaining metal–dye complexes. In a first experiment we added aqueous solutions of the dipeptides Val-Phe, Gly-Ala, His-Ala, Ala-His, Phe-Pro, and Pro-Gly to a mixture of the three dyes and the two metal salts (final [peptide] = 1.0 mM; [**1**] = [**2**] = [**3**] = 75 μM; [Cu] = [Ni] = 75 μM; 35 mM CHES buffer, pH 8.4). The changes in the UV/Vis spectra upon addition of the respective peptide are shown in Figure 2.

All six dipeptides can be easily distinguished by UV/Vis spectroscopy. An experiment of this kind can therefore be used to identify the dipeptide. It is interesting to note that His-Ala gave rise to a spectrum which was very different from that of the other peptides. This result can be explained by the fact that the side chain of the N-terminal His residue is able to coordinate to the metal ions. The spectrum of Ala-His, on the other hand, was more similar to the spectra found for simple dipeptides such as Val-Phe. This observation suggests that the side chains of a His residue at the C terminus is less important for metal coordination. Another distinctive spectrum was found for Phe-Pro, with rather weak color changes being

 © 2005 Wiley-VCH Verlag GmbH & Co. KGaA, Weinheim

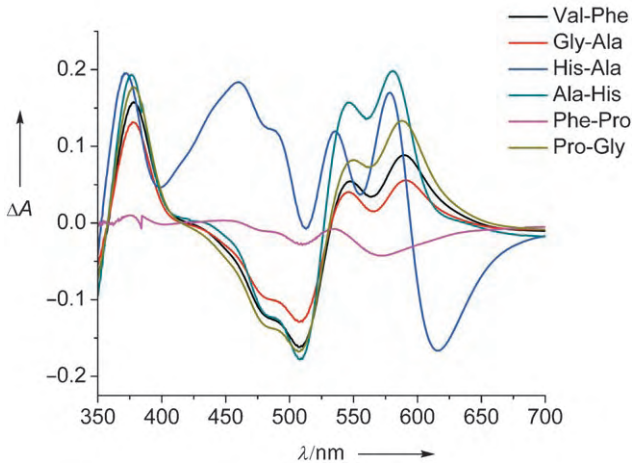

Figure 2. The changes in the UV/Vis spectra upon addition of different dipeptides (1.0 mM) to an aqueous solution containing a DCL sensor composed of the dyes **1**–**3** and the metal salts $CuCl_2$ and $NiCl_2$ ([**1**] = [**2**] = [**3**] = 75 μM, [Cu] = [Ni] = 75 μM, 35 mM CHES buffer, pH 8.4).

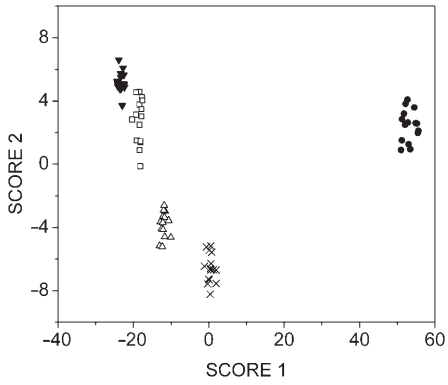

Figure 3. Two-dimensional LDA score plot for the analytes Gly-Ala (●), Val-Phe (□), Ala-Phe (▼), Phe-Ala (△), and D-Phe-Ala (×).

observed. This result highlights the importance of the amide bond for metal coordination.[9]

To test the scope of the DCL sensor we performed a second set of experiments with dipeptides which were structurally more closely related (Gly-Ala, Val-Phe, Ala-Phe, Phe-Ala, and D-Phe-Ala). As expected, the UV/Vis difference spectra were similar to each other, and we therefore used chemometrics[11] to classify the analytes. Fifteen UV/Vis measurements were performed for each dipeptide. To verify that the discrimination between the analytes did not arise from small differences in the concentrations of the peptide stock solutions we varied the peptide concentration for each analyte by ±5%. Thus, five measurements were performed with a peptide concentration of 1.00 mM, five with a concentration of 0.95 mM, and five with a concentration of 1.05 mM (the sensor composition was the same as that described in Figure 2). Data analysis was carried out with the help of the commercial statistics program SYSTAT (version 11.0).[12] A preselection was performed using an automatic variable selection algorithm (see the Supporting Information) to determine which wavelengths in the region between 350 and 700 nm were most relevant for the identification of the peptide. The data from the eight selected wavelengths were then classified by a linear discriminant analysis (LDA).[13] A graphical representation of this analysis in the form of a score plot is shown in Figure 3.

A 100% discrimination was achieved for a "jack-knifed" classification matrix, in which one measurement at a time was treated as an unknown and the rest of the data was used as the training set.[14] This result is quite remarkable, given the fact that none of the dipeptides contain coordinating side chains and that closely related analytes such as the regioisomers Ala-Phe and Phe-Ala as well as the stereoisomers L-Phe-Ala and D-Phe-Ala were used. The discriminative power of the sensor was lower when the complexity of the DCL was reduced by omitting one of the two metal salts: 7 out of the 75 measurements were misclassified for a DCL containing the dyes **1**–**3** and only $CuCl_2$, and 17 misclassifications were obtained for a DCL containing the dyes **1**–**3** and only $NiCl_2$ (see the Supporting Information). This observation shows that a certain library complexity is required to obtain a good differentiation.

The results described above clearly demonstrate the potential of DCLs as sensors. The present library was obtained by mixing commercially available dyes with two transition-metal salts. Despite this simplicity, it was possible to differentiate closely related analytes such as the steroisomers Phe-Ala and D-Phe-Ala. It should be noted that other adaptive systems which show a detectable response upon addition of an analyte can easily be envisioned. DCLs based on compounds with a distinct redox potential or fluorescence, for example, are potentially well suited. The response could then be used to identify a single component or to classify a complex matrix. The modular nature of a DCL makes it easy to optimize the response for a particular sensing problem by variation of the nature, the number, and/or the relative amount of its constituent building blocks. Given these advantages, it seems likely that DCL sensors may find various applications in analytical chemistry.

Received: August 9, 2005
Published online: November 10, 2005

Keywords: combinatorial chemistry · metal complexes · peptides · sensors · UV/Vis spectroscopy

[1] For recent reviews see: a) S. Otto, *J. Mater. Chem.* **2005**, *15*, 3357–3361; b) J. D. Cheeseman, A. D. Corbett, J. L. Gleason, R. J. Kazlauskas, *Chem. Eur. J.* **2005**, *11*, 1709–1716; c) J.-L. Reymond, *Angew. Chem.* **2004**, *116*, 5695–5697; *Angew. Chem. Int. Ed.* **2004**, *43*, 5577–5579; d) O. Ramström, T. Bunyapaiboonsri, S. Lohmann, J.-M. Lehn, *Biochim. Biophys. Acta* **2002**, *1572*, 178–186; e) J.-M. Lehn, *Proc. Natl. Acad. Sci. USA* **2002**, *99*, 4763–4768; f) S. J. Rowan, S. J. Cantrill, G. R. L. Cousins, J. K. M. Sanders, J. F. Stoddart, *Angew. Chem.* **2002**, *114*, 938–993; *Angew. Chem. Int. Ed.* **2002**, *41*, 898–952; g) S. Otto, R. L. E. Furlan, J. K. M. Sanders, *Curr. Opin. Chem. Biol.* **2002**, *6*, 321–327.

[2] For some selected recent publications see: a) P. T. Corbett, L. H. Tong, J. K. M. Sanders, S. Otto, *J. Am. Chem. Soc.* **2005**, *127*,

 © 2005 Wiley-VCH Verlag GmbH & Co. KGaA, Weinheim

8902 – 8903; b) N. Sreenivasachary, J.-M. Lehn, *Proc. Natl. Acad. Sci. USA* **2005**. *102*, 5938 – 5943; c) T. Hotchkiss, H. B. Kramer, K. J. Doores, D. P. Gamblin, N. J. Oldham, B. G. Davis, *Chem. Commun.* **2005**, 4264 – 4266; d) R. T. S. Lam, A. Belenguer, S. L. Roberts, C. Naumann, T. Jarrosson, S. Otto, J. K. M. Sanders, *Science* **2005**, *308*, 667 – 669; e) S. Zameo, B. Vauzeilles, J.-M. Beau, *Angew. Chem.* **2005**, *117*, 987 – 991; *Angew. Chem. Int. Ed.* **2005**, *44*, 965 – 969; f) A. Bugaut, J.-J. Toulmé, B. Rayner, *Angew. Chem.* **2004**, *116*, 2306 – 2309; *Angew. Chem. Int. Ed.* **2004**, *43*, 3144 – 3147; g) M. Albrecht, I. Janser, J. Runsink, G. Raabe, P. Weiss, R. Fröhlich, *Angew. Chem.* **2004**, *116*, 6832 – 6836; *Angew. Chem. Int. Ed.* **2004**, *43*, 6662 – 6666; h) R. Larsson, Z. Pei, O. Ramström, *Angew. Chem.* **2004**, *116*, 3802 – 3804; *Angew. Chem. Int. Ed.* **2004**, *43*, 3716 – 3718; i) K. Severin, *Chem. Eur. J.* **2004**, *10*, 2565 – 2580; j) W. G. Skene, J.-M. Lehn, *Proc. Natl. Acad. Sci. USA* **2004**. *101*, 8270 – 8275; k) Z. Grote, R. Scopelliti, K. Severin, *Angew. Chem.* **2003**, *115*, 3951 – 3955; *Angew. Chem. Int. Ed.* **2003**, *42*, 3821 – 3825.

[3] For a dynamic polymer which changes its optical properties upon addition of Zn^{2+} ions see: N. Guiseppone, J.-M. Lehn, *J. Am. Chem. Soc.* **2004**, *126*, 11448 – 11449.

[4] For metal complexes of arsenazo I see: a) M. B. Cingi, F. Bigoli, E. Leporati, M. A. Pellinghelli, *J. Chem. Soc. Dalton Trans.* **1982**, 1965 – 1970; b) H. Khalifa, Y. M. Issa, *Microchem. J.* **1975**, *20*, 287 – 291; c) A. A. Muk, R. Radosavljevic, *Croat. Chem. Acta* **1967**, *39*, 1 – 9; d) B. Budesinsky, *Z. Anal. Chem.* **1965**, *207*, 247 – 256; e) J. S. Fritz, M. Johnson-Richard, *Anal. Chim. Acta* **1959**, *20*, 164 – 171.

[5] For metal complexes of methylcalcein blue see: a) H. Yoshida, T. Ozawa, K. Jitsukawa, H. Einaga, *Polyhedron* **1993**, *12*, 1319 – 1328; b) H. G. Brittain, *Anal. Chem.* **1987**, *59*, 1122 – 1125; c) G. M. Huitink, H. Diehl, *Talanta* **1974**, *21*, 1193 – 1202.

[6] For metal complexes of glycine cresol red see: a) I. V. Pyatnitskii, L. L. Kolomiets, V. S. Barshchevskaya, *J. Anal. Chem. (Moscow)* **1989**, *44*, 450 – 454; b) B. Budesinsky, J. Gurovic, *Collect. Czech. Chem. Commun.* **1963**, *28*, 1154 – 1161.

[7] a) P. MacCarthy, *Anal. Chem.* **1978**, *50*, 2165; b) P. Job, *C. R. Hebd. Seances Acad. Sci.* **1925**, *180*, 928.

[8] For selected publications on sensors which are able to detect small peptides or amino acids in aqueous solution see: a) P. K. Sudeep, S. T. S. Joseph, K. G. Thomas, *J. Am. Chem. Soc.* **2005**, *127*, 6516 – 6517; b) M. Kruppa, C. Mandl, S. Miltschitzky, B. König, *J. Am. Chem. Soc.* **2005**, *127*, 3362 – 3365; c) A. Buryak, K. Severin, *J. Am. Chem. Soc.* **2005**, *127*, 3700 – 3701; d) A. Buryak, K. Severin, *Angew. Chem.* **2004**, *116*, 4875 – 4878; *Angew. Chem. Int. Ed.* **2004**, *43*, 4771 – 4774; e) C.-F. Chow, B. K. W. Chiu, M. H. W. Lam, W.-Y. Wong, *J. Am. Chem. Soc.* **2003**, *125*, 7802 – 7803; f) C.-Y. Lin, D.-F. Tai, T.-Z. Wu, *Chem. Eur. J.* **2003**, *9*, 5107 – 5110; g) M. A. Hortalá, L. Fabbrizzi, N. Marcotte, F. Stomeo, A. Taglietti, *J. Am. Chem. Soc.* **2003**, *125*, 20 – 21; h) K. E. S. Deam, G. Klein, O. Renaudet, J.-L. Reymond, *Bioorg. Med. Chem. Lett.* **2003**, *13*, 1653 – 1656; i) H. Aït-Haddou, S. L. Wiskur, V. M. Lynch, E. V. Anslyn, *J. Am. Chem. Soc.* **2001**, *123*, 11296 – 11297; j) G. Klein, J.-L. Reymond, *Angew. Chem.* **2001**, *113*, 1821 – 1823; *Angew. Chem. Int. Ed.* **2001**, *40*, 1771 – 1773.

[9] H. Sigel, R. B. Martin, *Chem. Rev.* **1982**, *82*, 385 – 426.

[10] For reviews on indicator displacement assays see: a) L. Fabbrizzi, M. Licchelli, A. Taglietti, *Dalton Trans.* **2003**, 3471 – 3479; b) C. Sukasai, T. Tuntulani, *Chem. Soc. Rev.* **2003**, *32*, 192 – 202; c) S. L. Wiskur, H. Aït-Haddou, J. J. Lavigne, E. V. Anslyn, *Acc. Chem. Res.* **2001**, *34*, 963 – 972.

[11] For recent reviews see: a) B. Lavine, J. J. Workman, Jr., *Anal. Chem.* **2004**, *76*, 3365 – 3372; b) P. Geladi, B. Sethson, J. Nyström, T. Lillhonga, T. Lestander, J. Burger, *Spectrochim. Acta Part B* **2004**, *59*, 1347 – 1357; c) A. de Juan, R. Tauler, *Anal. Chim. Acta* **2003**, *500*, 195 – 210; d) P. Geladi, *Spectrochim. Acta Part B* **2003**, *58*, 767 – 782; e) P. K. Hopke, *Anal. Chim. Acta* **2003**, *500*, 365 – 377.

[12] SYSTAT, version 11.0, Systat Software Inc., Richmond, California, USA.

[13] P. C. Jurs, G. A. Bakken, H. E. McClelland, *Chem. Rev.* **2000**, *100*, 2649 – 2678.

[14] A 97% discrimination was achieved in a cross-validation in which 50% of the measurements were taken out randomly and the rest of the data was used as the training set (see the Supporting information).

 © 2005 Wiley-VCH Verlag GmbH & Co. KGaA, Weinheim

Cluster Compounds

DOI: 10.1002/anie.200501807

Azine-Bridged Octanuclear Copper(II) Complexes Assembled with a One-Stranded Ditopic Thiocarbohydrazone Ligand**

Diana Dragancea, Vladimir B. Arion, Sergiu Shova, Eva Rentschler, and Nicolae V. Gerbeleu**

Multinuclear metal complexes are of interest in different fields of research. They are found in biological systems such as ferritin,[1,2] those with high-spin ground states can act as superparamagnets[3,4] and molecular nanomagnets,[5,6] and

[*] Prof. V. B. Arion
Institute of Inorganic Chemistry—Bioinorganic, Environmental and Radiochemistry
Faculty of Chemistry, University of Vienna
Waehringerstrasse 42, 1090 Vienna (Austria)
Fax: (+43) 1-427-752-680
E-mail: vladimir.arion@univie.ac.at

D. Dragancea, Prof. N. V. Gerbeleu
Institute of Chemistry of the Academy of Sciences of R. Moldova
strasse Academiei 3, 2028 Chisinau (Moldova)
Fax: (+373) 22-725-490
E-mail: garbalau@cc.acad.md

Dr. S. Shova
Department of Chemistry
Moldova State University
strasse Mateevici 60, 2009 Chisinau (Moldova)

Prof. E. Rentschler
Instutute of Inorganic and Analytical Chemistry
University of Mainz
Duesbergweg 10–14, 55099 Mainz (Germany)

[**] This work was supported by the University of Vienna and by INTAS Project Nr 03-51-4532. Mr. A. Göbels (MPI for Bioinorganic Chemistry, Mülheim an der Ruhr) is kindly acknowledged for carrying out the magnetic measurements. We also thank Dr. Euan Brechin for stimulating discussion.

Supporting information for this article is available on the WWW under http://www.angewandte.org or from the author.

WILEY InterScience DISCOVER SOMETHING GREAT
© 2005 Wiley-VCH Verlag GmbH & Co. KGaA, Weinheim

some exhibit spin-transition behavior[7] or manifest catalytic activity.[8] Like metal-template techniques,[9] self-assembly[10] can be used to build up beautiful molecular architectures,[6,11–13] often containing paramagnetic ions and endowed with unique properties.[14] A few octanuclear copper(II) complexes have been reported,[8,15–21] mostly synthesized in an "uncontrolled" assembly process starting from a large number of components in the presence of small bridging ligands such as hydroxide, oxide, methoxide, or halide.[21] A more attractive approach is the use of tailored single-stranded ligands for self-assembly, which makes the involvement of small bridging fragments unnecessary.[21,22] Two remarkable recent examples, reported by Thompson et al.[23] and Matthews et al.,[21] relied on linear ligands, one of which, $2poapH_2$, is tritopic, and the other, L′, tetratopic. Here we use a ditopic single-stranded thiocarbohydrazone ligand and show that further unusual multinuclear systems can be formed.

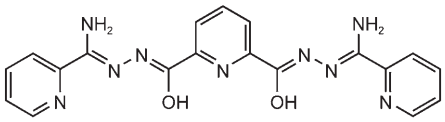

$2poapH_2$

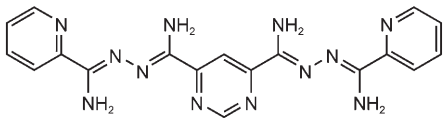

L′

Thiocarbohydrazones have previously served as building blocks in the self-assembly of tetranuclear molecular square structures. In particular, mixed-valent iron(II)–iron(III), nickel(II), zinc(II), and cadmium(II) clusters have been synthesized starting from 1,5-bis(2-acetylpyridine)thiocarbohydrazone or related derivatives.[24–26] Reactions of the same ligands with copper(II) produced dimers of dinuclear units held together by extraneous bridging ligands.[26,27]

We discovered that 1,5-bis(2-hydroxybenzaldehyde)thiocarbohydrazone (H_4L) reacts with copper(II) acetate monohydrate or copper(II) sulfate in dimethylformamide (DMF)/ethanol (1:10) in the presence of triethylamine to give the green-brown complex $[Cu_8L_4(DMF)_8(H_2O)]\cdot 3.5\,DMF\cdot 3\,H_2O$ (**1**·3.5 DMF·3 H_2O) with absorbance features at λ_{max} (ε_M) = 320 (118285), 413 (114660), 437 (136860), and 461 nm (113610 $M^{-1}cm^{-1}$). Recrystallization of the reaction product from dimethyl sulfoxide afforded the complex $[Cu_8L_4(dmso)_7]\cdot 6\,DMSO\cdot 1.32\,H_2O$ (**2**·6 DMSO·1.32 H_2O).

As for the parent thiocarbohydrazide, two tautomeric forms are possible for H_4L: thione form **A** and thiol form **B**, which are in equilibrium.[28] The thiol tautomer can adopt a syn (**B**) or anti (**B′**) configuration as a consequence of the double-bond character of the central N–C linkage.

X-ray diffraction studies showed the metal-free compound to crystallize in the thione form **A**.[29] Both thiol forms have been observed in metal complexes: in $[MoO_2(H_2L)(dmso)]$ the dianionic ligand adopts the *syn* configuration

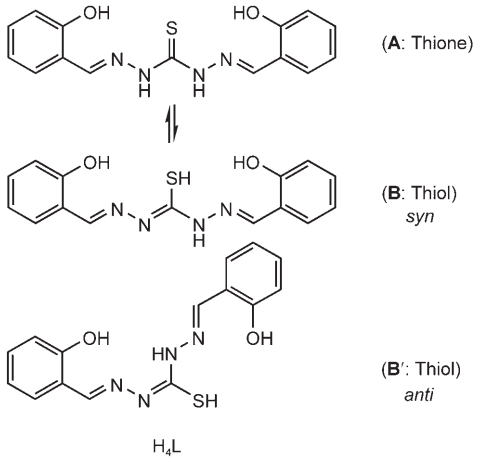

(**A**: Thione)

(**B**: Thiol) *syn*

(**B′**: Thiol) *anti*

H_4L

B,[28] while the *anti* configuration **B′** was found in $[MoO_2(H_2L)(CH_3OH)]$.[30] X-ray diffraction[31] revealed that in **1**·3.5 DMF·0.7 H_2O the four thiocarbohydrazone ligands adopt the thiol *anti* configuration **B′** and thus provide two contiguous tridentate pockets, one with NNO and the other with ONS donor atoms, each of which can accommodate one copper(II) ion (Figure 1). Thus, six of the seven donor atoms of a fully deprotonated ligand L^{4-} are linked with two metal ions to give a dicopper(II) unit $\{Cu_2L\}^0$. The assembly of four such units into a metallomacrocyclic array takes place by coordination of the seventh donor atom of each $\{Cu_2L\}$ unit to the copper(II) atom of the adjacent unit which resides in the ONS

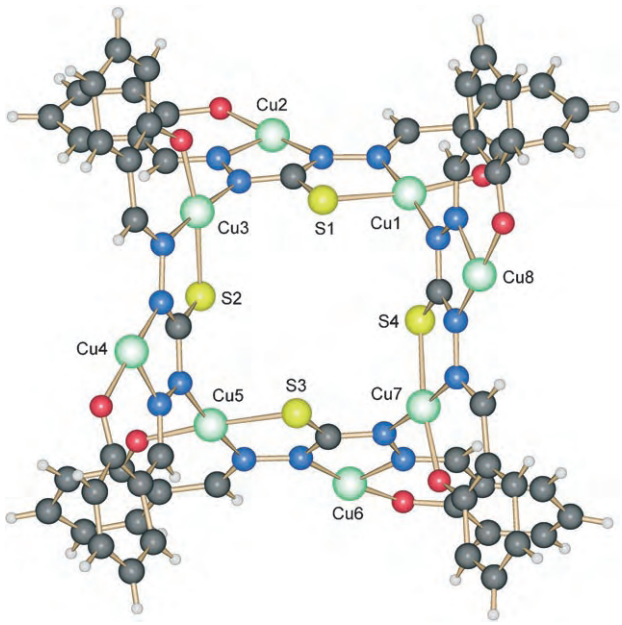

Figure 1. SCHAKAL representation of the charge-neutral copper(II) octanuclear species $\{Cu_8L_4\}^0$ with four ligands in nonparallel pairs in the crystal structure of **1**·3.5 DMF·0.7 H_2O. The DMF molecules coordinated to Cu2, Cu4, Cu6. and Cu8 are omitted for clarity. Gray C, red O, blue N, yellow S, white H, green Cu.

© 2005 Wiley-VCH Verlag GmbH & Co. KGaA, Weinheim

ligand pocket to achieve a square-planar geometry. In the resulting architecture (see Figure 1) four copper(II) atoms, Cu1, Cu3, Cu5, and Cu7, are four-coordinate, with two ligands L^{4-} filling all four coordination positions, while the other four copper(II) centers, Cu2, Cu4, Cu6, and Cu8, each accommodated in an ONN ligand pocket, require additional ligands (DMF or DMF and H_2O) to complete their coordination spheres, as shown for Cu2 in Figure 2. The coordination polyhedron for Cu2 is a trigonal bipyramid, while those for

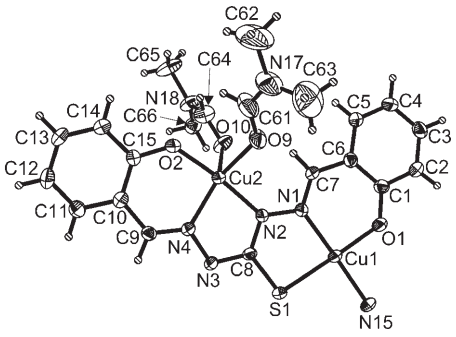

Figure 2. Structural representation of the $\{Cu_2L(dmf)_2\}$ fragment in **1**·3.5 DMF·0.7 H_2O. The atom N15 belongs to the second $\{Cu_2L\}$ unit, which is arranged perpendicular to the N1–Cu1 vector. Selected bond lengths [Å]: Cu1–O1 1.908(4), Cu1–N1 1.970(4), Cu1–S1 2.2527(15), Cu1–N15 2.007(4), Cu2–O2 1.887(4), Cu2–N2 1.965(4), Cu2–N4 1.957(4), Cu2–O9 2.109(4), Cu2–O10 2.159(4).

Cu4 and Cu8 can be better described as distorted square pyramids. Depending on the positions of the disordered components of DMF and H_2O molecules around Cu6 its coordination geometry changes between distorted trigonal-bipyramidal and distorted octahedral. In both cases a water molecule is involved in coordination to Cu6. The charge balance is in agreement with formation of species **1**. Sixteen negative charges provided by four fully deprotonated ligands are balanced by the sixteen positive charges of eight copper(II) ions. This unique assembly of eight copper(II) centers, four of which are four-coordinate and the other four five-coordinate, into an azine-bridged 24-membered metallomacrocycle is to our knowledge the first example in copper(II) coordination chemistry. It requires four heptadentate ligands which use their donor capacity in an unprecedented manner for thiocarbohydrazone coordination chemistry to bind eight metal ions with the number of solvent molecules required to fully satisfy the coordination preferences of the eight copper(II) centers. We note that **1**·3.5 DMF·3 H_2O has an insular molecular structure in which the shortest intermolecular copper–copper separation is about 7.6 Å.

Unlike **1**, the molecule of **2** has C_2 symmetry. Of four independent copper(II) atoms two (Cu1 and Cu3) are square-planar coordinated like in **1**, whereas the coordination polyhedra of Cu2 and Cu4 can be described as distorted trigonal-bipyramidal with DMSO molecules occupying the "axial" positions. While both DMSO molecules at Cu2 are bound through oxygen atoms (Cu2–O5 2.002(5), Cu2–O6 2.346(6) Å), the coordination behavior of the two DMSO ligands at Cu4 is different. One of them coordinates to Cu4 through the oxygen atom (Cu4–O8 1.948(6) Å), whereas the second is disordered over two positions, coordinating through O7 (Cu4–O7 2.378(11) Å) or S5 with a weak contact (Cu4–S5 at 3.257(2) Å) in an alternating fashion. As a result, this DMSO acts as a bridging ligand leading to association of the molecules of **2** in one-dimensional chains along [100] (Figure 3).

The magnetic behavior of a polycrystalline sample of **2**·6 DMSO·1.32 H_2O in the temperature range 2–290 K in a field of 1 T is shown in Figure 4. The value of $\chi_M T$ decreases from 1.48 $cm^3 K mol^{-1}$ at 300 K and reaches a plateau of 0.02 $cm^3 K mol^{-1}$ below 20 K. As the room-temperature value of $\chi_M T$ for an octanuclear unit of eight noninteracting $S = {}^1/_2$ Cu^{II} ions with $g = 2.0$ would be 3.00 $cm^3 K mol^{-1}$, this clearly reflects that the major interactions in **2**·6 DMSO·1.32 H_2O are antiferromagnetic in nature. To extract the magnitude of exchange interaction between the Cu^{II} ions we applied the spin Hamiltonian $\mathscr{H} = -2J \sum_{i=1}^{8} S_i S_{i+1}$. Best fits to the experimental data down to low temperature were obtained by using g values of 2.2 for the Cu^{II} ions and a coupling constant of $J = -145\ cm^{-1}$, taking additionally into account 0.66% of a paramagnetic impurity ($R = 1.6 \times 10^{-4}$). Since the formation of a dinuclear transition metal species with a related ligand

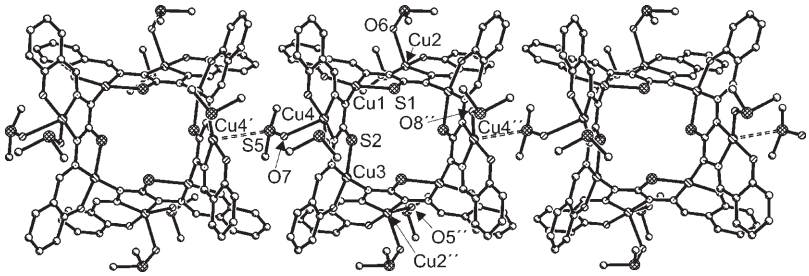

Figure 3. One-dimensional chain of molecules of **2** in **2**·6 DMSO·1.32 H_2O. The second position of the disordered bridging DMSO ligand is omitted for clarity; S5 atoms lie on special positions on twofold axes.

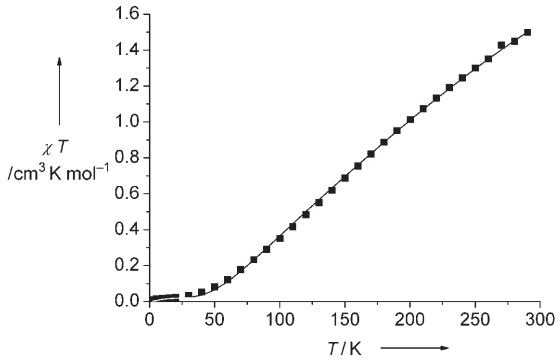

Figure 4. Magnetic data for **2**·6 DMSO·1.32 H_2O (see text for fitting parameters).

 © 2005 Wiley-VCH Verlag GmbH & Co. KGaA, Weinheim

has been observed,[32] the low-temperature behavior of the molar susceptibility was regarded not as a simple paramagnetic impurity but rather as 0.3% of a weakly coupled dimer of two copper ions in comparable ligand environments, and hence presumably having the same g values as in the main compound. The simulation of $\chi_M T$ versus T with these data is shown in Figure 4 as a solid line. The magnetic behavior of **1**·3.5 DMF·0.7 H_2O is very similar: the g value is 2.14, and the intramolecular coupling $J = -128$ cm^{-1}. Also here an impurity had to be considered. The preparation of **1** is very sensitive, and contributions of between 1 and 7% of a coupled side product were experimentally found. Independent of whether DMF or DMSO completed the coordination sphere for the copper atoms in **1**·3.5 DMF·0.7 H_2O and **2**·6 DMSO·1.32 H_2O, respectively, alternation of the bridging between the metal ions is not reflected in the magnetic measurements. In all cases the fitting of the data with a model containing only one exchange interaction constant was good. This seems reasonable, since all torsion angles Θ_{CuNNCu} (av. 176°) are very close to 180°. Interestingly, the intermolecular arrangement as a one-dimensional chain for **2**·6 DMSO·1.32 H_2O does not influence the magnetic properties of the octanuclear compound; it behaves magnetically like **1**·3.5 DMF·0.7 H_2O, which has shortest intermolecular contacts of about 7.6 Å.

In conclusion, the unprecedented octanuclear clusters **1** and **2** are formed by a unique heptadentate ligand that exhibits particular conformational and configurational flexibility, appropriate spatial arrangement of metal-binding sites, coordination ability, and acid–base properties which allow full use of its donor capacity to satisfy maximally the stereochemical demands of the metal ions with minimum strain energy. The assembled metallomacrocyclic array of eight azine-bridged copper(II) ions, four of which are square-planar and four of which are distorted square-pyramidal or distorted trigonal-bipyramidal, is also unique in copper(II) coordination chemistry. The isolation of **1** and **2** opens up exciting opportunities to construct multinuclear systems with a number of other redox active metal ions with similar stereochemical preferences. The construction of heteronuclear clusters is also a challenge. Substitution of solvent molecules by suitable bridging ligands will also permit the assembly of oligomeric or even polymeric chains of HSNC units. This work is underway in our laboratories.

Experimental Section

All reagents were used as received from Aldrich. 1,5-Bis(2-hydroxybenzaldehyde)thiocarbohydrazone[29] was prepared according to reported procedures.

1·3.5 DMF·3 H_2O: $Cu(CH_3COO)_2 \cdot H_2O$ (0.2 g, 1.0 mmol) in ethanol (20 mL) and triethylamine (3 mL) was added to a hot solution of 1,5-bis(2-hydroxybenzaldehyde)thiocarbohydrazone (0.16 g, 0.5 mmol) in DMF/ethanol (1:10, 22 mL). The resultant brown solution was heated at 100 °C for 1 h and allowed to cool to room temperature. The green-brown crude product was collected by filtration, washed with diethyl ether, and then dissolved in hot DMF (10 mL) and filtered. After 5 d the brown product crystallized from this solution at room temperature, was collected by filtration, washed with diethyl ether, and dried in air. Yield: 0.06 g, 19%. Elemental analysis (%): calcd for $C_{94.5}H_{144.5}N_{27.5}Cu_8O_{23.5}S_4$: C 42.38, H 5.44, N 14.38, S 4.79; found: C 41.99, H 5.60, N 14.09, S 4.92. IR (CsI): $\tilde{\nu} = 1651$, 1599, 1537, 1361, 1331, 1199, 757, 571, 527, 495, 472, 364, 323 cm^{-1}. Brown cubic crystals of 1·3.5 DMF·0.7 H_2O suitable for X-ray diffraction were obtained by recrystallization of **1**·3.5 DMF·3 H_2O from anhydrous DMF.

2·6 DMSO·1.32 H_2O: Recrystallization of the green-brown crude product (obtained as described above) from DMSO (5 mL) afforded green-brown prisms suitable for X-ray diffraction. Yield: 0.04 g. Elemental analysis (%): calcd for $C_{86}H_{120.67}N_{16}Cu_8O_{22.33}S_{17}$: C 37.03, H 4.32, N 8.03; found: C 37.03, H 3.97, N 8.11.

IR spectra were recorded on a Bruker FTIR VERTEX70 instrument in the region 4000–150 cm^{-1}. UV/Vis spectra were recorded on a Perkin-Elmer Lambda 20 UV/Vis spectrophotometer on samples dissolved in DMF. Magnetic susceptibility measurements were carried out with a Quantum Design MPMS SQUID magnetometer between 2 and 290 K in an applied field of 1 T. Diamagnetic corrections of -1370×10^{-6} and -1340×10^{-6} cm^3 mol^{-1} for **1**·3.5 DMF·3 H_2O and **2**·6 DMSO·1.32 H_2O, respectively, were estimated from Pascal's constants.[33]

Received: May 25, 2005
Revised: September 26, 2005
Published online: November 15, 2005

Keywords: cluster compounds · copper · magnetic properties · N ligands · self-assembly

[1] D. D. Awschalom, D. P. DiVincenzo, J. F. Smyth, *Science* **1992**, *258*, 414–417.
[2] S. Gider, D. D. Awschalom, T. Douglas, S. Mann, M. Charpala, *Science* **1995**, *267-270*, 77–80.
[3] M. A. Bolcar, S. M. J. Aubin, K. Folting, D. N. Hendrickson, G. Christou, *Chem. Commun.* **1997**, 1485–1486.
[4] C. Delfs, D. Gatteschi, L. Pardi, R. Sessoli, K. Wieghardt, D. Hanke, *Inorg. Chem.* **1993**, *32*, 3099–3103.
[5] a) R. Sessoli, D. Gatteschi, A. Caneschi, M. A. Novak, *Nature* **1993**, *365*, 141–143; b) L. Thomas, F. Lionti, R. Ballou, D. Gatteschi, R. Sessoli, B. Barbara, *Nature* **1996**, *383*, 145–147.
[6] a) E. K. Brechin, A. Graham, P. E. Y. Milne, M. Murrie, S. Parsons, R. E. P. Winpenny, *Philos. Trans. R. Soc. London Ser. A* **1999**, *357*, 3119–3137; b) R. E. P. Winpenny, *J. Chem. Soc. Dalton Trans.* **2001**, 1–10; c) "High Nuclearity Clusters: Clusters and Aggregates with Paramagnetic Centers: Oxygen and Nitrogen Bridged Systems": R. E. P. Winpenny in *Comprehensive Coordination Chemistry II* (Eds.: J. A. McCleverty, T. J. Meyer), Elsevier, Amsterdam, **2003**, chap. 7.3, pp. 125–175.
[7] M. Ruben, E. Breuning, J.-M. Lehn, V. Ksenofontov, F. Renz, P. Gütlich, G. B. M. Vaughan, *Chem. Eur. J.* **2003**, *9*, 4422–4429.
[8] a) A. Ardizzoia, M. A. Angarconi, G. LaMonica, F. Cariati, S. Cenini, M. Moret, N. Masciocchi, *Inorg. Chem.* **1991**, *30*, 4347–4353; b) S. Parsons, J. M. Rawson, D. Reed, R. E. P. Winpenny, *J. Chem. Soc. Dalton Trans.* **1995**, 163–175.
[9] N. V. Gerbeleu, V. B. Arion, J. Burgess, *Template Synthesis of Macrocyclic Compounds*, Wiley-VCH, Weinheim, **1999**, p. 565.
[10] J.-M. Lehn, *Supramolecular Chemistry: Concepts and Perspectives*, VCH, Weinheim, **1995**, chaps. 8, 9.
[11] a) P. N. W. Baxter, J.-M. Lehn, G. Baum, D. Fenske, *Chem. Eur. J.* **2000**, *6*, 4510–4517; b) M. Ruben, J. Rojo, F. J. Romero-Salguero, L. H. Uppadine, J.-M. Lehn, *Angew. Chem.* **2004**, *116*, 3728–3747 Angew. Chem. Int. Ed. **2004**, 43, 3644–3662; c) J. Rojo, J.-M. Lehn, G. Baum, D. Fenske, O. Waldmann, P. Müller, *Eur. J. Inorg. Chem.* **1999**, 517–522; d) P. J. Van Koningsbruggen, E. Müller, J. G. Haasnoot, J. Reedijk, *Inorg. Chim. Acta* **1993**, *208*, 37–42.
[12] M. Fujita, K. Umemoto, M. Yoshizawa, N. Fujita, T. Kusukawa, K. Biradha, *Chem. Commun.* **2001**, 509–518.

 © 2005 Wiley-VCH Verlag GmbH & Co. KGaA, Weinheim

[13] L. K. Thompson, *Coord. Chem. Rev.* **2002**, *233–234*, 193–206.
[14] a) O. Waldmann, J. Hassmann, P. Müller, G. S. Hanan, D. Volkmer, U. S. Schubert, J.-M. Lehn, *Phys. Rev. Lett.* **1997**, *78*, 3390–3393; b) M. Ruben, E. Breuning, J.-P. Gisselbrecht, J.-M. Lehn, *Angew. Chem.* **2000**, *112*, 4312–4315; *Angew. Chem. Int. Ed.* **2000**, *39*, 4139–4142; c) M. Ruben, E. Breuning, M. Barboiu, J.-P. Gisselbrecht, J.-M. Lehn, *Chem. Eur. J.* **2003**, *9*, 291–299.
[15] V. McKee, S. S. Tandon, *Inorg. Chem.* **1989**, *28*, 2901–2902.
[16] A. J. Blake, C. M. Grant, C. I. Gregory, S. Parsons, J. M. Rawson, D. Reed, R. E. P. Winpenny, *J. Chem. Soc. Dalton Trans.* **1995**, 163–175.
[17] V. Tangoulis, S. Passchalidou, E. G. Bakalbassis, S. P. Perlepes, C. P. Raptopoulou, A. Teris, *Chem. Commun.* **1996**, 1297–1298.
[18] Y. Zhang, L. K. Thompson, J. N. Bridson, M. Bubenic, *Inorg. Chem.* **1995**, *34*, 5870–5877.
[19] a) K. Geetha, M. Nethaji, A. R. Chakravarty, *Inorg. Chem.* **1997**, *36*, 6134–6137; b) A. Mukherjee, I. Rudra, M. Nethaji, S. Ramasesha, A. R. Chakravarty, *Inorg. Chem.* **2003**, *42*, 463–468.
[20] M.-L. Tong, H. K. Lee, Y.-X. Tong, X.-M. Chen, T. C. W. Mak, *Inorg. Chem.* **2000**, *39*, 4666–4669.
[21] S. T. Onions, S. L. Heath, D. J. Price, R. W. Harrington, W. Clegg, C. J. Matthews, *Angew. Chem.* **2004**, *116*, 1850–1853; *Angew. Chem. Int. Ed.* **2004**, *43*, 1814–1817.
[22] V. A. Milway, V. Niel, T. S. M. Abedin, Z. Xu, L. K. Thompson, H. Grove, D. O. Miller, S. R. Parsons, *Inorg. Chem.* **2004**, *43*, 1874–1884.
[23] Z. Xu, L. K. Thompson, D. O. Miller, *Chem. Commun.* **2001**, 1170–1171.
[24] H. Gang, G. Dong, D. Chun-Ying, M. Hong, M. Qing-jin, *New J. Chem.* **2002**, *26*, 1371–1377.
[25] M. Akbar Ali, P. V. Bernhardt, C. Lee Kiem, A. Huq Mirza, *Aust. J. Chem.* **2004**, *57*, 409–413.
[26] H. Cheng, D. Chun-ying, F. Chen-jie, L. Yong-jiang, M. Qing-jin, *J. Chem. Soc. Dalton Trans.* **2000**, 1207–1212.
[27] a) B. Moubaraki, K. S. Murray, J. D. Ranford, X. Wang, Y. Xu, *Chem. Commun.* **1998**, 353–354; b) B. Moubaraki, K. S. Murray, J. D. Ranford, J. J. Vittal, X. Wang, Y. Xu, *J. Chem. Soc. Dalton Trans.* **1999**, 3573–3578.
[28] C. Bustos, O. Burckhardt, R. Schrebler, D. Carillo, A. M. Arif, A. H. Cowley, C. M. Nunn, *Inorg. Chem.* **1990**, *29*, 3996–4001.
[29] R. Yanping, D. Rongbin, W. Liufang, W. Jigui, *Synth. Commun.* **1999**, *29*, 613–617.
[30] A. Rana, R. Dinda, P. Sengupta, S. Ghosh, L. R. Falvello, *Polyhedron* **2002**, *21*, 1023–1030.
[31] Crystal data for **1**·3.5 DMF·0.7 H_2O: $C_{94.5}H_{139.9}Cu_8N_{27.5}O_{21.2}S_4$, $M_r = 2620.83$, monoclinic, space group $P2_1/c$, $a = 19.431(4)$, $b = 28.279(6)$, $c = 26.838(9)$ Å, $\beta = 129.48(2)°$, $V = 11383(5)$ Å^3, $Z = 4$, $\rho_{calcd} = 1.529$ g cm^{-3}, $Mo_{K\alpha}$ radiation ($\lambda = 0.71073$ Å, $\mu = 1.615$ mm^{-1}), $T = 120$ K, $R = 0.0588$ ($F^2 > 2\sigma$), $R_w = 0.1746$ (for 22343 data and 1466 refined parameters). Crystal data for **2**·6 DMSO·1.32 H_2O: $C_{86}H_{120.67}Cu_8N_{16}O_{22.33}S_{17}$, $M_r = 2789.35$, monoclinic, space group $P2/c$, $a = 14.228(3)$, $b = 13.863(3)$, $c = 29.827(6)$ Å, $\beta = 102.75(3)°$, $V = 5738(2)$ Å^3, $Z = 2$, $\rho_{calcd} = 1.614$ g cm^{-3}, $Mo_{K\alpha}$ radiation ($\lambda = 0.71073$ Å, $\mu = 1.833$ mm^{-1}), $T = 120$ K, $R = 0.0820$ ($F^2 > 2\sigma$), $R_w = 0.2562$ (for 11279 data and 723 refined parameters). Data were collected on a Nonius Kappa CCD diffractometer. Single crystals were placed at 50 mm from the detector and 1267 and 942 frames were measured, each for 60 and 80 s over a 0.75 and 1° scan width for **1**·3.5 DMF·0.7 H_2O and **2**·6 DMSO·1.32 H_2O, respectively. The data were processed using Denzo-SMN software. The structure was solved by direct methods and refined by full-matrix least-squares techniques. Non-hydrogen atoms were refined with anisotropic displacement parameters. H atoms were placed at calculated positions and refined as riding atoms in the subsequent least-squares model refinements. Two DMF ligands coordinated to Cu6, as well as one of two DMF molecules coordinated to Cu4 and Cu8, were disordered over two positions, which could be resolved with close 0.5:0.5 occupancy. On the other hand, by taking into account the increased values of the thermal anisotropic factors, one of the DMF molecules of solvation was localized in a single position with 0.5 occupancy. Structure solution and refinement were performed with the SHELX program. CCDC-270851 (**1**·3.5 DMF·0.7 H_2O) and -281722 (**2**·6 DMSO·1.32 H_2O) contain the supplementary crystallographic data for this paper. These data can be obtained free of charge from The Cambridge Crystallographic Data Centre via www.ccdc.cam.ac.uk/data_request/cif.
[32] The reaction of $CuCl_2$ with 1,5-bis(2-hydroxybenzaldehyde)carbohydrazone (H_4L'') in 2:1 molar ratio in DMF/H_2O with subsequent recrystallization of the resulting precipitate from DMSO afforded the dinuclear complex $[Cu_2(HL'')Cl(dmso)_2]$·DMSO.
[33] For diamagnetic corrections (Pascal's constants) see, for example: R. L. Carlin, *Magnetochemistry*, Springer, Heidelberg, **1986**.

 © 2005 Wiley-VCH Verlag GmbH & Co. KGaA, Weinheim

Network Structures

DOI: 10.1002/anie.200502372

Interpenetrating Copper–Silver Cyanometallate Networks: Polymorphs and Topological Isomers**

Ann M. Chippindale, Simon M. Cheyne, and Simon J. Hibble**

Transition-metal cyanides have a long and fascinating history and exhibit a diverse and interesting range of chemical and physical properties leading to technological applications.[1] Many complex cyanometallate can be viewed as supramolecular compounds[2,3] constructed from $M(CN)_x$ structural building blocks that have independent existence. These include simple ions, for example, square planar $[Ni(CN)_4]^{2-}$ and octahedral $[Fe(CN)_6]^{4-}$, but can also include larger

[*] Dr. A. M. Chippindale, Dr. S. M. Cheyne, Dr. S. J. Hibble
School of Chemistry
University of Reading
Whiteknights, Reading, Berks RG6 6AD (UK)
Fax: (+44) 118-378-6331
E-mail: a.m.chippindale@rdg.ac.uk
s.j.hibble@rdg.ac.uk

[**] A.M.C. thanks the Leverhulme Trust for a Research Fellowship. We thank S. L. Jenkins (University of Reading) for IR microscopy measurements on single-crystal samples and especially thank the anonymous referee for helpful comments and analysis of the network found in form II.

Supporting information for this article is available on the WWW under http://www.angewandte.org or from the author.

WILEY InterScience DISCOVER SOMETHING GREAT
© 2005 Wiley-VCH Verlag GmbH & Co. KGaA, Weinheim

fragments, for example, -{CuCN}- chains. Such units are relatively robust, have well-defined topology and geometry, and can be assembled in at least a semirational manner to form new solids by combining with themselves, other complex metal ions, or organic species such as amines to generate 1-, 2-, and 3-dimensional frameworks.[2,4,5]

We have been investigating the use of CuCN, both as a source of infinite -{CuCN}- chains and as a precursor to other Cu^I cyano species, for use as alternative structural building blocks in the construction of new cyanide complexes. We have found that monatomic species, such as halide ions, are capable of producing new zeolitic and interpenetrating frameworks when alkali-metal halides and CuCN react under modest conditions.[6,7] Urban et al. recently achieved similar results using silver cyanide and cesium halides.[8] An extension of this approach is to replace the halides, which form bridges between copper–cyanide building units, with complex cyanide anions in the hope of producing framework materials with larger pore sizes. We selected $[Ag(CN)_2]^-$ as a bridging unit because it has been successfully used in the past to link other metal ions, for example, Mn^{II} and Cd^{II}, into 3D networks.[2,9,10] Employing $[Ag(CN)_2]^-$ has the additional attraction of providing a synthetic route to mixed Cu^I/Ag^I cyanides, which, despite the similarity in the chemistry of copper and silver in the +1 oxidation state, surprisingly remained unknown before this work. The Cu^I/Ag^I cyanide materials have the formula $A[Ag_2Cu(CN)_4]$ (A = K, Rb, Cs) and contain remarkable interpenetrating anionic networks assembled from $\{Cu(CN)_4\}^{3-}$ and $\{Ag(CN)_2\}^-$ units. These units are connected in different ways in the Rb and Cs compounds to produce two-dimensional (form I) and three-dimensional (form II) networks of the same formula. These materials challenge our views of what constitutes and distinguishes polymorphs and topological isomers.

Reaction of excess $K[Ag(CN)_2]$ with CuCN under hydrothermal conditions produced single crystals of $K[Ag_2Cu(CN)_4]$ (**1**, form I).[11] This material can also be made at room temperature by adding an aqueous solution of $K_3[Cu(CN)_4]$ to $AgNO_3$ in a 1:2 molar ratio. The Rb and Cs analogues $Rb[Ag_2Cu(CN)_4]$ (**2**, form I) and $Cs[Ag_2Cu(CN)_4]$ (**3**, form I) were also produced in hydrothermal reactions, but in each case, a second form, $Rb[Ag_2Cu(CN)_4]$ (**4**, form II) and $Cs[Ag_2Cu(CN)_4]$ (**5**, form II), predominated.[11]

Although form I of $A[Ag_2Cu(CN)_4]$ (**1**–**3**) has a two-dimensional network, and form II (**4**, **5**) a three-dimensional network, a good starting point for describing the structures is to view them both as derived from a (4,4)-connected net. Figure 1 shows the two different sheets found in these forms, both of which have this connectivity. Copper atoms are located at the 4-connected nodes in both forms.

In form I, all the copper atoms are identical and are linked by almost-linear bridging -{NC-Ag-CN}- units. In form II, there are two types of copper atoms: one type (Cu(1)) occurs at the nodes of the (4,4)-connected net and the second (Cu(2)) occurs within the -{NC-Cu(2)-NC-Ag(1)-CN}- unit that links the Cu(1) nodes. As a consequence of the tetrahedral coordination around the copper center, the sheets in both forms I and II are buckled. Neither of the resulting sheets fills the space very efficiently, and the

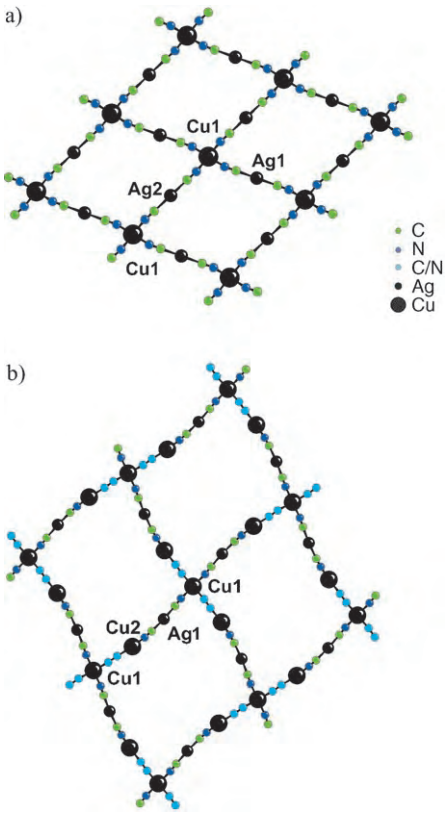

Figure 1. Portions of the sheets derived from a (4,4)-connected net for a) $A[Ag_2Cu(CN)_4]$ (form I, A = K, Rb, Cs) and b) $A[Ag_2Cu(CN)_4]$ (form II, A = Rb, Cs). The bridging cyanide groups bond through the carbon atom to silver, but are disordered when they bridge Cu(1) and Cu(2) atoms in (b).

structures formed from isolated sheets of these types, if they could be produced, would have very large free volumes. This situation is not the case in these materials. Instead, further copies of the sheets occupy the space (Figure 2). In form I, the structure consists of AAA-stacked layers of three identical interpenetrating sheets. In form II, four sheets can interpenetrate because the longer internode linkers (-{NC-Cu(2)-NC-Ag(1)-CN}- units) produce a larger mesh size than that found in form I. Figure 3 shows two layers formed from these interpenetrating sheets and clearly shows the buckling of the layers for each compound. In form I, the layers are sufficiently close together that the potassium ions within the layers also interact with cyanide groups in neighboring layers. The layers in form II, which stack in an ABAB pattern, are well separated, but, in contrast to form I, there are coordinatively unsaturated copper atoms on the outside of the layers. These Cu(2) atoms complete their tetrahedral coordination by forming bonds to two -{NC-Ag(2)-CN-Ag(3)-CN}- units external to the sheet. These units link sheets in adjacent layers to form a three-dimensional framework consisting of four identical interpenetrating networks. As in form I, the alkali-metal cations lie within the layers of buckled sheets.

Threefold parallel interpenetration of (4,4)-connected nets to form layers, as observed in form I, is very rare for coordinatively bonded networks[16,17] and this is the first

 © 2005 Wiley-VCH Verlag GmbH & Co. KGaA, Weinheim

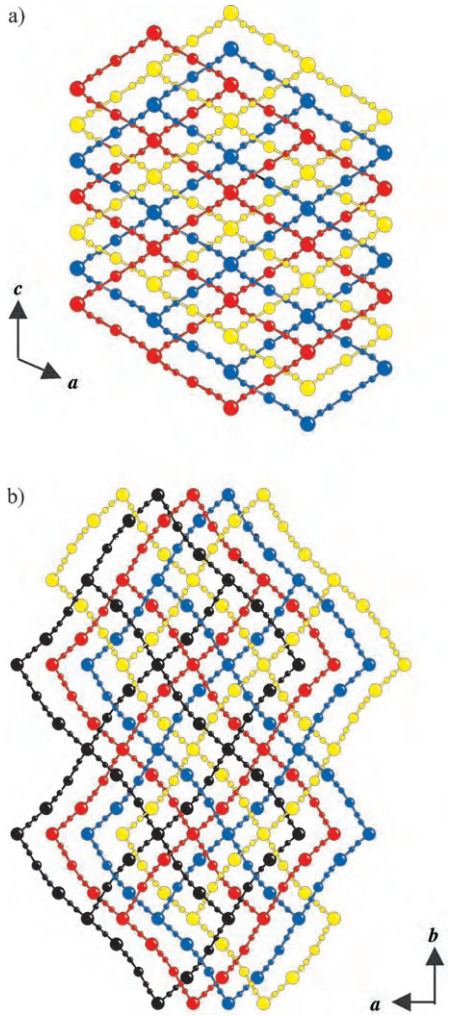

Figure 2. Layers derived from parallel interpenetration of a) three of the sheets shown in Figure 1 a) for $A[Ag_2Cu(CN)_4]$ (form I) and b) four of the sheets shown in Figure 1 b) for $A[Ag_2Cu(CN)_4]$ (form II). The different independent networks are shown in black, red, blue, and yellow.

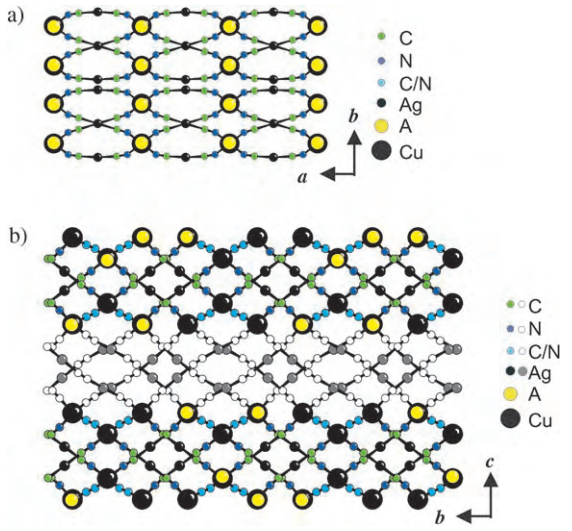

Figure 3. Side view showing the buckled sheets in a) $A[Ag_2Cu(CN)_4]$ (form I) forming a layered structure and b) $A[Ag_2Cu(CN)_4]$ (form II) forming a three-dimensional structure. The open and gray circles in (b) correspond to -{NC-Ag(2)-CN-Ag(3)-CN}- units that interlink the layers shown in Figure 2 b) to form the 3D structure containing four independent networks.

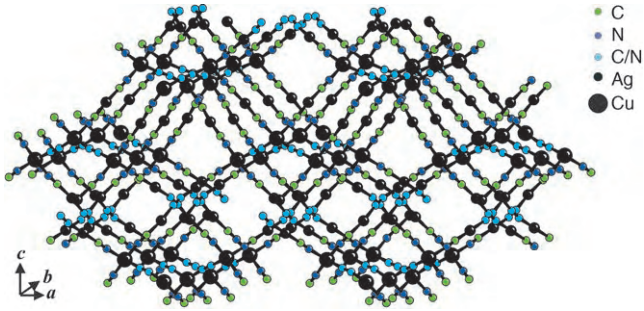

Figure 4. View of a single network found in $A[Ag_2Cu(CN)_4]$ (form II) showing self interpenetration.

totally inorganic example. Previous examples all have organic spacers between the metal centers at the nodes.[18–20] Form II, according to the recent classification of interpenetrating 3D networks by Blatov and co-workers,[21,22] belongs to Class Ia, which means that the four identical three-dimensional networks are related by simple translations ([1/2, 1/2, 1/2] (19.26 Å) and the symmetry-related operations). The 3D network found in form II[23] is, to the best of our knowledge, of a previously unknown type.[17,24,25] Moreover, this new network is self-penetrating (Figure 4) as rings containing six and eight copper atoms catenate within the structure. Interpenetration of self-penetrating networks is a rare combination[26] and, as is observed here, can lead to very complicated entangled structures.

It is remarkable that compounds of $A[Ag_2Cu(CN)_4]$ (A = Rb and Cs) form two distinct types of interpenetrating solid. These exceptional materials are true topological isomers because not only do they have frameworks of the same composition constructed from the same units, but their overall compositions are also identical. Most quoted examples of topological isomerism found in supramolecular chemistry involve the inclusion of different guest molecules, typically the solvent used in preparation,[27] and the overall compositions of the related compounds are therefore different. As the compositions of forms I and II are identical, and both are extended solids, they can also be classified as polymorphs according to the normal usage of that term.

Our experiments show that form II is the thermodynamically more stable phase of $Cs[Ag_2Cu(CN)_4]$ both under hydrothermal conditions and at atmospheric pressure at 300 K. Form I is the kinetically favored product, being formed immediately upon reaction between solutions containing A^+ (A = K and Cs), $Cu(CN)_4^{3-}$, and Ag^+, and also it appears as a minor phase in shorter hydrothermal reactions. It is interesting that $K[Ag_2Cu(CN)_4]$ has only been found in form I and does not convert to a form II analogue even on prolonged hydrothermal reaction. A further illustration of the

 © 2005 Wiley-VCH Verlag GmbH & Co. KGaA, Weinheim

thermodynamic stability of $Cs[Ag_2Cu(CN)_4]$ (form II) is that it can be formed by stirring a polycrystalline sample of $K[Ag_2Cu(CN)_4]$ in an aqueous solution of $CsNO_3$.

In summary, the first family of Cu^I/Ag^I cyanides has been prepared. The compounds of general formula $A[Ag_2Cu(CN)_4]$ (A = K, Rb and Cs) form curious interpenetrating two- and three-dimensional networks, the latter of which is also self penetrating. The two forms of the Rb and Cs compounds are both topological isomers and polymorphs. Further work will include analysis of the correlation between the uniaxial negative thermal expansion and the contraction of this axis upon increasing radius of the alkali-metal cation in all these materials. We are also attempting the preparation of $A[M_2M'(CN)_4]$ materials using other metals.

Experimental Section

$K[Ag_2Cu(CN)_4]$ (**1**, form I): Colorless rectangular plates[11] (IR: $\tilde{\nu} = \nu$(CN) 2135(vs), 2120(vs) cm^{-1}) were obtained by heating CuCN (0.09 g, 1 mmol) with $K[Ag(CN)_2]$ (1.39 g, 7 mmol) in H_2O (5 mL) in a teflon-lined autoclave at 453 K for 24 h and could be easily separated from a fernlike growth of metallic silver. A polycrystalline sample of **1** was prepared at 300 K by adding a solution of $K_3[Cu(CN)_4]$ (1.42 g, 5 mmol) in H_2O (5 mL) to $AgNO_3$ (1.75 g, 10 mmol) dissolved in H_2O (5 mL). A dark-gray precipitate formed immediately. In contrast, addition of the $AgNO_3$ solution to the $K_3[Cu(CN)_4]$ solution resulted in significant contamination by AgCN.

$Rb[Ag_2Cu(CN)_4]$ (**2**, form I and **4**, form II): Hydrothermal reaction of CuCN (0.09 g, 1 mmol), NaCN (0.15 g, 3 mmol), $RbNO_3$ (0.44 g, 3 mmol), and $AgNO_3$ (0.34 g, 2 mmol) in H_2O (5 mL) at 413 K for 3 days produced a mixture of colorless crystals—a majority of rectangular needles (**4**) and a minority of rectangular blocks (**2**)—which were easily separated for diffraction studies.[11]

Polycrystalline **2** was prepared at 300 K by adding $RbNO_3$ (0.44 g, 3 mmol) to a solution of $Na_3[Cu(CN)_4]$ (0.24 g, 1 mmol) in H_2O (2.5 mL). The resulting solution was then added to a solution of $AgNO_3$ (0.34 g, 2 mmol) in H_2O (2.5 mL) and a gray precipitate formed immediately. Compound **2** was the major component, together with a significant amount of AgCN. Allowing the precipitate to sit in the mother liquor at room temperature for 14 days led to the growth of single crystals of **2** (IR: $\tilde{\nu} = \nu$(CN) 2130(s), 2110(vs), 2089(s) cm^{-1}). Compound **4** was not produced in either room temperature reaction.

$Cs[Ag_2Cu(CN)_4]$ (**3**, form I and **5**, form II): Hydrothermal reaction of CuCN (0.23 g, 2.5 mmol), KCN (0.49 g, 7.5 mmol) $CsNO_3$ (1.46 g, 7.5 mmol), and $AgNO_3$ (0.85 g, 5 mmol) in H_2O (10 mL) at 413 K for 3 days produced colorless needles of **5** (IR: $\tilde{\nu} = \nu$(CN) 2168(vs), 2139(vs), 2115(vs), 2094(vs) cm^{-1}) as the major phase, together with a small quantity of colorless rectangular blocks of **3** (IR: $\tilde{\nu} = \nu$(CN) 2136(vs), 2114(vs), 2091(s) cm^{-1}).[11] Heating an identical mixture for 8 days produced a pure sample of **5**. Polycrystalline **3** was prepared at 300 K by adding $CsNO_3$ (1.46 g, 7.5 mmol) to $K_3[Cu(CN)_4]$ (1.42 g, 5 mmol) in H_2O (5 mL). The resulting solution was then added to $AgNO_3$ (0.85 g, 5 mmol) in H_2O (5 mL) and a gray precipitate formed immediately. Compound **3** was the major component, together with a small amount of AgCN. There was no evidence for the formation of **5** in this reaction.

Reactions of $K[Ag_2Cu(CN)_4]$ (**1**, form I): Stirring **1** (0.30 g, 0.70 mmol) in a solution of $CsNO_3$ (0.68 g, 3.5 mmol) in H_2O (5 mL) for 9 days at 300 K produced a change in the $[Ag_2Cu(CN)_4]^-$ framework to give $Cs[Ag_2Cu(CN)_4]$ (**5**, form II) as the major phase, together with small amounts of AgCN and Ag. The original $[Ag_2Cu(CN)_4]^-$ framework was, however, retained in a similar reaction in which $CsNO_3$ was replaced by KNO_3 (0.35 g, 3.5 mmol), although again some degradation to form AgCN occurred.

Received: July 7, 2005
Revised: September 21, 2005
Published online: November 15, 2005

Keywords: copper · cyanides · framework structures · polymorphism · silver

[1] K. R. Dunbar, R. A. Heintz, *Prog. Inorg. Chem.* **1997**, *45*, 283–391.
[2] T. Iwamoto in *Comprehensive Supramolecular Chemistry, Vol. 6* (Eds.: D. D. MacNicol, F. Toda, R. Bishop), Pergamon, Oxford, **1996**, pp. 643–690.
[3] J. Cernak, M. Orendac, I. Potocnak, J. Chomic, A. Orendacova, J. Skorsepa, A. Feher, *Coord. Chem. Rev.* **2002**, *224*, 51–66.
[4] J. Mühle, W. S. Sheldrick, *Z. Anorg. Allg. Chem.* **2003**, *629*, 2097–2102.
[5] D. J. Chesnut, D. Plewak, J. Zubieta, *J. Chem. Soc. Dalton Trans.* **2001**, 2567–2580.
[6] S. J. Hibble, S. G. Eversfield, A. R. Cowley, A. M. Chippindale, *Angew. Chem.* **2004**, *116*, 638–640; *Angew. Chem. Int. Ed.* **2004**, *43*, 628–630.
[7] A. M. Chippindale, S. J. Hibble, A. R. Cowley, *Inorg. Chem.* **2004**, *43*, 8040–8048.
[8] V. Urban, T. Pretsch, H. Hartl, *Angew. Chem.* **2005**, *117*, 2855–2858; *Angew. Chem. Int. Ed.* **2005**, *44*, 2794–2797.
[9] B. F. Hoskins, R. Robson, N. V. Y. Scarlett, *J. Chem. Soc. Chem. Commun.* **1994**, 2025–2026.
[10] U. Geiser, J. A. Schlueter, *Acta Crystallogr. Sect. C* **2003**, *59*, i21–i23.
[11] Crystal data for **1**–**5**: Enraf–Nonius Kappa CCD diffractometer (graphite monochromated $Mo_{K\alpha}$ radiation, $\lambda = 0.71073$ Å), 150 K, data processing and absorption correction (DENZO/SCALEPACK),[12] direct methods (SIR92),[13] full least-squares refinement against $|F|$ ($I > 3\sigma(I)$ cutoff) (CRYSTALS),[14] drawing package (CAMERON),[15] anisotropic thermal factors for all atoms, "head-to-tail" disorder of C/N atoms of the cyanide groups between Cu(1) and Cu(2) and Ag(2) and Ag(3) included for **4** and **5**. $A[Ag_2Cu(CN)_4]$ (form I, A = K **1**, Rb **2**, and Cs **3**), monoclinic, $P2/c$, $Z = 2$, **1**: $M_r = 422.45$, $a = 8.1480(4)$, $b = 7.1005(3)$, $c = 7.4533(3)$ Å, $\beta = 101.760(2)°$, $V = 422.16$ Å^3, $\rho_{calcd} = 3.323$ g cm^{-3}, $R = 0.0403$, $wR = 0.0455$ (1391 reflections). **2**: $M_r = 468.84$, $a = 7.9885(3)$, $b = 7.2945(3)$, $c = 7.7856(4)$ Å, $\beta = 102.5859(17)°$, $V = 442.78$ Å^3, $\rho_{calcd} = 3.516$ g cm^{-3}, $R = 0.0591$, $wR = 0.0606$ (804 reflections). **3**: $M_r = 516.28$, $a = 7.7266(3)$, $b = 7.6129(3)$, $c = 8.2541(3)$ Å, $\beta = 103.807(2)°$, $V = 471.49$ Å^3, $\rho_{calcd} = 3.637$ g cm^{-3}, $R = 0.0213$, $wR = 0.0242$ (931 reflections). $A[Ag_2Cu(CN)_4]$ (form II, A = Rb **4** and Cs **5**), orthorhombic, *Ibca*, $Z = 24$, **4**: $M_r = 1406.52$, $a = 8.1519(2)$, $b = 21.0135(7)$, $c = 31.2315(8)$ Å, $V = 5350.0$ Å^3, $\rho_{calcd} = 3.493$ g cm^{-3}, $R = 0.0368$, $wR = 0.0421$ (2280 reflections). **5**: $M_r = 1548.84$, $a = 8.5733(2)$, $b = 20.6076(5)$, $c = 31.5303(9)$ Å, $V = 5570.6$ Å^3, $\rho_{calcd} = 3.694$ g cm^{-3}, $R = 0.0264$, $wR = 0.0270$ (2196 reflections). Further details on the crystal structure investigation may be obtained from the Fachinformationszentrum Karlsruhe, 76344 Eggenstein-Leopoldshafen, Germany (fax: (+49) 7247-808-666; e-mail: crysdata@fiz-karlsruhe.de), on quoting the depository numbers CSD-415570 (**1**), -415571 (**2**), -415572 (**3**), -415573 (**4**), and -415574 (**5**). Note: Cell determinations at 298 K are given in the Supporting Information.
[12] Z. Otwinowski, W. Minor in *Methods in Enzymology, Vol. 276* (Eds.: C. W. Carter, R. M. Sweet), Academic Press, New York, **1997**, pp. 307–326.

 © 2005 Wiley-VCH Verlag GmbH & Co. KGaA, Weinheim

[13] A. Altomare, G. Cascarano, C. Giacovazzo, A. Guagliardi, M. C. Burla, G. Polidori, M. Camalli, *J. Appl. Crystallogr.* **1994**, *27*, 435.
[14] D. J. Watkin, C. K. Prout, J. R. Carruthers, P. W. Betteridge, R. I. Cooper, CRYSTALS, Issue 11, Chemical Crystallography Laboratory, Oxford, **2001**.
[15] D. J. Watkin, C. K. Prout, L. J. Pearce, CAMERON, Chemical Crystallography Laboratory, Oxford, **1996**.
[16] S. R. Batten, R. Robson, *Angew. Chem.* **1998**, *110*, 1558 – 1595; *Angew. Chem. Int. Ed.* **1998**, *37*, 1460 – 1494.
[17] S. R. Batten, *CrystEngComm* **2001**, *3*, 67 – 73.
[18] L. Carlucci, G. Ciani, D. M. Proserpio, S. Rizzato, *CrystEngComm* **2002**, *4*, 413 – 425.
[19] C.-H. Ge, X.-D. Zhang, P. Zhang, W. Guan, F. Guo, Q.-T. Liu, *Polyhedron* **2003**, *22*, 3493 – 3497.
[20] O. R. Evans, W. Lin, *Chem. Mater.* **2001**, *13*, 3009 – 3117.
[21] V. A. Blatov, L. Carlucci, G. Ciani, D. M. Proserpio, *CrystEngComm* **2004**, *6*, 377 – 395.
[22] I. A. Baburin, V. A. Blatov, L. Carlucci, G. Ciani, D. M. Proserpio, *J. Solid State Chem.* **2005**, *178*, 2452 – 2474.
[23] The single network in form II is a 4-connected net in which there are two nodal types, Cu(1) and Cu(2), with stoichiometry 1:2. Total Schläfli symbol: $(6^2\cdot8^4)(6^4\cdot8^2)_2$; Vertex symbol: $(6_2\cdot6_2\cdot8_3\cdot8_3\cdot8_3\cdot8_3)(6\cdot6\cdot6\cdot6\cdot8_2\cdot8_6)_2$.
[24] M. O'Keeffe, O. M. Yaghi, The Recticular Chemistry Structure Resource website: http://okeeffe-ws1.la.asu.edu/RCSR/home.htm.
[25] N. W. Ockwig, O. Delgado-Friedrichs, M. O'Keeffe, O. M. Yaghi, *Acc. Chem. Res.* **2005**, *38*, 176 – 182.
[26] L. Carlucci, G. Ciani, D. M. Proserpio, *Coord. Chem. Rev.* **2003**, *246*, 247 – 289.
[27] A. J. Blake, N. R. Brooks, N. R. Champness, M. Crew, A. Deveson, D. Fenske, D. H. Gregory, L. R. Hanton, P. Hubberstey, M. Schröder, *Chem. Commun.* **2001**, 1432 – 1433.

 © 2005 Wiley-VCH Verlag GmbH & Co. KGaA, Weinheim

Protein Chemistry

DOI: 10.1002/anie.200502431

Mild and Chemoselective Peptide-Bond Cleavage of Peptides and Proteins at Azido Homoalanine**

Jaap Willem Back, Olivier David, Gertjan Kramer, Géraldine Masson, Piotr T. Kasper, Leo J. de Koning, Luitzen de Jong, Jan H. van Maarseveen, and Chris G. de Koster*

The chemical cleavage of amide (peptide) bonds usually requires harsh conditions.[1] As a result, side reactions and the lack of specificity of chemical amide-bond hydrolysis limits its scope in chemical biology and synthetic applications. Herein, we disclose our results on the selective cleavage of amide bonds in peptides and proteins that is milder than any previously reported chemical method.

The azide functional group is well suited for the in vivo labeling of biomolecules.[2] Azides combine a high chemical stability under physiological conditions with a unique reactivity that enables mild and selective organic transformations, such as the Staudinger ligation[3] and the azide–alkyne [3+2] cycloaddition.[4] Azido-functionalized amino acids[5] and azido sugars[4e] have been introduced into biomacromolecules and have subsequently been derivatized with specific labels to enable their detection, thereby demonstrating full bioorthogonality.[2] It has been shown that azido homoalanine (**1**) is effectively incorporated into proteins by the native methionyl tRNA synthetase of *E. coli*, thus allowing specific modification reactions.[5a] Azides, however, are susceptible to reduc-

[*] Dr. J. W. Back, G. Kramer, P. T. Kasper, Dr. L. J. de Koning, Dr. L. de Jong, Prof. Dr. C. G. de Koster
Swammerdam Insitute for Life Sciences
Mass Spectrometry Group, University of Amsterdam
Nieuwe Achtergracht 166, 1018WV Amsterdam (The Netherlands)
Fax: (+31) 20-525-6971
E-mail: jwback@science.uva.nl

Dr. O. David
Laboratoire de Photochimie et Photophysique Supramoléculaire et Macromoléculaire
École Normale Supérieure de Cachan
61 Avenue du Président Wilson, 94235 Cachan (France)

Dr. G. Masson, Dr. J. H. van Maarseveen
van't Hoff Institute for Molecular Sciences
Department of Organic Cchemistry
University of Amsterdam
Nieuwe Achtergracht 129, 1018WS Amsterdam (The Netherlands)

[**] We gratefully acknowledge Dr. Michael van der Horst for the pHISP plasmid and assistance with cloning and purification of PYP and the Yale *E. coli* genetic stock center for providing *E. coli* strain CAG18491. This research was supported by a Horizon Breakthrough grant to J.W.B. from The Nationaal Regie Orgaan Genomics (NROG) of the Netherlands Organization for Scientific Research (NWO). The ESI-FTMS, MALDI-TOF, and QTOF mass spectrometers were largely funded by NWO-CW and NWO-MW.

Supporting information for this article is available on the WWW under http://www.angewandte.org or from the author.

WILEY InterScience DISCOVER SOMETHING GREAT
© 2005 Wiley-VCH Verlag GmbH & Co. KGaA, Weinheim

tion to amines with, for example, phosphines[3,6] and (di)thiols,[7] which are amongst the most widespread reagents to promote reduction in samples of biological origin, or that are present intracellularly (e.g., in the form of glutathione).

In our investigations into Cu^{I}-catalyzed [3+2] "click" cycloadditions of several different alkynes to peptides containing **1**,[4a–c] with the in situ reduction of Cu^{II} to Cu^{I}, we discovered that aside from the expected products smaller fragments were produced. Control experiments in which Cu^{II} or the alkyne moiety, or both, were omitted and a reducing agent was added showed a marked increase in peptidolysis, and so were chosen to investigate the underlying mechanism.

Two products were formed when the model octadecapeptide **P** (sequence: PPHHHHHHPPRGFG**1**GFR, synthesized by standard Fmoc chemistry) was incubated in buffers containing either tris(carboxyethyl)phosphine (TCEP), 2-mercaptoethanol (2ME), or dithiothreitol (DTT). As expected, a peak corresponding to the reduction of **1** to 2,4-diaminobutyrate (DAB) at *m*/*z* 2108.0 was observed under these conditions. Surprisingly, an additional product at *m*/*z* 1729.8 was observed. Low-energy collision-induced dissociation (CID) of this product in an ESI-Q-FT mass spectrometer revealed an N-terminal fragment of **P** that resulted from cleavage of the peptide bond C-terminal to element **1** together with the loss of the azide group.

To test the general occurrence of this cleavage reaction in proteins that contain **1** instead of methionine,[5a] we have produced His-tagged recombinant photoactive yellow protein (PYP) from *Ectothiorhodospira halophila* in methionine-auxotrophic *E. coli* grown on media containing **1**. A pure preparation of azido PYP (AzPYP), in which all six methionine residues have been replaced by **1**, was obtained, as detected by ESI mass-spectrometric analysis of the intact protein (see the Supporting Information) and MALDI-TOF mass-spectrometric analysis of a tryptic digest (data not shown). Reduction and cleavage of purified AzPYP by TCEP, 2ME, or DTT was analyzed by sodium dodecylsulfate polyacrylamide gel electrophoresis (SDS-PAGE) and mass spectrometry (Figure 1 a, b). It was found that TCEP was able to cleave the protein under all the conditions investigated, whereas both the rate and yield of the cleavage with DTT and 2ME increased drastically under denaturing conditions (4 M urea). Fragments N- or C-terminal to all positions of **1** in reductively treated AzPYP were detected (Figure 1 c).

All fragments, except for the C-terminal peptide that ends in valine, have a C-terminal residue with a mass of 83 Da which corresponds to **1** minus a HN_3 moiety, as confirmed by CID ESI Fourier Transform tandem mass spectroscopy (FTMSMS). Peptides with "missed cleavages" have masses that are in accordance with a reduction of the internal azidohomoalanine residues. The fact that reduction-induced cleavage occurs C terminal to all positions of element **1** in AzPYP indicates that the cleavage reaction apparently poses no special prerequisites to the residue C terminal to the scissile bond. This result underscores the high specificity and general applicability of this mild chemical cleavage reaction of peptide bonds C terminal to **1**.

Next, we carried out cleavage of peptide **P** by tris(carboxy ethyl)phosphine (TCEP) in 50% ^{18}O-enriched water, which

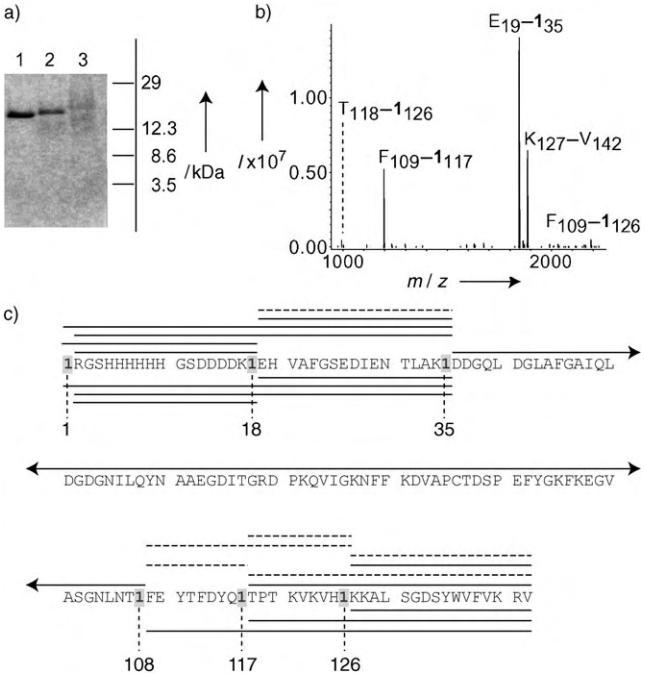

Figure 1. Recombinant AzPYP is cut by TCEP. a) Coomassie Blue stained gel containing equal amounts (23 μg) of AzPYP incubated without (lane 1) and with 10 mM (lane 2) and 100 mM (lane 3) TCEP at pH 5; the intact protein disappears and is cut into smaller fragments that do not resolve on the polyacrylamide gel. b) Deconvoluted ESI FTMS spectrum of TCEP-cleaved AzPYP. c) Sequence of His-tagged PYP from *E. halophila*. Intact molecular-mass and tryptic-peptide mapping confirmed >95% incorporation of **1** at methionine-coded residues. A coverage map obtained with TCEP (above the sequence) and DTT (below the sequence) is presented. Solid lines indicate peptides that result from cleavage that were detected with MALDI-TOF MS; dashed lines indicate peptides that were detected with ESI FTMS.

confirmed that the peptide bond C terminal to **1** is cleaved by hydrolysis, and indicated that only one ^{18}O atom is incorporated into the resulting C-terminal residue of the N-terminal peptide fragment (see the Supporting Information).

The C-terminal residue is considered to have a homoserine lactone structure based on the following observations: 1) When the cleavage product of peptide **P** was incubated under basic conditions, the mass of the product increased by 18 Da, which was added to the C-terminal residue as confirmed by CID; this addition could be reversed by incubation for one hour in anhydrous TFA.[8] 2) Incubation of the cleaved product of peptide **P**, or the cleaved products of AzPYP in butylamine, led to full conversion with an irreversible increase in the mass of the cleavage products by 73 Da, which is consistent with the addition of a C-terminal butylamine group,[8] as verified by CID. 3) It was found that both RP-HPLC retention times and CID MSMS analysis (see Figure 2 and the Supporting Information) of the presumed homoserine lactone ending peptides from TCEP-cleaved AzPYP and the corresponding homoserine lactone ending peptides from CNBr cleaved PYP were identical.

With TCEP, the reaction runs to completion in 100 min at 50 °C and pH 5, based on the disappearance of starting

 © 2005 Wiley-VCH Verlag GmbH & Co. KGaA, Weinheim

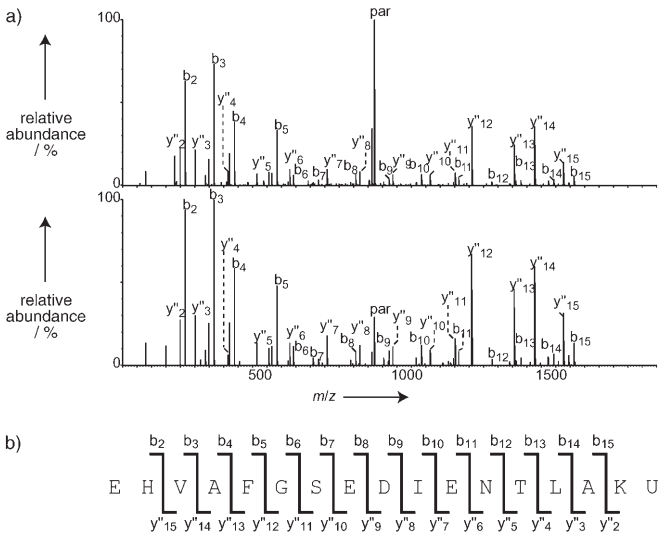

Figure 2. Comparison of the cleavage of AzPYP with TCEP and methionine-containing PYP with cyanogen bromide. Digests were loaded onto an LC–MSMS system (see Supporting Information). a) Charge-deconvoluted MSMS fragmentation spectra of the doubly charged ion of m/z 921.9 that eluted at identical retention times with annotation of fragment ions and parent ion (par). Identical fragment spectra verify the equivalence of both peptides. b) Sequence of the peptide and annotation of the retrieved fragment ions. U = homoserine lactone.

material. The ratio of cleaved/reduced product varied little as a function of pH value (the range of pH 3–11 was tested) or temperature, as quantified from RP-HPLC followed by MALDI-TOF-MS identification of the collected peak fractions. A maximized ratio at room temperature was accomplished at pH 5, thus resulting in 55% (±5%) cleavage, whereas at pH 9 approximately 40% (±5%) was cleaved (sum total of homoserine and homoserine lactone cleavage products).

With thiol reagents, the reaction only became significant at pH > 7, which is indicative of the requirement for the more nucleophilic thiolate anion. The peptide was significantly cleaved under these conditions, and a 30% (±8%) cleaved product was obtained with DTT within 16 hours with full conversion, whereas 84% of the azide compounds were still intact after 48 hours with 2ME. These results are consistent with the previously reported efficiencies of dithiols versus monothiols for azide reduction.[7a,9] In the case of 2ME, reduction into DAB (14%) predominated over cleavage (1%) as well. Cleaved peptides were mainly recovered with homoserine C termini, as could be expected at pH 9.2. Cleavage of AzPYP with thiols required unfolding of the protein with 4 M urea, which was not necessary for TCEP.

Peptide-bond hydrolysis that resulted in lactone formation can be rationalized by the mechanism depicted in Scheme 1. Phosphines attack at the electrophilic terminal nitrogen atom of azide **1**, initially forming intermediate **2**.[10] Water may add to **2** to give the postulated intermediate **3**, which fragments into the triazene **4** or lose dinitrogen to yield aza-ylide **5**.[10] It has been shown previously that triazenes may be substituted by suitable nucleophiles of either intra- or intermolecular origin.[9] It is worth mentioning that at elevated pH values conversion of **1** into homoserine without peptide cleavage occurs, which is indicative of direct hydroxide attack. The protonated triazene **6** may cyclize to imido ester **7** via an energetically favorable five-membered transition state, a pathway analogous to the cyanogen bromide induced cleavage of the methionine peptide bond.[11] Finally, hydrolysis of **7** liberates the homoserine lactone **8** and amine **9**.[1,8,11] This mechanism is supported by the above-discussed ^{18}O-labeling experimental results, which allow the carbonyl oxygen atom to be conserved in the lactone.

Alternatively, **5** can be hydrolyzed to an amine or may become protonated to generate intermediate **11**, which, through intramolecular S_N2 displacement involving the amide oxygen atom, yields the common imido ester intermediate **7**, which will then again hydrolyze to give **8** and **9**. The cleavage induced by (di)sulfides is presumed to be

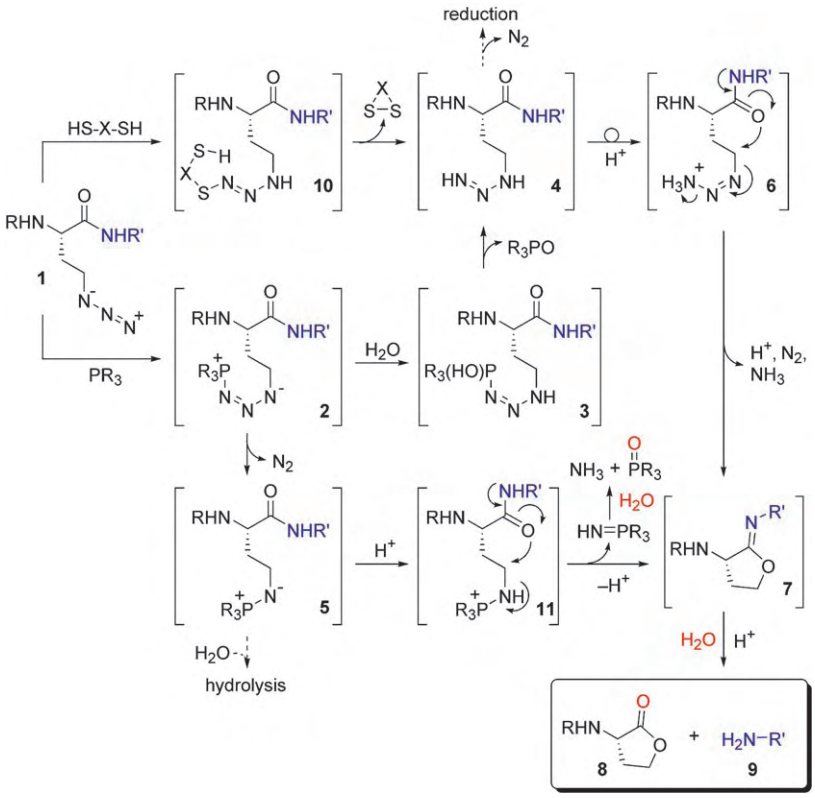

Scheme 1. Mechanism for peptide cleavage C terminal to **1**. Initiation of the reaction is by reduction of the azide **1** into triazene **4**. Intramolecular S_N2 reaction of the carbonyl oxygen atom displaces the reduced azide to yield imido ester **6**, which is hydrolyzed and liberates a homoserine lactone ending peptide **8** and a peptide with an N-terminal free amine **9**. X denotes a three- or four-carbon spacer that can be substituted (e.g., X = -CH_2-CHOH-CHOH-CH_2- for DTT).

 © 2005 Wiley-VCH Verlag GmbH & Co. KGaA, Weinheim

initiated by attack of the thiolate anion at either the α- or, as depicted, the γ-azide nitrogen atom (intermediate **10**).[7a] Loss of a cyclic disulfide from **10** gives the triazene **4**, which follows the pathway to **7** or fragments into DAB.

Lactones are amenable to further derivatization, for example, with amines in near quantitative yields,[8] as we have shown above for the cleaved peptide **P** and butylamine. As the cleavage reaction is not significantly affected by pH value, we were able to perform the cleavage reaction at elevated pH values (8–9) in the presence of amines. Under these conditions, we obtained products that were verified to be **P** cleaved C terminal to **1**, followed by addition of the selected amines (see the Supporting Information) and propose that the reaction proceeds as depicted in Scheme 2.

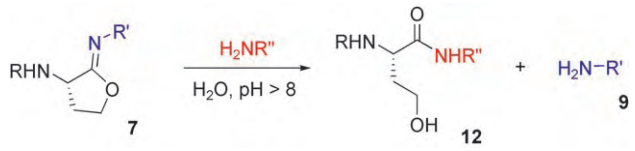

Scheme 2. Transamidation by exogeneous amines added to the reaction. Nucleophilic attack of an amine at the carbon atom of imido ester **7** may directly provide amide **12** while liberating amine **9**.

Other desired functionalities may similarly be installed with selected amines in a "one-pot" procedure. It is noteworthy that the stereocenter at C_α remains conserved, as is evident from the protein semisynthesis experiments with cyanogen bromide cleaved protein fragments.[12]

For optimal yield, however, the two-step alternative, in which first lactones are harvested and homoserine residues are closed by acid incubation,[8] may be preferred, as the initial yield of the TCEP-induced cleavage is higher at pH 5.

To our knowledge, this new cleavage reaction is milder than any chemical proteolysis described so far and, in contrast to I_2-induced allyl glycyl cleavage,[13] is directly applicable to overexpressed recombinant proteins. This report is also the first description of the use of an aza ylide as a leaving group amenable to intramolecular displacement by an amide group followed by hydrolysis to obtain an acid and amine. Until now, activated carboxylic acids were converted into amides using aza ylides and amidines were formed from amides,[3,14] the latter mainly in cyclization reactions. Performing this reaction in water has opened up a new pathway with far-reaching potential.

Direct application may be found in the preparation of isotope-labeled peptides by recombinant techniques, similar to the method described by Lindhout et al.[15] or protein semisynthesis from homoserine lactone,[8,12] but then after mild reduction-induced cleavage instead of CNBr. The yield of the cleavage reaction can be up to 60%; furthermore, a C-terminal function may be installed in a single step: an amine of choice elongates the cleaved polypeptide chain, thus providing the desired functionality.

Another powerful possibility lies in the targeted degradation of biopolymers.[16] However, as it is evident from earlier studies on azidothymidine (AZT) metabolism[9,17] and our findings that thiols reduce azides into highly reactive intermediates, one must remain conscious that the long-term intracellular presence of azides can lead to unintentional decomposition into unexpected products. On the other hand, methionines are often buried inside the protein core, and we have shown that degradation by thiols is accelerated under denaturing conditions, so at least for short-term experiments the azide function may be considered bio-orthogonal in vivo.

However, when phosphines or other reducing agents are added in subsequent reactions for the purpose of Staudinger ligations or to promote the in situ reduction of Cu^{II} to Cu^{I} for the catalysis of [3+2] azide–alkyne cycloadditions, it is conceivable that competitive nucleophilic substitutions at the (formerly) azide functionalized carbon atom may take place. The fate of intermediates **2** and **5** in Scheme 1, for example, will depend on the availability of suitable nucleophiles towards the phosphorane or the carbon nucleophilic center.[18] The proposal of using ultrapure Cu^{I} salts instead of the in situ reduction of Cu^{II} to catalyze the cycloadditions of azides and alkynes in biological samples[5c] may suppress reductive cleavage when this is not desired.

Received: July 12, 2005
Published online: November 10, 2005

Keywords: azides · nucleophilic substitution · phosphanes · proteolysis · triazenes

[1] B. J. Smith in *The Protein Protocols Handbook*, 2nd ed. (Ed.: J. M. Walker), Humana Press, Totowa, NJ, USA, **2002**, p. 485.
[2] a) J. A. Prescher, C. R. Bertozzi, *Nat. Chem. Biol.* **2005**, *1*, 13; b) J. H. Van Maarseveen, J. W. Back, *Angew. Chem.* **2003**, *115*, 6106; *Angew. Chem. Int. Ed.* **2003**, *42*, 5926.
[3] M. Kohn, R. Breinbauer, *Angew. Chem.* **2004**, *116*, 3168; *Angew. Chem. Int. Ed.* **2004**, *43*, 3106.
[4] a) V. V. Rostovtsev, L. G. Green, V. V. Fokin, K. B. Sharpless, *Angew. Chem.* **2002** *114*, 2708; *Angew. Chem. Int. Ed.* **2002**, *41*, 2596; b) C. W. Tornoe, C. Christensen, M. Meldal, *J. Org. Chem.* **2002**, *67*, 3057; c) R. Breinbauer, M. Kohn, *ChemBioChem* **2003**, *4*, 1147; d) H. C. Kolb, K. B. Sharpless, *Drug Discovery Today* **2003**, *8*, 1128; e) N. J. Agard, J. A. Prescher, C. R. Bertozzi, *J. Am. Chem. Soc.* **2004**, *126*, 15046; f) V. D. Bock, H. Hiemstra, J. H. van Maarseveen, **2005**, *Eur. J. Org. Chem.*, in press, DOI: 10.1002/ejoc.200500483.
[5] a) K. L. Kiick, E. Saxon, D. A. Tirrell, C. R. Bertozzi, *Proc. Natl. Acad. Sci. USA* **2002**, *99*, 19; b) J. W. Chin, T. A. Cropp, J. C. Anderson, M. Mukherji, Z. Zhang, P. G. Schultz, *Science* **2003**, *301*, 964; c) A. J. Link, M. K. Vink, D. A. Tirrell, *J. Am. Chem. Soc.* **2004**, *126*, 10598.
[6] H. Staudinger, E. Hauser, *Helv. Chim. Acta* **1921**, *4*, 861.
[7] a) I. Cartwright, D. Hutchinson, V. Armstrong, *Nucleic Acids Res.* **1976**, *3*, 2331; b) J. V. Staros, H. Bayley, D. N. Standring, J. R. Knowles, *Biochem. Biophys. Res. Commun.* **1978**, *80*, 568.
[8] J. B. C. Findlay, M. J. Geisow, *Protein Sequencing: A Practical Approach*, IRL, Oxford, **1989**.
[9] J. Reardon, R. Crouch, L. St. John-Williams, *J. Biol. Chem.* **1994**, *269*, 15999.
[10] a) W. Q. Tian, Y. A. Wang, *J. Org. Chem.* **2004**, *69*, 4299; b) F. L. Lin, H. M. Hoyt, H. van Halbeek, R. G. Bergman, C. R. Bertozzi, *J. Am. Chem. Soc.* **2005**, *127*, 2686.
[11] E. Gross, *Methods Enzymol.* **1967**, *11*, 238.

 © 2005 Wiley-VCH Verlag GmbH & Co. KGaA, Weinheim

[12] a) R. E. Offord, *Biochem. J.* **1972**, *129*, 499; b) C. J. Wallace, *Curr. Opin. Biotechnol.* **1995**, *6*, 403.
[13] B. Wang, K. C. Brown, M. Lodder, C. S. Craik, S. M. Hecht, *Biochemistry* **2002**, *41*, 2805.
[14] Y. G. Gololobov, L. F. Kasukhin, *Tetrahedron* **1992**, *48*, 1353.
[15] D. A. Lindhout, A. Thiessen, D. Schieve, B. D. Sykes, *Protein Sci.* **2003**, *12*, 1786.
[16] R. Langer, D. A. Tirrell, *Nature* **2004**, *428*, 487.
[17] F. Becher, A. G. Pruvost, D. D. Schlemmer, C. A. Creminon, C. M. Goujard, J. F. Delfraissy, H. C. Benech, J. J. Grassi, *Aids* **2003**, *17*, 555.
[18] It may be added that the templated Staudinger phosphine (*o*-(Ph_2P)$PhCO_2Me$; see E. Saxon, C. R. Bertozzi, *Science* **2000**, *287*, 2007) in water/MeOH (50:50) resulted in $>98\%$ conjugation of peptide **P** and less than 1% cleavage.

 © 2005 Wiley-VCH Verlag GmbH & Co. KGaA, Weinheim

Protein Folding

DOI: 10.1002/anie.200502723

Synthetic Substrates for an Endoplasmic Reticulum Protein-Folding Sensor, UDP-Glucose: Glycoprotein Glucosyltransferase**

*Kiichiro Totani, Yoshito Ihara, Ichiro Matsuo, Hiroyuki Koshino, and Yukishige Ito**

Proteins destined for secretory pathways are transported to the lumen of the endoplasmic reticulum (ER). The ER lumen is a machine for post-translational modifications that is equipped with a quality-control system.[1] It assists with the folding of proteins and prevents aggregation and transport to the Golgi apparatus of misfolded glycoproteins. Protein glycosylation with an Asn-linked (N-linked) oligosaccharide is a co-translational process that occurs in the ER. N-linked glycan is attached to nascent protein as a tetradecasaccharide (Glc3Man9GlcNAc2; Glc = D-glucose, Man = D-mannose, GlcNAc = *N*-acetyl-D-glucosamine), and is trimmed sequentially by glucosidase I (G-I) and glucosidase II (G-II) to tridecasaccharide (Glc2Man9GlcNAc2), dodecasaccharide (Glc1Man9GlcNAc2), and then to undecasaccharide (Man9GlcNAc2; Figure 1).

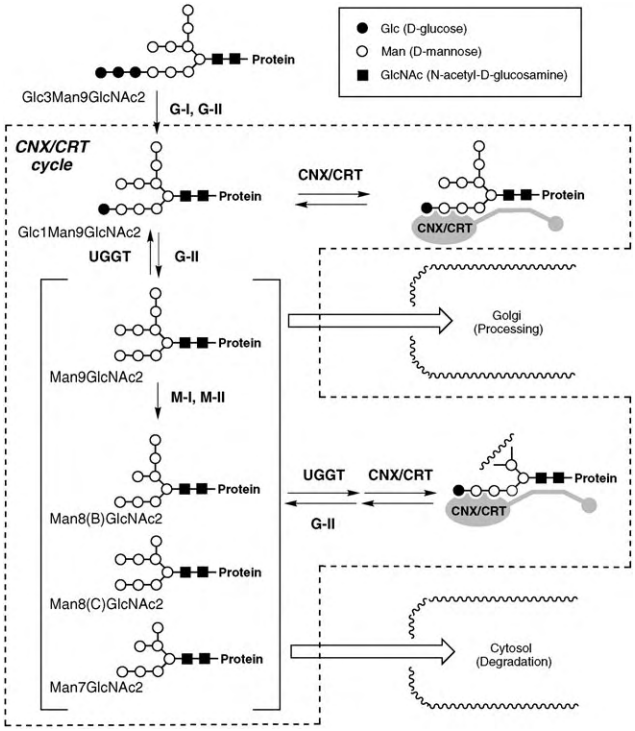

Figure 1. Processing of N-linked oligosaccharides in the ER.

The calnexin (CNX) cycle plays a central role in glycoprotein folding (Figure 1).[1] CNX and its soluble homologue calreticulin (CRT) are lectin chaperones, which have a similar specificity for monoglucosylated high-mannose-type glycans, such as the Glc1Man9GlcNAc2 of N-linked glycoproteins, as primary ligands. These chaperones assist with the folding of glycoproteins by recruiting the disulfide isomerase-like protein ERp57.[2] Clearly, CNX/CRT and G-II compete for the same glycan, and a certain proportion of glycoproteins may reach the nonglucosylated stage (Man9GlcNAc2) without being folded correctly.

Uridine 5′-diphosphate (UDP)-glucose:glycoprotein glucosyltransferase (UGGT) plays an important role in the CNX/CRT cycle as the "folding sensor".[3] It glucosylates the Man9GlcNAc2 of incompletely folded glycoproteins that arise from immature deglucosylation, and regenerates the CNX/CRT ligand Glc1Man9GlcNAc2. With repeated attempts at folding (CNX/CRT), deglucosylation (G-II), and reglucosylation (UGGT), this system maximizes the chance that newly formed glycoproteins will attain the correct structure. Successfully folded proteins escape from this cycle

[*] Dr. K. Totani, Dr. I. Matsuo, Dr. H. Koshino, Dr. Y. Ito
RIKEN (The Institute of Physical and Chemical Research)
2-1 Hirosawa, Wako, Saitama 351-0198 (Japan)
E-mail: yukito@riken.jp
Dr. K. Totani, Dr. I. Matsuo, Dr. Y. Ito
CREST, Japan Science and Technology Agency (JST)
Kawaguchi, Saitama 332-1102 (Japan)
Fax: (+81) 48-482-4680
Dr. Y. Ihara
Department of Biochemistry & Molecular Biology of Disease
Atomic Bomb Disease Institute
Nagasaki University Graduate School of Biomedical Sciences
1-12-4 Sakamoto, Nagasaki 852-8523 (Japan)

[**] This work was supported by the special postdoctoral researchers program at RIKEN. We thank A. Takahashi for technical assistance. Financial support from the Presidential Fund of RIKEN and the Ministry of Education, Culture, Sports, Science, and Technology (Grant-in-Aid for Young Scientists (B) No. 17750170 and Grant-in-Aid for Creative Scientific Research No. 17GS0420) is acknowledged. UDP = uridine 5′-diphosphate.

Supporting information for this article is available on the WWW under http://www.angewandte.org or from the author.

InterScience
© 2005 Wiley-VCH Verlag GmbH & Co. KGaA, Weinheim

and are transported to the Golgi apparatus for further processing and secretion, while misfolded proteins are retrotranslocated to the cytosol for degradation.[4] ER-resident α-mannosidases may digest Man9GlcNAc2 to Man8GlcNAc2, Man7GlcNAc2, and possibly Man6-5GlcNAc2.[5] UGGT also converts these glycans to monoglucosylated forms that can be CNX/CRT ligands, when protein folding is incomplete, thus constituting an intricate fail-safe system.

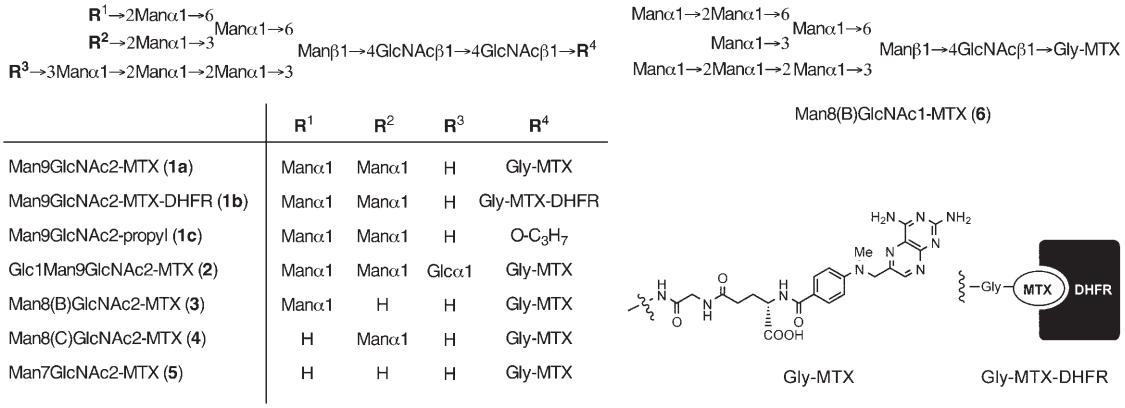

	R1	R2	R3	R4
Man9GlcNAc2-MTX (**1a**)	Manα1	Manα1	H	Gly-MTX
Man9GlcNAc2-MTX-DHFR (**1b**)	Manα1	Manα1	H	Gly-MTX-DHFR
Man9GlcNAc2-propyl (**1c**)	Manα1	Manα1	H	O-C_3H_7
Glc1Man9GlcNAc2-MTX (**2**)	Manα1	Manα1	Glcα1	Gly-MTX
Man8(B)GlcNAc2-MTX (**3**)	Manα1	H	H	Gly-MTX
Man8(C)GlcNAc2-MTX (**4**)	H	Manα1	H	Gly-MTX
Man7GlcNAc2-MTX (**5**)	H	H	H	Gly-MTX

Figure 2. Synthetic oligosaccharides used in this study.

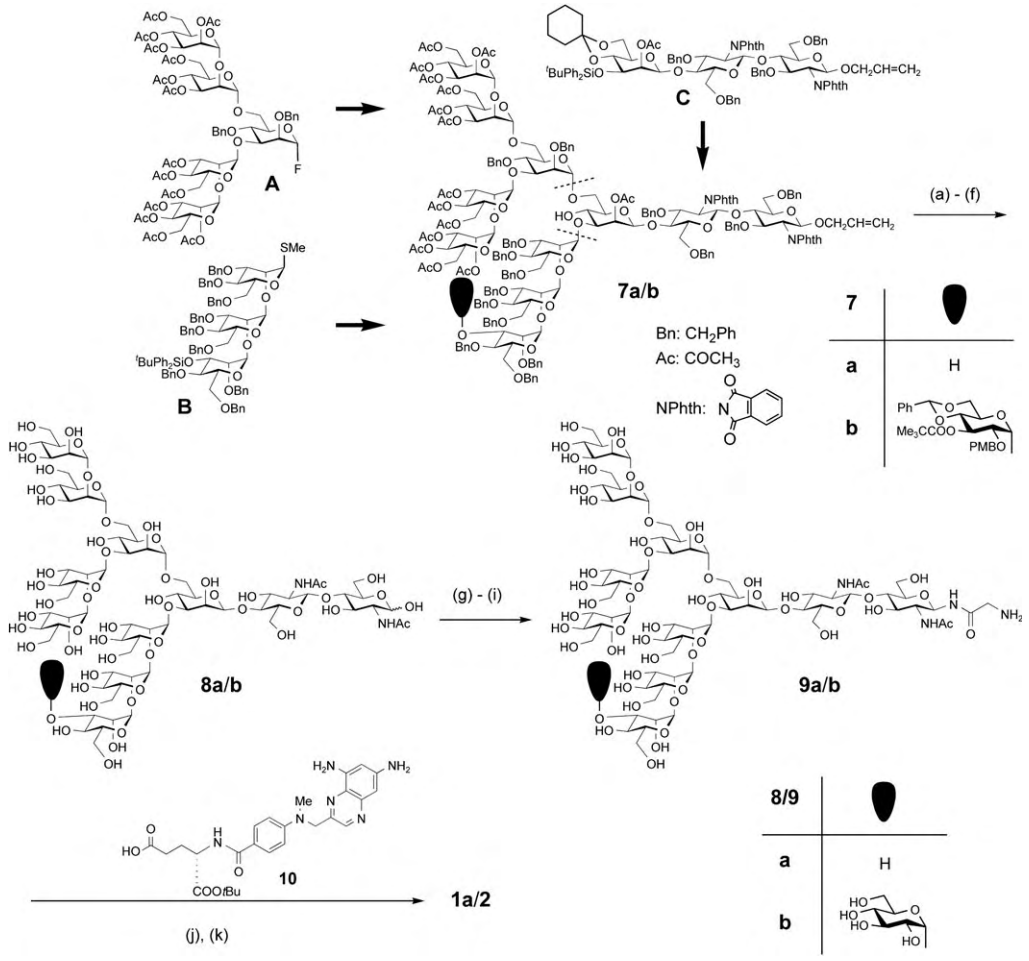

Scheme 1. Synthesis of CHO-MTX conjugates **1a** and **2**. Reagents and conditions: a) ethylenediamine, *n*BuOH, 70°C; b) Ac_2O, pyridine, DMAP; c) $[Ir(cod)(PMePh_2)_2]PF_6$, H_2, THF then I_2, $NaHCO_3$, H_2O; d) Ac_2O, pyridine, DMAP; e) $Pd(OH)_2$, H_2, 80% AcOH, RT; f) NaOMe/MeOH, RT (66% for **1a**, 81% for **2**, six steps); g) saturated aq. NH_4HCO_3, 40°C; h) FmocGlyCl, $NaHCO_3$, dioxane/H_2O (1:1), 0°C; i) piperidine, DMF (81% for **1a**, 79% for **2**, three steps); j) **10**, DMT-MM, MeOH/H_2O (1:1); k) CF_3COOH (62% for **1a**, 65% for **2**, two steps). DMAP = *N*,*N*-dimethylamino-4-pyridine, cod = 1,5-cyclooctadiene, DMT-MM = 4-(4,6-dimethoxy-1,3,5-thiazin-2-yl)-4-methylmorpholinium chloride.

 © 2005 Wiley-VCH Verlag GmbH & Co. KGaA, Weinheim

The detailed analysis of UGGT has been problematic because of its unusual specificity; it accepts unglucosylated high-mannose-type glycans only when they are covalently bound to incompletely folded proteins. Remarkably, UGGT rejects folded as well as severely misfolded glycoproteins, and prefers a native-like, compact, molten-globule-type conformation.[3,6,7] Previous studies of UGGT have been conducted using artificially denatured glycoproteins,[6,8] their tryptic digests,[8f] or neoglycopeptides.[7] The development of a simpler and better-defined substrate of UGGT is challenging, because this enzyme requires the coexistence of three separate elements: an acceptor (Manα1→2Man) element, a GlcNAcβ1→Asn element, and a cluster of hydrophobic amino acids exposed on the protein surface. Herein, we describe the first analysis of UGGT-catalyzed glucose transfer, by using chemically synthesized, fully defined, nonpeptidic substrates.

We have recently reported oligosaccharide–methotrexate conjugates (CHO-MTX) as the precursor of artificial glycoproteins having homogeneous carbohydrates.[9] MTX and its derivatives have been investigated as anticancer and antimicrobial drug candidates,[10] because of their inhibitory activity toward dihydrofolate reductase (DHFR), a key enzyme in the biosynthesis of nucleotide precursors of DNA. *Escherichia coli* DHFR is a relatively small (≈18 kDa) protein, which has been used as a tag for induced protein dimerization[11] and the in vitro labeling of proteins.[12] CHO-MTX can be converted to a tight-binding complex with DHFR, by virtue of the strong affinity ($K_A \approx 10^{10}\,M^{-1}$) between MTX and DHFR.[13] In the course of preparing a series of complexes of CHO-MTX and DHFR (Figure 2), we observed that CHO-MTX conjugate **1a** was an excellent acceptor substrate of UGGT.

The synthesis of Man9GlcNAc2-MTX (**1a**) was conducted as shown in Scheme 1. Thus, the protected undecasaccharide **7a**,[14] which was prepared from synthetic blocks **A**, **B**, and **C**, was deprotected to **8a** and converted to glycosylamine under the conditions proposed by Kochetkov et al.[15] Subsequent reaction with FmocGlyCl and removal of Fmoc afforded Man9GlcNAc2-Gly **9a**. Coupling with MTX-(α-*t*Bu)[9,16] was conducted under the conditions reported by Kunishima et al.[17] and cleavage of the *t*Bu ester afforded **1a**. Compound **1a** retained affinity for DHFR, which was confirmed by inhibition experiments[18] and lectin (Con A) binding experiments (see the Supporting Information). The expected UGGT product Glc1Man9GlcNAc2-MTX (**2**) was prepared from the protected dodecasaccharide **7b** in a similar manner.

Rat liver UGGT[19] and UDP-[^{3}H]Glc were used for the efficient glucosylation of **1a** (Figure 3a). Under the assay conditions (50 μM substrate), the reactivity of the synthetic substrate **1a** was at least comparable to that of denatured thyroglobulin, which has been used in conventional UGGT assays.[8a,19] Native thyroglobulin was completely inactive, as reported previously.[19b] We speculate that MTX mimics the property of unfolded proteins, and presumably has an exposed hydrophobic patch. In fact, Man9GlcNAc2 linked to a simpler and less hydrophobic aglycon (**1c**) was much less active, as was the complex Man9GlcNAc2-MTX-DHFR (**1b**).

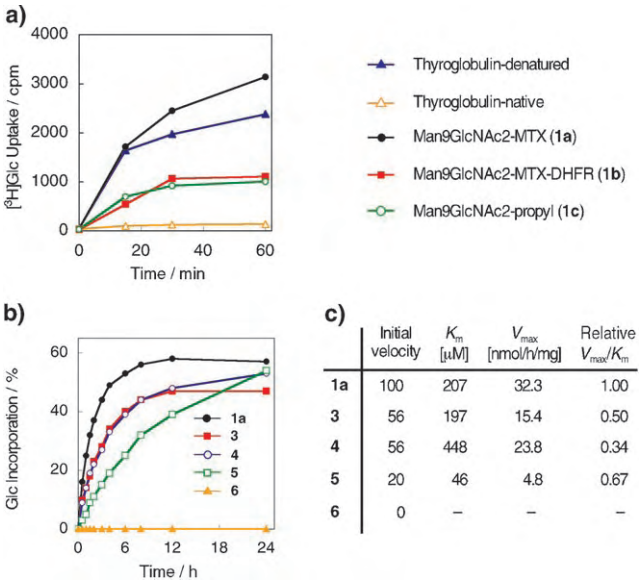

c)

	Initial velocity	K_m [μM]	V_{max} [nmol/h/mg]	Relative V_{max}/K_m
1a	100	207	32.3	1.00
3	56	197	15.4	0.50
4	56	448	23.8	0.34
5	20	46	4.8	0.67
6	0	–	–	–

Figure 3. Reaction of UGGT with the synthetic substrates. a) Time course of [^{3}H]Glc uptake; Man9GlcNAc2-MTX (**1a**), Man9GlcNAc2-MTX-DHFR (**1b**), Man9GlcNAc2-propyl (**1c**), denatured thyroglobulin, and native thyroglobulin. b) Time course of Glc incorporation; Man9-GlcNAc2-MTX (**1a**), Man8(B)GlcNAc2-MTX (**3**), Man8(C)GlcNAc2-MTX (**4**), Man7GlcNAc2-MTX (**5**), and Man8(B)GlcNAc1-MTX (**6**). c) Initial velocity (calculated from the value at 1 h incubation on (b)), K_m, and V_{max} values of **1a**, **3**, **4**, **5**, and **6**.

In the latter case, MTX may be buried in the folded protein, which makes it less accessible to UGGT.

The enzymatic transformation of **1a** to Glc1Man9GlcNAc2-MTX (II) was readily traced by HPLC and the characteristic UV absorption of MTX (Figure 4a). The product II was separated by preparative HPLC to achieve its characterization. Enzymatically produced II was identical to synthetic **2**, judging from MALDI-TOF mass spectrometry and ^{1}H NMR spectroscopy (1D, differential NOE, 2D TOCSY; see Figure 4b–d and the Supporting Information). Furthermore, when measured by isothermal titration calorimetry (ITC),[20] UGGT-generated II had a binding affinity for CRT with a K_A value ($5.17 \times 10^6\,M^{-1}$) essentially identical to that of the authentic **2** and previously reported Glc1Man9GlcNAc2-propyl[14,21] ($5.26 \times 10^6\,M^{-1}$). These results provided proof of the glycan structure of the UGGT product Glc1Man9GlcNAc2.

We then prepared a series of high-mannose glycan–MTX conjugates, Man8(B)GlcNAc2-MTX (**3**), Man8(C)GlcNA2-MTX (**4**), Man7GlcNAc2-MTX (**5**), and Man8(B)GlcNAc1-MTX (**6**; Figure 2), to examine the specificity of UGGT. As shown in Figure 3b and c, the order of reactivity was Man9 > Man8 > Man7, with relative values of initial velocity of 100, 56, and 20, respectively. These values were in good agreement with previously reported values that were estimated by using protease-digested thyroglobulin.[8a] The B and C isomers of Man8GlcNAc2-MTX had a similar reactivity. The K_m and V_{max} values for **1a**, **3**, **4**, and **5** (calculated from Lineweaver–Burk plots, see the Supporting Information) are provided in Figure 3c, and show that **1a** was the most reactive substrate. Interestingly, compound **6**, which had a single GlcNAc instead

 © 2005 Wiley-VCH Verlag GmbH & Co. KGaA, Weinheim

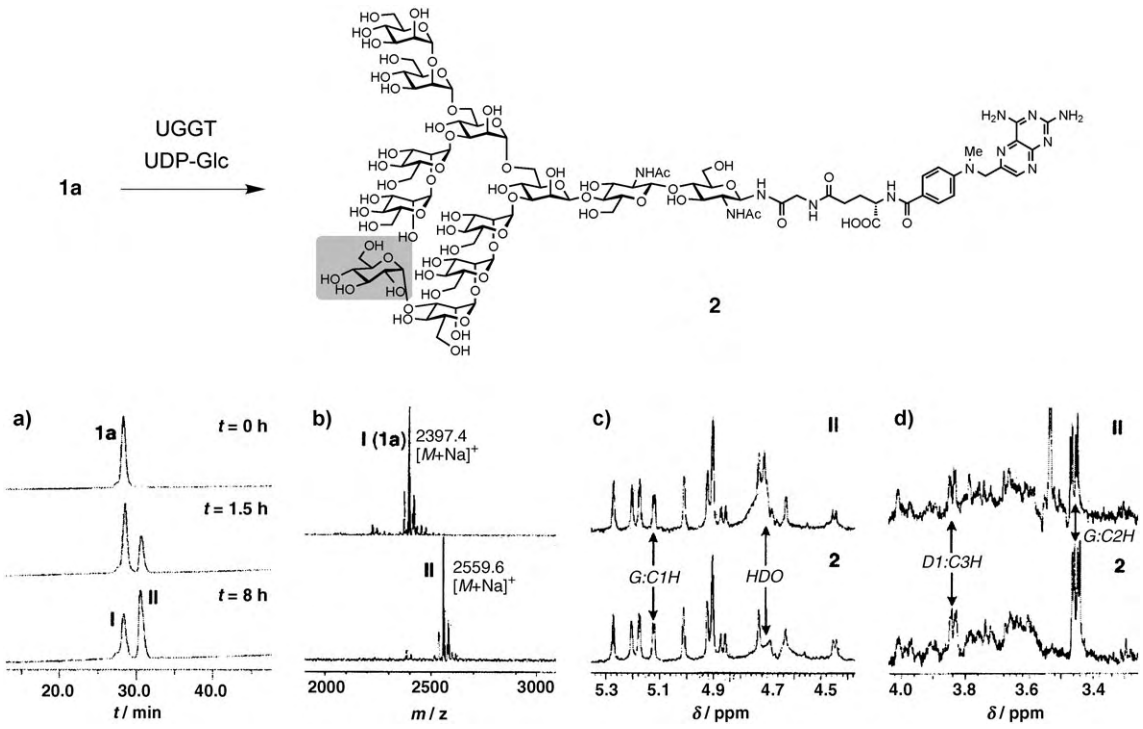

Figure 4. Characterization of the UGGT product. a) HPLC analysis of the glucosylation of Man9GlcNAc2-MTX (**1a**): TSK-GEL Amide-80 column (4.6 mmφ × 25 cm), mobile phase CH_3CN/3% AcOH-Et_3N, pH 7.3, linear gradient from 65:35 to 50:50 in 50 min, flow rate 1.0 mL min^{-1} at 40 °C. b) MALDI-TOF mass spectra of HPLC peaks of compounds **I** (**1a**) and **II** (corresponds to Glc1Man9GlcNAc2-MTX (**2**)). c) ^{1}H NMR spectra of synthetic **2** and the resulting UGGT product **II** in D_2O. The HDO signal was suppressed by DANTE (delays alternating with nutations for tailored excitation) presaturation. d) Differential NOE spectra (trace through the G:C1H resonance) of **2** and **II**.

of chitobiose ($GlcNAc_2$), was completely devoid of activity. UGGT was reported to recognize the innermost GlcNAc moiety,[8b] so the fact that **6** was not accepted might reflect an insufficient distance between the acceptor site Man and innermost GlcNAc.

Although Man7-9GlcNAc2-MTX were all accepted as substrates of UGGT, the glucosylation stopped at 50–60% conversion in every case. Addition of alkaline phosphatase had no effect, which suggests that the result was not caused by accumulated UDP. Interestingly, when recombinant CRT[22] (25 mol%) was added to the incubation mixture well after the reaction reached its plateau (150 h), the glucosylation was boosted (Figure 5a). We speculate that there was inhibition by glucosylated products; CRT trapped the products, segregated them from UGGT, and alleviated the inhibition. In line with this conjecture, a lectin-deficient CRT mutant (D135A)[23] had no effect (Figure 5b). For all the substrates examined (**1a**, **3**, and **4**), enhancement of the conversion (up to >70%) was observed in a dose-dependent manner (Figure 5c).

In summary, we have developed efficient substrates of UGGT that are completely synthetic. An unambiguous characterization of the UGGT product and the quantitative analysis of the specificity of UGGT for glycan were achieved with these substrates. Studies are in progress to systematically prepare various CHO-MTX conjugates. These compounds are expected to be valuable tools with which to investigate the

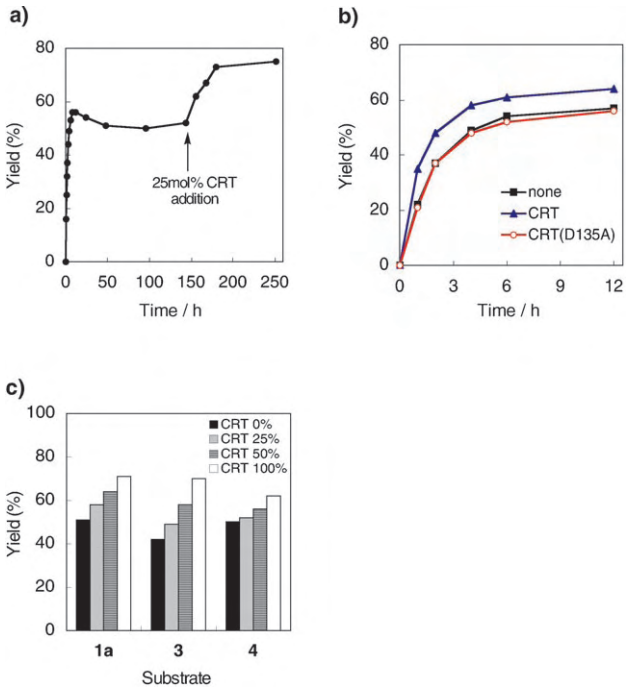

Figure 5. Effect of calreticulin (CRT). a) Effect of 25 mol% CRT addition on **1a**. b) Time course of Glc incorporation for **1a** in the presence or absence of 25 mol% CRT or CRT(D135A) mutant. c) CRT dose-dependent Glc incorporation for **1a**, **3**, and **4** after 48 h incubation at 37 °C.

 © 2005 Wiley-VCH Verlag GmbH & Co. KGaA, Weinheim

properties of UGGT and other proteins involved in the ER quality-control system.

Received: August 3, 2005
Published online: November 11, 2005

Keywords: glucose · glycoproteins · glycosylation · protein folding · quality control

[1] A. Helenius, M. Aebi, *Annu. Rev. Biochem.* **2004**, *73*, 1019–1049.
[2] E.-M. Frickel, P. Frei, M. Bouvier, W. F. Stafford, A. Helenius, *J. Biol. Chem.* **2004**, *279*, 18227–18287.
[3] E. S. Trombetta, A. J. Parodi, *Methods* **2005**, *35*, 328–337.
[4] a) Y. Yoshida, T. Chiba, F. Tokunaga, H. Kawasaki, K. Iwai, T. Suzuki, Y. Ito, K. Matsuoka, M. Yoshida, K. Tanaka, T. Tai, *Nature* **2002**, *418*, 438–442; b) Y. Oda, N. Hosokawa, I. Wada, K. Nagata, *Science* **2003**, *299*, 1394–1397; c) M. Molinari, K. K. Eriksson, V. Calanca, C. Galli, P. Cresswell, M. Michalak, A. Helenius, *Mol. Cell* **2004**, *13*, 125–135.
[5] Z. Frenkel, W. Gregory, S. Kornfeld, G. Z. Lederkremer, *J. Biol. Chem.* **2003**, *278*, 34119–34124.
[6] J. J. Caramelo, O. A. Castro, G. de Prat-Gay, A. Parodi, *J. Biol. Chem.* **2004**, *279*, 46280–46285.
[7] J. J. Caramelo, O. A. Castro, L. A. Alonso, G. de Prat-Gay, A. J. Parodi, *Proc. Natl. Acad. Sci. USA* **2003**, *100*, 86–91.
[8] a) M. C. Sousa, M. A. Ferrero-Garcia, A. J. Parodi, *Biochemistry* **1992**, *31*, 97–105; b) M. Sousa, A. Parodi, *EMBO J.* **1995**, *14*, 4196–4203; c) E. S. Trombetta, A. Helenius, *J. Cell Biol.* **2000**, *148*, 1123–1129; d) C. Ritter, A. Helenius, *Nat. Struct. Biol.* **2000**, *7*, 278–280; e) D. C. Tessier, D. Dignard, A. Zapun, A. Radominska-Pandya, A. J. Parodi, J. J. M. Bergeron, D. Y. Thomas, *Glycobiology* **2000**, *10*, 403–412; f) S. C. Taylor, A. D. Ferguson, J. J. M. Bergeron, D. Y. Thomas, *Nat. Struct. Mol. Biol.* **2004**, *11*, 128–134; g) S. M. Arnold, R. J. Kaufman, *J. Biol. Chem.* **2003**, *278*, 43320–43328.
[9] K. Totani, I. Matsuo, Y. Ito, *Bioorg. Med. Chem. Lett.* **2004**, *14*, 2285–2289.
[10] a) S. P. Ackland, R. L. Schlisky, *J. Clin. Oncol.* **1987**, *5*, 2017–2031; b) H. Zeng, Z.-S. Chen, M. G. Belinsky, P. A. Rea, G. D. Kruth, *Cancer Res.* **2001**, *61*, 7225–7232.
[11] a) S. Gendreizig, M. Kindermann, K. Johnsson, *J. Am. Chem. Soc.* **2003**, *125*, 14970–14971; b) H. Lin, W. M. Abida, R. T. Sauer, V. W. Cornish, *J. Am. Chem. Soc.* **2000**, *122*, 4247–4248.
[12] L. Miller, J. Sable, P. Goelet, M. P. Sheetz, V. W. Cornish, *Angew. Chem.* **2004**, *116*, 1704–1707; *Angew. Chem. Int. Ed.* **2004**, *43*, 1672–1675.
[13] a) J. R. Appleman, E. E. Howell, J. Kraut, M. Kuhl, R. L. Blakley, *J. Biol. Chem.* **1988**, *263*, 9187–9198; b) S. P. Sasso, R. M. Gilli, J. C. Sari, O. S. Rimet, C. M. Briand, *Biochim. Biophys. Acta* **1994**, *1207*, 74–79.
[14] I. Matsuo, M. Wada, S. Manabe, Y. Yamaguchi, K. Otake, K. Kato, Y. Ito, *J. Am. Chem. Soc.* **2003**, *125*, 3402–3403.
[15] a) L. M. Lihkosherstov, O. S. Novikoya, V. A. Dereviskaja, N. K. Kochetkov, *Carbohydr. Res.* **1986**, *146*, C1–C5; b) I. D. Manger, T. W. Rademacher, R. A. Dwek, *Biochemistry* **1992**, *31*, 10724–10732; c) H. J. Stubbs, M. A. Shia, K. G. Rice, *Anal. Biochem.* **1997**, *247*, 357–365.
[16] A. Rosowski, R. Forsch, J. Uren, M. Wick, *J. Med. Chem.* **1981**, *24*, 1450–1455.
[17] M. Kunishima, C. Kawachi, K. Hioki, K. Terao, S. Tani, *Tetrahedron* **2001**, *57*, 1551–1558.
[18] B. C. Widemann, F. M. Balis, P. C. Adamson, *Clin. Chem.* **1999**, *45*, 223–228.
[19] a) S. E. Trombetta, A. J. Parodi, *J. Biol. Chem.* **1992**, *267*, 9236–9240; b) S. E. Trombetta, M. Bosch, A. Parodi, *Biochemistry* **1989**, *28*, 8108–8116.
[20] T. K. Dam, C. F. Brewer, *Chem. Rev.* **2002**, *102*, 387–429.
[21] Y. Ito, S. Hagihara, M. A. Arai, I. Matsuo, M. Takatani, *Glycoconjugate J.* **2004**, *21*, 257–266.
[22] S. Baksh, M. Michalak, *J. Biol. Chem.* **1991**, *266*, 21458–21465.
[23] M. Kapoor, L. Ellgaard, J. Gopalakrishnapai, C. Schirra, E. Gemma, S. Oscarson, A. Helenius, A. Surolia, *Biochemistry* **2004**, *43*, 97–106.

 © 2005 Wiley-VCH Verlag GmbH & Co. KGaA, Weinheim

Self-Assembly

DOI: 10.1002/anie.200503040

Predictions, Synthetic Strategy, and Isolation of a Linear Tetrametallic Triple-Stranded Lanthanide Helicate**

Kornelia Zeckert, Josef Hamacek, Jean-Michel Senegas, Natalia Dalla-Favera, Sébastien Floquet, Gérald Bernardinelli, and Claude Piguet**

Dedicated to Professor Jean-Claude G. Bünzli

The majority of self-assembled linear multi-stranded helicates are bimetallic, with some extensions toward trimetallic analogues,[1] whilst those with four or more metal centers remain rare.[2] Although the regular arrangement of several metal ions in a single direction, thus forming a discrete chain, may induce novel and unusual electrochemical,[3] photophys-

[*] Dr. G. Bernardinelli
Laboratory of X-ray Crystallography
University of Geneva
24 Quai E. Ansermet, 1211 Geneva 4 (Switzerland)
Fax: (+41) 22-379-6108
E-mail: gerald.bernardinelli@cryst.unige.ch

Dr. K. Zeckert,[+] Dr. J. Hamacek, Dr. J.-M. Senegas, N. Dalla-Favera, Dr. S. Floquet,[++] Prof. Dr. C. Piguet
Department of Inorganic
Analytical and Applied Chemistry
University of Geneva
30 Quai E. Ansermet, 1211 Geneva 4 (Switzerland)
Fax: (+41) 22-379-6830
E-mail: claude.piguet@chiam.unige.ch

[+] Present address: Institut für Anorganische Chemie
der Universität Leipzig
Johannisallee 29, 04103 Leipzig (Germany)

[++] Present address: Institut Lavoisier, IREM, UMR 8637
Université de Versailles
45 Avenue des Etats-Unis, 78035 Versailles (France)

[**] This work was supported through grants from the Swiss National Science Foundation.

Supporting information for this article is available on the WWW under http://www.angewandte.org or from the author.

WILEY InterScience DISCOVER SOMETHING GREAT
© 2005 Wiley-VCH Verlag GmbH & Co. KGaA, Weinheim

ical,[4] or magnetic[5] properties, multimetallic linear helicates have been mainly investigated for their structural aspect, which is indebted to their undeniable aesthetic appeal. The recent expansion of (supra)molecular chemistry toward the nanosciences dramatically revealed the very limited quantitative predictions available for the design of large multicomponent assemblies,[6] despite the remarkable reports of major successes based on qualitative symmetry matching and stereochemical restrictions.[7] In this context, the assembly of simple mono-dimensional multimetallic helicates can bring some valuable contributions to the fundamental understanding and rationalization of thermodynamically driven multicomponent complexation processes. In two seminal reports,[8] Lehn and co-workers first proposed a thermodynamic model that accounted for the formation of trimetallic double-stranded helicates. Scatchard plots based on the classical two-parameter site-binding model,[9–11] which considers the total free energy of formation of the final complex as the sum of the connection energies of each metal ion to a single receptor modulated by intermetallic pair interactions, suggested the occurrence of thermodynamic complexation processes driven to completion by positive cooperativity—a landmark that deeply influenced the rationalization of metallosupramolecular self-assembly processes for more than a decade.[10] The recent reanalysis of these original data by Ercolani indicates that helicate formation cannot be modeled with pure intermolecular interactions and entropic corrections must be considered for adequately rationalizing intramolecular metal–ligand connections, which occur during the self-assembly processes.[11] An explicit treatment, which combines metal–ligand connections (intra- and intermolecular) and pair interactions (intermetallic and interligand) has been recently proposed, and the macroscopic formation constant $\beta_{m,n}^{M,L}$ of any supramolecular complex $[M_mL_n]$ [Eq. (1)] can be modeled with four microscopic parameters [Eq. (2), extended site-binding model]:[12]

$$m\,M + n\,L \rightleftharpoons [M_mL_n]\ \beta_{m,n}^{M,L} \quad (1)$$

$$\beta_{m,n}^{M,L} = \sigma_{chir}^{M,L}\,\omega_{m,n} \prod_{i=1}^{mn} (f_i^{M,L}) \prod_{i=1}^{mn-m-n+1} (c_i^{eff}) \prod_{i<j}{}'' (u_{ij}^{MM}) \prod_{k<l}{}''' (u_{kl}^{LL}) \quad (2)$$

1) $f_i^{M,L}$ represents the intermolecular microscopic affinity constant that characterizes the connection of a metal M to the binding site i of a ligand L (including desolvation); 2) $u_{ij}^{MM} = \exp(-\Delta E_{ij}^{MM}/RT)$ is the Boltzman factor that accounts for the intermetallic interaction ΔE_{ij}^{MM} (in terms of free energy), which occurs when two metal centers occupy two adjacent binding sites i and j of the same ligand; 3) $u_{kl}^{LL} = \exp(-\Delta E_{kl}^{LL}/RT)$ is the Boltzman factor that accounts for the interligand interactions ΔE_{kl}^{LL}, which results from the connection of two binding sites k and l to the same metal center; 4) $c_i^{eff} = \exp((\Delta S_{i,intra}^{M,L} - \Delta S_{i,inter}^{M,L})/R)$ is the "effective concentration" used for the correction of the entropy change observed between inter- and intramolecular binding processes; 5) the term $\sigma_{chir}^{M,L}\omega_{m,n}$ represents the degeneracy of the microscopic state, which must be evaluated for each microspecies by using standard statistical methods.[9–12] Finally, the two last products $\prod''$ and $\prod'''$ run over all the pairs of intermetallic (u^{MM}) or interligand (u^{LL}) interactions that occur in the $[M_mL_n]$ microspecies.[12] Obviously, the reliable estimation of these four parameters requires a large amount of independent macroscopic constants that characterize comparable complexation events, a situation which is met when the thermodynamic equilibria relevant to the formation of the bimetallic $[Eu_2(\mathbf{L1})_3]^{6+}$ and $[Eu_2(\mathbf{L2})_3]^{6+}$ and trimetallic $[Eu_3(\mathbf{L3})_3]^{9+}$ triple-stranded helicates are simultaneously considered (only two different tridentate binding units N_2O and N_3 are involved in these complexes; Scheme 1). A complete set of microscopic parameters $f_{N_2O}^{Eu}$, $f_{N_3}^{Eu}$, u^{EuEu}, u^{LL}, and c^{eff} results,[13] and Equation (2) can be then used to predict the stability constant of the unknown tetrametallic homologue $[Eu_4(\mathbf{L4})_3]^{12+}$ [Eq. (3)].

$$\beta_{4,3}^{Eu,L4} = 2\,(f_{N_2O}^{Eu})^6\,(f_{N_3}^{Eu})^6\,(u^{LL})^{12}\,(u^{EuEu})^{4.33}\,(c^{eff})^6 \quad (3)$$

We calculate $\log(\beta_{4,3}^{Eu,L4}) = 42.5$ for the saturated triple-stranded helicate $[Eu_4(\mathbf{L4})_3]^{12+}$ [Eq. (3)], which is much larger than $\log(\beta_{3,3}^{Eu,L4}) = 35.5$, $\log(\beta_{3,2}^{Eu,L4}) = 27.4$, and $\log(\beta_{4,2}^{Eu,L4}) = 31.5$ predicted for its decomposition products, respectively, in excess of ligand ($[Eu_3(\mathbf{L4})_3]^{9+}$) or in excess of metal ($[Eu_3(\mathbf{L4})_2]^{9+}$ and $[Eu_4(\mathbf{L4})_2]^{12+}$; detailed calculations are given in the Supporting Information). The associated predicted distribution curves for a total ligand concentration

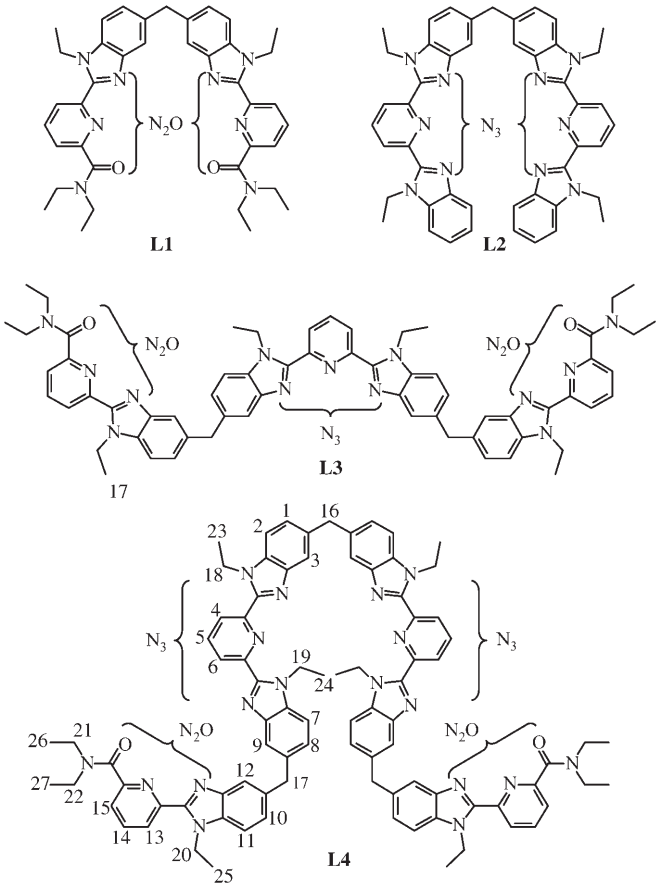

Scheme 1. Structures of the ligands **L1**–**L4**, with the common N_3 and N_2O tridentate binding sites highlighted and the numbering scheme used for the ^{1}H NMR spectroscopic analysis given.

 © 2005 Wiley-VCH Verlag GmbH & Co. KGaA, Weinheim

$|\mathbf{L4}|_{tot} = 10^{-3}$ M show that $[Eu_4(\mathbf{L4})_3]^{12+}$ corresponds to > 95% of the solution species for the stoichiometric ratio Eu/**L4** = 1.33, despite its high 12+ charge (see the Supporting Information). With this encouraging prediction in mind, we embarked upon a program to prepare the first stable tetrametallic lanthanide-containing triple-helical complex. Our ultimate goal is concerned with the exploration of the exact dependence of u^{MM} and c^{eff} on the intersite separation d, which is responsible for 1) the potential programming of local intermetallic dielectric constants (through $\Delta E^{MM} \propto 1/\varepsilon_r d$) and 2) the quantitative description of preorganization in self-assembled processes (through $c^{eff} \propto 1/d^n$).[6,11,12] Herein, we present the synthetic strategy, isolation, and structural and thermodynamic characterizations of the first tetrametallic lanthanide triple-stranded helicate $[Eu_4(\mathbf{L4})_3]^{12+}$. Following the original synthetic strategy developed for the preparation of **L3**,[14] we attempt to react the unsymmetrical *o*-nitroaminoarene **3**[14] with the diacid **2** (Scheme 2).[15]

However, **3** proved to be such a poor nucleophile that it does not react with the activated dicarbonyl chloride **2**-$(COCl)_2$ (Scheme 2, left). The remarkable C-shaped molecular structure of **3** observed in the solid state[16] may help to rationalize its poor nucleophilicity because 1) one face of the incriminated secondary ethyl amine N1 is blocked by the distal diethylcarboxamido group bound to the pyridine ring and 2) the H1 proton is involved in an intramolecular hydrogen bond with the adjacent nitro group N1–H1···O1 (N1···O1: 2.634(3) Å, ∢ N1–H1···O1: 130(2)°; Figure 1). Removing the terminal *N*,*N*-diethylcarboxamide pyridyl group in **1** sufficiently improves the nucleophilicity of the secondary amine to react with **2**-$(COCl)_2$ to give the bis(*o*-nitroaminoarene) **4**, which can be further successfully converted into **L4** (Scheme 2, right).

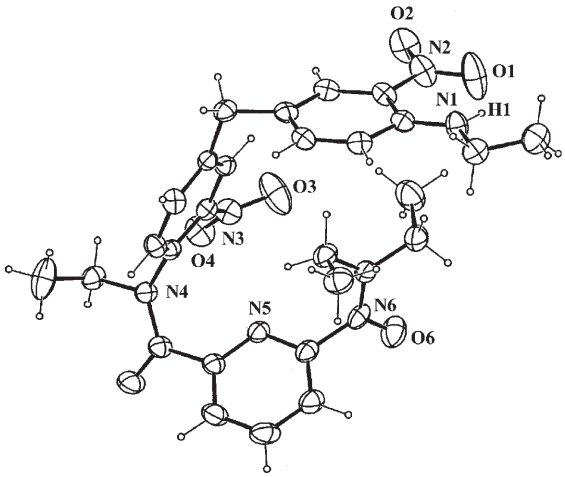

Figure 1. Perspective view of the C-shaped molecular structure of the *o*-nitroaminoarene synthon **3** with partial numbering. Ellipsoids are shown at the 50% probability level.

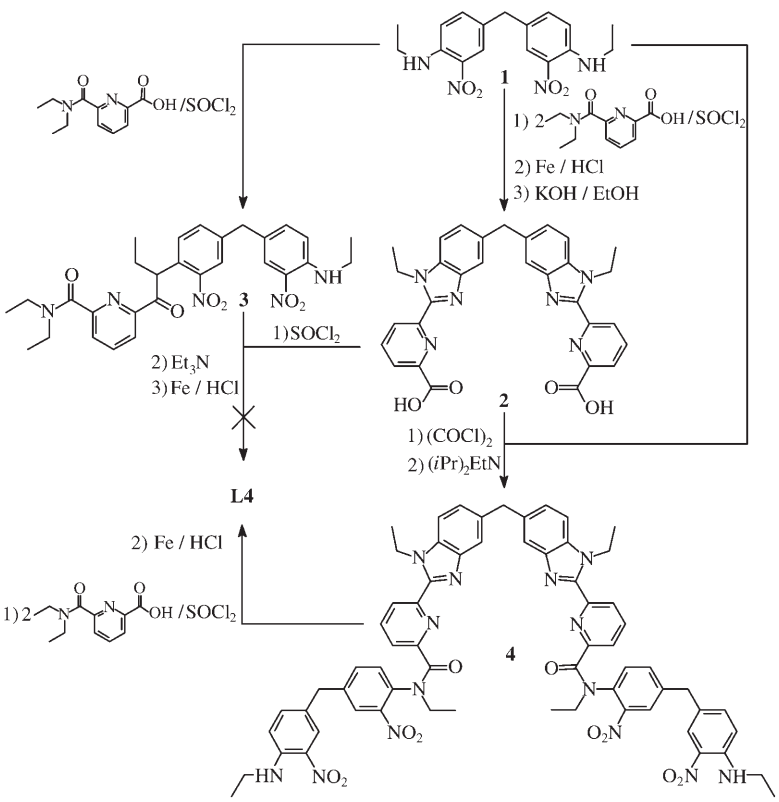

Scheme 2. Synthetic strategy for the preparation of **L4**.

ESI-MS titrations of **L4** (10^{-3} M) with $[Ln(CF_3SO_3)_3]\cdot x H_2O$ ($x = 3$–5) in acetonitrile (Ln = La, Eu, Lu) are dominated by the signals of the saturated species $[Ln_4(\mathbf{L4})_3(CF_3SO_3)_n]^{(12-n)+}$ ($n = 3$–9) together with minor signals (< 10%) that arise from the unsaturated intermediates $[Ln_3(\mathbf{L4})_3(CF_3SO_3)_n]^{(9-n)+}$ (excess of ligand, Ln/**L4** < 1.33) and $[Ln_3(\mathbf{L4})_2(CF_3SO_3)_n]^{(9-n)+}$ and $[Ln_4(\mathbf{L4})_2(CF_3SO_3)_n]^{(12-n)+}$ (excess of metal, Ln/**L4** > 1.33; see the Supporting Information). Parallel ^{1}H NMR titrations in CD_3CN/CD_2Cl_2 (9:1, $|\mathbf{L4}|_{tot} = 8 \times 10^{-3}$ M) confirm this behavior with the stepwise conversion of free **L4** into $[Ln_4(\mathbf{L4})_3]^{12+}$, which largely dominates the speciation in solution (only very weak signals are detected for some low-symmetrical intermediates; see the Supporting Information). The only species detected in solution for Ln/**L4** = 1.33 are $[Ln_4(\mathbf{L4})_3]^{12+}$, and their ^{1}H NMR spectra are compatible with D_3-symmetry (six equivalent half-ligand strands that lead to 15 different CH signals, an enantiotopic central methylene signal for H16,16′, and six diastereotopic methylene protons H17,17′–H22,22′; Figure 2). Finally, preliminary-batch spectrophotometric titrations show complicated variations of the absorption spectra for Eu/**L4** in the range 0.1–4.0 ($|\mathbf{L4}|_{tot} = 10^{-4}$ M, CH_3CN + 5% CH_2Cl_2; see the Supporting Information), which can be satisfyingly fitted with the four absorbing complexes $[Eu_3(\mathbf{L4})_3]^{9+}$, $[Eu_4(\mathbf{L4})_3]^{12+}$, $[Eu_3(\mathbf{L4})_2]^{9+}$, and $[Eu_4(\mathbf{L4})_2]^{12+}$. The associated macroscopic constants $\log(\beta_{3,3}^{Eu,L4}) = 36.2(1.9)$, $\log(\beta_{4,3}^{Eu,L4}) = 42.1(1.9)$, $\log(\beta_{3,2}^{Eu,L4}) = 27.9(1.4)$, and $\log(\beta_{4,2}^{Eu,L4}) = 32.0(1.7)$ match our predictions within experimental errors.

The diffusion of diethyl ether into a concentrated solution of $[Ln_4(\mathbf{L4})_3]^{12+}$ in methanol provides white microcrystals in 70–85% yield; the elemental analyses were shown to be compatible with $[Ln_4(\mathbf{L4})_3](CF_3SO_3)_{12}\cdot x H_2O\cdot y CH_3OH$ (Ln = La: $x = 8.1$,

 © 2005 Wiley-VCH Verlag GmbH & Co. KGaA, Weinheim

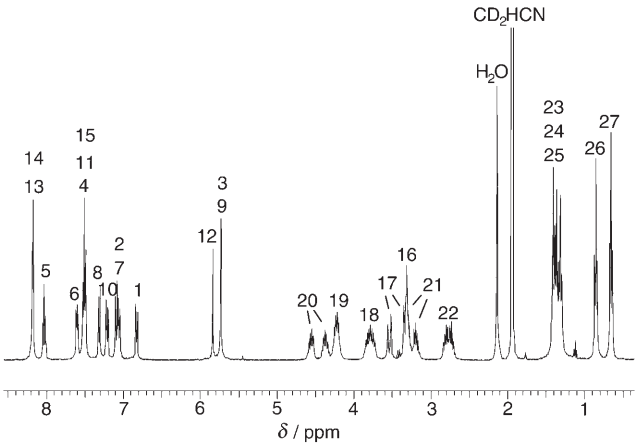

Figure 2. ^{1}H NMR spectrum of the D_3-symmetrical complex $[La_4(\mathbf{L4})_3]^{12+}$ in CD_3CN (298 K, numbering given in Scheme 1).

$y = 1.6$; Ln = Eu: $x = 5.0$, $y = 2.3$; Ln = Lu: $x = 9.6$, $y = 4.7$; see the Supporting Information). Their ESI-MS and ^{1}H NMR spectra obtained after redissolution in acetonitrile are identical with those obtained during the original titration processes (except for an extra peak in the ^{1}H NMR spectrum corresponding to CH_3OH), and slow recrystallization from methanol/diethyl ether gives prisms of $[Eu_4(\mathbf{L4})_3](CF_3SO_3)_{12}\cdot 5H_2O\cdot 5CH_3OH$ (**5**) suitable for X-ray diffraction studies.[17] The crystal structure of **5** is composed of the expected tetrametallic $[Eu_4(\mathbf{L4})_3]^{12+}$ cations together with 12 non-coordinated triflate anions and 10 interstitial solvent molecules. The pseudo-D_3-symmetrical triple-helical cation $[Eu_4(\mathbf{L4})_3]^{12+}$ shows only minor disorder that affects two peripheral ethyl groups, and its molecular structure (Figure 3a) can be best described as the packing of two terminal $\{EuN_6O_3\}$ and two central $\{EuN_9\}$ pseudo tricapped trigonal prismatic building blocks along the approximate threefold axis defined by the metal ions, as previously reported for $[Eu_3(\mathbf{L3})_3]^{9+}$.[14] The Eu–N and Eu–O bond lengths are standard, as are the bond angles (see the Supporting Information).

The four europium atoms are aligned along the pseudo threefold axis (∢Eu1···Eu2···Eu3: 170.71(1), ∢Eu2···Eu3···Eu4: 172.03(1)°) and regularly spaced by approximately 9.3 Å (Eu1···Eu2: 9.312(1), Eu2···Eu3: 9.054(1), Eu3···Eu4: 9.405(1) Å; Figure 3a). A detailed analysis of the 11 successive helical portions delimited by the 12 parallel facial planes containing the coordinated donor atoms (see Figure 3b and the Supporting Information) shows the usual tightening of the helical pitch about the complexed metal centers, and its relaxation within the intermetallic domains (see the Supporting Information). The total length of the helix amounts to 31 Å (3.1 nm according to modern semantics) for 2.22 turns (Figure 3c), which translates into an average helical pitch of 14.0 Å, comparable with 13.6 Å previously reported for the trimetallic analogous complex $[Eu_3(\mathbf{L3})_3]^{9+}$.[14]

We thus conclude that the incorporation of an additional central tridentate N_3 segment into **L3** to form **L4** is not deleterious for the extension of the helicate series and, in agreement with theoretical thermodynamic predictions, the tetrametallic complex $[Eu_4(\mathbf{L4})_3]^{12+}$ indeed dominates the speciation in solution for concentrations within the millimolar range. Its isolation in the solid state eventually demonstrates the formation of the expected linear triple-stranded helicate. Interestingly, the considerable intermetallic separation in these complexes limits destabilizing intramolecular intercationic repulsions, thus allowing the preparation of stable highly charged polymetallic cations. Although further work is required to address the exact dependence of u^{MM} and c^{eff} on the intersite separation, our novel synthetic strategy for the stepwise extension of the ligand strand offers remarkable perspectives for the design of higher homologues, a crucial

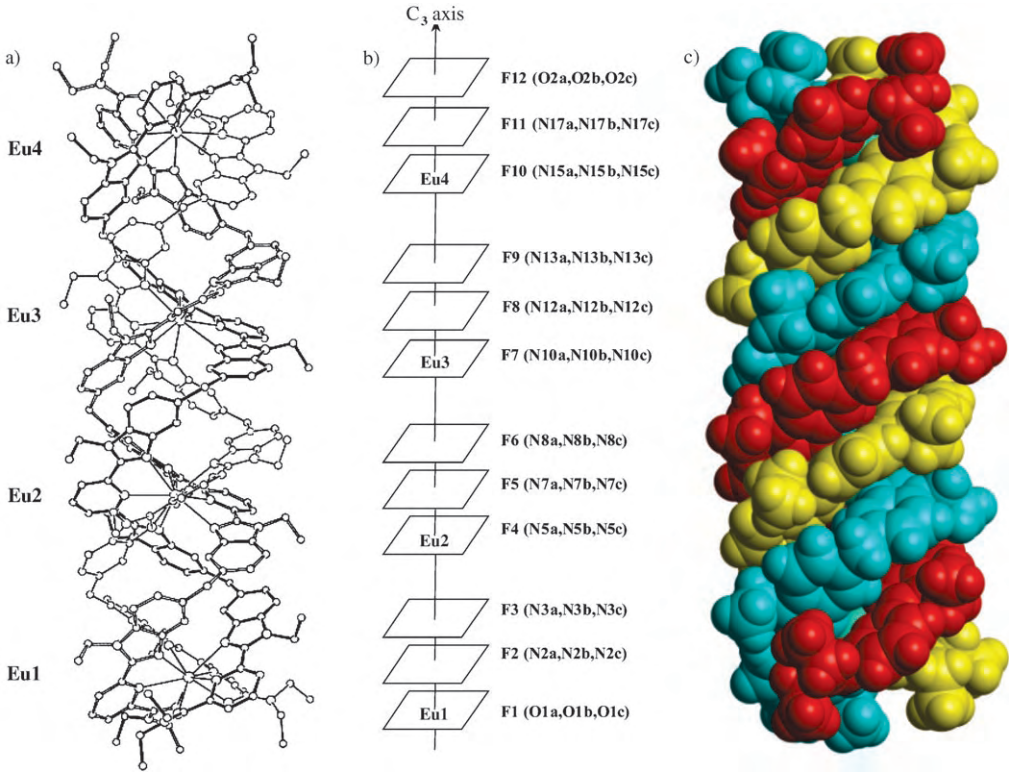

Figure 3. Perspective views of the cation $[Eu_4(\mathbf{L4})_3]^{12+}$ perpendicular to the pseudo threefold axis in the crystal structure of **5**. a) View of the metallic environments (hydrogen atoms have been omitted for clarity); b) schematic representations of the 12 facial planes containing the donor atoms; c) CPK view of the three ligand strands intertwined (represented with different colors).

© 2005 Wiley-VCH Verlag GmbH & Co. KGaA, Weinheim

point for unraveling reliable long-range intermetallic parameters (through u^{MM}) and long-range preorganization effects (through c^{eff}).

Received: August 26, 2005
Published online: November 17, 2005

Keywords: helical structures · lanthanides · polymetallic complexes · self-assembly

[1] a) C. Piguet, G. Bernardinelli, G. Hopfgartner, *Chem. Rev.* **1997**, *97*, 2005; b) M. Albrecht, *Chem. Rev.* **2001**, *101*, 3457; c) M. J. Hannon, L. J. Childs, *Supramol. Chem.* **2004**, *16*, 7.

[2] a) J.-M. Lehn, A. Rigault, *Angew. Chem.* **1988**, *100*, 1121; *Angew. Chem. Int. Ed. Engl.* **1988**, *27*, 1095; b) K. T. Potts, M. Keshavarz-K, F. S. Tham, K. A. Gheysen Raiford, C. Arana, H. D. Abruña, *Inorg. Chem.* **1993**, *32*, 5477; c) A. Marquis-Rigault, A. Dupont-Gervais, A. Van Dorsselaer, J.-M. Lehn, *Chem. Eur. J.* **1996**, *2*, 1395; d) C.-C. Wang, W.-C. Lo, C.-C. Chou, G.-H. Lee, J.-M. Chen, S.-M. Peng, *Inorg. Chem.* **1998**, *37*, 4059; e) R. Krämer, I. O. Fritsky, H. Pritzkow, L. A. Kovbasyuk, *J. Chem. Soc. Dalton Trans.* **2002**, 1307; f) C. J. Matthews, S. T. Onions, G. Morata, L. J. Davis, S. L. Heath, D. J. Price, *Angew. Chem.* **2003**, *115*, 3274; *Angew. Chem. Int. Ed.* **2003**, *42*, 3166.

[3] a) B. R. Serr, K. A. Andersen, C. M. Elliott, O. P. Anderson, *Inorg. Chem.* **1988**, *27*, 4499; b) K. T. Potts, M. Keshavarz-K, F. S. Tham, H. D. Abruña, C. Arana, *Inorg. Chem.* **1993**, *32*, 4422; c) K. T. Potts, M. Keshavarz-K, F. S. Tham, H. D. Abruña, C. Arana, *Inorg. Chem.* **1993**, *32*, 4436; d) K. T. Potts, M. Keshavarz-K, F. S. Tham, H. D. Abruña, C. Arana, *Inorg. Chem.* **1993**, *32*, 4450.

[4] J.-C. G. Bünzli, C. Piguet, *Chem. Rev.* **2002**, *102*, 1897, and references therein.

[5] a) R. Clérac, F. A. Cotton, K. R. Dunbar, C. A. Murillo, I. Pascual, X. Wang, *Inorg. Chem.* **1999**, *38*, 2655; b) J. K. Berra, K. R. Dunbar, *Angew. Chem.* **2002**, *114*, 4633; *Angew. Chem. Int. Ed.* **2002**, *41*, 4453.

[6] a) L. J. Prins, D. N. Reinhoudt, P. Timmerman, *Angew. Chem.* **2001**, *113*, 2446; *Angew. Chem. Int. Ed.* **2001**, *40*, 2382; b) A. Mulder, J. Huskens, D. N. Reinhoudt, *Org. Biomol. Chem.* **2004**, *2*, 3409, and references therein.

[7] For recent reviews, see: a) D. L. Caulder, K. N. Raymond, *Acc. Chem. Res.* **1999**, *32*, 975; b) S. Leininger, B. Olenyuk, P. J. Stang, *Chem. Rev.* **2000**, *100*, 853; c) B. J. Holliday, C. A. Mirkin, *Angew. Chem.* **2001**, *113*, 2076; *Angew. Chem. Int. Ed.* **2001**, *40*, 2022; d) M. Fujita, M. Tominaga, A. Hori, B. Therrien, *Acc. Chem. Res.* **2005**, *38*, 371.

[8] a) T. M. Garrett, U. Koert, J.-M. Lehn, *J. Phys. Org. Chem.* **1992**, *5*, 529; b) A. Pfeil, J.-M. Lehn, *J. Chem. Soc. Chem. Commun.* **1992**, 838.

[9] a) B. Perlmutter-Hayman, *Acc. Chem. Res.* **1986**, *19*, 90; b) M. Borkovec, J. Hamacek, C. Piguet, *Dalton Trans.* **2004**, 4096.

[10] For a recent review, see: C. Piguet, M. Borkovec, J. Hamacek, K. Zeckert, *Coord. Chem. Rev.* **2005**, *249*, 705.

[11] G. Ercolani, *J. Am. Chem. Soc.* **2003**, *125*, 16097.

[12] a) J. Hamacek, M. Borkovec, C. Piguet, *Chem. Eur. J.* **2005**, *11*, 5217; b) J. Hamacek, M. Borkovec, C. Piguet, *Chem. Eur. J.* **2005**, *11*, 5227.

[13] $f^{Eu}_{N_2O} = 5.9$, $f^{Eu}_{N_3} = 5.6$, $\log(u^{EuEu}) = -2.4$, $\log(u^{LL}) = -0.9$, and $\log(c^{eff}) = -0.9$; taken from Table S2 in reference [12b].

[14] S. Floquet, N. Ouali, B. Bocquet, G. Bernardinelli, D. Imbert, J.-C. G. Bünzli, G. Hopfgartner, C. Piguet, *Chem. Eur. J.* **2003**, *9*, 1860.

[15] M. Elhabiri, R. Scopelliti, J.-C. G. Bünzli, C. Piguet, *J. Am. Chem. Soc.* **1999**, *121*, 10747.

[16] Crystal data for **3**: $C_{28}H_{32}N_6O_6$, $M_r = 548.7$, $T = 200$ K, triclinic, $P\bar{1}$, $Z = 2$, $a = 8.1231(7)$, $b = 11.7582(10)$, $c = 15.4242(15)$ Å, $\alpha = 72.580(10)$, $\beta = 77.868(10)$, $\gamma = 89.854(10)°$, $V = 1367.9(2)$ Å^3; 16181 measured reflections, 5504 unique reflections ($R_{int} = 0.065$), $R = 0.039$, $\omega R = 0.038$ for 364 variables and 2764 contributing reflections ($|F_o| > 4\sigma(F_o)$). CCDC-282004 contains the supplementary crystallographic data for this paper. These data can be obtained free of charge from The Cambridge Crystallographic Data Centre via www.ccdc.cam.ac.uk/data_request/cif.

[17] Crystal data for **5**: $Eu_4C_{278}H_{288}N_{54}O_{52}S_{12}F_{36}$, $M_r = 6894.2$, $T = 200$ K, triclinic, $P\bar{1}$, $Z = 2$, $a = 16.9598(9)$, $b = 29.7098(17)$, $c = 34.8898(15)$ Å, $\alpha = 83.449(6)$, $\beta = 88.614(6)$, $\gamma = 88.695(7)°$, $V = 17457(2)$ Å^3; 113988 measured reflections, 50309 unique reflections ($R_{int} = 0.086$), $R = \omega R = 0.085$ for 3719 variables and 23103 contributing reflections ($|F_o| > 3\sigma(F_o)$). CCDC-282005 contains the supplementary crystallographic data for this paper. These data can be obtained free of charge from The Cambridge Crystallographic Data Centre via www.ccdc.cam.ac.uk/data_request/cif.

 © 2005 Wiley-VCH Verlag GmbH & Co. KGaA, Weinheim

Crown Compounds

DOI: 10.1002/anie.200502900

The Autoionization of $[TiF_4]$ by Cation Complexation with [15]Crown-5 To Give $[TiF_2([15]crown\text{-}5)][Ti_4F_{18}]$ Containing the Tetrahedral $[Ti_4F_{18}]^{2-}$ Ion**

Andreas Decken, H. Donald B. Jenkins, Carsten Knapp, Grigory B. Nikiforov, Jack Passmore,* and J. Mikko Rautiainen*

Crown ethers[1] promote the autoionization of elements and compounds leading to novel anions, driven by the complex-

[*] Prof. H. D. B. Jenkins
Department of Chemistry
University of Warwick
Coventry, CV4 7AL, West Midlands (UK)
Fax: (+44) 2476-466-747
Fax: (+44) 2476-524-112
E-mail: Don.Jenkins@warwick.ac.uk
Dr. A. Decken, Dr. C. Knapp, Dr. G. B. Nikiforov, Prof. J. Passmore, J. M. Rautiainen
Department of Chemistry
University of New Brunswick
Fredericton, N.B., E3B 6E2 (Canada)
Fax: (+1) 506-453-4981
E-mail: passmore@unb.ca

[**] We thank the Natural Science and Engineering Research Council (NSERC) of Canada for funding (J.P.), the Alexander von Humboldt Foundation in Germany for providing a Feodor Lynen Fellowship (C.K.), and the Ministry of Education in Finland for providing financial support (J.M.R.).

Supporting information (full experimental details for the preparation of **1** and full computational details) for this article is available on the WWW under http://www.angewandte.org or from the author (J.P.).

WILEY InterScience DISCOVER SOMETHING GREAT
© 2005 Wiley-VCH Verlag GmbH & Co. KGaA, Weinheim

ation energy of the corresponding cation. Examples include the autoionization of alkali metals M on reaction with crown ethers to give complexed M^+ as well as alkalides and electrides,[2] and the autoionization of main-group and transition-metal chlorides to give cationic crown ether complexes and metal chloro anions.[3] We report herein the reaction of TiF_4 and [15]crown-5 to give $[TiF_2([15]crown\text{-}5)][Ti_4F_{18}]\cdot 0.5\,MeCN$ (**1**). This is, as far as we are aware, the first autoionization of a metal fluoride on reaction with a crown ether, and suggests that this is a viable preparative route to other related binary fluoro metal anions. $[Ti_4F_{18}]^{2-}$ (Figure 1) has overall T_d symmetry and is the second example

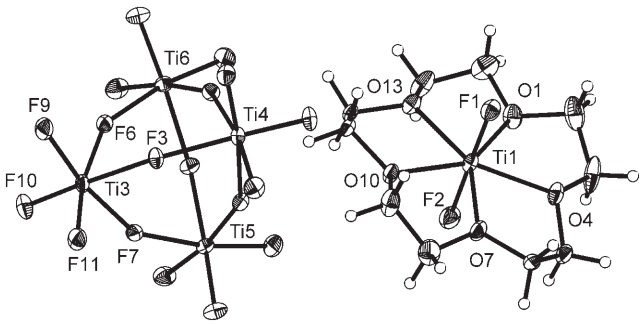

Figure 1. One of the two crystallographically independent dications and dianions in **1** (ellipsoids represent 30% thermal probability). Selected distances [Å] and angles [°]: dication: Ti1–F1 1.769(3), Ti1–F2 1.821(3), Ti1–O1 2.084(3), Ti1–O7 2.089(3), Ti1–O10 2.101(3), Ti1–O13 2.103(3), Ti1–O4 2.113(3); dianion: av $Ti-F_{terminal}$ 1.768 Å, av $Ti-F_{bridging}$ 1.987 Å, av $F_{bridging}$-Ti-$F_{bridging}$ 97.12 °, av $F_{terminal}$-Ti-$F_{terminal}$ 82.84 °.

of such a binary $[M_4X_{18}]^{2-}$ cage (M = metal, X = halogen), the first being $[W_4F_{18}]^{2-}$.[4] Its structure is related to the more-elaborate oxo complexes, for example, $[Ti_4F_{12}O_6]^{4-}$,[5] and $[Ti_4O_6(OSMe_2)_{12}]^{4+}$.[6] The related $[Ti_2F_9]^-$ ion was claimed to exist in solution,[7] and the salts $M[Ti_2F_9]$ (M = Cs, NF_4) have been reported,[8] although their X-ray crystal structures were not determined. We predict, on the basis of estimates of the corresponding energetics, that all monocation salts, with the possible exception of those having small cations, favor $[Ti_2F_9]^-$ ions, and salts of dications favor $[Ti_4F_{18}]^{2-}$ ions.

The structurally characterized binary Ti^{4+} fluorides are $[TiF_4]$,[9] $[TiF_6]^{2-}$,[10] $[TiF_7]^{3-}$,[11] $[Ti_2F_{11}]^{3-}$,[12] $[Ti_2F_{10}]^{2-}$,[13] $\{[Ti_8F_{33}]^-\}_n$,[14] and $\{[Ti_7F_{30}]^{2-}\}_n$.[15] Excess [15]crown-5 and titanium tetrafluoride react in MeCN to form $[TiF_2([15]crown\text{-}5)][Ti_4F_{18}]\cdot 0.5\,MeCN$ (**1**) in 90% yield according to reaction (1), thus effecting the autoionization of $[TiF_4]$ to $[TiF_2]^{2+}$ (stabilized by [15]crown-5) and $[Ti_4F_{18}]^{2-}$. This product is formed in contrast to the neutral adduct isolated from the reaction of $[TiF_4]$ with [18]crown-6, which yielded $[(TiF_4)_2([18]crown\text{-}6)]$.[16] This difference may be because [18]crown-6[17] has a cavity diameter of about 2.9 Å, which is large relative to the ionic diameter of Ti^{4+} (1.4 Å).[18] The diameter of the [15]crown-5 cavity is about 1.95 Å,[17] that is, slightly larger than the ionic diameter of Ti^{4+}, and hence, [15]crown-5 is well suited to promoting the formation of cationic and anionic titanium complexes.

$$5\,TiF_4 + [15]crown\text{-}5 \xrightarrow{MeCN} [TiF_2([15]crown\text{-}5)][Ti_4F_{18}]\cdot 0.5MeCN \quad (1)$$

The ^{19}F NMR spectrum of **1** formed in situ from the reaction of $[TiF_4]$ (4.2 equiv) and [15]crown-5 (1 equiv) in MeCN showed the resonance of the $[TiF_2([15]crown\text{-}5)]^{2+}$ ion at $\delta = 246.8$ ppm.[19] The X-ray crystal-structure determination (Figure 1) showed discrete $[TiF_2([15]crown\text{-}5)]^{2+}$ ions, with structure identical to that found in $[TiF_2([15]crown\text{-}5)][SbF_6]_2$,[19] and $[Ti_4F_{18}]^{2-}$ ions. This $[Ti_4F_{18}]^{2-}$ ion has almost T_d symmetry, with the four titanium atoms situated at the vertices of a tetrahedron, connected by six bridging fluorine atoms and capped by three terminal fluorine atoms each. The $Ti-F_{terminal}$ bond lengths (1.754(3)–1.777(3) Å, av 1.768 Å, 0.98 v.u. (valency units)[20]) and $Ti-F_{bridging}$ bond lengths (1.965(3)–2.010(3) Å, av 1.987 Å, 0.54 v.u.) are similar to those found in oligomeric Ti^{IV} fluoride complexes.[21] The $F_{terminal}$-Ti-$F_{terminal}$ angles (94.94(12)–98.03(13)°, av 97.12°) in **1** are greater than the $F_{bridging}$-Ti-$F_{bridging}$ angles (81.88(10)–83.40(10)°, av 82.84°), as expected from a VSEPR[22] and a ligand–ligand repulsion model.[23]

Consistent with the latter model, the $F_{bridging}\cdots F_{bridging}$ contacts (2.596(4)–2.641(3) Å) are almost equal to the $F_{terminal}\cdots F_{terminal}$ contacts (2.609(5)–2.671(4) Å) in $[Ti_4F_{18}]^{2-}$. We note that the F···F nonbonding distances in other oligomeric Ti–F complexes are very similar (e.g., $[TiF_4]$ ($F_{bridging}\cdots F_{bridging}$ 2.553–2.670 Å, $F_{terminal}\cdots F_{terminal}$ 2.603–2.638 Å),[9] $[Ti_7F_{30}]^{2-}$ ($F_{bridging}\cdots F_{bridging}$ 2.567–2.669 Å, $F_{terminal}\cdots F_{terminal}$ 2.631–2.744 Å),[15] $[TiF_6]^{2-}$(2.636 Å);[10e] the F-Ti-F angles are determined by the almost equal nonbonding F···F distances, in a similar way to various second and third row main group fluorides.[23]

To answer the question as to why $[Ti_4F_{18}]^{2-}$ and not $[Ti_2F_9]^-$ was formed, the optimized structures, vibrational spectra, and ^{19}F NMR shifts of $[Ti_2F_9]^-$ and $[Ti_4F_{18}]^{2-}$ were calculated (see Supporting Information). Unfortunately, the calculated spectroscopic properties were very similar for both anions. The similarity of spectroscopic properties is related to the similarity in the structures of $[Ti_2F_9]^-$ and $[Ti_4F_{18}]^{2-}$ from the perspective of the environments around the titanium and fluorine atoms, and a completely unambiguous distinction between the two is only possible experimentally by X-ray diffraction.

The calculated values of ΔH^{298} and ΔG^{298} for reactions (2)–(5) are given in Table 1. The formation of two $[Ti_2F_9]^-$ ions is favored in the gas phase over dimerization to the $[Ti_4F_{18}]^{2-}$ ion. The situation is less clear for solutions in acetonitrile and dichloromethane, and most likely both anions exist in equilibrium. The energetics in the solid state were estimated by using the equation of Jenkins et al. and applying the "volume-based" thermodynamic (VBT) approach.[24,25] Dimerization to the $[Ti_4F_{18}]^{2-}$ ion and formation of $[TiF_2([15]crown\text{-}5)][Ti_4F_{18}]$ is strongly favored in the solid state over the hypothetical $[TiF_2([15]crown\text{-}5)][Ti_2F_9]_2$ salt of the $[Ti_2F_9]^-$ ion, thus the $[Ti_4F_{18}]^{2-}$ ion is lattice-stabilized in the solid state.[26]

To investigate which conditions promote the formation of a stable salt of $[Ti_2F_9]^-$, the $\Delta H^{298}{}_{(s)}$ ($\approx \Delta G^{298}{}_{(s)}$) values of reactions (6) and (7) for salts containing mono- and dications of different sizes were compared (Figure 2).

 © 2005 Wiley-VCH Verlag GmbH & Co. KGaA, Weinheim

Table 1: Calculated and estimated thermodynamic enthalpies and free energies [kJ mol^{-1}] of the $[Ti_2F_9]^-$ and $[Ti_4F_{18}]^{2-}$ ions for the gas-phase, solid-state (as salts of $[TiF_2([15]crown-5)]$),[a,b] and solution dimerization[c] reactions.[d]

	Reaction	$\Delta G(n)^{298}$	$\Delta H(n)^{298}$
(2)	$2\,[Ti_2F_9]^-_{(g)} \rightarrow [Ti_4F_{18}]^{2-}_{(g)}$ [e]	215	160
(3)	$[TiF_2([15]crown-5)][Ti_2F_9]_{2(s)} \rightarrow [TiF_2([15]crown-5)][Ti_4F_{18}]_{(s)}$		−216
(4)	$2\,[Ti_2F_9]^- \rightarrow [Ti_4F_{18}]^{2-}$ (in MeCN)	−4[c]	
(5)	$2\,[Ti_2F_9]^- \rightarrow [Ti_4F_{18}]^{2-}$ (in CH_2Cl_2)	19[c]	

[a] $U_{lattice}\{[TiF_2([15]crown-5)][Ti_2F_9]_{2(s)}\}$ 1289 ± 5 kJ mol^{-1} (see Supporting Information). [b] $U_{lattice}\{[TiF_2([15]crown-5)][Ti_4F_{18}]_{(s)}\}$ 1665 ± 6 kJ mol^{-1} (see Supporting Information). [c] C-PCM solvation model. [d] Details for the estimation of the energetics in all three phases are included in the Supporting Information. [e] We note that the number of bridging and terminal bonds in $2\,[Ti_2F_9]^-$ and $[Ti_4F_{18}]^{2-}$ are the same. Thus the reaction is isodesmic and therefore the calculated energy is of good accuracy, ± ca. 10 kJ mol^{-1}. It is not trivial to establish the absolute error in such calculations. However, borderline cases of this kind can be used to obtain upper or lower limits of the gas phase calculated values, e.g. in the dimerization of $2\,S_2^+$ to S_4^{2+}.[35]

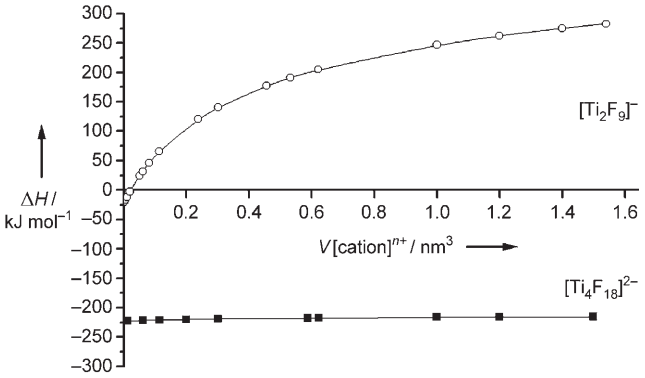

Figure 2. Plot of ΔH ($\approx \Delta G$) versus $V([cation]^{n+})$ for reactions (6) (○, $n=1$) and (7) (■, $n=2$). The data used in the calculation of this plot are included with the Supporting Information.

$$2\,[cation]^+[Ti_2F_9]^-_{(s)} \rightarrow [cation]^+_2[Ti_4F_{18}]^{2-}_{(s)} \quad (6)$$

$$[cation]^{2+}[Ti_2F_9]^-_{2\,(s)} \rightarrow [cation]^{2+}[Ti_4F_{18}]^{2-}_{(s)} \quad (7)$$

The VBT approach suggests that the monocations generally favor the formation of [cation][Ti_2F_9] (since $\Delta H(6)$ ($\approx \Delta G(6)$) is usually >0), whereas dications favor [cation]-[Ti_4F_{18}] (since $\Delta H(7)$ ($\approx \Delta G(7)$) <0, i.e., negative and almost independent of the size of the cation). We predict that the previously reported $[NF_4][Ti_2F_9]$ salt[8] ($\Delta G(6) = 32 \pm (10 + x)$ kJ mol^{-1} [x = uncertainty in the calculated dimerization energy of $2[Ti_2F_9]^-_{(g)}$ according to reaction (2)]) probably contains $[Ti_2F_9]^-$ ions; for $Cs[Ti_2F_9]$[8] ($\Delta G(6) = -3 \pm (10 + x)$ kJ mol^{-1}), however, with its slightly smaller Cs^+ ion, it is still an open question as to which anion is present. Notwithstanding borderline cases, this approach has the potential for rationalizing the underlying thermodynamics of related systems and to guide the synthesis of hitherto unknown anions.

Experimental Section

1: A solution of [15]crown-5 (0.54 g, 0.49 mL, 2.5 mmol) in MeCN (20 mL) was added to a solution of $[TiF_4]$ (1.244 g, 10.0 mmol) in MeCN (20 mL). Concentration of the resulting transparent mixture to approximately 20 mL and storage at room temperature for a period of several hours afforded colorless crystals (1.58 g, 90%). Elemental analysis (%): calcd for $C_{22}H_{43}F_{40}NO_{10}Ti_{10}$: C 15.34, H 2.50, Ti 27.90, F 44.14, N 0.81; found: C 15.47, H 2.40, Ti 27.10, F 43.54, N 0.82. Decomposition occurred above 120 °C without melting; ^{1}H NMR (400 MHz, MeCN, RT): $\delta = 4.61$ ppm (s, *trans*-$[TiF_2([15]crown-5)]^{2+}$); ^{19}F NMR (376.3 MHz, MeCN, RT): $\delta = 262.8$ (m, $12\,F_{terminal}$, $[Ti_4F_{18}]^{2-}$), 246.8 (s, 2F, *trans*-$[TiF_2([15]crown-5)]^{2+}$), −21.6 ppm (m, $6\,F_{bridging}$, $[Ti_4F_{18}]^{2-}$).

Data were collected on a Bruker AXS P4/SMART 1000 diffractometer ($\lambda(Mo_{K\alpha}) = 0.71073$ Å) by using ω and θ scans. The structure was solved by direct methods and refined against F^2 with non-hydrogen atoms anisotropic and hydrogen atoms in a riding model. The data were reduced (SAINT)[27] and corrected for absorption (SADABS).[28] All calculations were carried out with SHELXTL software,[29] and the structural drawing was prepared by using Diamond.[30] Crystallographic data for **1** ($C_{11}H_{21.50}F_{20}N_{0.50}O_5Ti_5$) at 198 K: $M_r = 860.29$, crystal dimensions $0.30 \times 0.275 \times 0.275$ mm^3, monoclinic, space group $P2_1/c$, $a = 8.3335(9)$, $b = 41.887(5)$, $c = 16.4117(18)$ Å, $\beta = 103.927(2)°$, $V = 5560.4(11)$ Å^3, $Z = 8$, $\rho_{calcd} = 2.055$ Mg m^{-3}, $\mu = 1.531$ mm^{-1}, of 28675 reflections measured ($2.33 < \theta < 25.00°$), 9761 were independent ($R_{int} = 0.0277$), $wR2 = 0.1445$ (all data), $R1 = 0.0482$ (for 7181 reflections with $I > 2\sigma(I)$), 734 parameters, GOF = 1.073. CCDC-272157 contains the supplementary crystallographic data. These data can be obtained free of charge from the Cambridge Crystallographic Data Centre via www.ccdc.cam.ac.uk/data_request/cif.

All theoretical calculations were performed by using the Gaussian 03 program[31] and the MPW91PW91 DFT functional[32] with the NASA AMES cc-pVTZ basis set[33] for titanium and the aug-cc-pVDZ basis set[34] (aug-cc-pVTZ for energy calculations) for fluorine. Solution energetics in acetonitrile and dichloromethane were calculated by using the C-PCM solvation model as implemented in Gaussian 03.[31] Details for all calculations are included in the Supporting Information.

Received: August 15, 2005
Published online: November 22, 2005

Keywords: anions · crown compounds · density functional calculations · fluorides · titanium

[1] See for review: G. W. Gokel, *Monographs in Supramolecular Chemistry, No. 4 Crown Ethers and Cryptands*, The Royal Society of Chemistry, Cambridge, **1994**.
[2] a) S. B. Dawes, D. L. Ward, O. Fussa-Rydel, R.-H. Huang, J. L. Dye, *Inorg. Chem.* **1989**, *28*, 2132–2136; b) R.-H. Huang, J. L. Eglin, S. Z. Huang, L. E. H. McMills, J. L. Dye, *J. Am. Chem. Soc.* **1993**, *115*, 9542–9546.
[3] V. K. Belsky, B. M. Bulychev, *Russ. Chem. Rev.* **1999**, *68*, 119–135; *Uspekhi Khimii* **1999**, *68*, 136–153, and references therein.
[4] T. S. Cameron, T. M. Klapötke, A. Schulz, J. Valkonen, *J. Chem. Soc. Dalton Trans.* **1993**, 659–662.
[5] J. Sala-Pala, J. Guerchais, A. Edwards, *Angew. Chem.* **1982**, *94*, 876–877; *Angew. Chem. Int. Ed. Engl.* **1982**, *21*, 870–871.
[6] S. Rabe, U. Müller, *Z. Naturforsch. B* **1997**, *52*, 1291–1295.
[7] a) J. A. Chandler, J. E. Wuller, R. S. Drago, *Inorg. Chem.* **1962**, *1*, 65–69; b) J. A. Chandler, R. S. Drago, *Inorg. Chem.* **1962**, *1*, 356–358; c) P. A. W. Dean, *Can. J. Chem.* **1973**, *51*, 4024–4030.
[8] K. O. Christe, C. J. Schack, *Inorg. Chem.* **1977**, *16*, 353–360.
[9] H. Bialowons, M. Müller, B. G. Müller, *Z. Anorg. Allg. Chem.* **1995**, *621*, 1227–1231.
[10] O. Göbel, *Acta Crystallogr. Sect. A* **2000**, *56*, 521–522.

 © 2005 Wiley-VCH Verlag GmbH & Co. KGaA, Weinheim

[11] a) B. Hofmann, *Z. Anorg. Allg. Chem.* **1979**, *458*, 151 – 162; b) R. Weiss, J. Fischer, B. Chevrier, *Acta Crystallogr.* **1967**, *23*, 1948 – 1953.

[12] L.-Q. Tang, M. S. Dadachov, X.-D. Zou, *Z. Kristallogr. New Cryst. Struct.* **2001**, *216*, 387 – 388.

[13] a) M. S. Dadachov, L.-Q. Tang, X.-D. Zou, *Z. Kristallogr. New Cryst. Struct.* **2000**, *215*, 605 – 606; b) H. Akutsu, K. Ozeki, T. Ozaki, K. Nozawa, M. Kinoshita, K. Kozawa, T. Uchida, *Bull. Chem. Soc. Jpn.* **1996**, *69*, 1869 – 1873.

[14] H. Bialowons, B. G. Müller, *Z. Anorg. Allg. Chem.* **1995**, *621*, 1223 – 1226.

[15] B. G. Müller, *J. Fluorine Chem.* **1981**, *17*, 489 – 499.

[16] T. S. Cameron, A. Decken, E. G. Ilyin, G. B. Nikiforov, J. Passmore, *Eur. J. Inorg. Chem.* **2004**, 3865 – 3872, and references therein.

[17] a) H. K. Frensdorff, *J. Am. Chem. Soc.* **1971**, *93*, 600 – 606; b) J. J. Christensen, D. J. Eatough, R. M. Izatt, *Chem. Rev.* **1974**, *74*, 351 – 384.

[18] L. Pauling, *The Nature of the Chemical Bond, 3rd ed.*, Cornell University Press, Ithaca N.Y., **1960**, p. 514.

[19] A. Decken, E. G. Ilyin, H. D. B. Jenkins, G. B. Nikiforov, J. Passmore, *Dalton. Trans.* **2005**, 3039 – 3050

[20] The values used (i.e., Ti–F $R_o = 1.76$, $B = 0.37$) are available from: a) I. D. Brown, *The Chemical Bond in Inorganic Chemistry—The Bond Valence Model*, Oxford, **2002**; and b) http://ccp14.sims.nrc.ca/ccp/web-mirrors/i_d_brown/bond_valence_param/.

[21] a) H. W. Roesky, I. Haiduc, *J. Chem. Soc. Dalton Trans.* **1999**, 2249 – 2264; b) E. F. Murphy, R. Murugavel, H. W. Roesky, *Chem. Rev.* **1997**, *97*, 3425 – 3468.

[22] R. J. Gillespie, I. Hargittai, *The VSEPR Model of Molecular Geometry*, Allyn and Bacon, Boston, **1991**.

[23] a) E. A. Robinson, R. J. Gillespie, *Inorg. Chem.* **2003**, *42*, 3865 – 3872; b) R. J. Gillespie, E. A. Robinson, *Chem. Soc. Rev.* **2005**, *34*, 396 – 407.

[24] a) H. D. B. Jenkins, H. K. Roobottom, J. Passmore, L. Glasser, *Inorg. Chem.* **1999**, *38*, 3609 – 3620; b) H. D. B. Jenkins, D. Tudela, L. Glasser, *Inorg. Chem.* **2002**, *41*, 2364 – 2367.

[25] H. D. B. Jenkins, L. Glasser, *J. Am. Chem. Soc.* **2004**, *126*, 15809 – 15817, and references therein.

[26] A similar situation has been found in other doubly charged ions, for example, $[S_2I_4][MF_6]_2$ (M = As, Sb); see: S. Brownridge, T. S. Cameron, H. Du, C. Knapp, R. Köppe, J. Passmore, J. M. Rautiainen, H. Schnöckel, *Inorg. Chem.* **2005**, *44*, 1660 – 1671.

[27] *SAINT 6.02*, **1997–1999**, Bruker AXS, Inc., Madison, Wisconsin, USA.

[28] *SADABS*, G. Sheldrick, **1999**, Bruker AXS, Inc., Madison, Wisconsin, USA.

[29] *SHELXTL 5.1*, G. Sheldrick, **1997**, Bruker AXS, Inc., Madison, Wisconsin, USA.

[30] *Diamond 3.0c*, Crystal Impact, Bonn, Germany.

[31] *Gaussian 03*, *Revision C.02*, M. J. Frisch et al., Gaussian, Inc., Wallingford CT, **2004**.

[32] a) C. Adamo, V. Barone, *Chem. Phys. Lett.* **1997**, *274*, 242 – 250; b) C. Adamo, V. Barone, *J. Chem. Phys.* **1998**, *108*, 664 – 675.

[33] a) C. W. Bauschlicher, Jr., *Theor. Chem. Acc.* **1999**, *103*, 141 – 145; b) C. W. Bauschlicher, Jr., *Theor. Chim. Acta* **1995**, *92*, 183 – 198.

[34] a) R. A. Kendall, T. H. Dunning, Jr., R. J. Harrison, *J. Chem. Phys.* **1992**, *96*, 6796 – 6806; b) T. H. Dunning, Jr., *J. Chem. Phys.* **1989**, *90*, 1007 – 1023.

[35] a) T. S. Cameron, I. Dionne, H. D. B. Jenkins, S. Parsons, J. Passmore, H. K. Roobottom, *Inorg. Chem.* **2000**, *39*, 2042 – 2052; b) H. D. B. Jenkins, L. C. Jitariu, I. Krossing, J. Passmore, R. Suontamo, *J. Comput. Chem.* **2000**, *21*, 218 – 226.

 © 2005 Wiley-VCH Verlag GmbH & Co. KGaA, Weinheim

Multicomponent Arylation

DOI: 10.1002/anie.200502636

Phenol Ugi–Smiles Systems: Strategies for the Multicomponent N-Arylation of Primary Amines with Isocyanides, Aldehydes, and Phenols

Laurent El Kaïm, Laurence Grimaud,* and Julie Oble*

Since the pioneering work of Passerini and Ugi, the use of isocyanides has been strongly associated with the success achieved by multicomponent reactions (MCRs) in the creation of molecular diversity.[1] The high efficiency of isocyanides in MCRs lies in their ability to create bonds in a reversible manner by extending their valence. In the Ugi four-component reaction (U-4CR), equilibria between primary amines, isocyanides, carbonyl compounds, and carboxylic acids are displaced by a final irreversible Mumm-type rearrangement (Scheme 1).

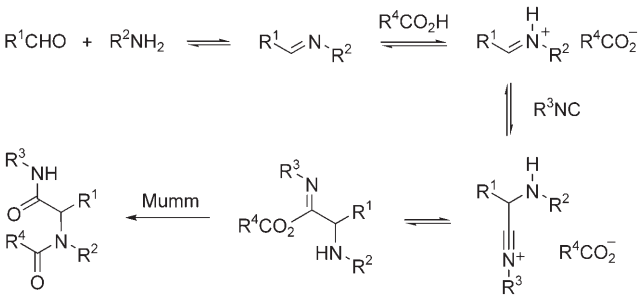

Scheme 1. Ugi reaction mechanism.

The replacement of the carboxylic acid by other acidic compounds has found limited success since the discovery of the reaction. The ideal surrogate for the carboxylic acid should be sufficiently acidic to activate the imine toward the moderately nucleophilic isocyanide, and its counter anion should give a reversible addition to the nitrilium intermediate and induce an irreversible rearrangement in the final step. Ultimately, the acidic compound has to be integrated in the structure so that the final adduct retains sufficient stability (to heat, and for compounds of biological interest, to enzymatic hydrolysis).

Besides carboxylic acids, the most useful acidic components (water, hydrazoic acid, carbonic acid monoesters,

[*] Dr. L. El Kaïm, Dr. L. Grimaud, J. Oble
Laboratoire de Chimie Organique, UMR CNRS 7652
Ecole Nationale Supérieure des Techniques Avancées
32 Bd Victor, 75015 Paris (France)
Fax: (+33) 1-4552-8322
E-mail: laurent.elkaim@ensta.fr
laurence.grimaud@ensta.fr

Supporting information for this article is available on the WWW under http://www.angewandte.org or from the author.

© 2005 Wiley-VCH Verlag GmbH & Co. KGaA, Weinheim

hydrogen sulfide, hydrogen selenide, cyanate,[2] thiocyanate,[2] and thiosulfate[2])[3] were examined by Ugi shortly after his description of the U-4CR process. Recently, in analogy to the formation of carbonic acid from CO_2 and alcohols, COS and CS_2 have also been employed for the preparation of thio derivatives.[4] More significantly, the use of thio acids has led to some elegant heterocyclic syntheses.[5] There has since been no major development in this direction.

The scope of MCRs using isocyanides has been widely extended through the intramolecular trapping of the nitrilium intermediates. Among the most recent and useful examples, the [4+1] cycloaddition of 2-iminopyridines[6] and the formation of isoxazole from isocyanoacetamides[7] are worth noting. In these cases, intramolecular conditions and final aromatization allow good yields even with nucleophiles that perform poorly in the normal U-4CR process (oxygen atoms of amides for instance). However, their intramolecular nature limits the scope of these reactions to three-component couplings with a consequent lower molecular diversity.[8] Herein, we report a highly flexible multicomponent reaction between electron-deficient phenols, amines, carbonyl compounds, and isocyanides to form *N*-aryl amines in phenol Ugi–Smiles systems.

While searching for new acidic partners in the Ugi reaction, we thought that a suitable electron-withdrawing group on a phenol could trigger both the imine activation and the irreversible rearrangement in the key step of the reaction. Indeed, we were delighted to find that *o*-nitrophenol reacts with cyclohexyl isocyanide (1 equiv), *p*-chlorobenzylamine (1 equiv), and propionaldehyde (1 equiv) by a very efficient four-component reaction. This reaction proceeds smoothly at 40 °C in methanol (1 M) within a few hours to provide the desired *N*-aryl amine **1** in 74 % yield (Scheme 2).

The high yield, simple reaction protocol, and originality of this tandem process prompted us to explore the reaction more widely (Table 1). Aliphatic aldehydes are good substrates for this process and react with various amines and isocyanides. Aromatic aldehydes give the expected adducts in moderate

Table 1: The reagents used in the multicomponent reactions and the resulting products.

Entry	RCHO	Amine	RNC	Phenol	Reaction time	Product	Yields[%][a]
1	EtCHO	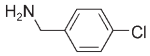	BnNC	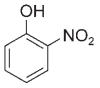	4 h	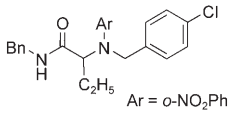	96
2	$C_6H_{13}CHO$	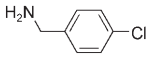	*t*BuNC	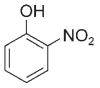	4 h	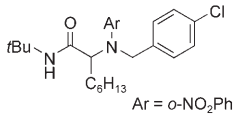	79
3	EtCHO	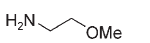	CyNC	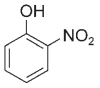	4 h	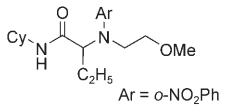	71
4							35
5	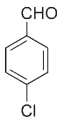	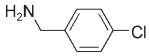	CyNC	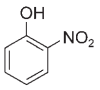	20 h	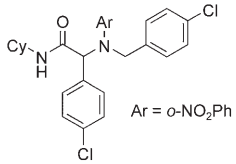	73[b]
6	EtCHO	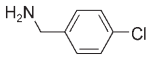	CyNC	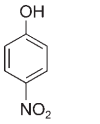	16 h	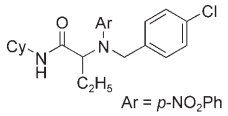	72
7	*i*BuCHO		*t*BuNC	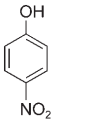	48 h	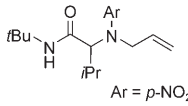	98[c]
8	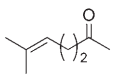	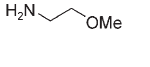	CyNC	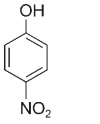	10 days	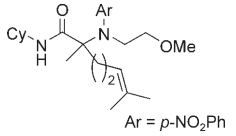	46[c]
9		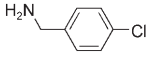	CyNC	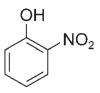	6 days	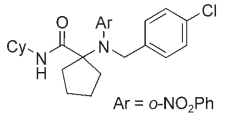	33[c]

[a] Yields of isolated product. [b] A catalytic amount (15 mol %) of $MgClO_4$ was added. [c] The mixture was heated at 60 °C in methanol. Cy = cyclohexyl.

 © 2005 Wiley-VCH Verlag GmbH & Co. KGaA, Weinheim

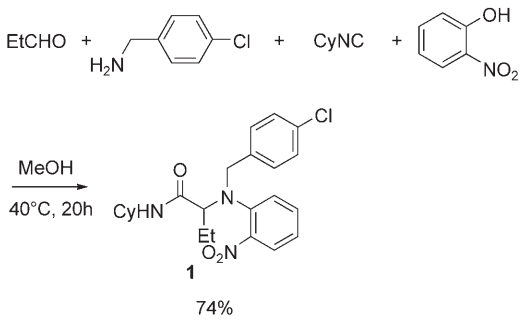

Scheme 2. Multicomponent N-arylation of chlorobenzylamine with nitrophenol. Cy = cyclohexyl.

yields under these conditions. However, the use of a catalytic amount (15 mol %) of magnesium perchlorate improves the yield considerably (entries 4 and 5, Table 1). *p*-Nitrophenol, which has a comparable acidity, undergoes this coupling process equally efficiently (entries 6 and 7, Table 1). Ketones are less reactive than aldehydes and need much longer reaction times to afford the desired products in moderate yield (entries 8 and 9, Table 1).

Although no detailed mechanistic studies have been carried out, a reaction sequence leading to *N*-aryl amines can be proposed (Scheme 3). It seems that the acidity of nitrophenols (pK_a values from 7 to 9) provokes sufficient

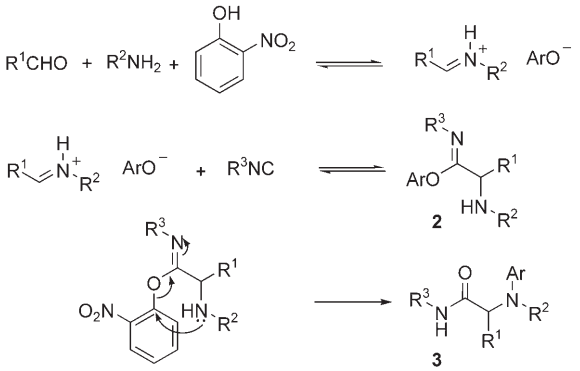

Scheme 3. Proposed mechanism for the phenol Ugi–Smiles reaction.

protonation of the imine to induce isocyanide addition. The phenoxide is nucleophilic enough to trap the resulting nitrilium intermediate, thus forming imidate **2**. At 40 °C, the latter undergoes a Smiles rearrangement[9] to provide the more stable *N*-aryl amine **3** (Scheme 3). This last rearrangement probably constitutes the only irreversible step in the whole process, and drives all the preceding equilibria toward the desired product in high yields.

Imidates are known to undergo a Mumm-type rearrangement or an electrocyclic reaction (in the case of hydrazoic acid).[10] However, to the best of our knowledge, this reaction constitutes the first example of a Smiles rearrangement intervening in an Ugi-type reaction. Moreover, the reaction can be extended to other weak phenolic acids. As an example, the reaction of methyl salicylate, propionaldehyde, cyclohexyl isocyanide, and *p*-chlorobenzylamine provides the desired *N*-aryl amine in 74 % yield (Scheme 4). The reaction proceeds smoothly in methanol at 60 °C within 2 days. This result indicates that a wide range of phenols could participate successfully in this new four-component reaction.

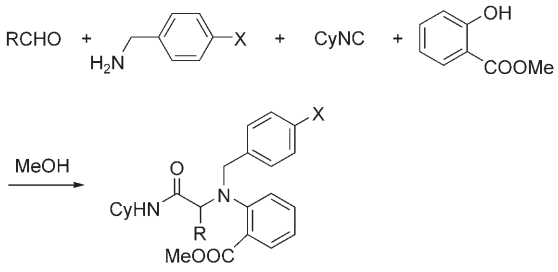

R = Et	X = Cl	40°C, 16h	38%
		40°C, 48h	57%
		60°C, 48h	74%
R = *i*Bu	X = OMe	60°C, 48h	76%

Scheme 4. Salicylic ester as the phenol in the Ugi–Smiles reaction. Cy = cyclohexyl.

The presence of the nitro or ester group on the final adduct allows interesting applications to heterocyclic synthesis. Thus, we accomplished an efficient one-pot synthesis of benzopyrazinone **4** by hydrogenolysis (H_2, Pd/C, methanol) and subsequent acidic cyclization (*para*-toluenesulfonic acid (TsOH), methanol) of the aryl amine **5** (Scheme 5).

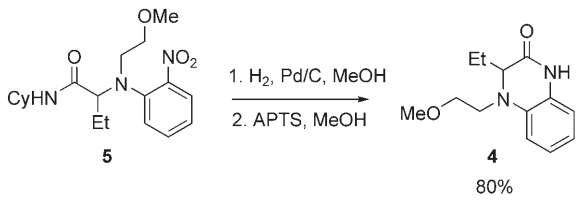

Scheme 5. Application to the synthesis of benzopyrazinone. Cy = cyclohexyl.

In conclusion, we have developed a novel and very efficient four-component reaction from readily available substrates. The creation of four bonds that should be reasonably resistant to hydrolysis makes this process particularly attractive for the design of pharmaceutical and agrochemical libraries. Moreover, a straightforward elaboration of these adducts gives easy access to various heterocyclic structures. Further studies are under way to examine more thoroughly the scope and limitations of this MCR system.

Experimental Section

Synthesis of benzopyrazinone **4**: 2-Methoxy-1-ethylamine (1.0 equiv), cyclohexyl isocyanide (1.0 equiv), and *o*-nitrophenol (1.0 equiv) were added to a solution of propionaldehyde in methanol (1 M). The resulting mixture was stirred at 40 °C under an inert atmosphere for 20 h and concentrated in vacuo. The crude product was then purified by flash chromatography on silica gel.

 © 2005 Wiley-VCH Verlag GmbH & Co. KGaA, Weinheim

A catalytic amount of Pd/C (10%) was added to a solution of the resulting aryl amine in methanol (0.3 M), and the mixture was stirred at room temperature (RT) under a hydrogen atmosphere for 24 h. Hydrogen was then replaced by argon and a catalytic amount of *p*-toluenesulfonic acid was added. The resulting mixture was stirred at RT for 24 h. After addition of a saturated aqueous solution of $NaHCO_3$, filtration, and extraction with diethyl ether, the combined organic layers were washed with brine, dried over anhydrous $MgSO_4$, filtered, and concentrated in vacuo. The crude product was purified by flash chromatography on silica gel (80:20 ether/petroleum ether) to give the desired benzopyrazinone **4** in 81% yield. ^{1}H NMR ($CDCl_3$, 400 MHz): $\delta = 8.62$ (br s, 1H), 7.02–6.96 (m, 1H), 6.80–6.70 (m, 3H), 3.86 (t, 1H, $J = 6.8$ Hz), 3.73–3.63 (m, 1H), 3.57 (t, 2H, $J = 6.8$ Hz), 3.37 (s, 3H), 3.41–3.31 (m, 1H), 1.72–1.60 (m, 2H), 0.95 ppm (t, 3H, $J = 7.3$ Hz). ^{13}C NMR ($CDCl_3$, 100.6 MHz): $\delta = 168.9$, 134.2, 126.7, 124.5, 119.1, 115.9, 113.5, 70.5, 64.6, 59.4, 50.1, 24.1, 10.4 ppm. IR (thin film): $\tilde{\nu} = 3200$, 2925, 1675, 1117, 745 cm^{-1}. MS (DI, CI NH_3) *m*/*z* 235.

Received: July 27, 2005
Published online: November 15, 2005

Keywords: amines · arylation · multicomponent reaction · phenols · rearrangement

[1] For recent reviews, see: a) L. Banfi, R. Riva, *Org. React.* **2005**, *65*, 1–140; b) J. Zhu, *Eur. J. Org. Chem.* **2003**, 1133–1144; c) I. Ugi, B. Werner, A. Dömling, *Molecules* **2003**, *8*, 53–66; d) C. Hulme, V. Gore, *Curr. Med. Chem.* **2003**, *10*, 51–80; e) H. Bienaymé, C. Hulme, G. Oddon, P. Schmitt, *Chem. Eur. J.* **2000**, *6*, 3321–3329; f) A. Dömling, I. Ugi, *Angew. Chem.* **2000**, *112*, 3300–3344; *Angew. Chem. Int. Ed.* **2000**, *39*, 3168–3210.

[2] These salts are usually added to the reaction mixture in association with amine hydrochlorides; see ref. [3c].

[3] a) I. Ugi, R. Meyr, U. Fetzer, C. Steinbrückner, *Angew. Chem.* **1959**, *71*, 386; b) I. Ugi, C. Steinbrückner, *Angew. Chem.* **1960**, *72*, 267–268; c) I. Ugi, F. K. Rosendahl, F. Bodesheim, *Justus Liebigs Ann. Chem.* **1963**, *666*, 54–61; d) I. Ugi, *Angew. Chem.* **1962**, *74*, 9–22; *Angew. Chem. Int. Ed. Engl.* **1962**, *1*, 8–21.

[4] T. A. Keating, R. W. Armstrong, *J. Org. Chem.* **1998**, *63*, 867–871.

[5] S. Heck, A. Dömling, *Synlett* **2000**, 424–426.

[6] a) H. Bienaymé, K. Bouzid, *Angew. Chem.* **1998**, *110*, 2349–2352; *Angew. Chem. Int. Ed.* **1998**, *37*, 2234–2237; b) C. Blackburn, B. Guan, P. Fleming, K. Shiosaki, S. Tsai, *Tetrahedron Lett.* **1998**, *39*, 3665–3668; c) K. Groebke, L. Weber, F. Mehlin, *Synlett* **1998**, 661–663.

[7] a) X. Sun, P. Janvier, G. Zhao, H. Bienaymé, J. Zhu, *Org. Lett.* **2001**, *3*, 877–880; b) P. Janvier, X. Sun, H. Bienaymé, J. Zhu, *J. Am. Chem. Soc.* **2002**, *124*, 2560–2567; c) A. Fayol, J. Zhu, *Angew. Chem.* **2002**, *114*, 3785–3787; *Angew. Chem. Int. Ed.* **2002**, *41*, 3633–3635.

[8] If tandem reactions using the heterocyclic core are involved, more components can be included in the process; see ref. [7b,c].

[9] For examples of Smiles rearrangements, see: a) J. F. Bunnet, R. E. Zahler, *Chem. Rev.* **1951**, *49*, 273–308; b) N. Selvakumar, D. Srinivas, A. M. Azhagan, *Synthesis* **2002**, 2421–2425; c) L. H. Mitchell, N. C. Barvian, *Tetrahedron Lett.* **2004**, *45*, 5669–5671; d) V. J. Huber, R. A. Bartsch, *Tetrahedron* **1998**, *54*, 9281–9288.

[10] Formation of tetrazoles when performing Ugi reactions with azides involves the cyclization of an azidoimidoyl intermediate. For a recent example using $TMSN_3$ (trimethylsilyl azide), see: T. Nixey, M. Kelly, D. Semin, C. Hulme, *Tetrahedron Lett.* **2002**, *43*, 3681–3684.

 © 2005 Wiley-VCH Verlag GmbH & Co. KGaA, Weinheim

Organogels

DOI: 10.1002/anie.200502809

Gelation of Helical Polypeptide–Random Coil Diblock Copolymers by a Nanoribbon Mechanism**

Kyoung Taek Kim, Chiyoung Park, Guido W. M. Vandermeulen, David A. Rider, Chulhee Kim, Mitchell A. Winnik, and Ian Manners**

The polypeptide poly(γ-benzyl-L-glutamate) (PBLG) serves as a model rod-like polymer in solution and in the solid state because of its rigid α-helix conformation.[1,2] The stiff rod-like conformation of the PBLG helix is a crucial prerequisite for its unique solution behavior such as liquid crystalline ordering[3,4] and thermoreversible gelation.[5] Nematic ordering (orientational order of rod-like molecules) is responsible for the thermoreversible gelation of PBLG in dilute solution. Diblock copolymers of PBLG and flexible organic polymers are unable to form a nematic phase due to the presence of a block with a bulky random-coil conformation. Here we report the discovery of thermoreversible gelation of diblock copolymers of PBLG in dilute solution which has not been observed previously despite many studies of such materials.[6] We also explain the gel formation of PBLG-based diblock copolymers in solution by a mechanism which is distinct from the current understanding of PBLG self-assembly.[7] Based on our findings, we describe the formation of self-assembled functional scaffolds with precisely aligned fluorescent labels. The results illustrate a novel and general mode of self-assembly for block copolymers of PBLG and presumably other helical polypeptides and demonstrate an attractive new approach to nanostructured supramolecular materials derived from biological and synthetic polymers.

Our initial studies involved the synthesis of poly(ferrocenylsilane)-*b*-poly(γ-benzyl-L-glutamate) (PFS-*b*-PBLG), conjugates of an organometallic polymer and polypeptides with narrow molecular weight distributions (Figure 1a, Table 1).

[*] K. T. Kim, G. W. M. Vandermeulen, D. A. Rider, Prof. M. A. Winnik, Prof. I. Manners
Department of Chemistry
University of Toronto
80 St. George Street, Toronto, Ontario M5S 3H6 (Canada)
Fax: (+1) 416-978-6157
E-mail: mwinnik@chem.utoronto.ca
imanners@chem.utoronto.ca
C. Park, Prof. C. Kim
Hyperstructured Organic Materials Research Center
Department of Polymer Science and Engineering
Inha University
Incheon 402-751 (South Korea)

[**] This work was supported by the Emerging Materials Network of Materials and Manufacturing Ontario. K.T.K. thanks Jian Yang for the fluorescence experiments. C.K. and C.P. thank HOMRC for support. G.V. thanks the Deutsche Forschungsgemeinschaft (DFG) for a postdoctoral research scholarship. I.M. thanks the Canadian Government for a Research Chair.

 WILEY InterScience DISCOVER SOMETHING GREAT

© 2005 Wiley-VCH Verlag GmbH & Co. KGaA, Weinheim

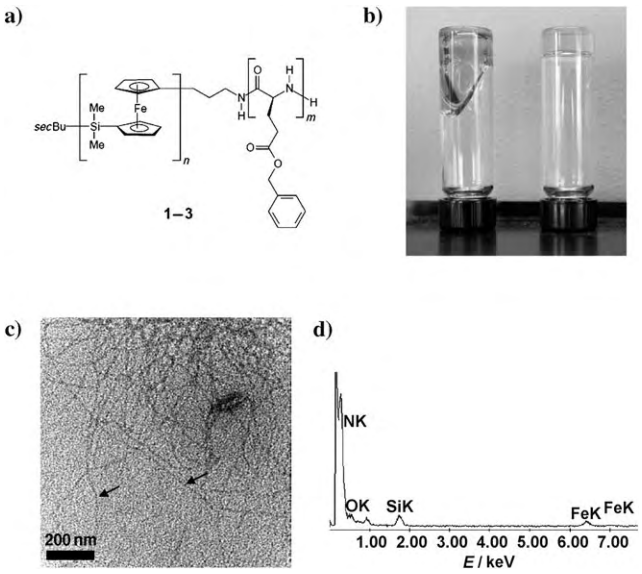

Figure 1. a) Chemical structure of PFS-*b*-PBLG. Subscripts *n* and *m* denote the average number of repeating units in the polymer backbones. b) Toluene solution of **1** (3 wt%) below the critical gelation concentration (3.3 wt%) (left) and toluene gel of **2** at 0.2 wt% (right). c) TEM image of the toluene gel of **2** (1 wt%). Arrows in the picture indicate the individual fibers with about 20 nm width. d) EDX spectrum of the unstained toluene gel of **2**.

Table 1: Characterization and gelation characteristics of block copolymers.

Block copolymers[a]	M_n[b] [g mol^{-1}]	M_w/M_n[c]	C_{gel}[d] [wt%]	T_{gel}[e] [°C]	L_{helix}[f] [nm]	W_{ribbon}[g] [nm]
PFS_{38}-$PBLG_{69}$ (**1**)	24500	1.14	3.3	48	10.3	14.9
PFS_{38}-$PBLG_{95}$ (**2**)	30200	1.13	0.2	50	14.2	15.8
PFS_{19}-$PBLG_{48}$ (**3**)	15300	1.21	1.9	46	7.2	9.7
PS_{93}-$PBLG_{76}$ (**4**)	26700	1.14	0.3	48	11.4	19.0
PEG_{227}-$PBLG_{56}$ (**5**)	22300	1.18	0.5	45	8.4	16.0

[a] Subscripts indicate the average number of repeating units of the polymer determined by ^{1}H NMR integration. PFS: poly(ferrocenyldimethylsilane), PS: polystyrene, PEG: poly(ethylene glycol), PBLG: poly(γ-benzyl-L-glutamate). [b] Molecular weights of the block copolymers measured by ^{1}H NMR integration. [c] Polydispersity indices of molecular weights of block copolymers obtained by GPC with THF/$[Bu_4N]Br$ (0.003 M) as the eluent. [d] The apparent critical gelation concentrations for the toluene solutions of the block copolymers. [e] The gel–solution transition temperature measured with the toluene gels at C_{gel}. [f] Calculated length of the PBLG helix of the block copolymers. L_{helix} (in nm) = $N_{PBLG} \times 0.15$ nm where N_{PBLG} is the average number of residues in the PBLG helix determined by ^{1}H NMR. [g] The width of the ribbon in the dried gels measured by SAXS.

These materials were synthesized by ring-opening polymerization (ROP) of γ-benzyl-L-glutamate-*N*-carboxyanhydride (γ-Bz-L-Glu-α-NCA) with amine-terminated PFS (amino-PFS) as a macroinitiator.[8] Amino-PFSs were prepared by living anionic ROP of a strained [1]-silaferrocenophane monomer.[9,10] The PFS-*b*-PBLG block copolymers were very soluble in common organic solvents such as chloroform and tetrahydrofuran (THF), but only sparingly soluble in hot *N*,*N*-dimethylformamide (DMF).

We found that PFS-*b*-PBLG block copolymers are soluble in hot toluene and, to our surprise, form optically transparent gels upon cooling to ambient temperature. The gelation was thermally reversible in all cases. The apparent critical concentration for the gelation (C_{gel}), below which the solution exists as a viscous fluid (Figure 1b), strongly depends on the chain length of the PBLG block (see Experimental Section for details of the measurement). For example, block copolymers **1** and **2**, which differ only in the number of γ-Bz-L-Glu residues (69 for **1** and 98 for **2**) in the PBLG block, have a considerably different C_{gel} (3.3 wt% for **1** and 0.2 wt% for **2**). This result indicates that the interaction between the PBLG helices is a crucial factor in the gelation process. The lower C_{gel} of block copolymer **3** as compared to that of **1** (Table 1) suggests that the chain length ratio between the PFS and the PBLG blocks might also be a factor in the gelation process. In addition, for PFS_{38}-*b*-$PBLG_{133}$ (38.5 kDa), where the chain length ratio between the PFS and the PBLG exceeds 1:3, incomplete gelation was observed (macroscopic phase separation into a dense block copolymer gel and the free solution phase) regardless of the concentration of the block copolymer in toluene. Significantly, the gels retained their shape and thermoreversibility on the addition of methanol (5 vol% to toluene). This suggests that there is no end-to-end intermolecular hydrogen bonding between the PBLG blocks, as methanol can readily disrupt the hydrogen bonding between the PBLG chains.[11,12] This result indicates that hydrogen bonding is not a key factor for the gelation.

PBLG homopolypeptide is known to form thermoreversible gels in various solvents such as toluene and benzyl alcohol,[13] which has led to challenging questions on the origin of this phenomenon.[14] PBLG differs from other gel-forming polymers[15] because its rigid-rod conformation does not allow the formation of chain–chain entanglements. One aspect of the current understanding of the gelation of PBLG in solution is based on phase separation.[16] The PBLG homopolypeptide undergoes microscopic phase separation when a warm homogeneous solution in the dilute concentration regime (< 2 wt%) is cooled. Phase separation increases the concentration of PBLG locally, and the increased concentration forces the rods to order in a liquid crystalline phase where PBLG rods align parallel to the long axis of the phase-separated domains. Strong dipolar π–π interactions between the phenyl groups of the PBLG rods consequently stabilize the microfibers that are intertwined into a 3-D network structure.

Based on the mechanism described above, it is difficult to imagine that block copolymers of PBLG and a random-coil polymer could form a gel since the block copolymers can not be ordered in a liquid crystalline phase in dilute solution due to the presence of the bulky random-coil polymer chain at the end of PBLG helix. Our findings reported here imply that a different mechanism of gelation is required to explain the self-assembly behavior of PBLG–random coil diblock copolymers in solution. Therefore, we studied the detailed structure of the gels of PFS-*b*-PBLG in toluene with transmission electron microscopy (TEM), atomic force microscopy (AFM), and small-angle X-ray scattering (SAXS). TEM images of the dried gel of **2** formed in toluene (Figure 1c)

 © 2005 Wiley-VCH Verlag GmbH & Co. KGaA, Weinheim

show a network of fibrous structures, where each individual fiber has a width of about 20 nm. Energy- dispersive X-ray spectroscopy (EDX) clearly evidenced the presence of both the PBLG block and PFS block in the structure (Figure 1d). AFM experiments were carried out to determine the lateral dimension and the height profiles of the fiber (Figure 2a and b). Analysis of the AFM height profiles (Figure 2b) revealed

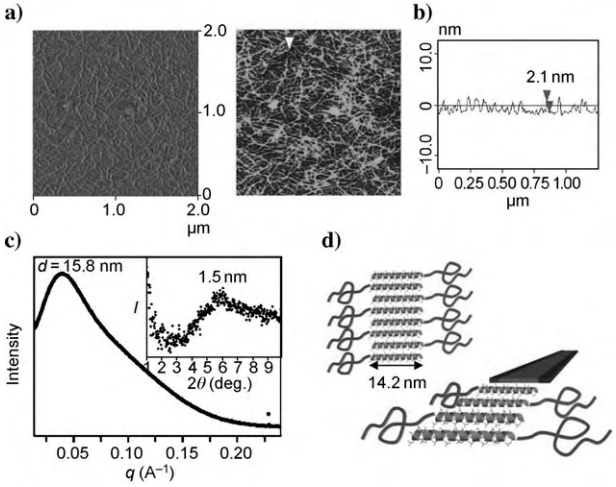

Figure 2. a) AFM phase (left) and height (right) images of the toluene gel of **2** (0.1 wt%). b) AFM height profile of the nanoribbons. c) SAXS profile of the dried gel of **2** showing the width of the ribbon (15.8 nm). The inset denotes the diffraction at 1.5 nm indicating the distance between two PBLG helices obtained by PXRD. d) A schematic presentation of the nanoribbon formed in the network structure of the toluene gel of **2**. 14.2 nm indicates the calculated length of the PBLG helix.

a height of 2.1 ± 0.2 nm, and a lateral dimension of about 23 nm. This suggests that the individual fibrous structure is not cylindrical but has a ribbon or tape-like morphology. SAXS measurements were carried out on the dried gel because all gels showed strong birefringence when examined by polarized optical microscopy, indicating the presence of regular structures (Figure 2c). The results corroborated TEM and AFM observations of the width of the individual fibers by showing a diffraction peak at 15.8 nm. This lateral dimension of the fiber obtained on SAXS has not been observed in the gels of the PBLG homopolypeptide due to the lack of order in the diameters of fibers.[17] Powder X-ray diffraction (PXRD) of the dried gels of PFS-*b*-PBLG also showed a diffraction peak at 1.5 nm, which indicates the distance between PBLG helices.[4]

Based on the TEM, AFM, SAXS, and PXRD results, a mechanism for the gelation of **2** was conceived. From the experimental data and the molecular dimensions of block copolymer **2**, containing a PBLG helix of 14.2 nm length and 1.5 nm diameter, we propose that the observed fibers are nanoribbons assembled from the 1-dimensional stacking of the block copolymers in a monolayer fashion (Figure 2d).[18] This self-assembly mechanism is reminiscent of that proposed for nanoribbons derived from dendron rod-coil molecules[19] but with two differences. First, in our case, the self-organizing motifs are high molecular weight block copolymers, and second, hydrogen bonding interactions, which have been shown to be essential for dendron rod-coil self-assembly, are not involved. We propose that strong dipolar π–π interactions involving phenyl groups between the PBLG helices stabilize the structure and could be the driving force for the self-assembly.[20] The long axis of the PBLG helix is parallel to the plane of the ribbon. The PFS block protrudes outside of the ribbon due to its high solubility in toluene and prevents the aggregation between nanoribbons in the solution. In the nanoribbon, the PBLG chains are most probably oriented in an anti-parallel fashion. In this orientation the dipole moments of the PBLG helices are oriented in a favorable manner, and the steric repulsion between the PFS chains is minimized.[21] The nanoribbon mechanism proposed here explains the dependence of C_{gel} of the block copolymers on the length of the PBLG helix and the independence of gelation on the presence of hydrogen bonding disrupting solvents such as methanol.

The proposed mechanism is potentially applicable to other diblock copolymers when the appropriate structural requirements are met: a stable α-helical conformation of the PBLG polypeptide block and a random-coil block which is soluble in the given solvent. To establish the generality of the mechanism, we prepared two block copolymers, polystyrene-*b*-PBLG (PS-*b*-PBLG) **4** and poly(ethylene glycol)-*b*-PBLG (PEG-*b*-PBLG) **5**. We chose PS and PEG because these polymers possess a random-coil conformation in solution and are readily soluble in toluene. In addition, amino-functionalized PS and PEG are commercially available, and the block copolymers, PS-*b*-PBLG and PEG-*b*-PBLG, have been previously synthesized.[22,23] Both diblock copolymers formed stable transparent thermoreversible gels in toluene at concentrations as low as 0.3 wt% (Figure 3a and c). A detailed structural characterization of gels in toluene of both block copolymers also showed structures of the fibers identical to those described for the PFS-*b*-PBLG gels. TEM observations and SAXS experiments revealed that both block copolymers self-assemble in a manner that is consistent with the nanoribbon mechanism described above (Figure 3b and d). In addition to our work, diblock copolypeptides containing both random-coil and α-helical peptide blocks have been shown by Deming and co-workers to form hydrogels in aqueous solution.[24] Our results together with those of Deming strongly suggest that the gelation of the diblock copolymers with an α-helix and a random-coil block in an appropriate solvent (toluene for the PBLG block copolymers) is a general phenomenon, and the concept could be expanded to numerous block copolymers containing a helical polypeptide block other than the PBLG.

The ROP of α-NCA yields an amino end group at the polypeptide chain. This amino group could be further functionalized by reacting guest molecules such as fluorescent dyes, nanoparticles, and other functional species. The resulting self-assembled structures of the labeled block copolymers would then be functional scaffolds with precise alignment of the labels in the nanostructures. To test this idea, we labeled PEG-*b*-PBLG with a pyrene (Py) chromophore using an *N*-hydroxysuccinimide activated pyrene derivative (Figure 4a

 © 2005 Wiley-VCH Verlag GmbH & Co. KGaA, Weinheim

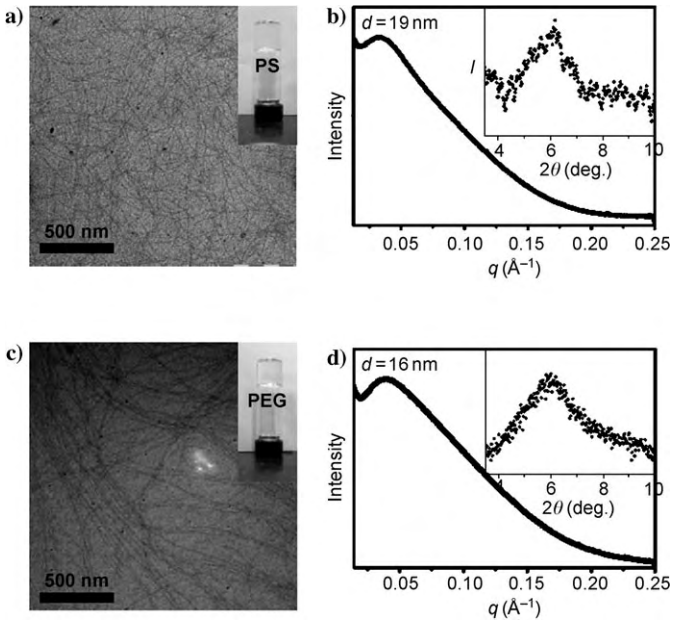

Figure 3. a, c) Energy-filtered TEM (EF-TEM) images of 1 wt% toluene gels of PS-*b*-PBLG **4** (a) and PEG-*b*-PBLG **5** (c). Insets show the transparent gels of the respective block copolymers formed at the critical gelation concentrations. b, d) SAXS profiles of dried gel for PS-PBLG **4** (b) and PEG-PBLG **5** (d). Insets are PXRD results of the dried gels indicating the distance between PBLG helices (1.5 nm) in the nanoribbon structure.

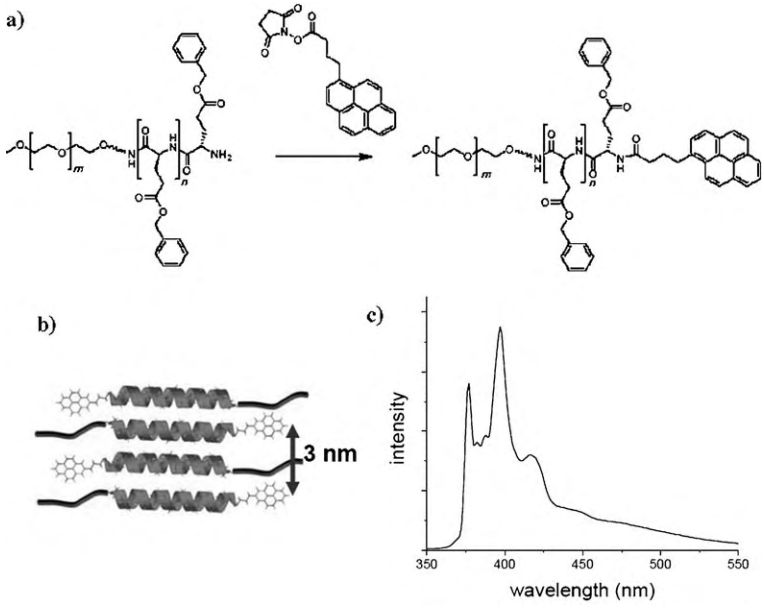

Figure 4. a) N-terminal labeling of PEG-*b*-PBLG. b) Graphic representation of the self-assembled nanoribbon of pyrene-labeled PEG-*b*-PBLG. c) Fluorescence emission spectrum (excitation at 340 nm) of toluene gel of pyrene-labeled PEG-*b*-PBLG.

and Experimental Section).[25] The functionalized PEG-*b*-PBLG formed a transparent thermoreversible organogel at 2.5 wt% in toluene. This indicates that the incorporation of bulky guest molecules such as pyrene does not hamper the self-assembling ability of the block copolymer and the self-assembled structure can accommodate numerous functional molecules and nanoparticles with 1-D alignment at the defined location. For Py, the fluorescence emission spectrum reveals information about its micro-environment. Based on the mechanism proposed here, Py groups would be segregated in the nanoribbon structure by a 3 nm distance and shielded from one another by flexible PEG chain. Despite the high local concentration of Py groups, the structural model predicts that excimer formation should be strongly inhibited (Figure 4b). The excimer sandwich requires close proximity of two Py molecules (ca. 4 Å), achieved either through pre-association or diffusive motion of Py groups in the medium.[26] The fluorescence emission spectrum of the organogels of pyrene-labeled PEG-*b*-PBLG shows only characteristic monomeric emission peaks of pyrene (377 nm, 397 nm, and 416 nm) and no noticeable excimer emission at about 480 nm. This result provides strong support for the proposed mechanism. In addition, the unique self-assembly mechanism allows labeling species to be incorporated in the block copolymer without interfering with the self-assembly process. The labeled organogels based on random coil–helical polypeptide block copolymers could be utilized as scaffolds for catalysis.

The studies described here show that synthetic polymers with a defined conformation can play a role as well-defined building blocks for self-assembly. It is remarkable that the random coil–helical polypeptide diblock copolymers behave with the same precision as well-defined small molecules that form organogels (organogelators)[27] although the size of the block copolymer building blocks is orders of magnitude larger. This dimension regime is comparable to that of proteins that form elaborate 1-D structures such as F-actin.[28] Our findings could facilitate the development of synthetic polymeric systems that self-assemble precisely into well-defined nanostructures by adopting stable polymer conformations. Furthermore, fine-tuning of the properties and chemical functionality of organogels made of helix–random coil diblock copolymers should be possible based on the mechanism proposed here. The potential development of PFS-*b*-PBLG gels as magnetic and redox-active scaffolds where the additional functionality arises from the presence of metal atoms is particularly attractive.[29,30]

Experimental Section

Synthesis of the block copolymers, gel characterization, and labeling experiments: Amino-PFSs and block copolymers of PBLG were synthesized as previously reported.[8] Amino-polystyrene ($M_n = 10500\ g\,mol^{-1}$, PDI = 1.05) and amino-poly(ethylene glycol) ($M_n = 10000\ g\,mol^{-1}$, PDI = 1.08) were purchased from Polymer Source. For organogels, block copolymers and toluene were mixed in a sealed vial and heated until the mixture became a homogeneous solution. The homogeneous solution was stored at 22 °C for 24 h. After 24 h, the organogel was subjected to gravity for 24 h. When no flow was observed, we defined the state as a gel. The lowest concentration of gelation in this condition was determined as C_{gel}. T_{gel}

 © 2005 Wiley-VCH Verlag GmbH & Co. KGaA, Weinheim

was measured by the procedure reported by Hirst et al.[31] All C_{gel} and T_{gel} values were measured three times. Pyrene labeling of the block copolymer was achieved by means of an amidation reaction between PEG-*b*-PBLG and *N*-hydroxysuccinidal pyrene butyric acid (fivefold excess to the block copolymer) in THF at room temperature for 24 h. The completion of the reaction was monitored by ^{1}H NMR integration. Labeled block copolymer was purified by repeated precipitations in diethyl ether and washings over acetone until the washings show no presence of pyrene by UV/Vis absorption. Organogels of the labeled block copolymer were prepared in sealed quartz cells. Fluorescence emission spectrum of the organogel were taken on a Flurolog 322 fluorescence spectrophotometer with a 340 nm excitation wavelength.

Microscopy and X-ray experiments: Transmission electron microscopy (TEM) images were obtained on a Philips CM200 microscope operated at an acceleration voltage of 80 kV. The TEM specimen was prepared by gently placing a carbon-coated copper grid on the fraction of organogel. The TEM grid was removed after 30 sec and air-dried for 1 h. When necessary, the sample specimen was shadowed with Au/Pd (7–8 Å thickness at 20° tilting angle). Zero-loss bright field images were obtained on the energy-filtering TEM microscope Carl Zeiss Leo 912 Omega at an acceleration voltage of 120 kV. Small angle X-ray scattering (SAXS) experiments were carried out at the 4C1 X-ray beamline of Pohang Accelerator Laboratory (Pohang, Korea). The scattered data were collected using a 2-D CCD detector and the X-ray wavelength was 1.608 Å ($Co_{K\alpha}$ radiation). Powder X-ray diffraction data were collected on a Rigaku RINT-2000 counter diffractometer with a $Cu_{K\alpha}$ radiation source (operated at 40 kV, 40 mA). For X-ray experiments, organogels were slowly dried under air for 24 h. Atomic force microscopy was performed on a NanoScope III in the tapping mode. The sample preparation for AFM measurement was identical to the preparation of the TEM specimen. Fresh cleaved mica was used as a substrate. The height and width values of the fiber were determined from ten different locations.

Received: August 8, 2005
Published online: November 15, 2005

Keywords: block copolymers · organogels · polypeptides · self-assembly

[1] H. Block, *Poly(γ-benzyl-L-glutamate) and Other Glutamic Acid Containing Polymers*, Gordon and Breach, New York, **1983**.
[2] P. J. Flory, *Proc. R. Soc. London Ser. A* **1956**, *234*, 73 – 89.
[3] C. Robinson, J. C. Ward, *Nature* **1957**, *180*, 1183 – 1184.
[4] S. M. Yu, V. P. Conticello, G. Zhang, C. Kayser, M. J. Fournier, T. L. Mason, D. A. Tirrell, *Nature* **1997**, *389*, 167 – 170.
[5] K. Tohyama, W. G. Miller, *Nature* **1981**, *289*, 813 – 814.
[6] B. Gallot, *Prog. Polym. Sci.* **1996**, *21*, 1035 – 1088.
[7] R. Tadmor, R. L. Khalfin, Y. Cohen, *Langmuir* **2002**, *18*, 7146 – 7150.
[8] K. T. Kim, G. W. M. Vandermeulen, M. A. Winnik, I. Manners, *Macromolecules* **2005**, *38*, 4958 – 4961.
[9] Y. Ni, R. Rulkens, I. Manners, *J. Am. Chem. Soc.* **1996**, *118*, 4102 – 4114.
[10] K. Kulbaba, I. Manners, *Macromol. Rapid Commun.* **2001**, *22*, 711 – 724.
[11] P. Rohrer, H.-G. Elias, *Makromol. Chem.* **1972**, *151*, 281 – 283.
[12] C. Kim, K. T. Kim, Y. Chang, H. H. Song, T.-Y. Cho, H.-J. Jeon, *J. Am. Chem. Soc.* **2001**, *123*, 5586 – 5587.
[13] P. Doty, J. H. Bradbury, A. M. Holtzer, *J. Am. Chem. Soc.* **1956**, *78*, 947 – 954.
[14] S. Schmidtke, P. Russo, J. Nakamatsu, E. Buyuktanir, B. Turfan, E. Temyanko, *Macromolecules* **2000**, *33*, 4427 – 4432.
[15] J.-M. Guenet, *Thermoreversible Gelation of Polymers and Biopolymers*, Academic Press, London, **1992**.
[16] W. G. Miller, K. Lee, K. Tohyama, V. Voltaggio, *J. Polym. Sci. Polym. Symp.* **1978**, *65*, 91 – 106.
[17] Y. Cohen, *J. Polym. Sci. Part B: Polym. Phys.* **1996**, *34*, 57 – 64.
[18] J. M. Smeenk, M. B. J. Otten, J. Thies, D. A. Tirrell, H. G. Stunnenberg, J. C. M. van Hest, *Angew. Chem.* **2005**, *117*, 2004 – 2007; *Angew. Chem. Int. Ed.* **2005**, *44*, 1968 – 1971.
[19] E. R. Zubarev, M. U. Pralle, E. D. Sone, S. I. Stupp, *J. Am. Chem. Soc.* **2001**, *123*, 4105 – 4106.
[20] M. Lee, B.-K. Cho, W.-C. Zin, *Chem. Rev.* **2001**, *101*, 3869 – 3892; in toluene, the interaction between PBLG helices could be more stabilized by a solvent-mediated "co-crystallization" of PBLG helices. For details, see ref. [7].
[21] S. Ludwigs, G. Krausch, G. Reiter, M. Losik, M. Antonietti, H. Schlaad, *Macromolecules* **2005**, *38*, 7532 – 7535.
[22] H.-A. Klok, J. F. Langenwalter, S. Lecommandoux, *Macromolecules* **2000**, *33*, 7819 – 7826.
[23] J.-F. Lutz, D. Schütt, S. Kubowicz, *Macromol. Rapid Commun.* **2005**, *26*, 23 – 28.
[24] A. P. Nowak, V. Breedveld, L. Pakstis, B. Ozbas, D. J. Pine, D. Pochan, T. J. Deming, *Nature* **2002**, *417*, 424 – 428.
[25] Q, Wang, T. Lin, T. L. Tang, J. E. Johnson, M. G. Finn, *Angew. Chem.* **2002**, *114*, 477 – 480; *Angew. Chem. Int. Ed.* **2002**, *41*, 459 – 462.
[26] F. M. Winnik, *Chem. Rev.* **1993**, *93*, 587 – 614.
[27] P. Terech, R. G. Weiss, *Chem. Rev.* **1997**, *97*, 3133 – 3159.
[28] K. C. Holmes, D. Popp, W. Gebhard, W. Kabsch, *Nature* **1990**, *347*, 44 – 49.
[29] M. J. MacLachlan, M. Ginzburg, N. Coombs, T. W. Coyle, N. P. Raju, J. E. Greedan, G. A. Ozin, I. Manners *Science* **2000**, *287*, 1460 – 1463.
[30] I. Manners, *Science* **2001**, *294*, 1664 – 1666.
[31] A. R. Hirst, D. K. Smith, M. C. Feiters, H. P. M. Geurts, A. C. Wright, *J. Am. Chem. Soc.* **2003**, *125*, 9010 – 9011.

 © 2005 Wiley-VCH Verlag GmbH & Co. KGaA, Weinheim

Switchable Nanostructures

DOI: 10.1002/anie.200502236

Springlike Nanohelical Structures in Chiral Block Copolymers**

Yeo-Wan Chiang, Rong-Ming Ho, Bao-Tsan Ko, and Chu-Chien Lin*

Helical structures are probably the most fascinating morphologies in nature, and they have been intensively studied as a result of their specific functions in the formation of biological architectures. Helical-chain conformations, such as single-strand α-helical peptides and double-stranded DNA, are regarded as the fundamental motifs for the hierarchical organization of proteins. A variety of origins for the formation of helical structures, such as hydrogen bonds,[1] solvophobic interactions,[2] π–π interactions,[3] cholesteric liquid crystal formation,[4] relative incompatibility,[5] and chirality,[6] have all been demonstrated. Biomimicking nature, helical morphologies have been obtained on different length scales by the interplay of noncovalent bonding interactions (that is, secondary forces). Block copolymers that consist of two chemically different components are able to self-assemble into various ordered nanostructures, such as spheres, cylinders, gyroids, and lamellae, as a consequence of the incompatibility of the constituent blocks.[7] Therefore, the self-assembled nanostructures in block copolymers appear promising in applications that employ the bottom-up approach.[8] In contrast to the helical superstructures in the hierarchical organization of chiral molecules, helical nanostructures have been obtained from the self-assembly of block copolymers that consist of achiral and chiral blocks, for example, polystyrene-*b*-poly(isocyanopeptide), in buffer solutions.[6a] However, a three-dimensionally packed nanohelical structure phase was found in the self-assembled chiral diblock copolymer, polystyrene-*b*-poly(L-lactide) (PS-PLLA), in the bulk.[9] Contrary to the conventional phase morphology of diblock copolymers, the formation of a nanohelical structure phase is attributed to the chirality of the constituent PLLA block.[9] Furthermore, a significant change, from long-pitch to short-pitch nanohelices, was found in the nanohelical phase upon annealing.[10] Thus, the structural geometries of the nanohelices might be strongly affected by applying stimulation. Herein, we report the internal and external stimuli, such as crystallization and shearing, respectively, which act on the nanohelical morphology so that the microphase-separated PLLA nanohelices exhibit springlike behavior in a PS matrix in response to the applied stimulus. Consequently, switchable nanostructures can be obtained by interplay of vitrification, crystallization, and microphase separation as well as shearing.

Bulk samples of block copolymers were prepared by solution casting of PS280-PLLA127 ($f^{v}_{PLLA} = 0.35$) in dichloromethane (CH_2Cl_2; 10 wt%) at room temperature. As evidenced by transmission electron microscopy (TEM) and small-angle X-ray scattering (SAXS), a nanohelical structure phase quenched from microphase-separated melt at 165 °C (melting point of PLLA, ca. 160 °C) can be obtained from the self-assembly of PS-PLLA, and is packed in a hexagonal lattice.[9] In contrast to the racemic block copolymer, polystyrene-*b*-poly(D,L-lactide) (PS-PLA),[11] the formation of the nanohelical structures in PS-PLLA is attributed to the interplay of chirality and immiscibility of the constituent blocks.[9] As a result, the self-assembly of helical curvature is induced by the formation of specific conformations of PLLA chains arising from the interactions of chiral entities.

Considering their origin, the self-assembled nanohelical structures are expected to be affected by the changes of PLLA chain conformation. Notably, the PLLA component is intrinsically a crystallizable polymer as a result of the regularity of the chiral configuration. The crystallization of PLLA in PS-PLLA might give rise to significant changes in the self-assembly morphology and is thus considered as a driving force (namely, an internal stimulus) for manipulating the intrinsic nanohelical structure. The final morphology of crystalline block copolymers is strongly dependent on the experimental temperature, with respect to the order–disorder transition temperature (T_{ODT}), the crystallization temperature of the crystallizing block (T_c^c), the glass transition temperature of the amorphous block (T_g^a), and the crystallization rate.[12] Consequently, the microphase-separated morphology is determined by the crystallization temperature of PLLA that also justifies the degree of vitrification of the confined environment (that is, the PS matrix). The dividing confined environments—hard confinement ($T_c^c < T_g^a$) and soft confinement ($T_c^c \geq T_g^a$)—dictate the final morphology of crystallized PS-PLLA. For a system with $T_c^c < T_g^a$, the ordered nanostructure can be preserved because of the vitrified microdomains of the PS blocks. By contrast, if $T_c^c \geq T_g^a$, the effect of crystallization may lead to a change of microphase-separated morphology.

To examine the crystallization effect, the amorphous nanohelices (intrinsic nanohelices) of PS-PLLA were crystallized from hard ($T_{c,PLLA} < T_{g,PS} = 99.2$ °C) to soft ($T_{c,PLLA} \geq T_{g,PS}$) confinement. The nanohelical morphology remained

[*] Y.-W. Chiang, Prof. Dr. R.-M. Ho
Department of Chemical Engineering
National Tsing Hua University
Hsinchu 30013 (Taiwan)
E-mail: rmho@mx.nthu.edu.tw
Prof. Dr. R.-M. Ho, B.-T. Ko
Industrial Technology Research Institute
Union Chemical Laboratory
Hsinchu 30013 (Taiwan)
Fax: (+886) 3-571-5408
Prof. Dr. C.-C. Lin
Department of Chemistry, National Chung-Hsing University
Taichung 40227 (Taiwan)

[**] We thank Dr. B. S. Hsiao of the Chemistry Department, State University of New York at Stony Brook, and Drs. I. Sics and C. A. Avila-Orta of the National Synchrotron Light Source, Brookhaven National Laboratory, for their help in synchrotron SAXS experiments. We also thank Ms. P.-C. Chao of the Regional Instruments Center at NCHU for her help in TEM experiments.

Supporting information for this article is available on the WWW under http://www.angewandte.org or from the author.

 © 2005 Wiley-VCH Verlag GmbH & Co. KGaA, Weinheim

while PLLA crystallization was carried out under hard confinement (for instance, $T_{c,PLLA} = 80\,^{\circ}C$; see Figure 1a). The microdomains of the PS component became dark after staining with RuO_4, whereas those of the PLLA component appeared light. The crystallization of PLLA was restricted within confined microdomains because of the vitrification of the PS matrix, which preserved the helical morphology. Also, as evidenced by the one-dimensional (1D) SAXS profile (Figure 2a and b), the diffraction peaks occurred at q^* ratios of $1:\sqrt{4}:\sqrt{7}:\sqrt{13}$, consistent with the hexagonally packed phase structure. As a result, the packing geometry of the crystalline nanohelices remained as a hexagonal lattice under hard confinement.

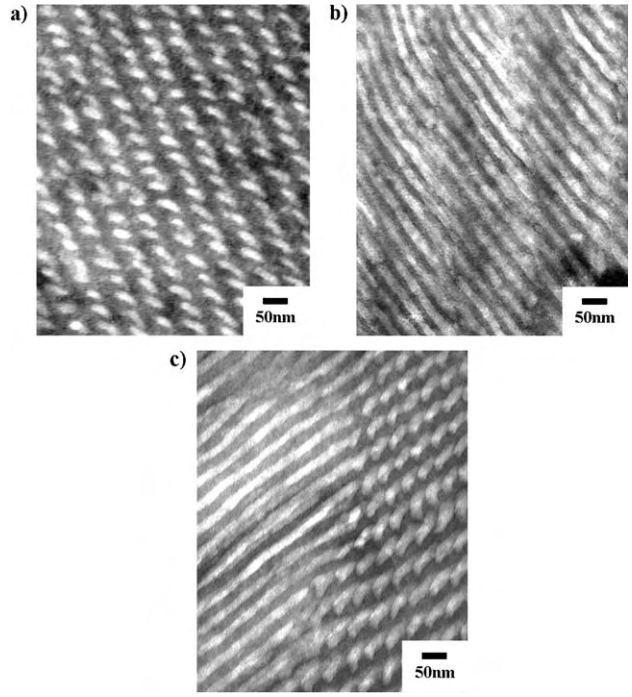

Figure 1. TEM micrographs of nanohelical structures in PS280-PLLA127 ($f^{v}_{PLLA} = 0.35$) bulk samples quenched from microphase-separated melt (165 °C), then a) crystallized at 80 °C for 120 min and b) crystallized at 110 °C for 120 min. c) TEM micrograph for phase transformation from helices to cylinders during crystallization at 110 °C.

By contrast, the nanohelices were transformed into a cylindrical phase when crystallization was carried out under soft confinement, while $T_{c,PLLA} > T_{g,PS}$ (for instance, $T_{c,PLLA} = 110\,^{\circ}C$; see Figure 1b). The developing stage of phase transformation can be clearly observed (Figure 1c). The helical structure was stretched and transformed into a crystalline cylinder along the long axes of the helices (or cylinders), so that the hexagonal packing remained regardless of the transformation (Figure 2c). The significant effect of crystallization on the microphase-separated phase is attributed to the stress-induced structural change when crystallization is carried out above $T_{g,PS}$.[12] As a result, the nanohelical structure behaves like a spring in response to a crystallization event, and the springlike PLLA microdomain can be modified as a crystalline spring under hard confinement, or a fully extended spring under soft confinement, by tuning the crystallization temperature.

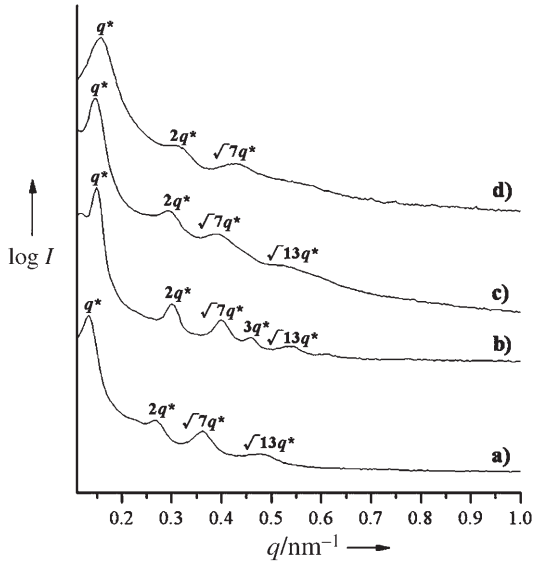

Figure 2. One-dimensional SAXS profiles for self-assembly of PS280-PLLA127 ($f^{v}_{PLLA} = 0.35$) with different geometries. a) Intrinsic nanohelices; b) crystalline nanohelices under hard confinement; c) stretched nanohelices (crystalline cylinders) under soft confinement; d) stretched nanohelices (amorphous cylinders) after shearing.

It is well-known that shear-induced orientation of block copolymers is one of the most convenient ways to generate a well-oriented morphology for bulk samples in practical applications.[13] Considering the springlike behavior of the nanohelical phase, shearing (an external stimulus as compared to crystallization) is expected to achieve the orientation of nanohelices and modify the morphology. Flow-induced alignment of the nanohelical phase was thus conducted by using a lubricated-channel die based on the design of Khan and Larson.[14] Molding and shearing of the intrinsic nanohelices were performed on a microphase-separated melt at 180 °C for 1 min, and then the processed strip was held in the die at the shearing temperature for 1 min before quenching with liquid nitrogen to eliminate the residual shear stress. The shear (velocity), vorticity, and velocity gradient directions were assigned as the x, y, and z directions, respectively. After quenching from the shearing melt, a hexagonally packed cylinder morphology was found in the y–z plane (Figure 3a). Also, a longitudinal cylinder morphology was observed along the y direction (Figure 3b), whereas the 2D SAXS pattern along the y direction appeared as a well-defined diffraction from oriented microdomains (inset of Figure 3b). The 1D SAXS profile indicated the unchanged hexagonally packed structures after shearing (Figure 2d). Thus, oriented cylinders were obtained, and the nanohelices also exhibited springlike behavior in response to shearing. Contrary to crystallization-induced cylinders, the shear-induced cylinders appeared as an amorphous entity.

The nanohelical phase with PLLA helices embedded in the PS matrix acted with springlike behavior upon internal and external stimulation. The stress-induced phase trans-

 © 2005 Wiley-VCH Verlag GmbH & Co. KGaA, Weinheim

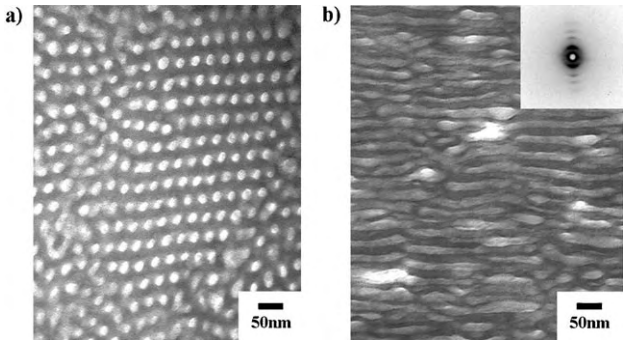

Figure 3. TEM micrographs of nanohelical structures in PS280-PLLA127 ($f^{v}_{PLLA}=0.35$) bulk samples after shearing at 180 °C (above the m.p. of PLLA (≈160 °C) and $T_{g,PS}$ (99.2 °C)) viewed a) parallel, and b) perpendicular to the shear axis. The inset shows the 2D SAXS pattern normal to the cylindrical axis.

formation from nanohelices to cylinders was driven either by crystallization or shearing. Considering the springlike behavior, a reversible process comprising transformation from stretched nanohelices (that is, cylinders) to intrinsic nanohelices would be expected once the stress-induced morphology was thermally treated to release the built-in stress. Figure 4 shows the reversible morphology at which the

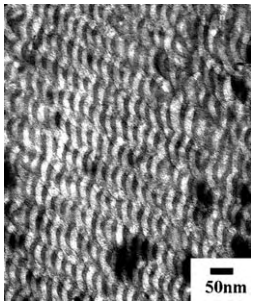

Figure 4. TEM micrograph of crystalline cylinders of PS280-PLLA127 ($f^{v}_{PLLA}=0.35$) bulk samples after annealing at 130 °C for 60 min from 165 °C (microphase-separated melt).

crystalline cylinders gradually revert to the original nanohelical structures through undulation, once the crystallized samples are remelted (at 165 °C) and then annealed at a temperature (130 °C) above the glass transition temperature of PS ($T_{g,PS}=99.2$ °C). Similar results can also be obtained in shear-induced, amorphous cylinders, which progressively transform into an intrinsic structure once the shearing samples are annealed at a temperature (130 °C) above the glass transition temperature of PS (see the Supporting Information).

In conclusion, a variety of self-assembled nanohelices in chiral block copolymers were observed by applying internal and external stimuli (that is, crystallization and shearing). The amorphous nanohelices in the bulk transform into crystalline nanohelices and cylinders by crystallization, and into amorphous cylinders by shearing. The crystallization-induced cylinders were thermally reversible, and able to revert to the original nanohelices upon remelting and annealing. In contrast to crystallized nanohelices, the reversible phase behavior can also be found in shear-induced cylinders by simple thermal annealing. As a result, the hexagonally packed nanohelical structure of the PLLA in the PS matrix of chiral PS-PLLA block copolymers has springlike behavior in response to the applied stimulus. This unique phase behavior thus might provide a technique for manipulating tunable nanohelical structures in practical applications. Consequently, switchable nanohelices from chiral block copolymers can be manipulated by the interplay of vitrification, crystallization, and microphase separation as well as shearing.

Experimental Section

PS-PLLA samples were prepared by using living free radical and ring-opening polymerizations in sequence. Detailed synthetic routes were described in our previous paper.[9]

The number-average molecular weight of PS and polydispersity index (PDI) of PS-PLLA were obtained by gel permeation chromatography. The molecular weight of the PLLA block was measured by ^{1}H NMR analysis. On the basis of molecular weight and volume ratio, the PS-PLLA is designated as PSx-PLLAy ($f^{v}_{PLLA}=z$); x and y represent the numbers of repeating units of PS and PLLA, respectively, and z indicates the volume fraction of PLLA calculated by assuming that the densities of PS and PLLA are 1.02 and 1.18 g cm^{-3}, respectively. The number-average molecular weights of PS and PLLA and the PDI of PS280-PLLA127 ($f^{v}_{PLLA}=0.35$) were 29400 g mol^{-1}, 18300 g mol^{-1}, and 1.21, respectively.

The thermal behavior of PS-PLLA was examined by differential scanning calorimetry (DSC). The sample was first heated to 165 °C and then cooled to −50 °C at a rate of 150 K min^{-1}. The glass transition temperatures of the PLLA and PS blocks were clearly identified as 51.4 and 99.2 °C, respectively.

Received: June 25, 2005
Revised: September 28, 2005
Published online: November 10, 2005

Keywords: block copolymers · chirality · helical structures · nanostructures · self-assembly

[1] J. J. L. M. Cornelissen, J. J. J. M. Donners, R. E. Gelder, W. S. Graswinckel, G. A. Metselaar, A. E. Rowan, N. A. J. M. Sommerdijk, R. J. M. Nolte, *Science* **2001**, *293*, 676.
[2] a) J. C. Nelson, J. G. Saven, J. S. Moore, P. G. Wolynes, *Science* **1997**, *277*, 1793; b) M. J. Mio, R. B. Prince, J. S. Moore, C. Kuebel, D. C. Martin, *J. Am. Chem. Soc.* **2000**, *122*, 6134; c) R. B. Prince, L. Brunsveld, E. W. Meijer, J. S. Moore, *Angew. Chem.* **2000**, *112*, 234; *Angew. Chem. Int. Ed.* **2000**, *39*, 228.
[3] a) R. S. Lokey, B. L. Iverson, *Nature* **1995**, *375*, 303; b) G. S. Hanan, J.-M. Lehn, N. Kyritsakas, J. Fischer, *J. Chem. Soc. Chem. Commun.* **1995**, 765; c) J. C. Nelson, J. G. Saven, J. S. Moore, P. G. Wolynes, *Science* **1997**, *277*, 1793; d) D. M. Bassani, J.-M. Lehn, G. Baum, D. Fenske, *Angew. Chem.* **1997**, *109*, 1931; *Angew. Chem. Int. Ed. Engl.* **1997**, *36*, 1845.
[4] a) C. Y. Li, S. Z. D. Cheng, J. J. Ge, F. Bai, J. Z. Zhang, I. K. Mann, F. W. Harris, L.-C. Chien, D. Yan, T. He, B. Lotz, *Phys. Rev. Lett.* **1999**, *83*, 4558; b) C. Y. Li, S. Z. D. Cheng, J. J. Ge, F. Bai, J. Z. Zhang, I. K. Mann, L.-C. Chien, F. W. Harris, B. Lotz, *J. Am. Chem. Soc.* **2000**, *122*, 72.
[5] a) R. Stadler, C. Auschra, J. Beckmann, U. Krappe, I. Voigt-Martin, L. Leibler, *Macromolecules* **1995**, *28*, 3080; b) U.

 © 2005 Wiley-VCH Verlag GmbH & Co. KGaA, Weinheim

Krappe, R. Stadler, I. Voigt-Martin, *Macromolecules* **1995**, *28*, 4558; c) T. Goldacker, V. Abetz, R. Stadler, I. Erukhimovich, L. Leibler, *Nature* **1999**, *398*, 137.
[6] a) E. Yashima, S. Huang, T. Matsushima, Y. Okamoto, *Macromolecules* **1995**, *28*, 4184; b) E. Yashima, T. Matsushima, Y. Okamoto, *J. Am. Chem. Soc.* **1997**, *119*, 6345; c) J. J. L. M. Cornelissen, M. Fischer, N. A. J. M. Sommerdijk, R. J. M. Nolte, *Science* **1998**, *280*, 1427; d) S.-I. Sakurai, K. Kuroyanagi, K. Morino, M. Kunitake, E. Yashima, *Macromolecules* **2003**, *36*, 9670.
[7] F. S. Bates, G. H. Fredrickson, *Annu. Rev. Phys. Chem.* **1990**, *41*, 525.
[8] C. Park, J. Yoon, E. L. Thomas, *Polymer* **2003**, *44*, 6725.
[9] R.-M. Ho, Y.-W. Chiang, C.-C. Tsai, C.-C. Lin, B.-T. Ko, B.-H. Huang, *J. Am. Chem. Soc.* **2004**, *126*, 2704.
[10] R.-M. Ho, Y.-W. Chiang, C. Burger, B. S. Hsiao, C.-C. Lin, B.-T. Ko, unpublished results.
[11] A. S. Zalusky, R. Olayo-Valles, J. H. Wolf, M. A. Hillmyer, *J. Am. Chem. Soc.* **2002**, *124*, 12761.
[12] R.-M. Ho, F.-H. Lin, C.-C. Tsai, C.-C. Lin, B.-T. Ko, B. S. Hsiao, I. Sics, *Macromolecules* **2004**, *37*, 5985.
[13] C. C. Honeker, E. L. Thomas, *Chem. Mater.* **1996**, *8*, 1702.
[14] S. A. Khan, R. G. Larson, *Rheol. Acta* **1991**, *30*, 1.

 © 2005 Wiley-VCH Verlag GmbH & Co. KGaA, Weinheim

Synthetic Methods

DOI: 10.1002/anie.200502387

Controlled Autocatalytic Nitration of Phenol in a Microreactor

Laurent Ducry and Dominique M. Roberge**

Nitration reactions can often show extremely exothermic behavior, and this, combined with the decomposition or explosion potential of many nitro compounds, places them amongst the most hazardous industrial processes.[1] In this context, continuous processes are attractive for safety reasons because of the much smaller reaction volumes used.[2] Continuous production is of commercial importance for very fast nitrations, such as that of phenol (Scheme 1).[3] Moreover, microreactors[4] should allow better control of the reaction thanks to their efficient mixing and heat transfer, as already described for nitration reactions.[5] The nitration of phenol (**1**) was chosen as a model reaction to investigate the potential of microreactors from both a chemical and a safety point of view.

The general mechanism for the acid-catalyzed nitration of aromatic compounds is electrophilic and involves the nitronium ion (NO_2^+) as the reactive species.[6] The nitration of phenol (**1**) and other aromatic substrates activated toward electrophilic substitution is, however, essentially different in that it is catalyzed by nitrous acid.[7] The rate of phenol nitration by nitric acid in water was first reported by Martinsen, who showed that the reaction is autocatalyzed by the nitrous acid it produces.[8] The importance of the presence of HNO_2 could suggest that the nitrosonium ion (NO^+) acts as the reactive species. Catalysis by nitrous acid can not, however, involve a nitrosation followed by an oxidation by HNO_3, since nitrosation is *para*-selective whereas nitration affords a mixture of *ortho*- and *para*-nitrophenols.[9] Evidence has since been gained that phenol nitration mainly occurs by a radical mechanism involving a single electron-transfer reaction.[10]

The autocatalytic nature of phenol nitration was first verified by carrying out the reaction in a Mettler RC1 calorimeter (Table 1, entries 1 and 2). The addition of 65% HNO_3 to a 23% phenol solution in CH_3CO_2H (6%, used to increase the phenol solubility) and water (71%) was carried out in two portions (Figure 1). Essentially no reaction took place during the addition of the first HNO_3 portion (corresponding to 0.67 equiv). The small heat signal observed during this addition corresponds to the slightly exothermic dilution of the acid. A first exothermic reaction (35 kJ mol^{-1}) was observed shortly after the first addition. Once this reaction was over, the HNO_3 addition was resumed; again, the reaction did not start immediately. It was only towards the end of the second addition (2.0 equiv HNO_3 added in total) that the strongly exothermic reaction took place (170 kJ mol^{-1}; 115 °C total adiabatic temperature rise). It is important to note that despite the relatively small reaction volume (< 1 L) and the efficient cooling system of the calorimeter, a significant temperature rise occurred (55 °C). Scaling-up such a semibatch reaction would almost certainly be impracticable for safety reasons. Analysis of the final organic phase by differential scanning calorimetry (DSC) showed a small exotherm starting at 104 °C (30 J g^{-1}) followed

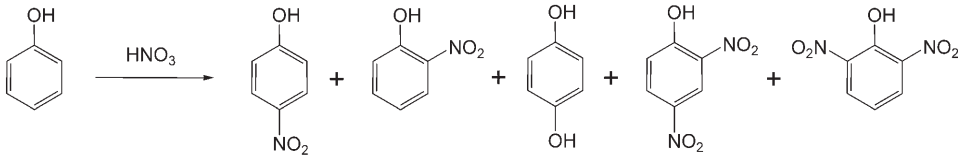

Scheme 1. Nitration of phenol (**1**) affords the mononitro isomers **2** and **3** as main products. Some hydroquinone (**4**), dinitrophenols (**5** and **6**), and polymeric side-products are also formed. *para*-Nitrophenol (**2**) is the most valuable regioisomer commercially.

[*] Dr. L. Ducry, Dr. D. M. Roberge
Lonza Ltd.
Valais Works
3930 Visp (Switzerland)
Fax: (+41) 27-948-6067
E-mail: laurent.ducry@lonza.com
dominique.roberge@lonza.com

InterScience
© 2005 Wiley-VCH Verlag GmbH & Co. KGaA, Weinheim

Table 1: Phenol nitration in semibatch or in continuous mode (microreactor, MR).[a]

Entry	Equipment	T [°C]	HNO_3 [equiv]	CH_3CO_2H [%]	H_2O [%]	Yield [%]	Ratio **2**/**3**	Purity [wt%]	**1** [wt%]	**4** [area%]	**5** [area%]	**6** [area%]	Polymers [area%]
1	RC1	25	1.5	6	71	54	1.2	56.5	0.1	0.6	0.5	0.0	32.3
2	RC1	25	2.0	6	71	55	1.2	57.8	0.0	0.0	0.0	1.9	32.2
3	MR	35	1.5	6	71	70	1.1	71.1	0.1	0.8	0.0	0.0	18.0
4	MR	45	1.1	6	71	65	1.2	65.8	4.6	0.8	0.0	0.0	18.8
5	MR	45	1.2	6	71	68	1.2	67.4	0.6	1.6	0.0	0.0	20.4
6	MR	45	1.5	6	71	73	1.1	74.8	0.0	1.4	0.6	0.0	13.2
7	MR	45	1.8	6	71	75	1.1	79.4	0.0	1.6	0.0	0.6	9.0
8	MR	60	1.6	6	71	76	1.0	78.2	0.0	2.4	0.8	0.0	8.6
9	batch	0	2.0	0	78	30	1.2	25.3	0.0	0.0	0.0	0.0	64.7
10	batch	10	2.0	0	78	32	0.7	17.9	0.0	0.0	0.0	0.0	72.1
11	batch	20	2.0	0	78	21	0.6	12.8	0.0	0.0	0.0	0.0	77.2
12	MR	20	1.4	0	10	77	1.0	74.6	0.3	3.8	4.2	1.9	7.1
13	MR	20	2.0	0	10	69	1.0	73.9	0.4	2.3	6.8	2.7	6.6
14	MR	20	2.3	0	10	65	0.9	72.4	0.4	2.0	7.8	3.0	7.4
15	MR	5	1.7	0	10	74	0.9	77.4	0.0	2.9	3.2	0.0	6.5
16	MR	15	1.7	0	10	70	0.9	75.7	0.3	2.9	4.2	1.3	6.9
17	MR	25	1.7	0	10	70	0.9	74.5	0.3	3.1	5.5	1.9	6.6
18	MR	35	1.7	0	10	69	0.9	73.1	0.3	3.2	6.6	2.3	6.8
29	MR	45	1.7	0	10	65	0.9	70.7	0.4	2.8	7.4	2.4	8.7
20	MR	55	1.7	0	10	65	0.9	69.3	0.4	3.1	8.7	2.8	8.5

[a] The nitrated solution was analyzed by GC (quantitative results for **1**, **2** and **3**, area% for the side-products). The yield (calcd) and purity correspond to the total amount of mononitro products **2** and **3**. The water concentration does not take into account the water contained in nitric acid.

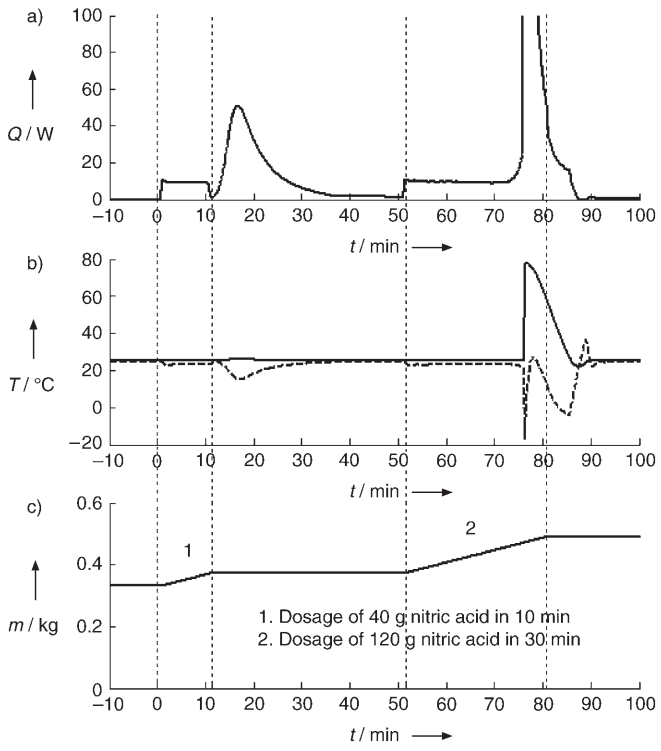

Figure 1. Semibatch nitration of phenol at 25 °C with acetic acid (Table 1, entry 2): a) heat signal (Q, positive values denote exothermic reactions); b) reaction temperature (T, ——) and temperature of the cooling system (T, -----); c) addition rate (m) versus reaction time (t).

by a large one at 185 °C (1500 $J\,g^{-1}$), which actually corresponds to a thermal runaway scenario.

A glass microreactor with a 10×0.5-mm channel width and 2.0 mL internal volume was next used for the nitration experiments (entries 3–8). The phenol solution (23%) in a mixture of CH_3CO_2H (6%) and water (71%, feed 1) and the 65% HNO_3 solution (feed 2) were continuously pumped through the mixer at a total flow rate of approximately 21 $g\,min^{-1}$ (phenol throughput of 3.7 $g\,min^{-1}$). The split between the phenol (**1**) and the nitric acid solutions was varied between 3.9:1 and 2.3:1, which corresponds to 1.1 to 1.8 equivalents of HNO_3. The efficient cooling of the microreactor allowed safe control of the exothermic reaction. With 1.5 equivalents of HNO_3, a one-minute delay was observed at 45 °C before the start of the autocatalysis (Figure 2). The autocatalysis started immediately at a higher temperature with 1.5 equivalents of HNO_3 (entry 8), whereas at lower temperatures the autocatalysis did not start at all, was extinguished, or partially took place outside the microreactor. Similar trends were also observed on variation of the amount of HNO_3: the nitration was completed within the microreactor with 1.8 equivalents of HNO_3 (entry 7), while the reaction proved slower and occurred partially outside the reactor (residence time: 7 s) at a lower stoichiometry. One advantage of a glass microreactor is the possibility to observe the reaction as it takes place. After the start of the autocatalysis, the violent evolution of a colorless gas suggests that gaseous nitrogen dioxide (N_2O_4) is formed in the catalytic cycle. However, the true reactive species for this reaction is presumably the dissociated nitrogen dioxide radical ($NO_2^{\bullet}$) which couples with the radical cation from the phenol in a single electron-transfer mechanism.[10]

Reduced amounts of polymeric side-products, increased purities, and up to 20% higher yields were obtained when performing the reaction continuously in a microreactor. Only

 © 2005 Wiley-VCH Verlag GmbH & Co. KGaA, Weinheim

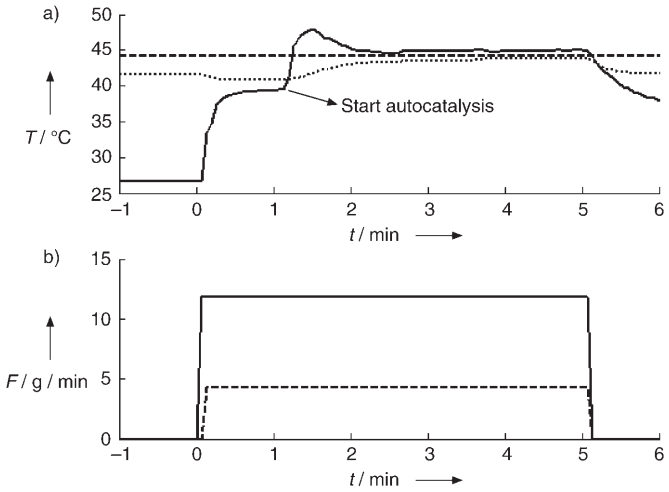

Figure 2. Phenol nitration in a microreactor at 45 °C with acetic acid (Table 1, entry 6): a) temperature of the thermal fluid inlet (*T*, -----), temperature of the thermal fluid outlet (*T*, •••••), and temperature of the reaction mixture outlet (*T*, ——); b) phenol addition rate (*F*, ——) and nitric acid addition rate (*F*, -----) versus time on stream (*t*).

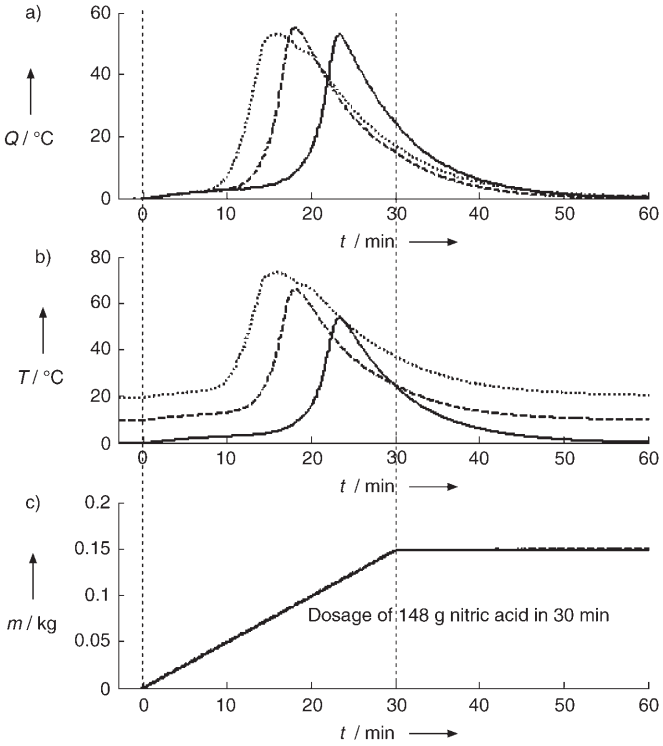

Figure 3. Batchwise phenol nitration at 0 (——), 10 (-----), and 20 °C (•••••) without acetic acid (Table 1, entries 9–11): a) heat signal (*Q*) obtained from the difference of the reactor and jacket temperatures; b) reaction temperatures (*T*); c) mass of nitric acid added (*m*) versus reaction time (*t*).

about 9 % of polymers were formed when 1.6 and 1.8 equivalents of HNO_3 were used (entries 7 and 8). Lower HNO_3 stoichiometries resulted in intermediate amounts of polymers, possibly reflecting the part of the nitration which took place outside the microreactor (batch instead of flow reaction). While the *para* isomer **2** was slightly favored in batch reactions, especially at lower temperature, no significant regioselectivity was observed with the microreactor.

In a second set of experiments, phenol nitration was studied without CH_3CO_2H. For comparison purposes, the reaction was again first performed batchwise in a jacketed 100-mL reactor. Continuous addition of 65 % HNO_3 to a 24 % aqueous phenol solution was carried out at various temperatures (Figure 3). These conditions correspond to a liquid–liquid biphasic system where the phenol (**1**) is dispersed as a fine emulsion. The reactions only started after a delay of 15, 18, and 24 minutes at 20, 10, and 0 °C, respectively, as judged by the heat signal. Not surprisingly, the lower the temperature, the longer the time required to start the autocatalysis. In each case, the exotherm was such that a 50 °C temperature rise occurred. These conditions led mainly to polymer formation and only 21–32 % yield of nitrophenols **2** and **3** (entries 9–11).

The phenol nitration without CH_3CO_2H was next investigated using the microreactor. The phenol concentration was increased to 90 % (feed 1) because of the difficulty to continuously dose a liquid–liquid emulsion. The HNO_3 solution (feed 2) was first diluted with water to obtain the same concentration as in the batch experiments. Based on the good temperature control obtained with the microreactor, the concentration of the nitric acid solution was increased stepwise and commercial 65 % HNO_3 solution was finally used (entries 12–20). Thus, these experiments were performed solvent-free, except for the 10 % water used to liquefy the phenol and the water present in the nitric acid. The flow rate was reduced to about 8 $g\,min^{-1}$ (1.6:1 split, phenol throughput of 2.8 $g\,min^{-1}$). Under these concentrated conditions the autocatalysis always started spontaneously in the mixing zone of the microreactor, thus allowing safe control of the reaction. The amount of polymeric components decreased by a factor of 10 compared to batch experiments, with the yield of the mononitro products **2** and **3** increasing correspondingly. However, the amount of hydroquinone (**4**) and of dinitro compounds **5** and **6** also increased. The best yield (77 %) and purity (74.6 %) of nitrophenols **2** and **3** were obtained with 1.4 equivalents of nitric acid at 20 °C (entry 12). Some unreacted phenol remained at lower stoichiometries, presumably a consequence of HNO_3 consumption in overnitration and oxidation reactions. In contrast to the series with acetic acid, *ortho* isomer **3** was slightly favored.

The results described above indicate that higher yields of nitrophenols are obtained when the nitration of phenol is performed in a microreactor (both with and without CH_3CO_2H). Enhanced heat exchange, good mixing properties, and very rapid radical propagation in a confined volume account for this result. In addition to the small reacting volumes present at any given time, continuous phenol nitration in a microreactor allows for better control of the exothermic reactions. Running the nitration under more concentrated conditions, almost solvent-free and without H_2SO_4 or CH_3CO_2H, is important to ensure that the nitration takes place within the microreactor. Thus, the resulting improved yields and enhanced process safety make micro-

 © 2005 Wiley-VCH Verlag GmbH & Co. KGaA, Weinheim

reactor technology attractive to operate autocatalytic reactions such as nitrations on an industrial scale.

Received: July 8, 2005
Published online: November 10, 2005

Keywords: autocatalysis · microreactor · nitration · oxidation · synthetic methods

[1] a) A. Lunghi, P. Cardillo, *Riv. Combust.* **1997**, *51*, 1–2; b) J. Barton, R. Rogers, *Chemical Reaction Hazards*, IChemE, Trowbridge, **1997**.
[2] N. G. Anderson, *Org. Process Res. Dev.* **2001**, *5*, 613–621.
[3] M. Baudouin, J.-L. Bougeois, S. Ratton, J.-P. Lecouve, Patent US 5030769, **1991**.
[4] a) W. Ehrfeld, V. Essel, H. Löwe, *Microreactors*, Wiley-VCH, Weinheim, **2000**; b) P. D. I. Fletcher, S. J. Haswell, E. Pombo-Villar, B. H. Warrington, P. Watts, S. Y. F. Wong, X. Zhang, *Tetrahedron* **2002**, *58*, 4735–4757; c) K. Jähnisch, V. Hessel, H. Löwe, M. Baerns, *Angew. Chem.* **2004**, *116*, 410–451; *Angew. Chem. Int. Ed.* **2004**, *43*, 406–446.
[5] a) H. Wurziger, J. Stoldt, K. Fabian, N. Schwesinger, Patent DE 19935692A1, **2001**; b) G. Panke, T. Schwalbe, W. Stirner, S. Taghavi-Moghadam, G. Wille, *Synthesis* **2003**, 2827–2830; c) J. Antes, D. Boskovic, H. Krause, S. Loebbecke, N. Lutz, T. Tuercke, W. Schweikert, *Trans. IChemE A* **2003**, *81*, 760–765.
[6] G. A. Olah, R. Malhotra, S. C. Narang, *Nitration: Methods and Mechanisms*, VCH, New York, **1989**.
[7] C. A. Bunton, E. D. Hughes, C. K. Ingold, D. I. H. Jacobs, M. H. Jones, G. J. Minkoff, R. I. Reed, *J. Chem. Soc.* **1950**, 2628–2656.
[8] H. Martinsen, *Z. Phys. Chem.* **1904**, *50*, 385–435.
[9] D. S. Ross, G. P. Hum, W. G. Blucher, *J. Chem. Soc. Chem. Commun.* **1980**, 532–533.
[10] a) V. D. Pokhodenko, V. A. Khizhnyi, V. G. Koshechko, O. I. Shkrebtii, *Zh. Org. Khim.* **1975**, *11*, 1883–1886; b) C. L. Perrin, *J. Am. Chem. Soc.* **1977**, *99*, 5516–5518; c) U. Al-Obaidi, R. B. Moodie, *J. Chem. Soc. Perkin Trans. 2* **1985**, 467–472.

 © 2005 Wiley-VCH Verlag GmbH & Co. KGaA, Weinheim

Asymmetric Synthesis

DOI: 10.1002/anie.200502646

Phase-Transfer-Catalyzed Asymmetric Aza-Henry Reaction Using *N*-Carbamoyl Imines Generated In Situ from α-Amido Sulfones**

Francesco Fini, Valentina Sgarzani, Daniel Pettersen, Raquel P. Herrera, Luca Bernardi,* and Alfredo Ricci*

Nucleophilic addition to the C=N bond of imine derivatives is of paramount importance in organic chemistry for the synthesis of functionalized amines and related nitrogen-containing compounds.[1] In this transformation, the substituent on the nitrogen atom of the imine often plays a crucial role, thus strongly affecting the electrophilicity.[2] In principle, as well as guaranteeing sufficient reactivity, this *N*-substituent should be easily removable after the reaction has taken place. Both requirements are fulfilled by carbamoyl groups, such as *tert*-butoxycarbonyl (Boc) or benzyloxycarbonyl (Cbz).[3] However, because of their inherent high reactivity, *N*-carbamoyl imines are rather sensitive to moisture, their purification (though often not necessary) is rather troublesome, and their storage requires some precautions. Furthermore, the isolation of *N*-carbamoyl imines derived from aliphatic enolizable aldehydes has not been reported, as they readily tautomerize to the corresponding ene carbamate,[4] thus resulting in a considerable limitation to the generality of their applications. A possible way to overcome these drawbacks is the in situ generation of the imine through the use of carbamates with a good leaving group at the carbon atom α to the nitrogen atom. Among the suitable imine precursors available, α-amido sulfones **1** are particularly attractive as they are bench-stable solids and can be very easily obtained by the condensation of a carbamate and a sodium aryl sulfinate with the appropriate aldehyde.[5] As α-amido

[*] Dr. R. P. Herrera[+]
Departamento de Química Orgánica
Universidad de Alicante
Apdo 99, 03080 Alicante (Spain)
Fax: (+39) 051-209-3654
E-mail: rph@alu.ua.es

F. Fini, V. Sgarzani, Dr. D. Pettersen, Dr. L. Bernardi, Prof. A. Ricci
Dipartimento di Chimica Organica "A. Mangini"
Università di Bologna
Viale Risorgimento 4, 40136, Bologna (Italy)
Fax: (+39) 051-209-3654
E-mail: nacca@ms.fci.unibo.it

[+] Current address: Dipartimento di Chimica Organica "A. Mangini"
Università di Bologna
Viale Risorgimento 4, 40136 Bologna (Italy)

[**] We acknowledge financial support from the National Project "Stereoselezione in Sintesi Organica. Metodologie ed Applicazioni, 2003" and by the RTN project "Design, Analysis and Computation for Catalytic Organic Reactions", contract HPRN-CT-2001-00172, which also provided a postdoctoral fellowship to R.P.H. and D.P.

Supporting information for this article is available on the WWW under http://www.angewandte.org or from the author.

© 2005 Wiley-VCH Verlag GmbH & Co. KGaA, Weinheim

sulfones **1** furnish the corresponding imine when treated with a base,[6] they have been widely used in combination with hard organometallic reagents or metal-stabilized enolates.[7] The formation of the imine in situ can also be achieved by using a phase-transfer catalyst in combination with an inorganic base. Despite the considerable benefits of the latter approach, which combines the operational simplicity and the mild reaction conditions typical of phase-transfer catalysis (PTC)[8] with the convenience and the generality of the use of α-amido sulfones **1** as imine surrogates, this reaction has been only occasionally reported.[9]

Bearing in mind the impressive applications of PTC in enantioselective transformations,[8] we decided to employ this strategy in the catalytic asymmetric nucleophilic addition of nitromethane to *N*-carbamoyl imines (aza-Henry reaction) generated in situ from α-amido sulfones **1**[10] using cinchona-derived quaternary ammonium salts as catalysts.[11] The aza-Henry reaction,[12] and especially its catalytic asymmetric variants,[13] has received a lot of attention in recent years, the resulting β-nitroamines being readily converted into highly valuable chiral compounds, such as α-amino acids and vicinal diamines. After the first pioneering reports on metal-catalyzed asymmetric aza-Henry reactions,[14] a few organocatalytic protocols have been reported.[15] Despite the remarkable results in terms of enantioselectivity and catalytic efficiency, all methods show a considerable limitation in the variability of the imine partner because preformed imines are employed. We felt that our approach could significantly extend the scope of the reaction, besides providing a new and convenient protocol for this asymmetric transformation.[16]

To test the feasibility of our approach, we thought it convenient to first explore the capability of phase-transfer catalysts derived from cinchona alkaloids to impart an appreciable asymmetric induction in the addition of nitromethane to *N*-carbamoyl imines. For this purpose, *N*-Boc imine **2a** was treated in the presence of catalytic amounts of several cinchona-derived quaternary ammonium salts and KF as a base under the solid–liquid PTC conditions used for the enantioselective addition of nitromethane to chalcones and for the Henry reaction (Scheme 1).[17] Among the catalysts tested (see the Supporting Information), the commercially available *N*-benzyl quininium chloride **4** proved to be the most effective, thus furnishing the corresponding β-nitroamine **3a** after 18 h in good yield of isolated product and with moderate, but promising, enantiomeric excess (Scheme 1). Encouraged by this result, we turned our attention to the possibility of using **1a** directly in the reaction with nitromethane. After a thorough screening of different

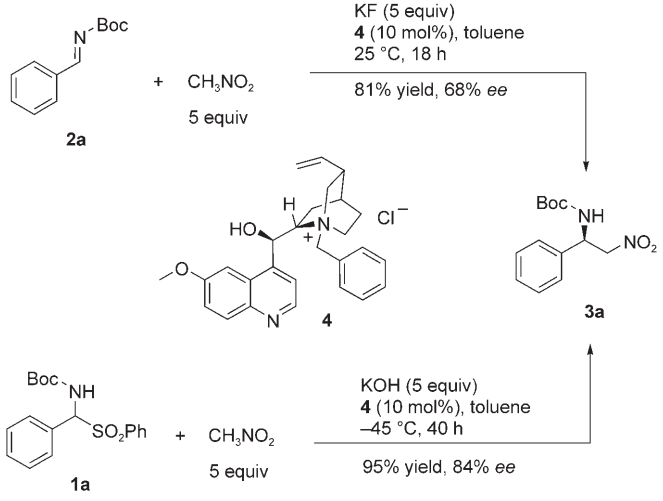

Scheme 1. PTC aza-Henry reaction using imine **2** and α-amido sulfone **1a**.

reaction conditions (see the Supporting Information), we found that the reaction proceeded smoothly even at low temperature when a stronger base, such as solid KOH, was used, thus furnishing the product **3a** directly from **1a** at −45 °C in good yield and with useful enantiomeric excess (Scheme 1).

We next investigated the generality of this new catalytic enantioselective addition of nitromethane to *N*-carbamoyl imines generated in situ from **1** by varying both the substituent of the starting compound **1** and the protecting group (PG) on the nitrogen atom (Table 1). A few α-amido sulfones **1a–e** derived from aromatic and heteroaromatic

Table 1: Catalytic asymmetric addition of nitromethane to *N*-carbamoyl imines generated in situ from α-amido sulfones **1a–l** under PTC.[a]

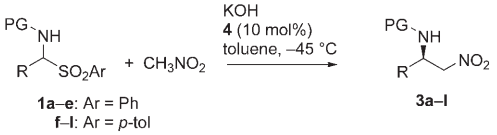

Entry	**1**	R group	PG	**3**	*t* [h]	Yield [%][b]	*ee* [%][c]
1	**1a**	Ph	Boc	**3a**	40	95	84 (>99)[e]
2	**1b**	*o*-BrC_6H_4	Boc	**3b**	64	70	76
3	**1c**	*p*-$MeOC_6H_4$	Boc	**3c**	60	75[d]	88 (>99)[e]
4	**1d**	1-naphtyl	Boc	**3d**	44	95	84
5	**1e**	2-furyl	Boc	**3e**	25	81	75
6	**1f**	$PhCH_2CH_2$	Boc	**3f**	40	98	95
7	**1g**	Cy	Boc	**3g**	42	84	98
8	**1h**	*i*Pr	Boc	**3h**	40	95	95
9	**1i**	Et	Boc	**3i**	40	92	94
10	**1j**	Me	Boc	**3j**	43	86	92
11	**1k**	Ph	Cbz	**3k**	44	53[f]	73
12	**1l**	Cy	Cbz	**3l**	40	96[f]	93

[a] Experimental conditions: finely ground KOH (0.5 mmol) was added to a cooled mixture (−45 °C) of **1** (0.1 mmol), **4** (0.01 mmol), and CH_3NO_2 (0.5 mmol) in toluene (1 mL), and the reaction mixture vigorously stirred for the stated time. [b] Yield of the isolated product after chromatography on silica gel. [c] Determined by chiral stationary-phase HPLC. [d] aqueous KOH (50% w/w) was used in the reaction. [e] After a single crystallization. [f] A mixture of toluene/CH_2Cl_2 (1:1) was used as the solvent. Cy = cyclohexyl.

 © 2005 Wiley-VCH Verlag GmbH & Co. KGaA, Weinheim

aldehydes were treated with nitromethane under the optimized reaction conditions, thus furnishing the corresponding optically active *N*-Boc β-nitroamines **3a–e** in fairly good yield and enantiomeric excess (entries 1–5). It is noteworthy that **3a** and **3c** could be obtained in essentially enantiopure form after a single crystallization (entries 1 and 3). Moreover, we found that this new strategy for the catalytic enantioselective aza-Henry reaction was particularly effective for the synthesis of *N*-Boc α-alkyl β-nitroamines, which cannot be obtained by the previously reported methods. As a matter of fact, **1f–j**, derived from both linear and branched aliphatic aldehydes, all gave the corresponding β-nitroamines **3f–j** in very good yields and enantioselectivities (entries 6–10). The efficiency of the present method for this class of substrates is well accounted for by the high enantiofacial discrimination in the imine derived from **1j** (entry 10) bearing a proton and a small methyl group. Variation of the protecting group on the nitrogen atom was then shortly investigated using **1k** and **1l** bearing a Cbz moiety (entries 11 and 12), thus demonstrating that the present method is not restricted to obtaining *N*-Boc-protected β-nitroamines. Also in this case, **1l**, derived from an aliphatic aldehyde, gave better results with respect to **1k**.

The absolute configuration of the products was determined by comparison of the HPLC retention time and optical rotation of **3a** with reported values[15b,c] and by reduction of **3h** (see the Supporting Information) to the known diamine derivative.[18] Attack on the *Si* face of the intermediate imine by the nitronate and quininium ion pair accounts for the *R* configuration at the stereogenic centre observed in both cases.

In summary, we have developed a new catalytic enantioselective approach to the asymmetric nucleophilic addition of nitromethane to *N*-carbamoyl imines generated in situ from α-amido sulfones. The chiral phase-transfer catalyst acts in a dual fashion,[19] first promoting the formation of the imine under mild reaction conditions and then activating the nucleophile for asymmetric addition. The potential of this approach was demonstrated in the reaction of nitromethane with α-amido sulfones, which could be efficiently catalyzed by a simple and commercially available quininium salt. Besides the mild reaction conditions and the operational simplicity, this new method allows *N*-carbamoyl imines derived from enolizable aldehydes in a catalytic asymmetric aza-Henry reaction to be used for the first time, thus extending the generality of this asymmetric transformation.

Received: July 27, 2005
Published online: November 15, 2005

Keywords: α-amido sulfones · asymmetric synthesis · aza-Henry reaction · nucleophilic addition · phase-transfer catalysis

[1] For recent reviews, see: a) R. A. Volkmann, *Nucleophilic Addition to Imines and Imine Derivatives* in *Comprehensive Organic Synthesis, Vol. I* (Eds.: B. M. Trost, I. Fleming, S. L. Schreiber), 1st ed., Pergamon, Oxford, **1991**, p. 355; b) D. Enders, U. Reinhold, *Tetrahedron: Asymmetry* **1997**, 1895; c) R. Bloch, *Chem. Rev.* **1998**, *98*, 1407; d) S. Kobayashi, H. Ishitani, *Chem. Rev.* **1999**, *99*, 1069; e) A. Córdova, *Acc. Chem. Res.* **2004**, *37*, 102.

[2] S. M. Weinreb, *Top. Curr. Chem.* **1997**, *190*, 131.

[3] a) H. A. Zuagg, *Synthesis* **1984**, 85; b) H. A. Zuagg, *Synthesis* **1984**, 181; for recent applications of *N*-carbamoyl and *N*-acyl imines, see for example; c) A. M. Kanazawa, J.-N. Denis, A. E. Greene, *J. Org. Chem.* **1994**, *59*, 1238; d) A. Okada, T. Shibuguchi, T. Ohshima, H. Masu, K. Yamaguchi, M. Shibasaki, *Angew. Chem.* **2005**, *117*, 4640; *Angew. Chem. Int. Ed.* **2005**, *44*, 4564; e) T. B. Poulsen, C. Alemparte, S. Saaby, M. Bella, K. A. Jørgensen, *Angew. Chem.* **2005**, *117*, 2956; *Angew. Chem. Int. Ed.* **2005**, *44*, 2896; f) D. Uraguchi, K. Sorimachi, M. Terada, *J. Am. Chem. Soc.* **2004**, *126*, 11804; g) R. Matsubara, Y. Nakamura, S. Kobayashi, *Angew. Chem.* **2004**, *116*, 1711; *Angew. Chem. Int. Ed.* **2004**, *43*, 1679; h) A. G. Wenzel, E. N. Jacobsen, *J. Am. Chem. Soc.* **2002**, *124*, 12964.

[4] T. Mecozzi, M. Petrini, *Synlett* **2000**, 73.

[5] a) J. B. F. N. Engberts, J. Strating, *Recl. Trav. Chim. Pys-Bas* **1965**, *84*, 942; b) W. H. Pearson, A. C. Lindbeck, J. W. Kampf, *J. Am. Chem. Soc.* **1993**, *115*, 2622.

[6] A method for the synthesis of aromatic *N*-Boc imines involves the treatment of α-amido sulfones with K_2CO_3 in THF at reflux for several hours; see reference [3c].

[7] a) J. Morton, A. Rahim, E. R. H. Walker, *Tetrahedron Lett.* **1982**, *23*, 4122; b) N. Hermanns, S. Dahmen, C. Bolm, S. Bräse, *Angew. Chem.* **2002**, *114*, 3844; *Angew. Chem. Int. Ed.* **2002**, *41*, 3692; c) D. Enders, S. Oberbörsch, *Synlett* **2002**, 471; d) C. Palomo, M. Oiarbide, A. Landa, M. C. González-Rego, J. M. García, A. González, J. M. Odriozola, M. Martin-Pastor, A. Linden, *J. Am. Chem. Soc.* **2002**, *124*, 8637; e) C. Palomo, M. Oiarbide, C. González-Rego, A. K. Sharma, J. M. García, A. González, C. Landa, A. Linden, *Angew. Chem.* **2000**, *112*, 1105; *Angew. Chem. Int. Ed.* **2000**, *39*, 1063; f) M. Petrini, R. Profeta, P. Righi, *J. Org. Chem.* **2002**, *67*, 4530; g) N. Giri, M. Petrini, R. Profeta, *J. Org. Chem.* **2004**, *69*, 7303, and references therein.

[8] For recent reviews, see: a) A. Nelson, *Angew. Chem.* **1999**, *111*, 1685; *Angew. Chem. Int. Ed.* **1999**, *38*, 1583; b) K. Maruoka, T. Ooi, *Chem. Rev.* **2003**, *103*, 3013; c) B. Lygo, B. I. Andrews, *Acc. Chem. Res.* **2004**, *37*, 518; d) M. J. O'Donnell, *Acc. Chem. Res.* **2004**, *37*, 506.

[9] a) R. Kimura, T. Nagano, H. Kinoshita, *Bull. Chem. Soc. Jpn.* **2002**, *75*, 2517; b) V. Banphavichit, S. Chaleawlertumpon, W. Bhanthumnavin, T. Vilaivan, *Synth. Commun.* **2004**, *34*, 3147.

[10] For a reaction of nitromethane with α-amido sulfones, see: a) R. Ballini, M. Petrini, *Tetrahedron Lett.* **1999**, *40*, 4449; b) E. Foresti, G. Palmieri, M. Petrini, R. Profeta, *Org. Biomol. Chem.* **2003**, *1*, 4275.

[11] a) H. Wynberg, *Top. Stereochem.* **1986**, *16*, 87; b) K. Kacprzak, J. Gawroñski, *Synthesis* **2001**, 961.

[12] a) H. Adams, J. C. Anderson, S. Peace, A. M. K. Pennell, *J. Org. Chem.* **1998**, *63*, 9932; b) Z. Li, C.-J. Li, *J. Am. Chem. Soc.* **2005**, *127*, 3672; c) J. C. Anderson, A. J. Blake, J. P. Howell, C. Wilson, *J. Org. Chem.* **2005**, *70*, 549; d) L. Bernardi, B. F. Bonini, E. Capitò, M. Comes-Franchini, G. Dessole, M. Fochi, A. Ricci, *J. Org. Chem.* **2004**, *69*, 8168, and references therein.

[13] For an overview, see: B. Westermann, *Angew. Chem.* **2003**, *115*, 161; *Angew. Chem. Int. Ed.* **2003**, *42*, 151.

[14] a) K.-i. Yamada, S. J. Harwood, H. Gröger, M. Shibasaki, *Angew. Chem.* **1999**, *111*, 3713; *Angew. Chem. Int. Ed.* **1999**, *38*, 3504; b) K.-i. Yamada, G. Moll, M. Shibasaki, *Synlett* **2001**, 980; c) N. Nishiwaki, K. R. Knudsen, K. V. Gothelf, K. A. Jørgensen, *Angew. Chem.* **2001**, *113*, 3080; *Angew. Chem. Int. Ed.* **2001**, *40*, 2992; d) K. R. Knudsen, T. Risgaard, N. Nishiwaki, K. V. Gothelf, K. A. Jørgensen, *J. Am. Chem. Soc.* **2001**, *123*, 5843.

[15] a) T. Okino, S. Nakamura, T. Furukawa, Y. Takemoto, *Org. Lett.* **2004**, *6*, 625; b) B. M. Nugent, R. A. Yoder, J. N. Johnston, *J. Am.*

 © 2005 Wiley-VCH Verlag GmbH & Co. KGaA, Weinheim

Chem. Soc. **2004**, *126*, 3418; c) T. P. Yoon, E. N. Jacobsen, *Angew. Chem.* **2005**, *117*, 470; *Angew. Chem. Int. Ed.* **2005**, *44*, 466; d) L. Bernardi, F. Fini, R. P. Herrera, A. Ricci, V. Sgarzani, *Tetrahedron*, in press DOI: 10.1016/j.tet.2005.09.076.

[16] Very recently, an asymmetric aza-Henry reaction of two aliphatic *N-para*-methoxyphenyl imines with preformed *O*-silyl propionitronate, which makes use of a chiral Cu^{II} complex as a catalyst, has been reported: J. C. Anderson, G. P. Howell, R. M. Lawrence, C. S. Wilson, *J. Org. Chem.* **2005**, *70*, 5665.

[17] a) S. Colonna, H. Hiemstra, H. Wynberg, *J. Chem. Soc. Chem. Commun.* **1978**, 238; b) E. J. Corey, F.-Y. Zhang, *Org. Lett.* **2000**, *2*, 4257; c) E. J. Corey, F.-Y. Zhang, *Angew. Chem.* **1999**, *111*, 2057; *Angew. Chem. Int. Ed.* **1999**, *38*, 1931.

[18] D. Enders, J. Wiedemann, *Synthesis* **1996**, 1443.

[19] For another example of two sequential processes carried out using a cinchona-derived phase-transfer catalyst, see: B. Lygo, D. C. M. To, *Chem. Commun.* **2002**, 2360.

 © 2005 Wiley-VCH Verlag GmbH & Co. KGaA, Weinheim

Catalyst Research

DOI: 10.1002/anie.200503169

Quasi-Homogeneous Methanol Synthesis Over Highly Active Copper Nanoparticles**

*Sascha Vukojević, Oliver Trapp, Jan-Dierk Grunwaldt, Christoph Kiener, and Ferdi Schüth**

Heterogeneously catalyzed methanol synthesis from synthesis gas over $Cu/ZnO/Al_2O_3$ is one of the most important processes in the chemical industry, with a world production capacity of more than 28 million tons per year.[1] Despite the enormous number of publications on methanol synthesis over copper-based catalysts, however, the nature of the active site(s), the reaction mechanism, the role of Cu and ZnO in the solid catalyst,[2] and further issues remain highly controversial. This is partly due to the problems associated with the analysis of a complex solid catalyst. However, a homogeneous model system for the methanol synthesis catalyst, which would help to address these questions, is lacking so far.[3] We have now succeeded in the development of a quasi-homogeneous version of the process which uses aluminum-stabilized copper colloids with a size of about 5 nm. This catalyst, rather surprisingly, has a productivity that is very high in spite of the absence of ZnO. Consequently, the intrinsic activity of copper in this reaction is much higher than previously thought. Mechanistic studies suggest that the reaction proceeds in a similar manner as on the solid catalyst, which opens new roads for a detailed understanding of one of the most important commercial catalytic systems.

There are several reports in the literature on homogeneously catalyzed methanol synthesis;[4] they typically use catalysts based on transition metals such as Ru,[5,6] Ni,[7,8] or Re.[7] However, these catalysts bear no resemblance to the technically used $Cu/ZnO/Al_2O_3$ system. The homogeneous analog of this process—methanol synthesis over copper-based catalysts—has not been described up to now. Indeed, our attempts with simple copper complexes in solution did not result in the formation of methanol from synthesis gas. However, copper nanoparticles synthesized by reduction of copper acetylacetonate with trialkylaluminum were found to be highly active in this reaction. This shows that copper can have a very high intrinsic activity for methanol synthesis, and opens the door to mechanistic studies of the process with techniques known from homogeneous catalysis.

In the present study colloidal copper nanoparticles were obtained by reduction of copper acetylacetonate in THF with a triorganoaluminum reagent.[9] The organoaluminum compounds also stabilizes the colloid by forming an organometallic protecting shell around the nanoparticles.[10] The resulting copper nanoparticle solutions were deep-red and stable for months in the absence of air. The copper particle size can be tuned in the 3–5 nm range, with a narrow size distribution, by varying the alkyl groups of the aluminum reagent. Figure 1 a shows a TEM image of roughly spherical, isolated copper nanoparticles with sizes of (4.5 ± 1.5) nm. The nano-

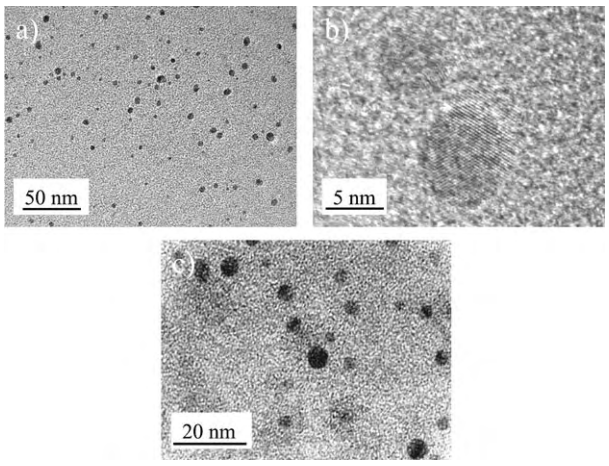

Figure 1. TEM images of trioctylaluminum-stabilized copper nanoparticles: a) freshly prepared (multiple nanoparticles), b) high-resolution TEM, c) after catalysis at 150 °C.

[*] Dipl.-Chem. S. Vukojević, Dr. O. Trapp, Dr. C. Kiener, Prof. Dr. F. Schüth
Max-Planck-Institut für Kohlenforschung
Kaiser-Wilhelm-Platz 1, 45470 Mülheim (Germany)
Fax: (+49) 208-306-2995
E-mail: schueth@mpi-muelheim.mpg.de
Dr. J.-D. Grunwaldt
ETH Hönggerberg
8093 Zürich (Switzerland)

[**] We thank the Max-Planck-Institut für Kohlenforschung and the Deutsche Forschungsgemeinschaft (SFB 558) for financial support. The ESRF (beamlines SNBL and DUBBLE) is gratefully acknowledged for granting beamtime for the development of the new liquid EXAFS cell and the measurements at the Cu K-edge. We thank Mr. A. Dreier and Mr. B. Spliethoff (MPI für Kohlenforschung) for TEM measurements, Prof. Dr. H. Bönnemann for helpful discussions, and Dr. N. Theyssen (MPI für Kohlenforschung) for technical advice.

InterScience
© 2005 Wiley-VCH Verlag GmbH & Co. KGaA, Weinheim

particles are protected against aggregation by a layer of condensed triorganoaluminum molecules. High-resolution TEM images (Figure 1b) revealed that the nanoparticles are crystalline, and upon closer inspection some of the particles were found to consist of one single-crystal domain, while others seemed to be composed of several domains. Lattice fringes with a lattice spacing of about 2.17 Å, which corresponds to the Cu (111) plane, can be resolved in the HRTEM images of Cu nanocrystals (Figure 1b).

The Cu nanoparticles were also subjected to a Cu K-edge EXAFS analysis to obtain complementary insight into the structure of the Cu nanoparticles in solution, especially the oxidation state and the Cu–Cu distance. Figure 2 displays the extracted EXAFS functions at the Cu K-edge and the corresponding radial distribution functions of trioctylaluminum-stabilized copper colloids compared with that of copper foil.

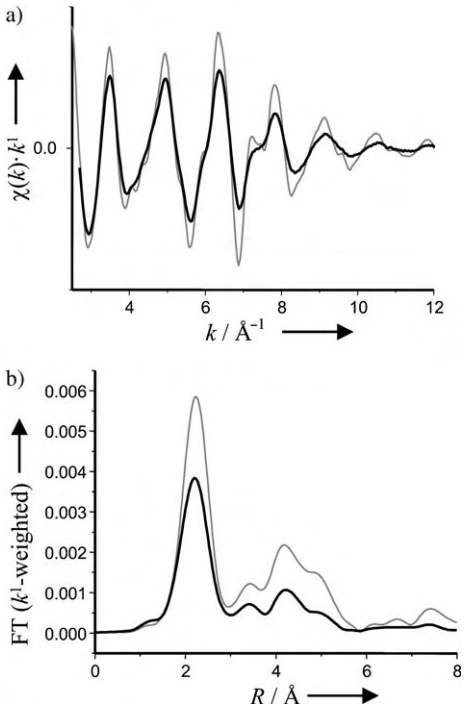

Figure 2. EXAFS function at the Cu K-edge in terms of a) the k^1-weighted $\chi(k)$-function and b) the corresponding radial distribution functions (Fourier-transformed k^1-weighted EXAFS spectra, not corrected for the phase shift) of trioctylaluminum-stabilized copper colloids (black line) in comparison to copper foil as reference (gray line).

The EXAFS experiment confirmed the zero-valent state of copper in the colloids. In the $\chi(k)$-extracted EXAFS functions the same frequency was observed for Cu foil, as reference, and the Cu colloids. The relatively lower amplitude of the function representing the Cu colloids is due to the small size of the Cu nanoparticles (Figure 2a). The Fourier-transformed EXAFS spectra show mainly the first Cu–Cu shell (Figure 2b). Fitting of the EXAFS spectra resulted in a Cu–Cu distance of 2.53 Å, compared to 2.55 Å in bulk copper, which is shorter because of the small size of the Cu nanoparticles.[11,12] This is also supported by the fact that the next nearest neighbors ($R > 4$ Å) give a smaller contribution in the Fourier-transformed EXAFS spectrum. No oxygen shells were detected. The coordination number is significantly lower than in bulk copper (10.9 for trioctylaluminum-stabilized copper colloids and 12 for copper foil) and corresponds to a particle size of about 3 nm.

Freshly synthesized copper colloids dissolved in THF were tested for methanol formation in a laboratory-made, high-pressure, stainless-steel autoclave in a quasi-homogeneous phase. Quantitative online analysis of the reaction mixture was performed with a gas chromatograph coupled directly to the high-pressure autoclave. The ratio of gases in the reaction gas mixture was adjusted to correspond to the typical gas-phase composition ($H_2/CO/CO_2 = 74:20:6$), although the different solubility of the reaction gases in THF resulted in a gas-phase composition with a different molar ratio ($H_2/CO/CO_2 = 86:10:4$). In a typical procedure, the high-pressure autoclave was charged with copper colloid solution (40 mL, 9.8 mM Cu) followed by sequential pressurization with synthesis gas (H_2/CO) and CO_2 at room temperature. The reaction mixture was heated with a ramp of 0.5 K min^{-1} to the desired reaction temperature. Surprisingly, methanol formation started already at 130 °C. The results of the methanol formation under these reaction conditions at temperatures with trioctylaluminum-stabilized copper colloids as catalyst are summarized in Figure 3.

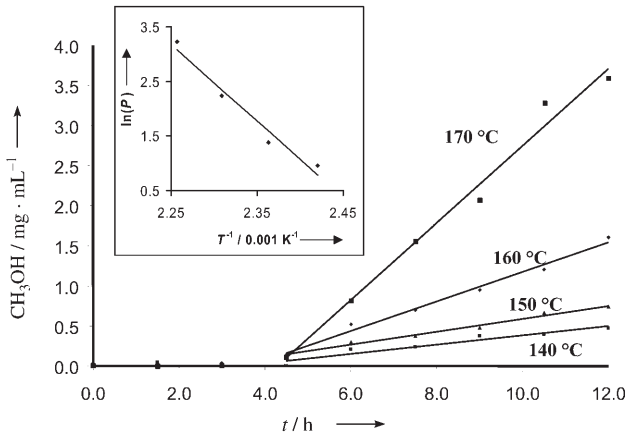

Figure 3. Formation of methanol at temperatures between 140 and 170 °C. Inset: Arrhenius plot for the determination of the apparent activation energy.

The productivity of the methanol formation ($mol_{methanol}/(kg_{Cu}\,h)$) was obtained from the slope of the linear regression of these data points (the first three data points show the methanol formation during the heating period and were not considered in the linear regression). Productivities, P, as high as 25.2 $mol_{methanol}/(kg_{Cu}\,h)$ were observed at elevated reaction-gas pressure and temperature. The results of the temperature-dependent catalytic experiments over trioctylaluminum-stabilized copper colloids are summarized in Table 1 and show an increase in productivity with increasing reaction temperature. From these, turnover

 © 2005 Wiley-VCH Verlag GmbH & Co. KGaA, Weinheim

Table 1: Catalytic performance of trioctylaluminum-stabilized copper colloids at different temperatures.

T [°C]	P [$mol_{methanol}/(kg_{Cu}\,h)$]	TOF [$10^{-4}\ s^{-1}$]
140.0	2.6	3.2
150.0	4.0	4.9
160.0	9.3	11.3
170.0	25.2	30.7

frequencies (TOF) were calculated assuming spherical Cu particles with a diameter of 5 nm and approximately 800 Cu surface atoms per particle. From the temperature-dependent experiments an apparent activation energy of 116 $kJ\,mol^{-1}$ was calculated from the slope of an Arrhenius plot (see inset in Figure 3).

An isotope-labeling experiment with deuterium instead of hydrogen was performed to confirm methanol formation from the reaction gases and to gain further information on the catalytic process. At 150 °C and a gas-phase composition of $D_2/CO/CO_2 = 86:9:5$ at an initial pressure of 11.2 MPa a productivity of 6.8 $mol_{methanol}/(kg_{Cu}\,h)$ was determined. GC-MS analysis revealed the formation of deuterated methanol (CD_3OH; -OD to -OH exchange occured during the separation process) and perdeuterated methyl formate. Methyl formate is often observed as a by-product in the heterogeneously catalyzed synthesis of methanol. It has to be noted, though, that after an initial increase the concentration of methyl formate remained constant throughout the entire run in all experiments. This indicates that methyl formate reaches a steady-state concentration and may therefore not be a by-product but rather an intermediate. To elucidate the role of the methyl formate, the following experiments were conducted: 1) catalysis was performed with synthesis gas only, excluding CO_2. In this experiment, only negligible formation of methanol was observed ($P = 0.4$ $mol_{methanol}/(kg_{Cu}\,h)$); 2) the reaction was carried out with H_2 and CO_2 only, which gave initial methanol formation with the production dropping to zero after 10 h. The initial productivity was determined to be 1.7 $mol_{methanol}/(kg_{Cu}\,h)$ at 140 °C; 3) the reaction was performed with synthesis gas and a trace amount of methyl formate (50 μL in 40 mL of Cu colloid solution), which gave fast initial formation of methanol ($P = 4.2$ $mol_{methanol}/(kg_{Cu}\,h)$). The concentration of methyl formate reaches a steady state due to hydrogenolysis of methyl formate and simultaneous conversion of synthesis gas into methanol via methyl formate. It should be noted that the stability of the Cu colloids in experiment 3 was greater than in experiments where CO_2 was present in the gas phase. Productivity differences were within a margin of error of ± 1.6 $mol_{methanol}/(kg_{Cu}\,h)$.

These experiments with our model Cu catalyst suggest that the reduction of CO_2 to methyl formate is the initial step for methanol formation. However, more detailed studies are necessary to distinguish between different mechanistic pathways.

To exclude the remote possibility that methanol is formed from the acetylacetonate ligands of the copper precursor some of the experiments were repeated with copper colloids synthesized from copper bis(hexafluoroacetylacetonate) by reduction with trioctylaluminum. The resulting Cu colloids were less stable than those synthesized from the non-fluorinated Cu precursor, but were also active in methanol production, although with a reduced productivity $P =$ 2.0 $mol_{methanol}/(kg_{Cu}\,h)$ at 150 °C. No fluorinated by-products or fragments beside hexafluoroacetylacetonate were detected, which, together with the results of the experiments with deuterium as a synthesis gas component, proves that methanol is indeed formed from the synthesis gas.

In an effort to compare these data with the results for a commercially available methanol synthesis catalyst (ICI Katalco 51-8, powder, < 125 μm, same copper amount as in colloidal solution), this catalyst was reduced under H_2 at 250 °C, following the prescribed protocol, and suspended in THF solution. Catalytic testing was performed in a stainless-steel reactor in batch mode at 150 °C with the same reaction conditions as described above. A methanol productivity of 5.5 $mol_{methanol}/(kg_{Cu}\,h)$ was determined after a reaction time of 20 h. This is higher than with the Cu colloids described here. However, it should be kept in mind that the Cu colloids do not contain any Zn species, which are thought to improve the catalytic activity.[2b] Studies of the catalytic activity of commercial catalysts cannot be compared directly to the value measured here for the $Cu/ZnO/Al_2O_3$ system (ICI Katalco 51-8) since these investigations are typically performed at appreciably lower pressures at different temperatures and in the gas phase.

Our study shows that copper nanoparticles are remarkably active catalysts in the quasi-homogeneous phase for methanol synthesis from synthesis gas without any solid support. Similar results have been obtained in independent studies on colloidal Cu/ZnO particles by Fischer.[13] Our results show, in particular, that the ZnO component of the technical catalyst is not absolutely necessary to induce high activity for methanol synthesis, since the colloids without a Zn compound display similar activities as the commercial catalyst, which is in agreement with surface science studies on polycrystalline or single-crystal copper surfaces.[14–16]

Experimental Section

All preparations were carried out in anhydrous THF as solvent under an argon atmosphere.

Organoaluminum-stabilized Cu colloids were synthesized by the dropwise addition of Al(*n*-octyl)$_3$ (7.3 mL, 16.5 mmol) or Al(*n*-butyl)$_3$ (6.7 mL, 27.5 mmol) in THF (30 mL) to a solution of [Cu(acac)$_2$] (1.45 g, 5.5 mmol) in THF (400 mL) at room temperature with mechanical stirring. After 2–3 h the deep-red solution was filtered through a glass frit and stored under argon.

To determine the effective copper concentration an aliquot of the copper colloid solution was dissolved in hydrochloric acid and titrated with ethylenediaminetetraacetic acid solution (0.1M) using murexide as indicator at pH 8.0.

Safety warning: Experiments using large amounts of compressed gases, especially CO, are potentially hazardous and must only be carried out with the appropriate equipment and safety precautions.

The catalytic experiments were carried out in a laboratory-built, stainless-steel, high-pressure autoclave connected to a microvolume high-pressure valve system (0.2 μL) and an online GC analysis setup equipped with a fused-silica column coated with poly(dimethylsiloxane) SE30 (ID 250 μm, film thickness 500 nm). Typically, the Cu colloid solution (40 mL) was placed under argon in the 225-mL,

 © 2005 Wiley-VCH Verlag GmbH & Co. KGaA, Weinheim

window-equipped autoclave together with *n*-heptane (50 μL) as internal standard. A preformed H_2/CO gas mixture (molar ratio 9:1) was prepared in a 5-L autoclave at 25.0 MPa and used throughout the experiments. The reactor was pressurized to the desired starting pressure (10.0–14.0 MPa) whilst stirring vigorously and CO_2 gas (0.6 MPa) was added. The pressurized system was heated to the reaction temperature with a ramp of 0.5 K min^{-1} (pressure at reaction temperature was 17.5–21.5 MPa). Samples were automatically analyzed every 90 min. After the reaction, the reactor was vented to ambient pressure and the collected samples were analyzed by GC, GC-MS, and TEM.

XAS data were collected at the European Synchrotron Radiation Facility (ESRF, Grenoble, France, beamlines SNBL and DUBBLE) using a specially designed cell for liquid samples. The XAS data were obtained in transmission geometry using a Si(111) channel-cut monochromator. For XAS measurements at the Cu K-edge (8.980 keV) the incident and transmitted X-rays were recorded with ionization chambers. Three ionization chambers, located before and after the spectroscopic cell as well as after a Cu foil for energy calibration, were used to measure the incident and output X-ray intensities. The colloidal solution, prepared as above, was introduced into the liquid cell under argon. Kapton windows allowed transmission of the X-rays, and due to appropriate sealing the cell could be dried and evacuated before filling with exclusion of air (for details see ref. [17]). The EXAFS spectra were extracted after background correction, normalization, and energy correction with the WINAXS 3.1 software.[18] Fourier transformation was applied in the region 3 to 12.5 $Å^{-1}$ (the distance scale in the Fourier-transformed EXAFS spectra was not phase-shift corrected) and data fitting was performed in R-space using theoretical phase and amplitude functions calculated with the FEFF 6.0 code.[19]

TEM studies were performed with a Hitachi 7500 and Hitachi HF2000 microscope. Samples were prepared by placing a drop of the dispersed colloidal solution onto a carbon-coated Ni grid. The samples were prepared in a glove box to prevent exposure to air.

Received: September 6, 2005
Published online: November 22, 2005

Keywords: colloids · copper · EXAFS spectroscopy · homogeneous catalysis · nanoparticles

[1] B. Cornils, W. A. Herrmann, R. Schlögl, C.-H. Wong, *Catalysis from A to Z*, Wiley-VCH, Weinheim, **2003**.
[2] a) M. Schur, B. Bems, A. Dassenoy, I. Kassatkine, J. Urban, H. Wilmes, O. Hinrichsen, M. Muhler, R. Schlögl, *Angew. Chem.* **2003**, *115*, 3945 – 3947; *Angew. Chem. Int. Ed.* **2003**, *42*, 3815 – 3817; b) M. Kurtz, J. Strunk, O. Hinrichsen, M. Muhler, K. Fink, B. Meyer, C. Wöll, *Angew. Chem.* **2005**, *117*, 2850 – 2854; *Angew. Chem. Int. Ed.* **2005**, *44*, 2790 – 2794.
[3] T. Ressler, B. L. Kniep, I. Kasatkin, R. Schlögl, *Angew. Chem.* **2005**, *117*, 4782 – 4785; *Angew. Chem. Int. Ed.* **2005**, *44*, 4704 – 4707.
[4] G. Henrici-Olivé, S. Olivé, *The Chemistry of the Catalyzed Hydrogenation of Carbon Monoxide*, Springer, Berlin, **1983**.
[5] P. G. Jessop, T. Ikariya, R. Noyori, *Chem. Rev.* **1995**, *95*, 259 – 272.
[6] K. Tominaga, Y. Sasaki, M. Kawai, T. Watanabe, *J. Chem. Soc. Chem. Commun.* **1993**, 629 – 631.
[7] M. Marchionna, L. Basini, A. Argano, M. Lami, F. Ancillotti, *J. Mol. Catal.* **1992**, *75*, 147 – 151.
[8] D. Mahajan, *Top. Catal.* **2005**, *32*, 209 – 214.
[9] H. Bönnemann, S. S. Botha, B. Bladergroen, V. M. Linkov, *Appl. Organomet. Chem.* **2005**, *19*, 768 – 773.
[10] H. Bönnemann, N. Waldöfner, H.-G. Haubold, T. Vad, *Chem. Mater.* **2002**, *14*, 1115 – 1120.
[11] J.-D. Grunwaldt, A. M. Molenbroek, N.-Y. Topsøe, H. Topsøe, B. S. Clausen, *J. Catal.* **2000**, *194*, 452 – 460.
[12] J.-D. Grunwaldt, B. S. Clausen, *Top. Catal.* **2002**, *19*, 37 – 43.
[13] R. Fischer, private communication.
[14] P. B. Rasmussen, P. M. Holmblad, T. S. Askgaard, C. V. Ovesen, P. Stoltze, J. K. Nørskov, I. Chorkendorff, *Catal. Lett.* **1994**, *26*, 373 – 381.
[15] T. Fujitani, I. Nakamura, T. Watanabe, T. Uchijima, J. Nakamura, *Catal. Lett.* **1995**, *35*, 297 – 302.
[16] J. Yoshihara, C. T. J. Campbell, *J. Catal.* **1996**, *161*, 776.
[17] S. Vukojević, J.-D. Grunwaldt, F. Schüth, unpublished results.
[18] T. Ressler, *J. Synchrotron Radiat.* **1998**, *5*, 118 – 122.
[19] S. I. Zabinsky, J. J. Rehr, A. Ankudinov, R. C. Albers, M. J. Eller, *Phys. Rev.* **1995**, *52*, 2995.

 © 2005 Wiley-VCH Verlag GmbH & Co. KGaA, Weinheim

Natural Product Synthesis

DOI: 10.1002/anie.200502763

Total Synthesis of (−)-Samaderine Y from (*S*)-(+)-Carvone**

Tony K. M. Shing and Ying Y. Yeung*

Quassinoids, a group of heavily oxygenated terpenoid bitter compounds isolated from the *Simaroubaceae* plant family, display a wide range of biological activities[1] and have attracted interest with respect to their synthesis during the past decades.[2] (−)-Samaderine Y (**1**), a pentacyclic quassinoid isolated from *Quassia indica*, was shown to exhibit in

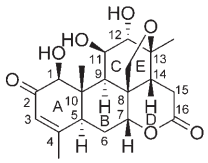

(−)-samaderine Y (**1**)

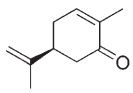

(*S*)-(+)-carvone (**2**)

[*] Prof. Dr. T. K. M. Shing, Y. Y. Yeung
Department of Chemistry
The Chinese University of Hong Kong
Shatin, NT, Hong Kong (China)
Fax: (+852) 2603-5057
E-mail: tonyshing@cuhk.edu.hk

[**] This work was financially supported by a CUHK direct grant. We thank Professor M. Kobayashi (Osaka University) for kindly providing the ^{1}H and ^{13}C NMR spectra of natural (−)-samaderine Y for comparison.

Supporting information for this article is available on the WWW under http://www.angewandte.org or from the author.

© 2005 Wiley-VCH Verlag GmbH & Co. KGaA, Weinheim

vitro cytotoxicity ($IC_{50} = 0.10\ \mu g\,mL^{-1}$) against KB cells[3] and contains stereogenic centers common to many pentacyclic quassinoids as well as structural requirements and functionalities that are essential for cytotoxicity and solid tumor selectivity.[1] Herein, we report the first short, efficient, and enantiospecific total synthesis of (−)-samaderine Y (**1**) from (*S*)-(+)-carvone (**2**).

On the basis of our previous synthetic endeavors toward pentacyclic quassinoids, we reasoned that the hydroxy group at C11 in ring C of **1** should be secured before the construction of the pentacyclic skeleton.[4] The known enone **3**, which is readily available from (*S*)-(+)-carvone (**2**) in two steps that involve an aldol reaction with formaldehyde and acetonation in an overall yield of 75%,[4] was considered a good starting material for our synthesis (Scheme 1). After extensive experimentation, enone **3** was oxidized regioselectively with CrO_3 and 3,5-dimethylpyrazole[5] at the allylic position at C11 (quassinoid numbering scheme) to give ene-dione **4**. Regio- and stereoselective hydride reduction of the less congested keto group in **4** under Luche conditions[6] from the less hindered α face provided a β-alcohol, which was silylated to give silyl ether **5** in good overall yield. Alkaline hydroperoxide epoxidation of enone **5** at the less hindered α face afforded the α-epoxide, which was subjected to chelation-controlled hydride reduction of the remaining keto group to yield epoxy alcohol **6**. Acid-catalyzed shift of the acetonide diol protecting group accompanied by epoxide-ring opening with an internal hydroxy function in a one-pot procedure furnished ether-bridged **7**. The structure of **7** was confirmed by an X-ray crystallographic study,[7] and the stereocenters in rings C and E were thereby established. Protection of the hydroxy group at C12 in **7** gave disilyl ether **8**. Acid hydrolysis of the acetonide in **8** followed by TPAP-catalyzed[8] oxidation of the resultant 1,3-diol gave rise to keto-aldehyde **9** in 78% overall yield from **7**.

Construction of the AB ring system involved the addition of a six-carbon-atom diene to aldehyde **9** to form the Diels–Alder precursor (Scheme 2). Addition of Grignard reagent **10**[4] to aldehyde **9** generated the 1,4-diene **11** as a single diastereomer (the 1,3-cycloadduct). The stereochemistry of the hydroxy group in **11** was confirmed at a later stage. Fortunately, subsequent [1,3]-sigmatropic rearrangement[9] of 1,4-diene **11** furnished the desired 1,3-diene **12** also as a single diastereomer, in which the alcohol group at C7 was then protected as an acetate to give **13**. The AB ring was constructed by an intramolecular Diels–Alder reaction. Heating triene **13** in toluene at 180 °C afforded *trans*- and *cis*-fused tetracyclic keto-acetate **14** in 2:1 ratio based on ^{1}H NMR spectroscopic studies.[10] Variation of the reaction temperature (140–220 °C), reaction time (48–150 h), and solvent (benzene and benzonitrile) did not affect the ratio of *trans* and *cis* isomers. The two diastereomers could not be separated by column chromatography at this stage but were separated later. Our next aim was to invert the configuration at C7 to the desired α-acetate—the stereochemistry found in natural (−)-samaderine Y (**1**). Base-catalyzed hydrolysis of β-acetate **14** afforded alcohol **15**, which was esterified to give triflate **16**. Nucleophilic substitution of triflate **16** with nBu$_4$NOAc[11] provided α-acetate **17**. No *cis*-fused tetracyclic acetate was obtained. Instead, *cis*-fused tetracyclic 1,4-diene **18** was

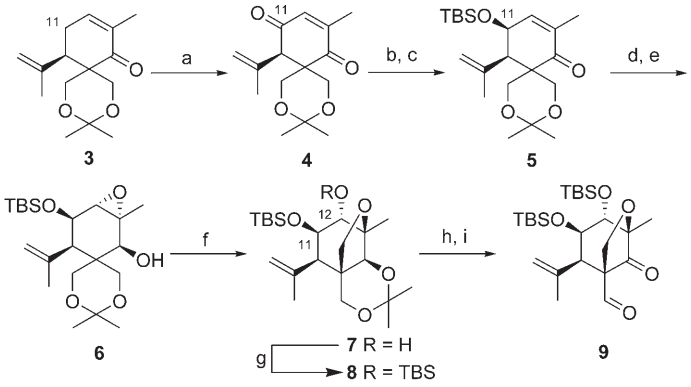

Scheme 1. Construction of the CE ring system. Reagents and conditions: a) CrO_3, 3,5-dimethylpyrazole, CH_2Cl_2, reflux, 70% yield (70% conversion); b) $NaBH_4$, $CeCl_3 \cdot 7H_2O$, MeOH, 0 °C; c) TBSOTf, Et_3N, CH_2Cl_2, room temperature, 87% from **4**; d) TBHP, 2 N NaOH, MeOH, 40 °C; e) $NaBH_4$, $CeCl_3 \cdot 7H_2O$, MeOH, 0 °C; f) 1. TFA, CH_2Cl_2, room temperature; 2. 2,2-dimethoxypropane, *p*TsOH, room temperature, 73% from **6**; g) TBSOTf, Et_3N, CH_2Cl_2, 100%; h) TFA, H_2O, CH_2Cl_2, room temperature, 92%; i) NMO, TPAP, 3 Å MS, CH_2Cl_2, room temperature, 85%. TBS = *tert*-butyldimethylsilyl; Tf = trifluoromethanesulfonyl; TBHP = *tert*-butylhydroperoxide; TFA = trifluoroacetic acid; Ts = *p*-toluenesulfonyl; NMO = *N*-methylmorpholine *N*-oxide; TPAP = tetrapropylammonium perruthenate; MS = molecular sieves.

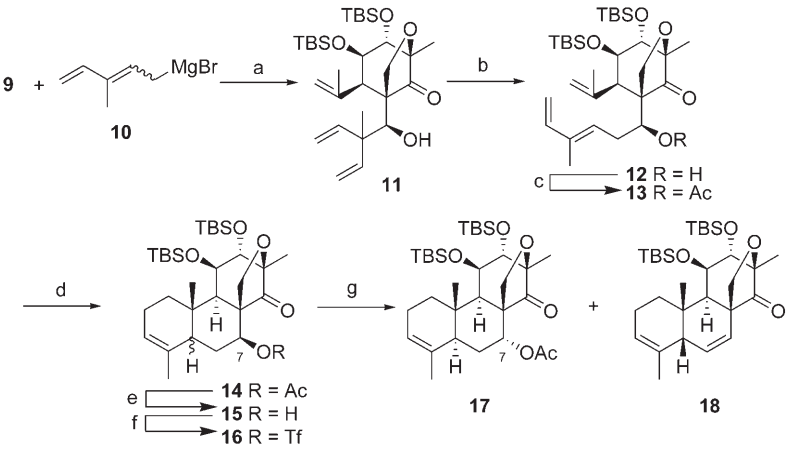

Scheme 2. Construction of the AB ring system. a) Et_2O, 0 °C, 78%; b) NaH, 4-methylbenzo[15]crown-5, THF, room temperature; c) Ac_2O, Et_3N, DMAP, CH_2Cl_2, room temperature, 83% from **11**; d) methylene blue, toluene, 180 °C, 92% (2:1 *trans*:*cis*); e) NaOH, MeOH, room temperature; f) Tf_2O, pyridine, DMAP, CH_2Cl_2, room temperature; g) nBu$_4$NOAc, THF, room temperature, **17** (65% from **15**), **18** (31% from **15**). DMAP = 4-(*N*,*N*-dimethylamino)pyridine.

 © 2005 Wiley-VCH Verlag GmbH & Co. KGaA, Weinheim

isolated, attributable to hindrance imposed by ring A in which substitution could not proceed smoothly. At this stage, compounds **17** and **18** could be separated by column chromatography.

The construction of ring D was our next objective. Intramolecular aldol reaction of acetate **17** gave lactone **19**. The chirality at C14 was introduced in a three-step sequence. Dehydration of the alcohol in **19** afforded α,β-unsaturated lactone **20**. Conjugated reduction[12] of **20** gave rise to the corresponding lactol, which was subjected to acid-catalyzed acetalization with methanol in a one-pot procedure to yield methyl acetal **21** (Scheme 3).

Our remaining task was the functionalization of ring A, and tetracycle **17** was used for model studies (Scheme 4). Oxidation of **17** with classic chromium reagents[13] did not afford enone **28**. After several trials, allylic oxidation of tetracycle **17** did furnish enone **28**.[14] α-Keto acetoxylation[15] of enone **28** gave diacetate **29**, whose structure was confirmed by X-ray crystallography.[7] Following the successful functionalization of ring A of tetracycle **17**, the same procedure was applied to pentacycle **21**.

Allylic oxidation[14] of **21** provided enone **22**, which was subjected to α-keto acetoxylation[15] to give α-acetate **23** as anticipated. The stereogenic center at C1 in **23** had to be inverted before further manipulation could take place. Base hydrolysis of acetate **23** gave alcohol **24**. Acid- or base-catalyzed epimerization of **24** from OH1α to OH1β were unsuccessful. After extensive experimentation, we investigated an oxidation–reduction sequence. Dess–Martin oxidation[16] of alcohol **24** yielded an unstable diketone **25**. Regio- and stereoselective hydride reduction of the carbonyl at C1 in diketone **25** afforded β-alcohol **26**. Acid hydrolysis of acetal **26** gave rise to the corresponding lactol, which was oxidized with Ag_2CO_3 on celite[17] to yield lactone **27**.

Our last objective was the removal of the two silyl ethers, however, conventional desilylation conditions were unsuccessful. After extensive experimentation, the use of concentrated HCl with TFA as the solvent at room temperature led to the smooth removal of the silyl ether groups and gave the target molecule (−)-samaderine Y (**1**) in 61% yield. The physical and spectral data of synthetic **1** were in full accordance with those reported in the literature in all respects.[3]

In summary, (−)-samaderine Y (**1**) was constructed in 21 steps from (*S*)-(+)-carvone (**2**), with an average yield of 81% for each step. This relatively short synthesis opens feasible avenues for the preparation of other optically active pentacyclic quassinoids and analogues for biological evaluation. Research aimed in this direction is in progress.

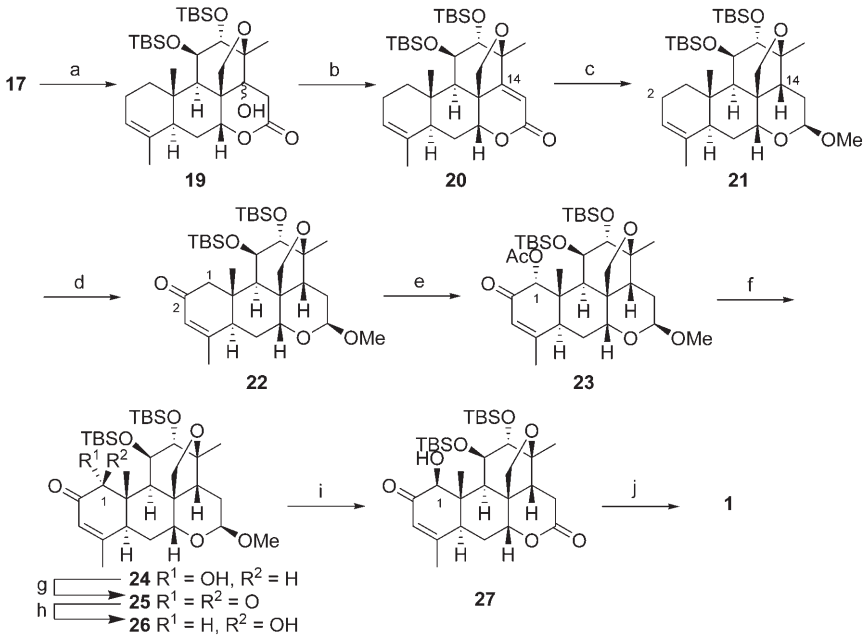

Scheme 3. Synthesis of (−)-samaderine Y (**1**). a) LDA, THF, −78 °C, 88%; b) $SOCl_2$, pyridine, CH_2Cl_2, 45 °C, 94%; c) 1. $NaBH_4$, $NiCl_2 \cdot 6H_2O$, MeOH, room temperature; 2. conc. HCl, room temperature, 78%; d) 10 mol% $Mn(OAc)_3 \cdot 2H_2O$, TBHP, 3 Å MS, EtOAc, room temperature, 72%; e) $Mn(OAc)_3 \cdot 2H_2O$, benzene, reflux, 78%; f) K_2CO_3, MeOH, room temperature, 90%; g) Dess–Martin periodinane, CH_2Cl_2, room temperature; h) $NaBH_4$, THF, MeOH, 0 °C, 80% from **24**; i) 1. conc. HCl, H_2O, THF, 45 °C; 2. Ag_2CO_3/celite, benzene, reflux, 68%; j) conc. HCl, TFA, room temperature, 61%. LDA = lithium diisopropylamide.

Received: August 5, 2005
Published online: November 10, 2005

Keywords: antitumor agents · fused-ring systems · natural products · quassinoids · total synthesis

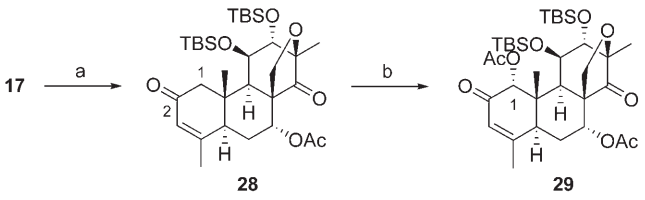

Scheme 4. Functionalization of ring A. a) 10 mol% $Mn(OAc)_3 \cdot 2H_2O$, TBHP, 3 Å MS, EtOAc, room temperature, 70%; b) $Mn(OAc)_3 \cdot 2H_2O$, benzene, reflux, 78%.

[1] For a recent review, see: Z. Guo, S. Vangapandu, R. W. Sindelar, L. A. Walker, R. D. Sindelar, *Curr. Med. Chem.* **2005**, *12*, 173–190.

[2] For some reports of total syntheses of pentacyclic quassinoids, see: a) (*dl*)-samaderine B: P. A. Grieco, M. M. Piñeiro-Nuñez, *J. Am. Chem. Soc.* **1994**, *116*, 7606–7615; b) (−)-chaparrinone, (−)-glaucarubolone, and (+)-glaucarubinone: P. A. Grieco, J. L. Collins, E. D. Moher, T. J. Fleck, R. S. Gross, *J. Am. Chem. Soc.*

 © 2005 Wiley-VCH Verlag GmbH & Co. KGaA, Weinheim

1993, *115*, 6078 – 6093; c) simalikalactone D: E. D. Moher, J. L. Collins, P. A. Grieco, *J. Am. Chem. Soc.* **1992**, *114*, 2764 – 2765.
[3] a) I. Kitagawa, T. Mahmud, K. Yokota, S. Nakagawa, T. Mayumi, M. Kobayashi, H. Shibuya, *Chem. Pharm. Bull.* **1996**, *44*, 2009 – 2014; b) H. Aono, K. Koike, J. Kaneko, T. Ohmoto, *Phytochemistry* **1994**, *37*, 579 – 584.
[4] a) T. K. M. Shing, X. Y. Zhu, Y. Y. Yeung, *Chem. Eur. J.* **2003**, *9*, 5489 – 5500; b) T. K. M. Shing, Q. Jiang, *Tetrahedron Lett.* **2001**, *42*, 5271 – 5273.
[5] W. G. Salmond, M. A. Barta, J. L. Havens, *J. Org. Chem.* **1978**, *43*, 2057 – 2059.
[6] J. L. Luche, L. Rodriguez-Hahn, P. Crabbe, *J. Chem. Soc. Chem. Commun.* **1978**, *14*, 601 – 602.
[7] CCDC 235459 (**7**) and 266924 (**29**) contain the supplementary crystallographic data for this paper. These data can be obtained free of charge from The Cambridge Crystallographic Data Centre via www.ccdc.cam.ac.uk/data_request/cif.
[8] S. V. Ley, J. Norman, W. P. Griffith, S. P. Marsden, *Synthesis* **1994**, *7*, 639 – 666.
[9] S. R. Wilson, D. T. Mao, K. M. Jernberg, S. T. Ezmirly, *Tetrahedron Lett.* **1977**, *18*, 2559 – 2562.
[10] K. Shishido, T. Omodani, M. Shibuya, *J. Chem. Soc. Perkin Trans. 1* **1991**, *9*, 2285 – 2287.
[11] T. K. M. Shing, V. E. F. Tai, *J. Org. Chem.* **1995**, *60*, 5332 – 5334.
[12] T. K. M. Shing, Y. Tang, *J. Chem. Soc. Perkin Trans. 1* **1994**, *12*, 1625 – 1631.
[13] J. Muzart, *Chem. Rev.* **1992**, *92*, 113 – 140.
[14] T. K. M. Shing, Y. Y. Yeung, P. L. So, unpublished results.
[15] R. C. Cambie, M. P. Hay, L. Larsen, C. E. F. Rickard, P. S. Rutledge, P. D. Woodgate, *Aust. J. Chem.* **1991**, *44*, 821 – 842.
[16] D. B. Dess, J. C. Martin, *J. Am. Chem. Soc.* **1991**, *113*, 7277 – 7287.
[17] a) M. Fetizon, M. Golfier, *C. R. Acad. Sci. Ser. C* **1968**, *267*, 900 – 903; b) M. Fetizon, M. Golfier, J. M. Louis, *J. Chem. Soc. D* **1969**, *19*, 1102; c) M. Fetizon, M. Golfier, P. Mourgues, *Tetrahedron Lett.* **1972**, *13*, 4445 – 4448.

 © 2005 Wiley-VCH Verlag GmbH & Co. KGaA, Weinheim

Substituted Fullerenes

DOI: 10.1002/anie.200502419

High-Temperature Synthesis of the Surprisingly Stable C_1-$C_{70}(CF_3)_{10}$ Isomer with a *para*^{7}–*meta*–*para* Ribbon of Nine $C_6(CF_3)_2$ Edge-Sharing Hexagons**

Ivan E. Kareev, Igor V. Kuvychko, Alexey A. Popov, Sergey F. Lebedkin, Susie M. Miller, Oren P. Anderson, Steven H. Strauss, and Olga V. Boltalina**

With one exception, isolable $C_{70}X_{10}$ derivatives, which include $C_{70}H_{10}$,[1] $C_{70}Me_{10}$,[2] $C_{70}Ph_{10}$,[3] $C_{70}Ph_9(OH)$,[4] $C_{70}Ph_8(OH)_2$,[4] $C_{70}Cl_{10}$,[5] and $C_{70}Br_{10}$,[6] have the "equatorial-belt" C_s structure shown in Figure 1, with the ten substituents[7] positioned on a closed loop of ten edge-sharing hexagons, nine of which are *para*-C_6X_2 fragments and one of which is an *ortho*-C_6X_2 fragment (p^9o(loop)).[8–10] The exception is the recently described compound $C_{70}(t\text{BuOO})_{10}$, which has the C_2 structure also shown in Figure 1 with an all-*para* ribbon of nine edge-sharing $C_6(t\text{BuOO})_2$ hexagons (p^9), presumably because the *t*BuOO groups are too large to be on adjacent cage C atoms.[11]

We recently reported the synthesis of batches (more than 10 mg) of a single isomer of $C_{70}(CF_3)_{10}$ at 470 °C in 27 % overall yield based on converted C_{70}.[12] A combination of 1D- and 2D-COSY ^{19}F NMR spectroscopy showed that this derivative has C_1 symmetry and, by analogy with the structure of a spectroscopically similar C_1 isomer of $C_{60}(CF_3)_{10}$, most probably has its ten CF_3 groups arranged in the form of a ribbon of nine *meta*-$C_6(CF_3)_2$ and/or *para*-$C_6(CF_3)_2$ edge-sharing hexagons.[12] We now report an X-ray diffraction study of this high-yield, high-temperature C_1-$C_{70}(CF_3)_{10}$ isomer, which demonstrates that the ribbon of hexagons is the

[*] I. V. Kuvychko, S. M. Miller, Prof. O. P. Anderson, Prof. S. H. Strauss, Dr. O. V. Boltalina
Department of Chemistry
Colorado State University
Fort Collins, CO 80523 (USA)
Fax: (+1) 970-491-1801
E-mail: steven.strauss@colostate.edu
ovbolt@lamar.colostate.edu

I. E. Kareev, Dr. S. F. Lebedkin
Forschungszentrum Karlsruhe
Institut für Nanotechnologie
Postfach 3640, 76021 Karlsruhe (Germany)

I. E. Kareev
Institute of Problems of Chemical Physics
Russian Academy of Sciences
Chernogolovka 142432 (Russia)

Dr. A. A. Popov
Chemistry Department
Moscow State University
Moscow 119899 (Russia)

[**] This work was supported by the Volkswagen Foundation (I-77/855) and the US National Science Foundation. We thank Prof. M. Kappes for his generous support of this work.

 InterScience © 2005 Wiley-VCH Verlag GmbH & Co. KGaA, Weinheim

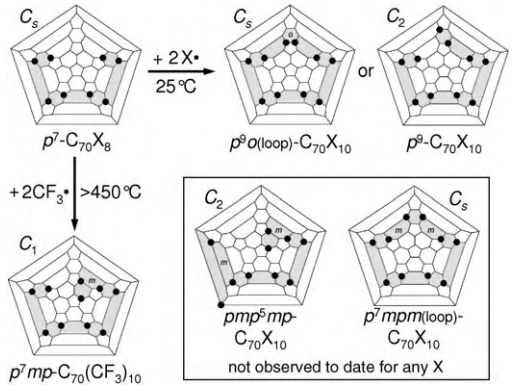

Figure 1. The transformation of C_s-p^7-$C_{70}X_8$, the structure of which has been proven by single-crystal X-ray diffraction (XRD) for X = Me, into either C_s-p^9o(loop)-$C_{70}X_{10}$ (proven by XRD for X = Br; proven by ^{13}C NMR for X = H, Cl, and Ph), C_2-p^9-$C_{70}X_{10}$ (proven by ^{13}C NMR for X = *t*BuOO), or C_1-p^7mp-$C_{70}(CF_3)_{10}$ (proven by XRD; this work). The inset shows the structures of two $C_{70}X_{10}$ isomers that have not yet been observed for any isolable compound. See text for references.

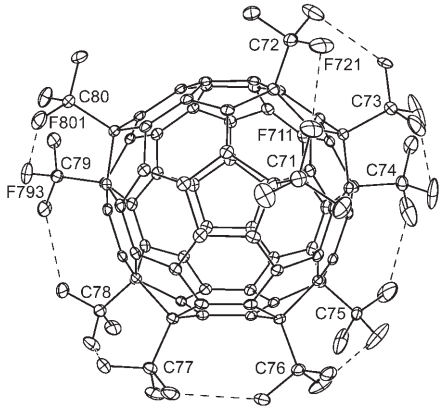

Figure 2. Drawing of C_1-$C_{70}(CF_3)_{10}$ looking down the former C_5 axis of the empty C_{70} cage (50% probability ellipsoids; only one of the two disordered CF_3 conformers is shown for each of the C73 and C74 CF_3 groups). Starting with the C80 CF_3 group, the CF_3 groups are arranged on a *para*^{7}–*meta*–*para* ribbon of $C_6(CF_3)_2$ edge-sharing hexagons. Atoms C71–C80 are connected to the fullerene cage at C25, C10, C1, C4, C19, C41, C60, C69, C66, and C49, respectively. The F801···F793 and F711···F721 distances are 2.570(2) and 2.744(2) Å, respectively.

unprecedented C_1-symmetric p^7mp ribbon shown in Figure 1. Like the hypothetical C_s-p^9o(loop)- and C_2-p^9-$C_{70}(CF_3)_{10}$ structures, the C_1-p^7mp-$C_{70}(CF_3)_{10}$ structure includes the C_s-p^7-$C_{70}X_8$ motif that has been observed for $C_{70}Me_8$[13] and $C_{70}Ph_8$.[3]

A thermal-ellipsoid plot, excluding the molecule of lattice-bound toluene, is shown in Figure 2. The poly(trifluoromethyl)fullerene itself is not disordered. The CF_3 groups containing C73 and C74 each exhibit a two-fold librational disorder; the other CF_3 groups, including the four CF_3 groups on the two *p*-$C_6(CF_3)_2$ hexagons at opposite ends of the ribbon, exhibit unexceptional F-atom thermal ellipsoids. Distances and angles within the ordered CF_3 groups are normal. The estimated standard deviations (esds) for individual C–C and C–F distances in this structure are all 0.003 Å (except for the C–F distances in the two disordered CF_3 groups), making this one of the most precisely determined C_{70}-containing structures reported to date (the ranges of esd's for C–C bonds within the cage of known structures include 0.002–0.004 Å for two Diels–Alder monoadducts,[14] 0.004–0.006 and 0.006–0.007 Å for $C_{70}(CH_3)_8$[13] and $C_{70}F_{38}$,[15] respectively, and 0.02–0.03 Å for $C_{70}Br_{10}$,[6] $C_{70}(IrCl(PPh_3)_2)$,[16] and $C_{70}(Ru_3(CO)_9)$[17]).

In addition to further supporting[12] our earlier conclusion[18] that fullerene$(CF_3)_n$ compounds in general have their CF_3 groups arranged on *m*- and *p*-$C_6(CF_3)_2$ hexagons (most of which form a continuous ribbon through edge sharing) and are not arranged on adjacent (i.e., *ortho*) cage C atoms as suggested by others,[19–21] the structure of C_1-$C_{70}(CF_3)_{10}$ has revealed several interesting and unanticipated aspects of $C_{70}X_n$ stereochemistry. In 1999, Clare and Kepert predicted the relative ΔH_f^0 values for a (necessarily) limited number of isomers of $C_{70}X_{10}$ at the AM1 level of theory, including the C_s-p^9o(loop) and C_2-p^9 isomers for X = H, F, Br, Ph, and *t*Bu.[10] They did not consider any $C_{70}X_{10}$ isomer with one or more *m*-C_6X_2 hexagons. Except for X = *t*Bu, the C_s-p^9o(loop) isomer was found to be more stable than the C_2-p^9 isomer for these substituents (Table 1; Schlegel diagrams for the five isomers are shown in Figure 1). However, all isolable C_s-p^9o(loop)-$C_{70}X_{10}$ compounds[1,3–6] and the one isolable C_2-p^9-$C_{70}X_{10}$ compound, $C_{70}(t\text{BuOO})_{10}$,[11] were prepared at 25 °C and may, at least in some cases, be a kinetically stable isomer and not the isomer with the lowest ΔH_f^0 value. On the other hand, C_1-$C_{70}(CF_3)_{10}$ was prepared at 470 °C,[12] a temperature that may be high enough for facile CF_3 migration to occur on the fullerene surface, a process that could conceivably result in the transformation of a less stable isomer to a more stable

Table 1: AM1 relative enthalpies ΔH_f^0 [kJ mol^{-1}] of formation of $C_{70}X_{10}$ isomers.[a]

X	C_s-p^9o(loop)	C_2-p^9	C_1-p^7mp	C_s-p^7mpm(loop)	C_2-pmp^5mp
CF_3	0.0	−14.1	−36.2[b]	132.0	−17.2
Ph	0.0 [0.0][b]	6.2 [3.1]	−16.0	156.5	2.8
Br	0.0 [0.0][b]	11.6 [11.6]	−2.9	145.1	20.6
Cl	0.0[b]	13.7	0.6	149.7	26.2
H	0.0 [0.0][b]	26.8 [26.9[c]]	14.4	158.4	40.7
F	0.0 [0.0]	33.7 [33.7]	20.3	183.9	47.8
*t*BuOO	0.0	24.7[b]	13.7		
*t*Bu	0.0 [0.0]	−230.2 [−230.0]	−202.2		

[a] All values from this work except values in square brackets, which are from reference [10]. The lowest relative ΔH_f^0 value for each composition is underlined. [b] The principal or only isomer observed by X-ray crystallography or ^{13}C NMR spectroscopy. [c] The next most stable structure reported in reference [10], $p^4opopop$(loop)-$C_{70}H_{10}$, had a relative ΔH_f^0 value of 46.4 kJ mol^{-1}.

 © 2005 Wiley-VCH Verlag GmbH & Co. KGaA, Weinheim

one. The facile migration of F atoms on the surface of $C_{60}F_n$ isomers at 300–350 °C is well documented.[22]

The relative stabilities of various fullerene$(CF_3)_n$ isomers are determined by at least four factors: 1) the degree of delocalization/aromatization of the remaining fullerene π bonds; 2) the presence or absence of double bonds in pentagons; 3) steric repulsions between proximate substituents; and, in the case of nonlinear polyatomic substituents such as CF_3 groups, 4) the rotational conformation of each substituent with respect to its underlying cage C–C bonds. To examine the possibility that C_1-p^7mp-$C_{70}(CF_3)_{10}$ is truly more stable than the alternative C_s-p^9o(loop) and C_2-p^9 isomers, we also carried out calculations at the AM1 level of theory. The AM1-predicted relative ΔH_f^0 values for five isomers of $C_{70}(CF_3)_{10}$ and selected $C_{70}X_{10}$ derivatives (X = H, F, Cl, Br, Ph, *t*BuOO, and *t*Bu) are also listed in Table 1. (We also optimized the geometry of C_1-p^7mp-$C_{70}(CF_3)_{10}$ at the DFT level of theory for comparison with the X-ray structure.) Note that C_1-p^7mp-$C_{70}(CF_3)_{10}$ is predicted to be 36 kJ mol^{-1} more stable than the C_s-p^9o(loop) isomer and 22 kJ mol^{-1} more stable than the C_2-p^9 isomer, despite the fact that the C_s and C_2 isomers do not have any double bonds in pentagons and the C_1 isomer has several (the three shortest 6–5 junctions in C_1-p^7mp-$C_{70}(CF_3)_{10}$ are C8-C9 (1.347(3) Å X-ray, 1.357 Å DFT), C6-C7 (1.397(3) Å X-ray, 1.403 Å DFT), and C11-C29 (1.391(3) Å X-ray, 1.399 Å DFT)).

The difference in energy between the C_1 and C_2 isomers may be explained by the fact that two bulky CF_3 groups can be farther apart on a *p*-$C_6(CF_3)_2$ hexagon in the more highly curved polar region of the C_{70} cage than on a relatively flat equatorial hexagon. For example, the $F_3C\cdots CF_3$ distance is 4.412(3) Å for the end-of-ribbon polar *p*-$C_6(CF_3)_2$ hexagon (i.e., C71···C72) and 3.935(3) Å for the end-of-ribbon equatorial *p*-$C_6(CF_3)_2$ hexagon (C79···C80); the corresponding DFT distances are 4.502 and 3.992 Å, respectively. Consistent with this, the X-ray and DFT results reveal that every other CF_3 group on the equatorial part of the ribbon of *p*-$C_6(CF_3)_2$ edge-sharing hexagons in C_1-p^7mp-$C_{70}(CF_3)_{10}$ is partially or very-nearly eclipsed, in contrast to the [60]fullerene derivative C_1-pmp^3mpmp-$C_{60}(CF_3)_{10}$, in which all but one of the CF_3 groups along the ribbon are staggered or nearly so.[12] Note that both of the CF_3 groups on the end-of-ribbon polar hexagon in the structure of C_1-$C_{70}(CF_3)_{10}$ adopt the staggered conformation.

Surprisingly, the relative ΔH_f^0 results in Table 1 suggest that the isolable and well-characterized C_s-p^9o(loop) isomers of $C_{70}Br_{10}$ and $C_{70}Ph_{10}$ may only be kinetically stable with respect to their respective, thermodynamically more stable, C_1-p^7mp isomers. Even more surprisingly, it appears that C_2-p^9-C_{70}(*t*BuOO)$_{10}$[11] may be a kinetic isomer with respect to *both* C_1-p^7mp-C_{70}(*t*BuOO)$_{10}$ and C_s-p^9o(loop)-C_{70}(*t*BuOO)$_{10}$, and would ultimately rearrange to C_s-p^9o(loop)-C_{70}(*t*BuOO)$_{10}$ if sufficient activation energy were available (and if the compound did not decompose when that activation energy was added). It is also possible that C_2-p^9-$C_{70}(CF_3)_{10}$, like C_2-p^9-C_{70}(*t*BuOO)$_{10}$, is formed during the reaction of C_{70} and the X· precursor (CF_3I or *t*BuOOH) and rearranges to the high-yield product C_1-p^7mp-$C_{70}(CF_3)_{10}$ at 470 °C.[12] These and other issues relating to the mechanisms of multiple additions to C_{70}, including the kinetic vs. thermodynamic importance of the density of unpaired spins on the various C atoms of putative $C_{70}X_9$· radical intermediates,[9] will be addressed in future experimental work and with additional calculations at the DFT level.

It is significant that the stability of C_1-p^7mp-$C_{70}(CF_3)_{10}$ relative to the hypothetical isomers C_s-p^9o-$C_{70}(CF_3)_{10}$ and C_2-p^9-$C_{70}(CF_3)_{10}$ would not have been discovered were it not for the fact that poly(trifluoromethyl)fullerenes are thermally stable at 400–500 °C,[12,18] a property that is unparalleled in exohedral fullerene chemistry except for a few fluorofullerenes.[23] Therefore, we expect that the study of poly(perfluoroalkyl)fullerenes at high temperatures will reveal additional unanticipated aspects of kinetically vs. thermodynamically controlled addition reactions for C_{60} and higher fullerenes.

We have also calculated ΔH_f^0 values at the AM1 level for two loop/ribbon $C_{70}X_{10}$ isomers that have not been observed experimentally, the equatorial C_s-p^7mpm(loop) isomer and the "pole-to-pole" C_2-pmp^5mp isomer. The C_s-p^7mpm(loop) isomer is $\geq$140 kJ mol^{-1} less stable than the most stable isomer listed in Table 1 for X = H, F, Cl, Br, Ph, and CF_3. This extreme instability is because the formation of C_s-p^7mpm-(loop)-$C_{70}X_{10}$ from C_s-$C_{70}X_8$ requires the pyramidalization of two triple-hexagon junctions, the most planar C atoms in C_{70}.[24] In the structure of C_s-p^7-$C_{70}Me_8$,[13] for example, the triple-hexagon-junction C atoms are only 0.19 Å above the least-squares planes formed by their three nearest-neighbor cage C atoms. Other sp^2 C atoms involved in forming the four other isomers in Table 1 are displaced 0.26–0.31 Å from their respective nearest-neighbor planes (the largest values in this range are for the C atoms that comprise the polar pentagons). For comparison, out-of-plane displacements for the sp^3 cage C atoms are 0.58–0.59 Å in $C_{70}Me_8$ and are 0.583(3) and 0.561(3) for C25 and C49 in C_1-$C_{70}(CF_3)_{10}$. The high energy cost involved in adding X groups to the triple-hexagon junctions of C_{70} was previously noted.[10] The pole-to-pole isomers C_2-pmp^5mp-$C_{70}(CF_3)_{10}$ and -$C_{70}Ph_{10}$ are marginally more stable than the all-*para*, all-equatorial ribbon isomers C_2-p^9-C_{70}-$(CF_3)_{10}$ and -$C_{70}Ph_{10}$. They are not more stable than the C_1-p^7mp isomers, possibly because the formation of the pole-to-pole isomer would disrupt the polar corannulene-like π system of C_1-p^7mp-$C_{70}(CF_3)_{10}$.

The two *p*-$C_6(CF_3)_2$ hexagons at opposite ends of the ribbon of edge-sharing hexagons in C_1-$C_{70}(CF_3)_{10}$ give rise to two different F···F distances between nearest-neighbor CF_3 groups, 2.744(2) Å for the polar end-of-ribbon hexagon and 2.570(2) Å for the equatorial end-of-ribbon hexagon. These F···F distances are fully consistent with different through-space Fermi-contact $^7J_{FF}$ values reported earlier for the two terminal CF_3 groups in C_1-$C_{70}(CF_3)_{10}$, 10.3 and 15.9 Hz,[12] which can now be assigned to the polar and equatorial end-of-ribbon CF_3 groups, respectively. Note that one of the end-of-ribbon *p*-$C_6(CF_3)_2$ hexagons in C_1-$C_{60}(CF_3)_{10}$ exhibited an F···F distance of 2.640(3) Å and a $^7J_{FF}$ value of 12.8 Hz,[12] both intermediate values when compared with the above-listed values for C_1-$C_{70}(CF_3)_{10}$. The conclusions reached by others, that through-space J_{FF} coupling in fullerene$(CF_3)_n$ derivatives is unimportant[19,20] and that, in general, 1,4-addition of CF_3 groups to C_{70} "does not account for the large coupling

 © 2005 Wiley-VCH Verlag GmbH & Co. KGaA, Weinheim

constant variations" (i.e., $J_{FF} = 9.1–17.7$ Hz),[19,21] are not supported by the data presented here.

In summary, the precise structure of C_1-$C_{70}(CF_3)_{10}$ and the new computational results have added significant new information to the small but growing fullerene$(CF_3)_n$ and $C_{70}X_{10}$ databases. More importantly, it has shown that low-temperature exohedral addition on C_{70} may frequently produce kinetic, not thermodynamic, products.

Experimental Section

The compound C_1-$C_{70}(CF_3)_{10}$ was prepared as previously described (no other isomers of this composition were obtained).[12] Crystals suitable for X-ray diffraction were grown by slow evaporation of a toluene solution. Diffraction data from a single crystal were recorded on a Bruker SMART CCD diffractometer employing MoK_α radiation (graphite monochromator). Unit cell parameters were obtained from a least-squares fit to the angular coordinates of all reflections. An empirical absorption correction was applied by using SADABS.[25] The structure was solved by using direct methods and was refined (on F^2, using all data) by a full-matrix, weighted least-squares process.[26] All C and F atoms were refined using anisotropic atomic displacement parameters. Two of the CF_3 groups (C73, C74) were treated as disordered by rotation about the C–C bond connecting them to the fullerene cage. The disorder model allowed for variation of the C-F distance within each disordered group while preserving the tetrahedral geometry about the C atom. Standard Bruker software was employed for structure solution, refinement, and graphics.[27]

The DFT-optimized structure of C_1-p^7mp-$C_{70}(CF_3)_{10}$ was determined with the PRIRODA package[28] using the GGA functional of Perdew, Burke, and Ernzerhof (PBE)[29] and the TZ2P {6,1,1,1,1,1/4,1,1/1,1} basis set. Semi-empirical AM1 calculations were performed with the PC version[30] of the GAMESS(US) package.[31]

Received: July 11, 2005
Published online: November 15, 2005

Keywords: fullerenes · structure elucidation · trifluoromethylation

[1] H. P. Spielmann, B. R. Weedon, M. S. Meier, *J. Org. Chem.* **2000**, *65*, 2755–2758.
[2] H. Al-Matar, A. K. A. Sada, A. G. Avent, R. Taylor, X. W. Wei, *J. Chem. Soc. Perkin Trans. 2* **2002**, 1251–1256.
[3] A. G. Avent, P. R. Birkett, A. D. Darwish, H. W. Kroto, R. Taylor, D. R. M. Walton, *Tetrahedron* **1996**, *52*, 5235–5246.
[4] A. G. Avent, P. R. Birkett, A. D. Darwish, H. W. Kroto, R. Taylor, D. R. M. Walton, *J. Chem. Soc. Perkin Trans. 2* **2001**, 68–72.
[5] P. R. Birkett, A. G. Avent, A. D. Darwish, H. W. Kroto, R. Taylor, D. R. M. Walton, *J. Chem. Soc. Chem. Commun.* **1995**, 683–684.
[6] S. I. Troyanov, A. A. Popov, N. I. Denisenko, O. V. Boltalina, L. N. Sidorov, E. Kemnitz, *Angew. Chem.* **2003**, *115*, 2497–2500; *Angew. Chem. Int. Ed.* **2003**, *42*, 2395–2398.
[7] W. H. Powell, F. Cozzi, G. P. Moss, C. Thilgen, R. J. R. Hwu, A. Yerin, *Pure Appl. Chem.* **2002**, *74*, 629–695.
[8] S. J. Austin, P. W. Fowler, J. P. B. Sandall, P. R. Birkett, A. G. Avent, A. D. Darwish, H. W. Kroto, R. Taylor, D. R. M. Walton, *J. Chem. Soc. Perkin Trans. 2* **1995**, 1027–1028.
[9] K. M. Rogers, P. W. Fowler, *Chem. Commun.* **1999**, 2357–2358.
[10] B. W. Clare, D. L. Kepert, *J. Mol. Struct.* **1999**, *491*, 249–264.
[11] Z. Xiao, F. D. Wang, S. H. Huang, L. B. Gan, J. Zhou, G. Yuan, M. J. Lu, J. Q. Pan, *J. Org. Chem.* **2005**, *70*, 2060–2066.
[12] I. E. Kareev, I. V. Kuvychko, S. F. Lebedkin, S. M. Miller, O. P. Anderson, K. Seppelt, S. H. Strauss, O. V. Boltalina, *J. Am. Chem. Soc.* **2005**, *127*, 8362–8375.
[13] A. D. Darwish, P. de Guio, R. Taylor, *Fullerene Sci. Technol.* **2002**, *10*, 261–272.
[14] P. Seiler, A. Herrmann, F. Diederich, *Helv. Chim. Acta* **1995**, *78*, 344–354.
[15] P. B. Hitchcock, A. G. Avent, N. Martsinovich, P. A. Troshin, R. Taylor, *Org. Lett.* **2005**, *7*, 1975–1978.
[16] A. L. Balch, V. J. Catalano, J. W. Lee, M. M. Olmstead, S. R. Parkin, *J. Am. Chem. Soc.* **1991**, *113*, 8953–8955.
[17] H.-F. Hsu, S. R. Wilson, J. R. Shapley, *Chem. Commun.* **1997**, 1125–1126.
[18] a) A. A. Goryunkov, I. V. Kuvychko, I. N. Ioffe, D. L. Dick, L. N. Sidorov, S. H. Strauss, O. V. Boltalina, *J. Fluorine Chem.* **2003**, *124*, 61–64; b) A. A. Goryunkov, I. N. Ioffe, I. V. Kuvychko, T. S. Yankova, V. Y. Markov, A. V. Streletskii, D. L. Dick, L. N. Sidorov, O. V. Boltalina, S. H. Strauss, *Fullerenes Nanotubes Carbon Nanostruct.* **2004**, *12*, 181–185; c) I. E. Kareev, S. F. Lebedkin, V. P. Bubnov, E. B. Yagubskii, I. N. Ioffe, P. A. Khavrel, I. V. Kuvychko, S. H. Strauss, O. V. Boltalina, *Angew. Chem.* **2005**, *117*, 1880–1883; *Angew. Chem. Int. Ed.* **2005**, *44*, 1846–1849.
[19] A. D. Darwish, A. G. Avent, A. K. Abdul-Sada, R. Taylor, *Chem. Commun.* **2003**, 1374–1375.
[20] A. D. Darwish, A. K. Abdul-Sada, A. G. Avent, V. I. Lyakhovetsky, E. A. Shilova, R. Taylor, *Org. Biomol. Chem.* **2003**, *1*, 3102–3110.
[21] A. D. Darwish, A. K. Abdul-Sada, A. G. Avent, N. Martsinovich, J. M. Street, R. Taylor, *J. Fluorine Chem.* **2004**, *125*, 1383–1391.
[22] A. A. Gakh, A. A. Tuinman, *Tetrahedron Lett.* **2001**, *42*, 7137–7139; O. V. Boltalina, M. Buhl, A. Khong, M. Saunders, J. M. Street, R. Taylor, *J. Chem. Soc. Perkin Trans. 2* **1999**, 1475–1479.
[23] O. V. Boltalina, S. H. Strauss in *Dekker Encyclopedia of Nanoscience and Nanotechnology* (Eds.: J. A. Schwarz, C. Contescu, K. Putyera), Marcel Dekker, New York, **2004**, pp. 1175–1190.
[24] H.-B. Burgi, P. Venugopalan, D. Schwarzenbach, F. Diederich, C. Thilgen, *Helv. Chim. Acta* **1993**, *76*, 2155–2159.
[25] G. M. Sheldrick, *SADABS—A program for area detector absorption corrections.*
[26] For C_1-$C_{70}(CF_3)_{10}$: $0.31 \times 0.26 \times 0.12$ mm; monoclinic; $P2_1/c$; $a = 20.9959(14)$, $b = 16.0478(13)$, $c = 17.0276(11)$ Å, $\beta = 100.628(7)°$; $V = 5638.8(7)$ Å^3 ($Z = 4$); $\rho_{calcd} = 1.912$ Mg m^{-3}; $2\theta_{max} = 28.32°$; $-27 \le h \le 28$, $-21 \le k \le 21$, $-22 \le l \le 22$; $\lambda = 0.71073$ Å; $T = 100(1)$ K; number of reflections = 53979; number of independent reflections = 13877 (R(int) = 0.0571); restraints/parameters = 24/1077; full-matrix least-squares refinement on F^2; semi-empirical absorption correction from equivalents; $\mu = 0.181$ mm^{-1}; final R indices ($I > 2\sigma(I)$) are $R_1 = 0.0568$ and $wR_2 = 0.1324$; largest difference peak and hole = 1.174 and -1.008e Å^{-3}. CCDC-277466 contains the supplementary crystallographic data for this paper. These data can be obtained free of charge from the Cambridge Crystallographic Data Centre via www.ccdc.cam.ac.uk/data_request/cif.
[27] G. M. Sheldrick, *SHELXTL*, version 6.14, Bruker AXS, Madison, WI, **2004**.
[28] D. N. Laikov, *Chem. Phys. Lett.* **1997**, *281*, 151–156.
[29] J. P. Perdew, K. Burke, M. Ernzerhof, *Phys. Rev. Lett.* **1996**, *77*, 3865–3868.
[30] A. A. Granovsky, PC GAMESS url: http://classic.chem.msu.su-/gran/gamess/index.html.
[31] M. W. Schmidt, K. K. Baldridge, J. A. Boatz, S. T. Elbert, M. S. Gordon, J. H. Jensen, S. Koseki, N. Matsunaga, K. A. Nguyen, S. J. Su, T. L. Windus, M. Dupuis, J. A. Montgomery, *J. Comput. Chem.* **1993**, *14*, 1347.

 © 2005 Wiley-VCH Verlag GmbH & Co. KGaA, Weinheim

Photofunctional Materials

DOI: 10.1002/anie.200502514

An Unexpected Photoelectronic Effect from $[Co(en)_3]_2(Zr_2F_{12})(SiF_6)\cdot 4H_2O$, a Compound Containing an H-Bonded Assembly of Discrete $[Co(en)_3]^{3+}$, $(Zr_2F_{12})^{4-}$, and $(SiF_6)^{2-}$ Ions**

Yu Du, Min Yang, Jihong Yu, Qinhe Pan, and Ruren Xu**

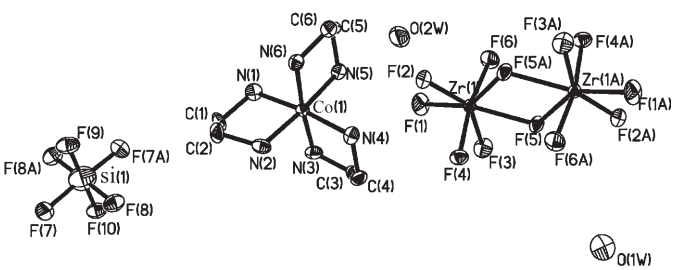

Figure 1. Thermal ellipsoid plot (50%) of $[Co(en)_3]_2(Zr_2F_{12})(SiF_6)\cdot 4H_2O$ (**1**).

Photofunctional materials are important because of their unique optical and electrical properties and are widely used in solar-energy conversion, semiconductor surface sensitization and modification, and nanoelectronics.[1–5] In recent decades, much effort has been directed toward the synthesis of pnictide- and chalcogenide-based inorganic semiconductor materials such as GaN,[6] SiC,[7] ZnO_2,[8] and SnO_2[9] because of their comparatively wide HOMO–LUMO gaps. There has been little investigation, however, of the photoelectronic properties of molecular solids.

Recently, by using an optically pure or a racemic mixture of a chiral cobalt complex such as $[Co(en)_3Cl_3]$ or $[Co(dien)_2Cl_3]$ as the template, we prepared a series of open-framework metal phosphates and oxides with chiral structure characters.[10,11] In order to explore new metal fluorides formed with a chiral cobalt complex as the template, we prepared a new cobalt complex-containing zirconium–silicon compound, namely $[Co(en)_3]_2(Zr_2F_{12})(SiF_6)\cdot 4H_2O$ (**1**), which contains an H-bonded network of discrete $[Co(en)_3]^{3+}$, $[Zr_2F_{12}]^{4-}$, and $[SiF_6]^{2-}$ ions. Unexpectedly, this new compound exhibits intriguing photoelectronic effects in the near-UV region.

A single-crystal X-ray diffraction analysis[12] indicated that **1** crystallizes in a monoclinic unit cell with space group *C*2/*c* (no. 15). Each asymmetric unit (Figure 1) contains one unique Co atom, one unique Zr atom, and one unique Si atom that is located on the two-fold axis. Two $[ZrF_7]^{3-}$ units share edges through difluoro bridges to form a $[Zr_2F_{12}]^{4-}$ pentagonal-bipyramid cluster with Zr–F bond lengths in the range of 1.988(4)–2.213(3) Å. The $[Co(en)_3]^{3+}$ cation and $[SiF_6]^{2-}$ anion display a disordered and a near regular octahedral geometry, respectively, with the Co–N and Si–F distances in the range of 1.965(6)–1.984(5) and 1.660(6)–1.742(6) Å, respectively. Each asymmetric unit also contains two H_2O molecules. As seen in Figure 2a, an extensive H-bonding network exists connecting the discrete $[Zr_2F_{12}]^{4-}$, $[Co(en)_3]^{3+}$, and $[SiF_6]^{2-}$ ions, in which the N atoms serve as H-bond donors and the F atoms as H-bond acceptors. As seen in Figure 2b, each $[Zr_2F_{12}]^{4-}$ unit interacts with six nearby complex cations through H-bonds. The N···F distances are in the range of 2.766(7)–3.106(7) Å, with angles in the range of 111.60–170.83°, both of which are typical values for H-bonding interactions between F and N atoms observed in a variety of metal fluorides.[13] The six complex cations are three pairs of enantiomers of the chiral $[Co(en)_3]^{3+}$ ion with *C*2 point symmetry; they are related by an inversion center.

The UV/Vis absorption spectrum of **1** shows three bands with maxima at approximately 237, 337, and 465 nm (Fig-

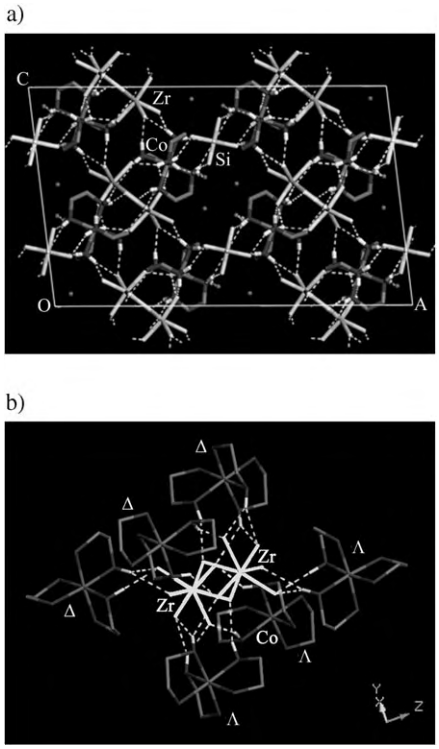

Figure 2. a) H-bonding network of discrete $[Co(en)_3]^{3+}$, $[Zr_2F_{12}]^{4-}$, and $[SiF_6]^{2-}$ ions viewed along the *b* axis. b) One $[Zr_2F_{12}]^{4-}$ unit interacts with six complex cations through H-bonds.

[*] Y. Du, M. Yang, Prof. J. Yu, Q. Pan, Prof. R. Xu
State Key Laboratory of Inorganic Synthesis and Preparative Chemistry
College of Chemistry
Jilin University
Changchun 130012 (P. R. China)
Fax: (+86) 431-516-8608
E-mail: jihong@mail.jlu.edu.cn

[**] This work was supported by the National Natural Science Foundation of China and the State Basic Research Project of China (G2000077507). The authors thank Prof. Dejun Wang and Prof. Yubai Bai for their helpful discussions.

Supporting information for this article is available on the WWW under http://www.angewandte.org or from the author.

InterScience
© 2005 Wiley-VCH Verlag GmbH & Co. KGaA, Weinheim

ure 3a). The two absorptions at 337 and 465 nm are d–d transitions characteristic of the $[Co(en)_3]^{3+}$ complex cation,[14] whereas that at about 237 nm, which is absent in $K_4Zr_2F_{12}$ but is commonly found in many zirconium-containing compounds,[15] is tentatively assigned to a ligand-to-metal charge-transfer (LMCT) from the fluoride to the zirconium center. As $K_4Zr_2F_{12}$ itself does not absorb at wavelengths longer than 200 nm, the absorption at about 237 nm in **1** suggests that the HOMO–LUMO gap of $[Zr_2F_{12}]^{4-}$ in **1** may be smaller than that in $K_4Zr_2F_{12}$.

Studies by surface photovoltage spectroscopy (SPS) revealed that compound **1** possesses unusual photoelectronic properties (Figure 3b). When illuminated in absence of an external electric field, **1** shows a signal for the surface photovoltage (SPV) at 337 nm that is coincidental with one of the UV/Vis adsorption transitions of the $[Co(en)_3]^{3+}$ ions (Figure 3a). In contrast, no photovoltage response is generated when either $[Co(en)_3Cl_3]$ or $K_4Zr_2F_{12}$ are illuminated by photons with wavelengths longer than 300 nm. It is supposed that the electrons of the $[Zr_2F_{12}]^{4-}$ ion in $K_4Zr_2F_{12}$ are unable to transfer from the HOMO to the LUMO energy levels upon illumination by light of 337 nm. In $[Co(en)_3Cl_3]$, even though the $[Co(en)_3]^{3+}$ ion can be excited by light of this wavelength, electron–hole pairs cannot be effectively separated because no perfect energy band is formed, and, as a result, no photovoltage signal is generated. Furthermore, the fact that the intensity of the SPV response increases with increasing positive electric-field strength is indicative of its *n*-type conduction character[8] (inset of Figure 3b).

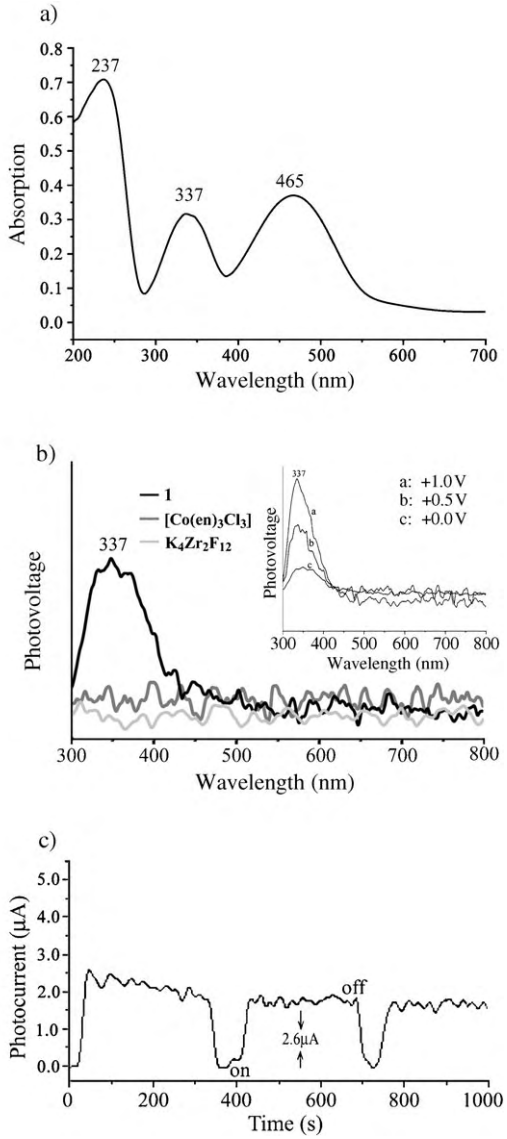

Figure 3. a) UV/Vis absorption spectrum of **1**. b) SPS of $[Co(en)_3Cl_3]$ (dark gray line), $K_4Zr_2F_{12}$ (light gray line), and **1** (black line). Inset: FISPS of compound **1** under positive field. c) Transient photocurrent response of compound **1** at 0.4 V versus SCE. (↑ and ↓ indicate when the light was turned on and off).

Figure 3c shows the transient photocurrent response of **1** recorded for several on–off cycles of illumination. The current reaches a steady-state value in approximately 300 s. The trace shows that an anodic photocurrent of about 2.6 μA is generated at a constant applied voltage of 0.4 V versus SCE, which is much higher than that of $(ZnO)_2(UO_2)_3(NA)_4(OAC)_2$ (0.2 μA) under the same measurement conditions.[16] In contrast to conventional oxide semiconductors,[17] the current density of compound **1** is very low. However, the lower current density, in combination with its lower electrical conductivity ($< 10^{-5}$ S cm^{-1}), suggests that compound **1** might contain a controlled carrier density[18] similar to that of $(ZnO)_2(UO_2)_3(NA)_4(OAC)_2$.

We believe that a cooperative behavior between discrete $[Co(en)_3]^{3+}$ and $[Zr_2F_{12}]^{4-}$ ions through interionic interactions might be responsible for this unexpected photoelectric phenomenon in **1**. As expected, we have also observed an interesting photoelectric phenomenon in another cobalt complex-containing zirconium fluoride compound, namely $[Co(chxn)_3](ZrF_6)Cl{\cdot}3.5\,H_2O$ (**2**; chxn = 1,2-diaminocyclohexane).[19] Compound **2** is built up from discrete $[Co(chxn)_3]^{3+}$ and $[ZrF_6]^{2-}$ ions (see Supporting Information). As with **1**, there are extensive H-bonds between the $[Co(chxn)_3]^{3+}$ and $[ZrF_6]^{2-}$ ions in **2**. Upon illumination in absence of an external electric field, **2** shows a signal for the surface photovoltage at 357 nm, which is also coincidental with one of the UV/Vis adsorption transitions of the $[Co(chxn)_3]^{3+}$ ions (see Supporting Information).

In summary, compounds **1** and **2** both exhibit unusual photoelectric properties. The fact that the signal of the surface photovoltage is coincident with one of the UV/Vis absorption transitions of the cobalt complex implies that a charge transfer from the excited cobalt complex cation to the zirconium fluoride anion may occur upon illumination. The successful synthesis of compounds **1** and **2** and the discovery of their unusual physical properties as a result of the cooperative behavior between their component species will open-up new vistas in the search for materials with useful photoelectric properties. Further investigation of the mechanism of this intriguing photoelectric effect is ongoing.

Experimental Section

In a typical hydrothermal synthesis of **1**, zirconium tetrachloride (0.233 g, 1.00 mmol) was dissolved in distilled water (10 mL) and

 © 2005 Wiley-VCH Verlag GmbH & Co. KGaA, Weinheim

tris(ethylenediamine)cobalt(III) chloride (0.172 g, 0.50 mmol) and phosphoric acid (0.272 mL, 85 wt.%, 4 mmol) were added whilst stirring. Finally, hydrofluoric acid (HF, 0.5 mL, 40 wt.% aqueous solution, 10 mmol) and tetraethylorthosilicate (0.10 mL, 97 wt.% aqueous solution, 0.43 mmol) were added to the above reaction mixture. After stirring for 30 min, the final reaction mixture with a pH value of about 1.0 was transferred into a Teflon-lined, stainless-steel autoclave (20 mL) and heated at 130 °C for six days. The resulting orange, rod-like crystals were isolated by filtration, washed with deionized water, and dried in the air. The phase purity of **1** was checked by recording its X-ray powder diffraction pattern, which was consistent with that simulated on the basis of the single-crystal structure data. XRD studies indicated that compound **1** is thermally stable below 200 °C. Inductively coupled plasma (ICP) analysis indicated a Zr:Co:Si molar ratio of 1:1:0.5 for **1**.

Received: July 19, 2005
Revised: September 14, 2005
Published online: November 15, 2005

Keywords: cobalt · hydrogen bonds · hydrothermal synthesis · materials science · photoelectronic effect

[1] J. Ferber, J. Luther, *J. Phys. Chem. B* **2001**, *105*, 4895 – 4903.
[2] F. Pichot, B. A. Gregg, *J. Phys. Chem. B* **2000**, *104*, 6 – 10.
[3] S. Capone, S. Mongelli, R. Rella, P. Siciliano, L. Valli, *Langmuir* **1999**, *15*, 1748 – 1753.
[4] M. Grätzel, *Prog. Photovoltaics* **2000**, *8*, 171 – 185.
[5] L. Kronik, Y. Shapira, *Surf. Interface Anal.* **2001**, *31*, 954 – 965.
[6] S. Arulkumaran, M. Sakai, Y. Kuraoka, *Appl. Phys. Lett.* **2002**, *81*, 1131 – 1133.
[7] S. Harada, S. Suzuki, J. Senzaki, *Mater. Sci. Forum* **2002**, 389 – 393; S. Harada, S. Suzuki, J. Senzaki, *Mater. Sci. Forum* **2002**, 1069 – 1072.
[8] Y. Lin, D. Wang, *J. Phys. Chem. B* **2004**, *108*, 3202 – 3206.
[9] M. W. Prins, R. P. Weening, R. M. Wolf, *Appl. Phys. Lett.* **1996**, *68*, 3650 – 3652.
[10] Y. Wang, J. Yu, M. Guo, *Angew. Chem.* **2003**, *115*, 4223 – 4226; *Angew. Chem. Int. Ed.* **2003**, *42*, 4089 – 4092.
[11] Y. Wang, J. Yu, Q. Pan, *Inorg. Chem.* **2004**, *43*, 559 – 565.
[12] Crystal data: $0.30 \times 0.20 \times 0.08\ mm^3$, $C_{12}H_{56}N_{12}O_4F_{18}Co_2SiZr_2$, $M_r = 1103.08$, monoclinic, space group, $C2/c$ (no. 15), $a = 26.782(14)$, $b = 8.218(3)$, $c = 16.546(8)$ Å, $\beta = 96.630(19)°$, $V = 3617(3)$ Å^3, $Z = 4$, $\rho_{calcd} = 2.025\ g\,cm^{-3}$, $\mu = 1.629\ mm^{-1}$, $T = 293(2)$ K. A total of 4611 reflections were collected, of which 3044 were independent ($R_{int} = 0.0683$). Final R indices [$I > 2\sigma(I)$]: $R_1 = 0.0474$, $wR_2 = 0.1128$, GOF = 1.020. CCDC-266808 contains the supplementary crystallographic data for this paper. These data can be obtained free of charge from the Cambridge Crystallographic Data Center via www.ccdc.cam.ac.uk/data - request/cif.
[13] U. Bertrup, M. Feist, E. Kemnitz, *Prog. Solid St. Chem.* **1999**, *27*, 75 – 129.
[14] S. M. Jörgensen, *J. Prakt. Chem.* **1889**, *39*, 8 – 11.
[15] R. Hart, W. Levason, *J. Chem. Soc. Dalton Trans.* **2002**, 3153 – 3159.
[16] W. Chen, H. Yuan, J. Wang, J. Chen, *J. Am. Chem. Soc.* **2003**, *125*, 9266 – 9267.
[17] M. W. J. Prins, S. E. Zinnemers, J. F. M. Cillessen, J. B. Giesbers, *Appl. Phys. Lett.* **1997**, *70*, 458 – 460.
[18] K. Nomura, H. Ohta, K. Ueda, T. Kamiya, M. Hirano, *Science* **2003**, *300*, 1269 – 1272.
[19] Compound **2** was obtained from a reaction mixture with a molar composition of $1\,ZrCl_4{:}3\,H_3PO_4{:}0.5\,Co(chxn)_3Cl_3{:}10\,HF{:}404\,H_2O$ at 110 °C for six days. The resulting orange-yellow, block-shaped crystals were isolated by filtration, washed with deionized water, and dried under ambient conditions.

 © 2005 Wiley-VCH Verlag GmbH & Co. KGaA, Weinheim

Author Index

The entry for correspondence authors includes the complete information regarding the article. For the coauthors, the type of article and the page numbers are listed. The page numbers in square brackets refer to the German edition [*Angew. Chem.* **2005**, *117*] of *Angewandte Chemie*.

(C) = Communication (E) = Essay (H) = Highlight (L) = Correspondence (M) = Minireview (O) = Obituary (R) = Review Article (T) = Meeting Review

Abad, A. (C) 4066 – 4069 [4134 – 4137]
Abad, J. A. (C) 6001 – 6004 [6155 – 6158]
Abakumov, G. A.
– Reversible Binding of Dioxygen by a Non-Transition-Metal Complex
(C) 2767 – 2771 [2827 – 2831]
DOI: 10.1002/anie.200462503
Abakumova, L. G. (C) 2767 – 2771 [2827 – 2831]
Abbas, H. (C) 3415 – 3419 [3481 – 3485]
Abboud, K. A. (C) 892 – 896 [914 – 918], 897 – 901 [919 – 923], 5834 – 5838 [5984 – 5988]
Abe, M.
– Photoconversion of a Redox-Active Self-Assembled Monolayer: In Situ Probing of Photoinduced CO Dissociation from a Triruthenium Cluster Center on Gold
(C) 416 – 419 [420 – 423]
DOI: 10.1002/anie.200460651
Abele, B. C. (C) 3136 – 3139 [3196 – 3199]
Abid, M. (C) 3086 – 3089 [3146 – 3149]
Abu-Omar, M. M.
– On the Mechanism of the Reaction of Organic Azides with Transition Metals: Evidence for Triplet Nitrene Capture
(C) 6203 – 6207 [6359 – 6363]
DOI: 10.1002/anie.200462647
Acharya, H. P. (C) 3481 – 3484 [3547 – 3550]
Ackermann, L.
– Efficient Aryl – (Hetero)Aryl Coupling by Activation of C–Cl and C–F Bonds Using Nickel Complexes of Air-Stable Phosphine Oxides
(C) 7216 – 7219 [7382 – 7386]
DOI: 10.1002/anie.200501860
– Modular Diamino- and Dioxophosphine Oxides and Chlorides as Ligands for Transition-Metal-Catalyzed C–C and C–N Couplings with Aryl Chlorides
(C) 2444 – 2447 [2497 – 2500]
DOI: 10.1002/anie.200462371
– Titanium-Catalyzed Intermolecular Hydroamination of Vinylarenes
(C) 5972 – 5974 [6126 – 6128]
DOI: 10.1002/anie.200501423
Acquah, S. F. A. (C) 325 – 328 [329 – 332]
Adams, R. D.
– A Highly Unsaturated Platinum – Rhenium Cluster Complex that Adds an Unusually Large Amount of Hydrogen
(C) 2531 – 2533 [2587 – 2589]
DOI: 10.1002/anie.200500086
Adibekian, A. (C) 7605 – 7607 [7777 – 7780]
Adolfsson, H.
– Organocatalytic Hydride Transfers: A New Concept in Asymmetric Hydrogenations
(H) 3340 – 3342 [3404 – 3406]
DOI: 10.1002/anie.200500827
Adolph, S. (C) 2806 – 2808 [2866 – 2869]
Adrian, M. (C) 1388 – 1392 [1412 – 1416]
Adzic, R. R.
– Controlling the Catalytic Activity of Platinum-Monolayer Electrocatalysts for Oxygen Reduction with Different Substrates
(C) 2132 – 2135 [2170 – 2173]
DOI: 10.1002/anie.200462335
Affronte, M.
– Linking Rings through Diamines and Clusters: Exploring Synthetic Methods for Making Magnetic Quantum Gates
(C) 6496 – 6500 [6654 – 6658]
DOI: 10.1002/anie.200502505
Agarrabeitia, A. R. (C) 7739 – 7741 [7917 – 7919]
Aggarwal, V. K.
– Enantioselective α-Arylation of Cyclohexanones with Diaryl Iodonium Salts: Application to the Synthesis of (–)-Epibatidine
(C) 5516 – 5519 [5652 – 5655]
DOI: 10.1002/anie.200501745
– On the Importance of Leaving Group Ability in Reactions of Ammonium, Oxonium, Phosphonium, and Sulfonium Ylides
(C) 5468 – 5471 [5604 – 5607]
DOI: 10.1002/anie.200501526
– Reevaluation of the Mechanism of the Baylis – Hillman Reaction: Implications for Asymmetric Catalysis
(C) 1706 – 1708 [1734 – 1736]
DOI: 10.1002/anie.200462462
Aggeli, A. (C) 1965 – 1968 [2001 – 2004]
Aguilar, A. (C) 5989 – 5992 [6143 – 6146]
Aguilar, E. (C) 5875 – 5878 [6025 – 6028]
Ahijado, M. (C) 6947 – 6951 [7107 – 7111]
Ahlrichs, R. (C) 3932 – 3936 [4002 – 4005]
Ahn, J.-H. (C) 328 – 332 [332 – 336]
Ai, X.-C. (C) 747 – 750 [757 – 760]
Aida, T.
– Fully Plastic Actuator through Layer-by-Layer Casting with Ionic-Liquid-Based Bucky Gel
(C) 2410 – 2413 [2462 – 2465]
DOI: 10.1002/anie.200462318
– Planar or Perpendicular? Conformational Preferences of π-Conjugated Metalloporphyrin Dimers and Trimers in Supramolecular Tubular Arrays
(C) 4884 – 4888 [4962 – 4966]
DOI: 10.1002/anie.200500887
Aida, T. (C) 419 – 423 [423 – 427]
Aikawa, K. (C) 7257 – 7260 [7423 – 7426]
Aime, S.
– Highly Sensitive MRI Chemical Exchange Saturation Transfer Agents Using Liposomes
(C) 5513 – 5515 [5649 – 5651]
DOI: 10.1002/anie.200501473
– Tunable Imaging of Cells Labeled with MRI-PARACEST Agents
(C) 1813 – 1815 [1847 – 1849]
DOI: 10.1002/anie.200462566
Aizenberg, J.
– Template-Dependent Morphogenesis of Oriented Calcite Crystals in the Presence of Magnesium Ions
(C) 2386 – 2390 [2438 – 2442]
DOI: 10.1002/anie.200462296
Ajikumar, P. K. (C) 5476 – 5479 [5612 – 5615]
Akagi, K.
– Optically Active Conjugated Polymers Prepared from Achiral Monomers by Polycondensation in a Chiral Nematic Solvent
(C) 4322 – 4328 [4396 – 4402]
DOI: 10.1002/anie.200462859
Akasaka, T.
– 2D NMR Characterization of the La@C_{82} Anion
(C) 3282 – 3285 [3346 – 3349]
DOI: 10.1002/anie.200500039
– S-Heterocyclic Carbene with a Disilane Backbone
(C) 7567 – 7570 [7739 – 7742]
DOI: 10.1002/anie.200502971
Åkermark, B. Corrigendum: 506
Akita, M. (C) 4899 – 4903 [4977 – 4981]
Akiyama, K.
– Study of Anisotropic Interfacial Electron Transfer Across a Semiconductor/Solution Interface by Time-Resolved EPR Spectroscopy
(C) 3591 – 3594 [3657 – 3660]
DOI: 10.1002/anie.200461681
Akiyama, R. (C) 2732 – 2737 [2792 – 2797]
Akutagawa, T.
– Molecularly Assembled Nanostructures of a Redox-Active Organogelator
(C) 7283 – 7287 [7449 – 7453]
DOI: 10.1002/anie.200502336
Akutagawa, T. (C) 292 – 295 [296 – 299]
Akutsu, H. (C) 292 – 295 [296 – 299]
Akutsu-Sato, A. (C) 292 – 295 [296 – 299]
Al-Harrasi, A. (C) 6227 – 6231 [6383 – 6387]
Al-Hashimi, H. M.
– Evidence that Electrostatic Interactions Dictate the Ligand-Induced Arrest of RNA Global Flexibility
(C) 3412 – 3415 [3478 – 3481]
DOI: 10.1002/anie.200500075
Alam, M. S. (C) 803 – 806 [813 – 817], 7896 – 7900 [8109 – 8113]
Albinati, A. (C) 5701 – 5705 [5847 – 5851]
Albini, A.
– Metal-Free Cross-Coupling Reactions of Aryl Sulfonates and Phosphates through Photoheterolysis of Aryl – Oxygen Bonds
(C) 1232 – 1236 [1258 – 1262]
DOI: 10.1002/anie.200461444

DOI: 10.1002/anie.200512345
© 2005 Wiley-VCH Verlag GmbH & Co. KGaA, Weinheim

– Photo-Cross-Coupling Reaction of Electron-Rich Aryl Chlorides and Aryl Esters with Alkynes: A Metal-Free Alkynylation (C) 5675 – 5678 [5821 – 5824] DOI: 10.1002/anie.200501541
Albinsson, B. (C) 7591 – 7594 [7763 – 7766]
Albonetti, C. (C) 888 – 892 [910 – 914]
Albouy, P. A. (C) 4589 – 4592 [4665 – 4668]
Albrecht, M.
– Artificial Molecular Double-Stranded Helices (H) 6448 – 6451 [6606 – 6609] DOI: 10.1002/anie.200501472
Albrecht-Gary, A.-M.
– Supramolecular Click Chemistry with a Bisammonium-C_{60} Substrate and a Ditopic Crown Ether Host (C) 5338 – 5341 [5472 – 5475] DOI: 10.1002/anie.200501249
Albrecht-Schmitt, T. E.
– Actinide Materials Adopt Curvature: Nanotubules and Nanospheres (H) 4836 – 4838 [4914 – 4916] DOI: 10.1002/anie.200500936
Albu-Yaron, A. (C) 4169 – 4172 [4241 – 4244]
Alcalde, M. (C) 7553 – 7557 [7725 – 7729]
Alcaraz, C. (C) 5630 – 5634 [5774 – 5779]
Aldaba, E. (C) 2903 – 2907 [2963 – 2967]
Aldabergerova, S. (C) 7463 – 7465 [7629 – 7632]
Aldridge, S.
– Cationic Terminal Borylene Complexes: A Synthetic and Mechanistic Investigation of M=B Metathesis Chemistry (C) 7457 – 7460 [7623 – 7626] DOI: 10.1002/anie.200502343
– Selective Electrochemical Detection of Hydrogen Fluoride by Ambiphilic Ferrocene Derivatives (C) 3606 – 3609 [3672 – 3675] DOI: 10.1002/anie.200500527
Alemparte, C. (C) 2896 – 2899 [2956 – 2959]
Alexakis, A.
– Enantioselective Copper-Catalyzed Conjugate Addition to Trisubstituted Cyclohexenones: Construction of Stereogenic Quaternary Centers (C) 1376 – 1378 [1400 – 1402] DOI: 10.1002/anie.200462137
Aliaga-Alcalde, N. (C) 2908 – 2912 [2968 – 2972]
Allemann, R. K.
– Photochemical Regulation of DNA-Binding Specificity of MyoD (C) 7778 – 7782 [7956 – 7960] DOI: 10.1002/anie.200502666
Allix, M. M. B. (C) 7733 – 7736 [7911 – 7914]
Alonso, I. (C) 5670 – 5674 [5816 – 5820]
Alonso, J. L. (C) 3840 – 3844 [3908 – 3912], 6311 – 6315 [6469 – 6473]
Alonso-Gómez, J. L. (C) 5074 – 5078 [5203 – 5207]
Alsfasser, R.
– The Deposition of Metallopeptide-Based Coordination Polymers on Graphite Substrates: Effects of Side-Chain Functional Groups and Local Surface Structure (C) 803 – 806 [813 – 817] DOI: 10.1002/anie.200461274
Alteheld, A. (C) 1188 – 1192 [1212 – 1216]
Altmann, K.-H.
– Scaffolds for Microtubule Inhibition through Extensive Modification of the Epothilone Template (C) 7469 – 7473 [7636 – 7640] DOI: 10.1002/anie.200501760
Altus, E. (C) 7432 – 7435 [7598 – 7601]
Alvarez, S. (C) 2711 – 2715 [2771 – 2775]
Alves de Sousa, R. (C) 6162 – 6165 [6318 – 6321]
Amann, C. M. (C) 6546 – 6549 [6704 – 6707]
Amaranatha Reddy, R. (C) 774 – 778 [784 – 788]
Ambhaikar, N. B. (C) 606 – 609 [612 – 615], 3892 – 3895 [3960 – 3963]
Amenitsch, H. (C) 4589 – 4592 [4665 – 4668]
Amir, E. (C) 7374 – 7378 [7540 – 7544]
Amir, R. J. (C) 4378 – 4381 [4452 – 4455]
Amo-Ochoa, P. (C) 5670 – 5674 [5816 – 5820]
Amorín, M. (C) 5710 – 5713 [5856 – 5859]
Amorós, P. (C) 2918 – 2922 [2978 – 2982]
Amouri, H.
– Host – Guest Interactions: Design Strategy and Structure of an Unusual Cobalt Cage That Encapsulates a Tetrafluoroborate Anion (C) 4543 – 4546 [4619 – 4622] DOI: 10.1002/anie.200500786
Amslinger, S. (C) 7114 – 7118 [7276 – 7280]
An, H. (C) 5100 – 5103 [5230 – 5233]
An, M. H. (C) 4929 – 4932 [5009 – 5012]
Anagho, L. E. (C) 3271 – 3275 [3335 – 3339]
Anand, V. G. (C) 7244 – 7248 [7410 – 7414]
Ananda, K. (C) 4972 – 4975 [5052 – 5055]
Anderson, K. W. (C) 6173 – 6177 [6329 – 6333]
Anderson, M. W.
– A New Minimal Surface and the Structure of Mesoporous Silicas (C) 3243 – 3248 [3307 – 3312] DOI: 10.1002/anie.200462295
Anderson, O. P. (C) 7984 – 7987 [8198 – 8201]
Anderson, T. M. (C) 3540 – 3544 [3606 – 3610]
Andersson, M. (C) 7269 – 7273 [7435 – 7439]
Ando, H.
– 1,5-Lactamized Sialyl Acceptors for Various Disialoside Syntheses: Novel Method for the Synthesis of Glycan Portions of Hp-s6 and HLG-2 Gangliosides (C) 6759 – 6763 [6917 – 6921] DOI: 10.1002/anie.200501608
Andréasson, J.
– Molecular AND Logic Gate Based on Electric Dichroism of a Photochromic Dihydroindolizine (C) 7591 – 7594 [7763 – 7766] DOI: 10.1002/anie.200502420
Andreitchenko, E. V. (C) 6348 – 6354 [6506 – 6512]
Andrés, J. (C) 904 – 909 [926 – 931]
Andrews, C. G. (C) 7453 – 7456 [7619 – 7622]
Andrews, L.
– [H_2C=ZrH_2]: The Simplest Carbene Hydride Complex, Agostic Bonding, and C–H Activation of CH_4 to Form [$(CH_3)_2ZrH_2$] (C) 113 – 116 [115 – 118] DOI: 10.1002/anie.200461526
Andrikopoulos, P. C. (C) 3459 – 3462 [3525 – 3528]
Andruniów, T. (C) 6077 – 6081 [6231 – 6235]
Anselmetti, D.
– Single-Molecule Experiments in Synthetic Biology: An Approach to the Affinity Ranking of DNA-Binding Peptides (C) 3921 – 3924 [3989 – 3993] DOI: 10.1002/anie.200500152
– Supramolecular Chemistry at the Single-Molecule Level (C) 484 – 488 [489 – 492] DOI: 10.1002/anie.200461382
Anslyn, E. V.
– A Functional Assay for Heparin in Serum Using a Designed Synthetic Receptor (C) 5679 – 5682 [5825 – 5828] DOI: 10.1002/anie.200501437
– Differential Receptors Create Patterns That Distinguish Various Proteins (C) 6375 – 6378 [6533 – 6536] DOI: 10.1002/anie.200501137
Anson, C. E. (C) 4187 – 4192 [4259 – 4264], 5242 – 5246 [5376 – 5381], 6678 – 6682 [6836 – 6840], 7048 – 7053 [7210 – 7215]
Antipin, M. Yu. (C) 3400 – 3402 [3466 – 3468]
Antoine, T. (C) 1350 – 1352 [1374 – 1376]
Antonenko, Yu. N. (C) 1195 – 1198 [1219 – 1223]
Antonietti, M. (C) 4087 – 4092 [4156 – 4161], (R) 5576 – 5591 [5714 – 5730], (C) 6004 – 6009 [6158 – 6163]
Antonijevic, S.
– A Synthetic Zwitterionic Water Channel: Characterization in the Solid State by X-ray Crystallography and NMR Spectroscopy (C) 5720 – 5725 [5866 – 5871] DOI: 10.1002/anie.200500207
Antonijevic, S. (C) 2935 – 2938 [2995 – 2998]
Antonio, M. R. (C) 2135 – 2139 [2173 – 2177]
Antoniotti, S. (C) 4949 – 4953 [5029 – 5033]
Anwander, R.
– Trimethylyttrium and Trimethyllutetium (C) 5303 – 5306 [5437 – 5440] DOI: 10.1002/anie.200463109
Aoki, M. (C) 7447 – 7450 [7613 – 7616]
Aoun, R. (C) 2021 – 2023 [2057 – 2059]
Apeloig, Y.
– Nonsolvated, Aggregated 1,1-Dilithiosilane and the Derived Silyl Radicals (C) 739 – 743 [749 – 753] DOI: 10.1002/anie.200461765
Apostol, M. (C) 2580 – 2582 [2636 – 2638]
Appelhagen, A.
– Calculation of Clathrate-Like Water Clusters Including H_2O-Buckminsterfullerene (C) 811 – 815 [821 – 826] DOI: 10.1002/anie.200460899
Aquilanti, V. (C) 2356 – 2360 [2408 – 2412]
Arad, T. (C) 4169 – 4172 [4241 – 4244]
Arai, K. (C) 761 – 764 [771 – 774]
Arai, S. (C) 5459 – 5464 [5595 – 5600]
Arai, T. (C) 1546 – 1548 [1570 – 1572]
Arakawa, Y. (C) 3861 – 3864 [3929 – 3932]
Aranzaes, J. R. (R) 7852 – 7872 [8062 – 8083]
Aratani, N. (C) 6899 – 6901 [7059 – 7061]
Arceo, E. (C) 6187 – 6190 [6343 – 6346]
Archuleta, J. G. (C) 737 – 739 [747 – 749]
Ardeli-Tzaraf, Y. (C) 2885 – 2887 [2945 – 2947]
Arduengo III, A. J.
– The Generation of a Metallocene-Fused Imidazol-2-ylidene and Its Mercury Complex (C) 7240 – 7244 [7406 – 7410] DOI: 10.1002/anie.200502814
Arduini, A.
– Selective Synthesis of Two Constitutionally Isomeric Oriented Calix[6]arene-Based Rotaxanes (C) 278 – 281 [282 – 285] DOI: 10.1002/anie.200461336
Arduini, A. (C) 2913 – 2916 [2973 – 2976]
Arenz, S. (C) 5485 – 5488 [5621 – 5624]

 © 2005 Wiley-VCH Verlag GmbH & Co. KGaA, Weinheim

Arif, A. M. (C) 3129 – 3132 [3189 – 3192], 6546 – 6549 [6704 – 6707]
Arihara, R. (C) 2245 – 2249 [2285 – 2289]
Arik, I. C. (C) 400 – 403 [404 – 407]
Arikawa, Y. (C) 5509 – 5513 [5645 – 5649]
Arion, V. B.
– Azine-Bridged Octanuclear Copper(II) Complexes Assembled with a One-Stranded Ditopic Thiocarbohydrazone Ligand
(C) 7938 – 7942 [8152 – 8156]
DOI: 10.1002/anie.200501807
Armes, S. P. (C) 4795 – 4798 [4873 – 4876]
Armesto, D.
– The Effects of Triplet Sensitizers' Energies on the Photoreactivity of β,γ-Unsaturated Methyl Ketones
(C) 7739 – 7741 [7917 – 7919]
DOI: 10.1002/anie.200502619
Armstrong, D. R. (C) 3459 – 3462 [3525 – 3528]
Arndt, S. (C) 7473 – 7477 [7640 – 7644]
Arnesano, F. (C) 6341 – 6344 [6499 – 6502]
Aromí, G.
– [$GdNi_6$] and [$LaNi_6$]: High-Field EPR Spectroscopy and Magnetic Studies of Exchange-Coupled Octahedral Clusters
(C) 1997 – 2001 [2033 – 2037]
DOI: 10.1002/anie.200462401
Arora, P. S.
– Enhanced Metabolic Stability and Protein-Binding Properties of Artificial α Helices Derived from a Hydrogen-Bond Surrogate: Application to Bcl-xL
(C) 6525 – 6529 [6683 – 6687]
DOI: 10.1002/anie.200501603
Arrieta, A. (C) 2903 – 2907 [2963 – 2967]
Arrio, M.-A. (C) 4798 – 4801 [4876 – 4879]
Artaud, I.
– Direct Synthesis of a Thiolato-S and Sulfinato-S Co^{III} Complex Related to the Active Site of Nitrile Hydratase: A Pathway to the Post-Translational Oxidation of the Protein
(C) 6162 – 6165 [6318 – 6321]
DOI: 10.1002/anie.200500814
Arya, P.
– Stereocontrolled Solid-Phase Synthesis of a 90-Membered Library of Indoline-Alkaloid-like Polycycles from an Enantioenriched Aminoindoline Scaffold
(C) 1366 – 1368 [1390 – 1392]
DOI: 10.1002/anie.200462298
Arzoumanian, A. (C) 1984 – 1987 [2020 – 2023]
Asai, M. (C) 1257 – 1261 [1283 – 1287]
Asaka, K. (C) 2410 – 2413 [2462 – 2465]
Asao, N.
– Direct Mannich and Nitro-Mannich Reactions with Non-Activated Imines: AgOTf-Catalyzed Addition of Pronucleophiles to *ortho*-Alkynylaryl Aldimines Leading to 1,2-Dihydroisoquinolines
(C) 5526 – 5528 [5662 – 5664]
DOI: 10.1002/anie.200500795
Ashkenasy, N. (C) 1401 – 1404 [1425 – 1428]
Asmis, K. R.
– Polyhedral Vanadium Oxide Cages: Infrared Spectra of Cluster Anions and Size-Induced d Electron Localization
(C) 3122 – 3125 [3182 – 3185]
DOI: 10.1002/anie.200462894
Aßmann, J. (C) 917 – 920 [939 – 942]
Astruc, D.
– Efficient Mono- and Bifunctionalization of Polyolefin Dendrimers by Olefin Metathesis
(C) 7399 – 7404 [7565 – 7570]
DOI: 10.1002/anie.200502848
– Nanoparticles as Recyclable Catalysts: The Frontier between Homogeneous and Heterogeneous Catalysis
(R) 7852 – 7872 [8062 – 8083]
DOI: 10.1002/anie.200500766
Ataka, K. (C) 2413 – 2416 [2465 – 2468]
Atilla, G. E. (C) 1984 – 1987 [2020 – 2023]
Atrian, S. (C) 4618 – 4622 [4694 – 4698]
Atwood, J. L.
– Diffusion of Water in a Nonporous Hydrophobic Crystal
(C) 3848 – 3851 [3916 – 3919]
DOI: 10.1002/anie.200500749
– Hydrogen-Bonded Supramolecular Assemblies as Robust Templates in the Synthesis of Large Metal-Coordinated Capsules
(C) 5733 – 5736 [5879 – 5882]
DOI: 10.1002/anie.200501491
Aubele, D. L. (C) 3485 – 3488 [3551 – 3554]
Aubert, C.
– Chemo-, Regio-, and Stereoselective Cobalt-Mediated [2 + 2 + 2] Cycloaddition of Alkynyl Boronates to Alkenes: 1,3- and 1,4-Diboryl-1,3-cyclohexadienes
(C) 7114 – 7118 [7276 – 7280]
DOI: 10.1002/anie.200502038
Auclair, K.
– Regio- and Chemoselective 6′-N-Derivatization of Aminoglycosides: Bisubstrate Inhibitors as Probes To Study Aminoglycoside 6′-*N*-Acetyltransferases
(C) 6859 – 6862 [7019 – 7022]
DOI: 10.1002/anie.200501399
Auer, G. (C) 7620 – 7624 [7793 – 7797]
Aukauloo, A.
– A Biomimetic Model of the Electron Transfer between P_{680} and the TyrZ–His190 Pair of PSII
(C) 1536 – 1540 [1560 – 1564]
DOI: 10.1002/anie.200461948
Autrey, T.
– Nanoscaffold Mediates Hydrogen Release and the Reactivity of Ammonia Borane
(C) 3578 – 3582 [3644 – 3648]
DOI: 10.1002/anie.200462602
Avram, L. (R) 520 – 554 [524 – 560]
Axel, R.
– Scents and Sensibility: A Molecular Logic of Olfactory Perception (Nobel Lecture)
(R) 6110 – 6127 [6264 – 6282]
DOI: 10.1002/anie.200501726
Axtell, A. T. (C) 5834 – 5838 [5984 – 5988]
Azov, V. A. (C) 4635 – 4638 [4711 – 4715]
Azzaroni, O. (C) 4578 – 4581 [4654 – 4657]

Baasov, T.
– Dual Effect of Synthetic Aminoglycosides: Antibacterial Activity against *Bacillus anthracis* and Inhibition of Anthrax Lethal Factor
(C) 447 – 452 [451 – 456]
DOI: 10.1002/anie.200462003
Baati, R. (C) 2008 – 2011 [2044 – 2047]
Babai, A. (C) 5485 – 5488 [5621 – 5624]
Bacciu, D. (C) 5282 – 5284 [5416 – 5418]
Baceiredo, A. (C) 1700 – 1703 [1728 – 1731], 5497 – 5500 [5633 – 5636]
Bach, B. (C) 632 – 634 [638 – 640]
Bach, T.
– Synthesis of the Heterocyclic Core of the GE2270 Antibiotics and Structure Elucidation of a Major Degradation Product
(C) 1199 – 1201 [1223 – 1226]
DOI: 10.1002/anie.200461715
Back, J. W.
– Mild and Chemoselective Peptide-Bond Cleavage of Peptides and Proteins at Azido Homoalanine
(C) 7946 – 7950 [8160 – 8164]
DOI: 10.1002/anie.200502431
Bacskai, B. J. (C) 5452 – 5456 [5588 – 5592]
Badger, P. D. (C) 2508 – 2512 [2564 – 2568]
Bae, A.-H. (C) 2030 – 2033 [2066 – 2069]
Bae, C. (C) 6410 – 6413 [6568 – 6571]
Baettig, O. M. (C) 6859 – 6862 [7019 – 7022]
Bagno, A.
– Vicinal Tungsten – Tungsten Coupling Constants in Polyoxotungstates: DFT Calculations Challenge an Empirical Rule
(C) 2023 – 2026 [2059 – 2062]
DOI: 10.1002/anie.200462292
Bai, C.-L.
– Mass Production and High Photocatalytic Activity of ZnS Nanoporous Nanoparticles
(C) 1269 – 1273 [1295 – 1299]
DOI: 10.1002/anie.200462057
Baik, M.-H.
– A Unique Approach to Metal-Induced Bergman Cyclization: Long-Range Enediyne Activation by Ligand-to-Metal Charge Transfer
(C) 592 – 595 [598 – 601]
DOI: 10.1002/anie.200461825
Baiker, A. (C) 5643 – 5647 [5787 – 5792]
Bakac, A.
– Aqueous Fe^{IV}=O: Spectroscopic Identification and Oxo-Group Exchange
(C) 6871 – 6874 [7031 – 7034]
DOI: 10.1002/anie.200502686
Bakardjiev, M. (C) 6222 – 6226 [6378 – 6382]
Balagurusamy, V. S. K. (C) 4739 – 4745 [4817 – 4823]
Balamurugan, S. S. (C) 4872 – 4876 [4950 – 4954]
Balaram, P.
– C_9 Helices and Ribbons in γ-Peptides: Crystal Structures of Gabapentin Oligomers
(C) 4972 – 4975 [5052 – 5055]
DOI: 10.1002/anie.200501055
Balasubramanian, S.
– Targeting Nucleic Acid Secondary Structures with Polyamides Using an Optimized Dynamic Combinatorial Approach
(C) 5736 – 5739 [5882 – 5885]
DOI: 10.1002/anie.200501450
Balaz, M. (C) 4006 – 4009 [4074 – 4077]
Balázs, G. (C) 4920 – 4924 [4999 – 5003]
Balbo Block, M. A. (H) 6986 – 6989 [7146 – 7149]
Baldacchino, G. (C) 110 – 112 [112 – 114]
Baldamus, J. (C) 962 – 965 [984 – 987]
Baldus, M.
– A Concept for Rapid Protein-Structure Determination by Solid-State NMR Spec-

 © 2005 Wiley-VCH Verlag GmbH & Co. KGaA, Weinheim

troscopy
(C) 2089 – 2092 [2125 – 2129]
DOI: 10.1002/anie.200462516
Baldus, M. (C) 7072 – 7074 [7234 – 7236]
Ball, L. J.
– Recognition of Proline-Rich Motifs by Protein – Protein-Interaction Domains
(R) 2852 – 2869 [2912 – 2930]
DOI: 10.1002/anie.200400618
Ball, M. (C) 5433 – 5438 [5569 – 5574]
Ballano, G. (C) 396 – 399 [400 – 403]
Ballesteros, Alfredo (C) 4981 – 4983 [5061 – 5063]
Ballesteros, Antonio (C) 7553 – 7557 [7725 – 7729]
Balzani, V.
– Tweezering the Core of a Dendrimer: A Photophysical and Electrochemical Study
(C) 4574 – 4578 [4650 – 4654]
DOI: 10.1002/anie.200501025
Banci, L. (C) 6341 – 6344 [6499 – 6502]
Bando, Y. (C) 576 – 579 [582 – 585], 2140 – 2144 [2178 – 2182], 7929 – 7932 [8143 – 8146], 7932 – 7935 [8146 – 8149]
Banerjee, Rahul (C) 2515 – 2520 [2571 – 2576]
Banerjee, Rajkumar
– 17β-Estradiol-Associated Stealth-Liposomal Delivery of Anticancer Gene to Breast Cancer Cells
(C) 6723 – 6727 [6881 – 6885]
DOI: 10.1002/anie.200501793
Bang, D. (C) 3852 – 3856 [3920 – 3924]
Banner, D. W.
– Quantification of Cation – π Interactions in Protein – Ligand Complexes: Crystal-Structure Analysis of Factor Xa Bound to a Quaternary Ammonium Ion Ligand
(C) 4400 – 4404 [4474 – 4479]
DOI: 10.1002/anie.200500883
Bansal, G. (C) 3710 – 3714 [3776 – 3780]
Banser, D. (C) 6311 – 6315 [6469 – 6473]
Bantchev, G. B. (C) 4872 – 4876 [4950 – 4954]
Bao, J. (C) 6054 – 6057 [6208 – 6211]
Bao, W. (C) 952 – 955 [974 – 977]
Bar-Sadan, M. (C) 4169 – 4172 [4241 – 4244]
Baran, P. S.
– A Remarkable Ring Contraction En Route to the Chartelline Alkaloids
(C) 3714 – 3717 [3780 – 3783]
DOI: 10.1002/anie.200500522
– Direct Coupling of Pyrroles with Carbonyl Compounds: Short Enantioselective Synthesis of (*S*)-Ketorolac
(C) 609 – 612 [615 – 618]
DOI: 10.1002/anie.200462048
– Short, Enantioselective Total Synthesis of Stephacidin A
(C) 606 – 609 [612 – 615]
DOI: 10.1002/anie.200461864
– Total Synthesis of Avrainvillamide (CJ-17,665) and Stephacidin B
(C) 3892 – 3895 [3960 – 3963]
DOI: 10.1002/anie.200500655
Baratta, W.
– Ruthenium(II) Terdentate CNN Complexes: Superlative Catalysts for the Hydrogen-Transfer Reduction of Ketones by Reversible Insertion of a Carbonyl Group into the Ru–H Bond
(C) 6214 – 6219 [6370 – 6375]
DOI: 10.1002/anie.200502118
Barbara, P. F.
– Single-Molecule Studies of Electronic Energy Transfer in a Diblock Conjugated Polymer
(C) 6207 – 6210 [6363 – 6366]
DOI: 10.1002/anie.200501388
Barbas III, C. F.
– Direct Asymmetric α-Fluorination of Aldehydes
(C) 3706 – 3710 [3772 – 3776]
DOI: 10.1002/anie.200500571
Barbas III, C. F. (C) 716 – 720 [726 – 730], 4378 – 4381 [4452 – 4455]
Barbe, J.-M.
– Organic – Inorganic Hybrid Sol – Gel Materials Incorporating Functionalized Cobalt(III) Corroles for the Selective Detection of CO
(C) 3103 – 3106 [3163 – 3166]
DOI: 10.1002/anie.200463009
Barbet, J. (C) 4058 – 4061 [4126 – 4129]
Barbier, B. (C) 5630 – 5634 [5774 – 5779]
Barbosa, F. (C) 2390 – 2393 [2442 – 2445]
Barbour, L. J.
– Diffusion of Water in a Nonporous Hydrophobic Crystal
(C) 3848 – 3851 [3916 – 3919]
DOI: 10.1002/anie.200500749
Barenholz, Y. (C) 2885 – 2887 [2945 – 2947]
Baret, P. (C) 2580 – 2582 [2636 – 2638]
Barker, P. D.
– Controlling Self-Assembly by Linking Protein Folding, DNA Binding, and the Redox Chemistry of Heme
(C) 6337 – 6341 [6495 – 6499]
DOI: 10.1002/anie.200463035
Barker, W. (C) 5830 – 5833 [5980 – 5983]
Barley, H. R. L. (C) 6018 – 6021 [6172 – 6175]
Barlow, J. S. (C) 2732 – 2737 [2792 – 2797]
Barluenga, J.
– Formal Alkyne Insertion into Alkoxycarbene Complexes: Simple Access to Enantiopure Group 6 Alkynyl(alkoxy)carbene Complexes
(C) 4981 – 4983 [5061 – 5063]
DOI: 10.1002/anie.200501400
– Lithium Benzocyclobuteneoxide as a Precursor of a Vinylogous Enolate: Solvent-Controlled Synthesis of Highly Functionalized Seven-Membered Benzocarbocycles
(C) 5875 – 5878 [6025 – 6028]
DOI: 10.1002/anie.200501468
– New Iodination Reactions of Saturated Hydrocarbons
(C) 5851 – 5854 [6001 – 6004]
DOI: 10.1002/anie.200501195
– Tandem [$W(CO)_5$]-Catalyzed Cycloisomerization – Cyclopropanation Reactions Directed toward the Synthesis of Eight-Membered Carbocycles
(C) 126 – 128 [128 – 130]
DOI: 10.1002/anie.200461414
– Uncatalyzed Mukaiyama – Michael Reaction: Rapid Access to Simple and Complex Enantiopure γ-Butenolides
(C) 6583 – 6585 [6741 – 6743]
DOI: 10.1002/anie.200501746
Barma, D. K. (C) 2008 – 2011 [2044 – 2047]
Baro, A. (C) 820 – 822 [831 – 833]
Baron, G. V. (C) 400 – 403 [404 – 407]
Baron, O. (C) 3133 – 3135 [3193 – 3195]
Baron, R. (C) 4010 – 4015 [4078 – 4083]
Baroni, S. (C) 6142 – 6145 [6298 – 6301]
Barra, A.-L. (C) 1876 – 1879 [1910 – 1913], 3613 – 3616 [3679 – 3682]
Barral, M. C. (C) 305 – 307 [309 – 311]
Barth, J. V.
– Mesoscopic Metallosupramolecular Texturing by Hierarchic Assembly
(C) 7294 – 7297 [7460 – 7463]
DOI: 10.1002/anie.200501906
– Two-Dimensional Adatom Gas Bestowing Dynamic Heterogeneity on Surfaces
(C) 1488 – 1491 [1512 – 1515]
DOI: 10.1002/anie.200461390
Barth, M. (C) 1560 – 1563 [1584 – 1588]
Bartoli, G.
– Organocatalytic Asymmetric α-Halogenation of 1,3-Dicarbonyl Compounds
(C) 6219 – 6222 [6375 – 6378]
DOI: 10.1002/anie.200502134
Bartsch, A. (C) 2957 – 2959 [3016 – 3019]
Basak, Amit
– Activation of Macrocyclic Enediynes by Transannular Cyclization
(C) 132 – 135 [134 – 137]
DOI: 10.1002/anie.200460831
Basak, Arindrajit (C) 4389 – 4391 [4463 – 4465]
Basch, H. (C) 7432 – 7435 [7598 – 7601]
Basché, T. (C) 2437 – 2440 [2490 – 2493]
Basnar, B. (C) 78 – 83 [80 – 85]
Basosi, R. (C) 2390 – 2393 [2442 – 2445]
Bassan, A.
– Two Faces of a Biomimetic Non-Heme HO–Fe^{V}=O Oxidant: Olefin Epoxidation versus *cis*-Dihydroxylation
(C) 2939 – 2941 [2999 – 3001]
DOI: 10.1002/anie.200463072
Bassan, A. (C) 7028 – 7032 [7190 – 7194]
Bassani, D. M.
– Hydrogen-Bonded CdS Nanoparticle Assemblies on Electrodes for Photoelectrochemical Applications
(C) 4010 – 4015 [4078 – 4083]
DOI: 10.1002/anie.200463055
Bassani, D. M. (C) 1072 – 1075 [1096 – 1099]
Basset, J.-M.
– Development of Tungsten-Based Heterogeneous Alkane Metathesis Catalysts Through a Structure – Activity Relationship
(C) 6755 – 6758 [6913 – 6916]
DOI: 10.1002/anie.200501382
Bates, G. W. (C) 2537 – 2542 [2593 – 2598]
Batey, H. D. (C) 1712 – 1714 [1740 – 1742]
Bath, J.
– A Free-Running DNA Motor Powered by a Nicking Enzyme
(C) 4358 – 4361 [4432 – 4435]
DOI: 10.1002/anie.200501262
Bats, J. W. (C) 2798 – 2801 [2858 – 2861]
Batten, S. R. (C) 5471 – 5475 [5607 – 5611]
Bau, R.
– A Neutron Diffraction Study of [$OsClH_3(PPh_3)_3$]: A Complex Containing a Highly "Stretched" Dihydrogen Ligand
(C) 7227 – 7230 [7393 – 7396]
DOI: 10.1002/anie.200502297
Bau, R. (C) 1860 – 1865 [1894 – 1899]
Bauer, H. (R) 690 – 715 [698 – 724]
Bauer, J. (C) 7542 – 7545 [7714 – 7717]
Bauer, M. (C) 6381 – 6384 [6539 – 6542]
Bauer, R. (C) 2447 – 2451 [2501 – 2505]
Bauer, R. E. (C) 6348 – 6354 [6506 – 6512]
Bauer, W. (C) 1564 – 1567 [1588 – 1592]
Baumann, D. (C) 3548 – 3552 [3614 – 3618]
Baumann, K. (C) 7208 – 7212 [7374 – 7379]
Baumann, W. (C) 1184 – 1188 [1208 – 1212]
Baussard, J.-F. (C) 5262 – 5265 [5397 – 5400]
Bawendi, M. G.
– A Microfabricated Gas – Liquid Segmented Flow Reactor for High-Temperature Synthesis: The Case of CdSe Quan-

 © 2005 Wiley-VCH Verlag GmbH & Co. KGaA, Weinheim

tum Dots
(C) 5447 – 5451 [5583 – 5587]
DOI: 10.1002/anie.200500792
Bayley, H.
– Single Protein Pores Containing Molecular Adapters at High Temperatures
(C) 1495 – 1499 [1519 – 1523]
DOI: 10.1002/anie.200461885
Bayley, H. (C) 1401 – 1404 [1425 – 1428]
Baylies, C. J. (C) 6909 – 6912 [7069 – 7072]
Bazan, G. C.
– Remote Activation of Nickel Catalysts for Ethylene Oligomerization
(C) 1108 – 1112 [1132 – 1136]
DOI: 10.1002/anie.200461630
Beau, J.-M.
– Dynamic Combinatorial Chemistry: Lysozyme Selects an Aromatic Motif That Mimics a Carbohydrate Residue
(C) 965 – 969 [987 – 991]
DOI: 10.1002/anie.200462150
Beauchesne, F. (C) 3475 – 3477 [3541 – 3543]
Beaufils, F. (C) 5273 – 5275 [5407 – 5409]
Becher, J. (C) 7283 – 7287 [7449 – 7453]
Bechtel, H. A. (C) 2382 – 2385 [2434 – 2437]
Beck, M. (C) 7612 – 7615 [7784 – 7788]
Beck, R. (C) 975 – 977 [997 – 999]
Becker, A. (C) 3921 – 3924 [3989 – 3993]
Becker, C. F. W.
– Direct Readout of Protein – Protein Interactions by Mass Spectrometry from Protein – DNA Microarrays
(C) 7635 – 7639 [7808 – 7812]
DOI: 10.1002/anie.200502908
Becker, J. Y.
– A Rigid Neutral Molecule Involving TTF and TCNQ Moieties with Intrinsic Charge- and Electron-Transfer Properties that Depend on the Polarity of the Solvent
(C) 4015 – 4018 [4083 – 4086]
DOI: 10.1002/anie.200500812
Becker, S.
– A Concept for Rapid Protein-Structure Determination by Solid-State NMR Spectroscopy
(C) 2089 – 2092 [2125 – 2129]
DOI: 10.1002/anie.200462516
Becker, S. (C) 7776 – 7778 [7954 – 7956]
Beckerle, K. (C) 7473 – 7477 [7640 – 7644]
Behenna, D. C. (C) 6924 – 6927 [7084 – 7087]
Bejot, R. (C) 2008 – 2011 [2044 – 2047]
Belakhov, V. (C) 447 – 452 [451 – 456]
Belder, D.
– Microfluidics with Droplets
(H) 3521 – 3522 [3587 – 3588]
DOI: 10.1002/anie.200500620
Belderrain, T. R. (C) 5284 – 5288 [5418 – 5422]
Bell, M. (C) 1965 – 1968 [2001 – 2004]
Bell, S. G. (C) 4029 – 4032 [4097 – 4100]
Bella, M. (C) 2896 – 2899 [2956 – 2959]
Belle, C. (C) 438 – 441 [442 – 445]
Bellemin-Laponnaz, S.
– C_3 Chirality in Polymerization Catalysis: A Highly Active Dicationic Scandium(III) Catalyst for the Isoselective Polymerization of 1-Hexene
(C) 1668 – 1671 [1696 – 1699]
DOI: 10.1002/anie.200462804
Beller, M.
– An Efficient and General Iron-Catalyzed Arylation of Benzyl Alcohols and Benzyl Carboxylates
(C) 3913 – 3917 [3981 – 3985]
DOI: 10.1002/anie.200462522
– Catalysts for Cross-Coupling Reactions with Non-activated Alkyl Halides
(M) 674 – 688 [680 – 695]
DOI: 10.1002/anie.200461432
– Transition-Metal-Catalyzed Benzylation of Arenes and Heteroarenes
(C) 238 – 242 [242 – 246]
DOI: 10.1002/anie.200460666
Bello, I. (C) 4749 – 4753 [4827 – 4831]
Beltrán, D. (C) 2918 – 2922 [2978 – 2982]
Ben Yahia, M. (C) 7542 – 7545 [7714 – 7717]
Bendig, J. (C) 1195 – 1198 [1219 – 1223]
Benhmid, A. (C) 6771 – 6774 [6929 – 6933]
Benincasa, M. (C) 6358 – 6362 [6516 – 6520]
Benisvy, L.
– Phenoxyl Radicals Hydrogen-Bonded to Imidazolium: Analogues of Tyrosyl $D^{\cdot}$ of Photosystem II: High-Field EPR and DFT Studies
(C) 5314 – 5317 [5448 – 5451]
DOI: 10.1002/anie.200501132
Benkovic, S. J.
– Genetically Selected Cyclic-Peptide Inhibitors of AICAR Transformylase Homodimerization
(C) 2760 – 2763 [2820 – 2823]
DOI: 10.1002/anie.200500417
Benndorf, K. (C) 7887 – 7891 [8099 – 8104]
Bennett, J. S. (C) 6685 – 6689 [6843 – 6847]
Bensch, W. (C) 5643 – 5647 [5787 – 5792]
Bensel, N. (C) 6863 – 6866 [7023 – 7026]
Benz, J. (C) 4400 – 4404 [4474 – 4479]
Bera, T. K. (C) 4739 – 4745 [4817 – 4823]
Bérar, J.-F. (C) 1725 – 1729 [1753 – 1757]
Berg, A. M. (C) 1821 – 1823 [1855 – 1857]
Berg, T.
– Cellular Profiling of Small-Molecule Bioactivities: an Alternative Tool for Chemical Biology
(H) 5008 – 5011 [5134 – 5137]
DOI: 10.1002/anie.200500721
Berger, R. (C) 3623 – 3626 [3689 – 3693]
Berghuis, A. M. (C) 6859 – 6862 [7019 – 7022]
Berkessel, A.
– Highly Efficient Dynamic Kinetic Resolution of Azlactones by Urea-Based Bifunctional Organocatalysts
(C) 807 – 811 [817 – 821]
DOI: 10.1002/anie.200461442
– Kinetic Resolution of Oxazinones: An Organocatalytic Approach to Enantiomerically Pure β-Amino Acids
(C) 7466 – 7469 [7632 – 7635]
DOI: 10.1002/anie.200502003
Berlicka, A. (C) 5288 – 5291 [5422 – 5425]
Bermejo, M. R.
– Route to Cluster Helicates
(C) 4182 – 4187 [4254 – 4259]
DOI: 10.1002/anie.200500840
Bermel, W. (C) 3089 – 3092 [3149 – 3152]
Bernardi, J. (C) 4917 – 4920 [4996 – 4999]
Bernardi, L.
– Phase-Transfer-Catalyzed Asymmetric Aza-Henry Reaction Using *N*-Carbamoyl Imines Generated In Situ from α-Amido Sulfones
(C) 7975 – 7978 [8189 – 8192]
DOI: 10.1002/anie.200502646
Bernardi, L. (C) 6576 – 6579 [6734 – 6737]
Bernardinelli, G.
– Predictions, Synthetic Strategy, and Isolation of a Linear Tetrametallic Triple-Stranded Lanthanide Helicate
(C) 7954 – 7958 [8168 – 8172]
DOI: 10.1002/anie.200503040
Bernardinelli, G. (C) 1879 – 1883 [1913 – 1917], 5060 – 5064 [5188 – 5192]
Berndt, A.
– Derivatives of the Simplest Polyhedral Carborane Anion: Structures at the Borderline between Two- and Three-Dimensional Aromatic Compounds
(C) 1643 – 1646 Corrigendum: 2471 [1670 – 1673 Corrigendum: 2525]
DOI: 10.1002/anie.200462397
Bernhard, W. A.
– 2-Deoxyribonolactone Lesions in X-ray-Irradiated DNA: Quantitative Determination by Catalytic 5-Methylene-2-furanone Release
(C) 6210 – 6213 [6366 – 6369]
DOI: 10.1002/anie.200501956
Bernhardt, P. (C) 2742 – 2746 [2802 – 2806]
Bernsmann, H. (C) 4209 – 4212 [4281 – 4284]
Berova, N.
– A Cationic Zinc Porphyrin as a Chiroptical Probe for Z-DNA
(C) 4006 – 4009 [4074 – 4077]
DOI: 10.1002/anie.200501149
Berry, A. (C) 2109 – 2112 [2147 – 2150]
Berry, V. (C) 6668 – 6673 [6826 – 6831]
Bertagnolli, E. (C) 3419 – 3422 [3485 – 3488]
Bertermann, R. (C) 5292 – 5295 [5426 – 5429]
Berthod, M. (C) 5130 – 5133 [5260 – 5263]
Bertini, I.
– Complete Assignment of Heteronuclear Protein Resonances by Protonless NMR Spectroscopy
(C) 3089 – 3092 [3149 – 3152]
DOI: 10.1002/anie.200461794
– NMR Spectroscopic Detection of Protein Protons and Longitudinal Relaxation Rates between 0.01 and 50 MHz
(C) 2223 – 2225 [2263 – 2265]
DOI: 10.1002/anie.200462344
– Structural Interplay between Calcium(II) and Copper(II) Binding to S100A13 Protein
(C) 6341 – 6344 [6499 – 6502]
DOI: 10.1002/anie.200500540
Bertrán, J. (C) 904 – 909 [926 – 931]
Bertrand, G.
– A Rigid Cyclic (Alkyl)(amino)carbene Ligand Leads to Isolation of Low-Coordinate Transition-Metal Complexes
(C) 7236 – 7239 [7402 – 7405]
DOI: 10.1002/anie.200502566
– A Stable P-Heterocyclic Carbene
(C) 1700 – 1703 [1728 – 1731]
DOI: 10.1002/anie.200462239
– Dimerization of a Cyclo-1σ^4,3σ^2,4σ^2-Triphosphapentadienyl Radical: Evidence for Phosphorus – Phosphorus Odd-Electron Bonds
(C) 5497 – 5500 [5633 – 5636]
DOI: 10.1002/anie.200501369
– Stable Cyclic (Alkyl)(Amino)Carbenes as Rigid or Flexible, Bulky, Electron-Rich Ligands for Transition-Metal Catalysts: A Quaternary Carbon Atom Makes the Difference
(C) 5705 – 5709 [5851 – 5855]
DOI: 10.1002/anie.200501841
Besenbacher, F.
– Guanine Quartet Networks Stabilized by Cooperative Hydrogen Bonds
(C) 2270 – 2275 [2310 – 2315]
DOI: 10.1002/anie.200461586
Besong, G. E. (C) 6403 – 6406 [6561 – 6564]
Bessho, Y. (C) 7287 – 7290 [7453 – 7456]
Betson, M. S. (C) 1241 – 1244 [1267 – 1270]

 © 2005 Wiley-VCH Verlag GmbH & Co. KGaA, Weinheim

Beutner, G. L. (R) 4682 – 4698 [4760 – 4777]
Beyermann, M. (C) 4631 – 4635 [4707 – 4711]
Bhalla, G. (C) 1540 – 1543 [1564 – 1567]
Bhatia, B. (C) 7761 – 7764 [7939 – 7942]
Bhatt, A. (C) 7075 – 7078 [7237 – 7240]
Bhatt, P. M. (C) 2515 – 2520 [2571 – 2576]
Bhattacharyya, S. (C) 592 – 595 [598 – 601]
Bialy, L. (R) 3814 – 3839 [3880 – 3906]
Bianco, A.
– Targeted Delivery of Amphotericin B to Cells by Using Functionalized Carbon Nanotubes
(C) 6358 – 6362 [6516 – 6520]
DOI: 10.1002/anie.200501613
Bickley, J. F. (C) 3271 – 3275 [3335 – 3339]
Biel, M. (R) 3186 – 3216 [3248 – 3280], (C) 4975 – 4980 [5055 – 5060]
Bienert, M. (C) 4631 – 4635 [4707 – 4711], 5252 – 5255 [5386 – 5389]
Biesalski, M.
– Peptide – Polymer Hybrid Nanotubes
(C) 3297 – 3301 [3361 – 3365]
DOI: 10.1002/anie.200462993
Bigeault, J. (C) 4753 – 4757 [4831 – 4835]
Bill, E. (C) 2908 – 2912 [2968 – 2972]
Binder, W. H.
– Supramolecular Assembly of Nanoparticles at Liquid – Liquid Interfaces
(H) 5172 – 5175 [5300 – 5304]
DOI: 10.1002/anie.200501220
Bindu, S. Corrigendum: 1907
Binks, B. P.
– Aqueous Foams Stabilized Solely by Silica Nanoparticles
(C) 3722 – 3725 [3788 – 3791]
DOI: 10.1002/anie.200462470
– Inversion of Emulsions Stabilized Solely by Ionizable Nanoparticles
(C) 441 – 444 [445 – 448]
DOI: 10.1002/anie.200461846
– Temperature-Induced Inversion of Nanoparticle-Stabilized Emulsions
(C) 4795 – 4798 [4873 – 4876]
DOI: 10.1002/anie.200501073
Bircher, R. (C) 4239 – 4242 [4311 – 4314]
Biron, J.-P. (C) 6731 – 6734 [6889 – 6892]
Biscarini, F.
– Magnetic Information Storage on Polymers by Using Patterned Single-Molecule Magnets
(C) 888 – 892 [910 – 914]
DOI: 10.1002/anie.200461554
Bishop, K. J. M. (C) 7263 – 7269 [7429 – 7435]
Biswas, K. (C) 2232 – 2234 [2272 – 2274]
Bitter, J. H.
– Physicochemical Characterization of Porous Materials: Spatially Resolved Accessibility of Zeolite Crystals
(C) 1360 – 1363 [1384 – 1387]
DOI: 10.1002/anie.200460966
Bittl, R. (C) 5314 – 5317 [5448 – 5451]
Bittner, E. W. (C) 72 – 75 [74 – 77]
Björling, T. (C) 7269 – 7273 [7435 – 7439]
Bjørnholm, T.
– Structural Evidence of Mechanical Shuttling in Condensed Monolayers of Bistable Rotaxane Molecules
(C) 7035 – 7039 [7197 – 7201]
DOI: 10.1002/anie.200501538
Blackmond, D. G.
– Reaction Progress Kinetic Analysis: A Powerful Methodology for Mechanistic Studies of Complex Catalytic Reactions
(R) 4302 – 4320 [4374 – 4393]
DOI: 10.1002/anie.200462544
Blackmore, I. J. (C) 6746 – 6750 [6904 – 6908]
Blagden, N. (C) 7032 – 7035 [7194 – 7197]
Blais, J.-C. (C) 7399 – 7404 [7565 – 7570]
Blanc, A. (C) 5130 – 5133 [5260 – 5263]
Blasco, T.
– Establishing a Molecular Mechanism for the Beckmann Rearrangement of Oximes over Microporous Molecular Sieves
(C) 2370 – 2373 [2422 – 2425]
DOI: 10.1002/anie.200462737
Blechert, S.
– Intramolecular Hydroamination of Functionalized Alkenes and Alkynes with a Homogenous Zinc Catalyst
(C) 7794 – 7798 [7972 – 7976]
DOI: 10.1002/anie.200502006
Bleuzen, A.
– The Co Ligand Field: A Key Parameter in Photomagnetic CoFe Prussian Blue Derivatives
(C) 4798 – 4801 [4876 – 4879]
DOI: 10.1002/anie.200500647
Blight, B. A. (C) 1499 – 1504 [1523 – 1528]
Blom, R. (C) 6354 – 6358 [6512 – 6516]
Blomberg, M. R. A. (C) 2939 – 2941 [2999 – 3001]
Blommers, M. J. J. (C) 4172 – 4175 [4244 – 4247]
Blondin, G. (C) 1876 – 1879 [1910 – 1913]
Blount, K. F. (C) 927 – 932 [949 – 954], 5329 – 5334 [5463 – 5468]
Blüm, M.-C.
– Conservation of Chirality in a Hierarchical Supramolecular Self-Assembled Structure with Pentagonal Symmetry
(C) 5334 – 5337 [5468 – 5471]
DOI: 10.1002/anie.200501467
Blumenstein, M. (C) 4242 – 4244 [4314 – 4316]
Bo, C. (C) 7230 – 7233 [7396 – 7399]
Boatz, J. A. (C) 1860 – 1865 [1894 – 1899]
Bobadova-Parvanova, P. (C) 7101 – 7103 [7263 – 7265]
Bocharova, V. (C) 6391 – 6394 [6549 – 6552]
Bockrath, B. C. (C) 72 – 75 [74 – 77]
Bocola, M. (C) 4192 – 4196 [4264 – 4268]
Bode, H. B. (R) 6828 – 6846 [6988 – 7007]
Boden, N.
– Adsorption and Self-Assembly of Peptides on Mica Substrates
(C) 1965 – 1968 [2001 – 2004]
DOI: 10.1002/anie.200462160
Bodenhausen, G.
– High-Resolution NMR Spectroscopy in Solids by Truly Magic-Angle Spinning
(C) 2935 – 2938 [2995 – 2998]
DOI: 10.1002/anie.200463049
Bodenhausen, G. (C) 5720 – 5725 [5866 – 5871]
Bodtke, A. (C) 5255 – 5259 [5389 – 5393]
Bodyagin, M. (C) 774 – 778 [784 – 788]
Boer, J. (C) 927 – 932 [949 – 954]
Boezio, A. A. (C) 6046 – 6050 [6200 – 6204]
Bofill, R. (C) 4939 – 4944 [5019 – 5024]
Boga, C. (C) 3285 – 3289 [3349 – 3353]
Bogani, L. (C) 5817 – 5821 [5967 – 5971]
Bögge, H. (C) 3857 – 3861 [3925 – 3929], 7757 – 7761 [7935 – 7939]
Böhme, D. K.
– Gas-Phase Catalysis by Atomic and Cluster Metal Ions: The Ultimate Single-Site Catalysts
(R) 2336 – 2354 [2388 – 2406]
DOI: 10.1002/anie.200461698
Bohn, A. (R) 3358 – 3393 [3422 – 3458]
Boissière, C. (C) 4589 – 4592 [4665 – 4668]
Boisson, C.
– Alternating Copolymerization of Ethylene and Butadiene with a Neodymocene Catalyst
(C) 2593 – 2596 [2649 – 2652]
DOI: 10.1002/anie.200462019
Böker, A. (C) 2420 – 2426 [2472 – 2478]
Bolbach, G. (C) 4244 – 4247 [4316 – 4319]
Boldron, C. (C) 3585 – 3587 [3651 – 3653]
Bollinger, J. C. (C) 6689 – 6693 [6847 – 6851]
Bollot, G. (C) 6154 – 6157 [6310 – 6313]
Bolm, C.
– Diphenylphosphanylsulfoximines as Ligands in Iridium-Catalyzed Asymmetric Imine Hydrogenations
(C) 7564 – 7567 [7736 – 7739]
DOI: 10.1002/anie.200502482
– Protonated Chiral Catalysts: Versatile Tools for Asymmetric Synthesis
(H) 1758 – 1763 [1788 – 1793]
DOI: 10.1002/anie.200500154
Boltalina, O. V.
– High-Temperature Synthesis of the Surprisingly Stable C_1-$C_{70}(CF_3)_{10}$ Isomer with a *para*^{7} – *meta* – *para* Ribbon of Nine $C_6(CF_3)_2$ Edge-Sharing Hexagons
(C) 7984 – 7987 [8198 – 8201]
DOI: 10.1002/anie.200502419
– Trifluoromethylated Endohedral Metallofullerenes: Synthesis and Characterization of $Y@C_{82}(CF_3)_5$
(C) 1846 – 1849 [1880 – 1883]
DOI: 10.1002/anie.200461497
Bolte, M. (C) 7783 – 7786 [7961 – 7964]
Bominaar, E. L. (C) 6871 – 6874 [7031 – 7034]
Bonchio, M. (C) 2023 – 2026 [2059 – 2062]
Bone, N. (C) 325 – 328 [329 – 332]
Bonhommeau, S. (C) 4069 – 4073 [4137 – 4141]
Bonino, F. (C) 4774 – 4777 [4852 – 4855]
Bonneviot, L.
– Organometallic Chemistry Inside the Pore Walls of Mesostructured Silica Materials
(C) 3475 – 3477 [3541 – 3543]
DOI: 10.1002/anie.200500454
Bonvallet, P. A. (C) 3050 – 3055 [3110 – 3115]
Boogers, J. A. F. (C) 4209 – 4212 [4281 – 4284]
Booker-Milburn, K. I.
– Enantioselective Reduction of β-Keto Acids with Engineered *Streptomyces coelicolor*
(C) 1121 – 1125 [1145 – 1149]
DOI: 10.1002/anie.200462076
Boons, G.-J.
– Stereoselective Glycosylation Reactions with Chiral Auxiliaries
(C) 947 – 949 [969 – 971]
DOI: 10.1002/anie.200461745
– Towards a Fully Synthetic Carbohydrate-Based Anticancer Vaccine: Synthesis and Immunological Evaluation of a Lipidated Glycopeptide Containing the Tumor-Associated Tn Antigen
(C) 5985 – 5988 [6139 – 6142]
DOI: 10.1002/anie.200501818
Boos, D. (C) 4707 – 4712 [4785 – 4791]
Bordiga, S. (C) 4774 – 4777 [4852 – 4855]
Borel, A. (C) 1480 – 1484 [1504 – 1508]
Born, R. (C) 2444 – 2447 [2497 – 2500], 7216 – 7219 [7382 – 7386]
Bornand, M. (C) 7909 – 7911 [8123 – 8125]
Boronat, M. (C) 2370 – 2373 [2422 – 2425]

 © 2005 Wiley-VCH Verlag GmbH & Co. KGaA, Weinheim

Borsato, G.
– "Hexacarboxytrindanes": Benzene Rings with Homotopic Faces as Scaffolds for the Construction of D_3 Chiral Architectures (C) 7435 – 7439 [7601 – 7605] DOI: 10.1002/anie.200502262
Borse, P. H. (C) 4585 – 4589 [4661 – 4665]
Borst, M. L. G. (C) 3289 – 3293 [3353 – 3357]
Bosco, M. (C) 6219 – 6222 [6375 – 6378]
Bosso, C. (C) 1350 – 1352 [1374 – 1376]
Bostock, J. M. (C) 6403 – 6406 [6561 – 6564]
Bothe, E. (C) 5314 – 5317 [5448 – 5451]
Botoshansky, M. (C) 739 – 743 [749 – 753], 5087 – 5089 [5217 – 5219]
Böttcher, C.
– Switchable Supramolecular Organization of Structurally Defined Micelles Based on an Amphiphilic Fullerene (C) 2976 – 2979 [3036 – 3039] DOI: 10.1002/anie.200462465
Böttcher, J. (C) 3140 – 3144 [3200 – 3204]
Boudebous, H. (C) 4073 – 4075 [4141 – 4143]
Boulatov, R. (C) 5682 – 5686 [5828 – 5832]
Boulfelfel, S. E. (C) 7542 – 7545 [7714 – 7717]
Bourgeois, D. (C) 618 – 621 [624 – 627]
Bourke, S. C. (R) 5016 – 5036 [5142 – 5163], (C) 5886 – 5890 [6036 – 6040]
Bourles, E. (C) 6162 – 6165 [6318 – 6321]
Bourne, H. O. (C) 1221 – 1222 [1247 – 1248]
Bouschen, W. (C) 7635 – 7639 [7808 – 7812]
Bousseksou, A.
– One Shot Laser Pulse Induced Reversible Spin Transition in the Spin-Crossover Complex $[Fe(C_4H_4N_2)\{Pt(CN)_4\}]$ at Room Temperature (C) 4069 – 4073 [4137 – 4141] DOI: 10.1002/anie.200500717
Boyd, J. W. (C) 944 – 946 [966 – 968]
Brabec, V. (C) 2885 – 2887 [2945 – 2947]
Bracco, S. (C) 1816 – 1820 [1850 – 1854]
Brace, G. N. (C) 403 – 406 [407 – 410]
Brack, A. (C) 5630 – 5634 [5774 – 5779]
Brady, S. F.
– Cloning and Heterologous Expression of Isocyanide Biosynthetic Genes from Environmental DNA (C) 7063 – 7065 [7225 – 7227] DOI: 10.1002/anie.200501941
– Systematic Investigation of the *Escherichia coli* Metabolome for the Biosynthetic Origin of an Isocyanide Carbon Atom (C) 7045 – 7048 [7207 – 7210] DOI: 10.1002/anie.200501942
Brakke, K. A. (C) 3243 – 3248 [3307 – 3312]
Brand, H. (C) 3929 – 3932 [3998 – 4001]
Brand, S. (C) 452 – 455 [456 – 459]
Branda, N. R.
– Photoswitching of Stereoselectivity in Catalysis Using a Copper Dithienylethene Complex (C) 2019 – 2021 [2055 – 2057] DOI: 10.1002/anie.200462538
Brandès, S. (C) 3103 – 3106 [3163 – 3166]
Brandt, B. (C) 7601 – 7605 [7773 – 7777]
Bräse, S.
– Asymmetric Conjugate Addition of Organozinc Compounds to α,β-Unsaturated Aldehydes and Ketones with [2.2]Paracyclophaneketimine Ligands without Added Copper Salts (C) 7879 – 7881 [8091 – 8093] DOI: 10.1002/anie.200501732
– Organic Azides: An Exploding Diversity of a Unique Class of Compounds (R) 5188 – 5240 [5320 – 5374] DOI: 10.1002/anie.200400657
Braun, T.
– Oxidative Addition of NH_3 to a Transition-Metal Complex: A Key Step for the Metal-Mediated Derivatization of Ammonia? (H) 5012 – 5014 [5138 – 5140] DOI: 10.1002/anie.200501505
– Rhodium-Mediated Formation of Peroxides from Dioxygen: Isolation of Hydroperoxo, Silylperoxo, and Methylperoxo Intermediates (C) 6947 – 6951 [7107 – 7111] DOI: 10.1002/anie.200501615
Braunschweig, H.
– A Boryl Bridged Complex: An Unusual Coordination Mode of the BR_2 Ligand (C) 1192 – 1194 [1217 – 1219] DOI: 10.1002/anie.200462444
– A T-Shaped Platinum(II) Boryl Complex as the Precursor to a Platinum Compound with a Base-Stabilized Borylene Ligand (C) 5651 – 5654 [5796 – 5799] DOI: 10.1002/anie.200501588
– Boron—A Meeting Point (T) 7826 – 7828 [8036 – 8038] DOI: 10.1002/anie.200503703
– Boron as a Bridging Ligand (C) 1658 – 1661 [1685 – 1688] DOI: 10.1002/anie.200463026
– Synthesis of *ansa*-[2]Boracyclopentadienylcycloheptatrienylchromium and Its Reaction to the *ansa*-Platinabis(boryl) Complex by Oxidative Addition of the Boron–Boron Bond (C) 5647 – 5651 [5792 – 5796] DOI: 10.1002/anie.200500686
– Synthesis of Borirenes by Photochemical Borylene Transfer from $[(OC)_5M{=}BN(SiMe_3)_2]$ (M = Cr, Mo) to Alkynes (C) 7461 – 7463 [7627 – 7629] DOI: 10.1002/anie.200502524
– Terminal Borylene Complexes Stabilized by a Transition-Metal Base (C) 3763 – 3766 [3829 – 3832] DOI: 10.1002/anie.200500302
Braunton, A. (C) 3703 – 3706 [3769 – 3772]
Bravo-Zhivotovskii, D.
– Nonsolvated, Aggregated 1,1-Dilithiosilane and the Derived Silyl Radicals (C) 739 – 743 [749 – 753] DOI: 10.1002/anie.200461765
Brayshaw, S. K. (C) 6875 – 6878 [7035 – 7038]
Brea, R. J. (C) 5710 – 5713 [5856 – 5859]
Brechin, E. K.
– Linking Centered Manganese Triangles into Larger Clusters: A $\{Mn_{32}\}$ Truncated Cube (C) 6540 – 6543 [6698 – 6701] DOI: 10.1002/anie.200501881
Bredehöft, J. H. (C) 5630 – 5634 [5774 – 5779]
Bregman, H. (C) 1984 – 1987 [2020 – 2023]
Breher, F.
– Distannenes Turned Inside Out: Bis(stannylenes) with an Unusual Structural Motif (C) 473 – 477 [477 – 481] DOI: 10.1002/anie.200460910
Breher, F. (C) 4397 – 4400 [4471 – 4474], 6318 – 6323 [6477 – 6481], 6325 – 6329 [6483 – 6487]
Breit, B.
– Enantioselective Total Synthesis and Determination of the Absolute Configuration of the 4,6,8,10,16,18-Hexamethyldocosane from *Antitrogus parvulus* (C) 5267 – 5269 [5401 – 5403] DOI: 10.1002/anie.200501612
– Self-Assembly of Bidentate Ligands for Combinatorial Homogeneous Catalysis Based on an A – T Base-Pair Model (C) 1640 – 1643 [1666 – 1669] DOI: 10.1002/anie.200462499
– Supramolecular Approaches to Generate Libraries of Chelating Bidentate Ligands for Homogeneous Catalysis (M) 6816 – 6825 [6976 – 6986] DOI: 10.1002/anie.200501798
Brennessel, W. W. (C) 3690 – 3694 [3756 – 3760]
Bresner, C. (C) 3606 – 3609 [3672 – 3675]
Bretonnière, Y. (C) 7595 – 7598 [7767 – 7770]
Breuker, K.
– The Thermal Unfolding of Native Cytochrome *c* in the Transition from Solution to Gas Phase Probed by Native Electron Capture Dissociation (C) 4911 – 4914 [4989 – 4992] DOI: 10.1002/anie.200500668
Breuning, M.
– Atroposelective Synthesis of Axially Chiral Biaryl Compounds (R) 5384 – 5427 [5518 – 5563] DOI: 10.1002/anie.200462661
Brezesinski, T. (C) 4589 – 4592 [4665 – 4668]
Briand, J.-P. (C) 6358 – 6362 [6516 – 6520]
Bridgeman, A. J. (C) 6746 – 6750 [6904 – 6908]
Bringmann, G.
– Atroposelective Synthesis of Axially Chiral Biaryl Compounds (R) 5384 – 5427 [5518 – 5563] DOI: 10.1002/anie.200462661
Brinkley, D. W. (C) 7273 – 7276 [7439 – 7442]
Brinkmann, A. (C) 1346 – 1349 [1370 – 1373]
Brittain, D. E. A. (C) 2732 – 2737 [2792 – 2797]
Brock, R. (C) 1560 – 1563 [1584 – 1588]
Broersma, A. (C) 1360 – 1363 [1384 – 1387]
Brooks, S. J. (C) 2537 – 2542 [2593 – 2598]
Bross, M. (C) 2957 – 2959 [3016 – 3019]
Brouwer, A. M.
– Patterning through Controlled Submolecular Motion: Rotaxane-Based Switches and Logic Gates that Function in Solution and Polymer Films (C) 3062 – 3067 [3122 – 3127] DOI: 10.1002/anie.200500101
Brown, A. M. (C) 4207 – 4209 [4279 – 4281]
Brown, D. J. A. (C) 2382 – 2385 [2434 – 2437]
Brown, E. C. (C) 7745 – 7748 [7923 – 7926]
Brown, E. J. (C) 1392 – 1395 [1416 – 1419]
Brown, M. K. (C) 5306 – 5310 [5440 – 5444]
Brown, P. D.
– Metallic Nanowires of Nb_3Te_4: A Nanostructured Chalcogenide (C) 3555 – 3558 [3621 – 3624] DOI: 10.1002/anie.200500157
Brown, R. C. D.
– Developments in Furan Syntheses (H) 850 – 852 [872 – 874] DOI: 10.1002/anie.200461668
Brown, S. H. (C) 5687 – 5690 [5833 – 5836]
Bruce, P. G.
– Synthesis of Nanowire and Mesoporous Low-Temperature $LiCoO_2$ by a Post-Templating Reaction (C) 6550 – 6553 [6708 – 6711] DOI: 10.1002/anie.200501663
Bruckbauer, A. (C) 6854 – 6859 [7014 – 7019]

 © 2005 Wiley-VCH Verlag GmbH & Co. KGaA, Weinheim

Brückner, R.
– Novel Strategy for the Synthesis of the Butenolide Moiety of Peridinin
(C) 1553 – 1557 [1577 – 1581]
DOI: 10.1002/anie.200460259
Bruggesser, H. (C) 1504 – 1508 [1528 – 1532]
Brümmer, M. (C) 3122 – 3125 [3182 – 3185]
Brune, H. (C) 7294 – 7297 [7460 – 7463]
Bruneau, C.
– Concomitant Monoreduction and Hydrogenation of Unsaturated Cyclic Imides to Lactams Catalyzed by Ruthenium Compounds
(C) 2021 – 2023 [2057 – 2059]
DOI: 10.1002/anie.200462996
– Electrophilic Activation and Cycloisomerization of Enynes: A New Route to Functional Cyclopropanes
(M) 2328 – 2334 [2380 – 2386]
DOI: 10.1002/anie.200462568
Brüning, J. (C) 7783 – 7786 [7961 – 7964]
Brunner, G. (C) 99 – 101 [101 – 103]
Brust, M.
– Molecular Recognition by Calix[4]arene-Modified Gold Nanoparticles in Aqueous Solution
(C) 2913 – 2916 [2973 – 2976]
DOI: 10.1002/anie.200462909
Bryce, M. R.
– Molecules with Exceptionally Small HOMO – LUMO Gaps
(H) 5370 – 5373 [5504 – 5507]
DOI: 10.1002/anie.200500413
Brydson, R. (C) 1965 – 1968 [2001 – 2004]
Brynda, M. (C) 2546 – 2549 [2602 – 2605]
Bu, X. (C) 5299 – 5303 [5433 – 5437]
Bubnov, V. P. (C) 1846 – 1849 [1880 – 1883]
Bucher, G. (C) 3289 – 3293 [3353 – 3357]
Buchner, J. (C) 5247 – 5251 [5381 – 5386]
Buchwald, S. L.
– Dynamic Kinetic Resolution of α,β-Unsaturated Lactones through Asymmetric Copper-Catalyzed Conjugate Reduction: Application to the Total Synthesis of Eupomatilone-3
(C) 6177 – 6180 [6333 – 6336]
DOI: 10.1002/anie.200501890
– General Catalysts for the Suzuki – Miyaura and Sonogashira Coupling Reactions of Aryl Chlorides and for the Coupling of Challenging Substrate Combinations in Water
(C) 6173 – 6177 [6329 – 6333]
DOI: 10.1002/anie.200502017
Buck, L. B.
– Unraveling the Sense of Smell (Nobel Lecture)
(R) 6128 – 6140 [6283 – 6296]
DOI: 10.1002/anie.200501120
Buckner, F. S. (C) 4903 – 4906 [4981 – 4984]
Buevich, A. (C) 7024 – 7028 [7186 – 7190]
Bukowski, M. R. (C) 584 – 587 [590 – 593]
Bulger, P. G. (R) 4442 – 4489 [4516 – 4563], 4490 – 4527 [4564 – 4601]
Buma, W. J.
– Patterning through Controlled Submolecular Motion: Rotaxane-Based Switches and Logic Gates that Function in Solution and Polymer Films
(C) 3062 – 3067 [3122 – 3127]
DOI: 10.1002/anie.200500101
Bundle, D. R.
– Thiooligosaccharide Conjugate Vaccines Evoke Antibodies Specific for Native Antigens
(C) 7725 – 7729 [7903 – 7907]
DOI: 10.1002/anie.200502179
Bunel, E. E. (C) 5269 – 5272 [5403 – 5406]
Bunkóczi, G. (C) 1340 – 1342 [1364 – 1366]
Buñuel, E. (C) 6146 – 6148 [6302 – 6304]
Buono, G.
– [2 + 1] Cycloadditions of Terminal Alkynes to Norbornene Derivatives Catalyzed by Palladium Complexes with Phosphinous Acid Ligands
(C) 4753 – 4757 [4831 – 4835]
DOI: 10.1002/anie.200500879
Burchard, W.
– Macromolecules: *Walter Hugo Stockmayer*
(O) 1754 – 1755 [1782 – 1783]
DOI: 10.1002/anie.200500381
Burda, C.
– PbTe Nanorods by Sonoelectrochemistry
(C) 5855 – 5857 [6005 – 6007]
DOI: 10.1002/anie.200501282
Burford, N.
– Facile Synthetic Methods for the Diversification of Catena-Polyphosphorus Cations
(C) 2364 – 2367 [2416 – 2419]
DOI: 10.1002/anie.200462997
– Small Cyclopolyphosphinophosphonium Cations: Systematic Development of Fundamental *catena*-Phosphorus Frameworks
(C) 6196 – 6199 [6352 – 6355]
DOI: 10.1002/anie.200501850
Burgert, R. (C) 265 – 269 [270 – 274], 6956 – 6960 [7117 – 7121]
Burgess, J. D. (C) 5855 – 5857 [6005 – 6007]
Burghardt, S. (C) 2976 – 2979 [3036 – 3039]
Burguete, M. I. (C) 6504 – 6508 [6662 – 6666]
Burkart, M. D. (R) 192 – 212 [196 – 217]
Burkholder, L. (C) 4572 – 4574 [4648 – 4650]
Burley, G. A.
– Trannulenes with "In-Plane" Aromaticity: Candidates for Harvesting Light Energy
(H) 3176 – 3178 [3238 – 3240]
DOI: 10.1002/anie.200500362
Burlina, F.
– Quantification of the Cellular Uptake of Cell-Penetrating Peptides by MALDI-TOF Mass Spectrometry
(C) 4244 – 4247 [4316 – 4319]
DOI: 10.1002/anie.200500477
Burns, D. C. (C) 7778 – 7782 [7956 – 7960]
Burns, P. C.
– Actinyl Peroxide Nanospheres
(C) 2135 – 2139 [2173 – 2177]
DOI: 10.1002/anie.200462445
Burschka, C. (C) 5292 – 5295 [5426 – 5429]
Buryak, A. (C) 7935 – 7938 [8149 – 8152]
Buschmann, H. (C) 1184 – 1188 [1208 – 1212]
Buskas, T. (C) 5985 – 5988 [6139 – 6142]
Butenschön, H.
– Organometallics at Lake Geneva
(T) 5556 – 5558 [5692 – 5695]
DOI: 10.1002/anie.200502598
Butterworth, S. (C) 4766 – 4768 [4844 – 4846]
Büttner, T. (C) 6318 – 6323 [6477 – 6481]
Bytschkov, I. (C) 2951 – 2954 [3011 – 3013]

Caballero, A. (C) 1977 – 1981 [2013 – 2017]
Cacace, F. (C) 462 – 465 [466 – 469]
Cachoux, F. (C) 7469 – 7473 [7636 – 7640]
Caggiano, L. (C) 588 – 591 [594 – 597], 7221 – 7223 [7387 – 7389]
Cahill, S. M. (C) 4242 – 4244 [4314 – 4316]
Cai, Q. J. (C) 1104 – 1107 [1128 – 1131]
Caille, J.-R. (C) 1101 – 1104 [1125 – 1128], 3439 – 3442 [3505 – 3508]
Calaza, F. (C) 4572 – 4574 [4648 – 4650]
Calderon-Moreno, J. (C) 6560 – 6563 [6718 – 6721]
Calderone, C. T. (C) 7383 – 7386 [7549 – 7552]
Calhorda, M. J. (C) 4397 – 4400 [4471 – 4474]
Calle, C. (C) 3301 – 3303 [3365 – 3367]
Calzaferri, G.
– Förster-Type Energy Transfer along a Specified Axis
(C) 5325 – 5329 [5459 – 5463]
DOI: 10.1002/anie.200500431
Camadanli, S. (C) 975 – 977 [997 – 999]
Camden, J. P. (C) 2382 – 2385 [2434 – 2437]
Caminal, C. (C) 6030 – 6032 [6184 – 6186]
Caminati, W.
– Isotopomeric Conformational Change in Anisole – Water
(C) 603 – 606 [609 – 612]
DOI: 10.1002/anie.200461860
– Weak CH···F Bridges and Internal Dynamics in the $CH_3F \cdot CHF_3$ Molecular Complex
(C) 3840 – 3844 [3908 – 3912]
DOI: 10.1002/anie.200500775
Campagna, S.
– The Structural and Functional Roles of Rhodium(II) – Rhodium(II) Dimers in Multinuclear Ruthenium(II) Complexes
(C) 4881 – 4884 [4959 – 4962]
DOI: 10.1002/anie.200500392
Campanera, J. M. (C) 7230 – 7233 [7396 – 7399]
Campbell, C. J. (C) 7263 – 7269 [7429 – 7435]
Campo, M. (C) 1873 – 1875 [1907 – 1909]
Campos-Gómez, E. (C) 5851 – 5854 [6001 – 6004]
Canac, Y. (C) 5705 – 5709 [5851 – 5855], 7236 – 7239 [7402 – 7405]
Cañada, F. J. (C) 296 – 298 [300 – 302]
Canard, G. (C) 3103 – 3106 [3163 – 3166]
Candini, A. (C) 6496 – 6500 [6654 – 6658]
Cane, D. E.
– Chain Elongation, Macrolactonization, and Hydrolysis of Natural and Reduced Hexaketide Substrates by the Picromycin/Methymycin Polyketide Synthase
(C) 7557 – 7560 [7729 – 7732]
DOI: 10.1002/anie.200502246
Caneschi, A. (C) 3429 – 3432 [3495 – 3498], 4187 – 4192 [4259 – 4264]
Cannizzaro, C. (C) 3548 – 3552 [3614 – 3618]
Cano, J. (C) 5828 – 5830 [5978 – 5980]
Cao, A.-M. (C) 1269 – 1273 [1295 – 1299], 4391 – 4395 [4465 – 4469]
Cao, B.-X. (C) 6544 – 6546 [6702 – 6704]
Cao, M. (C) 4197 – 4201 [4269 – 4273]
Cao, Y. C.
– Synthesis of CdSe and CdTe Nanocrystals without Precursor Injection
(C) 6712 – 6715 [6870 – 6873]
DOI: 10.1002/anie.200502279
Capdevila, M.
– Zn– and Cd – Metallothionein Recombinant Species from the Most Diverse Phyla May Contain Sulfide (S^{2-}) Ligands
(C) 4618 – 4622 [4694 – 4698]
DOI: 10.1002/anie.200501183
Capek, R. (C) 5997 – 6001 [6151 – 6155]

 © 2005 Wiley-VCH Verlag GmbH & Co. KGaA, Weinheim

Cappel, D. (C) 3617 – 3620 [3683 – 3686]
Cappelletti, D.
– Glory-Scattering Measurement of Water – Noble-Gas Interactions: The Birth of the Hydrogen Bond
(C) 2356 – 2360 [2408 – 2412]
DOI: 10.1002/anie.200462704
Caprioli, R. M.
– Mass Spectrometric Profiling of Intact Biological Tissue by Using Desorption Electrospray Ionization
(C) 7094 – 7097 [7256 – 7259]
DOI: 10.1002/anie.200502362
Captain, B. (C) 2531 – 2533 [2587 – 2589]
Caravan, P.
– Multilocus Binding Increases the Relaxivity of Protein-Bound MRI Contrast Agents
(C) 6766 – 6769 [6924 – 6927]
DOI: 10.1002/anie.200502245
Carballeira, J. D. (C) 4192 – 4196 [4264 – 4268]
Cárdenas, D. J. (C) 6146 – 6148 [6302 – 6304]
Cardona, F. (H) 7832 – 7835 [8042 – 8045]
Carell, T.
– A Highly DNA-Duplex-Stabilizing Metal – Salen Base Pair
(C) 7204 – 7208 [7370 – 7374]
DOI: 10.1002/anie.200501589
Carenzi, G. E. A. (C) 3895 – 3899 [3963 – 3967]
Cariati, E. (C) 7922 – 7925 [8136 – 8139]
Carl, P. (C) 2420 – 2426 [2472 – 2478]
Carlomagno, T.
– The INPHARMA Method: Protein-Mediated Interligand NOEs for Pharmacophore Mapping
(C) 4172 – 4175 [4244 – 4247]
DOI: 10.1002/anie.200500503
Carlomagno, T. (C) 7776 – 7778 [7954 – 7956]
Carlone, A. (C) 6219 – 6222 [6375 – 6378]
Carlucci, L.
– Entangled Coordination Networks with Inherent Features of Polycatenation, Polythreading, and Polyknotting
(C) 5824 – 5827 [5974 – 5977]
DOI: 10.1002/anie.200501373
Carmichael, A. J. (C) 3062 – 3067 [3122 – 3127]
Carmona, E.
– Theoretical and Synthetic Studies on $[Zn_2(\eta^5\text{-}C_5Me_5)_2]$: Analysis of the Zn–Zn Bonding Interaction
(C) 1244 – 1247 [1270 – 1273]
DOI: 10.1002/anie.200462175
Caro, J. (C) 6906 – 6909 [7066 – 7069]
Carpenter, G. B. (C) 7710 – 7715 [7888 – 7893]
Carrascal, T. (C) 2903 – 2907 [2963 – 2967]
Carreira, E. M.
– Conformationally Restricted Aza-Bodipy: A Highly Fluorescent, Stable, Near-Infrared-Absorbing Dye
(C) 1677 – 1679 [1705 – 1707]
DOI: 10.1002/anie.200461868
– Convenient Transformation of Optically Active Nitroalkanes into Chiral Aldoximes and Nitriles
(C) 612 – 615 [618 – 621]
DOI: 10.1002/anie.200461879
– 1,2,4-Oxadiazolidinones as Configurationally Stable Chiral Building Blocks
(C) 936 – 938 [958 – 960]
DOI: 10.1002/anie.200461934
– Total Synthesis of Erythronolide A by Mg^{II}-Mediated Cycloadditions of Nitrile Oxides
(C) 4036 – 4038 [4104 – 4106]
DOI: 10.1002/anie.200500172
Carreon, J. R. (C) 2542 – 2546 [2598 – 2602]
Carrera, C. (C) 1813 – 1815 [1847 – 1849]
Carret, S. (C) 5130 – 5133 [5260 – 5263]
Carretta, S. (C) 6496 – 6500 [6654 – 6658]
Carrettin, S. (C) 2242 – 2245 [2282 – 2285], 4778 – 4781 [4856 – 4859]
Cartier dit Moulin, C. (C) 4798 – 4801 [4876 – 4879]
Cartoni, A. (C) 462 – 465 [466 – 469]
Caruso, F.
– Nanoporous Polyelectrolyte Spheres Prepared by Sequentially Coating Sacrificial Mesoporous Silica Spheres
(C) 2888 – 2892 [2948 – 2952]
DOI: 10.1002/anie.200462135
Carver, G. (C) 4239 – 4242 [4311 – 4314]
Casas, J. (C) 1343 – 1345 [1367 – 1369]
Casati, N.
– Staggered to Eclipsed Conformational Rearrangement of $[Co_2(CO)_6(PPh_3)_2]$ in the Solid State: An X-ray Diffraction Study at High Pressure and Low Temperature
(C) 7736 – 7739 [7914 – 7917]
DOI: 10.1002/anie.200502241
Casci, J. L. (C) 3243 – 3248 [3307 – 3312]
Casson, I. (C) 6496 – 6500 [6654 – 6658]
Castaldi, M. P. (C) 3432 – 3435 [3498 – 3501]
Castaño, O. (C) 5828 – 5830 [5978 – 5980]
Castarlenas, R. (C) 2576 – 2579 [2632 – 2635]
Castedo, L. (C) 5710 – 5713 [5856 – 5859]
Castellani, F. (C) 6151 – 6154 [6307 – 6310]
Castoldi, D. (C) 588 – 591 [594 – 597]
Cativiela, C. (C) 396 – 399 [400 – 403]
Catlow, C. R. A.
– Oligomerization and Cyclization Processes in the Nucleation of Microporous Silicas
(C) 3082 – 3086 [3142 – 3146]
DOI: 10.1002/anie.200462524
Cavallini, M. (C) 888 – 892 [910 – 914]
Ćavar, E. (C) 5334 – 5337 [5468 – 5471]
Cave, G. W. V. (C) 5733 – 5736 [5879 – 5882]
Cavell, K. J.
– Platinum-Mediated Oxidative Addition and Reductive Elimination of Imidazolium Salts at C4 and C5
(C) 5282 – 5284 [5416 – 5418]
DOI: 10.1002/anie.200500884
Cavell, K. J. (C) 2026 – 2029 [2062 – 2065]
Cavell, R. G.
– Water-Induced Rearrangement of a Platinacyclic Carbene Produces a Platinacyclic Carbaphosphazene with an Intraannular Pt–C Bond in a Pt–N–P–N–P–C Ring
(C) 2005 – 2008 [2041 – 2044]
DOI: 10.1002/anie.200461525
Ceola, S. (C) 3289 – 3293 [3353 – 3357]
Ceroni, P. (C) 4574 – 4578 [4650 – 4654]
Cha, J. K.
– Rapid Access to the "in,out"-Tetracyclic Core of Ingenol
(C) 121 – 123 [123 – 125]
DOI: 10.1002/anie.200461807
Cha, J. N. (C) 7574 – 7580 [7746 – 7752]
Chaboussant, G. (C) 4239 – 4242 [4311 – 4314]
Chadha, R. K. (C) 5846 – 5851 [5996 – 6001]
Chai, J. (C) 5090 – 5093 [5220 – 5223]
Chaigneau, J. (C) 6488 – 6491 [6646 – 6649]
Chakrabarti, D. (C) 4903 – 4906 [4981 – 4984]
Chakrabarti, S. (R) 4844 – 4870 [4922 – 4949]
Champion, G. (C) 4798 – 4801 [4876 – 4879]
Chan, C. Y. (C) 4749 – 4753 [4827 – 4831]
Chan, H.-S. (C) 2128 – 2131 [2166 – 2169]
Chan, K. H.-Y. (C) 791 – 794 [801 – 804]
Chan, T.-M. (C) 7024 – 7028 [7186 – 7190]
Chan, T. W. D. (C) 6399 – 6403 [6557 – 6561]
Chandrasekhar, V. (C) 281 – 284 [285 – 288]
Chanéac, C. (C) 5691 – 5694 [5837 – 5840]
Chang, C.-C.
– Aluminum – Magnesium Complexes with Linearly Bridging Carbon Dioxide
(C) 7418 – 7420 [7584 – 7586]
DOI: 10.1002/anie.200502400
Chang, H.-C. (C) 2700 – 2704 [2760 – 2764]
Chang, H.-H. (C) 7450 – 7453 [7616 – 7619]
Chang, J.-S.
– Microwave Fabrication of MFI Zeolite Crystals with a Fibrous Morphology and Their Applications
(C) 556 – 560 [562 – 566]
DOI: 10.1002/anie.200461403
Chang, K.-J. (C) 7926 – 7929 [8140 – 8143]
Chang, S.
– Cooperative Catalysis by Ru and Pd for the Direct Coupling of a Chelating Aldehyde with Iodoarenes or Organostannanes
(C) 455 – 457 [459 – 461]
DOI: 10.1002/anie.200462006
– Tetraarylphosphonium Halides as Arylating Reagents in Pd-Catalyzed Heck and Cross-Coupling Reactions
(C) 6166 – 6169 [6322 – 6325]
DOI: 10.1002/anie.200501582
Chang, S.-Y. (C) 4903 – 4906 [4981 – 4984]
Chang, T.-H. (C) 7418 – 7420 [7584 – 7586]
Charbonnière, L. J.
– Quantum Dots as Efficient Energy Acceptors in a Time-Resolved Fluoroimmunoassay
(C) 7612 – 7615 [7784 – 7788]
DOI: 10.1002/anie.200501552
Charlot, M.-F. (C) 1536 – 1540 [1560 – 1564]
Charmant, J. P. H. (C) 6878 – 6881 [7038 – 7041]
Chassaing, G. (C) 4244 – 4247 [4316 – 4319]
Chastanet, G. (C) 5044 – 5048 [5172 – 5176]
Chatelet, F. (C) 4058 – 4061 [4126 – 4129]
Chatgilialoglu, C.
– Tautomers of One-Electron-Oxidized Guanosine
(C) 6030 – 6032 [6184 – 6186]
DOI: 10.1002/anie.200501087
Chatterton, N. (C) 7595 – 7598 [7767 – 7770]
Chatziefthimiou, S. (C) 5097 – 5100 [5227 – 5230]
Chavez, D. E. (C) 7089 – 7094 [7251 – 7256]
Che, S. (C) 5317 – 5322 [5451 – 5456]
Chebny, V. J. (C) 2771 – 2774 [2831 – 2834]
Chechik, V.
– Radical Mechanism of a Place-Exchange Reaction of Au Nanoparticles
(C) 3720 – 3722 [3786 – 3788]
DOI: 10.1002/anie.200500518
Cheedrala, R. K. (C) 6913 – 6915 [7073 – 7075]
Cheetham, A. K.
– A High-Throughput Investigation of the Role of pH, Temperature, Concentration, and Time on the Synthesis of Hybrid Inorganic – Organic Materials
(C) 7608 – 7611 [7780 – 7784]
DOI: 10.1002/anie.200501766
Cheley, S. (C) 1495 – 1499 [1519 – 1523]
Chellappan, K. (C) 2899 – 2903 [2959 – 2963]
Chelucci, G. (C) 6214 – 6219 [6370 – 6375]
Chen, B.
– High H_2 Adsorption in a Microporous Metal – Organic Framework with Open

 © 2005 Wiley-VCH Verlag GmbH & Co. KGaA, Weinheim

Metal Sites
(C) 4745 – 4749 [4823 – 4827]
DOI: 10.1002/anie.200462787
Chen, C.-H.
– Nickel-Foam-Supported Reticular CoO – Li_2O Composite Anode Materials for Lithium Ion Batteries
(C) 7085 – 7089 [7247 – 7251]
DOI: 10.1002/anie.200501905
Chen, C.-L. (C) 6673 – 6677 [6831 – 6835]
Chen, Changneng Corrigendum: 506
Chen, Chuo (C) 2249 – 2252 [2289 – 2292]
Chen, Da-W. (C) 2144 – 2148 [2182 – 2186]
Chen, E.-Q. (C) 6025 – 6029 [6179 – 6183]
Chen, F. (C) 7771 – 7775 [7949 – 7953]
Chen, G. Y. J. (C) 1048 – 1053 [1072 – 1077]
Chen, H. (C) 1517 – 1520 [1541 – 1544]
Chen, H.-L.
– Iodine-Assisted Assembly of Helical Coordination Polymers of Cucurbituril and Asymmetric Copper(II) Complexes
(C) 3402 – 3407 [3468 – 3473]
DOI: 10.1002/anie.200463071
Chen, H.-T. (C) 1826 – 1830 [1860 – 1864]
Chen, J.-C. (C) 5471 – 5475 [5607 – 5611]
Chen, J.-Y. (C) 6888 – 6892 [7048 – 7052]
Chen, Jian (C) 7414 – 7418 [7580 – 7584]
Chen, Jingyi (C) 2589 – 2592 [2645 – 2648], 3596 – 3600 [3662 – 3666], 7913 – 7917 [8127 – 8131]
Chen, Jinping (C) 2782 – 2785 [2842 – 2845]
Chen, K. X.
– Proline-Based Macrocyclic Inhibitors of the Hepatitis C Virus: Stereoselective Synthesis and Biological Activity
(C) 7024 – 7028 [7186 – 7190]
DOI: 10.1002/anie.200501553
Chen, Ming (C) 4368 – 4372 [4442 – 4446]
Chen, Mingwei (C) 4002 – 4006 [4070 – 4074]
Chen, Peng (C) 2715 – 2719 [2775 – 2779]
Chen, Peter
– Mechanism-Based Design of a ROMP Catalyst for Sequence-Selective Copolymerization
(C) 7909 – 7911 [8123 – 8125]
DOI: 10.1002/anie.200502606
Chen, S. (C) 4731 – 4735 [4809 – 4813]
Chen, W. (C) 6009 – 6012 [6163 – 6166]
Chen, W.-M. (C) 2124 – 2127 [2162 – 2165]
Chen, X.-M.
– Spin Canting and Metamagnetism in a 3D Homometallic Molecular Material Constructed by Interpenetration of Two Kinds of Cobalt(II)-Coordination-Polymer Sheets
(C) 3079 – 3082 [3139 – 3142]
DOI: 10.1002/anie.200462463
Chen, Xiao (C) 2112 – 2115 [2150 – 2153], 7420 – 7424 [7586 – 7590]
Chen, Xiaowei (C) 5488 – 5492 [5624 – 5628]
Chen, Xuecheng (C) 1517 – 1520 [1541 – 1544]
Chen, Y.-G. (C) 3072 – 3075 [3132 – 3135]
Chen, Y.-M. (C) 5814 – 5817 [5964 – 5967]
Chen, Yaofeng (C) 1108 – 1112 [1132 – 1136], 7721 – 7725 [7899 – 7903]
Chen, Yi (C) 4355 – 4358 [4429 – 4432], 6694 – 6696 [6852 – 6854]
Chen, Yonggang (C) 3478 – 3481 [3544 – 3547]
Chen, Z. (C) 1078 – 1082 [1102 – 1106]
Chen, Z.-Da
– Two Molecular Tapes Consisting of Serial or Parallel Azido-Bridged Eight-Membered Copper Rings
(C) 5841 – 5846 [5991 – 5996]
DOI: 10.1002/anie.200501327
Cheng, H. (C) 598 – 603 [604 – 609]
Cheng, X. (C) 1118 – 1121 [1142 – 1145]
Cheng, X. H. (C) 2801 – 2805 [2862 – 2866]
Cherkasov, V. K. (C) 2767 – 2771 [2827 – 2831]
Cheyne, S. M. (C) 7942 – 7946 [8156 – 8160]
Chiang, Y.-W. (C) 7969 – 7972 [8183 – 8186]
Chiappe, C. (C) 1412 – 1416 [1437 – 1441]
Chippindale, A. M.
– Interpenetrating Copper – Silver Cyanometalate Networks: Polymorphs and Topological Isomers
(C) 7942 – 7946 [8156 – 8160]
DOI: 10.1002/anie.200502372
Chisholm, M. H.
– Oligothiophenes Incorporating Metal – Metal Quadruple Bonds
(C) 6537 – 6540 [6695 – 6698]
DOI: 10.1002/anie.200500138
Chiu, M. E. (C) 1213 – 1217 [1239 – 1243]
Chivers, T.
– An Unusual Ditelluride: Synthesis and Molecular and Electronic Structures of the Dimer of the Tellurium-Centered Radical $[TeP\textit{i}Pr_2N\textit{i}Pr_2PTe]^{\cdot}$
(C) 4953 – 4956 [5033 – 5036]
DOI: 10.1002/anie.200501138
Chmielewski, P. J.
– Synthesis and Characterization of a Cyclic Bis-silver(I) Assembly of Four 2-Aza-21-carbaporphyrinatosilver(III) Subunits
(C) 6417 – 6420 [6575 – 6578]
DOI: 10.1002/anie.200502208
Cho, B. K. (C) 1096 – 1101 [1120 – 1125]
Cho, H.-G. (C) 113 – 116 [115 – 118]
Cho, M.-H.
– Multifunctional Nanoparticles Possessing A "Magnetic Motor Effect" for Drug or Gene Delivery
(C) 1068 – 1071 [1092 – 1095]
DOI: 10.1002/anie.200461910
Cho, W.-S. (C) 2537 – 2542 [2593 – 2598], 5989 – 5992 [6143 – 6146]
Choi, K.-S.
– Directing the Architecture of Cuprous Oxide Crystals during Electrochemical Growth
(C) 3218 – 3223 [3282 – 3287]
DOI: 10.1002/anie.200463018
Choi, S. (C) 6685 – 6689 [6843 – 6847]
Choi, S.-h. (C) 1383 – 1385 [1407 – 1409]
Choi, W. (C) 4585 – 4589 [4661 – 4665]
Choi, W. S. (C) 1096 – 1101 [1120 – 1125]
Chopra, I. (C) 6403 – 6406 [6561 – 6564]
Chou, J. (C) 4735 – 4739 [4813 – 4817]
Chou, T.-C. (M) 2838 – 2850 [2898 – 2910]
Choudary, B. M.
– Hydrogen Processing by Fe^{III}-Exchanged Montmorillonite: A Unique Geochemical Protocol
(C) 322 – 325 [326 – 329]
DOI: 10.1002/anie.200461070
Choudhary, V. R.
– Simultaneous Conversion of Methane and Methanol into Gasoline over Bifunctional Ga-, Zn-, In-, and/or Mo-Modified ZSM-5 Zeolites
(C) 4381 – 4385 [4455 – 4459]
DOI: 10.1002/anie.200500694
Chow, Y. L. (C) 1265 – 1268 [1291 – 1294]
Christe, K. O.
– Polyazide Chemistry: The First Binary Group 6 Azides, $Mo(N_3)_6$, $W(N_3)_6$, $[Mo(N_3)_7]^-$, and $[W(N_3)_7]^-$, and the $[NW(N_3)_4]^-$ and $[NMo(N_3)_4]^-$ Ions
(C) 1860 – 1865 [1894 – 1899]
DOI: 10.1002/anie.200462740
Christmann, M.
– New Developments in the Asymmetric Stetter Reaction
(H) 2632 – 2634 [2688 – 2690]
DOI: 10.1002/anie.200500761
Christmann, U. (M) 366 – 374 [370 – 378]
Christou, G.
– DFT Computational Rationalization of an Unusual Spin Ground State in an Mn_{12} Single-Molecule Magnet with a Low-Symmetry Loop Structure
(C) 897 – 901 [919 – 923]
DOI: 10.1002/anie.200461820
– New Structural Motifs in Manganese Single-Molecule Magnetism from the Use of Triethanolamine Ligands
(C) 892 – 896 [914 – 918]
DOI: 10.1002/anie.200461703
Christou, G. (C) 6540 – 6543 [6698 – 6701]
Chu, G. (C) 1994 – 1997 [2030 – 2033]
Chu, L.-Y.
– Negatively Thermoresponsive Membranes with Functional Gates Driven by Zipper-Type Hydrogen-Bonding Interactions
(C) 2124 – 2127 [2162 – 2165]
DOI: 10.1002/anie.200462687
Chu, Qian (C) 4352 – 4355 [4426 – 4429]
Chu, Qianli (C) 3569 – 3572 [3635 – 3638]
Chubukov, V. A. (C) 7263 – 7269 [7429 – 7435]
Chung, H. (C) 6410 – 6413 [6568 – 6571]
Chung, T. S. (C) 4782 – 4785 [4860 – 4863]
Chung, W. R. (C) 7574 – 7580 [7746 – 7752]
Cid, M. M.
– Shape-Persistent Chiral Alleno-Acetylenic Macrocycles and Cyclophanes by Acetylenic Scaffolding with 1,3-Diethynylallenes
(C) 5074 – 5078 [5203 – 5207]
DOI: 10.1002/anie.200501621
Ciechanover, A.
– Intracellular Protein Degradation: From a Vague Idea, through the Lysosome and the Ubiquitin – Proteasome System, and onto Human Diseases and Drug Targeting (Nobel Lecture)
(R) 5944 – 5967 [6095 – 6119]
DOI: 10.1002/anie.200501428
Ciesa, F. (C) 278 – 281 [282 – 285]
Cinellu, M. A.
– Reactions of Gold(III) Oxo Complexes with Cyclic Alkenes
(C) 6892 – 6895 [7052 – 7055]
DOI: 10.1002/anie.200501754
Cipollini, R. (C) 462 – 465 [466 – 469]
Ciriano, M. A. (C) 3267 – 3271 [3331 – 3335]
Císařová, I. (C) 6222 – 6226 [6378 – 6382]
Cladera, J. (C) 1065 – 1067 [1089 – 1091]
Clair, S. (C) 7294 – 7297 [7460 – 7463]
Clardy, J. (C) 7045 – 7048 [7207 – 7210], 7063 – 7065 [7225 – 7227]
Claridge, J. B. (C) 7733 – 7736 [7911 – 7914]
Clark, C. G., Jr. (C) 6348 – 6354 [6506 – 6512]
Clark, J. S.
– Rapid Two-Directional Synthesis of the F – J Fragment of the Gambieric Acids by Iterative Double Ring-Closing Metathesis
(C) 6157 – 6162 [6313 – 6318]
DOI: 10.1002/anie.200501925
Clarke, R. W. (C) 3747 – 3750 [3813 – 3816]

 © 2005 Wiley-VCH Verlag GmbH & Co. KGaA, Weinheim

Classen, T.
– Templated Growth of Metal–Organic Coordination Chains at Surfaces
(C) 6142 – 6145 [6298 – 6301]
DOI: 10.1002/anie.200502007
Claus, P.
– Direct Conversion of Linoleic Acid over Silver Catalysts in the Presence of H_2: An Unusual Way towards Conjugated Linoleic Acids
(C) 7800 – 7804 [7979 – 7983]
DOI: 10.1002/anie.200501852
Clay, M. D. (C) 4039 – 4042 [4107 – 4110]
Clayden, J.
– Using Dipoles to Control the Directionality of Functional Groups: *Syn*- and *Anti*-Oriented Benzene-1,3-dicarboxamides
(C) 1241 – 1244 [1267 – 1270]
DOI: 10.1002/anie.200461787
Cleemann, F. (C) 807 – 811 [817 – 821], 7466 – 7469 [7632 – 7635]
Clegg, W. (C) 6018 – 6021 [6172 – 6175]
Clement, B.
– A Two-Step Synthesis of Cytostatically Active Benzo[*c*]phenanthridine Derivatives
(C) 635 – 638 [641 – 645]
DOI: 10.1002/anie.200461969
Clement, N. D. (C) 2026 – 2029 [2062 – 2065]
Clements, D. J. (C) 6685 – 6689 [6843 – 6847]
Clérac, R. (C) 2711 – 2715 [2771 – 2775], 6678 – 6682 [6836 – 6840]
Clever, G. H. (C) 7204 – 7208 [7370 – 7374]
Clough, C. R. (C) 2560 – 2563 [2616 – 2619]
Cloutet, E. (C) 7399 – 7404 [7565 – 7570]
Cobley, C. J. (C) 5834 – 5838 [5984 – 5988]
Cocco, F. (C) 6892 – 6895 [7052 – 7055]
Cocinero, E. J. (C) 6311 – 6315 [6469 – 6473]
Cohen, Y.
– Diffusion NMR Spectroscopy in Supramolecular and Combinatorial Chemistry: An Old Parameter—New Insights
(R) 520 – 554 [524 – 560]
DOI: 10.1002/anie.200300637
Cokoja, M. (C) 2943 – 2946 [3003 – 3007]
Colasson, B. (C) 116 – 120 [118 – 122]
Cölfen, H.
– Crystalline, Porous Microspheres Made from Amino Acids by Using Polymer-Induced Liquid Precursor Phases
(C) 4087 – 4092 [4156 – 4161]
DOI: 10.1002/anie.200462467
– Mesocrystals: Inorganic Superstructures Made by Highly Parallel Crystallization and Controlled Alignment
(R) 5576 – 5591 [5714 – 5730]
DOI: 10.1002/anie.200500496
– Synthesis of Stable Aragonite Superstructures by a Biomimetic Crystallization Pathway
(C) 6004 – 6009 [6158 – 6163]
DOI: 10.1002/anie.200500081
Comes, M. (C) 2918 – 2922 [2978 – 2982]
Comotti, A. (C) 1816 – 1820 [1850 – 1854]
Compton, R. G.
– Fabrication of Random Assemblies of Metal Nanobands: A General Method
(C) 6491 – 6496 [6649 – 6654]
DOI: 10.1002/anie.200502128
– Nanotrench Arrays Reveal Insight into Graphite Electrochemistry
(C) 5121 – 5126 [5251 – 5256]
DOI: 10.1002/anie.200462750
Concepción, P. (C) 4066 – 4069 [4134 – 4137]
Connon, S. J.
– Urea- and Thiourea-Substituted Cinchona Alkaloid Derivatives as Highly Efficient Bifunctional Organocatalysts for the Asymmetric Addition of Malonate to Nitroalkenes: Inversion of Configuration at C9 Dramatically Improves Catalyst Performance.
(C) 6367 – 6370 [6525 – 6528]
DOI: 10.1002/anie.200501721
Conroy, K. D. (R) 5016 – 5036 [5142 – 5163]
Constant, S. (C) 5060 – 5064 [5188 – 5192]
Contreras, D. S. (C) 4745 – 4749 [4823 – 4827]
Converso, A. (C) 3443 – 3447 [3509 – 3513], 3447 – 3452 [3513 – 3518]
Cooke, M. W. (C) 4881 – 4884 [4959 – 4962]
Cooks, R. G.
– Direct Characterization of Enzyme–Substrate Complexes by Using Electrosonic Spray Ionization Mass Spectrometry
(C) 913 – 916 [935 – 938]
DOI: 10.1002/anie.200461672
– Mass Spectrometric Profiling of Intact Biological Tissue by Using Desorption Electrospray Ionization
(C) 7094 – 7097 [7256 – 7259]
DOI: 10.1002/anie.200502362
Cookson, D. (C) 2420 – 2426 [2472 – 2478]
Copéret, C. (C) 6755 – 6758 [6913 – 6916]
Coppens, P.
– An Unstable Ligand-Unsupported Cu^{I} Dimer Stabilized in a Supramolecular Framework
(C) 4614 – 4617 [4690 – 4693]
DOI: 10.1002/anie.200501154
– Charge Densities Come of Age
(H) 6810 – 6811 [6970 – 6972]
DOI: 10.1002/anie.200501734
Coppo, P. (C) 1806 – 1810 [1840 – 1844]
Coquerel, Y. (C) 5130 – 5133 [5260 – 5263]
Corbí, A. L.
– 1D Saturation Transfer Difference NMR Experiments on Living Cells: The DC-SIGN/Oligomannose Interaction
(C) 296 – 298 [300 – 302]
DOI: 10.1002/anie.200461574
Córdova, A.
– Direct Amino Acid Catalyzed Asymmetric Synthesis of Polyketide Sugars
(C) 1343 – 1345 [1367 – 1369]
DOI: 10.1002/anie.200461400
– Direct Catalytic Enantioselective Aza-Diels–Alder Reactions
(C) 4877 – 4880 [4955 – 4958]
DOI: 10.1002/anie.200500811
– The Origin of Stereoselectivity in Primary Amino Acid Catalyzed Intermolecular Aldol Reactions
(C) 7028 – 7032 [7190 – 7194]
DOI: 10.1002/anie.200502388
Corma, A.
– A Collaborative Effect between Gold and a Support Induces the Selective Oxidation of Alcohols
(C) 4066 – 4069 [4134 – 4137]
DOI: 10.1002/anie.200500382
– CO Oxidation Catalyzed by Supported Gold: Cooperation between Gold and Nanocrystalline Rare-Earth Supports Forms Reactive Surface Superoxide and Peroxide Species
(C) 4778 – 4781 [4856 – 4859]
DOI: 10.1002/anie.200500659
– Supported Gold Catalyzes the Homocoupling of Phenylboronic Acid with High Conversion and Selectivity
(C) 2242 – 2245 [2282 – 2285]
DOI: 10.1002/anie.200462560
Corma, A. (C) 2370 – 2373 [2422 – 2425]
Cornejo, A. (C) 458 – 461 [462 – 465]
Cornelissen, J. J. L. M.
– Acid-Initiated Stereospecific Polymerization of Isocyanopeptides
(C) 1990 – 1993 [2026 – 2029]
DOI: 10.1002/anie.200462417
– Synthesis and Self-Assembly of Rod–Rod Hybrid Poly(γ-benzyl L-glutamate)-*block*-Polyisocyanide Copolymers
(C) 4349 – 4352 [4423 – 4426]
DOI: 10.1002/anie.200500877
Cornicchi, E. (C) 2356 – 2360 [2408 – 2412]
Correa-Duarte, M. A. (C) 4375 – 4378 [4449 – 4452]
Cossío, F. P.
– Application of Stereocontrolled Stepwise [3 + 2] Cycloadditions to the Preparation of Inhibitors of $\alpha_4\beta_1$-Integrin-Mediated Hepatic Melanoma Metastasis
(C) 2903 – 2907 [2963 – 2967]
DOI: 10.1002/anie.200462497
Costa, A. M. (C) 588 – 591 [594 – 597]
Costantini, G. (C) 6142 – 6145 [6298 – 6301]
Costantino, F. (C) 4187 – 4192 [4259 – 4264]
Costuas, K. (C) 4362 – 4365 [4436 – 4439]
Cotlet, M. (C) 560 – 564 [566 – 570]
Coucouvanis, D.
– Metal Clusters as Ligands: Substitution of Fe ions in Fe/Mo/S Clusters by Thiophilic Cu^{I} Ions To Give Clusters with $[Cu_4Mo_2Fe_2S_8]^{4+}$ and $[Cu_5Mo_3Fe_4S_{11}]^{6+}$ Cores
(C) 1971 – 1974 [2007 – 2010]
DOI: 10.1002/anie.200462596
Couet, J. (C) 3297 – 3301 [3361 – 3365]
Coulembier, O. (C) 4964 – 4968 [5044 – 5048]
Courtois, J. (C) 3902 – 3906 [3970 – 3974]
Couve-Bonnaire, S. (C) 1366 – 1368 [1390 – 1392]
Cozzi, P. G.
– Highly Enantioselective One-Pot, Three-Component Imino-Reformatsky Reaction
(C) 3600 – 3603 [3666 – 3669]
DOI: 10.1002/anie.200462757
Crabtree, R. H. (C) 444 – 447 [448 – 451]
Craig, D.
– Synthesis of Homoallylic Sulfones through a Decarboxylative Claisen Rearrangement Reaction
(C) 618 – 621 [624 – 627]
DOI: 10.1002/anie.200462023
Craig, S. L.
– Strong Means Slow: Dynamic Contributions to the Bulk Mechanical Properties of Supramolecular Networks
(C) 2746 – 2748 [2806 – 2808]
DOI: 10.1002/anie.200500026
Cramer, C. J.
– Structures of Nonheme Oxoiron(IV) Complexes from X-ray Crystallography, NMR Spectroscopy, and DFT Calculations
(C) 3690 – 3694 [3756 – 3760]
DOI: 10.1002/anie.200500485
Cramer, N. (C) 820 – 822 [831 – 833]
Cravatt, B. F.
– Class Assignment of Sequence-Unrelated Members of Enzyme Superfamilies by Activity-Based Protein Profiling
(C) 2400 – 2403 [2452 – 2455]
DOI: 10.1002/anie.200463098

 © 2005 Wiley-VCH Verlag GmbH & Co. KGaA, Weinheim

– Protein-Reactive Natural Products
(R) 5788 – 5809 [5936 – 5958]
DOI: 10.1002/anie.200500900
Crawford, M.-J.
– UN_{21}^{3-}: A Structurally Characterized Binary Actinide Heptaazide Anion
(C) 7874 – 7878 [8086 – 8090]
DOI: 10.1002/anie.200502484
Crawford, N. R. M. (C) 2549 – 2553 [2605 – 2609]
Crean, C. (C) 5057 – 5060 [5185 – 5188]
Crego-Calama, M.
– Ditopic Complexation and Release of Neutral Guest Molecules by a Hydrogen-Bonded "*Endo* – *Exo*" Receptor
(C) 3248 – 3253 [3312 – 3317]
DOI: 10.1002/anie.200500134
Créminon, C. (C) 6863 – 6866 [7023 – 7026]
Crespo, M. D. (C) 4939 – 4944 [5019 – 5024]
Crihan, D. (C) 917 – 920 [939 – 942]
Crisma, M. (C) 7435 – 7439 [7601 – 7605]
Cronin, L.
– Confined Electron-Transfer Reactions within a Molecular Metal Oxide "Trojan Horse"
(C) 3415 – 3419 [3481 – 3485]
DOI: 10.1002/anie.200500541
– Polyoxometalate Nanostructures, Superclusters, and Colloids: From Functional Clusters to Chemical Aesthetics
(T) 844 – 846 [866 – 868]
DOI: 10.1002/anie.200462662
Crump, M. P. (C) 298 – 302 [302 – 306]
Crutchley, R. J.
– Charge-Transfer Isomers and Mixed-Valence Properties
(H) 6452 – 6454 [6610 – 6612]
DOI: 10.1002/anie.200501598
Cuadrado-Peinado, M. L. (C) 6708 – 6711 [6866 – 6869]
Cuenca, T.
– Carbon Dioxide Activation Assisted by a Bis(chlorodimethylsilyl)cyclopentadienyl Titanium Compound
(C) 5828 – 5830 [5978 – 5980]
DOI: 10.1002/anie.200500716
Cuerva, J. M. (C) 319 – 322 [323 – 326]
Cuevas, G.
– The Origin of One-Bond C – H Coupling Constants in OCH Fragments: Not Primarily $n_O \rightarrow \sigma^*_{CH}$ Delocalization
(C) 2360 – 2364 [2412 – 2416]
DOI: 10.1002/anie.200461583
Cui, A.-L. (C) 7742 – 7745 [7920 – 7923]
Cui, D. (C) 959 – 962 [981 – 984]
Cui, H.-B. (C) 6508 – 6512 [6666 – 6670]
Cui, Y. (C) 72 – 75 [74 – 77]
Culkin, D. A. (C) 4964 – 4968 [5044 – 5048]
Cummins, C. C.
– A Ligand Composed of Dinitrogen and Methyldiphenylphosphane in a Cationic Molybdenum Complex
(C) 2560 – 2563 [2616 – 2619]
DOI: 10.1002/anie.200463057
– Triatomic EP_2 Triangles (E = Ge, Sn, Pb) as μ_2:η^3,η^3-Bridging Ligands
(C) 4592 – 4596 [4668 – 4672]
DOI: 10.1002/anie.200500707
Cumpstey, I. (C) 5110 – 5112 [5240 – 5242]
Cundari, T. R. (C) 4907 – 4910 [4985 – 4988]
Cuny, E. (C) 4944 – 4948 [5024 – 5028]
Curran, D. P.
– Solution-Phase Mixture Synthesis with Double-Separation Tagging: Double Demixing of a Single Mixture Provides a Stereoisomer Library of 16 Individual Murisolins
(C) 6938 – 6940 [7098 – 7100]
DOI: 10.1002/anie.200501989
Custelcean, R. (C) 2537 – 2542 [2593 – 2598]
Cutting, G. A. (C) 1543 – 1545 [1567 – 1569]
Czekelius, C. (C) 612 – 615 [618 – 621]
Czerski, I. (C) 1230 – 1232 [1256 – 1258]

da Silva, G. F. Z. (C) 5501 – 5504 [5637 – 5640]
da Silva, M. F. C. G. (C) 4345 – 4349 [4419 – 4423]
Dagneau, P. (C) 3874 – 3879 [3942 – 3947]
Dahl, L. F.
– Nanosized $[Pd_{52}(CO)_{36}(PEt_3)_{14}]$ and $[Pd_{66}(CO)_{45}(PEt_3)_{16}]$ Clusters Based on a Hypothetical Pd_{38} Vertex-Truncated v_3 Octahedron
(C) 6848 – 6854 [7008 – 7014]
DOI: 10.1002/anie.200502307
– The First Trimetallic Pd/Tl/Co Carbonyl Cluster, Trigonal $[Pd_9\{\mu_3\text{-}TlCo(CO)_3L\}(\mu_2\text{-}CO)_6(\mu_3\text{-}CO)_3L_6]$: Ligand-Stabilization of the Trigonal-Bipyramidal $[TlCo(CO)_3L]$ Entity
(C) 786 – 790 [796 – 800]
DOI: 10.1002/anie.200461124
Dahse, H.-M. (C) 1202 – 1205 [1226 – 1230]
Dai, B. (C) 6022 – 6024 [6176 – 6178]
Dai, H.
– Deterministic One-to-One Synthesis of Germanium Nanowires and Individual Gold Nanoseed Patterning for Aligned Nanowire Arrays
(C) 2925 – 2929 [2985 – 2989]
DOI: 10.1002/anie.200500291
Dai, L.-X. (C) 6544 – 6546 [6702 – 6704]
Dai, Q.
– Rapid I^-/I_3^- Diffusion in a Molecular-Plastic-Crystal Electrolyte for Potential Application in Solid-State Photoelectrochemical Cells
(C) 313 – 316 [317 – 320]
DOI: 10.1002/anie.200460871
Dai, S. (C) 274 – 278 [278 – 282]
Dale, S. H. (C) 6018 – 6021 [6172 – 6175]
Dalla-Favera, N. (C) 7954 – 7958 [8168 – 8172]
Dall'Asta, C. (C) 5126 – 5130 [5256 – 5260]
Damin, A. (C) 4774 – 4777 [4852 – 4855]
Danheiser, R. L.
– Stereoselective Synthesis of Highly Substituted Cyclopentenones through [4 + 1] Annulations of Trialkylsilyl Vinyl Ketenes with α-Benzotriazolyl Organolithium Compounds
(C) 5867 – 5870 [6017 – 6020]
DOI: 10.1002/anie.200501579
Danishefsky, S. J.
– A Synthetic Pathway to Either Enantiomer of Merrilactone A
(C) 1511 – 1513 [1535 – 1537]
DOI: 10.1002/anie.200462509
– On the Remarkable Antitumor Properties of Fludelone: How We Got There
(M) 2838 – 2850 [2898 – 2910]
DOI: 10.1002/anie.200461751
Darensbourg, D. J. (C) 1217 – 1220 [1243 – 1246]
Darensbourg, M. Y.
– N_2S_2Ni Metallothiolates as a Class of Ligands that Support Organometallic and Bioorganometallic Reactivity
(C) 1217 – 1220 [1243 – 1246]
DOI: 10.1002/anie.200461747
Darragh, M. (C) 3698 – 3702 [3764 – 3768]
Das, A. (C) 3237 – 3240 [3301 – 3304]
Dathe, M. (C) 5252 – 5255 [5386 – 5389]
Daub, J.
– Multiple Switching and Photogated Electrochemiluminescence Expressed by a Dihydroazulene/Boron Dipyrromethene Dyad
(C) 6943 – 6947 [7104 – 7107]
DOI: 10.1002/anie.200501573
– "Turn ON/OFF your LOV light": Boron-dipyrromethene – Flavin Dyads as Biomimetic Switches Derived from the LOV Domain
(C) 2288 – 2291 [2328 – 2331]
DOI: 10.1002/anie.200462377
Daugulis, O.
– Anilide *ortho*-Arylation by Using C–H Activation Methodology
(C) 4046 – 4048 [4114 – 4116]
DOI: 10.1002/anie.200500589
d'Augustin, M. (C) 1376 – 1378 [1400 – 1402]
Daura, X.
– Stability of SIV gp32 Fusion-Peptide Single-Layer Protofibrils as Monitored by Molecular-Dynamics Simulations
(C) 1065 – 1067 [1089 – 1091]
DOI: 10.1002/anie.200461935
Davey, R. J.
– Polymorphism in Benzamide
(C) 7032 – 7035 [7194 – 7197]
DOI: 10.1002/anie.200501146
David, O. (C) 7946 – 7950 [8160 – 8164]
David, W. I. F. (C) 7032 – 7035 [7194 – 7197]
Davie, C. P. (C) 5867 – 5870 [6017 – 6020]
Davies, H. M. L.
– Direct Synthesis of (+)-Erogorgiaene through a Kinetic Enantiodifferentiating Step
(C) 1733 – 1735 [1761 – 1763]
DOI: 10.1002/anie.200462227
– Recent Advances in Catalytic Intramolecular C–H Aminations
(H) 3518 – 3520 [3584 – 3586]
DOI: 10.1002/anie.200500554
Davies, T. J. (C) 5121 – 5126 [5251 – 5256], 6491 – 6496 [6649 – 6654]
Davis, A. P.
– Carbohydrate Recognition in Water by a Tricyclic Polyamide Receptor
(C) 298 – 302 [302 – 306]
DOI: 10.1002/anie.200461409
– Spiraling Steroids: Organic Crystals with Asymmetric Nanometer-Scale Channels
(C) 6878 – 6881 [7038 – 7041]
DOI: 10.1002/anie.200502330
Davis, B. G.
– Glycoviruses: Chemical Glycosylation Retargets Adenoviral Gene Transfer
(C) 1057 – 1061 [1081 – 1085]
DOI: 10.1002/anie.200461832
Davisson, V. J. (C) 913 – 916 [935 – 938]
Day, J. K. (C) 7457 – 7460 [7623 – 7626]
Day, P.
– The First Proton-Conducting Metallic Ion-Radical Salts

(C) 292 – 295 [296 – 299]
DOI: 10.1002/anie.200461686
Dayal, S. (C) 5855 – 5857 [6005 – 6007]
De Angelis, F. (C) 6077 – 6081 [6231 – 6235]
De Brabander, J. K.
– Synthesis of Functionalized Salicylate Esters and Amides by Photochemical Acylation
(C) 1696 – 1699 [1724 – 1727]
DOI: 10.1002/anie.200462577
De Carolis, M. (C) 1232 – 1236 [1258 – 1262]
De Cola, L.
– White-Light Emission from an Assembly Comprising Luminescent Iridium and Europium Complexes
(C) 1806 – 1810 [1840 – 1844]
DOI: 10.1002/anie.200461953
de Frémont, P. (C) 5284 – 5288 [5418 – 5422]
de Gironcoli, S. (C) 6142 – 6145 [6298 – 6301]
de Groot, B. L.
– Molecular Dynamics Simulations of Protein G Challenge NMR-Derived Correlated Backbone Motions
(C) 3394 – 3399 [3460 – 3465]
DOI: 10.1002/anie.200462957
de Jong, J. J. D. (C) 2373 – 2376 [2425 – 2428]
de Jong, K. P. (C) 1360 – 1363 [1384 – 1387]
de Jong, L. (C) 7946 – 7950 [8160 – 8164]
de Kanter, F. J. J. (C) 6579 – 6582 [6737 – 6740]
de Koning, L. J. (C) 7946 – 7950 [8160 – 8164]
de Koster, C. G. (C) 7946 – 7950 [8160 – 8164]
de la Rosa, G. (C) 6521 – 6525 [6679 – 6683]
de la Rúa, R. B. (C) 4981 – 4983 [5061 – 5063]
de Loos, M. (C) 2373 – 2376 [2425 – 2428]
De Lucchi, O. (C) 7435 – 7439 [7601 – 7605]
de Mallmann, A. (C) 6755 – 6758 [6913 – 6916]
de Meijere, A.
– Adolf von Baeyer: Winner of the Nobel Prize for Chemistry 1905
(E) 7836 – 7840 [8046 – 8050]
DOI: 10.1002/anie.200503351
– C–C Bond Activation by Octacarbonyldicobalt: [3 + 1] Cocyclizations of Methylenecyclopropanes with Carbon Monoxide
(C) 7881 – 7884 [8093 – 8096]
DOI: 10.1002/anie.200502596
– Versatile Direct Synthesis of Oligosubstituted Pyrroles by Cycloaddition of α-Metalated Isocyanides to Acetylenes
(C) 5664 – 5667 [5809 – 5813]
DOI: 10.1002/anie.200502140
De Napoli, M. (C) 4006 – 4009 [4074 – 4077]
de Noronha, R. G. (C) 4925 – 4929 [5005 – 5009]
de Petris, G.
– Experimental Detection of Theoretically Predicted N_2CO
(C) 462 – 465 [466 – 469]
DOI: 10.1002/anie.200460310
de Prado, A. (C) 6583 – 6585 [6741 – 6743]
de Sáa, D. (C) 4981 – 4983 [5061 – 5063]
de Schryver, F. C. (C) 560 – 564 [566 – 570]
De Vos, D. E.
– Gold Redox Catalysis for Selective Oxidation of Methane to Methanol
(H) 30 – 32 [30 – 32]
DOI: 10.1002/anie.200461561
De Vos, D. E. (C) 310 – 313 [314 – 317]
de Vries, A. H. M. (C) 4209 – 4212 [4281 – 4284]
de Vries, J. G.
– Achiral Ligands Dramatically Enhance Rate and Enantioselectivity in the Rh/Phosphoramidite-Catalyzed Hydrogenation of α,β-Disubstituted Unsaturated Acids
(C) 4209 – 4212 [4281 – 4284]
DOI: 10.1002/anie.200500784
de Vries, J. G. (C) 7442 – 7447 [7608 – 7613]
Deacon, G. B. (C) 5871 – 5875 [6021 – 6025]
DeBeer George, S. (C) 2908 – 2912 [2968 – 2972]
Debuigne, A. (C) 1101 – 1104 [1125 – 1128], 3439 – 3442 [3505 – 3508]
Decher, G. (C) 3260 – 3264 [3324 – 3328]
Dechert, S. (C) 7111 – 7114 [7273 – 7276]
Deck, P. (C) 4975 – 4980 [5055 – 5060]
Decken, A. (C) 2364 – 2367 [2416 – 2419], 6196 – 6199 [6352 – 6355], 7958 – 7961 [8172 – 8175]
Decker, A. (C) 2252 – 2255 [2292 – 2295]
Decker, B. (C) 484 – 488 [489 – 492]
Décout, J.-L.
– DNA Detection through Signal Amplification by Using NADH:Flavin Oxidoreductase and Oligonucleotide – Flavin Conjugates as Cofactors
(C) 2764 – 2767 [2824 – 2827]
DOI: 10.1002/anie.200461145
Decurtins, S. (C) 2711 – 2715 [2771 – 2775]
Degrado, S. J. (C) 5306 – 5310 [5440 – 5444]
DeGrado, W. F.
– The Design and Evaluation of Heparin-Binding Foldamers
(C) 6685 – 6689 [6843 – 6847]
DOI: 10.1002/anie.200501279
Deguchi, K. (C) 91 – 96 [93 – 98]
Dehaen, W. (C) 4731 – 4735 [4809 – 4813]
Dehner, A. (C) 5247 – 5251 [5381 – 5386]
DeHope, A. (C) 7236 – 7239 [7402 – 7405]
Dei, A.
– Photomagnetic Effects in Polycyanometalate Compounds: An Intriguing Future Chemically Based Technology?
(H) 1160 – 1163 [1184 – 1187]
DOI: 10.1002/anie.200461413
Dekowski, B. (C) 7887 – 7891 [8099 – 8104]
del Amo Sanchez, V. (C) 6878 – 6881 [7038 – 7041]
del Campo, A. (C) 4707 – 4712 [4785 – 4791]
del Río, D. (C) 1244 – 1247 [1270 – 1273], 3429 – 3432 [3495 – 3498]
del Río, M. P. (C) 3267 – 3271 [3331 – 3335]
Del Vecchio, E. (C) 3285 – 3289 [3349 – 3353]
Delbecq, F. (C) 5279 – 5282 [5413 – 5416]
Delli Castelli, D. (C) 1813 – 1815 [1847 – 1849], 5513 – 5515 [5649 – 5651]
Dellios, C. C. (C) 3447 – 3452 [3513 – 3518]
Delmau, L. H. (C) 2537 – 2542 [2593 – 2598]
Demachy, I. (C) 5310 – 5313 [5444 – 5447]
Demchenko, A. V.
– Development of an Arming Participating Group for Stereoselective Glycosylation and Chemoselective Oligosaccharide Synthesis
(C) 7123 – 7126 [7285 – 7288]
DOI: 10.1002/anie.200502694
Demeshko, S. (C) 7111 – 7114 [7273 – 7276]
Demurtas, D. (C) 1221 – 1222 [1247 – 1248]
Demuru, D. (C) 2913 – 2916 [2973 – 2976]
Demydchuk, Y. A. (C) 7075 – 7078 [7237 – 7240]
Denayer, J. F. M.
– Rotational Entropy Driven Separation of Alkane/Isoalkane Mixtures in Zeolite Cages
(C) 400 – 403 [404 – 407]
DOI: 10.1002/anie.200454058
Dénès, F. (C) 5273 – 5275 [5407 – 5409]
Deng, G. (C) 4042 – 4045 [4110 – 4113]
Deng, H. (C) 2782 – 2785 [2842 – 2845]
Deng, Li
– Catalytic Enantioselective Total Syntheses of Bisorbicillinolide, Bisorbicillinol, and Bisorbibutenolide
(C) 3478 – 3481 [3544 – 3547]
DOI: 10.1002/anie.200500480
– Stereocontrolled Creation of Adjacent Quaternary and Tertiary Stereocenters by a Catalytic Conjugate Addition
(C) 105 – 108 [107 – 110]
DOI: 10.1002/anie.200461923
Deng, Liang (C) 2128 – 2131 [2166 – 2169]
Deng, S. (C) 3755 – 3758 [3821 – 3825]
Deng, Z. (C) 3582 – 3585 [3648 – 3651], 6694 – 6696 [6852 – 6854]
Denifl, S. (C) 1647 – 1650 [1673 – 1676], 6941 – 6943 [7101 – 7103]
Denmark, S. E.
– Catalytic, Enantioselective, Vinylogous Aldol Reactions
(R) 4682 – 4698 [4760 – 4777]
DOI: 10.1002/anie.200462338
– Synthesis of *cis*,*cis*,*cis*,*cis*-[5.5.5.4]-1-Azafenestrane with Discovery of an Unexpected Dyotropic Rearrangement
(C) 3732 – 3736 [3798 – 3802]
DOI: 10.1002/anie.200500367
Deprés, J.-P.
– Approach to the Blues: A Highly Flexible Route to the Azulenes
(C) 5130 – 5133 [5260 – 5263]
DOI: 10.1002/anie.200501276
Desbiens, N. (C) 5310 – 5313 [5444 – 5447]
Desbrières, J. (C) 2580 – 2582 [2636 – 2638]
Desiraju, G. R.
– Structural Studies of the System Na(saccharinate)·$n$$H_2O$: A Model for Crystallization
(C) 2515 – 2520 [2571 – 2576]
DOI: 10.1002/anie.200462967
Despotopoulou, C. (C) 1654 – 1658 [1682 – 1685]
Desvergne, J.-P.
– Photorelease of an Organic Molecule in Solution: Light-Triggered Blockage of a Hydrogen-Bonding Receptor Site
(C) 1072 – 1075 [1096 – 1099]
DOI: 10.1002/anie.200461946
Detert, H.
– *cis*-Bromination of Alkynes without Cationic Intermediates
(C) 1412 – 1416 [1437 – 1441]
DOI: 10.1002/anie.200461632
Detmer, I. (C) 4712 – 4715 [4791 – 4794]
Detrembleur, C. (C) 3439 – 3442 [3505 – 3508]
Devadoss, A. (C) 5855 – 5857 [6005 – 6007]
Di, Y. (C) 2563 – 2568 [2619 – 2624]
Dias, H. V. R.
– Monomeric Thallium(I) Complexes of Fluorinated Triazapentadienyl Ligands
(C) 4907 – 4910 [4985 – 4988]
DOI: 10.1002/anie.200500401
– Supramolecular Features of Calixarene-Based Synthetic Nanotubes
(C) 3043 – 3047 [3103 – 3107]
DOI: 10.1002/anie.200500057
Díaz, N. (C) 3260 – 3264 [3324 – 3328]
Diaz, S. L. (C) 2400 – 2403 [2452 – 2455]
Díaz-Requejo, M. M.
– A Gold Catalyst for Carbene-Transfer Reactions from Ethyl Diazoacetate

 © 2005 Wiley-VCH Verlag GmbH & Co. KGaA, Weinheim

(C) 5284 – 5288 [5418 – 5422]
DOI: 10.1002/anie.200501056
Diederich, F.
– Editorial: Reviews in *Angewandte Chemie*: Influence, Language, Competition
2308 – 2309 [2360 – 2361]
DOI: 10.1002/anie.200500233
– Geometrically Precisely Defined Multinanometer Expansion/Contraction Motions in a Resorcin[4]arene Cavitand Based Molecular Switch
(C) 4635 – 4638 [4711 – 4715]
DOI: 10.1002/anie.200500970
– Orthogonal Multipolar Interactions in Structural Chemistry and Biology
(R) 1788 – 1805 [1820 – 1839]
DOI: 10.1002/anie.200462213
– Quantification of Cation – π Interactions in Protein – Ligand Complexes: Crystal-Structure Analysis of Factor Xa Bound to a Quaternary Ammonium Ion Ligand
(C) 4400 – 4404 [4474 – 4479]
DOI: 10.1002/anie.200500883
– Shape-Persistent Chiral Alleno-Acetylenic Macrocycles and Cyclophanes by Acetylenic Scaffolding with 1,3-Diethynylallenes
(C) 5074 – 5078 [5203 – 5207]
DOI: 10.1002/anie.200501621
Diéguez, A. (C) 126 – 128 [128 – 130]
Diele, S. (C) 774 – 778 [784 – 788]
Dietrich, H. M. (C) 5303 – 5306 [5437 – 5440]
Dietzel, P. D. C.
– An In Situ High-Temperature Single-Crystal Investigation of a Dehydrated Metal – Organic Framework Compound and Field-Induced Magnetization of One-Dimensional Metal – Oxygen Chains
(C) 6354 – 6358 [6512 – 6516]
DOI: 10.1002/anie.200501508
Díez, E. (C) 580 – 584 [586 – 590]
Dikarev, E. V.
– Heterobimetallic Main-Group – Transition-Metal Paddle-Wheel Carboxylates
(C) 1721 – 1724 [1749 – 1752]
DOI: 10.1002/anie.200462433
Ding, K.
– Heterogenization of Shibasaki's Binol/La Catalyst for Enantioselective Epoxidation of α,β-Unsaturated Ketones with Multitopic Binol Ligands: The Impact of Bridging Spacers
(C) 6362 – 6366 [6520 – 6524]
DOI: 10.1002/anie.200501676
Ding, S.
– A Small-Molecule Agonist of the Wnt Signaling Pathway
(C) 1987 – 1990 [2023 – 2026]
DOI: 10.1002/anie.200462552
Ding, Yaping (C) 1517 – 1520 [1541 – 1544]
Ding, Yi (C) 4002 – 4006 [4070 – 4074]
Dingerdissen, U. (C) 6771 – 6774 [6929 – 6933]
Dinh, L. V. (C) 4095 – 4097 [4164 – 4167]
Dinnebier, R. E. (C) 770 – 773 [780 – 783]
Diwald, O. (C) 4917 – 4920 [4996 – 4999]
Dixneuf, P. H.
– Alkenylcarbene Ruthenium Arene Complexes as Initiators of Alkene Metathesis: An Enyne Creates a Catalyst that Promotes Its Selective Transformation
(C) 2576 – 2579 [2632 – 2635]
DOI: 10.1002/anie.200462865
Dixneuf, P. H. (C) 2021 – 2023 [2057 – 2059]
Dixon, D. J. (C) 580 – 584 [586 – 590]
Djanhan, J. E. (C) 7783 – 7786 [7961 – 7964]
Dmitriev, A. (C) 1488 – 1491 [1512 – 1515]
Do, Y. (C) 6166 – 6169 [6322 – 6325]
Dochnahl, M. (C) 7794 – 7798 [7972 – 7976]
Dohi, T. (C) 6193 – 6196 [6349 – 6352]
Doi, M. (C) 4352 – 4355 [4426 – 4429]
Dolle, R. E.
– Solid/Solution-Phase Annulation Reagents: Single-Step Synthesis of Cyclic Amine Derivatives
(C) 5830 – 5833 [5980 – 5983]
DOI: 10.1002/anie.200501665
Domènech, J. (C) 4618 – 4622 [4694 – 4698]
Dominiak, P. (C) 2115 – 2119 [2153 – 2157]
Donath, E.
– Engineering Virus Functionalities on Colloidal Polyelectrolyte Lipid Composites
(C) 2892 – 2895 [2952 – 2955]
DOI: 10.1002/anie.200460763
Dondas, H. A. (C) 7570 – 7574 [7742 – 7746]
Dondoni, A.
– Hybrid Solution/Solid-Phase Synthesis of Oligosaccharides by Using Trichloroacetyl Isocyanate as Sequestration-Enabling Reagent of Sugar Alcohols
(C) 1672 – 1676 [1700 – 1704]
DOI: 10.1002/anie.200462422
Dong, S. (C) 4018 – 4021 [4086 – 4089]
Dong, X. (C) 5083 – 5087 [5213 – 5217]
Donnadieu, B. (C) 5705 – 5709 [5851 – 5855], 7236 – 7239 [7402 – 7405]
Donnell, A. F. (C) 6715 – 6718 [6873 – 6876]
Donohoe, T. J.
– Oxidative Cyclization of Diols Derived from 1,5-Dienes: Formation of Enantiopure *cis*-Tetrahydrofurans by Using Catalytic Osmium Tetroxide; Formal Synthesis of (+)-*cis*-Solamin
(C) 4766 – 4768 [4844 – 4846]
DOI: 10.1002/anie.200500513
Donovan, P. M. (C) 7549 – 7553 [7721 – 7725]
Dopfer, O.
– Real-Time Observation of Ionization-Induced Hydrophobic → Hydrophilic Switching
(C) 6149 – 6151 [6305 – 6307]
DOI: 10.1002/anie.200501430
Döring, S. Corrigendum: 506
Dorlet, P.
– A Biomimetic Model of the Electron Transfer between P_{680} and the TyrZ – His190 Pair of PSII
(C) 1536 – 1540 [1560 – 1564]
DOI: 10.1002/anie.200461948
Dossena, A. (C) 5126 – 5130 [5256 – 5260]
Dötz, F. (C) 1247 – 1250 [1273 – 1276]
Doundoulakis, T. (C) 765 – 769 [775 – 779]
Dove, A. P. (C) 4964 – 4968 [5044 – 5048]
Doye, S.
– Hydroamination/Hydrosilylation Sequence Catalyzed by Titanium Complexes
(C) 2951 – 2954 [3011 – 3013]
DOI: 10.1002/anie.200462250
Doyle, A. M. (C) 629 – 631 [635 – 637]
Dragancea, D. (C) 7938 – 7942 [8152 – 8156]
Drago, C. (C) 7221 – 7223 [7387 – 7389]
Dragota, S. (C) 5292 – 5295 [5426 – 5429]
Drahl, C. (R) 5788 – 5809 [5936 – 5958], (C) 6533 – 6537 [6691 – 6695]
Dremov, Viacheslav (C) 7896 – 7900 [8109 – 8113]
Dremov, Viatcheslav (C) 803 – 806 [813 – 817]
Dressel, M. (C) 3857 – 3861 [3925 – 3929]
Dreuw, A.
– Molecular Mechanism of the Solid-State Fluorescence Behavior of the Organic Pigment Yellow 101 and Its Derivatives
(C) 7783 – 7786 [7961 – 7964]
DOI: 10.1002/anie.200501781
Drexler, H.-J. (C) 1184 – 1188 [1208 – 1212]
Driess, M.
– A Novel Type of Pentacoordinate Silicon Complexes and Unusual Ligand Coupling by Intramolecular Electron Transfer
(C) 6738 – 6741 [6896 – 6899]
DOI: 10.1002/anie.200501997
– Formation of a Bowl-Shaped, Pentacyclic Phosphonium Cage by Methylation of a Nucleophilic Phosphinidene
(C) 6734 – 6737 [6892 – 6895]
DOI: 10.1002/anie.200501990
Driess, M. (C) 7892 – 7896 [8104 – 8109]
Drillon, M. (C) 6488 – 6491 [6646 – 6649]
Dronskowski, R.
– Predicting New Ferromagnetic Nitrides from Electronic Structure Theory: $IrFe_3N$ and $RhFe_3N$
(C) 1205 – 1210 [1230 – 1235]
DOI: 10.1002/anie.200462247
– Synthesis, Crystal Structure, and Magnetic Properties of the Semihard Itinerant Ferromagnet $RhFe_3N$
(C) 7212 – 7215 [7379 – 7382]
DOI: 10.1002/anie.200502579
Dryfe, R. A. W.
– Electrochemically Controlled Ion Exchange: Proton Exchange with Sodium Zeolite Y
(C) 3075 – 3078 [3135 – 3138]
DOI: 10.1002/anie.200463036
D'Souza, D. M. (C) 153 – 158 [156 – 161]
Du, Yu (C) 7988 – 7990 [8202 – 8204]
Du, Yunchen (C) 2563 – 2568 [2619 – 2624]
Duan, H. (C) 1717 – 1720 [1745 – 1748]
Duan, T. (C) 2973 – 2975 [3033 – 3036]
Duan, W.-L. (C) 4611 – 4614 [4687 – 4690]
Duati, M. (C) 1806 – 1810 [1840 – 1844]
Dubbaka, S. R. (M) 7674 – 7684 [7848 – 7859]
Duboc, C. (C) 438 – 441 [442 – 445]
Dubois, G. (C) 7574 – 7580 [7746 – 7752]
Dubois, P.
– Latent, Thermally Activated Organic Catalysts for the On-Demand Living Polymerization of Lactide
(C) 4964 – 4968 [5044 – 5048]
DOI: 10.1002/anie.200500723
Dubruel, P. (C) 5505 – 5509 [5641 – 5645]
Ducry, L.
– Controlled Autocatalytic Nitration of Phenol in a Microreactor
(C) 7972 – 7975 [8186 – 8189]
DOI: 10.1002/anie.200502387
Duer, M. J. (C) 5729 – 5733 [5875 – 5879]
Dueymes, C. (C) 2764 – 2767 [2824 – 2827]
Dufaud, V.
– Organometallic Chemistry Inside the Pore Walls of Mesostructured Silica Materials
(C) 3475 – 3477 [3541 – 3543]
DOI: 10.1002/anie.200500454
Duhme-Klair, A.-K.
– A Metal-Based Lumophore Tailored To Sense Biologically Relevant Oxometalates
(C) 1712 – 1714 [1740 – 1742]
DOI: 10.1002/anie.200462306
– The First μ_6-Peroxide Transition-Metal Complex: $[Ni_8(L)_{12}(O_2)]^{2+}$
(C) 1392 – 1395 [1416 – 1419]
DOI: 10.1002/anie.200461892

 © 2005 Wiley-VCH Verlag GmbH & Co. KGaA, Weinheim

Dulcey, A. E. (C) 6516 – 6521 [6674 – 6679]
Duma, L. (C) 3089 – 3092 [3149 – 3152]
Dumesic, J. A.
– Preferential Oxidation of CO in H_2 by Aqueous Polyoxometalates over Metal Catalysts
(C) 778 – 782 [788 – 792]
DOI: 10.1002/anie.200461601
Dumrongchai, N. (C) 7570 – 7574 [7742 – 7746]
Duncan, R.
– Polymer Therapeutics Designed for a Combination Therapy of Hormone-Dependent Cancer
(C) 4061 – 4066 [4129 – 4134]
DOI: 10.1002/anie.200462960
Dunitz, J. D.
– Molecular Recognition in Organic Crystals: Directed Intermolecular Bonds or Nonlocalized Bonding?
(R) 1766 – 1787 [1796 – 1819]
DOI: 10.1002/anie.200460157
Dunsch, L.
– Magnetic Moments of the Endohedral Cluster Fullerenes $Ho_3N@C_{80}$ and $Tb_3N@C_{80}$: The Role of Ligand Fields
(C) 3306 – 3309 [3371 – 3374]
DOI: 10.1002/anie.200461500
Dunsch, L. (C) 1557 – 1560 [1581 – 1584]
Duppen, K.
– Light-Driven Dynamic Pattern Formation
(C) 2373 – 2376 [2425 – 2428]
DOI: 10.1002/anie.200462500
Duran, M. (C) 1876 – 1879 [1910 – 1913]
Durbin, M. J. (C) 1543 – 1545 [1567 – 1569]
Durón, S. G. (R) 192 – 212 [196 – 217]
Durrant, J. R. (C) 5740 – 5744 [5886 – 5890]
Dwars, T. (R) 7174 – 7199 [7338 – 7364]
Dyker, C. A. (C) 2364 – 2367 [2416 – 2419], 6196 – 6199 [6352 – 6355]
Dyson, P. J.
– A Synthetic Zwitterionic Water Channel: Characterization in the Solid State by X-ray Crystallography and NMR Spectroscopy
(C) 5720 – 5725 [5866 – 5871]
DOI: 10.1002/anie.200500207
– Hydrogen Sponge? A Heteronuclear Cluster That Absorbs Large Quantities of Hydrogen
(H) 5772 – 5774 [5918 – 5921]
DOI: 10.1002/anie.200501549
Dziadek, S. (C) 7624 – 7630 [7798 – 7803], 7630 – 7635 [7803 – 7808]

Eames, J.
– Recent Developments in the Transfer of Chirality within Enolate Alkylation Reactions
(H) 186 – 189 [190 – 193]
DOI: 10.1002/anie.200461617
Ebata, N. (C) 5439 – 5441 [5575 – 5577]
Ebitani, K. (C) 3423 – 3426 [3489 – 3492]
Ebizuka, Y. (C) 1121 – 1125 [1145 – 1149]
Echavarren, A. M.
– Couplings with Monoorganotin Compounds: A "Radical" Twist from the Original Stille Reaction
(H) 3962 – 3965 [4028 – 4031]
DOI: 10.1002/anie.200500918
– Divergent Mechanisms for the Skeletal Rearrangement and [2 + 2] Cycloaddition of Enynes Catalyzed by Gold
(C) 6146 – 6148 [6302 – 6304]
DOI: 10.1002/anie.200501937
Eckel, R. (C) 484 – 488 [489 – 492], 3921 – 3924 [3989 – 3993]
Eckert, D. (C) 3306 – 3309 [3371 – 3374]
Eckert, M. (C) 2576 – 2579 [2632 – 2635]
Edén, M. (C) 7269 – 7273 [7435 – 7439]
Edlund, U. (C) 6516 – 6521 [6674 – 6679]
Edwards, H. K. (C) 3555 – 3558 [3621 – 3624]
Edwards, N. Y. (C) 6203 – 6207 [6359 – 6363]
Egger, C. C. (C) 3243 – 3248 [3307 – 3312]
Ehlers, A. W. (C) 3289 – 3293 [3353 – 3357], 6579 – 6582 [6737 – 6740]
Eichelbaum, M. (C) 7905 – 7909 [8118 – 8122]
Eichhöfer, A. (C) 5242 – 5246 [5376 – 5381]
Eichhorn, B.
– Pt – Cu Core – Shell and Alloy Nanoparticles for Heterogeneous NO_x Reduction: Anomalous Stability and Reactivity of a Core – Shell Nanostructure
(C) 4539 – 4543 [4615 – 4619]
DOI: 10.1002/anie.200500919
Eichhorst, J. (C) 7887 – 7891 [8099 – 8104]
Eichler, B. E. (C) 2546 – 2549 [2602 – 2605]
Eichmüller, C. (C) 2284 – 2288 [2324 – 2328]
Eikey, R. A. (C) 6203 – 6207 [6359 – 6363]
Eisler, D. J. (C) 4953 – 4956 [5033 – 5036]
El-Aziz, A. M. (C) 2080 – 2084 [2116 – 2120]
El-Boulifi, N. (C) 7739 – 7741 [7917 – 7919]
El Kaïm, L.
– Phenol Ugi – Smiles Systems: Strategies for the Multicomponent N-Arylation of Primary Amines with Isocyanides, Aldehydes, and Phenols
(C) 7961 – 7964 [8175 – 8178]
DOI: 10.1002/anie.200502636
Elborough, K. (C) 7553 – 7557 [7725 – 7729]
Elhabiri, M. (C) 5338 – 5341 [5472 – 5475]
Eller, L. R. (C) 5989 – 5992 [6143 – 6146]
Ellern, A. (C) 4960 – 4963 [5040 – 5043], 7874 – 7878 [8086 – 8090]
Elliott, M. I. (C) 1392 – 1395 [1416 – 1419]
Elsegood, M. R. J. (C) 1850 – 1853 [1884 – 1887]
Elsevier, C. J.
– Palladium – (N-Heterocyclic Carbene) Hydrogenation Catalysts
(C) 2026 – 2029 [2062 – 2065]
DOI: 10.1002/anie.200462930
Elson-Schwab, L. (C) 927 – 932 [949 – 954]
Emrick, T. (C) 2420 – 2426 [2472 – 2478]
Emsley, L. (C) 3089 – 3092 [3149 – 3152]
Enders, D.
– Asymmetric Synthesis of Selectively Protected Amino Sugars and Derivatives by a Direct Organocatalytic Mannich Reaction
(C) 4079 – 4083 [4147 – 4151]
DOI: 10.1002/anie.200500810
– Asymmetric Synthesis of the 1-*epi* Aglycon of the Cripowellins A and B
(C) 3766 – 3769 [3832 – 3835]
DOI: 10.1002/anie.200500556
– Direct Organocatalytic De Novo Synthesis of Carbohydrates
(C) 1210 – 1212 [1235 – 1238]
DOI: 10.1002/anie.200462428
– The Dihydroxyacetone Unit—A Versatile C_3 Building Block in Organic Synthesis
(R) 1304 – 1325 [1330 – 1351]
DOI: 10.1002/anie.200400659
Endo, K. (C) 7248 – 7251 [7414 – 7417]
Endo, M.
– DNA Tube Structures Controlled by a Four-Way-Branched DNA Connector
(C) 6074 – 6077 [6228 – 6231]
DOI: 10.1002/anie.200501034
Engelborghs, Y. (C) 560 – 564 [566 – 570]
Engelhard, M.
– Direct Readout of Protein – Protein Interactions by Mass Spectrometry from Protein – DNA Microarrays
(C) 7635 – 7639 [7808 – 7812]
DOI: 10.1002/anie.200502908
Engelhardt, L. (C) 3857 – 3861 [3925 – 3929]
Engels, J. W.
– Gene Synthesis on Microchips
(H) 7166 – 7169 [7328 – 7331]
DOI: 10.1002/anie.200501896
Englert, U.
– Crystal-to-Crystal Transformation from a Chain Polymer to a Two-Dimensional Network at Low Temperatures
(C) 2281 – 2283 [2321 – 2323]
DOI: 10.1002/anie.200462100
Engqvist, M. (C) 1343 – 1345 [1367 – 1369]
Enkelmann, V. (C) 1247 – 1250 [1273 – 1276], 2801 – 2805 [2862 – 2866]
Ensling, J. (C) 7787 – 7790 [7965 – 7968]
Epergyes, A. (C) 7059 – 7062 [7221 – 7224]
Epstein, A. J.
– Oligothiophenes Incorporating Metal – Metal Quadruple Bonds
(C) 6537 – 6540 [6695 – 6698]
DOI: 10.1002/anie.200500138
Epstein, O. L. (C) 121 – 123 [123 – 125]
Erhardt, S. (C) 1078 – 1082 [1102 – 1106]
Eriksson, L. (C) 4877 – 4880 [4955 – 4958]
Erlebacher, J.
– Epitaxial Casting of Nanotubular Mesoporous Platinum
(C) 4002 – 4006 [4070 – 4074]
DOI: 10.1002/anie.200463106
Ernst, M. (C) 2441 – 2444 [2494 – 2497]
Ernsting, N. P.
– Ultrafast Solvation of *N*-Methyl-6-quinolone Probes Local IR Spectrum
(C) 5635 – 5639 [5779 – 5783]
DOI: 10.1002/anie.200501397
Errington, R. J.
– Covalent Immobilization of a TiW_5 Polyoxometalate on Derivatized Silicon Surfaces
(C) 1254 – 1257 [1280 – 1283]
DOI: 10.1002/anie.200461065
Ertl, G. (C) 139 – 142 [141 – 144]
Escax, V. (C) 4798 – 4801 [4876 – 4879]
Escolano, C.
– Stephacidin B, The Avrainvillamide Dimer: A Formidable Synthetic Challenge
(H) 7670 – 7673 [7844 – 7847]
DOI: 10.1002/anie.200502383
Espindola, P. (C) 2447 – 2451 [2501 – 2505]
Espinosa, A. (C) 1977 – 1981 [2013 – 2017]
Esquibel, J. (C) 3086 – 3089 [3146 – 3149]
Esteves da Silva, J. C. G.
– Synthesis of Luciferyl Coenzyme A: A Bioluminescent Substrate for Firefly Luciferase in the Presence of AMP
(C) 3427 – 3429 [3493 – 3495]
DOI: 10.1002/anie.200462934
Estévez, R. E. (C) 319 – 322 [323 – 326]

 © 2005 Wiley-VCH Verlag GmbH & Co. KGaA, Weinheim

Estrada, A. A. (C) 1378 – 1382 [1402 – 1406], 3736 – 3740 [3802 – 3806]
Evangelisti, M. (C) 6496 – 6500 [6654 – 6658]
Evans, D. A.
– Polycyclic Molecules from Linear Precursors: Stereoselective Synthesis of Clavolonine and Related Complex Structures (C) 6038 – 6042 [6192 – 6196] DOI: 10.1002/anie.200502296
Evans, S. T. (C) 778 – 782 [788 – 792]
Exner, K. (C) 2433 – 2437 [2485 – 2490]
Expert, D. (C) 2580 – 2582 [2636 – 2638]
Eychmüller, A.
– Aerogels from Semiconductor Nanomaterials (H) 4839 – 4841 [4917 – 4919] DOI: 10.1002/anie.200501052
– Selective Fabrication of Ordered Bimetallic Nanostructures with Hierarchical Porosity (C) 5997 – 6001 [6151 – 6155] DOI: 10.1002/anie.200501471

F

Faber, K.
– Highly Enantioselective *sec*-Alkyl Sulfatase Activity of the Marine Planctomycete *Rhodopirellula baltica* Shows Retention of Configuration (C) 6381 – 6384 [6539 – 6542] DOI: 10.1002/anie.200501955
Fabian, H.
– ^{13}C-Labeled Tyrosine Residues as Local IR Probes for Monitoring Conformational Changes in Peptides and Proteins (C) 4631 – 4635 [4707 – 4711] DOI: 10.1002/anie.200500547
Fabris, S.
– Templated Growth of Metal – Organic Coordination Chains at Surfaces (C) 6142 – 6145 [6298 – 6301] DOI: 10.1002/anie.200502007
Fabrizi de Biani, F. (C) 5701 – 5705 [5847 – 5851]
Facchetti, A. (C) 7922 – 7925 [8136 – 8139]
Fagnoni, M.
– Metal-Free Cross-Coupling Reactions of Aryl Sulfonates and Phosphates through Photoheterolysis of Aryl – Oxygen Bonds (C) 1232 – 1236 [1258 – 1262] DOI: 10.1002/anie.200461444
– Photo-Cross-Coupling Reaction of Electron-Rich Aryl Chlorides and Aryl Esters with Alkynes: A Metal-Free Alkynylation (C) 5675 – 5678 [5821 – 5824] DOI: 10.1002/anie.200501541
Falck, J. R.
– Stereoselective Transformations of Trihalomethylcarbinols Induced by Chromous Chloride (C) 2008 – 2011 [2044 – 2047] DOI: 10.1002/anie.200461884
Fallis, A. G.
– Acetylenic Allenophanes: An Asymmetric Synthesis of a Bis(alleno)-bis(butadiynyl)-*meta*-cyclophane (C) 4039 – 4042 [4107 – 4110] DOI: 10.1002/anie.200500484
Fallis, I. A.
– Selective Electrochemical Detection of Hydrogen Fluoride by Ambiphilic Ferrocene Derivatives (C) 3606 – 3609 [3672 – 3675] DOI: 10.1002/anie.200500527
Fallis, I. A. (C) 5282 – 5284 [5416 – 5418]
Fan, C.
– Nanoparticle PCR: Nanogold-Assisted PCR with Enhanced Specificity (C) 5100 – 5103 [5230 – 5233] DOI: 10.1002/anie.200500403
Fan, Hongjun (C) 5090 – 5093 [5220 – 5223]
Fan, Huizhi (C) 615 – 617 [621 – 623]
Fan, J.-Q.
– Rational Design and Synthesis of Highly Potent β-Glucocerebrosidase Inhibitors (C) 7450 – 7453 [7616 – 7619] DOI: 10.1002/anie.200502662
Fan, Y. (C) 6067 – 6074 [6221 – 6228]
Fañanás, F. J. (C) 126 – 128 [128 – 130]
Fang, H. (C) 2737 – 2742 [2797 – 2802]
Fang, J. (C) 1965 – 1968 [2001 – 2004]
Fang, M. (C) 2005 – 2008 [2041 – 2044]
Fang, Q. (C) 3845 – 3848 [3913 – 3916]
Fang, X. (C) 3540 – 3544 [3606 – 3610]
Fang, Y. (C) 3562 – 3565 [3628 – 3631]
Fantacci, S.
– Mechanism of the Initial Conformational Transition of a Photomodulable Peptide (C) 6077 – 6081 [6231 – 6235] DOI: 10.1002/anie.200501145
Fantoni, A. (C) 6341 – 6344 [6499 – 6502]
Faraoni, R. (C) 3874 – 3879 [3942 – 3947]
Farès, C. (C) 7776 – 7778 [7954 – 7956]
Farhan, T. (C) 4578 – 4581 [4654 – 4657]
Farjon, J. (C) 427 – 429 [431 – 433]
Fässler, T. F.
– $[Pb_5\{Mo(CO)_3\}_2]^{4-}$: A Complex Containing a Planar Pb_5 Unit (C) 2092 – 2096 [2129 – 2133] DOI: 10.1002/anie.200462342
Faul, C. F. J.
– Self-Assembly and Electrical Conductivity Transitions in Conjugated Oligoaniline – Surfactant Complexes (C) 751 – 756 [761 – 766] DOI: 10.1002/anie.200460928
Fedorov, V. E.
– $[Re_{12}CS_{17}(CN)_6]^{n-}$ ($n = 6$, 8): A Sulfido – Cyanide Rhenium Cluster with an Interstitial Carbon Atom (C) 6867 – 6871 [7027 – 7031] DOI: 10.1002/anie.200501911
Fehlner, T. P.
– Borane Mimics of Classic Organometallic Compounds: $[(Cp^*Ru)B_8H_{14}(RuCp^*)]^{0,+}$, Isoelectronic Analogues of Dinuclear Pentalene Complexes (C) 6568 – 6571 [6726 – 6729] DOI: 10.1002/anie.200502212
– Borane Mimics of C_1–M_m Organometallic Complexes (H) 2056 – 2058 [2092 – 2094] DOI: 10.1002/anie.200500054
– Synthesis and Characterization of [*exo*-$BH_2(Cp^*M)_2B_9H_{14}$] (M = Ru, Re), and the Conversion of the Ruthenaborane into $[(Cp^*Ru)_2B_{10}H_{16}]$ with an Open Cluster Framework Based on a Capped Truncated Tetrahedron (C) 2916 – 2918 [2976 – 2978] DOI: 10.1002/anie.200500343
Fehrmann, R. (C) 815 – 819 [826 – 830]
Fei, Z. (C) 5720 – 5725 [5866 – 5871]
Feil, F. (C) 6537 – 6540 [6695 – 6698]
Feldmann, J. (C) 1520 – 1525 [1544 – 1549]
Felli, I. C. (C) 3089 – 3092 [3149 – 3152]
Feng, J. (C) 5083 – 5087 [5213 – 5217]
Feng, P.
– Open-Framework Chalcogenides as Visible-Light Photocatalysts for Hydrogen Generation from Water (C) 5299 – 5303 [5433 – 5437] DOI: 10.1002/anie.200500346
Feng, X. (C) 5115 – 5118 [5245 – 5248]
Feng, Yakai (C) 1188 – 1192 [1212 – 1216]
Feng, Yefei (C) 2563 – 2568 [2619 – 2624]
Fenske, D.
– Phosphine-Stabilized Copper – Antimony Clusters: Syntheses, Structures, and Theoretical Investigations of $[Cu_{12}(SbSiMe_3)_6(PiPr_3)_6]$, $[Cu_{40}Sb_{12}(PMe_3)_{20}]$, and $[Cu_{45}Sb_{16}(PEt_2Me)_{16}]$ (C) 3932 – 3936 [4002 – 4005] DOI: 10.1002/anie.200500593
– Syntheses and Crystal Structures of $[Ag_{123}S_{35}(StBu)_{50}]$ and $[Ag_{344}S_{124}(StBu)_{96}]$ (C) 5242 – 5246 [5376 – 5381] DOI: 10.1002/anie.200501414
Férey, G. (C) 6488 – 6491 [6646 – 6649]
Ferguson, M. J. (C) 2005 – 2008 [2041 – 2044], 3603 – 3606 [3669 – 3672]
Feringa, B. L.
– Achiral Ligands Dramatically Enhance Rate and Enantioselectivity in the Rh/Phosphoramidite-Catalyzed Hydrogenation of α,β-Disubstituted Unsaturated Acids (C) 4209 – 4212 [4281 – 4284] DOI: 10.1002/anie.200500784
– Copper-Catalyzed Enantioselective Conjugate Addition of Grignard Reagents to α,β-Unsaturated Esters (C) 2752 – 2756 [2812 – 2816] DOI: 10.1002/anie.200500317
– DNA-Based Asymmetric Catalysis (C) 3230 – 3232 [3294 – 3296] DOI: 10.1002/anie.200500298
– Light-Driven Dynamic Pattern Formation (C) 2373 – 2376 [2425 – 2428] DOI: 10.1002/anie.200462500
Fernández, A. B. (C) 2370 – 2373 [2422 – 2425]
Fernández, I. (C) 4397 – 4400 [4471 – 4474]
Fernández-Alonso, M. del C. (C) 2360 – 2364 [2412 – 2416]
Fernández-Rodríguez, M. A. (C) 5875 – 5878 [6025 – 6028]
Fernández Sanz, J. (C) 3429 – 3432 [3495 – 3498]
Ferraris, J. P. (C) 6207 – 6210 [6363 – 6366]
Ferré, N. (C) 6077 – 6081 [6231 – 6235]
Ferrer, M.
– Conversion of a Carboxylesterase into a Triacylglycerol Lipase by a Random Mutation (C) 7553 – 7557 [7725 – 7729] DOI: 10.1002/anie.200502461
Ferretti, L. (C) 1816 – 1820 [1850 – 1854]
Ferrigno, R. (C) 5682 – 5686 [5828 – 5832]
Fery, A. (C) 2420 – 2426 [2472 – 2478]
Fessner, W.-D.
– Reversible Substrate Anchoring: NC-SPOS as a Sustainable Approach to Solid-Supported Organic Synthesis (C) 4724 – 4728 [4802 – 4806] DOI: 10.1002/anie.200462278
Feussner, I. (C) 158 – 161 [161 – 164]
Fialkowski, M. (C) 7263 – 7269 [7429 – 7435]

 © 2005 Wiley-VCH Verlag GmbH & Co. KGaA, Weinheim

Fiebig, T.
– Real-Time Spectroscopic and Chemical Probing of Reductive Electron Transfer in DNA
(C) 1636 – 1639 [1662 – 1666]
DOI: 10.1002/anie.200462592
Fiedler, J. (C) 2103 – 2106 [2140 – 2143], 5655 – 5658 [5800 – 5803]
Fielenbach, D. (C) 794 – 797 [804 – 807], 3703 – 3706 [3769 – 3772]
Fierro-Gonzalez, J. C. (C) 4778 – 4781 [4856 – 4859]
Figueroa, J. S. (C) 2560 – 2563 [2616 – 2619], 4592 – 4596 [4668 – 4672]
Filippou, A. C.
– Ge_2 Trapped by Triple Bonds between Two Metal Centers: The Germylidyne Complexes *trans,trans*-[Cl(depe)$_2$M≡Ge–Ge≡M(depe)$_2$Cl] (M = Mo, W) and Bonding Analyses of the M≡Ge–Ge≡M Chain
(C) 5979 – 5985 [6133 – 6139]
DOI: 10.1002/anie.200501968
Fingerhut, B. (C) 5972 – 5974 [6126 – 6128]
Fini, F. (C) 7975 – 7978 [8189 – 8192]
Fink, H.-P.
– Cellulose: Fascinating Biopolymer and Sustainable Raw Material
(R) 3358 – 3393 [3422 – 3458]
DOI: 10.1002/anie.200460587
Fink, K.
– Active Sites on Oxide Surfaces: ZnO-Catalyzed Synthesis of Methanol from CO and H_2
(C) 2790 – 2794 [2850 – 2854]
DOI: 10.1002/anie.200462374
Fink, T. (C) 1504 – 1508 [1528 – 1532]
Finn, M. G.
– Head-to-Tail Peptide Cyclodimerization by Copper-Catalyzed Azide – Alkyne Cycloaddition
(C) 2215 – 2220 [2255 – 2260]
DOI: 10.1002/anie.200461656
– Mechanism of the Ligand-Free Cu^I-Catalyzed Azide – Alkyne Cycloaddition Reaction
(C) 2210 – 2215 [2250 – 2255]
DOI: 10.1002/anie.200461496
Finn, M. G. (C) 3275 – 3279 [3339 – 3343]
Fischer, A. (C) 3906 – 3909 [3974 – 3977]
Fischer, C. (C) 1184 – 1188 [1208 – 1212]
Fischer, Gerd (C) 7884 – 7887 [8096 – 8099]
Fischer, Gunter
– The Architecture of Protein – Ligand Binding Sites Revealed through Template-Assisted Intramolecular Peptide – Peptide Interactions
(C) 1408 – 1412 [1432 – 1437]
DOI: 10.1002/anie.200460991
Fischer, P. (C) 6231 – 6234 [6387 – 6390]
Fischer, R. (C) 1560 – 1563 [1584 – 1588]
Fischer, R. A.
– C–H Activated Isomers of [M(AlCp*)$_5$] (M = Fe, Ru)
(C) 2943 – 2946 [3003 – 3007]
DOI: 10.1002/anie.200462834
– Metal@MOF: Loading of Highly Porous Coordination Polymers Host Lattices by Metal Organic Chemical Vapor Deposition
(C) 6237 – 6241 [6394 – 6397]
DOI: 10.1002/anie.200462515
Fischer, R. W. (C) 6237 – 6241 [6394 – 6397]
Fischlechner, M. (C) 2892 – 2895 [2952 – 2955]
Fish, S. (C) 2694 – 2700 [2754 – 2760]
Fisher, K. D. (C) 1057 – 1061 [1081 – 1085]
Fishwick, C. W. G.
– A De Novo Designed Inhibitor of D-Ala – D-Ala Ligase from *E. coli*
(C) 6403 – 6406 [6561 – 6564]
DOI: 10.1002/anie.200501662
Fishwick, C. W. G. (C) 1965 – 1968 [2001 – 2004], 7570 – 7574 [7742 – 7746]
Fjellvåg, H. (C) 6354 – 6358 [6512 – 6516]
Flasche, W. (C) 5635 – 5639 [5779 – 5783]
Flicker, S. (C) 815 – 819 [826 – 830]
Flomenbom, O. (C) 560 – 564 [566 – 570]
Flood, A. H. (C) 7035 – 7039 [7197 – 7201]
Floquet, S. (C) 7954 – 7958 [8168 – 8172]
Floreancig, P. E.
– Total Synthesis of (+)-Dactylolide through an Efficient Sequential Peterson Olefination and Prins Cyclization Reaction
(C) 3485 – 3488 [3551 – 3554]
DOI: 10.1002/anie.200500564
Florence, G. J. (C) 1130 – 1133 [1154 – 1157]
Flörke, U. (C) 975 – 977 [997 – 999]
Foguet-Albiol, D. (C) 897 – 901 [919 – 923]
Fokin, A. A.
– The Protonation of Cubane Revisited
(C) 146 – 149 [148 – 152]
DOI: 10.1002/anie.200461042
Fokin, V. V.
– Mechanism of the Ligand-Free Cu^I-Catalyzed Azide – Alkyne Cycloaddition Reaction
(C) 2210 – 2215 [2250 – 2255]
DOI: 10.1002/anie.200461496
Fokin, V. V. (C) 3275 – 3279 [3339 – 3343]
Foley, S. (C) 110 – 112 [112 – 114]
Fontaine, P. (C) 2749 – 2752 [2809 – 2812]
Fontecave, M.
– DNA Detection through Signal Amplification by Using NADH:Flavin Oxidoreductase and Oligonucleotide – Flavin Conjugates as Cofactors
(C) 2764 – 2767 [2824 – 2827]
DOI: 10.1002/anie.200461145
Fontes, R. (C) 3427 – 3429 [3493 – 3495]
Ford, W. (C) 2015 – 2018 [2051 – 2054]
Forlani, L.
– Evidence for Carbon – Carbon Meisenheimer – Wheland Complexes between Superelectrophilic and Supernucleophilic Carbon Reagents
(C) 3285 – 3289 [3349 – 3353]
DOI: 10.1002/anie.200500238
Forniés, J.
– Reversible Transformation of Two Diphenylphosphanido Ligands into the Neutral Tetraphenyldiphosphane Ligand
(C) 2407 – 2410 [2459 – 2462]
DOI: 10.1002/anie.200462498
Forster, P. M. (C) 7608 – 7611 [7780 – 7784]
Forsyth, M. (C) 313 – 316 [317 – 320]
Fortuño, C. (C) 2407 – 2410 [2459 – 2462]
Fossi, M. (C) 6151 – 6154 [6307 – 6310]
Fournié-Zaluski, M.-C. (C) 4058 – 4061 [4126 – 4129]
Fox, A. R. (C) 7729 – 7733 [7907 – 7911]
Fox, D. J. (C) 1870 – 1873 Corrigendum: 2471 [1904 – 1907 Corrigendum: 2525]
Foxman, B. M. (C) 105 – 108 [107 – 110], 7420 – 7424 [7586 – 7590]
Fraga, H. (C) 3427 – 3429 [3493 – 3495]
Fragassi, M. (C) 278 – 281 [282 – 285]
Fraile, J. M. (C) 458 – 461 [462 – 465]
Francisco, J. S.
– The SF_5O_x Radicals, $x = 0 – 3$
(C) 253 – 257 [258 – 261]
DOI: 10.1002/anie.200461235
Franck, E. U. (R) 2672 – 2692 [2730 – 2752]
Franckevicius, V. (C) 1870 – 1873 Corrigendum: 2471 [1904 – 1907 Corrigendum: 2525]
Frantz, R. (C) 5060 – 5064 [5188 – 5192]
Franz, A. (C) 1564 – 1567 [1588 – 1592]
Fraser-Reid, B.
– Synthesis of a Lipomannan Component of the Cell-Wall Complex of *Mycobacterium tuberculosis* Is Based on Paulsen's Concept of Donor/Acceptor "Match"
(C) 5894 – 5898 [6044 – 6048]
DOI: 10.1002/anie.200500505
Fratesi, G. (C) 6142 – 6145 [6298 – 6301]
Frech, C. M. (C) 1709 – 1711 [1737 – 1739]
Fréchet, J. M. J.
– One-Pot Reaction Cascades Using Star Polymers with Core-Confined Catalysts
(C) 6384 – 6387 [6542 – 6545]
DOI: 10.1002/anie.200502095
Frederiksen, M. U. (C) 308 – 310 [312 – 314], (R) 6630 – 6666 [6788 – 6825]
Freixa, Z.
– Activity of SPANphos Rhodium Dimers in Methanol Carbonylation
(C) 4385 – 4388 [4459 – 4462]
DOI: 10.1002/anie.200500226
Frenking, G.
– Aromatic Boron Wheels with More than One Carbon Atom in the Center: C_2B_8, $C_3B_9^{3+}$, and $C_5B_{11}^{+}$
(C) 1078 – 1082 [1102 – 1106]
DOI: 10.1002/anie.200461970
– Direct Estimate of the Conjugative and Hyperconjugative Stabilization in Diynes, Dienes, and Related Compounds
(C) 3617 – 3620 [3683 – 3686]
DOI: 10.1002/anie.200500452
Frenking, G. (C) 2943 – 2946 [3003 – 3007]
Freudenberger, J. C. (C) 423 – 426 [427 – 430]
Freund, H.-J. (C) 629 – 631 [635 – 637], 7601 – 7605 [7773 – 7777]
Frey, W. (C) 2798 – 2801 [2858 – 2861]
Fridman, M. (C) 447 – 452 [451 – 456]
Friedman, S. H.
– Light-Activated RNA Interference
(C) 1328 – 1332 [1352 – 1356]
DOI: 10.1002/anie.200461458
Frieman, B. A. (C) 6345 – 6348 [6503 – 6506]
Frigoli, M. (C) 5048 – 5052 [5176 – 5180]
Frisch, A. C. (M) 674 – 688 [680 – 695]
Frisch, K. (C) 6058 – 6063 [6212 – 6217]
Frish, L. (R) 520 – 554 [524 – 560]
Froelich, J. M. (C) 2694 – 2700 [2754 – 2760]
Fröhlich, R. (C) 5492 – 5496 [5629 – 5632]
Frohn, H. J. (C) 406 – 409 [410 – 413]
Fronczek, F. R. (C) 3047 – 3050 [3107 – 3110]
Fructos, M. R. (C) 5284 – 5288 [5418 – 5422]
Fruk, L. (C) 2603 – 2606 [2659 – 2662]
Frutos, L. M. (C) 5828 – 5830 [5978 – 5980]
Fry, C. G. (C) 786 – 790 [796 – 800]
Fryer, B. J. (C) 2135 – 2139 [2173 – 2177]
Fu, D. (C) 5520 – 5523 [5656 – 5659]
Fu, G. C.
– Catalytic Asymmetric Couplings of Ketenes with Aldehydes To Generate Enol Esters
(C) 4606 – 4608 [4682 – 4684]
DOI: 10.1002/anie.200501434
– Nucleophile-Catalyzed Asymmetric Acylations of Silyl Ketene Imines: Application to the Enantioselective Synthesis of Verapamil
(C) 949 – 952 [971 – 974]
DOI: 10.1002/anie.200461886

 © 2005 Wiley-VCH Verlag GmbH & Co. KGaA, Weinheim

Fu, G. D. (C) 1104 – 1107 [1128 – 1131]
Fu, L.-M. (C) 747 – 750 [757 – 760]
Fu, Y. (C) 4731 – 4735 [4809 – 4813]
Fuchigami, T.
– An Electrolytic System That Uses Solid-Supported Bases for In Situ Generation of a Supporting Electrolyte from Acetic Acid Solvent
(C) 4760 – 4763 [4838 – 4841]
DOI: 10.1002/anie.200500977
Fuchs, A. H.
– Water Condensation in Hydrophobic Nanopores
(C) 5310 – 5313 [5444 – 5447]
DOI: 10.1002/anie.200501250
Fuhr, O. (C) 5242 – 5246 [5376 – 5381]
Fujii, E. (C) 5857 – 5860 [6007 – 6010]
Fujii, M.
– Real-Time Observation of Ionization-Induced Hydrophobic → Hydrophilic Switching
(C) 6149 – 6151 [6305 – 6307]
DOI: 10.1002/anie.200501430
Fujii, S. (C) 4795 – 4798 [4873 – 4876]
Fujioka, H.
– A Double Iodoetherification of σ-Symmetric Diene Acetals for Installing Four Stereogenic Centers in a Single Operation: Short Asymmetric Total Synthesis of Rubrenolide
(C) 734 – 737 [744 – 747]
DOI: 10.1002/anie.200461584
Fujioka, H. (C) 5857 – 5860 [6007 – 6010]
Fujisawa, Y. (C) 596 – 598 [602 – 604]
Fujita, K.
– Synthesis of a Cycloallin Derivative from β-Cyclodextrin: Heptakis(2,3-dideoxy-2,3-epithio)-β-cycloallin
(C) 4201 – 4204 [4273 – 4276]
DOI: 10.1002/anie.200462678
Fujita, M.
– A Two-in-One Crystal: Uptake of Two Different Guests into Two Distinct Channels of a Biporous Coordination Network
(C) 1962 – 1964 [1998 – 2000]
DOI: 10.1002/anie.200462201
– Discrete Stacking of Large Aromatic Molecules within Organic-Pillared Coordination Cages
(C) 1810 – 1813 [1844 – 1847]
DOI: 10.1002/anie.200462171
– In Situ Observation of a Reversible Single-Crystal-to-Single-Crystal Apical-Ligand-Exchange Reaction in a Hydrogen-Bonded 2D Coordination Network
(C) 2151 – 2154 [2189 – 2192]
DOI: 10.1002/anie.200462214
– pH-Switchable Through-Space Interaction of Organic Radicals within a Self-Assembled Coordination Cage
(C) 5322 – 5325 [5456 – 5459]
DOI: 10.1002/anie.200501568
– Ultramacrocyclization through Reversible Catenation
(C) 4896 – 4899 [4974 – 4977]
DOI: 10.1002/anie.200501559
Fujita, N. (C) 1257 – 1261 [1283 – 1287]
Fujita, T. (C) 5523 – 5526 [5659 – 5662]
Fujiwara, H. (C) 1951 – 1954 [1987 – 1990]
Fukin, G. K. (C) 2767 – 2771 [2827 – 2831]
Fukudome, M. (C) 4201 – 4204 [4273 – 4276]
Fukui, Kôichi (C) 5459 – 5464 [5595 – 5600]
Fukui, Kozo (C) 7277 – 7280 [7443 – 7446]
Fukushima, T. (C) 2410 – 2413 [2462 – 2465]
Fukuyama, T. (C) 1075 – 1078 [1099 – 1102]
Fulford, S. Y. (C) 1706 – 1708 [1734 – 1736]
Fumoto, M. (C) 91 – 96 [93 – 98], 2534 – 2537 [2590 – 2593]
Funabiki, T. (C) 7104 – 7106 [7266 – 7268]
Funeriu, D.-P.
– A Feast of Supramolecular Chemistry
(T) 6442 – 6444 [6600 – 6602]
DOI: 10.1002/anie.200503161
Fung, M. K. (C) 4749 – 4753 [4827 – 4831]
Fung, Y. M. E. (C) 6399 – 6403 [6557 – 6561]
Fürstner, A.
– Chasing a Phantom by Total Synthesis: The Butylcycloheptylprodigiosin Case
(C) 2777 – 2781 [2837 – 2841]
DOI: 10.1002/anie.200462215
– Concise and Practical Synthesis of Latrunculin A by Ring-Closing Enyne – Yne Metathesis
(C) 3462 – 3466 [3528 – 3532]
DOI: 10.1002/anie.200500390
Fürtig, B. (C) 2600 – 2603 [2656 – 2659]
Furukawa, K. (C) 6899 – 6901 [7059 – 7061]
Furukawa, S. (C) 2700 – 2704 [2760 – 2764]
Furusho, Y.
– A Modular Strategy to Artificial Double Helices
(C) 3867 – 3870 [3935 – 3938]
DOI: 10.1002/anie.200501028
Futatsugi, K. (C) 1484 – 1487 [1508 – 1511], (R) 1924 – 1942 [1958 – 1977]

Gabriel, S. (C) 5505 – 5509 [5641 – 5645]
Gade, L. H.
– C_3 Chirality in Polymerization Catalysis: A Highly Active Dicationic Scandium(III) Catalyst for the Isoselective Polymerization of 1-Hexene
(C) 1668 – 1671 [1696 – 1699]
DOI: 10.1002/anie.200462804
– Controlling Molecular Assembly in Two Dimensions: The Concentration Dependence of Thermally Induced 2D Aggregation of Molecules on a Metal Surface
(C) 7394 – 7398 [7560 – 7564]
DOI: 10.1002/anie.200502316
Gagnon, J. E. (C) 2135 – 2139 [2173 – 2177]
Gai, H. (C) 5107 – 5110 [5237 – 5240]
Gai, X. (C) 7570 – 7574 [7742 – 7746]
Gaillard, C. (C) 4957 – 4960 [5037 – 5040]
Gaisberger, R. (C) 4700 – 4704 [4778 – 4782]
Gaisser, S. (C) 4757 – 4760 [4835 – 4838]
Galan, M. C. (C) 4596 – 4599 [4672 – 4675]
Galardon, E. (C) 6162 – 6165 [6318 – 6321]
Galaverna, G. (C) 5126 – 5130 [5256 – 5260]
Gale, J. D. (C) 1213 – 1217 [1239 – 1243]
Gale, P. A.
– Calix[4]pyrrole: An Old yet New Ion-Pair Receptor
(C) 2537 – 2542 [2593 – 2598]
DOI: 10.1002/anie.200462945
Galet, A. (C) 4069 – 4073 [4137 – 4141]
Galindo, A.
– Supramolecular Interactions as Determining Factors of the Geometry of Metallic Building Blocks: Tetracarboxylate Dimanganese Species
(C) 3429 – 3432 [3495 – 3498]
DOI: 10.1002/anie.200462965
– Theoretical and Synthetic Studies on $[Zn_2(\eta^5\text{-}C_5Me_5)_2]$: Analysis of the Zn–Zn Bonding Interaction
(C) 1244 – 1247 [1270 – 1273]
DOI: 10.1002/anie.200462175
Galindo, F.
– Synthetic Macrocyclic Peptidomimetics as Tunable pH Probes for the Fluorescence Imaging of Acidic Organelles in Live Cells
(C) 6504 – 6508 [6662 – 6666]
DOI: 10.1002/anie.200501920
Galka, C. H. (C) 7394 – 7398 [7560 – 7564]
Gallimore, A. R. (C) 7075 – 7078 [7237 – 7240]
Gallucci, J. C. (C) 6537 – 6540 [6695 – 6698]
Gamez, P. (C) 3585 – 3587 [3651 – 3653]
Gan, Z. (C) 1366 – 1368 [1390 – 1392]
Gandelman, M. (C) 2393 – 2397 [2445 – 2449]
Gandhi, B. A. (C) 5269 – 5272 [5403 – 5406]
Gandon, V. (C) 7114 – 7118 [7276 – 7280]
Ganesan, R. (C) 6557 – 6560 [6715 – 6718]
Gao, F. (C) 6859 – 6862 [7019 – 7022]
Gao, J. (C) 3118 – 3122 [3178 – 3182]
Gao, M.
– Preparation of Water-Soluble Magnetite Nanocrystals from Hydrated Ferric Salts in 2-Pyrrolidone: Mechanism Leading to Fe_3O_4
(C) 123 – 126 [125 – 128]
DOI: 10.1002/anie.200460715
Gao, S.
– Two Molecular Tapes Consisting of Serial or Parallel Azido-Bridged Eight-Membered Copper Rings
(C) 5841 – 5846 [5991 – 5996]
DOI: 10.1002/anie.200501327
Gao, S. (C) 4197 – 4201 [4269 – 4273]
Gao, W. (C) 1687 – 1689 [1715 – 1717]
Gaponik, N. (C) 5997 – 6001 [6151 – 6155]
Garcia, C. B. W. (C) 1226 – 1229 [1252 – 1255]
García, F. (C) 3456 – 3459 [3522 – 3525], 5729 – 5733 [5875 – 5879]
García, G. (C) 102 – 105 [104 – 107]
García, H. (C) 4066 – 4069 [4134 – 4137]
García, J. I.
– Asymmetric versus C_2-Symmetric Ligands: Origin of the Enantioselectivity in Ruthenium – Pybox-Catalyzed Cyclopropanation Reactions
(C) 458 – 461 [462 – 465]
DOI: 10.1002/anie.200461418
García, J. M. (C) 6187 – 6190 [6343 – 6346]
Garcia-Bennett, A. E.
– Synthesis of Mesocage Structures by Kinetic Control of Self-Assembly in Anionic Surfactants
(C) 5317 – 5322 [5451 – 5456]
DOI: 10.1002/anie.200500113
García-García, P. (C) 5875 – 5878 [6025 – 6028]
García Segovia, A. B. (C) 6231 – 6234 [6387 – 6390]
Garneau-Tsodikova, S. (R) 7342 – 7372 [7508 – 7539]
Garner, C. D. (C) 5314 – 5317 [5448 – 5451]
Garner, J. (R) 5384 – 5427 [5518 – 5563]
Garozzo, D. (C) 4892 – 4896 [4970 – 4974]
Garric, J. (C) 1954 – 1958 [1990 – 1994]
Garrido-Hernandez, H. (C) 765 – 769 [775 – 779]
Garstecki, P. (C) 724 – 728 Corrigendum: 3799 [734 – 738 Corrigendum: 3865]
Gast, K. (C) 5252 – 5255 [5386 – 5389]

Gates, B. C. (C) 4778 – 4781 [4856 – 4859]
Gatteschi, D.
– Molecular Engineering for Single-Chain-Magnet Behavior in a One-Dimensional Dysprosium – Nitronyl Nitroxide Compound
(C) 5817 – 5821 [5967 – 5971]
DOI: 10.1002/anie.200500464
Gatto, G. J., Jr. (R) 7342 – 7372 [7508 – 7539]
Gattuso, G. (C) 4892 – 4896 [4970 – 4974]
Gaunt, M. J.
– Palladium-Catalyzed Intermolecular Alkenylation of Indoles by Solvent-Controlled Regioselective C–H Functionalization
(C) 3125 – 3129 [3185 – 3189]
DOI: 10.1002/anie.200500468
Gaunt, M. J. (C) 5433 – 5438 [5569 – 5574]
Gauntlett, C. (C) 3125 – 3129 [3185 – 3189]
Gautier, R. (C) 1363 – 1365 [1387 – 1389]
Gavezzotti, A.
– Molecular Recognition in Organic Crystals: Directed Intermolecular Bonds or Nonlocalized Bonding?
(R) 1766 – 1787 [1796 – 1819]
DOI: 10.1002/anie.200460157
Gavrilovic, J. (C) 6504 – 6508 [6662 – 6666]
Ge, C. (C) 7742 – 7745 [7920 – 7923]
Ge, X. (C) 2563 – 2568 [2619 – 2624]
Geacintov, N. E. (C) 5057 – 5060 [5185 – 5188]
Gedanken, A.
– Rapid Synthesis in Ionic Liquids of Room-Temperature-Conducting Solid Microsilica Spheres
(C) 6560 – 6563 [6718 – 6721]
DOI: 10.1002/anie.200501446
Gehring, T. (H) 5776 – 5777 [5922 – 5924]
Gehrke, N. (C) 6004 – 6009 [6158 – 6163]
Geib, S. J. (C) 2508 – 2512 [2564 – 2568]
Geier, J.
– In-Plane Bishomoaromaticity in Tetranitrogen Dianions: Solid-State, Solution, and Electronic Structures
(C) 2433 – 2437 [2485 – 2490]
DOI: 10.1002/anie.200462126
Geiseler, G. (C) 1643 – 1646 Corrigendum: 2471 [1670 – 1673 Corrigendum: 2525]
Geissbuehler, I. (C) 1388 – 1392 [1412 – 1416]
Geißelmann, A. (C) 924 – 927 [946 – 949]
Geißler, D. (C) 1195 – 1198 [1219 – 1223], 7887 – 7891 [8099 – 8104]
Geissler, M. (C) 3596 – 3600 [3662 – 3666]
Gelb, M. (C) 4903 – 4906 [4981 – 4984]
Geldbach, T. J. (C) 5720 – 5725 [5866 – 5871]
Gemel, C. (C) 2943 – 2946 [3003 – 3007]
Genêt, J.-P.
– An Ir^{I}-Catalyzed *exo*-Selective Tandem Cycloisomerization/Hydroalkoxylation of Bis-Homopropargylic Alcohols at Room Temperature
(C) 4949 – 4953 [5029 – 5033]
DOI: 10.1002/anie.200501150
Genin, E. (C) 4949 – 4953 [5029 – 5033]
Geninatti Crich, S. (C) 1813 – 1815 [1847 – 1849]
Gennari, C.
– A Formal Total Synthesis of Eleutherobin Through an Unprecedented Kinetically Controlled Ring-Closing-Metathesis Reaction of a Densely Functionalized Diene
(C) 588 – 591 [594 – 597]
DOI: 10.1002/anie.200461767
Gennaro, R. (C) 6358 – 6362 [6516 – 6520]
Georgi, P. (C) 3306 – 3309 [3371 – 3374]
Gerbeleu, N. V.
– Azine-Bridged Octanuclear Copper(II) Complexes Assembled with a One-Stranded Ditopic Thiocarbohydrazone Ligand
(C) 7938 – 7942 [8152 – 8156]
DOI: 10.1002/anie.200501807
Gerber, F. (C) 2749 – 2752 [2809 – 2812]
Gerber, S. (C) 7787 – 7790 [7965 – 7968]
Ghadiri, M. R.
– Recognizing a Single Base in an Individual DNA Strand: A Step Toward DNA Sequencing in Nanopores
(C) 1401 – 1404 [1425 – 1428]
DOI: 10.1002/anie.200462114
Ghiggino, K. P.
– Star-Shaped Light-Harvesting Polymers Incorporating an Energy Cascade
(C) 4368 – 4372 [4442 – 4446]
DOI: 10.1002/anie.200462796
Ghosh, Suhrit (C) 5441 – 5447 [5577 – 5583]
Ghosh, Sundargopal
– Borane Mimics of Classic Organometallic Compounds: $[(Cp^*Ru)B_8H_{14}(RuCp^*)]^{0,+}$, Isoelectronic Analogues of Dinuclear Pentalene Complexes
(C) 6568 – 6571 [6726 – 6729]
DOI: 10.1002/anie.200502212
Ghosh, Sundargopal (C) 2916 – 2918 [2976 – 2978]
Giannis, A.
– Development and Biological Evaluation of Acyl Protein Thioesterase 1 (APT1) Inhibitors
(C) 4975 – 4980 [5055 – 5060]
DOI: 10.1002/anie.200462625
– Epigenetics—An Epicenter of Gene Regulation: Histones and Histone-Modifying Enzymes
(R) 3186 – 3216 [3248 – 3280]
DOI: 10.1002/anie.200461346
Giansante, C. (C) 4574 – 4578 [4650 – 4654]
Giastas, P. (C) 5097 – 5100 [5227 – 5230]
Gibson, D.
– Structure and Unique Interactions with DNA of a Cationic *Trans*-Platinum Complex with the Nonplanar Bicyclic Piperidinopiperidine Ligand
(C) 2885 – 2887 [2945 – 2947]
DOI: 10.1002/anie.200462389
Gibson, S. E.
– Introduction of Multiple Elements of Chirality around an Aromatic Core and an Approach to Enantiomerically Pure C_3-Symmetric Ligands
(C) 3432 – 3435 [3498 – 3501]
DOI: 10.1002/anie.200500020
– The Intermolecular Pauson – Khand Reaction
(R) 3022 – 3037 [3082 – 3097]
DOI: 10.1002/anie.200462235
Giernoth, R. (C) 5485 – 5488 [5621 – 5624]
Giersig, M. (C) 4375 – 4378 [4449 – 4452]
Giese, B.
– Mechanism of the Norrish – Yang Photocyclization Reaction of an Alanine Derivative in the Singlet State: Origin of the Chiral-Memory Effect
(C) 2390 – 2393 [2442 – 2445]
DOI: 10.1002/anie.200461898
– Multistep Electron Transfer in Oligopeptides: Direct Observation of Radical Cation Intermediates
(C) 4073 – 4075 [4141 – 4143]
DOI: 10.1002/anie.200500391
Giese, S. (C) 6546 – 6549 [6704 – 6707]
Gil, C. (R) 5188 – 5240 [5320 – 5374]
Gil, M. J. (C) 458 – 461 [462 – 465]
Gilardi, R. D. (C) 7089 – 7094 [7251 – 7256]
Gilardoni, F. (C) 7764 – 7767 [7942 – 7945]
Gilbert, B. (C) 5505 – 5509 [5641 – 5645]
Gilbert, B. C. (C) 3720 – 3722 [3786 – 3788]
Gilch, P.
– The Photochemistry of *o*-Nitrobenzaldehyde as Seen by Femtosecond Vibrational Spectroscopy
(C) 7901 – 7904 [8114 – 8118]
DOI: 10.1002/anie.200501642
Giles, I. D. (C) 3129 – 3132 [3189 – 3192]
Gill, R. (C) 4554 – 4557 [4630 – 4633]
Gillan, R. (C) 1121 – 1125 [1145 – 1149]
Giller, K. (C) 2089 – 2092 [2125 – 2129]
Gillon, B. (C) 2711 – 2715 [2771 – 2775]
Gimbert, Y.
– Lewis Base Promoters in the Pauson – Khand Reaction: A Different Scenario
(C) 5717 – 5719 [5863 – 5865]
DOI: 10.1002/anie.200500955
Gin, M. S.
– A Highly Active Anion-Selective Aminocyclodextrin Ion Channel
(C) 7584 – 7587 [7756 – 7759]
DOI: 10.1002/anie.200501625
Giordano, L. (C) 4753 – 4757 [4831 – 4835]
Giorgi, M. (C) 6162 – 6165 [6318 – 6321]
Giovannelli, J. L. (C) 5141 – 5144 [5271 – 5274]
Giri, R. (C) 2112 – 2115 [2150 – 2153], 7420 – 7424 [7586 – 7590]
Giri, S. (C) 5038 – 5044 [5166 – 5172]
Gitlin, I. (C) 724 – 728 Corrigendum: 3799 [734 – 738 Corrigendum: 3865]
Giuliano, B. M. (C) 603 – 606 [609 – 612]
Gjoni, M. (C) 4957 – 4960 [5037 – 5040]
Gladiali, S. (C) 6214 – 6219 [6370 – 6375]
Gladysz, J. A.
– "Catalyst-on-a-Tape"—Teflon: A New Delivery and Recovery Method for Homogeneous Fluorous Catalysts
(C) 4095 – 4097 [4164 – 4167]
DOI: 10.1002/anie.200500237
– Fluorous Chemistry and Technology—A Symposium Showcases Ever-Broadening Frontiers
(T) 5766 – 5768 [5912 – 5914]
DOI: 10.1002/anie.200502639
Glasser, G. (C) 262 – 265 [267 – 270]
Glenn, M. P. (C) 4903 – 4906 [4981 – 4984]
Glieder, A.
– Carving the Active Site of Almond *R*-HNL for Increased Enantioselectivity
(C) 4700 – 4704 [4778 – 4782]
DOI: 10.1002/anie.200500435
Glöckner, F. O. (C) 6381 – 6384 [6539 – 6542]
Gnanou, Y.
– Tri- and Tetracarbanionic Initiators by a Lithium/Halide Exchange Reaction: Application to Star-Polymer Synthesis
(C) 284 – 287 [288 – 291]
DOI: 10.1002/anie.200461056
Göbel, C. (C) 158 – 161 [161 – 164]
Goddard, R. (C) 412 – 415 [416 – 419]
Godfrey, C. R. A. (C) 3125 – 3129 [3185 – 3189]
Godin, B. (C) 3072 – 3075 [3132 – 3135]
Goedel, W. A.
– The Preparation of Mesoscopic Rings in Colloidal Crystal Templates
(C) 2084 – 2088 [2121 – 2125]
DOI: 10.1002/anie.200460584

 © 2005 Wiley-VCH Verlag GmbH & Co. KGaA, Weinheim

Goeke, A.
– Alkyl Aluminum Halide Promoted Intramolecular Cyclization of ω-Allyl-cycloalk-2-enones: Access to Bridged Bi- and Tricyclic Compounds
(C) 99 – 101 [101 – 103]
DOI: 10.1002/anie.200461207
Goforth, A. M. (C) 6673 – 6677 [6831 – 6835]
Gogoll, A.
– Ligand-Induced Formation of an Adamantanoid Hexanuclear (π-Allyl)Pd^{II}(μ_3-Hydroxo) Cluster Stacked as Hydrogen-Bonded Double Strands
(C) 4729 – 4731 [4807 – 4809]
DOI: 10.1002/anie.200500750
Goh, S. H. (C) 4782 – 4785 [4860 – 4863]
Gohda, K. (C) 6180 – 6183 [6336 – 6339]
Gohlke, S. (C) 1647 – 1650 [1673 – 1676]
Goicoechea, J. M. (C) 4026 – 4028 [4094 – 4096]
Golberg, D. (C) 576 – 579 [582 – 585], 2140 – 2144 [2178 – 2182], 7929 – 7932 [8143 – 8146], 7932 – 7935 [8146 – 8149]
Goldmann, M. (C) 2749 – 2752 [2809 – 2812]
Goldsmith, P. J. (C) 2232 – 2234 [2272 – 2274], 2235 – 2237 [2275 – 2277]
Gölitz, P.
– Editorial: Open Access and *Angewandte Chemie*
4 – 7 [4 – 7]
DOI: 10.1002/anie.200462726
– Editorial: Who Is Going to Read all This?
5538 – 5541 [5674 – 5677]
DOI: 10.1002/anie.200502730
Gologan, B. (C) 913 – 916 [935 – 938]
Golyshin, P. N. (C) 7553 – 7557 [7725 – 7729]
Gomez-Segura, J. (C) 888 – 892 [910 – 914]
Gong, B. Corrigendum: 1907
Gong, B.
– Template-Assisted Cross Olefin Metathesis
(C) 1352 – 1356 [1376 – 1380]
DOI: 10.1002/anie.200461777
Gong, H. (C) 7069 – 7071 [7231 – 7233]
Gong, X.
– Experimental and Theoretical Investigation of the Electronic and Geometrical Structures of the Au_{32} Cluster
(C) 7119 – 7123 [7281 – 7285]
DOI: 10.1002/anie.200502795
Gonsalvi, L. (C) 2568 – 2572 [2624 – 2628]
González, A. (C) 6187 – 6190 [6343 – 6346]
González, J. M. (C) 5851 – 5854 [6001 – 6004]
González-Bobes, F. (C) 5851 – 5854 [6001 – 6004]
González-Noya, A. M. (C) 4182 – 4187 [4254 – 4259]
Goody, R. S. (C) 7635 – 7639 [7808 – 7812]
Gooßen, L. J.
– Ru-Catalyzed Anti-Markovnikov Addition of Amides to Alkynes: A Regio- and Stereoselective Synthesis of Enamides
(C) 4042 – 4045 [4110 – 4113]
DOI: 10.1002/anie.200462844
Gopalakrishnan, G. (C) 4957 – 4960 [5037 – 5040]
Gorlov, M. (C) 3906 – 3909 [3974 – 3977]
Görls, H. (C) 5255 – 5259 [5389 – 5393]
Görner, W. (C) 7905 – 7909 [8118 – 8122]
Gornitzka, H. (C) 1700 – 1703 [1728 – 1731], 5497 – 5500 [5633 – 5636]
Gösele, U. (C) 6050 – 6054 [6204 – 6208]
Gossage, R. A.
– Hetero-Aggregate Compounds of Aryl and Alkyl Lithium Reagents: A Structurally Intriguing Aspect of Organolithium Chemistry
(M) 1448 – 1454 [1472 – 1478]
DOI: 10.1002/anie.200462103
Goti, A.
– The Discovery of Novel Metal-Induced Reactions of Nitrones: Not Only Electrophiles and Reagents for [3 + 2] Cycloadditions
(H) 7832 – 7835 [8042 – 8045]
DOI: 10.1002/anie.200502640
Goto, Hidekazu (C) 4164 – 4168 [4236 – 4240]
Goto, Hiromasa (C) 4322 – 4328 [4396 – 4402]
Goto, M. (C) 3861 – 3864 [3929 – 3932]
Goto, S. (C) 406 – 409 [410 – 413]
Gotoh, H. (C) 4212 – 4215 [4284 – 4287]
Gougeon, P.
– $Ba_4Mo_{12}S_{18}$: A Superconductor Containing the Dimeric Unit $(Mo_6)_2S_{24}$, the Missing Link between the Mo_6S_{14} and Mo_9S_{17} Units
(C) 1363 – 1365 [1387 – 1389]
DOI: 10.1002/anie.200461255
Goundry, W. R. F. (C) 6715 – 6718 [6873 – 6876]
Gourier, C. (C) 1683 – 1687 [1711 – 1715]
Gouzerh, P.
– Coordination Chemistry of the Hexavacant Tungstophosphate $[H_2P_2W_{12}O_{48}]^{12-}$ with Fe^{III} Ions: Towards Original Structures of Increasing Size and Complexity
(C) 3072 – 3075 [3132 – 3135]
DOI: 10.1002/anie.200463033
Govorov, A. O. (C) 7439 – 7442 [7605 – 7608]
Gower, L. (C) 639 – 644 [645 – 650]
Goze, C. (C) 3694 – 3698 [3760 – 3764]
Grabow, J.-U.
– The Internuclear Potential, Electronic Structure, and Chemical Bond of Tellurium Selenide
(C) 6311 – 6315 [6469 – 6473]
DOI: 10.1002/anie.200501658
Grabow, J.-U. (C) 3840 – 3844 [3908 – 3912]
Grachev, M. (C) 6928 – 6931 [7088 – 7091]
Gradinaru, J. (C) 7764 – 7767 [7942 – 7945]
Grady, M. J. W. (C) 5269 – 5272 [5403 – 5406]
Graham, D. V. (C) 3459 – 3462 [3525 – 3528]
Graham, E. M. (C) 6512 – 6516 [6670 – 6674]
Granja, J. R.
– Methyl-Blocked Dimeric α,γ-Peptide Nanotube Segments: Formation of a Peptide Heterodimer through Backbone – Backbone Interactions
(C) 5710 – 5713 [5856 – 5859]
DOI: 10.1002/anie.200501555
Grapperhaus, C. A.
– Carbon – Sulfur Bond Formation between a Ruthenium-Coordinated Thiyl Radical and Methyl Ketones
(C) 1883 – 1887 [1917 – 1921]
DOI: 10.1002/anie.200462713
Grätzel, M. (C) 6413 – 6417 [6571 – 6575]
Gray, T. G. (C) 1721 – 1724 [1749 – 1752]
Greaves, N. (C) 944 – 946 [966 – 968]
Greco, F. (C) 4061 – 4066 [4129 – 4134]
Green, J. C. (C) 6875 – 6878 [7035 – 7038]
Green, S. J. (C) 4358 – 4361 [4432 – 4435]
Greenberg, B. (C) 2715 – 2719 [2775 – 2779]
Greene, A. E. (C) 5130 – 5133 [5260 – 5263], 5717 – 5719 [5863 – 5865]
Greene, G. L. (C) 5480 – 5483 [5616 – 5619]
Greenfield, M. T. (C) 6766 – 6769 [6924 – 6927]
Gregory, D. H.
– Metallic Nanowires of Nb_3Te_4: A Nanostructured Chalcogenide
(C) 3555 – 3558 [3621 – 3624]
DOI: 10.1002/anie.200500157
Gregory, M. A. (C) 4757 – 4760 [4835 – 4838]
Greim, H.
– Chemicals with Endocrine-Disrupting Potential: A Threat to Human Health?
(E) 5568 – 5574 [5704 – 5711]
DOI: 10.1002/anie.200502138
Grennberg, H. (C) 4729 – 4731 [4807 – 4809]
Gresser, M. J. (R) 5384 – 5427 [5518 – 5563]
Grey, J. K. (C) 6207 – 6210 [6363 – 6366]
Griebenow, N. (C) 3140 – 3144 [3200 – 3204]
Griesinger, C.
– A DMSO-Compatible Orienting Medium: Towards the Investigation of the Stereochemistry of Natural Products
(C) 427 – 429 [431 – 433]
DOI: 10.1002/anie.200461267
– Side-Chain Orientation and Hydrogen-Bonding Imprint Supra-τ_c Motion on the Protein Backbone of Ubiquitin
(C) 7776 – 7778 [7954 – 7956]
DOI: 10.1002/anie.200502573
– The INPHARMA Method: Protein-Mediated Interligand NOEs for Pharmacophore Mapping
(C) 4172 – 4175 [4244 – 4247]
DOI: 10.1002/anie.200500503
Griffin, A. M. E. (C) 6878 – 6881 [7038 – 7041]
Griffin, M. J. (C) 6375 – 6378 [6533 – 6536]
Griffith, C. S. (C) 3038 – 3043 [3098 – 3103]
Griffiths, P. C (C) 4061 – 4066 [4129 – 4134]
Griffiths-Jones, C. M. (C) 2732 – 2737 [2792 – 2797]
Grigg, R.
– Stereoselective Palladium-Catalyzed Four-Component Cascade Synthesis of Pyrrolidinyl-, Pyrazolidinyl-, and Isoxazolidinyl Isoquinolines
(C) 7570 – 7574 [7742 – 7746]
DOI: 10.1002/anie.200502066
Grill, V. (C) 1647 – 1650 [1673 – 1676]
Grimaud, L.
– Phenol Ugi – Smiles Systems: Strategies for the Multicomponent N-Arylation of Primary Amines with Isocyanides, Aldehydes, and Phenols
(C) 7961 – 7964 [8175 – 8178]
DOI: 10.1002/anie.200502636
Grimsdale, A. C. (C) 1520 – 1525 [1544 – 1549], (R) 5592 – 5629 [5732 – 5772]
Grimster, N. P. (C) 3125 – 3129 [3185 – 3189]
Grirrane, A. (C) 3429 – 3432 [3495 – 3498]
Gröger, H. (C) 7787 – 7790 [7965 – 7968]
Grondal, C. (C) 1210 – 1212 [1235 – 1238], 4079 – 4083 [4147 – 4151]
Gross, B. A. (C) 3885 – 3889 [3953 – 3957]
Gross, D. (C) 2537 – 2542 [2593 – 2598]
Grosso, D. (C) 4589 – 4592 [4665 – 4668]
Grote, D. (C) 3289 – 3293 [3353 – 3357]
Grötzl, B. (C) 3609 – 3613 [3675 – 3679]
Groves, J. T.
– Molecular Organization and Signal Transduction at Intermembrane Junctions
(R) 3524 – 3538 [3590 – 3605]
DOI: 10.1002/anie.200461014
Gruaz-Guyon, A.
– A Labeled Neutral Endopeptidase Inhibitor as a Potential Tool for Tumor Diagnosis and Prognosis
(C) 4058 – 4061 [4126 – 4129]
DOI: 10.1002/anie.200500700

 © 2005 Wiley-VCH Verlag GmbH & Co. KGaA, Weinheim

Gruber, K.
– Carving the Active Site of Almond *R*-HNL for Increased Enantioselectivity
(C) 4700 – 4704 [4778 – 4782]
DOI: 10.1002/anie.200500435
Gruber, K. (C) 2284 – 2288 [2324 – 2328]
Grubert, L. (C) 3925 – 3928 [3993 – 3997]
Grubmüller, H. (C) 3394 – 3399 [3460 – 3465]
Grundy, J. (C) 1082 – 1084 [1106 – 1108]
Gruner, M. (C) 6231 – 6234 [6387 – 6390]
Gruner, S. M. (C) 1226 – 1229 [1252 – 1255]
Grunova, E. V. (C) 2767 – 2771 [2827 – 2831]
Grunwaldt, J.-D. (C) 5643 – 5647 [5787 – 5792], 7978 – 7981 [8192 – 8195]
Grupče, O. (C) 1251 – 1254 [1277 – 1280]
Grützmacher, H.
– Diamido Rhodates(1 –)
(C) 6325 – 6329 [6483 – 6487]
DOI: 10.1002/anie.200502036
– Heterolytic Splitting of Hydrogen with Rhodium(I) Amides
(C) 6318 – 6323 [6477 – 6481]
DOI: 10.1002/anie.200500773
Grützmacher, H. (C) 2433 – 2437 [2485 – 2490]
Grzybowski, B. A.
– Architecture and Evolution of Organic Chemistry
(C) 7263 – 7269 [7429 – 7435]
DOI: 10.1002/anie.200502272
Gschösser, S. (C) 2284 – 2288 [2324 – 2328]
Gschwind, R. M.
– Residual Dipolar Couplings—A Valuable NMR Parameter for Small Organic Molecules
(H) 4666 – 4668 [4744 – 4746]
DOI: 10.1002/anie.200500634
Gu, D. (C) 7053 – 7059 [7215 – 7221]
Gu, L.-Q. (C) 1495 – 1499 [1519 – 1523]
Gu, X. (C) 7119 – 7123 [7281 – 7285]
Gu, Z. (C) 5275 – 5278 [5409 – 5412], (M) 7512 – 7517 [7680 – 7685]
Guan, X. (C) 3698 – 3702 [3764 – 3768]
Guan, Z.
– Saccharide – Peptide Hybrid Copolymers as Biomaterials
(C) 6529 – 6533 [6687 – 6691]
DOI: 10.1002/anie.200501944
Guardigli, M. (C) 3694 – 3698 [3760 – 3764]
Güdel, H.-U.
– Effect of Pressure on the Magnetic Anisotropy in the Single-Molecule Magnet Mn_{12}-Acetate: An Inelastic Neutron Scattering Study
(C) 4239 – 4242 [4311 – 4314]
DOI: 10.1002/anie.200500171
Gudipati, V. (C) 6938 – 6940 [7098 – 7100]
Guerra, M. (C) 6030 – 6032 [6184 – 6186]
Guerrero, C. A. (C) 606 – 609 [612 – 615], 3892 – 3895 [3960 – 3963]
Guerrero, L. (C) 7778 – 7782 [7956 – 7960]
Guilard, R.
– Organic – Inorganic Hybrid Sol – Gel Materials Incorporating Functionalized Cobalt(III) Corroles for the Selective Detection of CO
(C) 3103 – 3106 [3163 – 3166]
DOI: 10.1002/anie.200463009
Guillaudeu, S. J. (C) 6384 – 6387 [6542 – 6545]
Guillemin, J.-C.
– Synthesis and Characterization of 2,4-Pentadiynenitrile—A Key Compound in Space Science
(C) 7224 – 7226 [7390 – 7392]
DOI: 10.1002/anie.200502122
Guillou, N. (C) 6488 – 6491 [6646 – 6649]
Guimond, S. (C) 7601 – 7605 [7773 – 7777]
Guldi, D. M.
– Hydrogen-Bonding Motifs in Fullerene Chemistry
(M) 5374 – 5382 [5508 – 5516]
DOI: 10.1002/anie.200500321
– Single-Wall Carbon Nanotubes as Integrative Building Blocks for Solar-Energy Conversion
(C) 2015 – 2018 [2051 – 2054]
DOI: 10.1002/anie.200462416
Gunchenko, P. A. (C) 146 – 149 [148 – 152]
Gunda, P. Corrigendum: 1154
Günther, A. (C) 5447 – 5451 [5583 – 5587]
Guo, C. (C) 105 – 108 [107 – 110], 7420 – 7424 [7586 – 7590]
Guo, H. (C) 4771 – 4774 [4849 – 4852]
Guo, J.-C. (C) 2158 – 2161 [2196 – 2199]
Guo, X.-L. (C) 4242 – 4244 [4314 – 4316]
Guo, Y.
– Probing the Mechanism of the Palladium-Catalyzed Addition of Organoboronic Acids to Allenes in the Presence of AcOH by ESI-FTMS
(C) 4771 – 4774 [4849 – 4852]
DOI: 10.1002/anie.200463101
Guo, Y.-G. (C) 1269 – 1273 [1295 – 1299]
Gupta, Y. K. (C) 2223 – 2225 [2263 – 2265]
Gust, D.
– Molecular AND Logic Gate Based on Electric Dichroism of a Photochromic Dihydroindolizine
(C) 7591 – 7594 [7763 – 7766]
DOI: 10.1002/anie.200502420
Gutierrez, J. J. (C) 6207 – 6210 [6363 – 6366]
Gütlich, P. (C) 7787 – 7790 [7965 – 7968]
Gutowska, A. (C) 3578 – 3582 [3644 – 3648]
Gutowski, M.
– Finding Adiabatically Bound Anions of Guanine through a Combinatorial Computational Approach
(C) 6585 – 6588 [6743 – 6746]
DOI: 10.1002/anie.200501671
Gutowski, M. (C) 3578 – 3582 [3644 – 3648]
Gutta, P. (C) 2719 – 2723 [2779 – 2783]
Guyard-Duhayon, C. (C) 4543 – 4546 [4619 – 4622]
Guzei, I. A. (C) 2771 – 2774 [2831 – 2834], 5269 – 5272 [5403 – 5406]
Guzman, J. (C) 2242 – 2245 [2282 – 2285], 4778 – 4781 [4856 – 4859]

Haas, M. (C) 1084 – 1088 [1108 – 1112]
Haba, K. (C) 716 – 720 [726 – 730]
Haberz, P. (C) 427 – 429 [431 – 433]
Hachikubo, A. (C) 6928 – 6931 [7088 – 7091]
Hackeng, T. M. (C) 5052 – 5057 [5180 – 5185]
Haddleton, D. M.
– Patterning through Controlled Submolecular Motion: Rotaxane-Based Switches and Logic Gates that Function in Solution and Polymer Films
(C) 3062 – 3067 [3122 – 3127]
DOI: 10.1002/anie.200500101
Hafensteiner, B. D. (C) 606 – 609 [612 – 615], 3892 – 3895 [3960 – 3963]
Haga, R. (C) 6553 – 6556 [6711 – 6714]
Hagen, V.
– (Coumarin-4-yl)methyl Esters as Highly Efficient, Ultrafast Phototriggers for Protons and Their Application to Acidifying Membrane Surfaces
(C) 1195 – 1198 [1219 – 1223]
DOI: 10.1002/anie.200461567
– Coumarinylmethyl Esters for Ultrafast Release of High Concentrations of Cyclic Nucleotides upon One- and Two-Photon Photolysis
(C) 7887 – 7891 [8099 – 8104]
DOI: 10.1002/anie.200502411
Hagenbuch, P. (C) 6588 – 6592 [6746 – 6750]
Hagiwara, J. (C) 3744 – 3746 [3810 – 3812]
Hagiwara, Y. (C) 7260 – 7263 [7426 – 7429]
Hahn, F. E.
– Template Synthesis of a Coordinated Tetracarbene Ligand with Crown Ether Topology
(C) 3759 – 3763 [3825 – 3829]
DOI: 10.1002/anie.200462690
Hahn, U. (C) 477 – 480 [481 – 485], 4574 – 4578 [4650 – 4654], 5338 – 5341 [5472 – 5475]
Haiges, R.
– Polyazide Chemistry: The First Binary Group 6 Azides, $Mo(N_3)_6$, $W(N_3)_6$, $[Mo(N_3)_7]^-$, and $[W(N_3)_7]^-$, and the $[NW(N_3)_4]^-$ and $[NMo(N_3)_4]^-$ Ions
(C) 1860 – 1865 [1894 – 1899]
DOI: 10.1002/anie.200462740
Hainard, A. (C) 2600 – 2603 [2656 – 2659]
Hajra, A. (C) 7248 – 7251 [7414 – 7417]
Hålenius, U. (C) 7269 – 7273 [7435 – 7439]
Halet, J.-F.
– Structural Preference versus Metal within the MB_2C_2 (M = Mg, Sc, Ca, Y, Ln) Phases: The Coloring Problem Revisited by DFT Calculations
(C) 7542 – 7545 [7714 – 7717]
DOI: 10.1002/anie.200503080
Halet, J.-F. (C) 4362 – 4365 [4436 – 4439]
Halfen, H. L. (C) 584 – 587 [590 – 593]
Halfen, J. A.
– Spin-State Rationale for the Peroxo-Stabilizing Role of the Thiolate Ligand in Superoxide Reductase
(C) 584 – 587 [590 – 593]
DOI: 10.1002/anie.200461527
Hall, A. J.
– An Artificial Riboflavin Receptor Prepared by a Template Analogue Imprinting Strategy
(C) 3902 – 3906 [3970 – 3974]
DOI: 10.1002/anie.200500342
Hall, L. M. (C) 1226 – 1229 [1252 – 1255]
Hamacek, J. (C) 7954 – 7958 [8168 – 8172]
Hamaguchi, H. (C) 1513 – 1517 [1537 – 1541]
Hamamoto, H. (C) 4536 – 4538 [4612 – 4614]
Hamashima, Y. (C) 1525 – 1529 [1549 – 1553]
Hamberg, A. (C) 4582 – 4585 [4658 – 4661]
Hamid, S. B. A. (C) 5488 – 5492 [5624 – 5628]
Hamilton, A. D.
– Strategies for Targeting Protein – Protein Interactions With Synthetic Agents
(R) 4130 – 4163 [4200 – 4235]
DOI: 10.1002/anie.200461786
– Structurally Simple Farnesyltransferase Inhibitors Arrest the Growth of Malaria Parasites
(C) 4903 – 4906 [4981 – 4984]
DOI: 10.1002/anie.200500674

 © 2005 Wiley-VCH Verlag GmbH & Co. KGaA, Weinheim

– Terphenyl-Based Helical Mimetics That Disrupt the p53/HDM2 Interaction
(C) 2704 – 2707 [2764 – 2767]
DOI: 10.1002/anie.200462316
Hamman, S. (C) 438 – 441 [442 – 445]
Hammer, B. (C) 2270 – 2275 [2310 – 2315]
Hammond, G. B.
– Difluoroallenyl Bromide as a Wide-Ranging Difluoromethylene Cation Equivalent: S_N2 Substitution of Difluoropropargyl Bromide through Sequential S_E2' and S_N2' Reactions
(C) 7404 – 7407 [7570 – 7573]
DOI: 10.1002/anie.200502807
Hammond, P. T.
– A Family of Hierarchically Self-Assembling Linear-Dendritic Hybrid Polymers for Highly Efficient Targeted Gene Delivery
(C) 6704 – 6708 [6862 – 6866]
DOI: 10.1002/anie.200502152
Han, L. (C) 6484 – 6487 [6642 – 6645]
Han, M.
– Aminolysis Route to Monodisperse Titania Nanorods with Tunable Aspect Ratio
(C) 3466 – 3470 [3532 – 3536]
DOI: 10.1002/anie.200500410
Han, Q. (C) 2694 – 2700 [2754 – 2760], 5329 – 5334 [5463 – 5468]
Han, X.-D. (C) 4328 – 4333 [4402 – 4407]
Han, Y. (C) 288 – 292 [292 – 296]
Han, Y.-J. (C) 2386 – 2390 [2438 – 2442]
Hanan, G. S.
– The Structural and Functional Roles of Rhodium(II) – Rhodium(II) Dimers in Multinuclear Ruthenium(II) Complexes
(C) 4881 – 4884 [4959 – 4962]
DOI: 10.1002/anie.200500392
Hanashima, S. (C) 4218 – 4224 [4290 – 4296]
Hanauer, T. (C) 7200 – 7204 [7366 – 7370]
Handa, Samantha (C) 5740 – 5744 [5886 – 5890]
Handa, Shinya (C) 4365 – 4368 [4439 – 4442]
Hania, P. R. (C) 2373 – 2376 [2425 – 2428]
Hanrath, T. (C) 3573 – 3577 [3639 – 3643]
Hansen, S. (C) 5247 – 5251 [5381 – 5386]
Hao, J.
– An Onion Phase in Salt-Free Zero-Charged Catanionic Surfactant Solutions
(C) 4018 – 4021 [4086 – 4089]
DOI: 10.1002/anie.200500353
Hao, Y. (C) 4778 – 4781 [4856 – 4859]
Haque, S. A.
– Supermolecular Control of Charge Transfer in Dye-Sensitized Nanocrystalline TiO_2 Films: Towards a Quantitative Structure – Function Relationship
(C) 5740 – 5744 [5886 – 5890]
DOI: 10.1002/anie.200500363
Harada, A. (C) 419 – 423 [423 – 427]
Harada, N.
– Conclusive Determination of the Absolute Configuration of Chiral C_{60}-Fullerene *cis*-3 Bisadducts by X-ray Crystallography and Circular Dichroism
(C) 2262 – 2265 [2302 – 2305]
DOI: 10.1002/anie.200462811
Harada, S. (C) 4365 – 4368 [4439 – 4442]
Haraguchi, K.
– Control of the Coil-to-Globule Transition and Ultrahigh Mechanical Properties of PNIPA in Nanocomposite Hydrogels
(C) 6500 – 6504 [6658 – 6662]
DOI: 10.1002/anie.200502004
Harańczyk, M. (C) 6585 – 6588 [6743 – 6746]
Harano, K. (C) 2727 – 2731 [2787 – 2791]
Hardie, M. J.
– Capsules and Star-Burst Polyhedra: An $[Ag_2L_2]$ Capsule and a Tetrahedral $[Ag_4L_4]$ Metallosupramolecular Prism with Cyclotriveratrylene-Type Ligands
(C) 6395 – 6399 [6553 – 6557]
DOI: 10.1002/anie.200501358
Harding, L. P. (C) 6909 – 6912 [7069 – 7072]
Hardy, J. G. (C) 2556 – 2559 [2612 – 2615]
Harms, M. (C) 639 – 644 [645 – 650]
Harned, A. M. (C) 6924 – 6927 [7084 – 7087]
Harran, P. G.
– Spirocycloisomerization of Tethered Alkylidene Glycocyamidines: Synthesis of a Base Template Common to the Palau'-amine Family of Alkaloids
(C) 765 – 769 [775 – 779]
DOI: 10.1002/anie.200462069
Harris, J. R. (C) 3057 – 3061 [3117 – 3121]
Harris, N. (C) 6746 – 6750 [6904 – 6908]
Harris, N. K. (C) 6410 – 6413 [6568 – 6571]
Harrison, B. A. (C) 6533 – 6537 [6691 – 6695]
Harrity, J. P. A.
– Synthesis of Highly Substituted Pyridazines through Alkynyl Boronic Ester Cycloaddition Reactions
(C) 3889 – 3892 [3957 – 3960]
DOI: 10.1002/anie.200500288
Harrowven, D. C.
– Total Synthesis of Cavicularin and Riccardin C: Addressing the Synthesis of an Arene That Adopts a Boat Configuration
(C) 3899 – 3901 [3967 – 3969]
DOI: 10.1002/anie.200500466
– Total Synthesis of (−)-Colombiasin A and (−)-Elisapterosin B
(C) 1221 – 1222 [1247 – 1248]
DOI: 10.1002/anie.200462268
Hartl, H.
– From AgCN Chains to a Fivefold Helix and a Fishnet-Shaped Framework Structure
(C) 2794 – 2797 [2855 – 2858]
DOI: 10.1002/anie.200462793
Hartwig, J. F.
– Highly Reactive, General, and Long-Lived Catalysts for Coupling Heteroaryl and Aryl Chlorides with Primary Nitrogen Nucleophiles
(C) 1371 – 1375 [1395 – 1399]
DOI: 10.1002/anie.200462629
– Regiospecific Side-Chain Functionalization of Linear Low-Density Polyethylene with Polar Groups
(C) 6410 – 6413 [6568 – 6571]
DOI: 10.1002/anie.200501837
Harutyunyan, S. R. (C) 2752 – 2756 [2812 – 2816]
Harvey, B. M. (C) 7075 – 7078 [7237 – 7240]
Harvey, J. N.
– On the Importance of Leaving Group Ability in Reactions of Ammonium, Oxonium, Phosphonium, and Sulfonium Ylides
(C) 5468 – 5471 [5604 – 5607]
DOI: 10.1002/anie.200501526
Hasegawa, H. (C) 7283 – 7287 [7449 – 7453]
Hasegawa, M. (C) 6682 – 6685 [6840 – 6843]
Hasegawa, Tatsuo (C) 7283 – 7287 [7449 – 7453]
Hasegawa, Teruaki (C) 2030 – 2033 [2066 – 2069]
Hashimoto, Shinji (C) 3591 – 3594 [3657 – 3660]
Hashimoto, Shunichi
– Direct and Stereoselective Synthesis of 2-Acetamido-2-deoxy-β-D-glycopyranosides by Using the Phosphite Method
(C) 2245 – 2249 [2285 – 2289]
DOI: 10.1002/anie.200461988
Hashmi, A. S. K.
– Gold Catalysis: Proof of Arene Oxides as Intermediates in the Phenol Synthesis
(C) 2798 – 2801 [2858 – 2861]
DOI: 10.1002/anie.200462672
– The Catalysis Gold Rush: New Claims
(H) 6990 – 6993 [7150 – 7154]
DOI: 10.1002/anie.200502735
Hasselmann, D.
– Dynamic Effects on [3,3] and [1,3] Shifts of 6-Methylenebicyclo[3.2.0]hept-2-ene
(C) 3548 – 3552 [3614 – 3618]
DOI: 10.1002/anie.200500027
Hata, H. (C) 932 – 935 [954 – 957], 6899 – 6901 [7059 – 7061]
Hata, K. (C) 5857 – 5860 [6007 – 6010]
Hauber, S.-O. (C) 5871 – 5875 [6021 – 6025]
Haukka, M. (C) 4345 – 4349 [4419 – 4423]
Haumann, M. (C) 815 – 819 [826 – 830]
Häussermann, U.
– SrAlSiH: A Polyanionic Semiconductor Hydride
(C) 7269 – 7273 [7435 – 7439]
DOI: 10.1002/anie.200502090
Hawker, C. J.
– One-Pot Reaction Cascades Using Star Polymers with Core-Confined Catalysts
(C) 6384 – 6387 [6542 – 6545]
DOI: 10.1002/anie.200502095
Hayami, S.
– Reverse Spin Transition Triggered by a Structural Phase Transition
(C) 4899 – 4903 [4977 – 4981]
DOI: 10.1002/anie.200500316
Hayashi, Takaaki (C) 4212 – 4215 [4284 – 4287]
Hayashi, Tamio
– Chiral Phosphine – Olefin Bidentate Ligands in Asymmetric Catalysis: Rhodium-Catalyzed Asymmetric 1,4-Addition of Aryl Boronic Acids to Maleimides
(C) 4611 – 4614 [4687 – 4690]
DOI: 10.1002/anie.200501305
– Highly Chemo- and Enantioselective Arylative Cyclization of Alkyne-Tethered Electron-Deficient Olefins Catalyzed by Rhodium Complexes with Chiral Dienes
(C) 3909 – 3912 [3977 – 3980]
DOI: 10.1002/anie.200500843
– Rhodium-Catalyzed Asymmetric 1,6-Addition of Aryl Zinc Reagents to Dienones
(C) 4224 – 4227 [4296 – 4299]
DOI: 10.1002/anie.200500678
Hayashi, Y.
– Determination by Asymmetric Total Synthesis of the Absolute Configuration of Lucilactaene, a Cell-Cycle Inhibitor in p53-Transfected Cancer Cells
(C) 3110 – 3115 [3170 – 3175]
DOI: 10.1002/anie.200500060
– Diphenylprolinol Silyl Ethers as Efficient Organocatalysts for the Asymmetric Michael Reaction of Aldehydes and Nitroalkenes
(C) 4212 – 4215 [4284 – 4287]
DOI: 10.1002/anie.200500599

 © 2005 Wiley-VCH Verlag GmbH & Co. KGaA, Weinheim

Hayden, O.
– Nanophotonic Light Sources for Fluorescence Spectroscopy and Cellular Imaging (C) 1395 – 1398 [1419 – 1422] DOI: 10.1002/anie.200462120
Haynes, R. K.
– Reply to Comments on "Highly Antimalaria-Active Artemisinin Derivatives: Biological Activity Does Not Correlate with Chemical Reactivity" (L) 2064 – 2065 [2100 – 2101] DOI: 10.1002/anie.200462723
Hayward, R. C. (C) 332 – 336 [336 – 340]
He, C.-B. (C) 4782 – 4785 [4860 – 4863]
He, Cheng (C) 5090 – 5093 [5220 – 5223]
He, Chengjiang Corrigendum: 506
He, Chuan
– An Exceptionally Selective Lead(II)-Regulatory Protein from *Ralstonia Metallidurans*: Development of a Fluorescent Lead(II) Probe (C) 2715 – 2719 [2775 – 2779] DOI: 10.1002/anie.200462443
He, Jiangtao (C) 7298 – 7301 [7464 – 7467]
He, Jinbo (C) 2420 – 2426 [2472 – 2478]
He, Jing (C) 1202 – 1205 [1226 – 1230]
He, Q. (C) 5275 – 5278 [5409 – 5412]
He, W. (C) 7557 – 7560 [7729 – 7732]
He, X. (C) 6742 – 6746 [6900 – 6904]
He, Y. (C) 4355 – 4358 [4429 – 4432], 6694 – 6696 [6852 – 6854]
Hechavarria Fonseca, M. T. (C) 108 – 110 [110 – 112]
Hecht, S.
– Wrapping Peptide Tubes: Merging Biological Self-Assembly and Polymer Synthesis (H) 6986 – 6989 [7146 – 7149] DOI: 10.1002/anie.200502436
Heckel, A.
– Photoinduced Transcription by Using Temporarily Mismatched Caged Oligonucleotides (C) 471 – 473 [475 – 477] DOI: 10.1002/anie.200461779
Heckmann, D. (C) 423 – 426 [427 – 430]
Heckmann, G. (C) 1199 – 1201 [1223 – 1226]
Hedrick, J. L.
– Latent, Thermally Activated Organic Catalysts for the On-Demand Living Polymerization of Lactide (C) 4964 – 4968 [5044 – 5048] DOI: 10.1002/anie.200500723
– Oriented Nanoporous Lamellar Organosilicates Templated from Topologically Unsymmetrical Dendritic-Linear Block Copolymers (C) 7574 – 7580 [7746 – 7752] DOI: 10.1002/anie.200501577
Heeger, A. J. (C) 5456 – 5459 [5592 – 5595]
Heemstra, J. R., Jr. (R) 4682 – 4698 [4760 – 4777]
Heil, M. (C) 7208 – 7212 [7374 – 7379]
Heimann, A. C. (C) 1130 – 1133 [1154 – 1157]
Heine, A. (C) 3140 – 3144 [3200 – 3204], 3620 – 3623 [3686 – 3689]
Heinekey, D. M. (C) 2512 – 2515 [2568 – 2571]
Heinemann, F. W. (C) 803 – 806 [813 – 817]
Heiney, P. A. (C) 4739 – 4745 [4817 – 4823], 6516 – 6521 [6674 – 6679]
Heinz, D. W.
– Much Anticipated—The Bioactive Conformation of Epothilone and Its Binding to Tubulin (H) 1298 – 1301 [1324 – 1327] DOI: 10.1002/anie.200462241
Heinze, J.
– 3D-Hybrid Networks with Controllable Electrical Conductivity from the Electrochemical Deposition of Terthiophene-Functionalized Polyphenylene Dendrimers (C) 2447 – 2451 [2501 – 2505] DOI: 10.1002/anie.200462378
Heller, D.
– Are β-Acylaminoacrylates Hydrogenated in the Same Way as α-Acylaminoacrylates? (C) 1184 – 1188 [1208 – 1212] DOI: 10.1002/anie.200461716
Helliwell, M. (C) 1241 – 1244 [1267 – 1270], 7546 – 7549 [7718 – 7721]
Helm, M. D. (C) 3889 – 3892 [3957 – 3960]
Helms, B. (C) 6384 – 6387 [6542 – 6545]
Henderson, J. R. (C) 1965 – 1968 [2001 – 2004]
Hensel, F.
– Fluids at High Pressures and Supercritical Temperatures: *Ernst-Ulrich Franck* (O) 1156 [1180] DOI: 10.1002/anie.200500097
Herber, C. (C) 5267 – 5269 [5401 – 5403]
Herberhold, M. (C) 259 – 262 [264 – 267]
Herbert, D. E. (C) 5886 – 5890 [6036 – 6040]
Herbertz, T. (C) 5830 – 5833 [5980 – 5983]
Herbst, T. (C) 7461 – 7463 [7627 – 7629]
Herges, R.
– *cis*-Bromination of Alkynes without Cationic Intermediates (C) 1412 – 1416 [1437 – 1441] DOI: 10.1002/anie.200461632
Herler, S. (C) 7790 – 7793 [7968 – 7971]
Hermann, T.
– Molecular Recognition by Glycoside Pseudo Base Pairs and Triples in an Apramycin – RNA Complex (C) 2694 – 2700 [2754 – 2760] DOI: 10.1002/anie.200500028
– Molecular Recognition of RNA by Neomycin and a Restricted Neomycin Derivative (C) 5329 – 5334 [5463 – 5468] DOI: 10.1002/anie.200500903
Hermatschweiler, R. (C) 4397 – 4400 [4471 – 4474]
Hermes, S. (C) 6237 – 6241 [6394 – 6397]
Héroguez, V. (C) 284 – 287 [288 – 291]
Herrera, R. P.
– Phase-Transfer-Catalyzed Asymmetric Aza-Henry Reaction Using *N*-Carbamoyl Imines Generated In Situ from α-Amido Sulfones (C) 7975 – 7978 [8189 – 8192] DOI: 10.1002/anie.200502646
Herrera, R. P. (C) 6576 – 6579 [6734 – 6737]
Herrero, S. (C) 305 – 307 [309 – 311]
Herricks, T. (C) 2589 – 2592 [2645 – 2648]
Herrmann, J.-S. (C) 7794 – 7798 [7972 – 7976]
Herschbach, H. (C) 5338 – 5341 [5472 – 5475]
Herse, C. (C) 1879 – 1883 [1913 – 1917]
Hershko, A.
– The Ubiquitin System for Protein Degradation and Some of Its Roles in the Control of the Cell-Division Cycle (Nobel Lecture) (R) 5932 – 5943 [6082 – 6094] DOI: 10.1002/anie.200501724
Hertweck, C.
– Mutasynthesis of Aureonitrile: An Aureothin Derivative with Significantly Improved Cytostatic Effect (C) 1202 – 1205 [1226 – 1230] DOI: 10.1002/anie.200461990
– Sequential Enzymatic Oxidation of Aminoarenes to Nitroarenes via Hydroxylamines (C) 4083 – 4087 [4152 – 4155] DOI: 10.1002/anie.200500365
Hess, K. (C) 1412 – 1416 [1437 – 1441]
Heuberger, B. D. (C) 1529 – 1532 [1553 – 1556]
Heublein, B. (R) 3358 – 3393 [3422 – 3458]
Heutling, A. (C) 2951 – 2954 [3011 – 3013]
Hevia, E.
– Alkali-Metal-Mediated Zincation of Ferrocene: Synthesis, Structure, and Reactivity of a Lithium Tmp/Zincate Reagent (C) 6018 – 6021 [6172 – 6175] DOI: 10.1002/anie.200501560
Hevia, E. (C) 68 – 72 [70 – 74], 3459 – 3462 [3525 – 3528]
Hey-Hawkins, E.
– From Racemic Primary Aminoalkyl(phosphanyl)ferrocene Complexes to a Lithium – Phosphorus *closo* Cluster (C) 2965 – 2969 [3025 – 3029] DOI: 10.1002/anie.200462543
– Synthesis and Molecular Structure of the Cu_4P_8 Cage Compound $[Cu_4(P_4Ph_4)_2(PCyp_3)_3]$ (C) 6241 – 6244 [6398 – 6401] DOI: 10.1002/anie.200501607
Heyraud, A. (C) 1350 – 1352 [1374 – 1376]
Hibble, S. J.
– Interpenetrating Copper – Silver Cyanometalate Networks: Polymorphs and Topological Isomers (C) 7942 – 7946 [8156 – 8160] DOI: 10.1002/anie.200502372
Hibino, M. (C) 797 – 802 [807 – 812]
Hidehira, Y. (C) 7136 – 7138 [7298 – 7300]
Higashi, T. (C) 3861 – 3864 [3929 – 3932]
Hikishima, S. (C) 596 – 598 [602 – 604]
Hildebrandt, N.
– Quantum Dots as Efficient Energy Acceptors in a Time-Resolved Fluoroimmunoassay (C) 7612 – 7615 [7784 – 7788] DOI: 10.1002/anie.200501552
Hill, C. L.
– Enantiomerically Pure Polytungstates: Chirality Transfer through Zirconium Coordination Centers to Nanosized Inorganic Clusters (C) 3540 – 3544 [3606 – 3610] DOI: 10.1002/anie.200500415
Hill, J. P. (C) 4187 – 4192 [4259 – 4264], 7048 – 7053 [7210 – 7215]
Hill, M. S.
– Dimerization of Indanediyl Fragments: An Alkene Analogue for Group 13? (C) 4231 – 4235 [4303 – 4307] DOI: 10.1002/anie.200500764
Hillmyer, M. A.
– Regiospecific Side-Chain Functionalization of Linear Low-Density Polyethylene with Polar Groups (C) 6410 – 6413 [6568 – 6571] DOI: 10.1002/anie.200501837
Himmel, H.-J.
– Subvalent Compounds Featuring Direct Metal – Metal Bonds: The Zn–Zn Bond in $[Cp^*_2Zn_2]$ (H) 3006 – 3008 [3066 – 3068] DOI: 10.1002/anie.200500597
Himo, F.
– The Origin of Stereoselectivity in Primary Amino Acid Catalyzed Intermolecular

 © 2005 Wiley-VCH Verlag GmbH & Co. KGaA, Weinheim

Aldol Reactions
(C) 7028 – 7032 [7190 – 7194]
DOI: 10.1002/anie.200502388
Hinatsu, Y. (C) 720 – 724 [730 – 734]
Hinou, H. (C) 91 – 96 [93 – 98], 2534 – 2537 [2590 – 2593]
Hinrichsen, O.
– Active Sites on Oxide Surfaces: ZnO-Catalyzed Synthesis of Methanol from CO and H_2
(C) 2790 – 2794 [2850 – 2854]
DOI: 10.1002/anie.200462374
Hioki, K. (C) 7254 – 7257 [7420 – 7423]
Hiraki, K. (C) 5509 – 5513 [5645 – 5649]
Hirano, S. (C) 1854 – 1856 [1888 – 1890]
Hiraoka, S. (C) 2727 – 2731 [2787 – 2791]
Hirayama, T. (C) 3293 – 3296 [3357 – 3360]
Hiroaki, H. (C) 6180 – 6183 [6336 – 6339]
Hirose, H. (C) 734 – 737 [744 – 747]
Hirota, S. (C) 435 – 438 [439 – 442]
Hiroto, S. (C) 6763 – 6766 [6921 – 6924]
Hirsch, A.
– Complete Self-Assembly of Discrete Supramolecular Dendrimers
(C) 1564 – 1567 [1588 – 1592]
DOI: 10.1002/anie.200462104
– Switchable Supramolecular Organization of Structurally Defined Micelles Based on an Amphiphilic Fullerene
(C) 2976 – 2979 [3036 – 3039]
DOI: 10.1002/anie.200462465
Hirsch, T. (C) 6775 – 6778 [6933 – 6936]
Hisaki, I. (C) 6763 – 6766 [6921 – 6924]
Hiskey, M. A.
– Preparation of Nitrogen-Rich Nanolayered, Nanoclustered, and Nanodendritic Carbon Nitrides
(C) 737 – 739 [747 – 749]
DOI: 10.1002/anie.200461758
– Tetraazapentalene Chemistry: Unexpected Intramolecular Electron Rearrangement Induced by Highly Reactive ψ-Dinitroso Substituents
(C) 7089 – 7094 [7251 – 7256]
DOI: 10.1002/anie.200502342
Hitchcock, P. B. (C) 4231 – 4235 [4303 – 4307]
Hiyama, T.
– Modern Synthetic Methods for Fluorine-Substituted Target Molecules
(R) 214 – 231 [218 – 234]
DOI: 10.1002/anie.200460441
Hiyama, T. (C) 7136 – 7138 [7298 – 7300]
Hnyk, D. (C) 6222 – 6226 [6378 – 6382]
Ho, C. (C) 5141 – 5144 [5271 – 5274]
Ho, N. T. (C) 5141 – 5144 [5271 – 5274]
Ho, R.-M.
– Springlike Nanohelical Structures in Chiral Block Copolymers
(C) 7969 – 7972 [8183 – 8186]
DOI: 10.1002/anie.200502236
Ho, S.-T. (C) 7922 – 7925 [8136 – 8139]
Hoashi, Y. (C) 4032 – 4035 [4100 – 4103]
Höbartner, C. (C) 7305 – 7309 [7471 – 7475]
Hobel, A. (C) 7630 – 7635 [7803 – 7808]
Hochgesand, A. (C) 6588 – 6592 [6746 – 6750]
Hodeau, J.-L.
– Direct Localization of Atoms in Mixed-Occupancy Powders by Resonant Contrast Diffraction
(C) 1725 – 1729 [1753 – 1757]
DOI: 10.1002/anie.200461642
Hoen, R. (C) 4209 – 4212 [4281 – 4284]
Hofacker, A. L. (C) 1053 – 1057 [1077 – 1081]
Höfener, S. (C) 7879 – 7881 [8091 – 8093]
Hoffart, D. J. (C) 901 – 904 [923 – 926]
Hoffman, T. Z. (C) 2144 – 2148 [2182 – 2186]
Hoffmann, H. M. R.
– [4 + 3] Cycloadducts from Lewis Acid Mediated Reactions of Acroleins with Cyclopentadiene
(H) 26 – 29 [26 – 29]
DOI: 10.1002/anie.200461313
Hoffmann, R.
– Squeezing C–C Bonds
(C) 7549 – 7553 [7721 – 7725]
DOI: 10.1002/anie.200502721
Hoffmann, R. W.
– Redox Catalysts for Reduction with Base Metals
(H) 6277 – 6279 [6433 – 6435]
DOI: 10.1002/anie.200501951
Hoffmann, S. (C) 7424 – 7427 [7590 – 7593]
Hoffmann, S. D. (C) 2092 – 2096 [2129 – 2133]
Hoffmann, S. V. (C) 5630 – 5634 [5774 – 5779]
Hofkens, J.
– Single-Enzyme Kinetics of CALB-Catalyzed Hydrolysis
(C) 560 – 564 [566 – 570]
DOI: 10.1002/anie.200460625
Höfle, G.
– Much Anticipated—The Bioactive Conformation of Epothilone and Its Binding to Tubulin
(H) 1298 – 1301 [1324 – 1327]
DOI: 10.1002/anie.200462241
Hofmann, J. (C) 2892 – 2895 [2952 – 2955]
Hofmann, M. (C) 1643 – 1646 Corrigendum: 2471 [1670 – 1673 Corrigendum: 2525]
Hofstraat, J. W. (C) 1806 – 1810 [1840 – 1844]
Höger, S.
– Discotic Liquid Crystals with an Inverted Structure
(C) 2801 – 2805 [2862 – 2866]
DOI: 10.1002/anie.200462319
– Shape-Persistent Phenylene-Acetylene Macrocycles: Large Rings—Low Yield?
(H) 3806 – 3808 [3872 – 3875]
DOI: 10.1002/anie.200500681
Holdaway, M. A. (C) 6746 – 6750 [6904 – 6908]
Hollmann, D. (C) 7794 – 7798 [7972 – 7976]
Holmes, A. E. (C) 4006 – 4009 [4074 – 4077]
Holmes, E. (C) 4939 – 4944 [5019 – 5024]
Holmes, I. P. (C) 403 – 406 [407 – 410]
Holmes, K. E. (C) 1850 – 1853 [1884 – 1887]
Holmes, S. M. (C) 3075 – 3078 [3135 – 3138]
Holub, J. (C) 6222 – 6226 [6378 – 6382]
Honda, K. (C) 3559 – 3562 Corrigendum: 4282 [3625 – 3628 Corrigendum: 4354]
Honda, S. (C) 7929 – 7932 [8143 – 8146], 7932 – 7935 [8146 – 8149]
Honeyman, G. W. (C) 68 – 72 [70 – 74], 6018 – 6021 [6172 – 6175]
Hong, A. (C) 4048 – 4052 [4116 – 4120]
Hong, M.-K. (C) 328 – 332 [332 – 336]
Hong, R. (C) 3478 – 3481 [3544 – 3547]
Hong, W. (C) 6544 – 6546 [6702 – 6704]
Honjo, T. (C) 5838 – 5841 [5988 – 5991]
Honma, I. (C) 797 – 802 [807 – 812]
Hook, D. F. (C) 5433 – 5438 [5569 – 5574]
Hopfgartner, G. (C) 1879 – 1883 [1913 – 1917]
Hoppe, Diana (C) 7616 – 7619 [7788 – 7792]
Hoppe, Dieter
– Solid-State Structure and Enantioselective Reactions of a Complex of a 1-Thio-Substituted Propargyllithium and (–)-Sparteine
(C) 5492 – 5496 [5629 – 5632]
DOI: 10.1002/anie.200501142
Höppe, H. A. (C) 567 – 570 [573 – 576]
Hopwood, D. A. (C) 1121 – 1125 [1145 – 1149]
Hor, T. S. A.
– Ethylene Oligomerization at Coordinatively and Electronically Unsaturated Low-Valent Nickel
(C) 7560 – 7564 [7732 – 7736]
DOI: 10.1002/anie.200502532
Horai, M. (C) 5857 – 5860 [6007 – 6010]
Hori, A. (C) 4896 – 4899 [4974 – 4977]
Horne, D. A.
– Biomimetic Synthesis of Grossularines-1
(C) 3280 – 3282 [3344 – 3346]
DOI: 10.1002/anie.200500055
Horný, C. (C) 4903 – 4906 [4981 – 4984]
Horozov, T. S. (C) 3722 – 3725 [3788 – 3791]
Horrocks, B. R. (C) 1254 – 1257 [1280 – 1283]
Horton, P. N. (C) 1072 – 1075 [1096 – 1099]
Hoshino, A. (C) 4550 – 4554 [4626 – 4630]
Hoshino, T. (C) 468 – 470 [472 – 474]
Hoshino, Y. (C) 4389 – 4391 [4463 – 4465]
Hoskin, A. (C) 1405 – 1408 [1429 – 1432]
Hotta, D. (C) 1525 – 1529 [1549 – 1553]
Hou, Hairong (C) 5275 – 5278 [5409 – 5412]
Hou, Hongwei
– Metal Ions Play Different Roles in the Third-Order Nonlinear Optical Properties of d^{10} Metal – Organic Clusters
(C) 6067 – 6074 [6221 – 6228]
DOI: 10.1002/anie.200463004
Hou, J.-L. (C) 5725 – 5729 [5871 – 5875]
Hou, X.-L.
– Highly Enantioselective Pd-Catalyzed Allylic Alkylations of Acyclic Ketones
(C) 6544 – 6546 [6702 – 6704]
DOI: 10.1002/anie.200502020
Hou, Zhaomin
– Alternating Ethylene – Norbornene Copolymerization Catalyzed by Cationic Half-Sandwich Scandium Complexes
(C) 962 – 965 [984 – 987]
DOI: 10.1002/anie.200461971
– Lanthanide – Imido Complexes and Their Reactions with Benzonitrile
(C) 959 – 962 [981 – 984]
DOI: 10.1002/anie.200461939
Hou, Zhenshan (C) 1346 – 1349 [1370 – 1373]
Houben, A. (C) 7212 – 7215 [7379 – 7382]
Houk, K. N.
– Dynamic Effects on [3,3] and [1,3] Shifts of 6-Methylenebicyclo[3.2.0]hept-2-ene
(C) 3548 – 3552 [3614 – 3618]
DOI: 10.1002/anie.200500027
– Origins of Stereoselectivity in Strain-Release Allylations
(C) 938 – 941 [960 – 963]
DOI: 10.1002/anie.200462130
Houlton, A. (C) 1254 – 1257 [1280 – 1283]
Hoveyda, A. H.
– Highly Enantioselective Cu-Catalyzed Conjugate Additions of Dialkylzinc Reagents to Unsaturated Furanones and Pyranones: Preparation of Air-Stable and Catalytically Active Cu – Peptide Complexes
(C) 5306 – 5310 [5440 – 5444]
DOI: 10.1002/anie.200501251
Hovius, R. (C) 1388 – 1392 [1412 – 1416], 4957 – 4960 [5037 – 5040]
Howard, J. A. K. (C) 292 – 295 [296 – 299]
Howes, P. D. (C) 3899 – 3901 [3967 – 3969]
Howlett, P. C. (C) 313 – 316 [317 – 320]
Hoyer, J. R. (C) 3698 – 3702 [3764 – 3768]
Hoyer, R. (C) 2080 – 2084 [2116 – 2120]

 © 2005 Wiley-VCH Verlag GmbH & Co. KGaA, Weinheim

Hoz, S.
– Harder than Diamond: Determining the Cross-Sectional Area and Young's Modulus of Molecular Rods
(C) 7432 – 7435 [7598 – 7601]
DOI: 10.1002/anie.200502448
Hsieh, R. W. (C) 5480 – 5483 [5616 – 5619]
Hsu, C.-Y. (C) 1665 – 1668 [1693 – 1696]
Hu, Changwen
– Single-Crystal Dendritic Micro-Pines of Magnetic α-Fe_2O_3: Large-Scale Synthesis, Formation Mechanism, and Properties
(C) 4197 – 4201 [4269 – 4273]
DOI: 10.1002/anie.200500448
Hu, Chunhua (C) 632 – 634 [638 – 640], 2281 – 2283 [2321 – 2323]
Hu, H. (C) 4884 – 4888 [4962 – 4966]
Hu, H.-M. (C) 3864 – 3867 [3932 – 3935]
Hu, J.-S. (C) 1269 – 1273 [1295 – 1299], 4391 – 4395 [4465 – 4469]
Hu, Jinbo
– Facile Synthesis of Chiral α-Difluoromethyl Amines from *N*-(*tert*-Butylsulfinyl)aldimines
(C) 5882 – 5886 [6032 – 6036]
DOI: 10.1002/anie.200501769
Hu, Jun
– Nanoparticle PCR: Nanogold-Assisted PCR with Enhanced Specificity
(C) 5100 – 5103 [5230 – 5233]
DOI: 10.1002/anie.200500403
Hu, Junqing (C) 2140 – 2144 [2178 – 2182]
Hu, S. (C) 5471 – 5475 [5607 – 5611]
Hu, X.
– Highly Efficient $NaNO_2$-Catalyzed Destruction of Trichlorophenol Using Molecular Oxygen
(C) 5520 – 5523 [5656 – 5659]
DOI: 10.1002/anie.200501470
Hu, Y. (C) 1048 – 1053 [1072 – 1077]
Hua, F. Corrigendum: 1907
Huang, C.-H. (C) 4010 – 4015 [4078 – 4083]
Huang, Jianguo (C) 4532 – 4535 [4608 – 4611]
Huang, Jiehuan (C) 5100 – 5103 [5230 – 5233]
Huang, X. (C) 7251 – 7254 [7417 – 7420]
Huang, X.-C. (C) 4175 – 4178 [4247 – 4250]
Huang, Y. (C) 6025 – 6029 [6179 – 6183]
Huber, M. (C) 3289 – 3293 [3353 – 3357]
Huber, V. (C) 3147 – 3151 [3208 – 3212]
Hübner, C. (C) 2437 – 2440 [2490 – 2493]
Huc, I.
– Molecular Apple Peels
(C) 1954 – 1958 [1990 – 1994]
DOI: 10.1002/anie.200462898
Huch, V. (C) 5968 – 5971 [6122 – 6126], 7884 – 7887 [8096 – 8099]
Huck, W. T. S.
– Locking and Unlocking of Polyelectrolyte Brushes: Toward the Fabrication of Chemically Controlled Nanoactuators
(C) 4578 – 4581 [4654 – 4657]
DOI: 10.1002/anie.200500228
Hucke, O. (C) 4903 – 4906 [4981 – 4984]
Huels, M. A. (C) 1647 – 1650 [1673 – 1676]
Huh, S. (C) 1826 – 1830 [1860 – 1864]
Hult, K.
– An *S*-Selective Lipase Was Created by Rational Redesign and the Enantioselectivity Increased with Temperature
(C) 4582 – 4585 [4658 – 4661]
DOI: 10.1002/anie.200500971
Hult, K. (C) 2742 – 2746 [2802 – 2806]
Humbert, N. (C) 7764 – 7767 [7942 – 7945]
Humphrey, S. M. (C) 3456 – 3459 [3522 – 3525]
Humphries, J. (C) 1057 – 1061 [1081 – 1085]
Hung, L.-L. (C) 3107 – 3110 [3167 – 3170]
Hung, S.-C.
– $Cu(OTf)_2$ as an Efficient and Dual-Purpose Catalyst in the Regioselective Reductive Ring Opening of Benzylidene Acetals
(C) 1665 – 1668 [1693 – 1696]
DOI: 10.1002/anie.200462172
Huntley, D. R.
– Squeezing C–C Bonds
(C) 7549 – 7553 [7721 – 7725]
DOI: 10.1002/anie.200502721
Huo, Z. (C) 6054 – 6057 [6208 – 6211]
Hursthouse, M. B. (C) 1072 – 1075 [1096 – 1099]
Hussain, F. (C) 3773 – 3777 [3839 – 3843]
Huynh, M. H. V.
– Preparation of Nitrogen-Rich Nanolayered, Nanoclustered, and Nanodendritic Carbon Nitrides
(C) 737 – 739 [747 – 749]
DOI: 10.1002/anie.200461758
– Tetraazapentalene Chemistry: Unexpected Intramolecular Electron Rearrangement Induced by Highly Reactive ψ-Dinitroso Substituents
(C) 7089 – 7094 [7251 – 7256]
DOI: 10.1002/anie.200502342
Hwang, I. (C) 87 – 91 [89 – 93]
Hwang, I.-C.
– A Calix[4]imidazolium[2]pyridine as an Anion Receptor
(C) 2899 – 2903 [2959 – 2963]
DOI: 10.1002/anie.200500119
Hwang, J.-S. (C) 556 – 560 [562 – 566]
Hwang, L. K. (C) 6166 – 6169 [6322 – 6325]
Hwang, N.-M. (C) 2872 – 2877 [2932 – 2937]
Hwang, Y. (C) 2872 – 2877 [2932 – 2937], 7427 – 7432 [7593 – 7598]
Hwang, Y. K. (C) 556 – 560 [562 – 566]
Hyde, J. R.
– "Hydrogen-Catalyzed" Dehydrogenation: A Supercritical Conundrum
(C) 7588 – 7591 [7760 – 7763]
DOI: 10.1002/anie.200502049
Hyde, M. E. (C) 5121 – 5126 [5251 – 5256], 6491 – 6496 [6649 – 6654]
Hyeon, T.
– Large-Scale Nonhydrolytic Sol–Gel Synthesis of Uniform-Sized Ceria Nanocrystals with Spherical, Wire, and Tadpole Shapes
(C) 7411 – 7414 [7577 – 7580]
DOI: 10.1002/anie.200500992
– One-Nanometer-Scale Size-Controlled Synthesis of Monodisperse Magnetic Iron Oxide Nanoparticles
(C) 2872 – 2877 [2932 – 2937]
DOI: 10.1002/anie.200461665
– Preparation of a Magnetically Switchable Bio-electrocatalytic System Employing Cross-linked Enzyme Aggregates in Magnetic Mesocellular Carbon Foam
(C) 7427 – 7432 [7593 – 7598]
DOI: 10.1002/anie.200502995
Hyman, B. T. (C) 5452 – 5456 [5588 – 5592]

I

Ibáñez, S. (C) 2407 – 2410 [2459 – 2462]
Ibberson, R. M. (C) 7733 – 7736 [7911 – 7914]
Ibrahem, I. (C) 1343 – 1345 [1367 – 1369], 4877 – 4880 [4955 – 4958]
Ichikawa, S. (C) 1854 – 1856 [1888 – 1890]
Ichikawa, Y.
– Total Synthesis of Glycocinnasperimicin D
(C) 4372 – 4375 [4446 – 4449]
DOI: 10.1002/anie.200500892
Ichinohe, M. (C) 6378 – 6381 [6536 – 6539]
Ichinose, I.
– Dried Foam Films: Self-Standing, Water-Free, Reversed Bilayers of Amphiphilic Compounds
(C) 4532 – 4535 [4608 – 4611]
DOI: 10.1002/anie.200500036
Ichinose, I. (C) 7048 – 7053 [7210 – 7215]
Ichinose, K. (C) 1121 – 1125 [1145 – 1149]
Iddles, D. M. (C) 7733 – 7736 [7911 – 7914]
Ienco, A. (C) 3429 – 3432 [3495 – 3498]
Igarashi, H. (C) 2774 – 2777 [2834 – 2837]
Igarashi, S. (C) 1997 – 2001 [2033 – 2037]
Igashira-Kamiyama, A. (C) 1088 – 1092 [1112 – 1116]
Ihara, Y. (C) 7950 – 7954 [8164 – 8168]
Ihori, Y. (C) 761 – 764 [771 – 774]
Iida, H. (C) 1704 – 1706 [1732 – 1734]
Ikariya, T.
– *N*-Methylhydroxylamido(1 –)- and Nitrosomethaneruthenium Complexes Derived from Nitrosyl Complexes: Reversible N-Protonation of an N-Coordinated Nitrosoalkane
(C) 6406 – 6409 [6564 – 6567]
DOI: 10.1002/anie.200501916
Ikegami, S.
– A Recyclable Catalytic System Based on a Temperature-Responsive Catalyst
(C) 4536 – 4538 [4612 – 4614]
DOI: 10.1002/anie.200500574
Ikeno, T. (C) 2524 – 2527 [2580 – 2583]
Ikeue, T. (C) 6899 – 6901 [7059 – 7061]
Ikkala, O. (C) 751 – 756 [761 – 766]
Ikoma, T. (C) 3591 – 3594 [3657 – 3660]
Ilies, M. (C) 6516 – 6521 [6674 – 6679]
Illenberger, E.
– Bond- and Site-Selective Loss of H Atoms from Nucleobases by Very-Low-Energy Electrons (< 3 eV)
(C) 6941 – 6943 [7101 – 7103]
DOI: 10.1002/anie.200502040
Illenberger, E. (C) 1647 – 1650 [1673 – 1676]
Im, S. H. (C) 2154 – 2157 [2192 – 2195]
Imada, H. (C) 7254 – 7257 [7420 – 7423]
Imada, Y.
– An Aerobic, Organocatalytic, and Chemoselective Method for Baeyer – Villiger Oxidation
(C) 1704 – 1706 [1732 – 1734]
DOI: 10.1002/anie.200462429
Imai, H.
– The Hierarchical Architecture of Nacre and Its Mimetic Material
(C) 6571 – 6575 [6729 – 6733]
DOI: 10.1002/anie.200500338
Imam, M. R. (C) 4739 – 4745 [4817 – 4823]

 © 2005 Wiley-VCH Verlag GmbH & Co. KGaA, Weinheim

Imanishi, T.
– Adjustment of the γ Dihedral Angle of an Oligonucleotide P3′ → N5′ Phosphoramidate Enhances Its Binding Affinity towards Complementary Strands
(C) 1944 – 1947 [1980 – 1983]
DOI: 10.1002/anie.200461942
Immel, S. (C) 4201 – 4204 [4273 – 4276]
Inaba, K. (C) 7447 – 7450 [7613 – 7616]
Inada, Y. (C) 7715 – 7717 [7893 – 7895]
Inazu, T. (C) 2534 – 2537 [2590 – 2593]
Ingale, S. (C) 5985 – 5988 [6139 – 6142]
Ingendoh, A. (C) 5242 – 5246 [5376 – 5381]
Ingleson, M. J. (C) 6875 – 6878 [7035 – 7038]
Inokuma, Y. (C) 1856 – 1860 [1890 – 1894]
Inoue, Katsunari (C) 7059 – 7062 [7221 – 7224]
Inoue, Katsuya (C) 4899 – 4903 [4977 – 4981]
Inoue, Y.
– Circular Dichroism of a Chiral Tethered Donor – Acceptor System: Enhanced Anisotropy Factors in Charge-Transfer Transitions by Dimer Formation and by Confinement
(C) 2582 – 2585 [2638 – 2641]
DOI: 10.1002/anie.200462071
Insley, A. (C) 4029 – 4032 [4097 – 4100]
Ioffe, I. N. (C) 234 – 237 [238 – 241], 1846 – 1849 [1880 – 1883]
Ionita, P. (C) 3720 – 3722 [3786 – 3788]
Iovel, I. (C) 238 – 242 [242 – 246], 3913 – 3917 [3981 – 3985]
Irgum, K. (C) 3902 – 3906 [3970 – 3974]
Irie, M.
– Conformational Control of Photochromic Reactivity in a Diarylethene Single Crystal
(C) 2148 – 2151 [2186 – 2189]
DOI: 10.1002/anie.200462426
Isaacs, L.
– The Cucurbit[*n*]uril Family
(R) 4844 – 4870 [4922 – 4949]
DOI: 10.1002/anie.200460675
Isarno, T. (C) 7469 – 7473 [7636 – 7640]
Ishibashi, Y. (C) 7287 – 7290 [7453 – 7456]
Ishida, H. (C) 6759 – 6763 [6917 – 6921]
Ishii, Y.
– Hydroxylation of Benzene to Phenol under Air and Carbon Monoxide Catalyzed by Molybdovanadophosphoric Acid
(C) 2586 – 2588 [2642 – 2644]
DOI: 10.1002/anie.200462769
Ishikawa, K. (C) 1948 – 1951 [1984 – 1987]
Ishikawa, N.
– Quantum Tunneling of Magnetization in Lanthanide Single-Molecule Magnets: Bis(phthalocyaninato)terbium and Bis(phthalocyaninato)dysprosium Anions
(C) 2931 – 2935 [2991 – 2995]
DOI: 10.1002/anie.200462638
– The Effect of the f – f Interaction on the Dynamic Magnetism of a Coupled $4f^8$ System in a Dinuclear Terbium Complex with Phthalocyanines
(C) 731 – 733 [741 – 743]
DOI: 10.1002/anie.200461546
Ishimaru, T. (C) 4204 – 4207 [4276 – 4279]
Ishimura, K. (C) 6553 – 6556 [6711 – 6714]
Ishitani, H. (C) 761 – 764 [771 – 774]
Ishiuchi, S.-i. (C) 6149 – 6151 [6305 – 6307]
Ismagilov, R. F.
– A Microfluidic Approach for Screening Submicroliter Volumes against Multiple Reagents by Using Preformed Arrays of Nanoliter Plugs in a Three-Phase Liquid/Liquid/Gas Flow
(C) 2520 – 2523 [2576 – 2579]
DOI: 10.1002/anie.200462857
Isobe, M. (C) 4372 – 4375 [4446 – 4449]
Itagaki, Y. (C) 7097 – 7100 [7259 – 7262]
Ito, H. (C) 4547 – 4549 [4623 – 4625]
Ito, T. (C) 2534 – 2537 [2590 – 2593]
Ito, Y.
– Divergent Synthesis of Sialylated Glycan Chains: Combined Use of Polymer Support, Resin Capture – Release, and Chemoenzymatic Strategies
(C) 4218 – 4224 [4290 – 4296]
DOI: 10.1002/anie.200500777
– Synthetic Substrates for an Endoplasmic Reticulum Protein-Folding Sensor, UDP-Glucose: Glycoprotein Glucosyltransferase
(C) 7950 – 7954 [8164 – 8168]
DOI: 10.1002/anie.200502723
Itoh, M. (C) 7104 – 7106 [7266 – 7268]
Itoh, N. (C) 2922 – 2925 [2982 – 2985]
Itzhaki, L. (C) 7432 – 7435 [7598 – 7601]
Iuchi, M. (C) 5103 – 5106 [5233 – 5236]
Ivanov, I. (C) 6685 – 6689 [6843 – 6847]
Ivanov, S. A. (C) 6848 – 6854 [7008 – 7014]
Ivanova, A. (C) 7764 – 7767 [7942 – 7945]
Iwakura, I. (C) 2524 – 2527 [2580 – 2583]
Iwamoto, M.
– Improvement in Photocyclization Efficiency of Diaryl Ethenes by Adjusting the Pore Size of Mesoporous Silica
(C) 7233 – 7236 [7399 – 7402]
DOI: 10.1002/anie.200501992
Iwasawa, N.
– Complexation-Initiated Intramolecular [4 + 2] Cycloaddition: Construction of Bridged-Type Cycloadducts
(C) 7447 – 7450 [7613 – 7616]
DOI: 10.1002/anie.200502313
– Rhenium(I)-Catalyzed Intramolecular Geminal Carbofunctionalization of Alkynes: Tandem Cyclization of ω-Acetylenic Dienol Silyl Ethers
(C) 468 – 470 [472 – 474]
DOI: 10.1002/anie.200461559
Iwata, K. (C) 4568 – 4571 [4644 – 4647]
Iwata, Y. (C) 1532 – 1536 [1556 – 1560], 5094 – 5097 [5224 – 5227]
Iyer, R. G. (C) 3552 – 3555 [3618 – 3621]

Jackson, G. (C) 4539 – 4543 [4615 – 4619]
Jackson, R. F. W.
– Vanadium-Catalyzed Sulfur Oxidation/Kinetic Resolution in the Synthesis of Enantiomerically Pure Alkyl Aryl Sulfoxides
(C) 7221 – 7223 [7387 – 7389]
DOI: 10.1002/anie.200503046
Jacob, D. S. (C) 6560 – 6563 [6718 – 6721]
Jacob, J. (C) 1520 – 1525 [1544 – 1549]
Jacobs, P. A.
– Bromide-Assisted Oxidation of Substituted Phenols with Hydrogen Peroxide to the Corresponding *p*-Quinol and *p*-Quinol Ethers over WO_4^{2-}-Exchanged Layered Double Hydroxides
(C) 310 – 313 [314 – 317]
DOI: 10.1002/anie.200461555
Jacobs, P. A. (C) 5687 – 5690 [5833 – 5836]
Jacobsen, E. N.
– Efficient Total Syntheses of (−)-Colombiasin A and (−)-Elisapterosin B: Application of the Cr-Catalyzed Asymmetric Quinone Diels – Alder Reaction
(C) 6046 – 6050 [6200 – 6204]
DOI: 10.1002/anie.200502178
– Enantioselective Thiourea-Catalyzed Acyl-Mannich Reactions of Isoquinolines
(C) 6700 – 6704 [6858 – 6862]
DOI: 10.1002/anie.200502277
– Highly Enantio- and Regioselective Quinone Diels – Alder Reactions Catalyzed by a Tridentate [(Schiff Base)Cr^{III}] Complex
(C) 6043 – 6046 [6197 – 6200]
DOI: 10.1002/anie.200502176
– Highly Enantioselective Catalytic Conjugate Addition of N-Heterocycles to α,β-Unsaturated Ketones and Imides
(C) 2393 – 2397 [2445 – 2449]
DOI: 10.1002/anie.200463058
– Highly Enantioselective Thiourea-Catalyzed Nitro-Mannich Reactions
(C) 466 – 468 Corrigendum: 7327 [470 – 472 Corrigendum: 7493]
DOI: 10.1002/anie.200461814
Jacques, O. (C) 4073 – 4075 [4141 – 4143]
Jacques, S. (C) 7725 – 7729 [7903 – 7907]
Jacquot, D. E. N. (C) 2295 – 2298 [2336 – 2338]
Jahreis, G. (C) 1408 – 1412 [1432 – 1437]
Jain, A. (C) 1226 – 1229 [1252 – 1255]
Jäkle, F.
– Reversible Expansion and Contraction of a 1,2-Diborylated Ferrocene Dimer Promoted by Redox Chemistry and Nucleophile Binding
(C) 5428 – 5433 [5564 – 5569]
DOI: 10.1002/anie.200502148
Jamison, T. F.
– Catalytic Reductive Coupling of Epoxides and Aldehydes: Epoxide-Ring Opening Precedes Carbonyl Reduction
(C) 129 – 132 [131 – 134]
DOI: 10.1002/anie.200461705
Jana, S. (C) 4804 – 4808 [4882 – 4886]
Janardanan, D. (C) 5655 – 5658 [5800 – 5803]
Jancik, V. (C) 5090 – 5093 [5220 – 5223], 6016 – 6018 [6170 – 6172]
Janda, K. D.
– Enzymatic Incorporation of an Antibody-Activated Blue Fluorophore into DNA
(C) 2144 – 2148 [2182 – 2186]
DOI: 10.1002/anie.200461143
Janey, J. M.
– Recent Advances in Catalytic, Enantioselective α Aminations and α Oxygenations of Carbonyl Compounds
(M) 4292 – 4300 [4364 – 4372]
DOI: 10.1002/anie.200462314
Jang, W.-D. (C) 419 – 423 [423 – 427]
Jansen, M.
– Dibariumplatinide: $(Ba^{2+})_2Pt^{2-}\cdot 2e^-$ and Its Relation to the Alkaline-Earth-Metal Subnitrides
(C) 770 – 773 [780 – 783]
DOI: 10.1002/anie.200462055
– $[Tl_8]^{6-}$ in Cs_8Tl_8O: A Naked Eight-Vertex *closo*-Deltaeder as a Cluster Anion
(C) 7639 – 7643 [7813 – 7816]
DOI: 10.1002/anie.200502283
Jansen, M. (C) 4169 – 4172 [4241 – 4244]

 © 2005 Wiley-VCH Verlag GmbH & Co. KGaA, Weinheim

Jansson, K. (C) 7269 – 7273 [7435 – 7439]
Janzen, M. C. (C) 4528 – 4532 [4604 – 4608]
Jaroniec, J. (C) 2723 – 2727 [2783 – 2787]
Jarvo, E. R. (C) 6043 – 6046 [6197 – 6200], 6046 – 6050 [6200 – 6204]
Jastrzebski, J. T. B. H. (M) 1448 – 1454 [1472 – 1478]
Jayaprakash, K. N. (C) 5894 – 5898 [6044 – 6048]
Jayaprakash, P. (C) 5878 – 5882 [6028 – 6032]
Jeffery, J. C. (C) 6909 – 6912 [7069 – 7072]
Jeffery, S. P. (C) 1217 – 1220 [1243 – 1246]
Jeitschko, W.
– The Metal Flux: A Preparative Tool for the Exploration of Intermetallic Compounds (R) 6996 – 7023 [7156 – 7184] DOI: 10.1002/anie.200462170
Jelinek, R.
– Visualization of Membrane Processes in Living Cells by Surface-Attached Chromatic Polymer Patches (C) 1092 – 1096 [1116 – 1120] DOI: 10.1002/anie.200462393
Jenkins, H. D. B.
– The Autoionization of $[TiF_4]$ by Cation Complexation with [15]Crown-5 To Give $[TiF_2([15]crown\text{-}5)][Ti_4F_{18}]$ Containing the Tetrahedral $[Ti_4F_{18}]^{2-}$ Ion (C) 7958 – 7961 [8172 – 8175] DOI: 10.1002/anie.200502900
Jennings, M. C. (C) 1499 – 1504 [1523 – 1528]
Jensen, F.
– Singlet Oxygen: *Christopher S. Foote* (O) 6268 [6424] DOI: 10.1002/anie.200502934
Jensen, K. F.
– A Microfabricated Gas – Liquid Segmented Flow Reactor for High-Temperature Synthesis: The Case of CdSe Quantum Dots (C) 5447 – 5451 [5583 – 5587] DOI: 10.1002/anie.200500792
Jeon, W. S. (C) 87 – 91 [89 – 93]
Jeong, B.-S. (C) 1383 – 1385 [1407 – 1409]
Jeong, K.-S.
– Indole-Based Macrocycles as a Class of Receptors for Anions (C) 7926 – 7929 [8140 – 8143] DOI: 10.1002/anie.200503121
Jeong, U. (C) 3099 – 3103 [3159 – 3163]
Jérôme, C.
– Electrografting of Poly(ethylene glycol) Acrylate: A One-Step Strategy for the Synthesis of Protein-Repellent Surfaces (C) 5505 – 5509 [5641 – 5645] DOI: 10.1002/anie.200500639
Jérôme, R.
– Effective Cobalt Mediation of the Radical Polymerization of Vinyl Acetate in Suspension (C) 3439 – 3442 [3505 – 3508] DOI: 10.1002/anie.200500112
– Highly Efficient Cobalt-Mediated Radical Polymerization of Vinyl Acetate (C) 1101 – 1104 [1125 – 1128] DOI: 10.1002/anie.200461333
Jérôme, R. (C) 5505 – 5509 [5641 – 5645]
Jeso, V. (C) 3895 – 3899 [3963 – 3967]
Jessani, N. (C) 2400 – 2403 [2452 – 2455]
Jesse, W. (C) 4349 – 4352 [4423 – 4426]
Jessiman, A. S. (C) 5433 – 5438 [5569 – 5574]
Jestin, J. (C) 3260 – 3264 [3324 – 3328]
Jew, S.-s.
– Highly Enantioselective Epoxidation of 2,4-Diarylenones by Using Dimeric Cinchona Phase-Transfer Catalysts: Enhancement of Enantioselectivity by Surfactants (C) 1383 – 1385 [1407 – 1409] DOI: 10.1002/anie.200462254
Jhung, S. H. (C) 556 – 560 [562 – 566]
Ji, M. (C) 7119 – 7123 [7281 – 7285]
Ji, Y. (C) 6025 – 6029 [6179 – 6183]
Jia, C.-J. (C) 4328 – 4333 [4402 – 4407]
Jia, G.
– A Neutron Diffraction Study of $[OsClH_3(PPh_3)_3]$: A Complex Containing a Highly "Stretched" Dihydrogen Ligand (C) 7227 – 7230 [7393 – 7396] DOI: 10.1002/anie.200502297
Jia, X. (C) 4018 – 4021 [4086 – 4089]
Jia, X.-R.
– A Dendron Based on Natural Amino Acids: Synthesis and Behavior as an Organogelator and Lyotropic Liquid Crystal (C) 6025 – 6029 [6179 – 6183] DOI: 10.1002/anie.200500359
Jiang, D.-L. (C) 419 – 423 [423 – 427]
Jiang, H. (C) 7922 – 7925 [8136 – 8139]
Jiang, J. (C) 2291 – 2295 [2331 – 2335]
Jiang, Lei
– The Fabrication and Switchable Superhydrophobicity of TiO_2 Nanorod Films (C) 5115 – 5118 [5245 – 5248] DOI: 10.1002/anie.200501337
Jiang, Ling (C) 4338 – 4342 [4412 – 4416]
Jiang, X. (C) 4749 – 4753 [4827 – 4831]
Jiang, X.-K. (C) 5725 – 5729 [5871 – 5875]
Jiang, Xuan (C) 4782 – 4785 [4860 – 4863]
Jiang, Xuefeng (C) 5275 – 5278 [5409 – 5412]
Jiang, Y. (C) 6387 – 6391 [6545 – 6549]
Jiang, Z. (C) 4092 – 4095 [4161 – 4164]
Jiao, F. (C) 6550 – 6553 [6708 – 6711]
Jicsinsky, L. (C) 4092 – 4095 [4161 – 4164]
Jiménez, A. I.
– First Observation of Two Consecutive γ Turns in a Crystalline Linear Dipeptide (C) 396 – 399 [400 – 403] DOI: 10.1002/anie.200461230
Jiménez, O. (C) 6521 – 6525 [6679 – 6683]
Jiménez-Aparicio, R.
– A Spin-Admixed Ruthenium Complex (C) 305 – 307 [309 – 311] DOI: 10.1002/anie.200461463
Jiménez-Barbero, J.
– 1D Saturation Transfer Difference NMR Experiments on Living Cells: The DC-SIGN/Oligomannose Interaction (C) 296 – 298 [300 – 302] DOI: 10.1002/anie.200461574
Jiménez-Barbero, J. (C) 2360 – 2364 [2412 – 2416]
Jin, E. (C) 952 – 955 [974 – 977]
Jin, G.-X.
– Formation of Ir–Rh and Ir–Mo Bonds by Using an Ancillary *ortho*-Carborane-1,2-diselenolato Ligand (C) 259 – 262 [264 – 267] DOI: 10.1002/anie.200461348
Jin, J. (C) 4532 – 4535 [4608 – 4611]
Jin, S. (C) 7427 – 7432 [7593 – 7598]
Jin, W. (C) 3885 – 3889 [3953 – 3957]
Jin, X. (C) 5275 – 5278 [5409 – 5412]
Jisr, R. M. (C) 782 – 785 [792 – 795]
Jitsukawa, K. (C) 5698 – 5701 [5844 – 5847]
Jo, K. (C) 2774 – 2777 [2834 – 2837]
Jockusch, S. (C) 7097 – 7100 [7259 – 7262]
Johansson, M. P. (C) 1843 – 1846 [1877 – 1880]
John, H. (C) 2447 – 2451 [2501 – 2505]
John, M. P. (C) 1543 – 1545 [1567 – 1569]
Johnson, A. P.
– A De Novo Designed Inhibitor of D-Ala – D-Ala Ligase from *E. coli* (C) 6403 – 6406 [6561 – 6564] DOI: 10.1002/anie.200501662
Johnson, J. S.
– Metallophosphite-Induced Nucleophilic Acylation of α,β-Unsaturated Amides: Facilitated Catalysis by a Diastereoselective Retro [1,4] Brook Rearrangement (C) 2377 – 2379 Corrigendum: 4660 [2429 – 2431 Corrigendum: 4735] DOI: 10.1002/anie.200462795
Johnston, S. M. (C) 1830 – 1833 [1864 – 1867]
Jois, S. D. S. (C) 5476 – 5479 [5612 – 5615], 6333 – 6337 [6491 – 6495]
Jolivet, J.-P. (C) 5691 – 5694 [5837 – 5840]
Jonas, A. M. (C) 5505 – 5509 [5641 – 5645]
Jonas, U.
– Surface Modification with Orthogonal Photosensitive Silanes for Sequential Chemical Lithography and Site-Selective Particle Deposition (C) 4707 – 4712 [4785 – 4791] DOI: 10.1002/anie.200500092
Jones, A. C.
– Quantitative Spatial Mapping of Mixing in Microfluidic Systems (C) 6512 – 6516 [6670 – 6674] DOI: 10.1002/anie.200500558
Jones, C. (C) 3606 – 3609 [3672 – 3675]
Jones, D. D. (C) 6337 – 6341 [6495 – 6499]
Jones, N. D. (C) 2005 – 2008 [2041 – 2044]
Jones, P. G. (C) 6001 – 6004 [6155 – 6158]
Joo, J. (C) 7411 – 7414 [7577 – 7580]
Joppek, W. Corrigendum: 506
Jørgensen, K. A.
– Direct Organocatalytic and Highly Enantio- and Diastereoselective Mannich Reactions of α-Substituted α-Cyanoacetates (C) 2896 – 2899 [2956 – 2959] DOI: 10.1002/anie.200500144
– Enantioselective Formation of Stereogenic Carbon – Fluorine Centers by a Simple Catalytic Method (C) 3703 – 3706 [3769 – 3772] DOI: 10.1002/anie.200500395
– Enantioselective Organocatalyzed α Sulfenylation of Aldehydes (C) 794 – 797 [804 – 807] DOI: 10.1002/anie.200462101
– Organocatalytic Diastereo- and Enantioselective Annulation Reactions—Construction of Optically Active 1,2-Dihydroisoquinoline and 1,2-Dihydrophthalazine Derivatives (C) 6058 – 6063 [6212 – 6217] DOI: 10.1002/anie.200501900
Joseph, A. (C) 6560 – 6563 [6718 – 6721]
Jovanovski, G. (C) 1251 – 1254 [1277 – 1280]
Joyce, G. F.
– A DNA-Templated Aldol Reaction as a Model for the Formation of Pentose Sugars in the RNA World (C) 7580 – 7583 [7752 – 7755] DOI: 10.1002/anie.200503387
Juanico, M. P. (C) 4187 – 4192 [4259 – 4264]
Juaristi, E. (C) 2360 – 2364 [2412 – 2416]
Jung, T. A. (C) 7394 – 7398 [7560 – 7564]
Jung, V. (C) 2806 – 2808 [2866 – 2869]
Jure, M.
– Efficiency in Nonenzymatic Kinetic Resolution (R) 3974 – 4001 [4040 – 4069] DOI: 10.1002/anie.200460842

 © 2005 Wiley-VCH Verlag GmbH & Co. KGaA, Weinheim

Jusélius, J. (C) 1843 – 1846 [1877 – 1880]
Juskowiak, B. (C) 5067 – 5070 [5195 – 5198]
Jux, N. (C) 2015 – 2018 [2051 – 2054]

Kabalka, G. W.
– Organoboranes: *Herbert C. Brown*
(O) 1438 [1462 – 1463]
DOI: 10.1002/anie.200500286
Kabir, N. (C) 6504 – 6508 [6662 – 6666]
Kaden, P. (C) 1636 – 1639 [1662 – 1666]
Kadish, K. M.
– Reductive N Alkylation of Cyclo[8]pyrroles
(C) 83 – 87 [85 – 89]
DOI: 10.1002/anie.200461801
Kadodwala, M.
– Going Beyond the Physical: Instilling Chirality onto the Electronic Structure of a Metal
(C) 1830 – 1833 [1864 – 1867]
DOI: 10.1002/anie.200462265
Kadoh, Y. (C) 5113 – 5115 [5243 – 5245]
Kaftory, M. (C) 5087 – 5089 [5217 – 5219]
Kahlenberg, V. (C) 1134 – 1136 [1158 – 1160]
Kaim, W.
– Theoretical and Experimental Evidence for a New Kind of Spin-Coupled Singlet Species: Isomeric Mixed-Valent Complexes Bridged by a Radical Anion Ligand
(C) 5655 – 5658 [5800 – 5803]
DOI: 10.1002/anie.200501075
– Three-Spin System with a Twist: A Bis(semiquinonato)copper Complex with a Nonplanar Configuration at the Copper(II) Center
(C) 2103 – 2106 [2140 – 2143]
DOI: 10.1002/anie.200462339
Kaindl, R. (C) 1134 – 1136 [1158 – 1160]
Kaiser, F. (C) 3447 – 3452 [3513 – 3518]
Kaitner, B. (C) 1251 – 1254 [1277 – 1280]
Kaizer, J. (C) 3690 – 3694 [3756 – 3760]
Kaizu, Y.
– The Effect of the f – f Interaction on the Dynamic Magnetism of a Coupled $4f^8$ System in a Dinuclear Terbium Complex with Phthalocyanines
(C) 731 – 733 [741 – 743]
DOI: 10.1002/anie.200461546
Kakeya, H. (C) 3110 – 3115 [3170 – 3175]
Kakiuchi, K. (C) 7283 – 7287 [7449 – 7453]
Kakuno, H. (C) 7257 – 7260 [7423 – 7426]
Kalevaru, V. N. (C) 6771 – 6774 [6929 – 6933]
Kalisch, A. (C) 96 – 98 [98 – 100]
Kallitsis, I. (C) 284 – 287 [288 – 291]
Kálmán, F. K. (C) 6920 – 6923 [7080 – 7083]
Kamata, K. (C) 5136 – 5141 [5266 – 5271]
Kamata, Y. (C) 6928 – 6931 [7088 – 7091]
Kamer, P. C. J. (C) 4385 – 4388 [4459 – 4462]
Kameyama, A. (C) 4547 – 4549 [4623 – 4625]
Kameyama, K. (C) 4763 – 4766 [4841 – 4844]
Kamienska-Trela, K. (C) 1230 – 1232 [1256 – 1258]
Kamijo, S.
– Oxindole Synthesis through Intramolecular Nucleophilic Addition of Vinylpalladiums to Aryl Isocyanates
(C) 7718 – 7721 [7896 – 7899]
DOI: 10.1002/anie.200502252
Kamitani, R. (C) 91 – 96 [93 – 98]
Kamiya, M. (C) 5439 – 5441 [5575 – 5577]
Kammler, D. C. (C) 6715 – 6718 [6873 – 6876]
Kanamori, D. (C) 969 – 972 [991 – 994]
Kanatzidis, M. G.
– $\{Sn[Zn_4Sn_4S_{17}]\}^{6-}$: A Robust Open Framework Based on Metal-Linked Penta-Supertetrahedral $[Zn_4Sn_4S_{17}]^{10-}$ Clusters with Ion-Exchange Properties
(C) 3552 – 3555 [3618 – 3621]
DOI: 10.1002/anie.200500214
– The Metal Flux: A Preparative Tool for the Exploration of Intermetallic Compounds
(R) 6996 – 7023 [7156 – 7184]
DOI: 10.1002/anie.200462170
Kanazawa, C. (C) 7718 – 7721 [7896 – 7899]
Kaneda, K.
– Heterotrimetallic RuMnMn Species on a Hydrotalcite Surface as Highly Efficient Heterogeneous Catalysts for Liquid-Phase Oxidation of Alcohols with Molecular Oxygen
(C) 3423 – 3426 [3489 – 3492]
DOI: 10.1002/anie.200462600
Kaneko, H. (C) 7887 – 7891 [8099 – 8104]
Kaneko, K. (C) 2030 – 2033 [2066 – 2069]
Kaneko, M. (C) 1336 – 1340 [1360 – 1364]
Kanemasa, S. (C) 4204 – 4207 [4276 – 4279]
Kang, B. (C) 455 – 457 [459 – 461]
Kang, E.-T.
– GaAs – Polymer Hybrids Formed by Surface-Initiated Atom-Transfer Radical Polymerization of Methyl Methacrylate
(C) 1104 – 1107 [1128 – 1131]
DOI: 10.1002/anie.200461570
Kang, H. (C) 7922 – 7925 [8136 – 8139]
Kang, J. (C) 6902 – 6905 [7062 – 7065]
Kang, M. (C) 2872 – 2877 [2932 – 2937]
Kang, T. S. (C) 6333 – 6337 [6491 – 6495]
Kang, X.-f. (C) 1495 – 1499 [1519 – 1523]
Kang, Y. (C) 409 – 412 [413 – 416]
Kang, Y.-J. (C) 4053 – 4055 [4121 – 4123]
Kano, K.
– Dioxygen Binding to a Simple Myoglobin Model in Aqueous Solution
(C) 435 – 438 [439 – 442]
DOI: 10.1002/anie.200461609
Kano, K. (C) 7104 – 7106 [7266 – 7268]
Kano, T. (C) 3055 – 3057 [3115 – 3117]
Kanoh, N. (C) 3559 – 3562 Corrigendum: 4282 [3625 – 3628 Corrigendum: 4354]
Kantam, M. L. (C) 322 – 325 [326 – 329]
Kaper, H. (H) 3809 – 3811 [3876 – 3878]
Kapitan, P. (C) 3609 – 3613 [3675 – 3679]
Kappe, C. O.
– All the Rave in Microwaves
(T) 7666 – 7669 [7840 – 7843]
DOI: 10.1002/anie.200503543
Kareev, I. E.
– Trifluoromethylated Endohedral Metallofullerenes: Synthesis and Characterization of $Y@C_{82}(CF_3)_5$
(C) 1846 – 1849 [1880 – 1883]
DOI: 10.1002/anie.200461497
Kareev, I. E. (C) 7984 – 7987 [8198 – 8201]
Karimata, H. (C) 3740 – 3744 [3806 – 3810]
Karpov, A. (C) 770 – 773 [780 – 783], 7639 – 7643 [7813 – 7816]
Karpov, A. S. (C) 6951 – 6956 [7112 – 7117]
Kasatkin, I. (C) 4704 – 4707 [4782 – 4785]
Kaspar, L. T. (C) 5972 – 5974 [6126 – 6128]
Kasparkova, J. (C) 2885 – 2887 [2945 – 2947]
Kasper, P. T. (C) 7946 – 7950 [8160 – 8164]
Kassel, W. S. (C) 5428 – 5433 [5564 – 5569]
Katagiri, H. (C) 3867 – 3870 [3935 – 3938]
Kataoka, K.
– A Synthetic Block Copolymer Regulates S1 Nuclease Fragmentation of Supercoiled Plasmid DNA
(C) 3544 – 3548 [3610 – 3614]
DOI: 10.1002/anie.200500201
– Supramolecular Nanocarrier of Anionic Dendrimer Porphyrins with Cationic Block Copolymers Modified with Polyethylene Glycol to Enhance Intracellular Photodynamic Efficacy
(C) 419 – 423 [423 – 427]
DOI: 10.1002/anie.200461603
Katayama, K. (C) 2922 – 2925 [2982 – 2985]
Katayev, E. A. (C) 7386 – 7390 [7552 – 7556]
Katayose, S. (C) 3544 – 3548 [3610 – 3614]
Kato, Hideki (C) 3565 – 3568 [3631 – 3634]
Kato, Hirohisa (C) 3871 – 3874 [3939 – 3942]
Kato, K. (C) 920 – 923 [942 – 945], 4899 – 4903 [4977 – 4981]
Kato, M. (C) 5097 – 5100 [5227 – 5230], 7301 – 7304 [7467 – 7470]
Kato, N. (C) 7301 – 7304 [7467 – 7470]
Kato, Tatsuhisa
– The Importance of a β – β Bond for Long-Range Antiferromagnetic Coupling in Directly Linked Copper(II) and Silver(II) Diporphyrins
(C) 6899 – 6901 [7059 – 7061]
DOI: 10.1002/anie.200501943
Kato, Tatsuhisa (C) 3282 – 3285 [3346 – 3349]
Kato, Tsuyoshi (C) 5497 – 5500 [5633 – 5636]
Katsuki, T.
– Construction of Pseudo-Heterochiral and Homochiral Di-μ-oxotitanium(Schiff base) Dimers and Enantioselective Epoxidation Using Aqueous Hydrogen Peroxide
(C) 4935 – 4939 [5015 – 5019]
DOI: 10.1002/anie.200501318
– Synthesis of an Optically Active C_1-Symmetric Al(salalen) Complex and Its Application to the Catalytic Hydrophosphonylation of Aldehydes
(C) 4600 – 4602 [4676 – 4678]
DOI: 10.1002/anie.200501008
Katterle, M. (C) 3147 – 3151 [3208 – 3212]
Katz, E. (C) 4554 – 4557 [4630 – 4633], 4791 – 4794 [4869 – 4872]
Katz, T. J.
– Olefin Metatheses and Related Reactions Initiated by Carbene Derivatives of Metals in Low Oxidation States
(M) 3010 – 3019 [3070 – 3079]
DOI: 10.1002/anie.200462442
Kaufman, T. S.
– The Quest for Quinine: Those Who Won the Battles and Those Who Won the War
(R) 854 – 885 [876 – 907]
DOI: 10.1002/anie.200400663
Kaufmann, G. F. (C) 2144 – 2148 [2182 – 2186]
Kaupp, M.
– $[Pb_5\{Mo(CO)_3\}_2]^{4-}$: A Complex Containing a Planar Pb_5 Unit
(C) 2092 – 2096 [2129 – 2133]
DOI: 10.1002/anie.200462342
Kawaguchi, H. (C) 4352 – 4355 [4426 – 4429]
Kawaguchi, T. (C) 2413 – 2416 [2465 – 2468]
Kawahara, S. (C) 5433 – 5438 [5569 – 5574]
Kawajiri, R. (C) 4899 – 4903 [4977 – 4981]
Kawakami, Y. (C) 1336 – 1340 [1360 – 1364]
Kawamoto, T. (C) 1088 – 1092 [1112 – 1116]

 © 2005 Wiley-VCH Verlag GmbH & Co. KGaA, Weinheim

Kawano, M.
– A Two-in-One Crystal: Uptake of Two Different Guests into Two Distinct Channels of a Biporous Coordination Network (C) 1962 – 1964 [1998 – 2000] DOI: 10.1002/anie.200462201
– In Situ Observation of a Reversible Single-Crystal-to-Single-Crystal Apical-Ligand-Exchange Reaction in a Hydrogen-Bonded 2D Coordination Network (C) 2151 – 2154 [2189 – 2192] DOI: 10.1002/anie.200462214
– pH-Switchable Through-Space Interaction of Organic Radicals within a Self-Assembled Coordination Cage (C) 5322 – 5325 [5456 – 5459] DOI: 10.1002/anie.200501568
Kawano, M. (C) 1810 – 1813 [1844 – 1847]
Kawasaki, T. (C) 2774 – 2777 [2834 – 2837]
Kawase, T.
– A Hexapentaene-Extended Quinocumulene Cyclotrimerized to a Tricyclobutabenzene Derivative (C) 316 – 319 [320 – 323] DOI: 10.1002/anie.200461608
– Allenophane and Allenoacetylenic Macrocycles: A New Class of Chiral Cyclophanes (H) 7334 – 7336 [7500 – 7502] DOI: 10.1002/anie.200502474
Kawashima, Y. (C) 6149 – 6151 [6305 – 6307]
Kawauchi, S. (C) 419 – 423 [423 – 427]
Kay, B. D. (C) 3578 – 3582 [3644 – 3648]
Kaynak, B. (C) 1343 – 1345 [1367 – 1369]
Kays, D. L. (née Coombs) (C) 7457 – 7460 [7623 – 7626]
Kazlauskas, R. J.
– Molecular Basis of Perhydrolase Activity in Serine Hydrolases (C) 2742 – 2746 [2802 – 2806] DOI: 10.1002/anie.200463006
Kazmaier, U.
– Amino Acids—Valuable Organocatalysts in Carbohydrate Synthesis (H) 2186 – 2188 Corrigendum: 3509 [2224 – 2226 Corrigendum: 3575] DOI: 10.1002/anie.200462873
– Efficient 1,5-Chirality Transfer in Palladium-Catalyzed Allylic Alkylations of Chelated Amino Acid Ester Enolates (C) 3303 – 3306 [3368 – 3371] DOI: 10.1002/anie.200500095
Keegan, N. (C) 4801 – 4804 [4879 – 4882]
Keizer, T. S. (C) 2403 – 2406 [2455 – 2458]
Kelch, S. (C) 1188 – 1192 [1212 – 1216]
Keller, P. A. (R) 5384 – 5427 [5518 – 5563]
Keller, S.
– Membrane-Mimetic Nanocarriers Formed by a Dipalmitoylated Cell-Penetrating Peptide (C) 5252 – 5255 [5386 – 5389] DOI: 10.1002/anie.200500519
Keller, S. (C) 1195 – 1198 [1219 – 1223], 7887 – 7891 [8099 – 8104]
Kelley, S. O.
– Phototoxicity of Peptidoconjugates Modulated by a Single Amino Acid (C) 2542 – 2546 [2598 – 2602] DOI: 10.1002/anie.200462836
Kellogg, R. M. (C) 2373 – 2376 [2425 – 2428]
Kelly, T. R.
– Molecular Motors: Synthetic DNA-Based Walkers Inspired by Kinesin (H) 4124 – 4127 [4194 – 4198] DOI: 10.1002/anie.200500568
Kemnitz, E. (C) 234 – 237 [238 – 241], 432 – 435 [436 – 439]
Kemper, J. (C) 4914 – 4917 [4993 – 4995]
Kempter, A. (C) 2943 – 2946 [3003 – 3007]
Kennedy, A. R. (C) 68 – 72 [70 – 74], 3459 – 3462 [3525 – 3528], 6018 – 6021 [6172 – 6175]
Kent, S. B.
– Total Chemical Synthesis and X-ray Crystal Structure of a Protein Diastereomer: [D-Gln35]Ubiquitin (C) 3852 – 3856 [3920 – 3924] DOI: 10.1002/anie.200463040
Kerckhoffs, J. M. C. A. (C) 3248 – 3253 [3312 – 3317]
Kern, K.
– Templated Growth of Metal – Organic Coordination Chains at Surfaces (C) 6142 – 6145 [6298 – 6301] DOI: 10.1002/anie.200502007
– Two-Dimensional Adatom Gas Bestowing Dynamic Heterogeneity on Surfaces (C) 1488 – 1491 [1512 – 1515] DOI: 10.1002/anie.200461390
Kern, K. (C) 7294 – 7297 [7460 – 7463]
Kervio, E. (C) 6588 – 6592 [6746 – 6750]
Kesanli, B. (C) 72 – 75 [74 – 77]
Kessler, H.
– Cooperative Binding of p53 to DNA: Regulation by Protein – Protein Interactions through a Double Salt Bridge (C) 5247 – 5251 [5381 – 5386] DOI: 10.1002/anie.200501887
Kessler, H. (C) 423 – 426 [427 – 430], 3145 – 3147 Corrigendum: 3509 [3205 – 3207 Corrigendum: 3575]
Kettle, J. (C) 944 – 946 [966 – 968]
Khairallah, G. N. (C) 728 – 731 [738 – 741]
Khan, S. I. (C) 3050 – 3055 [3110 – 3115]
Khan, T. A. (C) 1356 – 1360 [1380 – 1384]
Khavrel, P. A. (C) 1846 – 1849 [1880 – 1883]
Khazanov, E. (C) 2885 – 2887 [2945 – 2947]
Khlystov, O. (C) 6928 – 6931 [7088 – 7091]
Khodeir, L. (C) 6237 – 6241 [6394 – 6397]
Khodorkovsky, V.
– A Rigid Neutral Molecule Involving TTF and TCNQ Moieties with Intrinsic Charge- and Electron-Transfer Properties that Depend on the Polarity of the Solvent (C) 4015 – 4018 [4083 – 4086] DOI: 10.1002/anie.200500812
Khosla, C. (C) 7557 – 7560 [7729 – 7732]
Khrustalev, V. N. (C) 7386 – 7390 [7552 – 7556]
Kibler, L. A.
– Tuning Reaction Rates by Lateral Strain in a Palladium Monolayer (C) 2080 – 2084 [2116 – 2120] DOI: 10.1002/anie.200462127
Kickelbick, G.
– The Diverse World of Silicon Chemistry (T) 6804 – 6806 [6964 – 6966] DOI: 10.1002/anie.200503350
Kida, M. (C) 6928 – 6931 [7088 – 7091]
Kiebach, R. (C) 5643 – 5647 [5787 – 5792]
Kiener, C. (C) 7978 – 7981 [8192 – 8195]
Kienle, L. (C) 3917 – 3921 [3985 – 3989]
Kienle, M. (C) 3096 – 3099 [3156 – 3159]
Kikuchi, K. (C) 7254 – 7257 [7420 – 7423]
Kikuchi, M. (C) 419 – 423 [423 – 427]
Kilner, C. (C) 7570 – 7574 [7742 – 7746]
Kim, B. G. (C) 1068 – 1071 [1092 – 1095]
Kim, Cheolkyu (C) 6142 – 6145 [6298 – 6301]
Kim, Chulhee (C) 7964 – 7968 [8178 – 8182]
Kim, D. S. (C) 556 – 560 [562 – 566]
Kim, D. W. (C) 4925 – 4929 [5005 – 5009]
Kim, D. Y. (C) 6207 – 6210 [6363 – 6366]
Kim, Do-Youn (C) 7749 – 7752 [7927 – 7930]
Kim, Dong-Yu
– "Grafting-From" Polymerization inside a Polyelectrolyte Hollow-Capsule Microreactor (C) 1096 – 1101 [1120 – 1125] DOI: 10.1002/anie.200460971
Kim, E. (C) 87 – 91 [89 – 93]
Kim, H.-C.
– Oriented Nanoporous Lamellar Organosilicates Templated from Topologically Unsymmetrical Dendritic-Linear Block Copolymers (C) 7574 – 7580 [7746 – 7752] DOI: 10.1002/anie.200501577
Kim, H. G. (C) 4585 – 4589 [4661 – 4665]
Kim, H.-S.
– Preparation of a Magnetically Switchable Bio-electrocatalytic System Employing Cross-linked Enzyme Aggregates in Magnetic Mesocellular Carbon Foam (C) 7427 – 7432 [7593 – 7598] DOI: 10.1002/anie.200502995
Kim, Hee-Joon (C) 87 – 91 [89 – 93]
Kim, Heechul (C) 1840 – 1843 [1874 – 1877]
Kim, Ho-Joong (C) 5810 – 5814 [5960 – 5964]
Kim, Hyoseok (C) 2929 – 2931 [2989 – 2991]
Kim, Hyunseok (C) 1840 – 1843 [1874 – 1877]
Kim, J.-H. (C) 947 – 949 [969 – 971]
Kim, J. H. (C) 1261 – 1265 [1287 – 1291]
Kim, J.-K. (C) 328 – 332 [332 – 336]
Kim, J. S. (C) 1068 – 1071 [1092 – 1095]
Kim, Jae-Young (C) 2872 – 2877 [2932 – 2937]
Kim, Jaeyun (C) 7427 – 7432 [7593 – 7598]
Kim, Jinheung
– Mechanistic Insight into Alcohol Oxidation by High-Valent Iron – Oxo Complexes of Heme and Nonheme Ligands (C) 4235 – 4239 [4307 – 4311] DOI: 10.1002/anie.200500623
Kim, Jongseong (C) 1333 – 1336 [1357 – 1360]
Kim, Ju-Young (C) 1096 – 1101 [1120 – 1125]
Kim, Jungbae
– Preparation of a Magnetically Switchable Bio-electrocatalytic System Employing Cross-linked Enzyme Aggregates in Magnetic Mesocellular Carbon Foam (C) 7427 – 7432 [7593 – 7598] DOI: 10.1002/anie.200502995
Kim, K.
– Molecular Loop Lock: A Redox-Driven Molecular Machine Based on a Host-Stabilized Charge-Transfer Complex (C) 87 – 91 [89 – 93] DOI: 10.1002/anie.200461806
Kim, K. S.
– A Calix[4]imidazolium[2]pyridine as an Anion Receptor (C) 2899 – 2903 [2959 – 2963] DOI: 10.1002/anie.200500119
Kim, K. T. (C) 7964 – 7968 [8178 – 8182]
Kim, M. (C) 1840 – 1843 [1874 – 1877]
Kim, M.-J. (C) 1383 – 1385 [1407 – 1409]
Kim, M. S.
– A Dramatic Spin – Orbit Effect Observed in the Vibrational Frequencies of the Chloroiodomethane Cation (C) 2929 – 2931 [2989 – 2991] DOI: 10.1002/anie.200463090
Kim, N. (C) 6913 – 6915 [7073 – 7075]
Kim, P. H. (C) 1529 – 1532 [1553 – 1556]
Kim, S. B. (C) 7710 – 7715 [7888 – 7893]
Kim, S. C. (C) 2872 – 2877 [2932 – 2937]

 © 2005 Wiley-VCH Verlag GmbH & Co. KGaA, Weinheim

Kim, S.-J.
– $[Re_{12}CS_{17}(CN)_6]^{n-}$ ($n=6$, 8): A Sulfido–Cyanide Rhenium Cluster with an Interstitial Carbon Atom
(C) 6867 – 6871 [7027 – 7031]
DOI: 10.1002/anie.200501911
Kim, S.-Y. (C) 87 – 91 [89 – 93]
Kim, Sangmo (C) 6183 – 6186 [6339 – 6342]
Kim, Sunggak
– Tin-Free Radical Carbonylation: Thiol Ester Synthesis Using Alkyl Allyl Sulfone Precursors, Phenyl Benzenethiosulfonate, and CO
(C) 6183 – 6186 [6339 – 6342]
DOI: 10.1002/anie.200501606
Kim, W. Corrigendum: 1907
Kim, W. B. (C) 778 – 782 [788 – 792]
Kim, Y.-P. (C) 7427 – 7432 [7593 – 7598]
Kimber, M. C. (C) 6157 – 6162 [6313 – 6318]
Kimberley, M. (C) 1121 – 1125 [1145 – 1149]
Kimura, S.
– A Helical Molecule That Exhibits Two Lengths in Response to an Applied Potential
(C) 6330 – 6333 [6488 – 6491]
DOI: 10.1002/anie.200502240
Kindermann, M. (C) 6750 – 6755 [6908 – 6913]
King, F. (C) 3407 – 3411 [3473 – 3477]
King, N. P. (C) 618 – 621 [624 – 627]
Kingston, J. V. (C) 4960 – 4963 [5040 – 5043]
Kini, R. M.
– Effect of C-Terminal Amidation on Folding and Disulfide-Pairing of α-Conotoxin ImI
(C) 6333 – 6337 [6491 – 6495]
DOI: 10.1002/anie.200502300
Kini, R. M. (C) 5476 – 5479 [5612 – 5615]
Kinoshita, H. (C) 2397 – 2400 [2449 – 2452]
Kinscherf, R. (C) 2429 – 2432 [2481 – 2485]
Kintner, C. (C) 1987 – 1990 [2023 – 2026]
Kiran, B. (C) 4968 – 4972 [5048 – 5052], 7251 – 7254 [7417 – 7420]
Kirchner, M. T. (C) 2515 – 2520 [2571 – 2576]
Kirchner, N. (C) 1876 – 1879 [1910 – 1913]
Kirillov, A. M. (C) 4345 – 4349 [4419 – 4423]
Kirillova, M. V. (C) 4345 – 4349 [4419 – 4423]
Kiriy, A.
– Polypyrrole Nanowires Grown from Single Adsorbed Polyelectrolyte Molecules
(C) 6391 – 6394 [6549 – 6552]
DOI: 10.1002/anie.200501354
Kirmse, W.
– Incarcerated Carbenes
(H) 2476 – 2479 [2530 – 2533]
DOI: 10.1002/anie.200500546
Kirsch-Rodeschini, H. (C) 5310 – 5313 [5444 – 5447]
Kirschhock, C. E. A. (C) 400 – 403 [404 – 407]
Kischel, J. (C) 238 – 242 [242 – 246], 3913 – 3917 [3981 – 3985]
Kishida, H. (C) 3240 – 3243 [3304 – 3307], 6484 – 6487 [6642 – 6645]
Kiso, M.
– 1,5-Lactamized Sialyl Acceptors for Various Disialoside Syntheses: Novel Method for the Synthesis of Glycan Portions of Hp-s6 and HLG-2 Gangliosides
(C) 6759 – 6763 [6917 – 6921]
DOI: 10.1002/anie.200501608
Kison, C. (C) 5662 – 5664 [5807 – 5809]
Kita, Y.
– A Double Iodoetherification of σ-Symmetric Diene Acetals for Installing Four Stereogenic Centers in a Single Operation: Short Asymmetric Total Synthesis of Rubrenolide
(C) 734 – 737 [744 – 747]
DOI: 10.1002/anie.200461584
– Domino Reaction of 2,3-Epoxy-1-alcohols and PIFA in the Presence of H_2O and the Concise Synthesis of (+)-Tanikolide
(C) 5857 – 5860 [6007 – 6010]
DOI: 10.1002/anie.200501686
– Versatile Hypervalent-Iodine(III)-Catalyzed Oxidations with *m*-Chloroperbenzoic Acid as a Cooxidant
(C) 6193 – 6196 [6349 – 6352]
DOI: 10.1002/anie.200501688
Kitagawa, K. (C) 6330 – 6333 [6488 – 6491]
Kitagawa, S.
– Effect of the Metal-Assisted Assembling Mode on the Redox States of Hexaazatriphenylene Hexacarbonitrile
(C) 2700 – 2704 [2760 – 2764]
DOI: 10.1002/anie.200462962
Kitagawa, S. (C) 920 – 923 [942 – 945]
Kitagawa, T.
– Generation and Properties of an Alkylated C_{70} Cation
(C) 1398 – 1401 [1422 – 1425]
DOI: 10.1002/anie.200462696
Kitagishi, H. (C) 435 – 438 [439 – 442]
Kitamura, Masanori (C) 625 – 628 [631 – 634], 1549 – 1551 [1573 – 1575]
Kitamura, Masato
– Catalytic Dehydrative Allylation of Alcohols
(C) 1730 – 1732 [1758 – 1760]
DOI: 10.1002/anie.200462513
– Origin of the Minor Enantiomeric Product in a Noyori Asymmetric Hydrogenation: Evidence for Pathways Different to the Major Mechanism
(C) 7287 – 7290 [7453 – 7456]
DOI: 10.1002/anie.200502463
Kitamura, Mitsuru (C) 3871 – 3874 [3939 – 3942]
Kitaura, R. (C) 920 – 923 [942 – 945]
Kiyohara, K. (C) 4547 – 4549 [4623 – 4625]
Kjaer, K. (C) 7035 – 7039 [7197 – 7201]
Kjærsgaard, A. (C) 3703 – 3706 [3769 – 3772]
Kjeldsen, F.
– Facile Disulfide Bond Cleavage in Gaseous Peptide and Protein Cations by Ultraviolet Photodissociation at 157 nm
(C) 6399 – 6403 [6557 – 6561]
DOI: 10.1002/anie.200501533
Klafter, J. (C) 560 – 564 [566 – 570]
Klapötke, T. M. (C) 4254 – 4257 [4326 – 4330]
Klärner, F.-G.
– Tweezering the Core of a Dendrimer: A Photophysical and Electrochemical Study
(C) 4574 – 4578 [4650 – 4654]
DOI: 10.1002/anie.200501025
Klärner, F.-G. (C) 477 – 480 [481 – 485]
Klebe, G.
– An Old Target Revisited: Two New Privileged Skeletons and an Unexpected Binding Mode For HIV-Protease Inhibitors
(C) 3140 – 3144 [3200 – 3204]
DOI: 10.1002/anie.200462643
Klebe, G. (C) 3620 – 3623 [3686 – 3689]
Klein, C. D. P.
– Metal Ions as Cofactors for the Binding of Inhibitors to Methionine Aminopeptidase: A Critical View of the Relevance of In Vitro Metalloenzyme Assays
(C) 3620 – 3623 [3686 – 3689]
DOI: 10.1002/anie.200500592
Klein, Cédric (C) 6413 – 6417 [6571 – 6575]
Klein, Christian (C) 5247 – 5251 [5381 – 5386]
Klein, E. (C) 298 – 302 [302 – 306]
Klein, G. (C) 7764 – 7767 [7942 – 7945]
Klein, H.-F.
– Cyclometalation of Substrates Containing Imine and Pyridyl Anchoring Groups by Iron and Cobalt Complexes
(C) 975 – 977 [997 – 999]
DOI: 10.1002/anie.200460978
Klein, M. L. (C) 6685 – 6689 [6843 – 6847]
Klein, P. S. (C) 1984 – 1987 [2020 – 2023]
Klein-Hofmann, A. (C) 5488 – 5492 [5624 – 5628]
Klemm, D.
– Cellulose: Fascinating Biopolymer and Sustainable Raw Material
(R) 3358 – 3393 [3422 – 3458]
DOI: 10.1002/anie.200460587
Klenerman, D.
– Trapping of Proteins under Physiological Conditions in a Nanopipette
(C) 3747 – 3750 [3813 – 3816]
DOI: 10.1002/anie.200500196
– Two-Component Graded Deposition of Biomolecules with a Double-Barreled Nanopipette
(C) 6854 – 6859 [7014 – 7019]
DOI: 10.1002/anie.200502338
Kline, T. R. (C) 744 – 746 [754 – 756]
Klinker, E. J. (C) 3690 – 3694 [3756 – 3760]
Klitgaard, S. (C) 3613 – 3616 [3679 – 3682]
Kloo, L.
– One-Step Synthesis of a Platinum(0) – Gallium(III) Chrysene Complex
(C) 3906 – 3909 [3974 – 3977]
DOI: 10.1002/anie.200462373
Klosin, J.
– Highly Regio- and Enantioselective Asymmetric Hydroformylation of Olefins Mediated by 2,5-Disubstituted Phospholane Ligands
(C) 5834 – 5838 [5984 – 5988]
DOI: 10.1002/anie.200501478
Klüfers, P.
– Carbohydrate – Metal Interactions Shaped by Supramolecular Assembling
(C) 924 – 927 [946 – 949]
DOI: 10.1002/anie.200460079
Klumpp, C. (C) 6358 – 6362 [6516 – 6520]
Klunk, W. E. (C) 5452 – 5456 [5588 – 5592]
Knapp, C. (C) 7958 – 7961 [8172 – 8175]
Knapp, M. (C) 917 – 920 [939 – 942]
Kneifel, A. N. (C) 96 – 98 [98 – 100]
Kneisel, F. F. (C) 4627 – 4631 [4703 – 4707]
Knepper, K. (R) 5188 – 5240 [5320 – 5374]
Kniep, B. L. (C) 4704 – 4707 [4782 – 4785]
Knobler, C. M. (C) 1965 – 1968 [2001 – 2004]
Knochel, P.
– Cobalt(II)-Catalyzed Cross-Coupling of Polyfunctional Aryl Copper Reagents with Aryl Bromides and Chlorides
(C) 2947 – 2951 [3007 – 3010]
DOI: 10.1002/anie.200500099
– Highly Enantioselective Preparation of Tertiary Alcohols and Amines by Copper-Mediated Diastereoselective Allylic S_N2' Substitutions
(C) 4627 – 4631 [4703 – 4707]
DOI: 10.1002/anie.200500672
– Iron-Catalyzed Aryl – Aryl Cross-Couplings with Magnesium-Derived Copper Reagents
(C) 1654 – 1658 [1682 – 1685]
DOI: 10.1002/anie.200462013

 © 2005 Wiley-VCH Verlag GmbH & Co. KGaA, Weinheim

– Preparation and Selective Reactions of Mixed Bimetallic Aromatic and Heteroaromatic Boron–Magnesium Reagents
(C) 3133–3135 [3193–3195]
DOI: 10.1002/anie.200462928
– Preparation of Functionalized Aryl Magnesium Reagents by the Addition of Magnesium Aryl Thiolates and Amides to Arynes
(C) 4258–4261 [4330–4333]
DOI: 10.1002/anie.200500443
Knör, S. (C) 423–426 [427–430]
Knözinger, E.
– Size-Dependent Optical Properties of MgO Nanocubes
(C) 4917–4920 [4996–4999]
DOI: 10.1002/anie.200500663
Ko, B.-T. (C) 7969–7972 [8183–8186]
Ko, S. (C) 455–457 [459–461]
Ko, Y. H. (C) 87–91 [89–93]
Kobaru, S. (C) 5523–5526 [5659–5662]
Kobatake, S.
– Conformational Control of Photochromic Reactivity in a Diarylethene Single Crystal
(C) 2148–2151 [2186–2189]
DOI: 10.1002/anie.200462426
Kobayashi, A. (C) 6508–6512 [6666–6670]
Kobayashi, H.
– Dielectric Properties of Porous Molecular Crystals That Contain Polar Molecules
(C) 6508–6512 [6666–6670]
DOI: 10.1002/anie.200501867
Kobayashi, K. (C) 3282–3285 [3346–3349]
Kobayashi, M. (C) 4164–4168 [4236–4240]
Kobayashi, Shigeya (C) 7040–7044 [7202–7206]
Kobayashi, Shū
– A Novel Dinuclear Chiral Niobium Complex for Lewis Acid Catalyzed Enantioselective Reactions: Design of a Tridentate Ligand and Elucidation of the Catalyst Structure
(C) 761–764 [771–774]
DOI: 10.1002/anie.200462204
– *N*-Acylhydrazones as Versatile Electrophiles for the Synthesis of Nitrogen-Containing Compounds
(M) 5176–5186 [5306–5317]
DOI: 10.1002/anie.200500691
Kobayashi, T. C. (C) 920–923 [942–945]
Kobayashi, Y.
– Total Synthesis of 2-(5,6-Epoxyisoprostane A_2)phosphorylcholine and Elucidation of the Relative Configuration of the Isoprostane Moiety
(C) 3481–3484 [3547–3550]
DOI: 10.1002/anie.200500534
Kobuke, Y.
– Highly Fluorescent Self-Coordinated Phthalocyanine Dimers
(C) 4763–4766 [4841–4844]
DOI: 10.1002/anie.200501199
Kobzar, K. (C) 423–426 [427–430], 3145–3147 Corrigendum: 3509 [3205–3207 Corrigendum: 3575]
Koch, K. (C) 265–269 [270–274]
Kocher, N. (C) 6947–6951 [7107–7111]
Kochi, J. K.
– Through-Space (Cofacial) π-Delocalization among Multiple Aromatic Centers: Toroidal Conjugation in Hexaphenylbenzene-like Radical Cations
(C) 5133–5136 [5263–5266]
DOI: 10.1002/anie.200501005
Kociok-Köhn, G. (C) 6875–6878 [7035–7038]
Kock, I. (C) 635–638 [641–645]
Kodera, M.
– A Diiron Center Stabilized by a Bis-TPA Ligand as a Model of Soluble Methane Monooxygenase: Predominant Alkene Epoxidation with H_2O_2
(C) 7104–7106 [7266–7268]
DOI: 10.1002/anie.200501825
Kodera, M. (C) 435–438 [439–442]
Kofink, C. C. (C) 1654–1658 [1682–1685]
Koftis, T. V. (C) 3447–3452 [3513–3518]
Kögerler, P.
– Polyoxometalate Nanostructures, Superclusters, and Colloids: From Functional Clusters to Chemical Aesthetics
(T) 844–846 [866–868]
DOI: 10.1002/anie.200462662
Kögerler, P. (C) 3415–3419 [3481–3485]
Koh, L. L. (C) 7560–7564 [7732–7736]
Köhler, K. (C) 3310–3314 [3375–3379]
Köhler, T. (C) 83–87 [85–89]
Köhler, V. (C) 4888–4891 [4966–4969]
Kohno, J. (C) 4204–4207 [4276–4279]
Koike, Y. (C) 6759–6763 [6917–6921]
Koizumi, S. (C) 6759–6763 [6917–6921]
Koizumi, T.-a. (C) 2229–2232 [2269–2272], 5891–5894 [6041–6044]
Kojima, T. (C) 720–724 [730–734]
Kolaric, B. (C) 7635–7639 [7808–7812]
Kolb, D. M. (C) 2080–2084 [2116–2120]
Kolb, H. C.
– In Situ Click Chemistry: Enzyme-Generated Inhibitors of Carbonic Anhydrase II
(C) 116–120 [118–122]
DOI: 10.1002/anie.200461580
Kolb, H. C. (C) 3275–3279 [3339–3343]
Kolb, L. (C) 429–432 [433–436]
Kolb, U. (C) 262–265 [267–270], 2120–2123 [2158–2161]
Koller, F. (C) 7901–7904 [8114–8118]
Koltypin, Yu. (C) 6560–6563 [6718–6721]
Kolusheva, S. (C) 1092–1096 [1116–1120]
Komatsu, K.
– Generation and Properties of an Alkylated C_{70} Cation
(C) 1398–1401 [1422–1425]
DOI: 10.1002/anie.200462696
Komatsu, K. (C) 1981–1983 [2017–2019]
Komiya, N. (C) 6931–6933 [7091–7093]
Kondo, H. (C) 91–96 [93–98], 2534–2537 [2590–2593]
Kondo, T. (C) 416–419 [420–423]
Kong, L.-Y. (C) 4352–4355 [4426–4429]
Kongkathip, B. (C) 7570–7574 [7742–7746]
Kongkathip, N. (C) 7570–7574 [7742–7746]
König, P. (C) 5968–5971 [6122–6126]
Konno, T.
– A Rock-Salt-Like Lattice Structure Consisting of Monocationic and Monoanionic $Au^{I}Ag^{I}Cu^{II}$ Supramolecular Cages of D-Penicillaminate
(C) 1088–1092 [1112–1116]
DOI: 10.1002/anie.200462205
Koo, H. Y. (C) 1096–1101 [1120–1125]
Kool, E. T.
– Assembly of the Complete Eight-Base Artificial Genetic Helix, xDNA, and Its Interaction with the Natural Genetic System
(C) 3118–3122 [3178–3182]
DOI: 10.1002/anie.200500069
Kopatz, E. J. (C) 2771–2774 [2831–2834]
Koposov, A. Y. (C) 7127–7131 [7289–7293]
Kopylovich, M. N. (C) 4345–4349 [4419–4423]
Kopyshev, A. (C) 3297–3301 [3361–3365]
Korber, N.
– Chemical Bond in the Cyclic Anions P_6^{4-} and As_6^{4-}: Synthesis, Crystal Structure, and Electron Localization Function of $\{Rb[18]crown\text{-}6)\}_2Rb_2As_6\cdot 6NH_3$
(C) 7200–7204 [7366–7370]
DOI: 10.1002/anie.200502535
Korchev, Yu. E. (C) 6854–6859 [7014–7019]
Korgel, B. A.
– The Role of Precursor-Decomposition Kinetics in Silicon-Nanowire Synthesis in Organic Solvents
(C) 3573–3577 [3639–3643]
DOI: 10.1002/anie.200463001
Korn, T. J. (C) 2947–2951 [3007–3010]
Kornath, A.
– Synthesis of Fluorodihydroxysulfonium Hexafluoroantimonate $[FS(OH)_2]^+[SbF_6]^-$
(C) 973–975 [995–997]
DOI: 10.1002/anie.200461847
Kornowski, A. (C) 5997–6001 [6151–6155]
Kortus, J. (C) 7896–7900 [8109–8113]
Kortz, U.
– The Ball-Shaped Heteropolytungstates $[\{Sn(CH_3)_2(H_2O)\}_{24}\{Sn(CH_3)_2\}_{12}(A\text{-}XW_9O_{34})_{12}]^{36-}$
(C) 3773–3777 [3839–3843]
DOI: 10.1002/anie.200500548
– The Wheel-Shaped Cu_{20} Tungstophosphate $[Cu_{20}Cl(OH)_{24}(H_2O)_{12}(P_8W_{48}O_{184})]^{25-}$ Ion
(C) 3777–3780 [3843–3846]
DOI: 10.1002/anie.200500682
Kosaka, A. (C) 2410–2413 [2462–2465]
Kosaka, S. (C) 1513–1517 [1537–1541]
Koshima, H. (C) 2774–2777 [2834–2837]
Koshino, H. (C) 7950–7954 [8164–8168]
Kossiakoff, A. A. (C) 3852–3856 [3920–3924]
Kostiainen, M. A. (C) 2556–2559 [2612–2615]
Kosuge, J. (C) 5439–5441 [5575–5577]
Kosugi, Y. (C) 4389–4391 [4463–4465]
Kotani, M. (C) 5136–5141 [5266–5271]
Kotov, N. A.
– Nanoparticle Assemblies with Molecular Springs: A Nanoscale Thermometer
(C) 7439–7442 [7605–7608]
DOI: 10.1002/anie.200501264
Kötz, R. (R) 2190–2209 [2228–2248]
Kou, H.-Z.
– $[Mn^{III}(salen)]_6[Fe^{III}(bpmb)(CN)_2]_6\cdot 7H_2O$: A Cyanide-Bridged Nanosized Molecular Wheel
(C) 7742–7745 [7920–7923]
DOI: 10.1002/anie.200502699
Koutmos, M. (C) 1971–1974 [2007–2010]
Koutsantonis, G. A.
– Reaction of Ruthenium Ethyne-1,2-diyl Compounds with Bis(trimethylsilyl)acetylene Complexes of Titanocene and Zirconocene: Remarkable Transfer of a C_2 Ligand
(C) 3038–3043 [3098–3103]
DOI: 10.1002/anie.200500224
Kovalenko, S. A. (C) 5635–5639 [5779–5783]
Kowalczyk, D. (C) 7624–7630 [7798–7803]
Kowenicki, R. A. (C) 3456–3459 [3522–3525], 5729–5733 [5875–5879]
Koyama, H. (C) 419–423 [423–427]
Kozaki, M. (C) 4056–4058 [4124–4126]

 © 2005 Wiley-VCH Verlag GmbH & Co. KGaA, Weinheim

Kozhevnikov, V. N. (C) 1806 – 1810 [1840 – 1844]
Kozlova, S. G. (C) 6867 – 6871 [7027 – 7031]
Krafft, M. P.
– Preventing Crystallization of Phospholipids in Monolayers: A New Approach to Lung-Surfactant Therapy
(C) 2749 – 2752 [2809 – 2812]
DOI: 10.1002/anie.200462978
Kragol, G. (C) 4975 – 4980 [5055 – 5060]
Kramer, G. (C) 7946 – 7950 [8160 – 8164]
Kranz, C.
– AFM-Tip-Integrated Amperometric Microbiosensors: High-Resolution Imaging of Membrane Transport
(C) 3419 – 3422 [3485 – 3488]
DOI: 10.1002/anie.200461556
Krapp, A. (C) 2943 – 2946 [3003 – 3007], 3617 – 3620 [3683 – 3686]
Kratky, C.
– B_{12}-*retro*-Riboswitches: Constitutional Switching of B_{12} Coenzymes Induced by Nucleotides
(C) 2284 – 2288 [2324 – 2328]
DOI: 10.1002/anie.200462085
Kraus, F. (C) 7200 – 7204 [7366 – 7370]
Krause, M.
– Gadolinium Nitride Gd_3N in Carbon Cages: The Influence of Cluster Size and Bond Strength
(C) 1557 – 1560 [1581 – 1584]
DOI: 10.1002/anie.200461441
Krause, M. (C) 3306 – 3309 [3371 – 3374]
Krause, N.
– Elucidation of the Mechanism of the 1,6-Cuprate Addition to Acceptor-Substituted Enynes through ^{13}C Kinetic Isotope Effects: Experimental and Theoretical Studies
(C) 4715 – 4719 [4795 – 4798]
DOI: 10.1002/anie.200462976
Krauth-Siegel, R. L.
– Dithiol Proteins as Guardians of the Intracellular Redox Milieu in Parasites: Old and New Drug Targets in Trypanosomes and Malaria-Causing Plasmodia
(R) 690 – 715 [698 – 724]
DOI: 10.1002/anie.200300639
Kräutler, B.
– A High-Precision Switch on an RNA Message
(H) 4288 – 4290 [4360 – 4362]
DOI: 10.1002/anie.200500774
– B_{12}-*retro*-Riboswitches: Constitutional Switching of B_{12} Coenzymes Induced by Nucleotides
(C) 2284 – 2288 [2324 – 2328]
DOI: 10.1002/anie.200462085
Krautscheid, H.
– $(Pr_4N)_4[Ag_3Fe_2(ECN)_{12}]$—Anionic Network Structures with Mutual Interpenetration
(C) 7787 – 7790 [7965 – 7968]
DOI: 10.1002/anie.200502287
Kravtsov, V. C. (C) 2877 – 2880 [2937 – 2940]
Kreich, M. (C) 7800 – 7804 [7979 – 7983]
Kresse, H. (C) 774 – 778 [784 – 788]
Krill, S. (C) 6579 – 6582 [6737 – 6740]
Krische, M. J.
– Hydrogen-Bond-Mediated Self-Assembly of Aminopyrazolones: Macrocyclic Quartets—Single and Stacked One-Dimensional Motifs
(C) 7069 – 7071 [7231 – 7233]
DOI: 10.1002/anie.200502539
Krivokapič, I. (C) 3613 – 3616 [3679 – 3682]
Krivovichev, S. V.
– Nanoscale Tubules in Uranyl Selenates
(C) 1134 – 1136 [1158 – 1160]
DOI: 10.1002/anie.200462356
Kröck, L. (C) 471 – 473 [475 – 477]
Kroll, P.
– Prediction of Novel Phases of Tantalum(v) Nitride and Tungsten(vi) Nitride That Can Be Synthesized under High Pressure and High Temperature
(C) 4249 – 4254 [4321 – 4326]
DOI: 10.1002/anie.200462980
Kroll, P. (C) 567 – 570 [573 – 576]
Kronberg, M. (C) 253 – 257 [258 – 261]
Kropfgans, C. (C) 924 – 927 [946 – 949]
Kros, A.
– Synthesis and Self-Assembly of Rod – Rod Hybrid Poly(γ-benzyl L-glutamate)-*block*-Polyisocyanide Copolymers
(C) 4349 – 4352 [4423 – 4426]
DOI: 10.1002/anie.200500877
Kroto, H. W. (C) 325 – 328 [329 – 332]
Krotz, O. (C) 2427 – 2428 Corrigendum: 3955 [2479 – 2480]
Krylova, O. O. (C) 1195 – 1198 [1219 – 1223]
Krzystek, J. (C) 1997 – 2001 [2033 – 2037]
Kuang, M. (C) 1717 – 1720 [1745 – 1748]
Kubatko, K.-A. (C) 2135 – 2139 [2173 – 2177]
Kubiak, C. P.
– A Trihydroxy Tin Group That Resists Oligomerization in the Trinuclear Nickel Cluster $[Ni_3(\mu\text{-}P,P'\text{-}PPh_2CH_2PPh_2)_3(\mu_3\text{-}L)(\mu_3\text{-}Sn(OH)_3)]$
(C) 1125 – 1128 [1149 – 1152]
DOI: 10.1002/anie.200462129
Kubo, T.
– Synthesis, Intermolecular Interaction, and Semiconductive Behavior of a Delocalized Singlet Biradical Hydrocarbon
(C) 6564 – 6568 [6722 – 6726]
DOI: 10.1002/anie.200502303
Kubota, Y.
– Direct Observation of Hydrogen Molecules Adsorbed onto a Microporous Coordination Polymer
(C) 920 – 923 [942 – 945]
DOI: 10.1002/anie.200461895
Kubowicz, S. (C) 5262 – 5265 [5397 – 5400]
Kucharski, C. (C) 3710 – 3714 [3776 – 3780]
Kudo, A.
– Visible-Light-Induced H_2 Evolution from an Aqueous Solution Containing Sulfide and Sulfite over a $ZnS – CuInS_2 – AgInS_2$ Solid-Solution Photocatalyst
(C) 3565 – 3568 [3631 – 3634]
DOI: 10.1002/anie.200500314
Kuemmel, M. (C) 4589 – 4592 [4665 – 4668]
Kueng, A. (C) 3419 – 3422 [3485 – 3488]
Kuhlenbeck, H. (C) 7601 – 7605 [7773 – 7777]
Kuhlmann, J.
– Development and Biological Evaluation of Acyl Protein Thioesterase 1 (APT1) Inhibitors
(C) 4975 – 4980 [5055 – 5060]
DOI: 10.1002/anie.200462625
Kühne, R. (R) 2852 – 2869 [2912 – 2930]
Kujawa, D. P. (C) 2144 – 2148 [2182 – 2186]
Kulkarni, S. S. (C) 1665 – 1668 [1693 – 1696]
Kumacheva, E.
– Generation of Monodisperse Particles by Using Microfluidics: Control over Size, Shape, and Composition
(C) 724 – 728 Corrigendum: 3799 [734 – 738 Corrigendum: 3865]
DOI: 10.1002/anie.200462226
Kumagai, N. (C) 3470 – 3474 [3536 – 3540]
Kumaki, J.
– AFM Snapshots of Synthetic Multifunctional Pores with Polyacetylene Blockers: Pseudorotaxanes and Template Effects
(C) 6154 – 6157 [6310 – 6313]
DOI: 10.1002/anie.200501886
Kumazawa, K. (C) 1810 – 1813 [1844 – 1847]
Kunishima, M.
– Unusual Rate Enhancement of Bimolecular Dehydrocondensation To Form Amides at the Interface of Micelles of Fatty Acid Salts
(C) 7254 – 7257 [7420 – 7423]
DOI: 10.1002/anie.200502594
Kunwar, A. C.
– 9/11 Mixed Helices in α/β Peptides Derived from C-Linked Carbo-β-Amino Acid and L-Ala Repeats
(C) 5878 – 5882 [6028 – 6032]
DOI: 10.1002/anie.200501247
Kunz, H.
– A Fully Synthetic Vaccine Consisting of a Tumor-Associated Glycopeptide Antigen and a T-Cell Epitope for the Induction of a Highly Specific Humoral Immune Response
(C) 7630 – 7635 [7803 – 7808]
DOI: 10.1002/anie.200501594
– Nestor of Preparative Organic Chemistry: *Leopold Horner*
(O) 7664 – 7665 [7838 – 7839]
DOI: 10.1002/anie.200503637
– Synthetic Vaccines Consisting of Tumor-Associated MUC1 Glycopeptide Antigens and Bovine Serum Albumin
(C) 7624 – 7630 [7798 – 7803]
DOI: 10.1002/anie.200501593
Kupferschmidt, N. (C) 5317 – 5322 [5451 – 5456]
Kura, S. (C) 6406 – 6409 [6564 – 6567]
Kurahashi, T. (C) 7881 – 7884 [8093 – 8096]
Kuramoto, K. (C) 596 – 598 [602 – 604]
Kurata, H. (C) 316 – 319 [320 – 323]
Kuratsu, M. (C) 4056 – 4058 [4124 – 4126]
Kuroda, R. (C) 2527 – 2531 [2583 – 2587]
Kuroda, S.-i. (C) 4164 – 4168 [4236 – 4240]
Kurogi, K. (C) 3453 – 3456 [3519 – 3522]
Kurogochi, M. (C) 91 – 96 [93 – 98], 2534 – 2537 [2590 – 2593]
Kurosaki, H.
– Irreversible Inhibition of Metallo-β-lactamase (IMP-1) by 3-(3-Mercaptopropionylsulfanyl)propionic Acid Pentafluorophenyl Ester
(C) 3861 – 3864 [3929 – 3932]
DOI: 10.1002/anie.200500835
Kurskii, Y. A. (C) 2767 – 2771 [2827 – 2831]
Kurth, D. G. (C) 1717 – 1720 [1745 – 1748]
Kurtz, M. (C) 2790 – 2794 [2850 – 2854]
Kusama, H. (C) 468 – 470 [472 – 474]
Kutzelnigg, W.
– Ligand Field Theory: *Hans Bethe*
(O) 3800 – 3801 [3866 – 3867]
DOI: 10.1002/anie.200501634
Kuvychko, I. V. (C) 1846 – 1849 [1880 – 1883], 7984 – 7987 [8198 – 8201]
Kuwahara, H. (C) 7929 – 7932 [8143 – 8146], 7932 – 7935 [8146 – 8149]
Kuwahara, M. (C) 6682 – 6685 [6840 – 6843]
Kuwahara, S. (C) 2262 – 2265 [2302 – 2305]

 © 2005 Wiley-VCH Verlag GmbH & Co. KGaA, Weinheim

Kuwata, S.
– *N*-Methylhydroxylamido(1 –)- and Nitrosomethaneruthenium Complexes Derived from Nitrosyl Complexes: Reversible N-Protonation of an N-Coordinated Nitrosoalkane
(C) 6406 – 6409 [6564 – 6567]
DOI: 10.1002/anie.200501916
Kuzelka, J. (C) 2215 – 2220 [2255 – 2260]
Kwak, J. H. (C) 7427 – 7432 [7593 – 7598]
Kwok, W.-M. (C) 3436 – 3439 [3502 – 3505]
Kwon, M. S. (C) 6913 – 6915 [7073 – 7075]
Kwon, Y.-U. (C) 556 – 560 [562 – 566]
Kyushin, S. (C) 7567 – 7570 [7739 – 7742]

Labinger, J. A.
– Controversy in Chemistry: How Do You Prove a Negative?—The Cases of Phlogiston and Cold Fusion
(E) 1916 – 1922 [1950 – 1956]
DOI: 10.1002/anie.200462084
Lachaud, F. (C) 1536 – 1540 [1560 – 1564]
Lacour, J.
– Fluorinated TRISPHAT Anions: Spectroscopic Probes for Detailed Asymmetric Ion Pairing Studies
(C) 5060 – 5064 [5188 – 5192]
DOI: 10.1002/anie.200500862
– Resolution of [4]Heterohelicenium Dyes with Unprecedented Pummerer-like Chemistry
(C) 1879 – 1883 [1913 – 1917]
DOI: 10.1002/anie.200462321
Ladame, S. (C) 5736 – 5739 [5882 – 5885]
Ladislaw, J. (C) 6516 – 6521 [6674 – 6679]
Ladziata, U. (C) 7127 – 7131 [7289 – 7293]
Lægsgaard, E. (C) 2270 – 2275 [2310 – 2315]
Lagona, J. (R) 4844 – 4870 [4922 – 4949]
Lah, M. S. (C) 1383 – 1385 [1407 – 1409], 7926 – 7929 [8140 – 8143]
Lahav, M.
– Solvent Effect on Crystal Polymorphism: Why Addition of Methanol or Ethanol to Aqueous Solutions Induces the Precipitation of the Least Stable β Form of Glycine
(C) 3226 – 3229 [3290 – 3293]
DOI: 10.1002/anie.200500164
Lahiri, G. K.
– Theoretical and Experimental Evidence for a New Kind of Spin-Coupled Singlet Species: Isomeric Mixed-Valent Complexes Bridged by a Radical Anion Ligand
(C) 5655 – 5658 [5800 – 5803]
DOI: 10.1002/anie.200501075
Lahoz, F. J. (C) 3267 – 3271 [3331 – 3335]
Lai, Y.-N. (C) 6888 – 6892 [7048 – 7052]
Laimgruber, S. (C) 7901 – 7904 [8114 – 8118]
Laitinen, T. (C) 751 – 756 [761 – 766]
Lakey, J. H.
– Circular Dichroism Spectroscopy of Folding in a Protein Monolayer
(C) 4801 – 4804 [4879 – 4882]
DOI: 10.1002/anie.200462977
Lakomek, N. A. (C) 7776 – 7778 [7954 – 7956]
Lakshman, M. K. Corrigendum: 1154
Lakshminarayanan, R. (C) 5476 – 5479 [5612 – 5615]
Laleu, B. (C) 1879 – 1883 [1913 – 1917]
Lalic, G. (C) 2259 – 2261 [2299 – 2301]
Lam, H. K. (C) 1241 – 1244 [1267 – 1270]
Lama, M. (C) 2527 – 2531 [2583 – 2587]
Lambert, C.
– Hexaarylbenzenes—Prospects for Toroidal Delocalization of Charge and Energy
(H) 7337 – 7339 [7503 – 7505]
DOI: 10.1002/anie.200502105
Lambert, R. M.
– An Electrochemically Driven and Electrochemically Regenerated NO_x Trap
(C) 3730 – 3732 [3796 – 3798]
DOI: 10.1002/anie.200500393
Lami, A. (C) 5118 – 5121 [5248 – 5251]
Lammertsma, K.
– Infrared, UV/Vis, and W-band EPR Spectroscopic Characterization and Photochemistry of Triplet Mesitylphosphinidene
(C) 3289 – 3293 [3353 – 3357]
DOI: 10.1002/anie.200462862
– Valence Isomerization of 2-Phosphabicyclo[1.1.0]butanes
(C) 6579 – 6582 [6737 – 6740]
DOI: 10.1002/anie.200502248
Lanci, M. P. (C) 7273 – 7276 [7439 – 7442]
Landa, A. (C) 6058 – 6063 [6212 – 6217]
Landskron, K. (C) 2107 – 2109 [2145 – 2147]
Lane, I. (C) 1830 – 1833 [1864 – 1867]
Lang, P. (C) 7635 – 7639 [7808 – 7812]
Lange, A. (C) 2089 – 2092 [2125 – 2129]
Lange, O. F. (C) 3394 – 3399 [3460 – 3465]
Langenhahn, V. (C) 3759 – 3763 [3825 – 3829]
Langer, P.
– 3,5,7,9-Tetraphenylhexaazaacridine: A Highly Stable, Weakly Antiaromatic Species with 16 π Electrons
(C) 5255 – 5259 [5389 – 5393]
DOI: 10.1002/anie.200500831
Langer, R.
– A Family of Hierarchically Self-Assembling Linear-Dendritic Hybrid Polymers for Highly Efficient Targeted Gene Delivery
(C) 6704 – 6708 [6862 – 6866]
DOI: 10.1002/anie.200502152
Langhals, H.
– A Novel Fluorescent Dye with Strong, Anisotropic Solid-State Fluorescence, Small Stokes Shift, and High Photostability
(C) 2427 – 2428 Corrigendum: 3955 [2479 – 2480]
DOI: 10.1002/anie.200461610
Larhed, M.
– All the Rave in Microwaves
(T) 7666 – 7669 [7840 – 7843]
DOI: 10.1002/anie.200503543
Larionov, O. V. (C) 5664 – 5667 [5809 – 5813]
Larionova, J. (C) 2711 – 2715 [2771 – 2775]
Larock, R. C.
– Consecutive Vinylic to Aryl to Allylic Palladium Migration and Multiple C–H Activation Processes
(C) 1873 – 1875 [1907 – 1909]
DOI: 10.1002/anie.200462327
Laromaine, A. (C) 2220 – 2222 [2260 – 2262]
Larsen, T. (H) 4432 – 4434 [4506 – 4508]
Laschat, S.
– Enantioselective Total Synthesis of Cylindramide
(C) 820 – 822 [831 – 833]
DOI: 10.1002/anie.200461823
Laschewsky, A.
– Multicompartment Micelles Formed by Self-Assembly of Linear ABC Triblock Copolymers in Aqueous Medium
(C) 5262 – 5265 [5397 – 5400]
DOI: 10.1002/anie.200500584
Laso, A. (C) 3881 – 3884 [3949 – 3952]
Latos-Grażyński, L.
– Dithiaethyneporphyrin: An Atypical [18]Triphyrin(4.1.1) Frame for Contracted Porphyrins
(C) 5288 – 5291 [5422 – 5425]
DOI: 10.1002/anie.200501635
Laubender, G. (C) 3623 – 3626 [3689 – 3693]
Lauffer, R. B. (C) 6766 – 6769 [6924 – 6927]
Laurent, S. A.-L. (L) 2060 – 2063 [2096 – 2099]
Laurin, M. (C) 7601 – 7605 [7773 – 7777]
Laursen, B. W. (C) 1879 – 1883 [1913 – 1917], 7035 – 7039 [7197 – 7201]
Lauterbur, P. C.
– All Science Is Interdisciplinary—From Magnetic Moments to Molecules to Men (Nobel Lecture)
(R) 1004 – 1011 [1026 – 1034]
DOI: 10.1002/anie.200462400
Lavallo, V. (C) 5705 – 5709 [5851 – 5855], 7236 – 7239 [7402 – 7405]
Lavilla, R.
– Straightforward Access to a Structurally Diverse Set of Oxacyclic Scaffolds through a Four-Component Reaction
(C) 6521 – 6525 [6679 – 6683]
DOI: 10.1002/anie.200501548
Law, G.-L. (C) 3436 – 3439 [3502 – 3505]
Lawrence, B. M. (C) 6043 – 6046 [6197 – 6200], 6046 – 6050 [6200 – 6204]
Lawrence, D. S.
– Design, Construction, and Intracellular Activation of an Intramolecularly Self-Silenced Signal Transduction Inhibitor
(C) 4242 – 4244 [4314 – 4316]
DOI: 10.1002/anie.200462004
Lax, P. (C) 5670 – 5674 [5816 – 5820]
Le Floch, P. (C) 6318 – 6323 [6477 – 6481]
Le Roux, E. (C) 6755 – 6758 [6913 – 6916]
Le Van, D. (C) 3759 – 3763 [3825 – 3829]
Leadlay, P. F.
– Accumulation of an *E*,*E*,*E*-Triene by the Monensin-Producing Polyketide Synthase when Oxidative Cyclization is Blocked
(C) 7075 – 7078 [7237 – 7240]
DOI: 10.1002/anie.200501757
Leadlay, P. F. (C) 4757 – 4760 [4835 – 4838]
Lebedkin, S. F. (C) 1846 – 1849 [1880 – 1883], 7984 – 7987 [8198 – 8201]
Leboeuf, D. (C) 7114 – 7118 [7276 – 7280]
Lebreton, A. (C) 284 – 287 [288 – 291]
Leca, F. (C) 4362 – 4365 [4436 – 4439]
Lecea, B. (C) 2903 – 2907 [2963 – 2967]
Lednik, J. (C) 4029 – 4032 [4097 – 4100]
Lee, A. (C) 5682 – 5686 [5828 – 5832]
Lee, C. (C) 910 – 913 [932 – 935]
Lee, C.-H.
– A Benzodipyrrole-Derived Sapphyrin
(C) 4053 – 4055 [4121 – 4123]
DOI: 10.1002/anie.200500944
Lee, D. C. (C) 3573 – 3577 [3639 – 3643]
Lee, Dohoon (C) 7427 – 7432 [7593 – 7598]
Lee, Dongwhan
– Escape from a Nonporous Solid: Mechanically Coupled Biconcave Molecules
(C) 6689 – 6693 [6847 – 6851]
DOI: 10.1002/anie.200501888
Lee, E. (C) 2872 – 2877 [2932 – 2937]
Lee, G. (C) 2723 – 2727 [2783 – 2787]
Lee, G.-H. (C) 7418 – 7420 [7584 – 7586]
Lee, G.-i. (C) 2704 – 2707 [2764 – 2767]

 © 2005 Wiley-VCH Verlag GmbH & Co. KGaA, Weinheim

Lee, H.
– Structural Transition and Tuning of *tert*-Butylamine Hydrate
(C) 7749 – 7752 [7927 – 7930]
DOI: 10.1002/anie.200502376
Lee, J.-K.
– Multifunctional Nanoparticles Possessing A "Magnetic Motor Effect" for Drug or Gene Delivery
(C) 1068 – 1071 [1092 – 1095]
DOI: 10.1002/anie.200461910
Lee, J. S.
– Photocatalytic Nanodiodes for Visible-Light Photocatalysis
(C) 4585 – 4589 [4661 – 4665]
DOI: 10.1002/anie.200500064
– Tungsten Carbide Microspheres as a Noble-Metal-Economic Electrocatalyst for Methanol Oxidation
(C) 6557 – 6560 [6715 – 6718]
DOI: 10.1002/anie.200501272
Lee, J. T. (C) 83 – 87 [85 – 89], 5989 – 5992 [6143 – 6146]
Lee, J.-w. (C) 7749 – 7752 [7927 – 7930]
Lee, J. W. (C) 87 – 91 [89 – 93], 2899 – 2903 [2959 – 2963]
Lee, Jaebeom (C) 7439 – 7442 [7605 – 7608]
Lee, Jeong-Hee (C) 1383 – 1385 [1407 – 1409]
Lee, Jihye (C) 1383 – 1385 [1407 – 1409]
Lee, Jinwoo (C) 7427 – 7432 [7593 – 7598]
Lee, Jung-Hoon (C) 5810 – 5814 [5960 – 5964]
Lee, Junseong (C) 6166 – 6169 [6322 – 6325]
Lee, K. H. (C) 910 – 913 [932 – 935]
Lee, Kooyeon (C) 1840 – 1843 [1874 – 1877], 3253 – 3256 [3317 – 3320]
Lee, Kyungjae (C) 1383 – 1385 [1407 – 1409]
Lee, L. V. (C) 116 – 120 [118 – 122], 447 – 452 [451 – 456]
Lee, M.-r. (C) 2881 – 2884 [2941 – 2944]
Lee, Mina (C) 2929 – 2931 [2989 – 2991]
Lee, Myongsoo
– Liquid-Crystalline Assembly from Rigid Wedge – Flexible Coil Diblock Molecules
(C) 328 – 332 [332 – 336]
DOI: 10.1002/anie.200461623
– Stimuli-Responsive Gels from Reversible Coordination Polymers
(C) 5810 – 5814 [5960 – 5964]
DOI: 10.1002/anie.200501270
Lee, P. H.
– Intermolecular Tandem Pd-Catalyzed Cross-Coupling/[4 + 4] and [4 + 2] Cycloadditions: A One-Pot, Five-Component Assembly of Bicyclo[6.4.0]dodecanes
(C) 3253 – 3256 [3317 – 3320]
DOI: 10.1002/anie.200461957
– The Indium-Mediated Selective Introduction of Allenyl and Propargyl Groups at the C4-Position of 2-Azetidinones and the $AuCl_3$-Catalyzed Cyclization of 4-Allenyl-2-azetidinones
(C) 1840 – 1843 [1874 – 1877]
DOI: 10.1002/anie.200462512
Lee, S.
– Bulk Preparation of Si – SiO_x Hierarchical Structures: High-Density Radially Oriented Amorphous Silica Nanowires on a Single-Crystal Silicon Nanocore
(C) 6934 – 6937 [7094 – 7097]
DOI: 10.1002/anie.200501960
Lee, S. (C) 4749 – 4753 [4827 – 4831]
Lee, S.-H. (C) 3582 – 3585 [3648 – 3651]
Lee, S. H. (C) 1378 – 1382 [1402 – 1406], 3736 – 3740 [3802 – 3806]
Lee, S.-Y. (C) 4242 – 4244 [4314 – 4316]
Lee, V. Y. (C) 6378 – 6381 [6536 – 6539], 7574 – 7580 [7746 – 7752]
Lee, W.
– A Template-Based Electrochemical Method for the Synthesis of Multisegmented Metallic Nanotubes
(C) 6050 – 6054 [6204 – 6208]
DOI: 10.1002/anie.200501341
Lee, Y.-J. (C) 1383 – 1385 [1407 – 1409]
Lee, Y. J. (C) 6207 – 6210 [6363 – 6366]
Lee, Y. S. (C) 2929 – 2931 [2989 – 2991]
Lee, Y. T. (C) 2154 – 2157 [2192 – 2195]
Lee, Yangsoo (C) 1398 – 1401 [1422 – 1425]
Lee, Youngu (C) 4228 – 4231 [4300 – 4303]
Leffler, H. (C) 5110 – 5112 [5240 – 5242]
Léger, J.-M. (C) 1954 – 1958 [1990 – 1994]
Lehmen, K. (C) 3136 – 3139 [3196 – 3199]
Lehn, J.-M.
– Addressing the Metal Centers of [2 × 2] Co^{II}_4 Grid-Type Complexes by STM/STS
(C) 7896 – 7900 [8109 – 8113]
DOI: 10.1002/anie.200502743
Lei, J.-G. (C) 7420 – 7424 [7586 – 7590]
Leibeling, G. (C) 7111 – 7114 [7273 – 7276]
Leibl, W.
– A Biomimetic Model of the Electron Transfer between P_{680} and the TyrZ – His190 Pair of PSII
(C) 1536 – 1540 [1560 – 1564]
DOI: 10.1002/anie.200461948
Leigh, D. A.
– Patterning through Controlled Submolecular Motion: Rotaxane-Based Switches and Logic Gates that Function in Solution and Polymer Films
(C) 3062 – 3067 [3122 – 3127]
DOI: 10.1002/anie.200500101
– Rare and Diverse Binding Modes Introduced through Mechanical Bonding
(C) 4557 – 4564 [4633 – 4640]
DOI: 10.1002/anie.200500004
Leighton, J. L. (C) 938 – 941 [960 – 963]
Leiserowitz, L.
– Solvent Effect on Crystal Polymorphism: Why Addition of Methanol or Ethanol to Aqueous Solutions Induces the Precipitation of the Least Stable β Form of Glycine
(C) 3226 – 3229 [3290 – 3293]
DOI: 10.1002/anie.200500164
Leitner, W.
– A Cartridge System for Organometallic Catalysis: Sequential Catalysis and Separation Using Supercritical Carbon Dioxide to Switch Phases
(C) 2291 – 2295 [2331 – 2335]
DOI: 10.1002/anie.200461768
– Biphasic Aerobic Oxidation of Alcohols Catalyzed by Poly(ethylene glycol)-Stabilized Palladium Nanoparticles in Supercritical Carbon Dioxide
(C) 1346 – 1349 [1370 – 1373]
DOI: 10.1002/anie.200461493
Leize, E. (C) 5338 – 5341 [5472 – 5475]
Lendlein, A.
– Biodegradable, Amorphous Copolyester-Urethane Networks Having Shape-Memory Properties
(C) 1188 – 1192 [1212 – 1216]
DOI: 10.1002/anie.200461360
Lennon, D. (C) 1830 – 1833 [1864 – 1867]
Lenoir, D.
– *cis*-Bromination of Alkynes without Cationic Intermediates
(C) 1412 – 1416 [1437 – 1441]
DOI: 10.1002/anie.200461632
Lentz, D.
– Synthesis and Structure Determination of Tellurium Tetracyanide Solvates: Pseudopolymorphism of $Te(CN)_4$ and TeF_4
(C) 5079 – 5082 [5207 – 5211]
DOI: 10.1002/anie.200500168
Lenzen, A. (R) 1304 – 1325 [1330 – 1351], (C) 3766 – 3769 [3832 – 3835]
León, S. (C) 3062 – 3067 [3122 – 3127]
Leong, K. W. (C) 4782 – 4785 [4860 – 4863]
Leoni, P.
– Redox Control of Light-Induced Platinum-Cluster-to-Iron Charge Transfer in a Bis(ferrocenylethynyl)-Substituted Hexanuclear Platinum Derivative
(C) 5701 – 5705 [5847 – 5851]
DOI: 10.1002/anie.200501714
Leonova, E. (C) 7269 – 7273 [7435 – 7439]
Leontiev, A. V. (C) 3043 – 3047 [3103 – 3107]
Lerner, R. A.
– Enzymatic Incorporation of an Antibody-Activated Blue Fluorophore into DNA
(C) 2144 – 2148 [2182 – 2186]
DOI: 10.1002/anie.200461143
Lerner, R. A. (C) 716 – 720 [726 – 730], 4378 – 4381 [4452 – 4455]
Lesarri, A. (C) 6311 – 6315 [6469 – 6473]
Lescop, C. (C) 4362 – 4365 [4436 – 4439]
Leukel, D. (C) 975 – 977 [997 – 999]
Leuser, H. (C) 4627 – 4631 [4703 – 4707]
Leusser, D. (C) 250 – 253 [254 – 257]
Lewis, D. W.
– Oligomerization and Cyclization Processes in the Nucleation of Microporous Silicas
(C) 3082 – 3086 [3142 – 3146]
DOI: 10.1002/anie.200462524
Lewis, D. W. (R) 6456 – 6482 [6614 – 6641]
Lewis, P. (C) 724 – 728 Corrigendum: 3799 [734 – 738 Corrigendum: 3865]
Lex, J. (C) 807 – 811 [817 – 821]
Ley, S. V.
– The Total Synthesis of the Annonaceous Acetogenin 10-Hydroxyasimicin
(C) 580 – 584 [586 – 590]
DOI: 10.1002/anie.200462264
– Total Synthesis of Antascomicin B
(C) 2732 – 2737 [2792 – 2797]
DOI: 10.1002/anie.200500174
– Total Synthesis of Spongistatin 1: A Synthetic Strategy Exploiting Its Latent Pseudo-Symmetry
(C) 5433 – 5438 [5569 – 5574]
DOI: 10.1002/anie.200502008
Li, B. (C) 1721 – 1724 [1749 – 1752]
Li, Chuang (C) 5725 – 5729 [5871 – 5875]
Li, Chun (C) 2030 – 2033 [2066 – 2069], 6371 – 6374 [6529 – 6532]
Li, D.-S. (C) 3864 – 3867 [3932 – 3935]
Li, Dan
– Twelve-Connected Net with Face-Centered Cubic Topology: A Coordination Polymer Based on $[Cu_{12}(\mu_4\text{-}SCH_3)_6]^{6+}$ Clusters and CN^- Linkers
(C) 4175 – 4178 [4247 – 4250]
DOI: 10.1002/anie.200500290
Li, Dongfei (C) 3466 – 3470 [3532 – 3536]
Li, Donglin (C) 797 – 802 [807 – 812]
Li, H.-J. (C) 6500 – 6504 [6658 – 6662]
Li, Haikuo (C) 5100 – 5103 [5230 – 5233]
Li, Hanying (C) 4333 – 4338 [4407 – 4412]
Li, Hao (C) 1369 – 1371 [1393 – 1395]
Li, Hongming (C) 105 – 108 [107 – 110]
Li, J.-J. (C) 7420 – 7424 [7586 – 7590]
Li, Jing (C) 4342 – 4345 [4416 – 4419]

 © 2005 Wiley-VCH Verlag GmbH & Co. KGaA, Weinheim

Li, Jixue (C) 262 – 265 [267 – 270], 2120 – 2123 [2158 – 2161]
Li, Jun
– Experimental and Theoretical Investigation of the Electronic and Geometrical Structures of the Au_{32} Cluster (C) 7119 – 7123 [7281 – 7285] DOI: 10.1002/anie.200502795
Li, L.-s. (C) 1833 – 1836 [1867 – 1870]
Li, Linke (C) 6067 – 6074 [6221 – 6228]
Li, Liyu (C) 3578 – 3582 [3644 – 3648]
Li, M. (C) 6362 – 6366 [6520 – 6524]
Li, P. (C) 7771 – 7775 [7949 – 7953]
Li, Q. (C) 765 – 769 [775 – 779]
Li, S. (C) 7450 – 7453 [7616 – 7619]
Li, S.-D.
– $[(\eta^6\text{-}B_6X)_2M]$ (X = C, N; M = Mn, Fe, Co, Ni): A New Class of Transition-Metal Sandwich-Type Complexes (C) 2158 – 2161 [2196 – 2199] DOI: 10.1002/anie.200462476
Li, X. S. (C) 3578 – 3582 [3644 – 3648]
Li, Xi (C) 7119 – 7123 [7281 – 7285]
Li, Xiaodong (C) 2249 – 2252 [2289 – 2292]
Li, Xiaofang (C) 962 – 965 [984 – 987]
Li, Xiaoguang (C) 2959 – 2962 [3019 – 3021], 2962 – 2964 [3022 – 3024], 3407 – 3411 [3473 – 3477]
Li, Xiaolin (C) 2782 – 2785 [2842 – 2845]
Li, Y.-G. (C) 5824 – 5827 [5974 – 5977]
Li, Y. (Sichuan) (C) 2124 – 2127 [2162 – 2165]
Li, Y. (Tianjin) (C) 6387 – 6391 [6545 – 6549]
Li, Y.-Z. (C) 3402 – 3407 [3468 – 3473]
Li, Ya (C) 5882 – 5886 [6032 – 6036]
Li, Yadong
– Fluorescence Resonant Energy Transfer Biosensor Based on Upconversion-Luminescent Nanoparticles (C) 6054 – 6057 [6208 – 6211] DOI: 10.1002/anie.200501907
– Monodisperse Magnetic Single-Crystal Ferrite Microspheres (C) 2782 – 2785 [2842 – 2845] DOI: 10.1002/anie.200462551
Li, Yadong (C) 7742 – 7745 [7920 – 7923]
Li, Yafeng (C) 2012 – 2015 [2048 – 2051]
Li, Yingfu
– A DNA – Protein Nanoengine for "On-Demand" Release and Precise Delivery of Molecules (C) 5464 – 5467 [5600 – 5603] DOI: 10.1002/anie.200501214
– In Vitro Selection of Structure-Switching Signaling Aptamers (C) 1061 – 1065 [1085 – 1089] DOI: 10.1002/anie.200461848
Li, Yongsheng (C) 5083 – 5087 [5213 – 5217]
Li, Z.-B. (C) 1690 – 1693 [1718 – 1721]
Li, Z.-T.
– F···H–N Hydrogen Bonding Driven Foldamers: Efficient Receptors for Dialkylammonium Ions (C) 5725 – 5729 [5871 – 5875] DOI: 10.1002/anie.200500982
Li, Z.-Y. (C) 7913 – 7917 [8127 – 8131]
Li, Zhen (C) 123 – 126 [125 – 128]
Li, Zheng (C) 7053 – 7059 [7215 – 7221]
Liang, C.-G. (C) 6544 – 6546 [6702 – 6704]
Liang, F. (C) 4242 – 4244 [4314 – 4316]
Liang, F.-S. (C) 447 – 452 [451 – 456]
Liang, H.-P. (C) 1269 – 1273 [1295 – 1299], 4391 – 4395 [4465 – 4469]
Liang, J. (C) 7420 – 7424 [7586 – 7590]
Liang, X.
– Highly Efficient $NaNO_2$-Catalyzed Destruction of Trichlorophenol Using Molecular Oxygen (C) 5520 – 5523 [5656 – 5659] DOI: 10.1002/anie.200501470
Liao, J. H. (C) 3552 – 3555 [3618 – 3621]
Liao, M.-C. (C) 7418 – 7420 [7584 – 7586]
Liao, W. (C) 6525 – 6529 [6683 – 6687]
Liao, Y. (C) 4771 – 4774 [4849 – 4852]
Libuda, J.
– Oxygen Storage at the Metal/Oxide Interface of Catalyst Nanoparticles (C) 7601 – 7605 [7773 – 7777] DOI: 10.1002/anie.200502160
Lichtenshtein, A. (C) 1092 – 1096 [1116 – 1120]
Lichtenthaler, F. W.
– A Concise and General Method for Doubly Attaching 2-Ketosugars to Aglycon Diols: Synthesis of the Gomphosides and Spectinomycin (C) 4944 – 4948 [5024 – 5028] DOI: 10.1002/anie.200500434
Lidrissi, C. (C) 2568 – 2572 [2624 – 2628]
Lie, L. H. (C) 1254 – 1257 [1280 – 1283]
Lieser, G. (C) 6348 – 6354 [6506 – 6512]
Lifshitz, Y. (C) 4749 – 4753 [4827 – 4831]
Light, M. E. (C) 2537 – 2542 [2593 – 2598]
Lilie, H. (C) 3140 – 3144 [3200 – 3204]
Lill, R. E. (C) 4757 – 4760 [4835 – 4838]
Lim, Y. H. (C) 7917 – 7921 [8131 – 8135]
Limberg, C.
– ADHOC 2005 in Cologne: The Latest in Dioxygen Activation and Homogeneous Catalytic Oxidation (T) 6102 – 6104 Corrigendum: 6440 [6256 – 6258] DOI: 10.1002/anie.200502936
– Molecular Compounds with Mo-O-Bi Moieties (C) 5259 – 5262 [5393 – 5397] DOI: 10.1002/anie.200500375
Lin, B.
– Correlations between Molecular Numbers and Molecular Masses in an Evanescent Field and Their Applications in Probing Molecular Interactions (C) 5107 – 5110 [5237 – 5240] DOI: 10.1002/anie.200500461
Lin, C. (C) 4333 – 4338 [4407 – 4412]
Lin, C.-C. (C) 7969 – 7972 [8183 – 8186]
Lin, D. W. (C) 609 – 612 [615 – 618]
Lin, J. (C) 1690 – 1693 [1718 – 1721]
Lin, L.-G. (C) 6063 – 6067 [6217 – 6221]
Lin, N.
– Two-Dimensional Adatom Gas Bestowing Dynamic Heterogeneity on Surfaces (C) 1488 – 1491 [1512 – 1515] DOI: 10.1002/anie.200461390
Lin, V. S.-Y.
– Cooperative Catalysis by General Acid and Base Bifunctionalized Mesoporous Silica Nanospheres (C) 1826 – 1830 [1860 – 1864] DOI: 10.1002/anie.200462424
– Stimuli-Responsive Controlled-Release Delivery System Based on Mesoporous Silica Nanorods Capped with Magnetic Nanoparticles (C) 5038 – 5044 [5166 – 5172] DOI: 10.1002/anie.200501819
Lin, Wenbin
– Highly Interpenetrated Metal – Organic Frameworks for Hydrogen Storage (C) 72 – 75 [74 – 77] DOI: 10.1002/anie.200461214
– Highly Porous, Homochiral Metal – Organic Frameworks: Solvent-Exchange-Induced Single-Crystal to Single-Crystal Transformations (C) 1958 – 1961 [1994 – 1997] DOI: 10.1002/anie.200462711
Lin, Wenwei (C) 1654 – 1658 [1682 – 1685], 4258 – 4261 [4330 – 4333]
Lin, X. (C) 135 – 138 [137 – 140]
Lin, Y. (C) 2420 – 2426 [2472 – 2478]
Lin, Z.-E. (C) 6881 – 6884 [7041 – 7044]
Lindel, T.
– Total Synthesis of the Marine Natural Product *rac*-Dibromophakellstatin (C) 2295 – 2298 [2336 – 2338] DOI: 10.1002/anie.200462252
Linden, A. (C) 6187 – 6190 [6343 – 6346]
Linder, M. R. (C) 2732 – 2737 [2792 – 2797]
Lindner, T. (C) 3303 – 3306 [3368 – 3371]
Linehan, J. C. (C) 3578 – 3582 [3644 – 3648]
Ling, C.-C. (C) 7725 – 7729 [7903 – 7907]
Linghu, X. (C) 2377 – 2379 Corrigendum: 4660 [2429 – 2431 Corrigendum: 4735]
Link, A.
– A Timely Reassessment of Early Prediction in the Bioavailability of Orally Administered Drugs (H) 4432 – 4434 [4506 – 4508] DOI: 10.1002/anie.200462888
Lippert, B.
– Models of Putative (AH)G(AH)G Nucleobase Quartets (C) 5670 – 5674 [5816 – 5820] DOI: 10.1002/anie.200500896
Lipshutz, B. H.
– CuH in a Bottle: A Convenient Reagent for Asymmetric Hydrosilylations (C) 6345 – 6348 [6503 – 6506] DOI: 10.1002/anie.200500800
Liron, F. (C) 4627 – 4631 [4703 – 4707]
Lis, T. (C) 5288 – 5291 [5422 – 5425]
Lissner, F. (C) 2103 – 2106 [2140 – 2143], 5871 – 5875 [6021 – 6025]
List, B.
– A Powerful Brønsted Acid Catalyst for the Organocatalytic Asymmetric Transfer Hydrogenation of Imines (C) 7424 – 7427 [7590 – 7593] DOI: 10.1002/anie.200503062
– Metal-Free, Organocatalytic Asymmetric Transfer Hydrogenation of α,β-Unsaturated Aldehydes (C) 108 – 110 [110 – 112] DOI: 10.1002/anie.200462432
Little, S. R. (C) 6704 – 6708 [6862 – 6866]
Littrell, K. (C) 2420 – 2426 [2472 – 2478]
Litvinchuk, S. (C) 6154 – 6157 [6310 – 6313]
Liu, B. (C) 1265 – 1268 [1291 – 1294]
Liu, D. (C) 1687 – 1689 [1715 – 1717]
Liu, D. R.
– Ordered Multistep Synthesis in a Single Solution Directed by DNA Templates (C) 7379 – 7382 [7545 – 7548] DOI: 10.1002/anie.200502879
– Small-Molecule Diversification from Iterated Branching Reaction Pathways Enabled by DNA-Templated Synthesis (C) 7383 – 7386 [7549 – 7552] DOI: 10.1002/anie.200502899
Liu, H. (C) 3118 – 3122 [3178 – 3182]
Liu, H.-w.
– Biosynthesis of TDP-D-Desosamine: Identification of a Strategy for C4 Deoxygena-

 © 2005 Wiley-VCH Verlag GmbH & Co. KGaA, Weinheim

tion
(C) 6742 – 6746 [6900 – 6904]
DOI: 10.1002/anie.200501998
Liu, J.-G. (C) 1836 – 1840 [1870 – 1874]
Liu, Jianhui Corrigendum: 506
Liu, Juewen (C) 7290 – 7293 [7456 – 7459]
Liu, Jun (C) 1987 – 1990 [2023 – 2026]
Liu, M. T. H. (C) 7567 – 7570 [7739 – 7742]
Liu, P. (C) 3864 – 3867 [3932 – 3935]
Liu, Q.-T.
– Iodine-Assisted Assembly of Helical Coordination Polymers of Cucurbituril and Asymmetric Copper(II) Complexes
(C) 3402 – 3407 [3468 – 3473]
DOI: 10.1002/anie.200463071
Liu, R.
– Highly Efficient $NaNO_2$-Catalyzed Destruction of Trichlorophenol Using Molecular Oxygen
(C) 5520 – 5523 [5656 – 5659]
DOI: 10.1002/anie.200501470
Liu, S. (C) 3466 – 3470 [3532 – 3536]
Liu, Tianbo (C) 4018 – 4021 [4086 – 4089]
Liu, Tianfu (C) 4197 – 4201 [4269 – 4273]
Liu, W.
– An Onion Phase in Salt-Free Zero-Charged Catanionic Surfactant Solutions
(C) 4018 – 4021 [4086 – 4089]
DOI: 10.1002/anie.200500353
Liu, Xiaofeng (C) 105 – 108 [107 – 110]
Liu, Xuejun (C) 1994 – 1997 [2030 – 2033]
Liu, Y.-H. (C) 6063 – 6067 [6217 – 6221]
Liu, Yan (C) 4333 – 4338 [4407 – 4412]
Liu, Ye
– Polyethylenimine-Grafted Multiwalled Carbon Nanotubes for Secure Noncovalent Immobilization and Efficient Delivery of DNA
(C) 4782 – 4785 [4860 – 4863]
DOI: 10.1002/anie.200500042
Liu, Yi (C) 3050 – 3055 [3110 – 3115]
Liu, Yong (C) 7107 – 7110 [7269 – 7272]
Liu, Zhifu (C) 7922 – 7925 [8136 – 8139]
Liu, Zhongfan
– Finely Tuning Metallic Nanogap Size with Electrodeposition by Utilizing High-Frequency Impedance in Feedback
(C) 7771 – 7775 [7949 – 7953]
DOI: 10.1002/anie.200502680
Liu, Zongwen (C) 2140 – 2144 [2178 – 2182]
Livage, C.
– A Three-Dimensional Metal – Organic Framework with an Unprecedented Octahedral Building Unit
(C) 6488 – 6491 [6646 – 6649]
DOI: 10.1002/anie.200502185
Livneh, E. (C) 1092 – 1096 [1116 – 1120]
Livramento, J. B. (C) 1480 – 1484 [1504 – 1508]
Liz-Marzán, L. M.
– Aligning Au Nanorods by Using Carbon Nanotubes as Templates
(C) 4375 – 4378 [4449 – 4452]
DOI: 10.1002/anie.200500581
Lizos, D. E. (C) 4925 – 4929 [5005 – 5009]
Lloveras, V. (C) 1977 – 1981 [2013 – 2017]
Lloyd, A. J. (C) 6403 – 6406 [6561 – 6564]
Lloyd, G. O. (C) 3848 – 3851 [3916 – 3919]
Lloyd, N. C. (C) 941 – 944 [963 – 966]
Lloyd-Jones, G. C.
– Rate Enhancement by Ethylene in the Ru-Catalyzed Ring-Closing Metathesis of Enynes: Evidence for an "Ene-then-Yne" Pathway that Diverts through a Second Catalytic Cycle
(C) 7442 – 7447 [7608 – 7613]
DOI: 10.1002/anie.200502243
– Reevaluation of the Mechanism of the Baylis – Hillman Reaction: Implications for Asymmetric Catalysis
(C) 1706 – 1708 [1734 – 1736]
DOI: 10.1002/anie.200462462
Lo, K. Y. (C) 7127 – 7131 [7289 – 7293]
Lo, L.-C.
– Design of a Mechanism-Based Probe for Neuraminidase To Capture Influenza Viruses
(C) 6888 – 6892 [7048 – 7052]
DOI: 10.1002/anie.200501738
Lo, M. M.-C. (C) 2249 – 2252 [2289 – 2292]
Locatelli, M. (C) 6219 – 6222 [6375 – 6378]
Loeb, S. J.
– Metal – Organic Rotaxane Frameworks: Three-Dimensional Polyrotaxanes from Lanthanide-Ion Nodes, Pyridinium *N*-Oxide Axles, and Crown-Ether Wheels
(C) 901 – 904 [923 – 926]
DOI: 10.1002/anie.200461707
Löffler, E. (C) 917 – 920 [939 – 942]
Loffreda, D.
– Catalytic Hydrogenation of Unsaturated Aldehydes on Pt(111): Understanding the Selectivity from First-Principles Calculations
(C) 5279 – 5282 [5413 – 5416]
DOI: 10.1002/anie.200500913
Löhmannsröben, H.-G. (C) 7612 – 7615 [7784 – 7788]
Löhnwitz, K. (C) 7794 – 7798 [7972 – 7976]
Lohr, A. (C) 5071 – 5074 [5199 – 5202]
Lohse-Fraefel, N. (C) 4036 – 4038 [4104 – 4106]
Loiseau, F. (C) 4881 – 4884 [4959 – 4962]
Loizidou, E. (C) 3447 – 3452 [3513 – 3518]
Londesborough, M. G. S. (C) 6222 – 6226 [6378 – 6382]
London, G. (C) 3086 – 3089 [3146 – 3149]
Long, De-L. (C) 3415 – 3419 [3481 – 3485]
Long, J. R.
– Synthesis and Characterization of the Nitrogen-Centered Trigonal Prismatic Clusters $[W_6NCl_{18}]^{n-}$ ($n = 1 – 3$)
(C) 2549 – 2553 [2605 – 2609]
DOI: 10.1002/anie.200462585
Long, M. S. (H) 3518 – 3520 [3584 – 3586]
Longbottom, D. A. (C) 4925 – 4929 [5005 – 5009]
Lönnecke, P. (C) 2965 – 2969 [3025 – 3029]
Looper, R. E. (C) 3879 – 3881 [3947 – 3949]
Loos, D. (C) 560 – 564 [566 – 570]
López, C. (C) 1865 – 1869 [1899 – 1903]
López, F. (C) 2752 – 2756 [2812 – 2816]
López, J. C. (C) 3840 – 3844 [3908 – 3912]
Lopez, N. (C) 1824 – 1826 [1858 – 1860]
López, R. (C) 6187 – 6190 [6343 – 6346]
López, S. (C) 6146 – 6148 [6302 – 6304]
López-Cortés, N. (C) 7553 – 7557 [7725 – 7729]
López-Mora, N. (C) 2360 – 2364 [2412 – 2416]
López-Sáez, M.-J. (C) 6001 – 6004 [6155 – 6158]
Lorenz, D. (C) 7887 – 7891 [8099 – 8104]
Lorenz, L. (C) 7783 – 7786 [7961 – 7964]
Lou, Y. (C) 5855 – 5857 [6005 – 6007]
Lough, A. J. (C) 5886 – 5890 [6036 – 6040]
Loveless, D. M. (C) 2746 – 2748 [2806 – 2808]
Lovrinovic, M. (H) 3179 – 3183 [3241 – 3246]
Lowndes, D. H.
– Germanium-Catalyzed Growth of Zinc Oxide Nanowires: A Semiconductor Catalyst for Nanowire Synthesis
(C) 274 – 278 [278 – 282]
DOI: 10.1002/anie.200460043
Lu, C. (C) 598 – 603 [604 – 609]
Lu, C.-P. (C) 6888 – 6892 [7048 – 7052]
Lu, F. (R) 7852 – 7872 [8062 – 8083]
Lu, H. (C) 6938 – 6940 [7098 – 7100]
Lu, J. (C) 5894 – 5898 [6044 – 6048]
Lu, K.-L.
– Crystal Engineering: Toward Intersecting Channels from a Neutral Network with a bcu-Type Topology
(C) 6063 – 6067 [6217 – 6221]
DOI: 10.1002/anie.200462674
Lu, Lehui (C) 5997 – 6001 [6151 – 6155]
Lu, Lianghua (C) 5275 – 5278 [5409 – 5412]
Lu, P. (C) 5275 – 5278 [5409 – 5412]
Lu, Yi
– Proofreading and Error Removal in a Nanomaterial Assembly
(C) 7290 – 7293 [7456 – 7459]
DOI: 10.1002/anie.200501815
Lu, Yunfeng
– General Synthetic Route toward Functional Hollow Spheres with Double-Shelled Structures
(C) 6727 – 6730 [6885 – 6888]
DOI: 10.1002/anie.200501556
Luan, X.-J. (C) 3864 – 3867 [3932 – 3935]
Luban, M. (C) 3857 – 3861 [3925 – 3929]
Lubin, A. A. (C) 5456 – 5459 [5592 – 5595]
Lucas, L. N. (C) 2373 – 2376 [2425 – 2428]
Lucchini, V.
– "Hexacarboxytrindanes": Benzene Rings with Homotopic Faces as Scaffolds for the Construction of D_3 Chiral Architectures
(C) 7435 – 7439 [7601 – 7605]
DOI: 10.1002/anie.200502262
Luchinat, C. (C) 2223 – 2225 [2263 – 2265]
Lücke, B. (C) 6771 – 6774 [6929 – 6933]
Luckhurst, G. R.
– V-Shaped Molecules: New Contenders for the Biaxial Nematic Phase
(H) 2834 – 2836 [2894 – 2897]
DOI: 10.1002/anie.200500709
Ludolph, B. (C) 4975 – 4980 [5055 – 5060]
Ludwig, K. (C) 2976 – 2979 [3036 – 3039]
Ludwig, R.
– Calculation of Clathrate-Like Water Clusters Including H_2O-Buckminsterfullerene
(C) 811 – 815 [821 – 826]
DOI: 10.1002/anie.200460899
Luedtke, N. W. (C) 927 – 932 [949 – 954]
Lueken, H. (C) 7212 – 7215 [7379 – 7382]
Luger, P.
– Electron Density and Bonding at Inverted Carbon Atoms: An Experimental Study of a [1.1.1]Propellane Derivative
(C) 3925 – 3928 [3993 – 3997]
DOI: 10.1002/anie.200500169
Lügger, T. (C) 3759 – 3763 [3825 – 3829]
Lugstein, A. (C) 3419 – 3422 [3485 – 3488]
Luis, S. V.
– Synthetic Macrocyclic Peptidomimetics as Tunable pH Probes for the Fluorescence Imaging of Acidic Organelles in Live Cells
(C) 6504 – 6508 [6662 – 6666]
DOI: 10.1002/anie.200501920
Lukin, O. (R) 1456 – 1477 [1480 – 1501]
Lumsden, M. (C) 6196 – 6199 [6352 – 6355]
Lundgren, E. (C) 917 – 920 [939 – 942]
Luo, F. (C) 4328 – 4333 [4402 – 4407]
Luo, J. (C) 2553 – 2556 [2609 – 2612]
Luo, T.-T. (C) 6063 – 6067 [6217 – 6221]
Luo, Y.-F. (C) 6025 – 6029 [6179 – 6183]

 © 2005 Wiley-VCH Verlag GmbH & Co. KGaA, Weinheim

Luong, N. (C) 6207 – 6210 [6363 – 6366]
Lupton, J. M.
– Counting Chromophores in Conjugated Polymers
(C) 1520 – 1525 [1544 – 1549]
DOI: 10.1002/anie.200461784
Lusby, P. J. (C) 4557 – 4564 [4633 – 4640]
Lutz, J.-F. (C) 5262 – 5265 [5397 – 5400]
Lutz, Martin (C) 4385 – 4388 [4459 – 4462], 6579 – 6582 [6737 – 6740]
Lutz, Matthias (C) 5647 – 5651 [5792 – 5796]
Lützen, A.
– Self-Assembled Molecular Capsules—Even More Than Nano-Sized Reaction Vessels
(H) 1000 – 1002 [1022 – 1025]
DOI: 10.1002/anie.200462272
Luy, B.
– Stretched Gelatin Gels as Chiral Alignment Media for the Discrimination of Enantiomers by NMR Spectroscopy
(C) 3145 – 3147 Corrigendum: 3509 [3205 – 3207 Corrigendum: 3575]
DOI: 10.1002/anie.200462736
– Stretched Poly(vinyl acetate) Gels as NMR Alignment Media for the Measurement of Residual Dipolar Couplings in Polar Organic Solvents
(C) 423 – 426 [427 – 430]
DOI: 10.1002/anie.200461241
Lv, J. (C) 5100 – 5103 [5230 – 5233]
Lynch, J. (C) 1725 – 1729 [1753 – 1757]
Lynch, V. M. (C) 83 – 87 [85 – 89], 5989 – 5992 [6143 – 6146], 7386 – 7390 [7552 – 7556]
Lyon, L. A.
– Photoswitchable Microlens Arrays
(C) 1333 – 1336 [1357 – 1360]
DOI: 10.1002/anie.200461538
– Soft Nanotechnology with Soft Nanoparticles
(R) 7686 – 7708 [7862 – 7886]
DOI: 10.1002/anie.200501321
Lysetska, M. (C) 3147 – 3151 [3208 – 3212], 5071 – 5074 [5199 – 5202]
Lyubovskaya, R. N. (C) 234 – 237 [238 – 241]

Ma, C. T. L. (C) 4178 – 4182 [4250 – 4254]
Ma, D.
– Total Synthesis of Halipeptin A: A Potent Antiinflammatory Cyclic Depsipeptide
(C) 135 – 138 [137 – 140]
DOI: 10.1002/anie.200461239
Ma, J.-A. (C) 412 – 415 [416 – 419]
Ma, Jiming (C) 598 – 603 [604 – 609]
Ma, Jin (C) 6727 – 6730 [6885 – 6888]
Ma, R. (C) 576 – 579 [582 – 585]
Ma, S.
– 1,4-Migration of Rhodium and Palladium in Catalytic Organometallic Reactions
(M) 7512 – 7517 [7680 – 7685]
DOI: 10.1002/anie.200501298
– Probing the Mechanism of the Palladium-Catalyzed Addition of Organoboronic Acids to Allenes in the Presence of AcOH by ESI-FTMS
(C) 4771 – 4774 [4849 – 4852]
DOI: 10.1002/anie.200463101
– What Can a Metal Catalyst Do with Allenes? One-Step Formation of Steroid Scaffolds from Readily Available Starting Materials
(C) 5275 – 5278 [5409 – 5412]
DOI: 10.1002/anie.200501350
Ma, X. (C) 7072 – 7074 [7234 – 7236]
Ma, Y.
– Correlations between Molecular Numbers and Molecular Masses in an Evanescent Field and Their Applications in Probing Molecular Interactions
(C) 5107 – 5110 [5237 – 5240]
DOI: 10.1002/anie.200500461
Macak, J. M. (C) 7463 – 7465 [7629 – 7632]
Macák, J. M. (C) 2100 – 2102 [2136 – 2139]
McAllister, L. A. (C) 452 – 455 [456 – 459]
McCarley, R. L.
– Highly Water-Soluble Thermally Responsive Poly(thiophene)-Based Brushes
(C) 4872 – 4876 [4950 – 4954]
DOI: 10.1002/anie.200500867
Macchi, P. (C) 7736 – 7739 [7914 – 7917]
Macchioni, A. (C) 7922 – 7925 [8136 – 8139]
McCleskey, S. C. (C) 6375 – 6378 [6533 – 6536]
McCleskey, T. M.
– Stable, Soluble Beryllium Aluminum Citrate Complexes Inspired by the Emerald Mineral Structure
(C) 2403 – 2406 [2455 – 2458]
DOI: 10.1002/anie.200462531
McCooey, S. H. (C) 6367 – 6370 [6525 – 6528]
McCormick, R. A. (C) 452 – 455 [456 – 459]
McCusker, C. (C) 2732 – 2737 [2792 – 2797]
McDevitt, J. T.
– Differential Receptors Create Patterns That Distinguish Various Proteins
(C) 6375 – 6378 [6533 – 6536]
DOI: 10.1002/anie.200501137
Macdonald, C. L. B.
– Crown Ether Ligation: An Approach to Low-Oxidation-State Indium Compounds
(C) 7453 – 7456 [7619 – 7622]
DOI: 10.1002/anie.200502901
McDonald, R. (C) 2005 – 2008 [2041 – 2044], 3603 – 3606 [3669 – 3672]
Macdonald, S. J. F. (C) 1870 – 1873 Corrigendum: 2471 [1904 – 1907 Corrigendum: 2525]
McErlean, C. S. P. (C) 6157 – 6162 [6313 – 6318]
McFarland, E. W.
– Benzene Formation at 70 °C by Coupling of Propylene on Supported Pd Nanoclusters
(C) 4735 – 4739 [4813 – 4817]
DOI: 10.1002/anie.200500022
MacFarlane, D. R. (C) 313 – 316 [317 – 320]
McGarvey, J. J. (C) 4069 – 4073 [4137 – 4141]
MacGillivray, L. R.
– A Single-Crystal-to-Single-Crystal Transformation Mediated by Argentophilic Forces Converts a Finite Metal Complex into an Infinite Coordination Network
(C) 3569 – 3572 [3635 – 3638]
DOI: 10.1002/anie.200500400
Mach, R. (C) 3609 – 3613 [3675 – 3679]
Machotta, A. B. (C) 149 – 152 [152 – 155]
McIlwrath, K. (C) 4539 – 4543 [4615 – 4619]
McIndoe, J. S.
– Hydrogen Sponge? A Heteronuclear Cluster That Absorbs Large Quantities of Hydrogen
(H) 5772 – 5774 [5918 – 5921]
DOI: 10.1002/anie.200501549
McIndoe, J. S. (C) 6875 – 6878 [7035 – 7038]
McInnes, E. J. L. (C) 3456 – 3459 [3522 – 3525]
McIntyre, G. J. (C) 7227 – 7230 [7393 – 7396]
Mackay, A. C. (C) 1130 – 1133 [1154 – 1157]
McKenzie, C. J.
– Water Oxidation Catalyzed by a Dinuclear Mn Complex: A Functional Model for the Oxygen-Evolving Center of Photosystem II
(C) 6916 – 6920 [7076 – 7080]
DOI: 10.1002/anie.200502114
McKeown, N. B.
– A Phthalocyanine Clathrate of Cubic Symmetry Containing Interconnected Solvent-Filled Voids of Nanometer Dimensions
(C) 7546 – 7549 [7718 – 7721]
DOI: 10.1002/anie.200502668
McKinlay, R. M. (C) 5733 – 5736 [5879 – 5882]
MacLachlan, M. J.
– Supramolecular Assembly and Coordination-Assisted Deaggregation of Multimetallic Macrocycles
(C) 4178 – 4182 [4250 – 4254]
DOI: 10.1002/anie.200500058
McLachlan, M. M. (C) 580 – 584 [586 – 590]
McLafferty, F. W. (C) 4911 – 4914 [4989 – 4992]
McLellan, J. M. (C) 3596 – 3600 [3662 – 3666]
MacLeod, C. (C) 5830 – 5833 [5980 – 5983]
MacLeod, N. (C) 3730 – 3732 [3796 – 3798]
McMaster, J. (C) 5314 – 5317 [5448 – 5451]
McMurdo, M. (C) 6384 – 6387 [6542 – 6545]
McMurry, T. J. (C) 6766 – 6769 [6924 – 6927]
McPartlin, M. (C) 3456 – 3459 [3522 – 3525], 3932 – 3936 [4002 – 4005], 5729 – 5733 [5875 – 5879]
Madhavan, N. (C) 7584 – 7587 [7756 – 7759]
Madison, V. (C) 7024 – 7028 [7186 – 7190]
Mae, K. (C) 2413 – 2416 [2465 – 2468]
Maeda, A. (C) 6484 – 6487 [6642 – 6645]
Maeda, H.
– 2,4-Dinitrobenzenesulfonyl Fluoresceins as Fluorescent Alternatives to Ellman's Reagent in Thiol-Quantification Enzyme Assays
(C) 2922 – 2925 [2982 – 2985]
DOI: 10.1002/anie.200500114
Maeda, Yonezo (C) 4899 – 4903 [4977 – 4981]
Maeda, Yutaka (C) 3282 – 3285 [3346 – 3349], 7567 – 7570 [7739 – 7742]
Maekawara, N. (C) 1532 – 1536 [1556 – 1560]
Maestro, M. A. (C) 1865 – 1869 [1899 – 1903]
Magbitang, T. (C) 7574 – 7580 [7746 – 7752]
Magda, D. J.
– Synthesis, Anion-Binding Properties, and In Vitro Anticancer Activity of Prodigiosin Analogues
(C) 5989 – 5992 [6143 – 6146]
DOI: 10.1002/anie.200501740
Magennis, S. W. (C) 6512 – 6516 [6670 – 6674]
Maggard, P. A.
– Pillared Hybrid Solids with Access to Coordinatively Unsaturated Metal Sites: An Alternative Strategy
(C) 2553 – 2556 [2609 – 2612]
DOI: 10.1002/anie.200462715
Magnusson, A. O. (C) 4582 – 4585 [4658 – 4661]
Magro, G. (C) 6878 – 6881 [7038 – 7041]
Magull, J. (C) 281 – 284 [285 – 288]
Mahajan, S. (C) 1226 – 1229 [1252 – 1255]
Mahesh, M. (C) 1356 – 1360 [1380 – 1384]
Maheswaran, S. (C) 5044 – 5048 [5172 – 5176]

 © 2005 Wiley-VCH Verlag GmbH & Co. KGaA, Weinheim

Mainolfi, N. (R) 3022 – 3037 [3082 – 3097]
Maire, P. (C) 6318 – 6323 [6477 – 6481], 6325 – 6329 [6483 – 6487]
Maiti, S. (C) 6529 – 6533 [6687 – 6691]
Majd, S. (C) 6697 – 6700 [6855 – 6858]
Majima, T.
– DNA Tube Structures Controlled by a Four-Way-Branched DNA Connector (C) 6074 – 6077 [6228 – 6231] DOI: 10.1002/anie.200501034
Majima, T. (C) 3591 – 3594 [3657 – 3660]
Makhatadze, G. I. (C) 3852 – 3856 [3920 – 3924]
Makhluf, S. (C) 6560 – 6563 [6718 – 6721]
Makhseed, S. (C) 7546 – 7549 [7718 – 7721]
Makino, M. (C) 4608 – 4611 [4684 – 4687]
Mal, S. S. (C) 3777 – 3780 [3843 – 3846]
Malacria, M. (C) 7114 – 7118 [7276 – 7280]
Malda, H. (C) 5052 – 5057 [5180 – 5185]
Malek, N. (C) 4021 – 4025 [4089 – 4093]
Malesevic, M. (C) 1408 – 1412 [1432 – 1437]
Malik, S. (C) 7048 – 7053 [7210 – 7215]
Mallah, T.
– Very Large Ising-Type Magnetic Anisotropy in a Mononuclear Ni^{II} Complex (C) 1876 – 1879 [1910 – 1913] DOI: 10.1002/anie.200462294
Mallah, T. (C) 5044 – 5048 [5172 – 5176]
Mallenahalli, S. P. (C) 6560 – 6563 [6718 – 6721]
Mallet, J.-M. (C) 1683 – 1687 [1711 – 1715]
Mallinson, P. M. (C) 7733 – 7736 [7911 – 7914]
Mallouk, T. E. (C) 744 – 746 [754 – 756]
Malo, J. (C) 3057 – 3061 [3117 – 3121]
Mammana, A. (C) 4006 – 4009 [4074 – 4077]
Mamula, O.
– A Trinuclear Eu^{III} Array within a Diastereoselectively Self-Assembled Helix Formed by Chiral Bipyridine-Carboxylate Ligands (C) 2527 – 2531 [2583 – 2587] DOI: 10.1002/anie.200500094
Manabe, S. (C) 4218 – 4224 [4290 – 4296]
Manassero, M. (C) 6892 – 6895 [7052 – 7055]
Mandal, Subrata (C) 132 – 135 [134 – 137]
Mandal, Sunil (C) 3443 – 3447 [3509 – 3513]
Manesiotis, P. (C) 3902 – 3906 [3970 – 3974]
Mann, B. E. (C) 4543 – 4546 [4619 – 4622]
Manners, I.
– Gelation of Helical Polypeptide – Random Coil Diblock Copolymers by a Nanoribbon Mechanism (C) 7964 – 7968 [8178 – 8182] DOI: 10.1002/anie.200502809
– Reversible, Strain-Controlled Haptotropic Shifts of Cyclopentadienyl Ligands in [1]- and [2]Metallocenophanes (C) 5886 – 5890 [6036 – 6040] DOI: 10.1002/anie.200501155
Manos, M. J. (C) 3552 – 3555 [3618 – 3621]
Mansfeld, D. (C) 245 – 249 [250 – 254]
Mao, B.-W. (C) 1265 – 1268 [1291 – 1294]
Mao, C.
– A DNAzyme That Walks Processively and Autonomously along a One-Dimensional Track (C) 4355 – 4358 [4429 – 4432] DOI: 10.1002/anie.200500703
– DNA-Encoded Self-Assembly of Gold Nanoparticles into One-Dimensional Arrays (C) 3582 – 3585 [3648 – 3651] DOI: 10.1002/anie.200463096
– Sequence Symmetry as a Tool for Designing DNA Nanostructures (C) 6694 – 6696 [6852 – 6854] DOI: 10.1002/anie.200502193
Marchelli, R. (C) 5126 – 5130 [5256 – 5260]
Marchetti, L. (C) 5701 – 5705 [5847 – 5851]
Marcos, M. D. (C) 2918 – 2922 [2978 – 2982], 4405 – 4407 [4479 – 4482]
Mareda, J. (C) 6154 – 6157 [6310 – 6313]
Margue, R. G. (C) 7442 – 7447 [7608 – 7613]
Mari, S. (C) 296 – 298 [300 – 302]
Marigo, M. (C) 794 – 797 [804 – 807], 3703 – 3706 [3769 – 3772]
Maris, T. (C) 4021 – 4025 [4089 – 4093]
Mark, A. E. (C) 1065 – 1067 [1089 – 1091]
Märk, T. D. (C) 1647 – 1650 [1673 – 1676], 6941 – 6943 [7101 – 7103]
Markopoulos, G. (C) 7549 – 7553 [7721 – 7725]
Marks, T. J.
– Exceptional Molecular Hyperpolarizabilities in Twisted π-Electron System Chromophores (C) 7922 – 7925 [8136 – 8139] DOI: 10.1002/anie.200501581
Markwick, P. R. L.
– Local Structure and Anisotropic Backbone Dynamics from Cross-Correlated NMR Relaxation in Proteins (C) 3232 – 3237 [3296 – 3301] DOI: 10.1002/anie.200462495
Marquínez, F. (C) 102 – 105 [104 – 107]
Marra, A.
– Hybrid Solution/Solid-Phase Synthesis of Oligosaccharides by Using Trichloroacetyl Isocyanate as Sequestration-Enabling Reagent of Sugar Alcohols (C) 1672 – 1676 [1700 – 1704] DOI: 10.1002/anie.200462422
Marshall, W. J. (C) 7240 – 7244 [7406 – 7410]
Marszalek, P. E.
– Direct Detection of Inter-residue Hydrogen Bonds in Polysaccharides by Single-Molecule Force Spectroscopy (C) 2723 – 2727 [2783 – 2787] DOI: 10.1002/anie.200462067
Martens, J. A.
– Tailored Catalytic Propene Trimerization over Acidic Zeolites with Tubular Pores (C) 5687 – 5690 [5833 – 5836] DOI: 10.1002/anie.200463045
Martens, J. A. (C) 400 – 403 [404 – 407]
Martí, S. (C) 904 – 909 [926 – 931]
Martín, A. (C) 2407 – 2410 [2459 – 2462]
Martin, A. (C) 6771 – 6774 [6929 – 6933]
Martin, D. (C) 1700 – 1703 [1728 – 1731]
Martin, M. R. (C) 2382 – 2385 [2434 – 2437]
Martín, N.
– Hydrogen-Bonding Motifs in Fullerene Chemistry (M) 5374 – 5382 [5508 – 5516] DOI: 10.1002/anie.200500321
Martin, R. E.
– Joint Meeting on Medicinal Chemistry in Vienna (T) 5364 – 5366 [5498 – 5500] DOI: 10.1002/anie.200502439
Martinez, K. L. (C) 1388 – 1392 [1412 – 1416]
Martínez-Máñez, R.
– A Regenerative Chemodosimeter Based on Metal-Induced Dye Formation for the Highly Selective and Sensitive Optical Determination of Hg^{2+} Ions (C) 4405 – 4407 [4479 – 4482] DOI: 10.1002/anie.200500583
– Host Solids Containing Nanoscale Anion-Binding Pockets and Their Use in Selective Sensing Displacement Assays (C) 2918 – 2922 [2978 – 2982] DOI: 10.1002/anie.200461511
Martínez-Mayorga, K. (C) 2360 – 2364 [2412 – 2416]
Martínez-Merino, V. (C) 458 – 461 [462 – 465]
Martinez-Teipel, B. (C) 5830 – 5833 [5980 – 5983]
Martoňák, R. (C) 3769 – 3773 [3835 – 3839]
Maruoka, K.
– Design of an Axially Chiral Amino Acid with a Binaphthyl Backbone as an Organocatalyst for a Direct Asymmetric Aldol Reaction (C) 3055 – 3057 [3115 – 3117] DOI: 10.1002/anie.200500408
– Dramatic Rate Enhancement of Asymmetric Phase-Transfer-Catalyzed Alkylations (C) 625 – 628 [631 – 634] DOI: 10.1002/anie.200462035
– Powerful Chiral Phase-Transfer Catalysts for the Asymmetric Synthesis of α-Alkyl- and α,α-Dialkyl-α-amino Acids (C) 1549 – 1551 [1573 – 1575] DOI: 10.1002/anie.200462257
Maruyama, A. (C) 6193 – 6196 [6349 – 6352]
Marvilliers, A. (C) 1876 – 1879 [1910 – 1913]
Marx, A.
– Enhanced Fidelity in Mismatch Extension by DNA Polymerase through Directed Combinatorial Enzyme Design (C) 4712 – 4715 [4791 – 4794] DOI: 10.1002/anie.200500047
– Genotyping—From Genomic DNA to Genotype in a Single Tube (M) 7842 – 7849 [8052 – 8060] DOI: 10.1002/anie.200501444
Mas-Marzá, E. (C) 444 – 447 [448 – 451]
Masaoka, N. (C) 1398 – 1401 [1422 – 1425]
Masaoka, S. (C) 2700 – 2704 [2760 – 2764]
Mase, N. (C) 3706 – 3710 [3772 – 3776]
Mashiko, S. (C) 7283 – 7287 [7449 – 7453]
Mashuta, M. S. (C) 1883 – 1887 [1917 – 1921]
Mason, S. A. (C) 7227 – 7230 [7393 – 7396]
Maspoch, D. (C) 6013 – 6015 [6167 – 6169]
Massa, W. (C) 1643 – 1646 Corrigendum: 2471 [1670 – 1673 Corrigendum: 2525]
Massi, A.
– Hybrid Solution/Solid-Phase Synthesis of Oligosaccharides by Using Trichloroacetyl Isocyanate as Sequestration-Enabling Reagent of Sugar Alcohols (C) 1672 – 1676 [1700 – 1704] DOI: 10.1002/anie.200462422
Massi, M. (C) 888 – 892 [910 – 914]
Masson, G. (C) 7946 – 7950 [8160 – 8164]
Mastuzaki, H.
– Vapochromic Behavior Accompanied by Phase Transition between Charge-Polarization and Charge-Density-Wave States in a Quasi-One-Dimensional Iodine-Bridged Dinuclear Platinum Compound (C) 3240 – 3243 [3304 – 3307] DOI: 10.1002/anie.200500091
Masu, H. (C) 4564 – 4567 [4640 – 4643]
Masuda, H.
– Preparation of a Hydroperoxo Zinc(II) Intermediate (C) 5698 – 5701 [5844 – 5847] DOI: 10.1002/anie.200501157
Masuda, M. (C) 2275 – 2279 [2315 – 2319]
Masuda, T. (C) 416 – 419 [420 – 423]
Masuo, S. (C) 560 – 564 [566 – 570]

 © 2005 Wiley-VCH Verlag GmbH & Co. KGaA, Weinheim

Mateos-Timoneda, M. A. (C) 3248 – 3253 [3312 – 3317]
Mathey, F.
– One-Pot Conversion of Phospholide Ions into β-Functional Phosphinines (C) 1082 – 1084 [1106 – 1108] DOI: 10.1002/anie.200462020
Mathison, C. J. N. (C) 5992 – 5997 [6146 – 6151]
Mathur, A. (C) 4002 – 4006 [4070 – 4074]
Mathys, G. M. (C) 5687 – 5690 [5833 – 5836]
Matile, S.
– AFM Snapshots of Synthetic Multifunctional Pores with Polyacetylene Blockers: Pseudorotaxanes and Template Effects (C) 6154 – 6157 [6310 – 6313] DOI: 10.1002/anie.200501886
Matmour, R. (C) 284 – 287 [288 – 291]
Matsubara, H. (C) 1075 – 1078 [1099 – 1102]
Matsubara, S.
– Preparation of Enolate – Homoenolate Species as (*Z*)-γ-Siloxyallylmetal Equivalents: Sequential 1,4-Addition of Bis(iodozincio)methane to 1,4-Dicarbonylbutenes and Cyclopropanation (C) 3293 – 3296 [3357 – 3360] DOI: 10.1002/anie.200500133
– Stereospecific and Stereoselective Preparation of 2-(1-Hydroxyalkyl)-1-alkylcyclopropanols from α,β-Epoxy Ketones and Bis(iodozincio)methane (C) 5860 – 5863 [6010 – 6013] DOI: 10.1002/anie.200501644
Matsubara, Y. (C) 7040 – 7044 [7202 – 7206]
Matsubayashi, H. (C) 1336 – 1340 [1360 – 1364]
Matsuda, A.
– Synthesis of 1,8-Naphthyridine C-Nucleosides and Their Base-Pairing Properties in Oligodeoxynucleotides: Thermally Stable Naphthyridine:Imidazopyridopyrimidine Base-Pairing Motifs (C) 596 – 598 [602 – 604] DOI: 10.1002/anie.200461857
– Total Synthesis of Caprazol, a Core Structure of the Caprazamycin Antituberculosis Antibiotics (C) 1854 – 1856 [1888 – 1890] DOI: 10.1002/anie.200462439
Matsuda, R. (C) 920 – 923 [942 – 945]
Matsuda, S. (C) 5857 – 5860 [6007 – 6010]
Matsuda, T. (C) 4608 – 4611 [4684 – 4687]
Matsueda, S. (C) 3861 – 3864 [3929 – 3932]
Matsukawa, Y.
– Palladium(0)-Catalyzed Hydroalkoxylation of Hexafluoropropene: Synthesis of Hydrofluoroethers under Neutral Conditions (C) 1128 – 1130 [1152 – 1154] DOI: 10.1002/anie.200462200
Matsumoto, A. (C) 7059 – 7062 [7221 – 7224]
Matsumoto, H.
– S-Heterocyclic Carbene with a Disilane Backbone (C) 7567 – 7570 [7739 – 7742] DOI: 10.1002/anie.200502971
Matsumoto, Kazuhiro (C) 4935 – 4939 [5015 – 5019]
Matsumoto, Kazuko
– Paramagnetic Platinum – Rhodium Octamers Bridged by Halogen Ions To Afford a Quasi-1D System (C) 5459 – 5464 [5595 – 5600] DOI: 10.1002/anie.200501049
Matsumoto, T. (C) 2262 – 2265 [2302 – 2305]
Matsumoto, Y. (C) 2148 – 2151 [2186 – 2189]
Matsunaga, Satoshi (C) 3240 – 3243 [3304 – 3307]
Matsunaga, Shigeki
– Direct Catalytic Asymmetric Mannich-Type Reactions of *N*-(2-Hydroxyacetyl)-pyrrole as an Ester-Equivalent Donor (C) 4365 – 4368 [4439 – 4442] DOI: 10.1002/anie.200501180
– Non-C_2-Symmetric, Chirally Economical, and Readily Tunable Linked-binols: Design and Application in a Direct Catalytic Asymmetric Mannich-Type Reaction (C) 3470 – 3474 [3536 – 3540] DOI: 10.1002/anie.200500425
Matsunari, T. (C) 1856 – 1860 [1890 – 1894]
Matsuno, H. (C) 2922 – 2925 [2982 – 2985]
Matsuo, I. (C) 7950 – 7954 [8164 – 8168]
Matsushita, T. (C) 91 – 96 [93 – 98], 2534 – 2537 [2590 – 2593]
Mattausch, H. (C) 3917 – 3921 [3985 – 3989]
Mattay, J.
– Supramolecular Chemistry at the Single-Molecule Level (C) 484 – 488 [489 – 492] DOI: 10.1002/anie.200461382
Maue, M. (C) 2265 – 2270 [2305 – 2310]
Maunders, B. M. (C) 6755 – 6758 [6913 – 6916]
Mavridis, I. M. (C) 5097 – 5100 [5227 – 5230]
Mavrikakis, M.
– Controlling the Catalytic Activity of Platinum-Monolayer Electrocatalysts for Oxygen Reduction with Different Substrates (C) 2132 – 2135 [2170 – 2173] DOI: 10.1002/anie.200462335
Mayama, H. (C) 3453 – 3456 [3519 – 3522]
Mayer, J. M.
– Comments on "How Single and Bifurcated Hydrogen Bonds Influence Proton-Migration Rate Constants, Redox, and Electronic Properties of Phenoxyl Radicals" (L) 1598 – 1599 [1624 – 1625] DOI: 10.1002/anie.200461977
Mayer, M.
– Hydrogel Stamping of Arrays of Supported Lipid Bilayers with Various Lipid Compositions for the Screening of Drug – Membrane and Protein – Membrane Interactions (C) 6697 – 6700 [6855 – 6858] DOI: 10.1002/anie.200502189
Mayer, P. (C) 924 – 927 [946 – 949], 2427 – 2428 Corrigendum: 3955 [2479 – 2480], 3929 – 3932 [3998 – 4001], 6234 – 6237 [6391 – 6393], 7790 – 7793 [7968 – 7971], 7874 – 7878 [8086 – 8090], 7884 – 7887 [8096 – 8099]
Mayer-Enthart, E. (C) 1636 – 1639 [1662 – 1666]
Mayoral, J. A. (C) 458 – 461 [462 – 465]
Mayr, H.
– Ambident Reactivity of the Cyanide Ion: A Failure of the HSAB Principle (C) 142 – 145 [145 – 148] DOI: 10.1002/anie.200461640
– Ambident Reactivity of the Nitrite Ion Revisited (C) 4623 – 4626 [4699 – 4703] DOI: 10.1002/anie.200501274
Mazet, C. (C) 4888 – 4891 [4966 – 4969]
Mazzanti, A. (C) 3285 – 3289 [3349 – 3353]
Mazzanti, M.
– An Efficient Design for the Rigid Assembly of Four Bidentate Chromophores in Water-Stable Highly Luminescent Lanthanide Complexes (C) 7595 – 7598 [7767 – 7770] DOI: 10.1002/anie.200502231
Mazzola, R. D., Jr. (C) 6546 – 6549 [6704 – 6707]
Mealli, C.
– Supramolecular Interactions as Determining Factors of the Geometry of Metallic Building Blocks: Tetracarboxylate Dimanganese Species (C) 3429 – 3432 [3495 – 3498] DOI: 10.1002/anie.200462965
Mecking, S.
– Aqueous Dispersions of Extraordinarily Small Polyethylene Nanoparticles (C) 429 – 432 [433 – 436] DOI: 10.1002/anie.200460455
Mednikov, E. G.
– Nanosized $[Pd_{52}(CO)_{36}(PEt_3)_{14}]$ and $[Pd_{66}(CO)_{45}(PEt_3)_{16}]$ Clusters Based on a Hypothetical Pd_{38} Vertex-Truncated v_3 Octahedron (C) 6848 – 6854 [7008 – 7014] DOI: 10.1002/anie.200502307
Mednikov, E. G. (C) 786 – 790 [796 – 800]
Mee, J. M. (C) 2144 – 2148 [2182 – 2186]
Meetsma, A. (C) 2752 – 2756 [2812 – 2816], 4209 – 4212 [4281 – 4284]
Meggers, E.
– Switching on a Signaling Pathway with an Organoruthenium Complex (C) 1984 – 1987 [2020 – 2023] DOI: 10.1002/anie.200462501
Meguro, A. (C) 7567 – 7570 [7739 – 7742]
Mehl, G. H.
– Multiple Addressing in a Hybrid Biphotochromic System (C) 5048 – 5052 [5176 – 5180] DOI: 10.1002/anie.200462575
– Quasi-Periodic Organization in Soft Self-Assembling Matter (H) 672 – 673 [678 – 679] DOI: 10.1002/anie.200461639
Mehring, M.
– From a Monomeric Bismuth Silanolate to a Molecular Bismuth Oxo Cluster: $[Bi_{22}O_{26}(OSiMe_2tBu)_{14}]$ (C) 245 – 249 [250 – 254] DOI: 10.1002/anie.200461476
Meier, B. H.
– High-Resolution Solid-State NMR Spectroscopy of the Prion Protein HET-s in Its Amyloid Conformation (C) 2441 – 2444 [2494 – 2497] DOI: 10.1002/anie.200462952
Meier, H.
– Conjugated Oligomers with Terminal Donor – Acceptor Substitution (R) 2482 – 2506 [2536 – 2561] DOI: 10.1002/anie.200461146
Meierhenrich, U. J.
– Asymmetric Vacuum UV photolysis of the Amino Acid Leucine in the Solid State (C) 5630 – 5634 [5774 – 5779] DOI: 10.1002/anie.200501311
Meijer, E. W.
– Chiral Amplification in the Transcription of Supramolecular Helicity into a Polymer Backbone (C) 2275 – 2279 [2315 – 2319] DOI: 10.1002/anie.200462347
– Multivalent Peptide and Protein Dendrimers Using Native Chemical Ligation

 © 2005 Wiley-VCH Verlag GmbH & Co. KGaA, Weinheim

(C) 5052 – 5057 [5180 – 5185]
DOI: 10.1002/anie.200500635
Meijler, M. M. (C) 2144 – 2148 [2182 – 2186]
Meiler, J.
– Side-Chain Orientation and Hydrogen-Bonding Imprint Supra-τ_c Motion on the Protein Backbone of Ubiquitin
(C) 7776 – 7778 [7954 – 7956]
DOI: 10.1002/anie.200502573
Meiler, J. (C) 4172 – 4175 [4244 – 4247]
Melamed, S. (C) 739 – 743 [749 – 753]
Melchiorre, P.
– Organocatalytic Asymmetric α-Halogenation of 1,3-Dicarbonyl Compounds
(C) 6219 – 6222 [6375 – 6378]
DOI: 10.1002/anie.200502134
Meldrum, J. K. (C) 4939 – 4944 [5019 – 5024]
Mendoza, L. (C) 2903 – 2907 [2963 – 2967]
Meng, Xiangmin (C) 4749 – 4753 [4827 – 4831], 6934 – 6937 [7094 – 7097]
Meng, Xiaoyu (C) 1517 – 1520 [1541 – 1544]
Meng, Y. (C) 7053 – 7059 [7215 – 7221]
Meng, Z. (C) 1511 – 1513 [1535 – 1537]
Merbach, A. E. (C) 1480 – 1484 [1504 – 1508]
Merino, I. (C) 5875 – 5878 [6025 – 6028]
Merkul, E. (C) 6951 – 6956 [7112 – 7117]
Merkx, M.
– Multivalent Peptide and Protein Dendrimers Using Native Chemical Ligation
(C) 5052 – 5057 [5180 – 5185]
DOI: 10.1002/anie.200500635
Mermerian, A. H. (C) 949 – 952 [971 – 974]
Merrill, W. A. (C) 5090 – 5093 [5220 – 5223]
Mersdorf, E. (C) 1134 – 1136 [1158 – 1160]
Mertins, K. (C) 238 – 242 [242 – 246], 3913 – 3917 [3981 – 3985]
Mertl, D. (C) 99 – 101 [101 – 103]
Méry, D. (C) 7399 – 7404 [7565 – 7570]
Merz, K. (C) 6734 – 6737 [6892 – 6895], 6738 – 6741 [6896 – 6899]
Mésini, P. J.
– Self-Assembled Diamide Nanotubes in Organic Solvents
(C) 3260 – 3264 [3324 – 3328]
DOI: 10.1002/anie.200500536
Mespouille, L. (C) 4964 – 4968 [5044 – 5048]
Messerschmidt, M. (C) 3925 – 3928 [3993 – 3997], 4614 – 4617 [4690 – 4693]
Metselaar, G. A. (C) 1990 – 1993 [2026 – 2029], 4349 – 4352 [4423 – 4426]
Metz, P.
– A General Sultone Route to the Pamamycin Macrodiolides—Total Synthesis of Pamamycin-621A and Pamamycin-635B
(C) 6231 – 6234 [6387 – 6390]
DOI: 10.1002/anie.200501511
Metz, T. (C) 7783 – 7786 [7961 – 7964]
Metzke, M. (C) 6529 – 6533 [6687 – 6691]
Metzler-Nolte, N.
– A Cobaltocenium – Peptide Bioconjugate Shows Enhanced Cellular Uptake and Directed Nuclear Delivery
(C) 2429 – 2432 [2481 – 2485]
DOI: 10.1002/anie.200462519
Meunier, B.
– C10-Modified Artemisinin Derivatives: Efficient Heme-Alkylating Agents
(L) 2060 – 2063 [2096 – 2099]
DOI: 10.1002/anie.200462556
Mews, A.
– CdSe/ZnS Nanocrystals with Dye-Functionalized Polymer Ligands Containing Many Anchor Groups
(C) 2437 – 2440 [2490 – 2493]
DOI: 10.1002/anie.200462236
Meyer, B. (C) 2790 – 2794 [2850 – 2854]
Meyer, D. (C) 7216 – 7219 [7382 – 7386]
Meyer, F.
– Hysteretic Magnetic Bistability Based on a Molecular Azide Switch
(C) 7111 – 7114 [7273 – 7276]
DOI: 10.1002/anie.200501987
Meyer, H.-J.
– Mass Spectrometric Investigations of the Dissociation of $[C@W_6Cl_{17}]^-$ Ions in the Gas Phase
(C) 265 – 269 [270 – 274]
DOI: 10.1002/anie.200460972
Meyer, N. (C) 5662 – 5664 [5807 – 5809]
Mezzato, S. (C) 1650 – 1654 [1677 – 1681]
Mhadgut, S. C. (C) 3086 – 3089 [3146 – 3149]
Mi, L. (C) 6067 – 6074 [6221 – 6228]
Mialocq, J.-C. (C) 110 – 112 [112 – 114]
Miao, C.-Q. (C) 2158 – 2161 [2196 – 2199]
Miao, Q. (C) 7390 – 7394 [7556 – 7560]
Michailovski, A. (C) 5643 – 5647 [5787 – 5792]
Michel, F. (C) 438 – 441 [442 – 445]
Michelet, V.
– An Ir^I-Catalyzed *exo*-Selective Tandem Cycloisomerization/Hydroalkoxylation of Bis-Homopropargylic Alcohols at Room Temperature
(C) 4949 – 4953 [5029 – 5033]
DOI: 10.1002/anie.200501150
Mieda, E. (C) 3717 – 3720 [3783 – 3786]
Mienert, B. (C) 2908 – 2912 [2968 – 2972]
Mihovilovic, M. D.
– Family Clustering of Baeyer – Villiger Monooxygenases Based on Protein Sequence and Stereopreference
(C) 3609 – 3613 [3675 – 3679]
DOI: 10.1002/anie.200462964
Mikami, K.
– Enantiodiscrimination and Enantiocontrol of Neutral and Cationic Pt^{II} Complexes Bearing the *Tropos* Biphep Ligand: Application to Asymmetric Lewis Acid Catalysis
(C) 7257 – 7260 [7423 – 7426]
DOI: 10.1002/anie.200502682
Milet, A.
– Lewis Base Promoters in the Pauson – Khand Reaction: A Different Scenario
(C) 5717 – 5719 [5863 – 5865]
DOI: 10.1002/anie.200500955
Miller, A. K. (C) 4602 – 4606 [4678 – 4682]
Miller, J. A. (C) 3885 – 3889 [3953 – 3957]
Miller, J. S.
– Building Blocks for 2D Molecule-Based Magnets: The Diruthenium Tetrapivalate Monocation $[Ru^{II/III}_2(O_2CtBu)_4]^+$
(C) 2416 – 2419 [2468 – 2471]
DOI: 10.1002/anie.200462546
– The Myth of Cyanide Always Being a Strong-Field Ligand: Synthesis and Structural Characterization of Homoleptic $S = 2$ Pentacyanochromate(II), $[Cr^{II}(CN)_5]^{3-}$, and Nonacyanodichromate(II), $[Cr^{II}_2(CN)_9]^{5-}$
(C) 3129 – 3132 [3189 – 3192]
DOI: 10.1002/anie.200462763
Miller, R. D. (C) 7574 – 7580 [7746 – 7752]
Miller, S. M. (C) 7984 – 7987 [8198 – 8201]
Millward, A. R. (C) 4745 – 4749 [4823 – 4827]
Milne, J. E. (C) 6177 – 6180 [6333 – 6336]
Milstein, D.
– Redox-Induced Collapse and Regeneration of a Pincer-Type Complex Framework: A Nonplanar Coordination Mode of Palladium(II)
(C) 1709 – 1711 [1737 – 1739]
DOI: 10.1002/anie.200462386
Mimassi, L. (C) 4543 – 4546 [4619 – 4622]
Min, D.-H. (C) 5480 – 5483 [5616 – 5619]
Minakawa, N.
– Synthesis of 1,8-Naphthyridine C-Nucleosides and Their Base-Pairing Properties in Oligodeoxynucleotides: Thermally Stable Naphthyridine:Imidazopyridopyrimidine Base-Pairing Motifs
(C) 596 – 598 [602 – 604]
DOI: 10.1002/anie.200461857
Minami, H. (C) 6928 – 6931 [7088 – 7091]
Minami, Y. (C) 316 – 319 [320 – 323]
Ming, L.-J.
– Alzheimer's Disease Related Copper(II)-β-Amyloid Peptide Exhibits Phenol Monooxygenase and Catechol Oxidase Activities
(C) 5501 – 5504 [5637 – 5640]
DOI: 10.1002/anie.200501013
Minghetti, G. (C) 6892 – 6895 [7052 – 7055]
Minkowski, C. (C) 5325 – 5329 [5459 – 5463]
Minkwitz, R. (C) 973 – 975 [995 – 997]
Minnaard, A. J.
– Achiral Ligands Dramatically Enhance Rate and Enantioselectivity in the Rh/Phosphoramidite-Catalyzed Hydrogenation of α,β-Disubstituted Unsaturated Acids
(C) 4209 – 4212 [4281 – 4284]
DOI: 10.1002/anie.200500784
Minnaard, A. J. (C) 2752 – 2756 [2812 – 2816]
Mino, T. (C) 5523 – 5526 [5659 – 5662]
Mioskowski, C.
– Stereoselective Transformations of Trihalomethylcarbinols Induced by Chromous Chloride
(C) 2008 – 2011 [2044 – 2047]
DOI: 10.1002/anie.200461884
Mirkin, C. A.
– Heteroligated Rh^I Tweezer Complexes
(C) 4207 – 4209 [4279 – 4281]
DOI: 10.1002/anie.200500689
– Nanoarrays of Single Virus Particles
(C) 6013 – 6015 [6167 – 6169]
DOI: 10.1002/anie.200501978
– Sacrificial Biological Templates for the Formation of Nanostructured Metallic Microshells
(C) 5064 – 5067 [5192 – 5195]
DOI: 10.1002/anie.200500988
Mironov, Yu. V. (C) 6867 – 6871 [7027 – 7031]
Mirsky, V. M.
– Size-Controlled Electrochemical Synthesis of Metal Nanoparticles on Monomolecular Templates
(C) 6775 – 6778 [6933 – 6936]
DOI: 10.1002/anie.200500912
Misasa, N. (C) 720 – 724 [730 – 734]
Misumi, S. (C) 3861 – 3864 [3929 – 3932]
Mita, S. (C) 2586 – 2588 [2642 – 2644]
Mitani, T. (C) 4899 – 4903 [4977 – 4981]
Mitchell, B. (C) 1987 – 1990 [2023 – 2026]
Mitchell, J. C. (C) 3057 – 3061 [3117 – 3121]
Mitrikas, G. (C) 3301 – 3303 [3365 – 3367]
Mitsos, C. A. (C) 3714 – 3717 [3780 – 3783]
Mitsumi, M.
– A Neutral Mixed-Valent Conducting Polymer Formed by Electron Transfer between Metal d and Ligand π Orbitals
(C) 4164 – 4168 [4236 – 4240]
DOI: 10.1002/anie.200501189
Miura, N. (C) 91 – 96 [93 – 98], 571 – 575 [577 – 581]
Miura, T. (C) 7598 – 7600 [7770 – 7772]
Miyabe, H. (C) 6190 – 6193 [6346 – 6349]
Miyake, F. Y. (C) 3280 – 3282 [3344 – 3346]

 © 2005 Wiley-VCH Verlag GmbH & Co. KGaA, Weinheim

Miyamoto, K. (C) 75 – 78 [77 – 80], 6896 – 6899 [7056 – 7059]
Miyamura, K. (C) 5113 – 5115 [5243 – 5245]
Miyasaka, H. (C) 3240 – 3243 [3304 – 3307]
Miyashita, M.
– Pd-Catalyzed Stereospecific Azide Substitution of α,β-Unsaturated γ,δ-Epoxy Esters with Double Inversion of Configuration
(C) 5094 – 5097 [5224 – 5227]
DOI: 10.1002/anie.200500838
– Tetramic Acid Antibiotics: Stereoselective Synthesis of Streptolic Acid and Tirandalydigin
(C) 1532 – 1536 [1556 – 1560]
DOI: 10.1002/anie.200462300
Miyata, H. (C) 2413 – 2416 [2465 – 2468]
Miyata, M.
– Multicomponent Organic Alloys Based on Organic Layered Crystals
(C) 7059 – 7062 [7221 – 7224]
DOI: 10.1002/anie.200501678
Miyata, O. (C) 6190 – 6193 [6346 – 6349]
Miyauchi, M.
– Electrochromism of Titanate-Based Nanotubes
(C) 1974 – 1977 [2010 – 2013]
DOI: 10.1002/anie.200462448
Miyazawa, M. (C) 5094 – 5097 [5224 – 5227]
Miyoshi, D. (C) 3740 – 3744 [3806 – 3810]
Mizaikoff, B. (C) 3419 – 3422 [3485 – 3488]
Mizorogi, N. (C) 3282 – 3285 [3346 – 3349], 7567 – 7570 [7739 – 7742]
Mizugaki, T. (C) 3423 – 3426 [3489 – 3492]
Mizukado, J. (C) 1128 – 1130 [1152 – 1154]
Mizuki, M. (C) 3744 – 3746 [3810 – 3812]
Mizuno, N.
– Polyoxovanadometalate-Catalyzed Selective Epoxidation of Alkenes with Hydrogen Peroxide
(C) 5136 – 5141 [5266 – 5271]
DOI: 10.1002/anie.200500491
Mizuno, T. (C) 6180 – 6183 [6336 – 6339]
Mizutani, Taiku (C) 5094 – 5097 [5224 – 5227]
Mizutani, Tsuyoshi (C) 5113 – 5115 [5243 – 5245]
Mobian, P. (C) 1879 – 1883 [1913 – 1917]
Mobin, S. M. (C) 5655 – 5658 [5800 – 5803]
Mocharla, V. P. (C) 116 – 120 [118 – 122]
Moessner, C. (C) 7564 – 7567 [7736 – 7739]
Mohanty, J. (C) 3750 – 3754 [3816 – 3820]
Mohr, J. T. (C) 6924 – 6927 [7084 – 7087]
Mohr, P. (T) 5364 – 5366 [5498 – 5500]
Möhwald, H.
– EUCHEM: Nanoscale Surface Self-Assembly
(T) 5920 – 5921 [6070 – 6071]
DOI: 10.1002/anie.200502935
Möhwald, H. (C) 1717 – 1720 [1745 – 1748], 3310 – 3314 [3375 – 3379], 7767 – 7770 [7945 – 7948]
Moix Teixidor, M. (C) 2356 – 2360 [2408 – 2412]
Molard, Y. (C) 1072 – 1075 [1096 – 1099]
Molina, L. M. (C) 2270 – 2275 [2310 – 2315]
Molina, P.
– An Electroactive Nitrogen-Rich [4.4]Ferrocenophane Displaying Redox-Switchable Behavior: Selective Sensing, Complexation, and Decomplexation of Mg^{2+} ions
(C) 1977 – 1981 [2013 – 2017]
DOI: 10.1002/anie.200462521
Molinaro, C. (C) 129 – 132 [131 – 134]
Moliner, V.
– Towards a Rational Design of Antibody Catalysts through Computational Chemistry
(C) 904 – 909 [926 – 931]
DOI: 10.1002/anie.200461325
Möller, D. (C) 480 – 484 [485 – 488], 2969 – 2973 [3029 – 3033]
Molnár, G. (C) 4069 – 4073 [4137 – 4141]
Mönch, I. (C) 6391 – 6394 [6549 – 6552]
Mondal, K. C. (C) 4381 – 4385 [4455 – 4459]
Monde, K. (C) 91 – 96 [93 – 98], 571 – 575 [577 – 581]
Mondeshki, M. (C) 2801 – 2805 [2862 – 2866]
Monteil, V. (C) 429 – 432 [433 – 436], 2593 – 2596 [2649 – 2652]
Montgomery, J. I. (C) 3732 – 3736 [3798 – 3802]
Moon, D. (C) 7926 – 7929 [8140 – 8143]
Moon, H. R. (C) 1261 – 1265 [1287 – 1291]
Moon, R. (C) 6909 – 6912 [7069 – 7072]
Moonen, K. (C) 7407 – 7411 [7573 – 7577]
Moore, A. L.
– Molecular AND Logic Gate Based on Electric Dichroism of a Photochromic Dihydroindolizine
(C) 7591 – 7594 [7763 – 7766]
DOI: 10.1002/anie.200502420
Moore, J. E. (C) 3889 – 3892 [3957 – 3960]
Moore, T. A.
– Molecular AND Logic Gate Based on Electric Dichroism of a Photochromic Dihydroindolizine
(C) 7591 – 7594 [7763 – 7766]
DOI: 10.1002/anie.200502420
Moorefield, C. N. (C) 1679 – 1683 [1707 – 1711]
Moorthy, J. N.
– Corundum, Diamond, and PtS Metal – Organic Frameworks with a Difference: Self-Assembly of a Unique Pair of 3-Connecting D_{2d}-Symmetric 3,3′,5,5′-Tetrakis(4-pyridyl)bimesityl
(C) 2115 – 2119 [2153 – 2157]
DOI: 10.1002/anie.200461625
Mora-Fonz, M. J. (C) 3082 – 3086 [3142 – 3146]
Morales, G. M. (C) 4228 – 4231 [4300 – 4303]
Morales, M. Á. F. (C) 3062 – 3067 [3122 – 3127]
Moreno, R. M. (C) 1865 – 1869 [1899 – 1903]
Morgan, H. W. (C) 941 – 944 [963 – 966]
Morgenthaler, M. (C) 4400 – 4404 [4474 – 4479]
Mori, S.
– Elucidation of the Mechanism of the 1,6-Cuprate Addition to Acceptor-Substituted Enynes through ^{13}C Kinetic Isotope Effects: Experimental and Theoretical Studies
(C) 4715 – 4719 [4795 – 4798]
DOI: 10.1002/anie.200462976
Mori, Tadashi
– Circular Dichroism of a Chiral Tethered Donor – Acceptor System: Enhanced Anisotropy Factors in Charge-Transfer Transitions by Dimer Formation and by Confinement
(C) 2582 – 2585 [2638 – 2641]
DOI: 10.1002/anie.200462071
Mori, Takehiko (C) 292 – 295 [296 – 299]
Morimoto, H. (C) 3470 – 3474 [3536 – 3540]
Morimoto, K. (C) 6193 – 6196 [6349 – 6352]
Morimoto, Y. (C) 419 – 423 [423 – 427]
Morishita, J.-i. (C) 5509 – 5513 [5645 – 5649]
Morisue, M. (C) 4763 – 4766 [4841 – 4844]
Morita, T. (C) 6330 – 6333 [6488 – 6491]
Morita, Yasushi
– Spin Transfer and Solvato-/Thermochromism Induced by Intramolecular Electron Transfer in a Purely Organic Open-Shell System
(C) 7277 – 7280 [7443 – 7446]
DOI: 10.1002/anie.200502180
Morita, Yasushi (C) 6564 – 6568 [6722 – 6726]
Morita, Yusuke (C) 6354 – 6358 [6512 – 6516]
Morokuma, K.
– Elucidation of the Mechanism of the 1,6-Cuprate Addition to Acceptor-Substituted Enynes through ^{13}C Kinetic Isotope Effects: Experimental and Theoretical Studies
(C) 4715 – 4719 [4795 – 4798]
DOI: 10.1002/anie.200462976
– How Many Methyl Groups in $[\{(\eta^5\text{-}C_5Me_nH_{5-n})_2Zr\}_2(\mu_2,\eta^2,\eta^2\text{-}N_2)]$ Are Needed for Dinitrogen Hydrogenation? A Theoretical Study
(C) 7101 – 7103 [7263 – 7265]
DOI: 10.1002/anie.200501371
Moseriti, A. (C) 5126 – 5130 [5256 – 5260]
Mosquera, M. (C) 5635 – 5639 [5779 – 5783]
Mosquera, M. E. G. (C) 102 – 105 [104 – 107], 5828 – 5830 [5978 – 5980]
Moss, R. A.
– Fluorophenoxycarbene inside a Hemicarcerand: A Bottled Singlet Carbene
(C) 1994 – 1997 [2030 – 2033]
DOI: 10.1002/anie.200462633
Moss, S. J. (C) 4757 – 4760 [4835 – 4838]
Motokura, K. (C) 3423 – 3426 [3489 – 3492]
Moulton, B. (C) 897 – 901 [919 – 923]
Mountford, D. M. (C) 618 – 621 [624 – 627]
Moya, S. (C) 4578 – 4581 [4654 – 4657]
Moyano, A.
– Oxazoline-Mediated Interannular Cyclopalladation of Ferrocene: Chiral Palladium(II) Catalysts for the Enantioselective Aza-Claisen Rearrangement
(C) 1865 – 1869 [1899 – 1903]
DOI: 10.1002/anie.200462434
Moyer, B. A.
– Calix[4]pyrrole: An Old yet New Ion-Pair Receptor
(C) 2537 – 2542 [2593 – 2598]
DOI: 10.1002/anie.200462945
Mrksich, M.
– Label-Free Detection of Protein – Protein Interactions on Biochips
(C) 5480 – 5483 [5616 – 5619]
DOI: 10.1002/anie.200501363
Mruk, R. (C) 2437 – 2440 [2490 – 2493]
Msayib, K. J. (C) 7546 – 7549 [7718 – 7721]
Mudring, A.-V.
– The "Noncoordinating" Anion Tf_2N^- Coordinates to Yb^{2+}: A Structurally Characterized Tf_2N^- Complex from the Ionic Liquid [mppyr][Tf_2N]
(C) 5485 – 5488 [5621 – 5624]
DOI: 10.1002/anie.200501297
Muhler, M.
– Understanding the Structural Deactivation of Ruthenium Catalysts on an Atomic Scale under both Oxidizing and Reducing Conditions
(C) 917 – 920 [939 – 942]
DOI: 10.1002/anie.200461805
Muhler, M. (C) 2790 – 2794 [2850 – 2854], 6237 – 6241 [6394 – 6397]
Mühling, O. (C) 6778 – 6781 [6936 – 6940]

 © 2005 Wiley-VCH Verlag GmbH & Co. KGaA, Weinheim

Muir, T. W.
– A Ligation and Photorelease Strategy for the Temporal and Spatial Control of Protein Function in Living Cells
(C) 5713 – 5717 [5859 – 5863]
DOI: 10.1002/anie.200501244
Mukherjee, S. (C) 807 – 811 [817 – 821], 7466 – 7469 [7632 – 7635]
Mukhopadhyay, P. (R) 4844 – 4870 [4922 – 4949]
Mulazzani, Q. G. (C) 6030 – 6032 [6184 – 6186]
Mulchandani, A. (C) 6009 – 6012 [6163 – 6166]
Muldoon, J. (C) 3275 – 3279 [3339 – 3343]
Mulla, S. A. R. (C) 4381 – 4385 [4455 – 4459]
Müllen, K.
– Carbonization of Disclike Molecules in Porous Alumina Membranes: Toward Carbon Nanotubes with Controlled Graphene-Layer Orientation
(C) 2120 – 2123 [2158 – 2161]
DOI: 10.1002/anie.200460986
– 3D-Hybrid Networks with Controllable Electrical Conductivity from the Electrochemical Deposition of Terthiophene-Functionalized Polyphenylene Dendrimers
(C) 2447 – 2451 [2501 – 2505]
DOI: 10.1002/anie.200462378
– "Double-Concave" Graphene: Permethoxylated Hexa-*peri*-hexabenzocoronene and Its Cocrystals with Hexafluorobenzene and Fullerene
(C) 1247 – 1250 [1273 – 1276]
DOI: 10.1002/anie.200461445
– Pushing the Synthetic Limit: Polyphenylene Dendrimers with "Exploded" Branching Units—22-nm-Diameter, Monodisperse, Stiff Macromolecules
(C) 6348 – 6354 [6506 – 6512]
DOI: 10.1002/anie.200501368
– The Chemistry of Organic Nanomaterials
(R) 5592 – 5629 [5732 – 5772]
DOI: 10.1002/anie.200500805
Müllen, K. (C) 1520 – 1525 [1544 – 1549]
Müller, A.
– Porous Capsules Allow Pore Opening and Closing That Results in Cation Uptake
(C) 7757 – 7761 [7935 – 7939]
DOI: 10.1002/anie.200502202
– Triangular Geometrical and Magnetic Motifs Uniquely Linked on a Spherical Capsule Surface
(C) 3857 – 3861 [3925 – 3929]
DOI: 10.1002/anie.200500697
Müller, G. (C) 3140 – 3144 [3200 – 3204]
Müller, I. M.
– Rational Design of a Coordination Cage with a Trigonal-Bipyramidal Shape Constructed from 33 Building Units
(C) 2969 – 2973 [3029 – 3033]
DOI: 10.1002/anie.200463034
– Rational Design of Tightly Closed Coordination Tetrahedra that are Stable in the Solid State, in Solution, and in the Gas Phase
(C) 480 – 484 [485 – 488]
DOI: 10.1002/anie.200461800
Müller, K.
– Orthogonal Multipolar Interactions in Structural Chemistry and Biology
(R) 1788 – 1805 [1820 – 1839]
DOI: 10.1002/anie.200462213
Müller, K.-H. (C) 3306 – 3309 [3371 – 3374]
Müller, L. (C) 5247 – 5251 [5381 – 5386]
Müller, Mario
– Stimulating Chemistry and Strong Bonds (T) 3000 – 3001 [3060 – 3061]
DOI: 10.1002/anie.200501340
Müller, Markus (C) 4917 – 4920 [4996 – 4999]
Müller, Michael
– Chemoenzymatic Synthesis of Building Blocks for Statin Side Chains
(H) 362 – 365 [366 – 369]
DOI: 10.1002/anie.200460852
Müller, O. (C) 7635 – 7639 [7808 – 7812]
Müller, P.
– Addressing the Metal Centers of $[2 \times 2]$ Co^{II}_4 Grid-Type Complexes by STM/STS
(C) 7896 – 7900 [8109 – 8113]
DOI: 10.1002/anie.200502743
Müller, P. (Aachen) (C) 7212 – 7215 [7379 – 7382]
Müller, P. (Erlangen)
– The Deposition of Metallopeptide-Based Coordination Polymers on Graphite Substrates: Effects of Side-Chain Functional Groups and Local Surface Structure
(C) 803 – 806 [813 – 817]
DOI: 10.1002/anie.200461274
Müller, Ralf (C) 7905 – 7909 [8118 – 8122]
Müller, Rolf
– The Impact of Bacterial Genomics on Natural Product Research
(R) 6828 – 6846 [6988 – 7007]
DOI: 10.1002/anie.200501080
Müller, T. (C) 632 – 634 [638 – 640]
Müller, T. J. J.
– A Domino Sequence Consisting of Insertion, Coupling, Isomerization, and Diels – Alder Steps Yields Highly Fluorescent Spirocycles
(C) 153 – 158 [156 – 161]
DOI: 10.1002/anie.200461489
– Concise Syntheses of Meridianins by Carbonylative Alkynylation and a Four-Component Pyrimidine Synthesis
(C) 6951 – 6956 [7112 – 7117]
DOI: 10.1002/anie.200501703
Müller, T. N. (C) 807 – 811 [817 – 821]
Müller-Dethlefs, K.
– Real-Time Observation of Ionization-Induced Hydrophobic → Hydrophilic Switching
(C) 6149 – 6151 [6305 – 6307]
DOI: 10.1002/anie.200501430
Mulligan, A. (C) 1830 – 1833 [1864 – 1867]
Mulvey, R. E.
– Alkali-Metal-Mediated Zincation of Ferrocene: Synthesis, Structure, and Reactivity of a Lithium Tmp/Zincate Reagent
(C) 6018 – 6021 [6172 – 6175]
DOI: 10.1002/anie.200501560
– Selective *Meta*-Deprotonation of Toluene by Using Alkali-Metal-Mediated Magnesiation
(C) 3459 – 3462 [3525 – 3528]
DOI: 10.1002/anie.200500379
– Synergic Monodeprotonation of Bis(benzene)chromium by Using Mixed Alkali Metal – Magnesium Amide Bases and Structural Characterization of the Heterotrimetallic Products
(C) 68 – 72 [70 – 74]
DOI: 10.1002/anie.200460637
Münck, E.
– Aqueous Fe^{IV}=O: Spectroscopic Identification and Oxo-Group Exchange
(C) 6871 – 6874 [7031 – 7034]
DOI: 10.1002/anie.200502686
Muñiz, K.
– Bifunctional Metal – Ligand Catalysis: Hydrogenations and New Reactions within the Metal – (Di)amine Scaffold
(H) 6622 – 6627 [6780 – 6785]
DOI: 10.1002/anie.200501787
Muñoz, M. P. (C) 6146 – 6148 [6302 – 6304]
Murahashi, S.-I.
– An Aerobic, Organocatalytic, and Chemoselective Method for Baeyer – Villiger Oxidation
(C) 1704 – 1706 [1732 – 1734]
DOI: 10.1002/anie.200462429
– Ruthenium-Catalyzed Oxidative Cyanation of Tertiary Amines with Hydrogen Peroxide and Sodium Cyanide
(C) 6931 – 6933 [7091 – 7093]
DOI: 10.1002/anie.200501496
Murahashi, T. (C) 2560 – 2563 [2616 – 2619]
Murai, K. (C) 734 – 737 [744 – 747]
Murakami, M.
– Acyl 1,3-Migration in Rhodium-Catalyzed Reactions of Acetylenic β-Ketoesters with Aryl Boronic Acids: Application to Two-Carbon-Atom Ring Expansions
(C) 7598 – 7600 [7770 – 7772]
DOI: 10.1002/anie.200502650
– Palladium-Catalyzed Addition of Cyanoboranes to Alkynes: Regio- and Stereoselective Synthesis of α,β-Unsaturated β-Boryl Nitriles
(C) 2380 – 2382 [2432 – 2434]
DOI: 10.1002/anie.200462961
– Synthesis of Seven-Membered-Ring Ketones by Arylative Ring Expansion of Alkyne-Substituted Cyclobutanones
(C) 4608 – 4611 [4684 – 4687]
DOI: 10.1002/anie.200500799
Murakami, R. (C) 4795 – 4798 [4873 – 4876]
Murakami, Y. (C) 2708 – 2711 [2768 – 2771]
Murata, M. (C) 1981 – 1983 [2017 – 2019]
Murata, Y. (C) 1981 – 1983 [2017 – 2019]
Muresan, N. (C) 6734 – 6737 [6892 – 6895], 6738 – 6741 [6896 – 6899]
Muri, D. (C) 4036 – 4038 [4104 – 4106]
Muroi, M. (C) 3559 – 3562 Corrigendum: 4282 [3625 – 3628 Corrigendum: 4354]
Murphy, J. A.
– Highly Efficient Reduction of Unactivated Aryl and Alkyl Iodides by a Ground-State Neutral Organic Electron Donor
(C) 1356 – 1360 [1380 – 1384]
DOI: 10.1002/anie.200462038
Murugesu, M. (C) 892 – 896 [914 – 918], 6540 – 6543 [6698 – 6701], 6678 – 6682 [6836 – 6840]
Muryn, C. A. (C) 6496 – 6500 [6654 – 6658]
Musaev, D. G.
– How Many Methyl Groups in $[\{(\eta^5\text{-}C_5Me_nH_{5-n})_2Zr\}_2(\mu_2,\eta^2,\eta^2\text{-}N_2)]$ Are Needed for Dinitrogen Hydrogenation? A Theoretical Study
(C) 7101 – 7103 [7263 – 7265]
DOI: 10.1002/anie.200501371
Mutka, H. (C) 4239 – 4242 [4311 – 4314]
Myasoedov, B. F. (C) 1134 – 1136 [1158 – 1160]
Myers, M. (C) 7390 – 7394 [7556 – 7560]

 © 2005 Wiley-VCH Verlag GmbH & Co. KGaA, Weinheim

N

Na, Y. (C) 6166 – 6169 [6322 – 6325]
Nache, V. (C) 7887 – 7891 [8099 – 8104]
Nagae, S. (C) 5509 – 5513 [5645 – 5649]
Nagahori, N. (C) 571 – 575 [577 – 581]
Nagano, M. (C) 2774 – 2777 [2834 – 2837]
Nagano, Takashi (C) 4611 – 4614 [4687 – 4690]
Nagano, Tetsuo
– Extension of the Applicable Range of Fluorescein: A Fluorescein-Based Probe for Western Blot Analysis
(C) 5439 – 5441 [5575 – 5577]
DOI: 10.1002/anie.200501542
Nagao, J. (C) 6928 – 6931 [7088 – 7091]
Nagao, M. (C) 1810 – 1813 [1844 – 1847]
Nagao, Y.
– Highly Enantioselective Catalytic Thiolysis of Prochiral Cyclic Dicarboxylic Anhydrides Utilizing a Bifunctional Chiral Sulfonamide
(C) 5838 – 5841 [5988 – 5991]
DOI: 10.1002/anie.200501408
Nagarathinam, M. (C) 2237 – 2241 [2277 – 2281]
Nagase, S.
– 2D NMR Characterization of the La@C_{82} Anion
(C) 3282 – 3285 [3346 – 3349]
DOI: 10.1002/anie.200500039
– S-Heterocyclic Carbene with a Disilane Backbone
(C) 7567 – 7570 [7739 – 7742]
DOI: 10.1002/anie.200502971
Nagase, S. (C) 6553 – 6556 [6711 – 6714]
Nagatoishi, S. (C) 5067 – 5070 [5195 – 5198]
Nagendar, P. (C) 5878 – 5882 [6028 – 6032]
Naggar, I. C. (C) 7420 – 7424 [7586 – 7590]
Nahm, M. R. (C) 2377 – 2379 Corrigendum: 4660 [2429 – 2431 Corrigendum: 4735]
Nahon, L.
– Asymmetric Vacuum UV photolysis of the Amino Acid Leucine in the Solid State
(C) 5630 – 5634 [5774 – 5779]
DOI: 10.1002/anie.200501311
Nair, V. Corrigendum: 1907
Naito, T.
– Tandem Radical-Addition – Aldol-Type Reaction of an α,β-Unsaturated Oxime Ether
(C) 6190 – 6193 [6346 – 6349]
DOI: 10.1002/anie.200502263
Najajreh, Y. (C) 2885 – 2887 [2945 – 2947]
Nájera, C.
– Catalytic Enantioselective 1,3-Dipolar Cycloaddition Reaction of Azomethine Ylides and Alkenes: The Direct Strategy To Prepare Enantioenriched Highly Substituted Proline Derivatives
(H) 6272 – 6276 [6428 – 6432]
DOI: 10.1002/anie.200501074
Nakabayashi, K. (C) 5322 – 5325 [5456 – 5459]
Nakadai, M. (C) 765 – 769 [775 – 779]
Nakagawa, H. (C) 91 – 96 [93 – 98]
Nakagawa, J. (C) 1810 – 1813 [1844 – 1847]
Nakagawa, Y. (C) 5136 – 5141 [5266 – 5271]
Nakahara, Y. (C) 4547 – 4549 [4623 – 4625]
Nakahodo, T. (C) 7567 – 7570 [7739 – 7742]
Nakajima, N. (C) 7233 – 7236 [7399 – 7402]
Nakamura, A. (C) 2527 – 2531 [2583 – 2587]
Nakamura, E.
– Mechanism of Remote Conjugate Addition of a Lithium Organocuprate to a Polyconjugated Carbonyl Compound
(C) 4721 – 4723 [4799 – 4801]
DOI: 10.1002/anie.200501107
– Synthesis of Chiral α-Fluoroketones through Catalytic Enantioselective Decarboxylation
(C) 7248 – 7251 [7414 – 7417]
DOI: 10.1002/anie.200502703
– Ultra-rapid Synthesis of ^{15}O-Labeled 2-Deoxy-D-glucose for Positron Emission Tomography (PET)
(C) 2708 – 2711 [2768 – 2771]
DOI: 10.1002/anie.200500044
Nakamura, M.
– Synthesis of Chiral α-Fluoroketones through Catalytic Enantioselective Decarboxylation
(C) 7248 – 7251 [7414 – 7417]
DOI: 10.1002/anie.200502703
Nakamura, Seiichi (C) 2245 – 2249 [2285 – 2289]
Nakamura, Shuichi (C) 4204 – 4207 [4276 – 4279]
Nakamura, T.
– Molecularly Assembled Nanostructures of a Redox-Active Organogelator
(C) 7283 – 7287 [7449 – 7453]
DOI: 10.1002/anie.200502336
Nakamura, T. (C) 292 – 295 [296 – 299]
Nakanishi, K.
– Superoxidation of Bisretinoids
(C) 7097 – 7100 [7259 – 7262]
DOI: 10.1002/anie.200501346
Nakanishi, K. (C) 4006 – 4009 [4074 – 4077]
Nakano, K. (C) 7136 – 7138 [7298 – 7300]
Nakano, M. (C) 6564 – 6568 [6722 – 6726]
Nakasuji, K.
– Spin Transfer and Solvato-/Thermochromism Induced by Intramolecular Electron Transfer in a Purely Organic Open-Shell System
(C) 7277 – 7280 [7443 – 7446]
DOI: 10.1002/anie.200502180
– Synthesis, Intermolecular Interaction, and Semiconductive Behavior of a Delocalized Singlet Biradical Hydrocarbon
(C) 6564 – 6568 [6722 – 6726]
DOI: 10.1002/anie.200502303
Nakatani, K.
– Binding of Naphthyridine Carbamate Dimer to the $(CGG)_n$ Repeat Results in the Disruption of the G – C Base Pairing
(C) 7280 – 7283 [7446 – 7449]
DOI: 10.1002/anie.200502282
Nakayama, S. (C) 7447 – 7450 [7613 – 7616]
Nakazawa, J. (C) 3744 – 3746 [3810 – 3812]
Nam, W.
– Mechanistic Insight into Alcohol Oxidation by High-Valent Iron – Oxo Complexes of Heme and Nonheme Ligands
(C) 4235 – 4239 [4307 – 4311]
DOI: 10.1002/anie.200500623
Nancollas, G. H.
– Control of Biomineralization Dynamics by Interfacial Energies
(C) 3698 – 3702 [3764 – 3768]
DOI: 10.1002/anie.200500153
Nandakumar, M. V. (C) 3115 – 3118 [3175 – 3178]
Naota, T.
– An Aerobic, Organocatalytic, and Chemoselective Method for Baeyer – Villiger Oxidation
(C) 1704 – 1706 [1732 – 1734]
DOI: 10.1002/anie.200462429
Napp, M. (C) 4073 – 4075 [4141 – 4143]
Narayan, S. (C) 3275 – 3279 [3339 – 3343]
Nardis, S. (C) 3047 – 3050 [3107 – 3110]
Narimatsu, H.
– Molecular-Weight-Tagged Glycopeptide Library: Efficient Construction and Applications
(C) 4547 – 4549 [4623 – 4625]
DOI: 10.1002/anie.200500802
Narkhede, V. (C) 917 – 920 [939 – 942]
Naruta, Y.
– A Functional Model of the Cytochrome *c* Oxidase Active Site: Unique Conversion of a Heme – μ-peroxo – Cu^{II} Intermediate into Heme– superoxo/Cu^{I}
(C) 1836 – 1840 [1870 – 1874]
DOI: 10.1002/anie.200462582
– Size-Selective and Reversible Encapsulation of Single Small Hydrocarbon Molecules by a Cavitand – Porphyrin Species
(C) 3744 – 3746 [3810 – 3812]
DOI: 10.1002/anie.200500732
Naseri, V. (C) 5729 – 5733 [5875 – 5879]
Nassif, N.
– Synthesis of Stable Aragonite Superstructures by a Biomimetic Crystallization Pathway
(C) 6004 – 6009 [6158 – 6163]
DOI: 10.1002/anie.200500081
Nasveschuk, C. G. (C) 3264 – 3267 [3328 – 3331]
Natarajan, R. (C) 2115 – 2119 [2153 – 2157]
Nathan, I. (C) 1092 – 1096 [1116 – 1120]
Nattrass, G. L. (C) 580 – 584 [586 – 590]
Nau, W. M.
– Ultrastable Rhodamine with Cucurbituril
(C) 3750 – 3754 [3816 – 3820]
DOI: 10.1002/anie.200500502
Naumann, D. (C) 4631 – 4635 [4707 – 4711]
Naumov, N. G. (C) 6867 – 6871 [7027 – 7031]
Naumov, P.
– Solid-State Structure and Temperature/Evacuation-Induced Dehydration of Sodium Saccharinate 1.875 Hydrate
(C) 1251 – 1254 [1277 – 1280]
DOI: 10.1002/anie.200461043
Nayak, S. (R) 7686 – 7708 [7862 – 7886]
Nazaraly, M. (C) 5691 – 5694 [5837 – 5840]
Neese, F.
– Phenoxyl Radicals Hydrogen-Bonded to Imidazolium: Analogues of Tyrosyl D· of Photosystem II: High-Field EPR and DFT Studies
(C) 5314 – 5317 [5448 – 5451]
DOI: 10.1002/anie.200501132
– The Geometric and Electronic Structure of $[(cyclam\text{-}acetato)Fe(N)]^{+}$: A Genuine Iron(v) Species with a Ground-State Spin $S = 1/2$
(C) 2908 – 2912 [2968 – 2972]
DOI: 10.1002/anie.200462368
Nehete, U. N. (C) 281 – 284 [285 – 288]
Nelson, A.
– Creation of a Tailored Aldolase for the Parallel Synthesis of Sialic Acid Mimetics
(C) 2109 – 2112 [2147 – 2150]
DOI: 10.1002/anie.200462733
Nelson, E. (C) 6529 – 6533 [6687 – 6691]
Nelson, K. J. (C) 3129 – 3132 [3189 – 3192]

 © 2005 Wiley-VCH Verlag GmbH & Co. KGaA, Weinheim

Nemykin, V. N.
– Synthesis, Structure, and Chemoselective Reactivity of *N*-(2-Iodylphenyl)acylamides: Hypervalent Iodine Reagents Bearing a Pseudo-Six-Membered Ring Scaffold (C) 7127 – 7131 [7289 – 7293] DOI: 10.1002/anie.200502707
Nendel, M. (C) 3548 – 3552 [3614 – 3618]
Neoh, K.-G. (C) 1104 – 1107 [1128 – 1131]
Nesterov, E. E. (C) 5452 – 5456 [5588 – 5592]
Neuhaus, C. (C) 4077 – 4079 [4145 – 4147]
Neumann, B. (C) 6947 – 6951 [7107 – 7111]
Neumann, C. S. (C) 2249 – 2252 [2289 – 2292]
Neurock, M. (C) 4572 – 4574 [4648 – 4650]
Nevado, C. (C) 6146 – 6148 [6302 – 6304]
Newkome, G. R.
– Nanofabrication: Reversible Self-Assembly of an Imbedded Hexameric Metallomacrocycle within a Macromolecular Superstructure (C) 1679 – 1683 [1707 – 1711] DOI: 10.1002/anie.200462379
Ng, S. W. (C) 1251 – 1254 [1277 – 1280]
Nguyen, Q. T. (C) 1084 – 1088 [1108 – 1112]
Nguyen, S. T.
– Axial Ligand Effects: Utilization of Chiral Sulfoxide Additives for the Induction of Asymmetry in (Salen)ruthenium(II) Olefin Cyclopropanation Catalysts (C) 3885 – 3889 [3953 – 3957] DOI: 10.1002/anie.200460887
Ni, Z.-H. (C) 7742 – 7745 [7920 – 7923]
Nicholson, B. K.
– The Composition of Ehrlich's Salvarsan: Resolution of a Century-Old Debate (C) 941 – 944 [963 – 966] DOI: 10.1002/anie.200461471
Nicholson, R. I. (C) 4061 – 4066 [4129 – 4134]
Nicolaou, K. C.
– A Catalytic Asymmetric Three-Component 1,4-Addition/Aldol Reaction: Enantioselective Synthesis of the Spirocyclic System of Vannusal A (C) 3874 – 3879 [3942 – 3947] DOI: 10.1002/anie.200500789
– A Mild and Selective Method for the Hydrolysis of Esters with Trimethyltin Hydroxide (C) 1378 – 1382 [1402 – 1406] DOI: 10.1002/anie.200462207
– Biomimetic Total Synthesis of Gambogin and Rate Acceleration of Pericyclic Reactions in Aqueous Media (C) 756 – 761 [766 – 771] DOI: 10.1002/anie.200462211
– Chasing Molecules That Were Never There: Misassigned Natural Products and the Role of Chemical Synthesis in Modern Structure Elucidation (R) 1012 – 1044 Corrigendum: 2050 [1036 – 1069 Corrigendum: 2086] DOI: 10.1002/anie.200460864
– Construction of Highly Functionalized Medium-Sized Rings: Synthesis of Hyperforin and Perforatumone Model Systems (C) 3895 – 3899 [3963 – 3967] DOI: 10.1002/anie.200500776
– Construction of Substituted *N*-Hydroxyindoles: Synthesis of a Nocathiacin I Model System (C) 3736 – 3740 [3802 – 3806] DOI: 10.1002/anie.200500724
– Metathesis Reactions in Total Synthesis (R) 4490 – 4527 [4564 – 4601] DOI: 10.1002/anie.200500369
– Palladium-Catalyzed Cross-Coupling Reactions in Total Synthesis (R) 4442 – 4489 [4516 – 4563] DOI: 10.1002/anie.200500368
– Studies toward the Synthesis of Azadirachtin, Part 2: Construction of Fully Functionalized ABCD Ring Frameworks and Unusual Intramolecular Reactions Induced by Close-Proximity Effects (C) 3447 – 3452 [3513 – 3518] DOI: 10.1002/anie.200500217
– Studies toward the Synthesis of Azadirachtin, Part 1: Total Synthesis of a Fully Functionalized ABC Ring Framework and Coupling with a Norbornene Domain (C) 3443 – 3447 [3509 – 3513] DOI: 10.1002/anie.200500216
– Synthesis of Imides, *N*-Acyl Vinylogous Carbamates and Ureas, and Nitriles by Oxidation of Amides and Amines with Dess – Martin Periodinane (C) 5992 – 5997 [6146 – 6151] DOI: 10.1002/anie.200501853
– The Cytoskyrin Cascade: A Facile Entry into Cytoskyrin A, Deoxyrubroskyrin, Rugulin, Skyrin, and Flavoskyrin Model Systems (C) 5846 – 5851 [5996 – 6001] DOI: 10.1002/anie.200502011
– Total Synthesis of Halipeptins A and D and Analogues (C) 4925 – 4929 [5005 – 5009] DOI: 10.1002/anie.200500702
– Total Synthesis of (+)-Rugulosin and (+)-2,2′-*epi*-Cytoskyrin A through Cascade Reactions (C) 7917 – 7921 [8131 – 8135] DOI: 10.1002/anie.200503678
Nicolaou, S. (C) 5989 – 5992 [6143 – 6146]
Nie, Y. (C) 632 – 634 [638 – 640]
Nie, Z. (C) 724 – 728 Corrigendum: 3799 [734 – 738 Corrigendum: 3865]
Niecke, E.
– Cyclic Bis(phosphanyl)carbenium Ion by Protonation of a 1,3-Diphosphacyclobutane-2,4-diyl (C) 1405 – 1408 [1429 – 1432] DOI: 10.1002/anie.200462032
Nieger, M. (C) 1405 – 1408 [1429 – 1432], 5668 – 5670 [5813 – 5815]
Nielsch, K. (C) 6050 – 6054 [6204 – 6208]
Niemeyer, C. M.
– Covalent Hemin – DNA Adducts for Generating a Novel Class of Artificial Heme Enzymes (C) 2603 – 2606 [2659 – 2662] DOI: 10.1002/anie.200462567
– DNA Microarrays as Decoding Tools in Combinatorial Chemistry and Chemical Biology (H) 3179 – 3183 [3241 – 3246] DOI: 10.1002/anie.200500645
Niemeyer, C. M. (C) 7635 – 7639 [7808 – 7812]
Niemeyer, M.
– Stabilization of Aryl – Calcium, –Strontium, and –Barium Compounds by Designed Steric and π-Bonding Encapsulation (C) 5871 – 5875 [6021 – 6025] DOI: 10.1002/anie.200501494
Niemeyer, M. (C) 5655 – 5658 [5800 – 5803]
Nierengarten, J.-F.
– Dendrimers: Platforms for Chemical Functionality (T) 2830 – 2831 [2890 – 2891] DOI: 10.1002/anie.200501226
– Supramolecular Click Chemistry with a Bisammonium-C_{60} Substrate and a Ditopic Crown Ether Host (C) 5338 – 5341 [5472 – 5475] DOI: 10.1002/anie.200501249
Niess, B. (H) 26 – 29 [26 – 29]
Nieto-Oberhuber, C. (C) 6146 – 6148 [6302 – 6304]
Niewa, R. (C) 7212 – 7215 [7379 – 7382]
Nihei, M. (C) 6484 – 6487 [6642 – 6645]
Nihira, T. (C) 1948 – 1951 [1984 – 1987]
Niikura, K. (C) 91 – 96 [93 – 98]
Nijhuis, T. A.
– The Role of Gold in Gold – Titania Epoxidation Catalysts (C) 1115 – 1118 [1139 – 1142] DOI: 10.1002/anie.200462043
Nikawa, H. (C) 7567 – 7570 [7739 – 7742]
Nikiforov, G. B. (C) 7958 – 7961 [8172 – 8175]
Nilges, M. (C) 6151 – 6154 [6307 – 6310]
Nilsson, U. J.
– C_2-Symmetrical Thiodigalactoside Bis-Benzamido Derivatives as High-Affinity Inhibitors of Galectin-3: Efficient Lectin Inhibition through Double Arginine – Arene Interactions (C) 5110 – 5112 [5240 – 5242] DOI: 10.1002/anie.200500627
Nishi, Y. (C) 406 – 409 [410 – 413], 6896 – 6899 [7056 – 7059]
Nishibayashi, Y.
– Asymmetric Carboselenenylation Reaction of Alkenes with Aromatic Compounds (C) 3588 – 3591 [3654 – 3657] DOI: 10.1002/anie.200500573
– Ruthenium-Catalyzed Asymmetric Propargylic Substitution Reactions of Propargylic Alcohols with Acetone (C) 7715 – 7717 [7893 – 7895] DOI: 10.1002/anie.200502981
Nishibori, E. (C) 4568 – 4571 [4644 – 4647]
Nishida, J. (C) 7254 – 7257 [7420 – 7423]
Nishida, S. (C) 7277 – 7280 [7443 – 7446]
Nishigaki, N. (C) 316 – 319 [320 – 323]
Nishikata, T. (C) 6682 – 6685 [6840 – 6843]
Nishikawa, H. (C) 5459 – 5464 [5595 – 5600]
Nishimura, S. (C) 2708 – 2711 [2768 – 2771]
Nishimura, S.-I.
– Direct Observation of Sugar – Protein, Sugar – Sugar, and Sugar – Water Complexes by Cold-Spray Ionization Time-of-Flight Mass Spectrometry (C) 571 – 575 [577 – 581] DOI: 10.1002/anie.200461867
– High-Throughput Protein Glycomics: Combined Use of Chemoselective Glycoblotting and MALDI-TOF/TOF Mass Spectrometry (C) 91 – 96 [93 – 98] DOI: 10.1002/anie.200461685
– Molecular Transporter Between Polymer Platforms: Highly Efficient Chemoenzymatic Glycopeptide Synthesis by the Combined Use of Solid-Phase and Water-Soluble Polymer Supports (C) 2534 – 2537 [2590 – 2593] DOI: 10.1002/anie.200463065
Nishiura, M. (C) 959 – 962 [981 – 984]
Nishiyama, N. (C) 419 – 423 [423 – 427]
Nishiyama, T. (C) 4372 – 4375 [4446 – 4449]
Nitz, M. (C) 7725 – 7729 [7903 – 7907]
Njoroge, F. G. (C) 7024 – 7028 [7186 – 7190]
Noble, C. (C) 3613 – 3616 [3679 – 3682]

 © 2005 Wiley-VCH Verlag GmbH & Co. KGaA, Weinheim

Nobuta, O. (C) 1075 – 1078 [1099 – 1102]
Nogami, T. (C) 5526 – 5528 [5662 – 5664]
Nogami, Y. (C) 4201 – 4204 [4273 – 4276]
Noguchi, K. (C) 7260 – 7263 [7426 – 7429]
Noh, H.-J. (C) 2872 – 2877 [2932 – 2937]
Noh, K. (C) 1840 – 1843 [1874 – 1877]
Nojima, T. (C) 5067 – 5070 [5195 – 5198]
Nolan, S. P.
– A Gold Catalyst for Carbene-Transfer Reactions from Ethyl Diazoacetate
(C) 5284 – 5288 [5418 – 5422]
DOI: 10.1002/anie.200501056
– An Electron-Deficient Iridium(III) Dihydride Complex Capable of Intramolecular C–H Activation
(C) 2512 – 2515 [2568 – 2571]
DOI: 10.1002/anie.200463000
Noll, B. C. (C) 2916 – 2918 [2976 – 2978], 6568 – 6571 [6726 – 6729]
Nolte, R. J. M. (C) 560 – 564 [566 – 570], 1990 – 1993 [2026 – 2029]
Noltemeyer, M. (C) 5090 – 5093 [5220 – 5223], 7072 – 7074 [7234 – 7236]
Nomura, K. (C) 5860 – 5863 [6010 – 6013]
Noor, F. (C) 2429 – 2432 [2481 – 2485]
Noréus, D. (C) 7269 – 7273 [7435 – 7439]
Nørgaard, K. (C) 7035 – 7039 [7197 – 7201]
Noro, S.-i. (C) 7283 – 7287 [7449 – 7453]
Nørskov, J. K. (C) 1824 – 1826 [1858 – 1860]
Norsten, T. B. (C) 2019 – 2021 [2055 – 2057]
Notti, A. (C) 4892 – 4896 [4970 – 4974]
Novak, B. M.
– A Thermal and Solvocontrollable Cylindrical Nanoshutter Based on a Single Screw-Sense Helical Polyguanidine
(C) 7298 – 7301 [7464 – 7467]
DOI: 10.1002/anie.200501977
Noveski, D. (C) 6947 – 6951 [7107 – 7111]
Novokmet, S. (C) 803 – 806 [813 – 817]
Nozaki, K.
– Stereospecific Synthesis of Hetero[7]helicenes by Pd-Catalyzed Double *N*-Arylation and Intramolecular *O*-Arylation
(C) 7136 – 7138 [7298 – 7300]
DOI: 10.1002/anie.200502855
Nuckolls, C.
– Molecular Wires from Contorted Aromatic Compounds
(C) 7390 – 7394 [7556 – 7560]
DOI: 10.1002/anie.200502142
Numata, M. (C) 2030 – 2033 [2066 – 2069], 6371 – 6374 [6529 – 6532]
Nutiu, R. (C) 1061 – 1065 [1085 – 1089], 5464 – 5467 [5600 – 5603]
Nyffeler, P. T. (R) 192 – 212 [196 – 217]
Nygaard, S. (C) 7035 – 7039 [7197 – 7201]
Nyulászi, L.
– Cyclic Bis(phosphanyl)carbenium Ion by Protonation of a 1,3-Diphosphacyclobutane-2,4-diyl
(C) 1405 – 1408 [1429 – 1432]
DOI: 10.1002/anie.200462032

O

Oaki, Y. (C) 6571 – 6575 [6729 – 6733]
Obata, K. (C) 2262 – 2265 [2302 – 2305]
Oberhuber, M. (C) 7580 – 7583 [7752 – 7755]
Obika, S. (C) 1944 – 1947 [1980 – 1983]
Oble, J. (C) 7961 – 7964 [8175 – 8178]
O'Brien, T. A. (C) 897 – 901 [919 – 923]
Obst-Sander, U. (C) 4400 – 4404 [4474 – 4479]
Ocakoglu, R. A. (C) 400 – 403 [404 – 407]
Ochiai, M.
– 1-Alkynyl(aryl)(tetrafluoroborato)-λ^3-bromanes as Highly Efficient Michael Acceptors: Uncatalyzed Conjugate Addition of 1-Alkynyl(trialkyl)stannanes To Yield Symmetrical and Unsymmetrical 1,3-Butadiynes
(C) 406 – 409 [410 – 413]
DOI: 10.1002/anie.200461985
– Synthesis, Characterization, and Reaction of Crown Ether Complexes of Aqua(hydroxy)(aryl)iodonium Ions
(C) 75 – 78 [77 – 80]
DOI: 10.1002/anie.200461375
– Thiazole Synthesis by Cyclocondensation of 1-Alkynyl(phenyl)-λ^3-iodanes with Thioureas and Thioamides
(C) 6896 – 6899 [7056 – 7059]
DOI: 10.1002/anie.200502438
Ockwig, N. W. (C) 4745 – 4749 [4823 – 4827]
O'Connor, N. (C) 6529 – 6533 [6687 – 6691]
Oda, M.
– A Hexapentaene-Extended Quinocumulene Cyclotrimerized to a Tricyclobutabenzene Derivative
(C) 316 – 319 [320 – 323]
DOI: 10.1002/anie.200461608
Oda, T. (C) 1948 – 1951 [1984 – 1987]
Odermatt, S. (C) 5074 – 5078 [5203 – 5207]
Oeckler, O. (C) 567 – 570 [573 – 576], 3917 – 3921 [3985 – 3989]
Oehme, G.
– Reactions in Micellar Systems
(R) 7174 – 7199 [7338 – 7364]
DOI: 10.1002/anie.200501365
Oeser, T. (C) 632 – 634 [638 – 640]
Oestreich, M.
– Catalytic Desymmetrizing Intramolecular Heck Reaction: Evidence for an Unusual Hydroxy-Directed Migratory Insertion
(C) 149 – 152 [152 – 155]
DOI: 10.1002/anie.200460921
– Kaleidoscope of Catalysis: Heidelberg Forum of Molecular Catalysis 2005
(T) 5166 – 5167 [5296 – 5297]
DOI: 10.1002/anie.200502426
– Kinetic Resolution of Chiral Secondary Alcohols by Dehydrogenative Coupling with Recyclable Silicon-Stereogenic Silanes
(C) 7620 – 7624 [7793 – 7797]
DOI: 10.1002/anie.200502631
– Strategies for Catalytic Asymmetric Electrophilic α Halogenation of Carbonyl Compounds
(H) 2324 – 2327 [2376 – 2379]
DOI: 10.1002/anie.200500478
– Swiss Delight: Bürgenstock 2005
(T) 3512 – 3513 [3578 – 3580]
DOI: 10.1002/anie.200501433
– "True" Chirality Transfer from Silicon to Carbon: Asymmetric Amplification in a Reagent-Controlled Palladium-Catalyzed Hydrosilylation
(C) 1661 – 1664 [1688 – 1691]
DOI: 10.1002/anie.200462355
Ogawa, M. (C) 596 – 598 [602 – 604]
Ogilby, P. R.
– Singlet Oxygen: *Christopher S. Foote*
(O) 6268 [6424]
DOI: 10.1002/anie.200502934
Oh, E. (C) 7427 – 7432 [7593 – 7598]
Oh, N. Y. (C) 4235 – 4239 [4307 – 4311]
O'Hair, R. A. J.
– Gas-Phase Synthesis of $[Ag_4H]^+$ and Its Mediation of the C–C Coupling of Allyl Bromide
(C) 728 – 731 [738 – 741]
DOI: 10.1002/anie.200461328
O'Hara, C. T. (C) 3459 – 3462 [3525 – 3528]
Ohba, Y. (C) 734 – 737 [744 – 747]
Ohmi, M. (C) 2756 – 2760 [2816 – 2820]
Ohmichi, T. (C) 6682 – 6685 [6840 – 6843]
Ohmiya, H. (C) 2368 – 2370 [2420 – 2422], 3488 – 3490 [3554 – 3556]
Ohmori, K. (C) 3871 – 3874 [3939 – 3942]
Ohmori, O. (C) 1962 – 1964 [1998 – 2000]
Ohno, H.
– Bromoallenes as Allyl Dication Equivalents in the Absence of Palladium(0): Synthesis of Bicyclic Sulfamides by Tandem Cyclization of Bromoallenes
(C) 1513 – 1517 [1537 – 1541]
DOI: 10.1002/anie.200462557
– Palladium-Catalyzed Tandem Cyclization of Bromoenynes through Aromatic C–H Bond Functionalization
(C) 5103 – 5106 [5233 – 5236]
DOI: 10.1002/anie.200500159
– Thermal Intramolecular [2 + 2] Cycloaddition of Allenenes and Allenynes: Diastereoselective Access to Bicyclic Nitrogen Heterocycles
(C) 5113 – 5115 [5243 – 5245]
DOI: 10.1002/anie.200501413
Ohshima, T.
– Enantio- and Diastereoselective Catalytic Mannich-Type Reaction of a Glycine Schiff Base Using a Chiral Two-Center Phase-Transfer Catalyst
(C) 4564 – 4567 [4640 – 4643]
DOI: 10.1002/anie.200500927
Ohta, T. (C) 2534 – 2537 [2590 – 2593]
Ohtsu, C. (C) 720 – 724 [730 – 734]
Oiarbide, M. (C) 3881 – 3884 [3949 – 3952], 6187 – 6190 [6343 – 6346]
Okada, Akihiro (C) 4564 – 4567 [4640 – 4643]
Okada, Atsushi (C) 4611 – 4614 [4687 – 4690]
Okada, H. (C) 7233 – 7236 [7399 – 7402]
Okada, K.
– 2,2′:6′,2″:6″,6-Trioxytriphenylamine: Synthesis and Properties of the Radical Cation and Neutral Species
(C) 4056 – 4058 [4124 – 4126]
DOI: 10.1002/anie.200500397
Okamoto, H.
– Vapochromic Behavior Accompanied by Phase Transition between Charge-Polarization and Charge-Density-Wave States in a Quasi-One-Dimensional Iodine-Bridged Dinuclear Platinum Compound
(C) 3240 – 3243 [3304 – 3307]
DOI: 10.1002/anie.200500091
Okamoto, H. (C) 6484 – 6487 [6642 – 6645]
Okamoto, Kazuhiro (C) 3909 – 3912 [3977 – 3980]
Okamoto, Kazuki (C) 3588 – 3591 [3654 – 3657]
Okamura, T.-a. (C) 969 – 972 [991 – 994], 4352 – 4355 [4426 – 4429]
Okano, S. (C) 316 – 319 [320 – 323]
Okano, Y. (C) 6508 – 6512 [6666 – 6670]
Okino, T. (C) 4032 – 4035 [4100 – 4103]
Oku, J.-i. (C) 6180 – 6183 [6336 – 6339]
Okubo, H. (C) 3282 – 3285 [3346 – 3349]
Okubo, T. (C) 2700 – 2704 [2760 – 2764]

 © 2005 Wiley-VCH Verlag GmbH & Co. KGaA, Weinheim

Okuda, J.
– Cationic Yttrium Methyl Complexes as Functional Models for Polymerization Catalysts of 1,3-Dienes
(C) 7473 – 7477 [7640 – 7644]
DOI: 10.1002/anie.200502915
Olah, G. A.
– Beyond Oil and Gas: The Methanol Economy
(E) 2636 – 2639 [2692 – 2696]
DOI: 10.1002/anie.200462121
Olivucci, M.
– A Tiny Excited-State Barrier Can Induce a Multiexponential Decay of the Retinal Chromophore: A Quantum Dynamics Investigation
(C) 5118 – 5121 [5248 – 5251]
DOI: 10.1002/anie.200501236
– Mechanism of the Initial Conformational Transition of a Photomodulable Peptide
(C) 6077 – 6081 [6231 – 6235]
DOI: 10.1002/anie.200501145
– Mechanism of the Norrish – Yang Photocyclization Reaction of an Alanine Derivative in the Singlet State: Origin of the Chiral-Memory Effect
(C) 2390 – 2393 [2442 – 2445]
DOI: 10.1002/anie.200461898
Olmstead, M. M. (C) 2546 – 2549 [2602 – 2605]
Olofsson, B. (C) 5516 – 5519 [5652 – 5655]
Olpp, T. (C) 1553 – 1557 [1577 – 1581]
Oltra, J. E.
– Enantiospecific Strategy Towards Oxygen-Bridged Terpenoids: Tandem Transannular-Cyclization and Ring-Contraction Processes
(C) 319 – 322 [323 – 326]
DOI: 10.1002/anie.200461210
Onclin, S. (R) 6282 – 6304 [6438 – 6462]
Onishi, M.
– Formation of an Unsymmetrical Dinuclear Ruthenium Complex with μ-H, μ-OH, and μ-κ^2-CO_2 Bridges and Multiple Reactive Sites
(C) 5509 – 5513 [5645 – 5649]
DOI: 10.1002/anie.200501335
– Unusual Magnetic Properties of the Edge-Sharing Bioctahedral Dirhenium(IV) Complex of Pyridine-2-thiolate
(C) 720 – 724 [730 – 734]
DOI: 10.1002/anie.200460532
Onizawa, Y. (C) 468 – 470 [472 – 474]
Ono, N.
– A Doubly N-Fused Benzohexaphyrin and Its Rearrangement to a Fluorescent Macrocycle upon DDQ Oxidation
(C) 1856 – 1860 [1890 – 1894]
DOI: 10.1002/anie.200462815
Onopriyenko, A. (C) 4010 – 4015 [4078 – 4083]
Ooi, L.-L. (C) 3606 – 3609 [3672 – 3675], 7457 – 7460 [7623 – 7626], 7546 – 7549 [7718 – 7721]
Ooi, L.-l. (C) 5282 – 5284 [5416 – 5418]
Ooi, T. (C) 625 – 628 [631 – 634]
Oorui, M. (C) 3871 – 3874 [3939 – 3942]
Opatz, T.
– An Aldimine Cross-Coupling for the Diastereoselective Synthesis of Unsymmetrical 1,2-Diamines
(C) 5662 – 5664 [5807 – 5809]
DOI: 10.1002/anie.200501705
Organo, V. G. (C) 3043 – 3047 [3103 – 3107]
Oriol, L. (H) 6618 – 6621 [6776 – 6779]
Orlandini, A. (C) 3429 – 3432 [3495 – 3498]
Orlov, A. V. (C) 7892 – 7896 [8104 – 8109]
Orme, C. A. (C) 3698 – 3702 [3764 – 3768]
Ornelas, C. (C) 7399 – 7404 [7565 – 7570]
Oro, L. A. (C) 3267 – 3271 [3331 – 3335]
Orsini, P. (C) 5433 – 5438 [5569 – 5574]
Ortiz, C. G. (C) 1217 – 1220 [1243 – 1246]
Ortiz, M. J.
– The Effects of Triplet Sensitizers' Energies on the Photoreactivity of β,γ-Unsaturated Methyl Ketones
(C) 7739 – 7741 [7917 – 7919]
DOI: 10.1002/anie.200502619
Orynbayeva, Z. (C) 1092 – 1096 [1116 – 1120]
Osada, H.
– Photo-Cross-Linked Small-Molecule Affinity Matrix for Facilitating Forward and Reverse Chemical Genetics
(C) 3559 – 3562 Corrigendum: 4282 [3625 – 3628 Corrigendum: 4354]
DOI: 10.1002/anie.200462370
Osada, H. (C) 3110 – 3115 [3170 – 3175]
Osada, K. (C) 3544 – 3548 [3610 – 3614]
Osaka, K. (C) 4899 – 4903 [4977 – 4981]
Osawa, M.
– Current Oscillations during Formic Acid Oxidation on a Pt Electrode: Insight into the Mechanism by Time-Resolved IR Spectroscopy
(C) 5694 – 5698 [5840 – 5844]
DOI: 10.1002/anie.200501009
Osborne, V. L. (C) 4578 – 4581 [4654 – 4657]
Oschkinat, H.
– Recognition of Proline-Rich Motifs by Protein – Protein-Interaction Domains
(R) 2852 – 2869 [2912 – 2930]
DOI: 10.1002/anie.200400618
– SOLARIA: A Protocol for Automated Cross-Peak Assignment and Structure Calculation for Solid-State Magic-Angle Spinning NMR Spectroscopy
(C) 6151 – 6154 [6307 – 6310]
DOI: 10.1002/anie.200501884
Oschkinat, H. (C) 4631 – 4635 [4707 – 4711]
Oshima, K.
– Cobalt-Catalyzed *syn* Hydrophosphination of Alkynes
(C) 2368 – 2370 [2420 – 2422]
DOI: 10.1002/anie.200500255
– Recent Progress in Asymmetric Allylic Substitutions Catalyzed by Chiral Copper Complexes
(H) 4435 – 4439 [4509 – 4513]
DOI: 10.1002/anie.200500653
– Regio- and Stereoselective Approach to 1,2-Di- and 1,1,2-Trisilylethenes by Cobalt-Mediated Reaction of Silyl-Substituted Dibromomethanes with Silylmethylmagnesium Reagents
(C) 3488 – 3490 [3554 – 3556]
DOI: 10.1002/anie.200500576
– Synthesis of (*E*)-1,2-Diphosphanylethene Derivatives from Alkynes by Radical Addition of Tetraorganodiphosphane Generated In Situ
(C) 1694 – 1696 [1722 – 1724]
DOI: 10.1002/anie.200462603
– Synthesis of Medium- and Large-Sized Lactones in an Aqueous – Organic Biphasic System
(C) 2397 – 2400 [2449 – 2452]
DOI: 10.1002/anie.200462677
Oshima, K. (C) 3293 – 3296 [3357 – 3360], 5860 – 5863 [6010 – 6013]
Oshio, H.
– Two-Step Spin Conversion in a Cyanide-Bridged Ferrous Square
(C) 6484 – 6487 [6642 – 6645]
DOI: 10.1002/anie.200502216
Oshio, H. (C) 5459 – 5464 [5595 – 5600]
Osswald, P. (C) 250 – 253 [254 – 257]
Osuka, A.
– A Doubly N-Fused Benzohexaphyrin and Its Rearrangement to a Fluorescent Macrocycle upon DDQ Oxidation
(C) 1856 – 1860 [1890 – 1894]
DOI: 10.1002/anie.200462815
– Anthracene-Bridged Z-Shaped [26]Hexaphyrin(1.1.1.1.1.1.1) Dimer from the Regioselective Diels – Alder Reaction of a Hexaphyrin with Bis-*o*-xylylene Equivalents
(C) 932 – 935 [954 – 957]
DOI: 10.1002/anie.200462231
– Dicopper and Disilver Complexes of Octaphyrin(1.1.1.1.1.1.1): Reversible Hydrolytic Cleavage of the Pyrrolic Ring to a Keto – Imine
(C) 3726 – 3729 [3792 – 3795]
DOI: 10.1002/anie.200500676
– Internally 1,4-Phenylene-Bridged *meso* Aryl-Substituted Expanded Porphyrins: The Decaphyrin and Octaphyrin Cases
(C) 7244 – 7248 [7410 – 7414]
DOI: 10.1002/anie.200502769
– *meso*-Aryl-Substituted [26]Hexaphyrin(1.1.0.1.1.0) and [38]Nonaphyrin(1.1.0.1.1.0.1.1.0) from Oxidative Coupling of a Tripyrrane
(C) 2225 – 2229 [2265 – 2269]
DOI: 10.1002/anie.200463054
– Synthesis of Corrole Derivatives through Regioselective Ir-Catalyzed Direct Borylation
(C) 6763 – 6766 [6921 – 6924]
DOI: 10.1002/anie.200502335
– The Importance of a β – β Bond for Long-Range Antiferromagnetic Coupling in Directly Linked Copper(II) and Silver(II) Diporphyrins
(C) 6899 – 6901 [7059 – 7061]
DOI: 10.1002/anie.200501943
Oswald, R. B. (C) 7072 – 7074 [7234 – 7236]
Otero, R. (C) 2270 – 2275 [2310 – 2315]
Otsuka, N. (C) 6183 – 6186 [6339 – 6342]
Otsuka, S. (C) 731 – 733 [741 – 743]
Otte, R. (C) 5492 – 5496 [5629 – 5632]
Otten, M. B. J. (C) 1968 – 1971 [2004 – 2007]
Ou, Z. (C) 83 – 87 [85 – 89]
Ovchinnikov, M. V. (C) 4207 – 4209 [4279 – 4281]
Over, H.
– Understanding the Structural Deactivation of Ruthenium Catalysts on an Atomic Scale under both Oxidizing and Reducing Conditions
(C) 917 – 920 [939 – 942]
DOI: 10.1002/anie.200461805
Owens, R. W. (C) 1965 – 1968 [2001 – 2004]
Ozanne-Beaudenon, A. (C) 7065 – 7069 [7227 – 7231]
Ozawa, Y. (C) 2262 – 2265 [2302 – 2305], 4164 – 4168 [4236 – 4240]
Ozeki, T. (C) 1810 – 1813 [1844 – 1847]
Ozin, G. A.
– Periodic Mesoporous Organosilicas: Self-Assembly from Bridged Cyclic Silsesquioxane Precursors
(C) 2107 – 2109 [2145 – 2147]
DOI: 10.1002/anie.200462279

 © 2005 Wiley-VCH Verlag GmbH & Co. KGaA, Weinheim

P

Päch, M. (C) 6734 – 6737 [6892 – 6895]
Paetzold, E. (R) 7174 – 7199 [7338 – 7364]
Pagani, A. (C) 4618 – 4622 [4694 – 4698]
Palais, L. (C) 1376 – 1378 [1400 – 1402]
Palancher, H. (C) 1725 – 1729 [1753 – 1757]
Palmer, W. (T) 5364 – 5366 [5498 – 5500]
Palomares, E. (C) 5740 – 5744 [5886 – 5890]
Palomo, C.
– Enantioselective Henry Reactions under Dual Lewis Acid/Amine Catalysis Using Chiral Amino Alcohol Ligands
(C) 3881 – 3884 [3949 – 3952]
DOI: 10.1002/anie.200463075
– Lewis Acid Catalyzed Asymmetric Cycloadditions of Nitrones: α′-Hydroxy Enones as Efficient Reaction Partners
(C) 6187 – 6190 [6343 – 6346]
DOI: 10.1002/anie.200502308
Pan, C.-Y. (C) 6881 – 6884 [7041 – 7044]
Pan, F. (C) 5841 – 5846 [5991 – 5996]
Pan, Q. (C) 7988 – 7990 [8202 – 8204]
Pan, X. (C) 135 – 138 [137 – 140]
Pan, Z. W. (C) 274 – 278 [278 – 282]
Panda, P. K (C) 4053 – 4055 [4121 – 4123]
Panek, J. S.
– Total Synthesis of (+)-Leucascandrolide A
(C) 1223 – 1225 [1249 – 1251]
DOI: 10.1002/anie.200462408
Pang, K. (C) 7390 – 7394 [7556 – 7560]
Pang, Y.-C. (C) 4328 – 4333 [4402 – 4407]
Panigada, L. (C) 588 – 591 [594 – 597]
Pankau, W. M. (C) 6750 – 6755 [6908 – 6913]
Pantos, G. D. (C) 7386 – 7390 [7552 – 7556]
Paolesse, R.
– Hemiporphycene from the Expansion of a Corrole Ring
(C) 3047 – 3050 [3107 – 3110]
DOI: 10.1002/anie.200500481
Papafilippopoulos, A. (C) 1412 – 1416 [1437 – 1441]
Papageorgiou, C. D. (C) 5846 – 5851 [5996 – 6001], 7917 – 7921 [8131 – 8135]
Pape, T. (C) 3759 – 3763 [3825 – 3829], 7798 – 7800 [7976 – 7979]
Pappalardo, A. (C) 4892 – 4896 [4970 – 4974]
Pappalardo, S.
– A Calix[5]arene-Based Heterotetratopic Host for Molecular Recognition of Long-Chain, Ion-Paired α,ω-Alkanediyldiammonium Salts
(C) 4892 – 4896 [4970 – 4974]
DOI: 10.1002/anie.200500985
Parigi, G. (C) 2223 – 2225 [2263 – 2265]
Parisi, M. F.
– A Calix[5]arene-Based Heterotetratopic Host for Molecular Recognition of Long-Chain, Ion-Paired α,ω-Alkanediyldiammonium Salts
(C) 4892 – 4896 [4970 – 4974]
DOI: 10.1002/anie.200500985
Park, C. (C) 7964 – 7968 [8178 – 8182]
Park, H.-g.
– Highly Enantioselective Epoxidation of 2,4-Diarylenones by Using Dimeric Cinchona Phase-Transfer Catalysts: Enhancement of Enantioselectivity by Surfactants
(C) 1383 – 1385 [1407 – 1409]
DOI: 10.1002/anie.200462254
Park, H. S. (C) 2704 – 2707 [2764 – 2767]
Park, I. S. (C) 6913 – 6915 [7073 – 7075]
Park, J.-G. (C) 2872 – 2877 [2932 – 2937], 7427 – 7432 [7593 – 7598]
Park, Jae-Hoon (C) 2872 – 2877 [2932 – 2937]
Park, Jaiwook
– Recyclable Palladium Catalyst for Highly Selective α Alkylation of Ketones with Alcohols
(C) 6913 – 6915 [7073 – 7075]
DOI: 10.1002/anie.200502422
Park, Jeong-Ho (C) 1096 – 1101 [1120 – 1125]
Park, Jongnam (C) 2872 – 2877 [2932 – 2937]
Park, M. J. (C) 4235 – 4239 [4307 – 4311]
Park, M. S. (C) 556 – 560 [562 – 566]
Park, S.-E.
– Microwave Fabrication of MFI Zeolite Crystals with a Fibrous Morphology and Their Applications
(C) 556 – 560 [562 – 566]
DOI: 10.1002/anie.200461403
Park, Y. I. (C) 7411 – 7414 [7577 – 7580]
Parkes, A. L. (C) 6731 – 6734 [6889 – 6892]
Parquette, J. R.
– Dendrimer Folding in Aqueous Media: An Example of Solvent-Mediated Chirality Switching
(C) 1053 – 1057 [1077 – 1081]
DOI: 10.1002/anie.200460943
Parrinello, M. (C) 3769 – 3773 [3835 – 3839]
Parsons, S. (C) 1876 – 1879 [1910 – 1913], 6540 – 6543 [6698 – 6701]
Pascal, R.
– Expeditious, Potentially Primordial, Aminoacylation of Nucleotides
(C) 6731 – 6734 [6889 – 6892]
DOI: 10.1002/anie.200501591
Pascoe, D. D. (C) 1221 – 1222 [1247 – 1248]
Pask, C. M. (C) 3456 – 3459 [3522 – 3525]
Pasquali, M. (C) 5701 – 5705 [5847 – 5851]
Passmore, J.
– The Autoionization of $[TiF_4]$ by Cation Complexation with [15]Crown-5 To Give $[TiF_2([15]crown\text{-}5)][Ti_4F_{18}]$ Containing the Tetrahedral $[Ti_4F_{18}]^{2-}$ Ion
(C) 7958 – 7961 [8172 – 8175]
DOI: 10.1002/anie.200502900
Pastor, A. (C) 3429 – 3432 [3495 – 3498]
Pastorin, G. (C) 6358 – 6362 [6516 – 6520]
Patarin, J. (C) 5310 – 5313 [5444 – 5447]
Patel, D. J. (C) 3412 – 3415 [3478 – 3481]
Patel, U. (C) 1715 – 1717 [1743 – 1745]
Paterson, I.
– Stereocontrolled Total Synthesis of (−)-Aurisides A and B
(C) 1130 – 1133 [1154 – 1157]
DOI: 10.1002/anie.200462267
Patole, S. N. (C) 1254 – 1257 [1280 – 1283]
Patolsky, F. (C) 4554 – 4557 [4630 – 4633]
Patra, S. (C) 5655 – 5658 [5800 – 5803]
Patricelli, M. P. (C) 2400 – 2403 [2452 – 2455]
Patrick, D. L.
– Preparation of Chiral Surfaces from Achiral Molecules by Controlled Symmetry Breaking
(C) 1821 – 1823 [1855 – 1857]
DOI: 10.1002/anie.200461833
Patthey, F. (C) 5334 – 5337 [5468 – 5471]
Patwardhan, A. P. (C) 6169 – 6172 [6325 – 6328]
Pätzel, M. (C) 3925 – 3928 [3993 – 3997]
Patzke, G. R.
– Studying the Solvothermal Formation of MoO_3 Fibers by Complementary In Situ EXAFS/EDXRD Techniques
(C) 5643 – 5647 [5787 – 5792]
DOI: 10.1002/anie.200500514
Paul, A. (C) 4061 – 4066 [4129 – 4134]
Paulini, R. (R) 1788 – 1805 [1820 – 1839], (C) 4400 – 4404 [4474 – 4479]
Paulmann, C. (C) 3925 – 3928 [3993 – 3997]
Paululat, T. (C) 423 – 426 [427 – 430]
Paxton, W. F. (C) 744 – 746 [754 – 756]
Payer, D. (C) 1488 – 1491 [1512 – 1515]
Payne, C. K.
– Nanophotonic Light Sources for Fluorescence Spectroscopy and Cellular Imaging
(C) 1395 – 1398 [1419 – 1422]
DOI: 10.1002/anie.200462120
Payne, E. K. (C) 5064 – 5067 [5192 – 5195]
Payne, G. A. (C) 2704 – 2707 [2764 – 2767]
Peacock, A. F. A. (C) 1712 – 1714 [1740 – 1742]
Pearce, O. M. T. (C) 1057 – 1061 [1081 – 1085]
Pécaut, J. (C) 7595 – 7598 [7767 – 7770]
Pedireddi, V. R.
– Nucleobases in Molecular Recognition: Molecular Adducts of Adenine and Cytosine with COOH Functional Groups
(C) 7752 – 7757 [7930 – 7935]
DOI: 10.1002/anie.200502434
Pedrido, R. M. (C) 4182 – 4187 [4254 – 4259]
Pélaprat, D. (C) 4058 – 4061 [4126 – 4129]
Pèlegrin, A. (C) 4058 – 4061 [4126 – 4129]
Pellegrin, Y. (C) 1536 – 1540 [1560 – 1564]
Pellois, J.-P. (C) 5713 – 5717 [5859 – 5863]
Pelzl, G.
– Field-Induced Switching of Chirality in Undulated Ferroelectric and Antiferroelectric SmCP Phases Formed by Bent-Core Mesogens
(C) 774 – 778 [784 – 788]
DOI: 10.1002/anie.200461490
Pendyala, P. R. (C) 4903 – 4906 [4981 – 4984]
Pendzialek, D. (C) 4975 – 4980 [5055 – 5060]
Peng, K. (C) 2737 – 2742 [2797 – 2802]
Peng, Q. (C) 2782 – 2785 [2842 – 2845], 6054 – 6057 [6208 – 6211]
Peng, S.-M. (C) 3864 – 3867 [3932 – 3935], 7418 – 7420 [7584 – 7586]
Peng, T. (C) 7280 – 7283 [7446 – 7449]
Peng, Z.
– Molecular and Polymeric Hybrids Based on Covalently Linked Polyoxometalates and Transition-Metal Complexes
(C) 6902 – 6905 [7062 – 7065]
DOI: 10.1002/anie.200501924
Percec, V.
– Self-Assembly of Semifluorinated Janus-Dendritic Benzamides into Bilayered Pyramidal Columns
(C) 4739 – 4745 [4817 – 4823]
DOI: 10.1002/anie.200501254
– The Internal Structure of Helical Pores Self-Assembled from Dendritic Dipeptides is Stereochemically Programmed and Allosterically Regulated
(C) 6516 – 6521 [6674 – 6679]
DOI: 10.1002/anie.200501331
Perekalin, D. S. (C) 6222 – 6226 [6378 – 6382]
Perepichka, D. F.
– Molecules with Exceptionally Small HOMO – LUMO Gaps
(H) 5370 – 5373 [5504 – 5507]
DOI: 10.1002/anie.200500413

 © 2005 Wiley-VCH Verlag GmbH & Co. KGaA, Weinheim

Perez, E.
– The Natural Lewis^X-Bearing Lipids Promote Membrane Adhesion: Influence of Ceramide on Carbohydrate–Carbohydrate Recognition
(C) 1683–1687 [1711–1715]
DOI: 10.1002/anie.200461224
Pérez, E. M. (C) 3062–3067 [3122–3127]
Perez, J. M. (C) 2885–2887 [2945–2947]
Perez, M. (C) 4892–4896 [4970–4974]
Pérez, P. J.
– A Gold Catalyst for Carbene-Transfer Reactions from Ethyl Diazoacetate
(C) 5284–5288 [5418–5422]
DOI: 10.1002/anie.200501056
Perez del Valle, C. (C) 5717–5719 [5863–5865]
Pérez-Juste, J. (C) 4375–4378 [4449–4452]
Pérez Lustres, J. L. (C) 5635–5639 [5779–5783]
Pérez-Ramírez, J.
– Perovskite Membranes in Ammonia Oxidation: Towards Process Intensification in Nitric Acid Manufacture
(C) 1112–1115 [1136–1139]
DOI: 10.1002/anie.200462024
Periana, R. A.
– C–H Activation of Alkanes and Arenes Catalyzed by an O-Donor Bis(tropolonato)iridium(III) Complex
(C) 1540–1543 [1564–1567]
DOI: 10.1002/anie.200462065
Peris, E.
– An N-Heterocyclic Carbene/Iridium Hydride Complex from the Oxidative Addition of a Ferrocenyl–Bisimidazolium Salt: Implications for Synthesis
(C) 444–447 [448–451]
DOI: 10.1002/anie.200461918
Perrin, C. L.
– The Origin of One-Bond C–H Coupling Constants in OCH Fragments: Not Primarily $n_O \rightarrow \sigma^*_{CH}$ Delocalization
(C) 2360–2364 [2412–2416]
DOI: 10.1002/anie.200461583
Perron, M.-È. (C) 4021–4025 [4089–4093]
Perrone, S. (C) 4627–4631 [4703–4707]
Persau, C. (C) 5242–5246 [5376–5381]
Perumalla, S. R. (C) 7752–7757 [7930–7935]
Perutz, R. N.
– A Metal-Based Lumophore Tailored To Sense Biologically Relevant Oxometalates
(C) 1712–1714 [1740–1742]
DOI: 10.1002/anie.200462306
Peruzzini, M.
– Stable, Water-Soluble Pta-Based Ru–Ag Organometallic Polymers
(C) 2568–2572 [2624–2628]
DOI: 10.1002/anie.200462790
Pestovsky, O. (C) 6871–6874 [7031–7034]
Peter, K. (C) 5740–5744 [5886–5890]
Peterca, M. (C) 4739–4745 [4817–4823], 6516–6521 [6674–6679]
Peters, H. (C) 2777–2781 [2837–2841]
Peters, M. (C) 4249–4254 [4321–4326]
Petkar, S. S. (C) 1254–1257 [1280–1283]
Petkovic, H. (C) 4757–4760 [4835–4838]
Petoud, S.
– Sensitization of Near-Infrared-Emitting Lanthanide Cations in Solution by Tropolonate Ligands
(C) 2508–2512 [2564–2568]
DOI: 10.1002/anie.200463081
Petrovic, G. (C) 3447–3452 [3513–3518]
Pettersen, D. (C) 7975–7978 [8189–8192]
Pettinger, B.
– Tip-Enhanced Raman Spectroscopy of Benzenethiol Adsorbed on Au and Pt Single-Crystal Surfaces
(C) 139–142 [141–144]
DOI: 10.1002/anie.200460656
Pfaltz, A.
– Chiral Boron-Bridged Bisoxazolines: Readily Available Anionic Ligands for Asymmetric Catalysis
(C) 4888–4891 [4966–4969]
DOI: 10.1002/anie.200501111
Philippopoulos, A. I. (C) 5979–5985 [6133–6139]
Phillips, D. L.
– Simultaneous Observation of Green Multiphoton Upconversion and Red and Blue NLO Processes from Polymeric Terbium(III) Complexes
(C) 3436–3439 [3502–3505]
DOI: 10.1002/anie.200500031
Philouze, C. (C) 438–441 [442–445]
Picardi, G. (C) 139–142 [141–144]
Piccio, V. J.-D. (C) 1543–1545 [1567–1569]
Pichardo, J. (C) 7024–7028 [7186–7190]
Pichon, C. (C) 1725–1729 [1753–1757]
Pierattelli, R. (C) 3089–3092 [3149–3152]
Pierre, J.-L.
– Self-Assembly of an Amphiphilic Iron(III) Chelator: Mimicking Iron Acquisition in Marine Bacteria
(C) 2580–2582 [2636–2638]
DOI: 10.1002/anie.200462841
Pierre, J.-L. (C) 438–441 [442–445]
Piers, W. E.
– Borinium, Borenium, and Boronium Ions: Synthesis, Reactivity, and Applications
(R) 5016–5036 [5142–5163]
DOI: 10.1002/anie.200500402
Piguet, C.
– Predictions, Synthetic Strategy, and Isolation of a Linear Tetrametallic Triple-Stranded Lanthanide Helicate
(C) 7954–7958 [8168–8172]
DOI: 10.1002/anie.200503040
Pin, S. (C) 110–112 [112–114]
Pincet, F. (C) 1683–1687 [1711–1715]
Pink, M. (C) 592–595 [598–601]
Pinna, N. (C) 6004–6009 [6158–6163]
Pinto, A. (C) 5060–5064 [5188–5192]
Pinto, M. (C) 2572–2576 [2628–2632]
Piotrowski, H. (C) 924–927 [946–949]
Piper, J. L. (C) 5846–5851 [5996–6001], 7917–7921 [8131–8135]
Pirani, F. (C) 2356–2360 [2408–2412]
Pirkle, W. (C) 6537–6540 [6695–6698]
Pisagatti, I. (C) 4892–4896 [4970–4974]
Pitsch, S.
– Kinetics of Photoinduced RNA Refolding by Real-Time NMR Spectroscopy
(C) 2600–2603 [2656–2659]
DOI: 10.1002/anie.200462724
Pitt, S. W. (C) 3412–3415 [3478–3481]
Pivetta, M. (C) 5334–5337 [5468–5471]
Plant, A. (C) 3889–3892 [3957–3960]
Plaxco, K. W.
– Label-Free Electronic Detection of Thrombin in Blood Serum by Using an Aptamer-Based Sensor
(C) 5456–5459 [5592–5595]
DOI: 10.1002/anie.200500989
Plenio, H.
– Redox-Switchable Phase Tags for Recycling of Homogeneous Catalysts
(C) 6885–6888 [7045–7048]
DOI: 10.1002/anie.200502182
Plötner, J. (C) 7783–7786 [7961–7964]
Plou, F. J. (C) 7553–7557 [7725–7729]
Plutowski, U. (C) 621–625 [627–631], 6588–6592 [6746–6750]
Poblet, J. M.
– General Rule for the Stabilization of Fullerene Cages Encapsulating Trimetallic Nitride Templates
(C) 7230–7233 [7396–7399]
DOI: 10.1002/anie.200501791
Pochini, A.
– Molecular Recognition by Calix[4]arene-Modified Gold Nanoparticles in Aqueous Solution
(C) 2913–2916 [2973–2976]
DOI: 10.1002/anie.200462909
Pochini, A. (C) 278–281 [282–285]
Poddel'sky, A. I. (C) 2767–2771 [2827–2831]
Podlech, J.
– New Aspects of Soai's Asymmetric Autocatalysis
(H) 5776–5777 [5922–5924]
DOI: 10.1002/anie.200501742
Pohl, M.-M. (C) 6771–6774 [6929–6933]
Pohl, P. (C) 1195–1198 [1219–1223]
Pohlki, F. (C) 2951–2954 [3011–3013]
Pohnert, G.
– Unprecedented Lipoxygenase/Hydroperoxide Lyase Pathways in the Moss *Physcomitrella patens*
(C) 158–161 [161–164]
DOI: 10.1002/anie.200460686
– Wound Closure in the Invasive Green Alga *Caulerpa taxifolia* by Enzymatic Activation of a Protein Cross-Linker
(C) 2806–2808 [2866–2869]
DOI: 10.1002/anie.200462276
Polaina, J. (C) 7553–7557 [7725–7729]
Polarz, S.
– Molecular Encoding at the Nanoscale: From Complex Cubes to Bimetallic Oxides
(C) 7892–7896 [8104–8109]
DOI: 10.1002/anie.200501212
Polášek, M. (C) 6708–6711 [6866–6869]
Polavarapu, P. L.
– A Thermal and Solvocontrollable Cylindrical Nanoshutter Based on a Single Screw-Sense Helical Polyguanidine
(C) 7298–7301 [7464–7467]
DOI: 10.1002/anie.200501977
Polborn, K. (C) 2427–2428 Corrigendum: 3955 [2479–2480], 7204–7208 [7370–7374]
Poliakoff, M.
– "Hydrogen-Catalyzed" Dehydrogenation: A Supercritical Conundrum
(C) 7588–7591 [7760–7763]
DOI: 10.1002/anie.200502049
Polysuk, C. (C) 7570–7574 [7742–7746]
Pombeiro, A. J. L.
– Multinuclear Copper Triethanolamine Complexes as Selective Catalysts for the Peroxidative Oxidation of Alkanes under Mild Conditions
(C) 4345–4349 [4419–4423]
DOI: 10.1002/anie.200500585
Ponder, J. B. (C) 4528–4532 [4604–4608]
Pongs, O. (C) 2089–2092 [2125–2129]
Pongtavornpinyo, R. (C) 4231–4235 [4303–4307]
Pons, S. (C) 7294–7297 [7460–7463]
Pons, V. (C) 2512–2515 [2568–2571]
Pophristic, V. (C) 6685–6689 [6843–6847]

 © 2005 Wiley-VCH Verlag GmbH & Co. KGaA, Weinheim

Popkirova, B. (C) 4975 – 4980 [5055 – 5060]
Popkov, M. (C) 716 – 720 [726 – 730], 4378 – 4381 [4452 – 4455]
Popov, A. A. (C) 432 – 435 [436 – 439], 4215 – 4218 [4287 – 4290], 7984 – 7987 [8198 – 8201]
Popovitz-Biro, R. (C) 4169 – 4172 [4241 – 4244]
Poppe, L. (R) 3668 – 3688 [3734 – 3754]
Porco, J. A., Jr.
– Synthesis of the Tetracyclic Core of the Tetrapetalones through Transannular Oxidative [4 + 3] Cyclization
(C) 3067 – 3071 [3127 – 3131]
DOI: 10.1002/anie.200500247
Pornsuriyasak, P. (C) 7123 – 7126 [7285 – 7288]
Porzelle, A. (C) 4724 – 4728 [4802 – 4806]
Pöschl, U.
– Atmospheric Aerosols: Composition, Transformation, Climate and Health Effects
(R) 7520 – 7540 [7690 – 7712]
DOI: 10.1002/anie.200501122
Potapova, I. (C) 2437 – 2440 [2490 – 2493]
Potel, M. (C) 1363 – 1365 [1387 – 1389]
Potnick, J. R. (C) 2377 – 2379 Corrigendum: 4660 [2429 – 2431 Corrigendum: 4735]
Pöttgen, R.
– The Metal Flux: A Preparative Tool for the Exploration of Intermetallic Compounds
(R) 6996 – 7023 [7156 – 7184]
DOI: 10.1002/anie.200462170
Poturovic, S. (C) 1883 – 1887 [1917 – 1921]
Poulsen, A. K. (C) 6916 – 6920 [7076 – 7080]
Poulsen, T. B. (C) 2896 – 2899 [2956 – 2959]
Powell, A. K.
– Hierarchical Assembly of $\{Fe_{13}\}$ Oxygen-Bridged Clusters into a Close-Packed Superstructure
(C) 6678 – 6682 [6836 – 6840]
DOI: 10.1002/anie.200500208
– Supramolecular Coordination Assemblies of Dinuclear Fe^{III} Complexes
(C) 4187 – 4192 [4259 – 4264]
DOI: 10.1002/anie.200500516
– Thermolysis of a Hybrid Organic – Inorganic Supramolecular Coordination Assembly: Templating the Formation of Nanostructured Fibrous Materials and Carbon-Based Microcapsules
(C) 7048 – 7053 [7210 – 7215]
DOI: 10.1002/anie.200501748
Powell, D. R. (C) 6902 – 6905 [7062 – 7065]
Power, P. P.
– Metal-Rich, Neutral and Cationic Organotin Clusters
(C) 2546 – 2549 [2602 – 2605]
DOI: 10.1002/anie.200500117
– $Tl_2[Aryl_2P_4]$: A Thallium Complexed Diaryltetraphosphabutadienediide and its Two-Electron Oxidation to a Diaryltetraphosphabicyclobutane, $Aryl_2P_4$
(C) 7729 – 7733 [7907 – 7911]
DOI: 10.1002/anie.200502865
Power, P. P. (C) 5090 – 5093 [5220 – 5223]
Poyatos, M. (C) 444 – 447 [448 – 451]
Prakash, G. K. S.
– Highly Enantioselective Organocatalytic Hydroxyalkylation of Indoles with Ethyl Trifluoropyruvate
(C) 3086 – 3089 [3146 – 3149]
DOI: 10.1002/anie.200462877
Präsang, C. (C) 1643 – 1646 Corrigendum: 2471 [1670 – 1673 Corrigendum: 2525], 5705 – 5709 [5851 – 5855]
Prato, M. (C) 2015 – 2018 [2051 – 2054], 6358 – 6362 [6516 – 6520]
Pratt, R. C. (C) 4964 – 4968 [5044 – 5048]
Pregosin, P. S.
– Ruthenium-Catalyzed Allylic Alkylation Reactions: Carbonate-Based Catalysts and Intermediates
(C) 4397 – 4400 [4471 – 4474]
DOI: 10.1002/anie.200500967
Prestwich, E. G. (C) 2542 – 2546 [2598 – 2602]
Pretsch, T. (C) 2794 – 2797 [2855 – 2858]
Price, T. (C) 7733 – 7736 [7911 – 7914]
Price Mortimer, A. J. (R) 5384 – 5427 [5518 – 5563]
Prieto, O. (C) 2232 – 2234 [2272 – 2274]
Prilutski, D. (C) 2885 – 2887 [2945 – 2947]
Prinzbach, H.
– In-Plane Bishomoaromaticity in Tetranitrogen Dianions: Solid-State, Solution, and Electronic Structures
(C) 2433 – 2437 [2485 – 2490]
DOI: 10.1002/anie.200462126
Prior, Y. (C) 4169 – 4172 [4241 – 4244]
Pritzkow, H. (C) 632 – 634 [638 – 640]
Probert, M. R. (C) 292 – 295 [296 – 299]
Probst, W. (C) 1226 – 1229 [1252 – 1255]
Procter, D. J.
– A Fluorous-Phase Pummerer Cyclative-Capture Strategy for the Synthesis of Nitrogen Heterocycles
(C) 452 – 455 [456 – 459]
DOI: 10.1002/anie.200461930
Prongay, A. (C) 7024 – 7028 [7186 – 7190]
Protti, S. (C) 1232 – 1236 [1258 – 1262], 5675 – 5678 [5821 – 5824]
Pruski, M. (C) 1826 – 1830 [1860 – 1864]
Ptasińska, S. (C) 1647 – 1650 [1673 – 1676], 6941 – 6943 [7101 – 7103]
Pu, L.
– A Cyclohexyl-1,2-diamine-Derived Bis(binaphthyl) Macrocycle: Enhanced Sensitivity and Enantioselectivity in the Fluorescent Recognition of Mandelic Acid
(C) 1690 – 1693 [1718 – 1721]
DOI: 10.1002/anie.200462471
Puchta, R. (C) 6033 – 6038 [6187 – 6192]
Pugžlys, A. (C) 2373 – 2376 [2425 – 2428]
Pulgam, V. R. (C) 6169 – 6172 [6325 – 6328]
Pulham, C. R. (C) 7032 – 7035 [7194 – 7197]
Punna, S. (C) 2215 – 2220 [2255 – 2260]
Puolitaival, S. M. (C) 7094 – 7097 [7256 – 7259]
Purrello, R.
– A Cationic Zinc Porphyrin as a Chiroptical Probe for Z-DNA
(C) 4006 – 4009 [4074 – 4077]
DOI: 10.1002/anie.200501149
Putaux, J.-L. (C) 2580 – 2582 [2636 – 2638]

Qi, L.
– Morphosynthesis of Rhombododecahedral Silver Cages by Self-Assembly Coupled with Precursor Crystal Templating
(C) 598 – 603 [604 – 609]
DOI: 10.1002/anie.200461859
Qian, R. (C) 4771 – 4774 [4849 – 4852]
Qian, W. (C) 952 – 955 [974 – 977]
Qin, C. (C) 5824 – 5827 [5974 – 5977]
Qin, S. (C) 2015 – 2018 [2051 – 2054]
Qing, Q. (C) 7771 – 7775 [7949 – 7953]
Qiu, S.
– A Metal – Organic Framework with the Zeolite MTN Topology Containing Large Cages of Volume 2.5 nm^3
(C) 3845 – 3848 [3913 – 3916]
DOI: 10.1002/anie.200462260
Qiu, X. (C) 5855 – 5857 [6005 – 6007]
Qu, Da-H. (C) 5296 – 5299 [5430 – 5433]
Quack, M.
– Isotopic Chirality and Molecular Parity Violation
(C) 3623 – 3626 [3689 – 3693]
DOI: 10.1002/anie.200462088
Quan, H.-d. (C) 1128 – 1130 [1152 – 1154]
Quaranta, A. (C) 1536 – 1540 [1560 – 1564]
Quarez, E. (C) 3552 – 3555 [3618 – 3621]
Quarton, M. (C) 5691 – 5694 [5837 – 5840]
Que, L., Jr.
– Aqueous Fe^{IV}=O: Spectroscopic Identification and Oxo-Group Exchange
(C) 6871 – 6874 [7031 – 7034]
DOI: 10.1002/anie.200502686
– Axial Coordination of Carboxylate Activates the Non-heme Fe^{IV}=O Unit
(C) 2255 – 2258 [2295 – 2298]
DOI: 10.1002/anie.200462631
– Spin-State Rationale for the Peroxo-Stabilizing Role of the Thiolate Ligand in Superoxide Reductase
(C) 584 – 587 [590 – 593]
DOI: 10.1002/anie.200461527
– Structures of Nonheme Oxoiron(IV) Complexes from X-ray Crystallography, NMR Spectroscopy, and DFT Calculations
(C) 3690 – 3694 [3756 – 3760]
DOI: 10.1002/anie.200500485
– Two Faces of a Biomimetic Non-Heme HO–Fe^{V}=O Oxidant: Olefin Epoxidation versus *cis*-Dihydroxylation
(C) 2939 – 2941 [2999 – 3001]
DOI: 10.1002/anie.200463072
Quebatte, L. (C) 1084 – 1088 [1108 – 1112]
Quevillon, S. (C) 1366 – 1368 [1390 – 1392]
Quideau, S.
– Regioselective Hypervalent-Iodine(III)-Mediated Dearomatizing Phenylation of Phenols through Direct Ligand Coupling
(C) 7065 – 7069 [7227 – 7231]
DOI: 10.1002/anie.200501638

Raabe, G. (C) 3766 – 3769 [3832 – 3835], 4079 – 4083 [4147 – 4151]
Rabu, P. (C) 6488 – 6491 [6646 – 6649]
Radacki, K. (C) 1192 – 1194 [1217 – 1219], 1658 – 1661 [1685 – 1688], 5647 – 5651 [5792 – 5796], 5651 – 5654 [5796 – 5799]
Rademann, J.
– Reversible Cross-Linking of Hyperbranched Polymers: A Strategy for the Combinatorial Decoration of Multivalent

 © 2005 Wiley-VCH Verlag GmbH & Co. KGaA, Weinheim

Scaffolds
(C) 1560 – 1563 [1584 – 1588]
DOI: 10.1002/anie.200460559
Rademann, K.
– On the Chemistry of Gold in Silicate Glasses: Studies on a Nonthermally Activated Growth of Gold Nanoparticles
(C) 7905 – 7909 [8118 – 8122]
DOI: 10.1002/anie.200502174
Radha Krishna, P. (C) 5878 – 5882 [6028 – 6032]
Radkowski, K. (C) 2777 – 2781 [2837 – 2841]
Radnik, J.
– Deactivation of Pd Acetoxylation Catalysts: Direct Observations by XPS Investigations
(C) 6771 – 6774 [6929 – 6933]
DOI: 10.1002/anie.200501650
Radtke, M. (C) 7905 – 7909 [8118 – 8122]
Rae, A. D. (C) 1251 – 1254 [1277 – 1280]
Raehm, L. (C) 4543 – 4546 [4619 – 4622]
Raendler, C. (C) 1712 – 1714 [1740 – 1742]
Rager, M. N. (C) 4543 – 4546 [4619 – 4622]
Raguin, O. (C) 4058 – 4061 [4126 – 4129]
Rahman, G. M. A. (C) 2015 – 2018 [2051 – 2054], 7567 – 7570 [7739 – 7742]
Raimondi, F. (R) 2190 – 2209 [2228 – 2248]
Rainka, M. P. (C) 6177 – 6180 [6333 – 6336]
Rais, D. (C) 1192 – 1194 [1217 – 1219], 3763 – 3766 [3829 – 3832], 5651 – 5654 [5796 – 5799], 7461 – 7463 [7627 – 7629], (T) 7826 – 7828 [8036 – 8038]
Raiteri, P.
– Exploring Polymorphism: The Case of Benzene
(C) 3769 – 3773 [3835 – 3839]
DOI: 10.1002/anie.200462760
Raithby, P. R. (C) 6875 – 6878 [7035 – 7038]
Raja, R. (R) 6456 – 6482 [6614 – 6641]
Rajaraman, G. (C) 2711 – 2715 [2771 – 2775]
Rajendran, R. G. (C) 564 – 567 [570 – 573]
Rakow, N. A. (C) 4528 – 4532 [4604 – 4608]
Ramakrishna, K. V. S. (C) 5878 – 5882 [6028 – 6032]
Ramakrishnan, S.
– Small-Molecule-Induced Folding of a Synthetic Polymer
(C) 5441 – 5447 [5577 – 5583]
DOI: 10.1002/anie.200501448
Ramminger, A.-D. (C) 2801 – 2805 [2862 – 2866]
Rammo, A. (C) 5968 – 5971 [6122 – 6126]
Ramón, D. J. (R) 1602 – 1634 [1628 – 1661]
Rampersad, M. V. (C) 1217 – 1220 [1243 – 1246]
Ranganath, K. V. S. (C) 322 – 325 [326 – 329]
Rangarajan, S. (C) 1328 – 1332 [1352 – 1356]
Rankin, M. A. (C) 3603 – 3606 [3669 – 3672]
Rantanen, T. (H) 1758 – 1763 [1788 – 1793]
Rao, K. K. (C) 322 – 325 [326 – 329]
Rao, L.
– Optical Absorption and Structure of a Highly Symmetrical Neptunium(v) Diamide Complex
(C) 6200 – 6203 [6356 – 6359]
DOI: 10.1002/anie.200501281
Rao, Z.
– The Heme Monooxygenase Cytochrome $P450_{cam}$ Can Be Engineered to Oxidize Ethane to Ethanol
(C) 4029 – 4032 [4097 – 4100]
DOI: 10.1002/anie.200462630
Rapp, A. (C) 2801 – 2805 [2862 – 2866]
Ratajczyk, T. (C) 1230 – 1232 [1256 – 1258]
Rathore, R.
– Redox-Induced Transformation from an Extended to a π-Stacked Conformer in Acyclic Bis(catecholacetal)s of Acetylacetone
(C) 2771 – 2774 [2831 – 2834]
DOI: 10.1002/anie.200463103
Rattke, J. (C) 2806 – 2808 [2866 – 2869]
Raudaschl-Sieber, G. (C) 5303 – 5306 [5437 – 5440]
Rauhaus, J. E. (C) 4042 – 4045 [4110 – 4113]
Rautiainen, J. M. (C) 7958 – 7961 [8172 – 8175]
Ravoo, B. J.
– Engineering Silicon Oxide Surfaces Using Self-Assembled Monolayers
(R) 6282 – 6304 [6438 – 6462]
DOI: 10.1002/anie.200500633
Rawiso, M. (C) 3260 – 3264 [3324 – 3328]
Rawson, J. M. (C) 3456 – 3459 [3522 – 3525]
Razskazovskiy, Y. (C) 6210 – 6213 [6366 – 6369]
Real, J.-A. (C) 4069 – 4073 [4137 – 4141]
Réau, R.
– Bridging Phosphanes: Exotic or Versatile Binucleating Ligands?
(C) 4362 – 4365 [4436 – 4439]
DOI: 10.1002/anie.200500529
Rebek, J., Jr.
– Simultaneous Encapsulation: Molecules Held at Close Range
(R) 2068 – 2078 [2104 – 2115]
DOI: 10.1002/anie.200462839
Rebilly, J.-N. (C) 1876 – 1879 [1910 – 1913]
Rebours, B. (C) 1725 – 1729 [1753 – 1757]
Reddy, B. G. (C) 2001 – 2004 [2037 – 2040]
Reddy, B. S. (C) 6723 – 6727 [6881 – 6885]
Reddy, L. M. (C) 2008 – 2011 [2044 – 2047]
Reddy, P. T. (C) 1366 – 1368 [1390 – 1392]
Redshaw, C.
– Synthesis of Hexa- and Dodecanuclear Organoaluminum Ring Structures Incorporating the "Magic" $Ph_2C(X)$ Group (X = O^-, NH^-)
(C) 1850 – 1853 [1884 – 1887]
DOI: 10.1002/anie.200461627
Reedijk, J.
– Copper-Mediated Selective Oxidation of a C–H Bond
(C) 3585 – 3587 [3651 – 3653]
DOI: 10.1002/anie.200462946
Reese, M. (C) 4172 – 4175 [4244 – 4247]
Reetz, M. T.
– Binol-Derived Monodentate Phosphites and Phosphoramidites with Phosphorus Stereogenic Centers: Novel Ligands for Transition-Metal Catalysis
(C) 412 – 415 [416 – 419]
DOI: 10.1002/anie.200461624
– Expanding the Range of Substrate Acceptance of Enzymes: Combinatorial Active-Site Saturation Test
(C) 4192 – 4196 [4264 – 4268]
DOI: 10.1002/anie.200500767
– Mixtures of Configurationally Stable and Fluxional Atropisomeric Monodentate P Ligands in Asymmetric Rh-Catalyzed Olefin Hydrogenation
(C) 2959 – 2962 [3019 – 3021]
DOI: 10.1002/anie.200462612
– The Influence of Mixtures of Monodentate Achiral Ligands on the Regioselectivity of Transition-Metal-Catalyzed Hydroformylation
(C) 2962 – 2964 [3022 – 3024]
DOI: 10.1002/anie.200462613
Reglier, M. (C) 7104 – 7106 [7266 – 7268]
Reibenspies, J. H. (C) 1217 – 1220 [1243 – 1246]
Reiber, A. (C) 262 – 265 [267 – 270]
Reicke, M. (C) 3773 – 3777 [3839 – 3843]
Reimold, M. (C) 6750 – 6755 [6908 – 6913]
Reingold, J. A. (C) 7710 – 7715 [7888 – 7893]
Reinhold, J. (C) 2965 – 2969 [3025 – 3029]
Reinhoudt, D. N.
– Ditopic Complexation and Release of Neutral Guest Molecules by a Hydrogen-Bonded "*Endo* – *Exo*" Receptor
(C) 3248 – 3253 [3312 – 3317]
DOI: 10.1002/anie.200500134
– Engineering Silicon Oxide Surfaces Using Self-Assembled Monolayers
(R) 6282 – 6304 [6438 – 6462]
DOI: 10.1002/anie.200500633
Reiser, O.
– Helical Chirality in Pentacoordinate Zinc Complexes—Selective Access to Both Pseudoenantiomers with One Ligand Configuration
(C) 242 – 245 [246 – 249]
DOI: 10.1002/anie.200460843
Reißig, H.-U.
– Synthesis of Enantiopure Carbohydrate Mimetics by Lewis Acid Catalyzed Rearrangement of 1,3-Dioxolanyl-Substituted 1,2-Oxazines
(C) 6227 – 6231 [6383 – 6387]
DOI: 10.1002/anie.200501127
Remediakis, I. N.
– CO Oxidation on Rutile-Supported Au Nanoparticles
(C) 1824 – 1826 [1858 – 1860]
DOI: 10.1002/anie.200461699
Ren, B.
– Tip-Enhanced Raman Spectroscopy of Benzenethiol Adsorbed on Au and Pt Single-Crystal Surfaces
(C) 139 – 142 [141 – 144]
DOI: 10.1002/anie.200460656
Ren, B. (C) 1265 – 1268 [1291 – 1294]
Ren, C.-T. (C) 6888 – 6892 [7048 – 7052]
Ren, G.-M. (C) 2158 – 2161 [2196 – 2199]
Ren, Jimin (C) 6920 – 6923 [7080 – 7083]
Ren, Jinsong
– Molecular Recognition of Basic Fibroblast Growth Factor by Polyoxometalates
(C) 4048 – 4052 [4116 – 4120]
DOI: 10.1002/anie.200500108
Ren, L.-L. (C) 1269 – 1273 [1295 – 1299]
Ren, S.-F. (C) 5725 – 5729 [5871 – 5875]
Renaud, J.-L. (C) 2021 – 2023 [2057 – 2059]
Renaud, P.
– Dimethyl Phosphite Mediated Hydrogen Atom Abstraction: A Tin-Free Procedure for the Preparation of Cyclopentane Derivatives
(C) 5273 – 5275 [5407 – 5409]
DOI: 10.1002/anie.200501309
Renault, J.-P.
– Radiolysis of Confined Water: Production and Reactivity of Hydroxyl Radicals
(C) 110 – 112 [112 – 114]
DOI: 10.1002/anie.200460284
Rendler, S. (C) 1661 – 1664 [1688 – 1691], 7620 – 7624 [7793 – 7797]
Rentschler, E. (C) 7938 – 7942 [8152 – 8156]
Resa, I. (C) 1244 – 1247 [1270 – 1273]
Reshetova, M. D. (C) 7386 – 7390 [7552 – 7556]

 © 2005 Wiley-VCH Verlag GmbH & Co. KGaA, Weinheim

Ressler, T.
– The Microstructure of Copper Zinc Oxide Catalysts: Bridging the Materials Gap (C) 4704 – 4707 [4782 – 4785] DOI: 10.1002/anie.200462942
Rétey, J.
– Friedel – Crafts-Type Mechanism for the Enzymatic Elimination of Ammonia from Histidine and Phenylalanine (R) 3668 – 3688 [3734 – 3754] DOI: 10.1002/anie.200461377
Reyes, E. (C) 7028 – 7032 [7190 – 7194]
Reyes-Duarte, D. (C) 7553 – 7557 [7725 – 7729]
Reymond, J.-L.
– Virtual Exploration of the Small-Molecule Chemical Universe below 160 Daltons (C) 1504 – 1508 [1528 – 1532] DOI: 10.1002/anie.200462457
Rheingold, A. L. (C) 1508 – 1510 [1532 – 1534], 5428 – 5433 [5564 – 5569]
Rhile, I. J. (L) 1598 – 1599 [1624 – 1625]
Ribas, J. (C) 1997 – 2001 [2033 – 2037]
Ribbe, A. E. (C) 3582 – 3585 [3648 – 3651], 6694 – 6696 [6852 – 6854]
Ribot, F.
– The First Structure of a Cerium(IV) Phosphate: Ab Initio Rietveld Analysis of $Ce^{IV}(PO_4)(HPO_4)_{0.5}(H_2O)_{0.5}$ (C) 5691 – 5694 [5837 – 5840] DOI: 10.1002/anie.200501871
Ricard, L. (C) 1876 – 1879 [1910 – 1913]
Ricci, A.
– Catalytic Enantioselective Friedel – Crafts Alkylation of Indoles with Nitroalkenes by Using a Simple Thiourea Organocatalyst (C) 6576 – 6579 [6734 – 6737] DOI: 10.1002/anie.200500227
Ricci, A. (C) 7975 – 7978 [8189 – 8192]
Rice, C. R.
– Allosteric-Controlled Metal Specificity of a Ditopic Ligand (C) 6909 – 6912 [7069 – 7072] DOI: 10.1002/anie.200502571
Rich, J. R. (C) 7725 – 7729 [7903 – 7907]
Richards, A. F. (C) 2546 – 2549 [2602 – 2605]
Richert, C.
– A Direct Glimpse of Cross-Hybridization: Background-Passified Microarrays That Allow Mass-Spectrometric Detection of Captured Oligonucleotides (C) 621 – 625 [627 – 631] DOI: 10.1002/anie.200461212
– Chemical Primer Extension: Efficiently Determining Single Nucleotides in DNA (C) 6588 – 6592 [6746 – 6750] DOI: 10.1002/anie.200501794
Richert, C. (C) 5242 – 5246 [5376 – 5381]
Richter, C. (C) 820 – 822 [831 – 833]
Richter, J. M. (C) 609 – 612 [615 – 618]
Riddle, J. A. (C) 6689 – 6693 [6847 – 6851]
Rider, D. A. (C) 7964 – 7968 [8178 – 8182]
Riedel, S. (C) 2092 – 2096 [2129 – 2133]
Riedle, E. (C) 4623 – 4626 [4699 – 4703]
Riehm, T. (C) 7394 – 7398 [7560 – 7564]
Riek, R. (C) 2441 – 2444 [2494 – 2497]
Riera, V. (C) 102 – 105 [104 – 107]
Riesemeier, H. (C) 7905 – 7909 [8118 – 8122]
Righetto, S. (C) 7922 – 7925 [8136 – 8139]
Rigo, P. (C) 6214 – 6219 [6370 – 6375]
Riis-Johannessen, T. (C) 6909 – 6912 [7069 – 7072]
Riisager, A.
– Very Stable and Highly Regioselective Supported Ionic-Liquid-Phase (SILP) Catalysis: Continuous-Flow Fixed-Bed Hydroformylation of Propene (C) 815 – 819 [826 – 830] DOI: 10.1002/anie.200461534
Ríos-Moreno, G. (C) 3267 – 3271 [3331 – 3335]
Ripmeester, J. A. (C) 7749 – 7752 [7927 – 7930]
Rissanen, K.
– Very Large Container Molecules (H) 3652 – 3654 [3718 – 3720] DOI: 10.1002/anie.200500714
Rissing, P.-J. (C) 3548 – 3552 [3614 – 3618]
Ritch, J. S. (C) 4953 – 4956 [5033 – 5036]
Ritter, C. (C) 2441 – 2444 [2494 – 2497]
Ritter, H. Corrigendum: 6099
Ritter, H.
– Unusual Solubility Properties of Polymethacrylamides as a Result of Supramolecular Interactions with Cyclodextrin (C) 5658 – 5661 [5803 – 5806] DOI: 10.1002/anie.200501374
Ritter, T. (C) 936 – 938 [958 – 960]
Rivalta, E. (C) 3600 – 3603 [3666 – 3669]
Rivard, E. (C) 7729 – 7733 [7907 – 7911]
Rivas, K. (C) 4903 – 4906 [4981 – 4984]
Rivera, D. G. (C) 4785 – 4790 [4863 – 4868]
Rivkin, A. (M) 2838 – 2850 [2898 – 2910]
Rizzato, S. (C) 5701 – 5705 [5847 – 5851]
Rmaile, H. H. (C) 782 – 785 [792 – 795]
Roberge, D. M.
– Controlled Autocatalytic Nitration of Phenol in a Microreactor (C) 7972 – 7975 [8186 – 8189] DOI: 10.1002/anie.200502387
Robert, A.
– C10-Modified Artemisinin Derivatives: Efficient Heme-Alkylating Agents (L) 2060 – 2063 [2096 – 2099] DOI: 10.1002/anie.200462556
Robert, E. C. (C) 7584 – 7587 [7756 – 7759]
Robertson, J. (C) 6157 – 6162 [6313 – 6318]
Robiette, R. (C) 5468 – 5471 [5604 – 5607]
Rocker, F. (C) 262 – 265 [267 – 270]
Rocquefelte, X.
– Structural Preference versus Metal within the MB_2C_2 (M = Mg, Sc, Ca, Y, Ln) Phases: The Coloring Problem Revisited by DFT Calculations (C) 7542 – 7545 [7714 – 7717] DOI: 10.1002/anie.200503080
Roda, A. (C) 3694 – 3698 [3760 – 3764]
Rodionov, V. O. (C) 2210 – 2215 [2250 – 2255]
Rodolfa, K. T. (C) 6854 – 6859 [7014 – 7019]
Rodrigues, J. A. (C) 441 – 444 [445 – 448]
Rodríguez, D. (C) 5851 – 5854 [6001 – 6004]
Rodríguez, F. (C) 126 – 128 [128 – 130]
Rodriguez, J. M. (C) 2704 – 2707 [2764 – 2767]
Rodriguez-Carvajal, J. (C) 1725 – 1729 [1753 – 1757]
Rodríguez-López, G. (C) 2918 – 2922 [2978 – 2982]
Rodriguez-Rivera, G. J. (C) 778 – 782 [788 – 792]
Rodriguez-Sanz, E. (C) 4362 – 4365 [4436 – 4439]
Roe, M. J. (C) 3555 – 3558 [3621 – 3624]
Roecker, A. J. (C) 3443 – 3447 [3509 – 3513], 3447 – 3452 [3513 – 3518]
Roelfes, G.
– DNA-Based Asymmetric Catalysis (C) 3230 – 3232 [3294 – 3296] DOI: 10.1002/anie.200500298
Roemer, E. L. (C) 737 – 739 [747 – 749]
Roesky, H. W.
– A Stable Aluminacyclopropene $LAl(\eta^2\text{-}C_2H_2)$ and Its End-On Azide Insertion to an Aluminaazacyclobutene (C) 5090 – 5093 [5220 – 5223] DOI: 10.1002/anie.200500899
– Janus-Faced Aluminum: A Demonstration of Unique Lewis Acid and Lewis Base Behavior of the Aluminum Atom in $[LAlB(C_6F_5)_3]$ (C) 7072 – 7074 [7234 – 7236] DOI: 10.1002/anie.200502251
– Preparation of Heterobimetallic Oxide – Hydroxide – Hydrogensulfides $[LAl(OH)(\mu\text{-}O)MCp_2(SH)]$ (M = Ti, Zr) (C) 6016 – 6018 [6170 – 6172] DOI: 10.1002/anie.200501509
– The Formal Conversion of SiOH Protons into Hydrides by Germanium(II) Species Leads to the Formation of the Germanium(IV) Hydride Cluster $[(RSiO_3GeH)_4]$ (C) 281 – 284 [285 – 288] DOI: 10.1002/anie.200460849
Roesky, P. W.
– Intramolecular Hydroamination of Functionalized Alkenes and Alkynes with a Homogenous Zinc Catalyst (C) 7794 – 7798 [7972 – 7976] DOI: 10.1002/anie.200502006
Rogez, G.
– Very Large Ising-Type Magnetic Anisotropy in a Mononuclear Ni^{II} Complex (C) 1876 – 1879 [1910 – 1913] DOI: 10.1002/anie.200462294
Roggan, S. (C) 5259 – 5262 [5393 – 5397]
Roginskaya, M. (C) 6210 – 6213 [6366 – 6369]
Rohde, J.-U. (C) 2255 – 2258 [2295 – 2298]
Röhr, H. (C) 6943 – 6947 [7104 – 7107]
Roithová, J. (C) 3092 – 3096 [3152 – 3156]
Roitzsch, M. (C) 5670 – 5674 [5816 – 5820]
Romano, C. (C) 2715 – 2719 [2775 – 2779]
Romero, M. J. (C) 4182 – 4187 [4254 – 4259]
Romerosa, A.
– Stable, Water-Soluble Pta-Based Ru – Ag Organometallic Polymers (C) 2568 – 2572 [2624 – 2628] DOI: 10.1002/anie.200462790
Romieu, A. (C) 4058 – 4061 [4126 – 4129]
Rominger, F. (C) 153 – 158 [156 – 161], 6951 – 6956 [7112 – 7117]
Rompel, A. (C) 6916 – 6920 [7076 – 7080]
Ronimus, R. S. (C) 941 – 944 [963 – 966]
Rooms, J. F. (C) 6746 – 6750 [6904 – 6908]
Roper, D. I. (C) 6403 – 6406 [6561 – 6564]
Röper, S. (C) 116 – 120 [118 – 122]
Roques, B. P.
– A Labeled Neutral Endopeptidase Inhibitor as a Potential Tool for Tumor Diagnosis and Prognosis (C) 4058 – 4061 [4126 – 4129] DOI: 10.1002/anie.200500700
Ros, R. (C) 484 – 488 [489 – 492], 3921 – 3924 [3989 – 3993]
Ros-Lis, J. V. (C) 4405 – 4407 [4479 – 4482]
Rosales, A. (C) 319 – 322 [323 – 326]
Rose, I.
– Ubiquitin at Fox Chase (Nobel Lecture) (R) 5927 – 5931 [6077 – 6081] DOI: 10.1002/anie.200500995
Rosen, B. M. (C) 6516 – 6521 [6674 – 6679]
Rosi, M. (C) 462 – 465 [466 – 469]
Rosi, N. L. (C) 5064 – 5067 [5192 – 5195]
Rosokha, S. V. (C) 5133 – 5136 [5263 – 5266]
Rosol, M. (C) 1865 – 1869 [1899 – 1903]
Ross, S. (C) 5314 – 5317 [5448 – 5451]

 © 2005 Wiley-VCH Verlag GmbH & Co. KGaA, Weinheim

Rosseinsky, M. J.
– $Ba_8CoNb_6O_{24}$: A d^0 Dielectric Oxide Host Containing Ordered d^7 Cation Layers 1.88 nm Apart
(C) 7733 – 7736 [7911 – 7914]
DOI: 10.1002/anie.200500135
Roth, J. P.
– Structures of Transition States in Metal-Mediated O_2-Activation Reactions
(C) 7273 – 7276 [7439 – 7442]
DOI: 10.1002/anie.200502096
Roth, S. (C) 4623 – 4626 [4699 – 4703]
Rothenberger, A. (C) 3932 – 3936 [4002 – 4005]
Rotureau, P. (C) 110 – 112 [112 – 114]
Rouleau, C. M. (C) 274 – 278 [278 – 282]
Rousseau, G. B. D. (C) 1830 – 1833 [1864 – 1867]
Rovira, C. (C) 888 – 892 [910 – 914], 1977 – 1981 [2013 – 2017]
Rovis, T.
– Stereoselective Lewis Acid Mediated [1,3] Ring Contraction of 2,5-Dihydrooxepins as a Route to Polysubstituted Cyclopentenes
(C) 3264 – 3267 [3328 – 3331]
DOI: 10.1002/anie.200500088
Rowan, A. E.
– Acid-Initiated Stereospecific Polymerization of Isocyanopeptides
(C) 1990 – 1993 [2026 – 2029]
DOI: 10.1002/anie.200462417
– Single-Enzyme Kinetics of CALB-Catalyzed Hydrolysis
(C) 560 – 564 [566 – 570]
DOI: 10.1002/anie.200460625
Rowan, S. J.
– Metallomesogens
(T) 4830 – 4832 [4908 – 4910]
DOI: 10.1002/anie.200502405
Rowsell, J. L. C. (M) 4670 – 4679 [4748 – 4758]
Roy, S. K. (C) 132 – 135 [134 – 137]
Royo, P.
– Carbon Dioxide Activation Assisted by a Bis(chlorodimethylsilyl)cyclopentadienyl Titanium Compound
(C) 5828 – 5830 [5978 – 5980]
DOI: 10.1002/anie.200500716
Rozen, S.
– Synthesis of [all]-*S*,*S*-Dioxide Oligothiophenes Using $HOF \cdot CH_3CN$
(C) 7374 – 7378 [7540 – 7544]
DOI: 10.1002/anie.200501681
Ruan, J. (C) 6719 – 6723 [6877 – 6881]
Ruan, M. (C) 5083 – 5087 [5213 – 5217]
Ruben, M.
– Addressing the Metal Centers of $[2 \times 2]$ Co^{II}_4 Grid-Type Complexes by STM/STS
(C) 7896 – 7900 [8109 – 8113]
DOI: 10.1002/anie.200502743
– Squaring the Interface: "Surface-Assisted" Coordination Chemistry
(H) 1594 – 1596 [1620 – 1623]
DOI: 10.1002/anie.200462064
Ruck, M.
– Fibrous Red Phosphorus
(C) 7616 – 7619 [7788 – 7792]
DOI: 10.1002/anie.200503017
Ruckenstein, E. Corrigendum: 1907
Rudd, M. (C) 3432 – 3435 [3498 – 3501]
Rudd, M. T. (R) 6630 – 6666 [6788 – 6825]
Ruderfer, I. (C) 739 – 743 [749 – 753]
Rudinger, N. Z. (C) 4712 – 4715 [4791 – 4794]
Rudkevich, D. M.
– Supramolecular Features of Calixarene-Based Synthetic Nanotubes
(C) 3043 – 3047 [3103 – 3107]
DOI: 10.1002/anie.200500057
Rudolph, M. (C) 2798 – 2801 [2858 – 2861]
Rudroff, F. (C) 3609 – 3613 [3675 – 3679]
Rüegger, H. (C) 473 – 477 [477 – 481]
Ruhlmann, L. (C) 3072 – 3075 [3132 – 3135]
Ruiz, E.
– Symmetry and Topology Determine the Mo^V – CN – Mn^{II} Exchange Interactions in High-Spin Molecules
(C) 2711 – 2715 [2771 – 2775]
DOI: 10.1002/anie.200500129
Ruiz, J.
– Imidazoline-Functionalized Diphosphines: Models for N-Heterocyclic Carbene – Diphosphinocarbene Coupling
(C) 102 – 105 [104 – 107]
DOI: 10.1002/anie.200461120
Ruiz Aranzaes, J. (C) 7399 – 7404 [7565 – 7570]
Ruiz-Molina, D. (C) 888 – 892 [910 – 914]
Ruloff, R. (C) 1480 – 1484 [1504 – 1508]
Runnegar, M. T. C. (C) 3879 – 3881 [3947 – 3949]
Rurack, K.
– A Regenerative Chemodosimeter Based on Metal-Induced Dye Formation for the Highly Selective and Sensitive Optical Determination of Hg^{2+} Ions
(C) 4405 – 4407 [4479 – 4482]
DOI: 10.1002/anie.200500583
– Multiple Switching and Photogated Electrochemiluminescence Expressed by a Dihydroazulene/Boron Dipyrromethene Dyad
(C) 6943 – 6947 [7104 – 7107]
DOI: 10.1002/anie.200501573
– "Turn ON/OFF your LOV light": Borondipyrromethene – Flavin Dyads as Biomimetic Switches Derived from the LOV Domain
(C) 2288 – 2291 [2328 – 2331]
DOI: 10.1002/anie.200462377
Rusbandi, U. E. (C) 7764 – 7767 [7942 – 7945]
Russell, A. T.
– Alkene – Arene *meta* Photocycloadditions with a Four-Carbon-Atom Tether: Efficient Approach toward the Polycyclic Ring Systems of Aphidicolin and Stemodinone
(C) 944 – 946 [966 – 968]
DOI: 10.1002/anie.200461661
Russell, D. A.
– Synthetic Macrocyclic Peptidomimetics as Tunable pH Probes for the Fluorescence Imaging of Acidic Organelles in Live Cells
(C) 6504 – 6508 [6662 – 6666]
DOI: 10.1002/anie.200501920
Russell, J. T. (C) 2420 – 2426 [2472 – 2478]
Russell, T. P.
– Self-Assembly and Cross-Linking of Bionanoparticles at Liquid – Liquid Interfaces
(C) 2420 – 2426 [2472 – 2478]
DOI: 10.1002/anie.200462653
Russon, L. M. Corrigendum: 1154
Rusu, M. (C) 3857 – 3861 [3925 – 3929]
Ruud, K.
– The Importance of Molecular Vibrations: The Sign Change of the Optical Rotation of Methyloxirane
(C) 3594 – 3596 [3660 – 3662]
DOI: 10.1002/anie.200500642
Rúveda, E. A. (R) 854 – 885 [876 – 907]
Ryadnov, M. G. (C) 325 – 328 [329 – 332]
Rydz, J. (C) 3609 – 3613 [3675 – 3679]
Ryu, C. Y. Corrigendum: 1907
Ryu, I.
– Alkyne Carbonylation by Radicals: Tin-Radical-Catalyzed Synthesis of α-Methylene Amides from 1-Alkynes, Carbon Monoxide, and Amines
(C) 1075 – 1078 [1099 – 1102]
DOI: 10.1002/anie.200461954
– Tin-Free Radical Carbonylation: Thiol Ester Synthesis Using Alkyl Allyl Sulfone Precursors, Phenyl Benzenethiosulfonate, and CO
(C) 6183 – 6186 [6339 – 6342]
DOI: 10.1002/anie.200501606

Saaby, S. (C) 2896 – 2899 [2956 – 2959], 6058 – 6063 [6212 – 6217]
Saburi, H. (C) 1730 – 1732 [1758 – 1760]
Sada, K.
– Multicomponent Organic Alloys Based on Organic Layered Crystals
(C) 7059 – 7062 [7221 – 7224]
DOI: 10.1002/anie.200501678
Sadowski, O. Corrigendum: 6099
Saeki, K. (C) 2922 – 2925 [2982 – 2985]
Saendig, N. (C) 2356 – 2360 [2408 – 2412]
Safina, B. S. (C) 1378 – 1382 [1402 – 1406]
Sagan, S. (C) 4244 – 4247 [4316 – 4319]
Sahade, D. A. (C) 1948 – 1951 [1984 – 1987]
Sahin, Y. (C) 1643 – 1646 Corrigendum: 2471 [1670 – 1673 Corrigendum: 2525]
Saillard, J.-Y.
– Structural Preference versus Metal within the MB_2C_2 (M = Mg, Sc, Ca, Y, Ln) Phases: The Coloring Problem Revisited by DFT Calculations
(C) 7542 – 7545 [7714 – 7717]
DOI: 10.1002/anie.200503080
Saint-Aman, E. (C) 438 – 441 [442 – 445]
Saito, A. (C) 5523 – 5526 [5659 – 5662]
Saito, B. (C) 4600 – 4602 [4676 – 4678], 4935 – 4939 [5015 – 5019]
Saito, M.
– The Aromaticity of the Stannole Dianion
(C) 6553 – 6556 [6711 – 6714]
DOI: 10.1002/anie.200501632
Saito, S. (C) 7244 – 7248 [7410 – 7414]
Saiz, C. G. (C) 3062 – 3067 [3122 – 3127]
Sakagami, H. (C) 6928 – 6931 [7088 – 7091]
Sakaguchi, S. (C) 2586 – 2588 [2642 – 2644]
Sakai, K. (C) 4935 – 4939 [5015 – 5019]
Sakai, M. (C) 6149 – 6151 [6305 – 6307]
Sakamoto, Maki (C) 6564 – 6568 [6722 – 6726]
Sakamoto, Masami
– Asymmetric Photocycloaddition in Solution of a Chiral Crystallized Naphthamide
(C) 5523 – 5526 [5659 – 5662]
DOI: 10.1002/anie.200501156
Sakamoto, T. (C) 2586 – 2588 [2642 – 2644]
Sakamoto, Y. (C) 5317 – 5322 [5451 – 5456]
Sakanaka, O. (C) 4944 – 4948 [5024 – 5028]
Sakata, M. (C) 920 – 923 [942 – 945], 4568 – 4571 [4644 – 4647]
Sakurai, K. (C) 2030 – 2033 [2066 – 2069]
Sakurai, Y. (C) 6180 – 6183 [6336 – 6339]

Salaita, K. (C) 6013 – 6015 [6167 – 6169]
Saleh, N. N. R. (C) 5255 – 5259 [5389 – 5393]
Salloum, D. (C) 1363 – 1365 [1387 – 1389]
Salvatella, L. (C) 458 – 461 [462 – 465]
Salyer, P. A. (C) 3555 – 3558 [3621 – 3624]
Samain, E.
– Highly Efficient Biosynthesis of the Oligosaccharide Moiety of the GD3 Ganglioside by Using Metabolically Engineered *Escherichia coli*
(C) 1350 – 1352 [1374 – 1376]
DOI: 10.1002/anie.200461507
Sambri, L. (C) 6219 – 6222 [6375 – 6378]
Samia, A. C. S. (C) 5855 – 5857 [6005 – 6007]
Samjeské, G. (C) 5694 – 5698 [5840 – 5844]
Samorì, B.
– DNA Codes for Nanoscience
(R) 1166 – 1181 [1190 – 1206]
DOI: 10.1002/anie.200400652
Samuel, J. D. J. S. (C) 3297 – 3301 [3361 – 3365]
Sanaú, M. (C) 444 – 447 [448 – 451]
Sanaur, S. (C) 7390 – 7394 [7556 – 7560]
Sancenón, F. (C) 2918 – 2922 [2978 – 2982]
Sanchez, C.
– Thermally Stable Nanocrystalline γ-Alumina Layers with Highly Ordered 3D Mesoporosity
(C) 4589 – 4592 [4665 – 4668]
DOI: 10.1002/anie.200500037
Sánchez, L. (M) 5374 – 5382 [5508 – 5516]
Sánchez-Iglesias, A. (C) 4375 – 4378 [4449 – 4452]
Sánchez-Pedregal, V. M. (C) 4172 – 4175 [4244 – 4247]
Sánchez-Quesada, J. (C) 1401 – 1404 [1425 – 1428]
Sander, W.
– 1,2,3-Tridehydrobenzene
(C) 6306 – 6311 [6464 – 6469]
DOI: 10.1002/anie.200501912
Sander, W. (C) 3289 – 3293 [3353 – 3357]
Sangregorio, C. (C) 5817 – 5821 [5967 – 5971]
Sanji, T.
– Helical Folding in a Helical Channel: Chiroptical Transcription of Helical Information through Chiral Wrapping
(C) 7301 – 7304 [7467 – 7470]
DOI: 10.1002/anie.200502073
Sano, S. (C) 5838 – 5841 [5988 – 5991]
Sansano, J. M.
– Catalytic Enantioselective 1,3-Dipolar Cycloaddition Reaction of Azomethine Ylides and Alkenes: The Direct Strategy To Prepare Enantioenriched Highly Substituted Proline Derivatives
(H) 6272 – 6276 [6428 – 6432]
DOI: 10.1002/anie.200501074
Santamaría, D. (C) 5828 – 5830 [5978 – 5980]
Santamaría, J. (C) 6583 – 6585 [6741 – 6743]
Santambrogio, G. (C) 3122 – 3125 [3182 – 3185]
Santer, S. (C) 3297 – 3301 [3361 – 3365]
Santoro, F.
– A Tiny Excited-State Barrier Can Induce a Multiexponential Decay of the Retinal Chromophore: A Quantum Dynamics Investigation
(C) 5118 – 5121 [5248 – 5251]
DOI: 10.1002/anie.200501236
Sanz Miguel, P. J. (C) 5670 – 5674 [5816 – 5820]
Saoud, M. (C) 2568 – 2572 [2624 – 2628]
Sapelza, G. (C) 6234 – 6237 [6391 – 6393]
Sapountzis, I. (C) 1654 – 1658 [1682 – 1685], 4258 – 4261 [4330 – 4333]
Saraf, R. F.
– Self-Assembly of Nanoparticles on Live Bacterium: An Avenue to Fabricate Electronic Devices
(C) 6668 – 6673 [6826 – 6831]
DOI: 10.1002/anie.200501711
Sarkar, B. (C) 2103 – 2106 [2140 – 2143], 5655 – 5658 [5800 – 5803]
Sarlah, D. (R) 4442 – 4489 [4516 – 4563], 4490 – 4527 [4564 – 4601]
Sasaki, K. (C) 1951 – 1954 [1987 – 1990]
Sasaki, N. (C) 6682 – 6685 [6840 – 6843]
Sasaki, Yoichi
– Photoconversion of a Redox-Active Self-Assembled Monolayer: In Situ Probing of Photoinduced CO Dissociation from a Triruthenium Cluster Center on Gold
(C) 416 – 419 [420 – 423]
DOI: 10.1002/anie.200460651
Sasaki, Yuya (C) 7718 – 7721 [7896 – 7899]
Sasamori, T. (C) 3717 – 3720 [3783 – 3786]
Sasamoto, N. (C) 1525 – 1529 [1549 – 1553]
Sasmal, P. K. (C) 3443 – 3447 [3509 – 3513], 3447 – 3452 [3513 – 3518]
Satake, A. (C) 4763 – 4766 [4841 – 4844]
Sato, A. (C) 1694 – 1696 [1722 – 1724]
Sato, I. (C) 2774 – 2777 [2834 – 2837]
Sato, Kazuhiko (C) 7929 – 7932 [8143 – 8146], 7932 – 7935 [8146 – 8149]
Sato, Kazunobu (C) 6564 – 6568 [6722 – 6726], 7277 – 7280 [7443 – 7446]
Sato, O.
– $[Mn^{III}(salen)]_6[Fe^{III}(bpmb)(CN)_2]_6 \cdot 7H_2O$: A Cyanide-Bridged Nanosized Molecular Wheel
(C) 7742 – 7745 [7920 – 7923]
DOI: 10.1002/anie.200502699
Sato, T. (C) 4547 – 4549 [4623 – 4625]
Sattler, M.
– Local Structure and Anisotropic Backbone Dynamics from Cross-Correlated NMR Relaxation in Proteins
(C) 3232 – 3237 [3296 – 3301]
DOI: 10.1002/anie.200462495
Sauer, I. (C) 5252 – 5255 [5386 – 5389]
Sauer, J.
– Polyhedral Vanadium Oxide Cages: Infrared Spectra of Cluster Anions and Size-Induced d Electron Localization
(C) 3122 – 3125 [3182 – 3185]
DOI: 10.1002/anie.200462894
– Protonated Isobutene in Zeolites: *tert*-Butyl Cation or Alkoxide?
(C) 4769 – 4771 [4847 – 4849]
DOI: 10.1002/anie.200501002
Sauer, M.
– Branching Out of Single-Molecule Fluorescence Spectroscopy: Challenges for Chemistry and Influence on Biology
(R) 2642 – 2671 [2698 – 2728]
DOI: 10.1002/anie.200300647
Sauer, N. N. (C) 2403 – 2406 [2455 – 2458]
Sauers, R. R.
– Fluorophenoxycarbene inside a Hemicarcerand: A Bottled Singlet Carbene
(C) 1994 – 1997 [2030 – 2033]
DOI: 10.1002/anie.200462633
Sautet, P. (C) 5279 – 5282 [5413 – 5416]
Savitha, G. (C) 2115 – 2119 [2153 – 2157]
Sawa, H.
– Floating Single Hydrogen Molecule in an Open-Cage Fullerene
(C) 1981 – 1983 [2017 – 2019]
DOI: 10.1002/anie.200462850
Sawada, T. (C) 4896 – 4899 [4974 – 4977]
Sawada, Y. (C) 4935 – 4939 [5015 – 5019]
Sawai, H. (C) 6682 – 6685 [6840 – 6843]
Scarborough, C. C. (C) 5269 – 5272 [5403 – 5406]
Schacht, E. (C) 5505 – 5509 [5641 – 5645]
Schade, B. (C) 2976 – 2979 [3036 – 3039]
Schaefer, C. (C) 4606 – 4608 [4682 – 4684]
Schäffer, C. (C) 7757 – 7761 [7935 – 7939]
Schaffrath, Manuela (C) 1650 – 1654 [1677 – 1681]
Schaffrath, Markus (C) 7798 – 7800 [7976 – 7979]
Schakel, M. (C) 6579 – 6582 [6737 – 6740]
Schalley, C. A.
– Gas-Phase Host – Guest Chemistry of Dendritic Viologens and Molecular Tweezers: A Remarkably Strong Effect on Dication Stability
(C) 477 – 480 [481 – 485]
DOI: 10.1002/anie.200461872
Schalley, C. A. (C) 480 – 484 [485 – 488]
Schalow, T. (C) 7601 – 7605 [7773 – 7777]
Schanze, K. (C) 2572 – 2576 [2628 – 2632]
Schärer, K. (C) 4400 – 4404 [4474 – 4479]
Schauermann, S. (C) 7601 – 7605 [7773 – 7777]
Scheer, M.
– Antimony – Tungsten Triple Bond: A Stable Complex with a Terminal Antimony Ligand
(C) 4920 – 4924 [4999 – 5003]
DOI: 10.1002/anie.200500781
– Tetraphosphacyclopentadienyl and Triphosphaallyl Ligands in Iron Complexes
(C) 3755 – 3758 [3821 – 3825]
DOI: 10.1002/anie.200500194
Scheerer, J. R. (C) 6038 – 6042 [6192 – 6196]
Scheffer, J. R.
– Orbital-Overlap Control of the Reactivity of a Bicyclic 1-Hydroxy-1,4-Biradical
(C) 5087 – 5089 [5217 – 5219]
DOI: 10.1002/anie.200500983
Scheiber, J. (C) 7208 – 7212 [7374 – 7379]
Scheier, P.
– Bond-Selective H^- Ion Abstraction from Thymine
(C) 1647 – 1650 [1673 – 1676]
DOI: 10.1002/anie.200461739
Scheier, P. (C) 6941 – 6943 [7101 – 7103]
Scheins, S. (C) 3925 – 3928 [3993 – 3997]
Schenk, K. J. (C) 4957 – 4960 [5037 – 5040]
Scherer, G. G. (R) 2190 – 2209 [2228 – 2248]
Scherer, O. J. (C) 3755 – 3758 [3821 – 3825]
Scherf, U. (C) 1520 – 1525 [1544 – 1549]
Scheschkewitz, D.
– A Molecular Silicon Cluster with a "Naked" Vertex Atom
(C) 2954 – 2956 [3014 – 3016]
DOI: 10.1002/anie.200462730
Scheschkewitz, D. (C) 1658 – 1661 [1685 – 1688], 5651 – 5654 [5796 – 5799]
Schiene-Fischer, C. (C) 1408 – 1412 [1432 – 1437]
Schiestel, T. (C) 6906 – 6909 [7066 – 7069]
Schiffers, I. (H) 1758 – 1763 [1788 – 1793]
Schiffmann, R. (C) 3620 – 3623 [3686 – 3689]
Schildbach, D. (C) 3136 – 3139 [3196 – 3199]
Schindler, F. (C) 1520 – 1525 [1544 – 1549]
Schirmer, R. H.
– Dithiol Proteins as Guardians of the Intracellular Redox Milieu in Parasites: Old and New Drug Targets in Trypanosomes and

 © 2005 Wiley-VCH Verlag GmbH & Co. KGaA, Weinheim

Malaria-Causing Plasmodia
(R) 690 – 715 [698 – 724]
DOI: 10.1002/anie.200300639
Schlatter, D. (C) 4400 – 4404 [4474 – 4479]
Schlawe, D. (C) 4925 – 4929 [5005 – 5009]
Schlegel, A. (C) 4635 – 4638 [4711 – 4715]
Schleid, T. (C) 2103 – 2106 [2140 – 2143]
Schlenoff, J. B.
– Hydrophobic and Ultrahydrophobic Multilayer Thin Films from Perfluorinated Polyelectrolytes
(C) 782 – 785 [792 – 795]
DOI: 10.1002/anie.200461645
Schleyer, P. von R.
– Aromatic Boron Wheels with More than One Carbon Atom in the Center: C_2B_8, $C_3B_9^{3+}$, and $C_5B_{11}^{+}$
(C) 1078 – 1082 [1102 – 1106]
DOI: 10.1002/anie.200461970
Schlögl, R. (C) 4704 – 4707 [4782 – 4785], 5488 – 5492 [5624 – 5628]
Schlörb, C. (C) 2223 – 2225 [2263 – 2265]
Schlosser, M.
– The 2×3 Toolbox of Organometallic Methods for Regiochemically Exhaustive Functionalization
(R) 376 – 393 [380 – 398]
DOI: 10.1002/anie.200300645
Schmedt auf der Günne, J. (C) 7790 – 7793 [7968 – 7971]
Schmid, B. (C) 3578 – 3582 [3644 – 3648]
Schmid, M. (C) 917 – 920 [939 – 942]
Schmid, R. (C) 6237 – 6241 [6394 – 6397]
Schmidhammer, U. (C) 4623 – 4626 [4699 – 4703]
Schmidt, H.-G. (C) 5090 – 5093 [5220 – 5223], 7072 – 7074 [7234 – 7236]
Schmidt, L. D.
– Renewable Olefins from Biodiesel by Autothermal Reforming
(C) 302 – 305 [306 – 309]
DOI: 10.1002/anie.200460790
Schmidt, M. A. (C) 5447 – 5451 [5583 – 5587]
Schmidt, M. U.
– Molecular Mechanism of the Solid-State Fluorescence Behavior of the Organic Pigment Yellow 101 and Its Derivatives
(C) 7783 – 7786 [7961 – 7964]
DOI: 10.1002/anie.200501781
Schmidt, R. (C) 1195 – 1198 [1219 – 1223], 7887 – 7891 [8099 – 8104]
Schmidt, T. (C) 1184 – 1188 [1208 – 1212]
Schmidt-Mende, L. (C) 6413 – 6417 [6571 – 6575]
Schmidtmann, M. (C) 3857 – 3861 [3925 – 3929]
Schmitt, E. (C) 7630 – 7635 [7803 – 7808]
Schmitt, W.
– Supramolecular Coordination Assemblies of Dinuclear Fe^{III} Complexes
(C) 4187 – 4192 [4259 – 4264]
DOI: 10.1002/anie.200500516
– Thermolysis of a Hybrid Organic – Inorganic Supramolecular Coordination Assembly: Templating the Formation of Nanostructured Fibrous Materials and Carbon-Based Microcapsules
(C) 7048 – 7053 [7210 – 7215]
DOI: 10.1002/anie.200501748
Schmitz, S. (C) 5658 – 5661 [5803 – 5806]
Schmuck, C.
– Charge Interactions Do the Job: A Combined Statistical and Combinatorial Approach to Finding Artificial Receptors for Binding Tetrapeptides in Water
(C) 7208 – 7212 [7374 – 7379]
DOI: 10.1002/anie.200501812
Schmuki, P.
– High-Aspect-Ratio TiO_2 Nanotubes by Anodization of Titanium
(C) 2100 – 2102 [2136 – 2139]
DOI: 10.1002/anie.200462459
– Smooth Anodic TiO_2 Nanotubes
(C) 7463 – 7465 [7629 – 7632]
DOI: 10.1002/anie.200502781
Schmutz, M. (C) 3260 – 3264 [3324 – 3328]
Schnakenburg, G. (C) 5979 – 5985 [6133 – 6139]
Schneider, S. (C) 1860 – 1865 [1894 – 1899]
Schneider, W.-D. (C) 5334 – 5337 [5468 – 5471]
Schneider-Mergener, J. (R) 2852 – 2869 [2912 – 2930]
Schnell, I. (C) 2801 – 2805 [2862 – 2866]
Schnell, M. (C) 6311 – 6315 [6469 – 6473]
Schnepf, A.
– Subvalent Compounds Featuring Direct Metal – Metal Bonds: The Zn–Zn Bond in $[Cp^*_2Zn_2]$
(H) 3006 – 3008 [3066 – 3068]
DOI: 10.1002/anie.200500597
Schnick, W.
– $SrSi_6N_8$—A Reduced Nitridosilicate with a Si–Si Bond
(C) 567 – 570 [573 – 576]
DOI: 10.1002/anie.200461633
Schnöckel, H.
– $Al_{20}Cp^*_8X_{10}$ (X = Cl, Br): Snapshots of the Formation of Metalloid Clusters from Polyhedral Al_nX_m Molecules?
(C) 6956 – 6960 [7117 – 7121]
DOI: 10.1002/anie.200500671
– $Ga_{10}Br_{10}$(4-*tert*-Butylpyridine)$_{10}$: A Mixed-Valent Gallium(I) Subhalide as an Intermediate during the Formation of Elemental Gallium?
(C) 2973 – 2975 [3033 – 3036]
DOI: 10.1002/anie.200462075
– Mass Spectrometric Investigations of the Dissociation of $[C@W_6Cl_{17}]^-$ Ions in the Gas Phase
(C) 265 – 269 [270 – 274]
DOI: 10.1002/anie.200460972
– The Molecules AlO_2, $Al(O_2)_2$, and $Al(O_2)_3$: Experimental and Quantum-Chemical Investigations on the Oxidation of Aluminum Atoms
(C) 4261 – 4264 [4334 – 4336]
DOI: 10.1002/anie.200500512
Schöck, M. (C) 2270 – 2275 [2310 – 2315]
Schoeller, W. W. (C) 1700 – 1703 [1728 – 1731], 5497 – 5500 [5633 – 5636]
Scholz, R. (C) 6050 – 6054 [6204 – 6208]
Schönherr, H.
– Stretching and Rupturing Individual Supramolecular Polymer Chains by AFM
(C) 956 – 959 [978 – 981]
DOI: 10.1002/anie.200460963
Schoop, A. (C) 3140 – 3144 [3200 – 3204]
Schrader, Thomas
– A Color Sensor for Catecholamines
(C) 2265 – 2270 [2305 – 2310]
DOI: 10.1002/anie.200462702
Schrader, Tobias (C) 7901 – 7904 [8114 – 8118]
Schrader, W. Corrigendum: 506
Schrader, W.
– Atmosphere, a Chemical Reactor—Formation Pathways of Secondary Organic Aerosols
(H) 1444 – 1446 [1468 – 1470]
DOI: 10.1002/anie.200461611
Schreiber, S. L.
– Convergent Diversity-Oriented Synthesis of Small-Molecule Hybrids
(C) 2249 – 2252 [2289 – 2292]
DOI: 10.1002/anie.200462798
Schreier, W. J. (C) 7901 – 7904 [8114 – 8118]
Schreiner, P. R.
– 3,5,7,9-Tetraphenylhexaazaacridine: A Highly Stable, Weakly Antiaromatic Species with 16 π Electrons
(C) 5255 – 5259 [5389 – 5393]
DOI: 10.1002/anie.200500831
– The Protonation of Cubane Revisited
(C) 146 – 149 [148 – 152]
DOI: 10.1002/anie.200461042
Schröder, D.
– Generation of the Elusive *meta*-Benzoquinone in the Gas Phase
(C) 3092 – 3096 [3152 – 3156]
DOI: 10.1002/anie.200461783
– Stability of Gaseous Thallium Monofluoride as TlF^0, TlF^+, and TlF^{2+}
(C) 4254 – 4257 [4326 – 4330]
DOI: 10.1002/anie.200461334
Schröder, M. W. (C) 774 – 778 [784 – 788]
Schrodt, C. (C) 3932 – 3936 [4002 – 4005]
Schroeder, H. (C) 7635 – 7639 [7808 – 7812]
Schroer, T. (C) 1860 – 1865 [1894 – 1899]
Schröter, M.-K. (C) 6237 – 6241 [6394 – 6397]
Schröter, T. (C) 4249 – 4254 [4321 – 4326]
Schubert, W.-D. (H) 1298 – 1301 [1324 – 1327]
Schultz, P. G.
– A Small-Molecule Agonist of the Wnt Signaling Pathway
(C) 1987 – 1990 [2023 – 2026]
DOI: 10.1002/anie.200462552
– Expanding the Genetic Code
(R) 34 – 66 [34 – 68]
DOI: 10.1002/anie.200460627
Schulz, A.
– A Triazadiphosphole
(C) 7790 – 7793 [7968 – 7971]
DOI: 10.1002/anie.200502475
– Nitro(nitroso)cyanomethanides
(C) 3929 – 3932 [3998 – 4001]
DOI: 10.1002/anie.200500495
Schulz, S.
– Synthesis of Thermolabile Zinc – Pentel Compounds under Kinetically Controlled Reaction Conditions
(C) 5668 – 5670 [5813 – 5815]
DOI: 10.1002/anie.200500688
Schulz-Dobrick, M.
– European Conference on Solid-State Chemistry in Sheffield
(T) 7160 – 7162 [7322 – 7324]
DOI: 10.1002/anie.200503352
Schulzke, C. (C) 7072 – 7074 [7234 – 7236]
Schurig, V.
– Modified Linear Dextrins ("Acyclodextrins") as New Chiral Selectors for the Gas-Chromatographic Separation of Enantiomers
(C) 4092 – 4095 [4161 – 4164]
DOI: 10.1002/anie.200500509
Schürmann, M. (C) 245 – 249 [250 – 254]
Schüßeler, T. (C) 7718 – 7721 [7896 – 7899]
Schuster, R. (C) 139 – 142 [141 – 144]
Schüth, F.
– Quasi-Homogeneous Methanol Synthesis Over Highly Active Copper Nanoparticles
(C) 7978 – 7981 [8192 – 8195]
DOI: 10.1002/anie.200503169

 © 2005 Wiley-VCH Verlag GmbH & Co. KGaA, Weinheim

Schutkowski, M. (C) 1408 – 1412 [1432 – 1437]
Schütz, M. (C) 242 – 245 [246 – 249]
Schwabacher, A. W. (C) 4572 – 4574 [4648 – 4650]
Schwaiger, M. (C) 5247 – 5251 [5381 – 5386]
Schwalbe, H.
– Kinetics of Photoinduced RNA Refolding by Real-Time NMR Spectroscopy (C) 2600 – 2603 [2656 – 2659] DOI: 10.1002/anie.200462724
Schwalbe, H. (C) 820 – 822 [831 – 833], 2223 – 2225 [2263 – 2265]
Schwarz, H.
– Gas-Phase Catalysis by Atomic and Cluster Metal Ions: The Ultimate Single-Site Catalysts (R) 2336 – 2354 [2388 – 2406] DOI: 10.1002/anie.200461698
Schwarz, H. (C) 3092 – 3096 [3152 – 3156], 4254 – 4257 [4326 – 4330]
Schweiger, A.
– Asymmetric Spin Density Distribution in the Copper(II) Complex of N-Confused Tetraphenylporphyrin: A Multifrequency Continuous-Wave and Pulse EPR Study (C) 3301 – 3303 [3365 – 3367] DOI: 10.1002/anie.200500155
Scolaro, A. (C) 5433 – 5438 [5569 – 5574]
Scopelliti, R. (C) 1084 – 1088 [1108 – 1112], 2527 – 2531 [2583 – 2587], 5720 – 5725 [5866 – 5871]
Scott, B. L. (C) 2403 – 2406 [2455 – 2458]
Scott, L. T. (C) 7549 – 7553 [7721 – 7725]
Scott, N. M. (C) 2512 – 2515 [2568 – 2571], 5284 – 5288 [5418 – 5422]
Scott, R. T. W. (C) 6540 – 6543 [6698 – 6701]
Searle, M. S.
– Engineering Enhanced Protein Stability through β-Turn Optimization: Insights for the Design of Stable Peptide β-Hairpin Systems (C) 4939 – 4944 [5019 – 5024] DOI: 10.1002/anie.200500577
Seayad, A. M. (C) 7424 – 7427 [7590 – 7593]
Sebastian, M. (C) 1405 – 1408 [1429 – 1432]
Sebti, S. M. (C) 2704 – 2707 [2764 – 2767], 4903 – 4906 [4981 – 4984]
Secchi, A. (C) 278 – 281 [282 – 285], 2913 – 2916 [2973 – 2976]
Seeberger, P. H.
– Short De Novo Synthesis of Fully Functionalized Uronic Acid Monosaccharides (C) 7605 – 7607 [7777 – 7780] DOI: 10.1002/anie.200502742
– Total Synthesis of Antigen *Bacillus Anthracis* Tetrasaccharide—Creation of an Anthrax Vaccine Candidate (C) 6315 – 6318 [6474 – 6476] DOI: 10.1002/anie.200502615
Seelbinder, R. (C) 973 – 975 [995 – 997]
Seeler, F. (C) 7461 – 7463 [7627 – 7629]
Seeman, N. C. (C) 6074 – 6077 [6228 – 6231]
Segura, J.-M. (C) 4957 – 4960 [5037 – 5040]
Seiche, W. (C) 1640 – 1643 [1666 – 1669]
Seida, P. R. (C) 5830 – 5833 [5980 – 5983]
Seidel, D. (C) 83 – 87 [85 – 89]
Seidel, K. (C) 2089 – 2092 [2125 – 2129]
Seidel, R. (C) 7635 – 7639 [7808 – 7812]
Seidel, W. W.
– Can Acetylenedithiolate Act as a Tetradentate Bridging Ligand? (C) 7798 – 7800 [7976 – 7979] DOI: 10.1002/anie.200502489
Seifert, G. (C) 7616 – 7619 [7788 – 7792]
Seigal, B. A. (C) 4929 – 4932 [5009 – 5012]
Seiler, P. (C) 5074 – 5078 [5203 – 5207]
Seitsonen, A. P. (C) 917 – 920 [939 – 942]
Seitz, M. (C) 242 – 245 [246 – 249]
Sekiguchi, A.
– Hexakis(trimethylsilyl)tetrahedranyltetrahedrane (C) 5821 – 5823 [5971 – 5973] DOI: 10.1002/anie.200501605
– $SiGe_2$ and Ge_3: Cyclic Digermenes that Undergo Unexpected Ring-Expansion Reactions (C) 6378 – 6381 [6536 – 6539] DOI: 10.1002/anie.200501885
Sekiguchi, M. (C) 1944 – 1947 [1980 – 1983]
Sekiya, A. (C) 1128 – 1130 [1152 – 1154]
Selçuki, C. (C) 3548 – 3552 [3614 – 3618]
Sellergren, B.
– An Artificial Riboflavin Receptor Prepared by a Template Analogue Imprinting Strategy (C) 3902 – 3906 [3970 – 3974] DOI: 10.1002/anie.200500342
Sels, B. F. (H) 30 – 32 [30 – 32], (C) 310 – 313 [314 – 317]
Selva, M. (C) 4774 – 4777 [4852 – 4855]
Sempere-Culler, F. (C) 149 – 152 [152 – 155]
Sen, Avijit (C) 4528 – 4532 [4604 – 4608]
Sen, Ayusman
– Catalytic Nanomotors: Remote-Controlled Autonomous Movement of Striped Metallic Nanorods (C) 744 – 746 [754 – 756] DOI: 10.1002/anie.200461890
Senegas, J.-M. (C) 7954 – 7958 [8168 – 8172]
Senker, J. (C) 567 – 570 [573 – 576]
Sentman, A. C. (C) 4964 – 4968 [5044 – 5048]
Senyushkina, T. (C) 5635 – 5639 [5779 – 5783]
Seo, M. (C) 724 – 728 Corrigendum: 3799 [734 – 738 Corrigendum: 3865]
Seo, M. S. (C) 4235 – 4239 [4307 – 4311]
Seo, S. H. (C) 6913 – 6915 [7073 – 7075]
Seo, Y. S. (C) 910 – 913 [932 – 935]
Seo, Y.-T. (C) 7749 – 7752 [7927 – 7930]
Seomoon, D. (C) 1840 – 1843 [1874 – 1877]
Serpe, M. J. (C) 1333 – 1336 [1357 – 1360]
Serrano, J. L.
– Metal-Containing Nanostructured Materials through In Situ Polymerization of Reactive Metallomesogens (H) 6618 – 6621 [6776 – 6779] DOI: 10.1002/anie.200501880
Serrano-Gómez, D. (C) 296 – 298 [300 – 302]
Serrano-Ruiz, M. (C) 2568 – 2572 [2624 – 2628]
Serratrice, G. (C) 2580 – 2582 [2636 – 2638]
Sessler, J. L.
– Anion-Induced Synthesis and Combinatorial Selection of Polypyrrolic Macrocycles (C) 7386 – 7390 [7552 – 7556] DOI: 10.1002/anie.200502393
– Calix[4]pyrrole: An Old yet New Ion-Pair Receptor (C) 2537 – 2542 [2593 – 2598] DOI: 10.1002/anie.200462945
– Reductive N Alkylation of Cyclo[8]pyrroles (C) 83 – 87 [85 – 89] DOI: 10.1002/anie.200461801
– Synthesis, Anion-Binding Properties, and In Vitro Anticancer Activity of Prodigiosin Analogues (C) 5989 – 5992 [6143 – 6146] DOI: 10.1002/anie.200501740
Sessoli, R.
– Phosphonate Ligands Stabilize Mixed-Valent $\{Mn^{III}_{20-x}Mn^{II}_{x}\}$ Clusters with Large Spin and Coercivity (C) 5044 – 5048 [5172 – 5176] DOI: 10.1002/anie.200501265
Sessoli, R. (C) 5817 – 5821 [5967 – 5971]
Severin, K.
– Atom-Transfer Radical Reactions under Mild Conditions with $[\{RuCl_2(1,3,5\text{-}C_6H_3iPr_3)\}_2]$ and PCy_3 as the Catalyst Precursors (C) 1084 – 1088 [1108 – 1112] DOI: 10.1002/anie.200462037
– Dynamic Combinatorial Libraries of Dye Complexes as Sensors (C) 7935 – 7938 [8149 – 8152] DOI: 10.1002/anie.200502827
Sevov, S. C.
– $[(Ni\text{-}Ni\text{-}Ni)@(Ge_9)_2]^{4-}$: A Linear Triatomic Nickel Filament Enclosed in a Dimer of Nine-Atom Germanium Clusters (C) 4026 – 4028 [4094 – 4096] DOI: 10.1002/anie.200500600
Sewald, N.
– Single-Molecule Experiments in Synthetic Biology: An Approach to the Affinity Ranking of DNA-Binding Peptides (C) 3921 – 3924 [3989 – 3993] DOI: 10.1002/anie.200500152
Seymour, L. W.
– Glycoviruses: Chemical Glycosylation Retargets Adenoviral Gene Transfer (C) 1057 – 1061 [1081 – 1085] DOI: 10.1002/anie.200461832
Sforza, S.
– Alternate Isotope-Coded Derivatization Assay: An Isotope Dilution Method Applied to the Quantification of Zearalenone in Maize Flour (C) 5126 – 5130 [5256 – 5260] DOI: 10.1002/anie.200500148
Sgarlata, V. (C) 3043 – 3047 [3103 – 3107]
Sgarzani, V. (C) 6576 – 6579 [6734 – 6737], 7975 – 7978 [8189 – 8192]
Shabat, D.
– Prodrug Activation Gated by a Molecular "OR" Logic Trigger (C) 4378 – 4381 [4452 – 4455] DOI: 10.1002/anie.200500842
– Single-Triggered Trimeric Prodrugs (C) 716 – 720 [726 – 730] DOI: 10.1002/anie.200461657
Shafirovich, V.
– Oxidation of Guanine and 8-oxo-7,8-Dihydroguanine by Carbonate Radical Anions: Insight from Oxygen-18 Labeling Experiments (C) 5057 – 5060 [5185 – 5188] DOI: 10.1002/anie.200500991
Shah, Samit (C) 1328 – 1332 [1352 – 1356]
Shah, Shilen (C) 6878 – 6881 [7038 – 7041]
Shaikhutdinov, S. K.
– Surface-Bonded Precursor Determines Particle Size Effects for Alkene Hydrogenation on Palladium (C) 629 – 631 [635 – 637] DOI: 10.1002/anie.200461614
Shaikhutdinov, S. K. (C) 7601 – 7605 [7773 – 7777]
Shair, M. D.
– Dynamic Kinetic Resolution during a Cascade Reaction on Substrates with Chiral All-Carbon Quaternary Centers

 © 2005 Wiley-VCH Verlag GmbH & Co. KGaA, Weinheim

(C) 2259 – 2261 [2299 – 2301]
DOI: 10.1002/anie.200462039
Shaju, K. M. (C) 6550 – 6553 [6708 – 6711]
Shamala, N.
– C_9 Helices and Ribbons in γ-Peptides: Crystal Structures of Gabapentin Oligomers
(C) 4972 – 4975 [5052 – 5055]
DOI: 10.1002/anie.200501055
Shames, A. (C) 4015 – 4018 [4083 – 4086]
Shamis, M. (C) 716 – 720 [726 – 730]
Shan, W. (C) 615 – 617 [621 – 623]
Shan, X. (C) 6871 – 6874 [7031 – 7034]
Shankland, K. (C) 7032 – 7035 [7194 – 7197]
Shanmugam, S. (C) 6560 – 6563 [6718 – 6721]
Shapiro, L. (C) 4015 – 4018 [4083 – 4086]
Shaporenko, A. (C) 6775 – 6778 [6933 – 6936]
Sharma, G. V. M.
– 9/11 Mixed Helices in α/β Peptides Derived from C-Linked Carbo-β-Amino Acid and L-Ala Repeats
(C) 5878 – 5882 [6028 – 6032]
DOI: 10.1002/anie.200501247
Sharon, O. (C) 588 – 591 [594 – 597]
Sharpless, K. B.
– "On Water": Unique Reactivity of Organic Compounds in Aqueous Suspension
(C) 3275 – 3279 [3339 – 3343]
DOI: 10.1002/anie.200462883
Sharpless, K. B. (C) 116 – 120 [118 – 122]
Shaw, W. (C) 3578 – 3582 [3644 – 3648]
Shay, D. T. (C) 1508 – 1510 [1532 – 1534]
Shchukin, D. G.
– Gas-Filled Polyelectrolyte Capsules
(C) 3310 – 3314 [3375 – 3379]
DOI: 10.1002/anie.200462889
Sheehan, S. M. (C) 2259 – 2261 [2299 – 2301]
Sheeney-Haj-Ichia, L. (C) 78 – 83 [80 – 85]
Shekhar, S. (C) 1371 – 1375 [1395 – 1399]
Sheldrick, G. M.
– The Antiviral Antibiotic Feglymycin: First Direct-Methods Solution of a 1000+ Equal-Atom Structure
(C) 1340 – 1342 [1364 – 1366]
DOI: 10.1002/anie.200461933
Shen, Q. (C) 1371 – 1375 [1395 – 1399]
Shen, W. (C) 5083 – 5087 [5213 – 5217]
Shenvi, R. A. (C) 3714 – 3717 [3780 – 3783]
Sheridan, R. M.
– Mutasynthesis of Rapamycin Analogues through the Manipulation of a Gene Governing Starter Unit Biosynthesis
(C) 4757 – 4760 [4835 – 4838]
DOI: 10.1002/anie.200462784
Sherratt, D. J. (C) 3057 – 3061 [3117 – 3121]
Sherrington, D. C.
– Transfer of Chirality from (−)-Sparteine Zinc(II) (Meth)acrylate Complexes to the Main Chains of Their (Meth)acrylate Polymer Derivatives
(C) 4804 – 4808 [4882 – 4886]
DOI: 10.1002/anie.200501308
Sherrington, D. C. (C) 68 – 72 [70 – 74]
Sherry, A. D.
– Selective Sensing of Zinc Ions with a PARACEST Contrast Agent
(C) 6920 – 6923 [7080 – 7083]
DOI: 10.1002/anie.200502173
Sheth, K. A. (C) 7450 – 7453 [7616 – 7619]
Shi, H. (C) 7132 – 7135 [7294 – 7297]
Shi, J.
– Stimuli-Responsive Controlled Drug Release from a Hollow Mesoporous Silica Sphere/Polyelectrolyte Multilayer Core – Shell Structure
(C) 5083 – 5087 [5213 – 5217]
DOI: 10.1002/anie.200501500
Shi, L. (C) 6362 – 6366 [6520 – 6524]
Shi, Q.-Z. (C) 3864 – 3867 [3932 – 3935]
Shi, W. (C) 6934 – 6937 [7094 – 7097]
Shi, Y. (C) 7053 – 7059 [7215 – 7221]
Shibasaki, M.
– Direct Catalytic Asymmetric Mannich-Type Reactions of *N*-(2-Hydroxyacetyl)-pyrrole as an Ester-Equivalent Donor
(C) 4365 – 4368 [4439 – 4442]
DOI: 10.1002/anie.200501180
– Enantio- and Diastereoselective Catalytic Mannich-Type Reaction of a Glycine Schiff Base Using a Chiral Two-Center Phase-Transfer Catalyst
(C) 4564 – 4567 [4640 – 4643]
DOI: 10.1002/anie.200500927
– Non-C_2-Symmetric, Chirally Economical, and Readily Tunable Linked-binols: Design and Application in a Direct Catalytic Asymmetric Mannich-Type Reaction
(C) 3470 – 3474 [3536 – 3540]
DOI: 10.1002/anie.200500425
Shibata, N.
– Highly Enantioselective Catalytic Fluorination and Chlorination Reactions of Carbonyl Compounds Capable of Two-Point Binding
(C) 4204 – 4207 [4276 – 4279]
DOI: 10.1002/anie.200501041
Shibuguchi, T. (C) 4564 – 4567 [4640 – 4643]
Shie, C.-R. (C) 1665 – 1668 [1693 – 1696]
Shields, C. E. (C) 6203 – 6207 [6359 – 6363]
Shigeyoshi, Y. (C) 4899 – 4903 [4977 – 4981]
Shimada, M. (C) 7598 – 7600 [7770 – 7772]
Shimazaki, Y. (C) 3744 – 3746 [3810 – 3812]
Shimizu, A. (C) 6564 – 6568 [6722 – 6726]
Shimizu, H. (C) 761 – 764 [771 – 774]
Shimizu, M. (R) 214 – 231 [218 – 234]
Shimizu, S. (C) 2225 – 2229 [2265 – 2269], 3726 – 3729 [3792 – 3795], 7244 – 7248 [7410 – 7414]
Shimon, L. J. W. (C) 1709 – 1711 [1737 – 1739]
Shin, C.-H. (C) 7427 – 7432 [7593 – 7598]
Shin, I.
– Fabrication of Chemical Microarrays by Efficient Immobilization of Hydrazide-Linked Substances on Epoxide-Coated Glass Surfaces
(C) 2881 – 2884 [2941 – 2944]
DOI: 10.1002/anie.200462720
Shin, Y. (C) 3578 – 3582 [3644 – 3648]
Shing, T. K. M.
– Total Synthesis of (−)-Samaderine Y from (*S*)-(+)-Carvone
(C) 7981 – 7984 [8195 – 8198]
DOI: 10.1002/anie.200502763
Shinkai, S.
– A Sensitive Colorimetric and Fluorescent Probe Based on a Polythiophene Derivative for the Detection of ATP
(C) 6371 – 6374 [6529 – 6532]
DOI: 10.1002/anie.200501823
– 1D Arrangement of Au Nanoparticles by the Helical Structure of Schizophyllan: A Unique Encounter of a Natural Product with Inorganic Compounds
(C) 2030 – 2033 [2066 – 2069]
DOI: 10.1002/anie.200462810
– Formation of [60]Fullerene Nanoclusters with Controlled Size and Morphology through the Aid of Supramolecular Rod – Coil Diblock Copolymers
(C) 1257 – 1261 [1283 – 1287]
DOI: 10.1002/anie.200461174
Shinohara, H.
– An Anomalous Endohedral Structure of Eu@C_{82} Metallofullerenes
(C) 4568 – 4571 [4644 – 4647]
DOI: 10.1002/anie.200500876
Shinokubo, H.
– Anthracene-Bridged Z-Shaped [26]Hexaphyrin(1.1.1.1.1.1.1) Dimer from the Regioselective Diels – Alder Reaction of a Hexaphyrin with Bis-*o*-xylylene Equivalents
(C) 932 – 935 [954 – 957]
DOI: 10.1002/anie.200462231
– Synthesis of Corrole Derivatives through Regioselective Ir-Catalyzed Direct Borylation
(C) 6763 – 6766 [6921 – 6924]
DOI: 10.1002/anie.200502335
– Synthesis of Medium- and Large-Sized Lactones in an Aqueous – Organic Biphasic System
(C) 2397 – 2400 [2449 – 2452]
DOI: 10.1002/anie.200462677
Shinokubo, H. (C) 6899 – 6901 [7059 – 7061]
Shintani, R. (C) 3909 – 3912 [3977 – 3980], 4611 – 4614 [4687 – 4690]
Shiomi, D. (C) 6564 – 6568 [6722 – 6726], 7277 – 7280 [7443 – 7446]
Shionoya, M.
– Quantitative Dynamic Interconversion between Ag^I-Mediated Capsule and Cage Complexes Accompanying Guest Encapsulation/Release
(C) 2727 – 2731 [2787 – 2791]
DOI: 10.1002/anie.200462394
Shirakawa, E.
– Easy Access to Aryl- and Heteroaryl-Annulated[*a*]carbazoles by the Indium-Catalyzed Reaction of 2-Arylindoles with Propargyl Ethers
(C) 1336 – 1340 [1360 – 1364]
DOI: 10.1002/anie.200462280
Shirakawa, S. (C) 625 – 628 [631 – 634], 1549 – 1551 [1573 – 1575]
Shiratani, T. (C) 4201 – 4204 [4273 – 4276]
Shiro, M. (C) 75 – 78 [77 – 80], 2727 – 2731 [2787 – 2791], 5838 – 5841 [5988 – 5991]
Shiromo, K. (C) 1948 – 1951 [1984 – 1987]
Shirshova, N. (C) 6004 – 6009 [6158 – 6163]
Shoji, H.
– Lattice Expansion of Clathrate Hydrates of Methane Mixtures and Natural Gas
(C) 6928 – 6931 [7088 – 7091]
DOI: 10.1002/anie.200501845
Shoji, M. (C) 3110 – 3115 [3170 – 3175], 4212 – 4215 [4284 – 4287]
Sholl, D. S.
– Enantiospecific Chemisorption of Small Molecules on Intrinsically Chiral Cu Surfaces
(C) 7761 – 7764 [7939 – 7942]
DOI: 10.1002/anie.200501655
Shova, S. (C) 7938 – 7942 [8152 – 8156]
Shui, J.-L. (C) 7085 – 7089 [7247 – 7251]
Shukla, A. D. (C) 3237 – 3240 [3301 – 3304]
Shum, W. W. (C) 3129 – 3132 [3189 – 3192]
Shustova, N. B. (C) 234 – 237 [238 – 241], 432 – 435 [436 – 439]
Si, R. (C) 3256 – 3260 [3320 – 3324]
Sicherl, F. (C) 2096 – 2099 [2133 – 2136]
Sicoli, G. (C) 4092 – 4095 [4161 – 4164]
Sidorov, L. N. (C) 432 – 435 [436 – 439]
Sieben, A. (C) 3623 – 3626 [3689 – 3693]
Sieber, A. (C) 4239 – 4242 [4311 – 4314]

 © 2005 Wiley-VCH Verlag GmbH & Co. KGaA, Weinheim

Siebert, W.
– Ruthenocene Analogues with a Novel C_5B_2 Ligand: (η^7-4-Borataborepine)(η^5-pentamethylcyclopentadienyl)ruthenium Complexes
(C) 632 – 634 [638 – 640]
DOI: 10.1002/anie.200461719
Siega, K. (C) 6214 – 6219 [6370 – 6375]
Siegbahn, P. E. M. (C) 2939 – 2941 [2999 – 3001]
Siegfried, M. J. (C) 3218 – 3223 [3282 – 3287]
Siegrist, T. (C) 2386 – 2390 [2438 – 2442]
Siemer, A. B. (C) 2441 – 2444 [2494 – 2497]
Sierka, M. (C) 3755 – 3758 [3821 – 3825], 4920 – 4924 [4999 – 5003]
Sigmon, G. (C) 2135 – 2139 [2173 – 2177]
Sijbesma, R. P.
– Chiral Amplification in the Transcription of Supramolecular Helicity into a Polymer Backbone
(C) 2275 – 2279 [2315 – 2319]
DOI: 10.1002/anie.200462347
Silivra, O. A. (C) 6399 – 6403 [6557 – 6561]
Sill, K. (C) 2420 – 2426 [2472 – 2478]
Silla, E. (C) 904 – 909 [926 – 931]
Silverman, S. K.
– Efficient One-Step Synthesis of Biologically Related Lariat RNAs by a Deoxyribozyme
(C) 5863 – 5866 [6013 – 6016]
DOI: 10.1002/anie.200501643
– Modulation of RNA Tertiary Folding by Incorporation of Caged Nucleotides
(C) 7305 – 7309 [7471 – 7475]
DOI: 10.1002/anie.200502928
Simizu, S. (C) 3559 – 3562 Corrigendum: 4282 [3625 – 3628 Corrigendum: 4354]
Simon, A.
– Cluster Disorder and Ordering Principles in Al-Stabilized "LaI"
(C) 3917 – 3921 [3985 – 3989]
DOI: 10.1002/anie.200500594
Simon, F.-X. (C) 3260 – 3264 [3324 – 3328]
Simon, Paul (C) 7616 – 7619 [7788 – 7792]
Simon, Philippe (C) 2764 – 2767 [2824 – 2827]
Simón-Manso, E. (C) 1125 – 1128 [1149 – 1152]
Simonsen, K. B. (C) 2694 – 2700 [2754 – 2760]
Simonutti, R. (C) 1816 – 1820 [1850 – 1854]
Simpson, E. R. (C) 4939 – 4944 [5019 – 5024]
Sinaÿ, P. (C) 1683 – 1687 [1711 – 1715]
Singh, H. B.
– Synthesis of a Metallophilic Metallamacrocycle: A $Hg^{II}\cdots Cu^{I}\cdots Hg^{II}\cdots Hg^{II}\cdots Cu^{I}\cdots Hg^{II}$ Interaction
(C) 1715 – 1717 [1743 – 1745]
DOI: 10.1002/anie.200462487
Singh, N. J. (C) 2899 – 2903 [2959 – 2963]
Singh, S. (C) 4907 – 4910 [4985 – 4988]
Sinha, A. K.
– Three-Dimensional Mesoporous Chromium Oxide: A Highly Efficient Material for the Elimination of Volatile Organic Compounds
(C) 271 – 273 [275 – 277]
DOI: 10.1002/anie.200461284
Sinha, S. (C) 1529 – 1532 [1553 – 1556]
Sinicropi, A. (C) 2390 – 2393 [2442 – 2445]
Sironi, A.
– Staggered to Eclipsed Conformational Rearrangement of $[Co_2(CO)_6(PPh_3)_2]$ in the Solid State: An X-ray Diffraction Study at High Pressure and Low Temperature
(C) 7736 – 7739 [7914 – 7917]
DOI: 10.1002/anie.200502241
Sisson, A. L. (C) 6878 – 6881 [7038 – 7041]
Sitzmann, H.
– Phenolate Complexes of Iron(II) in Different Spin States
(C) 2597 – 2599 [2653 – 2655]
DOI: 10.1002/anie.200462153
Skelton, B. W. (C) 3038 – 3043 [3098 – 3103]
Skoch, J. (C) 5452 – 5456 [5588 – 5592]
Skourski, Y. (C) 3306 – 3309 [3371 – 3374]
Skranc, W. (C) 4700 – 4704 [4778 – 4782]
Slater, B.
– Simulating the Dissolution and Growth of Zeolite Beta C
(C) 1213 – 1217 [1239 – 1243]
DOI: 10.1002/anie.200461545
Slater, B. (C) 6719 – 6723 [6877 – 6881]
Slawin, A. M. Z.
– Patterning through Controlled Submolecular Motion: Rotaxane-Based Switches and Logic Gates that Function in Solution and Polymer Films
(C) 3062 – 3067 [3122 – 3127]
DOI: 10.1002/anie.200500101
Slawin, A. M. Z. (C) 4557 – 4564 [4633 – 4640]
Slootweg, J. C. (C) 6579 – 6582 [6737 – 6740]
Slovokhotova, I. V. (C) 6848 – 6854 [7008 – 7014]
Smarsly, B.
– Liquid Inorganic – Organic Nanocomposites: Novel Electrolytes and Ferrofluids
(H) 3809 – 3811 [3876 – 3878]
DOI: 10.1002/anie.200500690
Smarsly, B. (C) 751 – 756 [761 – 766], 4589 – 4592 [4665 – 4668]
Smart, O. S. (C) 7778 – 7782 [7956 – 7960]
Smeenk, J. M. (C) 1968 – 1971 [2004 – 2007]
Smet, M. (C) 4731 – 4735 [4809 – 4813]
Smirnov, V. V. (C) 7273 – 7276 [7439 – 7442]
Smith, A. (C) 1057 – 1061 [1081 – 1085]
Smith, A. M. (C) 325 – 328 [329 – 332]
Smith, D. A. (C) 1965 – 1968 [2001 – 2004]
Smith, D. K.
– High-Affinity Multivalent DNA Binding by Using Low-Molecular-Weight Dendrons
(C) 2556 – 2559 [2612 – 2615]
DOI: 10.1002/anie.200500066
Smith, M. R. (C) 72 – 75 [74 – 77]
Smith, Mark D. (C) 6673 – 6677 [6831 – 6835]
Smith, Martin D. (C) 2732 – 2737 [2792 – 2797]
Smith, R. S. (C) 3578 – 3582 [3644 – 3648]
Smoot, J. T. (C) 7123 – 7126 [7285 – 7288]
Snaith, H. J.
– Ion-Coordinating Sensitizer in Solid-State Hybrid Solar Cells
(C) 6413 – 6417 [6571 – 6575]
DOI: 10.1002/anie.200502009
Snajdrova, R. (C) 3609 – 3613 [3675 – 3679]
Snapper, M. L.
– Intramolecular [2 + 2 + 1] Cycloadditions with (Cyclobutadiene)tricarbonyliron
(C) 4929 – 4932 [5009 – 5012]
DOI: 10.1002/anie.200501100
Snyder, S. A. (R) 1012 – 1044 Corrigendum: 2050 [1036 – 1069 Corrigendum: 2086]
Snyder, T. M. (C) 7379 – 7382 [7545 – 7548]
Soai, K.
– Asymmetric Amplification Using Chiral Cocrystals Formed from Achiral Organic Molecules by Asymmetric Autocatalysis
(C) 2774 – 2777 [2834 – 2837]
DOI: 10.1002/anie.200462963
Sodeoka, M.
– Catalytic Asymmetric Addition of β-Ketoesters to Various Imines by Using Chiral Palladium Complexes
(C) 1525 – 1529 [1549 – 1553]
DOI: 10.1002/anie.200462202
Soderholm, L. (C) 2135 – 2139 [2173 – 2177]
Soga, K. (C) 3861 – 3864 [3929 – 3932]
Sokolov, M. (C) 720 – 724 [730 – 734]
Sola, E. (C) 3267 – 3271 [3331 – 3335]
Solari, E. (C) 1084 – 1088 [1108 – 1112]
Solinas, M. (C) 2291 – 2295 [2331 – 2335]
Solomon, E. I.
– Comparison of Fe^{IV}=O Heme and Nonheme Species: Electronic Structures, Bonding, and Reactivities
(C) 2252 – 2255 [2292 – 2295]
DOI: 10.1002/anie.200462182
Soloviev, V. (C) 6928 – 6931 [7088 – 7091]
Soltani, O. (C) 1696 – 1699 [1724 – 1727]
Somei, H. (C) 1525 – 1529 [1549 – 1553]
Somfai, P.
– 1,3-Dipolar Cycloadditions of Carbonyl Ylides to Aldimines: A Three-Component Approach to *syn*-α-Hydroxy-β-amino Esters
(C) 3096 – 3099 [3156 – 3159]
DOI: 10.1002/anie.200500296
Somjing, R. (C) 1944 – 1947 [1980 – 1983]
Sommer, K. M. (C) 257 – 259 [262 – 264]
Son, S. U. (C) 7710 – 7715 [7888 – 7893]
Sonar, P. (C) 2447 – 2451 [2501 – 2505]
Song, A. (C) 4018 – 4021 [4086 – 4089]
Song, B. (C) 4731 – 4735 [4809 – 4813]
Song, M. (C) 7032 – 7035 [7194 – 7197]
Song, Y. (C) 6067 – 6074 [6221 – 6228]
Sorace, L. (C) 1876 – 1879 [1910 – 1913]
Sorensen, E. J.
– A Diels – Alder Macrocyclization Enables an Efficient Asymmetric Synthesis of the Antibacterial Natural Product Abyssomicin C
(C) 6533 – 6537 [6691 – 6695]
DOI: 10.1002/anie.200502119
– Protein-Reactive Natural Products
(R) 5788 – 5809 [5936 – 5958]
DOI: 10.1002/anie.200500900
Sörgel, T.
– European Conference on Solid-State Chemistry in Sheffield
(T) 7160 – 7162 [7322 – 7324]
DOI: 10.1002/anie.200503352
Soto, J. (C) 2918 – 2922 [2978 – 2982], 4405 – 4407 [4479 – 4482]
Soto, P. (C) 1065 – 1067 [1089 – 1091]
Soulard, M. (C) 5310 – 5313 [5444 – 5447]
Sour, A. (C) 1480 – 1484 [1504 – 1508]
Sozzani, P.
– Methane and Carbon Dioxide Storage in a Porous van der Waals Crystal
(C) 1816 – 1820 [1850 – 1854]
DOI: 10.1002/anie.200461704
Spaniol, T. P. (C) 7473 – 7477 [7640 – 7644]
Spannenberg, A. (C) 1184 – 1188 [1208 – 1212]
Spatz, J. H. (C) 7216 – 7219 [7382 – 7386]
Specker, E. (C) 3140 – 3144 [3200 – 3204]
Spek, A. L. (C) 3585 – 3587 [3651 – 3653], 4385 – 4388 [4459 – 4462], 6579 – 6582 [6737 – 6740]
Spencer, J. B.
– A Method for Trapping Intermediates of Polyketide Biosynthesis with a Nonhydrolyzable Malonyl-Coenzyme A Analogue

 © 2005 Wiley-VCH Verlag GmbH & Co. KGaA, Weinheim

(C) 7079 – 7082 [7241 – 7244]
DOI: 10.1002/anie.200501670
Spencer, J. B. (C) 7075 – 7078 [7237 – 7240]
Spengler, B. (C) 7635 – 7639 [7808 – 7812]
Spiess, H. W. (C) 4707 – 4712 [4785 – 4791]
Spiller, M. (C) 6766 – 6769 [6924 – 6927]
Spiteller, D. (C) 7079 – 7082 [7241 – 7244]
Spiteller, M. (C) 2957 – 2959 [3016 – 3019]
Spiteller, P. (C) 2957 – 2959 [3016 – 3019]
Spitz, R. (C) 2593 – 2596 [2649 – 2652]
Sprangers, R. (C) 3232 – 3237 [3296 – 3301]
Sprengers, J. W. (C) 2026 – 2029 [2062 – 2065]
Spring, D. R.
– Synthesis of Medium-Ring and Iodinated Biaryl Compounds by Organocuprate Oxidation
(C) 1870 – 1873 Corrigendum: 2471 [1904 – 1907 Corrigendum: 2525]
DOI: 10.1002/anie.200462642
Sreekumar, V. Corrigendum: 1907
Sridharan, V. (C) 7570 – 7574 [7742 – 7746]
Stacchiola, D. (C) 4572 – 4574 [4648 – 4650]
Stadelmann, P. A. (C) 4957 – 4960 [5037 – 5040]
Stadler, F. (C) 567 – 570 [573 – 576]
Stadler, F. L. (C) 6142 – 6145 [6298 – 6301]
Stahl, I. (C) 6750 – 6755 [6908 – 6913]
Stahl, J. (C) 6775 – 6778 [6933 – 6936]
Stahl, L.
– Synthesis and Solid-State Structure of a Metal Complex of a Diphosphineimine
(C) 3271 – 3275 [3335 – 3339]
DOI: 10.1002/anie.200462588
Stahl, S. S.
– Pd^{II} Complexes Possessing a Seven-Membered N-Heterocyclic Carbene Ligand
(C) 5269 – 5272 [5403 – 5406]
DOI: 10.1002/anie.200501522
Stalder, H. (T) 5364 – 5366 [5498 – 5500]
Stalke, D. (C) 250 – 253 [254 – 257], 6947 – 6951 [7107 – 7111]
Stambuli, J. P. (C) 1371 – 1375 [1395 – 1399]
Stamm, M. (C) 6391 – 6394 [6549 – 6552]
Stammler, A. (C) 7757 – 7761 [7935 – 7939]
Stammler, H.-G. (C) 6947 – 6951 [7107 – 7111]
Stamou, D. (C) 4957 – 4960 [5037 – 5040]
Stankic, S. (C) 4917 – 4920 [4996 – 4999]
Stark, C. B. W. (C) 7075 – 7078 [7237 – 7240]
Starke, K. (C) 7072 – 7074 [7234 – 7236]
Starr, D. E. (C) 7601 – 7605 [7773 – 7777]
Staunton, J. (C) 7075 – 7078 [7237 – 7240]
Stead, M. L. (C) 3456 – 3459 [3522 – 3525], 5729 – 5733 [5875 – 5879]
Stébé, M.-J. (C) 2580 – 2582 [2636 – 2638]
Stecker, F. (C) 257 – 259 [262 – 264]
Steed, J. W. (C) 944 – 946 [966 – 968]
Stefanelli, M. (C) 3047 – 3050 [3107 – 3110]
Steglich, W.
– Birnbaumin A and B: Two Unusual 1-Hydroxyindole Pigments from the "Flower Pot Parasol" *Leucocoprinus birnbaumii*
(C) 2957 – 2959 [3016 – 3019]
DOI: 10.1002/anie.200500082
Steigerwald, M. L. (C) 7390 – 7394 [7556 – 7560]
Stein, R. S. (C) 5729 – 5733 [5875 – 5879]
Steiner, A.
– Synthesis and Solid-State Structure of a Metal Complex of a Diphosphineimine
(C) 3271 – 3275 [3335 – 3339]
DOI: 10.1002/anie.200462588
Steiner, D. D. (C) 3706 – 3710 [3772 – 3776]
Steinke, T. (C) 2943 – 2946 [3003 – 3007]
Stellmaker, M. P. (C) 5038 – 5044 [5166 – 5172]
Stelzer, O. (C) 2291 – 2295 [2331 – 2335]
Stempfhuber, S. (C) 242 – 245 [246 – 249]
Stensgaard, I. (C) 2270 – 2275 [2310 – 2315]
Stephenson, G. R. (C) 1121 – 1125 [1145 – 1149]
Stephenson, M. J. (C) 3075 – 3078 [3135 – 3138]
Stepputat, M. (C) 262 – 265 [267 – 270]
Stern, C. L. (C) 7922 – 7925 [8136 – 8139]
Sterrer, M. (C) 4917 – 4920 [4996 – 4999]
Stevens, C. V.
– One-Pot Tandem 1,4 – 1,2-Addition of Phosphites to α,β-Unsaturated Imines for the Synthesis of Glutamic Acid Analogues
(C) 7407 – 7411 [7573 – 7577]
DOI: 10.1002/anie.200501830
Stevens, E. D. (C) 2512 – 2515 [2568 – 2571]
Stevens, M. S. P. (C) 325 – 328 [329 – 332]
Štíbr, B.
– Structural Dualism in the Zwitterionic 7-RR′NH-*nido*-7,8,9-$C_3B_8H_{10}$ Tricarbollide Series: An Example of Absolute Tautomerism
(C) 6222 – 6226 [6378 – 6382]
DOI: 10.1002/anie.200501018
Stihle, M. (C) 4400 – 4404 [4474 – 4479]
Stoccoro, S. (C) 6892 – 6895 [7052 – 7055]
Stock, N.
– A High-Throughput Investigation of the Role of pH, Temperature, Concentration, and Time on the Synthesis of Hybrid Inorganic – Organic Materials
(C) 7608 – 7611 [7780 – 7784]
DOI: 10.1002/anie.200501766
Stoddart, J. F.
– Donor – Acceptor Pretzelanes and a Cyclic Bis[2]catenane Homologue
(C) 3050 – 3055 [3110 – 3115]
DOI: 10.1002/anie.200500041
Stoddart, J. F. (C) 7035 – 7039 [7197 – 7201]
Stoeckli-Evans, H. (C) 2527 – 2531 [2583 – 2587]
Stohner, J. (C) 3623 – 3626 [3689 – 3693]
Stöhr, M.
– Controlling Molecular Assembly in Two Dimensions: The Concentration Dependence of Thermally Induced 2D Aggregation of Molecules on a Metal Surface
(C) 7394 – 7398 [7560 – 7564]
DOI: 10.1002/anie.200502316
Stoian, S. (C) 6871 – 6874 [7031 – 7034]
Stoltz, B. M.
– Deracemization of Quaternary Stereocenters by Pd-Catalyzed Enantioconvergent Decarboxylative Allylation of Racemic β-Ketoesters
(C) 6924 – 6927 [7084 – 7087]
DOI: 10.1002/anie.200502018
Stone, H. A. (C) 724 – 728 Corrigendum: 3799 [734 – 738 Corrigendum: 3865]
Stone, K. L. (C) 7273 – 7276 [7439 – 7442]
Stößer, G. (C) 2973 – 2975 [3033 – 3036], 4261 – 4264 [4334 – 4336]
Stradiotto, M.
– Coordinatively Unsaturated Cationic and Zwitterionic [Cp*Ru(κ^2-P,N)] Complexes: Ligand-Assisted Double-Geminal C–H Bond Activation and Reversible a-H Elimination at Ruthenium
(C) 3603 – 3606 [3669 – 3672]
DOI: 10.1002/anie.200500528
Straub, B. F.
– Origin of the High Activity of Second-Generation Grubbs Catalysts
(C) 5974 – 5978 [6129 – 6132]
DOI: 10.1002/anie.200501114
Strauss, H. (C) 5252 – 5255 [5386 – 5389]
Strauss, S. H.
– High-Temperature Synthesis of the Surprisingly Stable C_1-$C_{70}(CF_3)_{10}$ Isomer with a *para*[7]–*meta*–*para* Ribbon of Nine $C_6(CF_3)_2$ Edge-Sharing Hexagons
(C) 7984 – 7987 [8198 – 8201]
DOI: 10.1002/anie.200502419
Strauss, S. H. (C) 1846 – 1849 [1880 – 1883]
Strerath, M. (M) 7842 – 7849 [8052 – 8060]
Stride, J. (C) 2711 – 2715 [2771 – 2775]
Strohmann, C.
– A Highly Diastereomerically Enriched, Silyl-Substituted Alkyl Lithium, Configurationally Stable at Room Temperature
(C) 3136 – 3139 [3196 – 3199]
DOI: 10.1002/anie.200462141
Strömsdörfer, S. (C) 7896 – 7900 [8109 – 8113]
Strunk, J. (C) 2790 – 2794 [2850 – 2854]
Strunskus, T. (C) 1488 – 1491 [1512 – 1515]
Stubbings, W. (C) 6403 – 6406 [6561 – 6564]
Stucky, G. D.
– Single-Crystal Mesoporous Silica Ribbons
(C) 332 – 336 [336 – 340]
DOI: 10.1002/anie.200461296
Studer, A.
– Stable Reagents for the Generation of N-Centered Radicals: Hydroamination of Norbornene
(C) 4914 – 4917 [4993 – 4995]
DOI: 10.1002/anie.200463032
Studt, F. (C) 5639 – 5642 [5783 – 5787]
Stunnenberg, H. G. (C) 1968 – 1971 [2004 – 2007]
Stupp, S. I.
– One-Dimensional Assembly of Lipophilic Inorganic Nanoparticles Templated by Peptide-Based Nanofibers with Binding Functionalities
(C) 1833 – 1836 [1867 – 1870]
DOI: 10.1002/anie.200462142
Su, C.-C. (C) 6063 – 6067 [6217 – 6221]
Su, C.-Y. (C) 6673 – 6677 [6831 – 6835]
Su, D. S.
– Hierarchically Structured Carbon: Synthesis of Carbon Nanofibers Nested inside or Immobilized onto Modified Activated Carbon
(C) 5488 – 5492 [5624 – 5628]
DOI: 10.1002/anie.200500685
Su, L. (C) 2420 – 2426 [2472 – 2478]
Su, Q. (C) 1223 – 1225 [1249 – 1251]
Su, X. (C) 1870 – 1873 Corrigendum: 2471 [1904 – 1907 Corrigendum: 2525]
Su, Z.-M.
– Entangled Coordination Networks with Inherent Features of Polycatenation, Polythreading, and Polyknotting
(C) 5824 – 5827 [5974 – 5977]
DOI: 10.1002/anie.200501373
Subramanian, R. (C) 302 – 305 [306 – 309]
Sud, D. (C) 2019 – 2021 [2055 – 2057]
Suefuji, T. (C) 75 – 78 [77 – 80]
Sugai, T. (C) 4568 – 4571 [4644 – 4647]
Suggate, M. J. (H) 186 – 189 [190 – 193]
Sugimoto, N.
– Drastic Effect of a Single Base Difference between Human and *Tetrahymena* Telomere Sequences on Their Structures under Molecular Crowding Conditions
(C) 3740 – 3744 [3806 – 3810]
DOI: 10.1002/anie.200462667

 © 2005 Wiley-VCH Verlag GmbH & Co. KGaA, Weinheim

– Nucleic Acid with Guanidinium Modification Exhibits Efficient Cellular Uptake
(C) 6682 – 6685 [6840 – 6843]
DOI: 10.1002/anie.200500904
Sugino, H. (C) 6190 – 6193 [6346 – 6349]
Suginome, M.
– Palladium-Catalyzed Addition of Cyanoboranes to Alkynes: Regio- and Stereoselective Synthesis of α,β-Unsaturated β-Boryl Nitriles
(C) 2380 – 2382 [2432 – 2434]
DOI: 10.1002/anie.200462961
Sugita, M. (C) 2931 – 2935 [2991 – 2995]
Sugiura, K.-i. (C) 3240 – 3243 [3304 – 3307]
Sugiura, M. (M) 5176 – 5186 [5306 – 5317]
Suh, M. P.
– Redox-Active Porous Metal – Organic Framework Producing Silver Nanoparticles from Ag^{I} Ions at Room Temperature
(C) 1261 – 1265 [1287 – 1291]
DOI: 10.1002/anie.200461408
Suh, Y. (C) 4235 – 4239 [4307 – 4311]
Suhrada, C. P. (C) 3548 – 3552 [3614 – 3618]
Sui, X. (C) 5141 – 5144 [5271 – 5274]
Sui-Seng, C. (C) 7721 – 7725 [7899 – 7903]
Sukhorukov, G. B. (C) 3310 – 3314 [3375 – 3379]
Sumby, C. J. (C) 6395 – 6399 [6553 – 6557]
Summerer, D. (C) 4712 – 4715 [4791 – 4794]
Sun, A. (C) 1184 – 1188 [1208 – 1212]
Sun, B. (C) 2563 – 2568 [2619 – 2624]
Sun, B.-Y. (C) 4568 – 4571 [4644 – 4647]
Sun, C. (C) 2144 – 2148 [2182 – 2186]
Sun, D. (C) 5133 – 5136 [5263 – 5266]
Sun, G. (C) 4197 – 4201 [4269 – 4273]
Sun, J. (C) 3845 – 3848 [3913 – 3916]
Sun, L. Corrigendum: 506
Sun, L.-D.
– Single-Crystalline Iron Oxide Nanotubes
(C) 4328 – 4333 [4402 – 4407]
DOI: 10.1002/anie.200463038
Sun, Q. (C) 123 – 126 [125 – 128]
Sun, S. (C) 4735 – 4739 [4813 – 4817]
Sun, W.-Y.
– Copper(II) and Zinc(II) Complexes Can Fix Atmospheric Carbon Dioxide
(C) 4352 – 4355 [4426 – 4429]
DOI: 10.1002/anie.200500587
Sun, X. (C) 4933 – 4935 [5013 – 5015]
Sun, X.-W. (C) 3443 – 3447 [3509 – 3513], 3447 – 3452 [3513 – 3518]
Sun, X.-Z. (C) 3079 – 3082 [3139 – 3142]
Sun, Y. (C) 747 – 750 [757 – 760]
Sun, Y.-Q. (C) 5814 – 5817 [5964 – 5967]
Sundén, H. (C) 4877 – 4880 [4955 – 4958]
Sundholm, D.
– Sphere Currents of Buckminsterfullerene
(C) 1843 – 1846 [1877 – 1880]
DOI: 10.1002/anie.200462348
Sundin, A. (C) 5110 – 5112 [5240 – 5242]
Sunley, G. J. (C) 6755 – 6758 [6913 – 6916]
Sunoj, R. B. (C) 5655 – 5658 [5800 – 5803]
Suresh, E. (C) 7752 – 7757 [7930 – 7935]
Surry, D. S. (C) 1870 – 1873 Corrigendum: 2471 [1904 – 1907 Corrigendum: 2525]
Suslick, K. S.
– Molecular Recognition and Discrimination of Amines with a Colorimetric Array
(C) 4528 – 4532 [4604 – 4608]
DOI: 10.1002/anie.200500939
Süßner, M. (C) 6885 – 6888 [7045 – 7048]
Sutherland, J. D.
– Expeditious, Potentially Primordial, Aminoacylation of Nucleotides
(C) 6731 – 6734 [6889 – 6892]
DOI: 10.1002/anie.200501591
Suzuki, Keisuke
– Regio- and Stereocontrolled Total Synthesis of Benanomicin B
(C) 3871 – 3874 [3939 – 3942]
DOI: 10.1002/anie.200501210
Suzuki, Kenichirou (C) 271 – 273 [275 – 277]
Suzuki, Y. (C) 4536 – 4538 [4612 – 4614]
Swager, T. M.
– In Vivo Optical Imaging of Amyloid Aggregates in Brain: Design of Fluorescent Markers
(C) 5452 – 5456 [5588 – 5592]
DOI: 10.1002/anie.200500845
Sweigart, D. A.
– Lithium Alkoxide $\{Li_4O_4\}$ Cubanes Bridged by Rhodium – Quinonoid Organometalloligands
(C) 7710 – 7715 [7888 – 7893]
DOI: 10.1002/anie.200503050
Swenson, D. C. (C) 3569 – 3572 [3635 – 3638]
Switek, K. A. (C) 6410 – 6413 [6568 – 6571]
Switzer, C.
– A Purine-like Nickel(II) Base Pair for DNA
(C) 1529 – 1532 [1553 – 1556]
DOI: 10.1002/anie.200462047
Synowsky, S. A. (C) 5052 – 5057 [5180 – 5185]
Szeimies, G. (C) 3925 – 3928 [3993 – 3997]
Szu, P.-h. (C) 6742 – 6746 [6900 – 6904]
Szwak, M. (C) 5079 – 5082 [5207 – 5211]
Szymanski, S.
– ^{1}J(C,H) Couplings to the Individual Protons in a Methyl Group: Evidence of the Methyl Protons' Engagement in Hydrogen Bonds
(C) 1230 – 1232 [1256 – 1258]
DOI: 10.1002/anie.200461383

Tabata, H. (C) 4536 – 4538 [4612 – 4614]
Tachibana, Y. (C) 571 – 575 [577 – 581]
Tacke, R.
– A Zwitterionic Spirocyclic Pentacoordinate Silicon Compound Synthesized in Water by Si–O and Si–C Bond Cleavage
(C) 5292 – 5295 [5426 – 5429]
DOI: 10.1002/anie.200501164
Tadano, G. (C) 5094 – 5097 [5224 – 5227]
Taghavi, S. (C) 2715 – 2719 [2775 – 2779]
Taguchi, T. (C) 1121 – 1125 [1145 – 1149]
Tajima, T. (C) 4760 – 4763 [4838 – 4841]
Takahashi, H. (C) 4536 – 4538 [4612 – 4614]
Takahashi, Kazuyuki (C) 6508 – 6512 [6666 – 6670]
Takahashi, Keita (C) 7136 – 7138 [7298 – 7300]
Takahashi, N. (C) 6928 – 6931 [7088 – 7091]
Takai, J. (C) 3055 – 3057 [3115 – 3117]
Takai, K. (C) 4204 – 4207 [4276 – 4279]
Takaishi, S. (C) 3240 – 3243 [3304 – 3307]
Takamatsu, H. (C) 2708 – 2711 [2768 – 2771]
Takanishi, Y. (C) 1948 – 1951 [1984 – 1987]
Takaoka, K. (C) 2151 – 2154 [2189 – 2192]
Takata, M. (C) 920 – 923 [942 – 945], 4568 – 4571 [4644 – 4647], 4899 – 4903 [4977 – 4981]
Takáts, Z. (C) 913 – 916 [935 – 938], 7094 – 7097 [7256 – 7259]
Takatsuka, K.
– Methyl Group Rotation Driven by Proton Transfer through a Long-Range Chemical Interaction
(C) 1237 – 1240 [1263 – 1266]
DOI: 10.1002/anie.200461459
Takaya, K. (C) 571 – 575 [577 – 581]
Takeda, A. (C) 6149 – 6151 [6305 – 6307]
Takeda, N. (C) 3717 – 3720 [3783 – 3786]
Takeda, S. (C) 292 – 295 [296 – 299]
Takemoto, Y.
– Enantioselective Michael Addition to α,β-Unsaturated Imides Catalyzed by a Bifunctional Organocatalyst
(C) 4032 – 4035 [4100 – 4103]
DOI: 10.1002/anie.200500459
Takenaka, S.
– A Pyrene-Labeled G-Quadruplex Oligonucleotide as a Fluorescent Probe for Potassium Ion Detection in Biological Applications
(C) 5067 – 5070 [5195 – 5198]
DOI: 10.1002/anie.200501506
Takeuchi, M. (C) 6371 – 6374 [6529 – 6532]
Takeya, S.
– Lattice Expansion of Clathrate Hydrates of Methane Mixtures and Natural Gas
(C) 6928 – 6931 [7088 – 7091]
DOI: 10.1002/anie.200501845
Takezoe, H.
– Finite Enantiomeric Excess Nucleated in an Achiral Banana Mesogen by Chiral Alignment Surfaces
(C) 1948 – 1951 [1984 – 1987]
DOI: 10.1002/anie.200461881
Takimoto, A. (C) 2534 – 2537 [2590 – 2593]
Takizawa, K. (C) 3240 – 3243 [3304 – 3307]
Takui, T.
– Spin Transfer and Solvato-/Thermochromism Induced by Intramolecular Electron Transfer in a Purely Organic Open-Shell System
(C) 7277 – 7280 [7443 – 7446]
DOI: 10.1002/anie.200502180
Takui, T. (C) 6564 – 6568 [6722 – 6726]
Takwa, M. (C) 4582 – 4585 [4658 – 4661]
Talbot, A. C. (C) 5433 – 5438 [5569 – 5574]
Talmard, C. (C) 3459 – 3462 [3525 – 3528]
Tamiya, M. (C) 3871 – 3874 [3939 – 3942]
Tamura, M. (C) 1128 – 1130 [1152 – 1154]
Tan, W.
– Direct Synthesis of an Oligonucleotide – Poly(phenylene ethynylene) Conjugate with a Precise One-to-One Molecular Ratio
(C) 2572 – 2576 [2628 – 2632]
DOI: 10.1002/anie.200462431
Tanabe, M. (C) 5886 – 5890 [6036 – 6040]
Tanaka, A. (C) 7059 – 7062 [7221 – 7224]
Tanaka, D. (C) 2700 – 2704 [2760 – 2764]
Tanaka, H. (C) 4164 – 4168 [4236 – 4240]
Tanaka, Ken
– Rhodium-Catalyzed Regio- and Enantioselective Intermolecular [4 + 2] Carbocyclization of 4-Alkynals with *N*,*N*-Dialkyl Acrylamides
(C) 7260 – 7263 [7426 – 7429]
DOI: 10.1002/anie.200502380
Tanaka, Koji
– Electrochemical Hydrogenation of $[Ru(bpy)_2(napy\text{-}\kappa N)(CO)]^{2+}$: Inhibition of Reductive Ru–CO Bond Cleavage by a Ruthenacycle

 © 2005 Wiley-VCH Verlag GmbH & Co. KGaA, Weinheim

(C) 2229 – 2232 [2269 – 2272]
DOI: 10.1002/anie.200462486
– Reversible Hydride Generation and Release from the Ligand of [Ru(pbn)(bpy)$_2$](PF$_6$)$_2$ Driven by a pbn-Localized Redox Reaction
(C) 5891 – 5894 [6041 – 6044]
DOI: 10.1002/anie.200500760
Tanaka, Masanobu (C) 5821 – 5823 [5971 – 5973]
Tanaka, Masato
– Helical Folding in a Helical Channel: Chiroptical Transcription of Helical Information through Chiral Wrapping
(C) 7301 – 7304 [7467 – 7470]
DOI: 10.1002/anie.200502073
Tanaka, R. (C) 4884 – 4888 [4962 – 4966]
Tanaka, S. (C) 1730 – 1732 [1758 – 1760]
Tanaka, Tetsuaki
– Bromoallenes as Allyl Dication Equivalents in the Absence of Palladium(0): Synthesis of Bicyclic Sulfamides by Tandem Cyclization of Bromoallenes
(C) 1513 – 1517 [1537 – 1541]
DOI: 10.1002/anie.200462557
– Palladium-Catalyzed Tandem Cyclization of Bromoenynes through Aromatic C–H Bond Functionalization
(C) 5103 – 5106 [5233 – 5236]
DOI: 10.1002/anie.200500159
– Thermal Intramolecular [2 + 2] Cycloaddition of Allenenes and Allenynes: Diastereoselective Access to Bicyclic Nitrogen Heterocycles
(C) 5113 – 5115 [5243 – 5245]
DOI: 10.1002/anie.200501413
Tanaka, Tomoyuki (C) 7059 – 7062 [7221 – 7224]
Tanaka, Toshihiro (C) 7233 – 7236 [7399 – 7402]
Tanaka, Toshiki
– High Thermal Stability Imparted by a Designed Tandem Arg – Trp Stretch in an α-Helical Coiled Coil
(C) 6180 – 6183 [6336 – 6339]
DOI: 10.1002/anie.200500806
Tanaka, Yasuo (C) 3726 – 3729 [3792 – 3795]
Tanaka, Yasutaka
– The Structural and Functional Roles of Rhodium(II) – Rhodium(II) Dimers in Multinuclear Ruthenium(II) Complexes
(C) 4881 – 4884 [4959 – 4962]
DOI: 10.1002/anie.200500392
Tanaka, Yoshie (C) 3867 – 3870 [3935 – 3938]
Tananaev, I. G. (C) 1134 – 1136 [1158 – 1160]
Tang, C.
– Cerium Phosphate Nanotubes: Synthesis, Valence State, and Optical Properties
(C) 576 – 579 [582 – 585]
DOI: 10.1002/anie.200461171
Tang, C. (C) 7929 – 7932 [8143 – 8146], 7932 – 7935 [8146 – 8149]
Tang, H.-Z. (C) 7298 – 7301 [7464 – 7467]
Tang, L. (C) 105 – 108 [107 – 110]
Tang, M. (C) 6067 – 6074 [6221 – 6228]
Tang, R. (C) 3698 – 3702 [3764 – 3768]
Tang, T.
– Synthesis of Multiwalled Carbon Nanotubes by Catalytic Combustion of Polypropylene
(C) 1517 – 1520 [1541 – 1544]
DOI: 10.1002/anie.200461506
Tang, Weihua (C) 7771 – 7775 [7949 – 7953]
Tang, Wenjun (C) 3874 – 3879 [3942 – 3947]
Tang, Y.
– Enrichment of Low-Abundance Peptides and Proteins on Zeolite Nanocrystals for Direct MALDI-TOF MS Analysis
(C) 615 – 617 [621 – 623]
DOI: 10.1002/anie.200460741
Tangirala, R. (C) 2420 – 2426 [2472 – 2478]
Tani, F. (C) 1836 – 1840 [1870 – 1874], 3744 – 3746 [3810 – 3812]
Tani, M. (C) 2586 – 2588 [2642 – 2644]
Tani, S. (C) 7254 – 7257 [7420 – 7423]
Taniguchi, R. (C) 2225 – 2229 [2265 – 2269]
Tanino, K. (C) 1532 – 1536 [1556 – 1560], 5094 – 5097 [5224 – 5227]
Tanner, H. R. (C) 5433 – 5438 [5569 – 5574]
Tantillo, D. J.
– Proton Sandwiches: Nonclassical Carbocations with Tetracoordinate Protons
(C) 2719 – 2723 [2779 – 2783]
DOI: 10.1002/anie.200461915
Taoufik, M.
– Development of Tungsten-Based Heterogeneous Alkane Metathesis Catalysts Through a Structure – Activity Relationship
(C) 6755 – 6758 [6913 – 6916]
DOI: 10.1002/anie.200501382
Tapu, D. (C) 7240 – 7244 [7406 – 7410]
Taran, F.
– Sandwich Immunoassay as a High-Throughput Screening Method for Cross-Coupling Reactions
(C) 6863 – 6866 [7023 – 7026]
DOI: 10.1002/anie.200501641
Tárraga, A. (C) 1977 – 1981 [2013 – 2017]
Taton, T. A.
– Core/Shell Gold Nanoparticles by Self-Assembly and Crosslinking of Micellar, Block-Copolymer Shells
(C) 409 – 412 [413 – 416]
DOI: 10.1002/anie.200461119
Tauer, K. (C) 6004 – 6009 [6158 – 6163]
Tavassoli, A. (C) 2760 – 2763 [2820 – 2823]
Taveira, L. (C) 7463 – 7465 [7629 – 7632]
Taylor, A. M. (C) 4073 – 4075 [4141 – 4143]
Taylor, M. S. (C) 6700 – 6704 [6858 – 6862]
Teat, S. J. (C) 2235 – 2237 [2275 – 2277], 5044 – 5048 [5172 – 5176], 6496 – 6500 [6654 – 6658]
Teixidor, F. (C) 2220 – 2222 [2260 – 2262]
Tejel, C.
– Dimetallic Dioxygen Activation Leading to a Doubly Oxygen-Bridged Dirhodium Complex
(C) 3267 – 3271 [3331 – 3335]
DOI: 10.1002/anie.200463073
Telfer, S. G. (C) 2527 – 2531 [2583 – 2587]
Tenne, R.
– Preparation and Structural Characterization of Stable Cs$_2$O Closed-Cage Structures
(C) 4169 – 4172 [4241 – 4244]
DOI: 10.1002/anie.200500356
Tenori, L. (C) 6341 – 6344 [6499 – 6502]
Teo, S. (C) 7560 – 7564 [7732 – 7736]
Tepper, E. Corrigendum: 6099
Terai, H. (C) 6931 – 6933 [7091 – 7093]
Terasaki, O.
– Structure Elucidation of the Highly Active Titanosilicate Catalyst Ti-YNU-1
(C) 6719 – 6723 [6877 – 6881]
DOI: 10.1002/anie.200501939
Terasaki, O. (C) 5317 – 5322 [5451 – 5456]
Terazono, Y. (C) 7591 – 7594 [7763 – 7766]
Tereshko, V. (C) 3852 – 3856 [3920 – 3924]
Tero-Kubota, S. (C) 3591 – 3594 [3657 – 3660]
Terreno, E. (C) 1813 – 1815 [1847 – 1849], 5513 – 5515 [5649 – 5651]
Teutloff, C. (C) 5314 – 5317 [5448 – 5451]
Thallapally, P. K. (C) 3848 – 3851 [3916 – 3919], 5733 – 5736 [5879 – 5882]
Thampi, K. R. (C) 1388 – 1392 [1412 – 1416]
Thanawala, M. S. (C) 2386 – 2390 [2438 – 2442]
Thang, S. H. (C) 4368 – 4372 [4442 – 4446]
Thayer, D. A. (C) 4596 – 4599 [4672 – 4675]
Thelakkat, M. (C) 5740 – 5744 [5886 – 5890]
Theopold, K. H.
– Intramolecular C–H Activation by an Open-Shell Cobalt(III) Imido Complex
(C) 1508 – 1510 [1532 – 1534]
DOI: 10.1002/anie.200462529
Therese, H. A. (C) 262 – 265 [267 – 270]
Theyssen, N. (C) 1346 – 1349 [1370 – 1373]
Thiele, C. M.
– Scaling the Alignment of Small Organic Molecules in Substituted Polyglutamates by Variable-Angle Sample Spinning
(C) 2787 – 2790 [2847 – 2850]
DOI: 10.1002/anie.200461532
Thies, J. (C) 1968 – 1971 [2004 – 2007]
Thivolle-Cazat, J. (C) 6755 – 6758 [6913 – 6916]
Thiyagarajan, P. (C) 2420 – 2426 [2472 – 2478]
Thomann, R. (C) 429 – 432 [433 – 436]
Thomas, Fabrice
– An Unprecedented Bridging Phenoxyl Radical in Dicopper(II) Complexes: Evidence for an $S = 3/2$ Spin State
(C) 438 – 441 [442 – 445]
DOI: 10.1002/anie.200461462
Thomas, Florian (C) 5668 – 5670 [5813 – 5815]
Thomas, J. M.
– A Revolution in Electron Microscopy
(H) 5563 – 5566 [5699 – 5702]
DOI: 10.1002/anie.200501466
– Single-Site Heterogeneous Catalysts
(R) 6456 – 6482 [6614 – 6641]
DOI: 10.1002/anie.200462473
Thomas-Oates, J. E. (C) 1392 – 1395 [1416 – 1419]
Thompson, E. L. (C) 6746 – 6750 [6904 – 6908]
Thomson, D. W. (C) 1356 – 1360 [1380 – 1384]
Thomson, N. H. (C) 1965 – 1968 [2001 – 2004]
Thuilliez, J. (C) 2593 – 2596 [2649 – 2652]
Thünemann, A. F. (C) 5262 – 5265 [5397 – 5400]
Tian, Ge (C) 2563 – 2568 [2619 – 2624]
Tian, Guoxin (C) 6200 – 6203 [6356 – 6359]
Tian, H.
– A Half Adder Based on a Photochemically Driven [2]Rotaxane
(C) 5296 – 5299 [5430 – 5433]
DOI: 10.1002/anie.200501215
Tian, Y. (C) 3582 – 3585 [3648 – 3651], 4355 – 4358 [4429 – 4432], 6694 – 6696 [6852 – 6854]
Tian, Z.-Q.
– A Controllable Electrochemical Fabrication of Metallic Electrodes with a Nanometer/Angstrom-Sized Gap Using an Electric Double Layer as Feedback
(C) 1265 – 1268 [1291 – 1294]
DOI: 10.1002/anie.200461797
Tiddy, G. J. T. (C) 3243 – 3248 [3307 – 3312]
Tidwell, T. T.
– Catalytic Asymmetric Esterification of Ketenes
(H) 6812 – 6814 [6973 – 6975]
DOI: 10.1002/anie.200501849

 © 2005 Wiley-VCH Verlag GmbH & Co. KGaA, Weinheim

– The First Century of Ketenes (1905–2005): The Birth of a Versatile Family of Reactive Intermediates
(E) 5778–5785 [5926–5933]
DOI: 10.1002/anie.200500098
Tiemersma-Wegman, T. D. (C) 4209–4212 [4281–4284]
Tietze, L. F.
– Palladium-Catalyzed Enantioselective Domino Reaction for the Efficient Synthesis of Vitamin E
(C) 257–259 [262–264]
DOI: 10.1002/anie.200461629
Tikhov, M. S. (C) 3730–3732 [3796–3798]
Tilley, R. D.
– Water-Soluble Photoluminescent Silicon Quantum Dots
(C) 4550–4554 [4626–4630]
DOI: 10.1002/anie.200501256
Timco, G. A.
– Linking Rings through Diamines and Clusters: Exploring Synthetic Methods for Making Magnetic Quantum Gates
(C) 6496–6500 [6654–6658]
DOI: 10.1002/anie.200502505
Timmer, M. S. M. (C) 7605–7607 [7777–7780]
Timmins, P. L. (C) 1392–1395 [1416–1419]
Timmis, K. N. (C) 7553–7557 [7725–7729]
Timpe, O. (C) 5488–5492 [5624–5628]
Tinnefeld, P.
– Branching Out of Single-Molecule Fluorescence Spectroscopy: Challenges for Chemistry and Influence on Biology
(R) 2642–2671 [2698–2728]
DOI: 10.1002/anie.200300647
Tío, L. (C) 4618–4622 [4694–4698]
Tirrell, D. A. (C) 1968–1971 [2004–2007]
Tishkov, A. A. (C) 142–145 [145–148], 4623–4626 [4699–4703]
Tisserand, S. (C) 2008–2011 [2044–2047]
Tissler, A. (C) 6237–6241 [6394–6397]
Tkachenko, B. A. (C) 146–149 [148–152]
Toda, F.
– Control of Differential Inclusion Complexation in the Solid State by Seed Crystals
(C) 5097–5100 [5227–5230]
DOI: 10.1002/anie.200501364
Todea, A. M. (C) 3857–3861 [3925–3929]
Todesco, P. E. (C) 3285–3289 [3349–3353]
Toh, N. L. (C) 2237–2241 [2277–2281]
Tohma, H. (C) 6193–6196 [6349–6352]
Tohnai, N. (C) 7059–7062 [7221–7224]
Tojo, S. (C) 3591–3594 [3657–3660]
Tokitoh, N.
– Telluradistibirane and Telluradibismirane: Three-Membered Heterocycles of Heavier Main Group Elements
(C) 3717–3720 [3783–3786]
DOI: 10.1002/anie.200462122
Tokuda, O. (C) 3055–3057 [3115–3117]
Tokudome, H. (C) 1974–1977 [2010–2013]
Tokunaga, N. (C) 4224–4227 [4296–4299], 6700–6704 [6858–6862]
Tolman, W. B.
– Characterization of a Complex Comprising a $\{Cu_2(S_2)_2\}^{2+}$ Core: Bis(μ-S_2^{2-})dicopper(III) or Bis(μ-$S_2^{\cdot-}$)dicopper(II)?
(C) 7745–7748 [7923–7926]
DOI: 10.1002/anie.200503134
Toma, L. (C) 7757–7761 [7935–7939]
Tomás, M. (C) 4981–4983 [5061–5063], 6583–6585 [6741–6743]
Tominaga, M. (C) 2151–2154 [2189–2192]
Tomon, T. (C) 2229–2232 [2269–2272]
Tong, M.-L.
– Cu^{2+}-Mediated Dehydrogenative Coupling and Hydroxylation of an N-Heterocyclic Ligand: From Generation of a New Tetratopic Ligand to the Designed Assembly of Three-Dimensional Copper(I) Coordination Polymers
(C) 5471–5475 [5607–5611]
DOI: 10.1002/anie.200501753
Toniutti, M. (C) 6214–6219 [6370–6375]
Tooke, D. M. (C) 3585–3587 [3651–3653]
Toom, L. (C) 4729–4731 [4807–4809]
Toombes, G. E. S. (C) 1226–1229 [1252–1255]
Tor, Y.
– RNA-Selective Modification by a Platinum(II) Complex Conjugated to Amino- and Guanidinoglycosides
(C) 927–932 [949–954]
DOI: 10.1002/anie.200461182
Tor, Y. (C) 5329–5334 [5463–5468]
Torbeev, V. Yu. (C) 3226–3229 [3290–3293]
Torelli, S. (C) 438–441 [442–445]
Toriumi, K.
– A Neutral Mixed-Valent Conducting Polymer Formed by Electron Transfer between Metal d and Ligand π Orbitals
(C) 4164–4168 [4236–4240]
DOI: 10.1002/anie.200501189
Toriumi, K. (C) 2262–2265 [2302–2305]
Török, B.
– Highly Enantioselective Organocatalytic Hydroxyalkylation of Indoles with Ethyl Trifluoropyruvate
(C) 3086–3089 [3146–3149]
DOI: 10.1002/anie.200462877
Török, M. (C) 3086–3089 [3146–3149]
Torres, M. R. (C) 305–307 [309–311]
Torssell, S. (C) 3096–3099 [3156–3159]
Toru, T.
– Highly Enantioselective Catalytic Fluorination and Chlorination Reactions of Carbonyl Compounds Capable of Two-Point Binding
(C) 4204–4207 [4276–4279]
DOI: 10.1002/anie.200501041
Toshimitsu, A.
– Asymmetric Carboselenenylation Reaction of Alkenes with Aromatic Compounds
(C) 3588–3591 [3654–3657]
DOI: 10.1002/anie.200500573
Totani, K. (C) 7950–7954 [8164–8168]
Tóth, É.
– High Relaxivity Confined to a Small Molecular Space: A Metallostar-Based, Potential MRI Contrast Agent
(C) 1480–1484 [1504–1508]
DOI: 10.1002/anie.200461875
Touge, T. (C) 1546–1548 [1570–1572]
Toyota, A. (C) 1088–1092 [1112–1116]
Toyota, S. (C) 5097–5100 [5227–5230]
Trabolsi, A. (C) 5338–5341 [5472–5475]
Trapp, O. (C) 7978–7981 [8192–8195]
Trauner, D.
– Mining the Tetraene Manifold: Total Synthesis of Complex Pyrones from *Placobranchus ocellatus*
(C) 4602–4606 [4678–4682]
DOI: 10.1002/anie.200500488
Tregenna-Piggott, P.
– Anisotropic Hyperfine Interaction in the Manganese(III) Hexaaqua Ion
(C) 3613–3616 [3679–3682]
DOI: 10.1002/anie.200463084
Tremel, W.
– VS_2 Nanotubes Containing Organic-Amine Templates from the NT-VO_x Precursors and Reversible Copper Intercalation in NT-VS_2
(C) 262–265 [267–270]
DOI: 10.1002/anie.200461326
Tremmel, S.
– ^{13}C-Labeled Tyrosine Residues as Local IR Probes for Monitoring Conformational Changes in Peptides and Proteins
(C) 4631–4635 [4707–4711]
DOI: 10.1002/anie.200500547
Trewyn, B. G. (C) 5038–5044 [5166–5172]
Trieflinger, C. (C) 2288–2291 [2328–2331], 6943–6947 [7104–7107]
Trifonov, A. (C) 1636–1639 [1662–1666]
Troiani, A. (C) 462–465 [466–469]
Trokowski, R. (C) 6920–6923 [7080–7083]
Trolez, Y. (C) 7224–7226 [7390–7392]
Tronc, E. (C) 5691–5694 [5837–5840]
Troshin, P. A.
– Synthesis and Structure of the Highly Chlorinated [60]Fullerene $C_{60}Cl_{30}$ with a Drum-Shaped Carbon Cage
(C) 234–237 [238–241]
DOI: 10.1002/anie.200461531
Trost, B. M.
– Palladium-Catalyzed Asymmetric Allylation of Prochiral Nucleophiles: Synthesis of 3-Allyl-3-Aryl Oxindoles
(C) 308–310 [312–314]
DOI: 10.1002/anie.200460335
– Ruthenium-Catalyzed Reactions—A Treasure Trove of Atom-Economic Transformations
(R) 6630–6666 [6788–6825]
DOI: 10.1002/anie.200500136
Troyanov, S. I.
– A [70]Fullerene Chloride, $C_{70}Cl_{16}$, Obtained by the Attempted Bromination of C_{70} in $TiCl_4$
(C) 4215–4218 [4287–4290]
DOI: 10.1002/anie.200500476
– Preparation and Structural Characterization of Two Kinetically Stable Chlorofullerenes, $C_{60}Cl_{28}$ and $C_{60}Cl_{30}$
(C) 432–435 [436–439]
DOI: 10.1002/anie.200462139
– Synthesis and Structure of the Highly Chlorinated [60]Fullerene $C_{60}Cl_{30}$ with a Drum-Shaped Carbon Cage
(C) 234–237 [238–241]
DOI: 10.1002/anie.200461531
Tsai, H.-L. (C) 6063–6067 [6217–6221]
Tschirschwitz, S. (C) 2965–2969 [3025–3029]
Tseng, H.-R. (C) 7035–7039 [7197–7201]
Tshikhudo, T. R. (C) 2913–2916 [2973–2976]
Tsiperman, E. (C) 4015–4018 [4083–4086]
Tsipis, A. C. (C) 2407–2410 [2459–2462]
Tsipis, C. A.
– Reversible Transformation of Two Diphenylphosphanido Ligands into the Neutral Tetraphenyldiphosphane Ligand
(C) 2407–2410 [2459–2462]
DOI: 10.1002/anie.200462498
Tsitsilianis, C. (C) 284–287 [288–291]
Tsuchida, Y. (C) 6149–6151 [6305–6307]
Tsuchimoto, T.
– Easy Access to Aryl- and Heteroaryl-Annulated[*a*]carbazoles by the Indium-Catalyzed Reaction of 2-Arylindoles with Propargyl Ethers

 © 2005 Wiley-VCH Verlag GmbH & Co. KGaA, Weinheim

(C) 1336 – 1340 [1360 – 1364]
DOI: 10.1002/anie.200462280
Tsuchiya, H. (C) 2100 – 2102 [2136 – 2139], 7463 – 7465 [7629 – 7632]
Tsuchiya, T. (C) 3282 – 3285 [3346 – 3349], 7567 – 7570 [7739 – 7742]
Tsuda, A.
– Planar or Perpendicular? Conformational Preferences of π-Conjugated Metalloporphyrin Dimers and Trimers in Supramolecular Tubular Arrays
(C) 4884 – 4888 [4962 – 4966]
DOI: 10.1002/anie.200500887
Tsuji, I. (C) 3565 – 3568 [3631 – 3634]
Tsujii, K.
– Environmentally Stable Super Water-Repellent Poly(alkylpyrrole) Films
(C) 3453 – 3456 [3519 – 3522]
DOI: 10.1002/anie.200500266
– Rapid Swelling/Collapsing Behavior of Thermoresponsive Poly(*N*-isopropylacrylamide) Gel Containing Poly(2-(methacryloyloxy)decyl phosphate) Surfactant
(C) 1951 – 1954 [1987 – 1990]
DOI: 10.1002/anie.200462288
Tsukamoto, M. (C) 7287 – 7290 [7453 – 7456]
Tsumori, N. (C) 4338 – 4342 [4412 – 4416]
Tsung, C.-K. (C) 332 – 336 [336 – 340]
Tsurusaki, A. (C) 3909 – 3912 [3977 – 3980]
Tu, B. (C) 7053 – 7059 [7215 – 7221]
Tu, R. (C) 2925 – 2929 [2985 – 2989]
Tucker, J. H. R.
– Photorelease of an Organic Molecule in Solution: Light-Triggered Blockage of a Hydrogen-Bonding Receptor Site
(C) 1072 – 1075 [1096 – 1099]
DOI: 10.1002/anie.200461946
Tuczek, F.
– Energetics and Mechanism of a Room-Temperature Catalytic Process for Ammonia Synthesis (Schrock Cycle): Comparison with Biological Nitrogen Fixation
(C) 5639 – 5642 [5783 – 5787]
DOI: 10.1002/anie.200501485
Tüllmann, S. (C) 3617 – 3620 [3683 – 3686]
Tuma, C. (C) 4769 – 4771 [4847 – 4849]
Tumanskii, B. (C) 739 – 743 [749 – 753]
Tundo, P. (C) 4774 – 4777 [4852 – 4855]
Tuñón, I.
– Towards a Rational Design of Antibody Catalysts through Computational Chemistry
(C) 904 – 909 [926 – 931]
DOI: 10.1002/anie.200461325
Tuononen, H. M. (C) 4953 – 4956 [5033 – 5036]
Turberfield, A. J.
– Engineering a 2D Protein – DNA Crystal
(C) 3057 – 3061 [3117 – 3121]
DOI: 10.1002/anie.200463027
Turberfield, A. J. (C) 4358 – 4361 [4432 – 4435]
Tureček, F.
– Specific Generation of 1-Methylcytosine Radicals in the Gas Phase
(C) 6708 – 6711 [6866 – 6869]
DOI: 10.1002/anie.200502363
Turet, L. (C) 3462 – 3466 [3528 – 3532]
Turkyilmaz, S. (C) 6938 – 6940 [7098 – 7100]
Turner, S. S. (C) 292 – 295 [296 – 299]
Turro, N. J.
– Superoxidation of Bisretinoids
(C) 7097 – 7100 [7259 – 7262]
DOI: 10.1002/anie.200501346
Tysoe, W. T.
– Elucidation of the Reaction Mechanism for the Palladium-Catalyzed Synthesis of Vinyl Acetate
(C) 4572 – 4574 [4648 – 4650]
DOI: 10.1002/anie.200500782
Tzeng, Z.-H. (C) 1665 – 1668 [1693 – 1696]

Uang, B.-J. (C) 1665 – 1668 [1693 – 1696]
Uchida, T. (C) 6928 – 6931 [7088 – 7091]
Ueda, M. (C) 6190 – 6193 [6346 – 6349]
Uemura, K. (C) 5459 – 5464 [5595 – 5600]
Uemura, S. (C) 3588 – 3591 [3654 – 3657], 7715 – 7717 [7893 – 7895]
Ueng, C.-H. (C) 6063 – 6067 [6217 – 6221]
Uenishi, J.'i.
– Total Synthesis of (−)-Laulimalide: Pd-Catalyzed Stereospecific Ring Construction of the Substituted 3,6-Dihydro[2*H*]-pyran Units
(C) 2756 – 2760 [2816 – 2820]
DOI: 10.1002/anie.200500029
Uenoyama, Y. (C) 1075 – 1078 [1099 – 1102]
Uerdingen, M. (C) 4715 – 4719 [4795 – 4798]
Ueyama, N.
– Linear-to-Turn Conformational Switching Induced by Deprotonation of Unsymmetrically Linked Phenolic Oligoamides
(C) 969 – 972 [991 – 994]
DOI: 10.1002/anie.200461842
Ueyama, N. (C) 4352 – 4355 [4426 – 4429]
Ugo, R. (C) 7922 – 7925 [8136 – 8139]
Ui, M. (C) 6484 – 6487 [6642 – 6645]
Ulrich, G.
– Pyrromethene Dialkynyl Borane Complexes for "Cascatelle" Energy Transfer and Protein Labeling
(C) 3694 – 3698 [3760 – 3764]
DOI: 10.1002/anie.200500808
Uludağ, H.
– A Dendritic Tetra(bisphosphonic acid) for Improved Targeting of Proteins to Bone
(C) 3710 – 3714 [3776 – 3780]
DOI: 10.1002/anie.200500350
Umakoshi, K.
– Unusual Magnetic Properties of the Edge-Sharing Bioctahedral Dirhenium(IV) Complex of Pyridine-2-thiolate
(C) 720 – 724 [730 – 734]
DOI: 10.1002/anie.200460532
Umebayashi, N. (C) 1525 – 1529 [1549 – 1553]
Umebayashi, S. (C) 4164 – 4168 [4236 – 4240]
Un, S. (C) 1536 – 1540 [1560 – 1564]
Uno, H.
– A Doubly N-Fused Benzohexaphyrin and Its Rearrangement to a Fluorescent Macrocycle upon DDQ Oxidation
(C) 1856 – 1860 [1890 – 1894]
DOI: 10.1002/anie.200462815
Uno, T. (C) 3110 – 3115 [3170 – 3175]
Unosawa, A. (C) 5523 – 5526 [5659 – 5662]
Unverzagt, C.
– An Orthogonal Double-Linker Resin Facilitates the Efficient Solid-Phase Synthesis of Complex-Type N-Glycopeptide Thioesters Suitable for Native Chemical Ligation
(C) 1650 – 1654 [1677 – 1681]
DOI: 10.1002/anie.200461125
Uosaki, K.
– Photoconversion of a Redox-Active Self-Assembled Monolayer: In Situ Probing of Photoinduced CO Dissociation from a Triruthenium Cluster Center on Gold
(C) 416 – 419 [420 – 423]
DOI: 10.1002/anie.200460651
Urano, Y. (C) 5439 – 5441 [5575 – 5577]
Urban, V. (C) 2794 – 2797 [2855 – 2858]
Urbanos, F. A. (C) 305 – 307 [309 – 311]
Uruichi, M. (C) 6564 – 6568 [6722 – 6726]
Ushida, M. (C) 2922 – 2925 [2982 – 2985]
Ushiyama, H.
– Methyl Group Rotation Driven by Proton Transfer through a Long-Range Chemical Interaction
(C) 1237 – 1240 [1263 – 1266]
DOI: 10.1002/anie.200461459
Ustynyuk, Yu. A. (C) 7386 – 7390 [7552 – 7556]
Uttinger, K. (C) 3763 – 3766 [3829 – 3832]

Vaissermann, J. (C) 3072 – 3075 [3132 – 3135]
Valiyaveettil, S.
– Mimicking the Function of Eggshell Matrix Proteins: The Role of Multiplets of Charged Amino Acid Residues and Self-Assembly of Peptides in Biomineralization
(C) 5476 – 5479 [5612 – 5615]
DOI: 10.1002/anie.200500261
van Baal, I. (C) 5052 – 5057 [5180 – 5185]
van den Berg, M. W. E. (C) 7892 – 7896 [8104 – 8109]
van den Berg, T. A. (C) 584 – 587 [590 – 593]
van der Boom, M. E.
– Electrochemical Addressing of the Optical Properties of a Monolayer on a Transparent Conducting Substrate
(C) 3237 – 3240 [3301 – 3304]
DOI: 10.1002/anie.200461958
van der Lelie, D. (C) 2715 – 2719 [2775 – 2779]
van Dongen, J. L. J. (C) 5052 – 5057 [5180 – 5185]
van Donk, S. (C) 1360 – 1363 [1384 – 1387]
Van Dorsselaer, A.
– Supramolecular Click Chemistry with a Bisammonium-C_{60} Substrate and a Ditopic Crown Ether Host
(C) 5338 – 5341 [5472 – 5475]
DOI: 10.1002/anie.200501249
van Eikema Hommes, N. J. R. (C) 6033 – 6038 [6187 – 6192]
van Eldik, R.
– Transition-State Effects of Ionic Liquids in Substitution Reactions of Pt^{II} Complexes
(C) 6033 – 6038 [6187 – 6192]
DOI: 10.1002/anie.200501329
van Esch, J. H.
– Light-Driven Dynamic Pattern Formation
(C) 2373 – 2376 [2425 – 2428]
DOI: 10.1002/anie.200462500
van Hal, R. (C) 815 – 819 [826 – 830]

van Hest, J. C. M.
– Controlled Assembly of Macromolecular β-Sheet Fibrils
(C) 1968 – 1971 [2004 – 2007]
DOI: 10.1002/anie.200462415
van Koten, G.
– Hetero-Aggregate Compounds of Aryl and Alkyl Lithium Reagents: A Structurally Intriguing Aspect of Organolithium Chemistry
(M) 1448 – 1454 [1472 – 1478]
DOI: 10.1002/anie.200462103
van Leeuwen, P. W. N. M. (C) 4385 – 4388 [4459 – 4462]
van Maarseveen, J. H. (C) 7946 – 7950 [8160 – 8164]
Van Meenen, E. (C) 7407 – 7411 [7573 – 7577]
Van Noortwyk, K. A. (C) 1499 – 1504 [1523 – 1528]
van Rossum, B.-J.
– SOLARIA: A Protocol for Automated Cross-Peak Assignment and Structure Calculation for Solid-State Magic-Angle Spinning NMR Spectroscopy
(C) 6151 – 6154 [6307 – 6310]
DOI: 10.1002/anie.200501884
van Slageren, J. (C) 1876 – 1879 [1910 – 1913], 2103 – 2106 [2140 – 2143], 3857 – 3861 [3925 – 3929]
Van Voorhis, W. C. (C) 4903 – 4906 [4981 – 4984]
van Wüllen, C.
– Stability of Gaseous Thallium Monofluoride as TlF^0, TlF^+, and TlF^{2+}
(C) 4254 – 4257 [4326 – 4330]
DOI: 10.1002/anie.200461334
Vancso, G. J.
– Stretching and Rupturing Individual Supramolecular Polymer Chains by AFM
(C) 956 – 959 [978 – 981]
DOI: 10.1002/anie.200460963
Vandamme, T. F. (C) 2749 – 2752 [2809 – 2812]
Vandermeulen, G. W. M. (C) 7964 – 7968 [8178 – 8182]
Vankar, Y. D.
– The Synthesis of Hybrids of D-Galactose with 1-Deoxynojirimycin Analogues as Glycosidase Inhibitors
(C) 2001 – 2004 [2037 – 2040]
DOI: 10.1002/anie.200462413
Varga, P. (C) 917 – 920 [939 – 942]
Varki, A. (C) 2400 – 2403 [2452 – 2455]
Varughese, B. (C) 4539 – 4543 [4615 – 4619]
Varzatskii, O. A. (C) 3400 – 3402 [3466 – 3468]
Vasisht, S. K. (C) 7884 – 7887 [8096 – 8099]
Vasos, P. R. (C) 3089 – 3092 [3149 – 3152]
Vasudev, P. G. (C) 4972 – 4975 [5052 – 5055]
Vaupel, E.
– Arthur Eichengrün—Tribute to a Forgotten Chemist, Entrepreneur, and German Jew
(E) 3344 – 3355 [3408 – 3419]
DOI: 10.1002/anie.200462959
Vauzeilles, B.
– Dynamic Combinatorial Chemistry: Lysozyme Selects an Aromatic Motif That Mimics a Carbohydrate Residue
(C) 965 – 969 [987 – 991]
DOI: 10.1002/anie.200462150
Vázquez, M. (C) 4182 – 4187 [4254 – 4259]
Veciana, J.
– An Electroactive Nitrogen-Rich [4.4]Ferrocenophane Displaying Redox-Switchable Behavior: Selective Sensing, Complexation, and Decomplexation of Mg^{2+} ions
(C) 1977 – 1981 [2013 – 2017]
DOI: 10.1002/anie.200462521
– Magnetic Information Storage on Polymers by Using Patterned Single-Molecule Magnets
(C) 888 – 892 [910 – 914]
DOI: 10.1002/anie.200461554
Vedejs, E.
– Efficiency in Nonenzymatic Kinetic Resolution
(R) 3974 – 4001 [4040 – 4069]
DOI: 10.1002/anie.200460842
Vega, R. A. (C) 6013 – 6015 [6167 – 6169]
Veiros, L. F. (C) 4397 – 4400 [4471 – 4474]
Veith, M.
– Cubane-Like Li_4H_4 and $Li_3H_3Li(OH)$: Stabilized in Molecular Adducts with Alanes
(C) 5968 – 5971 [6122 – 6126]
DOI: 10.1002/anie.200501864
Veith, M. (C) 7884 – 7887 [8096 – 8099]
Velasco, M. D. (C) 1977 – 1981 [2013 – 2017]
Velonia, K.
– Single-Enzyme Kinetics of CALB-Catalyzed Hydrolysis
(C) 560 – 564 [566 – 570]
DOI: 10.1002/anie.200460625
Vemparala, S. (C) 6685 – 6689 [6843 – 6847]
Vénien-Bryan, C. (C) 3057 – 3061 [3117 – 3121]
Venkataramani, S. (C) 6306 – 6311 [6464 – 6469]
Venkatasubbaiah, K. (C) 5428 – 5433 [5564 – 5569]
Verberckmoes, A. (C) 1360 – 1363 [1384 – 1387]
Verdaguer, M. (C) 3072 – 3075 [3132 – 3135]
Verhaelen, C. (C) 477 – 480 [481 – 485], 4574 – 4578 [4650 – 4654]
Verkade, J. G.
– A Stable Structurally Characterized Phosphorus-Bound Isocyanide and Its Thermal and Catalyzed Isomerization to the Corresponding Cyanide
(C) 4960 – 4963 [5040 – 5043]
DOI: 10.1002/anie.200501401
– One-Pot Sequential N and C Arylations: An Efficient Methodology for the Synthesis of *trans* 4-*N*,*N*-Diaryl Aminostilbenes
(C) 3115 – 3118 [3175 – 3178]
DOI: 10.1002/anie.200462938
Verlinde, C. L. M. J. (C) 4903 – 4906 [4981 – 4984]
Verrelst, W. H. (C) 5687 – 5690 [5833 – 5836]
Versluijs-Helder, M. (C) 1360 – 1363 [1384 – 1387]
Vértesy, L. (C) 1340 – 1342 [1364 – 1366]
Verwée, A. (C) 7407 – 7411 [7573 – 7577]
Vibulbhan, B. (C) 7024 – 7028 [7186 – 7190]
Vicennati, P. (C) 6863 – 6866 [7023 – 7026]
Vicent, M. J.
– Polymer Therapeutics Designed for a Combination Therapy of Hormone-Dependent Cancer
(C) 4061 – 4066 [4129 – 4134]
DOI: 10.1002/anie.200462960
Vicente, J.
– Reactivity of *ortho*-Palladated Phenol Derivatives with Unsaturated Molecules: Insertion of Nitriles into a Late-Transition-Metal – Carbon Bond
(C) 6001 – 6004 [6155 – 6158]
DOI: 10.1002/anie.200501202
Vicente, M. G. H. (C) 3047 – 3050 [3107 – 3110]
Viciano, M. (C) 444 – 447 [448 – 451]
Vicinelli, V. (C) 4574 – 4578 [4650 – 4654]
Vidal-Gancedo, J. (C) 1977 – 1981 [2013 – 2017]
Vidal-Vanaclocha, F. (C) 2903 – 2907 [2963 – 2967]
Viezzoli, M. S. (C) 6341 – 6344 [6499 – 6502]
Vigara, L. (C) 6504 – 6508 [6662 – 6666]
Vigeland, B. (C) 1112 – 1115 [1136 – 1139]
Vigné, F. (C) 5279 – 5282 [5413 – 5416]
Vignola, N. (C) 108 – 110 [110 – 112]
Vignon, S. A. (C) 3050 – 3055 [3110 – 3115]
Vilar, R.
– Monoligated Palladium Species as Catalysts in Cross-Coupling Reactions
(M) 366 – 374 [370 – 378]
DOI: 10.1002/anie.200461189
Villaescusa, L. A. (C) 2918 – 2922 [2978 – 2982]
Villarreal, L. (C) 4618 – 4622 [4694 – 4698]
Villinger, A. (C) 7790 – 7793 [7968 – 7971]
Vimolratana, M. (C) 765 – 769 [775 – 779]
Viñas, C.
– Carbon Extrusion in 1,2-Dicarba-*closo*-dodecaboranes: Regioselective Boron Substitution in Ten-Vertex *closo*-Monocarbaborane Anions
(C) 2220 – 2222 [2260 – 2262]
DOI: 10.1002/anie.200462209
Vincent, S. P. (R) 192 – 212 [196 – 217]
Vinzelberg, H. (C) 6391 – 6394 [6549 – 6552]
Visser, T. (C) 1115 – 1118 [1139 – 1142]
Vittal, J. J.
– Topochemical Photodimerization in the Coordination Polymer $[\{(CF_3CO_2)(\mu\text{-}O_2CCH_3)Zn\}_2(\mu\text{-bpe})_2]_n$ through Single-Crystal to Single-Crystal Transformation
(C) 2237 – 2241 [2277 – 2281]
DOI: 10.1002/anie.200462673
Vivanco, S. (C) 2903 – 2907 [2963 – 2967]
Vivekanandan, S. (C) 5476 – 5479 [5612 – 5615], 6333 – 6337 [6491 – 6495]
Vodopyanov, K. (C) 2382 – 2385 [2434 – 2437]
Vogel, A. (C) 4192 – 4196 [4264 – 4268]
Vogel, H.
– Lipid-Coated Nanocrystals as Multifunctionalized Luminescent Scaffolds for Supramolecular Biological Assemblies
(C) 1388 – 1392 [1412 – 1416]
DOI: 10.1002/anie.200461491
– Synthesis of Nanoscopic Optical Fibers Using Lipid Membranes as Templates
(C) 4957 – 4960 [5037 – 5040]
DOI: 10.1002/anie.200500386
Vogel, P.
– Organosulfur Compounds: Electrophilic Reagents in Transition-Metal-Catalyzed Carbon – Carbon Bond-Forming Reactions
(M) 7674 – 7684 [7848 – 7859]
DOI: 10.1002/anie.200463007
Vögtle, F.
– Knotting and Threading of Molecules: Chemistry and Chirality of Molecular Knots and Their Assemblies
(R) 1456 – 1477 [1480 – 1501]
DOI: 10.1002/anie.200460312
– Tweezering the Core of a Dendrimer: A Photophysical and Electrochemical Study
(C) 4574 – 4578 [4650 – 4654]
DOI: 10.1002/anie.200501025
Vögtle, F. (C) 477 – 480 [481 – 485]
Voigt, B. (C) 4785 – 4790 [4863 – 4868]
Voith, M. (R) 1304 – 1325 [1330 – 1351]

 © 2005 Wiley-VCH Verlag GmbH & Co. KGaA, Weinheim

Voitl, T. (C) 778 – 782 [788 – 792]
Volkert, C. A. (C) 7048 – 7053 [7210 – 7215]
Volkmer, D.
– Morphosynthesis of Nacre-Type Laminated $CaCO_3$ Thin Films and Coatings (C) 639 – 644 [645 – 650] DOI: 10.1002/anie.200461386
Volksen, W. (C) 7574 – 7580 [7746 – 7752]
Vollet, J. (C) 6956 – 6960 [7117 – 7121]
Vollhardt, K. P. C. (C) 7114 – 7118 [7276 – 7280]
Voloshin, Y. Z.
– Tuning a Metal's Oxidation State: The Potential of Clathrochelate Systems (C) 3400 – 3402 [3466 – 3468] DOI: 10.1002/anie.200463070
von Ahsen, S. (C) 253 – 257 [258 – 261]
von Appen, J. (C) 1205 – 1210 [1230 – 1235], 7212 – 7215 [7379 – 7382]
von Berlepsch, H. (C) 5262 – 5265 [5397 – 5400]
von Kiedrowski, G.
– Systems Chemistry: Kinetic and Computational Analysis of a Nearly Exponential Organic Replicator (C) 6750 – 6755 [6908 – 6913] DOI: 10.1002/anie.200501527
von Schnering, H. G. (C) 265 – 269 [270 – 274]
Vorontsov, I. I. (C) 3400 – 3402 [3466 – 3468]
Vos, T. E. (C) 2416 – 2419 [2468 – 2471]
Vourloumis, D. (C) 2694 – 2700 [2754 – 2760]
Vrettou, M. (C) 4079 – 4083 [4147 – 4151]
Vu, H. (C) 5299 – 5303 [5433 – 5437]
Vukmirovic, M. B. (C) 2132 – 2135 [2170 – 2173]
Vukojević, S. (C) 7978 – 7981 [8192 – 8195]

Wabnitz, T. C. (C) 794 – 797 [804 – 807]
Wachtveitl, J. (C) 7783 – 7786 [7961 – 7964]
Wacker, R. (C) 7635 – 7639 [7808 – 7812]
Wada, A. (C) 5698 – 5701 [5844 – 5847]
Waelchli, M. (C) 3282 – 3285 [3346 – 3349]
Wagenknecht, H.-A.
– Real-Time Spectroscopic and Chemical Probing of Reductive Electron Transfer in DNA (C) 1636 – 1639 [1662 – 1666] DOI: 10.1002/anie.200462592
Wagner, A. (C) 6863 – 6866 [7023 – 7026]
Wagner, M. (C) 4975 – 4980 [5055 – 5060]
Wahl, B. (C) 7616 – 7619 [7788 – 7792]
Wahl, M. (C) 7394 – 7398 [7560 – 7564]
Wakabayashi, Y. (C) 1981 – 1983 [2017 – 2019]
Wakahara, T. (C) 3282 – 3285 [3346 – 3349], 7567 – 7570 [7739 – 7742]
Wakamiya, T. (C) 7040 – 7044 [7202 – 7206]
Wakeshima, M. (C) 720 – 724 [730 – 734]
Waldmann, H.
– Development and Biological Evaluation of Acyl Protein Thioesterase 1 (APT1) Inhibitors (C) 4975 – 4980 [5055 – 5060] DOI: 10.1002/anie.200462625
– Inhibitors of Protein Tyrosine Phosphatases: Next-Generation Drugs? (R) 3814 – 3839 [3880 – 3906] DOI: 10.1002/anie.200461517
Waldmann, O. (C) 4239 – 4242 [4311 – 4314]
Walji, A. M. (C) 1733 – 1735 [1761 – 1763]
Walker, D. B. (C) 4557 – 4564 [4633 – 4640]
Walker, G. S. (C) 3555 – 3558 [3621 – 3624]
Wall, D. (C) 2694 – 2700 [2754 – 2760]
Wallace, D. J.
– Relay Ring-Closing Metathesis—A Strategy for Achieving Reactivity and Selectivity in Metathesis Chemistry (H) 1912 – 1915 [1946 – 1949] DOI: 10.1002/anie.200462753
Wallasch, M. (C) 2597 – 2599 [2653 – 2655]
Wallez, G. (C) 5691 – 5694 [5837 – 5840]
Wallner, S. R. (C) 6381 – 6384 [6539 – 6542]
Walsh, B. (C) 7588 – 7591 [7760 – 7763]
Walsh, C. T.
– Protein Posttranslational Modifications: The Chemistry of Proteome Diversifications (R) 7342 – 7372 [7508 – 7539] DOI: 10.1002/anie.200501023
Walton, D. R. M. (C) 325 – 328 [329 – 332]
Walton, P. H.
– The First μ_6-Peroxide Transition-Metal Complex: $[Ni_8(L)_{12}(O_2)]^{2+}$ (C) 1392 – 1395 [1416 – 1419] DOI: 10.1002/anie.200461892
Wan, L.-J.
– Mass Production and High Photocatalytic Activity of ZnS Nanoporous Nanoparticles (C) 1269 – 1273 [1295 – 1299] DOI: 10.1002/anie.200462057
– Self-Assembled Vanadium Pentoxide (V_2O_5) Hollow Microspheres from Nanorods and Their Application in Lithium-Ion Batteries (C) 4391 – 4395 [4465 – 4469] DOI: 10.1002/anie.200500946
Wan, S. (C) 3485 – 3488 [3551 – 3554]
Wang, B. (C) 5471 – 5475 [5607 – 5611]
Wang, B.-B. (C) 6025 – 6029 [6179 – 6183]
Wang, C. M. (C) 3578 – 3582 [3644 – 3648]
Wang, Chengxin (C) 7414 – 7418 [7580 – 7584]
Wang, Chunjiang (C) 1687 – 1689 [1715 – 1717], 4933 – 4935 [5013 – 5015]
Wang, D.-H. (C) 7420 – 7424 [7586 – 7590]
Wang, Dayang
– Colloidally Stable Amphibious Nanocrystals Derived from Poly{[2-(dimethylamino)ethyl] Methacrylate} Capping (C) 1717 – 1720 [1745 – 1748] DOI: 10.1002/anie.200461023
– Decoration of Microspheres with Gold Nanodots—Giving Colloidal Spheres Valences (C) 7767 – 7770 [7945 – 7948] DOI: 10.1002/anie.200502117
Wang, Deyun (C) 6525 – 6529 [6683 – 6687]
Wang, Dunwei (C) 2925 – 2929 [2985 – 2989]
Wang, E.-B.
– Entangled Coordination Networks with Inherent Features of Polycatenation, Polythreading, and Polyknotting (C) 5824 – 5827 [5974 – 5977] DOI: 10.1002/anie.200501373
Wang, G.-M. (C) 6881 – 6884 [7041 – 7044]
Wang, H.-L. (C) 7574 – 7580 [7746 – 7752]
Wang, Haihui
– Perovskite Hollow-Fiber Membranes for the Production of Oxygen-Enriched Air (C) 6906 – 6909 [7066 – 7069] DOI: 10.1002/anie.200501914
Wang, Hui (C) 6934 – 6937 [7094 – 7097]
Wang, J.-Q. (C) 259 – 262 [264 – 267]
Wang, Jian (C) 1369 – 1371 [1393 – 1395]
Wang, Jianfang (C) 332 – 336 [336 – 340]
Wang, Ju (C) 4048 – 4052 [4116 – 4120]
Wang, L.-S.
– Experimental and Theoretical Investigation of the Electronic and Geometrical Structures of the Au_{32} Cluster (C) 7119 – 7123 [7281 – 7285] DOI: 10.1002/anie.200502795
– Intramolecular Rotation through Proton Transfer: $[Fe(\eta^5\text{-}C_5H_4CO_2^-)_2]$ versus $[(\eta^5\text{-}C_5H_4CO_2^-)Fe(\eta^5\text{-}C_5H_4CO_2H)]$ (C) 6022 – 6024 [6176 – 6178] DOI: 10.1002/anie.200501564
– Observation of d-Orbital Aromaticity (C) 7251 – 7254 [7417 – 7420] DOI: 10.1002/anie.200502678
– Observation of Weak C–H···O Hydrogen Bonding to Unactivated Alkanes (C) 4968 – 4972 [5048 – 5052] DOI: 10.1002/anie.200501349
Wang, L.-X. (C) 1118 – 1121 [1142 – 1145]
Wang, Lei (R) 34 – 66 [34 – 68]
Wang, Leyu (C) 6054 – 6057 [6208 – 6211]
Wang, Lun (C) 6054 – 6057 [6208 – 6211]
Wang, M. Corrigendum: 506
Wang, P. (C) 1679 – 1683 [1707 – 1711]
Wang, Q.-C. (C) 5296 – 5299 [5430 – 5433]
Wang, Qi (C) 5107 – 5110 [5237 – 5240]
Wang, Qian
– Self-Assembly and Cross-Linking of Bionanoparticles at Liquid – Liquid Interfaces (C) 2420 – 2426 [2472 – 2478] DOI: 10.1002/anie.200462653
Wang, Qian (C) 2215 – 2220 [2255 – 2260]
Wang, Qinfang (C) 7101 – 7103 [7263 – 7265]
Wang, R.-J. (C) 7742 – 7745 [7920 – 7923]
Wang, W.
– Direct, Highly Enantioselective Pyrrolidine Sulfonamide Catalyzed Michael Addition of Aldehydes to Nitrostyrenes (C) 1369 – 1371 [1393 – 1395] DOI: 10.1002/anie.200461959
Wang, W.-M. (C) 6888 – 6892 [7048 – 7052]
Wang, X.-B. (C) 4968 – 4972 [5048 – 5052], 6022 – 6024 [6176 – 6178]
Wang, X.-L. (C) 5824 – 5827 [5974 – 5977]
Wang, Xiang (C) 3067 – 3071 [3127 – 3131]
Wang, Xiaoyan (C) 615 – 617 [621 – 623]
Wang, Xingwang (C) 6362 – 6366 [6520 – 6524]
Wang, Xuefeng (C) 113 – 116 [115 – 118]
Wang, Xun (C) 2782 – 2785 [2842 – 2845], 6054 – 6057 [6208 – 6211]
Wang, Y.-Y.
– Self-Assembly of an Interlaced Triple-Stranded Molecular Braid with an Unprecedented Topology through Hydrogen-Bonding Interactions (C) 3864 – 3867 [3932 – 3935] DOI: 10.1002/anie.200500744
Wang, Yajun (C) 2888 – 2892 [2948 – 2952]
Wang, Yangming (C) 5863 – 5866 [6013 – 6016]
Wang, Yi (C) 105 – 108 [107 – 110]
Wang, Yuan
– Efficient Two-Photon-Sensitized Luminescence of a Europium(III) Complex (C) 747 – 750 [757 – 760] DOI: 10.1002/anie.200462382
Wang, Yuekui (C) 7616 – 7619 [7788 – 7792]
Wang, Z. L.
– Single-Crystal Dendritic Micro-Pines of Magnetic α-Fe_2O_3: Large-Scale Synthesis,

 © 2005 Wiley-VCH Verlag GmbH & Co. KGaA, Weinheim

Formation Mechanism, and Properties
(C) 4197 – 4201 [4269 – 4273]
DOI: 10.1002/anie.200500448
Wang, Zhaohui (C) 1247 – 1250 [1273 – 1276]
Wang, Zheming (C) 5841 – 5846 [5991 – 5996], 6508 – 6512 [6666 – 6670]
Wang, Zhen Corrigendum: 506
Wang, Zhenqiang (C) 2877 – 2880 [2937 – 2940]
Wang, Zhenxin (C) 2913 – 2916 [2973 – 2976]
Wang, Zhiqiang (C) 4731 – 4735 [4809 – 4813]
Ward, B. D. (C) 1668 – 1671 [1696 – 1699]
Ward, T. R.
– Tailoring the Active Site of Chemzymes by Using a Chemogenetic-Optimization Procedure: Towards Substrate-Specific Artificial Hydrogenases Based on the Biotin – Avidin Technology
(C) 7764 – 7767 [7942 – 7945]
DOI: 10.1002/anie.200502000
Warmuth, R.
– A "Through-Shell" Binding Isotope Effect
(C) 7107 – 7110 [7269 – 7272]
DOI: 10.1002/anie.200501840
– Fluorophenoxycarbene inside a Hemicarcerand: A Bottled Singlet Carbene
(C) 1994 – 1997 [2030 – 2033]
DOI: 10.1002/anie.200462633
Warner, J. H. (C) 4550 – 4554 [4626 – 4630]
Warren, J. E. (C) 7546 – 7549 [7718 – 7721]
Wartmann, M. (C) 756 – 761 [766 – 771], 7469 – 7473 [7636 – 7640]
Wascholowski, V. (R) 3186 – 3216 [3248 – 3280]
Washington, I. (C) 7097 – 7100 [7259 – 7262]
Wassenaar, J. (C) 2026 – 2029 [2062 – 2065]
Wasserscheid, P.
– Very Stable and Highly Regioselective Supported Ionic-Liquid-Phase (SILP) Catalysis: Continuous-Flow Fixed-Bed Hydroformylation of Propene
(C) 815 – 819 [826 – 830]
DOI: 10.1002/anie.200461534
Wasserscheid, P. (C) 6033 – 6038 [6187 – 6192]
Watanabe, M. (C) 4881 – 4884 [4959 – 4962]
Waterman, C. L. (C) 7079 – 7082 [7241 – 7244]
Waymouth, R. M.
– Latent, Thermally Activated Organic Catalysts for the On-Demand Living Polymerization of Lactide
(C) 4964 – 4968 [5044 – 5048]
DOI: 10.1002/anie.200500723
Weber, C. F. (C) 6033 – 6038 [6187 – 6192]
Weber, T. (C) 3917 – 3921 [3985 – 3989]
Wecker, P. (C) 6381 – 6384 [6539 – 6542]
Weckhuysen, B. M. (C) 1115 – 1118 [1139 – 1142]
Wedig, U. (C) 770 – 773 [780 – 783]
Wei, H.-Y. (C) 5841 – 5846 [5991 – 5996]
Wei, J. (C) 5275 – 5278 [5409 – 5412]
Wei, Yen
– A Dendron Based on Natural Amino Acids: Synthesis and Behavior as an Organogelator and Lyotropic Liquid Crystal
(C) 6025 – 6029 [6179 – 6183]
DOI: 10.1002/anie.200500359
Wei, Yen (C) 3845 – 3848 [3913 – 3916]
Wei, Yongge (C) 6902 – 6905 [7062 – 7065]
Wei, Yongli (C) 6067 – 6074 [6221 – 6228]
Wei, Z. (C) 751 – 756 [761 – 766]
Weibel, D. B. (C) 724 – 728 Corrigendum: 3799 [734 – 738 Corrigendum: 3865], 5682 – 5686 [5828 – 5832]
Weide, M. (C) 635 – 638 [641 – 645]
Weidemann, N. (C) 5979 – 5985 [6133 – 6139]
Weidenbruch, M.
– Molecules with a Genuine Si–Si Triple Bond and a Stable Derivative of $[SiH]^+$
(H) 514 – 516 [518 – 520]
DOI: 10.1002/anie.200462273
Weigand, J. J. (C) 3929 – 3932 [3998 – 4001], 7790 – 7793 [7968 – 7971]
Weihe, H.
– Anisotropic Hyperfine Interaction in the Manganese(III) Hexaaqua Ion
(C) 3613 – 3616 [3679 – 3682]
DOI: 10.1002/anie.200463084
Weinberg, G. (C) 5488 – 5492 [5624 – 5628]
Weingärtner, H.
– Supercritical Water as a Solvent
(R) 2672 – 2692 [2730 – 2752]
DOI: 10.1002/anie.200462468
Weininger, S. J.
– Controversy in Chemistry: How Do You Prove a Negative?—The Cases of Phlogiston and Cold Fusion
(E) 1916 – 1922 [1950 – 1956]
DOI: 10.1002/anie.200462084
Weis, R. (C) 4700 – 4704 [4778 – 4782]
Weiss, D. (C) 6775 – 6778 [6933 – 6936]
Weissbuch, I.
– Solvent Effect on Crystal Polymorphism: Why Addition of Methanol or Ethanol to Aqueous Solutions Induces the Precipitation of the Least Stable β Form of Glycine
(C) 3226 – 3229 [3290 – 3293]
DOI: 10.1002/anie.200500164
Weisser, M. (C) 265 – 269 [270 – 274]
Weissflog, W. (C) 774 – 778 [784 – 788]
Welch, E. J. (C) 2549 – 2553 [2605 – 2609]
Weller, A. S.
– Holding onto Lots of Hydrogen: A 12-Hydride Rhodium Cluster That Reversibly Adds Two Molecules of H_2
(C) 6875 – 6878 [7035 – 7038]
DOI: 10.1002/anie.200502221
Wen, T. B. (C) 7227 – 7230 [7393 – 7396]
Wen, X. (C) 3562 – 3565 [3628 – 3631]
Wen, X.-F. (C) 747 – 750 [757 – 760]
Wendt, K. U.
– Enzyme Mechanisms for Triterpene Cyclization: New Pieces of the Puzzle
(H) 3966 – 3971 [4032 – 4037]
DOI: 10.1002/anie.200500804
Weng, L.-H. (C) 259 – 262 [264 – 267]
Weng, Z. (C) 7560 – 7564 [7732 – 7736]
Wenter, P. (C) 2600 – 2603 [2656 – 2659]
Wenthold, P. G.
– Toward the Systematic Decomposition of Benzene
(H) 7170 – 7172 [7332 – 7334]
DOI: 10.1002/anie.200502644
Wernette, D. P. (C) 7290 – 7293 [7456 – 7459]
Wernsdorfer, W.
– Quantum Tunneling of Magnetization in Lanthanide Single-Molecule Magnets: Bis(phthalocyaninato)terbium and Bis(phthalocyaninato)dysprosium Anions
(C) 2931 – 2935 [2991 – 2995]
DOI: 10.1002/anie.200462638
Wernsdorfer, W. (C) 892 – 896 [914 – 918], 897 – 901 [919 – 923], 5044 – 5048 [5172 – 5176], 6496 – 6500 [6654 – 6658], 6540 – 6543 [6698 – 6701], 6678 – 6682 [6836 – 6840]
Werth, S. (C) 6906 – 6909 [7066 – 7069]
Werz, D. B. (C) 6315 – 6318 [6474 – 6476]
Wessig, P.
– 1,2-Chirality Transfer in the Synthesis of Cyclopropanes
(C) 6778 – 6781 [6936 – 6940]
DOI: 10.1002/anie.200501481
Wessjohann, L. A.
– Diversity Oriented One-Pot Synthesis of Complex Macrocycles: Very Large Steroid – Peptoid Hybrids from Multiple Multicomponent Reactions Including Bifunctional Building Blocks
(C) 4785 – 4790 [4863 – 4868]
DOI: 10.1002/anie.200500019
West, F. G.
– Unexpected Participation of an Unconjugated Olefin during Nazarov Cyclization of Bridged Bicyclic Dienones
(C) 6546 – 6549 [6704 – 6707]
DOI: 10.1002/anie.200501737
Westerhausen, M.
– Activation of a Zinc-Bound Ethyl Group by Formation of a Zn-C_{Et}-Ba Moiety and Crystal Structure of $[\{(Me_3Si)_2N\}Ba(thf)Zn_2(\mu\text{-}Et)(\mu_3\text{-}PSitBu_3)_2]_2$ with Bridging Ethyl Substituents
(C) 6234 – 6237 [6391 – 6393]
DOI: 10.1002/anie.200501899
– (*Z*)-Bis(alkylzinc)imido-1,2-di(2-pyridyl)-ethene: Intramolecular Stabilization of a Bis(alkylzinc)imide
(C) 96 – 98 [98 – 100]
DOI: 10.1002/anie.200461356
Westermann, B.
– Dihydroxyacetone in Amino Acid Catalyzed Mannich-Type Reactions
(C) 4077 – 4079 [4145 – 4147]
DOI: 10.1002/anie.200500297
Weston, C. J. (C) 7778 – 7782 [7956 – 7960]
Weyrauch, J. P. (C) 2798 – 2801 [2858 – 2861]
White, A. H. (C) 3038 – 3043 [3098 – 3103]
White, A. J. P. (C) 3432 – 3435 [3498 – 3501]
White, P. S. (C) 2377 – 2379 Corrigendum: 4660 [2429 – 2431 Corrigendum: 4735]
White, S. S. (C) 3747 – 3750 [3813 – 3816]
Whitehead, M. (C) 6909 – 6912 [7069 – 7072]
Whitehouse, C.
– Adsorption and Self-Assembly of Peptides on Mica Substrates
(C) 1965 – 1968 [2001 – 2004]
DOI: 10.1002/anie.200462160
Whiteker, G. T. (C) 5834 – 5838 [5984 – 5988]
Whitesides, G. M.
– Generation of Monodisperse Particles by Using Microfluidics: Control over Size, Shape, and Composition
(C) 724 – 728 Corrigendum: 3799 [734 – 738 Corrigendum: 3865]
DOI: 10.1002/anie.200462226
– Modeling the Anodic Half-Cell of a Low-Temperature Coal Fuel Cell
(C) 5682 – 5686 [5828 – 5832]
DOI: 10.1002/anie.200501192
Whitney, A. M. (C) 5736 – 5739 [5882 – 5885]
Whittell, G. R. (C) 1192 – 1194 [1217 – 1219], 1658 – 1661 [1685 – 1688]
Whitwood, A. C. (C) 1712 – 1714 [1740 – 1742]
Wibbeling, B. (C) 5492 – 5496 [5629 – 5632]
Wiberg, N.
– $Si_8(SitBu_3)_6$: A Hitherto Unknown Cluster Structure in Silicon Chemistry
(C) 7884 – 7887 [8096 – 8099]
DOI: 10.1002/anie.200501289
Wichard, T. (C) 158 – 161 [161 – 164]
Wieber, S. (C) 3932 – 3936 [4002 – 4005]
Wieckowski, S. (C) 6358 – 6362 [6516 – 6520]

 © 2005 Wiley-VCH Verlag GmbH & Co. KGaA, Weinheim

Wieghardt, K.
– The Geometric and Electronic Structure of [(cyclam-acetato)Fe(N)]$^{+}$: A Genuine Iron(v) Species with a Ground-State Spin $S = 1/2$
(C) 2908 – 2912 [2968 – 2972]
DOI: 10.1002/anie.200462368
Wiench, J. W. (C) 1826 – 1830 [1860 – 1864]
Wiesner, B. (C) 1195 – 1198 [1219 – 1223], 7887 – 7891 [8099 – 8104]
Wiesner, U.
– Direct Access to Bicontinuous Skeletal Inorganic Plumber's Nightmare Networks from Block Copolymers
(C) 1226 – 1229 [1252 – 1255]
DOI: 10.1002/anie.200461156
Wilcox, C. S.
– Solution-Phase Mixture Synthesis with Double-Separation Tagging: Double Demixing of a Single Mixture Provides a Stereoisomer Library of 16 Individual Murisolins
(C) 6938 – 6940 [7098 – 7100]
DOI: 10.1002/anie.200501989
Wiley, B. (C) 2154 – 2157 [2192 – 2195], 7913 – 7917 [8127 – 8131]
Wilking, S. D. (C) 3921 – 3924 [3989 – 3993]
Wilkinson, B. (C) 4757 – 4760 [4835 – 4838]
Wille, H. (C) 3057 – 3061 [3117 – 3121]
Willeke, M. (C) 3623 – 3626 [3689 – 3693]
Willging, J. (C) 7127 – 7131 [7289 – 7293]
Williams, D. R.
– Total Synthesis of (+)-Apiosporamide: Assignment of Relative and Absolute Configuration
(C) 6715 – 6718 [6873 – 6876]
DOI: 10.1002/anie.200502015
Williams, D. S. (C) 1984 – 1987 [2020 – 2023]
Williams, F. J. (C) 3730 – 3732 [3796 – 3798]
Williams, G. (C) 2109 – 2112 [2147 – 2150]
Williams, K. R. (C) 6712 – 6715 [6870 – 6873]
Williams, R. M.
– Synthesis of the Putative Structure of 7-Deoxycylindrospermopsin: C7 Oxygenation Is Not Required for the Inhibition of Protein Synthesis
(C) 3879 – 3881 [3947 – 3949]
DOI: 10.1002/anie.200500520
Willis, M. C.
– Palladium-Catalyzed Tandem Alkenyl and Aryl C–N Bond Formation: A Cascade N-Annulation Route to 1-Functionalized Indoles
(C) 403 – 406 [407 – 410]
DOI: 10.1002/anie.200461598
– The Direct Catalytic Enantioselective Synthesis of Protected Aryl β-Hydroxy-α-Amino Acids
(C) 1543 – 1545 [1567 – 1569]
DOI: 10.1002/anie.200462125
Willner, H.
– The SF_5O_x Radicals, $x = 0 – 3$
(C) 253 – 257 [258 – 261]
DOI: 10.1002/anie.200461235
Willner, I.
– Efficient Generation of Photocurrents by Using CdS/Carbon Nanotube Assemblies on Electrodes
(C) 78 – 83 [80 – 85]
DOI: 10.1002/anie.200461666
– Electrochemical Control of the Photocurrent Direction in Intercalated DNA/CdS Nanoparticle Systems
(C) 4554 – 4557 [4630 – 4633]
DOI: 10.1002/anie.200500830
– Hydrogen-Bonded CdS Nanoparticle Assemblies on Electrodes for Photoelectrochemical Applications
(C) 4010 – 4015 [4078 – 4083]
DOI: 10.1002/anie.200463055
– Switching of Directions of Bioelectrocatalytic Currents and Photocurrents at Electrode Surfaces by Using Hydrophobic Magnetic Nanoparticles
(C) 4791 – 4794 [4869 – 4872]
DOI: 10.1002/anie.200501126
Wilson, A. J. (C) 2275 – 2279 [2315 – 2319]
Wilson, C. (C) 6157 – 6162 [6313 – 6318]
Wilson, G. J. (C) 4368 – 4372 [4442 – 4446]
Winkler, J. D. (C) 6685 – 6689 [6843 – 6847]
Winkler, M. (C) 6306 – 6311 [6464 – 6469]
Winkler, R. (C) 4083 – 4087 [4152 – 4155]
Winnik, M. A.
– Gelation of Helical Polypeptide – Random Coil Diblock Copolymers by a Nanoribbon Mechanism
(C) 7964 – 7968 [8178 – 8182]
DOI: 10.1002/anie.200502809
Winpenny, R. E. P.
– Linking Rings through Diamines and Clusters: Exploring Synthetic Methods for Making Magnetic Quantum Gates
(C) 6496 – 6500 [6654 – 6658]
DOI: 10.1002/anie.200502505
– Phosphonate Ligands Stabilize Mixed-Valent $\{Mn^{III}_{20-x}Mn^{II}_{x}\}$ Clusters with Large Spin and Coercivity
(C) 5044 – 5048 [5172 – 5176]
DOI: 10.1002/anie.200501265
Wirsching, P. (C) 2144 – 2148 [2182 – 2186]
Wirth, T.
– Hypervalent Iodine Chemistry in Synthesis: Scope and New Directions
(M) 3656 – 3665 [3722 – 3731]
DOI: 10.1002/anie.200500115
Wirz, J. (C) 4073 – 4075 [4141 – 4143]
Wiseman, J. M. (C) 913 – 916 [935 – 938], 7094 – 7097 [7256 – 7259]
Wisner, J. A.
– [2]Pseudorotaxanes through Second-Sphere Coordination
(C) 1499 – 1504 [1523 – 1528]
DOI: 10.1002/anie.200462380
Wittenhagen, L. M. (C) 2542 – 2546 [2598 – 2602]
Wittmann, V.
– Orthogonally Protected Sugar Diamino Acids as Building Blocks for Linear and Branched Oligosaccharide Mimetics
(C) 2096 – 2099 [2133 – 2136]
DOI: 10.1002/anie.200462595
Wohlrab, S. (C) 4087 – 4092 [4156 – 4161]
Wöhrle, D.
– Macromolecular Metal Complexes: Materials for Various Applications
(T) 7500 – 7502 [7668 – 7670]
DOI: 10.1002/anie.200503544
Wojcik, J.
– ^{1}J(C,H) Couplings to the Individual Protons in a Methyl Group: Evidence of the Methyl Protons' Engagement in Hydrogen Bonds
(C) 1230 – 1232 [1256 – 1258]
DOI: 10.1002/anie.200461383
Wokaun, A.
– Nanoparticles in Energy Technology: Examples from Electrochemistry and Catalysis
(R) 2190 – 2209 [2228 – 2248]
DOI: 10.1002/anie.200460466
Wolf, M. (C) 3306 – 3309 [3371 – 3374]
Wolf, R. (C) 6241 – 6244 [6398 – 6401]
Wolfbeis, O. S. (C) 6775 – 6778 [6933 – 6936]
Wölfle, M. (C) 2798 – 2801 [2858 – 2861]
Wöll, C. (C) 1488 – 1491 [1512 – 1515], 2790 – 2794 [2850 – 2854]
Wolmershäuser, G. (C) 1715 – 1717 [1743 – 1745], 2597 – 2599 [2653 – 2655]
Wolschendorf, U. (C) 635 – 638 [641 – 645]
Wong, C.-H.
– A General Strategy toward S-Linked Glycopeptides
(C) 4596 – 4599 [4672 – 4675]
DOI: 10.1002/anie.200500090
– Dual Effect of Synthetic Aminoglycosides: Antibacterial Activity against *Bacillus anthracis* and Inhibition of Anthrax Lethal Factor
(C) 447 – 452 [451 – 456]
DOI: 10.1002/anie.200462003
– Selectfluor: Mechanistic Insight and Applications
(R) 192 – 212 [196 – 217]
DOI: 10.1002/anie.200400648
Wong, C.-H. (C) 116 – 120 [118 – 122]
Wong, J. K. Y. (C) 3062 – 3067 [3122 – 3127]
Wong, K.-L. (C) 3436 – 3439 [3502 – 3505]
Wong, K. M.-C. (C) 791 – 794 [801 – 804], 3107 – 3110 [3167 – 3170]
Wong, L.-L.
– The Heme Monooxygenase Cytochrome $P450_{cam}$ Can Be Engineered to Oxidize Ethane to Ethanol
(C) 4029 – 4032 [4097 – 4100]
DOI: 10.1002/anie.200462630
Wong, W.-T.
– Simultaneous Observation of Green Multiphoton Upconversion and Red and Blue NLO Processes from Polymeric Terbium(III) Complexes
(C) 3436 – 3439 [3502 – 3505]
DOI: 10.1002/anie.200500031
Woo, H.-K. (C) 4968 – 4972 [5048 – 5052], 6022 – 6024 [6176 – 6178]
Wood, K. C. (C) 6704 – 6708 [6862 – 6866]
Woodcock, T. (C) 3899 – 3901 [3967 – 3969]
Woodhall, T. (C) 2109 – 2112 [2147 – 2150]
Woodrum, N. L. (C) 3690 – 3694 [3756 – 3760]
Woods, A. D.
– Quadruple Deprotonation of 2-Aminophenylphosphane with a p-Block-Metal/Alkali-Metal Base
(C) 3456 – 3459 [3522 – 3525]
DOI: 10.1002/anie.200500340
Woodward, S.
– Enantioselective Preparation of β,β-Disubstituted α-Methylenepropionates by MAO Promotion of the Zinc Schlenk Equilibrium
(C) 2235 – 2237 [2275 – 2277]
DOI: 10.1002/anie.200463028
– Organocopper for the Craftsman Cunning at His Trade
(H) 5560 – 5562 [5696 – 5698]
DOI: 10.1002/anie.200501204
– Remarkably Stable $(Me_3Al)_2 \cdot$DABCO and Stereoselective Nickel-Catalyzed AlR_3 (R = Me, Et) Additions to Aldehydes
(C) 2232 – 2234 [2272 – 2274]
DOI: 10.1002/anie.200462569
Woolfson, D. N.
– Polar Assembly in a Designed Protein Fiber
(C) 325 – 328 [329 – 332]
DOI: 10.1002/anie.200461599

 © 2005 Wiley-VCH Verlag GmbH & Co. KGaA, Weinheim

Woolley, G. A. (C) 7778 – 7782 [7956 – 7960]
Wozniak, K. (C) 2115 – 2119 [2153 – 2157]
Wright, A. T. (C) 5679 – 5682 [5825 – 5828], 6375 – 6378 [6533 – 6536]
Wright, D. S.
– Inverse Coordination of an Ionic Lattice by a Metal Host (C) 5729 – 5733 [5875 – 5879] DOI: 10.1002/anie.200501198
– Quadruple Deprotonation of 2-Aminophenylphosphane with a p-Block-Metal/Alkali-Metal Base (C) 3456 – 3459 [3522 – 3525] DOI: 10.1002/anie.200500340
Wright, J. E. I. (C) 3710 – 3714 [3776 – 3780]
Wright, N. G. (C) 4801 – 4804 [4879 – 4882]
Wright, R. J. (C) 7729 – 7733 [7907 – 7911]
Wu, B. (C) 615 – 617 [621 – 623]
Wu, C.-De (C) 1958 – 1961 [1994 – 1997]
Wu, De-C. (C) 4782 – 4785 [4860 – 4863]
Wu, F. (C) 105 – 108 [107 – 110]
Wu, G. (C) 1108 – 1112 [1132 – 1136]
Wu, H. (C) 6712 – 6715 [6870 – 6873]
Wu, Jiaquan (C) 7557 – 7560 [7729 – 7732]
Wu, Jishan (C) 2120 – 2123 [2158 – 2161]
Wu, P. (C) 6719 – 6723 [6877 – 6881]
Wu, Q. (C) 4048 – 4052 [4116 – 4120]
Wu, S. (C) 6934 – 6937 [7094 – 7097]
Wu, S.-H.
– Design of a Mechanism-Based Probe for Neuraminidase To Capture Influenza Viruses (C) 6888 – 6892 [7048 – 7052] DOI: 10.1002/anie.200501738
Wu, S.-T. (C) 1265 – 1268 [1291 – 1294]
Wu, T. (C) 4175 – 4178 [4247 – 4250]
Wu, W. (C) 6358 – 6362 [6516 – 6520]
Wu, Xiaofeng (C) 3407 – 3411 [3473 – 3477]
Wu, Xinglong (C) 4197 – 4201 [4269 – 4273]
Wu, Xu (C) 1987 – 1990 [2023 – 2026]
Wu, Y.-S. (C) 747 – 750 [757 – 760]
Wu, Yin (C) 2737 – 2742 [2797 – 2802]
Wu, Yiying (C) 332 – 336 [336 – 340]
Wu, Z. (C) 7771 – 7775 [7949 – 7953]
Wuest, J. D.
– Molecular Tectonics: Porous Cleavable Networks Constructed by Dipole-Directed Stacking of Hydrogen-Bonded Sheets (C) 4021 – 4025 [4089 – 4093] DOI: 10.1002/anie.200500198
Wulff, W. D.
– Highly Diastereoselective Alkylation of Aziridine-2-carboxylate Esters: Enantioselective Synthesis of LFA-1 Antagonist BIRT-377 (C) 6169 – 6172 [6325 – 6328] DOI: 10.1002/anie.200500923
Würdemann, C. (C) 6381 – 6384 [6539 – 6542]
Wurpel, G. W. H. (C) 3062 – 3067 [3122 – 3127]
Wurst, K. (C) 1977 – 1981 [2013 – 2017]
Würthner, F.
– Perylene Bisimide Based Macrocycles: Effective Probes for the Assessment of Conformational Effects on Optical Properties (C) 250 – 253 [254 – 257] DOI: 10.1002/anie.200461585
– Reversible Self-Organization of Semisynthetic Zinc Chlorins into Well-Defined Rod Antennae (C) 3147 – 3151 [3208 – 3212] DOI: 10.1002/anie.200462762
– Supramolecular Stereomutation in Kinetic and Thermodynamic Self-Assembly of Helical Merocyanine Dye Nanorods (C) 5071 – 5074 [5199 – 5202] DOI: 10.1002/anie.200500640
Wüstholz, A. (C) 2429 – 2432 [2481 – 2485]
Wysocki, L. M. (C) 2386 – 2390 [2438 – 2442]

Xia, W. (C) 5087 – 5089 [5217 – 5219]
Xia, Y.
– Corrosion-Based Synthesis of Single-Crystal Pd Nanoboxes and Nanocages and Their Surface Plasmon Properties (C) 7913 – 7917 [8127 – 8131] DOI: 10.1002/anie.200502722
– Large-Scale Synthesis of Silver Nanocubes: The Role of HCl in Promoting Cube Perfection and Monodispersity (C) 2154 – 2157 [2192 – 2195] DOI: 10.1002/anie.200462208
– Photonic Crystals with Thermally Switchable Stop Bands Fabricated from $Se@Ag_2Se$ Spherical Colloids (C) 3099 – 3103 [3159 – 3163] DOI: 10.1002/anie.200462906
– Polyol Synthesis of Platinum Nanostructures: Control of Morphology through the Manipulation of Reduction Kinetics (C) 2589 – 2592 [2645 – 2648] DOI: 10.1002/anie.200462668
– Side-by-Side Patterning of Multiple Alkanethiolate Monolayers on Gold by Edge-Spreading Lithography (C) 3596 – 3600 [3662 – 3666] DOI: 10.1002/anie.200500421
Xiang, J. (C) 1265 – 1268 [1291 – 1294]
Xiao, F.-S.
– Design and Size Control of Uniform Zeolite Nanocrystals Synthesized in Adjustable Confined Voids Formed by Recyclable Monodisperse Polymer Spheres (C) 2563 – 2568 [2619 – 2624] DOI: 10.1002/anie.200462187
Xiao, J.
– Insight into and Practical Application of pH-Controlled Asymmetric Transfer Hydrogenation of Aromatic Ketones in Water (C) 3407 – 3411 [3473 – 3477] DOI: 10.1002/anie.200500023
Xiao, S. (C) 7390 – 7394 [7556 – 7560]
Xiao, Y. (C) 5456 – 5459 [5592 – 5595]
Xie, J.-H. (C) 1118 – 1121 [1142 – 1145]
Xie, L. (C) 4242 – 4244 [4314 – 4316]
Xie, S. (C) 7085 – 7089 [7247 – 7251]
Xie, Y. (C) 6384 – 6387 [6542 – 6545]
Xie, Z.
– Synthesis, Reactivity, and Structural Characterization of a 14-Vertex Carborane (C) 2128 – 2131 [2166 – 2169] DOI: 10.1002/anie.200462708
Xiong, Y. (C) 7913 – 7917 [8127 – 8131]
Xu, B.-Q.
– Catalysis by Gold: Isolated Surface Au^{3+} Ions are Active Sites for Selective Hydrogenation of 1,3-Butadiene over Au/ZrO_2 Catalysts (C) 7132 – 7135 [7294 – 7297] DOI: 10.1002/anie.200502101
Xu, Bo (C) 7404 – 7407 [7570 – 7573]
Xu, Bubin (C) 6902 – 6905 [7062 – 7065]
Xu, F. (C) 4029 – 4032 [4097 – 4100]
Xu, G.-Z. (C) 3402 – 3407 [3468 – 3473]
Xu, H. (C) 756 – 761 [766 – 771]
Xu, J. (C) 6200 – 6203 [6356 – 6359]
Xu, K. (C) 2259 – 2261 [2299 – 2301]
Xu, Lianbin (C) 6009 – 6012 [6163 – 6166]
Xu, Lin (C) 5824 – 5827 [5974 – 5977]
Xu, N.
– Thermodynamic Stability and Ultrasmall-Size Effect of Nanodiamonds (C) 7414 – 7418 [7580 – 7584] DOI: 10.1002/anie.200501495
Xu, Q.
– *cyclo*-$Ti_3[\eta^2(\mu_2\text{-}C,O)]_3$: A Side-on-Bonded Polycarbonyl Titanium Cluster with Potentially Antiaromatic Character (C) 4338 – 4342 [4412 – 4416] DOI: 10.1002/anie.200500364
Xu, R.
– An Unexpected Photoelectronic Effect from $[Co(en)_3]_2(Zr_2F_{12})(SiF_6)\cdot 4H_2O$, a Compound Containing an H-Bonded Assembly of Discrete $[Co(en)_3]^{3+}$, $(Zr_2F_{12})^{4-}$, and $(SiF_6)^{2-}$ Ions (C) 7988 – 7990 [8202 – 8204] DOI: 10.1002/anie.200502514
Xu, R. (C) 3845 – 3848 [3913 – 3916]
Xu, S. (C) 724 – 728 Corrigendum: 3799 [734 – 738 Corrigendum: 3865]
Xu, Ye (C) 2132 – 2135 [2170 – 2173]
Xu, Ying (C) 2737 – 2742 [2797 – 2802]
Xu, Yingqi (C) 5141 – 5144 [5271 – 5274]
Xue, C. (C) 5064 – 5067 [5192 – 5195]
Xue, M. (C) 3845 – 3848 [3913 – 3916]

Yadav, R. D. (C) 6063 – 6067 [6217 – 6221]
Yaghi, O. M.
– High H_2 Adsorption in a Microporous Metal – Organic Framework with Open Metal Sites (C) 4745 – 4749 [4823 – 4827] DOI: 10.1002/anie.200462787
– Strategies for Hydrogen Storage in Metal – Organic Frameworks (M) 4670 – 4679 [4748 – 4758] DOI: 10.1002/anie.200462786
Yagubskii, E. B. (C) 1846 – 1849 [1880 – 1883]
Yajima, T. (C) 3402 – 3407 [3468 – 3473]
Yakushi, K. (C) 6564 – 6568 [6722 – 6726]
Yakushijin, K. (C) 3280 – 3282 [3344 – 3346]
Yam, V. W.-W.
– Luminescent Gold(III) Alkynyl Complexes: Synthesis, Structural Characterization, and Luminescence Properties (C) 3107 – 3110 [3167 – 3170] DOI: 10.1002/anie.200500253
– Polymer-Induced Self-Assembly of Alkynylplatinum(II) Terpyridyl Complexes by Metal···Metal/π···π Interactions (C) 791 – 794 [801 – 804] DOI: 10.1002/anie.200461261
Yamabe, H. (C) 468 – 470 [472 – 474]
Yamada, K. (C) 2534 – 2537 [2590 – 2593]

 © 2005 Wiley-VCH Verlag GmbH & Co. KGaA, Weinheim

Yamada, T.
– A DFT Study on Hetero-Diels–Alder Reactions Catalyzed by Cobalt Complexes: Lewis Acidity Enhancement as a Consequence of Spin Transition Caused by Lewis Base Coordination
(C) 2524–2527 [2580–2583]
DOI: 10.1002/anie.200460836
Yamada, Y. M. A. (C) 4536–4538 [4612–4614]
Yamagata, Y. (C) 3861–3864 [3929–3932]
Yamaguchi, J. (C) 3110–3115 [3170–3175]
Yamaguchi, Kazuya (C) 5136–5141 [5266–5271]
Yamaguchi, Kentaro (C) 4564–4567 [4640–4643]
Yamaguchi, S. (C) 5698–5701 [5844–5847]
Yamaguchi, T. (C) 1088–1092 [1112–1116]
Yamaguchi, Y. (Kumamoto) (C) 3861–3864 [3929–3932]
Yamaguchi, Y. (Osaka)
– Banana-Shaped Oligo(aryleneethynylene)s: Synthesis and Light-Emitting Characteristics
(C) 7040–7044 [7202–7206]
DOI: 10.1002/anie.200502214
Yamamoto, A. (C) 2380–2382 [2432–2434]
Yamamoto, Hisashi
– Catalytic Asymmetric Nitroso-Diels–Alder Reaction with Acyclic Dienes
(C) 7082–7085 [7244–7247]
DOI: 10.1002/anie.200501345
– "Designer Acids": Combined Acid Catalysis for Asymmetric Synthesis
(R) 1924–1942 [1958–1977]
DOI: 10.1002/anie.200460394
– Enantioselective Epoxidation of Allylic Alcohols by a Chiral Complex of Vanadium: An Effective Controller System and a Rational Mechanistic Model
(C) 4389–4391 [4463–4465]
DOI: 10.1002/anie.200500938
– Oxazaborolidine-Derived Lewis Acid Assisted Lewis Acid as a Moisture-Tolerant Catalyst for Enantioselective Diels–Alder Reactions
(C) 1484–1487 [1508–1511]
DOI: 10.1002/anie.200461319
Yamamoto, Hitoshi (C) 969–972 [991–994]
Yamamoto, Kenichiro (C) 625–628 [631–634]
Yamamoto, Kenji (C) 4550–4554 [4626–4630]
Yamamoto, Masami (C) 5439–5441 [5575–5577]
Yamamoto, Mio (C) 5103–5106 [5233–5236]
Yamamoto, S. (C) 4224–4227 [4296–4299]
Yamamoto, Yoshinori
– Oxindole Synthesis through Intramolecular Nucleophilic Addition of Vinylpalladiums to Aryl Isocyanates
(C) 7718–7721 [7896–7899]
DOI: 10.1002/anie.200502252
Yamamoto, Yoshinori (C) 5526–5528 [5662–5664]
Yamamoto, Yuhei (C) 7082–7085 [7244–7247]
Yamanoi, S. (C) 5433–5438 [5569–5574]
Yamasaki, Y. (C) 3544–3548 [3610–3614]
Yamashita, K.-i. (C) 4896–4899 [4974–4977]
Yamashita, M. (C) 3240–3243 [3304–3307]
Yamashita, Taketomo (C) 1257–1261 [1283–1287]
Yamashita, Tatsuya (C) 4721–4723 [4799–4801]
Yamashita, Y. (C) 761–764 [771–774]
Yamato, K. Corrigendum: 1907
Yamauchi, O.
– Iodine-Assisted Assembly of Helical Coordination Polymers of Cucurbituril and Asymmetric Copper(II) Complexes
(C) 3402–3407 [3468–3473]
DOI: 10.1002/anie.200463071
Yan, B. (C) 2553–2556 [2609–2612]
Yan, C.-H.
– Rare-Earth Oxide Nanopolyhedra, Nanoplates, and Nanodisks
(C) 3256–3260 [3320–3324]
DOI: 10.1002/anie.200462573
– Single-Crystalline Iron Oxide Nanotubes
(C) 4328–4333 [4402–4407]
DOI: 10.1002/anie.200463038
Yan, D.
– Real-Time Membrane Fission of Giant Polymer Vesicles
(C) 3223–3226 [3287–3290]
DOI: 10.1002/anie.200462622
Yan, F. (C) 2084–2088 [2121–2125]
Yan, Hao
– Aptamer-Directed Self-Assembly of Protein Arrays on a DNA Nanostructure
(C) 4333–4338 [4407–4412]
DOI: 10.1002/anie.200501089
Yan, Hu
– Environmentally Stable Super Water-Repellent Poly(alkylpyrrole) Films
(C) 3453–3456 [3519–3522]
DOI: 10.1002/anie.200500266
– Rapid Swelling/Collapsing Behavior of Thermoresponsive Poly(*N*-isopropylacrylamide) Gel Containing Poly(2-(methacryloyloxy)decyl phosphate) Surfactant
(C) 1951–1954 [1987–1990]
DOI: 10.1002/anie.200462288
Yan, P. (C) 3086–3089 [3146–3149]
Yan, R. (C) 6054–6057 [6208–6211]
Yan, X. (C) 6859–6862 [7019–7022]
Yan, X.-P.
– Interfacing Capillary Electrophoresis and Electrothermal Atomic Absorption Spectroscopy To Study Metal Speciation and Metal–Biomolecule Interactions
(C) 6387–6391 [6545–6549]
DOI: 10.1002/anie.200501245
Yan, X.-X. (C) 6544–6546 [6702–6704]
Yan, Y.
– Reversible Conversion of Conducting Polymer Films from Superhydrophobic to Superhydrophilic
(C) 6009–6012 [6163–6166]
DOI: 10.1002/anie.200500868
Yan, Y.-X. (C) 5471–5475 [5607–5611]
Yan, Z.-G. (C) 4328–4333 [4402–4407]
Yanagisawa, A.
– Enantioselective Protonation of Silyl Enolates Catalyzed by a Binap·AgF Complex
(C) 1546–1548 [1570–1572]
DOI: 10.1002/anie.200462325
Yang, C. (C) 5087–5089 [5217–5219]
Yang, C. J. (C) 2572–2576 [2628–2632]
Yang, D.
– Mapping Protein–Protein Interfaces on the Basis of Proton Density Difference
(C) 5141–5144 [5271–5274]
DOI: 10.1002/anie.200501209
Yang, F.-Z. (C) 1265–1268 [1291–1294]
Yang, G.
– Thermodynamic Stability and Ultrasmall-Size Effect of Nanodiamonds
(C) 7414–7418 [7580–7584]
DOI: 10.1002/anie.200501495
Yang, G.-Y.
– A 3D Coordination Framework Based on Linkages of Nanosized Hydroxo Lanthanide Clusters and Copper Centers by Isonicotinate Ligands
(C) 1385–1388 [1409–1412]
DOI: 10.1002/anie.200461424
– A Germanate Framework Containing 24-Ring Channels, Ni–Ge Bonds, and Chiral $[Ni@Ge_{14}O_{24}(OH)_3]$ Cluster Motifs Transferred from Chiral Metal Complexes
(C) 6881–6884 [7041–7044]
DOI: 10.1002/anie.200502432
– Porous Lanthanide–Organic Open Frameworks with Helical Tubes Constructed from Interweaving Triple-Helical and Double-Helical Chains
(C) 5814–5817 [5964–5967]
DOI: 10.1002/anie.200500453
Yang, Hai (C) 947–949 [969–971]
Yang, Haifeng (C) 7053–7059 [7215–7221]
Yang, Heyi (C) 4242–4244 [4314–4316]
Yang, J. (C) 598–603 [604–609]
Yang, J. W. (C) 108–110 [110–112]
Yang, Min (C) 7988–7990 [8202–8204]
Yang, Mu (C) 6727–6730 [6885–6888]
Yang, P.
– Enrichment of Low-Abundance Peptides and Proteins on Zeolite Nanocrystals for Direct MALDI-TOF MS Analysis
(C) 615–617 [621–623]
DOI: 10.1002/anie.200460741
Yang, S.
– Synthesis of Ultrathin Zinc Nanowires and Nanotubes by Vapor Transport
(C) 3562–3565 [3628–3631]
DOI: 10.1002/anie.200500438
Yang, S.-L. (C) 6063–6067 [6217–6221]
Yang, Xiaowu Corrigendum: 1907
Yang, Xiaowu (C) 1352–1356 [1376–1380]
Yang, Xiaoyu (C) 2563–2568 [2619–2624]
Yang, Y. A. (C) 6712–6715 [6870–6873]
Yang, Yu (C) 7922–7925 [8136–8139]
Yang, Yuming (C) 4872–4876 [4950–4954]
Yang, Z.-Y.
– Copolymerization of Ethylene, Tetrafluoroethylene, and an Olefin-Containing Fluorosulfonyl Fluoride: Synthesis of High-Proton-Conductive Membranes for Fuel-Cell Applications
(C) 564–567 [570–573]
DOI: 10.1002/anie.200461104
Yang, Zhenzhong
– General Synthetic Route toward Functional Hollow Spheres with Double-Shelled Structures
(C) 6727–6730 [6885–6888]
DOI: 10.1002/anie.200501556
Yang, Zhi (C) 7072–7074 [7234–7236]
Yao, C. (C) 6708–6711 [6866–6869]
Yao, S. Q.
– Activity-Based High-Throughput Screening of Enzymes by Using a DNA Microarray
(C) 1048–1053 [1072–1077]
DOI: 10.1002/anie.200461612
Yap, G. P. A. (C) 1508–1510 [1532–1534]
Yashima, E.
– A Modular Strategy to Artificial Double Helices
(C) 3867–3870 [3935–3938]
DOI: 10.1002/anie.200501028
Yashima, E. (C) 6154–6157 [6310–6313]

 © 2005 Wiley-VCH Verlag GmbH & Co. KGaA, Weinheim

Yasuda, H. (C) 6378 – 6381 [6536 – 6539]
Yasuda, K. (C) 2732 – 2737 [2792 – 2797]
Yasuda, N. (C) 2262 – 2265 [2302 – 2305]
Yates, C. M. (C) 2377 – 2379 Corrigendum: 4660 [2429 – 2431 Corrigendum: 4735]
Ye, C. (C) 6025 – 6029 [6179 – 6183]
Ye, S. (C) 2103 – 2106 [2140 – 2143]
Yen, B. K. H. (C) 5447 – 5451 [5583 – 5587]
Yeo, W.-S. (C) 5480 – 5483 [5616 – 5619]
Yeung, Y. Y. (C) 7981 – 7984 [8195 – 8198]
Yi, H.-P. (C) 5725 – 5729 [5871 – 5875]
Yin, H. (C) 2704 – 2707 [2764 – 2767], (R) 4130 – 4163 [4200 – 4235]
Yin, L. (C) 2140 – 2144 [2178 – 2182]
Yin, P. (C) 4355 – 4358 [4429 – 4432]
Yin, Y. (C) 7913 – 7917 [8127 – 8131]
Ying, J. Y.
– Generalized Fluorocarbon-Surfactant-Mediated Synthesis of Nanoparticles with Various Mesoporous Structures (C) 288 – 292 [292 – 296] DOI: 10.1002/anie.200460892
Ying, L.
– Trapping of Proteins under Physiological Conditions in a Nanopipette (C) 3747 – 3750 [3813 – 3816] DOI: 10.1002/anie.200500196
Yokota, M. (C) 6484 – 6487 [6642 – 6645]
Yokota, Y. (C) 75 – 78 [77 – 80]
Yokoyama, K. (C) 4903 – 4906 [4981 – 4984]
Yokoyama, T. (C) 4164 – 4168 [4236 – 4240]
Yong, L. (C) 2092 – 2096 [2129 – 2133]
Yoo, M.-S. (C) 1383 – 1385 [1407 – 1409]
Yoo, S. (C) 1491 – 1494 [1515 – 1518]
Yoon, K. B.
– 1:1 and 2:1 Charge-Transfer Complexes between Aromatic Hydrocarbons and Dry Titanium Dioxide (C) 910 – 913 [932 – 935] DOI: 10.1002/anie.200461972
Yoon, T.-J. (C) 1068 – 1071 [1092 – 1095]
Yoon, T. P. (C) 466 – 468 Corrigendum: 7327 [470 – 472 Corrigendum: 7493]
Yorimitsu, H. (Kyoto)
– Recent Progress in Asymmetric Allylic Substitutions Catalyzed by Chiral Copper Complexes (H) 4435 – 4439 [4509 – 4513] DOI: 10.1002/anie.200500653
Yorimitsu, H. (Kyoto) (C) 3488 – 3490 [3554 – 3556]
Yorimitsu, H. (Tokyo) (C) 1694 – 1696 [1722 – 1724], 2368 – 2370 [2420 – 2422], 2708 – 2711 [2768 – 2771]
York, J. T. (C) 7745 – 7748 [7923 – 7926]
Yoshida, J.-i.
– Room-Temperature Swern Oxidations by Using a Microscale Flow System (C) 2413 – 2416 [2465 – 2468] DOI: 10.1002/anie.200462466
Yoshida, K. (C) 2262 – 2265 [2302 – 2305]
Yoshida, T. (C) 3470 – 3474 [3536 – 3540]
Yoshida, Z.-i.
– Banana-Shaped Oligo(aryleneethynylene)s: Synthesis and Light-Emitting Characteristics (C) 7040 – 7044 [7202 – 7206] DOI: 10.1002/anie.200502214
Yoshikai, N. (C) 4721 – 4723 [4799 – 4801]
Yoshimura, Masahiro (C) 7287 – 7290 [7453 – 7456]
Yoshimura, Misaki (C) 6193 – 6196 [6349 – 6352]
Yoshioka, M. (C) 6553 – 6556 [6711 – 6714]
Yoshizawa, K. (C) 5097 – 5100 [5227 – 5230]
Yoshizawa, M. (C) 1810 – 1813 [1844 – 1847]
You, L.-P. (C) 3256 – 3260 [3320 – 3324], 4328 – 4333 [4402 – 4407]
Youfu, K. (C) 3726 – 3729 [3792 – 3795]
Young, J. A. (C) 2400 – 2403 [2452 – 2455]
Young, N. A.
– Experimental Evidence for a Jahn – Teller Distortion in $AuCl_3$ (C) 6746 – 6750 [6904 – 6908] DOI: 10.1002/anie.200502503
Yount, W. C. (C) 2746 – 2748 [2806 – 2808]
Yousufuddin, M. (C) 1860 – 1865 [1894 – 1899], 7227 – 7230 [7393 – 7396]
Yu, A. (C) 2888 – 2892 [2948 – 2952]
Yu, C. L. (C) 2549 – 2553 [2605 – 2609]
Yu, Chao (C) 1408 – 1412 [1432 – 1437]
Yu, Chengzhong (C) 7053 – 7059 [7215 – 7221]
Yu, Cong (C) 791 – 794 [801 – 804]
Yu, H. N. (C) 4596 – 4599 [4672 – 4675], 7725 – 7729 [7903 – 7907]
Yu, J.
– An Unexpected Photoelectronic Effect from $[Co(en)_3]_2(Zr_2F_{12})(SiF_6)\cdot 4H_2O$, a Compound Containing an H-Bonded Assembly of Discrete $[Co(en)_3]^{3+}$, $(Zr_2F_{12})^{4-}$, and $(SiF_6)^{2-}$ Ions (C) 7988 – 7990 [8202 – 8204] DOI: 10.1002/anie.200502514
Yu, J.-Q.
– Palladium-Catalyzed Asymmetric Iodination of Unactivated C–H Bonds under Mild Conditions (C) 2112 – 2115 [2150 – 2153] DOI: 10.1002/anie.200462884
– Pd-Catalyzed Stereoselective Oxidation of Methyl Groups by Inexpensive Oxidants under Mild Conditions: A Dual Role for Carboxylic Anhydrides in Catalytic C–H Bond Oxidation (C) 7420 – 7424 [7586 – 7590] DOI: 10.1002/anie.200502767
Yu, K. N. (C) 1068 – 1071 [1092 – 1095]
Yu, L.
– Self-Assembled Monolayers of Isocyanides on Nickel Electrodes (C) 4228 – 4231 [4300 – 4303] DOI: 10.1002/anie.200500942
Yu, S. (C) 135 – 138 [137 – 140]
Yu, T. (C) 7411 – 7414 [7577 – 7580]
Yu, X. (C) 615 – 617 [621 – 623]
Yu, Y. (C) 7085 – 7089 [7247 – 7251]
Yuan, De-Q. (C) 4201 – 4204 [4273 – 4276]
Yudha S., S. (C) 5526 – 5528 [5662 – 5664]
Yukawa, Y.
– $[GdNi_6]$ and $[LaNi_6]$: High-Field EPR Spectroscopy and Magnetic Studies of Exchange-Coupled Octahedral Clusters (C) 1997 – 2001 [2033 – 2037] DOI: 10.1002/anie.200462401
Yumoto, H. (C) 3861 – 3864 [3929 – 3932]
Yus, M.
– Asymmetric Multicomponent Reactions (AMCRs): The New Frontier (R) 1602 – 1634 [1628 – 1661] DOI: 10.1002/anie.200460548

Z

Zabel, M. (C) 242 – 245 [246 – 249]
Zacchigna, M. (C) 4798 – 4801 [4876 – 4879]
Zaitsev, V. G. (C) 4046 – 4048 [4114 – 4116]
Zak, M. (C) 1378 – 1382 [1402 – 1406], 3736 – 3740 [3802 – 3806]
Zakeeruddin, S. M. (C) 6413 – 6417 [6571 – 6575]
Zakharov, L. N. (C) 1508 – 1510 [1532 – 1534], 5428 – 5433 [5564 – 5569]
Zaleski, J. M.
– A Unique Approach to Metal-Induced Bergman Cyclization: Long-Range Enediyne Activation by Ligand-to-Metal Charge Transfer (C) 592 – 595 [598 – 601] DOI: 10.1002/anie.200461825
Zambon, A. (C) 7435 – 7439 [7601 – 7605]
Zameo, S. (C) 965 – 969 [987 – 991]
Zamora, F.
– Models of Putative (AH)G(AH)G Nucleobase Quartets (C) 5670 – 5674 [5816 – 5820] DOI: 10.1002/anie.200500896
Zanasi, R. (C) 3594 – 3596 [3660 – 3662]
Zanello, P.
– Redox Control of Light-Induced Platinum-Cluster-to-Iron Charge Transfer in a Bis(ferrocenylethynyl)-Substituted Hexanuclear Platinum Derivative (C) 5701 – 5705 [5847 – 5851] DOI: 10.1002/anie.200501714
Zanette, M. (C) 6214 – 6219 [6370 – 6375]
Zangrando, E. (C) 6214 – 6219 [6370 – 6375]
Zani, L. (H) 1758 – 1763 [1788 – 1793]
Zanotti-Gerosa, A. (C) 5834 – 5838 [5984 – 5988]
Zapf, A. (C) 238 – 242 [242 – 246], 3913 – 3917 [3981 – 3985]
Zapf, C. W. (C) 6533 – 6537 [6691 – 6695]
Zare, R. N.
– Effects of Bending Excitation on the Reaction of Chlorine Atoms with Methane (C) 2382 – 2385 [2434 – 2437] DOI: 10.1002/anie.200462837
Zargarian, D.
– Tetraphenylborate as a Novel Bridging Ligand in a Zwitterionic Nickel(I) Dimer (C) 7721 – 7725 [7899 – 7903] DOI: 10.1002/anie.200502905
Zaworotko, M. J.
– Ternary Nets formed by Self-Assembly of Triangles, Squares, and Tetrahedra (C) 2877 – 2880 [2937 – 2940] DOI: 10.1002/anie.200500156
Zaworotko, M. J. (C) 897 – 901 [919 – 923]
Zayats, M. (C) 4010 – 4015 [4078 – 4083]
Zecchina, A.
– Dimethyl Carbonate in the Supercages of NaY Zeolite: The Role of Local Fields in Promoting Methylation and Carboxymethylation Activity (C) 4774 – 4777 [4852 – 4855] DOI: 10.1002/anie.200500110
Zeckert, K. (C) 7954 – 7958 [8168 – 8172]
Zeimentz, P. M. (C) 7473 – 7477 [7640 – 7644]

 © 2005 Wiley-VCH Verlag GmbH & Co. KGaA, Weinheim

Zeitler, K.
– Extending Mechanistic Routes in Heterazolium Catalysis – Promising Concepts for Versatile Synthetic Methods
(H) 7506 – 7510 [7674 – 7678]
DOI: 10.1002/anie.200502617
Zeng, H. C.
– Size Tuning, Functionalization, and Reactivation of Au in TiO_2 Nanoreactors
(C) 4342 – 4345 [4416 – 4419]
DOI: 10.1002/anie.200500394
Zeng, J. (C) 6054 – 6057 [6208 – 6211]
Zeng, M.-H. (C) 3079 – 3082 [3139 – 3142]
Zeng, X. C.
– Motif Transition in Growth Patterns of Small to Medium-Sized Silicon Clusters
(C) 1491 – 1494 [1515 – 1518]
DOI: 10.1002/anie.200461753
Zenneck, U. (C) 2943 – 2946 [3003 – 3007]
Zentel, R. (C) 2437 – 2440 [2490 – 2493]
Zerbetto, F.
– Patterning through Controlled Submolecular Motion: Rotaxane-Based Switches and Logic Gates that Function in Solution and Polymer Films
(C) 3062 – 3067 [3122 – 3127]
DOI: 10.1002/anie.200500101
Zettl, H. (C) 2420 – 2426 [2472 – 2478]
Zha, D. (C) 4192 – 4196 [4264 – 4268]
Zhai, H.-J. (C) 7251 – 7254 [7417 – 7420]
Zhai, J. (C) 5115 – 5118 [5245 – 5248]
Zhan, J.
– Fabrication of Metal – Semiconductor Nanowire Heterojunctions
(C) 2140 – 2144 [2178 – 2182]
DOI: 10.1002/anie.200462813
Zhang, Chen (C) 259 – 262 [264 – 267]
Zhang, Chengliang (C) 6727 – 6730 [6885 – 6888]
Zhang, Feng (C) 3402 – 3407 [3468 – 3473]
Zhang, Fuqiang (C) 7053 – 7059 [7215 – 7221]
Zhang, G. (C) 7767 – 7770 [7945 – 7948]
Zhang, G.-D. (C) 419 – 423 [423 – 427]
Zhang, J.-P.
– Efficient Two-Photon-Sensitized Luminescence of a Europium(III) Complex
(C) 747 – 750 [757 – 760]
DOI: 10.1002/anie.200462382
Zhang, Jian (C) 2508 – 2512 [2564 – 2568]
Zhang, Jie (C) 1385 – 1388 [1409 – 1412], 5814 – 5817 [5964 – 5967], 6881 – 6884 [7041 – 7044]
Zhang, Junliang (C) 2132 – 2135 [2170 – 2173]
Zhang, L.-F. (C) 7742 – 7745 [7920 – 7923]
Zhang, Li (C) 2925 – 2929 [2985 – 2989]
Zhang, Ling (C) 4048 – 4052 [4116 – 4120]
Zhang, M.-B. (C) 1385 – 1388 [1409 – 1412]
Zhang, Q. (Ann Arbor) (C) 3412 – 3415 [3478 – 3481]
Zhang, Q. (Tianjin) (C) 1118 – 1121 [1142 – 1145]
Zhang, Qing (C) 5520 – 5523 [5656 – 5659]
Zhang, Qingmin (C) 2723 – 2727 [2783 – 2787]
Zhang, Siyan (C) 4735 – 4739 [4813 – 4817]
Zhang, Songlin (C) 1184 – 1188 [1208 – 1212]
Zhang, T. Y. (C) 5520 – 5523 [5656 – 5659]
Zhang, W. (C) 4389 – 4391 [4463 – 4465]
Zhang, W.-De (C) 4782 – 4785 [4860 – 4863]
Zhang, W. J.
– The Mechanism of Chemical Vapor Deposition of Cubic Boron Nitride Films from Fluorine-Containing Species
(C) 4749 – 4753 [4827 – 4831]
DOI: 10.1002/anie.200500320
Zhang, W.-X. (C) 3079 – 3082 [3139 – 3142]
Zhang, Xi
– The Introduction of π – π Stacking Moieties for Fabricating Stable Micellar Structure: Formation and Dynamics of Disklike Micelles
(C) 4731 – 4735 [4809 – 4813]
DOI: 10.1002/anie.200500980
Zhang, Xiaodong (C) 5100 – 5103 [5230 – 5233]
Zhang, Xiaofeng Corrigendum: 506
Zhang, Xiaohong
– Bulk Preparation of Si – SiO_x Hierarchical Structures: High-Density Radially Oriented Amorphous Silica Nanowires on a Single-Crystal Silicon Nanocore
(C) 6934 – 6937 [7094 – 7097]
DOI: 10.1002/anie.200501960
Zhang, Xin (C) 7132 – 7135 [7294 – 7297]
Zhang, Xiyun (C) 938 – 941 [960 – 963]
Zhang, Xumu
– Enantioselective Hydrogenation of Allylphthalimides: An Efficient Method for the Synthesis of β-Methyl Chiral Amines
(C) 4933 – 4935 [5013 – 5015]
DOI: 10.1002/anie.200501332
– Practical Synthesis of Enantiopure γ-Amino Alcohols by Rhodium-Catalyzed Asymmetric Hydrogenation of β-Secondary-Amino Ketones
(C) 1687 – 1689 [1715 – 1717]
DOI: 10.1002/anie.200462178
Zhang, Y. (Paris) (C) 1683 – 1687 [1711 – 1715]
Zhang, Y.-W.
– Rare-Earth Oxide Nanopolyhedra, Nanoplates, and Nanodisks
(C) 3256 – 3260 [3320 – 3324]
DOI: 10.1002/anie.200462573
Zhang, Y.-Z. (C) 5841 – 5846 [5991 – 5996]
Zhang, Y. (Zhejiang)
– Clean and Highly Selective Oxidation of Alcohols in an Ionic Liquid by Using an Ion-Supported Hypervalent Iodine(III) Reagent
(C) 952 – 955 [974 – 977]
DOI: 10.1002/anie.200461889
Zhang, Yahong (C) 615 – 617 [621 – 623]
Zhang, Yan (C) 6544 – 6546 [6702 – 6704]
Zhang, Yonglai (C) 2563 – 2568 [2619 – 2624]
Zhang, Yu (C) 6169 – 6172 [6325 – 6328]
Zhang, Z.-H. (C) 4352 – 4355 [4426 – 4429]
Zhang, Z.-Y.
– Design, Construction, and Intracellular Activation of an Intramolecularly Self-Silenced Signal Transduction Inhibitor
(C) 4242 – 4244 [4314 – 4316]
DOI: 10.1002/anie.200462004
Zhang, Ze (C) 4328 – 4333 [4402 – 4407]
Zhang, Zhaoda (C) 6766 – 6769 [6924 – 6927]
Zhang, Zhihua (C) 3466 – 3470 [3532 – 3536]
Zhang, Zhizhou
– Nanoparticle PCR: Nanogold-Assisted PCR with Enhanced Specificity
(C) 5100 – 5103 [5230 – 5233]
DOI: 10.1002/anie.200500403
Zhao, Dongbin (C) 5720 – 5725 [5866 – 5871]
Zhao, Dongyuan
– Ordered Mesoporous Polymers and Homologous Carbon Frameworks: Amphiphilic Surfactant Templating and Direct Transformation
(C) 7053 – 7059 [7215 – 7221]
DOI: 10.1002/anie.200501561
Zhao, F. (C) 5329 – 5334 [5463 – 5468]
Zhao, J. (C) 1873 – 1875 [1907 – 1909]
Zhao, J.-T. (C) 6881 – 6884 [7041 – 7044]
Zhao, L. (C) 6742 – 6746 [6900 – 6904]
Zhao, Q. (C) 2694 – 2700 [2754 – 2760], 5329 – 5334 [5463 – 5468]
Zhao, W. (C) 1677 – 1679 [1705 – 1707]
Zharnikov, M. (C) 6775 – 6778 [6933 – 6936]
Zhdankin, V. V.
– Synthesis, Structure, and Chemoselective Reactivity of *N*-(2-Iodylphenyl)acylamides: Hypervalent Iodine Reagents Bearing a Pseudo-Six-Membered Ring Scaffold
(C) 7127 – 7131 [7289 – 7293]
DOI: 10.1002/anie.200502707
Zheng, B. (C) 2520 – 2523 [2576 – 2579]
Zheng, N. (C) 5299 – 5303 [5433 – 5437]
Zheng, S.-L.
– An Unstable Ligand-Unsupported Cu^{I} Dimer Stabilized in a Supramolecular Framework
(C) 4614 – 4617 [4690 – 4693]
DOI: 10.1002/anie.200501154
Zheng, S.-T. (C) 1385 – 1388 [1409 – 1412], 6881 – 6884 [7041 – 7044]
Zhi, C.
– Characteristics of Boron Nitride Nanotube – Polyaniline Composites
(C) 7929 – 7932 [8143 – 8146]
DOI: 10.1002/anie.200502591
– Covalent Functionalization: Towards Soluble Multiwalled Boron Nitride Nanotubes
(C) 7932 – 7935 [8146 – 8149]
DOI: 10.1002/anie.200502846
Zhi, L. (C) 2120 – 2123 [2158 – 2161]
Zhong, Xiaoyan (C) 2737 – 2742 [2797 – 2802]
Zhong, Xinhua (C) 3466 – 3470 [3532 – 3536]
Zhong, Z. (C) 5679 – 5682 [5825 – 5828], 6375 – 6378 [6533 – 6536]
Zhou, D. (C) 3747 – 3750 [3813 – 3816], 6854 – 6859 [7014 – 7019]
Zhou, H.
– A Self-Ordered, Crystalline – Glass, Mesoporous Nanocomposite for Use as a Lithium-Based Storage Device with Both High Power and High Energy Densities
(C) 797 – 802 [807 – 812]
DOI: 10.1002/anie.200460937
Zhou, Q.-F. (C) 6025 – 6029 [6179 – 6183]
Zhou, Q.-L.
– Highly Rigid Diphosphane Ligands with a Large Dihedral Angle Based on a Chiral Spirobifluorene Backbone
(C) 1118 – 1121 [1142 – 1145]
DOI: 10.1002/anie.200462072
Zhou, R. (C) 4175 – 4178 [4247 – 4250]
Zhou, S.-z. (C) 1356 – 1360 [1380 – 1384]
Zhou, Shaomin (C) 6934 – 6937 [7094 – 7097]
Zhou, Shenghu (C) 4539 – 4543 [4615 – 4619]
Zhou, X.-P. (C) 4175 – 4178 [4247 – 4250]
Zhou, Y. (C) 3223 – 3226 [3287 – 3290]
Zhu, F. R. (C) 1104 – 1107 [1128 – 1131]
Zhu, G.
– A Metal – Organic Framework with the Zeolite MTN Topology Containing Large Cages of Volume 2.5 nm^3
(C) 3845 – 3848 [3913 – 3916]
DOI: 10.1002/anie.200462260
Zhu, H. (C) 5090 – 5093 [5220 – 5223], 7072 – 7074 [7234 – 7236]
Zhu, H.-F. (C) 4352 – 4355 [4426 – 4429]
Zhu, J.
– Uniform, Axial-Orientation Alignment of One-Dimensional Single-Crystal Silicon Nanostructure Arrays

 © 2005 Wiley-VCH Verlag GmbH & Co. KGaA, Weinheim

(C) 2737 – 2742 [2797 – 2802]
DOI: 10.1002/anie.200462995
Zhu, J.-H. (C) 2124 – 2127 [2162 – 2165]
Zhu, N. (C) 3107 – 3110 [3167 – 3170]
Zhu, P. (C) 7922 – 7925 [8136 – 8139]
Zhu, S.-Z. (C) 5725 – 5729 [5871 – 5875]
Zhu, Xiaodong (C) 6902 – 6905 [7062 – 7065]
Zhu, Xiaoxiang (C) 7450 – 7453 [7616 – 7619]
Zhu, Y. (C) 5083 – 5087 [5213 – 5217]
Zhu, Z. (C) 1683 – 1687 [1711 – 1715]
Zhuravel, M. A. (C) 3885 – 3889 [3953 – 3957]
Ziegler, A. (C) 639 – 644 [645 – 650]
Ziehl, M. (C) 1202 – 1205 [1226 – 1230]
Ziemer, B. (C) 5259 – 5262 [5393 – 5397]
Ziessel, R.
– Pyrromethene Dialkynyl Borane Complexes for "Cascatelle" Energy Transfer and Protein Labeling
(C) 3694 – 3698 [3760 – 3764]
DOI: 10.1002/anie.200500808
Ziessel, R. F. (C) 7612 – 7615 [7784 – 7788]
Zimmerman, T. (C) 2903 – 2907 [2963 – 2967]
Zimmermann, V. (R) 5188 – 5240 [5320 – 5374]
Zinngrebe, J. (C) 257 – 259 [262 – 264]
Zinth, W. (C) 7901 – 7904 [8114 – 8118]
Zöllinger, M. (C) 2295 – 2298 [2336 – 2338]
Zou, S. (C) 956 – 959 [978 – 981]
Zou, W. (C) 7028 – 7032 [7190 – 7194]
Zou, X.
– SU-16: A Three-Dimensional Open-Framework Borogermanate with a Novel Zeolite Topology
(C) 2012 – 2015 [2048 – 2051]
DOI: 10.1002/anie.200461911
Zschörnig, O. (C) 2892 – 2895 [2952 – 2955]
Zubarev, R. A.
– Facile Disulfide Bond Cleavage in Gaseous Peptide and Protein Cations by Ultraviolet Photodissociation at 157 nm
(C) 6399 – 6403 [6557 – 6561]
DOI: 10.1002/anie.200501533
Zubia, A. (C) 2903 – 2907 [2963 – 2967]
Zucca, A. (C) 6892 – 6895 [7052 – 7055]
Zuccaccia, C. (C) 7922 – 7925 [8136 – 8139]
Zuccheri, G. (R) 1166 – 1181 [1190 – 1206]
Zulys, A. (C) 7794 – 7798 [7972 – 7976]
zur Loye, H.-C.
– $[Co_2(ppca)_2(H_2O)(V_4O_{12})_{0.5}]$: A Framework Material Exhibiting Reversible Shrinkage and Expansion through a Single-Crystal-to-Single-Crystal Transformation Involving a Change in the Cobalt Coordination Environment
(C) 6673 – 6677 [6831 – 6835]
DOI: 10.1002/anie.200502309
Zvyagin, S. A. (C) 1997 – 2001 [2033 – 2037]
Zwick, A. (C) 4069 – 4073 [4137 – 4141]

 © 2005 Wiley-VCH Verlag GmbH & Co. KGaA, Weinheim

Reviews and Minireviews

The name of the correspondence author is in boldface and it is accompanied by the title of the publication and all coauthors.

Antonietti, M., see *Cölfen, H.* 5576
Aranzaes, J. R., see *Astruc, D.* 7852
Astruc, D., *Lu, F.*, and *Aranzaes, J. R.*, Nanoparticles as Recyclable Catalysts: The Frontier between Homogeneous and Heterogeneous Catalysis 7852
Avram, L., see *Cohen, Y.* 520
Axel, R., Scents and Sensibility: A Molecular Logic of Olfactory Perception (Nobel Lecture) 6110
Ball, L. J., see *Oschkinat, H.* 2852
Bauer, H., see *Schirmer, R. H.* 690
Frisch, A. C. and ***Beller, M.***, Catalysts for Cross-Coupling Reactions with Non-activated Alkyl Halides . 674
Beutner, G. L., see *Denmark, S. E.* 4682
Bialy, L., see *Waldmann, H.* 3814
Biel, M., see *Giannis, A.* 3186
Blackmond, D. G., Reaction Progress Kinetic Analysis: A Powerful Methodology for Mechanistic Studies of Complex Catalytic Reactions 4302
Bode, H. B., see *Müller, Rolf* 6828
Böhme, D. K., see *Schwarz, H.* 2336
Bohn, A., see *Fink, H.-P.* 3358
Bourke, S. C., see *Piers, W. E.* 5016
Bräse, S., *Gil, C.*, *Knepper, K.*, and *Zimmermann, V.*, Organic Azides: An Exploding Diversity of a Unique Class of Compounds 5188
Breit, B., Supramolecular Approaches to Generate Libraries of Chelating Bidentate Ligands for Homogeneous Catalysis 6816
Bringmann, G., *Price Mortimer, A. J.*, *Keller, P. A.*, *Gresser, M. J.*, *Garner, J.*, and ***Breuning, M.***, Atroposelective Synthesis of Axially Chiral Biaryl Compounds 5384
Bringmann, G., see *Breuning, M.* 5384
Bruneau, C., Electrophilic Activation and Cycloisomerization of Enynes: A New Route to Functional Cyclopropanes 2328
Buck, L. B., Unraveling the Sense of Smell (Nobel Lecture) 6128
Bulger, P. G., see *Nicolaou, K. C.* 4442, 4490
Burkart, M. D., see *Wong, C.-H.* 192
Chakrabarti, S., see *Isaacs, L.* 4844
Chou, T.-C., see *Danishefsky, S. J.* 2838
Christmann, U., see *Vilar, R.* 366
Ciechanover, A., Intracellular Protein Degradation: From a Vague Idea, through the Lysosome and the Ubiquitin–Proteasome System, and onto Human Diseases and Drug Targeting (Nobel Lecture) 5944
Cohen, Y., *Avram, L.*, and *Frish, L.*, Diffusion NMR Spectroscopy in Supramolecular and Combinatorial Chemistry: An Old Parameter—New Insights 520
Cölfen, H. and *Antonietti, M.*, Mesocrystals: Inorganic Superstructures Made by Highly Parallel Crystallization and Controlled Alignment 5576
Conroy, K. D., see *Piers, W. E.* 5016
Drahl, C., ***Cravatt, B. F.***, and *Sorensen, E. J.*, Protein-Reactive Natural Products 5788
Rivkin, A., *Chou, T.-C.*, and ***Danishefsky, S. J.***, On the Remarkable Antitumor Properties of Fludelone: How We Got There 2838
Denmark, S. E., *Heemstra, Jr., J. R.*, and *Beutner, G. L.*, Catalytic, Enantioselective, Vinylogous Aldol Reactions 4682
Diederich, F., see *Müller, K.* 1788
Drahl, C., see *Cravatt, B. F.* 5788
Dubbaka, S. R., see *Vogel, P.* 7674
Dunitz, J. D., see *Gavezzotti, A.* 1766
Durón, S. G., see *Wong, C.-H.* 192
Dwars, T., see *Oehme, G.* 7174
Enders, D., *Voith, M.*, and *Lenzen, A.*, The Dihydroxyacetone Unit—A Versatile C_3 Building Block in Organic Synthesis 1304
Klemm, D., *Heublein, B.*, ***Fink, H.-P.***, and *Bohn, A.*, Cellulose: Fascinating Biopolymer and Sustainable Raw Material 3358
Franck, E. U., see *Weingärtner, H.* 2672
Frederiksen, M. U., see *Trost, B. M.* 6630
Frisch, A. C., see *Beller, M.* 674
Frish, L., see *Cohen, Y.* 520
Futatsugi, K., see *Yamamoto, Hisashi* 1924
Garneau-Tsodikova, S., see *Walsh, C. T.* 7342
Garner, J., see *Breuning, M.* 5384
Gatto, Jr., G. J., see *Walsh, C. T.* 7342
Dunitz, J. D. and ***Gavezzotti, A.***, Molecular Recognition in Organic Crystals: Directed Intermolecular Bonds or Nonlocalized Bonding? 1766
Biel, M., *Wascholowski, V.*, and ***Giannis, A.***, Epigenetics—An Epicenter of Gene Regulation: Histones and Histone-Modifying Enzymes 3186
Gibson, S. E. and *Mainolfi, N.*, The Intermolecular Pauson–Khand Reaction 3022
Gil, C., see *Bräse, S.* 5188
Gossage, R. A., see *van Koten, G.* 1448
Gresser, M. J., see *Breuning, M.* 5384
Grimsdale, A. C., see *Müllen, K.* 5592
Groves, J. T., Molecular Organization and Signal Transduction at Intermembrane Junctions 3524
Gu, Z., see *Ma, S.* 7512
Guldi, D. M., see *Martín, N.* 5374
Yin, H. and ***Hamilton, A. D.***, Strategies for Targeting Protein–Protein Interactions With Synthetic Agents 4130
Heemstra, Jr., J. R., see *Denmark, S. E.* 4682
Hershko, A., The Ubiquitin System for Protein Degradation and Some of Its Roles in the Control of the Cell-Division Cycle (Nobel Lecture) 5932
Heublein, B., see *Fink, H.-P.* 3358
Shimizu, M. and ***Hiyama, T.***, Modern Synthetic Methods for Fluorine-Substituted Target Molecules 214

 © 2005 Wiley-VCH Verlag GmbH & Co. KGaA, Weinheim DOI: 10.1002/anie.200512345

Lagona, J., Mukhopadhyay, P., Chakrabarti, S., and ***Isaacs, L.***, The Cucurbit[*n*]uril Family 4844
Janey, J. M., Recent Advances in Catalytic, Enantioselective α Aminations and α Oxygenations of Carbonyl Compounds 4292
Jastrzebski, J. T. B. H., see *van Koten, G.* 1448
Jeitschko, W., see *Pöttgen, R.* 6996
Vedejs, E. and ***Jure, M.***, Efficiency in Nonenzymatic Kinetic Resolution 3974
Kanatzidis, M. G., see *Pöttgen, R.* 6996
Katz, T. J., Olefin Metatheses and Related Reactions Initiated by Carbene Derivatives of Metals in Low Oxidation States 3010
Kaufman, T. S. and *Rúveda, E. A.,* The Quest for Quinine: Those Who Won the Battles and Those Who Won the War 854
Keller, P. A., see *Breuning, M.* 5384
Klemm, D., see *Fink, H.-P.* 3358
Knepper, K., see *Bräse, S.* 5188
Sugiura, M. and ***Kobayashi, Shū***, *N*-Acylhydrazones as Versatile Electrophiles for the Synthesis of Nitrogen-Containing Compounds 5176
Kötz, R., see *Wokaun, A.* 2190
Krauth-Siegel, R. L., see *Schirmer, R. H.* 690
Kühne, R., see *Oschkinat, H.* 2852
Lagona, J., see *Isaacs, L.* 4844
Lauterbur, P. C., All Science Is Interdisciplinary—From Magnetic Moments to Molecules to Men (Nobel Lecture) 1004
Lenzen, A., see *Enders, D.* 1304
Lewis, D. W., see *Thomas, J. M.* 6456
Lu, F., see *Astruc, D.* 7852
Lukin, O., see *Vögtle, F.* 1456
Nayak, S. and ***Lyon, L. A.***, Soft Nanotechnology with Soft Nanoparticles 7686
Ma, S. and *Gu, Z.,* 1,4-Migration of Rhodium and Palladium in Catalytic Organometallic Reactions .. 7512
Mainolfi, N., see *Gibson, S. E.* 3022
Sánchez, L., ***Martín, N.***, and *Guldi, D. M.,* Hydrogen-Bonding Motifs in Fullerene Chemistry 5374
Strerath, M. and ***Marx, A.***, Genotyping—From Genomic DNA to Genotype in a Single Tube 7842
Meier, H., Conjugated Oligomers with Terminal Donor–Acceptor Substitution 2482
Mukhopadhyay, P., see *Isaacs, L.* 4844
Grimsdale, A. C. and ***Müllen, K.***, The Chemistry of Organic Nanomaterials 5592
Paulini, R., ***Müller, K.***, and *Diederich, F.,* Orthogonal Multipolar Interactions in Structural Chemistry and Biology 1788
Bode, H. B. and ***Müller, Rolf***, The Impact of Bacterial Genomics on Natural Product Research 6828
Nayak, S., see *Lyon, L. A.* 7686
Nicolaou, K. C., *Bulger, P. G.,* and *Sarlah, D.,* Metathesis Reactions in Total Synthesis 4490
Nicolaou, K. C., *Bulger, P. G.,* and *Sarlah, D.,* Palladium-Catalyzed Cross-Coupling Reactions in Total Synthesis 4442
Nicolaou, K. C. and *Snyder, S. A.,* Chasing Molecules That Were Never There: Misassigned Natural Products and the Role of Chemical Synthesis in Modern Structure Elucidation 1012
Nyffeler, P. T., see *Wong, C.-H.* 192
Dwars, T., Paetzold, E., and ***Oehme, G.***, Reactions in Micellar Systems 7174
Onclin, S., see *Ravoo, B. J.* 6282
Ball, L. J., Kühne, R., Schneider-Mergener, J., and ***Oschkinat, H.***, Recognition of Proline-Rich Motifs by Protein–Protein-Interaction Domains 2852
Paetzold, E., see *Oehme, G.* 7174
Paulini, R., see *Müller, K.* 1788
Piers, W. E., *Bourke, S. C.,* and *Conroy, K. D.,* Borinium, Borenium, and Boronium Ions: Synthesis, Reactivity, and Applications 5016
Poppe, L., see *Rétey, J.* 3668
Pöschl, U., Atmospheric Aerosols: Composition, Transformation, Climate and Health Effects 7520
Kanatzidis, M. G., ***Pöttgen, R.***, and *Jeitschko, W.,* The Metal Flux: A Preparative Tool for the Exploration of Intermetallic Compounds 6996
Price Mortimer, A. J., see *Breuning, M.* 5384
Raimondi, F., see *Wokaun, A.* 2190
Raja, R., see *Thomas, J. M.* 6456
Ramón, D. J., see *Yus, M.* 1602
Onclin, S., ***Ravoo, B. J.***, and *Reinhoudt, D. N.,* Engineering Silicon Oxide Surfaces Using Self-Assembled Monolayers 6282
Rebek, Jr., J., Simultaneous Encapsulation: Molecules Held at Close Range 2068
Reinhoudt, D. N., see *Ravoo, B. J.* 6282
Poppe, L. and ***Rétey, J.***, Friedel–Crafts-Type Mechanism for the Enzymatic Elimination of Ammonia from Histidine and Phenylalanine 3668
Rivkin, A., see *Danishefsky, S. J.* 2838
Rose, I., Ubiquitin at Fox Chase (Nobel Lecture) ... 5926
Rowsell, J. L. C., see *Yaghi, O. M.* 4670
Rudd, M. T., see *Trost, B. M.* 6630
Rúveda, E. A., see *Kaufman, T. S.* 854
Samorì, B. and *Zuccheri, G.,* DNA Codes for Nanoscience 1166
Sánchez, L., see *Martín, N.* 5374
Sarlah, D., see *Nicolaou, K. C.* 4442, 4490
Tinnefeld, P. and ***Sauer, M.***, Branching Out of Single-Molecule Fluorescence Spectroscopy: Challenges for Chemistry and Influence on Biology 2642
Scherer, G. G., see *Wokaun, A.* 2190
Krauth-Siegel, R. L., Bauer, H., and ***Schirmer, R. H.***, Dithiol Proteins as Guardians of the Intracellular Redox Milieu in Parasites: Old and New Drug Targets in Trypanosomes and Malaria-Causing Plasmodia 690
Schlosser, M., The 2 × 3 Toolbox of Organometallic Methods for Regiochemically Exhaustive Functionalization 376
Schneider-Mergener, J., see *Oschkinat, H.* 2852

 © 2005 Wiley-VCH Verlag GmbH & Co. KGaA, Weinheim

Wang, Lei and ***Schultz, P. G.***, Expanding the Genetic Code 34
Böhme, D. K. and ***Schwarz, H.***, Gas-Phase Catalysis by Atomic and Cluster Metal Ions: The Ultimate Single-Site Catalysts 2336
Shimizu, M., see *Hiyama, T.* 214
Snyder, S. A., see *Nicolaou, K. C.* 1012
Sorensen, E. J., see *Cravatt, B. F.* 5788
Strerath, M., see *Marx, A.* 7842
Sugiura, M., see *Kobayashi, Shū* 5176
Thomas, J. M., *Raja, R.*, and *Lewis, D. W.*, Single-Site Heterogeneous Catalysts 6456
Tinnefeld, P., see *Sauer, M.* 2642
Trost, B. M., *Frederiksen, M. U.*, and *Rudd, M. T.*, Ruthenium-Catalyzed Reactions—A Treasure Trove of Atom-Economic Transformations 6630
Gossage, R. A., *Jastrzebski, J. T. B. H.*, and ***van Koten, G.***, Hetero-Aggregate Compounds of Aryl and Alkyl Lithium Reagents: A Structurally Intriguing Aspect of Organolithium Chemistry 1448
Vedejs, E., see *Jure, M.* 3974
Christmann, U. and ***Vilar, R.***, Monoligated Palladium Species as Catalysts in Cross-Coupling Reactions . 366
Vincent, S. P., see *Wong, C.-H.* 192
Dubbaka, S. R. and ***Vogel, P.***, Organosulfur Compounds: Electrophilic Reagents in Transition-Metal-Catalyzed Carbon–Carbon Bond-Forming Reactions 7674
Lukin, O. and ***Vögtle, F.***, Knotting and Threading of Molecules: Chemistry and Chirality of Molecular Knots and Their Assemblies 1456
Voith, M., see *Enders, D.* 1304
Bialy, L. and ***Waldmann, H.***, Inhibitors of Protein Tyrosine Phosphatases: Next-Generation Drugs? .. 3814
Walsh, C. T., *Garneau-Tsodikova, S.*, and *Gatto, Jr., G. J.*, Protein Posttranslational Modifications: The Chemistry of Proteome Diversifications 7342
Wang, Lei, see *Schultz, P. G.* 34
Wascholowski, V., see *Giannis, A.* 3186
Weingärtner, H. and *Franck, E. U.*, Supercritical Water as a Solvent 2672
Wirth, T., Hypervalent Iodine Chemistry in Synthesis: Scope and New Directions 3656
Raimondi, F., Scherer, G. G., Kötz, R., and ***Wokaun, A.***, Nanoparticles in Energy Technology: Examples from Electrochemistry and Catalysis 2190
Nyffeler, P. T., Durón, S. G., Burkart, M. D., Vincent, S. P., and ***Wong, C.-H.***, Selectfluor: Mechanistic Insight and Applications 192
Rowsell, J. L. C. and ***Yaghi, O. M.***, Strategies for Hydrogen Storage in Metal–Organic Frameworks ... 4670
Yamamoto, Hisashi and *Futatsugi, K.*, "Designer Acids": Combined Acid Catalysis for Asymmetric Synthesis 1924
Yin, H., see *Hamilton, A. D.* 4130
Ramón, D. J. and ***Yus, M.***, Asymmetric Multicomponent Reactions (AMCRs): The New Frontier 1602
Zimmermann, V., see *Bräse, S.* 5188
Zuccheri, G., see *Samorì, B.* 1166

Essays

de Meijere, A., Adolf von Baeyer: Winner of the Nobel Prize for Chemistry 1905 7836
Greim, H., Chemicals with Endocrine-Disrupting Potential: A Threat to Human Health? 5568
Labinger, J. A., see *Weininger, S. J.* 1916
Olah, G. A., Beyond Oil and Gas: The Methanol Economy 2636
Tidwell, T. T., The First Century of Ketenes (1905–2005): The Birth of a Versatile Family of Reactive Intermediates 5778
Vaupel, E., Arthur Eichengrün—Tribute to a Forgotten Chemist, Entrepreneur, and German Jew .. 3344
Labinger, J. A. and ***Weininger, S. J.***, Controversy in Chemistry: How Do You Prove a Negative?—The Cases of Phlogiston and Cold Fusion 1916

 © 2005 Wiley-VCH Verlag GmbH & Co. KGaA, Weinheim

Highlights

Adolfsson, H., Organocatalytic Hydride Transfers: A New Concept in Asymmetric Hydrogenations 3340
Albrecht, M., Artificial Molecular Double-Stranded Helices 6448
Albrecht-Schmitt, T. E., Actinide Materials Adopt Curvature: Nanotubules and Nanospheres 4836
Balbo Block, M. A., see *Hecht, S.* 6986
Belder, D., Microfluidics with Droplets 3521
Berg, T., Cellular Profiling of Small-Molecule Bioactivities: an Alternative Tool for Chemical Biology 5008
Binder, W. H., Supramolecular Assembly of Nanoparticles at Liquid–Liquid Interfaces 5172
Bolm, C., *Rantanen, T., Schiffers, I.*, and *Zani, L.*, Protonated Chiral Catalysts: Versatile Tools for Asymmetric Synthesis 1758
Braun, T., Oxidative Addition of NH_3 to a Transition-Metal Complex: A Key Step for the Metal-Mediated Derivatization of Ammonia? 5012
Brown, R. C. D., Developments in Furan Syntheses 850
Perepichka, D. F. and ***Bryce, M. R.***, Molecules with Exceptionally Small HOMO–LUMO Gaps 5370
Burley, G. A., Trannulenes with "In-Plane" Aromaticity: Candidates for Harvesting Light Energy 3176
Cardona, F., see *Goti, A.* 7832
Christmann, M., New Developments in the Asymmetric Stetter Reaction 2632
Coppens, P., Charge Densities Come of Age 6810
Crutchley, R. J., Charge-Transfer Isomers and Mixed-Valence Properties 6452
Davies, H. M. L. and *Long, M. S.*, Recent Advances in Catalytic Intramolecular C–H Aminations 3518
De Vos, D. E. and *Sels, B. F.*, Gold Redox Catalysis for Selective Oxidation of Methane to Methanol 30
Dei, A., Photomagnetic Effects in Polycyanometalate Compounds: An Intriguing Future Chemically Based Technology? 1160
Dyson, P. J., see *McIndoe, J. S.* 5772
Eames, J. and *Suggate, M. J.*, Recent Developments in the Transfer of Chirality within Enolate Alkylation Reactions 186
Echavarren, A. M., Couplings with Monoorganotin Compounds: A "Radical" Twist from the Original Stille Reaction 3962
Engels, J. W., Gene Synthesis on Microchips 7166
Escolano, C., Stephacidin B, The Avrainvillamide Dimer: A Formidable Synthetic Challenge 7670
Eychmüller, A., Aerogels from Semiconductor Nanomaterials 4839
Fehlner, T. P., Borane Mimics of C_1–M_m Organometallic Complexes 2056
Gehring, T., see *Podlech, J.* 5776
Cardona, F. and ***Goti, A.***, The Discovery of Novel Metal-Induced Reactions of Nitrones: Not Only Electrophiles and Reagents for [3+2] Cycloadditions 7832
Gschwind, R. M., Residual Dipolar Couplings—A Valuable NMR Parameter for Small Organic Molecules 4666
Hashmi, A. S. K., The Catalysis Gold Rush: New Claims 6990
Balbo Block, M. A. and ***Hecht, S.***, Wrapping Peptide Tubes: Merging Biological Self-Assembly and Polymer Synthesis 6986
Heinz, D. W., see *Höfle, G.* 1298
Schnepf, A. and ***Himmel, H.-J.***, Subvalent Compounds Featuring Direct Metal–Metal Bonds: The Zn–Zn Bond in $[Cp^*_2Zn_2]$ 3006
Niess, B. and ***Hoffmann, H. M. R.***, [4+3] Cycloadducts from Lewis Acid Mediated Reactions of Acroleins with Cyclopentadiene 26
Hoffmann, R. W., Redox Catalysts for Reduction with Base Metals 6277
Heinz, D. W., Schubert, W.-D., and ***Höfle, G.***, Much Anticipated—The Bioactive Conformation of Epothilone and Its Binding to Tubulin 1298
Höger, S., Shape-Persistent Phenylene-Acetylene Macrocycles: Large Rings—Low Yield? 3806
Kaper, H., see *Smarsly, B.* 3809
Kawase, T., Allenophane and Allenoacetylenic Macrocycles: A New Class of Chiral Cyclophanes 7334
Kazmaier, U., Amino Acids—Valuable Organocatalysts in Carbohydrate Synthesis 2186
Kelly, T. R., Molecular Motors: Synthetic DNA-Based Walkers Inspired by Kinesin 4124
Kirmse, W., Incarcerated Carbenes 2476
Kräutler, B., A High-Precision Switch on an RNA Message 4288
Lambert, C., Hexaarylbenzenes—Prospects for Toroidal Delocalization of Charge and Energy 7337
Larsen, T., see *Link, A.* 4432
Larsen, T. and ***Link, A.***, A Timely Reassessment of Early Prediction in the Bioavailability of Orally Administered Drugs 4432
Long, M. S., see *Davies, H. M. L.* 3518
Lovrinovic, M., see *Niemeyer, C. M.* 3179
Luckhurst, G. R., V-Shaped Molecules: New Contenders for the Biaxial Nematic Phase 2834
Lützen, A., Self-Assembled Molecular Capsules—Even More Than Nano-Sized Reaction Vessels 1000
Dyson, P. J. and ***McIndoe, J. S.***, Hydrogen Sponge? A Heteronuclear Cluster That Absorbs Large Quantities of Hydrogen 5772
Mehl, G. H., Quasi-Periodic Organization in Soft Self-Assembling Matter 672
Müller, Michael, Chemoenzymatic Synthesis of Building Blocks for Statin Side Chains 362
Muñiz, K., Bifunctional Metal–Ligand Catalysis: Hydrogenations and New Reactions within the Metal–(Di)amine Scaffold 6622
Nájera, C., see *Sansano, J. M.* 6272

 DOI: 10.1002/anie.200512345 © 2005 Wiley-VCH Verlag GmbH & Co. KGaA, Weinheim

1298

Lovrinovic, M. and ***Niemeyer, C. M.***, DNA Microarrays as Decoding Tools in Combinatorial Chemistry and Chemical Biology 3179
Niess, B., see *Hoffmann, H. M. R.* 26
Oestreich, M., Strategies for Catalytic Asymmetric Electrophilic α Halogenation of Carbonyl Compounds 2324
Oriol, L., see *Serrano, J. L.* 6618
Yorimitsu (Kyoto), H. and ***Oshima, K.***, Recent Progress in Asymmetric Allylic Substitutions Catalyzed by Chiral Copper Complexes 4435
Perepichka, D. F., see *Bryce, M. R.* 5370
Podlech, J. and *Gehring, T.*, New Aspects of Soai's Asymmetric Autocatalysis 5776
Rantanen, T., see *Bolm, C.* 1758
Rissanen, K., Very Large Container Molecules 3652
Ruben, M., Squaring the Interface: "Surface-Assisted" Coordination Chemistry 1594
Nájera, C. and ***Sansano, J. M.***, Catalytic Enantioselective 1,3-Dipolar Cycloaddition Reaction of Azomethine Ylides and Alkenes: The Direct Strategy To Prepare Enantioenriched Highly Substituted Proline Derivatives 6272
Schiffers, I., see *Bolm, C.* 1758
Schnepf, A., see *Himmel, H.-J.* 3006
Schrader, W., Atmosphere, a Chemical Reactor—Formation Pathways of Secondary Organic Aerosols . 1444
Schubert, W.-D., see *Höfle, G.* .....
Sels, B. F., see *De Vos, D. E.* 30
Oriol, L. and ***Serrano, J. L.***, Metal-Containing Nanostructured Materials through In Situ Polymerization of Reactive Metallomesogens 6618
Smarsly, B. and *Kaper, H.*, Liquid Inorganic–Organic Nanocomposites: Novel Electrolytes and Ferrofluids 3809
Suggate, M. J., see *Eames, J.* 186
Thomas, J. M., A Revolution in Electron Microscopy 5563
Tidwell, T. T., Catalytic Asymmetric Esterification of Ketenes 6812
Wallace, D. J., Relay Ring-Closing Metathesis—A Strategy for Achieving Reactivity and Selectivity in Metathesis Chemistry 1912
Weidenbruch, M., Molecules with a Genuine Si–Si Triple Bond and a Stable Derivative of $[SiH]^+$ 514
Wendt, K. U., Enzyme Mechanisms for Triterpene Cyclization: New Pieces of the Puzzle 3966
Wenthold, P. G., Toward the Systematic Decomposition of Benzene 7170
Woodward, S., Organocopper for the Craftsman Cunning at His Trade 5560
Yorimitsu (Kyoto), H., see *Oshima, K.* 4435
Zani, L., see *Bolm, C.* 1758
Zeitler, K., Extending Mechanistic Routes in Heterazolium Catalysis–Promising Concepts for Versatile Synthetic Methods 7506

 © 2005 Wiley-VCH Verlag GmbH & Co. KGaA, Weinheim

Book and Website Reviews

For book reviews authors/editors, book titles, and reviewers are given, for website reviews subjects and reviewers.

Books

Autobiography/Biography

Stoltzenberg, D.	Fritz Haber: Chemist, Nobel Laureate, German, Jew	Friedrich, B.	3957
Hargittai, I.	Our Lives	Schroth, W.	5169
Büttner, J.	The Life and Work of Friedrich Wöhler (1800–1882)	Hopf, H.	5168

Encyclopedia/Handbook/Reference Book

Enghag, P.	Encyclopedia of the Elements	Fink, G.	3174
Blümich, B.	Essential NMR	Lützen, A.	6445
Hartmann, R. K., Bindereif, A., Schön, A., Westhof, E.	Handbook of RNA Biochemistry	Saenger, W.	5367

Industrial Chemistry

Lawrence, S. A.	Amines	North, M.	2053
Sundmacher, K., Kienle, A., Seidel-Morgenstern, A.	Integrated Chemical Processes	Cornils, B.	6807
Larsen, R. D.	Organometallics in Process Chemistry	Bröring, M.	360
Hawthorne, F.	The Merck Druggernaut	Kleemann, A.	4834

Monograph/Research Report in Analytical Chemistry

Kellner, R., Mermet, J.-M., Otto, M., Valcárel, M., Widmer, H. M.	Analytical Chemistry	Bettmer, J.	4286
Duer, M. J.	Introduction to Solid-State NMR Spectroscopy	Baldus, M.	2473
Noble, R. D., Terry, P. A.	Principles of Chemical Separations with Environmental Applications	Frimmel, F. H.	183
Kambhampati, D.	Protein Microarray Technology	Eppinger, J.	5770

Monograph/Research Report in Biochemistry/Bioorganic Chemistry

Breslow, R.	Artificial Enzymes	Meldal, M.	7829
Buchholz, K., Kasche, V., Bornscheuer, U. T.	Biocatalysts and Enzyme Technology	May, O.	5367
Niemeyer, C. M.	Bioconjugation Protocols	Kraatz, H.-B.	847
Walz, D., Teissié, J., Milazzo, G.	Bioelectrochemistry of Membranes	Terrettaz, S.	1590
Bäuerlein, E.	Biomineralization	Weiner, S.	4833
Kubinyi, H., Müller, G.	Chemogenomics in Drug Discovery	Börjesson, U.	2832
Oprea, T. I.	Chemoinformatics in Drug Discovery	Engel, T.	7163
Copeland, R. A.	Evaluation of Enzyme Inhibitors in Drug Discovery	Breinbauer, R.	6445
Brakmann, S., Schwienhorst, A.	Evolutionary Methods in Biotechnology	Budisa, N.	3649
Nierhaus, K. H., Wilson, D. N.	Protein Synthesis and Ribosome Structure	Sprinzl, M.	2182
Schepers, U.	RNA Interference in Practice	Polacek, N.	3003
Choi, S.-K.	Synthetic Multivalent Molecules	Rojo, J.	2629
Nursten, H.	The Maillard Reaction	Steinhart, H.	7503

Monograph/Research Report in Inorganic Chemistry

Karlin, K. D., Stiefel, E. I.	Dithiolene Chemistry	Leigh, G. J.	23

Monograph/Research Report in Materials Science

Elias, H.-G.	An Introduction to Plastics	Voit, B.	848
Tadros, T. F.	Applied Surfactants	Engberts, J. B. F. N.	5922
Teipel, U.	Energetic Materials	Crawford, M.-J., Klapötke, T. M., Welch, J.	1909
Jackson, K. A.	Kinetic Processes	Munoz, A. G.	1756
Miller, J. S., Drillon, M.	Magnetism: Molecules to Materials V	Plass, W.	5922
Kumar, C. S. S. R., Hormes, J., Leuschner, C.	Nanofabrication Towards Biomedical Applications	Katz, E.	4429
Roth, S., Carroll, D.	One-Dimensional Metals	Swager, T. M.	2473
Advincula, R. C., Brittain, W. J., Caster, K. C., Rühe, J.	Polymer Brushes	van Hest, J. C. M.	1294

DOI: 10.1002/anie.200512345
© 2005 Wiley-VCH Verlag GmbH & Co. KGaA, Weinheim

Manners, I.	Synthetic Metal-Containing Polymers	Bergbreiter, D.	24
Fecht, H.-J., Werner, M.	The Nano-Micro Interface	Cao, G.	3514

Monograph/Research Report in Organic Chemistry

Diederich, F., Stang, P. J., Tykwinski, R. R.	Acetylene Chemistry	Hirsch, A.	3803
Olah, G. A., Prakash, G. K. S.	Carbocation Chemistry	Lenoir, D.	3003
Rowe, D. J.	Chemistry and Technology of Flavors and Fragrances	Herrmann, A.	3650
Bajorath, J.	Chemoinformatics	Schneider, G.	511
Inoue, Y., Ramamurthy, V.	Chiral Photochemistry	von Zelewsky, A.	3515
Sierra, M. A., de la Torre, M. C.	Dead Ends and Detours	Baran, P. S.	3338
Chambers, R. D.	Fluorine in Organic Chemistry	Prakash, G. K. S.	2322
Gladysz, J. A., Curran, D. P., Horváth, I.	Handbook of Fluorous Chemistry	Haufe, G.	4121
Yamamoto, Hisashi, Oshima, K.	Main Group Metals in Organic Synthesis	Andrews, P.	3173
de Meijere, A., Diederich, F.	Metal-Catalyzed Cross-Coupling Reactions	Glorius, F.	1157
Takahashi, T.	Metallocenes in Regio- and Stereoselective Synthesis	Nishimura, T.	6807
Mahrwald, R.	Modern Aldol Reactions	Breuning, M.	2053
Krause, N., Hashmi, S. K.	Modern Allene Chemistry	Maas, G.	1909
Gleiter, R., Hopf, H.	Modern Cyclophane Chemistry	Bunz, U. H.	5005
Kirsch, P.	Modern Fluoroorganic Chemistry	Prakash, G. K. S.	1439
Bäckvall, J.-E.	Modern Oxidation Methods	Recupero, F.	2321
Evans, P. A.	Modern Rhodium-Catalyzed Organic Reactions	Schmidt, B.	3802
Zhu, J., Bienyamé, H.	Multicomponent Reactions	Nair, V.	5769
Shibasaki, M., Yamamoto, Yoshinori	Multimetallic Catalysts in Organic Synthesis	Kreidler, B.	1295
Fujita, S.	Organic Chemistry of Photography	Tausch, M. W.	2629
Schäfer, H. J.	Organic Electrochemistry	Holze, R.	2832
Kocieński, P. J.	Protecting Groups	Vogel, C.	183
Murahashi, S.-I.	Ruthenium in Organic Synthesis	Tam, W.	6269
Kürti, L., Czako, B.	Strategic Applications of Named Reactions in Organic Synthesis	Waldvogel, S. R.	5005
Griesbeck, A. G., Mattay, J.	Synthetic Organic Photochemistry	Döpp, D.	4120
Kündig, E. P.	Transition Metal Arene π-Complexes in Organic Synthesis and Catalysis	Butenschön, H.	1591
Beller, M., Bolm, C.	Transition Metals for Organic Synthesis	Tsogoeva, S. B.	3337

Monograph/Research Report in Physical/Theoretical Chemistry

Kaupp, M., Bühl, M., Malkin, V. G.	Calculation of NMR and EPR Parameters	Ochsenfeld, C.	359
Wales, D. J.	Energy Landscapes	Heuer, A.	1756

Monograph/Research Report in the History of Science

Buckingham, J.	Chasing the Molecule	Maaß, F.	3002
Ramberg, P. J.	Chemical Structure, Spatial Arrangement	Reggelin, M.	669
Klein, U.	Experiments, Models, Paper Tools	Berson, J. A.	1157
Djerassi, C., Pinner, D.	Newton's Darkness	Kauffman, G. B., Kauffman, L. M.	1440
Archer, M., Haley, C.	The 1702 Chair of Chemistry at Cambridge	Rouvray, D. H.	4663

Monograph/Research Report on Catalysis

Berkessel, A., Gröger, H.	Asymmetric Organocatalysis	Krische, M. J.	4285
Wieckowski, A., Savinova, E. R., Vayenas, C. G.	Catalysis and Electrocatalysis at Nanoparticle Surfaces	Imbihl, R.	359
Hagemeyer, A., Strasser, P., Volpe, A. F., Jr.	High-Throughput Screening in Chemical Catalysis	Markert, C.	2183
Tsuji., J.	Palladium Reagents and Catalysts	Stahl, S. S.	997

Monograph/Research Report on Spectroscopic Methods

Ellis, A., Feher, M., Wright, T.	Electronic and Photoelectron Spectroscopy	Hohlneicher, G.	6983
Quin, L. D., Williams, A. J.	Practical Interpretation of P-31 NMR Spectra and Computer Assisted Structure Verification	Klein, H.-F.	7331

Popular Science Book

Limberg, C.	Books for the (Chemical) Senses	Kraft, P.	6105
Mann, J.	Life Saving Drugs	Prien, O.	6615
Emsley, J.	The Elements of Murder	Jacob, V.	7332

 © 2005 Wiley-VCH Verlag GmbH & Co. KGaA, Weinheim

Text Book

Cooper, A.	Biophysical Chemistry	Kahms, M.	998
Waldmann, H., Janning, P.	Chemical Biology	Breyhan, H., Kolter, T.	511
Chorkendorff, I., Niemantsverdriet, J. W.	Concepts of Modern Catalysis and Kinetics	Sermon, P. A.	2323
Bunker, P. R., Jensen, P.	Fundamentals of Molecular Symmetry	Bettermann, H.	6616
van Leeuwen, P. W. N. M.	Homogeneous Catalysis	Zapf, A.	1295
Jean, Y.	Molecular Orbitals of Transition Metal Complexes	Hey-Hawkins, E.	7163
Levine, R. D.	Molecular Reaction Dynamics	Vasyutinskii, O. S.	4664
Doonan, S.	Nucleic Acids	Cosstick, R.	184
Zaragoza-Dörwald, F.	Side Reactions in Organic Synthesis	Sierra, M. A.	4430

Websites

Literature searches
Wallenwein, R. 1292
Weise, C. 182

History of science
Cintas, P. 3648

Protein structures
Heinz, D. W., Schubert, W.-D. 4428

Pheromones
Schulz, S. 4118

Correspondences

Laurent, S. A.-L., Robert, A., Meunier, B.	Comments on "Highly Antimalaria-Active Artemisinin Derivatives: Biological Activity Does Not Correlate with Chemical Reactivity"s	2060
Rhile, I. J., Mayer, J. M.	Comments on "How Single and Bifurcated Hydrogen Bonds Influence Proton-Migration Rate Constants, Redox, and Electronic Properties of Phenoxyl Radicals"	1598
Haynes, R. K.	Reply to Comments on "Highly Antimalaria-Active Artemisinin Derivatives: Biological Activity Does Not Correlate with Chemical Reactivity"	2064

Obituaries

Hensel, F.	Fluids at High Pressures and Supercritical Temperatures: *Ernst-Ulrich Franck*	1156
Kutzelnigg, W.	Ligand Field Theory: *Hans Bethe*	3800
Burchard, W.	Macromolecules: *Walter Hugo Stockmayer*	1754
Kunz, H.	Nestor of Preparative Organic Chemistry: *Leopold Horner*	7664
Kabalka, G. W.	Organoboranes: *Herbert C. Brown*	1438
Jensen, F., Ogilby, P. R.	Singlet Oxygen: *Christopher S. Foote*	6268

 © 2005 Wiley-VCH Verlag GmbH & Co. KGaA, Weinheim